

PERRY'S CHEMICAL ENGINEERS' HANDBOOK

8TH EDITION



DON W. GREEN
ROBERT H. PERRY

**Perry's
Chemical
Engineers'
Handbook**

ABOUT THE EDITORS

Don W. Green is Deane E. Ackers Distinguished Professor of Chemical and Petroleum Engineering and codirector of the Tertiary Oil Recovery Project at the University of Kansas in Lawrence, Kansas, where he has taught since 1964. He received his doctorate in chemical engineering in 1963 from the University of Oklahoma, where he was Dr. Perry's first doctoral student. Dr. Green has won several teaching awards at the University of Kansas, and he is a Fellow of the American Institute of Chemical Engineers and an Honorary Member of the Society of Petroleum Engineers. He is the author of numerous articles in technical journals.

The late **Robert H. Perry** served as chairman of the Department of Chemical Engineering at the University of Oklahoma and program director for graduate research facilities at the National Science Research Foundation. He was a consultant to various United Nations and other international organizations. From 1973 until his death in 1978, Dr. Perry devoted his time to a study of the cross impact of technologies within the next half century. The subjects under his investigation on a global basis were energy, minerals and metals, transportation and communications, medicine, food production, and the environment.

PERRY'S CHEMICAL ENGINEERS' HANDBOOK

EIGHTH EDITION

McGraw-Hill

New York
Chicago
San Francisco
Lisbon
London
Madrid
Mexico City
Milan
New Delhi
San Juan
Seoul
Singapore
Sydney
Toronto

**Prepared by a staff of specialists
under the editorial direction of**

Editor-in-Chief

Don W. Green

Deane E. Ackers Distinguished Professor of
Chemical and Petroleum Engineering,
University of Kansas

Late Editor

Robert H. Perry

Copyright © 2008, 1997, 1984, 1973, 1963, 1950, 1941, 1934 by The McGraw-Hill Companies, Inc. All rights reserved. Manufactured in the United States of America. Except as permitted under the United States Copyright Act of 1976, no part of this publication may be reproduced or distributed in any form or by any means, or stored in a database or retrieval system, without the prior written permission of the publisher.

0-07-159313-6

The material in this eBook also appears in the print version of this title: 0-07-142294-3.

All trademarks are trademarks of their respective owners. Rather than put a trademark symbol after every occurrence of a trademarked name, we use names in an editorial fashion only, and to the benefit of the trademark owner, with no intention of infringement of the trademark. Where such designations appear in this book, they have been printed with initial caps.

McGraw-Hill eBooks are available at special quantity discounts to use as premiums and sales promotions, or for use in corporate training programs. For more information, please contact George Hoare, Special Sales, at george_hoare@mcgraw-hill.com or (212) 904-4069.

TERMS OF USE

This is a copyrighted work and The McGraw-Hill Companies, Inc. (“McGraw-Hill”) and its licensors reserve all rights in and to the work. Use of this work is subject to these terms. Except as permitted under the Copyright Act of 1976 and the right to store and retrieve one copy of the work, you may not decompile, disassemble, reverse engineer, reproduce, modify, create derivative works based upon, transmit, distribute, disseminate, sell, publish or sublicense the work or any part of it without McGraw-Hill’s prior consent. You may use the work for your own noncommercial and personal use; any other use of the work is strictly prohibited. Your right to use the work may be terminated if you fail to comply with these terms.

THE WORK IS PROVIDED “AS IS.” MCGRAW-HILL AND ITS LICENSORS MAKE NO GUARANTEES OR WARRANTIES AS TO THE ACCURACY, ADEQUACY OR COMPLETENESS OF OR RESULTS TO BE OBTAINED FROM USING THE WORK, INCLUDING ANY INFORMATION THAT CAN BE ACCESSED THROUGH THE WORK VIA HYPERLINK OR OTHERWISE, AND EXPRESSLY DISCLAIM ANY WARRANTY, EXPRESS OR IMPLIED, INCLUDING BUT NOT LIMITED TO IMPLIED WARRANTIES OF MERCHANTABILITY OR FITNESS FOR A PARTICULAR PURPOSE. McGraw-Hill and its licensors do not warrant or guarantee that the functions contained in the work will meet your requirements or that its operation will be uninterrupted or error free. Neither McGraw-Hill nor its licensors shall be liable to you or anyone else for any inaccuracy, error or omission, regardless of cause, in the work or for any damages resulting therefrom. McGraw-Hill has no responsibility for the content of any information accessed through the work. Under no circumstances shall McGraw-Hill and/or its licensors be liable for any indirect, incidental, special, punitive, consequential or similar damages that result from the use of or inability to use the work, even if any of them has been advised of the possibility of such damages. This limitation of liability shall apply to any claim or cause whatsoever whether such claim or cause arises in contract, tort or otherwise.

DOI: 10.1036/0071422943



Professional



Want to learn more?

We hope you enjoy this McGraw-Hill eBook! If you'd like more information about this book, its author, or related books and websites, please [click here](#).

Contents

For the detailed contents of any section, consult the title page of that section. See also the alphabetical index in the back of the handbook.

	Section
Conversion Factors and Mathematical Symbols <i>James O. Maloney</i>	1
Physical and Chemical Data <i>Bruce E. Poling, George H. Thomson, Daniel G. Friend, Richard L. Rowley, W. Vincent Wilding</i>	2
Mathematics <i>Bruce A. Finlayson, Lorenz T. Biegler</i>	3
Thermodynamics <i>Hendrick C. Van Ness, Michael M. Abbott</i>	4
Heat and Mass Transfer <i>Hoyt C. Hottel, James J. Noble, Adel F. Sarofim, Geoffrey D. Silcox, Phillip C. Wankat, Kent S. Knaebel</i>	5
Fluid and Particle Dynamics <i>James N. Tilton</i>	6
Reaction Kinetics <i>Tiberiu M. Leib, Carmo J. Pereira</i>	7
Process Control <i>Thomas F. Edgar, Cecil L. Smith, F. Greg Shinskey, George W. Gassman, Andrew W. R. Waite, Thomas J. McAvoy, Dale E. Seborg</i>	8
Process Economics <i>James R. Couper, Darryl W. Hertz, (Francis) Lee Smith</i>	9
Transport and Storage of Fluids <i>Meherwan P. Boyce, Victor H. Edwards, Terry W. Cowley, Timothy Fan, Hugh D. Kaiser, Wayne B. Geyer, David Nadel, Larry Skoda, Shawn Testone, Kenneth L. Walter</i>	10
Heat-Transfer Equipment <i>Richard L. Shilling, Patrick M. Bernhagen, Victor M. Goldschmidt, Predrag S. Hrnjak, David Johnson, Klaus D. Timmerhaus</i>	11
Psychrometry, Evaporative Cooling, and Solids Drying <i>Larry R. Genskow, Wayne E. Beimesch, John P. Hecht, Ian C. Kemp, Tim Langrish, Christian Schwartzbach, (Francis) Lee Smith</i>	12
Distillation <i>M. F. Doherty, Z. T. Fidkowski, M. F. Malone, R. Taylor</i>	13
Equipment for Distillation, Gas Absorption, Phase Dispersion, and Phase Separation <i>Henry Z. Kister, Paul M. Mathias, D. E. Steinmeyer, W. R. Penney, B. B. Crocker, James R. Fair</i>	14
Liquid-Liquid Extraction and Other Liquid-Liquid Operations and Equipment <i>Timothy C. Frank, Lise Dahuron, Bruce S. Holden, William D. Prince, A. Frank Seibert, Loren C. Wilson</i>	15
Adsorption and Ion Exchange <i>M. Douglas LeVan, Giorgio Carta</i>	16
Gas-Solid Operations and Equipment <i>Mel Pell, James B. Dunson, Ted M. Knowlton</i>	17

vi CONTENTS

Liquid-Solid Operations and Equipment	Wayne J. Genck, David S. Dickey, Frank A. Baczek, Daniel C. Bedell, Kent Brown, Wu Chen, Daniel E. Ellis, Peter Harriott, Tim J. Laros, Wenping Li, James K. McGillicuddy, Terence P. McNulty, James Y. Oldshue, Fred Schoenbrunn, Julian C. Smith, Donald C. Taylor, Daniel R. Wells, Todd W. Wisdom	18
Reactors	Carmo J. Pereira, Tiberiu M. Leib	19
Alternative Separation Processes	Michael E. Prudich, Huanlin Chen, Tingyue Gu, Ram B. Gupta, Keith P. Johnston, Herb Lutz, Guanghui Ma, Zhiguo Su	20
Solid-Solid Operations and Processing	Bryan J. Ennis, Wolfgang Witt, Ralf Weinekötter, Douglas Sphar, Erik Gommeran, Richard H. Snow, Terry Allen, Grantges J. Raymus, James D. Litster	21
Waste Management	Louis Theodore, Kenneth N. Weiss, John D. McKenna, (Francis) Lee Smith, Robert R. Sharp, Joseph J. Santoleri, Thomas F. McGowan	22
Process Safety	Daniel A. Crowl, Laurence G. Britton, Walter L. Frank, Stanley Grossel, Dennis Hendershot, W. G. High, Robert W. Johnson, Trevor A. Kletz, Joseph C. Leung, David A. Moore, Robert Ormsby, Jack E. Owens, Richard W. Prugh, Carl A. Schiappa Richard Siwek, Thomas O. Spicer III, Angela Summers, Ronald Willey, John L. Woodward	23
Energy Resources, Conversion, and Utilization	Walter F. Podolski, David K. Schmalzer, Vincent Conrad, Douglas E. Lowenhaupt, Richard A. Winschel, Edgar B. Klunder, Howard G. McIlvried III, Massood Ramezan, Gary J. Stiegel, Rameshwar D. Srivastava, John Winslow, Peter J. Loftus, Charles E. Benson, John M. Wheeldon, Michael Krumpelt, (Francis) Lee Smith	24
Materials of Construction	Oliver W. Siebert, Kevin M. Brooks, Laurence J. Craigie, F. Galen Hodge, L. Theodore Hutton, Thomas M. Laronge, J. Ian Munro, Daniel H. Pope, Simon J. Scott, John G. Stoecker II	25

Index follows Section 25

Contributors

- Michael M. Abbott, Ph.D.** *Deceased; Professor Emeritus, Howard P. Isermann Department of Chemical and Biological Engineering, Rensselaer Polytechnic Institute (Sec. 4, Thermodynamics)*
- Terry Allen, Ph.D.** *Senior Research Associate (retired), DuPont Central Research and Development (Sec. 21, Solid-Solid Operations and Processing)*
- Frank A. Baczek, B.S.Ch.E.&Chem.** *Manager, Paste and Sedimentation Technology, Dorr-Oliver EIMCO (Sec. 18, Liquid-Solid Operations and Equipment)*
- Daniel C. Bedell, B.S.Ch.E.** *Global Market Manager E-CAT & Sedimentation, Dorr-Oliver EIMCO (Sec. 18, Liquid-Solid Operations and Equipment)*
- Wayne E. Beimesch, Ph.D.** *Technical Associate Director, Corporate Engineering, The Procter & Gamble Company (Sec. 12, Psychrometry, Evaporative Cooling, and Solids Drying)*
- Charles E. Benson, M.Eng.** *Principal, ENVIRON International Corp. (Sec. 24, Energy Resources, Conversion, and Utilization)*
- Patrick M. Bernhagen, P.E., B.S.M.E.** *Sales Manager—Fired Heater, Foster Wheeler North America Corp. (Sec. 11, Heat-Transfer Equipment)*
- Lorenz T. Biegler, Ph.D.** *Bayer Professor of Chemical Engineering, Carnegie Mellon University (Sec. 3, Mathematics)*
- Meherwan P. Boyce, Ph.D., P.E.** *Chairman and Principal Consultant, The Boyce Consultancy Group, LLC (Sec. 10, Transport and Storage of Fluids)*
- Laurence G. Britton, Ph.D.** *Process Safety Consultant; Consulting Scientist, Neolytica, Inc. (Sec. 23, Process Safety)*
- Kevin M. Brooks, P.E., B.S.Ch.E.** *Vice President Engineering and Construction, Koch Knight LLC (Sec. 25, Materials of Construction)*
- Kent Brown, B.S.Civ.E.** *Sedimentation Product Manager N.A., Dorr-Oliver EIMCO (Sec. 18, Liquid-Solid Operations and Equipment)*
- Giorgio Carta, Ph.D.** *Professor, Department of Chemical Engineering, University of Virginia (Sec. 16, Adsorption and Ion Exchange)*
- Huanlin Chen, M.Sc.** *Professor of Chemical and Biochemical Engineering, Zhejiang University (Sec. 20, Alternative Separation Processes)*

viii CONTRIBUTORS

Wu Chen, Ph.D. *Fluid/Particle Specialist, Dow Chemical Company* (Sec. 18, Liquid-Solid Operations and Equipment)

Vincent Conrad, Ph.D. *Group Leader, Technical Services Development, CONSOL Energy Inc.* (Sec. 24, Energy Resources, Conversion, and Utilization)

James R. Couper, D.Sc. *Professor Emeritus, The Ralph E. Martin Department of Chemical Engineering, University of Arkansas—Fayetteville* (Sec. 9, Process Economics)

Terry W. Cowley, B.S., M.A. *Consultant, DuPont Engineering* (Sec. 10, Transport and Storage of Fluids)

Laurence J. Craigie, B.S.Chem. *Composite Resources, LLC* (Sec. 25, Materials of Construction)

B. B. Crocker, P.E., S.M. *Consulting Chemical Engineer* (Sec. 14, Equipment for Distillation, Gas Absorption, Phase Dispersion, and Phase Separation)

Daniel A. Crowl, Ph.D. *Professor of Chemical Engineering, Michigan Technological University* (Sec. 23, Process Safety)

Lise Dahuron, Ph.D. *Sr. Research Specialist, The Dow Chemical Company* (Sec. 15, Liquid-Liquid Extraction and Other Liquid-Liquid Operations and Equipment)

David S. Dickey, Ph.D. *Senior Consultant, MixTech, Inc.* (Sec. 18, Liquid-Solid Operations and Equipment)

M. F. Doherty, Ph.D. *Professor of Chemical Engineering, University of California—Santa Barbara* (Sec. 13, Distillation)

James B. Dunson, M.S. *Principal Division Consultant (retired), E. I. duPont de Nemours & Co.* (Sec. 17, Gas-Solid Operations and Equipment)

Thomas F. Edgar, Ph.D. *Professor of Chemical Engineering, University of Texas—Austin* (Sec. 8, Process Control)

Victor H. Edwards, Ph.D., P.E. *Process Director, Aker Kvaerner, Inc.* (Sec. 10, Transport and Storage of Fluids)

Daniel E. Ellis, B.S.Ch.E. *Product Manager, Sedimentation Centrifuges and Belt Presses, Krauss Maffei Process Technology, Inc.* (Sec. 18, Liquid-Solid Operations and Equipment)

Bryan J. Ennis, Ph.D. *President, E&G Associates, Inc., and CEO, iPowder Systems, Inc.* (Sec. 21, Solid-Solid Operations and Processing)

James R. Fair, Ph.D., P.E. *Professor of Chemical Engineering, University of Texas* (Sec. 14, Equipment for Distillation, Gas Absorption, Phase Dispersion, and Phase Separation)

Timothy Fan, P.E., M.Sc. *Chief Project Engineer, Foster Wheeler USA* (Sec. 10, Transport and Storage of Fluids)

Z. T. Fidkowski, Ph.D. *Process Engineer, Air Products and Chemicals Inc.* (Sec. 13, Distillation)

Bruce A. Finlayson, Ph.D. *Rehnberg Professor, Department of Chemical Engineering, University of Washington* (Sec. 3, Mathematics)

Timothy C. Frank, Ph.D. *Research Scientist and Sr. Technical Leader, The Dow Chemical Company* (Sec. 15, Liquid-Liquid Extraction and Other Liquid-Liquid Operations and Equipment)

Walter L. Frank, P.E., B.S.Ch.E. *Senior Consultant, ABS Consulting* (Sec. 23, Process Safety)

Daniel G. Friend *National Institute of Standards and Technology* (Sec. 2, Physical and Chemical Data)

George W. Gassman, B.S.M.E. *Senior Research Specialist, Final Control Systems, Fisher Controls International, Inc.* (Sec. 8, Process Control)

Wayne J. Genck, Ph.D. *President, Genck International* (Sec. 18, Liquid-Solid Operations and Equipment)

Larry R. Genskow *Technical Director, Corporate Engineering Technologies, The Procter & Gamble Company* (Sec. 12, Psychrometry, Evaporative Cooling, and Solids Drying)

Wayne B. Geyer, P.E. *Executive Vice President, Steel Tank Institute and Steel Plate Fabricators Association* (Sec. 10, Transport and Storage of Fluids)

Victor M. Goldschmidt, Ph.D., P.E. *Professor Emeritus, Mechanical Engineering, Purdue University* (Sec. 11, Heat-Transfer Equipment)

Erik Gommeran, Dr. sc. techn. *Research Associate, DuPont Central Research and Development* (Sec. 21, Solid-Solid Operations and Processing)

Stanley Grossel, M.S.Ch.E. *President, Process Safety & Design* (Sec. 23, Process Safety)

Tingyue Gu, Ph.D. *Associate Professor of Chemical Engineering, Ohio University* (Sec. 20, Alternative Separation Processes)

Ram B. Gupta, Ph.D. *Alumni (Chair) Professor of Chemical Engineering, Department of Chemical Engineering, Auburn University* (Sec. 20, Alternative Separation Processes)

Peter Harriott, Ph.D. *Professor Emeritus, School of Chemical Engineering, Cornell University* (Sec. 18, Liquid-Solid Operations and Equipment)

John P. Hecht, Ph.D. *Senior Engineer, The Procter & Gamble Company* (Sec. 12, Psychrometry, Evaporative Cooling, and Solids Drying)

Dennis Hendershot, M.S.Ch.E. *Principal Process Safety Specialist, Chilworth Technology, Inc.* (Sec. 23, Process Safety)

Darryl W. Hertz, B.S. *Manager, Front-End Loading and Value-Improving Practices Group, KBR* (Sec. 9, Process Economics)

W. G. High, C.Eng., B.Sc., F.I.Mech.E. *Consultant, Burgoyne Consultants* (Sec. 23, Process Safety)

F. Galen Hodge, Ph.D. (Materials Engineering), P. E. *Associate Director, Materials Technology Institute* (Sec. 25, Materials of Construction)

Bruce S. Holden, M.S. *Process Research Leader, The Dow Chemical Company* (Sec. 15, Liquid-Liquid Extraction and Other Liquid-Liquid Operations and Equipment)

Hoyt C. Hottel, S.M. *Deceased; Professor Emeritus of Chemical Engineering, Massachusetts Institute of Technology* (Sec. 5, Heat and Mass Transfer)

Predrag S. Hrnjak, Ph.D., V.Res. *Assistant Professor, University of Illinois at Urbana-Champaign; Principal Investigator—U of I Air Conditioning and Refrigeration Center; Assistant Professor, University of Belgrade* (Sec. 11, Heat-Transfer Equipment)

L. Theodore Hutton, B.S.Mech.&Ind.Eng. *Senior Business Development Engineer, ARKEMA, Inc.* (Sec. 25, Materials of Construction)

David Johnson, P.E., M.S.C.E. *Heat Exchanger Specialist, A&A Technology, B.P. p.l.c.* (Sec. 11, Heat-Transfer Equipment)

Robert W. Johnson, M.S.Ch.E. *President, Unwin Company* (Sec. 23, Process Safety)

Keith P. Johnston, Ph.D., P.E. *M. C. (Bud) and Mary Beth Baird Endowed Chair and Professor of Chemical Engineering, University of Texas (Austin)* (Sec. 20, Alternative Separation Processes)

Hugh D. Kaiser, P.E., B.S., MBA *Principal Engineer, PB Energy Storage Services, Inc.* (Sec. 10, Transport and Storage of Fluids)

Ian C. Kemp, M.A. (Cantab), C.Eng. *Senior Technical Manager, GlaxoSmithKline* (Sec. 12, Psychrometry, Evaporative Cooling, and Solids Drying)

Henry Z. Kister, M.E., C.Eng., C.Sc. *Senior Fellow and Director of Fractionation Technology, Fluor Corporation* (Sec. 14, Equipment for Distillation, Gas Absorption, Phase Dispersion, and Phase Separation)

x CONTRIBUTORS

Trevor A. Kletz, D.Sc. *Visiting Professor, Department of Chemical Engineering, Loughborough University (U.K.); Adjunct Professor, Department of Chemical Engineering, Texas A&M University (Sec. 23, Process Safety)*

Edgar B. Klunder, Ph.D. *Project Manager, National Energy Technology Laboratory, U.S. Department of Energy (Sec. 24, Energy Resources, Conversion, and Utilization)*

Kent S. Knaebel, Ph.D. *President, Adsorption Research, Inc. (Sec. 5, Heat and Mass Transfer)*

Ted M. Knowlton, Ph.D. *Technical Director, Particulate Solid Research, Inc. (Sec. 17, Gas-Solid Operations and Equipment)*

Michael Krumpelt, Ph.D. *Manager, Fuel Cell Technology, Argonne National Laboratory (Sec. 24, Energy Resources, Conversion, and Utilization)*

Tim Langrish, D.Phil. *School of Chemical and Biomolecular Engineering, The University of Sydney (Australia) (Sec. 12, Psychrometry, Evaporative Cooling, and Solids Drying)*

Thomas M. Laronge, M.S.Phys.Chem. *Director, Thomas M. Laronge, Inc. (Sec. 25, Materials of Construction)*

Tim J. Laros, M.S. *Senior Process Consultant, Dorr-Oliver EIMCO (Sec. 18, Liquid-Solid Operations and Equipment)*

Tiberiu M. Leib, Ph.D. *Principal Consultant, DuPont Engineering Research and Technology, E. I. du Pont de Nemours and Company (Sec. 7, Reaction Kinetics; Sec. 19, Reactors)*

Joseph C. Leung, Ph.D. *President, Leung Inc. (Sec. 23, Process Safety)*

M. Douglas LeVan, Ph.D. *J. Lawrence Wilson Professor of Engineering, Department of Chemical Engineering, Vanderbilt University (Sec. 16, Adsorption and Ion Exchange)*

Wenping Li, Ph.D. *R&D Manager, Agrilectric Research Company (Sec. 18, Liquid-Solid Operations and Equipment)*

James D. Litster, Ph.D. *Professor, Department of Chemical Engineering, University of Queensland (Sec. 21, Solid-Solid Operations and Processing)*

Peter J. Loftus, D.Phil. *Principal, ENVIRON International Corp. (Sec. 24, Energy Resources, Conversion, and Utilization)*

Douglas E. Lowenhaupt, M.S. *Group Leader, Coke Laboratory, CONSOL Energy Inc. (Sec. 24, Energy Resources, Conversion, and Utilization)*

Herb Lutz *Consulting Engineer, Millipore Corporation (Sec. 20, Alternative Separation Processes)*

Guanghui Ma, Ph.D. *Professor, State Key Laboratory of Biochemical Engineering, Institute of Process Engineering, CAS, Beijing, China (Sec. 20, Alternative Separation Processes)*

M. F. Malone, Ph.D. *Professor of Chemical Engineering and Dean of Engineering, University of Massachusetts—Amherst (Sec. 13, Distillation)*

James O. Maloney, Ph.D., P.E. *Emeritus Professor of Chemical Engineering, University of Kansas (Sec. 1, Conversion Factors and Mathematical Symbols)*

Paul M. Mathias, Ph.D. *Technical Director, Fluor Corporation (Sec. 14, Equipment for Distillation, Gas Absorption, Phase Dispersion, and Phase Separation)*

Thomas J. McAvoy, Ph.D. *Professor of Chemical Engineering, University of Maryland—College Park (Sec. 8, Process Control)*

James K. McGillicuddy, B.S.M.E. *Product Manager, Filtration Centrifuges and Filters, Krauss Maffei Process Technology, Inc. (Sec. 18, Liquid-Solid Operations and Equipment)*

Thomas F. McGowan, P.E. *President, TMTS Associates (Sec. 22, Waste Management)*

- Howard G. McIlvried III, Ph.D.** *Consulting Engineer, Science Applications International Corporation, National Energy Technology Laboratory* (Sec. 24, Energy Resources, Conversion, and Utilization)
- John D. McKenna, Ph.D.** *President and Chairman, ETS International, Inc.* (Sec. 22, Waste Management)
- Terence P. McNulty, Ph.D.** *President, T. P. McNulty and Associates, Inc.* (Sec. 18, Liquid-Solid Operations and Equipment)
- David A. Moore, MBA, B.Sc.** *President, AcuTech Consulting Group* (Sec. 23, Process Safety)
- J. Ian Munro, P.E., B.A.Sc.E.E.** *Senior Consultant, Corrosion Probes, Inc.* (Sec. 25, Materials of Construction)
- David Nadel, P.E., M.S.** *Senior Principal Mechanical Engineer, Aker Kvaerner, Inc.* (Sec. 10, Transport and Storage of Fluids)
- James J. Noble, Ph.D., P.E., CE [UK]** *Research Affiliate, Department of Chemical Engineering, Massachusetts Institute of Technology* (Sec. 5, Heat and Mass Transfer)
- James Y. Oldshue, Ph.D.** *Deceased; President, Oldshue Technologies International, Inc.; Adjunct Professor of Chemical Engineering at Beijing Institute of Chemical Technology, Beijing, China* (Sec. 18, Liquid-Solid Operations and Equipment)
- Robert Ormsby, M.S.Ch.E.** *Process Safety Consultant* (Sec. 23, Process Safety)
- Jack E. Owens, B.E.E.** *Electrostatics Consultant, E. I. Dupont de Nemours and Co.* (Sec. 23, Process Safety)
- Mel Pell, Ph.D.** *President, ESD Consulting Services* (Sec. 17, Gas-Solid Operations and Equipment)
- W. R. Penney, Ph.D., P.E.** *Professor of Chemical Engineering, University of Arkansas* (Sec. 14, Equipment for Distillation, Gas Absorption, Phase Dispersion, and Phase Separation)
- Carmo J. Pereira, Ph.D., MBA** *DuPont Fellow, DuPont Engineering Research and Technology, E. I. du Pont de Nemours and Company* (Sec. 7, Reaction Kinetics; Sec. 19, Reactors)
- Walter F. Podolski, Ph.D.** *Chemical Engineer, Electrochemical Technology Program, Argonne National Laboratory* (Sec. 24, Energy Resources, Conversion, and Utilization)
- Bruce E. Poling** *Department of Chemical Engineering, University of Toledo* (Sec. 2, Physical and Chemical Data)
- Daniel H. Pope, Ph.D. (Microbiology)** *President and Owner, Bioindustrial Technologies, Inc.* (Sec. 25, Materials of Construction)
- William D. Prince, M.S.** *Process Engineering Associate, The Dow Chemical Company* (Sec. 15, Liquid-Liquid Extraction and Other Liquid-Liquid Operations and Equipment)
- Michael E. Prudich, Ph.D.** *Professor of Chemical Engineering, Ohio University* (Sec. 20, Alternative Separation Processes)
- Richard W. Prugh, M.S.P.E., C.S.P.** *Senior Process Safety Specialist, Chilworth Technology, Inc.* (Sec. 23, Process Safety)
- Massood Ramezan, Ph.D., P.E.** *Program Manager, Science Applications International Corporation, National Energy Technology Laboratory* (Sec. 24, Energy Resources, Conversion, and Utilization)
- Grantges J. Raymus, M.E., M.S.** *President, Raymus Associates, Inc.; Manager of Packaging Engineering (retired), Union Carbide Corporation* (Sec. 21, Solid-Solid Operations and Processing)
- Richard L. Rowley** *Department of Chemical Engineering, Brigham Young University* (Sec. 2, Physical and Chemical Data)
- Joseph J. Santoleri, P.E.** *Senior Consultant, RMT Inc. & Santoleri Associates* (Sec. 22, Waste Management)

xii CONTRIBUTORS

Adel F. Sarofim, Sc.D. *Presidential Professor of Chemical Engineering, Combustion, and Reactors, University of Utah (Sec. 5, Heat and Mass Transfer)*

Carl A. Schiappa, B.S.Ch.E. *Retired, The Dow Chemical Company (Sec. 23, Process Safety)*

David K. Schmalzer, Ph.D., P.E. *Fossil Energy Program Manager, Argonne National Laboratory (Sec. 24, Energy Resources, Conversion, and Utilization)*

Fred Schoenbrunn, B.S.Ch.E. *Product Manager for Minerals Sedimentation, Dorr-Oliver EIMCO (Sec. 18, Liquid-Solid Operations and Equipment)*

Christian Schwartzbach, M.Sc. *Manager, Technology Development (retired), Niro A/S (Sec. 12, Psychrometry, Evaporative Cooling, and Solids Drying)*

Simon J. Scott, B.S.Ch.E. *President and Principal, Scott & Associates (Sec. 25, Materials of Construction)*

Dale E. Seborg, Ph.D. *Professor of Chemical Engineering, University of California—Santa Barbara (Sec. 8, Process Control)*

A. Frank Seibert, Ph.D., P.E. *Technical Manager, Separations Research Program, The University of Texas at Austin (Sec. 15, Liquid-Liquid Extraction and Other Liquid-Liquid Operations and Equipment)*

Robert R. Sharp, Ph.D., P.E. *Professor of Environmental Engineering, Manhattan College; Environmental Consultant (Sec. 22, Waste Management)*

Richard L. Shilling, P.E., B.S.M., B.E.M.E. *Vice President of Engineering, Koch Heat Transfer Company LP (Sec. 11, Heat-Transfer Equipment)*

F. Greg Shinskey, B.S.Ch.E. *Consultant (retired from Foxboro Co.) (Sec. 8, Process Control)*

Oliver W. Siebert, P.E., B.S.M.E. *Affiliate Professor of Chemical Engineering, Washington University, St. Louis, Mo.; Director, North Central Research Institute; President and Principal, Siebert Materials Engineering, Inc. (Sec. 25, Materials of Construction)*

Geoffrey D. Silcox, Ph.D. *Professor of Chemical Engineering, Combustion, and Reactors, University of Utah (Sec. 5, Heat and Mass Transfer)*

Richard Siwek, M.S. *Managing Director, President, FireEx Consultant Ltd. (Sec. 23, Process Safety)*

Larry Skoda, P.E. *Principal Piping Engineer, Aker Kvaerner, Inc. (Sec. 10, Transport and Storage of Fluids)*

Cecil L. Smith, Ph.D. *Principal, Cecil L. Smith Inc. (Sec. 8, Process Control)*

(Francis) Lee Smith, Ph.D., M.Eng. *Principal, Wilcrest Consulting Associates, Houston, Texas (Sec. 9, Process Economics; Sec. 12, Psychrometry, Evaporative Cooling, and Solids Drying; Sec. 22, Waste Management; Sec. 24, Energy Resources, Conversion, and Utilization)*

Julian C. Smith, B.Chem.&Ch.E. *Professor Emeritus, School of Chemical Engineering, Cornell University (Sec. 18, Liquid-Solid Operations and Equipment)*

Richard H. Snow, Ph.D. *Engineering Advisor, IIT Research Institute (retired) (Sec. 21, Solid-Solid Operations and Processing)*

Douglas Sphar, Ph.D. *Research Associate, DuPont Central Research and Development (Sec. 21, Solid-Solid Operations and Processing)*

Thomas O. Spicer III, Ph.D., P.E. *Professor and Head, Ralph E. Martin Department of Chemical Engineering, University of Arkansas (Sec. 23, Process Safety)*

Rameshwar D. Srivastava, Ph.D. *Principal Engineer, Science Applications International Corporation, National Energy Technology Laboratory (Sec. 24, Energy Resources, Conversion, and Utilization)*

D. E. Steinmeyer, P.E., M.A., M.S. *Distinguished Fellow, Monsanto Company (retired) (Sec. 14, Equipment for Distillation, Gas Absorption, Phase Dispersion, and Phase Separation)*

- Gary J. Stiegel, P.E., M.S.** *Technology Manager, National Energy Technology Laboratory, U.S. Department of Energy (Sec. 24, Energy Resources, Conversion, and Utilization)*
- John G. Stoecker II, B.S.M.E.** *Principal Consultant, Stoecker & Associates (Sec. 25, Materials of Construction)*
- Zhiguo Su, Ph.D.** *Professor and Director, State Key Laboratory of Biochemical Engineering, Institute of Process Engineering, CAS, Beijing, China (Sec. 20, Alternative Separation Processes)*
- Angela Summers, Ph.D., P.E.** *President, SIS-TECH; Adjunct Professor, Department of Environmental Management, University of Houston—Clear Lake (Sec. 23, Process Safety)*
- Donald C. Taylor, B.S.Eng.Geol., M.S.Civ.E.** *Process Manager Industrial Water & Wastewater Technology, Dorr-Oliver EIMCO (Sec. 18, Liquid-Solid Operations and Equipment)*
- R. Taylor, Ph.D.** *Professor of Chemical Engineering, Clarkson University (Sec. 13, Distillation)*
- Shawn Testone** *Product Manager, De Dietrich Process Systems (Sec. 10, Transport and Storage of Fluids)*
- Louis Theodore, Eng.Sc.D.** *Professor of Chemical Engineering, Manhattan College (Sec. 22, Waste Management)*
- George H. Thomson** *AICHE Design Institute for Physical Properties (Sec. 2, Physical and Chemical Data)*
- James N. Tilton, Ph.D., P.E.** *Principal Consultant, Process Engineering, E. I. du Pont de Nemours & Co. (Sec. 6, Fluid and Particle Dynamics)*
- Klaus D. Timmerhaus, Ph.D., P.E.** *Professor and President's Teaching Scholar, University of Colorado (Sec. 11, Heat-Transfer Equipment)*
- Hendrick C. Van Ness, D.Eng.** *Howard P. Isermann Department of Chemical and Biological Engineering, Rensselaer Polytechnic Institute (Sec. 4, Thermodynamics)*
- Andrew W. R. Waite, P.Eng.** *Principal Process Control Consultant, EnTech Control, a Division of Emerson Electric Canada (Sec. 8, Process Control)*
- Kenneth L. Walter, Ph.D.** *Process Manager—Technology, Aker Kvaerner, Inc. (Sec. 10, Transport and Storage of Fluids)*
- Phillip C. Wankat, Ph.D.** *Clifton L. Lovell Distinguished Professor of Chemical Engineering, Purdue University (Sec. 5, Heat and Mass Transfer)*
- Ralf Weinekötter, Dr. sc. techn.** *Managing Director, Gericke AG, Switzerland (Sec. 21, Solid-Solid Operations and Processing)*
- Kenneth N. Weiss, P.E., Diplomate AAEE** *Partner and North American Director of Compliance Assurance, ERM (Sec. 22, Waste Management)*
- Daniel R. Wells, B.S.Ind.E., MBA** *Product Manager Sedimentation Products, Dorr-Oliver EIMCO (Sec. 18, Liquid-Solid Operations and Equipment)*
- John M. Wheeldon, Ph.D.** *Electric Power Research Institute (Sec. 24, Energy Resources, Conversion, and Utilization)*
- W. Vincent Wilding** *Department of Chemical Engineering, Brigham Young University (Sec. 2, Physical and Chemical Data)*
- Ronald Willey, Ph.D., P.E.** *Professor, Department of Chemical Engineering, Northeastern University (Sec. 23, Process Safety)*
- Loren C. Wilson, B.S.** *Sr. Research Specialist, The Dow Chemical Company (Sec. 15, Liquid-Liquid Extraction and Other Liquid-Liquid Operations and Equipment)*
- Richard A. Winschel, B.S.** *Director, Research Services, CONSOL Energy Inc. (Sec. 24, Energy Resources, Conversion, and Utilization)*

xiv CONTRIBUTORS

John Winslow, M.S. *Technology Manager, National Energy Technology Laboratory, U.S. Department of Energy (Sec. 24, Energy Resources, Conversion, and Utilization)*

Todd W. Wisdom, M.S.Ch.E. *Global Filtration Product Manager, Dorr-Oliver EIMCO (Sec. 18, Liquid-Solid Operations and Equipment)*

Wolfgang Witt, Dr. rer. nat. *Technical Director, Sympatec GmbH–System Partikel Technik (Sec. 21, Solid-Solid Operations and Processing)*

John L. Woodward, Ph.D. *Senior Principal Consultant, Baker Engineering and Risk Consultants, Inc. (Sec. 23, Process Safety)*

Preface to the Eighth Edition

Perry's has been an important source of information related to the fundamentals and practice of chemical engineering since it was first published in 1934, with John H. Perry both the initiator and editor. Several chemical engineers, serving as editor- or coeditor-in-chief, have guided the preparation of the different editions over the years. These include John H. Perry (first to third editions), Robert H. Perry (fourth to sixth editions), Cecil H. Chilton (fourth and fifth editions), Sidney D. Kirkpatrick (fourth edition), Don W. Green (sixth to eighth editions) and James O. Maloney (sixth and seventh editions). Robert H. Perry was also listed as an editor for the seventh edition, and is listed again as an editor for the current edition, although his tragic death occurred during the preparation of the sixth edition. Many of the ideas developed through his leadership during preparation of earlier editions carried over to the seventh and eighth editions. I owe much to the friendship and mentoring of Bob Perry.

The organization of this eighth edition is much the same as for the seventh edition, although content changes are extensive. The first group of sections includes comprehensive tables with units conversions and fundamental constants, physical and chemical data, methods to predict properties, and fundamentals of mathematics most useful to engineers. The second group, comprising the fourth through the ninth sections, covers fundamentals of chemical engineering. The third and largest group of sections deals with processes, such as heat-transfer operations, distillation, gas-liquid processes, chemical reactors, and liquid-liquid processes. The last group covers auxiliary information including waste management, safety and the handling of hazardous materials, energy sources, and materials of construction. All sections have been updated to cover the latest advances in technology related to chemical engineering. As there are a significant number of new section editors, the material in the *Handbook* has been extensively revised. Section 2, which covers physical and chemical data, has been expanded by well over 100 pages to include, among other new information, data from the AIChE Design Institute for Physical Properties.

A large number of section editors and contributors worked on this eighth edition, and these persons and their affiliations are listed as a part of the front material. Many of these authors are Fellows of the AIChE. I would like to recognize two of these colleagues, Dr. Michael M. Abbott and Dr. James Y. Oldshue, who passed away while this work was being prepared. They will be missed. A number of chemical engineering students at the University of Kansas assisted in the preparation of the index. They are Jonathan Ashley, Andrew Becker, Jonathan Bunn, Don Claus, Andrew Duncan, Meghan Easter, Bill Eckman, Justin Ellrich, Mehrdad Hosni, Kaitlyn Kelly, Jennifer Lawrence, Casey Morris, Chris Roatch, Chris Sharpe, Jeremy Steeley, Daniel Theimer, and Nick Willis. In addition, Maxine Younes, Susan Bolton, and my wife Patricia Green provided extensive secretarial assistance.

DON W. GREEN
Editor-in-Chief
University of Kansas

This page intentionally left blank

SECTION 1

Conversion
Factors and
Mathematical
Symbols

PERRY'S CHEMICAL ENGINEERS' HANDBOOK

8TH EDITION



JAMES O. MALONEY

Copyright © 2008, 1997, 1984, 1973, 1963, 1950, 1941, 1934 by The McGraw-Hill Companies, Inc. All rights reserved. Manufactured in the United States of America. Except as permitted under the United States Copyright Act of 1976, no part of this publication may be reproduced or distributed in any form or by any means, or stored in a database or retrieval system, without the prior written permission of the publisher.

0-07-154208-6

The material in this eBook also appears in the print version of this title: 0-07-151124-5.

All trademarks are trademarks of their respective owners. Rather than put a trademark symbol after every occurrence of a trademarked name, we use names in an editorial fashion only, and to the benefit of the trademark owner, with no intention of infringement of the trademark. Where such designations appear in this book, they have been printed with initial caps.

McGraw-Hill eBooks are available at special quantity discounts to use as premiums and sales promotions, or for use in corporate training programs. For more information, please contact George Hoare, Special Sales, at george_hoare@mcgraw-hill.com or (212) 904-4069.

TERMS OF USE

This is a copyrighted work and The McGraw-Hill Companies, Inc. (“McGraw-Hill”) and its licensors reserve all rights in and to the work. Use of this work is subject to these terms. Except as permitted under the Copyright Act of 1976 and the right to store and retrieve one copy of the work, you may not decompile, disassemble, reverse engineer, reproduce, modify, create derivative works based upon, transmit, distribute, disseminate, sell, publish or sublicense the work or any part of it without McGraw-Hill’s prior consent. You may use the work for your own noncommercial and personal use; any other use of the work is strictly prohibited. Your right to use the work may be terminated if you fail to comply with these terms.

THE WORK IS PROVIDED “AS IS.” MCGRAW-HILL AND ITS LICENSORS MAKE NO GUARANTEES OR WARRANTIES AS TO THE ACCURACY, ADEQUACY OR COMPLETENESS OF OR RESULTS TO BE OBTAINED FROM USING THE WORK, INCLUDING ANY INFORMATION THAT CAN BE ACCESSED THROUGH THE WORK VIA HYPERLINK OR OTHERWISE, AND EXPRESSLY DISCLAIM ANY WARRANTY, EXPRESS OR IMPLIED, INCLUDING BUT NOT LIMITED TO IMPLIED WARRANTIES OF MERCHANTABILITY OR FITNESS FOR A PARTICULAR PURPOSE. McGraw-Hill and its licensors do not warrant or guarantee that the functions contained in the work will meet your requirements or that its operation will be uninterrupted or error free. Neither McGraw-Hill nor its licensors shall be liable to you or anyone else for any inaccuracy, error or omission, regardless of cause, in the work or for any damages resulting therefrom. McGraw-Hill has no responsibility for the content of any information accessed through the work. Under no circumstances shall McGraw-Hill and/or its licensors be liable for any indirect, incidental, special, punitive, consequential or similar damages that result from the use of or inability to use the work, even if any of them has been advised of the possibility of such damages. This limitation of liability shall apply to any claim or cause whatsoever whether such claim or cause arises in contract, tort or otherwise.

DOI: 10.1036/0071511245

Conversion Factors and Mathematical Symbols*

James O. Maloney, Ph.D., P.E. *Emeritus Professor of Chemical Engineering, University of Kansas; Fellow, American Institute of Chemical Engineering; Fellow, American Association for the Advancement of Science; Member, American Chemical Society; Member, American Society for Engineering Education*

CONVERSION FACTORS

Table 1-1	SI Base and Supplementary Quantities and Units	1-2
Table 1-2a	Derived Units of SI that Have Special Names	1-2
Table 1-2b	Additional Common Derived Units of SI	1-2
Table 1-3	SI Prefixes	1-2
Table 1-4	Conversion Factors: U.S. Customary and Commonly Used Units to SI Units	1-3
Table 1-5	Metric Conversion Factors as Exact Numerical Multiples of SI Units	1-12
Table 1-6	Alphabetical Listing of Common Conversions	1-14
Table 1-7	Common Units and Conversion Factors	1-17
Table 1-8	Kinematic-Viscosity Conversion Formulas	1-17

Table 1-9	Values of the Gas-Law Constant	1-17
Table 1-10	United States Customary System of Weights and Measures	1-18
Table 1-11	Temperature Conversion	1-18
Table 1-12	Greek Alphabet	1-18
Table 1-13	Specific Gravity, Degrees Baumé, Degrees API, Degrees Twaddell, Pounds per Gallon, Pounds per Cubic Foot	1-19
Table 1-14	Fundamental Physical Constants	1-20

CONVERSION OF VALUES FROM U.S. CUSTOMARY UNITS TO SI UNITS

* Much of the material was taken from Sec. 1. of the fifth edition. The contribution of Cecil H. Chilton in developing that material is acknowledged.

TABLE 1-1 SI Base and Supplementary Quantities and Units

Quantity or "dimension"	SI unit	SI unit symbol ("abbreviation"); Use roman (upright) type
Base quantity or "dimension"		
length	meter	m
mass	kilogram	kg
time	second	s
electric current	ampere	A
thermodynamic temperature	kelvin	K
amount of substance	mole ^o	mol
luminous intensity	candela	cd
Supplementary quantity or "dimension"		
plane angle	radian	rad
solid angle	steradian	sr

^o When the mole is used, the elementary entities must be specified; they may be atoms, molecules, ions, electrons, other particles, or specified groups of such particles.

TABLE 1-2a Derived Units of SI that Have Special Names

Quantity	Unit	Symbol	Formula
frequency (of a periodic phenomenon)	hertz	Hz	1/s
force	newton	N	(kg·m)/s ²
pressure, stress	pascal	Pa	N/m ²
energy, work, quantity of heat	joule	J	N·m
power, radiant flux	watt	W	J/s
quantity of electricity, electric charge	coulomb	C	A·s
electric potential, potential difference, electromotive force	volt	V	W/A
capacitance	farad	F	C/V
electric resistance	ohm	Ω	V/A
conductance	siemens	S	A/V
magnetic flux	weber	Wb	V·s
magnetic-flux density	tesla	T	Wb/m ²
inductance	henry	H	Wb/A
luminous flux	lumen	lm	cd·sr
illuminance	lux	lx	lm/m ²
activity (of radionuclides)	becquerel	Bq	1/s
absorbed dose	gray	Gy	J/kg

TABLE 1-2b Additional Common Derived Units of SI

Quantity	Unit	Symbol
acceleration	meter per second squared	m/s ²
angular acceleration	radian per second squared	rad/s ²
angular velocity	radian per second	rad/s
area	square meter	m ²
concentration (of amount of substance)	mole per cubic meter	mol/m ³
current density	ampere per square meter	A/m ²
density, mass	kilogram per cubic meter	kg/m ³
electric-charge density	coulomb per cubic meter	C/m ³
electric-field strength	volt per meter	V/m
electric-flux density	coulomb per square meter	C/m ²
energy density	joule per cubic meter	J/m ³
entropy	joule per kelvin	J/K
heat capacity	joule per kelvin	J/K
heat-flux density, irradiance	watt per square meter	W/m ²
luminance	candela per square meter	cd/m ²
magnetic-field strength	ampere per meter	A/m
molar energy	joule per mole	J/mol
molar entropy	joule per mole-kelvin	J/(mol·K)
molar-heat capacity	joule per mole-kelvin	J/(mol·K)
moment of force	newton-meter	N·m
permeability	henry per meter	H/m
permittivity	farad per meter	F/m
radiance	watt per square-meter-steradian	W/(m ² ·sr)
radiant intensity	watt per steradian	W/sr
specific-heat capacity	joule per kilogram-kelvin	J/(kg·K)
specific energy	joule per kilogram	J/kg
specific entropy	joule per kilogram-kelvin	J/(kg·K)
specific volume	cubic meter per kilogram	m ³ /kg
surface tension	newton per meter	N/m
thermal conductivity	watt per meter-kelvin	W/(m·K)
velocity	meter per second	m/s
viscosity, dynamic	pascal-second	Pa·s
viscosity, kinematic	square meter per second	m ² /s
volume	cubic meter	m ³
wave number	1 per meter	1/m

TABLE 1-3 SI Prefixes

Multiplication factor	Prefix	Symbol
1 000 000 000 000 000 000 = 10 ¹⁸	exa	E
1 000 000 000 000 000 = 10 ¹⁵	peta	P
1 000 000 000 000 = 10 ¹²	tera	T
1 000 000 000 = 10 ⁹	giga	G
1 000 000 = 10 ⁶	mega	M
1 000 = 10 ³	kilo	k
100 = 10 ²	hecto ^o	h
10 = 10 ¹	deka ^o	da
0.1 = 10 ⁻¹	deci ^o	d
0.01 = 10 ⁻²	centi	c
0.001 = 10 ⁻³	milli	m
0.000 001 = 10 ⁻⁶	micro	μ
0.000 000 001 = 10 ⁻⁹	nano	n
0.000 000 000 001 = 10 ⁻¹²	pico	p
0.000 000 000 000 001 = 10 ⁻¹⁵	femto	f
0.000 000 000 000 000 001 = 10 ⁻¹⁸	atto	a

^o Generally to be avoided.

TABLE 1-4 Conversion Factors: U.S. Customary and Commonly Used Units to SI Units

Quantity	Customary or commonly used unit	SI unit	Alternate SI unit	Conversion factor; multiply customary unit by factor to obtain SI unit
Space, † time				
Length	naut mi	km		1.852° E + 00
	mi	km		1.609 344° E + 00
	chain	m		2.011 68° E + 01
	link	m		2.011 68° E - 01
	fathom	m		1.828 8° E + 00
	yd	m		9.144° E - 01
	ft	m		3.048° E - 01
		cm		3.048° E + 01
	in	mm		2.54° E + 01
	in	cm		2.54 E + 00
	mil	µm		2.54° E + 01
Length/length	ft/mi	m/km		1.893 939 E - 01
Length/volume	ft/U.S. gal	m/m ³		8.051 964 E + 01
	ft/ft ³	m/m ³		1.076 391 E + 01
	ft/bbl	m/m ³		1.917 134 E + 00
Area	mi ²	km ²		2.589 988 E + 00
	section	ha		2.589 988 E + 02
	acre	ha		4.046 856 E - 01
	ha	m ²		1.000 000° E + 04
	yd ²	m ²		8.361 274 E - 01
	ft ²	m ²		9.290 304° E - 02
	in ²	mm ²		6.451 6° E + 02
	cm ²		6.451 6° E + 00	
Area/volume	ft ² /in ³	m ² /cm ³		5.699 291 E - 03
	ft ² /ft ³	m ² /m ³		3.280 840 E + 00
Volume	cubem	km ³		4.168 182 E + 00
	acre-ft	m ³		1.233 482 E + 03
		ha·m		1.233 482 E - 01
	yd ³	m ³		7.645 549 E - 01
	bbl (42 U.S. gal)	m ³		1.589 873 E - 01
	ft ³	m ³		2.831 685 E - 02
		dm ³	L	2.831 685 E + 01
	U.K. gal	m ³		4.546 092 E - 03
		dm ³	L	4.546 092 E + 00
	U.S. gal	m ³		3.785 412 E - 03
		dm ³	L	3.785 412 E + 00
	U.K. qt	dm ³	L	1.136 523 E + 00
	U.S. qt	dm ³	L	9.463 529 E - 01
	U.S. pt	dm ³	L	4.731 765 E - 01
	U.K. fl oz	cm ³		2.841 307 E + 01
	U.S. fl oz	cm ³		2.957 353 E + 01
		in ³	cm ³	1.638 706 E + 01
Volume/length (linear displacement)	bbl/in	m ³ /m		6.259 342 E + 00
	bbl/ft	m ³ /m		5.216 119 E - 01
	ft ³ /ft	m ³ /m		9.290 304° E - 02
	U.S. gal/ft	m ³ /m		1.241 933 E - 02
		L/m		1.241 933 E + 01
Plane angle	rad	rad		1
	deg (°)	rad		1.745 329 E - 02
	min (′)	rad		2.908 882 E - 04
	sec (″)	rad		4.848 137 E - 06
Solid angle	sr	sr		1
Time	year	a		1
	week	d		7.0° E + 00
	h	s		3.6° E + 03
		min		6.0° E + 01
	min	s		6.0° E + 01
		h		1.666 667 E - 02
	mµs	ns		1
Mass, amount of substance				
Mass	U.K. ton	Mg	t	1.016 047 E + 00
	U.S. ton	Mg	t	9.071 847 E - 01
	U.K. cwt	kg		5.080 234 E + 01
	U.S. cwt	kg		4.535 924 E + 01
	lbm	kg		4.535 924 E - 01
	oz (troy)	g		3.110 348 E + 01
	oz (av)	g		2.834 952 E + 01
	gr	mg		6.479 891 E + 01

TABLE 1-4 Conversion Factors: U.S. Customary and Commonly Used Units to SI Units (Continued)

Quantity	Customary or commonly used unit	SI unit	Alternate SI unit	Conversion factor; multiply customary unit by factor to obtain SI unit		
Amount of substance	lbm-mol	kmol		4.535 924	E - 01	
	std m ³ (0°C, 1 atm)	kmol		4.461 58	E - 02	
	std ft ³ (60°F, 1 atm)	kmol		1.195 30	E - 03	
Enthalpy, calorific value, heat, entropy, heat capacity						
Calorific value, enthalpy (mass basis)	Btu/lbm	MJ/kg		2.326 000	E - 03	
		kJ/kg	J/g	2.326 000	E + 00	
	cal/g cal/lbm	kWh/kg		6.461 112	E - 04	
		kJ/kg J/kg	J/g	4.184°	E + 00	
Caloric value, enthalpy (mole basis)	kcal/(g-mol)	kJ/kmol		4.184°	E + 03	
	Btu/(lb-mol)	kJ/kmol		2.326 000	E + 00	
Calorific value (volume basis—solids and liquids)	Btu/U.S. gal	MJ/m ³	kJ/dm ³	2.787 163	E - 01	
		kJ/m ³		2.787 163	E + 02	
		kWh/m ³		7.742 119	E - 02	
	Btu/U.K. gal	MJ/m ³	kJ/dm ³	2.320 800	E - 01	
		kJ/m ³		2.320 800	E + 02	
	Btu/ft ³	kWh/m ³		6.446 667	E - 02	
		MJ/m ³	kJ/dm ³	3.725 895	E - 02	
		kJ/m ³		3.725 895	E + 01	
		kWh/m ³		1.034 971	E - 02	
		cal/mL (ft-lbf)/U.S. gal	MJ/m ³ kJ/m ³		4.184° 3.581 692	E + 00 E - 01
Caloric value (volume basis—gases)	cal/mL	kJ/m ³	J/dm ³	4.184°	E + 03	
	kcal/m ³	kJ/m ³	J/dm ³	4.184°	E + 00	
	Btu/ft ³	kJ/m ³	J/dm ³	3.725 895	E + 01	
		kWh/m ³		1.034 971	E - 02	
Specific entropy	Btu/(lbm-°R)	kJ/(kg-K)	J/(g-K)	4.186 8°	E + 00	
	cal/(g-K)	kJ/(kg-K)	J/(g-K)	4.184°	E + 00	
	kcal/(kg-°C)	kJ/(kg-K)	J/(g-K)	4.184°	E + 00	
Specific-heat capacity (mass basis)	kWh/(kg-°C)	kJ/(kg-K)	J/(g-K)	3.6°	E + 03	
	Btu/(lbm-°F)	kJ/(kg-K)	J/(g-K)	4.186 8°	E + 00	
	kcal/(kg-°C)	kJ/(kg-K)	J/(g-K)	4.184°	E + 00	
Specific-heat capacity (mole basis)	Btu/(lb-mol-°F)	kJ/(kmol-K)		4.186 8°	E + 00	
	cal/(g-mol-°C)	kJ/(kmol-K)		4.184°	E + 00	
Temperature, pressure, vacuum						
Temperature (absolute)	°R	K		5/9		
	K	K		1		
Temperature (traditional)	°F	°C		5/9(°F - 32)		
Temperature (difference)	°F	K, °C		5/9		
Pressure	atm (760 mmHg at 0°C or 14,696 psi)	MPa		1.013 250°	E - 01	
		kPa		1.013 250°	E + 02	
		bar		1.013 250°	E + 00	
		bar	MPa		1.0°	E - 01
			kPa		1.0°	E + 02
			MPa		6.894 757	E - 03
	mmHg (0°C) = torr	kPa		6.894 757	E + 00	
		bar		6.894 757	E - 02	
		kPa		3.376 85	E + 00	
		kPa		2.488 4	E - 01	
		mmHg = torr (0°C)	kPa		1.333 224	E - 01
		cmH ₂ O (4°C)	kPa		9.806 38	E - 02
	μmHg (0°C) μ bar	lb/ft ² (psf)	kPa		4.788 026	E - 02
		mHg (0°C)	Pa		1.333 224	E - 01
		bar	Pa		1.0°	E + 05
		dyn/cm ²	Pa		1.0°	E - 01
Vacuum, draft		inHg (60°F)	kPa		3.376 85	E + 00
		inH ₂ O (39.2°F)	kPa		2.490 82	E - 01
	inH ₂ O (60°F)	kPa		2.488 4	E - 01	
	mmHg (0°C) = torr	kPa		1.333 224	E - 01	
	cmH ₂ O (4°C)	kPa		9.806 38	E - 02	
Liquid head	ft	m		3.048°	E - 01	
	in	mm		2.54°	E + 01	
		cm		2.54°	E + 00	
Pressure drop/length	psi/ft	kPa/m		2.262 059	E + 01	

TABLE 1-4 Conversion Factors: U.S. Customary and Commonly Used Units to SI Units (Continued)

Quantity	Customary or commonly used unit	SI unit	Alternate SI unit	Conversion factor; multiply customary unit by factor to obtain SI unit
Density, specific volume, concentration, dosage				
Density	lbm/ft ³	kg/m ³		1.601 846 E + 01
		g/m ³		1.601 846 E + 04
	lbm/U.S. gal	kg/m ³		1.198 264 E + 02
		g/cm ³		1.198 264 E - 01
	lbm/U.K. gal	kg/m ³		9.977 633 E + 01
	lbm/ft ³	kg/m ³		1.601 846 E + 01
		g/cm ³		1.601 846 E - 02
	g/cm ³	kg/m ³		1.0° E + 03
	lbm/ft ³	kg/m ³		1.601 846 E + 01
Specific volume	ft ³ /lbm	m ³ /kg		6.242 796 E - 02
		m ³ /g		6.242 796 E - 05
	ft ³ /lbm	dm ³ /kg		6.242 796 E + 01
	U.K. gal/lbm	dm ³ /kg	cm ³ /g	1.002 242 E + 01
U.S. gal/lbm	dm ³ /kg	cm ³ /g	8.345 404 E + 00	
Specific volume (mole basis)	L/(g·mol)	m ³ /kmol		1
	ft ³ /(lb·mol)	m ³ /kmol		6.242 796 E - 02
Specific volume	bbl/U.S. ton	m ³ /t		1.752 535 E - 01
	bbl/U.K. ton	m ³ /t		1.564 763 E - 01
Yield	bbl/U.S. ton	dm ³ /t	L/t	1.752 535 E + 02
	bbl/U.K. ton	dm ³ /t	L/t	1.564 763 E + 02
	U.S. gal/U.S. ton	dm ³ /t	L/t	4.172 702 E + 00
	U.S. gal/U.K. ton	dm ³ /t	L/t	3.725 627 E + 00
Concentration (mass/mass)	wt %	kg/kg		1.0° E - 02
		g/kg		1.0° E + 01
	wt ppm	mg/kg		1
Concentration (mass/volume)	lbm/bbl	kg/m ³	g/dm ³	2.853 010 E + 00
	g/U.S. gal	kg/m ³		2.641 720 E - 01
	g/U.K. gal	kg/m ³	g/L	2.199 692 E - 01
	lbm/1000 U.S. gal	g/m ³	mg/dm ³	1.198 264 E + 02
	lbm/1000 U.K. gal	g/m ³	mg/dm ³	9.977 633 E + 01
	gr/U.S. gal	g/m ³	mg/dm ³	1.711 806 E + 01
	gr/ft ³	mg/m ³		2.288 351 E + 03
	lbm/1000 bbl	g/m ³	mg/dm ³	2.853 010 E + 00
	mg/U.S. gal	g/m ³	mg/dm ³	2.641 720 E - 01
	gr/100 ft ³	mg/m ³		2.288 351 E + 01
Concentration (volume/volume)	ft ³ /ft ³	m ³ /m ³		1
	bbl/(acre-ft)	m ³ /m ³		1.288 931 E - 04
	vol%	m ³ /m ³		1.0° E - 02
	U.K. gal/ft ³	dm ³ /m ³	L/m ³	1.605 437 E + 02
	U.S. gal/ft ³	dm ³ /m ³	L/m ³	1.336 806 E + 02
	mL/U.S. gal	dm ³ /m ³	L/m ³	2.641 720 E - 01
	mL/U.K. gal	dm ³ /m ³	L/m ³	2.199 692 E - 01
	vol ppm	cm ³ /m ³		1
		dm ³ /m ³	L/m ³	1.0° E - 03
	U.K. gal/1000 bbl	cm ³ /m ³		2.859 403 E + 01
	U.S. gal/1000 bbl	cm ³ /m ³		2.380 952 E + 01
	U.K. pt/1000 bbl	cm ³ /m ³		3.574 253 E + 00
	Concentration (mole/volume)	(lb·mol)/U.S. gal	kmol/m ³	
(lb·mol)/U.K. gal		kmol/m ³		9.977 644 E + 01
(lb·mol)/ft ³		kmol/m ³		1.601 846 E + 01
std ft ³ (60°F, 1 atm)/bbl		kmol/m ³		7.518 21 E - 03
Concentration (volume/mole)	U.S. gal/1000 std ft ³ (60°F/60°F)	dm ³ /kmol	L/kmol	3.166 91 E + 00
	bbl/million std ft ³ (60°F/60°F)	dm ³ /kmol	L/kmol	1.330 10 E - 01
Facility throughput, capacity				
Throughput (mass basis)	U.K. ton/year	t/a		1.016 047 E + 00
	U.S. ton/year	t/a		9.071 847 E - 01
	U.K. ton/day	t/d		1.016 047 E + 00
		t/h		4.233 529 E - 02
	U.S. ton/day	t/d		9.071 847 E - 01
		t/h		3.779 936 E - 02
	U.K. ton/h	t/h		1.016 047 E + 00
	U.S. ton/h	t/h		9.071 847 E - 01
	lbm/h	kg/h		4.535 924 E - 01

TABLE 1-4 Conversion Factors: U.S. Customary and Commonly Used Units to SI Units (Continued)

Quantity	Customary or commonly used unit	SI unit	Alternate SI unit	Conversion factor; multiply customary unit by factor to obtain SI unit
Throughput (volume basis)	bbl/day	t/a		5.803 036 E + 01
		m ³ /d		1.589 873 E - 01
	ft ³ /day	m ³ /h		1.179 869 E - 03
	bbl/h	m ³ /h		1.589 873 E - 01
	ft ³ /h	m ³ /h		2.831 685 E - 02
	U.K. gal/h	m ³ /h		4.546 092 E - 03
		L/s		1.262 803 E - 03
	U.S. gal/h	m ³ /h		3.785 412 E - 03
		L/s		1.051 503 E - 03
	U.K. gal/min	m ³ /h		2.727 655 E - 01
	L/s		7.576 819 E - 02	
U.S. gal/min	m ³ /h		2.271 247 E - 01	
	L/s		6.309 020 E - 02	
Throughput (mole basis)	(lbm-mol)/h	kmol/h		4.535 924 E - 01
		kmol/s		1.259 979 E - 04
Flow rate				
Flow rate (mass basis)	U.K. ton/min	kg/s		1.693 412 E + 01
	U.S. ton/min	kg/s		1.511 974 E + 01
	U.K. ton/h	kg/s		2.822 353 E - 01
	U.S. ton/h	kg/s		2.519 958 E - 01
	U.K. ton/day	kg/s		1.175 980 E - 02
	U.S. ton/day	kg/s		1.049 982 E - 02
	million lbm/year	kg/s		5.249 912 E + 00
	U.K. ton/year	kg/s		3.221 864 E - 05
	U.S. ton/year	kg/s		2.876 664 E - 05
	lbm/s	kg/s		4.535 924 E - 01
	lbm/min	kg/s		7.559 873 E - 03
	lbm/h	kg/s		1.259 979 E - 04
	Flow rate (volume basis)	bbl/day	m ³ /d	
		L/s		1.840 131 E - 03
ft ³ /day		m ³ /d		2.831 685 E - 02
		L/s		3.277 413 E - 04
bbl/h		m ³ /s		4.416 314 E - 05
		L/s		4.416 314 E - 02
ft ³ /h		m ³ /s		7.865 791 E - 06
		L/s		7.865 791 E - 03
U.K. gal/h		dm ³ /s	L/s	1.262 803 E - 03
U.S. gal/h		dm ³ /s	L/s	1.051 503 E - 03
U.K. gal/min		dm ³ /s	L/s	7.576 820 E - 02
U.S. gal/min		dm ³ /s	L/s	6.309 020 E - 02
ft ³ /min		dm ³ /s	L/s	4.719 474 E - 01
ft ³ /s	dm ³ /s	L/s	2.831 685 E + 01	
Flow rate (mole basis)	(lb-mol)/s	kmol/s		4.535 924 E - 01
	(lb-mol)/h	kmol/s		1.259 979 E - 04
	million scf/D	kmol/s		1.383 45 E - 02
Flow rate/length (mass basis)	lbm/(s-ft)	kg/(s-m)		1.488 164 E + 00
	lbm/(h-ft)	kg/(s-m)		4.133 789 E - 04
Flow rate/length (volume basis)	U.K. gal/(min-ft)	m ² /s	m ³ /(s-m)	2.485 833 E - 04
	U.S. gal/(min-ft)	m ² /s	m ³ /(s-m)	2.069 888 E - 04
	U.K. gal/(h-in)	m ² /s	m ³ /(s-m)	4.971 667 E - 05
	U.S. gal/(h-in)	m ² /s	m ³ /(s-m)	4.139 776 E - 05
	U.K. gal/(h-ft)	m ² /s	m ³ /(s-m)	4.143 055 E - 06
	U.S. gal/(h-ft)	m ² /s	m ³ /(s-m)	3.449 814 E - 06
Flow rate/area (mass basis)	lbm/(s-ft ²)	kg/(s-m ²)		4.882 428 E + 00
	lbm/(h-ft ²)	kg/(s-m ²)		1.356 230 E - 03
Flow rate/area (volume basis)	ft ³ /(s-ft ²)	m/s	m ³ /(s-m ²)	3.048° E - 01
	ft ³ /(min-ft ²)	m/s	m ³ /(s-m ²)	5.08° E - 03
	U.K. gal/(h-in ²)	m/s	m ³ /(s-m ²)	1.957 349 E - 03
	U.S. gal/(h-in ²)	m/s	m ³ /(s-m ²)	1.629 833 E - 03
	U.K. gal/(min-ft ²)	m/s	m ³ /(s-m ²)	8.155 621 E - 04
	U.S. gal/(min-ft ²)	m/s	m ³ /(s-m ²)	6.790 972 E - 04
	U.K. gal/(h-ft ²)	m/s	m ³ /(s-m ²)	1.359 270 E - 05
	U.S. gal/(h-ft ²)	m/s	m ³ /(s-m ²)	1.131 829 E - 05

TABLE 1-4 Conversion Factors: U.S. Customary and Commonly Used Units to SI Units (Continued)

Quantity	Customary or commonly used unit	SI unit	Alternate SI unit	Conversion factor; multiply customary unit by factor to obtain SI unit
Energy, work, power				
Energy, work	therm	MJ		1.055 056 E + 02
		kJ		1.055 056 E + 05
		kWh		2.930 711 E + 01
	U.S. tonf·mi hp·h	MJ		1.431 744 E + 01
		MJ		2.684 520 E + 00
		kJ		2.684 520 E + 03
	ch·h or CV·h	kWh		7.456 999 E - 01
		MJ		2.647 780 E + 00
		kJ		2.647 780 E + 03
	kWh	kWh		7.354 999 E - 01
		MJ		3.6° E + 00
		kJ		3.6° E + 03
	Chu	kJ		1.899 101 E + 00
		kWh		5.275 280 E - 04
	Btu	kJ		1.055 056 E + 00
		kWh		2.930 711 E - 04
	kcal	kJ		4.184° E + 00
cal		kJ	4.184° E - 03	
ft·lbf		kJ	1.355 818 E - 03	
lbf·ft		kJ	1.355 818 E - 03	
J		kJ	1.0° E - 03	
(lbf·ft ²)/s ²		kJ	4.214 011 E - 05	
erg		J	1.0° E - 07	
Impact energy	kgf·m	J	9.806 650° E + 00	
	lbf·ft	J	1.355 818 E + 00	
Surface energy	erg/cm ²	mJ/m ²	1.0° E + 00	
Specific-impact energy	(kgf·m)/cm ²	J/cm ²	9.806 650° E - 02	
	(lbf·ft)/in ²	J/cm ²	2.101 522 E - 03	
Power	million Btu/h	MW	2.930 711 E - 01	
	ton of refrigeration	kW	3.516 853 E + 00	
	Btu/s	kW	1.055 056 E + 00	
	kW	kW	1	
	hydraulic horsepower—hhp	kW	7.460 43 E - 01	
	hp (electric)	kW	7.46° E - 01	
	hp [(550 ft·lbf)/s]	kW	7.456 999 E - 01	
	ch or CV	kW	7.354 999 E - 01	
	Btu/min	kW	1.758 427 E - 02	
	(ft·lbf)/s	kW	1.355 818 E - 03	
	kcal/h	W	1.162 222 E + 00	
	Btu/h	W	2.930 711 E - 01	
(ft·lbf)/min	W	2.259 697 E - 02		
Power/area	Btu/(s·ft ²)	kW/m ²	1.135 653 E + 01	
	cal/(h·cm ²)	kW/m ²	1.162 222 E - 02	
	Btu/(h·ft ²)	kW/m ²	3.154 591 E - 03	
Heat-release rate, mixing power	hp/ft ³	kW/m ³	2.633 414 E + 01	
	cal/(h·cm ³)	kW/m ³	1.162 222 E + 00	
	Btu/(s·ft ³)	kW/m ³	3.725 895 E + 01	
	Btu/(h·ft ³)	kW/m ³	1.034 971 E - 02	
Cooling duty (machinery)	Btu/(bhp·h)	W/kW	3.930 148 E - 01	
Specific fuel consumption (mass basis)	lbm/(hp·h)	mg/J	1.689 659 E - 01	
		kg/kWh	6.082 774 E - 01	
Specific fuel consumption (volume basis)	m ³ /kWh	dm ³ /MJ	2.777 778 E + 02	
	U.S. gal/(hp·h)	dm ³ /MJ	1.410 089 E + 00	
	U.K. pt/(hp·h)	dm ³ /MJ	2.116 806 E - 01	
Fuel consumption	U.K. gal/mi	dm ³ /100 km	L/100 km	2.824 807 E + 02
	U.S. gal/mi	dm ³ /100 km	L/100 km	2.352 146 E + 02
	mi/U.S. gal	km/dm ³	km/L	4.251 437 E - 01
	mi/U.K. gal	km/dm ³	km/L	3.540 064 E - 01

TABLE 1-4 Conversion Factors: U.S. Customary and Commonly Used Units to SI Units (Continued)

Quantity	Customary or commonly used unit	SI unit	Alternate SI unit	Conversion factor; multiply customary unit by factor to obtain SI unit
Velocity (linear), speed	knot	km/h		1.852° E + 00
	mi/h	km/h		1.609 344° E + 00
	ft/s	m/s		3.048° E - 01
		cm/s		3.048° E + 01
	ft/min	m/s		5.08° E - 03
	ft/h	mm/s		8.466 667 E - 02
	ft/day	mm/s		3.527 778 E - 03
		m/d		3.048° E - 01
	in/s	mm/s		2.54° E + 01
	in/min	mm/s		4.233 333 E - 01
Corrosion rate	in/year (ipy)	mm/a		2.54° E + 01
	mil/year	mm/a		2.54° E - 02
Rotational frequency	r/min	r/s		1.666 667 E - 02
		rad/s		1.047 198 E - 01
Acceleration (linear)	ft/s ²	m/s ²		3.048° E - 01
		cm/s ²		3.048° E + 01
Acceleration (rotational)	rpm/s	rad/s ²		1.047 198 E - 01
Momentum	(lbm·ft)/s	(kg·m)/s		1.382 550 E - 01
Force	U.K. tonf	kN		9.964 016 E + 00
	U.S. tonf	kN		8.896 443 E + 00
	kgf (kp)	N		9.806 650° E + 00
	lbf	N		4.448 222 E + 00
	dyn	mN		1.0 E - 02
Bending moment, torque	U.S. tonf·ft	kN·m		2.711 636 E + 00
	kgf·m	N·m		9.806 650° E + 00
	lbf·ft	N·m		1.355 818 E + 00
	lbf·in	N·m		1.129 848 E - 01
Bending moment/length	(lbf·ft)/in	(N·m)/m		5.337 866 E + 01
	(lbf·in)/in	(N·m)/m		4.448 222 E + 00
Moment of inertia	lbm·ft ²	kg·m ²		4.214 011 E - 02
Stress	U.S. tonf/in ²	MPa	N/mm ²	1.378 951 E + 01
	kgf/mm ²	MPa	N/mm ²	9.806 650° E + 00
	U.S. tonf/ft ²	MPa	N/mm ²	9.576 052 E - 02
	lbf/in ² (psi)	MPa	N/mm ²	6.894 757 E - 03
	lbf/ft ² (psf)	kPa		4.788 026 E - 02
	dyn/cm ²	Pa		1.0° E - 01
Mass/length	lbm/ft	kg/m		1.488 164 E + 00
Mass/area structural loading, bearing capacity (mass basis)	U.S. ton/ft ²	Mg/m ²		9.764 855 E + 00
	lbm/ft ²	kg/m ²		4.882 428 E + 00
Miscellaneous transport properties				
Diffusivity	ft ² /s	m ² /s		9.290 304° E - 02
	m ² /s	mm ² /s		1.0° E + 06
	ft ² /h	m ² /s		2.580 64° E - 05
Thermal resistance	(°C·m ² ·h)/kcal	(K·m ²)/kW		8.604 208 E + 02
	(°F·ft ² ·h)/Btu	(K·m ²)/kW		1.761 102 E + 02
Heat flux	Btu/(h·ft ²)	kW/m ²		3.154 591 E - 03
Thermal conductivity	(cal·cm)/(s·cm ² ·°C)	W/(m·K)		4.184° E + 02
	(Btu·ft)/(h·ft ² ·°F)	W/(m·K)		1.730 735 E + 00
		(kJ·m)/(h·m ² ·K)		6.230 646 E + 00
	(kcal·m)/(h·m ² ·°C)	W/(m·K)		1.162 222 E + 00
	(Btu·in)/(h·ft ² ·°F)	W/(m·K)		1.442 279 E - 01
	(cal·cm)/(h·cm ² ·°C)	W/(m·K)		1.162 222 E - 01
Heat-transfer coefficient	cal/(s·cm ² ·°C)	kW/(m ² ·K)		4.184° E + 01
	Btu/(s·ft ² ·°F)	kW/(m ² ·K)		2.044 175 E + 01
	cal/(h·cm ² ·°C)	kW/(m ² ·K)		1.162 222 E - 02
	Btu/(h·ft ² ·°F)	kW/(m ² ·K)		5.678 263 E - 03
		kJ/(h·m ² ·K)		2.044 175 E + 01
		Btu/(h·ft ² ·°R)	kW/(m ² ·K)	
	kcal/(h·m ² ·°C)	kW/(m ² ·K)		1.162 222 E - 03

TABLE 1-4 Conversion Factors: U.S. Customary and Commonly Used Units to SI Units (Continued)

Quantity	Customary or commonly used unit	SI unit	Alternate SI unit	Conversion factor; multiply customary unit by factor to obtain SI unit
Volumetric heat-transfer coefficient	Btu/(s·ft ³ ·°F)	kW/(m ³ ·K)		6.706 611 E + 01
	Btu/(h·ft ³ ·°F)	kW/(m ³ ·K)		1.862 947 E - 02
Surface tension	dyn/cm	mN/m		1
Viscosity (dynamic)	(lbf·s)/in ²	Pa·s	(N·s)/m ²	6.894 757 E + 03
	(lbf·s)/ft ²	Pa·s	(N·s)/m ²	4.788 026 E + 01
	(kgf·s)/m ²	Pa·s	(N·s)/m ²	9.806 650° E + 00
	lbm/(ft·s)	Pa·s	(N·s)/m ²	1.488 164 E + 00
	(dyn·s)/cm ²	Pa·s	(N·s)/m ²	1.0° E - 01
	cP	Pa·s	(N·s)/m ²	1.0° E - 03
Viscosity (kinematic)	lbm/(ft·h)	Pa·s	(N·s)/m ²	4.133 789 E - 04
	ft ² /s	m ² /s		9.290 304° E - 02
	in ² /s	mm ² /s		6.451 6° E + 02
	m ² /h	mm ² /s		2.777 778 E + 02
	ft ² /h	m ² /s		2.580 64° E - 05
Permeability	darcy	μm ²		9.869 233 E - 01
	millidarcy	μm ²		9.869 233 E - 04
Thermal flux	Btu/(h·ft ²)	W/m ²		3.152 E + 00
	Btu/(s·ft ²)	W/m ²		1.135 E + 04
	cal/(s·cm ²)	W/m ²		4.184 E + 04
Mass-transfer coefficient	(lb·mol)/(h·ft ² (lb·mol/ft ³))	m/s		8.467 E - 05
	(g·mol)/(s·m ² (g·mol/L))	m/s		1.0 E + 01
Electricity, magnetism				
Admittance	S	S		1
Capacitance	μF	μF		1
Charge density	C/mm ³	C/mm ³		1
Conductance	S	S		1
	Ω (mho)	S		1
Conductivity	S/m	S/m		1
	Ω/m	S/m		1
	mΩ/m	mS/m		1
Current density	A/mm ²	A/mm ²		1
Displacement	C/cm ²	C/cm ²		1
Electric charge	C	C		1
Electric current	A	A		1
Electric-dipole moment	C·m	C·m		1
Electric-field strength	V/m	V/m		1
Electric flux	C	C		1
Electric polarization	C/cm ²	C/cm ²		1
Electric potential	V	V		1
	mV	mV		1
Electromagnetic moment	A·m ²	A·m ²		1
Electromotive force	V	V		1
Flux of displacement	C	C		1
Frequency	cycles/s	Hz		1
Impedance	Ω	Ω		1
Linear-current density	A/mm	A/mm		1
Magnetic-dipole moment	Wb·m	Wb·m		1
Magnetic-field strength	A/mm	A/mm		1
	Oe	A/m		7.957 747 E + 01
	gamma	A/m		7.957 747 E - 04
Magnetic flux	mWb	mWb		1

TABLE 1-4 Conversion Factors: U.S. Customary and Commonly Used Units to SI Units (Continued)

Quantity	Customary or commonly used unit	SI unit	Alternate SI unit	Conversion factor; multiply customary unit by factor to obtain SI unit
Magnetic-flux density	mT	mT		1
	G	T		1.0° E - 04
	gamma	nT		1
Magnetic induction	mT	mT		1
Magnetic moment	A·m ²	A·m ²		1
Magnetic polarization	mT	mT		1
Magnetic potential difference	A	A		1
Magnetic-vector potential	Wb/mm	Wb/mm		1
Magnetization	A/mm	A/mm		1
Modulus of admittance	S	S		1
Modulus of impedance	Ω	Ω		1
Mutual inductance	H	H		1
Permeability	μH/m	μH/m		1
Permeance	H	H		1
Permittivity	μF/m	μF/m		1
Potential difference	V	V		1
Quantity of electricity	C	C		1
Reactance	Ω	Ω		1
Reluctance	H ⁻¹	H ⁻¹		1
Resistance	Ω	Ω		1
Resistivity	Ω·cm	Ω·cm		1
	Ω·m	Ω·m		1
Self-inductance	mH	mH		1
Surface density of charge	mC/m ²	mC/m ²		1
Susceptance	S	S		1
Volume density of charge	C/mm ³	C/mm ³		1
Acoustics, light, radiation				
Absorbed dose	rad	Gy		1.0° E - 02
Acoustical energy	J	J		1
Acoustical intensity	W/cm ²	W/m ²		1.0° E + 04
Acoustical power	W	W		1
Sound pressure	N/m ²	N/m ²		1.0°
Illuminance	fc	lx		1.076 391 E + 01
Illumination	fc	lx		1.076 391 E + 01
Irradiance	W/m ²	W/m ²		1
Light exposure	fc·s	lx·s		1.076 391 E + 01
Luminance	cd/m ²	cd/m ²		1
Luminous efficacy	lm/W	lm/W		1
Luminous exitance	lm/m ²	lm/m ²		1
Luminous flux	lm	lm		1
Luminous intensity	cd	cd		1
Radiance	W/m ² ·sr	W/m ² ·sr		1
Radiant energy	J	J		1
Radiant flux	W	W		1
Radiant intensity	W/sr	W/sr		1
Radiant power	W	W		1

TABLE 1-4 Conversion Factors: U.S. Customary and Commonly Used Units to SI Units (Concluded)

Quantity	Customary or commonly used unit	SI unit	Alternate SI unit	Conversion factor; multiply customary unit by factor to obtain SI unit	
Wavelength	Å	nm		1.0°	E - 01
Capture unit	10 ⁻³ cm ⁻¹	m ⁻¹		1.0°	E + 01
	m ⁻¹	m ⁻¹	10 ⁻³ cm ⁻¹	1	1
Radioactivity	Ci	Bq		3.7°	E + 10

° An asterisk indicates that the conversion factor is exact.

† Conversion factors for length, area, and volume are based on the international foot. The international foot is longer by 2 parts in 1 million than the U.S. Survey foot (land-measurement use).

NOTE: The following unit symbols are used in the table:

Unit symbol	Name	Unit symbol	Name
A	ampere	lm	lumen
a	annum (year)	lx	lux
Bq	becquerel	m	meter
C	coulomb	min	minute
cd	candela	'	minute
Ci	curie	N	newton
d	day	naut mi	U.S. nautical mile
°C	degree Celsius	Oe	oersted
°	degree	Ω	ohm
dyn	dyne	Pa	pascal
F	farad	rad	radian
fc	footcandle	r	revolution
G	gauss	S	siemens
g	gram	s	second
gr	grain	"	second
Gy	gray	sr	steradian
H	henry	St	stokes
h	hour	T	tesla
ha	hectare	t	tonne
Hz	hertz	V	volt
J	joule	W	watt
K	kelvin	Wb	weber
L, ℓ, l	liter		

NOTE: Copyright SPE-AIME, *The SI Metric System of Units and SPE's Tentative Metric Standard*, Society of Petroleum Engineers, Dallas, 1977.

TABLE 1-5 Metric Conversion Factors as Exact Numerical Multiples of SI Units

The first two digits of each numerical entry represent a power of 10. For example, the entry “-02 2.54” expresses the fact that 1 in = 2.54 × 10⁻² m.

To convert from	To	Multiply by	To convert from	To	Multiply by
abampere	ampere	+01 1.00	fluid ounce (U.S.)	meter ³	-05 2.957 352
abcoumb	coulomb	+01 1.00	foot	meter	-01 3.048
abfarad	farad	+09 1.00	foot (U.S. survey)	meter	-01 3.048 006
abhenry	henry	-09 1.00	foot of water (39.2°F)	newton/meter ²	+03 2.988 98
abmho	mho	+09 1.00	footcandle	lumen/meter ²	+01 1.076 391
abohm	ohm	-09 1.00	footlambert	candela/meter ²	+00 3.426 259
abvolt	volt	-08 1.00	furlong	meter	+02 2.011 68
acre	meter ²	+03 4.046 856	gal (galileo)	meter/second ²	-02 1.00
ampere (international of 1948)	ampere	-01 9.998 35	gallon (U.K. liquid)	meter ³	-03 4.546 087
angstrom	meter	-10 1.00	gallon (U.S. dry)	meter ³	-03 4.404 883
are	meter ²	+02 1.00	gallon (U.S. liquid)	meter ³	-03 3.785 411
astronomical unit	meter	+11 1.495 978	gamma	tesla	-09 1.00
atmosphere	newton/meter ²	+05 1.013 25	gauss	tesla	-04 1.00
bar	newton/meter ²	+05 1.00	gilbert	ampere turn	-01 7.957 747
barn	meter ²	-28 1.00	gill (U.K.)	meter ³	-04 1.420 652
barrel (petroleum 42 gal)	meter ³	-01 1.589 873	gill (U.S.)	meter ³	-04 1.182 941
barye	newton/meter ²	-01 1.00	grad	degree (angular)	-01 9.00
British thermal unit (ISO/TC 12)	joule	+03 1.055 06	grad	radian	-02 1.570 796
British thermal unit (International Steam Table)	joule	+03 1.055 04	grain	kilogram	-05 6.479 891
British thermal unit (mean)	joule	+03 1.055 87	gram	kilogram	-03 1.00
British thermal unit (thermochemical)	joule	+03 1.054 350	hand	meter	-01 1.016
British thermal unit (39°F)	joule	+03 1.059 67	hectare	meter ²	+04 1.00
British thermal unit (60°F)	joule	+03 1.054 68	henry (international of 1948)	henry	+00 1.000 495
bushel (U.S.)	meter ³	-02 3.523 907	hogshead (U.S.)	meter ³	-01 2.384 809
cable	meter	+02 2.194 56	horsepower (550 ft lbf/s)	watt	+02 7.456 998
caliber	meter	-04 2.54	horsepower (boiler)	watt	+03 9.809 50
calorie (International Steam Table)	joule	+00 4.1868	horsepower (electric)	watt	+02 7.46
calorie (mean)	joule	+00 4.190 02	horsepower (metric)	watt	+02 7.354 99
calorie (thermochemical)	joule	+00 4.184	horsepower (U.K.)	watt	+02 7.457
calorie (15°C)	joule	+00 4.185 80	horsepower (water)	watt	+02 7.460 43
calorie (20°C)	joule	+00 4.181 90	hour (mean solar)	second (mean solar)	+03 3.60
calorie (kilogram, International Steam Table)	joule	+03 4.186 8	hour (sidereal)	second (mean solar)	+03 3.590 170
calorie (kilogram, mean)	joule	+03 4.190 02	hundredweight (long)	kilogram	+01 5.080 234
calorie (kilogram, thermochemical)	joule	+03 4.184	hundredweight (short)	kilogram	+01 4.535 923
carat (metric)	kilogram	-04 2.00	inch	meter	-02 2.54
Celsius (temperature)	kelvin	$t_K = t_c + 273.15$	inch of mercury (32°F)	newton/meter ²	+03 3.386 389
centimeter of mercury (0°C)	newton/meter ²	+03 1.333 22	inch of mercury (60°F)	newton/meter ²	+03 3.376 85
centimeter of water (4°C)	newton/meter ²	+01 9.806 38	inch of water (39.2°F)	newton/meter ²	+02 2.490 82
chain (engineer's)	meter	+01 3.048	inch of water (60°F)	newton/meter ²	+02 2.4884
chain (surveyor's or Gunter's)	meter	+01 2.011 68	joule (international of 1948)	joule	+00 1.000 165
circular mil	meter ²	-10 5.067 074	kayser	1/meter	+02 1.00
cord	meter ³	+00 3.624 556	kilocalorie (International Steam Table)	joule	+03 4.186 74
coulomb (international of 1948)	coulomb	-01 9.998 35	kilocalorie (mean)	joule	+03 4.190 02
cubit	meter	-01 4.572	kilocalorie (thermochemical)	joule	+03 4.184
cup	meter ³	-04 2.365 882	kilogram mass	kilogram	+00 1.00
curie	disintegration/second	+10 3.70	kilogram-force (kgf)	newton	+00 9.806 65
day (mean solar)	second (mean solar)	+04 8.64	kilopond-force	newton	+00 9.806 65
day (sidereal)	second (mean solar)	+04 8.616 409	kip	newton	+03 4.448 221
degree (angle)	radian	-02 1.745 329	knot (international)	meter/second	-01 5.144 444
denier (international)	kilogram/meter	-07 1.111 111	lambert	candela/meter ²	+04 1/π
dram (avoirdupois)	kilogram	-03 1.771 845	lambert	candela/meter ²	+03 3.183 098
dram (troy or apothecary)	kilogram	-03 3.887 934	langley	joule/meter ²	+04 4.184
dram (U.S. fluid)	meter ³	-06 3.696 691	lbf (pound-force, avoirdupois)	newton	+00 4.448 221
dyne	newton	-05 1.00	lbm (pound-mass, avoirdupois)	kilogram	-01 4.535 923
electron volt	joule	-19 1.602 10	league (British nautical)	meter	+03 5.559 552
erg	joule	-07 1.00	league (international nautical)	meter	+03 5.556
Fahrenheit (temperature)	kelvin	$t_K = (5/9)(t_F + 459.67)$	league (statute)	meter	+03 4.828 032
Fahrenheit (temperature)	Celsius	$t_c = (5/9)(t_F - 32)$	light-year	meter	+15 9.460 55
farad (international of 1948)	farad	-01 9.995 05	link (engineer's)	meter	-01 3.048
faraday (based on carbon 12)	coulomb	+04 9.648 70	link (surveyor's or Gunter's)	meter	-01 2.011 68
faraday (chemical)	coulomb	+04 9.649 57	liter	meter ³	-03 1.00
faraday (physical)	coulomb	+04 9.652 19	lux	lumen/meter ²	+00 1.00
fathom	meter	+00 1.828 8	maxwell	weber	-08 1.00
fermi (femtometer)	meter	-15 1.00	meter	wavelengths Kr 86	+06 1.650 763
			micrometer	meter	-06 1.00
			mil	meter	-05 2.54
			mile (U.S. statute)	meter	+03 1.609 344
			mile (U.K. nautical)	meter	+03 1.853 184
			mile (international nautical)	meter	+03 1.852
			mile (U.S. nautical)	meter	+03 1.852
			millibar	newton/meter ²	+02 1.00
			millimeter of mercury (0°C)	newton/meter ²	+02 1.333 224

TABLE 1-5 Metric Conversion Factors as Exact Numerical Multiples of SI Units (Concluded)

The first two digits of each numerical entry represent a power of 10. For example, the entry “-02 2.54” expresses the fact that 1 in = 2.54 × 10⁻².

To convert from	To	Multiply by	To convert from	To	Multiply by
minute (angle)	radian	-04 2.908 882	second (ephemeris)	second	+00 1.000 000
minute (mean solar)	second (mean solar)	+01 6.00	second (mean solar)	second (ephemeris)	Consult
minute (sidereal)	second (mean solar)	+01 5.983 617		American	
month (mean calendar)	second (mean solar)	+06 2.628		Ephemeris	
nautical mile (international)	meter	+03 1.852		and Nautical	
nautical mile (U.S.)	meter	+03 1.852		Almanac	
nautical mile (U.K.)	meter	+03 1.853 184	second (sidereal)	second (mean solar)	-01 9.972 695
oersted	ampere/meter	+01 7.957 747	section	meter ²	+06 2.589 988
ohm (international of 1948)	ohm	+00 1.000 495	scruple (apothecary)	kilogram	-03 1.295 978
ounce-force (avoirdupois)	newton	-01 2.780 138	shake	second	-08 1.00
ounce-mass (avoirdupois)	kilogram	-02 2.834 952	skein	meter	+02 1.097 28
ounce-mass (troy or apothecary)	kilogram	-02 3.110 347	slug	kilogram	+01 1.459 390
ounce (U.S. fluid)	meter ³	-05 2.957 352	span	meter	-01 2.286
pace	meter	-01 7.62	statampere	ampere	-10 3.335 640
parsec	meter	+16 3.083 74	statcoulomb	coulomb	-10 3.335 640
pascal	newton/meter ²	+00 1.00	statfarad	farad	-12 1.112 650
peck (U.S.)	meter ³	-03 8.809 767	stathenry	henry	+11 8.987 554
pennyweight	kilogram	-03 1.555 173	statmho	mho	-12 1.112 650
perch	meter	+00 5.0292	statohm	ohm	+11 8.987 554
phot	lumen/meter ²	+04 1.00	statute mile (U.S.)	meter	+03 1.609 344
pica (printer's)	meter	-03 4.217 517	statvolt	volt	+02 2.997 925
pint (U.S. dry)	meter ³	-04 5.506 104	stere	meter ³	+00 1.00
pint (U.S. liquid)	meter ³	-04 4.731 764	still	candela/meter ²	+04 1.00
point (printer's)	meter	-04 3.514 598	stoke	meter ² /second	-04 1.00
poise	(newton-second)/meter ²	-01 1.00	tablespoon	meter ³	-05 1.478 676
pole	meter	+00 5.0292	teaspoon	meter ³	-06 4.928 921
pound-force (lbf)	newton	+00 4.448 221	ton (assay)	kilogram	-02 2.916 666
avoirdupois)			ton (long)	kilogram	+03 1.016 046
pound-mass (lbm)	kilogram	-01 4.535 923	ton (metric)	kilogram	+03 1.00
avoirdupois)			ton (nuclear equivalent of TNT)	joule	+09 4.20
pound-mass (troy or	kilogram	-01 3.732 417	ton (register)	meter ³	+00 2.831 684
apothecary)			ton (short, 2000 lb)	kilogram	+02 9.071 847
poundal	newton	-01 1.382 549	tonne	kilogram	+03 1.00
quart (U.S. dry)	meter ³	-03 1.101 220	torr (0°C)	newton/meter ²	+02 1.333 22
quart (U.S. liquid)	meter ³	-04 9.463 529	township	meter ²	+07 9.323 957
rad (radiation dose	joule/kilogram	-02 1.00	unit pole	weber	-07 1.256 637
absorbed)			volt (international of 1948)	volt	+00 1.000 330
Rankine (temperature)	kelvin	$t_K = (5/9)t_R$	watt (international of 1948)	watt	+00 1.000 165
rayleigh (rate of photon	1/second-meter ²	+10 1.00	yard	meter	-01 9.144
emission)			year (calendar)	second (mean solar)	+07 3.1536
rhe	meter ² /(newton-	+01 1.00	year (sidereal)	second (mean solar)	+07 3.155 815
	second)		year (tropical)	second (mean solar)	+07 3.155 692
rod	meter	+00 5.0292	year 1900, tropical, Jan., day	second (ephemeris)	+07 3.155 692
roentgen	coulomb/kilogram	-04 2.579 76	0, hour 12		
rutherford	disintegration/second	+06 1.00	year 1900, tropical, Jan., day	second	+07 3.155 692
second (angle)	radian	-06 4.848 136	0, hour 12		

TABLE 1-6 Alphabetical Listing of Common Conversions

To convert from	To	Multiply by	To convert from	To	Multiply by
Acres	Square feet	43,560	Drams (avoirdupois)	Grams	1.7719
Acres	Square meters	4074	Dynes	Newtons	1×10^{-5}
Acres	Square miles	0.001563	Ergs	Joules	1×10^{-7}
Acre-feet	Cubic meters	1233	Faradays	Coulombs (abs.)	96,500
Ampere-hours (absolute)	Coulombs (absolute)	3600	Fathoms	Feet	6
Angstrom units	Inches	3.937×10^{-9}	Feet	Meters	0.3048
Angstrom units	Meters	1×10^{-10}	Feet per minute	Centimeters per second	0.5080
Angstrom units	Microns	1×10^{-4}	Feet per minute	Miles per hour	0.011364
Atmospheres	Millimeters of mercury at 32°F	760	Feet per (second) ²	Meters per (second) ²	0.3048
Atmospheres	Dynes per square centimeter	1.0133×10^6	Feet of water at 39.2°F.	Newtons per square meter	2989
Atmospheres	Newtons per square meter	101,325	Foot-poundals	B.t.u.	3.995×10^{-5}
Atmospheres	Feet of water at 39.1°F	33.90	Foot-poundals	Joules	0.04214
Atmospheres	Grams per square centimeter	1033.3	Foot-poundals	Liter-atmospheres	4.159×10^{-4}
Atmospheres	Inches of mercury at 32°F	29.921	Foot-pounds	B.t.u.	0.0012856
Atmospheres	Pounds per square foot	2116.3	Foot-pounds	Calories, gram	0.3239
Atmospheres	Pounds per square inch	14.696	Foot-pounds	Foot-poundals	32.174
Bags (cement)	Pounds (cement)	94	Foot-pounds	Horsepower-hours	5.051×10^{-7}
Barrels (cement)	Pounds (cement)	376	Foot-pounds	Kilowatt-hours	3.766×10^{-7}
Barrels (oil)	Cubic meters	0.15899	Foot-pounds	Liter-atmospheres	0.013381
Barrels (oil)	Gallons	42	Foot-pounds force	Joules	1.3558
Barrels (U.S. liquid)	Cubic meters	0.11924	Foot-pounds per second	Horsepower	0.0018182
Barrels (U.S. liquid)	Gallons	31.5	Foot-pounds per second	Kilowatts	0.0013558
Barrels per day	Gallons per minute	0.02917	Furlongs	Miles	0.125
Bars	Atmospheres	0.9869	Gallons (U.S. liquid)	Barrels (U.S. liquid)	0.03175
Bars	Newtons per square meter	1×10^5	Gallons	Cubic meters	0.003785
Bars	Pounds per square inch	14.504	Gallons	Cubic feet	0.13368
Board feet	Cubic feet	$\frac{1}{2}$	Gallons	Gallons (Imperial)	0.8327
Boiler horsepower	B.t.u. per hour	33,480	Gallons	Liters	3.785
Boiler horsepower	Kilowatts	9.803	Gallons	Ounces (U.S. fluid)	128
B.t.u.	Calories (gram)	252	Gallons per minute	Cubic feet per hour	8.021
B.t.u.	Centigrade heat units (c.h.u. or p.c.u.)	0.55556	Gallons per minute	Cubic feet per second	0.002228
B.t.u.	Foot-pounds	777.9	Grains	Grams	0.06480
B.t.u.	Horsepower-hours	3.929×10^{-4}	Grains	Pounds	$\frac{1}{7000}$
B.t.u.	Joules	1055.1	Grains per cubic foot	Grams per cubic meter	2.2884
B.t.u.	Liter-atmospheres	10.41	Grains per gallon	Parts per million	17.118
B.t.u.	Pounds carbon to CO ₂	6.88×10^{-5}	Grains	Drams (avoirdupois)	0.5644
B.t.u.	Pounds water evaporated from and at 212°F	0.001036	Grains	Drams (troy)	0.2572
B.t.u.	Cubic foot-atmospheres	0.3676	Grains	Grains	15.432
B.t.u.	Kilowatt-hours	2.930×10^{-4}	Grains	Kilograms	0.001
B.t.u. per cubic foot	Joules per cubic meter	37,260	Grains	Pounds (avoirdupois)	0.0022046
B.t.u. per hour	Watts	0.29307	Grains	Pounds (troy)	0.002679
B.t.u. per minute	Horsepower	0.02357	Grams per cubic centimeter	Pounds per cubic foot	62.43
B.t.u. per pound	Joules per kilogram	2326	Grams per cubic centimeter	Pounds per gallon	8.345
B.t.u. per pound per degree Fahrenheit	Calories per gram per degree centigrade	1	Grams per liter	Grains per gallon	58.42
B.t.u. per pound per degree Fahrenheit	Joules per kilogram per degree Kelvin	4186.8	Grams per liter	Pounds per cubic foot	0.0624
B.t.u. per second	Watts	1054.4	Grams per square centimeter	Pounds per square foot	2.0482
B.t.u. per square foot per hour	Joules per square meter per second	3.1546	Grams per square centimeter	Pounds per square inch	0.014223
B.t.u. per square foot per minute	Kilowatts per square foot	0.1758	Hectares	Acres	2.471
B.t.u. per square foot per second for a temperature gradient of 1°F. per inch	Calories, gram (15°C.), per square centimeter per second for a temperature gradient of 1°C. per centimeter	1.2405	Hectares	Square meters	10,000
			Horsepower (British)	B.t.u. per minute	42.42
			Horsepower (British)	B.t.u. per hour	2545
			Horsepower (British)	Foot-pounds per minute	33,000
			Horsepower (British)	Foot-pounds per second	550
			Horsepower (British)	Watts	745.7

B.t.u. (60°F) per degree Fahrenheit	Calories per degree centigrade	453.6	Horsepower (British)	Horsepower (metric)	1.0139
Bushels (U.S. dry)	Cubic feet	1.2444	Horsepower (British)	Pounds carbon to CO ₂ per hour	0.175
Bushels (U.S. dry)	Cubic meters	0.03524	Horsepower (British)	Pounds water evaporated per hour at 212°F	2.64
Calories, gram	B.t.u.	3.968×10^{-3}	Horsepower (metric)	Foot-pounds per second	542.47
Calories, gram	Foot-pounds	3.087	Horsepower (metric)	Kilogram-meters per second	75.0
Calories, gram	Joules	4.1868	Hours (mean solar)	Seconds	3600
Calories, gram	Liter-atmospheres	4.130×10^{-2}	Inches	Meters	0.0254
Calories, gram	Horsepower-hours	1.5591×10^{-6}	Inches of mercury at 60°F	Newtons per square meter	3376.9
Calories, gram, per gram per degree C.	Joules per kilogram per degree Kelvin	4186.8	Inches of water at 60°F	Newtons per square meter	248.84
Calories, kilogram	Kilowatt-hours	0.0011626	Joules (absolute)	B.t.u. (mean)	9.480×10^{-4}
Calories, kilogram per second	Kilowatts	4.185	Joules (absolute)	Calories, gram (mean)	0.2389
Candle power (spherical)	Lumens	12.556	Joules (absolute)	Cubic foot-atmospheres	0.3485
Carats (metric)	Grams	0.2	Joules (absolute)	Foot-pounds	0.7376
Centigrade heat units	B.t.u.	1.8	Joules (absolute)	Kilowatt-hours	2.7778×10^{-7}
Centimeters	Angstrom units	1×10^8	Joules (absolute)	Liter-atmospheres	0.009869
Centimeters	Feet	0.03281	Kilocalories	Joules	4186.8
Centimeters	Inches	0.3937	Kilograms	Pounds (avoirdupois)	2.2046
Centimeters	Meters	0.01	Kilograms force	Newtons	9.807
Centimeters	Microns	10,000	Kilograms per square centimeter	Pounds per square inch	14.223
Centimeters of mercury at 0°C.	Atmospheres	0.013158	Kilometers	Miles	0.6214
Centimeters of mercury at 0°C.	Feet of water at 39.1°F.	0.4460	Kilowatt-hours	B.t.u.	3414
Centimeters of mercury at 0°C.	Newtons per square meter	1333.2	Kilowatts	Foot-pounds	2.6552×10^6
Centimeters of mercury at 0°C.	Pounds per square foot	27.845	Knots (international)	Horsepower	1.3410
Centimeters of mercury at 0°C.	Pounds per square inch	0.19337	Knots (nautical miles per hour)	Meters per second	0.5144
Centimeters per second	Feet per minute	1.9685	Lamberts	Miles per hour	1.1516
Centimeters of water at 4°C.	Newtons per square meter	98.064	Liter-atmospheres	Candles per square inch	2.054
Centistokes	Square meters per second	1×10^{-6}	Liter-atmospheres	Cubic foot-atmospheres	0.03532
Circular mils	Square centimeters	5.067×10^{-6}	Liters	Foot-pounds	74.74
Circular mils	Square inches	7.854×10^{-7}	Liters	Cubic feet	0.03532
Circular mils	Square mils	0.7854	Liters	Cubic meters	0.001
Cords	Cubic feet	128	Lumens	Gallons	0.26418
Cubic centimeters	Cubic feet	3.532×10^{-5}	Micromicrons	Watts	0.001496
Cubic centimeters	Gallons	2.6417×10^{-4}	Microns	Microns	1×10^{-6}
Cubic centimeters	Ounces (U.S. fluid)	0.03381	Microns	Angstrom units	1×10^4
Cubic centimeters	Quarts (U.S. fluid)	0.0010567	Miles (nautical)	Meters	1×10^{-6}
Cubic feet	Bushels (U.S.)	0.8036	Miles (nautical)	Feet	6080
Cubic feet	Cubic centimeters	28,317	Miles	Miles (U.S. statute)	1.1516
Cubic feet	Cubic meters	0.028317	Miles	Feet	5280
Cubic feet	Cubic yards	0.03704	Miles per hour	Meters	1609.3
Cubic feet	Gallons	7.481	Miles per hour	Feet per second	1.4667
Cubic feet	Liters	28.316	Milliliters	Meters per second	0.4470
Cubic foot-atmospheres	Foot-pounds	2116.3	Millimeters	Cubic centimeters	1
Cubic foot-atmospheres	Liter-atmospheres	28.316	Millimeters of mercury at 0°C.	Meters	0.001
Cubic feet of water (60°F.)	Pounds	62.37	Millimicrons	Newtons per square meter	133.32
Cubic feet per minute	Cubic centimeters per second	472.0	Mils	Microns	0.001
Cubic feet per minute	Gallons per second	0.1247	Mils	Inches	0.001
Cubic feet per second	Gallons per minute	448.8	Minims (U.S.)	Meters	2.54×10^{-5}
Cubic feet per second	Million gallons per day	0.64632	Minutes (angle)	Cubic centimeters	0.06161
Cubic inches	Cubic meters	1.6387×10^{-5}	Minutes (mean solar)	Radians	2.909×10^{-4}
Cubic yards	Cubic meters	0.76456	Newtons	Seconds	60
Curies	Disintegrations per minute	2.2×10^{12}	Ounces (avoirdupois)	Kilograms	0.10197
Curies	Coulombs per minute	1.1×10^{12}	Ounces (avoirdupois)	Kilograms	0.02835
Degrees	Radians	0.017453	Ounces (U.S. fluid)	Ounces (troy)	0.9115
Drams (apothecaries' or troy)	Grams	3.888	Ounces (troy)	Cubic meters	2.957×10^{-5}
				Ounces (apothecaries')	1.000

TABLE 1-6 Alphabetical Listing of Common Conversions (Concluded)

To convert from	To	Multiply by	To convert from	To	Multiply by
Pints (U.S. liquid)	Cubic meters	4.732×10^{-4}	Square centimeters	Square feet	0.0010764
Poundals	Newtons	0.13826	Square feet	Square meters	0.0929
Pounds (avoirdupois)	Grains	7000	Square feet per hour	Square meters per second	2.581×10^{-5}
Pounds (avoirdupois)	Kilograms	0.45359	Square inches	Square centimeters	6.452
Pounds (avoirdupois)	Pounds (troy)	1.2153	Square inches	Square meters	6.452×10^{-4}
Pounds per cubic foot	Grams per cubic centimeter	0.016018	Square yards	Square meters	0.8361
Pounds per cubic foot	Kilograms per cubic meter	16.018	Stokes	Square meters per second	1×10^{-4}
Pounds per square foot	Atmospheres	4.725×10^{-4}	Tons (long)	Kilograms	1016
Pounds per square foot	Kilograms per square meter	4.882	Tons (long)	Pounds	2240
Pounds per square inch	Atmospheres	0.06805	Tons (metric)	Kilograms	1000
Pounds per square inch	Kilograms per square centimeter	0.07031	Tons (metric)	Pounds	2204.6
Pounds per square inch	Newtons per square meter	6894.8	Tons (metric)	Tons (short)	1.1023
Pounds force	Newtons	4.4482	Tons (short)	Kilograms	907.18
Pounds force per square foot	Newtons per square meter	47.88	Tons (short)	Pounds	2000
Pounds water evaporated from and at 212°F.	Horsepower-hours	0.379	Tons (refrigeration)	B.t.u. per hour	12,000
Pound-centigrade units (p.c.u.)	B.t.u.	1.8	Tons (British shipping)	Cubic feet	42.00
Quarts (U.S. liquid)	Cubic meters	9.464×10^{-4}	Tons (U.S. shipping)	Cubic feet	40.00
Radians	Degrees	57.30	Torr (mm. mercury, 0°C.)	Newtons per square meter	133.32
Revolutions per minute	Radians per second	0.10472	Watts	B.t.u. per hour	3.413
Seconds (angle)	Radians	4.848×10^{-6}	Watts	Joules per second	1
Slugs	Gee pounds	1	Watts	Kilogram-meters per second	0.10197
Slugs	Kilograms	14.594	Watt-hours	Joules	3600
Slugs	Pounds	32.17	Yards	Meters	0.9144

TABLE 1-7 Common Units and Conversion Factors*

Mass (M)	1 pound mass = 453.5924 grams = 0.45359 kilograms = 7000 grains 1 slug = 32.174 pounds mass 1 ton (short) = 2000 pounds mass 1 ton (long) = 2240 pounds mass 1 ton (metric) = 1000 kilograms = 2204.62 pounds mass 1 pound mole = 453.59 gram moles	1 atm = 760 millimeters of mercury at 0°C (density 13.5951 g/cm ³) = 29.921 inches of mercury at 32°F = 14.696 pounds force/square inch = 33.899 feet of water at 39.1°F = 1.01325 × 10 ⁶ dynes/square centimeter = 1.01325 × 10 ⁵ Newtons/square meter
Length (L)	1 foot = 30.480 centimeters = 0.3048 meters 1 inch = 2.54 centimeters = 0.0254 meters 1 mile (U.S.) = 1.60935 kilometers 1 yard = 0.9144 meters	Density (M/L ³) 1 pound mass/cubic foot = 0.01601846 grams/cubic centimeter = 16.01846 kilogram/cubic meter
Area (L ²)	1 square foot = 929.0304 square centimeters = 0.09290304 square meters 1 square inch = 6.4516 square centimeters 1 square yard = 0.836127 square meters	Energy (H or FL) 1 British thermal unit = 251.98 calories = 1054.4 joules = 777.97 foot-pounds force = 10.409 liter-atmospheres = 0.2930 watt-hour
Volume (L ³)	1 cubic foot = 28,316.85 cubic centimeters = 0.02831685 cubic meters = 28.31685 liters = 7.481 gallons (U.S.) 1 gallon = 3.7853 liters = 231 cubic inches	Diffusivity (L ² /θ) 1 square foot/hour = 0.258 cm ² /s = 2.58 × 10 ⁻⁵ m ² /s
Time (θ)	1 hour = 60 minutes = 3600 seconds	Viscosity (M/Lθ) 1 pound mass/foot hour = 0.00413 g/cm s = 0.000413 kg/m s 1 centipoise = 0.01 poise = 0.01 g/cm s = 0.001 kg/m s = 0.000672 lbm/ft s = 0.0000209 lbf _s /ft ²
Temperature (T)	1 centigrade or Celsius degree = 1.8 Fahrenheit degree Temperature, Kelvin = T°C + 273.15 Temperature, Rankine = T°F + 459.7 Temperature, Fahrenheit = 9/5 T°C + 32 Temperature, centigrade or Celsius = 5/9 (T°F - 32) Temperature, Rankine = 1.8 T K	Thermal conductivity [H/θL ² (T/L)] 1 Btu/hr ft ² (°F/ft) = 0.00413 cal/s cm ² (°C/cm) = 1.728 J/s m ² (°C/m)
Force (F)	1 pound force = 444,822.2 dynes = 4.448222 Newtons = 32.174 pounds	Heat transfer coefficient 1 Btu/hr ft ² °F = 5.678 J/s m ² °C
Pressure (F/L ²)	Normal atmospheric pressure	Heat capacity (H/MT) 1 Btu/lbm °F = 1 cal/g °C = 4184 J/kg °C
		Gas constant 1.987 Btu/lbm mole °R = 1.987 cal/mol K = 82.057 atm cm ³ /mol K = 0.7302 atm ft ³ /lb mole °F = 10.73 (lb _f /in. ²) (ft ³)/lb mole °R = 1545 (lb _f /ft ²) (ft ³)/lb mole °R = 8.314 (N/m ²) (m ³)/mol K
		Gravitational acceleration g = 9.8066 m/s ² = 32.174 ft/s ²

NOTE: U.S. customary units, or British units, on left and SI units on right.
 *Adapted from Faust et al., *Principles of Unit Operations*, John Wiley and Sons, 1980.

TABLE 1-8 Kinematic-Viscosity Conversion Formulas

Viscosity scale	Range of t, sec	Kinematic viscosity, stokes
Saybolt Universal	32 < t < 100	0.00226t - 1.95/t
	t > 100	0.00220t - 1.35/t
Saybolt Furol	25 < t < 40	0.0224t - 1.84/t
	t > 40	0.0216t - 0.60/t
Redwood No. 1	34 < t < 100	0.00260t - 1.79/t
	t > 100	0.00247t - 0.50/t
Redwood Admiralty Engler		0.027t - 20/t
		0.00147t - 3.74/t

TABLE 1-9 Values of the Gas-Law Constant

Temp. scale	Press. units	Vol. units	Wt. units	Energy units*	R
Kelvin			g-moles	calories	1.9872
			g-moles	joules (abs)	8.3144
			g-moles	joules (int)	8.3130
		atm.	cm ³	g-moles atm cm ³	82.057
		atm.	liters	g-moles atm liters	0.08205
		mm. Hg	liters	g-moles mm Hg-liters	62.361
		bar	liters	g-moles bar-liters	0.08314
		kg/cm ²	liters	g-moles kg/(cm ²)(liters)	0.08478
		atm	ft ³	lb-moles atm-ft ³	1.314
		mm Hg	ft ³	lb-moles mm Hg-ft ³	998.9
				lb-moles chu or pcu	1.9872
				lb-moles Btu	1.9872
Rankine			lb-moles	hp-hr	0.0007805
			lb-moles	kw-hr	0.0005819
			lb-moles	atm-ft ³	0.7302
	atm	ft ³	lb-moles	in Hg-ft ³	21.85
	in Hg	ft ³	lb-moles	mm Hg-ft ³	555.0
	mm Hg	ft ³	lb-moles	(lb)/(ft ²)/in ²	10.73
	lb/m ² abs	ft ³	lb-moles	ft-lb	1545.0
	lb/ft ² abs	ft ³	lb-moles		

*Energy units are the product of pressure units and volume units.

TABLE 1-10 United States Customary System of Weights and Measures

Linear Measure	
12 inches (in) or (") = 1 foot (ft) or (')	
3 feet = 1 yard (yd)	
16.5 feet } = 1 rod (rd)	
5.5 yards } = 1 mile (mi)	
5280 feet } = 1 mile (mi)	
320 rods } = 1 mile (mi)	
1 mil = 0.001 inch	
<i>Nautical:</i>	
6080.2 feet = 1 nautical mile	
6 feet = 1 fathom	
120 fathoms = 1 cable length	
1 knot = 1 nautical mile per hour	
60 nautical miles = 1° of latitude	
Square Measure	
144 sq. inches (sq. in) or (in ²) or (□") = 1 sq. foot (ft ²) or (□')	
9 sq. feet (ft ²) (□') = 1 sq. yard (yd ²)	
30.25 sq. yards = 1 sq. rod, pole, or perch	
160 sq. rods = $\left\{ \begin{array}{l} 10 \text{ sq. chains} \\ 43,560 \text{ sq. ft} \end{array} \right\} = 1 \text{ acre}$	
640 acres = 1 sq. mile = 1 section	
1 circular inch (area of circle of 1 inch diameter) = 0.7854 sq. inch	
1 sq. inch = 1.2732 circular inch	
1 circular mil = area of circle of 0.001 inch diameter	
1,000,000 circular mils = 1 circular inch	
Circular Measure	
60 seconds (") (sec) = 1 minute (min) or (')	
60 minutes (') = 1 degree (°)	
90 degrees (°) = 1 quadrant	
360 degrees (°) = 1 circumference	
57.29578 degrees $\left\{ \begin{array}{l} = 1 \text{ radian (rad.)} \\ = 57^\circ 17' 44.81'' \end{array} \right.$	
Volume Measure	
<i>Solid:</i>	
1728 cubic in (cu. in) (in ³) = 1 cubic foot (cu. ft)(ft ³)	
27 cu. ft = 1 cubic yard (cu. yd)	
<i>Dry Measure:</i>	
2 pints = 1 quart	
8 quarts = 1 peck	
4 pecks = 1 bushel	
1 United States Winchester bushel = 2150.42 cubic inches	
<i>Liquid:</i>	
4 gills = 1 pint (pt)	
2 pints = 1 quart (qt)	
4 quarts = 1 gallon (gal)	
7.4805 gallons = 1 cubic foot	
<i>Apothecaries' Liquid:</i>	
60 minims (min. or \mathfrak{m}) = 1 fluid dram or drachm	
8 drams (℥) = 1 fluid ounce	
16 ounces (oz. ℥) = 1 pint	
Avoirdupois Weight	
16 drams = 437.5 grains = 1 ounce (oz)	
16 ounces = 7000 grains = 1 pound (lb)	
100 pounds = 1 hundredweight (cwt)	
2000 pounds = 1 short ton: 2240 pounds = 1 long ton	
Troy Weight	
24 grains = 1 pennyweight (dwt)	
20 pennyweights = 1 ounce (oz)	
12 ounces = 1 pound (lb)	
Apothecaries' Weight	
20 grains (gr) = 1 scruple (℞)	
3 scruples = 1 dram (℥)	
8 drams = 1 ounce (℥)	
12 ounces = 1 pound (lb)	

TABLE 1-11 Temperature Conversion Formulas

°F = (°C × 5/9) + 32
°C = (°F - 32) × 5/9
°R = °F + 459.69
°K = °C + 273.15
°K = °R × 5/9
Temperature difference, ΔT
°F = °C × 9/5
NOTE: An extensive table of temperature conversions may be found in the sixth edition of the <i>Handbook</i> (Table 1-12).

TABLE 1-12 Greek Alphabet

Alpha = A, α = A, a	Nu = N, ν = N, n
Beta = B, β = B, b	Xi = Ξ, ξ = X, x
Gamma = Γ, γ = G, g	Omicron = O, ο = O, o
Delta = Δ, δ = D, d	Pi = Π, π = P, p
Epsilon = Ε, ε = E, e	Rho = Ρ, ρ = R, r
Zeta = Ζ, ζ = Z, z	Sigma = Σ, σ = S, s
Eta = Η, η = E, e	Tau = Τ, τ = T, t
Theta = Θ, θ = Th, th	Upsilon = Υ, υ = U, u
Iota = Ι, ι = I, i	Phi = Φ, φ = Ph, ph
Kappa = Κ, κ = K, k	Chi = Χ, χ = Ch, ch
Lambda = Λ, λ = L, l	Psi = Ψ, ψ = Ps, ps
Mu = Μ, μ = M, m	Omega = Ω, ω = O, o

TABLE 1-14 Fundamental Physical Constants

1 sec = 1.00273791 sidereal seconds	sec = mean solar second
$g_0 = 9.80665 \text{ m/sec}^2$	Definition: g_0 = standard gravity
1 liter = 0.001 cu. m	
1 atm = 101,325 newtons/sq m	Definition: atm = standard atmosphere
1 mm Hg (pressure) = $(1/760) \text{ atm}$	mm Hg (pressure) = standard millimeter mercury
= 133.3224 newtons/sq m	
1 int ohm = 1.000495 ± 0.000015 abs ohm	int = international; abs = absolute
1 int amp = 0.999835 ± 0.000025 abs amp	amp = ampere
1 int coul = 0.999835 ± 0.000025 abs coul	coul = coulomb
1 int volt = 1.000330 ± 0.000029 abs volt	
1 int watt = 1.000165 ± 0.000052 abs watt	
1 int joule = 1.000165 ± 0.000052 abs joule	
$T_{0^\circ\text{C}} = 273.150 \pm 0.010^\circ\text{K}$	Absolute temperature of the ice point, 0°C
$(PV)_{0^\circ\text{C}}^{P=0} = (RT)_{0^\circ\text{C}} = 2271.16 \pm 0.04$ abs joule/mole	PV product for ideal gas at 0°C
= 22,414.6 \pm 0.4 cu. cm atm/mole	
= 22.4146 \pm 0.0004 liter atm/mole	R = gas constant per mole
$R = 8.31439 \pm 0.00034$ abs joule/deg mole	
= 1.98719 \pm 0.00013 cal/deg mole	
= 82.0567 \pm 0.0034 cu. cm atm/deg mole	
= 0.0820567 \pm 0.0000034 liter atm/deg mole	
$\ln 10 = 2.302585$	\ln = natural logarithm (base e)
$R \ln 10 = 19.14460 \pm 0.00078$ abs joule/deg mole	
= 4.57567 \pm 0.00030 cal/deg mole	
$N = (6.02283 \pm 0.0022) \times 10^{23}$ /mole	N = Avogadro number
$h = (6.6242 \pm 0.0044) \times 10^{-34}$ joule sec	h = Planck constant
$c = (2.99776 \pm 0.00008) \times 10^8$ m/sec	c = velocity of light
$(h^2/8\pi^2k) = (4.0258 \pm 0.0037) \times 10^{-39}$ g sq cm deg	Constant in rotational partition function of gases
$(h/8\pi^2c) = (2.7986 \pm 0.0018) \times 10^{-39}$ g cm	Constant relating wave number and moment of inertia
$Z = Nhc = 11.9600 \pm 0.0036$ abs joule cm/mole	Z = constant relating wave number and energy per mole
= 2.85851 \pm 0.0009 cal cm/mole	
$(Z/R) = (hc/k) = c_2 = 1.43847 \pm 0.00045$ cm deg	c_2 = second radiation constant
$\mathcal{F} = 96,501.2 \pm 10.0$ int coul/g-equiv or int joule/int volt g-equiv	\mathcal{F} = Faraday constant
= 96,485.3 \pm 10.0 abs coul/g-equiv or abs joule/abs volt g-equiv	
= 23,068.1 \pm 2.4 cal/int volt g-equiv	
= 23,060.5 \pm 2.4 cal/abs volt g-equiv	
$e = (1.60199 \pm 0.00060) \times 10^{-19}$ abs coul	e = electronic charge
= $(1.60199 \pm 0.00060) \times 10^{-20}$ abs emu	
= $(4.80239 \pm 0.00180) \times 10^{-10}$ abs esu	
1 int electron-volt/molecule = 96,501.2 \pm 10 int joule/mole	
= 23,068.1 \pm 2.4 cal/mole	
1 abs electron-volt/molecule = 96,485.3 \pm 10. abs joule/mole	
= 23,060.5 \pm 2.4 cal/mole	
1 int electron-volt = $(1.60252 \pm 0.00060) \times 10^{-12}$ erg	
1 abs electron-volt = $(1.60199 \pm 0.00060) \times 10^{-12}$ erg	
$hc = (1.23916 \pm 0.00032) \times 10^{-4}$ int electron-volt cm	Constant relating wave number and energy per molecule
= $(1.23957 \pm 0.00032) \times 10^{-4}$ abs electron-volt cm	
$k = (8.61442 \pm 0.00100) \times 10^{-5}$ int electron-volt/deg	k = Boltzmann constant
= $(8.61727 \pm 0.00100) \times 10^{-5}$ abs electron-volt/deg	
= $(R/N) = (1.38048 \pm 0.00050) \times 10^{-23}$ joule/deg	
1 IT cal = $(1/860) = 0.00116279$ int watt-hr	Definition of IT cal: IT = International steam tables
= 4.18605 int joule	
= 4.18674 abs joule	
= 1.000654 cal	
1 cal = 4.1840 abs joule	cal = thermochemical calorie
= 4.1833 int joule	Definition: cal = thermochemical calorie
= 41.2929 \pm 0.0020 cu. cm atm	
= 0.0412929 \pm 0.0000020 liter atm	
1 IT cal/g = 1.8 Btu/lb	Definition of Btu: Btu = IT British Thermal Unit
1 Btu = 251.996 IT cal	
= 0.293018 int watt-hr	
= 1054.866 int joule	
= 1055.040 abs joule	
= 252.161 cal	
1 horsepower = 550 ft-lb (wt)/sec	cal = thermochemical calorie
= 745.578 int watt	Definition of horsepower (mechanical): lb (wt) = weight of 1 lb
= 745.70 abs watt	at standard gravity
1 in = $(1/0.3937) = 2.54$ cm	Definition of in: in = U.S. inch
1 ft = 0.304800610 m	ft = U.S. foot (1 ft = 12 in)
1 lb = 453.5924277 g	
1 gal = 231 cu. in	Definition; lb = avoirdupois pound
= 0.133680555 cu. ft	Definition; gal = U.S. gallon
= 3.785412×10^{-3} cu. m	
= 3.785412 liter	

CONVERSION OF VALUES FROM U.S. CUSTOMARY UNITS TO SI UNITS

American engineers are probably more familiar with the magnitude of physical entities in U.S. customary units than in SI units. Consequently, errors made in the conversion from one set of units to the other may go undetected. The following six examples will show how to convert the elements in six dimensionless groups. Proper conversions will result in the same numerical value for the dimensionless number. The dimensionless numbers used as examples are the Reynolds, Prandtl, Nusselt, Grashof, Schmidt, and Archimedes numbers.

Table 1-7 provides a number of useful conversion factors. To make a conversion of an element in U.S. customary units to SI units, one multiplies the value of the U.S. customary unit, found on the left side in the table, by the equivalent value on the right side. For example, to convert 10 British thermal units to joules, one multiplies 10 by 1054.4 to obtain 10544 joules.

In each example, the initial values of the factors are expressed in U.S. customary units, and the dimensionless value is calculated. Then the factors are converted to SI units, and the dimensionless value is recalculated. The two dimensionless values will be approximately the same. (Small variations occur due to the number of significant figures carried in the solution.)

Example 1. Calculation of a Reynolds Number

$$N_{Re} = \frac{DV\rho}{\mu}$$

U.S. customary units

$$D = 3 \text{ in.} = \frac{3}{12} \text{ ft}$$

$$V = 6 \text{ ft/s}$$

$$\rho = 0.08 \text{ lbm/ft}^3$$

$$\mu = 0.015 \text{ cp} = (0.015)(0.000672) \text{ lbm/ft-s}$$

$$N_{Re} = \frac{(3/12)(6)(0.08)}{(0.015)(0.000672)} = 11,904$$

SI units

$$D = (3)(0.0254) \text{ m}$$

$$V = (6)(0.3048) \text{ m/s}$$

$$\rho = (0.08)(16.018) \text{ kg/m}^3$$

$$\mu = (0.015)(0.001) \text{ kg/m-s}$$

$$N_{Re} = \frac{(3 \times 0.0254)(6 \times 0.3048)(0.08 \times 16.018)}{(0.015)(0.001)} = 11,904$$

Example 2. Calculation of a Prandtl Number

$$N_{Pr} = \frac{C_p \mu}{k}$$

U.S. customary units

$$\gamma_p = 0.47 \text{ Btu/lbm } ^\circ\text{F}$$

$$\mu = 15 \text{ centipoise} = (15)(0.000672) (3600) \text{ lbm/ft-hr}$$

$$k = 0.065 \text{ Btu/hr-ft}^2 (^\circ\text{F/ft})$$

$$N_{Pr} = \frac{(0.47)(15 \times 0.000672 \times 3600)}{0.065} = 262.4$$

SI units

$$\gamma = (0.47)(4184) \text{ J/kg } ^\circ\text{C}$$

$$\mu = (15)(0.001) \text{ kg/m-s}$$

$$k = (0.065)(1.728) \text{ J/s-m}^2 (^\circ\text{C/m})$$

$$N_{Pr} = \frac{(0.47)(4184)(15)(0.001)}{(0.065)(1.728)} = 262.6$$

(Difference due to rounding)

Example 3. Calculation of a Nusselt Number

$$N_{Nu} = \frac{hD}{k}$$

U.S. customary units

$$h = 200 \text{ Btu/hr-ft}^2 \cdot ^\circ\text{F}$$

$$D = 1.5 \text{ in.} = 1.5/12 \text{ ft}$$

$$k = 0.07 \text{ Btu/hr-ft}^2 (^\circ\text{F/ft})$$

$$N_{Nu} = \frac{(200)(1.5/12)}{0.07} = 357.1$$

SI units

$$h = (200)(5.678) \text{ J/(s-m}^2 \cdot ^\circ\text{C)}$$

$$D = (1.5)(0.0254) \text{ m}$$

$$k = (0.07)(1.728) \text{ J/s-m}^2 (^\circ\text{C/m})$$

$$N_{Nu} = \frac{(200)(5.678)(1.5)(0.0254)}{(0.07)(1.728)} = 357.7$$

(Difference due to rounding)

Example 4. Calculation of a Grashof Number

$$N_{Gr} = L^3 \rho^2 g \beta (\Delta T) / \mu^2$$

U.S. Customary units

$$L = 3 \text{ ft}$$

$$\rho = 0.0725 \text{ lbm/ft}^3$$

$$g = 32.174 \text{ ft/s}^2$$

$$\beta = 0.00168 / ^\circ\text{R}$$

$$\Delta T = 99 \text{ } ^\circ\text{R}$$

$$\mu = 0.019 \text{ centipoise} = 0.019 \times 0.000672 \text{ lbm/ft-s}$$

$$= 1.277 \times 10^{-5} \text{ lbm/ft-s}$$

$$N_{Gr} = \frac{(3^3)(0.0725)^2(32.174)(0.00168)(99)}{(1.277 \times 10^{-5})^2} = 4.66 \times 10^9$$

SI units

$$L = (3)(0.3048) = 0.9144 \text{ m}$$

$$\rho = (0.0725)(16.018) = 1.1613 \text{ kg/m}^3$$

$$g = 9.807 \text{ m/s}^2$$

$$\beta = (0.00168)/(1.8) = 0.000933 / ^\circ\text{K}$$

$$\Delta T = (99)(1.8) = 178.2 \text{ } ^\circ\text{K}$$

$$\mu = (0.019)(0.001) = 1.9 \times 10^{-5} \text{ kg/m-s}$$

$$N_{Gr} = \frac{(0.9144)^3(1.1613)^2(9.807)(0.000933)(178.2)}{(1.9 \times 10^{-5})^2} = 4.66 \times 10^9$$

Example 5. Calculation of a Schmidt Number

$$N_{Sc} = \frac{\mu}{\rho D}$$

U.S. customary units

$$\mu = 0.02 \text{ centipoise} = (0.02)(2.42) \text{ lbm/ft-hr}$$

$$\rho = 0.08 \text{ lbm/ft}^3$$

$$D = 1.0 \text{ ft}^2/\text{hr} \text{ (diffusivity)}$$

$$N_{Sc} = \frac{(0.02)(2.42)}{(0.08)(1.0)} = 0.605$$

SI units

$$\mu = (0.02)(0.001) \text{ kg/m-s}$$

$$\rho = (0.08)(16.02) \text{ kg/m}^3$$

$$D = (1.0)(2.58 \times 10^{-5}) \text{ m}^2/\text{s}$$

$$N_{Sc} = \frac{(0.02)(0.001)}{(0.08)(16.02)(1.0)(2.58 \times 10^{-5})} = 0.605$$

Example 6. Calculation of an Archimedes Number

$$N_{Ar} = \frac{d^3 \rho_f (\rho_p - \rho_f) g}{\mu^2}$$

U.S. customary units

$$d = 2 \text{ mm} = 2 / [(1000)(0.3048)] = 0.00656 \text{ ft}$$

$$\rho_f = 0.0175 \text{ lbm/ft}^3$$

$$\rho_p = 168.5 \text{ lbm/ft}^3$$

$$g = 32.174 \text{ ft/s}^2$$

$$\mu = 0.04 \text{ centipoise} = 0.04 \times 0.000672 = 2.688 \times 10^{-5} \text{ lbm/ft-s}$$

$$N_{Ar} = \frac{(0.00656)^3 (0.0175) (168.5 - 0.0175) (32.174)}{(2.688 \times 10^{-5})^2} = 37,064$$

SI units

$$d = 2/1000 \text{ m}$$

$$\rho_p = 168.5 \times 16.02 = 2699.37 \text{ kg/m}^3$$

$$\rho_f = 0.0175 \times 16.02 = 0.2804 \text{ g/m}^3$$

$$g = 9.807 \text{ m/s}^2$$

$$\mu = 0.04 \times 0.001 = 4 \times 10^{-5} \text{ kg/m-s}$$

$$N_{Ar} = \frac{(2/1000)^3 (0.2804) (2699.37 - 0.28) (9.807)}{(4 \times 10^{-5})^2} = 37,118$$

(Difference due to rounding)

SECTION 2

Physical and
Chemical Data

PERRY'S CHEMICAL ENGINEERS' HANDBOOK

8TH EDITION



BRUCE E. POLING, GEORGE H. THOMSON
DANIEL G. FRIEND, RICHARD L. ROWLEY
W. VINCENT WILDING

Copyright © 2008, 1997, 1984, 1973, 1963, 1950, 1941, 1934 by The McGraw-Hill Companies, Inc. All rights reserved. Manufactured in the United States of America. Except as permitted under the United States Copyright Act of 1976, no part of this publication may be reproduced or distributed in any form or by any means, or stored in a database or retrieval system, without the prior written permission of the publisher.

0-07-154209-4

The material in this eBook also appears in the print version of this title: 0-07-151125-3.

All trademarks are trademarks of their respective owners. Rather than put a trademark symbol after every occurrence of a trademarked name, we use names in an editorial fashion only, and to the benefit of the trademark owner, with no intention of infringement of the trademark. Where such designations appear in this book, they have been printed with initial caps.

McGraw-Hill eBooks are available at special quantity discounts to use as premiums and sales promotions, or for use in corporate training programs. For more information, please contact George Hoare, Special Sales, at george_hoare@mcgraw-hill.com or (212) 904-4069.

TERMS OF USE

This is a copyrighted work and The McGraw-Hill Companies, Inc. (“McGraw-Hill”) and its licensors reserve all rights in and to the work. Use of this work is subject to these terms. Except as permitted under the Copyright Act of 1976 and the right to store and retrieve one copy of the work, you may not decompile, disassemble, reverse engineer, reproduce, modify, create derivative works based upon, transmit, distribute, disseminate, sell, publish or sublicense the work or any part of it without McGraw-Hill’s prior consent. You may use the work for your own noncommercial and personal use; any other use of the work is strictly prohibited. Your right to use the work may be terminated if you fail to comply with these terms.

THE WORK IS PROVIDED “AS IS.” McGRAW-HILL AND ITS LICENSORS MAKE NO GUARANTEES OR WARRANTIES AS TO THE ACCURACY, ADEQUACY OR COMPLETENESS OF OR RESULTS TO BE OBTAINED FROM USING THE WORK, INCLUDING ANY INFORMATION THAT CAN BE ACCESSED THROUGH THE WORK VIA HYPERLINK OR OTHERWISE, AND EXPRESSLY DISCLAIM ANY WARRANTY, EXPRESS OR IMPLIED, INCLUDING BUT NOT LIMITED TO IMPLIED WARRANTIES OF MERCHANTABILITY OR FITNESS FOR A PARTICULAR PURPOSE. McGraw-Hill and its licensors do not warrant or guarantee that the functions contained in the work will meet your requirements or that its operation will be uninterrupted or error free. Neither McGraw-Hill nor its licensors shall be liable to you or anyone else for any inaccuracy, error or omission, regardless of cause, in the work or for any damages resulting therefrom. McGraw-Hill has no responsibility for the content of any information accessed through the work. Under no circumstances shall McGraw-Hill and/or its licensors be liable for any indirect, incidental, special, punitive, consequential or similar damages that result from the use of or inability to use the work, even if any of them has been advised of the possibility of such damages. This limitation of liability shall apply to any claim or cause whatsoever whether such claim or cause arises in contract, tort or otherwise.

DOI: 10.1036/0071511253

Physical and Chemical Data*

Bruce E. Poling *Department of Chemical Engineering, University of Toledo (Physical and Chemical Data)*

George H. Thomson *AIChE Design Institute for Physical Properties (Physical and Chemical Data)*

Daniel G. Friend *National Institute of Standards and Technology (Physical and Chemical Data)*

Richard L. Rowley *Department of Chemical Engineering, Brigham Young University (Prediction and Correlation of Physical Properties)*

W. Vincent Wilding *Department of Chemical Engineering, Brigham Young University (Prediction and Correlation of Physical Properties)*

GENERAL REFERENCES

PHYSICAL PROPERTIES OF PURE SUBSTANCES

Tables		
2-1	Physical Properties of the Elements and Inorganic Compounds	2-7
2-2	Physical Properties of Organic Compounds	2-28

VAPOR PRESSURES OF PURE SUBSTANCES

Units Conversions		2-48
Additional References		2-48
Tables		
2-3	Vapor Pressure of Water Ice from 0 to -40 °C	2-48
2-4	Vapor Pressure of Supercooled Liquid Water from 0 to -40 °C	2-48
2-5	Vapor Pressure (MPa) of Liquid Water from 0 to 100 °C	2-48
2-6	Substances in Tables 2-8, 2-32, 2-141, 2-150, 2-153, 2-155, 2-156, 2-179, 2-312, 2-313, 2-314, and 2-315 Sorted by Chemical Family	2-49
2-7	Formula Index of Substances in Tables 2-8, 2-32, 2-141, 2-150, 2-153, 2-155, 2-156, 2-179, 2-312, 2-313, 2-314, and 2-315	2-52
2-8	Vapor Pressure of Inorganic and Organic Liquids, $\ln P = C1 + C2/T + C3 \ln T + C4 T^{C5}$, P in Pa	2-55
2-9	Vapor Pressures of Inorganic Compounds, up to 1 atm	2-61

2-10	Vapor Pressures of Organic Compounds, up to 1 atm	2-65
------	---------------------------------------------------	------

VAPOR PRESSURES OF SOLUTIONS

Units Conversions		2-80
Tables		
2-11	Partial Pressures of Water over Aqueous Solutions of HCl	2-80
2-12	Partial Pressures of HCl over Aqueous Solutions of HCl	2-80
	Vapor Pressures of H ₃ PO ₄ Aqueous: Partial Pressure of H ₂ O Vapor (Fig. 2-1)	2-81
	Vapor Pressures of H ₃ PO ₄ Aqueous: Weight of H ₂ O in Saturated Air (Fig. 2-2)	2-81
2-13	Partial Pressures of H ₂ O and SO ₂ over Aqueous Solutions of Sulfur Dioxide	2-81
2-14	Water Partial Pressure, bar, over Aqueous Sulfuric Acid Solutions	2-82
2-15	Sulfur Trioxide Partial Pressure, bar, over Aqueous Sulfuric Acid Solutions	2-84
2-16	Sulfuric Acid Partial Pressure, bar, over Aqueous Sulfuric Acid	2-86
2-17	Total Pressure, bar, of Aqueous Sulfuric Acid Solutions	2-87
2-18	Partial Pressures of HNO ₃ and H ₂ O over Aqueous Solutions of HNO ₃	2-88
2-19	Partial Pressures of H ₂ O and HBr over Aqueous Solutions of HBr at 20 to 55 °C	2-89

*Contribution in part of the National Institute of Standards and Technology; not subject to copyright in the United States.

2-2 PHYSICAL AND CHEMICAL DATA

2-20	Partial Pressures of HI over Aqueous Solutions of HI at 25 °C	2-89
2-21	Vapor Pressures of the System: Water-Sulfuric Acid-Nitric Acid	2-89
2-22	Total Vapor Pressures of Aqueous Solutions of CH ₃ COOH	2-89
	Vapor Pressure of Aqueous Diethylene Glycol Solutions (Fig. 2-3)	2-89
2-23	Partial Pressure of H ₂ O over Aqueous Solutions of NH ₃ (psia)	2-90
2-24	Mole Percentages of H ₂ O over Aqueous Solutions of NH ₃	2-91
2-25	Partial Pressures of NH ₃ over Aqueous Solutions of NH ₃ (psia)	2-92
2-26	Total Vapor Pressures of Aqueous Solutions of NH ₃ (psia)	2-93
2-27	Partial Pressures of H ₂ O over Aqueous Solutions of Sodium Carbonate	2-94
2-28	Partial Pressures of H ₂ O and CH ₃ OH over Aqueous Solutions of Methyl Alcohol	2-94
2-29	Partial Pressures of H ₂ O over Aqueous Solutions of Sodium Hydroxide	2-94

WATER-VAPOR CONTENT OF GASES

Chart for Gases at High Pressures	2-95
Water Content of Air (Fig. 2-4)	2-95

DENSITIES OF PURE SUBSTANCES

Tables		
2-30	Density (kg/m ³) of Saturated Liquid Water from the Triple Point to the Critical Point	2-96
2-31	Density (kg/m ³) of Mercury from 0 to 350°C	2-97
2-32	Densities of Inorganic and Organic Liquids (mol/dm ³)	2-98

DENSITIES OF AQUEOUS INORGANIC SOLUTIONS AT 1 ATM

Units and Units Conversions	2-104	
Additional References	2-104	
Tables		
2-33	Aluminum Sulfate [Al ₂ (SO ₄) ₃]	2-104
2-34	Ammonia (NH ₃)	2-104
2-35	Ammonium Acetate (CH ₃ COONH ₄)	2-104
2-36	Ammonium Bichromate [(NH ₄) ₂ Cr ₂ O ₇]	2-104
2-37	Ammonium Chloride (NH ₄ Cl)	2-104
2-38	Ammonium Chromate [(NH ₄) ₂ CrO ₄]	2-104
2-39	Ammonium Nitrate (NH ₄ NO ₃)	2-104
2-40	Ammonium Sulfate [(NH ₄) ₂ SO ₄]	2-104
2-41	Arsenic Acid (H ₃ AsO ₄)	2-104
2-42	Barium Chloride (BaCl ₂)	2-105
2-43	Cadmium Nitrate [Cd(NO ₃) ₂]	2-105
2-44	Calcium Chloride (CaCl ₂)	2-105
2-45	Calcium Hydroxide [Ca(OH) ₂]	2-105
2-46	Calcium Hypochlorite (CaOCl ₂)	2-105
2-47	Calcium Nitrate [Ca(NO ₃) ₂]	2-105
2-48	Chromic Acid (CrO ₃)	2-105
2-49	Chromium Chloride (CrCl ₃)	2-105
2-50	Copper Nitrate [Cu(NO ₃) ₂]	2-105
2-51	Copper Sulfate (CuSO ₄)	2-105
2-52	Cuprous Chloride (CuCl ₂)	2-105
2-53	Ferric Chloride (FeCl ₃)	2-105
2-54	Ferric Sulfate [Fe ₂ (SO ₄) ₃]	2-106
2-55	Ferric Nitrate [Fe(NO ₃) ₃]	2-106
2-56	Ferrous Sulfate (FeSO ₄)	2-106
2-57	Hydrogen Bromide (HBr)	2-106
2-58	Hydrogen Cyanide (HCN)	2-106
2-59	Hydrogen Chloride (HCl)	2-106
2-60	Hydrogen Fluoride (HF)	2-106
2-61	Hydrogen Peroxide (H ₂ O ₂)	2-106
2-62	Hydrofluosilic Acid (H ₂ SiF ₆)	2-106
2-63	Magnesium Chloride (MgCl ₂)	2-106
2-64	Magnesium Sulfate (MgSO ₄)	2-106
2-65	Nickel Chloride (NiCl ₂)	2-106
2-66	Nickel Nitrate [Ni(NO ₃) ₂]	2-106
2-67	Nickel Sulfate (NiSO ₄)	2-106
2-68	Nitric Acid (HNO ₃)	2-107
2-69	Perchloric Acid (HClO ₄)	2-108
2-70	Phosphoric Acid (H ₃ PO ₄)	2-108
2-71	Potassium Bicarbonate (KHCO ₃)	2-108
2-72	Potassium Bromide (KBr)	2-108

2-73	Potassium Carbonate (K ₂ CO ₃)	2-109
2-74	Potassium Chromate (K ₂ CrO ₄)	2-109
2-75	Potassium Chlorate (KClO ₃)	2-109
2-76	Potassium Chloride (KCl)	2-109
2-77	Potassium Chrome Alum [K ₂ Cr ₂ (SO ₄) ₄]	2-109
2-78	Potassium Hydroxide (KOH)	2-109
2-79	Potassium Nitrate (KNO ₃)	2-109
2-80	Potassium Dichromate (K ₂ Cr ₂ O ₇)	2-109
2-81	Potassium Sulfate (K ₂ SO ₄)	2-109
2-82	Potassium Sulfite (K ₂ SO ₃)	2-109
2-83	Sodium Acetate (NaC ₂ H ₃ O ₂)	2-109
2-84	Sodium Arsenate (Na ₃ AsO ₄)	2-109
2-85	Sodium Bichromate (Na ₂ Cr ₂ O ₇)	2-109
2-86	Sodium Bromide (NaBr)	2-109
2-87	Sodium Formate (HCOONa)	2-109
2-88	Sodium Carbonate (Na ₂ CO ₃)	2-110
2-89	Sodium Chlorate (NaClO ₃)	2-110
2-90	Sodium Chloride (NaCl)	2-110
2-91	Sodium Chromate (Na ₂ CrO ₄)	2-110
2-92	Sodium Hydroxide (NaOH)	2-110
2-93	Sodium Nitrate (NaNO ₃)	2-110
2-94	Sodium Nitrite (NaNO ₂)	2-110
2-95	Sodium Silicates	2-110
2-96	Sodium Sulfate (Na ₂ SO ₄)	2-111
2-97	Sodium Sulfide (Na ₂ S)	2-111
2-98	Sodium Sulfite (Na ₂ SO ₃)	2-111
2-99	Sodium Thiosulfate (Na ₂ S ₂ O ₃)	2-111
2-100	Sodium Thiosulfate Pentahydrate (Na ₂ S ₂ O ₅ ·5H ₂ O)	2-111
2-101	Stannic Chloride (SnCl ₄)	2-111
2-102	Stannous Chloride (SnCl ₂)	2-111
2-103	Sulfuric Acid (H ₂ SO ₄)	2-112
2-104	Zinc Bromide (ZnBr ₂)	2-114
2-105	Zinc Chloride (ZnCl ₂)	2-114
2-106	Zinc Nitrate [Zn(NO ₃) ₂]	2-114
2-107	Zinc Sulfate (ZnSO ₄)	2-114

DENSITIES OF AQUEOUS ORGANIC SOLUTIONS

Units and Units Conversions	2-114	
Tables		
2-108	Formic Acid (HCOOH)	2-114
2-109	Acetic Acid (CH ₃ COOH)	2-115
2-110	Oxalic Acid (H ₂ C ₂ O ₄)	2-116
2-111	Methyl Alcohol (CH ₃ OH)	2-116
2-112	Ethyl Alcohol (C ₂ H ₅ OH)	2-117
2-113	Densities of Mixtures of C ₂ H ₅ OH and H ₂ O at 20°C	2-118
2-114	Specific Gravity {60°/60°F [(15.56°/15.56°C)]} of Mixtures by Volume of C ₂ H ₅ OH and H ₂ O	2-119
2-115	n-Propyl Alcohol (C ₃ H ₇ OH)	2-120
2-116	Isopropyl Alcohol (C ₃ H ₇ OH)	2-120
2-117	Glycerol	2-121
2-118	Hydrazine (N ₂ H ₄)	2-121
2-119	Densities of Aqueous Solutions of Miscellaneous Organic Compounds	2-122

DENSITIES OF MISCELLANEOUS MATERIALS

Tables		
2-120	Approximate Specific Gravities and Densities of Miscellaneous Solids and Liquids	2-124
2-121	Density (kg/m ³) of Selected Elements as a Function of Temperature	2-125

SOLUBILITIES

Units Conversions	2-125	
Tables		
2-122	Solubilities of Inorganic Compounds in Water at Various Temperatures	2-126
2-123	Solubility as a Function of Temperature and Henry's Constant at 25°C for Gases in Water	2-130
2-124	Henry's Constant H for Various Compounds in Water at 25°C	2-130
2-125	Henry's Constant H for Various Compounds in Water at 25°C from Infinite Dilution Activity Coefficients	2-131
2-126	Air	2-131
2-127	Ammonia-Water at 10 and 20°C	2-131
2-128	Carbon Dioxide (CO ₂)	2-131
2-129	Carbonyl Sulfide (COS)	2-131
2-130	Chlorine (Cl ₂)	2-132
2-131	Chlorine Dioxide (ClO ₂)	2-132

2-132	Hydrogen Chloride (HCl)	2-132
2-133	Hydrogen Sulfide (H ₂ S)	2-132
2-134	Partial Vapor Pressure of Sulfur Dioxide over Water, mmHg	2-133

THERMAL EXPANSION

Units Conversions	2-133	
Additional References	2-133	
Thermal Expansion of Gases	2-133	
Tables		
2-135	Linear Expansion of the Solid Elements	2-134
2-136	Linear Expansion of Miscellaneous Substances	2-135
2-137	Volume Expansion of Liquids	2-136
2-138	Volume Expansion of Solids	2-136

JOULE-THOMSON EFFECT

Units Conversions	2-137	
Tables		
2-139	Additional References Available for the Joule-Thomson Coefficient	2-137
2-140	Approximate Inversion-Curve Locus in Reduced Coordinates ($T_r = T/T_c$, $P_r = P/P_c$)	2-137

CRITICAL CONSTANTS

Additional References	2-138	
Table		
2-141	Critical Constants and Acentric Factors of Inorganic and Organic Compounds	2-138

COMPRESSIBILITIES

Introduction	2-143	
Units conversions	2-143	
Tables		
2-142	Composition of Selected Refrigerant Mixtures	2-143
2-143	Compressibility Factors for R 407A (Klea 60)	2-143
2-144	Compressibility Factors for R 407B (Klea 61)	2-143
2-145	Compressibilities of Liquids	2-144
2-146	Compressibilities of Solids	2-144

LATENT HEATS

Units Conversions	2-144	
Tables		
2-147	Heats of Fusion and Vaporization of the Elements and Inorganic Compounds	2-145
2-148	Heats of Fusion of Miscellaneous Materials	2-147
2-149	Heats of Fusion of Organic Compounds	2-148
2-150	Heats of Vaporization of Inorganic and Organic Liquids (J/kmol)	2-150

SPECIFIC HEATS OF PURE COMPOUNDS

Units Conversions	2-156	
Additional References	2-156	
Tables		
2-151	Heat Capacities of the Elements and Inorganic Compounds	2-156
2-152	Specific Heat [kJ/(kg·K)] of Selected Elements	2-164
2-153	Heat Capacities of Inorganic and Organic Liquids [J/(kmol·K)]	2-165
2-154	Specific Heats of Organic Solids	2-171
2-155	Heat Capacity at Constant Pressure of Inorganic and Organic Compounds in the Ideal Gas State Fit to a Polynomial Cp [J/(kmol·K)]	2-174
2-156	Heat Capacity at Constant Pressure of Inorganic and Organic Compounds in the Ideal Gas State Fit to Hyperbolic Functions Cp [J/(kmol·K)]	2-176
2-157	C _p /C _v Ratios of Specific Heats of Gases at 1 atm Pressure	2-182

SPECIFIC HEATS OF AQUEOUS SOLUTIONS

Units Conversions	2-183	
Additional References	2-183	
Tables		
2-158	Acetic Acid (at 38°C)	2-183
2-159	Ammonia	2-183
2-160	Aniline (at 20°C)	2-183
2-161	Copper Sulfate	2-183

2-162	Ethyl Alcohol	2-183
2-163	Glycerol	2-183
2-164	Hydrochloric Acid	2-183
2-165	Methyl Alcohol	2-183
2-166	Nitric Acid	2-183
2-167	Phosphoric Acid	2-183
2-168	Potassium Chloride	2-184
2-169	Potassium Hydroxide (at 19°C)	2-184
2-170	Normal Propyl Alcohol	2-184
2-171	Sodium Carbonate	2-184
2-172	Sodium Chloride	2-184
2-173	Sodium Hydroxide (at 20°C)	2-184
2-174	Sulfuric Acid	2-184
2-175	Zinc Sulfate	2-184

SPECIFIC HEATS OF MISCELLANEOUS MATERIALS

Tables		
2-176	Specific Heats of Miscellaneous Liquids and Solids	2-185
2-177	Oils (Animal, Vegetable, Mineral Oils)	2-185

PROPERTIES OF FORMATION AND COMBUSTION REACTIONS

Units Conversions	2-185	
Table		
2-178	Heats and Free Energies of Formation of Inorganic Compounds	2-186
2-179	Enthalpies and Gibbs Energies of Formation, Entropies, and Net Enthalpies of Combustion of Inorganic and Organic Compounds at 298.15 K	2-195
2-180	Ideal Gas Sensible Enthalpies, $h_T - h_{298}$ (kJ/kmol), of Combustion Products	2-201
2-181	Ideal Gas Entropies s° , kJ/(kmol·K), of Combustion Products	2-202

HEATS OF SOLUTION

Tables		
2-182	Heats of Solution of Inorganic Compounds in Water	2-203
2-183	Heats of Solution of Organic Compounds in Water (at Infinite Dilution and Approximately Room Temperature)	2-206

THERMODYNAMIC PROPERTIES

Explanation of Tables	2-207	
Notation	2-207	
Units Conversions	2-207	
Additional References	2-207	
Tables		
2-184	List of Substances for Which Thermodynamic Property Tables Were Generated from NIST Standard Reference Database 23	2-208
2-185	Thermodynamic Properties of Acetone	2-209
2-186	Saturated Acetylene	2-210
2-187	Thermodynamic Properties of Air Pressure-Enthalpy Diagram for Dry Air (Fig. 2-5)	2-215
	Air, Moist	2-216
2-188	Air, Moist	2-216
2-189	Thermodynamic Properties of Ammonia Pressure-Enthalpy Diagram for Ammonia (Fig. 2-6)	2-217
	Enthalpy-Concentration Diagram for Aqueous Ammonia (Fig. 2-7)	2-219
2-190	Thermodynamic Properties of Argon	2-220
2-191	Liquid-Vapor Equilibrium Data for the Argon-Nitrogen-Oxygen System	2-221
2-192	Thermodynamic Properties of the International Standard Atmosphere	2-224
2-193	Thermodynamic Properties of Benzene	2-228
2-194	Saturated Bromine	2-229
2-195	Thermodynamic Properties of Butane	2-231
2-196	Thermodynamic Properties of 1-Butene	2-232
2-197	Thermodynamic Properties of <i>cis</i> -2-Butene	2-234
2-198	Thermodynamic Properties of <i>trans</i> -2-Butene	2-236
2-199	Thermodynamic Properties of Carbon Dioxide	2-238
2-200	Thermodynamic Properties of Carbon Monoxide Temperature-Entropy Diagram for Carbon Monoxide (Fig. 2-8)	2-240
	Thermodynamic Properties of Saturated Carbon Tetrachloride	2-242
2-201	Thermophysical Properties of Saturated Carbon Tetrachloride	2-244

2-4 PHYSICAL AND CHEMICAL DATA

Tables

2-202	Saturated Carbon Tetrafluoride (R14)	2-245	2-258	Thermodynamic Properties of R-41, Fluoromethane	2-348
2-203	Thermodynamic Properties of Carbonyl Sulfide	2-246	2-259	Saturated R-401A (SUVA MP 39)	2-350
2-204	Saturated Cesium	2-248	2-260	R-401A (SUVA MP 39) at Atmospheric Pressure	2-350
2-205	Thermophysical Properties of Saturated Chlorine	2-249	2-261	Thermodynamic Properties of Saturated R-407A (Klea 60)	2-351
	Enthalpy-Log-Pressure Diagram for Chlorine (Fig. 2-9)	2-250	2-262	Thermodynamic Properties of Saturated R-407B (Klea 61)	2-351
2-206	Saturated Chloroform (R20)	2-251		Enthalpy-Log-Pressure Diagram for R-407A (Klea 60)	
2-207	Thermodynamic Properties of Cyclohexane	2-252		(Fig. 2-22)	2-352
2-208	Thermodynamic Properties of Decane	2-254		Enthalpy-Log-Pressure Diagram for R-407B (Klea 61)	
2-209	Thermodynamic Properties of Deuterium Oxide (Heavy Water)	2-256	2-263	(Fig. 2-23)	2-353
			2-264	Saturated R-404A (SUVA HP 62)	2-354
2-210	Thermodynamic Properties of 2,2-Dimethylpropane (Neopentane)	2-258		R-404A (SUVA HP 62) at Atmospheric Pressure	2-354
2-211	Saturated Diphenyl	2-260	2-265	Enthalpy-Log-Pressure Diagram for Refrigerant 123	
2-212	Thermodynamic Properties of Dodecane	2-261	2-266	Saturated R-401B (SUVA MP 66)	2-355
2-213	Thermodynamic Properties of Ethane	2-263	2-267	R-401B (SUVA MP 66) at Atmospheric Pressure	2-355
2-214	Thermodynamic Properties of Ethanol	2-265	2-267	Saturated R-402A (SUVA HP 80)	2-355
	Enthalpy-Concentration Diagram for Aqueous Ethyl Alcohol (Fig. 2-10)	2-267	2-268	R-402A (SUVA HP 80) at Atmospheric Pressure	2-356
2-215	Thermodynamic Properties of Ethylene	2-268	2-269	Saturated R-402B (SUVA HP 81)	2-356
2-216	Thermodynamic Properties of Fluorine	2-270	2-270	R-402B (SUVA HP 81) at Atmospheric Pressure	2-356
2-217	Flutec	2-271	2-271	Thermodynamic Properties of R-113, 1,1,2-Trichlorotrifluoroethane	2-357
2-218	Halon	2-271	2-272	Thermodynamic Properties of R-114, 1,2-Dichlorotetrafluoroethane	2-359
2-219	Thermodynamic Properties of Helium	2-272	2-273	Saturated Refrigerant 115, Chloropentafluoroethane	2-361
2-220	Thermodynamic Properties of Heptane	2-274	2-274	Thermodynamic Properties of R-116, Hexafluoroethane	2-362
2-221	Thermodynamic Properties of Hexane	2-276	2-275	Thermodynamic Properties of R-123, 2,2-Dichloro-1,1,1-Trifluoroethane	2-365
2-222	Saturated Hydrazine	2-278		Enthalpy-Log-Pressure Diagram for Refrigerant 123	
2-223	Thermodynamic Properties of Normal Hydrogen	2-279		(Fig. 2-24)	2-366
2-224	Thermodynamic Properties of <i>para</i> -Hydrogen	2-281	2-276	Thermodynamic Properties of R-124, 2-Chloro-1,1,1,2-Tetrafluoroethane	2-367
2-225	Saturated Hydrogen Peroxide	2-282	2-277	Thermodynamic Properties of R-125, Pentafluoroethane	2-369
2-226	Thermodynamic Properties of Hydrogen Sulfide	2-283		Enthalpy-Log-Pressure Diagram for Refrigerant 125 (Fig. 2-25)	2-371
	Enthalpy-Concentration Diagram for Aqueous Hydrogen Chloride at 1 atm (Fig. 2-11)	2-285	2-278	Thermodynamic Properties of R-134a, 1,1,1,2-Tetrafluoroethane	2-372
2-227	Thermodynamic Properties of Isobutane	2-286		Pressure-Enthalpy Diagram for Refrigerant 134a (Fig. 2-26)	2-374
2-228	Thermodynamic Properties of Isobutene (2-Methyl 1-Propene)	2-288	2-279	Thermodynamic Properties of R-141b, 1,1-Dichloro-1-Fluoroethane	2-375
2-229	Thermodynamic Properties of Krypton	2-290	2-280	Thermodynamic Properties of R-142b, 1-Chloro-1,1-Difluoroethane	2-377
2-230	Saturated Lithium	2-292	2-281	Thermodynamic Properties of R-143a, 1,1,1-Trifluoroethane	2-379
2-231	Lithium Bromide—Water Solutions	2-292	2-282	Thermodynamic Properties of R-152a, 1,1-Difluoroethane	2-381
2-232	Saturated Mercury	2-293	2-283	Saturated Refrigerant 216a, 1,3-Dichloro-1,1,2,2,3,3-Hexafluoropropane	2-383
	Enthalpy-Log-Pressure Diagram for Mercury (Fig. 2-12)	2-295	2-284	Thermodynamic Properties of R-218, Octafluoropropane	2-384
2-233	Thermodynamic Properties of Methane	2-296	2-285	Thermodynamic Properties of R-227ea, 1,1,1,2,3,3,3-Heptafluoropropane	2-386
2-234	Thermodynamic Properties of Methanol	2-298	2-286	Saturated Refrigerant 245cb, 1,1,1,2,2-Pentafluoropropane	2-388
2-235	Thermodynamic Properties of 2-Methyl Butane (Isopentane)	2-300	2-287	Refrigerant RC 318, Octafluorocyclobutane	2-388
2-236	Thermodynamic Properties of 2-Methyl Pentane (Isohexane)	2-302	2-288	Thermodynamic Properties of R-404A	2-389
		2-304	2-289	Thermodynamic Properties of R-407C	2-391
2-237	Saturated Methyl Chloride	2-304		Pressure-Enthalpy Diagram for Refrigerant 407C (Fig. 2-27)	2-393
2-238	Thermodynamic Properties of Neon	2-305	2-290	Thermodynamic Properties of R-410A	2-394
2-239	Thermodynamic Properties of Nitrogen	2-307	2-291	Saturated Refrigerant 500	2-396
	Pressure-Enthalpy Diagram for Nitrogen (Fig. 2-13)	2-309	2-292	Saturated Refrigerant 502	2-396
2-240	Saturated Nitrogen Tetroxide	2-310	2-293	Saturated Refrigerant 503	2-397
2-241	Thermodynamic Properties of Nitrogen Trifluoride	2-311	2-294	Saturated Refrigerant 504	2-397
2-242	Thermodynamic Properties of Nitrous Oxide	2-313	2-295	Thermodynamic Properties of Refrigerant 507	2-397
	Mollier Diagram for Nitrous Oxide (Fig. 2-14)	2-315	2-296	Thermodynamic Properties of R-507A	2-398
2-243	Thermodynamic Properties of Nonane	2-316	2-297	Saturated Rubidium	2-400
2-244	Thermodynamic Properties of Octane	2-318	2-298	Thermophysical Properties of Saturated Seawater	2-400
2-245	Thermodynamic Properties of Oxygen	2-320	2-299	Saturated Sodium	2-401
	Pressure-Enthalpy Diagram for Oxygen (Fig. 2-15)	2-322		Mollier Diagram for Sodium (Fig. 2-28)	2-402
	Enthalpy-Concentration Diagram for Oxygen-Nitrogen Mixture at 1 atm (Fig. 2-16)	2-323	2-300	Enthalpy-Concentration Diagram for Aqueous Sodium Hydroxide at 1 atm (Fig. 2-29)	2-403
2-246	Thermodynamic Properties of Pentane	2-324	2-301	Thermodynamic Properties of Sulfur Dioxide	2-404
2-247	Saturated Potassium	2-326		Thermodynamic Properties of Sulfur Hexafluoride	2-406
	Mollier Diagram for Potassium (Fig. 2-17)	2-326		Pressure-Enthalpy Diagram for Sulfur Hexafluoride (SF ₆) (Fig. 2-30)	2-408
2-248	Thermodynamic Properties of Propane	2-327	2-302	Saturated SUVA AC 9000	2-409
2-249	Thermodynamic Properties of Propylene	2-329		Enthalpy-Concentration Diagram for Aqueous Sulfuric Acid at 1 atm (Fig. 2-31)	2-409
2-250	Thermodynamic Properties of R-11, Trichlorofluoromethane	2-331	2-303	Thermodynamic Properties of Toluene	2-410
	Pressure-Enthalpy Diagram for Refrigerant 11 (Fig. 2-18)	2-333	2-304	Saturated Solid/Vapor Water	2-412
2-251	Thermodynamic Properties of R-12, Dichlorodifluoromethane	2-334	2-305	Thermodynamic Properties of Water	2-413
	Pressure-Enthalpy Diagram for Refrigerant 12 (Fig. 2-19)	2-336	2-306	Thermodynamic Properties of Water Substance along the Melting Line	2-416
2-252	Thermodynamic Properties of R-13, Chlorotrifluoromethane	2-337	2-307	Thermodynamic Properties of Xenon	2-417
Refrigerant 20		2-339	2-308	Surface Tension (N/m) of Saturated Liquid Refrigerants	2-419
Refrigerant 14		2-339	2-309	Surface Tension σ (dyn/cm) of Various Liquids	2-419
2-253	Saturated Refrigerant 13B1, Bromotrifluoromethane	2-339			
2-254	Saturated Refrigerant 21, Dichlorodifluoromethane	2-339			
2-255	Thermodynamic Properties of R-22, Chlorodifluoromethane	2-340			
	Pressure-Enthalpy Diagram for Refrigerant 22 (Fig. 2-20)	2-342			
2-256	Thermodynamic Properties of R-23, Trifluoromethane	2-343			
2-257	Thermodynamic Properties of R-32, Difluoromethane	2-345			
	Pressure-Enthalpy Diagram for Refrigerant 32 (Fig. 2-21)	2-347			

TRANSPORT PROPERTIES

Introduction 2-420
 Units Conversions 2-420
 Additional References 2-420
 Tables
 2-310 Velocity of Sound (m/s) in Gaseous Refrigerants
 at Atmospheric Pressure 2-420
 2-311 Velocity of Sound (m/s) in Saturated Liquid Refrigerants .. 2-420
 2-312 Vapor Viscosity of Inorganic and Organic Substances (Pa·s) 2-421
 2-313 Viscosity of Inorganic and Organic Liquids (Pa·s) 2-427
 2-314 Vapor Thermal Conductivity of Inorganic and Organic
 Substances [W/(m·K)] 2-433
 2-315 Thermal Conductivity of Inorganic and Organic Liquids
 [W/(m·K)] 2-439
 2-316 Transport Properties of Selected Gases at Atmospheric
 Pressure 2-445
 2-317 Lower and Upper Flammability Limits,
 Flash Point, and Autoignition Temperature for
 Selected Hydrocarbons 2-446
 2-318 Viscosities of Liquids: Coordinates for Use with Fig. 2-32 .. 2-448
 Nomograph for Viscosities of Liquids at 1 atm (Fig. 2-32) .. 2-449
 Tables
 2-319 Viscosity of Sucrose Solutions 2-450
 Nomograph for Thermal Conductivity of Organic Liquids
 (Fig. 2-33) 2-450
 2-320 Thermal Conductivity Nomograph Coordinates 2-450
 2-321 Prandtl Number of Air 2-451
 2-322 Prandtl Number of Liquid Refrigerants 2-451
 2-323 Thermophysical Properties of Miscellaneous Saturated
 Liquids 2-452
 2-324 Diffusivities of Pairs of Gases and Vapors (1 atm) 2-454
 2-325 Diffusivities in Liquids (25°C) 2-456
 2-326 Thermal Conductivities of Some Building and Insulating
 Materials 2-459
 2-327 Thermal-Conductivity-Temperature for Metals 2-460
 2-328 Thermal Conductivity of Chromium Alloys 2-461
 2-329 Thermal Conductivity of Some Alloys at High Temperature 2-461
 2-330 Thermal Conductivities of Some Materials for
 Refrigeration and Building Insulation 2-461
 2-331 Thermal Conductivities of Insulating Materials at High
 Temperatures 2-461
 2-332 Thermal Conductivities of Insulating Materials at
 Moderate Temperatures (Nusselt) 2-462
 2-333 Thermal Conductivities of Insulating Materials
 at Low Temperatures (Gröber) 2-462
 2-334 Thermal Diffusivity (m²/s) of Selected Elements 2-462
 2-335 Thermophysical Properties of Selected Nonmetallic Solid
 Substances 2-463

PREDICTION AND CORRELATION OF PHYSICAL PROPERTIES

Introduction 2-463
 Units 2-464
 Classification of Estimation Methods 2-467
 Theory and Empirical Extension of Theory 2-467
 Corresponding States (CS) 2-467
 Group Contributions (GC) 2-467
 Computational Chemistry (CC) 2-468
 Empirical QSPR Correlations 2-468
 Molecular Simulations 2-468
 Physical Constants 2-468
 Critical Properties 2-468
 Tables
 2-336 Ambrose Group Contributions for Critical Constants 2-469
 2-337 Joback Group Contributions for Critical Constants 2-470
 Normal Melting Point 2-471
 Normal Boiling Point 2-471
 2-338 Fedors Method Atomic and Structural Contributions 2-471
 2-339 First-Order Groups and Their Contributions for Melting
 Point 2-472
 2-340 Second-Order Groups and Their Contributions for Melting
 Point 2-472
 Characterizing and Correlating Constants 2-473

2-341 Group Contributions for the Nannoolal Method for
 Normal Boiling Point 2-474
 2-342 Intermolecular Interaction Corrections for the
 Nannoolal et al. Method for Normal Boiling Point 2-476
 Vapor Pressure 2-477
 Liquids 2-477
 Solids 2-478
 Thermal Properties 2-478
 Enthalpy of Formation 2-478
 2-343 Domalski-Hearing Group Contribution Values for
 Standard State Thermal Properties 2-479
 Entropy 2-485
 Gibbs' Energy of Formation 2-486
 Latent Enthalpy 2-486
 Enthalpy of Vaporization 2-486
 Enthalpy of Fusion 2-487
 Enthalpy of Sublimation 2-488
 2-344 Cs (C—H) Group Values for Chickos Estimation of ΔH_{fus} 2-488
 2-345 Ct (Functional) Group Values for Chickos Estimation of ΔH_{fus} 2-488
 Heat Capacity 2-489
 Gases 2-489
 2-346 Group Contributions and Corrections for ΔH_{sub} 2-489
 Liquids 2-490
 2-347 Benson and CHETAH Group Contributions for Ideal Gas
 Heat Capacity 2-491
 Solids 2-495
 2-348 Liquid Heat Capacity Group Parameters for
 Ruzicka-Domalski Method 2-496
 Mixtures 2-497
 Density 2-497
 Gases 2-497
 2-349 Group Values and Nonlinear Correction Terms for
 Estimation of Solid Heat Capacity with the Goodman et al.
 Method 2-498
 2-350 Element Contributions to Solid Heat Capacity for the
 Modified Kopp's Rule 2-498
 2-351 Simple Fluid Compressibility Factors $Z^{(0)}$ 2-500
 2-352 Acentric Deviations $Z^{(1)}$ from the Simple Fluid
 Compressibility Factor 2-501
 2-353 Constants for the Two Reference Fluids Used in Lee-Kesler
 Method 2-502
 2-354 Relationships for Eq. (2-66) for Common Cubic EoS 2-502
 Solids 2-503
 Mixtures 2-503
 Viscosity 2-504
 Gases 2-504
 2-355 Reichenberg Group Contribution Values 2-505
 Liquids 2-506
 Liquid Mixtures 2-506
 2-356 Group Contributions for the Hsu et al. Method 2-507
 2-357 UNIFAC-VISCO Group Interaction Parameters α_{mm} 2-509
 Thermal Conductivity 2-509
 Gases 2-510
 Liquids 2-510
 2-358 Correlation Parameters for Baroncini et al. Method for
 Estimation of Thermal Conductivity 2-511
 2-359 Sastri-Rao Group Contributions for Liquid Thermal
 Conductivity at the Normal Boiling Point 2-511
 Liquid Mixtures 2-512
 Surface Tension 2-513
 Pure Liquids 2-513
 Liquid Mixtures 2-514
 2-360 Knotts Group Contributions for the Parachor in Estimating
 Surface Tension 2-514
 Flammability Properties 2-515
 2-361 Group Contributions for Pintar Flammability Limits
 Method for Organic Compounds 2-516
 2-362 Group Contributions for Pintar Flammability Limits
 Method for Inorganic Compounds 2-516
 2-363 Group Contributions for Pintar Autoignition Temperature
 Method for Organic Compounds 2-517
 2-364 Group Contributions for Pintar Autoignition Temperature
 Method for Inorganic Compounds 2-517

GENERAL REFERENCES

Considerations of reader interest, space availability, the system or systems of units employed, copyright considerations, etc., have all influenced the revision of material in previous editions for the present edition. Reference is made at numerous places to various specialized works and, when appropriate, to more general works. A listing of general works may be useful to readers in need of further information.

ASHRAE Handbook—Fundamentals, SI edition, ASHRAE, Atlanta, 2005; Benedek, P., and F. Olti, *Computer-Aided Chemical Thermodynamics of Gases and Liquids*, Wiley, New York, 1985; Brule, M. R., L. L. Lee, and K. E. Starling, *Chem. Eng.*, **86**, 25, Nov. 19, 1979, pp. 155–164; Cox, J. D., and G. Pilcher, *Thermochemistry of Organic and Organometallic Compounds*, Academic Press, New York, 1970; Cox, J. D., D. D. Wagman, and V. A. Medvedev, *CODATA Key Values for Thermodynamics*, Hemisphere Publishing Corp., New York, 1989; Daubert, T. E., R. P. Danner, H. M. Sibel, and C. C. Stebbins, *Physical and Thermodynamic Properties of Pure Chemicals: Data Compilation*, Taylor & Francis, Washington, 1997; Domalski, E. S., and E. D. Hearing, Heat capacities and entropies of organic compounds in the condensed phase, vol. 3, *J. Phys. Chem. Ref. Data* 25(1):1–525, Jan-Feb 1996; Dykij, J., and M. Repas, Saturated vapor pressures of organic compounds, *Veda*, Bratislava, 1979 (Slovak); Dykij, J., M. Repas, and J. Svoboda, Saturated vapor pressures of organic compounds, *Veda*, Bratislava, 1984 (Slovak); Glushko, V. P., Ed., *Thermal Constants of Compounds*, Issues 1–X., Moscow, 1965–1982 (Russian only); Gmehling, J., *Azeotropic Data*, 2 vols., VCH Weinheim, Germany, 1994; Gmehling, J., and U. Onken, *Vapor-Liquid Equilibrium Data Collection*, Dechema Chemistry Data Series, Frankfurt, 1977–1978; International Data Series, *Selected Data on Mixtures*, Series A: Thermodynamics Research Center, National Institute of Standards and Technology, Boulder, Colo.; Kaye, S. M., *Encyclopedia of Explosives and Related Items*, U.S. Army R&D command, Dover, N.J., 1980; King, M. B., *Phase Equilibrium in Mixtures*, Pergamon, Oxford, 1969; Landolt-Boernstein, Numerical Data and Functional Relationships in Science and Technology (New Series), <http://www.springeronline.com/sgw/cda/frontpage/0,11855,4-10113-2-95859-0,00.html>; Lide, D. R., *CRC Handbook of Chemistry and Physics*, 86th ed., CRC Press, Boca Raton, Fla., 2005; Lyman, W. J., W. F. Reehl, and D. H. Rosenblatt, *Handbook of Chemical Property Estimation Methods*, McGraw-Hill, New York, 1990; Majer, V., and V. Svoboda, *Enthalpies of Vaporization of Organic Compounds: A Critical Review and Data Compilation*, Blackwell Science, 1985; Majer, V., V. Svoboda, and J. Pick, *Heats of Vaporization of Fluids*, Elsevier, Amsterdam, 1989 (general discussion); Marsh, K. N., *Recommended Reference Materials for the Realization of Physicochemical Properties*, Blackwell Science, 1987; NIST-IUPAC Solubility Data Series, Pergamon Press, <http://www.iupac.org/publications/ci/1999/march/solubility.html>; Olse, R. W., and H. von Tippelskirch, *High Temp.—High Press.*, **9**:367–385, 1977; Olse, R. W., *Handbook of Thermodynamic and Transport Properties of Alkali Metals*, Blackwell Science Pubs., Oxford, England, 1985; Pedley, J. B., R. D. Naylor, and S. P. Kirby, *Thermochemical Data of Organic Compounds*, Chapman and Hall, New York, 1986; *Physical Property Data for the Design Engineer*, Hemisphere, New York, 1989; Poling, B. E., J. M. Prausnitz, and J. P. O'Connell, *The Properties of*

Gases and Liquids, 5th ed., McGraw-Hill, New York, 2001; Rothman, D., et al., Max Planck Inst. f. Stromungsforschung, Ber 6, 1978; Smith, B. D., and R. Srivastava, *Thermodynamic Data for Pure Compounds*, Part A: *Hydrocarbons and Ketones*, Elsevier, Amsterdam, 1986, Physical sciences data 25, http://www.elsevier.com/wps/find/bookseriesdescription.librarians/BS_PSD/description; Sterbacek, Z., B. Biskup, and P. Tausk, *Calculation of Properties Using Corresponding States Methods*, Elsevier, Amsterdam, 1979; Stull, D. R., E. F. Westrum, and G. C. Sink, *The Chemical Thermodynamics of Organic Compounds*, Wiley, New York, 1969; *TRC Thermodynamic Tables—Hydrocarbons*, Thermodynamics Research Center, National Institute of Standards and Technology, Boulder, Colo.; *TRC Thermodynamic Tables—Non-Hydrocarbons*, Thermodynamics Research Center, National Institute of Standards and Technology, Boulder, Colo.; Young, D. A., "Phase Diagrams of the Elements," UCRL Rep. 51902, 1975 republished in expanded form by the University of California Press, 1991; Zabransky, M., V. Ruzicka, Jr., V. Majer, and E. S. Domalski, Heat Capacity of Liquids: Critical Review and Recommended Values, *J. Phys. Chem. Ref. Data*, Monograph No. 6, 1996.

CRITICAL DATA ARE COMPILED IN:

Ambrose, D., "Vapor-Liquid Critical Properties," N. P. L. Teddington, Middlesex, Rep. 107, 1980; Kudchaker, A. P., G. H. Alani, and B. J. Zwolinski, *Chem. Revs.* **68**:659–735, 1968; Matthews, J. F., *Chem. Revs.* **72**:71–100, 1972; Simmrock, K., R. Janowsky, and A. Ohnsorge, *Critical Data of Pure Substances*, Parts 1 and 2, Dechema Chemistry Data Series, 1986; Other recent references for critical data can be found in Lide, D. R., *CRC Handbook of Chemistry and Physics*, 86th ed., CRC Press, Boca Raton, Fla., 2005.

PUBLICATIONS ON THERMOCHEMISTRY

Pedley, J. B., *Thermochemical Data and Structures of Organic Compounds*, 1, Thermodynamic Research Center, Texas A&M Univ., 1994 (976 pp., 3000 cpds.); Frenkel, M., et al., *Thermodynamics of Organic Compounds in the Gas State*, 2 vols., Thermodynamic Research Center, Texas A&M Univ., 1994 (1825 pp., 2000 cpds.); Barin, I., *Thermochemical Data of Pure Substances*, 2 vols., 2d ed., VCH Weinheim, Germany, 1993 (1834 pp., 2400 substances); Gurvich, L.V., et al., *Thermodynamic Properties of Individual Substances*, 3 vols., 4th ed., Hemisphere, New York, 1989, 1990, and 1993 (2520 pp.); Lide, D. R., and G. W. A. Milne, *Handbook of Data on Organic Compounds*, 7 vols., 3d ed., Chemical Rubber, Miami, 1993 (7000 pp.); Daubert, T. E., et al., *Physical and Thermodynamic Properties of Pure Chemicals: Data Compilation*, extant 1995, Taylor & Francis, Bristol, Pa., 1995; Database 11, NIST, Gaithersburg, Md. U.S. Bureau of Mines publications include Bulletins 584, 1960 (232 pp.); 592, 1961 (149 pp.); 595, 1961 (68 pp.); 654, 1970 (26 pp.); Chase, M. W., et al., *JANAF Thermochemical Tables*, 3d ed., *J. Phys. Chem. Ref. Data* 14 suppl 1., 1986 (1896 pp.); *Journal of Physical and Chemical Reference Data* is available online at <http://listserv.nd.edu/cgi-bin/wa?A2=ind0501&L=pamnet&F=&S=&P=8490> and at <http://www.nist.gov/srd/reprints.htm>

PHYSICAL PROPERTIES OF PURE SUBSTANCES

TABLE 2-1 Physical Properties of the Elements and Inorganic Compounds*

Abbreviations Used in the Table

a., acid A., specific gravity with reference to air = 1 abs., absolute ac., acetic acid act., acetone al., 95 percent ethyl alcohol alk, alkali (<i>i.e.</i> , aq. NaOH or KOH) am., amyl (C ₅ H ₁₁) amor., amorphous anh., anhydrous aq., aqueous or water aq. reg., aqua regia	atm., atmosphere or 760 mm. of mercury pressure bk., black brn., brown bz., benzene c., cold cb., cubic cc, cubic centimeter chl., chloroform col., colorless or white conc., concentrated cr., crystals or crystalline d., decomposes D., specific gravity with reference to hydrogen = 1	d. 50, decomposes at 50°C; 50 d., melts at 50°C with decomposition delq., deliquescent dil., dilute dk., dark eff., effloresces or efflorescent et., ethyl ether expl., explodes gel., gelatinous gly., glycerol (glycerin) gn., green h., hot hex., hexagonal	hyg., hygroscopic i., insoluble ign., ignites lq., liquid lt., light m. al., methyl alcohol mn., monoclinic nd., needles NH ₃ , liquid ammonia NH ₄ OH, ammonium hydroxide solution oct., octahedral or., orange pd., powder	pl., plates pr., prisms or prismatic pyr., pyridine rhb., rhombic (orthorhombic) s., soluble satd., saturated sl., slightly soln., solution subl., sublimes sulf., sulfides tart. a., tartaric acid tet., tetragonal tr., transition tri., triclinic	trig., trigonal v., very vac., in vacuo vl., violet volt., volatile or volatilizes wh., white yell., yellow ∞, soluble in all proportions <, less than >, greater than 42±, about or near 42 -3H ₂ O, 100, loses 3 moles of water per formula weight at 100°C
-------------------------------------------------------------------------------------------------------------------------------------------------------------------------------------------------------------------------------------------------------------------------------------------------------------------------------------------	--------------------------------------------------------------------------------------------------------------------------------------------------------------------------------------------------------------------------------------------------------------------------------------------------------------------------------	-------------------------------------------------------------------------------------------------------------------------------------------------------------------------------------------------------------------------------------------------------------------------------------------------	----------------------------------------------------------------------------------------------------------------------------------------------------------------------------------------------------------------------------------------------------------------------------------------	---------------------------------------------------------------------------------------------------------------------------------------------------------------------------------------------------------------------------------------------------------------------------------------------	-----------------------------------------------------------------------------------------------------------------------------------------------------------------------------------------------------------------------------------------------------------------------------------------------------------

Formula weights are based upon the International Atomic Weights in "Atomic Weights of the Elements 2001," *Pure Appl. Chem.*, **75**, 1107, 2003, and are computed to the nearest hundredth.

Refractive index, where given for a uniaxial crystal, is for the ordinary (α) ray; where given for a biaxial crystal, the index given is for the median (β) value. Unless otherwise specified, the index is given for the sodium D-line (λ = 589.3 mμ).

Specific gravity values are given at room temperatures (15 to 20 °C) unless otherwise indicated by the small figures which follow the value: thus, "5.6^{18°C}" indicates a specific gravity of 5.6 for the substance at 18 °C referred to water at 4 °C. In this table the values for the specific gravity of gases are given with reference to air (A) = 1, or hydrogen (D) = 1.

Melting point is recorded in a certain case as "82 d." and in some other case as "d. 82," the distinction being made in this manner to indicate that the former is a melting point with decomposition at 82°C, while in the latter decomposition only occurs at 82 °C. Where a value such as "-2H₂O, 82" is given it indicates loss of 2 moles of water per formula weight of the compound at a temperature of 82 °C.

Boiling point is given at atmospheric pressure (760 mm. of mercury) unless otherwise indicated; thus, "82^{15mm.}" indicates the boiling point is 82°C when the pressure is 15 mm.

Solubility is given in parts by weight (of the formula shown at the extreme left) per 100 parts by weight of the solvent; the small superscript indicates the temperature. In the case of gases the solubility is often expressed in some manner as "5^{10°} cc" which indicates that at 10 °C, 5 cc. of the gas are soluble in 100 g of the solvent. The symbols of the common mineral acids: H₂SO₄, HNO₃, HCl, etc., represent dilute aqueous solutions of these acids. See also special tables on Solubility.

REFERENCES: The information given in this table has been collected mainly from the following sources: Mellor, *A Comprehensive Treatise on Inorganic and Theoretical Chemistry*, Longmans, New York, 1922. Abegg, *Handbuch der anorganischen Chemie*, S. Hirzel, Leipzig, 1905. Gmelin-Kraut, *Handbuch der anorganischen Chemie*, 7th ed., Carl Winter, Heidelberg; 8th ed., Verlag Chemie, Berlin, 1924. Friend, *Textbook of Inorganic Chemistry*, Griffin, London, 1914. Winchell, *Microscopic Character of Artificial Inorganic Solid Substances or Artificial Minerals*, Wiley, New York, 1931. *International Critical Tables*, McGraw-Hill, New York, 1926. *Tables annuelles internationales de constantes et donnees numeriques*, McGraw-Hill, New York. *Annual Tables of Physical Constants and Numerical Data*, National Research Council, Princeton, N.J., 1943. Comey and Hahn, *A Dictionary of Chemical Solubilities*, Macmillan, New York, 1921. Seidell, *Solubilities of Inorganic and Metal Organic Compounds*, Van Nostrand, New York, 1940.

Name	Formula	Formula weight	Color, crystalline form and refractive index	Specific gravity	Melting point, °C	Boiling point, °C	Solubility in 100 parts		
							Cold water	Hot water	Other reagents
Aluminum	Al	26.98	silv., cb.	2.70 ^{20°}	660	2056	i.	i.	s. HCl, H ₂ SO ₄ , alk.
acetate, normal	Al(C ₂ H ₃ O ₂) ₃	204.11	wh. pd.		d. 200		s.	d.	
acetate, basic	Al(OH)(C ₂ H ₃ O ₂) ₂	162.08	wh., amor.		d.		i.		s.a.; i. NH ₄ salts
bromide	AlBr ₃	266.69	trig.	3.01 ^{25°} / ₄	97.5	268	s.		s.al., act., CS ₂
bromide	AlBr ₃ ·6H ₂ O	374.78	col., delq. cr.		d. 100		s.	s.	s. al., CS ₂
carbide	Al ₄ C ₃	143.96	yel., hex., 2.70	2.95	d. >2200		d. to CH ₄		s. a.; i. act.
chloride	AlCl ₃	133.34	wh., delq., hex.	2.44 ^{25°} / ₄	194 ^{3.2atm.}	182.7 ^{752mm.} , subl. 178	69.87 ^{15°}	s. d.	s. et., chl., CCl ₄ ; i. bz.
chloride	AlCl ₃ ·6H ₂ O	241.43	col., delq., trig., 1.560				400	v. s.	50 al.; s. et.
fluoride (fluellite)	AlF ₃ ·H ₂ O	101.99	col., rhb., 1.490	2.17	d.		sl. s.		
fluoride	Al ₂ F ₆ ·7H ₂ O	294.06	wh., cr. pd.		-4H ₂ O, 120	-6H ₂ O, 250	i.	sl. s.	
hydroxide	Al(OH) ₃	78.00	wh., mn.	2.42	-2H ₂ O, 300		0.000104 ^{18°}	i.	s. a., alk.; i. a.
nitrate	Al(NO ₃) ₃ ·9H ₂ O	375.13	rhb., delq.		73	d. 134	v. s.	v. s. d.	s. al., CS ₂
nitride	Al ₂ N ₂	81.98	yel., hex.	3.05 ^{25°} / ₄	2150 ^{4atm.}	d. >1400	d. slowly		s. alk. d.
oxide	Al ₂ O ₃	101.96	col., hex., 1.67-8	3.99	1999 to 2032		i.	i.	v. sl. s. a., alk.
oxide (corundum)	Al ₂ O ₃	101.96	wh., trig., 1.768	4.00	1999 to 2032	2210	i.	i.	v. sl. s. a., alk.
phosphate	AlPO ₄	121.95	col., hex.	2.59			i.	i.	s. a., alk.; i. ac.

*By N. A. Lange, Ph.D., Handbook Publishers, Inc., Sandusky, Ohio. Abridged from table of Physical Constants of Inorganic Compounds in *Lange's Handbook of Chemistry*.

TABLE 2-1 Physical Properties of the Elements and Inorganic Compounds (Continued)

Name	Formula	Formula weight	Color, crystalline form and refractive index	Specific gravity	Melting point, °C	Boiling point, °C	Solubility in 100 parts		
							Cold water	Hot water	Other reagents
Aluminum (<i>Cont.</i>)									
potassium silicate (muscovite)	3Al ₂ O ₃ ·K ₂ O·6SiO ₂ ·2H ₂ O	796.61	mn., 1.590	2.9	d.		i.		
potassium silicate (orthoclase)	Al ₂ O ₃ ·K ₂ O·6SiO ₂	556.66	col., mn., 1.524	2.56	1450 (1150)		i.		
Aluminum potassium tartrate	AlK(C ₄ H ₄ O ₆) ₂	362.22	col.				s.	s.	
sodium fluorite (cryolite)	AlF ₃ ·3NaF	209.94	wh., mn., 1.3389	2.90	1000		sl. s.		i. HCl
sodium silicate	Al ₂ O ₃ ·Na ₂ O·6SiO ₂	524.44	col., tri., 1.529	2.61	1100		i.	i.	d. a.
sulfate	Al ₂ (SO ₄) ₃	342.15	wh. cr.	2.71	d. 770		31.3 ^{90°}	89 ^{100°}	
Alum, ammonium (tschermigite)	Al ₂ (SO ₄) ₃ ·(NH ₄) ₂ SO ₄ ·24H ₂ O	906.66	col., oct., 1.4594	1.64 ^{20°} / _{4°}	93.5	-20H ₂ O, 120; -24H ₂ O, 200	3.9 ^{90°}	∞ 100°	i. al.
ammonium chrome	Cr ₂ (SO ₄) ₃ ·(NH ₄) ₂ SO ₄ ·24H ₂ O	956.69	gn. or vl., oct., 1.4842	1.72	100 d.		21.2 ^{25°}		s. al.
ammonium iron	Fe ₂ (SO ₄) ₃ ·(NH ₄) ₂ SO ₄ ·24H ₂ O	964.38	vl., oct., 1.485	1.71	40		124 ^{25°}		i. al.
potassium (kalinite)	Al ₂ (SO ₄) ₃ ·K ₂ SO ₄ ·24H ₂ O	948.78	col., mn., 1.4564	1.76 ^{26°} / _{4°}	92	-18H ₂ O, 64.5	5.7 ^{10°}	∞ ^{93°}	
potassium chrome	Cr ₂ (SO ₄) ₃ ·K ₂ SO ₄ ·24H ₂ O	998.81	red or gn., cb., 1.4814	1.83	89		20	50	i. al.
sodium	Al ₂ (SO ₄) ₃ ·Na ₂ SO ₄ ·24H ₂ O	916.56	col., oct., 1.4388	1.675 ^{20°} / _{4°}	61		106.4 ^{90°}	121.7 ^{45°}	i. al.
Ammonia†	NH ₃	17.03	col. gas, 1.325 (lq.)	0.817 ^{-79°} 0.5971 (A)	-77.7	-33.4	89.9 ^{90°}	7.4 ^{96°}	14.8 ^{20°} al.; s. et.
Ammonium acetate	NH ₄ C ₂ H ₃ O ₂	77.08	wh., hyg. cr.	1.073	114	d.	148 ^{45°}		s. al.; sl. s. act.
auricyanide	NH ₄ CN·Au(CN) ₃ ·H ₂ O	337.09	pl.		d. 200		s.	v. s.	i. al.
bicarbonate	NH ₄ HCO ₃	79.06	mn. or rhb., 1.5358	1.573	d. 35-60		11.9 ^{90°}	27 ^{30°}	i. al.
bromide	NH ₄ Br	97.94	col., cb., 1.7108	2.327 ^{15°} / _{4°}	subl. 542		68 ^{10°}	145.6 ^{100°}	s. al., et., act.
carbonate	(NH ₄) ₂ CO ₃ ·H ₂ O	114.10	col. pl.		d. 58		100 ^{15°}		i. al., CS ₂ , NH ₃
carbonate, carbamate	NH ₄ HCO ₃ ·NH ₄ CO ₂ NH ₄ †	157.13	wh. cr.		subl.		25 ^{15°}	67 ^{65°}	
carbonate, sesqui-	(NH ₄) ₂ CO ₃ ·2NH ₄ HCO ₃ ·H ₂ O	272.21	wh.		d.		20 ^{15°}	50 ^{49°}	
chloride (salammoniac)	NH ₄ Cl	53.49	wh., cb., 1.639, 1.6426	1.53 ^{17°}	d. 350	subl. 520	29.4 ^{90°}	77.3 ^{100°}	s. NH ₃ ; sl. s. al., m. al.
chloroplatinate	(NH ₄) ₂ PtCl ₆	443.87	yel., cb.	3.065	d.		0.7 ^{15°}	1.25 ^{100°}	0.005 al.
chloroplatinite	(NH ₄) ₂ PtCl ₄	372.97	tet.		d.		s.		
chlorostannate	(NH ₄) ₂ SnCl ₆	367.50	pink., cb.	2.4			33.3 ^{15°}		
chromate	(NH ₄) ₂ CrO ₄	152.07	yel., mn.	1.917 ^{12°}	d. 180		40.5 ^{30°}		sl. s. act., NH ₃ ; i. al.
cyanide	NH ₄ CN	44.06	col., cb.	0.79 ^{100°} (A)	36		s.	v. s.	s. al.
dichromate	(NH ₄) ₂ Cr ₂ O ₇	252.06	or., mn.	2.15	d. 185		47.2 ^{30°}	v. s.	s. al.; i. act.
ferrocyanide	(NH ₄) ₄ Fe(CN) ₆ ·6H ₂ O	392.19	mn.		d.		s.		i. al.
fluoride	NH ₄ F	37.04	wh., hex.				v. s.	d.	s. al.; i. NH ₃
fluoride, acid	NH ₄ F·HF	57.04	wh., rhb., 1.390	2.21 ^{12°} / _{12°}			v. s.		
formate	HCO ₂ NH ₄	63.06	col., mn., delq.	1.266	114-116	d. 180; subl. in vac. subl. 120	102 ^{90°}	531 ^{80°}	s. al.
hydrosulfide	NH ₄ HS	51.11	col., rhb.		d.		v. s.		s. al.
hydroxide	NH ₄ OH	35.05	in soln. only				s.		
molybdate	(NH ₄) ₂ MoO ₄	196.01	mn.	2.27	d.		d.	d.	i. al., NH ₃
molybdate, hepta-	(NH ₄) ₆ Mo ₇ O ₂₄ ·4H ₂ O†	1235.86	col., mn.				44 ^{25°}		i. al.
nitrate (α), stable -16° to 32°	NH ₄ NO ₃	80.04	col., tet., 1.611	1.66 ^{25°} / _{4°}	169.6	d. 210	118.3 ^{90°}	241.8 ^{30°}	3.8 ^{20°} al., 17.1 ^{20°} m. al.; v. s. NH ₃
nitrate (β), stable 32° to 84°	NH ₄ NO ₃	80.04	col., rhb. or mn.	1.725 ^{25°} / _{4°}		d. 210	365.8 ^{35°}	580 ^{80°}	
nitrite	NH ₄ NO ₂	64.04	wh. nd.	1.69	expl.		s.	d.	s. al.
osmochloride	(NH ₄) ₂ OsCl ₆	439.02	cb.	2.93 ^{20°} / _{4°}					
oxalate	(NH ₄) ₂ C ₂ O ₄ ·H ₂ O	142.11	col., rhb.	1.501			2.5 ^{90°}	11.8 ^{50°}	sl. s. al.; i. NH ₃
oxalate, acid	NH ₄ H ₂ C ₂ O ₄ ·H ₂ O	125.08	col., trimetric	1.556	d.		s.		
perchlorate	NH ₄ ClO ₄	117.49	col., rhb., 1.4833	1.95	d.		10.9 ^{90°}	46.9 ^{100°}	2 ^{20°} al.; s. act.; i. et.
persulfate	(NH ₄) ₂ S ₂ O ₈	228.20	wh., mn., 1.5016	1.98	d. 120		58.2 ^{90°}	d.	
phosphate, monobasic	NH ₄ H ₂ PO ₄	115.03	col., tet., 1.5246	1.803 ^{19°} / _{4°}			22.7 ^{90°}	173.2 ^{100°}	i. ac.

phosphate, dibasic	(NH ₄) ₂ HPO ₄	132.06	col., mn., 1.53	1.619			131 ^{15°}		i. act.
phosphate, meta-	(NH ₄) ₄ P ₂ O ₁₂	388.04	col., mn.	2.21			s.		
Ammonium phosphomolybdate	(NH ₄) ₃ PO ₄ ·12MoO ₃ ·3H ₂ O (?)	1930.39	yel.		d.		0.03 ^{15°}	i.	s. alk.; i. al., HNO ₃
silicofluoride	(NH ₄) ₂ SIF ₆	178.15	cb., 1.3696	2.01		subl.	18.5 ^{17.5°}	55.5	s. al.; i. act.
sulfamate	NH ₄ ·SO ₃ NH ₂	114.12	col. pl.		132	d. 160	134 ^{0°}	357 ^{50°}	
sulfate (mascagnite)	(NH ₄) ₂ SO ₄	132.14	col., rhb., 1.5230	1.769 ^{20°}	235 d.		70.6 ^{0°}	103.3 ^{100°}	i. al., act., CS ₂
sulfate, acid	NH ₄ HSO ₄	115.11	col., rhb., 1.480	1.78	146.9	490	100		v. sl. s. al.; i. act.
sulfide	(NH ₄) ₂ S	68.14	yel.-wh.		d.		v. s.		120 ^{25°} NH ₃
sulfide, penta-	(NH ₄) ₂ S ₅	196.40	or.-red pr.				s.		
sulfite	(NH ₄) ₂ SO ₃ ·H ₂ O	134.16	col., mn.	1.41		d.	100 ^{12°}		i. al., act.
sulfite, acid	NH ₄ HSO ₃	99.11	rhb.	2.03 ^{12°}		d.	s.		
tartrate	(NH ₄) ₂ C ₄ H ₄ O ₆	184.15	col., mn.	1.60		d.	45 ^{0°}	87 ^{60°}	sl. s. al.
thiocyanate	NH ₄ CNS	76.12	col., mn., 1.685±	1.305	149.6	d. 170	120 ^{0°}	170 ^{20°}	s. al., act., NH ₃ , SO ₂
vanadate, meta-	NH ₄ VO ₃	116.98	col. cr.	2.326		d.	0.44 ^{18°}	3.05 ^{70°}	i. al., NH ₄ Cl
Antimony	Sb	121.76	tin wh., trig.	6.684 ^{25°}	630.5	1380	i.	i.	s. aq. reg., h. conc.
chloride, tri- (butter of antimony) ^o	SbCl ₃	228.12	col., rhb., delq.	3.14 ^{20°}	73.4	220.2	601.6 ^{0°}	∞ ^{72°}	H ₂ SO ₄ s. al., HCl, HBr H ₂ C ₄ H ₄ O ₆ s. HCl, KOH, H ₂ C ₄ H ₄ O ₆
oxide, tri- (valentinite)	Sb ₂ O ₃	291.52	rhb., 2.35	5.67	656	1570	v. sl. s.	sl. s.	
oxide, tri- (senarmontite)	Sb ₂ O ₃	291.52	cb., 2.087	5.2	652				
sulfide, tri- (stibnite)	Sb ₂ S ₃	339.72	bk., rhb., 4.046	4.64	550		0.00017 ^{18°}	d.	s. HCl; alk., NH ₄ HS, K ₂ S; i. ac.
sulfide, penta-	Sb ₂ S ₅	403.85	golden	4.120 ^{0°}	-2S, 135		i.	i.	s. HCl, alk., NH ₄ HS
telluride, tri-	Sb ₂ Te ₃	626.32	gray		629				
Antimonyl potassium tartrate (tartar emetic)	(SbO)KC ₄ H ₄ O ₆ ·½H ₂ O	333.94	wh., rhb.	2.60	-½H ₂ O, 100		5.26 ^{8.7°}	35.7 ^{100°}	s. gly.; i. al.
sulfate, normal	(SbO) ₂ SO ₄	371.58	wh. pd.	4.89			d.	d.	
sulfate, basic	(SbO) ₂ SO ₄ ·Sb ₂ (OH) ₄	683.20	wh. pd.				i.	d.	5.15 ^{15°} gly.
Argon	Ar	39.95	col. gas	1.65 ^{-288°} ; 1.402 ^{-185.7°} ; 1.38 (A)	-189.2	-185.7	5.6 ^{0°} cc	2.23 ^{50°} cc	24 ^{25°} cc al.
Arsenic (crystalline) (α)	As ₄	299.69	met., hex.	5.727 ^{14°}	814 ^{36atm.}	subl. 615	i.	i.	s. HNO ₃
Arsenic (black) (β)	As ₄	299.69	bk., amor.	4.7 ^{20°}			i.	i.	s. HNO ₃ , aq. reg., aq. Cl ₂ , h. alk.
Arsenic (yellow)(γ)	As ₄	299.69	yel., cb.	2.0 ^{20°}	d. 358				
acid, ortho-	H ₃ AsO ₄ ·½H ₂ O	150.95	col., hyg.	2.0-2.5	35.5	-H ₂ O, 160	16.7	50	s. alk.
acid, meta-	HAsO ₃	123.93	wh., hyg.		d.		d. to form	H ₃ AsO ₄	
acid, pyro-	H ₄ As ₂ O ₇	265.87	col.		d. 206		d. to form	H ₃ AsO ₄	
pentoxide	As ₂ O ₅	229.84	wh., amor.	4.086		d.	59.5 ^{0°}	76.7 ^{100°}	s. alk., al.
sulfide, di- (realgar)	As ₂ S ₂	213.97	red, mn., 2.68	(α)3.506 ^{19°} ; (β)3.254 ^{19°}	(α)tr. 267; (β)307	565	i.	d.	s. K ₂ S, NaHCO ₃
sulfide, penta-	As ₂ S ₅	310.17	yel.			d. 500	0.000136 ^{0°}	i.	s. HNO ₃ , alk.
Arsenious chloride (butter of arsenic)	AsCl ₃	181.28	oily lq.	lq. 2.163	-18	130	d.	d.	s. HCl, HBr, PCl ₃
hydride (arsine)	AsH ₃	77.95	col. gas	2.695 (A)	-113.5	-55; d. 230	20 cc	sl. s.	sl. s. alk.
oxide (arsenolite)	As ₂ O ₃	197.84	col., cb., fibrous, 1.755	3.865 ^{25°}	subl.		sl. s.	sl. s.	i. al., et.
oxide (claudetite)	As ₂ O ₃	197.84	col., mn., 1.92	3.85	subl.		sl. s.	sl. s.	i. al., et.
oxide	As ₂ O ₃	197.84	amor. or vitreous	3.738	315		1.21 ^{0°}	2.93 ^{40°}	s. HCl, alk., Na ₂ CO ₃ ; i. al., et.
Auric chloride	AuCl ₃ ·2H ₂ O	339.36	or. cr.		d.		v. s.	v. s.	s. HCl, al., et.; sl. s. NH ₃
cyanide	Au(CN) ₃ ·6H ₂ O	383.11			d. 50		v. s.	v. s.	s. al.
Aurous chloride	AuCl	232.42	yel. cr.	7.4	AuCl ₃ , 170	d. 290	d.	d.	s. HCl, HBr; d. al.
cyanide	AuCN	222.98	yel. cr.		d.		i.	i.	s. KCN; i. al., et.
Barium	Ba	137.33	silv. met.	3.5	850	1140	d.	d.	s. a.; d. al.
acetate	Ba(C ₂ H ₃ O ₂) ₂	255.42	col.	2.468			58.8 ^{0°}	75.0 ^{100°}	
acetate	Ba(C ₂ H ₃ O ₂) ₂ ·H ₂ O	273.43	wh., tri. pr., 1.517	2.19	-H ₂ O, 41		75 ^{30°} (anh.)	79 ^{40°} (anh.)	i. al.
bromide	BaBr ₂	297.14	col.	4.781 ^{24°}	847	d.	98 ^{0°}	149 ^{100°}	v. s. m. al.; v. sl. s. act.

^o Usually the solution.

† See special tables.

‡ Usual commercial form.

TABLE 2-1 Physical Properties of the Elements and Inorganic Compounds (Continued)

Name	Formula	Formula weight	Color, crystalline form and refractive index	Specific gravity	Melting point, °C	Boiling point, °C	Solubility in 100 parts		
							Cold water	Hot water	Other reagents
Barium (<i>Cont.</i>)									
bromide	BaBr ₂ ·2H ₂ O	333.17	col., mn., 1.7266	3.69	-2H ₂ O, 100	d.	v. s.	v. s.	s. al.
carbonate (witherite)	BaCO ₃	197.34	wh., rhb., 1.676	4.29	tr. 811 to α	d. 1450	0.0022 ^{18°}	0.0065 ^{100°}	s. a.; i. al.
carbonate (α)	BaCO ₃	197.34	wh., hex.		tr. 982 to β				
carbonate (β)	BaCO ₃	197.34	wh.		1740 ^{90atm}		0.0022 ^{18°}	0.0065 ^{100°}	s. a.; i. al.
Barium chlorate	Ba(ClO ₃) ₂	304.23	col.		414		20.35 ^{0°}	84.8 ^{80°}	
chlorate	Ba(ClO ₃) ₂ ·H ₂ O ^o	322.24	col., mn., 1.577	3.179	d. 120		s.	s.	sl. s. al., act.
chloride	BaCl ₂	208.23	col., mn., 1.7361	3.856 ^{34°}	tr. 925	1560	31 ^{0°}	59 ^{100°}	sl. s. HCl, HNO ₃ ; i. al.
chloride	BaCl ₂	208.23	col., cb.		962	1560			
chloride	BaCl ₂ ·2H ₂ O†	244.26	col., mn., 1.646	3.097 ^{34°}	-2H ₂ O, 100		39.3 ^{0°}	76.8 ^{100°}	sl. s. HCl, HNO ₃ ; i. al.
hydroxide	Ba(OH) ₂	171.34	col., mn.	4.495			1.67 ^{0°}	101.4 ^{80°}	
hydroxide	Ba(OH) ₂ ·8H ₂ O	315.46	col., mn., 1.5017	2.188 ^{16°}	77.9	-8H ₂ O, 550	5.6 ^{15°}		v. sl. s. al.; i. et.
nitrate (nitrobarite)	Ba(NO ₃) ₂	261.34	col., cb., 1.572	3.244 ^{28°}	592	d.	5.0 ^{0°}	34.2 ^{100°}	sl. s. a.; i. al.
oxalate	BaC ₂ O ₄	225.35	wh. cr.	2.658			0.0016 ^{8°}	0.0024 ^{24°}	s. a., NH ₄ Cl; i. al.
oxide	BaO	153.33	col., cb., 1.98	5.72	1923	2000±	1.5 ^{0°}	90.8 ^{80°}	s. HCl, HNO ₃ , abs. al.; i. NH ₃ , act.
peroxide	BaO ₂ ^o	169.33	gray or wh. pd.	4.958	-O, 800		v. sl. s.	d.	s. dil. a.; i. act.
peroxide	BaO ₂ ·8H ₂ O	313.45	pearly sc.		-8H ₂ O, 100		0.168	d.	s. dil. a.; i. al., et., act.
phosphate, monobasic	BaH ₄ (PO ₄) ₂	331.30	tri.	2.9 ^{4°}			d.	d.	s. a.
phosphate, dibasic	BaHPO ₄	233.31	wh., rhb. nd., 1.635	4.165 ^{15°}			0.015		s. a., NH ₄ salts
phosphate, tribasic	Ba ₃ (PO ₄) ₂	601.92	wh., cb.	4.1 ^{16°}			i.		s. a.
phosphate, pyro-	Ba ₂ P ₂ O ₇	448.60	wh., rhb.	3.9 ^{20°}			0.01		s. a., NH ₄ salts
silicofluoride	BaSiF ₆	279.40	pr.	4.279 ^{15°}			0.026 ^{17°}	0.09 ^{100°}	sl. s. HCl, NH ₄ Cl; i. al.
sulfate (barite, barytes)	BaSO ₄	233.39	col., rhb., 1.636	4.499 ^{15°}	1580 d.	tr. to mn. 1149	0.000115 ^{0°}	0.000285 ^{30°}	s. conc. H ₂ SO ₄ ; 0.006, 3% HCl
sulfide, mono-	BaS	169.39	col., cb., 2.155	4.25 ^{15°}			d.	d.	d. HCl; i. al.
sulfide, tri-	BaS ₃	233.52	yel.-gn.		d. 400		s.	s.	
sulfide, tetra-	BaS ₄ ·2H ₂ O	301.62	red, rhb.	2.988 ^{20°}	d. 200		41 ^{15°}	v. s.	i. al., CS ₂
Beryllium (glucinum)	Be(Gl)	9.01	gray, met., hex.	1.816	1284	2767	i.	sl. s. d.	s. dil. a., alk.
Bismuth	Bi	208.98	silv. wh. or reddish, hex.	9.80 ^{20°}	271	1450	i.	i.	s. aq. reg., conc. H ₂ SO ₄ , HNO ₃
carbonate, sub-	Bi ₂ O ₃ ·CO ₂ ·H ₂ O	527.98	wh. pd.	6.86	d.		i.	i.	s. a.
chloride, di-	BiCl ₃ (?)	279.89	bk. nd.	4.86	163	d. 300	d.	d.	
chloride, tri-	BiCl ₃ ^o	315.34	wh. cr.	4.75	230	447	d.	d.	s. al.
nitrate	Bi(NO ₃) ₃ ·5H ₂ O	485.07	col., tri.	2.82	d. 30	-5H ₂ O, 80	d.	d.	42 ^{19°} act.; s. a.; i. al.
nitrate, sub-	BiONO ₃ ·H ₂ O	305.00	hex. pl.	4.928 ^{15°}	d. 260		i.	i.	s. a.
oxide, tri-	Bi ₂ O ₃	465.96	yel., rhb.	8.9	820	1900±	i.	i.	s. a.
oxide, tri-	Bi ₂ O ₃	465.96	yel., tet.	8.55	860		i.	i.	s. a.
oxide, tri-	Bi ₂ O ₃	465.96	yel., cb.	8.20	tr. 704		i.	i.	s. a.
oxychloride	BiOCl	260.43	wh., amor.	7.72 ^{15°}			sl. s.	sl. s.	s. a.; i. act., NH ₃ , H ₂ C ₄ H ₄ O ₆
Boric acid	H ₃ BO ₃	61.83	wh., tri.	1.435 ^{15°}	185 d.		2.66 ^{0°}	40.2 ^{100°}	22.2 ^{20°} gly., 0.24 ^{25°} et.; s. al.
Boron	B	10.81	gray or bk., amor. or mn.	2.32	2300	2550	i.	i.	s. HNO ₃ ; i. al.
carbide	B ₄ C	55.25	bk. cr.	2.54	2450	>3500	i.	i.	i. a.
oxide	B ₂ O ₃	69.62	col. glass, 1.459	1.85	577	>1500	1.1 ^{0°}	15.7 ^{100°}	s. a., al., gly.
oxide (sassolite)	B ₂ O ₃ ·3H ₂ O	123.67	tri., 1.456	1.49	d.		sl. s.	s.	
Bromic acid	HBrO ₃	128.91	col.; in soln. only		d. 100		v. s.	d.	
Bromine	Br ₂	159.81	rhb., or red liq.	3.119 ^{30°} ; 5.87 (A)	-7.2	58.78	4.22 ^{0°}	3.13 ^{30°}	s. al., et., alk., CS ₂
hydrate	Br ₂ ·10H ₂ O	339.96	red, oct.		d. 6.8		s.		
Cadmium	Cd	112.41	silv. met., hex.	8.65 ^{20°}	320.9	767	i.	i.	s. a., NH ₄ NO ₃
acetate	Cd(C ₂ H ₃ O ₂) ₂	230.50	col.	2.31	256	d.	v. s.	s. m. al.	
acetate	Cd(C ₂ H ₃ O ₂) ₂ ·2H ₂ O ^o	266.53	col., mn.	2.041	-H ₂ O, 130		v. s.	s. al.	
carbonate	CdCO ₃	172.42	wh., trig.	4.258 ^{4°}	d. <500		i.	i.	s. a., KCN, NH ₄ salts; i. NH ₃
chloride	CdCl ₂	183.32	wh., cb.	4.047 ^{25°}	568	960	90 ^{0°}	147 ^{100°}	1.52 ^{15°} al.; i. et., act.

chloride	CdCl ₂ ·2½H ₂ O	228.36	col., mn., 1.6513	3.327	tr. 34		168 ^{20°}	180 ^{100°}	2.05 ^{15°} m. al.
cyanide	Cd(CN) ₂	164.45			d. >200		0.0247 ^{15°}		s. a.; NH ₄ OH, KCN
hydroxide	Cd(OH) ₂	146.43	wh., trig.	4.79 ^{15°}	d. 300		0.00026 ^{25°}		s. a., NH ₄ salts; i. alk.
nitrate	Cd(NO ₃) ₂	236.42	col.		350		109.7 ^{0°}	326 ^{59.5°}	v. s. a.
nitrate	Cd(NO ₃) ₂ ·4H ₂ O*	308.48	col. nd.	2.455 ^{17°}	59.4	132	215 ^{0°}		s. al., NH ₃ ; i. HNO ₃
oxide	CdO	128.41	brn., cb.	8.15			i.	i.	s. a., NH ₄ salts; i. alk.
oxide	CdO	128.41	brn., amor. 2.49	6.95	d. 900–1000		i.	i.	s. a., NH ₄ salts; i. alk.
oxide, sub-	Cd ₂ O	240.82	gn., amor.	8.192 ^{18°}	d.				d. a., alk.
Cadmium sulfate	CdSO ₄	208.47	rhb.	4.691 ^{24°}	1000		76.5 ^{0°}	60.8 ^{100°}	i.act., NH ₃
sulfate	CdSO ₄ ·H ₂ O	226.49	mn.	3.786 ^{20°}	tr. 108		s.	s.	
sulfate	3CdSO ₄ ·8H ₂ O*	769.54	col., mn., 1.565	3.09	tr. 41.5		114.2 ^{0°}	127.6 ^{50°}	i. al.
sulfate	CdSO ₄ ·4H ₂ O	280.53	col.	3.05			s.	s.	i. al.
sulfate	CdSO ₄ ·7H ₂ O	334.58	mn.	2.48 ^{20°}	tr. 4		350 ^{-5°}		i. al.
sulfide (greenockite)	CdS	144.48	yel.-or., hex., 2.506	4.58	1750 ^{100atm}	subl. in N ₂ , 980	0.000001	Colloidal	s. a.; v. s. NH ₄ OH
Calcium	Ca	40.08	silv. met., cb.	1.55 ^{20°}	810	1200 ± 30	d.	d.	s. a.; sl. s. al.
acetate	Ca(C ₂ H ₃ O ₂) ₂ ·H ₂ O	176.18	wh. nd.		d.		52 ^{0°}	45.5 ^{50°}	sl. s. al.
aluminate	Ca(AlO ₂) ₂	158.04	col., rhb. or mn.	3.67 ^{20°}	1600		d.		s. HCl
aluminum silicate (anorthite)	CaO·Al ₂ O ₃ ·2SiO ₂	278.21	tri., 1.5832	2.765	1551				
arsenate	Ca ₃ (AsO ₄) ₂	398.07	wh. pd.				0.013 ^{25°}	i.	s. dil. a.
bromide	CaBr ₂	199.89	delq. nd.	3.353 ^{25°}	760	1810	125 ^{0°}	312 ^{105°}	s. al., act.; sl. s. NH ₃
carbonate (aragonite)	CaCO ₃	100.09	col., rhb., 1.6809	2.93	d. 825		0.0012 ^{20°} †	0.002 ^{100°}	s. a., NH ₄ Cl
carbonate (calcite)	CaCO ₃	100.09	col., hex., 1.550	2.711 ^{25°}	1339 ^{103atm}		0.0014 ^{25°}	0.002 ^{100°}	s. a., NH ₄ Cl
chloride (hydrophilite)	CaCl ₂ *	110.98	wh., delq., cb. 1.52	2.152 ^{15°}	772	>1600	59.5 ^{0°}	347 ^{260°}	s. al.
chloride	CaCl ₂ ·H ₂ O	129.00	col., delq.				s.	s.	s. al.
chloride	CaCl ₂ ·6H ₂ O	219.08	col., trig., 1.417	1.68 ^{17°}	29.92	-6H ₂ O, 200	v. s.	v. s.	s. al.
citrate	Ca ₃ (C ₆ H ₅ O ₇) ₂ ·4H ₂ O	570.49	col. nd.		-2H ₂ O, 130		0.085 ^{18°}	0.096 ^{26°}	0.0065 ^{18°} al.
cyanamide	CaCN ₂	80.10	col., rhombohedral				s. d.	d.	
ferrocyanide	Ca ₂ Fe(CN) ₆ ·12H ₂ O	508.29	yel., tri., 1.5818	1.7			s.	150 ^{90°}	i. al.
fluoride (fluorite)	CaF ₂	78.07	wh., cb., 1.4339	3.180 ^{30°}	1330		0.0016 ^{18°}	0.0017 ^{26°}	sl. s. a.
formate	Ca(HCO ₂) ₂	130.11	col., rhb.	2.015	d.		16.1 ^{0°}	18.4 ¹⁰⁰	i. al., et.
hydride	CaH ₂	42.09	wh. cr. or pd.	1.7	d. 675		d.		d. a.; i. bz.
hydroxide	Ca(OH) ₂	74.09	col., hex., 1.574	2.2	-H ₂ O, 580		0.185 ^{0°}	0.077 ^{100°}	s. NH ₄ Cl
hypochlorite	Ca(ClO) ₂ ·4H ₂ O	215.04	wh., feathery cr.		d.		delq.; d.	d.	d. a.
hypophosphate	Ca ₃ P ₂ O ₆ ·2H ₂ O	274.13	granular		-2H ₂ O, 200		i.		s. HCl, H ₄ P ₂ O ₆
lactate	Ca(C ₃ H ₅ O ₃) ₂ ·5H ₂ O	308.29	col., eff.		-3H ₂ O, 100		10.5	∞	∞h. al.; i. et.
magnesium carbonate (dolomite)	CaO·MgO·2CO ₂	184.40	trig., 1.68174	2.872	d. 730–760		0.032 ^{18°}		
magnesium silicate (diopside)	CaO·MgO·2SiO ₂	216.55	wh., mn.	3.3	1391		i.	i.	
nitrate (nitrocalcite)	Ca(NO ₃) ₂	164.09	col., cb.	2.36	561		102 ^{0°}	376 ^{151°}	14 ^{15°} al.; s. amyl al., NH ₃
nitrate	Ca(NO ₃) ₂ ·4H ₂ O*	236.15	col., mn., 1.498	1.82	42.7		266 ^{0°}	v. s.	
nitride	Ca ₃ N ₂	148.25	brn. cr.	2.63 ^{17°}	900		d.	d.	s. dil. a.; i. abs. al.
nitrite	Ca(NO ₂) ₂ ·H ₂ O	150.10	delq., hex.	2.23 ^{34°}			77 ^{0°}	417 ^{90°}	s. 90% al.
oxalate	CaC ₂ O ₄	128.10	col., cb.	2.2 ^{4°}	d.		0.00067 ^{13°}	0.0014 ^{95°}	s. a.; i. ac.
oxalate	CaC ₂ O ₄ ·H ₂ O	146.11	col.	2.2	-H ₂ O, 200		i.	i.	s. a.; i. ac
oxide	CaO	56.08	col., cb., 1.837	3.32	2570	2850	Forms Ca(OH) ₂		s. a.; i. al.
peroxide	CaO ₂ ·8H ₂ O	216.20	pearly, tet.		-8H ₂ O, 100	expl. 275	sl. s.	d.	s. a. d.; i. al., et.
phosphate, monobasic	CaH ₄ (PO ₄) ₂ ·H ₂ O	252.07	wh., tri.	2.220 ^{16°}	-H ₂ O, 100	d. 200	d.	d.	
phosphate, dibasic	CaHPO ₄ ·2H ₂ O	172.09	wh., mn. pl.	2.306 ^{16°}	d.		0.02 ^{24.5°}	0.075 ^{100°}	
phosphate, tribasic	Ca ₃ (PO ₄) ₂	310.18	wh., amor.	3.14	1670		0.0025	d.	s. a.; i. al., ac.
phosphate, meta-	Ca(PO ₃) ₂	198.02	wh., tet., 1.588	2.82	975		i.	i.	i. a.
phosphate, pyro-	Ca ₂ P ₂ O ₇	254.10	col., biaxial, 1.60	3.09	1230		i.		s. a.
phosphate, pyro- (brushite)	Ca ₂ P ₂ O ₇ ·5H ₂ O	344.18	wh., mn.	2.25			sl. s.		s. a.; i. NH ₄ Cl
phosphide	Ca ₃ P ₂	182.18	red cr.	2.51 ^{15°}	>1600		d.		s. dil. a.; i. al., et.
silicate (α) (pseudowollastonite)	CaSiO ₃	116.16	col., pseudo hex., 1.6150 or mn.(?)	2.905	1540		0.0095 ^{17°}		s. HCl
silicate (β) (wollastonite)	CaSiO ₃	116.16	col., mn., 1.610	2.915	tr. 1190 to α				
sulfate (anhydrite)	CaSO ₄	136.14	col., rhb., 1.576, or mn. 1.50	2.96	1450(mn.)	tr. 1193 to rhb.	0.298 ^{20°}	0.1619 ^{100°}	s. a., Na ₂ S ₂ O ₃ , NH ₄ salts

* Usual commercial form.

† The solubility of CaCO₃ in H₂O is greatly increased by increasing the amount of CO₂ in the H₂O.

TABLE 2-1 Physical Properties of the Elements and Inorganic Compounds (Continued)

Name	Formula	Formula weight	Color, crystalline form and refractive index	Specific gravity	Melting point, °C	Boiling point, °C	Solubility in 100 parts		
							Cold water	Hot water	Other reagents
Calcium (<i>Cont.</i>) sulfate (gypsum)	CaSO ₄ ·2H ₂ O	172.17	col., mn., 1.5226	2.32	-1½H ₂ O, 128	-2H ₂ O, 163	0.223 ^{0°}	0.257 ^{50°}	s. a., gly., Na ₂ S ₂ O ₃ , NH ₄ salts
sulfhydrate	Ca(SH) ₂ ·6H ₂ O	214.32	col. pr.		d. 15		v. s.	v. s.	s. al.
sulfide (oldhamite)	CaS	72.14	col., cb.	2.8 ^{15°}			d.	d.	s. a.
sulfite	CaSO ₃ ·2H ₂ O	156.17	wh., cr., 1.595		-2H ₂ O, 100	d. 650	0.0043 ^{18°}	0.0027 ^{90°}	s. H ₂ SO ₃
tartrate	CaC ₄ H ₄ O ₆ ·4H ₂ O	260.21	col., rhb.		d.		0.037 ^{0°}	0.22 ^{35°}	sl. s. al.
thiocyanate	Ca(CNS) ₂ ·3H ₂ O	210.29	wh., delq. cr.				s.	v. s.	v. s. al.
thiosulfate	CaS ₂ O ₃ ·6H ₂ O	260.30	col., tri., 1.56	1.873 ^{16°}		d.	71.2 ^{9°}	d.	i. al.
tungstate (scheelite)	CaWO ₄	287.92	wh., tet., 1.9200	6.06			0.2		s. NH ₄ Cl; i. a.
Carbon, <i>cf.</i> table of organic compounds									
Carbon, amorphous	C	12.01	bk., amor.	1.8-2.1	>3500	4200	i.	i.	i. a., alk.
Carbon, diamond	C	12.01	col., cb., 2.4195	3.51 ^{20°}	>3500	4200	i.	i.	i. a., alk.
Carbon, graphite	C	12.01	bk., hex.	2.26 ^{20°}	>3500	4200	i.	i.	i. a., alk.
dioxide	CO ₂	44.01	col. gas	lq. 1.101 ^{-87°} ; 1.53 (A); solid 1.56 ^{-79°}	-56.6 ^{5,2atm.}	subl. -78.5	179.7 ^{0°} cc	90.1 ^{20°} cc	s. a., alk.
disulfide	CS ₂	76.14	col. lq.	lq. 1.261 ^{22°} ; 2.63 (A)	-108.6	46.3	0.2 ^{0°}	0.014 ^{50°}	s. al.; et.
monoxide	CO	28.01	col., poisonous, odorless gas	lq. 0.814 ^{-195°} ; 0.968 (A)	-207	-192	0.0044 ^{0°} ; 3.5 ^{0°} cc	0.0018 ^{50°} ; 2.32 ^{20°} cc	s. al., Cu ₂ Cl ₂
oxychloride (phosgene)	COCl ₂	98.92	poisonous gas	1.392 ^{49°}	-104	8.2 ^{756mm}	v. s. sl. d.	d.	s. ac., CCl ₄ , bs.; d. a.
oxysulfide	COS	60.08	gas	lq. 1.24 ^{-87°} ; 2.10 (A)	-138.2	-50.2 ^{760mm}	133 ^{0°} cc	40.3 ^{30°} cc	v. s. alk., al.
suboxide	C ₃ O ₂	68.03	gas	lq. 1.114 ^{0°}	-107	7 ^{761mm}	d.		s. et.
thionyl chloride	S ₂ Cl ₂	114.98	yel.-red lq.	1.509 ^{15°}		73.5			
Ceric hydroxide	2CeO ₂ ·3H ₂ O	398.28	yel., gelatinous						s. a.; sl. s. alk. carb.; i. alk
hydroxynitrate	Ce(OH)(NO ₃) ₃ ·3H ₂ O	397.18	red, mn.				d.		
oxide	CeO ₂	172.11	wh. or pa. yel., cb.	7.3	1950		i.	i.	s. H ₂ SO ₄ , HCl
sulfate	Ce(SO ₄) ₂ ·4H ₂ O	404.30	yel., rhb.	3.91			s. d.		s. dil. H ₂ SO ₄
Cerium	Ce	140.12	steel gray, cb. or hex.	6.9 ^{30°} cb.; 6.7 hex.	645	1400	i.	Slowly oxidized	s. dil. a.; i. al.
Cerous sulfate	Ce ₂ (SO ₄) ₃	568.42	wh., mn. or rhb.	3.91			18.98 ^{0°}	0.4 ^{100°}	
sulfate	Ce ₂ (SO ₄) ₃ ·8H ₂ O	712.54	tri.	2.886 ^{17°}	-8H ₂ O, 630		25 ^{0°}	7.6 ^{40°}	
Cesium	Cs	132.91	silv. met., hex.	1.90 ^{20°}	28.5	670	d.		s. a., al., NH ₃
Chloric acid	HClO ₃ ·7H ₂ O	210.57	lq.	1.282 ^{14.2°}	<-20	d. 40	v. s.		
Chlorine	Cl ₂	70.91	rhb., or gn.-yel. gas	lq. 1.56 ^{-33.6°} ; 2.49 ^{0°} (A)	-101.6	-34.6	1.46 ^{0°} ; 310 ^{10°} cc	0.57 ^{30°} ; 177 ^{30°} cc	s. alk.
hydrate	Cl ₂ ·8H ₂ O	215.03	rhb.	1.23	d. 9.6		s.		s. alk.
Chloroplatinic acid	H ₂ PtCl ₆ ·6H ₂ O	517.90	red-brn., delq.	2.431	60		v. s.	v. s.	s. al., et.
Chlorostannic acid	H ₂ SnCl ₆ ·6H ₂ O	441.54	delq.	1.971 ^{28°}	19.2		s.		
Chlorosulfonic acid	HO·SO ₂ ·Cl	116.52	col. lq.	1.787 ^{25°}	-80	151.5 ^{765mm}	d.		d. al.; i. CS ₂
Chromic acetate	Cr ₂ (C ₂ H ₃ O ₂) ₆ ·2H ₂ O	494.29	gn.				s.		4.76 ^{15°} m. al.
chloride	CrCl ₃	158.36	pink, trig.	2.757 ^{15°}		1200-1500 d.	i. §	sl. s.	i. a., act., CS ₂
chloride	CrCl ₃ ·6H ₂ O ^o	266.45	vl. or gn., hex. pl.	1.835 ^{25°}			v. s. d.		s. al.; i. et.
fluoride	CrF ₃	108.99	gn., rhb.	3.8		d.	i.		sl. s. a.; i. al., NH ₃
hydroxide	Cr(OH) ₃	103.02	gn. or blue, gelatinous				i.		s. a., alk.; sl. s. NH ₃
hydroxide	Cr(OH) ₃ ·2H ₂ O	139.05	gn.		-2H ₂ O, 100		i.	i.	s. a., alk.
nitrate	Cr(NO ₃) ₃ ·9H ₂ O ^o	400.15	purple pr.			d. 100	s.	s.	s. a., alk., al., act.
nitrate	Cr(NO ₃) ₃ ·7½H ₂ O	373.13	purple, mn.			d.	s.	s.	
oxide	Cr ₂ O ₃	151.99	dark gn., hex.	5.21	1900		i.	i.	sl. s. a.
sulfate	Cr ₂ (SO ₄) ₃	392.18	rose pd.	3.012			i. †		i. a.
sulfate	Cr ₂ (SO ₄) ₃ ·5H ₂ O	482.26	gn.				s.		s. al., H ₂ SO ₄
sulfate	Cr ₂ (SO ₄) ₃ ·15H ₂ O	662.41	vl.	1.867 ^{17°}	100	-10H ₂ O, 100	s.	d. 67°	sl. s. al.
sulfate	Cr ₂ (SO ₄) ₃ ·18H ₂ O	716.46	vl., cb., 1.564	1.7 ^{22°}		-12H ₂ O, 100	120 ^{20°}	d.	s. al.
sulfide	Cr ₂ S ₃	200.19	brn.-bk. pd.	3.77 ^{19°}	-S, 1350		i.	d.	s. h. HNO ₃

Chromium	Cr	52.00	gray, met., cb.	7.1	1615	2200	i.	i.	s. HCl, dil. H ₂ SO ₄ ; i. HNO ₃
trioxide (chromic acid)	CrO ₃	99.99	red, rhb.	2.70	197 d.		164.9 ^{0°}	206.7 ^{100°}	s. H ₂ SO ₄ , al., et. sl. s. al.; i. et.
Chromous chloride	CrCl ₃	122.90	wh., delq.	2.75			v. s.	v. s.	s. conc. a.
hydroxide	Cr(OH) ₃	86.01	yel.-brn.		d.		d.		i. dil. HNO ₃
oxide	CrO	68.00	bk. pd.				i.	i.	sl. s. al.
sulfate	CrSO ₄ ·7H ₂ O	274.17	blue				12.35 ⁰		v. s. a.
sulfide (daubrelite)	CrS	84.06	bk. pd.	3.97	1550		i.		s. et.
Chromyl chloride	CrO ₂ Cl ₂	154.90	dark red lq.	1.92	-96.5	117.6	d.		s. a.
Cobalt	Co	58.93	silv. met., cb.	8.9 ^{20°}	1480	2900	i.	i.	s. al., et., CS ₂
carbonyl	Co(CO) ₄	170.97	or. cr.	1.73 ^{18°}	51	d. 52	i.	d.	s. HNO ₃ , aq. reg.
sulfide, di-	CoS ₂	123.06	bk., cb.	4.269			i.		
Cobaltic chloride	CoCl ₃	165.29	red cr.	2.94	subl.		s.	s.	
chloride, dichro	Co(NH ₃) ₃ Cl ₃ ·H ₂ O	234.40					s.		s. a.; al.
chloride, luteo	Co(NH ₃) ₆ Cl ₃	267.48	or., mn.	1.7016 ^{20°}			4.26 ^{0°}	12.74 ^{46.5°}	i. al., NH ₄ OH
chloride, praseo	Co(NH ₃) ₄ Cl ₃ ·H ₂ O	251.43	gn., rhb.	1.847			v. s.		s. a.; i. al.
Cobaltic chloride, purpureo	Co(NH ₃) ₅ Cl ₃	250.44	rhb.	1.819 ^{25°/25°}			0.232 ^{0°}	1.031 ^{46.5°}	i. al.
chloride, roseo	Co(NH ₃) ₅ Cl ₃ ·H ₂ O	268.46	brick red		d. 100		16.12 ^{0°}	24.87 ^{16°}	sl. s. HCl
hydroxide	Co(OH) ₃	109.96	bk.		-1½H ₂ O, 100		i.	i.	s. a.; i. al.
oxide	Co ₂ O ₃	165.86	bk.	5.18	d. 900		i.	i.	s. a.
sulfate	Co ₂ (SO ₄) ₃	406.05	blue cr.				d.		s. H ₂ SO ₄
sulfide	Co ₂ S ₃	214.06	bk. cr.	4.8			i.		d. a.
Cobalto-cobaltic oxide	Co ₃ O ₄	240.80	bk., cb.	6.07			i.	i.	s. H ₂ SO ₄ ; i. HCl, HNO ₃
Cobaltous acetate	Co(C ₂ H ₃ O ₂) ₂ ·4H ₂ O	249.08	red-vl., mn., 1.542	1.7053 ^{15.7°}	-4H ₂ O, 140		s.	s.	s. a., al.
chloride	CoCl ₂	129.84	blue cr.	3.356	subl.	1049	45 ^{7°}	105 ^{96°}	31 al.; 8.6 act.
chloride	CoCl ₂ ·6H ₂ O*	237.93	red, mn.	1.924 ^{25°}	86	-6H ₂ O, 110	116.5 ^{0°}	177 ^{80°}	v. s. et., act.
nitrate	Co(NO ₃) ₂ ·6H ₂ O	291.03	red, mn., 1.4	1.883 ^{25°}	<100	d.	84.03 ^{0°} (anh.)	334.9 ^{90°}	100 ^{12.5°} al.; s. act.; sl. s. NH ₃
oxide	CoO	74.93	brn., cb.	5.68	d. 1800		i.	i.	s. a., NH ₄ OH; i. al.
sulfate	CoSO ₄	155.00	red pd.	3.710 ^{25°}	d. 880		25.6 ^{0°}	83 ^{100°}	1.04 ^{18°} m. al.; i. NH ₃
sulfate	CoSO ₄ ·H ₂ O	173.01	red pd., mn.(?), 1.639	3.13	d.		s.	s.	
sulfate (biebeorite)	CoSO ₄ ·7H ₂ O*	281.10	red, mn., 1.483	1.948 ^{25°}	96.8	-7H ₂ O, 420	33 ^{80°}	s.	2.5 ^{8°} al.
sulfide (syeporite)	CoS	91.00	brn. nd.	5.45 ^{15°}	>1100		0.00038 ^{18°}		s. a., aq. reg.
Copper	Cu	63.55	yel.-red met., cb.		1083	2300	i.	i.	s. HNO ₃ , h. H ₂ SO ₄
Cupric acetate	Cu(C ₂ H ₃ O ₂) ₂	181.63		1.930 ^{20°/4°}			s.		
acetate	Cu(C ₂ H ₃ O ₂) ₂ ·H ₂ O	199.65	dark gn., mn.	1.882	115	240 d.	7.2	20	7 al.; s. et.; gly.
aceto-arsenite (Paris green)	(CuOAs ₂ O ₃) ₃ · Cu(C ₂ H ₃ O ₂) ₂ *	1013.79	gn.				i.		s. a., NH ₄ OH
ammonium chloride	CuCl ₂ ·2NH ₄ Cl·2H ₂ O	277.47	blue, tet., 1.670, 1.744	1.98	d. 110		33.8 ^{0°}	99.3 ^{90°}	s. a.
ammonium sulfate	CuSO ₄ ·4NH ₃ ·H ₂ O	245.75	blue, rhb.	1.81	d. 150		18.05 ^{21.5°}	d.	i. al.
carbonate, basic (azurite)	2CuCO ₃ ·Cu(OH) ₂	344.67	blue, mn., 1.758	3.88	d. 220		i.	d.	s. NH ₄ OH, h. aq. NaHCO ₃
carbonate, basic (malachite)	CuCO ₃ ·Cu(OH) ₂	221.12	dark gn., mn., 1.875	3.9	d.		i.	d.	s. KCN; 0.03 aq. CO
chloride (eriochalcite)	CuCl ₂	134.45	brn.-yel. pd.	3.054	498	Forms Cu ₂ Cl ₂ 993	70.7 ^{0°}	107.9 ^{100°}	53 ^{15°} al.; 68 ^{15°} m. al.
chloride	CuCl ₂ ·2H ₂ O	170.48	gn., rhb., 1.684	2.39 ^{22.4°}	-2H ₂ O, 110	d.	110.4 ^{0°}	192.4 ^{100°}	s. al.; et., NH ₄ Cl
chromate, basic	CuCrO ₄ ·2CuO·2H ₂ O	374.66	yel.-brn.		-2H ₂ O, 260		i.		s. HNO ₃ , NH ₄ OH
cyanide	Cu(CN) ₂	115.58	yel.-gn.		d.		i.		s. KCN, C ₆ H ₅ N
dichromate	CuCr ₂ O ₇ ·2H ₂ O	315.56	bk., tri.	2.286 ^{18°}	-2H ₂ O, 100		sl. s.	d.	s. a.; NH ₄ OH
ferrocyanide	Cu ₃ [Fe(CN) ₆] ₂	614.54	yel.-gn.				i.		s. NH ₄ OH; i. HCl
ferrocyanide	Cu ₂ Fe(CN) ₆ ·7H ₂ O	465.15	red-brn.				i.	i.	s. NH ₄ OH; i. a., NH ₃
formate	Cu(HCO ₂) ₂	153.58	blue, mn.	1.831			12.5	d.	0.25 al.
hydroxide	Cu(OH) ₂	97.56	blue, gelatinous	3.368	-H ₂ O		i.	d.	s. a., NH ₄ OH, KCN, al.
lactate	Cu(C ₃ H ₃ O ₃) ₂ ·2H ₂ O	277.72	dark blue, mn.				16.7	45 ^{100°}	sl. s. al.
nitrate	Cu(NO ₃) ₂ ·3H ₂ O*	241.60	blue, delq.	2.047 ^{3.9°}	114.5	-HNO ₃ , 170	381 ^{40°}	666 ^{90°}	100 ^{12.5°} al.
nitrate	Cu(NO ₃) ₂ ·6H ₂ O	295.65	blue, rhb.	2.074	-3H ₂ O, 26.4		243.7 ^{0°}	∞	s. al.

*Usual commercial form.

†Also a soluble modification.

TABLE 2-1 Physical Properties of the Elements and Inorganic Compounds (Continued)

Name	Formula	Formula weight	Color, crystalline form and refractive index	Specific gravity	Melting point, °C	Boiling point, °C	Solubility in 100 parts		
							Cold water	Hot water	Other reagents
Cupric acetate (<i>Cont.</i>)									
oxide (paramelaconite)	CuO	79.55	bk., cb.	6.40	d. 1026		i.	i.	s. a.; KCN, NH ₄ Cl
oxide (tenorite)	CuO	79.55	bk., tri., 2.63	6.45	d. 1026		i.	i.	s. a.; KCN, NH ₄ Cl
oxychloride	CuCl ₂ ·2CuO·4H ₂ O	365.60	blue-gn.		-3H ₂ O, 140		i.		s. a.
phosphide	Cu ₃ P ₂	252.59	bk.	6.35	d.		i.		s. HNO ₃ ; i. HCl
sulfate (hydrocyanite)	CuSO ₄	159.61	gn.-wh., rhb., 1.733	3.606 ^{15°}	d. >600	Forms CuO, 650	14.3 ^{0°}	75.4 ^{100°}	i. al.
sulfate (blue vitriol or chalcanthite)	CuSO ₄ ·5H ₂ O	249.69	blue, tri., 1.5368	2.286 ^{15.6°} / ₄	-4H ₂ O, 110	-5H ₂ O, 250	24.3 ^{0°}	205 ^{100°}	1.1 [°] al.
sulfide (covellite)	CuS	95.61	blue, hex. or mn., 1.45	4.6	tr. 103	d. 220	0.000033 ^{18°}		s. HNO ₃ , KCN
tartate	Cu ₂ C ₄ H ₄ O ₆ ·3H ₂ O	265.66	1 gn. pd.		d.		0.02 ^{15°}	0.14 ^{85°}	s. a., KOH
Cuprous ammonium iodide	CuI·NH ₄ I·H ₂ O	353.41	rhb. pl.				d.		s. NH ₄ I
carbonate	Cu ₂ CO ₃	187.10	yel.	4.4	d.		i.	i.	s. a., NH ₄ OH
chloride (nantokite)	Cu ₂ Cl ₂	198.00	wh., cb., 1.973	3.53	422	1366	1.52 ^{25°}		s. HCl, NH ₄ OH, al.
cyanide	Cu ₂ (CN) ₂	179.13	wh., mn.	2.9	474.5	d.	i.	i.	s. KCN, HCl, NH ₄ OH; sl. s. NH ₃
ferricyanide	Cu ₃ Fe(CN) ₆	402.59	brn.-red				i.		s. NH ₄ OH; i. HCl
ferrocyanide	Cu ₄ Fe(CN) ₆	466.13	brn.-red				i.		s. NH ₄ OH; i. NH ₄ Cl
fluoride	Cu ₂ F ₂	165.09	red cr.		908	subl. 1100	i.		s. HF, HCl, HNO ₃ ; i. al.
hydroxide	CuOH	80.55	yel.	3.4	-½H ₂ O, 360		i.	i.	s. a., NH ₄ OH
oxide (cuprite)	Cu ₂ O	143.09	red, cb., 2.705	6.0	1235	-O, 1800	i.	i.	s. HCl, NH ₄ Cl, NH ₄ OH
Cuprous phosphide	Cu ₆ P ₂	443.22	gray-bk.	6.4 to 6.8			i.		s. HNO ₃ ; i. HCl
sulfide (chalcocite)	Cu ₂ S	159.16	bk., rhb.	5.6	1100		0.0005 ^{18°}		s. HNO ₃ , NH ₄ OH; i. act.
sulfide	Cu ₂ S	159.16	bk., cb.	5.80	1130		0.0005 ^{18°}		s. HNO ₃ , NH ₄ OH; i. act.
Cyanogen	C ₂ N ₂	52.03	poisonous gas	lq. 0.866 ^{-17.2°} ; 1.806 (A)	-34.4		-20.5	450 ^{30°} cc	2300 ^{20°} cc al.; 500 ^{18°} cc et.
Cyanogen compounds, <i>cf.</i> table of organic compounds									
Ferric acetate, basic ammonium sulfate, <i>cf.</i> Alum chloride (molysite)	Fe(OH)(C ₂ H ₃ O ₂) ₂	190.94	brn., amor.				i.		s. a.; al.
chloride	FeCl ₃	162.20	bk.-brn., hex. delq.	2.804 ^{11°}	282	315	74.4 ^{0°}	535.8 ^{100°}	v. s. al.; et. +HCl
ferrocyanide (Prussian blue)	FeCl ₃ ·6H ₂ O	270.30	red-yel., delq.		37	280	246 ^{0°}	∞	s. al., act., gly.
hydroxide	Fe(OH) ₃	106.87	red-brn.	3.4 to 3.9		-½H ₂ O, 500	i.	i.	s. a.; i. al., et.
lactate	Fe(C ₃ H ₅ O ₃) ₃	323.06	brn., amor., delq.				v. s.	v. s.	i. et.
nitrate	Fe(NO ₃) ₃ ·6H ₂ O	349.95	rhb., delq.	1.684 ^{20°}	35	d.	150 ^{0°}	∞	s. al., act.
oxide (hematite)	Fe ₂ O ₃	159.69	red or bk., trig., 3.042	5.12	1560 d.		i.		s. HCl
sulfate	Fe ₂ (SO ₄) ₃	399.88	rhb., 1.814	3.097 ^{15°}	d. 480		sl. s.	d.	i. H ₂ SO ₄ , NH ₃
sulfate (coquimbite)	Fe ₂ (SO ₄) ₃ ·9H ₂ O	562.02	yel., trig.	2.1			440	d.	s. abs. al.
Ferroso-ferric chloride	FeCl ₂ ·2FeCl ₃ ·18H ₂ O	775.43	yel., delq.		d. 50		s.	s.	
ferricyanide (Prussian green)	Fe ^{III} Fe ^{II} [Fe(CN) ₆] ₆	1662.61	gn.		d. 180		i.		s. d. h. HCl
oxide (magnetite; magnetic iron oxide)	Fe ₃ O ₄	231.53	bk., cb., 2.42	5.2	1538 d.		i.	i.	i. al.
oxide, hydrated	Fe ₃ O ₄ ·4H ₂ O	303.59	bk.		d.		i.	i.	s. a.
Ferrous ammonium sulfate	FeSO ₄ ·(NH ₄) ₂ SO ₄ · 6H ₂ O	392.14	blue-gn., mn., 1.4915	1.864	d.		18 ^{0°}	100 ^{75°}	i. al.
chloride (lawrencite)	FeCl ₂	126.75	gn.-yel., hex., 1.567	2.7		delq.	64.4 ^{10°}	105.7 ^{100°}	100 al.; s. act.; i. et.
chloroplatinate	FePtCl ₆ ·6H ₂ O	571.73	yel., hex.	2.714			v. s.	v. s.	
ferricyanide (Turnbull's blue)	Fe ₃ [Fe(CN) ₆] ₂	591.43	dark blue		d.		i.		i. dil. a., al.
ferrocyanide	Fe ₂ Fe(CN) ₆	323.64	blue-wh., amor.				i.		
formate	Fe(HCO ₂) ₂ ·2H ₂ O	181.91			d.		sl. s.		
hydroxide	Fe(OH) ₂	89.86	lt. gn.	3.4			0.00067		s. a., NH ₄ Cl
nitrate	Fe(NO ₃) ₂ ·6H ₂ O	287.95	cr.		60.5		200 ^{0°}	300 ^{25°}	
oxide	FeO	71.84	bk.	5.7	1420		i.	i.	s. a.; i. alk.

phosphate (vivianite)	$\text{Fe}_3(\text{PO}_4)_2 \cdot 8\text{H}_2\text{O}$	501.60	blue, mn., 1.592, 1.603	2.58 3.5				i.	i.	s. a.; i. ac.
silicate	FeSiO_3	131.93	mn.	2.58	1550					
sulfate (siderotilite)	$\text{FeSO}_4 \cdot 5\text{H}_2\text{O}$	241.98	gn., tri., 1.536	2.2						
sulfate (copperas)	$\text{FeSO}_4 \cdot 7\text{H}_2\text{O}^*$	278.01	blue-gn., mn.	1.899 ^{14,50}	64	-5H ₂ O, 300	s.	s.		i. al.
sulfide	FeS	87.91	bk., hex.	4.84	1193	-7H ₂ O, 300 d.	32.8 ⁰⁰ 0.000616 ¹⁸⁰	149 ⁵⁰⁰		s. a.; i. NH ₃
<i>cf.</i> also under iron										
Fluoboric acid	HBF_4	87.81	col. lq.			130 d.	∞	∞		s. al.
Fluorine	F_2	38.00	gn.-yel. gas	lq. 1.51 ⁻¹⁸⁷⁰ ; 1.31 ¹⁵⁰ (A)	-223	-187	d.			
Fluosilicic acid	H_2SiF_6	144.09					s.	s.		
Gadolinium	Gd	157.25								
Callium bromide	GaBr_3	309.44	delq. cr.				s.	s.		
Glucinum <i>cf.</i> Beryllium										
Gold	Au	196.97	yel. met., cb.	19.3 ²⁰⁰	1063	2600	i.	i.		s. aq. reg., KCN; i. a.
Gold, colloidal	Au	196.97	blue to vl.				s.			s. aq. reg., KCN; i. a.
Gold salts <i>cf.</i> under Auric and Aurous										
Hafnium	Hf	178.49	hex.	12.1	>1700	>3200(?)				
Helium	He	4.00	col. gas	0.1368 (A)	<-272.2	-268.9	0.97 ⁰⁰ cc	1.08 ⁵⁰⁰ cc		Absorbed by Pt
Hydrazine	N_2H_4	32.05	col. lq.	1.011 ¹²⁰ ₄	1.4	113.5	∞	∞		s. al.
formate	$\text{N}_2\text{H}_4 \cdot 2\text{HCO}_2\text{H}$	124.10	cb.		128		s.			
hydrate	$\text{N}_2\text{H}_4 \cdot \text{H}_2\text{O}$	50.06	col.	1.03 ²¹⁰	-40	118.5 ^{739.5mm}	∞	∞		∞ al.; i. et.
hydrochloride	$\text{N}_2\text{H}_4 \cdot \text{HCl}$	68.51	yel. lq.				v. s.	v. s.		sl. s. al.
hydrochloride, di-	$\text{N}_2\text{H}_4 \cdot 2\text{HCl}$	104.97	wh., cb.	1.42	198		s.	v. s.		s. al.
nitrate	$\text{N}_2\text{H}_4 \cdot \text{HNO}_3$	95.06	cr.		70.7	subl. 140	174.9 ¹⁰⁰	v. s.		
nitrate, di-	$\text{N}_2\text{H}_4 \cdot 2\text{HNO}_3$	158.07	nd.		104	d.	v. s.			
sulfate	$\text{N}_2\text{H}_4 \cdot \frac{1}{2}\text{H}_2\text{SO}_4$	81.08	delq. pl.		85		v. s.			i. al.
sulfate	$\text{N}_2\text{H}_4 \cdot \text{H}_2\text{SO}_4$	130.12	rhb.	1.378	254		3.055 ²²⁰	27.65 ⁶⁰⁰		v. sl. s. abs. al.
Hydrazoic acid (azoimide)	HN_3	43.03	col. lq.		-80	37	∞	∞		∞ al.
Hydriodic acid	HI	127.91	col. gas	4.4 ⁰⁰ (A)	-50.8	-35.5	42500 ¹⁰⁰ cc	v. s.		s. al.
Hydriodic acid	$\text{HI} \cdot \text{H}_2\text{O}$	145.93	col. lq.	1.7 ¹⁵⁰		127 ^{774mm}	∞	∞		∞ al.
Hydriodic acid	$\text{HI} \cdot 2\text{H}_2\text{O}$	163.94	col. lq.		-43		∞	∞		s. al.
Hydriodic acid	$\text{HI} \cdot 3\text{H}_2\text{O}$	181.96	col. lq.		-48		∞	∞		s. al.
Hydriodic acid	$\text{HI} \cdot 4\text{H}_2\text{O}$	199.97	col. lq.		-36.5		∞	∞		s. al.
Hydrobromic acid	HBr	80.91	col. gas; 1.325 (lq.)	2.71 ⁰⁰ (A)	-86	-67	221 ⁰⁰	130 ¹⁰⁰⁰		s. al.
Hydrobromic acid	$\text{HBr} \cdot \text{H}_2\text{O}$	98.93	col. lq.	1.78						Stable at -15.5° and 1 atm., and at -11.3° and 2.5 atm.
Hydrobromic acid	HBr (47.8% in H ₂ O)	80.91	col. lq.	1.486		126	∞			s. al.
Hydrobromic acid	$\text{HBr} \cdot 2\text{H}_2\text{O}$	118.96	wh. cr.	2.11 ⁻¹⁵⁰	-11		s.	s.		
Hydrochloric acid	HCl†	36.46	col. gas; 1.256 (lq.)	1.268 ⁰⁰ (A)	-111	-85	82.3 ⁰⁰	56.1 ⁶⁰⁰		s. al., et.
Hydrochloric acid	HCl (45.2% in H ₂ O)	36.46	col. lq.	1.48	-15.35		∞			s. al.
Hydrochloric acid	$\text{HCl} \cdot 2\text{H}_2\text{O}$	72.49	col. lq.	1.46 ^{-18.30} ₄	0	d.	∞	∞		s. al.
Hydrochloric acid	$\text{HCl} \cdot 3\text{H}_2\text{O}$	90.51	col. lq.		-24.4	d.	∞	∞		s. al.
Hydrocyanic acid (prussic acid)	HCN	27.03	poisonous gas or col. lq., 1.254	0.697 ¹⁸⁰	-14	26	∞	∞		∞ al., et.
Hydrofluoric acid	HF	20.01	gas or col. lq.	0.988 ^{13.60}	-83	19.4	∞ 0° to 19.4°	v. s.		
Hydrofluoric acid	HF (35.35% in H ₂ O)	20.01	col. lq.	1.15	-35	120	v. s.			
Hydrogen	H ₂	2.02	col. gas or cb.	lq. 0.0709 ^{-252.70} 0.06948 (A)	-259.1	-252.7	2.1 ⁰⁰ cc	0.85 ⁵⁰⁰ cc		sl. s. Fe, Pd, Pt
peroxide	H_2O_2 ‡	34.01	col. lq., 1.333	1.438 ²⁰⁰ ₄	-0.89	151.4 ^{760mm}	∞			s. a., et.; i. petr. et
selenide	H_2Se	80.98	col. gas	2.12 ⁻¹²⁰	-64	-42	377 ⁴⁰ cc	270 ^{22.50} cc		s. CS ₂ , COCl ₂
sulfide	H_2S	34.08	col. gas	1.1895 (A)	-82.9	-59.6	437 ⁰⁰ cc	186 ⁴⁰⁰ cc		9.54 ¹⁵⁰ cc al.; s. CS ₂
Hydroxylamine	NH_2OH	33.03	rhb., delq.	1.35 ¹⁸⁰	34	56.5 ^{22mm}	s.	d.		s. a., al.
hydrochloride	$\text{NH}_2\text{OH} \cdot \text{HCl}$	69.49	col., mn.	1.67 ¹⁷⁰	151	d.	83.3 ¹⁷⁰	v. s.		s. al.; i. et.
nitrate	$\text{NH}_2\text{OH} \cdot \text{HNO}_3$	96.04	col. cr.		48	d. <100	v. s.	d.		v. s. abs. al.
sulfate	$\text{NH}_2\text{OH} \cdot \frac{1}{2}\text{H}_2\text{SO}_4$	82.07	col., mn.		170 d.		32.9 ⁰⁰	68.5 ⁵⁰⁰		v. sl. s. al.; i. et., abs. al.

*Usual commercial form.

†Usual commercial form about 31 percent.

‡Usual commercial forms 3 or 30 percent.

TABLE 2-1 Physical Properties of the Elements and Inorganic Compounds (Continued)

Name	Formula	Formula weight	Color, crystalline form and refractive index	Specific gravity	Melting point, °C	Boiling point, °C	Solubility in 100 parts		
							Cold water	Hot water	Other reagents
Hypobromous acid	HBrO	96.91	yel.			40 ^{50mm}	s.	d.	
Indium	In	114.82	soft, tet. met.	7.3 ^{20°}	155	1450	i.	i.	s. a.
Iodic acid	HIO ₃	175.91	col., rhb.	4.629 ^{0°}	110 d.		286 ^{0°}	576 ^{101°}	v. s. 87% al.; i. abs. al. et., chl.
Iodine	I ₂	253.81	blue-bk., rhb.	4.93 ^{20°}	113.5	184.35	0.0162 ^{0°}	0.09566 ^{60°}	s. al., KI, et.
oxide, penta-	I ₂ O ₅	333.81	wh., trimetric	4.799 ^{25°} ₄	d. 300		187.4 ^{12°}		i. abs. al., et., chl.
Iodoplatinic acid	H ₂ PtI ₆ ·9H ₂ O	1120.66	brn., delq. mn.				s. d.		
Iridium	Ir	192.22	wh. met., cb.	22.4 ^{20°}	2350	>4800	i.	i.	sl. s. aq. reg., aq. Cl ₂
Iron, cast†	Fe	55.85	gray	7.03	1275		i.	i.	s. a.; i. alk.
pure	Fe	55.85	silv. met., cb.	7.86 ^{20°}	1535	3000	i.	i.	s. a.; i. alk.
steel	Fe	55.85	silv. gray	7.6 to 7.8	1375		i.	i.	s. a.; i. alk.
white pig	Fe	55.85	gray	7.6 to 7.8	1075		i.	i.	s. a.; i. alk.
wrought	Fe	55.85	gray	7.86	1505		i.	i.	s. a.; i. alk.
carbide (cementite)	Fe ₃ C	179.55	pseudo hex.	7.4	1837		i.	i.	s. a.
carbonyl	Fe(CO) ₅	195.90	pa. yel. lq.	1.457 ^{21°}	-21	102.5 ^{760mm}	i.		s. al., H ₂ SO ₄ , alk.
nitride	Fe ₂ N	125.70	gray	6.35	d. >560		d.		s. HCl, H ₂ SO ₄
silicide	FeSi	83.93	yel.-gray, oct.	6.1 ^{20°} ₄			i.	i.	i. aq. reg.
sulfide, di- (marcasite)	FeS ₂	119.98	yel., rhb.	4.87	tr. 450	d.	0.00049		i. dil. a.
sulfide, di- (pyrite)	FeS ₂	119.98	yel., cb.	5.0	1171	d.	0.0005		i. dil. a.
sulfide (pyrrhotite)	Fe ₇ S ₈	647.44	hex.	4.6 ^{20°} ₄	d. >700		i.		
Cf. also under ferric and ferrous									
Krypton	Kr	83.80	col. gas	2.818 (A)	-169	-151.8	11.05 ^{0°} cc	3.57 ^{60°} cc	sl. s. al., bz.
Lanthanum	La	138.91	lead gray	6.15 ^{20°}	826	1800	d.		s. a.
Lead	Pb	207.20	silv. met., cb.	11.337 ^{20°} ₂₀	327.5	1620	i.	i.	s. HNO ₃ ; i. c. HCl, H ₂ SO ₄
acetate	Pb(C ₂ H ₃ O ₂) ₂	325.29	wh. cr.	3.251 ^{20°} ₄	280		19.7 ^{0°}	221 ^{50°}	s. gly.; v. sl. s. al.
acetate (sugar of lead)	Pb(C ₂ H ₃ O ₂) ₂ ·3H ₂ O†	379.33	wh., mn.	2.55	-3H ₂ O, 75		45.64 ^{15°}	200 ^{100°}	s. gly.; sl. s. al.
acetate	Pb(C ₂ H ₃ O ₂) ₂ ·10H ₂ O	505.44	wh., rhb.	1.689	22		s.	s.	
acetate, basic	Pb ₂ (C ₂ H ₃ O ₂) ₃ OH	608.54	wh.				v. s.		sl. s. al.
acetate, basic	Pb(C ₂ H ₃ O ₂) ₂ ·Pb(OH) ₂ ·H ₂ O	584.52	wh. nd.				v. s.		s. al.
acetate, basic	Pb(C ₂ H ₃ O ₂) ₂ ·2Pb(OH) ₂	807.72	wh. nd.				5.55	18.2	s. al.
arsenate, monobasic	PbH ₂ (AsO ₄) ₂	489.07	tri., 1.82	4.46 ^{15°}	d. 140		d.		s. HNO ₃
arsenate, dibasic (schultenite)	PbHASO ₄	347.13	wh., mn., 1.9097	5.94	d. >200	-H ₂ O, 280	i.	sl. s.	s. HNO ₃ , NaOH
arsenate, meta-	Pb(AsO ₃) ₂	453.04	hex.	6.42 ^{15°}			d.		s. HNO ₃
arsenate, pyro-	Pb ₃ As ₂ O ₇	676.24	rhb., 2.03	6.85 ^{15°} ₁₅	802		i.	d.	s. HCl, HNO ₃ ; i. sc.
Lead azide	PbN ₆	291.24	col. nd.		expl. 350		i.	0.05 ^{100°}	v. s. ac.; i. NH ₄ OH
bromide	PbBr ₂	367.01	col., rhb.	6.66	373	918	0.4554 ^{0°}	4.75 ^{100°}	s. a., KBr; sl. s. NH ₃ ; i. al.
carbonate (cerussite)	PbCO ₃	267.21	wh., rhb., 2.0763	6.6	d. 315		0.00011 ^{20°}	d.	s. a., alk.; i. NH ₃ , al.
carbonate, basic (hydrocerussite; white lead)	2PbCO ₃ ·Pb(OH) ₂ †	775.63	wh., hex.	6.14	d. 400		i.	i.	s. ac.; sl. s. aq. CO ₂
chloride (cotunnite)	PbCl ₂	278.11	wh., rhb., 2.2172	5.80	501	954 ^{760mm}	0.673 ^{0°}	3.34 ^{100°}	sl. s. dil. HCl, NH ₃ , i. al.
chromate (crocoite)	PbCrO ₄	323.19	yel., mn., 2.42	6.12	844	d.	0.000007 ^{20°}	i.	s. a., alk.; i. NH ₃ , ac.
chromate, basic	PbCrO ₄ ·PbO	546.39	or.-yel. nd.				i.	i.	s. a., alk.
formate	Pb(HCO ₂) ₂	297.23	wh., rhb.	4.56	d. 190		1.6 ^{16°}	18 ^{100°} d.	i. al.
hydroxide	3PbO·H ₂ O	687.61	cb.	7.592	-H ₂ O, 130		0.014		s. a., alk.
nitrate	Pb(NO ₃) ₂	331.21	col., cb. or mn., 1.7815	4.53	d. 470		38.8 ^{0°}	138.8 ^{100°}	8.8 ^{23°} al.
oxide, sub-	Pb ₂ O	430.40	bk., amor.	8.34	d. red heat		i.	i.	s. a., alk.
oxide, mono- (litharge)	PbO	223.20	yel., tet.	9.53	888		0.0068 ^{18°}		s. alk., PbAc, NH ₄ Cl, CaCl ₂
oxide, mono (massicotite)	PbO	223.20	yel., rhb., 2.61	8.0					

oxide, mono-	PbO	223.20	amor.	9.2 to 9.5			i.	i.	s. alk., PbAc, NH ₄ Cl, CaCl ₂
oxide, red (minium)	Pb ₃ O ₄	685.60	red, amor.	9.1	d. 500		i.	i.	s. ac., h. HCl
oxide, sesqui-	Pb ₂ O ₃	462.40	red-yel., amor.		d. 360		i.	i.	s. a., alk.
oxide, di- (plattnerite)	PbO ₂	239.20	brn., tet., 2.229	9.375	d. 290		i.	i.	s. ac., h. alk.; i. al.
silicate	PbSiO ₃	283.28	col., mn., 1.961	6.49	766		i.		s. a.
sulfate (anglesite)	PbSO ₄	303.26	wh., mn. or rhb., 1.8823						
			cr.	6.2	1170		0.0028 ⁹⁰	0.0056 ⁴⁰	s. conc. a., NH ₄ salts; i. al.
sulfate, acid	Pb(HSO ₄) ₂ ·H ₂ O	419.36			d.		0.0001 ¹⁸		sl. s. H ₂ SO ₄
sulfate, basic (lanarkite)	PbSO ₄ ·PbO	526.46	col., mn.	6.92	977		0.0004 ¹⁸		sl. s. H ₂ SO ₄
sulfide (galena)	PbS	239.27	lead gray, cb., 3.912	7.5	1120		0.00009 ¹⁸	i.	s. a.; i. alk.
thiocyanate	Pb(CNS) ₂	323.36	col., mn.	3.82	d. 190		0.05 ²⁰	s.	s. KCNS, HNO ₃
Lithium	Li	6.94	silv. met. cb.	0.53 ²⁰	186	1336 ± 5	d.	d.	s. a., NH ₃
benzoate	LiC ₇ H ₅ O ₂	128.05	wh. leaflets				33 ²⁵	40 ¹⁰⁰	7.7 ²⁵ , 10 ³⁸ al.
bromide	LiBr	86.85	wh., delq., cb., 1.784	3.464 ²⁵	547	1265	143 ⁹⁰ (2H ₂ O)	266 ¹⁰⁰	s. al., act.
			wh. pr.		44		246 ²⁰		s. al.
bromide	LiBr·2H ₂ O	122.88					1.54 ⁹⁰	0.72 ¹⁰⁰	s. dil. a.; i. al., act., NH ₃
carbonate	Li ₂ CO ₃	73.89	col., mn., 1.567	2.11 ⁹⁰	618	d.	67 ⁹⁰	127.5 ¹⁰⁰	2.48 ¹⁵ al.; s. et.
chloride	LiCl	42.39	wh., delq., cb., 1.662	2.068 ²⁵	614	1360			
			wh. cr.		d.		61.2 ¹⁵	66.7 ¹⁰⁰	sl. s. al., et.
citrate	Li ₃ C ₆ H ₅ O ₇ ·4H ₂ O	281.98		2.295 ^{21.5}	870	1670	0.27 ¹⁵	0.135 ³⁵	s. HF; i. act.
fluoride	LiF	25.94	wh., cb., 1.3915	1.46	-H ₂ O, 94		49.2 ⁹⁰	346.6 ¹⁰⁴	sl. s. al., et.
formate	LiHCO ₂ ·H ₂ O	69.97	col., rhb.	0.820	680		d.		i. et.
hydride	LiH	7.95	wh., cb.	2.54	445	925 ±	12.7 ⁹⁰	17.5 ¹⁰⁰	sl. s. al.
hydroxide	LiOH	23.95	wh. cr.	1.83		d.	22.3 ¹⁰	26.8 ⁹⁰	sl. s. al.
hydroxide	LiOH·H ₂ O	41.96	col., mn.	2.38	261		53.4 ⁹⁰	194 ⁷⁰	sl. s. al.
nitrate	LiNO ₃	68.95	col., trig., 1.735		29.88		v. s.	∞	s. al., NH ₃
nitrate	LiNO ₃ ·3H ₂ O	122.99	col.	2.013 ²⁵		subl. <1000	forms LiOH		
oxide	Li ₂ O	29.88	col., 1.644	2.461	>100				
phosphate, monobasic	LiH ₂ PO ₄	103.93	col.	2.537 ^{17.5}	837		0.034 ¹⁸	v. sl. s.	s. a., NH ₄ Cl; i. act.
phosphate, tribasic	Li ₃ PO ₄	115.79	wh., rhb.	1.645	100		v. sl. s.	v. sl. s.	
phosphate, tribasic	Li ₃ PO ₄ ·12H ₂ O	331.98	wh., trig.		d.		128 ²⁶		v. s. al.
salicylate	LiC ₇ H ₅ O ₃	144.05	col.	2.22	860		35.34 ⁹⁰	29.9 ¹⁰⁰	i. act., 80% al.
sulfate	Li ₂ SO ₄	109.94	col., mn., 1.465	2.06	-H ₂ O, 130		43.6 ⁹⁰	35 ¹⁰⁰	i. 80% al.
sulfate	Li ₂ SO ₄ ·H ₂ O†	127.96	col., mn., 1.477	2.123 ¹³	170.5		d.		
sulfate, acid	LiHSO ₄	104.01	pr.						
Lutecium	Lu	174.97		1.74 ²⁰	651	1110	i.	sl. s. d.	s. a., NH ₄ salts
Magnesium	Mg	24.31	silv. met., hex.	1.42	323		v. s.	v. s.	5.25 ¹⁵ m. al.
acetate	Mg(C ₂ H ₃ O ₂) ₂	142.39	wh.	1.454	80		v. s.	v. s.	v. s. al.
acetate	Mg(C ₂ H ₃ O ₂) ₂ ·4H ₂ O†	214.45	wh., mn. pr., 1.491	3.6	2135		i.		v. sl. s. dil. HCl; i. dil. HNO ₃
aluminate (spinel)	MgO·Al ₂ O ₃	142.26	col. cb., 1.718–23						
ammonium chloride	MgCl ₂ ·NH ₄ Cl·6H ₂ O	256.79	wh., rhb., delq.	1.456	-4H ₂ O, 195		16.7	s.	
ammonium phosphate (struvite)	MgNH ₄ PO ₄ ·6H ₂ O	245.41	col., rhb., 1.496	1.715	d. 100		0.0231 ⁹⁰	0.0195 ⁸⁰	s. a.; i. al.
ammonium sulfate (boussingaultite)	MgSO ₄ ·(NH ₄) ₂ SO ₄ ·6H ₂ O	360.60	col., mn.	1.72	>120		16.86 ⁹⁰	130 ¹⁰⁰	
benzoate	Mg(C ₇ H ₅ O ₂) ₂ ·3H ₂ O	320.58	wh. pd.		-3H ₂ O, 110		4.5 ²⁵ (anh.)	s.	s. act.
carbonate (magnesite)	MgCO ₃	84.31	wh., trig., 1.700	3.037	d. 350		0.0106		s. a., aq. CO ₂ ; i. act., NH ₃
carbonate (nesquehonite)	MgCO ₃ ·3H ₂ O	138.36	col., rhb., 1.501	1.852	-H ₂ O, 100		0.1518 ¹⁹	d.	s. a., aq. CO ₂
carbonate, basic (hydromagnesite)	3MgCO ₃ ·Mg(OH) ₂ ·3H ₂ O	365.31	wh., rhb., 1.530	2.16	d.		0.04	0.011	s. a., NH ₄ salts; i. al.
Magnesium chloride (chloromagnesite)	MgCl ₂	95.21	col., hex., 1.675	2.325 ²⁵	712	1412	52.8 ⁹⁰	73 ¹⁰⁰	50 al.
chloride (bischofite)	MgCl ₂ ·6H ₂ O†	203.30	wh., delq., mn., 1.507	1.56	118 d.	d.	281 ⁹⁰	918 ¹⁰⁰	50 al.
hydroxide (brucite)	Mg(OH) ₂	58.32	wh., trig., 1.5617	2.4	d.		0.0009 ¹⁸		s. NH ₄ salts, dil. a.
nitride	Mg ₃ N ₂	100.93	gn.-yel., amor.		d.		i.	d.	s. a.; i. al.
oxide (magnesia; periclase)	MgO	40.30	col., cb., 1.7364	3.65	2800	3600	0.00062		s. a., NH ₄ salts; i. al.
perchlorate	Mg(ClO ₄) ₂ †	223.21	wh., delq.	2.60 ²⁵	d.		99.6 ²⁵	v. s.	24 ²⁵ al., 51.8 ²⁵ m. al.; 0.29 et.

*See also a table of alloys.

†Usual commercial form.

TABLE 2-1 Physical Properties of the Elements and Inorganic Compounds (Continued)

Name	Formula	Formula weight	Color, crystalline form and refractive index	Specific gravity	Melting point, °C	Boiling point, °C	Solubility in 100 parts		
							Cold water	Hot water	Other reagents
Magnesium chloride (<i>Cont.</i>)									
peroxide	MgO ₂	56.30	wh. pd.		expl. 275		i.	i.	s. a.
phosphate, pyro-	Mg ₂ P ₂ O ₇	222.55	col., mn., 1.604	2.598 ^{22°}	1383		i.	i.	s. a.; i. alk.
phosphate, pyro-	Mg ₂ P ₂ O ₇ ·3H ₂ O	276.60	wh., amor.	2.56	-3H ₂ O, 100		i.	sl. s.	s. a.; i. al.
potassium chloride (carnallite)	MgCl ₂ ·KCl·6H ₂ O	277.85	delq., rhb., 1.475	1.60 ^{19.4°}	265		64.5 ^{19°}	d.	d. al.
potassium sulfate (picromerite)	MgSO ₄ ·K ₂ SO ₄ ·6H ₂ O	402.72	mn., 1.4629	2.15	d. 72		19.26 ^{0°}		81.7 ^{75°}
silicofluoride	MgSiF ₆ ·6H ₂ O	274.47	col., trig., 1.3439	1.788 ^{17.5°}	d.		64.8 ^{17.5°}	s.	d. HF
sodium chloride	MgCl ₂ ·NaCl·H ₂ O	171.67	col.				s.	s.	
sulfate	MgSO ₄	120.37	col.	2.66	1185		26.9 ^{0°}	68.3 ^{100°}	s. al.
sulfate (epsom salt; epsomite)	MgSO ₄ ·7H ₂ O	246.47	col., rhb., 1.4554	1.68	70 d.		72.4 ^{0°}	178 ^{40°}	s. al.
Manganese	Mn	54.94	gray-pink met.	7.2 ^{20°}	1260	1900	d.	s.	s. dil. a.
acetate	Mn(C ₂ H ₃ O ₂) ₂	173.03		1.74 ^{20°}			s.	s.	
acetate	Mn(C ₂ H ₃ O ₂) ₂ ·4H ₂ O	245.09	pa. pink, mn.	1.589			s.	64.5 ^{50°}	s. al., m. al.
carbonate (rhodocrosite)	MnCO ₃	114.95	rose, trig., 1.817	3.125	d.		0.0065 ^{25°}		s. aq. CO ₂ , dil. a.; l. NH ₃ , al.
chloride (scacchite)	MnCl ₂	125.84	rose, delq., cb.	2.977 ^{25°}	650	1190	63.4 ^{0°}	123.8 ^{100°}	s. al.; i. et., NH ₃
chloride	MnCl ₂ ·4H ₂ O	197.91	rose red, delq., mn. 1.575	2.01	58.0	-H ₂ O, 106; -4H ₂ O, 200	151 ^{8°}	∞	s. al.; i. et.
chloride, per-	MnCl ₄	196.75	gn.				s.	s.	s. al., et.
hydroxide (ous) (pyrochroite)	Mn(OH) ₂	88.95	wh., trig.	3.258 ^{18°}	d.		0.002 ^{20°}		s. a., NH ₃ salts; i. alk.
hydroxide (ic) (manganite)	Mn ₂ O ₃ ·H ₂ O	175.89	brn., rhb., 2.24	3.258	d.		i.	i.	s. h. H ₂ SO ₄
nitrate	Mn(NO ₃) ₂ ·6H ₂ O	287.04	rose red, mn.	1.82 ^{21°}	25.8	129.5	426 ^{0°}	∞	v. s. al.
oxide (ous) (manganosite)	MnO	70.94	gray-gn., cb., 2.16	5.18	1650		i.	i.	s. a., NH ₄ Cl
oxide (ic)	Mn ₂ O ₃	157.87	brn.-bk., cb.	4.81	-0, 1080		i.	i.	s. a.; i. act.
oxide, di- (pyrolusite; polianite)	MnO ₂	86.94	bk., rhb.	5.026	-0, >230		i.	i.	s. HCl; i. HNO ₃ , act.
sulfate (ous)	MnSO ₄	151.00	red-wh.	3.235	700	d. 850	53 ^{0°}	73 ^{50°}	s. al.; i. et.
sulfate (ous) (szmikite)	MnSO ₄ ·H ₂ O	169.02	pa. pink, mn., 1.595	2.87	Stable 57 to 117		98.47 ^{48°}	79.77 ^{100°}	
sulfate (ous)	MnSO ₄ ·2H ₂ O	187.03		2.526 ^{15°}	Stable 40 to 57		85.27 ^{35°}	106.6 ^{55°}	
sulfate (ous)	MnSO ₄ ·3H ₂ O	205.05		2.356 ^{15°}	Stable 30 to 40		74.22 ^{5°}	99.31 ^{57°}	
sulfate (ous)	MnSO ₄ ·4H ₂ O	223.06	pink, rhb. or mn., 1.518	2.107	Stable 18 to 30	-4H ₂ O, 450	136 ^{16°}	169 ^{50°}	i. al.
sulfate (ous)	MnSO ₄ ·5H ₂ O	241.08	pink, tri., 1.508	2.103 ^{15°}	Stable 8 to 18		142 ^{5°}	200 ^{35°}	
sulfate (ous)	MnSO ₄ ·6H ₂ O	259.09			Stable -5 to +8		204 ^{0°}	247 ^{0°}	
sulfate (ous)	MnSO ₄ ·7H ₂ O	277.11	pink, mn. or rhb.	2.092	Stable -10 to -5; 19 d.	-7H ₂ O, 280	176 ^{0°}	251 ^{14°}	
sulfate (ic)	Mn ₂ (SO ₄) ₃	398.06	gn., delq. cr.	3.24	d. 160		v. s.	d.	s. HCl, dil. H ₂ SO ₄ ; l. conc. H ₂ SO ₄ , HNO ₃
Mercuric acetate	Hg(C ₂ H ₃ O ₂) ₂	318.68	wh. pl.	3.270	d.		25 ^{10°}	100 ^{100°}	s. al. sl. d.
bromide	HgBr ₂	360.40	wh., rhb.	6.053	237	322	0.5 ^{20°}	25 ^{100°}	25.2 ^{0°} al.; v. sl. s. et.
carbonate, basic	HgCO ₃ ·2HgO	693.78	brn.-red				i.		s. aq. CO ₂ , NH ₄ Cl
chloride (corrosive sublimate)	HgCl ₂	271.50	wh., rhb., 1.859	5.44	277	304	3.6 ^{0°}	61.3 ^{100°}	33 ^{25°} 99% al.; 33 et.
fulminate	Hg(CNO) ₂	284.62	cb.	4.42	expl.		sl. s.		s. NH ₄ OH, al.
hydroxide	Hg(OH) ₂	234.60							
oxide (montroydite)	HgO	216.59	yel. or red, rhb., 2.5	11.14	-H ₂ O, 175		i.	i.	s. a.
oxychloride (kleinite)	HgCl ₂ ·3HgO	921.26	yel., hex.	7.93	d. 100		0.0052 ^{25°}	0.041 ^{100°}	s. a.; i. al.
silicofluoride, basic	HgSiF ₆ ·HgO·3H ₂ O	613.30	yel. nd.		d. 260		i.	d.	s. HCl
sulfate	HgSO ₄	296.65	wh., rhb.	6.47	d.		d.		s. a.
sulfate, basic (turpeth)	HgSO ₄ ·2HgO	729.83	yel., tet.	6.44			0.005	0.167 ^{100°}	s. a.; i. al., act., NH ₃
Mercurous acetate	Hg ₂ C ₂ H ₃ O ₂	259.63	wh. sc.		d.		0.75 ^{13°}	d.	s. H ₂ SO ₄ , HNO ₃ ; i. al.
bromide	HgBr	280.49	wh., tet.	7.307	subl. 345		7 × 10 ⁻⁹	i.	s. a.; i. al., act.
carbonate	Hg ₂ CO ₃	461.19	yel. pd.		d. 130		i.	d.	s. NH ₄ Cl

chloride (calomel)	HgCl	236.04	wh., tet., 1.9733	7.150	302	383.7	0.0014 ⁹⁰	0.0007 ⁴³⁰	s. aq. reg., Hg(NO ₃) ₂ ; sl. s. HNO ₃ , HCl; i. al., etc.
iodide	HgI	327.49	yel., tet.	7.70	290 d.	subl. 140; 310d.	2 × 10 ⁻⁸	v. sl. s.	s. KI; i. al.
nitrate	HgNO ₃ ·H ₂ O	280.61	wh. mn.	4.785 ³⁹⁰	70	expl.	v. s.	d.	s. HNO ₃ ; i. al., et.
Mercurous oxide	Hg ₂ O	417.18	bk.	9.8	d. 100		i.	0.0007	s. h. ac.; i. alk., dil. HCl, NH ₃
sulfate	Hg ₂ SO ₄	497.24	wh., mn.	7.56	d.		0.055 ¹⁶⁵⁰	0.092 ¹⁰⁰⁰	s. H ₂ SO ₄ , HNO ₃
Mercury†	Hg	200.59	silv. lq. or hex.(?)	13.546 ²⁰⁰	-38.87	356.9	i.	i.	s. HNO ₃ ; i. HCl
Molybdenum	Mo	95.94	gray. cb.	10.2	2620 ± 10	3700	i.	i.	s. h. conc. H ₂ SO ₄ ; i. HCl, HF, NH ₃ , dil. H ₂ SO ₄ , Hg
chloride, di-	MoCl ₂	166.85	yel., amor.	3.714 ²⁵²	d.		i.	i.	s. HCl, H ₂ SO ₄ , NH ₄ OH, al., et.
chloride, tri-	MoCl ₃	202.30	dark red pd.	3.578 ²⁵³	d.		i.	d.	s. HNO ₃ , H ₂ SO ₄ ; v. sl. s. al., et.
chloride, tetra-	MoCl ₄	237.75	brn., delq.		volt.	d.	s.	d.	s. HNO ₃ , H ₂ SO ₄ ; sl. s. al., et.
chloride, penta-	MoCl ₅	273.21	bk. cr.	2.928 ²⁵³	194	268	s.	d.	s. HNO ₃ , H ₂ SO ₄ ; i. abs. al., et.
oxide, tri- (molybdate)	MoO ₃	143.94	col., rhb.	4.50 ¹⁹⁵⁰	795	subl.	0.107 ¹⁸⁰	2.106 ⁷⁹⁰	s. a., NH ₄ OH
sulfide, di- (molybdenite)	MoS ₂	160.07	bk., hex., 4.7	4.801 ¹⁴⁰	1185		i.	i.	s. H ₂ SO ₄ , aq. reg.
sulfide, tri-	MoS ₃	192.14	red-brn.		d.		sl. s.	s.	s. alk. sulfides
sulfide, tetra-	MoS ₄	224.20	brn. pd.		d.		i.	i.	s. alk. sulfides; i. NH ₃
Molybdic acid	H ₂ MoO ₄	161.95	yel-wh., hex.		d. 115		v. sl. s.	sl. s.	s. NH ₄ OH, H ₂ SO ₄ ; i. NH ₃
Molybdic acid	H ₂ MoO ₄ ·H ₂ O	161.95	yel., mn.	3.124 ¹⁵⁰	-H ₂ O, 70	-2H ₂ O, 200	0.133 ¹⁸⁰	2.13 ⁷⁰⁰	s. a., NH ₄ OH, NH ₄ , salts
Neodymium	Nd	144.24	yellowish	6.9 ²⁰⁰	840		d.	d.	
Neon	Ne	20.18	col. gas	lq. 1.204 ^{-245.90} 0.674 (A)	-248.67	-245.9	2.6 ⁰⁰ cc	1.1 ⁴⁵⁰ cc	s. lq. O ₂ , al., act., bz.
Neptunium	Np ²³⁹	239.05				Produced by Neutron bombardment of U ²³⁸			
Nickel	Ni	58.69	silv. met., cb.	8.90 ²⁰	1452	2900	i.	i.	s. dil. HNO ₃ ; sl. s. H ₂ SO ₄ , HCl; i. NH ₃ i. al.
acetate	Ni(C ₂ H ₃ O ₂) ₂	176.78	gn. pr.	1.798	d.		16.6		
ammonium chloride	NiCl ₂ ·NH ₄ Cl·6H ₂ O	291.18	gn., delq., mn.	1.645			150 ²⁵⁰	v. s.	
ammonium sulfate	NiSO ₄ ·(NH ₄) ₂ SO ₄ · 6H ₂ O	394.99	blue-gn., mn., 1.5007	1.923			2.5 ^{3.50}	39.2 ⁸⁸⁰	v. sl. s. (NH ₄) ₂ SO ₄
bromate	Ni(BrO ₃) ₂ ·6H ₂ O	422.59	gn., cb.	2.575	d.		28		s. NH ₄ OH
bromide	NiBr ₂	218.50	yel., delq.	4.64 ²⁸⁰	d.		112.8 ⁹⁰	156 ¹⁰⁰⁰	s. al., et., NH ₄ OH
bromide	NiBr ₂ ·3H ₂ O	272.55	gn., delq.			-3H ₂ O, 200	199 ⁹⁰	316 ¹⁰⁰⁰	s. al., et., NH ₄ OH
bromide, ammonia	NiBr ₂ ·6NH ₃	320.68	vl. pd.	1.837			v. s.	d.	i. c. NH ₄ OH
bromoplatinate	NiPtBr ₆ ·6H ₂ O	841.29	trig.	3.715					
carbonate	NiCO ₃	118.70	lt. gn., rhb.		d.		0.0093 ²⁵⁰	i.	s. a.
carbonate, basic	2NiCO ₃ ·3Ni(OH) ₂ · 4H ₂ O	587.59	lt. gn.		d.		i.	d.	s. a., NH ₄ salts
carbonyl	Ni(CO) ₄	170.73	lq.	1.31 ¹⁷⁰	-25	43 ^{751mm}	0.018 ^{9.80}	i.	s. aq. reg., HNO ₃ , al., et.
chloride	NiCl ₂	129.60	yel., delq.	3.544	subl.	973	53.8 ⁹⁰	87.6 ¹⁰⁰⁰	s. NH ₄ OH, al.; i. NH ₃
chloride	NiCl ₂ ·6H ₂ O*	237.69	gn., delq., mn., 1.57 ±				180	v. s.	v. s. al.
chloride, ammonia	NiCl ₂ ·6NH ₃	231.78					s.	d.	s. NH ₄ OH; i. al.
cyanide	Ni(CN) ₂ ·4H ₂ O	182.79	gn. pl.			-4H ₂ O, 200	i.	i.	s. KCN; i. dil. KCl
dimethylglyoxime	NiC ₈ H ₁₄ O ₄ N ₄	288.91	scarlet red cr.			subl. 250	i.	i.	s. abs. al., a.; i. ac., NH ₄ OH
formate	Ni(HCO ₂) ₂ ·2H ₂ O	184.76	gn. cr.	2.154	d.		s.		
hydroxide (ic)	Ni(OH) ₂	109.72	bk.		d.		i.	i.	s. a., NH ₄ OH, NH ₄ Cl
hydroxide (ous)	Ni(OH) ₂ ·¼H ₂ O	97.21	lt. gn.	4.36	d.		v. sl. s.	v. sl. s.	s. a., NH ₄ OH; i. alk.
nitrate	Ni(NO ₃) ₂ ·6H ₂ O	290.79	gn., mn.	2.05	56.7	136.7	243.0 ⁹⁰	∞ ^{56.70}	s. NH ₄ OH; i. abs. al.
nitrate, ammonia	Ni(NO ₃) ₂ ·4NH ₃ ·2H ₂ O	286.86					v. s.	i. al.	i. al.
oxide, mono- (bunsenite)	NiO	74.69	gn.-bk., cb., 2.37	7.45	Forms Ni ₂ O ₃ at 400		i.	i.	s. a., NH ₄ OH
potassium cyanide	Ni(CN) ₂ ·2KCN·H ₂ O	258.97	red yel., mn.	1.875 ¹¹⁰	-H ₂ O, 100		s.	d. a.	d. a.
sulfate	NiSO ₄	154.76	yel., cb.	3.68		-SO ₃ , 840	27.2 ⁹⁰	76.7 ¹⁰⁰⁰	i. al., et., act.

*Usual commercial form.

†See also Tables 2-28 and 2-280.

TABLE 2-1 Physical Properties of the Elements and Inorganic Compounds (Continued)

Name	Formula	Formula weight	Color, crystalline form and refractive index	Specific gravity	Melting point, °C	Boiling point, °C	Solubility in 100 parts			
							Cold water	Hot water	Other reagents	
Nickel (<i>Cont.</i>) sulfate	NiSO ₄ ·6H ₂ O ^o	262.85	gn. mn. or blue, tet., 1.5109	2.07	tr. 53.3	-6H ₂ O, 280	131 ^{50°}	280 ^{100°}	v. s. NH ₄ OH, al.	
sulfate (morenosite)	NiSO ₄ ·7H ₂ O	280.86	gn., rhb., 1.4893	1.948	98-100	-6H ₂ O, 103	63.5 ^{50°}	117.8 ^{30°}	s. al.	
Nitric acid	HNO ₃	63.01	col. lq.	1.502	-42	86	∞	∞	expl. with al.	
Nitric acid	HNO ₃ ·H ₂ O	81.03	col. lq.		-38		∞	∞	d. al.	
Nitric acid	HNO ₃ ·3H ₂ O	117.06	col. lq.		-18.5		263 ^{-20°}	∞	d. al.	
Nitro acid sulfite	NO ₂ HSO ₃	127.08	col., rhb.		73 d.		d.		s. H ₂ SO ₄	
Nitrogen	N ₂	28.01	col. gas or cb. cr.	1.026 ^{-252.5°} 0.805 ^{-195.8°} 12.5 ^{0°} (D) lq. 1.226 ^{-89°} 1.530 (A)		-209.86		2.35 ^{0°} cc	1.55 ^{20°} cc	sl. s. al.
Nitrogen oxide, mono- (ous)	N ₂ O	44.01	col. gas		-102.3	-90.7	130.52 ^{0°} cc	60.82 ^{24°} cc	s. H ₂ SO ₄ , al.	
oxide, di- (ic)	NO or (NO) ₂	30.01 60.01	col. gas		-161	-151	7.34 ^{0°} cc	0.0 ^{100°}	26.6 cc al.; 3.5 cc H ₂ SO ₄ ; s. aq. FeSO ₄	
oxide, tri-	N ₂ O ₃	76.01	red-brn. gas or blue lq. or solid	1.447 ^{2°}	-102	3.5	s.		s. a., et.	
oxide, tetra- (per- or di-)	NO ₂ or (NO ₂) ₂	46.01 92.01	yel. lq., col. solid, red-brn. gas	1.448 ^{20°}	-9.3	21.3	d.		s. HNO ₃ , H ₂ SO ₄ , chl., CS ₂	
oxide, penta-	N ₂ O ₅	108.01	wh., rhb.	1.63 ^{18°}	30	47	s.	Forms HNO ₃		
oxybromide	NOBr	109.91	brn. lq.	>1.0	-55.5	-2	d.			
oxychloride	NOCl	65.46	red-yel. lq. or gas	1.417 ^{-12°} 2.31 (A) lq. 1.32 ^{14°} 22.48 ^{20°}	-64.5	-5.5	d.		s. fuming H ₂ SO ₄	
Nitroxyl chloride	NO ₂ Cl	81.46	yel.-brn. gas		<-30	5	d.			
Osmium chloride, di-	Os	190.23	blue, hex.		2700	>5300	i.	i.	sl. s. aq. reg., HNO ₃ ; i. NH ₃	
chloride, tri-	OsCl ₂	261.14	gn., delq.				s. d.		s. NaCl, al., et.	
chloride, tetra-	OsCl ₃	296.59	brn., cb.			d. 560-600	sl. s.		s. a., alk., al.; sl. s. et.	
Oxygen	OsCl ₄	332.04	red-yel. nd.				s. d.		s. HCl, al.	
	O ₂	32.00	col. gas or hex. solid	1.14 ^{-188°} 1.426 ^{-252.5°} 1.1053 (A)		-218.4	-183	4.89 ^{0°} cc	2.6 ^{30°} cc 1.7 ^{100°} cc	sl. s. al., s. fused Ag
Ozone	O ₃	48.00	col. gas	1.71 ^{-183°} 3.03 ^{-80°} 1.658 (A)		-251	-112	0.494 ^{0°} cc	0 ^{60°} cc	s. oil turp., oil cinn.
Palladium	Pd	106.42	silv. met., cb.	12.0 ^{20°} 11 ^{1550°}		1555	2200	i.	i.	s. aq. reg., h. H ₂ SO ₄ ; i. NH ₃
bromide (ous)	PdBr ₂	266.23	brn.				i.	i.	s. HBr	
chloride	PdCl ₂	177.33	brn., cb.		500 d.		s.	s.	s. HCl, act., al.	
chloride	PdCl ₂ ·2H ₂ O	213.36	brn. pr.				s.	s.	s. HCl, act., al.	
cyanide	Pd(CN) ₂	158.45	yel.		d.		i.	i.	s. HCN, KCN, NH ₄ OH; i. dil. a.	
hydride	Pd ₂ H	213.85	met.	11.06	d.					
Palladous dichlorodiammine	Pd(NH ₃) ₂ Cl ₂	211.39	red or yel., tet.	2.5			s.		s. a., NH ₄ OH	
Perchloric acid	HClO ₄	100.46	unstable, col. lq.	1.768 ^{22°} 1.88	-112	16 ^{18mm}	s.	s.		
Perchloric acid	HClO ₄ ·H ₂ O	118.47	fairly stable nd.	1.71 ^{25°}	50	d.	s.			
Perchloric acid	HClO ₄ ·2H ₂ O ^o 73.6% anh.	136.49	stable lq., col.		-17.8	200	v. s.		s. al.	
Periodic acid	HIO ₄	191.91	wh. cr.		d. 138	subl. 110	s.			
Periodic acid	HIO ₄ ·2H ₂ O	227.94	delq., mn.		d. 110		v. s.	v. s.	sl. s. al., et.	
Permanganic acid	HMnO ₄	119.94	exists only in solution				v. s.	d.	d. al.	
Permolybdic acid	HMoO ₄ ·2H ₂ O	196.98	wh. cr.				v. s.	v. s.		
Persulfuric acid	H ₂ S ₂ O ₈	194.14	hyg. cr.		<60		v. s.	d.		
Phosphamic acid	PONH ₂ ·(OH) ₂	97.01	cb.		d.		v. s.	v. s. d.	i. al.	
Phosphatomolybdic acid	H ₂ P(Mo ₂ O ₇) ₆ ·28H ₂ O	2365.71	yel. cb.		78	-25H ₂ O, 140	s.		s. HNO ₃	
Phosphine	PH ₃	34.00	col. gas	lq. 0.746 ^{-90°} 1.146 (A)	-132.5	-85	26 ^{17°} cc	i. ^{100°}	s. Cu ₂ Cl ₂ , al., et.	
Phosphonium chloride	PH ₄ Cl	70.46	wh., cb.		28 ^{46atm}	subl.	d.			

Phosphoric acid, hypo-	H ₃ P ₂ O ₆	161.98	cr.		55	d. 70	s.	450 ^{62°}	
Phosphoric acid, meta-	HPO ₃	79.98	vitreous, delq.	2.2–2.5	subl.		s.	Forms H ₃ PO ₄	i. lq. CO ₂
Phosphoric acid, ortho-	H ₃ PO ₄ †	98.00	col., rhb.	1.834 ^{18,2°}	42.35	–½H ₂ O, 213	2340 ^{26°}	v. s.	s. al.
Phosphoric acid, pyro-	H ₄ P ₂ O ₇	177.98	wh. nd.		61		800 ^{25°}	Forms H ₃ PO ₄	v. s. al., et.
Phosphorous acid, hypo-	H ₃ PO ₃	66.00	syrupey	1.493 ^{18,8°}	26.5	d.	∞	∞	
Phosphorous acid, ortho-	H ₃ PO ₃	82.00	col.	1.651 ^{21,2°}	74	d. 200	307.3 ^{9°}	730 ^{40°}	
Phosphorous acid, pyro-	H ₄ P ₂ O ₅	145.98	nd.		38	d. 130	d.		
Phosphorus, black	P ₄	123.90	rhombohedral	2.69		ign. in air, 400	i.	i.	i. CS ₂
Phosphorus, red	P ₄	123.90	red, cb.	2.20 ^{20°}	590 ^{43atm}	ign. in air, 725	i.	i.	s. alk.; i. CS ₂ , NH ₃ , et.
Phosphorus, yellow	P ₄	123.90	yel., hex., 2.1168	1.82 ^{20°} ; lq. 1.745 ^{44,5°}	44.1; ign. 34	280	0.0003	sl. s.	0.4 al.; 1000 ^{10°} CS ₂ ; 1.5 ^{9°} , 10 ^{81°} bs.; s. NH ₃
chloride, tri-	PCl ₃	137.33	col., fuming lq.	1.574 ^{20,8°}	–111.8	75.95 ^{760mm}	d.	d.	s. et., chl., CS ₂
chloride, penta-	PCl ₅	208.24	delq., tet.	solid 1.6; 3.60 ^{29,5°} (A)	148 under pressure	subl. 160	d.	Forms H ₃ PO ₄	s. CS ₂ , C ₆ H ₅ COCl
oxide, penta-	P ₂ O ₅	141.94	wh., delq., amor.	2.387	subl. 250			v. s.	s. H ₂ SO ₄ ; i. NH ₃ , act.
oxychloride	POCl ₃	153.33	col., fuming lq.	1.675	2	107.2 ^{760mm}	d.	d.	d. al.
Phosphotungstic acid	H ₃ PO ₄ ·12WO ₃ ·xH ₂ O	2880.05	yel.-gn. cr.				s.	s.	s. al., et.
Platinum	Pt	195.08	silv. met., cb.	21.45 ^{20°} lq. 19 ^{1755°}	1755	4300	i.	i.	s. aq. reg., fused alk.
chloride (ic)	PtCl ₄	336.89	brn.		d. 370		140 ^{25°}	v. s.	s. al., act.; sl. s. NH ₂ ;
chloride (ous)	PtCl ₂	265.98	brn.	5.87 ^{11°}	d. 581		i.	i.	i. et.
chloride (ic)	PtCl ₄ ·8H ₂ O	481.01	red. mn.	2.43	–4H ₂ O, 100		v. s.	v. s.	s. HCl, NH ₄ OH; sl. s. NH ₃ ; i. al., et.
cyanide (ous)	Pt(CN) ₂	247.11	yel.-brn.				i.	i.	s. al., et.
Plutonium	Pu	238.05		Produced by deuteron bombardment on U ²³⁸					
Plutonium	Pu	239.05		Produced by neutron bombardment on U ²³⁸					
Potassium	K	39.10	silv. met., cb.	0.86 ^{20°} lq. 0.83 ^{42°}	62.3	760	d.	Forms KOH 396 ^{90°}	s. a., al., Hg
acetate	KC ₂ H ₃ O ₂	98.14	wh. pd.	1.8	292		217 ^{0°}		33 al.; i. et.
acetate, acid	KH(C ₂ H ₃ O ₂) ₂	158.19	delq. nd. or pl.		148	d. 200	d.	s. ac.	s. ac.
aluminate	K ₂ (AlO ₂) ₂ ·3H ₂ O	250.20	cr.				s.	d.	s. alk.; i. al.
amide	KNH ₂	55.12	yel.-grm.		338	subl. 400	d.		d. al.; 3.6 ^{25°} NH ₃
arsenate (monobasic)	KH ₂ AsO ₄	180.03	col., tet., 1.5674	2.867	288		18.87 ^{6°}	v. s.	i. al.
auricyanide	KAu(CN) ₄ ·1.5H ₂ O	367.16	pl.		d. 200		s.	v. s.	s. al.
aurocyanide	KAu(CN) ₂	288.10	rhb.				14.3	20.0 ^{100°}	sl. s. al.; i. et.
bicarbonate	KHCO ₃	100.12	mn., 1.482	2.17	d. 100–200		22.4 ^{0°}	60 ^{90°}	i. satd. K ₂ CO ₃ , al.
bisulfate	KHSO ₄	136.17	rhb., or mn., 1.480	2.35	210	d.	36.3 ^{0°}	121.6 ^{100°}	d. al.
bromate	KBrO ₃	167.00	trig.	3.27 ^{17,5°}	370 d.		3.11 ^{0°}	49.75 ^{100°}	sl. s. al.; i. act.
bromide	KBr	119.00	col., cb., 1.5594	2.75 ^{25°}	730	1380	53.5 ^{0°}	104 ^{100°}	sl. s. al., et.
carbonate	K ₂ CO ₃	138.21	wh., delq. pd., 1.531	2.29	891	d.	105.5 ^{0°}	156 ^{100°}	i. al.
carbonate	K ₂ CO ₃ ·2H ₂ O	174.24	rhb.	2.043			183 ^{10°}	331 ^{100°}	
carbonate	2K ₂ CO ₃ ·3H ₂ O	330.46	mn.	2.13			129.4 ^{0°}	268 ^{100°}	
chlorate	KClO ₃	122.55	col., mn., 1.5167	2.32	368	d. 400	3.3 ^{0°}	57 ^{100°}	0.83 al.; s. alk.
chloride (sylvite)	KCl	74.55	col., cb., 1.4904	1.988	790	1500	27.6 ^{0°}	56.7 ^{100°}	s. al., alk.
chloroplatinate	K ₂ PtCl ₆	485.99	yel., cb., 1.825±	3.499	d. 250		0.74 ^{0°}	5.2 ^{100°}	i. al., et.
chromate (tarapacait)	K ₂ CrO ₄	194.19	yel., rhb., 1.7261	2.732 ^{18°}	975		58.0 ^{0°}	75.6 ^{100°}	i. al.
cyanate	KCN	81.12	wh., tet.	2.048			s.	d.	v. sl. s. al.
cyanide	KCN	65.12	wh., cb., delq., 1.410	1.52 ^{16°}	634.5		s.	122.2 ^{108,8°}	s. gly.; 0.9 ^{19,5°} al.; 1.3 h. al.
dichromate	K ₂ Cr ₂ O ₇	294.18	red, tri.	2.69	398	d.	4.9 ^{0°}	80 ^{100°}	i. al.
ferricyanide	K ₃ Fe(CN) ₆	329.24	red. mn. pr., 1.5689	1.84	d.		33 ^{4,4°}	77.5 ^{100°}	s. act.; sl. s. al.; i. NH ₃
ferrocyanide	K ₄ Fe(CN) ₆ ·3H ₂ O	422.39	yel., mn., 1.5772	1.853 ^{17°}	–3HO ₂ , 70		27.8 ^{12,2°}	90.6 ^{96,8°}	s. act.; i. NH ₃ , al., et.
formate	KHCO ₂	84.12	col., rhb.	1.91	167.5	d.	331 ^{18°}	657 ^{90°}	sl. s. al.; i. et.
hydride	KH	40.11	cb., 1.453	0.80	d.		d.		i. et., bz., CS ₂
hydrosulfide	KHS	72.17	wh., delq., rhb.	2.0	455		s.	s. d.	s. al.
hydroxide	KOH	56.11	wh., delq., rhb.	2.044	380	1320	97 ^{0°}	178 ^{100°}	v. s. al., et.; i. NH ₃
iodate	KIO ₃	214.00	col., mn.	3.89	560		4.73 ^{0°}	32.2 ^{100°}	s. KI; i. al., NH ₃
iodide	KI	166.00	wh., cb., 1.6670	3.13	723	1330	127.5 ^{0°}	208 ^{100°}	4 ^{20°} al.; s. NH ₃ ; sl. s. et.

*One commercial form 70 to 72 per cent.

†Common commercial form 85 per cent H₃PO₄ in aqueous solution.

TABLE 2-1 Physical Properties of the Elements and Inorganic Compounds (Continued)

Name	Formula	Formula weight	Color, crystalline form and refractive index	Specific gravity	Melting point, °C	Boiling point, °C	Solubility in 100 parts		
							Cold water	Hot water	Other reagents
Potassium (<i>Cont.</i>)									
iodide, tri-	KI ₃	419.81	dark blue, delq., mn.	3.498	45	d. 225	v. s.		s. KI, al.
iodoplatinate	K ₂ PtI ₆	1034.70	cb.	5.18			s.		
manganate	K ₂ MnO ₄	197.13	gn., rhb.		d. 190		d.		s. KOH
metabisulfite	K ₂ S ₂ O ₅	222.32	mn., pl.		d. 150		25 ^{0°}	120 ^{94°}	sl. s. al.; i. et.
nitrate (saltpeter)	KNO ₃	101.10	col., rhb., 1.5038	2.11 ^{100°}	tr. 129; 333	d. 400	13.3 ^{0°}	246 ^{100°}	0.1 ^{30°} al.; i. et.
nitrite	KNO ₂	85.10	pr.	1.915	297	d. 350	281 ^{0°}	413 ^{100°}	v. s. NH ₃ ; sl. s. al.
oxalate	K ₂ C ₂ O ₄ ·H ₂ O	184.23	wh., mn.	2.13	d.		28.7 ^{0°}	83.2 ^{100°}	
oxalate, acid	KHC ₂ O ₄ [°]	128.13	mn., 1.545	2.0	d.		14.3 ^{30°}	48.1 ^{100°}	
oxalate, acid	KHC ₂ O ₄ ·½H ₂ O	137.13	trimetric		d.		2.2 ^{0°}	51.5 ^{100°}	
oxide	K ₂ O	94.20	wh., cb.	2.32 ^{30°}			Forms KOH	v. s.	s. al., et.
perchlorate	KClO ₄	138.55	col., rhb., 1.4737	2.524 ^{11°}	d. 400		0.75 ^{0°}	21.8 ^{100°}	0.105 ^{20°} m. al.; i. et.
permanganate	KMnO ₄	158.03	purple, rhb.	2.703	d. <240		2.83 ^{0°}	32.35 ^{75°}	s. H ₂ SO ₄ ; d. al.
persulfate	K ₂ S ₂ O ₈	190.32	wh., tri., 1.4669		d. <100		1.77 ^{0°}	10 ^{40°}	i. al.
phosphate, monobasic	KH ₂ PO ₄	136.09	col., delq., tet., 1.5095	2.338	256		14.8 ^{0°}	83.5 ^{90°}	i. al.
phosphate, dibasic	K ₂ HPO ₄	174.18	wh., delq.		d.		33 ^{25°}	v. s.	sl. s. al.
phosphate, tribasic	K ₃ PO ₄	212.27	wh., rhb.	2.564 ^{17°}	1340		193.1 ^{25°}	v. s.	i. al.
phosphate, meta-	KPO ₃	118.07	wh. pd.	2.258 ^{14.5°}	tr. 450; 798	1320	s.	s.	
phosphate, meta-	K ₄ P ₂ O ₇ ·2H ₂ O	508.31	amor.	2.264 ^{14.5°}	-2H ₂ O, 100	d.	s.	83	s. a.
phosphate, pyro-	K ₂ P ₂ O ₇ ·3H ₂ O	384.38	delq.	2.33	-2H ₂ O, 180	-3H ₂ O, 300	s.	v. s.	i. al.
phthalate, acid	KHC ₈ H ₄ O ₄	204.22	wh. cr.	1.63	d.		10.2 ^{25°}	36	
platinocyanide	K ₂ Pt(CN) ₄ ·3H ₂ O	431.39	yel., rhb., 1.62±	2.45 ^{16°}			sl. s.	v. s.	s. al., et.
silicate	K ₂ SiO ₃	154.28	hyg. 1.521±		976		s.	s.	i. al.
silicate, tetra-	K ₄ Si ₃ O ₉ ·H ₂ O	352.55	rhb., 1.530	2.417	d. 400		s.	s.	i. al.
sulfate (arcanite)	K ₂ SO ₄	174.26	col., rhb., 1.4947	2.662	tr. 588		7.35 ^{0°}	24.1 ^{100°}	i. al., act., CS ₂
Potassium sulfate, pyro-	K ₂ S ₂ O ₇	254.32	col.	2.277	300		s.	d.	
sulfide, mono-	K ₂ S·5H ₂ O	200.34	rhb., delq.		60	-3H ₂ O, 150	s.		s. al., gly.; i. et.
sulfite	K ₂ SO ₃ ·2H ₂ O	194.29	wh., rhb.		d.		100	>100	sl. s. al.; i. NH ₃
sulfite, acid	KHSO ₃	120.17	wh., mn.		d. 190		45.5 ^{15°}	91.5 ^{75°}	i. abs. al.
tartrate	K ₂ C ₄ H ₄ O ₆ ·½H ₂ O	235.28	col., mn., 1.526	1.98		d.	12.5 ^{17.5°}	278 ^{100°}	sl. s. al.
tartrate, acid	KHC ₄ H ₄ O ₆ [°]	188.18	col., rhb.	1.956			0.37 ^{0°}	6.1 ^{100°}	s. a., alk.; i. al., ac.
thiocyanate	KCNS	97.18	col., delq., mn., 1.660±	1.886	172.3	d. 500	177 ^{0°}	217 ^{20°}	20.8 ^{22°} act.; s. al.
thiosulfate	K ₂ S ₂ O ₃	190.32	col., cb.		d. 400		96.1 ^{0°}	311.2 ^{90°}	
thiosulfate	3K ₂ S ₂ O ₃ ·H ₂ O	588.99	delq., mn.	2.23	-H ₂ O, 180	d.			i. al.
Praseodymium	Pr	140.91	yel.	6.5 ^{30°}	940		d.		
Radium	Ra	226.03	wh., met.	5 [°]	960	1140	d. +H ₂		d. a.
bromide	RaBr ₂	385.83	wh., mn.	5.79	728	subl. 900	70 ^{20°}	s.	s. al.
Radon (Niton)	Rn	222.02	gas	lq. 5.5; 111 (D)	-71	-62	51 ^{0°} cc	8.5 ^{60°} cc	
Rhenium	Re	186.21	hex.		3440				i. HF, HCl; s. H ₂ SO ₄ ; HNO ₃
Rhodium	Rh	102.91	gray-wh., cb.	12.5	1955	>2500	i.	i.	sl. s. aq. reg., a.
chloride	RhCl ₃	209.26	red		d. 450	subl. 800±	i.	i.	v. sl. s. alk.; i. aq. reg., a.
chloride	RhCl ₃ ·4H ₂ O	281.33	dark red				v. s.		s. HCl, al.; i. et.
Rubidium	Rb	85.47	silv. wh.	lq. 1.475 ^{88.5°} , 1.53 ^{30°}	38.5	700	d.		s. a., al.
Ruthenium	Ru	101.07	bk., porous	8.6	>1950		i.	i.	sl. s. aq. reg., a.
Ruthenium	Ru	101.07	gray, hex.	12.2 ^{20°}	2450	>2700	i.	i.	
Samarium	Sm (also Sa)	150.36		7.7	>1300				
Scandium	Sc	44.96		2.5 [°]	1200	2400			
Selenic acid	H ₂ SeO ₄	144.97	hex. pr.	2.950 ^{15°}	58	260	1300 ^{30°}	∞ ^{60°}	s. H ₂ SO ₄ ; d. al.; i. NH ₃
Selenic acid	H ₂ SeO ₄ ·H ₂ O	162.99	nd.	2.627 ^{15°}	26	205	v. s.		
Selenium	Se ₈	631.68	red pd., amor., 2.92	4.26 ^{25°}	50	688	i.	i.	s. CS ₂ , H ₂ SO ₄ , CH ₂ I ₂
Selenium	Se ₈	631.68	gray, trig., 3.00; red, hex.	4.80; 4.50	220	688	i.	i.	s. CS ₂ , H ₂ SO ₄

Selenium	Se ₈	631.68	steel gray	4.8 ^{25°}	217	688	i.	i.	i. CS ₂ ; s. H ₂ SO ₄
Selenous acid	H ₂ SeO ₃	128.97	hex.	3.004 ^{15°}	d.		90 ^{0°}	400 ^{90°}	v. s. al.; i. NH ₃
Silicic acid, meta-	H ₂ SiO ₃	78.10	amor., 1.41	2.1–2.3			i.	i.	s. alk.; i. NH ₄ Cl
Silicic acid, ortho-	H ₄ SiO ₄	96.11	amor.	1.576 ^{17°}			sl. s.	sl. s.	s. alk.; i. NH ₄ Cl
Silicon, crystalline	Si	28.09	gray, cb., 3.736	2.4 ^{20°}	1420	2600	i.	i.	s. HNO ₃ + HF, Ag; sl. s. Pb, Zn; i. HF
Silicon, graphitic	Si	28.09	cr.	2.0–2.5		2600	i.	i.	s. HNO ₃ + HF, fused alk.; i. HF
Silicon, amorphous	Si	28.09	brn., amor.	2		2600	i.	i.	s. HF, KOH
carbide	SiC	40.10	blue-bk., trig., 2.654	3.17	>2700	subl. 2200	i.	i.	s. fused alk.; i. a.
chloride, tri-	Si ₂ Cl ₆	268.89	lf. or lq.	1.58 ^{0°}	–1	144 ^{760mm}	d.	d.	d. alk.
chloride, tetra-	SiCl ₄	169.90	col., fuming lq., 1.412	1.50	–70	57.6	d.	d.	d. conc. H ₂ SO ₄ , al.
fluoride	SiF ₄	104.08	gas	3.57 (A)	–95.7	–65 ^{1810mm}	v. s. d.		s. HNO ₃ , al., et.
hydride (silane)	SiH ₄	32.12	col. gas	lq. 0.68 ^{–185°}	–185	–112 ^{760mm}	i.		i. al., et.; d. KOH
oxide, di- (opal)	SiO ₂ ·xH ₂ O		iridescent, amor.	2.2	1600–1750	subl. 1750	i.	i.	s. HF, h. alk., fused CaCl ₂
oxide, di- (cristobalite)	SiO ₂	60.08	col., cb. or tet., 1.487	2.32	1710	2230	i.	i.	s. HF; i. alk.
oxide, di- (lechatelierite)	SiO ₂	60.08		2.20		2230	i.	i.	s. HF; i. alk.
oxide, di- (quartz)	SiO ₂	60.08	hex., 1.5442	2.650 ^{20°}	tr. <1425	2230	i.	i.	s. HF; i. alk.
oxide, di- (tridymite)	SiO ₂	60.08	trig., rhb., 1.469	2.26	tr. 1670	2230	i.		s. HF; i. alk.
Silver	Ag	107.87	silv. met., cb.	10.5 ^{20°}	960.5	1950	i.	i.	s. HNO ₃ , h. H ₂ SO ₄ ; i. alk.
bromide (bromyrite)	AgBr	187.77	pa. yel., cb., 2.252	6.473 ^{25°}	434	d. 700	0.00002 ^{20°}	0.00037 ^{100°}	0.51 ^{18°} NH ₄ OH; s. KCN, Na ₂ S ₂ O ₃
carbonate	Ag ₂ CO ₃	275.75	yel. pd.	6.077	218 d.		0.003 ^{20°}	0.05 ^{100°}	s. NH ₄ OH, Na ₂ S ₂ O ₃ ; i. al.
chloride (cerargyrite)	AgCl	143.32	wh., cb., 2.071	5.56	455	1550	0.000089 ^{10°}	0.00217 ^{100°}	s. NH ₄ OH, KCN; sl. s. HCl
cyanide	AgCN	133.89	wh., 1.685±	3.95	–(CN) ₂ , 320		0.000022 ^{20°}		s. NH ₄ OH, KCN, HNO ₃
nitrate (lunar caustic)	AgNO ₃	169.87	col., rhb., 1.744	4.352 ^{19°}	212	444 d.	122 ^{0°}	952 ^{100°}	s. gly.; v. sl. s. al.
Sodium	Na	22.99	silv. met. cb.	0.97 ^{20°}	97.5	880	d., forms NaOH		i. bz.; d. al.
acetate	NaC ₂ H ₃ O ₂	82.03	wh., mn., 1.464	1.528	324		46.5 ^{20°}	170 ^{100°}	2.1 ^{18°} al.
acetate	NaC ₂ H ₃ O ₂ ·3H ₂ O	136.08	wh., mn.	1.45	58	–3H ₂ O, 120	v. s.	v. s.	7.8 ^{25°} abs. al.
aluminate	NaAlO ₂	81.97	amor.		1650		s.	v. s.	i. al.
amide	NaNH ₂	39.01	olive gn.		210	400	d.	d.	d. al.
Sodium ammonium phosphate	NaNH ₄ HPO ₄ ·4H ₂ O	209.07	col., mn.	1.574	79 d.		16.7	100	i. al.
antimonate, meta-	2NaSbO ₃ ·7H ₂ O	511.60	cb.				0.031 ^{12,8°}		sl. s. al., NH ₄ salts; i. ac.
arsenate	Na ₃ AsO ₄ ·12H ₂ O	424.07	hex., 1.4589	1.759	86.3		26.7 ^{17°}		1.67 al., 50 ^{15°} gly.
arsenate, acid (monobasic)	NaH ₂ AsO ₄ ·H ₂ O	181.94	rhb., 1.5535	2.535	d. 100		s.		
arsenate, acid (dibasic)	Na ₂ HAsO ₄ ·7H ₂ O°	312.01	col., mn., 1.4658	1.871	125	–7H ₂ O, 100	61 ^{15°}	v. s.	sl. s. al.
arsenate, acid (dibasic)	Na ₂ HAsO ₄ ·12H ₂ O	402.09	mn., 1.4496	1.871	28	–12H ₂ O, 100	5.59 ^{0,1°}	140.7 ^{30°}	sl. s. al.
arsenite, acid	Na ₂ HAsO ₃	169.91	col.	1.87			v. s.		
benzoate	NaC ₇ H ₅ O ₂	144.10	col. cr.				62.5 ^{25°}	76.9 ^{100°}	2.3 ^{25°} , 8.3 ^{78°} al.
bicarbonate	NaHCO ₃	84.01	wh., mn., 1.500	2.20	–CO ₂ , 270		6.9 ^{0°}	16.4 ^{60°}	i. al.
bifluoride	NaHF ₂	61.99	col. cr.		d.		3.7 ^{20°}	s.	
bisulfate	NaHSO ₄	120.06	col., tri.	2.742	>315	d., –H ₂ O	50 ^{0°}	100 ^{100°}	d. al.; i. NH ₃
bisulfite	NaHSO ₃	104.06	col., mn., 1.526	1.48	d.		sl. s.	s.	i. al., act.
borate, tetra-	Na ₂ B ₄ O ₇	201.22		2.367	741		1.3 ^{0°}	8.79 ^{40°}	i. al.
borate, tetra	Na ₂ B ₄ O ₇ ·5H ₂ O	291.30	col., rhb., 1.461	1.815			22 ^{92°} (anh.)	52.3 ^{100°} (anh.)	
borate, tetra- (borax)	Na ₂ B ₄ O ₇ ·10H ₂ O°	381.37	wh., mn., 1.4694	1.73	75	–10H ₂ O, 200	1.3 ^{0,5} (anh.)	20.3 ^{90°} (anh.)	s. gly.; i. abs. al.
bromate	NaBrO ₃	150.89	col., cb.	3.339 ^{17,5°}	381		27.5 ^{0°}	90.9 ^{100°}	i. al.
bromide	NaBr	102.89	col., cb., 1.6412	3.205 ^{17,5°}	755	1390	90 ^{20°}	121 ^{100°}	sl. s. al.
bromide	NaBr·2H ₂ O	138.92	col., mn.	2.176	50.7		79.5 ^{0°} (anh.)	118.3 ^{90°} (anh.)	sl. s. al.
carbonate (soda ash)	Na ₂ CO ₃	105.99	wh. pd., 1.535	2.533	851	d.	7.1 ^{0°}	48.5 ^{104°}	i. al., et.
carbonate	Na ₂ CO ₃ ·H ₂ O	124.00	wh., rhb., 1.506–1.509	1.55	–H ₂ O, 100		s.	s.	s. gly.; i. al., et.
carbonate	Na ₂ CO ₃ ·7H ₂ O	232.10	rhb. or trig.	1.51	d. 35.1		s.	s.	
carbonate (sal soda)	Na ₂ CO ₃ ·10H ₂ O	286.14	wh., mn., 1.425	1.46			21.5 ^{0°}	238 ^{30°}	i. al.

⁰Usual commercial form.

TABLE 2-1 Physical Properties of the Elements and Inorganic Compounds (Continued)

Name	Formula	Formula weight	Color, crystalline form and refractive index	Specific gravity	Melting point, °C	Boiling point, °C	Solubility in 100 parts		
							Cold water	Hot water	Other reagents
Sodium ammonium phosphate (Cont.)									
carbonate, sesqui- (trona)	$\text{Na}_3\text{H}(\text{CO}_3)_2 \cdot 2\text{H}_2\text{O}$	226.03	wh., mn., 1.5073	2.112	d.		13°	42 ^{100°}	
chlorate	NaClO_3	106.44	wh., cb., or trig., 1.5151	2.490 ^{15°}	248	d.	79°	230 ^{100°}	s. al.
chloride	NaCl	58.44	col., cb., 1.5443	2.163	800.4	1413	35.7°	39.8 ^{100°}	sl. s. al.; i. conc. HCl
chromate	Na_2CrO_4	161.97	yel., rhb.	2.723	392		32°	126 ^{100°}	
chromate	$\text{Na}_2\text{CrO}_4 \cdot 10\text{H}_2\text{O}$	342.13	yel., delq., mn.	1.483	19.9		v. s.	∞	sl. s. al.
citrate	$2\text{Na}_3\text{C}_6\text{H}_5\text{O}_7 \cdot 11\text{H}_2\text{O}$	714.31	wh., rhb.	1.857 ^{$\frac{23.5^\circ}{4}$}	-11H ₂ O, 150	d.	91 ^{25°}	250 ^{100°}	i. al.
cyanide	NaCN	49.01	wh., cb., 1.452		563.7	1496	48 ^{10°}	82 ^{35°}	s. NH ₃ ; sl. s. al.
dichromate	$\text{Na}_2\text{Cr}_2\text{O}_7 \cdot 2\text{H}_2\text{O}$	298.00	red, mn., 1.6994	2.52 ^{18°}	-2H ₂ O, 84.6; 356 (anh.)	d. 400	238°	508 ^{80°}	
ferricyanide	$\text{Na}_3\text{Fe}(\text{CN})_6 \cdot \text{H}_2\text{O}$	298.93	red, delq.				18.9°	67 ^{100°}	i. al.
ferrocyanide	$\text{Na}_4\text{Fe}(\text{CN})_6 \cdot 10\text{H}_2\text{O}$	484.06	yel., mn.	1.458			17.9 ^{20°} (anh.)	63 ^{38.5°} (anh.)	i. al.
fluoride (villiumite)	NaF	41.99	tet., 1.3258	2.79	992		4°	5 ^{100°}	v. sl. s. al.
formate	NaHCO_2	68.01	wh., mn.	1.919	253		44°	160 ^{100°}	sl. s. al.; i. et.
hydride	NaH	24.00	silv. nd., 1.470	0.92	d. 800		d.		i. bz., CS ₂ , CCl ₄ , NH ₃ ; s. molten metal
hydrosulfide	$\text{NaSH} \cdot 2\text{H}_2\text{O}$	92.09	col., delq., nd.		d.		s.	s.	s. al.; d. a.
hydrosulfide	$\text{NaSH} \cdot 3\text{H}_2\text{O}$	110.11	rhb.		22	d.	s.	s.	s. al.; d. a.
hydrosulfite	$\text{Na}_2\text{S}_2\text{O}_4 \cdot 2\text{H}_2\text{O}$	210.14	col. cr.		d.		22 ^{20°}	d.	i. al.
hydroxide	NaOH	40.00	wh., delq.	2.130	318.4	1390	42°	347 ^{100°}	v. s. al., et., gly.; i. act.
hydroxide	$\text{NaOH} \cdot 3\frac{1}{2}\text{H}_2\text{O}$	103.05	mn.		15.5		s.	v. s.	
hypochlorite	NaOCl	74.44	pa. yel., in soln. only		d.		26°	158 ^{56°}	
iodide	NaI^*	149.89	col., cb., 1.7745	3.667 ^{0°}	651	1300	158.7°	302 ^{100°}	v. s. al., act.
iodide	$\text{NaI} \cdot 2\text{H}_2\text{O}$	185.92	col., mn.	2.448			v. s.	v. s.	v. s. NH ₃
lactate	$\text{NaC}_3\text{H}_5\text{O}_3$	112.06	col., amor.		d.		v. s.	v. s.	s. al.; i. et.
nitrate (soda niter)	NaNO_3	84.99	col., trig., 1.5874	2.257	308	d. 380	73°	180 ^{100°}	s. NH ₃ ; sl. s. gly., al.
nitrite	NaNO_2	69.00	pa. yel., rhb.	2.168 ^{0°}	271	d. 320	72.1°	163.2 ^{100°}	0.3 ^{20°} et.; 0.3 abs. al.; 4.4 ^{20°} m. al.; v. s. NH ₃
oxide	Na_2O	61.98	wh., delq.	2.27	subl.		Forms NaOH		d. al.
perborate	$\text{NaBO}_3 \cdot \text{H}_2\text{O}$	99.81	wh. pd.		d. 40		sl. s.	d.	s. gly., alk.
perchlorate	NaClO_4	122.44	rhb., 1.4617		482 d.		170°	320 ^{100°}	s. al.; 51 m. al.; 52 act.; i. et.
perchlorate	$\text{NaClO}_4 \cdot \text{H}_2\text{O}$	140.46	hex.	2.02	d. 130		209 ^{15°}	284 ^{50°}	s. al.
peroxide	Na_2O_2^*	77.98	yel.-wh. pd.	2.805	d.		s. d.	d.	s. dil. a.
peroxide	$\text{Na}_2\text{O}_2 \cdot 8\text{H}_2\text{O}$	222.10	wh., hex.		d. 30		s. d.	d.	
phosphate, monobasic	$\text{NaH}_2\text{PO}_4 \cdot \text{H}_2\text{O}^*$	137.99	col., rhb., 1.4852	2.040	-H ₂ O, 100	d. 200	71°	390 ^{83°}	i. al.
phosphate, monobasic	$\text{NaH}_2\text{PO}_4 \cdot 2\text{H}_2\text{O}$	156.01	col., rhb., 1.4629	1.91	60		91.1°	308 ^{40°}	
phosphate, dibasic	$\text{Na}_2\text{HPO}_4 \cdot 7\text{H}_2\text{O}$	268.07	col., mn., 1.4424	1.679	d.		185 ^{40°}	2000 ^{100°}	
phosphate, dibasic	$\text{Na}_2\text{HPO}_4 \cdot 12\text{H}_2\text{O}$	358.14	col., mn., 1.4361	1.52	34.6	-12H ₂ O, 180	4.3°	76.7 ^{30°}	i. al.
phosphate, tribasic	Na_3PO_4	163.94	wh.	2.537 ^{17.5°}	1340		4.5°	77 ^{100°}	
phosphate, tribasic	$\text{Na}_3\text{PO}_4 \cdot 12\text{H}_2\text{O}^*$	380.12	wh., trig., 1.4458	1.62	73.4	-11H ₂ O, 100	28.3 ^{15°}	∞	i. CS ₂
phosphate, meta-	$\text{Na}_4\text{P}_2\text{O}_7$	407.85	col.	2.476	616 d.		s.	∞	s. a., alk.
phosphate, pyro-	$\text{Na}_4\text{P}_2\text{O}_7^*$	265.90	wh.	2.45	988		2.26°	45 ^{96°}	d. a.
phosphate, pyro-	$\text{Na}_4\text{P}_2\text{O}_7 \cdot 10\text{H}_2\text{O}$	446.06	mn., 1.4525	1.82	d.		5.4°	93 ^{100°}	i. al., NH ₃
phosphate (pyrosodium)	$\text{Na}_2\text{H}_2\text{P}_2\text{O}_7$	221.94	col., mn., 1.510	1.862	d. 220		4.5°	21 ^{40°}	
phosphate (pyrosodium)	$\text{Na}_2\text{H}_2\text{P}_2\text{O}_7 \cdot 6\text{H}_2\text{O}$	330.03	col., mn., 1.4645	1.848			6.9°	36 ^{40°}	
potassium tartrate	$\text{NaKC}_4\text{H}_4\text{O}_6 \cdot 4\text{H}_2\text{O}$	282.22	rhb., 1.493	1.790	70 to 80	-4H ₂ O, 215	26°	66 ^{36°}	sl. s. al.
silicate, meta-	Na_3SiO_3	122.06	col., rhb., 1.520		1088		s.	s. d.	i. Na or K salts, al.
Sodium silicate, meta-	$\text{Na}_2\text{SiO}_3 \cdot 9\text{H}_2\text{O}$	284.20	rhb.		47	-6H ₂ O, 100	v. s.	v. s.	29 ^{18°} , $\frac{1}{2}\text{N}$ NaOH
silicate, ortho-	Na_4SiO_4	184.04	col., hex., 1.530		1018		s.	s.	
silicofluoride	Na_2SiF_6	188.06	wh., hex., 1.312	2.679	d.		0.44°	2.45 ^{100°}	i. al.
stannate	$\text{Na}_2\text{SnO}_3 \cdot 3\text{H}_2\text{O}$	266.73	hex. tablets		d. 140		50°	67 ^{50°}	i. al., act.
sulfate (thenardite)	Na_2SO_4	142.04	col., rhb., 1.477	2.698	tr. 100 to mn.		5°	42 ^{100°}	i. al.
sulfate	Na_2SO_4	142.04	col., mn.		tr. 500 to hex.		48.8 ^{40°}	42.5 ^{100°}	d. HI; s. H ₂ SO ₄

sulfate	Na ₂ SO ₄	142.04	col., hex.		884		19.4 ^{20p}	45.3 ^{60p}	
sulfate	Na ₂ SO ₄ ·7H ₂ O	268.15	tet.				44.9 ^{9p}	202.6 ^{26p}	
sulfate (Glauber's salt)	Na ₂ SO ₄ ·10H ₂ O	322.19	col., mn., 1.396	1.464	32.4	-10H ₂ O, 100	36 ^{15s}	412 ^{34a}	i. al.
sulfide, mono-	Na ₂ S	78.04	pink or wh., amor.	1.856			15.4 ^{10p}	57.3 ^{90p}	sl. s. al.; i. et.
sulfide, tetra-	Na ₂ S ₄	174.24	yel., cb.				s.	s.	s. al.
sulfide, penta-	Na ₂ S ₅	206.30	yel.				s.	s.	s. al.
sulfite	Na ₂ SO ₃	126.04	hex. pr., 1.565	2.633 ^{15s}	d.		13.9 ^{9p}	28.3 ^{84a}	i. al., NH
sulfite	Na ₂ SO ₃ ·7H ₂ O	252.15	mn.	1.561		-7H ₂ O, 150	34.7 ^{2p}	67.8 ^{18s}	i. al.
tartrate	Na ₂ C ₄ H ₄ O ₆ ·2H ₂ O	230.08	rhb.	1.818			29 ^{9p}	66 ^{43s}	i. al.
thiocyanate	NaCNS	81.07	delq., rhb., 1.625±		287		110 ^{10p}	225 ^{100p}	v. s. al.
thiosulfate	Na ₂ S ₂ O ₃	158.11	mn.	1.667			50 ^{9p}	231 ^{80p}	
thiosulfate (hypo)	Na ₂ S ₂ O ₃ ·5H ₂ O	248.18	mn. pr., 1.5079	1.685	d. 48.0		74.7 ^{7p}	301.8 ^{60p}	s. NH ₃ ; v. sl. s. al.
tungstate	Na ₂ WO ₄	293.82	wh., rhb.	4.179	692		57.5 ^{8p}	97 ^{100p}	
tungstate	Na ₂ WO ₄ ·2H ₂ O	329.85	wh., rhb.	3.245		-2H ₂ O, 100	88 ^{9p}	123.5 ^{100p}	sl. s. NH ₃ ; i. a., al.
tungstate, para-	Na ₆ W ₇ O ₂₄ ·16H ₂ O	2097.05	wh., tri.	3.987 ^{14p}		-16H ₂ O, 300	8	d.	
uranate	Na ₂ UO ₄	348.01	yel.				i.	i.	s. alk. carb., dil. a.
vanadate	Na ₃ VO ₄ ·16H ₂ O	472.15	col. nd.		866 (anh.)		v. s.	d.	i. al.
vanadate, pyro-	Na ₄ V ₂ O ₇	305.84	hex.		654		s.	i. al.	
Stannic chloride	SnCl ₄	260.52	col., fuming lq.	2.226	-30.2	114.1	s.	d.	s. abs. al., act., NH ₃ ; s. ∞ CS ₂
oxide (cassiterite)	SnO ₂	150.71	wh., tet., 1.9968	7.0	1127		i.	i.	s. conc. H ₂ SO ₄ ; i. alk.; NH ₄ OH, NH ₃
sulfate	Sn(SO ₄) ₂ ·2H ₂ O	346.87	col., delq., hex.				v. s.	d.	s. dil. H ₂ SO ₄ , HCl; d. abs. al.
Stannous bromide	SnBr ₂	278.52	yel., rhb.	5.12 ^{17p}	215.5	620	s.	d.	s. C ₆ H ₅ N
chloride	SnCl ₂	189.62	wh., rhb.		246.8	623	83.9 ^{9p}	269.8 ^{15p}	s. alk., abs. al., et.
chloride (tin salt)	SnCl ₂ ·2H ₂ O*	225.65	wh., tri.	2.71 ^{15.5p}	37.7	d.	118.7 ^{0p}	∞	s. tart. a., alk., al.
sulfate	SnSO ₄	214.77	wh. cr.		-SO ₂ , 360		19 ^{19p}	18 ^{100p}	s. H ₂ SO ₄
Strontium	Sr	87.62	silv. met.	2.6	800	1150	d.	Forms Sr(OH) ₂	s. al., a.
acetate	Sr(C ₂ H ₃ O ₂) ₂	205.71	wh. cr.	2.099		d.	36.9 ^{9p}	36.4 ^{47p}	0.26 ^{15p} m. al.
carbonate (strontianite)	SrCO ₃	147.63	wh., rhb., 1.664	3.70	149 ^{760atm}	-CO ₂ , 1350	0.0011 ^{18s}	0.065 ^{100p}	s. a., NH ₃ salts, aq. CO ₂
chloride	SrCl ₂	158.53	wh., cb., 1.6499	3.052	873		43.5 ^{9p}	100.6 ^{100p}	v. sl. s. act., abs. al.; i. NH ₃
chloride	SrCl ₂ ·6H ₂ O*	266.62	wh., rhb., 1.5364	1.933 ^{17p}	-4H ₂ O, 61	-6H ₂ O, 100	104 ^{9p}	198 ^{40p}	
hydroxide	Sr(OH) ₂	121.63	wh., delq.	3.625	375		0.41 ^{9p}	21.83 ^{100p}	s. NH ₄ Cl
hydroxide	Sr(OH) ₂ ·8H ₂ O*	265.76	col., tet., 1.499	1.90	-7H ₂ O in dry air		0.90 ^{9p}	47.7 ^{100p}	s. NH ₄ Cl; i. act.
nitrate	Sr(NO ₃) ₂ *	211.63	col., cb., 1.5878	2.986	570		40 ^{9p}	100 ^{89p}	s. NH ₃ ; 0.012 abs. al.
nitrate	Sr(NO ₃) ₂ ·4H ₂ O	283.69	wh., mn.	2.2			62.2 ^{9p}	124 ^{20p}	i. HNO ₃
oxide (strontia)	SrO	103.62	col., cb., 1.870	4.7	2430		Forms Sr(OH) ₂		sl. s. al.; i. et.
peroxide	SrO ₂	119.62	wh. pd.		d.		0.008 ^{20p}	d.	s. al., NH ₄ Cl; i. act.
peroxide	SrO ₂ ·8H ₂ O	263.74	wh. cr.		-8H ₂ O, 100		0.018 ^{20p}	d.	s. al.; i. NH ₄ OH
sulfate (celestite)	SrSO ₄	183.68	col., rhb., 1.6237	3.96	1580 d.	d.	0.0113 ^{9p}	0.0114 ^{32p}	sl. s. a.; i. dil. H ₂ SO ₄ , al.
sulfate, acid	Sr(HSO ₄) ₂	281.76	col., granular		d.		d.		14 ^{70p} H ₂ SO ₄
Sulfamic acid	NH ₂ SO ₃ H	97.09	wh., rhb.	2.03 ^{13p}	205 d.		20 ^{9p}	40 ^{70p}	sl. s. al., act.; i. et.
Sulfur, amorphous	S	32.07	pa. yel. pd., 2.0-2.9	2.046	120	444.6	i.	i.	sl. s. CS ₂
Sulfur, monoclinic	S ₈	256.52	pa. yel., mn.	1.96	119.0	444.6	i.	i.	s. CS ₂ , al.
Sulfur, rhombic	S ₈	256.52	pa. yel., rhb.	2.07	112.8	444.6	i.	i.	24 ^{40p} , 181 ^{55p} CS ₂
Sulfur bromide, mono-	S ₂ Br ₂	223.94	red, fuming lq.	2.635	-46	54 ^{0.18mm}	d.	d.	
chloride, mono-	S ₂ Cl ₂	135.04	red-yel. lq.	1.687	-80	138	d.	d.	s. CS ₂ , et., bz.
chloride, di-	SCL ₂	102.97	dark red fuming lq.	1.621 ^{15s}	-78	59	d.	d.	d. al.
chloride, tetra-	SCL ₄	173.88	yel.-brn. lq.		-30		d.	d.	
oxide, di-	SO ₂	64.06	col. gas		-75.5	-10.0	d.	22.8 ^{9p}	s. H ₂ SO ₄ ; al., ac.
oxide, tri-(α)	SO ₃	80.06	col. pr.		lq., 1.434 ^{9p} ; 2.264 (A)	16.83	d.		s. H ₂ SO ₄
oxide, tri-(β)	(SO ₃) ₂	160.13	col., silky, nd.		lq., 1.923; 2.75 (A)				
Sulfuric acid	H ₂ SO ₄ *	98.08	col., viscous lq.		1.97 ^{20p}	50	Forms H ₂ SO ₄	∞	s. H ₂ SO ₄
Sulfuric acid	H ₂ SO ₄ ·H ₂ O	116.09	pr. or lq.		1.834 ^{18s}	10.49	d. 340	∞	d. al.
					1.842 ^{15s}	8.62	290	∞	d. al.

*Usual commercial form.

TABLE 2-1 Physical Properties of the Elements and Inorganic Compounds (Concluded)

Name	Formula	Formula weight	Color, crystalline form and refractive index	Specific gravity	Melting point, °C	Boiling point, °C	Solubility in 100 parts		
							Cold water	Hot water	Other reagents
Sulfuric acid	H ₂ SO ₄ ·2H ₂ O	134.11	col. lq.	1.650 ⁴	-38.9	167	∞	∞	d. al.
Sulfuric acid, pyro-	H ₂ S ₂ O ₇	178.14	cr.	1.9 ²⁰	35	d.	d.		d. al.
Sulfuric oxychloride	SO ₂ Cl ₂	134.97	col. lq.	1.667 ²⁰	-54.1	69.1 ^{760mm}	d.		s. ac.; d. al.
Sulfurous oxybromide	SOBr ₂	207.87	or.-yel. lq.	2.68 ¹⁸	-50	68 ^{40mm}	d.		s. bz., CS ₂ , CCl ₄ ; d. act.
Sulfurous oxychloride	SOCl ₂	118.97	col. lq.	1.638	-104.5	78.8	d.		s. bz., chl.
Tantalum	Ta	180.95	bk.-gray, cb.	16.6	2850	>4100	i.	i.	s. fused alk., HF; i. HCl, HNO ₃ , H ₂ SO ₄
Tellurium	Te	127.60	met., hex.	(α) 6.24; (β) 6.00	452	1390	i.	i.	s. H ₂ SO ₄ , HNO ₃ , KCN, KOH, aq. reg.; i. CS ₂
Terbium	Tb	158.93							
Thallium	Tl	204.38	blue-wh., tet.	11.85	303.5	1650	i.	i.	s. HNO ₃ , H ₂ SO ₄ ; i. NH ₃
acetate	TlC ₂ H ₃ O ₂	263.43	silky nd.	3.68	110		v. s.		v. s. al.
chloride, mono-	TlCl	239.84	wh., cb.	7.00	430	806	0.21 ⁰	1.8 ¹⁰⁰	sl. s. HCl; i. al., NH ₄ OH
chloride, sesqui-	Tl ₂ Cl ₃	515.13	yel., hex.	5.9	400-500	d.	0.26 ¹⁵	1.9 ¹⁰⁰	
chloride, tri-	TlCl ₃	310.74	hex. pl.		25	d.	v. s.		s. al., et.
chloride, tri-	TlCl ₃ ·4H ₂ O	382.80	nd.		37	-4H ₂ O, 100	86.2 ¹⁷	d.	s. al., et.
sulfate (ic)	Tl ₂ (SO ₄) ₃ ·7H ₂ O	823.06	lf.		-6H ₂ O, 200	d.	d.	d.	s. dil. H ₂ SO ₄
sulfate (ous)	Tl ₂ SO ₄	504.83	col., rhb., 1.8671	6.77	632	d.	2.70 ⁰	18.45 ¹⁰⁰	
sulfate, acid	TlHSO ₄	301.45	trimorphous		115 d.				v. sl. s. dil. H ₂ SO ₄
Thio, cf. sulfo or sulfur									
Thorium	Th	232.04	cb.	11.2	1845	>3000	i.	i.	s. HCl, H ₂ SO ₄ ; sl. s. HNO ₃ ; i. HF, alk.
oxide, di- (thorianite)	ThO ₂	264.04	wh., cb.	9.69	>2800	4400	i.		s. h. H ₂ SO ₄ ; i. alk.
sulfate	Th(SO ₄) ₂	424.16		4.225 ¹⁷			0.74 ⁰	5.22 ⁵⁰	
sulfate	Th(SO ₄) ₂ ·9H ₂ O	586.30	mn. pr.	2.77	-9H ₂ O, 400		sl. s.	sl. s.	
Thulium	Tm	168.93					i.	i.	
Tin	Sn	118.71	silv. met., tet.	7.31	231.85	2260	i.	i.	s. HCl, H ₂ SO ₄ , dil. HNO ₃
Tin	Sn	118.71	gray, cb.	5.750	Stable -163 to +18	2260	i.	i.	h. aq. KOH s. a., h. alk. solns.
Tin salts, cf. stannic and stannous									
Titanic acid	H ₂ TiO ₃	97.88	wh. pd.				i.	i.	s. alk.; v. sl. s. dil. a.; i. al.
Titanium	Ti	47.87	dark gray, cb.	4.50 ^{17.5}	1800	>3000	i.	d.	s. a.
chloride, di-	TiCl ₂	118.77	bk., delq.		Unstable in air		d.		i. CS ₂ , et., chl.
chloride, tri-	TiCl ₃	154.23	vl., delq.		d. 440		s.	s.	
chloride, tetra-	TiCl ₄ ⁰	189.68	col. lq.	lq., 1.726	-30	136.4	s.	d.	s. dil. HCl
oxide, di- (anatase)	TiO ₂	79.87	brn. or bk., tet., 2.534-2.564	3.84			i.	i.	sl. s. alk.
oxide, di- (brookite)	TiO ₂	79.87	brn. or bk., rhb., 2.586	4.17			i.	i.	
oxide, di- (rutile)	TiO ₂	79.87	col. if pure, tet., 2.615	4.26	1640 d.	<3000	i.	i.	s. H ₂ SO ₄ , alk.
Tungsten	W	183.84	gray-bk., cb.	19.3	3370	5900	i.	i.	s. h. conc. KOH; sl. s. NH ₃ , HNO ₃ , aq. reg.
carbide	WC	195.85	gray pd., cb.	15.7 ¹⁸	2777	6000	i.	i.	s. F ₂ ; i. a.
carbide	W ₂ C	379.69	iron gray	16.06 ¹⁸	2877	6000	i.	i.	s. h. HNO ₃ ; sl. s. HCl, H ₂ SO ₄
oxide, tri-	WO ₃	231.84	yel., rhb.	7.16	>2130		i.	i.	s. alk.; i. a.
Tungstic acid (tungstite)	H ₂ WO ₄	249.85	yel., rhb. 2.24	5.5	-½H ₂ O, 100; 1473		i.	sl. s.	s. HF, alk., NH ₃
Uranic acid	H ₂ UO ₄	304.04	yel. pd.	5.926 ¹⁵	-H ₂ O, 250 to 300		i.	i.	s. a., alk. carb.; i. alk.
Uranium	U	238.03	wh. cr.	18.485 ¹³	1133	3500	i.	i.	s. a.; i. alk.
carbide	U ₂ C ₃	512.09	cr.	11.28	2400		d.	d.	d. a.
oxide, di- (uraninite)	UO ₂	270.03	bk., rhb.	10.9	2176		i.	i.	s. HNO ₃ , conc. H ₂ SO ₄

oxide (pitchblende)	U ₃ O ₈	842.08	olive gn.	7.31	d.		i.	i.	s. HNO ₃ , H ₂ SO ₄
sulfate (ous)	U(SO ₄) ₂ ·4H ₂ O	502.22	gn., rhb.		−4H ₂ O, 300		23 ^{11°}	9 ^{63°}	s. dil. a.
Uranyl acetate	UO ₂ (C ₂ H ₃ O ₂) ₂ ·2H ₂ O	424.15	yel., rhb.	2.89 ^{15°}	−2H ₂ O, 110		9.2 ^{17°}	d.	s. al., act.
carbonate (rutherfordine)	UO ₂ CO ₃	330.04	tet.	5.6					
nitrate	UO ₂ (NO ₃) ₂ ·6H ₂ O	502.13	yel., rhb., 1.4967	2.807	60.2	118	170.3 ^{30°}	∞ ^{60°}	v. s. ac., al., et.; i. dil., alk.
sulfate	UO ₂ SO ₄ ·3H ₂ O	420.14	yel. cr.	3.28 ^{16.5°}	d. 100		18.9 ^{13.2°}	230 ^{25°}	4 al.; s. a.
Vanadic acid, meta-	HVO ₃	99.95	yel. scales				i.		s. a., alk.; i. NH ₃
Vanadic acid, pyro-	H ₄ V ₂ O ₇	217.91	pa. yel., amor.				i.		s. a., alk., NH ₄ OH
Vanadium	V	50.94	lt. gray. cb.	5.96	1710	3000	i.	i.	s. HNO ₃ , H ₂ SO ₄ ; i. aq., alk.
chloride, di-	VCl ₂	121.85	gn., hex., delq.	3.23 ^{18°}			s.	d.	s. al., et.
chloride, tri-	VCl ₃	157.30	pink, tabular, delq.	3.00 ^{18°}	d.		s.	d.	s. abs. al., et.
chloride, tetra-	VCl ₄	192.75	red lq.	1.816 ^{30°}	−109	148.5 ^{75.5mm}	s. d.		s. abs. al., et., chl., ac.
oxide, di-	V ₂ O ₃	133.88	lt. gray cr.	3.64	ign.		i.	i.	s. a.
oxide, tri-	V ₂ O ₃	149.88	bk. cr.	4.87 ^{18°}	1970		sl. s.	s.	s. HNO ₃ , HF, alk.
oxide, tetra-	V ₂ O ₄	165.88	blue cr.	4.399	1967		i.	i.	s. a., alk.
oxide, penta-	V ₂ O ₅	181.88	red-yel., rhb.	3.357 ^{18°}	800	d. 1750	0.8 ^{20°}		s. a., alk.; i. abs. al.
oxychloride, mono-	VOCl	86.39	brn. pd.	2.824			i.		v. s. HNO ₃
Vanadyl chloride	(VO) ₂ Cl	169.33	yel. cr.	3.64	d. in air		i.		s. HNO ₃
chloride, di-	VOCl ₂	137.85	gn., delq.	2.88 ^{13°}			d.		s. abs. al., dil. HNO ₃
chloride, tri-	VOCl ₃	173.30	yel. lq.	1.829	<−15	127.19	s. d.		s. al., et., ∞Br ₂
Water†	H ₂ O	18.02	col. lq., 1.33300 ^{20°} ; hex. solid, 1.309 col. lq., 1.32844 ^{20°}	1.00 ^{4°} (lq.); 0.915 ^{0°} (ice)	0	100			∞ al.; sl. s. et.
Water, heavy	D ₂ O	20.029		1.107 ^{20°}	3.82	101.42	∞	∞	∞ al.; sl. s. et.
Xenon	Xe	131.29	col. gas	lq., 3.06 ^{−109.1} 2.7 ^{−140°} 4.53 (A)	−140	−109.1	24.2 ^{0°} cc	7.3 ^{50°} cc	
Ytterbium	Yb	173.04							
Yttrium	Y	88.91	dark gray, hex.	5.51	1490	2500	sl. d.	d.	v. s. dil. a., h. KOH
Zinc	Zn	65.41	silv. met., hex.	7.140	419.4	907	i.	i.	s. a., ac., alk.
acetate	Zn(C ₂ H ₃ O ₂) ₂	183.50	mn.	1.840	242	subl. in vac.	30 ^{25°}	44.6 ^{100°}	2.8 ^{25°} , 166 ^{70°} al.
acetate	Zn(C ₂ H ₃ O ₂) ₂ ·2H ₂ O*	219.53	wh., mn., 1.494	1.735	237	−2H ₂ O, 100	40 ^{25°}	66.6 ^{100°}	v. s. al.
bromide	ZnBr ₂	225.22	rhb.	4.219 ^{4°}	394	650	390 ^{0°}	670 ^{100°}	v. s. NH ₄ OH, al., et.
carbonate	ZnCO ₃	125.42	wh., trig., 1.818	4.42	−CO ₂ , 300		0.001 ^{15°}		s. a., alk., NH ₄ salts;
chloride	ZnCl ₂	136.32	wh., delq., 1.687, uniaxial	2.91 ^{35°}	283	732	432 ^{25°}	615 ^{100°}	i. act., NH ₃ 100 ^{12.5°} al.; v. s. et.; i.
cyanide	Zn(CN) ₂	117.44	col., rhb.		d. 80		0.0005 ^{15°}	sl. s.	s. KCN, NH ₃ , alk.; i. al.
hydroxide	Zn(OH) ₂	99.42	col., rhb.	3.053	d. 125		0.00052 ^{15°}		s. a., alk., NH ₄ OH
iodide	ZnI ₂	319.22	cb.	4.666 ^{14.2°}	446	624	430 ^{0°}	510 ^{100°}	s. a., al., NH ₃ , aq. (NH ₄) ₂ CO ₃
nitrate	Zn(NO ₃) ₂ ·6H ₂ O	297.51	col., tet.	2.065 ^{14°}	36.4	−6H ₂ O, 105	324.5	∞ ^{36.4°}	v. s. al.
oxide (zincite)	ZnO	81.41	wh., hex., 2.004	5.606	>1800		0.00042 ^{15°}		s. a., alk., NH ₄ Cl; i. NH ₃
oxide	ZnO	81.41	wh., amor.	5.47	>1800		0.00042 ^{15°}		
peroxide	ZnO ₂	97.41	yel.	1.571	expl. 212		0.0022		i. NH ₄ OH; d. a.
phosphide	Zn ₃ P ₂	258.17	steel gray, cb.	4.55 ^{13°}	>420	1100	i.		s. dil. a.
silicate	ZnSiO ₃	141.49	hex. or rhb.; glass, 1.650	3.52	1437		i.		
sulfate (zincosite)	ZnSO ₄	161.47	wh., rhb., 1.669	3.74 ^{15°}	d. 740		42 ^{0°}	61 ^{100°}	sl. s. al.; s. gly.
sulfate	ZnSO ₄ ·H ₂ O	179.49	col.	3.28 ^{15°}	d. 238		s.	89.5 ^{100°}	
sulfate	ZnSO ₄ ·6H ₂ O	269.56	mn.	2.072 ^{15°}	−5H ₂ O, 70		s.	s.	sl. s. al.; i. act.; NH ₃
sulfate (goslarite)	ZnSO ₄ ·7H ₂ O*	287.58	rhb., 1.4801	1.966 ^{16.5°}	tr. 39	−7H ₂ O, 280	115.2 ^{0°}	653.6 ^{100°}	sl. s. al.; i. act.; NH ₃
sulfide (α) (wurzite)	ZnS	97.47	wh., hex., 2.356	4.087	1850 ^{150atm}	subl. 1185	0.00069 ^{15°}	i.	v. s. a.; i. ac.
sulfide (β) (sphalerite)	ZnS	97.47	wh., cb.; glass (?) 2.18–2.25	4.102 ^{25°}	tr. 1020		i.	i.	s. a.
sulfide (blende)	ZnS	97.47	wh., granular	4.04			i.	i.	v. s. a.; i. ac.
sulfite	ZnSO ₃ ·2½H ₂ O	190.51	mn.		−2½H ₂ O, 100	d. 200	0.16	d.	s. H ₂ SO ₃ , NH ₄ OH; i. al.
Zirconium	Zr	91.22	cb., pd. ign. easily	6.4	1700	>2900	i.	i.	s. HF, aq. reg.; sl. s. a.
oxide, di- (baddeleyite)	ZrO ₂	123.22	yel. or brn., mn., 2.19	5.49	2700		i.	i.	s. H ₂ SO ₄ , HF
oxide, di- (free from Hf)	ZrO ₂	123.22	wh., mn.	5.73		4300	i.	i.	s. H ₂ SO ₄ , HF

*Usual commercial form.

†Cf. special tables on water and steam, Tables 2-3, 2-4, 2-5, 2-185, 2-186 and 2-351 through 2-357.

NOTE: °F = 9/5 °C + 32.

TABLE 2-2 Physical Properties of Organic Compounds*

Abbreviations Used in the Table

(A), density referred to air	cr., crystalline	i-, iso-, containing the group	nd., needles	s-, sec-, secondary	v. s., very soluble
al., ethyl alcohol	d., decomposes	(CH ₃) ₂ CH-	o-, ortho	silv., silvery	v. sl. s., very slightly soluble
amor., amorphous	d-, dextrorotatory	i-, insoluble	or., orange	sl., slightly	wh., white
aq., aqua, water	dl-, dextro-laevorotatory	ign., ignites	p-, para	subl., sublimes	yel., yellow
brn., brown	et., ethyl ether	l-, laevorotatory	pd., powder	sym., symmetrical	(+), right rotation
bz., benzene	expl., explodes	lf., leaflets	pet., petroleum ether	t-, tertiary	>, greater than
c., cubic	gn., green	lq., liquid	pl., plates	tet., tetragonal	<, less than
cc., cubic centimeter	h., hot	m-, meta	pr., prisms	tri., triclinic	∞, infinitely
chl., chloroform	hex., hexagonal	mn., monoclinic	rhb., rhombic	uns., unsymmetrical	
col., colorless		n-, normal	s., soluble	v., very	

This table of the physical properties includes the organic compounds of most general interest. For the properties of other organic compounds, reference must be made to larger tables in Lange's *Handbook of Chemistry* (Handbook Publishers), *Handbook of Chemistry and Physics* (Chemical Rubber Publishing Co.), Van Nostrand's *Chemical Annual*, *International Critical Tables* (McGraw-Hill), and similar works.

The **molecular weights** are based on the atomic weight values in "Atomic weights of the Elements 2001," *PURE Appl. Chem.*, **75**, 1107, 2003. The **densities** are given for the temperature indicated and

are usually referred to water at 4°C, e.g., 1.028^{95/4} a density of 1.028 at 95° C referred to water at 4° C, the 4 being omitted when it is not clear whether the reference is to water at 4° C or at the temperature indicated by the upper figure. The melting and boiling points given have been selected from available data as probably the most accurate. The **solubility** is given in grams of the substance in 100 of the solvent. In the case of gases, the solubility is often expressed in some manner as "5¹⁰ cc." which indicates that, at 10° C, 5 cc. of the gas are soluble in 100 of the solvent.

Name	Synonym	Formula	Formula weight	Form and color	Specific gravity	Melting point, °C	Boiling point, °C	Solubility in 100 parts		
								Water	Alcohol	Ether
Abietic acid	sylvic acid, abietinic acid	C ₂₀ H ₃₀ O ₂	302.45	lf.		182		i.	v. s.	v. s.
Acenaphthene	naphthylene ethylene	C ₁₀ H ₈ (CH ₂) ₂	154.21	rhb./al.	1.069 ^{95/95}	95	278-9	i.	s. h.	s. chl.
Acetal	acetaldehyde diethylacetal	CH ₃ CH(OC ₂ H ₅) ₂	118.17	lq.	0.821 ^{22/4}		102.2	6 ²⁵	∞	∞
Acet-aldehyde	ethanal	CH ₃ CHO	44.05	col. lq.	0.783 ^{18/4}	-123.5	20.2	∞	∞	∞
-aldehyde, par-	paraldehyde	(C ₂ H ₄ O) ₃	132.16	col. cr.	0.994 ^{20/4}	10.5-12	124.4 ⁷⁵²	12 ¹³	∞	∞
-aldehyde ammonia		CH ₃ CHOHNH ₂	61.08	col. cr.		97	100-10 d.	v. s.	v. s.	sl. s.
-amide	ethanamide	CH ₃ CONH ₂	59.07	col. cr.	1.159	81(69.4)	222	s.		v. sl. s.
-anilide	antifebrin	C ₆ H ₅ NHCOCH ₃	135.16	rhb./al.	1.21 ⁴	113-4	305	0.5 ⁹	21 ²⁰	7 ²⁵
-phenetidine (o-)	o-ethoxyacetanilide	CH ₃ CONHC ₆ H ₄ OC ₂ H ₅	179.22	lf./al.		79	>250	i.	s.	
(m-)	acetyl-m-phenetidine	CH ₃ CONHC ₆ H ₄ OC ₂ H ₅	179.22	lf./al.		96-7		sl. s.	s.	
-toluidide (o-)	N-tolylacetamide	CH ₃ C ₆ H ₄ NHCOCH ₃	149.19	rhb.	1.168 ¹⁵	110	296	0.86 ¹⁹		s.
(p-)	N-tolylacetamide	CH ₃ C ₆ H ₄ NHCOCH ₃	149.19	rhb. or mn.	1.212 ¹⁵	153	306-7	0.09 ²²	10 ²⁵	s.
Acetic acid	ethanoic acid, vinegar acid	CH ₃ CO ₂ H	60.05	col. lq.	1.049 ^{20/4}	16.7	118.1	∞	∞	∞
anhydride	acetyl oxide, acetic oxide	(CH ₃ CO) ₂ O	102.09	col. lq.	1.082 ^{20/4}	-73	139.6	12 c.	∞	∞
nitrile	methyl cyanide	CH ₃ CN	41.05	col. lq.	0.783 ^{20/4}	-41	81.6-2.0	∞	∞	∞
Acetone	propanone, dimethyl ketone	CH ₃ COCH ₃	58.08	col. lq.	0.792 ^{20/4}	-94.6	56.5	∞	∞	∞
Acetonyl urea	dimethyl hydantoin	<NHCONHCO>(CH ₃) ₂	128.13	tri./al.		175	subl.	s.	s.	s.
Acetophenone benzoyl hydride	methyl-phenyl ketone	CH ₃ COC ₆ H ₅	120.15	lf.	1.033 ^{15/15}	20.5	202.3 ⁷⁴⁹	i.	s.	s.
Acetyl-chloride	ethanoyl chloride	CH ₃ COCl	78.50	col. lq.	1.105 ^{20/4}	-112.0	51-2	d.	d.	∞
-phenylenediamine (p-)	amino-acetanilide (p)	C ₆ H ₄ ONHC ₆ H ₄ NH ₂	150.18	nd./aq.		162		s. h.	v. s.	v. s.
Acetylene	ethyne; ethine	HC≡CH	26.04	col. gas	(A) 0.906	-81.5 ⁸⁹¹	-84 ⁷⁶⁰	100 cc. ¹⁸	600 cc. ¹⁸	v. s.
dichloride (cis)	1,2-dichloroethene	CHCl:CHCl	96.94	col. lq.	1.291 ^{15/4}	-80.5	60.3	0.35 ²⁰	∞	∞
(trans)	dioform	CHCl:CHCl	96.94	col. lq.	1.265 ^{15/4}	-50	48.4	0.63 ³⁰	∞	∞
Aconitic acid	equisetie acid; citridic acid	C ₃ H ₄ (CO ₂ H) ₃	174.11	cr./aq.		192 d.		33 ¹⁵	∞	∞
Acridine		C ₆ H ₇ < (CH)(N) > C ₆ H ₄	179.22	rhb./aq. al.		110-1	346	sl. s. h.	s.	v. sl. s.
Acrolein ethylene aldehyde	acrylic aldehyde, propenal	CH ₂ :CH-CHO	56.06	col. lq.	0.841 ^{20/4}	-87.7	52.5	40	∞	s.
Acrylic acid	propenoic acid	CH ₂ :CH-CO ₂ H	72.06	col. lq.	1.062 ^{16/4}	12-13	141-2	∞	∞	∞
nitrile	vinyl cyanide	CH ₂ :CH-CN	53.06	col. lq.	0.811 ²⁰	-82	78-9	s.		
Adipic acid	hexandioic acid, adipinic acid	(CH ₂ CH ₂ CO ₂ H) ₂	146.14	mn. pr.	1.360 ^{25/4}	151-3	265 ¹⁰	1.4 ¹⁵	v. s.	0.6 ¹⁵
amide		(CH ₂ CH ₂ CONH ₂) ₂	144.17	cr. pd.		226-7		0.4 ¹²		
nitrile	tetramethylene	(CH ₂ CH ₂ CN) ₂	108.14	col. oil	0.951 ^{19/19}	1	295	v. sl. s.	s.	v. sl. s.
Adrenaline (1-) (3,4,1)	1-suprarenine	C ₉ H ₉ (OH) ₂ (CHOHCH ₂ NHCH ₃)	183.20	col. pd.		d. 207-11		0.03 ²⁰	v. sl. s.	i.
Alanine (α) (dl-)		CH ₃ CH(NH ₂)CO ₂ H	89.09	nd./aq.		295 d.	subl. >200	22 ¹⁷	v. sl. s.	i.
Aldol acetaldo	2-hydroxybutyraldehyde	CH ₃ CH(OH)CH ₂ COH	88.11	col. lq.	1.103 ^{20/4}		83 ²⁰	∞	v. sl. s.	s.
Alizarin	Anthraquinone acid	C ₆ H ₄ (CO) ₂ C ₆ H ₃ (OH) ₂	240.21	red rhb.		289-90	430	0.03 ¹⁰⁰	v. s.	v. s.
Allyl alcohol	propen-1-ol-3, propenyl alcohol	CH ₂ :CH-CH ₂ OH	58.08	col. lq.	0.854 ^{20/4}	-129	96.6	∞	∞	∞
bromide	3-bromo-propene-1	CH ₂ :CH-CH ₂ Br	120.98	lq.	1.398 ^{20/4}	-119.4	70-1 ⁷⁵³	i.	∞	∞
chloride	3-chloro-propene-1	CH ₂ :CH-CH ₂ Cl	76.52	col. lq.	0.938 ^{20/4}	-136.4	44.6	<0.1	∞	∞
thiocyanate (i)	mustard oil	CH ₂ :CH-CH ₂ SCN	99.15	col. oil	1.013 ^{20/4}	-80	152	0.2	∞	∞
thiourea	thiosinamide	CH ₂ :CH-CH ₂ NHCSNH ₂	116.18	col. pr.	1.219 ^{20/20}	77-8		3 ⁰	s.	v. sl. s.
Aluminum ethoxide		Al(OCH ₂ CH ₃) ₃	162.16	pd.	1.142 ^{20/0}	150-60	200-5 ¹⁰	d.	i.	v. sl. s.
Amino-anthraquinone (α)		C ₆ H ₄ (CO) ₂ C ₆ H ₃ NH ₂	223.23	red nd.		256	subl.	i.	s.	s.
(β)		C ₆ H ₄ (CO) ₂ C ₆ H ₃ NH ₂	223.23	red nd.		302	subl.	i.	s.	i.
-azobenzene		C ₆ H ₅ :N=N:C ₆ H ₅ NH ₂	197.24	yel. mn.		126-7	225 ¹²⁰	sl. s. h.	s. h.	s.
-benzoic acid (m-)		H ₂ N-C ₆ H ₄ CO ₂ H	137.14	nd./aq.	1.511 ⁴⁷	173-4		v. sl. s.	2 ¹⁰	1.8 ⁶
(p-)	aminodracylic acid	H ₂ N-C ₆ H ₄ CO ₂ H	137.14	mn. pr.		187-8		0.3 ¹³	11 ¹⁰	8.2 ⁶

Amino-diphenylamine (<i>p</i> -)		$\text{H}_2\text{N}\cdot\text{C}_6\text{H}_4\text{NH}\cdot\text{C}_6\text{H}_5$	184.24	nd./aq. al.	67	354	sl. s.	s.	s.
-G-acid (2-)-(6-,8-), Na_2 salt		$\text{C}_{10}\text{H}_5(\text{NH}_2)(\text{SO}_3\text{Na})_2$	347.28				v. sl. s.		
-mono-potassium salt		$\text{C}_{10}\text{H}_5(\text{NH}_2)\text{S}_2\text{O}_6\text{HK}$	341.40				12.8 ²⁰		
-sodium salt		$\text{C}_{10}\text{H}_5(\text{NH}_2)\text{S}_2\text{O}_6\text{HNa}$	325.29				2.7 ¹⁸		
-J-acid (2-)-(5-,7-)		$\text{C}_{10}\text{H}_5(\text{NH}_2)(\text{SO}_3\text{H})_2$	303.31				10.0 ²⁰		
-mono-potassium salt		$\text{C}_{10}\text{H}_5(\text{NH}_2)\text{S}_2\text{O}_6\text{HK}$	341.40				3.4 ¹⁸		
-naphthol sulfonic (1-,2-,4-)(α -)		$\text{C}_{10}\text{H}_5\text{OHNH}_2\text{SO}_3\text{H}\cdot\frac{1}{2}\text{H}_2\text{O}$	248.26				v. s.		
(1-,8-,4-)		$\text{NH}_2(\text{OH})\text{C}_{10}\text{H}_5\text{SO}_3\text{H}$	239.25				v. sl. s.		
-phenol (<i>o</i> -)	2-aminophenol	$\text{H}_2\text{N}\cdot\text{C}_6\text{H}_4\cdot\text{OH}$	109.13	col. nd.	173	subl.	1.7 ⁹	4.3 ⁹	v. s.
(<i>m</i> -)	3-aminophenol	$\text{H}_2\text{N}\cdot\text{C}_6\text{H}_4\cdot\text{OH}$	109.13	pr.	122-3		2.6 ⁹	s.	sl. s.
(<i>p</i> -)	<i>p</i> -hydroxyaniline	$\text{H}_2\text{N}\cdot\text{C}_6\text{H}_4\cdot\text{OH}$	109.13	lf.	184-6 d.	subl.	1.1 ⁹	4 ⁹	sl. s.
-toluene sulfonic acid (1-,2-,3-)		$\text{C}_6\text{H}_4(\text{CH}_3)(\text{NH}_2)\text{SO}_3\text{H}$	187.22	nd.			0.97 ¹¹		i. bz.
(1-,4-,2-)		$\text{C}_6\text{H}_4(\text{CH}_3)(\text{NH}_2)\text{SO}_3\text{H}\cdot\text{H}_2\text{O}$	205.23	mn.	d.		0.5 ²⁰	i.	
(1-,4-,3-)		$\text{C}_6\text{H}_3(\text{CH}_3)(\text{NH}_2)\text{SO}_3\text{H}\cdot\frac{1}{2}\text{H}_2\text{O}$	196.22	nd.			0.47		
(1-,2-,5-)		$\text{C}_6\text{H}_3(\text{CH}_3)(\text{NH}_2)\text{SO}_3\text{H}\cdot\text{H}_2\text{O}$	205.23	tri./aq.		-H ₂ O, 120	3 ¹¹	i.	
Amyl acetate (<i>n</i> -)		$\text{CH}_3\text{CO}_2\text{CH}_2(\text{CH}_2)_3\text{CH}_3$	130.18	col. lq.	0.879 ^{20/20}	-70.8	148.4 ⁷³⁷	v. sl. s.	∞
(<i>i</i> -)	common amyl acetate	$\text{CH}_3\text{CO}_2\text{CH}_2\text{CH}_2\text{CH}(\text{CH}_3)_2$	130.18	col. lq.	0.876 ^{15/4}		142 ⁷³⁷	0.3 ¹⁵	∞
		$\text{CH}_3\text{CO}_2\text{CH}_2\text{CH}(\text{CH}_3)\text{C}_2\text{H}_5$	130.18	col. lq.	0.880 ¹³		141-2	v. sl. s.	∞
(<i>s</i> -)	α -Me-Bu-acetate	$\text{CH}_3\text{CO}_2\text{CH}(\text{CH}_3)\text{C}_2\text{H}_5$	130.18	col. lq.	0.922 ⁹		133.5	sl. s.	∞
(<i>s</i> -)	di Et-carbinol acetate	$\text{CH}_3\text{CO}_2\text{CH}(\text{C}_2\text{H}_5)_2$	130.18	col. lq.	0.871 ^{20/4}		133	sl. s.	∞
(<i>t</i> -)		$\text{CH}_3\text{CO}_2\text{C}(\text{CH}_3)_2\text{C}_2\text{H}_5$	130.18	col. lq.	0.874 ¹⁹		124.5 ⁷⁴⁹	v. sl. s.	∞
alcohol (<i>n</i> -) fusel oil,	pentanol-1	$\text{CH}_3(\text{CH}_2)_4\text{OH}$	88.15	col. lq.	0.817 ^{20/20}	-78.5	137.9	2.7 ²²	∞
(<i>s</i> - <i>n</i> -) methyl-propyl carbinol,	pentanol-2	$\text{C}_2\text{H}_5\text{CH}_2\text{CH}(\text{OH})\text{CH}_3$	88.15	col. lq.	0.810 ^{20/20}		119.5	4 ²⁰	∞
(prim-, <i>t</i> -) isobutyl carbinol,	2-methyl-butanol-4	$(\text{CH}_3)_2\text{CHCH}_2\text{CH}_2\text{OH}$	88.15	col. lq.	0.813 ^{15/4}	-117.2	132.0	2 ¹⁴	∞
(<i>s</i> - <i>i</i> -)	2-methyl-butanol-3	$(\text{C}_2\text{H}_5)_2\text{CHOH}$	88.15	col. lq.	0.815 ^{25/4}		115.6	5.5 ³⁰	∞
(<i>t</i> -)	2-methyl-butanol-2	$(\text{CH}_3)_2\text{CCH}(\text{OH})\text{CH}_3$	88.15	col. lq.	0.819 ¹⁹	-11.9	113-4	2.8 ³⁰	∞
		$(\text{CH}_3)_2\text{C}(\text{OH})\text{C}_2\text{H}_5$	88.15	col. lq.	0.809 ^{20/4}	52-3	102	sl. s.	s.
(<i>d</i> -)	active amyl alcohol	$(\text{CH}_3)_3\text{CCH}_2\text{OH}$	88.15	cr.			113-4	sl. s.	∞
-amine (<i>n</i> -)		$\text{C}_2\text{H}_5\text{CH}(\text{CH}_3)\text{CH}_2\text{OH}$	88.15	col. lq.	0.816 ^{20/4}		128	3.6 ³⁰	∞
(<i>s</i> - <i>n</i> -)		$\text{CH}_3(\text{CH}_2)_4\text{NH}_2$	87.16	col. lq.	0.766 ¹⁹	-55	103-4	s.	s.
(<i>i</i> -)		$(\text{C}_2\text{H}_5)_2\text{CHCH}_2\text{NH}_2$	87.16	col. lq.	0.749 ^{20/4}		91-2	∞	∞
(<i>t</i> -)		$(\text{CH}_3)_2\text{CH}(\text{CH}_2)_2\text{NH}_2$	87.16	col. lq.	0.751 ^{15/4}		95	∞	∞
		$(\text{C}_2\text{H}_5)_2\text{CH}_2\text{CNH}_2$	87.16	col. lq.	0.731 ^{25/4}	-105	77-8	∞	∞
	1-NH ₂ -2-Me-butane	$\text{C}_2\text{H}_5\text{CH}(\text{CH}_3)\text{CH}_2\text{NH}_2$	87.16	col. lq.	0.755 ¹⁸		95-6	∞	∞
	3-amino pentane	$(\text{C}_2\text{H}_5)_2\text{CHNH}_2$	87.16	col. lq.	0.749 ^{20/4}		90-1	∞	∞
	3-NH ₂ -2-Me-butane	$(\text{CH}_3)_2\text{CHCH}(\text{CH}_3)\text{NH}_2$	87.16	col. lq.	0.757 ¹⁸		83-4	∞	∞
aniline (<i>i</i> -)		$\text{C}_6\text{H}_5\text{NHC}_2\text{H}_5$	163.26	lq.	0.928 ^{15/4}		254.5	i.	∞
benzoate (<i>i</i> -)		$\text{C}_6\text{H}_5\text{CO}_2\text{C}_2\text{H}_5$	192.25	col. lq.	0.992 ^{4/14}		261 ⁷⁴⁶	i.	∞
bromide (<i>n</i> -)	1-bromopentane	$\text{CH}_3(\text{CH}_2)_4\text{Br}$	151.04	col. lq.	1.218 ^{80/4}	-95	129.7	i.	s.
(<i>i</i> -)	4-Br-2-Me-butane	$(\text{CH}_3)_2\text{CH}(\text{CH}_2)_2\text{Br}$	151.04	col. lq.	1.220 ^{17/15}		120 ⁷⁴⁵	0.02 ¹⁶	s.
(<i>t</i> -)	2-Br-2-Me-butane	$(\text{CH}_3)_2\text{C}(\text{Br})\text{C}_2\text{H}_5$	151.04	lq.	1.216 ^{80/0}		108 ⁷⁶⁵	i.	s.
<i>n</i> -butyrate (<i>n</i> -)		$\text{C}_2\text{H}_5\text{CH}_2\text{CO}_2(\text{CH}_2)_3\text{CH}_3$	158.24	col. lq.	0.871 ^{15/4}	-73.2	186.4	0.05 ³⁰	∞
(<i>i</i> -)		$\text{C}_2\text{H}_5\text{CH}_2\text{CO}_2\text{C}_2\text{H}_5$	158.24	col. lq.	0.866 ^{19/15}		178.6	i.	∞
(<i>t</i> -)		$\text{C}_2\text{H}_5\text{CO}_2\text{C}(\text{CH}_3)_2\text{C}_2\text{H}_5$	158.24	col. lq.	0.865 ^{15/0}		164	sl. s.	∞
<i>i</i> -butyrate (<i>i</i> -)		$(\text{CH}_3)_2\text{CHCO}_2\text{C}_2\text{H}_5$	158.24	lq.	0.876 ^{9/4}		168.8	i.	s.
chloride (<i>n</i> -)	1-chloropentane	$\text{CH}_3(\text{CH}_2)_4\text{Cl}$	106.59	col. lq.	0.878 ^{20/4}	-99	108.4	i.	s.
(<i>s</i> -)	2-chloropentane	$\text{C}_2\text{H}_5\text{CH}_2\text{CH}_2\text{Cl}$	106.59	lq.	0.870 ^{20/4}		96.7	i.	s.
(<i>s</i> -)	3-chloropentane	$(\text{C}_2\text{H}_5)_2\text{CHCl}$	106.59	col. lq.	0.895 ²¹		97.3	i.	∞
(<i>i</i> -)	4-Cl-2-Me-butane	$(\text{CH}_3)_2\text{CH}(\text{CH}_2)_2\text{Cl}$	106.59	col. lq.	0.893 ^{20/4}		99.7 ⁷⁵⁸	i.	s.
(<i>s</i> - <i>i</i> -)	3-Cl-2-Me-butane	$(\text{CH}_3)_2\text{CHCH}_2\text{Cl}$	106.59	lq.	0.883 ⁹		91 ⁷³³	i.	s.
(<i>t</i> -)	2-Cl-2-Me-butane	$(\text{CH}_3)_2\text{CClC}_2\text{H}_5$	106.59	lq.	0.871 ^{20/4}	-72.9	85.7	i.	s.
	1-Cl-2-Me-butane	$(\text{CH}_3)(\text{C}_2\text{H}_5)\text{CHCH}_2\text{Cl}$	106.59	lq.	0.881 ^{17/5}		98-9	i.	s.
<i>i</i> -cyanide (<i>i</i> -)	iso-caproic iso-nitrile	$(\text{CH}_3)_2\text{CH}(\text{CH}_2)_2\text{NC}$	97.16	lq.			137-9	i.	s.
formate (<i>n</i> -)		$\text{HCO}_2\text{CH}_2(\text{CH}_2)_4\text{CH}_3$	116.16	lq.	0.902 ⁹	-73.5	132	v. sl. s.	∞
(<i>i</i> -)		$\text{HCO}_2\text{CH}_2\text{CH}_2\text{CH}(\text{CH}_3)_2$	116.16	lq.	0.882 ^{20/4}	-93.5	123.5	0.3 ²²	∞
iodide (<i>n</i> -)	1-iodopentane	$\text{CH}_3(\text{CH}_2)_4\text{I}$	198.05	lq.	1.510 ^{20/4}	-86	157.0	i.	s.
(<i>i</i> -)	4-I-2-Me-butane	$(\text{CH}_3)_2\text{CHCH}_2\text{CH}_2\text{I}$	198.05	lq.	1.515 ^{18/4}		147 ⁷⁶⁵	i.	∞
(<i>s</i> - <i>n</i> -)	2-iodopentane	$\text{C}_2\text{H}_5\text{CH}_2\text{CH}_2\text{CH}_2\text{I}$	198.05	lq.	1.507 ^{17/4}		144.5	i.	∞
(<i>t</i> -)	2-I-2-Me-butane	$(\text{CH}_3)_2\text{CIC}_2\text{H}_5$	198.05	lq.	1.471 ^{19/15}		127 ⁷⁶⁵	i.	∞
		$\text{C}_2\text{H}_5\text{CH}(\text{CH}_3)\text{CH}_2\text{I}$	198.05	lq.	1.524 ^{20/4}		148	i.	∞
mercaptan (<i>n</i> -)	pentanthiol-1	$\text{CH}_3(\text{CH}_2)_4\text{SH}$	104.21	lq.	0.857 ²⁰		126 ⁷⁶⁷	i.	∞
(<i>n</i> -)	pentanthiol-3	$(\text{C}_2\text{H}_5)_2\text{CHSH}$	104.21	col. lq.			105	i.	∞
(<i>i</i> -)	2-Me-butanthiol-4	$(\text{CH}_3)_2\text{CH}(\text{CH}_2)_2\text{SH}$	104.21	lq.	0.835 ^{20/4}		120	i.	∞
phenol (<i>t</i> -)(<i>p</i> -)	pentaphen	$\text{C}_5\text{H}_9\cdot\text{C}_6\text{H}_5\text{OH}$	164.24	cr.		93	265-7	sl. s.	s.
propionate (<i>n</i> -)		$\text{C}_2\text{H}_5\text{CO}_2(\text{CH}_2)_3\text{CH}_3$	144.21	lq.	0.876 ^{15/4}	-73.1	168.7	i.	∞
(<i>i</i> -)		$\text{C}_2\text{H}_5\text{CO}_2\text{CH}_2\text{CH}(\text{CH}_3)_2$	144.21	col. lq.	0.870 ^{20/4}		160.2	0.1 ²⁵	∞
(act.)		$\text{C}_2\text{H}_5\text{CO}_2\text{C}_2\text{H}_5$	144.21	col. lq.	0.866 ^{20/4}		58 ¹⁶	v. sl. s.	∞
salicylate (<i>n</i> -)		$\text{HOC}_6\text{H}_4\text{CO}_2\text{C}_2\text{H}_5$	208.25	lq.	1.065 ¹⁵		265	i.	∞
Amyl <i>i</i> -valerate (<i>i</i> -)		$\text{C}_4\text{H}_9\text{CO}_2\text{C}_5\text{H}_{11}$	172.26	col. lq.	0.858 ^{20/15}		194	v. sl. s.	∞
		$\text{C}_4\text{H}_9\text{CO}_2\text{C}_3\text{H}_7$	172.26	col. lq.	0.861 ^{14/0}		173-4	sl. s.	s.

*By N. A. Lange, Ph.D., Handbook Publishers, Inc., Sandusky, Ohio. Abridged from table of Physical Constants of Organic Compounds in *Lange's Handbook of Chemistry*.

TABLE 2-2 Physical Properties of Organic Compounds (Continued)

Name	Synonym	Formula	Formula weight	Form and color	Specific gravity	Melting point, °C	Boiling point, °C	Solubility in 100 parts		
								Water	Alcohol	Ether
Amylene (<i>n</i> -)(α -) (<i>i</i> -) (α -) (<i>n</i> -)(β -) (<i>i</i> -)(β -)	pentene-1	C ₅ H ₈ CH ₂ CH:CH ₂	70.13	lq.	0.644 ²⁰		30-1	i.	∞	∞
	2-methyl-butene-3	(CH ₃) ₂ CHCH:CH ₂	70.13	col. lq.	0.632 ¹⁵	-135	20.5 ⁷⁷¹	i.	∞	∞
	2-methyl-butene-1	(C ₆ H ₅)(CH ₃)C:CH ₂	70.13	col. lq.	0.667 ⁰⁰		31-2 ⁷⁸⁵	i.	∞	∞
	pentene-2	C ₅ H ₈ CH:CHCH ₃	70.13	col. lq.	0.650 ^{20/4}	-139	36.4	v. sl. s.	∞	∞
	2-methyl-butene-2	(CH ₃) ₂ C:CHCH ₃	70.13	col. lq.	0.663 ^{10/4}	-124	37-8	i.	s.	∞
Anethole (<i>p</i> -)	<i>p</i> -propenyl anisole	CH ₃ CH ₂ CH:C ₆ H ₄ OCH ₃	148.20	lf./al.	0.991 ^{20/20}	22.5	235.3	v. sl. s.	s.	∞
Anhydroformal-aniline	methylene aniline	(CH ₂ NC ₆ H ₅) ₂	315.41	pr./al.		143	185	i.	sl. s.	s.
Aniline	amino benzene, phenyl amine, cyanol	C ₆ H ₅ NH ₂	93.13	col. oil	1.022 ^{20/4}	-6.2	184.4	3.6 ¹⁸	∞	∞
	hydrochloride	C ₆ H ₅ NH ₂ ·HCl	129.59	cr.	1.222 ⁴	198	245	18 ¹⁵	s.	i.
	nitrate	C ₆ H ₅ NH ₂ ·HNO ₃	156.14	rhb.	1.356 ⁴	d. 190		s.	s.	sl. s.
	sulfate	(C ₆ H ₅ NH ₂) ₂ ·H ₂ SO ₄	284.33	lf./al.	1.377 ⁴	d.		5 ¹⁴	sl. s.	i.
Anisal-acetone (<i>p</i> -)	MeO-benzalacetone	CH ₃ OC ₆ H ₄ CH:CHCOCH ₃	176.21	lf./et.		73-4		i.	v. s.	v. s.
Anisic acid (<i>p</i> -)		CH ₃ OC ₆ H ₄ CO ₂ H	152.15	mm./aq.	1.385 ⁴	184.2	275-80	0.03 ¹⁹	v. s.	v. s.
aldehyde (<i>p</i> -)		CH ₃ OC ₆ H ₄ CHO	136.15	col. oil	1.123 ^{20/4}	2.5	247-8	∞	v. sl. s.	∞
Anisidine (<i>o</i> -)	2-amino-anisole	CH ₃ OC ₆ H ₄ NH ₂	123.15	col. lq.	1.098 ^{15/15}	5.2	225	v. sl. s.	∞	∞
	MeO-aniline(<i>m</i>)	CH ₃ OC ₆ H ₄ NH ₂	123.15	oil	1.096 ^{20/4}	<-12	251	v. sl. s.	s.	s.
	(<i>m</i> -)	CH ₃ OC ₆ H ₄ NH ₂	123.15	pl./aq.	1.089 ^{35/55}	57.2	243	s. h.	s.	s.
	(<i>p</i> -)	CH ₃ OC ₆ H ₄ NH ₂	108.14	col. lq.	0.990 ^{22/4}	-37.3	154-5	i.	s.	s.
Anisole	methyl phenyl ether	C ₆ H ₅ OCH ₃	108.14	col. mm.	1.25 ^{27/4}	217-8		i.	1.5 ²⁰	
Anthracene	paranaphthalene, anthracin green oil	C ₆ H ₄ :(CH ₂) ₂ :C ₆ H ₄	178.23							
	α -amino-anthracene	C ₆ H ₄ :(CH ₂) ₂ :C ₆ H ₃ NH ₂	193.24	yel./al.		130±		i.	s.	
	β -amino-anthracene	C ₆ H ₄ :(CH ₂) ₂ :C ₆ H ₃ NH ₂	193.24	yel./al.		238	subl.	sl. s.	sl. s.	sl. s.
Anthranil		C ₆ H ₄ :(NH)CO	119.12	col. oil	1.187 ^{15/4}	<-18	d. >215	sl. s. h.	s.	s.
Anthranilic acid (<i>o</i> -)		H ₂ NC ₆ H ₄ CO ₂ H	137.14	col. rhb.		144-5	subl.	0.35 ¹⁴	11 ¹⁰	16 ⁷
Anthrapurpurin (1-,2-,7-)		C ₁₁ H ₇ O ₃ (OH) ₃	256.21	or. nd./al.		369	462	v. s. h.	sl. s.	sl. s.
Anthraquinone	diphenyleneketone, dihydrodiketoanthracene	C ₆ H ₄ :(CO) ₂ :C ₆ H ₄	208.21	yel. rhb.	1.438 ^{20/4}	286	379-81	i.	0.05 ¹⁸	v. sl. s.
	disulfonate Na ₂ (1-,5-)	C ₁₄ H ₆ O ₃ (SO ₃ Na) ₂ ·5H ₂ O	502.38	yel. lf.				v. s.	i.	i.
	(1-,8-)	C ₁₄ H ₆ O ₃ (SO ₃ Na) ₂ ·4H ₂ O	484.36	yel. pr.				sl. s.		
	(2-,6-)	C ₁₄ H ₆ O ₃ (SO ₃ Na) ₂ ·7H ₂ O	538.41	col. cr.				3.9 ²⁰		
	(2-,7-)	C ₁₄ H ₆ O ₃ (SO ₃ Na) ₂ ·4H ₂ O	484.36	cr.				30.5 ²⁰	v. sl. s.	i.
	sulfonate Na (1-)	C ₁₄ H ₇ O ₃ SO ₃ Na	310.26	yel. lf.				0.53 ²⁰		i.
	(2-)	C ₁₄ H ₇ O ₃ SO ₃ Na	310.26	silv. lf.				0.84 ²⁵	i.	i.
Anthrarufin (1-,5-)		C ₁₄ H ₇ O ₃ (OH) ₂	240.21	yel. lf.		280	subl.	i.	sl. s.	s.
Antipyrène	1-ph-2,3-diMepyrzalone-5	C ₁₁ H ₁₂ O ₂ N ₂	188.23	mm./aq.	1.088 ^{113/4}	113(109)	319 ¹⁷⁴	100 ²⁵	100	sl. s.
Apiole	1-allyl-2,5-diMeO-3,4 methylenedioxybenzene	C ₁₂ H ₁₄ O ₄	222.24	col. nd.	1.02 ^{20/4}	30	294	i.	s.	s.
		CH ₂ OH(CHOH) ₃ CHO	150.13	rhb. pr.	1.585 ^{20/4}	159.5		46 ⁰	0.5 ⁰⁷	i.
		CH ₂ OH(CHOH) ₃ CHO	150.13			164.5		16.9 ¹⁰		
Arachidic acid	eicosanoic acid	CH ₃ (CH ₂) ₁₈ CO ₂ H	312.53	col. lf.		77	328	i.	s. h.	v. s.
Arsanilic acid (<i>p</i> -)		H ₂ N·C ₆ H ₄ ·AsO ₃ H ₂	217.05	nd./aq.		232		v. s. h.	v. s. h.	i.
Asparagine (<i>l</i> -)		HO ₂ C·C ₆ H ₄ (NH ₂) ₂ ·CONH ₂	132.12	rhb.	1.543 ^{15/4}	227-35	d. 235	3.1 ²⁸	i. c.	
Aspirin (<i>o</i> -)		C ₉ H ₇ CO ₂ ·C ₆ H ₄ ·CO ₂ H	180.16	nd./aq.		135-6		1 ³⁷	s.	5 ²⁰
Atropic acid	α -phenyl acrylic acid	C ₆ H ₅ C:(CH ₂)·CO ₂ H	148.16	nd./aq.		106-7	267 d.	0.1 c.	s.	s.
Auramine	4,4'-dimethylaminobenzenophenonide	[(CH ₃) ₂ NC ₆ H ₄] ₂ C:NH	267.37	col./al.		136-7		i.	7 ²⁰	2.3 ²⁰
		(HOC ₆ H ₄) ₂ C:C ₆ H ₄ O	290.31	red		310 d.		i.	s.	s.
Aurine, coralline (4-,4')		(CH ₃ O·C ₆ H ₄ N) ₂	242.27	or. pr.		153		i.	s.	s.
Azo-anisole (2-,2')	diMeO-azobenzene	C ₆ H ₅ N=N·C ₆ H ₅	182.22	or. mn.	1.203 ^{20/4}	68	297	i.	4.2 ²⁰	
benzene	diphenyldiimide	(C ₆ H ₅) ₂ N ₂ O	198.22	yel. rhb.	1.248 ^{20/20}	36	d.	i.	11.4 ¹⁵	
Azoxybenzene		CO ₂ :(NHCO) ₂ :CH ₂ ·2H ₂ O	164.12	col./aq.		d. 245		s. h.	sl. s.	s.
Barbituric acid	malonyl urea		146.19	pl.	1.035 ^{20/20}	41-2	260-2	i.	s.	s.
Benzal acetone	Me-cinnamyl ketone	C ₆ H ₅ CH:CHCOCH ₃	106.12	col. lq.	1.046 ^{20/4}	-26	179	0.3	∞	∞
Benzaldehyde	artificial almond oil	C ₆ H ₅ CHO	121.14	col. pr.	1.341	130	290	1.35 ²⁵	∞	sl. s.
Benzamide		C ₆ H ₅ CONH ₂	121.14	col. pr.	1.341	130	290	1.35 ²⁵	∞	sl. s.
Benzanilide		C ₆ H ₅ CONHC ₆ H ₅	197.23	lf./al.	1.31 ⁴	163	117-9 ¹⁰	i.	4 ³⁰	sl. s.
Benzene	benzol, phenyl hydride, cyclohexatriene	C ₆ H ₆	78.11	col. lq.	0.879 ^{20/4}	5.5	80.1	0.07 ²²	s.	∞
	sulfonic acid	C ₆ H ₅ SO ₃ H	142.18	pr./aq.		83-4	d. > 100	v. s. h.	v. s.	v. s.
	sulfonic acid	C ₆ H ₅ SO ₃ H	158.18	col. nd.		65-6	d.	v. s.	v. s.	i.
	sulfonic amide	C ₆ H ₅ SO ₂ NH ₂	157.19	mm./aq.		156		0.43 ¹⁶	v. s.	v. s.
	sulfonic chloride	C ₆ H ₅ SO ₂ Cl	176.62	cr.	1.384 ^{15/15}	14.5	251.5	i.	v. s.	s.
Benzidine (4-,4')		NH ₂ ·C ₆ H ₄ ·C ₆ H ₄ ·NH ₂	184.24	cr./aq.		128-9	400 ⁷⁰⁰	1 h.	1 h.	2
disulfonic acid (2-,2')		(·C ₆ H ₃ (NH ₂)SO ₂ H) ₂ ·3H ₂ O	398.41	pr./aq.		d. >175		0.09 ²⁵	i.	i.
	(3-,3')	(·C ₆ H ₃ (NH ₂)SO ₂ H) ₂	344.36					v. sl. s.		
Benzil	dibenzoyl	C ₆ H ₅ CO·COC ₆ H ₅	210.23	pr.	1.23 ¹⁵	95	348 d.	i.	v. s.	v. s.
Benzoic acid		C ₆ H ₅ CO ₂ H	122.12	mm. pr.	1.266 ^{15/4}	121.7	249.2	0.2 ¹⁷	46 ¹⁵	66 ¹⁵
anhydride		(C ₆ H ₅ CO) ₂ O	226.23	rhb./et.	1.199 ^{15/4}	42	360	i.	s.	s.
nitrile	phenyl cyanide	C ₆ H ₅ CN	103.12	col. lq.	1.001 ^{25/6}	-12.9	190.7	1 ¹⁰⁰	∞	∞

Benzoin (<i>dl</i> -)		$C_6H_5CO \cdot CHOHC_6H_5$	212.24	mn.		133-7	344 ⁷⁶⁸	v. sl. s.	s. h.	sl. s.
Benzophenone	diphenyl ketone	$C_6H_5COC_6H_5$	182.22	col. rhb.	1.083 ⁵⁴	48.5	305.4	i.	6.5 ¹⁵	15 ¹³
Benzotrichloride	phenyl chloroform	$C_6H_5CCl_3$	195.47	col. lq.	1.380 ⁴⁴	-4.75	197.7	i.	s.	s.
Benzoyl-benzoic acid (<i>o</i> -)		$C_6H_5COC_6H_4CO_2H \cdot H_2O$	244.24	tri./aq.		93(128)		sl. s.		
-chloride		C_6H_5COCl	140.57	col. lq.	1.212 ^{20/4}	-0.5	197.2	d.	d. h.	∞
-peroxide		$(C_6H_5CO)_2O_2$	242.23	rhb./et.		108 d.	expl.	i.	s. h.	s.
Benzyl acetate		$CH_3CO_2CH_2C_6H_5$	150.17	col. lq.	1.057 ¹⁷	-51.5	213.5	i.	∞	∞
alcohol	phenyl carbinol	$C_6H_5CH_2OH$	108.14	col. lq.	1.043 ^{20/4}	-15.3	204.7	417	∞	∞
amine	ω -amino toluene	$C_6H_5CH_2NH_2$	107.15	lq.	0.982 ^{20/4}		184.5	∞	∞	∞
aniline	phenyl-benzylamine	$C_6H_5CH_2NHC_6H_5$	183.25	mn. pr.	1.065 ^{25/25}	37-8	306 ⁷⁵⁰	i.	∞	s.
benzoate		$C_6H_5CO_2CH_2C_6H_5$	212.24	nd.	1.12 ^{20/4}	21	323-4	i.	∞	∞
butyrate		$C_2H_5CH_2CO_2CH_2C_6H_5$	178.23	col. lq.	1.016 ^{16/18}	238-40	i.	v. s.	v. s.	∞
chloride	ω -chlorotoluene	$C_6H_5CH_2Cl$	126.58	col. lq.	1.100 ^{20/20}	-39	179.4	i.	∞	∞
ether	dibenzyl ether	$(C_6H_5CH_2)_2O$	198.26	lq.	1.036 ¹⁵		295-8	i.	s. h.	s.
formate		$HCO_2CH_2C_6H_5$	136.15	col. lq.	1.081 ²³	3.6	202-3 ⁷⁴⁷	i.	s.	∞
propionate		$C_2H_5CO_2CH_2C_6H_5$	164.20	lq.	1.036 ^{16/17}		220-2	i.	∞	∞
Berberonic acid (2-,4-,5-)		$C_5H_5N(CO_2H)_3 \cdot 2H_2O$	247.16	tri.		243		v. sl. s.	sl. s. h.	i.
Biuret	allopnanamide	$NH(CONH_2)_2$	103.08	nd./al.		192-3 d.	1.3 ⁹	v. sl. s.	s.	∞
Borneol (<i>dl</i> -)		$C_{10}H_{17}OH$	154.25	col. cr.	1.011 ^{20/4}	210.5	subl.	v. sl. s.		
(<i>d</i> - or <i>l</i> -)		$C_{10}H_{17}OH$	154.25	col. cr.	1.011 ^{20/4}	208-9	212-3	v. sl. s.	v. s.	v. s.
(iso-)		$C_{10}H_{17}OH$	154.25	col. cr.		212		i.		∞
Bornyl acetate (<i>d</i> -)		$CH_3CO_2C_{10}H_{17}$	196.29	rhb./pet.	0.991 ¹⁵	29	226-7	i.	s.	s.
Bromo-aniline (<i>p</i> -)		$BrC_6H_4NH_2$	172.02	rhb.	1.8 ²⁰	63-4		i. c.	v. s.	v. s.
-benzene	phenyl bromide	C_6H_5Br	157.01	col. lq.	1.495 ^{20/4}	-30.6	156.2	i.	s.	∞
-camphor (3-)(<i>d</i> -)	α -bromocamphor	$BrC_{10}H_{15}O$	231.13	cr.	1.449 ^{20/4}	77-8	274	i.	20 ²⁶	v. s.
-diphenyl (<i>p</i> -)		$BrC_6H_4 \cdot C_6H_5$	233.10	cr./al.		90-1	310	i.	s.	34 ²⁵
-naphthalene (α -)	α -naphthyl bromide	$C_{10}H_7Br$	207.07	col. oil	1.482 ^{20/4}	5-6	281.1	i.	s.	∞
(β -)	β -naphthyl bromide	$C_{10}H_7Br$	207.07	lf./al.	1.605 ⁹	59	281-2	i.	6 ²⁰	v. s.
-phenol (<i>o</i> -)		BrC_6H_4OH	173.01	col. lq.	1.553 ²⁰	5.6	194-5	s.	∞	∞
(<i>m</i> -)		BrC_6H_4OH	173.01	cr.		32-3	236-7	s.	s.	s.
(<i>p</i> -)		BrC_6H_4OH	173.01	tet. cr.	1.588 ²⁰	63.5	238	1.4 ¹⁵	v. s.	v. s.
-styrene (ω)(1)		$C_6H_5CH=CHBr$	183.05	lq.	1.422 ^{20/4}	7	221	i.	∞	∞
(2)		$C_6H_5CH=CHBr$	183.05	lq.	1.427 ^{20/4}	-7.5	108 ²⁶	i.	∞	∞
-toluene (<i>o</i> -)	<i>o</i> -tolyl bromide	$CH_3 \cdot C_6H_4Br$	171.03	col. lq.	1.422 ^{20/4}	-28	181.8	i.	s.	∞ ²⁵
(<i>m</i> -)		$CH_3 \cdot C_6H_4Br$	171.03	col. lq.	1.410 ^{20/4}	-39.8	183.7	i.	s.	s.
(<i>p</i> -)		$CH_3 \cdot C_6H_4Br$	171.03	cr./al.	1.390 ^{20/4}	28.5	184-5	i.	s.	∞ ²⁵
Bromoform	tribromo-methane	$CHBr_3$	252.73	col. lq.	2.890 ^{20/4}	8-9	150.5	0.1 c.	∞	∞
Butadiene (1-,2-)	methyl-allene	$CH_3CH=C:CH_2$	54.09	lq.			18-9	i.	∞	∞
(1-,3-)	erythrene	$CH_2=CHCH=CH_2$	54.09	col. gas	0.621 ^{20/4}	-108.9	-4.41	i.	∞	∞
Butadienyl acetylene		$CH_2=(CH)_2CH:C:CH$	78.11	col. lq.	0.773 ^{20/4}		83-6	i.	∞	∞
Butane	diethyl	$CH_3CH_2CH_2CH_3$	58.12	col. gas	0.60 ⁰	-135	-0.6	i.	s.	s.
(<i>i</i> -)	trimethyl-methane	$(CH_3)_3CH$	58.12	col. gas	0.60 ⁰	-145	-10	i.	s.	s.
Butyl acetate (<i>n</i> -)		$CH_3CO_2(CH_2)_3C_2H_5$	116.16	col. lq.	0.882 ²⁰	-76.3	125 ⁷⁴⁰	0.7	∞	∞
(<i>s</i> -)		$CH_3CO_2CH(CH_3)C_2H_5$	116.16	col. lq.	0.865 ^{25/4}		112 ⁷⁴⁴	i.	∞	∞
(<i>i</i> -)		$CH_3CO_2CH_2CH(CH_3)_2$	116.16	col. lq.	0.871 ^{20/4}	-98.9	118	0.6 ²⁵	∞	∞
(<i>tert</i> -)		$CH_3CO_2C(CH_3)_3$	116.16	col. lq.	0.866 ^{20/4}		95-6 ⁷⁶⁰	i.	∞	∞
alcohol (<i>n</i> -)	butanol-1	C_4H_9OH	74.12	col. lq.	0.810 ^{20/4}	-79.9	117	915	∞	∞
(<i>s</i> -)	butanol-2	C_4H_9OH	74.12	col. lq.	0.808 ^{20/4}	-114.7	99.5	12.5 ²⁰	∞	∞
(<i>i</i> -)	2-methyl-propanol-1	$(CH_3)_2CHCH_2OH$	74.12	col. lq.	0.805 ^{17.5}	-108	107-8	10 ¹⁵	∞	∞
(<i>tert</i> -)	2-methyl-propanol-2	$(CH_3)_3COH$	74.12	lq.	0.779 ²⁶	25.5	82.9	∞	∞	∞
amine (<i>n</i> -)		$C_2H_5CH_2CH_2NH_2$	73.14	col. lq.	0.739 ^{25/4}	-50	77.8	∞	∞	∞
(<i>s</i> -)		$C_3H_7CH(NH_2)CH_3$	73.14	col. lq.	0.724 ^{20/4}	-104	66 ⁷⁷²	∞	∞	∞
(<i>i</i> -)		$(CH_3)_2CHCH_2NH_2$	73.14	col. lq.	0.732 ^{20/20}	-85	68-9	∞	∞	∞
(<i>t</i> -)		$(CH_3)_3CNH_2$	73.14	col. lq.	0.698 ^{18/4}	-67.5	45.2	∞	∞	∞
<i>p</i> -aminophenol (<i>N</i>)(<i>n</i>)		$C_6H_4NH_2 \cdot C_6H_4OH$	165.23			71		i.		
(<i>N</i>)(<i>i</i> -)		$C_6H_4NH_2 \cdot C_6H_4OH$	165.23			79		i.		
aniline (<i>n</i> -)		$C_6H_5NH_2$	149.23	lq.			235 ⁷²⁰	i.	v. s.	v. s.
(<i>i</i> -)		$C_6H_5NH_2$	149.23	oil	0.940 ^{20/4}		231-2	i.	0.01 ¹⁵	v. s.
arsonic acid (<i>n</i> -)		$C_6H_5AsO(OH)_2$	182.05	col. lf.		158-9		s.	s.	i.
benzoate (<i>n</i> -)		$C_6H_5CO_2C_6H_5$	178.23	col. oil	1.005 ^{25/25}	-22	249-50	i.	s.	s.
(<i>i</i> -)		$C_6H_5CO_2C_6H_5$	178.23	col. oil	0.997 ^{25/25}		241.5	i.	∞	∞
bromide (<i>n</i> -)	1-bromo-butane	C_4H_9Br	137.02	lq.	1.277 ^{20/4}	-112.4	101.6	0.06 ¹⁶	∞	∞
(<i>s</i> -)	2-bromo-butane	C_4H_9Br	137.02	lq.	1.251 ^{25/4}	-112	91.3	i.	∞	∞
(<i>i</i> -)	1-Br-2-Me-propane	$(CH_3)_2CHCH_2Br$	137.02	lq.	1.258 ^{25/4}	-118.5	91.5	0.06 ¹⁸	∞	∞
(<i>t</i> -)	2-Br-2-Me-propane	$(CH_3)_3CBr$	137.02	lq.	1.211 ^{20/4}	-16.2	73.3	i.	∞	∞
butyrate (<i>n</i> -)(<i>n</i> -)		$C_2H_5CH_2CO_2CH_2CH_2C_2H_5$	144.21	col. lq.	0.872 ^{20/20}		165.7 ⁷³⁶	i.	∞	∞
(<i>n</i> -)(<i>i</i> -)		$C_2H_5CH_2CO_2CH_2CH(CH_3)_2$	144.21	col. lq.	0.863 ^{18/4}		156.9	i.	∞	∞
(<i>i</i> -)(<i>i</i> -)		$(CH_3)_2CHCO_2CH_2CH(CH_3)_2$	144.21	col. lq.	0.875 ^{10/4}	-80.7	148-9	i.	∞	∞
caproate		$CH_3(CH_2)_4CO_2C_6H_5$	172.26	col. lq.	0.882 ²⁰		204.3	i.	∞	∞
carbamate (<i>i</i> -)		$NH_2CO_2CH_2CH(CH_3)_2$	117.15	col. lf.	0.956 ^{16/4}	65	206-7	i.	s.	s.
cellosolve (<i>n</i> -)	2-BuO-ethanol-1	$C_4H_9OCH_2CH_2OH$	118.17	col. lq.	0.903 ^{20/4}		171.2	∞	∞	∞

TABLE 2-2 Physical Properties of Organic Compounds (Continued)

Name	Synonym	Formula	Formula weight	Form and color	Specific gravity	Melting point, °C	Boiling point, °C	Solubility in 100 parts				
								Water	Alcohol	Ether		
chloride (<i>n</i> -)	1-chloro-butane	C ₄ H ₉ CH ₂ CH ₂ Cl	92.57	col. lq.	0.887 ²⁰	-123.1	77.9 ⁷⁶³	0.07 ¹⁸	∞	∞		
	(<i>s</i> -)	2-chloro-butane	C ₄ H ₉ :CHCl-CH ₃	92.57	col. lq.	0.871 ^{20/4}	67.8 ⁷⁶⁷	∞	∞	∞		
	(<i>i</i> -)	1-Cl ₂ -2-Me-propane	(CH ₃) ₂ CHCH ₂ Cl	92.57	col. lq.	0.884 ¹⁵	-131.2	68.9	∞	∞		
	(<i>t</i> -)	2-Cl ₂ -2-Me-propane	(CH ₃) ₂ CCl ₂	92.57	col. lq.	0.847 ¹⁵	-26.5	51-2	∞	∞		
dimethylbenzene (<i>t</i> -)(1-,3-,5-)	formate (<i>n</i> -)	(CH ₃) ₂ C:C ₆ H ₄ :(CH ₃) ₂	162.27	col. lq.			200-2 ¹⁴⁷	i.				
		HCO ₂ CH ₂ CH ₂ C ₆ H ₄	102.13	lq.	0.911 ⁹		106.9	v. sl. s.	∞	∞		
		HCO ₂ CH(CH ₃)C ₆ H ₅	102.13	lq.	0.882 ^{20/4}		97	sl. s.	∞	∞		
		HCO ₂ CH ₂ CH(CH ₃) ₂	102.13	lq.	0.885 ^{20/4}		98.2	1.1 ²²	∞	∞		
furoate (<i>n</i> -)	iodide (<i>n</i> -)	OC ₄ H ₇ CO ₂ C ₄ H ₉	168.19	col. lq.	1.056 ^{20/4}	-95.3	118-20 ²⁵	i.	∞	∞		
		C ₂ H ₅ CH ₂ CH ₂ I	184.02	lq.	1.617 ^{20/4}	-103.5	129.9	i.	∞	∞		
		C ₂ H ₅ CHICH ₃	184.02	lq.	1.595 ²⁰	-104	118-9	i.	∞	∞		
		(<i>s</i> -)	1-iodo-2-Me-propane	(CH ₃) ₂ CHCH ₂ I	184.02	lq.	1.606 ^{20/4}	-90.7	120	i.	∞	
(<i>i</i> -)	2-iodo-2-Me-propane	(CH ₃) ₂ CCl	184.02	lq.	1.370 ^{19/15}	-34	99	i.	∞			
lactate (<i>n</i> -)	mercaptan (<i>n</i> -)	CH ₃ CH(OH)CO ₂ C ₄ H ₉	146.18	col. lq.	0.968		75-6 ⁵	sl. s.				
		C ₂ H ₅ CH ₂ CH ₂ SH	90.19	col. lq.	0.837 ^{25/4}	-116	97-8	sl. s.	v. s.	v. s.		
		(<i>i</i> -)	2-Me-propanthiol-1	(CH ₃) ₂ CHCH ₂ SH	90.19	lq.	0.836 ^{20/4}	<-79	88	v. sl. s.	s.	
		(<i>t</i> -)		(CH ₃) ₂ CSH	90.19	lq.			65-7			
methacrylate (<i>n</i> -)	phenol (<i>p</i> -)(<i>t</i> -)	CH ₂ :C(CH ₃)CO ₂ C ₄ H ₉	142.20	lq.	0.889 ^{15,6}		155	i.				
		(<i>i</i> -)	CH ₂ :C(CH ₃)CO ₂ C ₄ H ₉	142.20	lq.	0.889 ^{15,6}		155	i.			
		(<i>s</i> -)	(CH ₃) ₂ C:C ₆ H ₄ :OH	150.22	nd./aq.	0.908 ^{112/4}	99	236-8	sl. s.	s.	s.	
		(<i>t</i> -)										
propionate (<i>n</i> -)	stearate (<i>n</i> -)	C ₂ H ₅ CO ₂ C ₄ H ₉	130.18	col. lq.	0.883 ¹⁵	-89.55	146	i.	∞	∞		
		(<i>s</i> -)	C ₂ H ₅ CO ₂ C ₄ H ₉	130.18	col. lq.	0.866 ^{20/4}		132.5	i.	∞		
		(<i>i</i> -)	C ₂ H ₅ CO ₂ C ₄ H ₉	130.18	col. lq.	0.888 ^{20/4}	-71.4	136.8	i.	∞		
		(<i>t</i> -)	CH ₃ (CH ₂) ₁₆ CO ₂ C ₄ H ₉	340.58	col. lq.	0.855 ^{25/25}	27.5	220-5 ²⁵	0.3 ²⁵	∞	s.	
iso-thiocyanate (<i>n</i> -)	iso-Bu mustard oil	CH ₃ (CH ₂) ₁₆ CO ₂ C ₄ H ₉	340.58	wax			25	i.				
		(<i>i</i> -)	C ₂ H ₅ CH ₂ CH ₂ :N:CS	115.20	lq.	0.956 ¹¹		165 ⁷²⁴	i.	s.	s.	
		(<i>s</i> -)(<i>d</i> -)	(CH ₃) ₂ CHCH ₂ :N:CS	115.20	lq.	0.964 ^{14/4}		162	i.	s.	s.	
		(<i>t</i> -)	C ₄ H ₉ :N:CS	115.20	lq.	0.943 ^{20/4}		159-63	i.	s.	s.	
valerate (<i>n</i> -)(<i>n</i> -)	valerate (<i>i</i> -)(<i>n</i> -)	(CH ₃) ₂ C:N:CS	115.20	lq.	0.919 ¹⁰	10.5	140 ⁷²⁰	i.	s.	s.		
		(<i>i</i> -)(<i>n</i> -)	CH ₃ (CH ₂) ₃ CO ₂ (CH ₂) ₃ CH ₃	158.24	lq.	0.870 ^{15/4}	-93	186	v. sl. s.	∞	∞	
		(<i>i</i> -)(<i>s</i> -)	(CH ₃) ₂ CHCH ₂ CO ₂ (CH ₂) ₃ CH ₃	158.24	lq.	0.862 ^{25/4}		168.8	i.	∞	∞	
		(<i>i</i> -)(<i>i</i> -)	(CH ₃) ₂ CHCH ₂ CO ₂ C ₄ H ₉	158.24	col. lq.	0.848 ^{20/4}		163-4 ⁷³²	i.	∞	∞	
Butylene (α-)	butene-2	C ₄ H ₈ CO ₂ C ₄ H ₉	158.24	col. lq.	0.874 ^{20/4}		168.7	i.	∞	∞		
		(β-)	C ₂ H ₅ CH:CH ₂	56.11	col. gas	0.6 ⁹	-130	-5 ⁷⁸⁵	i.	v. s.	v. s.	
			CH ₃ CH:CHCH ₃	56.11	col. gas			3 ⁷⁴⁶				
			CH ₂ CH ₂ CH ₂ CHO	72.11	col. lq.	0.817 ^{20/4}	-99	75.7	4	∞	∞	
Butyraldehyde (<i>n</i> -)	Butyric acid (<i>n</i> -)	(<i>i</i> -)	(CH ₃) ₂ CHCHO	72.11	col. lq.	0.794 ^{20/4}	-65.9	64 ⁷³⁷	11 ²⁰	∞	∞	
		(<i>i</i> -)	butanoic acid	C ₄ H ₈ CH ₂ CO ₂ H	88.11	col. lq.	0.964 ^{20/4}	-4.7	163.5 ⁷⁵⁷	∞	∞	
		(<i>i</i> -)	2-Me-propanoic acid	(CH ₃) ₂ CHCO ₂ H	88.11	col. lq.	0.949 ^{20/4}	-47	154.5	20 ³⁰	∞	∞
		(<i>i</i> -)	amide (<i>n</i> -)	<i>n</i> -butyramide	C ₄ H ₉ CONH ₂	87.12	rhb.	1.032	115-6	216	16.3 ¹⁵	s.
anhydride (<i>n</i> -)	anilide (<i>n</i> -)	iso-butyramide	(CH ₃) ₂ CHCONH ₂	87.12	mn. pl.	1.013	129-30	216-20	v. s.	∞	sl. s.	
			(C ₂ H ₅ CH ₂ CO) ₂ O	158.19	col. lq.	0.968 ^{20/20}	-75	199.5	d.	d.	∞	
			[(CH ₃) ₂ CHCO] ₂ O	158.19	col. lq.	0.950 ^{25/4}	-53.5	181.5 ⁷³⁴	d.	d.	∞	
			<i>n</i> -butyranilide	C ₈ H ₉ CONHC ₆ H ₅	163.22	mn. pr.	1.134	92	189 ¹⁵	i.	s.	s.
Caffeic acid (3-,4-)	Caffeine	(HO) ₂ C ₆ H ₃ C ₂ H ₅ CO ₂ H	180.16	yel./aq.		195-213	d.	s. h.	s.	sl. s.		
			C ₈ H ₁₀ O ₂ N ₄ :H ₂ O	212.21	nd./al.	1.23 ¹⁹	237	subl.	2	2	0.3	
			C ₁₀ H ₁₆	136.23	cr.	0.822 ⁷⁵	50	160	i.	s.	s.	
			C ₁₀ H ₁₆	136.23	cr.	0.845 ^{20/4}	42.7	159.6	i.	s.	s.	
Camphene (<i>dl</i> -)	Camphor (<i>d</i> -)	(<i>d</i> - or <i>l</i> -)	C ₁₀ H ₁₆ O	152.23	trig.	0.990 ^{9/9}	178-9	209.1 ⁷⁵⁹	0.1	120 ¹²	v. s.	
			C ₈ H ₁₄ (CO ₂ H) ₂	200.23	mn.	1.186	187		0.6 ¹²	s.		
			C ₁₀ H ₁₂ O ₄	196.20	cr.		212		0.003			
			decanoic acid	CH ₃ (CH ₂) ₈ CO ₂ H	172.26	col. nd.	0.889 ⁹⁷	31.5	268-70	0.003	s.	s.
Caproic acid (<i>n</i> -)	Caprylic acid (<i>n</i> -)	hexanoic acid	CH ₃ (CH ₂) ₆ CO ₂ H	116.16	col. lq.	0.922 ^{20/4}	-1.5	202 ⁷⁶¹	1.1 ²⁰	s.	s.	
		(<i>i</i> -)	2-Me-pentanoic-5 acid	(CH ₃) ₂ CH(CH ₂) ₂ CO ₂ H	116.16	col. oil	0.925 ^{20/4}	-35	207.7	v. sl. s.	s.	
			octanoic acid	CH ₃ (CH ₂) ₈ CO ₂ H	144.21	col. lf.	0.910 ^{20/4}	16	237.5	0.07 ¹⁵	s.	s.
			Carbazole	(C ₆ H ₄) ₂ NH	167.21	lf.		244.8	354.8	i.	0.92 ¹⁴	sl. s.
Carbitol	Carbon disulfide	diethylene glycol mono-Et ether	C ₂ H ₅ O(CH ₂) ₂ O(CH ₂) ₂ OH	134.17	col. lq.	0.990 ^{20/20}	201.9	201.9	∞	v. s.	s.	
		monoxide	CS ₂	76.14	col. lq.	1.263 ^{20/4}	-108.6	46.3	0.2 ⁹	∞	∞	
		suboxide	CO	28.01	col. gas	0.81-1 ^{95/4}	-207	-192	3.5 ⁹ cc.	s.		
		tetrabromide	OC:C:CO	68.03	gas	1.114 ⁹	-107	7 ⁷⁶¹	d.		s.	
tetrachloride	tetrafluoride	tetrabromomethane	CBr ₄	331.63	col. mn.	3.42	90.1(48)	189.5	0.02 ³⁰	s.	s.	
		tetrachloromethane	CCl ₄	153.82	col. lq.	1.595 ^{20/4}	-22.6	76.8	0.08 ³⁰	∞	∞	
		tetrafluoride	CF ₄	88.00	gas			-128	sl. s.			
		Carbonyl sulfide	COS	60.08	col. gas	1.24-5 ⁷	-138.2	-50.2 ⁷⁶⁰	80 ¹⁴ cc.	s.	s.	
Carminic acid	Carvacrol (1-,2-,4-)	C ₂₂ H ₂₀ O ₁₃	492.39	red pd.		d. 136		s.	s.	v. sl. s.		
		CH ₃ C ₆ H ₃ (OH)CH(CH ₃) ₂	150.22	col. lq.	0.977 ^{20/4}	0.5	238	v. sl. s.	∞	∞		

Carvacrylamine (2-,1-,4-)	$H_2NC_6H_4(CH_3)C_3H_7$	149.23	oil	0.994 ²⁰	-16	241	v. sl. s.	s.	s.
Carvone (<i>d</i> -)	$C_{10}H_{16}O$	150.22	col. lq.	0.961 ^{20/4}		230 ⁷⁶⁶	i.	∞	∞
Cellulosolve	$C_2H_5O(CH_2)_2OH$	90.12	col. lq.	0.931 ^{20/4}	-70	135.1	∞	∞	∞
acetate	$CH_3CO_2CH_2CH_2OC_2H_5$	132.16	col. lq.	0.975 ^{20/4}		156.3	22	∞	∞
Cellulose	$(C_6H_{10}O_5)_x$	162.14	amor.	1.3-1.4		i.	i.	i.	∞
Cetyl acetate	$CH_3CO_2(CH_2)_{15}CH_3$	284.48	nd.	0.858 ²⁰	22-3	200 ¹⁵	i.	v. sl. s. c.	
alcohol	$CH_3(CH_2)_{14}CH_2OH$	242.44	lf.	0.818 ^{20/4}	49-50	189.5 ¹⁵	i.	s.	s.
Chloral	$CCl_3 \cdot CHO$	147.39	col. lq.	1.505 ^{25/4}	-57	97.6 ⁷⁶⁸	v. s.	∞	∞
hydrate	$CCl_3 \cdot CH(OH)_2$	165.40	mn. pr.	1.619 ^{20/4}	51.7	d. 98	d. 98	474 ¹⁷	v. s.
Chloranil	$OC_2(CCl_2CCl)_2CO$	245.88	yel./bz.		290	subl.	i.	i. c.	i. c.
Chloreton	$Cl_3C \cdot C(OH)(CH_3)_2$	177.46	col. cr.		97	167	0.8 c.	111	111
Chloro-acetanilide (<i>p</i> -)	$CH_3CONHC_6H_4Cl$	169.61	rhb.	1.385 ²²	175-6		sl. s.	s.	v. s.
-acetic acid	$ClCH_2CO_2H$	94.50	col. cr.	1.58 ^{20/20}	61.2	189.5	61.2	s.	s.
-acetone	CH_3COCH_2Cl	92.52	col. lq.	1.162 ¹⁶	-44.5	121	∞	∞	∞
-acetophenone (<i>o</i> -)	$C_6H_5COCH_2Cl$	154.59	rhb.	1.324 ¹⁵	58-9	245-7	0.11	v. s.	v. s.
-acetyl chloride	$ClCH_2COCl$	112.94	col. lq.	1.498 ^{20/20}		105	d.	d.	∞
-aniline (<i>o</i> -)	$ClC_6H_4NH_2$	127.57	lq.	1.213 ^{20/4}	0	210.5	i.	i.	s.
(<i>m</i> -)	$ClC_6H_4NH_2$	127.57	lq.	1.216 ^{20/4}	-10.4	230 ⁷⁶⁷	i.	s.	s.
(<i>p</i> -)	$ClC_6H_4NH_2$	127.57	rhb.	1.427 ¹⁹	70-1	230-1	s. h.	s.	s.
-anthraquinone (1-)	$C_{14}H_8(O)_2$	242.66	yel. nd.		162	subl.	i.	sl. s. h.	
(2-)	$C_6H_4(CO)_2C_6H_4Cl$	242.66	nd./al.		208-9		i.		
-benzaldehyde (<i>o</i> -)	ClC_6H_4CHO	140.57	nd.	1.29 ⁸	11	208 ⁷⁴⁸	v. sl. s.	v. s.	v. s.
(<i>m</i> -)	ClC_6H_4CHO	140.57	pr.	1.250 ¹⁵	17-8	213-4	v. sl. s.	v. s.	v. s.
(<i>p</i> -)	ClC_6H_4CHO	140.57	pr.	1.196 ⁶¹	47.8	213 ⁷⁴⁸	s. h.	v. s.	v. s.
-benzene	C_6H_6	112.56	col. lq.	1.107 ^{20/4}	-45.2	132.1	0.049 ²⁰	∞	∞
-benzoic acid (<i>o</i> -)	$ClC_6H_4CO_2H$	156.57	mn./aq.	1.544 ^{25/4}	141-2		0.208 ²⁵	s.	s.
(<i>m</i> -)	$ClC_6H_4CO_2H$	156.57	pr.	1.496 ^{25/4}	158		0.041 ²⁵	s.	s.
(<i>p</i> -)	$ClC_6H_4CO_2H$	156.57	tri.	1.541 ²⁴	242-3		0.008 ²⁵	s.	s.
-buta-1,3-diene (2-)	$CH_2=CCl \cdot CH=CH_2$	88.54	col. lq.	0.958 ^{20/20}		59.4	v. sl. s.	∞	∞
(1-)	$CH_2=CH \cdot CH=CHCl$	88.54	col. lq.	0.965 ^{20/20}		69	v. sl. s.	∞	∞
-buta-1,2-diene (4-)	$CH_2=C \cdot CH=CH_2Cl$	88.54	col. lq.	0.991 ^{20/20}		88	d.	d.	∞
-dimethylhydantoin	$—C(CH_3)_2N(Cl)CON(Cl)CO—$	197.02		1.5 ^{20/20}	130		0.21 ²⁵		
-dinitrobenzene (α)(1-,2-)(4-)	$ClC_6H_3(NO_2)_2$	202.55	cr./et.		39(36)	315 d.	i.	v. s. h.	v. s.
(α)(1-,3-)(4-)	$ClC_6H_3(NO_2)_2$	202.55	rhb./et.	1.697 ²²	53(43)	315 d.	i.	s. h.	s.
-diphenyl (<i>o</i> -)	$C_6H_5 \cdot C_6H_4Cl$	188.65	cr.		34	267-8	i.		
(<i>m</i> -)	$C_6H_5 \cdot C_6H_4Cl$	188.65	cr.		89	284-5	i.		
(<i>p</i> -)	$C_6H_5 \cdot C_6H_4Cl$	188.65	lf.		77.5	282	i.		
-hydroquinone	$ClC_6H_4(OH)_2$	144.56	mn.		106	263 sl. d.	v. s.	v. s.	v. s.
-naphthalene (α -)	$C_{10}H_8$	162.62	col. lq.	1.194 ^{20/4}	-20	259.3	i.	s.	∞
(β -)	$C_{10}H_8$	162.62	lf./al.	1.266 ¹⁶	56-7	264 ⁷⁵¹	i.	v. s.	v. s.
-nitrobenzene (<i>o</i> -)	$ClC_6H_4NO_2$	157.55	mn. nd.	1.305 ^{20/4}	32.5	245.5 ⁷⁵³	i.	s. h.	s.
(<i>m</i> -)	$ClC_6H_4NO_2$	157.55	yel./al.	1.343 ^{20/4}	44.4(24)	235.6	i.	v. s. h.	v. s.
(<i>p</i> -)	$ClC_6H_4NO_2$	157.55	mn. pr.	1.298 ⁹¹	83-4	242 ⁷⁶¹	i.	v. s. h.	v. s.
-nitrotoluene (2-,4-)	$CH_3C_6H_4(NO_2)(Cl)$	171.58	cr.	1.256 ⁹⁰	38.2	240 ⁷¹⁸	i.		
(2-,6-)	$CH_3C_6H_3(NO_2)(Cl)$	171.58	cr.		37.5	238	i.		
-phenol (<i>o</i> -)	ClC_6H_4OH	128.56	col. lq.	1.241 ^{18/15}	7(0)	175-6	2.85 ²⁰	s.	s.
(<i>m</i> -)	ClC_6H_4OH	128.56	nd.	1.268 ²⁵	32-3	214	2.60 ²⁰	s.	s.
(<i>p</i> -)	ClC_6H_4OH	128.56	nd.	1.306 ^{20/4}	41-3	217	2.71 ²⁰	v. s.	v. s.
-propionic acid (α)(dl-)	$CH_3 \cdot CHCl \cdot CO_2H$	108.52	col. lq.	1.306 ⁹	<-20	186	∞	∞	∞
-toluene (<i>o</i> -)	$CH_3 \cdot C_6H_4Cl$	126.58	col. lq.	1.082 ^{20/4}	-34	159.5	i.	s.	∞
(<i>m</i> -)	$CH_3 \cdot C_6H_4Cl$	126.58	col. lq.	1.072 ^{20/4}	-47.8	161.6	i.	s.	∞
(<i>p</i> -)	$CH_3 \cdot C_6H_4Cl$	126.58	col. lq.	1.070 ^{20/4}	7.5	162.2	i.	s.	∞
Chloroform	$CHCl_3$	119.38	col. lq.	1.489 ²⁰	-63.5	61.2	0.82 ²⁰	∞	∞
Chlorophyll (α -)	$C_{57}H_{72}O_5N_4Mg$	893.49			d.	i.	s.		
Chloropicrin	Cl_3CNO_2	164.38	lq.	1.651 ^{23/4}	-64	112.3 ⁷⁶⁶	0.17 ¹⁸	s.	s.
Cholesterol	$C_{27}H_{48}OH \cdot H_2O$	404.67	rhb./al.	1.067	149-51	subl.	0.26 ²⁰	1.1 ¹⁷	18
Chrysen	$C_{18}H_{12}$	228.29	col. rhb.		253-4	448	i.	0.1 ¹⁶	v. sl. s.
Chrysoidine (2-,4-)	$C_6H_5 \cdot N \cdot C_6H_3(NH_2)_2$	212.25	yel. cr.		117.5		sl. s. h.	s.	s.
Chrysophanic acid	$C_{14}H_8(OH)_2(CH_3)_2O_2$	254.24	yel./al.		195	subl.	i. c.	s. h.	sl. s.
Cinchomeric acid (3-,4-)	$C_5H_3N(CO_2H)_2$	167.12	cr./HCl		258-9 d.	subl. d.	v. sl. s.	sl. s.	i.
Cineole, eucalyptole	$C_{10}H_{18}O$	154.25	col. oil	0.927 ²⁰	1.5	176-7	1.9 ¹⁵	∞	∞
Cinnamic acid (<i>cis</i> -)	$C_6H_5CH=CHCO_2H$	148.16	mn. pr.	1.284 ⁴	68	125 ¹⁹			
(<i>trans</i> -)	$C_6H_5CH=CHCO_2H$	148.16	mn. pr.	1.245	133	300	0.04 ¹⁸	24 ²⁰	v. s.
aldehyde	$C_6H_5CH=CHCHO$	132.16	lq.	1.110 ^{20/20}	-7.5	252 sl. d.	v. sl. s.	s.	∞
Cinnamyl alcohol	$C_6H_5CH_2CH=CH_2OH$	134.18	nd.	1.040 ^{25/35}	33	257.5	sl. s.	v. s.	v. s.
cinnamate	$C_6H_5 \cdot CO_2C_6H_5$	264.32	nd. or pr.	1.085 ^{16,5}	44		i.	4 c.	33
Citraconic acid (<i>cis</i> -)	$CH_3C(CO_2H) \cdot CHCO_2H$	130.10	nd.	1.617	92-3		360 ²⁵	s.	s.
Citral (α)	$C_9H_{16}CHO$	152.23	col. oil	0.890 ^{17/4}		229	i.	∞	s.
Citric acid	$C_3H_4(OH)(CO_2H)_3$	192.12	cr.	1.542 ^{20/4}	153	d.	207.7 ²⁵	76 ¹⁵	2 ¹⁵
Citronellal (<i>d</i> -)	$C_9H_{17} \cdot CHO$	154.25	col. oil	0.855 ^{17,5}		204-8	v. sl. s.	∞	∞
Citronellol (<i>d</i> -)	$C_{10}H_{20}O$	156.27	col. oil	0.848 ^{20/4}		224-5	v. sl. s.	∞	∞
Comiine (<i>d</i> -)(2-)	$C_3H_7 \cdot C_9H_{10}N$	127.23	col. lq.	0.847 ¹⁷	-2	166-7	1.1	v. s.	v. s.

TABLE 2-2 Physical Properties of Organic Compounds (Continued)

Name	Formula	Formula weight	Form and color	Specific gravity	Melting point, °C	Boiling point, °C	Solubility in 100 parts		
							Water	Alcohol	Ether
Coumaric acid (<i>o</i> -)	$\text{HOOC}_6\text{H}_4\text{CH}_2\text{CHCO}_2\text{H}$	164.16	nd./aq.		207-8	subl.	sl. s. c.	s.	v. sl. s.
	$\text{HOC}_6\text{H}_4\text{CH}_2\text{CHCO}_2\text{H}$	164.16	cr./aq.		206-7 d.		s. h.	v. s. h.	v. s.
Coumarin	$\text{C}_9\text{H}_6\text{O}_2$	146.14	rhb./et.	0.935 ^{20/4}	70	290-1	0.3 c.	v. s.	s.
Coumarone	$\text{C}_9\text{H}_8\text{O}$	118.13	oil	1.078 ^{15/15}	<-18	173-4	i.		s.
Creatine	$\text{C}_4\text{H}_7\text{N}_3\text{O}_2 \cdot \text{H}_2\text{O}$	149.15	mn./aq.		295		1.4 ¹⁸	0.01 ¹⁷	i.
Creatinine	$\text{C}_4\text{H}_7\text{N}_3\text{O}$	113.12	mn.		260 d.		8.7 ¹⁶	1 ¹⁶	
Creosol (3-,1-,4-)	$\text{CH}_3\text{O} \cdot \text{C}_6\text{H}_3(\text{CH}_3)\text{OH}$	138.16	pr.	1.092 ^{20/20}	5.5	221-2 ⁷⁶⁵	v. sl. s.	∞	∞
Cresidine (1-,2-,4-)	$\text{CH}_3(\text{NH}_2)\text{C}_6\text{H}_3\text{OCH}_3$	137.18	nd./pet.		93-4	235	v. sl. s.	s.	s.
Cresol (<i>o</i> -)	$\text{CH}_3\text{C}_6\text{H}_4\text{OH}$	108.14	cr.	1.048 ^{20/4}	30.8	190.8	2.5	∞ ³⁰	∞ ³⁰
	$\text{CH}_3\text{C}_6\text{H}_4\text{OH}$	108.14	lq.	1.034 ^{20/4}	10.9	202.8	0.5	∞	∞
	$\text{CH}_3\text{C}_6\text{H}_4\text{OH}$	108.14	pr.	1.035 ^{20/4}	35-6	202	1.8	∞ ³⁶	∞ ³⁶
Cresyl benzoate (<i>o</i> -)	$\text{C}_6\text{H}_5\text{CO}_2\text{C}_6\text{H}_4\text{CH}_3$	212.24	lq.			308	i.		
	$\text{C}_6\text{H}_5\text{CO}_2\text{C}_6\text{H}_4\text{CH}_3$	212.24	cr.		55	314	i.		
	$\text{C}_6\text{H}_5\text{CO}_2\text{C}_6\text{H}_4\text{CH}_3$	212.24	cr.		71.5	316	i.		
Crotonic acid (α -)	$\text{CH}_3\text{CH}_2\text{CHCO}_2\text{H}$	86.09	col. mn.	0.964 ^{29,7}	72	189	8.3 ¹⁵		
acid (β -)(<i>cis</i> -)	$\text{CH}_3\text{CH}_2\text{CHCO}_2\text{H}$	86.09	nd.	1.031 ^{15/4}	15.5	170-1 d.	∞ ²⁵	s.	
aldehyde (α)	$\text{CH}_3\text{CH}_2\text{CHCHO}$	70.09	col. lq.	0.853 ^{20/20}	-69	102.2	18	∞	∞
Cumene	$\text{C}_6\text{H}_5\text{CH}(\text{CH}_3)_2$	120.19	col. lq.	0.862 ^{20/4}	-96.9	152.5	i.	∞	∞
Cumic acid (<i>p</i> -)	$(\text{CH}_3)_2\text{CH} \cdot \text{C}_6\text{H}_4\text{CO}_2\text{H}$	164.20	tri.	1.162 ⁴	116-7	subl.	0.02 ²⁵	s.	s.
Cumidine (<i>p</i> -)	$(\text{CH}_3)_2\text{CH} \cdot \text{C}_6\text{H}_4\text{NH}_2$	135.21	lq.	0.953	<-20	225 ^{70/1}	i.		
Cyanamide	$\text{H}_2\text{N} \cdot \text{CN}$	42.04	col. nd.	1.073 ^{28/4}	44-5	140 ¹⁹	v. s.	v. s.	v. s.
Cyanoic acid	HOCN or HNCO	43.02	gas	1.140 ⁹	-80	-64 ⁰	sl. s.		
Cyanoacetic acid	$\text{CH}_2(\text{CN})\text{CO}_2\text{H}$	85.06	col. lq.		65-6	108 ^{0,2}	s.	s.	
Cyanogen	$(\text{CN})_2$	52.03	col. gas	0.866 ¹⁷	-34.4	-21	450 ²⁰ cc.	2300 ²⁰ cc.	500 ²⁰ cc.
bromide	BrCN	105.92	nd.	2.015 ^{20/4}	52	61.3 ⁷⁵⁰	s.	s.	s.
chloride	ClCN	61.47	gas	1.222 ⁹	-6.5	12.5-13	v. s.	v. s.	5000 ²⁰ cc.
Cyanuric acid	$\text{C}_3\text{H}_3\text{O}_3\text{N}_3 \cdot 2\text{H}_2\text{O}$	165.10	mn./aq.	1.768 ^{9/4}	>360	d.	0.27 ¹⁷	0.1 ²²	
Cyclo-butane	$\text{CH}_2 < (\text{CH}_2)_2 > \text{CH}_2$	56.11	col. gas	0.703 ^{9/4}	-50	11-12 ⁷³⁶	i.	v. s.	
-heptane	$\text{CH}_2 < (\text{CH}_2\text{CH}_2\text{CH}_2)_2 >$	98.19	oil	0.810 ^{20/4}	-12	118-20	i.		
-hexane	$\text{CH}_2 < (\text{CH}_2\text{CH}_2)_2 > \text{CH}_2$	84.16	col. lq.	0.779 ^{20/4}	6.5	80-1	i.	∞	∞
-hexanol	$\text{CH}_2 < (\text{CH}_2\text{CH}_2)_2 > \text{CHOH}$	100.16	col. nd.	0.962 ^{20/4}	23.9	160-1	3.6 ²⁰	∞	s.
-hexanone	$\text{CH}_2 < (\text{CH}_2\text{CH}_2)_2 > \text{CO}$	98.14	col. oil	0.947 ^{19/4}	-45	155-6	s.	v. s.	v. s.
-hexene	$(\cdot\text{CH}_2 \cdot \text{CH}_2\text{CH}_2 \cdot)_2$	82.14	lq.	0.810 ^{20/4}	-103.7	83.3	v. sl. s.	v. s.	v. s.
-hexyl acetate	$\text{CH}_3\text{CO}_2\text{C}_6\text{H}_{11}$	142.20	oil	0.985 ^{9/4}		174 ⁷⁵⁰	i.	∞	∞
amine	$\text{CH}_2 < (\text{CH}_2\text{CH}_2)_2 > \text{CHNH}_2$	99.17	col. lq.	0.865 ^{20/20}		134	i.	∞	∞
bromide	$\text{CH}_2 < (\text{CH}_2\text{CH}_2)_2 > \text{CHBr}$	163.06	col. lq.	1.324 ^{20/20}		165 ⁷¹⁴	i.	s.	s.
chloride	$\text{CH}_2 < (\text{CH}_2\text{CH}_2)_2 > \text{CHCl}$	118.60	col. lq.	0.977 ^{18/4}	-43.9	142	i.	∞	∞
-pentadiene (1-,3-)	$\text{CH}_2 < (\text{CH} \cdot \text{CH})_2 >$	66.10	col. lq.	0.805 ^{19/4}	-85	41-2	i.	∞	∞
-pentane	$\text{CH}_2 < (\text{CH}_2\text{CH}_2)_2 >$	70.13	col. oil	0.745 ^{20/4}	-93.3	49-50	i.		
-pentanone	$< (\text{CH}_2\text{CH}_2)_2 > \text{CO}$	84.12	col. oil	0.948 ²⁰	-58.2	129-30	v. sl. s.		
-propane	$< \text{CH}_2\text{CH}_2\text{CH}_2 >$	42.08	col. gas	0.720 ^{20/70}	-126.6	-34 ⁷³⁰	i.	s.	s.
Cymene (<i>o</i> -)	$\text{CH}_3 \cdot \text{C}_6\text{H}_4\text{CH}(\text{CH}_3)_2$	134.22	col. lq.	0.875 ^{20/4}		177	i.	s.	s.
	$\text{CH}_3 \cdot \text{C}_6\text{H}_4\text{CH}(\text{CH}_3)_2$	134.22	col. lq.	0.862 ^{20/4}	<-25	175-6	i.	s.	s.
	$\text{CH}_3 \cdot \text{C}_6\text{H}_4\text{CH}(\text{CH}_3)_2$	134.22	col. lq.	0.857 ^{20/4}	-73.5	176-7	i.	s.	s.
Cystine (<i>L</i> -)	$[\cdot\text{SCH}_2\text{CH}(\text{NH}_2)\text{CO}_2\text{H}]_2$	240.30	pl.		d. 258-61		0.01 ¹⁹	i.	
Dambose	$\text{C}_6\text{H}_6(\text{OH})_6$	180.16	mn./aq.	1.752	253	319 ¹⁵	2 ¹²	i.	i.
Decahydronaphthalene (<i>cis</i> -)	$\text{C}_{10}\text{H}_{18}$	138.25	lq.	0.895 ^{18/4}	-51	193.3	i.	s.	s.
	$\text{C}_{10}\text{H}_{18}$	138.25	lq.	0.872 ^{20/4}	-32	185.3	i.	s.	s.
Decane (<i>n</i> -)	$\text{CH}_3(\text{CH}_2)_8\text{CH}_3$	142.28	col. lq.	0.730 ²	-29.7	174.0	i.	∞	∞
Decyl alcohol	$\text{CH}_3(\text{CH}_2)_9\text{CH}_2\text{OH}$	158.28	col. oil	0.830 ^{20/4}	7	232.9	i.	s.	
Dextrin	$(\text{C}_6\text{H}_{10}\text{O}_5)_x$	162.14	amor.	1.038			s.	i.	i.
Diacetone alcohol	$(\text{CH}_3)_2\text{C}(\text{OH}) \cdot \text{CH}_2\text{COCH}_3$	116.16	lq.	0.931 ²⁵	-47	167.9	∞	∞	∞
Diamino-benzophenone (4-,4'-)	$\text{H}_2\text{NC}_6\text{H}_4\text{COC}_6\text{H}_4\text{NH}_2$	212.25	yel. nd.		237-9		sl. s. h.	∞	s.
-diphenylamine (4-,4'-)	$\text{H}_2\text{NC}_6\text{H}_4\text{NHC}_6\text{H}_4\text{NH}_2$	199.25	lf./aq.		158	d.	sl. s.	s.	s.
-diphenylmethane (4-,4'-)	$\text{H}_2\text{NC}_6\text{H}_4\text{CH}_2\text{C}_6\text{H}_4\text{NH}_2$	198.26	nd./aq.		93-4	249-53 ¹⁵	sl. s. c.	s.	s.
-diphenylurea (4-,4'-)	$(\text{H}_2\text{NC}_6\text{H}_4\text{NH})_2\text{CO}$	242.28	cr.			subl. 310	v. sl. s.		
Diamyl-amine (<i>i</i> -)	$[(\text{CH}_3)_2\text{CHCH}_2\text{CH}_2]_2\text{NH}$	157.30	col. lq.	0.767 ^{21/4}	-44	188-90	sl. s.	s.	∞
ether (<i>n</i> -)	$(\text{C}_6\text{H}_5\text{CH}_2\text{CH}_2\text{CH}_2)_2\text{O}$	158.28	col. lq.	0.774 ^{20/4}	-69	190	i.	∞	∞
(<i>i</i> -)	$[(\text{CH}_3)_2\text{CH}(\text{CH}_2)_2]_2\text{O}$	158.28	col. lq.	0.777 ^{20/4}		173.4	i.	∞	∞
Diamyl ketone (<i>i</i> -)	$[(\text{CH}_3)_2\text{CHCH}_2\text{CH}_2]_2\text{CO}$	170.29	yel. oil	0.821 ^{25/4}	14.6	228	i.	s.	s.
phthalate (<i>n</i> -)	$\text{C}_6\text{H}_4(\text{CO}_2\text{C}_5\text{H}_{11})_2$	306.40	col. lq.			204-6 ¹¹	i.	s.	s.
(<i>i</i> -)	$\text{C}_6\text{H}_4(\text{CO}_2\text{C}_5\text{H}_{11})_2$	306.40	col. lq.	1.03		225 ⁴⁰	i.	s.	s.
tartrate (<i>i</i> -)	$(\text{HOCH} \cdot \text{CO}_2\text{C}_5\text{H}_{11})_2$	290.35	lq.	1.063 ^{15/4}		195 ¹⁶	i.		
Dianisidine (<i>o</i> -)(4-,3-)	$[\text{NH}_2(\text{OCH}_3)\text{C}_6\text{H}_3]_2$	244.29	col. lf.		131.5		i.	s.	s.
Diazo-aminobenzene	$\text{C}_6\text{H}_5\text{N} \cdot \text{N} \cdot \text{NHC}_6\text{H}_5$	197.24	yel. lf.		96-8	expl.	i.	s. h.	v. s.
-aminotoluene (2-,2'-)	$\text{C}_7\text{H}_7\text{N} \cdot \text{N} \cdot \text{NHC}_7\text{H}_7$	225.29	or. cr.		51		0.05		
-methane	$\text{CH}_2 \cdot \text{N}_2$	42.04	gas		-145	-23	d.		s.

Dibenzothiazyl-disulfide (2-,2'-)	(C ₆ H ₄ N ₂ SC ₂) ₂ S ₂	332.49	cr.	1.50	180	d.	i.			
Dibenzoyl methane	(C ₆ H ₅ CO) ₂ CH ₂	224.25	rhb./al.		78	219–21 ¹⁸	i.			
Dibenzyl-amine	(C ₆ H ₅ CH ₂) ₂ NH ₂	197.28	col. oil	1.028 ^{25/25}	-26	268–71 ²⁵⁰	i.		4.4 ²⁰	s.
-aniline	C ₆ H ₅ N(CH ₂ C ₆ H ₅) ₂	273.37	pr./al.		70–1	>300	i.		s.	s.
ketone	(C ₆ H ₅ CH ₂) ₂ CO	210.27	cr.		34–5	330.6	i.		v. s. h.	s.
phthalate (o-)	C ₆ H ₄ (CO ₂ CH ₂ C ₆ H ₅) ₂	346.38	pr./al.		42–3	274 ¹²	v. sl. s.		s.	s.
succinate	(-CH ₂ CO ₂ CH ₂ C ₆ H ₅) ₂	298.33	lf./al.		45–6	238 ¹⁴	i.		s.	s.
Dibromo-benzene (o-)	C ₆ H ₃ Br ₂	235.90	col. lq.	1.956 ^{20/4}	1.8	221–2	i.		s.	s.
(m-)	C ₆ H ₃ Br ₂	235.90	col. lq.	1.952 ^{20/4}	-6.9	219 ⁷⁵⁵	i.		s.	s.
(p-)	C ₆ H ₃ Br ₂	235.90	pl./al.	2.261 ¹⁵	87–8	218.6 ⁷⁵⁵	i.		1.6	71 ²⁵
-diphenyl (4-,4'-)	BrC ₆ H ₄ ·C ₆ H ₄ ·Br	312.00	mn. pr.	1.897	164–5	355–60	i.		v. sl. s. h.	
Dibutyl-adipate (n-)	(-CH ₂ CH ₂ CO ₂ C ₆ H ₁₃) ₂	258.35	col. lq.	0.965 ^{20/4}	-38	183 ¹⁴	i.		∞	∞
(i-)	(-CH ₂ CH ₂ CO ₂ C ₆ H ₉) ₂	258.35	col. lq.	0.950 ²⁵	-20	278–50	i.		∞	∞
-amine (n-)	(C ₂ H ₅ CH ₂ CH ₂) ₂ NH ₂	129.24	col. lq.	0.768 ^{20/20}		159 ⁷⁶¹	∞		∞	∞
(i-)	[(CH ₃) ₂ CHCH ₂] ₂ NH ₂	129.24	col. lq.	0.741 ^{25/4}	-70	139–40	v. sl. s.		s.	s.
-p-aminophenol (s-)	(C ₆ H ₄) ₂ N·C ₆ H ₄ ·OH	221.34	lq.			170 ¹⁰	i.		∞	∞
-aniline (n-)	C ₆ H ₅ N(C ₆ H ₅) ₂	205.34	lq.			262.8	i.		∞	∞
carbonate (n-)	CO(OC ₂ H ₅) ₂	174.24	col. lq.	0.924 ^{20/4}		207 ⁷⁴⁰	i.		s.	
(i-)	CO(OC ₄ H ₉) ₂	174.24	col. lq.	0.919 ¹⁵		190	i.			
(s-)	CO(OC ₆ H ₁₃) ₂	174.24	col. lq.			178–80				
ether (n-)	(C ₂ H ₅ CH ₂ CH ₂) ₂ O	130.23	lq.	0.769 ^{20/20}	-98	142.4	<0.05		∞	∞
(i-)	[(CH ₃) ₂ CHCH ₂] ₂ O	130.23	lq.	0.762 ¹⁵		122.5	i.		∞	∞
(s-)	[C ₂ H ₅ (CH ₂) ₂ CH] ₂ O	130.23	lq.	0.756 ²¹		121	i.		∞	∞
ketone (n-)	(C ₂ H ₅ CH ₂ CH ₂) ₂ CO	142.24	lq.	0.827 ^{15/4}	-5.9	187.7	i.		s.	v. s.
(i-)	[(CH ₃) ₂ CHCH ₂] ₂ CO	142.24	oil	0.805 ^{21/4}		168.1	<0.06		∞	∞
malate (l-)(n-)	C ₂ H ₄ O(CO ₂ C ₆ H ₉) ₂	246.30	lq.	1.038 ^{20/4}		170–1 ¹⁸	v. sl. s.		∞	∞
oxalate (n-)	(-CO ₂ C ₆ H ₉) ₂	202.25	col. lq.	0.986 ^{20/4}	-29.6	245.5	i.		s.	s.
phthalate (n-)	C ₆ H ₄ (CO ₂ C ₆ H ₉) ₂	278.34	col. lq.	1.045 ²¹		340	0.04 ²⁵		∞	∞
tartrate (d-)(n-)	(CHOHCOC ₂ H ₄) ₂	262.30	pr.	1.098 ¹⁵	22–2.5	200–3 ¹⁸	i.			
(d-)(i-)	(CHOHCOC ₄ H ₉) ₂	262.30	cr.	1.031 ^{75/4}	73–4	323–5	v. sl. s.			
Dichloro-acetic acid	Cl ₂ CH·CO ₂ H	128.94	lq.	1.560 ^{25/25}	9.7(–4)	194.4	∞		∞	∞
-acetone (αα-)	Cl ₂ CHCO ₂ CH ₃	126.97	lq.	1.234 ¹⁵		120	v. sl. s.		s.	s.
-aniline (2-,5-)	Cl ₂ C ₆ H ₃ NH ₂	162.02	nd.			251	v. sl. s.		s.	s.
-anthraquinone (1-,3-)	C ₁₀ H ₆ (CO) ₂ ·C ₆ H ₄ Cl ₂	277.10	yel. nd.			50	i.			
(1-,4-)	C ₆ H ₄ (CO) ₂ ·C ₆ H ₄ Cl ₂	277.10	yel. nd.			208–9	i.			
(1-,5-)	C ₆ H ₃ Cl(CO) ₂ ·C ₆ H ₄ Cl ₂	277.10	yel. nd.			187.5	i.		v. sl. s.	v. sl. s.
(1-,6-)	C ₆ H ₃ Cl ₂ (CO) ₂ ·C ₆ H ₄ Cl	277.10	yel. nd.			251	i.		sl. s.	
(1-,8-)	C ₆ H ₃ Cl ₂ (CO) ₂ ·C ₆ H ₃ Cl	277.10	yel. nd.			203–4	i.			
(2-,3-)	C ₆ H ₄ (CO) ₂ ·C ₆ H ₂ Cl ₂	277.10	yel. nd.			202–3	i.		sl. s.	
(2-,6-)	C ₆ H ₃ Cl(CO) ₂ ·C ₆ H ₂ Cl ₂	277.10	yel. nd.			268–70	i.		sl. s.	
(2-,7-)	C ₆ H ₃ Cl ₂ (CO) ₂ ·C ₆ H ₃ Cl	277.10	yel. nd.			282	i.			
-benzene (o-)	C ₆ H ₄ Cl ₂	147.00	col. lq.	1.305 ^{20/4}		210–11	i.			
(m-)	C ₆ H ₄ Cl ₂	147.00	col. lq.	1.288 ^{20/4}	-24.8	179	i.		∞	∞
(p-)	C ₆ H ₄ Cl ₂	147.00	col. mn.	1.458 ²¹		172 ⁷⁶⁶	i.		s.	s.
-butane (n-)(1-,4-)	ClCH ₂ (CH ₂) ₂ CH ₂ Cl	127.01	lq.			174 ⁷⁶⁴	i.		v. s.	v. s.
-diphenyl (4-,4'-)	ClC ₆ H ₄ ·C ₆ H ₄ ·Cl	223.10	pr.	1.442 ^{0/4}		161–3	i.			
-ethane (1-,2-)	ClCH ₂ ·CH ₂ Cl	98.96	col. lq.	1.256 ^{20/20}	-35.3	315–9	i.		v. sl. s.	4 ²⁵
-naphthalene (β-)(1-,4-)	C ₁₀ H ₆ Cl ₂	197.06	nd./al.	1.300 ^{76/4}	67–8	83.7	0.9 ⁹		∞	∞
(γ-)(1-,5-)	C ₁₀ H ₆ Cl ₂	197.06	lf./al.			286–7 ⁷⁴⁰	i.		v. sl. s.	
-nitrobenzene (2-,5-)	Cl ₂ C ₆ H ₃ NO ₂	192.00	tri./al.	1.669 ²²	54.6	107	i.		s.	s.
-pentane (1-,5-)	ClCH ₂ (CH ₂) ₃ CH ₂ Cl	141.04	col. lq.	1.094 ^{25/4}		266	i.		v. s. h.	
-phenol (2-,4-)	Cl ₂ C ₆ H ₃ OH	163.00	nd.	1.383 ^{90/25}		180–1	i.		s.	s.
Dichloramine T (p-)	CH ₂ Cl ₂ NHCl	240.11	cr.			209–10	0.45 ²⁰		v. s.	v. s.
Dicyandiamide	H ₂ N·C(=NH)·NH·C(=NH) ₂	84.08	mn. pl.	1.40 ¹⁴	207–8	83	sl. s.			
Diethanolamine	HN(CH ₂ CH ₂ OH) ₂	105.14	pr.	1.097 ^{20/4}		d.	2.3 ¹⁵		1.3 ¹⁵	0.01 ¹⁵
Diethyl adipate	(-CH ₂ CH ₂ CO ₂ C ₂ H ₅) ₂	202.25	col. lq.	1.009 ^{20/4}	-21	270 ⁷⁴⁸	∞			v. sl. s.
-amine	(C ₂ H ₅) ₂ NH	73.14	col. lq.	0.712 ^{15/15}	-38.9	239–41 ⁷⁶¹	0.43 ⁸⁰		s.	s.
-aminophenol (m-)	(C ₂ H ₅) ₂ N·C ₆ H ₄ ·OH	165.23	rhb.			55.5 ⁷⁵⁹	v. s.		∞	∞
-aniline	(C ₂ H ₅) ₂ N·C ₆ H ₅	149.23	oil	0.934 ^{20/4}	-34.4	276–80	i.		1.4 ¹²	s.
sulfonic acid (m-)	(C ₂ H ₅) ₂ N·C ₆ H ₄ ·SO ₃ H	229.30	cr.			216	s.			
carbonate	OC(OC ₂ H ₅) ₂	118.13	col. lq.	0.975 ^{20/4}	-43	126 ⁷⁵⁹	i.		∞	∞
diethyl malonate	(C ₂ H ₅) ₂ C(CO ₂ C ₂ H ₅) ₂	216.27	col. lq.	0.985 ^{20/4}		230	i.		∞	∞
Diethyl dimethyl malonate	(CH ₃) ₂ C(CO ₂ C ₂ H ₅) ₂	188.22	col. lq.	0.994 ^{25/25}		196.7	i.		∞	∞
glutarate	CH ₂ (CH ₂ CO ₂ C ₂ H ₅) ₂	188.22	syrrup	1.025 ²¹	-24	237	0.88 ²⁰		v. s.	s.
ketone	(C ₂ H ₅) ₂ CO	86.13	col. lq.	0.816 ^{19/4}	-42	101.7	4.7 ²⁰		∞	∞
malonate	CH ₂ (CO ₂ C ₂ H ₅) ₂	160.17	col. lq.	1.055 ^{20/4}	-49.8	198.9	2.08 ²⁰		∞	∞
-malonic acid	(C ₂ H ₃) ₂ C(CO ₂ H) ₂	160.17	pr./aq.			d. 170–80	65 ¹⁶		v. s.	v. s.
-naphthylamine (α-)	C ₁₀ H ₇ N(C ₂ H ₅) ₂	199.29	col. oil	1.005		285–90	i.		∞	∞
(β-)	C ₁₀ H ₇ N(C ₂ H ₅) ₂	199.29	col. oil	1.026		318	i.		∞	∞
oxalate	(-CO ₂ C ₂ H ₅) ₂	146.14	col. lq.	1.079 ^{20/4}	-40.6	186	v. sl. s.		∞	∞
phthalate (o-)	C ₆ H ₄ (CO ₂ C ₂ H ₅) ₂	222.24	col. lq.	1.121 ^{25/25}		298–9	i.		∞	∞
sulfate	O ₂ S(OC ₂ H ₅) ₂	154.18	col. lq.	1.172 ^{25/4}	-25	210	i.		s.	∞
sulfide	(C ₂ H ₅) ₂ S	90.19	col. lq.	0.837 ^{20/4}	-99.5	92–3 ⁷⁵⁴	0.31 ²⁰		∞	∞

TABLE 2-2 Physical Properties of Organic Compounds (Continued)

Name	Formula	Formula weight	Form and color	Specific gravity	Melting point, °C	Boiling point, °C	Solubility in 100 parts		
							Water	Alcohol	Ether
tartrate (<i>d</i> -)	(CHOH·CO ₂ C ₂ H ₅) ₂	206.19	lq.	1.204 ^{20/4}	17	280	sl. s.	∞	∞
-toluidine (<i>o</i> -)	CH ₃ ·C ₆ H ₄ ·N(C ₂ H ₅) ₂	163.26	lq.			208–9 ⁷⁵⁵	i.	s.	s.
(<i>m</i> -)	CH ₃ ·C ₆ H ₄ ·N(C ₂ H ₅) ₂	163.26	lq.			231–2	i.	s.	s.
(<i>p</i> -)	CH ₃ ·C ₆ H ₄ ·N(C ₂ H ₅) ₂	163.26	lq.	0.924 ^{15.5}		228–9	i.		
Diethyleneglycol dinitrate	O(CH ₂ CH ₂ ONO ₂) ₂	196.12	lq.	1.377 ^{25/4}	-11.3		i.		
Diffurordichloromethane	F ₂ CCl ₂	120.91	gas	1.486 ³⁰	-155	-29.2	5.7 cc. ²⁶	s.	s.
Diglycerol	[(HO) ₂ C ₃ H ₅] ₂ O	166.17	lq.			220–30 ¹⁰	s. h.		i.
Dihydroxy-dinaphthyl (α -)	(HO·C ₁₀ H ₆) ₂	286.32	pl./al.			300	i.	s.	v. s.
(-2,-2',-1,-1')	(HO·C ₁₀ H ₆) ₂	286.32	nd./al.			218	i.	s.	v. s.
-diphenyl (4,-4')	(HO·C ₆ H ₄) ₂	186.21	rhb./al.	1.25		270–2	subl.	v. s.	v. s.
-ethyl formal (β -)	CH ₃ (OCH ₂ CH ₂ OH) ₂	136.15	lq.	1.154 ²⁵		264	∞		
-naphthalene (1,-5)	C ₁₀ H ₆ (OH) ₂	160.17	pr./aq.			258–60	sl. s.	s.	v. s.
(1,-8)	C ₁₀ H ₆ (OH) ₂	160.17	nd.			140	sl. s. h.		v. s.
Dimethoxy-benzene (<i>p</i> -)	(CH ₃ O) ₂ C ₆ H ₄	138.16	lf.	1.053 ^{25/55}		56	v. sl. s.	v. s.	v. s.
-diphenylamine (4,-4')	HN(C ₆ H ₅ OCH ₃) ₂	229.27	cr.			103	i.		
-ethyl adipate	(CH ₂) ₄ (CO ₂ C ₂ H ₅ OCH ₃) ₂	262.30	lq.	1.075 ^{15.6}		145–50 ²	5		
Dimethyl adipate	[(CH ₃) ₂ CO ₂ CH ₃] ₂	174.19	col. lq.	1.063 ^{20/4}		115 ¹⁸	i.		
-amine	(CH ₃) ₂ NH	45.08	col. lq.	0.680 ^{9/4}		-96	v. s.	s.	s.
-aminoasobenzene (<i>p</i> -)	C ₆ H ₅ N=N·C ₆ H ₄ N(CH ₃) ₂	225.29	yel./al.			116–7	d.	s.	s.
-aminoethanol	(CH ₃) ₂ NCH ₂ CH ₂ OH	89.14	col. lq.	0.887 ^{20/4}			∞		
-aminophenol (<i>m</i> -)	(CH ₃) ₂ NCH ₆ H ₄ OH	137.18	nd.			85	sl. s. h.	s.	s.
-aniline	(CH ₃) ₂ NCH ₆ H ₅	121.18	yel. lq.	0.956 ^{20/4}		2.5	i.	s.	s.
sulfonic acid (<i>m</i> -)	(CH ₃) ₂ NCH ₆ H ₄ SO ₃ H	201.24	cr.			d. 266	s.		
(<i>p</i> -)	(CH ₃) ₂ NCH ₆ H ₄ SO ₃ H·H ₂ O	219.26	pr.			257	s. h.	v. sl. s.	v. sl. s.
carbonate	OC(OCH ₃) ₂	90.08	col. lq.	1.070 ^{20/4}		0.5	89–90	∞	∞
ether	CH ₃ OCH ₃	46.07	gas			-138.5	i.	3700 cc. ¹⁸	s.
-formamide	HCON(CH ₃) ₂	73.09	lq.	0.945 ²⁵		-58.3	∞		
fumarate	(C ₂ H ₃ CO ₂ CH ₃) ₂	144.13	col. tri.			102	i.	sl. s.	sl. s.
glutarate	(CH ₂) ₂ (CO ₂ CH ₃) ₂	160.17	lq.	1.089 ^{15.6}		-37	130 ⁵⁰		
glyoxime	(CH ₃ ·C:NOH) ₂	116.12	col. cr.			240–6	0.06 ²⁰	v. s.	v. s.
-naphthalene (1,-4)	C ₁₀ H ₆ (CH ₃) ₂	156.22	lq.	1.016 ^{20/4}		<-18	i.		
(2,-3)	C ₁₀ H ₆ (CH ₃) ₂	156.22	lf./al.			104	265 ⁷⁰⁷		
-naphthylamine (α -)	C ₁₀ H ₇ N(CH ₃) ₂	171.24	col. oil	1.042 ²⁰		274.5 ⁷¹¹	i.	sl. s.	s.
(β -)	C ₁₀ H ₇ N(CH ₃) ₂	171.24	col. cr.	1.039 ^{70/70}		46	i.	s.	s.
oxalate	(-CO ₂ CH ₃) ₂	118.09	col. mn.	1.148 ^{5/4}		54	6	s.	s.
phthalate (<i>o</i> -)	C ₆ H ₄ (CO ₂ CH ₃) ₂	194.18	col. lq.	1.189 ^{25/25}		280 ⁷³⁴	0.43		
sulfate	(CH ₃ O) ₂ SO ₂	126.13	col. oil	1.352 ^{20/4}		188.3	v. sl. s.	∞	∞
sulfide	(CH ₃) ₂ S	62.13	oil	0.846 ^{21/4}		-83.2	37.3	i.	s.
tartrate (<i>d</i> -)	(CHOH·CO ₂ CH ₃) ₂	178.14	cr.	1.328 ^{20/4}		61.5	280	s.	200 ¹⁵
-vinyl-ethyl carbinol	(CH ₃) ₂ COH·C ₂ H ₅	110.15	lq.	0.887 ^{20/4}		150	6 ²⁰		
Dinaphthyl ($\alpha\alpha$ -)	C ₁₀ H ₇ ·C ₁₀ H ₇	254.33	lf./al.			160	240–4 ¹²	i.	s. h.
-methane ($\alpha\alpha'$ -)	(C ₁₀ H ₇) ₂ CH ₂	268.35	pr./al.			109	>360	i.	0.8 c.
($\beta\beta'$ -)	(C ₁₀ H ₇) ₂ CH ₂	268.35	nd./al.			92		i.	s.
Dinitro-anisole (1-)(2,-4-)	CH ₃ OC ₆ H ₃ (NO ₂) ₂	198.13	col. mn.	1.341 ²⁰		94–5	sl. s. h.	1.5 ²⁰	
-benzene (<i>o</i> -)	C ₆ H ₄ (NO ₂) ₂	168.11	col. mn.	1.591 ¹⁸		117–8	0.01 c.	1.9 ²¹	
(<i>m</i> -)	C ₆ H ₄ (NO ₂) ₂	168.11	col. rhb.	1.575 ^{20/4}		89.8	300–2	0.3 ⁹⁹	3 ²⁰
(<i>p</i> -)	C ₆ H ₄ (NO ₂) ₂	168.11	col. mn.	1.625 ¹⁸		173–4	299 ⁷⁷⁷	0.18 ¹⁰⁰	0.18 ²¹
sulfonic acid (2,-4-)(1-)	(NO ₂) ₂ C ₆ H ₃ SO ₃ H·3H ₂ O	302.22	pr.			106–8	s.		v. sl. s.
-benzoic acid (2,-4)	(NO ₂) ₂ C ₆ H ₃ CO ₂ H	212.12	cr./aq.			179–80	1.85 ²⁵	s.	
(3,-5)	(NO ₂) ₂ C ₆ H ₃ CO ₂ H	212.12	mn. pr.			204–5	s. h.	v. s.	sl. s.
-benzophenone (4,-4')	(NO ₂ C ₆ H ₄) ₂ CO	272.21	col. nd.			189	i.		
-diphenyl (4,-4')	(NO ₂ C ₆ H ₄) ₂	244.20	nd./al.	1.445		233	i.	1.5 ²⁰	
(2,-4')	(NO ₂ C ₆ H ₄) ₂	244.20	mn.	1.474		93.5	i.	v. s. h.	
-naphthalene (1,-5)	C ₁₀ H ₆ (NO ₂) ₂	218.17	nd.			216	subl.		
(1,-8)	C ₁₀ H ₆ (NO ₂) ₂	218.17	rhb.			170–2	d.	i.	0.2 c.
Dinitro-phenol (2,-3)	(NO ₂) ₂ C ₆ H ₃ OH	184.11	yel. mn.	1.681 ²⁰		144–5	sl. s.	v. s. h.	v. s.
(2,-4)	(NO ₂) ₂ C ₆ H ₃ OH	184.11	yel. rhb.	1.683 ²⁴		114–5	0.5 c.	4 ²⁰	v. s. h.
(2,-6)	(NO ₂) ₂ C ₆ H ₃ OH	184.11	yel. rhb.			63–4	s. h.	s. h.	s.
-salicylic acid (3,-5)	(NO ₂) ₂ C ₆ H ₃ (OH)CO ₂ H·H ₂ O	246.13	pl./aq.			173 d.	s. c.	v. s.	v. s.
-stilbene (4,-4')	(NO ₂ C ₆ H ₄ CH ₂) ₂	270.24	yel. lf.			210–6	i.	v. sl. s.	v. sl. s.
-toluene (2,-4)	(NO ₂) ₂ C ₆ H ₃ CH ₃	182.13	nd.	1.321 ⁷¹		70	0.03 ²²	1.2 ¹⁵	9 ¹⁶
(3,-4)	(NO ₂) ₂ C ₆ H ₃ CH ₃	182.13	nd.	1.259 ¹¹¹		60–1	i.		
(3,-5)	(NO ₂) ₂ C ₆ H ₃ CH ₃	182.13	mn. pr.	1.277 ¹¹¹		92–3	subl.	sl. s.	s.
Dioxane	O < (CH ₂ ·CH ₂) ₂ > O	88.11	col. lq.	1.033 ^{20/4}		9.5–10.5	∞	s. h.	s.
Dipentene	C ₁₀ H ₁₆	136.23	col. lq.	0.865 ¹⁸		178	i.		

Diphenyl	C_6H_5 ; C_6H_5	154.21	col. mn.	0.992 ^{73/4}	69–70	254.9	i.	10 ²⁰	6.6 ²⁰
-amine	C_6H_5NH ; C_6H_5	169.22	col. mn.	1.160 ^{20/20}	52.9	302	0.03 ²⁵	56 ^{10,5}	s.
carbonate	CO (OC_6H_5) ₂	214.22	nd./al.	1.272 ¹⁴	80	302–6	i.	v. s.	s.
-chloroarsine	(C_6H_5) ₂ AsCl	264.58	rhb.	1.583 ¹⁰	43–4	d. 327	0.2 d.	20	s.
-ethane	($C_6H_5CH_2$) ₂	182.26	col. pr.	0.978 ^{20/50}	52–3	284	i.	s.	v. s.
ether	$C_6H_5OC_6H_5$	170.21	col. rhh.	1.073 ²⁰	27	259	v. sl. s.	s.	∞
guanidine	(C_6H_5NH) ₂ C:NH	211.26	mn./al.		147–8	d. > 170	v. sl. s.	9 ²⁰	sl. s.
-methane	(C_6H_5) ₂ CH ₂	168.23	col. pr.	1.001 ^{20/4}	26–7	265	i.	v. s.	v. s.
phenylenediamine (<i>p</i> -)	(C_6H_5NH) ₂ C ₆ H ₄	260.33	cr.		152		i.		
succinate	(-CH ₂ CO ₂ C ₆ H ₅) ₂	270.28	lf./al.		122–3	330	i.		s.
sulfide	(C_6H_5) ₂ S	186.27	col. lq.	1.119 ^{15/15}	<–40	296–7	sl. s. h.	s. h.	∞
sulfone	(C_6H_5) ₂ SO ₂	218.27	nd./aq.	1.248 ^{25/4}	128–9	379	sl. s. h.	s. h.	∞
urea (uns.)	(C_6H_5) ₂ NCONH ₂	212.25	rhb.	1.276	189		v. sl. s.	s.	v. s.
Diphenylene oxide	< (C_6H_4) ₂ O	168.19	lf./al.		86–7	287–8	i.	s. h.	v. s.
Dipropyl adipate (<i>n</i> -)	(-CH ₂ CH ₂ CO ₂ C ₃ H ₇) ₂	230.30	col. lq.	0.979 ^{20/4}	-20.3	143–5 ¹⁰	i.	s.	s.
-amine (<i>n</i> -)	($C_3H_7CH_2$) ₂ NH	101.19	col. lq.	0.739 ^{20/4}	-39.6	110–1	s.	∞	∞
(<i>i</i> -)	[(CH ₃) ₂ CH] ₂ NH	101.19	col. lq.	0.722 ²²	-61	83.5 ¹⁴³	s.	s.	
aniline (<i>n</i> -)	C_6H_5N (C_3H_7) ₂	177.29	yel. oil	0.910 ²⁰		245.4	i.	s.	s.
carbonate (<i>n</i> -)	CO (OCH ₂ C ₆ H ₅) ₂	146.18	col. lq.	0.968 ²²		168.2	v. sl. s.		
ether (<i>n</i> -)	($C_3H_7CH_2$) ₂ O	102.17	col. lq.	0.744 ^{21/0}	-122	91	sl. s.	∞	∞
(<i>i</i> -)	[(CH ₃) ₂ CH] ₂ O	102.17	col. lq.	0.725 ^{21/0}	-60	69	0.2	∞	∞
ketone (<i>n</i> -)	($C_3H_7CH_2$) ₂ CO	114.19	col. lq.	0.822 ^{20/4}	-32.6	144.2	0.43	∞	∞
(<i>i</i> -)	[(CH ₃) ₂ CH] ₂ CO	114.19	col. lq.	0.806 ^{20/4}		123.7	v. sl. s.	∞	∞
oxalate (<i>n</i> -)	($CO_2CH_2C_3H_7$) ₂	174.19	col. lq.	1.038 ^{20/0}	-51.7	213.5	d. h.		
(<i>i</i> -)	[CO ₂ CH(CH ₃) ₂] ₂	174.19	col. lq.			190			
Disalicylal ethylenediamine	[HO C_6H_4 CH=CH(CH ₂) ₂] ₂	268.31	cr.	1.34	125–6		0.03 ²⁵		
Ditolyl guanidine (<i>o</i> -)	(C_6H_7NH) ₂ C:NH	239.32	cr.	1.10 ^{20/4}	178–9		v. sl. s.	s. h.	s.
Divinyl acetylene	(H ₂ C:CH:C:) ₂	78.11	lq.	0.776 ^{20/4}		85	i.		
Docosane (<i>n</i> -)	CH ₃ (CH ₂) ₂₀ CH ₃	310.60	cr.	0.778 ^{14/4}	44.5	224.5 ¹⁵	i.	4 h.	v. s.
Dodecane (<i>n</i> -)	CH ₃ (CH ₂) ₁₀ CH ₃	170.33	lq.	0.751 ^{20/4}	-9.6	214.5	i.	v. s.	v. s.
Dulcitol	CH ₂ OH(CHOH) ₄ CH ₂ OH	182.17	mn.	1.466 ¹⁵	189	290–5 ³	3.2 ¹⁵	v. sl. s.	i.
Durene (1-,2-,4-,5-)	(CH ₃) ₄ C ₆ H ₂	134.22	mn.	0.838 ^{11/4}	79–80	193–5	i.	s.	s.
Elaidic acid	C_8H_{17} CH:CH(CH ₂) ₇ CO ₂ H	282.46	lf./al.	0.851 ^{79/4}	51–2	288 ¹⁰⁰	i.	v. s.	v. s.
Eosine	$C_{20}H_8O_6Br_4$	647.89	col. cr.			40	i.	s.	∞
Ephedrine (<i>L</i> -)	$C_9H_{13}CHOHCH(CH_3)NHCH_3$	165.23	cr./et.		40	255	5	500	∞
Epichlorhydrin (α -)	C_2H_5O -CH ₂ Cl	92.52	lq.	1.183 ^{25/25}	-25.6	117 ⁷⁵⁶	<5	∞	s.
Epidichlorohydrin ($\alpha\alpha$ -)	CH ₂ :CCl-CH ₂ Cl	110.97	col. lq.	1.204 ²⁵		94	i.	∞	∞
Erythritol (<i>dl</i> -)	CH ₂ OH(CHOH) ₂ CH ₂ OH	122.12	tet. pr.	1.451 ^{20/4}	126	329–31	60	sl. s. c.	i.
tetranitrate	$C_4H_6(ONO_2)_4$	302.11	lf./al.		61	expl.	i. c.	s.	s.
Ethane	CH ₃ CH ₃	30.07	col. gas	0.546 ⁻⁸⁸	-172	-88.6	4.7 cc. ²⁰	150 cc.	
Ethanol-amine	HOCH ₂ CH ₂ NH ₂	61.08	col. oil	1.022 ²⁰	10.5	171 ⁷⁵⁷	∞	∞	1
formamide	HCONHCH ₂ CH ₂ OH	89.09	lq.	1.169 ²⁵	<–40	d.	∞	∞	
Ether	(CH ₃ CH ₂) ₂ O	74.12	col. lq.	0.708 ^{25/4}	-116.3	34.6	7.5 ²⁰	∞	
Ethyl abietate	$C_{19}H_{20}CO_2$; $C_9C_2H_5$	330.50	lq.	1.020 ^{20/20}		200 ⁴	i.		
acetate	CH ₃ CO ₂ C ₂ H ₅	88.11	col. lq.	0.901 ^{20/4}	-82.4	77.1	8.5 ¹⁵	∞	∞
acetate	CH ₃ COCH ₂ CO ₂ C ₂ H ₅	130.14	col. lq.	1.025 ^{20/4}	-45	180 ⁷⁵⁵	13 ¹⁷	∞	∞
alcohol	CH ₃ CH ₂ OH	46.07	col. lq.	0.789 ^{20/4}	-112	78.4	∞	∞	∞
-amine	$C_2H_5NH_2$	45.08	col. lq.	0.689 ^{15/15}	-80.6	16.6	∞	∞	∞
hydrochloride	$C_2H_5NH_2$ ·HCl	81.54	mn.	1.216	108–9		240 ¹⁷	v. s.	i.
aniline	$C_6H_5NH_2$	121.18	lq.	0.963 ^{20/4}	-63.5	204	i.	∞	∞
sulfonic acid (<i>m</i> -)	$C_6H_5NHC_6H_4SO_3H$	201.24	nd./aq.		d. 294		2.15 ¹⁵		
anisate (<i>p</i> -)	CH ₃ OC ₆ H ₄ CO ₂ C ₂ H ₅	180.20	lq.	1.103 ^{25/25}	7–8	269–70	s.	s.	s.
anthranilate (<i>o</i> -)	NH ₂ C ₆ H ₄ CO ₂ C ₂ H ₅	165.19	cr.	1.117 ^{20/4}	13	266–8	v. sl. s.	s.	s.
benzene	C_6H_6 ; C_6H_6	106.17	col. lq.	0.867 ^{20/4}	-94.4	136.2	0.01 ¹⁵	∞	∞
benzoate	$C_6H_5CO_2C_2H_5$	150.17	col. lq.	1.052 ^{15/15}	-34.6	211–2	0.08 ²⁰	∞	∞
-benzyl-aniline	$C_6H_5N(C_2H_5)CH_2C_6H_5$	211.30	yel. oil	1.034 ^{18,5}		285 ¹⁰	i.	18	∞
bromide	C_2H_5Br	108.97	col. lq.	1.431 ^{20/4}	-117.8	38.4	1.06 ⁰	∞	∞
butyrate (<i>n</i> -)	$C_3H_7CH_2CO_2C_2H_5$	116.16	col. lq.	0.879 ^{20/4}	-93.3	120–1	0.68 ²⁵	∞	∞
(<i>i</i> -)	(CH ₃) ₂ CHCO ₂ C ₂ H ₅	116.16	col. lq.	0.871 ^{20/4}	-88.2	110–1	sl. s.	∞	∞
caprate (<i>n</i> -)	CH ₃ (CH ₂) ₈ CO ₂ C ₂ H ₅	200.32	lq.	0.859 ²⁵	-20	244.6 ⁷⁵⁸	0.002 ²⁰	∞	∞
Ethyl caproate (<i>n</i> -)	CH ₃ (CH ₂) ₆ CO ₂ C ₂ H ₅	144.21	col. lq.	0.873 ^{20/20}	-67.5	165–6 ⁷⁵⁶	i.	∞	∞
caprylate (<i>n</i> -)	CH ₃ (CH ₂) ₈ CO ₂ C ₂ H ₅	172.26	col. lq.	0.878 ¹⁷	-45	207–8 ⁷⁵³	i.	∞	∞
chloride	CH ₂ CH ₂ Cl	64.51	col. lq.	0.917 ^{6/6}	-139	13	0.45 ⁹	∞	∞
chloroacetate	ClCH ₂ CO ₂ C ₂ H ₅	122.55	col. lq.	1.159 ^{20/4}	-26	144	i.	∞	∞
chlorocarbonate	ClCO ₂ CH ₂ CH ₃	108.52	col. lq.	1.138 ^{20/4}	-80.6	94–5	d.	∞	∞
cinnamate (<i>trans</i> -)	$C_6H_5CH=CHCO_2C_2H_5$	176.21	col. lq.	1.049 ^{20/4}	12	271	i.	∞	∞
cianoacetate	CH ₂ (CN)CO ₂ C ₂ H ₅	113.11	col. lq.	1.062 ^{20/4}	-22.5	208 ⁷⁵³	2 ²⁵	∞	∞
formate	HCO ₂ CH ₂ CH ₃	74.08	col. lq.	0.923 ^{20/4}	-79	54 ⁷⁸⁰	11 ¹⁸	∞	∞
furoate (α)	OC ₄ H ₃ CO ₂ C ₂ H ₅	140.14	lf.	1.117 ^{20/20}	34	195 ⁷⁶⁶	i.	∞	∞
heptoate	CH ₃ (CH ₂) ₆ CO ₂ C ₂ H ₅	158.24	col. lq.	0.872 ^{20/20}	-66.1	187–8	0.029 ²⁰	∞	∞
hypochlorite	ClOCH ₂ CH ₃	80.51	yel. lq.	1.013 ^{4/4}		expl.		∞	∞
iodide	CH ₃ CH ₂ I	155.97	col. lq.	1.933 ^{20/4}	-105	72.4	0.4 ²⁰	∞	∞
lactate	CH ₃ CH(OH)CO ₂ C ₂ H ₅	118.13	oil	1.030 ^{25/4}		155	∞	∞	∞

TABLE 2-2 Physical Properties of Organic Compounds (Continued)

Name	Formula	Formula weight	Form and color	Specific gravity	Melting point, °C	Boiling point, °C	Solubility in 100 parts		
							Water	Alcohol	Ether
laurate	CH ₃ (CH ₂) ₁₀ CO ₂ C ₂ H ₅	228.37	oil	0.868 ^{13/4}	-10.7	269	i.	s.	∞
mercaptopan	CH ₃ CH ₂ SH	62.13	lq.	0.839 ^{20/4}	-121	36-7	1.5	s.	s.
methacrylate	CH ₂ =C(CH ₃)CO ₂ C ₂ H ₅	114.14	col. lq.	0.913 ^{15/6}		118	i.	s.	s.
naphthylamine (α-)	C ₁₀ H ₇ NH ₂ C ₂ H ₅	171.24	oil	1.060 ^{20/4}		303 ^{7/23}	i.	s.	s.
naphthyl ether (α-)	C ₁₀ H ₇ OC ₂ H ₅	172.22	cr.	1.061 ^{20/20}	5.5	276.4	i.	s.	s.
nitrate	C ₂ H ₅ ONO ₂	91.07	col. lq.	1.100 ^{25/4}	-102	87-8	1.3 ⁵⁵	∞	∞
nitrite	C ₂ H ₅ ONO	75.07	lq.	0.900 ^{15/5}		17	v. sl. s.	∞	∞
oleate	C ₁₇ H ₃₃ CO ₂ C ₂ H ₅	310.51	oil	0.867 ²⁵	<-15	216-8 ¹⁵	i.	∞	∞
palmitate	CH ₃ (CH ₂) ₁₄ CO ₂ C ₂ H ₅	284.48	col. nd.	0.858 ^{25/4}	24-5	191 ¹⁰	i.	s.	s.
pelargonate	CH ₃ (CH ₂) ₇ CO ₂ C ₂ H ₅	186.29	col. lq.	0.866 ^{17/5}	-44.5	227-8 ^{7/27}	i.	∞	∞
propionate	CH ₃ CH ₂ CO ₂ C ₂ H ₅	102.13	col. lq.	0.891 ^{20/4}	-72.6	99.1	∞	∞	∞
salicylate (o-)	HOC ₆ H ₄ CO ₂ C ₂ H ₅	166.17	col. lq.	1.136 ^{15/4}	1.3	233-4	i.	∞	∞
stearate	CH ₃ (CH ₂) ₁₆ CO ₂ C ₂ H ₅	312.53	col. cr.	0.848 ^{36/3}	33.4(31)	201 ¹⁰	i.	s.	s.
toluate (o-)	CH ₃ -C ₆ H ₄ -CO ₂ C ₂ H ₅	164.20	lq.	1.032 ^{25/25}	<-10	227	i.	∞	∞
(m-)	CH ₃ -C ₆ H ₄ -CO ₂ C ₂ H ₅	164.20	lq.	1.030 ^{20/20}		231 ^{7/50}	i.	∞	∞
toluene sulfonate (p-)	CH ₃ -C ₆ H ₄ -SO ₂ -C ₂ H ₅	200.25	pr./al.	1.166 ^{48/4}	33-4	221.3	i.	s.	s.
toluidine (o-)	CH ₃ -C ₆ H ₄ NH ₂ C ₂ H ₅	135.21	lq.	0.948 ^{25/4}	<-15	215-6	i.		
(p-)	CH ₃ -C ₆ H ₄ NH ₂ C ₂ H ₅	135.21	lq.	0.942 ^{25/4}		217	i.		
urea	C ₂ H ₅ NH-CO-NH ₂	88.11	nd.	1.213 ¹⁸	92		v. s.	80	i.
valerate (n-)	CH ₃ (CH ₂) ₃ CO ₂ C ₂ H ₅	130.18	col. lq.	0.877 ²⁰	-91.2	145.5	∞	∞	∞
(i-)	(CH ₂) ₂ CH(CH ₂)CO ₂ C ₂ H ₅	130.18	col. lq.	0.867 ^{20/4}	-99.3	135	0.17 ²⁰	∞	∞
Ethylal	CH ₂ (OC ₂ H ₅) ₂	104.15	lq.	0.824 ^{25/4}	-66.5	89	9 ¹⁸	∞	∞
Ethylene	H ₂ C:CH ₂	28.05	col. gas	0.57 ^{-102/4}	-169	-103.9	26 cc. ⁰	360 cc.	s.
bromide	BrCH ₂ -CH ₂ Br	187.86	col. lq.	2.180 ^{20/4}	10	131.5	∞	∞	∞
bromohydrin	BrCH ₂ -CH ₂ OH	124.96	col. lq.	1.772 ^{20/4}		150.3	sl. s.	s.	
chlorobromide	ClCH ₂ -CH ₂ Br	143.41	lq.	1.689 ¹⁹	-16.6	106.7	0.69 ⁸⁰		
chlorohydrin	ClCH ₂ -CH ₂ OH	80.51	col. lq.	1.213 ^{20/4}	-69	128.8	∞	∞	∞
diamine	H ₂ NCH ₂ -CH ₂ NH ₂	60.10	col. lq.	0.900 ^{20/20}	8.5	117.2	∞	∞	0.3
oxide	<(CH ₂) ₂ >O	44.05	lq.	0.887 ^{7/4}	-111.3	13.5 ⁴⁷	∞	∞	v. s.
Ethylidene diacetate	CH ₃ CH(O ₂ CCH ₃) ₂	146.14	col. lq.	1.061 ¹²	18.85	168 ⁴⁰	sl. s.	∞	
Eugenol (1-4,3-)	C ₃ H ₂ -C ₆ H ₃ (OH)OCH ₃	164.20	oil	1.070 ^{15/15}	10.3	253.5	v. sl. s.	∞	∞
(i-)(1-3,4-)	C ₃ H ₂ -C ₆ H ₃ (OCH ₃)OH	164.20	oil	1.091 ^{15/15}	-10	267.5	v. sl. s.	∞	∞
Fenchyl alcohol (dl-)	C ₁₀ H ₁₇ OH	154.25	col. cr.	0.935 ⁴⁰	35	201	sl. s.		
(d-)(α-)	C ₁₀ H ₁₇ OH	154.25	col. pr.	0.964 ^{20/4}	45-7	201-2	sl. s.	s.	s.
(i-)(l-)	C ₁₀ H ₁₇ OH	154.25	col. cr.	0.961	61-2	201-2	i.		
Ferric dimethyl-dithiocarbamate	Fe[SSCN(CH ₃) ₂] ₃	416.49	cr.		d. 100-30	ign. >150	v. sl. s.		
Fluorene	(C ₆ H ₄) ₂ >CH ₂	166.22	cr./al.	1.203 ^{9/4}	115-6	293-5	i.	s. h.	s.
Fluorescein	C ₂₀ H ₁₂ O ₅	332.31	yel. red		d. > 290		v. sl. s. h.	s. h.	
Fluoro-dichloromethane	FCHCl ₂	102.92	gas	1.426 ⁹	-127	14.5	i.	s.	∞
-trichloromethane	Cl ₃ CF	137.37	col. lq.	1.494 ^{17/2}		24.9	i.	∞	∞
Formaldehyde	HCHO	30.03	gas	0.815 ⁻²⁰	-92	-21	v. s.	v. s.	v. s.
(m-)	(CH ₂ O) ₃	90.08	wh.	1.17 ⁶⁵	64	114.5 ⁷⁵⁹	21 ²⁵	v. s.	s.
(p-)	(CH ₂ O) _x ·xH ₂ O	(30.03)	amor.		150-60	subl.	20-30 ¹⁵	i.	i.
Formamide	HCONH ₂	45.04	lq.	1.139 ^{20/4}	2	193	∞	∞	v. sl. s.
Formanilide	HCONHC ₆ H ₅	121.14	mm.	1.147 ^{15/15}	47	216 ¹²⁰	sl. s.	v. s.	s.
Formic acid	HO ₂ H	46.03	col. lq.	1.220 ^{20/4}	8.6	100.8	∞	∞	∞
Fructose	CH ₂ OH(CHOH) ₃ COCH ₂ OH	180.16	nd./aq.	1.669 ^{17/5}	95-105		v. s.	8 ¹⁸	
Fuchsin	C ₂₀ H ₁₉ N ₃ HCl	337.85	red	1.22	d. >200		0.3	s.	i.
Fulminic acid	C:NOH	43.02							
Fumaric acid (trans-)	HO ₂ CCH:CHCO ₂ H	116.07	col. pr.	1.635 ^{20/4}	286-7	290	0.7 ¹⁷	5.8 ³⁰	0.7 ²⁵
Furfural	C ₄ H ₃ O-CHO	96.08	lq.	1.159 ^{20/4}	-38.7	161.7 ⁷⁶⁰	9.1 ¹³	∞	∞
Furfuran	C ₄ H ₄ O	68.07	col. lq.	0.937 ^{20/4}		31-2 ⁷⁵⁶	i.	s.	s.
Furfuryl acetate	CH ₃ CO ₂ CH ₂ C ₄ H ₃ O	140.14	col. oil	1.118 ^{20/4}		175-7	i.	s.	s.
alcohol	C ₄ H ₃ O-CH ₂ OH	98.10	oil	1.129 ^{25/4}		169.5 ⁷⁵²	∞	s.	s.
butyrate	C ₃ H ₇ CO ₂ CH ₂ -C ₄ H ₃ O	168.19	col. lq.	1.053 ^{20/4}		212-3	v. sl. s.	s.	∞
propionate	C ₂ H ₅ CO ₂ CH ₂ -C ₄ H ₃ O	154.16	col. lq.	1.109 ^{20/4}		195-6	v. sl. s.	s.	∞
Furoic acid	C ₄ H ₃ O-CO ₂ H	112.08	mm. pr.		133-4	230-2	3.6 ¹⁵	s.	s.
G-acid, K salt (2-)(6-8-)	HOC ₁₀ H ₇ (SO ₃ K) ₂	380.48	cr.				8 ²⁵		
Na salt (2-)(6-8-)	HOC ₁₀ H ₇ (SO ₂ Na) ₂	348.26	cr.				34 ²⁰		
Galactose (d-)(α-)	C ₆ H ₁₂ O ₆ ·CHO	180.16	pr.		165.5		10.3 ⁰	0.6 ⁴⁰	
Gallic acid (3-4,5-)	(HO) ₃ C ₆ H ₃ CO ₂ H·H ₂ O	188.13	mm./aq.	1.694 ^{4/4}	d. 220		1 ¹³	28 ¹⁵	2.5 ¹⁵
Gamma acid (2-,8-,6-)	C ₁₀ H ₈ (NH ₂)(OH)SO ₃ H	239.25	cr.						
Geraniol	C ₉ H ₁₆ CH ₂ OH	154.25	col. lq.	0.883 ¹⁵	<-15	230	i.	∞	∞
Glucose (d-)(α-)	C ₆ H ₁₂ O ₆ ·CHO	180.16	rhb.	1.544 ²⁵	146		82 ^{17/5}	sl. s.	i.
(d-)(β-)	C ₆ H ₁₂ O ₆ ·H ₂ O	198.17	cr.	1.562 ^{18/4}	150		154 ¹⁵		
Glucuronic acid	CHO(CHOH) ₄ CO ₂ H	194.14	cr.		154	d.	v. s.		
Glutaminic acid (dl-)	[·CHNH ₂ (CH ₂) ₂ ·](CO ₂ H) ₂	147.13	cr./aq.	1.460	199 d.		1.5 ²⁰	v. sl. s.	v. sl. s.

Glutaric acid	$\text{CH}_3(\text{CH}_2\text{CO}_2\text{H})_2$	132.11	col. cr.	1.429 ¹⁵	97.5	200 ²⁰	63.9 ²⁰	v. s.	v. s.
Glycerol	$\text{CH}_2\text{OH}\cdot\text{CHOH}\cdot\text{CH}_2\text{OH}$	92.09	col. liq.	1.260 ^{90/4}	17.9	290	∞	∞	i.
acetate (mono-)	$\text{C}_5\text{H}_{10}\text{O}_4$	134.13	col. oil	1.20 ^{20/4}		158 ^{16/5}	v. s.	v. s.	sl. s.
(di-)	$(\text{CH}_2\text{CO}_2)_2\text{C}_3\text{H}_5\text{OH}$	176.17	col. liq.	1.178 ^{15/15}	40	175-6 ⁴⁰	s.	s.	sl. s.
nitrate (mono-) (α -)	$\text{CH}_2\text{OH}\cdot\text{CHOH}\cdot\text{CH}_2\text{NO}_3$	137.09	col. pr.	1.40 ¹⁵	58-9	155-60	70 ¹⁵	v. s.	v. sl. s.
(β -)	$\text{CH}_2\text{OH}\cdot\text{CHNO}_2\cdot\text{CH}_2\text{OH}$	137.09	lf.	1.40 ¹⁵	54	155-60		v. s.	sl. s.
dinitrate (1,3-)	$\text{CHOH}(\text{CH}_2\text{ONO}_2)_2$	182.09	oil	1.47 ^{17/4}	<-30	146-3 ¹⁵		v. s.	v. s.
Glyceryl triacetate	$(\text{CH}_2\text{CO}_2)_3\text{C}_3\text{H}_5$	218.20	col. liq.	1.161 ^{17/4}	-78	258-9	7.17 ¹⁵	∞	∞
tribenzoate	$(\text{C}_6\text{H}_5\text{CO}_2)_3\text{C}_3\text{H}_5$	404.41	nd.	1.228 ¹²	75-6		i.	s. h.	s.
tributyrate	$(\text{C}_4\text{H}_9\text{CH}_2\text{CO}_2)_3\text{C}_3\text{H}_5$	302.36	col. liq.	1.032 ^{20/4}	<-75	305-9	i.	s.	s.
tricaprate	$[\text{CH}_3(\text{CH}_2)_4\text{CO}_2]_3\text{C}_3\text{H}_5$	554.84	col. cr.	0.921 ^{40/4}	31(25)		i.	s. h.	v. s.
tricaproate	$[\text{CH}_3(\text{CH}_2)_2\text{CO}_2]_3\text{C}_3\text{H}_5$	386.52	col. liq.	0.987 ^{20/4}	-25		i.	s.	v. s.
tricaprylate	$[\text{CH}_3(\text{CH}_2)_6\text{CO}_2]_3\text{C}_3\text{H}_5$	470.68	col. liq.	0.954 ^{20/4}	8.3(-21)		i.	s.	s.
trilaurate	$[\text{CH}_3(\text{CH}_2)_{10}\text{CO}_2]_3\text{C}_3\text{H}_5$	639.00	col. nd.	0.894 ^{40/4}	45-6		i.	sl. s. c.	v. s.
trimyristate	$[\text{CH}_3(\text{CH}_2)_{12}\text{CO}_2]_3\text{C}_3\text{H}_5$	723.16	lf.	0.885 ^{40/6}	56.5		i.	s.	∞
trinitrate	$\text{CH}_2\text{NO}_3\cdot\text{CHNO}_2\cdot\text{CH}_2\text{NO}_3$	227.09	yel. oil	1.601 ¹⁵	13.3(2)	160 ¹⁵	0.18 ²⁰	50 ²⁰	∞
trinitrite	$\text{CH}_2\text{NO}_2\cdot\text{CHNO}_2\cdot\text{CH}_2\text{NO}_2$	179.09	yel. liq.	1.291 ^{10/16}		150 sl. d.	d.	d.	s.
trioleate	$(\text{C}_{17}\text{H}_{33}\text{CO}_2)_3\text{C}_3\text{H}_5$	885.43	col. oil	0.915 ¹⁵	-4	240 ¹⁸	i.	sl. s.	v. s.
tripalmitate	$[\text{CH}_3(\text{CH}_2)_{14}\text{CO}_2]_3\text{C}_3\text{H}_5$	807.32	col. nd.	0.866 ^{30/4}	65.1	310-20 ¹¹	i.	0.004 ²¹	v. s.
tristearate	$[\text{CH}_3(\text{CH}_2)_{18}\text{CO}_2]_3\text{C}_3\text{H}_5$	891.48	col. pr.	0.862 ^{30/4}	70.8(55)		i.	s. h.	s. h.
Glycide	$\text{C}_3\text{H}_6\text{O}\cdot\text{CH}_2\text{OH}$	74.08	col. liq.	1.114 ^{16/16}		166 sl. d.	∞	∞	∞
Glycine, Glycocol	$\text{NH}_2\text{CH}_2\cdot\text{CO}_2\text{H}$	75.07	mn.	1.161	232-6 d.		23 c.	0.1 c.	i.
Glycol	$\text{CH}_2\text{OH}\cdot\text{CH}_2\text{OH}$	62.07	col. liq.	1.113 ^{19/4}	-15.6	197.4	∞	∞	1.0
diacetate	$(\text{CH}_3\text{CO}_2\text{CH}_2)_2$	146.14	col. liq.	1.109 ^{14/4}	-31	190.5	14.3 ²²	∞	∞
dibenzoate	$(\text{C}_6\text{H}_5\text{CO}_2\text{CH}_2)_2$	270.28	rhb./et.			>360	i.	∞	s.
dibutyrate	$(\text{C}_4\text{H}_9\text{CO}_2\text{CH}_2)_2$	202.25	col. liq.	1.024 ⁹		240	i.	v. s.	v. s.
dicaprylate	$(\text{C}_7\text{H}_{15}\text{CO}_2\text{CH}_2)_2$	314.46	liq.			22	i.		
diformate	$(\text{HCO}_2\text{CH}_2)_2$	118.09	liq.			174	v. sl. s.		
dilaurate	$(\text{C}_{11}\text{H}_{23}\text{CO}_2\text{CH}_2)_2$	426.67	amor.		52-4	188 ²⁰	i.	v. s.	v. s.
dinitrate	$(\text{ONO}\cdot\text{CH}_2)_2$	152.06	yel. liq.	1.482 ^{21/2}	-20	expl. 114	0.92 ²⁵	s.	∞
dinitrite	$(\text{ONO}\cdot\text{CH}_2)_2$	120.06	liq.	1.216 ⁹	<-15	96-8	i.	s. d.	s.
dipalmitate	$(\text{C}_{16}\text{H}_{33}\text{CO}_2\text{CH}_2)_2$	538.89	nd.		71-2	260 ¹¹	i.	s.	s.
dipropionate	$(\text{C}_3\text{H}_7\text{CO}_2\text{CH}_2)_2$	174.19	liq.	1.045 ²⁵		211-2	sl. s.	∞	∞
ether	$(\text{HO}\cdot\text{CH}_2\text{CH}_2)_2\text{O}$	106.12	liq.	1.118 ^{20/20}	-10.5	244.8	∞	∞	i.
formal	$<\text{O}\cdot\text{CH}_2\text{CH}_2\text{CO}_2\text{H}>$	74.08	liq.	1.060 ^{20/4}		75-6	∞	∞	∞
formate (mono-)	$\text{HCO}_2\text{CH}_2\text{CH}_2\text{OH}$	90.08	liq.	1.199 ^{15/4}		180	∞	∞	∞
Glycolic acid	$\text{HOCH}_2\text{CO}_2\text{H}$	76.05	nd./aq.		79(63)	d.	∞	90 ²⁵	v. s.
Guaiacol (o-)	$\text{C}_7\text{H}_5\text{O}\cdot\text{C}_6\text{H}_4\text{OH}$	124.14	pr.	1.140 ^{15/15}		28.3	1.7 ¹⁵	v. s.	v. s.
Guanidine	$\text{NH}_2\text{C}(\text{NH}_2)_2$	59.07	col. cr.		50		v. s.	s.	
H-acid, Na salt (1-,8-,3-,6-)	$\text{C}_{10}\text{H}_8\text{O}_7\text{NS}_2\text{Na}\cdot\frac{1}{2}\text{H}_2\text{O}$	368.32	cr.				0.17 ²⁰	∞	∞
Heptacosane (n-)	$\text{CH}_3(\text{CH}_2)_{25}\text{CH}_3$	380.73	col. cr.	0.780 ^{90/4}	59.5	270 ¹⁵	i.		∞
Heptane (n-)	$\text{CH}_3(\text{CH}_2)_6\text{CH}_3$	100.20	col. liq.	0.684 ^{20/4}	-90.6	98.4 ⁶⁰	0.005 ¹⁵	sl. s.	∞
(i-)	$(\text{CH}_2)_7\text{CH}(\text{CH}_2)_6\text{CH}_3$	100.20	col. liq.	0.679 ^{20/4}	-118.2	90.0	i.	s.	∞
	$\text{C}_3\text{H}_7\cdot\text{CH}(\text{CH}_3)\cdot\text{C}_6\text{H}_5$	100.20	col. liq.	0.687 ^{20/4}	-119.4	91.8	i.	s.	∞
	$(\text{CH}_2)_3\text{C}\cdot\text{CH}_2\cdot\text{C}_2\text{H}_5$	100.20	col. liq.	0.674 ^{20/4}	-125	79.1	i.	s.	∞
	$[(\text{CH}_3)_2\text{CH}]_2\text{CH}_2$	100.20	col. liq.	0.675 ^{20/4}	-119.4	80.8	i.	s.	∞
	$(\text{CH}_3)_2\text{C}(\text{C}_2\text{H}_5)_2$	100.20	col. liq.	0.693 ^{20/4}	-135.0	86.0	i.	s.	∞
	$(\text{C}_2\text{H}_5)_3\text{CH}$	100.20	col. liq.	0.698 ^{20/4}	-118.7	93.5	i.	s.	∞
	$(\text{CH}_3)_3\text{C}\cdot\text{CH}(\text{CH}_3)_2$	100.20	col. liq.	0.690 ^{20/4}	-25	80.8	i.	s.	∞
Heptoic acid	$\text{CH}_3(\text{CH}_2)_5\text{CO}_2\text{H}$	130.18	col. liq.	0.918 ²⁰	-10	221-2	0.25 ¹⁵	s.	s.
aldehyde	$\text{CH}_3(\text{CH}_2)_5\text{CHO}$	114.19	col. liq.	0.850 ^{20/6}	-42	155	0.02 ²⁰	∞	∞
Heptyl acetate (n-)	$\text{CH}_3\text{CO}_2\text{CH}_2(\text{CH}_2)_6\text{CH}_3$	158.24	col. liq.	0.874 ^{16/16}		191.5 ⁷⁵⁰	i.	s.	s.
alcohol (n-)	$\text{CH}_3(\text{CH}_2)_6\text{CH}_2\text{OH}$	116.20	col. liq.	0.824 ^{20/4}	-34	175 ⁷⁵⁶	0.18 ²⁵	∞	∞
	$[(\text{CH}_3)_2\text{CH}]_2\text{CHOH}$	116.20	col. liq.	0.829 ^{20/4}		140	v. sl. s.	∞	∞
	$(\text{C}_6\text{H}_5\cdot\text{CH}_2)_3\text{CHOH}$	116.20	liq.	0.820 ^{20/4}	-37	156	i.	s.	s.
mercaptan	$\text{CH}_3\text{CH}(\text{SH})\cdot\text{C}_5\text{H}_{11}$	132.27	liq.	0.835 ²⁰		174-5 ⁷⁶⁵	i.		
Hexachloro-benzene	C_6Cl_6	284.78	mn.	2.044 ²⁴	228-31	309 ⁷⁴²	i.	v. sl. s. h.	s. h.
-ethane	$\text{CCl}_3\cdot\text{CCl}_3$	236.74	rhb.	2.091 ^{20/4}	186-7	186 ⁷⁷⁷	0.005 ²²	v. s.	v. s.
Hexacosane (n-)	$\text{CH}_3(\text{CH}_2)_{24}\text{CH}_3$	366.71	cr.	0.779 ^{77/4}	56.6	262 ¹⁵	i.	v. sl. s.	∞
Hexadecane (n-)	$\text{CH}_3(\text{CH}_2)_{14}\text{CH}_3$	226.44	lf.	0.774 ^{20/4}	18.5	287.5	i.	∞	∞
Hexaethylbenzene	$\text{C}_6(\text{C}_2\text{H}_5)_6$	246.43	pr./al.	0.831 ^{130/4}	130	298.3	i.	0.75 ²⁵	8 ²⁵
Hexamethylbenzene	$\text{C}_6(\text{CH}_3)_6$	162.27	pl./al.		166	265	i.	0.2 ⁹	v. s.
Hexamethylene-diamine	$\text{NH}_2(\text{CH}_2)_6\text{NH}_2$	116.20	lf.		42	204-5	v. s.	s.	
-diisocyanate	$\text{OCN}(\text{CH}_2)_6\text{NCO}$	168.19	liq.	1.04 ²⁵		143-4 ²⁰	d.	d.	
-glycol	$\text{HO}(\text{CH}_2)_6\text{OH}$	118.17	nd./aq.		42	250	s.	s.	sl. s. h.
tetramine	$(\text{CH}_2)_6\text{N}_4$	140.19	col. rhb.		subl.		81 ¹²	3	v. sl. s.
Hexane (n-)	$\text{CH}_3(\text{CH}_2)_4\text{CH}_3$	86.18	col. liq.	0.659 ^{20/4}	-94	69	0.014 ¹⁵	50 ³³	∞
(i-)	$(\text{CH}_2)_5\text{CH}(\text{CH}_2)_2\text{CH}_3$	86.18	liq.	0.654 ^{20/4}	-153.7	60.2	i.	s.	s.
(neo-)	$(\text{CH}_3)_3\text{C}\cdot\text{C}_2\text{H}_5$	86.18	liq.	0.649 ^{20/20}	-98.2	49.7	i.	s.	s.
	$(\text{CH}_3)_2\text{CH}\cdot\text{CH}(\text{CH}_3)_2$	86.18	liq.	0.662 ^{20/4}	-129.8	58.0 ⁷⁶⁰	i.	s.	s.
	$(\text{C}_2\text{H}_5)_2\text{CHCH}_3$	86.18	liq.	0.664 ^{20/4}	-118	63.2	i.	s.	s.

TABLE 2-2 Physical Properties of Organic Compounds (Continued)

Name	Formula	Formula weight	Form and color	Specific gravity	Melting point, °C	Boiling point, °C	Solubility in 100 parts		
							Water	Alcohol	Ether
Hexyl acetate (<i>n</i> -)	CH ₃ CO ₂ (CH ₂) ₅ CH ₃	144.21	col. lq.	0.890 ⁹⁰		169.2	i.	v. s.	v. s.
alcohol (<i>n</i> -)	CH ₃ (CH ₂) ₄ CH ₂ OH	102.17	col. lq.	0.820 ^{20/20}	-51.6	157.2	0.6 ²⁰	∞	∞
	(CH ₃) ₂ CH-C(CH ₃) ₂ OH	102.17	lq.	0.821 ^{20/20}	-14	120-1	v. sl. s.	∞	∞
	(CH ₃) ₂ COH-CH ₂ C ₆ H ₅	102.17	lq.	0.809 ^{20/4}	-107	123 ^{76/2}	v. sl. s.	∞	∞
formate (<i>n</i> -)	HCO ₂ CH ₂ (CH ₂) ₄ CH ₃	130.18	lq.	0.898 ⁹		153.6	∞	∞	∞
resorcinol (2-,4-)	CH ₃ (CH ₂) ₂ C ₆ H ₃ (OH) ₂	194.27	col. nd.		68-70	179 ⁷	0.05	v. s.	s.
Hippuric acid	C ₈ H ₇ CONHCH ₂ CO ₂ H	179.17	rhb.	1.371 ^{20/4}	187-8	d.	0.4 ²⁰	v. s. h.	0.25 ¹⁸
Histidine (<i>l</i> -)	C ₆ H ₇ O ₂ N ₃	155.15	lf./aq.		d. 287		s.	v. sl. s.	i.
Homophthalic acid (<i>o</i> -)	HO ₂ C-C ₆ H ₄ -CH ₂ CO ₂ H	180.16	cr./aq.		175-80		s. h.	v. s.	sl. s.
Hydracrylic acid	HOCH ₂ CH ₂ CO ₂ H	90.08	syrup			d.			
Hydro-cyanic acid	HCN	27.03	lq.	0.697 ¹⁸	-12	25-6	∞	∞	∞
-quinone (<i>p</i> -)	C ₆ H ₄ (OH) ₂	110.11	cr.	1.332 ¹⁵	170.3	285 ²⁰	6 ¹⁵	v. s.	v. s.
Hydroxy-benzaldehyde (<i>p</i> -)	HO-C ₆ H ₄ -CHO	122.12	nd./aq.	1.129 ³⁰	116-7	subl.	1.35 ³¹		
-benzamide (<i>o</i> -)	HO-C ₆ H ₄ -CONHC ₆ H ₅	213.23	pr./al.		135	d.	v. sl. s. h.	s.	s.
-quinoline (2-)(<i>α</i> -)	C ₉ H ₆ N-OH	145.16	pr./al.		199-200	subl.	s. h.	v. s.	v. s.
(8-)(<i>o</i> -)	C ₉ H ₆ N-OH	145.16	pr.		75-6	266.6 ^{75/2}	v. sl. s. c.	s.	sl. s.
Indigo	[C ₁₆ H ₄ (CO)(NH)C] ₂	262.26	cr.	1.35	390-2	subl.	i.	i.	i.
White	C ₁₆ H ₁₂ O ₂ N ₂	264.28	gray				i.	s.	s.
Indole	C ₈ H ₇ N	117.15	lf./aq.		52	253-4	s. h.	s. h.	s.
Indoxyl	C ₈ H ₆ NOH	133.15	yel. pr.		85	110	s.	s.	s.
Iodo-benzene	C ₆ H ₅ I	204.01	col. lq.	1.824 ^{25/4}	-28.5	188.6	0.034 ²⁰	s.	∞
-phenol (<i>p</i> -)	IC ₆ H ₄ OH	220.01	nd./aq.	1.857 ^{11/2}	93-4	d.	sl. s.	v. s.	v. s.
Iodoform	CHI ₃	393.73	yel. hex.	4.008 ¹⁷	119	subl.	0.01 ²⁵	1.5 ¹⁷	13.6 ²⁵
Ionone (<i>α</i> -)	C ₁₀ H ₁₆ :CHCOCH ₃	192.30	col. oil	0.930 ²⁰		136.1 ¹⁷	sl. s.	∞	∞
(<i>β</i> -)	C ₁₀ H ₁₆ :CHCOCH ₃	192.30	col. oil	0.944 ²⁰		140 ¹⁸	sl. s.	∞	∞
Iron (β-)	C ₁₄ H ₂₂ O	206.32	col. oil	0.939 ²⁰		144 ¹⁶	v. sl. s.	v. s.	v. s.
Isatin	C ₆ H ₄ < (CO)(N) > COH	147.13	yel. red		200-1	subl.	s. h.	v. s. h.	sl. s.
Isoprene	CH ₂ :CH-C(CH ₃):CH ₂	68.12	col. lq.	0.681 ^{20/4}	-120	34	i.	∞	∞
Ketene	H ₂ C:CO	42.04	col. gas		-151	-56	d.	d.	s.
Koch acid (1-)(3-,6-,8-)	C ₁₀ H ₄ (NH ₂) ₃ S ₃ O ₃ HN ₂	427.34	cr.				7.2 ²⁰		
Lactic acid (<i>dl</i> -)	CH ₃ CH(OH)CO ₂ H	90.08	hyg.	1.249 ^{15/4}	16.8	122 ¹⁴	∞	∞	∞
anhydride	C ₆ H ₁₀ O ₃	162.14	yel. oil			d. 250	v. sl. s.	s.	s.
Lactide (<i>dl</i> -)	C ₆ H ₈ O ₄	144.13	tri./al.	0.862 ^{10/4}	124.5	255 ^{75/7}	v. sl. s.	v. sl. s. c.	
Lactose	C ₁₂ H ₂₂ O ₁₁ ·H ₂ O	360.31	col. rhb.	1.525 ²⁰	202	d.	17 ¹⁰	i.	i.
Lauric acid	CH ₃ (CH ₂) ₁₀ CO ₂ H	200.32	col. nd.	0.869 ^{20/4}	48(44)	225 ¹⁰⁰	i.	s.	s.
Laurone	[CH ₃ (CH ₂) ₁₀] ₂ CO	338.61	pl.	0.809 ^{20/4}	69-70		i.	i. c.	
Lauryl alcohol	CH ₃ (CH ₂) ₁₀ CH ₂ OH	186.33	lf.	0.831 ^{24/4}	24	255-9	i.	s.	s.
Lead tetraethyl	Pb(CH ₂ CH ₃) ₄	323.44	col. lq.	1.659 ^{18/4}	-136	152 ^{20/1}	i.	sl. s.	∞
tetramethyl	Pb(CH ₃) ₄	267.34	col. lq.	1.995 ^{20/4}	-27.5	110 ^{70/0}	i.	∞	∞
Lepidine (<i>py</i> -4)	C ₈ H ₆ N-CH ₃	143.19	lq.	1.086 ²⁰	9-10	216-3	sl. s.	∞	∞
Leucine (<i>l</i> -)	(CH ₃) ₂ CHCH ₂ CH(NH ₂)CO ₂ H	131.17	cr.	1.293 ¹⁸	295	subl.	2.2 ¹⁸		
Levulinic acid	CH ₃ CO(CH ₂) ₂ CO ₂ H	116.12	lf.	1.140 ^{20/20}	33.5	245-6	v. s.	v. s.	v. s.
Limonene (<i>d</i> - or <i>l</i> -)	C ₁₀ H ₁₆	136.23	lq.	0.842 ^{20/4}	-96.9	177	i.	∞	∞
Linalool (<i>d</i> - or <i>l</i> -)	C ₁₀ H ₁₇ OH	154.25	col. oil	0.868 ²⁰		198-200	v. sl. s.	s.	∞
Linalyl acetate	CH ₃ CO ₂ C ₁₀ H ₁₇	196.29	col. lq.	0.895 ²⁰		220 ^{76/2} d.	v. sl. s.	∞	∞
Linoleic acid	C ₁₇ H ₃₁ CO ₂ H	280.45	yel. oil	0.903 ^{15/4}	-9.5	229-30 ¹⁶	i.	∞	∞
Malic acid	HO ₂ C-CH-CH-CH ₂ CO ₂ H	116.07	mn.	1.609	130.5	135 d.	79 ²⁵	70 ³⁰	8 ²⁵
anhydride	< (-CHCO) ₂ > O	98.06	cr.	1.5	57-60	202	16.3 ⁸⁰		
Malic acid (<i>dl</i> -)	HO ₂ CCH ₂ CH(OH)CO ₂ H	134.09	col. cr.	1.601 ^{20/4}	128-9	150 d.	144 ²⁰	v. s.	v. s.
(<i>d</i> - or <i>l</i> -)	HO ₂ CCH ₂ CH(OH)CO ₂ H	134.09	col. cr.	1.595 ^{20/4}	99-100	140 d.	v. s.	v. s.	8.4 ¹⁵
Malonic acid	H ₂ C(CO ₂ H) ₂	104.06	col. tri.	1.631 ¹⁵	130-5 d.		138 ¹⁶	42 ²⁵	8 ¹⁵
Maltose	C ₁₂ H ₂₂ O ₁₁ ·H ₂ O	360.31	col. nd.	1.540 ¹⁷	d.		108 ²⁵	v. sl. s. c.	i.
Mandelic acid (<i>dl</i> -)	C ₆ H ₅ CH(OH)CO ₂ H	152.15	rhb./aq.	1.300 ^{20/4}	118.1	d.	16 ²⁰	s.	s.
Mannitol (<i>d</i> -)	CH ₂ OH(CHOH) ₄ CH ₂ OH	182.17	col. rhb.	1.489 ^{20/4}	166	290-5 ³	13 ¹⁴	0.01 ¹⁴	i.
Mannose (<i>d</i> -)	CH ₂ OH(CHOH) ₄ CHO	180.16	rhb.	1.539 ^{20/4}	132		248 ¹⁷	v. sl. s.	i.
Margaric acid	CH ₃ (CH ₂) ₁₅ CO ₂ H	270.45	col. pl.	0.853 ⁹⁰	60-1	227 ¹⁰⁰	i.	32 ²⁸	v. s.
Mellitic acid	C ₆ (CO ₂ H) ₆	342.17	nd./al.		286-8	d.	v. s.	v. s.	
Menthol (1-)(<i>α</i> -)	C ₁₀ H ₁₉ OH	156.27	col. cr.	0.890 ^{15/15}	42-3	212	0.04 c.	v. s.	v. s.
Mercapto-benzothiazole (2-)	< C ₆ H ₄ N:C(SH)S >	167.25	nd.	1.42 ^{20/4}	179	d.	i.	s.	sl. s.
-thiazoline (2-)	< CH ₂ N:C(SH)SCH ₂ >	119.21	cr.	1.50	106		1.6 ⁶⁰		
Mercuric cyanide	Hg(CN) ₂	252.62	cr.	4.003 ²²	d. 320		12.5 ¹⁵		
fulminate	Hg(ONC) ₂ ·½H ₂ O	293.63	cr./aq.	4.4	d.		0.07 ¹²	s.	
Mesityl oxide	(CH ₃) ₂ C:CHCOCH ₃	98.14	lq.	0.858 ^{20/4}	-59	130 ^{75/0}	3 ²⁰	∞	∞
Mesitylene (1-,3-,5-)	C ₆ H ₃ (CH ₃) ₃	120.19	col. lq.	0.865 ^{20/4}	-45(-52)	164.8	i.	s.	∞
Metanilic acid (<i>m</i> -)	H ₂ NC ₆ H ₄ SO ₃ H	173.19	col. nd.		d.		2 ¹⁵	v. sl. s.	v. sl. s.
Methane	CH ₄	16.04	gas	0.415 ^{-16/4}	-182.6	-161.4	0.4 ²⁰ cc.	47 ²⁰ cc.	104 ¹⁰ cc.

Methoxy-methoxyethanol	$\text{CH}_3(\text{OCH}_2)_2\text{CH}_2\text{OH}$	106.12	lq.	1.038 ²⁵	<-70	167.5	∞	∞	∞
Methyl acetate	$\text{CH}_3\text{CO}_2\text{CH}_3$	74.08	col. lq.	0.924 ^{20/4}	-98.7	57.1	33 ²²	∞	∞
acrylic acid (α -)	$\text{CH}_2=\text{C}(\text{CH}_3)\text{CO}_2\text{H}$	86.09	pr.	1.015 ^{20/4}	15-16	161-3	s. h.	∞	∞
alcohol	CH_3OH	32.04	col. lq.	0.792 ^{20/4}	-97-8	64.7	∞	∞	∞
-amine	CH_3NH_2	31.06	col. gas	0.699 ⁻¹¹	-92.5	-6.7 ⁷⁵⁸	v. s.	v. s.	∞
-amine hydrochloride	$\text{CH}_3\text{NH}_2\cdot\text{HCl}$	67.52	pl./al.	1.23	226-8	230 ¹⁵	v. s.	23 h.	i.
aniline	$\text{C}_6\text{H}_5\text{NHCH}_3$	107.15	lq.	0.989 ^{20/4}	-57	195.5	0.01 ²⁵	∞	∞
anthracene (α -)	$\text{C}_6\text{H}_4:(\text{CH}_2)_2\text{C}_6\text{H}_4\text{CH}_3$	192.26	lf./al.	1.047 ^{20/4}	86		i.		
(β -)	$\text{C}_6\text{H}_4:(\text{CH}_2)_2\text{C}_6\text{H}_3\text{CH}_3$	192.26	col. lf.	1.181 ^{9/4}	207		i.	v. sl. s.	v. sl. s.
anthranilate (o -)	$\text{NH}_2\text{C}_6\text{H}_4\text{CO}_2\text{CH}_3$	151.16	col. lq.	1.168 ^{19/4}	24	135.5 ¹⁵	sl. s.	s.	s.
anthraquinone (2-)	$\text{C}_6\text{H}_2:(\text{CO})_2\text{C}_6\text{H}_3\text{CH}_3$	222.24	col. nd.		176-7		subl.	s.	s.
benzoate	$\text{C}_6\text{H}_5\text{CO}_2\text{CH}_3$	136.15	col. lq.	1.087 ^{25/25}	-12.5	198-9	0.02 ³⁰	∞	∞
benzylamine	$\text{C}_6\text{H}_5\text{N}(\text{CH}_2)\text{CH}_2\text{C}_6\text{H}_5$	197.28	lq.		9.2	305-6	i.	s.	s.
bromide	CH_3Br	94.94	gas	1.732 ^{9/0}	-93	4.5 ⁷⁵⁸	v. sl. s.	s.	s.
butyrate (n -)	$\text{CH}_3(\text{CH}_2)_2\text{CO}_2\text{CH}_3$	102.13	col. lq.	0.898 ^{20/4}	<-95	102.3	1.7	∞	∞
(i -)	$(\text{CH}_3)_2\text{CHCO}_2\text{CH}_3$	102.13	col. lq.	0.891 ^{20/4}	-84.7	92.6	v. sl. s.	∞	∞
caprate	$\text{CH}_3(\text{CH}_2)_8\text{CO}_2\text{CH}_3$	186.29	lq.		-18	223-4	i.	∞	∞
caproate (n -)	$\text{CH}_3(\text{CH}_2)_4\text{CO}_2\text{CH}_3$	130.18	col. lq.	0.904 ^{9/0}		149.5	i.	∞	∞
caprylate	$\text{CH}_3(\text{CH}_2)_6\text{CO}_2\text{CH}_3$	158.24	col. lq.	0.887 ¹⁸	-40	192-4	i.	∞	∞
cellosolve	$\text{CH}_3\text{OCH}_2\text{CH}_2\text{OH}$	76.09	col. lq.	0.965 ^{20/4}		124-5	∞	∞	∞
chloride	CH_2Cl	50.49	gas	0.952 ⁹	-97.7	-24	280 ¹⁶ cc.	v. s.	v. s.
chloroacetate	$\text{ClCH}_2\text{CO}_2\text{CH}_3$	108.52	col. lq.	1.236 ^{20/4}	-32.7	130 ^{7/40}	v. sl. s.	∞	∞
chloroformate	ClCO_2CH_3	94.50	col. lq.	1.236 ¹⁵		71-2	d.	∞	∞
cinnamate	$\text{C}_6\text{H}_5\text{CH}=\text{CHCO}_2\text{CH}_3$	162.19	cr.	1.042 ^{36/0}	33.4	263	i.	v. s.	v. s.
cyclohexane	$\text{CH}_2 < (\text{CH}_2)_4 > \text{CHCH}_3$	98.19	col. lq.	0.769 ^{20/4}	-126.3	101	i.	s.	s.
ethyl carbonate	$\text{CH}_3\text{O}-\text{CO}-\text{OC}_2\text{H}_5$	104.10	lq.	1.002 ²⁷	-14.5	109.2	i.	∞	∞
ethyl ketone	$\text{CH}_3\text{CO}-\text{C}_2\text{H}_5$	72.11	col. lq.	0.805 ^{20/4}	-85.9	79.6	35 ¹⁰	∞	∞
ethyl oxalate	$\text{CH}_3\text{OCO}-\text{CO}_2\text{C}_2\text{H}_5$	132.11	lq.	1.156 ^{9/0}		173.7	i.	v. s.	v. s.
formate	HCO_2CH_3	60.05	lq.	0.974 ^{20/4}	-99.8	32	30 ²⁰	∞	∞
furoate	$\text{C}_6\text{H}_4\text{O}-\text{CO}_2\text{CH}_3$	126.11	col. lq.	1.179 ^{21/4}		181.3	i.	∞	∞
glucamine	$\text{CH}_2\text{OH}(\text{CHOH})_4\text{CH}_2\text{NHCH}_3$	195.21							
glycolate	$\text{HOCH}_2\text{CO}_2\text{CH}_3$	90.08	lq.	1.168 ¹⁸		151.2			
heptoate	$\text{CH}_3(\text{CH}_2)_5\text{CO}_2\text{CH}_3$	144.21	lq.	0.881 ^{15/4}		172-3	i.		
hypochlorite	ClOCH_3	66.49	gas		-64.4	12 ⁷²⁶	1.8 ¹⁵	∞	∞
iodide	CH_3I	141.94	col. lq.	2.279 ^{20/4}		42.4	∞	∞	∞
lactate	$\text{CH}_3\text{CH}(\text{OH})\text{CO}_2\text{CH}_3$	104.10	lq.	1.090 ¹⁹		144.8	∞	s.	s.
laurate	$\text{CH}_3(\text{CH}_2)_{10}\text{CO}_2\text{CH}_3$	214.34	lq.		5	148 ¹⁵	i.	∞	∞
mercaptan	CH_3SH	48.11	gas	0.896 ⁹	-121	5.8 ⁷⁵²	s.	v. s.	v. s.
methacrylate	$\text{CH}_2=\text{C}(\text{CH}_3)\text{CO}_2\text{CH}_3$	100.12	lq.	0.950 ^{15/6}	-48	100.3	i.	∞	∞
myristate	$\text{CH}_3(\text{CH}_2)_{12}\text{CO}_2\text{CH}_3$	242.40	cr./al.		18-9	295 ⁷¹⁵	i.	∞	∞
naphthalene (α -)	$\text{C}_{10}\text{H}_7\text{CH}_3$	142.20	oil	1.025 ^{14/4}	-19	244.6	i.	v. s.	v. s.
(β -)	$\text{C}_{10}\text{H}_7\text{CH}_3$	142.20	mn.	0.994 ^{40/4}	35-6	241-2	i.	v. s.	v. s.
nitrate	CH_3ONO_2	77.04	lq.	1.203 ²⁵	expl.	65	sl. s.	s.	s.
nitrite	CH_3ONO	61.04	gas	0.991 ¹⁵		-12		s.	s.
nonyl ketone (n -)	$\text{CH}_3(\text{CH}_2)_8\text{COCH}_3$	170.29	col. oil	0.828 ^{20/20}	13.5	228	i.	s.	s.
oleate	$\text{C}_{17}\text{H}_{33}\text{CO}_2\text{CH}_3$	296.49	oil	0.879 ¹⁸		190-1 ¹⁰	i.	∞	∞
orange	$(\text{CH}_3)_2\text{NC}_6\text{H}_4\text{N}_2\text{C}_6\text{H}_4\text{SO}_3\text{Na}$	327.33	red pd.				0.2 c.	∞	∞
palmitate	$\text{CH}_3(\text{CH}_2)_{14}\text{CO}_2\text{CH}_3$	270.45	col. cr.		30-1	196 ¹⁵	i.	s.	s.
phosphine	CH_3PH_2	48.02	gas			-14 ⁷⁵⁹	i.	sl. s.	∞
propionate	$\text{CH}_3\text{CH}_2\text{CO}_2\text{CH}_3$	88.11	col. lq.	0.915 ^{20/4}	-87.5	79.7	0.5 ²⁰	∞	∞
propyl ketone (n -)	$\text{CH}_3\text{COCH}_2\text{CH}_2\text{CH}_3$	86.13	col. lq.	0.812 ^{15/15}	-77.8	102	v. sl. s.	∞	∞
salicylate (o -)	$\text{HO}-\text{C}_6\text{H}_4\text{CO}_2\text{CH}_3$	152.15	col. lq.	1.182 ^{25/25}	-8.3	222.2	0.07 ³⁰	∞	∞
stearate	$\text{CH}_3(\text{CH}_2)_{16}\text{CO}_2\text{CH}_3$	298.50	col. cr.		38-9	215 ¹⁵	i.	s.	s.
toluate (o -)	$\text{CH}_3-\text{C}_6\text{H}_4\text{CO}_2\text{CH}_3$	150.17	col. lq.	1.073 ¹⁵	<-50	213	i.	∞	∞
(m -)	$\text{CH}_3-\text{C}_6\text{H}_4\text{CO}_2\text{CH}_3$	150.17	col. lq.	1.066 ¹⁵		215	i.	∞	∞
(p -)	$\text{CH}_3-\text{C}_6\text{H}_4\text{CO}_2\text{CH}_3$	150.17	cr.		33-4	217	i.	v. s.	v. s.
Methyl toluidine (o -)	$\text{CH}_3-\text{C}_6\text{H}_4\text{NHCH}_3$	121.18	lq.	0.973 ¹⁵		206-7	i.	∞	∞
(m -)	$\text{CH}_3-\text{C}_6\text{H}_4\text{NHCH}_3$	121.18	lq.			206-7	i.	∞	∞
(p -)	$\text{CH}_3-\text{C}_6\text{H}_4\text{NHCH}_3$	121.18	lq.	0.935 ^{25/4}		211 ⁷⁶¹	i.	∞	∞
valerate (n -)	$\text{CH}_3(\text{CH}_2)_3\text{CO}_2\text{CH}_3$	116.16	lq.	0.895 ^{15/4}	-91	127.3	v. sl. s.	∞	∞
(i -)	$(\text{CH}_3)_2\text{CHCH}_2\text{CO}_2\text{CH}_3$	116.16	col. lq.	0.881 ^{20/4}		116.7 ⁷⁶⁴	v. sl. s.	∞	∞
vinyl ketone	$\text{CH}_2=\text{C}(\text{OCH}_3)\text{CH}_2$	70.09	lq.	0.836 ^{20/4}		81	>85	∞	∞
Methylal	$\text{HCH}(\text{OCH}_3)_2$	76.09	col. lq.	0.866 ^{15/4}	-104.8	42-3	33	∞	∞
Methylene-bis-(phenyl-4-isocyanate)	$(\text{OCN}-\text{C}_6\text{H}_4)_2\text{CH}_2$	250.25	lq.	1.222 ²⁰		210-2 ¹³	d.	d.	∞
bromide	CH_2Br_2	173.83	col. lq.	2.495 ^{20/4}	-52.8	98.5 ⁷⁵⁶	1.17 ⁰	∞	∞
chloride	CH_2Cl_2	84.93	col. lq.	1.336 ^{20/4}	-96.7	40-1	2 ²⁰	∞	∞
dianiline	$(\text{C}_6\text{H}_5\text{NH})_2\text{CH}_2$	198.26	cr.		65	208-9 d.	i.	s.	s.
iodide	CH_2I_2	267.84	col. lq.	3.325 ^{20/4}	5.7	180 d.	1.4 ²⁰	∞	∞
Michler's hydrol (p -, p' -)	$[(\text{CH}_3)_2\text{NC}_6\text{H}_4]_2\text{CHOH}$	270.37	gn.		96-7		i.	s. h.	∞
ketone	$[(\text{CH}_3)_2\text{NC}_6\text{H}_4]_2\text{CO}$	268.35	lf./al.		174	>360 d.	i.	sl. s.	v. sl. s.
Morphine	$\text{C}_{17}\text{H}_{19}\text{O}_3\text{N}\cdot\text{H}_2\text{O}$	303.35	pr./al.	1.317	254 d.		0.02 ²⁰	sl. s.	∞
Mucic acid	$(-\text{CHOHCH}(\text{OHCO}_2\text{H})_2)$	210.14	pd.		206-14		0.33 ¹⁴	i.	i.

TABLE 2-2 Physical Properties of Organic Compounds (Continued)

Name	Formula	Formula weight	Form and color	Specific gravity	Melting point, °C	Boiling point, °C	Solubility in 100 parts		
							Water	Alcohol	Ether
Mustard gas	(ClCH ₂ :CH ₂) ₂ S	159.08	oil	1.275 ^{20/4}	13–4	217	0.07 ²⁵	s.	s.
Myrcyl alcohol	C ₉ H ₁₆ O(OH)(?)	452.84	cr.	0.777 ^{7/5}	88		i.	v. sl. s.	v. s.
Myristic acid	CH ₃ (CH ₂) ₁₂ CO ₂ H	228.37	col. lf.	0.853 ^{20/4}	57–8	250.5 ¹⁰⁰	i.	v. s.	v. s.
Myristyl alcohol	CH ₃ (CH ₂) ₁₂ CH ₂ OH	214.39	cr.	0.824 ^{25/4}	38	167 ¹⁵	<0.02	sl. s.	v. s.
Naphthalene	C ₁₀ H ₈	128.17	pl./al.	1.145 ^{20/4}	80.2	217.9	0.003 ²⁵	9.5 ²⁰	v. s.
disulfonic acid (1-,5-)	C ₁₀ H ₆ (SO ₃ H) ₂	288.30	lf.		d.		102 ²⁰	s.	i.
(1-,6-)	C ₁₀ H ₆ (SO ₃ H) ₂	288.30	cr.		d. 125		164 ²⁰	s.	i.
sulfonic acid (α-)	C ₁₀ H ₇ SO ₃ H·2H ₂ O	244.26	cr.		90		v. s.	v. s.	sl. s.
(β-)	C ₁₀ H ₇ SO ₃ H·H ₂ O	226.25	cr.		125		77 ²⁰		
Naphthasultam (1-,8-)	C ₁₀ H ₇ O ₂ NS	205.23	nd.		177–8		s. h.	sl. s.	s.
disulfonate Na (1-,8-)	C ₁₀ H ₅ O ₂ NS ₂ Na ₂ ·2H ₂ O	445.35	cr.				v. s.		
(2-,4-)	C ₁₀ H ₄ O ₂ NS ₂ Na ₂ ·8½H ₂ O	584.43	lf.				v. s.	sl. s.	
Naphthoic acid (α-)	C ₁₀ H ₇ CO ₂ H	172.18	nd.		160–1	300	v. sl. s. h.	sl. s.	s.
(β-)	C ₁₀ H ₇ CO ₂ H	172.18	mn.	1.077 ^{100/4}	184	>300	0.007 ²⁵	s.	s.
Naphthol (α-)	C ₁₀ H ₇ OH	144.17	mn.	1.224 ⁴	96	278–80	sl. s. h.	v. s.	v. s.
(β-)	C ₁₀ H ₇ OH	144.17	mn.	1.217 ⁴	122–3	285–6	0.074 ²⁵	v. s.	v. s.
sulfonic acid (α-)(1-,2-)	HO·C ₁₀ H ₆ SO ₃ H	224.23	pl./aq.		>250		v. s. h.		i.
(β-)(2-,6-)	HO·C ₁₀ H ₆ SO ₃ H	224.23	lf.		125		v. s.	v. s.	
Naphthyl acetate (α-)	CH ₃ CO ₂ C ₁₀ H ₇	186.21	nd./al.		46–9		sl. s. h.	s.	s.
(β-)	CH ₃ CO ₂ C ₁₀ H ₇	186.21	nd./al.		69–70		i.	s.	s.
amine (α-)	C ₁₀ H ₇ NH ₂	143.19	rhb.	1.123 ^{25/25}	50	300.8	0.17 c.	v. s.	v. s.
(β-)	C ₁₀ H ₇ NH ₂	143.19	lf./aq.	1.061 ^{98/4}	111–2		v. s. h.	s.	s.
amine hydrochloride (α-)	C ₁₀ H ₇ NH ₂ ·HCl	179.65	nd.			subl.	3.8 ²⁰	s.	s.
(β-)	C ₁₀ H ₇ NH ₂ ·HCl	179.65	lf.				v. s.	v. s.	
amine sulfonic acid (1-,4-)	NH ₂ ·C ₁₀ H ₆ ·SO ₃ H	223.25	nd.		d.		0.2 ¹⁰⁰	i.	i.
(1-,5-)	NH ₂ ·C ₁₀ H ₆ ·SO ₃ H·H ₂ O	241.26	cr.				sl. s.		
(1-,7-)	NH ₂ ·C ₁₀ H ₆ ·SO ₃ H·H ₂ O	241.26	cr.				0.46 ²⁵		
(1-,8-)	NH ₂ ·C ₁₀ H ₆ ·SO ₃ H·H ₂ O	241.26	cr.				0.42 ¹⁰⁰		
(2-,5-)	NH ₂ ·C ₁₀ H ₆ ·SO ₃ H	223.25	cr.				0.08		
(2-,6-)	NH ₂ ·C ₁₀ H ₆ ·SO ₃ H·H ₂ O	241.26	cr.				0.38 ¹⁰⁰		
(2-,7-)	NH ₂ ·C ₁₀ H ₆ ·SO ₃ H·H ₂ O	241.26	cr.				0.28 ¹⁰⁰		
isocyanate (α-)	C ₁₀ H ₇ N:CO	169.18	col. lq.	1.18		269–70	d.	s.	s.
Nicotine	C ₁₀ H ₁₄ N ₂	162.23	oil	1.009 ^{20/4}	<–80	246 ⁷³⁰	s.	∞	∞
Nicotinic acid (3-)	C ₆ H ₄ NCO ₂ H	123.11	nd./al.		235.2	subl.	s. h.	s. h.	v. sl. s.
(i-)(4-)	C ₆ H ₄ NCO ₂ H	123.11	nd./aq.		317	d.	s. h.	sl. s. h.	v. sl. s.
Nitro-acetanilide (p-)	CH ₃ CONHC ₆ H ₄ NO ₂	180.16	rhb.		215–6		s. h.	s.	s.
-acetophenone (m-)	CH ₃ COC ₆ H ₄ NO ₂	165.15	nd.		80–1	202	i.	s.	
-aminoanisole (4-,1-,2-)	NO ₂ ·C ₆ H ₃ (OCH ₃)NH ₂	168.15	red nd.	1.207 ¹⁵⁶	118		i.	s.	
(5-,1-,2-)	NO ₂ ·C ₆ H ₃ (OCH ₃)NH ₂	168.15	yel. nd.	1.211 ¹⁵⁶	139–40				
(3-,1-,4-)	NO ₂ ·C ₆ H ₃ (OCH ₃)NH ₂	168.15	red		123		sl. s.	s.	s.
-aminophenol (4-,2-,1-)	NO ₂ ·C ₆ H ₃ (NH ₂)OH	154.12	or. pr.		142–3		sl. s. c.	v. s.	v. s.
-aniline (o-)	NO ₂ ·C ₆ H ₄ NH ₂	138.12	yel. rhb.	1.442 ¹⁵	71.5	284.1	s. h.	v. s.	v. s.
(m-)	NO ₂ ·C ₆ H ₄ NH ₂	138.12	yel. rhb.	1.43	114	306.4	0.11 ²⁰	7.1 ²⁰	7.9 ²⁰
(p-)	NO ₂ ·C ₆ H ₄ NH ₂	138.12	yel. mn.	1.437 ¹⁴	146–7	331.7	0.08 ¹⁹	5.8 ²⁰	6.1 ²⁰
-anisole (o-)	CH ₃ OOC ₆ H ₄ NO ₂	153.14	col. cr.	1.254 ^{20/4}	9.4	272–3	0.17 ³⁰	∞	∞
(p-)	CH ₃ OOC ₆ H ₄ NO ₂	153.14	pr./al.	1.233 ²⁰	54	274	0.06 ³⁰	v. s.	v. s.
-anthraquinone (α-)	C ₁₄ H ₈ (CO) ₂ ·C ₆ H ₃ NO ₂	253.21	nd.		230	270 ⁷	i.	sl. s.	v. sl. s.
-anthraquinone sulfonic acid (1-,5-)	NO ₂ ·C ₁₄ H ₇ O ₂ ·SO ₃ H	333.27	yel. cr.				s.	i.	i.
-benzal chloride (m-)	NO ₂ ·C ₆ H ₄ ·CHCl ₂	206.03	mn.		65		i.	v. s. h.	v. s.
-benzaldehyde (m-)	NO ₂ ·C ₆ H ₄ ·CHO	151.12	nd./aq.		58	164 ²³	1.95 ¹¹²	v. s. h.	v. s.
Nitro-benzene	C ₆ H ₅ NO ₂	123.11	yel. lq.	1.205 ^{18/4}	5.7	210.9	0.19 ²⁰	v. s.	∞
-benzidine (2-)	NH ₂ ·C ₆ H ₄ ·C ₆ H ₃ (NH ₂)NO ₂	229.23	red nd.		143		sl. s. h.		
-benzoic acid (o-)	NO ₂ ·C ₆ H ₄ ·CO ₂ H	167.12	tri./aq.	1.575 ^{4/4}	147.5		0.65 ²⁰	28 ¹¹	22 ¹¹
(m-)	NO ₂ ·C ₆ H ₄ ·CO ₂ H	167.12	mn.	1.494 ^{4/4}	140–1		0.24 ¹⁶⁵	31 ¹²	25 ¹⁰
(p-)	NO ₂ ·C ₆ H ₄ ·CO ₂ H	167.12	yel. mn.	1.550 ^{22/4}	240–2	subl.	0.02 ¹⁵	0.9 ¹⁰	2.2 ¹⁸
-benzyl alcohol (m-)	NO ₂ ·C ₆ H ₄ ·CH ₂ OH	153.14	cr.		27	175–80 ³			
-benzyl bromide (p-)	NO ₂ ·C ₆ H ₄ ·CH ₂ Br	216.03	nd./al.		99–100		i.	2 ¹⁹	v. s.
-chlorotoluene (1-,2-,6-)	CH ₃ ·C ₆ H ₃ (NO ₂)Cl	171.58	cr.		37.5	238	i.		
-cresol (1-,3-,4-)	CH ₃ ·C ₆ H ₃ (NO ₂)OH	153.14	yel.	1.240 ^{89/4}	32	125 ²²	v. sl. s.	v. s.	v. s.
-cymene (1-,2-,4-)	CH ₃ ·C ₆ H ₃ (NO ₂)CH(CH ₃) ₂	179.22	oil	1.067 ^{20/4}		152 ¹⁵	i.		
-dimethylaniline (o-)	NO ₂ ·C ₆ N ₂ (CH ₃) ₂	166.18	yel. oil	1.179 ^{20/4}		151–3 ⁸⁰	v. sl. s.	v. s.	v. s.
(m-)	NO ₂ ·C ₆ H ₄ N(CH ₃) ₂	166.18	red mn.	1.313 ¹⁷	60–1	280–5	i.	s.	s.
(p-)	NO ₂ ·C ₆ H ₄ N(CH ₃) ₂	166.18	yel. nd.		163–4		i.	s. h.	
-diphenyl (o-)	C ₆ H ₅ ·C ₆ H ₄ NO ₂	199.21	rhb.	1.44	37	320	i.	s.	v. s.
(p-)	C ₆ H ₅ ·C ₆ H ₄ NO ₂	199.21	nd./al.		113–4	340	i.	sl. s. c.	v. s.
-diphenylamine (o-)	C ₆ H ₅ ·NH·C ₆ H ₄ NO ₂	214.22	or. cr.		75–6				
-guanidine	H ₂ NC(NH)NHNO ₂	104.07	nd./aq.		246–7		9 ¹⁰⁰	sl. s.	v. sl. s.

-naphthalene (α -)	$C_{10}H_7NO_2$	173.17	yel./al.	1.223 ⁶²	59-60	304	i.	s.	s.
(β -)	$C_{10}H_7NO_2$	173.17	col./al.		79	165 ¹⁵	i.	v. s.	v. s.
-phenol (<i>o</i> -)	$NO_2 \cdot C_6H_4 \cdot OH$	139.11	yel. mn.	1.295 ⁴⁵	44-5	214.5	1.08 ¹⁰⁰	v. s.	v. s.
(<i>m</i> -)	$NO_2 \cdot C_6H_4 \cdot OH$	139.11	col. mn.	1.485 ³⁰	96-7	194 ⁷⁰	1.35 ²⁰	v. s.	v. s.
(<i>p</i> -)	$NO_2 \cdot C_6H_4 \cdot OH$	139.11	yel. pr.	1.479 ²⁰	113-4	subl.	1.6 ²⁵	v. s.	v. s.
-phenol sulfonic acid (1-,4-,2-)	$HO \cdot C_6H_3(NO_2)SO_3H \cdot 3H_2O$	273.22	nd.		d. 110		v. s.	v. s.	sl. s.
(1-,2-,4-)	$HO \cdot C_6H_3(NO_2)SO_3H \cdot 3H_2O$	273.22	nd./aq.		51.5		v. s.	v. s.	
-phthalic acid (3-)	$NO_2 \cdot C_6H_3(CO_2H)_2$	211.13	yel./aq.		222		2.05 ²⁵	v. s. h.	sl. s.
(4-)	$NO_2 \cdot C_6H_3(CO_2H)_2$	211.13	yel. cr.		164-5		v. s.	v. s.	
-toluene (<i>o</i> -)	$CH_3 \cdot C_6H_4NO_2$	137.14	yel. lq.	1.163 ^{20/4}	-4.1	222.3	0.07 ⁸⁰	∞	∞
(<i>m</i> -)	$CH_3 \cdot C_6H_4NO_2$	137.14	lq.	1.160 ^{18/4}	15-16	230-1	0.05 ⁸⁰	∞	∞
(<i>p</i> -)	$CH_3 \cdot C_6H_4NO_2$	137.14	rhb.	1.139 ^{55/55}	51.9	237.7	0.04 ⁸⁰	8.6 ¹⁵	80.8 ¹⁵
-toluene sulfonic acid (1-,4-,2-)	$CH_3 \cdot C_6H_3(NO_2)SO_3H \cdot 2H_2O$	253.23	pl./aq.		130		47.7 ²⁵	v. s.	v. s.
-toluidine (4-,1-,2-)	$NO_2 \cdot C_6H_3(CH_3)NH_2$	152.15	yel. mn.	1.365 ¹⁵	105-7		v. sl. s.	s.	s.
(3-,1-,4-)	$NO_2 \cdot C_6H_3(CH_3)NH_2$	152.15	red mn.	1.312 ¹⁷	116-7		sl. s. h.	s.	s.
Nitron	$C_{20}H_{16}N_4$	312.37	yel. lf.		189-90 d.		i.	s. h.	v. sl. s.
Nitroso-dimethylaniline (<i>p</i> -)	$ON \cdot C_6H_4N(CH_3)_2$	150.18	gn. tri.		86-7		i.	s.	s.
-naphthol (β -)(1-)	$ON \cdot C_{10}H_7OH$	173.17	brn. pr.		109.5		0.1 ²⁰	2.4 ¹⁸	
Nonadecane (<i>n</i> -)	$CH_3(CH_2)_{17}CH_3$	268.52	cr.	0.777 ^{32/4}	32	330	i.	sl. s.	s.
Nonane (<i>n</i> -)	$CH_3(CH_2)_7CH_3$	128.26	col. lq.	0.718 ^{20/4}	-53.7	150.5 ^{75/9}	i.	sl. s.	s.
Octadecane (<i>n</i> -)	$CH_3(CH_2)_{16}CH_3$	254.49	cr.	0.775 ^{25/4}	28	317	i.	sl. s.	s.
Octane (<i>n</i> -)	$CH_3(CH_2)_6CH_3$	114.23	col. lq.	0.703 ^{20/4}	-56.5	125.7	0.002 ¹⁶	sl. s.	s.
(iso-)	$(CH_3)_2CCH_2CH_2CH_3$	114.23	col. lq.	0.692 ^{20/4}	-107.4	99.3 ^{70/0}	i.	sl. s.	s.
Octyl acetate (<i>n</i> -)	$CH_3CO_2CH_2(CH_2)_6CH_3$	172.26	col. lq.	0.885 ^{0/4}	-38.5	210	i.	s.	s.
(<i>sec</i> -)	$CH_3CO_2CH(CH_3)(CH_2)_5CH_3$	172.26	col. lq.	0.863 ^{14/4}		195	i.	s.	s.
alcohol (<i>n</i> -)	$CH_3(CH_2)_6CH_2OH$	130.23	col. lq.	0.827 ^{27/20/4}	-16	194-5	0.054 ²⁵	∞	∞
(<i>sec</i> -)	$CH_3(CH_2)_5CH(OH)CH_3$	130.23	col. lq.	0.822 ^{20/4}	-38.6	179-80	0.096 ²⁵	∞	∞
Octylene (<i>n</i> -)	$CH_3(CH_2)_5CH_2CH_2$	111.21	lq.	0.721 ^{18/4}		126	i.	∞	∞
Oleic acid	$C_8H_{17} \cdot CH \cdot CH(CH_2)_7 \cdot CO_2H$	282.46	col. nd.	0.854 ^{78/4}	14	285-6 ¹⁰⁰	i.	∞	∞
Orcinol (1-,3-,5-)	$(HO)_2C_6H_3 \cdot CH_3$	124.14	pr./bz.	1.290 ⁴	107-8	287-90	v. s.	v. s.	v. s.
Oxalic acid	$HO_2C \cdot CO_2H \cdot 2H_2O$	126.07	col. mn.	1.653 ^{19/4}	101.5	subl.	s.	v. s.	1.3
Palmitic acid	$CH_3(CH_2)_{14}CO_2H$	256.42	col. pl.	0.849 ^{70/4}	63-4	271.5 ¹⁰⁰	i.	9 ³⁰	s.
Pelargonic acid	$CH_3(CH_2)_7CO_2H$	158.24	col. oil	0.906 ^{20/4}	12.5	253-4	v. sl. s.	s.	s.
Penta-chloroethane	$CHCl_2 \cdot CCl_3$	202.29	col. lq.	1.671 ^{25/4}	-22	162	0.05 ²⁰	∞	∞
-decane (<i>n</i> -)	$CH_3(CH_2)_{10}CH_3$	212.41	col. lq.	0.770 ^{20/4}	10	270.5	i.	v. s.	v. s.
-erythritol	$C(CH_2OH)_4$	136.15	cr.		262	276 ³⁰	5.6 ¹⁵	v. sl. s.	i.
Pentandiol	$HOCH_2(CH_2)_3CH_2OH$	104.15	lq.	0.994 ^{20/4}		239.4	∞	∞	∞
Pentane (<i>n</i> -)	$CH_3(CH_2)_3CH_3$	72.15	col. lq.	0.630 ^{18/4}	-129.7	36.3	0.036 ¹⁶	∞	∞
(<i>i</i> -)	$(CH_3)_2CHCH_2CH_3$	72.15	col. lq.	0.621 ¹⁹	-160.0	27.95	i.	∞	∞
(neo-)	$(CH_3)_3C(CH_3)_2$	72.15	col. lq.	0.613 ^{20/4}	-20	9.5	i.	s.	s.
Phenacetin	$C_8H_9O_2C_6H_4NHCOCOCH_3$	179.22	col. mn.		134-5	d.	0.7 ²⁰	40 h.	1.6 ²⁵
Phenanthrene	$> (C_6H_4CH)_2$	178.23	pl./al.	1.179 ²⁵	99-100	340	i.	10 h.	v. s.
Phenetidine (<i>o</i> -)	$C_8H_9O \cdot C_6H_4 \cdot NH_2$	137.18	oil		<-21	228-9	i.	s.	s.
(<i>p</i> -)	$C_8H_9O \cdot C_6H_4 \cdot NH_2$	137.18	lq.	1.061 ¹⁵	3-4	254-5	i.	s.	s.
Phenetole	$C_8H_9O \cdot C_6H_5$	122.16	col. lq.	0.967 ^{20/4}	-30.2	172	i.	∞	∞
Phenol	C_6H_5OH	94.11	col. nd.	1.071 ^{25/4}	42-3	181.4	8.2 ¹⁵	∞	∞
-phthalein	$C_{20}H_{14}O_4$	318.32	col. rhb.	1.299 ^{25/4}	261-2		0.2 ²⁰	10 ²⁵	5.9 c.
-sulfonic acid (<i>o</i> -)	$HO \cdot C_6H_4SO_3H \cdot 3/4H_2O$	187.69	cr.		50 d.		v. s.	v. s.	
Phenyl acetaldehyde	$C_6H_5CH_2CHO$	120.15	lq.	1.025 ³⁰		193-4	v. sl. s.	∞	∞
acetic acid	$C_6H_5CH_2CO_2H$	136.15	lf.	1.081 ^{30/4}	76-7	265.5	1.66 ²⁰	v. s.	v. s.
-acetylene	$C_6H_5C \cdot CH$	102.13	col. lq.	0.930 ^{20/4}	-43	142-3	i.	∞	∞
aniline (<i>o</i> -)	$C_6H_5 \cdot C_6H_4 \cdot NH_2$	169.22	cr.		45-6	299 ^{70/0}	v. sl. s.	s.	s.
(<i>p</i> -)	$C_6H_5 \cdot C_6H_4 \cdot NH_2$	169.22	lf.		50-2	302	s. h.	s.	s.
Phenyl-ethyl alcohol	$C_6H_5CH_2CH_2OH$	122.16	col. oil	1.023 ^{18/4}		219-21 ^{70/0}	1.6 ²⁰	s.	sl. s.
-glycine	$C_6H_5NHCH_2CO_2H$	151.16	cr.		127		s.	s.	sl. s.
-hydrazine	$C_6H_5NH \cdot NH_2$	108.14	yel. oil	1.097 ^{23/4}	19.6	243.5	sl. s. h.	∞	∞
-hydrazine sulfonic acid (<i>p</i> -)	$H_2NNHC_6H_4SO_3H$	188.20	cr./al.		286		0.6 ¹²	sl. s.	∞
isocyanate	$C_6H_5N \cdot CO$	119.12	lq.	1.096 ^{20/4}		166 ^{70/0}	d.	d.	v. s.
-methylpyrazolone (3-)(<i>N</i> -)	$C_6H_5ON_2 \cdot C_6H_5$	174.20	pr./aq.		128	191 ¹⁷	1 ²⁰	v. s. h.	v. sl. s.
-mustard oil	$C_6H_5N \cdot CS$	135.19	col. lq.	1.138 ^{15/15}	-21	219-20	i.	s.	v. s.
naphthalene (α -)	$C_{10}H_7 \cdot C_6H_5$	204.27	waxy		45	336-7	i.	v. s.	v. s.
(β -)	$C_{10}H_7 \cdot C_6H_5$	204.27	lf./al.		102.5	345-6	i.	sl. s.	sl. s.
naphthylamine (α -)	$C_{10}H_7NHC_6H_5$	219.28	pr./al.	1.17	62	335 ^{25/8}	0.08 ⁶⁰	s.	s.
(β -)	$C_{10}H_7NHC_6H_5$	219.28	rhb.	1.18	107-8	399.5	0.4 ⁶⁰	v. s. h.	v. s. h.
phenol (<i>o</i> -)	$C_6H_5 \cdot C_6H_4OH$	170.21	nd.		56-7	275	i.	s.	s.
(<i>p</i> -)	$C_6H_5 \cdot C_6H_4OH$	170.21	nd.		164-5	305-8	i.	s.	s.
propyl alcohol (γ -)	$C_6H_5(CH_2)_3OH$	136.19	oil	1.008 ^{20/4}	<-18	235-7	sl. s.	∞	∞
quinoline (2-)(α -)	$C_8H_5 \cdot C_6H_6N$	205.25	nd.		86	363	sl. s.	s. h.	s.
(8-)(0-)	$C_8H_5 \cdot C_6H_6N$	205.25	lq.			283 ¹⁸⁷	sl. s.	s.	s.
salicylate, salol	$HO \cdot C_6H_4CO_2C_6H_5$	214.22	rhb./al.	1.250 ^{20/4}	42-3	172-3 ¹²	0.015 ²⁵	v. s.	s.
stearate	$CH_3(CH_2)_{16}CO_2C_6H_5$	360.57	cr.		52	267 ¹⁵	i.		
urethane	$C_6H_5NHCOCO_2C_6H_5$	165.19	pl./al.	1.106 ^{20/4}	52-3	237-8	i. c.	s.	s.

TABLE 2-2 Physical Properties of Organic Compounds (Continued)

Name	Formula	Formula weight	Form and color	Specific gravity	Melting point, °C	Boiling point, °C	Solubility in 100 parts		
							Water	Alcohol	Ether
Phenylene-diamine (<i>o</i> -)	$C_6H_4(NH_2)_2$	108.14	lf./aq.		103-4	256-8	733 ⁸¹	v. s.	v. s.
(<i>m</i> -)	$C_6H_4(NH_2)_2$	108.14	rhb.	1.139 ^{15/15}	62.8	284-7	35.1 ²⁵	v. s.	v. s.
(<i>p</i> -)	$C_6H_4(NH_2)_2$	108.14	mn.		140	267	669 ¹⁰⁷	s.	s.
Phloroglucinol (1-,3-,5-)	$C_6H_3(OH)_3 \cdot 2H_2O$	162.14	rhb.		117	subl.	1.13 ²⁵	v. s.	v. s.
Phorone	$[(CH_3)_2C \cdot CH]_2CO$	135.21	yel. pr.	0.885 ^{20/4}	28	197.2 ⁷⁴³	0.1 ⁹⁰	s.	s.
Phosgene	$COCl_2$	98.92	gas	1.392 ^{19/4}	-104	8.2 ⁷⁵⁶	v. sl. s.		
Phthalic acid (<i>o</i> -)	$C_6H_4(CO_2H)_2$	166.13	mn./aq.	1.593 ^{20/4}	208	d.	0.70 ²⁵	12 ¹⁸	0.68 ¹⁵
(<i>m</i> -)(iso-)	$C_6H_4(CO_2H)_2$	166.13	nd./aq.		330	subl.	0.2 ⁹⁰	s.	
anhydride (<i>o</i> -)	$C_6H_4 < (CO)_2 > O$	148.12	rhb.	1.527 ⁴	130.8	284.5	v. sl. s.	s.	sl. s.
nitrile (<i>o</i> -)	$C_6H_4(CN)_2$	128.13	cr.		141		sl. s. c.		
Phthalide	$C_8H_7(CH_2)(CO) > O$	134.13	nd./aq.	1.164 ^{99/4}	73(65)	290	v. sl. s.	s.	
Phthalimide (<i>o</i> -)	$C_8H_5 < (CO)_2 > NH$	147.13	cr./et.		238	subl.	0.04 ²⁵	5	s. h.
Picoline (α -)	$C_5H_4N \cdot CH_3$	93.13	col. lq.	0.950 ^{15/4}	-70	128.8	v. s.	∞	∞
(β -)	$C_5H_4N \cdot CH_3$	93.13	col. lq.	0.961 ^{15/4}		143.5	∞	∞	∞
(γ -)	$C_5H_4N \cdot CH_3$	93.13	lq.	0.957 ^{15/4}		143.1	∞	∞	∞
Picramic acid (1-,2-,4-,6-)	$HO \cdot C_6H_3(NH_2)(NO_2)_2$	199.12	red nd.		169		0.14 ²²	s.	sl. s.
Picric acid (2-,4-,6-)	$HO \cdot C_6H_2(NO_2)_3$	229.10	yel. rhb.	1.763 ^{20/4}	121.8	expl.	1.23 ²⁰	6 ²⁰	1 ¹³
Picryl chloride (2-,4-,6-)	$ClC_6H_2(NO_2)_3$	247.55	yel. mn.	1.797 ²⁰	83	d.	0.018 ¹⁵	4.8 ¹⁷	7 ¹⁷
Pinacol	$[(CH_3)_2C \cdot OH]_2$	118.17	col. nd.	0.967 ¹⁵	43(38)	171-2 ⁷⁹⁰	sl. s. c.	v. s.	v. s.
Pinacolone	$CH_3COC(CH_3)_3$	100.16	col. lq.	0.800 ¹⁶	-52.5	106.2	2.5 ¹⁵	s.	v. s.
Pinene (α -)(<i>dl</i> -)	$C_{10}H_{16}$	136.23	col. lq.	0.878 ^{20/4}	-55	154-6	v. sl. s.	s.	∞
hydrochloride	$C_{10}H_{17}Cl$	172.69	lf.		131-2	207-8	i.	33	s.
Pinol (<i>dl</i> -)	$C_{10}H_{16}O$	152.23	lq.	0.953 ^{20/20}		183-4	s.	s.	s.
Piperidine	$CH_2 < (CH_2CH_2)_2 > NH$	85.15	lq.	0.860 ^{20/4}	-9		∞	∞	∞
carboxylic acid (α -)(<i>dl</i> -)	$HO_2C \cdot CH < (CH_2CH_2)_2 > NH$	129.16	cr.		264		s.		
Piperidinium pentamethylene dithiocarbamate	$(CH_2)_5CS_2HN(CH_2)_5$	232.43	cr.	1.13	175		6 ²⁸		
Propane	$CH_3CH_2CH_3$	44.10	gas	0.585 ^{-45/4}	-187.1	-42.2	6.5 ¹⁸ cc.	s.	v. s.
Propionic acid	$CH_3CH_2CO_2H$	74.08	col. lq.	0.992 ^{20/4}	-22	141.1	∞	∞	∞
aldehyde	CH_3CH_2CHO	58.08	col. lq.	0.807 ^{20/4}	-81	49.5 ⁷⁴⁰	20 ²⁰	∞	∞
anhydride	$(CH_3CH_2CO)_2O$	130.14	col. lq.	1.012 ^{20/4}	-45	168.8 ⁷⁵⁰	d.	d.	∞
Propyl acetate (<i>n</i> -)	$CH_3CO_2CH_2CH_2CH_3$	102.13	col. lq.	0.886 ^{20/4}	-92.5	101.6	1.6 ¹⁶	∞	∞
(<i>i</i> -)	$CH_3CO_2CH(CH_3)_2$	102.13	col. lq.	0.874 ^{20/20}	-73.4	88.4	3 ²⁰	∞	∞
alcohol (<i>n</i> -)	$CH_3CH_2CH_2OH$	60.10	col. lq.	0.804 ^{20/4}	-127	97.8	∞	∞	∞
(<i>i</i> -)	$(CH_3)_2CHOH$	60.10	col. lq.	0.789 ^{20/4}	-85.8	82.5	∞	∞	∞
amine (<i>n</i> -)	$CH_3CH_2CH_2NH_2$	59.11	col. lq.	0.718 ^{20/20}	-83	49-50 ⁷⁶¹	∞	∞	∞
(<i>i</i> -)	$(CH_3)_2CHNH_2$	59.11	col. lq.	0.694 ^{15/4}	-101	33-4	∞	∞	∞
aniline (<i>n</i> -)	$C_6H_5NHCH_2CH_2CH_3$	135.21	lq.	0.949 ¹⁸	222	i.	v. s.	v. s.	v. s.
benzoate (<i>n</i> -)	$C_6H_5CO_2CH_2CH_2CH_3$	164.20	col. lq.	1.021 ^{25/25}	-51.6	231	i.	s.	s.
(<i>i</i> -)	$C_6H_5CO_2CH(CH_3)_2$	164.20	col. lq.	1.010 ^{25/25}		218.5	i.	s.	s.
bromide (<i>n</i> -)	$CH_3CH_2CH_2Br$	122.99	col. lq.	1.353 ^{20/4}	-109.9	70.8	0.25 ²⁰	∞	∞
(<i>i</i> -)	$(CH_3)_2CHBr$	122.99	col. lq.	1.310 ^{20/4}	-89	60	0.32 ²⁰	∞	∞
<i>n</i> -butyrate (<i>n</i> -)	$C_3H_7CH_2CO_2CH_2C_2H_5$	130.18	col. lq.	0.879 ¹⁵	-95.2	142.7	∞	∞	∞
<i>i</i> -butyrate (<i>n</i> -)	$(CH_3)_2CHCO_2CH_2C_2H_5$	130.18	col. lq.	0.884 ^{9/4}		134-5	v. sl. s.		
<i>n</i> -butyrate (<i>i</i> -)	$C_3H_7CH_2CO_2CH(CH_3)_2$	130.18	col. lq.	0.865 ¹⁸		128	v. sl. s.		
<i>i</i> -butyrate (<i>i</i> -)	$(CH_3)_2CHCO_2CH(CH_3)_2$	130.18	col. lq.	0.869 ^{9/4}		120.8	v. sl. s.		
chloride (<i>n</i> -)	$CH_3CH_2CH_2Cl$	78.54	col. lq.	0.890 ^{20/4}	-122.8	46.4	0.27 ²⁰	∞	∞
(<i>i</i> -)	$(CH_3)_2CHCl$	78.54	col. lq.	0.859 ²⁰	-117	36.5	0.31 ²⁰	∞	∞
Propyl formate (<i>n</i> -)	$HCO_2CH_2CH_2CH_3$	88.11	col. lq.	0.901 ^{20/4}	-92.9	81.3	12.2 ²²	∞	∞
(<i>i</i> -)	$HCO_2CH(CH_3)_2$	88.11	col. lq.	0.873 ^{20/4}		68-71 ⁷⁵¹	2.1 ²²	∞	∞
furoate (<i>n</i> -)	$C_6H_5O \cdot CO_2C_3H_7$	154.16	col. lq.	1.075 ^{26/4}		211	v. sl. s.	s.	∞
lactate (<i>n</i> -)	$CH_3CH(OH)CO_2CH_2C_2H_5$	132.16	col. lq.			122-3 ¹⁵⁰	s.	s.	s.
(<i>i</i> -)	$CH_3CH(OH)CO_2CH(CH_3)_2$	132.16	col. lq.			167.5	s.	s.	s.
mercaptan (<i>n</i> -)	$CH_3CH_2CH_2SH$	76.16	lq.	0.836 ^{25/4}	-112	67-8	v. sl. s.	s.	s.
(<i>i</i> -)	$(CH_3)_2CHSH$	76.16	lq.	0.809 ^{25/4}	-130.7	58-60	v. sl. s.	∞	∞
propionate (<i>n</i> -)	$C_3H_7CO_2CH_2C_2H_5$	116.16	col. lq.	0.883 ^{20/4}	-76	122-3	0.56 ²⁵	∞	∞
(<i>i</i> -)	$C_3H_7CO_2CH(CH_3)_2$	116.16	col. lq.	0.893 ⁹		109-11 ⁷⁵⁰	0.6 ²⁵	∞	∞
thiocyanate (<i>i</i> -)	$(CH_3)_2CH \cdot CNS$	101.17	lq.	0.963 ²⁰		152-3 ⁷⁵⁴	i.	∞	∞
<i>n</i> -valerate (<i>n</i> -)	$CH_3(CH_2)_4CO_2CH_2C_2H_5$	144.21	lq.	0.874 ¹⁵	-70.7	67.5	i.	∞	∞
<i>i</i> -valerate (<i>n</i> -)	$(CH_3)_2CHCH_2CO_2C_3H_7$	144.21	col. lq.	0.863 ^{20/4}		155.9	i.	∞	∞
<i>i</i> -valerate (<i>i</i> -)	$(CH_3)_2CHCH_2CO_2C_3H_7$	144.21	col. lq.	0.854 ¹⁷		142 ⁷⁵⁶	i.	∞	∞
Propylene	$CH_3CH \cdot CH_2$	42.08	gas	0.609 ^{-47/4}	-185	-48 ⁷⁴⁰	44.6 cc.	1200 cc.	
bromide	$CH_3CHBrCH_2Br$	201.89	col. lq.	1.933 ^{20/4}	-55.5	141.6	0.25 ²⁰	s.	v. s.
chlorohydrin	$CH_3CHClCH_2OH$	94.54	col. lq.	1.103 ²⁰		133-4	s.	s.	s.
chloride	$CH_3CHClCH_2Cl$	112.99	col. lq.	1.159 ^{20/20}	<-70	96.8	0.27 ²⁰	v. s.	v. s.
glycol	$CH_3CH(OH)CH_2OH$	76.09	col. oil	1.040 ^{19/4}		188-9	∞	∞	§
oxide	$CH_3(CH_2)_2O$	58.08	col. lq.	0.831 ^{20/20}		35	33 ²⁰	∞	∞
Protocatechuic acid (3-,4-)	$(HO)_2C_6H_3CO_2H \cdot H_2O$	172.14	nd./aq.	1.542 ^{1/4}	199 d.		1.82 ¹⁴	v. s.	s.

Pulegol (iso-)(<i>d</i> -)	C ₁₀ H ₁₇ OH	154.25	col. lq.	0.911 ^{20/4}		86-9 ¹⁰	v. sl. s.		
Pulegone	C ₁₀ H ₁₆ O	152.23	col. lq.	0.932 ^{20/20}		224 ^{75/4}	i.	∞	∞
Pyrazole	—NH·N·CH·CH·CH—	68.08	nd./et.		70	186-8	s.	s.	s.
Pyrazoline	—NH·N·CH·CH ₂ CH ₂ —	70.09	lq.			144	∞	∞	sl. s.
Pyrazolone	—NH·CO·CH ₂ CH·N—	84.08	nd.		165	subl. d.	s.	v. s.	v. sl. s.
Pyrene	C ₁₆ H ₁₀	202.25	vel. pr.	1.277 ^{70/4}	149-50	>360	i.	3 h.	v. s.
Pyridazine	N ₂ < (CHCH) ₂ >	80.09	lq.	1.107 ^{20/4}		208	∞	∞	s.
Pyridine	CH < (CHCH) ₂ > N	79.10	col. lq.	0.982 ^{20/4}	-42	115-6	∞	∞	s.
Pyrocatechol (<i>o</i> -)	C ₆ H ₄ (OH) ₂	110.11	nd./aq.	1.344 ⁴	104-5	240-5	45.1 ²⁰	v. s.	v. s.
Pyrogallol (1-,2-,3-)	C ₆ H ₃ (OH) ₃	126.11	nd.	1.453 ⁴	133-4	309	40 ¹³	s.	s.
Pyrone	CO < (CHCH) ₂ > O	96.08	cr.	1.190 ^{40/3}	32.5	215-7	v. sl. s.	s.	v. s.
Pyrrole	< (CH·CH) ₂ > NH	67.09	lq.	0.948 ^{20/4}		131	i.	s.	s.
Pyrrolidine	< (CH ₂ ·CH) ₂ > NH	71.12	lq.	0.852 ^{22/5}		87-8	∞	∞	∞
Pyrroline	< (CH·CH ₂) ₂ > NH	69.11	lq.	0.910 ^{20/4}		90-1	v. s.	∞	∞
Pyruvic acid	CH ₃ COCO ₂ H	88.06	col. lq.	1.267 ^{20/4}	13.6	165	∞	∞	∞
Quercitrin	C ₂₅ H ₃₀ O ₁₁ ·2H ₂ O	484.41	vel. nd.		182-5		0.04 ²⁰	∞	sl. s.
Quinaldine (py-2)	CH ₃ ·C ₉ H ₆ N	143.19	lq.	1.059 ^{20/4}	-1	244-5 ^{75/0}	v. sl. s.	s.	s.
Quinoline	C ₉ H ₇ N	129.16	lq.	1.095 ²⁰	-15	237.1 ^{74/7}	6	∞	∞
(iso-)	C ₉ H ₇ N	129.16	pl.	1.099 ^{21/4}	24.6	240.5 ^{76/3}	sl. s.		s.
-diol (1-,3-)	—C ₆ H ₄ ·CH·C(OH)N·C(OH)—	161.16	cr.		237		v. sl. s.		
Quinone (<i>p</i> -)	CO < (CHCH) ₂ > CO	108.09	yel. mn.	1.318 ^{20/4}	115.7	subl.	sl. s. h.	s.	s.
R-acid Ca salt (2-)(3-,6-)	HOC ₁₀ H ₇ (SO ₃) ₂ Ca	342.36	cr.				30.6 ²⁵		
K salt	HOC ₁₀ H ₇ (SO ₃ K) ₂	380.48	cr.				29.5 ²⁵		
Na salt	HOC ₁₀ H ₇ (SO ₃ Na) ₂	348.26	cr.				25.2 ²⁵		
Raffinose	C ₁₈ H ₃₂ O ₁₆ ·5H ₂ O	594.51	cr./aq.	1.465 ⁹	119	d. 130	14.3 ²⁰	0.1 ²⁰	
Resorcinol (<i>m</i> -)	C ₆ H ₄ (OH) ₂	110.11	col. rhb.	1.272 ¹⁵	110.7	276.5	147 ¹²		v. s.
Retene	C ₁₈ H ₁₈	234.34	lf./al.	1.13 ^{16/5}	98-9	390-4	i.	69 h.	v. s. h.
Rhamnose (β-)	CH ₃ (CHOH) ₄ CHO·H ₂ O	182.17	col. mn.	1.471 ^{20/4}	126		60.8 ²¹		i.
Ricinoleic acid	C ₁₇ H ₃₂ (OH)CO ₂ H	298.46	lq.	0.954 ¹⁶	4-5	226-8 ¹⁰	i.	∞	∞
Rosaniline	C ₂₀ H ₂₁ ON ₃	319.40	col. nd.		186 d.		v. sl. s.	sl. s.	i.
Rosolic acid	C ₂₀ H ₁₆ O ₃	304.34	red lf.		308-10 d.		0.12 ²⁵	v. s. h.	sl. s.
Saccharin	C ₆ H ₄ (CO)(SO ₂) > NH	183.18	mn.		225-8	subl.	0.4 ²⁵	3.1 c.	1.05 c.
Safrole (1-,3-,4-)	CH ₂ :CHCH ₂ :C ₆ H ₃ :O ₂ CH ₂	162.19	col. mn.	1.100 ^{20/4}	11-2	233-4	i.	s.	∞
(iso-)(1-,3-,4-)	CH ₃ :CH:CH·C ₆ H ₃ :O ₂ CH ₂	162.19	col. lq.	1.122 ^{20/4}	6-7	252-3	i.	∞	∞
Salicylic acid (<i>o</i> -)	HO·C ₆ H ₄ ·CO ₂ H	138.12	mn.	1.443 ^{20/4}	159	211 ²⁰	0.2 ²³	49 ¹⁵	51 ¹⁵
aldehyde (<i>o</i> -)	HO·C ₆ H ₄ ·CHO	122.12	col. oil	1.153 ^{25/4}	-7	196.5	∞	∞	∞
Saligenin	HO·C ₆ H ₃ ·CH ₂ OH	124.14	rhb./aq.	1.161 ²⁵	86-7	subl.	6.6 ¹⁵	v. s.	v. s.
Schaeffer's salt, Ca	(HOC ₁₀ H ₆ SO ₃) ₂ Ca·5H ₂ O	576.60	cr.				4.76 ²⁰		
K	HOC ₁₀ H ₆ SO ₃ K	262.32	cr.				3.46 ²⁵		
Na	HOC ₁₀ H ₆ SO ₃ Na	246.21	cr.				6.29 ²⁵		
Semicarbazide	NH ₂ ·CO·NH·NH ₂	75.07	pr./al.		96		v. s.	v. s.	i.
hydrochloride	NH ₂ ·CO·NH·NH ₂ Cl	111.53	pr.		173 d.		v. s.	sl. s.	i.
Skatole (3-)	CH ₃ ·C ₆ H ₆ N	131.17	lf.		95	265-6 ^{75/5}	0.05 c.	s.	s.
Sodium methylate	CH ₃ ONa	54.02	pd.		d. 300		d.		
Sorbitol	[CH ₂ OH(CHOH) ₂] ₂	182.17	cr.		110-2		v. s.	v. s. h.	
Sorbose (<i>d</i> - or <i>l</i> -)	C ₆ H ₁₂ O ₆	180.16	rhb.	1.654 ¹⁵	165		55 ¹⁷	sl. s.	
Starch	(C ₆ H ₁₀ O ₅) _x	162.14	amor.	1.50 ²¹	d.		i.	i.	i.
Stearic acid	CH ₃ (CH ₂) ₁₆ CO ₂ H	284.48	mn.	0.847 ^{69/3}	70-1	291 ¹¹⁰	0.03 ²⁵	2 ²⁰	6 ⁶
amide	CH ₃ (CH ₂) ₁₆ CONH ₂	283.49	col. cr.		108-9	251 ¹²	i.	s. h.	s. h.
Styrene	C ₆ H ₅ CH=CH ₂	104.15	col. lq.	0.903 ^{20/4}	-31	145-6	v. sl. s.	∞	∞
Suberic acid	H ₂ O ₂ C(CH ₂) ₆ CO ₂ H	174.19	nd./aq.	1.266 ^{25/4}	140-4	279 ¹⁰⁰	0.14 ¹⁶	s.	0.8 ¹⁵
Succinic acid	H ₂ O ₂ C(CH ₂) ₂ CO ₂ H	118.09	col. mn.	1.572 ^{25/4}	189-90	235 d.	6.8 ²⁰	9.9 ¹⁵	1.2 ¹⁵
Sucrose	C ₁₂ H ₂₂ O ₁₁	342.30	col. mn.	1.588 ¹⁵	170-86 d.		179 ⁰	0.9	i.
Sulfanilic acid (<i>p</i> -)	H ₂ N·C ₆ H ₄ ·SO ₂ H	173.19	col. cr.		d. > 280		0.8 ¹⁰	v. sl. s.	v. sl. s.
Sylvestrene (<i>d</i> -)	C ₁₀ H ₁₆	136.23	lq.	0.863 ^{20/4}		176-7			
Tartaric acid (meso-)	(CHOHCO ₂ H) ₂	150.09	cr.	1.737	159-60		120 ¹⁵		
(racemic)	(CHOHCO ₂ H) ₂ ·H ₂ O	168.10	tri.	1.697 ^{20/4}	205-6		20.6 ²⁰	2 ⁹	0.09
(<i>d</i> - or <i>l</i> -)	(CHOHCO ₂ H) ₂	150.09	mn.	1.760 ^{20/4}	168-70	d.	139 ²⁰	25 ¹⁵	0.4 ¹⁵
Tartronic acid	CH(OH)(CO ₂ H) ₂ ·½H ₂ O	129.07	pr./aq.		d. 155-8	subl.	v. s.	v. s.	i.
Terephthalic acid (<i>p</i> -)	C ₆ H ₄ (CO ₂ H) ₂	166.13	cr.	1.510			0.001 c.	sl. s. h.	i.
Terpin hydrate (<i>cis</i> -)	C ₁₀ H ₂₀ O ₂ ·H ₂ O	190.28	rhb.		117	d.	0.4 ¹⁵	10 ¹⁵	1 ¹⁵
Terpineol (α-)(<i>d</i> - or <i>l</i> -)	C ₁₀ H ₁₈ O	154.25	col. cr.	0.935 ¹⁵	38-40	219-21	i.	v. s.	v. s.
(<i>d</i> -)	C ₁₀ H ₁₈ O	154.25	col. cr.	0.935 ^{20/20}	35	218-9 ^{75/2}	i.	v. s.	v. s.
Terpinyl acetate (α-)(<i>dl</i> -)	CH ₃ CO ₂ ·C ₁₀ H ₁₇	196.29	lq.	0.966 ^{20/4}	< -50	220 d.	i.	20	
Tetrabromo-ethane (sym)	Br ₂ CH·CHBr ₂	345.65	col. lq.	2.964 ^{20/4}	-1.0	151 ³⁴	i.	∞	∞
(uns)	Br ₂ C·CH ₂ Br	345.65	col. lq.	2.875 ^{20/4}	0	104 ¹³	i.	s.	∞
Tetrachloro-ethane (sym)	Cl ₂ CH·CHCl ₂	167.85	col. lq.	1.600 ^{20/4}	-36	146.3	0.29 ²⁰	∞	∞
(uns)	Cl ₃ C·CH ₂ Cl	167.85	lq.	1.588 ^{20/4}		129-30	i.	∞	∞
-ethylene	Cl ₂ C·CCl ₂	165.83	col. lq.	1.624 ^{15/4}	-19	120.8	0.02 ²⁰	∞	∞
Tetracosane (<i>n</i> -)	CH ₃ (CH ₂) ₂₂ CH ₃	338.65	cr.	0.779 ^{11/4}	51.1	324		∞	s.
Tetradecane (<i>n</i> -)	CH ₃ (CH ₂) ₁₂ CH ₃	198.39	col. lq.	0.765 ^{20/4}	5.5	252.5	i.	v. s.	v. s.
Tetraethyl-thiuram disulfide	[(C ₂ H ₅) ₂ NCS] ₂ S ₂	296.54	cr.	1.17	70		i.		

TABLE 2-2 Physical Properties of Organic Compounds (Concluded)

Name	Formula	Formula weight	Form and color	Specific gravity	Melting point, °C	Boiling point, °C	Solubility in 100 parts		
							Water	Alcohol	Ether
Tetrafluoro-ethylene	F ₂ C:CF ₂	100.02	gas	1.58 ⁻⁷⁸	-142.5	-76.3	0.01 ³⁰		
Tetrahydro-furan	—CH ₂ (CH ₂) ₂ CH ₂ O—	72.11	col. lq.	0.888 ^{21/4}	-65	65-6	s.	s.	s.
-furfuryl alcohol	C ₄ H ₄ O:CH ₂ OH	102.13	col. lq.	1.050 ^{20/4}		177-8 ⁷⁴³	∞	∞	∞
-pyran	—CH ₂ (CH ₂) ₂ CH ₂ O—	86.13	lq.	0.881 ^{20/4}		88	s.		
Tetralin	—C ₆ H ₄ CH ₂ (CH ₂) ₂ CH ₂ —	132.20	col. lq.	0.973 ^{18/4}	-31	206 ⁷⁶⁴	i.	s.	s.
Tetramethyl-thiuram disulfide	[(CH ₃) ₂ NCS] ₂ S ₂	240.43	cr.	1.29	155-6		i.		
Tetryl (2-,4-,6-)	(NO ₂) ₃ C ₆ H ₂ :N(CH ₃)NO ₂	287.14	yel. mn.	1.57 ¹⁹	130.5	expl.	i.	s. h.	s.
Theobromine	C ₇ H ₈ O ₂ N ₄	180.16	rhb.		330		0.06 ¹⁵	0.06 c.	0.03 h.
Thio-acetic acid	CH ₃ :CO:SH	76.12	yel. lq.	1.074 ¹⁰	< -17	93	s.	∞	∞
-aniline (4-, 4'-)	(NH ₂ :C ₆ H ₄) ₂ S	216.30	nd./aq.		108		sl. s. h.	s.	s.
-carbanilide	(C ₆ H ₅ :NH) ₂ CS	228.31	rhb./al.	1.3 ²⁴	154	d.	i.	v. s.	v. s.
-naphthol (β-)	C ₁₀ H ₇ :SH	160.24	cr./al.		81	286-8	v. sl. s.	v. s.	v. s.
-phenol	C ₆ H ₅ :SH	110.18	col. lq.	1.074 ^{23/4}		168-9	v. sl. s.	v. s.	∞
-salicylic acid (o-)	HS:C ₆ H ₄ :CO ₂ H	154.19	yel. nd.		164	subl.	sl. s. h.	s.	
-urea	NH ₂ :CS:NH ₂	76.12	rhb./al.	1.405 ^{20/4}	180-2	d.	9.2 ¹³	s.	sl. s.
Thiophene	<(CH:CH) ₂ > S	84.14	col. lq.	1.070 ^{15/4}	-30	84	i.	s.	
Thymol (5-,2-,1-)	(CH ₃)(C ₃ H ₇)C ₆ H ₃ OH	150.22	cr.	0.972 ^{25/5}	51.5	232 ⁷⁵²	0.09 ¹⁹	v. s.	v. s.
Tolidine (0-)(3-,3'-,4-,4'-)	[CH ₃ (NH ₂) ₂ C ₆ H ₄] ₂	212.29	lf.		128-9		v. sl. s.	s.	s.
Toluene	C ₆ H ₅ :CH ₃	92.14	col. lq.	0.866 ^{20/4}	-95	110.8	0.05 ¹⁶	s.	∞
sulfonic acid (o-)	CH ₃ :C ₆ H ₄ SO ₃ H:2H ₂ O	208.23	cr.			128.8 ⁰	v. s.	s.	
(p-)	CH ₃ :C ₆ H ₄ SO ₃ H:H ₂ O	190.22	mn.		104-5		v. s.	s.	
sulfonic amide (p-)	CH ₃ :C ₆ H ₄ SO ₂ NH ₂	171.22	mn.		137	146-7 ⁰	0.2 ⁹	7.4 ⁵	
sulfonic chloride (p-)	CH ₃ :C ₆ H ₄ :SO ₂ Cl	190.65	tri.		69	134.5 ¹⁰	i.	s.	s.
Toluic acid (o-)	CH ₃ :C ₆ H ₄ :CO ₂ H	136.15	cr./aq.	1.062 ^{115/4}	104-5	259 ⁷⁵¹	1.06 ²	2.17 ¹⁰⁰	v. s.
(m-)	CH ₃ :C ₆ H ₄ :CO ₂ H	136.15	pr./aq.	1.054 ^{112/4}	110-1	263	1.6 ¹⁰⁰	v. s.	v. s.
(p-)	CH ₃ :C ₆ H ₄ :CO ₂ H	136.15	cr./aq.		179-80	274-5	1.3 ¹⁰⁰	v. s.	v. s.
Toluidine (o-)	CH ₃ :C ₆ H ₄ :NH ₂	107.15	col. lq.	0.999 ^{20/4}	-16.3	199.7	1.5 ²⁵	∞	∞
(m-)	CH ₃ :C ₆ H ₄ :NH ₂	107.15	col. lq.	0.989 ^{20/4}	-31.5	203.3	sl. s.	∞	∞
(p-)	CH ₃ :C ₆ H ₄ :NH ₂	107.15	cr.	1.046 ^{20/4}	44-5	200.3	0.74 ²¹	v. s.	v. s.
hydrochloride (o-)	CH ₃ :C ₆ H ₄ :NH ₃ Cl	143.61	mn. pr.		218-20	242	s.	sl. s.	
sulfonic acid (1-,2-,3-)	CH ₃ (NH ₂)C ₆ H ₃ SO ₃ H	187.22	cr.		157-22		0.97 ¹¹		
Tolyleneediamine (1-,2-,4-)	CH ₃ :C ₆ H ₃ (NH ₂) ₂	122.17	rhb.		99	283-5	s. h.	s.	s.
Tolylene diisocyanate (1-,2-,4-)	CH ₃ :C ₆ H ₃ (NCO) ₂	174.16	lq.	1.23 ²⁸		134.5 ²⁰	d.	d.	
Trehalose	C ₁₂ H ₂₂ O ₁₁ :2H ₂ O	378.33	rhb./al.		97		s. h.	sl. s. h.	i.
Triamylamine (n-)	[CH ₃ (CH ₂) ₅ CH ₂] ₃ N	227.43	lq.			240-5	i.		
(i-)	[(CH ₃) ₂ CH(CH ₂) ₂] ₃ N	227.43	col. lq.	0.786 ^{20/4}		235	i.		
Tributyl-amine (n-)	[CH ₃ (CH ₂) ₃ CH ₂] ₃ N	185.35	col. lq.	0.778 ^{20/20}		216.5 ⁷⁶¹	i.	s.	∞
phosphite	[CH ₃ (CH ₂) ₃ O] ₃ P	250.31	lq.	0.925 ^{20/4}		122-3 ¹²	i.		
Trichloro-acetic acid	Cl ₃ C:CO ₂ H	163.39	cr.	1.617 ^{46/15}	58	193.5 ⁷⁵⁴	120 ²⁵	s.	s.
-benzene (s-)(1-,3-,5-)	C ₆ H ₂ Cl ₃	181.45	nd.		63.5	208.5 ⁷⁶⁴	i.	sl. s.	
-ethane (1-,1-,1-)	Cl ₃ C:CH ₃	133.40	lq.	1.325 ^{26/4}		74.1	i.	∞	∞
-ethylene	Cl ₃ C:CHCl	131.39	col. lq.	1.466 ^{29/20}	-73	87.2	0.1 ³⁵	∞	∞
-phenol	Cl ₃ C:H ₂ OH	197.45	nd.	1.490 ^{75/4}	68-9	246	0.09 ²⁵	v. s.	v. s.
Tricosane (n-)	CH ₃ (CH ₂) ₂₁ CH ₃	324.63	lf.	0.779 ^{28/4}	47.7	234 ¹⁵	i.		
Tricresyl phosphate (o-)	OP(O)(OC ₆ H ₄ CH ₃) ₃	368.36	lq.				i.		
Tridecane (n-)	CH ₃ (CH ₂) ₁₁ CH ₃	184.36	col. lq.	0.757 ^{20/4}	-6.2	234	i.	v. s.	v. s.
Triethanol amine	(HOCH ₂ CH ₂) ₃ N	149.19	col. lq.	1.126 ^{20/20}	20-1	277-9 ¹⁵⁰	∞	∞	sl. s.
Triethyl-amine	(CH ₃ CH ₂) ₃ N	101.19	col. oil	0.729 ^{20/20}	-114.8	89.4	∞ > 19 ⁰	∞	∞
-benzene (1-,3-,5-)	(C ₂ H ₅) ₃ C ₆ H ₃	162.27	lq.	0.861 ^{20/4}		215	i.	s.	s.
(1-,2-,4-)	(C ₂ H ₅) ₃ C ₆ H ₃	162.27	lq.	0.882 ^{17/4}		217-8 ⁷⁵⁵	i.	s.	s.
borate	B(OCH ₂ CH ₃) ₃	145.99	lq.	0.864 ^{20/20}		120	d.		
citrate	HOOC ₃ H ₄ (CO ₂ C ₂ H ₅) ₃	276.28	oil	1.137 ^{20/4}		294	i.	∞	∞
Triethylene glycol	(-CH ₂ OCH ₂ CH ₂ OH) ₂	150.17	col. lq.	1.125 ^{20/20}	-5	290	∞	∞	v. sl. s.
Trifluoro-chloromethane	CF ₃ Cl	104.46	gas	1.726 ¹³⁰	-182	-80			
-chloroethylene	F ₃ C:CFCl	116.47	gas		-157.5		d.		
-trichloroethane	Cl ₃ CF:CClF	187.38	lq.	1.576 ^{20/4}	-35	47.6	i.	∞	∞
Trimethoxybutane (1-,3-,3-)	CH ₃ (OCH ₃) ₂ CH ₂ C(OCH ₃) ₂ CH ₃	145.20	lq.	0.932		63-5 ²⁵	d.		
Trimethylamine	(CH ₃) ₃ N	59.11	gas	0.662 ⁻⁵	-124	3.5	41 ¹⁹	s.	s.
Trimethylene bromide	Br:CH ₂ :CH ₂ :CH ₂ :Br	201.89	lq.	1.987 ^{15/4}	-34.4	167.5	0.17 ³⁰	s.	s.
chloride	Cl:CH ₂ :CH ₂ :CH ₂ :Cl	112.99	lq.	1.201 ¹⁵		123-5	0.27 ²⁵	s.	s.
glycol	HOCH ₂ CH ₂ CH ₂ OH	76.09	oil	1.060 ^{20/4}	∞	214	∞	∞	
Trinitro-benzene (1-,3-,5-)	C ₆ H ₃ (NO ₂) ₃	213.10	col. rhb.	1.688 ^{20/4}	121	d.	0.03 ¹⁵	1.9 ¹⁸	1.5 ¹⁸
-benzoic acid (2-,4-,6-)	(NO ₂) ₃ C ₆ H ₂ CO ₂ H	257.11	rhb./aq.		210-20 d.		2.05 ²⁴		
-tert-butylxylene	(NO ₂) ₃ C ₆ (CH ₃) ₂ C ₆ H ₃	297.26	nd./al.		110		i.	sl. s.	s.
-naphthalene (α-)(1-,3-,5-)	C ₁₀ H ₅ (NO ₂) ₃	263.16	rhb.		122-3		i.	s.	
(β-)(1-,3-,8-)	C ₁₀ H ₅ (NO ₂) ₃	263.16	cr./al.		218-9		0.02 ¹⁰⁰	0.05 ²³	0.13 ¹⁵
(γ-)(1-,4-,5-)	C ₁₀ H ₅ (NO ₂) ₃	263.16	yel. cr.		148-9		i.	0.11 ¹⁹	0.4 ¹⁹

-phenol (2-,3-,6-)	(NO ₂) ₂ C ₆ H ₃ OH	229.10	nd.		117-8		s. h.	v. s.	v. s.
-toluene (β-)(2-,3-,4-)	CH ₃ C ₆ H ₄ (NO ₂) ₃	227.13	cr.	1.620 ^{20/4}	112	expl.	i.	sl. s. c.	s.
(γ-)(2-,4-,5-)	CH ₃ C ₆ H ₃ (NO ₂) ₃	227.13	ye l. pl.	1.620 ^{20/4}	104	expl.	i.	s. h.	v. s.
(α-)(2-,4-,6-)	CH ₃ C ₆ H ₃ (NO ₂) ₃	227.13	cr/al.	1.654	80.8	expl.	0.01 ³⁰	1.5 ³²	5 ³³
Triional	(C ₅ H ₃ SO ₂ C ₄ H ₉) ₂	242.36	pl./al.	1.199 ^{5/4}	76	d.	0.3 ¹⁵	5 ⁹	6.6 ¹⁵
Triphenyl-arsine	(C ₆ H ₅) ₃ As	306.23	pl.	1.306	59-60	>360	i.	s.	v. s.
carbinol	(C ₆ H ₅) ₃ COH	260.33	cr.	1.188 ^{20/4}	162.5	>360	i.	v. s.	v. s.
guanidine (α-)	C ₆ H ₅ N·C(NHC ₆ H ₅) ₂	287.36	rhb./al.	1.13	144-5	d.	i.	4 ⁹	
methane	(C ₆ H ₅) ₃ CH	244.33	cr.	1.014 ^{90/4}	93.4	359 ^{75/4}	i.	v. s. h.	v. s.
methyl	(C ₆ H ₅) ₃ C . . .	243.32	col. cr.		145-7	d.	i.	sl. s. h.	
phosphate	OP(OC ₆ H ₅) ₃	326.28	pr./al.	1.206 ^{90/4}	49-50	245 ¹¹	i.	155 ²⁵	v. s.
Tripropylamine (n-)	(CH ₂ CH ₂ CH ₂) ₃ N	143.27	col. lq.	0.757 ^{20/4}	-93.5	156.5	v. sl. s.	∞	∞
Undecane (n-)	CH ₃ (CH ₂) ₉ CH ₃	156.31	col. lq.	0.741 ^{20/4}	-25.6	194.5	i.	∞	∞
Urea	H ₂ N·CO·NH ₂	60.06	col. pr.	1.335 ^{20/4}	132.7	d.	100 ¹⁷	20 ²⁰	sl. s.
nitrate	CO(NH ₂) ₂ ·HNO ₃	123.07	col. mm.		152 d.		v. s. h.	s.	
Uric acid	C ₅ H ₄ O ₃ N ₄	168.11	cr.	1.893 ²⁰	d.		0.06 h.	i.	i.
Valeric acid (n-)	C ₅ H ₉ CH ₂ CH ₂ CO ₂ H	102.13	col. lq.	0.939 ^{20/4}	-34.5	187	3.3 ¹⁶	∞	∞
(i-)	(CH ₃) ₂ CHCH ₂ CO ₂ H	102.13	col. lq.	0.931 ^{20/20}	-37.6	176	4.2 ²⁰	∞	∞
aldehyde (n-)	C ₅ H ₉ CH ₂ CH ₂ CHO	86.13	lq.	0.819 ¹¹	-92	103.4	v. sl. s.	s.	s.
(i-)	(CH ₃) ₂ CHCH ₂ CHO	86.13	col. lq.	0.803 ¹⁷	-51	92.5	sl. s.	s.	s.
amide (n-)	C ₅ H ₉ CH ₂ CH ₂ CONH ₂	101.15	mm. pl.	1.023	106		v. s.	v. s.	v. s.
(i-)	(CH ₃) ₂ CHCH ₂ CONH ₂	101.15	mm.	0.965 ^{20/4}	135-7	232	s.	s.	s.
Vanillic acid (3-,4-,1-)	H ₂ C(O)(OH)C ₆ H ₃ CO ₂ H	168.15	nd./aq.		207	subl.	0.12 ¹⁴	v. s.	v. s.
alcohol (3-,4-,1-)	CH ₃ O(OH)C ₆ H ₃ CH ₂ OH	154.16	mm./aq.		115	d.	v. s. h.	v. s.	v. s.
hyl-thiuram disulfide	[(C ₂ H ₅) ₂ NCS] ₂ S ₂	296.54	cr.	1.17	70		i.		
Vanillin (3-,4-,1-)	CH ₃ O(OH)C ₆ H ₃ CHO	152.15	mm.	1.056	81-2	285	1 ¹⁴	v. s.	v. s.
Veratrole (o-)	C ₆ H ₄ (OCH ₃) ₂	138.16	cr.	1.091 ^{15/15}	22.5	207.1	v. sl. s.	s.	s.
Vinyl acetate	CH ₃ CO ₂ CH ₂ CH ₂	86.09	col. lq.	0.932 ^{20/4}	< -60	72-3	2 ²⁰	∞	∞
(poly-)	(CH ₂ CO ₂ CH ₂ CH ₂) _x	(86.09)		1.19 ²⁰	100-25		i.		
acetic acid	CH ₃ ·CH ₂ ·CH ₂ CO ₂ H	86.09	col. lq.	1.013 ^{15/15}	-39	163	s.	∞	∞
acetylene	CH ₃ ·CH·C·CH	52.07	gas	0.705 ^{1.5}		5.5	0.67 ^{0.6}		
alcohol	CH ₃ ·CHOH	44.05							
(poly-)	(CH ₂ ·CHOH) _x	(44.05)		1.3 ²⁰	d. >200		s.		
chloride	CH ₂ ·CHCl	62.50	gas	0.908 ^{25/25}	-160	-12	sl. s.	s.	v. s.
propionate	C ₃ H ₇ CO ₂ CH·CH ₂	100.12	lq.		93-5		v. sl. s.		
Xylene (o-)	C ₆ H ₄ (CH ₃) ₂	106.17	col. lq.	0.881 ^{20/4}	-25	144	i.	s.	∞
(m-)	C ₆ H ₄ (CH ₃) ₂	106.17	col. lq.	0.867 ^{17/4}	-47.4	139.3	i.	s.	∞
(p-)	C ₆ H ₄ (CH ₃) ₂	106.17	col. lq.	0.861 ^{20/4}	13.2	138.5	i.	s.	v. s.
sulfonic acid (1-,4-,2-)	(CH ₃) ₂ C ₆ H ₃ SO ₃ H·2H ₂ O	222.26	col. lf.		86	149 ^{0/1}	s.		
Xylidine (1:2)(3-)	(CH ₃) ₂ C ₆ H ₃ NH ₂	121.18	lq.	0.991 ¹⁵	< -15	223	v. sl. s.	s.	s.
(1:2)(4-)	(CH ₃) ₂ C ₆ H ₃ NH ₂	121.18	pr.	1.076 ^{17.5}	49-50	224-6	v. sl. s.		
(1:3)(2-)	(CH ₃) ₂ C ₆ H ₃ NH ₂	121.18	lq.	0.980 ¹⁵		216-7	v. sl. s.		
(1:3)(4-)	(CH ₃) ₂ C ₆ H ₃ NH ₂	121.18	lq.	0.978 ^{20/4}		213-4	v. sl. s.		
(1:3)(5-)	(CH ₃) ₂ C ₆ H ₃ NH ₂	121.18	oil	0.972 ^{20/4}		221-2	v. sl. s.		
(1:4)(2-)	(CH ₃) ₂ C ₆ H ₃ NH ₂	121.18	oil	0.979 ^{21/4}		215 ^{79/9}	v. sl. s.		
Xylose (l-)(+)	CH ₂ OH(CHOH) ₃ CHO	150.13	nd.	1.535 ⁹	153-4		117 ²⁰		
Xylylene dichloride (p-)	C ₆ H ₄ (CH ₂ Cl) ₂	175.06	mm.	1.417 ⁹	100.5	240-5 d.	i.	s.	v. sl. s.
Zinc diethyl	Zn(CH ₂ CH ₃) ₂	123.53	col. lq.	1.182 ¹⁸	-28	118	d.	d.	
dimethyl	Zn(CH ₃) ₂	95.48	col. lq.	1.386 ¹¹	-40	46	d.	d.	
dimethyl-dithiocarbamate	Zn[S ₂ CN(CH ₂) ₂] ₂	305.84		2.00 ^{10/4}	248-50		i.		

NOTE: °F = % °C + 32.

VAPOR PRESSURES OF PURE SUBSTANCES

TABLE 2-3 Vapor Pressure of Water Ice from 0 to -40 °C

t, °C	Vapor pressure		t, °C	Vapor pressure		t, °C	Vapor pressure	
	mmHg	kPa		mmHg	kPa		mmHg	kPa
0	4.584	0.6112	-13.5	1.423	0.1897	-27.0	0.3881	0.05174
-0.5	4.399	0.5865	-14.0	1.359	0.1812	-27.5	0.3688	0.04918
-1.0	4.220	0.5627	-14.5	1.298	0.1731	-28.0	0.3505	0.04673
-1.5	4.049	0.5398	-15.0	1.240	0.1653	-28.5	0.3330	0.04439
-2.0	3.883	0.5177	-15.5	1.184	0.1578	-29.0	0.3162	0.04216
-2.5	3.724	0.4965	-16.0	1.130	0.1507	-29.5	0.3003	0.04004
-3.0	3.571	0.4761	-16.5	1.079	0.1438	-30.0	0.2851	0.03801
-3.5	3.423	0.4564	-17.0	1.029	0.1372	-30.5	0.2706	0.03608
-4.0	3.281	0.4375	-17.5	0.9822	0.1310	-31.0	0.2568	0.03424
-4.5	3.145	0.4193	-18.0	0.9370	0.1249	-31.5	0.2437	0.03249
-5.0	3.013	0.4018	-18.5	0.8937	0.1191	-32.0	0.2311	0.03082
-5.5	2.887	0.3849	-19.0	0.8522	0.1136	-32.5	0.2192	0.02923
-6.0	2.766	0.3687	-19.5	0.8125	0.1083	-33.0	0.2078	0.02771
-6.5	2.649	0.3532	-20.0	0.7745	0.1033	-33.5	0.1970	0.02627
-7.0	2.537	0.3382	-20.5	0.7381	0.09841	-34.0	0.1867	0.02490
-7.5	2.429	0.3238	-21.0	0.7034	0.09377	-34.5	0.1769	0.02359
-8.0	2.325	0.3100	-21.5	0.6701	0.08934	-35.0	0.1676	0.02235
-8.5	2.225	0.2967	-22.0	0.6383	0.08510	-35.5	0.1587	0.02116
-9.0	2.130	0.2839	-22.5	0.6078	0.08104	-36.0	0.1503	0.02004
-9.5	2.038	0.2717	-23.0	0.5787	0.07716	-36.5	0.1423	0.01897
-10.0	1.949	0.2599	-23.5	0.5509	0.07345	-37.0	0.1347	0.01796
-10.5	1.865	0.2486	-24.0	0.5243	0.06991	-37.5	0.1274	0.01699
-11.0	1.783	0.2377	-24.5	0.4989	0.06652	-38.0	0.1206	0.01607
-11.5	1.705	0.2273	-25.0	0.4747	0.06329	-38.5	0.1140	0.01520
-12.0	1.630	0.2173	-25.5	0.4515	0.06020	-39.0	0.1078	0.01437
-12.5	1.558	0.2077	-26.0	0.4294	0.05725	-39.5	0.1019	0.01359
-13.0	1.489	0.1985	-26.5	0.4083	0.05443	-40.0	0.0963	0.01284

SOURCE: Formulation of Wagner, Saul, and Pruss, *J. Phys. Chem. Ref. Data*, **23**, 515 (1994), implemented in Harvey, Peskin, and Klein, *NIST/ASME Steam Properties*, NIST Standard Reference Database 10, Version 2.2, National Institute of Standards and Technology, Gaithersburg, Md., 2000. This source provides data down to 190 K (-83.15 °C). A formula extending to 110 K may be found in Murphy and Koop, *Q. J. R. Meteorol. Soc.*, **131**, 1539 (2005).

TABLE 2-4 Vapor Pressure of Supercooled Liquid Water from 0 to -40 °C*

t, °C	Vapor pressure		t, °C	Vapor pressure		t, °C	Vapor pressure	
	mmHg	kPa		mmHg	kPa		mmHg	kPa
0	4.584	0.6112	-13.5	1.623	0.2163	-27.0	0.5051	0.06734
-0.5	4.421	0.5894	-14.0	1.558	0.2077	-27.5	0.4824	0.06431
-1.0	4.262	0.5682	-14.5	1.495	0.1993	-28.0	0.4606	0.06141
-1.5	4.108	0.5477	-15.0	1.435	0.1913	-28.5	0.4397	0.05862
-2.0	3.959	0.5279	-15.5	1.377	0.1836	-29.0	0.4197	0.05595
-2.5	3.816	0.5087	-16.0	1.321	0.1761	-29.5	0.4005	0.05339
-3.0	3.676	0.4901	-16.5	1.267	0.1689	-30.0	0.3820	0.05094
-3.5	3.542	0.4722	-17.0	1.215	0.1620	-30.5	0.3644	0.04858
-4.0	3.411	0.4548	-17.5	1.165	0.1553	-31.0	0.3475	0.04633
-4.5	3.285	0.4380	-18.0	1.117	0.1489	-31.5	0.3313	0.04417
-5.0	3.163	0.4218	-18.5	1.070	0.1427	-32.0	0.3158	0.04210
-5.5	3.046	0.4061	-19.0	1.026	0.1367	-32.5	0.3009	0.04012
-6.0	2.932	0.3909	-19.5	0.9827	0.1310	-33.0	0.2867	0.03822
-6.5	2.822	0.3762	-20.0	0.9414	0.1255	-33.5	0.2731	0.03640
-7.0	2.715	0.3620	-20.5	0.9016	0.1202	-34.0	0.2600	0.03467
-7.5	2.612	0.3483	-21.0	0.8633	0.1151	-34.5	0.2476	0.03300
-8.0	2.513	0.3351	-21.5	0.8265	0.1102	-35.0	0.2356	0.03141
-8.5	2.417	0.3223	-22.0	0.7911	0.1055	-35.5	0.2242	0.02989
-9.0	2.324	0.3099	-22.5	0.7571	0.1009	-36.0	0.2133	0.02844
-9.5	2.235	0.2980	-23.0	0.7244	0.0965	-36.5	0.2029	0.02705
-10.0	2.149	0.2865	-23.5	0.6930	0.0923	-37.0	0.1929	0.02572
-10.5	2.065	0.2753	-24.0	0.6628	0.08836	-37.5	0.1834	0.02445
-11.0	1.985	0.2646	-24.5	0.6337	0.08449	-38.0	0.1743	0.02324
-11.5	1.907	0.2542	-25.0	0.6059	0.08078	-38.5	0.1656	0.02208
-12.0	1.832	0.2442	-25.5	0.5791	0.07721	-39.0	0.1573	0.02098
-12.5	1.760	0.2346	-26.0	0.5534	0.07379	-39.5	0.1494	0.01992
-13.0	1.690	0.2253	-26.5	0.5288	0.07050	-40.0	0.1419	0.01891

*SOURCE: Murphy and Koop, *Q. J. R. Meteorol. Soc.*, **131**, 1539 (2005). The formula in the reference extends down to 123 K (-150.15 °C), although in practice pure liquid water cannot be supercooled below about 235 K.

UNITS CONVERSIONS

For this subsection, the following units conversions are applicable:

$$^{\circ}\text{F} = \% \text{ } ^{\circ}\text{C} + 32.$$

To convert millimeters of mercury to pounds-force per square inch, multiply by 0.01934.

ADDITIONAL REFERENCES

Additional vapor-pressure data may be found in major thermodynamic property databases, such as those produced by the AIChE's DIPPER program (www.aiche.org/dipper), NIST's Thermodynamics Research Center (trc.nist.gov), the Dortmund Databank (www.ddb.tu-berlin.de), and the Physical Property Data Service (www.ppps.co.uk). Additional sources include the *NIST Chemistry Webbook* (webbook.nist.gov/chemistry/); Boublik, Fried, and Hala, *The Vapor Pressures of Pure Substances*, 2d ed., Elsevier, Amsterdam, 1984; Poling, Prausnitz, and O'Connell, *The Properties of Gases and Liquids*, 5th ed., McGraw-Hill, New York, 2001; *Vapor Pressure of Chemicals* (Subvolumes A, B, and C), vol. IV/20 in Landolt-Bornstein: *Numerical Data and Functional Relationships in Science and Technology—New Series*, Springer-Verlag, Berlin, 1999–2001. The most recent work on water may be found at The International Association for the Properties of Water and Steam website <http://iapws.org>.

TABLE 2-5 Vapor Pressure (MPa) of Liquid Water from 0 to 100 °C

t, °C	P _{vp} , MPa	t, °C	P _{vp} , MPa	t, °C	P _{vp} , MPa
0.01	0.00061165	34	0.0053251	68	0.028599
1	0.00065709	35	0.0056290	69	0.029876
2	0.00070599	36	0.0059479	70	0.031201
3	0.00075808	37	0.0062823	71	0.032575
4	0.00081355	38	0.0066328	72	0.034000
5	0.00087258	39	0.0070002	73	0.035478
6	0.00093536	40	0.0073849	74	0.037009
7	0.0010021	41	0.0077878	75	0.038595
8	0.0010730	42	0.0082096	76	0.040239
9	0.0011483	43	0.0086508	77	0.041941
10	0.0012282	44	0.0091124	78	0.043703
11	0.0013130	45	0.0095950	79	0.045527
12	0.0014028	46	0.010099	80	0.047414
13	0.0014981	47	0.010627	81	0.049367
14	0.0015990	48	0.011177	82	0.051387
15	0.0017058	49	0.011752	83	0.053476
16	0.0018188	50	0.012352	84	0.055635
17	0.0019384	51	0.012978	85	0.057867
18	0.0020647	52	0.013631	86	0.060173
19	0.0021983	53	0.014312	87	0.062556
20	0.0023393	54	0.015022	88	0.065017
21	0.0024882	55	0.015762	89	0.067558
22	0.0026453	56	0.016533	90	0.070182
23	0.0028111	57	0.017336	91	0.072890
24	0.0029858	58	0.018171	92	0.075684
25	0.0031699	59	0.019041	93	0.078568
26	0.0033639	60	0.019946	94	0.081541
27	0.0035681	61	0.020888	95	0.084608
28	0.0037831	62	0.021867	96	0.087771
29	0.0040092	63	0.022885	97	0.091030
30	0.0042470	64	0.023943	98	0.094390
31	0.0044969	65	0.025042	99	0.097852
32	0.0047596	66	0.026183	100	0.10142
33	0.0050354	67	0.027368		

From E. W. Lemmon, M. O. McLinden, and D. G. Friend, "Thermophysical Properties of Fluid Systems" in *NIST Chemistry WebBook*, NIST Standard Reference Database Number 69, Eds. P. J. Linstrom and W. G. Mallard, June 2005, National Institute of Standards and Technology, Gaithersburg, Md. (<http://webbook.nist.gov>) and Wagner, W., and A., Pruss, "The IAPWS Formulation 1995 for the Thermodynamic Properties of Ordinary Water Substance for General and Scientific Use," *J. Phys. Chem. Ref. Data* **31**(2):387–535, 2002.

The website mentioned above allows users to generate their own tables of thermodynamic properties. The user can select the units as well as the temperatures and/or pressures for which properties are to be generated. The results can then be copied into spreadsheets or other files.

TABLE 2-6 Substances in Tables 2-8, 2-32, 2-141, 2-150, 2-153, 2-155, 2-156, 2-179, 2-312, 2-313, 2-314, and 2-315 Sorted by Chemical Family

Name	Cmpd. No.	Formula	Name	Cmpd. No.	Formula
Paraffins			Acetylenes		
Methane	193	CH ₄	1-Octyne	273	C ₈ H ₁₄
Ethane	125	C ₂ H ₆	1-Nonyne	262	C ₉ H ₁₆
Propane	295	C ₃ H ₈	1-Decyne	79	C ₁₀ H ₁₈
Butane	31	C ₄ H ₁₀	Methyl acetylene	197	C ₃ H ₄
Pentane	279	C ₅ H ₁₂	Vinyl acetylene	339	C ₄ H ₄
Hexane	171	C ₆ H ₁₄	Dimethyl acetylene	105	C ₄ H ₆
Heptane	160	C ₇ H ₁₆	2-Methyl-1-butene-3-yne	207	C ₅ H ₆
Octane	265	C ₈ H ₁₈	3-Methyl-1-butyne	210	C ₅ H ₈
Nonane	256	C ₉ H ₂₀	Aromatics		
Decane	74	C ₁₀ H ₂₂	Benzene	16	C ₆ H ₆
Undecane	336	C ₁₁ H ₂₄	Toluene	325	C ₇ H ₈
Dodecane	123	C ₁₂ H ₂₆	Styrene	312	C ₈ H ₈
Tridecane	327	C ₁₃ H ₂₈	Ethylbenzene	129	C ₈ H ₁₀
Tetradecane	319	C ₁₄ H ₃₀	<i>m</i> -Xylene	343	C ₈ H ₁₀
Pentadecane	277	C ₁₅ H ₃₂	<i>o</i> -Xylene	344	C ₈ H ₁₀
Hexadecane	169	C ₁₆ H ₃₄	<i>p</i> -Xylene	345	C ₈ H ₁₀
Heptadecane	158	C ₁₇ H ₃₆	alpha-Methyl styrene	243	C ₉ H ₁₀
Octadecane	263	C ₁₈ H ₃₈	Cumene	62	C ₉ H ₁₂
Nonadecane	254	C ₁₉ H ₄₀	Propylbenzene	304	C ₉ H ₁₂
Eicosane	124	C ₂₀ H ₄₂	1,2,3-Trimethylbenzene	330	C ₉ H ₁₂
2-Methylpropane	236	C ₄ H ₁₀	1,2,4-Trimethylbenzene	331	C ₉ H ₁₂
2-Methylbutane	202	C ₅ H ₁₂	Naphthalene	246	C ₁₀ H ₈
2,3-Dimethylbutane	107	C ₆ H ₁₄	1,2,3,4-Tetrahydronaphthalene	321	C ₁₀ H ₁₂
2-Methylpentane	234	C ₆ H ₁₄	Butylbenzene	40	C ₁₀ H ₁₄
2,3-Dimethylpentane	114	C ₇ H ₁₆	Biphenyl	24	C ₁₂ H ₁₀
2,2,3,3-Tetramethylbutane	323	C ₈ H ₁₈	Phenanthrene	290	C ₁₄ H ₁₀
2,2,4-Trimethylpentane	332	C ₈ H ₁₈	<i>o</i> -Terphenyl	318	C ₁₈ H ₁₄
2,3,3-Trimethylpentane	333	C ₈ H ₁₈	Aldehydes		
Cyclopropane	71	C ₃ H ₆	Formaldehyde	153	CH ₂ O
Cyclobutane	64	C ₄ H ₈	Acetaldehyde	1	C ₂ H ₄ O
Cyclopentane	69	C ₅ H ₁₀	Propionaldehyde	299	C ₃ H ₆ O
Cyclohexane	65	C ₆ H ₁₂	Butyraldehyde	44	C ₄ H ₈ O
Methylcyclopentane	217	C ₆ H ₁₂	Pentanal	278	C ₅ H ₁₀ O
Ethylcyclopentane	134	C ₇ H ₁₄	Hexanal	170	C ₆ H ₁₂ O
Methylcyclohexane	213	C ₇ H ₁₄	Heptanal	159	C ₇ H ₁₄ O
1,1-Dimethylcyclohexane	108	C ₈ H ₁₆	Octanal	264	C ₈ H ₁₆ O
<i>cis</i> -1,2-Dimethylcyclohexane	109	C ₈ H ₁₆	Nonanal	255	C ₉ H ₁₈ O
<i>trans</i> -1,2-Dimethylcyclohexane	110	C ₈ H ₁₆	Decanal	73	C ₁₀ H ₂₀ O
Ethylcyclohexane	133	C ₈ H ₁₆	Ketones		
Olefins			Acrolein	8	C ₃ H ₄ O
Ethylene	135	C ₂ H ₄	Acetone	5	C ₃ H ₆ O
Propylene	305	C ₃ H ₆	Methylethyl ketone	222	C ₄ H ₈ O
1-Butene	36	C ₄ H ₈	Methylisopropyl ketone	229	C ₅ H ₁₀ O
<i>cis</i> -2-Butene	37	C ₄ H ₈	2-Pentanone	283	C ₅ H ₁₀ O
<i>trans</i> -2-Butene	38	C ₄ H ₈	3-Pentanone	284	C ₅ H ₁₀ O
Cyclopentene	70	C ₅ H ₈	Quinone	310	C ₆ H ₄ O ₂
1-Pentene	285	C ₅ H ₁₀	Cyclohexanone	67	C ₆ H ₁₀ O
Cyclohexene	68	C ₆ H ₁₀	Ethylisopropyl ketone	144	C ₆ H ₁₂ O
1-Hexene	177	C ₆ H ₁₂	2-Hexanone	175	C ₆ H ₁₂ O
1-Heptene	166	C ₇ H ₁₄	3-Hexanone	176	C ₆ H ₁₂ O
1-Octene	271	C ₈ H ₁₆	Methylisobutyl ketone	226	C ₆ H ₁₂ O
1-Nonene	260	C ₉ H ₁₈	Diisopropyl ketone	102	C ₇ H ₁₄ O
1-Decene	77	C ₁₀ H ₂₀	3-Heptanone	164	C ₇ H ₁₄ O
2-Methyl propene	238	C ₄ H ₈	2-Heptanone	165	C ₇ H ₁₄ O
2-Methyl-1-butene	205	C ₅ H ₁₀	2-Octanone	269	C ₈ H ₁₆ O
2-Methyl-2-butene	206	C ₅ H ₁₀	3-Octanone	270	C ₈ H ₁₆ O
1-Methylcyclopentene	218	C ₆ H ₁₀	Benzophenone	20	C ₁₃ H ₁₀ O
3-Methylcyclopentene	219	C ₆ H ₁₀	Heterocyclics		
Propenylcyclohexene	298	C ₉ H ₁₄	Furan	156	C ₄ H ₄ O
Propadiene	294	C ₃ H ₄	Thiophene	324	C ₄ H ₄ S
1,2-Butadiene	29	C ₄ H ₆	Tetrahydrofuran	320	C ₄ H ₈ O
1,3-Butadiene	30	C ₄ H ₆	Tetrahydrothiophene	322	C ₄ H ₈ S
3-Methyl-1,2-butadiene	201	C ₅ H ₈	Elements		
Acetylenes			Argon	14	Ar
Acetylene	7	C ₂ H ₂	Bromine	25	Br ₂
1-Butyne	43	C ₄ H ₆	Chlorine	52	Cl ₂
1-Pentyne	288	C ₅ H ₈	Deuterium	80	D ₂
2-Pentyne	289	C ₅ H ₈	Fluorine	149	F ₂
3-Hexyne	178	C ₆ H ₁₀			
1-Hexyne	180	C ₆ H ₁₀			
2-Hexyne	181	C ₆ H ₁₀			
1-Heptyne	168	C ₇ H ₁₂			

2-50 PHYSICAL AND CHEMICAL DATA
TABLE 2-6 Substances in Tables 2-8, 2-32, 2-141, 2-150, 2-153, 2-155, 2-156, 2-179, 2-312, 2-313, 2-314, and 2-315 Sorted by Chemical Family (Continued)

Name	Cmpd. No.	Formula	Name	Cmpd. No.	Formula
Elements			Acids		
Hydrogen	183	H ₂	Methacrylic acid	192	C ₄ H ₆ O ₂
Helium-4	157	He	Acetic anhydride	4	C ₄ H ₆ O ₃
Nitrogen	249	N ₂	Succinic acid	313	C ₄ H ₆ O ₄
Neon	247	Ne	Butyric acid	45	C ₄ H ₈ O ₂
Oxygen	275	O ₂	Isobutyric acid	189	C ₄ H ₈ O ₂
Alcohols			2-Methylbutanoic acid	203	C ₅ H ₁₀ O ₂
Methanol	194	CH ₄ O	Pentanoic acid	280	C ₅ H ₁₀ O ₂
Ethanol	126	C ₂ H ₆ O	2-Ethyl butanoic acid	131	C ₆ H ₁₂ O ₂
1-Propanol	296	C ₃ H ₈ O	Hexanoic acid	172	C ₆ H ₁₂ O ₂
2-Propanol	297	C ₃ H ₈ O	Benzoic acid	18	C ₇ H ₆ O ₂
1-Butanol	34	C ₄ H ₁₀ O	Heptanoic acid	161	C ₇ H ₁₄ O ₂
2-Butanol	35	C ₄ H ₁₀ O	Phthalic anhydride	293	C ₈ H ₄ O ₃
1-Pentanol	281	C ₅ H ₁₂ O	Terephthalic acid	317	C ₈ H ₆ O ₄
2-Pentanol	282	C ₅ H ₁₂ O	2-Ethyl hexanoic acid	141	C ₈ H ₁₆ O ₂
Cyclohexanol	66	C ₆ H ₁₂ O	Octanoic acid	266	C ₈ H ₁₆ O ₂
1-Hexanol	173	C ₆ H ₁₄ O	2-Methyloctanoic acid	233	C ₉ H ₁₈ O ₂
2-Hexanol	174	C ₆ H ₁₄ O	Nonanoic acid	257	C ₉ H ₁₈ O ₂
1-Heptanol	162	C ₇ H ₁₆ O	Decanoic acid	75	C ₁₀ H ₂₀ O ₂
2-Heptanol	163	C ₇ H ₁₆ O	Esters		
1-Octanol	267	C ₈ H ₁₈ O	Methyl formate	224	C ₂ H ₄ O ₂
2-Octanol	268	C ₈ H ₁₈ O	Ethyl formate	140	C ₃ H ₆ O ₂
1-Nonanol	258	C ₉ H ₂₀ O	Methyl acetate	196	C ₃ H ₆ O ₂
2-Nonanol	259	C ₉ H ₂₀ O	Methyl acrylate	198	C ₄ H ₆ O ₂
1-Decanol	76	C ₁₀ H ₂₂ O	Vinyl acetate	338	C ₄ H ₆ O ₂
1-Undecanol	337	C ₁₁ H ₂₄ O	Ethyl acetate	127	C ₄ H ₈ O ₂
2-Methyl-2-propanol	237	C ₄ H ₁₀ O	Methyl propionate	239	C ₄ H ₈ O ₂
3-Methyl-1-butanol	204	C ₅ H ₁₂ O	Propyl formate	306	C ₄ H ₈ O ₂
Benzyl alcohol	21	C ₇ H ₈ O	Methyl methacrylate	232	C ₅ H ₈ O ₂
1-Methylcyclohexanol	214	C ₇ H ₁₄ O	Ethyl propionate	146	C ₅ H ₁₀ O ₂
<i>cis</i> -2-Methylcyclohexanol	215	C ₇ H ₁₄ O	Methyl butyrate	211	C ₅ H ₁₀ O ₂
<i>trans</i> -2-Methylcyclohexanol	216	C ₇ H ₁₄ O	Propyl acetate	302	C ₅ H ₁₀ O ₂
Ethylene glycol	137	C ₂ H ₆ O ₂	Butyl acetate	39	C ₆ H ₁₂ O ₂
1,2-Propylene glycol	309	C ₃ H ₈ O ₂	Ethyl butyrate	132	C ₆ H ₁₂ O ₂
1,2-Butanediol	32	C ₄ H ₁₀ O ₂	Methyl benzoate	200	C ₈ H ₈ O ₂
1,3-Butanediol	33	C ₄ H ₁₀ O ₂	Ethyl benzoate	130	C ₉ H ₁₀ O ₂
Phenols			Dimethyl phthalate	115	C ₁₀ H ₁₀ O ₄
Phenol	291	C ₆ H ₆ O	Dimethyl terephthalate	119	C ₁₀ H ₁₀ O ₄
<i>m</i> -Cresol	59	C ₇ H ₈ O	Amines		
<i>o</i> -Cresol	60	C ₇ H ₈ O	Methyl amine	199	CH ₃ N
<i>p</i> -Cresol	61	C ₇ H ₈ O	Ethyleneimine	138	C ₂ H ₅ N
Ethers			Dimethyl amine	106	C ₂ H ₇ N
Dimethyl ether	112	C ₂ H ₆ O	Ethyl amine	128	C ₂ H ₇ N
Methyl vinyl ether	245	C ₃ H ₆ O	Ethylenediamine	136	C ₂ H ₆ N ₂
Methylethyl ether	221	C ₃ H ₈ O	Isopropyl amine	190	C ₃ H ₉ N
1,4-Dioxane	120	C ₄ H ₈ O ₂	Propyl amine	303	C ₃ H ₉ N
Diethyl ether	95	C ₄ H ₁₀ O	Trimethyl amine	329	C ₃ H ₉ N
Methylpropyl ether	240	C ₄ H ₁₀ O	Diethyl amine	94	C ₄ H ₁₁ N
Methylisopropyl ether	228	C ₄ H ₁₀ O	Diethanol amine	93	C ₄ H ₁₁ NO ₂
1,1-Dimethoxyethane	103	C ₄ H ₁₀ O ₂	Di-isopropyl amine	100	C ₆ H ₁₅ N
Methylbutyl ether	208	C ₅ H ₁₂ O	Dipropyl amine	122	C ₆ H ₁₅ N
Methylisobutyl ether	225	C ₅ H ₁₂ O	Triethyl amine	328	C ₆ H ₁₅ N
Methyl <i>tert</i> -butyl ether	244	C ₅ H ₁₂ O	Amides		
Ethylpropyl ether	147	C ₅ H ₁₂ O	Formamide	154	CH ₃ NO
Ethylisopropyl ether	143	C ₅ H ₁₂ O	Acetamide	2	C ₂ H ₅ NO
1,2-Dimethoxypropane	104	C ₅ H ₁₂ O ₂	<i>N,N</i> -Dimethyl formamide	113	C ₃ H ₇ NO
Di-isopropyl ether	101	C ₆ H ₁₄ O	<i>N</i> -Methyl acetamide	195	C ₃ H ₇ NO
Methyl pentyl ether	235	C ₆ H ₁₄ O	Benzamide	15	C ₇ H ₇ NO
Anisole	13	C ₇ H ₈ O	Nitriles		
Dibutyl ether	84	C ₈ H ₁₈ O	Acetonitrile	6	C ₂ H ₃ N
Ethylhexyl ether	142	C ₈ H ₁₈ O	Cyanogen	63	C ₂ N ₂
Benzyl ethyl ether	22	C ₉ H ₁₆ O	Acrylonitrile	10	C ₃ H ₃ N
Diphenyl ether	121	C ₁₂ H ₁₀ O	Propionitrile	301	C ₃ H ₅ N
Acids			Butyronitrile	46	C ₄ H ₇ N
Formic acid	155	CH ₂ O ₂	Benzonitrile	19	C ₇ H ₅ N
Oxalic acid	274	C ₂ H ₂ O ₄	Nitro Compounds		
Acetic acid	3	C ₂ H ₄ O ₂	Nitromethane	251	CH ₃ NO ₂
Acrylic acid	9	C ₃ H ₄ O ₂	Nitroethane	248	C ₂ H ₅ NO ₂
Malonic acid	191	C ₃ H ₄ O ₄			
Propionic acid	300	C ₃ H ₆ O ₂			

TABLE 2-6 Substances in Tables 2-8, 2-32, 2-141, 2-150, 2-153, 2-155, 2-156, 2-179, 2-312, 2-313, 2-314, and 2-315 Sorted by Chemical Family (Concluded)

Name	Cmpd. No.	Formula	Name	Cmpd. No.	Formula
Nitro Compounds			Halogenated Hydrocarbons		
1,3,5-Trinitrobenzene	334	C ₆ H ₃ N ₃ O ₆	1,2-Dichloroethane	89	C ₂ H ₄ Cl ₂
2,4,6-Trinitrotoluene	335	C ₇ H ₅ N ₃ O ₆	1,1-Difluoroethane	97	C ₂ H ₄ F ₂
Isocyanates			1,2-Difluoroethane	98	C ₂ H ₄ F ₂
Methyl isocyanate	227	C ₂ H ₃ NO	Bromoethane	27	C ₂ H ₅ Br
Phenyl isocyanate	292	C ₇ H ₅ NO	Chloroethane	54	C ₂ H ₅ Cl
Mercaptans			Fluoroethane	151	C ₂ H ₅ F
Methyl mercaptan	231	CH ₄ S	1,1-Dichloropropane	91	C ₃ H ₆ Cl ₂
Ethyl mercaptan	145	C ₂ H ₆ S	1,2-Dichloropropane	92	C ₃ H ₆ Cl ₂
Propyl mercaptan	308	C ₃ H ₈ S	1-Chloropropane	57	C ₃ H ₇ Cl
2-Propyl mercaptan	307	C ₃ H ₈ S	2-Chloropropane	58	C ₃ H ₇ Cl
Butyl mercaptan	41	C ₄ H ₁₀ S	<i>m</i> -Dichlorobenzene	85	C ₆ H ₄ Cl ₂
<i>sec</i> -Butyl mercaptan	42	C ₄ H ₁₀ S	<i>o</i> -Dichlorobenzene	86	C ₆ H ₄ Cl ₂
Pentyl mercaptan	287	C ₅ H ₁₂ S	<i>p</i> -Dichlorobenzene	87	C ₆ H ₄ Cl ₂
2-Pentyl mercaptan	286	C ₅ H ₁₂ S	Bromobenzene	26	C ₆ H ₅ Br
Benzenethiol	17	C ₆ H ₆ S	Chlorobenzene	53	C ₆ H ₅ Cl
Cyclohexyl mercaptan	72	C ₆ H ₁₂ S	Fluorobenzene	150	C ₆ H ₅ F
Hexyl mercaptan	179	C ₆ H ₁₄ S	Silanes		
Benzyl mercaptan	23	C ₇ H ₈ S	Methylsilane	242	CH ₄ Si
Heptyl mercaptan	167	C ₇ H ₁₆ S	Methylchlorosilane	212	CH ₃ ClSi
Octyl mercaptan	272	C ₈ H ₁₈ S	Methyldichlorosilane	220	CH ₂ Cl ₂ Si
Nonyl mercaptan	261	C ₉ H ₂₀ S	Vinyl trichlorosilane	341	C ₂ H ₃ Cl ₃ Si
Decyl mercaptan	78	C ₁₀ H ₂₂ S	Ethyltrichlorosilane	148	C ₂ H ₅ Cl ₃ Si
Sulfides			Dimethylsilane	116	C ₂ H ₆ Si
Dimethyl sulfide	117	C ₂ H ₆ S	Silicon tetrafluoride	311	F ₄ Si
Dimethyl disulfide	111	C ₂ H ₆ S ₂	Light Gases		
Methylethyl sulfide	223	C ₃ H ₈ S	Hydrogen cyanide	186	CHN
Diethyl sulfide	96	C ₄ H ₁₀ S	Carbon monoxide	49	CO
Methylisopropyl sulfide	230	C ₄ H ₁₀ S	Carbon dioxide	47	CO ₂
Methylpropyl sulfide	241	C ₄ H ₁₀ S	Carbon disulfide	48	CS ₂
Methylbutyl sulfide	209	C ₅ H ₁₂ S	Nitrogen trifluoride	250	F ₃ N
Halogenated Hydrocarbons			Sulfur hexafluoride	315	F ₆ S
Carbon tetrachloride	50	CCl ₄	Hydrogen bromide	184	HBr
Carbon tetrafluoride	51	CF ₄	Hydrogen chloride	185	HCl
Chloroform	55	CHCl ₃	Hydrogen fluoride	187	HF
Dibromomethane	83	CH ₂ Br ₂	Hydrogen sulfide	188	H ₂ S
Dichloromethane	90	CH ₂ Cl ₂	Ammonia	12	H ₃ N
Difluoromethane	99	CH ₂ F ₂	Hydrazine	182	H ₂ N ₂
Bromomethane	28	CH ₃ Br	Nitric oxide	253	NO
Chloromethane	56	CH ₃ Cl	Nitrous oxide	252	N ₂ O
Fluoromethane	152	CH ₃ F	Sulfur dioxide	314	O ₂ S
Vinyl chloride	340	C ₂ H ₃ Cl	Ozone	276	O ₃
1,1,2-Trichloroethane	326	C ₂ H ₃ Cl ₃	Sulfur trioxide	316	O ₃ S
1,1-Dibromoethane	81	C ₂ H ₄ Br ₂	Others		
1,2-Dibromoethane	82	C ₂ H ₄ Br ₂	Air	11	Mixture
1,1-Dichloroethane	88	C ₂ H ₄ Cl ₂	Ethylene oxide	139	C ₂ H ₄ O
			Dimethyl sulfoxide	118	C ₂ H ₆ OS
			Water	342	H ₂ O

2-52 PHYSICAL AND CHEMICAL DATA

TABLE 2-7 Formula Index of Substances in Tables 2-8, 2-32, 2-141, 2-150, 2-153, 2-155, 2-156, 2-179, 2-312, 2-313, 2-314, and 2-315

Formula	No.	Name	Formula	No.	Name
Ar	11	Air	C ₃ H ₆ Cl ₂	92	1,2-Dichloropropane
Br ₂	14	Argon	C ₃ H ₆ O	5	Acetone
CCl ₄	25	Bromine	C ₃ H ₆ O	245	Methyl vinyl ether
CF ₄	50	Carbon tetrachloride	C ₃ H ₆ O	299	Propionaldehyde
CHCl ₃	51	Carbon tetrafluoride	C ₃ H ₆ O ₂	140	Ethyl formate
CHN	55	Chloroform	C ₃ H ₆ O ₂	196	Methyl acetate
CH ₂ Br ₂	186	Hydrogen cyanide	C ₃ H ₆ O ₂	300	Propionic acid
CH ₂ Cl ₂	83	Dibromomethane	C ₃ H ₇ Cl	57	1-Chloropropane
CH ₂ F ₂	90	Dichloromethane	C ₃ H ₇ Cl	58	2-Chloropropane
CH ₂ O	99	Diffluoromethane	C ₃ H ₇ NO	113	N,N-Dimethyl formamide
CH ₂ O ₂	153	Formaldehyde	C ₃ H ₇ NO	195	N-Methyl acetamide
CH ₃ Br	155	Formic acid	C ₃ H ₈	295	Propane
CH ₃ Cl	28	Bromomethane	C ₃ H ₈ O	221	Methylethyl ether
CH ₃ F	56	Chloromethane	C ₃ H ₈ O	296	1-Propanol
CH ₃ NO	152	Fluoromethane	C ₃ H ₈ O	297	2-Propanol
CH ₃ NO ₂	154	Formamide	C ₃ H ₈ O ₂	309	1,2-Propylene glycol
CH ₄	251	Nitromethane	C ₃ H ₈ S	223	Methylethyl sulfide
CH ₄ Cl ₂ Si	193	Methane	C ₃ H ₈ S	308	Propyl mercaptan
CH ₄ O	220	Methyldichlorosilane	C ₃ H ₈ S	307	2-Propyl mercaptan
CH ₄ S	194	Methanol	C ₃ H ₉ N	190	Isopropyl amine
CH ₅ ClSi	231	Methyl mercaptan	C ₃ H ₉ N	303	Propyl amine
CH ₅ NO	212	Methylchlorosilane	C ₃ H ₉ N	329	Trimethyl amine
CH ₆ Si	199	Methyl amine	C ₄ H ₄	339	Vinyl acetylene
CO	242	Methylsilane	C ₄ H ₄ O	156	Furan
CO ₂	49	Carbon monoxide	C ₄ H ₄ S	324	Thiophene
CS ₂	47	Carbon dioxide	C ₄ H ₆	29	1,2-Butadiene
C ₂ H ₂	48	Carbon disulfide	C ₄ H ₆	30	1,3-Butadiene
C ₂ H ₂ O ₄	7	Acetylene	C ₄ H ₆	43	1-Butyne
C ₂ H ₃ Cl	274	Oxalic acid	C ₄ H ₆	105	Dimethyl acetylene
C ₂ H ₃ Cl ₃	340	Vinyl chloride	C ₄ H ₆ O ₂	192	Methacrylic acid
C ₂ H ₃ Cl ₃ Si	326	1,1,2-Trichloroethane	C ₄ H ₆ O ₂	198	Methyl acrylate
C ₂ H ₃ Cl ₃ Si	341	Vinyl trichlorosilane	C ₄ H ₆ O ₂	338	Vinyl acetate
C ₂ H ₃ N	6	Acetonitrile	C ₄ H ₆ O ₃	4	Acetic anhydride
C ₂ H ₃ NO	227	Methyl Isocyanate	C ₄ H ₆ O ₄	313	Succinic acid
C ₂ H ₄	135	Ethylene	C ₄ H ₇ N	46	Butyronitrile
C ₂ H ₄ Br ₂	81	1,1-Dibromoethane	C ₄ H ₈	36	1-Butene
C ₂ H ₄ Br ₂	82	1,2-Dibromoethane	C ₄ H ₈	37	<i>cis</i> -2-Butene
C ₂ H ₄ Cl ₂	88	1,1-Dichloroethane	C ₄ H ₈	38	<i>trans</i> -2-Butene
C ₂ H ₄ Cl ₂	89	1,2-Dichloroethane	C ₄ H ₈	64	Cyclobutane
C ₂ H ₄ F ₂	97	1,1-Difluoroethane	C ₄ H ₈	238	2-Methyl propene
C ₂ H ₄ F ₂	98	1,2-Difluoroethane	C ₄ H ₈ O	44	Butyraldehyde
C ₂ H ₄ O	1	Acetaldehyde	C ₄ H ₈ O	222	Methylethyl ketone
C ₂ H ₄ O	139	Ethylene oxide	C ₄ H ₈ O	320	Tetrahydrofuran
C ₂ H ₄ O ₂	3	Acetic acid	C ₄ H ₈ O ₂	45	Butyric acid
C ₂ H ₄ O ₂	224	Methyl formate	C ₄ H ₈ O ₂	120	1,4-Dioxane
C ₂ H ₅ Br	27	Bromoethane	C ₄ H ₈ O ₂	127	Ethyl acetate
C ₂ H ₅ Cl	54	Chloroethane	C ₄ H ₈ O ₂	189	Isobutyric acid
C ₂ H ₅ Cl ₃ Si	148	Ethyltrichlorosilane	C ₄ H ₈ O ₂	239	Methyl propionate
C ₂ H ₅ F	151	Fluoroethane	C ₄ H ₈ O ₂	306	Propyl formate
C ₂ H ₅ N	138	Ethyleneimine	C ₄ H ₈ S	322	Tetrahydrothiophene
C ₂ H ₅ NO	2	Acetamide	C ₄ H ₁₀	31	Butane
C ₂ H ₅ NO ₂	248	Nitroethane	C ₄ H ₁₀	236	2-Methylpropane
C ₂ H ₆	125	Ethane	C ₄ H ₁₀ O	34	1-Butanol
C ₂ H ₆ O	112	Dimethyl ether	C ₄ H ₁₀ O	35	2-Butanol
C ₂ H ₆ O	126	Ethanol	C ₄ H ₁₀ O	95	Diethyl ether
C ₂ H ₆ O ₂	137	Ethylene glycol	C ₄ H ₁₀ O	237	2-Methyl-2-propanol
C ₂ H ₆ OS	118	Dimethyl sulfoxide	C ₄ H ₁₀ O	240	Methylpropyl ether
C ₂ H ₆ S	117	Dimethyl sulfide	C ₄ H ₁₀ O	228	Methylisopropyl ether
C ₂ H ₆ S	145	Ethyl mercaptan	C ₄ H ₁₀ O ₂	32	1,2-Butanediol
C ₂ H ₆ S ₂	111	Dimethyl disulfide	C ₄ H ₁₀ O ₂	33	1,3-Butanediol
C ₂ H ₇ N	106	Dimethyl amine	C ₄ H ₁₀ O ₂	103	1,1-Dimethoxyethane
C ₂ H ₇ N	128	Ethyl amine	C ₄ H ₁₀ S	41	Butyl mercaptan
C ₂ H ₈ N ₂	136	Ethylenediamine	C ₄ H ₁₀ S	42	<i>sec</i> -Butyl mercaptan
C ₂ H ₈ Si	116	Dimethylsilane	C ₄ H ₁₀ S	96	Diethyl sulfide
C ₂ N ₂	63	Cyanogen	C ₄ H ₁₀ S	230	Methylisopropyl sulfide
C ₃ H ₃ N	10	Acrylonitrile	C ₄ H ₁₀ S	241	Methylpropyl sulfide
C ₃ H ₄	197	Methyl acetylene	C ₄ H ₁₁ N	94	Diethyl amine
C ₃ H ₄	294	Propadiene	C ₄ H ₁₁ NO ₂	93	Diethanol amine
C ₃ H ₄ O	8	Acrolein	C ₅ H ₆	207	2-Methyl-1-butene-3-yne
C ₃ H ₄ O ₂	9	Acrylic acid	C ₅ H ₈	70	Cyclopentene
C ₃ H ₄ O ₄	191	Malonic acid	C ₅ H ₈	201	3-Methyl-1,2-butadiene
C ₃ H ₅ N	301	Propionitrile	C ₅ H ₈	210	3-Methyl-1-butyne
C ₃ H ₆	71	Cyclopropane	C ₅ H ₈	288	1-Pentyne
C ₃ H ₆	305	Propylene	C ₅ H ₈	289	2-Pentyne
C ₃ H ₆ Cl ₂	91	1,1-Dichloropropane	C ₅ H ₈ O ₂	232	Methyl methacrylate

TABLE 2-7 Formula Index of Substances in Tables 2-8, 2-32, 2-141, 2-150, 2-153, 2-155, 2-156, 2-179, 2-312, 2-313, 2-314, and 2-315 (Continued)

Formula	No.	Name	Formula	No.	Name
C ₅ H ₁₀	69	Cyclopentane	C ₇ H ₈	325	Toluene
C ₅ H ₁₀	205	2-Methyl-1-butene	C ₇ H ₈ O	13	Anisole
C ₅ H ₁₀	206	2-Methyl-2-butene	C ₇ H ₈ O	21	Benzyl alcohol
C ₅ H ₁₀	285	1-Pentene	C ₇ H ₈ O	59	<i>m</i> -Cresol
C ₅ H ₁₀ O	229	Methylisopropyl ketone	C ₇ H ₈ O	60	<i>o</i> -Cresol
C ₅ H ₁₀ O	278	Pentanal	C ₇ H ₈ O	61	<i>p</i> -Cresol
C ₅ H ₁₀ O	283	2-Pentanone	C ₇ H ₈ S	23	Benzyl mercaptan
C ₅ H ₁₀ O	284	3-Pentanone	C ₇ H ₁₂	168	1-Heptyne
C ₅ H ₁₀ O ₂	146	Ethyl propionate	C ₇ H ₁₄	134	Ethylcyclopentane
C ₅ H ₁₀ O ₂	203	2-Methylbutanoic acid	C ₇ H ₁₄	166	1-Heptene
C ₅ H ₁₀ O ₂	211	Methyl butyrate	C ₇ H ₁₄	213	Methylcyclohexane
C ₅ H ₁₀ O ₂	280	Pentanoic acid	C ₇ H ₁₄ O	102	Di-isopropyl ketone
C ₅ H ₁₀ O ₂	302	Propyl acetate	C ₇ H ₁₄ O	159	Heptanal
C ₅ H ₁₂	202	2-Methylbutane	C ₇ H ₁₄ O	164	3-Heptanone
C ₅ H ₁₂	279	Pentane	C ₇ H ₁₄ O	165	2-Heptanone
C ₅ H ₁₂ O	143	Ethylisopropyl ether	C ₇ H ₁₄ O	214	1-Methylcyclohexanol
C ₅ H ₁₂ O	147	Ethylpropyl ether	C ₇ H ₁₄ O	215	<i>cis</i> -2-Methylcyclohexanol
C ₅ H ₁₂ O	204	3-Methyl-1-butanol	C ₇ H ₁₄ O	216	<i>trans</i> -2-Methylcyclohexanol
C ₅ H ₁₂ O	208	Methylbutyl ether	C ₇ H ₁₄ O ₂	161	Heptanoic acid
C ₅ H ₁₂ O	225	Methylisobutyl ether	C ₇ H ₁₆	114	2,3-Dimethylpentane
C ₅ H ₁₂ O	244	Methyl <i>tert</i> -butyl ether	C ₇ H ₁₆	160	Heptane
C ₅ H ₁₂ O	281	1-Pentanol	C ₇ H ₁₆ O	162	1-Heptanol
C ₅ H ₁₂ O	282	2-Pentanol	C ₇ H ₁₆ O	163	2-Heptanol
C ₅ H ₁₂ O ₂	104	1,2-Dimethoxypropane	C ₇ H ₁₆ S	167	Heptyl mercaptan
C ₅ H ₁₂ S	209	Methylbutyl sulfide	C ₈ H ₄ O ₃	293	Phthalic anhydride
C ₅ H ₁₂ S	286	2-Pentyl mercaptan	C ₈ H ₆ O ₄	317	Terephthalic acid
C ₅ H ₁₂ S	287	Pentyl mercaptan	C ₈ H ₈	312	Styrene
C ₆ H ₃ N ₃ O ₆	334	1,3,5-Trinitrobenzene	C ₈ H ₈ O ₂	200	Methyl benzoate
C ₆ H ₄ Cl ₂	85	<i>m</i> -Dichlorobenzene	C ₈ H ₁₀	129	Ethylbenzene
C ₆ H ₄ Cl ₂	86	<i>o</i> -Dichlorobenzene	C ₈ H ₁₀	343	<i>m</i> -Xylene
C ₆ H ₄ Cl ₂	87	<i>p</i> -Dichlorobenzene	C ₈ H ₁₀	344	<i>o</i> -Xylene
C ₆ H ₄ O ₃	310	Quinone	C ₈ H ₁₀	345	<i>p</i> -Xylene
C ₆ H ₅ Br	26	Bromobenzene	C ₈ H ₁₄	273	1-Octyne
C ₆ H ₅ Cl	53	Chlorobenzene	C ₈ H ₁₆	108	1,1-Dimethylcyclohexane
C ₆ H ₅ F	150	Fluorobenzene	C ₈ H ₁₆	109	<i>cis</i> -1,2-Dimethylcyclohexane
C ₆ H ₆	16	Benzene	C ₈ H ₁₆	110	<i>trans</i> -1,2-Dimethylcyclohexane
C ₆ H ₆ O	291	Phenol	C ₈ H ₁₆	133	Ethylcyclohexane
C ₆ H ₆ S	17	Benzenethiol	C ₈ H ₁₆	271	1-Octene
C ₆ H ₁₀	218	1-Methylcyclopentene	C ₈ H ₁₆ O	264	Octanal
C ₆ H ₁₀	68	Cyclohexene	C ₈ H ₁₆ O	269	2-Octanone
C ₆ H ₁₀	178	3-Hexyne	C ₈ H ₁₆ O	270	3-Octanone
C ₆ H ₁₀	180	1-Hexyne	C ₈ H ₁₆ O ₂	141	2-Ethyl hexanoic acid
C ₆ H ₁₀	181	2-Hexyne	C ₈ H ₁₆ O ₂	266	Octanoic acid
C ₆ H ₁₀	219	3-Methylcyclopentene	C ₈ H ₁₈	265	Octane
C ₆ H ₁₀ O	67	Cyclohexanone	C ₈ H ₁₈	323	2,2,3,3-Tetramethylbutane
C ₆ H ₁₂	65	Cyclohexane	C ₈ H ₁₈	332	2,2,4-Trimethylpentane
C ₆ H ₁₂	177	1-Hexene	C ₈ H ₁₈	333	2,3,3-Trimethylpentane
C ₆ H ₁₂	217	Methylcyclopentane	C ₈ H ₁₈ O	84	Dibutyl ether
C ₆ H ₁₂ O	66	Cyclohexanol	C ₈ H ₁₈ O	142	Ethylhexyl ether
C ₆ H ₁₂ O	144	Ethylisopropyl ketone	C ₈ H ₁₈ O	267	1-Octanol
C ₆ H ₁₂ O	170	Hexanal	C ₈ H ₁₈ O	268	2-Octanol
C ₆ H ₁₂ O	175	2-Hexanone	C ₈ H ₁₈ S	272	Octyl mercaptan
C ₆ H ₁₂ O	176	3-Hexanone	C ₉ H ₁₀	243	alpha-Methyl styrene
C ₆ H ₁₂ O	226	Methylisobutyl ketone	C ₉ H ₁₀ O ₂	130	Ethyl benzoate
C ₆ H ₁₂ O ₂	39	Butyl acetate	C ₉ H ₁₂	62	Cumene
C ₆ H ₁₂ O ₂	131	2-Ethyl butanoic acid	C ₉ H ₁₂	304	Propylbenzene
C ₆ H ₁₂ O ₂	132	Ethyl butyrate	C ₉ H ₁₂	330	1,2,3-Trimethylbenzene
C ₆ H ₁₂ O ₂	172	Hexanoic acid	C ₉ H ₁₂	331	1,2,4-Trimethylbenzene
C ₆ H ₁₂ S	72	Cyclohexyl mercaptan	C ₉ H ₁₂ O	22	Benzyl ethyl ether
C ₆ H ₁₄	107	2,3-Dimethylbutane	C ₉ H ₁₄	298	Propenylcyclohexene
C ₆ H ₁₄	171	Hexane	C ₉ H ₁₆	262	1-Nonyne
C ₆ H ₁₄	234	2-Methylpentane	C ₉ H ₁₆	260	1-Nonene
C ₆ H ₁₄ O	101	Di-isopropyl ether	C ₉ H ₁₈ O	255	Nonanal
C ₆ H ₁₄ O	173	1-Hexanol	C ₉ H ₁₈ O ₂	233	2-Methyloctanoic acid
C ₆ H ₁₄ O	174	2-Hexanol	C ₉ H ₁₈ O ₂	257	Nonanoic acid
C ₆ H ₁₄ O	235	Methyl pentyl ether	C ₉ H ₂₀	256	Nonane
C ₆ H ₁₄ S	179	Hexyl mercaptan	C ₉ H ₂₀ O	258	1-Nonanol
C ₆ H ₁₅ N	100	Di-isopropyl amine	C ₉ H ₂₀ O	259	2-Nonanol
C ₆ H ₁₅ N	122	Dipropyl amine	C ₉ H ₂₀ S	261	Nonyl mercaptan
C ₆ H ₁₅ N	328	Triethyl amine	C ₁₀ H ₈	246	Naphthalene
C ₇ H ₅ N	19	Benzonitrile	C ₁₀ H ₁₀ O ₄	115	Dimethyl phthalate
C ₇ H ₅ N ₃ O ₆	335	2,4,6-Trinitrotoluene	C ₁₀ H ₁₀ O ₄	119	Dimethyl terephthalate
C ₇ H ₅ NO	292	Phenyl isocyanate	C ₁₀ H ₁₂	321	1,2,3,4-Tetrahydronaphthalene
C ₇ H ₆ O ₂	18	Benzoic acid	C ₁₀ H ₁₄	40	Butylbenzene
C ₇ H ₇ NO	15	Benzamide	C ₁₀ H ₁₈	79	1-Decyne

2-54 PHYSICAL AND CHEMICAL DATA
TABLE 2-7 Formula Index of Substances in Tables 2-8, 2-32, 2-141, 2-150, 2-153, 2-155, 2-156, 2-179, 2-312, 2-313, 2-314, and 2-315 (Concluded)

Formula	No.	Name	Formula	No.	Name
C ₁₀ H ₂₀	77	1-Decene	D ₂	80	Deuterium
C ₁₀ H ₂₀ O	73	Decanal	F ₂	149	Fluorine
C ₁₀ H ₂₀ O ₂	75	Decanoic acid	F ₃ N	250	Nitrogen trifluoride
C ₁₀ H ₂₂	74	Decane	F ₄ Si	311	Silicon tetrafluoride
C ₁₀ H ₂₂ O	76	1-Decanol	F ₆ S	315	Sulfur hexafluoride
C ₁₀ H ₂₂ S	78	Decyl mercaptan	HBr	184	Hydrogen bromide
C ₁₁ H ₂₄	336	Undecane	HCl	185	Hydrogen chloride
C ₁₁ H ₂₄ O	337	1-Undecanol	HF	187	Hydrogen fluoride
C ₁₂ H ₁₀	24	Biphenyl	H ₂	183	Hydrogen
C ₁₂ H ₁₀ O	121	Diphenyl ether	H ₂ O	342	Water
C ₁₂ H ₂₆	123	Dodecane	H ₂ S	188	Hydrogen sulfide
C ₁₃ H ₁₀ O	20	Benzophenone	H ₃ N	12	Ammonia
C ₁₃ H ₂₈	327	Tridecane	H ₄ N ₂	182	Hydrazine
C ₁₄ H ₁₀	290	Phenanthrene	He	157	Helium-4
C ₁₄ H ₃₀	319	Tetradecane	NO	253	Nitric oxide
C ₁₅ H ₃₂	277	Pentadecane	N ₂	249	Nitrogen
C ₁₆ H ₃₄	169	Hexadecane	N ₂ O	252	Nitrous oxide
C ₁₇ H ₃₆	158	Heptadecane	Ne	247	Neon
C ₁₈ H ₁₄	318	<i>o</i> -Terphenyl	O ₂	275	Oxygen
C ₁₈ H ₃₈	263	Octadecane	O ₂ S	314	Sulfur dioxide
C ₁₉ H ₄₀	254	Nonadecane	O ₃	276	Ozone
C ₂₀ H ₄₂	124	Eicosane	O ₃ S	316	Sulfur trioxide
Cl ₂	52	Chlorine			

TABLE 2-8 Vapor Pressure of Inorganic and Organic Liquids, $\ln P = C1 + C2/T + C3 \ln T + C4 T^{C5}$, P in Pa

No.	Name	Formula	CAS no.	C1	C2	C3	C4	C5	T_{min} , K	P at T_{min}	T_{max} , K	P at T_{max}
1	Acetaldehyde	C ₂ H ₄ O	75-07-0	193.69	-8,036.7	-29,502	4.3678E-02	1	150.15	3.23E-01	466	5.565E+06
2	Acetamide	C ₂ H ₅ NO	60-35-5	125.81	-12,376	-14,589	5.0824E-06	2	353.33	3.36E+02	761	6.569E+06
3	Acetic acid	C ₂ H ₄ O ₂	64-19-7	53.27	-6,304.5	-4,2985	8.8865E-18	6	289.81	1.28E+03	591.95	5.739E+06
4	Acetic anhydride	C ₄ H ₆ O ₃	108-24-7	100.95	-8,873.2	-11,451	6.1316E-06	2	200.15	2.20E-02	606	3.970E+06
5	Acetone	C ₃ H ₆ O	67-64-1	69.006	-5,599.6	-7,0985	6.2237E-06	2	178.45	2.79E+00	508.2	4.709E+06
6	Acetonitrile	C ₂ H ₃ N	75-05-8	58.302	-5,385.6	-5,4954	5.3634E-06	2	229.32	1.87E+02	545.5	4.852E+06
7	Acetylene	C ₂ H ₂	74-86-2	39.63	-2,552.2	-2,78	2.3930E-16	6	192.4	1.27E+05	308.3	6.106E+06
8	Acrolein	C ₃ H ₄ O	107-02-8	138.4	-7,122.7	-19,638	2.6447E-02	1	185.45	1.03E+01	506	5.020E+06
9	Acrylic acid	C ₃ H ₄ O ₂	79-10-7	46.745	-6,587.1	-3,2208	5.2253E-07	2	286.15	2.57E+02	615	5.661E+06
10	Acrylonitrile	C ₃ H ₃ N	107-13-1	87.604	-6,392.7	-10,101	1.0891E-05	2	189.63	3.68E+00	535	4.480E+06
11	Air	Mixture	132259-10-0	21.662	-692.39	-0.392	4.7574E-03	1	59.15	5.64E+03	132.45	3.793E+06
12	Ammonia	H ₃ N	7664-41-7	90.483	-4,669.7	-11,607	1.7194E-02	1	195.41	6.11E+03	405.65	1.130E+07
13	Anisole	C ₇ H ₈ O	100-66-3	128.06	-9,307.7	-16,693	1.4919E-02	1	235.65	2.45E+00	645.6	4.273E+06
14	Argon	Ar	7440-37-1	42.127	-1,093.1	-4,1425	5.7254E-05	2	83.78	6.87E+04	150.86	4.896E+06
15	Benzamide	C ₇ H ₇ NO	55-21-0	85.474	-11,932	-8,3348	1.2850E-18	6	403	3.55E+02	824	5.047E+06
16	Benzene	C ₆ H ₆	71-43-2	83.107	-6,486.2	-9,2194	6.9844E-06	2	278.68	4.76E+03	562.05	4.875E+06
17	Benzenethiol	C ₆ H ₆ S	108-98-5	77.765	-8,455.1	-7,7404	4.3089E-18	6	258.27	7.68E+00	689	4.728E+06
18	Benzoic acid	C ₇ H ₆ O ₂	65-85-0	88.513	-11,829	-8,6826	2.3248E-19	6	395.45	7.96E+02	751	4.469E+06
19	Benzonitrile	C ₇ H ₅ N	100-47-0	138.5	-11,195	-17,085	9.5641E-06	2	260.4	3.08E+00	699.35	4.243E+06
20	Benzophenone	C ₁₃ H ₁₀ O	119-61-9	88.404	-11,769	-8,9014	1.9334E-18	6	321.35	1.49E+00	830	3.357E+06
21	Benzyl alcohol	C ₇ H ₈ O	100-51-6	100.68	-11,059	-10,709	3.0582E-18	6	257.85	1.88E-01	720.15	4.372E+06
22	Benzyl ethyl ether	C ₉ H ₁₂ O	539-30-0	68.541	-7,886.2	-6,5804	2.4285E-06	2	275.65	2.31E+01	662	3.113E+06
23	Benzyl mercaptan	C ₇ H ₈ S	100-53-8	118.02	-10,527	-13,91	6.4794E-06	2	243.95	2.98E-01	718	4.074E+06
24	Biphenyl	C ₁₂ H ₁₀	92-52-4	77.314	-9,910.4	-7,5079	2.2385E-18	6	342.2	9.42E+01	773	3.407E+06
25	Bromine	Br ₂	7726-95-6	108.26	-6,592	-14,16	1.6043E-02	1	265.85	5.85E+03	584.15	1.028E+07
26	Bromobenzene	C ₆ H ₅ Br	108-86-1	63.749	-7,130.2	-5,879	5.2136E-18	6	242.43	7.84E+00	670.15	4.520E+06
27	Bromoethane	C ₂ H ₅ Br	74-96-4	62.217	-5,113.3	-5,9761	4.7174E-17	6	154.55	3.72E-01	503.8	6.290E+06
28	Bromomethane	CH ₃ Br	74-83-9	72.586	-4,698.6	-7,9966	1.1553E-05	2	179.47	1.95E+02	467	7.997E+06
29	1,2-Butadiene	C ₄ H ₆	590-19-2	39.714	-3,769.9	-2,6407	6.9379E-18	6	136.95	4.47E-01	452	4.361E+06
30	1,3-Butadiene	C ₄ H ₆	106-99-0	75.572	-4,621.9	-8,5323	1.2269E-05	2	164.25	6.92E+01	425	4.303E+06
31	Butane	C ₄ H ₁₀	106-97-8	66.343	-4,363.2	-7,046	9.4509E-06	2	134.86	6.74E-01	425.12	3.770E+06
32	1,2-Butanediol	C ₄ H ₁₀ O ₂	584-03-2	103.28	-11,548	-10,925	4.2560E-18	6	220	2.93E-04	680	5.202E+06
33	1,3-Butanediol	C ₄ H ₁₀ O ₂	107-88-0	123.22	-12,620	-13,986	3.9260E-06	2	196.15	3.74E-07	676	4.033E+06
34	1-Butanol	C ₄ H ₁₀ O	71-36-3	106.295	-9,866.4	-11,655	1.0832E-17	6	183.85	2.90E-04	563.1	4.401E+06
35	2-Butanol	C ₄ H ₁₀ O	78-92-2	114.68	-9,850.2	-6,1293	1.8738E-17	6	158.45	1.95E+06	535.9	4.182E+06
36	1-Butene	C ₄ H ₈	106-98-9	51.836	-4,019.2	-4,5229	4.8833E-17	6	87.8	6.94E-07	419.5	4.021E+06
37	cis-2-Butene	C ₄ H ₈	590-18-1	72.541	-4,691.2	-7,9776	1.0368E-05	2	134.26	2.72E-01	435.5	4.238E+06
38	trans-2-Butene	C ₄ H ₈	624-64-6	71.704	-4,563.1	-7,9053	1.1319E-05	2	167.62	7.45E+01	428.6	4.100E+06
39	Butyl acetate	C ₈ H ₁₆ O ₂	123-86-4	122.82	-9,253.2	-14,99	1.0470E-05	2	199.65	8.17E-02	575.4	3.087E+06
40	Butylbenzene	C ₁₀ H ₁₄	104-51-8	101.22	-9,255.4	-11,538	5.9208E-06	2	185.3	1.54E-04	660.5	2.882E+06
41	Butyl mercaptan	C ₈ H ₁₆ S	109-79-5	65.382	-6,262.4	-6,2585	1.4943E-17	6	157.46	2.35E-03	570.1	3.973E+06
42	sec-Butyl mercaptan	C ₈ H ₁₆ S	513-53-1	60.649	-5,785.9	-5,6113	1.5877E-17	6	133.02	3.40E-05	554	4.060E+06
43	1-Butyne	C ₄ H ₆	107-00-6	77.004	-5,054.5	-8,5665	1.0161E-05	2	147.43	1.18E+00	440	4.599E+06
44	Butyraldehyde	C ₄ H ₈ O	123-72-8	99.33	-7,083.6	-11,733	1.0027E-05	2	176.75	3.17E-01	537.2	4.323E+06
45	Butyric acid	C ₄ H ₈ O ₂	107-92-6	93.815	-9,942.2	-9,8019	9.3124E-18	6	267.95	6.78E+00	615.7	4.071E+06
46	Butyronitrile	C ₄ H ₇ N	109-74-0	66.32	-6,714.9	-6,3087	1.3516E-17	6	161.25	6.18E-04	582.25	3.787E+06
47	Carbon dioxide	CO ₂	124-38-9	140.54	-4,735	-21,268	4.0909E-02	1	216.58	5.19E+05	304.21	7.390E+06
48	Carbon disulfide	CS ₂	75-15-0	67.114	-4,820.4	-7,5303	9.1695E-03	1	161.11	1.49E+00	552	8.041E+06
49	Carbon monoxide	CO	630-08-0	45.698	-1,076.6	-4,8814	7.5673E-05	2	68.15	1.54E+04	132.92	3.494E+06
50	Carbon tetrachloride	CCl ₄	56-23-5	78.441	-6,128.1	-8,5766	6.8465E-06	2	250.33	1.12E+03	556.35	4.544E+06
51	Carbon tetrafluoride	CF ₄	75-73-0	61.89	-2,296.3	-7,086	3.4687E-05	2	89.56	1.08E+02	227.51	3.742E+06
52	Chlorine	Cl ₂	7782-50-5	71.334	-3,855	-8,5171	1.2378E-02	1	172.12	1.37E+03	417.15	7.793E+06
53	Chlorobenzene	C ₆ H ₅ Cl	108-90-7	54.144	-6,244.4	-4,5343	4.7030E-18	6	227.95	8.45E+00	632.35	4.529E+06
54	Chloroethane	C ₂ H ₅ Cl	75-00-3	65.988	-4,661.3	-6,8586	7.9404E-06	2	134.8	1.25E-01	460.35	5.327E+06
55	Chloroform	CHCl ₃	67-66-3	146.43	-7,792.3	-20,614	2.4578E-02	1	207.15	5.25E+01	536.4	5.554E+06
56	Chloromethane	CH ₃ Cl	74-87-3	64.697	-4,048.1	-6,8066	1.0371E-05	2	175.43	8.71E+02	416.25	6.691E+06
57	1-Chloropropane	C ₃ H ₇ Cl	540-54-5	79.24	-5,718.8	-8,789	8.4486E-06	2	150.35	6.96E-02	503.15	4.581E+06
58	2-Chloropropane	C ₃ H ₇ Cl	75-29-6	46.854	-4,445.5	-3,6533	1.3260E-17	6	155.97	9.08E-01	489	4.510E+06
59	m-Cresol	C ₇ H ₈ O	108-39-4	95.403	-10,581	-10,004	4.3032E-18	6	285.39	5.86E+00	705.85	4.522E+06
60	o-Cresol	C ₇ H ₈ O	95-48-7	210.88	-13,928	-29,483	2.5182E-02	1	304.19	6.53E+01	697.55	5.058E+06

TABLE 2-8 Vapor Pressure of Inorganic and Organic Liquids, $\ln P = C1 + C2/T + C3 \ln T + C4 T^{C5}$, P in Pa (Continued)

No.	Name	Formula	CAS no.	C1	C2	C3	C4	C5	T_{\min} , K	P at T_{\min}	T_{\max} , K	P at T_{\max}
61	<i>p</i> -Cresol	C ₇ H ₈ O	106-44-5	118.53	-11,957	-13.293	8.6988E-18	6	307.93	3.45E+01	704.65	5.151E+06
62	Cumene	C ₉ H ₁₂	98-82-8	102.81	-8,674.6	-11.922	7.0048E-06	2	177.14	4.71E-04	631	3.226E+06
63	Cyanogen	C ₂ N ₂	460-19-5	81.565	-4,808.9	-9.3748	1.3901E-05	2	245.25	7.390E+04	400.15	5.961E+06
64	Cyclobutane	C ₄ H ₈	287-23-0	85.899	-4,884.4	-10.883	1.4934E-02	1	182.48	1.80E+02	459.93	4.991E+06
65	Cyclohexane	C ₆ H ₁₂	110-82-7	51.087	-5,226.4	-4.2278	9.7554E-18	6	279.69	5.36E+03	553.8	4.094E+06
66	Cyclohexanol	C ₆ H ₁₂ O	108-93-0	189.19	-14,337	-24.148	1.0740E-05	2	296.6	7.65E+01	650.1	4.265E+06
67	Cyclohexanone	C ₆ H ₁₀ O	108-94-1	85.424	-7,944.4	-9.2862	4.9957E-06	2	242	6.80E+00	653	3.989E+06
68	Cyclohexene	C ₆ H ₁₀	110-83-8	88.184	-6,624.9	-10.059	8.2566E-06	2	169.67	1.04E-01	560.4	4.392E+06
69	Cyclopentane	C ₅ H ₁₀	287-92-3	66.341	-5,198.5	-6.8103	6.1930E-06	2	179.28	9.07E+00	511.7	4.513E+06
70	Cyclopentene	C ₅ H ₈	142-29-0	67.952	-5,187.5	-7.0785	6.8165E-06	2	138.13	1.28E-02	507	4.799E+06
71	Cyclopropane	C ₃ H ₆	75-19-4	40.608	-3,179.6	-2.8937	5.6131E-17	6	145.59	7.80E+01	398	5.494E+06
72	Cyclohexyl mercaptan	C ₆ H ₁₂ S	1569-69-3	85.146	-7,843.7	-9.2982	5.1788E-06	2	189.64	8.24E-03	664	3.970E+06
73	Decanal	C ₁₀ H ₂₀ O	112-31-2	201.64	-15,133	-26.264	1.4625E-05	2	267.15	4.86E-01	674.2	2.599E+06
74	Decane	C ₁₀ H ₂₂	124-18-5	112.73	-9,749.6	-13.245	7.1266E-06	2	243.51	1.39E+00	617.7	2.091E+06
75	Decanoic acid	C ₁₀ H ₂₀ O ₂	334-48-5	123.36	-14,680	-13.474	1.9491E-18	6	304.55	1.50E-01	722.1	2.233E+06
76	1-Decanol	C ₁₀ H ₂₂ O	112-30-1	156.239	-15,212	-18.424	8.5006E-18	6	280.05	1.51E-01	688	2.309E+06
77	1-Decene	C ₁₀ H ₂₀	872-05-9	68.401	-7,776.9	-6.4637	6.3750E-18	6	206.89	2.59E-02	616.6	2.223E+06
78	Decyl mercaptan	C ₁₀ H ₂₂ S	143-10-2	91.91	-10,565	-9.5957	5.7028E-18	6	247.56	2.59E-02	696	2.130E+06
79	1-Decyne	C ₁₀ H ₁₈	764-93-2	142.94	-11,119	-17.818	1.1020E-05	2	229.15	1.60E-01	619.85	2.363E+06
80	Deuterium	D ₂	7782-39-0	18.947	-154.47	-0.5723	3.8899E-02	1	18.73	1.72E+04	38.35	1.663E+06
81	1,1-Dibromoethane	C ₂ H ₄ Br ₂	557-91-5	62.711	-6,503.5	-5.7669	1.0427E-06	2	210.15	2.64E+00	628	6.034E+06
82	1,2-Dibromoethane	C ₂ H ₄ Br ₂	106-93-4	43.751	-5,587.7	-3.0891	8.2664E-07	2	282.85	5.37E+02	650.15	5.75E+06
83	Dibromomethane	CH ₂ Br ₂	74-95-3	86.295	-7,010.3	-9.5972	6.7794E-06	2	220.6	2.13E+01	611	7.170E+06
84	Dibutyl ether	C ₈ H ₁₈ O	142-96-1	72.227	-7,537.6	-7.0596	9.1442E-18	6	175.3	7.14E-04	584.1	2.459E+06
85	<i>m</i> -Dichlorobenzene	C ₆ H ₄ Cl ₂	541-73-1	53.187	-6,827.5	-4.3233	2.3112E-18	6	248.39	6.41E+00	683.95	4.070E+06
86	<i>o</i> -Dichlorobenzene	C ₆ H ₄ Cl ₂	95-50-1	77.105	-8,111.1	-7.8886	2.7267E-06	2	256.15	6.49E+00	705	4.074E+06
87	<i>p</i> -Dichlorobenzene	C ₆ H ₄ Cl ₂	106-46-7	88.31	-8,463.4	-9.6308	4.5833E-06	2	326.14	1.23E+03	684.75	4.070E+06
88	1,1-Dichloroethane	C ₂ H ₄ Cl ₂	75-34-3	66.611	-5,493.1	-6.7301	5.3579E-06	2	176.19	2.21E+00	523	5.106E+06
89	1,2-Dichloroethane	C ₂ H ₄ Cl ₂	107-06-2	92.355	-6,920.4	-10.651	9.1426E-06	2	237.49	2.37E+02	561.6	5.318E+06
90	Dichloromethane	CH ₂ Cl ₂	75-09-2	101.6	-6,541.6	-12.247	1.2311E-05	2	178.01	5.93E+00	510	6.093E+06
91	1,1-Dichloropropane	C ₃ H ₆ Cl ₂	78-99-9	83.495	-6,661.4	-9.2386	6.7652E-06	2	200	4.52E+00	560	4.239E+06
92	1,2-Dichloropropane	C ₃ H ₆ Cl ₂	78-87-5	65.955	-6,015.6	-6.5509	4.3172E-06	2	172.71	8.25E-02	572	4.232E+06
93	Diethanol amine	C ₄ H ₁₁ NO ₂	111-42-2	106.38	-13,714	-11.06	3.2645E-18	6	301.15	1.02E-01	736.6	4.260E+06
94	Diethyl amine	C ₄ H ₁₁ N	109-89-7	49.314	-4,949	-3.9256	9.1978E-18	6	223.35	3.74E+02	496.6	3.674E+06
95	Diethyl ether	C ₄ H ₁₀ O	60-29-7	136.9	-6,954.3	-19.254	2.4508E-02	1	156.85	3.95E+01	466.7	3.641E+06
96	Diethyl sulfide	C ₄ H ₁₀ S	352-93-2	46.705	-5,177.4	-3.5985	1.7147E-06	2	169.20	9.93E-02	557.15	3.961E+06
97	1,1-Difluoroethane	C ₂ H ₄ F ₂	75-37-6	73.491	-4,385.9	-8.1851	1.2978E-05	2	154.56	6.45E+01	386.44	4.507E+06
98	1,2-Difluoroethane	C ₂ H ₄ F ₂	624-72-6	84.625	-5,217.4	-9.871	1.3050E-05	2	215	2.83E+03	445	4.372E+06
99	Difluoromethane	CH ₂ F ₂	75-10-5	69.132	-3,847.7	-7.5868	1.5065E-05	2	136.95	5.43E+01	351.255	5.760E+06
100	Di-isopropyl amine	C ₆ H ₁₅ N	108-18-9	462.84	-18,227	-73.734	9.2794E-02	1	176.85	4.47E-03	523.1	3.199E+06
101	Di-isopropyl ether	C ₆ H ₁₄ O	108-20-3	41.631	-4,668.7	-2.8551	6.3693E-04	1	187.65	6.86E+00	500.05	2.869E+06
102	Di-isopropyl ketone	C ₇ H ₁₄ O	565-80-0	50.868	-6,036.5	-4.066	1.1326E-06	2	204.81	8.21E-01	576	3.017E+06
103	1,1-Dimethoxyethane	C ₄ H ₁₀ O ₂	534-15-6	53.637	-5,251.2	-4.5649	1.6754E-17	6	159.95	9.45E-02	507.8	3.773E+06
104	1,2-Dimethoxypropane	C ₅ H ₁₂ O ₂	7778-85-0	62.097	-6,174.9	-5.715	1.2323E-17	6	226.1	4.50E+01	543	3.447E+06
105	Dimethyl acetylene	C ₄ H ₆	503-17-3	66.592	-4,999.8	-6.8387	6.6793E-06	2	240.91	6.12E+03	473.2	4.870E+06
106	Dimethyl amine	C ₂ H ₇ N	124-40-3	71.738	-5,302	-7.3324	6.4200E-17	6	180.96	7.56E+01	437.2	5.258E+06
107	2,3-Dimethylbutane	C ₆ H ₁₄	79-29-8	77.161	-5,691.1	-8.501	8.0325E-06	2	145.19	1.52E-02	500	3.130E+06
108	1,1-Dimethylcyclohexane	C ₈ H ₁₆	590-66-9	81.184	-6,927	-8.8498	5.4580E-06	2	239.66	6.06E+01	591.15	2.939E+06
109	<i>cis</i> -1,2-Dimethylcyclohexane	C ₈ H ₁₆	2207-01-4	78.952	-7,075.4	-8.4344	4.5035E-06	2	223.16	6.41E+00	606.15	2.939E+06
110	<i>trans</i> -1,2-Dimethylcyclohexane	C ₈ H ₁₆	6876-23-9	78.429	-6,882.1	-8.4129	4.9831E-06	2	184.99	8.04E-02	596.15	2.938E+06
111	Dimethyl disulfide	C ₂ H ₆ S ₂	624-92-0	81.045	-6,941.3	-8.777	5.5501E-06	2	188.44	2.07E-01	615	5.363E+06
112	Dimethyl ether	C ₂ H ₆ O	115-10-6	44.704	-3,525.6	-3.4444	5.4574E-17	6	131.65	3.05E+00	400.1	5.274E+06
113	<i>N,N</i> -Dimethyl formamide	C ₃ H ₇ NO	68-12-2	82.762	-7,955.5	-8.8038	4.2431E-06	2	212.72	1.95E-01	649.6	4.365E+06
114	2,3-Dimethylpentane	C ₇ H ₁₆	565-59-3	78.335	-6,348.7	-8.5105	6.4311E-06	2	160	1.26E-02	537.3	2.882E+06
115	Dimethyl phthalate	C ₁₀ H ₁₀ O ₄	131-11-3	72.517	-10,415	-6.755	1.3269E-06	2	274.18	3.72E-02	766	2.780E+06
116	Dimethylsilane	C ₂ H ₆ Si	1111-74-6	63.08	-4,062.3	-6.425	1.5115E-16	6	122.93	4.15E-01	402	3.561E+06
117	Dimethyl sulfide	C ₂ H ₆ S	75-18-3	84.39	-5,740.6	-9.6454	1.0073E-05	2	174.88	7.86E+00	503.04	5.533E+06
118	Dimethyl sulfoxide	C ₂ H ₆ OS	67-68-5	56.273	-7,620.6	-4.6279	4.3819E-07	2	291.67	5.02E+01	729	5.648E+06
119	Dimethyl terephthalate	C ₁₀ H ₁₀ O ₄	120-61-6	43.541	-8,204.8	-2.7519	1.0466E-18	6	413.8	1.26E+03	772	2.778E+06
120	1,4-Dioxane	C ₄ H ₈ O ₂	123-91-1	44.494	-5,406.7	-3.1287	2.8913E-18	6	284.95	2.53E+03	587	5.158E+06

121	Diphenyl ether	C ₁₂ H ₁₀ O	101-84-8	59.969	-8,585.5	-5.1538	1.9983E-18	6	300.03	7.09E+00	766.8	3.097E+06
122	Dipropyl amine	C ₆ H ₁₅ N	142-84-7	54	-6,018.5	-4.4981	9.9684E-18	6	210.15	3.69E+00	550	3.111E+06
123	Dodecane	C ₁₂ H ₂₆	112-40-3	137.47	-11,976	-16.698	8.0906E-06	2	263.57	6.15E-01	658	1.822E+06
124	Eicosane	C ₂₀ H ₄₂	112-95-8	203.66	-19,441	-25.525	8.8382E-06	2	309.58	9.26E-03	768	1.175E+06
125	Ethane	C ₂ H ₆	74-84-0	51.857	-2,598.7	-5.1283	1.4913E-05	2	90.35	1.13E+00	305.32	4.852E+06
126	Ethanol	C ₂ H ₆ O	64-17-5	73.304	-7,122.3	-7.1424	2.8853E-06	2	159.05	4.96E-04	514	6.109E+06
127	Ethyl acetate	C ₄ H ₈ O ₂	141-78-6	66.824	-6,227.6	-6.41	1.7914E-17	6	189.6	1.43E+00	523.3	3.850E+06
128	Ethyl amine	C ₂ H ₇ N	75-04-7	81.56	-5,596.9	-9.0779	8.7920E-06	2	192.15	1.52E+02	456.15	5.594E+06
129	Ethylbenzene	C ₈ H ₁₀	100-41-4	89.063	-7,733.7	-9.917	5.9860E-06	2	178.2	3.91E-03	617.15	3.590E+06
130	Ethyl benzoate	C ₉ H ₁₀ O ₂	93-89-0	52.923	-7,531.7	-4.2347	1.1835E-06	2	238.45	1.69E-01	698	3.203E+06
131	2-Ethyl butanoic acid	C ₆ H ₁₂ O ₂	88-09-5	90.464	-10,243	-9.2836	5.2573E-18	6	258.15	4.63E-01	655	3.403E+06
132	Ethyl butyrate	C ₆ H ₁₂ O ₂	105-54-4	57.661	-6,346.5	-5.032	8.2534E-18	6	175.15	1.04E-02	571	2.935E+06
133	Ethylcyclohexane	C ₈ H ₁₆	1678-91-7	80.208	-7,203.2	-8.6023	4.5901E-06	2	161.84	3.57E-04	609.15	3.041E+06
134	Ethylcyclopentane	C ₇ H ₁₄	1640-89-7	88.671	-7,012.7	-10.045	7.4578E-06	2	134.71	3.71E-06	569.5	3.412E+06
135	Ethylene	C ₂ H ₄	74-85-1	53.963	-2,443	-5.5643	1.9079E-05	2	104	1.26E+02	282.34	5.032E+06
136	Ethylenediamine	C ₂ H ₆ N ₂	107-15-3	73.51	-7,572.7	-7.1435	1.2124E-17	6	284.29	6.78E+02	593	6.290E+06
137	Ethylene glycol	C ₂ H ₆ O ₂	107-21-1	84.09	-10,411	-8.1976	1.6536E-18	6	260.15	2.19E-01	720	8.257E+06
138	Ethyleneimine	C ₂ H ₅ N	151-56-4	66.51	-6,019.2	-6.3332	1.0394E-17	6	195.2	9.71E+00	537	6.850E+06
139	Ethylene oxide	C ₂ H ₄ O	75-21-8	91.944	-5,293.4	-11.682	1.4902E-02	1	160.65	7.79E+00	469.15	7.255E+06
140	Ethyl formate	C ₃ H ₆ O ₂	109-94-4	73.833	-5,817	-7.809	6.3200E-06	2	193.55	1.81E+01	508.4	4.708E+06
141	2-Ethyl hexanoic acid	C ₈ H ₁₆ O ₂	149-57-5	117.52	-12,991	-12.895	6.1306E-18	6	235	2.86E-04	674.6	2.788E+06
142	Ethylhexyl ether	C ₈ H ₁₈ O	5756-43-4	77.523	-7,978.8	-7.7757	1.0076E-17	6	180	7.60E-04	583	2.460E+06
143	Ethylisopropyl ether	C ₆ H ₁₂ O	625-54-7	57.723	-5,236.9	-5.2136	2.2998E-17	6	140	4.31E-03	489	3.415E+06
144	Ethylisopropyl ketone	C ₆ H ₁₂ O	565-69-5	57.459	-6,356.8	-4.9545	5.2015E-18	6	204.15	9.70E-01	567	3.293E+06
145	Ethyl mercaptan	C ₂ H ₆ S	75-08-1	65.551	-5,027.4	-6.6853	6.3208E-06	2	125.26	1.14E-03	499.15	5.492E+06
146	Ethyl propionate	C ₅ H ₁₀ O ₂	105-37-3	105.64	-8,007	-12.477	9.0000E-06	2	199.25	7.80E-01	546	3.337E+06
147	Ethylpropyl ether	C ₆ H ₁₂ O	628-32-0	86.898	-6,646.4	-9.5758	5.9615E-17	6	145.65	1.61E-03	500.23	3.372E+06
148	Ethyltrichlorosilane	C ₂ H ₅ Cl ₃ Si	115-21-9	62.614	-6,148.2	-5.84	1.0900E-17	6	167.55	1.85E-02	559.95	3.320E+06
149	Fluorine	F ₂	7782-41-4	42.393	-1,103.3	-4.1203	5.7815E-05	2	53.48	2.53E+02	144.12	5.167E+06
150	Fluorobenzene	C ₆ H ₅ F	462-06-6	51.915	-5,439	-4.2896	8.7527E-18	6	230.94	1.51E+02	560.09	4.544E+06
151	Fluoroethane	C ₂ H ₅ F	353-36-6	56.639	-3,576.5	-5.5801	9.8969E-06	2	129.95	8.37E+00	375.31	5.006E+06
152	Fluoromethane	CH ₃ F	593-53-3	59.123	-3,043.7	-6.1845	1.6637E-05	2	131.35	4.33E+02	317.42	5.875E+06
153	Formaldehyde	CH ₂ O	50-00-0	101.51	-4,917.2	-13.765	2.2031E-02	1	181.15	8.87E+02	408	6.594E+06
154	Formamide	CH ₃ NO	75-12-7	100.3	-10,763	-10.946	3.8503E-06	2	275.6	1.04E+00	771	7.751E+06
155	Formic acid	CH ₂ O ₂	64-18-6	50.323	-5,378.2	-4.203	3.4697E-06	2	281.45	2.40E+03	588	5.807E+06
156	Furan	C ₄ H ₄ O	110-00-9	74.738	-5,417	-8.0636	7.4700E-06	2	187.55	5.00E+01	490.15	5.550E+06
157	Helium-4	He	7440-59-7	11.533	-8.99	0.6724	2.7430E-01	1	1.76	1.46E+03	5.2	2.285E+05
158	Heptadecane	C ₁₇ H ₃₆	629-78-7	156.95	-15,557	-18.966	6.4559E-06	2	295.13	4.65E-02	736	1.344E+06
159	Heptanal	C ₇ H ₁₄ O	111-71-7	92.252	-8,349	-10.274	5.9252E-06	2	229.8	1.45E+00	616.8	3.155E+06
160	Heptane	C ₇ H ₁₆	142-82-5	87.829	-6,996.4	-9.8802	7.2099E-06	2	182.57	1.83E-01	540.2	2.719E+06
161	Heptanoic acid	C ₇ H ₁₄ O ₂	111-14-8	120.47	-13,106	-13.31	5.8384E-18	6	265.83	4.34E-02	677.3	3.039E+06
162	1-Heptanol	C ₇ H ₁₆ O	111-70-6	147.41	-13,466	-17.353	1.1284E-17	6	239.15	1.95E-02	632.3	3.013E+06
163	2-Heptanol	C ₇ H ₁₆ O	543-49-7	124.23	-11,637	-14.148	6.9486E-17	5.7	230	3.68E-02	608.3	2.995E+06
164	3-Heptanone	C ₇ H ₁₄ O	106-35-4	78.463	-8,077.2	-7.9062	8.0521E-18	6	234.15	2.30E+00	606.6	2.919E+06
165	2-Heptanone	C ₇ H ₁₄ O	110-43-0	75.494	-7,896.5	-7.5047	8.9130E-18	6	238.15	3.54E+00	611.4	2.946E+06
166	1-Heptene	C ₇ H ₁₄	592-76-7	65.922	-6,189	-6.3629	2.0091E-17	6	154.12	1.86E-03	537.4	2.921E+06
167	Heptyl mercaptan	C ₇ H ₁₆ S	1639-09-4	79.858	-8,501.8	-8.1043	8.1501E-18	6	229.92	3.05E-01	645	2.772E+06
168	1-Heptyne	C ₇ H ₁₂	628-71-7	59.083	-6,031.8	-5.3072	1.4357E-17	6	192.22	8.15E-01	547	3.209E+06
169	Hexadecane	C ₁₆ H ₃₄	544-76-3	156.06	-15,015	-18.941	6.8172E-06	2	291.31	9.23E-02	723	1.411E+06
170	Hexanal	C ₆ H ₁₂ O	66-25-1	81.507	-7,776.8	-8.4516	1.5143E-17	6	217.15	1.25E+00	591	3.461E+06
171	Hexane	C ₆ H ₁₄	110-54-3	104.65	-6,995.5	-12.702	1.2381E-05	2	177.83	9.02E-01	507.6	3.045E+06
172	Hexanoic acid	C ₆ H ₁₂ O ₂	142-62-1	114.05	-12,332	-12.45	5.6253E-18	6	269.25	2.43E-01	660.2	3.284E+06
173	1-Hexanol	C ₆ H ₁₄ O	111-27-3	135.421	-12,288	-15.732	1.2701E-17	6	228.55	2.25E-02	611.3	3.441E+06
174	2-Hexanol	C ₆ H ₁₄ O	626-93-7	109.42	-10,449	-12.051	2.6122E-46	16	223	7.44E-02	585.3	3.298E+06
175	2-Hexanone	C ₆ H ₁₂ O	591-78-6	107.44	-8,528.6	-12.679	8.4606E-06	2	217.35	1.45E+00	587.61	3.286E+06
176	3-Hexanone	C ₆ H ₁₂ O	589-38-8	73.155	-7,242.9	-7.2569	1.2741E-17	6	217.5	2.22E+00	582.82	3.322E+06
177	1-Hexene	C ₆ H ₁₂	592-41-6	51.024	-4,986.4	-4.2463	1.6768E-17	6	133.39	7.68E-04	504	3.212E+06
178	3-Hexyne	C ₆ H ₁₀	928-49-4	47.091	-5,104	-3.6371	5.1621E-04	1	170.05	2.20E-01	544	3.540E+06
179	Hexyl mercaptan	C ₆ H ₁₄ S	111-31-9	68.467	-7,390.5	-6.5456	7.7611E-18	6	192.62	1.31E-02	623	3.079E+06
180	1-Hexyne	C ₆ H ₁₀	693-02-7	133.2	-7,492.9	-18.405	2.2062E-02	1	141.25	3.92E-04	516.2	3.635E+06
181	2-Hexyne	C ₆ H ₁₀	764-35-2	123.71	-7,639	-16.451	1.6495E-02	1	183.65	5.40E-01	549	3.530E+06
182	Hydrazine	H ₂ N ₂	302-01-2	76.858	-7,245.2	-8.22	6.1557E-03	1	274.69	4.08E+02	653.15	1.473E+07
183	Hydrogen	H ₂	1333-74-0	12.69	-94.896	1.1125	3.2915E-04	2	13.95	7.21E+03	33.19	1.315E+06

TABLE 2-8 Vapor Pressure of Inorganic and Organic Liquids, $\ln P = C1 + C2/T + C3 \ln T + C4 T^{\text{CS}}$, P in Pa (Continued)

No.	Name	Formula	CAS no.	C1	C2	C3	C4	C5	T_{min} , K	P at T_{min}	T_{max} , K	P at T_{max}
184	Hydrogen bromide	HBr	10035-10-6	29.315	-2,424.5	-1.1354	2.3806E-18	6	185.15	2.95E+04	363.15	8.463E+06
185	Hydrogen chloride	HCl	7647-01-0	104.27	-3,731.2	-15.047	3.1340E-02	1	158.97	1.35E+04	324.65	8.356E+06
186	Hydrogen cyanide	HCN	74-90-8	36.75	-3,927.1	-2.1245	3.8948E-17	6	259.83	1.87E+04	456.65	5.353E+06
187	Hydrogen fluoride	HF	7664-39-3	59.544	-4,143.8	-6.1764	1.4161E-05	2	189.79	3.37E+02	461.15	6.487E+06
188	Hydrogen sulfide	H ₂ S	7783-06-4	85.584	-3,839.9	-11.199	1.8848E-02	1	187.68	2.29E+04	373.53	8.999E+06
189	Isobutyric acid	C ₄ H ₈ O ₂	79-31-2	110.38	-10,540	-12.262	1.4310E-17	6	227.15	7.82E-02	605	3.683E+06
190	Isopropyl amine	C ₃ H ₇ N	75-31-0	136.66	-7,201.5	-18.934	2.2255E-02	1	177.95	7.73E+00	471.85	4.540E+06
191	Malonic acid	C ₃ H ₄ O ₄	141-82-2	122.92	-16,258	-13.113	2.0609E-12	6	407.95	7.03E+01	805	5.652E+06
192	Methacrylic acid	C ₄ H ₆ O ₂	79-41-4	109.53	-10,410	-12.289	3.1990E-06	2	288.15	5.86E+01	662	4.812E+06
193	Methane	CH ₄	74-82-8	39.205	-1,324.4	-3.4366	3.1019E-05	2	90.69	1.17E+04	190.56	4.590E+06
194	Methanol	CH ₃ O	67-56-1	82.718	-6,904.5	-8.8622	7.4664E-06	2	175.47	1.11E-01	512.5	8.146E+06
195	N-Methyl acetamide	C ₃ H ₇ NO	79-16-3	79.128	-9,523.9	-7.7355	3.1616E-18	6	301.15	2.86E+01	718	4.997E+06
196	Methyl acetate	C ₃ H ₆ O ₂	79-20-9	61.267	-5,618.6	-5.6473	2.1080E-17	6	175.15	1.02E+00	506.55	4.695E+06
197	Methyl acetylene	C ₃ H ₄	74-99-7	50.242	-3,811.9	-4.2526	6.5326E-17	6	170.45	4.15E+02	402.4	5.619E+06
198	Methyl acrylate	C ₄ H ₆ O ₂	96-33-3	107.69	-7,027.2	-13.916	1.5185E-02	1	196.32	4.07E+00	536	4.277E+06
199	Methyl amine	CH ₅ N	74-89-5	75.206	-5,082.8	-8.0919	8.1130E-06	2	179.69	1.77E+02	430.05	7.414E+06
200	Methyl benzoate	C ₈ H ₈ O ₂	93-58-3	84.828	-9,334.7	-8.7063	6.1723E-18	6	260.75	1.81E+00	693	3.590E+06
201	3-Methyl-1,2-butadiene	C ₅ H ₈	598-25-4	66.575	-5,213.4	-6.7693	4.8106E-06	2	159.53	7.28E-01	490	3.831E+06
202	2-Methylbutane	C ₅ H ₁₂	78-78-4	71.308	-4,976	-7.7169	8.7271E-06	2	113.25	1.21E-04	460.4	3.366E+06
203	2-Methylbutanoic acid	C ₆ H ₁₀ O ₂	116-53-0	85.383	-9,575.4	-8.6164	5.6124E-18	6	193	6.94E-05	643	3.887E+06
204	3-Methyl-1-butanol	C ₅ H ₁₂ O	123-51-3	121.85	-10,976	-13.869	1.4283E-17	6	155.95	8.67E-09	577.2	3.916E+06
205	2-Methyl-1-butene	C ₅ H ₁₀	563-46-2	93.131	-5,525.4	-11.852	1.4205E-02	1	135.58	2.05E-02	465	3.465E+06
206	2-Methyl-2-butene	C ₅ H ₁₀	513-35-9	83.927	-5,640.5	-9.6453	1.1121E-05	2	139.39	1.94E-02	470	3.394E+06
207	2-Methyl-1-butene-3-yne	C ₅ H ₆	78-80-8	95.453	-5,448.8	-12.384	1.5643E-02	1	160.15	2.92E+00	492	4.669E+06
208	Methylbutyl ether	C ₅ H ₁₂ O	628-28-4	60.164	-5,621.7	-5.53	1.8629E-17	6	157.48	2.99E-02	512.74	3.377E+06
209	Methylbutyl sulfide	C ₅ H ₁₂ S	628-29-5	96.344	-7,856.3	-11.058	7.3080E-06	2	175.3	4.61E-03	593	3.464E+06
210	3-Methyl-1-butyne	C ₅ H ₈	598-23-2	69.459	-5,250	-7.1125	7.9289E-17	6	183.45	4.36E+01	463.2	4.199E+06
211	Methyl butyrate	C ₅ H ₁₀ O ₂	623-42-7	71.87	-6,885.7	-7.0944	1.4903E-17	6	187.35	1.34E-01	554.5	3.480E+06
212	Methylchlorosilane	CH ₃ ClSi	993-00-0	95.984	-5,401.7	-11.829	1.8092E-05	2	139.05	4.12E-01	442	4.170E+06
213	Methylcyclohexane	C ₇ H ₁₄	108-87-2	92.684	-7,080.8	-10.695	8.1366E-06	2	146.58	1.52E-04	572.1	3.486E+06
214	1-Methylcyclohexanol	C ₇ H ₁₄ O	590-67-0	134.63	-10,682	-16.511	8.4427E-06	2	299.15	2.57E+02	686	3.994E+06
215	cis-2-Methylcyclohexanol	C ₇ H ₁₄ O	7443-70-1	125.1	-10,288	-15.157	1.0918E-05	2	280.15	4.56E+01	614	3.808E+06
216	trans-2-Methylcyclohexanol	C ₇ H ₁₄ O	7443-52-9	54.179	-7,477.2	-4.22	3.5225E-18	6	269.15	1.62E+01	617	3.767E+06
217	Methylcyclopentane	C ₆ H ₁₂	96-37-7	55.368	-5,149.8	-5.0136	3.2220E-06	2	130.73	2.25E-04	532.7	3.759E+06
218	1-Methylcyclopentene	C ₆ H ₁₀	693-89-0	52.732	-5,286.9	-4.4509	1.0883E-17	6	146.62	3.98E-03	542	4.130E+06
219	3-Methylcyclopentene	C ₆ H ₁₀	1120-62-3	52.601	-5,120.3	-4.4554	1.3288E-17	6	115	2.12E-06	526	4.129E+06
220	Methyldichlorosilane	CH ₂ Cl ₂ Si	75-54-7	79.788	-5,420	-9.0702	1.1489E-05	2	182.55	2.58E+01	483	3.964E+06
221	Methylethyl ether	C ₃ H ₈ O	540-67-0	78.586	-5,176.3	-8.7501	9.1727E-06	2	160	7.85E+00	437.8	4.433E+06
222	Methylethyl ketone	C ₄ H ₈ O	78-93-3	72.698	-6,143.6	-7.5779	5.6476E-06	2	186.48	1.39E+00	535.5	4.120E+06
223	Methylethyl sulfide	C ₃ H ₈ S	624-89-5	79.07	-6,114.1	-8.631	6.5333E-06	2	167.23	2.25E-01	533	4.261E+06
224	Methyl formate	C ₂ H ₄ O ₂	107-31-3	77.184	-5,606.1	-8.392	7.8468E-06	2	174.15	6.88E+00	487.2	5.983E+06
225	Methylisobutyl ether	C ₆ H ₁₂ O	625-44-5	57.984	-5,339.6	-5.2362	2.0767E-17	6	150	2.13E-02	497	3.416E+06
226	Methylisobutyl ketone	C ₆ H ₁₂ O	108-10-1	80.503	-7,421.8	-8.379	1.8114E-17	6	189.15	6.99E-02	574.6	3.272E+06
227	Methyl Isocyanate	C ₂ H ₃ NO	624-83-9	57.612	-5,197.9	-5.1269	2.1702E-17	6	256.15	7.28E+03	488	5.480E+06
228	Methylisopropyl ether	C ₆ H ₁₂ O	598-53-8	53.867	-4,701	-4.7052	2.8791E-17	6	127.93	3.32E-03	464.48	3.764E+06
229	Methylisopropyl ketone	C ₆ H ₁₂ O	563-80-4	45.242	-5,324.4	-3.2551	3.0363E-18	6	180.15	2.95E-01	553.4	3.792E+06
230	Methylisopropyl sulfide	C ₆ H ₁₂ S	1551-21-9	52.82	-5,437.7	-4.442	9.5103E-18	6	171.64	1.80E-01	553.1	4.022E+06
231	Methyl mercaptan	CH ₃ S	74-93-1	54.15	-4,337.7	-4.8127	4.5000E-17	6	150.18	3.15E+00	469.95	7.231E+06
232	Methyl methacrylate	C ₅ H ₈ O ₂	80-62-6	107.36	-8,085.3	-12.72	8.3307E-06	2	224.95	1.91E+01	566	3.674E+06
233	2-Methyloctanoic acid	C ₉ H ₁₈ O ₂	3004-93-1	105.7	-12,458	-11.234	4.4629E-18	6	240	4.19E-04	694	2.545E+06
234	2-Methylpentane	C ₆ H ₁₄	107-83-5	53.579	-5,041.2	-4.6404	1.9443E-17	6	119.55	2.07E-05	497.7	3.044E+06
235	Methyl pentyl ether	C ₆ H ₁₄ O	628-80-8	61.907	-6,188.9	-5.706	1.1767E-17	6	176	6.33E-02	546.49	3.041E+06
236	2-Methylpropane	C ₄ H ₁₀	75-28-5	108.43	-5,039.9	-15.012	2.2725E-02	1	113.54	1.21E-02	407.8	3.630E+06
237	2-Methyl-2-propanol	C ₄ H ₁₀ O	75-65-0	172.27	-11,589	-22.113	1.3703E-05	2	298.97	5.88E+03	506.2	3.957E+06
238	2-Methyl propene	C ₄ H ₈	115-11-7	78.01	-4,634.1	-8.9575	1.3413E-05	2	132.81	6.45E-01	417.9	4.004E+06
239	Methyl propionate	C ₄ H ₈ O ₂	554-12-1	70.717	-6,439.7	-6.9845	2.0129E-17	6	185.65	6.34E-01	530.6	4.028E+06
240	Methylpropyl ether	C ₄ H ₁₀ O	557-17-5	67.942	-5,419.1	-6.8067	4.7778E-17	6	133.97	2.90E-03	476.25	3.802E+06
241	Methylpropyl sulfide	C ₄ H ₁₀ S	3877-15-4	83.711	-6,786.9	-9.2526	6.6666E-06	2	160.17	4.26E-03	565	3.972E+06
242	Methylsilane	CH ₃ Si	992-94-9	37.205	-2,590.3	-2.5993	6.0508E-06	2	116.34	1.43E+01	352.5	4.702E+06

243	α -Methyl styrene	C ₉ H ₁₀	98-83-9	56.485	-6,954.2	-4.7889	2.7753E-18	6	249.95	9.23E+00	654	3.341E+06
244	Methyl <i>tert</i> -butyl ether	C ₈ H ₁₂ O	1634-04-4	57.1511	-5,201.7	-5.1429	1.6529E-17	6	164.55	4.93E-01	497.1	3.285E+06
245	Methyl vinyl ether	C ₃ H ₆ O	107-25-5	51.085	-4,271	-4.307	3.0530E-17	6	151.15	3.37E+00	437	4.583E+06
246	Naphthalene	C ₁₀ H ₈	91-20-3	62.964	-8,137.5	-5.6317	2.2675E-18	6	353.43	9.91E+02	748.4	4.069E+06
247	Neon	Ne	7440-01-9	29.755	-2,710.6	-2.6081	5.2700E-04	2	24.56	4.38E+04	44.4	2.665E+06
248	Nitroethane	C ₂ H ₅ NO ₂	79-24-3	75.632	-7,202.3	-7.6464	1.8250E-17	6	183.63	3.18E-02	593	5.159E+06
249	Nitrogen	N ₂	7727-37-9	58.282	-1,084.1	-8.3144	4.4127E-02	1	63.15	1.25E+04	126.2	3.391E+06
250	Nitrogen trifluoride	F ₃ N	7783-54-2	68.149	-2,257.9	-8.9118	2.3233E-02	1	66.46	1.86E-01	234	4.500E+06
251	Nitromethane	CH ₃ NO ₂	75-52-5	57.278	-6,089	-4.9821	1.2154E-17	6	244.6	1.47E+02	588.15	6.309E+06
252	Nitrous oxide	N ₂ O	10024-97-2	96.512	-4,045	-12.277	2.8560E-05	2	182.3	8.69E+04	309.57	7.278E+06
253	Nitric oxide	NO	10102-43-9	72.974	-2,650	-8.261	9.7000E-15	6	109.5	2.20E+04	180.15	6.516E+06
254	Nonadecane	C ₁₉ H ₄₀	629-92-5	182.54	-17,897	-22.498	7.4008E-06	2	305.04	1.59E-02	758	1.208E+06
255	Nonanal	C ₉ H ₁₈ O	124-19-6	337.71	-18,506	-50.224	4.7345E-02	1	255.15	3.42E-01	658	2.743E+06
256	Nonane	C ₉ H ₂₀	111-84-2	109.35	-9,030.4	-12.882	7.8544E-06	2	219.66	4.31E-01	594.6	2.305E+06
257	Nonanoic acid	C ₉ H ₁₈ O ₂	112-05-0	137.6	-14,948	-15.618	5.5660E-18	6	285.55	4.71E-02	710.7	2.502E+06
258	1-Nonanol	C ₉ H ₂₀ O	143-08-8	162.854	-15,205	-19.424	1.0722E-17	6	268.15	8.55E-02	670.9	5.522E+06
259	2-Nonanol	C ₉ H ₂₀ O	628-99-9	146.46	-13,813	-17.158	8.6279E-40	14	238.15	4.32E-03	649.5	2.551E+06
260	1-Nonene	C ₉ H ₁₈	124-11-8	63.313	-7,040.4	-5.8055	7.5753E-18	6	191.91	2.04E-02	593.1	2.427E+06
261	Nonyl mercaptan	C ₉ H ₂₀ S	1455-21-6	106.2	-10,982	-11.696	8.8955E-18	6	253.05	1.47E-01	681	2.330E+06
262	1-Nonyne	C ₉ H ₁₆	3452-09-3	114.77	-9,430.8	-13.631	8.1918E-06	2	223.15	4.50E-01	598.05	2.620E+06
263	Octadecane	C ₁₈ H ₃₈	593-45-3	157.68	-16,093	-18.954	5.9272E-06	2	301.31	3.39E-02	747	1.256E+06
264	Octanal	C ₈ H ₁₆ O	124-13-0	83.601	-8,865.8	-8.5711	7.9446E-18	6	246	1.46E+01	638.9	2.951E+06
265	Octane	C ₈ H ₁₈	111-65-9	96.084	-7,900.2	-11.003	7.1802E-06	2	216.38	2.11E+00	568.7	2.467E+06
266	Octanoic acid	C ₈ H ₁₆ O ₂	124-07-2	140.16	-14,813	-16.004	6.4239E-18	6	289.65	1.83E-01	694.26	2.761E+06
267	1-Octanol	C ₈ H ₁₈ O	111-87-5	144.111	-13,667	-16.826	9.3666E-18	6	257.65	9.60E-02	652.3	2.782E+06
268	2-Octanol	C ₈ H ₁₈ O	123-96-6	133.41	-12,630	-15.369	2.9939E-41	14	241.55	4.04E-02	629.8	2.754E+06
269	2-Octanone	C ₈ H ₁₆ O	111-13-7	63.775	-7,711.3	-5.7359	3.0902E-18	6	252.85	4.68E+00	632.7	2.647E+06
270	3-Octanone	C ₈ H ₁₆ O	106-68-3	72.382	-8,054.8	-7.0002	5.8276E-18	6	255.55	7.84E+00	627.7	2.705E+06
271	1-Octene	C ₈ H ₁₆	111-66-0	74.936	-7,155.9	-7.5843	1.7106E-17	6	171.45	2.98E-03	566.9	2.663E+06
272	Octyl mercaptan	C ₈ H ₁₆ S	111-88-6	78.368	-8,855.4	-7.8202	5.6629E-18	6	223.95	3.05E-02	667.3	2.523E+06
273	1-Octyne	C ₈ H ₁₄	629-05-0	64.612	-6,802.5	-6.0261	1.1013E-17	6	193.55	1.04E-01	574	2.880E+06
274	Oxalic acid	C ₂ H ₂ O ₄	144-62-7	122.04	-16,050	-12.986	2.0871E-18	6	462.65	2.15E+03	804	7.060E+06
275	Oxygen	O ₂	7782-44-7	51.245	-1,200.2	-6.4361	2.8405E-02	1	54.36	1.48E+02	154.58	5.021E+06
276	Ozone	O ₃	10028-15-6	40.067	-2,204.8	-2.9351	7.7520E-16	6	80.15	7.35E-01	261	5.566E+06
277	Pentadecane	C ₁₅ H ₃₂	629-62-9	135.57	-13,478	-16.022	5.6136E-06	2	283.07	1.29E-01	708	1.474E+06
278	Pentanal	C ₅ H ₁₀ O	110-62-3	149.58	-8,890	-20.697	2.2101E-02	1	182	5.23E-02	566.1	3.969E+06
279	Pentane	C ₅ H ₁₂	109-66-0	78.741	-5,420.3	-8.8253	9.6171E-06	2	143.42	6.86E-02	469.7	3.364E+06
280	Pentanoic acid	C ₅ H ₁₀ O ₂	109-52-4	101.7	-10,955	-10.829	7.1880E-18	6	239.15	3.28E-02	639.16	3.589E+06
281	1-Pentanol	C ₅ H ₁₂ O	71-41-0	114.748	-10,643	-12.858	1.2491E-17	6	195.56	5.48E-04	588.1	3.896E+06
282	2-Pentanol	C ₅ H ₁₂ O	6032-29-7	122.26	-10,774	-13.943	1.0700E-42	15	200	4.15E-03	561	3.709E+06
283	2-Pentanone	C ₅ H ₁₀ O	107-87-9	84.635	-7,078.4	-9.3	6.2702E-06	2	196.29	7.52E-01	561.08	3.706E+06
284	3-Pentanone	C ₅ H ₁₀ O	96-22-0	44.286	-5,415.1	-3.0913	1.8580E-18	6	234.18	7.34E+01	560.95	3.699E+06
285	1-Pentene	C ₅ H ₁₀	109-67-1	46.994	-4,289.5	-3.7345	2.5424E-17	6	108.02	3.70E-05	464.8	3.562E+06
286	2-Pentyl mercaptan	C ₅ H ₁₂ S	2084-19-7	58.985	-6,193.1	-5.2746	7.3986E-18	6	160.75	1.77E-03	584.3	3.537E+06
287	Pentyl mercaptan	C ₅ H ₁₂ S	110-66-7	67.309	-6,880.8	-6.4449	1.0148E-17	6	197.45	2.01E-01	598	3.474E+06
288	1-Pentyne	C ₅ H ₈	627-19-0	82.805	-5,683.8	-9.4301	1.0767E-05	2	167.45	2.40E+00	481.2	4.170E+06
289	2-Pentyne	C ₅ H ₈	627-21-4	137.29	-7,447.1	-19.01	2.1415E-02	1	163.83	2.05E-01	519	4.020E+06
290	Phenanthrene	C ₁₄ H ₁₀	85-01-8	72.958	-10,943	-6.7902	1.0850E-18	6	372.38	2.93E+01	869	2.902E+06
291	Phenol	C ₆ H ₆ O	108-95-2	95.444	-10,113	-10.09	6.7603E-18	6	314.06	1.88E+02	694.25	6.059E+06
292	Phenyl isocyanate	C ₇ H ₅ NO	103-71-9	86.779	-8,101.8	-9.5303	6.1367E-06	2	243.15	4.33E+00	653	4.063E+06
293	Phthalic anhydride	C ₈ H ₄ O ₃	85-44-9	126.5	-12,551	-15.002	7.7521E-06	2	404.15	7.90E+02	791	4.734E+06
294	Propadiene	C ₃ H ₄	463-49-0	57.069	-3,682.7	-5.5662	6.5133E-06	2	136.87	1.83E+01	394	5.218E+06
295	Propane	C ₃ H ₈	74-98-6	59.078	-3,492.6	-6.0669	1.0919E-05	2	85.47	1.68E-04	369.83	4.214E+06
296	1-Propanol	C ₃ H ₈ O	71-23-8	84.6642	-8,307.2	-8.5767	7.5091E-18	6	146.95	4.28E-07	536.8	5.170E+06
297	2-Propanol	C ₃ H ₈ O	67-63-0	96.094	-8,575.4	-10.292	1.6665E-17	6	185.26	1.95E-02	508.3	4.783E+06
298	Propenylcyclohexene	C ₉ H ₁₄	13511-13-2	64.268	-7,298.9	-5.9109	4.8482E-18	6	199	2.48E-02	636	3.130E+06
299	Propionaldehyde	C ₃ H ₆ O	123-38-6	80.581	-5,896.1	-8.9301	8.2236E-06	2	170	1.31E+00	504.4	4.919E+06
300	Propionic acid	C ₃ H ₆ O ₂	79-09-4	54.552	-7,149.4	-4.2769	1.1843E-18	6	252.45	1.31E+01	600.81	4.608E+06
301	Propionitrile	C ₃ H ₅ N	107-12-0	82.699	-6,703.5	-9.1506	7.5424E-06	2	180.26	1.69E-01	564.4	4.191E+06
302	Propyl acetate	C ₅ H ₁₀ O ₂	109-60-4	115.16	-8,433.9	-13.934	1.0346E-05	2	178.15	1.71E-02	549.73	3.366E+06
303	Propyl amine	C ₃ H ₉ N	107-10-8	58.398	-5,312.7	-5.2876	1.9913E-06	2	188.36	1.30E+01	496.95	4.738E+06
304	Propylbenzene	C ₉ H ₁₂	103-65-1	91.379	-8,276.8	-10.176	5.6240E-06	2	173.55	1.81E-04	638.35	3.202E+06
305	Propylene	C ₃ H ₆	115-07-1	43.905	-3,097.8	-3.4425	9.9989E-17	6	87.89	1.17E-03	364.85	4.599E+06

TABLE 2-8 Vapor Pressure of Inorganic and Organic Liquids, $\ln P = C1 + C2/T + C3 \ln T + C4 T^{C5}$, P in Pa (Concluded)

No.	Name	Formula	CAS no.	C1	C2	C3	C4	C5	T_{\min} , K	P at T_{\min}	T_{\max} , K	P at T_{\max}
306	Propyl formate	C ₄ H ₈ O ₂	110-74-7	104.08	-7,535.9	-12.348	9.6020E-06	2	180.25	2.11E-01	538	4.031E+06
307	2-Propyl mercaptan	C ₃ H ₆ S	75-33-2	60.43	-5,276.9	-5.6572	2.6039E-17	6	142.61	9.73E-03	517	4.752E+06
308	Propyl mercaptan	C ₃ H ₆ S	107-03-9	62.165	-5,624	-5.8595	2.0597E-17	6	159.95	6.51E-02	536.6	4.627E+06
309	1,2-Propylene glycol	C ₃ H ₈ O ₂	57-55-6	212.8	-15,420	-28.109	2.1564E-05	2	213.15	9.29E-05	626	6.041E+06
310	Quinone	C ₆ H ₄ O ₂	106-51-4	48.651	-7,289.5	-3.4453	1.0068E-18	6	388.85	1.17E+04	683	5.925E+06
311	Silicon tetrafluoride	F ₄ Si	7783-61-1	272.85	-9,548.9	-40.089	6.3699E-15	6	186.35	2.21E+05	259	3.748E+06
312	Styrene	C ₈ H ₈	100-42-5	105.93	-8,685.9	-12.42	7.5583E-06	2	242.54	1.06E+01	636	3.823E+06
313	Succinic acid	C ₄ H ₆ O ₄	110-15-6	128.65	-16,958	-13.872	2.1559E-18	6	460.65	8.85E+02	806	4.727E+06
314	Sulfur dioxide	O ₂ S	7446-09-5	47.365	-4,084.5	-3.6469	1.7990E-17	6	197.67	1.67E+03	430.75	7.860E+06
315	Sulfur hexafluoride	F ₆ S	2551-62-4	29.16	-2,383.6	-1.1342			223.15	2.30E+05	318.69	3.771E+06
316	Sulfur trioxide	O ₃ S	7446-11-9	180.99	-12,060	-22.839	7.2350E-17	6	289.95	2.09E+04	490.85	8.192E+06
317	Terephthalic acid	C ₈ H ₆ O ₄	100-21-0	248.72	-32,238	-30.009	4.7950E-06	2	700.15	4.57E+03	1113	3.943E+06
318	<i>o</i> -Terphenyl	C ₁₈ H ₁₄	84-15-1	110.52	-14,045	-11.861	2.2121E-18	6	329.35	4.14E-01	857	2.974E+06
319	Tetradecane	C ₁₄ H ₃₀	629-59-4	140.47	-13,231	-16.859	6.5877E-06	2	279.01	2.53E-01	693	3.447E+06
320	Tetrahydrofuran	C ₄ H ₈ O	109-99-9	54.898	-5,305.4	-4.7627	1.4291E-17	6	164.65	1.96E-01	540.15	5.203E+06
321	1,2,3,4-Tetrahydronaphthalene	C ₁₀ H ₁₂	119-64-2	137.23	-10,620	-17.908	1.4506E-02	1	237.38	1.33E-01	720	3.624E+06
322	Tetrahydrothiophene	C ₄ H ₈ S	110-01-0	75.881	-6,910.6	-7.9499	4.4315E-06	2	176.99	1.54E-02	631.95	5.117E+06
323	2,2,3,3-Tetramethylbutane	C ₈ H ₁₈	594-82-1	57.963	-5,901.5	-5.2048	9.1301E-18	6	373.96	8.69E+04	568	2.871E+06
324	Thiophene	C ₄ H ₄ S	110-02-1	93.193	-7,001.5	-10.738	8.2308E-06	2	234.94	1.86E+02	579.35	5.702E+06
325	Toluene	C ₇ H ₈	108-88-3	76.945	-6,729.8	-8.179	5.3017E-06	2	178.18	4.75E-02	591.75	4.080E+06
326	1,1,2-Trichloroethane	C ₂ H ₃ Cl ₃	79-00-5	54.153	-6,041.8	-4.5383	4.9833E-18	6	236.5	4.47E+01	602	4.447E+06
327	Tridecane	C ₁₃ H ₂₈	629-50-5	137.45	-12,549	-16.543	7.1275E-06	2	267.76	2.51E-01	675	1.679E+06
328	Triethyl amine	C ₆ H ₁₅ N	121-44-8	56.55	-5,681.9	-4.9815	1.2363E-17	6	158.45	1.06E-02	535.15	3.037E+06
329	Trimethyl amine	C ₃ H ₉ N	75-50-3	134.68	-6,055.8	-19.415	2.8619E-02	1	156.08	9.92E+00	433.25	4.102E+06
330	1,2,3-Trimethylbenzene	C ₉ H ₁₂	526-73-8	78.341	-8,019.8	-8.1458	3.8971E-06	2	247.79	3.71E+00	664.5	3.447E+06
331	1,2,4-Trimethylbenzene	C ₉ H ₁₂	95-63-6	85.301	-8,215.9	-9.2166	4.7979E-06	2	229.33	6.93E-01	649.1	3.212E+06
332	2,2,4-Trimethylpentane	C ₈ H ₁₈	540-84-1	84.912	-6,722.2	-9.5157	7.2244E-06	2	165.78	1.71E-02	543.8	2.550E+06
333	2,3,3-Trimethylpentane	C ₈ H ₁₈	560-21-4	83.105	-6,903.7	-9.1858	6.4703E-06	2	172.22	1.68E-02	573.5	2.812E+06
334	1,3,5-Trinitrobenzene	C ₆ H ₃ N ₃ O ₆	99-35-4	506.33	-37,483	-69.22	2.7381E-05	2	398.4	8.50E+00	846	3.410E+06
335	2,4,6-Trinitrotoluene	C ₇ H ₅ N ₃ O ₆	118-96-7	302	-24,324	-40.13	1.7403E-05	2	354	9.36E-01	828	3.019E+06
336	Undecane	C ₁₁ H ₂₄	1120-21-4	131	-11,143	-15.855	8.1871E-06	2	247.57	4.08E-01	639	1.949E+06
337	1-Undecanol	C ₁₁ H ₂₄ O	112-42-5	182.571	-17,112	-22.125	1.12835E-17	6	288.45	1.26E-01	703.9	2.120E+06
338	Vinyl acetate	C ₄ H ₆ O ₂	108-05-4	57.406	-5,702.8	-5.0307	1.1042E-17	6	180.35	7.06E-01	519.13	3.930E+06
339	Vinyl acetylene	C ₄ H ₄	689-97-4	55.682	-4,439.3	-5.0136	1.9650E-17	6	173.15	6.69E+01	454	4.887E+06
340	Vinyl chloride	C ₂ H ₃ Cl	75-01-4	91.432	-5,141.7	-10.981	1.4318E-05	2	119.36	1.92E-02	432	5.750E+06
341	Vinyl trichlorosilane	C ₂ H ₃ Cl ₃ Si	75-94-5	54.571	-5,561.5	-4.712	1.0702E-17	6	178.35	3.54E-01	543.15	3.058E+06
342	Water	H ₂ O	7732-18-5	73.649	-7,258.2	-7.3037	4.1653E-06	2	273.16	6.11E+02	647.096	2.193E+07
343	<i>m</i> -Xylene	C ₈ H ₁₀	108-38-3	85.099	-7,615.9	-9.3072	5.5643E-06	2	225.3	3.18E+00	617	3.528E+06
344	<i>o</i> -Xylene	C ₈ H ₁₀	95-47-6	90.405	-7,955.2	-10.086	5.9594E-06	2	247.98	2.18E+01	630.3	3.741E+06
345	<i>p</i> -Xylene	C ₈ H ₁₀	106-42-3	88.72	-7,741.2	-9.8693	6.0770E-06	2	286.41	5.76E+02	616.2	3.501E+06

Vapor pressure P_v is calculated by

$$P_v = \exp(C1 + C2/T + C3 \ln T + C4 T^{C5})$$

where P_v is in Pa and T is in K. All substances are listed by chemical family in Table 2-6 and by formula in Table 2-7.

Values in this table were taken from the Design Institute for Physical Properties (DIPPR) of the American Institute of Chemical Engineers (AIChE), copyright 2007 AIChE and reproduced with permission of AIChE and of the DIPPR Evaluated Process Design Data Project Steering Committee. Their source should be cited as R. L. Rowley, W. V. Wilding, J. L. Oscarson, Y. Yang, N. A. Zundel, T. E. Daubert, R. P. Danner, DIPPR® Data Compilation of Pure Chemical Properties, Design Institute for Physical Properties, AIChE, New York (2007).

The number of digits provided for values at T_{\min} and T_{\max} was chosen for uniformity of appearance and formatting; these do not represent the uncertainties of the physical quantities, but are the result of calculations from the standard thermophysical property formulations within a fixed format.

TABLE 2-9 Vapor Pressures of Inorganic Compounds, up to 1 atm*

Compound		Pressure, mmHg										Melting point, °C
Name	Formula	1	5	10	20	40	60	100	200	400	760	
		Temperature, °C										
Aluminum	Al	1284	1421	1487	1555	1635	1684	1749	1844	1947	2056	660
borohydride	Al(BH ₄) ₃		-52.2	-42.9	-32.5	-20.9	-13.4	-3.9	+11.2	28.1	45.9	-64.
bromide	AlBr ₃	81.3	103.8	118.0	134.0	150.6	161.7	176.1	199.8	227.0	256.3	97.
chloride	Al ₂ Cl ₆	100.0	116.4	123.8	131.8	139.9	145.4	152.0	161.8	171.6	180.2	192.4
fluoride	AlF ₃	1238	1298	1324	1350	1378	1398	1422	1457	1496	1537	1040
iodide	AlI ₃	178.0	207.7	225.8	244.2	265.0	277.8	294.5	322.0	354.0	385.5	
oxide	Al ₂ O ₃	2148	2306	2385	2465	2549	2599	2665	2766	2874	2977	2050
Ammonia	NH ₃	-109.1	-97.5	-91.9	-85.8	-79.2	-74.3	-68.4	-57.0	-45.4	-33.6	-77.7
heavy	ND ₃						-74.0	-67.4	-57.0	-45.4	-33.4	-74.0
Ammonium bromide	NH ₄ Br	198.3	234.5	252.0	270.6	290.0	303.8	320.0	345.3	370.8	396.0	
carbamate	N ₂ H ₄ CO ₂	-26.1	-10.4	-2.9	+5.3	14.0	19.6	26.7	37.2	48.0	58.3	
chloride	NH ₄ Cl	160.4	193.8	209.8	226.1	245.0	256.2	271.5	293.2	316.5	337.8	520
cyanide	NH ₄ CN	-50.6	-35.7	-28.6	-20.9	-12.6	-7.4	-0.5	+9.6	20.5	31.7	36
hydrogen sulfide	NH ₄ HS	-51.1	-36.0	-28.7	-20.8	-12.3	-7.0	0.0	+10.5	21.8	33.3	
iodide	NH ₄ I	210.9	247.0	263.5	282.8	302.8	316.0	331.8	355.8	381.0	404.9	
Antimony	Sb	886	984	1033	1084	1141	1176	1223	1288	1364	1440	630.5
tribromide	SbBr ₃	93.9	126.0	142.7	158.3	177.4	188.1	203.5	225.7	250.2	275.0	96.6
trichloride	SbCl ₃	49.2	71.4	85.2	100.6	117.8	128.3	143.3	165.9	192.2	219.0	73.4
pentachloride	SbCl ₅	22.7	48.6	61.8	75.8	91.0	101.0	114.1				2.8
triiodide	SbI ₃	163.6	203.8	223.5	244.8	267.8	282.5	303.5	333.8	368.5	401.0	167
trioxide	Sb ₂ O ₆	574	626	666	729	812	873	957	1085	1242	1425	656
Argon	A	-218.2	-213.9	-210.9	-207.9	-204.9	-202.9	-200.5	-195.6	-190.6	-185.6	-189.2
Arsenic	As	372	416	437	459	483	498	518	548	579	610	814
Arsenic tribromide	AsBr ₃	41.8	70.6	85.2	101.3	118.7	130.0	145.2	167.7	193.6	220.0	
trichloride	AsCl ₃	-11.4	+11.7	+23.5	36.0	50.0	58.7	70.9	89.2	109.7	130.4	-18
trifluoride	AsF ₃					-2.5	+4.2	13.2	26.7	41.4	56.3	-5.9
pentafluoride	AsF ₅	-117.9	-108.0	-103.1	-98.0	-92.4	-88.5	-84.3	-75.5	-64.0	-52.8	-79.8
trioxide	As ₂ O ₃	212.5	242.6	259.7	279.2	299.2	310.3	332.5	370.0	412.2	457.2	312.8
Arsine	AsH ₃	-142.6	-130.8	-124.7	-117.7	-110.2	-104.8	-98.0	-87.2	-75.2	-62.1	-116.3
Barium	Ba	984	1049	1120	1195	1240	1301	1403	1518	1638	1768	850
Beryllium borohydride	Be(BH ₄) ₂	+1.0	19.8	28.1	36.8	46.2	51.7	58.6	69.0	79.7	90.0	123
bromide	BeBr ₂	289	325	342	361	379	390	405	427	451	474	490
chloride	BeCl ₂	291	328	346	365	384	395	411	435	461	487	405
iodide	BeI ₂	283	322	341	361	382	394	411	435	461	487	488
Bismuth	Bi	1021	1099	1136	1177	1217	1240	1271	1319	1370	1420	271
tribromide	BiBr ₃	261	282	305	327	340	360	392	425	461	501	218
trichloride	BiCl ₃	242	264	287	311	324	343	372	405	441	481	230
Diborane hydrobromide	B ₂ H ₂ Br	-93.3	-75.3	-66.3	-56.4	-45.4	-38.2	-29.0	-15.4	0.0	+16.3	-104.2
Borine carbonyl	BH ₃ CO	-139.2	-127.3	-121.1	-114.1	-106.6	-101.9	-95.3	-85.5	-74.8	-64.0	-137.0
triimine	B ₃ N ₃ H ₆	-63.0	-45.0	-35.3	-25.0	-13.2	-5.8	+4.0	18.5	34.3	50.6	-58.2
Boron hydrides												
dihydrodecaborane	B ₁₀ H ₁₄	60.0	80.8	90.2	100.0	117.4	127.8	142.3	163.8			99.6
dihydrodiborane	B ₂ H ₆	-159.7	-149.5	-144.3	-138.5	-131.6	-127.2	-120.9	-111.2	-99.6	-86.5	-169
dihydropentaborane	B ₅ H ₉		-40.4	-30.7	-20.0	-8.0	-0.4	+9.6	24.6	40.8	58.1	-47.0
tetrahydropentaborane	B ₄ H ₁₁	-50.2	-29.9	-19.9	-9.2	+2.7	10.2	20.1	34.8	51.2	67.0	
tetrahydrotriborane	B ₃ H ₁₀	-90.9	-73.1	-64.3	-54.8	-44.3	-37.4	-28.1	-14.0	+0.8	16.1	-119.9
Boron tribromide	BBr ₃	-41.4	-20.4	-10.1	+1.5	14.0	22.1	33.5	50.3	70.0	91.7	-45
trichloride	BCl ₃	-91.5	-75.2	-66.9	-57.9	-47.8	-41.2	-32.4	-18.9	-3.6	+12.7	-107
trifluoride	BF ₃	-154.6	-145.4	-141.3	-136.4	-131.0	-127.6	-123.0	-115.9	-108.3	-100.7	-126.8
Bromine	Br ₂	-48.7	-32.8	-25.0	-16.8	-8.0	-0.6	+9.3	24.3	41.0	58.2	-7.3
pentafluoride	BrF ₅	-69.3	-51.0	-41.9	-32.0	-21.0	-14.0	-4.5	+9.9	25.7	40.4	-61.4
Cadmium	Cd	394	455	484	516	553	578	611	658	711	765	320.9
chloride	CdCl ₂	618	656	695	736	762	797	847	908	967	1028	568
fluoride	CdF ₂	1112	1231	1286	1344	1400	1436	1486	1561	1651	1751	520
iodide	CdI ₂	416	481	512	546	584	608	640	688	742	796	385
oxide	CdO	1000	1100	1149	1200	1257	1295	1341	1409	1484	1559	
Calcium	Ca	926	983	1046	1111	1152	1207	1288	1388	1487	1587	851
Carbon (graphite)	C	3586	3828	3946	4069	4196	4273	4373	4516	4660	4827	
dioxide	CO ₂	-134.3	-124.4	-119.5	-114.4	-108.6	-104.8	-100.2	-93.0	-85.7	-78.2	-57.5
disulfide	CS ₂	-73.8	-54.3	-44.7	-34.3	-22.5	-15.3	-5.1	+10.4	28.0	46.5	-110.8
monoxide	CO	-222.0	-212.2	-215.0	-212.8	-210.0	-208.1	-205.7	-201.3	-196.3	-191.3	-205.0
oxyselenide	COSe	-117.1	-102.3	-95.0	-86.3	-76.4	-70.2	-61.7	-49.8	-35.6	-21.9	
oxysulfide	COS	-132.4	-119.8	-113.3	-106.0	-98.3	-93.0	-85.9	-75.0	-62.7	-49.9	-138.8
selenosulfide	CSeS	-47.3	-26.5	-16.0	-4.4	+8.6	17.0	28.3	45.7	65.2	85.6	-75.2
subulfide	C ₂ S ₂	14.0	41.2	54.9	69.3	85.6	96.0	109.9	130.8			+0.4
tetrabromide	CBR ₄					96.3	106.3	119.7	139.7	163.5	189.5	90.1
tetrachloride	CCl ₄	-50.0	-30.0	-19.6	-8.2	+4.3	12.3	23.0	38.3	57.8	76.7	-22.6
tetrafluoride	CF ₄	-184.6	-174.1	-169.3	-164.3	-158.8	-155.4	-150.7	-143.6	-135.5	-127.7	-183.7
Cesium	Cs	279	341	375	409	449	474	509	561	624	690	28.5
bromide	CsBr	748	838	887	938	993	1026	1072	1140	1221	1300	636
chloride	CsCl	744	837	884	934	989	1023	1069	1139	1217	1300	646
fluoride	CsF	712	798	844	893	947	980	1025	1092	1170	1251	683
iodide	CsI	738	828	873	923	976	1009	1055	1124	1200	1280	621

*Compiled from the extended tables published by D. R. Stull in *Ind. Eng. Chem.*, **39**, 517 (1947).

2-62 PHYSICAL AND CHEMICAL DATA

TABLE 2-9 Vapor Pressures of Inorganic Compounds, up to 1 atm (Continued)

Compound		Pressure, mmHg										Melting point, °C
Name	Formula	1	5	10	20	40	60	100	200	400	760	
		Temperature, °C										
Chlorine	Cl ₂	-118.0	-106.7	-101.6	-93.3	-84.5	-79.0	-71.7	-60.2	-47.3	-33.8	-100.7
fluoride	ClF		-143.4	-139.0	-134.3	-128.8	-125.3	-120.8	-114.4	-107.0	-100.5	-145
trifluoride	ClF ₃		-80.4	-71.8	-62.3	-51.3	-44.1	-34.7	-20.7	-4.9	+11.5	-83
monoxide	Cl ₂ O	-98.5	-81.6	-73.1	-64.3	-54.3	-48.0	-39.4	-26.5	-12.5	+2.2	-116
dioxide	ClO ₂		-59.0	-51.2	-42.8	-37.2	-29.4	-17.8	-4.0	+11.1	-59	
heptoxide	Cl ₂ O ₇	-45.3	-23.8	-13.2	-2.1	+10.3	+18.2	29.1	44.6	62.2	78.8	-91
Chlorosulfonic acid	HSO ₃ Cl	32.0	53.5	64.0	75.3	87.6	95.2	105.3	120.0	136.1	151.0	-80
Chromium	Cr	1616	1768	1845	1928	2013	2067	2139	2243	2361	2482	1615
carbonyl	Cr(CO) ₆	36.0	58.0	68.3	79.5	91.2	98.3	108.0	121.8	137.2	151.0	
oxychloride	CrO ₂ Cl ₂	-18.4	+3.2	13.8	25.7	38.5	46.7	58.0	75.2	95.2	117.1	
Cobalt chloride	CoCl ₂					770	801	843	904	974	1050	735
nitrosyl tricarboyl	Co(CO) ₃ NO				-1.3	+11.0	18.5	29.0	44.4	62.0	80.0	-11
Columbium fluoride	CbF ₅			86.3	103.0	121.5	133.2	148.5	172.2	198.0	225.0	75.5
Copper	Cu	1628	1795	1879	1970	2067	2127	2207	2325	2465	2595	1083
Cuprous bromide	Cu ₂ Br ₂	572	666	718	777	844	887	951	1052	1189	1355	504
chloride	Cu ₂ Cl ₂	546	645	702	766	838	886	960	1077	1249	1490	422
iodide	Cu ₂ I ₂		610	656	716	786	836	907	1018	1158	1336	605
Cyanogen	C ₂ N ₂	-95.8	-83.2	-76.8	-70.1	-62.7	-57.9	-51.8	-42.6	-33.0	-21.0	-34.4
bromide	CNBr	-35.7	-18.3	-10.0	-1.0	+8.6	14.7	22.6	33.8	46.0	61.5	58
chloride	CNCl	-76.7	-61.4	-53.8	-46.1	-37.5	-32.1	-24.9	-14.1	-2.3	+13.1	-6.5
fluoride	CNF	-134.4	-123.8	-118.5	-112.8	-106.4	-102.3	-97.0	-89.2	-80.5	-72.6	
Deuterium cyanide	DCN	-68.9	-54.0	-46.7	-38.8	-30.1	-24.7	-17.5	-5.4	+10.0	26.2	-12
Fluorine	F ₂	-223.0	-216.9	-214.1	-211.0	-207.7	-205.6	-202.7	-198.3	-193.2	-187.9	-223
oxide	F ₂ O	-196.1	-186.6	-182.3	-177.8	-173.0	-170.0	-165.8	-159.0	-151.9	-144.6	-223.9
Germanium bromide	GeBr ₄		43.3	56.8	71.8	88.1	98.8	113.2	135.4	161.6	189.0	26.1
chloride	GeCl ₄	-45.0	-24.9	-15.0	-4.1	+8.0	16.2	27.5	44.4	63.8	84.0	-49.5
hydride	GeH ₄	-163.0	-151.0	-145.3	-139.2	-131.6	-126.7	-120.3	-111.2	-100.2	-88.9	-165
Trichlorogermane	GeHCl ₃	-41.3	-22.3	-13.0	-3.0	+8.8	16.2	26.5	41.6	58.3	75.0	-71.1
Tetramethylgermane	Ge(CH ₃) ₄	-73.2	-54.6	-45.2	-35.0	-23.4	-16.2	-6.3	+8.8	26.0	44.0	-88
Digermane	Ge ₂ H ₆	-88.7	-69.8	-60.1	-49.9	-38.2	-30.7	-20.3	-4.7	+13.3	31.5	-109
Trigermane	Ge ₃ H ₈	-36.9	-12.8	-0.9	+11.8	26.3	35.5	47.9	67.0	88.6	110.8	-105.6
Gold	Au	1869	2059	2154	2256	2363	2431	2521	2657	2807	2966	1063
Helium	He	-271.7	-271.5	-271.3	-271.1	-270.7	-270.6	-270.3	-269.8	-269.3	-268.6	
para-Hydrogen	H ₂	-263.3	-261.9	-261.3	-260.4	-259.6	-258.9	-257.9	-256.3	-254.5	-252.5	-259.1
Hydrogen bromide	HBr	-138.8	-127.4	-121.8	-115.4	-108.3	-103.8	-97.7	-88.1	-78.0	-66.5	-87.0
chloride	HCl	-150.8	-140.7	-135.6	-130.0	-123.8	-119.6	-114.0	-105.2	-95.3	-84.8	-114.3
cyanide	HCN	-71.0	-55.3	-47.7	-39.7	-30.9	-25.1	-17.8	-5.3	+10.2	25.9	-13.2
fluoride	H ₂ F ₂		-74.7	-65.8	-56.0	-45.0	-37.9	-28.2	-13.2	+2.5	19.7	-83.7
iodide	HI	-123.3	-109.6	-102.3	-94.5	-85.6	-79.8	-72.1	-60.3	-48.3	-35.1	-50.9
oxide (water)	H ₂ O	-17.3	+1.2	11.2	22.1	34.0	41.5	51.6	65.5	83.0	100.0	0.0
sulfide	H ₂ S	-134.3	-122.4	-116.3	-109.7	-102.3	-97.9	-91.6	-82.3	-71.8	-60.4	-85.5
disulfide	HSSH	-43.2	-24.4	-15.2	-5.1	+6.0	12.8	22.0	35.3	49.6	64.0	-89.7
selenide	H ₂ Se	-115.3	-103.4	-97.9	-91.8	-84.7	-80.2	-74.2	-65.2	-53.6	-41.1	-64
telluride	H ₂ Te	-96.4	-82.4	-75.4	-67.8	-59.1	-53.7	-45.7	-32.4	-17.2	-2.0	-49.0
Iodine	I ₂	38.7	62.2	73.2	84.7	97.5	105.4	116.5	137.3	159.8	183.0	112.9
heptafluoride	IF ₇	-87.0	-70.7	-63.0	-54.5	-45.3	-39.4	-31.9	-20.7	-8.3	+4.0	5.5
Iron	Fe	1787	1957	2039	2128	2224	2283	2360	2475	2605	2735	1535
pentacarbonyl	Fe(CO) ₅		-6.5	+4.6	16.7	30.3	39.1	50.3	68.0	86.1	105.0	-21
Ferric chloride	Fe ₂ Cl ₆	194.0	221.8	235.5	246.0	256.8	263.7	272.5	285.0	298.0	319.0	304
Ferrous chloride	FeCl ₂			700	737	779	805	842	897	961	1026	
Krypton	Kr	-199.3	-191.3	-187.2	-182.9	-178.4	-175.7	-171.8	-165.9	-159.0	-152.0	-156.7
Lead	Pb	973	1099	1162	1234	1309	1358	1421	1519	1630	1744	327.5
bromide	PbBr ₂	513	578	610	646	686	711	745	796	856	914	373
chloride	PbCl ₂	547	615	648	684	725	750	784	833	893	954	501
fluoride	PbF ₂		861	904	950	1003	1036	1080	1144	1219	1293	855
iodide	PbI ₂	479	540	571	605	644	668	701	750	807	872	402
oxide	PbO	943	1039	1085	1134	1189	1222	1265	1330	1402	1472	890
sulfide	PbS	852	928	975	1005	1048	1074	1108	1160	1221	1281	1114
Lithium	Li	723	838	881	940	1003	1042	1097	1178	1273	1372	186
bromide	LiBr	748	840	888	939	994	1028	1076	1147	1226	1310	547
chloride	LiCl	783	880	932	987	1045	1081	1129	1203	1290	1382	614
fluoride	LiF	1047	1156	1211	1270	1333	1372	1425	1503	1591	1681	870
iodide	LiI	723	802	841	883	927	955	993	1049	1110	1171	446
Magnesium	Mg	621	702	743	789	838	868	909	967	1034	1107	651
chloride	MgCl ₂	778	877	930	988	1050	1088	1142	1223	1316	1418	712
Manganese	Mn	1292	1434	1505	1583	1666	1720	1792	1900	2029	2151	1260
chloride	MnCl ₂		736	778	825	879	913	960	1028	1108	1190	650
Mercury	Hg	126.2	164.8	184.0	204.6	228.8	242.0	261.7	290.7	323.0	357.0	-38.9
Mercuric bromide	HgBr ₂	136.5	165.3	179.8	194.3	211.5	221.0	237.8	262.7	290.0	319.0	-237
chloride	HgCl ₂	136.2	166.0	180.2	195.8	212.5	222.2	237.0	256.5	275.5	304.0	277
iodide	HgI ₂	157.5	189.2	204.5	220.0	238.2	249.0	261.8	291.0	324.2	354.0	259
Molybdenum	Mo	3102	3393	3535	3690	3859	3964	4109	4322	4553	4804	2622
hexafluoride	MoF ₆	-65.5	-49.0	-40.8	-32.0	-22.1	-16.2	-8.0	+4.1	17.2	36.0	17
oxide	MoO ₃	734	785	814	851	892	917	955	1014	1082	1151	795

TABLE 2-9 Vapor Pressures of Inorganic Compounds, up to 1 atm (Continued)

Compound		Pressure, mmHg										Melting point, °C
Name	Formula	1	5	10	20	40	60	100	200	400	760	
		Temperature, °C										
Neon	Ne	-257.3	-255.5	-254.6	-253.7	-252.6	-251.9	-251.0	-249.7	-248.1	-246.0	-248.7
Nickel	Ni	1810	1979	2057	2143	2234	2289	2364	2473	2603	2732	1452
carbonyl chloride	Ni(CO) ₄					-23.0	-15.9	-6.0	+8.8	25.8	42.5	-25
	NiCl ₂	671	731	759	789	821	840	866	904	945	987	1001
Nitrogen	N ₂	-226.1	-221.3	-219.1	-216.8	-214.0	-212.3	-209.7	-205.6	-200.9	-195.8	-210.0
Nitric oxide	NO	-184.5	-180.6	-178.2	-175.3	-171.7	-168.9	-166.0	-162.3	-156.8	-151.7	-161
Nitrogen dioxide	NO ₂	-55.6	-42.7	-36.7	-30.4	-23.9	-19.9	-14.7	-5.0	+8.0	21.0	-9.3
Nitrogen pentoxide	N ₂ O ₅	-36.8	-23.0	-16.7	-10.0	-2.9	+1.8	7.4	15.6	24.4	32.4	30
Nitrous oxide	N ₂ O	-143.4	-133.4	-128.7	-124.0	-118.3	-114.9	-110.3	-103.6	-96.2	-85.5	-90.9
Nitrosyl chloride	NOCl					-60.2	-54.2	-46.3	-34.0	-20.3	-6.4	-64.5
fluoride	NOF	-132.0	-120.3	-114.3	-107.8	-100.3	-95.7	-88.8	-79.2	-68.2	-56.0	-134
Osmium tetroxide (yellow)	OsO ₄	3.2	22.0	31.3	41.0	51.7	59.4	71.5	89.5	109.3	130.0	56
(white)	OsO ₄	-5.6	+15.6	26.0	37.4	50.5	59.4	71.5	89.5	109.3	130.0	42
Oxygen	O ₂	-219.1	-213.4	-210.6	-207.5	-204.1	-201.9	-198.8	-194.0	-188.8	-183.1	-218.7
Ozone	O ₃	-180.4	-168.6	-163.2	-157.2	-150.7	-146.7	-141.0	-132.6	-122.5	-111.1	-251
Phosgene	COCl ₂	-92.9	-77.0	-69.3	-60.3	-50.3	-44.0	-35.6	-22.3	-7.6	+8.3	-104
Phosphorus (yellow)	P	76.6	111.2	128.0	146.2	166.7	179.8	197.3	222.7	251.0	280.0	44.1
(violet)	P	237	271	287	306	323	334	349	370	391	417	590
tribromide	PBr ₃	7.8	34.4	47.8	62.4	79.0	89.8	103.6	125.2	149.7	175.3	-40
trichloride	PCl ₃	-51.6	-31.5	-21.3	-10.2	+2.3	10.2	21.0	37.6	56.9	74.2	-111.8
pentachloride	PCl ₅	55.5	74.0	83.2	92.5	102.5	108.3	117.0	131.3	147.2	162.0	
Phosphine	PH ₃					-129.4	-125.0	-118.8	-109.4	-98.3	-87.5	-132.5
Phosphonium bromide	PH ₄ Br	-43.7	-28.5	-21.2	-13.3	-5.0	+0.3	7.4	17.6	28.0	38.3	
chloride	PH ₄ Cl	-91.0	-79.6	-74.0	-68.0	-61.5	-57.3	-52.0	-44.0	-35.4	-27.0	-28.5
iodide	PH ₄ I	-25.2	-9.0	-1.1	+7.3	16.1	21.9	29.3	39.9	51.6	62.3	
Phosphorus trioxide	P ₂ O ₃		39.7	53.0	67.8	84.0	94.2	108.3	129.0	150.3	173.1	22.5
pentoxide	P ₂ O ₅	384	424	442	462	481	493	510	532	556	591	569
oxychloride	POCl ₃			2.0	13.6	27.3	35.8	47.4	65.0	84.3	105.1	2
thiobromide	PSBr ₃	50.0	72.4	83.6	95.5	108.0	116.0	126.3	141.8	157.8	175.0	38
thiochloride	PSCl ₃	-18.3	+4.6	16.1	29.0	42.7	51.8	63.8	82.0	102.3	124.0	-36.2
Platinum	Pt	2730	3007	3146	3302	3469	3574	3714	3923	4169	4407	1755
Potassium	K	341	408	443	483	524	550	586	643	708	774	62.3
bromide	KBr	795	892	940	994	1050	1087	1137	1212	1297	1383	730
chloride	KCl	821	919	968	1020	1078	1115	1164	1239	1322	1407	790
fluoride	KF	885	988	1039	1096	1156	1193	1245	1323	1411	1502	880
hydroxide	KOH	719	814	863	918	976	1013	1064	1142	1233	1327	380
iodide	KI	745	840	887	938	995	1030	1080	1152	1238	1324	723
Radon	Rn	-144.2	-132.4	-126.3	-119.2	-111.3	-106.2	-99.0	-87.7	-75.0	-61.8	-71
Rhenium heptoxide	Re ₂ O ₇	212.5	237.5	248.0	261.0	272.0	280.0	289.0	307.0	336.0	362.4	296
Rubidium	Rb	297	358	389	422	459	482	514	563	620	679	38.5
bromide	RbBr	781	876	923	975	1031	1066	1114	1186	1267	1352	682
chloride	RbCl	792	887	937	990	1047	1084	1133	1207	1294	1381	715
fluoride	RbF	921	982	1016	1052	1096	1123	1168	1239	1322	1408	760
iodide	RbI	748	839	884	935	991	1026	1072	1141	1223	1304	642
Selenium	Se	356	413	442	473	506	527	554	594	637	680	217
dioxide	SeO ₂	157.0	187.7	202.5	217.5	234.1	244.6	258.0	277.0	297.7	317.0	340
hexafluoride	SeF ₆	-118.6	-105.2	-98.9	-92.3	-84.7	-80.0	-73.9	-64.8	-55.2	-45.8	-34.7
oxychloride	SeOCl ₂	34.8	59.8	71.9	84.2	98.0	106.5	118.0	134.6	151.7	168.0	8.5
tetrachloride	SeCl ₄	74.0	96.3	107.4	118.1	130.1	137.8	147.5	161.0	176.4	191.5	
Silicon	Si	1724	1835	1888	1942	2000	2036	2083	2151	2220	2287	1420
dioxide	SiO ₂			1732	1798	1867	1911	1969	2053	2141	2227	1710
tetrachloride	SiCl ₄	-63.4	-44.1	-34.4	-24.0	-12.1	-4.8	+5.4	21.0	38.4	56.8	-68.8
tetrafluoride	SiF ₄	-144.0	-134.8	-130.4	-125.9	-120.8	-117.5	-113.3	-107.2	-100.7	-94.8	-90
Trichlorofluorosilane	SiFCl ₃	-92.6	-76.4	-68.3	-59.0	-48.8	-42.2	-33.2	-19.3	-4.0	+12.2	-120.8
Iodosilane	SiH ₃ I		-53.0	-47.7	-33.4	-21.8	-14.3	-4.4	+10.7	27.9	45.4	-57.0
Diiodosilane	SiH ₂ I ₂		3.8	18.0	34.1	52.6	64.0	79.4	101.8	125.5	149.5	-1.0
Disiloxan	(SiH ₃) ₂ O	-112.5	-95.8	-88.2	-79.8	-70.4	-64.2	-55.9	-43.5	-29.3	-15.4	-144.2
Trisilane	Si ₃ H ₈	-68.9	-49.7	-40.0	-29.0	-16.9	-9.0	+1.6	17.8	35.5	53.1	-117.2
Trisilazane	(SiH ₃) ₃ N	-68.7	-49.9	-40.4	-30.0	-18.5	-11.0	-1.1	+14.0	31.0	48.7	-105.7
Tetrasilane	Si ₄ H ₁₀	-27.7	-6.2	+4.3	15.8	28.4	36.6	47.4	63.6	81.7	100.0	-93.6
Octachlorotrisilane	Si ₃ Cl ₈	46.3	74.7	89.3	104.2	121.5	132.0	146.0	166.2	189.5	211.4	
Hexachlorodisiloxane	(SiCl ₃) ₂ O	-5.0	17.8	29.4	41.5	55.2	63.8	75.4	92.5	113.6	135.6	-33.2
Hexachlorodisilane	Si ₂ Cl ₆	+4.0	27.4	38.8	51.5	65.3	73.9	85.4	102.2	120.6	139.0	-1.2
Tribromosilane	SiHBr ₃	-30.5	-8.0	+3.4	16.0	30.0	39.2	51.6	70.2	90.2	111.8	-73.5
Trichlorosilane	SiHCl ₃	-80.7	-62.6	-53.4	-43.8	-32.9	-25.8	-16.4	-1.8	+14.5	31.8	-126.6
Trifluorosilane	SiHF ₃	-152.0	-142.7	-138.2	-132.9	-127.3	-123.7	-118.7	-111.3	-102.8	-95.0	-131.4
Dibromosilane	SiH ₂ Br ₂	-60.9	-40.0	-29.4	-18.0	-5.2	+3.2	14.1	31.6	50.7	70.5	-70.2
Difluorosilane	SiH ₂ F ₂	-146.7	-136.0	-130.4	-124.3	-117.6	-113.3	-107.3	-98.3	-87.6	-77.8	
Monobromosilane	SiH ₃ Br		-85.7	-77.3	-68.3	-57.8	-51.1	-42.3	-28.6	-13.3	+2.4	-93.9
Monochlorosilane	SiH ₃ Cl	-117.8	-104.3	-97.7	-90.1	-81.8	-76.0	-68.5	-57.0	-44.5	-30.4	
Monofluorosilane	SiH ₃ F	-153.0	-145.5	-141.2	-136.3	-130.8	-127.2	-122.4	-115.2	-106.8	-98.0	
Tribromofluorosilane	SiFBr ₃	-46.1	-25.4	-15.1	-3.7	+9.2	17.4	28.6	45.7	64.6	83.8	-82.5
Dichlorodifluorosilane	SiF ₂ Cl ₂	-124.7	-110.5	-102.9	-94.5	-85.0	-78.6	-70.3	-58.0	-45.0	-31.8	-139.7
Trifluorobromosilane	SiF ₃ Br								-69.8	-55.9	-41.7	-70.5

2-64 PHYSICAL AND CHEMICAL DATA

TABLE 2-9 Vapor Pressures of Inorganic Compounds, up to 1 atm (Concluded)

Compound		Pressure, mmHg										Melting point, °C
Name	Formula	1	5	10	20	40	60	100	200	400	760	
		Temperature, °C										
Trifluorochlorosilane	SiF ₂ Cl	-144.0	-133.0	-127.0	-120.5	-112.8	-108.2	-101.7	-91.7	-81.0	-70.0	-142
Hexafluorodisilane	Si ₂ F ₆	-81.0	-68.8	-63.1	-57.0	-50.6	-46.7	-41.7	-34.2	-26.4	-18.9	-18.6
Dichlorofluorobromosilane	SiFCl ₂ Br	-86.5	-68.4	-59.0	-48.8	-37.0	-29.0	-19.5	-3.2	+15.4	35.4	-112.3
Dibromochlorofluorosilane	SiFClBr ₂	-65.2	-45.5	-35.6	-24.5	-12.0	-4.7	+6.3	23.0	43.0	59.5	-99.3
Silane	SiH ₄	-179.3	-168.6	-163.0	-156.9	-150.3	-146.3	-140.5	-131.6	-122.0	-111.5	-185
Disilane	Si ₂ H ₆	-114.8	-99.3	-91.4	-82.7	-72.8	-66.4	-57.5	-44.6	-29.0	-14.3	-132.6
Silver	Ag	1357	1500	1575	1658	1743	1795	1865	1971	2090	2212	960.5
chloride	AgCl	912	1019	1074	1134	1200	1242	1297	1379	1467	1564	455
iodide	AgI	820	927	983	1045	1111	1152	1210	1297	1400	1506	552
Sodium	Na	439	511	549	589	633	662	701	758	823	892	97.5
bromide	NaBr	806	903	952	1005	1063	1099	1148	1220	1304	1392	755
chloride	NaCl	865	967	1017	1072	1131	1169	1220	1296	1379	1465	800
cyanide	NaCN	817	928	983	1046	1115	1156	1214	1302	1401	1497	564
fluoride	NaF	1077	1186	1240	1300	1363	1403	1455	1531	1617	1704	992
hydroxide	NaOH	739	843	897	953	1017	1057	1111	1192	1286	1378	318
iodide	NaI	767	857	903	952	1005	1039	1083	1150	1225	1304	651
Strontium	Sr		847	898	953	1018	1057	1111	1192	1285	1384	800
Strontium oxide	SrO	2068	2198	2262	2333	2410						2430
Sulfur	S	183.8	223.0	243.8	264.7	288.3	305.5	327.2	359.7	399.6	444.6	112.8
monochloride	S ₂ Cl ₂	-7.4	+15.7	27.5	40.0	54.1	63.2	75.3	93.5	115.4	138.0	-80
hexafluoride	SF ₆	-132.7	-120.6	-114.7	-108.4	-101.5	-96.8	-90.9	-82.3	-72.6	-63.5	-50.2
Sulfuryl chloride	SO ₂ Cl ₂		-35.1	-24.8	-13.4	-1.0	+7.2	17.8	33.7	51.3	69.2	-54.1
Sulfur dioxide	SO ₂	-95.5	-83.0	-76.8	-69.7	-60.5	-54.6	-46.9	-35.4	-23.0	-10.0	-73.2
trioxide (α)	SO ₃	-39.0	-23.7	-16.5	-9.1	-1.0	+4.0	10.5	20.5	32.6	44.8	16.8
trioxide (β)	SO ₃	-34.0	-19.2	-12.3	-4.9	+3.2	8.0	14.3	23.7	32.6	44.8	32.3
trioxide (γ)	SO ₃	-15.3	-2.0	+4.3	11.1	17.9	21.4	28.0	35.8	44.0	51.6	62.1
Tellurium	Te	520	605	650	697	753	789	838	910	997	1087	452
chloride	TeCl ₄			233	253	273	287	304	330	360	392	224
fluoride	TeF ₆	-111.3	-98.8	-92.4	-86.0	-78.4	-73.8	-67.9	-57.3	-48.2	-38.6	-37.8
Thallium	Tl	825	931	983	1040	1103	1143	1196	1274	1364	1457	3035
Thallos bromide	TlBr		490	522	559	598	621	653	703	759	819	460
chloride	TlCl		487	517	550	589	612	645	694	748	807	430
iodide	TlI	440	502	531	567	607	631	663	712	763	823	440
Thionyl bromide	SOBr ₂	-6.7	+18.4	31.0	44.1	58.8	68.3	80.6	99.0	119.2	139.5	-52.2
Thionyl chloride	SOCl ₂	-52.9	-32.4	-21.9	-10.5	+2.2	10.4	21.4	37.9	56.5	75.4	-104.5
Tin	Sn	1492	1634	1703	1777	1855	1903	1968	2063	2169	2270	231.9
Stannic bromide	SnBr ₄		58.3	72.7	88.1	105.5	116.2	131.0	152.8	177.7	204.7	31.0
Stannous chloride	SnCl ₂	316	366	391	420	450	467	493	533	577	623	246.8
Stannic chloride	SnCl ₄	-22.7	-1.0	+10.0	22.0	35.2	43.5	54.7	72.0	92.1	113.0	-30.2
iodide	SnI ₄		156.0	175.8	196.2	218.8	234.2	254.2	283.5	315.5	348.0	144.5
hydride	SnH ₄	-140.0	-125.8	-118.5	-111.2	-102.3	-96.6	-89.2	-78.0	-65.2	-52.3	-149.9
Tin tetramethyl	Sn(CH ₃) ₄	-51.3	-31.0	-20.6	-9.3	+3.5	11.7	22.8	39.8	58.5	78.0	
trimethyl-ethyl	Sn(CH ₃) ₃ C ₂ H ₅	-30.0	-7.6	+3.8	16.1	30.0	38.4	50.0	67.3	87.6	108.8	
trimethyl-propyl	Sn(CH ₃) ₃ C ₃ H ₇	-12.0	+10.7	21.8	34.0	48.5	57.5	69.8	88.0	109.6	131.7	
Titanium chloride	TiCl ₄	-13.9	+9.4	21.3	34.2	48.4	58.0	71.0	90.5	112.7	136.0	-30
Tungsten	W	3990	4337	4507	4690	4886	5007	5168	5403	5666	5927	3370
Tungsten hexafluoride	WF ₆	-71.4	-56.5	-49.2	-41.5	-33.0	-27.5	-20.3	-10.0	+1.2	17.3	-0.5
Uranium hexafluoride	UF ₆	-38.8	-22.0	-13.8	-5.2	+4.4	10.4	18.2	30.0	42.7	55.7	69.2
Vanadyl trichloride	VOCl ₃	-23.2	+0.2	12.2	26.6	40.0	49.8	62.5	82.0	103.5	127.2	
Xenon	Xe	-168.5	-158.2	-152.8	-147.1	-141.2	-137.7	-132.8	-125.4	-117.1	-108.0	-111.6
Zinc	Zn	487	558	593	632	673	700	736	788	844	907	419.4
chloride	ZnCl ₂	428	481	508	536	566	584	610	648	689	732	365
fluoride	ZnF ₂	970	1055	1086	1129	1175	1207	1254	1329	1417	1497	872
diethyl	Zn(C ₂ H ₅) ₂	-22.4	0.0	+11.7	24.2	38.0	47.2	59.1	77.0	97.3	118.0	-28
Zirconium bromide	ZrBr ₄	207	237	250	266	281	289	301	318	337	357	450
chloride	ZrCl ₄	190	217	230	243	259	268	279	295	312	331	437
iodide	ZrI ₄	264	297	311	329	344	355	369	389	409	431	499

TABLE 2-10 Vapor Pressures of Organic Compounds, up to 1 atm*

Compound		Pressure, mmHg										Melting point, °C
		1	5	10	20	40	60	100	200	400	760	
Name	Formula	Temperature, °C										
Acenaphthalene	C ₁₂ H ₁₀		114.8	131.2	148.7	168.2	181.2	197.5	222.1	250.0	277.5	95
Acetal	C ₆ H ₁₄ O ₂	-23.0	-2.3	+8.0	19.6	31.9	39.8	50.1	66.3	84.0	102.2	
Acetaldehyde	C ₂ H ₄ O	-81.5	-65.1	-56.8	-47.8	-37.8	-31.4	-22.6	-10.0	+4.9	20.2	-123.5
Acetamide	C ₂ H ₅ NO	65.0	92.0	105.0	120.0	135.8	145.8	158.0	178.3	200.0	222.0	81
Acetamidide	C ₈ H ₉ NO	114.0	146.6	162.0	180.0	199.6	211.8	227.2	250.5	277.0	303.8	113.5
Acetic acid	C ₂ H ₄ O ₂	-17.2	+6.3	17.5	29.9	43.0	51.7	63.0	80.0	99.0	118.1	16.7
anhydride	C ₄ H ₆ O ₃	1.7	24.8	36.0	48.3	62.1	70.8	82.2	100.0	119.8	139.6	-73
Acetone	C ₃ H ₆ O	-59.4	-40.5	-31.1	-20.8	-9.4	-2.0	+7.7	22.7	39.5	56.5	-94.6
Acetonitrile	C ₂ H ₃ N	-47.0	-26.6	-16.3	-5.0	+7.7	15.9	27.0	43.7	62.5	81.8	-41
Acetophenone	C ₈ H ₈ O	37.1	64.0	78.0	92.4	109.4	119.8	133.6	154.2	178.0	202.4	20.5
Acetyl chloride	C ₂ H ₃ Cl	-50.0	-35.0	-27.6	-19.6	-10.4	-4.5	+3.2	16.1	32.0	50.8	-112.0
Acetylene	C ₂ H ₂	-142.9	-133.0	-128.2	-122.8	-116.7	-112.8	-107.9	-100.3	-92.0	-84.0	-81.5
Acridine	C ₁₃ H ₉ N	129.4	165.8	184.0	203.5	224.2	238.7	256.0	284.0	314.3	346.0	110.5
Acrolein (2-propenal)	C ₃ H ₄ O	-64.5	-46.0	-36.7	-26.3	-15.0	-7.5	+2.5	17.5	34.5	52.5	-87.7
Acrylic acid	C ₃ H ₄ O ₂	+3.5	27.3	39.0	52.0	66.2	75.0	86.1	103.3	122.0	141.0	14
Adipic acid	C ₆ H ₁₀ O ₄	159.5	191.0	205.5	222.0	240.5	251.0	265.0	287.8	312.5	337.5	152
Allene (propadiene)	C ₃ H ₄	-120.6	-108.0	-101.0	-93.4	-85.2	-78.8	-72.5	-61.3	-48.5	-35.0	-136
Allyl alcohol (propen-1-ol-3)	C ₃ H ₆ O	-20.0	+0.2	10.5	21.7	33.4	40.3	50.0	64.5	80.2	96.6	-129
chloride (3-chloropropene)	C ₃ H ₅ Cl	-70.0	-52.0	-42.9	-32.8	-21.2	-14.1	-4.5	10.4	27.5	44.6	-136.4
isopropyl ether	C ₆ H ₁₂ O	-43.7	-23.1	-12.9	-1.8	+10.9	18.7	29.0	44.3	61.7	79.5	
isothiocyanate	C ₃ H ₃ NS	-2.0	+25.3	38.3	52.1	67.4	76.2	89.5	108.0	129.8	150.7	-80
<i>n</i> -propyl ether	C ₆ H ₁₂ O	-39.0	-18.2	-7.9	+3.7	16.4	25.0	35.8	52.6	71.4	90.5	
4-Allylveratrole	C ₁₁ H ₁₄ O ₂	85.0	113.9	127.0	142.8	158.3	169.6	183.7	204.0	226.2	248.0	
iso-Amyl acetate	C ₇ H ₁₄ O ₂	0.0	+23.7	35.2	47.8	62.1	71.0	83.2	101.3	121.5	142.0	
<i>n</i> -Amyl alcohol	C ₆ H ₁₂ O	+13.6	34.7	44.9	55.8	68.0	75.5	85.8	102.0	119.8	137.8	
iso-Amyl alcohol	C ₅ H ₁₂ O	+10.0	30.9	40.8	51.7	63.4	71.0	80.7	95.8	113.7	130.6	-117.2
<i>sec</i> -Amyl alcohol (2-pentanol)	C ₅ H ₁₂ O	+1.5	22.1	32.2	42.6	54.1	61.5	70.7	85.7	102.3	119.7	
<i>tert</i> -Amyl alcohol	C ₅ H ₁₂ O	-12.9	+7.2	17.2	27.9	38.8	46.0	55.3	69.7	85.7	101.7	-11.9
<i>sec</i> -Amylbenzene	C ₁₁ H ₁₆	29.0	55.8	69.2	83.8	100.0	110.4	124.1	145.2	168.0	193.0	
iso-Amyl benzoate	C ₁₂ H ₁₆ O ₂	72.0	104.5	121.6	139.7	158.3	171.4	186.8	210.2	235.8	262.0	
bromide (1-bromo-3-methylbutane)	C ₅ H ₁₁ Br	-20.4	+2.1	13.6	26.1	39.8	48.7	60.4	78.7	99.4	120.4	
<i>n</i> -butyrate	C ₉ H ₁₆ O ₂	21.2	47.1	59.9	74.0	90.0	99.8	113.1	133.2	155.3	178.6	
formate	C ₆ H ₁₂ O ₂	-17.5	+5.4	17.1	30.0	44.0	53.3	65.4	83.2	102.7	123.3	
iodide (1-iodo-3-methylbutane)	C ₅ H ₁₁ I	-2.5	+21.9	34.1	47.6	62.3	71.9	84.4	103.8	125.8	148.2	
isobutyrate	C ₈ H ₁₅ O ₂	14.8	40.1	52.8	66.6	81.8	91.7	104.4	124.2	146.0	168.8	
Amyl isopropionate	C ₈ H ₁₆ O ₂	+8.5	33.7	46.3	60.0	75.5	85.2	97.6	117.3	138.4	160.2	
iso-Amyl isovalerate	C ₁₀ H ₂₀ O ₂	27.0	54.4	68.6	83.8	100.6	110.3	125.1	146.1	169.5	194.0	
<i>n</i> -Amyl levulinate	C ₁₀ H ₁₈ O ₃	81.3	110.0	124.0	139.7	155.8	165.2	180.5	203.1	227.4	253.2	
iso-Amyl levulinate	C ₁₀ H ₁₈ O ₃	75.6	104.0	118.8	134.4	151.7	162.6	177.0	198.1	222.7	247.9	
nitrate	C ₈ H ₁₁ NO ₃	+5.2	28.8	40.3	53.5	67.6	76.3	88.6	106.7	126.5	147.5	
4- <i>tert</i> -Amylphenol	C ₁₁ H ₁₆ O		109.8	125.5	142.3	160.3	172.6	189.0	213.0	239.5	266.0	93
Anethole	C ₁₀ H ₁₂ O	62.6	91.6	106.0	121.8	139.3	149.8	164.2	186.1	210.5	235.3	22.5
Angelonitrile	C ₈ H ₇ N	-8.0	+15.0	28.0	41.0	55.8	65.2	77.5	96.3	117.7	140.0	
Aniline	C ₆ H ₇ N	34.8	57.9	69.4	82.0	96.7	106.0	119.9	140.1	161.9	184.4	-6.2
2-Anilinoethanol	C ₈ H ₁₁ NO	104.0	134.3	149.6	165.7	183.7	194.0	209.5	230.6	254.5	279.6	
Anisaldehyde	C ₈ H ₈ O ₂	73.2	102.6	117.8	133.5	150.5	161.7	176.7	199.0	223.0	248.0	2.5
<i>o</i> -Anisidine (2-methoxyaniline)	C ₇ H ₉ NO	61.0	88.0	101.7	116.1	132.0	142.1	155.2	175.3	197.3	218.5	5.2
Anthracene	C ₁₄ H ₁₀	145.0	173.5	187.2	201.9	217.5	231.8	250.0	279.0	310.2	342.0	217.5
Anthraquinone	C ₁₄ H ₈ O ₂	190.0	219.4	234.2	248.3	264.3	273.3	285.0	314.6	346.2	379.9	286
Azelaic acid	C ₉ H ₁₆ O ₄	178.3	210.4	225.5	242.4	260.0	271.8	286.5	309.6	332.8	356.5	106.5
Azelaldehyde	C ₉ H ₁₆ O	33.3	58.4	71.6	85.0	100.2	110.0	123.0	142.1	163.4	185.0	
Azobenzene	C ₁₂ H ₁₀ N ₂	103.5	135.7	151.5	168.3	187.9	199.8	216.0	240.0	266.1	293.0	68
Benzal chloride (α,α-Dichlorotoluene)	C ₇ H ₆ Cl ₂	35.4	64.0	78.7	94.3	112.1	123.4	138.3	160.7	187.0	214.0	-16.1
Benzaldehyde	C ₇ H ₆ O	26.2	50.1	62.0	75.0	90.1	99.6	112.5	131.7	154.1	179.0	-26
Benzanthrone	C ₁₇ H ₁₀ O	225.0	274.5	297.2	322.5	350.0	368.8	390.0	426.5			174
Benzene	C ₆ H ₆	-36.7	-19.6	-11.5	-2.6	+7.6	15.4	26.1	42.2	60.6	80.1	+5.5
Benzenesulfonylchloride	C ₆ H ₅ ClO ₂ S	65.9	96.5	112.0	129.0	147.7	158.2	174.5	198.0	224.0	251.5	14.5
Benzil	C ₁₄ H ₁₀ O ₂	128.4	165.2	183.0	202.8	224.5	238.2	255.8	283.5	314.3	347.0	95
Benzoic acid	C ₇ H ₆ O ₂	96.0	119.5	132.1	146.7	162.6	172.8	186.2	205.8	227.0	249.2	121.7
anhydride	C ₁₄ H ₁₀ O ₃	143.8	180.0	198.0	218.0	239.8	252.7	270.4	299.1	328.8	360.0	42
Benzoin	C ₁₄ H ₁₂ O ₂	135.6	170.2	188.1	207.0	227.6	241.7	258.0	284.4	313.5	343.0	132
Benzonitrile	C ₇ H ₅ N	28.2	55.3	69.2	83.4	99.6	109.8	123.5	144.1	166.7	190.6	-12.9
Benzophenone	C ₁₃ H ₁₀ O	108.2	141.7	157.6	175.8	195.7	208.2	224.4	249.8	276.8	305.4	48.5
Benzotrichloride (α,α,α-Trichlorotoluene)	C ₆ H ₂ Cl ₃	45.8	73.7	87.6	102.7	119.8	130.0	144.3	165.6	189.2	213.5	-21.2
Benzotrifluoride (α,α,α-Trifluorotoluene)	C ₆ H ₂ F ₃	-32.0	-10.3	-0.4	12.2	25.7	34.0	45.3	62.5	82.0	102.2	-29.3
Benzoyl bromide	C ₇ H ₅ BrO	47.0	75.4	89.8	105.4	122.6	133.4	147.7	169.2	193.7	218.5	0
chloride	C ₇ H ₅ ClO	32.1	59.1	73.0	87.6	103.8	114.7	128.0	149.5	172.8	197.2	-0.5
nitride	C ₈ H ₅ NO	44.5	71.7	85.5	100.2	116.6	127.0	141.0	161.3	185.0	208.0	33.5
Benzyl acetate	C ₉ H ₁₀ O ₂	45.0	73.4	87.6	102.3	119.6	129.8	144.0	165.5	189.0	213.5	-51.5
alcohol	C ₇ H ₈ O	58.0	80.8	92.6	105.8	119.8	129.3	141.7	160.0	183.0	204.7	-15.3

*Compiled from the extended tables published by D. R. Stull in *Ind. Eng. Chem.*, **39**, 517 (1947). For information on fuels see Hibbard, N.A.C.A. Research Mem. E56121, 1956. For methane see Johnson (ed.), WADD-TR-60-56, 1960.

TABLE 2-10 Vapor Pressures of Organic Compounds, up to 1 atm (Continued)

Compound		Pressure, mmHg										Melting point, °C
		1	5	10	20	40	60	100	200	400	760	
Name	Formula	Temperature, °C										
Benzylamine	C ₇ H ₉ N	29.0	54.8	67.7	81.8	97.3	107.3	120.0	140.0	161.3	184.5	
Benzyl bromide (α -bromotoluene)	C ₇ H ₇ Br	32.2	59.6	73.4	88.3	104.8	115.6	129.8	150.8	175.2	198.5	-4
chloride (α -chlorotoluene)	C ₇ H ₇ Cl	22.0	47.8	60.8	75.0	90.7	100.5	114.2	134.0	155.8	179.4	-39
cinnamate	C ₁₆ H ₁₄ O ₂	173.8	206.3	221.5	239.3	255.8	267.0	281.5	303.8	326.7	350.0	39
Benzylidichlorosilane	C ₇ H ₈ Cl ₂ Si	45.3	70.2	83.2	96.7	111.8	121.3	133.5	152.0	173.0	194.3	
Benzyl ethyl ether	C ₉ H ₁₂ O	26.0	52.0	65.0	79.6	95.4	105.5	118.9	139.6	161.5	185.0	
phenyl ether	C ₁₃ H ₁₈ O	95.4	127.7	144.0	160.7	180.1	192.6	209.2	233.2	259.8	287.0	
isothiocyanate	C ₈ H ₇ NS	79.5	107.8	121.8	137.0	153.0	163.8	177.7	198.0	220.4	243.0	
Biphenyl	C ₁₂ H ₁₀	70.6	101.8	117.0	134.2	152.5	165.2	180.7	204.2	229.4	254.9	69.5
1-Biphenyloxy-2,3-epoxypropane	C ₁₅ H ₁₄ O ₂	135.3	169.9	187.2	205.8	226.3	239.7	255.0	280.4	309.8	340.0	
<i>d</i> -Bornyl acetate	C ₁₂ H ₂₀ O ₂	46.9	75.7	90.2	106.0	123.7	135.7	149.8	172.0	197.5	223.0	29
Bornyl <i>n</i> -butyrate	C ₁₄ H ₂₄ O ₂	74.0	103.4	118.0	133.8	150.7	161.8	176.4	198.0	222.2	247.0	
formate	C ₁₁ H ₁₈ O ₂	47.0	74.8	89.3	104.0	121.2	131.7	145.8	166.4	190.2	214.0	
isobutyrate	C ₁₁ H ₂₀ O ₂	70.0	99.8	114.0	130.0	147.2	157.6	172.2	194.2	218.2	243.0	
propionate	C ₁₃ H ₂₂ O ₂	64.6	93.7	108.0	123.7	140.4	151.2	165.7	187.5	211.2	235.0	
Brassicic acid	C ₂₂ H ₄₂ O ₂	209.6	241.7	256.0	272.9	290.0	301.5	316.2	336.8	359.6	382.5	61.5
Bromoacetic acid	C ₂ H ₃ BrO ₂	54.7	81.6	94.1	108.2	124.0	133.8	146.3	165.8	186.7	208.0	49.5
4-Bromoanisole	C ₈ H ₇ BrO	48.8	77.8	91.9	107.8	125.0	136.0	150.1	172.7	197.5	223.0	12.5
Bromobenzene	C ₆ H ₅ Br	+2.9	27.8	40.0	53.8	68.6	78.1	90.8	110.1	132.3	156.2	-30.7
4-Bromobiphenyl	C ₁₂ H ₉ Br	98.0	133.7	150.6	169.8	190.8	204.5	221.8	248.2	277.7	310.0	90.5
1-Bromo-2-butanol	C ₄ H ₉ BrO	23.7	45.4	55.8	67.2	79.5	87.0	97.6	112.1	128.3	145.0	
1-Bromo-2-butanone	C ₄ H ₇ BrO	+6.2	30.0	41.8	54.2	68.2	77.3	89.2	107.0	126.3	147.0	
<i>cis</i> -1-Bromo-1-butene	C ₄ H ₇ Br	-44.0	-23.2	-12.8	-1.4	+11.5	19.8	30.8	47.8	66.8	86.2	
<i>trans</i> -1-Bromo-1-butene	C ₄ H ₇ Br	-38.4	-17.0	-6.4	+5.4	18.4	27.2	38.1	55.7	75.0	94.7	-100.3
2-Bromo-1-butene	C ₄ H ₇ Br	-47.3	-27.0	-16.8	-5.3	+7.2	15.4	26.3	42.8	61.9	81.0	-133.4
<i>cis</i> -2-Bromo-2-butene	C ₄ H ₇ Br	-39.0	-17.9	-7.2	+4.6	17.7	26.2	37.5	54.5	74.0	93.9	-111.2
<i>trans</i> -2-Bromo-2-butene	C ₄ H ₇ Br	-45.0	-24.1	-13.8	-2.4	+10.5	18.7	29.9	46.5	66.0	85.5	-114.6
1,4-Bromochlorobenzene	C ₆ H ₄ BrCl	32.0	59.5	72.7	87.8	103.8	114.8	128.0	149.5	172.6	196.9	
1-Bromo-1-chloroethane	C ₂ H ₄ BrCl	-36.0	-18.0	-9.4	0.0	+10.4	17.0	28.0	44.7	63.4	82.7	16.6
1-Bromo-2-chloroethane	C ₂ H ₄ BrCl	-28.8	-7.0	+4.1	16.0	29.7	38.0	49.5	66.8	86.0	106.7	-16.6
2-Bromo-4,6-dichlorophenol	C ₆ H ₃ BrCl ₂ O	84.0	115.6	130.8	147.7	165.8	177.6	193.2	216.5	242.0	268.0	68
1-Bromo-4-ethyl benzene	C ₈ H ₉ Br	30.4	42.5	74.0	90.2	108.5	121.0	135.5	156.5	182.0	206.0	-45.0
(2-Bromoethyl)-benzene	C ₈ H ₉ Br	48.0	76.2	90.5	105.8	123.2	133.8	148.2	169.8	194.0	219.0	
2-Bromoethyl 2-chloroethyl ether	C ₄ H ₈ BrClO	36.5	63.2	76.3	90.8	106.6	116.4	129.8	150.0	172.3	195.8	
(2-Bromoethyl)-cyclohexane	C ₈ H ₁₅ Br	38.7	66.6	80.5	95.8	113.0	123.7	138.0	160.0	186.2	213.0	
1-Bromoethylene	C ₂ H ₃ Br	-95.4	-77.8	-68.8	-58.8	-48.1	-41.2	-31.9	-17.2	-1.1	+15.8	-138
Bromoform (tribromomethane)	CHBr ₃	22.0	34.0	48.0	63.6	73.4	85.9	106.1	127.9	150.5	175.0	8.5
1-Bromonaphthalene	C ₁₀ H ₇ Br	84.2	117.5	133.6	150.2	170.2	183.5	198.8	224.2	252.0	281.1	5.5
2-Bromo-4-phenylphenol	C ₁₂ H ₉ BrO	100.0	135.4	152.3	171.8	193.8	207.0	224.5	251.0	280.2	311.0	95
3-Bromopyridine	C ₅ H ₄ BrN	16.8	42.0	55.2	69.1	84.1	94.1	107.8	127.7	150.0	173.4	
2-Bromotoluene	C ₇ H ₇ Br	24.4	49.7	62.3	76.0	91.0	100.0	112.0	133.6	157.3	181.8	-28
3-Bromotoluene	C ₇ H ₇ Br	14.8	50.8	64.0	78.1	93.9	104.1	117.8	138.0	160.0	183.7	39.8
4-Bromotoluene	C ₇ H ₇ Br	10.3	47.5	61.1	75.2	91.8	102.3	116.4	137.4	160.2	184.5	28.5
3-Bromo-2,4,6-trichlorophenol	C ₆ H ₂ BrCl ₃ O	112.4	146.2	163.2	181.8	200.5	213.0	229.3	253.0	278.0	305.8	
2-Bromo-1,4-xylene	C ₈ H ₉ Br	37.5	65.0	78.8	94.0	110.6	121.6	135.7	156.4	181.0	206.7	+9.5
1,2-Butadiene (methyl allene)	C ₄ H ₆	-89.0	-72.7	-64.2	-54.9	-44.3	-37.5	-28.3	-14.2	+1.8	18.5	
1,3-Butadiene	C ₄ H ₆	-102.8	-87.6	-79.7	-71.0	-61.3	-55.1	-46.8	-33.9	-19.3	-4.5	-108.9
<i>n</i> -Butane	C ₄ H ₁₀	-101.5	-85.7	-77.8	-68.9	-59.1	-52.8	-44.2	-31.2	-16.3	-0.5	-135
iso-Butane (2-methylpropane)	C ₄ H ₁₀	-109.2	-94.1	-86.4	-77.9	-68.4	-62.4	-54.1	-41.5	-27.1	-11.7	-145
1,3-Butanediol	C ₄ H ₁₀ O ₂	22.2	67.5	85.3	100.0	117.4	127.5	141.2	161.0	183.8	206.5	77
1,2,3-Butanetriol	C ₄ H ₁₀ O ₃	102.0	132.0	146.0	161.0	178.0	188.0	202.5	222.0	243.5	264.0	
1-Butene	C ₄ H ₈	-104.8	-89.4	-81.6	-73.0	-63.4	-57.2	-48.9	-36.2	-21.7	-6.3	-130
<i>cis</i> -2-Butene	C ₄ H ₈	-96.4	-81.1	-73.4	-64.6	-54.7	-48.4	-39.8	-26.8	-12.0	+3.7	-138.9
<i>trans</i> -2-Butene	C ₄ H ₈	-99.4	-84.0	-76.3	-67.5	-57.6	-51.3	-42.7	-29.7	-14.8	+0.9	-105.4
3-Butenenitrile	C ₄ H ₅ N	-19.6	+2.9	14.1	26.6	40.0	48.8	60.2	78.0	98.0	119.0	
iso-Butyl acetate	C ₆ H ₁₂ O ₂	-21.2	+1.4	12.8	25.5	39.2	48.0	59.7	77.6	97.5	118.0	-98.9
<i>n</i> -Butyl acrylate	C ₈ H ₁₂ O ₂	-0.5	+23.5	35.5	48.6	63.4	72.6	85.1	104.0	125.2	147.4	-64.6
alcohol	C ₄ H ₁₀ O	-1.2	+20.0	30.2	41.5	53.4	60.3	70.1	84.3	100.8	117.5	-79.9
iso-Butyl alcohol	C ₄ H ₁₀ O	-9.0	+11.6	21.7	32.4	44.1	51.7	61.5	75.9	91.4	108.0	-108
<i>sec</i> -Butyl alcohol	C ₄ H ₁₀ O	-12.2	+7.2	16.9	27.3	38.1	45.2	54.1	67.9	83.9	99.5	-114.7
<i>tert</i> -Butyl alcohol	C ₄ H ₁₀ O	-20.4	-3.0	+5.5	14.3	24.5	31.0	39.8	52.7	68.0	82.9	25.3
iso-Butyl amine	C ₄ H ₁₁ N	-50.0	-31.0	-21.0	-10.3	+1.3	8.8	18.8	32.0	50.7	68.6	-85.0
<i>n</i> -Butylbenzene	C ₁₀ H ₁₄	22.7	48.8	62.0	76.3	92.4	102.6	116.2	136.9	159.2	183.1	-88.0
iso-Butylbenzene	C ₁₀ H ₁₄	14.1	40.5	53.7	67.8	83.3	93.3	107.0	127.2	149.6	172.8	-51.5
<i>sec</i> -Butylbenzene	C ₁₀ H ₁₄	18.6	44.2	57.0	70.6	86.2	96.0	109.5	128.8	150.3	173.5	-75.5
<i>tert</i> -Butylbenzene	C ₁₀ H ₁₄	13.0	39.0	51.7	65.6	80.8	90.6	103.8	123.7	145.8	168.5	-58
iso-Butyl benzoate	C ₁₁ H ₁₄ O ₂	64.0	93.6	108.6	124.2	141.8	152.0	166.4	188.2	212.8	237.0	
<i>n</i> -Butyl bromide (1-bromobutane)	C ₄ H ₉ Br	-33.0	-11.2	-0.3	+11.6	24.8	33.4	44.7	62.0	81.7	101.6	-112.4
iso-Butyl <i>n</i> -butyrate	C ₈ H ₁₆ O ₂	+4.6	30.0	42.2	56.1	71.7	81.3	94.0	113.9	135.7	156.9	
carbamate	C ₅ H ₁₁ NO ₂		83.7	96.4	110.1	125.3	134.6	147.2	165.7	186.0	206.5	65
Butyl carbitol (diethylene glycol butyl ether)	C ₈ H ₁₈ O ₃	70.0	95.7	107.8	120.5	135.5	146.0	159.8	181.2	205.0	231.2	
<i>n</i> -Butyl chloride (1-chlorobutane)	C ₄ H ₉ Cl	-49.0	-28.9	-18.6	-7.4	+5.0	13.0	24.0	40.0	58.8	77.8	-123.1
iso-Butyl chloride	C ₄ H ₉ Cl	-53.8	-34.3	-24.5	-13.8	-1.9	+5.9	16.0	32.0	50.0	68.9	-131.2

TABLE 2-10 Vapor Pressures of Organic Compounds, up to 1 atm (Continued)

Compound		Pressure, mmHg										Melting point, °C
		1	5	10	20	40	60	100	200	400	760	
Name	Formula	Temperature, °C										
<i>sec</i> -Butyl chloride (2-Chlorobutane)	C ₄ H ₉ Cl	-60.2	-39.8	-29.2	-17.7	-5.0	+3.4	14.2	31.5	50.0	68.0	-131.3
<i>tert</i> -Butyl chloride	C ₄ H ₉ Cl					-19.0	-11.4	-1.0	+14.6	32.6	51.0	-26.5
<i>sec</i> -Butyl chloroacetate	C ₆ H ₁₁ ClO ₂	17.0	41.8	54.6	68.2	83.6	93.0	105.5	124.1	146.0	167.8	
2- <i>tert</i> -Butyl-4-cresol	C ₁₁ H ₁₆ O	70.0	98.0	112.0	127.2	143.9	153.7	167.0	187.8	210.0	232.6	
4- <i>tert</i> -Butyl-2-cresol	C ₁₁ H ₁₆ O	74.3	103.7	118.0	134.0	150.8	161.7	176.2	197.8	221.8	247.0	
iso-Butyl dichloroacetate	C ₆ H ₁₀ Cl ₂ O ₂	28.6	54.3	67.5	81.4	96.7	106.6	119.8	139.2	160.0	183.0	
2,3-Butylene glycol (2,3-butanediol)	C ₄ H ₁₀ O ₂	44.0	68.4	80.3	93.4	107.8	116.3	127.8	145.6	164.0	182.0	22.5
2-Butyl-2-ethylbutane-1,3-diol	C ₁₀ H ₂₂ O ₂	94.1	122.6	136.8	151.2	167.8	178.0	191.9	212.0	233.5	255.0	
2- <i>tert</i> -Butyl-4-ethylphenol	C ₁₂ H ₁₆ O	76.3	106.2	121.0	137.0	154.0	165.4	179.0	200.3	223.8	247.8	
<i>n</i> -Butyl formate	C ₅ H ₁₀ O ₂	-26.4	-4.7	+6.1	18.0	31.6	39.8	51.0	67.9	86.2	106.0	
iso-Butyl formate	C ₅ H ₁₀ O ₂	-32.7	-11.4	-0.8	+11.0	24.1	32.4	43.4	60.0	79.0	98.2	-95.3
<i>sec</i> -Butyl formate	C ₅ H ₁₀ O ₂	-34.4	-13.3	-3.1	+8.4	21.3	29.6	40.2	56.8	75.2	93.6	
<i>sec</i> -Butyl glycolate	C ₆ H ₁₂ O ₃	28.3	53.6	66.0	79.8	94.2	104.0	116.4	135.5	155.6	177.5	
iso-Butyl iodide (1-iodo-2-methylpropane)	C ₄ H ₉ I	-17.0	+5.8	17.0	29.8	42.8	51.8	63.5	81.0	100.3	120.4	-90.7
isobutyrate	C ₅ H ₁₀ O ₂	+4.1	28.0	39.9	52.4	67.2	75.9	88.0	106.3	126.3	147.5	-80.7
isovalerate	C ₆ H ₁₂ O ₂	16.0	41.2	53.8	67.7	82.7	92.4	105.2	124.8	146.4	168.7	
levulinate	C ₆ H ₁₂ O ₃	65.0	92.1	105.9	120.2	136.2	147.0	160.2	181.8	205.5	229.9	
naphthylketone (1-isovaleronaphthone)	C ₁₃ H ₁₆ O	136.0	167.9	184.0	201.6	219.7	231.5	246.7	269.7	294.0	320.0	
2- <i>sec</i> -Butylphenol	C ₁₀ H ₁₄ O	57.4	86.0	100.8	116.1	133.4	143.9	157.3	179.7	203.8	228.0	
2- <i>tert</i> -Butylphenol	C ₁₀ H ₁₄ O	56.6	84.2	98.1	113.0	129.2	140.0	153.5	173.8	196.3	219.5	
4-iso-Butylphenol	C ₁₀ H ₁₄ O	72.1	100.9	115.5	130.3	147.2	157.0	171.2	191.2	214.7	237.0	
4- <i>sec</i> -Butylphenol	C ₁₀ H ₁₄ O	71.4	100.5	114.8	130.3	147.8	157.9	172.4	194.3	217.6	242.1	
4- <i>tert</i> -Butylphenol	C ₁₀ H ₁₄ O	70.0	99.2	114.0	129.5	146.0	156.0	170.2	191.5	214.0	238.0	99
2-(4- <i>tert</i> -Butylphenoxy)ethyl acetate	C ₁₄ H ₂₀ O ₃	118.0	150.0	165.8	183.3	201.5	212.8	228.0	250.3	277.6	304.4	
4- <i>tert</i> -Butylphenyl dichlorophosphate	C ₁₀ H ₁₃ Cl ₂ O ₂ P	96.0	129.6	146.0	164.0	184.3	197.2	214.3	240.0	268.2	299.0	
<i>tert</i> -Butyl phenyl ketone (pivalophenone)	C ₁₁ H ₁₄ O	57.8	85.7	99.0	114.3	130.4	140.8	154.0	175.0	197.7	220.0	
iso-Butyl propionate	C ₇ H ₁₄ O ₂	-2.3	+20.9	32.3	44.8	58.5	67.6	79.5	97.0	116.4	136.8	-71
4- <i>tert</i> -Butyl-2,5-xyleneol	C ₁₂ H ₁₆ O	88.2	119.8	135.0	151.0	169.8	180.3	195.0	217.5	241.3	265.3	
4- <i>tert</i> -Butyl-2,6-xyleneol	C ₁₂ H ₁₆ O	74.0	103.9	119.0	135.0	152.2	163.6	176.0	196.0	217.8	239.8	
6- <i>tert</i> -Butyl-2,4-xyleneol	C ₁₂ H ₁₆ O	70.3	100.2	115.0	131.0	148.5	158.2	172.0	192.3	214.2	236.5	
6- <i>tert</i> -Butyl-3,4-xyleneol	C ₁₂ H ₁₆ O	83.9	113.6	127.0	143.0	159.7	170.0	184.0	204.5	226.7	249.5	
Butyric acid	C ₄ H ₈ O ₂	25.5	49.8	61.5	74.0	88.0	96.5	108.0	125.5	144.5	163.5	-74
iso-Butyric acid	C ₄ H ₈ O ₂	14.7	39.3	51.2	64.0	77.8	86.3	98.0	115.8	134.5	154.5	-47
Butyronitrile	C ₄ H ₇ N	-20.0	+2.1	13.4	25.7	38.4	47.3	59.0	76.7	96.8	117.5	
iso-Valerophenone	C ₁₁ H ₁₄ O	58.3	87.0	101.4	116.8	133.8	144.6	158.0	180.1	204.2	228.0	
Camphene	C ₁₀ H ₁₆			47.2	60.4	75.7	85.0	97.9	117.5	138.7	160.5	50
Campholenic acid	C ₁₀ H ₁₆ O ₂	97.6	125.7	139.8	153.9	170.0	180.0	193.7	212.7	234.0	256.0	
<i>d</i> -Camphor	C ₁₀ H ₁₆ O	41.5	68.6	82.3	97.5	114.0	124.0	138.0	157.9	182.0	209.2	178.5
Camphylamine	C ₁₀ H ₁₉ N	45.3	74.0	83.7	97.6	112.5	122.0	134.6	153.0	173.8	195.0	
Capraldehyde	C ₁₀ H ₂₀ O	51.9	78.8	92.0	106.3	122.2	132.0	145.3	164.8	186.3	208.5	
Capric acid	C ₁₀ H ₂₀ O ₂	125.0	142.0	152.2	165.0	179.9	189.8	200.0	217.1	240.3	268.4	31.5
<i>n</i> -Caproic acid	C ₆ H ₁₂ O ₂	71.4	89.5	99.5	111.8	125.0	133.3	144.0	160.8	181.0	202.0	-1.5
iso-Caproic acid	C ₆ H ₁₂ O ₂	66.2	83.0	94.0	107.0	120.4	129.6	141.4	158.3	181.0	207.7	-35
iso-Caprolactone	C ₆ H ₁₀ O ₂	38.3	66.4	80.3	95.7	112.3	123.2	137.2	157.8	182.1	207.0	
Capronitrile	C ₆ H ₁₁ N	9.2	34.6	47.5	61.7	76.9	86.8	99.8	119.7	141.0	163.7	
Capryl alcohol (2-octanol)	C ₈ H ₁₈ O	32.8	57.6	70.0	83.3	98.0	107.4	119.8	138.0	157.5	178.5	-38.6
Caprylaldehyde	C ₈ H ₁₆ O	73.4	92.0	101.2	110.2	120.0	126.0	133.9	145.4	156.5	168.5	
Caprylic acid (octanoic acid)	C ₈ H ₁₆ O ₂	92.3	114.1	124.0	136.4	150.6	160.0	172.2	190.3	213.9	237.5	16
Caprylonitrile	C ₈ H ₁₅ N	43.0	67.6	80.4	94.6	110.6	121.2	134.8	155.2	179.5	204.5	
Carbazole	C ₁₂ H ₉ N					248.2	265.0	292.5	323.0	354.8	244.8	
Carbon dioxide	CO ₂	-134.3	-124.4	-119.5	-114.4	-108.6	-104.8	-100.2	-93.0	-85.7	-78.2	-57.5
disulfide	CS ₂	-73.8	-54.3	-44.7	-34.3	-22.5	-15.3	-5.1	+10.4	28.0	46.5	-110.8
monoxide	CO	-222.0	-217.2	-215.0	-212.8	-210.0	-208.1	-205.7	-201.3	-196.3	-191.3	-205.0
oxyselenide (carbonyl selenide)	COSe	-117.1	-102.3	-95.0	-86.3	-76.4	-70.2	-61.7	-49.8	-35.6	-21.9	
oxysulfide (carbonyl sulfide)	COS	-132.4	-119.8	-113.3	-106.0	-98.3	-93.0	-85.9	-75.0	-62.7	-49.9	-138.8
tetrabromide	CBr ₄					96.3	106.3	119.7	139.7	163.5	189.5	90.1
tetrachloride	CCl ₄	-50.0	-30.0	-19.6	-8.2	+4.3	12.3	23.0	38.3	57.8	76.7	-22.6
tetrafluoride	CF ₄	-184.6	-174.1	-169.3	-164.3	-158.8	-155.4	-150.7	-143.6	-135.5	-127.7	-183.7
Carvacrol	C ₁₀ H ₁₄ O	70.0	98.4	113.2	127.9	145.2	155.3	169.7	191.2	213.8	237.0	+0.5
Carvone	C ₁₀ H ₁₄ O	57.4	86.1	100.4	116.1	133.0	143.8	157.3	179.6	203.5	227.5	
Chavibetol	C ₁₀ H ₁₄ O ₂	83.6	113.3	127.0	143.2	159.8	170.7	185.5	206.8	229.8	254.0	
Chloral (trichloroacetaldehyde)	C ₂ HCl ₃ O	-37.8	-16.0	-5.0	+7.2	20.2	29.1	40.2	57.8	77.5	97.7	-57
hydrate (trichloroacetaldehyde hydrate)	C ₂ H ₃ Cl ₃ O ₂	-9.8	+10.0	19.5	29.2	39.7	46.5	55.0	68.0	82.1	96.2	51.7
Chloranil	C ₆ Cl ₄ O ₂	70.7	89.3	97.8	106.4	116.1	122.0	129.5	140.3	151.3	162.6	290
Chloroacetic acid	C ₂ H ₃ ClO ₂	43.0	68.3	81.0	94.2	109.2	118.3	130.7	149.0	169.0	189.5	61.2
anhydride	C ₂ H ₂ Cl ₂ O ₃	67.2	94.1	108.0	122.4	138.2	148.0	159.8	177.8	197.0	217.0	46
2-Chloroaniline	C ₆ H ₆ ClN	46.3	72.3	84.8	99.2	115.6	125.7	139.5	160.0	183.7	208.8	0
3-Chloroaniline	C ₆ H ₆ ClN	63.5	89.8	102.0	116.7	133.6	144.1	158.0	179.5	203.5	228.5	-10.4
4-Chloroaniline	C ₆ H ₆ ClN	59.3	87.9	102.1	117.8	135.0	145.8	159.9	182.3	206.6	230.5	70.5
Chlorobenzene	C ₆ H ₅ Cl	-13.0	+10.6	22.2	35.3	49.7	58.3	70.7	89.4	110.0	132.2	-45.2
2-Chlorobenzotrithloride												
(2- α,α,α -tetrachlorotoluene)	C ₇ H ₄ Cl ₄	69.0	101.8	117.9	135.8	155.0	167.8	185.0	208.0	233.0	262.1	28.7

2-68 PHYSICAL AND CHEMICAL DATA

TABLE 2-10 Vapor Pressures of Organic Compounds, up to 1 atm (Continued)

Compound		Pressure, mmHg										Melting point, °C
		1	5	10	20	40	60	100	200	400	760	
Name	Formula	Temperature, °C										
2-Chlorobenzotrifluoride (2-chloro- α,α,α -trifluorotoluene)	C ₇ H ₄ ClF ₃	0.0	24.7	37.1	50.6	65.9	75.4	88.3	108.3	130.0	152.2	-6.0
2-Chlorobiphenyl	C ₁₂ H ₉ Cl	89.3	109.8	134.7	151.2	169.9	182.1	197.0	219.6	243.8	267.5	34
4-Chlorobiphenyl	C ₁₂ H ₉ Cl	96.4	129.8	146.0	164.0	183.8	196.0	212.5	237.8	264.5	292.9	75.5
α -Chlorocrotonic acid	C ₇ H ₅ ClO ₂	70.0	95.6	108.0	121.2	135.6	144.4	155.9	173.8	193.2	212.0	
Chlorodifluoromethane	CHClF ₂	-122.8	-110.2	-103.7	-96.5	-88.6	-83.4	-76.4	-65.8	-53.6	-40.8	-160
Chlorodimethylphenylsilane	C ₈ H ₁₁ ClSi	29.8	56.7	70.0	84.7	101.2	111.5	124.7	145.5	168.6	193.5	
1-Chloro-2-ethoxybenzene	C ₈ H ₉ ClO	45.8	72.8	86.5	101.5	117.8	127.8	141.8	162.0	185.5	208.0	
2-(2-Chloroethoxy) ethanol	C ₄ H ₉ ClO ₂	53.0	78.3	90.7	104.1	118.4	127.5	139.5	157.2	176.5	196.0	
bis-2-Chloroethyl acetacetal	C ₈ H ₁₂ Cl ₂ O ₂	56.2	83.7	97.6	112.2	127.8	138.0	150.7	169.8	190.5	212.6	
1-Chloro-2-ethylbenzene	C ₈ H ₉ Cl	17.2	43.0	56.1	70.3	86.2	96.4	110.0	130.2	152.2	177.6	-80.2
1-Chloro-3-ethylbenzene	C ₈ H ₉ Cl	18.6	45.2	58.1	73.0	89.2	99.6	113.6	133.8	156.7	181.1	-53.3
1-Chloro-4-ethylbenzene	C ₈ H ₉ Cl	19.2	46.4	60.0	75.5	91.8	102.0	116.0	137.0	159.8	184.3	-62.6
2-Chloroethyl chloroacetate	C ₄ H ₆ Cl ₂ O ₂	46.0	72.1	86.0	100.0	116.0	126.2	140.0	159.8	182.2	205.0	
2-Chloroethyl 2-chloroisopropyl ether	C ₅ H ₁₀ Cl ₂ O	24.7	50.1	63.0	77.2	92.4	102.2	115.8	135.7	156.5	180.0	
2-Chloroethyl 2-chloropropyl ether	C ₅ H ₁₀ Cl ₂ O	29.8	56.5	70.0	84.8	101.5	111.8	125.6	146.3	169.8	194.1	
2-Chloroethyl α -methylbenzyl ether	C ₁₀ H ₁₃ ClO	62.3	91.4	106.0	121.8	139.6	150.0	164.8	186.3	210.8	235.0	
Chloroform (trichloromethane)	CHCl ₃	-58.0	-39.1	-29.7	-19.0	-7.1	+0.5	10.4	25.9	42.7	61.3	-63.5
1-Chloronaphthalene	C ₁₀ H ₇ Cl	80.6	104.8	118.6	134.4	153.2	165.6	180.4	204.2	230.8	259.3	-20
4-Chlorophenethyl alcohol	C ₈ H ₉ ClO	84.0	114.3	129.0	145.0	162.0	173.5	188.1	210.0	234.5	259.3	
2-Chlorophenol	C ₆ H ₅ ClO	12.1	38.2	51.2	65.9	82.0	92.0	106.0	126.4	149.8	174.5	7
3-Chlorophenol	C ₆ H ₅ ClO	44.2	72.0	86.1	101.7	118.0	129.4	143.0	164.8	188.7	214.0	32.5
4-Chlorophenol	C ₆ H ₅ ClO	49.8	78.2	92.2	108.1	125.0	136.1	150.0	172.0	196.0	220.0	42
2-Chloro-3-phenylphenol	C ₁₂ H ₉ ClO	118.0	152.2	169.7	186.7	207.4	219.6	237.0	261.3	289.4	317.5	+6
2-Chloro-6-phenylphenol	C ₁₂ H ₉ ClO	119.8	153.7	170.7	189.8	208.2	220.0	237.1	261.6	289.5	317.0	
Chloropicrin (trichloronitromethane)	CCl ₃ NO ₂	-25.5	-3.3	+7.8	20.0	33.8	42.3	53.8	71.8	91.1	111.9	-64
1-Chloropropene	C ₃ H ₅ Cl	-81.3	-63.4	-54.1	-44.0	-32.7	-25.1	-15.1	+1.3	18.0	37.0	-99.0
2-Chloropyridine	C ₅ H ₄ ClN	13.3	38.8	51.7	65.8	81.7	91.6	104.6	125.0	147.7	170.2	
3-Chlorostyrene	C ₈ H ₇ Cl	25.3	51.3	65.2	80.0	96.5	107.2	121.2	142.2	165.7	190.0	
4-Chlorostyrene	C ₈ H ₇ Cl	28.0	54.5	67.5	82.0	98.0	108.5	122.0	143.5	166.0	191.0	-15.0
1-Chlorotetradecane	C ₁₄ H ₂₉ Cl	98.5	131.8	148.2	166.2	187.0	199.8	215.5	240.3	267.5	296.0	+0.9
2-Chlorotoluene	C ₇ H ₇ Cl	+5.4	30.6	43.2	56.9	72.0	81.8	94.7	115.0	137.1	159.3	
3-Chlorotoluene	C ₇ H ₇ Cl	+4.8	30.3	43.2	57.4	73.0	83.2	96.3	116.6	139.7	162.3	
4-Chlorotoluene	C ₇ H ₇ Cl	+5.5	31.0	43.8	57.8	73.5	83.3	96.6	117.1	139.8	162.3	+7.3
Chlorotriethylsilane	C ₆ H ₁₅ ClSi	-4.9	+19.8	32.0	45.5	60.2	69.5	82.3	101.6	123.6	146.3	
1-Chloro-1,2,2-trifluoroethylene	C ₂ ClF ₃	-116.0	-102.5	-95.9	-88.2	-79.7	-74.1	-66.7	-55.0	-41.7	-27.9	-157.5
Chlorotrifluoromethane	CClF ₃	-149.5	-139.2	-134.1	-128.5	-121.9	-117.3	-111.7	-102.5	-92.7	-81.2	
Chlorotrimethylsilane	C ₃ H ₉ ClSi	-62.8	-43.6	-34.0	-23.2	-11.4	-4.0	+6.0	21.9	39.4	57.9	
<i>trans</i> -Cinnamic acid	C ₉ H ₈ O ₂	127.5	157.8	173.0	189.5	207.1	217.8	232.4	253.3	276.7	300.0	133
Cinnamyl alcohol	C ₉ H ₁₀ O	72.6	102.5	117.8	133.7	151.0	162.0	177.8	199.8	224.6	250.0	33
Cinnamylaldehyde	C ₉ H ₈ O	76.1	105.8	120.0	135.7	152.2	163.7	177.7	199.3	222.4	246.0	-7.5
Citraconic anhydride	C ₈ H ₄ O ₃	47.1	74.8	88.9	103.8	120.3	131.3	145.4	165.8	189.8	213.5	
<i>cis</i> - α -Citral	C ₁₀ H ₁₆ O	61.7	90.0	103.9	119.4	135.9	146.3	160.0	181.8	205.0	228.0	
<i>d</i> -Citronellal	C ₁₀ H ₁₆ O	44.0	71.4	84.8	99.8	116.1	126.2	140.1	160.0	183.8	206.5	
Citronellol acid	C ₁₀ H ₁₈ O ₂	99.5	127.3	141.4	155.6	171.9	182.1	195.4	214.5	236.6	257.0	
Citronellol	C ₁₀ H ₂₀ O	66.4	93.6	107.0	121.5	137.2	147.2	159.8	179.8	201.0	221.5	
Citronellyl acetate	C ₁₂ H ₂₂ O ₂	74.7	100.2	113.0	126.0	140.5	149.7	161.0	178.8	197.8	217.0	
Coumarin	C ₉ H ₆ O ₂	106.0	137.8	153.4	170.0	189.0	200.5	216.5	240.0	264.7	291.0	70
<i>o</i> -Cresol (2-cresol; 2-methylphenol)	C ₇ H ₈ O	38.2	64.0	76.7	90.5	105.8	115.5	127.4	146.7	168.4	190.8	30.8
<i>m</i> -Cresol (3-cresol; 3-methylphenol)	C ₇ H ₈ O	52.0	76.0	87.8	101.4	116.0	125.8	138.0	157.3	179.0	202.8	10.9
<i>p</i> -Cresol (4-cresol; 4-methylphenol)	C ₇ H ₈ O	53.0	76.5	88.6	102.3	117.7	127.0	140.0	157.3	179.4	201.8	35.5
<i>cis</i> -Crotonic acid	C ₄ H ₆ O ₂	33.5	57.4	69.0	82.0	96.0	104.5	116.3	133.9	152.2	171.9	15.5
<i>trans</i> -Crotonic acid	C ₄ H ₆ O ₂			80.0	93.0	107.8	116.7	128.0	146.0	165.5	185.0	72
<i>cis</i> -Crotononitrile	C ₄ H ₅ N	-29.0	-7.1	+4.0	16.4	30.0	38.5	50.1	68.0	88.0	108.0	
<i>trans</i> -Crotononitrile	C ₄ H ₅ N	-19.5	+3.5	15.0	27.8	41.8	50.9	62.8	81.1	101.5	122.8	
Cumene	C ₉ H ₁₂	+2.9	26.8	38.3	51.5	66.1	75.4	88.1	107.3	129.2	152.4	-96.0
4-Cumidene	C ₉ H ₁₂ N	60.0	88.2	102.2	117.8	134.2	145.0	158.0	180.0	203.2	227.0	
Cuminal	C ₁₀ H ₁₄ O	58.0	87.3	102.0	117.9	135.2	146.0	160.0	182.8	206.7	232.0	
Cuminy alcohol	C ₁₀ H ₁₄ O	74.2	103.7	118.0	133.8	150.3	161.7	176.2	197.9	221.7	246.6	
2-Cyano-2- <i>n</i> -butyl acetate	C ₈ H ₁₁ NO ₂	42.0	68.7	82.0	96.2	111.8	121.5	133.8	152.2	173.4	195.2	
Cyanogen bromide	CBrN	-95.8	-83.2	-76.8	-70.1	-62.7	-57.9	-51.8	-42.6	-33.0	-21.0	-34.4
chloride	CClN	-35.7	-18.3	-10.0	-1.0	+8.6	14.7	22.6	33.8	46.0	61.5	58
iodide	CIN	-76.7	-61.4	-53.8	-46.1	-37.5	-32.1	-24.9	-14.1	-2.3	+13.1	-6.5
Cyclobutane	C ₄ H ₈	25.2	47.2	57.7	68.6	80.3	88.0	97.6	111.5	126.1	141.1	
Cyclobutene	C ₄ H ₆	-92.0	-76.0	-67.9	-58.7	-48.4	-41.8	-32.8	-18.9	-3.4	+12.9	-50
Cyclohexane	C ₆ H ₁₂	-99.1	-83.4	-75.4	-66.6	-56.4	-50.0	-41.2	-27.8	-12.2	+2.4	
Cyclohexaneethanol	C ₈ H ₁₆ O	-45.3	-25.4	-15.9	-5.0	+6.7	14.7	25.5	42.0	60.8	80.7	+6.6
Cyclohexanol	C ₆ H ₁₂ O	50.4	77.2	90.0	104.0	119.8	129.8	142.7	161.7	183.5	205.4	
Cyclohexanone	C ₆ H ₁₀ O	21.0	44.0	56.0	68.8	83.0	91.8	103.7	121.7	141.4	161.0	23.9
Cyclohexanone	C ₆ H ₁₀ O	+1.4	26.4	38.7	52.5	67.8	77.5	90.4	110.3	132.5	155.6	-45.0
2-Cyclohexyl-4,6-dinitrophenol	C ₁₂ H ₁₄ N ₂ O ₅	132.8	161.8	175.9	191.2	206.7	216.0	229.0	248.7	269.8	291.5	
Cyclopentane	C ₅ H ₁₀	-68.0	-49.6	-40.4	-30.1	-18.6	-11.3	-1.3	+13.8	31.0	49.3	-93.7
Cyclopropane	C ₃ H ₆	-116.8	-104.2	-97.5	-90.3	-82.3	-77.0	-70.0	-59.1	-46.9	-33.5	-126.6
Cymene	C ₁₀ H ₁₄	17.3	43.9	57.0	71.1	87.0	97.2	110.8	131.4	153.5	177.2	-68.2

TABLE 2-10 Vapor Pressures of Organic Compounds, up to 1 atm (Continued)

Compound		Pressure, mmHg										Melting point, °C
		1	5	10	20	40	60	100	200	400	760	
Name	Formula	Temperature, °C										
<i>cis</i> -Decalin	C ₁₀ H ₁₈	22.5	50.1	64.2	79.8	97.2	108.0	123.2	145.4	169.9	194.6	-43.3
<i>trans</i> -Decalin	C ₁₀ H ₁₈	-0.8	+30.6	47.2	65.3	85.7	98.4	114.6	136.2	160.1	186.7	-30.7
Decane	C ₁₀ H ₂₂	16.5	42.3	55.7	69.8	85.5	95.5	108.6	128.4	150.6	174.1	-29.7
Decan-2-one	C ₁₀ H ₂₀ O	44.2	71.9	85.8	100.7	117.1	127.8	142.0	163.2	186.7	211.0	+3.5
1-Decene	C ₁₀ H ₂₀	14.7	40.3	53.7	67.8	83.3	93.5	106.5	126.7	149.2	172.0	
Decyl alcohol	C ₁₀ H ₂₂ O	69.5	97.3	111.3	125.8	142.1	152.0	165.8	186.2	208.8	231.0	+7
Decyltrimethylsilane	C ₁₃ H ₃₀ Si	67.4	96.4	111.0	126.5	144.0	154.3	169.5	191.0	215.5	240.0	
Dehydroacetic acid	C ₈ H ₈ O ₄	91.7	122.0	137.3	153.0	171.0	181.5	197.5	219.5	244.5	269.0	
Desoxybenzoin	C ₁₄ H ₁₂ O	123.3	156.2	173.5	192.0	212.0	224.5	241.3	265.2	293.0	321.0	60
Diacetamide	C ₈ H ₇ NO ₂	70.0	95.0	108.0	122.6	138.2	148.0	160.6	180.8	202.0	223.0	78.5
Diacetylene (1,3-butadiyne)	C ₂ H ₂	-82.5	-68.0	-61.2	-53.8	-45.9	-41.0	-34.0	-20.9	-6.1	+9.7	-34.9
Diallyldichlorosilane	C ₆ H ₁₀ Cl ₂ Si	+9.5	34.8	47.4	61.3	76.4	86.3	99.7	119.4	142.0	165.3	
Diallyl sulfide	C ₆ H ₁₀ S	-9.5	+14.4	26.6	39.7	54.2	63.7	75.8	94.8	116.1	138.6	-83
Diisoamyl ether	C ₁₀ H ₂₀ O	18.6	44.3	57.0	70.7	86.3	96.0	109.6	129.0	150.3	173.4	
oxalate	C ₁₂ H ₂₂ O ₄	85.4	116.0	131.4	147.7	165.7	177.0	192.2	215.0	240.0	265.0	
sulfide	C ₁₀ H ₂₂ S	43.0	73.0	87.6	102.7	120.0	130.6	145.3	166.4	191.0	216.0	
Dibenzylamine	C ₁₄ H ₁₅ N	118.3	149.8	165.6	182.2	200.2	212.2	227.3	249.8	274.3	300.0	-26
Dibenzyl ketone (1,3-diphenyl-2-propanone)	C ₁₅ H ₁₄ O	125.5	159.8	177.6	195.7	216.6	229.4	246.6	272.3	301.7	330.5	34.5
1,4-Dibromobenzene	C ₆ H ₄ Br ₂	61.0	79.3	87.7	103.6	120.8	131.6	146.5	168.5	192.5	218.6	87.5
1,2-Dibromobutane	C ₄ H ₈ Br ₂	7.5	33.2	46.1	60.0	76.0	86.0	99.8	120.2	143.5	166.3	-64.5
<i>dl</i> -2,3-Dibromobutane	C ₄ H ₈ Br ₂	+5.0	30.0	41.6	56.4	72.0	82.0	95.3	115.7	138.0	160.5	
<i>meso</i> -2,3-Dibromobutane	C ₄ H ₈ Br ₂	+1.5	26.6	39.3	53.2	68.0	78.0	91.7	111.8	134.2	157.3	-34.5
1,2-Dibromodecane	C ₁₀ H ₂₀ Br ₂	95.7	123.6	137.3	151.0	167.4	177.5	190.2	209.6	229.8	250.4	
Di(2-bromoethyl) ether	C ₄ H ₈ Br ₂ O	47.7	75.3	88.5	103.6	119.8	130.0	144.0	165.0	188.0	212.5	
α,β-Dibromomaleic anhydride	C ₆ H ₂ Br ₂ O ₃	50.0	78.0	92.0	106.7	123.5	133.8	147.7	168.0	192.0	215.0	
1,2-Dibromo-2-methylpropane	C ₄ H ₈ Br ₂	-28.8	-3.0	+10.5	25.7	42.3	53.7	68.8	92.1	119.8	149.0	-70.3
1,3-Dibromo-2-methylpropane	C ₄ H ₈ Br ₂	14.0	40.0	53.0	67.5	83.5	93.7	107.4	117.8	150.6	174.6	
1,2-Dibromopentane	C ₅ H ₁₀ Br ₂	19.8	45.4	58.0	72.0	87.4	97.4	110.1	130.2	151.8	175.0	
1,2-Dibromopropane	C ₃ H ₆ Br ₂	-7.0	+17.3	29.4	42.3	57.2	66.4	78.7	97.8	118.5	141.6	-55.5
1,3-Dibromopropane	C ₃ H ₆ Br ₂	+9.7	35.4	48.0	62.1	77.8	87.8	101.3	121.7	144.1	167.5	-34.4
2,3-Dibromopropane	C ₃ H ₆ Br ₂	-6.0	+17.9	30.0	43.2	57.8	67.0	79.5	98.0	119.5	141.2	
2,3-Dibromo-1-propanol	C ₃ H ₆ Br ₂ O	57.0	84.5	98.2	113.5	129.8	140.0	153.0	173.8	196.0	219.0	
Diisobutylamine	C ₈ H ₁₉ N	-5.1	+18.4	30.6	43.7	57.8	67.0	79.2	97.6	118.0	139.5	-70
2,6-Ditert-butyl-4-cresol	C ₁₅ H ₂₄ O	85.8	116.2	131.0	147.0	164.1	175.2	190.0	212.8	237.6	262.5	
4,6-Ditert-butyl-2-cresol	C ₁₅ H ₂₄ O	86.2	117.3	132.4	149.0	167.4	179.0	194.0	217.5	243.4	269.3	
4,6-Ditert-butyl-3-cresol	C ₁₅ H ₂₄ O	103.7	135.2	150.0	167.0	185.3	196.1	211.0	233.0	257.1	282.0	
2,6-Ditert-butyl-4-ethylphenol	C ₁₆ H ₂₆ O	89.1	121.4	137.0	154.0	172.1	183.9	198.0	220.0	244.0	268.6	
4,6-Ditert-butyl-3-ethylphenol	C ₁₆ H ₂₆ O	111.5	142.6	157.4	174.0	192.3	204.4	218.0	241.7	264.6	290.0	
Diisobutyl oxalate	C ₁₀ H ₁₈ O ₄	63.2	91.2	105.3	120.3	137.5	147.8	161.8	183.5	205.8	229.5	
2,4-Ditert-butylphenol	C ₁₄ H ₂₂ O	84.5	115.4	130.0	146.0	164.3	175.8	190.0	212.5	237.0	260.8	
Dibutyl phthalate	C ₁₆ H ₂₂ O ₄	148.2	182.1	198.2	216.2	235.8	247.8	263.7	287.0	313.5	340.0	
sulfide	C ₈ H ₁₈ S	+21.7	51.8	66.4	80.5	96.0	105.8	118.6	138.0	159.0	182.0	-79.7
Diisobutyl <i>d</i> -tartrate	C ₁₂ H ₂₂ O ₆	117.8	151.8	169.0	188.0	208.5	221.6	239.5	264.7	294.0	324.0	73.5
Dicarvacryl-mono-(6-chloro-2-xylyl) phosphate	C ₂₀ H ₃₄ ClO ₄ P	204.2	234.5	249.3	264.5	280.5	290.7	304.9	323.8	342.0	361.0	
Dicarvacryl-2-tolyl phosphate	C ₂₇ H ₃₂ O ₄ P	180.2	209.3	221.8	237.0	251.5	260.3	272.5	290.0	309.8	330.0	
Dichloroacetic acid	C ₂ H ₂ Cl ₂ O ₂	44.0	69.8	82.6	96.3	111.8	121.5	134.0	152.3	173.7	194.4	9.7
1,2-Dichlorobenzene	C ₆ H ₄ Cl ₂	20.0	46.0	59.1	73.4	89.4	99.5	112.9	133.4	155.8	179.0	-17.6
1,3-Dichlorobenzene	C ₆ H ₄ Cl ₂	12.1	39.0	52.0	66.2	82.0	92.2	105.0	125.9	149.0	173.0	-24.2
1,4-Dichlorobenzene	C ₆ H ₄ Cl ₂			54.8	69.2	84.8	95.2	108.4	128.3	150.2	173.9	53.0
1,2-Dichlorobutane	C ₄ H ₈ Cl ₂	-23.6	-0.3	+11.5	24.5	37.7	47.8	60.2	79.7	100.8	123.5	
2,3-Dichlorobutane	C ₄ H ₈ Cl ₂	-25.2	-3.0	+8.5	21.2	35.0	43.9	56.0	74.0	94.2	116.0	-80.4
1,2-Dichloro-1,2-difluoroethylene	C ₂ Cl ₂ F ₂	-82.0	-65.6	-57.3	-48.3	-38.2	-31.8	-23.0	-10.0	+5.0	20.9	-112
Dichlorodifluoromethane	CCl ₂ F ₂	-118.5	-104.6	-97.8	-90.1	-81.6	-76.1	-68.6	-57.0	-43.9	-29.8	
Dichlorodiphenyl silane	C ₁₂ H ₁₀ Cl ₂ Si	109.6	142.4	158.0	176.0	195.5	207.5	223.8	248.0	275.5	304.0	
Dichlorodiisopropyl ether	C ₆ H ₁₂ Cl ₂ O	29.6	55.2	68.2	82.2	97.3	106.9	119.7	139.0	159.8	182.7	
Di(2-chloroethoxy) methane	C ₅ H ₁₀ Cl ₂ O ₂	53.0	80.4	94.0	109.5	125.5	135.8	149.6	170.0	192.0	215.0	
Dichloroethoxymethylsilane	C ₆ H ₈ Cl ₂ OSi	-33.8	-12.1	-1.3	+11.3	24.4	32.6	44.1	61.0	80.3	100.6	
1,2-Dichloro-3-ethylbenzene	C ₉ H ₈ Cl ₂	46.0	75.0	90.0	105.9	123.8	135.0	149.8	172.0	197.0	222.1	-40.8
1,2-Dichloro-4-ethylbenzene	C ₉ H ₈ Cl ₂	47.0	77.2	92.3	109.6	127.5	139.0	153.3	176.0	201.7	226.6	-76.4
1,4-Dichloro-2-ethylbenzene	C ₉ H ₈ Cl ₂	38.5	68.0	83.2	99.8	118.0	129.0	144.0	166.2	191.5	216.3	-61.2
<i>cis</i> -1,2-Dichloroethylene	C ₂ H ₂ Cl ₂	-58.4	-39.2	-29.9	-19.4	-7.9	-0.5	+9.5	24.6	41.0	59.0	-80.5
<i>trans</i> -1,2-Dichloroethylene	C ₂ H ₂ Cl ₂	-65.4	-47.2	-38.0	-28.0	-17.0	-10.0	-0.2	+14.3	30.8	47.8	-50.0
Di(2-chloroethyl) ether	C ₄ H ₈ Cl ₂ O	23.5	49.3	62.0	76.0	91.5	101.5	114.5	134.0	155.4	178.5	
Dichlorofluoromethane	CHCl ₂ F	-91.3	-75.5	-67.5	-58.6	-48.8	-42.6	-33.9	-20.9	-6.2	+8.9	-135
1,5-Dichlorohexamethyltrisiloxane	C ₆ H ₁₈ Cl ₂ O ₂ Si ₃	26.0	52.0	65.1	79.0	94.8	105.0	118.2	138.3	160.2	184.0	-53.0
Dichloromethylphenylsilane	C ₇ H ₈ Cl ₂ Si	35.7	63.5	77.4	92.4	109.5	120.0	134.2	155.5	180.2	205.5	
1,1-Dichloro-2-methylpropane	C ₄ H ₈ Cl ₂	-31.0	-8.4	+2.6	14.6	28.2	37.0	48.2	65.8	85.4	106.0	
1,2-Dichloro-2-methylpropane	C ₄ H ₈ Cl ₂	-25.8	-4.2	+6.7	18.7	32.0	40.2	51.7	68.9	87.8	108.0	
1,3-Dichloro-2-methylpropane	C ₄ H ₈ Cl ₂	-3.0	+20.6	32.0	44.8	58.6	67.5	78.8	96.1	115.4	135.0	
2,4-Dichlorophenol	C ₆ H ₄ Cl ₂ O	53.0	80.0	92.8	107.7	123.4	133.5	146.0	165.2	187.5	210.0	45.0
2,6-Dichlorophenol	C ₆ H ₄ Cl ₂ O	59.5	87.6	101.0	115.5	131.6	141.8	154.6	175.5	197.7	220.0	

2-70 PHYSICAL AND CHEMICAL DATA

TABLE 2-10 Vapor Pressures of Organic Compounds, up to 1 atm (Continued)

Compound		Pressure, mmHg										Melting point, °C
		1	5	10	20	40	60	100	200	400	760	
Name	Formula	Temperature, °C										
α,α -Dichlorophenylacetone	$C_8H_5Cl_2N$	56.0	84.0	98.1	113.8	130.0	141.0	154.5	176.2	199.5	223.5	
Dichlorophenylarsine	$C_6H_5AsCl_2$	61.8	100.0	116.0	133.1	151.0	163.2	178.9	202.8	228.8	256.5	
1,2-Dichloropropane	$C_3H_6Cl_2$	-38.5	-17.0	-6.1	+6.0	19.4	28.0	39.4	57.0	76.0	96.8	
2,3-Dichlorostyrene	$C_8H_8Cl_2$	61.0	90.1	104.6	120.5	137.8	149.0	163.5	185.7	210.0	235.0	
2,4-Dichlorostyrene	$C_8H_8Cl_2$	53.5	82.2	97.4	111.8	129.2	140.0	153.8	176.0	200.0	225.0	
2,5-Dichlorostyrene	$C_8H_8Cl_2$	55.5	83.9	98.2	114.0	131.0	142.0	155.8	178.0	202.5	227.0	
2,6-Dichlorostyrene	$C_8H_8Cl_2$	47.8	75.7	90.0	105.5	122.4	133.3	147.6	169.0	193.5	217.0	
3,4-Dichlorostyrene	$C_8H_8Cl_2$	57.2	86.0	100.4	116.2	133.7	144.6	158.2	181.5	205.7	230.0	
3,5-Dichlorostyrene	$C_8H_8Cl_2$	53.5	82.2	97.4	111.8	129.2	140.0	153.8	176.0	200.0	225.0	
1,2-Dichlorotetraethylbenzene	$C_{14}H_{20}Cl_2$	105.6	138.7	155.0	172.5	192.2	204.8	220.7	245.6	272.8	302.0	
1,4-Dichlorotetraethylbenzene	$C_{14}H_{20}Cl_2$	91.7	126.1	143.8	162.0	183.2	195.8	212.0	238.5	265.8	296.5	
1,2-Dichloro-1,1,2,2-tetrafluoroethane	$C_2Cl_2F_4$	-95.4	-80.0	-72.3	-63.5	-53.7	-47.5	-39.1	-26.3	-12.0	+3.5	-94
Dichloro-4-tolylsilane	$C_9H_8Cl_2Si$	46.2	71.7	84.2	97.8	113.2	122.6	135.5	153.5	175.2	196.3	
3,4-Dichloro- α,α,α -trifluorotoluene	$C_7H_5Cl_2F_3$	11.0	38.3	52.2	67.3	84.0	95.0	109.2	129.0	150.5	172.8	-12.1
Dicyclopentadiene	$C_{10}H_8$	34.1	47.6	62.0	77.9	98.0	107.7	121.8	144.2	166.6	193.9	32.9
Diethoxydimethylsilane	$C_6H_{16}O_2Si$	-19.1	+2.4	13.3	25.3	38.0	46.3	57.6	74.2	93.2	113.5	
Diethoxydiphenylsilane	$C_{16}H_{20}O_2Si$	111.5	142.8	157.6	174.3	193.2	205.0	220.0	243.8	259.7	296.0	
Diethyl adipate	$C_{10}H_{18}O_4$	74.0	106.6	123.0	138.3	154.6	165.8	179.0	198.2	219.1	240.0	-21
Diethylamine	$C_4H_{11}N$			-33.0	-22.6	-11.3	-4.0	+6.0	21.0	38.0	55.5	-38.9
N-Diethylaniline	$C_{10}H_{15}N$	49.7	78.0	91.9	107.2	123.6	133.8	147.3	168.2	192.4	215.5	-34.4
Diethyl arsanilate	$C_{10}H_{16}AsNO_3$		35.0	62.6	74.8	88.0	102.6	111.8	123.8	141.9	161.0	181.0
1,2-Diethylbenzene	$C_{10}H_{14}$	22.3	48.7	62.0	76.4	92.5	102.6	116.2	136.7	159.0	183.5	-31.4
1,3-Diethylbenzene	$C_{10}H_{14}$	20.7	46.8	59.9	74.5	90.4	100.7	114.4	134.8	156.9	181.1	-83.9
1,4-Diethylbenzene	$C_{10}H_{14}$	20.7	47.1	60.3	74.7	91.1	101.3	115.3	136.1	159.0	183.8	-43.2
Diethyl carbonate	$C_8H_{10}O_3$	-10.1	+12.3	23.8	36.0	49.5	57.9	69.7	86.5	105.8	125.8	-43
cis-Diethyl citraconate	$C_9H_{14}O_4$	59.8	88.3	103.0	118.2	135.7	146.2	160.0	182.3	206.5	230.3	
Diethyl dioxosuccinate	$C_8H_{10}O_6$	70.0	98.0	112.0	126.8	143.8	153.7	167.7	188.0	210.8	233.5	
Diethylene glycol	$C_4H_{10}O_3$	91.8	120.0	133.8	148.0	164.3	174.0	187.5	207.0	226.5	244.8	
Diethylene glycol-bis-chloroacetate	$C_8H_{12}Cl_2O_5$	148.3	180.0	195.8	212.0	229.0	239.5	252.0	271.5	291.8	313.0	
Diethylene glycol dimethyl ether												
Di(2-methoxyethyl) ether	$C_6H_{14}O_3$	13.0	37.6	50.0	63.0	77.5	86.8	99.5	118.0	138.5	159.8	
glycol ethyl ether	$C_6H_{14}O_3$	45.3	72.0	85.8	100.3	116.7	126.8	140.3	159.0	180.3	201.9	
Diethyl ether	$C_4H_{10}O$	-74.3	-56.9	-48.1	-38.5	27.7	-21.8	-11.5	+2.2	17.9	34.6	-116.3
ethylmalonate	$C_9H_{16}O_4$	50.8	77.8	91.6	106.0	122.4	132.4	146.0	166.0	188.7	211.5	
fumarate	$C_8H_{12}O_4$	53.2	81.2	95.3	110.2	126.7	137.7	151.1	172.2	195.8	218.5	+0.6
glutarate	$C_8H_{16}O_4$	65.6	94.7	109.7	125.4	142.8	153.2	167.8	189.5	212.8	237.0	
Diethylhexadecylamine	$C_{20}H_{42}N$	139.8	175.8	194.0	213.5	235.0	248.5	265.5	292.8	324.6	355.0	
Diethyl itaconate	$C_9H_{14}O_4$	51.3	80.2	95.2	111.0	128.2	139.9	154.3	177.5	203.1	227.9	
ketone (3-pentanone)	$C_5H_{10}O$	-12.7	+7.5	17.2	27.9	39.4	46.7	56.2	70.6	86.3	102.7	-42
malate	$C_8H_{14}O_5$	80.7	110.4	125.3	141.2	157.8	169.0	183.9	205.3	229.5	253.4	
maleate	$C_8H_{12}O_4$	57.3	85.6	100.0	115.3	131.8	142.4	156.0	177.8	201.7	225.0	
malonate	$C_7H_{12}O_4$	40.0	67.5	81.3	95.9	113.3	123.0	136.2	155.5	176.8	198.9	-49.8
mesaconate	$C_9H_{14}O_4$	62.8	91.0	105.3	120.3	137.3	147.9	161.6	183.2	205.8	229.0	
oxalate	$C_8H_{10}O_4$	47.4	71.8	83.8	96.8	110.6	119.7	130.8	147.9	166.2	185.7	-40.6
phthalate	$C_{10}H_{14}O_4$	108.8	140.7	156.0	173.6	192.1	204.1	219.5	243.0	267.5	294.0	
sebacate	$C_{14}H_{26}O_4$	125.3	156.2	172.1	189.8	207.5	218.4	234.4	255.8	280.3	305.5	1.3
2,5-Diethylstyrene	$C_{12}H_{16}$	49.7	78.4	92.6	108.5	125.8	136.8	151.0	173.2	198.0	223.0	
Diethyl succinate	$C_8H_{14}O_4$	54.6	83.0	96.6	111.7	127.8	138.2	151.1	171.7	193.8	216.5	-20.8
isosuccinate	$C_8H_{14}O_4$	39.8	66.7	80.0	94.7	111.0	121.4	134.8	155.1	177.7	201.3	
sulfate	$C_4H_{10}O_4S$	47.0	74.0	87.7	102.1	118.0	128.6	142.5	162.5	185.5	209.5	-25.0
sulfide	C_3H_8OS	-39.6	-18.6	-8.0	+3.5	16.1	24.2	35.0	51.3	69.7	88.0	-99.5
sulfite	$C_3H_8O_2S$	10.0	34.2	46.4	59.7	74.2	83.8	96.3	115.8	137.0	159.0	
d-Diethyl tartrate	$C_8H_{14}O_6$	102.0	133.0	148.0	164.2	182.3	194.0	208.5	230.4	254.8	280.0	17
dl-Diethyl tartrate	$C_8H_{14}O_6$	100.0	131.7	147.2	163.8	181.7	193.2	208.0	230.0	254.3	280.0	
3,5-Diethyltoluene	$C_{11}H_{16}$	34.0	61.5	75.3	90.2	107.0	117.7	131.7	152.4	176.5	200.7	
Diethylzinc	$C_6H_{10}Zn$	-22.4	0.0	+11.7	24.2	38.0	47.2	59.1	77.0	97.3	118.0	-28
1-Dihydrocarvone	$C_{10}H_{16}O$	46.6	75.5	90.0	106.0	123.7	134.7	149.7	171.8	197.0	223.0	
Dihydrocitronellol	$C_{10}H_{18}O$	68.0	91.7	103.0	115.0	127.6	136.7	145.9	160.2	176.8	193.5	
1,4-Dihydroxanthraquinone	$C_{14}H_8O_4$	196.7	239.8	259.8	282.0	307.4	323.3	344.5	377.8	413.0	450.0	194
Dimethylacetylene (2-butyne)	C_4H_6	-73.0	-57.9	-50.5	-42.5	-33.9	-27.8	-18.8	-5.0	+10.6	27.2	-32.5
Dimethylamine	C_2H_7N	-87.7	-72.2	-64.6	-56.0	-46.7	-40.7	-32.6	-20.4	-7.1	+7.4	-96
N,N-Diethylaniline	$C_8H_{11}N$	29.5	56.3	70.0	84.8	101.6	111.9	125.8	146.5	169.2	193.1	+2.5
Dimethyl arsanilate	$C_8H_{12}AsNO_3$	15.0	39.6	51.8	65.0	79.7	88.6	101.0	119.8	140.3	160.5	
Di(α -methylbenzyl) ether	$C_{16}H_{18}O$	96.7	128.3	144.0	160.3	179.6	191.5	206.8	229.7	254.8	281.0	
2,2-Dimethylbutane	C_6H_{14}	-69.3	-50.7	-41.5	-31.1	-19.5	-12.1	-2.0	+13.4	31.0	49.7	-99.8
2,3-Dimethylbutane	C_6H_{14}	-63.6	-44.5	-34.9	-24.1	-12.4	-4.9	+5.4	21.1	39.0	58.0	-128.2
Dimethyl citraconate	$C_7H_{10}O_4$	50.8	78.2	91.8	106.5	122.6	132.7	145.8	165.8	188.0	210.5	
1,1-Dimethylcyclohexane	C_8H_{16}	-24.4	-1.4	+10.3	23.0	37.3	45.7	57.9	76.2	97.2	119.5	-34
cis-1,2-Dimethylcyclohexane	C_8H_{16}	-15.9	+7.3	18.4	31.1	45.3	54.4	66.8	85.6	107.0	129.7	-50.0
trans-1,2-Dimethylcyclohexane	C_8H_{16}	-21.1	+1.7	13.0	25.6	39.7	48.7	61.0	79.6	100.9	123.4	-88.0
trans-1,3-Dimethylcyclohexane	C_8H_{16}	-19.4	+3.4	14.9	27.4	41.4	50.4	62.5	81.0	102.1	124.4	-92.0
cis-1,3-Dimethylcyclohexane	C_8H_{16}	-22.7	0.0	+11.2	23.6	37.5	46.4	58.5	76.9	97.8	120.1	-76.2
cis-1,4-Dimethylcyclohexane	C_8H_{16}	-20.0	+3.2	14.5	27.1	41.1	50.1	62.3	80.8	101.9	124.3	-87.4
trans-1,4-Dimethylcyclohexane	C_8H_{16}	-24.3	-1.7	+10.1	22.6	36.5	45.4	57.6	76.0	97.0	119.3	-36.9

TABLE 2-10 Vapor Pressures of Organic Compounds, up to 1 atm (Continued)

Compound		Pressure, mmHg										Melting point, °C
		1	5	10	20	40	60	100	200	400	760	
Name	Formula	Temperature, °C										
Dimethyl ether	C ₂ H ₆ O	-115.7	-101.1	-93.3	-85.2	-76.2	-70.4	-62.7	-50.9	-37.8	-23.7	-138.5
2,2-Dimethylhexane	C ₈ H ₁₈	-29.7	-7.9	+3.1	15.0	28.2	36.7	48.2	65.7	85.6	106.8	
2,3-Dimethylhexane	C ₈ H ₁₈	-23.0	-1.1	+9.9	22.1	35.6	44.2	56.0	73.8	94.1	115.6	
2,4-Dimethylhexane	C ₈ H ₁₈	-26.9	-5.3	+5.2	17.2	30.5	39.0	50.6	68.1	88.2	109.4	
2,5-Dimethylhexane	C ₈ H ₁₈	-26.7	-5.5	+5.3	17.2	30.4	38.9	50.5	68.0	87.9	109.1	-90.7
3,3-Dimethylhexane	C ₈ H ₁₈	-25.8	-4.4	+6.1	18.2	31.7	40.4	52.5	70.0	90.4	112.0	
3,4-Dimethylhexane	C ₈ H ₁₈	-22.1	+0.2	11.3	23.5	37.1	45.8	57.7	75.6	96.0	117.7	
Dimethyl itaconate	C ₇ H ₁₀ O ₄	69.3	94.0	106.6	119.7	133.7	142.6	153.7	171.0	189.8	208.0	38
1-Dimethyl malate	C ₆ H ₁₀ O ₅	75.4	104.0	118.3	133.8	150.1	160.4	175.1	196.3	219.5	242.6	
Dimethyl maleate	C ₆ H ₈ O ₄	45.7	73.0	86.4	101.3	117.2	127.1	140.4	160.0	182.2	205.0	
malonate	C ₅ H ₈ O ₄	35.0	59.8	72.0	85.0	100.0	109.7	121.9	140.0	159.8	180.7	-62
<i>trans</i> -Dimethyl mesaconate	C ₇ H ₁₀ O ₄	46.8	74.0	87.8	102.1	118.0	127.8	141.5	161.0	183.5	206.0	
2,7-Dimethyloctane	C ₁₀ H ₂₂	+6.3	30.5	42.3	55.8	71.2	80.8	93.9	114.0	136.0	159.7	-52.8
Dimethyl oxalate	C ₄ H ₆ O ₄	20.0	44.0	56.0	69.4	83.6	92.8	104.8	123.3	143.3	163.3	
2,2-Dimethylpentane	C ₇ H ₁₆	-49.0	-28.7	-18.7	-7.5	+5.0	13.0	23.9	40.3	59.2	79.2	-123.7
2,3-Dimethylpentane	C ₇ H ₁₆	-42.0	-20.8	-10.3	+1.1	13.9	22.1	33.3	50.1	69.4	89.8	-135
2,4-Dimethylpentane	C ₇ H ₁₆	-48.0	-27.4	-17.1	-5.9	+6.5	14.5	25.4	41.8	60.6	80.5	-119.5
3,3-Dimethylpentane	C ₇ H ₁₆	-45.9	-25.0	-14.4	-2.9	+9.9	18.1	29.3	46.2	65.5	86.1	-135.0
2,3-Dimethylphenol (2,3-xyleneol)	C ₈ H ₁₀ O	56.0	83.8	97.6	112.0	129.2	139.5	152.2	173.0	196.0	218.0	75
2,4-Dimethylphenol (2,4-xyleneol)	C ₈ H ₁₀ O	51.8	78.0	91.3	105.0	121.5	131.0	143.0	161.5	184.2	211.5	25.5
2,5-Dimethylphenol (2,5-xyleneol)	C ₈ H ₁₀ O	51.8	78.0	91.3	105.0	121.5	131.0	143.0	161.5	184.2	211.5	74.5
3,4-Dimethylphenol (3,4-xyleneol)	C ₈ H ₁₀ O	66.2	93.8	107.7	122.0	138.0	148.0	161.0	181.5	203.6	225.2	62.5
3,5-Dimethylphenol (3,5-xyleneol)	C ₈ H ₁₀ O	62.0	89.2	102.4	117.0	133.3	143.5	156.0	176.2	197.8	219.5	68
Dimethylphenylsilane	C ₈ H ₁₂ Si	+5.3	30.3	42.6	56.2	71.4	81.3	94.2	114.2	136.4	159.3	
Dimethyl phthalate	C ₁₀ H ₁₀ O ₄	100.3	131.8	147.6	164.0	182.8	194.0	210.0	232.7	257.8	283.7	
3,5-Dimethyl-1,2-pyrone	C ₈ H ₆ O ₂	78.6	107.6	122.0	136.4	152.7	163.8	177.5	198.0	221.0	245.0	51.5
4,6-Dimethylresorcinol	C ₈ H ₁₀ O ₂	49.0	76.8	90.7	105.8	122.5	133.2	147.3	167.8	192.0	215.0	
Dimethyl sebacate	C ₁₂ H ₂₂ O ₄	104.0	139.8	156.2	175.8	196.0	208.0	222.6	245.0	269.6	293.5	38
2,4-Dimethylstyrene	C ₁₀ H ₁₂	34.2	61.9	75.8	90.8	107.7	118.0	132.3	153.2	177.5	202.0	
2,5-Dimethylstyrene	C ₁₀ H ₁₂	29.0	55.9	69.0	84.0	100.2	110.7	124.7	145.6	168.7	193.0	
α,α -Dimethylsuccinic anhydride	C ₆ H ₈ O ₃	61.4	88.1	102.0	116.3	132.3	142.4	155.3	175.8	197.5	219.5	
Dimethyl sulfide	C ₂ H ₆ S	-75.6	-58.0	-49.2	-39.4	-28.4	-21.4	-12.0	+2.6	18.7	36.0	-83.2
<i>d</i> -Dimethyl tartrate	C ₆ H ₁₀ O ₆	102.1	133.2	148.2	164.3	182.4	193.8	208.8	230.5	255.0	280.0	61.5
<i>dl</i> -Dimethyl tartrate	C ₆ H ₁₀ O ₆	100.4	131.8	147.5	164.0	182.4	193.8	209.5	232.3	257.4	282.0	89
<i>N,N</i> -Dimethyl-2-toluidine	C ₉ H ₁₃ N	28.8	54.1	66.2	80.2	95.0	105.2	118.1	138.3	161.5	184.8	-61
<i>N,N</i> -Dimethyl-4-toluidine	C ₉ H ₁₃ N	50.1	74.3	86.7	100.0	116.3	126.4	140.3	161.6	185.4	209.5	
Di(nitrosomethyl) amine	C ₂ H ₅ N ₂ O ₂	+3.2	27.8	40.0	53.7	68.2	77.7	90.3	110.0	131.3	153.0	
Diosphenol	C ₁₀ H ₁₆ O ₂	66.7	95.4	109.0	124.0	141.2	151.3	165.6	186.2	209.5	232.0	
1,4-Dioxane	C ₄ H ₈ O ₂	-35.8	-12.8	-1.2	+12.0	25.2	33.8	45.1	62.3	81.8	101.1	10
Dipentene	C ₁₀ H ₁₆	14.0	40.4	53.8	68.2	84.3	94.6	108.3	128.2	150.5	174.6	
Diphenylamine	C ₁₂ H ₁₁ N	108.3	141.7	157.0	175.2	194.3	206.9	222.8	247.5	274.1	302.0	52.9
Diphenyl carbinol (benzhydrol)	C ₁₃ H ₁₅ O	110.0	145.0	162.0	180.9	200.0	212.0	227.5	250.0	275.6	301.0	68.5
chlorophosphate	C ₁₂ H ₁₀ ClPO ₃	121.5	160.5	182.0	203.8	227.9	244.2	265.0	299.5	337.2	378.0	
disulfide	C ₁₂ H ₁₀ S ₂	131.6	164.0	180.0	197.0	214.8	226.2	241.3	262.6	285.8	310.0	61
1,2-Diphenylethane (dibenzyl)	C ₁₄ H ₁₄	86.8	119.8	136.0	153.7	173.7	186.0	202.8	227.8	255.0	284.0	51.5
Diphenyl ether	C ₁₂ H ₁₀ O	66.1	97.8	114.0	130.8	150.0	162.0	178.8	203.3	230.7	258.5	27
1,1-Diphenylethylene	C ₁₄ H ₁₂	87.4	119.6	135.0	151.8	170.8	183.4	198.6	222.8	249.8	277.0	
<i>trans</i> -Diphenylethylene	C ₁₄ H ₁₂	113.2	145.8	161.0	179.8	199.0	211.5	227.4	251.7	278.3	306.5	124
1,1-Diphenylhydrazine	C ₁₂ H ₁₂ N ₂	126.0	159.3	176.1	194.0	213.5	225.9	242.5	267.2	294.0	322.2	44
Diphenylmethane	C ₁₃ H ₁₂	76.0	107.4	122.8	139.8	157.8	170.2	186.3	210.7	237.5	264.5	26.5
Diphenyl sulfide	C ₁₂ H ₁₀ S	96.1	129.0	145.0	162.0	182.8	194.8	211.8	236.8	263.9	292.5	
Diphenyl-2-tolyl thiophosphate	C ₁₈ H ₁₇ O ₃ PS	159.7	179.8	201.6	215.5	230.6	240.4	252.5	270.3	290.0	310.0	
1,2-Dipropoxyethane	C ₆ H ₁₂ O ₂	-38.8	-10.3	+5.0	22.3	42.3	55.8	74.2	103.8	140.0	180.0	
1,2-Diisopropylbenzene	C ₁₂ H ₁₈	40.0	67.8	81.8	96.8	114.0	124.3	138.7	159.8	184.3	209.0	
1,3-Diisopropylbenzene	C ₁₂ H ₁₈	34.7	62.3	76.0	91.2	107.9	118.2	132.3	153.7	177.6	202.0	-105
Dipropylene glycol	C ₆ H ₁₄ O ₃	73.8	102.1	116.2	131.3	147.4	156.5	169.9	189.9	210.5	231.8	
Dipropylene glycol monobutyl ether	C ₁₀ H ₂₀ O ₃	64.7	92.0	106.0	120.4	136.3	146.3	159.8	180.0	203.8	227.0	
isopropyl ether	C ₆ H ₁₄ O	46.0	72.8	86.2	100.8	117.0	126.8	140.3	160.0	183.1	205.6	
Di- <i>n</i> -propyl ether	C ₆ H ₁₄ O	-43.3	-22.3	-11.8	0.0	+13.2	21.6	33.0	50.3	69.5	89.5	-122
Diisopropyl ether	C ₆ H ₁₄ O	-57.0	-37.4	-27.4	-16.7	-4.5	+3.4	13.7	30.0	48.2	67.5	-60
Di- <i>n</i> -propyl ketone (4-heptanone)	C ₇ H ₁₄ O	23.0	44.4	55.0	66.2	78.1	85.8	96.0	111.2	127.3	143.7	-32.6
Di- <i>n</i> -propyl oxalate	C ₈ H ₁₄ O ₄	53.4	80.2	93.9	108.6	124.6	134.8	148.1	168.0	190.3	213.5	
Diisopropyl oxalate	C ₈ H ₁₄ O ₄	43.2	69.0	81.9	95.6	110.5	120.0	132.6	151.2	171.8	193.5	
Di- <i>n</i> -propyl succinate	C ₁₀ H ₁₈ O ₄	77.5	107.6	122.2	138.0	154.8	166.0	180.3	202.5	226.5	250.8	
Di- <i>n</i> -propyl <i>d</i> -tartrate	C ₁₀ H ₁₈ O ₆	115.6	147.7	163.5	180.4	199.7	211.7	227.0	250.1	275.6	303.0	
Diisopropyl <i>d</i> -tartrate	C ₁₀ H ₁₈ O ₆	103.7	133.7	148.2	164.0	181.8	192.6	207.3	228.2	251.8	275.0	
Divinyl acetylene (1,5-hexadiene-3-yne)	C ₆ H ₆	-45.1	-24.4	-14.0	-2.8	+10.0	18.1	29.5	46.0	64.4	84.0	
1,3-Divinylbenzene	C ₁₀ H ₁₀	32.7	60.0	73.8	88.7	105.5	116.0	130.0	151.4	175.2	199.5	-66.9
Docosane	C ₂₂ H ₄₆	157.8	195.4	213.0	233.5	254.5	268.3	286.0	314.2	343.5	376.0	44.5
<i>n</i> -Dodecane	C ₁₂ H ₂₆	47.8	75.8	90.0	104.6	121.7	132.1	146.2	167.2	191.0	216.2	-9.6
1-Dodecene	C ₁₂ H ₂₄	47.2	74.0	87.8	102.4	118.6	128.5	142.3	162.2	185.5	208.0	-31.5
<i>n</i> -Dodecyl alcohol	C ₁₂ H ₂₆ O	91.0	120.2	134.7	150.0	167.2	177.8	192.0	213.0	235.7	259.0	24
Dodecylamine	C ₁₂ H ₂₇ N	82.8	111.8	127.8	141.6	157.4	168.0	182.1	203.0	225.0	248.0	
Dodecyltrimethylsilane	C ₁₅ H ₃₄ Si	91.2	122.1	137.7	153.8	172.1	184.2	199.5	222.0	248.0	273.0	
Elaidic acid	C ₁₈ H ₃₄ O ₂	171.3	206.7	223.5	242.3	260.8	273.0	288.0	312.4	337.0	362.0	51.5

2-72 PHYSICAL AND CHEMICAL DATA

TABLE 2-10 Vapor Pressures of Organic Compounds, up to 1 atm (Continued)

Compound		Pressure, mmHg										Melting point, °C
		1	5	10	20	40	60	100	200	400	760	
Name	Formula	Temperature, °C										
Epichlorohydrin	C ₃ H ₅ ClO	-16.5	+5.6	16.6	29.0	42.0	50.6	62.0	79.3	98.0	117.9	-25.6
1,2-Epoxy-2-methylpropane	C ₄ H ₈ O	-69.0	-50.0	-40.3	-29.5	-17.3	-9.7	+1.2	17.5	36.0	55.5	
Erucic acid	C ₂₂ H ₄₂ O ₂	206.7	239.7	254.5	270.6	289.1	300.2	314.4	336.5	358.8	381.5	33.5
Estragole (<i>p</i> -methoxy allyl benzene)	C ₁₀ H ₁₂ O	52.6	80.0	93.7	108.4	124.6	135.2	148.5	168.7	192.0	215.0	
Ethane	C ₂ H ₆	-159.5	-148.5	-142.9	-136.7	-129.8	-125.4	-119.3	-110.2	-99.7	-88.6	-183.2
Ethoxydimethylphenylsilane	C ₁₀ H ₁₆ O ₂ Si	36.3	63.1	76.2	91.0	107.2	127.5	131.4	151.5	175.0	199.5	
Ethoxytrimethylsilane	C ₉ H ₁₄ O ₂ Si	-50.9	-31.0	-20.7	-9.8	+3.7	11.5	22.1	38.1	56.3	75.7	
Ethoxytriphenylsilane	C ₂₀ H ₂₀ O ₂ Si	167.0	198.2	213.5	230.0	247.0	258.3	273.5	295.0	319.5	344.0	
Ethyl acetate	C ₄ H ₈ O ₂	-43.4	-23.5	-13.5	-3.0	+9.1	16.6	27.0	42.0	59.3	77.1	-82.4
acetoacetate	C ₆ H ₁₀ O ₃	28.5	54.0	67.3	81.1	96.2	106.0	118.5	138.0	158.2	180.8	-45
Ethylacetylene (1-butyne)	C ₄ H ₆	-92.5	-76.7	-68.7	-59.9	-50.0	-43.4	-34.9	-21.6	-6.9	+8.7	-130
Ethyl acrylate	C ₈ H ₈ O ₂	-29.5	-8.7	+2.0	13.0	26.0	33.5	44.5	61.5	80.0	99.5	-71.2
α-Ethylacrylic acid	C ₆ H ₈ O ₂	47.0	70.7	82.0	94.4	108.1	116.7	127.5	144.0	160.7	179.2	
α-Ethylacrylonitrile	C ₆ H ₇ N	-29.0	-6.4	+5.0	17.7	31.8	40.6	53.0	71.6	92.2	114.0	
Ethyl alcohol (ethanol)	C ₂ H ₆ O	-31.3	-12.0	-2.3	+8.0	19.0	26.0	34.9	48.4	63.5	78.4	-112
Ethylamine	C ₂ H ₇ N	-82.3	-66.4	-58.3	-48.6	-39.8	-33.4	-25.1	-12.3	+2.0	16.6	-80.6
4-Ethylaniline	C ₈ H ₁₁ N	52.0	80.0	93.8	109.0	125.7	136.0	149.8	170.6	194.2	217.4	-4
<i>N</i> -Ethylaniline	C ₈ H ₁₁ N	38.5	66.4	80.6	96.0	113.2	123.6	137.3	156.9	180.8	204.0	-63.5
2-Ethylanisole	C ₉ H ₁₂ O	29.7	55.9	69.0	83.1	98.8	109.0	122.3	142.1	164.2	187.1	
3-Ethylanisole	C ₉ H ₁₂ O	33.7	60.3	73.9	88.5	104.8	115.5	129.2	149.7	172.8	196.5	
4-Ethylanisole	C ₉ H ₁₂ O	33.5	60.2	73.9	88.5	104.7	115.4	128.4	149.2	172.3	196.5	
Ethylbenzene	C ₈ H ₁₀	-9.8	+13.9	25.9	38.6	52.8	61.8	74.1	92.7	113.8	136.2	-94.9
Ethyl benzoate	C ₉ H ₁₀ O ₂	44.0	72.0	86.0	101.4	118.2	129.0	143.2	164.8	188.4	213.4	-34.6
benzoylacetate	C ₁₁ H ₁₂ O ₃	107.6	136.4	150.3	166.8	181.8	191.9	205.0	223.8	244.7	265.0	
bromide	C ₈ H ₉ Br	-74.3	-56.4	-47.5	-37.8	-26.7	-19.5	-10.0	+4.5	21.0	38.4	-117.8
α-bromoisobutyrate	C ₈ H ₁₁ BrO ₂	10.6	35.8	48.0	61.8	77.0	86.7	99.8	119.7	141.2	163.6	
<i>n</i> -butyrate	C ₈ H ₁₂ O ₂	-18.4	+4.0	15.3	27.8	41.5	50.1	62.0	79.8	100.0	121.0	-93.3
isobutyrate	C ₈ H ₁₂ O ₂	-24.3	-2.4	+8.4	20.6	33.8	42.3	53.5	71.0	90.0	110.0	-88.2
Ethylcamphoronic anhydride	C ₁₁ H ₁₆ O ₅	118.2	149.8	165.0	181.8	199.8	211.5	226.6	248.5	272.8	298.0	
Ethyl isocaproate	C ₈ H ₁₆ O ₂	11.0	35.8	48.0	61.7	76.3	85.8	98.4	117.8	139.2	160.4	
carbamate	C ₉ H ₇ NO ₂	65.8	77.8	91.0	105.6	114.8	126.2	144.2	164.0	184.0	207.0	49
carbanilate	C ₉ H ₁₁ NO ₂	107.8	131.8	143.7	155.5	168.8	177.3	187.9	203.8	220.0	237.0	52.5
Ethylcetylamine	C ₁₈ H ₃₉ N	133.2	168.2	186.0	205.5	226.5	239.8	256.8	283.3	313.0	342.0	
Ethyl chloride	C ₂ H ₅ Cl	-89.8	-73.9	-65.8	-56.8	-47.0	-40.6	-32.0	-18.6	-3.9	+12.3	-139
chloroacetate	C ₃ H ₇ ClO ₂	+1.0	25.4	37.5	50.4	65.2	74.0	86.0	103.8	123.8	144.2	-26
chloroglyoxylate	C ₃ H ₅ ClO ₃	-5.1	+18.0	29.9	42.0	56.0	65.2	76.6	94.5	114.7	135.0	
α-chloropropionate	C ₃ H ₅ ClO ₂	+6.6	30.2	41.9	54.3	68.2	77.3	89.3	107.2	126.2	146.5	
<i>trans</i> -cinnamate	C ₁₁ H ₁₂ O ₂	87.6	108.5	134.0	150.3	169.2	181.2	196.0	219.3	245.0	271.0	12
3-Ethylcumene	C ₁₁ H ₁₆	28.3	55.5	68.8	83.6	99.9	110.2	124.3	145.4	168.2	193.0	
4-Ethylcumene	C ₁₁ H ₁₆	31.5	58.4	72.0	86.7	103.3	113.8	127.2	148.3	171.8	195.8	
Ethyl cyanoacetate	C ₅ H ₇ NO ₂	67.8	93.5	106.0	119.8	133.8	142.1	152.8	169.8	187.8	206.0	
Ethylcyclohexane	C ₈ H ₁₆	-14.5	+9.2	20.6	33.4	47.6	56.7	69.0	87.8	109.1	131.8	-111.3
Ethylcyclopentane	C ₇ H ₁₄	-32.2	-10.8	-0.1	+11.7	25.0	33.4	45.0	62.4	82.3	103.4	-138.6
Ethyl dichloroacetate	C ₄ H ₆ Cl ₂ O ₂	9.6	34.0	46.3	59.5	74.0	83.6	96.1	115.2	135.9	156.5	
<i>N,N</i> -diethylloxamate	C ₆ H ₁₅ NO ₃	76.0	106.3	121.7	137.7	154.4	166.0	180.3	202.8	226.5	252.0	
<i>N</i> -Ethylidiphenylamine	C ₁₄ H ₁₅ N	98.3	130.2	146.0	162.8	182.0	193.7	209.8	233.0	258.8	286.0	
Ethylene	C ₂ H ₄	-168.3	-158.3	-153.2	-147.6	-141.3	-137.3	-131.8	-123.4	-113.9	-103.7	-169
Ethylene-bis-(chloroacetate)	C ₆ H ₈ Cl ₂ O ₄	112.0	142.4	158.0	173.5	191.0	201.8	215.0	237.3	259.5	283.5	
Ethylene chlorohydrin (2-chloroethanol)	C ₂ H ₄ ClO	-4.0	+19.0	30.3	42.5	56.0	64.1	75.0	91.8	110.0	128.8	-69
diamine (1,2-ethanediamine)	C ₂ H ₆ N ₂	-11.0	+10.5	21.5	33.0	45.8	53.8	62.5	81.0	99.0	117.2	8.5
dibromide (1,2-dibromethane)	C ₂ H ₄ Br ₂	-27.0	+4.7	18.6	32.7	48.0	57.9	70.4	89.8	110.1	131.5	10
dichloride (1,2-dichloroethane)	C ₂ H ₄ Cl ₂	-44.5	-24.0	-13.6	-2.4	+10.0	18.1	29.4	45.7	64.0	82.4	-35.3
glycol (1,2-ethanediol)	C ₂ H ₆ O ₂	53.0	79.7	92.1	105.8	120.0	129.5	141.8	158.5	178.5	197.3	-15.6
glycol diethyl ether	C ₆ H ₁₄ O ₂	-33.5	-10.2	+1.6	14.7	29.7	39.0	51.8	71.8	94.1	119.5	
(1,2-diethoxyethane)												
glycol dimethyl ether	C ₄ H ₁₀ O ₂	-48.0	-26.2	-15.3	-3.0	+10.7	19.7	31.8	50.0	70.8	93.0	
(1,2-dimethoxyethane)												
glycol monomethyl ether	C ₃ H ₈ O ₂	-13.5	+10.2	22.0	34.3	47.8	56.4	68.0	85.3	104.3	124.4	
(2-methoxyethanol)												
oxide	C ₂ H ₄ O	-89.7	-73.8	-65.7	-56.6	-46.9	-40.7	-32.1	-19.5	-4.9	+10.7	-111.3
Ethyl α-ethylacetoacetate	C ₈ H ₁₄ O ₃	40.5	67.3	80.2	94.6	110.3	120.6	133.8	153.2	175.6	198.0	
fluoride	C ₂ H ₅ F	-117.0	-103.8	-97.7	-90.0	-81.8	-76.4	-69.3	-58.0	-45.5	-32.0	
formate	C ₃ H ₆ O ₂	-60.5	-42.2	-33.0	-22.7	-11.5	-4.3	-5.4	20.0	37.1	54.3	-79
2-furoate	C ₇ H ₈ O ₃	37.6	63.8	77.1	91.5	107.5	117.5	130.4	150.1	172.5	195.0	34
glycolate	C ₃ H ₆ O ₃	14.3	38.8	50.5	63.9	78.1	87.6	99.8	117.8	138.0	158.2	
3-Ethylhexane	C ₈ H ₁₈	-20.0	+2.1	12.8	25.0	38.5	47.1	58.9	76.7	97.0	118.5	
2-Ethylhexyl acrylate	C ₁₁ H ₂₀ O ₂	50.0	77.7	91.8	106.3	123.7	134.0	147.9	168.2	192.2	216.0	
Ethylidene chloride (1,1-dichloroethane)	C ₂ H ₂ Cl ₂	-60.7	-41.9	-32.3	-21.9	-10.2	-2.9	+7.2	22.4	39.8	57.4	-96.7
fluoride (1,1-difluoroethane)	C ₂ H ₂ F ₂	-112.5	-98.4	-91.7	-84.1	-75.8	-70.4	-63.2	-52.0	-39.5	-26.5	-117
Ethyl iodide	C ₂ H ₅ I	-54.4	-34.3	-24.3	-13.1	-0.9	+7.2	18.0	34.1	52.3	72.4	-105
Ethyl <i>l</i> -leucinate	C ₈ H ₁₇ NO ₂	27.8	57.3	72.1	88.0	106.0	117.8	131.8	149.8	167.3	184.0	
Ethyl levulinate	C ₇ H ₁₂ O ₃	47.3	74.0	87.3	101.8	117.7	127.6	141.3	160.2	183.0	206.2	
Ethyl mercaptan (ethanethiol)	C ₂ H ₆ S	-76.7	-59.1	-50.2	-40.7	-29.8	-22.4	-13.0	+1.5	17.7	35.0	-121
Ethyl methylcarbamate	C ₄ H ₉ NO ₂	26.5	51.0	63.2	76.1	91.0	100.0	112.0	130.0	149.8	170.0	
Ethyl methyl ether	C ₃ H ₈ O	-91.0	-75.6	-67.8	-59.1	-49.4	-43.3	-34.8	-22.0	-7.8	+7.5	

TABLE 2-10 Vapor Pressures of Organic Compounds, up to 1 atm (Continued)

Compound		Pressure, mmHg										Melting point, °C
		1	5	10	20	40	60	100	200	400	760	
Name	Formula	Temperature, °C										
1-Ethynaphthalene	C ₁₂ H ₁₂	70.0	101.4	116.8	133.8	152.0	164.1	180.0	204.6	230.8	258.1	-27
Ethyl α-naphthyl ketone (1-propionaphthone)	C ₁₃ H ₁₂ O	124.0	155.5	171.0	188.1	206.9	218.2	233.5	255.5	280.2	306.0	
Ethyl 3-nitrobenzoate	C ₉ H ₉ N ₂ O ₄	108.1	140.2	155.0	173.6	192.6	205.0	220.3	244.6	270.6	298.0	47
3-Ethylpentane	C ₇ H ₁₆	-37.8	-17.0	-6.8	+4.7	17.5	25.7	36.9	53.8	73.0	93.5	-118.6
4-Ethylphenetole	C ₁₀ H ₁₄ O	48.5	75.7	89.5	103.8	119.8	129.8	143.5	163.2	185.7	208.0	
2-Ethylphenol	C ₈ H ₁₀ O	46.2	73.4	87.0	101.5	117.9	127.9	141.8	161.6	184.5	207.5	-45
3-Ethylphenol	C ₈ H ₁₀ O	60.0	86.8	100.2	114.5	130.0	139.8	152.0	171.8	193.3	214.0	-4
4-Ethylphenol	C ₈ H ₁₀ O	59.3	86.5	100.2	115.0	131.3	141.7	154.2	175.0	197.4	219.0	46.5
Ethyl phenyl ether (phenetole)	C ₉ H ₁₀ O	18.1	43.7	56.4	70.3	86.6	95.4	108.4	127.9	149.8	172.0	-30.2
Ethyl propionate	C ₅ H ₁₀ O ₂	-28.0	-7.2	+3.4	14.3	27.2	35.1	45.2	61.7	79.8	99.1	-72.6
Ethyl propyl ether	C ₅ H ₁₂ O	-64.3	-45.0	-35.0	-24.0	-12.0	-4.0	+6.8	23.3	41.6	61.7	
Ethyl salicylate	C ₉ H ₁₀ O ₃	61.2	90.0	104.2	119.3	136.7	147.6	161.5	183.7	207.0	231.5	1.3
3-Ethylstyrene	C ₁₀ H ₁₂	28.3	55.0	68.3	82.8	99.2	109.6	123.2	144.0	167.2	191.5	
4-Ethylstyrene	C ₁₀ H ₁₂	26.0	52.7	66.3	80.8	97.3	107.6	121.5	142.0	165.0	189.0	
Ethylisothiocyanate	C ₅ H ₅ NS	-13.2	+10.6	22.8	36.1	50.8	59.8	71.9	90.0	110.1	131.0	-5.9
2-Ethyltoluene	C ₉ H ₁₂	9.4	34.8	47.6	61.2	76.4	86.0	99.0	119.0	141.4	165.1	
3-Ethyltoluene	C ₉ H ₁₂	7.2	32.3	44.7	58.2	73.3	82.9	95.9	115.5	137.8	161.3	-95.5
4-Ethyltoluene	C ₉ H ₁₂	7.6	32.7	44.9	58.5	73.6	83.2	96.3	116.1	136.4	162.0	
Ethyl trichloroacetate	C ₇ H ₅ Cl ₃ O ₂	20.7	45.5	57.7	70.6	85.5	94.4	107.4	125.8	146.0	167.0	
Ethyltrimethylsilane	C ₅ H ₁₄ Si	-60.6	-41.4	-31.8	-21.0	-9.0	-1.2	+9.2	25.0	42.8	62.0	
Ethyltrimethyltin	C ₅ H ₁₄ Sn	-30.0	-7.6	+3.8	16.1	30.0	38.4	50.0	67.3	87.6	108.8	
Ethyl isovalerate	C ₈ H ₁₄ O ₂	-6.1	+17.0	28.7	41.3	55.2	64.0	75.9	93.8	114.0	134.3	-99.3
2-Ethyl-1,4-xylene	C ₁₀ H ₁₄	25.7	52.0	65.6	79.8	96.0	106.2	120.0	140.2	163.1	186.9	
4-Ethyl-1,3-xylene	C ₁₀ H ₁₄	26.3	53.0	66.4	80.6	97.2	107.4	121.2	141.8	164.4	188.4	
5-Ethyl-1,3-xylene	C ₁₀ H ₁₄	22.1	48.8	62.1	76.5	92.6	103.0	116.5	137.4	159.6	183.7	
Eugenol	C ₁₀ H ₁₂ O ₂	78.4	108.1	123.0	138.7	155.8	167.3	182.2	204.7	228.3	253.5	
iso-Eugenol	C ₁₀ H ₁₂ O ₂	86.3	117.0	132.4	149.0	167.0	178.2	194.0	217.2	242.3	267.5	-10
Eugenyl acetate	C ₁₂ H ₁₄ O ₃	101.6	132.3	148.0	164.2	183.0	194.0	209.7	232.5	257.4	282.0	295
Fencholic acid	C ₁₀ H ₁₆ O ₂	101.7	128.7	142.3	155.8	171.8	181.5	194.0	215.0	237.8	264.1	19
d-Fenchone	C ₁₀ H ₁₆ O	28.0	54.7	68.3	83.0	99.5	109.8	123.6	144.0	166.8	191.0	5
dl-Fenchyl alcohol	C ₁₀ H ₁₈ O	45.8	70.3	82.1	95.6	110.8	120.2	132.3	150.0	173.2	201.0	35
Fluorene	C ₁₃ H ₁₀	129.3	146.0	164.2	185.2	197.8	214.7	240.3	268.6	295.0	313	
Fluorobenzene	C ₆ H ₅ F	-43.4	-22.8	-12.4	-1.2	+11.5	19.6	30.4	47.2	65.7	84.7	-42.1
2-Fluorotoluene	C ₇ H ₇ F	-24.2	-2.2	+8.9	21.4	34.7	43.7	55.3	73.0	92.8	114.0	-80
3-Fluorotoluene	C ₇ H ₇ F	-22.4	-0.3	+11.0	23.4	37.0	45.8	57.5	75.4	95.4	116.0	-110.8
4-Fluorotoluene	C ₇ H ₇ F	-21.8	+0.3	11.8	24.0	37.8	46.5	58.1	76.0	96.1	117.0	
Formaldehyde	CH ₂ O			-88.0	-79.6	-70.6	-65.0	-57.3	-46.0	-33.0	-19.5	-92
Formamide	CH ₃ NO	70.5	96.3	109.5	122.5	137.5	147.0	157.5	175.5	193.5	210.5	
Formic acid	CH ₂ O ₂	-20.0	-5.0	+2.1	10.3	24.0	32.4	43.8	61.4	80.3	100.6	8.2
trans-Fumaryl chloride	C ₄ H ₂ Cl ₂ O ₂	+15.0	38.5	51.8	65.0	79.5	89.0	101.0	120.0	140.0	160.0	
Furfural (2-furaldehyde)	C ₅ H ₄ O ₂	18.5	42.6	54.8	67.8	82.1	91.5	103.4	121.8	141.8	161.8	
Furfuryl alcohol	C ₅ H ₆ O ₂	31.8	56.0	68.0	81.0	95.7	104.0	115.9	133.1	151.8	170.0	
Geraniol	C ₁₀ H ₁₈ O	69.2	96.8	110.0	125.6	141.8	151.5	165.3	185.6	207.8	230.0	
Geranyl acetate	C ₁₂ H ₂₀ O ₂	73.5	102.7	117.9	133.0	150.0	160.3	175.2	196.3	219.8	243.3	
Geranyl n-butylate	C ₁₄ H ₂₆ O ₂	96.8	125.2	139.0	153.8	170.1	180.2	193.8	214.0	235.0	257.4	
Geranyl isobutylate	C ₁₄ H ₂₆ O ₂	90.9	119.6	133.0	147.9	164.0	174.0	187.7	207.6	228.5	251.0	
Geranyl formate	C ₁₁ H ₁₈ O ₂	61.8	90.3	103.0	119.8	136.2	147.2	160.7	182.6	205.8	230.0	
Glutaric acid	C ₅ H ₈ O ₄	155.5	183.8	196.0	210.5	226.3	235.5	247.0	265.0	283.5	303.0	97.5
Glutaric anhydride	C ₅ H ₆ O ₃	100.8	133.3	149.5	166.0	185.5	196.2	212.5	236.5	261.0	287.0	
Glutaronitrile	C ₅ H ₆ N ₂	91.3	123.7	140.0	156.5	176.4	189.5	205.5	230.0	257.3	286.2	
Glutaryl chloride	C ₅ H ₆ Cl ₂ O ₂	56.1	84.0	97.8	112.3	128.3	139.1	151.8	172.4	195.3	217.0	
Glycerol	C ₃ H ₈ O ₃	125.5	153.8	167.2	182.2	198.0	208.0	220.1	240.0	263.0	290.0	17.9
Glycerol dichlorohydrin (1,3-dichloro-2-propanol)	C ₃ H ₆ Cl ₂ O	28.0	52.2	64.7	78.0	93.0	102.0	114.8	133.3	153.5	174.3	
Glycol diacetate	C ₆ H ₁₀ O ₄	38.3	64.1	77.1	90.8	106.1	115.8	128.0	147.8	168.3	190.5	-31
Glycolide (1,4-dioxane-2,6-dione)	C ₄ H ₆ O ₄	103.0	116.6	132.0	148.6	158.2	173.2	194.0	217.0	240.0	260.0	97
Guaicol (2-methoxyphenol)	C ₇ H ₈ O ₂	52.4	79.1	92.0	106.0	121.6	131.0	144.0	162.7	181.4	205.0	28.3
Heneicosane	C ₂₁ H ₄₄	152.6	188.0	205.4	223.2	243.4	255.3	272.0	296.5	323.8	350.5	40.4
Heptacosane	C ₂₇ H ₅₆	211.7	248.6	266.8	284.6	305.7	318.3	333.5	359.4	385.0	410.6	59.5
Heptadecane	C ₁₇ H ₃₆	115.0	145.2	160.0	177.7	195.8	207.3	223.0	247.8	274.5	303.0	22.5
Heptaldehyde (enanthaldehyde)	C ₇ H ₁₄ O	12.0	32.7	43.0	54.0	66.3	74.0	84.0	102.0	125.5	155.0	-42
n-Heptane	C ₇ H ₁₆	-34.0	-12.7	-2.1	+9.5	22.3	30.6	41.8	58.7	78.0	98.4	-90.6
Heptanoic acid (enanthic acid)	C ₇ H ₁₄ O ₂	78.0	101.3	113.2	125.6	139.5	148.5	160.0	179.5	199.6	221.5	-10
1-Heptanol	C ₇ H ₁₆ O	42.4	64.3	74.7	85.8	99.8	108.0	119.5	136.6	155.6	175.8	34.6
Heptanoyl chloride (enanthyl chloride)	C ₇ H ₁₃ ClO	34.2	54.6	64.6	75.0	86.4	93.5	102.7	116.3	130.7	145.0	
2-Heptene	C ₇ H ₁₄	-35.8	-14.1	-3.5	+8.3	21.5	30.0	41.3	58.6	78.1	98.5	
Heptylbenzene	C ₁₃ H ₂₀	64.0	94.6	110.0	126.0	144.0	154.8	170.2	193.3	217.8	244.0	
Heptyl cyanide (enanthonitrile)	C ₇ H ₁₃ N	21.0	47.8	61.6	76.3	92.6	103.0	116.8	137.7	160.0	184.6	
Hexachlorobenzene	C ₆ Cl ₆	114.4	149.3	166.4	185.7	206.0	219.0	235.5	258.5	283.5	309.4	230
Hexachloroethane	C ₂ Cl ₆	32.7	49.8	73.5	87.6	102.3	112.0	124.2	143.1	163.8	185.6	186.6
Hexacosane	C ₂₆ H ₅₄	204.0	240.0	257.4	275.8	295.2	307.8	323.2	348.4	374.6	399.8	56.6
Hexadecane	C ₁₆ H ₃₄	105.3	135.2	149.8	164.7	181.3	193.2	208.5	231.7	258.3	287.5	18.5
1-Hexadecene	C ₁₆ H ₃₂	101.6	131.7	146.2	162.0	178.8	190.8	205.3	226.8	250.0	274.0	4
n-Hexadecyl alcohol (cetyl alcohol)	C ₁₆ H ₃₄ O	122.7	158.3	177.8	197.8	219.8	234.3	251.7	280.2	312.7	344.0	49.3

2-74 PHYSICAL AND CHEMICAL DATA

TABLE 2-10 Vapor Pressures of Organic Compounds, up to 1 atm (Continued)

Compound		Pressure, mmHg										Melting point, °C
		1	5	10	20	40	60	100	200	400	760	
Name	Formula	Temperature, °C										
<i>n</i> -Hexadecylamine (cetylamine)	C ₁₆ H ₃₅ N	123.6	157.8	176.0	195.7	215.7	228.8	245.8	272.2	300.4	330.0	
Hexaethylbenzene	C ₁₈ H ₃₀		134.3	150.3	168.0	187.7	199.7	216.0	241.7	268.5	298.3	130
<i>n</i> -Hexane	C ₆ H ₁₄	-53.9	-34.5	-25.0	-14.1	-2.3	+5.4	15.8	31.6	49.6	68.7	-95.3
1-Hexanol	C ₆ H ₁₃ O	24.4	47.2	58.2	70.3	83.7	92.0	102.8	119.6	138.0	157.0	-51.6
2-Hexanol	C ₆ H ₁₃ O	14.6	34.8	45.0	55.9	67.9	76.0	87.3	103.7	121.8	139.9	
3-Hexanol	C ₆ H ₁₃ O	+2.5	25.7	36.7	49.0	62.2	70.7	81.8	98.3	117.0	135.5	
1-Hexene	C ₆ H ₁₂	-57.5	-38.0	-28.1	-17.2	-5.0	+2.8	13.0	29.0	46.8	66.0	-98.5
<i>n</i> -Hexyl levulinate	C ₁₁ H ₂₀ O ₃	90.0	120.0	134.7	150.2	167.8	179.0	193.6	215.7	241.0	266.8	
<i>n</i> -Hexyl phenyl ketone (enantiofenone)	C ₁₃ H ₁₈ O	100.0	130.3	145.5	161.0	178.9	189.8	204.2	225.0	248.3	271.3	
Hydrocinnamic acid	C ₉ H ₁₀ O ₂	102.2	133.5	148.7	165.0	183.3	194.0	209.0	230.8	255.0	279.8	48.5
Hydrogen cyanide (hydrocyanic acid)	CHN	-71.0	-55.3	-47.7	-39.7	-30.9	-25.1	-17.8	-5.3	+10.2	25.9	-13.2
Hydroquinone	C ₆ H ₆ O ₂	132.4	153.3	163.5	174.6	192.0	203.0	216.5	238.0	262.5	286.2	170.3
4-Hydroxybenzaldehyde	C ₇ H ₆ O ₂	121.2	153.2	169.7	186.8	206.0	217.5	233.5	256.8	282.6	310.0	115.5
α -Hydroxyisobutyric acid	C ₄ H ₆ O ₃	73.5	98.5	110.5	123.8	138.0	146.4	157.7	175.2	193.8	212.0	79
α -Hydroxybutyronitrile	C ₅ H ₉ NO	41.0	65.8	77.8	90.7	104.8	113.9	125.0	142.0	159.8	178.8	
4-Hydroxy-3-methyl-2-butanone	C ₅ H ₁₀ O ₂	44.6	69.3	81.0	94.0	108.2	117.4	129.0	146.5	165.5	185.0	
4-Hydroxy-4-methyl-2-pentanone	C ₆ H ₁₂ O ₂	22.0	46.7	58.8	72.0	86.7	96.0	108.2	126.8	147.5	167.9	-47
3-Hydroxypropionitrile	C ₃ H ₅ NO	58.7	87.8	102.0	117.9	134.1	144.7	157.7	178.0	200.0	221.0	
Indene	C ₉ H ₈	16.4	44.3	58.5	73.9	90.7	100.8	114.7	135.6	157.8	181.6	-2
Iodobenzene	C ₆ H ₅ I	24.1	50.6	64.0	78.3	94.4	105.0	118.3	139.8	163.9	188.6	-28.5
Iodononane	C ₉ H ₁₉ I	70.0	96.2	109.0	123.0	138.1	147.7	159.8	179.0	199.3	219.5	
2-Iodotoluene	C ₇ H ₇ I	37.2	65.9	79.8	95.6	112.4	123.8	138.1	160.0	185.7	211.0	
α -Ionone	C ₁₃ H ₂₀ O	79.5	108.8	123.0	139.0	155.6	166.3	181.2	202.5	225.2	250.0	
Isoprene	C ₅ H ₈	-79.8	-62.3	-53.3	-43.5	-32.6	-25.4	-16.0	-1.2	+15.4	32.6	-146.7
Lauraldehyde	C ₁₂ H ₂₂ O	77.7	108.4	123.7	140.2	157.8	168.7	184.5	207.8	231.8	257.0	44.5
Lauric acid	C ₁₂ H ₂₄ O ₂	121.0	150.6	166.0	183.6	201.4	212.7	227.5	249.8	273.8	299.2	48
Levulinialdehyde	C ₅ H ₈ O ₂	28.1	54.9	68.0	82.7	98.3	108.4	121.8	142.0	164.0	187.0	
Levulinic acid	C ₅ H ₈ O ₃	102.0	128.1	141.8	154.1	169.5	178.0	190.2	208.3	227.4	245.8	33.5
<i>d</i> -Limonene	C ₁₀ H ₁₆	14.0	40.4	53.8	68.2	84.3	94.6	108.3	128.5	151.4	175.0	-96.9
Linalyl acetate	C ₁₂ H ₂₀ O ₂	55.4	82.5	96.0	111.4	127.7	138.1	151.8	173.3	196.2	220.0	
Maleic anhydride	C ₄ H ₂ O ₃	44.0	63.4	78.7	95.0	111.8	122.0	135.8	155.9	179.5	202.0	58
Menthane	C ₁₀ H ₂₀	+9.7	35.7	48.3	62.7	78.3	88.6	102.1	122.7	146.0	169.5	
1-Menthol	C ₁₀ H ₂₀ O	56.0	83.2	96.0	110.3	126.1	136.1	149.4	168.3	190.2	212.0	42.5
Menthyl acetate	C ₁₂ H ₂₂ O ₂	57.4	85.8	100.0	115.4	132.1	143.2	156.7	178.8	202.8	227.0	
benzoate	C ₁₇ H ₂₂ O ₂	123.2	154.2	170.0	186.3	204.3	215.8	230.4	253.2	277.1	301.0	54.5
formate	C ₁₁ H ₂₀ O ₂	47.3	75.8	90.0	105.8	123.0	133.8	148.0	169.8	194.2	219.0	
Mesityl oxide	C ₈ H ₁₀ O	-8.7	+14.1	26.0	37.9	51.7	60.4	72.1	90.0	109.8	130.0	-59
Methacrylic acid	C ₄ H ₆ O ₂	25.5	48.5	60.0	72.7	86.4	95.3	106.6	123.9	142.5	161.0	15
Methacrylonitrile	C ₄ H ₅ N	-44.5	-23.3	-12.5	-0.6	+12.8	21.5	32.8	50.0	70.3	90.3	
Methane	CH ₄	-205.9	-199.0	-195.5	-191.8	-187.7	-185.1	-181.4	-175.5	-168.8	-161.5	-182.5
Methanethiol	CH ₃ S	-90.7	-75.3	-67.5	-58.8	-49.2	-43.1	-34.8	-22.1	-7.9	+6.8	-121
Methoxyacetic acid	C ₃ H ₆ O ₃	52.5	79.3	92.0	106.5	122.0	131.8	144.5	163.5	184.2	204.0	
<i>N</i> -Methylacetanilide	C ₉ H ₁₁ NO		103.8	118.6	135.1	152.2	164.2	179.8	202.3	227.4	253.0	102
Methyl acetate	C ₃ H ₆ O ₂	-57.2	-38.6	-29.3	-19.1	-7.9	-0.5	+9.4	24.0	40.0	57.8	-98.7
acetylene (propyne)	C ₃ H ₄	-111.0	-97.5	-90.5	-82.9	-74.3	-68.8	-61.3	-49.8	-37.2	-23.3	-102.7
acrylate	C ₄ H ₆ O ₂	-43.7	-23.6	-13.5	-2.7	+9.2	17.3	28.0	43.9	61.8	80.2	
alcohol (methanol)	CH ₃ O	-44.0	-25.3	-16.2	-6.0	+5.0	12.1	21.2	34.8	49.9	64.7	-97.8
Methylamine	CH ₃ N	-95.8	-81.3	-73.8	-65.9	-56.9	-51.3	-43.7	-32.4	-19.7	-6.3	-93.5
<i>N</i> -Methylaniline	C ₈ H ₉ N	36.0	62.8	76.2	90.5	106.0	115.8	129.8	149.3	172.0	195.5	-57
Methyl anthranilate	C ₈ H ₉ NO ₂	77.6	109.0	124.2	141.5	159.7	172.0	187.8	212.4	238.5	266.5	24
benzoate	C ₈ H ₈ O ₂	39.0	64.4	77.3	91.8	107.8	117.4	130.8	151.4	174.7	199.5	-12.5
2-Methylbenzothiazole	C ₈ H ₇ NS	70.0	97.5	111.2	125.5	141.2	150.4	163.9	183.2	204.5	225.5	15.4
α -Methylbenzyl alcohol	C ₈ H ₁₀ O	49.0	75.2	88.0	102.1	117.8	127.4	140.3	159.0	180.7	204.0	
Methyl bromide	CH ₃ Br	-96.3	-80.6	-72.8	-64.0	-54.2	-48.0	-39.4	-26.5	-11.9	+3.6	-93
2-Methyl-1-butene	C ₅ H ₁₀	-89.1	-72.8	-64.3	-54.8	-44.1	-37.3	-28.0	-13.8	+2.5	20.2	-135
2-Methyl-2-butene	C ₅ H ₁₀	-75.4	-57.0	-47.9	-37.9	-26.7	-19.4	-9.9	+4.9	21.6	38.5	-133
Methyl isobutyl carbinol (2-methyl-4-pentanol)	C ₆ H ₁₄ O	-0.3	+22.1	33.3	45.4	58.2	67.0	78.0	94.9	113.5	131.7	
<i>n</i> -butyl ketone (2-hexanone)	C ₆ H ₁₂ O	+7.7	28.8	38.8	50.0	62.0	69.8	79.8	94.3	111.0	127.5	-56.9
isobutyl ketone (4-methyl-2-pentanone)	C ₆ H ₁₂ O	-1.4	+19.7	30.0	40.8	52.8	60.4	70.4	85.6	102.0	119.0	-84.7
<i>n</i> -butyrate	C ₄ H ₁₀ O ₂	-26.8	-5.5	+5.0	16.7	29.6	37.4	48.0	64.3	83.1	102.3	
isobutyrate	C ₄ H ₁₀ O ₂	-34.1	-13.0	-2.9	+8.4	21.0	28.9	39.6	55.7	73.6	92.6	-84.7
caprate	C ₁₁ H ₂₂ O ₂	63.7	93.5	108.0	123.0	139.0	148.6	161.5	181.6	202.9	224.0	-18
caproate	C ₆ H ₁₂ O ₂	+5.0	30.0	42.0	55.4	70.0	79.7	91.4	109.8	129.8	150.0	
caprylate	C ₈ H ₁₆ O ₂	34.2	61.7	74.9	89.0	105.3	115.3	128.0	148.1	170.0	193.0	-40
chloride	CH ₃ Cl	-99.5	-92.4	-84.8	-76.0	-66.0	-56.0	-46.0	-36.0	-26.0	-16.0	-97.7
chloroacetate	C ₃ H ₅ ClO ₂	-2.9	19.0	30.0	41.5	54.5	63.0	73.5	90.5	109.5	130.3	-31.9
cinnamate	C ₁₀ H ₁₀ O ₂	77.4	108.1	123.0	140.0	157.9	170.0	185.8	209.6	235.0	263.0	33.4
α -Methylcinnamic acid	C ₁₀ H ₁₀ O ₂	125.7	155.0	169.8	185.2	201.8	212.0	224.8	245.0	266.8	288.0	
Methylcyclohexane	C ₇ H ₁₄	-35.9	-14.0	-3.2	+8.7	22.0	30.5	42.1	59.6	79.6	100.9	-126.4
Methylcyclopentane	C ₆ H ₁₂	-53.7	-33.8	-23.7	-12.8	-0.6	+7.2	17.9	34.0	52.3	71.8	-142.4
Methylcyclopropane	C ₄ H ₈	-96.0	-80.6	-72.8	-64.0	-54.2	-48.0	-39.3	-26.0	-11.3	+4.5	
Methyl <i>n</i> -decyl ketone (<i>n</i> -dodecan-2-one)	C ₁₂ H ₂₄ O	77.1	106.0	120.4	136.0	152.4	163.8	177.5	199.0	222.5	246.5	
dichloroacetate	C ₃ H ₄ Cl ₂ O ₂	3.2	26.7	38.1	50.7	64.7	73.6	85.4	103.2	122.6	143.0	
<i>N</i> -Methyldiphenylamine	C ₁₃ H ₁₃ N	103.5	134.0	149.7	165.8	184.0	195.4	210.1	232.8	257.0	282.0	-7.6

TABLE 2-10 Vapor Pressures of Organic Compounds, up to 1 atm* (Continued)

Compound		Pressure, mmHg										Melting point, °C
		1	5	10	20	40	60	100	200	400	760	
		Temperature, °C										
Methyl <i>n</i> -dodecyl ketone (2-tetradecanone)	C ₁₄ H ₂₈ O	99.3	130.0	145.5	161.3	179.8	191.4	206.0	228.2	253.3	278.0	
Methylene bromide (dibromomethane)	CH ₂ Br ₂	-35.1	-13.2	-2.4	+9.7	23.3	31.6	42.3	58.5	79.0	98.6	-52.8
chloride (dichloromethane)	CH ₂ Cl ₂	-70.0	-52.1	-43.3	-33.4	-22.3	-15.7	-6.3	+8.0	24.1	40.7	-96.7
Methyl ethyl ketone (2-butanone)	C ₄ H ₈ O	-48.3	-28.0	-17.7	-6.5	+6.0	14.0	25.0	41.6	60.0	79.6	-85.9
2-Methyl-3-ethylpentane	C ₈ H ₁₈	-24.0	-1.8	+9.5	21.7	35.2	43.9	55.7	73.6	94.0	115.6	-114.5
3-Methyl-3-ethylpentane	C ₈ H ₁₈	-23.9	-1.4	+9.9	22.3	36.2	45.0	57.1	75.3	96.2	118.3	-90
Methyl fluoride	CH ₃ F	-147.3	-137.0	-131.6	-125.9	-119.1	-115.0	-109.0	-99.9	-89.5	-78.2	
formate	C ₂ H ₄ O ₂	-74.2	-57.0	-48.6	-39.2	-28.7	-21.9	-12.9	+0.8	16.0	32.0	-99.8
α-Methylglutaric anhydride	C ₆ H ₈ O ₃	93.8	125.4	141.8	157.7	177.5	189.9	205.0	229.1	255.5	282.5	
Methyl glycolate	C ₃ H ₆ O ₃	+9.6	33.7	45.3	58.1	72.3	81.8	93.7	111.8	131.7	151.5	
2-Methylheptadecane	C ₁₈ H ₃₈	119.8	152.0	168.7	186.0	204.8	216.3	231.5	254.5	279.8	306.5	
2-Methylheptane	C ₈ H ₁₈	-21.0	+1.3	12.3	24.4	37.9	46.6	58.3	76.0	96.2	117.6	-109.5
3-Methylheptane	C ₈ H ₁₈	-19.8	+2.6	13.3	25.4	38.9	47.6	59.4	77.1	97.4	118.9	-120.8
4-Methylheptane	C ₈ H ₁₈	-20.4	+1.5	12.4	24.5	38.0	46.6	58.3	76.1	96.3	117.7	-121.1
2-Methyl-2-heptene	C ₈ H ₁₆	-16.1	+6.7	17.8	30.4	44.0	52.8	64.6	82.3	102.2	122.5	
6-Methyl-3-hepten-2-ol	C ₈ H ₁₆ O	41.6	65.0	76.7	89.3	102.7	111.5	122.6	139.5	156.6	175.5	
6-Methyl-5-hepten-2-ol	C ₈ H ₁₆ O	41.9	66.0	77.8	90.4	104.0	112.8	123.8	140.0	156.6	174.3	
2-Methylhexane	C ₇ H ₁₆	-40.4	-19.5	-9.1	+2.3	14.9	23.0	34.1	50.8	69.8	90.0	-118.2
3-Methylhexane	C ₇ H ₁₆	-39.0	-18.1	-7.8	+3.6	16.4	24.5	35.6	52.4	71.6	91.9	
Methyl iodide	CH ₃ I		-55.0	-45.8	-35.6	-24.2	-16.9	-7.0	+8.0	25.3	42.4	-64.4
laurate	C ₁₃ H ₂₆ O ₂	87.8	117.9	133.2	149.0	166.0	176.8	190.8				5
levulinic acid	C ₆ H ₁₀ O ₃	39.8	66.4	79.7	93.7	109.5	119.3	133.0	153.4	175.8	197.7	
methacrylate	C ₅ H ₈ O ₂	-30.5	-10.0	+1.0	11.0	25.5	34.5	47.0	63.0	82.0	101.0	
myristate	C ₁₅ H ₃₀ O ₂	115.0	145.7	160.8	177.8	195.8	207.5	222.6	245.3	269.8	295.8	18.5
α-naphthyl ketone (1-acetonaphthone)	C ₁₂ H ₁₀ O	115.6	146.3	161.5	178.4	196.8	208.6	223.8	246.7	270.5	295.5	
β-naphthyl ketone (2-acetonaphthone)	C ₁₂ H ₁₀ O	120.2	152.3	168.5	185.7	203.8	214.7	229.8	251.6	275.8	301.0	55.5
<i>n</i> -nonyl ketone (undecan-2-one)	C ₁₁ H ₂₂ O	68.2	95.5	108.9	123.1	139.0	148.6	161.0	181.2	202.3	224.0	15
palmitate	C ₁₇ H ₃₄ O ₂	134.3	166.8	184.3	202.0							30
<i>n</i> -pentadecyl ketone (2-heptadecanone)	C ₁₇ H ₃₄ O	129.6	161.6	178.0	196.4	214.3	226.7	242.0	265.8	291.7	319.5	
2-Methylpentane	C ₆ H ₁₄	-60.9	-41.7	-32.1	-21.4	-9.7	-1.9	+8.1	24.1	41.6	60.3	-154
3-Methylpentane	C ₆ H ₁₄	-59.0	-39.8	-30.1	-19.4	-7.3	+0.1	10.5	26.5	44.2	63.3	-118
2-Methyl-1-pentanol	C ₆ H ₁₄ O	15.4	38.0	49.6	61.6	74.7	83.4	94.2	111.3	129.8	147.9	
2-Methyl-2-pentanol	C ₆ H ₁₄ O	-4.5	+16.8	27.6	38.8	51.3	58.8	69.2	85.0	102.6	121.2	-103
Methyl <i>n</i> -pentyl ketone (2-heptanone)	C ₇ H ₁₄ O	19.3	43.6	55.5	67.7	81.2	89.8	100.0	116.1	133.2	150.2	
phenyl ether (anisole)	C ₇ H ₈ O	+5.4	30.0	42.2	55.8	70.7	80.1	93.0	112.3	133.8	155.5	-37.3
2-Methylpropene	C ₄ H ₈	-105.1	-96.5	-81.9	-73.4	-63.8	-57.7	-49.3	-36.7	-22.2	-6.9	-140.3
Methyl propionate	C ₄ H ₈ O ₂	-42.0	-21.5	-11.8	-1.0	+11.0	18.7	29.0	44.2	61.8	79.8	-87.5
4-Methylpropiophenone	C ₁₀ H ₁₂ O	59.6	89.3	103.8	120.2	138.0	149.3	164.2	187.4	212.7	238.5	
2-Methylpropiol bromide	C ₄ H ₇ BrO	13.5	38.4	50.6	64.1	79.4	88.8	101.6	120.5	141.7	163.0	
Methyl propyl ether	C ₄ H ₁₀ O	-72.2	-54.3	-45.4	-35.4	-24.3	-17.4	-8.1	+6.0	22.5	39.1	
<i>n</i> -propyl ketone (2-pentanone)	C ₅ H ₁₀ O	-12.0	+8.0	17.9	28.5	39.8	47.3	56.8	71.0	86.8	103.3	-77.8
isopropyl ketone (3-Methyl-2-butanone)	C ₅ H ₁₀ O	-19.9	-1.0	+8.3	18.3	29.6	36.2	45.5	59.0	73.8	88.9	-92
2-Methylquinoline	C ₁₀ H ₉ N	75.3	104.0	119.0	134.0	150.8	161.7	176.2	197.8	211.7	246.5	-1
Methyl salicylate	C ₈ H ₈ O ₃	54.0	81.6	95.3	110.0	126.2	136.7	150.0	172.6	197.5	223.2	-8.3
α-Methyl styrene	C ₉ H ₁₀	7.4	34.0	47.1	61.8	77.8	88.3	102.2	121.8	143.0	165.4	-23.2
4-Methyl styrene	C ₉ H ₁₀	16.0	42.0	55.1	69.2	85.0	95.0	108.6	128.7	151.2	175.0	
Methyl <i>n</i> -tetradecyl ketone (2-hexadecanone)	C ₁₆ H ₃₂ O	109.8	151.5	167.3	184.6	203.7	215.0	230.5	254.4	279.8	307.0	
thiocyanate	C ₃ H ₂ NS	-14.0	+9.8	21.6	34.5	49.0	58.1	70.4	89.8	110.8	132.9	-51
isothiocyanate	C ₃ H ₃ NS	-34.7	-8.3	+5.4	20.4	38.2	47.5	59.3	77.5	97.8	119.0	35.5
undecyl ketone (2-tridecanone)	C ₁₃ H ₂₆ O	86.8	117.0	131.8	147.8	165.7	176.6	191.5	214.0	238.3	262.5	28.5
isovalerate	C ₆ H ₁₂ O ₂	-19.2	+2.9	14.0	26.4	39.8	48.2	59.8	77.3	96.7	116.7	
Monovinylacetylene (butenyne)	C ₄ H ₄	-93.2	-77.7	-70.0	-61.3	-51.7	-45.3	-37.1	-24.1	-10.1	+5.3	
Myrcene	C ₁₀ H ₁₆	14.5	40.0	53.2	67.0	82.6	92.6	106.0	126.0	148.3	171.5	
Myristaldehyde	C ₁₄ H ₂₆ O	99.0	132.0	148.3	166.2	186.0	198.3	214.5	240.4	267.9	297.8	23.5
Myristic acid (tetradecanoic acid)	C ₁₄ H ₂₈ O ₂	142.0	174.1	190.8	207.6	223.5	237.2	250.5	272.3	294.6	318.0	57.5
Naphthalene	C ₁₀ H ₈	52.6	74.2	85.8	101.7	119.3	130.2	145.5	167.7	193.2	217.9	80.2
1-Naphthoic acid	C ₁₁ H ₈ O ₂	156.0	184.0	196.8	211.2	225.0	234.5	245.8	263.5	281.4	300.0	160.5
2-Naphthoic acid	C ₁₁ H ₈ O ₂	160.8	189.7	202.8	216.9	231.5	241.3	252.7	270.3	289.5	308.5	184
1-Naphthol	C ₁₀ H ₈ O	94.0	125.5	142.0	158.0	177.8	190.0	206.0	229.6	255.8	282.5	96
2-Naphthol	C ₁₀ H ₈ O		128.6	145.5	161.8	177.1	193.7	209.8	234.0	260.6	288.0	122.5
1-Naphthylamine	C ₁₀ H ₉ N	104.3	137.7	153.8	171.6	191.5	203.8	220.0	244.9	272.2	300.8	50
2-Naphthylamine	C ₁₀ H ₉ N	108.0	141.6	157.6	175.8	195.7	208.1	224.3	249.7	277.4	306.1	111.5
Nicotine	C ₁₀ H ₁₄ N ₂	61.8	91.8	107.2	123.7	142.1	154.7	169.5	193.8	219.8	247.3	
2-Nitroaniline	C ₆ H ₆ N ₂ O ₂	104.0	135.7	150.4	167.7	186.0	197.8	213.0	236.3	260.0	284.5	71.5
3-Nitroaniline	C ₆ H ₆ N ₂ O ₂	119.3	151.5	167.8	185.5	204.2	216.5	232.1	255.3	280.2	305.7	114
4-Nitroaniline	C ₆ H ₆ N ₂ O ₂	142.4	177.6	194.4	213.2	234.2	245.9	261.8	284.5	310.2	336.0	146.5
2-Nitrobenzaldehyde	C ₇ H ₅ NO ₃	85.8	117.7	133.4	150.0	168.8	180.7	196.2	220.0	246.8	273.5	40.9
3-Nitrobenzaldehyde	C ₇ H ₅ NO ₃	96.2	127.4	142.8	159.0	177.7	189.5	204.3	227.4	252.1	278.3	58
Nitrobenzene	C ₆ H ₅ NO ₂	44.4	71.6	84.9	99.3	115.4	125.8	139.9	161.2	185.8	210.6	+5.7
Nitroethane	C ₂ H ₅ NO ₂	-21.0	+1.5	12.5	24.8	38.0	46.5	57.8	74.8	94.0	114.0	-90
Nitroglycerin	C ₃ H ₅ N ₃ O ₃	127	167	188	210	235	251					11
Nitromethane	CH ₃ NO ₂	-29.0	-7.9	+2.8	14.1	27.5	35.5	46.6	63.5	82.0	101.2	-29
2-Nitrophenol	C ₆ H ₅ NO ₃	49.3	76.8	90.4	105.8	122.1	132.6	146.4	167.6	191.0	214.5	45
2-Nitrophenyl acetate	C ₈ H ₇ NO ₄	100.0	128.0	142.0	155.8	172.8	181.7	194.1	213.0	233.5	253.0	

2-76 PHYSICAL AND CHEMICAL DATA

TABLE 2-10 Vapor Pressures of Organic Compounds, up to 1 atm (Continued)

Compound		Pressure, mmHg										Melting point, °C
		1	5	10	20	40	60	100	200	400	760	
Name	Formula	Temperature, °C										
1-Nitropropane	C ₃ H ₇ NO ₂	-9.6	+13.5	25.3	37.9	51.8	60.5	72.3	90.2	110.6	131.6	-108
2-Nitropropane	C ₃ H ₇ NO ₂	-18.8	+4.1	15.8	28.2	41.8	50.3	62.0	80.0	99.8	120.3	-93
2-Nitrotoluene	C ₇ H ₇ NO ₂	50.0	79.1	93.8	109.6	126.3	137.6	151.5	173.7	197.7	222.3	-4.1
3-Nitrotoluene	C ₇ H ₇ NO ₂	50.2	81.0	96.0	112.8	130.7	142.5	156.9	180.3	206.8	231.9	15.5
4-Nitrotoluene	C ₇ H ₇ NO ₂	53.7	85.0	100.5	117.7	136.0	147.9	163.0	186.7	212.5	238.3	51.9
4-Nitro-1,3-xylene (4-nitro- <i>m</i> -xylene)	C ₈ H ₉ NO ₂	65.6	95.0	109.8	125.8	143.3	153.8	168.5	191.7	217.5	244.0	+2
Nonacosane	C ₂₉ H ₆₀	234.2	269.8	286.4	303.6	323.2	334.8	350.0	373.2	397.2	421.8	63.8
Nonadecane	C ₁₉ H ₄₀	133.2	166.3	183.5	200.8	220.0	232.8	248.0	271.8	299.8	330.0	32
<i>n</i> -Nonane	C ₉ H ₂₀	+1.4	25.8	38.0	51.2	66.0	75.5	88.1	107.5	128.2	150.8	-53.7
1-Nonanol	C ₉ H ₂₀ O	59.5	86.1	99.7	113.8	129.0	139.0	151.3	170.5	192.1	213.5	-5
2-Nonanone	C ₉ H ₁₈ O	32.1	59.0	72.3	87.2	103.4	113.8	127.4	148.2	171.2	195.0	-19
Octacosane	C ₂₈ H ₅₈	226.5	260.3	277.4	295.4	314.2	326.8	341.8	364.8	388.9	412.5	61.6
Octadecane	C ₁₈ H ₃₈	119.6	152.1	169.6	187.5	207.4	219.7	236.0	260.6	288.0	317.0	28
<i>n</i> -Octane	C ₈ H ₁₈	-14.0	+8.3	19.2	31.5	45.1	53.8	65.7	83.6	104.0	125.6	-56.8
<i>n</i> -Octanol (1-octanol)	C ₈ H ₁₈ O	54.0	76.5	88.3	101.0	115.2	123.8	135.2	152.0	173.8	195.2	-15.4
2-Octanone	C ₈ H ₁₆ O	23.6	48.4	60.9	74.3	89.8	99.0	111.7	130.4	151.0	172.9	-16
<i>n</i> -Octyl acrylate	C ₁₁ H ₂₀ O ₂	58.5	87.7	102.0	117.8	135.6	145.6	159.1	180.2	204.0	227.0	
iodide (1-Iodoctane)	C ₈ H ₁₇ I	45.8	74.8	90.0	105.9	123.8	135.4	150.0	173.3	199.3	225.5	-45.9
Oleic acid	C ₁₈ H ₃₄ O ₂	176.5	208.5	223.0	240.0	257.2	269.8	286.0	309.8	334.7	360.0	14
Palmitaldehyde	C ₁₆ H ₃₂ O	121.6	154.6	171.8	190.0	210.0	222.6	239.5	264.1	292.3	321.0	34
Palmitic acid	C ₁₆ H ₃₂ O ₂	153.6	188.1	205.8	223.8	244.4	256.0	271.5	298.7	326.0	353.8	64.0
Palmitonitrile	C ₁₆ H ₃₁ N	134.3	168.3	185.8	204.2	223.8	236.6	251.5	277.1	304.5	332.0	31
Pelargonic acid	C ₉ H ₁₈ O ₂	108.2	126.0	137.4	149.8	163.7	172.3	184.4	203.1	227.5	253.5	12.5
Pentachlorobenzene	C ₆ HCl ₅	98.6	129.7	144.3	160.0	178.5	190.1	205.5	227.0	251.6	276.0	85.5
Pentachloroethane	C ₂ HCl ₅	+1.0	27.2	39.8	53.9	69.9	80.0	93.5	114.0	137.2	160.5	-22
Pentachloroethylbenzene	C ₈ H ₅ Cl ₅	96.2	130.0	148.0	166.0	186.2	199.0	216.0	241.8	269.3	299.0	
Pentachlorophenol	C ₆ HCl ₅ O				192.2	211.2	223.4	239.6	261.8	285.0	309.3	188.5
Pentacosane	C ₂₅ H ₅₂	194.2	230.0	248.2	266.1	285.6	298.4	314.0	339.0	365.4	390.3	53.3
Pentadecane	C ₁₅ H ₃₂	91.6	121.0	135.4	150.2	167.7	178.4	194.0	216.1	242.8	270.5	10
1,3-Pentadiene	C ₅ H ₈	-71.8	-53.8	-45.0	-34.8	-23.4	-16.5	-6.7	+8.0	24.7	42.1	
1,4-Pentadiene	C ₅ H ₈	-83.5	-66.2	-57.1	-47.7	-37.0	-30.0	-20.6	-6.7	+8.3	26.1	
Pentaethylbenzene	C ₁₆ H ₂₆	86.0	120.0	135.8	152.4	171.9	184.2	200.0	224.1	250.2	277.0	
Pentaethylchlorobenzene	C ₁₆ H ₂₅ Cl	90.0	123.8	140.7	158.1	178.2	191.0	208.0	230.3	257.2	285.0	
<i>n</i> -Pentane	C ₅ H ₁₂	-76.6	-62.5	-50.1	-40.2	-29.2	-22.2	-12.6	+1.9	18.5	36.1	-129.7
iso-Pentane (2-methylbutane)	C ₅ H ₁₂	-82.9	-65.8	-57.0	-47.3	-36.5	-29.6	-20.2	-5.9	+10.5	27.8	-159.7
neo-Pentane (2,2-dimethylpropane)	C ₅ H ₁₂	-102.0	-85.4	-76.7	-67.2	-56.1	-49.0	-39.1	-23.7	-7.1	+9.5	-16.6
2,3,4-Pentanetriol	C ₅ H ₁₂ O ₃	155.0	189.3	204.5	220.5	239.6	249.8	263.5	284.5	307.0	327.2	
1-Pentene	C ₅ H ₁₀	-80.4	-63.3	-54.5	-46.0	-34.1	-27.1	-17.7	-3.4	+12.8	30.1	
α-Phellandrene	C ₁₀ H ₁₆	20.0	45.7	58.0	72.1	87.8	97.6	110.6	130.6	152.0	175.0	
Phenanthrene	C ₁₄ H ₁₀	118.2	154.3	173.0	193.7	215.8	229.9	249.0	277.1	308.0	340.2	99.5
Phenethyl alcohol (phenyl cellosolve)	C ₈ H ₁₀ O ₂	58.2	85.9	100.0	114.8	130.5	141.2	154.0	175.0	197.5	219.5	
2-Phenetidine	C ₈ H ₁₁ NO	67.0	94.7	108.6	123.7	139.9	149.8	163.5	184.0	207.0	228.0	
Phenol	C ₆ H ₆ O	40.1	62.5	73.8	86.0	100.1	108.4	121.4	139.0	160.0	181.9	40.6
2-Phenoxyethanol	C ₈ H ₁₀ O ₂	78.0	106.6	121.2	136.0	152.2	163.2	176.5	197.6	221.0	245.3	11.6
2-Phenoxyethyl acetate	C ₁₀ H ₁₂ O ₃	82.6	113.5	128.0	144.5	162.3	174.0	189.2	211.3	235.0	259.7	-6.7
Phenyl acetate	C ₈ H ₈ O ₂	38.2	64.8	78.0	92.3	108.1	118.1	131.6	151.2	173.5	195.9	
Phenylacetic acid	C ₈ H ₈ O ₂	97.0	127.0	141.3	156.0	173.6	184.5	198.2	219.5	243.0	265.5	76.5
Phenylacetone	C ₈ H ₈ O	60.0	89.0	103.5	119.4	136.3	147.7	161.8	184.2	208.5	233.5	-23.8
Phenylacetyl chloride	C ₈ H ₇ ClO	48.0	75.3	89.0	103.6	119.8	129.8	143.5	163.8	186.0	210.0	
Phenyl benzoate	C ₁₃ H ₁₀ O ₂	106.8	141.5	157.8	177.0	197.6	210.8	227.8	254.0	283.5	314.0	70.5
4-Phenyl-3-buten-2-one	C ₁₀ H ₁₀ O	81.7	112.2	127.4	143.8	161.3	172.6	187.8	211.0	235.4	261.0	41.5
Phenyl isocyanate	C ₇ H ₇ NO	10.6	36.0	48.5	62.5	77.7	87.7	100.6	120.8	142.7	165.6	
isocyanide	C ₇ H ₇ N	12.0	37.0	49.7	63.4	78.3	88.0	101.0	120.8	142.3	165.0	
Phenylcyclohexane	C ₁₂ H ₁₆	67.5	96.5	111.3	126.4	144.0	154.2	169.3	191.3	214.6	240.0	+7.5
Phenyl dichlorophosphate	C ₆ H ₅ Cl ₂ O ₂ P	66.7	95.9	110.0	125.9	143.4	153.6	168.0	189.8	213.0	239.5	
<i>m</i> -Phenylenediamine (1,3-phenylenediamine)	C ₆ H ₈ N ₂	99.8	131.2	147.0	163.8	182.5	194.0	209.9	233.0	259.0	285.5	62.8
Phenylglyoxal	C ₈ H ₆ O ₂	75.0	87.8	100.7	115.5	132.4	142.4	156.2	175.8	197.5	219.5	73
Phenylhydrazine	C ₈ H ₈ N ₂	71.8	101.6	115.8	131.5	148.2	158.7	173.5	195.4	218.2	243.5	19.5
<i>N</i> -Phenyliminodiethanol	C ₁₀ H ₁₅ NO ₂	145.0	179.2	195.8	213.4	233.0	245.3	260.6	284.5	311.3	337.8	
1-Phenyl-1,3-pentanedione	C ₁₁ H ₁₄ O ₂	98.0	128.5	144.0	159.9	178.0	189.8	204.5	226.7	251.2	276.5	
2-Phenylphenol	C ₁₂ H ₁₀ O	100.0	131.6	146.2	163.3	180.3	192.2	205.9	227.9	251.8	275.0	56.5
4-Phenylphenol	C ₁₂ H ₁₀ O			176.2	193.8	213.0	225.3	240.9	263.2	285.5	308.0	164.5
3-Phenyl-1-propanol	C ₉ H ₁₂ O	74.7	102.4	116.0	131.2	147.4	156.8	170.3	191.2	212.8	235.0	
Phenyl isothiocyanate	C ₇ H ₇ NS	47.2	75.6	89.8	115.5	122.5	133.3	147.7	169.6	194.0	218.5	-21.0
Phorone	C ₉ H ₁₄ O	42.0	68.3	81.5	95.6	111.3	121.4	134.0	153.5	175.3	197.2	28
iso-Phorone	C ₉ H ₁₄ O	38.0	66.7	81.2	96.8	114.5	125.6	140.6	163.3	188.7	215.2	
Phosgene (carbonyl chloride)	CCl ₂ O	-92.9	-77.0	-69.3	-60.3	-50.3	-44.0	-35.6	-22.3	-7.6	+8.3	-104
Phthalic anhydride	C ₈ H ₄ O ₃	96.5	121.3	134.0	151.7	172.0	185.3	202.3	228.0	256.8	284.5	130.8
Phthalide	C ₈ H ₆ O ₂	95.5	127.7	144.0	161.3	181.0	193.5	210.0	234.5	261.8	290.0	73
Phthaloyl chloride	C ₈ H ₄ Cl ₂ O ₂	86.3	118.3	134.2	151.0	170.0	182.2	197.8	222.0	248.3	275.8	88.5
2-Picoline	C ₈ H ₇ N	-11.1	+12.6	24.4	37.4	51.2	59.9	71.4	89.0	108.4	128.8	-70
Pimelic acid	C ₇ H ₁₂ O ₄	163.4	196.2	212.0	229.3	247.0	258.2	272.0	294.5	318.5	342.1	103
α-Pinene	C ₁₀ H ₁₆	-1.0	+24.6	37.3	51.4	66.8	76.8	90.1	110.2	132.3	155.0	-55
β-Pinene	C ₁₀ H ₁₆	+4.2	30.0	42.3	58.1	71.5	81.2	94.0	114.1	136.1	158.3	

TABLE 2-10 Vapor Pressures of Organic Compounds, up to 1 atm (Continued)

Compound		Pressure, mmHg										Melting point, °C
		1	5	10	20	40	60	100	200	400	760	
Name	Formula	Temperature, °C										
Piperidine	C ₅ H ₁₁ N		-7.0	+3.9	15.8	29.2	37.7	49.0	66.2	85.7	106.0	-9
Piperonal	C ₈ H ₆ O ₃	87.0	117.4	132.0	148.0	165.7	177.0	191.7	214.3	238.5	263.0	37
Propane	C ₃ H ₈	-128.9	-115.4	-108.5	-100.9	-92.4	-87.0	-79.6	-68.4	-55.6	-42.1	-187.1
Propenylbenzene	C ₉ H ₁₀	17.5	43.8	57.0	71.5	87.7	97.8	111.7	132.0	154.7	179.0	-30.1
Propionamide	C ₃ H ₇ NO	65.0	91.0	105.0	119.0	134.8	144.3	156.0	174.2	194.0	213.0	79
Propionic acid	C ₃ H ₆ O ₂	4.6	28.0	39.7	52.0	65.8	74.1	85.8	102.5	122.0	141.1	-22
anhydride	C ₆ H ₁₀ O ₃	20.6	45.3	57.7	70.4	85.6	94.5	107.2	127.8	146.0	167.0	-45
Propionitrile	C ₃ H ₅ N	-35.0	-13.6	-3.0	+8.8	22.0	30.1	41.4	58.2	77.7	97.1	-91.9
Propiophenone	C ₉ H ₁₀ O	50.0	77.9	92.2	107.6	124.3	135.0	149.3	170.2	194.2	218.0	21
<i>n</i> -Propyl acetate	C ₅ H ₁₀ O ₂	-26.7	-5.4	+5.0	16.0	28.8	37.0	47.8	64.0	82.0	101.8	-92.5
iso-Propyl acetate	C ₅ H ₁₀ O ₂	-38.3	-17.4	-7.2	+4.2	17.0	25.1	35.7	51.7	69.8	89.0	
<i>n</i> -Propyl alcohol (1-propanol)	C ₃ H ₈ O	-15.0	+5.0	14.7	25.3	36.4	43.5	52.8	66.8	82.0	97.8	-127
iso-Propyl alcohol (2-propanol)	C ₃ H ₈ O	-26.1	-7.0	+2.4	12.7	23.8	30.5	39.5	53.0	67.8	82.5	-85.8
<i>n</i> -Propylamine	C ₃ H ₉ N	-64.4	-46.3	-37.2	-27.1	-16.0	-9.0	+0.5	15.0	31.5	48.5	-83
Propylbenzene	C ₉ H ₁₂	6.3	31.3	43.4	56.8	71.6	81.1	94.0	113.5	135.7	159.2	-99.5
Propyl benzoate	C ₁₀ H ₁₂ O ₂	54.6	83.8	98.0	114.3	131.8	143.3	157.4	180.1	205.2	231.0	-51.6
<i>n</i> -Propyl bromide (1-bromopropane)	C ₃ H ₇ Br	-53.0	-33.4	-23.3	-12.4	-0.3	+7.5	18.0	34.0	52.0	71.0	-109.9
iso-Propyl bromide (2-bromopropane)	C ₃ H ₇ Br	-61.8	-42.5	-32.8	-22.0	-10.1	-2.5	+8.0	23.8	41.5	60.0	-89.0
<i>n</i> -Propyl <i>n</i> -butyrate	C ₇ H ₁₄ O ₂	-1.6	+22.1	34.0	47.0	61.5	70.3	82.6	101.0	121.7	142.7	-95.2
isobutyrate	C ₇ H ₁₄ O ₂	-6.2	+16.8	28.3	40.6	54.3	63.0	73.9	91.8	112.0	133.9	
iso-Propyl isobutyrate	C ₇ H ₁₄ O ₂	-16.3	+5.8	17.0	29.0	42.4	51.4	62.3	80.2	100.0	120.5	
Propyl carbamate	C ₆ H ₁₃ NO ₂	52.4	77.6	90.0	103.2	117.7	126.5	138.3	155.8	175.8	195.0	
<i>n</i> -Propyl chloride (1-chloropropane)	C ₃ H ₇ Cl	-68.3	-50.0	-41.0	-31.0	-19.5	-12.1	-2.5	+12.2	29.4	46.4	-122.8
iso-Propyl chloride (2-chloropropane)	C ₃ H ₇ Cl	-78.8	-61.1	-52.0	-42.0	-31.0	-23.5	-13.7	+1.3	18.1	36.5	-117
iso-Propyl chloroacetate	C ₅ H ₉ ClO ₂	+3.8	28.1	40.2	53.9	68.7	78.0	90.3	108.8	128.0	148.6	
Propyl chloroglyoxylate	C ₅ H ₇ ClO ₃	9.7	32.3	43.5	55.6	68.8	77.2	88.0	104.7	123.0	150.0	
Propylene	C ₃ H ₆	-131.9	-120.7	-112.1	-104.7	-96.5	-91.3	-84.1	-73.3	-60.9	-47.7	-185
Propylene glycol (1,2-Propanediol)	C ₃ H ₈ O ₂	45.5	70.8	83.2	96.4	111.2	119.9	132.0	149.7	168.1	188.2	
Propylene oxide	C ₃ H ₆ O	-75.0	-57.8	-49.0	-39.3	-28.4	-21.3	-12.0	+2.1	17.8	34.5	-112.1
<i>m</i> -Propyl formate	C ₄ H ₈ O ₂	-43.0	-22.7	-12.6	-1.7	+10.8	18.8	29.5	45.3	62.6	81.3	-92.9
iso-Propyl formate	C ₄ H ₈ O ₂	-52.0	-32.7	-22.7	-12.1	-0.2	+7.5	17.8	33.6	50.5	68.3	
4,4'-iso-Propylidenebisphenol	C ₁₅ H ₁₆ O ₂	193.0	224.2	240.8	255.5	273.0	282.9	297.0	317.5	339.0	360.5	
<i>n</i> -Propyl iodide (1-iodopropane)	C ₃ H ₇ I	-36.0	-13.5	-2.4	+10.0	23.6	32.1	43.8	61.8	81.8	102.5	-98.8
iso-Propyl iodide (2-iodopropane)	C ₃ H ₇ I	-43.3	-22.1	-11.7	0.0	+13.2	21.6	32.8	50.0	69.5	89.5	-90
<i>n</i> -Propyl levulinate	C ₈ H ₁₄ O ₃	59.7	86.3	99.9	114.0	130.1	140.6	154.0	175.6	198.0	221.2	
iso-Propyl levulinate	C ₈ H ₁₄ O ₃	48.0	74.5	88.0	102.4	118.1	127.8	141.8	161.6	185.2	208.2	
Propyl mercaptan (1-propanethiol)	C ₃ H ₆ S	-56.0	-36.3	-26.3	-15.4	-3.2	+4.6	15.3	31.5	49.2	67.4	-112
2-iso-Propylnaphthalene	C ₁₃ H ₁₄	76.0	107.9	123.4	140.3	159.0	171.4	187.6	211.8	238.5	266.0	
iso-Propyl β-naphthyl ketone (2-isobutyronaphthone)	C ₁₄ H ₁₄ O	133.2	165.4	181.0	197.7	215.6	227.0	242.3	264.0	288.2	313.0	
2-iso-Propylphenol	C ₉ H ₁₂ O	56.6	83.8	97.0	111.7	127.5	137.7	150.3	170.1	192.6	214.5	15.5
3-iso-Propylphenol	C ₉ H ₁₂ O	62.0	90.3	104.1	119.8	136.2	146.6	160.2	182.0	205.0	228.0	26
4-iso-Propylphenol	C ₉ H ₁₂ O	67.0	94.7	108.0	123.4	139.8	149.7	163.3	184.0	206.1	228.2	61
Propyl propionate	C ₈ H ₁₆ O ₂	-14.2	+8.0	19.4	31.6	45.0	53.8	65.2	82.7	102.0	122.4	-76
4-iso-Propylstyrene	C ₁₁ H ₁₄	34.7	62.3	76.0	91.2	108.0	118.4	132.8	153.9	178.0	202.5	
Propyl isovalerate	C ₈ H ₁₆ O ₂	+8.0	32.8	45.1	58.0	72.8	82.3	95.0	113.9	135.0	155.9	
Pulegone	C ₁₀ H ₁₆ O	58.3	82.5	94.0	106.8	121.7	130.2	143.1	162.5	189.8	221.0	
Pyridine	C ₅ H ₅ N	-18.9	+2.5	13.2	24.8	38.0	46.8	57.8	75.0	95.6	115.4	-42
Pyrocatechol	C ₆ H ₆ O ₂		104.0	118.3	134.0	150.6	161.7	176.0	197.7	221.5	245.5	105
Pyrocaltechol diacetate (1,2-phenylene diacetate)	C ₁₀ H ₁₀ O ₄	98.0	129.8	145.7	161.8	179.8	191.6	206.5	228.7	253.3	278.0	
Pyrogallol	C ₆ H ₆ O ₃		151.7	167.7	185.3	204.2	216.3	232.0	255.3	281.5	309.0	133
Pyrotartaric anhydride	C ₈ H ₆ O ₃	69.7	99.7	114.2	130.0	147.8	158.6	173.8	196.1	221.0	247.4	
Pyruvic acid	C ₃ H ₄ O ₃	21.4	45.8	57.9	70.8	85.3	94.1	106.5	124.7	144.7	165.0	13.6
Quinoline	C ₈ H ₇ N	59.7	89.6	103.8	119.8	136.7	148.1	163.2	186.2	212.3	237.7	-15
iso-Quinoline	C ₈ H ₇ N	63.5	92.7	107.8	123.7	141.6	152.0	167.6	190.0	214.5	240.5	24.6
Resorcinol	C ₆ H ₆ O ₂	108.4	138.0	152.1	168.0	185.3	195.8	209.8	230.8	253.4	276.5	110.7
Safrole	C ₁₀ H ₁₀ O ₂	63.8	93.0	107.6	123.0	140.1	150.3	165.1	186.2	210.0	233.0	11.2
Salicylaldehyde	C ₇ H ₆ O ₂	33.0	60.1	73.8	88.7	105.2	115.7	129.4	150.0	173.7	196.5	-7
Salicylic acid	C ₇ H ₆ O ₃	113.7	136.0	146.2	156.8	172.2	182.0	193.4	210.0	230.5	256.0	159
Sebacic acid	C ₁₀ H ₁₈ O ₄	183.0	215.7	232.0	250.0	268.2	279.8	294.5	313.2	332.8	352.3	134.5
Selenophene	C ₄ H ₄ Se	-39.0	-16.0	-4.0	+9.1	24.1	33.8	47.0	66.7	89.8	114.3	
Skatole	C ₉ H ₉ N	95.0	124.2	139.6	154.3	171.9	183.6	197.4	218.8	242.5	266.2	95
Stearaldehyde	C ₁₈ H ₃₆ O	140.0	174.6	192.1	210.6	230.8	244.2	260.0	285.0	313.8	342.5	63.5
Stearic acid	C ₁₈ H ₃₆ O ₂	173.7	209.0	225.0	243.4	263.3	275.5	291.0	316.5	343.0	370.0	69.3
Stearyl alcohol (1-octadecanol)	C ₁₈ H ₃₆ O	150.3	185.6	202.0	220.0	240.4	252.7	269.4	293.5	320.3	349.5	58.5
Styrene	C ₈ H ₈	-7.0	+18.0	30.8	44.6	59.8	69.5	82.0	101.3	122.5	145.2	-30.6
Styrene dibromide [(1,2-dibromoethyl) benzene]	C ₈ H ₈ Br ₂	86.0	115.6	129.8	145.2	161.8	172.2	186.3	207.8	230.0	254.0	
Suberic acid	C ₈ H ₁₄ O ₄	172.8	205.5	219.5	238.2	254.6	265.4	279.8	300.5	322.8	345.5	142
Succinic anhydride	C ₄ H ₆ O ₃	92.0	115.0	128.2	145.3	163.0	174.0	189.0	212.0	237.0	261.0	119.6
Succinimide	C ₄ H ₅ NO ₂	115.0	143.2	157.0	174.0	192.0	203.0	217.4	240.0	263.5	287.5	125.5
Succinyl chloride	C ₄ H ₄ Cl ₂ O ₂	39.0	65.0	78.0	91.8	107.5	117.2	130.0	149.3	170.0	192.5	17
α-Terpineol	C ₁₀ H ₁₈ O	52.8	80.4	94.3	109.8	126.0	136.3	150.1	171.2	194.3	217.5	35
Terpenoline	C ₁₀ H ₁₆	32.3	58.0	70.6	84.8	100.0	109.8	122.7	142.0	163.5	185.0	

2-78 PHYSICAL AND CHEMICAL DATA

TABLE 2-10 Vapor Pressures of Organic Compounds, up to 1 atm (Continued)

Compound		Pressure, mmHg										Melting point, °C
		1	5	10	20	40	60	100	200	400	760	
Name	Formula	Temperature, °C										
1,1,1,2-Tetrabromoethane	C ₂ H ₂ Br ₄	58.0	83.3	95.7	108.5	123.2	132.0	144.0	161.5	181.0	200.0	
1,1,2,2-Tetrabromoethane	C ₂ H ₂ Br ₄	65.0	95.5	110.0	126.0	144.0	155.1	170.0	192.5	217.5	243.5	
Tetraisobutylene	C ₁₀ H ₁₆	63.8	93.7	108.5	124.5	142.2	152.6	167.5	190.0	214.6	240.0	
Tetracosane	C ₂₄ H ₅₀	183.8	219.6	237.6	255.3	276.3	288.4	305.2	330.5	358.0	386.4	51.1
1,2,3,4-Tetrachlorobenzene	C ₆ H ₂ Cl ₄	68.5	99.6	114.7	131.2	149.2	160.0	175.7	198.0	225.5	254.0	46.5
1,2,3,5-Tetrachlorobenzene	C ₆ H ₂ Cl ₄	58.2	89.0	104.1	121.6	140.0	152.0	168.0	193.7	220.0	246.0	54.5
1,2,4,5-Tetrachlorobenzene	C ₆ H ₂ Cl ₄					146.0	157.7	173.5	196.0	220.5	245.0	139
1,1,2,2-Tetrachloro-1,2-difluoroethane	C ₂ Cl ₂ F ₂	-37.5	-16.0	-5.0	+6.7	19.8	28.1	38.6	55.0	73.1	92.0	26.5
1,1,1,2-Tetrachloroethane	C ₂ H ₂ Cl ₄	-16.3	+7.4	19.3	32.1	46.7	56.0	68.0	87.2	108.2	130.5	-68.7
1,1,2,2-Tetrachloroethane	C ₂ H ₂ Cl ₄	-3.8	+20.7	33.0	46.2	60.8	70.0	83.2	102.2	124.0	145.9	-36
1,2,3,5-Tetrachloro-4-ethylbenzene	C ₈ H ₆ Cl ₄	77.0	110.0	126.0	143.7	162.1	175.0	191.6	215.3	243.0	270.0	
Tetrachloroethylene	C ₂ Cl ₄	-20.6	+2.4	13.8	26.3	40.1	49.2	61.3	79.8	100.0	120.8	-19.0
2,3,4,6-Tetrachlorophenol	C ₆ H ₂ Cl ₄ O	100.0	130.3	145.3	161.0	179.1	190.0	205.2	227.2	250.4	275.0	69.5
3,4,5,6-Tetrachloro-1,2-xylene	C ₈ H ₆ Cl ₄	94.4	125.0	140.3	156.0	174.2	185.8	200.5	223.0	248.3	273.5	
Tetradecane	C ₁₄ H ₃₀	76.4	106.0	120.7	135.6	152.7	164.0	178.5	201.8	226.8	252.5	5.5
Tetradecylamine	C ₁₄ H ₃₁ N	102.6	135.8	152.0	170.0	189.0	200.2	215.7	239.8	264.6	291.2	
Tetradecyltrimethylsilane	C ₁₇ H ₃₅ Si	120.0	150.7	166.2	183.5	201.5	213.3	227.8	250.0	275.0	300.0	
Tetraethoxysilane	C ₈ H ₂₀ O ₄ Si	16.0	40.3	52.6	65.8	81.1	90.7	103.6	123.5	146.2	168.5	
1,2,3,4-Tetraethylbenzene	C ₁₄ H ₂₂	65.7	96.2	111.6	127.7	145.8	156.7	172.4	196.0	221.4	248.0	11.6
Tetraethylene glycol	C ₈ H ₁₈ O ₅	153.9	183.7	197.1	212.3	228.0	237.8	250.0	268.4	288.0	307.8	
Tetraethylene glycol chlorohydrin	C ₈ H ₁₇ ClO ₄	110.1	141.8	156.1	172.6	190.0	200.5	214.7	236.5	258.2	281.5	
Tetraethyllead	C ₈ H ₂₀ Pb	35.4	63.6	74.8	88.0	102.4	111.7	123.8	142.0	161.8	183.0	-136
Tetraethylsilane	C ₈ H ₂₀ Si	-1.0	+23.9	36.3	50.0	65.3	74.8	88.0	108.0	130.2	153.0	
Tetralin	C ₁₀ H ₁₂	38.0	65.3	79.0	93.8	110.4	121.3	135.3	157.2	181.8	207.2	-31.0
1,2,3,4-Tetramethylbenzene	C ₁₀ H ₁₄	42.6	68.7	81.8	95.8	111.5	121.8	135.7	155.7	180.0	204.4	-6.2
1,2,3,5-Tetramethylbenzene	C ₁₀ H ₁₄	40.6	65.8	77.8	91.0	105.8	115.4	128.3	149.9	173.7	197.9	-24.0
1,2,4,5-Tetramethylbenzene	C ₁₀ H ₁₄	45.0	65.0	74.6	88.0	104.2	114.8	128.1	149.5	172.1	195.9	79.5
2,2,3,3-Tetramethylbutane	C ₈ H ₁₈	-17.4	+3.2	13.5	24.6	36.8	44.5	54.8	70.2	87.4	106.3	-102.2
Tetramethylene dibromide (1,4-dibromobutane)	C ₄ H ₈ Br ₂	32.0	58.8	72.4	87.6	104.0	115.1	128.7	149.8	173.8	197.5	-20
Tetramethyllead	C ₄ H ₁₂ Pb	-29.0	-6.8	+4.4	16.6	30.3	39.2	50.8	68.8	89.0	110.0	-27.5
Tetramethyltin	C ₄ H ₁₂ Sn	-51.3	-31.0	-20.6	-9.3	+3.5	11.7	22.8	39.8	58.5	78.0	
Tetrapropylene glycol monoisopropyl ether	C ₁₅ H ₃₂ O ₅	116.6	147.8	163.0	179.8	197.7	209.0	223.3	245.0	268.3	292.7	
Thioacetic acid (mercaptoacetic acid)	C ₂ H ₄ O ₂ S	60.0	87.7	101.5	115.8	131.8	142.0	154.0				-16.5
Thiodiglycol (2,2'-thiodiethanol)	C ₄ H ₁₀ O ₂ S	42.0	96.0	128.0	165.0	210.0	240.5	285				
Thiophene	C ₄ H ₄ S	-40.7	-20.8	-10.9	0.0	+12.5	20.1	30.5	46.5	64.7	84.4	-38.3
Thiophenol (benzenethiol)	C ₆ H ₆ S	18.6	43.7	56.0	69.7	84.2	93.9	106.6	125.8	146.7	168.0	
α-Thujone	C ₁₀ H ₁₆ O	38.3	65.7	79.3	93.7	110.0	120.2	134.0	154.2	177.8	201.0	
Thymol	C ₁₀ H ₁₄ O	64.3	92.8	107.4	122.6	139.8	149.8	164.1	185.5	209.2	231.8	51.5
Tiglaldehyde	C ₅ H ₈ O	-25.0	-1.6	+10.0	23.2	37.0	45.8	57.7	75.4	95.5	116.4	
Tiglic acid	C ₅ H ₈ O ₂	52.0	77.8	90.2	103.8	119.0	127.8	140.5	158.0	179.2	198.5	64.5
Tiglonitrile	C ₅ H ₇ N	-25.5	-2.4	+9.2	22.1	36.7	46.0	58.2	77.8	99.7	122.0	
Toluene	C ₇ H ₈	-26.7	-4.4	+6.4	18.4	31.8	40.3	51.9	69.5	89.5	110.6	-95.0
Toluene-2,4-diamine	C ₇ H ₁₀ N ₂	106.5	137.2	151.7	167.9	185.7	196.2	211.5	232.8	256.0	280.0	99
2-Toluic nitrile (2-tolunitrile)	C ₈ H ₇ N	36.7	64.0	77.9	93.0	110.0	120.8	135.0	156.0	180.0	205.2	-13
4-Toluic nitrile (4-tolunitrile)	C ₈ H ₇ N	42.5	71.3	85.8	101.7	109.5	130.0	145.2	167.3	193.0	217.6	29.5
2-Toluidine	C ₇ H ₉ N	44.0	69.3	81.4	95.1	110.0	119.8	133.0	153.0	176.2	199.7	-16.3
3-Toluidine	C ₇ H ₉ N	41.0	68.0	82.0	96.7	113.5	123.8	136.7	157.6	180.6	203.3	-31.5
4-Toluidine	C ₇ H ₉ N	42.0	68.2	81.8	95.8	111.5	121.5	133.7	154.0	176.9	200.4	44.5
2-Tolyl isocyanide	C ₈ H ₇ N	25.2	51.0	64.0	78.2	94.0	104.0	117.7	137.8	159.9	183.5	
4-Tolylhydrazine	C ₇ H ₁₀ N ₂	82.4	110.0	123.8	138.6	154.1	165.0	178.0	198.0	219.5	242.0	65.5
Tribromoacetaldehyde	C ₂ HBr ₃ O	18.5	45.0	58.0	72.1	87.8	97.5	110.2	130.0	151.6	174.0	
1,1,2-Tribromobutane	C ₄ H ₇ Br ₃	45.0	73.5	87.8	103.2	120.2	131.6	146.0	167.8	192.0	216.2	
1,2,2-Tribromobutane	C ₄ H ₇ Br ₃	41.0	69.0	83.2	98.6	116.0	127.0	141.8	163.5	188.0	213.8	
2,2,3-Tribromobutane	C ₄ H ₇ Br ₃	38.2	66.0	79.8	94.6	111.8	122.2	136.3	157.8	182.2	206.5	
1,1,2-Tribromoethane	C ₂ H ₃ Br ₃	32.6	58.0	70.6	84.2	100.0	110.0	123.5	143.5	165.4	188.4	-26
1,2,3-Tribromopropane	C ₃ H ₅ Br ₃	47.5	75.8	90.0	105.8	122.8	134.0	148.0	170.0	195.0	220.0	16.5
Triisobutylamine	C ₁₂ H ₂₇ N	32.3	57.4	69.8	83.0	97.8	107.3	119.7	138.0	157.8	179.0	-22
Triisobutylene	C ₁₂ H ₂₄	18.0	44.0	56.5	70.0	86.7	96.7	110.0	130.2	153.0	179.0	
2,4,6-Trinitrobenzylphenol	C ₁₅ H ₉ O ₆	95.2	126.1	142.0	158.0	177.4	188.0	203.0	226.2	250.6	276.3	
Trichloroacetic acid	C ₂ HCl ₃ O ₂	51.0	76.0	88.2	101.8	116.3	125.9	137.8	155.4	175.2	195.6	57
Trichloroacetic anhydride	C ₄ Cl ₆ O ₃	56.2	85.3	99.6	114.3	131.2	141.8	155.2	176.2	199.8	223.0	
Trichloroacetyl bromide	C ₂ BrCl ₃ O	-7.4	+16.7	29.3	42.1	57.2	66.7	79.5	98.4	120.2	143.0	
2,4,6-Trichloroaniline	C ₆ H ₃ Cl ₃ N	134.0	157.8	170.0	182.6	195.8	204.5	214.6	229.8	246.4	262.0	78
1,2,3-Trichlorobenzene	C ₆ H ₃ Cl ₃	40.0	70.0	85.6	101.8	119.8	131.5	146.0	168.2	193.5	218.5	52.5
1,2,4-Trichlorobenzene	C ₆ H ₃ Cl ₃	38.4	67.3	81.7	97.2	114.8	125.7	140.0	162.0	187.7	213.0	17
1,3,5-Trichlorobenzene	C ₆ H ₃ Cl ₃		63.8	78.0	93.7	110.8	121.8	136.0	157.7	183.0	208.4	63.5
1,2,3-Trichlorobutane	C ₄ H ₇ Cl ₃	+0.5	27.2	40.0	55.0	71.5	82.0	96.2	118.0	143.0	169.0	
1,1,1-Trichloroethane	C ₂ HCl ₃	-52.0	-32.0	-21.9	-10.8	+1.6	9.5	20.0	36.2	54.6	74.1	-30.6
1,1,2-Trichloroethane	C ₂ H ₂ Cl ₃	-24.0	-2.0	+8.3	21.6	35.2	44.0	55.7	73.3	93.0	113.9	-36.7
Trichloroethylene	C ₂ HCl ₃	-43.8	-22.8	-12.4	-1.0	+11.9	20.0	31.4	48.0	67.0	86.7	-73
Trichlorofluoromethane	CCl ₃ F	-84.3	-67.6	-59.0	-49.7	-39.0	-32.3	-23.0	-9.1	+6.8	23.7	
2,4,5-Trichlorophenol	C ₆ H ₃ Cl ₃ O	72.0	102.1	117.3	134.0	151.5	162.5	178.0	201.5	226.5	251.8	62
2,4,6-Trichlorophenol	C ₆ H ₃ Cl ₃ O	76.5	105.9	120.2	135.8	152.2	163.5	177.8	199.0	222.5	246.0	68.5

TABLE 2-10 Vapor Pressures of Organic Compounds, up to 1 atm (Concluded)

Compound		Pressure, mmHg										Melting point, °C
		1	5	10	20	40	60	100	200	400	760	
		Temperature, °C										
Name	Formula											
Tri-2-chlorophenylthiophosphate	C ₁₈ H ₁₂ Cl ₃ O ₃ PS	188.2	217.2	231.2	246.7	261.7	271.5	283.8	302.8	322.0	341.3	
1,1,1-Trichloropropane	C ₃ H ₅ Cl ₃	-28.8	-7.0	+4.2	16.2	29.9	38.3	50.0	67.7	87.5	108.2	-77.7
1,2,3-Trichloropropane	C ₃ H ₅ Cl ₃	+9.0	33.7	46.0	59.3	74.0	83.6	96.1	115.6	137.0	158.0	-14.7
1,1,2-Trichloro-1,2,2-trifluoroethane	C ₂ Cl ₃ F ₃	-68.0	-49.4	-40.3	-30.0	-18.5	-11.2	-1.7	+13.5	30.2	47.6	-35
Tricosane	C ₂₃ H ₄₈	170.0	206.3	223.0	242.0	261.3	273.8	289.8	313.5	339.8	366.5	47.7
Tridecane	C ₁₃ H ₂₈	59.4	98.3	104.0	120.2	137.7	148.2	162.5	185.0	209.4	234.0	-6.2
Tridecanoic acid	C ₁₃ H ₂₆ O ₂	137.8	166.3	181.0	195.8	212.4	222.0	236.0	255.2	276.5	299.0	41
Triethoxymethylsilane	C ₇ H ₁₅ O ₃ Si	-1.5	+22.8	34.6	47.2	61.7	70.4	82.7	101.0	121.8	143.5	
Triethoxyphenylsilane	C ₁₂ H ₂₀ O ₃ Si	71.0	98.8	112.6	127.2	143.5	153.2	167.5	188.0	210.5	233.5	
1,2,4-Triethylbenzene	C ₁₂ H ₁₈	46.0	74.2	88.5	104.0	121.7	132.2	146.8	168.3	193.7	218.0	
1,3,4-Triethylbenzene	C ₁₂ H ₁₈	47.9	76.0	90.2	105.8	122.6	133.4	147.7	168.3	193.2	217.5	
Triethylborine	C ₆ H ₁₅ B			-148.0	-140.6	-131.4	-125.2	-116.0	-101.0	-81.0	-56.2	
Triethyl camphorinate citrate	C ₁₉ H ₂₈ O ₆		150.2	166.0	183.6	201.8	213.5	228.6	250.8	276.0	301.0	135
Triethyleneglycol	C ₆ H ₁₄ O ₄	107.0	138.7	144.0	171.1	190.4	202.5	217.8	242.2	267.5	294.0	
Triethylheptylsilane	C ₁₃ H ₃₀ Si	114.0	144.0	158.1	174.0	191.3	201.5	214.6	235.2	256.6	278.3	
Triethylcytolsilane	C ₁₄ H ₃₀ Si	70.0	99.8	114.6	130.3	148.0	158.2	174.0	196.0	221.0	247.0	
Triethyl orthoformate phosphate	C ₇ H ₁₆ O ₃ P	73.7	104.8	120.6	137.7	155.7	168.0	184.3	208.0	235.0	262.0	
Triethylthallium	C ₆ H ₁₅ Tl	+5.5	29.2	40.5	53.4	67.5	76.0	88.0	106.0	125.7	146.0	
Trifluorophenylsilane	C ₆ H ₅ F ₃ Si	39.6	67.8	82.1	97.8	115.7	126.3	141.6	163.7	187.0	211.0	
Trimethyl phosphate	C ₃ H ₉ O ₃ P	+9.3	37.6	51.7	67.7	85.4	95.7	112.1	136.0	163.5	192.1	-63.0
2,3,5-Trimethylacetophenone	C ₁₂ H ₂₁ PO ₄	-31.0	-9.7	+0.8	12.3	25.4	33.2	44.2	60.1	78.7	98.3	
Trimethylamine	C ₃ H ₉ N	93.7	131.0	149.8	169.8	192.0	207.0	225.7	255.0	288.5	324.0	
2,4,5-Trimethylaniline	C ₁₁ H ₁₁ O	79.0	108.0	122.3	137.5	154.2	165.7	179.7	201.3	224.3	247.5	
1,2,3-Trimethylbenzene	C ₉ H ₁₂	-97.1	-81.7	-73.8	-65.0	-55.2	-48.8	-40.3	-27.0	-12.5	+2.9	-117.1
1,2,4-Trimethylbenzene	C ₉ H ₁₂	68.4	95.9	109.0	123.7	139.8	149.5	162.0	182.3	203.7	234.5	67
1,3,5-Trimethylbenzene	C ₉ H ₁₂	16.8	42.9	55.9	69.9	85.4	95.3	108.8	129.0	152.0	176.1	-25.5
2,2,3-Trimethylbutane	C ₉ H ₁₈	13.6	38.3	50.7	64.5	79.8	89.5	102.8	122.7	145.4	169.2	-44.1
Trimethyl citrate	C ₉ H ₁₈ O ₇	9.6	34.7	47.4	61.0	76.1	85.8	98.9	118.6	141.0	164.7	-44.8
Triethyleneglycol (1,3-propanediol)	C ₆ H ₁₄ O ₂			-18.8	-7.5	+5.2	13.3	24.4	41.2	60.4	80.9	-25.0
1,2,4-Trimethyl-5-ethylbenzene	C ₁₁ H ₁₆	106.2	146.2	160.4	177.2	194.2	205.5	219.6	241.3	264.2	287.0	78.5
1,3,5-Trimethyl-2-ethylbenzene	C ₁₁ H ₁₆	59.4	87.2	100.6	115.5	131.0	141.1	153.4	172.8	193.8	214.2	
2,2,3-Trimethylpentane	C ₈ H ₁₈	43.7	71.2	84.6	99.7	106.0	126.3	140.3	160.3	184.5	208.1	
2,2,4-Trimethylpentane	C ₈ H ₁₈	38.8	67.0	80.5	96.0	113.2	123.8	137.9	158.4	183.5	208.0	
2,3,3-Trimethylpentane	C ₈ H ₁₈	-29.0	-7.1	+3.9	16.0	29.5	38.1	49.9	67.8	88.2	109.8	-112.3
2,3,4-Trimethylpentane	C ₈ H ₁₈	-36.5	-15.0	-4.3	+7.5	20.7	29.1	40.7	58.1	78.0	99.2	-107.3
2,2,4-Trimethyl-3-pentanone	C ₈ H ₁₈	-25.8	-3.9	+6.9	19.2	33.0	41.8	53.8	72.0	92.7	114.8	-101.5
Trimethyl phosphate	C ₆ H ₁₆ O	-26.3	-4.1	+7.1	19.3	32.9	41.6	53.4	71.3	91.8	113.5	-109.2
2,4,5-Trimethylstyrene	C ₈ H ₁₆ O	14.7	36.0	46.4	57.6	69.8	77.3	87.6	102.2	118.4	135.0	
2,4,6-Trimethylstyrene	C ₈ H ₁₆ O	26.0	53.7	67.8	83.0	100.0	110.0	124.0	145.0	167.8	192.7	
Trimethylsuccinic anhydride	C ₁₁ H ₁₄	48.1	77.0	91.6	107.1	124.2	135.5	149.8	171.8	196.1	221.2	
Triphenylmethane	C ₁₉ H ₁₆	37.5	65.7	79.7	94.8	111.8	122.3	136.8	157.8	183.2	207.0	
Triphenylphosphate	C ₁₉ H ₁₆ O ₃	53.5	82.6	97.4	113.8	131.0	142.2	156.5	179.8	205.5	231.0	
Tripropyleneglycol	C ₁₀ H ₁₆	169.7	188.4	197.0	206.8	215.5	221.2	228.4	239.7	249.8	259.2	93.4
Tripropyleneglycol monobutyl ether	C ₁₈ H ₃₂ O ₄	193.5	230.4	249.8	269.3	290.3	305.2	322.5	349.8	379.2	413.5	49.4
Tripropyleneglycol monoisopropyl ether	C ₁₃ H ₂₆ O ₄	96.0	125.7	140.5	155.8	173.7	184.6	199.0	220.2	244.3	267.2	
Tritolyl phosphate	C ₁₅ H ₂₆ O ₄	101.5	131.6	147.0	161.8	179.8	190.2	204.4	224.4	247.0	269.5	
Undecane	C ₁₂ H ₂₆ O	82.4	112.4	127.3	143.7	161.4	173.2	187.8	209.7	232.8	256.6	
Undecanoic acid	C ₁₁ H ₂₂ O ₂	154.6	184.2	198.0	213.2	229.7	239.8	252.2	271.8	292.7	313.0	
10-Undecenoic acid	C ₁₁ H ₂₀ O ₂	32.7	59.7	73.9	85.6	104.4	115.2	128.1	149.3	171.9	195.8	-25.6
Undecan-2-ol	C ₁₁ H ₂₂ O	101.4	133.1	149.0	166.0	185.6	197.2	212.5	237.8	262.8	290.0	29.5
<i>n</i> -Valeric acid	C ₁₁ H ₂₂ O	114.0	142.8	156.3	172.0	188.7	199.5	213.5	232.8	254.0	275.0	24.5
iso-Valeric acid	C ₁₁ H ₂₂ O	71.1	99.0	112.8	127.5	143.7	153.7	167.2	187.7	209.8	232.0	
γ -Valerolactone	C ₆ H ₁₀ O ₂	42.2	67.7	79.8	93.1	107.8	116.6	128.3	146.0	165.0	184.4	-34.5
Valeronitrile	C ₅ H ₁₀ O ₂	34.5	59.6	71.3	84.0	98.0	107.3	118.9	136.2	155.2	175.1	-37.6
Vanillin	C ₉ H ₁₀ O ₂	37.5	65.8	79.8	95.2	101.9	122.4	136.5	157.7	182.3	207.5	
Vinyl acetate	C ₅ H ₁₀ O	-6.0	+18.1	30.0	43.3	57.8	66.9	78.6	97.7	118.7	140.8	
2-Vinylanisole	C ₉ H ₁₀ O	107.0	138.4	154.0	170.5	188.7	199.8	214.5	237.3	260.0	285.0	81.5
3-Vinylanisole	C ₉ H ₁₀ O	-48.0	-28.0	-18.0	-7.0	+5.3	13.0	23.3	38.4	55.5	72.5	
4-Vinylanisole	C ₉ H ₁₀ O	41.9	68.0	81.0	94.7	110.0	119.8	132.3	151.0	172.1	194.0	
Vinyl chloride (1-chloroethylene)	C ₂ H ₃ Cl	43.4	69.9	83.0	97.2	112.5	122.3	135.3	154.0	175.8	197.5	
cyamide (acrylonitrile)	C ₃ H _{3.5} N	45.2	72.0	85.7	100.0	116.0	126.1	139.7	159.0	182.0	204.5	
fluoride (1-fluoroethylene)	C ₂ H ₃ F	-105.6	-90.8	-83.7	-75.7	-66.8	-61.1	-53.2	-41.3	-28.0	-13.8	-153.7
Vinylidene chloride (1,1-dichloroethene)	C ₂ H ₂ Cl ₂	-51.0	-30.7	-20.3	-9.0	+3.8	11.8	22.8	38.7	58.3	78.5	-82
4-Vinylphenetole	C ₁₀ H ₁₂ O	-149.3	-138.0	-132.2	-125.4	-118.0	-113.0	-106.2	-95.4	-84.0	-72.2	-160.5
2-Xenyl dichlorophosphate	C ₁₂ H ₁₀ Cl ₂ PO	-77.2	-60.0	-51.2	-41.7	-31.1	-24.0	-15.0	-1.0	+14.8	31.7	-122.5
2,4-Xyalddehyde	C ₈ H ₁₀ O	64.0	91.7	105.6	120.3	136.3	146.4	159.8	180.0	202.8	225.0	
2-Xylene (2-xylene)	C ₈ H ₁₀	138.2	171.1	187.0	205.0	223.8	236.0	251.5	275.3	301.5	328.5	
3-Xylene (3-xylene)	C ₈ H ₁₀	59.0	85.9	99.0	114.0	129.7	139.8	152.2	172.3	194.1	215.5	75
4-Xylene (4-xylene)	C ₈ H ₁₀	-3.8	+20.2	32.1	45.1	59.5	68.8	81.3	100.2	121.7	144.4	-25.2
2,4-Xyldine	C ₈ H ₁₁ N	-6.9	+16.8	28.3	41.1	55.3	64.4	76.8	95.5	116.7	139.1	-47.9
2,6-Xyldine	C ₈ H ₁₁ N	-8.1	+15.5	27.3	40.1	54.4	63.5	75.9	94.6	115.9	138.3	+13.3
	C ₈ H ₁₁ N	52.6	79.8	93.0	107.6	123.8	133.7	146.8	166.4	188.3	211.5	
	C ₈ H ₁₁ N	44.0	72.6	87.0	102.7	120.2	131.5	146.0	168.0	193.7	217.9	

VAPOR PRESSURES OF SOLUTIONS

UNITS CONVERSIONS

For this subsection, the following units conversions are applicable:

$$^{\circ}\text{F} = \%^{\circ}\text{C} + 32$$

To convert millimeters of mercury to pounds-force per square inch, multiply by 0.01934.

To convert cubic feet to cubic meters, multiply by 0.02832.
 To convert bars to pounds-force per square inch, multiply by 14.504.
 To convert bars to kilopascals, multiply by 1×10^2 .

TABLE 2-11 Partial Pressures of Water over Aqueous Solutions of HCl*

$\log_{10} p_{\text{mm}} = A - B/T$, (T in K), which, however, agrees only approximately with the table. The table is more nearly correct.
 Partial pressure of H_2O , mmHg, $^{\circ}\text{C}$

% HCl	A	B	0°	5°	10°	15°	20°	25°	30°	35°	40°	45°	50°	60°	70°	80°	90°	100°	110°
6	8.99156	2282	4.18	6.04	8.45	11.7	15.9	21.8	29.1	39.4	50.6	66.2	86.0	139	220	333	492	715	
10	8.99864	2295	3.84	5.52	7.70	10.7	14.6	20.0	26.8	35.5	47.0	61.5	80.0	130	204	310	463	677	960
14	8.97075	2300	3.39	4.91	6.95	9.65	13.1	18.0	24.1	31.9	42.1	55.3	72.0	116	185	273	425	625	892
18	8.98014	2323	2.87	4.21	5.92	8.26	11.3	15.4	20.6	27.5	36.4	47.9	62.5	102	162	248	374	550	783
20	8.97877	2334	2.62	3.83	5.40	7.50	10.3	14.1	19.0	25.1	33.3	43.6	57.0	93.5	150	230	345	510	729
22	9.02708	2363	2.33	3.40	4.82	6.75	9.30	12.6	17.1	22.8	30.2	39.8	52.0	85.6	138	211	317	467	670
24	8.96022	2356	2.05	3.04	4.31	6.03	8.30	11.4	15.4	20.4	27.1	35.7	46.7	77.0	124	194	290	426	611
26	9.01511	2390	1.76	2.60	3.71	5.21	7.21	9.95	13.5	18.0	24.0	31.7	41.5	69.0	112	173	261	387	555
28	8.97611	2395	1.50	2.24	3.21	4.54	6.32	8.75	11.8	15.8	21.1	27.9	36.5	60.7	99.0	154	234	349	499
30	9.00117	2422	1.26	1.90	2.73	3.88	5.41	7.52	10.2	13.7	18.4	24.3	32.0	53.5	87.5	136	207	310	444
32	9.03317	2453	1.04	1.57	2.27	3.25	4.55	6.37	8.70	11.7	15.7	21.0	27.7	46.5	76.5	120	184	275	396
34	9.07143	2487	0.85	1.29	1.87	2.70	3.81	5.35	7.32	9.95	13.5	18.1	24.0	40.5	66.5	104	161	243	355
36	9.11815	2526	0.68	1.03	1.50	2.19	3.10	4.41	6.08	8.33	11.4	15.4	20.4	34.8	57.0	90.0	140	212	311
38	9.20783	2579	0.53	0.81	1.20	1.75	2.51	3.60	5.03	6.92	9.52	13.0	17.4	29.6	49.1	77.5	120	182	266
40	9.33923	2647	0.41	0.63	0.94	1.37	2.00	2.88	4.09	5.68	7.85	10.7	14.5	25.0	42.1	67.3	105	158	230
42	9.44953	2709	0.31	0.48	0.72	1.06	1.56	2.30	3.28	4.60	6.45	8.90	12.1	21.2	35.8	57.2	89.2	135	195

*Uncertainty, ca. 2 percent for solutions of 15 to 30 percent HCl between 0 and 100°; for solutions of > 30 percent HCl the accuracy is ca. 5 percent at the lower temperatures and ca. 15 percent at the higher temperatures. Below 15 percent HCl, the uncertainty is ca. 5 percent at the lower temperatures and higher strengths to ca. 15 to 20 percent at the lower strengths and perhaps 15 to 20 percent at the higher temperatures and lower strengths.
International Critical Tables, vol. 3, p. 301.

TABLE 2-12 Partial Pressures of HCl over Aqueous Solutions of HCl*

$\log_{10} p_{\text{mm}} = A - B/T$, (T in K), which, however, agrees only approximately with the table. The table is more nearly correct. mmHg, $^{\circ}\text{C}$

% HCl	A	B	0°	5°	10°	15°	20°	25°	30°	35°	40°	45°	50°	60°	70°	80°	90°	100°	110°
2	11.8037	4736			0.0000117	0.000023	0.000044	0.000084	0.000151	0.000275	0.00047	0.00083	0.00140	0.00380	0.0100	0.0245	0.058	0.132	0.280
4	11.6400	4471	0.000018	0.000036	0.000069	0.000131	0.00024	0.00044	0.00077	0.00134	0.0023	0.00385	0.0064	0.0165	0.0405	0.095	.21	.46	.93
6	11.2144	4202	0.000066	0.000125	0.000234	0.000425	0.00076	0.00131	0.00225	0.0038	0.0062	0.0102	0.0163	0.040	0.094	0.206	.44	.92	1.78
8	11.0406	4042	0.000118	0.000223	0.000383	0.00064	0.00104	0.00178	0.0031	0.00515	0.0085	0.0136	0.022	0.0344	0.081	0.183	.39	.82	1.64
10	10.9311	3908	0.00042	0.00075	0.00134	0.00232	0.00395	0.0067	0.0111	0.0178	0.0282	0.045	0.069	0.157	0.35	0.73	1.48	2.9	5.4
12	10.7900	3765	0.00099	0.00175	0.00305	0.0052	0.0088	0.0145	0.0234	0.037	0.058	0.091	0.136	0.305	0.66	1.34	2.65	5.1	9.3
14	10.6954	3636	0.0024	0.00415	0.0071	0.0118	0.0196	0.0316	0.050	0.078	0.121	0.185	0.275	0.60	1.25	2.50	4.8	9.0	16.0
16	10.6261	3516	0.0056	0.0095	0.016	0.0265	0.0428	0.0685	0.106	0.163	0.247	0.375	0.55	1.17	2.40	4.66	8.8	16.1	28
18	10.4957	3376	0.0135	0.0225	0.037	0.060	0.095	0.148	0.228	0.345	0.515	0.77	1.11	2.3	4.55	8.6	15.7	28	48
20	10.3833	3245	0.0316	0.052	0.084	0.132	0.205	0.32	0.48	0.72	1.06	1.55	2.21	4.4	8.5	15.6	28.1	49	83
22	10.3172	3125	0.0734	0.119	0.187	0.294	0.45	0.68	1.02	1.50	2.18	3.14	4.42	8.6	16.3	29.3	52	90	146
24	10.2185	2995	0.175	0.277	0.43	0.66	1.00	1.49	2.17	3.14	4.5	6.4	8.9	16.9	31.0	54.5	94	157	253
26	10.1303	2870	0.41	0.64	0.98	1.47	2.17	3.20	4.56	6.50	9.2	12.7	17.5	32.5	58.5	100	169	276	436
28	10.0115	2732	1.0	1.52	2.27	3.36	4.90	7.05	9.90	13.8	19.1	26.4	35.7	64	112	188	309	493	760
30	9.8763	2593	2.4	3.57	5.23	7.60	10.6	15.1	21.0	28.6	39.4	53	71	124	208	340	542	845	
32	9.7523	2457	5.7	8.3	11.8	16.8	23.5	32.5	44.5	60.0	81	107	141	238	390	623	970		
34	9.6061	2316	13.1	18.8	26.4	36.8	50.5	68.5	92	122	161	211	273	450	720				
36	9.5262	2229	29.0	41.0	56.4	78	105.5	142	188	246	322	416	535	860					
38	9.4670	2094	63.0	87.0	117	158	210	277	360	465	598	758	955						
40	9.2156	1939	130	176	233	307	399	515	627	830									
42	8.9925	1800	253	332	430	560	709	900											
44	8.8621	1681	510	655	840														
46		940																	

*Uncertainty, ca. 2 percent for solutions of 15 to 30 percent HCl between 0 and 100°; for solutions of > 30 percent HCl the accuracy is ca. 5 percent at the lower temperatures and ca. 15 percent at the higher temperatures. Below 15 percent HCl, the uncertainty is ca. 5 percent at the lower temperatures and higher strengths to ca. 15 to 20 percent at the lower strengths and perhaps 15 to 20 percent at the higher temperatures and lower strengths.
International Critical Tables, vol. 3, p. 301.

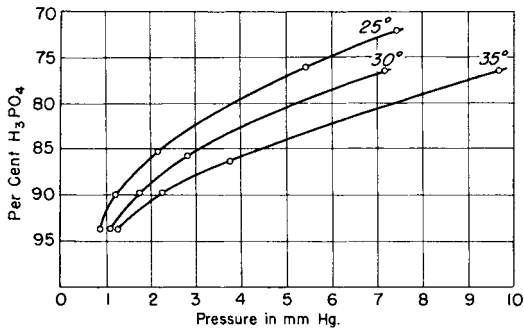


FIG. 2-1 Vapor pressures of H₃PO₄ aqueous: partial pressure of H₂O vapor. (Courtesy of Victor Chemical Works, Stauffer Chemical Company; measurements by W. H. Woodstock.)

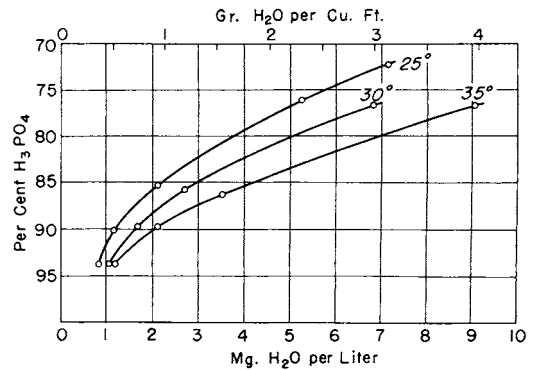


FIG. 2-2 Vapor pressures of H₃PO₄ aqueous: weight of H₂O in saturated air. (Courtesy of Victor Chemical Works, Stauffer Chemical Company; measurements by W. H. Woodstock.)

TABLE 2-13 Partial Pressures of H₂O and SO₂ over Aqueous Solutions of Sulfur Dioxide*
Partial pressures of H₂O and SO₂, mmHg, °C

g SO ₂ / 100 g H ₂ O	Temperature, °C								
	0	10	20	30	40	50	60	90	120
0.01	0.02	0.04	0.07	0.12	0.19	0.29	0.43	1.21	2.82
0.05	0.38	0.66	1.07	1.68	2.53	3.69	5.24	12.9	27.0
0.10	1.15	1.91	3.03	4.62	6.80	9.71	13.5	31.7	63.9
0.15	2.10	3.44	5.37	8.07	11.7	16.5	22.7	52.2	104
0.20	3.17	5.13	7.93	11.8	17.0	23.8	32.6	73.7	145
0.25	4.34	6.93	10.6	15.7	22.5	31.4	42.8	95.8	186
0.30	5.57	8.84	13.5	19.8	28.2	39.2	53.3	118	229
0.40	8.17	12.8	19.4	28.3	40.1	55.3	74.7	164	316
0.50	10.9	17.0	25.6	37.1	52.3	72.0	96.8	211	404
1.00	25.8	39.5	58.4	83.7	117	159	212	454	856
2.00	58.6	88.5	129	183	253	342	453	955	
3.00	93.2	139	202	285	393	530	700		
4.00	129	192	277	389	535	720			
5.00	165	245	353	496	679				
6.00	202	299	430	602	824				
8.00	275	407	585	818					
10.00	351	517	741						
15.00	542	796							
20.00	735								

*Extracted with permission from *J. Chem Eng. Data* 8, 1963: 333-336. Copyright 1963 American Chemical Society.

2-82 PHYSICAL AND CHEMICAL DATA

TABLE 2-14 Water Partial Pressure, bar, over Aqueous Sulfuric Acid Solutions*
Weight percent, H₂SO₄

°C	10.0	20.0	30.0	40.0	50.0	60.0	70.0	75.0	80.0	85.0
0	.582E-02	.534E-02	.448E-02	.326E-02	.193E-02	.836E-03	.207E-03	.747E-04	.197E-04	.343E-05
10	.117E-01	.107E-01	.909E-02	.670E-02	.405E-02	.180E-02	.467E-03	.175E-03	.490E-04	.952E-05
20	.223E-01	.205E-01	.174E-01	.130E-01	.802E-02	.367E-02	.995E-03	.388E-03	.115E-04	.245E-04
30	.404E-01	.373E-01	.319E-01	.241E-01	.151E-01	.710E-02	.201E-02	.811E-03	.253E-03	.589E-04
40	.703E-01	.649E-01	.558E-01	.427E-01	.272E-01	.131E-01	.387E-02	.162E-02	.531E-03	.133E-03
50	.117	.109	.939E-01	.725E-01	.470E-01	.232E-01	.715E-02	.309E-02	.106E-02	.286E-03
60	.189	.175	.152	.119	.782E-01	.395E-01	.127E-01	.565E-02	.204E-02	.584E-03
70	.296	.275	.239	.188	.126	.651E-01	.217E-01	.997E-02	.376E-02	.114E-02
80	.449	.417	.365	.290	.196	.104	.360E-01	.170E-01	.668E-02	.213E-02
90	.664	.617	.542	.434	.298	.161	.578E-01	.281E-01	.115E-01	.383E-02
100	.957	.891	.786	.634	.441	.244	.905E-01	.452E-01	.192E-01	.666E-02
110	1.349	1.258	1.113	.904	.638	.360	.138	.708E-01	.312E-01	.112E-01
120	1.863	1.740	1.544	1.264	.903	.519	.206	.108	.493E-01	.183E-01
130	2.524	2.361	2.101	1.732	1.253	.734	.301	.162	.760E-01	.291E-01
140	3.361	3.149	2.810	2.333	1.708	1.020	.481	.236	.115	.451E-01
150	4.404	4.132	3.697	3.090	2.289	1.392	.605	.339	.170	.682E-01
160	5.685	5.342	4.793	4.031	3.021	1.870	.837	.478	.246	.101
170	7.236	6.810	6.127	5.185	3.930	2.475	1.138	.662	.350	.147
180	9.093	8.571	7.731	6.584	5.045	3.233	1.525	.902	.489	.208
190	11.289	10.658	9.640	8.259	6.397	4.169	2.017	1.212	.673	.291
200	13.861	13.107	11.887	10.245	8.020	5.312	2.632	1.606	.913	.401
210	16.841	15.951	14.505	12.576	9.948	6.696	3.395	2.101	1.220	.542
220	20.264	19.225	17.529	15.287	12.217	8.354	4.331	2.714	1.609	.724
230	24.160	22.960	20.992	18.414	14.864	10.322	5.466	3.467	2.096	.952
240	28.561	27.188	24.927	21.992	17.929	12.641	6.831	4.381	2.699	1.237
250	33.494	31.939	29.364	26.056	21.452	15.351	8.458	5.480	3.435	1.587
260	38.984	37.240	34.334	30.642	25.472	18.496	10.382	6.788	4.326	2.012
270	45.055	43.116	39.865	35.784	30.030	22.121	12.640	8.333	5.395	2.525
280	51.726	49.590	45.984	41.514	35.168	26.274	15.269	10.142	6.663	3.136
290	59.015	56.681	52.715	47.865	40.926	31.003	18.311	12.242	8.155	3.857
300	66.934	64.407	60.081	54.868	47.346	36.360	21.808	14.665	9.897	4.701
310	75.495	72.781	68.100	62.553	54.470	42.395	25.804	17.438	11.912	5.680
320	84.705	81.816	76.792	70.947	62.337	49.164	30.343	20.591	14.227	6.806
330	94.567	91.518	86.172	80.077	70.988	56.721	35.473	24.153	16.867	8.093
340	105.083	101.894	96.252	89.969	80.463	65.123	41.240	28.154	19.855	9.551
350	116.251	112.946	107.043	100.646	90.802	74.426	47.692	32.622	23.217	11.193

*Vermeulen, Dong, Robinson, Nguyen, and Gmitro, AIChE meeting, Anaheim, Calif., 1982; and private communication from Prof. Theodore Vermeulen, Chemical Engineering Dept., University of California, Berkeley.

TABLE 2-14 Water Partial Pressure, bar, over Aqueous Sulfuric Acid Solutions (Concluded)
Weight percent, H₂SO₄

°C	90.0	92.0	94.0	96.0	97.0	98.0	98.5	99.0	99.5	100.0
0	.518E-06	.242E-06	.107E-06	.401E-07	.218E-07	.980E-08	.569E-08	.268E-08	.775E-09	.196E-09
10	.159E-05	.762E-06	.344E-06	.130E-06	.713E-07	.323E-07	.188E-07	.888E-08	.258E-08	.655E-09
20	.448E-05	.220E-05	.101E-05	.390E-06	.215E-06	.978E-07	.572E-07	.271E-07	.789E-08	.201E-08
30	.117E-04	.587E-05	.275E-05	.108E-05	.598E-06	.275E-06	.161E-06	.766E-07	.224E-07	.575E-08
40	.285E-04	.146E-04	.696E-05	.278E-05	.155E-05	.720E-06	.424E-06	.202E-06	.595E-07	.153E-07
50	.652E-04	.341E-04	.166E-04	.672E-05	.379E-05	.177E-05	.105E-05	.503E-06	.149E-06	.384E-07
60	.141E-03	.754E-04	.372E-04	.154E-04	.875E-05	.413E-05	.245E-05	.118E-05	.350E-06	.910E-07
70	.290E-03	.158E-03	.795E-04	.334E-04	.192E-04	.912E-05	.544E-05	.263E-05	.784E-06	.205E-06
80	.569E-03	.316E-03	.162E-03	.691E-04	.400E-04	.192E-04	.115E-04	.559E-05	.168E-05	.439E-06
90	.107E-02	.606E-03	.315E-03	.137E-03	.801E-04	.388E-04	.234E-04	.114E-04	.343E-05	.903E-06
100	.194E-02	.112E-02	.590E-03	.261E-03	.154E-03	.752E-04	.455E-04	.223E-04	.674E-05	.178E-05
110	.338E-02	.198E-02	.107E-02	.479E-03	.285E-03	.141E-03	.855E-04	.420E-04	.128E-04	.339E-05
120	.571E-02	.341E-02	.186E-02	.851E-03	.511E-03	.254E-03	.155E-03	.766E-04	.233E-04	.623E-05
130	.938E-02	.569E-02	.315E-02	.146E-02	.886E-03	.445E-03	.278E-03	.135E-03	.414E-04	.111E-04
140	.150E-01	.923E-02	.519E-02	.245E-02	.149E-02	.757E-03	.467E-03	.232E-03	.711E-04	.191E-04
150	.233E-01	.146E-01	.832E-02	.399E-02	.245E-02	.125E-02	.776E-03	.387E-03	.119E-03	.321E-04
160	.354E-01	.225E-01	.130E-01	.633E-02	.393E-02	.202E-02	.126E-02	.629E-03	.194E-03	.526E-04
170	.526E-01	.340E-01	.199E-01	.983E-02	.614E-02	.319E-02	.199E-02	.999E-03	.309E-03	.840E-04
180	.766E-01	.502E-01	.298E-01	.149E-01	.941E-02	.492E-02	.309E-02	.155E-02	.482E-03	.131E-03
190	.110	.729E-01	.438E-01	.222E-01	.141E-01	.744E-02	.469E-02	.236E-02	.735E-03	.201E-03
200	.154	.104	.631E-01	.325E-01	.208E-01	.110E-01	.698E-02	.352E-02	.110E-02	.300E-03
210	.213	.146	.894E-01	.467E-01	.300E-01	.161E-01	.102E-01	.516E-02	.161E-02	.442E-03
220	.290	.201	.125	.660E-01	.427E-01	.230E-01	.147E-01	.743E-02	.232E-02	.638E-03
230	.389	.273	.171	.918E-01	.598E-01	.325E-01	.208E-01	.105E-01	.329E-02	.906E-03
240	.514	.366	.232	.126	.825E-01	.451E-01	.290E-01	.147E-01	.460E-02	.127E-02
250	.673	.485	.310	.170	.112	.618E-01	.398E-01	.202E-01	.633E-02	.174E-02
260	.870	.635	.409	.227	.151	.835E-01	.540E-01	.274E-01	.858E-02	.237E-02
270	1.112	.822	.534	.300	.200	.111	.723E-01	.366E-01	.115E-01	.317E-02
280	1.407	1.052	.689	.391	.263	.147	.957E-01	.485E-01	.152E-01	.420E-02
290	1.763	1.335	.880	.505	.341	.192	.125	.634E-01	.199E-01	.548E-02
300	2.190	1.676	1.112	.646	.437	.248	.162	.820E-01	.257E-01	.708E-02
310	2.696	2.088	1.394	.817	.556	.316	.208	.105	.328E-01	.905E-02
320	3.292	2.578	1.732	1.025	.701	.400	.264	.133	.415E-01	.114E-01
330	3.990	3.159	2.133	1.274	.875	.502	.331	.167	.520E-01	.143E-01
340	4.801	3.843	2.608	1.571	1.083	.624	.413	.208	.646E-01	.178E-01
350	5.738	4.641	3.164	1.922	1.331	.770	.511	.256	.795E-01	.218E-01

2-84 PHYSICAL AND CHEMICAL DATA

TABLE 2-15 Sulfur Trioxide Partial Pressure, bar, over Aqueous Sulfuric Acid Solutions*
Weight percent, H₂SO₄

°C	10.0	20.0	30.0	40.0	50.0	60.0	70.0	75.0	80.0	85.0
0	.644E-29	.103E-27	.205E-26	.688E-25	.368E-23	.341E-21	.784E-19	.174E-17	.531E-16	.229E-14
10	.149E-27	.223E-26	.395E-25	.113E-23	.522E-22	.415E-20	.796E-18	.158E-16	.417E-15	.141E-13
20	.278E-26	.394E-25	.626E-24	.156E-22	.621E-21	.426E-19	.685E-17	.121E-15	.280E-14	.767E-13
30	.426E-25	.577E-24	.832E-23	.181E-21	.630E-20	.376E-18	.509E-16	.808E-15	.164E-13	.371E-12
40	.549E-24	.714E-23	.941E-22	.181E-20	.555E-19	.288E-17	.331E-15	.473E-14	.851E-13	.162E-11
50	.602E-23	.757E-22	.921E-21	.158E-19	.429E-18	.195E-16	.191E-14	.246E-13	.395E-12	.643E-11
60	.573E-22	.699E-21	.789E-20	.122E-18	.294E-17	.118E-15	.985E-14	.116E-12	.165E-11	.234E-10
70	.477E-21	.567E-20	.599E-19	.843E-18	.181E-16	.643E-15	.461E-13	.492E-12	.634E-11	.791E-10
80	.352E-20	.410E-19	.408E-18	.524E-17	.101E-15	.319E-14	.197E-12	.192E-11	.223E-10	.249E-09
90	.233E-19	.266E-18	.250E-17	.296E-16	.516E-15	.145E-13	.775E-12	.693E-11	.731E-10	.734E-09
100	.139E-18	.157E-17	.140E-16	.153E-15	.242E-14	.606E-13	.283E-11	.232E-10	.223E-09	.204E-08
110	.756E-18	.844E-17	.719E-16	.730E-15	.105E-13	.236E-12	.961E-11	.729E-10	.641E-09	.538E-08
120	.377E-17	.418E-16	.340E-15	.323E-14	.424E-13	.858E-12	.307E-10	.215E-09	.174E-08	.135E-07
130	.174E-16	.191E-15	.150E-14	.133E-13	.160E-12	.293E-11	.922E-10	.601E-09	.446E-08	.324E-07
140	.743E-16	.815E-15	.615E-14	.517E-13	.569E-12	.943E-11	.262E-09	.159E-08	.109E-07	.745E-07
150	.297E-15	.325E-14	.237E-13	.188E-12	.191E-11	.287E-10	.710E-09	.403E-08	.256E-07	.165E-06
160	.111E-14	.122E-13	.862E-13	.649E-12	.608E-11	.833E-10	.183E-08	.974E-08	.575E-07	.351E-06
170	.393E-14	.430E-13	.296E-12	.212E-11	.184E-10	.231E-09	.453E-08	.226E-07	.125E-06	.725E-06
180	.131E-13	.144E-12	.967E-12	.622E-11	.532E-10	.610E-09	.107E-07	.505E-07	.260E-06	.145E-05
190	.415E-13	.458E-12	.301E-11	.197E-10	.147E-09	.155E-08	.246E-07	.109E-06	.527E-06	.282E-05
200	.125E-12	.139E-11	.893E-11	.561E-10	.391E-09	.379E-08	.542E-07	.228E-06	.103E-05	.534E-05
210	.362E-12	.404E-11	.254E-10	.154E-09	.100E-08	.894E-08	.116E-06	.462E-06	.198E-05	.986E-05
220	.100E-11	.112E-10	.695E-10	.405E-09	.246E-08	.204E-07	.240E-06	.911E-06	.368E-05	.178E-04
230	.265E-11	.301E-10	.183E-09	.103E-08	.587E-08	.450E-07	.482E-06	.175E-05	.668E-05	.314E-04
240	.678E-11	.777E-10	.465E-09	.253E-08	.135E-07	.965E-07	.944E-06	.328E-05	.119E-04	.543E-04
250	.167E-10	.193E-09	.114E-08	.602E-08	.303E-07	.201E-06	.180E-05	.600E-05	.206E-04	.923E-04
260	.399E-10	.466E-09	.272E-08	.139E-07	.660E-07	.408E-06	.336E-05	.108E-04	.352E-04	.154E-03
270	.920E-10	.109E-08	.628E-08	.312E-07	.140E-06	.807E-06	.612E-05	.189E-04	.590E-04	.253E-03
280	.206E-09	.247E-08	.141E-07	.683E-07	.288E-06	.156E-05	.109E-04	.326E-04	.973E-04	.408E-03
290	.449E-09	.545E-08	.308E-07	.145E-06	.580E-06	.295E-05	.191E-04	.553E-04	.158E-03	.649E-03
300	.953E-09	.117E-07	.657E-07	.302E-06	.114E-05	.546E-05	.329E-04	.921E-04	.253E-03	.102E-02
310	.197E-08	.245E-07	.136E-06	.614E-06	.220E-05	.990E-05	.556E-04	.151E-03	.398E-03	.158E-02
320	.397E-08	.502E-07	.277E-06	.122E-05	.414E-05	.176E-04	.923E-04	.245E-03	.621E-03	.242E-02
330	.782E-08	.100E-06	.551E-06	.237E-05	.766E-05	.308E-04	.151E-03	.391E-03	.956E-03	.367E-02
340	.151E-07	.196E-06	.107E-05	.452E-05	.139E-04	.529E-04	.243E-03	.617E-03	.145E-02	.550E-02
350	.285E-07	.376E-06	.204E-05	.846E-05	.246E-04	.893E-04	.387E-03	.963E-03	.219E-02	.815E-02

*Vermeulen, Dong, Robinson, Nguyen, and Gmitro, AIChE meeting, Anaheim, Calif., 1982; and private communication from Prof. Theodore Vermeulen, Chemical Engineering Dept., University of California, Berkeley.

TABLE 2-15 Sulfur Trioxide Partial Pressure, bar, over Aqueous Sulfuric Acid Solutions (Concluded)
Weight percent, H₂SO₄

°C	90.0	92.0	94.0	96.0	97.0	98.0	98.5	99.0	99.5	100.0
0	.671E-13	.216E-12	.677E-12	.240E-11	.500E-11	.124E-10	.224E-10	.502E-10	.182E-09	.755E-09
10	.345E-12	.107E-11	.326E-11	.114E-10	.234E-10	.578E-10	.104E-09	.232E-09	.839E-09	.347E-08
20	.159E-11	.475E-11	.141E-10	.482E-10	.986E-10	.241E-09	.433E-09	.961E-09	.346E-08	.142E-07
30	.664E-11	.192E-10	.557E-10	.186E-09	.376E-09	.911E-09	.163E-08	.360E-08	.129E-07	.528E-07
40	.254E-10	.709E-10	.201E-09	.655E-09	.131E-08	.315E-08	.562E-08	.123E-07	.440E-07	.179E-06
50	.897E-10	.242E-09	.669E-09	.214E-08	.424E-08	.101E-07	.179E-07	.391E-07	.139E-06	.560E-06
60	.294E-09	.771E-09	.207E-08	.647E-08	.127E-07	.299E-07	.528E-07	.115E-06	.405E-06	.163E-05
70	.904E-09	.230E-08	.602E-08	.184E-07	.357E-07	.833E-07	.146E-06	.316E-06	.111E-05	.444E-05
80	.261E-08	.643E-08	.165E-07	.492E-07	.946E-07	.218E-06	.381E-06	.820E-06	.286E-05	.114E-04
90	.712E-08	.171E-07	.426E-07	.124E-06	.237E-06	.541E-06	.940E-06	.201E-05	.698E-05	.276E-04
100	.184E-07	.430E-07	.105E-06	.300E-06	.565E-06	.127E-05	.220E-05	.470E-05	.162E-04	.638E-04
110	.456E-07	.103E-06	.247E-06	.689E-06	.128E-05	.287E-05	.494E-05	.105E-04	.359E-04	.141E-03
120	.108E-06	.238E-06	.555E-06	.152E-05	.280E-05	.619E-05	.106E-04	.224E-04	.764E-04	.298E-03
130	.244E-06	.526E-06	.120E-05	.321E-05	.586E-05	.128E-04	.219E-04	.459E-04	.156E-03	.606E-03
140	.533E-06	.112E-05	.250E-05	.656E-05	.118E-04	.257E-04	.435E-04	.910E-04	.308E-03	.119E-02
150	.112E-05	.230E-05	.504E-05	.129E-04	.231E-04	.497E-04	.837E-04	.174E-03	.588E-03	.226E-02
160	.229E-05	.459E-05	.983E-05	.247E-04	.438E-04	.932E-04	.156E-03	.324E-03	.109E-02	.416E-02
170	.453E-05	.886E-05	.186E-04	.459E-04	.806E-04	.170E-03	.283E-03	.586E-03	.196E-02	.746E-02
180	.870E-05	.166E-04	.343E-04	.829E-04	.144E-03	.301E-03	.499E-03	.103E-02	.343E-02	.130E-01
190	.163E-04	.304E-04	.615E-04	.146E-03	.252E-03	.520E-03	.859E-03	.177E-02	.587E-02	.222E-01
200	.297E-04	.543E-04	.108E-03	.251E-03	.429E-03	.878E-03	.144E-02	.296E-02	.981E-02	.370E-01
210	.528E-04	.946E-04	.185E-03	.422E-03	.714E-03	.145E-02	.237E-02	.486E-02	.161E-01	.603E-01
220	.919E-04	.161E-03	.309E-03	.694E-03	.117E-02	.235E-02	.383E-02	.781E-02	.258E-01	.965E-01
230	.157E-03	.269E-03	.508E-03	.112E-02	.187E-02	.373E-02	.605E-02	.123E-01	.405E-01	.152
240	.261E-03	.441E-03	.819E-03	.178E-02	.293E-02	.582E-02	.939E-02	.191E-01	.627E-01	.234
250	.428E-03	.708E-03	.130E-02	.276E-02	.453E-02	.891E-02	.143E-01	.291E-01	.955E-01	.356
260	.690E-03	.112E-02	.202E-02	.423E-02	.688E-02	.134E-01	.215E-01	.437E-01	.143	.532
270	.109E-02	.174E-02	.309E-02	.638E-02	.103E-01	.200E-01	.319E-01	.646E-01	.212	.786
280	.170E-02	.266E-02	.466E-02	.948E-02	.152E-01	.293E-01	.465E-01	.943E-01	.309	1.144
290	.261E-02	.401E-02	.694E-02	.139E-01	.221E-01	.423E-01	.670E-01	.136	.444	1.646
300	.395E-02	.595E-02	.102E-01	.201E-01	.318E-01	.604E-01	.953E-01	.193	.632	2.339
310	.589E-02	.873E-02	.148E-01	.287E-01	.451E-01	.852E-01	.134	.272	.889	3.289
320	.868E-02	.126E-01	.211E-01	.405E-01	.632E-01	.119	.186	.378	1.236	4.575
330	.126E-01	.181E-01	.299E-01	.565E-01	.877E-01	.164	.256	.520	1.703	6.303
340	.181E-01	.255E-01	.418E-01	.780E-01	.120	.224	.348	.708	2.323	8.603
350	.258E-01	.357E-01	.578E-01	.107	.164	.303	.470	.956	3.142	11.640

TABLE 2-16 Sulfuric Acid Partial Pressure, bar, over Aqueous Sulfuric Acid*

°C	Weight percent, H ₂ SO ₄									
	10.0	20.0	30.0	40.0	50.0	60.0	70.0	75.0	80.0	85.0
0	.576E-21	.843E-20	.141E-18	.344E-17	.109E-15	.438E-14	.249E-12	.200E-11	.161E-10	.121E-09
10	.634E-20	.874E-19	.131E-17	.276E-16	.769E-15	.273E-13	.135E-11	.101E-10	.743E-10	.490E-09
20	.588E-19	.769E-18	.104E-16	.193E-15	.474E-14	.149E-12	.649E-11	.447E-10	.305E-09	.179E-08
30	.468E-18	.584E-17	.721E-16	.119E-14	.259E-13	.725E-12	.278E-10	.113E-09	.113E-08	.594E-08
40	.324E-17	.389E-16	.441E-15	.649E-14	.127E-12	.317E-11	.108E-09	.643E-09	.379E-08	.181E-07
50	.197E-16	.229E-15	.241E-14	.320E-13	.562E-12	.126E-10	.380E-09	.212E-08	.117E-07	.513E-07
60	.107E-15	.121E-14	.119E-13	.144E-12	.228E-11	.462E-10	.124E-08	.646E-08	.334E-07	.135E-06
70	.526E-15	.581E-14	.535E-13	.592E-12	.851E-11	.156E-09	.373E-08	.183E-07	.888E-07	.336E-06
80	.235E-14	.254E-13	.221E-12	.225E-11	.295E-10	.492E-09	.105E-07	.485E-07	.222E-06	.786E-06
90	.960E-14	.102E-12	.844E-12	.798E-11	.956E-10	.145E-08	.279E-07	.121E-06	.522E-06	.175E-05
100	.353E-13	.381E-12	.300E-11	.264E-10	.291E-09	.402E-08	.698E-07	.287E-06	.117E-05	.371E-05
110	.127E-12	.132E-11	.997E-11	.824E-10	.835E-09	.106E-07	.166E-06	.644E-06	.249E-05	.752E-05
120	.418E-12	.432E-11	.312E-10	.243E-09	.227E-08	.264E-07	.375E-06	.138E-05	.508E-05	.147E-04
130	.129E-11	.132E-10	.924E-10	.678E-09	.589E-08	.631E-07	.814E-06	.285E-05	.995E-05	.277E-04
140	.375E-11	.385E-10	.259E-09	.181E-08	.146E-07	.144E-06	.169E-05	.565E-05	.188E-04	.503E-04
150	.103E-10	.106E-09	.694E-09	.460E-08	.346E-07	.316E-06	.340E-05	.108E-04	.343E-04	.889E-04
160	.272E-10	.279E-09	.178E-08	.112E-07	.789E-07	.670E-06	.659E-05	.200E-04	.608E-04	.152E-03
170	.682E-10	.702E-09	.436E-08	.264E-07	.174E-06	.137E-05	.124E-04	.359E-04	.104E-03	.255E-03
180	.164E-09	.170E-08	.103E-07	.599E-07	.369E-06	.271E-05	.225E-04	.627E-04	.175E-03	.416E-03
190	.378E-09	.394E-08	.234E-07	.131E-06	.760E-06	.521E-05	.400E-04	.107E-03	.286E-03	.663E-03
200	.842E-09	.883E-08	.514E-07	.278E-06	.152E-05	.975E-05	.691E-04	.177E-03	.457E-03	.104E-02
210	.181E-08	.191E-07	.109E-06	.573E-06	.295E-05	.178E-04	.117E-03	.288E-03	.715E-03	.159E-02
220	.376E-08	.401E-07	.226E-06	.115E-05	.559E-05	.316E-04	.193E-03	.459E-03	.110E-02	.239E-02
230	.758E-08	.817E-07	.455E-06	.224E-05	.103E-04	.549E-04	.311E-03	.717E-03	.166E-02	.354E-02
240	.148E-07	.162E-06	.889E-06	.427E-05	.186E-04	.935E-04	.494E-03	.110E-02	.245E-02	.515E-02
250	.283E-07	.312E-06	.170E-05	.793E-05	.329E-04	.156E-03	.770E-03	.166E-02	.358E-02	.740E-02
260	.526E-07	.588E-06	.316E-05	.144E-04	.569E-04	.255E-03	.118E-02	.247E-02	.516E-02	.105E-01
270	.954E-07	.108E-05	.577E-05	.257E-04	.965E-04	.411E-03	.178E-02	.362E-02	.733E-02	.147E-01
280	.169E-06	.194E-05	.103E-04	.450E-04	.161E-03	.650E-03	.265E-02	.524E-02	.103E-01	.203E-01
290	.294E-06	.342E-05	.180E-04	.771E-04	.263E-03	.101E-02	.389E-02	.750E-02	.143E-01	.278E-01
300	.500E-06	.591E-05	.309E-04	.130E-03	.424E-03	.156E-02	.563E-02	.106E-01	.196E-01	.376E-01
310	.834E-06	.100E-04	.522E-04	.215E-03	.672E-03	.236E-02	.805E-02	.148E-01	.266E-01	.504E-01
320	.137E-05	.167E-04	.865E-04	.352E-03	.105E-02	.352E-02	.114E-01	.205E-01	.359E-01	.670E-01
330	.220E-05	.273E-04	.141E-03	.565E-03	.162E-02	.519E-02	.159E-01	.281E-01	.480E-01	.883E-01
340	.349E-05	.440E-04	.227E-03	.895E-03	.246E-02	.757E-02	.221E-01	.382E-01	.636E-01	.116
350	.544E-05	.698E-04	.360E-03	.140E-02	.369E-02	.109E-01	.303E-01	.516E-01	.836E-01	.150
°C	Weight percent, H ₂ SO ₄									
	90.0	92.0	94.0	96.0	97.0	98.0	98.5	99.0	99.5	100.0
0	.534E-09	.803E-09	.112E-08	.148E-08	.167E-08	.187E-08	.196E-08	.206E-08	.217E-08	.228E-08
10	.200E-08	.296E-08	.409E-08	.540E-08	.609E-08	.679E-08	.714E-08	.750E-08	.788E-08	.827E-08
20	.677E-08	.993E-08	.136E-07	.179E-07	.201E-07	.224E-07	.236E-07	.247E-07	.260E-07	.273E-07
30	.211E-07	.306E-07	.415E-07	.543E-07	.611E-07	.680E-07	.714E-07	.749E-07	.786E-07	.824E-07
40	.607E-07	.870E-07	.117E-06	.153E-06	.171E-06	.191E-06	.200E-06	.210E-06	.220E-06	.230E-06
50	.163E-06	.231E-06	.309E-06	.400E-06	.449E-06	.498E-06	.523E-06	.548E-06	.574E-06	.600E-06
60	.411E-06	.575E-06	.765E-06	.985E-06	.110E-05	.122E-05	.128E-05	.134E-05	.140E-05	.147E-05
70	.976E-06	.135E-05	.179E-05	.229E-05	.256E-05	.283E-05	.297E-05	.310E-05	.325E-05	.339E-05
80	.220E-05	.302E-05	.396E-05	.504E-05	.562E-05	.622E-05	.652E-05	.681E-05	.712E-05	.743E-05
90	.473E-05	.642E-05	.835E-05	.106E-04	.118E-04	.130E-04	.136E-04	.143E-04	.149E-04	.155E-04
100	.973E-05	.131E-04	.169E-04	.213E-04	.237E-04	.261E-04	.274E-04	.285E-04	.298E-04	.310E-04
110	.192E-04	.256E-04	.328E-04	.412E-04	.457E-04	.503E-04	.527E-04	.549E-04	.572E-04	.595E-04
120	.366E-04	.482E-04	.614E-04	.767E-04	.849E-04	.935E-04	.977E-04	.102E-03	.106E-03	.110E-03
130	.672E-04	.879E-04	.111E-03	.138E-03	.153E-03	.168E-03	.175E-03	.182E-03	.190E-03	.197E-03
140	.120E-03	.155E-03	.195E-03	.241E-03	.266E-03	.292E-03	.304E-03	.316E-03	.329E-03	.341E-03
150	.207E-03	.266E-03	.332E-03	.408E-03	.449E-03	.493E-03	.514E-03	.534E-03	.554E-03	.574E-03
160	.348E-03	.444E-03	.550E-03	.673E-03	.740E-03	.810E-03	.844E-03	.876E-03	.909E-03	.941E-03
170	.572E-03	.723E-03	.889E-03	.108E-02	.119E-02	.130E-02	.135E-02	.140E-02	.145E-02	.150E-02
180	.917E-03	.115E-02	.140E-02	.170E-02	.186E-02	.204E-02	.212E-02	.220E-02	.227E-02	.235E-02
190	.144E-02	.179E-02	.217E-02	.262E-02	.286E-02	.312E-02	.325E-02	.336E-02	.348E-02	.359E-02
200	.221E-02	.273E-02	.329E-02	.395E-02	.431E-02	.470E-02	.488E-02	.505E-02	.522E-02	.538E-02
210	.333E-02	.408E-02	.490E-02	.585E-02	.637E-02	.693E-02	.720E-02	.744E-02	.768E-02	.791E-02
220	.494E-02	.601E-02	.715E-02	.850E-02	.924E-02	.100E-01	.104E-01	.108E-01	.111E-01	.114E-01
230	.719E-02	.869E-02	.103E-01	.122E-01	.132E-01	.143E-01	.149E-01	.153E-01	.158E-01	.162E-01
240	.103E-01	.124E-01	.146E-01	.171E-01	.186E-01	.201E-01	.209E-01	.215E-01	.221E-01	.227E-01
250	.146E-01	.174E-01	.203E-01	.238E-01	.257E-01	.278E-01	.289E-01	.297E-01	.305E-01	.314E-01
260	.203E-01	.240E-01	.279E-01	.326E-01	.352E-01	.380E-01	.394E-01	.405E-01	.416E-01	.427E-01
270	.279E-01	.329E-01	.380E-01	.441E-01	.475E-01	.513E-01	.531E-01	.545E-01	.560E-01	.574E-01
280	.380E-01	.444E-01	.510E-01	.589E-01	.633E-01	.683E-01	.706E-01	.725E-01	.744E-01	.762E-01
290	.510E-01	.592E-01	.678E-01	.778E-01	.835E-01	.900E-01	.930E-01	.954E-01	.978E-01	.100
300	.678E-01	.782E-01	.888E-01	.102	.109	.117	.121	.124	.127	.130
310	.892E-01	.102	.115	.132	.141	.151	.156	.160	.164	.167
320	.116	.132	.149	.169	.180	.193	.199	.204	.209	.213
330	.150	.170	.190	.214	.228	.245	.252	.258	.263	.269
340	.192	.216	.240	.270	.287	.307	.317	.328	.330	.386
350	.243	.272	.301	.337	.358	.383	.394	.402	.410	.417

*Vermeulen, Dong, Robinson, Nguyen, and Gmitro, AIChE meeting, Anaheim, CA, 1982; and private communication from Prof. Theodore Vermeulen, Chemical Engineering Dept., University of California, Berkeley.

TABLE 2-17 Total Pressure, bar, of Aqueous Sulfuric Acid Solutions*

°C	Weight percent, H ₂ SO ₄									
	10.0	20.0	30.0	40.0	50.0	60.0	70.0	75.0	80.0	85.0
0	.582E-02	.534E-02	.448E-02	.326E-02	.193E-02	.836E-03	.207E-03	.747E-04	.197E-04	.343E-05
10	.117E-01	.107E-01	.909E-02	.670E-02	.405E-02	.180E-02	.467E-03	.175E-03	.490E-04	.952E-05
20	.223E-01	.205E-01	.174E-01	.130E-01	.802E-02	.367E-02	.995E-03	.388E-03	.115E-03	.245E-04
30	.404E-01	.373E-01	.319E-01	.241E-01	.151E-01	.710E-02	.201E-02	.811E-03	.253E-03	.589E-04
40	.703E-01	.649E-01	.558E-01	.427E-01	.272E-01	.131E-01	.387E-02	.162E-02	.531E-03	.134E-03
50	.117	.109	.939E-01	.725E-01	.470E-01	.232E-01	.715E-02	.309E-02	.106E-02	.286E-03
60	.189	.175	.152	.119	.782E-01	.395E-01	.127E-01	.565E-02	.204E-02	.584E-03
70	.296	.275	.239	.188	.126	.651E-01	.217E-01	.997E-01	.376E-02	.114E-02
80	.449	.417	.365	.290	.196	.104	.360E-01	.170E-01	.668E-02	.213E-02
90	.664	.617	.542	.434	.298	.161	.578E-01	.281E-01	.115E-01	.383E-02
100	.957	.891	.786	.634	.441	.244	.905E-01	.452E-01	.192E-01	.666E-02
110	1.349	1.258	1.113	.904	.638	.360	.138	.708E-01	.312E-01	.112E-01
120	1.863	1.740	1.544	1.264	.903	.519	.206	.108	.493E-01	.183E-01
130	2.524	2.361	2.101	1.732	1.253	.734	.301	.162	.760E-01	.291E-01
140	3.361	3.149	2.810	2.333	1.708	1.020	.431	.236	.115	.451E-01
150	4.404	4.132	3.697	3.090	2.289	1.392	.605	.339	.170	.683E-01
160	5.685	5.342	4.793	4.031	3.021	1.870	.837	.478	.246	.101
170	7.236	6.810	6.127	5.185	3.930	2.475	1.138	.662	.350	.147
180	9.093	8.571	7.731	6.584	5.045	3.233	1.525	.902	.489	.209
190	11.289	10.658	9.640	8.259	6.397	4.169	2.017	1.212	.673	.292
200	13.861	13.107	11.887	10.245	8.020	5.312	2.633	1.606	.913	.402
210	16.841	15.951	14.505	12.576	9.948	6.696	3.396	2.101	1.221	.544
220	20.264	19.225	17.529	15.287	12.217	8.354	4.331	2.715	1.610	.726
230	24.160	22.960	20.992	18.414	14.864	10.322	5.466	3.468	2.098	.956
240	28.561	27.188	24.927	21.992	17.929	12.641	6.832	4.382	2.701	1.242
250	33.494	31.939	29.364	26.056	21.452	15.351	8.459	5.481	3.439	1.594
260	38.984	37.240	34.334	30.642	25.472	18.496	10.384	6.791	4.332	2.023
270	45.055	43.116	39.865	35.784	30.030	22.122	12.642	8.337	5.402	2.540
280	51.726	49.590	45.984	41.514	35.168	26.275	15.272	10.147	6.673	3.157
290	59.015	56.681	52.715	47.866	40.926	31.004	18.315	12.250	8.170	3.886
300	66.934	64.407	60.081	54.869	47.347	36.361	21.814	14.675	9.916	4.740
310	75.495	72.781	68.101	62.553	54.470	42.398	25.812	17.453	11.939	5.732
320	84.705	81.816	76.792	70.947	62.338	49.168	30.355	20.611	14.264	6.876
330	94.567	91.518	86.172	80.078	70.990	56.727	35.489	24.182	16.916	8.185
340	105.083	101.894	96.252	89.970	80.466	65.130	41.262	28.193	19.920	9.672
350	116.251	112.947	107.043	100.647	90.806	74.437	47.723	32.674	23.303	11.351
°C	Weight percent, H ₂ SO ₄									
	90.0	92.0	94.0	96.0	97.0	98.0	98.5	99.0	99.5	100.0
0	.518E-06	.243E-06	.109E-06	.416E-07	.235E-07	.117E-07	.768E-08	.479E-08	.313E-08	.323E-08
10	.159E-05	.765E-06	.348E-06	.136E-06	.774E-07	.391E-07	.261E-07	.166E-07	.113E-07	.124E-07
20	.449E-05	.221E-05	.102E-05	.407E-06	.235E-06	.121E-06	.812E-07	.528E-07	.373E-07	.435E-07
30	.117E-04	.590E-05	.279E-05	.113E-05	.659E-06	.344E-06	.234E-06	.155E-06	.114E-06	.141E-06
40	.385E-04	.147E-04	.708E-05	.293E-05	.173E-05	.914E-06	.630E-06	.425E-06	.283E-06	.425E-06
50	.653E-04	.344E-04	.169E-04	.712E-05	.425E-05	.228E-05	.159E-05	.109E-05	.861E-06	.120E-05
60	.141E-03	.759E-04	.380E-04	.164E-04	.987E-05	.538E-05	.379E-05	.264E-05	.216E-05	.319E-05
70	.291E-03	.159E-03	.813E-04	.357E-04	.218E-04	.120E-04	.856E-05	.605E-05	.514E-05	.804E-05
80	.571E-03	.319E-03	.166E-03	.742E-04	.458E-04	.257E-04	.184E-04	.132E-04	.117E-04	.193E-04
90	.107E-02	.612E-03	.324E-03	.148E-03	.921E-04	.524E-04	.390E-04	.277E-04	.253E-04	.441E-04
100	.195E-02	.113E-02	.607E-03	.283E-03	.178E-03	.103E-03	.751E-04	.555E-04	.527E-04	.966E-04
110	.340E-02	.201E-02	.110E-02	.521E-03	.332E-03	.194E-03	.143E-03	.107E-03	.106E-03	.204E-03
120	.575E-02	.346E-02	.192E-02	.929E-03	.598E-03	.354E-03	.263E-03	.201E-03	.206E-03	.414E-03
130	.944E-02	.578E-02	.327E-02	.161E-02	.104E-02	.626E-03	.470E-03	.363E-03	.387E-03	.314E-03
140	.151E-01	.939E-02	.539E-02	.270E-02	.177E-02	.107E-02	.815E-03	.639E-03	.708E-03	.155E-02
150	.235E-01	.149E-01	.866E-02	.441E-02	.293E-02	.180E-02	.137E-02	.109E-02	.126E-02	.287E-02
160	.357E-01	.230E-01	.136E-01	.703E-02	.471E-02	.293E-02	.226E-02	.183E-02	.219E-02	.516E-02
170	.532E-01	.347E-01	.208E-01	.110E-01	.741E-02	.466E-02	.363E-02	.299E-02	.372E-02	.905E-02
180	.775E-01	.514E-01	.312E-01	.167E-01	.114E-01	.726E-02	.571E-02	.478E-02	.619E-02	.155E-01
190	.111	.747E-01	.460E-01	.250E-01	.172E-01	.111E-01	.880E-02	.749E-02	.101E-01	.260E-01
200	.156	.107	.665E-01	.367E-01	.255E-01	.166E-01	.133E-01	.115E-01	.161E-01	.427E-01
210	.216	.150	.944E-01	.530E-01	.371E-01	.245E-01	.198E-01	.175E-01	.253E-01	.687E-01
220	.295	.207	.132	.752E-01	.531E-01	.354E-01	.289E-01	.260E-01	.392E-01	.109
230	.396	.282	.182	.105	.749E-01	.505E-01	.417E-01	.382E-01	.596E-01	.169
240	.525	.379	.247	.145	.104	.710E-01	.592E-01	.553E-01	.895E-01	.258
250	.688	.503	.331	.197	.143	.985E-01	.830E-01	.790E-01	.132	.389
260	.881	.660	.439	.264	.193	.135	.115	.112	.193	.577
270	1.141	.856	.575	.351	.258	.153	.157	.156	.279	.846
280	1.447	1.099	.744	.460	.341	.245	.213	.215	.398	1.225
290	1.817	1.398	.954	.597	.446	.324	.285	.295	.562	1.751
300	2.261	1.761	1.211	.767	.578	.425	.379	.399	.785	2.476
310	2.791	2.199	1.524	.977	.742	.553	.498	.536	1.085	3.465
320	3.417	2.723	1.901	1.234	.944	.713	.649	.714	1.486	4.800
330	4.153	3.347	2.353	1.545	1.191	.911	.840	.944	2.018	6.586
340	5.011	4.084	2.889	1.919	1.491	1.156	1.078	1.239	2.718	8.957
350	6.006	4.949	3.523	2.366	1.852	1.456	1.374	1.614	3.631	12.079

*Vermeulen, Dong, Robinson, Nguyen, and Gmitro, AIChE meeting, Anaheim, Calif., 1982; and private communication from Prof. Theodore Vermeulen, Chemical Engineering Dept., University of California, Berkeley.

2-88 PHYSICAL AND CHEMICAL DATA

TABLE 2-18 Partial Pressures of HNO₃ and H₂O over Aqueous Solutions of HNO₃*

mmHg
Percentages are weight % HNO₃ in solution.

°C	20%		25%		30%		35%		40%		45%		50%	
	HNO ₃	H ₂ O	HNO ₃	H ₂ O	HNO ₃	H ₂ O	HNO ₃	H ₂ O	HNO ₃	H ₂ O	HNO ₃	H ₂ O	HNO ₃	H ₂ O
0		4.1		3.8		3.6		3.3		3.0		2.6		2.1
5		5.7		5.4		5.0		4.6		4.2		3.6		3.0
10		8.0		7.6		7.1		6.5		5.8		5.0	0.12	4.2
15		10.9		10.3		9.7		8.9		8.0	0.10	6.9	.18	5.8
20		15.2		14.2		13.2		12.0		10.8	.15	9.4	.27	7.9
25		20.6		19.2		17.8		16.2	0.12	14.6	.23	12.7	.39	10.7
30		27.6		25.7		23.8	0.09	21.7	.17	19.5	.33	16.9	.56	14.4
35		36.5		33.8		31.1	.13	28.3	.25	25.5	.48	22.3	.80	19.0
40		47.5		44	0.11	41	.20	37.7	.36	33.5	.68	29.3	1.13	25.0
45		62	0.09	57.5	.17	53	.28	48	.52	43	.96	38.0	1.57	32.5
50		80	.13	75	.25	69	.42	63	.75	56	1.35	49.5	2.18	42.5
55	0.09	100	.18	94	.35	87	.59	79	1.04	71	1.83	62.5	2.95	54
60	.13	128	.28	121	.51	113	.85	102	1.48	90	2.54	80	4.05	70
65	.19	162	.40	151	.71	140	1.18	127	2.05	114	3.47	100	5.46	88
70	.27	200	.54	187	1.00	174	1.63	159	2.80	143	4.65	126	7.25	110
75	.38	250	.77	234	1.38	217	2.26	198	3.80	178	6.20	158	9.6	138
80	.53	307	1.05	287	1.87	267	3.07	243	5.10	218	8.15	195	12.5	170
85	.74	378	1.44	352	2.53	325	4.15	297	6.83	268	10.7	240	16.3	211
90	1.01	458	1.95	426	3.38	393	5.50	359	9.0	325	13.7	292	20.9	258
95	1.37	555	2.62	517	4.53	478	7.32	436	11.7	394	17.8	355	26.8	315
100	1.87	675	3.50	628	6.05	580	9.7	530	15.5	480	23.0	430	34.2	383
105	2.50	800	4.65	745	7.90	690	12.7	631	20.0	573	29.2	520	43.0	463
110							16.5	755		688	37.0	625	54.5	560
115										810	46	740	67	665
120													84	785

°C	55%		60%		65%		70%		80%		90%		100%
	HNO ₃	H ₂ O	HNO ₃	H ₂ O	HNO ₃	H ₂ O	HNO ₃	H ₂ O	HNO ₃	H ₂ O	HNO ₃	H ₂ O	HNO ₃
0		1.8	0.19	1.5	0.41	1.3	0.79	1.1	2		5.5		11
5	0.14	2.5	.28	2.1	.60	1.8	1.12	1.6	3		8		15
10	.21	3.5	.41	3.0	.86	2.6	1.58	2.2	4	1.2	11		22
15	.31	4.9	.59	4.1	1.21	3.5	2.18	3.0	6	1.7	15		30
20	.45	6.7	.84	5.6	1.68	4.9	3.00	4.1	8	2.4	20		42
25	.66	9.1	1.21	7.7	2.32	6.6	4.10	5.5	10.5	3.2	27	1	57
30	.93	12.2	1.66	10.3	3.17	8.8	5.50	7.4	14	4	36	1.3	77
35	1.30	16.1	2.28	13.6	4.26	11.6	7.30	9.8	18.5	5.5	47	1.8	102
40	1.82	21.3	3.10	18.1	5.70	15.5	9.65	12.8	24.5	7	62	2.4	133
45	2.50	28.0	4.20	23.7	7.55	20.0	12.6	16.7	32	9.5	80	3	170
50	3.41	36.3	5.68	31	10.0	26.0	16.5	21.8	41	12	103	4	215
55	4.54	46	7.45	39	12.8	33.0	21.0	27.3	52	15	127	5	262
60	6.15	60	9.9	51	16.8	43.0	27.1	35.3	67	20	157	6.5	320
65	8.18	76	13.0	64	21.7	54.5	34.5	44.5	85	25	192	8	385
70	10.7	95	16.8	81	27.5	68	43.3	56	106	31	232	10	460
75	13.9	120	21.8	102	35.0	86	54.5	70	130	38	282	13	540
80	18.0	148	27.5	126	43.5	106	67.5	86	158	48	338	16	625
85	23.0	182	34.8	156	54.5	131	83	107	192	60	405	20	720
90	29.4	223	43.7	192	67.5	160	103	130	230	73	480	24	820
95	37.3	272	55.0	233	83.5	195	125	158	278	89	570	29	
100	47	331	69.5	285	103	238	152	192	330	108	675	35	
105	58.5	400	84.5	345	124	288	183	231	392	129	790	42	
110	73	485	103	417	152	345	221	278	465	155			
115	90	575	126	495	181	410	262	330	545	185			
120	110	685	156	590	218	490	312	393	640	219			
125			187	700	260	580	372	469					

*International Critical Tables, vol. 3, pp. 304-305.

TABLE 2-19 Partial Pressures of H₂O and HBr over Aqueous Solutions of HBr at 20 to 55°C*

		mmHg							
% HBr	20 °C		25 °C		50 °C		55 °C		
	HBr	H ₂ O	HBr	H ₂ O	HBr	H ₂ O	HBr	H ₂ O	
32			0.0016						
34			0.0022						
36			0.0033						
38			0.0061						
40			0.011						
42			0.023						
44			0.048						
46			0.10						
48	0.09	6.2	0.13	8.2	1.3	30.2	2.0	38	
50	0.23	4.5	0.37	6.1	3.2	24.3	4.6	31	
52	0.71	3.3	1.1	4.5	7.2	19.3	10.2	25	
54	2.2	2.4	3.2	3.3	17	16.0	23.0	21	
56	6.8	1.7	9.3	2.4	40	13.3	51	18	
58	21	1.3	27	1.9	91	10.4	115	14	
60							260	11.4	

*International Critical Tables, vol. 3, p. 306.

TABLE 2-20 Partial Pressures of HI over Aqueous Solutions of HI at 25°C*

		mmHg						
%HI		44	46	48	50	52	54	56
p_{HI}		0.00064	0.0010	0.0022	0.0050	0.013	0.035	0.10

*International Critical Tables, vol. 3, p. 306.

TABLE 2-21 Vapor Pressures of the System: Water-Sulfuric Acid-Nitric Acid

For these data reference must be made to the graphs of *International Critical Tables*, vol. 3, pp. 306-308.

TABLE 2-22 Total Vapor Pressures of Aqueous Solutions of CH₃COOH*

		Percentages of weight % acetic acid in the solution		
		mmHg		
°C		25%	50%	75%
20		16.3	15.7	15.3
25		22.1	21.4	20.8
30		29.6	28.8	27.8
35		39.4	38.3	36.6
40		51.7	50.2	48.1
45		67.0	65.0	62.0
50		87.2	85.0	80.1
55		110	107	102
60		141	138	130
65		178	172	162
70		223	216	203
75		277	269	251
80		342	331	310
85		419	407	376
90		510	497	458
95		618	602	550
100		743	725	666

*International Critical Tables, vol. 3, p. 306.

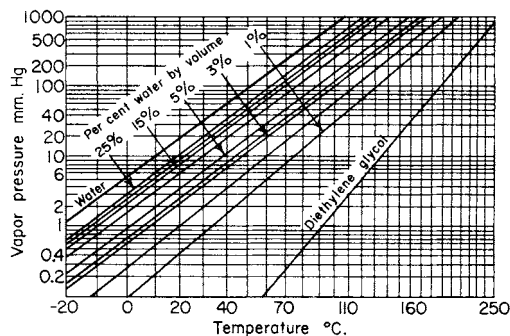


FIG. 2-3 Vapor pressure of aqueous diethylene glycol solutions. (Courtesy of Carbide and Carbon Chemicals Corp.)

TABLE 2-23 Partial Pressure of H₂O over Aqueous Solutions of NH₃ (psia)

t, °F	Liquid mole percent NH ₃ (liquid weight percent NH ₃)																			
	0	5	10	15	20	25	30	35	40	45	50	55	60	65	70	75	80	85	90	95
	(0)	(4.74)	(9.5)	(14.29)	(19.1)	(23.94)	(28.81)	(33.71)	(38.64)	(43.59)	(48.57)	(53.58)	(58.62)	(63.69)	(68.79)	(73.91)	(79.07)	(84.26)	(89.47)	(94.72)
32	0.089	0.083	0.077	0.071	0.063	0.055	0.047	0.039	0.031	0.025	0.019	0.014	0.011	0.008	0.006	0.004	0.003	0.002	0.002	0.001
40	0.122	0.115	0.106	0.097	0.087	0.077	0.065	0.054	0.044	0.035	0.027	0.021	0.016	0.012	0.009	0.007	0.005	0.004	0.002	0.001
50	0.178	0.168	0.156	0.143	0.129	0.113	0.097	0.081	0.066	0.053	0.041	0.032	0.025	0.019	0.014	0.011	0.008	0.006	0.004	0.002
60	0.256	0.242	0.225	0.207	0.186	0.164	0.142	0.119	0.098	0.079	0.062	0.049	0.038	0.030	0.023	0.018	0.014	0.010	0.007	0.004
70	0.363	0.343	0.320	0.294	0.266	0.235	0.204	0.172	0.143	0.116	0.093	0.073	0.058	0.045	0.036	0.028	0.022	0.016	0.011	0.006
80	0.507	0.479	0.448	0.413	0.374	0.332	0.289	0.245	0.205	0.168	0.136	0.109	0.087	0.069	0.055	0.043	0.034	0.025	0.018	0.010
90	0.699	0.661	0.618	0.571	0.518	0.462	0.403	0.345	0.290	0.240	0.196	0.159	0.128	0.103	0.083	0.066	0.052	0.040	0.028	0.015
100	0.951	0.899	0.843	0.780	0.710	0.634	0.556	0.479	0.405	0.338	0.279	0.228	0.186	0.152	0.123	0.100	0.079	0.061	0.043	0.024
110	1.277	1.209	1.135	1.052	0.960	0.861	0.758	0.656	0.559	0.470	0.392	0.324	0.268	0.220	0.181	0.148	0.119	0.092	0.065	0.036
120	1.695	1.607	1.510	1.402	1.283	1.154	1.021	0.889	0.763	0.647	0.544	0.455	0.380	0.316	0.263	0.217	0.176	0.137	0.099	0.056
130	2.226	2.112	1.988	1.850	1.696	1.532	1.361	1.192	1.030	0.881	0.747	0.632	0.532	0.448	0.376	0.313	0.257	0.202	0.147	0.083
140	2.893	2.748	2.591	2.415	2.221	2.012	1.796	1.582	1.376	1.186	1.016	0.867	0.738	0.628	0.532	0.448	0.371	0.295	0.216	0.124
150	3.723	3.540	3.343	3.122	2.879	2.618	2.347	2.078	1.821	1.582	1.367	1.177	1.013	0.870	0.746	0.634	0.529	0.425	0.314	0.183
160	4.747	4.519	4.273	4.000	3.698	3.374	3.039	2.706	2.387	2.090	1.821	1.584	1.376	1.194	1.033	0.887	0.748	0.607	0.453	0.267
170	6.000	5.717	5.416	5.079	4.709	4.312	3.902	3.493	3.101	2.736	2.405	2.110	1.851	1.622	1.418	1.229	1.047	0.858	0.647	0.386
180	7.520	7.174	6.807	6.397	5.947	5.465	4.968	4.472	3.995	3.551	3.148	2.787	2.468	2.184	1.928	1.688	1.451	1.201	0.917	0.555
190	9.350	8.931	8.488	7.994	7.452	6.873	6.275	5.680	5.107	4.573	4.086	3.650	3.262	2.914	2.598	2.297	1.994	1.669	1.290	0.793
200	11.538	11.035	10.504	9.916	9.270	8.580	7.869	7.160	6.479	5.842	5.262	4.740	4.275	3.856	3.470	3.098	2.718	2.300	1.802	1.129
210	14.136	13.538	12.910	12.213	11.449	10.635	9.796	8.962	8.160	7.410	6.725	6.110	5.559	5.061	4.598	4.146	3.675	3.147	2.502	1.600
220	17.201	16.496	15.758	14.941	14.047	13.095	12.115	11.141	10.205	9.331	8.534	7.817	7.175	6.592	6.045	5.504	4.932	4.277	3.455	2.262
230	20.796	19.971	19.111	18.162	17.124	16.020	14.886	13.760	12.679	11.672	10.754	9.930	9.192	8.522	7.889	7.255	6.573	5.777	4.751	3.196
240	24.986	24.029	23.037	21.943	20.748	19.479	18.179	16.889	15.654	14.506	13.463	12.530	11.696	10.938	10.221	9.496	8.703	7.759	6.508	4.520
250	29.844	28.744	27.607	26.358	24.996	23.549	22.070	20.608	19.212	17.917	16.748	15.708	14.783	13.946	13.153	12.346	11.452	10.369	8.891	6.413

The values in Tables 2-23 to 2-26 were generated from the NIST REFPROP software (Lemmon, E. W., McLinden, M. O., and Huber, M. L., NIST Standard Reference Database 23: Reference Fluid Thermodynamic and Transport Properties—REFPROP, Version 7.0, National Institute of Standards and Technology, Standard Reference Data Program, Gaithersburg, Md., 2002). The primary source for the properties of aqueous ammonia mixtures is R. Tillner-Roth and D. G. Friend, "A Helmholtz Free Energy Formulation of the Thermodynamic Properties of the Mixture {Water + Ammonia}," *J. Phys. Chem. Ref. Data* 27:63–96 (1998).

TABLE 2-24 Mole Percentages of H₂O over Aqueous Solutions of NH₃

<i>t</i> , °F	Liquid mole percent NH ₃ (liquid weight percent NH ₃)																			
	0	5	10	15	20	25	30	35	40	45	50	55	60	65	70	75	80	85	90	95
	(0)	(4.74)	(9.5)	(14.29)	(19.1)	(23.94)	(28.81)	(33.71)	(38.64)	(43.59)	(48.57)	(53.58)	(58.62)	(63.69)	(68.79)	(73.91)	(79.07)	(84.26)	(89.47)	(94.72)
32	100	32.046	14.173	7.263	3.959	2.202	1.226	0.679	0.375	0.207	0.116	0.067	0.039	0.024	0.015	0.010	0.007	0.005	0.003	0.001
40	100	33.233	15.064	7.842	4.321	2.427	1.365	0.765	0.428	0.240	0.137	0.080	0.048	0.030	0.019	0.013	0.009	0.006	0.004	0.002
50	100	34.709	16.192	8.588	4.797	2.727	1.554	0.883	0.502	0.287	0.167	0.100	0.061	0.039	0.026	0.017	0.012	0.008	0.005	0.003
60	100	36.172	17.334	9.359	5.299	3.050	1.760	1.015	0.587	0.342	0.203	0.123	0.077	0.050	0.034	0.023	0.016	0.011	0.007	0.004
70	100	37.619	18.489	10.154	5.828	3.396	1.985	1.162	0.683	0.405	0.245	0.152	0.097	0.064	0.044	0.030	0.021	0.015	0.010	0.005
80	100	39.047	19.653	10.974	6.382	3.765	2.231	1.325	0.791	0.478	0.294	0.186	0.121	0.081	0.056	0.040	0.028	0.020	0.013	0.007
90	100	40.455	20.827	11.816	6.963	4.160	2.497	1.505	0.913	0.561	0.351	0.226	0.149	0.102	0.072	0.051	0.037	0.026	0.017	0.009
100	100	41.840	22.007	12.681	7.571	4.580	2.786	1.703	1.049	0.655	0.418	0.273	0.184	0.127	0.091	0.066	0.048	0.034	0.023	0.012
110	100	43.201	23.194	13.567	8.205	5.027	3.098	1.920	1.201	0.763	0.494	0.328	0.224	0.158	0.114	0.084	0.062	0.044	0.030	0.016
120	100	44.537	24.385	14.475	8.867	5.501	3.434	2.158	1.370	0.884	0.582	0.393	0.273	0.195	0.142	0.106	0.079	0.057	0.039	0.021
130	100	45.849	25.580	15.404	9.557	6.002	3.796	2.419	1.558	1.020	0.682	0.467	0.329	0.238	0.177	0.133	0.100	0.073	0.050	0.027
140	100	47.136	26.779	16.353	10.273	6.532	4.184	2.702	1.766	1.173	0.796	0.554	0.396	0.290	0.218	0.166	0.126	0.094	0.064	0.035
150	100	48.398	27.979	17.322	11.017	7.091	4.600	3.010	1.994	1.344	0.925	0.653	0.473	0.352	0.268	0.206	0.158	0.118	0.082	0.045
160	100	49.636	29.182	18.310	11.789	7.680	5.044	3.344	2.246	1.534	1.071	0.767	0.563	0.425	0.327	0.254	0.197	0.149	0.104	0.058
170	100	50.849	30.385	19.317	12.587	8.298	5.517	3.705	2.521	1.746	1.236	0.897	0.668	0.509	0.396	0.312	0.245	0.187	0.132	0.074
180	100	52.038	31.588	20.341	13.413	8.948	6.021	4.094	2.822	1.981	1.421	1.045	0.788	0.609	0.479	0.381	0.302	0.233	0.166	0.094
190	100	53.204	32.792	21.383	14.266	9.628	6.557	4.513	3.151	2.240	1.628	1.212	0.926	0.724	0.576	0.463	0.371	0.288	0.209	0.120
200	100	54.347	33.994	22.442	15.146	10.340	7.124	4.963	3.508	2.526	1.859	1.402	1.083	0.857	0.690	0.561	0.453	0.357	0.261	0.153
210	100	55.468	35.196	23.517	16.052	11.083	7.725	5.445	3.896	2.840	2.116	1.615	1.263	1.011	0.823	0.676	0.552	0.439	0.326	0.195
220	100	56.567	36.395	24.607	16.985	11.858	8.359	5.961	4.316	3.184	2.401	1.854	1.468	1.187	0.977	0.811	0.669	0.539	0.406	0.248
230	100	57.645	37.592	25.711	17.943	12.665	9.028	6.512	4.769	3.560	2.716	2.122	1.699	1.390	1.156	0.969	0.809	0.660	0.506	0.317
240	100	58.702	38.787	26.830	18.927	13.503	9.732	7.098	5.258	3.970	3.064	2.421	1.960	1.621	1.363	1.155	0.975	0.806	0.629	0.406
250	100	59.740	39.978	27.962	19.936	14.374	10.471	7.722	5.784	4.416	3.447	2.754	2.254	1.884	1.601	1.371	1.171	0.982	0.783	0.524

The values in Tables 2-23 to 2-26 were generated from the NIST REFPROP software (Lemmon, E. W., McLinden, M. O., and Huber, M. L., NIST Standard Reference Database 23: Reference Fluid Thermodynamic and Transport Properties—REFPROP, Version 7.0, National Institute of Standards and Technology, Standard Reference Data Program, Gaithersburg, Md., 2002). The primary source for the properties of aqueous ammonia mixtures is R. Tillner-Roth and D. G. Friend, "A Helmholtz Free Energy Formulation of the Thermodynamic Properties of the Mixture [Water + Ammonia]," *J. Phys. Chem. Ref. Data* **27**:63–96 (1998).

TABLE 2-25 Partial Pressures of NH₃ over Aqueous Solutions of NH₃ (psia)

t, °F	Liquid mole percent NH ₃ (liquid weight percent NH ₃)																				
	0	5	10	15	20	25	30	35	40	45	50	55	60	65	70	75	80	85	90	95	100
	(0)	(4.74)	(9.5)	(14.29)	(19.1)	(23.94)	(28.81)	(33.71)	(38.64)	(43.59)	(48.57)	(53.58)	(58.62)	(63.69)	(68.79)	(73.91)	(79.07)	(84.26)	(89.47)	(94.72)	(100)
32	0	0.177	0.468	0.901	1.533	2.456	3.797	5.710	8.358	11.868	16.279	21.480	27.206	33.087	38.745	43.900	48.431	52.368	55.846	59.055	62.277
40	0	0.230	0.600	1.143	1.932	3.078	4.730	7.066	10.267	14.467	19.691	25.798	32.478	39.307	45.860	51.828	57.082	61.665	65.731	69.506	73.322
50	0	0.316	0.808	1.522	2.552	4.036	6.154	9.117	13.129	18.328	24.721	32.120	40.150	48.315	56.128	63.243	69.520	75.020	79.931	84.523	89.205
60	0	0.426	1.074	2.002	3.330	5.228	7.912	11.625	16.593	22.959	30.702	39.581	49.149	58.831	68.074	76.489	83.933	90.486	96.376	101.93	107.63
70	0	0.568	1.410	2.603	4.296	6.696	10.056	14.656	20.742	28.456	37.744	48.307	59.615	71.008	81.861	91.745	100.51	108.26	115.29	121.94	128.85
80	0	0.748	1.831	3.348	5.483	8.483	12.645	18.283	25.664	34.922	45.966	58.428	71.689	84.998	97.654	109.19	119.45	128.56	136.88	144.83	153.13
90	0	0.973	2.351	4.261	6.926	10.639	15.741	22.582	31.447	42.460	55.485	70.073	85.514	100.96	115.62	128.99	140.93	151.60	161.39	170.82	180.76
100	0	1.250	2.987	5.368	8.663	13.213	19.406	27.630	38.185	51.177	66.416	83.375	101.23	119.04	135.93	151.34	165.15	177.57	189.05	200.19	212.01
110	0	1.590	3.758	6.700	10.735	16.258	23.709	33.509	45.971	61.177	78.881	98.461	118.98	139.39	158.73	176.40	192.30	206.69	220.07	233.16	247.19
120	0	2.001	4.683	8.285	13.184	19.832	28.718	40.300	54.899	72.569	92.996	115.45	138.90	162.15	184.19	204.35	222.57	239.16	254.71	270.03	286.60
130	0	2.494	5.784	10.158	16.055	23.989	34.503	48.086	65.064	85.455	108.87	134.49	161.13	187.48	212.44	235.36	256.14	275.20	293.18	311.05	330.54
140	0	3.082	7.084	12.352	19.395	28.791	41.135	56.949	76.558	99.944	126.62	155.67	185.77	215.50	243.66	269.56	293.19	314.99	335.72	356.48	379.36
150	0	3.774	8.604	14.902	23.250	34.295	48.685	66.972	89.472	116.12	146.35	179.11	212.96	246.33	277.95	307.13	333.87	358.75	382.56	406.60	433.38
160	0	4.585	10.371	17.844	27.669	40.562	57.222	78.230	103.89	134.09	168.16	204.93	242.79	280.08	315.46	348.18	378.36	406.62	433.89	461.65	492.95
170	0	5.527	12.408	21.216	32.700	47.649	66.816	90.803	119.90	153.93	192.14	233.19	275.37	316.87	356.26	392.85	426.79	458.82	489.95	521.92	558.45
180	0	6.612	14.741	25.053	38.390	55.614	77.532	104.77	137.57	175.73	218.35	263.99	310.76	356.75	400.47	441.24	479.30	515.48	550.92	587.67	630.24
190	0	7.856	17.395	29.393	44.786	64.514	89.432	120.18	156.99	199.56	246.89	297.40	349.06	399.82	448.16	493.43	535.98	576.75	616.99	659.12	708.74
200	0	9.270	20.397	34.270	51.933	74.401	102.58	137.11	178.21	225.47	277.81	333.47	390.30	446.12	499.38	549.49	596.94	642.74	688.31	736.52	794.38
210	0	10.869	23.769	39.721	59.876	85.326	117.02	155.62	201.28	253.53	311.15	372.25	434.50	495.68	554.15	609.47	662.22	713.55	765.01	820.08	887.64
220	0	12.666	27.538	45.779	68.655	97.335	132.82	175.75	226.25	283.77	346.95	413.74	481.70	548.49	612.50	673.37	731.88	789.23	847.19	909.98	989.03
230	0	14.673	31.727	52.477	78.310	110.47	150.00	197.54	253.17	316.23	385.23	457.98	531.89	604.55	674.39	741.21	805.90	869.79	934.86	1006.3	1099.1
240	0	16.905	36.356	59.843	88.872	124.78	168.62	221.04	282.06	350.91	425.98	504.92	585.01	663.80	739.77	812.89	884.22	955.18	1028.0	1109.2	1218.7
250	0	19.371	41.449	67.906	100.38	140.28	188.70	246.26	312.93	387.82	469.20	554.55	641.05	726.18	808.55	888.35	966.78	1045.3	1126.5	1218.3	1348.5

The values in Tables 2-23 to 2-26 were generated from the NIST REFPROP software (Lemmon, E. W., McLinden, M. O., and Huber, M. L., NIST Standard Reference Database 23: Reference Fluid Thermodynamic and Transport Properties—REFPROP, Version 7.0, National Institute of Standards and Technology, Standard Reference Data Program, Gaithersburg, Md., 2002). The primary source for the properties of aqueous ammonia mixtures is R. Tillner-Roth and D. G. Friend, "A Helmholtz Free Energy Formulation of the Thermodynamic Properties of the Mixture [Water + Ammonia]," *J. Phys. Chem. Ref. Data* **27**:63–96 (1998).

TABLE 2-26 Total Vapor Pressures of Aqueous Solutions of NH₃ (psia)

t, °F	Liquid mole percent NH ₃ (liquid weight percent NH ₃)																				
	0	5	10	15	20	25	30	35	40	45	50	55	60	65	70	75	80	85	90	95	100
	(0)	(4.74)	(9.5)	(14.29)	(19.1)	(23.94)	(28.81)	(33.71)	(38.64)	(43.59)	(48.57)	(53.58)	(58.62)	(63.69)	(68.79)	(73.91)	(79.07)	(84.26)	(89.47)	(94.72)	(100)
32	0.089	0.260	0.545	0.971	1.596	2.512	3.844	5.749	8.389	11.893	16.298	21.494	27.217	33.095	38.751	43.904	48.434	52.371	55.848	59.056	62.277
40	0.122	0.345	0.706	1.240	2.020	3.155	4.795	7.120	10.311	14.502	19.718	25.819	32.494	39.319	45.869	51.835	57.087	61.669	65.734	69.507	73.322
50	0.178	0.483	0.964	1.665	2.680	4.149	6.251	9.198	13.195	18.381	24.762	32.152	40.175	48.334	56.143	63.254	69.528	75.026	79.935	84.526	89.205
60	0.256	0.668	1.299	2.209	3.516	5.392	8.053	11.744	16.691	23.038	30.764	39.630	49.187	58.860	68.097	76.507	83.946	90.496	96.383	101.93	107.63
70	0.363	0.911	1.730	2.898	4.562	6.931	10.260	14.828	20.885	28.572	37.837	48.381	59.673	71.053	81.897	91.773	100.53	108.28	115.30	121.95	128.85
80	0.507	1.227	2.279	3.761	5.857	8.815	12.934	18.528	25.869	35.090	46.102	58.537	71.776	85.067	97.709	109.23	119.48	128.59	136.90	144.84	153.13
90	0.699	1.633	2.969	4.832	7.445	11.101	16.144	22.927	31.737	42.700	55.680	70.232	85.642	101.06	115.70	129.06	140.98	151.64	161.42	170.84	180.76
100	0.951	2.149	3.830	6.148	9.373	13.847	19.962	28.109	38.590	51.514	66.695	83.603	101.42	119.19	136.05	151.44	165.23	177.63	189.09	200.21	212.01
110	1.277	2.799	4.893	7.751	11.694	17.119	24.467	34.165	46.530	61.647	79.273	98.785	119.25	139.61	158.91	176.55	192.42	206.78	220.14	233.20	247.19
120	1.695	3.608	6.194	9.688	14.467	20.986	29.739	41.189	55.662	73.216	93.540	115.91	139.28	162.47	184.45	204.57	222.75	239.30	254.81	270.09	286.60
130	2.226	4.607	7.773	12.008	17.752	25.521	35.864	49.278	66.094	86.336	109.62	135.12	161.66	187.93	212.82	235.67	256.40	275.40	293.33	311.13	330.54
140	2.893	5.830	9.674	14.767	21.616	30.803	42.931	58.531	77.934	101.13	127.64	156.54	186.51	216.13	244.19	270.01	293.56	315.29	335.94	356.60	379.36
150	3.723	7.315	11.947	18.024	26.129	36.913	51.032	69.050	91.292	117.70	147.72	180.29	213.97	247.20	278.70	307.76	334.40	359.17	382.87	406.78	433.38
160	4.747	9.104	14.644	21.844	31.367	43.936	60.262	80.937	106.28	136.18	169.98	206.51	244.16	281.28	316.49	349.07	379.11	407.23	434.34	461.92	492.95
170	6.000	11.244	17.824	26.295	37.409	51.961	70.718	94.297	123.00	156.67	194.54	235.30	277.22	318.49	357.68	394.08	427.84	459.68	490.60	522.31	558.45
180	7.520	13.786	21.548	31.450	44.337	61.079	82.499	109.24	141.57	179.28	221.50	266.78	313.23	358.94	402.40	442.93	480.75	516.68	551.84	588.22	630.24
190	9.350	16.787	25.883	37.387	52.238	71.387	95.708	125.86	162.10	204.13	250.98	301.05	352.32	402.74	450.76	495.73	537.98	578.42	618.28	659.91	708.74
200	11.538	20.305	30.901	44.186	61.203	82.981	110.45	144.27	184.69	231.31	283.07	338.21	394.57	449.98	502.85	552.59	599.66	645.04	690.11	737.65	794.38
210	14.136	24.407	36.679	51.934	71.325	95.961	126.82	164.58	209.44	260.94	317.88	378.36	440.06	500.74	558.75	613.62	665.90	716.70	767.51	821.68	887.64
220	17.201	29.162	43.296	60.720	82.702	110.43	144.93	186.89	236.46	293.10	355.49	421.56	488.88	555.08	618.54	678.88	736.81	793.51	850.64	912.24	989.03
230	20.796	34.644	50.838	70.639	95.434	126.49	164.89	211.30	265.85	327.90	395.98	467.91	541.08	613.07	682.28	748.46	812.47	875.57	939.61	1009.5	1099.1
240	24.986	40.934	59.393	81.786	109.62	144.26	186.80	237.93	297.71	365.42	439.44	517.45	596.71	674.74	749.99	822.39	892.93	962.94	1034.5	1113.7	1218.7
250	29.844	48.115	69.056	94.264	125.38	163.83	210.77	266.87	332.14	405.74	485.95	570.25	655.83	740.12	821.71	900.70	978.24	1055.7	1135.4	1224.7	1348.5

The values in Tables 2-23 to 2-26 were generated from the NIST REFPROP software (Lemmon, E. W., McLinden, M. O., and Huber, M. L., NIST Standard Reference Database 23: Reference Fluid Thermodynamic and Transport Properties—REFPROP, Version 7.0, National Institute of Standards and Technology, Standard Reference Data Program, Gaithersburg, Md., 2002). The primary source for the properties of aqueous ammonia mixtures is R. Tillner-Roth and D. G. Friend, "A Helmholtz Free Energy Formulation of the Thermodynamic Properties of the Mixture (Water + Ammonia)," *J. Phys. Chem. Ref. Data* 27:63–96 (1998).

2-94 PHYSICAL AND CHEMICAL DATA

TABLE 2-27 Partial Pressures of H₂O over Aqueous Solutions of Sodium Carbonate*

t, °C	mmHg						
	%Na ₂ CO ₃						
	0	5	10	15	20	25	30
0	4.5	4.5					
10	9.2	9.0	8.8				
20	17.5	17.2	16.8	16.3			
30	31.8	31.2	30.4	29.6	28.8	27.8	26.4
40	55.3	54.2	53.0	57.6	50.2	48.4	46.1
50	92.5	90.7	88.7	86.5	84.1	81.2	77.5
60	149.5	146.5	143.5	139.9	136.1	131.6	125.7
70	239.8	235	230.5	225	219	211.5	202.5
80	355.5	348	342	334	325	315	301
90	526.0	516	506	494	482	467	447
100	760.0	746	731	715	697	676	648

*International Critical Tables, vol. 3, p. 372.

TABLE 2-28 Partial Pressures of H₂O and CH₃OH over Aqueous Solutions of Methyl Alcohol*

Mole fraction CH ₃ OH	39.9 °C		Mole fraction CH ₃ OH	59.4 °C	
	P _{H₂O} , mmHg	P _{CH₃OH} , mmHg		P _{H₂O} , mmHg	P _{CH₃OH} , mmHg
	0	54.7		0	0
14.99	39.2	66.1	22.17	106.9	210.1
17.85	38.5	75.5	27.40	102.2	240.2
21.07	37.2	85.2	33.24	96.6	272.1
27.31	35.8	100.6	39.80	91.7	301.9
31.06	34.9	108.8	47.08	84.8	335.6
40.1	32.8	127.7	55.5	76.9	373.7
47.0	31.5	141.6	69.2	57.8	439.4
55.8	27.3	158.4	78.5	43.8	486.6
68.9	20.7	186.6	85.9	30.1	526.9
86.0	10.1	225.2	100.0	0	609.3
100.0	0	260.7			

*International Critical Tables, vol. 3, p. 290.

TABLE 2-29 Partial Pressures of H₂O over Aqueous Solutions of Sodium Hydroxide*

Conc. g NaOH/100 g H ₂ O	mmHg											
	Temperature, °C											
	0	20	40	60	80	100	120	160	200	250	300	350
0	4.6	17.5	55.3	149.5	355.5	760.0	1,489	4,633	11,647	29,771	64,200	123,600
5	4.4	16.9	53.2	143.5	341.5	730.0	1,430	4,450	11,200	28,600	61,800	118,900
10	4.2	16.0	50.6	137.0	325.5	697.0	1,365	4,260	10,750	27,500	59,300	114,100
20	3.6	13.9	44.2	120.5	288.5	621.0	1,225	3,860	9,800	25,300	54,700	105,400
30	2.9	11.3	36.6	101.0	246.0	537.0	1,070	3,460	8,950	23,300	50,800	98,000
40	2.2	8.7	28.7	81.0	202.0	450.0	920	3,090	8,150	21,500	47,200	91,600
50		6.3	20.7	62.5	160.5	368.0	770	2,690	7,400	19,900	44,100	85,800
60		4.4	15.5	47.0	124.0	294.0	635	2,340	6,750	18,400	41,200	80,700
70		3.0	10.9	34.5	94.0	231.0	515	2,030	6,100	17,100	38,700	76,000
80		2.0	7.6	24.5	70.5	179.0	415	1,740	5,500	15,800	36,300	71,900
90		1.3	5.2	17.5	53.0	138.0	330	1,490	5,000	14,700	34,200	68,100
100		0.9	3.6	12.5	38.5	105.0	262	1,300	4,500	13,650	32,200	64,600
120			1.7	6.3	20.5	61.0	164	915	3,650	11,800	28,800	58,600
140				3.0	11.0	35.5	102	765	2,980	10,300	25,900	53,400
160				1.5	6.0	20.5	63	470	2,430	8,960	23,300	49,000
180					3.5	12.0	40	340	1,980	7,830	21,200	45,100
200					2.0	7.0	25	245	1,620	6,870	19,200	41,800
250					0.5	2.0	8	110	985	5,000	15,400	35,000
300					0.1	0.5	2.7	50	610	3,690	12,500	29,800
350							0.9	23	380	2,750	10,300	25,700
400								11	240	2,080	8,600	22,400
500									100	1,210	6,100	17,500
700										440	3,300	11,500
1000											1,470	6,800
2000											150	1,760
4000												120
8000												7

*International Critical Tables, vol. 3, p. 370.

WATER-VAPOR CONTENT OF GASES

CHART FOR GASES AT HIGH PRESSURES

The accompanying figure is useful in determining the water-vapor content of air at high pressure in contact with liquid water.

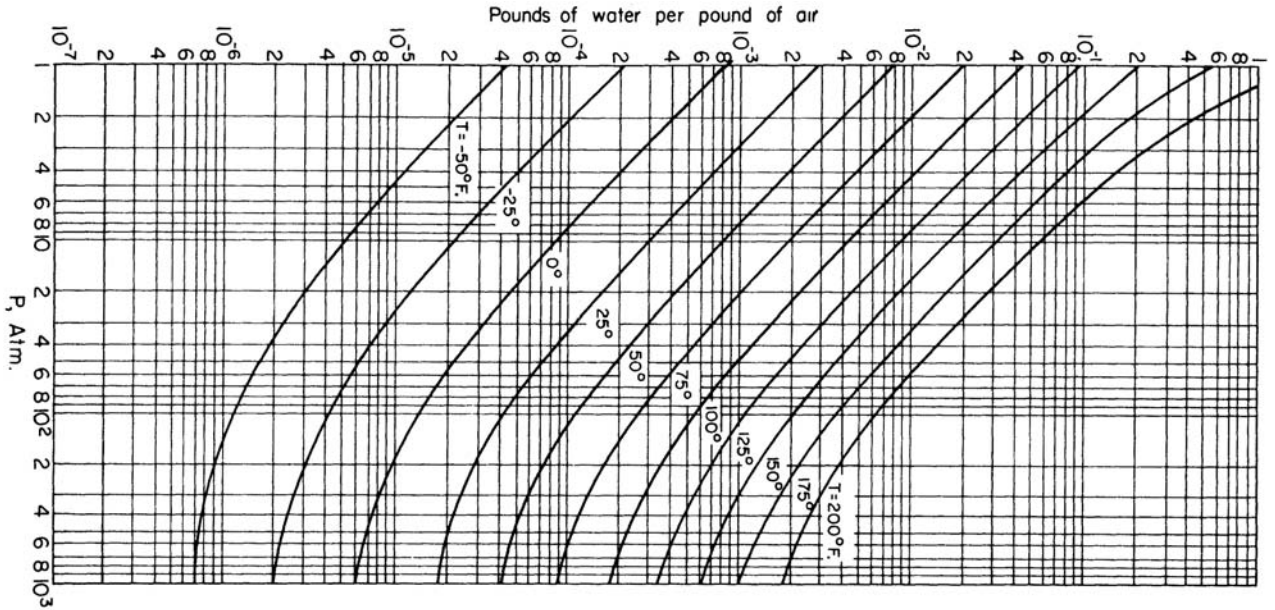


FIG. 2-4 Water content of air, °C = (°F - 32) × 5/9. (Landsbaum, Dadds, and Stutzman. Reprinted from vol. 47, January 1955 issue of Ind. Eng. Chem. [p. 192]. Copyright 1955 by the American Chemical Society and reproduced by permission of the copyright owner.)

DENSITIES OF PURE SUBSTANCES

TABLE 2-30 Density (kg/m³) of Saturated Liquid Water from the Triple Point to the Critical Point

T, K	ρ , kg/m ³	T, K	ρ , kg/m ³	T, K	ρ , kg/m ³	T, K	ρ , kg/m ³	T, K	ρ , kg/m ³
273.160 [°]	999.793	352	972.479	432	908.571	512	814.982	592	669.930
274	999.843	354	971.235	434	906.617	514	812.164	594	664.974
276	999.914	356	969.972	436	904.645	516	809.318	596	659.907
278	999.919	358	968.689	438	902.656	518	806.441	598	654.722
280	999.862	360	967.386	440	900.649	520	803.535	600	649.411
282	999.746	362	966.064	442	898.624	522	800.597	602	643.97
284	999.575	364	964.723	444	896.580	524	797.629	604	638.38
286	999.352	366	963.363	446	894.519	526	794.628	606	632.64
288	999.079	368	961.984	448	892.439	528	791.594	608	626.74
290	998.758	370	960.587	450	890.341	530	788.527	610	620.65
292	998.392	372	959.171	452	888.225	532	785.425	612	614.37
294	997.983	374	957.737	454	886.089	534	782.288	614	607.88
296	997.532	376	956.285	456	883.935	536	779.115	616	601.15
298	997.042	378	954.815	458	881.761	538	775.905	618	594.16
300	996.513	380	953.327	460	879.569	540	772.657	620	586.88
302	995.948	382	951.822	462	877.357	542	769.369	622	579.26
304	995.346	384	950.298	464	875.125	544	766.042	624	571.25
306	994.711	386	948.758	466	872.873	546	762.674	626	562.81
308	994.042	388	947.199	468	870.601	548	759.263	628	553.84
310	993.342	390	945.624	470	868.310	550	755.808	630	544.25
312	992.610	392	944.030	472	865.997	552	752.308	632	533.92
314	991.848	394	942.420	474	863.664	554	748.762	634	522.71
316	991.056	396	940.793	476	861.310	556	745.169	636	510.42
318	990.235	398	939.148	478	858.934	558	741.525	638	496.82
320	989.387	400	937.486	480	856.537	560	737.831	640	481.53
322	988.512	402	935.807	482	854.118	562	734.084	641	473.01
324	987.610	404	934.111	484	851.678	564	730.283	642	463.67
326	986.682	406	932.398	486	849.214	566	726.425	643	453.14
328	985.728	408	930.668	488	846.728	568	722.508	644	440.73
330	984.750	410	928.921	490	844.219	570	718.530	645	425.05
332	983.747	412	927.157	492	841.686	572	714.489	646	402.96
334	982.721	414	925.375	494	839.130	574	710.382	647	357.34
336	981.671	416	923.577	496	836.549	576	706.206	647.096†	322
338	980.599	418	921.761	498	833.944	578	701.959		
340	979.503	420	919.929	500	831.313	580	697.638		
342	978.386	422	918.079	502	828.658	582	693.238		
344	977.247	424	916.212	504	825.976	584	688.757		
346	976.086	426	914.328	506	823.269	586	684.190		
348	974.904	428	912.426	508	820.534	588	679.533		
350	973.702	430	910.507	510	817.772	590	674.781		

°Triple point

†Critical point

From Wagner, W., and Pruss, A., "The IAPWS Formulation 1995 for the Thermodynamic Properties of Ordinary Water Substance for General and Scientific Use," *J. Phys. Chem. Ref. Data* **31**(2):387-535, 2002.

TABLE 2-31 Density (kg/m³) of Mercury from 0 to 350°C*

t, °C	Density, kg/m ³									
	0	1	2	3	4	5	6	7	8	9
0	13595.08	13592.61	13590.14	13587.68	13585.21	13582.75	13580.29	13577.82	13575.36	13572.90
10	13570.44	13567.98	13565.52	13563.06	13560.60	13558.14	13555.69	13553.23	13550.78	13548.32
20	13545.87	13543.41	13540.96	13538.51	13536.06	13533.61	13531.16	13528.71	13526.26	13523.81
30	13521.36	13518.91	13516.47	13514.02	13511.58	13509.13	13506.69	13504.25	13501.80	13499.36
40	13496.92	13494.48	13492.04	13489.60	13487.16	13484.72	13482.29	13479.85	13477.41	13474.98
50	13472.54	13470.11	13467.67	13465.24	13462.81	13460.38	13457.94	13455.51	13453.08	13450.65
60	13448.22	13445.80	13443.37	13440.94	13438.51	13436.09	13433.66	13431.23	13428.81	13426.39
70	13423.96	13421.54	13419.12	13416.69	13414.27	13411.85	13409.43	13407.01	13404.59	13402.17
80	13399.75	13397.34	13394.92	13392.50	13390.08	13387.67	13385.25	13382.84	13380.42	13378.01
90	13375.59	13373.18	13370.77	13368.36	13365.94	13363.53	13361.12	13358.71	13356.30	13353.89
100	13351.5	13349.1	13346.7	13344.3	13341.9	13339.4	13337.0	13334.6	13332.2	13329.8
110	13327.4	13325.0	13322.6	13320.2	13317.8	13315.4	13313.0	13310.6	13308.2	13305.8
120	13303.4	13301.0	13298.6	13296.2	13293.8	13291.4	13289.0	13286.6	13284.2	13281.8
130	13279.4	13277.0	13274.6	13272.2	13269.8	13267.4	13265.0	13262.6	13260.2	13257.8
140	13255.4	13253.0	13250.6	13248.2	13245.8	13243.4	13241.0	13238.7	13236.3	13233.9
150	13231.5	13229.1	13226.7	13224.3	13221.9	13219.5	13217.1	13214.7	13212.4	13210.0
160	13207.6	13205.2	13202.8	13200.4	13198.0	13195.6	13193.2	13190.8	13188.5	13186.1
170	13183.7	13181.3	13178.9	13176.5	13174.1	13171.7	13169.4	13167.0	13164.6	13162.2
180	13159.8	13157.4	13155.0	13152.6	13150.3	13147.9	13145.5	13143.1	13140.7	13138.3
190	13136.0	13133.6	13131.2	13128.8	13126.4	13124.0	13121.7	13119.3	13116.9	13114.5
200	13112.1	13109.7	13107.4	13105.0	13102.6	13100.2	13097.8	13095.4	13093.1	13090.7
210	13088.3	13085.9	13083.5	13081.1	13078.8	13076.4	13074.0	13071.6	13069.2	13066.8
220	13064.5	13062.1	13059.7	13057.3	13054.9	13052.6	13050.2	13047.8	13045.4	13043.0
230	13040.6	13038.3	13035.9	13033.5	13031.1	13028.7	13026.4	13024.0	13021.6	13019.2
240	13016.8	13014.5	13012.1	13009.7	13007.3	13004.9	13002.5	13000.2	12997.8	12995.4
250	12993.0	12990.6	12988.3	12985.9	12983.5	12981.1	12978.7	12976.3	12974.0	12971.6
260	12969.2	12966.8	12964.4	12962.0	12959.7	12957.3	12954.9	12952.5	12950.1	12947.7
270	12945.4	12943.0	12940.6	12938.2	12935.8	12933.4	12931.1	12928.7	12926.3	12923.9
280	12921.5	12919.1	12916.7	12914.4	12912.0	12909.6	12907.2	12904.8	12902.4	12900.0
290	12897.7	12895.3	12892.9	12890.5	12888.1	12885.7	12883.3	12880.9	12878.5	12876.2
300	12873.8	12871.4	12869.0	12866.6	12864.2	12861.8	12859.4	12857.0	12854.6	12852.2
310	12849.9	12847.5	12845.1	12842.7	12840.3	12837.9	12835.5	12833.1	12830.7	12828.3
320	12825.9	12823.5	12821.1	12818.7	12816.3	12813.9	12811.5	12809.1	12806.7	12804.3
330	12801.9	12799.5	12797.1	12794.7	12792.3	12789.9	12787.5	12785.1	12782.7	12780.2
340	12777.8	12775.4	12773.0	12770.6	12768.2	12765.8	12763.4	12761.0	12758.6	12756.1
350	12753.7									

*From "Mercury—Density and Thermal Expansion at Atmospheric Pressure and Temperatures from 0 to 350 °C," *Tables of Standard Handbook Data*, Standartov, Moscow, 1978. The density values obtainable from those cited for the specific volume of the saturated liquid in the "Thermodynamic Properties" subsection show minor differences. No attempt was made to adjust either set.

TABLE 2-32 Densities of Inorganic and Organic Liquids (mol/dm³)

Cmpd. no.	Name	Formula	CAS no.	Mol. wt.	C1	C2	C3	C4	T _{min} , K	Density at T _{min}	T _{max} , K	Density at T _{max}
1	Acetaldehyde	C ₂ H ₄ O	75-07-0	44.053	1.6994	0.26167	466	0.2913	150.15	21.499	466.00	6.4944
2	Acetamide	C ₂ H ₅ NO	60-35-5	59.067	1.016	0.21845	761	0.26116	353.33	16.936	761.00	4.6509
3	Acetic acid	C ₂ H ₄ O ₂	64-19-7	60.052	1.4486	0.25892	591.95	0.2529	289.81	17.492	591.95	5.5948
4	Acetic anhydride	C ₄ H ₆ O ₃	108-24-7	102.089	0.86852	0.25187	606	0.31172	200.15	11.643	606.00	3.4483
5	Acetone	C ₃ H ₆ O	67-64-1	58.079	1.2332	0.25886	508.2	0.2913	178.45	15.683	508.20	4.7640
6	Acetonitrile	C ₂ H ₃ N	75-05-8	41.052	1.3064	0.22597	545.5	0.28678	229.32	20.628	545.50	5.7813
7	Acetylene	C ₂ H ₂	74-86-2	26.037	2.4507	0.27448	308.3	0.28752	192.40	23.692	308.30	8.9285
8	Acrolein	C ₃ H ₄ O	107-02-8	56.063	1.3261	0.26124	506	0.2489	185.45	16.822	506.00	5.0762
9	Acrylic acid	C ₃ H ₄ O ₂	79-10-7	72.063	1.2414	0.25822	615	0.30701	286.15	14.693	615.00	4.8075
10	Acrylonitrile	C ₃ H ₃ N	107-13-1	53.063	1.0816	0.2293	535	0.28939	189.63	17.265	535.00	4.7170
11	Air	Mixture	132259-10-0	28.960	2.8963	0.26733	132.45	0.27341	59.15	33.279	132.45	10.8340
12	Ammonia	H ₃ N	7664-41-7	17.031	3.5383	0.25443	405.65	0.2888	195.41	43.141	405.65	13.9070
13	Anisole	C ₇ H ₈ O	100-66-3	108.138	0.77488	0.26114	645.6	0.28234	235.65	9.668	645.60	2.9673
14	Argon	Ar	7440-37-1	39.948	3.8469	0.2881	150.86	0.29783	83.78	35.491	150.86	13.3530
15	Benzamide	C ₇ H ₇ NO	55-21-0	121.137	0.7371	0.25487	824	0.28571	403.00	8.938	824.00	2.8921
16	Benzene	C ₆ H ₆	71-43-2	78.112	1.0259	0.26666	562.05	0.28394	278.68	11.422	562.05	3.8472
17	Benzenethiol	C ₆ H ₆ S	108-98-5	110.177	0.83573	0.26326	689	0.30798	258.27	10.074	689.00	3.1745
18	Benzoic acid	C ₇ H ₆ O ₂	65-85-0	122.121	0.71587	0.24812	751	0.2857	395.45	8.894	751.00	2.8852
19	Benzonitrile	C ₇ H ₅ N	100-47-0	103.121	0.8552	0.26785	699.35	0.30523	260.40	10.011	699.35	3.1928
20	Benzophenone	C ₁₃ H ₁₀ O	119-61-9	182.118	0.43743	0.24833	830	0.27555	321.35	5.950	830.00	1.7615
21	Benzyl alcohol	C ₇ H ₈ O	100-51-6	108.138	0.59867	0.22849	720.15	0.23567	257.85	9.905	720.15	2.6201
22	Benzyl ethyl ether	C ₉ H ₁₂ O	539-30-0	136.191	0.60917	0.26925	662	0.2632	275.65	7.065	662.00	2.2625
23	Benzyl mercaptan	C ₇ H ₈ S	100-53-8	124.203	0.70797	0.25982	718	0.32144	243.95	8.862	718.00	2.7248
24	Biphenyl	C ₁₂ H ₁₀	92-52-4	154.208	0.52257	0.25833	773	0.27026	342.20	6.425	773.00	2.0229
25	Bromine	Br ₂	7726-95-6	159.808	2.1872	0.29527	584.15	0.3295	265.85	20.109	584.15	7.4075
26	Bromobenzene	C ₆ H ₅ Br	108-86-1	157.008	0.8226	0.26632	670.15	0.2821	242.43	9.909	670.15	3.0888
27	Bromoethane	C ₂ H ₅ Br	74-96-4	108.965	1.1908	0.25595	503.8	0.29152	154.55	15.833	503.80	4.6525
28	Bromomethane	CH ₃ Br	74-83-9	94.939	1.6762	0.26141	467	0.28402	179.47	20.640	467.00	6.4121
29	1,2-Butadiene	C ₄ H ₆	590-19-2	54.090	1.187	0.26114	452	0.3065	136.95	15.123	452.00	4.5455
30	1,3-Butadiene	C ₄ H ₆	106-99-0	54.090	1.2346	0.27216	425	0.28707	164.25	14.058	425.00	4.5363
31	Butane	C ₄ H ₁₀	106-97-8	58.122	1.0677	0.27188	425.12	0.28688	134.86	12.620	425.12	3.9271
32	1,2-Butanediol	C ₄ H ₁₀ O ₂	584-03-2	90.121	0.81696	0.24755	680	0.25435	220.00	11.734	680.00	3.3002
33	1,3-Butanediol	C ₄ H ₁₀ O ₂	107-88-0	90.121	0.81856	0.24967	676	0.22023	196.15	11.872	676.00	3.2786
34	1-Butanol	C ₄ H ₁₀ O	71-36-3	74.122	0.98279	0.26830	563.1	0.25488	183.85	12.035	563.10	3.6630
35	2-Butanol	C ₄ H ₁₀ O	78-92-2	74.122	0.9682	0.26244	535.9	0.26749	158.45	12.471	535.90	3.6892
36	1-Butene	C ₄ H ₈	106-98-9	56.106	1.0877	0.26454	419.5	0.2843	87.80	14.264	419.50	4.1117
37	cis-2-Butene	C ₄ H ₈	590-18-1	56.106	1.1591	0.27085	435.5	0.28116	134.26	13.894	435.50	4.2795
38	trans-2-Butene	C ₄ H ₈	624-64-6	56.106	1.1448	0.27154	428.6	0.28419	167.62	13.080	428.60	4.2160
39	Butyl acetate	C ₆ H ₁₂ O ₂	123-86-4	116.158	0.67794	0.2637	575.4	0.29318	199.65	8.337	575.40	2.5709
40	Butylbenzene	C ₁₀ H ₁₄	104-51-8	134.218	0.50812	0.25238	660.5	0.29373	185.30	7.026	660.50	2.0133
41	Butyl mercaptan	C ₄ H ₁₀ S	109-79-5	90.187	0.89458	0.27463	570.1	0.28512	157.46	10.585	570.10	3.2574
42	sec-Butyl mercaptan	C ₄ H ₁₀ S	513-53-1	90.187	0.89137	0.27365	554	0.2953	133.02	10.761	554.00	3.2573
43	1-Butyne	C ₄ H ₆	107-00-6	54.090	1.3409	0.27892	440	0.29661	147.43	14.901	440.00	4.8075
44	Butyraldehyde	C ₄ H ₈ O	123-72-8	72.106	1.0361	0.26731	537.2	0.28397	176.75	12.589	537.20	3.8760
45	Butyric acid	C ₄ H ₈ O ₂	107-92-6	88.105	0.88443	0.25828	615.7	0.248	267.95	11.087	615.70	3.4243
46	Butyronitrile	C ₄ H ₇ N	109-74-0	69.105	0.87533	0.24331	582.25	0.28586	161.25	13.047	582.25	3.5976
47	Carbon dioxide	CO ₂	124-38-9	44.010	2.768	0.26212	304.21	0.2908	216.58	26.828	304.21	10.5600
48	Carbon disulfide	CS ₂	75-15-0	76.141	1.7968	0.28749	552	0.3226	161.11	19.064	552.00	6.2500
49	Carbon monoxide	CO	630-08-0	28.010	2.897	0.27532	132.92	0.2813	68.15	30.180	132.92	10.5220
50	Carbon tetrachloride	CCl ₄	56-23-5	153.823	0.99835	0.274	556.35	0.287	250.33	10.843	556.35	3.6436
51	Carbon tetrafluoride	CF ₄	75-73-0	88.004	1.955	0.27884	227.51	0.28571	89.56	21.211	227.51	7.0112
52	Chlorine	Cl ₂	7782-50-5	70.906	2.23	0.27645	417.15	0.2926	172.12	24.242	417.15	8.0666
53	Chlorobenzene	C ₆ H ₅ Cl	108-90-7	112.557	0.8711	0.26805	632.35	0.2799	227.95	10.385	632.35	3.2498
54	Chloroethane	C ₂ H ₅ Cl	75-00-3	64.514	1.3	0.26019	460.35	0.27155	134.80	17.016	460.35	4.9963
55	Chloroform	CHCl ₃	67-66-3	119.378	1.0841	0.2581	536.4	0.2741	209.63	13.702	536.40	4.2003
56	Chloromethane	CH ₃ Cl	74-87-3	50.488	1.817	0.25877	416.25	0.2833	175.43	22.347	416.25	7.0217
57	1-Chloropropane	C ₃ H ₇ Cl	540-54-5	78.541	1.087	0.26832	503.15	0.28055	150.35	13.328	503.15	4.0511
58	2-Chloropropane	C ₃ H ₇ Cl	75-29-6	78.541	1.1202	0.27669	489	0.27646	155.97	12.855	489.00	4.0486
59	m-Cresol	C ₇ H ₈ O	108-39-4	108.138	0.9061	0.28268	705.85	0.2707	285.39	9.612	705.85	3.2054

60	<i>o</i> -Cresol	C ₇ H ₈ O	95-48-7	108.138	1.0861	0.30624	697.55	0.30587	304.19	9.575	697.55	3.5466
61	<i>p</i> -Cresol	C ₇ H ₈ O	106-44-5	108.138	1.1503	0.31861	704.65	0.30104	307.93	9.449	704.65	3.6104
62	Cumene	C ₉ H ₁₂	98-82-8	120.192	0.58711	0.25583	631	0.28498	177.14	7.939	631.00	2.2949
63	Cyanogen	C ₂ N ₂	460-19-5	52.035	1.0743	0.20948	400.15	0.20724	245.25	18.520	400.15	5.1284
64	Cyclobutane	C ₄ H ₆	287-23-0	56.106	1.3931	0.29255	459.93	0.24913	182.48	14.074	459.93	4.7619
65	Cyclohexane	C ₆ H ₁₂	110-82-7	84.159	0.88998	0.27376	553.8	0.28571	279.69	9.380	553.80	3.2509
66	Cyclohexanol	C ₆ H ₁₂ O	108-93-0	100.159	0.8243	0.26545	650.1	0.28495	296.60	9.469	650.10	3.1053
67	Cyclohexanone	C ₆ H ₁₀ O	108-94-1	98.143	0.86464	0.26888	653	0.29943	242.00	10.090	653.00	3.2157
68	Cyclohexene	C ₆ H ₁₀	110-83-8	82.144	0.92997	0.27056	560.4	0.28943	169.67	11.160	560.40	3.4372
69	Cyclopentane	C ₅ H ₁₀	287-92-3	70.133	1.0897	0.28356	511.7	0.25142	179.28	11.906	511.70	3.8429
70	Cyclopentene	C ₅ H ₈	142-29-0	68.117	1.1035	0.27035	507	0.28699	138.13	13.470	507.00	4.0817
71	Cyclopropane	C ₃ H ₆	75-19-4	42.080	1.7411	0.28205	398	0.29598	145.59	18.658	398.00	6.1730
72	Cyclohexyl mercaptan	C ₆ H ₁₂ S	1569-69-3	116.224	0.78578	0.27882	664	0.31067	189.64	8.905	664.00	2.8182
73	Decanal	C ₁₀ H ₂₀ O	112-31-2	156.265	0.46802	0.27146	674.2	0.26869	267.15	5.383	674.20	1.7241
74	Decane	C ₁₀ H ₂₂	124-18-5	142.282	0.41084	0.25175	617.7	0.28571	243.51	5.393	617.70	1.6320
75	Decanoic acid	C ₁₀ H ₂₀ O ₂	334-48-5	172.265	0.39348	0.2492	722.1	0.28571	304.55	5.181	722.10	1.5790
76	1-Decanol	C ₁₀ H ₂₂ O	112-30-1	158.281	0.38208	0.24645	688	0.26125	280.05	5.261	688.00	1.5503
77	1-Decene	C ₁₀ H ₂₀	872-05-9	140.266	0.43981	0.25661	616.6	0.29148	206.89	5.733	616.60	1.7139
78	Decyl mercaptan	C ₁₀ H ₂₂ S	143-10-2	174.347	0.44289	0.27636	696	0.27668	247.56	5.005	696.00	1.6026
79	1-Decyne	C ₁₀ H ₁₈	764-93-2	138.250	0.46877	0.25875	619.85	0.29479	229.15	5.895	619.85	1.8117
80	Deuterium	D ₂	7782-39-0	4.032	5.2115	0.315	38.35	0.28571	18.73	42.945	38.35	16.5440
81	1,1-Dibromoethane	C ₂ H ₄ Br ₂	557-91-5	187.861	0.95523	0.26364	628	0.29825	210.15	11.799	628.00	3.6232
82	1,2-Dibromoethane	C ₂ H ₄ Br ₂	106-93-4	187.861	1.0132	0.26634	650.15	0.28571	282.85	11.704	650.15	3.8042
83	Dibromomethane	CH ₂ Br ₂	74-95-3	173.835	1.1136	0.24834	611	0.27583	220.60	15.358	611.00	4.4842
84	Dibutyl ether	C ₈ H ₁₈ O	142-96-1	130.228	0.55941	0.27243	584.1	0.29932	175.30	6.607	584.10	2.0534
85	<i>m</i> -Dichlorobenzene	C ₆ H ₄ Cl ₂	541-73-1	147.002	0.74495	0.26147	683.95	0.31526	248.39	9.121	683.95	2.8491
86	<i>o</i> -Dichlorobenzene	C ₆ H ₄ Cl ₂	95-50-1	147.002	0.74404	0.26112	705	0.30815	256.15	9.166	705.00	2.8494
87	<i>p</i> -Dichlorobenzene	C ₆ H ₄ Cl ₂	106-46-7	147.002	0.74858	0.26276	684.75	0.30788	326.14	8.518	684.75	2.8489
88	1,1-Dichloroethane	C ₂ H ₄ Cl ₂	75-34-3	98.959	1.1055	0.26533	523	0.287	176.19	13.549	523.00	4.1665
89	1,2-Dichloroethane	C ₂ H ₄ Cl ₂	107-06-2	98.959	1.2591	0.27698	561.6	0.30492	237.49	13.462	561.60	4.5458
90	Dichloromethane	CH ₂ Cl ₂	75-09-2	84.933	1.3897	0.25678	510	0.2902	178.01	17.974	510.00	5.4120
91	1,1-Dichloropropane	C ₃ H ₆ Cl ₂	78-99-9	112.986	0.9551	0.27794	560	0.24132	200.00	10.862	560.00	3.4364
92	1,2-Dichloropropane	C ₃ H ₆ Cl ₂	78-87-5	112.986	0.89833	0.26142	572	0.2868	172.71	11.526	572.00	3.4363
93	Diethanol amine	C ₄ H ₁₁ NO ₂	111-42-2	105.136	0.68184	0.23796	736.6	0.2062	301.15	10.390	736.60	2.8654
94	Diethyl amine	C ₄ H ₁₁ N	109-89-7	73.137	0.85379	0.25675	496.6	0.27027	223.35	10.575	496.60	3.3254
95	Diethyl ether	C ₄ H ₁₀ O	60-29-7	74.122	0.9554	0.26847	466.7	0.2814	156.85	11.487	466.70	3.5587
96	Diethyl sulfide	C ₄ H ₁₀ S	352-93-2	90.187	0.82227	0.26314	557.15	0.27369	169.20	10.470	557.15	3.1248
97	1,1-Difluoroethane	C ₂ H ₄ F ₂	75-37-6	66.050	1.4345	0.25774	386.44	0.28178	154.56	18.006	386.44	5.5657
98	1,2-Difluoroethane	C ₂ H ₄ F ₂	624-72-6	66.050	1.173	0.22856	445	0.28571	215.00	17.424	445.00	5.1321
99	Difluoromethane	CH ₂ F ₂	75-10-5	52.023	1.9973	0.24653	351.26	0.28153	136.95	27.399	351.26	8.6070
100	Di-isopropyl amine	C ₆ H ₁₃ N	108-18-9	101.190	0.6181	0.25786	523.1	0.271	176.85	8.054	523.10	2.3970
101	Di-isopropyl ether	C ₆ H ₁₄ O	108-20-3	102.175	0.69213	0.26974	500.05	0.28571	187.65	8.067	500.05	2.5659
102	Di-isopropyl ketone	C ₇ H ₁₄ O	565-80-0	114.185	0.64619	0.26881	576	0.28036	204.81	7.680	576.00	2.4039
103	1,1-Dimethoxyethane	C ₄ H ₁₀ O ₂	534-15-6	90.121	0.89368	0.26599	507.8	0.28571	159.95	11.029	507.80	3.3598
104	1,2-Dimethoxypropane	C ₅ H ₁₂ O ₂	7778-85-0	104.148	0.76327	0.26742	543	0.28571	226.10	8.843	543.00	2.8542
105	Dimethyl acetylene	C ₄ H ₆	503-17-3	54.090	1.1717	0.25895	473.2	0.27289	240.91	13.767	473.20	4.5248
106	Dimethyl amine	C ₂ H ₇ N	124-40-3	45.084	1.5436	0.27784	437.2	0.2572	180.96	16.964	437.20	5.5557
107	2,3-Dimethylbutane	C ₆ H ₁₄	79-29-8	86.175	0.7565	0.27305	500	0.27408	145.19	9.031	500.00	2.7706
108	1,1-Dimethylcyclohexane	C ₈ H ₁₆	590-66-9	112.213	0.55873	0.25143	591.15	0.27758	239.66	7.342	591.15	2.2222
109	<i>cis</i> -1,2-Dimethylcyclohexane	C ₈ H ₁₆	2207-01-4	112.213	0.52953	0.24358	606.15	0.26809	223.16	7.578	606.15	2.1739
110	<i>trans</i> -1,2-Dimethylcyclohexane	C ₈ H ₁₆	6876-23-9	112.213	0.54405	0.25026	596.15	0.2658	184.99	7.626	596.15	2.1739
111	Dimethyl disulfide	C ₂ H ₆ S ₂	624-92-0	94.199	1.1058	0.27866	615	0.31082	188.44	12.413	615.00	3.9683
112	Dimethyl ether	C ₂ H ₆ O	115-10-6	46.068	1.5693	0.2679	400.1	0.2882	131.65	18.950	400.10	5.8578
113	<i>N,N</i> -Dimethyl formamide	C ₃ H ₇ NO	68-12-2	73.094	0.89615	0.23478	649.6	0.28091	212.72	13.954	649.60	3.8170
114	2,3-Dimethylpentane	C ₇ H ₁₆	565-59-3	100.202	0.72352	0.28629	537.3	0.27121	160.00	7.874	537.30	2.5272
115	Dimethyl phthalate	C ₁₀ H ₁₀ O ₄	131-11-3	194.184	0.47977	0.25428	766	0.30722	274.18	6.233	766.00	1.8868
116	Dimethylsilane	C ₂ H ₆ Si	1111-74-6	60.170	1.0214	0.26351	402	0.28421	122.93	12.898	402.00	3.8761
117	Dimethyl sulfide	C ₂ H ₆ S	75-18-3	62.134	1.4029	0.27991	503.04	0.2741	174.88	15.556	503.04	5.0120
118	Dimethyl sulfoxide	C ₂ H ₆ OS	67-68-5	78.133	1.1096	0.25189	729	0.3311	291.67	14.111	729.00	4.4051
119	Dimethyl terephthalate	C ₁₀ H ₁₀ O ₄	120-61-6	194.184	0.50824	0.26885	772	0.2612	413.80	5.538	772.00	1.8904
120	1,4-Dioxane	C ₄ H ₈ O ₂	123-91-1	88.105	1.1819	0.2813	587	0.3047	284.95	11.838	587.00	4.2016
121	Diphenyl ether	C ₁₂ H ₁₀ O	101-84-8	170.207	0.52133	0.26218	766.8	0.31033	300.03	6.265	766.80	1.9884
122	Dipropyl amine	C ₆ H ₁₅ N	142-84-7	101.190	0.659	0.26428	550	0.2766	210.15	7.993	550.00	2.4936

TABLE 2-32 Densities of Inorganic and Organic Liquids (mol/dm³) (Continued)

Cmpd. no.	Name	Formula	CAS no.	Mol. wt.	C1	C2	C3	C4	T _{min} , K	Density at T _{min}	T _{max} , K	Density at T _{max}
123	Dodecane	C ₁₂ H ₂₆	112-40-3	170.335	0.33267	0.24664	658	0.28571	263.57	4.521	658.00	1.3490
124	Eicosane	C ₂₀ H ₄₂	112-95-8	282.547	0.18166	0.23351	768	0.28571	309.58	2.729	768.00	0.7780
125	Ethane	C ₂ H ₆	74-84-0	30.069	1.9122	0.27937	305.32	0.29187	90.35	21.640	305.32	6.8447
126	Ethanol	C ₂ H ₆ O	64-17-5	46.068	1.6288	0.27469	514	0.23178	159.05	19.410	514.00	5.9296
127	Ethyl acetate	C ₄ H ₈ O ₂	141-78-6	88.105	0.8996	0.25856	523.3	0.278	189.60	11.478	523.30	3.4793
128	Ethyl amine	C ₂ H ₇ N	75-04-7	45.084	1.0936	0.22636	456.15	0.25522	192.15	17.588	456.15	4.8312
129	Ethylbenzene	C ₈ H ₁₀	100-41-4	106.165	0.70041	0.26162	617.15	0.28454	178.20	9.041	617.15	2.6772
130	Ethyl benzoate	C ₉ H ₁₀ O ₂	93-89-0	150.175	0.48864	0.23894	698	0.28421	238.45	7.291	698.00	2.0450
131	2-Ethyl butanoic acid	C ₈ H ₁₆ O ₂	88-09-5	116.158	0.66085	0.25707	655	0.31103	258.15	8.220	655.00	2.5707
132	Ethyl butyrate	C ₈ H ₁₆ O ₂	105-54-4	116.158	0.63566	0.25613	571	0.27829	175.15	8.491	571.00	2.4818
133	Ethylcyclohexane	C ₈ H ₁₆	1678-91-7	112.213	0.61587	0.26477	609.15	0.28054	161.84	7.868	609.15	2.3261
134	Ethylcyclopentane	C ₇ H ₁₄	1640-89-7	98.186	0.71751	0.26903	569.5	0.27733	134.71	9.018	569.50	2.6670
135	Ethylene	C ₂ H ₄	74-85-1	28.053	2.0961	0.27657	282.34	0.29147	104.00	23.326	282.34	7.5789
136	Ethylenediamine	C ₂ H ₆ N ₂	107-15-3	60.098	0.7842	0.20702	593	0.20254	284.29	15.055	593.00	3.7880
137	Ethylene glycol	C ₂ H ₆ O ₂	107-21-1	62.068	1.315	0.25125	720	0.21868	260.15	18.310	720.00	5.2338
138	Ethyleneimine	C ₂ H ₅ N	151-56-4	43.068	1.3462	0.23289	537	0.23357	195.20	21.450	537.00	5.7804
139	Ethylene oxide	C ₂ H ₄ O	75-21-8	44.053	1.836	0.26024	469.15	0.2696	160.65	23.477	469.15	7.0550
140	Ethyl formate	C ₃ H ₆ O ₂	109-94-4	74.079	1.1343	0.26168	508.4	0.2791	193.55	14.006	508.40	4.3347
141	2-Ethyl hexanoic acid	C ₈ H ₁₆ O ₂	149-57-5	144.211	0.47428	0.25028	674.6	0.25442	235.00	6.563	674.60	1.8950
142	Ethylhexyl ether	C ₈ H ₁₈ O	5756-43-4	130.228	0.55729	0.2714	583	0.29538	180.00	6.612	583.00	2.0534
143	Ethylisopropyl ether	C ₈ H ₁₈ O	625-54-7	88.148	0.8185	0.26929	489	0.30621	140.00	9.924	489.00	3.0395
144	Ethylisopropyl ketone	C ₈ H ₁₆ O	565-69-5	100.159	0.68162	0.25152	567	0.3182	204.15	8.975	567.00	2.7100
145	Ethyl mercaptan	C ₂ H ₆ S	75-08-1	62.134	1.3047	0.2694	499.15	0.27866	125.26	16.242	499.15	4.8430
146	Ethyl propionate	C ₅ H ₁₀ O ₂	105-37-3	102.132	0.7405	0.25563	546	0.2795	199.25	9.632	546.00	2.8968
147	Ethylpropyl ether	C ₈ H ₁₈ O	628-32-0	88.148	0.7908	0.266	500.23	0.292	145.65	9.847	500.23	2.9729
148	Ethyltrichlorosilane	C ₂ H ₅ Cl ₃ Si	115-21-9	163.506	0.58579	0.24246	559.95	0.29509	167.55	8.653	559.95	2.4160
149	Fluorine	F ₂	7782-41-4	37.997	4.2895	0.28587	144.12	0.28776	53.48	44.888	144.12	15.0050
150	Fluorobenzene	C ₆ H ₅ F	462-06-6	96.102	1.0146	0.27277	560.09	0.28291	230.94	11.374	560.09	3.7196
151	Fluoroethane	C ₂ H ₅ F	353-36-6	48.060	1.6525	0.27099	375.31	0.2442	129.95	19.785	375.31	6.0980
152	Fluoromethane	CH ₃ F	593-53-3	34.033	2.1854	0.24725	317.42	0.27558	131.35	29.526	317.42	8.8388
153	Formaldehyde	CH ₂ O	50-00-0	30.026	1.9415	0.22309	408	0.28571	181.15	30.945	408.00	8.7028
154	Formamide	CH ₃ NO	75-12-7	45.041	1.2486	0.20352	771	0.25178	275.60	25.488	771.00	6.1350
155	Formic acid	CH ₂ O ₂	64-18-6	46.026	1.938	0.24225	588	0.24435	281.45	26.806	588.00	8.0000
156	Furan	C ₄ H ₄ O	110-00-9	68.074	1.1339	0.24741	490.15	0.2612	187.55	15.702	490.15	4.5831
157	Helium-4	He	7440-59-7	4.003	7.2475	0.41865	5.2	0.24096	2.20	37.115	5.20	17.3120
158	Heptadecane	C ₁₇ H ₃₆	629-78-7	240.468	0.21897	0.23642	736	0.28571	295.13	3.219	736.00	0.9262
159	Heptanal	C ₇ H ₁₄ O	111-71-7	114.185	0.59006	0.25609	616.8	0.28384	229.80	7.600	616.80	2.3041
160	Heptane	C ₇ H ₁₆	142-82-5	100.202	0.61259	0.26211	540.2	0.28141	182.57	7.700	540.20	2.3371
161	Heptanoic acid	C ₇ H ₁₄ O ₂	111-14-8	130.185	0.53066	0.24729	677.3	0.28289	265.83	7.221	677.30	2.1459
162	1-Heptanol	C ₇ H ₁₆ O	111-70-6	116.201	0.55687	0.24725	632.3	0.31471	239.15	7.502	632.30	2.2523
163	2-Heptanol	C ₇ H ₁₆ O	543-49-7	116.201	0.57114	0.25534	608.3	0.26487	230.00	7.454	608.30	2.2368
164	3-Heptanone	C ₇ H ₁₄ O	106-35-4	114.185	0.59268	0.25663	606.6	0.27766	234.15	7.575	606.60	2.3095
165	2-Heptanone	C ₇ H ₁₄ O	110-43-0	114.185	0.58247	0.25279	611.4	0.29818	238.15	7.551	611.40	2.3042
166	1-Heptene	C ₇ H ₁₄	592-76-7	98.186	0.66016	0.26657	537.4	0.28571	154.12	8.226	537.40	2.4765
167	Heptyl mercaptan	C ₇ H ₁₆ S	1639-09-4	132.267	0.58622	0.2726	645	0.29644	229.92	6.728	645.00	2.1505
168	1-Heptyne	C ₇ H ₁₂	628-71-7	96.170	0.67304	0.26045	547	0.28388	192.22	8.492	547.00	2.5841
169	Hexadecane	C ₁₆ H ₃₄	544-76-3	226.441	0.23289	0.23659	723	0.28571	291.31	3.415	723.00	0.9844
170	Hexanal	C ₆ H ₁₂ O	66-25-1	100.159	0.71899	0.26531	591	0.27628	217.15	8.724	591.00	2.7100
171	Hexane	C ₆ H ₁₄	110-54-3	86.175	0.70824	0.26411	507.6	0.27537	177.83	8.747	507.60	2.6816
172	Hexanoic acid	C ₆ H ₁₂ O ₂	142-62-1	116.158	0.62833	0.25598	660.2	0.25304	269.25	8.096	660.20	2.4546
173	1-Hexanol	C ₆ H ₁₄ O	111-27-3	102.175	0.70093	0.26776	611.3	0.24919	228.55	8.456	611.30	2.6178
174	2-Hexanol	C ₆ H ₁₄ O	626-93-7	102.175	0.67393	0.25948	585.3	0.26552	223.00	8.518	585.30	2.5972
175	2-Hexanone	C ₆ H ₁₂ O	591-78-6	100.159	0.67816	0.25634	587.61	0.28365	217.35	8.732	587.61	2.6455
176	3-Hexanone	C ₆ H ₁₂ O	589-38-8	100.159	0.67666	0.25578	582.82	0.27746	217.50	8.763	582.82	2.6455
177	1-Hexene	C ₆ H ₁₂	592-41-6	84.159	0.76925	0.26809	504	0.28571	133.39	9.581	504.00	2.8694
178	3-Hexyne	C ₆ H ₁₀	928-49-4	82.144	0.78045	0.26065	544	0.28571	170.05	10.021	544.00	2.9942
179	Hexyl mercaptan	C ₆ H ₁₄ S	111-31-9	118.240	0.66372	0.27345	623	0.29185	192.62	7.773	623.00	2.4272
180	1-Hexyne	C ₆ H ₁₀	693-02-7	82.144	0.84427	0.27185	516.2	0.2771	141.25	10.230	516.20	3.1056
181	2-Hexyne	C ₆ H ₁₀	764-35-2	82.144	0.76277	0.25248	549	0.31611	183.65	10.133	549.00	3.0211

182	Hydrazine	H ₂ N ₂	302-01-2	32.045	1.0516	0.16613	653.15	0.1898	274.69	31.934	653.15	6.3300
183	Hydrogen	H ₂	1333-74-0	2.016	5.414	0.34893	33.19	0.2706	13.95	38.487	33.19	15.5160
184	Hydrogen bromide	HBr	10035-10-6	80.912	2.832	0.2832	363.15	0.28571	185.15	27.985	363.15	10.0000
185	Hydrogen chloride	HCl	7647-01-0	36.461	3.342	0.2729	324.65	0.3217	158.97	34.854	324.65	12.2460
186	Hydrogen cyanide	CHN	74-90-8	27.025	1.3413	0.18589	456.65	0.28206	259.83	27.202	456.65	7.2156
187	Hydrogen fluoride	HF	7664-39-3	20.006	2.5635	0.1766	461.15	0.3733	189.79	60.203	461.15	14.5160
188	Hydrogen sulfide	H ₂ S	7783-06-4	34.081	2.7672	0.27369	373.53	0.29015	187.68	29.130	373.53	10.1110
189	Isobutyric acid	C ₄ H ₈ O ₂	79-31-2	88.105	0.88575	0.25736	605	0.26265	227.15	11.420	605.00	3.4417
190	Isopropyl amine	C ₃ H ₉ N	75-31-0	59.110	1.2801	0.2828	471.85	0.2972	177.95	13.561	471.85	4.5265
191	Malonic acid	C ₃ H ₄ O ₄	141-82-2	104.061	0.84266	0.217	805	0.28571	407.95	13.533	805.00	3.8832
192	Methacrylic acid	C ₄ H ₆ O ₂	79-41-4	86.089	0.87025	0.24383	662	0.28571	288.15	11.834	662.00	3.5691
193	Methane	CH ₄	74-82-8	16.042	2.9214	0.28976	190.56	0.28881	90.69	28.180	190.56	10.0820
194	Methanol	CH ₃ O	67-56-1	32.042	2.3267	0.27073	512.5	0.24713	175.47	27.915	512.50	8.5942
195	N-Methyl acetamide	C ₃ H ₇ NO	79-16-3	73.094	0.88268	0.23568	718	0.27379	301.15	13.012	718.00	3.7452
196	Methyl acetate	C ₃ H ₆ O ₂	79-20-9	74.079	1.13	0.2593	506.55	0.2764	175.15	14.475	506.55	4.3579
197	Methyl acetylene	C ₂ H ₂	74-99-7	40.064	1.6085	0.26436	402.4	0.27987	170.45	19.031	402.40	6.0845
198	Methyl acrylate	C ₄ H ₆ O ₂	96-33-3	86.089	0.97286	0.26267	536	0.2508	196.32	12.203	536.00	3.7037
199	Methyl amine	CH ₃ N	74-89-5	31.057	1.39	0.21405	430.05	0.2275	179.69	25.378	430.05	6.4938
200	Methyl benzoate	C ₈ H ₈ O ₂	93-58-3	136.148	0.53382	0.23274	693	0.28147	260.75	8.220	693.00	2.2936
201	3-Methyl-1,2-butadiene	C ₅ H ₈	598-25-4	68.117	0.84623	0.24625	490	0.29041	159.53	11.994	490.00	3.4365
202	2-Methylbutane	C ₅ H ₁₂	78-78-4	72.149	0.91991	0.27815	460.4	0.28667	113.25	10.764	460.40	3.3072
203	2-Methylbutanoic acid	C ₅ H ₁₀ O ₂	116-53-0	102.132	0.72762	0.25244	643	0.28571	193.00	9.992	643.00	2.8823
204	3-Methyl-1-butanol	C ₅ H ₁₂ O	123-51-3	88.148	0.80828	0.26783	577.2	0.23588	155.95	10.254	577.20	3.0179
205	2-Methyl-1-butene	C ₅ H ₁₀	563-46-2	70.133	0.91619	0.26752	465	0.28164	135.58	11.332	465.00	3.4248
206	2-Methyl-2-butene	C ₅ H ₁₀	513-35-9	70.133	0.93391	0.27275	470	0.2578	139.39	11.216	470.00	3.4241
207	2-Methyl-1-butene-3-yne	C ₅ H ₆	78-80-8	66.101	1.1157	0.27671	492	0.30821	160.15	12.581	492.00	4.0320
208	Methylbutyl ether	C ₅ H ₁₂ O	628-28-4	88.148	0.8363	0.27514	512.74	0.27553	157.48	9.758	512.74	3.0395
209	Methylbutyl sulfide	C ₅ H ₁₂ S	628-29-5	104.214	0.75509	0.27183	593	0.29127	175.30	9.006	593.00	2.7778
210	3-Methyl-1-butyne	C ₅ H ₈	598-23-2	68.117	0.94575	0.26008	463.2	0.30807	183.45	11.519	463.20	3.6364
211	Methyl butyrate	C ₅ H ₁₀ O ₂	623-42-7	102.132	0.76983	0.26173	554.5	0.26879	187.35	9.764	554.50	2.9413
212	Methylchlorosilane	CH ₃ ClSi	993-00-0	80.589	1.0674	0.26257	442	0.26569	139.05	13.626	442.00	4.0652
213	Methylcyclohexane	C ₇ H ₁₄	108-87-2	98.186	0.73109	0.26971	572.1	0.29185	146.58	9.017	572.10	2.7107
214	1-Methylcyclohexanol	C ₇ H ₁₄ O	590-67-0	114.185	0.7013	0.266	686	0.28571	285.15	8.209	686.00	2.6365
215	cis-2-Methylcyclohexanol	C ₇ H ₁₄ O	7443-70-1	114.185	0.70973	0.26544	614	0.26016	280.15	8.293	614.00	2.6738
216	trans-2-Methylcyclohexanol	C ₇ H ₁₄ O	7443-52-9	114.185	0.72836	0.27241	617	0.2478	269.15	8.263	617.00	2.6738
217	Methylcyclopentane	C ₆ H ₁₂	96-37-7	84.159	0.84758	0.27037	532.7	0.28258	130.73	10.491	532.70	3.1349
218	1-Methylcyclopentene	C ₆ H ₁₀	693-89-0	82.144	0.88824	0.26914	542	0.27874	146.62	10.980	542.00	3.3003
219	3-Methylcyclopentene	C ₆ H ₁₀	1120-62-3	82.144	0.9109	0.276	526	0.26756	115.00	11.014	526.00	3.3004
220	Methyldichlorosilane	CH ₂ Cl ₂ Si	75-54-7	115.034	0.97608	0.28209	483	0.22529	182.55	10.789	483.00	3.4602
221	Methylethyl ether	C ₃ H ₈ O	540-67-0	60.095	1.2635	0.27878	437.8	0.2744	160.00	13.995	437.80	4.5322
222	Methylethyl ketone	C ₄ H ₈ O	78-93-3	72.106	0.93767	0.25035	535.5	0.29964	186.48	12.663	535.50	3.7454
223	Methylethyl sulfide	C ₃ H ₈ S	624-89-5	76.161	1.067	0.27102	533	0.29364	167.23	12.671	533.00	3.9370
224	Methyl formate	C ₂ H ₄ O ₂	107-31-3	60.052	1.525	0.2634	487.2	0.2806	174.15	18.811	487.20	5.7897
225	Methylisobutyl ether	C ₆ H ₁₂ O	625-44-5	88.148	0.84005	0.27638	497	0.27645	150.00	9.738	497.00	3.0395
226	Methylisobutyl ketone	C ₆ H ₁₂ O	108-10-1	100.159	0.71687	0.26453	574.6	0.28918	189.15	8.862	574.60	2.7100
227	Methyl isocyanate	C ₂ H ₃ N ₂ O	624-83-9	57.051	1.0228	0.20692	488	0.28571	256.15	17.666	488.00	4.9430
228	Methylisopropyl ether	C ₄ H ₁₀ O	598-53-8	74.122	0.97887	0.27017	464.48	0.28998	127.93	11.933	464.48	3.6232
229	Methylisopropyl ketone	C ₅ H ₁₀ O	563-80-4	86.132	0.86567	0.26836	553.4	0.28364	180.15	10.460	553.40	3.2258
230	Methylisopropyl sulfide	C ₄ H ₁₀ S	1551-21-9	90.187	0.78912	0.25915	553.1	0.26512	171.64	10.352	553.10	3.0450
231	Methyl mercaptan	CH ₃ S	74-93-1	48.107	1.9323	0.28018	469.95	0.28523	150.18	21.564	469.95	6.8966
232	Methyl methacrylate	C ₅ H ₈ O ₂	80-62-6	100.116	0.7761	0.25068	566	0.29773	224.95	10.176	566.00	3.0960
233	2-Methyloctanoic acid	C ₉ H ₁₈ O ₂	3004-93-1	158.238	0.4416	0.2521	694	0.28532	240.00	5.938	694.00	1.7517
234	2-Methylpentane	C ₆ H ₁₄	107-83-5	86.175	0.72701	0.26754	497.7	0.28268	119.55	9.204	497.70	2.7174
235	Methyl pentyl ether	C ₆ H ₁₄ O	628-80-8	102.175	0.71004	0.26981	546.49	0.29974	176.00	8.445	546.49	2.6316
236	2-Methylpropane	C ₄ H ₁₀	75-28-5	58.122	1.0631	0.27506	407.8	0.2758	113.54	12.574	407.80	3.8650
237	2-Methyl-2-propanol	C ₄ H ₁₀ O	75-65-0	74.122	0.92128	0.25442	506.2	0.27586	298.97	10.556	506.20	3.6211
238	2-Methyl propene	C ₄ H ₈	115-11-7	56.106	1.1446	0.2724	417.9	0.28172	132.81	13.507	417.90	4.2019
239	Methyl propionate	C ₄ H ₈ O ₂	554-12-1	88.105	0.9147	0.2594	530.6	0.2774	185.65	11.678	530.60	3.5262
240	Methylpropyl ether	C ₄ H ₁₀ O	557-17-5	74.122	0.96145	0.26536	476.25	0.30088	133.97	12.043	476.25	3.6232
241	Methylpropyl sulfide	C ₄ H ₁₀ S	3877-15-4	90.187	0.87496	0.26862	565	0.30259	160.17	10.689	565.00	3.2572
242	Methylsilane	CH ₃ Si	992-94-9	46.144	1.3052	0.26757	352.5	0.28799	116.34	15.791	352.50	4.8780
243	alpha-Methyl styrene	C ₉ H ₁₀	98-83-9	118.176	0.64856	0.25877	654	0.31444	249.95	8.010	654.00	2.5063
244	Methyl tert-butyl ether	C ₅ H ₁₂ O	1634-04-4	88.148	0.928	0.289	497.1	0.286	164.55	9.710	497.10	3.2111

TABLE 2-32 Densities of Inorganic and Organic Liquids (mol/dm³) (Concluded)

Cmpd. no.	Name	Formula	CAS no.	Mol. wt.	C1	C2	C3	C4	T _{min} , K	Density at T _{min}	T _{max} , K	Density at T _{max}
245	Methyl vinyl ether	C ₃ H ₆ O	107-25-5	58.079	1.2587	0.26433	437	0.25819	151.15	15.691	437.00	4.7619
246	Naphthalene	C ₁₀ H ₈	91-20-3	128.171	0.6348	0.25838	748.4	0.27727	333.15	7.755	425.00	2.4568
247	Neon	Ne	7440-01-9	20.180	7.3718	0.3067	44.4	0.2786	24.56	61.796	44.40	24.0360
248	Nitroethane	C ₂ H ₅ NO ₂	79-24-3	75.067	1.0024	0.23655	593	0.278	183.63	15.556	593.00	4.2376
249	Nitrogen	N ₂	7727-37-9	28.013	3.2091	0.2861	126.2	0.2966	63.15	31.063	126.20	11.2170
250	Nitrogen trifluoride	F ₃ N	7783-54-2	71.002	2.3736	0.2817	234	0.29529	66.46	26.555	234.00	8.4260
251	Nitromethane	CH ₃ NO ₂	75-52-5	61.040	1.3728	0.23793	588.15	0.29601	244.60	19.632	588.15	5.7698
252	Nitrous oxide	N ₂ O	10024-97-2	44.013	2.781	0.27244	309.57	0.2882	182.30	27.928	309.57	10.2080
253	Nitric oxide	NO	10102-43-9	30.006	5.246	0.3044	180.15	0.242	109.50	44.487	180.15	17.2340
254	Nonadecane	C ₁₉ H ₄₀	629-92-5	268.521	0.19199	0.23337	758	0.28571	305.04	2.889	758.00	0.8227
255	Nonanal	C ₉ H ₁₈ O	124-19-6	142.239	0.49587	0.26135	658	0.30736	255.15	6.017	658.00	1.8973
256	Nonane	C ₉ H ₂₀	111-84-2	128.255	0.46321	0.25444	594.6	0.28571	219.66	6.043	594.60	1.8210
257	Nonanoic acid	C ₉ H ₁₈ O ₂	112-05-0	158.238	0.41582	0.24284	710.7	0.30036	285.55	5.759	710.70	1.7123
258	1-Nonanol	C ₉ H ₂₀ O	143-08-8	144.255	0.43682	0.25161	670.9	0.2498	268.15	5.850	670.90	1.7361
259	2-Nonanol	C ₉ H ₂₀ O	628-99-9	144.255	0.41687	0.24056	649.5	0.2916	238.15	6.031	649.50	1.7329
260	1-Nonene	C ₉ H ₁₈	124-11-8	126.239	0.48661	0.25722	593.1	0.28571	191.91	6.372	593.10	1.8918
261	Nonyl mercaptan	C ₉ H ₂₀ S	1455-21-6	160.320	0.47377	0.27052	681	0.30284	253.05	5.453	681.00	1.7513
262	1-Nonyne	C ₉ H ₁₆	3452-09-3	124.223	0.52152	0.25918	598.05	0.29177	223.15	6.537	598.05	2.0122
263	Octadecane	C ₁₈ H ₃₈	593-45-3	254.494	0.20448	0.23474	747	0.28571	301.31	3.042	747.00	0.8711
264	Octanal	C ₈ H ₁₆ O	124-13-0	128.212	0.53636	0.26174	638.9	0.26348	246.00	6.664	638.90	2.0492
265	Octane	C ₈ H ₁₈	111-65-9	114.229	0.5266	0.25693	568.7	0.28571	216.38	6.705	568.70	2.0500
266	Octanoic acid	C ₈ H ₁₆ O ₂	124-07-2	144.211	0.48251	0.25196	694.26	0.26842	289.65	6.311	694.26	1.9150
267	1-Octanol	C ₈ H ₁₈ O	111-87-5	130.228	0.48979	0.24931	652.3	0.27824	257.65	6.574	652.30	1.9646
268	2-Octanol	C ₈ H ₁₈ O	123-96-6	130.228	0.50726	0.25972	629.8	0.22	241.55	6.563	629.80	1.9531
269	2-Octanone	C ₈ H ₁₆ O	111-13-7	128.212	0.50006	0.24851	632.7	0.29942	252.85	6.648	632.70	2.0122
270	3-Octanone	C ₈ H ₁₆ O	106-68-3	128.212	0.5108	0.25386	627.7	0.26735	255.55	6.628	627.70	2.0121
271	1-Octene	C ₈ H ₁₆	111-66-0	112.213	0.55449	0.25952	566.9	0.28571	171.45	7.216	566.90	2.1366
272	Octyl mercaptan	C ₈ H ₁₈ S	111-88-6	146.294	0.52577	0.27234	667.3	0.30063	223.95	6.099	667.30	1.9306
273	1-Octyne	C ₈ H ₁₄	629-05-0	110.197	0.58945	0.26052	574	0.28532	193.55	7.483	574.00	2.2626
274	Oxalic acid	C ₂ H ₂ O ₄	144-62-7	90.035	1.0501	0.215	804	0.28571	462.65	16.271	804.00	4.8842
275	Oxygen	O ₂	7782-44-7	31.999	3.9143	0.28772	154.58	0.2924	54.35	40.770	154.58	13.6050
276	Ozone	O ₃	10028-15-6	47.998	3.3592	0.29884	261	0.28523	80.15	33.361	261.00	11.2140
277	Pentadecane	C ₁₅ H ₃₂	629-62-9	212.415	0.25142	0.23837	708	0.28571	283.07	3.642	708.00	1.0550
278	Pentanol	C ₅ H ₁₂ O	110-62-3	86.132	0.83871	0.26252	566.1	0.29444	182.00	10.534	566.10	3.1948
279	Pentane	C ₅ H ₁₂	109-66-0	72.149	0.84947	0.26726	469.7	0.27789	143.42	10.474	469.70	3.1784
280	Pentanoic acid	C ₅ H ₁₀ O ₂	109-52-4	102.132	0.73455	0.25636	639.16	0.25522	239.15	9.587	639.16	2.8653
281	1-Pentanol	C ₅ H ₁₂ O	71-41-0	88.148	0.81754	0.26732	588.1	0.25348	195.56	10.061	588.10	3.0583
282	2-Pentanol	C ₅ H ₁₂ O	6032-29-7	88.148	0.79324	0.25806	561	0.28571	200.00	10.147	561.00	3.0739
283	2-Pentanone	C ₅ H ₁₀ O	107-87-9	86.132	0.90411	0.27207	561.08	0.30669	196.29	10.398	561.08	3.3231
284	3-Pentanone	C ₅ H ₁₀ O	96-22-0	86.132	0.71811	0.24129	560.95	0.27996	234.18	10.102	560.95	2.9761
285	1-Pentene	C ₅ H ₁₀	109-67-1	70.133	0.89816	0.26608	464.8	0.28571	108.02	11.521	464.80	3.3755
286	2-Pentyl mercaptan	C ₅ H ₁₂ S	2084-19-7	104.214	0.65858	0.25367	584.3	0.28571	160.75	9.073	584.30	2.5962
287	Pentyl mercaptan	C ₅ H ₁₂ S	110-66-7	104.214	0.75345	0.27047	598	0.30583	197.45	8.858	598.00	2.7857
288	1-Pentyne	C ₅ H ₈	627-19-0	68.117	0.8491	0.2352	481.2	0.353	167.45	12.532	481.20	3.6101
289	2-Pentyne	C ₅ H ₈	627-21-4	68.117	0.92099	0.25419	519	0.31077	163.83	12.240	519.00	3.6232
290	Phenanthrene	C ₁₄ H ₁₀	85-01-8	178.229	0.45554	0.2523	869	0.24841	372.38	5.985	869.00	1.8055
291	Phenol	C ₆ H ₆ O	108-95-2	94.111	1.3798	0.31598	694.25	0.32768	314.06	11.244	694.25	4.3667
292	Phenyl isocyanate	C ₇ H ₅ NO	103-71-9	119.121	0.63163	0.23373	653	0.28571	243.15	9.647	653.00	2.7024
293	Phthalic anhydride	C ₈ H ₄ O ₃	85-44-9	148.116	0.5393	0.22704	791	0.248	404.15	8.222	791.00	2.3754
294	Propadiene	C ₃ H ₄	463-49-0	40.064	1.6087	0.26543	394	0.29895	136.87	19.479	394.00	6.0607
295	Propane	C ₃ H ₈	74-98-6	44.096	1.3757	0.27453	369.83	0.29359	85.47	16.583	369.83	5.0111
296	1-Propanol	C ₃ H ₈ O	71-23-8	60.095	1.2457	0.27281	536.8	0.23994	146.95	15.206	536.80	4.5662
297	2-Propanol	C ₃ H ₈ O	67-63-0	60.095	1.1799	0.2644	508.3	0.24653	185.26	14.663	508.30	4.4626
298	Propenylcyclohexene	C ₉ H ₁₄	13511-13-2	122.207	0.61255	0.26769	636	0.28571	199.00	7.476	636.00	2.2883
299	Propionaldehyde	C ₃ H ₆ O	123-38-6	58.079	1.296	0.26439	504.4	0.29471	170.00	15.929	504.40	4.9018
300	Propionic acid	C ₃ H ₆ O ₂	79-09-4	74.079	1.0969	0.25568	600.81	0.26857	252.45	13.935	600.81	4.2901
301	Propionitrile	C ₃ H ₅ N	107-12-0	55.079	1.0224	0.23452	564.4	0.2804	180.26	16.027	564.40	4.3595
302	Propyl acetate	C ₅ H ₁₀ O ₂	109-60-4	102.132	0.73041	0.25456	549.73	0.27666	178.15	9.794	549.73	2.8693
303	Propyl amine	C ₃ H ₉ N	107-10-8	59.110	0.9195	0.23878	496.95	0.2461	188.36	13.764	496.95	3.8508

304	Propylbenzene	C ₉ H ₁₂	103-65-1	120.192	0.57233	0.25171	638.35	0.29616	173.55	7.982	638.35	2.2738
305	Propylene	C ₃ H ₆	115-07-1	42.080	1.4403	0.26852	364.85	0.28775	87.89	18.070	364.85	5.3638
306	Propyl formate	C ₇ H ₈ O ₂	110-74-7	88.105	0.915	0.26134	538	0.28	180.25	11.590	538.00	3.5012
307	2-Propyl mercaptan	C ₇ H ₈ S	75-33-2	76.161	1.093	0.27762	517	0.29781	142.61	12.610	517.00	3.9370
308	Propyl mercaptan	C ₇ H ₈ S	107-03-9	76.161	1.0714	0.27214	536.6	0.29481	159.95	12.716	536.60	3.9369
309	1,2-Propylene glycol	C ₃ H ₈ O ₂	57-55-6	76.094	1.0923	0.26106	626	0.20459	213.15	14.363	626.00	4.1841
310	Quinone	C ₆ H ₄ O ₂	106-51-4	108.095	0.83228	0.25385	683	0.23658	388.85	10.082	683.00	3.2786
311	Silicon tetrafluoride	F ₄ Si	7783-61-1	104.079	1.1945	0.24128	259	0.16693	186.35	15.635	259.00	4.9507
312	Styrene	C ₈ H ₈	100-42-5	104.149	0.7397	0.2603	636	0.3009	242.54	9.109	636.00	2.8417
313	Succinic acid	C ₄ H ₆ O ₄	110-15-6	118.088	0.70284	0.22268	806	0.28571	460.65	10.261	806.00	3.1563
314	Sulfur dioxide	O ₂ S	7446-09-5	64.064	2.106	0.25842	430.75	0.2895	197.67	25.298	430.75	8.1495
315	Sulfur hexafluoride	F ₆ S	2551-62-4	146.055	1.3587	0.2701	318.69	0.2921	223.15	12.631	318.69	5.0304
316	Sulfur trioxide	O ₃ S	7446-11-9	80.063	1.4969	0.19013	490.85	0.4359	289.95	24.241	490.85	7.8730
317	Terephthalic acid	C ₈ H ₆ O ₄	100-21-0	166.131	0.42685	0.181	1113	0.28571	700.15	8.546	1113.00	2.3583
318	<i>o</i> -Terphenyl	C ₁₈ H ₁₄	84-15-1	230.304	0.3448	0.25116	857	0.29268	329.35	4.553	857.00	1.3728
319	<i>o</i> -Terphenyl [use Eq. (2)]	C ₁₈ H ₁₄	84-15-1	230.304	5.7136	-0.003474			288.15	4.713	313.19	4.6256
320	Tetradecane	C ₁₄ H ₃₀	629-59-4	198.388	0.27248	0.24007	693	0.28571	279.01	3.889	693.00	1.1350
321	Tetrahydrofuran	C ₄ H ₈ O	109-99-9	72.106	1.2543	0.28084	540.15	0.2912	164.65	13.998	540.15	4.4662
322	1,2,3,4-Tetrahydronaphthalene	C ₁₀ H ₁₂	119-64-2	132.202	0.67717	0.27772	720	0.2878	237.38	7.638	720.00	2.4383
323	Tetrahydrothiophene	C ₄ H ₈ S	110-01-0	88.171	1.1628	0.28954	631.95	0.28674	176.99	12.408	631.95	4.0160
324	2,2,3,3-Tetramethylbutane	C ₈ H ₁₈	594-82-1	114.229	0.58988	0.27201	568	0.27341	373.96	5.724	568.00	2.1686
325	Thiophene	C ₄ H ₄ S	110-02-1	84.140	1.2874	0.28194	579.35	0.30781	234.94	13.430	579.35	4.5662
326	Toluene	C ₇ H ₈	108-88-3	92.138	0.8792	0.27136	591.75	0.29241	178.18	10.487	591.75	3.2400
327	1,1,2-Trichloroethane	C ₂ H ₃ Cl ₃	79-00-5	133.404	0.9062	0.25475	602	0.31	236.50	11.478	602.00	3.5572
328	Tridecane	C ₁₃ H ₂₈	629-50-5	184.361	0.29934	0.2433	675	0.28571	267.76	4.182	675.00	1.2300
329	Triethyl amine	C ₆ H ₁₅ N	121-44-8	101.190	0.7035	0.27386	535.15	0.2872	158.45	8.284	535.15	2.5688
330	Trimethyl amine	C ₃ H ₉ N	75-50-3	59.110	1.0116	0.25683	433.25	0.2696	156.08	13.144	433.25	3.9388
331	1,2,3-Trimethylbenzene	C ₉ H ₁₂	526-73-8	120.192	0.6531	0.27002	664.5	0.26268	243.15	7.728	664.50	2.4187
332	1,2,4-Trimethylbenzene	C ₉ H ₁₂	95-63-6	120.192	0.60394	0.25956	649.1	0.27713	229.33	7.689	649.10	2.3268
333	2,2,4-Trimethylpentane	C ₈ H ₁₈	540-84-1	114.229	0.59059	0.27424	543.8	0.2847	165.78	6.915	543.80	2.1536
334	2,3,3-Trimethylpentane	C ₈ H ₁₈	560-21-4	114.229	0.6028	0.27446	573.5	0.2741	172.22	7.093	573.50	2.1963
335	1,3,5-Trinitrobenzene	C ₆ H ₃ N ₃ O ₆	99-35-4	213.105	0.48195	0.23093	846	0.28571	398.40	7.083	846.00	2.0870
336	2,4,6-Trinitrotoluene	C ₇ H ₅ N ₃ O ₆	118-96-7	227.131	0.37378	0.21379	828	0.29905	354.00	6.452	828.00	1.7484
337	Undecane	C ₁₁ H ₂₄	1120-21-4	156.308	0.36703	0.24876	639	0.28571	247.57	4.945	639.00	1.4750
338	1-Undecanol	C ₁₁ H ₂₄ O	112-42-5	172.308	0.33113	0.23676	703.9	0.2762	288.45	4.859	703.90	1.3986
339	Vinyl acetate	C ₄ H ₆ O ₂	108-05-4	86.089	0.9591	0.2593	519.13	0.27448	180.35	12.287	519.13	3.6988
340	Vinyl acetylene	C ₄ H ₄	689-97-4	52.075	1.2703	0.26041	454	0.297	173.15	15.664	454.00	4.8781
341	Vinyl chloride	C ₂ H ₃ Cl	75-01-4	62.498	1.5115	0.2707	432	0.2716	119.36	18.481	432.00	5.5837
342	Vinyl trichlorosilane	C ₂ H ₃ Cl ₃ Si	75-94-5	161.490	0.59595	0.24314	543.15	0.24856	178.35	8.824	543.15	2.4511
344	Water [use Eq. (2)]	H ₂ O	7732-18-5	18.015	-13.851	0.64038	-0.00191	1.821E-06	273.16	55.497	353.15	54.0012
345	<i>m</i> -Xylene	C ₈ H ₁₀	108-38-3	106.165	0.68902	0.26086	617	0.27479	225.30	8.648	617.00	2.6413
346	<i>o</i> -Xylene	C ₈ H ₁₀	95-47-6	106.165	0.69962	0.26143	630.3	0.27365	247.98	8.623	630.30	2.6761
347	<i>p</i> -Xylene	C ₈ H ₁₀	106-42-3	106.165	0.67752	0.25887	616.2	0.27596	286.41	8.161	616.20	2.6172

Except for *o*-terphenyl and water, liquid density ρ is calculated by

$$\rho = C1/C2^{1+(1-T/C3)^{C4}}$$

where ρ is in mol/dm³ and T is in K. The pressure is equal to the vapor pressure for pressures greater than 1 atm and equal to 1 atm when the vapor pressure is less than 1 atm.

Equation (2), used for the limited temperature ranges as noted for *o*-terphenyl and water, is

$$\rho = C1 + C2T + C3T^2 + C4T^3$$

For water over the entire temperature range of 273.16 to 647.096 K, use

$$\rho = 17.863 + 58.606\tau^{0.35} - 95.396\tau^{0.3} + 213.89\tau - 141.26\tau^{4.3}$$

where $\tau = 1 - T/647.096$.

All substances are listed by chemical family in Table 2-6 and by formula in Table 2-7.

Values in this table were taken from the Design Institute for Physical Properties (DIPPR) of the American Institute of Chemical Engineers (AIChE), copyright 2007 AIChE and reproduced with permission of AIChE and of the DIPPR Evaluated Process Design Data Project Steering Committee. Their source should be cited as R. L. Rowley, W. V. Wilding, J. L. Oscarson, Y. Yang, N. A. Zundel, T. E. Daubert, R. P. Danner, DIPPR® Data Compilation of Pure Chemical Properties, Design Institute for Physical Properties, AIChE, New York (2007).

The number of digits provided for values at T_{\min} and T_{\max} was chosen for uniformity of appearance and formatting; these do not represent the uncertainties of the physical quantities, but are the result of calculations from the standard thermophysical property formulations within a fixed format.

DENSITIES OF AQUEOUS INORGANIC SOLUTIONS AT 1 ATM

UNITS AND UNITS CONVERSIONS

Most densities are given in grams per cubic centimeter. To convert to pounds per cubic foot, multiply by 62.43. °F = % °C + 32. Compositions are weight percent unless otherwise stated.

ADDITIONAL REFERENCES

For more detailed data on densities see *International Critical Tables*: tabular index, vol. 3, p. 1; abrasives, vol. 2, p. 87; air, moist, vol. 1, p. 71; building stones, vol. 2, p. 52; clays, vol. 2, p. 56; coals, vol. 2, p. 135; compounds, vol. 1, pp. 106, 176, 313, 341; elements, vol. 1, pp. 102, 340; fibers, vol. 2, p. 237; gases and vapors, vol. 3, pp. 3, 345; glass, vol. 2, p. 93; liquids and vitreous solids, vol. 3, p. 22; vol. 1, pp. 102, 340; vol. 2,

pp. 456, 463; vol. 3, pp. 20, 35; liquid coolants and saturated vapors are available from WADC-TR-59-598, 1959; plastics are collected in the *Handbook of Chemistry and Physics*, Chemical Rubber Publishing Co.; solid helium, neon, argon, fluorine, and methane data are given by Johnson (ed.), WADD-TR-60-56, 1960; temperatures of maximum solubility, vol. 3, p. 107; metals, vol. 2, p. 463; oils, fats, and waxes, vol. 2, p. 201; orthobaric, vol. 3, pp. 202, 228, 237, 244; petroleum, vol. 2, pp. 137, 144; plastics, vol. 2, p. 296; porcelains, vol. 2, pp. 68, 75; refrigerating brines, vol. 2, p. 327; rubber, vol. 2, pp. 255, 259; soaps, vol. 5, p. 447; metallic solid solutions, vol. 2, p. 358; solids, vol. 3, pp. 43, 45; vol. 2, p. 456; vol. 3, p. 21; solutions and mixtures, vol. 3, pp. 17, 51, 95, 104, 107, 111, 125, 130; woods, vol. 2, p. 1. Also see the *Handbook of Chemistry and Physics*, Chemical Rubber Publishing Co., 86th ed., etc.

TABLE 2-33 Aluminum Sulfate [Al₂(SO₄)₃]*

%	d ₄ ¹⁵	%	d ₄ ¹⁵
1	1.0093	16	1.1770
2	1.0195	20	1.2272
4	1.0404	24	1.2803
8	1.0837	26	1.3079
12	1.1293		

*International Critical Tables, vol. 3, p. 70.

TABLE 2-34 Ammonia (NH₃)*

%	-15 °C	-10 °C	-5 °C	0 °C	5 °C	10 °C	20 °C	25 °C	%	d ₄ ¹⁵
1		0.9943	0.9954	0.9959	0.9958	0.9955	0.9939	0.993	32	0.889
2		.9906	.9915	.9919	.9917	.9913	.9895	.988	36	.877
4		.9834	.9840	.9842	.9837	.9832	.9811	.980	40	.865
8	0.970	.9701	.9701	.9695	.9686	.9677	.9651	.964	45	.849
12	.958	.9576	.9571	.9561	.9548	.9534	.9501	.948	50	.832
16	.947	.9461	.9450	.9435	.9420	.9402	.9362	.934	60	.796
20		.9353	.9335	.9316	.9296	.9275	.9229		70	.755
24		.9249	.9226	.9202	.9179	.9155	.9101		80	.711
28		.9150	.9122	.9094	.9067	.9040	.8980		90	.665
30		.9101	.9070	.9040	.9012	.8983	.8920		100	.618

*International Critical Tables, vol. 3, p. 59.

TABLE 2-35 Ammonium Acetate* (CH₃COONH₄)

%	d ₄ ²⁵
1	0.9992
2	1.0013
4	1.0055
8	1.0136
12	1.0216
16	1.0294
20	1.0368
24	1.0439
28	1.0507
30	1.0540
35	1.0618
40	1.0691
45	1.0760

*International Critical Tables, vol. 3, p. 62.

For data at 16 °C for 3(1)52 percent see Atack, *Handbook of Chemical Data*, p. 33, Reinhold, New York, 1957.

TABLE 2-37 Ammonium Chloride (NH₄Cl)*

%	0 °C	10 °C	20 °C	30 °C	50 °C	80 °C	100 °C
1	1.0033	1.0029	1.0013	0.9987	0.9910	0.9749	0.9617
2	1.0067	1.0062	1.0045	1.0018	.9940	.9780	.9651
4	1.0135	1.0126	1.0107	1.0077	.9999	.9842	.9718
8	1.0266	1.0251	1.0227	1.0195	1.0116	.9963	.9849
12	1.0391	1.0370	1.0344	1.0310	1.0231	1.0081	.9975
16	1.0510	1.0485	1.0457	1.0422	1.0343	1.0198	1.0096
20	1.0625	1.0596	1.0567	1.0532	1.0454	1.0312	1.0213
24	1.0736	1.0705	1.0674	1.0641	1.0564	1.0426	1.0327

*International Critical Tables, vol. 3, p. 60.

TABLE 2-36 Ammonium Bichromate [(NH₄)₂Cr₂O₇]*

%	d ₄ ¹²
1	1.0051
2	1.0108
4	1.0223
8	1.0463
12	1.0715
16	1.0981
20	1.1263

*International Critical Tables, vol. 3, p. 70.

TABLE 2-38 Ammonium Chromate [(NH₄)₂CrO₄]*

%	°C	d ₄ ¹⁵
3.80	20	1.0219
10.52	13	1.0627
19.75	13.7	1.1189
28.04	19.6	1.1707

*International Critical Tables, vol. 3, p. 70.

TABLE 2-39 Ammonium Nitrate (NH₄NO₃)*

%	0 °C	10 °C	25 °C	40 °C	60 °C	80 °C
1.0	1.0043	1.0039	1.0011	0.9961	0.9870	0.9755
2.0	1.0088	1.0082	1.0051	1.0000	.9908	.9793
4.0	1.0178	1.0168	1.0132	1.0079	.9985	.9869
8.0	1.0358	1.0340	1.0297	1.0238	1.0142	1.0024
12.0	1.0539	1.0515	1.0464	1.0400	1.0301	1.0181
16.0	1.0721	1.0691	1.0633	1.0565	1.0462	1.0342
20.0	1.0905	1.0870	1.0806	1.0734	1.0627	1.0506
24.0	1.1090	1.1051	1.0982	1.0907	1.0796	1.0673
28.0	1.1277	1.1234	1.1161	1.1082	1.0968	1.0844
30.0	1.1371	1.1327	1.1252	1.1171	1.1055	1.0931
40.0	1.1862	1.1810	1.1727	1.1640	1.1515	1.1385
50.0	1.2380	1.2320	1.2229	1.2136	1.2006	1.1868

*International Critical Tables, vol. 3, p. 59.

TABLE 2-40 Ammonium Sulfate [(NH₄)₂SO₄]*

%	0 °C	20 °C	40 °C	80 °C	100 °C
1	1.0061	1.0041	0.9980	0.9777	0.9644
2	1.0124	1.0101	1.0039	.9836	.9705
4	1.0248	1.0220	1.0155	.9953	.9826
8	1.0495	1.0456	1.0387	1.0187	1.0066
12	1.0740	1.0691	1.0619	1.0421	1.0303
16	1.0980	1.0924	1.0849	1.0653	1.0539
20	1.1215	1.1154	1.1077	1.0883	1.0772
24	1.1448	1.1383	1.1304	1.1111	1.1003
28	1.1677	1.1609	1.1529	1.1338	1.1232
35	1.2072	1.2800	1.1919	1.1731	1.1629
40	1.2350	1.2277	1.2196	1.2011	1.1910
50	1.2899	1.2825	1.2745	1.2568	1.2466

*International Critical Tables, vol. 3, p. 60.

TABLE 2-41 Arsenic Acid (H₃AsO₄)*

%	d ₄ ¹⁵	%	d ₄ ¹⁵
1	1.0057	20	1.1447
2	1.0124	30	1.2331
6	1.0398	40	1.3370
10	1.0681	50	1.4602
16	1.1128	60	1.6070
		70	1.7811

*International Critical Tables, vol. 3, p. 61.

TABLE 2-42 Barium Chloride (BaCl₂)*

%	0 °C	20 °C	40 °C	60 °C	80 °C	100 °C
2	1.0181	1.0159	1.0096	1.0004	0.9890	0.9755
4	1.0368	1.0341	1.0275	1.0181	1.0066	.9931
8	1.0760	1.0721	1.0648	1.0551	1.0434	1.0299
12	1.1178	1.1128	1.1047	1.0948	1.0827	1.0692
16	1.1627	1.1564	1.1478	1.1373	1.1249	1.1113
20	1.2105	1.2031	1.1938	1.1828	1.1702	1.1563
24		1.2531	1.2430	1.2316	1.2186	1.2045
26		1.2793	1.2688	1.2571	1.2440	1.2298

*International Critical Tables, vol. 3, p. 75.

TABLE 2-43 Cadmium Nitrate [Cd(NO₃)₂]*

%	d ₄ ¹⁸	%	d ₄ ¹⁸
2	1.0154	20	1.1904
4	1.0326	25	1.2488
8	1.0683	30	1.3124
12	1.1061	40	1.4590
16	1.1468	50	1.6356

*International Critical Tables, vol. 3, p. 66.

TABLE 2-44 Calcium Chloride (CaCl₂)*

%	-5 °C	0 °C	20 °C	30 °C	40 °C	60 °C	80 °C	100 °C	120 °C†	140 °C
2		1.0171	1.0148	1.0120	1.0084	0.9994	0.9881	0.9748	0.9596	0.9428
4		1.0346	1.0316	1.0286	1.0249	1.0158	1.0046	0.9915	0.9765	0.9601
8	1.0708	1.0703	1.0659	1.0626	1.0586	1.0492	1.0382	1.0257	1.0111	0.9954
12	1.1083	1.1072	1.1015	1.0978	1.0937	1.0840	1.0730	1.0610	1.0466	1.0317
16	1.1471	1.1454	1.1386	1.1345	1.1301	1.1202	1.1092	1.0973	1.0835	1.0691
20	1.1874	1.1853	1.1775	1.1730	1.1684	1.1581	1.1471	1.1352	1.1219	1.1080
25		1.2376	1.2284	1.2236	1.2186	1.2079	1.1965	1.1846		
30		1.2922	1.2816	1.2764	1.2709	1.2597	1.2478	1.2359		
35			1.3373	1.3316	1.3255	1.3137	1.3013	1.2893		
40			1.3957	1.3895	1.3826	1.3700	1.3571	1.3450		

*International Critical Tables, vol. 3, pp. 72-73.

†Corrected to atmospheric pressure.

TABLE 2-45 Calcium Hydroxide [Ca(OH)₂]*

%	d ₄ ¹⁵	d ₄ ²⁵
0.05	0.99979	0.99773
.10	1.00044	.99838
.15	1.00110	.99904

*International Critical Tables, vol. 3, p. 72.

TABLE 2-46 Calcium Hypochlorite* (CaOCl₂)

% total salt	d ₄ ¹⁵
2	1.0169
4	1.0345
6	1.0520
8	1.0697
10	1.0876
12	1.1060

*International Critical Tables, vol. 3, p. 73.

CaOCl₂ = 89.15%

CaCl₂ = 7.31%

Ca(ClO₃)₂ = 0.26%

Ca(OH)₂ = 2.92%

TABLE 2-47 Calcium Nitrate [Ca(NO₃)₂]*

%	6 °C	18 °C	25 °C	30 °C
2*	1.0157	1.0137	1.0120	1.0105
4	1.0316	1.0291	1.0272	1.0256
8	1.0641	1.0608	1.0585	1.0565
12	1.0979	1.0937	1.0911	1.0887
16	1.1330	1.1279	1.1250	1.1224
20	1.1694	1.1636	1.1602	1.1575
25	1.2168	1.2106	1.2065	1.2032
30		1.260		
35		1.311		
40		1.365		
45		1.422		
68†		1.747	1.741	1.736

*International Critical Tables, vol. 3, pp. 73-74.

†Supercooled tetrahydrate (m.p. 41.4°C).

TABLE 2-48 Chromic Acid (CrO₃)*

%	d ₄ ¹⁵	%	d ₄ ¹⁵
1	1.006	20	1.163
2	1.014	26	1.220
6	1.045	30	1.260
10	1.076	40	1.371
16	1.127	50	1.505
		60	1.663

*International Critical Tables, vol. 3, p. 69.

TABLE 2-49 Chromium Chloride (CrCl₃)*

%	d ₄ ¹⁸		
	Violet	Green	Equilibrium mixture of violet and green
1	1.0076	1.0071	1.0075
2	1.0166	1.0157	1.0165
4	1.0349	1.0332	1.0347
8	1.0724	1.0691	1.0722
12	1.1114	1.1065	1.1111
14	1.1316		

*International Critical Tables, vol. 3, p. 69.

TABLE 2-50 Copper Nitrate [Cu(NO₃)₂]*

%	d ₄ ²⁰	%	d ₄ ²⁰
1	1.007	12	1.107
2	1.015	16	1.147
4	1.032	20	1.189
8	1.069	25	1.248

*International Critical Tables, vol. 3, p. 67.

TABLE 2-51 Copper Sulfate (CuSO₄)*

%	0 °C	20 °C	40 °C
1	1.0104	1.0086	1.0024
4	1.0429	1.0401	1.0332
8	1.0887	1.084	1.0764
12	1.1379	1.1308	1.1222
16		1.180	
18		1.206	

*International Critical Tables, vol. 3, p. 67.

TABLE 2-52 Cuprous Chloride (CuCl₂)*

%	0 °C	20 °C	40 °C
1	1.0095	1.0072	1.002
4	1.0387	1.036	1.0305
8	1.0788	1.0754	1.0682
12	1.1208	1.1165	1.107
16	1.1653	1.1595	1.151
20	1.2121	1.2052	1.1953

*International Critical Tables, vol. 3, p. 66.

TABLE 2-53 Ferric Chloride (FeCl₃)*

%	0 °C	10 °C	20 °C	30 °C
1	1.0086	1.0084	1.0068	1.0040
2	1.0174	1.0168	1.0152	1.0122
4	1.0347	1.0341	1.0324	1.0292
8	1.0703	1.0692	1.0669	1.0636
12	1.1088	1.1071	1.1040	1.1006
16	1.1475	1.1449	1.1418	1.1386
20	1.1870	1.1847	1.1820	1.1786
25	1.2400	1.2380	1.2340	1.2290
30	1.2970	1.2950	1.2910	1.2850
35	1.3605	1.3580	1.3530	1.3475
40	1.4280	1.4235	1.4175	1.4115
45		1.4920	1.4850	
50		1.5610	1.5510	

*International Critical Tables, vol. 3, p. 68.

2-106 PHYSICAL AND CHEMICAL DATA

TABLE 2-54 Ferric Sulfate
[Fe₂(SO₄)₃]*

%	<i>d</i> ₄ ^{17.5}
1	1.0072
2	1.0157
4	1.0327
8	1.0670
12	1.1028
16	1.1409
20	1.1811
30	1.3073
40	1.4487
50	1.6127
60	1.7983

*International Critical Tables, vol. 3, p. 68.

TABLE 2-56 Ferrous Sulfate (FeSO₄)*

%	15 °C	18 °C	20 °C
0.2		1.00068	1.0002
0.4		1.00275	1.0022
0.8		1.00645	1.0062
1.0	1.0090	1.0085	1.0082
4.0	1.0380	1.0375	
8.0	1.0790	1.0785	
12.0	1.1235	1.1220	
16.0	1.1690	1.1675	
20.0	1.2150	1.2135	

*International Critical Tables, vol. 3, p. 68.

TABLE 2-58 Hydrogen Cyanide (HCN)*

%	<i>d</i> ₄ ¹⁵
1	0.998
2	0.996
4	0.993
8	0.984
12	0.971
16	0.956
82	0.752
90	0.724
100	0.691

*International Critical Tables, vol. 3, p. 61.

TABLE 2-59 Hydrogen Chloride (HCl)

%	-5 °C	0 °C	10 °C	20 °C	40 °C	60 °C	80 °C	100 °C
1	1.0048	1.0052	1.0048	1.0032	0.9970	0.9881	0.9768	0.9636
2	1.0104	1.0106	1.0100	1.0082	1.0019	0.9930	0.9819	0.9688
4	1.0213	1.0213	1.0202	1.0181	1.0116	1.0026	0.9919	0.9791
6	1.0321	1.0319	1.0303	1.0279	1.0211	1.0121	1.0016	0.9892
8	1.0428	1.0423	1.0403	1.0376	1.0305	1.0215	1.0111	0.9992
10	1.0536	1.0528	1.0504	1.0474	1.0400	1.0310	1.0206	1.0090
12	1.0645	1.0634	1.0607	1.0574	1.0497	1.0406	1.0302	1.0188
14	1.0754	1.0741	1.0711	1.0675	1.0594	1.0502	1.0398	1.0286
16	1.0864	1.0849	1.0815	1.0776	1.0692	1.0598	1.0494	1.0383
18	1.0975	1.0958	1.0920	1.0878	1.0790	1.0694	1.0590	1.0479
20	1.1087	1.1067	1.1025	1.0980	1.0888	1.0790	1.0685	1.0574
22	1.1200	1.1177	1.1131	1.1083	1.0986	1.0886	1.0780	1.0668
24	1.1314	1.1287	1.1238	1.1187	1.1085	1.0982	1.0874	1.0761
26	1.1426	1.1396	1.1344	1.1290	1.1183	1.1076	1.0967	1.0853
28	1.1537	1.1505	1.1449	1.1392	1.1280	1.1169	1.1058	1.0942
30	1.1648	1.1613	1.1553	1.1493	1.1376	1.1260	1.1149	1.1030
32				1.1593				
34				1.1691				
36				1.1789				
38				1.1885				
40				1.1980				

*International Critical Tables, vol. 3, p. 54.

TABLE 2-55 Ferric Nitrate
[Fe(NO₃)₃]*

%	<i>d</i> ₄ ¹⁸
1	1.0065
2	1.0144
4	1.0304
8	1.0636
12	1.0989
16	1.1359
20	1.1748
25	1.2281

*International Critical Tables, vol. 3, p. 68.

TABLE 2-57 Hydrogen Bromide (HBr)*

%	<i>d</i> ₄ ⁴	<i>d</i> ₄ ¹⁰	<i>d</i> ₄ ²⁵
1.0	1.0073	1.0068	1.0041
2.0	1.0146	1.0139	1.0111
4.0	1.0295	1.0285	1.0255
6.0	1.0448	1.0435	1.0402
8.0	1.0604	1.0589	1.0552
10.0	1.0764	1.0747	1.0707
12.0	1.0928	1.0910	1.0867
14.0	1.1097	1.1078	1.1032
16.0	1.1272	1.1251	1.1202
18.0	1.1453	1.1430	1.1377
20.0	1.1640	1.1615	1.1557
22.0	1.1832	1.1806	1.1743
24.0	1.2030	1.2003	1.1935
26.0	1.2235	1.2206	1.2134
28.0	1.2446	1.2415	1.2340
30.0	1.2663	1.2630	1.2552
40.0	1.3877	1.3838	1.3736
50.0	1.5305	1.5257	1.5127
60.0	1.6950	1.6892	1.6731
65.0	1.7854	1.7792	1.7613

*International Critical Tables, vol. 3, p. 55.

TABLE 2-60 Hydrogen Fluoride (HF)*

%	<i>d</i> ₄ ⁰	<i>d</i> ₄ ²⁰
5	1.020	1.017
10	1.040	1.035
20	1.080	1.070
30	1.119	1.101
40	1.159	1.130
50	1.198	1.155
60	1.235	
70	1.258	
80	1.259	
90	1.178	
95	1.089	
100	1.0005	

*International Critical Tables, vol. 3, p. 54.

TABLE 2-61 Hydrogen Peroxide (H₂O₂)*

%	<i>d</i> ₄ ¹⁸	%	<i>d</i> ₄ ¹⁸
1	1.0022	26	1.0959
2	1.0058	28	1.1040
4	1.0131	30	1.1122
6	1.0204	35	1.1327
8	1.0277	40	1.1536
10	1.0351	45	1.1749
12	1.0425	50	1.1966
14	1.0499	55	1.2188
16	1.0574	60	1.2416
18	1.0649	70	1.2897
20	1.0725	80	1.3406
22	1.0802	90	1.3931
24	1.0880	100	1.4465

*International Critical Tables, vol. 3, p. 54.

TABLE 2-62 Hydrofluosilic Acid (H₂SiF₆)*

%	<i>d</i> ₄ ^{17.5}	%	<i>d</i> ₄ ^{17.5}
1	1.0080	16	1.1373
2	1.0161	20	1.1748
4	1.0324	25	1.2235
8	1.0661	30	1.2742
12	1.1011	34	1.3162

*O. Söhnel and P. Novotny, *Densities of Aqueous Solutions of Inorganic Substances*, Elsevier, 1985.

TABLE 2-63 Magnesium Chloride (MgCl₂)*

%	0 °C	20 °C	40 °C	60 °C	80 °C	100 °C
2	1.0168	1.0146	1.0084	0.9995	0.9883	0.9753
4	1.0338	1.0311	1.0248	1.0159	1.0050	0.9923
8	1.0683	1.0646	1.0580	1.0493	1.0388	1.0269
12	1.1035	1.0989	1.0921	1.0836	1.0735	1.0622
16	1.1395	1.1342	1.1272	1.1188	1.1092	1.0984
20	1.1764	1.1706	1.1635	1.1552	1.1460	1.1359
25	1.2246	1.2184	1.2111	1.2031	1.1942	1.1847
30	1.2754	1.2688	1.2614	1.2535	1.2451	1.2360

*International Critical Tables, vol. 3, p. 71.

TABLE 2-64 Magnesium Sulfate (MgSO₄)*

%	0 °C	20 °C	30 °C	40 °C	50 °C	60 °C	80 °C
2	1.0210	1.0186	1.0158	1.0123	1.0081	1.0032	0.9916
4	1.0423	1.0392	1.0362	1.0326	1.0283	1.0234	1.0118
8	1.0858	1.0816	1.0782	1.0743	1.0700	1.0650	1.0534
12	1.1309	1.1256	1.1220	1.1179	1.1135	1.1083	1.0968
16	1.1777	1.1717	1.1679	1.1637	1.1592		
20	1.2264	1.2198	1.2159	1.2117	1.2072		
26	1.3032	1.2961	1.2922	1.2879	1.2836		

*International Critical Tables, vol. 3, p. 72.

TABLE 2-65 Nickel Chloride (NiCl₂)*

%	<i>d</i> ₄ ¹⁸
1	1.0082
2	1.0179
4	1.0375
8	1.0785
12	1.1217
16	1.1674
20	1.2163
30	1.353

*International Critical Tables, vol. 3, p. 69.

TABLE 2-66 Nickel Nitrate [Ni(NO₃)₂]*

%	<i>d</i> ₄ ²⁰
1	1.0065
2	1.0150
4	1.0325
8	1.0688
12	1.1070
16	1.1480
20	1.191
30	1.311
35	1.377

*International Critical Tables, vol. 3, p. 69.

TABLE 2-67 Nickel Sulfate (NiSO₄)*

%	<i>d</i> ₄ ¹⁸
1	1.0091
2	1.0198
4	1.0415
8	1.0852
12	1.1325
16	1.1825
18	1.2090

*International Critical Tables, vol. 3, p. 69.

TABLE 2-68 Nitric Acid (HNO₃)*

%	0 °C	5 °C	10 °C	15 °C	20 °C	25 °C	30 °C	40 °C	50 °C	60 °C	80 °C	100 °C
1	1.0058	1.00572	1.00534	1.00464	1.00364	1.00241	1.0009	0.9973	0.9931	0.9882	0.9767	0.9632
2	1.0117	1.01149	1.01099	1.01018	1.00909	1.00778	1.0061	1.0025	0.9982	0.9932	0.9816	0.9681
3	1.0176	1.01730	1.01668	1.01576	1.01457	1.01318	1.0114	1.0077	1.0033	0.9982	0.9865	0.9730
4	1.0236	1.02315	1.02240	1.02137	1.02008	1.01861	1.0168	1.0129	1.0084	1.0033	0.9915	0.9779
5	1.0296	1.02904	1.02816	1.02702	1.02563	1.02408	1.0222	1.0182	1.0136	1.0084	0.9965	0.9829
6	1.0357	1.03497	1.03397	1.03272	1.03122	1.02958	1.0277	1.0235	1.0188	1.0136	1.0015	0.9879
7	1.0418	1.0410	1.0399	1.0385	1.0369	1.0352	1.0333	1.0289	1.0241	1.0188	1.0066	0.9929
8	1.0480	1.0471	1.0458	1.0443	1.0427	1.0409	1.0389	1.0344	1.0295	1.0241	1.0117	0.9980
9	1.0543	1.0532	1.0518	1.0502	1.0485	1.0466	1.0446	1.0399	1.0349	1.0294	1.0169	1.0032
10	1.0606	1.0594	1.0578	1.0561	1.0543	1.0523	1.0503	1.0455	1.0403	1.0347	1.0221	1.0083
11	1.0669	1.0656	1.0639	1.0621	1.0602	1.0581	1.0560	1.0511	1.0458	1.0401	1.0273	1.0134
12	1.0733	1.0718	1.0700	1.0681	1.0661	1.0640	1.0618	1.0567	1.0513	1.0455	1.0326	1.0186
13	1.0797	1.0781	1.0762	1.0742	1.0721	1.0699	1.0676	1.0624	1.0568	1.0509	1.0379	1.0238
14	1.0862	1.0845	1.0824	1.0803	1.0781	1.0758	1.0735	1.0681	1.0624	1.0564	1.0432	1.0289
15	1.0927	1.0909	1.0887	1.0865	1.0842	1.0818	1.0794	1.0739	1.0680	1.0619	1.0485	1.0341
16	1.0992	1.0973	1.0950	1.0927	1.0903	1.0879	1.0854	1.0797	1.0737	1.0675	1.0538	1.0393
17	1.1057	1.1038	1.1014	1.0989	1.0964	1.0940	1.0914	1.0855	1.0794	1.0731	1.0592	1.0444
18	1.1123	1.1103	1.1078	1.1052	1.1026	1.1001	1.0974	1.0913	1.0851	1.0787	1.0646	1.0496
19	1.1189	1.1168	1.1142	1.1115	1.1088	1.1062	1.1034	1.0972	1.0908	1.0843	1.0700	1.0547
20	1.1255	1.1234	1.1206	1.1178	1.1150	1.1123	1.1094	1.1031	1.0966	1.0899	1.0754	1.0598
21	1.1322	1.1300	1.1271	1.1242	1.1213	1.1185	1.1155	1.1090	1.1024	1.0956	1.0808	1.0650
22	1.1389	1.1366	1.1336	1.1306	1.1276	1.1247	1.1217	1.1150	1.1083	1.1013	1.0862	1.0701
23	1.1457	1.1433	1.1402	1.1371	1.1340	1.1310	1.1280	1.1210	1.1142	1.1070	1.0917	1.0753
24	1.1525	1.1501	1.1469	1.1437	1.1404	1.1374	1.1343	1.1271	1.1201	1.1127	1.0972	1.0805
25	1.1594	1.1569	1.1536	1.1503	1.1469	1.1438	1.1406	1.1332	1.1260	1.1185	1.1027	1.0857
26	1.1663	1.1638	1.1603	1.1569	1.1534	1.1502	1.1469	1.1394	1.1320	1.1244	1.1083	1.0910
27	1.1733	1.1707	1.1670	1.1635	1.1600	1.1566	1.1533	1.1456	1.1381	1.1303	1.1139	1.0963
28	1.1803	1.1777	1.1738	1.1702	1.1666	1.1631	1.1597	1.1519	1.1442	1.1362	1.1195	1.1016
29	1.1874	1.1847	1.1807	1.1770	1.1733	1.1697	1.1662	1.1582	1.1503	1.1422	1.1251	1.1069
30	1.1945	1.1917	1.1876	1.1838	1.1800	1.1763	1.1727	1.1645	1.1564	1.1482	1.1307	1.1122
31	1.2016	1.1988	1.1945	1.1906	1.1867	1.1829	1.1792	1.1708	1.1625	1.1542	1.1363	1.1175
32	1.2088	1.2059	1.2014	1.1974	1.1934	1.1896	1.1857	1.1772	1.1687	1.1602	1.1419	1.1228
33	1.2160	1.2131	1.2084	1.2043	1.2002	1.1963	1.1922	1.1836	1.1749	1.1662	1.1476	1.1281
34	1.2233	1.2203	1.2155	1.2113	1.2071	1.2030	1.1988	1.1901	1.1812	1.1723	1.1533	1.1335
35	1.2306	1.2275	1.2227	1.2183	1.2140	1.2098	1.2055	1.1966	1.1876	1.1784	1.1591	1.1390
36	1.2375	1.2344	1.2294	1.2249	1.2205	1.2163	1.2119	1.2028	1.1936	1.1842	1.1645	1.1440
37	1.2444	1.2412	1.2361	1.2315	1.2270	1.2227	1.2182	1.2089	1.1995	1.1899	1.1699	1.1490
38	1.2513	1.2479	1.2428	1.2381	1.2335	1.2291	1.2245	1.2150	1.2054	1.1956	1.1752	1.1540
39	1.2581	1.2546	1.2494	1.2446	1.2399	1.2354	1.2308	1.2210	1.2112	1.2013	1.1805	1.1589
40	1.2649	1.2613	1.2560	1.2511	1.2463	1.2417	1.2370	1.2270	1.2170	1.2069	1.1858	1.1638
41	1.2717	1.2680	1.2626	1.2576	1.2527	1.2480	1.2432	1.2330	1.2229	1.2126	1.1911	1.1687
42	1.2786	1.2747	1.2692	1.2641	1.2591	1.2543	1.2494	1.2390	1.2287	1.2182	1.1963	1.1735
43	1.2854	1.2814	1.2758	1.2706	1.2655	1.2606	1.2556	1.2450	1.2345	1.2238	1.2015	1.1783
44	1.2922	1.2880	1.2824	1.2771	1.2719	1.2669	1.2618	1.2510	1.2403	1.2294	1.2067	1.1831
45	1.2990	1.2947	1.2890	1.2836	1.2783	1.2732	1.2680	1.2570	1.2461	1.2350	1.2119	1.1879
46	1.3058	1.3014	1.2955	1.2901	1.2847	1.2795	1.2742	1.2630	1.2519	1.2406	1.2171	1.1927
47	1.3126	1.3080	1.3021	1.2966	1.2911	1.2858	1.2804	1.2690	1.2577	1.2462	1.2223	1.1976
48	1.3194	1.3147	1.3087	1.3031	1.2975	1.2921	1.2867	1.2750	1.2635	1.2518	1.2275	1.2024
49	1.3263	1.3214	1.3153	1.3096	1.3040	1.2984	1.2929	1.2811	1.2693	1.2575	1.2328	1.2073
50	1.3327	1.3277	1.3215	1.3157	1.3100	1.3043	1.2987	1.2867	1.2748	1.2628	1.2377	1.2118
51	1.3391	1.3339	1.3277	1.3218	1.3160	1.3102	1.3045	1.2923	1.2802	1.2680	1.2425	1.2163
52	1.3454	1.3401	1.3338	1.3278	1.3219	1.3160	1.3102	1.2978	1.2856	1.2731	1.2473	1.2208
53	1.3517	1.3462	1.3399	1.3338	1.3278	1.3218	1.3159	1.3033	1.2909	1.2782	1.2521	1.2252
54	1.3579	1.3523	1.3459	1.3397	1.3336	1.3275	1.3215	1.3087	1.2961	1.2833	1.2568	1.2296
55	1.3640	1.3583	1.3518	1.3455	1.3393	1.3331	1.3270	1.3141	1.3013	1.2883	1.2615	1.2339
56	1.3700	1.3642	1.3576	1.3512	1.3449	1.3386	1.3324	1.3194	1.3064	1.2932	1.2661	1.2382
57	1.3759	1.3700	1.3634	1.3569	1.3505	1.3441	1.3377	1.3246	1.3114	1.2981	1.2706	1.2424
58	1.3818	1.3757	1.3691	1.3625	1.3560	1.3495	1.3430	1.3298	1.3164	1.3029	1.2751	1.2466
59	1.3875	1.3813	1.3747	1.3680	1.3614	1.3548	1.3482	1.3348	1.3213	1.3077	1.2795	1.2507
60	1.3931	1.3868	1.3801	1.3734	1.3667	1.3600	1.3533	1.3398	1.3261	1.3124	1.2839	1.2547
61	1.3986	1.3922	1.3855	1.3787	1.3719	1.3651	1.3583	1.3447	1.3308	1.3169	1.2881	1.2587
62	1.4039	1.3975	1.3907	1.3838	1.3769	1.3700	1.3632	1.3494	1.3354	1.3213	1.2922	1.2625
63	1.4091	1.4027	1.3958	1.3888	1.3818	1.3748	1.3679	1.3540	1.3398	1.3255	1.2962	1.2661
64		1.4078	1.4007	1.3936	1.3866	1.3795	1.3725					

2-108 PHYSICAL AND CHEMICAL DATA

TABLE 2-68 Nitric Acid (HNO₃) (Concluded)

%	0 °C	5 °C	10 °C	15 °C	20 °C	25 °C	30 °C	40 °C	50 °C	60 °C	80 °C	100 °C
65		1.4128	1.4055	1.3984	1.3913	1.3841	1.3770					
66		1.4177	1.4103	1.4031	1.3959	1.3887	1.3814					
67		1.4224	1.4150	1.4077	1.4004	1.3932	1.3857					
68		1.4271	1.4196	1.4122	1.4048	1.3976	1.3900					
69		1.4317	1.4241	1.4166	1.4091	1.4019	1.3942					
70		1.4362	1.4285	1.4210	1.4134	1.4061	1.3983					
71		1.4406	1.4328	1.4252	1.4176	1.4102	1.4023					
72		1.4449	1.4371	1.4294	1.4218	1.4142	1.4063					
73		1.4491	1.4413	1.4335	1.4258	1.4182	1.4103					
74		1.4532	1.4454	1.4376	1.4298	1.4221	1.4142					
75		1.4573	1.4494	1.4415	1.4337	1.4259	1.4180					
76		1.4613	1.4533	1.4454	1.4375	1.4296	1.4217					
77		1.4652	1.4572	1.4492	1.4413	1.4333	1.4253					
78		1.4690	1.4610	1.4529	1.4450	1.4369	1.4288					
79		1.4727	1.4647	1.4565	1.4486	1.4404	1.4323					
80		1.4764	1.4683	1.4601	1.4521	1.4439	1.4357					
81		1.4800	1.4718	1.4636	1.4555	1.4473	1.4391					
82		1.4835	1.4753	1.4670	1.4589	1.4507	1.4424					
83		1.4869	1.4787	1.4704	1.4622	1.4540	1.4456					
84		1.4903	1.4820	1.4737	1.4655	1.4572	1.4487					
85		1.4936	1.4852	1.4769	1.4686	1.4603	1.4518					
86		1.4968	1.4883	1.4799	1.4716	1.4633	1.4548					
87		1.4999	1.4913	1.4829	1.4745	1.4662	1.4577					
88		1.5029	1.4942	1.4858	1.4773	1.4690	1.4605					
89		1.5058	1.4970	1.4885	1.4800	1.4716	1.4631					
90		1.5085	1.4997	1.4911	1.4826	1.4741	1.4656					
91		1.5111	1.5023	1.4936	1.4850	1.4766	1.4681					
92		1.5136	1.5048	1.4960	1.4873	1.4789	1.4704					
93		1.5156	1.5068	1.4979	1.4892	1.4807	1.4722					
94		1.5177	1.5088	1.4999	1.4912	1.4826	1.4741					
95		1.5198	1.5109	1.5019	1.4932	1.4846	1.4761					
96		1.5220	1.5130	1.5040	1.4952	1.4867	1.4781					
97		1.5244	1.5152	1.5062	1.4974	1.4889	1.4802					
98		1.5278	1.5187	1.5096	1.5008	1.4922	1.4835					
99		1.5327	1.5235	1.5144	1.5056	1.4969	1.4881					
100		1.5402	1.5310	1.5217	1.5129	1.5040	1.4952					

*International Critical Tables, vol. 3, pp. 58–59.

TABLE 2-69 Perchloric Acid (HClO₄)*

%	d ₄ ¹⁵	d ₄ ²⁰	d ₄ ²⁵	d ₄ ⁵⁰	%	d ₄ ¹⁵	d ₄ ²⁰	d ₄ ⁵⁰
1	1.0050		1.0020	0.9933	28	1.1900	1.1851	1.1645
2	1.0109		1.0070	0.9986	30	1.2067	1.2013	1.1800
4	1.0228		1.0169	0.9906	32	1.2239	1.2183	1.1960
6	1.0348		1.0270	1.0205	34	1.2418	1.2359	1.2130
8	1.0471		1.0372	1.0320	36	1.2603	1.2542	1.2310
10	1.0597		1.0475	1.0440	38	1.2794	1.2732	1.2490
12	1.0726			1.0560	40	1.2991	1.2927	1.2680
14	1.0589			1.0680	45	1.3521	1.3450	1.3180
16	1.0995			1.0810	50	1.4103	1.4018	1.3730
18	1.1135			1.0940	55	1.4733	1.4636	1.4320
20	1.1279			1.1070	60	1.5389	1.5298	1.4950
22	1.1428			1.1205	65	1.6059	1.5986	1.5620
24	1.1581			1.1345	70	1.6736	1.6680	1.6290
26	1.1738	1.1697		1.1490				

*International Critical Tables, vol. 3, p. 54.

TABLE 2-70 Phosphoric Acid (H₃PO₄)*

°C	2%	6%	14%	20%	26%	35%	50%	75%	100%
0	1.0113	1.0339	1.0811	1.1192					
10	1.0109	1.0330	1.0792	1.1167	1.1567	1.221	1.341		
20	1.0092	1.0309	1.0764	1.1134	1.1529	1.216	1.335	1.579	1.870
30	1.0065	1.0279	1.0728	1.1094	1.1484	1.211	1.329	1.572	1.862
40	1.0029	1.0241	1.0685	1.1048					

*International Critical Tables, vol. 3, p. 61.

TABLE 2-71 Potassium Bicarbonate (KHCO₃)*

°C	1%	2%	4%	6%	8%	10%
0	1.0066	1.0134	1.0270			
10	1.0064	1.0132	1.0268			
15	1.0058	1.0125	1.0260	1.0396	1.0534	1.0674
20	1.0049	1.0117	1.0252			
30	1.0024	1.0092	1.0228			
40	0.9990	1.0058	1.0195			
50	0.9949	1.0017	1.0154			
60	0.9901	0.9969	1.0106			
80	0.9786	0.9855	0.9993			
100	0.9653	0.9722	0.9860			

*International Critical Tables, vol. 3, p. 90.

TABLE 2-72 Potassium Bromide (KBr)*

%	d ₄ ²⁰
1	1.0054
2	1.0127
6	1.0426
12	1.0903
20	1.1601
30	1.2593
40	1.3746

*International Critical Tables, vol. 3, p. 87.

TABLE 2-73 Potassium Carbonate (K₂CO₃)*

%	0 °C	10 °C	20 °C	40 °C	60 °C	80 °C	100 °C
1	1.0094	1.0089	1.0072	1.0010	0.9919	0.9803	0.9670
2	1.0189	1.0182	1.0163	1.0098	1.0005	0.9889	0.9756
4	1.0381	1.0369	1.0345	1.0276	1.0180	1.0063	0.9951
8	1.0768	1.0746	1.0715	1.0640	1.0538	1.0418	1.0291
12	1.1160	1.1131	1.1096	1.1013	1.0906	1.0786	1.0663
16	1.1562	1.1530	1.1490	1.1399	1.1290	1.1170	1.1049
20	1.1977	1.1941	1.1898	1.1801	1.1690	1.1570	1.1451
24	1.2405	1.2366	1.2320	1.2219	1.2106	1.1986	1.1869
28	1.2846	1.2804	1.2756	1.2652	1.2538	1.2418	1.2301
30	1.3071	1.3028	1.2979	1.2873	1.2759	1.2640	1.2522
35	1.3646	1.3600	1.3548	1.3440	1.3324	1.3206	1.3089
40	1.4244	1.4195	1.4141	1.4029	1.3913	1.3795	1.3678
45	1.4867	1.4815	1.4759	1.4644	1.4528	1.4408	1.4290
50	1.5517	1.5462	1.5404	1.5285	1.5169	1.5048	1.4928

*International Critical Tables, vol. 3, p. 90.

TABLE 2-74 Potassium Chromate (K₂CrO₄)*

%	d ₄ ¹⁵	d ₄ ¹⁸
1	1.0073	1.0066
2	1.0155	1.0147
4	1.0321	1.0311
8	1.0659	1.0647
12	1.1009	1.0999
16		1.1366
20		1.1748
24		1.2147
28		1.2566
30		1.2784

*International Critical Tables, vol. 3, p. 92.

TABLE 2-75 Potassium Chlorate (KClO₃)*

°C	1%	2%	3%	4%
0	1.0061	1.0124	1.0189	1.0256
10	1.0059	1.0122	1.0187	1.0254
20	1.0045	1.0109	1.0174	1.0241
30	1.0020	1.0085	1.0151	1.0218
40	0.9986	1.0051	1.0116	1.0183
60	0.9895	0.9959	1.0024	1.0091
80	0.9781	0.9845	0.9910	0.9977
100	0.9646	0.9709	0.9774	0.9840

*International Critical Tables, vol. 3, p. 86.

TABLE 2-76 Potassium Chloride (KCl)*

%	0 °C	20 °C	25 °C	40 °C	60 °C	80 °C	100 °C
1.0	1.00661	1.00462	1.00342	0.99847	0.9894	0.9780	0.9646
2.0	1.01335	1.01103	1.00977	1.00471	0.9956	0.9842	0.9708
4.0	1.02690	1.02391	1.02255	1.01727	1.0080	0.9966	0.9634
8.0	1.05431	1.05003	1.04847	1.04278	1.0333	1.0219	1.0888
12.0	1.08222	1.07679	1.07506	1.06897	1.0592	1.0478	1.0350
16.0	1.11068	1.10434	1.10245	1.09600	1.0861	1.0746	1.0619
20.0	1.13973	1.13280	1.13072	1.12399	1.1138	1.1024	1.0897
24.0		1.16226	1.15995	1.15299	1.1425	1.1311	1.1185
28.0				1.18304	1.1723	1.1609	1.1483

%	110 °C	120 °C	130 °C	140 °C
3.79	0.9733	0.9663	0.9583	0.9502
7.45	0.9978	0.9899	0.9827	0.9745
13.62	1.0388	1.0313	1.0238	1.0159

*International Critical Tables, vol. 3, p. 87.

TABLE 2-77 Potassium Chrome Alum [K₂Cr₂(SO₄)₄]*

%	d ₄ ¹⁵
1	1.007
2	1.016
6	1.052
10	1.089
14	1.129
20	1.193
30	1.315
40	1.456
50	1.615

*International Critical Tables, vol. 3, p. 92.

TABLE 2-78 Potassium Hydroxide (KOH)*

%	d ₄ ¹⁵
1.0	1.0083
2.0	1.0175
4.0	1.0359
6.0	1.0544
8.0	1.0730
10.0	1.0918
15.0	1.1396
20.0	1.1884
25.0	1.2387
30.0	1.2905
35.0	1.3440
40.0	1.3991
45.0	1.4558
50.0	1.5143
51.7	1.5355 (sat'd. soln.)

*International Critical Tables, vol. 3, p. 86.

TABLE 2-79 Potassium Nitrate (KNO₃)*

%	0 °C	10 °C	20 °C	40 °C	60 °C	80 °C	100 °C
1	1.00654	1.00615	1.00447	0.99825	0.9890	0.9776	0.9641
2	1.01326	1.01262	1.01075	1.00430	0.9949	0.9834	0.9699
4	1.02677	1.02566	1.02344	1.01652	1.0068	0.9951	0.9816
8	1.05419	1.05226	1.04940	1.04152	1.0313	1.0192	1.0056
12	1.08221	1.07963	1.07620	1.06740	1.0567	1.0442	1.0304
16			1.10392	1.09432	1.0831	1.0703	1.0562
20			1.13261	1.12240	1.1106	1.0974	1.0831
24			1.16233	1.15175	1.1391	1.1256	1.1110

*International Critical Tables, vol. 3, p. 89.

TABLE 2-80 Potassium Dichromate (K₂Cr₂O₇)*

%	d ₄ ²⁰
1	1.0052
2	1.0122
4	1.0264
6	1.0408
8	1.0554
10	1.0703

*International Critical Tables, vol. 3, p. 92.

TABLE 2-81 Potassium Sulfate (K₂SO₄)*

%	d ₄ ²⁰
1	1.0063
2	1.0145
4	1.0310
6	1.0477
8	1.0646
10	1.0817

*International Critical Tables, vol. 3, p. 88.

TABLE 2-82 Potassium Sulfite (K₂SO₃)*

%	d ₄ ¹⁵
1	1.0073
2	1.0155
4	1.0322
8	1.0667
12	1.1026
16	1.1402
20	1.1793
24	1.2197
26	1.2404

*International Critical Tables, vol. 3, p. 87.

TABLE 2-83 Sodium Acetate (NaC₂H₃O₂)*

%	d ₄ ²⁰
1	1.0033
2	1.0084
4	1.0186
8	1.0392
12	1.0598
18	1.0807
20	1.1021
26	1.1351
28	1.1462

*International Critical Tables, vol. 3, p. 83.

TABLE 2-84 Sodium Arsenate (Na₃AsO₄)*

%	d ₄ ¹⁷
1	1.0097
2	1.0207
4	1.0431
8	1.0892
10	1.1130
12	1.1373

*International Critical Tables, vol. 3, p. 82.

TABLE 2-85 Sodium Bichromate (Na₂Cr₂O₇)*

%	d ₄ ¹⁵
1	1.006
2	1.013
4	1.027
8	1.056
12	1.084
16	1.112
20	1.140
24	1.166
28	1.193
30	1.207
35	1.244
40	1.279
45	1.312
50	1.342

*International Critical Tables, vol. 3, p. 86.

TABLE 2-86 Sodium Bromide (NaBr)*

%	d ₄ ²⁰
1	1.0060
2	1.0139
4	1.0298
8	1.0631
10	1.0803
12	1.0981
20	1.1745
30	1.2841
40	1.4138

*International Critical Tables, vol. 3, p. 80.

TABLE 2-87 Sodium Formate (HCOONa)*

%	d ₄ ²⁵
1	1.003
2	1.009
4	1.022
8	1.048
12	1.074
16	1.100
20	1.127
24	1.155
28	1.184
30	1.199
35	1.236
40	1.274

*International Critical Tables, vol. 3, p. 83.

2-110 PHYSICAL AND CHEMICAL DATA

TABLE 2-88 Sodium Carbonate (Na₂CO₃)*

%	0 °C	10 °C	20 °C	30 °C	40 °C	60 °C	80 °C	100 °C
1	1.0109	1.0103	1.0086	1.0058	1.0022	0.9929	0.9814	0.9683
2	1.0219	1.0210	1.0190	1.0159	1.0122	1.0027	0.9910	0.9782
4	1.0439	1.0423	1.0398	1.0363	1.0323	1.0223	1.0105	0.9980
8	1.0878	1.0850	1.0816	1.0775	1.0732	1.0625	1.0503	1.0380
12	1.1319	1.1284	1.1244	1.1200	1.1150	1.1039	1.0914	1.0787
14	1.1543	1.1506	1.1463	1.1417	1.1365	1.1251	1.1125	1.0996
16				1.1636				
18				1.1859				
20				1.2086				
24				1.2552				
28				1.3031				
30				1.3274				

*International Critical Tables, vol. 3, pp. 82–83.

TABLE 2-89 Sodium Chlorate (NaClO₃)*

%	d_4^{18}	%	d_4^{18}
1	1.0053	18	1.1288
2	1.0121	20	1.1449
4	1.0258	22	1.1614
6	1.0397	24	1.1782
8	1.0538	26	1.1953
10	1.0681	28	1.2128
12	1.0827	30	1.2307
14	1.0977	32	1.2491
16	1.1131	34	1.2680

*International Critical Tables, vol. 3, p. 80.

TABLE 2-90 Sodium Chloride (NaCl)*

%	0 °C	10 °C	25 °C	40 °C	60 °C	80 °C	100 °C
1	1.00747	1.00707	1.00409	0.99908	0.9900	0.9785	0.9651
2	1.01509	1.01442	1.01112	1.00593	0.9967	0.9852	0.9719
4	1.03038	1.02920	1.02530	1.01977	1.0103	0.9988	0.9855
8	1.06121	1.05907	1.05412	1.04798	1.0381	1.0264	1.0134
12	1.09244	1.08946	1.08365	1.07699	1.0667	1.0549	1.0420
16	1.12419	1.12056	1.11401	1.10688	1.0962	1.0842	1.0713
20	1.15663	1.15254	1.14533	1.13774	1.1268	1.1146	1.1017
24	1.18999	1.18557	1.17776	1.16971	1.1584	1.1463	1.1331
26	1.20709	1.20254	1.19443	1.18614	1.1747	1.1626	1.1492

*International Critical Tables, vol. 3, p. 79.

TABLE 2-91 Sodium Chromate (Na₂CrO₄)*

%	d_4^{18}
1	1.0074
2	1.0164
4	1.0344
8	1.0718
12	1.1110
16	1.1518
20	1.1942
24	1.2383
26	1.2611

*International Critical Tables, vol. 3, p. 86.

TABLE 2-95 Sodium Silicates*

Formula	Concentration, %												
	1	2	4	8	10	14	20	24	30	36	40	45	50
Na ₂ O/3.9SiO ₂	1.006	1.014	1.030	1.063	1.080	1.116	1.172	1.211	1.275				
Na ₂ O/3.36SiO ₂	1.006	1.014	1.030	1.065	1.083	1.120	1.179	1.222	1.290	1.365			
Na ₂ O/2.40SiO ₂	1.007	1.016	1.034	1.071	1.090	1.130							
Na ₂ O/2.44SiO ₂									1.309	1.387	1.445		
Na ₂ O/2.06SiO ₂	1.007	1.016	1.035	1.073	1.093	1.134	1.200	1.247	1.321	1.397	1.450	1.520	1.594
Na ₂ O/1.69SiO ₂	1.007	1.017	1.036	1.077	1.098	1.141	1.210	1.259	1.337	1.424			

*International Critical Tables, vol. 3, p. 85.

TABLE 2-92 Sodium Hydroxide (NaOH)*

%	0 °C	15 °C	20 °C	40 °C	60 °C	80 °C	100 °C
1	1.0124	1.01065	1.0095	1.0033	0.9941	0.9824	0.9693
2	1.0244	1.02198	1.0207	1.0139	1.0045	0.9929	0.9797
4	1.0482	1.04441	1.0428	1.0352	1.0254	1.0139	1.0009
8	1.0943	1.08887	1.0869	1.0780	1.0676	1.0560	1.0432
12	1.1399	1.13327	1.1309	1.1210	1.1101	1.0983	1.0855
16	1.1849	1.17761	1.1751	1.1645	1.1531	1.1408	1.1277
20	1.2296	1.22183	1.2191	1.2079	1.1960	1.1833	1.1700
24	1.2741	1.26582	1.2629	1.2512	1.2388	1.2259	1.2124
28	1.3182	1.3094	1.3064	1.2942	1.2814	1.2682	1.2546
32	1.3614	1.3520	1.3490	1.3362	1.3232	1.3097	1.2960
36	1.4030	1.3933	1.3900	1.3768	1.3634	1.3498	1.3360
40	1.4435	1.4334	1.4300	1.4164	1.4027	1.3889	1.3750
44	1.4825	1.4720	1.4685	1.4545	1.4405	1.4266	1.4127
48	1.5210	1.5102	1.5065	1.4922	1.4781	1.4641	1.4503
50	1.5400	1.5290	1.5253	1.5109	1.4967	1.4827	1.4690

*International Critical Tables, vol. 3, p. 79.

TABLE 2-93 Sodium Nitrate (NaNO₃)*

%	0 °C	20 °C	40 °C	60 °C	80 °C	100 °C
1	1.0071	1.0049	0.9986	0.9894	0.9779	0.9644
2	1.0144	1.0117	1.0050	0.9956	0.9840	0.9704
4	1.0290	1.0254	1.0180	1.0082	0.9964	0.9826
8	1.0587	1.0532	1.0447	1.0340	1.0218	1.0078
12	1.0891	1.0819	1.0724	1.0609	1.0481	1.0340
16	1.1203	1.1118	1.1013	1.0892	1.0757	1.0614
20	1.1526	1.1429	1.1314	1.1187	1.1048	1.0901
24	1.1860	1.1752	1.1629	1.1496	1.1351	1.1200
28	1.2204	1.2085	1.1955	1.1816	1.1667	1.1513
30	1.2380	1.2256	1.2122	1.1980	1.1830	1.1674
35	1.2834	1.2701	1.2560	1.2413	1.2258	1.2100
40	1.3316	1.3175	1.3027	1.2875	1.2715	1.2555
45		1.3683	1.3528	1.3371	1.3206	1.3044

*International Critical Tables, vol. 3, p. 82.

TABLE 2-94 Sodium Nitrite (NaNO₂)*

%	d_4^{15}
1	1.0058
2	1.0125
4	1.0260
8	1.0535
12	1.0816
16	1.1103
20	1.1394

*International Critical Tables, vol. 3, p. 82.

TABLE 2-96 Sodium Sulfate (Na₂SO₄)*

%	0 °C	20 °C	30 °C	40 °C	60 °C	80 °C	100 °C
1	1.0094	1.0073	1.0046	1.0010	0.9919	0.9805	0.9671
2	1.0189	1.0164	1.0135	1.0098	1.0007	0.9892	0.9758
4	1.0381	1.0348	1.0315	1.0276	1.0184	1.0068	0.9934
8	1.0773	1.0724	1.0682	1.0639	1.0544	1.0426	1.0292
12	1.1174	1.1109	1.1062	1.1015	1.0915	1.0795	1.0661
16	1.1585	1.1586	1.1456	1.1406	1.1299	1.1176	1.1042
20	1.2008	1.1915	1.1865	1.1813	1.1696	1.1569	
24	1.2443	1.2336	1.2292	1.2237			

*International Critical Tables, vol. 3, p. 81.

TABLE 2-97 Sodium Sulfide (Na₂S)*

%	d ₄ ¹⁸
1	1.0098
2	1.0211
4	1.0440
8	1.0907
12	1.1388
16	1.1885
18	1.2140

*International Critical Tables, vol. 3, p. 81.

TABLE 2-98 Sodium Sulfite (Na₂SO₃)*

%	d ₄ ¹⁹
1	1.0078
2	1.0172
4	1.0363
8	1.0751
12	1.1146
16	1.1549
18	1.1755

*International Critical Tables, vol. 3, p. 81.

TABLE 2-99 Sodium Thiosulfate (Na₂S₂O₃)*

%	d ₄ ²⁰
1	1.0065
2	1.0148
4	1.0315
8	1.0654
12	1.1003
16	1.1365
20	1.1740
24	1.2128
28	1.2532
30	1.2739
35	1.3273
40	1.3827

*International Critical Tables, vol. 3, p. 81.

TABLE 2-100 Sodium Thiosulfate Pentahydrate (Na₂S₂O₃·5H₂O)

%	d ₄ ¹⁹
1	1.0052
2	1.0105
4	1.0211
8	1.0423
12	1.0639
16	1.0863
20	1.1087
24	1.1322
28	1.1558
30	1.1676
40	1.2297
50	1.2954

TABLE 2-101 Stannic Chloride (SnCl₄)*

%	d ₄ ¹⁵
1	1.007
2	1.015
4	1.031
8	1.064
12	1.099
16	1.135
20	1.173
24	1.212
28	1.255
30	1.278
35	1.337
40	1.403
45	1.475
50	1.555
55	1.644
60	1.742
65	1.851
70	1.971

*International Critical Tables, vol. 3, p. 63.

TABLE 2-102 Stannous Chloride (SnCl₂)*

%	d ₄ ¹⁵
1	1.0068
2	1.0146
4	1.0306
8	1.0638
12	1.0986
16	1.1353
20	1.1743
24	1.2159
28	1.2603
30	1.2837
35	1.3461
40	1.4145
45	1.4897
50	1.5729
55	1.6656
60	1.7695
65	1.8865

*International Critical Tables, vol. 3, p. 63.

2-112 PHYSICAL AND CHEMICAL DATA

TABLE 2-103 Sulfuric Acid (H₂SO₄)*

%	0 °C	10 °C	15 °C	20 °C	25 °C	30 °C	40 °C	50 °C	60 °C	80 °C	100 °C
1	1.0074	1.0068	1.0060	1.0051	1.0038	1.0022	0.9986	0.9944	0.9895	0.9779	0.9645
2	1.0147	1.0138	1.0129	1.0118	1.0104	1.0087	1.0050	1.0006	0.9956	0.9839	0.9705
3	1.0219	1.0206	1.0197	1.0184	1.0169	1.0152	1.0113	1.0067	1.0017	0.9900	0.9766
4	1.0291	1.0275	1.0264	1.0250	1.0234	1.0216	1.0176	1.0129	1.0078	0.9961	0.9827
5	1.0364	1.0344	1.0332	1.0317	1.0300	1.0281	1.0240	1.0192	1.0140	1.0022	0.9888
6	1.0437	1.0414	1.0400	1.0385	1.0367	1.0347	1.0305	1.0256	1.0203	1.0084	0.9950
7	1.0511	1.0485	1.0469	1.0453	1.0434	1.0414	1.0371	1.0321	1.0266	1.0146	1.0013
8	1.0585	1.0556	1.0539	1.0522	1.0502	1.0481	1.0437	1.0386	1.0330	1.0209	1.0076
9	1.0660	1.0628	1.0610	1.0591	1.0571	1.0549	1.0503	1.0451	1.0395	1.0273	1.0140
10	1.0735	1.0700	1.0681	1.0661	1.0640	1.0617	1.0570	1.0517	1.0460	1.0338	1.0204
11	1.0810	1.0773	1.0753	1.0731	1.0710	1.0686	1.0637	1.0584	1.0526	1.0403	1.0269
12	1.0886	1.0846	1.0825	1.0802	1.0780	1.0756	1.0705	1.0651	1.0593	1.0469	1.0335
13	1.0962	1.0920	1.0898	1.0874	1.0851	1.0826	1.0774	1.0719	1.0661	1.0536	1.0402
14	1.1039	1.0994	1.0971	1.0947	1.0922	1.0897	1.0844	1.0788	1.0729	1.0603	1.0469
15	1.1116	1.1069	1.1045	1.1020	1.0994	1.0968	1.0914	1.0857	1.0798	1.0671	1.0537
16	1.1194	1.1145	1.1120	1.1094	1.1067	1.1040	1.0985	1.0927	1.0868	1.0740	1.0605
17	1.1272	1.1221	1.1195	1.1168	1.1141	1.1113	1.1057	1.0998	1.0938	1.0809	1.0674
18	1.1351	1.1298	1.1271	1.1243	1.1215	1.1187	1.1129	1.1070	1.1009	1.0879	1.0744
19	1.1430	1.1375	1.1347	1.1318	1.1290	1.1261	1.1202	1.1142	1.1081	1.0950	1.0814
20	1.1510	1.1453	1.1424	1.1394	1.1365	1.1335	1.1275	1.1215	1.1153	1.1021	1.0885
21	1.1590	1.1531	1.1501	1.1471	1.1441	1.1410	1.1349	1.1288	1.1226	1.1093	1.0957
22	1.1670	1.1609	1.1579	1.1548	1.1517	1.1486	1.1424	1.1362	1.1299	1.1166	1.1029
23	1.1751	1.1688	1.1657	1.1626	1.1594	1.1563	1.1500	1.1437	1.1373	1.1239	1.1102
24	1.1832	1.1768	1.1736	1.1704	1.1672	1.1640	1.1576	1.1512	1.1448	1.1313	1.1176
25	1.1914	1.1848	1.1816	1.1783	1.1750	1.1718	1.1653	1.1588	1.1523	1.1388	1.1250
26	1.1996	1.1929	1.1896	1.1862	1.1829	1.1796	1.1730	1.1665	1.1599	1.1463	1.1325
27	1.2078	1.2010	1.1976	1.1942	1.1909	1.1875	1.1808	1.1742	1.1676	1.1539	1.1400
28	1.2160	1.2091	1.2057	1.2023	1.1989	1.1955	1.1887	1.1820	1.1753	1.1616	1.1476
29	1.2243	1.2173	1.2138	1.2104	1.2069	1.2035	1.1966	1.1898	1.1831	1.1693	1.1553
30	1.2326	1.2255	1.2220	1.2185	1.2150	1.2115	1.2046	1.1977	1.1909	1.1771	1.1630
31	1.2409	1.2338	1.2302	1.2267	1.2232	1.2196	1.2126	1.2057	1.1988	1.1849	1.1708
32	1.2493	1.2421	1.2385	1.2349	1.2314	1.2278	1.2207	1.2137	1.2068	1.1928	1.1787
33	1.2577	1.2504	1.2468	1.2432	1.2396	1.2360	1.2289	1.2218	1.2148	1.2008	1.1866
34	1.2661	1.2588	1.2552	1.2515	1.2479	1.2443	1.2371	1.2300	1.2229	1.2088	1.1946
35	1.2746	1.2672	1.2636	1.2599	1.2563	1.2526	1.2454	1.2383	1.2311	1.2169	1.2027
36	1.2831	1.2757	1.2720	1.2684	1.2647	1.2610	1.2538	1.2466	1.2394	1.2251	1.2109
37	1.2917	1.2843	1.2805	1.2769	1.2732	1.2695	1.2622	1.2550	1.2477	1.2334	1.2192
38	1.3004	1.2929	1.2891	1.2855	1.2818	1.2780	1.2707	1.2635	1.2561	1.2418	1.2276
39	1.3091	1.3016	1.2978	1.2941	1.2904	1.2866	1.2793	1.2720	1.2646	1.2503	1.2361
40	1.3179	1.3103	1.3065	1.3028	1.2991	1.2953	1.2880	1.2806	1.2732	1.2589	1.2446
41	1.3268	1.3191	1.3153	1.3116	1.3079	1.3041	1.2967	1.2893	1.2819	1.2675	1.2532
42	1.3357	1.3280	1.3242	1.3205	1.3167	1.3129	1.3055	1.2981	1.2907	1.2762	1.2619
43	1.3447	1.3370	1.3332	1.3294	1.3256	1.3218	1.3144	1.3070	1.2996	1.2850	1.2707
44	1.3538	1.3461	1.3423	1.3384	1.3346	1.3308	1.3234	1.3160	1.3086	1.2939	1.2796
45	1.3630	1.3553	1.3515	1.3476	1.3437	1.3399	1.3325	1.3251	1.3177	1.3029	1.2886
46	1.3724	1.3646	1.3608	1.3569	1.3530	1.3492	1.3417	1.3343	1.3269	1.3120	1.2976
47	1.3819	1.3740	1.3702	1.3663	1.3624	1.3586	1.3510	1.3435	1.3361	1.3212	1.3067
48	1.3915	1.3835	1.3797	1.3758	1.3719	1.3680	1.3604	1.3528	1.3455	1.3305	1.3159
49	1.4012	1.3931	1.3893	1.3854	1.3814	1.3775	1.3699	1.3623	1.3549	1.3399	1.3253
50	1.4110	1.4029	1.3990	1.3951	1.3911	1.3872	1.3795	1.3719	1.3644	1.3494	1.3348
51	1.4209	1.4128	1.4088	1.4049	1.4009	1.3970	1.3893	1.3816	1.3740	1.3590	1.3444
52	1.4310	1.4228	1.4188	1.4148	1.4109	1.4069	1.3991	1.3914	1.3837	1.3687	1.3540
53	1.4412	1.4329	1.4289	1.4248	1.4209	1.4169	1.4091	1.4013	1.3936	1.3785	1.3637
54	1.4515	1.4431	1.4391	1.4350	1.4310	1.4270	1.4191	1.4113	1.4036	1.3884	1.3735
55	1.4619	1.4535	1.4494	1.4453	1.4412	1.4372	1.4293	1.4214	1.4137	1.3984	1.3834
56	1.4724	1.4640	1.4598	1.4557	1.4516	1.4475	1.4396	1.4317	1.4239	1.4085	1.3934
57	1.4830	1.4746	1.4703	1.4662	1.4621	1.4580	1.4500	1.4420	1.4342	1.4187	1.4035
58	1.4937	1.4852	1.4809	1.4768	1.4726	1.4685	1.4604	1.4524	1.4446	1.4290	1.4137
59	1.5045	1.4959	1.4916	1.4875	1.4832	1.4791	1.4709	1.4629	1.4551	1.4393	1.4240
60	1.5154	1.5067	1.5024	1.4983	1.4940	1.4898	1.4816	1.4735	1.4656	1.4497	1.4344
61	1.5264	1.5177	1.5133	1.5091	1.5048	1.5006	1.4923	1.4842	1.4762	1.4602	1.4449
62	1.5375	1.5287	1.5243	1.5200	1.5157	1.5115	1.5031	1.4950	1.4869	1.4708	1.4554
63	1.5487	1.5398	1.5354	1.5310	1.5267	1.5225	1.5140	1.5058	1.4977	1.4815	1.4660
64	1.5600	1.5510	1.5465	1.5421	1.5378	1.5335	1.5250	1.5167	1.5086	1.4923	1.4766

TABLE 2-103 Sulfuric Acid (H₂SO₄) (Concluded)

%	0 °C	10 °C	15 °C	20 °C	25 °C	30 °C	40 °C	50 °C	60 °C	80 °C	100 °C
65	1.5714	1.5623	1.5578	1.5533	1.5490	1.5446	1.5361	1.5277	1.5195	1.5031	1.4873
66	1.5828	1.5736	1.5691	1.5646	1.5602	1.5558	1.5472	1.5388	1.5305	1.5140	1.4981
67	1.5943	1.5850	1.5805	1.5760	1.5715	1.5671	1.5584	1.5499	1.5416	1.5249	1.5089
68	1.6059	1.5965	1.5920	1.5874	1.5829	1.5785	1.5697	1.5611	1.5528	1.5359	1.5198
69	1.6176	1.6081	1.6035	1.5989	1.5944	1.5899	1.5811	1.5724	1.5640	1.5470	1.5307
70	1.6293	1.6198	1.6151	1.6105	1.6059	1.6014	1.5925	1.5838	1.5753	1.5582	1.5417
71	1.6411	1.6315	1.6268	1.6221	1.6175	1.6130	1.6040	1.5952	1.5867	1.5694	1.5527
72	1.6529	1.6433	1.6385	1.6338	1.6292	1.6246	1.6155	1.6067	1.5981	1.5806	1.5637
73	1.6648	1.6551	1.6503	1.6456	1.6409	1.6363	1.6271	1.6182	1.6095	1.5919	1.5747
74	1.6768	1.6670	1.6622	1.6574	1.6526	1.6480	1.6387	1.6297	1.6209	1.6031	1.5857
75	1.6888	1.6789	1.6740	1.6692	1.6644	1.6597	1.6503	1.6412	1.6322	1.6142	1.5966
76	1.7008	1.6908	1.6858	1.6810	1.6761	1.6713	1.6619	1.6526	1.6435	1.6252	1.6074
77	1.7128	1.7026	1.6976	1.6927	1.6878	1.6829	1.6734	1.6640	1.6547	1.6361	1.6181
78	1.7247	1.7144	1.7093	1.7043	1.6994	1.6944	1.6847	1.6751	1.6657	1.6469	1.6286
79	1.7365	1.7261	1.7209	1.7158	1.7108	1.7058	1.6959	1.6862	1.6766	1.6575	1.6390
80	1.7482	1.7376	1.7323	1.7272	1.7221	1.7170	1.7069	1.6971	1.6873	1.6680	1.6493
81	1.7597	1.7489	1.7435	1.7383	1.7331	1.7279	1.7177	1.7077	1.6978	1.6782	1.6594
82	1.7709	1.7599	1.7544	1.7491	1.7437	1.7385	1.7281	1.7180	1.7080	1.6882	1.6692
83	1.7815	1.7704	1.7649	1.7594	1.7540	1.7487	1.7382	1.7279	1.7179	1.6979	1.6787
84	1.7916	1.7804	1.7748	1.7693	1.7639	1.7585	1.7479	1.7375	1.7274	1.7072	1.6878
85	1.8009	1.7897	1.7841	1.7786	1.7732	1.7678	1.7571	1.7466	1.7364	1.7161	1.6966
86	1.8095	1.7983	1.7927	1.7872	1.7818	1.7763	1.7657	1.7552	1.7449	1.7245	1.7050
87	1.8173	1.8061	1.8006	1.7951	1.7897	1.7842	1.7736	1.7632	1.7529	1.7324	1.7129
88	1.8243	1.8132	1.8077	1.8022	1.7968	1.7914	1.7809	1.7705	1.7602	1.7397	1.7202
89	1.8306	1.8195	1.8141	1.8087	1.8033	1.7979	1.7874	1.7770	1.7669	1.7464	1.7269
90	1.8361	1.8252	1.8198	1.8144	1.8091	1.8038	1.7933	1.7829	1.7729	1.7525	1.7331
91	1.8410	1.8302	1.8248	1.8195	1.8142	1.8090	1.7986	1.7883	1.7783	1.7581	1.7388
92	1.8453	1.8346	1.8293	1.8240	1.8188	1.8136	1.8033	1.7932	1.7832	1.7633	1.7439
93	1.8490	1.8384	1.8331	1.8279	1.8227	1.8176	1.8074	1.7974	1.7876	1.7681	1.7485
94	1.8520	1.8415	1.8363	1.8312	1.8260	1.8210	1.8109	1.8011	1.7914		
95	1.8544	1.8439	1.8388	1.8337	1.8286	1.8236	1.8137	1.8040	1.7944		
96	1.8560	1.8457	1.8406	1.8355	1.8305	1.8255	1.8157	1.8060	1.7965		
97	1.8569	1.8466	1.8414	1.8364	1.8314	1.8264	1.8166	1.8071	1.7977		
98	1.8567	1.8463	1.8411	1.8361	1.8310	1.8261	1.8163	1.8068	1.7976		
99	1.8551	1.8445	1.8393	1.8342	1.8292	1.8242	1.8145	1.8050	1.7958		
100	1.8517	1.8409	1.8357	1.8305	1.8255	1.8205	1.8107	1.8013	1.7922		

%	$d_4^{5.96}$	%	$d_4^{13.00}$	$d_4^{18.00}$
0.005	1.000 0140	0.05	0.999 810	0.999 028
.01	1.000 0576	0.1	1.000 185	0.999 400
.02	1.000 1434	0.2	1.000 912	1.000 119
.03	1.000 2276	0.3	1.001 623	1.000 820
.04	1.000 3104	0.4	1.002 326	1.001 512
.05	1.000 3920	0.5	1.003 023	1.002 197
.06	1.000 4726	0.6	1.003 716	1.002 877
.07	1.000 5523	0.8	1.005 090	1.004 227
.08	1.000 6313	1.0	1.006 452	1.005 570
.09	1.000 7098	1.2	1.007 807	1.006 909
.10	1.000 7880	1.4	1.009 159	1.008 247
.15	1.001 1732	1.6	1.010 510	1.009 583
.20	1.001 5514	1.8	1.011 860	1.010 918
.25	1.001 9254	2.0	1.013 209	1.012 252
.30	1.002 2961	2.2	1.014 557	1.013 586
.35	1.002 6639	2.4	1.015 904	1.014 919
.40	1.003 0292			
.45	1.003 3923			
.50	1.003 7534			

*International Critical Tables, vol. 3, pp. 56-57.

2-114 PHYSICAL AND CHEMICAL DATA

TABLE 2-104 Zinc Bromide (ZnBr₂)*

%	0 °C	20 °C	40 °C	60 °C	80 °C	100 °C
2	1.0188	1.0167	1.0102	1.0008	0.9890	0.9751
4	1.0381	1.0354	1.0285	1.0187	1.0065	0.9921
8	1.0777	1.0738	1.0660	1.0554	1.0422	1.0270
12	1.1186	1.1135	1.1046	1.0932	1.0789	1.0629
16	1.1609	1.1544	1.1445	1.1320	1.1169	1.1000
20	1.2043	1.1965	1.1855	1.1720	1.1560	1.1382
30	1.3288	1.3170	1.3030	1.2868	1.2688	1.2489
40	1.477	1.462	1.445	1.427	1.406	1.385
50	1.661	1.643	1.623	1.602	1.579	1.555
60	1.891	1.869	1.845	1.822	1.797	1.771
65	2.026	2.002	1.976	1.951	1.924	1.898

*International Critical Tables, vol. 3, p. 64.

TABLE 2-105 Zinc Chloride (ZnCl₂)*

%	0 °C	20 °C	40 °C	60 °C	80 °C	100 °C
2	1.0192	1.0167	1.0099	1.0003	0.9882	0.9739
4	1.0384	1.0350	1.0274	1.0172	1.0044	0.9894
8	1.0769	1.0715	1.0624	1.0508	1.0369	1.0211
12	1.1159	1.1085	1.0980	1.0853	1.0704	1.0541
16	1.1558	1.1468	1.1350	1.1212	1.1055	1.0888
20	1.1970	1.1866	1.1736	1.1590	1.1428	1.1255
30	1.3062	1.2928	1.2778	1.2614	1.2438	1.2252
40	1.4329	1.4173	1.4003	1.3824	1.3637	1.3441
50	1.5860	1.5681	1.5495	1.5300	1.5097	1.4892
60		1.749				
70		1.962				

*International Critical Tables, vol. 3, p. 64.

TABLE 2-106 Zinc Nitrate [Zn(NO₃)₂]*

%		18 °C	
2	1.0154	18	1.1652
4	1.0322	20	1.1865
6	1.0496	25	1.2427
8	1.0675	30	1.3029
10	1.0859	35	1.3678
12	1.1048	40	1.4378
14	1.1244	45	1.5134
16	1.1445	50	1.5944

*International Critical Tables, vol. 3, p. 65.

TABLE 2-107 Zinc Sulfate (ZnSO₄)*

%		20 °C	
2		2	1.019
4		4	1.0403
6		6	1.0620
8		8	1.0842
10		10	1.1071
12		12	1.1308
14		14	1.1553
16		16	1.1806

*International Critical Tables, vol. 3, p. 65.

DENSITIES OF AQUEOUS ORGANIC SOLUTIONS*

UNITS AND UNITS CONVERSIONS

Unless otherwise noted, densities are given in grams per cubic centimeter. To convert to pounds per cubic foot, multiply by 62.43.

$$^{\circ}\text{F} = \% \text{ }^{\circ}\text{C} + 32$$

From *International Critical Tables*, vol. 3, pp. 115–129 unless otherwise stated. All compositions are in weight percent in vacuo. All density values are $d_4^t = \text{g/mL}$ in vacuo.

*For gasoline and aircraft fuels see Hibbard, NACA Res. Mem. E56121 (declassified 1958).

TABLE 2-108 Formic Acid (HCOOH)

%				0 °C				15 °C				20 °C				30 °C			
0	0.9999	0.9991	0.9982	0.9957	25	1.0706	1.0627	1.0609	1.0540	50	1.1349	1.1225	1.1207	1.1098	75	1.1953	1.1794	1.1769	1.1636
1	1.0028	1.0019	1.0019	0.9980	26	1.0733	1.0652	1.0633	1.0564	51	1.1374	1.1248	1.1223	1.1120	76	1.1976	1.1816	1.1785	1.1656
2	1.0059	1.0045	1.0044	1.0004	27	1.0760	1.0678	1.0656	1.0587	52	1.1399	1.1271	1.1244	1.1142	77	1.1999	1.1837	1.1801	1.1676
3	1.0090	1.0072	1.0070	1.0028	28	1.0787	1.0702	1.0681	1.0609	53	1.1424	1.1294	1.1269	1.1164	78	1.2021	1.1859	1.1818	1.1697
4	1.0120	1.0100	1.0093	1.0053	29	1.0813	1.0726	1.0705	1.0632	54	1.1448	1.1318	1.1295	1.1186	79	1.2043	1.1881	1.1837	1.1717
5	1.0150	1.0124	1.0115	1.0075	30	1.0839	1.0750	1.0729	1.0654	55	1.1472	1.1341	1.1320	1.1208	80	1.2065	1.1902	1.1806	1.1737
6	1.0179	1.0151	1.0141	1.0101	31	1.0866	1.0774	1.0753	1.0676	56	1.1497	1.1365	1.1342	1.1230	81	1.2088	1.1924	1.1876	1.1758
7	1.0207	1.0177	1.0170	1.0125	32	1.0891	1.0798	1.0777	1.0699	57	1.1523	1.1388	1.1361	1.1253	82	1.2110	1.1944	1.1896	1.1778
8	1.0237	1.0204	1.0196	1.0149	33	1.0916	1.0821	1.0800	1.0721	58	1.1548	1.1411	1.1381	1.1274	83	1.2132	1.1965	1.1914	1.1798
9	1.0266	1.0230	1.0221	1.0173	34	1.0941	1.0844	1.0823	1.0743	59	1.1573	1.1434	1.1401	1.1295	84	1.2154	1.1985	1.1929	1.1817
10	1.0295	1.0256	1.0246	1.0197	35	1.0966	1.0867	1.0847	1.0766	60	1.1597	1.1458	1.1424	1.1317	85	1.2176	1.2005	1.1953	1.1837
11	1.0324	1.0281	1.0271	1.0221	36	1.0993	1.0892	1.0871	1.0788	61	1.1621	1.1481	1.1448	1.1338	86	1.2196	1.2025	1.1976	1.1856
12	1.0351	1.0306	1.0296	1.0244	37	1.1018	1.0916	1.0895	1.0810	62	1.1645	1.1504	1.1473	1.1360	87	1.2217	1.2045	1.1994	1.1875
13	1.0379	1.0330	1.0321	1.0267	38	1.1043	1.0940	1.0919	1.0832	63	1.1669	1.1526	1.1493	1.1382	88	1.2237	1.2064	1.2012	1.1893
14	1.0407	1.0355	1.0345	1.0290	39	1.1069	1.0964	1.0940	1.0854	64	1.1694	1.1549	1.1517	1.1403	89	1.2258	1.2084	1.2028	1.1910
15	1.0435	1.0380	1.0370	1.0313	40	1.1095	1.0988	1.0963	1.0876	65	1.1718	1.1572	1.1543	1.1425	90	1.2278	1.2102	1.2044	1.1927
16	1.0463	1.0405	1.0393	1.0336	41	1.1122	1.1012	1.0990	1.0898	66	1.1742	1.1595	1.1565	1.1446	91	1.2297	1.2121	1.2059	1.1945
17	1.0491	1.0430	1.0417	1.0358	42	1.1148	1.1036	1.1015	1.0920	67	1.1766	1.1618	1.1584	1.1467	92	1.2316	1.2139	1.2078	1.1961
18	1.0518	1.0455	1.0441	1.0381	43	1.1174	1.1060	1.1038	1.0943	68	1.1790	1.1640	1.1604	1.1489	93	1.2335	1.2157	1.2099	1.1978
19	1.0545	1.0480	1.0464	1.0404	44	1.1199	1.1084	1.1062	1.0965	69	1.1813	1.1663	1.1628	1.1510	94	1.2354	1.2174	1.2117	1.1994
20	1.0571	1.0505	1.0488	1.0427	45	1.1224	1.1109	1.1085	1.0987	70	1.1835	1.1685	1.1655	1.1531	95	1.2372	1.2191	1.2140	1.2008
21	1.0598	1.0532	1.0512	1.0451	46	1.1249	1.1133	1.1108	1.1009	71	1.1858	1.1707	1.1677	1.1552	96	1.2390	1.2208	1.2158	1.2022
22	1.0625	1.0556	1.0537	1.0473	47	1.1274	1.1156	1.1130	1.1031	72	1.1882	1.1729	1.1702	1.1573	97	1.2408	1.2224	1.2170	1.2036
23	1.0652	1.0580	1.0561	1.0496	48	1.1299	1.1179	1.1157	1.1053	73	1.1906	1.1751	1.1728	1.1595	98	1.2425	1.2240	1.2183	1.2048
24	1.0679	1.0604	1.0585	1.0518	49	1.1324	1.1202	1.1185	1.1076	74	1.1929	1.1773	1.1752	1.1615	99	1.2441	1.2257	1.2202	1.2061
															100	1.2456	1.2273	1.2212	1.2073

TABLE 2-109 Acetic Acid (CH₃COOH)

%	0°C	10°C	15°C	20°C	25°C	30°C	40°C	%	0°C	10°C	15°C	20°C	25°C	30°C	40°C
0	0.9999	0.9997	0.9991	0.9982	0.9971	0.9957	0.9922	50	1.0729	1.0654	1.0613	1.0575	1.0534	1.0492	1.0408
1	1.0016	1.0013	1.0006	0.9996	0.9987	0.9971	0.9934	51	1.0738	1.0663	1.0622	1.0582	1.0542	1.0499	1.0414
2	1.0033	1.0029	1.0021	1.0012	1.0000	0.9984	0.9946	52	1.0748	1.0671	1.0629	1.0590	1.0549	1.0506	1.0421
3	1.0051	1.0044	1.0036	1.0025	1.0013	0.9997	0.9958	53	1.0757	1.0679	1.0637	1.0597	1.0555	1.0512	1.0427
4	1.0070	1.0060	1.0051	1.0040	1.0027	1.0011	0.9970	54	1.0765	1.0687	1.0644	1.0604	1.0562	1.0518	1.0432
5	1.0088	1.0076	1.0066	1.0055	1.0041	1.0024	0.9982	55	1.0774	1.0694	1.0651	1.0611	1.0568	1.0525	1.0438
6	1.0106	1.0092	1.0081	1.0069	1.0055	1.0037	0.9994	56	1.0782	1.0701	1.0658	1.0618	1.0574	1.0531	1.0443
7	1.0124	1.0108	1.0096	1.0083	1.0068	1.0050	1.0006	57	1.0790	1.0708	1.0665	1.0624	1.0580	1.0536	1.0448
8	1.0142	1.0124	1.0111	1.0097	1.0081	1.0063	1.0018	58	1.0798	1.0715	1.0672	1.0631	1.0586	1.0542	1.0453
9	1.0159	1.0140	1.0126	1.0111	1.0094	1.0076	1.0030	59	1.0805	1.0722	1.0678	1.0637	1.0592	1.0547	1.0458
10	1.0177	1.0156	1.0141	1.0125	1.0107	1.0089	1.0042	60	1.0813	1.0728	1.0684	1.0642	1.0597	1.0552	1.0462
11	1.0194	1.0171	1.0155	1.0139	1.0120	1.0102	1.0054	61	1.0820	1.0734	1.0690	1.0648	1.0602	1.0557	1.0466
12	1.0211	1.0187	1.0170	1.0154	1.0133	1.0115	1.0065	62	1.0826	1.0740	1.0696	1.0653	1.0607	1.0562	1.0470
13	1.0228	1.0202	1.0184	1.0168	1.0146	1.0127	1.0077	63	1.0833	1.0746	1.0701	1.0658	1.0612	1.0566	1.0473
14	1.0245	1.0217	1.0199	1.0182	1.0159	1.0139	1.0088	64	1.0838	1.0752	1.0706	1.0662	1.0616	1.0571	1.0477
15	1.0262	1.0232	1.0213	1.0195	1.0172	1.0151	1.0099	65	1.0844	1.0757	1.0711	1.0666	1.0621	1.0575	1.0480
16	1.0278	1.0247	1.0227	1.0209	1.0185	1.0163	1.0110	66	1.0850	1.0762	1.0716	1.0671	1.0624	1.0578	1.0483
17	1.0295	1.0262	1.0241	1.0223	1.0198	1.0175	1.0121	67	1.0856	1.0767	1.0720	1.0675	1.0628	1.0582	1.0486
18	1.0311	1.0276	1.0255	1.0236	1.0210	1.0187	1.0132	68	1.0860	1.0771	1.0725	1.0678	1.0631	1.0585	1.0489
19	1.0327	1.0291	1.0269	1.0250	1.0223	1.0198	1.0142	69	1.0865	1.0775	1.0729	1.0682	1.0634	1.0588	1.0491
20	1.0343	1.0305	1.0283	1.0263	1.0235	1.0210	1.0153	70	1.0869	1.0779	1.0732	1.0685	1.0637	1.0590	1.0493
21	1.0358	1.0319	1.0297	1.0276	1.0248	1.0222	1.0164	71	1.0874	1.0783	1.0736	1.0687	1.0640	1.0592	1.0495
22	1.0374	1.0333	1.0310	1.0288	1.0260	1.0233	1.0174	72	1.0877	1.0786	1.0738	1.0690	1.0642	1.0594	1.0496
23	1.0389	1.0347	1.0323	1.0301	1.0272	1.0244	1.0185	73	1.0881	1.0789	1.0741	1.0693	1.0644	1.0595	1.0497
24	1.0404	1.0361	1.0336	1.0313	1.0283	1.0256	1.0195	74	1.0884	1.0792	1.0743	1.0694	1.0645	1.0596	1.0498
25	1.0419	1.0375	1.0349	1.0326	1.0295	1.0267	1.0205	75	1.0887	1.0794	1.0745	1.0696	1.0647	1.0597	1.0499
26	1.0434	1.0388	1.0362	1.0338	1.0307	1.0278	1.0215	76	1.0889	1.0796	1.0746	1.0698	1.0648	1.0598	1.0499
27	1.0449	1.0401	1.0374	1.0349	1.0318	1.0289	1.0225	77	1.0891	1.0797	1.0747	1.0699	1.0648	1.0598	1.0499
28	1.0463	1.0414	1.0386	1.0361	1.0329	1.0299	1.0234	78	1.0893	1.0798	1.0747	1.0700	1.0648	1.0598	1.0498
29	1.0477	1.0427	1.0399	1.0372	1.0340	1.0310	1.0244	79	1.0894	1.0798	1.0747	1.0700	1.0648	1.0597	1.0497
30	1.0491	1.0440	1.0411	1.0384	1.0350	1.0320	1.0253	80	1.0895	1.0798	1.0747	1.0700	1.0647	1.0596	1.0495
31	1.0505	1.0453	1.0423	1.0395	1.0361	1.0330	1.0262	81	1.0895	1.0797	1.0745	1.0699	1.0646	1.0594	1.0493
32	1.0519	1.0465	1.0435	1.0406	1.0372	1.0341	1.0272	82	1.0895	1.0796	1.0743	1.0698	1.0644	1.0592	1.0490
33	1.0532	1.0477	1.0446	1.0417	1.0382	1.0351	1.0281	83	1.0895	1.0795	1.0741	1.0696	1.0642	1.0589	1.0487
34	1.0545	1.0489	1.0458	1.0428	1.0392	1.0361	1.0289	84	1.0893	1.0793	1.0738	1.0693	1.0638	1.0585	1.0483
35	1.0558	1.0501	1.0469	1.0438	1.0402	1.0371	1.0298	85	1.0891	1.0790	1.0735	1.0689	1.0635	1.0582	1.0479
36	1.0571	1.0513	1.0480	1.0449	1.0412	1.0380	1.0306	86	1.0887	1.0787	1.0731	1.0685	1.0630	1.0576	1.0473
37	1.0584	1.0524	1.0491	1.0459	1.0422	1.0390	1.0314	87	1.0883	1.0783	1.0726	1.0680	1.0626	1.0571	1.0467
38	1.0596	1.0535	1.0501	1.0469	1.0432	1.0399	1.0322	88	1.0877	1.0778	1.0721	1.0675	1.0620	1.0564	1.0460
39	1.0608	1.0546	1.0512	1.0479	1.0441	1.0408	1.0330	89	1.0872	1.0773	1.0715	1.0668	1.0613	1.0557	1.0453
40	1.0621	1.0557	1.0522	1.0488	1.0450	1.0416	1.0338	90	1.0865	1.0766	1.0708	1.0661	1.0605	1.0549	1.0445
41	1.0633	1.0568	1.0532	1.0498	1.0460	1.0425	1.0346	91	1.0857	1.0758	1.0700	1.0652	1.0597	1.0541	1.0436
42	1.0644	1.0578	1.0542	1.0507	1.0469	1.0433	1.0353	92	1.0848	1.0749	1.0690	1.0643	1.0587	1.0530	1.0426
43	1.0656	1.0588	1.0551	1.0516	1.0477	1.0441	1.0361	93	1.0838	1.0739	1.0680	1.0632	1.0577	1.0518	1.0414
44	1.0667	1.0598	1.0561	1.0525	1.0486	1.0449	1.0368	94	1.0826	1.0727	1.0667	1.0619	1.0564	1.0506	1.0401
45	1.0679	1.0608	1.0570	1.0534	1.0495	1.0456	1.0375	95	1.0813	1.0714	1.0652	1.0605	1.0551	1.0491	1.0386
46	1.0689	1.0618	1.0579	1.0542	1.0503	1.0464	1.0382	96	1.0798	1.0700	1.0632	1.0588	1.0535	1.0473	1.0368
47	1.0699	1.0627	1.0588	1.0551	1.0511	1.0471	1.0389	97	1.0780	1.0681	1.0611	1.0570	1.0516	1.0454	1.0348
48	1.0709	1.0636	1.0597	1.0559	1.0518	1.0479	1.0395	98	1.0759	1.0660	1.0590	1.0549	1.0495	1.0431	1.0325
49	1.0720	1.0645	1.0605	1.0567	1.0526	1.0486	1.0402	99	1.0730	1.0631	1.0567	1.0524	1.0468	1.0407	1.0299
								100	1.0697		1.0545	1.0498	1.0440	1.0380	1.0271

TABLE 2-110 Oxalic Acid (H₂C₂O₄)

%	$d_4^{17.5}$	%	$d_4^{17.5}$
1	1.0035	8	1.0280
2	1.0070	10	1.0350
4	1.0140	12	1.0420

TABLE 2-111 Methyl Alcohol (CH₃OH)*

%	0°C	10°C	15.56°C	20°C	15°C	%	0°C	10°C	15.56°C	20°C	15°C	%	0°C	10°C	15.56°C	20°C	15°C
0	0.9999	0.9997	0.9990	0.9982	0.99913	35	0.9534	0.9484	0.9456	0.9433	0.94570	70	0.8869	0.8794	0.8748	0.8715	0.87507
1	0.9981	0.9980	0.9973	0.9965	0.99727	36	0.9520	0.9469	0.9440	0.9416	0.94404	71	0.8847	0.8770	0.8726	0.8690	0.87271
2	0.9963	0.9962	0.9955	0.9948	0.99543	37	0.9505	0.9453	0.9422	0.9398	0.94237	72	0.8824	0.8747	0.8702	0.8665	0.87033
3	0.9946	0.9945	0.9938	0.9931	0.99370	38	0.9490	0.9437	0.9405	0.9381	0.94067	73	0.8801	0.8724	0.8678	0.8641	0.86792
4	0.9930	0.9929	0.9921	0.9914	0.99198	39	0.9475	0.9420	0.9387	0.9363	0.93894	74	0.8778	0.8699	0.8653	0.8616	0.86546
5	0.9914	0.9912	0.9904	0.9896	0.99029	40	0.9459	0.9403	0.9369	0.9345	0.93720	75	0.8754	0.8676	0.8629	0.8592	0.86300
6	0.9899	0.9896	0.9889	0.9880	0.98864	41	0.9443	0.9387	0.9351	0.9327	0.93543	76	0.8729	0.8651	0.8604	0.8567	0.86051
7	0.9884	0.9881	0.9872	0.9863	0.98701	42	0.9427	0.9370	0.9333	0.9309	0.93365	77	0.8705	0.8626	0.8579	0.8542	0.85801
8	0.9870	0.9865	0.9857	0.9847	0.98547	43	0.9411	0.9352	0.9315	0.9290	0.93185	78	0.8680	0.8602	0.8554	0.8518	0.85551
9	0.9856	0.9849	0.9841	0.9831	0.98394	44	0.9395	0.9334	0.9297	0.9272	0.93001	79	0.8657	0.8577	0.8529	0.8494	0.85300
10	0.9842	0.9834	0.9826	0.9815	0.98241	45	0.9377	0.9316	0.9279	0.9252	0.92815	80	0.8634	0.8551	0.8503	0.8469	0.85048
11	0.9829	0.9820	0.9811	0.9799	0.98093	46	0.9360	0.9298	0.9261	0.9234	0.92627	81	0.8610	0.8527	0.8478	0.8446	0.84794
12	0.9816	0.9805	0.9796	0.9784	0.97945	47	0.9342	0.9279	0.9242	0.9214	0.92436	82	0.8585	0.8501	0.8452	0.8420	0.84536
13	0.9804	0.9791	0.9781	0.9768	0.97802	48	0.9324	0.9260	0.9223	0.9196	0.92242	83	0.8560	0.8475	0.8426	0.8394	0.84274
14	0.9792	0.9778	0.9766	0.9754	0.97660	49	0.9306	0.9240	0.9204	0.9176	0.92048	84	0.8535	0.8449	0.8400	0.8366	0.84009
15	0.9780	0.9764	0.9752	0.9740	0.97518	50	0.9287	0.9221	0.9185	0.9156	0.91852	85	0.8510	0.8422	0.8374	0.8340	0.83742
16	0.9769	0.9751	0.9738	0.9725	0.97377	51	0.9269	0.9202	0.9166	0.9135	0.91653	86	0.8483	0.8394	0.8347	0.8314	0.83475
17	0.9758	0.9739	0.9723	0.9710	0.97237	52	0.9250	0.9182	0.9146	0.9114	0.91451	87	0.8456	0.8367	0.8320	0.8286	0.83207
18	0.9747	0.9726	0.9709	0.9696	0.97096	53	0.9230	0.9162	0.9126	0.9094	0.91248	88	0.8428	0.8340	0.8294	0.8258	0.82937
19	0.9736	0.9713	0.9695	0.9681	0.96955	54	0.9211	0.9142	0.9106	0.9073	0.91044	89	0.8400	0.8314	0.8267	0.8230	0.82667
20	0.9725	0.9700	0.9680	0.9666	0.96814	55	0.9191	0.9122	0.9086	0.9052	0.90839	90	0.8374	0.8287	0.8239	0.8202	0.82396
21	0.9714	0.9687	0.9666	0.9651	0.96673	56	0.9172	0.9101	0.9065	0.9032	0.90631	91	0.8347	0.8261	0.8212	0.8174	0.82124
22	0.9702	0.9673	0.9652	0.9636	0.96533	57	0.9151	0.9080	0.9045	0.9010	0.90421	92	0.8320	0.8234	0.8185	0.8146	0.81849
23	0.9690	0.9660	0.9638	0.9622	0.96392	58	0.9131	0.9060	0.9024	0.8988	0.90210	93	0.8293	0.8208	0.8157	0.8118	0.81568
24	0.9678	0.9646	0.9624	0.9607	0.96251	59	0.9111	0.9039	0.9002	0.8968	0.89996	94	0.8266	0.8180	0.8129	0.8090	0.81285
25	0.9666	0.9632	0.9609	0.9592	0.96108	60	0.9090	0.9018	0.8980	0.8946	0.89781	95	0.8240	0.8152	0.8101	0.8062	0.80999
26	0.9654	0.9618	0.9595	0.9576	0.95963	61	0.9068	0.8998	0.8958	0.8924	0.89563	96	0.8212	0.8124	0.8073	0.8034	0.80713
27	0.9642	0.9604	0.9580	0.9562	0.95817	62	0.9046	0.8977	0.8936	0.8902	0.89341	97	0.8186	0.8096	0.8045	0.8005	0.80428
28	0.9629	0.9590	0.9565	0.9546	0.95668	63	0.9024	0.8955	0.8913	0.8879	0.89117	98	0.8158	0.8068	0.8016	0.7976	0.80143
29	0.9616	0.9575	0.9550	0.9531	0.95518	64	0.9002	0.8933	0.8890	0.8856	0.88890	99	0.8130	0.8040	0.7987	0.7948	0.79859
30	0.9604	0.9560	0.9535	0.9515	0.95366	65	0.8980	0.8911	0.8867	0.8834	0.88662	100	0.8102	0.8009	0.7959	0.7917	0.79577
31	0.9590	0.9546	0.9521	0.9499	0.95213	66	0.8958	0.8888	0.8844	0.8811	0.88433						
32	0.9576	0.9531	0.9505	0.9483	0.95056	67	0.8935	0.8865	0.8820	0.8787	0.88203						
33	0.9563	0.9516	0.9489	0.9466	0.94896	68	0.8913	0.8842	0.8797	0.8763	0.87971						
34	0.9549	0.9500	0.9473	0.9450	0.94734	69	0.8891	0.8818	0.8771	0.8738	0.87739						

*It should be noted that the values for 100 percent do not agree with some data available elsewhere, e.g., *American Institute of Physics Handbook*, McGraw-Hill, New York, 1957. Also, see *Attack, Handbook of Chemical Data*, Reinhold, New York, 1957. Also, see Tables 2-234 and 2-305 for pure component densities.

TABLE 2-112 Ethyl Alcohol (C₂H₅OH)*

%	10 °C	15 °C	20 °C	25 °C	30 °C	35 °C	40 °C	%	10 °C	15 °C	20 °C	25 °C	30 °C	35 °C	40 °C
0	0.99973	0.99913	0.99823	0.99708	0.99568	0.99406	0.99225	50	0.92126	0.91776	0.91384	0.90985	0.90580	0.90168	0.89750
1	785	725	636	520	379	217	034	51	0.91943	555	160	760	353	0.89940	519
2	602	542	453	336	194	031	0.98846	52	723	333	0.90936	534	125	710	258
3	426	365	275	157	014	0.98849	663	53	502	110	711	307	0.89896	479	056
4	258	195	103	0.98984	0.98839	672	485	54	279	0.90885	485	079	667	248	0.88823
5	098	032	0.98938	817	670	501	311	55	055	659	258	0.89850	437	016	589
6	0.98946	0.98877	780	656	507	335	142	56	0.90831	433	031	621	206	0.88784	356
7	801	729	627	500	347	172	0.97975	57	607	207	0.89803	392	0.88975	552	122
8	660	584	478	346	189	009	808	58	381	0.89980	574	162	744	319	0.87888
9	524	442	331	193	031	0.97846	641	59	154	752	344	0.88931	512	085	653
10	393	304	187	043	0.97875	685	475	60	0.89927	523	113	699	278	0.87851	417
11	267	171	047	0.97897	723	527	312	61	698	293	0.88882	446	044	615	180
12	145	041	0.97910	753	573	371	150	62	468	062	650	233	0.87809	379	0.86943
13	026	0.97914	775	611	424	216	0.96989	63	237	0.88830	417	0.87998	574	142	705
14	0.97911	790	643	472	278	063	829	64	006	597	183	763	337	0.86905	466
15	800	669	514	334	133	0.96911	670	65	0.88774	364	0.87948	527	100	667	227
16	692	552	387	199	0.96990	760	512	66	541	130	713	291	0.86863	429	0.85987
17	583	433	259	062	844	607	352	67	308	0.87895	477	054	625	190	747
18	473	313	129	0.96923	697	452	189	68	074	660	241	0.86817	387	0.85950	407
19	363	191	0.96997	782	547	294	023	69	0.87839	424	004	579	148	710	266
20	252	068	864	639	395	134	0.95856	70	602	187	0.86766	340	0.85908	470	025
21	139	0.96944	729	495	242	0.95973	687	71	365	0.86949	527	100	667	228	0.84783
22	024	818	592	348	087	809	516	72	127	710	287	0.85859	426	0.84986	540
23	0.96907	689	453	199	0.95929	643	343	73	0.86888	470	047	618	184	743	297
24	787	558	312	048	769	476	168	74	648	229	0.85806	376	0.84941	500	053
25	665	424	168	0.95895	607	306	0.94991	75	408	0.85988	564	134	698	257	0.83809
26	539	287	020	738	442	133	810	76	168	747	322	0.84891	455	013	564
27	406	144	0.95867	576	272	0.94955	625	77	0.85927	505	079	647	211	0.83768	319
28	268	0.95996	710	410	098	774	438	78	685	262	0.84835	403	0.83966	523	074
29	125	844	548	241	0.94922	590	248	79	442	018	590	158	720	277	0.82827
30	0.95977	686	382	067	741	403	055	80	197	0.84772	344	0.83911	473	029	578
31	823	524	212	0.94890	557	214	0.93860	81	0.84950	525	096	664	224	0.82780	329
32	665	357	038	709	370	021	662	82	702	277	0.83848	415	0.82974	530	079
33	502	186	0.94860	525	180	0.93825	461	83	453	028	599	164	724	279	0.81828
34	334	011	679	337	0.93986	626	257	84	203	0.83777	348	0.82913	473	027	576
35	162	0.94832	494	146	790	425	051	85	0.83951	525	095	660	220	0.81774	322
36	0.94986	650	306	0.93952	591	221	0.92843	86	697	271	0.82840	405	0.81965	519	067
37	805	464	114	756	390	016	634	87	441	014	583	148	708	262	0.80811
38	620	273	0.93919	556	186	0.92808	422	88	181	0.82754	323	0.81888	448	003	552
39	431	079	720	353	0.92979	597	208	89	0.82919	492	062	626	186	0.80742	291
40	238	0.93882	518	148	770	385	0.91992	90	654	227	0.81797	362	0.80922	478	028
41	042	682	314	0.92940	558	170	774	91	386	0.81959	529	094	655	211	0.79761
42	0.93842	478	107	729	344	0.91952	554	92	114	688	257	0.80823	384	0.79941	491
43	639	271	0.92897	516	128	733	332	93	0.81839	413	0.80983	549	111	669	220
44	433	062	685	301	0.91910	513	108	94	561	134	705	272	0.79835	393	0.78947
45	226	0.92852	472	085	692	291	0.90884	95	278	0.80852	424	0.79991	555	114	670
46	017	640	257	0.91868	472	069	660	96	0.80991	566	138	706	271	0.78831	388
47	0.92806	426	041	649	250	0.90845	434	97	698	274	0.79846	415	0.78981	542	100
48	593	211	0.91823	429	028	621	207	98	399	0.79975	547	117	684	247	0.77806
49	379	0.91995	604	208	0.90805	396	0.89979	99	094	670	243	0.78814	382	0.77946	507
								100	0.79784	360	0.78934	506	075	641	203

*For data from -78° to 78°C , see p. 2-142, Table 2N-5, *American Institute of Physics Handbook*, McGraw-Hill, New York, 1957. See Tables 2-214 and 2-305 for pure component densities.

2-118 PHYSICAL AND CHEMICAL DATA

TABLE 2-113 Densities of Mixtures of C₂H₅OH and H₂O at 20°C
g/mL

% alcohol by weight	Tenths of %									% alcohol by weight	Tenths of %										
	0	1	2	3	4	5	6	7	8		9	0	1	2	3	4	5	6	7	8	9
0	0.99823	804	785	766	748	729	710	692	673	655	50	0.91384	361	339	317	295	272	250	228	206	183
1	636	618	599	581	562	544	525	507	489	471	51	160	138	116	093	071	049	026	004	*981	*959
2	453	435	417	399	381	363	345	327	310	292	52	0.90936	914	891	869	846	824	801	779	756	734
3	275	257	240	222	205	188	171	154	137	120	53	711	689	666	644	621	598	576	553	531	508
4	103	087	070	053	037	020	003	*987	*971	*954	54	485	463	440	417	395	372	349	327	304	281
5	0.98938	922	906	890	874	859	843	827	811	796	55	258	236	213	190	167	145	122	099	076	054
6	780	765	749	734	718	703	688	673	658	642	56	031	008	*985	*962	*939	*917	*894	*871	*848	*825
7	627	612	597	582	567	553	538	523	508	493	57	0.89803	780	757	734	711	688	665	643	620	597
8	478	463	449	434	419	404	389	374	360	345	58	574	551	528	505	482	459	436	413	390	367
9	331	316	301	287	273	258	244	229	215	201	59	344	321	298	275	252	229	206	183	160	137
10	187	172	158	144	130	117	103	089	075	061	60	113	090	067	044	021	*998	*975	*951	*928	*905
11	047	033	019	006	*992	*978	*964	*951	*937	*923	61	0.88882	859	836	812	789	766	743	720	696	673
12	0.97910	896	883	869	855	842	828	815	801	788	62	650	626	603	580	557	533	510	487	463	440
13	775	761	748	735	722	709	696	683	670	657	63	417	393	370	347	323	300	277	253	230	206
14	643	630	617	604	591	578	565	552	539	526	64	183	160	136	113	089	066	042	019	*995	*972
15	514	501	488	475	462	450	438	425	412	400	65	0.87948	925	901	878	854	831	807	784	760	737
16	387	374	361	349	336	323	310	297	284	272	66	713	689	666	642	619	595	572	548	524	501
17	259	246	233	220	207	194	181	168	155	142	67	477	454	430	406	383	359	336	312	288	265
18	129	116	103	089	076	063	050	037	024	010	68	241	218	194	170	147	123	099	075	052	028
19	0.96997	984	971	957	944	931	917	904	891	877	69	004	*981	*957	*933	*909	*885	*862	*838	*814	*790
20	864	850	837	823	810	796	783	769	756	742	70	0.86766	742	718	694	671	647	623	599	575	551
21	729	716	702	688	675	661	647	634	620	606	71	527	503	479	455	431	407	383	359	335	311
22	592	578	564	551	537	523	509	495	481	467	72	287	263	239	215	191	167	143	119	095	071
23	453	439	425	411	396	382	368	354	340	326	73	047	022	*998	*974	*950	*926	*902	*878	*854	*830
24	312	297	283	269	254	240	225	211	196	182	74	0.85806	781	757	733	709	685	661	636	612	588
25	168	153	139	124	109	094	080	065	050	035	75	564	540	515	491	467	443	419	394	370	346
26	020	005	*990	*975	*959	*944	*929	*914	*898	*883	76	322	297	273	249	225	200	176	152	128	103
27	0.95867	851	836	820	805	789	773	757	742	726	77	079	055	031	006	*982	*958	*933	*909	*884	*860
28	710	694	678	662	646	630	613	597	581	565	78	0.84835	811	787	762	738	713	689	664	640	615
29	548	532	516	499	483	466	450	433	416	400	79	590	566	541	517	492	467	443	418	393	369
30	382	365	349	332	315	298	281	264	247	230	80	344	319	294	270	245	220	196	171	146	121
31	212	195	178	161	143	126	108	091	074	056	81	096	072	047	022	*997	*972	*947	*923	*898	*873
32	038	020	003	*985	*967	*950	*932	*914	*896	*878	82	0.83848	823	798	773	748	723	698	674	649	624
33	0.94860	842	824	806	788	770	752	734	715	697	83	599	574	549	523	498	473	448	423	398	373
34	679	660	642	624	605	587	568	550	531	512	84	348	323	297	272	247	222	196	171	146	120
35	494	475	456	438	419	400	382	363	344	325	85	095	070	044	019	*994	*968	*943	*917	*892	*866
36	306	287	268	249	230	211	192	172	153	134	86	0.82840	815	789	763	738	712	686	660	635	609
37	114	095	075	056	036	017	*997	*978	*958	*939	87	583	557	531	505	479	453	427	401	375	349
38	0.93919	899	879	859	840	820	800	780	760	740	88	323	297	271	245	219	193	167	140	114	088
39	720	700	680	660	640	620	599	579	559	539	89	062	035	009	*983	*956	*930	*903	*877	*850	*824
40	518	498	478	458	437	417	396	376	356	335	90	0.81797	770	744	717	690	664	637	610	583	556
41	314	294	273	253	232	212	191	170	149	129	91	529	502	475	448	421	394	366	339	312	285
42	107	086	065	044	023	002	*981	*960	*939	*918	92	257	230	203	175	148	120	093	066	038	010
43	0.92897	876	855	834	812	791	770	749	728	707	93	0.80983	955	928	900	872	844	817	789	761	733
44	685	664	642	621	600	579	557	536	515	493	94	705	677	649	621	593	565	537	509	480	452
45	472	450	429	408	386	365	343	322	300	279	95	424	395	367	338	310	281	253	224	195	166
46	257	236	214	193	171	150	128	106	085	063	96	138	109	080	051	022	*993	*963	*934	*905	*875
47	041	019	*997	*976	*954	*932	*910	*889	*867	*845	97	0.79846	816	787	757	727	698	668	638	608	578
48	0.91823	801	780	758	736	714	692	670	648	626	98	547	517	487	456	426	396	365	335	305	274
49	604	582	560	538	516	494	472	450	428	406	99	243	213	182	151	120	089	059	028	*997	*966
											100	0.78934									

*Indicates change in the first two decimal places.

TABLE 2-114 Specific Gravity {60°/60°F [(15.56°/15.56°C)]} of Mixtures by Volume of C₂H₅OH and H₂O

% alcohol by volume at 60°F	Tenths of %										% alcohol by volume at 60°F	Tenths of %									
	0	1	2	3	4	5	6	7	8	9		0	1	2	3	4	5	6	7	8	9
0	1.00000	*985	*970	*955	*940	*925	*910	*895	*880	865	50	0.93426	407	387	368	348	328	309	289	270	250
1	0.99850	835	820	806	791	776	761	747	732	717	51	230	210	190	171	151	131	111	091	071	051
2	703	688	674	659	645	630	616	602	587	573	52	031	011	*991	*971	*951	*931	*911	*890	*870	*850
3	559	545	531	516	502	488	474	460	446	432	53	0.92830	810	789	769	749	728	708	688	667	647
4	419	405	391	378	364	350	336	323	309	296	54	626	605	585	564	544	523	502	482	461	440
5	282	269	255	242	228	215	202	189	176	163	55	419	398	377	357	336	315	294	273	252	231
6	150	137	124	111	098	085	073	060	047	035	56	210	189	168	147	126	105	084	062	041	020
7	022	009	*997	*984	*972	*960	*947	*935	*923	*911	57	0.91999	978	956	935	914	892	871	849	827	806
8	0.98899	887	875	863	851	838	826	814	803	791	58	784	762	741	719	697	675	653	631	610	588
9	779	767	755	743	731	720	708	696	684	672	59	565	543	521	499	477	455	433	410	388	366
10	661	649	637	625	614	602	590	579	567	556	60	344	322	299	277	255	232	210	188	165	143
11	544	532	521	509	498	487	475	464	452	441	61	120	097	075	052	030	007	*984	*962	*939	*916
12	430	419	408	396	385	374	363	352	341	330	62	0.90893	870	847	825	802	779	756	733	710	687
13	319	308	297	286	275	264	254	243	232	221	63	664	641	618	595	572	549	526	503	480	457
14	210	200	190	179	168	157	147	136	125	115	64	434	411	388	365	341	318	295	272	249	225
15	104	093	083	072	062	051	040	030	019	009	65	202	179	155	132	108	085	061	038	014	*991
16	0.97998	988	977	967	956	946	936	925	915	905	66	0.89967	943	920	896	872	848	825	801	777	753
17	895	885	875	864	854	844	834	824	814	804	67	729	705	681	657	633	609	585	561	537	513
18	794	784	774	764	754	744	734	724	714	704	68	489	465	441	416	392	368	343	319	295	270
19	694	684	674	664	654	645	635	625	615	605	69	245	220	196	171	147	122	098	073	048	024
20	596	586	576	566	556	546	536	526	516	506	70	0.88999	974	950	925	900	875	850	825	801	776
21	496	486	476	466	456	446	436	425	415	405	71	751	725	700	675	650	625	600	574	549	524
22	395	385	375	365	354	344	334	324	313	303	72	499	474	448	423	397	372	346	321	296	270
23	293	283	272	262	252	241	231	221	210	200	73	244	218	193	167	141	116	090	064	039	013
24	189	179	168	158	147	137	126	116	105	095	74	0.87987	961	935	910	884	858	832	806	780	754
25	084	073	063	052	042	031	020	010	*999	*988	75	728	702	676	650	623	597	571	545	518	492
26	0.96978	967	957	946	935	924	914	903	892	881	76	465	439	412	386	359	332	306	279	252	226
27	870	859	848	837	826	815	804	793	782	771	77	199	172	145	118	092	065	038	011	*984	*957
28	760	749	738	727	715	704	693	682	671	659	78	0.86929	902	875	847	820	793	766	738	711	684
29	648	637	625	614	603	591	580	568	557	546	79	656	629	601	574	546	518	491	463	435	408
30	534	522	511	499	488	476	464	453	441	429	80	380	352	324	296	269	241	213	185	157	129
31	418	406	394	382	370	358	346	334	321	309	81	100	072	044	015	*987	*959	*931	*902	*874	*846
32	296	284	271	259	246	234	221	209	196	183	82	0.85817	789	760	732	703	674	646	617	588	560
33	170	157	144	132	119	106	093	080	067	054	83	531	502	473	444	415	386	357	328	299	270
34	041	028	015	002	*988	*975	*962	*948	*935	*921	84	240	211	181	152	122	093	063	033	004	*974
35	0.95908	894	881	867	854	840	826	812	798	784	85	0.84944	914	884	854	824	794	764	734	703	673
36	770	756	742	728	714	700	685	671	657	643	86	642	612	581	551	520	490	459	428	398	367
37	628	614	599	585	570	556	541	526	512	497	87	336	305	274	243	212	181	150	119	088	056
38	482	467	452	437	423	408	393	378	362	347	88	025	*994	*962	*930	*899	*867	*835	*803	*771	*739
39	332	317	302	286	271	256	240	225	209	194	89	0.83707	675	643	610	578	545	513	480	447	415
40	178	162	147	131	115	100	084	068	052	036	90	382	349	315	282	249	216	183	150	116	083
41	020	004	*988	*972	*956	*940	*923	*907	*891	*875	91	049	015	*981	*947	*913	*879	*845	*810	*776	*741
42	0.94858	842	825	809	792	776	759	743	726	710	92	0.82705	670	635	600	565	529	494	458	423	387
43	693	676	660	643	626	609	592	575	558	541	93	351	315	279	243	206	170	133	096	059	022
44	524	507	490	473	455	438	421	403	386	369	94	0.81984	947	909	871	834	796	757	719	681	642
45	351	334	316	298	281	263	245	228	210	192	95	603	564	525	486	446	407	367	327	287	247
46	174	156	138	120	102	084	066	048	030	011	96	206	165	125	084	042	001	*960	*918	*876	*834
47	0.93993	975	956	938	920	901	883	864	845	827	97	0.80792	750	707	664	620	577	533	489	445	401
48	808	789	771	752	733	714	695	676	657	638	98	356	311	265	219	173	127	080	033	*985	*937
49	619	600	581	562	543	523	504	485	465	446	99	0.79889	841	792	743	693	643	593	543	492	441
											100	389									

*Indicates change in first two decimal places.

2-120 PHYSICAL AND CHEMICAL DATA

TABLE 2-115 *n*-Propyl Alcohol (C₃H₇OH)

%	0°C	15°C	30°C	%	0°C	15°C	30°C	%	0°C	15°C	30°C	%	0°C	15°C	30°C	%	0°C	15°C	30°C
0	0.9999	0.9991	0.9957	20	0.9789	0.9723	0.9643	40	0.9430	0.9331	0.9226	60	0.9033	0.8922	0.8807	80	0.8634	0.8516	0.8394
1	0.9982	0.9974	0.9940	21	0.9776	0.9705	0.9622	41	0.9411	0.9310	0.9205	61	0.9013	0.8902	0.8786	81	0.8614	0.8496	0.8373
2	0.9967	0.9960	0.9924	22	0.9763	0.9688	0.9602	42	0.9391	0.9290	0.9184	62	0.8994	0.8882	0.8766	82	0.8594	0.8475	0.8352
3	0.9952	0.9944	0.9908	23	0.9748	0.9670	0.9583	43	0.9371	0.9269	0.9164	63	0.8974	0.8861	0.8745	83	0.8574	0.8454	0.8332
4	0.9939	0.9929	0.9893	24	0.9733	0.9651	0.9563	44	0.9352	0.9248	0.9143	64	0.8954	0.8841	0.8724	84	0.8554	0.8434	0.8311
5	0.9926	0.9915	0.9877	25	0.9717	0.9633	0.9543	45	0.9332	0.9228	0.9122	65	0.8934	0.8820	0.8703	85	0.8534	0.8413	0.8290
6	0.9914	0.9902	0.9862	26	0.9700	0.9614	0.9522	46	0.9311	0.9207	0.9100	66	0.8913	0.8800	0.8682	86	0.8513	0.8393	0.8269
7	0.9904	0.9890	0.9848	27	0.9682	0.9594	0.9501	47	0.9291	0.9186	0.9079	67	0.8894	0.8779	0.8662	87	0.8492	0.8372	0.8248
8	0.9894	0.9877	0.9834	28	0.9664	0.9576	0.9481	48	0.9272	0.9165	0.9057	68	0.8874	0.8759	0.8641	88	0.8471	0.8351	0.8227
9	0.9883	0.9864	0.9819	29	0.9646	0.9556	0.9460	49	0.9252	0.9145	0.9036	69	0.8854	0.8739	0.8620	89	0.8450	0.8330	0.8206
10	0.9874	0.9852	0.9804	30	0.9627	0.9535	0.9439	50	0.9232	0.9124	0.9015	70	0.8835	0.8719	0.8600	90	0.8429	0.8308	0.8185
11	0.9865	0.9840	0.9790	31	0.9608	0.9516	0.9418	51	0.9213	0.9104	0.8994	71	0.8815	0.8700	0.8580	91	0.8408	0.8287	0.8164
12	0.9857	0.9828	0.9775	32	0.9589	0.9495	0.9396	52	0.9192	0.9084	0.8973	72	0.8795	0.8680	0.8559	92	0.8387	0.8266	0.8142
13	0.9849	0.9817	0.9760	33	0.9570	0.9474	0.9375	53	0.9173	0.9064	0.8952	73	0.8776	0.8659	0.8539	93	0.8364	0.8244	0.8120
14	0.9841	0.9806	0.9746	34	0.9550	0.9454	0.9354	54	0.9153	0.9044	0.8931	74	0.8756	0.8639	0.8518	94	0.8342	0.8221	0.8098
15	0.9833	0.9793	0.9730	35	0.9530	0.9434	0.9333	55	0.9132	0.9023	0.8911	75	0.8736	0.8618	0.8497	95	0.8320	0.8199	0.8077
16	0.9825	0.9780	0.9714	36	0.9511	0.9413	0.9312	56	0.9112	0.9003	0.8890	76	0.8716	0.8598	0.8477	96	0.8296	0.8176	0.8054
17	0.9817	0.9768	0.9698	37	0.9491	0.9392	0.9289	57	0.9093	0.8983	0.8869	77	0.8695	0.8577	0.8456	97	0.8272	0.8153	0.8031
18	0.9808	0.9752	0.9680	38	0.9471	0.9372	0.9269	58	0.9073	0.8963	0.8849	78	0.8675	0.8556	0.8435	98	0.8248	0.8128	0.8008
19	0.9800	0.9739	0.9661	39	0.9450	0.9351	0.9247	59	0.9053	0.8942	0.8828	79	0.8655	0.8536	0.8414	99	0.8222	0.8104	0.7984
																100	0.8194	0.8077	0.7958

TABLE 2-116 Isopropyl Alcohol (C₃H₇OH)

%	0°C	15°C	15°C	20°C	30°C	%	0°C	15°C	15°C	20°C	30°C	%	0°C	15°C	15°C	20°C	30°C
0	0.9999	0.9991	0.99913	0.9982	0.9957	35	0.9557	0.9446	0.9419	0.9338	70	0.8761	0.8639	0.86346	0.8584	0.8511	
1	0.9980	0.9973	0.9972	0.9962	0.9939	36	0.9536	0.9424	0.9399	0.9315	71	0.8738	0.8615	0.8611	0.8560	0.8487	
2	0.9962	0.9956	0.9954	0.9944	0.9921	37	0.9514	0.9401	0.9377	0.9292	72	0.8714	0.8592	0.8588	0.8537	0.8464	
3	0.9946	0.9938	0.9936	0.9926	0.9904	38	0.9493	0.9379	0.9355	0.9269	73	0.8691	0.8568	0.8564	0.8513	0.8440	
4	0.9930	0.9922	0.9920	0.9909	0.9887	39	0.9472	0.9356	0.9333	0.9246	74	0.8668	0.8545	0.8541	0.8489	0.8416	
5	0.9916	0.9906	0.9904	0.9893	0.9871	40	0.9450	0.93333	0.9310	0.9224	75	0.8644	0.8521	0.8517	0.8464	0.8392	
6	0.9902	0.9892	0.9890	0.9877	0.9855	41	0.9428	0.9311	0.9287	0.9201	76	0.8621	0.8497	0.8493	0.8439	0.8368	
7	0.9890	0.9878	0.9875	0.9862	0.9839	42	0.9406	0.9288	0.9264	0.9177	77	0.8598	0.8474	0.8470	0.8415	0.8344	
8	0.9878	0.9864	0.9862	0.9847	0.9824	43	0.9384	0.9266	0.9239	0.9154	78	0.8575	0.8450	0.8446	0.8391	0.8321	
9	0.9866	0.9851	0.9849	0.9833	0.9809	44	0.9361	0.9243	0.9215	0.9130	79	0.8551	0.8426	0.8422	0.8366	0.8297	
10	0.9856	0.9838	0.98362	0.9820	0.9794	45	0.9338	0.9220	0.9191	0.9106	80	0.8528	0.8403	0.83979	0.8342	0.8273	
11	0.9846	0.9826	0.9824	0.9808	0.9778	46	0.9315	0.9197	0.9165	0.9082	81	0.8503	0.8379	0.8374	0.8317	0.8248	
12	0.9838	0.9813	0.9812	0.9797	0.9764	47	0.9292	0.9174	0.9141	0.9059	82	0.8479	0.8355	0.8350	0.8292	0.8224	
13	0.9829	0.9802	0.9800	0.9786	0.9750	48	0.9270	0.9150	0.9117	0.9036	83	0.8456	0.8331	0.8326	0.8268	0.8200	
14	0.9821	0.9790	0.9788	0.9776	0.9735	49	0.9247	0.9127	0.9093	0.9013	84	0.8432	0.8307	0.8302	0.8243	0.8175	
15	0.9814	0.9779	0.9777	0.9765	0.9720	50	0.9224	0.91043	0.9069	0.8990	85	0.8408	0.8282	0.8278	0.8219	0.8151	
16	0.9806	0.9768	0.9765	0.9754	0.9705	51	0.9201	0.9081	0.9044	0.8966	86	0.8384	0.8259	0.8254	0.8194	0.8127	
17	0.9799	0.9756	0.9753	0.9743	0.9690	52	0.9178	0.9058	0.9020	0.8943	87	0.8360	0.8234	0.8229	0.8169	0.8201	
18	0.9792	0.9745	0.9741	0.9731	0.9675	53	0.9155	0.9035	0.8996	0.8919	88	0.8336	0.8209	0.8205	0.8145	0.8078	
19	0.9784	0.9730	0.9728	0.9717	0.9658	54	0.9132	0.9011	0.8971	0.8895	89	0.8311	0.8184	0.8180	0.8120	0.8053	
20	0.9777	0.9719	0.97158	0.9703	0.9642	55	0.9109	0.8988	0.8946	0.8871	90	0.8287	0.8161	0.81553	0.8096	0.8029	
21	0.9768	0.9704	0.9703	0.9688	0.9624	56	0.9086	0.8964	0.8921	0.8847	91	0.8262	0.8136	0.8130	0.8072	0.8004	
22	0.9759	0.9690	0.9689	0.9669	0.9606	57	0.9063	0.8940	0.8896	0.8823	92	0.8237	0.8110	0.8104	0.8047	0.7979	
23	0.9749	0.9675	0.9674	0.9651	0.9587	58	0.9040	0.8917	0.8874	0.8800	93	0.8212	0.8085	0.8079	0.8023	0.7954	
24	0.9739	0.9660	0.9659	0.9634	0.9569	59	0.9017	0.8893	0.8850	0.8777	94	0.8186	0.8060	0.8052	0.7998	0.7929	
25	0.9727	0.9643	0.9642	0.9615	0.9549	60	0.8994	0.88690	0.8825	0.8752	95	0.8160	0.8034	0.8026	0.7973	0.7904	
26	0.9714	0.9626	0.9624	0.9597	0.9529	61	0.8970	0.8845	0.8800	0.8728	96	0.8133	0.8008	0.7999	0.7949	0.7878	
27	0.9699	0.9608	0.9605	0.9577	0.9509	62	0.8947	0.8829	0.8782	0.8707	97	0.8106	0.7981	0.7972	0.7925	0.7852	
28	0.9684	0.9590	0.9586	0.9558	0.9488	63	0.8924	0.8805	0.8758	0.8680	98	0.8078	0.7954	0.7945	0.7901	0.7826	
29	0.9669	0.9570	0.9568	0.9540	0.9467	64	0.8901	0.8781	0.8735	0.8656	99	0.8048	0.7926	0.7918	0.7877	0.7799	
30	0.9652	0.9551	0.95493	0.9520	0.9446	65	0.8878	0.8757	0.8712	0.8631	100	0.8016	0.7896	0.78913	0.7854	0.7770	
31	0.9634	0.9530	0.9500	0.9426	0.9351	66	0.8854	0.8733	0.8688	0.8607							
32	0.9615	0.9510	0.9481	0.9405	0.9330	67	0.8831	0.8710	0.8665	0.8583							
33	0.9596	0.9489	0.9460	0.9383	0.9308	68	0.8807	0.8686	0.8641	0.8559							
34	0.9577	0.9468	0.9440	0.9361	0.9286	69	0.8784	0.8662	0.8617	0.8535							

*Two different observers; see *International Critical Tables*, vol. 3, p. 120.

TABLE 2-117 Glycerol*

Glycerol, %	Density					Glycerol, %	Density					Glycerol, %	Density				
	15°C	15.5°C	20°C	25°C	30°C		15°C	15.5°C	20°C	25°C	30°C		15°C	15.5°C	20°C	25°C	30°C
100	1.26415	1.26381	1.26108	1.15802	1.25495	65	1.17030	1.17000	1.16750	1.16475	1.16195	30	1.07455	1.07435	1.07270	1.07070	1.06855
99	1.26160	1.26125	1.25850	1.25545	1.25235	64	1.16755	1.16725	1.16475	1.16200	1.15925	29	1.07195	1.07175	1.07010	1.06815	1.06605
98	1.25900	1.25865	1.25590	1.25290	1.24975	63	1.16480	1.16445	1.16205	1.15925	1.15650	28	1.06935	1.06915	1.06755	1.06560	1.06355
97	1.25645	1.25610	1.25335	1.25030	1.24710	62	1.16200	1.16170	1.15930	1.15655	1.15375	27	1.06670	1.06655	1.06495	1.06305	1.06105
96	1.25385	1.25350	1.25080	1.24770	1.24450	61	1.15925	1.15895	1.15655	1.15380	1.15100	26	1.06410	1.06390	1.06240	1.06055	1.05855
95	1.25130	1.25095	1.24825	1.24515	1.24190	60	1.15650	1.15615	1.15380	1.15105	1.14830	25	1.06150	1.06130	1.05980	1.05800	1.05605
94	1.24865	1.24830	1.24560	1.24250	1.23930	59	1.15370	1.15340	1.15105	1.14835	1.14555	24	1.05885	1.05870	1.05720	1.05545	1.05350
93	1.24600	1.24565	1.24300	1.23985	1.23670	58	1.15095	1.15065	1.14830	1.14560	1.14285	23	1.05625	1.05610	1.05465	1.05290	1.05100
92	1.24340	1.24305	1.24035	1.23725	1.23410	57	1.14815	1.14785	1.14555	1.14285	1.14010	22	1.05365	1.05350	1.05205	1.05035	1.04850
91	1.24075	1.24040	1.23770	1.23460	1.23150	56	1.14535	1.14510	1.14280	1.14015	1.13740	21	1.05100	1.05090	1.04950	1.04780	1.04600
90	1.23810	1.23775	1.23510	1.23200	1.22890	55	1.14260	1.14230	1.14005	1.13740	1.13470	20	1.04840	1.04825	1.04690	1.04525	1.04350
89	1.23545	1.23510	1.23245	1.22935	1.22625	54	1.13980	1.13955	1.13730	1.13465	1.13195	19	1.04590	1.04575	1.04440	1.04280	1.04105
88	1.23280	1.23245	1.22975	1.22665	1.22360	53	1.13705	1.13680	1.13455	1.13195	1.12925	18	1.04335	1.04325	1.04195	1.04035	1.03860
87	1.23015	1.22980	1.22710	1.22400	1.22095	52	1.13425	1.13400	1.13180	1.12920	1.12650	17	1.04085	1.04075	1.03945	1.03790	1.03615
86	1.22750	1.22710	1.22445	1.22135	1.21830	51	1.13150	1.13125	1.12905	1.12650	1.12380	16	1.03835	1.03825	1.03695	1.03545	1.03370
85	1.22485	1.22445	1.22180	1.21870	1.21565	50	1.12870	1.12845	1.12630	1.12375	1.12110	15	1.03580	1.03570	1.03450	1.03300	1.03130
84	1.22220	1.22180	1.21915	1.21605	1.21300	49	1.12600	1.12575	1.12360	1.12110	1.11845	14	1.03330	1.03320	1.03200	1.03055	1.02885
83	1.21955	1.21915	1.21650	1.21340	1.21035	48	1.12325	1.12305	1.12090	1.11840	1.11580	13	1.03080	1.03070	1.02955	1.02805	1.02640
82	1.21690	1.21650	1.21380	1.21075	1.20770	47	1.12055	1.12030	1.11820	1.11575	1.11320	12	1.02830	1.02820	1.02705	1.02560	1.02395
81	1.21425	1.21385	1.21115	1.20810	1.20505	46	1.11780	1.11760	1.11550	1.11310	1.11055	11	1.02575	1.02565	1.02455	1.02315	1.02150
80	1.21160	1.21120	1.20850	1.20545	1.20240	45	1.11510	1.11490	1.11280	1.11040	1.10795	10	1.02325	1.02315	1.02210	1.02070	1.01905
79	1.20885	1.20845	1.20575	1.20275	1.19970	44	1.11235	1.11215	1.11010	1.10775	1.10530	9	1.02085	1.02075	1.01970	1.01835	1.01670
78	1.20610	1.20570	1.20305	1.20005	1.19705	43	1.10960	1.10945	1.10740	1.10510	1.10265	8	1.01840	1.01835	1.01730	1.01600	1.01440
77	1.20335	1.20300	1.20030	1.19735	1.19435	42	1.10690	1.10670	1.10470	1.10240	1.10005	7	1.01600	1.01590	1.01495	1.01360	1.01205
76	1.20060	1.20025	1.19760	1.19465	1.19170	41	1.10415	1.10400	1.10200	1.09975	1.09740	6	1.01360	1.01350	1.01255	1.01125	1.00970
75	1.19785	1.19750	1.19485	1.19195	1.18900	40	1.10145	1.10130	1.09930	1.09710	1.09475	5	1.01120	1.01110	1.01015	1.00890	1.00735
74	1.19510	1.19480	1.19215	1.18925	1.18635	39	1.09875	1.09860	1.09665	1.09445	1.09215	4	1.00875	1.00870	1.00780	1.00655	1.00505
73	1.19235	1.19205	1.18940	1.18650	1.18365	38	1.09605	1.09590	1.09400	1.09180	1.08955	3	1.00635	1.00630	1.00540	1.00415	1.00270
72	1.18965	1.18930	1.18670	1.18380	1.18100	37	1.09340	1.09320	1.09135	1.08915	1.08690	2	1.00395	1.00385	1.00300	1.00180	1.00035
71	1.18690	1.18655	1.18395	1.18110	1.17830	36	1.09070	1.09050	1.08865	1.08655	1.08430	1	1.00155	1.00145	1.00060	0.99945	0.99800
70	1.18415	1.18385	1.18125	1.17840	1.17565	35	1.08800	1.08780	1.08600	1.08390	1.08165	0	0.99913	0.99905	0.99823	0.99708	0.99568
69	1.18135	1.18105	1.17850	1.17565	1.17290	34	1.08530	1.08515	1.08335	1.08125	1.07905						
68	1.17860	1.17830	1.17575	1.17295	1.17020	33	1.08265	1.08245	1.08070	1.07860	1.07645						
67	1.17585	1.17555	1.17300	1.17020	1.16745	32	1.07995	1.07975	1.07800	1.07600	1.07380						
66	1.17305	1.17275	1.17025	1.16745	1.16470	31	1.07725	1.07705	1.07535	1.07335	1.07120						

*Bosart and Snoddy, *Ind. Eng. Chem.*, **20**, (1928): 1378.

TABLE 2-118 Hydrazine (N₂H₄)*

%	d_4^{15}	%	d_4^{15}
1	1.0002	30	1.0305
2	1.0013	40	1.038
4	1.0034	50	1.044
8	1.0077	60	1.047
12	1.0121	70	1.046
16	1.0164	80	1.040
20	1.0207	90	1.030
24	1.0248	100	1.011
28	1.0286		

*International Critical Tables, vol. 3, p. 55.

2-122 PHYSICAL AND CHEMICAL DATA

TABLE 2-119 Densities of Aqueous Solutions of Miscellaneous Organic Compounds*

d , d_w , and d_s are the density of the solution, pure water, and pure liquid solute, respectively, all in g/mL. p_s is the wt % solute. 0.0₂255 means 2.55×10^{-4} .

Section A $d = d_w + Ap_s + Bp_s^2 + Cp_s^3$						
Name	Formula	t , °C	Range, p_s	A	B	C
Acetaldehyde	C ₂ H ₄ O	18	0– 30	+0.0 ₂ 255	-0.0 ₂ 16	
Acetamide	C ₂ H ₅ NO	15	0– 6	+0.0 ₂ 639	+0.0 ₂ 171	
Acetone	C ₃ H ₆ O	0	0–100	-0.0 ₂ 856	-0.0 ₂ 449	-0.0 ₂ 588
		4	0–100	-0.0 ₂ 7648	-0.0 ₂ 1193	+0.0 ₂ 272
		15	0–100	-0.0 ₂ 1009	-0.0 ₂ 9682	-0.0 ₂ 624
		20	0–100	-0.0 ₂ 1233	-0.0 ₂ 3529	-0.0 ₂ 5327
Acetonitrile	C ₂ H ₃ N	25	0–100	-0.0 ₂ 1171	-0.0 ₂ 904	-0.0 ₂ 56
		15	0– 16	-0.0 ₂ 1175	-0.0 ₂ 2024	
		0	0– 89	-0.0 ₂ 3729	-0.0 ₂ 1232	+0.0 ₂ 2984
		25	0– 0.6	+0.0 ₂ 5615	-0.0 ₂ 117	
Benzenepentacarboxylic acid	C ₁₁ H ₆ O ₁₀	25	0– 7.9	-0.0 ₂ 1651	+0.0 ₂ 285	
Butyl alcohol (<i>n</i> -)	C ₄ H ₁₀ O	20	0– 10	+0.0 ₂ 414	+0.0 ₂ 131	
Butyric acid (<i>n</i> -)	C ₄ H ₈ O ₂	18	0– 62	+0.0 ₂ 5135	-0.0 ₂ 166	+0.0 ₂ 11
		25	0– 70	+0.0 ₂ 4489	+0.0 ₂ 2802	-0.0 ₂ 1291
		0	0– 78	+0.0 ₂ 4455	+0.0 ₂ 2198	+0.0 ₂ 4366
Chloral hydrate	C ₂ H ₃ Cl ₃ O ₂	15	0– 90	+0.0 ₂ 4401	+0.0 ₂ 1887	+0.0 ₂ 6549
		30	0– 32	+0.0 ₂ 3648	+0.0 ₂ 302	
		20	0– 86	+0.0 ₂ 3602	+0.0 ₂ 552	+0.0 ₂ 22
Chloroacetic acid	C ₂ H ₃ ClO ₂	25	0– 50	+0.0 ₂ 3824	+0.0 ₂ 1141	+0.0 ₂ 17
Citric acid (hydrate)	C ₆ H ₈ O ₇ + H ₂ O	18	0– 30	+0.0 ₂ 4427	+0.0 ₂ 537	+0.0 ₂ 7534
Dichloroacetic acid	C ₂ H ₂ Cl ₂ O ₂	20	0– 97	+0.0 ₂ 4427	+0.0 ₂ 537	+0.0 ₂ 7534
Diethylamine hydrochloride	C ₈ H ₁₈ ClN	21	0– 36	+0.0 ₂ 34	+0.0 ₂ 76	
Ethylamine hydrochloride	C ₂ H ₅ ClN	21	0– 65	-0.0 ₂ 1193	-0.0 ₂ 307	-0.0 ₂ 47
Ethylene glycol	C ₂ H ₆ O ₂	0	0–100	+0.0 ₂ 1483	+0.0 ₂ 2992	-0.0 ₂ 5248
		15	0– 6	+0.0 ₂ 133	-0.0 ₂ 108	
		20	0– 5	-0.0 ₂ 221	+0.0 ₂ 48	
Ethyl ether	C ₄ H ₁₀ O	25	0– 4.5	-0.0 ₂ 221	+0.0 ₂ 35	
		15	0– 95	+0.0 ₂ 2367	+0.0 ₂ 358	-0.0 ₂ 6005
Formaldehyde	CH ₂ O	15	0– 40	+0.0 ₂ 2518	-0.0 ₂ 658	+0.0 ₂ 542
Formamide	CH ₃ NO	25	22– 96	+0.0 ₂ 1217	+0.0 ₂ 3199	-0.0 ₂ 2529
Furfural	C ₅ H ₄ O ₂	20	0– 8	+0.0 ₂ 1827	+0.0 ₂ 366	
		25	0– 8	+0.0 ₂ 1664	+0.0 ₂ 21	
Isoamyl alcohol	C ₇ H ₁₄ O	20	0– 2.5	+0.0 ₂ 155	+0.0 ₂ 3	
Isobutyl alcohol	C ₄ H ₁₀ O	15	0– 8	-0.0 ₂ 146	+0.0 ₂ 6	
		20	0– 8	-0.0 ₂ 169	+0.0 ₂ 38	
Isobutyric acid	C ₄ H ₈ O ₂	15	0– 9	+0.0 ₂ 52		
		18	0– 9	+0.0 ₂ 45		
		25	0– 12	+0.0 ₂ 37		
Isovaleric acid	C ₅ H ₁₀ O ₂	25	0– 5	+0.0 ₂ 253	-0.0 ₂ 282	
Lactic acid	C ₃ H ₆ O	25	0– 9	+0.0 ₂ 231	+0.0 ₂ 186	
Maleic acid	C ₄ H ₄ O ₄	25	0– 40	+0.0 ₂ 34	+0.0 ₂ 75	
Malic acid	C ₄ H ₆ O ₅	20	0– 40	+0.0 ₂ 3933	+0.0 ₂ 957	
		25	0– 40	+0.0 ₂ 3736	+0.0 ₂ 175	
Malonic acid	C ₃ H ₄ O ₄	20	0– 40	+0.0 ₂ 389	+0.0 ₂ 1066	
Methyl acetate	C ₃ H ₆ O ₂	20	0– 20	+0.0 ₂ 40	-0.0 ₂ 74	
		0	26– 51	+0.0 ₂ 3336	+0.0 ₂ 996	+0.01544
		30	26– 51	+0.0 ₂ 3151	+0.0 ₂ 975	+0.0 ₂ 978
Nicotine	C ₁₀ H ₁₄ N ₂	20	0– 60	+0.0 ₂ 642	+0.0 ₂ 454	-0.0 ₂ 687
Nitrophenol (<i>p</i> -)	C ₆ H ₅ NO ₃	15	0– 1.5	+0.0 ₂ 3216	-0.0 ₂ 55	
		0	0– 4	+0.0 ₂ 5898	-0.0 ₂ 3185	+0.0 ₂ 41
		15	0– 4	+0.0 ₂ 494	-0.0 ₂ 5	
Oxalic acid	C ₂ H ₂ O ₄	17.5	0– 9	+0.0 ₂ 494	-0.0 ₂ 5	
		20	0– 4	+0.0 ₂ 5264	-0.0 ₂ 1996	+0.0 ₂ 254
		25	0– 4	+0.0 ₂ 5108	-0.0 ₂ 1607	+0.0 ₂ 208
		15	0– 5	+0.0 ₂ 111	-0.0 ₂ 283	
Phenol	C ₆ H ₆ O	80	0– 65	+0.0 ₂ 462	-0.0 ₂ 86	
Phenylglycolic acid	C ₈ H ₈ O ₃	25	0– 11	+0.0 ₂ 207	+0.0 ₂ 23	
Picoline (α -)	C ₆ H ₇ N	25	0– 70	-0.0 ₂ 386	-0.0 ₂ 1405	-0.0 ₂ 4167
		(β -)	25	0– 60	-0.0 ₂ 683	-0.0 ₂ 13
Propionic acid	C ₃ H ₆ O ₂	18	0– 10	+0.0 ₂ 95	-0.0 ₂ 172	
		25	0– 40	+0.0 ₂ 9245	-0.0 ₂ 99	+0.0 ₂ 361
Pyridine	C ₅ H ₅ N	25	0– 60	+0.0 ₂ 229	-0.0 ₂ 204	-0.0 ₂ 28
Resorcinol	C ₆ H ₆ O ₂	18	0– 52	+0.0 ₂ 201	+0.0 ₂ 519	-0.0 ₂ 19
Succinic acid	C ₄ H ₆ O ₄	25	0– 5.5	+0.0 ₂ 304		
		15	0– 15	+0.0 ₂ 4482	+0.0 ₂ 185	
		17.5	0– 50	+0.0 ₂ 4455	+0.0 ₂ 185	
		20	0– 50	+0.0 ₂ 4432	+0.0 ₂ 1837	
		30	0– 50	+0.0 ₂ 4335	+0.0 ₂ 185	
		40	0– 50	+0.0 ₂ 4265	+0.0 ₂ 185	
Tartaric acid (<i>d</i> , <i>l</i> , or <i>dl</i>)	C ₄ H ₆ O ₆	50	0– 50	+0.0 ₂ 4205	+0.0 ₂ 185	
		60	0– 50	+0.0 ₂ 4155	+0.0 ₂ 185	

*From *International Critical Tables*, vol. 3, pp. 111–114.

TABLE 2-119 Densities of Aqueous Solutions of Miscellaneous Organic Compounds (Concluded)

Section A $d = d_w + Ap_s + Bp_s^2 + Cp_s^3$ (Cont.)							
Name	Formula	$t, ^\circ\text{C}$	Range, p_s	A	B	C	
Tetraethyl ammonium chloride	$\text{C}_8\text{H}_{20}\text{ClN}$	21	0-63	+0.0 ₃ 1884	+0.0 ₅ 6	+0.0 ₇ 122	
Thiourea	$\text{CH}_4\text{N}_2\text{S}$	15	0-7	+0.0 ₂ 2995	+0.0 ₃ 374		
Trichloroacetic acid	$\text{C}_2\text{HCl}_3\text{O}_2$	12.5	0-61	+0.0 ₄ 499	+0.0 ₁ 153		
		20	10-30	+0.0 ₂ 5053	+0.0 ₄ 1387		
		25	0-94	+0.0 ₂ 5051	+0.0 ₃ 6119	+0.0 ₆ 1038	
Triethylamine hydrochloride	$\text{C}_6\text{H}_{16}\text{ClN}$	21	0-54	+0.0 ₄ 6	+0.0 ₅ 558	-0.0 ₆ 69	
Trimethyl carbinol	$\text{C}_4\text{H}_{10}\text{O}$	20	0-100	-0.0 ₁ 117	-0.0 ₁ 1908	+0.0 ₉ 957	
		25	0-100	-0.0 ₂ 1286	-0.0 ₄ 176	+0.0 ₇ 887	
Urea	$\text{CH}_4\text{N}_2\text{O}$	14.8	0-12	+0.0 ₂ 3213	-0.0 ₄ 4802	+0.0 ₅ 1216	
		18	0-51	+0.0 ₂ 2718	+0.0 ₃ 1552	+0.0 ₂ 2573	
		20	0-35	+0.0 ₂ 2702	+0.0 ₃ 3712	-0.0 ₂ 2885	
		25	0-10	+0.0 ₂ 2728	-0.0 ₁ 1817	+0.0 ₅ 1379	
Urethane	$\text{C}_3\text{H}_7\text{NO}_2$	20	0-56	+0.0 ₂ 1278	-0.0 ₂ 245	-0.0 ₇ 3437	
Valeric acid (<i>n</i> -)	$\text{C}_5\text{H}_{10}\text{O}_2$	25	0-3	+0.0 ₃ 34	-0.0 ₄ 27		
Section B $d = d_s + Ap_w + Bp_w^2 + Cp_w^3$							
Name	Formula	d_s	$t, ^\circ\text{C}$	Range, p_w	A	B	C
Butyl alcohol (<i>n</i> -)	$\text{C}_4\text{H}_{10}\text{O}$	0.8097	20	0-20	+0.0 ₂ 2103	-0.0 ₄ 113	
Butyric acid (<i>n</i> -)	$\text{C}_4\text{H}_8\text{O}_2$	0.9534	25	0-38	+0.0 ₂ 1854	-0.0 ₂ 2314	
Ethyl ether	$\text{C}_4\text{H}_{10}\text{O}$	0.7077	25	0- 1.1	+0.0 ₂ 34	+0.0 ₃ 36	
Isobutyl alcohol	$\text{C}_4\text{H}_{10}\text{O}$	0.8170	0	0-14	+0.0 ₂ 2437	-0.0 ₂ 285	
		0.8055	15	0-16	+0.0 ₂ 224	-0.0 ₁ 129	
Isobutyric acid	$\text{C}_4\text{H}_8\text{O}_2$	0.9425	26	0-80	+0.0 ₂ 1808	-0.0 ₂ 2358	+0.0 ₆ 1253
Nicotine	$\text{C}_{10}\text{H}_{14}\text{N}_2$	1.0093	20	0-40	+0.0 ₂ 199	-0.0 ₄ 331	+0.0 ₇ 315
Picoline (α -)	$\text{C}_6\text{H}_7\text{N}$	0.9404	25	0-30	+0.0 ₂ 2715	-0.0 ₄ 393	
		0.9515	25	0-40	+0.0 ₂ 1925	-0.0 ₄ 352	+0.0 ₆ 25
Pyridine	$\text{C}_5\text{H}_5\text{N}$	0.9776	25	0-40	+0.0 ₂ 1157	-0.0 ₅ 536	-0.0 ₆ 2
Trimethyl carbinol	$\text{C}_4\text{H}_{10}\text{O}$	0.7856	20	0-20	+0.0 ₂ 2287	+0.0 ₂ 275	
Section C $d_t = d_o + At + Bt^2$							
Name	Formula	p_s	d_o	Range, $^\circ\text{C}$	A	B	
Allyl alcohol	$\text{C}_3\text{H}_6\text{O}$	76.60	0.9122	0-45	-0.0 ₃ 8	-0.0 ₂ 27	
Butyl alcohol (<i>n</i> -)	$\text{C}_4\text{H}_{10}\text{O}$	80.95	0.8614	0-43	-0.0 ₇ 292	-0.0 ₆ 75	
Chloral hydrate	$\text{C}_2\text{H}_3\text{Cl}_3\text{O}_2$	2.00	1.0094	7-80	-0.0 ₂ 2597	-0.0 ₄ 313	
		10.00	1.0476	7-80	-0.0 ₇ 955	-0.0 ₅ 4253	
Ethyl tartrate	$\text{C}_7\text{H}_{14}\text{O}_6$	5.00	1.0150	15-80	-0.0 ₂ 2103	-0.0 ₂ 2544	
		10.00	1.0270	15-80	-0.0 ₂ 2116	-0.0 ₂ 2929	
		25.00	1.0665	15-80	-0.0 ₄ 401	-0.0 ₂ 23	
Furfural	$\text{C}_5\text{H}_4\text{O}_2$	4.62	1.0125	22-74	-0.0 ₂ 232	-0.0 ₂ 254	
		5.69	1.0140	22-74	-0.0 ₂ 221	-0.0 ₂ 268	
		6.56	1.0155	22-74	-0.0 ₂ 211	-0.0 ₂ 290	
		9.34	1.0055	11-73	-0.0 ₄ 171	-0.0 ₃ 3615	
Pyridine	$\text{C}_5\text{H}_5\text{N}$	21.20	1.0115	14-73	-0.0 ₃ 378	-0.0 ₂ 248	
		29.50	1.0145	12-72	-0.0 ₄ 463	-0.0 ₂ 235	
		40.40	1.0182	9-74	-0.0 ₂ 605	-0.0 ₃ 167	

DENSITIES OF MISCELLANEOUS MATERIALS

TABLE 2-120 Approximate Specific Gravities and Densities of Miscellaneous Solids and Liquids*

Water at 4°C and normal atmospheric pressure taken as unity. For more detailed data on any material, see the section dealing with the properties of that material.

Substance	Sp. gr.	Aver. density lb/ft ³	Substance	Sp. gr.	Aver. density lb/ft ³	Substance	Sp. gr.	Aver. density lb/ft ³
Metals, Alloys, Ores			Timber, Air-dry			Dry Rubble Masonry		
Aluminum, cast-hammered	2.55-2.80	165	Apple	0.66-0.74	44	Granite, syenite, gneiss	1.9-2.3	130
bronze	7.7	481	Ash, black	0.55	34	Limestone, marble	1.9-2.1	125
Brass, cast-rolled	8.4-8.7	534	white	0.64-0.71	42	Sandstone, bluestone	1.8-1.9	110
Bronze, 7.9 to 14% Sn	7.4-8.9	509	Birch, sweet, yellow	0.71-0.72	44			
phosphor	8.88	554	Cedar, white, red	0.35	22	Brick Masonry		
Copper, cast-rolled	8.8-8.95	556	Cherry, wild red	0.43	27	Hard brick	1.8-2.3	128
ore, pyrites	4.1-4.3	262	Chestnut	0.48	30	Medium brick	1.6-2.0	112
German silver	8.58	536	Cypress	0.45-0.48	29	Soft brick	1.4-1.9	103
Gold, cast-hammered	19.25-19.35	1205	Elm, white	0.56	35	Sand-lime brick	1.4-2.2	112
coin (U.S.)	17.18-17.2	1073	Fir, Douglas	0.48-0.55	32			
Iridium	21.78-22.42	1383	balsam	0.40	25	Concrete Masonry		
Iron, gray cast	7.03-7.13	442	Hemlock	0.45-0.50	29	Cement, stone, sand	2.2-2.4	144
cast, pig	7.2	450	Hickory	0.74-0.80	48	slag, etc.	1.9-2.3	130
wrought	7.6-7.9	485	Locust	0.67-0.77	45	cinder, etc.	1.5-1.7	100
spiegeleisen	7.5	468	Mahogany	0.56-0.85	44	Various Building Materials		
ferro-silicon	6.7-7.3	437	Maple, sugar	0.68	43	Ashes, cinders	0.64-0.72	40-45
ore, hematite	5.2	325	white	0.53	33	Cement, Portland, loose	1.5	94
ore, limonite	3.6-4.0	237	Oak, chestnut	0.74	46	Lime, gypsum, loose	0.85-1.00	53-64
ore, magnetite	4.9-5.2	315	live	0.87	54	Mortar, lime, set	1.4-1.9	103
slag	2.5-3.0	172	red, black	0.64-0.71	42	Portland cement	2.08-2.25	94-135
Lead	11.34	710	white	0.77	48	Portland cement	3.1-3.2	196
ore, galena	7.3-7.6	465	Pine, Norway	0.55	34	Slags, bank slag	1.1-1.2	67-72
Manganese	7.42	475	Oregon	0.51	32	bank screenings	1.5-1.9	98-117
ore, pyrolusite	3.7-4.6	259	red	0.48	30	machine slag	1.5	96
Mercury	13.6	849	Southern	0.61-0.67	38-42	slag sand	0.8-0.9	49-55
			white	0.43	27	Earth, etc., Excavated		
Monel metal, rolled	8.97	555	Poplar	0.43	27	Clay, dry	1.0	63
Nickel	8.9	537	Redwood, California	0.42	26	damp plastic	1.76	110
Platinum, cast-hammered	21.5	1330	Spruce, white, red	0.45	28	and gravel, dry	1.6	100
Silver, cast-hammered	10.4-10.6	656	Teak, African	0.99	62	Earth, dry, loose	1.2	76
Steel, cold-drawn	7.83	489	Indian	0.66-0.88	48	dry, packed	1.5	95
machine	7.80	487	Walnut, black	0.59	37	moist, loose	1.3	78
tool	7.70-7.73	481	Willow	0.42-0.50	28	moist, packed	1.6	96
Tin, cast-hammered	7.2-7.5	459	Various Liquids			mud, flowing	1.7	108
cassiterite	6.4-7.0	418	Alcohol, ethyl (100%)	0.789	49	mud, packed	1.8	115
Tungsten	19.22	1200	methyl (100%)	0.796	50	Riprap, limestone	1.3-1.4	80-85
			Acid, muriatic, 40%	1.20	75	Riprap, sandstone	1.4	90
Zinc, cast-rolled	6.9-7.2	440	nitric, 91%	1.50	94	Riprap, shale	1.7	105
blende	3.9-4.2	253	sulfuric, 87%	1.80	112	Sand, gravel, dry, loose	1.4-1.7	90-105
Various Solids			Chloroform	1.500	95	gravel, dry, packed	1.6-1.9	100-120
Cereals, oats, bulk	0.51	26	Ether	0.736	46	gravel, wet	1.89-2.16	126
barley, bulk	0.62	39	Lye, soda, 66%	1.70	106	Excavations in Water		
corn, rye, bulk	0.73	45	Oils, vegetable	0.91-0.94	58	Clay	1.28	80
wheat, bulk	0.77	48	mineral, lubricants	0.88-0.94	57	River mud	1.44	90
Cork	0.22-0.26	15	Turpentine	0.861-0.867	54	Sand or gravel	0.96	60
Cotton, flax, hemp	1.47-1.50	93	Water, 4°C max. density	1.0	62.428	and clay	1.00	65
Fats	0.90-0.97	58	100°C	0.9584	59.830	Soil	1.12	70
Flour, loose	0.40-0.50	28	ice	0.88-0.92	56	Stone riprap	1.00	65
pressed	0.70-0.80	47	snow, fresh fallen	0.125	8	Minerals		
Glass, common	2.40-2.80	162	sea water	1.02-1.03	64	Asbestos	2.1-2.8	153
plate or crown	2.45-2.72	161	Ashlar Masonry			Barytes	4.50	281
crystal	2.90-3.00	184	Bluestone	2.3-2.6	153	Basalt	2.7-3.2	184
dint	3.2-4.7	247	Granite, syenite, gneiss	2.4-2.7	159	Bauxite	2.55	159
Hay and straw, bales	0.32	20	Limestone	2.1-2.8	153	Bluestone	2.5-2.6	159
Leather	0.86-1.02	59	Marble	2.4-2.8	162	Borax	1.7-1.8	109
Paper	0.70-1.15	58	Sandstone	2.0-2.6	143	Chalk	1.8-2.8	143
Potatoes, piled	0.67	44	Rubble Masonry			Clay, marl	1.8-2.6	137
Rubber, caoutchouc	0.92-0.96	59	Bluestone	2.2-2.5	147	Dolomite	2.9	181
goods	1.0-2.0	94	Granite, syenite, gneiss	2.3-2.6	153	Feldspar, orthoclase	2.5-2.7	162
Salt, granulated, piled	0.77	48	Limestone	2.0-2.7	147	Gneiss	2.7-2.9	175
			Marble	2.3-2.7	156	Granite	2.6-2.7	165
Saltpeter	1.07	67	Sandstone	1.9-2.5	137	Greenstone, trap	2.8-3.2	187
Starch	1.53	96				Gypsum, alabaster	2.3-2.8	159
Sulfur	1.93-2.07	125				Hornblende	3.0	187
Wool	1.32	82				Limestone	2.1-2.86	155
						Marble	2.6-2.86	170
						Magnesite	3.0	187
						Phosphate rock, apatite	3.2	200
						Porphyry	2.6-2.9	172

*From Marks' Standard Handbook for Mechanical Engineers, 10th ed., McGraw-Hill, 1996.

TABLE 2-120 Approximate Specific Gravities and Densities of Miscellaneous Solids and Liquids (Concluded)

Water at 4°C and normal atmospheric pressure taken as unity. For more detailed data on any material, see the section dealing with the properties of that material.

Substance	Sp. gr.	Aver. density lb/ft ³	Substance	Sp. gr.	Aver. density lb/ft ³	Substance	Sp. gr.	Aver. density lb/ft ³
Minerals (Cont.)			Bituminous Substances			Bituminous Substances (Cont.)		
Pumice, natural	0.37-0.90	40	Asphaltum	1.1-1.5	81	Petroleum	0.87	54
Quartz, flint	2.5-2.8	165	Coal, anthracite	1.4-1.8	97	refined (kerosene)	0.78-0.82	50
Sandstone	2.0-2.6	143	bituminous	1.2-1.5	84	benzine	0.73-0.75	46
Serpentine	2.7-2.8	171	lignite	1.1-1.4	78	gasoline	0.70-0.75	45
Shale, slate	2.6-2.9	172	peat, turf, dry	0.65-0.85	47	Pitch	1.07-1.15	69
						Tar, bituminous	1.20	75
Soapstone, talc	2.6-2.8	169	charcoal, pine	0.28-0.44	23	Coal and Coke, Piled		
Syenite	2.6-2.7	165	charcoal, oak	0.47-0.57	33	Coal, anthracite	0.75-0.93	47-58
			coke	1.0-1.4	75	bituminous, lignite	0.64-0.87	40-54
Stone, Quarried, Piled			Graphite	1.64-2.7	135	peat, turf	0.32-0.42	20-26
Basalt, granite, gneiss	1.5	96	Paraffin	0.87-0.91	56	charcoal	0.16-0.23	10-14
Greenstone, hornblende	1.7	107				coke	0.37-0.51	23-32
Limestone, marble, quartz	1.5	95						
Sandstone	1.3	82						
Shale	1.5	92						

NOTE: To convert pounds per cubic foot to kilograms per cubic meter, multiply by 16.02. °F = % °C + 32.

TABLE 2-121 Density (kg/m³) of Selected Elements as a Function of Temperature

Temperature, K°	Element symbol												
	Al	Be†	Cr	Cu	Au	Ir	Fe	Pb	Mo	Ni	Pt	Ag	Zn†
50	2736	3650	7160	9019	19,490	22,600	7910	11,570	10,260	8960	21,570	10,620	7280
100	2732	3640	7155	9009	19,460	22,580	7900	11,520	10,260	8950	21,550	10,600	7260
150	2726	3630	7150	8992	19,420	22,560	7890	11,470	10,250	8940	21,530	10,575	7230
200	2719	3620	7145	8973	19,380	22,540	7880	11,430	10,250	8930	21,500	10,550	7200
250	2710	3610	7140	8951	19,340	22,520	7870	11,380	10,250	8910	21,470	10,520	7170
300	2701	3600	7135	8930	19,300	22,500	7860	11,330	10,240	8900	21,450	10,490	7135
400	2681	3580	7120	8885	19,210	22,450	7830	11,230	10,220	8860	21,380	10,430	7070
500	2661	3555	7110	8837	19,130	22,410	7800	11,130	10,210	8820	21,330	10,360	7000
600	2639	3530	7080	8787	19,040	22,360	7760	11,010	10,190	8780	21,270	10,300	6935
800	2591	—	7040	8686	18,860	22,250	7690	10,430	10,160	8690	21,140	10,160	6430
1000	2365	—	7000	8568	18,660	22,140	7650	10,190	10,120	8610	21,010	10,010	6260
1200	2305	—	6945	8458	18,440	22,030	7620	9,940	10,080	8510	20,870	9,850	—
1400	2255	—	6890	7920	17,230	21,920	7520	—	10,040	8410	20,720	9,170	—
1600	—	—	6760	7750	16,950	21,790	7420	—	10,000	8320	20,570	8,980	—
1800	—	—	6700	7600	—	21,660	7320	—	9,950	7690	20,400	—	—
2000	—	—	7460	—	—	21,510	7030	—	9,900	7450	20,220	—	—

NOTE: Above the horizontal line the condensed phase is solid; below the line, it is liquid.

°R = % K.

† Polycrystalline form tabulated. Similar tables for an additional 45 elements appear in the *Handbook of Heat Transfer*, 2d ed., McGraw-Hill, New York, 1984.

SOLUBILITIES

UNITS CONVERSIONS

For this subsection, the following units conversions are applicable:

$$°F = \% °C + 32.$$

To convert cubic centimeters to cubic feet, multiply by 3.532×10^{-5} .

To convert millimeters of mercury to pounds-force per square inch, multiply by 0.01934.

To convert grams per liter to pounds per cubic foot, multiply by 6.243×10^{-2} .

A database containing solubilities originally published in the International Union for Pure and Applied Chemistry (IUPAC)-National Institute of Standards and Technology (NIST) Solubility Data Series is now available at no cost online at <http://srdata.nist.gov/solubility>.

TABLE 2-122 Solubilities of Inorganic Compounds in Water at Various Temperatures*

This table shows the grams of anhydrous substance that are soluble in 100 g of water at the temperature in degrees Celsius as indicated; when the name is followed by †, the value is expressed in grams of substance in 100 cm³ of saturated solution. Solid phase gives the hydrated form in equilibrium with the saturated solution.

	Substance	Formula	Solid phase	0 °C	10 °C	20 °C	30 °C	40 °C	50 °C	60 °C	70 °C	80 °C	90 °C	100 °C	
1	Aluminum chloride	AlCl ₃	6H ₂ O			69.86 ¹⁵⁰									1
2	sulfate	Al ₂ (SO ₄) ₃	18H ₂ O	31.2	33.5	36.4	40.4	46.1	52.2	59.2	66.1	73.0	80.8	89.0	2
3	Ammonium aluminum sulfate	(NH ₄) ₂ Al ₂ (SO ₄) ₄	24H ₂ O	2.1	4.99	7.74	10.94	14.88	20.10	26.70				109.7 ⁹⁶	3
4	bicarbonate	NH ₄ HCO ₃		11.9	15.8	21	27								4
5	bromide	NH ₄ Br		60.6	68	75.5	83.2	91.1	99.2	107.8	116.8	126	135.6	145.6	5
6	chloride	NH ₄ Cl		29.4	33.3	37.2	41.4	45.8	50.4	55.2	60.2	65.6	71.3	77.3	6
7	chloroplatinate	(NH ₄) ₂ PtCl ₆			0.7									1.25	7
8	chromate	(NH ₄) ₂ CrO ₄					40.4								8
9	chromium sulfate	(NH ₄) ₂ Cr ₂ (SO ₄) ₄	24H ₂ O			10.78 ²⁵									9
10	dichromate	(NH ₄) ₂ Cr ₂ O ₇					47.17								10
11	dihydrogen phosphite	NH ₄ H ₂ PO ₃		171		190 ¹⁴⁵⁰	260 ³¹⁰								11
12	hydrogen phosphate	(NH ₄) ₂ HPO ₄				131 ¹⁵									12
13	iodide	NH ₄ I		154.2	163.2	172.3	181.4	190.5	199.6	208.9	218.7	228.8		250.3	13
14	magnesium phosphate	NH ₄ MgPO ₄	6H ₂ O	0.023		0.052		0.036	0.030	0.040	0.016	0.019			14
15	manganese phosphate	NH ₄ MnPO ₄	7H ₂ O			0		0		0	0.005	0.007			15
16	nitrate	NH ₄ NO ₃		118.3		192	241.8	297.0	344.0	421.0	499.0	580.0	740.0	871.0	16
17	oxalate	(NH ₄) ₂ C ₂ O ₄	1H ₂ O	2.2	3.1	4.4	5.9	8.0	10.3						17
18	perchlorate†	NH ₄ ClO ₄ †		11.56		20.85		30.58		39.05		48.19		57.01	18
19	persulfate	(NH ₄) ₂ S ₂ O ₈		58.2			78.0	81.0		88.0		95.3		103.3	19
20	sulfate	(NH ₄) ₂ SO ₄		70.6	73.0	75.4	78.0	81.0		88.0		95.3		103.3	20
21	thiocyanate	NH ₄ CNS		119.8	144	170	207.7								21
22	vanadate (meta)	NH ₄ VO ₃				0.48	0.84	1.32	1.78		3.05				22
23	Antimonious fluoride	SbF ₃		384.7		444.7	563.6								23
24	sulfide	Sb ₂ S ₃				0.000175 ¹⁵⁰									24
25	Arsenic oxide	As ₂ O ₅		59.5	62.1	65.8	69.5	71.2		73.0		75.1		76.7	25
26	Arsenious sulfide	As ₂ S ₃		5.17 × 10 ⁻⁵ at 18°											26
27	Barium acetate	Ba(C ₂ H ₃ O ₂) ₂	3H ₂ O	59	63	71									27
28	acetate	Ba(C ₂ H ₃ O ₂) ₂	1H ₂ O				75	79	77	74	74			75	28
29	carbonate	BaCO ₃			0.0016 ⁹⁰	0.0022 ¹⁵⁰	0.0024 at 24.2°								29
30	chlorate	Ba(ClO ₃) ₂	1H ₂ O	20.34	26.95	33.80	41.70	49.61		66.81		84.84		104.9	30
31	chloride	BaCl ₂	2H ₂ O	31.6	33.3	35.7	38.2	40.7	43.6	46.4	49.4	52.4		58.8	31
32	chromate	BaCrO ₄		0.0002	0.00028	0.00037	0.00046								32
33	hydroxide	Ba(OH) ₂	8H ₂ O	1.67	2.48	3.59	5.59	8.22	13.12	20.94		101.4			33
34	iodide	BaI ₂	6H ₂ O	170.2	185.7	203.1	219.6								34
35	iodide	BaI ₂	2H ₂ O					231.9		247.3		261.0		271.7	35
36	nitrate	Ba(NO ₃) ₂		5.0	7.0	9.2	11.6	14.2	17.1	20.3		27.0		34.2	36
37	nitrite	Ba(NO ₂) ₂	1H ₂ O			67.5						205.8		300	37
38	oxalate	BaC ₂ O ₄			0.0016 ⁹⁰	0.0022 ¹⁵⁰	0.0024 at 24.2°								38
39	perchlorate	Ba(ClO ₄) ₂	3H ₂ O	205.8		289.1		358.7	426.3		495.2		562.3		39
40	sulfate	BaSO ₄		1.15 × 10 ⁻⁴	2.0 × 10 ⁻⁴	2.4 × 10 ⁻⁴	2.85 × 10 ⁻⁴								40
41	Beryllium sulfate	BeSO ₄	6H ₂ O				52		60.67						41
42	sulfate	BeSO ₄	4H ₂ O				43.78	46.74			62		83	100	42
43	sulfate	BeSO ₄	2H ₂ O									84.76	98	110	43
44	Boric acid	H ₃ BO ₃		2.66	3.57	5.04	6.60	8.72	11.54	14.81	16.73	23.75	30.38	40.25	44
45	Boron oxide	B ₂ O ₃		1.1	1.5	2.2	3.20	4.0		6.2		9.5		15.7	45
46	Bromine	Br ₂		4.22	3.4	3.20		3.13							46
47	Cadmium chloride	CdCl ₂	4H ₂ O	97.59	125.1										47
48	chloride	CdCl ₂	2½H ₂ O	90.01			132.1								48
49	chloride	CdCl ₂	1H ₂ O		135.1	134.5		135.3		136.5		140.4		147.0	49
50	cyanide	Cd(CN) ₂				1.7 ¹⁵⁰									50
51	hydroxide	Cd(OH) ₂					2.6 × 10 ⁻⁴ at 25°								51
52	sulfate	CdSO ₄		76.48	76.00	76.60		78.54		83.68			63.13	60.77	52
53	Calcium acetate	Ca(C ₂ H ₃ O ₂) ₂	2H ₂ O	37.4	36.0	34.7	33.8	33.2		32.7		33.5			53
54	acetate	Ca(C ₂ H ₃ O ₂) ₂	1H ₂ O										31.1	29.7	54

1	Calcium bicarbonate	Ca(HCO ₃) ₂		16.15		16.60		17.05		17.50		17.95		18.40	1
2	chloride	CaCl ₂	6H ₂ O	59.5	65.0	74.5	102								2
3	chloride	CaCl ₂	2H ₂ O							136.8	141.7	147.0	152.7	159	3
4	fluoride	CaF ₂				0.0016 ¹⁸⁰	0.0017 ²⁶⁰								4
5	hydroxide	Ca(OH) ₂		0.185	0.176	0.165	0.153	0.141	0.128	0.116	0.106	0.094	0.085	0.077	5
6	nitrate	Ca(NO ₃) ₂	4H ₂ O	102.0	115.3	129.3	152.6	195.9							6
7	nitrate	Ca(NO ₃) ₂	3H ₂ O					237.5	281.5						7
8	nitrate	Ca(NO ₃) ₂										358.7		363.6	8
9	nitrite	Ca(NO ₂) ₂	4H ₂ O	62.07		76.68									9
10	nitrite	Ca(NO ₂) ₂	2H ₂ O							132.6	151.9		244.8		10
11	oxalate	CaC ₂ O ₄			6.7 × 10 ⁻⁴	6.8 × 10 ⁻⁴	9.5 × 10 ⁻⁴	14 × 10 ⁻⁴							11
					at 13°	at 25°	at 50°	at 95°							
12	sulfate	CaSO ₄	2H ₂ O	0.1759	0.1928	0.2090	0.2097			0.2047	0.1966			0.1619	12
13	Carbon dioxide, 760 mm †	CO ₂		0.3346	0.2318	0.1688	0.1257	0.0973	0.0761	0.0576				0	13
14	monoxide, 760 mm †	CO		0.0044	0.0035	0.0028	0.0024	0.0021	0.0018	0.0015	0.0013	0.0010	0.0006	0	14
15	Cesium chloride	CsCl		161.4	174.7	186.5	197.3	208.0	218.5	229.7	239.5	250.0	260.1	270.5	15
16	nitrate	CsNO ₃		9.33	14.9	23.0	33.9	47.2	64.4	83.8	107.0	134.0	163.0	197.0	16
17	sulfate	Cs ₂ SO ₄		167.1	173.1	178.7	184.1	189.9	194.9	199.9	205.0	210.3	214.9	220.3	17
18	Chlorine, 760 mm †	Cl ₂		1.46	0.980	0.716	0.562	0.451	0.386	0.324	0.274	0.219	0.125	0	18
19	Chromic anhydride	CrO ₃		164.9				174.0	182.1				217.5	206.8	19
20	Cuprio chloride	CuCl ₂	2H ₂ O	70.7	73.76	77.0	80.34	83.8	87.44	91.2		99.2		107.9	20
21	nitrate	Cu(NO ₃) ₂	6H ₂ O	81.8	95.28	125.1									21
22	nitrate	Cu(NO ₃) ₂	3H ₂ O					159.8		178.8		207.8			22
23	sulfate	CuSO ₄	5H ₂ O	14.3	17.4	20.7	25	28.5	33.3	40		55		75.4	23
24	sulfide	CuS				3.3 × 10 ⁻⁵									24
						at 18°									
						1.52 ²⁵⁰									
25	Cuprous chloride	CuCl													25
26	Ferric chloride	FeCl ₃		74.4	81.9	91.8			315.1			525.8		535.7	26
27	Ferrous chloride	FeCl ₂	4H ₂ O		64.5		73.0	77.3	82.5	88.7		100			27
28	chloride	FeCl ₂											105.3	105.8	28
29	nitrate	Fe(NO ₃) ₂	6H ₂ O	71.02		83.8				165.6					29
30	sulfate	FeSO ₄	7H ₂ O	15.65	20.51	26.5	32.9	40.2	48.6						30
31	sulfate	FeSO ₄	1H ₂ O								50.9	43.6	37.3		31
32	Hydrobromic acid, 760 mm	HBr		221.2	210.3	198			171.5					130	32
33	Hydrochloric acid, 760 mm	HCl		82.3			67.3	63.3	59.6	56.1					33
34	Iodine	I ₂				0.029	0.04	0.056	0.078						34
35	Lead acetate	Pb(C ₂ H ₃ O ₂) ₂	3H ₂ O				55.04 ²⁵⁰								35
36	bromide	PbBr ₂		0.4554		0.85	1.15	1.53	1.94	2.36		3.34		4.75	36
37	carbonate	PbCO ₃				0.00011									37
38	chloride	PbCl ₂		0.6728		0.99	1.20	1.45	1.70	1.98		2.62		3.34	38
39	chromate	PbCrO ₄				7 × 10 ⁻⁶									39
40	fluoride	PbF ₂			0.060	0.064	0.068								40
41	nitrate	Pb(NO ₃) ₂		38.8	48.3	56.5	66	75	85	95		115		38.8	41
42	sulfate	PbSO ₄		0.0028	0.0035	0.0041	0.0049	0.0056							42
43	Magnesium bromide	MgBr ₂	6H ₂ O	91.0	94.5	96.5	99.2	101.6	104.1	107.5		113.7		120.2	43
44	chloride	MgCl ₂	6H ₂ O	52.8	53.5	54.5		57.5		61.0		66.0		73.0	44
45	hydroxide	Mg(OH) ₂				0.0009 ¹⁸⁰									45
46	nitrate	Mg(NO ₃) ₂	6H ₂ O	66.55				84.74					137.0		46
47	sulfate	MgSO ₄	7H ₂ O		30.9	35.5	40.8	45.6							47
48	sulfate	MgSO ₄	6H ₂ O	40.8	42.2	44.5	45.3		50.4	53.5	59.5	64.2	69.0	74.0	48
49	sulfate	MgSO ₄	1H ₂ O									62.9		68.3	49
50	Manganous sulfate	MnSO ₄	7H ₂ O	53.23	60.01										50
51	sulfate	MnSO ₄	5H ₂ O		59.5	62.9	67.76								51
52	sulfate	MnSO ₄	4H ₂ O			64.5	66.44	68.8	72.6						52
53	sulfate	MnSO ₄	1H ₂ O					58.17	55.0	52.0		48.0	42.5	34.0	53
54	Mercurous chloride	HgCl		0.00014		0.0002		0.0007							54
55	Molybdenic oxide	MoO ₃	2H ₂ O			0.138	0.264	0.476	0.687	1.206	2.055	2.106			55
56	Nickel chloride	NiCl ₂	6H ₂ O	53.9	59.5	64.2	68.9	73.3	78.3	82.2	85.2			87.6	56
57	nitrate	Ni(NO ₃) ₂	6H ₂ O	79.58		96.31		122.2							57
58	nitrate	Ni(NO ₃) ₂	3H ₂ O							163.1	169.1		235.1		58
59	sulfate	NiSO ₄	7H ₂ O	27.22	32		42.46								59
60	sulfate	NiSO ₄	6H ₂ O												60
61	Nitric oxide, 760 mm	NO		0.00984	0.00757	0.00618	0.00517	0.00440	0.00376	0.00324	0.00267	0.00199	0.00114	0	61
62	Nitrous oxide	N ₂ O			0.1705	0.1211									62

*By N. A. Lange; abridged from "Table of Solubilities of Inorganic Compounds in Water at Various Temperatures" in *Lange's Handbook of Chemistry*, 10th ed., McGraw-Hill, New York, 1961 (except for NaCl, which is from *CRC Handbook of Chemistry and Physics*, 86th ed., CRC Press, 2005). For tables of the solubility of gases in water at various temperatures, Atack (*Handbook of Chemical Data*, Reinhold, New York, 1957) gives values at closer temperature intervals, usually 1 or 5 °C, than are tabulated here. For materials marked by †, additional data are given in tables subsequent to this one. For the solubility of various hydrocarbons in water at high pressures see *J. Chem. Eng. Data*, **4**, 212 (1959).

TABLE 2-122 Solubilities of Inorganic Compounds in Water at Various Temperatures (Continued)

	Substance	Formula	Solid phase	0 °C	10 °C	20 °C	30 °C	40 °C	50 °C	60 °C	70 °C	80 °C	90 °C	100 °C	
1	Potassium acetate	KC ₂ H ₃ O ₂	1½H ₂ O	216.7	233.9	255.6	283.8	323.3							1
2	acetate	KC ₂ H ₃ O ₂	½H ₂ O						337.3	350	364.8	380.1	396.3		2
3	alum	K ₂ SO ₄ ·Al ₂ (SO ₄) ₃	24H ₂ O	3.0	4.0	5.9	8.39	11.70	17.00	24.75	40.0	71.0	109.0		3
4	bicarbonate	KHCO ₃		22.4	27.7	33.2	39.1	45.4		60.0					4
5	bisulfate	KHSO ₄		36.3		51.4		67.3						121.6	5
6	bitartrate	KHC ₄ H ₄ O ₆		0.32	0.40	0.53	0.90	1.32	1.83	2.46		4.6		6.95	6
7	carbonate	K ₂ CO ₃	2H ₂ O	105.5	108	110.5	113.7	116.9	121.2	126.8	133.1	139.8	147.5	155.7	7
8	chlorate	KClO ₃		3.3	5	7.4	10.5	14	19.3	24.5		38.5		57	8
9	chloride	KCl		27.6	31.0	34.0	37.0	40.0	42.6	45.5	48.3	51.1	54.0	56.7	9
10	chromate	K ₂ CrO ₄		58.2	60.0	61.7	63.4	65.2	66.8	68.6	70.4	72.1	73.9	75.6	10
11	dichromate	K ₂ Cr ₂ O ₇		5	7	12	20	26	34	43	52	61	70	80	11
12	ferricyanide	K ₃ Fe(CN) ₆		31	36	43	50	60		66				82.6 ¹⁰⁴	12
13	hydroxide	KOH	2H ₂ O	97	103	112	126								13
14	hydroxide	KOH	1H ₂ O						140					178	14
15	nitrate	KNO ₃		13.3	20.9	31.6	45.8	63.9	85.5	110.0	138	169	202	246	15
16	nitrite	KNO ₂		278.8		298.4		334.9						412.8	16
17	perchlorate	KClO ₄		0.75	1.05	1.80	2.6	4.4	6.5	9	11.8	14.8	18	21.8	17
18	permanganate	KMnO ₄		2.83	4.4	6.4	9.0	12.56	16.89	22.2					18
19	persulfate†	K ₂ S ₂ O ₈ †	†	1.62	2.60	4.49	7.19	9.89							19
20	sulfate	K ₂ SO ₄		7.35	9.22	11.11	12.97	14.76	16.50	18.17	19.75	21.4	22.8	24.1	20
21	thiocyanate	KCNS		177.0		217.5									21
22	Silver cyanide	AgCN				2.2 × 10 ⁻⁵									22
23	nitrate	AgNO ₃		122	170	222	300	376	455	525		669		952	23
24	sulfate	Ag ₂ SO ₄		0.573	0.695	0.796	0.888	0.979	1.08	1.15	1.22	1.30	1.36	1.41	24
25	Sodium acetate	NaC ₂ H ₃ O ₂	3H ₂ O	36.3	40.8	46.5	54.5	65.5	83	139					25
26	acetate	NaC ₂ H ₃ O ₂		119	121	123.5	126	129.5	134	139.5	146	153	161	170	26
27	bicarbonate	NaHCO ₃		6.9	8.15	9.6	11.1	12.7	14.45	16.4					27
28	carbonate	Na ₂ CO ₃	10H ₂ O	7	12.5	21.5		38.8							28
29	carbonate	Na ₂ CO ₃	1H ₂ O					50.5		46.4		45.8		45.5	29
30	chlorate	NaClO ₃		79	89	101	113	126	140	155	172	189		230	30
31	chloride	NaCl		35.65	35.72	35.89	36.09	36.37	36.69	37.04	37.46	37.93	38.47	38.99	31
32	chromate	Na ₂ CrO ₄	10H ₂ O	31.70	50.17	88.7									32
33	chromate	Na ₂ CrO ₄	4H ₂ O				88.7	95.96	104	114.6					33
34	chromate	Na ₂ CrO ₄									123.0	124.8		125.9	34
35	dichromate	Na ₂ Cr ₂ O ₇	2H ₂ O	163.0		177.8			244.8		316.7	376.2			35
36	dichromate	Na ₂ Cr ₂ O ₇												426.3	36
37	dihydrogen phosphate	NaH ₂ PO ₄	2H ₂ O	57.9	69.9	85.2	106.5	138.2							37
38	dihydrogen phosphate	NaH ₂ PO ₄	1H ₂ O						158.6						38
39	dihydrogen phosphate	NaH ₂ PO ₄								179.3	190.3	207.3	225.3	246.6	39
40	hydrogen arsenate	Na ₂ HAsO ₄	12H ₂ O	7.3	15.5	26.5	37	47				65	85		40
41	hydrogen phosphate	Na ₂ HPO ₄	12H ₂ O	1.67	3.6	7.7	20.8								41
42	hydrogen phosphate	Na ₂ HPO ₄	7H ₂ O					51.8							42
43	hydrogen phosphate	Na ₂ HPO ₄	2H ₂ O						80.2	82.9	88.1	92.4	102.9		43
44	hydrogen phosphate	Na ₂ HPO ₄												102.2	44
45	hydroxide	NaOH	4H ₂ O	42											45
46	hydroxide	NaOH	3½H ₂ O		51.5										46
47	hydroxide	NaOH	1H ₂ O			109	119	129	145	174					47
48	hydroxide	NaOH											313	347	48
49	nitrate	NaNO ₃		73	80	88	96	104	114	124		148		180	49
50	nitrite	NaNO ₂		72.1	78.0	84.5	91.6	98.4	104.1			132.6		163.2	50
51	oxalate	Na ₂ C ₂ O ₄				3.7								6.33	51
52	phosphate, tri-	Na ₃ PO ₄	12H ₂ O	1.5	4.1	11	20	31	43	55		81		108	52
53	pyrophosphate	Na ₄ P ₂ O ₇	10H ₂ O	3.16	3.95	6.23	9.95	13.50	17.45	21.83		30.04		40.26	53
54	sulfate	Na ₂ SO ₄	10H ₂ O	5.0	9.0	19.4	40.8								54
55	sulfate	Na ₂ SO ₄	7H ₂ O	19.5	30	44									55
56	sulfate	Na ₂ SO ₄						48.8	46.7	45.3		43.7		42.5	56
57	sulfide	Na ₂ S	9H ₂ O		15.42	18.8	22.5	28.5							57
58	sulfide	Na ₂ S	5½H ₂ O						39.82	42.69	45.73	51.40	59.23		58
59	sulfide	Na ₂ S	6H ₂ O						36.4	39.1	43.31	49.14	57.28		59
60	sulfite	Na ₂ SO ₃	7H ₂ O	13.9	20	26.9	36								60
61	sulfite	Na ₂ SO ₃						28	28.2	28.8		28.3			61
62	tetraborate	Na ₂ B ₄ O ₇	10H ₂ O	1.3	1.6	2.7	3.9		10.5	20.3					62
63	tetraborate	Na ₂ B ₄ O ₇	5H ₂ O								24.4	31.5	41	52.5	63
64	vanadate (meta)	NaVO ₃	2H ₂ O			15.3 ²⁵⁰		30.2		68.4					64

TABLE 2-122 Solubilities of Inorganic Compounds in Water at Various Temperatures (Concluded)

	Substance	Formula	Solid phase	0 °C	10 °C	20 °C	30 °C	40 °C	50 °C	60 °C	70 °C	80 °C	90 °C	100 °C	
1	Sodium vanadate (meta)	NaVO ₃				21.10 ^{25o}		26.23		32.97	36.9	38.8 ^{75o}			1
2	Stannous chloride	SnCl ₂		83.9		269.8 ^{15o}									2
3	sulfate	SnSO ₄				19								18	3
4	Strontium acetate	Sr(C ₂ H ₃ O ₂) ₂	4H ₂ O	36.9	43.61										4
5	acetate	Sr(C ₂ H ₃ O ₂) ₂	½H ₂ O		42.95	41.6	39.5		37.35		36.24	36.10		36.4	5
6	chloride	SrCl ₂	6H ₂ O	43.5	47.7	52.9	58.7	65.3	72.4	81.8					6
7	chloride	SrCl ₂	2H ₂ O								85.9	90.5		100.8	7
8	nitrate	Sr(NO ₃) ₂	1H ₂ O	52.7		64.0			83.8	97.2			130.4	139	8
9	nitrate	Sr(NO ₃) ₂	4H ₂ O	40.1		70.5									9
10	nitrate	Sr(NO ₃) ₂					88.6	90.1		93.8	96	98	100		10
11	sulfate	SrSO ₄		0.0113		0.0114	0.0114								11
12	Sulfur dioxide, 760 mm†	SO ₂		22.83	16.21	11.29	7.81	5.41	4.5						12
13	Thallium sulfate	Tl ₂ SO ₄		2.70	3.70	4.87	6.16		9.21	10.92	12.74	14.61	16.53	18.45	13
14	Thorium sulfate	Th(SO ₄) ₂	9H ₂ O	0.74	0.98	1.38	1.995	2.998	5.22						14
15	sulfate	Th(SO ₄) ₂	8H ₂ O	1.0	1.25	1.62									15
16	sulfate	Th(SO ₄) ₂	6H ₂ O	1.50		1.90	2.45			6.64					16
17	sulfate	Th(SO ₄) ₂	4H ₂ O					4.04	2.54	1.63	1.09				17
18	Zinc chlorate	ZnClO ₃	6H ₂ O	145.0	152.5										18
19	chlorate	ZnClO ₃	4H ₂ O			200.3	209.2	223.2	273.1						19
20	nitrate	Zn(NO ₃) ₂	6H ₂ O	94.78		118.3									20
21	nitrate	Zn(NO ₃) ₂	3H ₂ O					206.9							21
22	sulfate	ZnSO ₄	7H ₂ O	41.9	47	54.4									22
23	sulfate	ZnSO ₄	6H ₂ O					70.1	76.8						23
24	sulfate	ZnSO ₄	1H ₂ O									86.6	83.7	80.8	24

2-130 PHYSICAL AND CHEMICAL DATA

TABLE 2-123 Solubility as a Function of Temperature and Henry's Constant at 25°C for Gases in Water

Name	Formula	A	B	C	D	T range, K	H at 25°C, atm
Acetylene	C ₂ H ₂	-156.51	8,160.2	21.403	0	274-343	1,330
Carbon dioxide	CO ₂	-159.854	8,741.68	21.6694	-1.10261E-03	273-353	1,635
Carbon monoxide	CO	-171.764	8,296.9	23.3376	0	273-353	58,000
Ethane	C ₂ H ₆	-250.812	12,695.6	34.7413	0	275-323	29,400
Ethylene	C ₂ H ₄	-153.027	7,965.2	20.5248	0	287-346	11,726
Helium	He	-105.9768	4,259.62	14.0094	0	273-348	142,900
Hydrogen	H ₂	-125.939	5,528.45	16.8893	0	273-345	70,800
Methane	CH ₄	-338.217	13,282.1	51.9144	-0.0425831	273-523	39,200
Nitrogen	N ₂	-181.587	8,632.13	24.7981	0	273-350	84,600
Oxygen	O ₂	-171.2542	8,391.24	23.24323	0	273-333	43,400

The constants can be used to calculate solubility by the equation $\ln x = A + B/T + C \ln T + DT$, where T is in K and x is the mole fraction of the solute dissolved in water when the solute partial pressure is 1 atm. With the assumption that Henry's law is valid up to 1 atm, $H = 1/x$. Values of the constants are from P. G. T. Fogg and W. Gerrard, *Solubility of Gases in Liquids*, Wiley, 1991, New York, and *Solubility Data Series*, vol. 1, *Helium and Neon*, IUPAC, Pergamon Press, Oxford, 1979. For higher-temperature behavior and an up-to-date reference list, see R. Fernandez-Prini, J. L. Alvarez, and A. H. Harvey, *J. Phys. Chem. Ref. Data* **32**(2):903, 2003. To find H at temperatures other than 25°C, first find the solubility and then take the reciprocal.

TABLE 2-124 Henry's Constant H for Various Compounds in Water at 25°C

Compound	CAS no.	Formula	H, atm	Rating
<i>Paraffin Hydrocarbons</i>				
Methane	74828	CH ₄	36,600	4
Ethane	74840	C ₂ H ₆	26,700	3
Propane	74986	C ₃ H ₈	37,800	3
Butane	106978	C ₄ H ₁₀	51,100	3
Pentane	109660	C ₅ H ₁₂	70,000	3
Octane	111659	C ₈ H ₁₈	274,000	3
Nonane	111842	C ₉ H ₂₀	329,000	3
<i>Olefins</i>				
Ethylene	74851	C ₂ H ₄	11,700	3
Propylene	115071	C ₃ H ₆	11,700	4
<i>Aromatics</i>				
Benzene	71432	C ₆ H ₆	299	10
Toluene	108883	C ₇ H ₈	354	10
<i>o</i> -Xylene	95476	C ₈ H ₁₀	272	10
Cumene	98828	C ₉ H ₁₂	724	9
Phenol	108952	C ₆ H ₆ O	0.0394	7
<i>Aldehydes</i>				
Acetaldehyde	75,070	C ₂ H ₄ O	5.56	3
Propanal	123,386	C ₃ H ₆ O	4.36	4
<i>Ketones</i>				
Methyl ethyl ketone	78,933	C ₄ H ₈ O	2.59	5
<i>Esters</i>				
Methyl formate	107313	C ₂ H ₄ O ₂	13.6	3
Ethyl formate	109944	C ₃ H ₆ O ₂	13.6	3
Methyl acetate	79209	C ₃ H ₆ O ₂	5.04	3
Butyl acetate	123864	C ₆ H ₁₂ O ₂	13.6	3
<i>Chlorine Containing</i>				
Methyl chloride	74873	CH ₃ Cl	556	?
Chloroethane	75003	C ₂ H ₅ Cl	681	10
Chlorobenzene	108907	C ₆ H ₅ Cl	204	10
<i>Alcohols</i>				
Methanol	67561	CH ₃ O	0.272	4
Ethanol	64175	C ₂ H ₅ O	0.272	4
1-Propanol	71238	C ₃ H ₇ O	0.507	3
1-Butanol	71363	C ₄ H ₁₀ O	0.482	3
<i>Miscellaneous</i>				
Acrylonitrile	107131	C ₃ H ₃ N	5.54	3
Dimethyl sulfide	75183	C ₂ H ₆ S	121	3
Dimethyl disulfide	624920	C ₂ H ₆ S ₂	68.1	3
Methyl mercaptan	74931	CH ₃ S	177	3
Ethyl mercaptan	75081	C ₂ H ₅ S	161	3
Pyridine	110861	C ₅ H ₅ N	0.817	3

Values in this table were taken from the Design Institute for Physical Properties (DIPPR) of the American Institute of Chemical Engineers (AIChE), copyright 2007 AIChE and reproduced with permission of AIChE, the DIPPR Environmental Safety Property Data and Estimations Steering Committee and of the DIPPR Evaluated Process Design Data Project Steering Committee. Their source should be cited as T. N. Rogers, D. A. Zei, R. L. Rowley, W. V. Wilding, J. L. Oscarson, Y. Yang, N. A. Zundel, T. E. Daubert, R. P. Danner, DIPPR® Data Compilation of Pure Chemical Properties, Design Institute for Physical Properties, AIChE, New York (2007). Flammability limits are from B. Lewis and G. Von Elbe, *Combustion, Flames and Explosions of Gases*, New York: Harcourt Brace Jovanovich (1987). Flash point data are from N. I. Sax, *Dangerous Properties of Industrial Materials*, 6th ed, New York: Van Nostrand Reinhold (1984). Autoignition data are from I. Glassman, *Combustion*, 3d ed, New York: Academic Press (1996). The ratings reflect DIPPR® ESP's effort to provide a critical evaluation and quality assessment of each data point with 15

being the highest score possible. The rating is not directly correlated with the estimated experimental uncertainty. The ratings reflect DIPPR Project 911's effort to provide a critical evaluation and quality assessment of each data point, with 10 being the highest score possible. The rating is not directly correlated with the estimated experimental uncertainty. Henry's constant is a strong nonlinear function of temperature. A single value measured at one temperature, if used for calculation at a different temperature, can lead to serious errors. Procedures for extrapolation of single-point values over the ambient temperature range (4°C < T < 50°C) are presented in Sec. 22, p. 22-49, under "Estimating Henry's law constants." Estimation procedures for the larger range (4°C < T < 200°C) are presented in F. L. Smith and A. H. Harvey, "Avoid Common Pitfalls When Using Henry's Law," *Chem. Eng. Prog.*, **103**(9), 2007. See also Y.-L. Huang, J. D. Olson, and G. E. Keller II, "Steam Stripping for Removal of Organic Pollutants from Water. 2. Vapor-Liquid Equilibrium Data," *Ind. Eng. Chem. Res.*, **31**, pp. 1759-1768, 1992. (Also see the Supplementary Material, which contains the databank of 404 compounds of environmental interest and other useful property data.)

The H in Tables 2-123 to 2-134 is the proportionality constant in Henry's law, $p = Hx$, where x is the mole fraction of the solute in the aqueous liquid phase; p is the partial pressure in atm of the solute in the gas phase; and H is a proportionality constant, generally referred to as Henry's constant. Values of H often have considerable uncertainty and are strong functions of temperature. To convert values of H at 25°C from atm to atm/(mol/m³), divide by the molar density of water at 25°C, which is 55,342 mol/m³. Henry's law is valid only for dilute solutions.

Additional values of Henry's constant can be found in "Environmental Simulation Program": OLI Systems, Inc., Morris Plains, N.J.; "Estimated Henry's Law Constant," EPA Online Tools for Site Assessment Calculation (<http://www.epa.gov/athens/learn2model/part-two/onsite/esthenry.htm>); "Compilation of Henry's Law Constants for Inorganic and Organic Species of Potential Importance in Environmental Chemistry," Rolf Sander, Air Chemistry Department, Max-Planck Institute of Chemistry, Mainz, Germany; "Modeling Atmospheric Chemistry: Interactions between Gas-Phase Species and Liquid Cloud/Aerosol Particles," Rolf Sander, *Surv. Geophys.* **20**:1-31, 1999 (<http://www.henrys-law.org>).

TABLE 2-125 Henry's Constant H for Various Compounds in Water at 25 °C from Infinite Dilution Activity Coefficients

Compound	CAS no.	Formula	$H = \gamma^{\infty}P_{vp}$, atm
Pentane	109660	C ₅ H ₁₂	63700
Hexane	1100543	C ₆ H ₁₄	84600
Heptane	142825	C ₇ H ₁₆	120000
Benzene	71432	C ₆ H ₆	309
Toluene	108883	C ₇ H ₈	344
<i>o</i> -Xylene	95476	C ₈ H ₁₀	267
Cumene	98,828	C ₉ H ₁₂	613
Styrene	100425	C ₈ H ₈	145
Formaldehyde	50000	CH ₂ O	14.3
Acetaldehyde	75070	C ₂ H ₄ O	4.54
Propanal	123386	C ₃ H ₆ O	5.45
Acetone	67641	C ₃ H ₆ O	2.13
Methyl ethyl ketone	78933	C ₄ H ₈ O	3.11
Methyl <i>n</i> -propyl ketone	107879	C ₅ H ₁₀ O	4.60
Formic acid	64186	CH ₂ O ₂	0.0404
Methyl acetate	79209	C ₃ H ₆ O ₂	6.38
Ethyl acetate	141786	C ₄ H ₈ O ₂	8.01
Butyl acetate	123864	C ₆ H ₁₂ O ₂	12.3
Chloroethane	75003	C ₂ H ₅ Cl	626
1-Chloropropane	74986	C ₃ H ₇ Cl	792
Chlorobenzene	108907	C ₆ H ₅ Cl	219
Methanol	67561	CH ₃ O	0.263
Ethanol	64175	C ₂ H ₅ O	0.293
Pyridine	110861	C ₅ H ₅ N	0.544
Diethyl ether	60297	C ₄ H ₁₀ O	48.7
Thiophene	110021	C ₄ H ₄ S	160

Henry's constant H at 25 °C is the vapor pressure at 25 °C times the infinite dilution activity coefficient, also at 25 °C. Infinite dilution activity coefficients are from Mitchell and Jurs, *J. Chem. Inf. Comput. Sci.* **38**: 200 (1998). Henry's constant is a strong nonlinear function of temperature. A single value measured at one temperature, if used for calculation at a different temperature, can lead to serious errors. Procedures for extrapolation of single-point values over the ambient temperature range (4°C < T < 50°C) are presented in Sec. 22, p. 22–49, under "Estimating Henry's law constants." Estimation procedures for the larger range (4°C < T < 200°C) are presented in F. L. Smith and A. H. Harvey, "Avoid Common Pitfalls When Using Henry's Law," *Chem. Eng. Prog.*, **103**(9), 2007. See also Y.-L. Huang, J. D. Olson, and G. E. Keller II, "Steam Stripping for Removal of Organic Pollutants from Water. 2. Vapor-Liquid Equilibrium Data," *Ind. Eng. Chem. Res.*, **31**, pp. 1759–1768, 1992. (Also see the Supplementary Material, which contains the databank of 404 compounds of environmental interest and other useful property data.)

TABLE 2-128 Carbon Dioxide (CO₂)*

Total pressure, atm	Liquid mol fraction CO ₂ × 10 ³								
	0 °C	10 °C	15 °C	20 °C	25 °C	35 °C	50 °C	75 °C	100 °C
1	1.445	0.985	0.802	0.692	0.608	0.473	0.342	0.248	0.187
2	2.89	1.946	1.587	1.374	1.207	0.943	0.683	0.495	0.373
10	12.71	8.81	7.32	6.44	5.74	4.54	3.30	2.41	1.841
20	21.23	15.38	13.13	11.84	10.75	8.64	6.34	4.65	3.62
30	25.79	19.80	17.49	16.22	15.05	12.80	9.10	6.78	5.35
36		21.45	19.42	18.30	17.29	14.80	10.63	7.90	6.35

*Values selected from G. Houghton, A. M. McLean, and P. D. Ritchie, *Chem. Eng. Sci.* **6**:132–137, 1957.

TABLE 2-129 Carbonyl Sulfide (COS)*

t , °C	0	5	10	15	20	25	30
$10^{-3} \times H$	0.92	1.17	1.48	1.82	2.19	2.59	3.04

*International Critical Tables, vol. 3, p. 261.

TABLE 2-126 Air*

t , °C	0	5	10	15	20	25	30	35
$10^{-4} \times H$ †	4.32	4.88	5.49	6.07	6.64	7.20	7.71	8.23
t , °C	40	45	50	60	70	80	90	100
$10^{-4} \times H$ †	8.70	9.11	9.46	10.1	10.5	10.7	10.8	10.7

*International Critical Tables, vol. 3, p. 257.

† H is calculated from the absorption coefficients of O₂ and N₂, taking into consideration the correction for constant argon content.

TABLE 2-127 Ammonia-Water at 10 and 20 °C*

Mass fraction NH ₃ in liquid	10 °C		20 °C	
	P , kPa	Mass fraction NH ₃ in vapor	P , kPa	Mass fraction NH ₃ in vapor
0.0	1.23	0.0	2.34	0.0
0.00467	1.37	0.1		
0.00495			2.60	0.1
0.1	7.07	0.84164	11.95	0.82096
0.2	20.07	0.95438	32.34	0.94541
0.3	47.37	0.98565	73.85	0.98199
0.4	99.84	0.99544	150.56	0.99393
0.5	184.44	0.99848	269.50	0.99783
0.6	292.15	0.99943	416.63	0.99913
0.7	399.03	0.99975	560.61	0.99960
0.8	486.44	0.99988	678.61	0.99980
0.9	554.33	0.99995	771.87	0.99991
1.0	615.05	1.0	857.48	1.0

*Selected values from R. Tillner-Roth and D. G. Friend, *J. Phys. Chem. Ref. Data* **27**:63 (1998). This reference lists solubilities for temperatures from –70 to 340°C. Densities, enthalpies, and entropies are listed for both the two-phase and single-phase regions for pressures up to 40 MPa.

2-132 PHYSICAL AND CHEMICAL DATA

TABLE 2-130 Chlorine (Cl₂)

Partial pressure of Cl ₂ , mmHg	Solubility, g of Cl ₂ per liter					
	0 °C	10 °C	20 °C	30 °C	40 °C	50 °C
	5	0.488	0.451	0.438	0.424	0.412
10	0.679	0.603	0.575	0.553	0.532	0.512
30	1.221	1.024	0.937	0.873	0.821	0.781
50	1.717	1.354	1.210	1.106	1.025	0.962
100	2.79	2.08	1.773	1.573	1.424	1.313
150	3.81	2.73	2.27	1.966	1.754	1.599
200	4.78	3.35	2.74	2.34	2.05	1.856
250	5.71	3.95	3.19	2.69	2.34	2.09
300		4.54	3.63	3.03	2.61	2.31
350		5.13	4.06	3.35	2.86	2.53
400		5.71	4.48	3.69	3.11	2.74
450		6.26	4.88	3.98	3.36	2.94
500		6.85	5.29	4.30	3.61	3.14
550		7.39	5.71	4.60	3.84	3.33
600		7.97	6.12	4.91	4.08	3.52
650		8.52	6.52	5.21	4.32	3.71
700		9.09	6.90	5.50	4.54	3.89
750		9.65	7.29	5.80	4.77	4.07
800		10.21	7.69	6.08	4.99	4.27
900			8.46	6.68	5.44	4.62
1000				9.27	7.27	5.89
1200				10.84	8.42	6.81
1500				13.23	10.14	8.05
2000				17.07	13.02	10.22
2500				21.0	15.84	12.32
3000					18.73	14.47
3500					21.7	16.62
4000					24.7	18.84
4500					27.7	20.7
5000					30.8	23.3

Partial pressure of Cl ₂ , mmHg	Solubility, g of Cl ₂ per liter					
	60 °C	70 °C	80 °C	90 °C	100 °C	110 °C
	5	0.383	0.369	0.351	0.339	0.326
10	0.492	0.470	0.447	0.431	0.415	0.402
30	0.743	0.704	0.671	0.642	0.627	0.598
50	0.912	0.863	0.815	0.781	0.747	0.722
100	1.228	1.149	1.085	1.034	0.987	0.950
150	1.482	1.382	1.294	1.227	1.174	1.137
200	1.706	1.580	1.479	1.396	1.333	1.276
250	1.914	1.764	1.642	1.553	1.480	1.413
300	2.10	1.932	1.793	1.700	1.610	1.542
350	2.28	2.10	1.940	1.831	1.736	1.661
400	2.47	2.25	2.08	1.965	1.854	1.773
450	2.64	2.41	2.22	2.09	1.972	1.880
500	2.80	2.55	2.35	2.21	2.08	1.986
550	2.97	2.69	2.47	2.32	2.19	2.09
600	3.13	2.83	2.59	2.43	2.29	2.19
650	3.29	2.97	2.72	2.55	2.41	2.28
700	3.44	3.10	2.84	2.66	2.50	2.37
750	3.59	3.23	2.96	2.76	2.60	2.47
800	3.75	3.37	3.08	2.87	2.69	2.56
900	4.04	3.63	3.30	3.08	2.89	2.74
1000	4.36	3.88	3.53	3.28	3.07	2.91
1200	4.92	4.37	3.95	3.67	3.43	3.25
1500	5.76	5.09	4.58	4.23	3.95	3.74
2000	7.14	6.26	5.63	5.17	4.78	4.49
2500	8.48	7.40	6.61	6.05	5.59	5.25
3000	9.83	8.52	7.54	6.92	6.38	5.97
3500	11.22	9.65	8.53	7.79	7.16	6.72
4000	12.54	10.76	9.52	8.65	7.94	7.42
4500	13.88	11.91	10.46	9.49	8.72	8.13
5000	15.26	13.01	11.42	10.35	9.48	8.84

TABLE 2-131 Chlorine Dioxide (ClO₂)

Vol % of ClO ₂ in gas phase	Weight of ClO ₂ , grams per liter of solution						
	0 °C	5 °C	10 °C	15 °C	20 °C	30 °C	40 °C
1	2.00	1.50	1.25	1.00	0.90	0.60	0.46
3	6.00	4.7	3.85	3.20	2.70	1.95	1.30
5	10.0	7.8	6.30	5.25	4.30	3.20	2.25
7	14.0	10.9	8.95	7.35	6.15	4.40	3.20
10	20.0	15.5	12.8	10.5	8.80	6.30	4.50
11		17.0	14.0	11.7	9.70	7.00	5.00
12		18.6	15.3	12.8	10.55	7.50	5.45
13		20.3	16.6	13.8	11.5	8.20	5.85
14			18.0	14.9	12.3	8.80	6.35
15			19.2	16.0	13.2	9.50	6.80
16			20.3	17.0	14.2	10.1	7.20

Ishi, *Chem. Eng. (Japan)*, **22**:153 (1958).

TABLE 2-132 Hydrogen Chloride (HCl)

Weights of HCl per 100 weights of H ₂ O	Partial pressure of HCl, mmHg			
	0 °C	10 °C	20 °C	30 °C
78.6	510	840		
66.7	130	233		
56.3	29.0	56.4	399	627
47.0	5.7	11.8	105.5	188
38.9	1.0	2.27	23.5	44.5
31.6	0.175	0.43	1.00	2.17
25.0	0.0316	0.084	0.205	0.48
19.05	0.0056	0.016	0.0428	0.106
13.64	0.00099	0.00305	0.0088	0.0234
8.70	0.000118	0.000583	0.00178	0.00515
4.17	0.000018	0.000069	0.00024	0.00077
2.04		0.0000117	0.000044	0.000151

Weights of HCl per 100 weights of H ₂ O	Partial pressure of HCl, mm Hg		
	50 °C	80 °C	110 °C
78.6			
66.7			
56.3	535		
47.0	141	623	
38.9	35.7	188	760
31.6	8.9	54.5	253
25.0	2.21	15.6	83
19.05	0.55	4.66	28
13.64	0.136	1.34	9.3
8.70	0.0344	0.39	3.10
4.17	0.0064	0.095	0.93
2.04	0.00140	0.0245	0.280

Enthalpy and phase-equilibrium data for the binary system HCl-H₂O are given by Van Nuy, *Trans. Am. Inst. Chem. Engrs.*, **39**, 663 (1943).

TABLE 2-133 Hydrogen Sulfide (H₂S)

t, °C	0	5	10	15	20	25	30	35
10 ⁻² × H	2.68	3.15	3.67	4.23	4.83	5.45	6.09	6.76

t, °C	40	45	50	60	70	80	90	100
10 ⁻² × H	7.45	8.14	8.84	10.3	11.9	13.5	14.4	14.8

International Critical Tables, vol. 3, p. 259.

TABLE 2-134 Partial Vapor Pressure of Sulfur Dioxide over Water, mmHg

g SO ₂ / 100 g H ₂ O	Temperature, °C								
	0	10	20	30	40	50	60	90	120
0.01	0.02	0.04	0.07	0.12	0.19	0.29	0.43	1.21	2.82
0.05	0.38	0.66	1.07	1.68	2.53	3.69	5.24	12.9	27.0
0.10	1.15	1.91	3.03	4.62	6.80	9.71	13.5	31.7	63.9
0.15	2.10	3.44	5.37	8.07	11.7	16.5	22.7	52.2	104
0.20	3.17	5.13	7.93	11.8	17.0	23.8	32.6	73.7	145
0.25	4.34	6.93	10.6	15.7	22.5	31.4	42.8	95.8	186
0.30	5.57	8.84	13.5	19.8	28.2	39.2	53.3	118	229
0.40	8.17	12.8	19.4	28.3	40.1	55.3	74.7	164	316
0.50	10.9	17.0	25.6	37.1	52.3	72.0	96.8	211	404
1.00	25.8	39.5	58.4	83.7	117	159	212	454	856
2.00	58.6	88.5	129	183	253	342	453	955	
3.00	93.2	139	202	285	393	530	700		
4.00	129	192	277	389	535	720			
5.00	165	245	353	496	679				
6.00	202	299	430	602	824				
8.00	275	407	585	818					
10.00	351	517	741						
15.00	542	796							
20.00	735								

Condensed from Rabe, A. E. and Harris, J. F., *J. Chem. Eng. Data*, 8 (3), 333-336, 1963. Copyright © American Chemical Society and reproduced by permission of the copyright owner.

THERMAL EXPANSION

UNITS CONVERSIONS

For this subsection, the following units conversion is applicable:

$$^{\circ}\text{F} = \% ^{\circ}\text{C} + 32$$

ADDITIONAL REFERENCES

The tables given under this subject are reprinted by permission from the *Smithsonian Tables*. For more detailed data on thermal expansion, see *International Critical Tables*: tabular index, vol. 3, p. 1; abrasives, vol. 2, p. 87; alloys, vol. 2, p. 463; building stones, vol. 2, p. 54; carbons, vol. 2, p. 303; elements, vol. 1, p. 102; enamels, vol. 2, p. 115; glass, vol.

2, p. 93; metals, vol. 2, p. 459; petroleum, vol. 2, p. 145; porcelains, vol. 2, pp. 70, 78; refractory materials, vol. 2, p. 83; solid insulators, vol. 2, p. 310.

THERMAL EXPANSION OF GASES

No tables of the coefficients of thermal expansion of gases are given in this edition. The coefficient at constant pressure, $1/v(\partial v/\partial T)_p$, for an ideal gas is merely the reciprocal of the absolute temperature. For a real gas or liquid, both it and the coefficient at constant volume, $1/p(\partial p/\partial T)_v$, should be calculated either from the equation of state or from tabulated PVT data.

2-134 PHYSICAL AND CHEMICAL DATA

TABLE 2-135 Linear Expansion of the Solid Elements*

C is the true expansion coefficient at the given temperature; M is the mean coefficient between given temperatures; where one temperature is given, the true coefficient at that temperature is indicated; α and β are coefficients in formula $l_t = l_0(1 + \alpha t + \beta t^2)$; l_0 is length at 0 °C (unless otherwise indicated, when, if x is the reference temperature, $l_t = l_x[1 + \alpha(t - t_x) + \beta(t - t_x)^2]$; l_t is length at t °C).

Element	Temp., °C	C × 10 ⁴	Temp. range, °C	M × 10 ⁴	Temp. range, °C	$\alpha \times 10^4$	$\beta \times 10^6$
Aluminum	20	0.224	100	0.235	0, 500	0.22	0.009
Aluminum	300	0.284	500	0.311			
Antimony	20	0.136	20	0.080⊥			
Arsenic	20	0.05					
Bismuth	20	0.014	20	0.103⊥			
Cadmium	0	0.54	-180, -140	0.59	20, 100	0.526	
Cadmium	0	0.20⊥	-180, -140	0.117⊥	20, 100	0.214⊥	
Carbon, diamond	50	0.012					
graphite	50	0.06					
Chromium			20, 100	0.068	20, 500	0.086	
Cobalt	20	0.123			6, 121	0.121	0.0064
Copper	20	0.162	100	0.166	0, 625	0.161	0.0040
Copper	200	0.170	300	0.175			
Gold	20	0.140	17, 100	0.143	0, 520	0.142	0.0022
Gold			-191, 17	0.132			
Indium	40	0.417					
Iodine			-190, 17	0.837			
Iridium	20	0.065			0, 80	0.0636	0.0032
Iridium					1070, 1720	0.0679	0.0011
Iron, soft	40	0.1210	0, 100	0.11			
cast	20	0.118			0, 750	0.1158	0.0053
wrought	20	0.119			0, 750	0.1170	0.0053
steel	20	0.114			0, 750	0.1118	0.0053
Lead (99.9)			20, 100	0.291	100, 240	0.269	0.011
	100	0.291	20, 200	0.300			
	280	0.343					
Magnesium	20	0.254	-100, +20	0.240	+20, 500	0.2480	0.0096
			20, 100	0.260			
Manganese	20	0.233	0, 100	0.228			
			-190, 0	0.159	20, 300	0.216	0.0121
Molybdenum†	20	0.053	0, 100	0.052	-142, 19	0.0515	0.0057
			25, 100	0.049	19, +305	0.0501	0.0014
			25, 500	0.055			
Nickel	20	0.126	0, 100	0.130	-190, +20	0.1308	0.0166
					+20, +300	0.1236	0.0066
					500, 1000	0.1346	0.0033
Osmium	40	0.066					
Palladium	20	0.1173			-190, +100	0.1152	0.00517
					0, 1000	0.1167	0.0022
Platinum	20	0.0887			-190, -100	0.0875	0.00314
	20	0.0893			0, +80	0.0890	0.00121
					0, 1000	0.0887	0.00132
Potassium			0, 50	0.83			
Rhodium	40	0.0850	6, 21	0.0876	-75, -112	0.0746	
Ruthenium	40	0.0963					
Selenium	0	0.439	0, 100	0.660			
Silicon	40	0.0763	-3, +18	0.0249	-75, -67	0.0182	
Silver	20	0.1846	0, 100	0.197	0, 875	0.1827	0.00479
	20	0.195			20, 500	0.1939	0.00295
Sodium			-190, -17	0.622	0, 50	0.72	
Steel, 36.4Ni			20, 260	0.031	260, 500	0.144	
			20, 340	0.055	340, 500	0.136	
Tantalum†	20	0.065	-78, 0	0.059	20, 400	0.0646	0.0009
			0, 100	0.0655			
Tellurium	20	0.016	0, 20	0.272⊥			
Thallium	40	0.302					
Tin	20	0.214			8, 95	0.2033	0.0263
	20	0.305	20	0.154⊥			
Tungsten†	27	0.0444	0, 100	0.045	-105, +502	0.0428	0.00058
Zinc	20‡	0.643	-140, -100	0.656	+0, 400	0.354	0.010
	20‡	0.125⊥	+20, 100	0.639			
	20	0.358	+20, 100	0.141⊥			

*Smithsonian Tables. For more complete tabulations see Table 142, *Smithsonian Physical Tables*, 9th ed., 1954; *Handbook of Chemistry and Physics*, 40th ed., pp. 2239–2245. Chemical Rubber Publishing Co.; Goldsmith, and Waterman, WADC-TR-58-476, 1959; Johnson (ed.), WADD-TR-60-56, 1960, etc.

†Molybdenum, 300 to 2500 °C; $l_t = l_{300}[1 + 5.00 \times 10^{-6}(t - 300) + 10.5 \times 10^{-10}(t - 300)^2]$

Tantalum, 300 to 2800 °C; $l_t = l_{300}[1 + 6.60 \times 10^{-6}(t - 300) + 5.2 \times 10^{-10}(t - 300)^2]$

Tungsten, 300 to 2700 °C; $l_t = l_{300}[1 + 4.44 \times 10^{-6}(t - 300) + 4.5 \times 10^{-10}(t - 300)^2]$

Beryllium, 20 to 100 °C; 12.3×10^{-6} per °C.

Columbium, 0 to 100 °C; 7.2×10^{-6} per °C.

Tantalum, 20 to 100 °C; 6.6×10^{-6} per °C.

‡These values for zinc were taken from Grüneisen and Goens, *Z. Physik.*, **29**:141 (1924).

TABLE 2-136 Linear Expansion of Miscellaneous Substances*

The coefficient of cubical expansion may be taken as three times the linear coefficient. In the following table, t is the temperature or range of temperature, and C , the coefficient of expansion.

Substance	$t, ^\circ\text{C}$	$C \times 10^4$	Substance	$t, ^\circ\text{C}$	$C \times 10^4$	Substance	$t, ^\circ\text{C}$	$C \times 10^4$
Amber	0-30	0.50	Jena thermometer 59 ^{III}	0-100	0.058	Topas:		
	0-09	0.61	Jena thermometer 59 ^{III}	-191-+16	0.424	Parallel to lesser horizontal axis	0-100	0.0832
Bakelite, bleached	20-60	0.22	Gutta percha	20	1.983	Parallel to greater horizontal axis	0-100	0.0836
Brass:			Ice	-20-+1	0.51	Parallel to vertical axis	0-100	0.0472
Cast	0-100	0.1875	Iceland spar:			Tourmaline:		
Wire	0-100	0.1930	Parallel to axis	0-80	0.2631	Parallel to longitudinal axis	0-100	0.0937
Wire	0-100	0.1783-0.193	Perpendicular to axis	0-80	0.0544	Parallel to horizontal axis	0-100	0.0773
71.5 Cu + 27.7 Zn + 0.3 Sn + 0.5 Pb	40	0.1859	Lead tin (solder) 2 Pb + 1 Sn	0-100	0.2508	Type metal	16.6-25.4	0.1952
71 Cu + 29 Zn	0-100	0.1906	Limestone	25-100	0.09	Vulcanite	0-18	0.6360
Bronze:			Magnalium	12-39	0.238	Wedgwood ware	0-100	0.0890
3 Cu + 1 Sn	16.6-100	0.1844	Manganin		0.181	Wood:		
3 Cu + 1 Sn	16.6-350	0.2116	Marble	15-100	0.117	Parallel to fiber:		
3 Cu + 1 Sn	16.6-957	0.1737	Monel metal	25-100	0.14	Ash	0-100	0.0951
86.3 Cu + 9.7 Sn + 4 Zn	40	0.1782	Paraffin	0-16	1.0662	Beech	2.34	0.0257
97.6 Cu + hard	0-80	0.1713	Paraffin	16-38	1.3030	Chestnut	2.34	0.0649
2.2 Sn + soft	0-80	0.1708	Paraffin	38-49	4.7707	Elm	2.34	0.0565
0.2 P			Platinum-iridium, 10 Pt + 1 Ir	40	0.0884	Mahogany	2.34	0.0361
Caoutchouc		0.657-0.686	Platinum-silver, 1 Pt + 2 Ag	0-100	0.1523	Maple	2.34	0.0638
Caoutchouc	16.7-25.3	0.770	Porcelain	20-790	0.0413	Oak	2.34	0.0492
Celluloid	20-70	1.00	Porcelain Bayeux	1000-1400	0.0553	Pine	2.34	0.0541
Constantan	4-29	0.1523	Quartz:			Walnut	2.34	0.0658
Duralumin, 94Al	20-100	0.23	Parallel to axis	0-80	0.0797	Across the fiber:		
	20-300	0.25	Parallel to axis	-190 to + 16	0.0521	Beech	2.34	0.614
Ebonite	25.3-35.4	0.842	Perpend. to axis	0-80	0.1337	Chestnut	2.34	0.325
Fluorspar, CaF ₂	0-100	0.1950	Quartz glass	-190 to + 16	-0.0026	Elm	2.34	0.443
German silver	0-100	0.1836	Quartz glass	16 to 500	0.0057	Mahogany	2.34	0.404
Gold-platinum, 2 Au + 1 Pt	0-100	0.1523	Quartz glass	16 to 1000	0.0058	Maple	2.34	0.484
Gold-copper, 2 Au + 1 Cu	0-100	0.1552	Rock salt	40	0.4040	Oak	2.34	0.544
Glass:			Rubber, hard	0	0.691	Pine	2.34	0.341
Tube	0-100	0.0833	Rubber, hard	-160	0.300	Walnut	2.34	0.484
Tube	0-100	0.0828	Speculum metal	0-100	0.1933	Wax white	10-26	2.300
Plate	0-100	0.0891	Steel, 0.14 C, 34.5 Ni	25-100	0.037	Wax white	26-31	3.120
Crown (mean)	0-100	0.0897		25-600	0.136	Wax white	31-43	4.860
Crown (mean)	50-60	0.0954				Wax white	43-57	15.227
Flint	50-60	0.0788						
Jena thermometer 16 ^{III} normal	0-100	0.081						

* *Smithsonian Tables*. For a more complete tabulation see Tables 143, 144. *Smithsonian Physical Tables*. 9th ed., 1954, also reprinted in *American Institute of Physics Handbook*, McGraw-Hill, New York, 1957; *Handbook of Chemistry and Physics*, 40th ed., pp. 2239-2245, Chemical Rubber Publishing Co. For data on many solids prior to 1926, see Gruneisen, *Handbuch der Physik*, vol. 10, pp. 1-52, 1926, translation available as N.A.S.A. RE 2-18-59W, 1959. For eight plastic solids below 300 K, see Scott, *Cryogenic Engineering*, p. 331, Van Nostrand, Princeton, NJ, 1959. For 11 other materials to 300 K, see Scott, *loc. cit.*, p. 333. For quartz and silica, see Cook, *Brit. J. Appl. Phys.*, **7**, 285 (1956).

TABLE 2-137 Volume Expansion of Liquids*

If V_0 is the volume at 0° , then at t° the expansion formula is $V_t = V_0(1 + \alpha t + \beta t^2 + \gamma t^3)$. The table gives values of α , β , and γ , and of C , the true coefficient of volume expansion at 20° for some liquids and solutions. The temperature range of the observation is Δt . Values for the coefficient of volume expansion of liquids can be derived from the tables of specific volumes of the saturated liquid given as a function of temperature later in this section. $C = (dV/dt)/V_0$

Liquid	Range	$\alpha \times 10^3$	$\beta \times 10^6$	$\gamma \times 10^8$	$C \times 10^3$ at 20°
Acetic acid	16–107	1.0630	0.12636	1.0876	1.071
Acetone	0–54	1.3240	3.8090	-0.87983	1.487
Alcohol:					
Amyl	-15–80	0.9001	0.6573	1.18458	0.902
Ethyl, 30% by volume	18–39	0.2928	10.790	-11.87	
Ethyl, 50% by volume	0–39	0.7450	1.85	0.730	
Ethyl, 99.3% by volume	27–46	1.012	2.20		1.12
Ethyl, 500 atm pressure	0–40	0.866			
Ethyl, 3000 atm pressure	0–40	0.524			
Methyl	0–61	1.1342	1.3635	0.8741	1.199
Benzene	11–81	1.17626	1.27776	0.80648	1.237
Bromine	0–59	1.06218	1.87714	-0.30854	1.132
Calcium chloride:					
5.8% solution	18–25	0.07878	4.2742		0.250
40.9% solution	17–24	0.42383	0.8571		0.458
Carbon disulfide	-34–60	1.13980	1.37065	1.91225	1.218
500 atm pressure	0–50	0.940			
3000 atm pressure	0–50	0.581			
Carbon tetrachloride	0–76	1.18384	0.89881	1.35135	1.236
Chloroform	0–63	1.10715	4.66473	-1.74328	1.273
Ether	-15–38	1.51324	2.35918	4.00512	1.656
Glycerin		0.4853	0.4895		0.505
Hydrochloric acid, 33.2% solution	0–33	0.4460	0.215		0.455
Mercury	0–100	0.18182	0.0078		0.18186
Olive oil		0.6821	1.1405	-0.539	0.721
Pentane	0–33	1.4646	3.09319	1.6084	1.608
Potassium chloride, 24.3% solution	16–25	0.2695	2.080		0.353
Phenol	36–157	0.8340	0.10732	0.4446	1.090
Petroleum, 0.8467 density	24–120	0.8994	1.396		0.955
Sodium chloride, 20.6% solution	0–29	0.3640	1.237		0.414
Sodium sulfate, 24% solution	11–40	0.3599	1.258		0.410
Sulfuric acid:					
10.9% solution	0–30	0.2835	2.580		0.387
100.0%	0–30	0.5758	-0.432		0.558
Turpentine	-9–106	0.9003	1.9595	-0.44998	0.973
Water	0–33	-0.06427	8.5053	-6.7900	0.207

* *Smithsonian Tables*, Table 269. For a detailed discussion of mercury data, see Cook, *Brit. J. Appl. Phys.*, **7**, 285 (1956). For data on nitrogen and argon, see Johnson (ed.), WADD-TR-60-56, 1960.

Bromoform¹ 7.7–50 °C.

$$V_t = 0.34204[1 + 0.00090411(t - 7.7) + 0.000006766(t - 7.7)^2]$$

0.34204 is the specific volume of bromoform at 7.7 °C.

Glycerin² -62 to 0 °C.

$$\dot{V}_t = V_0(1 + 4.83 \times 10^{-4}t - 0.49 \times 10^{-6}t^2)$$

0–80 °C.

$$V_t = V_0(1 + 4.83 \times 10^{-4}t + 0.49 \times 10^{-6}t^2)$$

Mercury³ 0–300 °C.

$$V_t = V_0[1 + 10^{-8}(18,153.8t + 0.7548t^2 + 0.001533t^3 + 0.00000536t^4)]$$

¹Sherman and Sherman, *J. Am. Chem. Soc.*, **50**, 1119 (1928). (An obvious error in their equation has been corrected.)

²Samsoen, *Ann. phys.*, (10) **9**, 91 (1928).

³Harlow, *Phil. Mag.*, (7) **7**, 674 (1929).

TABLE 2-138 Volume Expansion of Solids*

If v_2 and v_1 are the volumes at t_2 and t_1 , respectively, then $v_2 = v_1(1 + C\Delta t)$, C being the coefficient of cubical expansion and Δt the temperature interval. Where only a single temperature is stated, C represents the true coefficient of volume expansion at that temperature.

Substance	t or Δt	$C \times 10^4$
Antimony	0–100	0.3167
Beryl	0–100	0.0105
Bismuth	0–100	0.3948
Copper†	0–100	0.4998
Diamond	40	0.0354
Emerald	40	0.0168
Galena	0–100	0.558
Glass, common tube	0–100	0.276
hard	0–100	0.214
Jena, borosilicate 59 III	20–100	0.156
pure silica	0–80	0.0129
Gold	0–100	0.4411
Ice	-20 to -1	1.1250
Iron	0–100	0.3550
Lead†	0–100	0.8399
Paraffin	20	5.88
Platinum	0–100	0.265
Porcelain, Berlin	20	0.0814
chloride	0–100	1.094
nitrate	0–100	1.967
sulfate	20	1.0754
Quartz	0–100	0.3840
Rock salt	50–60	1.2120
Rubber	20	4.87
Silver	0–100	0.5831
Sodium	20	2.13
Stearic acid	33.8–45.4	8.1
Sulfur, native	13.2–50.3	2.23
Tin	0–100	0.6889
Zinc†	0–100	0.8928

* *Smithsonian Tables*, Table 268.

† See additional data below.

Aluminum¹ 100–530 °C.

$$V = V_0(1 + 2.16 \times 10^{-5}t + 0.95 \times 10^{-8}t^2)$$

Cadmium¹ 130–270 °C.

$$V = V_0(1 + 8.04 \times 10^{-5}t + 5.9 \times 10^{-8}t^2)$$

Copper¹ 110–300 °C.

$$V = V_0(1 + 1.62 \times 10^{-5}t + 0.20 \times 10^{-8}t^2)$$

Colophony² 0–34 °C.

$$V = V_0(1 + 2.21 \times 10^{-4}t + 0.31 \times 10^{-6}t^2)$$

34–150 °C.

$$V = V_{34}[1 + 7.40 \times 10^{-4}(t - 34) + 5.91 \times 10^{-6}(t - 34)^2]$$

Lead¹ 100–280 °C.

$$V = V_0(1 + 1.60 \times 10^{-5}t + 3.2 \times 10^{-8}t^2)$$

Shellac² 0–46 °C.

$$V = V_0(1 + 2.73 \times 10^{-4}t + 0.39 \times 10^{-6}t^2)$$

46–100 °C.

$$V = V_{46}[1 + 13.10 \times 10^{-4}(t - 46) + 0.62 \times 10^{-6}(t - 46)^2]$$

Silica (vitreous)³ 0–300 °C.

$$V_t = V_0[1 + 10^{-8}(93.6t + 0.7776t^2 - 0.003315t^3 + 0.000005244t^4)]$$

Sugar (cane, amorphous)² 0–67 °C.

$$V_t = V_0(1 + 2.34 \times 10^{-4}t + 0.14 \times 10^{-6}t^2)$$

67–160 °C.

$$V_t = V_{67}[1 + 5.02 \times 10^{-4}(t - 67) + 0.43 \times 10^{-6}(t - 67)^2]$$

Zinc¹ 120–360 °C.

$$V_t = V_0(1 + 8.50 \times 10^{-5}t + 3.9 \times 10^{-8}t^2)$$

¹Uffelmann, *Phil. Mag.*, (7) **10**, 633 (1930).

²Samsoen, *Ann. phys.*, (10) **9**, 83 (1928).

³Harlow, *Phil. Mag.*, (7) **7**, 674 (1929).

JOULE-THOMSON EFFECT

UNITS CONVERSIONS

Joule-Thomson coefficients for substances listed in Table 2-184 are given in tables in the Thermodynamic Properties section.

For this subsection, the following units conversions are applicable:
 To convert the Joule-Thomson coefficient, μ , in degrees Celsius per atmosphere to degrees Fahrenheit per atmosphere, multiply by 1.8.

$$^{\circ}\text{F} = \% ^{\circ}\text{C} + 32; \text{ }^{\circ}\text{R} = \% \text{K}$$

To convert bars to pounds-force per square inch, multiply by 14.504; to convert bars to kilopascals, multiply by 1×10^2 .

TABLE 2-139 Additional References Available for the Joule-Thomson Coefficient

Gas	Pressure range, atm				Temp. range, °C		Other references
	0-10	10-50	50-200	>200	<0	0-300	
Air	12, 15, 16 19, 35	12, 15, 19 35	15, 19, 35		19, 35	12, 15, 16 19, 35	3, 4, 18
Ammonia	28					28	2, 3
Argon	39	39	39		39	39	
Benzene	31	31	31			31	31
Butane	26	26				26	
Carbon dioxide	7, 8, 28 37	7, 8, 37	7, 8, 37		7, 8, 37	7, 8, 9, 10 37	
Carbon monoxide	17	17			17	17	
Deuterium		22, 24, 25 1°	1°, 22, 24 25		1°, 22, 24, 25		
Dowtherm A	46	46				46	46
Ethane	45	45				45	
Ethylene						9, 10	
Helium	1, 38	1, 38	38		1, 38	38	48
Hydrogen	24, 30	22, 24, 25 30	24, 30		22, 24, 25 30	24	
Methane		6	6			6	
Mixtures						9, 11	
Natural gas			33	33	33	33	
Nitrogen	13, 28, 40	13, 40	13, 40	13	13, 40	9, 10, 13 28, 40	13
Nitrous oxide						9, 10	
Pentane	26, 34, 44	34	34			26, 34, 44	
Propane	41	43				43	
Steam	28, 29, 42	29, 42, 47	42, 47			28, 29, 42 45	29, 47

*See also 14 (generalized chart); 18 (review, to 1919); 20-22; 23 (review, to 1948); 27 (review, to 1905); 32, 36, 41, 50.

REFERENCES: 1. Baehr, *Z. Elektrochem.*, **60**, 515 (1956). 2. Beattie, *J. Math. Phys.*, **9**, 11 (1930). 3. Beattie, *Phys. Rev.*, **35**, 643 (1930). 4. Bradley and Hale, *Phys. Rev.*, **29**, 258 (1909). 5. Brown and Dean, *Bur. Stand. J. Res.*, **60**, 161 (1958). 6. Budenholzer, Sage, et al., *Ind. Eng. Chem.*, **29**, 658 (1937). 7. Burnett, *Phys. Rev.*, **22**, 590 (1923). 8. Burnett, Univ. Wisconsin Bull. 9(6), 1926. 9. Charnley, Ph.D. thesis, University of Manchester, 1952. 10. Charnley, Isles, et al., *Proc. R. Soc. (London)*, **A217**, 133 (1953). 11. Charnley, Rowlinson, et al., *Proc. R. Soc. (London)*, **A230**, 354 (1955). 12. Dalton, *Commun. Phys. Lab. Univ. Leiden*, no. 109c, 1909. 13. Deming and Deming, *Phys. Rev.*, **48**, 448 (1935). 14. Edmister, *Pet. Refiner*, **28**, 128 (1949). 15. Eucken, Clusius, et al., *Z. Tech. Phys.*, **13**, 267 (1932). 16. Eumorfopoulos and Rai, *Phil. Mag.*, **7**, 961 (1926). 17. Huang, Lin, et al., *Z. Phys.*, **100**, 594 (1936). 18. Hoxton, *Phys. Rev.*, **13**, 435 (1919). 19. Ishkin and Kaganev, *J. Tech. Phys. U.S.S.R.*, **26**, 2323 (1956). 20. Isles, Ph.D. thesis, Leeds University. 21. Jenkin and Pye, *Phil. Trans. R. Soc. (London)*, **A213**, 67 (1914); **A215**, 353 (1915). 22. Johnston, *J. Am. Chem. Soc.*, **68**, 2362 (1946). 23. Johnston, *Trans. Am. Soc. Mech. Eng.*, **70**, 651 (1948). 24. Johnston, Bezman, et al., *J. Am. Chem. Soc.*, **68**, 2367 (1946). 25. Johnston, Swanson, et al., *J. Am. Chem. Soc.*, **68**, 2373 (1946). 26. Kennedy, Sage, et al., *Ind. Eng. Chem.*, **28**, 718 (1936). 27. Kester, *Phys. Rev.*, **21**, 260 (1905). 28. Keyes and Collins, *Proc. Nat. Acad. Sci.*, **18**, 328 (1932). 29. Kleinschmidt, *Mech. Eng.*, **45**, 165 (1923); **48**, 155 (1926). 30. Koeppe, *Kältetechnik*, **8**, 275 (1956). 31. Lindsay and Brown, *Ind. Eng. Chem.*, **27**, 817 (1935). 32. Noell, dissertation, Munich, 1914, *Forschungsdienst*, 184, p. 1, 1916. 33. Palienko, *Tr. Inst. Ispol'z. Gaza, Akad. Nauk Ukr. SSR*, no. 4, p. 87, 1956. 34. Pattee and Brown, *Ind. Eng. Chem.*, **26**, 511, (1934). 35. Roebuck, *Proc. Am. Acad. Arts Sci.*, **60**, 537 (1925); **64**, 287 (1930). 36. Roebuck, see 49 below. 37. Roebuck and Murrell, *Phys. Rev.*, **55**, 240 (1939). 38. Roebuck and Osterberg, *Phys. Rev.*, **37**, 110 (1931); **43**, 60 (1933). 39. Roebuck and Osterberg, *Phys. Rev.*, **46**, 785 (1934). 40. Roebuck and Osterberg, *Phys. Rev.*, **48**, 450 (1935). 41. Roebuck, Murrell, et al., *J. Am. Chem. Soc.*, **64**, 400 (1942). 42. Sage, unpublished data, California Institute of Technology, 1959. 43. Sage and Lacy, *Ind. Eng. Chem.*, **27**, 1484 (1934). 44. Sage, Kennedy, et al., *Ind. Eng. Chem.*, **28**, 601 (1936). 45. Sage, Webster, et al., *Ind. Eng. Chem.*, **29**, 658 (1937). 46. Ullock, Gaffert, et al., *Trans. Am. Inst. Chem. Eng.*, **32**, 73 (1936). 47. Yang, *Ind. Eng. Chem.*, **45**, 786 (1953). 48. Zelmanov, *J. Phys. U.S.S.R.*, **3**, 43 (1940). 49. Roebuck, recalculated data. 50. Michels et al., van der Waals laboratory publications. Gunn, Cheuh, and Prausnitz, *Cryogenics*, **6**, 324 (1966), review equations relating the inversion temperatures and pressures. The ability of various equations of state to relate these was also discussed by Miller, *Ind. Eng. Chem. Fundam.*, **9**, 585 (1970); and Juris and Wenzel, *Am. Inst. Chem. Eng. J.*, **18**, 684 (1972). Perhaps the most detailed review is that of Hendricks, Peller, and Baron. NASA Tech. Note D 6807, 1972.

TABLE 2-140 Approximate Inversion-Curve Locus in Reduced Coordinates ($T_r = T/T_c$; $P_r = P/P_c$)^a

P_r	0	0.5	1	1.5	2	2.5	3	4
T_{rL}	0.782	0.800	0.818	0.838	0.859	0.880	0.903	0.953
T_{rU}	4.984	4.916	4.847	4.777	4.706	4.633	4.550	4.401
P_r	5	6	7	8	9	10	11	11.79
T_{rL}	1.01	1.08	1.16	1.25	1.35	1.50	1.73	2.24
T_{rU}	4.23	4.06	3.88	3.68	3.45	3.18	2.86	2.24

^aCalculated from the best three-constant equation recommended by Miller, *Ind. Eng. Chem. Fundam.*, **9**, 585 (1970). T_{rL} refers to the lower curve, and T_{rU} , to the upper curve.

CRITICAL CONSTANTS

ADDITIONAL REFERENCES

Other data and estimation techniques for the elements are contained in Gates and Thodos, *Am. Inst. Chem. Eng. J.*, **6** (1960):50-54; and Ohse and von Tippelskirch, *High Temperatures—High Pressures*, **9** (1977):367-385. For inorganic substances see Mathews, *Chem. Rev.*,

72 (1972):71-100; for organics see Kudchaker, Alani, and Zwolinski, *Chem. Rev.*, **68** (1968):659-735; and for fluorocarbons see *Advances in Fluorine Chemistry*, App. B, Butterworth, Washington, 1963, pp. 173-175. Pages 6-49 and 6-50 of the 84th edition of the *Handbook of Chemistry and Physics* provide an excellent list of references for critical properties.

TABLE 2-141 Critical Constants and Acentric Factors of Inorganic and Organic Compounds

Cmpd. no.	Name	Formula	CAS no.	Mol. wt.	T_c , K	P_c , MPa	V_c , m ³ /kmol	Z_c	Acentric factor
1	Acetaldehyde	C ₂ H ₄ O	75-07-0	44.053	466	5.55	0.154	0.221	0.2907
2	Acetamide	C ₂ H ₅ NO	60-35-5	59.067	761	6.6	0.215	0.224	0.4210
3	Acetic acid	C ₂ H ₄ O ₂	64-19-7	60.052	591.95	5.786	0.177	0.208	0.4665
4	Acetic anhydride	C ₄ H ₆ O ₃	108-24-7	102.089	606	4	0.29	0.23	0.4535
5	Acetone	C ₃ H ₆ O	67-64-1	58.079	508.2	4.701	0.209	0.233	0.3065
6	Acetonitrile	C ₂ H ₃ N	75-05-8	41.052	545.5	4.83	0.173	0.184	0.3379
7	Acetylene	C ₂ H ₂	74-86-2	26.037	308.3	6.138	0.112	0.268	0.1912
8	Acrolein	C ₃ H ₄ O	107-02-8	56.063	506	5	0.197	0.234	0.3198
9	Acrylic acid	C ₃ H ₄ O ₂	79-10-7	72.063	615	5.66	0.208	0.23	0.5383
10	Acrylonitrile	C ₃ H ₃ N	107-13-1	53.063	535	4.48	0.212	0.214	0.3498
11	Air	Mixture	132259-10-0	28.960	132.45	3.774	0.09147	0.313	
12	Ammonia	H ₃ N	7664-41-7	17.031	405.65	11.28	0.07247	0.242	0.2526
13	Anisole	C ₇ H ₈ O	100-66-3	108.138	645.6	4.25	0.337	0.267	0.3502
14	Argon	Ar	7440-37-1	39.948	150.86	4.898	0.07459	0.291	0.0000
15	Benzamide	C ₇ H ₇ NO	55-21-0	121.137	824	5.05	0.346	0.255	0.5585
16	Benzene	C ₆ H ₆	71-43-2	78.112	562.05	4.895	0.256	0.268	0.2103
17	Benzenethiol	C ₆ H ₆ S	108-98-5	110.177	689	4.74	0.315	0.261	0.2628
18	Benzoic acid	C ₇ H ₆ O ₂	65-85-0	122.121	751	4.47	0.344	0.246	0.6028
19	Benzonitrile	C ₇ H ₅ N	100-47-0	103.121	699.35	4.215	0.3132	0.227	0.3662
20	Benzophenone	C ₁₃ H ₁₀ O	119-61-9	182.218	830	3.352	0.5677	0.276	0.5019
21	Benzyl alcohol	C ₇ H ₈ O	100-51-6	108.138	720.15	4.374	0.382	0.279	0.3631
22	Benzyl ethyl ether	C ₉ H ₁₂ O	539-30-0	136.191	662	3.11	0.442	0.25	0.4332
23	Benzyl mercaptan	C ₇ H ₈ S	100-53-8	124.203	718	4.06	0.367	0.25	0.3126
24	Biphenyl	C ₁₂ H ₁₀	92-52-4	154.208	773	3.38	0.497	0.261	0.4029
25	Bromine	Br ₂	7726-95-6	159.808	584.15	10.3	0.135	0.286	0.1290
26	Bromobenzene	C ₆ H ₅ Br	108-86-1	157.008	670.15	4.519	0.324	0.263	0.2506
27	Bromoethane	C ₂ H ₅ Br	74-96-4	108.965	503.8	6.23	0.215	0.32	0.2548
28	Bromomethane	CH ₃ Br	74-83-9	94.939	467	8	0.156	0.321	0.1922
29	1,2-Butadiene	C ₄ H ₆	590-19-2	54.090	452	4.36	0.22	0.255	0.1659
30	1,3-Butadiene	C ₄ H ₆	106-99-0	54.090	425	4.32	0.221	0.27	0.1950
31	Butane	C ₄ H ₁₀	106-97-8	58.122	425.12	3.796	0.255	0.274	0.2002
32	1,2-Butanediol	C ₄ H ₁₀ O ₂	584-03-2	90.121	680	5.21	0.303	0.279	0.6305
33	1,3-Butanediol	C ₄ H ₁₀ O ₂	107-88-0	90.121	676	4.02	0.305	0.218	0.7043
34	1-Butanol	C ₄ H ₁₀ O	71-36-3	74.122	563.1	4.414	0.273	0.258	0.5883
35	2-Butanol	C ₄ H ₁₀ O	78-92-2	74.122	535.9	4.188	0.27	0.254	0.5692
36	1-Butene	C ₄ H ₈	106-98-9	56.106	419.5	4.02	0.241	0.278	0.1845
37	cis-2-Butene	C ₄ H ₈	590-18-1	56.106	435.5	4.21	0.234	0.272	0.2019
38	trans-2-Butene	C ₄ H ₈	624-64-6	56.106	428.6	4.1	0.238	0.274	0.2176
39	Butyl acetate	C ₆ H ₁₂ O ₂	123-86-4	116.158	575.4	3.09	0.389	0.251	0.4394
40	Butylbenzene	C ₁₀ H ₁₄	104-51-8	134.218	660.5	2.89	0.497	0.261	0.3941
41	Butyl mercaptan	C ₄ H ₁₀ S	109-79-5	90.187	570.1	3.97	0.307	0.257	0.2714
42	sec-Butyl mercaptan	C ₄ H ₁₀ S	513-53-1	90.187	554	4.06	0.307	0.271	0.2506
43	1-Butyne	C ₄ H ₆	107-00-6	54.090	440	4.6	0.208	0.262	0.2470
44	Butyraldehyde	C ₄ H ₈ O	123-72-8	72.106	537.2	4.32	0.258	0.25	0.2774
45	Butyric acid	C ₄ H ₈ O ₂	107-92-6	88.105	615.7	4.06	0.293	0.232	0.6805
46	Butyronitrile	C ₄ H ₇ N	109-74-0	69.105	582.25	3.79	0.278	0.218	0.3714
47	Carbon dioxide	CO ₂	124-38-9	44.010	304.21	7.383	0.094	0.274	0.2236
48	Carbon disulfide	CS ₂	75-15-0	76.141	552	7.9	0.16	0.275	0.1107
49	Carbon monoxide	CO	630-08-0	28.010	132.92	3.499	0.0944	0.299	0.0482
50	Carbon tetrachloride	CCl ₄	56-23-5	153.823	556.35	4.56	0.276	0.272	0.1926
51	Carbon tetrafluoride	CF ₄	75-73-0	88.004	227.51	3.745	0.143	0.283	0.1790
52	Chlorine	Cl ₂	7782-50-5	70.906	417.15	7.71	0.124	0.276	0.0688
53	Chlorobenzene	C ₆ H ₅ Cl	108-90-7	112.557	632.35	4.519	0.308	0.265	0.2499
54	Chloroethane	C ₂ H ₅ Cl	75-00-3	64.514	460.35	5.27	0.2	0.275	0.1902
55	Chloroform	CHCl ₃	67-66-3	119.378	536.4	5.472	0.239	0.293	0.2219
56	Chloromethane	CH ₃ Cl	74-87-3	50.488	416.25	6.68	0.143	0.276	0.1531
57	1-Chloropropane	C ₃ H ₇ Cl	540-54-5	78.541	503.15	4.58	0.247	0.27	0.2277
58	2-Chloropropane	C ₃ H ₇ Cl	75-29-6	78.541	489	4.54	0.247	0.276	0.1986
59	m-Cresol	C ₇ H ₈ O	108-39-4	108.138	705.85	4.56	0.312	0.242	0.4480
60	o-Cresol	C ₇ H ₈ O	95-48-7	108.138	697.55	5.01	0.282	0.244	0.4339
61	p-Cresol	C ₇ H ₈ O	106-44-5	108.138	704.65	5.15	0.277	0.244	0.5072
62	Cumene	C ₉ H ₁₂	98-82-8	120.192	631	3.209	0.434	0.265	0.3274
63	Cyanogen	C ₂ N ₂	460-19-5	52.035	400.15	5.98	0.195	0.351	0.2790
64	Cyclobutane	C ₄ H ₈	287-23-0	56.106	459.93	4.98	0.21	0.273	0.1847

TABLE 2-141 Critical Constants and Acentric Factors of Inorganic and Organic Compounds (Continued)

Cmpd. no.	Name	Formula	CAS no.	Mol. wt.	T_c , K	P_c , MPa	V_c , m ³ /kmol	Z_c	Acentric factor
65	Cyclohexane	C ₆ H ₁₂	110-82-7	84.159	553.8	4.08	0.308	0.273	0.2081
66	Cyclohexanol	C ₆ H ₁₂ O	108-93-0	100.159	650.1	4.26	0.322	0.254	0.3690
67	Cyclohexanone	C ₆ H ₁₀ O	108-94-1	98.143	653	4	0.311	0.229	0.2990
68	Cyclohexene	C ₆ H ₁₀	110-83-8	82.144	560.4	4.35	0.291	0.272	0.2123
69	Cyclopentane	C ₅ H ₁₀	287-92-3	70.133	511.7	4.51	0.26	0.276	0.1949
70	Cyclopentene	C ₅ H ₈	142-29-0	68.117	507	4.8	0.245	0.279	0.1961
71	Cyclopropane	C ₃ H ₆	75-19-4	42.080	398	5.54	0.162	0.271	0.1278
72	Cyclohexyl mercaptan	C ₆ H ₁₂ S	1569-69-3	116.224	664	3.97	0.355	0.255	0.2641
73	Decanal	C ₁₀ H ₂₀ O	112-31-2	156.265	674.2	2.6	0.58	0.269	0.5820
74	Decane	C ₁₀ H ₂₂	124-18-5	142.282	617.7	2.11	0.617	0.254	0.4923
75	Decanoic acid	C ₁₀ H ₂₀ O ₂	334-48-5	172.265	722.1	2.28	0.639	0.243	0.8126
76	1-Decanol	C ₁₀ H ₂₂ O	112-30-1	158.281	688	2.308	0.645	0.26	0.6070
77	1-Decene	C ₁₀ H ₂₀	872-05-9	140.266	616.6	2.223	0.584	0.253	0.4805
78	Decyl mercaptan	C ₁₀ H ₂₂ S	143-10-2	174.347	696	2.13	0.624	0.23	0.5874
79	1-Decyne	C ₁₀ H ₁₈	764-93-2	138.250	619.85	2.37	0.552	0.254	0.5178
80	Deuterium	D ₂	7782-39-0	4.032	38.35	1.6617	0.060263	0.314	-0.1449
81	1,1-Dibromoethane	C ₂ H ₄ Br ₂	557-91-5	187.861	628	6.03	0.276	0.319	0.1250
82	1,2-Dibromoethane	C ₂ H ₄ Br ₂	106-93-4	187.861	650.15	5.477	0.2616	0.265	0.2067
83	Dibromomethane	CH ₂ Br ₂	74-95-3	173.835	611	7.17	0.223	0.315	0.2095
84	Dibutyl ether	C ₈ H ₁₈ O	142-96-1	130.228	584.1	2.46	0.487	0.247	0.4476
85	<i>m</i> -Dichlorobenzene	C ₆ H ₄ Cl ₂	541-73-1	147.002	683.95	4.07	0.351	0.251	0.2790
86	<i>o</i> -Dichlorobenzene	C ₆ H ₄ Cl ₂	95-50-1	147.002	705	4.07	0.351	0.244	0.2192
87	<i>p</i> -Dichlorobenzene	C ₆ H ₄ Cl ₂	106-46-7	147.002	684.75	4.07	0.351	0.251	0.2846
88	1,1-Dichloroethane	C ₂ H ₄ Cl ₂	75-34-3	98.959	523	5.07	0.24	0.28	0.2339
89	1,2-Dichloroethane	C ₂ H ₄ Cl ₂	107-06-2	98.959	561.6	5.37	0.22	0.253	0.2866
90	Dichloromethane	CH ₂ Cl ₂	75-09-2	84.933	510	6.08	0.185	0.265	0.1986
91	1,1-Dichloropropane	C ₃ H ₆ Cl ₂	78-99-9	112.986	560	4.24	0.291	0.265	0.2529
92	1,2-Dichloropropane	C ₃ H ₆ Cl ₂	78-87-5	112.986	572	4.24	0.291	0.259	0.2564
93	Diethanol amine	C ₄ H ₁₁ NO ₂	111-42-2	105.136	736.6	4.27	0.349	0.243	0.9529
94	Diethyl amine	C ₄ H ₁₁ N	109-89-7	73.137	496.6	3.71	0.301	0.27	0.3039
95	Diethyl ether	C ₄ H ₁₀ O	60-29-7	74.122	466.7	3.64	0.28	0.263	0.2811
96	Diethyl sulfide	C ₄ H ₁₀ S	352-93-2	90.187	557.15	3.96	0.318	0.272	0.2900
97	1,1-Difluoroethane	C ₂ H ₄ F ₂	75-37-6	66.050	386.44	4.52	0.179	0.252	0.2751
98	1,2-Difluoroethane	C ₂ H ₄ F ₂	624-72-6	66.050	445	4.34	0.195	0.229	0.2224
99	Difluoromethane	CH ₂ F ₂	75-10-5	52.023	351.255	5.784	0.123	0.244	0.2771
100	Di-isopropyl amine	C ₆ H ₁₅ N	108-18-9	101.190	523.1	3.2	0.418	0.308	0.3883
101	Di-isopropyl ether	C ₆ H ₁₄ O	108-20-3	102.175	500.05	2.88	0.386	0.267	0.3387
102	Di-isopropyl ketone	C ₇ H ₁₄ O	565-80-0	114.185	576	3.02	0.416	0.262	0.4044
103	1,1-Dimethoxyethane	C ₄ H ₁₀ O ₂	534-15-6	90.121	507.8	3.773	0.297	0.263	0.3277
104	1,2-Dimethoxypropane	C ₅ H ₁₂ O ₂	7778-85-0	104.148	543	3.446	0.35	0.267	0.3522
105	Dimethyl acetylene	C ₄ H ₆	503-17-3	54.090	473.2	4.87	0.221	0.274	0.2385
106	Dimethyl amine	C ₂ H ₇ N	124-40-3	45.084	437.2	5.34	0.18	0.264	0.2999
107	2,3-Dimethylbutane	C ₆ H ₁₄	79-29-8	86.175	500	3.15	0.361	0.274	0.2493
108	1,1-Dimethylcyclohexane	C ₈ H ₁₆	590-66-9	112.213	591.15	2.938	0.45	0.269	0.2326
109	<i>cis</i> -1,2-Dimethylcyclohexane	C ₈ H ₁₆	2207-01-4	112.213	606.15	2.938	0.46	0.268	0.2324
110	<i>trans</i> -1,2-Dimethylcyclohexane	C ₈ H ₁₆	6876-23-9	112.213	596.15	2.938	0.46	0.273	0.2379
111	Dimethyl disulfide	C ₂ H ₆ S ₂	624-92-0	64.199	615	5.36	0.252	0.264	0.2059
112	Dimethyl ether	C ₂ H ₆ O	115-10-6	46.068	400.1	5.37	0.17	0.2744	0.2002
113	<i>N,N</i> -Dimethyl formamide	C ₃ H ₇ NO	68-12-2	73.094	649.6	4.42	0.26199	0.214	0.3177
114	2,3-Dimethylpentane	C ₇ H ₁₆	565-59-3	100.202	537.3	2.91	0.393	0.256	0.2964
115	Dimethyl phthalate	C ₁₀ H ₁₀ O ₄	131-11-3	194.184	766	2.78	0.53	0.231	0.6568
116	Dimethylsilane	C ₂ H ₆ Si	1111-74-6	60.170	402	3.56	0.258	0.275	0.1300
117	Dimethyl sulfide	C ₂ H ₆ S	75-18-3	62.134	503.04	5.53	0.201	0.266	0.1943
118	Dimethyl sulfoxide	C ₂ H ₆ OS	67-68-5	78.133	729	5.65	0.227	0.212	0.2806
119	Dimethyl terephthalate	C ₁₀ H ₁₀ O ₄	120-61-6	194.184	772	2.78	0.529	0.229	0.6371
120	1,4-Dioxane	C ₄ H ₈ O ₂	123-91-1	88.105	587	5.208	0.238	0.254	0.2793
121	Diphenyl ether	C ₁₂ H ₁₀ O	101-84-8	170.207	766.8	3.08	0.503	0.243	0.4389
122	Dipropyl amine	C ₆ H ₁₅ N	142-84-7	101.190	550	3.14	0.402	0.276	0.4497
123	Dodecane	C ₁₂ H ₂₆	112-40-3	170.335	658	1.82	0.755	0.251	0.5764
124	Eicosane	C ₂₀ H ₄₂	112-95-8	282.547	768	1.16	1.34	0.243	0.9069
125	Ethane	C ₂ H ₆	74-84-0	30.069	305.32	4.872	0.1455	0.279	0.0995
126	Ethanol	C ₂ H ₆ O	64-17-5	46.068	514	6.137	0.168	0.241	0.6436
127	Ethyl acetate	C ₄ H ₈ O ₂	141-78-6	88.105	523.3	3.88	0.286	0.256	0.3664
128	Ethyl amine	C ₂ H ₇ N	75-04-7	45.084	456.15	5.62	0.207	0.307	0.2848
129	Ethylbenzene	C ₈ H ₁₀	100-41-4	106.165	617.15	3.609	0.374	0.263	0.3035
130	Ethyl benzoate	C ₉ H ₁₀ O ₂	93-89-0	150.175	698	3.18	0.489	0.268	0.4771
131	2-Ethyl butanoic acid	C ₆ H ₁₂ O ₂	88-09-5	116.158	655	3.41	0.389	0.244	0.6326
132	Ethyl butyrate	C ₆ H ₁₂ O ₂	105-54-4	116.158	571	2.95	0.403	0.25	0.4011
133	Ethylcyclohexane	C ₈ H ₁₆	1678-91-7	112.213	609.15	3.04	0.43	0.258	0.2455
134	Ethylcyclopentane	C ₇ H ₁₄	1640-89-7	98.186	569.5	3.4	0.375	0.269	0.2701
135	Ethylene	C ₂ H ₄	74-85-1	28.053	282.34	5.041	0.131	0.281	0.0862
136	Ethylenediamine	C ₂ H ₆ N ₂	107-15-3	60.098	593	6.29	0.264	0.337	0.4724
137	Ethylene glycol	C ₂ H ₆ O ₂	107-21-1	62.068	720	8.2	0.191	0.262	0.5068
138	Ethyleneimine	C ₂ H ₅ N	151-56-4	43.068	537	6.85	0.173	0.265	0.2007
139	Ethylene oxide	C ₂ H ₄ O	75-21-8	44.053	469.15	7.19	0.140296	0.25876	0.1974
140	Ethyl formate	C ₃ H ₆ O ₂	109-94-4	74.079	508.4	4.74	0.229	0.257	0.2847

TABLE 2-141 Critical Constants and Acentric Factors of Inorganic and Organic Compounds (Continued)

Cmpd. no.	Name	Formula	CAS no.	Mol. wt.	T_c , K	P_c , MPa	V_c , m ³ /kmol	Z_c	Acentric factor
141	2-Ethyl hexanoic acid	C ₈ H ₁₆ O ₂	149-57-5	144.211	674.6	2.778	0.528	0.262	0.8067
142	Ethylhexyl ether	C ₈ H ₁₈ O	5756-43-4	130.228	583	2.46	0.487	0.247	0.4944
143	Ethylisopropyl ether	C ₇ H ₁₂ O	625-54-7	88.148	489	3.41	0.329	0.276	0.3056
144	Ethylisopropyl ketone	C ₈ H ₁₂ O	565-69-5	100.159	567	3.32	0.369	0.26	0.3891
145	Ethyl mercaptan	C ₂ H ₆ S	75-08-1	62.134	499.15	5.49	0.207	0.274	0.1878
146	Ethyl propionate	C ₇ H ₁₄ O ₂	105-37-3	102.132	546	3.362	0.345	0.256	0.3944
147	Ethylpropyl ether	C ₇ H ₁₂ O	628-32-0	88.148	500.23	3.37	0.339	0.275	0.3473
148	Ethyltrichlorosilane	C ₂ H ₅ Cl ₃ Si	115-21-9	163.506	559.95	3.33	0.414	0.296	0.2691
149	Fluorine	F ₂	7782-41-4	37.997	144.12	5.172	0.066547	0.287	0.0530
150	Fluorobenzene	C ₆ H ₅ F	462-06-6	96.102	560.09	4.551	0.269	0.263	0.2472
151	Fluoroethane	C ₂ H ₅ F	353-36-6	48.060	375.31	5.028	0.164	0.264	0.2200
152	Fluoromethane	CH ₃ F	593-53-3	34.033	317.42	5.875	0.113	0.252	0.1980
153	Formaldehyde	CH ₂ O	50-00-0	30.026	408	6.59	0.115	0.223	0.2818
154	Formamide	CH ₃ NO	75-12-7	45.041	771	7.8	0.163	0.198	0.4124
155	Formic acid	CH ₂ O ₂	64-18-6	46.026	588	5.81	0.125	0.149	0.3173
156	Furan	C ₄ H ₄ O	110-00-9	68.074	490.15	5.5	0.218	0.294	0.2015
157	Helium-4	He	7440-59-7	4.003	5.2	0.2275	0.0573	0.302	-0.3900
158	Heptadecane	C ₁₇ H ₃₆	629-78-7	240.468	736	1.34	1.11	0.244	0.7697
159	Heptanal	C ₇ H ₁₄ O	111-71-7	114.185	616.8	3.16	0.434	0.267	0.4279
160	Heptane	C ₇ H ₁₆	142-82-5	100.202	540.2	2.74	0.428	0.261	0.3495
161	Heptanoic acid	C ₇ H ₁₄ O ₂	111-14-8	130.185	677.3	3.043	0.466	0.252	0.7564
162	1-Heptanol	C ₇ H ₁₆ O	111-70-6	116.201	632.3	3.085	0.444	0.261	0.5621
163	2-Heptanol	C ₇ H ₁₆ O	543-49-7	116.201	608.3	3.001	0.447	0.265	0.5628
164	3-Heptanone	C ₇ H ₁₄ O	106-35-4	114.185	606.6	2.92	0.433	0.251	0.4076
165	2-Heptanone	C ₇ H ₁₄ O	110-43-0	114.185	611.4	2.94	0.434	0.251	0.4190
166	1-Heptene	C ₇ H ₁₄	592-76-7	98.186	537.4	2.92	0.402	0.263	0.3432
167	Heptyl mercaptan	C ₇ H ₁₆ S	1639-09-4	132.267	645	2.77	0.465	0.24	0.4226
168	1-Heptyne	C ₇ H ₁₂	628-71-7	96.170	547	3.21	0.387	0.273	0.3778
169	Hexadecane	C ₁₆ H ₃₄	544-76-3	226.441	723	1.4	1.04	0.243	0.7174
170	Hexanal	C ₆ H ₁₂ O	66-25-1	100.159	591	3.46	0.369	0.26	0.3872
171	Hexane	C ₆ H ₁₄	110-54-3	86.175	507.6	3.025	0.371	0.266	0.3013
172	Hexanoic acid	C ₆ H ₁₂ O ₂	142-62-1	116.158	660.2	3.308	0.408	0.246	0.7299
173	1-Hexanol	C ₆ H ₁₄ O	111-27-3	102.175	611.3	3.446	0.382	0.259	0.5586
174	2-Hexanol	C ₆ H ₁₄ O	626-93-7	102.175	585.3	3.311	0.385	0.262	0.5574
175	2-Hexanone	C ₆ H ₁₂ O	591-78-6	100.159	587.61	3.287	0.378	0.254	0.3846
176	3-Hexanone	C ₆ H ₁₂ O	589-38-8	100.159	582.82	3.32	0.378	0.259	0.3801
177	1-Hexene	C ₆ H ₁₂	592-41-6	84.159	504	3.21	0.348	0.267	0.2888
178	3-Hexyne	C ₆ H ₁₀	928-49-4	82.144	544	3.53	0.331	0.258	0.2183
179	Hexyl mercaptan	C ₆ H ₁₄ S	111-31-9	118.240	623	3.08	0.412	0.245	0.3681
180	1-Hexyne	C ₆ H ₁₀	693-02-7	82.144	516.2	3.62	0.322	0.272	0.3327
181	2-Hexyne	C ₆ H ₁₀	764-35-2	82.144	549	3.53	0.331	0.256	0.2214
182	Hydrazine	H ₄ N ₂	302-01-2	32.045	653.15	14.7	0.158	0.428	0.3143
183	Hydrogen	H ₂	1333-74-0	2.016	33.19	1.313	0.064147	0.305	-0.2160
184	Hydrogen bromide	HBr	10035-10-6	80.912	363.15	8.552	0.1	0.283	0.0734
185	Hydrogen chloride	HCl	7647-01-0	36.461	324.65	8.31	0.081	0.249	0.1315
186	Hydrogen cyanide	CHN	74-90-8	27.025	456.65	5.39	0.139	0.197	0.4099
187	Hydrogen fluoride	HF	7664-39-3	20.006	461.15	6.48	0.069	0.117	0.3823
188	Hydrogen sulfide	H ₂ S	7783-06-4	34.081	373.53	8.963	0.0985	0.284	0.0942
189	Isobutyric acid	C ₄ H ₈ O ₂	79-31-2	88.105	605	3.7	0.292	0.215	0.6141
190	Isopropyl amine	C ₃ H ₉ N	75-31-0	59.110	471.85	4.54	0.221	0.256	0.2759
191	Malonic acid	C ₃ H ₄ O ₄	141-82-2	104.061	805	5.64	0.258	0.217	0.9418
192	Methacrylic acid	C ₄ H ₆ O ₂	79-41-4	86.089	662	4.79	0.28	0.244	0.3318
193	Methane	CH ₄	74-82-8	16.042	190.564	4.599	0.0986	0.286	0.0115
194	Methanol	CH ₃ O	67-56-1	32.042	512.5	8.084	0.117	0.222	0.5658
195	N-Methyl acetamide	C ₃ H ₇ NO	79-16-3	73.094	718	4.98	0.267	0.223	0.4351
196	Methyl acetate	C ₃ H ₆ O ₂	79-20-9	74.079	506.55	4.75	0.228	0.257	0.3313
197	Methyl acetylene	C ₃ H ₄	74-99-7	40.064	402.4	5.63	0.164	0.276	0.2115
198	Methyl acrylate	C ₄ H ₆ O ₂	96-33-3	86.089	536	4.25	0.27	0.258	0.3423
199	Methyl amine	CH ₅ N	74-89-5	31.057	430.05	7.46	0.154	0.321	0.2814
200	Methyl benzoate	C ₈ H ₈ O ₂	93-58-3	136.148	693	3.59	0.436	0.272	0.4205
201	3-Methyl-1,2-butadiene	C ₅ H ₈	598-25-4	68.117	490	3.83	0.291	0.274	0.1874
202	2-Methylbutane	C ₅ H ₁₂	78-78-4	72.149	460.4	3.38	0.306	0.27	0.2279
203	2-Methylbutanoic acid	C ₅ H ₁₀ O ₂	116-53-0	102.132	643	3.89	0.347	0.252	0.5894
204	3-Methyl-1-butanol	C ₅ H ₁₂ O	123-51-3	88.148	577.2	3.93	0.329	0.269	0.5939
205	2-Methyl-1-butene	C ₅ H ₁₀	563-46-2	70.133	465	3.447	0.292	0.26	0.2341
206	2-Methyl-2-butene	C ₅ H ₁₀	513-35-9	70.133	470	3.42	0.292	0.256	0.2870
207	2-Methyl-1-butene-3-yne	C ₅ H ₈	78-80-8	66.101	492	4.38	0.248	0.266	0.1370
208	Methylbutyl ether	C ₅ H ₁₂ O	628-28-4	88.148	512.74	3.371	0.329	0.26	0.3130
209	Methylbutyl sulfide	C ₅ H ₁₂ S	628-29-5	104.214	593	3.47	0.36	0.253	0.3229
210	3-Methyl-1-butyne	C ₅ H ₈	598-23-2	68.117	463.2	4.2	0.275	0.3	0.3081
211	Methyl butyrate	C ₅ H ₁₀ O ₂	623-42-7	102.132	554.5	3.473	0.34	0.256	0.3775
212	Methylchlorosilane	CH ₃ ClSi	993-00-0	80.589	442	4.17	0.246	0.279	0.2252
213	Methylcyclohexane	C ₇ H ₁₄	108-87-2	98.186	572.1	3.48	0.369	0.27	0.2361
214	1-Methylcyclohexanol	C ₇ H ₁₄ O	590-67-0	114.185	686	4	0.374	0.262	0.2213
215	cis-2-Methylcyclohexanol	C ₇ H ₁₄ O	7443-70-1	114.185	614	3.79	0.374	0.278	0.6805
216	trans-2-Methylcyclohexanol	C ₇ H ₁₄ O	7443-52-9	114.185	617	3.79	0.374	0.276	0.6790

TABLE 2-141 Critical Constants and Acentric Factors of Inorganic and Organic Compounds (Continued)

Cmpd. no.	Name	Formula	CAS no.	Mol. wt.	T_c , K	P_c , MPa	V_c , m ³ /kmol	Z_c	Acentric factor
217	Methylcyclopentane	C ₆ H ₁₂	96-37-7	84.159	532.7	3.79	0.319	0.273	0.2288
218	1-Methylcyclopentene	C ₆ H ₁₀	693-89-0	82.144	542	4.13	0.303	0.278	0.2318
219	3-Methylcyclopentene	C ₆ H ₁₀	1120-62-3	82.144	526	4.13	0.303	0.286	0.2296
220	Methyldichlorosilane	CH ₂ Cl ₂ Si	75-54-7	115.034	483	3.95	0.289	0.284	0.2758
221	Methylethyl ether	C ₃ H ₈ O	540-67-0	60.095	437.8	4.4	0.221	0.267	0.2314
222	Methylethyl ketone	C ₄ H ₈ O	78-93-3	72.106	535.5	4.15	0.267	0.249	0.3234
223	Methylethyl sulfide	C ₃ H ₈ S	624-89-5	76.161	533	4.26	0.254	0.244	0.2091
224	Methyl formate	C ₂ H ₄ O ₂	107-31-3	60.052	487.2	6	0.172	0.255	0.2556
225	Methylisobutyl ether	C ₅ H ₁₂ O	625-44-5	88.148	497	3.41	0.329	0.272	0.3078
226	Methylisobutyl ketone	C ₆ H ₁₂ O	108-10-1	100.159	574.6	3.27	0.369	0.253	0.3557
227	Methyl Isocyanate	C ₂ H ₃ NO	624-83-9	57.051	488	5.48	0.202	0.273	0.3007
228	Methylisopropyl ether	C ₄ H ₁₀ O	598-53-8	74.122	464.48	3.762	0.276	0.269	0.2656
229	Methylisopropyl ketone	C ₅ H ₁₀ O	563-80-4	86.132	553.4	3.8	0.31	0.256	0.3208
230	Methylisopropyl sulfide	C ₄ H ₁₀ S	1551-21-9	90.187	553.1	4.021	0.328	0.28718	0.2461
231	Methyl mercaptan	CH ₃ S	74-93-1	48.107	469.95	7.23	0.145	0.268	0.1582
232	Methyl methacrylate	C ₅ H ₈ O ₂	80-62-6	100.116	566	3.68	0.323	0.253	0.2802
233	2-Methyloctanoic acid	C ₉ H ₁₈ O ₂	3004-93-1	158.238	694	2.54	0.572	0.252	0.7913
234	2-Methylpentane	C ₆ H ₁₄	107-83-5	86.175	497.7	3.04	0.368	0.27	0.2791
235	Methyl pentyl ether	C ₆ H ₁₄ O	628-80-8	102.175	546.49	3.042	0.38	0.254	0.3442
236	2-Methylpropane	C ₄ H ₁₀	75-28-5	58.122	407.8	3.64	0.259	0.278	0.1835
237	2-Methyl-2-propanol	C ₄ H ₁₀ O	75-65-0	74.122	506.2	3.972	0.275	0.26	0.6152
238	2-Methyl propene	C ₄ H ₈	115-11-7	56.106	417.9	4	0.239	0.275	0.1948
239	Methyl propionate	C ₄ H ₈ O ₂	554-12-1	88.105	530.6	4.004	0.282	0.256	0.3466
240	Methylpropyl ether	C ₄ H ₁₀ O	557-17-5	74.122	476.25	3.801	0.276	0.265	0.2770
241	Methylpropyl sulfide	C ₄ H ₁₀ S	3877-15-4	90.187	565	3.97	0.307	0.259	0.2737
242	Methylsilane	CH ₃ Si	992-94-9	46.144	352.5	4.7	0.205	0.329	0.1314
243	alpha-Methyl styrene	C ₉ H ₁₀	98-83-9	118.176	654	3.36	0.399	0.247	0.3230
244	Methyl <i>tert</i> -butyl ether	C ₅ H ₁₂ O	1634-04-4	88.148	497.1	3.287	0.314	0.25	0.2466
245	Methyl vinyl ether	C ₃ H ₆ O	107-25-5	58.079	437	4.67	0.21	0.27	0.2416
246	Naphthalene	C ₁₀ H ₈	91-20-3	128.171	748.4	4.05	0.407	0.265	0.3020
247	Neon	Ne	7440-01-9	20.180	44.4	2.653	0.0417	0.3	-0.0396
248	Nitroethane	C ₂ H ₅ NO ₂	79-24-3	75.067	593	5.16	0.236	0.247	0.3803
249	Nitrogen	N ₂	7727-37-9	28.013	126.2	3.4	0.08921	0.289	0.0377
250	Nitrogen trifluoride	F ₃ N	7783-54-2	71.002	234	4.461	0.11875	0.272	0.1200
251	Nitromethane	CH ₃ NO ₂	75-52-5	61.040	588.15	6.31	0.173	0.223	0.3480
252	Nitrous oxide	N ₂ O	10024-97-2	44.013	309.57	7.245	0.0974	0.274	0.1409
253	Nitric oxide	NO	10102-43-9	30.006	180.15	6.48	0.058	0.251	0.5829
254	Nonadecane	C ₁₉ H ₄₀	629-92-5	268.521	758	1.21	1.26	0.242	0.8522
255	Nonanal	C ₉ H ₁₈ O	124-19-6	142.239	658	2.73	0.527	0.263	0.5117
256	Nonane	C ₉ H ₂₀	111-84-2	128.255	594.6	2.29	0.551	0.255	0.4435
257	Nonanoic acid	C ₉ H ₁₈ O ₂	112-05-0	158.238	710.7	2.514	0.584	0.248	0.7724
258	1-Nonanol	C ₉ H ₂₀ O	143-08-8	144.255	670.9	2.527	0.576	0.261	0.5841
259	2-Nonanol	C ₉ H ₂₀ O	628-99-9	144.255	649.5	2.541	0.577	0.271	0.5911
260	1-Nonene	C ₉ H ₁₈	124-11-8	126.239	593.1	2.428	0.524	0.258	0.4367
261	Nonyl mercaptan	C ₉ H ₂₀ S	1455-21-6	160.320	681	2.31	0.571	0.233	0.5260
262	1-Nonyne	C ₉ H ₁₆	3452-09-3	124.223	598.05	2.61	0.497	0.261	0.4710
263	Octadecane	C ₁₈ H ₃₈	593-45-3	254.494	747	1.27	1.19	0.243	0.8114
264	Octanal	C ₈ H ₁₆ O	124-13-0	128.212	638.9	2.96	0.488	0.272	0.4636
265	Octane	C ₈ H ₁₈	111-65-9	114.229	568.7	2.49	0.486	0.256	0.3996
266	Octanoic acid	C ₈ H ₁₆ O ₂	124-07-2	144.211	694.26	2.779	0.523	0.252	0.7706
267	1-Octanol	C ₈ H ₁₈ O	111-87-5	130.228	652.3	2.783	0.509	0.261	0.5697
268	2-Octanol	C ₈ H ₁₈ O	123-96-6	130.228	629.8	2.749	0.512	0.269	0.5807
269	2-Octanone	C ₈ H ₁₆ O	111-13-7	128.212	632.7	2.64	0.497	0.249	0.4549
270	3-Octanone	C ₈ H ₁₆ O	106-68-3	128.212	627.7	2.704	0.497	0.257	0.4406
271	1-Octene	C ₈ H ₁₆	111-66-0	112.213	566.9	2.663	0.464	0.262	0.3921
272	Octyl mercaptan	C ₈ H ₁₈ S	111-88-6	146.294	667.3	2.52	0.518	0.235	0.4497
273	1-Octyne	C ₈ H ₁₄	629-05-0	110.197	574	2.88	0.442	0.267	0.4233
274	Oxalic acid	C ₂ H ₂ O ₄	144-62-7	90.035	804	7.02	0.205	0.215	0.9176
275	Oxygen	O ₂	7782-44-7	31.999	154.58	5.043	0.0734	0.288	0.0222
276	Ozone	O ₃	10028-15-6	47.998	261	5.57	0.089	0.228	0.2119
277	Pentadecane	C ₁₅ H ₃₂	629-62-9	212.415	708	1.48	0.969	0.244	0.6863
278	Pentanal	C ₅ H ₁₀ O	110-62-3	86.132	566.1	3.97	0.313	0.264	0.3472
279	Pentane	C ₅ H ₁₂	109-66-0	72.149	469.7	3.37	0.313	0.27	0.2515
280	Pentanoic acid	C ₅ H ₁₀ O ₂	109-52-4	102.132	639.16	3.63	0.35	0.239	0.7052
281	1-Pentanol	C ₅ H ₁₂ O	71-41-0	88.148	588.1	3.897	0.326	0.258	0.5748
282	2-Pentanol	C ₅ H ₁₂ O	6032-29-7	88.148	561	3.7	0.326	0.259	0.5549
283	2-Pentanone	C ₅ H ₁₀ O	107-87-9	86.132	561.08	3.694	0.301	0.238	0.3433
284	3-Pentanone	C ₅ H ₁₀ O	96-22-0	86.132	560.95	3.74	0.336	0.269	0.3448
285	1-Pentene	C ₅ H ₁₀	109-67-1	70.133	464.8	3.56	0.293	0.27	0.2372
286	2-Pentyl mercaptan	C ₅ H ₁₂ S	2084-19-7	104.214	584.3	3.536	0.385	0.28	0.2685
287	Pentyl mercaptan	C ₅ H ₁₂ S	110-66-7	104.214	598	3.47	0.359	0.251	0.3207
288	1-Pentyne	C ₅ H ₈	627-19-0	68.117	481.2	4.17	0.277	0.289	0.2899
289	2-Pentyne	C ₅ H ₈	627-21-4	68.117	519	4.03	0.276	0.258	0.1752
290	Phenanthrene	C ₁₄ H ₁₀	85-01-8	178.229	869	2.9	0.554	0.222	0.4707
291	Phenol	C ₆ H ₆ O	108-95-2	94.111	694.25	6.13	0.229	0.243	0.4435
292	Phenyl isocyanate	C ₇ H ₅ NO	103-71-9	119.121	653	4.06	0.37	0.277	0.4123

2-142 PHYSICAL AND CHEMICAL DATA
TABLE 2-141 Critical Constants and Acentric Factors of Inorganic and Organic Compounds (Concluded)

Cmpd. no.	Name	Formula	CAS no.	Mol. wt.	T_c , K	P_c , MPa	V_c , m ³ /kmol	Z_c	Acentric factor
293	Phthalic anhydride	C ₈ H ₄ O ₃	85-44-9	148.116	791	4.72	0.421	0.302	0.7025
294	Propadiene	C ₃ H ₄	463-49-0	40.064	394	5.25	0.165	0.264	0.1041
295	Propane	C ₃ H ₈	74-98-6	44.096	369.83	4.248	0.2	0.276	0.1523
296	1-Propanol	C ₃ H ₈ O	71-23-8	60.095	536.8	5.169	0.219	0.254	0.6209
297	2-Propanol	C ₃ H ₈ O	67-63-0	60.095	508.3	4.765	0.222	0.25	0.6544
298	Propenylcyclohexene	C ₉ H ₁₄	13511-13-2	122.207	636	3.12	0.437	0.258	0.3420
299	Propionaldehyde	C ₃ H ₆ O	123-38-6	58.079	504.4	4.92	0.204	0.239	0.2559
300	Propionic acid	C ₃ H ₆ O ₂	79-09-4	74.079	600.81	4.668	0.235	0.22	0.5796
301	Propionitrile	C ₃ H ₅ N	107-12-0	55.079	564.4	4.18	0.229	0.204	0.3243
302	Propyl acetate	C ₅ H ₁₀ O ₂	109-60-4	102.132	549.73	3.36	0.345	0.254	0.3889
303	Propyl amine	C ₃ H ₉ N	107-10-8	59.110	496.95	4.74	0.26	0.298	0.2798
304	Propylbenzene	C ₉ H ₁₂	103-65-1	120.192	638.35	3.2	0.44	0.265	0.3444
305	Propylene	C ₃ H ₆	115-07-1	42.080	364.85	4.6	0.185	0.281	0.1376
306	Propyl formate	C ₄ H ₈ O ₂	110-74-7	88.105	538	4.02	0.285	0.256	0.3088
307	2-Propyl mercaptan	C ₃ H ₇ S	75-33-2	76.161	517	4.75	0.254	0.281	0.2138
308	Propyl mercaptan	C ₃ H ₇ S	107-03-9	76.161	536.6	4.63	0.254	0.264	0.2318
309	1,2-Propylene glycol	C ₃ H ₈ O ₂	57-55-6	76.094	626	6.1	0.239	0.28	1.1065
310	Quinone	C ₆ H ₄ O ₂	106-51-4	108.095	683	5.96	0.291	0.305	0.4945
311	Silicon tetrafluoride	SiF ₄	7783-61-1	104.079	259	3.72	0.202	0.349	0.3858
312	Styrene	C ₈ H ₈	100-42-5	104.149	636	3.84	0.352	0.256	0.2971
313	Succinic acid	C ₄ H ₆ O ₄	110-15-6	118.088	806	4.71	0.317	0.223	0.9922
314	Sulfur dioxide	SO ₂	7446-09-5	64.064	430.75	7.884	0.122	0.269	0.2454
315	Sulfur hexafluoride	SF ₆	2551-62-4	146.055	318.69	3.76	0.19852	0.282	0.2151
316	Sulfur trioxide	SO ₃	7446-11-9	80.063	490.85	8.21	0.127	0.255	0.4240
317	Terephthalic acid	C ₈ H ₆ O ₄	100-21-0	166.131	1113	3.95	0.424	0.181	1.0591
318	<i>o</i> -Terphenyl	C ₁₈ H ₁₄	84-15-1	230.304	857	2.99	0.731	0.307	0.5513
319	Tetradecane	C ₁₄ H ₃₀	629-59-4	198.388	693	1.57	0.897	0.244	0.6430
320	Tetrahydrofuran	C ₄ H ₈ O	109-99-9	72.106	540.15	5.19	0.224	0.259	0.2254
321	1,2,3,4-Tetrahydronaphthalene	C ₁₀ H ₁₂	119-64-2	132.202	720	3.65	0.408	0.249	0.3353
322	Tetrahydrothiophene	C ₄ H ₈ S	110-01-0	88.171	631.95	5.16	0.249	0.245	0.1996
323	2,2,3,3-Tetramethylbutane	C ₈ H ₁₈	594-82-1	114.229	568	2.87	0.461	0.28	0.2450
324	Thiophene	C ₄ H ₄ S	110-02-1	84.140	579.35	5.69	0.219	0.259	0.1970
325	Toluene	C ₇ H ₈	108-88-3	92.138	591.75	4.108	0.316	0.264	0.2640
326	1,1,2-Trichloroethane	C ₂ H ₃ Cl ₃	79-00-5	133.404	602	4.48	0.281	0.252	0.2591
327	Tridecane	C ₁₃ H ₂₈	629-50-5	184.361	675	1.68	0.826	0.247	0.6174
328	Triethyl amine	C ₆ H ₁₅ N	121-44-8	101.190	535.15	3.04	0.39	0.266	0.3162
329	Trimethyl amine	C ₃ H ₉ N	75-50-3	59.110	433.25	4.07	0.254	0.287	0.2062
330	1,2,3-Trimethylbenzene	C ₉ H ₁₂	526-73-8	120.192	664.5	3.454	0.414	0.259	0.3666
331	1,2,4-Trimethylbenzene	C ₉ H ₁₂	95-63-6	120.192	649.1	3.232	0.43	0.258	0.3787
332	2,2,4-Trimethylpentane	C ₈ H ₁₈	540-84-1	114.229	543.8	2.57	0.468	0.266	0.3035
333	2,3,3-Trimethylpentane	C ₈ H ₁₈	560-21-4	114.229	573.5	2.82	0.455	0.269	0.2903
334	1,3,5-Trinitrobenzene	C ₆ H ₃ N ₃ O ₆	99-35-4	213.105	846	3.39	0.479	0.231	0.8623
335	2,4,6-Trinitrotoluene	C ₇ H ₅ N ₃ O ₆	118-96-7	227.131	828	3.04	0.572	0.253	0.8972
336	Undecane	C ₁₁ H ₂₄	1120-21-4	156.308	639	1.95	0.685	0.252	0.5303
337	1-Undecanol	C ₁₁ H ₂₄ O	112-42-5	172.308	703.9	2.119	0.715	0.259	0.6236
338	Vinyl acetate	C ₄ H ₆ O ₂	108-05-4	86.089	519.13	3.958	0.27	0.248	0.3513
339	Vinyl acetylene	C ₄ H ₄	689-97-4	52.075	454	4.86	0.205	0.264	0.1069
340	Vinyl chloride	C ₂ H ₃ Cl	75-01-4	62.498	432	5.67	0.179	0.283	0.1001
341	Vinyl trichlorosilane	C ₂ H ₃ Cl ₃ Si	75-94-5	161.490	543.15	3.06	0.408	0.276	0.2815
342	Water	H ₂ O	7732-18-5	18.015	647.096	22.064	0.0559472	0.229	0.3449
343	<i>m</i> -Xylene	C ₈ H ₁₀	108-38-3	106.165	617	3.541	0.375	0.259	0.3265
344	<i>o</i> -Xylene	C ₈ H ₁₀	95-47-6	106.165	630.3	3.732	0.37	0.264	0.3101
345	<i>p</i> -Xylene	C ₈ H ₁₀	106-42-3	106.165	616.2	3.511	0.378	0.259	0.3218

All substances are listed by chemical family in Table 2-6 and by formula in Table 2-7.

Values in this table were taken from the Design Institute for Physical Properties (DIPPR) of the American Institute of Chemical Engineers (AIChE), copyright 2007 AIChE and reproduced with permission of AIChE and of the DIPPR Evaluated Process Design Data Project Steering Committee. Their source should be cited as R. L. Rowley, W. V. Wilding, J. L. Oscarson, Y. Yang, N. A. Zundel, T. E. Daubert, R. P. Danner, DIPPR® Data Compilation of Pure Chemical Properties, Design Institute for Physical Properties, AIChE, New York (2007).

The number of digits provided for the acentric factor was chosen for uniformity of appearance and formatting; these do not represent the uncertainties of the physical quantities, but are the result of calculations from the standard thermophysical property formulations within a fixed format.

COMPRESSIBILITIES

INTRODUCTION

The compressibility factor Z can be calculated by using the defining equation $Z = PV/(RT)$, where P is pressure, V is molar volume, R is the gas constant, and T is absolute temperature. Values of P , V , and T for substances listed in Table 2-184 are given in tables in the Thermodynamic Properties section. For the units used in these tables, R is 0.008314472 MPa·dm³/(mol·K). Values at temperatures and pressures other than those in the tables can be generated for many of the substances in Table 2-184 by going to <http://webbook.nist.gov> and selecting NIST Chemistry WebBook, then Thermo-

physical Properties of Fluid Systems High Accuracy Data. Results can be pasted into a spreadsheet to facilitate calculation of the compressibility factor.

UNITS CONVERSIONS

For this subsection, the following units conversions are applicable:

$$^{\circ}\text{R} = \% \text{ K}$$

To convert bars to pounds-force per cubic inch, multiply by 14.504.
To convert bars to kilopascals, multiply by 1×10^2 .

TABLE 2-142 Composition of Selected Refrigerant Mixtures

Mixture	Tables	Composition (mass percent)			
		R-32	R-125	R-134a	R-143a
R-410A	2-290	50	50		
R-404A	2-288		44	4	52
R-507A	2-296		50		50
R-407C (Klea 66)	2-263, 2-264, 2-289	23	25	52	
R-407A (Klea 60)	2-143, 2-261	20	40	40	
R-407B (Klea 61)	2-144, 2-262	10	70	20	

TABLE 2-143 Compressibility Factors for R 407A (Klea 60)

T, K	Pressure, bar								Z_{dew}	P_{dew}
	1	5	10	15	20	25	30			
250	0.9691	0.0163	0.0325	0.0487	0.0648	0.0809	0.0970	0.9340	2.05	
260	0.9737	0.0161	0.0321	0.0480	0.0640	0.0798	0.0957	0.9136	3.08	
270	0.9773	0.4268	0.0318	0.0476	0.0633	0.0790	0.0947	0.8895	4.46	
280	0.9803	0.8932	0.0316	0.0473	0.0630	0.0785	0.0940	0.8614	6.28	
290	0.9828	0.9080	0.0360	0.0473	0.0629	0.0784	0.0938	0.8290	8.60	
300	0.9848	0.9199	0.8253	0.0476	0.0632	0.0787	0.0942	0.7916	11.53	
310	0.9866	0.9298	0.8495	0.7518	0.0641	0.0797	0.0952	0.7485	15.15	
320	0.9881	0.9380	0.8689	0.7889	0.5737	0.0816	0.0972	0.6983	19.58	
330	0.9893	0.9449	0.8847	0.8173	0.7386	0.6279	0.1011	0.6386	24.96	
340	0.9904	0.9509	0.8980	0.8401	0.7752	0.6993	0.6016	0.5641	31.46	
350	0.9914	0.9560	0.9092	0.8588	0.8038	0.7425	0.6713	0.4564	39.42	
Z_{dew}	0.9593	0.8809	0.8107	0.7502	0.6936	0.6381	0.5813			
T_{dew} , K	234.3	273.3	295.1	309.6	320.9	330.1	337.9			

The values in this table were generated from the NIST REFPROP software (Lemmon, E. W., McLinden, M. O., and Huber, M. L., NIST Standard Reference Database 23: Reference Fluid Thermodynamic and Transport Properties-REFPROP, National Institute of Standards and Technology, Standard Reference Data Program, Gaithersburg, Md., 2002, Version 7.1).

TABLE 2-144 Compressibility Factors for R 407B (Klea 61)

T, K	Pressure, bar								Z_{dew}	P_{dew}
	1	5	10	15	20	25	30			
250	0.9703	0.0180	0.0359	0.0538	0.0716	0.0894	0.1071	0.9251	2.40	
260	0.9745	0.0178	0.0355	0.0532	0.0708	0.0883	0.1058	0.9024	3.56	
270	0.9779	0.8785	0.0352	0.0527	0.0702	0.0875	0.1048	0.8757	5.10	
280	0.9808	0.8961	0.0351	0.0526	0.0699	0.0872	0.1043	0.8446	7.10	
290	0.9831	0.9101	0.5520	0.0527	0.0700	0.0872	0.1043	0.8085	9.64	
300	0.9851	0.9215	0.8290	0.0533	0.0707	0.0879	0.1050	0.7666	12.81	
310	0.9868	0.9310	0.8522	0.7569	0.0721	0.0895	0.1067	0.7178	16.71	
320	0.9883	0.9390	0.8709	0.7924	0.6949	0.0925	0.1098	0.6600	21.45	
330	0.9895	0.9457	0.8864	0.8200	0.7428	0.6453	0.1164	0.5890	27.18	
340	0.9906	0.9515	0.8993	0.8422	0.7784	0.7042	0.6108	0.4916	34.12	
350	0.9915	0.9565	0.9103	0.8606	0.8064	0.7462	0.6770			
Z_{dew}	0.9587	0.8774	0.8036	0.7389	0.6776	0.6164	0.5518			
T_{dew} , K	230.6	269.4	291.3	305.9	317.1	326.4	334.3			

The values in this table were generated from the NIST REFPROP software (Lemmon, E. W., McLinden, M. O., and Huber, M. L., NIST Standard Reference Database 23: Reference Fluid Thermodynamic and Transport Properties-REFPROP, National Institute of Standards and Technology, Standard Reference Data Program, Gaithersburg, Md., 2002, Version 7.1).

2-144 PHYSICAL AND CHEMICAL DATA

TABLE 2-145 Compressibilities of Liquids*

At the constant temperature T , the compressibility $\beta = (1/\bar{V}_0)(dV/dP)$. In general as P increases, β decreases rapidly at first and then slowly; the change of β with T is large at low pressures but very small at pressures above 1000 to 2000 megabars. 1 megabar = 0.987 atm = 10^6 dynes/cm² based upon the older usage, 1 bar = 1 dyne/cm².

Substance	Temp., °C	Pressure, megabars	Compressibility per megabar $\beta \times 10^6$	Substance	Temp., °C	Pressure, megabars	Compressibility per megabar $\beta \times 10^6$	Substance	Temp., °C	Pressure, megabars	Compressibility per megabar $\beta \times 10^6$
Acetone	14	23	111	Ethyl acetate	20	400	75	Methyl alcohol	15	23	103
Acetone	20	500	61	alcohol	14	23	100	alcohol	20	200	95
Acetone	20	1,000	52	alcohol	20	500	63	alcohol	20	400	80
Acetone	40	12,000	9	alcohol	20	1,000	54	alcohol	20	500	65
Amyl alcohol	14	23	88	alcohol	20	12,000	8	alcohol	20	1,000	54
alcohol, iso.	20	200	84	bromide	20	200	100	alcohol	20	12,000	8
alcohol, iso.	20	400	70	bromide	20	400	82	Nitric acid	0	17	32
alcohol, n	20	500	61	bromide	20	500	70	Oils:			
alcohol, n	20	1,000	46	bromide	20	1,000	54	Almond	15	5	53
alcohol, n	20	12,000	8	bromide	20	12,000	8	Castor	15	5	46
alcohol, n	40	12,000	8	chloride	15	23	151	Linseed	15	5	51
Benzene	17	5	89	chloride	20	500	102	Olive	15	5	55
Benzene	20	200	77	chloride	20	1,000	66	Rapeseed	20		59
Benzene	20	400	67	chloride	20	12,000	8	Phosphorus trichloride	10	250	71
Bromine	20	200	56	ether	25	23	188	trichloride	20	500	63
Bromine	20	400	51	ether	20	500	84	trichloride	20	1,000	47
Butyl alcohol, iso	18	8	97	ether	20	1,000	61	trichloride	20	12,000	8
alcohol, iso	20	200	81	ether	20	12,000	10	Propyl alcohol (n)	20	200	77
alcohol, iso	20	400	64	iodide	20	200	81	alcohol (n)	20	400	67
alcohol, iso	20	500	56	iodide	20	400	69	alcohol (n ?)	20	500	65
alcohol, iso	20	1,000	46	iodide	20	500	64	alcohol (n ?)	20	1,000	47
alcohol, iso	20	12,000	8	iodide	20	1,000	50	alcohol (n ?)	20	12,000	7
Carbon bisulfide	16	21	86	iodide	20	12,000	8	Toluene	20	200	74
bisulfide	20	500	57	Gallium	30	300	3.97	Toluene	20	400	64
bisulfide	20	1,000	48	Glycerol	15	5	22	Turpentine	20		74
bisulfide	20	12,000	6	Hexane	20	200	117	Water	20	13	49
tetrachloride	20	200	86	Hexane	20	400	91	Water	20	200	43
tetrachloride	20	400	73	Kerosene	20	500	55	Water	20	400	41
Chloroform	20	200	83	Kerosene	20	1,000	45	Water	20	500	39
Chloroform	20	400	70	Kerosene	20	12,000	8	Water	40	500	38
Dichloroethylsulfide	32	1,000	34	Mercury	20	300	3.95	Water	40	1,000	33
Dichloroethylsulfide	32	2,000	24	Mercury	22	500	3.97	Water	40	12,000	9
Ethyl acetate	13	23	103	Mercury	22	1,000	3.91	Xylene, meta	20	200	69
acetate	20	200	90	Mercury	22	12,000	2.37	meta	20	400	60

* *Smithsonian Tables*, Table 106.

Scott (*Cryogenic Engineering*, Van Nostrand, Princeton, N.J., 1959) gives data for liquid nitrogen (p. 283), oxygen (p. 276), and hydrogen (p. 303). For a convenient index to the high-pressure work of Bridgman, see *American Institute of Physics Handbook*, p. 2-163, McGraw-Hill, New York, 1957.

TABLE 2-146 Compressibilities of Solids

Many data on the compressibility of solids obtained prior to 1926 are contained in Gruneisen, *Handbuch der Physik*, vol. 10, Springer, Berlin, 1926, pp. 1-52; also available as translation, NASA RE 2-18-59W, 1959. See also Tables 271, 273, 276, 278, and other material in *Smithsonian Physical Tables*, 9th ed., 1954. For a review of high-pressure work to 1946, see Bridgman, *Rev. Mod. Phys.*, **18**, 1 (1946).

LATENT HEATS

UNITS CONVERSIONS

For this subsection, the following units conversions are applicable:

$$^{\circ}\text{F} = \frac{9}{5}^{\circ}\text{C} + 32$$

To convert calories per gram-mole to British thermal units per

pound-mole, multiply by 1.799; to convert calories per gram to British thermal units per pound, multiply by 1.799.

To convert millimeters of mercury to pounds-force per square inch, multiply by 1.934×10^{-2} .

TABLE 2-147 Heats of Fusion and Vaporization of the Elements and Inorganic Compounds*

Unless stated otherwise, the values have been taken from the compilations by K. K. Kelley on "Heats of Fusion of Inorganic Compounds," U.S. Bur. Mines Bull. 393 (1936), and "The Free Energies of Vaporization and Vapor Pressures of Inorganic Substances," U.S. Bur. Mines Bull. 383 (1935).

Substance	mp, °C	Heat of fusion, ^{a,b} cal/mol	bp at 1 atm, °C	Heat of vaporization, ^{a,b} cal/mol	Substance	mp, °C	Heat of fusion, ^{a,b} cal/mol	bp at 1 atm, °C	Heat of vaporization, ^{a,b} cal/mol
Aluminum					Carbon (Cont.)				
Al	660.0	2,550	2057	61,020	CNF			-72.8	5,780 ^f
Al ₂ Br ₆	97.5	5,420	256.4	10,920	CNI			141	13,980 ^f
Al ₂ Cl ₆	192.5	16,960	180.2 ^e	26,750 ^e	CO	-205.0	200	-191.5	1,444
AlF ₃ ·3NaF	1000	16,380			CO ₂	-57.5	1,900	-78.4 ^e	6,030 ^{c,r}
Al ₂ I ₆	191.0	7,960	385.5	15,360	COS	-138.8	1,129 ^t	-50.2	4,423 ^k
Al ₂ O ₃	2045	(26,000)	3000		COCl ₂			8.0	5,990
Antimony					CS ₂	-112.0	1,049 ^l		
Sb	630.5	4,770	1440	46,670	Cerium				
SbBr ₃	97	3,510			Ce	775	2,120		
SbCl ₃	73.4	3,030	219	10,360	Cesium				
SbCl ₅	4	2,400	172 ^l	11,570	Cs	28.4	500	690	16,320
Sb ₄ O ₆	655	(27,000)	1425	17,820	CsBr			1300	35,990
Sb ₄ S ₆	546	11,200			CsCl	642	3,600	1300	35,690
Argon					CsF	715	(2,450)	1251	34,330
A	-189.3	290	-185.8	1,590	CsI			1280	35,930
Arsenic					CsNO ₃	407	3,250		
As	814	(6,620)	610 ^e	31,000 ^e	Chlorine				
AsBr ₃	31	2,810			Cl ₂	-101.0	1,531 ^m	-34.1	4,878 ^m
AsCl ₃	-16	2,420	122	7,570	ClF			-101	
AsF ₃	-80.7	2,800	-52.8	4,980	ClF ₃			11.3	5,890
As ₄ O ₆	313	8,000	457.2	14,300	Cl ₂ O			2.0	6,280
Barium					ClO ₂			10.9	7,100
Ba	704	(1,400) ^e	1638	35,670	Cl ₂ O ₇			79	8,480
BaBr ₂	847	6,000			Chromium				
BaCl ₂	960	5,370			Cr	1550	3,930	2475	
BaF ₂	1287	3,000			CrO ₂ Cl ₂			117	8,250
Ba(NO ₃) ₂	595	(5,980)			Cobalt				
Ba ₃ (PO ₄) ₂	1730	18,600			Co	1490	3,660		
BaSO ₄	1350	9,700			CoCl ₂	727	7,390	1050	27,170
Beryllium					Copper				
Be	1280	2,500 ^e			Cu	1083.0	3,110	2595	72,810
Bismuth					Cu ₂ Br ₂			1355	16,310
Bi	271.3	2,505	1420	18,020	Cu ₂ Cl ₂	430	4,890	1490	11,920
BiBr ₃			461	17,350	CuI			1336	15,940
BiCl ₃	224	2,600	441		Cu ₂ (CN) ₂	473	(5,400)		
Bi ₂ O ₃	817	6,800			Cu ₂ O	1230	(13,400)		
Bi ₂ S ₅	747	8,900			CuO	1447	2,820		
Boron					Cu ₂ S	1127	5,500		
BBr ₃			91.3	7,300	Fluorine				
BCl ₃			12.5	5,680	F ₂	-223		-188.2	1,640
BF ₃	-128	480	-100.9	4,620	F ₂ O			-144.8	2,650
B ₂ H ₆	-165.5		-92.4	3,685	Gallium				
B ₂ H ₁₀	-119.8		16	6,470	Ga	29.8	1,336	2071	
B ₂ H ₉	-46.9		58	7,700	Germanium				
B ₂ H ₁₁			67	8,500	Ge	959	(8,300)		
B ₁₀ H ₁₄	99.7	7,800	<i>f</i>	11,600	GeH ₄	-165		-89.1	3,580
B ₂ H ₃ Br	-104		16	6,230	Ge ₂ H ₆	-109		31.4	5,900
B ₃ N ₃ H ₆	-58		50.4	7,670	Ge ₃ H ₈	-105.6		110.6	7,550
Bromine					GeHCl ₃	-71		75 ^e	8,000
Br ₂	-7.2	2,580	58.0	7,420	GeBr ₄	26.1		189	8,560
BrF ₅	-61.3	1,355	40.4	7,470	GeCl ₄	-49.5		84	7,030
Cadmium					Ge(CH ₃) ₄	-88		44	6,460
Cd	320.9	1,460	765	23,870	Gold				
CdBr ₂	568	(5,000)			Au	1063.0	3,030	2966	81,800
CdCl ₂	568	5,300	967	29,860	Helium				
CdF ₂	1110	(5,400)			He	-271.4		-268.4	22
CdI ₂	387	3,660	796	25,400	Hydrogen				
CdO			1559 ^e	53,820 ^e	H ₂	-259.2	28	-252.7	216
CdSO ₄	1000	4,790			HBr	-86.9	575	-66.7	4,210
Calcium					HCl	-114.2	476	-85.0	3,860
Ca	851	2,230	1487	36,580	HCN	-13.2	2,009 ^e	25.7	6,027 ^l
CaBr ₂	730	4,180			HF	-83.0	1,094	33.3	7,460
CaCO ₃	1282	(12,700)			(HF) ₆			51.2	5,020
CaCl ₂	782	6,100			HI	-50.8	686		
CaF ₂	1392	4,100			H ₂ O	0.0	1,436	100.0	9,729 ^{h,q}
Ca(NO ₃) ₂	561	5,120			H ₂ ² O (= D ₂ O)	3.8	1,501 ^t	101.4	9,945 ^q
CaO	2707	(12,240)			H ₂ O ₂	-2	2,520 ^e	158	10,270
CaO·Al ₂ O ₃ ·2SiO ₂	1550	29,400			HNO ₃	-47	600		
CaO·MgO·2SiO ₂	1392	(18,200)			H ₃ PO ₃	17.4	2,310		
CaO·SiO ₂	1512	13,400			H ₃ PO ₄	74	3,070		
CaSO ₄	1297	6,700			H ₃ PO ₄	42.4	2,520		
Carbon					H ₄ P ₂ O ₆	55	8,300		
C (graphite)	3600	11,000 ^e			H ₂ S	-85.5	568 ^e	-60.3	4,463 ^l
CBr ₄	90	1,050			H ₂ S ₂	-87.6	1,805		
CCl ₄	-24.0	644	77	7,280	H ₂ SO ₄	10.5	2,360		
CF ₄			-127.9	3,110	H ₂ Se			-41.3	4,880
CH ₄	-182.5	224	-161.4	2,040	H ₂ SeO ₄	58	3,450		
C ₂ N ₂	-27.8	1,938 ^e	-21.1	5,576 ^e	H ₂ Te	-48.9	1,670	-2.2	5,650
CNBr	52			11,010 ^e	Indium				
CNCl	-5	2,240	13	6,300	In	156.4	781		

*See also subsection "Thermodynamic Properties."

TABLE 2-147 Heats of Fusion and Vaporization of the Elements and Inorganic Compounds (Continued)

Substance	mp, °C	Heat of fusion, ^{a,b} cal/mol	bp at 1 atm, °C	Heat of vaporization, ^{a,b} cal/mol	Substance	mp, °C	Heat of fusion, ^{a,b} cal/mol	bp at 1 atm, °C	Heat of vaporization, ^{a,b} cal/mol
Iodine					Palladium				
I ₂	113.0	3,650	183	10,390	Pd	1554	4,120		
ICl(α)	17.2	2,660			Phosphorus				
ICl(β)	13.9	2,270			P ₄ (yellow)	44.2	615	280	12,520
IF ₇			4 ^c	7,460 ^c	P ₄ (violet)			417 ^c	25,600 ^c
Iron					P ₄ (black)			453 ^c	33,100
Fe	1530	3,560	2735	84,600	PCl ₃			74.2	7,280
FeCl ₂	677	7,800	1026	30,210	PH ₃	-133.8	270 ^c	-87.7	3,489 ^c
Fe ₂ Cl ₆	304	20,590	319	12,040	P ₂ O ₃	23.8	3,360	174	10,380
Fe(CO) ₅	-21	3,250	105	9,000	P ₄ O ₁₀ (α)	569	17,080	591	20,670
FeO	1380	(7,700)			P ₄ O ₁₀ (β)			358 ^c	
FeS	1195	5,000			POCl ₃	1.1	3,110	105.1	8,380
Krypton					P ₂ S ₅			508	
Kr	-157	360 ^c	152.9	2,310 ^c	Platinum				
Lead					Pt	1773.5	4,700	(4400)	(107,000)
Pb	327.4	1,224	1744	42,060	Potassium				
PbBr ₂	488	4,290	914	27,700	K	63.5	574	776	18,920
PbCl ₂	498	5,650	954	29,600	KBO ₂	947	(5,700)		
PbF ₂	824	1,860	1293	38,300	KBr	742	5,000	1383	37,060
PbI ₂	412	5,970	872	24,850	KCl	770	6,410	1407	38,840
PbMoO ₄	1065	(25,800)			KCN	623	(3,500)		
PbO	890	2,820	1472	51,310	KCNS	179	2,250		
PbS	1114	4,150	1281	(50,000)	K ₂ CO ₃	897	7,800		
PbSO ₄	1087	9,600			K ₂ CrO ₄	984	6,920		
PbWO ₄	1123	(15,200)			K ₂ Cr ₂ O ₇	398	8,770		
Lithium					KF	857	6,500		
Li	179	1,100	1372	32,250	KI	682	4,100	1324	34,690
LiBO ₂	845	(5,570)			K ₂ MoO ₄	922	(4,000)		
LiBr	552	2,900	1310	35,420	KNO ₃	338	2,840		
LiCl	614	3,200	1382	35,960	KOH	360	(2,000)	1327	30,850
LiF	847	(2,360)	1681	50,970	KPO ₃	817	2,110		
LiI	440	(1,420)	1171	40,770	K ₃ PO ₄	1340	8,900		
LiOH	462	2,480			K ₄ P ₂ O ₇	1092	14,000		
Li ₂ MoO ₄	705	4,200			K ₂ SO ₄	1074	8,100		
LiNO ₃					K ₂ TiO ₃	810	(10,600)		
Li ₂ SiO ₃	1177	7,210			K ₂ WO ₄	927	(4,400)		
Li ₂ SiO ₄	1249	7,430			Praseodymium				
Li ₂ SO ₄	857	3,040			Pr	932	2,700		
Li ₂ WO ₄	742	(6,700)			Radon				
Magnesium					Rn	-71		-61.8	4,010
Mg	650	2,160	1107	32,520	Rhenium				
MgBr ₂	711	8,300			Re	(3000)			
MgCl ₂	712	8,100	1418	32,690	Re ₂ O ₇	296	15,340	362.4	18,060
MgF ₂	1221	5,900			Re ₂ O ₈	147	3,800		
MgO	2642	18,500			Rubidium				
Mg ₃ (PO ₄) ₂	1184	(11,300)			Rb	39.1	525	679	18,110
MgSiO ₃	1524	14,700			RbBr	677	3,700	1352	37,120
MgSO ₄	1127	3,500			RbCl	717	4,400	1381	36,920
MgZn ₂	589	(8,270)			RbF	833	4,130	1408	39,510
Manganese					RbI	638	2,990	1304	35,960
Mn	1220	3,450	2152	55,150	RbNO ₃	305	1,340		
MnCl ₂	650	7,340	1190	29,630	Selenium				
MnSiO ₃	1274	(8,200)			Se ₂	217	1,220	753	25,490
MnTiO ₃	1404	(7,960)			Se ₈			736	20,600
Mercury					SeF ₆			-45.8 ^c	6,350 ^c
Hg	-38.9	557	361	13,980	SeO ₂			317 ^c	20,900
HgBr ₂	241	3,960	319	14,080	SeOCl ₂	10	1,010	168	
HgCl ₂	277	4,150	304	14,080	Silicon				
HgI ₂	250	4,500	354	14,260	Si	1427	9,470	2290	
HgSO ₄	850	(1,440)			SiCl ₄	-67.6	1,845	56.8	6,860
Molybdenum					Si ₂ Cl ₆	-1		139	
Mo	2622	(6,660)	(4800)	(128,000)	Si ₃ Cl ₈			211.4	12,340
MoF ₆	17	2,500	36	6,000	(SiCl ₃) ₂ O	-33		135.6	8,820
MoO ₃	745	(2,500)	1151		SiF ₄			-94.8 ^c	6,130 ^c
Neon					Si ₂ F ₆	-18.5	3,900	-18.9 ^c	10,400 ^c
Ne	-248.5	77	-246.0	440 ^c	SiF ₃ Cl	-138		-70.1	4,460
Nickel					SiF ₂ Cl ₂	-144		-31.5	5,080
Ni	1455	4,200	2730	87,300	SiH ₄	-185		-111.6	2,960
NiCl ₂			987 ^c	48,360 ^c	Si ₂ H ₆	-132.5		-14.3	5,110
Ni(CO) ₄			42.5	7,000	Si ₃ H ₈	-117		53.1	6,780
Ni ₂ S	645	(2,980)			Si ₄ H ₁₀	-93.5		100	8,890
Ni ₃ S ₂	790	5,800			SiH ₃ Br	-93.8		2.4	5,650
Nitrogen					SiH ₃ Br ₂	-70.0		70.5	6,840
N ₂	-210.0	172	-195.8	1,336	SiHCl ₃	-126.5		31.8	6,360
NF ₃			-129.0	3,000	(SiH ₃) ₂ N	-105.6		48.7	6,850
NH ₃	-77.7	1,352 ^c	-33.4	5,581 ^c	(SiH ₃) ₂ O	-144		-15.4	5,350
NH ₄ CNS	146	(4,700)			SiO ₂ (quartz)	1470	3,400	2230	
NH ₄ NO ₃	169.6	1,460			SiO ₂ (cristobalite)	1700	2,100		
N ₂ O	-90.8	1,563	-88.5	3,950	Silver				
NO	-163.6	550	-151.7	3,307	Ag	960.5	2,700	2212	60,720
N ₂ O ₄	-13	5,540	30	7,040	AgBr	430	2,180		
N ₂ O ₅			32.4	13,800 ^c	AgCl	455	3,155	1564	42,520
NOCl			-6.4	6,140	AgCN	350	2,750		
Osmium					AgI	557	2,250	1506	34,450
OsF ₈			47.4	6,840	AgNO ₃	209	2,755		
OsO ₄ (yellow)	56	4,060	130	9,450	Ag ₂ S	842	3,360		
OsO ₄ (white)	42	2,340			Ag ₂ SO ₄	657	(4,300)		
Oxygen					Sodium				
O ₂	-218.9	106	-183.0	1,629	Na	97.7	630	914	23,120
O ₃			-111	2,880	NaBO ₂	966	8,660		

TABLE 2-147 Heats of Fusion and Vaporization of the Elements and Inorganic Compounds (Concluded)

Substance	mp, °C	Heat of fusion, ^{a,b} cal/mol	bp at 1 atm, °C	Heat of vaporization, ^{a,b} cal/mol	Substance	mp, °C	Heat of fusion, ^{a,b} cal/mol	bp at 1 atm, °C	Heat of vaporization, ^{a,b} cal/mol
Sodium (Cont.)					Thallium				
NaBr	747	6,140	1392	37,950	Tl	302.5	1,030	1457	38,810
NaCl	800	7,220	1465	40,810	TlBr	460	5,990	819	23,800
NaClO ₃	255	5,290			TlCl	427	4,260	807	24,420
NaCN	562	(4,400)	1500	37,280	Tl ₂ CO ₃	273	4,400		
NaCNS	323	4,450			TlI	440	3,125	823	25,030
Na ₂ CO ₃	854	7,000			TlNO ₃	207	2,290		
NaF	992	7,000	1704	53,260	Tl ₂ S	449	3,000		
NaI	662	5,240			Tl ₂ SO ₄	632	5,500		
Na ₂ MoO ₄	687	3,600			Tin				
NaNO ₃	310	3,760			Sn	231.8	1,720	2270	68,000
NaOH	322	2,000	1378		SnBr ₂	232	(1,700)		
½Na ₂ O·½Al ₂ O ₃ ·3SiO ₂	1107	13,150			SnBr ₄	30	3,000		
NaPO ₃	988	(5,000)			SnCl ₂	247	3,050	623	20,740
Na ₄ P ₂ O ₇	970	(13,700)			SnCl ₄	-33.2	2,190	113	8,330
Na ₂ S	920	(1,200)			Sn(CH ₃) ₄			78.3	7,320
Na ₂ SiO ₃	1087	10,300			SnH ₄	-149.8		-52.3	4,420
Na ₂ Si ₂ O ₅	884	8,460			SnI ₄	143.5	(4,300)		
Na ₂ SO ₄	884	5,830			Titanium				
Na ₂ WO ₄	702	5,800			TiBr ₄	38.2	(2,060)		
Sr	757	2,190	1384	33,610	TiCl ₄	-23	2,240	136	8,350
SrBr ₂	643	4,780			TiO ₂	1825	(11,400)		
SrCl ₂	872	4,100			Tungsten				
SrF ₂	1400	4,260			W	3390	(8,400)	(5900)	(176,000)
Sr ₃ (PO ₄) ₂	1770	18,500			WF ₆	-0.4	1,800	17.3	6,350
Sulfur					Uranium				
S (rhombic)	112.8		444.6	2,200	UF ₆			55.1 ^c	9,990 ^c
S (monoclinic)	119.2				Xenon				
S ₂ Cl ₂			138	8,720	Xe	-111.5	740	-108.0	3,110
SF ₆			-63.5 ^d	5,600 ^e	Zinc				
SO ₂	-75.5	1,769 ^f	-5.0	5,960 ^f	Zn	419.5	1,595	907	27,430
SO ₃ (α)	17	2,060	44.8	10,190	ZnCl ₂	283	(5,500)	732	28,710
SO ₃ (β)	32.4	2,890			Zn(C ₂ H ₅) ₂			118	8,960
SO ₃ (γ)	62.2	6,310			ZnO	1975	4,470		
SOBr ₂			139.5	9,920	ZnS	1645	(9,000)		
SOCl ₂			75.4	7,600	Zirconium				
SO ₂ Cl ₂			69.2	7,760	ZrBr ₄			357 ^c	25,800 ^c
Tellurium					ZrCl ₄			311 ^c	25,290 ^c
Te	453	3,230	1090		ZrI ₄			431 ^c	29,030 ^c
TeCl ₄			392	16,830	ZrO ₂	2715	20,800		
TeF ₆			-38.6 ^g	6,700 ^g					

^a Values in parentheses are uncertain.
^b For the freezing point or the normal boiling point unless otherwise stated.
^c Sublimation.
^d Decomposes at about 75 °C; value obtained by extrapolation.
^e Bichowsky and Rossini, *Thermochemistry of the Chemical Substances*, Reinhold, New York (1936).
^f Decomposes before the normal boiling point is reached.
^g Decomposes at about 40 °C; value obtained by extrapolation.
^h See also pp. 2-304 through 2-307 on steam table.
ⁱ Giaque and Ruehrwein, *J. Am. Chem. Soc.*, **61** (1939): 2626.
^j Giaque and Egan, *J. Chem. Phys.*, **5** (1937): 45.

^k Kemp and Giaque, *J. Am. Chem. Soc.*, **59** (1937): 79.
^l Brown and Manov, *J. Am. Chem. Soc.*, **59** (1937): 500.
^m Giaque and Powell, *J. Am. Chem. Soc.*, **61** (1939): 1970.
ⁿ Overstreet and Giaque, *J. Am. Chem. Soc.*, **59** (1937): 254.
^o Stephenson and Giaque, *J. Chem. Phys.*, **5** (1937): 149.
^p Giaque and Stephenson, *J. Am. Chem. Soc.*, **60** (1938): 1389.
^q Osborne, Stimson, and Ginnings, *Bur. Standards J. Research*, **23**, 197 (1939): 261.
^r Miles and Menzies, *J. Am. Chem. Soc.*, **58** (1936): 1067.
^s Long and Kemp, *J. Am. Chem. Soc.*, **58** (1936): 1829.
^t Giaque and Blue, *J. Am. Chem. Soc.*, **58** (1936): 831.
^u Ruehrwein and Giaque, *J. Am. Chem. Soc.*, **61** (1939): 2940.

TABLE 2-148 Heats of Fusion of Miscellaneous Materials

Material	mp, °C	Heat of fusion, cal/g
Alloys		
30.5 Pb + 69.5 Sn	183	17
36.9 Pb + 63.1 Sn	179	15.5
63.7 Pb + 36.3 Sn	177.5	11.6
77.8 Pb + 22.2 Sn	176.5	9.54
1 Pb + 9 Sn	236	28
24 Pb + 27.3 Sn + 48.7 Bi	98.8	6.85
25.8 Pb + 14.7 Sn + 52.4 Bi + 7 Cd	75.5	8.4
Silicates		
Anorthite (CaAl ₂ Si ₂ O ₈)		100
Orthoclase (KAlSi ₃ O ₈)		100
Microcline (KAlSi ₃ O ₈)		83
Wollastonite (CaSiO ₃)		100
Malacolite (Ca ₈ MgSi ₄ O ₁₂)		94
Diopside (CaMgSi ₂ O ₄)		100
Olivine (Mg ₂ SiO ₄)		130
Fayalite (Fe ₂ SiO ₄)		85
Spermaceti	43.9	37.0
Wax (bees')	61.8	42.3

TABLE 2-149 Heats of Fusion of Organic Compounds

The values for the hydrocarbons are from the tables of the American Petroleum Institute Research Project 44 at the National Bureau of Standards, with some from Parks and Huffman, *Ind. Eng. Chem.*, **23**, 1138 (1931).

The values for the nonhydrocarbon compounds were recalculated from data in *International Critical Tables*, vol. 5.

Hydrocarbon compounds	Formula	mp, °C	Heat of fusion, cal/g	Hydrocarbon compounds	Formula	mp, °C	Heat of fusion, cal/g
Paraffins				Aromatics—(Cont.)			
Methane	CH ₄	-182.48	14.03	1-Methyl-3-ethylbenzene	C ₉ H ₁₂	-95.55	15.14
Ethane	C ₂ H ₆	-183.23	22.712	1-Methyl-4-ethylbenzene	C ₉ H ₁₂	-62.350	25.29
Propane	C ₃ H ₈	-187.65	19.100	1,2,3-Trimethylbenzene	C ₉ H ₁₂	-25.375	16.64
<i>n</i> -Butane	C ₄ H ₁₀	-138.33	19.167	1,2,4-Trimethylbenzene	C ₉ H ₁₂	-43.80	24.54
2-Methylpropane	C ₄ H ₁₀	-159.60	18.668	1,3,5-Trimethylbenzene	C ₉ H ₁₂	-44.720	18.97
<i>n</i> -Pentane	C ₅ H ₁₂	-129.723	27.874	Naphthalene	C ₁₀ H ₈	+80.0	36.0
2-Methylbutane	C ₅ H ₁₂	-159.890	17.076	Camphene	C ₁₀ H ₁₆	+51	57
2,2-Dimethylpropane	C ₅ H ₁₂	-16.6	10.786	Durene	C ₁₀ H ₁₄	+79.3	37.4
<i>n</i> -Hexane	C ₆ H ₁₄	-95.320	36.138	Isodurene	C ₁₀ H ₁₄	-24.0	23.0
2-Methylpentane	C ₆ H ₁₄	-153.680	17.407	Prehnitene	C ₁₀ H ₁₄	-7.7	20.0
2,2-Dimethylbutane	C ₆ H ₁₄	-99.73	1.607	<i>p</i> -Cymene	C ₁₀ H ₁₄	-68.9	17.1
2,3-Dimethylbutane	C ₆ H ₁₄	-128.41	2.251	<i>n</i> -Butyl benzene	C ₁₀ H ₁₄	-88.5	19.5
<i>n</i> -Heptane	C ₇ H ₁₆	-90.595	33.513	<i>tert</i> -Butyl benzene	C ₁₀ H ₁₄	-58.1	14.9
2-Methylhexane	C ₇ H ₁₆	-118.270	21.158	β -Methyl naphthalene	C ₁₁ H ₁₀	+34.1	20.1
3-Ethylpentane	C ₇ H ₁₆	-118.593	22.555	Diphenyl	C ₁₂ H ₁₀	+68.6	28.8
2,2-Dimethylpentane	C ₇ H ₁₆	-123.790	13.982	Hexamethyl benzene	C ₁₂ H ₁₈	+165.5	30.4
2,4-Dimethylpentane	C ₇ H ₁₆	-119.230	15.968	Diphenyl methane	C ₁₃ H ₁₂	+25.2	26.4
3,3-Dimethylpentane	C ₇ H ₁₆	-134.46	16.856	Anthracene	C ₁₄ H ₁₀	+216.5	38.7
2,2,3-Trimethylbutane	C ₇ H ₁₆	-24.96	5.250	Phenanthrene	C ₁₄ H ₁₀	+96.3	25.0
<i>n</i> -Octane	C ₈ H ₁₈	-56.798	43.169	Tolane	C ₁₁ H ₁₀	+60	28.7
2-Methylheptane	C ₈ H ₁₈	-109.04	21.458	Stilbene	C ₁₄ H ₁₂	+124	40.0
3-Methylheptane	C ₈ H ₁₈	-120.50	23.795	Dibenzil	C ₁₄ H ₁₄	+51.4	30.7
4-Methylheptane	C ₈ H ₁₈	-120.955	22.692	Triphenyl methane	C ₁₆ H ₁₆	+92.1	21.1
2,2-Dimethylhexane	C ₈ H ₁₈	-121.18	24.226	Alkyl cyclohexanes			
2,5-Dimethylhexane	C ₈ H ₁₈	-91.200	26.903	Cyclohexane	C ₆ H ₁₂	+6.67	7.569
3,3-Dimethylhexane	C ₈ H ₁₈	-126.10	14.9	Methylcyclohexane	C ₇ H ₁₄	-126.58	16.429
2-Methyl-3-ethylpentane	C ₈ H ₁₈	-114.960	23.690	Alkyl cyclopentanes			
3-Methyl-3-ethylpentane	C ₈ H ₁₈	-90.870	22.657	Cyclopentane	C ₅ H ₁₀	-93.80	2.068
2,2,3-Trimethylpentane	C ₈ H ₁₈	-112.27	18.061	Methylcyclopentane	C ₆ H ₁₂	-142.445	19.68
2,2,4-Trimethylpentane	C ₈ H ₁₈	-107.365	19.278	Ethylcyclopentane	C ₇ H ₁₄	-138.435	11.10
2,3,3-Trimethylpentane	C ₈ H ₁₈	-100.70	3.204	1,1-Dimethylcyclopentane	C ₇ H ₁₄	-69.73	3.36
2,3,4-Trimethylpentane	C ₈ H ₁₈	-109.210	19.392	<i>cis</i> -1,2-Dimethylcyclopentane	C ₇ H ₁₄	-53.85	3.87
2,2,3,3-Tetramethylbutane	C ₈ H ₁₈	+100.69	14.900	<i>trans</i> -1,2-Dimethylcyclopentane	C ₇ H ₁₄	-117.57	15.68
<i>n</i> -Nonane	C ₉ H ₂₀	-53.9	41.2	<i>trans</i> -1,3-Dimethylcyclopentane	C ₇ H ₁₄	-133.680	17.93
<i>n</i> -Decane	C ₁₀ H ₂₂	-30.0	48.3	Monoolefins			
<i>n</i> -Undecane	C ₁₁ H ₂₄	-25.9	34.1	Ethene (Ethylene)	C ₂ H ₄	-169.15	28.547
<i>n</i> -Dodecane	C ₁₂ H ₂₆	-9.6	51.3	Propene (Propylene)	C ₃ H ₆	-185.25	17.054
Eicosane	C ₂₀ H ₄₂	+36.4	52.0	1-Butene	C ₄ H ₈	-185.35	16.393
Pentacosane	C ₂₅ H ₅₂	+53.3	53.6	<i>cis</i> -2-Butene	C ₄ H ₈	-138.91	31.135
Tritriacontane	C ₃₃ H ₆₈	+71.1	54.0	<i>trans</i> -2-Butene	C ₄ H ₈	-105.55	41.564
Aromatics				2-Methylpropene (isobutene)	C ₄ H ₈	-140.35	25.265
Benzene	C ₆ H ₆	+5.533	30.100	1-Pentene	C ₅ H ₁₀	-165.27	16.82
Methylbenzene (Toluene)	C ₇ H ₈	-94.991	17.171	<i>cis</i> -2-pentene	C ₅ H ₁₀	-151.363	24.239
Ethylbenzene	C ₈ H ₁₀	-94.950	20.629	<i>trans</i> -2-pentene	C ₅ H ₁₀	-140.235	26.536
<i>o</i> -Xylene	C ₈ H ₁₀	-25.187	30.614	2-Methyl-1-butene	C ₆ H ₁₀	-137.560	26.879
<i>m</i> -Xylene	C ₈ H ₁₀	-47.872	26.045	3-Methyl-1-butene	C ₆ H ₁₀	-168.500	18.009
<i>p</i> -Xylene	C ₈ H ₁₀	+13.263	38.526	2-Methyl-2-butene	C ₆ H ₁₀	-133.780	25.738
<i>n</i> -Propylbenzene	C ₉ H ₁₂	-99.500	16.97	Acetylenes			
Isopropylbenzene	C ₉ H ₁₂	-96.028	19.22	Acetylene	C ₂ H ₂	-81.5	23.04
1-Methyl-2-ethylbenzene	C ₉ H ₁₂	-80.833	21.13	2-Butyne (dimethylacetylene)	C ₄ H ₆	-132.23	40.808
Nonhydrocarbon compounds	Formula	mp, °C	Heat of fusion, cal/g	Nonhydrocarbon compounds	Formula	mp, °C	Heat of fusion, cal/g
Acetic acid	C ₂ H ₄ O ₂	16.7	46.68	Butyl alcohol (<i>n</i> -)	C ₄ H ₁₀ O	-89.2	29.93
Acetone	C ₃ H ₆ O	-95.5	23.42	(<i>t</i> -)	C ₄ H ₁₀ O	25.4	21.88
Acrylic acid	C ₃ H ₄ O ₂	12.3	37.03	Butyric acid (<i>n</i> -)	C ₄ H ₈ O ₂	-5.7	30.04
Allo-cinnamic acid	C ₉ H ₈ O ₂	68	27.35	Capric acid (<i>n</i> -)	C ₁₀ H ₂₀ O ₂	31.99	38.87
Aminobenzoic acid (<i>o</i> -)	C ₇ H ₇ NO ₂	145	35.48	Caprylic acid (<i>n</i> -)	C ₈ H ₁₆ O ₂	16.3	35.40
(<i>m</i> -)	C ₇ H ₇ NO ₂	179.5	38.03	Carbazole	C ₁₂ H ₉ N	243	42.05
(<i>p</i> -)	C ₇ H ₇ NO ₂	188.5	36.46	Carbon tetrachloride	CCl ₄	-22.8	41.57
Amyl alcohol	C ₈ H ₁₈ O	-78.9	26.65	Carvoxime (<i>d</i> -)	C ₁₀ H ₁₅ NO	71.5	23.29
Anethole	C ₁₀ H ₁₂ O	22.5	25.80	(<i>l</i> -)	C ₁₀ H ₁₅ NO	71	23.41
Aniline	C ₆ H ₅ NH ₂	-6.3	27.09	(<i>dl</i> -)	C ₁₀ H ₁₅ NO	91	24.61
Anthraquinone	C ₁₄ H ₈ O ₂	284.8	37.48	Cetyl alcohol	C ₁₆ H ₃₄ O	49.27	33.80
Apiol	C ₁₂ H ₁₄ O ₄	29.5	25.80	Chloroacetic acid (α -)	C ₂ H ₃ ClO ₂	61.2	31.06
Azobenzene	C ₁₂ H ₁₀ N ₂	67.1	28.91	(β -)	C ₂ H ₂ ClO ₂	56	35.12
Azoxybenzene	C ₁₂ H ₁₀ N ₂ O	36	21.62	Chloral alcoholate	C ₂ H ₃ Cl ₂ O ₂	9	24.03
Benzil	C ₁₄ H ₁₀ O ₂	95.2	22.15	hydrate	C ₂ H ₃ Cl ₂ O ₂	47.4	33.18
Benzoic acid	C ₇ H ₆ O ₂	122.45	33.90	Chloroaniline (<i>p</i> -)	C ₆ H ₆ ClN	71	37.15
Benzophenone	C ₁₂ H ₁₀ O	47.85	23.53	Chlorobenzoic acid (<i>o</i> -)	C ₇ H ₅ ClO ₂	140.2	39.30
Benzylaniline	C ₁₅ H ₁₃ N	32.37	21.86	(<i>m</i> -)	C ₇ H ₅ ClO ₂	154.25	36.41
Bromocamphor	C ₁₀ H ₁₅ BrO	78	41.57	(<i>p</i> -)	C ₇ H ₅ ClO ₂	239.7	49.21
Bromochlorobenzene (<i>o</i> -)	C ₆ H ₄ BrCl	-12.6	15.41	Chloronitrobenzene (<i>m</i> -)	C ₆ H ₄ ClNO ₂	44.4	29.38
(<i>m</i> -)	C ₆ H ₄ BrCl	-21.2	15.29	(<i>p</i> -)	C ₆ H ₄ ClNO ₂	83.5	31.51
(<i>p</i> -)	C ₆ H ₄ BrCl	64.6	23.41	Cinnamic acid	C ₉ H ₈ O ₂	133	36.50
Bromiodobenzene (<i>o</i> -)	C ₆ H ₄ BrI	21	12.18	anhydride	C ₁₈ H ₁₄ O ₃	48	28.14
(<i>m</i> -)	C ₆ H ₄ BrI	9.3	10.27	Cresol (<i>p</i> -)	C ₇ H ₈ O	34.6	26.28
(<i>p</i> -)	C ₆ H ₄ BrI	90.1	16.60	Crotonic acid (α -)	C ₄ H ₆ O ₂	72	25.32
Bromol hydrate	C ₂ H ₃ Br ₂ O ₂	46	16.90	(<i>cis</i> -)	C ₄ H ₆ O ₂	71.2	34.90
Bromophenol (<i>p</i> -)	C ₆ H ₅ BrO	63.5	20.50	Cyanamide	CH ₃ N ₂	44	49.81
Bromotoluene (<i>p</i> -)	C ₇ H ₇ Br	28	20.86	Cyclohexanol	C ₆ H ₁₂ O	25.46	4.19

TABLE 2-149 Heats of Fusion of Organic Compounds (Concluded)

Nonhydrocarbon compounds	Formula	mp, °C	Heat of fusion, cal/g	Nonhydrocarbon compounds	Formula	mp, °C	Heat of fusion, cal/g
Dibromobenzene (<i>o</i> -)	C ₆ H ₄ Br ₂	1.8	12.78	Naphthol (α -)	C ₁₀ H ₈ O	95.0	38.94
(<i>m</i> -)	C ₆ H ₄ Br ₂	-6.9	13.38	(β -)	C ₁₀ H ₈ O	120.6	31.30
(<i>p</i> -)	C ₆ H ₄ Br ₂	86	20.55	Naphthylamine (α -)	C ₁₀ H ₉ N	50	22.34
Dibromophenol (2, 4-)	C ₆ H ₃ Br ₂ O	12	13.97	Nitroaniline (<i>o</i> -)	C ₆ H ₆ N ₂ O ₂	71.2	27.88
Dichloroacetic acid	C ₂ H ₂ Cl ₂ O ₂	-4(?)	14.21	(<i>m</i> -)	C ₆ H ₆ N ₂ O ₂	114.0	40.97
Dichlorobenzene (<i>o</i> -)	C ₆ H ₄ Cl ₂	-16.7	21.02	(<i>p</i> -)	C ₆ H ₆ N ₂ O ₂	147.3	36.46
(<i>m</i> -)	C ₆ H ₄ Cl ₂	-24.8	20.55	Nitrobenzene	C ₆ H ₅ NO ₂	5.85	22.52
(<i>p</i> -)	C ₆ H ₄ Cl ₂	53.13	29.67	Nitrobenzoic acid (<i>o</i> -)	C ₇ H ₅ NO ₄	145.8	40.06
Dihydroxybenzene (<i>o</i> -)	C ₆ H ₆ O ₂	104.3	49.40	(<i>m</i> -)	C ₇ H ₅ NO ₄	141.1	27.59
(<i>m</i> -)	C ₆ H ₆ O ₂	109.65	46.20	(<i>p</i> -)	C ₇ H ₅ NO ₄	239.2	52.80
(<i>p</i> -)	C ₆ H ₆ O ₂	172.3	58.77	Nitronaphthalene	C ₁₀ H ₇ NO ₂	56.7	25.44
Di-iodobenzene (<i>o</i> -)	C ₆ H ₄ I ₂	23.4	10.15	Nitrophenol (<i>o</i> -)	C ₆ H ₅ NO ₃	45.13	26.76
(<i>m</i> -)	C ₆ H ₄ I ₂	34.2	11.54	Palmitic acid	C ₁₆ H ₃₂ O ₂	61.82	39.18
(<i>p</i> -)	C ₆ H ₄ I ₂	129	16.20	Paraldehyde	C ₆ H ₁₂ O ₃	10.5	25.02
Dimethyl tartrate (<i>dl</i> -)	C ₈ H ₁₀ O ₆	87	35.12	Pelargic acid (<i>n</i> -) (β -)	C ₉ H ₁₈ O ₂		39.04
pyrone	C ₆ H ₄ O ₂	49	21.50	Pelargonic acid (<i>n</i> -) (α -)	C ₉ H ₁₈ O ₂	12.35	30.63
Dinitrobenzene (<i>o</i> -)	C ₆ H ₄ N ₂ O ₄	116.93	32.25	Phenol	C ₆ H ₆ O	40.92	29.03
(<i>m</i> -)	C ₆ H ₄ N ₂ O ₄	89.7	24.70	Phenylacetic acid	C ₈ H ₈ O ₂	76.7	25.44
(<i>p</i> -)	C ₆ H ₄ N ₂ O ₄	173.5	39.99	Phenylhydrazine	C ₈ H ₈ N ₂	19.6	36.31
Dinitrotoluene (2, 4-)	C ₇ H ₆ N ₂ O ₄	70.14	26.40	Propyl ether (<i>n</i>)	C ₆ H ₁₄ O	-126.1	20.66
Dioxane	C ₄ H ₈ O ₂	11.0	34.85	Quinone	C ₆ H ₄ O ₂	115.7	40.85
Diphenyl amine	C ₁₂ H ₁₁ N	52.98	25.23	Stearic acid	C ₁₈ H ₃₆ O ₂	68.82	47.54
Elaidic acid	C ₁₈ H ₃₄ O ₂	44.4	52.08	Succinic anhydride	C ₆ H ₈ O ₃	119	48.74
Ethyl acetate	C ₄ H ₈ O ₂	83.8	28.43	Succinonitrile	C ₄ H ₄ N ₂	54.5	11.71
alcohol	C ₂ H ₆ O	-114.4	25.76	Tetrachloroethylene (<i>o</i> -)	C ₂ Cl ₄	86	21.02
Ethylene dibromide	C ₂ H ₄ Br ₂	10.012	13.52	(<i>p</i> -)	C ₂ Cl ₄	95	22.10
Ethyl ether	C ₄ H ₁₀ O	-116.3	23.54	Thiophene	C ₄ H ₄ S	-39.4	14.11
Formic acid	CH ₂ O ₂	8.40	58.89	Thiosinamine	C ₇ H ₈ N ₂ S	77	33.45
Glutaric acid	C ₆ H ₈ O ₄	97.5	37.39	Thymol	C ₁₀ H ₁₄ O	51.5	27.47
Glycerol	C ₃ H ₈ O ₃	18.07	47.49	Toluic acid (<i>o</i> -)	C ₈ H ₈ O ₂	103.7	35.40
Glycol, ethylene	C ₂ H ₆ O ₂	-11.5	43.26	(<i>m</i> -)	C ₈ H ₈ O ₂	108.75	27.59
Hydrazo benzene	C ₁₂ H ₁₂ N ₂	134	22.89	(<i>p</i> -)	C ₈ H ₈ O ₂	179.6	39.90
Hydrocinnamic acid	C ₉ H ₁₀ O ₂	48	28.14	Tohidine (<i>p</i> -)	C ₇ H ₈ N	43.3	39.90
Hydroxyacetanilide	C ₈ H ₉ NO ₂	91.3	33.59	Tribromophenol (2, 4, 6-)	C ₆ H ₃ Br ₃ O	93	13.38
Iodotoluene (<i>p</i> -)	C ₇ H ₇ I	34	18.75	Trichloroacetic acid	C ₂ HCl ₃ O ₂	57.5	8.60
Isopropyl alcohol	C ₃ H ₈ O	-88.5	21.08	Trinitroglycerol	C ₃ H ₅ N ₃ O ₉	12.3	23.02
ether	C ₆ H ₁₄ O	-86.8	25.79	Trinitrotoluene (2, 4, 6-)	C ₇ H ₅ N ₃ O ₆	80.83	22.34
Lauric acid (<i>n</i> -)	C ₁₂ H ₂₄ O ₂	43.22	43.72	Tristearin	C ₅₇ H ₁₁₀ O ₆	70.8, 54.5	45.63
Levulinic acid	C ₅ H ₈ O ₃	33	18.97	Undecylic acid (α -) (<i>n</i> -)	C ₁₁ H ₂₂ O ₂	28.25	32.20
Menthol (<i>L</i> -) (α)	C ₁₀ H ₂₀ O	43.5	18.63	(β -) (<i>n</i> -)	C ₁₁ H ₂₂ O ₂		42.91
Methyl alcohol	CH ₄ O	-97.8	23.7	Urethane	C ₃ H ₇ NO ₂	48.7	40.85
Myristic acid	C ₁₄ H ₂₈ O ₂	53.86	47.49	Veratrol	C ₈ H ₁₀ O ₂	22.5	27.45
Methyl cinnamate	C ₁₀ H ₁₀ O ₂	36	26.53	Xylene dibromide (<i>o</i> -)	C ₈ H ₈ Br ₂	95	24.25
fumarate	C ₈ H ₈ O ₄	102	57.93	(<i>m</i> -)	C ₈ H ₈ Br ₂	77	21.45
oxalate	C ₄ H ₄ O ₄	54.35	42.64	dichloride (<i>o</i> -)	C ₈ H ₆ Cl ₂	55	29.03
phenylpropionate	C ₁₀ H ₈ O ₂	18	22.86	(<i>m</i> -)	C ₈ H ₆ Cl ₂	34	26.64
succinate	C ₈ H ₁₀ O ₄	19.5	35.72	(<i>p</i> -)	C ₈ H ₆ Cl ₂	100	32.73

TABLE 2-150 Heats of Vaporization of Inorganic and Organic Liquids (J/kmol)

Cmpd. no.	Name	Formula	CAS no.	Mol. wt.	C1 × 1E-07	C2	C3	C4	T _{min} , K	ΔH_v , at T _{min} × 1E-07	T _{max} , K	ΔH_v , at T _{max}
1	Acetaldehyde	C ₂ H ₄ O	75-07-0	44.053	3.8366	0.40081			150.15	3.2828	466.00	0
2	Acetamide	C ₂ H ₅ NO	60-35-5	59.067	8.107	0.42			353.15	6.2386	761.00	0
3	Acetic acid	C ₂ H ₄ O ₂	64-19-7	60.052	4.0179	2.6037	-5.0031	2.7069	289.81	2.3412	591.95	0
4	Acetic anhydride	C ₄ H ₆ O ₃	108-24-7	102.089	6.352	0.3986			200.15	5.4139	606.00	0
5	Acetone	C ₃ H ₆ O	67-64-1	58.079	4.215	0.3397			178.45	3.6390	508.20	0
6	Acetonitrile	C ₂ H ₃ N	75-05-8	41.052	4.3511	0.34765			229.32	3.5996	545.50	0
7	Acetylene	C ₂ H ₂	74-86-2	26.037	2.3214	0.35938			192.40	1.6333	308.30	0
8	Acrolein	C ₃ H ₄ O	107-02-8	56.063	3.8736	0.29335			185.45	3.3881	506.00	0
9	Acrylic acid	C ₃ H ₄ O ₂	79-10-7	72.063	4.3756	2.2571	-4.5116	2.5738	286.15	2.7965	615.00	0
10	Acrylonitrile	C ₃ H ₃ N	107-13-1	53.063	4.155	0.2733			189.63	3.6866	535.00	0
11	Air	Mixture	132259-10-0	28.960	0.8474	0.3822			59.15	0.6759	132.45	0
12	Ammonia	H ₃ N	7664-41-7	17.031	3.1523	0.3914	-0.2289	0.2309	195.41	2.5298	405.65	0
13	Anisole	C ₇ H ₈ O	100-66-3	108.138	5.8662	0.37127			235.65	4.9560	645.60	0
14	Argon	Ar	7440-37-1	39.948	0.87308	0.3526			83.78	0.6561	150.86	0
15	Benzamide	C ₇ H ₇ NO	55-21-0	121.137	8.7809	0.1933	0.30877	-0.14162	403.00	7.1286	824.00	0
16	Benzene	C ₆ H ₆	71-43-2	78.112	4.5346	0.39053			278.68	3.4705	562.05	0
17	Benzenethiol	C ₆ H ₆ S	108-98-5	110.177	6.225	0.4412			258.27	5.0597	689.00	0
18	Benzoic acid	C ₇ H ₆ O ₂	65-85-0	122.121	10.19	0.478			395.45	7.1277	751.00	0
19	Benzonitrile	C ₇ H ₅ N	100-47-0	103.121	6.8077	0.63344	-0.27365		260.40	5.3147	699.35	0
20	Benzophenone	C ₁₃ H ₁₀ O	119-61-9	182.218	10.523	0.87091	-0.45568		321.35	7.4895	830.00	0
21	Benzyl alcohol	C ₇ H ₈ O	100-51-6	108.138	8.4762	0.35251	0.43853	-0.3026	257.85	6.8800	720.15	0
22	Benzyl ethyl ether	C ₉ H ₁₂ O	539-30-0	136.191	6.228	0.3411			275.65	5.1829	662.00	0
23	Benzyl mercaptan	C ₇ H ₈ S	100-53-8	124.203	6.9642	0.44354			243.95	5.7930	718.00	0
24	Biphenyl	C ₁₂ H ₁₀	92-52-4	154.208	7.635	0.39182			342.20	6.0719	773.00	0
25	Bromine	Br ₂	7726-95-6	159.808	4	0.351			265.85	3.2323	584.15	0
26	Bromobenzene	C ₆ H ₅ Br	108-86-1	157.008	5.552	0.37694			242.43	4.6875	670.15	0
27	Bromoethane	C ₂ H ₅ Br	74-96-4	108.965	3.9004	0.38012			154.55	3.3933	503.80	0
28	Bromomethane	CH ₃ Br	74-83-9	94.939	3.169	0.3015			179.47	2.7379	467.00	0
29	1,2-Butadiene	C ₄ H ₆	590-19-2	54.090	3.522	0.395			136.95	3.0540	452.00	0
30	1,3-Butadiene	C ₄ H ₆	106-99-0	54.090	3.2632	0.3701			164.25	2.7235	425.00	0
31	Butane	C ₄ H ₁₀	106-97-8	58.122	3.6238	0.8337	-0.82274	0.39613	134.86	2.8684	425.12	0
32	1,2-Butanediol	C ₄ H ₁₀ O ₂	584-03-2	90.121	8.9754	0.45316			220.00	7.5185	680.00	0
33	1,3-Butanediol	C ₄ H ₁₀ O ₂	107-88-0	90.121	9.2247	0.42442			196.15	7.9759	676.00	0
34	1-Butanol	C ₄ H ₁₀ O	71-36-3	74.122	7.1274	0.0483	0.8966	-0.5116	183.85	6.3643	563.10	0
35	2-Butanol	C ₄ H ₁₀ O	78-92-2	74.122	7.9227	0.58361	0.02016	-0.08654	158.45	6.4607	535.90	0
36	1-Butene	C ₄ H ₈	106-98-9	56.106	3.3774	0.5107	-0.17304	0.05181	87.80	3.0197	419.50	0
37	cis-2-Butene	C ₄ H ₈	590-18-1	56.106	3.4358	0.38004			134.26	2.9867	435.50	0
38	trans-2-Butene	C ₄ H ₈	624-64-6	56.106	3.3191	0.36968			167.62	2.7630	428.60	0
39	Butyl acetate	C ₈ H ₁₆ O ₂	123-86-4	116.158	5.8276	0.38854			199.65	4.9384	575.40	0
40	Butylbenzene	C ₁₀ H ₁₄	104-51-8	134.218	6.3487	0.38222			185.30	5.5979	660.50	0
41	Butyl mercaptan	C ₄ H ₁₀ S	109-79-5	90.187	4.9702	0.41199			157.46	4.3505	570.10	0
42	sec-Butyl mercaptan	C ₄ H ₁₀ S	513-53-1	90.187	4.6432	0.399			133.02	4.1614	554.00	0
43	1-Butyne	C ₄ H ₆	107-00-6	54.090	3.6972	0.39168			147.43	3.1511	440.00	0
44	Butyraldehyde	C ₄ H ₈ O	123-72-8	72.106	4.6403	0.3849			176.75	3.9797	537.20	0
45	Butyric acid	C ₄ H ₈ O ₂	107-92-6	88.105	6.1947	1.6524	-2.8505	1.6285	250.00	4.1619	615.70	0
46	Butyronitrile	C ₃ H ₇ N	109-74-0	69.105	5.22	0.165	0.6692	-0.539	161.25	4.7223	582.25	0
47	Carbon dioxide	CO ₂	124-38-9	44.010	2.173	0.382	-0.4339	0.42213	216.58	1.5202	304.21	0
48	Carbon disulfide	CS ₂	75-15-0	76.141	3.496	0.2986			161.11	3.1537	552.00	0
49	Carbon monoxide	CO	630-08-0	28.010	0.8585	0.4921	-0.326	0.2231	68.13	0.6517	132.50	915,280
50	Carbon tetrachloride	CCl ₄	56-23-5	153.823	4.3252	0.37688			250.33	3.4528	556.35	0
51	Carbon tetrafluoride	CF ₄	75-73-0	88.004	1.9311	0.94983	-1.0615	0.51894	89.56	1.4215	227.51	0
52	Chlorine	Cl ₂	7782-50-5	70.906	3.068	0.8458	-0.9001	0.453	172.12	2.2878	417.15	0
53	Chlorobenzene	C ₆ H ₅ Cl	108-90-7	112.557	5.148	0.36614			227.95	4.3707	632.35	0
54	Chloroethane	C ₂ H ₅ Cl	75-00-3	64.514	3.524	0.3652			134.80	3.1052	460.35	0
55	Chloroform	CHCl ₃	67-66-3	119.378	4.186	0.3584			209.63	3.5047	536.40	0
56	Chloromethane	CH ₃ Cl	74-87-3	50.488	2.9745	0.353			175.43	2.4520	416.25	0
57	1-Chloropropane	C ₃ H ₇ Cl	540-54-5	78.541	3.989	0.37956			150.35	3.4862	503.15	0
58	2-Chloropropane	C ₃ H ₇ Cl	75-29-6	78.541	3.8871	0.38043			155.97	3.3586	489.00	0
59	m-Cresol	C ₇ H ₈ O	108-39-4	108.138	8.0082	0.45314			285.39	6.3326	705.85	0

60	<i>o</i> -Cresol	C ₇ H ₈ O	95-48-7	108.138	7.1979	0.40317			304.19	5.7135	697.55	0
61	<i>p</i> -Cresol	C ₇ H ₈ O	106-44-5	108.138	8.4942	0.50234			307.93	6.3649	704.65	0
62	Cumene	C ₉ H ₁₂	98-82-8	120.192	5.766	0.38939			177.14	5.0717	631.00	0
63	Cyanogen	C ₂ N ₂	460-19-5	52.035	3.384	0.3707			245.25	2.3803	400.15	0
64	Cyclobutane	C ₄ H ₈	287-23-0	56.106	3.334	0.3395			182.48	-2.8083	459.93	0
65	Cyclohexane	C ₆ H ₁₂	110-82-7	84.159	4.4902	0.39881			279.69	3.3920	553.80	0
66	Cyclohexanol	C ₆ H ₁₂ O	108-93-0	100.159	9.1791	0.6382			296.60	6.2221	650.10	0
67	Cyclohexanone	C ₆ H ₁₀ O	108-94-1	98.143	5.6772	0.37431			242.00	4.7739	653.00	0
68	Cyclohexene	C ₆ H ₁₀	110-83-8	82.144	4.4405	0.37479			169.67	3.8791	560.40	0
69	Cyclopentane	C ₅ H ₁₀	287-92-3	70.133	3.8911	0.36111			179.28	3.3299	511.70	0
70	Cyclopentene	C ₅ H ₈	142-29-0	68.117	3.8107	0.3543			138.13	3.4046	507.00	0
71	Cyclopropane	C ₃ H ₆	75-19-4	42.080	2.7672	0.35588			145.59	2.3532	398.00	0
72	Cyclohexyl mercaptan	C ₆ H ₁₂ S	1569-69-3	116.224	5.6067	0.38729			189.64	4.9220	664.00	0
73	Decanal	C ₁₀ H ₂₀ O	112-31-2	156.265	7.9073	0.4129			267.15	6.4201	674.20	0
74	Decane	C ₁₀ H ₂₂	124-18-5	142.282	6.6126	0.39797			243.51	5.4168	617.70	0
75	Decanoic acid	C ₁₀ H ₂₀ O ₂	334-48-5	172.265	13.107	1.0674	-0.97372	0.40491	304.55	8.7931	722.10	0
76	1-Decanol	C ₁₀ H ₂₂ O	112-30-1	158.281	7.9041	-1.36	4.0854	-2.3871	280.05	8.2959	688.00	0
77	1-Decene	C ₁₀ H ₂₀	872-05-9	140.266	6.6985	0.76944	-0.79975	0.42379	206.89	5.3524	616.60	0
78	Decyl mercaptan	C ₁₀ H ₂₂ S	143-10-2	174.347	8.0617	0.41045			247.56	6.7308	696.00	0
79	1-Decyne	C ₁₀ H ₁₈	764-93-2	138.250	6.9461	0.42109			229.15	5.7192	619.85	0
80	Deuterium	D ₂	7782-39-0	4.032	0.1657	0.352			18.73	0.1309	38.35	0
81	1,1-Dibromoethane	C ₂ H ₄ Br ₂	557-91-5	187.861	5.712	0.5255			210.15	4.6111	628.00	0
82	1,2-Dibromoethane	C ₂ H ₄ Br ₂	106-93-4	187.861	5.37	0.416			282.85	4.2346	650.15	0
83	Dibromomethane	CH ₂ Br ₂	74-95-3	173.835	4.82	0.3771			220.60	4.0709	611.00	0
84	Dibutyl ether	C ₈ H ₁₈ O	142-96-1	130.228	5.9616	0.38833			175.30	5.1902	584.10	0
85	<i>m</i> -Dichlorobenzene	C ₆ H ₄ Cl ₂	541-73-1	147.002	5.6899	0.35765			248.39	4.8419	683.95	0
86	<i>o</i> -Dichlorobenzene	C ₆ H ₄ Cl ₂	95-50-1	147.002	6.2117	0.42845			256.15	5.1191	705.00	0
87	<i>p</i> -Dichlorobenzene	C ₆ H ₄ Cl ₂	106-46-7	147.002	5.9765	0.38559			326.14	4.6573	684.75	0
88	1,1-Dichloroethane	C ₂ H ₄ Cl ₂	75-34-3	98.959	4.2117	0.36927			176.19	3.6189	523.00	0
89	1,2-Dichloroethane	C ₂ H ₄ Cl ₂	107-06-2	98.959	4.5507	0.34444			237.49	3.7657	561.60	0
90	Dichloromethane	CH ₂ Cl ₂	75-09-2	84.933	4.186	0.4092			178.01	3.5116	510.00	0
91	1,1-Dichloropropane	C ₃ H ₆ Cl ₂	78-99-9	112.986	4.774	0.39204			200.00	4.0147	560.00	0
92	1,2-Dichloropropane	C ₃ H ₆ Cl ₂	78-87-5	112.986	4.675	0.36529			172.71	4.0997	572.00	0
93	Diethanol amine	C ₄ H ₁₁ NO ₂	111-42-2	105.136	10.154	0.3403			301.15	8.4908	736.60	0
94	Diethyl amine	C ₄ H ₁₁ N	109-89-7	73.137	4.6133	0.42628			223.35	3.5761	496.60	0
95	Diethyl ether	C ₄ H ₁₀ O	60-29-7	74.122	4.06	0.3868			156.85	3.4651	466.70	0
96	Diethyl sulfide	C ₄ H ₁₀ S	352-93-2	90.187	4.7659	0.37987			169.20	4.1537	557.15	0
97	1,1-Difluoroethane	C ₂ H ₄ F ₂	75-37-6	66.050	3.2312	0.37653			154.56	2.6659	386.44	0
98	1,2-Difluoroethane	C ₂ H ₄ F ₂	624-72-6	66.050	3.4552	0.3499			215.00	2.7427	445.00	0
99	Difluoromethane	CH ₂ F ₂	75-10-5	52.023	2.8081	0.3364			136.95	2.3781	351.26	0
100	Di-isopropyl amine	C ₆ H ₁₅ N	108-18-9	101.190	5.007	0.4362			176.85	4.1823	523.10	0
101	Di-isopropyl ether	C ₆ H ₁₄ O	108-20-3	102.175	4.6117	0.4			187.65	3.8207	500.05	0
102	Di-isopropyl ketone	C ₇ H ₁₄ O	565-80-0	114.185	5.0256	0.29611			204.81	4.4125	576.00	0
103	1,1-Dimethoxyethane	C ₄ H ₁₀ O ₂	534-15-6	90.121	4.3872	0.56226	-0.60662	0.4202	159.95	3.7528	507.80	0
104	1,2-Dimethoxypropane	C ₅ H ₁₂ O ₂	7778-85-0	104.148	4.7999	0.30724	-0.024545	0.091361	226.10	4.0557	543.00	0
105	Dimethyl acetylene	C ₄ H ₆	503-17-3	54.090	3.856	0.2957			240.91	2.9577	473.20	0
106	Dimethyl amine	C ₂ H ₇ N	124-40-3	45.084	4.09	0.42005			180.96	3.2678	437.20	0
107	2,3-Dimethylbutane	C ₆ H ₁₄	79-29-8	86.175	4.1509	0.38383			145.19	3.6388	500.00	0
108	1,1-Dimethylcyclohexane	C ₈ H ₁₆	590-66-9	112.213	5.0402	0.4036			239.66	4.0862	591.15	0
109	<i>cis</i> -1,2-Dimethylcyclohexane	C ₈ H ₁₆	2207-01-4	112.213	5.2852	0.41607			223.16	4.3662	606.15	0
110	<i>trans</i> -1,2-Dimethylcyclohexane	C ₈ H ₁₆	6876-23-9	112.213	5.1194	0.405			184.99	4.4043	596.15	0
111	Dimethyl disulfide	C ₂ H ₆ S ₂	624-92-0	94.199	4.9825	0.3958			188.44	4.3108	615.00	0
112	Dimethyl ether	C ₂ H ₆ O	115-10-6	46.068	2.994	0.3505			131.65	2.6032	400.10	0
113	<i>N,N</i> -Dimethyl formamide	C ₃ H ₇ NO	68-12-2	73.094	5.9217	0.37996			212.72	5.0931	649.60	0
114	2,3-Dimethylpentane	C ₇ H ₁₆	565-59-3	100.202	4.6533	0.37577			160.00	4.0745	537.30	0
115	Dimethyl phthalate	C ₁₀ H ₁₀ O ₄	131-11-3	194.184	8.1578	0.29346			274.18	7.1632	766.00	0
116	Dimethylsilane	C ₂ H ₆ Si	1111-74-6	60.170	2.8365	0.35393			122.93	2.4928	402.00	0
117	Dimethyl sulfide	C ₂ H ₆ S	75-18-3	62.134	3.9022	0.37731			174.88	3.3213	503.04	0
118	Dimethyl sulfoxide	C ₂ H ₆ OS	67-68-5	78.133	6.629	0.4084			291.67	5.3804	729.00	0
119	Dimethyl terephthalate	C ₁₀ H ₁₀ O ₄	120-61-6	194.184	7.236	0.2424			413.80	6.0070	772.00	0
120	1,4-Dioxane	C ₄ H ₈ O ₂	123-91-1	88.105	5.051	0.3791			284.95	3.9263	587.00	0
121	Diphenyl ether	C ₁₂ H ₁₀ O	101-84-8	170.207	6.8243	0.30877			300.03	5.8546	766.80	0
122	Dipropyl amine	C ₆ H ₁₅ N	142-84-7	101.190	5.428	0.3665			210.15	4.5500	550.00	0

TABLE 2-150 Heats of Vaporization of Inorganic and Organic Liquids (J/kmol) (Continued)

Cmpd. no.	Name	Formula	CAS no.	Mol. wt.	C1 × 1E-07	C2	C3	C4	T _{min} , K	ΔH_v at T _{min} × 1E-07	T _{max} , K	ΔH_v at T _{max}
123	Dodecane	C ₁₂ H ₂₆	112-40-3	170.335	7.7337	0.40681			263.57	6.2802	658.00	0
124	Eicosane	C ₂₀ H ₄₂	112-95-8	282.547	12.86	0.50351	0.32986	-0.42184	309.58	9.5933	768.00	0
125	Ethane	C ₂ H ₆	74-84-0	30.069	2.1091	0.60646	-0.55492	0.32799	90.35	1.7879	305.32	0
126	Ethanol	C ₂ H ₆ O	64-17-5	46.068	5.5789	0.31245			159.05	4.9694	514.00	0
127	Ethyl acetate	C ₄ H ₈ O ₂	141-78-6	88.105	4.933	0.37804			189.60	4.1490	523.30	0
128	Ethyl amine	C ₂ H ₇ N	75-04-7	45.084	4.275	0.5857	-0.332	0.169	192.15	3.2955	456.15	0
129	Ethylbenzene	C ₈ H ₁₀	100-41-4	106.165	5.4805	0.39524			178.20	4.7900	617.15	0
130	Ethyl benzoate	C ₉ H ₁₀ O ₂	93-89-0	150.175	6.7093	0.33273			238.45	5.8382	698.00	0
131	2-Ethyl butanoic acid	C ₆ H ₁₂ O ₂	88-09-5	116.158	7.898	0.39445			258.15	6.4816	655.00	0
132	Ethyl butyrate	C ₆ H ₁₂ O ₂	105-54-4	116.158	5.6419	0.37985			175.15	4.9090	571.00	0
133	Ethylcyclohexane	C ₈ H ₁₆	1678-91-7	112.213	5.3832	0.41763			161.84	4.7318	609.15	0
134	Ethylcyclopentane	C ₇ H ₁₄	1640-89-7	98.186	4.8287	0.37804			134.71	4.3603	569.50	0
135	Ethylene	C ₂ H ₄	74-85-1	28.053	1.8844	0.36485			104.00	1.5936	282.34	0
136	Ethylenediamine	C ₂ H ₆ N ₂	107-15-3	60.098	5.7521	0.34513			284.29	4.5918	593.00	0
137	Ethylene glycol	C ₂ H ₆ O ₂	107-21-1	62.068	8.3518	0.42625			260.15	6.8989	720.00	0
138	Ethyleneimine	C ₂ H ₅ N	151-56-4	43.068	4.94	0.466			195.20	4.0022	537.00	0
139	Ethylene oxide	C ₂ H ₄ O	75-21-8	44.053	3.6652	0.37878			160.65	3.1271	469.15	0
140	Ethyl formate	C ₃ H ₆ O ₂	109-94-4	74.079	4.5909	0.4123			193.55	3.7679	508.40	0
141	2-Ethyl hexanoic acid	C ₈ H ₁₆ O ₂	149-57-5	144.211	11.184	0.86189	-0.47845	0.048646	235.00	8.2832	674.60	0
142	Ethylhexyl ether	C ₈ H ₁₈ O	5756-43-4	130.228	6.2786	0.39513			180.00	5.4262	583.00	0
143	Ethylisopropyl ether	C ₅ H ₁₂ O	625-54-7	88.148	4.258	0.37221			140.00	3.7556	489.00	0
144	Ethylisopropyl ketone	C ₆ H ₁₂ O	565-69-5	100.159	5.2207	0.34893			204.15	4.4677	567.00	0
145	Ethyl mercaptan	C ₂ H ₆ S	75-08-1	62.134	3.844	0.37534			125.26	3.4489	499.15	0
146	Ethyl propionate	C ₅ H ₁₀ O ₂	105-37-3	102.132	5.3325	0.401			199.25	4.4449	546.00	0
147	Ethylpropyl ether	C ₅ H ₁₂ O	628-32-0	88.148	5.438	0.60624			145.65	4.4140	500.23	0
148	Ethyltrichlorosilane	C ₂ H ₅ Cl ₃ Si	115-21-9	163.506	4.9482	0.39871			167.55	4.2942	559.95	0
149	Fluorine	F ₂	7782-41-4	37.997	0.88757	0.34072			53.48	0.7578	144.12	0
150	Fluorobenzene	C ₆ H ₅ F	462-06-6	96.102	4.582	0.3717			230.94	3.7605	560.09	0
151	Fluoroethane	C ₂ H ₅ F	353-36-6	48.060	2.7617	0.32162			129.95	2.4089	375.31	0
152	Fluoromethane	CH ₃ F	593-53-3	34.033	2.4708	0.37014			131.35	2.0276	317.42	0
153	Formaldehyde	CH ₂ O	50-00-0	30.026	3.076	0.2954			181.15	2.5863	408.00	0
154	Formamide	CH ₃ NO	75-12-7	45.041	7.358	0.3564			275.70	6.2844	771.00	0
155	Formic acid	CH ₂ O ₂	64-18-6	46.026	2.3195	1.9091	-5.0003	3.2641	250.00	1.8865	588.00	0
156	Furan	C ₄ H ₄ O	110-00-9	68.074	4.005	0.3995			196.29	3.2647	490.15	0
157	Helium-4	He	7440-59-7	4.003	0.012504	1.3038	-2.6954	1.7098	2.20	0.0097	5.20	0
158	Heptadecane	C ₁₇ H ₃₆	629-78-7	240.468	10.473	0.4374			295.13	8.3699	736.00	0
159	Heptanal	C ₇ H ₁₄ O	111-71-7	114.185	5.956	0.36474			229.80	5.0248	616.80	0
160	Heptane	C ₇ H ₁₆	142-82-5	100.202	5.0014	0.38795			182.57	4.2619	540.20	0
161	Heptanoic acid	C ₇ H ₁₄ O ₂	111-14-8	130.185	11.274	0.86047	-0.40661	-0.012644	265.83	7.9579	677.30	0
162	1-Heptanol	C ₇ H ₁₆ O	111-70-6	116.201	7.0236	-1.3652	3.987	-2.2545	239.15	7.6498	632.30	0
163	2-Heptanol	C ₇ H ₁₆ O	543-49-7	116.201	9.6433	0.783	-0.27273	0.038495	230.00	6.9638	608.30	0
164	3-Heptanone	C ₇ H ₁₄ O	106-35-4	114.185	6.3357	0.42167			234.15	5.1579	606.60	0
165	2-Heptanone	C ₇ H ₁₄ O	110-43-0	114.185	6.1425	0.39802			238.15	5.0471	611.40	0
166	1-Heptene	C ₇ H ₁₄	592-76-7	98.186	4.9437	0.35428	0.22149	-0.2353	154.12	4.3208	537.40	0
167	Heptyl mercaptan	C ₇ H ₁₆ S	1639-09-4	132.267	6.5473	0.40968			229.92	5.4656	645.00	0
168	1-Heptyne	C ₇ H ₁₂	628-71-7	96.170	4.8222	0.33858			192.22	4.1647	547.00	0
169	Hexadecane	C ₁₆ H ₃₄	544-76-3	226.441	10.156	0.45726			291.31	8.0225	723.00	0
170	Hexanal	C ₆ H ₁₂ O	66-25-1	100.159	5.6661	0.38533			217.15	4.7495	591.00	0
171	Hexane	C ₆ H ₁₄	110-54-3	86.175	4.4544	0.39002			177.83	3.7647	507.60	0
172	Hexanoic acid	C ₆ H ₁₂ O ₂	142-62-1	116.158	9.0746	0.8926	-0.75172	0.34378	269.25	6.4783	660.20	0
173	1-Hexanol	C ₆ H ₁₄ O	111-27-3	102.175	7.035	-0.9575	3.1431	-1.8066	228.55	7.1509	611.30	0
174	2-Hexanol	C ₆ H ₁₄ O	626-93-7	102.175	11.55	2.2877	-3.6724	2.1326	223.00	6.5014	585.30	0
175	2-Hexanone	C ₆ H ₁₂ O	591-78-6	100.159	5.6231	0.38207			217.35	4.7135	587.61	0
176	3-Hexanone	C ₆ H ₁₂ O	589-38-8	100.159	5.6232	0.39972			217.50	4.6655	582.82	0
177	1-Hexene	C ₆ H ₁₂	592-41-6	84.159	4.1429	0.49118	-0.44821	0.32105	133.39	3.6691	504.00	0
178	3-Hexyne	C ₆ H ₁₀	928-49-4	82.144	4.808	0.436			170.05	4.0831	544.00	0
179	Hexyl mercaptan	C ₆ H ₁₄ S	111-31-9	118.240	5.8422	0.38704			192.62	5.0630	623.00	0
180	1-Hexyne	C ₆ H ₁₀	693-02-7	82.144	4.574	0.3698			141.25	4.0640	516.20	0
181	2-Hexyne	C ₆ H ₁₀	764-35-2	82.144	4.911	0.4392			183.65	4.1067	549.00	0

182	Hydrazine	H ₂ N ₂	302-01-2	32.045	5.9794	0.9424	-1.398	0.8862	274.69	4.5238	653.15	0
183	Hydrogen	H ₂	1333-74-0	2.016	0.10127	0.698	-1.817	1.447	13.95	0.0913	33.19	0
184	Hydrogen bromide	HBr	10035-10-6	80.912	2.485	0.39			185.15	1.8817	363.15	0
185	Hydrogen chloride	HCl	7647-01-0	36.461	2.2093	0.3466			158.97	1.7498	324.65	0
186	Hydrogen cyanide	CHN	74-90-8	27.025	3.349	0.2053			259.83	2.8176	456.65	0
187	Hydrogen fluoride	HF	7664-39-3	20.006	13.451	13.36	-23.383	10.785	277.56	0.7104	461.15	0
188	Hydrogen sulfide	H ₂ S	7783-06-4	34.081	2.5676	0.37358			187.68	1.9782	373.53	0
189	Isobutyric acid	C ₄ H ₈ O ₂	79-31-2	88.105	4.0385	0.82698	-2.033	1.4769	227.15	3.5534	605.00	0
190	Isopropyl amine	C ₃ H ₇ N	75-31-0	59.110	4.4041	0.43325			177.95	3.5874	471.85	0
191	Malonic acid	C ₃ H ₄ O ₄	141-82-2	104.061	11.767	0.37877			407.95	9.0033	805.00	0
192	Methacrylic acid	C ₄ H ₆ O ₂	79-41-4	86.089	4.6095	0.23331			288.15	4.0342	662.00	0
193	Methane	CH ₄	74-82-8	16.042	1.0194	0.26087	-0.14694	0.22154	90.69	0.8724	190.56	0
194	Methanol	CH ₃ O	67-56-1	32.042	5.0451	0.33594			175.47	4.3825	512.50	0
195	N-Methyl acetamide	C ₃ H ₇ NO	79-16-3	73.094	7.3402	0.38974			301.15	5.9384	718.00	0
196	Methyl acetate	C ₃ H ₆ O ₂	79-20-9	74.079	4.492	0.3685			175.15	3.8418	506.55	0
197	Methyl acetylene	C ₃ H ₄	74-99-7	40.064	3.1889	0.37881			170.45	2.5882	402.40	0
198	Methyl acrylate	C ₄ H ₆ O ₂	96-33-3	86.089	4.68	0.349			196.32	3.9913	536.00	0
199	Methyl amine	CH ₃ N	74-89-5	31.057	3.858	0.404			179.69	3.1006	430.05	0
200	Methyl benzoate	C ₈ H ₈ O ₂	93-58-3	136.148	6.8504	0.38852			260.75	5.7026	693.00	0
201	3-Methyl-1,2-butadiene	C ₅ H ₈	598-25-4	68.117	4.1233	0.426			159.53	3.4864	490.00	0
202	2-Methylbutane	C ₅ H ₁₂	78-78-4	72.149	3.7593	0.39173			113.25	3.3657	460.40	0
203	2-Methylbutanoic acid	C ₅ H ₁₀ O ₂	116-53-0	102.132	7.48	0.3933			193.00	6.5004	643.00	0
204	3-Methyl-1-butanol	C ₅ H ₁₂ O	123-51-3	88.148	10.178	1.3211	-1.2234	0.44836	155.95	7.3738	577.20	0
205	2-Methyl-1-butene	C ₅ H ₁₀	563-46-2	70.133	3.9091	0.39866			135.58	3.4072	465.00	0
206	2-Methyl-2-butene	C ₅ H ₁₀	513-35-9	70.133	3.9248	0.36173			139.39	3.4558	470.00	0
207	2-Methyl-1-butene-3-yne	C ₅ H ₆	78-80-8	66.101	3.648	0.3863			160.15	3.1332	492.00	0
208	Methylbutyl ether	C ₅ H ₁₂ O	628-28-4	88.148	4.5302	0.37779			157.48	3.9438	512.74	0
209	Methylbutyl sulfide	C ₅ H ₁₂ S	628-29-5	104.214	5.3416	0.3835			175.30	4.6699	593.00	0
210	3-Methyl-1-butyne	C ₅ H ₈	598-23-2	68.117	3.792	0.3565			183.45	3.1681	463.20	0
211	Methyl butyrate	C ₅ H ₁₀ O ₂	623-42-7	102.132	5.3781	0.35923			187.35	4.5694	554.50	0
212	Methylchlorosilane	CH ₃ ClSi	993-00-0	80.589	3.2835	0.33116			139.05	2.8974	442.00	0
213	Methylcyclohexane	C ₇ H ₁₄	108-87-2	98.186	4.7528	0.39437			146.58	4.2291	572.10	0
214	1-Methylcyclohexanol	C ₇ H ₁₄ O	590-67-0	114.185	6.477	0.4853			299.15	4.9050	686.00	0
215	cis-2-Methylcyclohexanol	C ₇ H ₁₄ O	7443-70-1	114.185	7.8011	0.4172			280.15	6.0500	614.00	0
216	trans-2-Methylcyclohexanol	C ₇ H ₁₄ O	7443-52-9	114.185	7.8995	0.42479			269.15	6.1926	617.00	0
217	Methylcyclopentane	C ₆ H ₁₂	96-37-7	84.159	4.3595	0.38507			130.73	3.9115	532.70	0
218	1-Methylcyclopentene	C ₆ H ₁₀	693-89-0	82.144	4.3541	0.36805			146.62	3.8769	542.00	0
219	3-Methylcyclopentene	C ₆ H ₁₀	1120-62-3	82.144	4.209	0.36779			115.00	3.8439	526.00	0
220	Methyldichlorosilane	CH ₂ Cl ₂ Si	75-54-7	115.034	3.6756	0.31266			182.55	3.1686	483.00	0
221	Methylethyl ether	C ₃ H ₈ O	540-67-0	60.095	3.53	0.376			160.00	2.9751	437.80	0
222	Methylethyl ketone	C ₄ H ₈ O	78-93-3	72.106	4.622	0.355			186.48	3.9704	535.50	0
223	Methylethyl sulfide	C ₃ H ₈ S	624-89-5	76.161	4.4842	0.41151			167.23	3.8406	533.00	0
224	Methyl formate	C ₂ H ₄ O ₂	107-31-3	60.052	4.103	0.3825			174.15	3.4644	487.20	0
225	Methylisobutyl ether	C ₅ H ₁₂ O	625-44-5	88.148	4.2678	0.37995			150.00	3.7232	497.00	0
226	Methylisobutyl ketone	C ₆ H ₁₂ O	108-10-1	100.159	5.4687	0.40583			189.15	4.6507	574.60	0
227	Methyl Isocyanate	C ₂ H ₂ NO	624-83-9	57.051	4.2967	0.37922			256.15	3.2402	488.00	0
228	Methylisopropyl ether	C ₄ H ₁₀ O	598-53-8	74.122	3.8501	0.36453			127.93	3.4235	464.48	0
229	Methylisopropyl ketone	C ₅ H ₁₀ O	563-80-4	86.132	4.7075	0.33601			180.15	4.1240	553.40	0
230	Methylisopropyl sulfide	C ₄ H ₁₀ S	1551-21-9	90.187	4.5052	0.36493			171.64	3.9340	553.10	0
231	Methyl mercaptan	CH ₃ S	74-93-1	48.107	3.4448	0.37427			150.18	2.9825	469.95	0
232	Methyl methacrylate	C ₅ H ₈ O ₂	80-62-6	100.116	5.468	0.4472			224.95	4.3596	566.00	0
233	2-Methyloctanoic acid	C ₉ H ₁₈ O ₂	3004-93-1	158.238	10.53	0.7454	-0.39297	0.047214	240.00	8.1106	694.00	0
234	2-Methylpentane	C ₆ H ₁₄	107-83-5	86.175	4.2522	0.3807			119.55	3.8300	497.70	0
235	Methyl pentyl ether	C ₆ H ₁₄ O	628-80-8	102.175	5.0002	0.3781			176.00	4.3168	546.49	0
236	2-Methylpropane	C ₄ H ₁₀	75-28-5	58.122	3.188	0.39006			113.54	2.8070	407.80	0
237	2-Methyl-2-propanol	C ₄ H ₁₀ O	75-65-0	74.122	7.7646	0.56757			298.97	4.6771	506.20	0
238	2-Methyl propene	C ₄ H ₈	115-11-7	56.106	3.2614	0.38073			132.81	2.8195	417.90	0
239	Methyl propionate	C ₄ H ₈ O ₂	554-12-1	88.105	5.008	0.3959			185.65	4.2231	530.60	0
240	Methylpropyl ether	C ₄ H ₁₀ O	557-17-5	74.122	4.2719	0.43175			133.97	3.7041	476.25	0
241	Methylpropyl sulfide	C ₄ H ₁₀ S	3877-15-4	90.187	4.8253	0.38087			160.17	4.2499	565.00	0
242	Methylsilane	CH ₃ Si	992-94-9	46.144	2.2656	0.30269			116.34	2.0069	352.50	0
243	alpha-Methyl styrene	C ₉ H ₁₀	98-83-9	118.176	5.8071	0.37009			249.95	4.8591	654.00	0
244	Methyl tert-butyl ether	C ₅ H ₁₂ O	1634-04-4	88.148	3.872	0.044	0.448	-0.112	164.55	3.6017	497.10	0

TABLE 2-150 Heats of Vaporization of Inorganic and Organic Liquids (J/kmol) (Concluded)

Cmpd. no.	Name	Formula	CAS no.	Mol. wt.	C1 × 1E-07	C2	C3	C4	T_{\min} , K	ΔH_v at $T_{\min} \times 1E-07$	T_{\max} , K	ΔH_v at T_{\max}
245	Methyl vinyl ether	C ₃ H ₆ O	107-25-5	58.079	3.587	0.3769			151.15	3.0567	437.00	0
246	Naphthalene	C ₁₀ H ₈	91-20-3	128.171	7.0911	0.46468			353.43	5.2691	748.40	0
247	Neon	Ne	7440-01-9	20.180	0.2389	0.3494			24.56	0.1803	44.40	0
248	Nitroethane	C ₂ H ₅ NO ₂	79-24-3	75.067	5.1459	0.33017			183.63	4.5533	593.00	0
249	Nitrogen	N ₂	7727-37-9	28.013	0.74905	0.40406	-0.317	0.27343	63.15	0.6024	126.20	0
250	Nitrogen trifluoride	F ₃ N	7783-54-2	71.002	1.6402	0.36494			66.46	1.4519	234.00	0
251	Nitromethane	CH ₃ NO ₂	75-52-5	61.040	4.7417	0.3062			244.60	4.0220	588.15	0
252	Nitrous oxide	N ₂ O	10024-97-2	44.013	2.3215	0.384			182.30	1.6502	309.57	0
253	Nitric oxide	NO	10102-43-9	30.006	2.131	0.4056			109.50	1.4578	180.15	0
254	Nonadecane	C ₁₉ H ₄₀	629-92-5	268.521	11.674	0.45865			305.04	9.2185	758.00	0
255	Nonanal	C ₉ H ₁₈ O	124-19-6	142.239	7.3363	0.41735			255.15	5.9779	658.00	0
256	Nonane	C ₉ H ₂₀	111-84-2	128.255	6.037	0.38522			219.66	5.0545	594.60	0
257	Nonanoic acid	C ₉ H ₁₈ O ₂	112-05-0	158.238	12.38	0.69869	0.097854	-0.35082	285.55	8.7232	710.70	0
258	1-Nonanol	C ₉ H ₂₀ O	143-08-8	144.255	7.5429	-1.5966	4.6489	-2.7229	268.15	8.2411	670.90	0
259	2-Nonanol	C ₉ H ₂₀ O	628-99-9	144.255	7.9797	-1.0341	3.553	-2.1149	238.15	8.0370	649.50	0
260	1-Nonene	C ₉ H ₁₈	124-11-8	126.239	5.9054	0.61039	-0.54533	0.30683	191.91	4.9218	593.10	0
261	Nonyl mercaptan	C ₉ H ₂₀ S	1455-21-6	160.320	7.5239	0.3991			253.05	6.2506	681.00	0
262	1-Nonyne	C ₉ H ₁₆	3452-09-3	124.223	6.3337	0.3975			223.15	5.2606	598.05	0
263	Octadecane	C ₁₈ H ₃₈	593-45-3	254.494	10.969	0.44327			301.31	8.7246	747.00	0
264	Octanal	C ₈ H ₁₆ O	124-13-0	128.212	6.7735	0.40607			246.00	5.5600	638.90	0
265	Octane	C ₈ H ₁₈	111-65-9	114.229	5.518	0.38467			216.38	4.5898	568.70	0
266	Octanoic acid	C ₈ H ₁₆ O ₂	124-07-2	144.211	12.23	0.69294	0.12287	-0.36132	289.65	8.4658	694.26	0
267	1-Octanol	C ₈ H ₁₈ O	111-87-5	130.228	7.2468	-1.2464	3.6797	-2.0665	257.65	7.6793	652.30	0
268	2-Octanol	C ₈ H ₁₈ O	123-96-6	130.228	7.6376	-0.7612	2.7875	-1.6033	241.55	7.3759	629.80	0
269	2-Octanone	C ₈ H ₁₆ O	111-13-7	128.212	6.5363	0.38718			252.85	5.3646	632.70	0
270	3-Octanone	C ₈ H ₁₆ O	106-68-3	128.212	6.6142	0.58562	-0.40512	0.22144	255.55	5.2076	627.70	0
271	1-Octene	C ₈ H ₁₆	111-66-0	112.213	5.4859	0.26207	0.50642	-0.43873	171.45	4.7927	566.90	0
272	Octyl mercaptan	C ₈ H ₁₈ S	111-88-6	146.294	6.8907	0.40017			223.95	5.8506	667.30	0
273	1-Octyne	C ₈ H ₁₄	629-05-0	110.197	5.4046	0.35299			193.55	4.6743	574.00	0
274	Oxalic acid	C ₂ H ₂ O ₄	144-62-7	90.035	11.473	0.37238			462.65	8.3393	804.00	0
275	Oxygen	O ₂	7782-44-7	31.999	0.9008	0.4542	-0.4096	0.3183	54.36	0.7742	154.58	0
276	Ozone	O ₃	10028-15-6	47.998	1.8587	0.30416			80.15	1.6625	261.00	0
277	Pentadecane	C ₁₅ H ₃₂	629-62-9	212.415	9.6741	0.45399			283.07	7.6728	708.00	0
278	Pentanal	C ₅ H ₁₀ O	110-62-3	86.132	5.1478	0.37541			182.00	4.4502	566.10	0
279	Pentane	C ₅ H ₁₂	109-66-0	72.149	3.9109	0.38681			143.42	3.3968	469.70	0
280	Pentanoic acid	C ₅ H ₁₀ O ₂	109-52-4	102.132	7.3197	1.2093	-1.9114	1.1591	239.15	5.3813	639.16	0
281	1-Pentanol	C ₅ H ₁₂ O	71-41-0	88.148	7.39	-0.1464	1.4751	-0.9208	195.56	6.7005	588.10	0
282	2-Pentanol	C ₅ H ₁₂ O	6032-29-7	88.148	11.111	1.8011	-2.1801	1.0641	200.00	6.6655	561.00	0
283	2-Pentanone	C ₅ H ₁₀ O	107-87-9	86.132	5.174	0.39422			196.29	4.3663	561.08	0
284	3-Pentanone	C ₅ H ₁₀ O	96-22-0	86.132	5.2359	0.40465			234.18	4.2075	560.95	0
285	1-Pentene	C ₅ H ₁₀	109-67-1	70.133	3.5027	0.3481	-0.19672	0.22394	108.02	3.2232	464.80	0
286	2-Pentyl mercaptan	C ₅ H ₁₂ S	2084-19-7	104.214	5.0573	0.45827	-0.22568	0.16393	160.75	4.4343	584.30	0
287	Pentyl mercaptan	C ₅ H ₁₂ S	110-66-7	104.214	5.4315	0.3972			197.45	4.6322	598.00	0
288	1-Pentyne	C ₅ H ₈	627-19-0	68.117	3.954	0.3512			167.45	3.4025	481.20	0
289	2-Pentyne	C ₅ H ₈	627-21-4	68.117	4.4158	0.44347			163.83	3.7321	519.00	0
290	Phenanthrene	C ₁₄ H ₁₀	85-01-8	178.229	8.3482	0.33172			372.38	6.9340	869.00	0
291	Phenol	C ₆ H ₆ O	108-95-2	94.111	7.306	0.4246			314.06	5.6577	694.25	0
292	Phenyl isocyanate	C ₇ H ₅ NO	103-71-9	119.121	5.5769	0.30346			243.15	4.8418	653.00	0
293	Phthalic anhydride	C ₈ H ₆ O ₃	85-44-9	148.116	6.916	0.1755			404.15	6.1001	791.00	0
294	Propadiene	C ₃ H ₄	463-49-0	40.064	2.9535	0.41367			136.87	2.4755	394.00	0
295	Propane	C ₃ H ₈	74-98-6	44.096	2.9209	0.78237	-0.77319	0.39246	85.47	2.4787	369.83	0
296	1-Propanol	C ₃ H ₈ O	71-23-8	60.095	6.8988	0.6458	-0.5384	0.3317	146.95	5.8356	536.80	0
297	2-Propanol	C ₃ H ₈ O	67-63-0	60.095	7.2542	0.79137	-0.66092	0.34223	185.26	5.5370	508.30	0
298	Propenylcyclohexene	C ₉ H ₁₄	13511-13-2	122.207	5.8866	0.38533			199.00	5.0941	636.00	0
299	Propionaldehyde	C ₃ H ₆ O	123-38-6	58.079	4.1492	0.36751			170.00	3.5675	504.40	0
300	Propionic acid	C ₃ H ₆ O ₂	79-09-4	74.079	4	1.3936	-2.9465	1.794	252.45	3.0922	600.81	0
301	Propionitrile	C ₃ H ₅ N	107-12-0	55.079	4.9348	0.41873			180.26	4.2005	564.40	0
302	Propyl acetate	C ₅ H ₁₀ O ₂	109-60-4	102.132	5.4327	0.407			178.15	4.6322	549.73	0

303	Propyl amine	C ₃ H ₉ N	107-10-8	59.110	4.4488	0.39494			188.36	3.6857	496.95	0
304	Propylbenzene	C ₉ H ₁₂	103-65-1	120.192	5.8887	0.38534			173.55	5.2110	638.35	0
305	Propylene	C ₃ H ₆	115-07-1	42.080	2.5216	0.33721	-0.18399	0.22377	87.89	2.3177	364.85	0
306	Propyl formate	C ₄ H ₈ O ₂	110-74-7	88.105	4.9687	0.4025			180.25	4.2162	538.00	0
307	2-Propyl mercaptan	C ₃ H ₆ S	75-33-2	76.161	4.2191	0.41161			142.61	3.6942	517.00	0
308	Propyl mercaptan	C ₃ H ₈ S	107-03-9	76.161	4.4782	0.41073			159.95	3.8723	536.60	0
309	1,2-Propylene glycol	C ₃ H ₈ O ₂	57-55-6	76.094	8.07	0.295			213.15	7.1374	626.00	0
310	Quinone	C ₆ H ₄ O ₂	106-51-4	108.095	6.49	0.3112			388.85	4.9933	683.00	0
311	Silicon tetrafluoride	F ₄ Si	7783-61-1	104.079	2.4105	0.37988			186.35	1.4873	259.00	0
312	Styrene	C ₈ H ₈	100-42-5	104.149	5.726	0.4055			242.54	4.7128	636.00	0
313	Succinic acid	C ₄ H ₆ O ₄	110-15-6	118.088	12.018	0.37149			460.65	8.7719	806.00	0
314	Sulfur dioxide	O ₂ S	7446-09-5	64.064	3.676	0.4			197.67	2.8753	430.75	0
315	Sulfur hexafluoride	F ₆ S	2551-62-4	146.055	2.571	0.383			223.15	1.6208	318.69	0
316	Sulfur trioxide	O ₃ S	7446-11-9	80.063	7.337	0.5647			289.95	4.4303	490.85	0
317	Terephthalic acid	C ₈ H ₆ O ₄	100-21-0	166.131	8.824				298.15	8.8240	298.15	88,240,000
318	<i>o</i> -Terphenyl	C ₁₈ H ₁₄	84-15-1	230.304	8.7165	0.3224			329.35	7.4548	857.00	0
319	Tetradecane	C ₁₄ H ₃₀	629-59-4	198.388	9.0539	0.44467			279.01	7.2002	693.00	0
320	Tetrahydrofuran	C ₄ H ₈ O	109-99-9	72.106	4.3021	0.36972			164.65	3.7610	540.15	0
321	1,2,3,4-Tetrahydronaphthalene	C ₁₀ H ₁₂	119-64-2	132.202	6.8086	0.43054			237.38	5.7314	720.00	0
322	Tetrahydrothiophene	C ₄ H ₈ S	110-01-0	88.171	5.0642	0.38904			176.99	4.4565	631.95	0
323	2,2,3,3-Tetramethylbutane	C ₈ H ₁₈	594-82-1	114.229	4.9055	0.40678			373.96	3.1691	568.00	0
324	Thiophene	C ₄ H ₄ S	110-02-1	84.140	4.5854	0.38756			234.94	3.7484	579.35	0
325	Toluene	C ₇ H ₈	108-88-3	92.138	4.9507	0.37742			178.18	4.3246	591.75	0
326	1,1,2-Trichloroethane	C ₂ H ₃ Cl ₃	79-00-5	133.404	5.0929	0.36013			236.50	4.2130	602.00	0
327	Tridecane	C ₁₃ H ₂₈	629-50-5	184.361	8.4339	0.4257			267.76	6.8015	675.00	0
328	Triethyl amine	C ₆ H ₁₅ N	121-44-8	101.190	4.664	0.3663			158.45	4.1011	535.15	0
329	Trimethyl amine	C ₃ H ₉ N	75-50-3	59.110	3.305	0.354			156.08	2.8216	433.25	0
330	1,2,3-Trimethylbenzene	C ₉ H ₁₂	526-73-8	120.192	5.9996	0.35578			247.79	5.0818	664.50	0
331	1,2,4-Trimethylbenzene	C ₉ H ₁₂	95-63-6	120.192	5.9254	0.35709			229.33	5.0713	649.10	0
332	2,2,4-Trimethylpentane	C ₈ H ₁₈	540-84-1	114.229	4.7711	0.37949			165.78	4.1561	543.80	0
333	2,3,3-Trimethylpentane	C ₈ H ₁₈	560-21-4	114.229	4.991	0.383			172.22	4.3530	573.50	0
334	1,3,5-Trinitrobenzene	C ₆ H ₃ N ₃ O ₆	99-35-4	213.105	10.687	0.38			398.40	8.3906	846.00	0
335	2,4,6-Trinitrotoluene	C ₇ H ₅ N ₃ O ₆	118-96-7	227.131	10.686	0.40074			354.00	8.5455	828.00	0
336	Undecane	C ₁₁ H ₂₄	1120-21-4	156.308	7.2284	0.40607			247.57	5.9240	639.00	0
337	1-Undecanol	C ₁₁ H ₂₄ O	112-42-5	172.308	8.7274	-1.5834	5.0913	-3.2171	288.45	8.9007	703.90	0
338	Vinyl acetate	C ₄ H ₆ O ₂	108-05-4	86.089	4.77	0.3765			180.35	4.0619	519.13	0
339	Vinyl acetylene	C ₄ H ₄	689-97-4	52.075	3.649	0.4	0.043		173.15	2.9876	454.00	0
340	Vinyl chloride	C ₂ H ₃ Cl	75-01-4	62.498	3.4125	0.4513			119.36	2.9491	432.00	0
341	Vinyl trichlorosilane	C ₂ H ₃ Cl ₃ Si	75-94-5	161.490	4.5659	0.36278			178.35	3.9520	543.15	0
342	Water	H ₂ O	7732-18-5	18.015	5.2053	0.3199	-0.212	0.25795	273.16	4.4733	647.10	0
343	<i>m</i> -Xylene	C ₈ H ₁₀	108-38-3	106.165	5.4626	0.37289			225.30	4.6112	617.00	0
344	<i>o</i> -Xylene	C ₈ H ₁₀	95-47-6	106.165	5.5395	0.37788			247.98	4.5859	630.30	0
345	<i>p</i> -Xylene	C ₈ H ₁₀	106-42-3	106.165	5.3819	0.36695			286.41	4.2787	616.20	0

The heat of vaporization ΔH_v is calculated by

$$\Delta H_v = C1(1 - T_r)^{C2 + C3T_r + C4T_r^2 + C5T_r^3}$$

where $T_r = T/T_c$, T_c is the critical temperature from Table 2-141, ΔH_v is in J/kmol, and T is in K. All substances are listed by chemical family in Table 2-6 and by formula in Table 2-7.

Values in this table were taken from the Design Institute for Physical Properties (DIPPR) of the American Institute of Chemical Engineers (AIChE), copyright 2007 AIChE and reproduced with permission of AIChE and of the DIPPR Evaluated Process Design Data Project Steering Committee. Their source should be cited as R. L. Rowley, W. V. Wilding, J. L. Oscarson, Y. Yang, N. A. Zundel, T. E. Daubert, R. P. Danner, DIPPR® Data Compilation of Pure Chemical Properties, Design Institute for Physical Properties, AIChE, New York (2007).

The number of digits provided for values at T_{min} and T_{max} was chosen for uniformity of appearance and formatting; these do not represent the uncertainties of the physical quantities, but are the result of calculations from the standard thermophysical property formulations within a fixed format.

SPECIFIC HEATS OF PURE COMPOUNDS

UNITS CONVERSIONS

For this subsection, the following units conversions are applicable:

$$^{\circ}\text{F} = \% \text{ } ^{\circ}\text{C} + 32$$

$$^{\circ}\text{R} = 1.8 \text{ K}$$

To convert calories per gram-kelvin to British thermal units per pound-degree Rankine, multiply by 1.0; to convert calories per mole-kelvin to British thermal units per pound-mole-degree Rankine, multiply by 1.0.

To convert kilojoules per kilogram-kelvin to British thermal units per pound-degree Rankine, multiply by 0.2388.

ADDITIONAL REFERENCES

Additional data are contained in the subsection "Thermodynamic Properties." Data on water are also contained in that subsection. Additional tables for water are found in Eng. Sci. Data Item 68008, 251 Regent Street, London, England, which contains about 5000 values from 1 to 1000 bar, 0 to 1500 °C.

TABLE 2-151 Heat Capacities of the Elements and Inorganic Compounds*

Substance	State†	Heat capacity at constant pressure ($T = \text{K}$; $0^{\circ}\text{C} = 273.1 \text{ K}$), cal/(mol·K)	Range of temperature, K	Uncertainty, %
Aluminum ¹				
Al	<i>c</i>	$4.80 + 0.00322T$	273–931	1
	<i>l</i>	7.00	931–1273	5
AlBr ₃	<i>c</i>	$18.74 + 0.01866T$	273–370	3
	<i>l</i>	29.5	370–407	5
AlCl ₃	<i>c</i>	$13.25 + 0.02800T$	273–465	3
	<i>l</i>	31.2	465–504	3
AlCl ₃ ·6H ₂ O	<i>c</i>	76	288–327	?
AlF ₃	<i>c</i>	19.3	288–326	?
AlF ₃ ·3½H ₂ O	<i>c</i>	50.5	288–326	?
AlF ₃ ·3NaF	<i>c</i>	$38.63 + 0.04760T - 449200/T^2$	273–1273	2
	<i>l</i>	142	1273–1373	?
AlI ₃	<i>c</i>	$16.88 + 0.02266T$	273–464	3
	<i>l</i>	28.8	464–480	5
Al ₂ O ₃	<i>c</i>	$22.08 + 0.008971T - 522500/T^2$	273–1973	3
Al ₂ O ₃ ·SiO ₂	<i>c</i> , sillimanite	$40.79 + 0.004763T - 992800/T^2$	273–1573	3
	<i>c</i> , disthene	$41.81 + 0.005283T - 1211000/T^2$	273–1673	2
	<i>c</i> , andalusite	$43.96 + 0.001923T - 1086000/T^2$	273–1573	3
3Al ₂ O ₃ ·2SiO ₂	<i>c</i> , mullite	$59.65 + 0.0670T$	273–576	5
4Al ₂ O ₃ ·3SiO ₂	<i>c</i>	$113.2 + 0.0652T$	273–575	3
Al ₂ (SO ₄) ₃	<i>c</i>	63.5	273–373	?
Al ₂ (SO ₄) ₃ ·18H ₂ O	<i>c</i>	235	288–325	?
Antimony				
Sb	<i>c</i>	$5.51 + 0.00178T$	273–903	2
	<i>l</i>	7.15	903–1273	5
SbBr ₃	<i>c</i>	$17.2 + 0.0293T$	273–370	?
SbCl ₃	<i>c</i>	$10.3 + 0.0511T$	273–346	?
Sb ₂ O ₃	<i>c</i>	$19.1 + 0.0171T$	273–929	?
Sb ₂ O ₄	<i>c</i>	$22.6 + 0.0162T$	273–1198	?
Sb ₂ S ₃	<i>c</i>	$24.2 + 0.0132T$	273–821	?
Argon ²				
A	<i>g</i>	4.97	All	0
Arsenic				
As	<i>c</i>	$5.17 + 0.00234T$	273–1168	5
AsCl ₃	<i>l</i>	31.9	286–371	?
As ₂ O ₃	<i>c</i>	$8.37 + 0.0486T$	273–548	?
As ₂ S ₃	<i>c</i>	25.8	293–373	?
Barium				
BaCl ₂	<i>c</i>	$17.0 + 0.00334T$	273–1198	?
BaCl ₂ ·H ₂ O	<i>c</i>	28.2	273–307	?
BaCl ₂ ·2H ₂ O	<i>c</i>	37.3	273–307	?
Ba(ClO ₃) ₂ ·H ₂ O	<i>c</i>	51	289–320	?
BaCO ₃	<i>c</i> , α	$17.26 + 0.0131T$	273–1083	5
	<i>c</i> , β	30.0	1083–1255	15
BaMoO ₄	<i>c</i>	34	273–297	?
Ba(NO ₃) ₂	<i>c</i>	39.8	285–371	?
BaSO ₄	<i>c</i>	$21.35 + 0.0141T$	273–1323	5
Beryllium ^{3,4}				
Be	<i>c</i>	$4.698 + 0.001555T - 121000/T^2$	273–1173	1
BeO	<i>c</i>	$8.69 + 0.00365T - 313000/T^2$	273–1175	5
BeO·Al ₂ O ₃	<i>c</i>	25.4	273–373	?
BeSO ₄	<i>c</i>	20.8	273–373	?

*From Kelley, U.S. Bur. Mines Bull. 371, 1934. For a revision see Kelley, U.S. Bur. Mines Bull. 477, 1948. Data for many elements and compounds are given by Johnson (ed.), WADD-TR-60-56, 1960, for cryogenic temperatures. Tabulated data for gases can be obtained from many of the references cited in the "Thermodynamic Properties" subsection and other tables in this section. Thin, Duran, et al., *Hydrocarbon Process.*, **50**, 98 (January 1971), review previous equation fits and give newer fits for 408 hydrocarbons and related compounds. Later publications include Duran, Thin, et al., *Hydrocarbon Process.*, **55**, 153 (August 1976); Thompson, *J. Chem. Eng. Data*, **22**(4), 431 (1977); and Passut and Danner, *Ind. Eng. Chem. Process Des. Dev.*, **11**, 543 (1972); **13**, 193 (1974).

† The symbols in this column have the following meaning: *c*, crystal; *l*, liquid; *g*, gas; *gls*, glass.

TABLE 2-151 Heat Capacities of the Elements and Inorganic Compounds (Continued)

Substance	State†	Heat capacity at constant pressure ($T = K$; $0\text{ }^{\circ}\text{C} = 273.1\text{ K}$), cal/(mol·K)	Range of temperature, K	Uncertainty, %
Bismuth ⁴				
Bi	<i>c</i>	$5.38 + 0.00260T$	273–544	3
	<i>l</i>	7.60	544–1273	3
Bi ₂ O ₃	<i>c</i>	$23.27 + 0.01105T$	273–777	2
Bi ₂ S ₃	<i>c</i>	30.4	284–372	?
Boron				
B	<i>c</i>	$1.54 + 0.00440T$	273–1174	5
B ₂ O ₃	<i>gls</i>	$5.14 + 0.0320T$	273–513	3
	<i>gls</i>	30.4	513–623	3
BN	<i>c</i>	$1.61 + 0.00400T$	273–1173	5
Bromine				
Br ₂	<i>g</i>	9.00	300–2000	5
Cadmium				
Cd	<i>c</i>	$5.46 + 0.002466T$	273–594	1
	<i>l</i>	7.13	594–973	5
CdO	<i>c</i>	$9.65 + 0.00208T$	273–2086	?
CdS	<i>c</i>	$12.9 + 0.00090T$	273–1273	?
CdSO ₄ ·8/3H ₂ O	<i>c</i>	51.3	293	?
Calcium				
Ca	<i>c</i>	$5.31 + 0.00333T$	273–673	2
	<i>c</i>	$6.29 + 0.00140T$	673–873	2
CaCl ₂	<i>c</i>	$16.9 + 0.00386T$	273–1055	?
CaCO ₃	<i>c</i>	$19.68 + 0.01189T - 307600/T^2$	273–1033	3
CaF ₂	<i>c</i>	$14.7 + 0.00380T$	273–1651	?
CaMg(CO ₃) ₂	<i>c</i>	40.1	299–372	?
CaMoO ₄	<i>c</i>	33	273–297	?
CaO	<i>c</i>	$10.00 + 0.00484T - 108000/T^2$	273–1173	2
Ca(OH) ₂	<i>c</i>	21.4	276–373	?
CaO·Al ₂ O ₃ ·2SiO ₂	<i>c</i> , anorthite	$63.13 + 0.01500T - 1537000/T^2$	273–1673	1
	<i>gls</i>	$67.41 + 0.01048T - 1874000/T^2$	273–973	1
CaO·MgO·2SiO ₂	<i>c</i> , diopside	$54.46 + 0.005746T - 1500000/T^2$	273–1573	1
	<i>gls</i>	$51.68 + 0.009724T - 1308000/T^2$	273–973	1
CaO·SiO ₂	<i>c</i> , wollastonite	$27.95 + 0.002056T - 745600/T^2$	273–1573	1
	<i>c</i> , pseudowollastonite	$25.48 + 0.004132T - 488100/T^2$	273–1673	1
	<i>gls</i>	$23.16 + 0.009672T - 487100/T^2$	273–973	1
CaP ₂ O ₆	<i>c</i>	39.5	287–371	?
CaSO ₄	<i>c</i>	$18.52 + 0.02197T - 156800/T^2$	273–1373	5
CaSO ₄ ·2H ₂ O	<i>c</i>	46.8	282–373	?
CaWO ₄	<i>c</i>	27.9	292–322	?
Carbon ⁵				
C	<i>c</i> , graphite	$2.673 + 0.002617T - 116900/T^2$	273–1373	2
	<i>c</i> , diamond	$2.162 + 0.003059T - 130300/T^2$	273–1313	3
CH ₄	<i>g</i>	$5.34 + 0.0115T$	273–1200	2
CO ⁶	<i>g</i>	$6.60 + 0.00120T$	273–2500	1½
CO ₂	<i>g</i>	$10.34 + 0.00274T - 195500/T^2$	273–1200	1½
CS ₂	<i>l</i>	18.4	293	?
Cerium				
Ce	<i>c</i>	$5.88 + 0.00123T$	273–908	?
CeO ₂	<i>c</i>	15.1	273–373	?
Ce ₂ (MoO ₄) ₃	<i>c</i>	96	273–297	?
Ce ₂ (SO ₄) ₃	<i>c</i>	66.4	273–373	?
Ce ₂ (SO ₄) ₃ ·5H ₂ O	<i>c</i>	131.6	273–319	?
Cesium				
Cs	<i>c</i>	$1.96 + 0.0182T$	273–301	3
	<i>l</i>	8.00	302	3
	<i>g</i>	4.97	All	0
CsBr	<i>c</i>	$12.6 + 0.00259T$	273–909	?
CsCl	<i>c</i>	$11.7 + 0.00309T$	273–752	?
CsF	<i>c</i>	$11.3 + 0.00285T$	273–957	?
CsI	<i>c</i>	$11.6 + 0.00268T$	273–894	?
Chlorine				
Cl ₂	<i>g</i>	$8.28 + 0.00056T$	273–2000	1½
Chromium ⁴				
Cr	<i>c</i>	$4.84 + 0.00295T$	273–1823	5
	<i>l</i>	9.70	1823–1923	10
CrCl ₃	<i>c</i>	23	286–319	?
Cr ₂ O ₃	<i>c</i>	$26.0 + 0.00400T$	273–2263	?
CrSb	<i>c</i>	$12.3 + 0.00120T$	273–1383	?
CrSb ₂	<i>c</i>	$19.2 + 0.00184T$	273–949	?
Cr ₂ (SO ₄) ₃	<i>c</i>	67.4	273–373	?
Cobalt ⁴				
Co	<i>c</i>	$5.12 + 0.00333T$	273–1763	5
	<i>l</i>	8.40	1763–1873	5
CoAs ₂ ·CoS ₂	<i>c</i>	32.9	283–373	?
CoSb	<i>c</i>	$11.7 + 0.00156T$	273–1464	?
Co ₂ Sn	<i>c</i>	$15.83 + 0.00950T$	273–903	2
CoS	<i>c</i>	$10.6 + 0.00251T$	273–1373	?
CoSO ₄ ·7H ₂ O	<i>c</i>	96	286–303	?

TABLE 2-151 Heat Capacities of the Elements and Inorganic Compounds (Continued)

Substance	State†	Heat capacity at constant pressure ($T = K; 0^{\circ}C = 273.1 K$), cal/(mol·K)	Range of temperature, K	Uncertainty, %
Copper ⁷				
Cu	<i>c</i>	$5.44 + 0.001462T$	273–1357	1
	<i>l</i>	7.50	1357–1573	3
CuAl	<i>c</i>	$9.88 + 0.00500T$	273–733	2
CuAl ₂	<i>c</i>	$16.78 + 0.00366T$	273–773	2
Cu ₃ Al	<i>c</i>	$19.61 + 0.01054T$	273–775	2
CuI	<i>c</i>	$12.1 + 0.00286T$	273–675	?
CuI ₂	<i>c</i>	20.1	274–328	?
CuO	<i>c</i>	$10.87 + 0.003576T - 150600/T^2$	273–810	2
CuO·SiO ₂ ·H ₂ O	<i>c</i>	29	293–323	?
CuS	<i>c</i>	$10.6 + 0.00264T$	273–1273	?
Cu ₂ S	<i>c, α</i>	$9.38 + 0.0312T$	273–376	3
	<i>c, β</i>	20.9	376–1173	2
CuS·FeS	<i>c</i>	24	292–321	?
Cu ₂ Sb	<i>c</i>	$13.73 + 0.01350T$	273–573	2
Cu ₂ Sb	<i>c</i>	$21.79 + 0.00900T$	273–693	2
Cu ₂ Se	<i>c, α</i>	20.85	273–383	5
	<i>c, β</i>	20.35	383–488	5
Cu ₃ Si	<i>c</i>	$20.3 + 0.00587T$	273–1135	?
CuSO ₄	<i>c</i>	24.1	282	?
CuSO ₄ ·H ₂ O	<i>c</i>	31.3	282	?
CuSO ₄ ·3H ₂ O	<i>c</i>	49.0	282	?
CuSO ₄ ·5H ₂ O	<i>c</i>	67.2	282	?
Fluorine ⁸				
F ₂	<i>g</i>	$6.50 + 0.00100T$	300–3000	5
Gallium				
Ga ₂ O ₃	<i>c</i>	$18.2 + 0.0252T$	273–923	?
Ga ₂ (SO ₄) ₃	<i>c</i>	62.4	273–373	?
Germanium ¹				
Ge	<i>c</i>			
Gold				
Au	<i>c</i>	$5.61 + 0.00144T$	273–1336	2
	<i>l</i>	7.00	1336–1573	5
AuSb ₂	<i>c, α</i>	$17.12 + 0.00465T$	273–628	1
	<i>c, βγ</i>	$11.47 + 0.01756T$	628–713	?
Helium ⁹				
He	<i>g</i>	4.97	All	0
Hydrogen ¹⁰				
H	<i>g</i>	4.97	All	0
H ₂	<i>g</i>	$6.62 + 0.00081T$	273–2500	2
HBr	<i>g</i>	$6.80 + 0.00084T$	273–2000	2
HCl	<i>g</i>	$6.70 + 0.00084T$	273–2000	1½
HI	<i>g</i>	$6.93 + 0.00083T$	273–2000	2
H ₂ O	<i>l</i>	See Tables 2-153 and 2-305		
	<i>g</i>	$8.22 + 0.00015T + 0.00000134T^2$	300–2500	?
H ₂ S	<i>g</i>	$7.20 + 0.00360T$	300–600	8
H ₂ S ₂ O ₇	<i>c</i>	27	281	?
	<i>l</i>	58	308	?
Indium				
In	<i>c</i>			
Iodine				
I ₂	<i>g</i>	9.00	300–2000	5
Iridium				
Ir	<i>c</i>	$5.50 + 0.00148T$	273–1873	1
Iron ⁴				
Fe	<i>c, α</i>	$4.13 + 0.00638T$	273–1041	3
	<i>c, β</i>	$6.12 + 0.00336T$	1041–1179	3
	<i>c, γ</i>	8.40	1179–1674	5
	<i>c, δ</i>	10.0	1674–1803	5
	<i>l</i>	8.15	1803–1873	5
FeAs ₂	<i>c</i>	17.8	283–373	?
Fe ₃ C	<i>c</i>	$25.17 + 0.00223T$	273–1173	10
FeCO ₃	<i>c</i>	22.7	293–368	?
FeO	<i>c</i>	$12.62 + 0.001492T - 76200/T^2$	273–1173	2
Fe ₂ O ₃	<i>c</i>	$24.72 + 0.01604T - 423400/T^2$	273–1097	2
Fe ₃ O ₄	<i>c</i>	$41.17 + 0.01882T - 979500/T^2$	273–1065	2
Fe ₂ O ₃ ·3H ₂ O	<i>c</i>	47.8	286–373	?
FeS	<i>c, α</i>	$2.03 + 0.0390T$	273–411	5
	<i>c, β</i>	$12.05 + 0.00273T$	411–1468	3
FeS ₂	<i>c</i>	$10.7 + 0.01336T$	273–773	?
FeSi	<i>c</i>	$10.54 + 0.00458T$	273–903	2
Fe ₂ SiO ₄	<i>c</i>	$33.57 + 0.01907T - 879700/T^2$	273–1161	2
FeSO ₄	<i>c</i>	22	293–373	?
Fe ₂ (SO ₄) ₃	<i>c</i>	66.2	273–373	?
FeSO ₄ ·4H ₂ O	<i>c</i>	63.6	282	?
FeSO ₄ ·7H ₂ O	<i>c</i>	96	291–319	?
Krypton				
Kr	<i>g</i>	4.97	All	0

TABLE 2-151 Heat Capacities of the Elements and Inorganic Compounds (Continued)

Substance	State†	Heat capacity at constant pressure ($T = K$; $0\text{ }^{\circ}\text{C} = 273.1\text{ K}$), cal/(mol·K)	Range of temperature, K	Uncertainty, %
Lanthanum				
La	<i>c</i>	$5.91 + 0.00100T$	273–1009	?
La ₂ O ₃	<i>c</i>	$22.6 + 0.00544T$	273–2273	?
La ₂ (MoO ₄) ₃	<i>c</i>	86	273–307	?
La ₂ (SO ₄) ₃	<i>c</i>	66.9	273–373	?
La ₂ (SO ₄) ₃ ·9H ₂ O	<i>c</i>	152	273–319	?
Lead [‡]				
Pb	<i>c</i>	$5.77 + 0.00202T$	273–600	2
	<i>l</i>	6.8	600–1273	5
Pb ₃ (AsO ₄) ₂	<i>c</i>	65.5	286–370	?
PbB ₂ O ₄	<i>c</i>	26.5	288–371	?
PbB ₄ O ₇	<i>c</i>	41.4	289–371	?
PbBr ₂	<i>c</i>	$18.13 + 0.00310T$	273–761	2
	<i>l</i>	27.4	761–860	10
PbCl ₂	<i>c</i>	$15.88 + 0.00835T$	273–771	2
	<i>l</i>	27.2	771–851	10
2PbCl ₂ ·NH ₄ Cl	<i>c</i>	53.1	293	?
PbCO ₃	<i>c</i>	21.1	286–320	?
PbCrO ₄	<i>c</i>	29.1	292–323	?
PbF ₂	<i>c</i>	$16.5 + 0.00412T$	273–1091	?
PbI ₂	<i>c</i>	$18.66 + 0.00293T$	273–648	2
	<i>l</i>	32.3	648–776	20
PbMoO ₄	<i>c</i>	30.4	292–322	?
Pb(NO ₃) ₂	<i>c</i>	36.4	286–320	?
PbO	<i>c</i>	$10.33 + 0.00318T$	273–544	2
PbO ₂	<i>c</i>	$12.7 + 0.00780T$	273–?	?
Pb ₃ P ₂ O ₇	<i>c</i>	48.3	284–371	?
PbS	<i>c</i>	$10.63 + 0.00401T$	273–873	3
PbSO ₄	<i>c</i>	26.4	293–372	?
PbS ₂ O ₃	<i>c</i>	29	293–373	?
PbWO ₄	<i>c</i>	35	273–297	?
Lithium				
Li	<i>c</i>	$0.68 + 0.0180T$	273–459	10
	<i>g</i>	4.97	All	0
LiBr	<i>c</i>	$11.5 + 0.00302T$	273–825	?
LiBr·H ₂ O	<i>c</i>	22.6	278–318	?
LiCl	<i>c</i>	$11.0 + 0.00339T$	273–887	?
LiCl·H ₂ O	<i>c</i>	23.6	279–360	?
LiF	<i>c</i>	$8.20 + 0.00520T$	273–1117	?
LiI	<i>c</i>	$12.5 + 0.00208T$	273–723	?
LiI·H ₂ O	<i>c</i>	23.6	277–359	?
LiI·2H ₂ O	<i>c</i>	32.9	277–345	?
LiI·3H ₂ O	<i>c</i>	43.2	277–347	?
LiNO ₃	<i>c</i>	$9.17 + 0.0360T$	273–523	5
	<i>l</i>	26.8	523–575	5
Magnesium [‡]				
Mg	<i>c</i>	$6.20 + 0.00133T - 67800/T^2$	273–923	1
	<i>l</i>	7.4	923–1048	10
MgAg	<i>c</i>	$10.58 + 0.00412T$	273–905	2
Mg ₂ Al ₃	<i>c</i>	$34.4 + 0.0198T$	273–736	?
MgAu	<i>c</i>	$11.3 + 0.00189T$	273–1433	?
Mg ₂ Au	<i>c</i>	$16.2 + 0.00451T$	273–1073	?
Mg ₃ Au	<i>c</i>	$21.2 + 0.00614T$	273–1103	?
MgCl ₂	<i>c</i>	$17.3 + 0.00377T$	273–991	?
MgCl ₂ ·6H ₂ O	<i>c</i>	77.1	292–342	?
MgCO ₃	<i>c</i>	16.9	290	?
MgCu ₂	<i>c</i>	$14.96 + 0.00776T$	273–903	3
Mg ₂ Cu	<i>c</i>	$15.5 + 0.00652T$	273–843	?
MgNi ₂	<i>c</i>	$15.87 + 0.00692T$	273–903	2
MgO	<i>c</i>	$10.86 + 0.001197T - 208700/T^2$	273–2073	2
	<i>c</i>	28	288–319	?
MgO·Al ₂ O ₃	<i>c</i>	$25.60 + 0.004380T - 674200/T^2$	273–1373	1
MgO·SiO ₂	<i>c</i> , amphibole	$23.35 + 0.008062T - 558800/T^2$	273–773	1
	<i>c</i> , pyroxene	$23.30 + 0.007734T - 542000/T^2$	273–973	1
	<i>gls</i>	$58.7 + 0.408T$	273–538	5
6MgO·MgCl ₂ ·8B ₂ O ₃	<i>c</i> , α	$107.2 + 0.2876T$	538–623	5
	<i>c</i> , β	18.2	292–323	?
Mg(OH) ₂	<i>c</i>	$28.2 + 0.00560T$	273–1234	?
Mg ₃ Sb ₂	<i>c</i>	$15.4 + 0.00415T$	273–1343	?
Mg ₂ Si	<i>c</i>	26.7	296–372	?
MgSO ₄	<i>c</i>	33	282	?
MgSO ₄ ·H ₂ O	<i>c</i>	80	282	?
MgSO ₄ ·6H ₂ O	<i>c</i>	89	291–319	?
MgSO ₄ ·7H ₂ O	<i>c</i>			?

TABLE 2-151 Heat Capacities of the Elements and Inorganic Compounds (Continued)

Substance	State†	Heat capacity at constant pressure ($T = K$; $0\text{ }^{\circ}\text{C} = 273.1\text{ K}$), cal/(mol·K)	Range of temperature, K	Uncertainty, %
Manganese				
Mn	<i>c</i> , α	$3.76 + 0.00747T$	273–1108	5
	<i>c</i> , β	$5.06 + 0.00395T$	1108–1317	5
	<i>c</i> , γ	$4.80 + 0.00422T$	1317–1493	5
	<i>l</i>	11.0	1493–1673	10
MnCl ₂	<i>c</i>	$16.2 + 0.00520T$	273–923	?
MnCO ₃	<i>c</i>	$7.79 + 0.0421T + 0.0000090T^2$	273–773	?
MnO	<i>c</i>	$7.43 + 0.01038T - 0.00000362T^2$	273–1923	?
Mn ₂ O ₃	<i>c</i>	$10.33 + 0.0530T - 0.0000257T^2$	273–1173	?
Mn ₃ O ₄	<i>c</i>	$19.25 + 0.0538T - 0.0000209T^2$	273–1773	?
MnO ₂	<i>c</i>	$1.92 + 0.0471T - 0.0000297T^2$	273–773	?
Mn ₂ O ₃ ·H ₂ O	<i>c</i>	31	291–322	?
MnS	<i>c</i>	$10.21 + 0.00656T - 0.00000242T^2$	273–1883	?
MnSO ₄	<i>c</i>	27.5	293–373	?
MnSO ₄ ·5H ₂ O	<i>c</i>	78	290–319	?
Mercury ¹¹				
Hg	<i>l</i>	6.61	273–630	1
	<i>g</i>	4.97	All	0
Hg ₂	<i>g</i>	9.00	300–2000	5
HgCl	<i>c</i>	$11.05 + 0.00370T$	273–798	?
HgCl ₂	<i>c</i>	$15.3 + 0.0103T$	273–553	?
Hg(CN) ₂	<i>c</i>	25	285–319	?
HgI	<i>c</i>	$11.4 + 0.00461T$	273–563	?
HgI ₂	<i>c</i> , α	$17.4 + 0.004001T$	273–403	3
	<i>c</i> , β	20.2	403–523	3
HgO	<i>c</i>	11.5	278–371	?
HgS	<i>c</i>	$10.9 + 0.00365T$	273–853	?
Hg ₂ SO ₄	<i>c</i>	31.0	273–307	?
Molybdenum				
Mo	<i>c</i>	$5.69 + 0.00188T - 50300/T^2$	273–1773	5
MoO ₃	<i>c</i>	$15.1 + 0.0121T$	273–1068	?
MoS ₂	<i>c</i>	$19.7 + 0.00315T$	273–729	?
Neon ¹²				
Ne	<i>g</i>	4.97	All	0
Nickel ⁴				
Ni	<i>c</i> , α	$4.26 + 0.00640T$	273–626	2
	<i>c</i> , β	$6.99 + 0.000905T$	626–1725	5
	<i>l</i>	8.55	1725–1903	10
NiO	<i>c</i>	$11.3 + 0.00215T$	273–1273	?
NiS	<i>c</i>	$9.25 + 0.00640T$	273–597	3
Ni ₂ Si	<i>c</i>	$15.8 + 0.00329T$	273–1582	?
NiSi	<i>c</i>	$10.0 + 0.00312T$	273–1273	?
Ni ₃ Sn	<i>c</i>	$20.78 + 0.0102T$	273–904	2
NiSO ₄	<i>c</i>	33.4	293–373	?
NiSO ₄ ·6H ₂ O	<i>c</i>	82	291–325	?
NiTe	<i>c</i>	$11.00 + 0.00433T$	273–700	2
Nitrogen ¹³				
N ₂	<i>g</i>	$6.50 + 0.00100T$	300–3000	3
NH ₃	<i>g</i>	$6.70 + 0.00630T$	300–800	1½
NH ₄ Br	<i>c</i>	22.8	274–328	?
NH ₄ Cl	<i>c</i> , α	$9.80 + 0.0368T$	273–457	5
	<i>c</i> , β	$5.0 + 0.0340T$	457–523	5
NH ₄ I	<i>c</i>	17.8	273–328	?
NH ₄ NO ₃	<i>c</i>	31.8	273–293	?
(NH ₄) ₂ SO ₄	<i>c</i>	51.6	275–328	?
NO	<i>g</i>	$8.05 + 0.000233T - 156300/T^2$	300–5000	2
Osmium				
Os	<i>c</i>	$5.686 + 0.000875T$	273–1877	1
Oxygen ¹⁴				
O ₂	<i>g</i>	$8.27 + 0.000258T - 187700/T^2$	300–5000	1
Palladium				
Pd	<i>c</i>	$5.41 + 0.00184T$	273–1822	2
Phosphorus				
P	<i>c</i> , yellow	5.50	273–317	5
	<i>c</i> , red	$0.21 + 0.0180T$	273–472	10
	<i>l</i>	6.6	317–373	10
PCL ₃	<i>l</i>	28.7	284–371	?
P ₄ O ₁₀	<i>c</i>	$15.72 + 0.1092T$	273–631	2
	<i>g</i>	73.6	631–1371	3
Platinum ⁴				
Pt	<i>c</i>	$5.92 + 0.00116T$	273–1873	1
Potassium				
K	<i>c</i>	$5.24 + 0.00555T$	273–336	5
	<i>l</i>	7.7	336–373	5

TABLE 2-151 Heat Capacities of the Elements and Inorganic Compounds (Continued)

Substance	State†	Heat capacity at constant pressure ($T = K$; $0\text{ }^{\circ}\text{C} = 273.1\text{ K}$), cal/(mol·K)	Range of temperature, K	Uncertainty, %
Potassium—(Cont.)				
K	<i>g</i>	4.97	All	0
K ₂	<i>g</i>	9.00	300–2000	5
KAsO ₃	<i>c</i>	25.3	290–372	?
KBO ₂	<i>c</i>	12.6 + 0.0126 <i>T</i>	273–1220	?
K ₂ B ₄ O ₇	<i>c</i>	51.3	290–372	?
KBr	<i>c</i>	11.49 + 0.00360 <i>T</i>	273–543	2
KCl	<i>c</i>	10.93 + 0.00376 <i>T</i>	273–1043	2
KClO ₃	<i>c</i>	25.7	289–371	?
KClO ₄	<i>c</i>	26.3	287–318	?
2KCl·CuCl ₂ ·2H ₂ O	<i>c</i>	63	292–323	?
2KCl·PtCl ₄	<i>c</i>	55	286–319	?
2KCl·SnCl ₄	<i>c</i>	54.5	292–323	?
2KCl·ZnCl ₂	<i>c</i>	43.4	279–319	?
2KCN·Zn(CN) ₂	<i>c</i>	57.4	277–319	?
K ₂ CO ₃	<i>c</i>	29.9	296–372	?
K ₂ CrO ₄	<i>c</i>	35.9	289–371	?
K ₂ Cr ₂ O ₇	<i>c</i>	42.80 + 0.0410 <i>T</i>	273–671	5
	<i>l</i>	96.9	671–757	5
KF	<i>c</i>	10.8 + 0.00284 <i>T</i>	273–1129	?
K ₄ Fe(CN) ₆	<i>c</i>	80.1	273–319	?
K ₄ Fe(CN) ₆ ·3H ₂ O	<i>c</i>	114.5	273–310	?
KH ₂ AsO ₄	<i>c</i>	32	289–319	?
KH ₂ PO ₄	<i>c</i>	28.3	290–320	?
KHSO ₄	<i>c</i>	30	292–324	?
KMnO ₄	<i>c</i>	28	287–318	?
KNO ₃	<i>c</i>	6.42 + 0.0530 <i>T</i>	273–401	10
	<i>c</i>	28.8	401–611	5
	<i>l</i>	29.5	611–683	10
K ₂ O·Al ₂ O ₃ ·3SiO ₂	<i>c</i> , orthoclase	69.26 + 0.00821 <i>T</i> – 2331000/ <i>T</i> ²	273–1373	1½
	<i>g</i> ls, orthoclase	69.81 + 0.01053 – 2403000/ <i>T</i> ²	273–1373	1½
	<i>c</i> , microcline	65.65 + 0.01102 <i>T</i> – 1748000/ <i>T</i> ²	273–1373	1½
	<i>g</i> ls, microcline	64.83 + 0.01438 <i>T</i> – 1641000/ <i>T</i> ²	273–1373	1½
K ₄ P ₂ O ₇	<i>c</i>	63.1	290–371	?
K ₂ SO ₄	<i>c</i>	33.1	287–371	?
K ₂ S ₂ O ₃	<i>c</i>	37	293–373	?
K ₂ SO ₄ ·Al ₂ (SO ₄) ₃ ·24H ₂ O	<i>c</i>	352	292–322	?
K ₂ SO ₄ ·Cr ₂ (SO ₄) ₃ ·24H ₂ O	<i>c</i>	324	292–324	?
K ₂ SO ₄ ·MgSO ₄ ·6H ₂ O	<i>c</i>	106	292–323	?
K ₂ SO ₄ ·NiSO ₄ ·6H ₂ O	<i>c</i>	107	289–319	?
K ₂ SO ₄ ·ZnSO ₄ ·6H ₂ O	<i>c</i>	120	293–317	?
Promethium				
Pr	<i>c</i>			
Radon				
Rn	<i>g</i>	4.97	All	0
Rhenium				
Re	<i>c</i>	6.30 + 0.00053 <i>T</i>	273–2273	?
Rhodium				
Rh	<i>c</i>	5.40 + 0.00219 <i>T</i>	273–1877	2
Rubidium				
Rb	<i>c</i>	3.27 + 0.0131 <i>T</i>	273–312	2
	<i>l</i>	7.85	312–373	5
RbBr	<i>c</i>	11.6 + 0.00255 <i>T</i>	273–954	?
RbCl	<i>c</i>	11.5 + 0.00249 <i>T</i>	273–987	?
Rb ₂ CO ₃	<i>c</i>	28.4	291–320	?
RbF	<i>c</i>	11.3 + 0.00256 <i>T</i>	273–1048	?
RbI	<i>c</i>	11.6 + 0.00263 <i>T</i>	273–913	?
Scandium				
Sc ₂ O ₃	<i>c</i>	21.1	273–373	?
Sc ₂ (SO ₄) ₃	<i>c</i>	62.0	273–373	?
Selenium				
Se	<i>c</i>	4.53 + 0.00550 <i>T</i>	273–490	2
	<i>l</i>	8.35	490–570	3
Silicon				
Si	<i>c</i>	5.74 + 0.000617 <i>T</i> – 101000/ <i>T</i> ²	273–1174	2
SiC	<i>c</i>	8.89 + 0.00291 <i>T</i> – 284000/ <i>T</i> ²	273–1629	2
SiCl ₄	<i>l</i>	32.4	293–373	?
SiO ₂	<i>c</i> , quartz, α	10.87 + 0.008712 <i>T</i> – 241200/ <i>T</i> ²	273–848	1
	<i>c</i> , quartz, β	10.95 + 0.00550 <i>T</i>	848–1873	3½
	<i>c</i> , cristobalite, α	3.65 + 0.0240 <i>T</i>	273–523	2½
	<i>c</i> , cristobalite, β	17.09 + 0.000454 <i>T</i> – 897200/ <i>T</i> ²	523–1973	2
	<i>g</i> ls	12.80 + 0.00447 <i>T</i> – 302000/ <i>T</i> ²	273–1973	3½
Silver ⁴				
Ag	<i>c</i>	5.60 + 0.00150 <i>T</i>	273–1234	1
	<i>l</i>	8.2	1234–1573	3

TABLE 2-151 Heat Capacities of the Elements and Inorganic Compounds (Continued)

Substance	State†	Heat capacity at constant pressure ($T = K$; $0^\circ\text{C} = 273.1\text{ K}$), cal/(mol·K)	Range of temperature, K	Uncertainty, %
Silver—(Cont.)				
Ag ₃ Al	<i>c</i>	$22.56 + 0.00570T$	273–902	2
Ag ₅ Al	<i>c</i>	$16.85 + 0.00450T$	273–903	2
AgAl ₁₂	<i>c</i>	$58.62 + 0.0575T$	273–768	5
AgBr	<i>c</i>	$8.58 + 0.0141T$	273–703	6
	<i>l</i>	14.9	703–836	5
AgCl	<i>c</i>	$9.60 + 0.00929T$	273–728	2
	<i>l</i>	14.05	728–806	5
AgCNO	<i>c</i>	18.7	273–353	?
AgI	<i>c, α</i>	$8.58 + 0.0141T$	273–423	6
AgNO ₃	<i>c, α</i>	$18.83 + 0.0160T$	273–433	2
	<i>c, β</i>	25.7	433–482	5
	<i>l</i>	30.2	482–541	5
Ag ₃ PO ₄	<i>c</i>	37.5	293–325	?
Ag ₅ S	<i>c, α</i>	18.8	273–448	5
	<i>c, β</i>	21.8	448–597	5
Ag ₃ Sb	<i>c</i>	$19.53 + 0.0160T$	273–694	5
Ag ₃ Se	<i>c, α</i>	20.2	273–406	5
	<i>c, β</i>	20.4	406–460	5
Sodium ¹⁵				
Na	<i>c</i>	$5.01 + 0.00536T$	273–371	1½
	<i>l</i>	7.50	371–451	2
	<i>g</i>	4.97	All	0
NaBO ₂	<i>c</i>	$10.4 + 0.0199T$	273–1239	?
Na ₂ B ₄ O ₇	<i>c</i>	47.9	289–371	?
Na ₂ B ₄ O ₇ ·10H ₂ O	<i>c</i>	147	292–323	?
NaBr	<i>c</i>	$11.74 + 0.00233T$	273–543	2
NaCl	<i>c</i>	$10.79 + 0.00420T$	273–1074	2
	<i>l</i>	15.9	1073–1205	3
NaClO ₃	<i>c</i>	$9.48 + 0.0468T$	273–528	3
	<i>l</i>	31.8	528–572	5
NaCNO	<i>c</i>	13.1	273–353	?
Na ₂ CO ₃	<i>c</i>	28.9	288–371	?
NaF	<i>c</i>	$10.4 + 0.00289T$	273–1261	?
Na ₂ HPO ₄ ·7H ₂ O	<i>c</i>	86.6	275–307	?
Na ₂ HPO ₄ ·12H ₂ O	<i>c</i>	133.4	275–307	?
NaI	<i>c</i>	$12.5 + 0.00162T$	273–936	?
NaNO ₃	<i>c</i>	$4.56 + 0.0580T$	273–583	5
	<i>l</i>	37.2	583–703	10
Na ₂ O·Al ₂ O ₃ ·3SiO ₂	<i>c, albite</i>	$63.78 + 0.01171T - 1678000/T^2$	273–1373	1
	<i>gls</i>	$61.25 + 0.01768T - 1545000/T^2$	273–1173	1
NaPO ₃	<i>c</i>	22.1	290–319	?
Na ₄ P ₂ O ₇	<i>c</i>	60.7	290–371	?
Na ₂ SO ₄	<i>c</i>	32.8	289–371	?
Na ₂ S ₂ O ₃	<i>c</i>	34.9	273–307	?
Na ₂ S ₂ O ₃ ·5H ₂ O	<i>c</i>	86.2	273–307	?
Sodium-potassium alloys ¹⁵				
Strontium				
SrBr ₂	<i>c</i>	$18.1 + 0.00311T$	273–923	?
SrBr ₂ ·H ₂ O	<i>c</i>	28.9	277–370	?
SrBr ₂ ·6H ₂ O	<i>c</i>	82.1	276–327	?
SrCl ₂	<i>c</i>	$18.2 + 0.00244T$	273–1143	?
SrCl ₂ ·H ₂ O	<i>c</i>	28.7	276–365	?
SrCl ₂ ·2H ₂ O	<i>c</i>	38.3	277–366	?
SrCO ₃	<i>c</i>	21.8	281–371	?
SrI ₂	<i>c</i>	$18.6 + 0.00304T$	273–783	?
SrI ₂ ·H ₂ O	<i>c</i>	28.5	276–363	?
SrI ₂ ·2H ₂ O	<i>c</i>	39.1	275–336	?
SrI ₂ ·6H ₂ O	<i>c</i>	84.9	275–333	?
SrMoO ₄	<i>c</i>	37	273–297	?
Sr(NO ₃) ₂	<i>c</i>	38.3	290–320	?
SrSO ₄	<i>c</i>	26.2	293–369	?
Sulfur ¹⁶				
S	<i>c, rhombic</i>	$3.63 + 0.00640T$	273–368	3
	<i>c, monoclinic</i>	$4.38 + 0.00440T$	368–392	3
	<i>g</i>	$8.58 + 0.00030T$	300–2500	5
S ₂ Cl ₂	<i>l</i>	27.5	273–332	?
SO ₂	<i>g</i>	$7.70 + 0.00530T - 0.00000083T^2$	300–2500	2½
Tantalum				
Ta	<i>c</i>	$5.91 + 0.00099T$	273–1173	2
Tellurium				
Te	<i>c</i>	$5.19 + 0.00250T$	273–600	3
Thallium				
Tl	<i>c, α</i>	$5.32 + 0.00385T$	273–500	1
	<i>c, β</i>	8.12	500–576	1

TABLE 2-151 Heat Capacities of the Elements and Inorganic Compounds (Concluded)

Substance	State†	Heat capacity at constant pressure ($T = K$; $0\text{ }^{\circ}\text{C} = 273.1\text{ K}$), cal/(mol·K)	Range of temperature, K	Uncertainty, %
Thallium—(Cont.)				
Tl	<i>l</i>	7.12	576–773	3
TlBr	<i>c</i>	$12.53 + 0.00100T$	273–733	10
	<i>l</i>	16.0	733–800	10
TlCl	<i>c</i>	$12.56 + 0.00088T$	273–700	5
	<i>l</i>	14.2	700–803	10
Thorium				
Th	<i>c</i>	6.40	273–373	?
ThO ₂	<i>c</i>	$14.6 + 0.00507T$	273–1273	?
Th(SO ₄) ₂	<i>c</i>	41.2	273–373	?
Tin ⁴				
Sn	<i>c</i>	$5.05 + 0.00480T$	273–504	2
	<i>l</i>	6.6	504–1273	10
SnAu	<i>c</i>	$11.79 + 0.00233T$	273–581	1
SnCl ₂	<i>c</i>	$16.2 + 0.00926T$	273–520	?
SnCl ₄	<i>l</i>	38.4	286–371	?
SnO	<i>c</i>	$9.40 + 0.00362T$	273–1273	?
SnO ₂	<i>c</i>	$13.94 + 0.00565T - 252000/T^2$	273–1373	?
SnPt	<i>c</i>	$11.49 + 0.00190T$	273–1318	1
SnS	<i>c</i>	$12.1 + 0.00165T$	273–1153	?
SnS ₂	<i>c</i>	$20.5 + 0.00400T$	273–873	?
Titanium				
Ti	<i>c</i>	$8.91 + 0.00114T - 433000/T^2$	273–713	3
TiCl ₄	<i>l</i>	35.7	285–372	?
TiO ₂	<i>c</i>	$11.81 + 0.00754T - 41900/T^2$	273–713	3
Tungsten				
W	<i>c</i>	$5.65 + 0.00866$	273–2073	1
WO ₃	<i>c</i>	$16.0 + 0.00774T$	273–1550	?
Uranium				
U	<i>c</i>	6.64	273–372	?
U ₃ O ₈	<i>c</i>	59.8	276–314	?
Vanadium				
V	<i>c</i>	$5.57 + 0.00097T$	273–1993	?
Xenon				
Xe	<i>g</i>	4.97	All	0
Zinc ⁴				
Zn	<i>c</i>	$5.25 + 0.00270T$	273–692	1
	<i>l</i>	$7.59 + 0.00055T$	692–1122	3
ZnCl ₂	<i>c</i>	$15.9 + 0.00800T$	273–638	?
ZnO	<i>c</i>	$11.40 + 0.00145T - 182400/T^2$	273–1573	1
ZnS	<i>c</i>	$12.81 + 0.00095T - 194600/T^2$	273–1173	5
ZnSb	<i>c</i>	$11.5 + 0.00313T$	273–810	?
ZnSO ₄	<i>c</i>	28	293–373	?
ZnSO ₄ ·H ₂ O	<i>c</i>	34.7	282	?
ZnSO ₄ ·6H ₂ O	<i>c</i>	80.8	282	?
ZnSO ₄ ·7H ₂ O	<i>c</i>	100.2	273–307	?
Zirconium				
ZrO ₂	<i>c</i>	$11.62 + 0.01046T - 177700/T^2$	273–1673	5
ZrO ₂ ·SiO ₂	<i>c</i>	26.7	297–372	?

¹ See also Table 2-152. Data to 298 K are also given by Scott, *Cryogenic Engineering*, Van Nostrand, Princeton, N.J., 1959.

² For liquid and gas data, see Johnson (ed.), WADD-TR-60-56, 1960.

³ Stalder, NACA Tech. Note 4141, 1957 (Fig. 5), gives data from 400 to 2600°R.

⁴ See also Table 2-152.

⁵ For data from 400 to 5500°R see Stalder, NACA Tech. Note 4141, 1975 (Fig. 4).

⁶ For solid, liquid, and gas data, see Johnson (ed.), WADD-TR-60-56, 1960.

⁷ For data from 400 to 2350°R see Stalder, NACA Tech. Note 4141, 1957.

⁸ For solid, liquid, and gas data, see Johnson (ed.), WADD-TR-60-56, 1960.

⁹ For liquid and gas data, see Johnson (ed.), WADD-TR-60-56, 1960.

¹⁰ For solid, liquid, and gas data, see Johnson (ed.), WADD-TR-60-56, 1960.

¹¹ See also Table 2-152; Douglas, Ball, et al., *Bur. Stand. J. Res.*, **46** (1951): 334; Busey and Giaque, *J. Am. Chem. Soc.*, **75** (1953): 806; Sheldon, ASME Pap. 49-A-30, 1949.

¹² For solid, liquid, and gas data, see Johnson (ed.), WADD-TR-60-56, 1960.

¹³ For solid, liquid, and gas data, see Johnson (ed.), WADD-TR-60-56, 1960.

¹⁴ For solid, liquid, and gas data, see Johnson (ed.), WADD-TR-60-56, 1960. Ozone: For liquid see Brabets and Waterman, *J. Chem. Phys.*, **28** (1958): 1212.

¹⁵ For data on liquid Na-K alloys to 1500°F and for liquid Na to 1460°F, see Lubarsky and Kaufman, NACA Rep. 1270, 1956.

¹⁶ See also Evans and Wagman, *Bur. Stand. J. Res.*, **49** (1952): 141; Gratch, OTS PB 124957, 1950; Guthrie, Scott et al., *J. Am. Chem. Soc.*, **76** (1954): 1488.

2-164 PHYSICAL AND CHEMICAL DATA

TABLE 2-152 Specific Heat [kJ/(kg·K)] of Selected Elements

Symbol	Temperature, K														
	4	6	8	10	20	40	60	80	100	200	250	300	400	600	800
Al	0.00026	0.00050	0.00088	0.00140	0.0089	0.0775	0.214	0.357	0.481	0.797	0.859	0.902	0.949	1.042	1.134
Be	0.00008			0.00028	0.0014				0.195	1.109	1.537	1.840	2.191	2.605	2.823
Bi	0.00054	0.00220	0.00541	0.01040	0.0340	0.0729	0.092	0.102	0.109	0.120	0.121	0.122	0.123	0.142	0.136
Cr	0.00016	0.00029	0.00050	0.00081	0.0021	0.0107	0.059	0.127	0.190	0.382	0.424	0.450	0.501	0.565	0.611
Co	0.00036	0.00059	0.00085	0.00121	0.0048	0.0404	0.110	0.184	0.234	0.376	0.406	0.426	0.451	0.509	0.543
Cu	0.00011	0.00024	0.00048	0.00086	0.0076	0.059	0.137	0.203	0.254	0.357	0.377	0.386	0.396	0.431	0.448
Ge			0.00037	0.00081	0.0129	0.0619	0.108	0.153	0.192	0.286	0.305	0.323	0.343	0.364	0.377
Au	0.00018	0.00047	0.00126	0.00255	0.0163	0.0569	0.084	0.100	0.109	0.124	0.127	0.129	0.131	0.136	0.141
Ir				0.00032	0.0021				0.090	0.122	0.128	0.131	0.133	0.140	0.146
Fe	0.00038	0.00061	0.00090	0.00127	0.0039	0.0276	0.086	0.154	0.216	0.384	0.422	0.450	0.491	0.555	0.692
Pb	0.00075	0.00242	0.00747	0.01350	0.0531	0.0944	0.108	0.114	0.118	0.125	0.127	1.129	0.132	0.142	
Mg	0.00034	0.00080	0.00155	0.00172	0.0148	0.138	0.336	0.513	0.648	0.929	0.985	1.005	1.082	1.177	1.263
Hg	0.00417	0.01420	0.01820	0.02250	0.0515	0.0895	0.107	0.116	0.121	0.136	0.141	0.139	0.136	0.135	0.104
Mo	0.00011	0.00019	0.00032	0.00050	0.0029	0.0236	0.061	0.105	0.140	0.223	0.241	0.248	0.261	0.280	0.292
Ni	0.00054	0.00086	0.00121	0.00178	0.0058	0.0380	0.103	0.173	0.232	0.383	0.416	0.444	0.490	0.590	0.530
Pt	0.00019	0.00028	0.00067	0.00112	0.0077	0.0382	0.069	0.088	0.101	0.127	0.132	0.134	0.136	0.140	0.146
Ag	0.00016	0.00035	0.00093	0.00186	0.0159	0.0778	0.133	0.166	0.187	0.225	0.232	0.236	0.240	0.251	0.264
Sn	0.00024	0.00127	0.00423	0.00776	0.0400	0.108	0.149	0.173	0.189	0.214	0.220	0.222	0.245	0.257	0.257
Zn	0.00011	0.00029	0.00096	0.00250	0.0269	0.123	0.205	0.258	0.295	0.366	0.380	0.389	0.404	0.435	0.479

TABLE 2-153 Heat Capacities of Inorganic and Organic Liquids [J/(kmol·K)]

Cmpd. no.	Name	Formula	CAS no.	Mol. wt.	C1	C2	C3	C4	C5	T_{min} , K	C_p at T_{min} × 1E-05	T_{max} , K	C_p at T_{max} × 1E-05
1	Acetaldehyde	C ₂ H ₄ O	75-07-0	44.053	115,100	-433	1.425			150.15	0.8221	294.00	1.1097
2	Acetamide	C ₂ H ₅ NO	60-35-5	59.067	102,300	128.7				354.15	1.4788	571.00	1.7579
3	Acetic acid	C ₂ H ₄ O ₂	64-19-7	60.052	139,640	-320.8	0.8985			289.81	1.2213	391.05	1.5159
4	Acetic anhydride	C ₄ H ₆ O ₃	108-24-7	102.089	36,600	511				250.00	1.6435	350.00	2.1545
5	Acetone	C ₃ H ₆ O	67-64-1	58.079	135,600	-177	0.2837	0.000689		178.45	1.1696	329.44	1.3271
6	Acetonitrile	C ₂ H ₃ N	75-05-8	41.052	97,582	-122.2	0.34085			229.32	0.8748	354.75	0.9713
7	Acetylene	C ₂ H ₂	74-86-2	26.037	-122,020	3,082.7	-15.895	0.027732		192.40	0.8021	250.00	0.8853
8	Acrolein	C ₃ H ₄ O	107-02-8	56.063	103,090	-247.8	1.0343			253.00	1.0660	379.50	1.5801
9	Acrylic acid	C ₃ H ₄ O ₂	79-10-7	72.063	55,300	300				286.15	1.4114	375.00	1.6780
10	Acrylonitrile	C ₃ H ₃ N	107-13-1	53.063	109,900	-109.75	0.35441			189.63	1.0183	400.00	1.2271
11	Air	Mixture	132259-10-0	28.960	-214,460	9,185.1	-106.12	0.41616		75.00	0.5307	115.00	0.7132
12	Ammonia [use Eq. (2)]	H ₃ N	7664-41-7	17.031	61.289	80,925	799.4	-2,651		203.15	0.7575	401.15	4.1847
13	Anisole	C ₇ H ₈ O	100-66-3	108.138	150,940	93.455	0.23602			298.15	1.9978	484.20	2.5153
14	Argon	Ar	7440-37-1	39.948	134,390	-1,989.4	11.043			83.78	0.4523	135.00	0.6708
15	Benzamide	C ₇ H ₇ NO	55-21-0	121.137	161,440	260.66				403.00	2.6649	563.15	3.0823
16	Benzene	C ₆ H ₆	71-43-2	78.112	129,440	-169.5	0.64781			278.68	1.3251	353.24	1.5040
16	Benzene	C ₆ H ₆	71-43-2	78.112	162,940	-344.94	0.85562			278.68	1.3326	500.00	2.0437
17	Benzenethiol	C ₆ H ₆ S	108-98-5	110.177	119,780	180.34				258.27	1.6636	442.29	1.9954
18	Benzoic acid	C ₇ H ₆ O ₂	65-85-0	122.121	-5,480	647.12				395.45	2.5042	450.00	2.8572
19	Benzonitrile	C ₇ H ₅ N	100-47-0	103.121	93,383	242.61				260.40	1.5656	464.15	2.0599
20	Benzophenone	C ₁₃ H ₁₀ O	119-61-9	182.218	156,130	454.49				321.35	3.0218	640.00	4.4700
21	Benzyl alcohol	C ₇ H ₈ O	100-51-6	108.138	-334,997	3,644.21	-7.77514	0.00591102		257.85	1.8905	478.60	2.7617
22	Benzyl ethyl ether	C ₉ H ₁₀ O	539-30-0	136.191	87,500	640.20				275.65	2.1981	458.15	3.0741
23	Benzyl mercaptan	C ₇ H ₈ S	100-53-8	124.203	100,320	346.89				243.95	1.8494	472.03	2.6406
24	Biphenyl	C ₁₂ H ₁₀	92-52-4	154.208	121,770	429.3				342.20	2.6868	533.37	3.5075
25	Bromine	Br ₂	7726-95-6	159.808	179,400	-667.11	1.0701			265.90	0.7768	331.90	0.7587
26	Bromobenzene	C ₆ H ₅ Br	108-86-1	157.008	121,600	-9.45	0.358			293.15	1.4960	495.08	2.0467
27	Bromoethane	C ₂ H ₅ Br	74-96-4	108.965	94,364	-109.12	0.44032			160.00	0.8818	320.00	1.0453
28	Bromomethane	CH ₃ Br	74-83-9	94.939	129,730	-596.54	2.16	-0.0024234		184.45	0.7798	276.71	0.7870
29	1,2-Butadiene	C ₄ H ₆	590-19-2	54.090	135,150	-311.14	0.97007	-0.0001523		136.95	1.1034	290.00	1.2279
30	1,3-Butadiene	C ₄ H ₆	106-99-0	54.090	128,860	-323.1	1.015	0.000032		165.00	1.0333	350.00	1.4148
31	Butane	C ₄ H ₁₀	106-97-8	58.122	191,030	-1,675	12.5	-0.03874	4.6121E-05	134.86	1.1272	400.00	2.2237
32	1,2-Butanediol [use Eq. (2)]	C ₄ H ₁₀ O ₂	584-03-2	90.121	55.136	314,200	280.19	1,413.9		220.00	1.5590	670.00	5.2045
33	1,3-Butanediol [use Eq. (2)]	C ₄ H ₁₀ O ₂	107-88-0	90.121	42.152	324,580	517.35	1,449.5		196.15	0.6251	670.00	5.2437
34	1-Butanol	C ₄ H ₁₀ O	71-36-3	74.122	191,200	-730.4	2.2998			183.85	1.3465	391.90	2.5817
35	2-Butanol	C ₄ H ₁₀ O	78-92-2	74.122	426,790	-3,694.6	13.828	-0.0135		158.45	1.3485	372.90	2.7190
36	1-Butene	C ₄ H ₈	106-98-9	56.106	182,050	-1,611	11.963	-0.037454	4.5027E-05	87.80	1.1015	380.00	1.8103
37	cis-2-Butene	C ₄ H ₈	590-18-1	56.106	126,680	-65.47	-0.64	0.002912		134.26	1.1340	350.00	1.5022
38	trans-2-Butene	C ₄ H ₈	624-64-6	56.106	112,760	-104.7	0.5214			167.62	1.0986	274.03	1.2322
39	Butyl acetate	C ₆ H ₁₂ O ₂	123-86-4	116.158	111,850	384.52				298.15	2.2649	399.26	2.6537
40	Butylbenzene	C ₁₀ H ₁₄	104-51-8	134.218	182,470	-13,912	0.72897			185.30	2.0492	400.00	2.9354
41	Butyl mercaptan	C ₄ H ₁₀ S	109-79-5	90.187	232,190	-804.35	2.7063	-0.0023017		157.46	1.6365	390.00	1.9359
42	sec-Butyl mercaptan	C ₄ H ₁₀ S	513-53-1	90.187	197,890	-491.54	1.7219	-0.0012499		133.02	1.6003	370.00	1.8844
43	1-Butyne	C ₄ H ₆	107-00-6	54.090	136,340	-300.4	1.0216			147.43	1.1426	298.15	1.3759
44	Butyraldehyde	C ₄ H ₈ O	123-72-8	72.106	65,682	1,329.1	-7.1579	0.012755		176.75	1.4741	300.00	1.6459
45	Butyric acid	C ₄ H ₈ O ₂	107-92-6	88.105	237,700	-746.4	1.829			267.95	1.6902	436.42	2.6031
46	Butyronitrile	C ₄ H ₇ N	109-74-0	69.105	104,000	174				161.25	1.3206	390.75	1.7199
47	Carbon dioxide	CO ₂	124-38-9	44.010	-8,304,300	104,370	-433.33	0.60052		220.00	0.7827	290.00	1.6603
48	Carbon disulfide	CS ₂	75-15-0	76.141	85,600	-122	0.5605	-0.001452	2.008E-06	161.11	0.7577	552.00	1.3125
49	Carbon monoxide [use Eq. (2)]	CO	630-08-0	28.010	65.429	28,723	-847.39	1,959.6		68.15	0.5912	132.00	6.4799
50	Carbon tetrachloride	CCl ₄	56-23-5	153.823	-752,700	8,966.1	-30.394	0.034455		250.33	1.2763	388.71	1.6374
51	Carbon tetrafluoride	CF ₄	75-73-0	88.004	104,600	-500.6	2.2851			89.56	0.7810	145.10	0.8007
52	Chlorine	Cl ₂	7782-50-5	70.906	63,936	46.35	-0.1623			172.12	0.6711	239.12	0.6574
53	Chlorobenzene	C ₆ H ₅ Cl	108-90-7	112.557	-1,307,500	15,338	-53.974	0.063483		227.95	1.3617	360.00	1.8101
54	Chloroethane	C ₂ H ₅ Cl	75-00-3	64.514	127,900	-345.15	0.915			134.80	0.9800	340.00	1.1632
55	Chloroform	CHCl ₃	67-66-3	119.378	124,850	-166.34	0.43209			233.15	1.0956	366.48	1.2192
56	Chloromethane	CH ₃ Cl	74-87-3	50.488	96,910	-207.9	0.37456	0.000488		175.43	0.7460	373.15	0.9684
57	1-Chloropropane	C ₃ H ₇ Cl	540-54-5	78.541	132,280	-153.27	0.50836			150.35	1.2073	319.67	1.3523
58	2-Chloropropane	C ₃ H ₇ Cl	75-29-6	78.541	69,362	215.01				200.00	1.1236	308.85	1.3577

TABLE 2-153 Heat Capacities of Inorganic and Organic Liquids [J/(kmol·K)] (Continued)

Cmpd. no.	Name	Formula	CAS no.	Mol. wt.	C1	C2	C3	C4	C5	T_{\min} , K	C_p at T_{\min} $\times 1E-05$	T_{\max} , K	C_p at T_{\max} $\times 1E-05$
59	<i>m</i> -Cresol	C ₇ H ₈ O	108-39-4	108.138	-246,700	3,256.8	-7.4202	0.0060467		285.39	2.1895	400.00	2.5578
60	<i>o</i> -Cresol	C ₇ H ₈ O	95-48-7	108.138	-185,150	3,148	-8.0367	0.007254		304.20	2.3297	400.00	2.5243
61	<i>p</i> -Cresol	C ₇ H ₈ O	106-44-5	108.138	259,980	-1,112.3	4.9427	-0.0054367		307.93	2.2740	400.00	2.5794
62	Cumene	C ₉ H ₁₂	98-82-8	120.192	61,723	494.81				177.14	1.4937	425.56	2.7229
63	Cyanogen	C ₂ N ₂	460-19-5	52.035	65,516	144.7	0.063229			200.08	0.9700	300.08	1.1463
64	Cyclobutane	C ₄ H ₈	287-23-0	56.106	101,920	-215.81	0.8103			190.00	0.9017	298.15	1.0961
65	Cyclohexane	C ₆ H ₁₂	110-82-7	84.159	-220,600	3,118.3	-9.4216	0.010687		279.69	1.4836	400.00	2.0323
66	Cyclohexanol	C ₆ H ₁₂ O	108-93-0	100.159	-40,000	853				296.60	2.1300	434.00	3.3020
67	Cyclohexanone	C ₆ H ₁₀ O	108-94-1	98.143	6,110.4	600.94				290.00	1.8038	489.75	3.0042
68	Cyclohexene	C ₆ H ₁₀	110-83-8	82.144	105,850	-60	0.68			169.67	1.1525	356.12	1.7072
69	Cyclopentane	C ₅ H ₁₀	287-92-3	70.133	122,530	-403.8	1.7344	-0.0010975		179.28	0.9956	322.40	1.3584
70	Cyclopentene	C ₅ H ₈	142-29-0	68.117	125,380	-349.7	1.143			138.13	0.9888	317.38	1.2953
71	Cyclopropane	C ₃ H ₆	75-19-4	42.080	89,952	-196.63	0.65237			150.00	0.7514	298.15	0.8932
72	Cyclohexyl mercaptan	C ₆ H ₁₂ S	1569-69-3	116.224	177,560	-179.12	0.76723			189.64	1.7118	431.95	2.4334
73	Decanal	C ₁₀ H ₂₀ O	112-31-2	156.265	150,460	586.63				267.15	3.0718	488.15	4.3682
74	Decane	C ₁₀ H ₂₂	124-18-5	142.282	278,620	-197.91	1.0737			243.51	2.9409	460.00	4.1478
75	Decanoic acid	C ₁₀ H ₂₀ O ₂	334-48-5	172.265	219,840	140.41	0.9968			304.75	3.5521	543.15	5.9017
76	1-Decanol	C ₁₀ H ₂₂ O	112-30-1	158.281	4,988,500	-52,898	216.35	-0.37538	0.00023674	280.05	3.5373	503.00	5.0169
77	1-Decene	C ₁₀ H ₂₀	872-05-9	140.266	417,440	-1,616.5	5.3948	-0.004348		206.89	2.7541	443.75	3.8250
78	Decyl mercaptan	C ₁₀ H ₂₂ S	143-10-2	174.347	314,570	-160.93	0.95561			247.56	3.3330	512.35	4.8297
79	1-Decyne	C ₁₀ H ₁₈	764-93-2	138.250	276,900	-371.23	1.5774			229.15	2.7466	447.15	4.2629
80	Deuterium	D ₂	7782-39-0	4.032									
81	1,1-Dibromoethane	C ₂ H ₄ Br ₂	557-91-5	187.861	149,400	-231.8	0.5946			210.15	1.2695	381.15	1.4743
82	1,2-Dibromoethane	C ₂ H ₄ Br ₂	106-93-4	187.861	200,560	-491.44	0.9187			282.85	1.3506	410.00	1.5350
83	Dibromomethane	CH ₂ Br ₂	74-95-3	173.835	202,580	-726.3	1.3377			240.00	1.0532	370.10	1.1701
84	Diethyl ether	C ₄ H ₁₀ O	142-96-1	130.228	270,720	-259.83	0.95427			175.30	2.5450	450.00	3.4704
85	<i>m</i> -Dichlorobenzene	C ₆ H ₄ Cl ₂	541-73-1	147.002	114,880	187.25				248.39	1.6139	400.00	1.8978
86	<i>o</i> -Dichlorobenzene	C ₆ H ₄ Cl ₂	95-50-1	147.002	93,093	183.97	0.2314			273.15	1.6061	528.75	2.5506
87	<i>p</i> -Dichlorobenzene	C ₆ H ₄ Cl ₂	106-46-7	147.002	133,950	-24.84	0.48191			326.14	1.7711	513.56	2.4829
88	1,1-Dichloroethane	C ₂ H ₄ Cl ₂	75-34-3	98.959	126,340	-94.63	0.32			176.19	1.1960	330.45	1.3001
89	1,2-Dichloroethane	C ₂ H ₄ Cl ₂	107-06-2	98.959	179,170	-444.74	0.93009			237.49	1.2601	356.59	1.3885
90	Dichloromethane	CH ₂ Cl ₂	75-09-2	84.933	98,968	-62.941	0.23265			180.00	0.9518	320.00	1.0265
91	1,1-Dichloropropane	C ₃ H ₆ Cl ₂	78-99-9	112.986	144,560	-53.605	0.30617			180.00	1.4483	361.25	1.6515
92	1,2-Dichloropropane	C ₃ H ₆ Cl ₂	78-87-5	112.986	111,560	149.44				275.00	1.5266	369.52	1.6678
93	Diethanol amine	C ₄ H ₁₁ NO ₂	111-42-2	105.136	184,200	286				301.15	2.7033	541.54	3.3908
94	Diethyl amine	C ₄ H ₁₁ N	109-89-7	73.137	101,330	243.18				223.35	1.5564	328.60	1.8124
95	Diethyl ether	C ₄ H ₁₀ O	60-29-7	74.122	44,400	1,301	-5.5	0.008763		156.92	1.4698	460.00	3.3202
96	Diethyl sulfide	C ₄ H ₁₀ S	352-93-2	90.187	238,520	-1,038.4	4.0587	-0.0044691		181.95	1.5703	322.08	1.7579
97	1,1-Difluoroethane [use Eq. (2)]	C ₂ H ₄ F ₂	75-37-6	66.050	67,155	105,580	310.21	-490.54		154.56	0.9915	359.98	1.6874
98	1,2-Difluoroethane	C ₂ H ₄ F ₂	624-72-6	66.050	82,577	109.85				215.00	1.0619	283.65	1.1374
99	Difluoromethane	CH ₂ F ₂	75-10-5	52.023	263,980	-1,791.1	4.3666			200.00	0.8042	250.00	0.8912
100	Di-isopropyl amine	C ₆ H ₁₃ N	108-18-9	101.190	98,434	429.04				275.00	2.1642	357.05	2.5162
101	Di-isopropyl ether	C ₆ H ₁₄ O	108-20-3	102.175	163,000	-4.5	0.62			187.65	1.8399	341.45	2.3375
102	Di-isopropyl ketone	C ₇ H ₁₄ O	565-80-0	114.185	179,270	28.37	0.5375			204.81	2.0763	410.00	2.8126
103	1,1-Dimethoxyethane	C ₄ H ₁₀ O ₂	534-15-6	90.121	187,790	-313.41	1.1023			159.95	1.6586	337.45	2.0755
104	1,2-Dimethoxypropane	C ₅ H ₁₂ O ₂	7778-85-0	104.148	199,930	-191.5	0.87664			226.10	2.0145	366.15	2.4734
105	Dimethyl acetylene	C ₄ H ₆	503-17-3	54.090	88,153	124.16				240.91	1.1806	300.13	1.2542
106	Dimethyl amine	C ₂ H ₇ N	124-40-3	45.084	-214,870	3,787.2	-13.781	0.016924		180.96	1.1947	298.15	1.3779
107	2,3-Dimethylbutane	C ₆ H ₁₄	79-29-8	86.175	129,450	18.5	0.608			145.19	1.4495	331.13	2.0224
108	1,1-Dimethylcyclohexane	C ₈ H ₁₆	590-66-9	112.213	134,500	8,765	0.81151			239.66	1.8321	392.70	2.6309
109	<i>cis</i> -1,2-Dimethylcyclohexane	C ₈ H ₁₆	2207-01-4	112.213	150,130	-62.38	0.8851			223.16	1.8029	402.94	2.6870
110	<i>trans</i> -1,2-Dimethylcyclohexane	C ₈ H ₁₆	6876-23-9	112.213	155,560	-145.26	1.0932			184.99	1.6610	396.58	2.6989
111	Dimethyl disulfide	C ₂ H ₆ S ₂	624-92-0	94.199	171,580	-256.67	0.5727			188.44	1.4355	360.00	1.5340
112	Dimethyl ether	C ₂ H ₆ O	115-10-6	46.068	110,100	-157.47	0.51853			131.65	0.9836	250.00	1.0314
113	<i>N,N</i> -Dimethyl formamide	C ₃ H ₇ NO	68-12-2	73.094	147,900	-106	0.384			273.82	1.4767	466.44	1.8200
114	2,3-Dimethylpentane	C ₇ H ₁₆	565-59-3	100.202	146,420	59.2	0.604			90.00	1.5664	380.00	2.5613
115	Dimethyl phthalate	C ₁₀ H ₁₀ O ₄	131-11-3	194.184	206,560	325.75				274.16	2.9587	360.00	3.2383
116	Dimethylsilane	C ₂ H ₈ Si	1111-74-6	60.170	131,810					298.15	1.3181	298.15	1.3181

117	Dimethyl sulfide	C ₂ H ₆ S	75-18-3	62.134	146,950	-380.06	1.2035	-0.00084787		174.88	1.1276	310.48	1.1959
118	Dimethyl sulfoxide	C ₂ H ₆ OS	67-68-5	78.133	240,300	-595	1.013			291.67	1.5293	422.15	1.6965
119	Dimethyl terephthalate	C ₁₀ H ₁₀ O ₄	120-61-6	194.184	190,020	431.04				423.40	3.7252	466.35	3.9104
120	1,4-Dioxane	C ₄ H ₈ O ₂	123-91-1	88.105	956,860	-5,559.9	9.6124			284.95	1.5306	374.47	2.2277
121	Diphenyl ether	C ₁₂ H ₁₀ O	101-84-8	170.207	134,160	447.67				300.03	2.6847	570.00	3.8933
122	Dipropyl amine	C ₆ H ₁₅ N	142-84-7	101.190	49,120	562.24				277.90	2.0537	407.90	2.7846
123	Dodecane	C ₁₂ H ₂₆	112-40-3	170.335	508,210	-1,368.7	3.1015			263.57	3.6292	330.00	3.9429
124	Eicosane	C ₂₀ H ₄₂	112-95-8	282.547	352,720	807.32	0.2122			309.58	6.2299	616.93	9.3154
125	Ethane [use Eq. (2)]	C ₂ H ₆	74-84-0	30.069	44.009	89,718	918.77	-1.886		92.00	0.6855	290.00	1.2444
126	Ethanol	C ₂ H ₆ O	64-17-5	46.068	102,640	-139.63	-0.030341	0.0020386		159.05	0.8787	390.00	1.6450
127	Ethyl acetate	C ₄ H ₈ O ₂	141-78-6	88.105	226,230	-624.8	1.472			189.60	1.6068	350.21	1.8796
128	Ethyl amine	C ₂ H ₇ N	75-04-7	45.084	121,700	38,993				192.15	1.2919	289.73	1.3300
129	Ethylbenzene	C ₈ H ₁₀	100-41-4	106.165	154,040	-142.29	0.80539			178.20	1.5426	409.35	2.3075
130	Ethyl benzoate	C ₉ H ₁₀ O ₂	93-89-0	150.175	124,500	370.6				238.45	2.1287	486.55	3.0482
131	2-Ethyl butanoic acid	C ₆ H ₁₂ O ₂	88-09-5	116.158	56,359	603.02				258.15	2.1203	466.95	3.3794
132	Ethyl butyrate	C ₆ H ₁₂ O ₂	105-54-4	116.158	82,434	422.45	0.20992			285.50	2.2015	428.25	3.0185
133	Ethylcyclohexane	C ₈ H ₁₆	1678-91-7	112.213	132,360	72.74	0.64738			161.84	1.6109	404.95	2.6798
134	Ethylcyclopentane	C ₇ H ₁₄	1640-89-7	98.186	178,520	-518.35	2.3255	-0.0016818		134.71	1.4678	301.82	1.8767
135	Ethylene	C ₂ H ₄	74-85-1	28.053	247,390	-4,428	40.936	-0.1697	0.00026816	104.00	0.7012	252.70	0.9758
136	Ethylenediamine	C ₂ H ₈ N ₂	107-15-3	60.098	184,440	-150.2	0.37044			284.29	1.7168	390.41	1.8226
137	Ethylene glycol	C ₂ H ₆ O ₂	107-21-1	62.068	35,540	436.78	-0.18486			260.15	1.3666	493.15	2.0598
138	Ethyleneimine	C ₂ H ₅ N	151-56-4	43.068	46,848	205.35				250.00	0.9819	329.00	1.1441
139	Ethylene oxide	C ₂ H ₄ O	75-21-8	44.053	144,710	-758.87	2.8261	-0.003064		160.65	0.8303	283.85	0.8693
140	Ethyl formate	C ₃ H ₆ O ₂	109-94-4	74.079	80,000	223.6				254.20	1.3684	374.20	1.6367
141	2-Ethyl hexanoic acid	C ₈ H ₁₆ O ₂	149-57-5	144.211	207,670	-17.907	1.0493			235.00	2.6141	510.10	4.7157
142	Ethylhexyl ether	C ₈ H ₁₈ O	5756-43-4	130.228	146,040	458.22				298.15	2.8266	417.15	3.3719
143	Ethylisopropyl ether	C ₅ H ₁₂ O	625-54-7	88.148	106,250	292.15				298.15	1.9335	326.15	2.0153
144	Ethylisopropyl ketone	C ₆ H ₁₂ O	565-69-5	100.159	229,250	-404.54	1.1382			204.15	1.9410	386.55	2.4295
145	Ethyl mercaptan	C ₂ H ₆ S	75-08-1	62.134	134,670	-234.39	0.59656			125.26	1.1467	315.25	1.2007
146	Ethyl propionate	C ₅ H ₁₀ O ₂	105-37-3	102.132	76,330	400.1				298.15	1.9562	410.00	2.4037
147	Ethylpropyl ether	C ₅ H ₁₂ O	628-32-0	88.148	103,680	726.3	-2.6047	0.0040957		145.65	1.6686	320.00	2.0358
148	Ethyltrichlorosilane	C ₂ H ₅ Cl ₃ Si	115-21-9	163.506	105,150	0.46693	85.318			167.55	1.3255	371.05	2.0109
149	Fluorine	F ₂	7782-41-4	37.997	-94,585	7,529.9	-139.6	1.1301	-0.0033241	58.00	0.5541	98.00	0.5966
149	Fluorine	F ₂	7782-41-4	37.997	1724,400	-59,924	537.85			53.48	0.5798	56.00	0.5535
150	Fluorobenzene	C ₆ H ₅ F	462-06-6	96.102	-991,200	11,734	-40.669	0.047333		239.99	1.3675	319.99	1.5018
151	Fluoroethane	C ₂ H ₅ F	353-36-6	48.060	85,663	-118.56	0.55459			140.00	0.7994	240.00	0.8915
152	Fluoromethane	CH ₃ F	593-53-3	34.033	74,746	-132.32	0.53772			140.00	0.6676	220.00	0.7166
153	Formaldehyde	CH ₂ O	50-00-0	30.026	61,900	28.3				204.00	0.6767	234.00	0.6852
154	Formamide	CH ₃ NO	75-12-7	45.041	63,400	150.6				292.00	1.0738	493.00	1.3765
155	Formic acid	CH ₂ O ₂	64-18-6	46.026	78,060	71.54				281.45	0.9820	380.00	1.0525
156	Furan	C ₄ H ₄ O	110-00-9	68.074	114,370	-215.69	0.72691			187.55	0.9949	304.50	1.1609
157	Helium-4	He	7440-59-7	4.003	387,220	-465,570	211,800	-42,494	3212.9	2.20	0.1087	4.60	0.2965
157	Helium-4	He	7440-59-7	4.003	410,430	-464,890	135,100			1.80	0.1135	2.10	0.2995
158	Heptadecane	C ₁₇ H ₃₆	629-78-7	240.468	376,970	347.82	0.57895			295.13	5.3005	575.30	7.6869
159	Heptanal	C ₇ H ₁₄ O	111-71-7	114.185	222,360	-105.17	0.65074			229.80	2.3256	381.25	2.7685
160	Heptane [use Eq. (2)]	C ₇ H ₁₆	142-82-5	100.202	61.26	314,410	1,824.6	-2,547.9		182.57	1.9989	520.00	4.0657
161	Heptanoic acid	C ₇ H ₁₄ O ₂	111-14-8	130.185	194,570	-23.206	0.88395			265.83	2.5087	496.15	4.0065
162	1-Heptanol	C ₇ H ₁₆ O	111-70-6	116.201	2,416,800	-26.105	110.03	-0.19172	0.00011968	239.15	2.3590	448.60	3.8766
163	2-Heptanol	C ₇ H ₁₆ O	543-49-7	116.201	283,127	-1,037.63	3.44064			230.00	2.2649	432.90	4.7873
164	3-Heptanone	C ₇ H ₁₄ O	106-35-4	114.185	270,730	-399.89	1.0601			234.15	2.3522	480.00	3.2303
165	2-Heptanone	C ₇ H ₁₄ O	110-43-0	114.185	265,040	-375.68	1.0024			238.15	2.3242	490.00	3.2163
166	1-Heptene	C ₇ H ₁₄	592-76-7	98.186	267,950	-1,315.9	6.5242	-0.011994	9.3808E-06	154.12	1.8150	366.79	2.4096
167	Heptyl mercaptan	C ₇ H ₁₆ S	1639-09-4	132.267	236,870	-158.01	0.78982			229.92	2.4229	460.00	3.3131
168	1-Heptyne	C ₇ H ₁₂	628-71-7	96.170	46,798	761.13	-0.62882			200.00	1.7387	372.93	2.4319
169	Hexadecane	C ₁₆ H ₃₄	544-76-3	226.441	370,350	231.47	0.68632			291.31	4.9602	560.01	7.1521
170	Hexanal	C ₆ H ₁₂ O	66-25-1	100.159	117,700	329.52				217.15	1.8926	401.45	2.4999
171	Hexane	C ₆ H ₁₄	110-54-3	86.175	172,120	-183.78	0.88734			177.83	1.6750	460.00	2.7534
172	Hexanoic acid	C ₆ H ₁₂ O ₂	142-62-1	116.158	161,980	44.116	0.709			269.25	2.2526	478.85	3.4568
173	1-Hexanol	C ₆ H ₁₄ O	111-27-3	102.175	1,638,600	-17,261	71.721	-0.12026	0.000071087	228.55	1.9821	460.00	3.5197
174	2-Hexanol	C ₆ H ₁₄ O	626-93-7	102.175	267,628	-1,033.06	3.35185			223.00	2.0394	585.30	8.1124
175	2-Hexanone	C ₆ H ₁₂ O	591-78-6	100.159	208,250	-107.47	0.2062	0.00070293		217.35	2.0185	460.00	2.7087
176	3-Hexanone	C ₆ H ₁₂ O	589-38-8	100.159	235,960	-345.94	0.94278			217.50	2.0532	460.00	2.7632
177	1-Hexene	C ₆ H ₁₂	592-41-6	84.159	164,640	-200.37	0.8784			133.39	1.5354	336.63	1.9673

TABLE 2-153 Heat Capacities of Inorganic and Organic Liquids [J/(kmol·K)] (Continued)

Cmpd. no.	Name	Formula	CAS no.	Mol. wt.	C1	C2	C3	C4	C5	T_{\min} , K	C_p at T_{\min} $\times 1E-05$	T_{\max} , K	C_p at T_{\max} $\times 1E-05$
178	3-Hexyne	C ₆ H ₁₀	928-49-4	82.144	82,795	283.4				300.00	1.6781	354.35	1.8322
179	Hexyl mercaptan	C ₆ H ₁₄ S	111-31-9	118.240	303,320	-1,009	3.3885	-0.002762		192.62	2.1495	430.00	2.7639
180	1-Hexyne	C ₆ H ₁₀	693-02-7	82.144	93,000	326				200.00	1.5820	344.48	2.0530
181	2-Hexyne	C ₆ H ₁₀	764-35-2	82.144	94,860	254.15				300.00	1.7110	357.67	1.8576
182	Hydrazine	H ₄ N ₂	302-01-2	32.045	79,815	50,929	0.043379			274.69	0.9708	653.15	1.3158
183	Hydrogen [use Eq. (2)]	H ₂	1333-74-0	2.016	66,653	6,765.9	-123.63	478.27		13.95	0.1262	32.00	1.3122
184	Hydrogen bromide	HBr	10035-10-6	80.912	57,720	9.9				185.15	0.5955	206.45	0.5976
185	Hydrogen chloride	HCl	7647-01-0	36.461	47,300	90				165.00	0.6215	185.00	0.6395
186	Hydrogen cyanide	CHN	74-90-8	27.025	95,398	-197.52	0.3883			259.83	0.7029	298.85	0.7105
187	Hydrogen fluoride	HF	7664-39-3	20.006	62,520	-223.02	0.6297			189.79	0.4288	292.67	0.5119
188	Hydrogen sulfide [use Eq. (2)]	H ₂ S	7783-06-4	34.081	64,666	49,354	22.493	-1,623		187.68	0.6733	370.00	4.9183
189	Isobutyric acid	C ₄ H ₈ O ₂	79-31-2	88.105	127,540	-65.35	0.82867			270.00	1.7031	427.65	2.5114
190	Isopropyl amine	C ₃ H ₉ N	75-31-0	59.110	-32,469	1,977.1	-7.0145	0.0086913		177.95	1.4621	320.00	1.6671
191	Malonic acid	C ₃ H ₄ O ₄	141-82-2	104.061	157,850	-41,619	0.42817			407.95	2.1213	603.75	2.8880
192	Methacrylic acid	C ₄ H ₆ O ₂	79-41-4	86.089	146,290	-58.59	0.3582			288.15	1.5915	434.15	1.8837
193	Methane [use Eq. (2)]	CH ₄	74-82-8	16.042	65,708	38,883	-257.95	614.07		90.69	0.5361	190.00	14.9780
194	Methanol	CH ₃ O	67-56-1	32.042	105,800	-362.23	0.9379			175.47	0.7112	400.00	1.1097
195	N-Methyl acetamide	C ₃ H ₇ NO	79-16-3	73.094	62,600	243.4				359.00	1.4998	538.50	1.9367
196	Methyl acetate	C ₃ H ₆ O ₂	79-20-9	74.079	61,260	270.9				253.40	1.2991	373.40	1.6241
197	Methyl acetylene	C ₃ H ₄	74-99-7	40.064	79,791	89.49				200.00	0.9769	249.94	1.0216
198	Methyl acrylate	C ₄ H ₆ O ₂	96-33-3	86.089	275,500	-1,147	2.568			196.32	1.4930	353.35	1.9084
199	Methyl amine	CH ₃ N	74-89-5	31.057	92,520	37.45				179.69	0.9925	266.82	1.0251
200	Methyl benzoate	C ₈ H ₈ O ₂	93-58-3	136.148	125,630	279.75				260.75	1.9857	472.65	2.5785
201	3-Methyl-1,2-butadiene	C ₅ H ₈	598-25-4	68.117	135,370	-133.34	0.63868			159.53	1.3035	314.56	1.5662
202	2-Methylbutane	C ₅ H ₁₂	78-78-4	72.149	108,300	146	-0.292	0.00151		113.25	1.2328	310.00	1.7048
203	2-Methylbutanoic acid	C ₅ H ₁₀ O ₂	116-53-0	102.132	74,200	417.4				321.50	2.0839	481.50	2.7518
204	3-Methyl-1-butanol	C ₅ H ₁₂ O	123-51-3	88.148	247,870	-1,145	3.4223			155.95	1.5254	404.15	3.4411
205	2-Methyl-1-butene	C ₅ H ₁₀	563-46-2	70.133	149,510	-247.63	0.91849			135.58	1.3282	304.31	1.5921
206	2-Methyl-2-butene	C ₅ H ₁₀	513-35-9	70.133	151,600	-266.72	0.90847			139.39	1.3207	311.71	1.5673
207	2-Methyl-1-butene-3-yne	C ₆ H ₈	78-80-8	66.101	81,919	181.01				298.15	1.3589	305.40	1.3720
208	Methylbutyl ether	C ₅ H ₁₂ O	628-28-4	88.148	177,850	-171.57	0.74379			157.48	1.6928	343.31	2.0661
209	Methylbutyl sulfide	C ₅ H ₁₂ S	628-29-5	104.214	198,390	-220.35	0.76096			175.30	1.8315	510.00	2.8394
210	3-Methyl-1-butyne	C ₅ H ₈	598-23-2	68.117	105,200	191.1				200.00	1.4342	299.49	1.6243
211	Methyl butyrate	C ₅ H ₁₀ O ₂	623-42-7	102.132	102,930	129.1	0.62516			277.25	1.8678	415.87	2.6474
212	Methylchlorosilane	CH ₃ ClSi	993-00-0	80.589	47,726	338.4				250.00	1.3233	325.00	1.5771
213	Methylcyclohexane	C ₇ H ₁₄	108-87-2	98.186	131,340	-63.1	0.8125			146.58	1.3955	320.00	1.9435
214	1-Methylcyclohexanol	C ₇ H ₁₄ O	590-67-0	114.185	50,578	508.59				300.00	2.0315	441.15	2.7494
215	cis-2-Methylcyclohexanol	C ₇ H ₁₄ O	7443-70-1	114.185	118,600	447.07				300.00	2.5272	438.15	3.1448
216	trans-2-Methylcyclohexanol	C ₇ H ₁₄ O	7443-52-9	114.185	118,170	447.99				300.00	2.5257	440.15	3.1535
217	Methylcyclopentane	C ₆ H ₁₂	96-37-7	84.159	155,920	-490	2.1383	-0.0015585		130.73	1.2492	366.48	1.8682
218	1-Methylcyclopentene	C ₆ H ₁₀	693-89-0	82.144	53,271	327.92				200.00	1.1885	348.64	1.6760
219	3-Methylcyclopentene	C ₆ H ₁₀	1120-62-3	82.144	46,457	346.93				200.00	1.1584	338.05	1.6374
220	Methyldichlorosilane	CH ₂ Cl ₂ Si	75-54-7	115.034	27,030	413				250.00	1.3028	350.00	1.7158
221	Methylethyl ether	C ₃ H ₈ O	540-67-0	60.095	85,383	199.08	-0.061547			160.00	1.1566	280.50	1.3638
222	Methylethyl ketone	C ₄ H ₈ O	78-93-3	72.106	132,300	200.87	-0.9597	0.0019533		186.48	1.4905	373.15	1.7511
223	Methylethyl sulfide	C ₃ H ₈ S	624-89-5	76.161	161,240	-288.61	0.78179			167.23	1.3484	339.80	1.5344
224	Methyl formate	C ₂ H ₄ O ₂	107-31-3	60.052	130,200	-396	1.21			174.15	0.9793	304.90	1.2195
225	Methylisobutyl ether	C ₅ H ₁₂ O	625-44-5	88.148	92,919	324.43				298.15	1.8965	350.00	2.0647
226	Methylisobutyl ketone	C ₆ H ₁₂ O	108-10-1	100.159	183,650	-79,862	0.60769			189.15	1.9029	389.15	2.4460
227	Methyl Isocyanate	C ₂ H ₃ NO	624-83-9	57.051	149,770	-529.82	1.3499			256.15	1.0263	366.00	1.3668
228	Methylisopropyl ether	C ₄ H ₁₀ O	598-53-8	74.122	143,440	-154.07	0.7255			127.93	1.3560	310.00	1.6540
229	Methylisopropyl ketone	C ₅ H ₁₀ O	563-80-4	86.132	191,170	-331.04	0.98445			180.15	1.6348	440.00	2.3610
230	Methylisopropyl sulfide	C ₄ H ₁₀ S	1551-21-9	90.187	211,170	-661.97		-0.0021383		171.64	1.5808	357.91	1.8641
231	Methyl mercaptan	CH ₃ S	74-93-1	48.107	115,300	-263.23	0.60412			150.18	0.8939	298.15	0.9052
232	Methyl methacrylate	C ₅ H ₈ O ₂	80-62-6	100.116	255,100	-938.4	2.413			224.95	1.6611	373.45	2.4118
233	2-Methyloctanoic acid	C ₉ H ₁₈ O ₂	3004-93-1	158.238	226,650	15,421	1.0578			240.00	2.9128	518.15	5.1864
234	2-Methylpentane	C ₆ H ₁₄	107-83-5	86.175	142,220	-47.83	0.739			119.55	1.4706	333.41	2.0842
235	Methyl pentyl ether	C ₆ H ₁₄ O	628-80-8	102.175	251,890	-468.32	1.2209			176.00	2.0728	372.00	2.4663
236	2-Methylpropane	C ₄ H ₁₀	75-28-5	58.122	172,370	-1,783.9	14.759	-0.047909	0.00005805	113.54	0.9961	380.00	2.0725

237	2-Methyl-2-propanol	C ₄ H ₁₀ O	75-65-0	74.122	-925.460	7,894.9	-17.661	0.013617		298.96	2.2016	460.00	2.9455
238	2-Methyl propene	C ₄ H ₈	115-11-7	56.106	87.680	217.1	-0.9153	0.002266		132.81	1.0568	343.15	1.4596
239	Methyl propionate	C ₅ H ₈ O ₂	554-12-1	88.105	71.140	335.5				300.00	1.7179	390.00	2.0198
240	Methylpropyl ether	C ₆ H ₁₄ O	557-17-5	74.122	144.110	-102.09	0.58113			133.97	1.4086	312.20	1.6888
241	Methylpropyl sulfide	C ₆ H ₁₄ S	3877-15-4	90.187	179.850	-264.1	0.79202			160.17	1.5787	368.69	1.9014
242	Methylsilane	CH ₃ Si	992-94-9	46.144	113.470					298.15	1.1347	298.15	1.1347
243	alpha-Methyl styrene	C ₉ H ₁₀	98-83-9	118.176	76.822	421.6				249.95	1.8220	438.65	2.6176
244	Methyl <i>tert</i> -butyl ether	C ₇ H ₁₄ O	1634-04-4	88.148	134.300	94.356	-0.0032	0.0009795		164.55	1.5410	328.18	1.9954
245	Methyl vinyl ether	C ₅ H ₈ O	107-25-5	58.079	73.600	184.7				151.15	1.0152	278.65	1.2507
246	Naphthalene	C ₁₀ H ₈	91-20-3	128.171	29.800	527.5				353.43	2.1623	491.14	2.8888
247	Neon	Ne	7440-01-9	20.180	1,034,100	-138,770	7,154	-162.55	1.3841	24.56	0.3666	40.00	0.6980
248	Nitroethane	C ₂ H ₅ NO ₂	79-24-3	75.067	187.740	-497.6	1.0691			183.63	1.3242	387.22	1.5536
249	Nitrogen	N ₂	7727-37-9	28.013	281.970	-12,281	248	-2.2182	0.0074902	63.15	0.5593	112.00	0.7960
250	Nitrogen trifluoride	F ₃ N	7783-54-2	71.002	101.400	-682.11	3.8912			117.00	0.7486	175.50	1.0154
251	Nitromethane	CH ₃ NO ₂	75-52-5	61.040	116.270	-135.3	0.345			244.60	1.0382	473.15	1.2949
252	Nitrous oxide	N ₂ O	10024-97-2	44.013	67.556	54.373				182.30	0.7747	200.00	0.7843
253	Nitric oxide	NO	10102-43-9	30.006	-2,979.600	76.602	-652.59	1.8879		109.50	0.6229	150.00	1.9909
254	Nonadecane	C ₁₉ H ₄₀	629-92-5	268.521	342.570	762.08	0.20481			305.04	5.9409	603.05	8.7663
255	Nonanal	C ₉ H ₁₈ O	124-19-6	142.239	136.820	531.29				255.15	2.7238	468.15	3.8554
256	Nonane	C ₉ H ₂₀	111-84-2	128.255	383.080	-1,139.8	2.7101			219.66	2.6348	325.00	2.9890
257	Nonanoic acid	C ₉ H ₁₈ O ₂	112-05-0	158.238	224.336	49.726	0.9813			285.55	3.1855	528.75	5.2498
258	1-Nonanol	C ₉ H ₂₀ O	143-08-8	144.255	10,483.000	-115,220	476.87	-0.85381	0.00056246	310.00	3.5059	460.00	4.6494
259	2-Nonanol	C ₉ H ₂₀ O	628-99-9	144.255	329.641	-1,046.78	3.61823			238.15	2.8555	649.50	11.7608
260	1-Nonene	C ₉ H ₁₈	124-11-8	126.239	254.490	-298.06	1.1707			191.91	2.4041	420.02	3.3583
261	Nonyl mercaptan	C ₉ H ₂₀ S	1455-21-6	160.320	265.350	-46.22	0.79154			253.05	3.0434	492.95	4.3491
262	1-Nonyne	C ₉ H ₁₆	3452-09-3	124.223	253.580	-366.3	1.4881			223.15	2.4594	423.85	3.6566
263	Octadecane	C ₁₈ H ₃₈	593-45-3	254.494	399.430	374.64	0.58156			301.31	5.6511	589.86	8.2276
264	Octanal	C ₈ H ₁₆ O	124-13-0	128.212	130.650	463.61				246.00	2.4470	447.15	3.3795
265	Octane	C ₈ H ₁₈	111-65-9	114.229	224.830	-186.63	0.95891			216.38	2.2934	460.00	3.4189
266	Octanoic acid	C ₈ H ₁₆ O ₂	124-07-2	144.211	205.260	44.392	0.8956			289.65	2.9326	512.85	4.6358
267	1-Octanol	C ₈ H ₁₈ O	111-87-5	130.228	571.370	-4,849	19.725	-0.021532		250.00	2.5550	467.10	4.1566
268	2-Octanol	C ₈ H ₁₈ O	123-96-6	130.228	319.198	-1,042.21	3.52943			241.55	2.7338	452.90	5.7113
269	2-Octanone	C ₈ H ₁₆ O	111-13-7	128.212	300.400	-426.2	1.1172			252.86	2.6406	500.00	3.6660
270	3-Octanone	C ₈ H ₁₆ O	106-68-3	128.212	289.980	-417.2	1.2218			255.55	2.6314	440.65	3.4335
271	1-Octene	C ₈ H ₁₆	111-66-0	112.213	509.420	-4,279.1	21.477	-0.044462	3.5028E-05	171.45	2.1327	394.41	2.8235
272	Octyl mercaptan	C ₈ H ₁₈ S	111-88-6	146.294	240.040	-33.198	0.67889			240.00	2.7118	472.19	3.7573
273	1-Octyne	C ₈ H ₁₄	629-05-0	110.197	42.642	886.67	-0.69315			200.00	1.9225	399.35	2.8619
274	Oxalic acid	C ₂ H ₂ O ₄	144-62-7	90.035	175.510	-381.36	0.64623			462.65	1.3740	603.00	1.8052
275	Oxygen	O ₂	7782-44-7	31.999	175.430	-6,152.3	113.92	-0.92382	0.0027963	54.36	0.5365	142.00	0.9066
276	Ozone	O ₃	10028-15-6	47.998	60.046	281.16				90.00	0.8535	150.00	1.0222
277	Pentadecane	C ₁₅ H ₃₂	629-62-9	212.415	346.910	219.54	0.65632			283.07	4.6165	543.84	6.6042
278	Pentanal	C ₅ H ₁₀ O	110-62-3	86.132	112.050	257.78				200.00	1.6361	376.15	2.0901
279	Pentane	C ₅ H ₁₂	109-66-0	72.149	159.080	-270.5	0.99537			143.42	1.4076	390.00	2.0498
280	Pentanoic acid	C ₅ H ₁₀ O ₂	109-52-4	102.132	145.050	28.344	0.6372			239.15	1.8827	458.95	2.9228
281	1-Pentanol	C ₅ H ₁₂ O	71-41-0	88.148	201.200	-651.3	2.275			200.14	1.6198	389.15	2.9227
282	2-Pentanol	C ₅ H ₁₂ O	6032-29-7	88.148	251.596	-1,028.49	3.26306			200.00	1.7642	561.00	7.0158
283	2-Pentanone	C ₅ H ₁₀ O	107-87-9	86.132	194.590	-263.86	0.76808			196.29	1.7239	375.46	2.0380
284	3-Pentanone	C ₅ H ₁₀ O	96-22-0	86.132	193.020	-176.43	0.5669			234.18	1.8279	375.14	2.0661
285	1-Pentene	C ₅ H ₁₀	109-67-1	70.133	156.100	-456.94	2.255	-0.003163	0.00000238	108.02	1.2939	350.00	1.7251
286	2-Pentyl mercaptan	C ₇ H ₁₄ S	2084-19-7	104.214	188.200	-140.84	0.63581			160.75	1.8199	385.15	2.2827
287	Pentyl mercaptan	C ₅ H ₁₂ S	110-66-7	104.214	213.760	-324.4	0.9472			197.45	1.8664	399.79	2.3546
288	1-Pentyne	C ₅ H ₈	627-19-0	68.117	86.200	256.6				200.00	1.3752	313.33	1.6660
289	2-Pentyne	C ₅ H ₈	627-21-4	68.117	68.671	246.66				200.00	1.1800	329.27	1.4989
290	Phenanthrene	C ₁₄ H ₁₀	85-01-8	178.229	103.370	527.03				372.39	2.9963	500.00	3.6688
291	Phenol	C ₆ H ₆ O	108-95-2	94.111	101.720	317.61				314.06	2.0147	425.00	2.3670
292	Phenyl isocyanate	C ₇ H ₅ NO	103-71-9	119.121	60.834	215.89	0.29552			243.15	1.3080	489.75	2.3745
293	Phthalic anhydride	C ₈ H ₄ O ₃	85-44-9	148.116	145.400	252.4				404.15	2.4741	557.65	2.8615
294	Propadiene	C ₃ H ₄	463-49-0	40.064	66.230	98.275				200.00	0.8589	238.65	0.8968
295	Propane [use Eq. (2)]	C ₃ H ₈	74-98-6	44.096	62.983	113.630	633.21	-873.46		85.47	0.8488	360.00	2.6079
296	1-Propanol	C ₃ H ₈ O	71-23-8	60.095	158.760	-635	1.969			146.95	1.0797	400.00	2.1980
297	2-Propanol	C ₃ H ₈ O	67-63-0	60.095	471.710	-4,172.1	14.745	-0.0144		185.26	1.1329	355.30	2.0487
298	Propenylcyclohexene	C ₉ H ₁₄	13511-13-2	122.207	201.400	-450.6	1.7053			199.00	1.7926	431.65	3.2463
299	Propionaldehyde	C ₃ H ₆ O	123-38-6	58.079	99.306	115.73				200.00	1.2245	328.75	1.3735

TABLE 2-153 Heat Capacities of Inorganic and Organic Liquids [J/(kmol·K)] (Concluded)

Cmpd. no.	Name	Formula	CAS no.	Mol. wt.	C1	C2	C3	C4	C5	T_{\min} , K	C_p at T_{\min} $\times 1E-05$	T_{\max} , K	C_p at T_{\max} $\times 1E-05$
300	Propionic acid	C ₃ H ₆ O ₂	79-09-4	74.079	213,660	-702.7	1.6605			252.45	1.4209	414.32	2.0756
301	Propionitrile	C ₃ H ₅ N	107-12-0	55.079	118,190	-120.98	0.42075			180.26	1.1005	370.50	1.3112
302	Propyl acetate	C ₅ H ₁₀ O ₂	109-60-4	102.132	83,400	384.1				274.70	1.8891	404.70	2.3885
303	Propyl amine	C ₃ H ₉ N	107-10-8	59.110	139,530	78				188.36	1.5422	340.00	1.6605
304	Propylbenzene	C ₉ H ₁₂	103-65-1	120.192	174,380	-101.8	0.79			173.55	1.8051	432.39	2.7806
305	Propylene	C ₃ H ₆	115-07-1	42.080	114,140	-343.72	1.0905			87.89	0.9235	225.45	0.9208
306	Propyl formate	C ₄ H ₈ O ₂	110-74-7	88.105	75,700	326.1				298.15	1.7293	398.15	2.0554
307	2-Propyl mercaptan	C ₃ H ₂ S	75-33-2	76.161	135,390	-117.11	0.47059			142.61	1.3126	350.00	1.5505
308	Propyl mercaptan	C ₃ H ₇ S	107-03-9	76.161	167,330	-319.1	0.8127			159.95	1.3708	340.87	1.5299
309	1,2-Propylene glycol	C ₃ H ₈ O ₂	57-55-6	76.094	58,080	445.2				213.15	1.5297	460.75	2.6321
310	Quinone	C ₆ H ₄ O ₂	106-51-4	108.095	45,810	368.33				388.85	1.8904	683.00	2.9738
311	Silicon tetrafluoride	F ₄ Si	7783-61-1	104.079	829,380	-7,331.5	19.203			186.35	1.3000	253.15	2.0403
312	Styrene	C ₈ H ₈	100-42-5	104.149	113,340	290.2	-0.6051	0.0013567		242.54	1.6749	418.31	2.2816
313	Succinic acid	C ₄ H ₆ O ₄	110-15-6	118.088	244,770	-236.96	0.63148			460.65	2.6961	604.50	3.3228
314	Sulfur dioxide	O ₂ S	7446-09-5	64.064	85,743	5,7443				197.67	0.8688	350.00	0.8775
315	Sulfur hexafluoride	F ₆ S	2551-62-4	146.055	119,500					230.15	1.1950	230.15	1.1950
316	Sulfur trioxide	O ₃ S	7446-11-9	80.063	258,090					303.15	2.5809	303.15	2.5809
317	Terephthalic acid	C ₈ H ₆ O ₄	100-21-0	166.131									
318	<i>o</i> -Terphenyl	C ₁₈ H ₁₄	84-15-1	230.304	182,900	635.09				329.35	3.9207	609.15	5.6977
319	Tetradecane	C ₁₄ H ₃₀	629-59-4	198.388	353,140	29.13	0.86116			279.01	4.2831	526.73	6.0741
320	Tetrahydrofuran	C ₄ H ₈ O	109-99-9	72.106	171,730	-800.47	2.8934	-0.0025015		164.65	1.0721	339.12	1.3546
321	1,2,3,4-Tetrahydronaphthalene	C ₁₀ H ₁₂	119-64-2	132.202	81,760	455.38				237.38	1.8986	480.77	3.0069
322	Tetrahydrothiophene	C ₄ H ₈ S	110-01-0	88.171	123,300	-130.1	0.6229			176.98	1.1979	394.27	1.6883
323	2,2,3,3-Tetramethylbutane	C ₈ H ₁₈	594-82-1	114.229	43,326	630.73				375.41	2.8011	426.00	3.1202
324	Thiophene	C ₄ H ₄ S	110-02-1	84.140	84,864	91,725	0.13243			234.94	1.1372	357.31	1.3455
325	Toluene	C ₇ H ₈	108-88-3	92.138	140,140	-152.3	0.695			178.18	1.3507	500.00	2.3774
326	1,1,2-Trichloroethane	C ₂ H ₃ Cl ₃	79-00-5	133.404	103,350	159.3				236.50	1.4102	300.00	1.5114
327	Tridecane	C ₁₃ H ₂₈	629-50-5	184.361	350,180	-104.7	1.0022			267.76	3.9400	508.62	5.5619
328	Triethyl amine	C ₆ H ₁₅ N	121-44-8	101.190	111,480	368.13				200.00	1.8511	361.92	2.4471
329	Trimethyl amine	C ₃ H ₉ N	75-50-3	59.110	136,050	-288	0.9913			156.08	1.1525	276.02	1.3208
330	1,2,3-Trimethylbenzene	C ₉ H ₁₂	526-73-8	120.192	119,450	324.54				247.79	1.9987	449.27	2.6526
331	1,2,4-Trimethylbenzene	C ₉ H ₁₂	95-63-6	120.192	178,800	-128.47	0.83741			229.33	1.9338	350.00	2.3642
332	2,2,4-Trimethylpentane	C ₈ H ₁₈	540-84-1	114.229	95,275	696.7	-1.3765	0.0021734		165.78	1.8285	520.00	3.9095
333	2,3,3-Trimethylpentane	C ₈ H ₁₈	560-21-4	114.229	388,620	-1,439.5	3.2187			280.00	2.3791	320.00	2.5757
334	1,3,5-Trinitrobenzene	C ₆ H ₃ N ₃ O ₆	99-35-4	213.105	40,364	664.46				398.40	3.0508	475.47	3.5629
335	2,4,6-Trinitrotoluene	C ₇ H ₅ N ₃ O ₆	118-96-7	227.131	133,530	514.64				354.00	3.1571	475.00	3.7798
336	Undecane	C ₁₁ H ₂₄	1120-21-4	156.308	293,980	-114.98	0.96936			247.57	3.2493	433.42	4.2624
337	1-Undecanol	C ₁₁ H ₂₄ O	112-42-5	172.308	129,450	-3,039.5	27.927	-0.061847	4.3042E-05	289.05	3.9103	520.30	5.5127
338	Vinyl acetate	C ₄ H ₆ O ₂	108-05-4	86.089	136,300	-106.17	0.75175			259.56	1.5939	389.35	2.0892
339	Vinyl acetylene	C ₄ H ₄	689-97-4	52.075	68,720	135				200.00	0.9572	278.25	1.0628
340	Vinyl chloride	C ₂ H ₃ Cl	75-01-4	62.498	-10,320	322.8				200.00	0.5424	400.00	1.1880
341	Vinyl trichlorosilane	C ₂ H ₃ Cl ₃ Si	75-94-5	161.490	49,516	420.35				178.35	1.2449	363.85	2.0246
342	Water	H ₂ O	7732-18-5	18.015	276,370	-2,090.1	8.125	-0.014116	9.3701E-06	273.16	0.7615	533.15	0.8939
343	<i>m</i> -Xylene	C ₈ H ₁₀	108-38-3	106.165	133,860	7,8754	0.52265			217.00	1.6018	540.15	2.9060
344	<i>o</i> -Xylene	C ₈ H ₁₀	95-47-6	106.165	36,500	1,017.5	-2.63	0.00302		247.98	1.7314	417.58	2.2269
345	<i>p</i> -Xylene	C ₈ H ₁₀	106-42-3	106.165	-35,500	1,287.2	-2.599	0.002426		286.41	1.7697	600.00	3.2520

For the 11 substances, ammonia, 1,2-butanediol, 1,3-butanediol, carbon monoxide, 1,1-difluoroethane, ethane, heptane, hydrogen, hydrogen sulfide, methane, and propane, the liquid heat capacity C_{pL} is calculated with Eq. (2) below. For all other compounds, Eq. (1) is used. For benzene, fluorine, and helium, two sets of constants are given for Eq. (1) that cover different temperature ranges, as shown in the table.

$$(1) C_{pL} = C1 + C2T + C3T^2 + C4T^3 + C4T^4$$

$$(2) C_{pL} = \frac{C1^2}{t} + C2 - 2C1C3t - C1C4t^2 - \frac{C3^2t^3}{3} - \frac{C3C4t^4}{2} - \frac{C4^2t^5}{5}$$

where $t = 1 - T_r$, $T_r = T/T_c$, T_c is the critical temperature from Table 2-141. C_{pL} is in J/(kmol·K) and T is in K. All substances are listed by chemical family in Table 2-6 and by formula in Table 2-7. For temperatures less than the normal boiling point, the pressure is 1 atm. Above the normal boiling point, the pressure is the vapor pressure.

Values in this table were taken from the Design Institute for Physical Properties (DIPPR) of the American Institute of Chemical Engineers (AIChE), copyright 2007 AIChE and reproduced with permission of AIChE and of the DIPPR Evaluated Process Design Data Project Steering Committee. Their source should be cited as R. L. Rowley, W. V. Wilding, J. L. Oscarson, Y. Yang, N. A. Zundel, T. E. Daubert, R. P. Danner, DIPPR® Data Compilation of Pure Chemical Properties, Design Institute for Physical Properties, AIChE, New York (2007).

The number of digits provided for values at T_{\min} and T_{\max} was chosen for uniformity of appearance and formatting; these do not represent the uncertainties of the physical quantities, but are the result of calculations from the standard thermophysical property formulations within a fixed format.

TABLE 2-154 Specific Heats of Organic Solids

Recalculated from *International Critical Tables*, vol. 5, pp. 101-105

Compound	Formula	Temperature, °C	sp ht, cal/(g·°C)
Acetic acid	C ₂ H ₄ O ₂	-200 to +25	0.330 + 0.00080 <i>t</i>
Acetone	C ₃ H ₆ O	-210 to -80	0.540 + 0.0156 <i>t</i>
Aminobenzoic acid (<i>o</i> -)	C ₇ H ₇ NO ₂	85 to mp	0.254 + 0.00136 <i>t</i>
(<i>m</i> -)	C ₇ H ₇ NO ₂	120 to mp	0.253 + 0.00122 <i>t</i>
(<i>p</i> -)	C ₇ H ₇ NO ₂	128 to mp	0.287 + 0.00088 <i>t</i>
Aniline	C ₆ H ₇ N		0.741
Anthracene	C ₁₄ H ₁₀	50	0.308
		100	0.350
		150	0.382
Anthraquinone	C ₁₄ H ₈ O ₂	0 to 270	0.258 + 0.00069 <i>t</i>
Apiol	C ₁₂ H ₁₄ O ₄	10	0.299
Azobenzene	C ₁₂ H ₁₀ N ₂	28	0.330
Benzene	C ₆ H ₆	-250	0.0399
		-225	0.0908
		-200	0.124
		-150	0.170
		-100	0.227
		-50	0.299
		0	0.375
Benzoic acid	C ₇ H ₆ O ₂	20 to mp	0.287 + 0.00050 <i>t</i>
Benzophenone	C ₁₃ H ₁₀ O	-150	0.115
		-100	0.172
		-50	0.220
		0	0.275
		+20	0.303
Betol	C ₁₇ H ₁₂ O ₃	-150	0.129
		-100	0.167
		0	0.248
		+50	0.308
Bromiodobenzene (<i>o</i> -)	C ₆ H ₄ BrI	-50 to 0	0.143 + 0.00025 <i>t</i>
(<i>m</i> -)	C ₆ H ₄ BrI	-75 to -15	0.143
(<i>p</i> -)	C ₆ H ₄ BrI	-40 to 50	0.116 + 0.00032 <i>t</i>
Bromonaphthalene (β-)	C ₁₀ H ₇ Br	41	0.260
Bromophenol	C ₆ H ₅ BrO	32	0.263
Camphene	C ₁₀ H ₁₆	35	0.380
Capric acid	C ₁₀ H ₂₀ O ₂	8	0.695
Caprylic acid	C ₈ H ₁₆ O ₂	-2	0.628
Carbon tetrachloride	CCl ₄	-240	0.013
		-200	0.081
		-160	0.131
		-120	0.162
		-80	0.182
		-40	0.201
		15	0.387
Cerotic acid	C ₂₇ H ₅₄ O ₂	78	0.509
Chloral alcoholate hydrate	C ₂ H ₃ Cl ₃ O ₂	32	0.213
Chloroacetic acid	C ₂ H ₃ ClO ₂	60	0.363
Chlorobenzoic acid (<i>o</i> -)	C ₇ H ₅ ClO ₂	80 to mp	0.228 + 0.00084 <i>t</i>
(<i>m</i> -)	C ₇ H ₅ ClO ₂	94 to mp	0.232 + 0.00073 <i>t</i>
(<i>p</i> -)	C ₇ H ₅ ClO ₂	180 to mp	0.242 + 0.00055 <i>t</i>
Chlorobromobenzene (<i>o</i> -)	C ₆ H ₄ BrCl	-34	0.192
(<i>m</i> -)	C ₆ H ₄ BrCl	-52	0.150
(<i>p</i> -)	C ₆ H ₄ BrCl	-40	0.150
Crotonic acid	C ₄ H ₆ O ₂	38 to 70	0.520 + 0.00020 <i>t</i>
Cyamelide	C ₃ H ₃ N ₃ O ₃	40	0.263
Cyanamide	CH ₂ N ₂	20	0.547
Cyanuric acid	C ₃ H ₃ N ₃ O ₃	40	0.318
Dextrin	(C ₆ H ₁₀ O ₅) _x	0 to 90	0.291 + 0.00096 <i>t</i>
Dextrose	C ₆ H ₁₂ O ₆	-250	0.016
		-200	0.077
		-100	0.160
		0	0.277
		20	0.300
Dibenzyl	C ₁₄ H ₁₄	28	0.363
Dibromobenzene (<i>o</i> -)	C ₆ H ₄ Br ₂	-36	0.248
(<i>m</i> -)	C ₆ H ₄ Br ₂	-25	0.134
(<i>p</i> -)	C ₆ H ₄ Br ₂	-50 to +50	0.139 + 0.00038 <i>t</i>
Dichloroacetic acid	C ₂ H ₂ Cl ₂ O ₂		0.406
Dichlorobenzene (<i>o</i> -)	C ₆ H ₄ Cl ₂	-48.5	0.185
(<i>m</i> -)	C ₆ H ₄ Cl ₂	-52	0.186
(<i>p</i> -)	C ₆ H ₄ Cl ₂	-50 to +53	0.219 + 0.0021 <i>t</i>
Dicyandiamide	C ₂ H ₄ N ₄	0 to 204	0.456

TABLE 2-154 Specific Heats of Organic Solids (Continued)
 Recalculated from *International Critical Tables*, vol. 5, pp. 101-105

Compound	Formula	Temperature, °C	sp. ht., cal/(g·°C)	
Dihydroxybenzene (<i>o</i> -)	$C_6H_6O_2$	-163 to mp	0.278 + 0.00098 <i>t</i>	
		-160 to mp	0.269 + 0.00118 <i>t</i>	
		-250	0.025	
		-240	0.038	
		-220	0.061	
		-200	0.081	
Di-iodobenzene (<i>o</i> -)	$C_6H_4I_2$	-150 to mp	0.268 + 0.00093 <i>t</i>	
		-50 to +15	0.109 + 0.00026 <i>t</i>	
		-52 to -42	0.100 + 0.00026 <i>t</i>	
		-50 to +80	0.101 + 0.00026 <i>t</i>	
Dimethyl oxalate	$C_4H_6O_4$	10 to 50	0.212 + 0.0044 <i>t</i>	
		50	0.368	
Dimethylpyrene	$C_7H_8O_2$	50	0.368	
Dinitrobenzene (<i>o</i> -)	$C_6H_4N_2O_4$	-160 to mp	0.252 + 0.00083 <i>t</i>	
		-160 to mp	0.248 + 0.00077 <i>t</i>	
		119 to mp	0.259 + 0.00057 <i>t</i>	
Diphenyl	$C_{12}H_{10}$	40	0.385	
		26	0.337	
Diphenylamine	$C_{12}H_{11}N$	26	0.337	
Dulcitol	$C_6H_{14}O_6$	20	0.282	
Erythritol	$C_4H_{10}O_4$	60	0.351	
Ethyl alcohol	C_2H_6O (crystalline)	-190	0.232	
		-180	0.248	
		-160	0.282	
		-140	0.318	
		-130	0.376	
		(vitreous)	-190	0.260
		-180	0.296	
		-175	0.380	
		-170	0.399	
		-190 to -40	0.366 + 0.00110 <i>t</i>	
Ethylene glycol	$C_2H_6O_2$	-190 to -40	0.366 + 0.00110 <i>t</i>	
		-190 to -40	0.366 + 0.00110 <i>t</i>	
Formic acid	CH_2O_2	-22	0.387	
		0	0.430	
Glutaric acid	$C_5H_8O_4$	20	0.299	
Glycerol	$C_3H_8O_3$	-265	0.009	
		-260	0.022	
		-250	0.047	
		-220	0.085	
		-200	0.115	
		-100	0.217	
		0	0.330	
		0	0.330	
Hexachloroethane	C_2Cl_6	25	0.174	
Hexadecane	$C_{16}H_{34}$		0.495	
Hydroxyacetanilide	$C_8H_9NO_2$	41 to mp	0.249 + 0.00154 <i>t</i>	
Iodobenzene	C_6H_5I	40	0.191	
Isopropyl alcohol	C_3H_8O	-200 to -160	0.051 + 0.00165 <i>t</i>	
Lactose	$C_{12}H_{22}O_{11}$	20	0.287	
		20	0.299	
Lauric acid	$C_{12}H_{24}O_2$	-30 to +40	0.430 + 0.000027 <i>t</i>	
Levoglucofuranose	$C_6H_{10}O_5$	40	0.607	
Levulose	$C_6H_{12}O_6$	20	0.275	
Malonic acid	$C_3H_4O_4$	20	0.275	
Maltose	$C_{12}H_{22}O_{11}$	20	0.320	
Mannitol	$C_6H_{14}O_6$	0 to 100	0.313 + 0.00025 <i>t</i>	
Melamine	$C_3H_6N_6$	40	0.351	
Myristic acid	$C_{14}H_{28}O_2$	0 to 35	0.381 + 0.00545 <i>t</i>	
Naphthalene	$C_{10}H_8$	-130 to mp	0.281 + 0.00111 <i>t</i>	
Naphthol (α -)	$C_{10}H_8O$	50 to mp	0.240 + 0.00147 <i>t</i>	
		61 to mp	0.252 + 0.00128 <i>t</i>	
Naphthol (β -)	$C_{10}H_8O$	61 to mp	0.252 + 0.00128 <i>t</i>	
		0 to 50	0.270 + 0.0031 <i>t</i>	
Naphthylamine (α -)	$C_{10}H_9N$	0 to 50	0.270 + 0.0031 <i>t</i>	
Nitroaniline (<i>o</i> -)	$C_6H_6N_2O_2$	-160 to mp	0.269 + 0.000920 <i>t</i>	
		-160 to mp	0.275 + 0.000946 <i>t</i>	
Nitroaniline (<i>m</i> -)	$C_6H_6N_2O_2$	-160 to mp	0.275 + 0.000946 <i>t</i>	
		-160 to mp	0.276 + 0.001000 <i>t</i>	
Nitroaniline (<i>p</i> -)	$C_6H_6N_2O_2$	-160 to mp	0.276 + 0.001000 <i>t</i>	
		-160 to mp	0.276 + 0.001000 <i>t</i>	
Nitrobenzoic acid (<i>o</i> -)	$C_7H_5NO_4$	-163 to mp	0.256 + 0.00085 <i>t</i>	
		66 to mp	0.258 + 0.00091 <i>t</i>	
Nitrobenzoic acid (<i>m</i> -)	$C_7H_5NO_4$	66 to mp	0.258 + 0.00091 <i>t</i>	
		-160 to mp	0.247 + 0.00077 <i>t</i>	
Nitrobenzoic acid (<i>p</i> -)	$C_7H_5NO_4$	-160 to mp	0.247 + 0.00077 <i>t</i>	
		0 to 55	0.236 + 0.00215 <i>t</i>	
Nitronaphthalene	$C_{10}H_7NO_2$	0 to 55	0.236 + 0.00215 <i>t</i>	

TABLE 2-154 Specific Heats of Organic Solids (Concluded)
 Recalculated from *International Critical Tables*, vol. 5, pp. 101-105

Compound	Formula	Temperature, °C	sp ht, cal/(g·°C)
Oxalic acid	C ₂ H ₂ O ₄ C ₂ H ₂ O ₄ ·2H ₂ O	-200 to +50	0.259 + 0.00076 <i>t</i>
		-200	0.117
		-100	0.239
		0	0.338
		+50	0.385
		100	0.416
Palmitic acid	C ₁₆ H ₃₂ O ₂	-180	0.167
		-140	0.208
		-100	0.251
		-50	0.306
		0	0.382
		+20	0.430
Phenol	C ₆ H ₆ O	14 to 26	0.561
Phthalic acid	C ₈ H ₆ O ₄	20	0.232
Picric acid	C ₆ H ₃ N ₃ O ₇	-100	0.165
		0	0.240
		+50	0.263
		100	0.297
		120	0.332
Propionic acid	C ₃ H ₆ O ₂	-33	0.726
Propyl alcohol (<i>n</i> -)	C ₃ H ₈ O	-200	0.170
		-175	0.363
		-150	0.471
		-130	0.497
		20	0.301
Pyrotartaric acid	C ₆ H ₈ O ₄	20	0.301
		-250	0.017
		-225	0.061
		-200	0.098
		-100	0.191
Quinhydrone	C ₁₂ H ₁₀ O ₄	0	0.256
		-250	0.031
		-225	0.082
		-200	0.113
		-150 to mp	0.282 + 0.00083 <i>t</i>
Quinone	C ₆ H ₄ O ₂	32	0.289
		15	0.399
Salol	C ₁₃ H ₁₀ O ₃	15	0.399
Stearic acid	C ₁₈ H ₃₆ O ₂	0 to 160	0.248 + 0.00153 <i>t</i>
Succinic acid	C ₄ H ₆ O ₄	20	0.299
Sucrose	C ₁₂ H ₂₂ O ₁₁	22 to 51	0.301
Sugar (cane)	C ₁₂ H ₂₂ O ₁₁	22 to 51	0.301
Tartaric acid	C ₄ H ₆ O ₆	36	0.287
Tartaric acid	C ₄ H ₆ O ₆ ·H ₂ O	-150	0.112
		-100	0.170
		-50	0.231
		0	0.308
		+50	0.366
		-40 to 0	0.198 + 0.00018 <i>t</i>
		-100	0.182
Tetrachloroethylene	C ₂ Cl ₄	-100	0.182
		-50	0.199
		0	0.212
		+100	0.236
		-100 to +100	0.253 + 0.00072 <i>t</i>
Tetryl	C ₇ H ₅ N ₅ O ₈	-100	0.172
		0	0.280
		+50	0.325
		-100 to +100	0.253 + 0.00072 <i>t</i>
1 Tetryl + 1 picric acid	C ₁₃ H ₈ N ₈ O ₁₅	-100 to +100	0.172
1 Tetryl + 2 TNT	C ₂₁ H ₁₅ N ₁₁ O ₂₀	0	0.280
		+50	0.325
Thymol	C ₁₀ H ₁₄ O	0 to 49	0.315 + 0.0031 <i>t</i>
Toluic acid (<i>o</i> -)	C ₈ H ₈ O ₂	54 to mp	0.277 + 0.00120 <i>t</i>
		54 to mp	0.239 + 0.00195 <i>t</i>
		130 to mp	0.271 + 0.00106 <i>t</i>
Toluic acid (<i>m</i> -)	C ₈ H ₈ O ₂	130 to mp	0.271 + 0.00106 <i>t</i>
		0	0.337
Toluidine (<i>p</i> -)	C ₇ H ₉ N	20	0.387
		40	0.440
		solid	0.459
Trichloroacetic acid	C ₂ HCl ₃ O ₂	solid	0.459
Trimethyl carbinol	C ₄ H ₁₀ O	-4	0.559
Trinitrotoluene	C ₇ H ₅ N ₃ O ₆	-100	0.170
		-50	0.253
		0	0.311
		+100	0.385
		-185 to +23	0.241
Trinitroxylene	C ₈ H ₇ N ₃ O ₆	20 to 50	0.423
Triphenylmethane	C ₁₉ H ₁₆	0 to 91	0.189 + 0.0027 <i>t</i>
		0 to 91	0.189 + 0.0027 <i>t</i>
Urea	CH ₄ N ₂ O	20	0.320

TABLE 2-155 Heat Capacity at Constant Pressure of Inorganic and Organic Compounds in the Ideal Gas State Fit to a Polynomial C_p [J/(kmol·K)]

Cmpd. no.	Name	Formula	CAS no.	Mol. wt.	C1	C2	C3	C4 × 1E 05	C5 × 1E 10	T_{\min} , K	C_p at T_{\min} × 1E-05	T_{\max} , K	C_p at T_{\max} × 1E-05
1	Acetaldehyde	C ₂ H ₄ O	75-07-0	44.053	29,705	127.43	-0.21793			50	0.3553	200	0.4647
7	Acetylene	C ₂ H ₂	74-86-2	26.037	30,800	-53.08	0.384			50	0.2911	200	0.3554
8	Acrolein	C ₃ H ₄ O	107-02-8	56.063	30,702	80.95	0.191			50	0.3523	200	0.5453
14	Argon	Ar	7440-37-1	39.948	20,786	0	0			100	0.2079	1,500	0.2079
16	Benzene	C ₆ H ₆	71-43-2	78.112	35,978	-101.69	0.939			50	0.3324	200	0.5320
27	Bromoethane	C ₂ H ₅ Br	74-96-4	108.965	27,112	117.99	0			100	0.3891	200	0.5071
29	1,2-Butadiene	C ₄ H ₆	590-19-2	54.090	27,400	177.6	0			50	0.3628	200	0.6292
31	Butane	C ₄ H ₁₀	106-97-8	58.122	17,330	458.16	-0.816			50	0.3820	200	0.7632
34	1-Butanol	C ₄ H ₁₀ O	71-36-3	74.122	25,300	371.2	-0.461			50	0.4271	200	0.8110
37	cis-2-Butene	C ₄ H ₈	590-18-1	56.106	39,760	108.8	0			50	0.4520	200	0.6152
38	trans-2-Butene	C ₄ H ₈	624-64-6	56.106	20,908	324.73	-0.411			50	0.3612	200	0.6941
43	1-Butyne	C ₄ H ₆	107-00-6	54.090	25,300	183.2	0			50	0.3446	200	0.6194
59	m-Cresol	C ₇ H ₈ O	108-39-4	108.138	29,002	158.79	0.635			50	0.3853	200	0.8616
60	o-Cresol	C ₇ H ₈ O	95-48-7	108.138	16,192	469.81	-0.479			50	0.3849	200	0.9099
61	p-Cresol	C ₇ H ₈ O	106-44-5	108.138	29,090	166	0.616			50	0.3893	200	0.8693
64	Cyclobutane	C ₄ H ₈	287-23-0	56.106	31,863	37.226	0.23616			50	0.3432	200	0.4876
67	Cyclohexanone	C ₆ H ₁₀ O	108-94-1	98.143	32,182	116.87	0.547			50	0.3939	200	0.7744
81	1,1-Dibromoethane	C ₂ H ₄ Br ₂	557-91-5	187.861	20,560	285.2	-0.332			100	0.4576	200	0.6432
88	1,1-Dichloroethane	C ₂ H ₄ Cl ₂	75-34-3	98.959	19,560	249.01	-0.22187			100	0.4224	200	0.6049
95	Diethyl ether	C ₄ H ₁₀ O	60-29-7	74.122	26,040	388	-0.268			50	0.4477	200	0.9292
97	1,1-Difluoroethane	C ₂ H ₄ F ₂	75-37-6	66.050	29,736	72.364	0.228			50	0.3392	200	0.5333
98	1,2-Difluoroethane	C ₂ H ₄ F ₂	624-72-6	66.050	27,581	169.88	-0.1581			50	0.3568	200	0.5523
99	Difluoromethane	CH ₂ F ₂	75-10-5	52.023	33,851	-20.966	0.17584			50	0.3324	200	0.3669
112	Dimethyl ether	C ₂ H ₆ O	115-10-6	46.068	25,940	178.46	-0.186			50	0.3440	200	0.5419
120	1,4-Dioxane	C ₄ H ₈ O ₂	123-91-1	88.105	28,345	88.3	0.446			50	0.3388	200	0.6385
125	Ethane	C ₂ H ₆	74-84-0	30.069	31,742	26.567	0.12927			50	0.3339	200	0.4223
126	Ethanol	C ₂ H ₆ O	64-17-5	46.068	32,585	87.4	0.05			50	0.3708	200	0.5207
134	Ethylcyclopentane	C ₇ H ₁₄	1640-89-7	98.186	34,710	304.96	-0.084			50	0.4975	200	0.9234
145	Ethyl mercaptan	C ₂ H ₆ S	75-08-1	62.134	23,014	271.36	-0.4427			50	0.3548	200	0.5958
151	Fluoroethane	C ₂ H ₅ F	353-36-6	48.060	30,358	62.839	0.1067			50	0.3377	200	0.4719
156	Furan	C ₄ H ₄ O	110-00-9	68.074	40,860	-160.3	0.87			100	0.3353	200	0.4360
157	Helium-4	He	7440-59-7	4.003	20,786	0	0			100	0.2079	1,500	0.2079
182	Hydrazine	H ₂ N ₂	302-01-2	32.045	32,998	-5.2147	0.21379			50	0.3327	200	0.4051
183	Hydrogen	H ₂	1333-74-0	2.016	64,979	-788.17	5.8287	-1845.9	216400	50	0.3797	250	0.2834
190	Isopropyl amine	C ₃ H ₉ N	75-31-0	59.110	23,590	310.42	-0.274			50	0.3843	200	0.7471
194	Methanol	CH ₄ O	67-56-1	32.042	30,270	84.64	-0.188			50	0.3403	200	0.3968
197	Methyl acetylene	C ₃ H ₄	74-99-7	40.064	30,810	35.8	0.27			50	0.3328	200	0.4877
217	Methylcyclopentane	C ₆ H ₁₂	96-37-7	84.159	35,465	147.38	0.242			50	0.4344	200	0.7462
221	Methylethyl ether	C ₃ H ₈ O	540-67-0	60.095	23,337	309.03	-0.285			50	0.3508	200	0.7374
231	Methyl mercaptan	CH ₄ S	74-93-1	48.107	31,520	60.1	0			50	0.3453	200	0.4354
236	2-Methylpropane	C ₄ H ₁₀	75-28-5	58.122	21,380	271.2	-0.092			50	0.3471	200	0.7194

237	2-Methyl-2-propanol	C ₄ H ₁₀ O	75-65-0	74.122	17,080	381.7	-0.199			50	0.3567	200	0.8546
238	2-Methyl propene	C ₄ H ₈	115-11-7	56.106	24,970	211.8	0			50	0.3556	200	0.6733
243	alpha-Methyl styrene	C ₉ H ₁₀	98-83-9	118.176	37,735	112.94	0.846			50	0.4550	200	0.9416
246	Naphthalene	C ₁₀ H ₈	91-20-3	128.171	29,120	82.88	0.964			50	0.3567	200	0.8426
247	Neon	Ne	7440-01-9	20.180	20,786	0	0			100	0.2079	1,500	0.2079
248	Nitroethane	C ₂ H ₅ NO ₂	79-24-3	75.067	33,055	89.54	0.238			50	0.3813	200	0.6048
251	Nitromethane	CH ₃ NO ₂	75-52-5	61.040	38,782	-48.39	0.413			50	0.3740	200	0.4562
253	Nitric oxide	NO	10102-43-9	30.006	34,980	-35.32	0.07729	-5.7357	0.0014526	100	0.3217	1,500	0.3586
289	2-Pentyne	C ₅ H ₈	627-21-4	68.117	24,330	335.7	-0.37			50	0.4019	200	0.7667
290	Phenanthrene	C ₁₄ H ₁₀	85-01-8	178.229	27,700	210	1.24			50	0.4130	200	1.1930
294	Propadiene	C ₃ H ₄	463-49-0	40.064	31,690	17.1	0.282			50	0.3325	200	0.4639
295	Propane	C ₃ H ₈	74-98-6	44.096	26,675	147.04	0			50	0.3403	200	0.5608
296	1-Propanol	C ₃ H ₈ O	71-23-8	60.095	28,800	257	-0.35			50	0.4078	200	0.6620
304	Propylbenzene	C ₉ H ₁₂	103-65-1	120.192	22,880	538.46	-0.546			50	0.4844	200	1.0873
310	Quinone	C ₆ H ₄ O ₂	106-51-4	108.095	29,668	129.07	0.53105			50	0.3745	200	0.7672
320	Tetrahydrofuran	C ₄ H ₈ O	109-99-9	72.106	36,970	-12.28	0.444			50	0.3747	200	0.5227
321	1,2,3,4-Tetrahydronaphthalene	C ₁₀ H ₁₂	119-64-2	132.202	28,560	225.1	0.616			50	0.4136	200	0.9822
322	Tetrahydrothiophene	C ₄ H ₈ S	110-01-0	88.171	41,195	-88.3	0.942			50	0.3914	200	0.6122
324	Thiophene	C ₄ H ₄ S	110-02-1	84.140	36,765	-112.82	0.862			50	0.3328	200	0.4868
331	1,2,4-Trimethylbenzene	C ₉ H ₁₂	95-63-6	120.192	35,652	323.89	0.305			50	0.5261	200	1.1263

Constants in this table can be used in the following equation to calculate the ideal gas heat capacity C_p^0

$$C_p^0 = C_1 + C_2T + C_3T^2 + C_4T^3 + C_5T^4$$

where C_p^0 is in J/(kmol·K) and T is in K. All substances are listed by chemical family in Table 2-6 and by formula in Table 2-7.

Values in this table were taken from the Design Institute for Physical Properties (DIPPR) of the American Institute of Chemical Engineers (AIChE), copyright 2007 AIChE and reproduced with permission of AIChE and of the DIPPR Evaluated Process Design Data Project Steering Committee. Their source should be cited as R. L. Rowley, W. V. Wilding, J. L. Oscarson, Y. Yang, N. A. Zundel, T. E. Daubert, R. P. Danner, DIPPR® Data Compilation of Pure Chemical Properties, Design Institute for Physical Properties, AIChE, New York (2007).

The number of digits provided for values at T_{\min} and T_{\max} was chosen for uniformity of appearance and formatting; these do not represent the uncertainties of the physical quantities, but are the result of calculations from the standard thermophysical property formulations within a fixed format.

TABLE 2-156 Heat Capacity at Constant Pressure of Inorganic and Organic Compounds in the Ideal Gas State Fit to Hyperbolic Functions C_p [J/(kmol·K)]

Cmpd. no.	Name	Formula	CAS no.	Mol. wt.	C1 × 1E-05	C2 × 1E-05	C3 × 1E-03	C4 × 1E-05	C5	T_{\min} , K	C_p at T_{\min} × 1E-05	T_{\max} , K	C_p at T_{\max} × 1E-05
1	Acetaldehyde	C ₂ H ₄ O	75-07-0	44.053	0.4451	1.0687	1.6141	0.6135	737.8	200	0.4660	1500	1.2994
2	Acetamide	C ₂ H ₅ NO	60-35-5	59.067	0.342	1.294	1.075	0.64	502	100	0.3448	1500	1.4997
3	Acetic acid	C ₂ H ₄ O ₂	64-19-7	60.052	0.402	1.3675	1.262	0.7003	569.7	50	0.4020	1500	1.5756
4	Acetic anhydride	C ₄ H ₆ O ₃	108-24-7	102.089	0.713	2.222	1.6203	1.676	746.5	200	0.7665	1500	2.5675
5	Acetone	C ₃ H ₆ O	67-64-1	58.079	0.5704	1.632	1.607	0.968	731.5	200	0.6049	1500	1.8820
6	Acetonitrile	C ₂ H ₃ N	75-05-8	41.052	0.41914	0.8876	1.5818	0.5032	699.8	100	0.4192	1500	1.1285
7	Acetylene	C ₂ H ₂	74-86-2	26.037	0.3199	0.5424	1.594	0.4325	607.1	200	0.3566	1500	0.7575
8	Acrolein	C ₃ H ₄ O	107-02-8	56.063	0.48449	1.2546	1.3979	0.87243	633.26	200	0.5467	1500	1.5620
9	Acrylic acid	C ₃ H ₄ O ₂	79-10-7	72.063	0.6059	1.3703	1.6475	1.0446	751.49	250	0.6984	1500	1.7424
10	Acrylonitrile	C ₃ H ₃ N	107-13-1	53.063	0.4678	1.0366	1.3998	0.6536	629.35	200	0.5156	1500	1.3464
11	Air	Mixture	132259-10-0	28.960	0.28958	0.0939	3.012	0.0758	1484	50	0.2896	1500	0.3496
12	Ammonia	H ₃ N	7664-41-7	17.031	0.33427	0.4898	2.036	0.2256	882	100	0.3343	1500	0.6647
13	Anisole	C ₇ H ₈ O	100-66-3	108.138	0.7637	2.9377	1.6051	2.17	751.2	300	1.1302	1200	3.0226
15	Benzamide	C ₇ H ₇ NO	55-21-0	121.137	1.9581	1.7019	1.3257	-37.417	41.232	298.15	1.2745	1500	3.2501
16	Benzene	C ₆ H ₆	71-43-2	78.112	0.44767	2.3085	1.4792	1.6836	677.66	200	0.5358	1500	2.4157
17	Benzenethiol	C ₆ H ₆ S	108-98-5	110.177	0.6895	2.3275	1.512	1.7516	697.9	200	0.7689	1500	2.6739
18	Benzoic acid	C ₇ H ₆ O ₂	65-85-0	122.121	0.77594	2.6455	1.7925	2.2382	835.9	200	0.8126	1500	2.9712
19	Benzonitrile	C ₇ H ₅ N	100-47-0	103.121	0.7186	2.27	1.4669	1.693	680.77	200	0.8053	1500	2.6706
20	Benzophenone	C ₁₃ H ₁₀ O	119-61-9	182.218	1.0099	4.4898	1.311	2.8395	627.4	300	1.8001	1500	4.9311
21	Benzyl alcohol	C ₉ H ₈ O	100-51-6	108.138	0.84115	3.1428	1.9539	2.5743	850.06	298.15	1.1198	1500	3.2880
22	Benzyl ethyl ether	C ₉ H ₁₂ O	539-30-0	136.191	0.9521	2.8868	0.70207	1.6385	2002.6	300	1.5501	1500	4.3445
23	Benzyl mercaptan	C ₇ H ₈ S	100-53-8	124.203	0.99192	2.9633	1.5583	2.2116	719.16	300	1.4156	1200	3.2957
24	Biphenyl	C ₁₂ H ₁₀	92-52-4	154.208	1.0759	4.2105	1.9041	4.1785	828.81	200	1.1481	1500	4.5557
25	Bromine	Br ₂	7726-95-6	159.808	0.30113	0.08009	0.7514	0.1078	314.6	100	0.3090	1500	0.3794
26	Bromobenzene	C ₆ H ₅ Br	108-96-1	157.008	0.721	2.064	1.6504	1.687	765.3	200	0.7679	1500	2.4628
27	Bromoethane	C ₂ H ₅ Br	74-96-4	108.965	0.47191	1.2787	1.5957	0.85166	703.87	200	0.5089	1500	1.5121
28	Bromomethane	CH ₃ Br	74-83-9	94.939	0.3377	0.715	1.578	0.4175	691.4	100	0.3378	1500	0.9107
29	1,2-Butadiene	C ₄ H ₆	590-19-2	54.090	0.575	1.6476	1.527	0.99	677.3	200	0.6269	1500	1.9202
30	1,3-Butadiene	C ₄ H ₆	106-99-0	54.090	0.5095	1.705	1.5324	1.337	685.6	200	0.5756	1500	1.9555
31	Butane	C ₄ H ₁₀	106-97-8	58.122	0.7134	2.43	1.63	1.5033	730.42	200	0.7673	1500	2.6602
32	1,2-Butanediol	C ₄ H ₁₀ O ₂	584-03-2	90.121	1.0478	2.549	1.8776	1.875	833	298.15	1.2667	1500.1	3.0289
33	1,3-Butanediol	C ₄ H ₁₀ O ₂	107-88-0	90.121	1.066	2.575	1.967	1.951	860.5	298.15	1.2679	1500.15	3.0311
34	1-Butanol	C ₄ H ₁₀ O	71-36-3	74.122	0.7454	2.5907	1.6073	1.732	712.4	200	0.8162	1500	2.8509
35	2-Butanol	C ₄ H ₁₀ O	78-92-2	74.122	0.90878	2.5508	1.893	1.852	832.13	298.15	1.1257	1500	2.8730
36	1-Butene	C ₄ H ₈	106-98-9	56.106	0.64257	2.0618	1.6768	1.3324	757.06	250	0.7571	1500	2.2898
37	cis-2-Butene	C ₄ H ₈	590-18-1	56.106	0.5765	2.115	1.6299	1.2872	739.1	200	0.6199	1500	2.2715
38	trans-2-Butene	C ₄ H ₈	624-64-6	56.106	0.6592	2.07	1.6733	1.251	742.2	200	0.7004	1500	2.2904
39	Butyl acetate	C ₈ H ₁₆ O ₂	123-86-4	116.158	1.1684	3.769	1.956	2.818	811.2	300	1.5358	1200	3.6724
40	Butylbenzene	C ₁₀ H ₁₄	104-51-8	134.218	1.138	4.454	1.5507	3.0497	708.86	200	1.2659	1500	4.8435
41	Butyl mercaptan	C ₄ H ₁₀ S	109-79-5	90.187	0.92478	2.7795	1.6837	1.5974	758.68	200	0.9714	1500	3.1008
42	sec-Butyl mercaptan	C ₄ H ₁₀ S	513-53-1	90.187	0.92367	2.5166	1.6109	1.5641	739.2	200	0.9763	1500	2.9615
43	1-Butyne	C ₄ H ₆	107-00-6	54.090	0.5587	1.6694	1.5328	1.07	656	200	0.6238	1500	1.9209
44	Butyraldehyde	C ₄ H ₈ O	123-72-8	72.106	0.89657	2.3731	1.9754	1.5866	904.13	200	0.9119	1500	2.6775
45	Butyric acid	C ₄ H ₈ O ₂	107-92-6	88.105	1.488	1.3522	1.146	-678	6.98	298.15	1.1533	1500	2.5905
46	Butyronitrile	C ₄ H ₇ N	109-74-0	69.105	0.6906	1.9996	1.5494	1.3146	675	200	0.7607	1500	2.3273
47	Carbon dioxide	CO ₂	124-38-9	44.010	0.2937	0.3454	1.428	0.264	588	50	0.2937	5000	0.6335
48	Carbon disulfide	CS ₂	75-15-0	76.141	0.301	0.3338	0.896	0.2893	374.7	100	0.3100	1500	0.6148
49	Carbon monoxide	CO	630-08-0	28.010	0.29108	0.08773	3.0851	0.084553	1538.2	60	0.2911	1500	0.3521
50	Carbon tetrachloride	CCl ₄	56-23-5	153.823	0.37582	0.7054	0.5121	0.485	236.1	100	0.4730	1500	1.0662
51	Carbon tetrafluoride	CF ₄	75-73-0	88.004	0.92004	0.16446	1.0764	-5083.8	2.3486	298	0.6106	1500	1.0465
52	Chlorine	Cl ₂	7782-50-5	70.906	0.29142	0.09176	0.949	0.1003	425	50	0.2914	1500	0.3793
53	Chlorobenzene	C ₆ H ₅ Cl	108-90-7	112.557	0.8011	2.31	2.157	2.046	897.6	200	0.8219	1500	2.5327
54	Chloroethane	C ₂ H ₅ Cl	75-00-3	64.514	0.4568	1.2967	1.5992	0.859	708.8	100	0.4569	1500	1.5112
55	Chloroform	CHCl ₃	67-66-3	119.378	0.3942	0.6573	0.928	0.493	399.6	100	0.4048	1500	1.0063
56	Chloromethane	CH ₃ Cl	74-87-3	50.488	0.3409	0.7246	1.723	0.448	780.5	150	0.3424	1500	0.9097
57	1-Chloropropane	C ₃ H ₇ Cl	540-54-5	78.541	0.621	1.843	1.629	1.2337	724	200	0.6674	1500	2.1126
58	2-Chloropropane	C ₃ H ₇ Cl	75-29-6	78.541	0.61809	1.8023	1.5438	1.1893	685.93	200	0.6768	1500	2.1023
59	m-Cresol	C ₇ H ₈ O	108-39-4	108.138	0.7515	2.09	0.6666	1.212	2214	200	0.8701	1500	3.2075
60	o-Cresol	C ₇ H ₈ O	95-48-7	108.138	0.7988	2.853	1.4765	2.042	664.7	200	0.9158	1500	3.2163

61	<i>p</i> -Cresol	C ₇ H ₈ O	106-44-5	108.138	0.7384	2.908	1.4559	2.091	650.42	200	0.8707	1500	3.2102
62	Cumene	C ₉ H ₁₂	98-82-8	120.192	1.081	3.7932	1.7505	3.0027	794.8	200	1.1480	1500	4.1808
63	Cyanogen	C ₂ N ₂	460-19-5	52.035	0.3545	0.5015	1.057	0.452	396	100	0.3648	1500	0.8100
64	Cyclobutane	C ₄ H ₈	287-23-0	56.106	0.44004	2.3074	1.6283	1.5571	744.9	200	0.4903	1500	2.3234
65	Cyclohexane	C ₆ H ₁₂	110-82-7	84.159	0.432	3.735	1.192	1.635	530.1	100	0.4366	1500	3.6516
66	Cyclohexanol	C ₆ H ₁₂ O	108-93-0	100.159	0.9043	2.5771	0.7882	1.3068	1952.2	200	0.9648	1500	3.8251
67	Cyclohexanone	C ₆ H ₁₀ O	108-94-1	98.143	0.67384	3.2598	1.3955	2.0209	677.33	200	0.7802	1500	3.4743
68	Cyclohexene	C ₆ H ₁₀	110-83-8	82.144	0.58171	3.1717	1.5435	2.1273	701.62	150	0.5978	1500	3.2132
69	Cyclopentane	C ₅ H ₁₀	287-92-3	70.133	0.416	3.014	1.4617	1.8095	668.8	100	0.4165	1500	2.9298
70	Cyclopentene	C ₅ H ₈	142-29-0	68.117	0.48074	2.5159	1.5803	1.7454	718.37	150	0.4918	1500	2.5619
71	Cyclopropane	C ₃ H ₆	75-19-4	42.080	0.338	1.6894	1.6135	1.1768	722.8	100	0.3381	1500	1.7213
72	Cyclohexyl mercaptan	C ₆ H ₁₂ S	1569-69-3	116.224	0.54305	3.9962	1.3575	2.5623	618.54	300	1.2644	1200	3.7236
73	Decanal	C ₁₀ H ₂₀ O	112-31-2	156.265	1.9641	5.1412	1.8989	4.1278	862.51	200	2.0192	1500	6.0539
74	Decane	C ₁₀ H ₂₂	124-18-5	142.282	1.672	5.353	1.6141	3.782	742	200	1.7967	1500	6.0932
75	Decanoic acid	C ₁₀ H ₂₀ O ₂	334-48-5	172.265	0.24457	6.546	1.0899	4.8642	424	298.15	2.5232	1500	6.1099
76	1-Decanol	C ₁₀ H ₂₂ O	112-30-1	158.281	1.6984	5.392	1.568	3.938	720.5	200	1.8502	1500	6.2186
77	1-Decene	C ₁₀ H ₂₀	872-05-9	140.266	1.7101	5.2089	1.7265	3.5935	782.92	298.15	2.2304	1500	5.8745
78	Decyl mercaptan	C ₁₀ H ₂₂ S	143-10-2	174.347	1.931	5.4815	1.6085	3.74	754.75	200	2.0434	1500	6.4613
79	1-Decyne	C ₁₀ H ₁₈	764-93-2	138.250	1.5045	4.3794	1.3291	2.5557	632.01	298	2.1938	1500	5.2794
80	Deuterium	D ₂	7782-39-0	4.032	0.3029	0.0975	2.515	-0.0275	368	100	0.3020	1500	0.3425
81	1,1-Dibromoethane	C ₂ H ₄ Br ₂	557-91-5	187.861	0.5927	1.158	1.4931	0.8428	655.5	200	0.6442	1500	1.5673
82	1,2-Dibromoethane	C ₂ H ₄ Br ₂	106-93-4	187.861	0.74906	1.2725	1.981	0.9437	845.2	200	0.7635	1500	1.7041
83	Dibromomethane	CH ₂ Br ₂	74-95-3	173.835	0.391	0.648	1.194	0.42	501	100	0.3929	1500	0.9599
84	Dibutyl ether	C ₈ H ₁₈ O	142-96-1	130.228	1.6122	4.4777	1.6831	-2.918	781.6	200	1.6841	1500	5.2145
85	<i>m</i> -Dichlorobenzene	C ₆ H ₄ Cl ₂	541-73-1	147.002	0.7	2.0746	1.3664	1.5983	620.16	200	0.8245	1500	2.5161
86	<i>o</i> -Dichlorobenzene	C ₆ H ₄ Cl ₂	95-50-1	147.002	0.6948	2.0804	1.3632	1.594	619.2	200	0.8198	1500	2.5161
87	<i>p</i> -Dichlorobenzene	C ₆ H ₄ Cl ₂	106-46-7	147.002	0.6978	2.078	1.3635	1.5965	619.37	200	0.8228	1500	2.5175
88	1,1-Dichloroethane	C ₂ H ₄ Cl ₂	75-34-3	98.959	0.5521	1.205	1.502	0.8719	653.5	200	0.6061	1500	1.5615
89	1,2-Dichloroethane	C ₂ H ₄ Cl ₂	107-06-2	98.959	0.65271	1.1254	1.7376	0.878	795.45	200	0.6722	1500	1.5743
90	Dichloromethane	CH ₂ Cl ₂	75-09-2	84.933	0.3628	0.6804	1.256	0.4275	548	100	0.3637	1500	0.9543
91	1,1-Dichloropropane	C ₃ H ₆ Cl ₂	78-99-9	112.986	0.7145	1.7344	1.524	1.223	674.2	150	0.7268	1500	2.1609
92	1,2-Dichloropropane	C ₃ H ₆ Cl ₂	78-87-5	112.986	0.78658	1.7429	1.7157	1.2627	765.1	200	0.8217	1500	2.1894
93	Diethanol amine	C ₄ H ₁₁ NO ₂	111-42-2	105.136	1.208	3.066	2.089	2.343	891	298.15	1.4197	1500.1	3.4674
94	Diethyl amine	C ₄ H ₁₁ N	109-89-7	73.137	0.9102	2.674	1.719	1.7926	794.94	200	0.9502	1500	3.0519
95	Diethyl ether	C ₄ H ₁₀ O	60-29-7	74.122	0.8621	2.551	1.5413	1.437	688.9	200	0.9316	1500	2.9244
96	Diethyl sulfide	C ₄ H ₁₀ S	352-93-2	90.187	0.91273	2.41	1.6686	1.652	771.08	200	0.9567	1500	2.8724
97	1,1-Difluoroethane	C ₂ H ₄ F ₂	75-37-6	66.050	0.49653	1.2546	1.5394	0.87561	694.17	200	0.5373	1500	1.5424
98	1,2-Difluoroethane	C ₂ H ₄ F ₂	624-72-6	66.050	0.51889	1.2431	1.5048	0.76269	697.51	200	0.5536	1500	1.5510
99	Difluoromethane	CH ₂ F ₂	75-10-5	52.023	0.35489	0.71002	1.5936	0.4622	762	200	0.3681	1500	0.9419
100	Di-isopropyl amine	C ₆ H ₁₅ N	108-18-9	101.190	1.1384	2.5747	0.7384	1.62	2143	300	1.5995	1500	4.1941
101	Di-isopropyl ether	C ₆ H ₁₄ O	108-20-3	102.175	1.093	3.683	1.6057	2.342	699	298.15	1.5669	1500	4.0535
102	Di-isopropyl ketone	C ₇ H ₁₄ O	565-80-0	114.185	1.0869	4.054	1.7802	2.9786	791.6	300	1.5102	1500	4.3093
103	1,1-Dimethoxyethane	C ₄ H ₁₀ O ₂	534-15-6	90.121	1.1556	1.8305	0.95919	0.99605	2826.3	298.15	1.2777	1500	3.0678
104	1,2-Dimethoxypropane	C ₅ H ₁₂ O ₂	7778-85-0	104.148	1.0113	3.2393	1.5611	2.1501	689.3	298.15	1.4638	1500	3.6669
105	Dimethyl acetylene	C ₄ H ₆	503-17-3	54.090	0.6534	1.6179	1.7837	1.0242	821.4	200	0.6721	1500	1.9148
106	Dimethyl amine	C ₂ H ₇ N	124-40-3	45.084	0.5565	1.6384	1.7341	1.0899	793.04	200	0.5812	1500	1.8585
107	2,3-Dimethylbutane	C ₆ H ₁₄	79-29-8	86.175	0.7772	4.032	1.544	2.508	649.95	200	0.9363	1500	4.0353
108	1,1-Dimethylcyclohexane	C ₈ H ₁₆	590-66-9	112.213	1.0776	4.6718	1.654	3.3397	792.5	200	1.1535	1500	4.9543
109	<i>cis</i> -1,2-Dimethylcyclohexane	C ₈ H ₁₆	2207-01-4	112.213	1.1039	4.6445	1.6943	3.3949	798.35	200	1.1777	1500	4.9243
110	<i>trans</i> -1,2-Dimethylcyclohexane	C ₈ H ₁₆	6876-23-9	112.213	1.0991	4.6401	1.6679	3.3736	781.97	200	1.1820	1500	4.9275
111	Dimethyl disulfide	C ₂ H ₆ S ₂	624-92-0	94.199	0.7843	1.4364	1.5836	0.871	730.65	200	0.8155	1500	1.9523
112	Dimethyl ether	C ₂ H ₆ O	115-10-6	46.068	0.5148	1.442	1.6034	0.7747	725.4	200	0.5436	1500	1.6581
113	<i>N,N</i> -Dimethyl formamide	C ₃ H ₇ NO	68-12-2	73.094	0.722	1.783	1.532	1.31	762	200	0.7594	1500	2.2596
114	2,3-Dimethylpentane	C ₇ H ₁₆	565-59-3	100.202	0.85438	4.5772	1.5181	2.974	641.01	200	1.0550	1500	4.5983
115	Dimethyl phthalate	C ₁₀ H ₁₀ O ₄	131-11-3	194.184	1.396	4.78	2.19	3.9705	900.6	300	1.7481	1200	4.4740
116	Dimethylsilane	C ₂ H ₆ Si	1111-74-6	60.170	0.61453	1.7438	1.3418	1.0102	592.09	200	0.7095	1500	2.0944
117	Dimethyl sulfide	C ₂ H ₆ S	75-18-3	62.134	0.6037	1.3747	1.641	0.7988	743.5	200	0.6298	1500	1.6949
118	Dimethyl sulfoxide	C ₂ H ₆ OS	67-68-5	78.133	0.6949	1.524	1.6514	1.0658	722.2	200	0.7355	1500	1.9255
119	Dimethyl terephthalate	C ₁₀ H ₁₀ O ₄	120-61-6	194.184	1.174	5.32	2.105	4.1	818	298.15	1.6816	1000.15	4.1139
120	1,4-Dioxane	C ₄ H ₈ O ₂	123-91-1	88.105	0.56184	2.7034	1.5171	1.7658	700.76	200	0.6403	1500	2.8174
121	Diphenyl ether	C ₁₂ H ₁₀ O	101-84-8	170.207	1.0985	4.3412	1.6222	3.6455	743.62	300	1.7298	1200	4.5143
122	Dipropyl amine	C ₆ H ₁₅ N	142-84-7	101.190	1.2114	2.6127	0.78956	1.6903	2394.4	300	1.5900	1500	4.2484
123	Dodecane	C ₁₂ H ₂₆	112-40-3	170.335	2.1295	6.633	1.7155	4.5161	777.5	200	2.2442	1500	7.4325

TABLE 2-156 Heat Capacity at Constant Pressure of Inorganic and Organic Compounds in the Ideal Gas State Fit to Hyperbolic Functions C_p [J/(kmol·K)] (Continued)

Cmpd. no.	Name	Formula	CAS no.	Mol. wt.	C1 × 1E-05	C2 × 1E-05	C3 × 1E-03	C4 × 1E-05	C5	T_{\min} , K	C_p at T_{\min} × 1E-05	T_{\max} , K	C_p at T_{\max} × 1E-05
124	Eicosane	C ₂₀ H ₄₂	112-95-8	282.547	3.2481	11.09	1.636	7.45	726.27	200	3.5235	1500	12.2110
125	Ethane	C ₂ H ₆	74-84-0	30.069	0.40326	1.3422	1.6555	0.73223	752.87	200	0.4256	1500	1.4562
126	Ethanol	C ₂ H ₆ O	64-17-5	46.068	0.492	1.4577	1.6628	0.939	744.7	200	0.5224	1500	1.6576
127	Ethyl acetate	C ₄ H ₈ O ₂	141-78-6	88.105	0.9981	2.0931	2.0226	1.803	928.05	200	1.0126	1500	2.6594
128	Ethyl amine	C ₂ H ₇ N	75-04-7	45.084	0.594	1.618	1.812	1.078	820	200	0.6139	1500	1.8528
129	Ethylbenzene	C ₈ H ₁₀	100-41-4	106.165	0.7844	3.399	1.559	2.426	702	200	0.8912	1500	3.6147
130	Ethyl benzoate	C ₉ H ₁₀ O ₂	93-89-0	150.175	1.0944	4.1794	0.88375	-1.609	1183.1	300	1.4598	1500	4.2540
131	2-Ethyl butanoic acid	C ₈ H ₁₂ O ₂	88-09-5	116.158	1.0455	2.3148	0.71	1.471	2061.6	300	1.5102	1200.15	3.6330
132	Ethyl butyrate	C ₈ H ₁₂ O ₂	105-54-4	116.158	1.115	3.391	1.6705	2.518	733.6	298	1.5583	1200	3.6213
133	Ethylcyclohexane	C ₈ H ₁₆	1678-91-7	112.213	1.1059	4.6306	1.6628	3.299	781.1	200	1.1875	1500	4.9184
134	Ethylcyclopentane	C ₇ H ₁₄	1640-89-7	98.186	0.82052	4.0342	1.567	2.6697	715.52	200	0.9272	1500	4.1472
135	Ethylene	C ₂ H ₄	74-85-1	28.053	0.3338	0.9479	1.596	0.551	740.8	60	0.3338	1500	1.0987
136	Ethylenediamine	C ₂ H ₈ N ₂	107-15-3	60.098	0.7286	1.8436	1.688	1.199	767.3	300	0.9178	1500	2.2016
137	Ethylene glycol	C ₂ H ₆ O ₂	107-21-1	62.068	0.63012	1.4584	1.673	0.97296	773.65	300	0.7800	1500	1.8095
138	Ethyleneimine	C ₂ H ₅ N	151-56-4	43.068	0.343	1.427	1.638	1.037	744.7	150	0.3480	1500	1.5178
139	Ethylene oxide	C ₂ H ₄ O	75-21-8	44.053	0.3346	1.2116	1.6084	0.8241	737.3	50	0.3346	1500	1.3297
140	Ethyl formate	C ₃ H ₆ O ₂	109-94-4	74.079	0.537	1.886	1.207	0.864	496	100	0.5412	1500	2.1485
141	2-Ethyl hexanoic acid	C ₈ H ₁₆ O ₂	149-57-5	144.211	1.5777	4.4017	1.7494	3.2378	792.34	298.15	2.0279	1500	5.1201
142	Ethylhexyl ether	C ₈ H ₁₈ O	5756-43-4	130.228	1.634	4.5119	1.7532	3.1032	809.75	298.15	2.0360	1200	4.8744
143	Ethylisopropyl ether	C ₅ H ₁₂ O	625-54-7	88.148	1.0953	3.0032	1.7988	2.1311	817.35	298.15	1.3620	1200	3.2289
144	Ethylisopropyl ketone	C ₆ H ₁₂ O	565-69-5	100.159	1.24	3.2	1.967	2.346	896	298.15	1.4479	1200	3.4234
145	Ethyl mercaptan	C ₂ H ₆ S	75-08-1	62.134	0.5576	1.3617	1.5221	0.8073	687.5	200	0.5970	1500	1.6729
146	Ethyl propionate	C ₅ H ₁₀ O ₂	105-37-3	102.132	0.937	2.829	1.648	2.155	724.7	300	1.3377	1200	3.0569
147	Ethylpropyl ether	C ₅ H ₁₂ O	628-32-0	88.148	1.132	2.94	1.827	2.055	852	298.15	1.3538	1500	3.4535
148	Ethyltrichlorosilane	C ₂ H ₅ Cl ₃ Si	115-21-9	163.060	0.85105	1.0378	0.59737	0.94745	2122.7	167	0.8926	1500	2.2349
149	Fluorine	F ₂	7782-41-4	37.997	0.29122	0.10132	1.453	0.094101	662.91	50	0.2912	1500	0.3812
150	Fluorobenzene	C ₆ H ₅ F	462-06-6	96.102	0.62653	2.1646	1.564	1.7278	724.29	200	0.6914	1500	2.4736
151	Fluoroethane	C ₂ H ₅ F	353-36-6	48.060	0.44373	1.3119	1.6422	0.85441	738.77	200	0.4726	1500	1.5008
152	Fluoromethane	CH ₃ F	593-53-3	34.033	0.33289	0.73989	1.8639	0.46079	891.16	50	0.3329	1500	0.9024
153	Formaldehyde	CH ₂ O	50-00-0	30.026	0.3327	0.49542	1.8666	0.28075	934.9	50	0.3327	1500	0.7113
154	Formamide	CH ₃ NO	75-12-7	45.041	0.3822	0.93	1.845	0.69	850	150	0.3833	1500	1.1203
155	Formic acid	CH ₂ O ₂	64-18-6	46.026	0.3381	0.7593	1.1925	0.318	550	50	0.3381	1500	0.9933
156	Furan	C ₄ H ₄ O	110-00-9	68.074	0.3727	1.6606	1.5112	1.3145	686	200	0.4376	1500	1.7940
158	Heptadecane	C ₁₇ H ₃₆	629-78-7	240.468	2.7878	9.5247	1.6935	6.6651	744.57	200	3.0034	1500	10.4160
159	Heptanal	C ₇ H ₁₄ O	111-71-7	114.185	1.404	2.5907	0.8315	1.312	2201	200	1.4479	1500	4.2863
160	Heptane	C ₇ H ₁₆	142-82-5	100.202	1.2015	4.001	1.6766	2.74	756.4	200	1.2828	1500	4.4283
161	Heptanoic acid	C ₇ H ₁₄ O ₂	111-14-8	130.185	1.3135	2.3317	0.67567	1.824	1846	300	1.8497	1500	4.2941
162	1-Heptanol	C ₇ H ₁₆ O	111-70-6	116.201	1.2215	3.991	1.58	2.835	717.7	200	1.3330	1500	4.5346
163	2-Heptanol	C ₇ H ₁₆ O	543-49-7	116.201	1.4569	2.8252	0.81695	1.766	2537.2	298.15	1.8136	1500	4.6604
164	3-Heptanone	C ₇ H ₁₄ O	106-35-4	114.185	1.2768	3.381	1.3831	1.888	650.3	200	1.3968	1500	4.1386
165	2-Heptanone	C ₇ H ₁₄ O	110-43-0	114.185	1.2507	2.148	0.6912	1.619	1759.3	150	1.2688	1200	3.8446
166	1-Heptene	C ₇ H ₁₄	592-76-7	98.186	1.1851	3.6362	1.7359	2.5048	785.73	298.15	1.5434	1500	4.0836
167	Heptyl mercaptan	C ₇ H ₁₆ S	1639-09-4	132.267	1.442	4.1603	1.6603	2.6572	759.39	200	1.5191	1500	4.7831
168	1-Heptyne	C ₇ H ₁₂	628-71-7	96.170	1.0712	3.0258	1.5273	2.0975	689.62	200	1.1721	1500	3.5985
169	Hexadecane	C ₁₆ H ₃₄	544-76-3	226.441	2.6283	8.9733	1.6912	6.264	744.41	200	2.8312	1500	9.8182
170	Hexanal	C ₆ H ₁₂ O	66-25-1	100.159	1.232	2.2146	0.84	1.219	2205	200	1.2672	1500	3.7314
171	Hexane	C ₆ H ₁₄	110-54-3	86.175	1.044	3.523	1.6946	2.369	761.6	200	1.1117	1500	3.8620
172	Hexanoic acid	C ₆ H ₁₂ O ₂	142-62-1	116.158	1.1622	2.0708	0.68661	1.5355	1932.5	298.15	1.6107	1500	3.7636
173	1-Hexanol	C ₆ H ₁₄ O	111-27-3	102.175	1.0625	3.521	1.5835	2.462	715.75	200	1.1607	1500	3.9726
174	2-Hexanol	C ₆ H ₁₄ O	626-93-7	102.175	1.2615	3.5964	1.8445	2.594	819.17	298.15	1.5829	1500	4.0672
175	2-Hexanone	C ₆ H ₁₂ O	591-78-6	100.159	1.094	1.807	0.689	1.474	1772	200	1.1815	1200	3.3207
176	3-Hexanone	C ₆ H ₁₂ O	589-38-8	100.159	1.1237	2.936	1.401	1.601	650.5	150	1.1443	1500	3.5874
177	1-Hexene	C ₆ H ₁₂	592-41-6	84.159	1.0434	3.0749	1.7459	2.0728	793.53	298	1.3301	1500	3.4819
178	3-Hexyne	C ₆ H ₁₀	928-49-4	82.144	0.9376	3.015	1.9057	1.986	817	300	1.1909	1500	3.1889
179	Hexyl mercaptan	C ₆ H ₁₄ S	111-31-9	118.240	1.2662	3.7294	1.6574	2.308	757.8	200	1.3340	1500	4.2483
180	1-Hexyne	C ₆ H ₁₀	693-02-7	82.144	0.9129	2.5577	1.529	1.737	683	200	1.0004	1500	3.0371
181	2-Hexyne	C ₆ H ₁₀	764-35-2	82.144	1.036	3.009	2.116	2.106	902.4	300	1.2215	1500	3.1894
182	Hydrazine	H ₄ N ₂	302-01-2	32.045	0.38711	0.8576	1.7228	0.56635	733.53	200	0.4070	1500	1.0571
183	Hydrogen	H ₂	1333-74-0	2.016	0.27617	0.0956	2.466	0.0376	567.6	250	0.2843	1500	0.3225

184	Hydrogen bromide	HBr	10035-10-6	80.912	0.2912	0.0953	2.142	0.0157	1400	50	0.2912	1500	0.3479
185	Hydrogen chloride	HCl	7647-01-0	36.461	0.29157	0.09048	2.0938	-0.00107	120	50	0.2914	1500	0.3406
186	Hydrogen cyanide	HCN	74-90-8	27.025	0.30125	0.3171	1.6102	0.2179	626	100	0.3014	1500	0.5522
187	Hydrogen fluoride	HF	7664-39-3	20.006	0.29134	0.093252	2.905	1.95E-03	1.33E+03	50	0.2913	1500	0.3224
188	Hydrogen sulfide	H ₂ S	7783-06-4	34.081	0.33288	0.26086	0.9134	-0.17979	949.4	100	0.3329	1500	0.5143
189	Isobutyric acid	C ₄ H ₈ O ₂	79-31-2	88.105	0.74694	2.4356	1.715	1.8484	757.75	298.15	1.0427	1200	2.5383
190	Isopropyl amine	C ₃ H ₉ N	75-31-0	59.110	0.68545	2.1876	1.5831	1.3855	691.76	200	0.7510	1500	2.4540
191	Malonic acid	C ₃ H ₄ O ₄	141-82-2	104.061	0.49522	1.8718	1.2958	1.4852	569.96	300	0.9790	1200	2.0517
192	Methacrylic acid	C ₄ H ₆ O ₂	79-41-4	86.089	0.7251	2.089	1.8516	1.6483	798.43	298.15	0.9475	1200.1	2.2057
193	Methane	CH ₄	74-82-8	16.042	0.33298	0.79933	2.0869	0.41602	991.96	50	0.3330	1500	0.8890
194	Methanol	CH ₃ O	67-56-1	32.042	0.39252	0.879	1.9165	0.53654	896.7	200	0.3980	1500	1.0533
195	N-Methyl acetamide	C ₃ H ₇ NO	79-16-3	73.094	0.6116	2.029	1.7683	1.3302	835.5	300	0.7698	1500	2.2209
196	Methyl acetate	C ₃ H ₆ O ₂	79-20-9	74.079	0.555	1.782	1.26	0.853	752	298	0.8489	1500	2.0564
197	Methyl acetylene	C ₃ H ₄	74-99-7	40.064	0.4478	1.0917	1.5508	0.675	658.2	200	0.4882	1500	1.3293
198	Methyl acrylate	C ₄ H ₆ O ₂	96-33-3	86.089	0.1206	2.3766	1.0543	1.8186	418.8	298.15	0.9908	1200.1	2.1663
199	Methyl amine	CH ₃ N	74-89-5	31.057	0.41	1.0578	1.708	0.6836	735	150	0.4136	1500	1.2358
200	Methyl benzoate	C ₈ H ₈ O ₂	93-58-3	136.148	0.9396	2.559	0.825	1.36	3000	300	1.2586	1200	3.3569
201	3-Methyl-1,2-butadiene	C ₅ H ₈	598-25-4	68.117	0.671	2.222	1.421	1.194	614.7	150	0.6931	1500	2.5028
202	2-Methylbutane	C ₅ H ₁₂	78-78-4	72.149	0.746	3.265	1.545	1.923	666.7	200	0.8546	1500	3.3792
203	2-Methylbutanoic acid	C ₆ H ₁₀ O ₂	116-53-0	102.132	1.8458	1.743	1.22	-56.11	31.2	300	1.2793	1500	3.2262
204	3-Methyl-1-butanol	C ₅ H ₁₂ O	123-51-3	88.148	0.92165	3.3371	1.8365	2.4645	757.99	298.15	1.3135	1500	3.4856
205	2-Methyl-1-butene	C ₅ H ₁₀	563-46-2	70.133	0.87026	2.5556	1.7757	1.7636	807.82	200	0.9060	1500	2.8923
206	2-Methyl-2-butene	C ₅ H ₁₀	513-35-9	70.133	0.81924	2.6038	1.7593	1.7195	800.93	200	0.8559	1500	2.8709
207	2-Methyl-1-butene-3-yne	C ₅ H ₆	78-80-8	66.101	0.7906	1.656	1.6926	1.2167	788.4	298.15	0.9632	1500.15	2.1502
208	Methylbutyl ether	C ₈ H ₁₈ O	628-28-4	88.148	0.82051	3.0869	1.3864	1.7886	613.87	300	1.3300	1200	3.1994
209	Methylbutyl sulfide	C ₈ H ₁₈ S	628-29-5	104.214	1.0785	2.7388	1.5885	1.9067	749.6	273.15	1.3173	1200	3.1687
210	3-Methyl-1-butyne	C ₅ H ₈	598-23-2	68.117	0.8274	2.1377	1.755	1.5149	782	200	0.8646	1500	2.5255
211	Methyl butyrate	C ₈ H ₁₆ O ₂	623-42-7	102.132	0.894	2.91	1.57	2.073	678.3	298	1.3461	1200	3.0766
212	Methylchlorosilane	CH ₃ ClSi	993-00-0	80.589	0.59895	1.1636	1.565	0.81581	690.39	200	0.6380	1500	1.5593
213	Methylcyclohexane	C ₇ H ₁₄	108-87-2	98.186	0.9227	4.115	1.6504	2.9006	779.48	200	0.9953	1500	4.3180
214	1-Methylcyclohexanol	C ₇ H ₁₄ O	590-67-0	114.185	0.7959	2.596	0.6213	2.288	1698.6	300	1.5302	1200	4.1359
215	cis-2-Methylcyclohexanol	C ₇ H ₁₄ O	7443-70-1	114.185	0.92279	2.6709	0.68784	1.9847	1732.4	300	1.5099	1200	4.1467
216	trans-2-Methylcyclohexanol	C ₇ H ₁₄ O	7443-52-9	114.185	0.92279	2.6709	0.68784	1.9847	1732.4	300	1.5099	1200	4.1467
217	Methylcyclopentane	C ₆ H ₁₂	96-37-7	84.159	0.66456	3.507	1.5892	2.3526	727.13	200	0.7510	1500	3.5495
218	1-Methylcyclopentene	C ₆ H ₁₀	693-89-0	82.144	0.69411	3.0209	1.6903	2.1209	781.56	200	0.7464	1500	3.1496
219	3-Methylcyclopentene	C ₆ H ₁₀	1120-62-3	82.144	0.6422	3.0711	1.6387	2.1298	750.25	200	0.7083	1500	3.1549
220	Methyldichlorosilane	CH ₂ Cl ₂ Si	75-54-7	115.034	0.7283	1.0307	1.5429	0.7811	668.94	200	0.7717	1500	1.5893
221	Methylethyl ether	C ₃ H ₈ O	540-67-0	60.095	0.68681	1.9959	1.5534	1.1168	692.04	200	0.7396	1500	2.2931
222	Methylethyl ketone	C ₄ H ₈ O	78-93-3	72.106	0.784	2.1032	1.5488	1.1855	693	200	0.8397	1500	2.4816
223	Methylethyl sulfide	C ₃ H ₈ S	624-89-5	76.161	0.75083	1.9577	1.6424	1.1949	749.19	273.16	0.9004	1500	2.3178
224	Methyl formate	C ₂ H ₄ O ₂	107-31-3	60.052	0.506	1.219	1.637	0.894	743	250	0.5888	1500	1.5109
225	Methylisobutyl ether	C ₆ H ₁₂ O	625-44-5	88.148	0.7284	3.1713	1.352	1.8948	585.14	300	1.3200	1200	3.1987
226	Methylisobutyl ketone	C ₆ H ₁₂ O	108-10-1	100.159	1.227	2.195	0.842	1.191	2460	298.15	1.4755	1500.15	3.6532
227	Methyl Isocyanate	C ₂ H ₃ NO	624-83-9	57.051	0.474	1.226	2.188	0.85983	1008.2	298.15	0.5195	1500	1.3595
228	Methylisopropyl ether	C ₄ H ₁₀ O	598-53-8	74.122	0.89232	2.4765	1.696	1.5598	791.4	200	0.9280	1500	2.8696
229	Methylisopropyl ketone	C ₅ H ₁₀ O	563-80-4	86.132	1.5914	1.764	1.2076	-407.4	10.503	300	1.1291	1500	2.9991
230	Methylisopropyl sulfide	C ₄ H ₁₀ S	1551-21-9	90.187	0.99247	2.7275	2.003	1.8974	849.64	273	1.1377	1500	2.9952
231	Methyl mercaptan	CH ₃ S	74-93-1	48.107	0.4146	0.8307	1.589	0.4612	716.7	200	0.4329	1500	1.0781
232	Methyl methacrylate	C ₅ H ₈ O ₂	80-62-6	100.116	0.864	1.811	0.7543	0.8	2160	298.15	1.1621	1500	2.8637
233	2-Methyloctanoic acid	C ₈ H ₁₆ O ₂	3004-93-1	158.238	1.7483	4.9288	1.7384	3.5897	788.01	298.15	2.2567	1500	5.7177
234	2-Methylpentane	C ₆ H ₁₄	107-83-5	86.175	0.903	3.801	1.602	2.453	691.6	200	1.0192	1500	3.9617
235	Methyl pentyl ether	C ₆ H ₁₄ O	628-80-8	102.175	0.94326	3.5965	1.3533	2.0569	599.92	300	1.5600	1200	3.7409
236	2-Methylpropane	C ₄ H ₁₀	75-28-5	58.122	0.6549	2.4776	1.587	1.575	706.99	200	0.7218	1500	2.6656
237	2-Methyl-2-propanol	C ₄ H ₁₀ O	75-65-0	74.122	0.7704	2.539	1.5502	1.669	679.3	200	0.8567	1500	2.8508
238	2-Methyl propene	C ₄ H ₈	115-11-7	56.106	0.6125	2.066	1.545	1.2057	676	200	0.6763	1500	2.2814
239	Methyl propionate	C ₄ H ₈ O ₂	554-12-1	88.105	0.7765	2.442	1.714	1.818	716	300	1.1242	1200	2.5276
240	Methylpropyl ether	C ₄ H ₁₀ O	557-17-5	74.122	0.92151	2.3943	1.6936	1.4896	797.79	298	1.1251	1200	2.6391
241	Methylpropyl sulfide	C ₄ H ₁₀ S	3877-15-4	90.187	0.93775	2.6178	1.7291	1.6236	783.23	298.15	1.1728	1500	2.9904
242	Methylsilane	CH ₃ Si	992-94-9	46.144	0.46149	1.2781	1.4565	0.79115	643.23	200	0.5141	1500	1.5253
243	alpha-Methyl styrene	C ₉ H ₁₀	98-83-9	118.176	0.78548	3.5969	1.4342	2.5336	651.69	200	0.9445	1500	3.8592
244	Methyl tert-butyl ether	C ₅ H ₁₂ O	1634-04-4	88.148	0.9779	3.091	1.643	2.099	731.191	298	1.3522	1500	3.4779
245	Methyl vinyl ether	C ₃ H ₆ O	107-25-5	58.079	0.60865	1.5965	1.619	0.93783	739.55	300	0.7748	1500	1.8871
246	Naphthalene	C ₁₀ H ₈	91-20-3	128.171	0.6805	3.5494	1.4262	2.5984	650.1	200	0.8454	1500	3.7359

TABLE 2-156 Heat Capacity at Constant Pressure of Inorganic and Organic Compounds in the Ideal Gas State Fit to Hyperbolic Functions C_p [J/(kmol·K)] (Concluded)

Cmpd. no.	Name	Formula	CAS no.	Mol. wt.	C1	C2	C3	C4	C5	T_{min} , K	C_p at T_{min}	T_{max} , K	C_p at T_{max}
					× 1E-05	× 1E-05	× 1E-03	× 1E-05			× 1E-05		× 1E-05
248	Nitroethane	C ₂ H ₅ NO ₂	79-24-3	75.067	0.54619	1.6492	1.4803	1.0635	666.94	200	0.6062	1500	1.9237
249	Nitrogen	N ₂	7727-37-9	28.013	0.29105	0.086149	1.7016	0.0010347	909.79	50	0.2911	1500	0.3484
250	Nitrogen trifluoride	F ₃ N	7783-54-2	71.002	0.33284	0.49837	0.7093	0.23264	372.91	100	0.3404	1500	0.8092
251	Nitromethane	CH ₃ NO ₂	75-52-5	61.040	0.42267	1.0842	1.4885	0.68603	683.57	200	0.4571	1500	1.3280
252	Nitrous oxide	N ₂ O	10024-97-2	44.013	0.29338	0.3236	1.1238	0.2177	479.4	100	0.2948	1500	0.5828
254	Nonadecane	C ₁₉ H ₄₀	629-92-5	268.521	3.1062	10.575	0.76791	-4.5661	912.03	200	3.3533	1500	11.6130
255	Nonanal	C ₉ H ₁₈ O	124-19-6	142.239	1.7347	4.5115	1.712	3.3256	810.96	200	1.8005	1500	5.4439
256	Nonane	C ₉ H ₂₀	111-84-2	128.255	1.5175	4.915	1.6448	3.47	749.6	200	1.6257	1500	5.5407
257	Nonanoic acid	C ₉ H ₁₈ O ₂	112-05-0	158.238	0.1266	6.011	1.0815	4.5946	418.2	298.15	2.2953	1500	5.5267
258	1-Nonanol	C ₉ H ₂₀ O	143-08-8	144.255	1.54	4.936	1.578	3.588	721.11	200	1.6777	1500	5.6606
259	2-Nonanol	C ₉ H ₂₀ O	628-99-9	144.255	1.8197	3.5542	0.81514	2.1974	2508.8	298.15	2.2720	1500	5.8526
260	1-Nonene	C ₉ H ₁₈	124-11-8	126.239	1.5352	4.6844	1.7288	3.2304	783.67	298.15	2.0014	1500	5.2776
261	Nonyl mercaptan	C ₉ H ₂₀ S	1455-21-6	160.320	1.7646	5.044	1.6182	3.3857	755.48	200	1.8658	1500	5.9082
262	1-Nonyne	C ₉ H ₁₆	3452-09-3	124.223	1.6289	3.9708	1.8928	3.2136	855.52	298.15	1.9693	1500	4.7924
263	Octadecane	C ₁₈ H ₃₈	593-45-3	254.494	2.9502	10.034	0.77107	-4.3012	916.73	200	3.1800	1500	11.0160
264	Octanal	C ₈ H ₁₆ O	124-13-0	128.212	1.6088	4.218	1.9126	3.278	869	200	1.6504	1500	4.9286
265	Octane	C ₈ H ₁₈	111-65-9	114.229	1.3554	4.431	1.6356	3.054	746.4	200	1.4529	1500	4.9764
266	Octanoic acid	C ₈ H ₁₆ O ₂	124-07-2	144.211	1.4082	4.3436	1.4662	2.7687	659.38	298.15	2.0652	1500	5.0411
267	1-Octanol	C ₈ H ₁₈ O	111-87-5	130.228	1.3805	4.459	1.5751	3.2016	718.8	200	1.5055	1500	5.0965
268	2-Octanol	C ₈ H ₁₈ O	123-96-6	130.228	1.6383	3.1897	0.81595	1.9814	2521.3	298.15	2.0428	1500	5.2565
269	2-Octanone	C ₈ H ₁₆ O	111-13-7	128.212	1.3901	3.806	1.3717	2.2573	660.96	150	1.4162	1500	4.6547
270	3-Octanone	C ₈ H ₁₆ O	106-68-3	128.212	1.4952	4.4103	0.80211	-2.0958	981.95	200	1.5775	1500	4.9067
271	1-Octene	C ₈ H ₁₆	111-66-0	112.213	1.3599	4.1605	1.7317	2.8675	784.47	298.15	1.7723	1500	4.6807
272	Octyl mercaptan	C ₈ H ₁₈ S	111-88-6	146.294	1.5981	4.6063	1.6295	3.0301	756.28	200	1.6881	1500	5.3549
273	1-Octyne	C ₈ H ₁₄	629-05-0	110.197	1.2307	3.4942	1.528	2.4617	694.81	200	1.3448	1500	4.1604
274	Oxalic acid	C ₂ H ₂ O ₄	144-62-7	90.035	0.25751	1.1734	2.7969	0.65788	878.91	298.15	0.3201	1000.1	0.6502
275	Oxygen	O ₂	7782-44-7	31.999	0.29103	0.1004	2.5265	0.09356	1153.8	50	0.2910	1500	0.3653
276	Ozone	O ₃	10028-15-6	47.998	0.33483	0.29577	1.5217	0.27151	680.35	100	0.3349	1500	0.5928
277	Pentadecane	C ₁₅ H ₃₂	629-62-9	212.415	2.4679	8.4212	1.6865	5.8537	743.6	200	2.6586	1500	9.2209
278	Pentanal	C ₅ H ₁₀ O	110-62-3	86.132	1.0743	2.8363	1.9549	2.0146	890.44	200	1.0960	1500	3.2404
279	Pentane	C ₅ H ₁₂	109-66-0	72.149	0.8805	3.011	1.6502	1.892	747.6	200	0.9404	1500	3.2927
280	Pentanoic acid	C ₅ H ₁₀ O ₂	109-52-4	102.132	2.836	1.08	2.107	-3.56	283	298.15	1.3824	1500	3.2952
281	1-Pentanol	C ₅ H ₁₂ O	71-41-0	88.148	0.906	3.062	1.6054	2.115	717.97	200	0.9890	1500	3.4133
282	2-Pentanol	C ₅ H ₁₂ O	6032-29-7	88.148	1.0853	3.0747	1.8672	2.2271	825.4	298.15	1.3539	1500	3.4701
283	2-Pentanone	C ₅ H ₁₀ O	107-87-9	86.132	0.90053	2.7085	1.6592	1.8012	743.96	200	0.9591	1500	3.0797
284	3-Pentanone	C ₅ H ₁₀ O	96-22-0	86.132	0.96896	2.4907	1.4177	1.301	646.7	200	1.0536	1500	3.0358
285	1-Pentene	C ₅ H ₁₀	109-67-1	70.133	0.82523	2.5943	1.7291	1.768	778.7	298.15	1.0856	1500	2.8897
286	2-Pentyl mercaptan	C ₅ H ₁₂ S	2084-19-7	104.214	1.1327	2.947	1.7418	2.0987	795.78	298	1.4202	1500	3.4994
287	Pentyl mercaptan	C ₅ H ₁₂ S	110-66-7	104.214	1.0974	3.2959	1.6761	1.9486	757.67	200	1.1547	1500	3.6956
288	1-Pentyne	C ₅ H ₈	627-19-0	68.117	0.753	2.0905	1.5307	1.378	672.8	200	0.8276	1500	2.4754
289	2-Pentyne	C ₅ H ₈	627-21-4	68.117	0.70737	2.2229	1.557	1.3125	690.78	200	0.7700	1500	2.5052
290	Phenanthrene	C ₁₄ H ₁₀	85-01-8	178.229	0.9374	4.758	1.382	3.485	627.4	200	1.1959	1500	5.0645
291	Phenol	C ₆ H ₆ O	108-95-2	94.111	0.434	2.445	1.152	1.512	507	100	0.4401	1500	2.6045
292	Phenyl isocyanate	C ₇ H ₅ NO	103-71-9	119.121	0.59683	2.5533	1.2397	1.5519	576.78	298.15	1.1054	1500	2.8390
293	Phthalic anhydride	C ₈ H ₄ O ₃	85-44-9	148.116	0.7364	2.544	1.0852	0.808	573	298.15	1.0745	1000.15	2.6737
294	Propadiene	C ₃ H ₄	463-49-0	40.064	0.426	1.1194	1.5772	0.7546	680.8	200	0.4646	1500	1.3376
295	Propane	C ₃ H ₈	74-98-6	44.096	0.5192	1.9245	1.6265	1.168	723.6	200	0.5632	1500	2.0556
296	1-Propanol	C ₃ H ₈ O	71-23-8	60.095	0.619	2.0213	1.6293	1.2956	727.4	200	0.6665	1500	2.2458
297	2-Propanol	C ₃ H ₈ O	67-63-0	60.095	0.73145	2.0313	1.9375	1.4815	843.37	298.15	0.8966	1500	2.2760
298	Propenylcyclohexene	C ₉ H ₁₄	13511-13-2	122.207	1.0563	4.3397	1.6098	3.181	729.66	300	1.6392	1500	4.6527
299	Propionaldehyde	C ₃ H ₆ O	123-38-6	58.079	0.7174	1.914	2.0144	1.1708	930.6	200	0.7266	1500	2.1149
300	Propionic acid	C ₃ H ₆ O ₂	79-09-4	74.079	0.6959	1.7778	1.7098	1.2654	763.78	298.15	0.8938	1500	2.1248
301	Propionitrile	C ₃ H ₅ N	107-12-0	55.079	0.5357	1.4617	1.553	0.91197	678.2	200	0.5832	1500	1.7235
302	Propyl acetate	C ₅ H ₁₀ O ₂	109-60-4	102.132	1.7994	1.753	1.196	-4.12	108.2	298.15	1.3594	1500	3.2024
303	Propyl amine	C ₃ H ₉ N	107-10-8	59.110	0.76078	2.1049	1.7256	1.3936	789.03	200	0.7933	1500	2.4353

304	Propylbenzene	C ₉ H ₁₂	103-65-1	120.192	0.96885	3.7954	1.5168	2.6618	694.3	200	1.0927	1500	4.1613
305	Propylene	C ₃ H ₆	115-07-1	42.080	0.43852	1.506	1.3988	0.74754	616.46	130	0.4436	1500	1.6817
306	Propyl formate	C ₄ H ₈ O ₂	110-74-7	88.105	0.871	2.447	1.9254	1.888	821.3	298.15	1.1022	1500	2.7484
307	2-Propyl mercaptan	C ₃ H ₆ S	75-33-2	76.161	0.73815	1.9529	1.5954	1.2356	730.5	200	0.7825	1500	2.3287
308	Propyl mercaptan	C ₃ H ₆ S	107-03-9	76.161	0.7474	1.9523	1.631	1.2112	750.92	200	0.7848	1500	2.3216
309	1,2-Propylene glycol	C ₃ H ₈ O ₂	57-55-6	76.094	2.0114	0.8082	1.8656	-2.4404	279.98	298.15	1.0218	1000.15	2.1175
310	Quinone	C ₆ H ₄ O ₂	106-51-4	108.095	0.6487	2.1227	1.3491	1.514	614.8	200	0.7711	1500	2.4969
311	Silicon tetrafluoride	F ₄ Si	7783-61-1	104.079	0.3681	0.71245	0.65201	0.46721	286.03	100	0.4182	1500	1.0537
312	Styrene	C ₈ H ₈	100-42-5	104.149	0.893	2.1503	0.772	0.999	2442	100	0.8931	1500	3.2416
313	Succinic acid	C ₄ H ₆ O ₄	110-15-6	118.088	0.71806	2.2669	1.2739	1.7342	537.65	300	1.3370	1200	2.5823
314	Sulfur dioxide	O ₂ S	7446-09-5	64.064	0.33375	0.25864	0.9328	0.1088	423.7	100	0.3354	1500	0.5695
315	Sulfur hexafluoride	F ₆ S	2551-62-4	146.055	0.35256	1.227	0.67938	0.78407	351.27	100	0.3872	1500	1.5397
316	Sulfur trioxide	O ₃ S	7446-11-9	80.063	0.33408	0.49677	0.87322	0.28563	393.74	100	0.3408	1500	0.7967
317	Terephthalic acid	C ₈ H ₆ O ₄	100-21-0	166.131	0.945	2.526	0.829	0.5	2010	298.15	1.2478	1500	3.4444
318	<i>o</i> -Terphenyl	C ₁₈ H ₁₄	84-15-1	230.304	2.0719	6.2668	2.4044	6.345	967.71	298.15	2.4763	1500	6.6947
319	Tetradecane	C ₁₄ H ₃₀	629-59-4	198.388	2.3082	7.8678	1.6823	5.4486	743.1	200	2.4864	1500	8.6225
320	Tetrahydrofuran	C ₄ H ₈ O	109-99-9	72.106	0.46905	2.5314	1.5998	1.7051	740.64	200	0.5259	1500	2.5538
321	1,2,3,4-Tetrahydronaphthalene	C ₁₀ H ₁₂	119-64-2	132.202	0.8145	4.395	1.471	3.065	666.4	200	0.9881	1500	4.5348
322	Tetrahydrothiophene	C ₄ H ₆ S	110-01-0	88.171	0.51848	2.4535	1.5018	1.6871	665.31	200	0.6147	1500	2.5679
323	2,2,3,3-Tetramethylbutane	C ₈ H ₁₈	594-82-1	114.229	1.1352	5.6331	1.6211	3.3829	681.9	200	1.3069	1500	5.5784
324	Thiophene	C ₄ H ₄ S	110-02-1	84.140	0.40399	1.627	1.4562	1.322	648.81	200	0.4886	1500	1.8098
325	Toluene	C ₇ H ₈	108-88-3	92.138	0.5814	2.863	1.4406	1.898	650.43	200	0.7016	1500	3.0029
326	1,1,2-Trichloroethane	C ₂ H ₃ Cl ₃	79-00-5	133.404	0.66554	1.1257	1.5454	0.97196	717.04	298.15	0.8496	1500	1.6433
327	Tridecane	C ₁₃ H ₂₈	629-50-5	184.361	2.1496	7.3045	1.6695	4.9988	741.02	200	2.3156	1500	8.0251
328	Triethyl amine	C ₆ H ₁₅ N	121-44-8	101.190	1.2766	2.5559	0.80937	1.4829	2231.7	200	1.3278	1500	4.2046
329	Trimethyl amine	C ₃ H ₉ N	75-50-3	59.110	0.7107	1.5051	0.79662	0.84537	2187.6	200	0.7439	1500	2.4322
330	1,2,3-Trimethylbenzene	C ₉ H ₁₂	526-73-8	120.192	1.052	3.79	1.4814	2.331	667.3	200	1.1832	1500	4.1983
331	1,2,4-Trimethylbenzene	C ₉ H ₁₂	95-63-6	120.192	1.0106	3.8314	1.501	2.395	678.3	200	1.1354	1500	4.1854
332	2,2,4-Trimethylpentane	C ₈ H ₁₈	540-84-1	114.229	1.139	5.286	1.594	3.351	677.94	200	1.3139	1500	5.3769
333	2,3,3-Trimethylpentane	C ₈ H ₁₈	560-21-4	114.229	0.982	5.402	1.531	3.493	639.9	200	1.2194	1500	5.3754
334	1,3,5-Trinitrobenzene	C ₆ H ₃ N ₃ O ₆	99-35-4	213.105	2.0367	1.8181	1.2089	0.79777	1060.8	298.15	2.1054	1500	3.7585
335	2,4,6-Trinitrotoluene	C ₇ H ₅ N ₃ O ₆	118-96-7	227.131	2.154	2.4432	1.1126	0.58651	950.59	298.15	2.2726	1500	4.3560
336	Undecane	C ₁₁ H ₂₄	1120-21-4	156.308	1.9529	6.0998	1.7087	4.1302	775.4	200	2.0594	1500	6.8342
337	1-Undecanol	C ₁₁ H ₂₄ O	112-42-5	172.308	1.859	5.869	1.5718	4.326	722.7	200	2.0232	1500	6.7834
338	Vinyl acetate	C ₄ H ₆ O ₂	108-05-4	86.089	0.536	2.119	1.198	1.147	510	100	0.5404	1500	2.3750
339	Vinyl acetylene	C ₄ H ₄	689-97-4	52.075	0.55978	1.2141	1.6102	0.89079	710.4	200	0.5967	1500	1.5590
340	Vinyl chloride	C ₂ H ₃ Cl	75-01-4	62.498	0.42364	0.8735	1.6492	0.6556	739.07	200	0.4457	1500	1.1423
341	Vinyl trichlorosilane	C ₂ H ₃ Cl ₃ Si	75-94-5	161.490	0.84894	1.1471	1.38	0.9	644.61	298.15	1.0788	1500	1.8595
342	Water	H ₂ O	7732-18-5	18.015	0.33363	0.2679	2.6105	0.08896	1169	100	0.3336	2273.15	0.5276
343	<i>m</i> -Xylene	C ₈ H ₁₀	108-38-3	106.165	0.7568	3.3924	1.496	2.247	675.9	200	0.8759	1500	3.5920
344	<i>o</i> -Xylene	C ₈ H ₁₀	95-47-6	106.165	0.8521	3.2954	1.4944	2.115	675.8	200	0.9643	1500	3.5965
345	<i>p</i> -Xylene	C ₈ H ₁₀	106-42-3	106.165	0.7512	3.397	1.4928	2.247	675.1	200	0.8710	1500	3.5923

Constants in this table can be used in the following equation to calculate the ideal gas heat capacity C_p^0 .

$$C_p^0 = C1 + C2 \left[\frac{C3/T}{\sinh(C3/T)} \right]^2 + C4 \left[\frac{C5/T}{\cosh(C5/T)} \right]^2$$

where C_p^0 is in J/(kmol-K) and T is in K. All substances are listed by chemical family in Table 2-6 and by formula in Table 2-7.

Values in this table were taken from the Design Institute for Physical Properties (DIPPR) of the American Institute of Chemical Engineers (AIChE), copyright 2007 AIChE and reproduced with permission of AIChE and of the DIPPR Evaluated Process Design Data Project Steering Committee. Their source should be cited as R. L. Rowley, W. V. Wilding, J. L. Oscarson, Y. Yang, N. A. Zundel, T. E. Daubert, R. P. Danner, DIPPR® Data Compilation of Pure Chemical Properties, Design Institute for Physical Properties, AIChE, New York (2007).

The number of digits provided for values at T_{\min} and T_{\max} was chosen for uniformity of appearance and formatting; these do not represent the uncertainties of the physical quantities, but are the result of calculations from the standard thermophysical property formulations within a fixed format.

2-182 PHYSICAL AND CHEMICAL DATA

TABLE 2-157 C_p/C_v : Ratios of Specific Heats of Gases at 1 atm Pressure*

Compound	Formula	Temperature, °C	Ratio of specific heats, $(\gamma) = C_p/C_v$	Compound	Formula	Temperature, °C	Ratio of specific heats, $(\gamma) = C_p/C_v$
Acetaldehyde	C ₂ H ₄ O	30	1.14	Hydrogen (<i>Cont.</i>)			
Acetic acid	C ₂ H ₄ O ₂	136	1.15	iodide	HI	20–100	1.40
Acetylene	C ₂ H ₂	15	1.26	sulfide	H ₂ S	15	1.332
		-71	1.31			-45	1.350
Air		925	1.36			-57	1.356
		17	1.403				
		-78	1.408	Iodine	I ₂	185	1.30
		-118	1.415	Isobutane	C ₄ H ₁₀	15	1.110
Ammonia	NH ₃	15	1.320				
Argon	Ar	15	1.670	Krypton	Kr	19	1.672
		-180	1.715				
		0–100	1.67	Mercury	Hg	360	1.67
				Methane	CH ₄	600	1.113
Benzene	C ₆ H ₆	90	1.10			300	1.196
Bromine	Br ₂	20–350	1.32			15	1.310
						-80	1.339
Carbon dioxide	CO ₂	15	1.299			-115	1.347
		-75	1.37	Methyl acetate	C ₃ H ₆ O ₂	15	1.14
disulfide	CS ₂	100	1.21	alcohol	CH ₃ O	77	1.237
monoxide	CO	15	1.402	ether	C ₂ H ₆ O	6–30	1.11
		-180	1.433	Methylal	C ₃ H ₈ O ₂	13	1.06
Chlorine	Cl ₂	15	1.355			40	1.09
Chloroform	CHCl ₃	100	1.15	Neon	Ne	19	1.667
Cyanogen	(CN) ₂	15	1.256	Nitric oxide	NO	15	1.400
Cyclohexane	C ₆ H ₁₂	80	1.315			-45	1.39
						-80	1.38
Dichlorodifluoromethane	CCl ₂ F ₂	25	1.139			15	1.402
				Nitrogen	N ₂	-181	1.433
Ethane	C ₂ H ₆	100	1.157			100	1.28
		15	1.200	Nitrous oxide	N ₂ O	15	1.303
		-82	1.28			-30	1.31
Ethyl alcohol	C ₂ H ₆ O	90	1.13			-70	1.34
ether	C ₄ H ₁₀ O	35	1.08				
		80	1.086	Oxygen	O ₂	15	1.398
Ethylene	C ₂ H ₄	100	1.201			-76	1.405
		15	1.253			-181	1.439
		-91	1.345				
Helium	He	-180	1.667	Pentane (<i>n</i> -)	C ₅ H ₁₂	86	1.071
Hexane (<i>n</i> -)	C ₆ H ₁₄	80	1.066	Phosphorus	P	300	1.17
Hydrogen	H ₂	15	1.407	Potassium	K	850	1.77
		-76	1.441				
		-181	1.607	Sodium	Na	750–920	1.68
bromide	HBr	20	1.42	Sulfur dioxide	SO ₂	15	1.290
chloride	HCl	15	1.41				
		100	1.40	Xenon	Xe	19	1.678
cyanide	HCN	65	1.31				
		140	1.28				
		210	1.24				

*For compounds that appear in Table 2-184, values are from E. W. Lemmon, M. O. McLinden, and D. G. Friend, "Thermophysical Properties of Fluid Systems" in *NIST Chemistry WebBook, NIST Standard Reference Database Number 69*, Eds. P. J. Linstrom and W. G. Mallard, June 2005, National Institute of Standards and Technology, Gaithersburg, Md. (<http://webbook.nist.gov>). Values for other compounds are from *International Critical Tables*, vol. 5, pp. 80–82.

SPECIFIC HEATS OF AQUEOUS SOLUTIONS

UNITS CONVERSIONS

For this subsection, the following units conversions are applicable:

$$^{\circ}\text{F} = \% \text{ }^{\circ}\text{C} + 32$$

To convert calories per gram-degree Celsius to British thermal units per pound-degree Fahrenheit, multiply by 1.0.

TABLE 2-158 Acetic Acid (at 38 °C)

Mole % acetic acid	0	6.98	30.9	54.5	100
Cal/(g·°C)	1.0	0.911	0.73	0.631	0.535

TABLE 2-159 Ammonia

Mole % NH ₃	Specific heat, cal/(g·°C)			
	2.4 °C	20.6 °C	41 °C	61 °C
0	1.01	1.0	0.995	1.0
10.5	0.98	0.995	1.06	1.02
20.9	0.96	0.99	1.03	
31.2	0.956	1.0		
41.4	0.985			

TABLE 2-160 Aniline (at 20 °C)

Mol % aniline	100	95	90.5	82.3	75.2
Cal/(g·°C)	0.497	0.52	0.53	0.56	0.581

TABLE 2-161 Copper Sulfate

Composition	Temperature	Specific heat, cal/(g·°C)
CuSO ₄ + 50H ₂ O	12 to 15 °C	0.848
CuSO ₄ + 200H ₂ O	12 to 14 °C	0.951
CuSO ₄ + 400H ₂ O	13 to 17 °C	0.975

TABLE 2-162 Ethyl Alcohol

Mole % C ₂ H ₅ OH	Specific heat, cal/(g·°C)		
	3 °C	23 °C	41 °C
4.16	1.05	1.02	1.02
11.5	1.02	1.03	1.03
37.0	0.805	0.86	0.875
61.0	0.67	0.727	0.748
100.0	0.54	0.577	0.621

TABLE 2-163 Glycerol

Mole % C ₃ H ₅ (OH) ₃	Specific heat, cal/(g·°C)	
	15 °C	32 °C
2.12	0.961	0.960
4.66	0.929	0.924
11.5	0.851	0.841
22.7	0.765	0.758
43.9	0.67	0.672
100.0	0.555	0.576

TABLE 2-164 Hydrochloric Acid

Mole % HCl	Specific heat, cal/(g·°C)				
	0 °C	10 °C	20 °C	40 °C	60 °C
0.0	1.00				
9.09	0.72	0.72	0.74	0.75	0.78
16.7	0.61	0.605	0.631	0.645	0.67
20.0	0.58	0.575	0.591	0.615	0.638
25.9	0.55				0.61

ADDITIONAL REFERENCES

Most of the tables below are from *International Critical Tables*, vol. 5, pp. 115–116, 122–125.

TABLE 2-165 Methyl Alcohol

Mole % CH ₃ OH	Specific heat, cal/(g·°C)		
	5 °C	20 °C	40 °C
5.88	1.02	1.0	0.995
12.3	0.975	0.982	0.98
27.3	0.877	0.917	0.92
45.8	0.776	0.811	0.83
69.6	0.681	0.708	0.726
100	0.576	0.60	0.617

TABLE 2-166 Nitric Acid

% HNO ₃ by Weight	Specific heat at 20 °C, cal/(g·°C)
0	1.000
10	0.900
20	0.810
30	0.730
40	0.675
50	0.650
60	0.640
70	0.615
80	0.575
90	0.515

TABLE 2-167 Phosphoric Acid*

%H ₂ PO ₄	C _p at 21.3 °C cal/(g·°C)	%H ₃ PO ₄	C _p at 21.3 °C cal/(g·°C)
2.50	0.9903	50.00	0.6350
3.80	0.9970	52.19	0.6220
5.33	0.9669	53.72	0.6113
8.81	0.9389	56.04	0.5972
10.27	0.9293	58.06	0.5831
14.39	0.8958	60.23	0.5704
16.23	0.8796	62.10	0.5603
19.99	0.8489	64.14	0.5460
22.10	0.8300	66.13	0.5349
24.56	0.8125	68.14	0.5242
25.98	0.8004	69.97	0.5157
28.15	0.7856	69.50	0.5160
29.96	0.7735	71.88	0.5046
32.09	0.7590	73.71	0.4940
33.95	0.7432	75.79	0.4847
36.26	0.7270	77.69	0.4786
38.10	0.7160	79.54	0.4680
40.10	0.7024	80.00	0.4686
42.08	0.6877	82.00	0.4593
44.11	0.6748	84.00	0.4500
46.22	0.6607	85.98	0.4419
48.16	0.6475	88.01	0.4359
49.79	0.6370	89.72	0.4206

*Z. Physik. Chem., A167, 42 (1933).

2-184 PHYSICAL AND CHEMICAL DATA
TABLE 2-168 Potassium Chloride

Mole % KCl	Specific heat, cal/(g·°C)			
	6 °C	20 °C	33 °C	40 °C
0.99	0.945	0.947	0.947	0.947
3.85	0.828	0.831	0.835	0.837
5.66	0.77	0.775	0.778	0.775
7.41		0.727		

TABLE 2-169 Potassium Hydroxide (at 19 °C)

Mole % KOH	0	0.497	1.64	4.76	9.09
Cal/(g·°C)	1.0	0.975	0.93	0.814	0.75

TABLE 2-170 Normal Propyl Alcohol

Mole % C ₃ H ₇ OH	Specific heat, cal/(g·°C)		
	5 °C	20 °C	40 °C
1.55	1.03	1.02	1.01
5.03	1.07	1.06	1.03
11.4	1.035	1.032	0.99
23.1	0.877	0.90	0.91
41.2	0.75	0.78	0.815
73.0	0.612	0.645	0.708
100.0	0.534	0.57	0.621

TABLE 2-171 Sodium Carbonate*

% Na ₂ CO ₃ by weight	Temperature, °C			
	17.6	30.0	76.6	98.0
0.00	0.9992	0.9986	1.0098	1.0084
1.498	0.9807			
2.000		0.9786		
2.901	0.9597			
4.000		0.9594		
5.000	0.9428		0.9761	
6.000		0.9392		
8.000	0.9183			
10.000	0.9086		0.9452	
13.790	0.8924			
13.840		0.8881		
20.000		0.8631	0.8936	
25.000			0.8615	0.8911

*J. Chem. Soc. 3062–3079 (1931).

TABLE 2-172 Sodium Chloride

Mole % NaCl	Specific heat, cal/(g·°C)			
	6 °C	20 °C	33 °C	57 °C
0.249		0.99		
0.99	0.96	0.97	0.97	
2.44	0.91	0.915	0.915	0.923
9.09	0.805	0.81	0.81	0.82

TABLE 2-173 Sodium Hydroxide (at 20 °C)

Mole % NaOH	0	0.5	1.0	9.09	16.7	28.6	37.5
Cal/(g·°C)	1.0	0.985	0.97	0.835	0.80	0.784	0.782

TABLE 2-174 Sulfuric Acid*

%H ₂ SO ₄	C _p at 20 °C, cal/(g·°C)	%H ₂ SO ₄	C _p at 20 °C, cal/(g·°C)
0.34	0.9968	35.25	0.7238
0.68	0.9937	37.69	.7023
1.34	0.9877	40.49	.6770
2.65	0.9762	43.75	.6476
3.50	0.9688	47.57	.6153
5.16	0.9549	52.13	.5801
9.82	0.9177	57.65	.5420
15.36	0.8767	64.47	.5012
21.40	0.8339	73.13	.4628
22.27	0.8275	77.91	.4518
23.22	0.8205	81.33	.4481
24.25	0.8127	82.49	.4467
25.39	0.8041	84.48	.4408
26.63	0.7945	85.48	.4346
28.00	0.7837	89.36	.4016
29.52	0.7717	91.81	.3787
30.34	0.7647	94.82	.3554
31.20	0.7579	97.44	.3404
33.11	0.7422	100.00	.3352

*Vinal and Craig, *Bur. Standards J. Research*, **24**, 475 (1940).

TABLE 2-175 Zinc Sulfate

Composition	Temperature	Specific heat, cal/(g·°C)
ZnSO ₄ + 5H ₂ O	20 to 52 °C	0.842
ZnSO ₄ + 200H ₂ O	20 to 52 °C	0.952

SPECIFIC HEATS OF MISCELLANEOUS MATERIALS

TABLE 2-176 Specific Heats of Miscellaneous Liquids and Solids

Material	Specific heat, cal/(g·°C)
Alumina	0.2 (100 °C); 0.274 (1500 °C)
Alundum	0.186 (100 °C)
Asbestos	0.25
Asphalt	0.22
Bakelite	0.3 to 0.4
Brickwork	About 0.2
Carbon	0.168 (26 to 76 °C) 0.314 (40 to 892 °C) 0.387 (56 to 1450 °C)
(gas retort) (see under Graphite)	0.204
Cellulose	0.32
Cement, Portland Clinker	0.186
Charcoal (wood)	0.242
Chrome brick	0.17
Clay	0.224
Coal	0.26 to 0.37
tar oils	0.34 (15 to 90 °C)
Coal tars	0.35 (40 °C); 0.45 (200 °C)
Coke	0.265 (21 to 400 °C) 0.359 (21 to 800 °C) 0.403 (21 to 1300 °C)
Concrete	0.156 (70 to 312 °F); 0.219 (72 to 1472 °F)
Cryolite	0.253 (16 to 55 °C)
Diamond	0.147
Fireclay brick	0.198 (100 °C); 0.298 (1500 °C)
Fluorspar	0.21 (30 °C)
Gasoline	0.53
Glass (crown) (flint) (pyrex) (silicate)	0.16 to 0.20 0.117 0.20 0.188 to 0.204 (0 to 100 °C) 0.24 to 0.26 (0 to 700 °C)
wool	0.157
Granite	0.20 (20 to 100 °C)
Graphite	0.165 (26 to 76 °C); 0.390 (56 to 1450 °C)
Gypsum	0.259 (16 to 46 °C)
Kerosene	0.47
Limestone	0.217
Litharge	0.055
Magnesia	0.234 (100 °C); 0.188 (1500 °C)
Magnesite brick	0.222 (100 °C); 0.195 (1500 °C)
Marble	0.21 (18 °C)
Porcelain, fired Berlin	0.189 (60 °C)
Porcelain, green Berlin	0.185 (60 °C)
Porcelain, fired earthenware	0.186 (60 °C)
Porcelain, green earthenware	0.181 (60 °C)

TABLE 2-176 Specific Heats of Miscellaneous Liquids and Solids (Concluded)

Material	Specific heat, cal/(g·°C)
Pyrex glass	0.20
Pyrites (copper)	0.131 (30 °C)
Pyrites (iron)	0.136 (30 °C)
Pyroxylin plastics	0.34 to 0.38
Quartz	0.17 (0 °C); 0.28 (350 °C)
Rubber (vulcanized)	0.415
Sand	0.191
Silica	0.316
Silica brick	0.202 (100 °C); 0.195 (1500 °C)
Silicon carbide brick	0.202 (100 °C)
Silk	0.33
Steel	0.12
Stone	about 0.2
Stoneware (common)	0.188 (60 °C)
Turpentine	0.42 (18 °C)
Wood (Oak)	0.570
Woods, miscellaneous	0.45 to 0.65
Wool	0.325
Zirconium oxide	0.11 (100 °C); 0.179 (1500 °C)

TABLE 2-177 Oils (Animal, Vegetable, Mineral Oils)

$$C_p[\text{cal}/(\text{g}\cdot^\circ\text{C})] = A/\sqrt{d^{15}} + B(t - 15)$$

where d = density, g/cm^3 .

$^\circ\text{F} = \frac{9}{5} ^\circ\text{C} + 32$; to convert calories per gram-degree Celsius to British thermal units per pound-degree Fahrenheit, multiply by 1.0; to convert grams per cubic centimeter to pounds per cubic foot, multiply by 62.43.

Oils	A	B
Castor	0.500	0.0007
Citron	(0.438 at 54 °C)	
Fatty drying	0.440	0.0007
nondrying	0.450	0.0007
semidrying	0.445	0.0007
oils (except castor)	0.450	0.0007
Naphthene base	0.405	0.0009
Olive	(0.47 at 7 °C)	
Paraffin base	0.425	0.0009
Petroleum oils	0.415	0.0009

PROPERTIES OF FORMATION AND COMBUSTION REACTIONS

UNITS CONVERSIONS

$^\circ\text{F} = \frac{9}{5} ^\circ\text{C} + 32$; to convert kilocalories per gram-mole to British thermal units per pound-mole, multiply by 1.799×10^{-3} .

TABLE 2-178 Heats and Free Energies of Formation of Inorganic Compounds

The values given in the following table for the heats and free energies of formation of inorganic compounds are derived from (a) Bichowsky and Rossini, "Thermochemistry of the Chemical Substances," Reinhold, New York, 1936; (b) Latimer, "Oxidation States of the Elements and Their Potentials in Aqueous Solution," Prentice-Hall, New York, 1938; (c) the tables of the American Petroleum Institute Research Project 44 at the National Bureau of Standards; and (d) the tables of Selected Values of Chemical Thermodynamic Properties of the National Bureau of Standards. The reader is referred to the preceding books and tables for additional details as to methods of calculation, standard states, and so on.

Compound	State†	Heat of formation‡§ ΔH (formation) at 25 °C, kcal/mol	Free energy of formation ¶ ΔF (formation) at 25 °C, kcal/mol	Compound	State†	Heat of formation‡§ ΔH (formation) at 25 °C, kcal/mol	Free energy of formation ¶ ΔF (formation) at 25 °C, kcal/mol
Aluminum				Barium (Cont.)			
Al	c	0.00	0.00	BaF ₂	c	-287.9	
AlBr ₃	c	-123.4		BaF ₂	aq, 1600	-284.6	-265.3
	aq	-209.5	-189.2	BaH ₂	c	-40.8	-31.5
Al ₂ C ₃	c	-30.8	-29.0	Ba(HCO ₃) ₂	aq	-459	-414.4
AlCl ₃	c	-163.8		BaI ₂	c	-144.6	
	aq, 600	-243.9	-209.5		aq, 400	-155.17	-158.52
AlF ₃	c	-329		Ba(IO ₃) ₂	c	-264.5	
	aq	-360.8	-312.6		aq	-237.50	-198.35
AlI ₃	c	-72.8		BaMoO ₄	c	-370	
	aq	-163.4	-152.5	Ba ₃ N ₂	c	-90.7	
AlN	c	-57.7	-50.4	Ba(NO ₂) ₂	c	-184.5	
Al(NH ₄)(SO ₄) ₂	c	-561.19	-486.17		aq	-179.05	-150.75
Al(NH ₄)(SO ₄) ₂ ·12H ₂ O	c	-1419.36	-1179.26	Ba(NO ₃) ₂	c	-236.99	-189.94
Al(NO ₃) ₃ ·6H ₂ O	c	-680.89	-526.32		aq, 600	-227.74	
Al(NO ₃) ₃ ·9H ₂ O	c	-897.59		BaO	c	-133.0	
Al ₂ O ₃	c, corundum	-399.09	-376.87	Ba(OH) ₂	c	-225.9	
Al(OH) ₃	c	-304.8	-272.9		aq, 400	-237.76	-209.02
Al ₂ O ₃ ·SiO ₂	c, sillimanite	-648.7		BaO·SiO ₂	c	-363	
Al ₂ O ₃ ·SiO ₂	c, disthene	-642.4		Ba ₃ (PO ₄) ₂	c	-992	
Al ₂ O ₃ ·SiO ₂	c, andalusite	-642.0		BaPtCl ₆	c	-284.9	
3Al ₂ O ₃ ·2SiO ₂	c, mullite	-1874		BaS	c	-111.2	
Al ₂ S ₃	c	-121.6		BaSO ₃	c	-282.5	
Al ₂ (SO ₄) ₃	c	-820.99	-739.53	BaSO ₄	c	-340.2	-313.4
	aq	-893.9	-759.3	BaWO ₄	c	-402	
Al ₂ (SO ₄) ₃ ·6H ₂ O	c	-1268.15	-1103.39	Beryllium			
Al ₂ (SO ₄) ₃ ·18H ₂ O	c	-2120		Be	c	0.00	0.00
Antimony				BeBr ₂	c	-79.4	
Sb	c	0.00	0.00		aq	-142	-127.9
SbBr ₃	c	-59.9		BeCl ₂	c	-112.6	
SbCl ₃	c	-91.3	-77.8		aq	-163.9	-141.4
SbCl ₅	l	-104.8		BeI ₂	c	-39.4	
SbF ₃	c	-216.6			aq	-112	-103.4
SbI ₃	c	-22.8		Be ₃ N ₂	c	-134.5	-122.4
Sb ₂ O ₃	c, I, orthorhombic	-165.4	-146.0	BeO	c	-145.3	-138.3
	c, II, octahedral	-166.6		Be(OH) ₂	c	-215.6	
Sb ₂ O ₄	c	-213.0	-186.6	BeS	c	-56.1	
Sb ₂ O ₅	c	-230.0	-196.1	BeSO ₄	c	-281	
Sb ₂ S ₃	c, black	-38.2	-36.9		aq		-254.8
Arsenic				Bismuth			
As	c	0.00	0.00	Bi	c	0.00	0.00
AsBr ₃	c	-45.9		BiCl ₃	c	-90.5	-76.4
AsCl ₃	l	-80.2	-70.5		aq	-101.6	
AsF ₃	l	-223.76	-212.27	BiI ₃	c	-24	
AsH ₃	g	43.6	37.7		aq	-27	
AsI ₃	c	-13.6		BiO	c	-49.5	-43.2
As ₂ O ₃	c	-154.1	-134.8	Bi ₂ O ₃	c	-137.1	-117.9
As ₂ O ₅	c	-217.9	-183.9	Bi(OH) ₃	c	-171.1	
As ₂ S ₃	c	-20	-20	Bi ₂ S ₃	c	-43.9	-39.1
	amorphous	-34.76		Bi ₂ (SO ₄) ₃	c	-607.1	
Barium				Boron			
Ba	c	0.00	0.00	B	c	0.00	0.00
BaBr ₂	c	-180.38		BBr ₃	l	-52.7	
	aq, 400	-185.67	-183.0		g	-44.6	-50.9
BaCl ₂	c	-205.25		BCl ₃	g	-94.5	-90.8
	aq, 300	-207.92	-196.5	BF ₃	g	-265.2	-261.0
Ba(ClO ₃) ₂	c	-176.6		B ₂ H ₆	g	7.5	19.9
	aq, 1600	-170.0	-134.4	BN	c	-32.1	-27.2
Ba(ClO ₄) ₂	c	-210.2		B ₂ O ₃	c	-302.0	-282.9
	aq, 800		-155.3		gls	-297.6	-280.3
Ba(CN) ₂	c	-48		B(OH) ₃	c	-260.0	-229.4
Ba(CNO) ₂	c	-212.1		B ₂ S ₃	c	-56.6	
	aq		-180.7	Bromine			
BaCN ₂	c	-63.6		Br ₂	l	0.00	0.00
BaCO ₃	c, witherite	-284.2	-271.4		g	7.47	0.931
BaCrO ₄	c	-342.2		BrCl	g	3.06	-0.63

*For footnotes see end of table.

TABLE 2-178 Heats and Free Energies of Formation of Inorganic Compounds (Continued)

Compound	State†	Heat of formation‡§ ΔH (formation) at 25 °C, kcal/mol	Free energy of formation‡¶ ΔF (formation) at 25 °C, kcal/mol	Compound	State†	Heat of formation‡§ ΔH (formation) at 25 °C, kcal/mol	Free energy of formation‡¶ ΔF (formation) at 25 °C, kcal/mol
Cadmium				Cesium (Cont.)			
Cd	c	0.00	0.00	Cs ₂ CO ₃	c	-271.88	
CdBr ₂	c	-75.8	-70.7	CsF	c	-131.67	
	aq, 400	-76.6	-67.6		aq, 400	-140.48	-135.98
CdCl ₂	c	-92.149	-81.889	CsH	c	-12	-7.30
	aq, 400	-96.44	-81.2	CsHCO ₃	c	-230.6	
Cd(CN) ₂	c	36.2			aq, 2000	-226.6	-210.56
CdCO ₃	c	-178.2	-163.2	CsI	c	-83.91	
CdI ₂	c	-48.40			aq, 400	-75.74	-82.61
	aq, 400	-47.46	-43.22	CsNH ₂	c	-28.2	
Cd ₃ N ₂	c	39.8		CsNO ₃	c	-121.14	
Cd(NO ₃) ₂	aq, 400	-115.67	-71.05		aq, 400	-111.54	-96.53
CdO	c	-62.35	-55.28	Cs ₂ O	c	-82.1	
Cd(OH) ₂	c	-135.0	-113.7	CsOH	c	-100.2	
CdS	c	-34.5	-33.6		aq, 200	-117.0	-107.87
CdSO ₄	c	-222.23		Cs ₂ S	c	-87	
	aq, 400	-232.635	-194.65	Cs ₂ SO ₄	c	-344.86	
					aq	-340.12	-316.66
Calcium				Chlorine			
Ca	c	0.00	0.00	Cl ₂	g	0.00	0.00
CaBr ₂	c	-162.20		ClF	g	-25.7	
	aq, 400	-187.19	-181.86	ClO	g	33	
CaC ₂	c	-14.8		ClO ₂	g	24.7	29.5
CaCl ₂	c	-190.6	-179.8	ClO ₃	g	37	
	aq	-209.15	-195.36	Cl ₂ O	g	18.20	22.40
CaCN ₂	c	-85		Cl ₂ O ₇	g	63	
Ca(CN) ₂	c	-43.3		Chromium			
	aq		-54.0	Cr	c	0.00	0.00
CaCO ₃	c, calcite	-289.5	-270.8	CrBr ₃	aq		-122.7
	c, aragonite	-289.54	-270.57	Cr ₃ C ₂	c	-21.008	-21.20
CaCO ₃ ·MgCO ₃	c	-558.8		Cr ₄ C	c	-16.378	-16.74
CaC ₂ O ₄	c	-332.2		CrCl ₂	c	-103.1	-93.8
Ca(C ₂ H ₃ O ₂) ₂	c	-356.3			aq		-102.1
	aq	-364.1	-311.3	CrF ₂	c	-152	
CaF ₂	c	-290.2		CrF ₃	c	-231	
	aq	-286.5	-264.1	CrI ₂	c	-63.7	
CaH ₂	c	-46	-35.7		aq		-64.1
CaI ₂	c	-128.49		CrO ₃	c	-139.3	
	aq, 400	-156.63	-157.37	Cr ₂ O ₃	c	-268.8	-249.3
Ca ₃ N ₂	c	-103.2	-88.2	Cr ₃ (SO ₄) ₃	aq		-626.3
Ca(NO ₃) ₂	c	-224.05	-177.38	Cobalt			
	aq, 400	-228.29		Co	c	0.00	0.00
Ca(NO ₃) ₂ ·2H ₂ O	c	-367.95	-293.57	CoBr ₂	c	-55.0	
Ca(NO ₃) ₂ ·3H ₂ O	c	-439.05	-351.58		aq	-73.61	-61.96
Ca(NO ₃) ₂ ·4H ₂ O	c	-509.43	-409.32	Co ₃ C	c	9.49	7.08
CaO	c	-151.7	-144.3	CoCl ₂	c	-76.9	-66.6
Ca(OH) ₂	c	-235.58	-213.9		aq, 400	-95.58	-75.46
	aq, 800	-239.2	-207.9	CoCO ₃	c	-172.39	-155.36
CaO·SiO ₂	c, II, wollastonite	-377.9	-357.5	CoF ₂	aq	-172.98	-144.2
	c, I, pseudo-wollastonite	-376.6	-356.6	CoI ₂	c	-24.2	
					aq	-43.15	-37.4
CaS	c	-114.3	-113.1	Co(NO ₃) ₂	c	-102.8	
CaSO ₄	c, insoluble form	-338.73	-311.9		aq	-114.9	-65.3
	c, soluble form α	-336.58	-309.8	CoO	c	-57.5	
	c, soluble form β	-335.52	-308.8	Co ₃ O ₄	c	-196.5	
CaSO ₄ ·½H ₂ O	c	-376.13		Co(OH) ₂	c	-131.5	-108.9
CaSO ₄ ·2H ₂ O	c	-479.33	-425.47	Co(OH) ₃	c	-177.0	-142.0
CaWO ₄	c	-387		CoS	c	-22.3	-19.8
Carbon				Co ₂ S ₃	c	-40.0	
C	c, graphite	0.00	0.00	CoSO ₄	c	-216.6	
	c, diamond	0.453	0.685		aq, 400		-188.9
CO	g	-26.416	-32.808	Columbium			
CO ₂	g	-94.052	-94.260	Cb	c	0.00	0.00
				Cb ₂ O ₅	c	-462.96	
Cerium				Copper			
Ce	c	0.00	0.00	Cu	c	0.00	0.00
CeN	c	-78.2	-70.8	CuBr	c	-26.7	-23.8
Cesium				CuBr ₂	c	-34.0	
Cs	c	0.00	0.00		aq	-42.4	-33.25
CsBr	c	-97.64		CuCl	c	-31.4	-24.13
	aq, 500	-91.39	-94.86	CuCl ₂	c	-48.83	
CsCl	c	-106.31			aq, 400	-64.7	
	aq, 400	-102.01	-101.61				

TABLE 2-178 Heats and Free Energies of Formation of Inorganic Compounds (Continued)

Compound	State†	Heat of formation‡§ ΔH (formation) at 25 °C, kcal/mol	Free energy of formation ¶ ΔF (formation) at 25 °C, kcal/mol	Compound	State†	Heat of formation‡§ ΔH (formation) at 25 °C, kcal/mol	Free energy of formation ¶ ΔF (formation) at 25 °C, kcal/mol
Copper (Cont.)				Hydrogen (Cont.)			
CuClO ₄	aq	-28.3	1.34	H ₂ CO ₃	aq	-167.19	-149.0
Cu(ClO ₃) ₂	aq, 400		15.4	HF	g	-64.2	-64.7
Cu(ClO ₄) ₂	aq		-5.5		aq, 200	-75.75	
CuI	c	-17.8	-16.66	HI	g	6.27	0.365
CuI ₂	c	-4.8			aq, 400	-13.47	-12.35
	aq	-11.9	-8.76	HIO	aq	-38	-23.33
Cu ₃ N	c	17.78		HIO ₃	c	-56.77	
Cu(NO ₃) ₂	c	-73.1			aq	-54.8	-32.25
	aq, 200	-83.6	-36.6	HN ₃	g	70.3	78.50
CuO	c	-38.5	-31.9	HNO ₃	l	-31.99	-17.57
Cu ₂ O	c	-43.00	-38.13		g	-41.35	-19.05
Cu(OH) ₂	c	-108.9	-85.5		l	-49.210	
CuS	c	-11.6	-11.69	HNO ₃ ·H ₂ O	aq, 400	-112.91	-78.36
Cu ₂ S	c	-18.97	-20.56	HNO ₃ ·3H ₂ O	l	-252.15	-193.70
CuSO ₄	c	-184.7	-158.3	H ₂ O	g	-57.7979	-54.6351
	aq, 800	-200.78	-160.19		l	-68.3174	-56.6899
Cu ₂ SO ₄	c	-179.6		H ₂ O ₂	l	-45.16	-28.23
	aq		-152.0		aq, 200	-45.80	-31.47
Erbium				H ₃ PO ₂	c	-145.5	
Er	c	0.00	0.00		aq	-145.6	-120.0
Er(OH) ₃	c	-326.8		H ₃ PO ₃	c	-232.2	
Fluorine					aq	-232.2	-204.0
F ₂	g	0.00	0.00	H ₃ PO ₄	c	-306.2	
F ₂ O	g	5.5	9.7		aq, 400	-309.32	-270.0
Gallium				H ₂ S	g	-4.77	-7.85
Ga	c	0.00	0.00		aq, 2000	-9.38	
GaBr ₃	c	-92.4		H ₂ S ₂	l	-3.6	
GaCl ₃	c	-125.4		H ₂ SO ₃	aq, 200	-146.88	-128.54
GaN	c	-26.2		H ₂ SO ₄	l	-193.69	
Ga ₂ O	c	-84.3			aq, 400	-212.03	
Ga ₂ O ₃	c	-259.9		H ₂ Se	g	20.5	17.0
Germanium					aq	18.1	18.4
Ge	c	0.00	0.00	H ₂ SeO ₃	c	-126.5	
Ge ₃ N ₄	c	-15.7			aq	-122.4	-101.36
GeO ₂	c	-128.6		H ₂ SeO ₄	c	-130.23	
Gold					aq, 400	-143.4	
Au	c	0.00	0.00	H ₂ SiO ₃	c	-267.8	-247.9
AuBr	c	-3.4		H ₄ SiO ₄	c	-340.6	
AuBr ₃	c	-14.5		H ₂ Te	g	36.9	33.1
	aq	-11.0	24.47	H ₂ TeO ₃	c	-145.0	-115.7
AuCl	c	-8.3			aq	-145.0	
AuCl ₃	c	-28.3		H ₂ TeO ₄	aq	-165.6	
	aq	-32.96	4.21	Indium			
AuI	c	0.2	-0.76	In	c	0.00	0.00
Au ₂ O ₃	c	11.0	18.71	InBr ₃	c	-97.2	
Au(OH) ₃	c	-100.6			aq	-112.9	-97.2
Hafnium				InCl ₃	c	-128.5	
Hf	c	0.00	0.00		aq	-145.6	-117.5
HfO ₂	c	-271.1	-258.2	InI ₃	c	-56.5	
Hydrogen					aq	-67.2	-60.5
H ₃ AsO ₃	aq	-175.6	-153.04	InN	aq	-4.8	
H ₃ AsO ₄	c	-214.9		In ₂ O ₃	c	-222.47	
	aq	-214.8	-183.93	Iodine			
HBr	g	-8.66	-12.72	I ₂	c	0.00	0.00
	aq, 400	-28.80	-24.58		g	14.88	4.63
HBrO	aq	-25.4	-19.90	IBr	g	10.05	1.24
HBrO ₃	aq	-11.51	5.00	ICl	g	4.20	-1.32
HCl	g	-22.063	-22.778	ICl ₃	c	-21.8	-6.05
	aq, 400	-39.85	-31.330	I ₂ O ₅	c	-42.5	
HCN	g	31.1	27.94	Iridium			
	aq, 100	24.2	26.55	Ir	c	0.00	0.00
HClO	aq, 400	-28.18	-19.11	IrCl	c	-20.5	-16.9
HClO ₃	aq	-23.4	-0.25	IrCl ₂	c	-40.6	-32.0
HClO ₄	aq, 660	-31.4	-10.70	IrCl ₃	c	-60.5	-46.5
HC ₂ H ₃ O ₂	l	-116.2	-93.56	IrF ₆	l	-130	
	aq, 400	-116.74	-96.8	IrO ₂	c	-40.14	
H ₂ C ₂ O ₄	c	-196.7		Iron			
	aq, 300	-194.6	-165.64	Fe	c, α	0.00	0.00
HCOOH	l	-97.8	-82.7	FeBr ₂	c	-57.15	
	aq, 200	-98.0	-85.1		aq, 540	-78.7	-69.47

TABLE 2-178 Heats and Free Energies of Formation of Inorganic Compounds (Continued)

Compound	State†	Heat of formation‡§ ΔH (formation) at 25 °C, kcal/mol	Free energy of formation ¶ ΔF (formation) at 25 °C, kcal/mol	Compound	State†	Heat of formation‡§ ΔH (formation) at 25 °C, kcal/mol	Free energy of formation ¶ ΔF (formation) at 25 °C, kcal/mol
Iron (Cont.)				Lithium (Cont.)			
FeBr ₃	aq	-95.5	-76.26	LiC ₂ H ₃ O ₂	aq	-183.9	-160.00
Fe ₃ C	c	5.69	4.24	Li ₂ CO ₃	c	-289.7	-269.8
Fe(CO) ₅	l	-187.6			aq, 1900	-293.1	-267.58
FeCO ₃	c, siderite	-172.4	-154.8	LiCl	c	-97.63	
FeCl ₂	c	-81.9	-72.6		aq, 278	-106.45	-102.03
	aq	-100.0	-83.0	LiClO ₃	aq	-87.5	-70.95
FeCl ₃	c	-96.4		LiClO ₄	aq	-106.3	-81.4
	aq, 2000	-128.5	-96.5	LiF	c	-145.57	
FeF ₂	aq, 1200	-177.2	-151.7		aq, 400	-144.85	-136.40
FeI ₂	c	-24.2		LiH	c	-22.9	
	aq	-47.7	-45	LiHCO ₃	aq, 2000	-231.1	-210.98
FeI ₃	aq	-49.7	-39.5	LiI	c	-65.07	
Fe ₄ N	c	-2.55	0.862		aq, 400	-80.09	-83.03
Fe(NO ₃) ₂	aq	-118.9	-72.8	LiIO ₃	aq	-121.3	-102.95
Fe(NO ₃) ₃	aq, 800	-156.5	-81.3	Li ₃ N	c	-47.45	-37.33
FeO	c	-64.62	-59.38	LiNO ₃	c	-115.350	
Fe ₂ O ₃	c	-198.5	-179.1		aq, 400	-115.88	-96.95
Fe ₃ O ₄	c	-266.9	-242.3	Li ₂ O	c	-142.3	
Fe(OH) ₂	c	-135.9	-115.7	Li ₂ O ₂	c	-151.9	-138.0
Fe(OH) ₃	c	-197.3	-166.3		aq	-159	
FeO·SiO ₂	c	-273.5		LiOH	c	-116.58	-106.44
Fe ₂ P	c	-13			aq, 400	-121.47	-108.29
FeSi	c	-19.0		LiOH·H ₂ O	c	-188.92	
FeS	c	-22.64	-23.23	Li ₂ O·SiO ₂	gls	-374	
FeS ₂	c, pyrites	-38.62	-35.93	Li ₂ Se	c	-84.9	
	c, marcasite	-33.0			aq	-95.5	-105.64
FeSO ₄	c	-221.3	-195.5	Li ₂ SO ₄	c	-340.23	-314.66
	aq, 400	-236.2	-196.4		aq, 400	-347.02	
Fe ₂ (SO ₄) ₃	aq, 400	-653.3	-533.4	Li ₂ SO ₄ ·H ₂ O	c	-411.57	-375.07
FeTiO ₃	c, ilmenite	-295.51	-277.06	Magnesium			
Lanthanum				Mg	c	0.00	0.00
La	c	0.00	0.00	Mg(AsO ₄) ₂	c	-731.3	
LaCl ₃	c	-253.1			aq	-749	-630.14
	aq	-284.7		MgBr ₂	c	-123.9	
La ₃ H ₈	c	-160			aq, 400	-167.33	-156.94
LaN	c	-72.0	-64.6	Mg(CN) ₂	aq	-39.7	-29.08
La ₂ O ₃	c	-539		MgCN ₂	c	-61	
LaS ₂	c	-148.3		Mg(C ₂ H ₃ O ₂) ₂	aq	-344.6	-286.38
La ₂ S ₃	c	-351.4		MgCO ₃	c	-261.7	-241.7
La ₂ (SO ₄) ₃	aq	-972		MgCl ₂	c	-153.220	-143.77
Lead					aq, 400	-189.76	
Pb	c	0.00		MgCl ₂ ·H ₂ O	c	-230.970	-205.93
PbBr ₂	c	-66.24	-62.06	MgCl ₂ ·2H ₂ O	c	-305.810	-267.20
	aq	-56.4	-54.97	MgCl ₂ ·4H ₂ O	c	-453.820	-387.98
PbCO ₃	c, cerussite	-167.6	-150.0	MgCl ₂ ·6H ₂ O	c	-597.240	-505.45
Pb(C ₂ H ₃ O ₂) ₂	c	-232.6		MgF ₂	c	-263.8	
	aq, 400	-234.2	-184.40	MgI ₂	c	-86.8	
PbC ₂ O ₄	c	-205.3			aq, 400	-136.79	-132.45
PbCl ₂	c	-85.68	-75.04	MgMoO ₄	c	-329.9	
	aq	-82.5	-68.47	Mg ₃ N ₂	c	-115.2	-100.8
PbF ₂	c	-159.5	-148.1	Mg(NO ₃) ₂	c	-188.770	-140.66
PbI ₂	c	-41.77	-41.47		aq, 400	-209.927	-160.28
Pb(NO ₃) ₂	c	-106.88		Mg(NO ₃) ₂ ·2H ₂ O	c	-336.625	
	aq, 400	-99.46	-58.3	Mg(NO ₃) ₂ ·6H ₂ O	c	-624.48	-496.03
PbO	c, red	-51.72	-45.53	MgO	c	-143.84	-136.17
	c, yellow	-50.86	-43.88	MgO·SiO ₂	c	-347.5	-326.7
PbO ₂	c	-65.0	-52.0	Mg(OH) ₂	c, ppt.	-221.90	-200.17
Pb ₃ O ₄	c	-172.4	-142.2		c, brucite	-223.9	-193.3
Pb(OH) ₂	c	-123.0	-102.2	MgS	c	-84.2	
PbS	c	-22.38	-21.98		aq	-108	
PbSO ₄	c	-218.5	-192.9	MgSO ₄	c	-304.94	-277.7
Lithium					aq, 400	-325.4	-283.88
Li	c	0.00	0.00	MgTe	c	-25	
LiBr	c	-83.75		MgWO ₄	c	-345.2	
	aq, 400	-95.40	-95.28	Manganese			
LiBrO ₃	aq	-77.9	-65.70	Mn	c, α	0.00	0.00
Li ₂ C ₂	c	-13.0		MnBr ₂	c	-91	
LiCN	aq	-31.4	-31.35		aq	-106	-97.8
LiCNO	aq	-101.2	-94.12	Mn ₃ C	c	1.1	1.26

2-190 PHYSICAL AND CHEMICAL DATA

TABLE 2-178 Heats and Free Energies of Formation of Inorganic Compounds (Continued)

Compound	State†	Heat of formation‡§ ΔH (formation) at 25 °C, kcal/mol	Free energy of formation ¶ ΔF (formation) at 25 °C, kcal/mol	Compound	State†	Heat of formation‡§ ΔH (formation) at 25 °C, kcal/mol	Free energy of formation ¶ ΔF (formation) at 25 °C, kcal/mol
Manganese (Cont.)				Nickel (Cont.)			
Mn(C ₂ H ₃ O ₂) ₂	c	-270.3		NiF ₂	aq, 400	-94.34	-74.19
	aq	-282.7	-227.2		c	-157.5	
MnCO ₃	c	-211	-192.5	NiI ₂	aq	-171.6	-142.9
MnC ₂ O ₄	c	-240.9			c	-22.4	
MnCl ₂	c	-112.0	-102.2		aq	-42.0	-36.2
	aq, 400	-128.9		Ni(NO ₃) ₂	c	-101.5	
MnF ₂	aq, 1200	-206.1	-180.0		aq, 200	-113.5	-64.0
MnI ₂	c	-49.8		NiO	c	-58.4	-51.7
	aq	-76.2	-73.3	Ni(OH) ₂	c	-129.8	-105.6
Mn ₃ N ₂	c	-57.77	-46.49	Ni(OH) ₃	c	-163.2	
Mn(NO ₃) ₂	c	-134.9		NiS	c	-20.4	
	aq, 400	-148.0	-101.1	NiSO ₄	c	-216	
Mn(NO ₃) ₂ ·6H ₂ O	c	-557.07	-441.2		aq, 200	-231.3	-187.6
MnO	c	-92.04	-86.77	Nitrogen			
MnO ₂	c	-124.58	-111.49	N ₂	g	0.00	0.00
Mn ₂ O ₃	c	-229.5	-209.9	NF ₃	g	-27	
Mn ₃ O ₄	c	-331.65	-306.22	NH ₃	g	-10.96	-3.903
MnO·SiO ₂	c	-301.3	-282.1		aq, 200	-19.27	
Mn(OH) ₂	c	-163.4	-143.1	NH ₄ Br	c	-64.57	
Mn(OH) ₃	c	-221	-190		aq	-60.27	-43.54
Mn ₃ (PO ₄) ₂	c	-736		NH ₄ C ₂ H ₃ O ₂	c	-148.1	
MnSe	c	-26.3	-27.5		aq, 400	-148.58	-108.26
MnS	c, green	-47.0	-48.0	NH ₄ CN	c	-0.7	
MnSO ₄	c	-254.18	-228.41		aq	3.6	20.4
	aq, 400	-265.2		NH ₄ CNS	c	-17.8	
Mn ₂ (SO ₄) ₃	c	-635			aq	-12.3	4.4
	aq	-657		(NH ₄) ₂ CO ₃	aq	-223.4	-164.1
Mercury				(NH ₄) ₂ C ₂ O ₄	c	-266.3	
Hg	l	0.00	0.00		aq	-260.6	-196.2
HgBr	g	23	18	NH ₄ Cl	c	-75.23	-48.59
HgBr ₂	c	-40.68	-38.8		aq, 400	-71.20	
	aq	-38.4	-9.74	NH ₄ ClO ₄	c	-69.4	
Hg(C ₂ H ₃ O ₂) ₂	c	-196.3			aq	-63.2	-21.1
	aq	-192.5	-139.2	(NH ₄) ₂ CrO ₄	c	-276.9	
HgCl ₂	c	-53.4	-42.2		aq	-271.3	-209.3
	aq	-50.3	-23.25	NH ₄ F	c	-111.6	
HgCl	g	19	14		aq	-110.2	-84.7
Hg ₂ Cl ₂	c	-63.13		NH ₄ I	c	-48.43	
Hg(CN) ₂	c	62.8			aq	-44.97	-31.3
	aq, 1110	66.25		NH ₄ NO ₃	c	-87.40	
HgC ₂ O ₄	c	-159.3			aq, 500	-80.89	
HgH	g	57.1	52.25	NH ₄ OH	aq	-87.59	
HgI ₂	c, red	-25.3	-24.0	(NH ₄) ₂ S	aq, 400	-55.21	-14.50
HgI	g	33	23	(NH ₄) ₂ SO ₄	c	-281.74	-215.06
Hg ₂ I ₂	c	-28.88	-26.53		aq, 400	-279.33	-214.02
Hg(NO ₃) ₂	aq	-56.8	-13.09	N ₂ H ₄	l	12.06	
Hg ₂ (NO ₃) ₂	aq	-58.5	-15.65	N ₂ H ₄ ·H ₂ O	l	-57.96	
HgO	c, red	-21.6	-13.94	N ₂ H ₄ ·H ₂ SO ₄	c	-232.2	
	c, yellow ppt.	-20.8		N ₂ O	g	19.55	24.82
Hg ₂ O	c	-21.6	-12.80	NO	g	21.600	20.719
HgS	c, black	-10.7	-8.80	NO ₂	g	7.96	12.26
HgSO ₄	c	-166.6		N ₂ O ₄	g	2.23	23.41
Hg ₂ SO ₄	c	-177.34	-149.12	N ₂ O ₅	c	-10.0	
Molybdenum				NOBr	l	11.6	19.26
Mo	c	0.00	0.00	NOCl	g	12.8	16.1
Mo ₂ C	c	4.36	2.91	Osmium			
Mo ₂ N	c	-8.3		Os	c	0.00	0.00
MoO ₂	c	-130	-118.0	OsO ₄	c	-93.6	-70.9
MoO ₃	c	-180.39	-162.01		g	-80.1	-68.1
MoS ₂	c	-56.27	-54.19	Oxygen			
MoS ₃	c	-61.48	-57.38	O ₂	g	0.00	0.00
Nickel				O ₃	g	33.88	38.86
Ni	c	0.00	0.00	Palladium			
NiBr ₂	c	-53.4		Pd	c	0.00	0.00
	aq	-72.6	-60.7	PdO	c	-20.40	
Ni ₃ C	c	9.2	8.88	Phosphorus			
Ni(C ₂ H ₃ O ₂) ₂	aq	-249.6	-190.1	P	c, white ("yellow")	0.00	0.00
Ni(CN) ₂	aq	230.9	66.3		c, red ("violet")	-4.22	-1.80
NiCl ₂	c	-75.0			g	150.35	141.88

TABLE 2-178 Heats and Free Energies of Formation of Inorganic Compounds (Continued)

Compound	State†	Heat of formation‡§ ΔH (formation) at 25 °C, kcal/mol	Free energy of formation ¶ ΔF (formation) at 25 °C, kcal/mol	Compound	State†	Heat of formation‡§ ΔH (formation) at 25 °C, kcal/mol	Free energy of formation ¶ ΔF (formation) at 25 °C, kcal/mol
Phosphorus (Cont.)				Potassium (Cont.)			
P ₂		33.82	24.60	KNH ₂	c	-28.25	
P ₄	l-g	13.2	5.89	KNO ₂	aq	-86.0	-75.9
PBr ₃	l-g	-45		KNO ₃	c	-118.08	-94.29
PBr ₅	c	-60.6			aq, 400	-109.79	-93.68
PCl ₃	l-g	-70.0	-65.2	K ₂ O	c	-86.2	
		-76.8	-63.3	K ₂ O·Al ₂ O ₃ ·SiO ₂	c, leucite	-1379.6	
PCl ₅	g	-91.0	-73.2		gls	-1368.2	
PH ₃	g	2.21	-1.45	K ₂ O·Al ₂ O ₃ ·SiO ₂	c, adularia	-1784.5	
PI ₃	c	-10.9			c, microcline	-1784.5	
P ₂ O ₃	c	-360.0			gls	-1747	
POCl ₃	g	-138.4	-127.2	KOH	c	-102.02	
Platinum					aq, 400	-114.96	-105.0
Pt	c	0.00	0.00	K ₃ PO ₃	aq	-397.5	
PtBr ₄	c	-40.6		K ₃ PO ₄	aq	-478.7	-443.3
	aq	-50.7		KH ₂ PO ₄	c	-362.7	-326.1
PtCl ₂	c	-34		K ₂ PtCl ₄	c	-254.7	
PtCl ₄	c	-62.6			aq	-242.6	-226.5
	aq	-82.3		K ₂ PtCl ₆	c	-299.5	-263.6
PtI ₄	c	-18			aq, 9400	-286.1	
Pt(OH) ₂	c	-87.5	-67.9	K ₂ Se	c	-74.4	
PtS	c	-20.18	-18.55		aq	-83.4	-99.10
PtS ₂	c	-26.64	-24.28	K ₂ SeO ₄	aq	-267.1	-240.0
Potassium				K ₂ S	c	-121.5	
K	c	0.00	0.00		aq, 400	-110.75	-111.44
K ₃ AsO ₃	aq	-323.0		K ₂ SO ₃	c	-267.7	
K ₃ AsO ₄	aq	-390.3	-355.7		aq	-269.7	-251.3
KH ₂ AsO ₄	c	-271.2	-236.7	K ₂ SO ₄	c	-342.65	-314.62
KBr	c	-94.06	-90.8		aq, 400	-336.48	-310.96
	aq, 400	-89.19	-92.0	K ₂ SO ₄ ·Al ₂ (SO ₄) ₃	c	-1178.38	-1068.48
KBrO ₃	c	-81.58	-60.30	K ₂ SO ₄ ·Al ₂ (SO ₄) ₃ ·24H ₂ O	c	-2895.44	-2455.68
	aq, 1667	-71.68		K ₂ S ₂ O ₆	c	-418.62	
KC ₂ H ₃ O ₂	c	-173.80		Rhenium			
	aq, 400	-177.38	-156.73	Re	c	0.00	0.00
KCl	c	-104.348	-97.76	ReF ₆	g	-274	
	aq, 400	-100.164	-98.76	Rhodium			
KClO ₃	c	-93.5	-69.30	Rh	c	0.00	0.00
	aq, 400	-81.34		RhO	c	-21.7	
KClO ₄	c	-103.8	-72.86	Rh ₂ O	c	-22.7	
	aq, 400	-101.14		Rh ₂ O ₃	c	-68.3	
KCN	c	-28.1		Rubidium			
	aq, 400	-25.3	-28.08	Rb	c	0.00	0.00
KCNO	c	-99.6		RbBr	c	-95.82	
	aq	-94.5	-90.85		g	-45.0	-52.50
KCNS	c	-47.0			aq, 500	-90.54	-93.38
	aq, 400	-41.07	-44.08	RbCN	aq	-25.9	
K ₂ CO ₃	c	-274.01		Rb ₂ CO ₃	c	-273.22	
	aq, 400	-280.90	-264.04		aq, 220	-282.61	-263.78
K ₂ C ₂ O ₄	c	-319.9		RbCl	c	-105.06	-98.48
	aq, 400	-315.5	-293.1		g	-53.6	-57.9
K ₂ CrO ₄	c	-333.4			aq, ∞	-101.06	-100.13
	aq, 400	-328.2	-306.3	RbF	c	-133.23	
K ₂ Cr ₂ O ₇	c	-488.5			aq, 400	-139.31	-134.5
	aq, 400	-472.1	-440.9	RbHCO ₃	c	-230.01	
KF	c	-134.50			aq, 2000	-225.59	-209.07
	aq, 180	-138.36	-133.13	RbI	c	-81.04	
K ₃ Fe(CN) ₆	c	-48.4			g	-31.2	-40.5
	aq	-34.5			aq, 400	-74.57	-81.13
K ₄ Fe(CN) ₆	c	-131.8		RbNH ₂	c	-27.74	
	aq	-119.9		RbNO ₃	c	-119.22	
KH	c	-10	-5.3		aq, 400	-110.52	-95.05
KHCO ₃	c	-229.8		Rb ₂ O	c	-82.9	
	aq, 2000	-224.85	-207.71	Rb ₂ O ₂	c	-107	
KI	c	-78.88	-77.37	RbOH	c	-101.3	
	aq, 500	-73.95	-79.76		aq, 200	-115.8	-106.39
KIO ₃	c	-121.69	-101.87	Ruthenium			
	aq, 400	-115.18	-99.68	Ru	c	0.00	0.00
KIO ₄	aq	-98.1		RuS ₂	c	-46.99	-44.11
KMnO ₄	c	-192.9	-169.1	Selenium			
	aq, 400	-182.5	-168.0	Se	c, I, hexagonal	0.00	0.00
K ₂ MoO ₄	aq, 880	-364.2	-342.9				

2-192 PHYSICAL AND CHEMICAL DATA

TABLE 2-178 Heats and Free Energies of Formation of Inorganic Compounds (Continued)

Compound	State†	Heat of formation‡§ ΔH (formation) at 25 °C, kcal/mol	Free energy of formation ¶ ΔF (formation) at 25 °C, kcal/mol	Compound	State†	Heat of formation‡§ ΔH (formation) at 25 °C, kcal/mol	Free energy of formation ¶ ΔF (formation) at 25 °C, kcal/mol
Selenium (Cont.)				Sodium (Cont.)			
	c, II, red, monoclinic	0.2			aq, 476	-97.66	-73.29
Se ₂ Cl ₂	l	-22.06	-13.73	Na ₂ CrO ₄	c	-319.8	
SeF ₆	g	-246	-222		aq, 800	-323.0	-296.58
SeO ₂	c	-56.33		Na ₂ Cr ₂ O ₇	aq, 1200	-465.9	-431.18
Silicon				NaF	c	-135.94	-129.0
Si	c	0.00	0.00		aq, 400	-135.711	-128.29
SiBr ₄	l	-93.0		NaH	c	-14	-9.30
SiC	c	-28	-27.4	NaHCO ₃	c	-226.0	-202.66
SiCl ₄	l	-150.0	-133.9		aq	-222.1	-202.87
	g	-142.5	-133.0	NaI	c	-69.28	
SiF ₄	g	-370	-360		aq, ∞	-71.10	-74.92
SiH ₄	g	-14.8	-9.4	NaIO ₃	aq, 400	-112.300	-94.84
SiI ₄	c	-29.8		Na ₂ MoO ₄	c	-364	
Si ₃ N ₄	c	-179.25	-154.74		aq	-358.7	-333.18
SiO ₂	c, cristobalite, 1600° form	-202.62		NaNO ₂	c	-86.6	
	c, cristobalite, 1100° form	-202.46			aq	-83.1	-71.04
	c, quartz	-203.35	-190.4	NaNO ₃	c	-111.71	-87.62
	c, tridymite	-203.23			aq, 400	-106.880	-88.84
Silver				Na ₂ O	c	-99.45	-90.06
Ag	c	0.00	0.00	Na ₂ O ₂	c	-119.2	-105.0
AgBr	c	-23.90	-23.02	Na ₂ O·SiO ₂	c	-383.91	-361.49
Ag ₂ C ₂	c	84.5		Na ₂ O·Al ₂ O ₃ ·3SiO ₂	c, natrolite	-1180	
AgC ₂ H ₃ O ₂	c	-95.9		Na ₂ O·Al ₂ O ₃ ·4SiO ₂	c	-1366	
	aq	-91.7	-70.86	NaOH	c	-101.96	-90.60
AgCN	c	33.8	38.70		aq, 400	-112.193	-100.18
Ag ₂ CO ₃	c	-119.5	-103.0	Na ₃ PO ₃	aq, 1000	-389.1	
Ag ₂ C ₂ O ₄	c	-158.7		Na ₃ PO ₄	c	-457	
AgCl	c	-30.11	-25.98		aq, 400	-471.9	-428.74
AgF	c	-48.7		Na ₃ PtCl ₄	aq	-237.2	-216.78
	aq, 400	-53.1	-47.26	Na ₃ PtCl ₆	c	-272.1	
AgI	c	-15.14	-16.17		aq	-280.9	
AgIO ₃	c	-42.02	-24.08	Na ₂ Se	c	-59.1	
AgNO ₂	c	-11.6	3.76		aq, 440	-78.1	-89.42
	aq	-2.9	9.99	Na ₂ SeO ₄	c	-254	
AgNO ₃	c	-29.4	-7.66		aq, 800	-261.5	-230.30
	aq, 6500	-24.02	-7.81	Na ₂ S	c	-89.8	
Ag ₂ O	c	-6.95	-2.23		aq, 400	-105.17	-101.76
Ag ₂ S	c	-5.5	-7.6	Na ₂ SO ₃	c	-261.2	-240.14
Ag ₂ SO ₄	c	-170.1	-146.8		aq, 800	-264.1	-241.58
	aq	-165.8	-139.22	Na ₂ SO ₄	c	-330.50	-302.38
Sodium				Na ₂ SO ₄ ·10H ₂ O	aq, 1100	-330.82	-301.28
Na	c	0.00	0.00		c	-1033.85	-870.52
Na ₃ AsO ₃	aq, 500	-314.61		Na ₂ WO ₄	c	-391	
Na ₃ AsO ₄	c	-366			aq	-381.5	-345.18
	aq, 500	-381.97	-341.17	Strontium			
NaBr	c	-86.72		Sr	c	0.00	0.00
	aq, 400	-86.33	-87.17	SrBr ₂	c	-171.0	
NaBrO	aq	-78.9			aq, 400	-187.24	-182.36
NaBrO ₃	aq, 400	-68.89	-57.59	Sr(C ₂ H ₃ O ₂) ₂	c	-358.0	
NaC ₂ H ₃ O ₂	c	-170.45			aq	-364.4	-311.80
	aq, 400	-175.450	-152.31	Sr(CN) ₂	aq	-59.5	-54.50
NaCN	c	-22.47		SrCO ₃	c	-290.9	-271.9
	aq, 200	-22.29	-23.24	SrCl ₂	c	-197.84	
NaCNO	c	-96.3			aq, 400	-209.20	-195.86
	aq	-91.7	-86.00	SrF ₂	c	-289.0	
NaCNS	c	-39.94		Sr(HCO ₃) ₂	aq	-459.1	-413.76
	aq, 400	-38.23	-39.24	SrI ₂	c	-136.1	
Na ₂ CO ₃	c	-269.46	-249.55		aq, 400	-156.70	-157.87
	aq, 1000	-275.13	-251.36	Sr ₃ N ₂	c	-91.4	-76.5
NaCO ₂ NH ₂	c	-142.17		Sr(NO ₃) ₂	c	-233.2	
Na ₂ C ₂ O ₄	c	-313.8			aq, 400	-228.73	-185.70
	aq, 600	-309.92	-283.42	SrO	c	-140.8	-133.7
NaCl	c	-98.321	-91.894	SrO·SiO ₂	gls	-364	
	aq, 400	-97.324	-93.92	SrO ₂	c	-153.3	-139.0
NaClO ₃	c	-83.59		Sr ₂ O	c	-153.6	
	aq, 400	-78.42	-62.84		c	-228.7	
NaClO ₄	c	-101.12		Sr(OH) ₂	c	-229.4	
					aq, 800	-239.4	-208.27
				Sr ₃ (PO ₄) ₂	c	-980	
					aq	-985	-881.54
				SrS	c	-113.1	

TABLE 2-178 Heats and Free Energies of Formation of Inorganic Compounds (Continued)

Compound	State†	Heat of formation‡§ ΔH (formation) at 25 °C, kcal/mol	Free energy of formation ¶ ΔF (formation) at 25 °C, kcal/mol	Compound	State†	Heat of formation‡§ ΔH (formation) at 25 °C, kcal/mol	Free energy of formation ¶ ΔF (formation) at 25 °C, kcal/mol
Strontium (Cont.)				Tin			
SrSO ₄	aq	-120.4	-109.78	Sn	c, II, tetragonal	0.00	0.00
	c	-345.3			c, III, "gray," cubic	0.6	1.1
	aq, 400	-345.0	-309.30	SnBr ₂	c	-61.4	
SrWO ₄	c	-393			aq	-60.0	-55.43
Sulfur				SnBr ₄	c	-94.8	
S	c, rhombic	0.00	0.00		aq	-110.6	-97.66
	c, monoclinic	-0.071	0.023	SnCl ₂	c	-83.6	
	l, λ	0.257	0.072		aq	-81.7	-68.94
	l, λμ equilibrium		0.071	SnCl ₄	l	-127.3	-110.4
	g	53.25	43.57		aq	-157.6	-124.67
S ₂	g	31.02	19.36	SnI ₂	c	-38.9	
S ₆	g	27.78	13.97		aq	-33.3	-30.95
S ₈	g	27.090	12.770	SnO	c	-67.7	-60.75
S ₂ Br ₂	l	-4		SnO ₂	c	-138.1	-123.6
SCL ₄	l	-13.7		Sn(OH) ₂	c	-136.2	-115.95
S ₂ Cl ₂	l	-14.2	-5.90	Sn(OH) ₄	c	-268.9	-226.00
S ₂ Cl ₄	l	-24.1		SnS	c	-18.61	
SF ₆	g	-262	-237	Titanium			
SO	g	19.02	12.75	Ti	c	0.00	0.00
SO ₂	g	-70.94	-71.68	TiC	c	-110	-109.2
SO ₃	g	-94.39	-88.59	TiCl ₄	l	-181.4	-165.5
	l	-103.03	-88.28	TiN	c	-80.0	-73.17
	c, α	-105.09	-88.22	TiO ₂	c, III, rutil	-225.0	-211.9
	c, β	-105.92	-88.34		amorphous	-214.1	-201.4
	c, γ	-109.34	-88.98	Tungsten			
SO ₂ Cl ₂	g	-82.04	-74.06	W	c	0.00	0.00
	l	-89.80	-75.06	WO ₂	c	-130.5	-118.3
Tantalum				WO ₃	c	-195.7	-177.3
Ta	c	0.00	0.00	WS ₂	c	-84	
TaN	c	-51.2	-45.11	Uranium			
Ta ₂ O ₅	c	-486.0	-453.7	U	c	0.00	0.00
Tellurium				UC ₂	c	-29	
Te	c	0.00	0.00	UCl ₃	c	-213	
TeBr ₄	c	-49.3		UCl ₄	c	-251	
TeCl ₄	c	-77.4	-57.4	U ₃ N ₄	c	-274	-249.6
TeF ₆	g	-315	-292	UO ₂	c	-256.6	-242.2
TeO ₂	c	-77.56	-64.66	UO ₂ (NO ₃) ₂ ·6H ₂ O	c	-756.8	-617.8
Thallium				UO ₃	c	-291.6	
Tl	c	0.00	0.00	U ₃ O ₈	c	-845.1	
TlBr	c	-41.5	-39.43	Vanadium			
	aq	-28.0	-32.34	V	c	0.00	0.00
TlCl	c	-49.37	-44.46	VCl ₂	c	-147	
	aq	-38.4	-39.09	VCl ₃	l	-187	
TlCl ₃	c	-82.4		VCl ₄	l	-165	
	aq	-91.0	-44.25	VN	c	-41.43	-35.08
TlF	aq	-77.6	-73.46	V ₂ O ₂	c	-195	
TlI	c	-31.1	-31.3	V ₂ O ₃	c	-296	-277
	aq	-12.7	-20.09	V ₂ O ₄	c	-342	-316
TlNO ₃	c	-58.2	-36.32	V ₂ O ₅	c	-373	-342
	aq	-48.4	-34.01	Zinc			
Tl ₂ O	c	-43.18		Zn	c	0.00	0.00
Tl ₂ O ₃	c	-120		ZnSb	c	-3.6	-3.88
TlOH	c	-57.44	-45.54	ZnBr ₂	c	-77.0	-72.9
	aq	-53.9	-45.35		aq, 400	-93.6	
Tl ₂ S	c	-22		Zn(C ₂ H ₃ O ₂) ₂	c	-259.4	
Tl ₂ SO ₄	c	-222.8	-197.79		aq, 400	-269.4	-214.4
	aq, 800	-214.1	-191.62	Zn(CN) ₂	c	17.06	
Thorium				ZnCO ₃	c	-192.9	-173.5
Th	c	0.00	0.00	ZnCl ₂	c	-99.9	-88.8
ThBr ₄	c	-281.5			aq, 400	-115.44	
	aq	-352.0	-295.31	ZnF ₂	aq	-192.9	-166.6
ThC ₂	c	-45.1		ZnI ₂	c	-50.50	-49.93
ThCl ₄	c	-335			aq	-61.6	
	aq	-392	-322.32	Zn(NO ₃) ₂	aq, 400	-134.9	-87.7
ThI ₄	aq	-292.0	-246.33	ZnO	c, hexagonal	-83.36	-76.19
Th ₃ N ₄	c	-309.0	-282.3	ZnO·SiO ₂	c	-282.6	
ThO ₂	c	-291.6	-280.1	Zn(OH) ₂	c, rhombic	-153.66	
Th(OH) ₄	c, "soluble"	-336.1		ZnS	c, wurtzite	-45.3	-44.2
Th(SO ₄) ₂	c	-632		ZnSO ₄	c	-233.4	
	aq	-668.1	-549.2		aq, 400	-252.12	-211.28

2-194 PHYSICAL AND CHEMICAL DATA

TABLE 2-178 Heats and Free Energies of Formation of Inorganic Compounds (Concluded)

Compound	State†	Heat of formation‡§ ΔH (formation) at 25 °C, kcal/mol	Free energy of formation ¶ ΔF (formation) at 25 °C, kcal/mol	Compound	State†	Heat of formation‡§ ΔH (formation) at 25 °C, kcal/mol	Free energy of formation ¶ ΔF (formation) at 25 °C, kcal/mol
Zirconium				Zirconium (Cont.)			
Zr	c	0.00	0.00	ZrO ₂	c, monoclinic	-258.5	-244.6
ZrC	c	-29.8	-34.6	Zr(OH) ₄	c	-411.0	
ZrCl ₄	c	-268.9		ZrO(OH) ₂	c	-337	-307.6
ZrN	c	-82.5	-75.9				

† The physical state is indicated as follows: *c*, crystal (solid); *l*, liquid; *g*, gas; *gls*, glass or solid supercooled liquid; *aq*, in aqueous solution. A number following the symbol *aq* applies only to the values of the heats of formation (not to those of free energies of formation); and indicates the number of moles of water per mole of solute; when no number is given, the solution is understood to be dilute. For the free energy of formation of a substance in aqueous solution, the concentration is always that of the hypothetical solution of unit molality.

‡ The increment in heat content, ΔH , is the reaction of forming the given substance from its elements in their standard states. When ΔH is negative, heat is evolved in the process, and, when positive, heat is absorbed.

§ The heat of solution in water of a given solid, liquid, or gaseous compound is given by the difference in the value for the heat of formation of the given compound in the solid, liquid, or gaseous state and its heat of formation in aqueous solution. The following two examples serve as an illustration of the procedure: (1) For NaCl(*c*) and NaCl(*aq*, 400H₂O), the values of ΔH (formation) are, respectively, -98.321 and -97.324 kcal/mol. Subtraction of the first value from the second gives $\Delta H = 0.998$ kcal/mol for the reaction of dissolving crystalline sodium chloride in 400 mol of water. When this process occurs at a constant pressure of 1 atm, 0.998 kcal of energy are absorbed. (2) For HCl(*g*) and HCl(*aq*, 400H₂O), the values for ΔH (formation) are, respectively, -22.06 and -39.85 kcal/mol. Subtraction of the first from the second gives $\Delta H = -17.79$ kcal/mol for the reaction of dissolving gaseous hydrogen chloride in 400 mol of water. At a constant pressure of 1 atm, 17.79 kcal of energy are evolved in this process.

|| The increment in the free energy, ΔF , is the reaction of forming the given substance in its standard state from its elements in their standard states. The standard states are: for a gas, fugacity (approximately equal to the pressure) of 1 atm; for a pure liquid or solid, the substance at a pressure of 1 atm; for a substance in aqueous solution, the hypothetical solution of unit molality, which has all the properties of the infinitely dilute solution except the property of concentration.

¶ The free energy of solution of a given substance from its normal standard state as a solid, liquid, or gas to the hypothetical one molal state in aqueous solution may be calculated in a manner similar to that described in footnote § for calculating the heat of solution.

TABLE 2-179 Enthalpies and Gibbs Energies of Formation, Entropies, and Net Enthalpies of Combustion of Inorganic and Organic Compounds at 298.15 K

Cmpd. no.	Name	Formula	CAS no.	Mol. wt.	Ideal gas enthalpy of formation, J/kmol × 1E-07	Ideal gas Gibbs energy of formation, J/kmol × 1E-07	Ideal gas entropy, J/(kmol·K) × 1E-05	Standard net enthalpy of combustion, J/kmol × 1E-09
1	Acetaldehyde	C ₂ H ₄ O	75-07-0	44.053	-16.64	-13.33	2.642	-1.1045
2	Acetamide	C ₂ H ₅ NO	60-35-5	59.067	-23.83	-15.96	2.722	-1.0741
3	Acetic acid	C ₂ H ₄ O ₂	64-19-7	60.052	-46.11	-40.3	2.825	-0.7866
4	Acetic anhydride	C ₄ H ₆ O ₃	108-24-7	102.089	-57.25	-47.34	3.899	-1.675
5	Acetone	C ₃ H ₆ O	67-64-1	58.079	-21.57	-15.13	2.954	-1.659
6	Acetonitrile	C ₂ H ₃ N	75-05-8	41.052	7.404	9.1868	2.4329	-1.19043
7	Acetylene	C ₂ H ₂	74-86-2	26.037	22.82	21.068	2.0081	-1.257
8	Acrolein	C ₃ H ₄ O	107-02-8	56.063	-8.18	-5.68	2.97	-1.5468
9	Acrylic acid	C ₃ H ₄ O ₂	79-10-7	72.063	-35.591	-30.6	3.15	-1.32717
10	Acrylonitrile	C ₃ H _{3.5} N	107-13-1	53.063	18.37	19.37	2.753	-1.69
11	Air	Mixture	132259-10-0	28.960	0	0	1.99	0
12	Ammonia	H ₃ N	7664-41-7	17.031	-4.5898	-1.64	1.9266	-0.31683
13	Anisole	C ₇ H ₈ O	100-66-3	108.138	-6.79	2.27	3.61	-3.6072
14	Argon	Ar	7440-37-1	39.948	0	0	1.54737	0
15	Benzamide	C ₇ H ₇ NO	55-21-0	121.137	-10.09	-0.211	3.641	-3.39877
16	Benzene	C ₆ H ₆	71-43-2	78.112	8.288	12.96	2.693	-3.136
17	Benzenethiol	C ₆ H ₆ S	108-98-5	110.177	11.15	14.76	3.369	-3.4474
18	Benzoic acid	C ₇ H ₆ O ₂	65-85-0	122.121	-29.41	-21.42	3.69	-3.0951
19	Benzonitrile	C ₇ H ₅ N	100-47-0	103.121	21.57	25.78	3.21	-3.5238
20	Benzophenone	C ₁₃ H ₁₀ O	119-61-9	182.218	5.68	17.3	4.4	-6.2876
21	Benzyl alcohol	C ₈ H ₈ O	100-51-6	108.138	-9.025	-0.254	3.713	-3.56
22	Benzyl ethyl ether	C ₈ H ₁₀ O	539-30-0	136.191	-11.5	3.37	4.39	-4.83
23	Benzyl mercaptan	C ₇ H ₈ S	100-53-8	124.203	9.33	16.3	3.607	-4.06
24	Biphenyl	C ₁₂ H ₁₀	92-52-4	154.208	17.849	27.63	3.9367	-6.248
25	Bromine	Br ₂	7726-95-6	159.808	3.091	0.314	2.4535	0
26	Bromobenzene	C ₆ H ₅ Br	108-86-1	157.008	10.5018	13.8532	3.24386	-3.01917
27	Bromoethane	C ₂ H ₅ Br	74-96-4	108.965	-6.36	-2.582	2.873	-1.285
28	Bromomethane	CH ₃ Br	74-83-9	94.939	-9.37	-2.819	2.458	-0.70542
29	1,2-Butadiene	C ₄ H ₆	590-19-2	54.090	16.23	19.86	2.93	-2.4617
30	1,3-Butadiene	C ₄ H ₆	106-99-0	54.090	10.924	14.972	2.7859	-2.409
31	Butane	C ₄ H ₁₀	106-97-8	58.122	-12.579	-1.67	3.0991	-2.65732
32	1,2-Butanediol	C ₄ H ₁₀ O ₂	584-03-2	90.121	-44.58	-30.44	4.065	-2.2678
33	1,3-Butanediol	C ₄ H ₁₀ O ₂	107-88-0	90.121	-43.32	-29.18	4.065	-2.2824
34	1-Butanol	C ₄ H ₁₀ O	71-36-3	74.122	-27.51	-15.07	3.618	-2.454
35	2-Butanol	C ₄ H ₁₀ O	78-92-2	74.122	-29.29	-16.7	3.566	-2.446
36	1-Butene	C ₄ H ₈	106-98-9	56.106	-0.05	7.041	3.074	-2.5408
37	<i>cis</i> -2-Butene	C ₄ H ₈	590-18-1	56.106	-0.74	6.536	3.012	-2.5339
38	<i>trans</i> -2-Butene	C ₄ H ₈	624-64-6	56.106	-1.1	6.32	2.965	-2.53
39	Butyl acetate	C ₆ H ₁₂ O ₂	123-86-4	116.158	-48.56	-31.26	4.425	-3.28
40	Butylbenzene	C ₁₀ H ₁₄	104-51-8	134.218	-1.314	14.54	4.3949	-5.5644
41	Butyl mercaptan	C ₄ H ₁₀ S	109-79-5	90.187	-8.78	1.139	3.752	-2.9554
42	<i>sec</i> -Butyl mercaptan	C ₄ H ₁₀ S	513-53-1	90.187	-9.66	0.512	3.667	-2.949
43	1-Butyne	C ₄ H ₆	107-00-6	54.090	16.52	20.225	2.9039	-2.4647
44	Butyraldehyde	C ₄ H ₈ O	123-72-8	72.106	-20.7	-11.63	3.4365	-2.3035
45	Butyric acid	C ₄ H ₈ O ₂	107-92-6	88.105	-47.58	-36	3.601	-2.008
46	Butyronitrile	C ₄ H ₇ N	109-74-0	69.105	3.40578	10.8658	3.25432	-2.4148
47	Carbon dioxide	CO ₂	124-38-9	44.010	-39.351	-39.437	2.13677	0
48	Carbon disulfide	CS ₂	75-15-0	76.141	11.69	6.68	2.379	-1.0769
49	Carbon monoxide	CO	630-08-0	28.010	-11.053	-13.715	1.97556	-0.283
50	Carbon tetrachloride	CCl ₄	56-23-5	153.823	-9.581	-5.354	3.0991	-0.2653
51	Carbon tetrafluoride	CF ₄	75-73-0	88.004	-92.21	-87.76	2.62	0.5286
52	Chlorine	Cl ₂	7782-50-5	70.906	0	0	2.22972	0
53	Chlorobenzene	C ₆ H ₅ Cl	108-90-7	112.557	5.109	9.829	3.1403	-2.976
54	Chloroethane	C ₂ H ₅ Cl	75-00-3	64.514	-11.226	-6.0499	2.7578	-1.2849
55	Chloroform	CHCl ₃	67-66-3	119.378	-10.29	-7.01	2.956	-0.38
56	Chloromethane	CH ₃ Cl	74-87-3	50.488	-8.196	-5.844	2.3418	-0.67538
57	1-Chloropropane	C ₃ H ₇ Cl	540-54-5	78.541	-13.318	-5.261	3.1547	-1.867
58	2-Chloropropane	C ₃ H ₇ Cl	75-29-6	78.541	-14.477	-6.136	3.0594	-1.863

TABLE 2-179 Enthalpies and Gibbs Energies of Formation, Entropies, and Net Enthalpies of Combustion of Inorganic and Organic Compounds at 298.15 K (Continued)

Cmpd. no.	Name	Formula	CAS no.	Mol. wt.	Ideal gas enthalpy of formation, J/kmol × 1E-07	Ideal gas Gibbs energy of formation, J/kmol × 1E-07	Ideal gas entropy, J/(kmol·K) × 1E-05	Standard net enthalpy of combustion, J/kmol × 1E-09
59	<i>m</i> -Cresol	C ₇ H ₈ O	108-39-4	108.138	-13.23	-4.019	3.5604	-3.52783
60	<i>o</i> -Cresol	C ₇ H ₈ O	95-48-7	108.138	-12.857	-3.543	3.5259	-3.528
61	<i>p</i> -Cresol	C ₇ H ₈ O	106-44-5	108.138	-12.535	-3.166	3.5075	-3.52256
62	Cumene	C ₉ H ₁₂	98-82-8	120.192	0.4	13.79	3.86	-4.951
63	Cyanogen	C ₂ N ₂	460-19-5	52.035	30.9072	29.7598	2.14163	-1.0961
64	Cyclobutane	C ₄ H ₈	287-23-0	56.106	2.85	11.22	2.64396	-2.5678
65	Cyclohexane	C ₆ H ₁₂	110-82-7	84.159	-12.33	3.191	2.97276	-3.656
66	Cyclohexanol	C ₆ H ₁₂ O	108-93-0	100.159	-28.62	-10.95	3.277	-3.4639
67	Cyclohexanone	C ₆ H ₁₀ O	108-94-1	98.143	-22.61	-9.028	3.3426	-3.299
68	Cyclohexene	C ₆ H ₁₀	110-83-8	82.144	-0.46	10.77	3.10518	-3.532
69	Cyclopentane	C ₅ H ₁₀	287-92-3	70.133	-7.703	3.885	2.929	-3.0709
70	Cyclopentene	C ₅ H ₈	142-29-0	68.117	3.23	11.05	2.91267	-2.9393
71	Cyclopropane	C ₃ H ₆	75-19-4	42.080	5.33	10.44	2.37378	-1.9593
72	Cyclohexyl mercaptan	C ₆ H ₁₂ S	1569-69-3	116.224	-9.602	4.886	3.646	-3.968
73	Decanal	C ₁₀ H ₂₀ O	112-31-2	156.265	-33.17	-6.739	5.7912	-5.959
74	Decane	C ₁₀ H ₂₂	124-18-5	142.282	-24.946	3.318	5.457	-6.29422
75	Decanoic acid	C ₁₀ H ₂₀ O ₂	334-48-5	172.265	-59.43	-30.5	5.99	-5.72
76	1-Decanol	C ₁₀ H ₂₂ O	112-30-1	158.281	-39.85	-10.02	5.971	-6.116
77	1-Decene	C ₁₀ H ₂₀	872-05-9	140.266	-12.21	12.27	5.433	-6.1809
78	Decyl mercaptan	C ₁₀ H ₂₂ S	143-10-2	174.347	-21.09	6.165	6.116	-6.6161
79	1-Decyne	C ₁₀ H ₁₈	764-93-2	138.250	4.1	25.16	5.263	-6.1037
80	Deuterium	D ₂	7782-39-0	4.032	0	0	1.4486	-0.24625
81	1,1-Dibromoethane	C ₂ H ₄ Br ₂	557-91-5	187.861	-4.08	-1.181	3.276	-1.16
82	1,2-Dibromoethane	C ₂ H ₄ Br ₂	106-93-4	187.861	-3.89	-1.054	3.297	-1.1769
83	Dibromomethane	CH ₂ Br ₂	74-95-3	173.835			2.92964	
84	Dibutyl ether	C ₈ H ₁₈ O	142-96-1	130.228	-33.34	-8.827	5.014	-4.94691
85	<i>m</i> -Dichlorobenzene	C ₆ H ₄ Cl ₂	541-73-1	147.002	2.57	7.79	3.4353	-2.825
86	<i>o</i> -Dichlorobenzene	C ₆ H ₄ Cl ₂	95-50-1	147.002	3.02	8.29	3.4185	-2.826
87	<i>p</i> -Dichlorobenzene	C ₆ H ₄ Cl ₂	106-46-7	147.002	2.25	7.67	3.3674	-2.802
88	1,1-Dichloroethane	C ₂ H ₄ Cl ₂	75-34-3	98.959	-12.941	-7.259	3.0501	-1.1104
89	1,2-Dichloroethane	C ₂ H ₄ Cl ₂	107-06-2	98.959	-12.979	-7.3945	3.0828	-1.105
90	Dichloromethane	CH ₂ Cl ₂	75-09-2	84.933	-9.552	-6.896	2.7018	-0.51388
91	1,1-Dichloropropane	C ₃ H ₆ Cl ₂	78-99-9	112.986	-15.08	-6.52	3.448	-1.72
92	1,2-Dichloropropane	C ₃ H ₆ Cl ₂	78-87-5	112.986	-16.28	-8.018	3.548	-1.707
93	Diethanol amine	C ₄ H ₁₁ NO ₂	111-42-2	105.136	-40.847	-22.574	4.29	-2.4105
94	Diethyl amine	C ₄ H ₁₁ N	109-89-7	73.137	-7.142	7.308	3.522	-2.8003
95	Diethyl ether	C ₄ H ₁₀ O	60-29-7	74.122	-25.21	-12.21	3.423	-2.5035
96	Diethyl sulfide	C ₄ H ₁₀ S	352-93-2	90.187	-8.356	1.774	3.681	-2.9607
97	1,1-Difluoroethane	C ₂ H ₄ F ₂	75-37-6	66.050	-49.7	-43.9485	2.824	-0.773662
98	1,2-Difluoroethane	C ₂ H ₄ F ₂	624-72-6	66.050	-44.77	-39.19	2.88194	-0.823
99	Difluoromethane	CH ₂ F ₂	75-10-5	52.023	-45.23	-42.4747	2.4658	-0.183031
100	Di-isopropyl amine	C ₆ H ₁₅ N	108-18-9	101.190	-14.38	6.42	4.12	-3.99
101	Di-isopropyl ether	C ₆ H ₁₄ O	108-20-3	102.175	-31.92	-12.48	3.989	-3.70261
102	Di-isopropyl ketone	C ₇ H ₁₄ O	565-80-0	114.185	-31.14	-12.37	4.27	-4.095
103	1,1-Dimethoxyethane	C ₄ H ₁₀ O ₂	534-15-6	90.121	-38.97	-23.8	3.726	-2.394
104	1,2-Dimethoxypropane	C ₅ H ₁₂ O ₂	7778-85-0	104.148	-38.42	-20.11	4.038	-2.996
105	Dimethyl acetylene	C ₄ H ₆	503-17-3	54.090	14.57	18.49	2.833	-2.4189
106	Dimethyl amine	C ₂ H ₇ N	124-40-3	45.084	-1.845	6.839	2.7296	-1.6146
107	2,3-Dimethylbutane	C ₆ H ₁₄	79-29-8	86.175	-17.68	-0.3125	3.6592	-3.84761
108	1,1-Dimethylcyclohexane	C ₈ H ₁₆	590-66-9	112.213	-18.1	3.52293	3.65012	-4.8639
109	<i>cis</i> -1,2-Dimethylcyclohexane	C ₈ H ₁₆	2207-01-4	112.213	-17.2172	4.12124	3.7451	-4.87084
110	<i>trans</i> -1,2-Dimethylcyclohexane	C ₈ H ₁₆	6876-23-9	112.213	-17.9996	3.44761	3.70912	-4.86436
111	Dimethyl disulfide	C ₂ H ₆ S ₂	624-92-0	94.199	-2.42	1.516	3.35291	-2.0441
112	Dimethyl ether	C ₂ H ₆ O	115-10-6	46.068	-18.41	-11.28	2.667	-1.3284
113	<i>N,N</i> -Dimethyl formamide	C ₃ H ₇ NO	68-12-2	73.094	-19.17	-8.84	3.26	-1.78871
114	2,3-Dimethylpentane	C ₇ H ₁₆	565-59-3	100.202	-19.41	0.5717	4.1455	-4.46075
115	Dimethyl phthalate	C ₁₀ H ₁₀ O ₄	131-11-3	194.184	-60.5	-46.7749	6.6	-4.4662
116	Dimethylsilane	C ₂ H ₆ Si	1111-74-6	60.170	-9.47	-1.925	2.9953	-2.569

117	Dimethyl sulfide	C ₂ H ₆ S	75-18-3	62.134	-3.724	0.7302	2.8585	-1.7443
118	Dimethyl sulfoxide	C ₂ H ₆ OS	67-68-5	78.133	-15.046	-8.1441	3.0627	-1.6054
119	Dimethyl terephthalate	C ₁₀ H ₁₀ O ₄	120-61-6	194.184	-64.4	-47.4	5.5	-4.4115
120	1,4-Dioxane	C ₄ H ₈ O ₂	123-91-1	88.105	-31.58	-18.16	3.0012	-2.1863
121	Diphenyl ether	C ₁₂ H ₁₀ O	101-84-8	170.207	5.2	4.13	4.13	-5.8939
122	Dipropyl amine	C ₆ H ₁₅ N	142-84-7	101.190	-11.6	8.68	4.29	-4.0189
123	Dodecane	C ₁₂ H ₂₆	112-40-3	170.335	-29.072	4.981	6.2415	-7.51368
124	Eicosane	C ₂₀ H ₄₂	112-95-8	282.547	-45.646	11.57	9.3787	-12.3908
125	Ethane	C ₂ H ₆	74-84-0	30.069	-8.382	-3.192	2.2912	-1.42864
126	Ethanol	C ₂ H ₆ O	64-17-5	46.068	-23.495	-16.785	2.8064	-1.235
127	Ethyl acetate	C ₄ H ₈ O ₂	141-78-6	88.105	-44.45	-32.8	3.597	-2.061
128	Ethyl amine	C ₂ H ₇ N	75-04-7	45.084	-4.715	3.616	2.848	-1.5874
129	Ethylbenzene	C ₈ H ₁₀	100-41-4	106.165	2.992	13.073	3.6063	-4.3448
130	Ethyl benzoate	C ₉ H ₁₀ O ₂	93-89-0	150.175	-32.6	-19.05	4.55	-4.41
131	2-Ethyl butanoic acid	C ₆ H ₁₂ O ₂	88-09-5	116.158	-53.78	-35.9	4.23	-3.21203
132	Ethyl butyrate	C ₆ H ₁₂ O ₂	105-54-4	116.158	-48.55	-31.22	4.417	-3.284
133	Ethylcyclohexane	C ₈ H ₁₆	1678-91-7	112.213	-17.15	3.955	3.826	-4.87051
134	Ethylcyclopentane	C ₇ H ₁₄	1640-89-7	98.186	-12.69	4.48	3.783	-4.2839
135	Ethylene	C ₂ H ₄	74-85-1	28.053	5.251	6.844	2.192	-1.323
136	Ethylenediamine	C ₂ H ₈ N ₂	107-15-3	60.098	-1.73	10.3	3.21833	-1.691
137	Ethylene glycol	C ₂ H ₆ O ₂	107-21-1	62.068	-39.22	-30.18	3.04891	-1.0527
138	Ethyleneimine	C ₂ H ₅ N	151-56-4	43.068	12.3428	17.7987	2.5062	-1.481
139	Ethylene oxide	C ₂ H ₄ O	75-21-8	44.053	-5.263	-1.323	2.4299	-1.218
140	Ethyl formate	C ₃ H ₆ O ₂	109-94-4	74.079	-38.83	3.282	3.282	-1.50696
141	2-Ethyl hexanoic acid	C ₈ H ₁₆ O ₂	149-57-5	144.211	-55.95	-32.5	5.1	-4.448
142	Ethylhexyl ether	C ₈ H ₁₈ O	5756-43-4	130.228	-33.37	-9.042	5.076	-4.943
143	Ethylisopropyl ether	C ₅ H ₁₂ O	625-54-7	88.148	-28.58	-12.64	3.8	-3.103
144	Ethylisopropyl ketone	C ₆ H ₁₂ O	565-69-5	100.159	-28.61	-13.3	4.069	-3.4863
145	Ethyl mercaptan	C ₂ H ₆ S	75-08-1	62.134	-4.63	-0.4814	2.961	-1.7366
146	Ethyl propionate	C ₅ H ₁₀ O ₂	105-37-3	102.132	-46.36	-31.93	4.025	-2.674
147	Ethylpropyl ether	C ₅ H ₁₂ O	628-32-0	88.148	-27.22	-11.52	3.881	-3.12
148	Ethyltrichlorosilane	C ₂ H ₅ Cl ₃ Si	115-21-9	163.506	-59.54	-51.01	4.07	-1.671
149	Fluorine	F ₂	7782-41-4	37.997	0	0	2.02682	
150	Fluorobenzene	C ₆ H ₅ F	462-06-6	96.102	-11.6566	-6.9036	3.02629	-2.81451
151	Fluoroethane	C ₂ H ₅ F	353-36-6	48.060	-26.44	-21.23	2.644	-1.127
152	Fluoromethane	CH ₃ F	593-53-3	34.033	-23.43	-21.04	2.22734	-0.5219
153	Formaldehyde	CH ₂ O	50-00-0	30.026	-10.86	-10.26	2.1866	-0.5268
154	Formamide	CH ₃ NO	75-12-7	45.041	-19.22	-14.71	2.4857	-0.5021
155	Formic acid	CH ₂ O ₂	64-18-6	46.026	-40.55	-37.78	2.487	-0.2115
156	Furan	C ₄ H ₄ O	110-00-9	68.074	-3.48	0.08225	2.6714	-1.9959
157	Helium-4	He	7440-59-7	4.003	0	0	1.26044	0
158	Heptadecane	C ₁₇ H ₃₆	629-78-7	240.468	-39.445	9.083	8.2023	-10.5618
159	Heptanal	C ₇ H ₁₄ O	111-71-7	114.185	-26.94	-9.191	4.6138	-4.136
160	Heptane	C ₇ H ₁₆	142-82-5	100.202	-18.765	0.8165	4.2798	-4.46473
161	Heptanoic acid	C ₇ H ₁₄ O ₂	111-14-8	130.185	-53.62	-33.4	4.8	-3.839
162	1-Heptanol	C ₇ H ₁₆ O	111-70-6	116.201	-33.68	-12.55	4.795	-4.285
163	2-Heptanol	C ₇ H ₁₆ O	543-49-7	116.201	-35.54	-14.25	4.74	-4.282
164	3-Heptanone	C ₇ H ₁₄ O	106-35-4	114.185	-30.1	-12.25	4.58	-4.098
165	2-Heptanone	C ₇ H ₁₄ O	110-43-0	114.185	-30.0453	-11.96	4.486	-4.09952
166	1-Heptene	C ₇ H ₁₄	592-76-7	98.186	-6.289	9.482	4.252	-4.3499
167	Heptyl mercaptan	C ₇ H ₁₆ S	1639-09-4	132.267	-14.95	3.622	4.939	-4.7865
168	1-Heptyne	C ₇ H ₁₂	628-71-7	96.170	10.3	22.7	4.085	-4.2717
169	Hexadecane	C ₁₆ H ₃₄	544-76-3	226.441	-37.417	8.216	7.8102	-9.95145
170	Hexanal	C ₆ H ₁₂ O	66-25-1	100.159	-24.86	-10.005	4.2214	-3.52
171	Hexane	C ₆ H ₁₄	110-54-3	86.175	-16.694	-0.006634	3.8874	-3.8551
172	Hexanoic acid	C ₆ H ₁₂ O ₂	142-62-1	116.158	-51.19	-33.8	4.41	-3.23
173	1-Hexanol	C ₆ H ₁₄ O	111-27-3	102.175	-31.62	-13.39	4.402	-3.675
174	2-Hexanol	C ₆ H ₁₄ O	626-93-7	102.175	-33.46	-15.06	4.349	-3.67
175	2-Hexanone	C ₆ H ₁₂ O	591-78-6	100.159	-27.9826	-13.0081	4.17856	-3.49
176	3-Hexanone	C ₆ H ₁₂ O	589-38-8	100.159	-27.76	-12.6	4.092	-3.492
177	1-Hexene	C ₆ H ₁₂	592-41-6	84.159	-4.167	8.7	3.863	-3.7397
178	3-Hexyne	C ₆ H ₁₀	928-49-4	82.144	10.6	19.9	3.76	-3.64
179	Hexyl mercaptan	C ₆ H ₁₄ S	111-31-9	118.240	-12.92	2.759	4.546	-4.1762

TABLE 2-179 Enthalpies and Gibbs Energies of Formation, Entropies, and Net Enthalpies of Combustion of Inorganic and Organic Compounds at 298.15 K (Continued)

Cmpd. no.	Name	Formula	CAS no.	Mol. wt.	Ideal gas enthalpy of formation, J/kmol × 1E-07	Ideal gas Gibbs energy of formation, J/kmol × 1E-07	Ideal gas entropy, J/(kmol·K) × 1E-05	Standard net enthalpy of combustion, J/kmol × 1E-09
180	1-Hexyne	C ₆ H ₁₀	693-02-7	82.144	12.37	21.85	3.694	-3.661
181	2-Hexyne	C ₆ H ₁₀	764-35-2	82.144	10.5	19.9	3.72	-3.64
182	Hydrazine	H ₄ N ₂	302-01-2	32.045	9.5353	15.917	2.3861	-0.5342
183	Hydrogen	H ₂	1333-74-0	2.016	0	0	1.30571	-0.24182
184	Hydrogen bromide	HBr	10035-10-6	80.912	-3.629	-5.334	1.98591	-0.06904
185	Hydrogen chloride	HCl	7647-01-0	36.461	-9.231	-9.53	1.86786	-0.0286
186	Hydrogen cyanide	CHN	74-90-8	27.025	13.5143	12.4725	2.01719	-0.62329
187	Hydrogen fluoride	HF	7664-39-3	20.006	-27.33	-27.54	1.7367	0.1524
188	Hydrogen sulfide	H ₂ S	7783-06-4	34.081	-2.063	-3.344	2.056	-0.518
189	Isobutyric acid	C ₄ H ₈ O ₂	79-31-2	88.105	-48.41	-36.21	3.412	-2.0004
190	Isopropyl amine	C ₃ H ₉ N	75-31-0	59.110	-8.38	3.192	3.124	-2.1566
191	Malonic acid	C ₃ H ₄ O ₄	141-82-2	104.061	-76.68	-67	3.7	-0.7732
192	Methacrylic acid	C ₄ H ₆ O ₂	79-41-4	86.089	-36.8	-28.8	3.5	-1.93
193	Methane	CH ₄	74-82-8	16.042	-7.452	-5.049	1.8627	-0.80262
194	Methanol	CH ₄ O	67-56-1	32.042	-20.094	-16.232	2.3988	-0.6382
195	N-Methyl acetamide	C ₃ H ₇ NO	79-16-3	73.094	-24	-13.5	3.2	-1.71
196	Methyl acetate	C ₃ H ₆ O ₂	79-20-9	74.079	-41.19	-32.42	3.198	-1.461
197	Methyl acetylene	C ₃ H ₄	74-99-7	40.064	18.49	19.384	2.4836	-1.8487
198	Methyl acrylate	C ₄ H ₆ O ₂	96-33-3	86.089	-33.3	-25.7	3.66	-1.9303
199	Methyl amine	CH ₅ N	74-89-5	31.057	-2.297	3.207	2.433	-0.97508
200	Methyl benzoate	C ₈ H ₈ O ₂	93-58-3	136.148	-28.79	-18.1	4.14	-3.772
201	3-Methyl-1,2-butadiene	C ₅ H ₈	598-25-4	68.117	12.908	19.75	3.2151	-3.032
202	2-Methylbutane	C ₅ H ₁₂	78-78-4	72.149	-15.37	-1.405	3.4374	-3.23954
203	2-Methylbutanoic acid	C ₅ H ₁₀ O ₂	116-53-0	102.132	-49.8	-34.99	3.9	-2.622
204	3-Methyl-1-butanol	C ₅ H ₁₂ O	123-51-3	88.148	-30.3	-14.1	3.869	-3.062
205	2-Methyl-1-butene	C ₅ H ₁₀	563-46-2	70.133	-3.53	6.668	3.395	-3.1159
206	2-Methyl-2-butene	C ₅ H ₁₀	513-35-9	70.133	-4.18	6.045	3.386	-3.1088
207	2-Methyl-1-butene-3-yne	C ₅ H ₈	78-80-8	66.101	26	30.25	2.78	-2.93
208	Methylbutyl ether	C ₅ H ₁₂ O	628-28-4	88.148	-25.81	-10.17	3.901	-3.12818
209	Methylbutyl sulfide	C ₅ H ₁₂ S	628-29-5	104.214	-10.2	2.691	4.118	-3.5723
210	3-Methyl-1-butyne	C ₅ H ₈	598-23-2	68.117	13.8	20.72	3.189	-3.046
211	Methyl butyrate	C ₅ H ₁₀ O ₂	623-42-7	102.132	-45.07	-30.53	3.988	-2.686
212	Methylchlorosilane	CH ₃ ClSi	993-00-0	80.589	-21.5	-16.61	2.98277	-1.693
213	Methylcyclohexane	C ₇ H ₁₄	108-87-2	98.186	-15.48	2.733	3.433	-4.25714
214	1-Methylcyclohexanol	C ₇ H ₁₄ O	590-67-0	114.185	-33.2	-12.9	3.75	-4.058
215	cis-2-Methylcyclohexanol	C ₇ H ₁₄ O	7443-70-1	114.185	-32.7	-12.68	3.853	-4.0574
216	trans-2-Methylcyclohexanol	C ₇ H ₁₄ O	7443-52-9	114.185	-35.26	-15.24	3.853	-4.0318
217	Methylcyclopentane	C ₆ H ₁₂	96-37-7	84.159	-10.62	3.63	3.399	-3.6741
218	1-Methylcyclopentene	C ₆ H ₁₀	693-89-0	82.144	-0.38	10.38	3.264	-3.534
219	3-Methylcyclopentene	C ₆ H ₁₀	1120-62-3	82.144	0.74	11.38	3.305	-3.5464
220	Methyldichlorosilane	CH ₂ Cl ₂ Si	75-54-7	115.034	-40.2	-34.83	3.287	-1.357
221	Methylethyl ether	C ₃ H ₈ O	540-67-0	60.095	-21.64	-11.71	3.0881	-1.9314
222	Methylethyl ketone	C ₄ H ₈ O	78-93-3	72.106	-23.9	-14.7	3.394	-2.268
223	Methylethyl sulfide	C ₃ H ₈ S	624-89-5	76.161	-5.96	1.147	3.332	-2.354
224	Methyl formate	C ₂ H ₄ O ₂	107-31-3	60.052	-35.24	-29.5	2.852	-0.8924
225	Methylisobutyl ether	C ₅ H ₁₂ O	625-44-5	88.148	-26.6	-10.7	3.81	-3.122
226	Methylisobutyl ketone	C ₆ H ₁₂ O	108-10-1	100.159	-28.64	-13.51	4.129	-3.4762
227	Methyl Isocyanate	C ₂ H ₃ NO	624-83-9	57.051	-6.24	0.0244	1.955	-1.06
228	Methylisopropyl ether	C ₄ H ₁₀ O	598-53-8	74.122	-25.2	-12.18	3.416	-2.5311
229	Methylisopropyl ketone	C ₅ H ₁₀ O	563-80-4	86.132	-26.26	-13.93	3.699	-2.877
230	Methylisopropyl sulfide	C ₄ H ₁₀ S	1551-21-9	90.187	-8.96	1.4509	3.59	-2.957
231	Methyl mercaptan	CH ₄ S	74-93-1	48.107	-2.29	-0.98	2.55	-1.1517
232	Methyl methacrylate	C ₅ H ₈ O ₂	80-62-6	100.116	-36	-25.4	4.01	-2.54
233	2-Methyloctanoic acid	C ₉ H ₁₈ O ₂	3004-93-1	158.238	-57.95	-31.8	5.533	-5.056
234	2-Methylpentane	C ₆ H ₁₄	107-83-5	86.175	-17.455	-0.5338	3.8089	-3.84915
235	Methyl pentyl ether	C ₆ H ₁₄ O	628-80-8	102.175	-27.8	-9.35	4.32	-3.739
236	2-Methylpropane	C ₄ H ₁₀	75-28-5	58.122	-13.499	-2.144	2.955	-2.64895
237	2-Methyl-2-propanol	C ₄ H ₁₀ O	75-65-0	74.122	-31.24	-17.76	3.263	-2.4239

238	2-Methyl propene	C ₄ H ₈	115-11-7	56.106	-1.71	5.808	2.9309	-2.5242
239	Methyl propionate	C ₄ H ₈ O ₂	554-12-1	88.105	-42.75	-31.1	3.596	-2.078
240	Methylpropyl ether	C ₄ H ₁₀ O	557-17-5	74.122	-23.82	-11.1	3.52	-2.51739
241	Methylpropyl sulfide	C ₄ H ₁₀ S	3877-15-4	90.187	-8.23	1.793	3.717	-2.962
242	Methylsilane	CH ₃ Si	992-94-9	46.144	-2.91	1.853	2.565	-1.999
243	alpha-Methyl styrene	C ₉ H ₁₀	98-83-9	118.176	11.83	21.73	3.725	-4.8214
244	Methyl <i>tert</i> -butyl ether	C ₅ H ₁₂ O	1634-04-4	88.148	-28.32	-11.7	3.578	-3.105
245	Methyl vinyl ether	C ₃ H ₆ O	107-25-5	58.079	-10.8	-4.73	3.08	-1.77431
246	Naphthalene	C ₁₀ H ₈	91-20-3	128.171	15.058	22.408	3.3315	-4.9809
247	Neon	Ne	7440-01-9	20.180	0	0	1.46219	0
248	Nitroethane	C ₂ H ₅ NO ₂	79-24-3	75.067	-10.21	-0.6125	3.168	-1.25
249	Nitrogen	N ₂	7727-37-9	28.013	0	0	1.915	
250	Nitrogen trifluoride	F ₃ N	7783-54-2	71.002	-13.2089	-9.06	2.6062	
251	Nitromethane	CH ₃ NO ₂	75-52-5	61.040	-7.47	-0.6934	2.751	-0.6432
252	Nitrous oxide	N ₂ O	10024-97-2	44.013	8.205	10.416	2.1985	-0.0820482
253	Nitric oxide	NO	10102-43-9	30.006	30.006	9.025	2.106	-0.0902489
254	Nonadecane	C ₁₉ H ₄₀	629-92-5	268.521	-43.579	10.74	8.9866	-11.7812
255	Nonanal	C ₉ H ₁₈ O	124-19-6	142.239	-31.09	-7.553	5.3988	-5.35
256	Nonane	C ₉ H ₂₀	111-84-2	128.255	-22.874	2.498	5.064	-5.68455
257	Nonanoic acid	C ₉ H ₁₈ O ₂	112-05-0	158.238	-57.73	-31.7	5.59	-5.061
258	1-Nonanol	C ₉ H ₂₀ O	143-08-8	144.255	-37.79	-10.86	5.579	-5.506
259	2-Nonanol	C ₉ H ₂₀ O	628-99-9	144.255	-39.71	-12.61	5.523	-5.506
260	1-Nonene	C ₉ H ₁₈	124-11-8	126.239	-10.35	11.23	5.041	-5.5716
261	Nonyl mercaptan	C ₉ H ₂₀ S	1455-21-6	160.320	-19.08	5.28	5.724	-6.006
262	1-Nonyne	C ₉ H ₁₆	3452-09-3	124.223	6.17	24.34	4.8699	-5.493
263	Octadecane	C ₁₈ H ₃₈	593-45-3	254.494	-41.512	9.91	8.5945	-11.1715
264	Octanal	C ₈ H ₁₆ O	124-13-0	128.212	-29.02	-8.377	5.0063	-4.74
265	Octane	C ₈ H ₁₈	111-65-9	114.229	-20.875	1.6	4.6723	-5.07415
266	Octanoic acid	C ₈ H ₁₆ O ₂	124-07-2	144.211	-55.6	-32.5	5.2	-4.448
267	1-Octanol	C ₈ H ₁₈ O	111-87-5	130.228	-35.73	-11.7	5.187	-4.895
268	2-Octanol	C ₈ H ₁₈ O	123-96-6	130.228	-37.62	-13.43	5.132	-4.894
269	2-Octanone	C ₈ H ₁₆ O	111-13-7	128.212	-32.16	-11.38	4.962	-4.6984
270	3-Octanone	C ₈ H ₁₆ O	106-68-3	128.212	-33.9	-12.81	4.879	-4.711
271	1-Octene	C ₈ H ₁₆	111-66-0	112.213	-8.194	10.57	4.637	-4.961
272	Octyl mercaptan	C ₈ H ₁₈ S	111-88-6	146.294	-17.01	4.457	5.331	-5.3962
273	1-Octyne	C ₈ H ₁₄	629-05-0	110.197	8.23	23.5	4.478	-4.88145
274	Oxalic acid	C ₂ H ₂ O ₄	144-62-7	90.035	-72.37	-66.14	3.433	-0.1989
275	Oxygen	O ₂	7782-44-7	31.999	0	0	2.05043	0
276	Ozone	O ₃	10028-15-6	47.998	14.2671	16.3164	2.38823	-0.142671
277	Pentadecane	C ₁₅ H ₃₂	629-62-9	212.415	-35.311	7.426	7.4181	-9.34237
278	Pentanal	C ₅ H ₁₀ O	110-62-3	86.132	-22.78	-10.71	3.8289	-2.91
279	Pentane	C ₅ H ₁₂	109-66-0	72.149	-14.676	-0.8813	3.4945	-3.24494
280	Pentanoic acid	C ₅ H ₁₀ O ₂	109-52-4	102.132	-49.13	-34.7	4.02	-2.617
281	1-Pentanol	C ₅ H ₁₂ O	71-41-0	88.148	-29.57	-14.23	4.01	-3.064
282	2-Pentanol	C ₅ H ₁₂ O	6032-29-7	88.148	-31.37	-15.88	3.958	-3.058
283	2-Pentanone	C ₅ H ₁₀ O	107-87-9	86.132	-25.92	-13.83	3.786	-2.87956
284	3-Pentanone	C ₅ H ₁₀ O	96-22-0	86.132	-25.79	-13.44	3.7	-2.8804
285	1-Pentene	C ₅ H ₁₀	109-67-1	70.133	-2.162	7.837	3.462	-3.13037
286	2-Pentyl mercaptan	C ₅ H ₁₂ S	2084-19-7	104.214	-11.3	1.814	4.05	-3.564
287	Pentyl mercaptan	C ₅ H ₁₂ S	110-66-7	104.214	-10.84	1.94408	4.154	-3.5641
288	1-Pentyne	C ₅ H ₈	627-19-0	68.117	14.44	21.03	3.298	-3.051
289	2-Pentyne	C ₅ H ₈	627-21-4	68.117	12.89	19.45	3.3084	-3.0291
290	Phenanthrene	C ₁₄ H ₁₀	85-01-8	178.229	20.12	30.219	3.945	-6.8282
291	Phenol	C ₆ H ₆ O	108-95-2	94.111	-9.6399	-3.2637	3.1481	-2.921
292	Phenyl isocyanate	C ₇ H ₅ NO	103-71-9	119.121	-1.454	4.87212	3.527	-3.298
293	Phthalic anhydride	C ₈ H ₄ O ₃	85-44-9	148.116	-37.14	-30.7001	3.995	-3.1715
294	Propadiene	C ₃ H ₄	463-49-0	40.064	19.05	20.08	2.439	-1.8563
295	Propane	C ₃ H ₈	74-98-6	44.096	-10.468	-2.439	2.702	-2.04311
296	1-Propanol	C ₃ H ₈ O	71-23-8	60.095	-25.46	-15.99	3.226	-1.844
297	2-Propanol	C ₃ H ₈ O	67-63-0	60.095	-27.21	-17.52	3.175	-1.834
298	Propenylcyclohexene	C ₉ H ₁₄	13511-13-2	122.207	4.677	20.85	4.233	-5.232
299	Propionaldehyde	C ₃ H ₆ O	123-38-6	58.079	-18.63	-12.46	3.044	-1.6857
300	Propionic acid	C ₃ H ₆ O ₂	79-09-4	74.079	-47.99	-38.5	2.949	-1.395

TABLE 2-179 Enthalpies and Gibbs Energies of Formation, Entropies, and Net Enthalpies of Combustion of Inorganic and Organic Compounds at 298.15 K (Concluded)

Cmpd. no.	Name	Formula	CAS no.	Mol. wt.	Ideal gas enthalpy of formation, J/kmol × 1E-07	Ideal gas Gibbs energy of formation, J/kmol × 1E-07	Ideal gas entropy, J/(kmol·K) × 1E-05	Standard net enthalpy of combustion, J/kmol × 1E-09
301	Propionitrile	C ₃ H ₅ N	107-12-0	55.079	5.18	9.74949	2.8614	-1.8007
302	Propyl acetate	C ₅ H ₁₀ O ₂	109-60-4	102.132	-46.48	-32.04	4.023	-2.672
303	Propyl amine	C ₃ H ₇ N	107-10-8	59.110	-7.05	4.17	3.242	-2.165
304	Propylbenzene	C ₉ H ₁₂	103-65-1	120.192	0.79	13.76	4.0014	-4.95415
305	Propylene	C ₃ H ₆	115-07-1	42.080	2.023	6.264	2.67	-1.9262
306	Propyl formate	C ₄ H ₈ O ₂	110-74-7	88.105	-40.76	-29.36	3.678	-2.041
307	2-Propyl mercaptan	C ₃ H ₆ S	75-33-2	76.161	-7.59	-0.218	3.243	-2.3398
308	Propyl mercaptan	C ₃ H ₈ S	107-03-9	76.161	-6.75	0.2583	3.365	-2.3458
309	1,2-Propylene glycol	C ₃ H ₈ O ₂	57-55-6	76.094	-42.15	-30.4	3.52	-1.6476
310	Quinone	C ₆ H ₄ O ₂	106-51-4	108.095	-12.29	-6.92	3.205	-2.658
311	Silicon tetrafluoride	F ₄ Si	7783-61-1	104.079	-161.494	-157.27	2.82651	0.7055
312	Styrene	C ₈ H ₈	100-42-5	104.149	14.74	21.39	3.451	-4.219
313	Succinic acid	C ₄ H ₆ O ₄	110-15-6	118.088	-82.29	-69.73	4.034	-1.3591
314	Sulfur dioxide	O ₂ S	7446-09-5	64.064	-29.684	-30.012	2.481	
315	Sulfur hexafluoride	F ₆ S	2551-62-4	146.055	-122.047	-111.653	2.91625	0.924
316	Sulfur trioxide	O ₃ S	7446-11-9	80.063	-39.572	-37.095	2.5651	0.1422
317	Terephthalic acid	C ₈ H ₆ O ₄	100-21-0	166.131	-71.79	-59.9	4.48	-3.0576
318	<i>o</i> -Terphenyl	C ₁₈ H ₁₄	84-15-1	230.304	27.66	42.3	5.263	-9.053
319	Tetradecane	C ₁₄ H ₃₀	629-59-4	198.388	-33.244	6.599	7.0259	-8.73282
320	Tetrahydrofuran	C ₄ H ₈ O	109-99-9	72.106	-18.418	-7.969	2.9729	-2.325
321	1,2,3,4-Tetrahydronaphthalene	C ₁₀ H ₁₂	119-64-2	132.202	2.661	16.71	3.6964	-5.3575
322	Tetrahydrothiophene	C ₄ H ₈ S	110-01-0	88.171	-3.376	4.59	3.1	-2.76549
323	2,2,3,3-Tetramethylbutane	C ₈ H ₁₈	594-82-1	114.229	-22.56	2.239	3.893	-5.0639
324	Thiophene	C ₄ H ₄ S	110-02-1	84.140	11.544	12.67	2.784	-2.4352
325	Toluene	C ₇ H ₈	108-88-3	92.138	9.017	12.22	3.2099	-3.734
326	1,1,2-Trichloroethane	C ₂ H ₂ Cl ₃	79-00-5	133.404	-14.2	-8.097	3.371	-0.9685
327	Tridecane	C ₁₃ H ₂₈	629-50-5	184.361	-31.177	5.771	6.6337	-8.1229
328	Triethyl amine	C ₆ H ₁₅ N	121-44-8	101.190	-9.58	11.41	4.054	-4.0405
329	Trimethyl amine	C ₃ H ₉ N	75-50-3	59.110	-2.431	9.899	2.87	-2.2449
330	1,2,3-Trimethylbenzene	C ₉ H ₁₂	526-73-8	120.192	-0.95	12.61	3.805	-4.934
331	1,2,4-Trimethylbenzene	C ₉ H ₁₂	95-63-6	120.192	-1.38	11.71	3.961	-4.9307
332	2,2,4-Trimethylpentane	C ₈ H ₁₈	540-84-1	114.229	-22.401	1.394	4.2296	-5.06528
333	2,3,3-Trimethylpentane	C ₈ H ₁₈	560-21-4	114.229	-21.845	1.828	4.2702	-5.06876
334	1,3,5-Trinitrobenzene	C ₆ H ₃ N ₃ O ₆	99-35-4	213.105	6.24	26.79	4.435	-2.6867
335	2,4,6-Trinitrotoluene	C ₇ H ₅ N ₃ O ₆	118-96-7	227.131	4.34	28.44	4.607	-3.2959
336	Undecane	C ₁₁ H ₂₄	1120-21-4	156.308	-27.043	4.116	5.8493	-6.9036
337	1-Undecanol	C ₁₁ H ₂₄ O	112-42-5	172.308	-41.9	-9.177	6.363	-6.726
338	Vinyl acetate	C ₄ H ₆ O ₂	108-05-4	86.089	-31.49	-22.79	3.28	-1.95
339	Vinyl acetylene	C ₄ H ₄	689-97-4	52.075	30.46	30.6	2.794	-2.362
340	Vinyl chloride	C ₂ H ₃ Cl	75-01-4	62.498	2.845	4.195	2.7354	-1.178
341	Vinyl trichlorosilane	C ₂ H ₃ Cl ₃ Si	75-94-5	161.490	-48.116	-42.5514	3.73966	-1.544
342	Water	H ₂ O	7732-18-5	18.015	-24.1814	-22.859	1.88724	
343	<i>m</i> -Xylene	C ₈ H ₁₀	108-38-3	106.165	1.732	11.876	3.5854	-4.3318
344	<i>o</i> -Xylene	C ₈ H ₁₀	95-47-6	106.165	1.908	12.2	3.5383	-4.333
345	<i>p</i> -Xylene	C ₈ H ₁₀	106-42-3	106.165	1.803	12.14	3.52165	-4.333

The compounds are considered to be formed from the elements in their standard states at 298.15 K and 101,325 Pa. These include C (graphite) and S (rhombic). Enthalpy of combustion is the net value for the compound in its standard state at 298.15 K and 101,325 Pa. Products of combustion are taken to be CO₂ (gas), H₂O (gas), Cl₂ (gas), Br₂ (gas), I₂ (gas), SO₂ (gas), N₂ (gas), P₄O₁₀ (crystalline), SiO₂ (cristobalite), and Al₂O₃ (crystal, alpha).

Values in this table were taken from the Design Institute for Physical Properties (DIPPR) of the American Institute of Chemical Engineers (AIChE), copyright 2007 AIChE and reproduced with permission of AIChE and of the DIPPR Evaluated Process Design Data Project Steering Committee. Their source should be cited as R. L. Rowley, W. V. Wilding, J. L. Oscarson, Y. Yang, N. A. Zundel, T. E. Daubert, R. P. Daner, DIPPR® Data Compilation of Pure Chemical Properties, Design Institute for Physical Properties, AIChE, New York (2007).

TABLE 2-180 Ideal Gas Sensible Enthalpies, $h_T - h_{298}$ (kJ/kmol), of Combustion Products

Temperature, K	CO	CO ₂	H	OH	H ₂	N	NO	NO ₂	N ₂	N ₂ O	O	O ₂	SO ₂	H ₂ O
200	-2858	-3414	-2040	-2976	-2774	-2040	-2951	-3495	-2857	-3553	-2186	-2868	-3736	-3282
240	-1692	-2079	-1209	-1756	-1656	-1209	-1743	-2104	-1692	-2164	-1285	-1703	-2258	-1948
260	-1110	-1383	-793	-1150	-1091	-793	-1142	-1392	-1110	-1438	-840	-1118	-1496	-1279
280	-529	-665	-377	-546	-522	-378	-543	-672	-528	-692	-398	-533	-718	-609
298.15	0	0	0	0	0	0	0	0	0	0	0	0	0	0
300	54	69	38	55	53	38	55	68	54	72	41	54	74	62
320	638	823	454	654	630	454	652	816	636	854	478	643	881	735
340	1221	1594	870	1251	1209	870	1248	1571	1219	1654	913	1234	1702	1410
360	1805	2382	1285	1847	1791	1286	1845	2347	1802	2470	1346	1828	2538	2088
380	2389	3184	1701	2442	2373	1701	2442	3130	2386	3302	1777	2425	3387	2769
400	2975	4003	2117	3035	2959	2117	3040	3927	2971	4149	2207	3025	4250	3452
420	3563	4835	2532	3627	3544	2533	3638	4735	3557	5010	2635	3629	5126	4139
440	4153	5683	2948	4219	4131	2949	4240	5557	4143	5884	3063	4236	6015	4829
460	4643	6544	3364	4810	4715	3364	4844	6392	4731	6771	3490	4847	6917	5523
480	5335	7416	3779	5401	5298	3780	5450	7239	5320	7670	3918	5463	7831	6222
500	5931	8305	4196	5992	5882	4196	6059	8099	5911	8580	4343	6084	8758	6925
550	7428	10572	5235	7385	6760	5235	7592	10340	7395	10897	5402	7653	11123	8699
600	8942	12907	6274	8943	8811	6274	9144	12555	8894	13295	6462	9244	13544	10501
650	10477	15303	7314	10423	10278	7314	10716	14882	10407	15744	7515	10859	16022	12321
700	12023	17754	8353	11902	11749	8353	12307	17250	11937	18243	8570	12499	18548	14192
750	13592	20260	9392	13391	13223	9329	13919	19671	13481	20791	9620	14158	21117	16082
800	15177	22806	10431	14880	14702	10431	15548	22136	15046	23383	10671	15835	23721	18002
850	16781	25398	11471	16384	16186	11471	17195	24641	16624	26014	11718	17531	26369	19954
900	18401	28030	12510	17888	17676	12510	18858	27179	18223	28681	12767	19241	29023	21938
950	20031	30689	13550	19412	19175	13550	20537	29749	19834	31381	13812	20965	31714	23954
1000	21690	33397	14589	20935	20680	14589	22229	32344	21463	34110	14860	22703	34428	26000
1100	25035	38884	16667	24024	23719	16667	25653	37605	24760	39647	16950	26212	39914	30191
1200	28430	44473	18746	27160	26797	18746	29120	42946	28109	45274	19039	29761	45464	34506
1300	31868	50148	20824	30342	29918	20824	32626	48351	31503	50976	21126	33344	51069	38942
1400	35343	55896	22903	33569	33082	22903	36164	53808	34936	56740	23212	36957	56718	43493
1500	38850	61705	24982	36839	36290	24982	39729	59309	38405	62557	25296	40599	62404	48151
1600	42385	67569	27060	40151	39541	27060	43319	64846	41904	68420	27381	44266	68123	52908
1700	45945	73480	29139	43502	42835	29139	46929	70414	45429	74320	29464	47958	73870	57758
1800	49526	79431	31217	46889	46169	31218	50557	76007	48978	80254	31547	51673	79642	62693
1900	53126	85419	33296	50310	49541	33296	54201	81624	52548	86216	33630	55413	85436	67706
2000	56744	91439	35375	53762	52951	35375	57859	87259	56137	92203	35713	59175	91250	72790
2100	60376	97488	37453	57243	56397	37454	61530	92911	59742	98212	37796	62961	97081	77941
2200	64021	103562	39532	60752	59876	39534	65212	98577	63361	104240	39878	66769	102929	83153
2300	67683	109660	41610	64285	63387	41614	68904	104257	66995	110284	41962	70600	108792	88421
2400	71324	115779	43689	67841	66928	43695	72606	109947	70640	116344	44045	74453	114669	93741
2500	74985	121917	45768	71419	70498	45777	76316	115648	74296	122417	46130	78328	120559	99108
2600	78673	128073	47846	75017	74096	47860	80034	121357	77963	128501	48216	82224	126462	104520
2700	82369	134246	49925	78633	77720	49945	83759	127075	81639	134596	50303	86141	132376	109973
2800	86074	140433	52004	82267	81369	52033	87491	132799	85323	140701	52391	90079	138302	115464
2900	89786	146636	54082	85918	85043	54124	91229	138530	89015	146814	54481	94036	144238	120990
3000	93504	152852	56161	89584	88740	56218	94973	144267	92715	152935	56574	98013	150184	126549
3500	112185	184109	66554	108119	107555	66769	113768	173020	111306	183636	67079	118165	180057	154768
4000	130989	215622	75947	126939	126874	77532	132671	201859	130027	214453	77675	188705	210145	183552
4500	149895	247354	87340	145991	146660	88614	151662	230756	148850	245348	88386	159572	240427	212764
5000	168890	279283	97733	165246	166876	100111	170730	259692	167763	276299	99222	180749	270893	242313

Converted and usually rounded off from JANAF Thermochemical Tables, NSRDS-NBS-37, 1971 (1141 pp.).

2-202 PHYSICAL AND CHEMICAL DATA

TABLE 2-181 Ideal Gas Entropies s° , kJ/(kmol·K), of Combustion Products

Temperature, K	CO	CO ₂	H	OH	H ₂	N	NO	NO ₂	N ₂	N ₂ O	O	O ₂	SO ₂	H ₂ O
200	186.0	200.0	106.4	171.6	119.4	145.0	198.7	225.9	180.0	205.6	152.2	193.5	233.0	175.5
240	191.3	206.0	110.1	177.1	124.5	148.7	204.1	232.2	185.2	211.9	156.2	198.7	239.9	181.4
260	193.7	208.8	111.8	179.5	126.8	150.4	206.6	235.0	187.6	214.8	158.0	201.1	242.8	184.1
280	195.3	211.5	113.3	181.8	129.2	151.9	208.8	237.7	189.8	217.5	159.7	203.3	245.8	186.6
298.15	197.7	213.8	114.7	183.7	130.7	153.3	210.8	240.0	191.6	220.0	161.1	205.1	248.2	188.8
300	197.8	214.0	114.8	183.9	130.9	153.4	210.9	240.3	191.8	220.2	161.2	205.3	248.5	189.0
320	199.7	216.5	116.2	185.9	132.8	154.8	212.9	242.7	193.7	222.7	162.6	207.2	251.1	191.2
340	201.5	218.8	117.4	187.7	134.5	156.0	214.7	245.0	195.5	225.2	163.9	209.0	253.6	193.3
360	203.2	221.0	118.6	189.4	136.2	157.2	216.4	247.2	197.2	227.5	165.2	210.7	256.0	195.2
380	204.7	223.2	119.7	191.0	137.7	158.3	218.0	249.3	198.7	229.7	166.3	212.5	258.2	197.1
400	206.2	225.3	120.8	192.5	139.2	159.4	219.5	251.3	200.2	231.9	167.4	213.8	260.4	198.8
420	207.7	227.3	121.8	194.0	140.6	160.4	221.0	253.2	201.5	234.0	168.4	215.3	262.5	200.5
440	209.0	229.3	122.8	195.3	141.9	161.4	222.3	255.1	202.9	236.0	169.4	216.7	264.6	202.0
460	210.4	231.2	123.7	196.6	143.2	162.3	223.7	257.0	204.2	238.0	170.4	218.0	266.6	203.6
480	211.6	233.1	124.6	197.9	144.5	163.1	225.0	258.8	205.5	239.9	171.3	219.4	268.5	205.1
500	212.8	234.9	125.5	199.1	145.7	164.0	226.3	260.6	206.7	241.8	172.2	220.7	270.5	206.5
550	215.7	239.2	127.5	201.8	148.6	166.0	229.1	264.7	209.4	246.2	174.2	223.7	274.9	210.5
600	218.3	243.3	129.3	204.4	151.1	167.8	231.9	268.8	212.2	250.4	176.1	226.5	279.2	213.1
650	220.8	247.1	131.0	206.8	153.4	169.4	234.4	272.6	214.6	254.3	177.7	229.1	283.1	215.9
700	223.1	250.8	132.5	209.0	155.6	171.0	236.8	276.0	216.9	258.0	179.3	231.5	286.9	218.7
750	225.2	255.4	133.9	211.1	157.6	172.5	239.0	279.3	219.0	261.5	180.7	233.7	290.4	221.3
800	227.3	257.5	135.2	213.0	159.5	173.8	241.1	282.5	221.0	264.8	182.1	235.9	293.8	223.8
850	229.2	260.6	136.4	214.8	161.4	175.1	243.0	285.5	223.0	268.0	183.4	237.9	297.0	226.2
900	231.1	263.6	137.7	216.5	163.1	176.3	245.0	288.4	224.8	271.1	184.6	239.9	300.1	228.5
950	232.8	266.5	138.8	218.1	164.7	177.4	246.8	291.3	226.5	274.0	185.7	241.8	303.0	230.6
1000	234.5	269.3	139.9	219.7	166.2	178.5	248.4	293.9	228.2	276.8	186.8	243.6	305.8	232.7
1100	237.7	274.5	141.9	222.7	169.1	180.4	251.8	298.9	231.3	282.1	188.8	246.9	311.0	236.7
1200	240.7	279.4	143.7	225.4	171.8	182.2	254.8	303.6	234.2	287.0	190.6	250.0	315.8	240.5
1300	243.4	283.9	145.3	228.0	174.3	183.9	257.6	307.9	236.9	291.5	192.3	252.9	320.3	244.0
1400	246.0	288.2	146.9	230.3	176.6	185.4	260.2	311.9	239.5	295.8	193.8	255.6	324.5	247.4
1500	248.4	292.2	148.3	232.6	178.8	186.9	262.7	315.7	241.9	299.8	195.3	258.1	328.4	250.6
1600	250.7	296.0	149.6	234.7	180.9	188.2	265.0	319.3	244.1	303.6	196.6	260.4	332.1	253.7
1700	252.9	299.6	150.9	236.8	182.9	189.5	267.2	322.7	246.3	307.2	197.9	262.7	335.6	256.6
1800	254.9	303.0	152.1	238.7	184.8	190.7	269.3	325.9	248.3	310.6	199.1	264.8	338.9	259.5
1900	256.8	306.2	153.2	240.6	186.7	191.8	271.3	328.9	250.2	313.8	200.2	266.8	342.0	262.2
2000	258.7	309.3	154.3	242.3	188.4	192.9	273.1	331.8	252.1	316.9	201.3	268.7	345.0	264.8
2100	260.5	312.2	155.3	244.0	190.1	193.9	274.9	334.5	253.8	319.8	202.3	270.6	347.9	267.3
2200	262.2	315.1	156.3	245.7	191.7	194.8	276.6	337.2	255.5	322.6	203.2	272.4	350.6	269.7
2300	263.8	317.8	157.2	247.2	193.3	195.8	278.3	339.7	257.1	325.3	204.2	274.1	353.2	272.0
2400	265.4	320.4	158.1	248.7	194.8	196.7	279.8	342.1	258.7	327.9	205.0	275.7	355.7	274.3
2500	266.9	322.9	158.9	250.2	196.2	197.5	281.4	344.5	260.2	330.4	205.9	277.3	358.1	276.5
2600	268.3	325.3	159.7	251.6	197.7	198.3	282.8	346.7	261.6	332.7	206.7	278.8	360.4	278.6
2700	269.7	327.6	160.5	253.0	199.0	199.1	284.2	348.9	263.0	335.0	207.5	280.3	362.6	280.7
2800	271.0	329.9	161.3	254.3	200.3	199.9	285.6	350.9	264.3	337.3	208.3	281.7	364.8	282.7
2900	272.3	332.1	162.0	255.6	201.6	200.6	286.9	352.9	265.6	339.4	209.0	283.1	366.9	284.6
3000	273.6	334.2	162.7	256.8	202.9	201.3	288.2	354.9	266.9	341.5	209.7	284.4	368.9	286.5
3500	279.4	343.8	165.9	262.5	208.7	204.6	294.0	363.8	272.6	350.9	212.9	290.7	378.1	295.2
4000	284.4	352.2	168.7	267.6	213.8	207.4	299.0	371.5	277.6	359.2	215.8	296.2	386.1	302.9
4500	288.8	359.7	171.1	272.1	218.5	210.1	303.5	378.3	282.1	366.5	218.3	301.1	393.3	309.8
5000	292.8	366.4	173.3	276.1	222.8	212.5	307.5	384.4	286.0	373.0	220.6	305.5	399.7	316.0

Usually rounded off from JANAF Thermochemical Tables, NSRDS-NBS-37, 1971 (1141 pp.). Equilibrium constants can be calculated by combining Δh_f° values from Table 2-179, $h_T - h_{298}$ from Table 2-180, and s° values from the above, using the formula $\ln K_p = -\Delta G/(RT)$, where $\Delta G = \Delta h_f^\circ + (h_T - h_{298}) - T^\circ$.

HEATS OF SOLUTION

TABLE 2-182 Heats of Solution of Inorganic Compounds in Water

Heat evolved, in kilocalories per gram formula weight, on solution in water at 18 °C. Computed from data in Bichowsky and Rossini, *Thermochemistry of Chemical Substances*, Reinhold, New York, 1936.

Substance	Dilution ^o	Formula	Heat, kcal/mol	Substance	Dilution ^o	Formula	Heat, kcal/mol
Aluminum bromide	aq	AlBr ₃	+85.3	Calcium—(Cont.)			
	chloride	600	AlCl ₃		+77.9	∞	CaBr ₂
fluoride	600	AlCl ₃ ·6H ₂ O	+13.2	∞	CaBr ₂ ·6H ₂ O	-0.9	
	aq	AlF ₃	+31	∞	CaCl ₂	+4.9	
	aq	AlF ₃ ·½H ₂ O	+19.0	∞	CaCl ₂ ·H ₂ O	+12.3	
	aq	AlF ₃ ·3½H ₂ O	-1.7	∞	CaCl ₂ ·2H ₂ O	+12.5	
iodide	aq	AlI ₃	+89.0	∞	CaCl ₂ ·4H ₂ O	+2.4	
	sulfate	aq	Al ₂ (SO ₄) ₃	+126	∞	CaCl ₂ ·6H ₂ O	-4.11
Ammonium bromide	aq	Al ₂ (SO ₄) ₃ ·6H ₂ O	+56.2	400	Ca(CHO ₂) ₂	+0.7	
	aq	Al ₂ (SO ₄) ₃ ·18H ₂ O	+6.7	∞	CaI ₂	+28.0	
	∞	NH ₄ Br	-4.45	∞	CaI ₂ ·5H ₂ O	+1.8	
	∞	NH ₄ Cl	-3.82	∞	Ca(NO ₃) ₂	+4.1	
	aq	(NH ₄) ₂ CrO ₄	-5.82	∞	Ca(NO ₃) ₂ ·H ₂ O	+0.7	
	600	(NH ₄) ₂ Cr ₂ O ₇	-12.9	∞	Ca(NO ₃) ₂ ·2H ₂ O	-3.2	
	aq	NH ₄ I	-3.56	∞	Ca(NO ₃) ₂ ·3H ₂ O	-4.2	
	∞	NH ₄ NO ₃	-6.47	∞	Ca(NO ₃) ₂ ·4H ₂ O	-7.99	
	aq	NH ₄ BO ₃ ·H ₂ O	-9.0	aq	Ca(H ₂ PO ₄) ₂ ·H ₂ O	-0.6	
	∞	(NH ₄) ₂ SO ₄	-2.75	aq	CaHPO ₄ ·2H ₂ O	-1	
sulfate, acid	800	NH ₄ HSO ₄	+0.56	∞	CaSO ₄	+5.1	
sulfite	aq	(NH ₄) ₂ SO ₃	-1.2	∞	CaSO ₄ ·½H ₂ O	+3.6	
Antimony fluoride	aq	(NH ₄) ₂ SO ₃ ·H ₂ O	-4.13	∞	CaSO ₄ ·2H ₂ O	-0.18	
	aq	SbF ₃	-1.7	aq	CrCl ₂	+18.6	
	aq	SbI ₃	-0.8	Chromous chloride	aq	CrCl ₂ ·3H ₂ O	+5.3
Arsenic acid	aq	H ₃ AsO ₄	-0.4		aq	CrCl ₂ ·4H ₂ O	+2.0
Barium bromate	∞	Ba(BrO ₃) ₂ ·H ₂ O	-15.9	aq	CrI ₂	+5.7	
	bromide	∞	BaBr ₂	+5.3	aq	CoBr ₂	+18.4
chlorate	∞	BaBr ₂ ·H ₂ O	-0.8	aq	CoBr ₂ ·6H ₂ O	-1.25	
	∞	BaBr ₂ ·2H ₂ O	-3.87	400	CoCl ₂	+18.5	
	∞	Ba(ClO ₃) ₂	-6.7	400	CoCl ₂ ·2H ₂ O	+9.8	
	∞	Ba(ClO ₃) ₂ ·H ₂ O	-10.6	400	CoCl ₂ ·6H ₂ O	-2.9	
chloride	∞	BaCl ₂	+2.4	aq	CoI ₂	+18.8	
	∞	BaCl ₂ ·H ₂ O	-2.17	400	CoSO ₄	+15.0	
	∞	BaCl ₂ ·2H ₂ O	-4.5	400	CoSO ₄ ·6H ₂ O	-1.4	
	∞	BaCl ₂ ·2H ₂ O	-4.5	400	CoSO ₄ ·7H ₂ O	-3.6	
cyanide	aq	Ba(CN) ₂	+1.5	aq	Cu(C ₂ H ₃ O ₂) ₂	+2.4	
	aq	Ba(CN) ₂ ·H ₂ O	-2.4	aq	Cu(CHO ₂) ₂	+0.5	
	aq	Ba(CN) ₂ ·2H ₂ O	-4.9	200	Cu(NO ₃) ₂	+10.3	
iodate	∞	Ba(IO ₃) ₂	-9.1	200	Cu(NO ₃) ₂ ·3H ₂ O	-2.6	
	∞	Ba(IO ₃) ₂ ·H ₂ O	-11.3	200	Cu(NO ₃) ₂ ·6H ₂ O	-10.7	
iodide	∞	BaI ₂	+10.5	800	CuSO ₄	+15.9	
	∞	BaI ₂ ·H ₂ O	+2.7	∞	CuSO ₄ ·H ₂ O	+9.3	
	∞	BaI ₂ ·2H ₂ O	+0.14	∞	CuSO ₄ ·3H ₂ O	+3.65	
	∞	BaI ₂ ·2½H ₂ O	-0.58	∞	CuSO ₄ ·5H ₂ O	-2.85	
	∞	BaI ₂ ·7H ₂ O	-6.61	∞	Cu ₂ SO ₄	+11.6	
	∞	Ba(NO ₃) ₂	-10.2	Cuprous sulfate	aq		
	∞	Ba(ClO ₄) ₂	-2.8		1000	FeCl ₃	+31.7
	∞	Ba(ClO ₄) ₂ ·3H ₂ O	-10.5	1000	FeCl ₃ ·2½H ₂ O	+21.0	
∞	BaS	+7.2	1000	FeCl ₃ ·6H ₂ O	+5.6		
Beryllium bromide	aq	BeBr ₂	+62.6	800	Fe(NO ₃) ₃ ·9H ₂ O	-9.1	
	chloride	aq	BeCl ₂	+51.1	aq	FeBr ₂	+18.0
iodide	aq	BeI ₂	+72.6	400	FeCl ₂	+17.9	
	sulfate	aq	BeSO ₄	+18.1	400	FeCl ₂ ·2H ₂ O	+8.7
	aq	BeSO ₄ ·H ₂ O	+13.5	400	FeCl ₂ ·4H ₂ O	+2.7	
	aq	BeSO ₄ ·2H ₂ O	+7.9	aq	FeI ₂	+23.3	
	aq	BeSO ₄ ·4H ₂ O	+1.1	400	FeSO ₄	+14.7	
Bismuth iodide	aq	BiI ₃	+3	400	FeSO ₄ ·H ₂ O	+7.35	
Boric acid	aq	H ₃ BO ₃	-5.4	400	FeSO ₄ ·4H ₂ O	+1.4	
				400	FeSO ₄ ·7H ₂ O	-4.4	
Cadmium bromide	400	CdBr ₂	+0.4	Lead acetate	400	Pb(C ₂ H ₃ O ₂) ₂	+1.4
	chloride	400	CdBr ₂ ·4H ₂ O		-7.3	400	Pb(C ₂ H ₃ O ₂) ₂ ·3H ₂ O
nitrate	400	CdCl ₂	+3.1	aq	PbBr ₂	-10.1	
	400	CdCl ₂ ·H ₂ O	+0.6	aq	PbCl ₂	-3.4	
	400	CdCl ₂ ·2½H ₂ O	-3.00	aq	Pb(CHO ₂) ₂	-6.9	
	400	Cd(NO ₃) ₂ ·H ₂ O	+4.17	400	Pb(NO ₃) ₂	-7.61	
sulfate	400	Cd(NO ₃) ₂ ·4H ₂ O	-5.08	∞	LiBr	+11.54	
	400	CdSO ₄	+10.69	∞	LiBr·H ₂ O	+5.30	
Calcium acetate	400	CdSO ₄ ·H ₂ O	+6.05	∞	LiBr·2H ₂ O	+2.05	
	400	CdSO ₄ ·2½H ₂ O	+2.51	∞	LiBr·3H ₂ O	-1.59	
	∞	Ca(C ₂ H ₃ O ₂) ₂	+7.6	∞	LiCl	+8.66	
∞	Ca(C ₂ H ₃ O ₂) ₂ ·H ₂ O	+6.5	∞				

^oThe numbers represent moles of water used to dissolve 1 g formula weight of substance; ∞ means "infinite dilution"; and aq means "aqueous solution of unspecified dilution."

2-204 PHYSICAL AND CHEMICAL DATA

TABLE 2-182 Heats of Solution of Inorganic Compounds in Water (Continued)

Substance	Dilution ^o	Formula	Heat, kcal/mol	Substance	Dilution ^o	Formula	Heat, kcal/mol
Lithium—(Cont.)				Phosphoric acid, ortho-	400	H ₃ PO ₄	+2.79
	∞	LiCl·H ₂ O	+4.45		400	H ₃ PO ₄ ·½H ₂ O	-0.1
	∞	LiCl·2H ₂ O	+1.07		aq	H ₃ P ₂ O ₇	+25.9
	∞	LiCl·3H ₂ O	-1.98		aq	H ₄ P ₂ O ₇ ·1½H ₂ O	+4.65
fluoride	∞	LiF	-0.74	Potassium acetate	∞	KC ₂ H ₃ O ₂	+3.55
hydroxide	∞	LiOH	+4.74	aluminum sulfate	600	KAl(SO ₄) ₂	+48.5
	∞	LiOH·½H ₂ O	+4.39		600	KAl(SO ₄) ₂ ·3H ₂ O	+26.6
	∞	LiOH·H ₂ O	+9.6			KAl(SO ₄) ₂ ·12H ₂ O	-10.1
iodide	∞	LiI	+14.92	bicarbonate	2000	KHCO ₃	-5.1
	∞	LiI·½H ₂ O	+10.08	bromate	∞	KBrO ₃	-10.13
	∞	LiI·H ₂ O	+6.93	bromide	∞	KBr	-5.13
	∞	LiI·2H ₂ O	+3.43	carbonate	∞	K ₂ CO ₃	+6.58
	∞	LiI·3H ₂ O	-0.17			K ₂ CO ₃ ·½H ₂ O	+4.25
nitrate	∞	LiNO ₃	+0.466			K ₂ CO ₃ ·1½H ₂ O	-0.43
	∞	LiNO ₃ ·3H ₂ O	-7.87	chlorate	∞	KClO ₃	-10.31
sulfate	∞	Li ₂ SO ₄	+6.71	chloride	∞	KCl	-4.404
	∞	Li ₂ SO ₄ ·H ₂ O	+3.77	chromate	2185	K ₂ CrO ₄	-4.9
				chrome sulfate	600	KCr(SO ₄) ₂	+55
Magnesium bromide	∞	MgBr ₂	+43.7			KCr(SO ₄) ₂ ·H ₂ O	+42
	∞	MgBr ₂ ·H ₂ O	+35.9			KCr(SO ₄) ₂ ·2H ₂ O	+33
	∞	MgBr ₂ ·6H ₂ O	+19.8			KCr(SO ₄) ₂ ·6H ₂ O	+7
chloride	∞	MgCl ₂	+36.3			KCr(SO ₄) ₂ ·12H ₂ O	-9.5
	∞	MgCl ₂ ·2H ₂ O	+20.8	cyanide	200	KCN	-3.0
	∞	MgCl ₂ ·4H ₂ O	+10.5	dichromate	1600	K ₂ Cr ₂ O ₇	-17.8
	∞	MgCl ₂ ·6H ₂ O	+3.4	fluoride	∞	KF	+3.96
iodide	∞	MgI ₂	+50.2		∞	KF·2H ₂ O	-1.85
nitrate	∞	Mg(NO ₃) ₂ ·6H ₂ O	-3.7		∞	KF·4H ₂ O	-6.05
phosphate	aq	Mg ₃ (PO ₄) ₂	+10.2	hydrosulfide	∞	KHS	+0.86
sulfate	∞	MgSO ₄	+21.1		∞	KHS·½H ₂ O	+1.21
	∞	MgSO ₄ ·H ₂ O	+14.0	hydroxide	∞	KOH	+12.91
	∞	MgSO ₄ ·2H ₂ O	+11.7		∞	KOH·¾H ₂ O	+4.27
	∞	MgSO ₄ ·4H ₂ O	+4.9		∞	KOH·H ₂ O	+3.48
	∞	MgSO ₄ ·6H ₂ O	+0.55		∞	KOH·7H ₂ O	+0.86
	∞	MgSO ₄ ·7H ₂ O	-3.18	iodate	∞	KIO ₃	-6.93
sulfide	aq	MgS	+25.8	iodide	∞	KI	-5.23
Manganic nitrate	400	Mn(NO ₃) ₂	+12.9	nitrate	∞	KNO ₃	-8.633
	400	Mn(NO ₃) ₂ ·3H ₂ O	-3.9	oxalate	400	K ₂ C ₂ O ₄	-4.6
	400	Mn(NO ₃) ₂ ·6H ₂ O	-6.2			K ₂ C ₂ O ₄ ·H ₂ O	-7.5
sulfate	aq	Mn ₂ (SO ₄) ₃	+22	perchlorate	∞	KClO ₄	-12.94
Manganous acetate	aq	Mn(C ₂ H ₃ O ₂) ₂	+12.2	permanganate	400	KMnO ₄	-10.4
	aq	Mn(C ₂ H ₃ O ₂) ₂ ·4H ₂ O	+1.6	phosphate, dihydrogen	aq	KH ₂ PO ₄	+4.7
bromide	aq	MnBr ₂	+15	pyrosulfite	aq	K ₂ S ₂ O ₅	-11.0
	aq	MnBr ₂ ·H ₂ O	+14.4		aq	K ₂ S ₂ O ₅ ·½H ₂ O	-10.22
	aq	MnBr ₂ ·4H ₂ O	+16.1	sulfate	∞	K ₂ SO ₄	-6.32
chloride	400	MnCl ₂	+16.0	sulfate, acid	800	KHSO ₄	-3.10
	400	MnCl ₂ ·2H ₂ O	+8.2	sulfide	∞	K ₂ S	-11.0
	400	MnCl ₂ ·4H ₂ O	+1.5	sulfite	aq	K ₂ SO ₃	+1.8
formate	aq	Mn(CHO ₂) ₂	+4.3		aq	K ₂ SO ₃ ·H ₂ O	+1.37
	aq	Mn(CHO ₂) ₂ ·2H ₂ O	-2.9	thiocyanate	∞	KCNS	-6.08
iodide	aq	MnI ₂	+26.2	thionate, di-	aq	K ₂ S ₂ O ₆	-13.0
	aq	MnI ₂ ·H ₂ O	+24.1	thiosulfate	∞	K ₂ S ₂ O ₃	-4.5
	aq	MnI ₂ ·2H ₂ O	+22.7				
	aq	MnI ₂ ·4H ₂ O	+19.9	Silver acetate	aq	AgC ₂ H ₃ O ₂	-5.4
	aq	MnI ₂ ·6H ₂ O	+21.2	nitrate	200	AgNO ₃	-4.4
sulfate	400	MnSO ₄	+13.8	Sodium acetate	∞	NaC ₂ H ₃ O ₂	+4.085
	400	MnSO ₄ ·H ₂ O	+11.9		∞	NaC ₂ H ₃ O ₂ ·3H ₂ O	-4.665
	400	MnSO ₄ ·7H ₂ O	-1.7	arsenate	500	Na ₃ AsO ₄	+15.6
Mercuric acetate	aq	Hg(C ₂ H ₃ O ₂) ₂	-4.0		500	Na ₃ AsO ₄ ·12H ₂ O	-12.61
bromide	aq	HgBr ₂	-2.4	bicarbonate	1800	NaHCO ₃	-4.1
chloride	aq	HgCl ₂	-3.3	borate, tetra-	900	Na ₂ B ₄ O ₇	+10.0
nitrate	aq	Hg(NO ₃) ₂ ·½H ₂ O	-0.7		900	Na ₂ B ₄ O ₇ ·10H ₂ O	+16.8
Mercurous nitrate	aq	Hg ₂ (NO ₃) ₂ ·2H ₂ O	-11.5	bromide	∞	NaBr	-0.58
					∞	NaBr·2H ₂ O	-4.57
Nickel bromide	aq	NiBr ₂	+19.0	carbonate	∞	Na ₂ CO ₃	+5.57
	aq	NiBr ₂ ·3H ₂ O	+0.2		∞	Na ₂ CO ₃ ·H ₂ O	+2.19
Nickel chloride	800	NiCl ₂	+19.23		∞	Na ₂ CO ₃ ·7H ₂ O	-10.81
	800	NiCl ₂ ·2H ₂ O	+10.4		∞	Na ₂ CO ₃ ·10H ₂ O	-16.22
	800	NiCl ₂ ·4H ₂ O	+4.2	chlorate	∞	NaClO ₃	-5.37
	800	NiCl ₂ ·6H ₂ O	-1.15	chloride	∞	NaCl	-1.164
iodide	aq	NiI ₂	+19.4	chromate	800	Na ₂ CrO ₄	+2.50
nitrate	200	Ni(NO ₃) ₂	+11.8		800	Na ₂ CrO ₄ ·4H ₂ O	-7.52
	200	Ni(NO ₃) ₂ ·6H ₂ O	-7.5		800	Na ₂ CrO ₄ ·10H ₂ O	-16.0
sulfate	200	NiSO ₄	+15.1	cyanide	200	NaCN	-0.37
	200	NiSO ₄ ·7H ₂ O	-4.2		200	NaCN·½H ₂ O	-0.92

TABLE 2-182 Heats of Solution of Inorganic Compounds in Water (Concluded)

Substance	Dilution ^o	Formula	Heat, kcal/mol	Substance	Dilution ^o	Formula	Heat, kcal/mol
Sodium—(Cont.)				Sodium—(Cont.)			
fluoride	200	NaCN·2H ₂ O	-4.41	thionate, di-	aq	Na ₂ S ₂ O ₆	-5.80
hydrosulfide	∞	NaF	-0.27		aq	Na ₂ S ₂ O ₆ ·2H ₂ O	-11.86
	∞	NaHS	+4.62	Sodium thiosulfate	aq	Na ₂ S ₂ O ₃	+2.0
	∞	NaHS·2H ₂ O	-1.49		aq	Na ₂ S ₂ O ₃ ·5H ₂ O	-11.30
Sodium hydroxide	∞	NaOH	+10.18	Stannic bromide	aq	SnBr ₄	+15.5
	∞	NaOH·½H ₂ O	+5.17	Stannous bromide	aq	SnBr ₂	-1.6
	∞	NaOH·¾H ₂ O	+7.08	iodide	aq	SnI ₂	-5.8
	∞	NaOH·¾H ₂ O	+6.48	Strontium acetate	∞	Sr(C ₂ H ₃ O ₂) ₂	+6.2
	∞	NaOH·H ₂ O	+5.17		∞	Sr(C ₂ H ₃ O ₂) ₂ ·½H ₂ O	+5.9
iodide	∞	NaI	+1.57	bromide	∞	SrBr ₂	+16.4
	∞	NaI·2H ₂ O	-3.89		∞	SrBr ₂ ·H ₂ O	+9.25
metaphosphate	600	NaPO ₃	+3.97		∞	SrBr ₂ ·2H ₂ O	+6.5
nitrate	∞	NaNO ₃	-5.05		∞	SrBr ₂ ·4H ₂ O	+0.4
nitrite	aq	NaNO ₂	-3.6		∞	SrBr ₂ ·6H ₂ O	-6.1
perchlorate	∞	NaClO ₄	-4.15	chloride	∞	SrCl ₂	+11.54
phosphate di-	1600	Na ₂ HPO ₄	+5.21		∞	SrCl ₂ ·H ₂ O	+6.4
tri-	1600	Na ₃ PO ₄	+13		∞	SrCl ₂ ·2H ₂ O	+2.95
phosphate di-	1600	Na ₃ PO ₄ ·12H ₂ O	-15.3		∞	SrCl ₂ ·6H ₂ O	-7.1
di-	1600	Na ₂ HPO ₄ ·2H ₂ O	-0.82	iodide	∞	SrI ₂	+20.7
	1600	Na ₂ HPO ₄ ·7H ₂ O	-12.04		∞	SrI ₂ ·H ₂ O	+12.65
	1600	Na ₂ HPO ₄ ·12H ₂ O	-23.18		∞	SrI ₂ ·2H ₂ O	+10.4
phosphite, mono-	600	NaH ₂ PO ₃	+0.90		∞	SrI ₂ ·6H ₂ O	-4.5
	600	NaH ₂ PO ₃ ·2½H ₂ O	-5.29	nitrate	∞	Sr(NO ₃) ₂	-4.8
di-	800	Na ₂ HPO ₃	+9.30		∞	Sr(NO ₃) ₂ ·4H ₂ O	-12.4
	800	Na ₂ HPO ₃ ·5H ₂ O	-4.54	sulfate	∞	SrSO ₄	+0.5
pyrophosphate	1600	Na ₄ P ₂ O ₇	+11.9	Sulfuric acid, pyro-	∞	H ₂ S ₂ O ₇	-18.08
	1600	Na ₄ P ₂ O ₇ ·10H ₂ O	-11.7				
di-	1200	Na ₂ H ₂ P ₂ O ₇	-2.2	Zinc acetate	400	Zn(C ₂ H ₃ O ₂) ₂	+9.8
	1200	Na ₂ H ₂ P ₂ O ₇ ·6H ₂ O	-14.0		400	Zn(C ₂ H ₃ O ₂) ₂ ·H ₂ O	+7.0
sulfate	∞	Na ₂ SO ₄	+0.28		400	Zn(C ₂ H ₃ O ₂) ₂ ·2H ₂ O	+3.9
	∞	Na ₂ SO ₄ ·10H ₂ O	-18.74	bromide	400	ZnBr ₂	+15.0
sulfate, acid	800	NaHSO ₄	+1.74	chloride	400	ZnCl ₂	+15.72
	800	NaHSO ₄ ·H ₂ O	+0.15	iodide	aq	ZnI ₂	+11.6
sulfide	∞	Na ₂ S	+15.2	nitrate	400	Zn(NO ₃) ₂ ·3H ₂ O	-5
	∞	Na ₂ S·4½H ₂ O	+0.09		400	Zn(NO ₃) ₂ ·6H ₂ O	-6.0
	∞	Na ₂ S·5H ₂ O	-6.54	sulfate	400	ZnSO ₄	+18.5
	∞	Na ₂ S·9H ₂ O	-16.65		400	ZnSO ₄ ·H ₂ O	+10.0
sulfite	∞	Na ₂ SO ₃	+2.8		400	ZnSO ₄ ·6H ₂ O	-0.8
	∞	Na ₂ SO ₃ ·7H ₂ O	-11.1		400	ZnSO ₄ ·7H ₂ O	-4.3
thiocyanate	∞	NaCNS	-1.83				

NOTE: To convert kilocalories per mole to British thermal units per pound-mole, multiply by 1.799 × 10⁻³.

TABLE 2-183 Heats of Solution of Organic Compounds in Water (at Infinite Dilution and Approximately Room Temperature)Recalculated and rearranged from *International Critical Tables*, vol. 5, pp. 148–150. cal/mol = Btu/(lb·mol) × 1.799.

Solute	Heat of solution, cal/mol solute ^a	Solute	Heat of solution, cal/mol solute ^a
Acetic acid (solid), C ₂ H ₄ O ₂	-2,251	Oxalic acid, C ₂ H ₂ O ₄	-2,290
Acetylacetone, C ₈ H ₈ O ₂	-641	(2H ₂ O)	-8,485
Acetylurea, C ₃ H ₆ N ₂ O ₂	-6,812	Phenol (solid), C ₆ H ₆ O	-2,605
Aconitic acid, C ₆ H ₆ O ₅	-4,206	Phthalic acid, C ₈ H ₆ O ₄	-4,871
Ammonium benzoate, C ₇ H ₅ NO ₂	-2,700	Picric acid, C ₆ H ₃ N ₃ O ₇	-7,098
picrate	-8,700	Piperic acid, C ₁₂ H ₁₀ O ₄	-10,492
succinate (<i>n</i> -)	-3,489	Piperonylic acid, C ₈ H ₆ O ₄	-9,106
Aniline, hydrochloride, C ₆ H ₅ ClN	-2,732	Potassium benzoate	-1,506
Barium picrate	-4,708	citrate	2,820
Benzoic acid, C ₇ H ₆ O ₂	-6,501	tartrate (<i>n</i> -) (0.5 H ₂ O)	-5,562
Camphoric acid, C ₁₀ H ₁₆ O ₄	-502	Pyrogallol, C ₆ H ₆ O ₃	-3,705
Citric acid, C ₆ H ₈ O ₇	-5,401	Pyrotartaric acid	-5,019
Dextrin, C ₁₂ H ₂₀ O ₁₀	268	Quinone	-3,991
Fumaric acid, C ₄ H ₄ O ₄	-5,903	Raffinose, C ₁₈ H ₃₂ O ₁₆ (5H ₂ O)	-9,703
Hexamethylenetetramine, C ₆ H ₁₂ N ₄	4,780	Resorcinol, C ₆ H ₆ O ₂	-3,960
Hydroxybenzamide (<i>m</i> -), C ₇ H ₇ NO ₂	-4,161	Silver malonate (<i>n</i> -)	-9,799
(<i>m</i> -), (HCl)	-7,003	Sodium citrate (tri-)	5,270
(<i>o</i> -), C ₇ H ₇ NO ₂	-4,340	picrate	-6,441
(<i>p</i> -)	-5,392	potassium tartrate	-1,817
Hydroxybenzoic acid (<i>o</i> -), C ₇ H ₆ O ₃	-6,350	(4H ₂ O)	-12,342
(<i>p</i> -), C ₇ H ₆ O ₃	-5,781	succinate (<i>n</i> -)	2,390
Hydroxybenzyl alcohol (<i>o</i> -), C ₇ H ₈ O ₂	-3,203	(6H ₂ O)	-10,994
Inulin, C ₃₆ H ₆₂ O ₃₁	-96	tartrate (<i>n</i> -)	-1,121
Isosuccinic acid, C ₄ H ₆ O ₄	-3,420	(2H ₂ O)	-5,882
Itaconic acid, C ₅ H ₆ O ₄	-5,922	Strontium picrate	7,887
Lactose, C ₁₂ H ₂₂ O ₁₁ ·H ₂ O	-3,705	(6H ₂ O)	-14,412
Lead picrate	-7,098	Succinic acid, C ₄ H ₆ O ₄	-6,405
(2H ₂ O)	-13,193	Succinimide, C ₄ H ₅ NO ₂	-4,302
Magnesium picrate	14,699	Sucrose, C ₁₂ H ₂₂ O ₁₁	-1,319
(8H ₂ O)	-15,894	Tartaric acid (<i>d</i> -)	-3,451
Maleic acid, C ₄ H ₄ O ₄	-4,441	Thiourea, CH ₄ N ₂ S	-5,330
Malic acid, C ₄ H ₆ O ₅	-3,150	Urea, CH ₂ N ₂ O	-3,609
Malonic acid, C ₃ H ₄ O ₄	-4,493	acetate	-8,795
Mandelic acid, C ₈ H ₈ O ₃	-3,090	formate	-7,194
Mannitol, C ₆ H ₁₄ O ₆	-5,260	nitrate	-10,803
Menthol, C ₁₀ H ₂₀ O	0	oxalate	-17,806
Nicotine dihydrochloride, C ₁₀ H ₁₆ Cl ₂ N ₂	6,561	Vanillic acid	-5,160
Nitrobenzoic acid (<i>m</i> -), C ₇ H ₅ NO ₄	-5,593	Vanillin	-5,210
(<i>o</i> -), C ₇ H ₅ NO ₄	-5,306	Zinc picrate	-11,496
(<i>p</i> -), C ₇ H ₅ NO ₄	-8,891	(8H ₂ O)	-15,894
Nitrophenol (<i>m</i> -), C ₆ H ₅ NO ₃	-5,210		
(<i>o</i> -), C ₆ H ₅ NO ₃	-6,310		
(<i>p</i> -), C ₆ H ₅ NO ₃	-4,493		

^a + denotes heat evolved, and - denotes heat absorbed. The data in the *International Critical Tables* were calculated by E. Anderson.

THERMODYNAMIC PROPERTIES

EXPLANATION OF TABLES

The following subsection presents information on the thermodynamic properties of a number of fluids. In some cases transport properties are also included.

Properties for the compounds listed in Table 2-184 were generated by using the NIST REFPROP software (Lemmon, E. W., McLinden, M. O., and Huber, M. L., NIST Standard Reference Database 23: Reference Fluid Thermodynamic and Transport Properties—REFPROP, National Institute of Standards and Technology, Standard Reference Data Program, Gaithersburg, Md., 2002, Version 7.1). Megan Friend's help in generating these tables is acknowledged and gratefully appreciated. The number of digits provided in these tables was chosen for uniformity of appearance and formatting; these do not represent the uncertainties of the physical quantities, but are the result of calculations from the standard thermophysical property formulations within a fixed format.

Properties for many of these compounds can also be generated by going to <http://webbook.nist.gov> and selecting NIST Chemistry WebBook, then Thermophysical Properties of Fluid Systems High Accuracy Data. This site allows the user to generate tables of thermodynamic properties. The user can select the units as well as the temperatures and/or pressure increments for which properties are to be generated. The resulting table can be copied into a spreadsheet. Because of this capability, properties for the compounds listed in Table 2-184 are not tabulated at as many temperatures and pressures as might otherwise be the case.

Notation

- c_p = isobaric specific heat
- c_v = isochoric specific heat
- e = specific internal energy
- h = enthalpy
- k = thermal conductivity
- p = pressure
- s = specific entropy
- t = temperature
- T = absolute temperature
- u = specific internal energy
- μ = viscosity
- v = specific volume
- f = subscript denoting saturated liquid
- g = subscript denoting saturated vapor

UNITS CONVERSIONS

For this subsection, the following units conversions are applicable:

- c_p , specific heat: To convert kilojoules per kilogram-kelvin to British thermal units per pound-degree Fahrenheit, multiply by 0.23885.
- e , internal energy: To convert kilojoules per kilogram to British thermal units per pound, multiply by 0.42992.
- g , gravity acceleration: To convert meters per second squared to feet per second squared, multiply by 3.2808.

h , enthalpy: To convert kilojoules per kilogram to British thermal units per pound, multiply by 0.42992.

k , thermal conductivity: To convert watts per meter-kelvin to British thermal unit-feet per hour-square foot-degree Fahrenheit, multiply by 0.57779.

p , pressure: To convert bars to kilopascals, multiply by 1×10^5 ; to convert bars to pounds-force per square inch, multiply by 14.504; and to convert millimeters of mercury to pounds-force per square inch, multiply by 0.01934.

s , entropy: to convert kilojoules per kilogram-kelvin to British thermal units per pound-degree Rankine, multiply by 0.23885.

t , temperature: $^{\circ}\text{F} = \frac{9}{5} ^{\circ}\text{C} + 32$.

T , absolute temperature: $^{\circ}\text{R} = \frac{9}{5} \text{K}$.

u , internal energy: to convert kilojoules per kilogram to British thermal units per pound, multiply by 0.42992.

μ , viscosity: to convert pascal-seconds to pound-force-seconds per square foot, multiply by 0.020885; to convert pascal-seconds to c_p , multiply by 1000.

v , specific volume: to convert cubic meters per kilogram to cubic feet per pound, multiply by 16.018.

ρ , density: to convert kilograms per cubic meter to pounds per cubic foot, multiply by 0.062428.

ADDITIONAL REFERENCES

Bretsznajder, *Prediction of Transport and Other Physical Properties of Fluids*, Pergamon, New York, 1971. D'Ans and Lax, *Handbook for Chemists and Physicists* (in German), 3 vols., Springer-Verlag, Berlin. *Engineering Data Book*, Natural Gas Processors Suppliers Association, Tulsa, Okla. Ganic, Hartnett, and Rohsenow, *Handbook of Heat Transfer*, 2d ed., McGraw-Hill, New York, 1984. Gray, *American Institute of Physics Handbook*, 3d ed., McGraw-Hill, New York, 1972. Kay and Laby, *Tables of Physical and Chemical Constants*, Longman, London, various editions and dates. Landolt-Börnstein *Tables*, many volumes and dates, Springer-Verlag, Berlin. Lange, *Handbook of Chemistry*, McGraw-Hill, New York, various editions and dates. Partington, *Advanced Treatise on Physical Chemistry*, 5 vols., Longman, London, 1950. Raznjevic, *Handbook of Thermodynamic Tables and Charts*, McGraw-Hill, New York, 1976 and other editions. Reynolds, *Thermodynamic Properties in SI*, Department of Mechanical Engineering, Stanford University, 1979. Stephan and Lucas, *Viscosity of Dense Fluids*, Plenum, New York and London, 1979. *Selected Values of Properties of Chemical Compounds and Selected Values of the Properties of Hydrocarbons and Related Compounds*, Thermodynamics Research Center, NIST, Boulder, Colo., looseleaf, periodic publication. Vargaftik, *Tables of the Thermophysical Properties of Gases and Liquids*, Wiley, New York, 1975. Vargaftik, Filippov, Tarzimanov, and Totskiy, *Thermal Conductivity of Liquids and Gases* (in Russian), Standartov, Moscow, 1978. Weast, *Handbook of Chemistry and Physics*, Chemical Rubber Co., Boca Raton, FL, annually.

TABLE 2-184 List of Substances for Which Thermodynamic Property Tables Were Generated from NIST Standard Reference Database 23

Table no.	Name	Chemical formula	Alternate name
2-185	Acetone	C ₃ H ₆ O	
2-187	Air		
2-189	Ammonia	NH ₃	
2-190	Argon	Ar	
2-193	Benzene	C ₆ H ₆	
2-195	Butane	C ₄ H ₁₀	
2-196	1-Butene	C ₄ H ₈	
2-197	<i>cis</i> -2-Butene	C ₄ H ₈	
2-198	<i>trans</i> -2-butene	C ₄ H ₈	
2-199	Carbon dioxide	CO ₂	
2-200	Carbon monoxide	CO	
2-203	Carbonyl sulfide	COS	
2-207	Cyclohexane	C ₆ H ₁₂	
2-208	Decane	C ₁₀ H ₂₂	
2-209	Deuterium oxide	D ₂ O	Heavy water
2-210	2,2-Dimethylpropane	C ₅ H ₁₄	Neopentane
2-212	Dodecane	C ₁₂ H ₂₆	
2-213	Ethane	C ₂ H ₆	
2-214	Ethanol	C ₂ H ₆ O	
2-215	Ethylene	C ₂ H ₄	
2-216	Fluorine	F ₂	
2-219	Helium	He	
2-220	Heptane	C ₇ H ₁₆	
2-221	Hexane	C ₆ H ₁₄	
2-223	Normal hydrogen	H ₂	
2-224	<i>para</i> -Hydrogen	H ₂	
2-226	Hydrogen sulfide	H ₂ S	
2-227	Isobutane	C ₄ H ₁₀	
2-228	Isobutene	C ₄ H ₈	2-methyl propene
2-229	Krypton	Kr	
2-233	Methane	CH ₄	
2-234	Methanol	CH ₄ O	
2-235	2-Methylbutane	C ₅ H ₁₂	Isopentane
2-236	2-Methylpentane	C ₆ H ₁₄	Isohexane
2-238	Neon	Ne	
2-239	Nitrogen	N ₂	
2-241	Nitrogen trifluoride	NF ₃	
2-242	Nitrous oxide	N ₂ O	
2-243	Nonane	C ₉ H ₂₀	
2-244	Octane	C ₈ H ₁₈	
2-245	Oxygen	O ₂	
2-246	Pentane	C ₅ H ₁₂	
2-248	Propane	C ₃ H ₈	
2-249	Propylene	C ₃ H ₆	
2-250	R-11	CCl ₃ F	Trichlorofluoromethane
2-251	R-12	CCL ₂ F ₂	Dichlorodifluoromethane
2-252	R-13	CClF ₃	Chlorotrifluoromethane
2-255	R-22	CHClF ₂	Chlorodifluoromethane
2-256	R-23	CHF ₃	Trifluoromethane
2-257	R-32	CH ₂ F ₂	Difluoromethane
2-258	R-41	CH ₃ F	Fluoromethane
2-271	R-113	C ₂ Cl ₃ F ₃	1,1,2-Trichlorotrifluoroethane
2-272	R-114	C ₂ Cl ₂ F ₄	1,2-Dichlorotetrafluoroethane
2-274	R-116	C ₂ F ₆	Hexafluoroethane
2-275	R-123	C ₂ HF ₅	2,2-Dichloro-1,1,1-trifluoroethane
2-276	R-124	C ₂ HClF ₄	1-Chloro-1,2,2,2-tetrafluoroethane
2-277	R-125	C ₂ HF ₅	Pentafluoroethane
2-278	R-134a	C ₂ H ₂ F ₄	1,1,1,2-Tetrafluoroethane
2-279	R-141b	C ₂ H ₂ ClF	1,1-Dichloro-1-fluoroethane
2-280	R-142b	C ₂ H ₂ ClF ₂	1-Chloro-1,1-difluoroethane
2-281	R-143a	C ₂ H ₃ F ₃	1,1,1-Trifluoroethane
2-282	R-152a	C ₂ H ₄ F ₂	1,1-Difluoroethane
2-284	R-218	C ₃ F ₈	Octafluoropropane
2-285	R227ea	C ₃ HF ₇	1,1,1,2,3,3,3-Heptafluoropropane
2-288	R-404A		
2-289	R-407C		
2-290	R-410A		
2-296	R-507A		
2-300	Sulfur dioxide	SO ₂	
2-301	Sulfur hexafluoride	SF ₆	
2-303	Toluene	C ₇ H ₈	
2-305	Water	H ₂ O	
2-307	Xenon	Xe	

TABLE 2-185 Thermodynamic Properties of Acetone

Temperature K	Pressure MPa	Density mol/dm ³	Volume dm ³ /mol	Int. energy kJ/mol	Enthalpy kJ/mol	Entropy kJ/(mol·K)	C _v kJ/(mol·K)	C _p kJ/(mol·K)	Sound speed m/s	Joule- Thomson K/MPa
Saturated Properties										
178.50	2.3265E-06	15.723	0.063601	0.47366	0.47366	0.0080825	0.082500	0.11544	1765.7	-0.43351
180.00	2.8743E-06	15.695	0.063715	0.64687	0.64687	0.0090488	0.082598	0.11550	1757.0	-0.43308
195.00	1.9454E-05	15.416	0.064868	2.3835	2.3835	0.018316	0.083407	0.11604	1672.3	-0.42849
210.00	9.6588E-05	15.141	0.066048	4.1282	4.1282	0.026935	0.084076	0.11660	1591.8	-0.42274
225.00	0.00037556	14.867	0.067264	5.8823	5.8823	0.035003	0.084758	0.11731	1514.4	-0.41520
240.00	0.0012008	14.593	0.068525	7.6487	7.6488	0.042602	0.085541	0.11825	1439.4	-0.40545
255.00	0.0032765	14.319	0.069840	9.4311	9.4314	0.049806	0.086468	0.11946	1366.3	-0.39322
270.00	0.0078514	14.041	0.071218	11.234	11.234	0.056674	0.087553	0.12094	1294.8	-0.37827
285.00	0.016899	13.760	0.072673	13.060	13.062	0.063259	0.088794	0.12270	1224.5	-0.36033
300.00	0.033259	13.474	0.074217	14.915	14.918	0.069601	0.090180	0.12474	1155.2	-0.33907
315.00	0.060720	13.181	0.075867	16.802	16.807	0.075739	0.091697	0.12704	1086.7	-0.31399
330.00	0.10404	12.880	0.077643	18.725	18.733	0.081702	0.093329	0.12962	1018.8	-0.28437
345.00	0.16891	12.568	0.079569	20.687	20.701	0.087517	0.095063	0.13249	951.24	-0.24915
360.00	0.26188	12.243	0.081677	22.693	22.714	0.093209	0.096886	0.13568	883.84	-0.20678
375.00	0.39033	11.904	0.084008	24.746	24.779	0.098798	0.098794	0.13924	816.36	-0.15495
390.00	0.56235	11.545	0.086616	26.852	26.900	0.10431	0.10078	0.14328	748.57	-0.090162
405.00	0.78681	11.163	0.089578	29.015	29.085	0.10975	0.10286	0.14794	680.21	-0.0069455
420.00	1.0733	10.753	0.093001	31.243	31.343	0.11516	0.10504	0.15350	610.99	0.10371
435.00	1.4324	10.304	0.097051	33.546	33.685	0.12056	0.10736	0.16042	540.51	0.25760
450.00	1.8759	9.8043	0.10200	35.938	36.130	0.12599	0.10986	0.16967	468.19	0.48516
465.00	2.4172	9.2319	0.10832	38.445	38.707	0.13150	0.11265	0.18350	392.99	0.85357
480.00	3.0725	8.5423	0.11706	41.117	41.476	0.13720	0.11600	0.20893	312.66	1.5474
495.00	3.8632	7.6072	0.13145	44.096	44.604	0.14341	0.12077	0.28551	221.66	3.3240
508.10	4.6924	4.7000	0.21277	49.249	50.247	0.15437			0	14.310
178.50	2.3265E-06	1.5677E-06	637.900	36.689	38.173	0.21928	0.050120	0.058440	172.60	3845.4
180.00	2.8743E-06	1.9207E-06	520.660	36.764	38.260	0.21801	0.050280	0.058600	173.29	3637.4
195.00	1.9454E-05	1.2001E-05	83.324	37.528	39.149	0.20686	0.051928	0.060265	179.95	2139.7
210.00	9.6588E-05	5.5355E-05	18.065	38.314	40.059	0.19803	0.053740	0.062119	186.29	1312.0
225.00	0.00037556	0.00020108	4.973.1	39.121	40.989	0.19103	0.055800	0.064267	192.29	834.10
240.00	0.0012008	0.00060385	1.656.0	39.947	41.936	0.18546	0.058169	0.066795	197.94	547.82
255.00	0.0032765	0.0015555	642.89	40.790	42.897	0.18104	0.060883	0.069763	203.19	370.79
270.00	0.0078514	0.0035368	282.74	41.649	43.869	0.17754	0.063945	0.073198	207.99	258.27
285.00	0.016899	0.0072603	137.74	42.522	44.849	0.17479	0.067329	0.077094	212.26	184.97
300.00	0.033259	0.013699	72.996	43.406	45.834	0.17266	0.070988	0.081429	215.93	136.14
315.00	0.060720	0.024107	41.482	44.302	46.821	0.17102	0.074863	0.086172	218.90	102.93
330.00	0.10404	0.040034	24.979	45.207	47.806	0.16980	0.078895	0.091302	221.08	79.878
345.00	0.16891	0.063362	15.782	46.119	48.784	0.16892	0.083030	0.096822	222.35	63.590
360.00	0.26188	0.096367	10.377	47.033	49.751	0.16831	0.087227	0.10277	222.60	51.884
375.00	0.39033	0.14184	7.0503	47.946	50.698	0.16791	0.091459	0.10927	221.70	43.343
390.00	0.56235	0.20329	4.9192	48.849	51.615	0.16768	0.095718	0.11649	219.53	37.032
405.00	0.78681	0.28530	3.5050	49.733	52.490	0.16754	0.10001	0.12481	215.94	32.325
420.00	1.0733	0.39420	2.5368	50.582	53.305	0.16745	0.10438	0.13483	210.76	28.797
435.00	1.4324	0.53918	1.8547	51.376	54.033	0.16734	0.10887	0.14772	203.80	26.154
450.00	1.8759	0.73472	1.3611	52.083	54.636	0.16711	0.11357	0.16583	194.82	24.184
465.00	2.4172	1.0061	0.99393	52.648	55.050	0.16664	0.11865	0.19480	183.50	22.717
480.00	3.0725	1.4051	0.71168	52.968	55.154	0.16569	0.12436	0.25197	169.39	21.551
495.00	3.8632	2.0767	0.48154	52.771	54.631	0.16367	0.13126	0.42947	151.36	20.240
508.10	4.6924	4.7000	0.21277	49.249	50.247	0.15437			0	14.310
Single-Phase Properties										
200.00	0.10000	15.325	0.065254	2.9626	2.9691	0.021248	0.083638	0.11621	1645.6	-0.42678
250.00	0.10000	14.411	0.069389	8.8328	8.8397	0.047436	0.086143	0.11902	1391.1	-0.39768
300.00	0.10000	13.475	0.074210	14.913	14.921	0.069594	0.090180	0.12473	1155.7	-0.33922
328.84	0.10000	12.903	0.077500	18.575	18.583	0.081247	0.093199	0.12941	1024.0	-0.28685
328.84	0.10000	0.038565	25.930	45.137	47.730	0.16988	0.078579	0.090892	220.94	81.384
350.00	0.10000	0.035712	28.002	46.843	49.643	0.17552	0.079533	0.090386	229.44	58.339
400.00	0.10000	0.030709	32.563	50.998	54.255	0.18783	0.085418	0.094849	246.85	30.192
450.00	0.10000	0.027083	36.923	55.474	59.166	0.19939	0.092823	0.10175	262.23	18.173
500.00	0.10000	0.024272	41.200	60.316	64.436	0.21049	0.10033	0.10903	276.40	12.201
550.00	0.10000	0.022008	45.437	65.522	70.066	0.22122	0.10753	0.11612	289.72	8.8355
200.00	1.0000	15.333	0.065220	2.9486	3.0138	0.021178	0.083649	0.11619	1649.7	-0.42708
250.00	1.0000	14.423	0.069336	8.8130	8.8824	0.047357	0.086152	0.11896	1396.0	-0.39848
300.00	1.0000	13.491	0.074123	14.885	14.959	0.069499	0.090182	0.12460	1162.0	-0.34115
350.00	1.0000	12.483	0.080107	21.312	21.392	0.089316	0.095644	0.13326	936.35	-0.24033
400.00	1.0000	11.308	0.088431	28.263	28.351	0.10788	0.10213	0.14605	707.25	-0.042437
416.48	1.0000	10.852	0.092149	30.714	30.806	0.11389	0.10452	0.15210	627.32	0.074613
416.48	1.0000	0.36582	2.7336	50.387	53.120	0.16747	0.10335	0.13228	212.13	29.536
450.00	1.0000	0.31254	3.1996	54.081	57.281	0.17709	0.10087	0.11921	233.76	20.211
500.00	1.0000	0.26538	3.7681	59.388	63.156	0.18947	0.10402	0.11743	256.99	12.984
550.00	1.0000	0.23391	4.2751	64.832	69.107	0.20081	0.10950	0.12100	275.55	9.1542

2-210 PHYSICAL AND CHEMICAL DATA

TABLE 2-185 Thermodynamic Properties of Acetone (Concluded)

Temperature K	Pressure MPa	Density mol/dm ³	Volume dm ³ /mol	Int. energy kJ/mol	Enthalpy kJ/mol	Entropy kJ/(mol·K)	C _v kJ/(mol·K)	C _p kJ/(mol·K)	Sound speed m/s	Joule- Thomson K/MPa
Single-Phase Properties										
200.00	5.0000	15.367	0.065073	2.8871	3.2125	0.020868	0.083704	0.11609	1667.9	-0.42837
250.00	5.0000	14.471	0.069106	8.7271	9.0726	0.047011	0.086197	0.11871	1417.7	-0.40187
300.00	5.0000	13.560	0.073747	14.762	15.130	0.069085	0.090197	0.12408	1189.0	-0.34909
350.00	5.0000	12.588	0.079439	21.128	21.525	0.088784	0.095584	0.13214	972.15	-0.25988
400.00	5.0000	11.490	0.087035	27.958	28.393	0.10711	0.10186	0.14320	759.27	-0.10136
450.00	5.0000	10.123	0.098782	35.450	35.944	0.12488	0.10898	0.16059	538.79	0.26123
500.00	5.0000	7.8139	0.12798	44.435	45.075	0.14406	0.11961	0.23343	262.33	2.3418
550.00	5.0000	1.7344	0.57657	60.563	63.446	0.17943	0.12191	0.17820	205.69	10.650
200.00	10.000	15.410	0.064894	2.8125	3.4614	0.020488	0.083781	0.11598	1689.9	-0.42983
250.00	10.000	14.528	0.068831	8.6237	9.3120	0.046589	0.086264	0.11843	1443.6	-0.40569
300.00	10.000	13.641	0.073307	14.616	15.349	0.068589	0.090234	0.12351	1220.9	-0.35775
350.00	10.000	12.709	0.078687	20.916	21.703	0.088163	0.095554	0.13100	1013.1	-0.27983
400.00	10.000	11.683	0.085592	27.629	28.485	0.10626	0.10166	0.14066	815.03	-0.15336
450.00	10.000	10.491	0.095320	34.864	35.818	0.12352	0.10827	0.15332	622.74	0.080235
500.00	10.000	8.9733	0.11144	42.815	43.930	0.14060	0.11552	0.17314	433.48	0.63674
550.00	10.000	6.6600	0.15015	52.079	53.581	0.15896	0.12442	0.22174	255.34	2.7218
250.00	100.00	15.320	0.065276	7.2620	13.790	0.040421	0.088285	0.11631	1791.8	-0.43634
300.00	100.00	14.657	0.068228	12.852	19.675	0.061873	0.092127	0.11946	1616.6	-0.42000
350.00	100.00	14.023	0.071312	18.631	25.763	0.080632	0.097243	0.12424	1466.4	-0.39555
400.00	100.00	13.409	0.074574	24.654	32.112	0.097579	0.10299	0.12980	1337.4	-0.36734
450.00	100.00	12.813	0.078044	30.941	38.745	0.11320	0.10892	0.13553	1226.9	-0.33807
500.00	100.00	12.234	0.081739	37.489	45.663	0.12777	0.11478	0.14112	1133.0	-0.30922
550.00	100.00	11.674	0.085664	44.286	52.852	0.14147	0.12045	0.14639	1053.8	-0.28171
450.00	500.00	15.616	0.064037	27.237	59.256	0.097266	0.11562	0.13393	2201.1	-0.39010
500.00	500.00	15.306	0.065335	33.413	66.081	0.11164	0.12123	0.13909	2129.8	-0.37710
550.00	500.00	15.012	0.066615	39.856	73.163	0.12514	0.12669	0.14416	2067.5	-0.36510

The values in this table were generated from the NIST REFPROP software (Lemmon, E. W., McLinden, M. O., and Huber, M. L., NIST Standard Reference Database 23: Reference Fluid Thermodynamic and Transport Properties—REFPROP, National Institute of Standards and Technology, Standard Reference Data Program, Gaithersburg, Md., 2002, Version 7.1). The primary source for the thermodynamic properties is Lemmon, E. W., and Span, R., "Short Fundamental Equations of State for 20 Industrial Fluids," *J. Chem. Eng. Data*, **51**(3):785–850, 2006. Validated equations for the viscosity and thermal conductivity are not currently available for this fluid.

Properties at the triple point temperature and the critical point temperature are given in the first and last entries of the saturation tables, respectively. In the single-phase table, when the temperature range for a given isobar includes a vapor-liquid phase boundary, the temperature of phase equilibrium is noted, and properties for both the saturated liquid and saturated vapor are given (with liquid properties given in the upper line). Lines are omitted from the temperature-pressure grid of the single-phase table, when the system would be in the solid phase or if there are potential problems with the source property surface.

The uncertainties in the equation of state are 0.1% in the saturated liquid density between 280 and 310 K, 0.5% in density in the liquid phase below 380 K, and 1% in density elsewhere, including all states at pressures above 100 MPa. The uncertainties in vapor pressure are 0.5% above 270 K (0.25% between 290 and 390 K), and the uncertainties in heat capacities and speeds of sound are 1%. These uncertainties (in caloric properties and sound speeds) may be higher at pressures above the saturation pressure and at temperatures above 320 K in the liquid phase and at supercritical conditions.

TABLE 2-186 Saturated Acetylene*

Temperature, K	Pressure, bar	v _{cond} , m ³ /kg	v _g , m ³ /kg	h _{cond} , kJ/kg	h _g , kJ/kg	s _{cond} , kJ/(kg·K)	s _g , kJ/(kg·K)
162.0	0.101		5.081	158	983	2.967	8.062
169.3	0.203		2.644	173	994	3.039	7.889
173.9	0.304		1.805	182	999	3.095	7.797
180.0	0.507		1.116	194	1007	3.161	7.672
184.3	0.709		0.810	203	1011	3.216	7.596
189.1	1.013		0.5780	214	1015	3.272	7.511
192.4 ^a	1.283		0.4617	221	1018	3.312	7.455
192.4 ^c	1.283	0.00164	0.4617	378	1018	4.127	7.455
200.9	2.027	0.00165	0.3011	411	1027	4.296	7.362
209.4	3.040	0.00169	0.2074	445	1035	4.461	7.280
221.5	5.066	0.00174	0.1264	493	1046	4.684	7.180
230.4	7.093	0.00179	0.0907	528	1052	4.837	7.111
240.7	10.13	0.00186	0.0635	565	1058	4.990	7.037
253.2	15.20	0.00195	0.0420	602	1061	5.133	6.947
263.0	20.27	0.00204	0.0309	628	1061	5.231	6.878
271.6	25.33	0.00213	0.0240	654	1060	5.326	6.822
278.9	30.40	0.00223	0.0193	680	1057	5.414	6.767
284.9	35.46	0.00232	0.0159	704	1051	5.494	6.716
290.4	40.53	0.00242	0.0133	727	1041	5.576	6.658
300.0	50.66	0.00270	0.0093	778	1017	5.737	6.534
307.8	60.80	0.00335	0.0061	850	968	5.965	6.351
308.7 ^c	62.47	0.00434	0.0043	908	908	6.158	6.158

*Values recalculated into SI units from those of Din, *Thermodynamic Functions of Gases*, vol. 2, Butterworth, London, 1956. Above the solid line the condensed phase is solid; below the line it is liquid. t = triple point; c = critical point.

TABLE 2-187 Thermodynamic Properties of Air

Temperature K	Pressure MPa	Density mol/dm ³	Volume dm ³ /mol	Int. energy kJ/mol	Enthalpy kJ/mol	Entropy kJ/(mol·K)	C _v kJ/(mol·K)	C _p kJ/(mol·K)	Sound speed m/s	Joule- Thomson K/MPa	Therm. cond. mW/(m·K)	Viscosity μPa·s
Saturated Properties												
59.75	0.005265	33.067	0.030242	-1.0619	-1.0617	-0.01536	0.034011	0.055064	1030.3	-0.40785	171.43	376.64
60	0.005546	33.031	0.030275	-1.0481	-1.0480	-0.01513	0.033955	0.055062	1028.3	-0.40743	171.02	371.92
61	0.006797	32.888	0.030406	-0.99308	-0.99287	-0.01422	0.033731	0.055060	1020.3	-0.40565	169.40	353.83
62	0.008270	32.745	0.030539	-0.93803	-0.93778	-0.01333	0.033512	0.055062	1012.2	-0.40375	167.78	336.91
63	0.009994	32.601	0.030674	-0.88298	-0.88267	-0.01245	0.033298	0.055069	1004.0	-0.40173	166.16	321.09
64	0.012000	32.457	0.030810	-0.82792	-0.82755	-0.01158	0.033089	0.055081	995.77	-0.39958	164.53	306.27
65	0.014320	32.312	0.030949	-0.77286	-0.77241	-0.01073	0.032884	0.055098	987.48	-0.39729	162.91	292.39
66	0.016988	32.166	0.031089	-0.71777	-0.71725	-0.00989	0.032683	0.055120	979.13	-0.39485	161.28	279.38
67	0.020042	32.020	0.031231	-0.66267	-0.66205	-0.00906	0.032486	0.055148	970.72	-0.39227	159.65	267.17
68	0.023520	31.873	0.031375	-0.60755	-0.60681	-0.00824	0.032294	0.055181	962.24	-0.38952	158.01	255.71
69	0.027461	31.725	0.031521	-0.55239	-0.55152	-0.00744	0.032105	0.055220	953.70	-0.38660	156.37	244.94
70	0.031908	31.576	0.031669	-0.49720	-0.49619	-0.00664	0.031920	0.055266	945.10	-0.38352	154.73	234.81
71	0.036905	31.427	0.031820	-0.44196	-0.44079	-0.00586	0.031739	0.055317	936.43	-0.38024	153.09	225.28
72	0.042498	31.277	0.031972	-0.38669	-0.38533	-0.00508	0.031562	0.055376	927.70	-0.37677	151.44	216.31
73	0.048733	31.126	0.032127	-0.33135	-0.32979	-0.00432	0.031388	0.055441	918.90	-0.37310	149.79	207.85
74	0.055659	30.974	0.032285	-0.27597	-0.27417	-0.00357	0.031217	0.055514	910.04	-0.36922	148.14	199.88
75	0.063326	30.821	0.032445	-0.22051	-0.21846	-0.00282	0.031050	0.055594	901.11	-0.36511	146.49	192.35
76	0.071786	30.668	0.032608	-0.16499	-0.16265	-0.00209	0.030886	0.055682	892.11	-0.36076	144.83	185.23
77	0.081091	30.513	0.032773	-0.10939	-0.10673	-0.00136	0.030725	0.055779	883.05	-0.35616	143.16	178.51
78	0.091294	30.357	0.032941	-0.05371	-0.05070	-0.00064	0.030568	0.055884	873.91	-0.35130	141.50	172.14
79	0.10245	30.200	0.033112	0.002063	0.005456	6.86E-05	0.030413	0.055988	864.71	-0.34616	139.83	166.11
80	0.11462	30.042	0.033287	0.057934	0.061749	0.000772	0.030262	0.056122	855.44	-0.34074	138.15	160.39
81	0.12785	29.883	0.033464	0.11391	0.11819	0.001467	0.030113	0.056256	846.09	-0.33500	136.48	154.96
82	0.14221	29.722	0.033645	0.17000	0.17478	0.002156	0.029968	0.056400	836.67	-0.32894	134.80	149.80
83	0.15775	29.560	0.033829	0.22621	0.23155	0.002838	0.029826	0.056556	827.18	-0.32254	133.11	144.90
84	0.17453	29.397	0.034017	0.28255	0.28849	0.003513	0.029686	0.056723	817.61	-0.31577	131.42	140.23
85	0.19262	29.232	0.034209	0.33903	0.34562	0.004181	0.029550	0.056902	807.96	-0.30862	129.78	135.78
86	0.21207	29.066	0.034404	0.39566	0.40296	0.004844	0.029417	0.057094	798.24	-0.30107	128.11	131.54
87	0.23295	28.898	0.034604	0.45245	0.46051	0.005501	0.029286	0.057300	788.44	-0.29308	126.44	127.50
88	0.25531	28.729	0.034808	0.50940	0.51829	0.006153	0.029158	0.057521	778.56	-0.28464	124.76	123.63
89	0.27922	28.558	0.035017	0.56653	0.57631	0.006799	0.029033	0.057757	768.59	-0.27572	123.07	119.93
90	0.30475	28.385	0.035230	0.62386	0.63459	0.007440	0.028911	0.058009	758.55	-0.26628	121.38	116.38
91	0.33196	28.210	0.035449	0.68138	0.69315	0.008077	0.028792	0.058278	748.42	-0.25629	119.69	112.98
92	0.36091	28.033	0.035672	0.73912	0.75199	0.008708	0.028676	0.058566	738.20	-0.24573	118.00	109.72
93	0.39166	27.854	0.035901	0.79709	0.81115	0.009336	0.028563	0.058874	727.90	-0.23455	116.30	106.59
94	0.42429	27.673	0.036137	0.85529	0.87062	0.009960	0.028453	0.059202	717.51	-0.22270	114.61	103.58
95	0.45886	27.489	0.036378	0.91375	0.93044	0.010579	0.028346	0.059553	707.03	-0.21016	112.91	100.68
96	0.49543	27.304	0.036625	0.97248	0.99063	0.011195	0.028241	0.059928	696.46	-0.19686	111.21	97.879
97	0.53408	27.115	0.036880	1.0315	1.0512	0.011808	0.028140	0.060329	685.80	-0.18275	109.51	95.179
98	0.57486	26.924	0.037142	1.0908	1.1122	0.012418	0.028042	0.060757	675.05	-0.16779	107.81	92.571
99	0.61786	26.730	0.037411	1.1505	1.1736	0.013025	0.027948	0.061216	664.20	-0.15189	106.11	90.048
100	0.66313	26.533	0.037688	1.2104	1.2354	0.013630	0.027856	0.061707	653.26	-0.13501	104.41	87.605
101	0.71074	26.333	0.037975	1.2708	1.2978	0.014232	0.027768	0.062232	642.22	-0.11705	102.71	85.236
102	0.76077	26.130	0.038270	1.3315	1.3606	0.014833	0.027684	0.062796	631.08	-0.09794	101.01	82.937
103	0.81329	25.923	0.038575	1.3926	1.4240	0.015431	0.027603	0.063401	619.84	-0.07758	99.316	80.703
104	0.86836	25.713	0.038891	1.4542	1.4880	0.016029	0.027525	0.064052	608.50	-0.05588	97.623	78.529
105	0.92606	25.499	0.039217	1.5162	1.5525	0.016625	0.027452	0.064753	597.06	-0.03271	95.933	76.412
106	0.98645	25.281	0.039556	1.5787	1.6177	0.017221	0.027383	0.065508	585.51	-0.00795	94.247	74.347
107	1.0496	25.058	0.039908	1.6417	1.6836	0.017816	0.027317	0.066323	573.85	0.018543	92.565	72.331
108	1.1156	24.831	0.040273	1.7053	1.7502	0.018411	0.027256	0.067206	562.09	0.046927	90.888	70.361
109	1.1845	24.598	0.040653	1.7695	1.8176	0.019006	0.027200	0.068163	550.21	0.077386	89.216	68.432
110	1.2564	24.361	0.041050	1.8343	1.8858	0.019602	0.027149	0.069205	538.21	0.11012	87.551	66.542
111	1.3314	24.118	0.041464	1.8997	1.9549	0.020200	0.027103	0.070341	526.10	0.14538	85.893	64.688
112	1.4095	23.868	0.041896	1.9659	2.0250	0.020799	0.027062	0.071585	513.86	0.18342	84.242	62.867
113	1.4908	23.613	0.042350	2.0329	2.0960	0.021400	0.027028	0.072951	501.48	0.22456	82.599	61.075
114	1.5753	23.350	0.042826	2.1007	2.1682	0.022004	0.027000	0.074459	488.97	0.26917	80.965	59.311

TABLE 2-187 Thermodynamic Properties of Air (Continued)

Temperature K	Pressure MPa	Density mol/dm ³	Volume dm ³ /mol	Int. energy kJ/mol	Enthalpy kJ/mol	Entropy kJ/(mol·K)	C _v kJ/(mol·K)	C _p kJ/(mol·K)	Sound speed m/s	Joule- Thomson K/MPa	Therm. cond. mW/(m·K)	Viscosity μPa·s
Saturated Properties												
115	1.6633	23.080	0.043328	2.1695	2.2415	0.022611	0.026979	0.076131	476.31	0.31767	79.340	57.571
116	1.7546	22.801	0.043857	2.2392	2.3161	0.023223	0.026965	0.077996	463.48	0.37057	77.724	55.852
117	1.8495	22.514	0.044417	2.3100	2.3922	0.023840	0.026961	0.080090	450.49	0.42848	76.119	54.152
118	1.9479	22.217	0.045011	2.3821	2.4697	0.024462	0.026966	0.082459	437.29	0.49214	74.523	52.467
119	2.0499	21.908	0.045645	2.4554	2.5490	0.025092	0.026982	0.085163	423.88	0.56243	72.938	50.794
120	2.1557	21.588	0.046323	2.5303	2.6302	0.025731	0.027010	0.088280	410.23	0.64047	71.363	49.130
121	2.2653	21.253	0.047052	2.6069	2.7135	0.026380	0.027053	0.091919	396.30	0.72765	69.798	47.469
122	2.3787	20.903	0.047841	2.6854	2.7992	0.027041	0.027113	0.096227	382.04	0.82574	68.243	45.809
123	2.4960	20.534	0.048700	2.7662	2.8878	0.027717	0.027194	0.10142	367.40	0.93703	66.700	44.141
124	2.6173	20.144	0.049643	2.8496	2.9796	0.028412	0.027300	0.10781	352.31	1.0646	65.170	42.460
125	2.7427	19.727	0.050691	2.9363	3.0753	0.029131	0.027438	0.11589	336.67	1.2125	63.658	40.755
126	2.8721	19.278	0.051871	3.0269	3.1759	0.029880	0.027618	0.12645	320.36	1.3865	62.176	39.013
127	3.0055	18.788	0.053225	3.1227	3.2827	0.030668	0.027855	0.14089	303.21	1.5951	60.751	37.215
128	3.1431	18.242	0.054818	3.2253	3.3976	0.031512	0.028171	0.16186	285.00	1.8510	59.445	35.332
129	3.2845	17.616	0.056765	3.3379	3.5243	0.032436	0.028607	0.19519	265.37	2.1752	58.409	33.316
130	3.4295	16.863	0.059300	3.4661	3.6695	0.033492	0.029242	0.25624	243.75	2.6058	58.054	31.072
131	3.5770	15.869	0.063015	3.6243	3.8497	0.034804	0.030266	0.40151	219.07	3.2246	59.591	28.384
132	3.7228	14.198	0.070432	3.8680	4.1302	0.036863	0.032343	1.0148	189.12	4.2808	67.802	24.467
132.63	3.7858	10.448	0.095715	4.4004	4.7627	0.041603			0	6.3978		
59.75	0.002432	0.004907	203.80	4.8774	5.3730	0.096708	0.020805	0.029217	154.83	58.283	5.2938	4.2197
60	0.002584	0.005192	192.59	4.8825	5.3800	0.096323	0.020809	0.029225	155.14	57.634	5.3199	4.2382
61	0.003274	0.006475	154.45	4.9025	5.4081	0.094825	0.020825	0.029261	156.38	55.151	5.4244	4.3119
62	0.004111	0.008005	124.93	4.9225	5.4361	0.093392	0.020843	0.029302	157.60	52.832	5.5291	4.3855
63	0.005120	0.009817	101.86	4.9424	5.4639	0.092020	0.020864	0.029348	158.81	50.666	5.6340	4.4590
64	0.006325	0.011948	83.693	4.9621	5.4915	0.090705	0.020886	0.029399	159.99	48.640	5.7391	4.5324
65	0.007756	0.014438	69.263	4.9817	5.5189	0.089445	0.020911	0.029455	161.16	46.742	5.8444	4.6057
66	0.009442	0.017326	57.715	5.0012	5.5461	0.088235	0.020938	0.029518	162.30	44.963	5.9500	4.6788
67	0.011416	0.020659	48.406	5.0205	5.5731	0.087074	0.020968	0.029587	163.42	43.293	6.0559	4.7519
68	0.013713	0.024481	40.849	5.0397	5.5998	0.085959	0.021000	0.029663	164.53	41.724	6.1621	4.8248
69	0.016372	0.028841	34.673	5.0587	5.6263	0.084887	0.021035	0.029746	165.60	40.248	6.2688	4.8976
70	0.019431	0.033789	29.595	5.0774	5.6525	0.083855	0.021072	0.029836	166.66	38.858	6.3759	4.9703
71	0.022933	0.039379	25.394	5.0960	5.6784	0.082862	0.021113	0.029934	167.69	37.548	6.4835	5.0429
72	0.026921	0.045664	21.899	5.1144	5.7040	0.081906	0.021156	0.030040	168.70	36.313	6.5917	5.1154
73	0.031443	0.052702	18.975	5.1326	5.7292	0.080983	0.021201	0.030155	169.69	35.146	6.7005	5.1878
74	0.036547	0.060550	16.515	5.1505	5.7541	0.080094	0.021250	0.030278	170.65	34.043	6.8099	5.2602
75	0.042282	0.069268	14.437	5.1682	5.7786	0.079235	0.021302	0.030410	171.58	32.999	6.9202	5.3325
76	0.048702	0.078918	12.671	5.1856	5.8027	0.078406	0.021356	0.030552	172.49	32.010	7.0312	5.4048
77	0.055859	0.089564	11.165	5.2028	5.8264	0.077604	0.021414	0.030703	173.37	31.072	7.1431	5.4771
78	0.063810	0.10127	9.8746	5.2196	5.8497	0.076828	0.021474	0.030865	174.23	30.183	7.2560	5.5494
79	0.072611	0.11410	8.7639	5.2362	5.8726	0.076076	0.021538	0.031037	175.05	29.337	7.3700	5.6217
80	0.082321	0.12813	7.8043	5.2525	5.8949	0.075348	0.021605	0.031220	175.85	28.534	7.4851	5.6940
81	0.093001	0.14343	6.9721	5.2684	5.9169	0.074643	0.021674	0.031415	176.62	27.769	7.6014	5.7664
82	0.10471	0.16006	6.2475	5.2841	5.9383	0.073957	0.021747	0.031621	177.36	27.041	7.7192	5.8389
83	0.11751	0.17811	5.6145	5.2994	5.9591	0.073292	0.021822	0.031840	178.07	26.346	7.8384	5.9116
84	0.13147	0.19765	5.0595	5.3143	5.9795	0.072645	0.021901	0.032072	178.75	25.684	7.9591	5.9844
85	0.14665	0.21875	4.5715	5.3289	5.9993	0.072016	0.021983	0.032317	179.40	25.051	8.0817	6.0574
86	0.16312	0.24150	4.1408	5.3431	6.0185	0.071403	0.022068	0.032577	180.02	24.447	8.2060	6.1307
87	0.18094	0.26598	3.7597	5.3569	6.0372	0.070806	0.022155	0.032851	180.61	23.869	8.3324	6.2043
88	0.20018	0.29228	3.4214	5.3703	6.0552	0.070224	0.022246	0.033141	181.17	23.316	8.4610	6.2781
89	0.22091	0.32048	3.1203	5.3832	6.0726	0.069655	0.022340	0.033447	181.69	22.786	8.5919	6.3524
90	0.24320	0.35068	2.8516	5.3958	6.0893	0.069099	0.022436	0.033770	182.19	22.278	8.7254	6.4272
91	0.26712	0.38298	2.6111	5.4079	6.1054	0.068556	0.022536	0.034111	182.65	21.791	8.8616	6.5024
92	0.29273	0.41747	2.3954	5.4195	6.1207	0.068024	0.022638	0.034472	183.08	21.324	9.0008	6.5782
93	0.32011	0.45426	2.2014	5.4307	6.1354	0.067503	0.022744	0.034853	183.47	20.875	9.1433	6.6547
94	0.34934	0.49345	2.0265	5.4413	6.1492	0.066991	0.022852	0.035256	183.84	20.446	9.2893	6.7318
95	0.38047	0.53517	1.8686	5.4514	6.1624	0.066489	0.022964	0.035681	184.17	20.031	9.4390	6.8098
96	0.41359	0.57953	1.7255	5.4610	6.1747	0.065995	0.023078	0.036132	184.46	19.632	9.5929	6.8887

97	0.44878	0.62667	1.5957	5.4701	6.1862	0.065510	0.023196	0.036610	184.72	19.249	9.7513	6.9686
98	0.48609	0.67671	1.4777	5.4785	6.1968	0.065031	0.023317	0.037116	184.95	18.879	9.9145	7.0495
99	0.52562	0.72980	1.3702	5.4864	6.2066	0.064560	0.023441	0.037654	185.14	18.523	10.083	7.1317
100	0.56742	0.78609	1.2721	5.4936	6.2154	0.064094	0.023568	0.038225	185.30	18.180	10.257	7.2153
101	0.61159	0.84575	1.1824	5.5002	6.2233	0.063633	0.023698	0.038834	185.42	17.848	10.438	7.3003
102	0.65820	0.90895	1.1002	5.5060	6.2302	0.063177	0.023833	0.039483	185.51	17.528	10.626	7.3870
103	0.70732	0.97587	1.0247	5.5112	6.2360	0.062726	0.023970	0.040176	185.55	17.218	10.821	7.4755
104	0.75903	1.0467	0.95535	5.5156	6.2408	0.062277	0.024112	0.040918	185.57	16.918	11.024	7.5659
105	0.81341	1.1217	0.89147	5.5193	6.2444	0.061832	0.024258	0.041714	185.54	16.628	11.237	7.6586
106	0.87055	1.2011	0.83254	5.5221	6.2469	0.061389	0.024400	0.042570	185.48	16.346	11.459	7.7537
107	0.93052	1.2852	0.77810	5.5240	6.2481	0.060947	0.024563	0.043492	185.38	16.072	11.693	7.8514
108	0.9934	1.3742	0.72772	5.5250	6.2480	0.060506	0.024722	0.044490	185.24	15.805	11.939	7.9521
109	1.0593	1.4684	0.68102	5.5251	6.2465	0.060065	0.024887	0.045573	185.07	15.546	12.198	8.0560
110	1.1282	1.5682	0.63767	5.5241	6.2436	0.059623	0.025058	0.046751	184.85	15.292	12.473	8.1634
111	1.2004	1.6740	0.59737	5.5221	6.2391	0.059180	0.025234	0.048038	184.60	15.044	12.764	8.2749
112	1.2757	1.7862	0.55985	5.5188	6.2330	0.058735	0.025418	0.049450	184.30	14.800	13.074	8.3907
113	1.3545	1.9053	0.52486	5.5143	6.2252	0.058286	0.025608	0.051005	183.97	14.561	13.406	8.5114
114	1.4366	2.0318	0.49217	5.5085	6.2156	0.057833	0.025807	0.052727	183.59	14.324	13.762	8.6375
115	1.5223	2.1664	0.46160	5.5012	6.2039	0.057375	0.026015	0.054644	183.17	14.090	14.145	8.7696
116	1.6115	2.3097	0.43296	5.4924	6.1901	0.056910	0.026232	0.056790	182.71	13.856	14.559	8.9086
117	1.7045	2.4625	0.40608	5.4819	6.1740	0.056437	0.026461	0.059209	182.21	13.623	15.008	9.0552
118	1.8013	2.6259	0.38082	5.4695	6.1554	0.055955	0.026701	0.061956	181.66	13.388	15.499	9.2104
119	1.9020	2.8009	0.35702	5.4550	6.1341	0.055461	0.026956	0.065102	181.08	13.151	16.039	9.3755
120	2.0067	2.9889	0.33457	5.4383	6.1097	0.054954	0.027226	0.068738	180.45	12.909	16.635	9.5518
121	2.1156	3.1913	0.31335	5.4190	6.0819	0.054432	0.027514	0.072988	179.78	12.661	17.298	9.7412
122	2.2287	3.4103	0.29323	5.3969	6.0504	0.053890	0.027823	0.078015	179.06	12.405	18.042	9.9456
123	2.3462	3.6481	0.27412	5.3715	6.0147	0.053326	0.028155	0.084052	178.31	12.137	18.884	10.168
124	2.4682	3.9078	0.25590	5.3424	5.9740	0.052735	0.028516	0.091426	177.51	11.854	19.849	10.411
125	2.5949	4.1934	0.23847	5.3089	5.9277	0.052112	0.028910	0.10063	176.68	11.553	20.968	10.681
126	2.7266	4.5101	0.22173	5.2701	5.8746	0.051448	0.029344	0.11241	175.81	11.229	22.288	10.982
127	2.8633	4.8653	0.20554	5.2248	5.8133	0.050732	0.029827	0.12801	174.91	10.874	23.877	11.324
128	3.0055	5.2697	0.18976	5.1713	5.7417	0.049950	0.030371	0.14959	173.96	10.480	25.841	11.720
129	3.1536	5.7405	0.17420	5.1069	5.6563	0.049076	0.030994	0.18134	172.98	10.033	28.367	12.191
130	3.3084	6.3074	0.15854	5.0268	5.5513	0.048067	0.031726	0.23261	171.93	9.5119	31.807	12.775
131	3.4712	7.0343	0.14216	4.9209	5.4143	0.046830	0.032619	0.32992	170.79	8.8740	37.001	13.553
132	3.6462	8.1273	0.12304	4.7566	5.2053	0.045064	0.033814	0.59804	169.40	7.9854	46.996	14.798
132.63	3.7858	10.448	0.095715	4.4004	4.7627	0.041603			0	6.3978		

Single-Phase Properties

100	0.1	0.12283	8.1414	5.6800	6.4941	0.080463	0.021087	0.030116	198.24	17.423	9.4692	7.1068
300	0.1	0.040103	24.936	9.8544	12.348	0.11269	0.020796	0.029149	347.36	2.2510	26.384	18.537
500	0.1	0.024046	41.586	14.072	18.231	0.12770	0.021504	0.029830	446.40	0.50305	39.944	27.090
700	0.1	0.017175	58.223	18.500	24.323	0.13794	0.022817	0.031137	523.89	-0.12430	51.755	34.176
900	0.1	0.013359	74.855	23.201	30.686	0.14593	0.024150	0.032467	589.60	-0.41124	62.543	40.394
1100	0.1	0.010931	91.486	28.145	37.293	0.15255	0.025246	0.033562	648.15	-0.56194	72.680	46.051
1300	0.1	0.009249	108.12	33.282	44.094	0.15823	0.026091	0.034406	701.76	-0.64963	82.351	51.325
1500	0.1	0.008016	124.75	38.568	51.042	0.16320	0.026734	0.035049	751.59	-0.70457	91.781	56.325
1700	0.1	0.007073	141.38	43.966	58.104	0.16762	0.027229	0.035544	798.38	-0.74078	100.97	61.127
1900	0.1	0.006329	158.00	49.453	65.253	0.17160	0.027619	0.035934	842.62	-0.76547	110.01	65.783
100	1	26.593	0.037604	1.2007	1.2383	0.013532	0.027868	0.061355	658.25	-0.14308	104.97	88.326
106.22	1	25.232	0.039632	1.5924	1.6321	0.017351	0.027368	0.065680	582.97	-0.00232	93.879	73.903
108.1	1	1.3836	0.72278	5.5251	6.2479	0.060461	0.024739	0.044597	185.23	15.779	11.965	7.9625
300	1	0.40205	2.4873	9.8022	12.289	0.093372	0.020859	0.029563	348.45	2.1789	26.684	18.672
500	1	0.23974	4.1711	14.046	18.218	0.10851	0.021526	0.029954	448.46	0.47425	40.110	27.179
700	1	0.17119	5.8415	18.485	24.326	0.11877	0.022830	0.031194	525.96	-0.13809	51.868	34.242
900	1	0.13319	7.5079	23.190	30.698	0.12677	0.024159	0.032498	591.54	-0.41899	62.628	40.446
1100	1	0.10902	9.1727	28.138	37.311	0.13340	0.025253	0.033582	649.96	-0.56686	72.748	46.094
1300	1	0.092279	10.837	33.278	44.114	0.13908	0.026096	0.034419	703.44	-0.65304	82.438	51.361
1500	1	0.079999	12.500	38.565	51.065	0.14405	0.026738	0.035057	753.17	-0.70711	91.830	56.357
1700	1	0.070604	14.163	43.964	58.128	0.14847	0.027233	0.035550	799.86	-0.74278	101.01	61.155
1900	1	0.063185	15.827	49.451	65.278	0.15245	0.027622	0.035939	844.02	-0.76711	110.05	65.808
100	5	27.222	0.036735	1.0983	1.2820	0.012483	0.028034	0.058181	710.56	-0.21837	111.13	96.436
300	5	2.0232	0.49426	9.5710	12.042	0.079244	0.021131	0.031423	355.63	1.8817	28.389	19.420

TABLE 2-187 Thermodynamic Properties of Air (Concluded)

2-214

Temperature K	Pressure MPa	Density mol/dm ³	Volume dm ³ /mol	Int. energy kJ/mol	Enthalpy kJ/mol	Entropy kJ/(mol·K)	C _v kJ/(mol·K)	C _p kJ/(mol·K)	Sound speed m/s	Joule- Thomson K/MPa	Therm. cond. mW/(m·K)	Viscosity μPa·s
Single Phase Properties												
500	5	1.1814	0.84642	13.935	18.167	0.094907	0.021621	0.030478	458.30	0.36370	40.969	27.606
700	5	0.84321	1.1859	18.417	24.347	0.10529	0.022885	0.031434	535.45	-0.19118	52.433	34.545
900	5	0.65711	1.5218	23.146	30.755	0.11334	0.024197	0.032632	600.34	-0.44905	63.045	40.682
1100	5	0.53874	1.8562	28.107	37.388	0.11999	0.025282	0.033664	658.10	-0.58606	73.076	46.287
1300	5	0.45667	2.1898	33.256	44.205	0.12568	0.026119	0.034473	711.01	-0.66646	82.707	51.523
1500	5	0.39636	2.5229	38.550	51.165	0.13066	0.026757	0.035095	760.23	-0.71716	92.057	56.497
1700	5	0.35015	2.8559	43.954	58.234	0.13509	0.027249	0.035577	806.49	-0.75073	101.21	61.278
1900	5	0.31361	3.1887	49.445	65.389	0.13907	0.027636	0.035958	850.28	-0.77366	110.22	65.917
100	10	27.863	0.035889	0.99444	1.3533	0.011382	0.028284	0.055716	763.47	-0.27969	117.77	105.78
300	10	4.0370	0.24771	9.2885	11.766	0.072612	0.021441	0.033664	369.50	1.5212	31.116	20.637
500	10	2.3157	0.43183	13.802	18.120	0.088894	0.021733	0.031078	471.81	0.25100	42.260	28.194
700	10	1.6542	0.60452	18.336	24.382	0.099422	0.022952	0.031710	547.83	-0.24405	53.257	34.944
900	10	1.2922	0.77388	23.092	30.831	0.10752	0.024243	0.032786	611.64	-0.47890	63.641	40.985
1100	10	1.0618	0.94184	28.070	37.489	0.11420	0.025317	0.033760	668.47	-0.60517	73.538	46.531
1300	10	0.90165	1.1091	33.231	44.321	0.11990	0.026146	0.034537	720.60	-0.67990	83.082	51.728
1500	10	0.78374	1.2759	38.532	51.292	0.12489	0.026780	0.035139	769.17	-0.72730	92.372	56.673
1700	10	0.69321	1.4426	43.943	58.368	0.12932	0.027268	0.035608	814.87	-0.75881	101.48	61.432
1900	10	0.62149	1.6090	49.438	65.528	0.13330	0.027653	0.035981	858.18	-0.78039	110.45	66.054
100	100	33.161	0.030156	0.24746	3.2631	0.001378	0.031980	0.048218	1192.4	-0.47290	179.20	252.46
300	100	21.138	0.047309	7.0356	11.767	0.049067	0.023981	0.038366	818.47	-0.49747	86.312	53.642
500	100	15.089	0.066273	12.371	18.999	0.067619	0.023117	0.034686	772.41	-0.55640	71.549	42.159
700	100	11.803	0.084722	17.367	25.840	0.079134	0.023855	0.034011	790.14	-0.62591	73.572	43.339
900	100	9.7481	0.10258	22.408	32.667	0.087711	0.024903	0.034331	821.78	-0.67702	79.057	46.948
1100	100	8.3307	0.12004	27.580	39.584	0.09465	0.025831	0.034845	857.40	-0.71435	85.797	51.158
1300	100	7.2877	0.13722	32.880	46.602	0.10051	0.026565	0.035323	894.00	-0.74281	93.151	55.511
1500	100	6.4847	0.15421	38.287	53.708	0.10559	0.027131	0.035723	930.40	-0.76506	100.84	59.875
1700	100	5.8456	0.17107	43.779	60.886	0.11009	0.027569	0.036049	966.13	-0.78264	108.75	64.208
1900	100	5.3239	0.18783	49.340	68.123	0.11411	0.027915	0.036317	1001.0	-0.79653	116.78	68.504
300	500	34.106	0.029320	6.2145	20.875	0.033155	0.028875	0.039265	1678.8	-0.57656	208.23	181.12
500	500	29.826	0.033528	11.583	28.348	0.052311	0.026614	0.036111	1573.6	-0.65015	178.50	120.62
700	500	26.714	0.037433	16.768	35.484	0.064323	0.026496	0.035494	1514.8	-0.67879	161.67	97.470
900	500	24.283	0.041180	22.008	42.598	0.073261	0.026991	0.035702	1482.8	-0.68796	151.95	86.531
1100	500	22.305	0.044833	27.358	49.775	0.080460	0.027539	0.036073	1468.3	-0.69130	146.88	81.387
1300	500	20.651	0.048423	32.814	57.025	0.086515	0.028000	0.036415	1465.1	-0.69354	144.95	79.311
1500	500	19.243	0.051966	38.354	64.337	0.091746	0.028336	0.036693	1469.3	-0.69594	145.84	79.412
1700	500	18.027	0.055473	43.961	71.698	0.096353	0.02864	0.036911	1478.5	-0.69875	148.48	80.393
1900	500	16.963	0.058952	49.623	79.098	0.10047	0.02886	0.037085	1491.1	-0.70188	152.39	82.251
300	1000	40.130	0.024919	6.8286	31.747	0.024761	0.032271	0.041510	2208.5	-0.50493	274.96	337.76
500	1000	36.567	0.027347	12.271	39.618	0.044944	0.029334	0.037843	2104.7	-0.57316	247.30	219.41
700	1000	33.895	0.029503	17.554	47.057	0.057468	0.028754	0.036801	2033.9	-0.60504	230.60	174.51
900	1000	31.736	0.031510	22.890	54.399	0.066695	0.028917	0.036702	1984.7	-0.61882	219.72	149.43
1100	1000	29.916	0.033427	28.327	61.754	0.074073	0.029215	0.036558	1951.3	-0.62560	212.46	133.76
1300	1000	28.338	0.035288	33.857	69.145	0.080246	0.029476	0.037051	1929.3	-0.62968	207.70	123.58
1500	1000	26.946	0.037111	39.461	76.573	0.085561	0.029675	0.037224	1915.7	-0.63251	204.81	116.94
1700	1000	25.701	0.038909	45.123	84.032	0.090229	0.029821	0.037369	1908.3	-0.63465	203.41	112.74
1900	1000	24.577	0.040688	50.830	91.519	0.094392	0.029928	0.037491	1905.8	-0.63632	203.25	110.27

This table was generated for a standard three-component dry air containing mole fractions 0.7812 nitrogen, 0.2096 oxygen, and 0.0092 argon. The values in this table were generated from the NIST REFPROP software (Lemmon, E. W., McLinden, M. O., and Huber, M. L., NIST Standard Reference Database 23: Reference Fluid Thermodynamic and Transport Properties—REFPROP, National Institute of Standards and Technology, Standard Reference Data Program, Gaithersburg, Md., 2002, Version 7.1). The primary source for the thermodynamic properties is Lemmon, E. W., Jacobsen, R. T., Penoncello, S. G., and Friend, D. G., "Thermodynamic Properties of Air and Mixtures of Nitrogen, Argon, and Oxygen from 60 to 2000 K at Pressures to 2000 MPa," *J. Phys. Chem. Ref. Data* **29**(3):331–385, 2000. The source for viscosity and thermal conductivity is Lemmon, E. W., and Jacobsen, R. T., "Viscosity and Thermal Conductivity Equations for Nitrogen, Oxygen, Argon, and Air," *Int. J. Thermophys.* **25**:21–69, 2004.

Properties at the freezing point temperature and the critical point temperature are given in the first and last entries of the saturation tables, respectively. In the single-phase table, when the temperature range for a given isobar includes a vapor-liquid phase boundary, the temperature of phase equilibrium is noted, and properties for both the saturated liquid and saturated vapor are given (with liquid properties given in the upper line). Lines are omitted from the temperature-pressure grid of the single-phase table, when the system would be in the solid phase or if there are potential problems with the source property surface.

In the range from the solidification point to 873 K at pressures to 70 MPa, the estimated uncertainty of density values calculated with the equation of state is 0.1%. The estimated uncertainty of calculated speed of sound values is 0.2% and that for calculated heat capacities is 1%. At temperatures above 873 K and 70 MPa, the estimated uncertainty of calculated density values is 0.5%, increasing to 1.0% at 2000 K and 2000 MPa. For viscosity, the uncertainty is 1% in the dilute gas. The uncertainty is around 2% between 270 and 300 K and increases to 5% outside of this region. There are very few measurements between 130 and 270 K for air to validate this claim, and the uncertainties may be even higher in this supercritical region. For thermal conductivity, the uncertainty for the dilute gas is 2% with increasing uncertainties near the triple points. The uncertainties range from 3% between 140 and 300 K to 5% at the triple point and at high temperatures. The uncertainties above 100 MPa are not known due to a lack of experimental data.

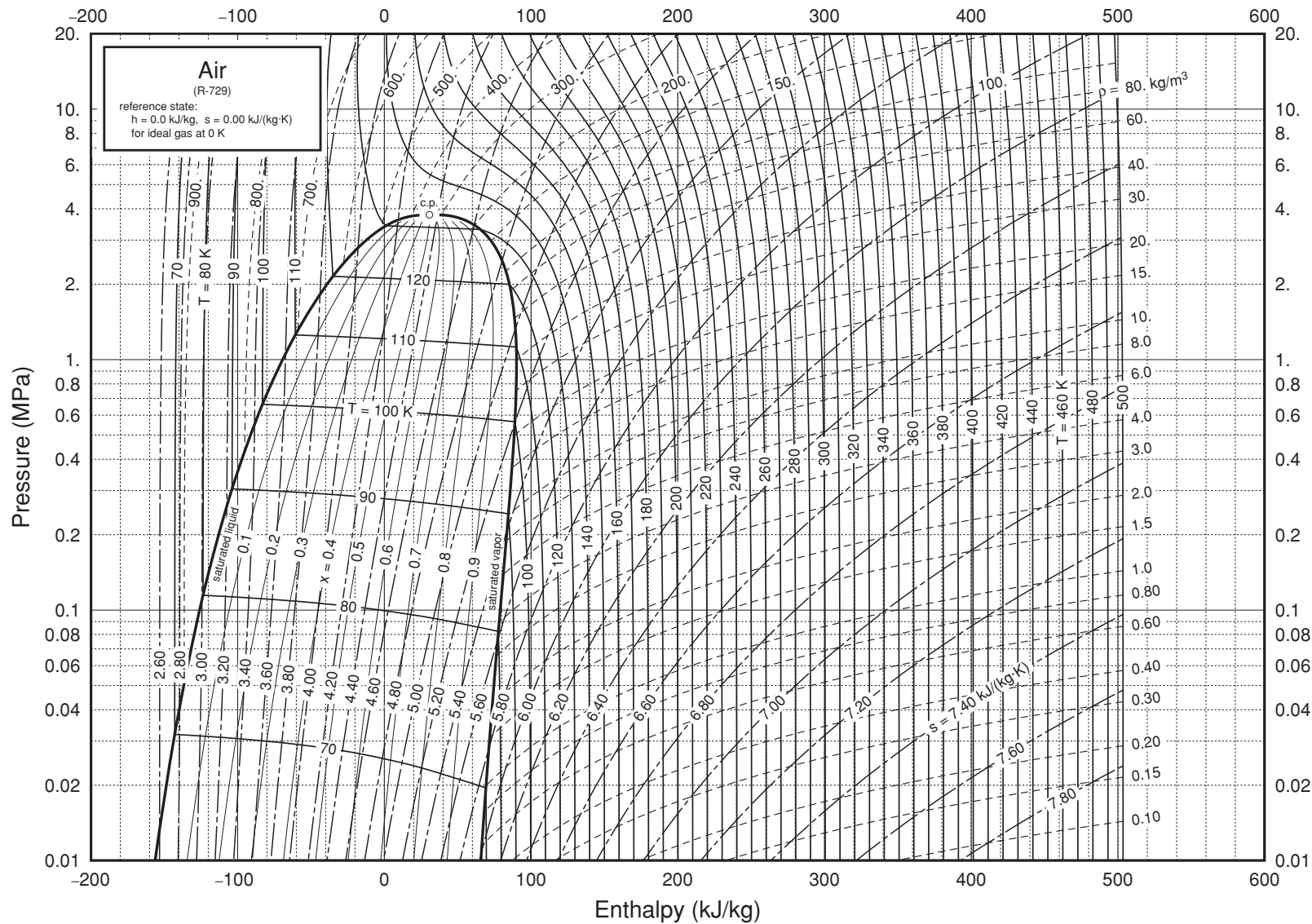


FIG. 2-5 Pressure-enthalpy diagram for dry air. Properties computed with the NIST REFPROP Database, Version 7.0 (Lemmon, E. W., McLinden, M. O., and Huber, M. L., 2002, NIST Standard Reference Database 23, NIST Reference Fluid Thermodynamic and Transport Properties—REFPROP, Version 7.0, Standard Reference Data Program, National Institute of Standards and Technology), based on the equation of state of Lemmon, E. W., Jacobsen, R. T., Penoncello, S. G., and Friend, D. G., "Thermodynamic Properties of Air and Mixtures of Nitrogen, Argon, and Oxygen from 60 to 2000 K at Pressures to 2000 MPa," *J. Phys. Chem. Ref. Data* **29**:331–355, 2000.

2-216 PHYSICAL AND CHEMICAL DATA

TABLE 2-188 Air

Other tables include Stewart, R. B., S. G. Penoncello, et al., University of Idaho CATS report, 85-5, 1985 (0.1–700 bar, 85–750 K), and Lemmon, E. W., Jacobsen, R. T., Penoncello, S. G., and Friend, D. G., *Thermodynamic Properties of Air and Mixtures of Nitrogen, Argon, and Oxygen from 60 to 2000 K at Pressures to 2000 MPa*, J. Phys. Chem. Ref. Data, **29**(3): 331–385, 2000. Tables including reactions with hydrocarbons include Gordon, S., NASA Techn. Paper 1907, 4 vols., 1982. See also Gupta, R. N., K-P. Lee, et al., NASA RP 1232, 1990 (89 pp.) and RP 1260, 1991 (75 pp.). Analytic expressions for high temperatures were given by Matsuzaki, R., *Jap. J. Appl. Phys.*, **21**, 7 (1982): 1009–1013 and Japanese National Aerospace Laboratory report NAL TR 671, 1981 (45 pp.). Functions from 1500 to 15,000 K were tabulated by Hilsenrath, J. and M. Klein, AEDC-TR-65-58 = AD 612 301, 1965 (333 pp.). Tables from 10000 to 10,000,000 K were authored by Gilmore, F. R., Lockheed rept. 3-27-67-1, vol 1., 1967 (340 pp.), also published as *Radiative Properties of Air*, IFI/Plenum, New York, 1969 (648 pp.). Saturation and superheat tables and a chart to 7000 psia, 660°R appear in Stewart, R. B., R. T. Jacobsen, et al., *Thermodynamic Properties of Refrigerants*, ASHRAE, Atlanta, Ga, 1986 (521 pp.). For specific heat, thermal conductivity, and viscosity see *Thermophysical Properties of Refrigerants*, ASHRAE, 1993.

AIR, MOIST

An ASHRAE publication, *Thermodynamic Properties of Dry Air and Water and S. I. Psychrometric Charts*, 1983 (360 pp.), extensively reviews moist air properties. Candiduson, P., *Chem. Eng.*, Oct. 29, 1984 gives on page 118 a nomograph from 50 to 120°F, while equations in SI units were given by Nelson, B., *Chem. Eng. Progr.* **76**, 5 (May 1980): 83–85. Liley, P. E., *2000 Solved Problems in M.E. Thermodynamics*, McGraw-Hill, New York, 1989, gives four simple equations with which most calculations can be made. Devres, Y.O., *Appl. Energy* **48** (1994): 1–18 gives equations with which three known properties can be used to determine four others. Klappert, M. T. and G. F. Schilling, Rand RM-4244-PR = AD 604 856, 1984 (40 pp.) gives tables from 100 to 270 K, while programs from –60 to 2°F are given by Sando, F. A., *ASHRAE Trans.*, **96**, 2 (1990): 299–308.

Viscosity references include Kestin, J. and J. H. Whitelaw, *Int. J. Ht. Mass Transf.* **7**, 11 (1964): 1245–1255; Studnokov, E. L., *Inz.-Fiz. Zhur.* **19**, 2 (1970): 338–340; Hochrainer, D. and F. Munczak, *Setzb. Ost. Acad. Wiss II* **175**, 10 (1966): 540–550. For thermal conductivity see, for instance, Mason, E. A. and L. Monchick, *Humidity and Moisture Control in Science and Industry*, Reinhold, New York, 1965 (257–272).

TABLE 2-189 Thermodynamic Properties of Ammonia

Temperature K	Pressure MPa	Density mol/dm ³	Volume dm ³ /mol	Int. energy kJ/mol	Enthalpy kJ/mol	Entropy kJ/(mol·K)	C _v kJ/(mol·K)	C _p kJ/(mol·K)	Sound speed m/s	Joule-Thomson K/MPa	Therm. cond. mW/(m·K)	Viscosity μPa·s
Saturated Properties												
195.50	0.0060912	43.035	0.023237	0.00000	0.00014154	0.00000	0.049972	0.071565	2124.2	-0.23362	818.99	559.57
200.00	0.0086509	42.754	0.023389	0.32333	0.32353	0.0016351	0.049837	0.071988	2080.2	-0.22917	803.14	507.28
210.00	0.017739	42.111	0.023747	1.0480	1.0484	0.0051707	0.049521	0.072971	1992.7	-0.21883	768.02	414.98
220.00	0.033790	41.442	0.024130	1.7825	1.7833	0.0085874	0.049207	0.073950	1913.7	-0.20813	733.17	346.68
230.00	0.060407	40.748	0.024541	2.5265	2.5279	0.011894	0.048906	0.074883	1839.2	-0.19712	698.50	294.94
240.00	0.10223	40.032	0.024980	3.2793	3.2818	0.015098	0.048613	0.075764	1766.9	-0.18561	665.09	254.85
250.00	0.16494	39.293	0.025450	4.0403	4.0445	0.018205	0.048327	0.076608	1695.6	-0.17327	632.16	223.08
260.00	0.25531	38.533	0.025952	4.8093	4.8160	0.021222	0.048047	0.077448	1624.5	-0.15963	600.07	197.34
270.00	0.38107	37.748	0.026491	5.5862	5.5963	0.024154	0.047774	0.078328	1553.1	-0.14414	568.55	176.06
280.00	0.55092	36.939	0.027072	6.3712	6.3861	0.027010	0.047511	0.079296	1481.0	-0.12612	538.50	158.12
290.00	0.77436	36.101	0.027700	7.1651	7.1866	0.029797	0.047266	0.080412	1407.8	-0.10470	508.99	142.74
300.00	1.0617	35.230	0.028385	7.9691	7.9993	0.032525	0.047044	0.081747	1333.2	-0.078790	480.25	129.33
310.00	1.4240	34.320	0.029138	8.7850	8.8265	0.035203	0.046856	0.083390	1256.7	-0.046923	452.23	117.49
320.00	1.8728	33.363	0.029973	9.6153	9.6714	0.037843	0.046715	0.085465	1177.9	-0.0070718	424.83	106.91
330.00	2.4205	32.350	0.030912	10.463	10.538	0.040458	0.046636	0.088145	1096.5	0.043673	397.96	97.325
340.00	3.0802	31.264	0.031986	11.333	11.432	0.043065	0.046642	0.091701	1011.8	0.10967	371.51	88.555
350.00	3.8660	30.087	0.033237	12.232	12.361	0.045682	0.046767	0.096576	923.38	0.19774	345.32	80.430
360.00	4.7929	28.788	0.034737	13.169	13.335	0.048339	0.047064	0.10357	830.62	0.31928	319.25	72.796
370.00	5.8778	27.321	0.036602	14.158	14.373	0.051075	0.047619	0.11435	732.78	0.49497	293.07	65.493
380.00	7.1402	25.606	0.039054	15.224	15.503	0.053961	0.048589	0.13314	628.75	0.76738	266.57	58.315
390.00	8.6045	23.465	0.042616	16.424	16.790	0.057149	0.050319	0.17550	515.88	1.2455	239.65	50.877
400.00	10.305	20.232	0.049426	17.969	18.478	0.061223	0.054109	0.38707	384.58	2.3557	216.00	41.802
405.40	11.339	13.212	0.075690	20.640	21.499	0.068559			0	5.0513		
195.50	0.0060912	0.0037635	265.71	23.661	25.279	0.12931	0.026510	0.035130	354.12	171.13	19.636	6.8396
200.00	0.0086509	0.0052305	191.19	23.770	25.424	0.12714	0.026650	0.035345	357.91	152.55	19.684	6.9515
210.00	0.017739	0.010249	97.573	24.006	25.737	0.12273	0.027053	0.035961	365.94	120.01	19.860	7.2115
220.00	0.033790	0.018721	53.415	24.233	26.038	0.11884	0.027583	0.036783	373.38	96.215	20.132	7.4846
230.00	0.060407	0.032214	31.043	24.450	26.325	0.11536	0.028245	0.037836	380.19	78.430	20.503	7.7679
240.00	0.10223	0.052667	18.987	24.655	26.596	0.11224	0.029043	0.039142	386.30	64.852	20.978	8.0587
250.00	0.16494	0.082417	12.133	24.846	26.847	0.10942	0.029978	0.040728	391.66	54.280	21.560	8.3552
260.00	0.25531	0.12421	8.0506	25.021	27.077	0.10684	0.031050	0.042623	396.20	45.905	22.258	8.6558
270.00	0.38107	0.18126	5.5168	25.179	27.281	0.10447	0.032253	0.044859	399.86	39.175	23.079	8.9595
280.00	0.55092	0.25729	3.8867	25.317	27.459	0.10227	0.033581	0.047476	402.59	33.701	24.034	9.2664
290.00	0.77436	0.35664	2.8040	25.435	27.606	0.10021	0.035028	0.050530	404.30	29.207	25.138	9.5771
300.00	1.0617	0.48448	2.0641	25.528	27.720	0.098259	0.036584	0.054099	404.95	25.489	26.408	9.8938
310.00	1.4240	0.64702	1.5455	25.595	27.796	0.096395	0.038244	0.058320	404.45	22.391	27.872	10.220
320.00	1.8728	0.85202	1.1737	25.632	27.830	0.094589	0.040004	0.063320	402.70	19.794	29.568	10.561
330.00	2.4205	1.1094	0.90139	25.634	27.816	0.092817	0.041868	0.069443	399.61	17.599	31.559	10.927
340.00	3.0802	1.4325	0.69810	25.595	27.746	0.091046	0.043844	0.077150	395.05	15.728	33.945	11.330
350.00	3.8660	1.8399	0.54350	25.505	27.606	0.089242	0.045954	0.087280	388.86	14.112	36.900	11.792
360.00	4.7929	2.3598	0.42377	25.350	27.381	0.087355	0.048233	0.10141	380.83	12.690	40.752	12.346
370.00	5.8778	3.0375	0.32922	25.107	27.042	0.085316	0.050744	0.12286	370.69	11.400	46.149	13.053
380.00	7.1402	3.9558	0.25279	24.734	26.539	0.083003	0.053589	0.16000	357.96	10.172	54.556	14.025
390.00	8.6045	5.2979	0.18875	24.144	25.768	0.080169	0.056957	0.24170	341.67	8.9038	70.114	15.527
400.00	10.305	7.6973	0.12992	23.047	24.386	0.075992	0.061281	0.59477	318.22	7.3513	113.54	18.529
405.40	11.339	13.212	0.075690	20.640	21.499	0.068559			0	5.0513		

TABLE 2-189 Thermodynamic Properties of Ammonia (Concluded)

Temperature K	Pressure MPa	Density mol/dm ³	Volume dm ³ /mol	Int. energy kJ/mol	Enthalpy kJ/mol	Entropy kJ/(mol·K)	C _v kJ/(mol·K)	C _p kJ/(mol·K)	Sound speed m/s	Joule-Thomson K/MPa	Therm. cond. mW/(m·K)	Viscosity μPa·s
Single-Phase Properties												
200.00	0.10000	42.756	0.023388	0.32270	0.32504	0.0016320	0.049842	0.071983	2080.3	-0.22921	803.24	507.47
239.56	0.10000	40.064	0.024960	3.2461	3.2486	0.014960	0.048626	0.075726	1770.0	-0.18613	666.56	256.42
239.56	0.10000	0.051595	19.382	24.646	26.584	0.11237	0.029005	0.039079	386.05	65.377	20.955	8.0459
300.00	0.10000	0.040502	24.690	26.378	28.847	0.12080	0.028021	0.036849	434.39	27.493	25.100	10.161
400.00	0.10000	0.030171	33.144	29.297	32.612	0.13162	0.030417	0.038883	497.93	10.681	37.215	13.971
500.00	0.10000	0.024091	41.509	32.514	36.665	0.14065	0.033897	0.042280	550.96	5.5276	53.119	17.863
600.00	0.10000	0.020060	49.849	36.096	41.081	0.14869	0.037731	0.046083	597.69	3.2702	68.607	21.682
700.00	0.10000	0.017188	58.179	40.068	45.885	0.15609	0.041678	0.050015	640.16	2.0841	78.312	25.391
200.00	1.0000	42.774	0.023379	0.31651	0.33989	0.0016010	0.049890	0.071938	2081.5	-0.22959	804.23	509.28
298.05	1.0000	35.403	0.028246	7.8111	7.8393	0.031996	0.047085	0.081465	1347.9	-0.084271	485.81	131.82
298.05	1.0000	0.45697	2.1883	25.512	27.700	0.098633	0.036271	0.053356	404.91	26.163	26.145	9.8313
300.00	1.0000	0.45215	2.2117	25.592	27.804	0.098979	0.035866	0.052493	407.16	25.620	26.308	9.9115
400.00	1.0000	0.31157	3.2095	29.019	32.229	0.11177	0.031641	0.041627	488.94	10.494	38.087	13.927
500.00	1.0000	0.24426	4.0940	32.359	36.453	0.12119	0.034312	0.043338	546.79	5.4884	53.750	17.877
600.00	1.0000	0.20197	4.9513	35.994	40.945	0.12937	0.037928	0.046628	595.60	3.2544	69.123	21.717
700.00	1.0000	0.17248	5.7977	39.994	45.792	0.13684	0.041791	0.050341	639.15	2.0746	78.751	25.434
200.00	5.0000	42.852	0.023336	0.28942	0.40611	0.0014649	0.050097	0.071739	2086.8	-0.23126	808.60	517.30
300.00	5.0000	35.450	0.028209	7.8852	8.0263	0.032243	0.047090	0.080899	1361.2	-0.089577	487.57	132.49
362.03	5.0000	28.505	0.035081	13.365	13.540	0.048887	0.047152	0.10538	811.17	0.34968	313.94	71.291
362.03	5.0000	2.4828	0.40277	25.309	27.323	0.086956	0.048722	0.10501	378.95	12.419	41.693	12.475
400.00	5.0000	1.8706	0.53459	27.540	30.213	0.094581	0.038466	0.061581	441.81	9.6373	45.730	14.036
500.00	5.0000	1.3046	0.76650	31.630	35.462	0.10634	0.036193	0.048779	528.14	5.2830	57.294	18.073
600.00	5.0000	1.0412	0.96040	35.527	40.329	0.11521	0.038798	0.049210	586.79	3.1693	71.791	21.941
700.00	5.0000	0.87563	1.1420	39.662	45.373	0.12298	0.042289	0.051836	635.17	2.0254	80.941	25.662
200.00	10.000	42.947	0.023284	0.25644	0.48928	0.0012980	0.050342	0.071495	2093.5	-0.23328	814.02	527.29
300.00	10.000	35.714	0.028000	7.7848	8.0648	0.031903	0.047164	0.079960	1394.2	-0.10159	496.50	136.36
398.32	10.000	20.945	0.047744	17.655	18.132	0.060394	0.053149	0.30653	409.04	2.0704	218.73	43.632
398.32	10.000	7.1390	0.14008	23.303	24.704	0.076892	0.060447	0.46915	323.12	7.6606	101.04	17.793
400.00	10.000	6.5455	0.15278	23.801	25.329	0.078458	0.057611	0.30552	336.28	7.7633	95.455	17.230
500.00	10.000	2.8656	0.34897	30.616	34.106	0.098525	0.038603	0.057806	505.64	4.9335	63.922	18.722
600.00	10.000	2.1650	0.46190	34.920	39.539	0.10844	0.039862	0.052806	577.38	3.0278	76.053	22.393
700.00	10.000	1.7835	0.56069	39.241	44.848	0.11663	0.042896	0.053796	631.50	1.9491	84.235	26.035
300.00	100.00	38.995	0.025644	6.5830	9.1474	0.027511	0.048894	0.072740	1774.7	-0.19551	622.86	193.71
400.00	100.00	33.105	0.030207	13.432	16.453	0.048523	0.046636	0.073557	1378.2	-0.11309	431.98	96.237
500.00	100.00	27.067	0.036945	20.212	23.907	0.065147	0.045999	0.075495	1081.8	0.049919	305.65	60.386
600.00	100.00	21.518	0.046473	26.825	31.472	0.078942	0.046723	0.075193	918.11	0.23722	234.79	46.188
700.00	100.00	17.303	0.057794	33.074	38.854	0.090326	0.048331	0.072317	861.52	0.32753	196.04	41.237
300.00	500.00	45.670	0.021896	4.7114	15.660	0.018023	0.052877	0.067831	2597.1	-0.25055	989.00	376.31
400.00	500.00	42.416	0.023576	10.633	22.421	0.037482	0.051527	0.066802	2353.2	-0.25064	804.05	188.46
500.00	500.00	39.515	0.025307	16.367	29.021	0.052215	0.050431	0.065418	2176.9	-0.25260	674.00	120.77
600.00	500.00	36.909	0.027094	22.007	35.554	0.064127	0.050614	0.065476	2044.6	-0.24722	582.63	91.251
700.00	500.00	34.550	0.028943	27.680	42.152	0.074295	0.051816	0.066615	1943.8	-0.23682	511.57	77.538
300.00	1000.0	49.944	0.020022	4.1818	24.204	0.011750	0.055176	0.065784	3230.2	-0.25989	1324.0	554.62
400.00	1000.0	47.551	0.021030	9.8612	30.891	0.030984	0.054864	0.066677	2997.6	-0.25431	1138.9	274.91
500.00	1000.0	45.362	0.022045	15.432	37.477	0.045686	0.053323	0.065150	2842.8	-0.26084	996.49	174.11
600.00	1000.0	43.378	0.023053	20.911	44.964	0.057514	0.052940	0.064819	2728.6	-0.26235	887.73	129.02
700.00	1000.0	41.556	0.024064	26.418	50.481	0.067559	0.053649	0.065697	2639.0	-0.25820	797.25	107.14

The values in these tables were generated from the NIST REFPROP software (Lemmon, E. W., McLinden, M. O., and Huber, M. L., NIST Standard Reference Database 23: Reference Fluid Thermodynamic and Transport Properties—REFPROP, National Institute of Standards and Technology, Standard Reference Data Program, Gaithersburg, Md., 2002, Version 7.1). The primary source for the thermodynamic properties is Tillner-Roth, R., Harms-Watzenberg, F., and Baehr, H. D., "Eine neue Fundamentalgleichung fuer Ammoniak," *DKV-Tagungsbericht*, **20**:167–181, 1993. The source for viscosity is Fenghour, A., Wakeham, W. A., Vesovic, V., Watson, J. T. R., Millat, J., and Vogel, E., "The Viscosity of Ammonia," *J. Phys. Chem. Ref. Data* **24**:1649–1667, 1995. The source for thermal conductivity is Tufeu, R., Ivanov, D. Y., Garrabos, Y., and Le Neindre, B., "Thermal Conductivity of Ammonia in a Large Temperature and Pressure Range Including the Critical Region," *Ber. Bunsenges. Phys. Chem.* **88**:422–427, 1984.

Properties at the triple point temperature and the critical point temperature are given in the first and last entries of the saturation tables, respectively. In the single-phase table, when the temperature range for a given isobar includes a vapor-liquid phase boundary, the temperature of phase equilibrium is noted, and properties for both the saturated liquid and saturated vapor are given (with liquid properties given in the upper line). Lines are omitted from the temperature-pressure grid of the single-phase table, when the system would be in the solid phase or if there are potential problems with the source property surface.

The uncertainties of the equation of state are 0.2% in density, 2% in heat capacity, and 2% in the speed of sound, except in the critical region. The uncertainty in vapor pressure is 0.2%. The uncertainty varies from 0.5% for the viscosity of the dilute gas phase at moderate temperatures to about 5% for the viscosity at high pressures and temperatures. The uncertainty in thermal conductivity is 2%.

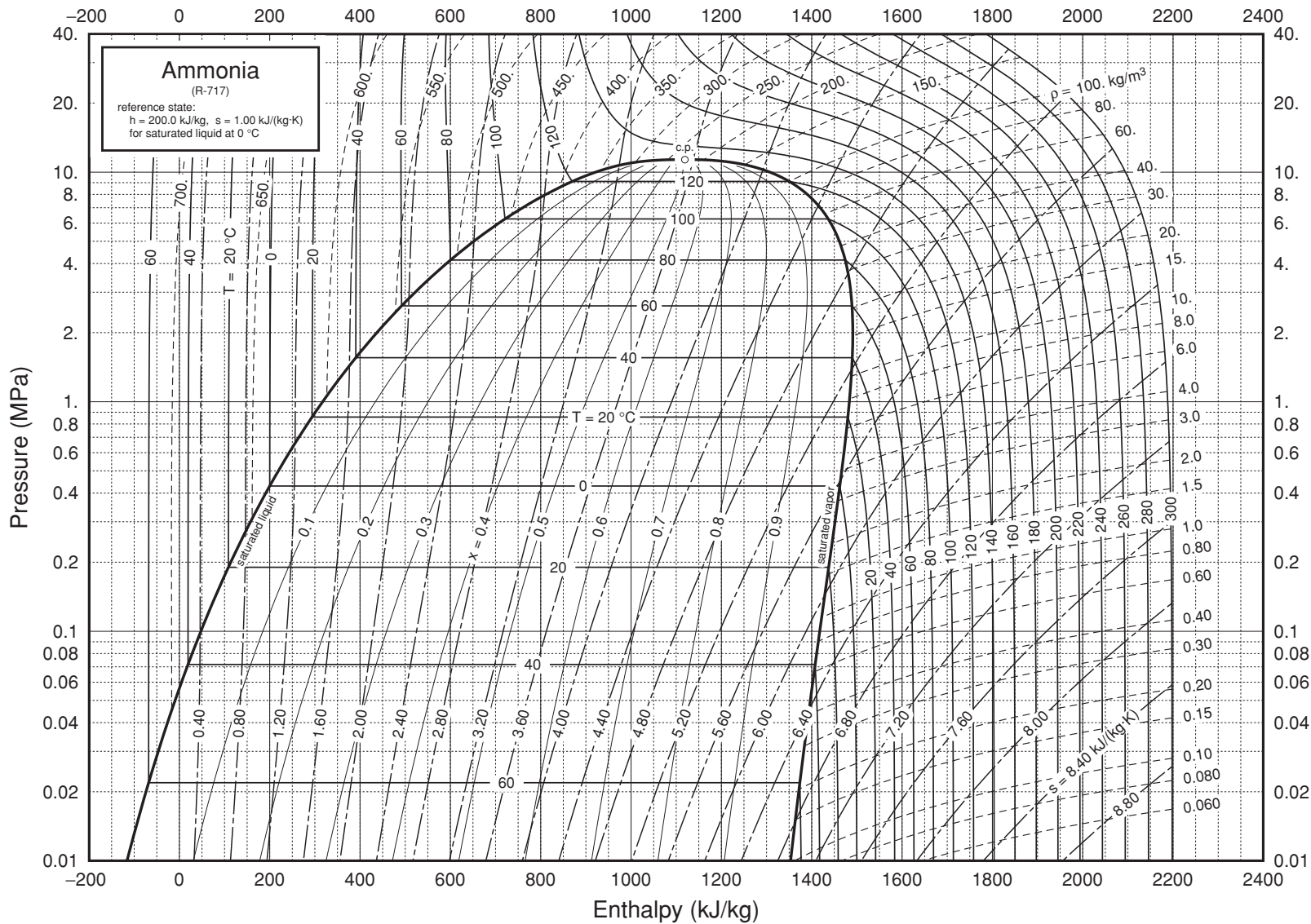


FIG. 2-6 Pressure-enthalpy diagram for ammonia. Properties computed with the NIST REFPROP Database, Version 7.0 (Lemmon, E. W., McLinden, M. O., and Huber, M. L., 2002, NIST Standard Reference Database 23, NIST Reference Fluid Thermodynamic and Transport Properties—REFPROP, Version 7.0, Standard Reference Data Program, National Institute of Standards and Technology), based on the equation of state of Tillner-Roth, R., Harms-Watzenberg, F., and Baehr, H. D., "Eine neue Fundamentalgleichung für Ammoniak, *DKV-Tagungsbericht* 20(II):167–181, 1993.

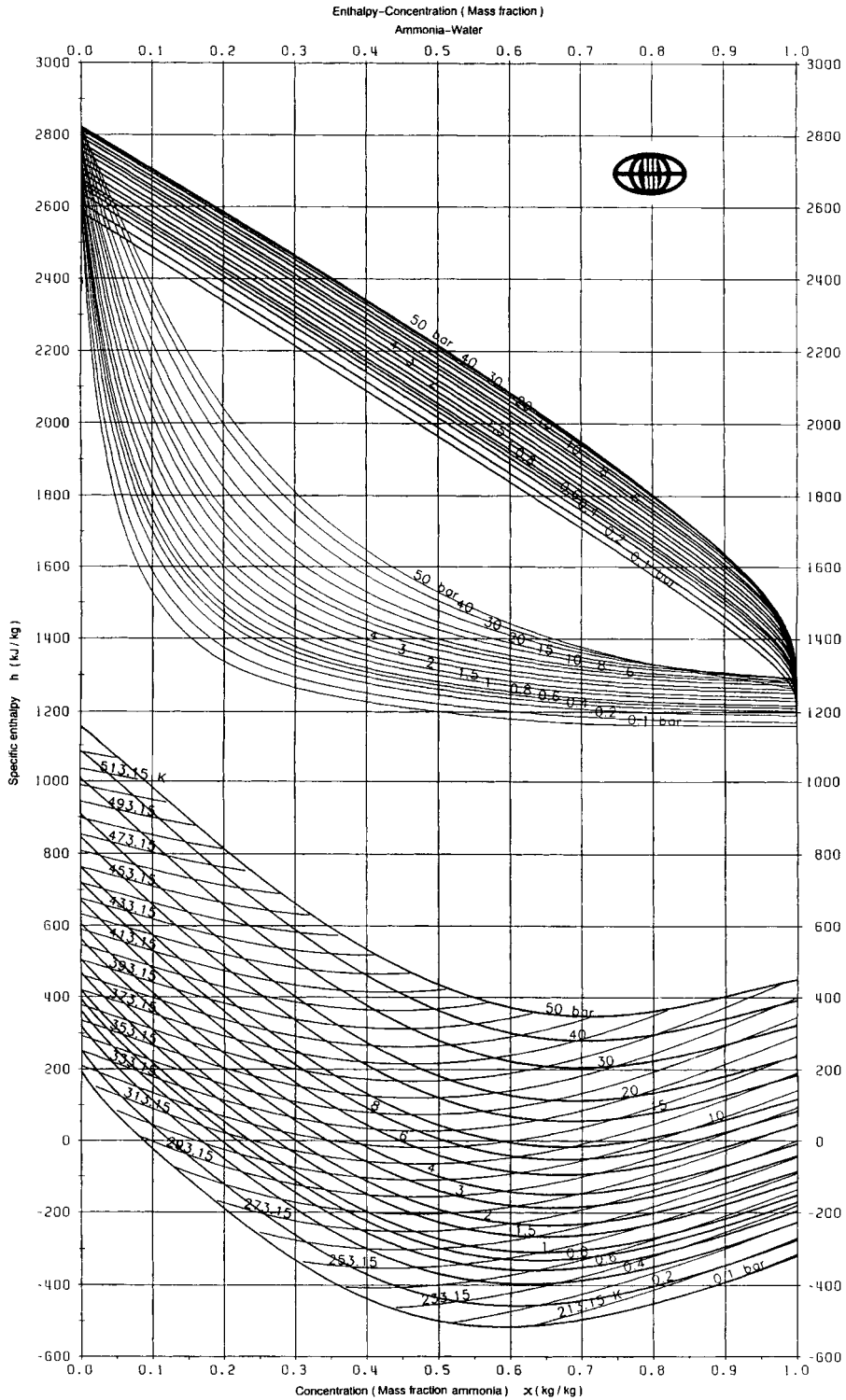


FIG. 2-7 Enthalpy-concentration diagram for aqueous ammonia. From *Thermodynamic and Physical Properties NH₃-H₂O*, Int. Inst. Refrigeration, Paris, France, 1994 (88 pp.). Reproduced by permission. In order to determine equilibrium compositions, draw a vertical from any liquid composition on any boiling line (the lowest plots) to intersect the appropriate auxiliary curve (the intermediate curves). A horizontal then drawn from this point to the appropriate dew line (the upper curves) will establish the vapor composition. The Int. Inst. Refrigeration publication also gives extensive P - v - x tables from -50 to 316°C . Other sources include Park, Y. M. and Sonntag, R. E., *ASHRAE Trans.*, **96**, 1 (1990): 150–159 (x , h , s , tables, 360 to 640 K); Ibrahim, O. M. and S. A. Klein, *ASHRAE Trans.*, **99**, 1 (1993): 1495–1502 (Eqs., 0.2 to 110 bar, 293 to 413 K); Smolen, T. M., D. B. Manley, et al., *J. Chem. Eng. Data*, **36** (1991): 202–208 (p - x correlation, 0.9 to 450 psia, 293–413 K); Ruiter, J. P., *Int. J. Refrig.*, **13** (1990): 223–236 gives ten sub-routines for computer calculations.

TABLE 2-190 Thermodynamic Properties of Argon

Temperature K	Pressure MPa	Density mol/dm ³	Volume dm ³ /mol	Int. energy kJ/mol	Enthalpy kJ/mol	Entropy kJ/(mol·K)	C _v kJ/(mol·K)	C _p kJ/(mol·K)	Sound speed m/s	Joule-Thomson K/MPa	Therm. cond. mW/(m·K)	Viscosity μPa·s
Saturated Properties												
83.806	0.068891	35.465	0.028197	-4.8531	-4.8512	0.053110	0.021956	0.044570	862.43	-0.40500	133.63	290.17
85.000	0.078897	35.284	0.028342	-4.8000	-4.7977	0.053740	0.021764	0.044571	854.24	-0.40120	131.86	279.46
87.000	0.098131	34.977	0.028590	-4.7110	-4.7082	0.054774	0.021461	0.044620	840.43	-0.39386	128.91	262.70
89.000	0.12078	34.667	0.028846	-4.6220	-4.6185	0.055787	0.021178	0.044720	826.48	-0.38530	125.97	247.29
91.000	0.14723	34.353	0.029109	-4.5328	-4.5285	0.056778	0.020912	0.044869	812.39	-0.37551	123.06	233.09
93.000	0.17785	34.035	0.029381	-4.4433	-4.4380	0.057752	0.020662	0.045063	798.14	-0.36447	120.16	219.98
95.000	0.21305	33.713	0.029662	-4.3534	-4.3471	0.058708	0.020424	0.045301	783.72	-0.35214	117.28	207.87
97.000	0.25323	33.386	0.029953	-4.2632	-4.2556	0.059649	0.020198	0.045583	769.14	-0.33847	114.44	196.65
99.000	0.29882	33.054	0.030254	-4.1725	-4.1634	0.060575	0.019982	0.045909	754.37	-0.32336	111.63	186.24
101.000	0.35023	32.715	0.030567	-4.0812	-4.0705	0.061489	0.019777	0.046282	739.40	-0.30671	108.82	176.58
103.000	0.40789	32.371	0.030892	-3.9893	-3.9767	0.062391	0.019580	0.046705	724.21	-0.28840	106.03	167.58
105.000	0.47224	32.020	0.031230	-3.8968	-3.8820	0.063283	0.019393	0.047181	708.81	-0.26827	103.26	159.18
107.000	0.54371	31.662	0.031584	-3.8034	-3.7862	0.064165	0.019214	0.047715	693.16	-0.24614	100.50	151.32
109.000	0.62276	31.296	0.031953	-3.7092	-3.6893	0.065039	0.019044	0.048313	677.26	-0.22181	97.768	143.96
111.000	0.70982	30.921	0.032340	-3.6141	-3.5912	0.065906	0.018883	0.048984	661.08	-0.19503	95.055	137.04
113.000	0.80535	30.538	0.032747	-3.5180	-3.4916	0.066767	0.018731	0.049737	644.60	-0.16549	92.363	130.52
115.000	0.90981	30.144	0.033174	-3.4207	-3.3905	0.067623	0.018589	0.050584	627.79	-0.13284	89.695	124.35
117.000	1.0237	29.739	0.033626	-3.3222	-3.2878	0.068477	0.018458	0.051541	610.64	-0.096667	87.049	118.50
119.000	1.1473	29.322	0.034104	-3.2223	-3.1831	0.069328	0.018337	0.052626	593.11	-0.056465	84.428	112.93
121.000	1.2814	28.891	0.034613	-3.1208	-3.0764	0.070179	0.018229	0.053865	575.16	-0.011619	81.832	107.61
123.000	1.4262	28.446	0.035155	-3.0175	-2.9674	0.071031	0.018134	0.055288	556.75	0.038624	79.260	102.49
125.000	1.5823	27.983	0.035735	-2.9123	-2.8558	0.071886	0.018056	0.056938	537.83	0.095199	76.711	97.565
127.000	1.7503	27.502	0.036361	-2.8049	-2.7413	0.072747	0.017995	0.058870	518.34	0.15298	74.185	92.791
129.000	1.9305	26.999	0.037039	-2.6949	-2.6234	0.073616	0.017955	0.061161	498.21	0.23236	71.679	88.143
131.000	2.1237	26.471	0.037778	-2.5820	-2.5018	0.074496	0.017941	0.063916	477.36	0.31637	69.190	83.595
133.000	2.3303	25.913	0.038591	-2.4655	-2.3756	0.075392	0.017957	0.067291	455.69	0.41386	66.713	79.119
135.000	2.5509	25.320	0.039495	-2.3449	-2.2442	0.076309	0.018011	0.071519	433.10	0.52823	64.243	74.689
137.000	2.7862	24.683	0.040513	-2.2192	-2.1063	0.077253	0.018109	0.076964	409.47	0.66427	61.773	70.276
139.000	3.0369	23.993	0.041678	-2.0871	-1.9605	0.078235	0.018264	0.084237	384.62	0.82889	59.297	65.850
141.000	3.3037	23.233	0.043041	-1.9468	-1.8046	0.079268	0.018501	0.094443	358.17	1.0326	56.816	61.374
143.000	3.5876	22.379	0.044686	-1.7953	-1.6350	0.080375	0.018882	0.10982	329.41	1.2928	54.352	56.802
145.000	3.8896	21.385	0.046762	-1.6277	-1.4458	0.081593	0.019546	0.13580	297.06	1.6405	52.009	52.060
147.000	4.2111	20.163	0.049597	-1.4335	-1.2247	0.083001	0.020842	0.18993	258.79	2.1416	50.224	46.982
149.000	4.5541	18.446	0.054213	-1.1822	-0.93533	0.084835	0.023975	0.37941	209.33	2.9836	51.152	41.002
150.69	4.8630	13.407	0.074586	-0.53575	-0.17304	0.089789			0	5.2503		
83.806	0.068891	0.10150	9.8526	1.0103	1.6891	0.13115	0.012972	0.022172	168.12	35.712	5.3590	6.8558
85.000	0.078897	0.11492	8.7019	1.0212	1.7078	0.13028	0.013015	0.022310	169.08	34.706	5.4485	6.9622
87.000	0.098131	0.14035	7.1253	1.0388	1.7380	0.12887	0.013092	0.022563	170.64	33.127	5.6006	7.1414
89.000	0.12078	0.16979	5.8895	1.0554	1.7668	0.12753	0.013176	0.022845	172.12	31.668	5.7559	7.3219
91.000	0.14723	0.20365	4.9104	1.0710	1.7939	0.12626	0.013267	0.023159	173.52	30.315	5.9147	7.5039
93.000	0.17785	0.24233	4.1266	1.0855	1.8194	0.12504	0.013364	0.023506	174.85	29.056	6.0776	7.6877
95.000	0.21305	0.28625	3.4935	1.0988	1.8431	0.12387	0.013469	0.023892	176.11	27.883	6.2452	7.8736
97.000	0.25323	0.33587	2.9774	1.1108	1.8648	0.12275	0.013580	0.024318	177.29	26.785	6.4180	8.0617
99.000	0.29882	0.39165	2.5533	1.1216	1.8845	0.12167	0.013700	0.024789	178.39	25.755	6.5969	8.2524
101.000	0.35023	0.45412	2.2021	1.1309	1.9021	0.12062	0.013828	0.025310	179.41	24.786	6.7825	8.4461
103.000	0.40789	0.52379	1.9092	1.1387	1.9174	0.11962	0.013964	0.025887	180.36	23.873	6.9760	8.6432
105.000	0.47224	0.60126	1.6632	1.1449	1.9303	0.11864	0.014108	0.026526	181.22	23.009	7.1783	8.8440
107.000	0.54371	0.68714	1.4553	1.1494	1.9406	0.11769	0.014263	0.027235	182.01	22.189	7.3908	9.0492
109.000	0.62276	0.78213	1.2786	1.1521	1.9483	0.11676	0.014427	0.028024	182.71	21.410	7.6149	9.2592
111.000	0.70982	0.88696	1.1274	1.1528	1.9531	0.11585	0.014602	0.028904	183.33	20.667	7.8524	9.4749
113.000	0.80535	1.0025	0.99752	1.1515	1.9549	0.11497	0.014789	0.029890	183.87	19.955	8.1054	9.6969
115.000	0.90981	1.1296	0.88525	1.1480	1.9534	0.11409	0.014989	0.030998	184.33	19.272	8.3764	9.9262
117.000	1.0237	1.2694	0.78776	1.1421	1.9485	0.11323	0.015203	0.032251	184.70	18.615	8.6685	10.164
119.000	1.1473	1.4231	0.70269	1.1336	1.9398	0.11238	0.015432	0.033674	184.98	17.979	8.9853	10.411
121.000	1.2814	1.5920	0.62813	1.1223	1.9271	0.11153	0.015679	0.035305	185.17	17.361	9.3315	10.670
123.000	1.4262	1.7778	0.56248	1.1079	1.9101	0.11069	0.015945	0.037186	185.27	16.758	9.7128	10.942
125.000	1.5823	1.9824	0.50443	1.0901	1.8883	0.10984	0.016234	0.039377	185.28	16.167	10.136	11.228

TABLE 2-190 Thermodynamic Properties of Argon (Concluded)

Temperature K	Pressure MPa	Density mol/dm ³	Volume dm ³ /mol	Int. energy kJ/mol	Enthalpy kJ/mol	Entropy kJ/(mol·K)	C _v kJ/(mol·K)	C _p kJ/(mol·K)	Sound speed m/s	Joule-Thomson K/MPa	Therm. cond. mW/(m·K)	Viscosity μPa·s
Saturated Properties												
127.00	1.7503	2.2081	0.45288	1.0685	1.8612	0.10899	0.016549	0.041958	185.18	15.585	10.611	11.533
129.00	1.9305	2.4576	0.40690	1.0428	1.8283	0.10813	0.016892	0.045036	184.98	15.007	11.150	11.860
131.00	2.1237	2.7345	0.36570	1.0122	1.7888	0.10725	0.017269	0.048764	184.68	14.430	11.768	12.212
133.00	2.3303	3.0431	0.32861	0.97615	1.7419	0.10635	0.017684	0.053370	184.27	13.851	12.487	12.596
135.00	2.5509	3.3893	0.29505	0.93360	1.6862	0.10542	0.018152	0.059209	183.74	13.262	13.337	13.018
137.00	2.7862	3.7806	0.26451	0.88331	1.6203	0.10445	0.018697	0.066854	183.03	12.655	14.363	13.489
139.00	3.0369	4.2280	0.23652	0.82353	1.5418	0.10343	0.019352	0.077279	182.09	12.019	15.633	14.022
141.00	3.3037	4.7471	0.21066	0.75170	1.4476	0.10233	0.020167	0.092257	180.81	11.341	17.255	14.638
143.00	3.5876	5.3629	0.18647	0.66386	1.3328	0.10113	0.021213	0.11542	179.05	10.606	19.424	15.370
145.00	3.8896	6.1190	0.16342	0.55308	1.1887	0.099762	0.022619	0.15563	176.57	9.7892	22.530	16.274
147.00	4.2111	7.1057	0.14073	0.40516	0.99779	0.098120	0.024694	0.24158	172.74	8.8407	27.572	17.475
149.00	4.5541	8.5869	0.11646	0.17894	0.70930	0.095873	0.028532	0.54500	165.39	7.6233	38.688	19.366
150.69	4.8630	13.407	0.074586	-0.53575	-0.17304	0.089789			133.87	0		
Single-Phase Properties												
100.00	0.10000	0.12304	8.1275	1.2122	2.0249	0.13179	0.012807	0.021852	184.16	25.048	6.4504	8.2341
200.00	0.10000	0.060310	16.581	2.4833	4.1414	0.14649	0.012497	0.020918	263.21	7.4099	12.539	15.998
300.00	0.10000	0.040115	24.928	3.7351	6.2279	0.15495	0.012479	0.020834	322.67	3.6153	17.837	22.741
400.00	0.10000	0.030069	33.257	4.9842	8.3099	0.16094	0.012475	0.020810	372.65	1.9970	22.516	28.704
500.00	0.10000	0.024050	41.580	6.2324	10.390	0.16559	0.012474	0.020801	416.64	1.1105	26.726	34.077
600.00	0.10000	0.020041	49.899	7.4803	12.470	0.16938	0.012473	0.020796	456.40	0.55603	30.573	38.997
700.00	0.10000	0.017177	58.217	8.7279	14.550	0.17258	0.012473	0.020793	492.95	0.17948	34.134	43.556
100.00	1.0000	32.955	0.030345	-4.1375	-4.1072	0.060927	0.019909	0.045870	751.59	-0.32095	110.85	183.08
116.60	1.0000	29.821	0.033533	-3.3421	-3.3086	0.068305	0.018483	0.051339	614.12	-0.10424	87.579	119.65
116.60	1.0000	1.2403	0.80628	1.1435	1.9497	0.11340	0.015159	0.031986	184.63	18.745	8.6079	10.115
200.00	1.0000	0.61937	1.6145	2.3849	3.9995	0.12686	0.012725	0.022195	261.59	7.2269	12.995	16.256
300.00	1.0000	0.40331	2.4795	3.6807	6.1603	0.13563	0.012545	0.021266	323.44	3.5287	18.142	22.901
400.00	1.0000	0.30073	3.3252	4.9476	8.2728	0.14171	0.012507	0.021025	374.06	1.9489	22.749	28.817
500.00	1.0000	0.24013	4.1644	6.2054	10.370	0.14639	0.012493	0.020928	418.25	1.0808	26.915	34.163
600.00	1.0000	0.19997	5.0007	7.4592	12.460	0.15020	0.012487	0.020879	458.06	0.53628	30.733	39.065
700.00	1.0000	0.17137	5.8354	8.7110	14.546	0.15342	0.012483	0.020851	494.61	0.16568	34.272	43.612
100.00	5.0000	33.343	0.029992	-4.1962	-4.0463	0.060330	0.020096	0.044750	777.34	-0.35058	114.41	193.32
200.00	5.0000	3.5342	0.28295	1.8892	3.3039	0.11098	0.013847	0.030481	257.20	6.1700	16.132	18.205
300.00	5.0000	2.0596	0.48554	3.4362	5.8640	0.12145	0.012825	0.023284	328.37	3.1276	19.721	23.850
400.00	5.0000	1.5022	0.66567	4.7860	8.1144	0.12793	0.012643	0.021972	381.06	1.7370	23.882	29.440
500.00	5.0000	1.1914	0.83938	6.0868	10.284	0.13277	0.012578	0.021480	425.81	0.95180	27.811	34.619
600.00	5.0000	0.98986	1.0102	7.3671	12.418	0.13667	0.012547	0.021239	465.68	0.45113	31.477	39.420
700.00	5.0000	0.84774	1.1796	8.6370	14.535	0.13993	0.012530	0.021104	502.09	0.10636	34.910	43.899
100.00	10.000	33.779	0.029604	-4.2615	-3.9654	0.059648	0.020331	0.043670	805.91	-0.37991	118.60	205.82
200.00	10.000	8.4545	0.11828	1.1163	2.2991	0.10142	0.015240	0.048544	267.70	4.1966	23.573	23.429
300.00	10.000	4.1955	0.23835	3.1284	5.5119	0.11472	0.013145	0.025892	338.42	2.6066	22.192	25.583
400.00	10.000	2.9896	0.33449	4.5884	7.9333	0.12170	0.012803	0.023107	391.51	1.4795	25.505	30.479
500.00	10.000	2.3554	0.42455	5.9428	10.188	0.12674	0.012681	0.022129	436.14	0.79870	29.044	35.348
600.00	10.000	1.9532	0.51198	7.2556	12.375	0.13073	0.012621	0.021662	475.69	0.35092	32.479	39.971
700.00	10.000	1.6722	0.59801	8.5473	14.527	0.13404	0.012587	0.021400	511.73	0.036761	35.757	44.338

200.00	100.00	30.368	0.032930	-1.9234	1.3696	0.077319	0.017598	0.034137	854.48	-0.51219	99.994	120.12
300.00	100.00	24.152	0.041404	0.48428	4.6247	0.090561	0.015534	0.031005	733.39	-0.45856	70.273	75.589
400.00	100.00	19.710	0.050736	2.5103	7.5839	0.099092	0.014579	0.028287	690.42	-0.45296	59.077	61.649
500.00	100.00	16.607	0.060216	4.2850	10.307	0.10518	0.014048	0.026288	683.08	-0.49513	54.952	57.655
600.00	100.00	14.372	0.069578	5.9046	12.862	0.10984	0.013716	0.024915	690.94	-0.55858	53.635	57.185
700.00	100.00	12.695	0.078769	7.4268	15.304	0.11361	0.013492	0.023969	705.52	-0.62622	53.660	58.260
200.00	500.00	41.639	0.024016	-2.6867	9.3214	0.063085	0.022923	0.032604	1519.6	-0.60932	218.05	504.85
300.00	500.00	38.382	0.026054	-0.59281	12.434	0.075743	0.019980	0.029872	1443.8	-0.67083	184.82	259.42
400.00	500.00	35.672	0.028033	1.3125	15.329	0.084083	0.018316	0.028142	1393.0	-0.71809	161.66	183.29
500.00	500.00	33.368	0.029969	3.0950	18.079	0.090226	0.017262	0.026929	1358.5	-0.75700	145.02	151.69
600.00	500.00	31.379	0.031868	4.7903	20.724	0.095050	0.016535	0.026007	1334.9	-0.79113	132.94	135.48
700.00	500.00	29.643	0.033734	6.4198	23.287	0.099002	0.016000	0.025273	1318.8	-0.82207	124.11	125.84
300.00	1000.0	44.836	0.022304	-0.13952	22.164	0.068356	0.022820	0.030815	1866.0	-0.61332	267.67	666.74
400.00	1000.0	42.715	0.023411	1.7386	25.150	0.076958	0.020840	0.029020	1823.7	-0.65733	243.17	410.53
500.00	1000.0	40.856	0.024476	3.5106	27.987	0.083293	0.019528	0.027790	1791.9	-0.69220	223.98	297.24
600.00	1000.0	39.201	0.025510	5.2086	30.718	0.088276	0.018596	0.026881	1767.8	-0.72129	208.59	239.91
700.00	1000.0	37.711	0.026518	6.8515	33.369	0.092364	0.017896	0.026165	1749.3	-0.74683	196.06	207.86

The values in these tables were generated from the NIST REFPROP software (Lemmon, E. W., McLinden, M. O., and Huber, M. L., NIST Standard Reference Database 23: Reference Fluid Thermodynamic and Transport Properties—REFPROP, National Institute of Standards and Technology, Standard Reference Data Program, Gaithersburg, Md., 2002, Version 7.1). The primary source for the thermodynamic properties is Tegeler, Ch., Span, R., and Wagner, W., "A New Equation of State for Argon Covering the Fluid Region for Temperatures from the Melting Line to 700 K at Pressures up to 1000 MPa," *J. Phys. Chem. Ref. Data* **28**(3):779–850, 1999. The source for viscosity and thermal conductivity is Lemmon, E. W., and Jacobsen, R. T., "Viscosity and Thermal Conductivity Equations for Nitrogen, Oxygen, Argon, and Air," *Int. J. Thermophys.* **25**:21–69, 2004.

Properties at the triple point temperature and the critical point temperature are given in the first and last entries of the saturation tables, respectively. In the single-phase table, when the temperature range for a given isobar includes a vapor-liquid phase boundary, the temperature of phase equilibrium is noted, and properties for both the saturated liquid and saturated vapor are given (with liquid properties given in the upper line). Lines are omitted from the temperature-pressure grid of the single-phase table, when the system would be in the solid phase or if there are potential problems with the source property surface.

The estimated uncertainty in density is less than 0.02% for pressures up to 12 MPa and temperatures up to 340 K with the exception of the critical region and less than 0.03% for pressures up to 30 MPa and temperatures between 235 and 520 K. Elsewhere, the uncertainty in density is generally within 0.2%. In the region with densities up to one-half the critical density and for temperatures between 90 and 450 K, the estimated uncertainty of calculated speeds of sound is in general less than 0.02%. In the liquid and supercritical regions, the uncertainty is less than 1%. The uncertainty in heat capacities is within 0.3% for the vapor and 2% for the liquid. The formulation gives reasonable extrapolation behavior up to very high pressures (50 GPa) and temperatures (17,000 K).

For viscosity, the uncertainty is 0.5% in the dilute gas. Away from the dilute gas (pressures greater than 1 MPa and in the liquid), the uncertainties are as low as 1% between 270 and 300 K at pressures less than 100 MPa, and increase outside that range. The uncertainties are around 2% at temperatures of 180 K and higher. Below this and away from the critical region, the uncertainties steadily increase to around 5% at the triple points of the fluids. The uncertainties in the critical region are higher.

For thermal conductivity, the uncertainty for the dilute gas is 2% with increasing uncertainties near the triple point. For the nondilute gas, the uncertainty is 2% for temperatures greater than 170 K. The uncertainty is 3% at temperatures less than the critical point and 5% in the critical region, except for states very near the critical point.

TABLE 2-191 Liquid-Vapor Equilibrium Data for the Argon-Nitrogen-Oxygen System

Liquid mole fraction				Vapor mole fraction			Temperature K	Relative volatility			p^0 (kPa)			Activity coefficient			Enthalpy kJ/kmol		Isobaric specific heat, kJ/(kmol·K)	
$N_2/(N_2+O_2)$	Ar	N_2	O_2	Ar	N_2	O_2		N_2/Ar	N_2/O_2	Ar/O_2	Ar	N_2	O_2	Ar	N_2	O_2	Liquid	Vapor	Liquid	Vapor
Pressure, 101.325 kPa (1 atm)																				
0.00	0.00	0.00	1.00	0.00000	0.0000	1.0000	90.188	—	—	1.606	136.010	366.29	101.33	1.196	—	1.000	-4268	2550	54.378	31.061
0.00	0.01	0.00	0.99	0.01590	0.0000	0.9841	90.128	—	—	1.600	135.210	364.42	100.69	1.192	—	1.000	-4271	2536	54.269	30.929
0.00	0.02	0.00	0.98	0.03151	0.0000	0.96855	90.070	—	—	1.594	134.430	362.62	100.08	1.188	—	1.001	-4275	2523	54.160	30.871
0.00	0.03	0.00	0.97	0.04684	0.0000	0.9532	90.013	—	—	1.589	133.680	360.86	99.49	1.183	—	1.001	-4278	2510	54.052	30.674
0.00	0.04	0.00	0.96	0.06189	0.0000	0.9381	89.956	—	—	1.583	132.930	359.10	98.89	1.179	—	1.001	-4282	2497	53.944	30.550
0.00	0.05	0.00	0.95	0.07667	0.0000	0.9233	89.901	—	—	1.578	132.200	357.41	98.32	1.175	—	1.002	-4285	2484	53.837	30.429
0.00	0.07	0.00	0.93	0.10548	0.0000	0.8945	89.794	—	—	1.567	130.810	354.14	97.22	1.167	—	1.002	-4292	2460	53.622	30.192
0.00	0.10	0.00	0.90	0.14692	0.0000	0.8531	89.640	—	—	1.550	128.810	349.47	95.65	1.156	—	1.004	-4302	2425	53.302	29.851
0.00	0.20	0.00	0.80	0.27211	0.0000	0.7279	89.183	—	—	1.495	123.040	335.88	91.10	1.120	—	1.012	-4336	2320	52.253	28.822
0.00	0.40	0.00	0.60	0.48104	0.0000	0.5190	88.470	—	—	1.390	114.430	315.46	84.35	1.065	—	1.039	-4409	2147	50.224	27.089
0.00	0.60	0.00	0.40	0.65969	0.0000	0.3403	87.948	—	—	1.292	108.420	301.10	79.66	1.028	—	1.082	-4491	2004	48.281	25.578
0.00	0.80	0.00	0.20	0.82774	0.0000	0.1723	87.566	—	—	1.201	104.180	290.90	76.35	1.006	—	1.143	-4586	1873	46.417	24.123
0.00	0.90	0.00	0.10	0.91247	0.0000	0.0875	87.420	—	—	1.158	102.590	287.07	75.12	1.001	—	1.181	-4638	1808	45.515	23.378
0.10	0.00	0.10	0.90	0.0000	0.3150	0.6850	87.546	2.573	4.138	1.608	103.960	290.37	76.18	1.193	1.099	1.012	-4235	2471	54.388	30.764
0.10	0.01	0.10	0.89	0.0122	0.3108	0.6771	87.529	2.579	4.131	1.602	103.780	289.93	76.04	1.188	1.097	1.013	-4238	2461	54.281	30.669
0.10	0.02	0.10	0.88	0.0242	0.3066	0.6692	87.512	2.584	4.124	1.596	103.590	289.48	75.89	1.184	1.095	1.013	-4241	2452	54.175	30.576
0.10	0.03	0.10	0.87	0.0361	0.3025	0.6614	87.495	2.589	4.117	1.590	103.410	289.03	75.75	1.180	1.093	1.013	-4244	2443	54.068	30.484
0.10	0.04	0.10	0.86	0.0479	0.2985	0.6536	87.479	2.595	4.110	1.584	103.230	288.61	75.61	1.176	1.092	1.014	-4248	2434	53.962	30.392
0.10	0.05	0.10	0.86	0.0596	0.2945	0.6459	87.463	2.600	4.103	1.578	103.060	288.19	75.48	1.172	1.090	1.014	-4251	2425	53.856	30.302
0.10	0.10	0.09	0.84	0.0826	0.2866	0.6308	87.432	2.611	4.089	1.566	102.720	287.38	75.22	1.164	1.086	1.015	-4257	2408	53.645	30.123
0.10	0.17	0.09	0.81	0.1164	0.2751	0.6086	87.389	2.627	4.068	1.549	102.260	286.26	74.86	1.153	1.082	1.017	-4266	2382	53.330	29.861
0.10	0.20	0.08	0.72	0.2230	0.2390	0.5380	87.270	2.680	3.999	1.492	100.980	283.17	73.87	1.119	1.069	1.025	-4300	2302	52.291	29.029
0.10	0.40	0.06	0.54	0.4179	0.1749	0.4072	87.121	2.790	3.866	1.386	99.401	279.34	72.64	1.065	1.057	1.052	-4378	2157	50.269	27.486
0.10	0.60	0.04	0.36	0.6027	0.1167	0.2807	87.077	2.904	3.742	1.288	98.938	278.22	72.28	1.029	1.062	1.093	-4469	2023	48.319	25.986
0.10	0.80	0.02	0.18	0.7916	0.0598	0.1486	87.132	3.023	3.625	1.199	99.517	279.63	72.73	1.008	1.084	1.150	-4575	1889	46.440	24.404
0.10	0.90	0.01	0.09	0.8923	0.0306	0.0771	87.201	3.085	3.569	1.157	100.250	281.40	73.30	1.002	1.101	1.185	-4633	1818	45.527	23.542
0.20	0.00	0.20	0.80	0.0000	0.5104	0.4896	85.511	2.606	4.170	1.600	83.506	240.35	60.37	1.188	1.076	1.027	-4176	2409	54.481	30.819
0.20	0.01	0.20	0.79	0.0098	0.5050	0.4853	85.519	2.611	4.162	1.594	83.580	240.53	60.42	1.184	1.074	1.027	-4179	2403	54.374	30.742
0.20	0.02	0.20	0.78	0.0195	0.4995	0.4810	85.526	2.616	4.154	1.588	83.645	240.69	60.47	1.180	1.073	1.028	-4183	2396	54.267	30.665
0.20	0.03	0.19	0.78	0.0292	0.4941	0.4767	85.534	2.621	4.146	1.582	83.719	240.88	60.53	1.176	1.071	1.028	-4186	2389	54.161	30.588
0.20	0.04	0.19	0.77	0.0388	0.4888	0.4724	85.542	2.626	4.139	1.576	83.793	241.06	60.59	1.172	1.070	1.029	-4190	2383	54.054	30.512
0.20	0.05	0.19	0.76	0.0484	0.4835	0.4682	85.551	2.631	4.131	1.570	83.876	241.27	60.65	1.169	1.069	1.029	-4193	2376	53.948	30.436
0.20	0.07	0.19	0.74	0.0674	0.4729	0.4597	85.568	2.641	4.115	1.558	84.033	241.66	60.77	1.161	1.066	1.030	-4200	2363	53.736	30.285
0.20	0.10	0.18	0.72	0.0957	0.4573	0.4470	85.594	2.656	4.092	1.541	84.274	242.25	60.96	1.150	1.063	1.032	-4211	2344	53.420	30.061
0.20	0.20	0.16	0.64	0.1879	0.4069	0.4052	85.695	2.707	4.017	1.484	85.216	244.59	61.68	1.117	1.054	1.040	-4250	2282	52.376	29.328
0.20	0.40	0.12	0.48	0.3685	0.3108	0.3206	85.947	2.812	3.878	1.379	87.602	250.48	63.52	1.066	1.048	1.066	-4340	2161	50.337	27.881
0.20	0.60	0.08	0.32	0.5541	0.2158	0.2302	86.280	2.921	3.750	1.284	90.832	258.43	66.01	1.030	1.057	1.104	-4444	2038	48.366	26.371
0.20	0.80	0.04	0.16	0.7583	0.1150	0.1267	86.717	3.033	3.630	1.197	95.211	269.15	69.39	1.009	1.082	1.157	-4563	1903	46.464	24.673
0.20	0.90	0.02	0.08	0.8729	0.0599	0.0671	86.987	3.090	3.572	1.156	97.996	275.93	71.55	1.003	1.101	1.188	-4628	1827	45.539	23.701
0.40	0.00	0.40	0.60	0.0000	0.7339	0.2661	82.557	2.639	4.138	1.568	—	179.50	42.12	—	1.036	1.067	-4012	2320	54.860	31.014
0.40	0.01	0.40	0.59	0.0070	0.7285	0.2646	82.590	2.644	4.131	1.562	—	180.11	42.29	—	1.035	1.067	-4017	2316	54.749	30.957
0.40	0.02	0.39	0.59	0.0139	0.7230	0.2630	82.623	2.649	4.123	1.557	—	180.72	42.47	—	1.034	1.067	-4022	2313	54.637	30.899
0.40	0.03	0.39	0.58	0.0209	0.7176	0.2615	82.656	2.654	4.116	1.551	—	181.33	42.65	—	1.033	1.068	-4028	2309	54.526	30.841
0.40	0.04	0.38	0.58	0.0279	0.7121	0.2600	82.689	2.659	4.108	1.545	—	181.95	42.82	—	1.033	1.068	-4033	2305	54.415	30.783
0.40	0.05	0.38	0.57	0.0349	0.7067	0.2585	82.722	2.664	4.101	1.540	—	182.56	43.00	—	1.032	1.068	-4038	2301	54.304	30.724
0.40	0.07	0.37	0.56	0.0490	0.6957	0.2553	82.789	2.673	4.087	1.529	—	183.81	43.37	—	1.031	1.069	-4049	2294	54.083	30.607
0.40	0.10	0.36	0.54	0.0702	0.6792	0.2506	82.890	2.688	4.066	1.513	—	185.71	43.92	—	1.029	1.071	-4066	2282	53.752	30.431
0.40	0.20	0.32	0.48	0.1424	0.6237	0.2340	83.238	2.738	3.998	1.460	—	192.37	45.87	—	1.027	1.077	-4123	2243	52.662	29.830
0.40	0.40	0.24	0.36	0.2971	0.5066	0.1963	83.994	2.842	3.871	1.362	70.40	207.45	50.35	1.069	1.031	1.097	-4250	2158	50.537	28.539
0.40	0.60	0.16	0.24	0.4762	0.3743	0.1496	84.870	2.947	3.753	1.273	77.76	226.01	55.96	1.034	1.049	1.129	-4389	2056	48.489	27.042
0.40	0.80	0.08	0.12	0.6988	0.2133	0.0880	85.936	3.052	3.637	1.192	87.50	250.22	63.43	1.012	1.079	1.171	-4538	1926	46.520	25.171
0.40	0.90	0.04	0.06	0.8364	0.1153	0.0483	86.573	3.101	3.577	1.153	93.75	265.58	68.26	1.004	1.100	1.196	-4616	1844	45.566	24.005
0.60	0.00	0.60	0.40	0.0000	0.8586	0.1414	80.441	2.657	4.047	1.523	—	143.61	31.97	—	1.010	1.121	-3821	2256	55.455	31.192
0.60	0.01	0.59	0.40	0.0054	0.8538	0.1408	80.485	2.661	4.041	1.519	—	144.30	32.16	—	1.009	1.121	-3828	2254	55.334	31.145
0.60	0.02	0.59	0.39	0.0108	0.8489	0.1402	80.530	2.666	4.036	1.514	—	145.00	32.35	—	1.009	1.120	-3836	2252	55.214	31.097
0.60	0.03	0.58	0.39	0.0163	0.8441	0.1396	80.574	2.671	4.030	1.509	—	145.69	32.54	—	1.009	1.121				

0.60	0.04	0.58	0.38	0.0218	0.8392	0.1390	80.619	2.676	4.024	1.504	—	146.40	32.74	—	1.008	1.121	-3851	2247	54.973	31.002
0.60	0.05	0.57	0.38	0.0273	0.8343	0.1384	80.664	2.681	4.018	1.499	—	147.12	32.94	—	1.008	1.121	-3859	2245	54.853	30.954
0.60	0.07	0.56	0.37	0.0384	0.8244	0.1372	80.755	2.690	4.007	1.489	—	148.56	33.34	—	1.008	1.121	-3874	2240	54.614	30.857
0.60	0.10	0.54	0.36	0.0554	0.8094	0.1352	80.893	2.705	3.991	1.475	—	150.78	33.95	—	1.007	1.121	-3898	2233	54.257	30.709
0.60	0.20	0.48	0.32	0.1145	0.7573	0.1282	81.368	2.756	3.938	1.429	—	158.60	36.14	—	1.008	1.123	-3978	2207	53.083	30.196
0.60	0.40	0.36	0.24	0.2487	0.6402	0.1112	82.415	2.860	3.839	1.342	—	176.90	41.36	—	1.019	1.135	-4148	2147	50.811	29.035
0.60	0.60	0.24	0.16	0.4170	0.4949	0.0881	83.658	2.967	3.743	1.262	—	200.64	48.32	—	1.041	1.155	-4327	2066	48.644	27.586
0.60	0.80	0.12	0.08	0.6475	0.2979	0.0546	85.216	3.068	3.640	1.186	80.82	233.67	58.30	1.015	1.077	1.186	-4512	1945	46.584	25.615
0.60	0.90	0.06	0.04	0.8025	0.1665	0.0310	86.175	3.111	3.581	1.151	89.80	255.91	65.21	1.006	1.099	1.204	-4604	1858	45.595	24.292
0.80	0.00	0.80	0.20	0.0000	0.9404	0.0596	78.768	2.673	3.942	1.475	—	119.30	25.42	—	0.998	1.189	-3620	2205	56.237	31.347
0.80	0.01	0.79	0.20	0.0044	0.9362	0.0594	78.820	2.677	3.938	1.471	—	120.01	25.60	—	0.998	1.188	-3630	2204	56.103	31.306
0.80	0.02	0.78	0.20	0.0089	0.9319	0.0592	78.871	2.682	3.934	1.467	—	120.70	25.79	—	0.998	1.187	-3640	2202	55.970	31.266
0.80	0.03	0.78	0.19	0.0133	0.9276	0.0590	78.923	2.687	3.930	1.463	—	121.41	25.97	—	0.998	1.187	-3650	2201	55.836	31.225
0.80	0.04	0.77	0.19	0.0179	0.9233	0.0588	78.974	2.691	3.926	1.459	—	122.12	26.16	—	0.998	1.186	-3660	2200	55.704	31.183
0.80	0.05	0.76	0.19	0.0224	0.9190	0.0586	79.027	2.696	3.921	1.455	—	122.85	26.35	—	0.997	1.186	-3670	2198	55.571	31.142
0.80	0.07	0.74	0.19	0.0317	0.9102	0.0581	79.132	2.705	3.913	1.447	—	124.31	26.74	—	0.997	1.185	-3691	2195	55.307	31.058
0.80	0.10	0.72	0.18	0.0458	0.8967	0.0575	79.292	2.720	3.901	1.434	—	126.55	27.34	—	0.997	1.183	-3721	2191	54.914	30.929
0.80	0.20	0.64	0.16	0.0958	0.8492	0.0550	79.848	2.769	3.863	1.395	—	134.60	29.51	—	0.999	1.179	-3825	2175	53.625	30.476
0.80	0.40	0.48	0.12	0.2139	0.7375	0.0486	81.090	2.874	3.793	1.320	—	153.99	34.85	—	1.011	1.178	-4039	2133	51.154	29.417
0.80	0.60	0.32	0.08	0.3708	0.5897	0.0396	82.596	2.982	3.723	1.249	—	180.22	42.32	—	1.036	1.185	-4261	2069	48.829	28.030
0.80	0.80	0.16	0.04	0.6029	0.3716	0.0255	84.549	3.082	3.639	1.181	74.99	219.07	53.85	1.018	1.074	1.201	-4483	1960	46.656	26.011
0.80	0.90	0.08	0.02	0.7712	0.2139	0.0149	85.793	3.121	3.584	1.148	86.14	246.87	62.39	1.008	1.098	1.212	-4591	1872	45.625	24.563
0.90	0.00	0.90	0.10	0.0000	0.9722	0.0278	78.036	2.683	3.891	1.450	—	109.71	22.91	—	0.998	1.228	-3519.2	2182.4	56.7	31.418
0.90	0.01	0.89	0.10	0.0040	0.9683	0.0277	78.090	2.687	3.888	1.447	—	110.4	23.088	—	0.997	1.227	-3530.4	2181.5	56.6	31.380
0.90	0.02	0.88	0.10	0.0081	0.9643	0.0276	78.144	2.692	3.884	1.443	—	111.09	23.267	—	0.997	1.226	-3541.6	2180.5	56.4	31.342
0.90	0.03	0.87	0.10	0.0122	0.9603	0.0275	78.199	2.696	3.881	1.439	—	111.79	23.45	—	0.997	1.225	-3552.8	2179.5	56.3	31.303
0.90	0.04	0.86	0.10	0.0164	0.9562	0.0274	78.254	2.701	3.877	1.436	—	112.5	23.634	—	0.997	1.224	-3564.1	2178.5	56.1	31.264
0.90	0.05	0.86	0.10	0.0206	0.9521	0.0273	78.309	2.705	3.874	1.432	—	113.22	23.82	—	0.997	1.223	-3575.3	2177.5	56.0	31.225
0.90	0.07	0.84	0.09	0.0291	0.9438	0.0271	78.420	2.714	3.867	1.425	—	114.67	24.198	—	0.996	1.221	-3598	2175.3	55.7	31.146
0.90	0.10	0.81	0.09	0.0421	0.9310	0.0268	78.589	2.728	3.857	1.414	—	116.9	24.783	—	0.996	1.219	-3632.1	2172	55.3	31.024
0.90	0.20	0.72	0.08	0.0886	0.8857	0.0257	79.177	2.776	3.825	1.378	—	124.93	26.908	—	0.998	1.211	-3747.3	2159.4	53.9	30.594
0.90	0.40	0.54	0.06	0.1999	0.7772	0.0229	80.497	2.880	3.768	1.308	—	144.49	32.209	—	1.009	1.202	-3983.9	2124.8	51.3	29.578
0.90	0.60	0.36	0.04	0.3513	0.6299	0.0189	82.110	2.988	3.711	1.242	—	171.42	39.784	—	1.034	1.201	-4226.4	2068.5	48.9	28.223
0.90	0.80	0.18	0.02	0.5828	0.4049	0.0124	84.233	3.088	3.638	1.178	72.35	212.4	51.833	1.020	1.073	1.209	-4468.2	1965.6	46.7	26.192
0.90	0.90	0.09	0.01	0.7563	0.2364	0.0073	85.608	3.125	3.585	1.147	84.404	242.58	61.055	1.009	1.097	1.216	-4584.8	1877.8	45.6	24.692
0.97	0.00	0.97	0.03	0.0000	0.9921	0.0080	77.555	2.691	3.857	1.433	—	103.74	21.375	—	0.999	1.257	-3448.5	2167.6	57.0	31.465
0.97	0.01	0.96	0.03	0.0038	0.9883	0.0079	77.610	2.695	3.854	1.430	—	104.41	21.546	—	0.999	1.256	-3460.5	2166.9	56.9	31.429
0.97	0.02	0.95	0.03	0.0077	0.9844	0.0079	77.666	2.700	3.851	1.426	—	105.09	21.722	—	0.998	1.254	-3472.5	2166.1	56.7	31.392
0.97	0.03	0.94	0.03	0.0116	0.9806	0.0079	77.722	2.704	3.848	1.423	—	105.78	21.898	—	0.998	1.253	-3484.6	2165.3	56.6	31.355
0.97	0.04	0.93	0.03	0.0155	0.9767	0.0079	77.779	2.708	3.844	1.420	—	106.49	22.079	—	0.998	1.252	-3496.6	2164.5	56.5	31.318
0.97	0.05	0.92	0.03	0.0195	0.9727	0.0078	77.836	2.712	3.841	1.416	—	107.2	22.261	—	0.998	1.251	-3508.7	2163.7	56.3	31.280
0.97	0.07	0.90	0.03	0.0275	0.9647	0.0078	77.950	2.721	3.835	1.409	—	108.62	22.629	—	0.998	1.249	-3533	2162.1	56.0	31.203
0.97	0.10	0.87	0.03	0.0399	0.9524	0.0077	78.125	2.735	3.826	1.399	—	110.85	23.204	—	0.997	1.245	-3569.5	2159.4	55.6	31.086
0.97	0.20	0.78	0.02	0.0842	0.9084	0.0074	78.734	2.781	3.798	1.366	—	118.85	25.294	—	0.998	1.235	-3692.7	2149.1	54.2	30.670
0.97	0.40	0.58	0.02	0.1912	0.8022	0.0066	80.104	2.884	3.750	1.300	—	138.44	30.551	—	1.009	1.219	-3944.8	2119.2	51.5	29.681
0.97	0.60	0.39	0.01	0.3389	0.6557	0.0055	81.786	2.992	3.702	1.237	—	165.73	38.159	—	1.033	1.212	-4202.1	2068.1	49.0	28.347
0.97	0.80	0.19	0.01	0.5694	0.4270	0.0036	84.018	3.092	3.636	1.176	70.593	207.94	50.496	1.022	1.072	1.215	-4457.7	1969.5	46.7	26.313
0.97	0.90	0.10	0.00	0.7462	0.2516	0.0022	85.481	3.128	3.585	1.146	83.23	239.66	60.153	1.009	1.097	1.219	-4580.2	1881.9	45.7	24.780
1.00	0.00	1.00	0.00	0.0000	1.0000	0.0000	77.355	2.695	—	—	—	101.33	20.762	—	1.000	—	-3418.2	2161.5	57.2	31.485
1.00	0.01	0.99	0.00	0.0037	0.9963	0.0000	77.411	2.699	—	—	—	102	20.932	—	1.000	—	-3430.5	2160.8	57.0	31.449
1.00	0.02	0.98	0.00	0.0075	0.9925	0.0000	77.468	2.703	—	—	—	102.68	21.106	—	0.999	—	-3442.9	2160.1	56.9	31.413
1.00	0.03	0.97	0.00	0.0113	0.9887	0.0000	77.525	2.708	—	—	—	103.37	21.282	—	0.999	—	-3455.3	2159.4	56.7	31.377
1.00	0.04	0.96	0.00	0.0151	0.9849	0.0000	77.582	2.712	—	—	—	104.06	21.459	—	0.999	—	-3467.7	2158.7	56.6	31.340
1.00	0.05	0.95	0.00	0.0190	0.9810	0.0000	77.640	2.716	—	—	—	104.77	21.64	—	0.999	—	-3480.2	2158	56.4	31.303
1.00	0.07	0.93	0.00	0.0269	0.9731	0.0000	77.756	2.725	—	—	—	106.2	22.006	—	0.998	—	-3505.1	2156.5	56.2	31.227
1.00	0.10	0.90	0.00	0.0390	0.9610	0.0000	77.933	2.738	—	—	—	108.41	22.574	—	0.998	—	-3542.7	2154.1	55.7	31.112
1.00	0.20	0.80	0.00	0.0824	0.9176	0.0000	78.550	2.784	—	—	—	116.38	24.647	—	0.999	—	-3669.3	2144.7	54.3	30.701
1.00	0.40	0.60	0.00	0.1877	0.8123	0.0000	79.941	2.885	—	—	—	135.99	29.883	—	1.009	—	-3927.9	2116.8	51.6	29.723
1.00	0.60	0.40	0.00	0.3338	0.6662	0.0000	81.650	2.994	—	—	—	163.38	37.493	—	1.033	—	-4191.7	2067.7	49.0	28.398
1.00	0.80	0.20	0.00	0.5639																

TABLE 2-191 Liquid-Vapor Equilibrium Data for the Argon-Nitrogen-Oxygen System (Concluded)

Liquid mole fraction				Vapor mole fraction			Temperature K	Relative volatility			p^0 (kPa)			Activity coefficient			Enthalpy kJ/kmol		Isobaric specific heat, kJ/(kmol·K)	
$N_2/(N_2+O_2)$	Ar	N_2	O_2	Ar	N_2	O_2		N_2/Ar	N_2/O_2	Ar/O_2	Ar	N_2	O_2	Ar	N_2	O_2	Liquid	Vapor	Liquid	Vapor
Pressure, 405.3 kPa (4 atm)																				
0.00	0.02	0.00	0.98	0.0275	0.0000	0.9725	105.790	—	—	1.385	499.6	1138.3	401.72	1.115	—	1.001	-3402.6	2829.5	56.5	33.534
0.00	0.03	0.00	0.97	0.0410	0.0000	0.9590	105.740	—	—	1.381	497.83	1134.8	400.22	1.112	—	1.001	-3407.8	2816.1	56.4	33.431
0.00	0.04	0.00	0.96	0.0543	0.0000	0.9457	105.680	—	—	1.378	495.72	1130.5	398.43	1.110	—	1.002	-3412.9	2802.8	56.3	33.329
0.00	0.05	0.00	0.95	0.0675	0.0000	0.9326	105.630	—	—	1.374	493.96	1127	396.94	1.107	—	1.002	-3418	2789.7	56.2	33.229
0.00	0.07	0.00	0.93	0.0933	0.0000	0.9067	105.520	—	—	1.367	490.12	1119.3	393.68	1.102	—	1.004	-3428.3	2764	56.0	33.031
0.00	0.10	0.00	0.90	0.1310	0.0000	0.8690	105.370	—	—	1.357	484.91	1108.8	389.27	1.095	—	1.005	-3443.6	2726.7	55.7	32.744
0.00	0.20	0.00	0.80	0.2484	0.0000	0.7516	104.900	—	—	1.322	468.86	1076.5	375.67	1.074	—	1.014	-3495.1	2611.3	54.6	31.846
0.00	0.40	0.00	0.60	0.4556	0.0000	0.5445	104.150	—	—	1.255	444.04	1026.3	354.7	1.040	—	1.037	-3601.7	2411.9	52.5	30.249
0.00	0.60	0.00	0.40	0.6412	0.0000	0.3588	103.590	—	—	1.191	426.16	989.9	339.63	1.016	—	1.071	-3716.7	2238.3	50.5	28.788
0.00	0.80	0.00	0.20	0.8190	0.0000	0.1810	103.190	—	—	1.131	413.71	964.49	329.15	1.003	—	1.115	-3842.6	2076.7	48.6	27.354
0.00	0.90	0.00	0.10	0.9084	0.0000	0.0916	103.030	—	—	1.102	408.8	954.46	325.03	1.001	—	1.142	-3910.1	1997.2	47.6	26.620
0.10	0.00	0.10	0.90	0.0000	0.2399	0.7601	103.430	2.045	2.840	1.389	421.14	979.68	335.41	1.129	0.992	1.021	-3351.1	2779.8	56.8	33.931
0.10	0.01	0.10	0.89	0.0117	0.2369	0.7515	103.400	2.048	2.837	1.385	420.21	977.77	334.62	1.127	0.992	1.022	-3356.1	2769.2	56.7	33.841
0.10	0.02	0.10	0.88	0.0233	0.2339	0.7429	103.380	2.051	2.833	1.381	419.59	976.5	334.1	1.124	0.990	1.022	-3361.1	2758.7	56.5	33.752
0.10	0.03	0.10	0.87	0.0348	0.2309	0.7343	103.360	2.054	2.830	1.378	418.97	975.23	333.57	1.121	0.989	1.022	-3366.1	2748.2	56.4	33.663
0.10	0.04	0.10	0.86	0.0462	0.2280	0.7259	103.340	2.057	2.827	1.374	418.34	973.97	333.05	1.118	0.988	1.022	-3371.1	2737.9	56.3	33.575
0.10	0.05	0.10	0.86	0.0575	0.2251	0.7174	103.320	2.060	2.823	1.370	417.72	972.7	332.53	1.116	0.987	1.023	-3376.2	2727.6	56.2	33.488
0.10	0.07	0.09	0.84	0.0799	0.2193	0.7008	103.280	2.066	2.817	1.363	416.49	970.17	331.49	1.111	0.985	1.024	-3386.3	2707.4	56.0	33.315
0.10	0.10	0.09	0.81	0.1129	0.2109	0.6762	103.220	2.075	2.807	1.352	414.63	966.38	329.93	1.104	0.983	1.026	-3401.7	2677.6	55.7	33.059
0.10	0.20	0.08	0.72	0.2186	0.1841	0.5973	103.060	2.105	2.774	1.317	409.72	956.33	325.8	1.081	0.975	1.032	-3454.5	2583	54.6	32.238
0.10	0.40	0.06	0.54	0.4159	0.1352	0.4489	102.840	2.166	2.709	1.251	403.04	942.64	320.19	1.046	0.968	1.052	-3568	2409.5	52.6	30.684
0.10	0.60	0.04	0.36	0.6047	0.0899	0.3054	102.740	2.229	2.648	1.188	400.02	936.47	317.66	1.021	0.972	1.082	-3693.2	2247.1	50.6	29.163
0.10	0.80	0.02	0.18	0.7958	0.0456	0.1586	102.760	2.294	2.591	1.129	400.62	937.7	318.16	1.006	0.986	1.122	-3830.8	2086.1	48.6	27.585
0.10	0.90	0.01	0.09	0.8955	0.0232	0.0813	102.820	2.328	2.563	1.101	402.43	941.41	319.68	1.002	0.997	1.146	-3904.2	2003.1	47.6	26.748
0.20	0.00	0.20	0.80	0.0000	0.4159	0.5841	101.340	2.061	2.848	1.382	359.58	853.02	283.81	1.138	0.988	1.043	-3293.1	2714.9	56.9	34.186
0.20	0.01	0.20	0.79	0.0101	0.4114	0.5785	101.340	2.064	2.845	1.378	359.58	853.02	283.81	1.135	0.987	1.043	-3298.4	2706.6	56.8	34.106
0.20	0.02	0.20	0.78	0.0201	0.4069	0.5730	101.340	2.067	2.841	1.375	359.58	853.02	283.81	1.132	0.986	1.044	-3303.7	2698.3	56.6	34.026
0.20	0.03	0.19	0.78	0.0301	0.4025	0.5674	101.350	2.070	2.837	1.371	359.85	853.59	284.04	1.129	0.985	1.043	-3309.1	2690.1	56.5	33.946
0.20	0.04	0.19	0.77	0.0400	0.3981	0.5619	101.350	2.072	2.834	1.367	359.85	853.59	284.04	1.127	0.984	1.044	-3314.5	2681.9	56.4	33.867
0.20	0.05	0.19	0.76	0.0499	0.3937	0.5564	101.350	2.075	2.830	1.364	359.85	853.59	284.04	1.124	0.984	1.045	-3319.9	2673.7	56.3	33.787
0.20	0.07	0.19	0.74	0.0696	0.3849	0.5455	101.360	2.081	2.823	1.356	360.13	854.17	284.27	1.119	0.982	1.045	-3330.8	2657.6	56.1	33.630
0.20	0.10	0.18	0.72	0.0989	0.3720	0.5291	101.380	2.089	2.812	1.346	360.69	855.32	284.74	1.111	0.979	1.046	-3347.5	2633.6	55.8	33.395
0.20	0.20	0.16	0.64	0.1948	0.3300	0.4753	101.440	2.118	2.777	1.311	362.36	858.79	286.13	1.089	0.973	1.052	-3405.2	2555.4	54.7	32.622
0.20	0.40	0.12	0.48	0.3822	0.2496	0.3682	101.640	2.176	2.711	1.246	367.98	870.43	290.82	1.052	0.968	1.069	-3530.2	2404.5	52.6	31.093
0.20	0.60	0.08	0.32	0.5719	0.1706	0.2575	101.940	2.237	2.649	1.185	376.52	888.1	297.97	1.026	0.973	1.095	-3668.1	2253.6	50.6	29.517
0.20	0.80	0.04	0.16	0.7738	0.0889	0.1373	102.350	2.299	2.592	1.127	388.44	912.66	307.94	1.009	0.987	1.129	-3818.6	2094.6	48.6	27.809
0.20	0.90	0.02	0.08	0.8829	0.0457	0.0713	102.610	2.330	2.564	1.100	396.13	928.48	314.4	1.004	0.998	1.150	-3898.3	2008.8	47.6	26.873
0.40	0.00	0.40	0.60	0.0000	0.6538	0.3462	97.997	2.082	2.832	1.360	275.25	675.50	213.91	1.156	0.981	1.093	-3143.7	2610.3	57.346	34.697
0.40	0.01	0.40	0.59	0.0079	0.6484	0.3438	98.032	2.084	2.829	1.357	276.05	677.21	214.57	1.153	0.980	1.093	-3150.5	2605.1	57.232	34.629
0.40	0.02	0.39	0.59	0.0157	0.6429	0.3414	98.067	2.087	2.825	1.354	276.85	678.92	215.23	1.150	0.979	1.093	-3157.4	2599.8	57.118	34.560
0.40	0.03	0.39	0.58	0.0236	0.6375	0.3389	98.101	2.090	2.822	1.350	277.63	680.58	215.87	1.148	0.978	1.093	-3164.4	2594.5	57.004	34.492
0.40	0.04	0.38	0.58	0.0315	0.6321	0.3364	98.136	2.092	2.818	1.347	278.43	682.30	216.53	1.145	0.978	1.093	-3171.3	2589.2	56.891	34.423
0.40	0.05	0.38	0.57	0.0394	0.6267	0.3340	98.172	2.095	2.815	1.344	279.26	684.07	217.21	1.142	0.977	1.093	-3178.3	2584.0	56.778	34.354
0.40	0.07	0.37	0.56	0.0552	0.6159	0.3290	98.242	2.100	2.808	1.337	280.88	687.51	218.54	1.137	0.976	1.093	-3192.4	2573.4	56.551	34.217
0.40	0.10	0.36	0.54	0.0790	0.5996	0.3214	98.350	2.108	2.798	1.327	283.38	692.86	220.61	1.130	0.974	1.094	-3213.9	2557.4	56.212	34.009
0.40	0.20	0.32	0.48	0.1595	0.5449	0.2956	98.721	2.136	2.765	1.295	292.12	711.44	227.81	1.106	0.970	1.096	-3287.5	2503.3	55.091	33.304
0.40	0.40	0.24	0.36	0.3285	0.4320	0.2396	99.531	2.192	2.704	1.234	311.88	753.27	244.15	1.067	0.968	1.105	-3444.6	2389.2	52.889	31.817
0.40	0.60	0.16	0.24	0.5155	0.3092	0.1752	100.460	2.249	2.647	1.177	335.75	803.38	263.96	1.037	0.975	1.121	-3613.8	2261.2	50.745	30.162
0.40	0.80	0.08	0.12	0.7330	0.1691	0.0979	101.570	2.307	2.592	1.124	366.00	866.34	289.17	1.015	0.989	1.143	-3793.2	2109.2	48.673	28.233
0.40	0.90	0.04	0.06	0.8588	0.0891	0.0521	102.200	2.335	2.564	1.098	384.05	903.62	304.26	1.007	0.999	1.157	-3886.1	2019.4	47.668	27.117
0.60	0.00	0.60	0.40	0.0000	0.8073	0.1927	95.398	2.095	2.793	1.333	220.63	557.21	169.24	1.180	0.979	1.154	-2969.3	2527.7	58.120	35.181
0.60	0.01	0.59	0.40	0.0064	0.8019	0.1916	95.451	2.097	2.790	1.330	221.66	559.46	170.08	1.177	0.978	1.153	-2978.2	2524.3	57.994	35.120
0.60	0.02	0.59	0.39	0.0129	0.7966	0.1906	95.503	2.100	2.787	1.327	222.67	561.68	170.90	1.174	0.978	1.153	-2987.2	2520.9	57.869	35.057
0.60	0.03	0.58	0.39	0.0194	0.7912	0.1895	95.556	2.102	2.784	1.324	223.70	563.94	171.74	1.172	0.977	1.152	-2996.2	2517.5	57.743	34.995
0.60	0.04	0.58	0.38	0.0259	0.7857	0.1883														

0.60	0.07	0.56	0.37	0.0457	0.7694	0.1850	95.771	2.113	2.773	1.312	227.93	573.19	175.17	1.160	0.975	1.150	-3032.6	2503.5	57.243	34.742
0.60	0.10	0.54	0.36	0.0657	0.7528	0.1815	95.934	2.121	2.765	1.304	231.17	580.27	177.81	1.152	0.974	1.149	-3060.2	2492.8	56.870	34.550
0.60	0.20	0.48	0.32	0.1350	0.6957	0.1694	96.496	2.148	2.738	1.275	242.61	605.18	187.15	1.127	0.971	1.146	-3154.0	2455.3	55.639	33.887
0.60	0.40	0.36	0.24	0.2878	0.5707	0.1415	97.721	2.203	2.688	1.220	269.02	662.15	208.79	1.084	0.970	1.145	-3349.9	2369.9	53.233	32.433
0.60	0.60	0.24	0.16	0.4690	0.4239	0.1070	99.133	2.260	2.641	1.169	302.05	732.50	236.01	1.049	0.977	1.149	-3554.9	2263.2	50.938	30.730
0.60	0.80	0.12	0.08	0.6962	0.2417	0.0622	100.820	2.314	2.592	1.120	345.35	823.43	271.95	1.021	0.991	1.158	-3766.5	2121.1	48.741	28.628
0.60	0.90	0.06	0.04	0.8358	0.1303	0.0339	101.810	2.339	2.565	1.096	372.80	880.41	294.86	1.010	1.000	1.164	-3873.6	2029.2	47.694	27.351
0.80	0.00	0.80	0.20	0.0000	0.9165	0.0835	93.251	2.106	2.744	1.303	182.01	471.46	138.01	1.212	0.985	1.226	-2783.0	2458.2	59.157	35.652
0.80	0.01	0.79	0.20	0.0055	0.9114	0.0831	93.315	2.108	2.742	1.301	183.08	473.86	138.88	1.209	0.984	1.225	-2794.3	2456.1	59.014	35.593
0.80	0.02	0.78	0.20	0.0110	0.9063	0.0827	93.380	2.111	2.740	1.298	184.17	476.32	139.75	1.205	0.984	1.224	-2805.5	2454.0	58.871	35.533
0.80	0.03	0.78	0.19	0.0165	0.9012	0.0823	93.445	2.113	2.738	1.296	185.27	478.78	140.64	1.202	0.983	1.223	-2816.8	2451.8	58.729	35.474
0.80	0.04	0.77	0.19	0.0221	0.8961	0.0819	93.510	2.116	2.736	1.293	186.37	481.25	141.53	1.199	0.983	1.221	-2828.1	2449.7	58.586	35.414
0.80	0.05	0.76	0.19	0.0277	0.8909	0.0815	93.576	2.118	2.734	1.291	187.50	483.77	142.43	1.196	0.982	1.220	-2839.4	2447.5	58.444	35.354
0.80	0.07	0.74	0.19	0.0390	0.8804	0.0806	93.708	2.123	2.729	1.286	189.76	488.84	144.26	1.190	0.981	1.218	-2862.1	2443.0	58.161	35.232
0.80	0.10	0.72	0.18	0.0563	0.8643	0.0793	93.910	2.131	2.723	1.278	193.27	496.68	147.09	1.181	0.980	1.215	-2896.3	2436.0	57.739	35.047
0.80	0.20	0.64	0.16	0.1171	0.8082	0.0747	94.605	2.157	2.704	1.254	205.71	524.32	157.14	1.153	0.976	1.205	-3011.9	2410.8	56.353	34.405
0.80	0.40	0.48	0.12	0.2562	0.6801	0.0637	96.135	2.212	2.667	1.206	235.21	589.09	181.11	1.104	0.975	1.189	-3249.2	2348.3	53.683	32.970
0.80	0.60	0.32	0.08	0.4302	0.5204	0.0494	97.925	2.268	2.631	1.160	273.62	672.00	212.57	1.062	0.981	1.178	-3492.7	2261.3	51.165	31.234
0.80	0.80	0.16	0.04	0.6627	0.3076	0.0297	100.110	2.321	2.590	1.116	326.60	844.23	256.36	1.028	0.994	1.174	-3738.8	2130.7	48.820	28.996
0.80	0.90	0.08	0.02	0.8139	0.1696	0.0165	101.420	2.343	2.565	1.095	361.80	857.63	285.67	1.013	1.002	1.172	-3860.8	2038.1	47.724	27.577
0.90	0.00	0.90	0.10	0.0000	0.9607	0.0393	92.292	2.111	2.719	1.288	166.50	436.43	125.58	1.231	0.991	1.267	-2687.7	2426.8	59.774	35.885
0.90	0.01	0.89	0.10	0.0051	0.9558	0.0391	92.361	2.114	2.717	1.286	167.59	438.89	126.45	1.227	0.991	1.265	-2700.1	2425.2	59.619	35.827
0.90	0.02	0.88	0.10	0.0102	0.9509	0.0389	92.431	2.116	2.716	1.283	168.69	441.39	127.33	1.224	0.990	1.264	-2712.5	2423.6	59.466	35.768
0.90	0.03	0.87	0.10	0.0153	0.9459	0.0387	92.501	2.119	2.714	1.281	169.79	443.90	128.22	1.221	0.989	1.262	-2724.9	2422.0	59.312	35.709
0.90	0.04	0.86	0.10	0.0205	0.9409	0.0385	92.571	2.121	2.712	1.279	170.91	446.42	129.11	1.218	0.989	1.261	-2737.3	2420.3	59.159	35.650
0.90	0.05	0.86	0.10	0.0258	0.9359	0.0384	92.642	2.123	2.710	1.276	172.04	448.99	130.02	1.214	0.988	1.259	-2749.8	2418.6	59.007	35.590
0.90	0.07	0.84	0.09	0.0364	0.9256	0.0380	92.784	2.128	2.707	1.272	174.33	454.16	131.85	1.208	0.987	1.256	-2774.7	2415.2	58.703	35.469
0.90	0.10	0.81	0.09	0.0526	0.9100	0.0374	93.001	2.136	2.702	1.265	177.86	462.14	134.69	1.199	0.985	1.251	-2812.4	2409.7	58.250	35.286
0.90	0.20	0.72	0.08	0.1099	0.8548	0.0354	93.751	2.161	2.686	1.242	190.51	490.50	144.86	1.169	0.981	1.237	-2939.0	2389.6	56.769	34.648
0.90	0.40	0.54	0.06	0.2429	0.7267	0.0304	95.408	2.216	2.655	1.198	220.83	557.64	169.40	1.115	0.978	1.212	-3197.3	2337.1	53.939	33.216
0.90	0.60	0.36	0.04	0.4131	0.5631	0.0238	97.360	2.272	2.625	1.156	261.03	644.98	202.23	1.069	0.983	1.194	-3460.7	2259.1	51.297	31.467
0.90	0.80	0.18	0.02	0.6471	0.3384	0.0145	99.771	2.324	2.589	1.114	317.92	765.99	249.16	1.031	0.995	1.181	-3724.5	2134.7	48.865	29.170
0.90	0.90	0.09	0.01	0.8034	0.1884	0.0082	101.230	2.346	2.565	1.094	356.53	846.69	281.27	1.015	1.002	1.176	-3854.3	2042.2	47.740	27.687
0.97	0.00	0.97	0.03	0.0000	0.9887	0.0113	91.656	2.116	2.702	1.277	156.79	414.28	117.83	1.245	0.997	1.298	-2620.4	2405.9	60.245	36.049
0.97	0.01	0.96	0.03	0.0048	0.9839	0.0113	91.728	2.118	2.700	1.275	157.87	416.75	118.68	1.242	0.996	1.296	-2633.6	2404.6	60.082	35.990
0.97	0.02	0.95	0.03	0.0097	0.9791	0.0112	91.801	2.120	2.699	1.273	158.97	419.26	119.56	1.238	0.996	1.294	-2646.8	2403.3	59.920	35.932
0.97	0.03	0.94	0.03	0.0146	0.9742	0.0112	91.874	2.123	2.697	1.271	160.07	421.78	120.44	1.235	0.995	1.292	-2660.0	2402.0	59.758	35.873
0.97	0.04	0.93	0.03	0.0196	0.9693	0.0111	91.948	2.125	2.696	1.268	161.20	424.35	121.34	1.231	0.994	1.290	-2673.3	2400.6	59.596	35.813
0.97	0.05	0.92	0.03	0.0246	0.9643	0.0111	92.022	2.128	2.694	1.266	162.33	426.93	122.24	1.228	0.993	1.288	-2686.5	2399.3	59.436	35.754
0.97	0.07	0.90	0.03	0.0347	0.9543	0.0110	92.171	2.132	2.691	1.262	164.62	432.16	124.08	1.221	0.992	1.284	-2713.1	2396.5	59.115	35.634
0.97	0.10	0.87	0.03	0.0503	0.9389	0.0108	92.397	2.140	2.687	1.256	168.15	440.17	126.90	1.212	0.990	1.279	-2753.1	2392.0	58.639	35.450
0.97	0.20	0.78	0.02	0.1053	0.8845	0.0102	93.182	2.165	2.673	1.235	180.86	468.87	137.09	1.180	0.985	1.261	-2887.4	2375.1	57.084	34.814
0.97	0.40	0.58	0.02	0.2344	0.7567	0.0088	94.921	2.219	2.647	1.193	211.56	537.25	161.88	1.123	0.981	1.230	-3160.7	2329.1	54.131	33.381
0.97	0.60	0.39	0.01	0.4019	0.5911	0.0070	96.979	2.274	2.621	1.152	252.78	627.20	195.47	1.074	0.984	1.205	-3437.9	2257.3	51.395	31.622
0.97	0.80	0.19	0.01	0.6366	0.3591	0.0043	99.538	2.326	2.588	1.112	312.06	753.64	244.29	1.034	0.995	1.187	-3714.4	2137.3	48.897	29.289
0.97	0.90	0.10	0.00	0.7962	0.2014	0.0024	101.100	2.347	2.565	1.093	352.96	839.27	278.29	1.016	1.003	1.179	-3849.7	2045.0	47.752	27.763
1.00	0.00	1.00	0.00	0.0000	1.0000	0.0000	91.391	2.118	—	—	152.87	405.30	114.70	1.252	1.000	—	-2591.4	2397.1	60.458	36.119
1.00	0.01	0.99	0.00	0.0047	0.9953	0.0000	91.465	2.120	—	—	153.96	407.79	115.57	1.248	0.999	—	-2605.0	2396.0	60.291	36.060
1.00	0.02	0.98	0.00	0.0095	0.9905	0.0000	91.539	2.122	—	—	155.05	410.30	116.44	1.245	0.998	—	-2618.5	2394.8	60.124	36.002
1.00	0.03	0.97	0.00	0.0143	0.9857	0.0000	91.613	2.125	—	—	156.15	412.81	117.31	1.241	0.998	—	-2632.1	2393.6	59.959	35.943
1.00	0.04	0.96	0.00	0.0192	0.9808	0.0000	91.688	2.127	—	—	157.27	415.38	118.21	1.238	0.997	—	-2645.7	2392.4	59.793	35.883
1.00	0.05	0.95	0.00	0.0241	0.9759	0.0000	91.763	2.129	—	—	158.39	417.95	119.10	1.234	0.996	—	-2659.3	2391.2	59.629	35.824
1.00	0.07	0.93	0.00	0.0341	0.9659	0.0000	91.915	2.134	—	—	160.69	423.20	120.94	1.228	0.995	—	-2686.6	2388.6	59.301	35.704
1.00	0.10	0.90	0.00	0.0493	0.9507	0.0000	92.146	2.141	—	—	164.24	431.27	123.77	1.217	0.993	—	-2727.6	2384.6	58.814	35.520
1.00	0.20	0.80	0.00	0.1035	0.8965	0.0000	92.945	2.166	—	—	176.95	460.07	133.95	1.185	0.987	—	-2865.3	2369.0	57.225	34.883
1.00	0.40	0.60	0.00	0.2310	0.7690	0.0000	94.718	2.220	—	—	207.79	528.92	158.82	1.126	0.982	—	-3144.8	2325.6	54.217	33.450
1.00	0.60	0.40																		

2-228 PHYSICAL AND CHEMICAL DATA

TABLE 2-192 Thermodynamic Properties of the International Standard Atmosphere*

Z, m	T, K	P, bar	ρ , kg/m ³	g, m/s ²	M	a, m/s	μ , Pa·s	k, W/(m·K)	λ , m	H, m
0	288.15	1.01325	1.2250	9.80665	28.964	340.29	1.79.-5	2.54.-5	6.63.-8	0
1,000	281.65	0.89876	1.1117	9.8036	28.964	336.43	1.76.-5	2.49.-5	7.31.-8	1,000
2,000	275.15	0.79501	1.0066	9.8005	28.964	332.53	1.73.-5	2.43.-5	8.07.-8	2,999
3,000	268.66	0.70121	0.90925	9.7974	28.964	328.58	1.69.-5	2.38.-5	8.94.-8	2,999
4,000	262.17	0.61660	0.81935	9.7943	28.964	324.59	1.66.-5	2.33.-5	9.92.-8	3,997
5,000	255.68	0.54048	0.73643	9.7912	28.964	320.55	1.63.-5	2.28.-5	1.10.-7	4,996
6,000	249.19	0.47217	0.66011	9.7882	28.964	316.45	1.59.-5	2.22.-5	1.23.-7	5,994
7,000	242.70	0.41105	0.59002	9.7851	28.964	312.31	1.56.-5	2.17.-5	1.38.-7	6,992
8,000	236.22	0.35651	0.52579	9.7820	28.964	308.11	1.53.-5	2.12.-5	1.55.-7	7,990
9,000	229.73	0.30800	0.46706	9.7789	28.964	303.85	1.49.-5	2.06.-5	1.74.-7	8,987
10,000	223.25	0.26499	0.41351	9.7759	28.964	299.53	1.46.-5	2.01.-5	1.97.-7	9,984
15,000	216.65	0.12111	0.19476	9.7605	28.964	295.07	1.42.-5	1.95.-5	4.17.-7	14,965
20,000	216.65	0.05529	0.08891	9.7452	28.964	295.07	1.42.-5	1.95.-5	9.14.-7	19,937
25,000	221.55	0.02549	0.04008	9.7300	28.964	298.39	1.45.-5	1.99.-5	2.03.-6	24,902
30,000	226.51	0.01197	0.01841	9.7147	28.964	301.71	1.48.-5	2.04.-5	4.42.-6	29,859
40,000	250.35	2.87.-3	4.00.-3	9.6844	28.964	317.19	1.60.-5	2.23.-5	2.03.-5	39,750
50,000	270.65	8.00.-4	1.03.-3	9.6542	28.964	329.80	1.70.-5	2.40.-5	7.91.-5	49,610
60,000	247.02	2.20.-4	3.10.-4	9.6241	28.964	315.07	1.58.-5	2.21.-5	2.62.-4	59,439
70,000	219.59	5.22.-5	8.28.-5	9.5942	28.964	297.06	1.44.-5	1.98.-5	9.81.-4	69,238
80,000	198.64	1.05.-5	1.85.-5	9.5644	28.964	282.54	1.32.-5	1.80.-5	4.40.-3	79,006
90,000	186.87	1.84.-6	3.43.-6	9.5348	28.95				2.37.-2	88,744
100,000	195.08	3.20.-7	5.60.-7	9.5052	28.40				0.142	98,451
150,000	634.39	4.54.-9	2.08.-9	9.3597	24.10				33	146,542
200,000	854.56	8.47.-10	2.54.-10	9.2175	21.30				240	193,899
250,000	941.33	2.48.-10	6.07.-11	9.0785	19.19				890	240,540
300,000	976.01	8.77.-11	1.92.-11	8.9427	17.73				2600	286,480
400,000	995.83	1.45.-11	2.80.-12	8.6799	15.98				1.6.+4	376,320
500,000	999.24	3.02.-12	5.22.-13	8.4286	14.33				7.7.+4	463,540
600,000	999.85	8.21.-13	1.14.-13	8.1880	11.51				2.8.+5	548,252
800,000	999.99	1.70.-13	1.14.-14	7.7368	5.54				1.4.+6	710,574
1,000,000	1000.00	7.51.-14	3.56.-15	7.3218	3.94				3.1.+6	864,071

*Extracted from *U.S. Standard Atmosphere, 1976, National Oceanic and Atmospheric Administration, National Aeronautics and Space Administration and the U.S. Air Force, Washington, 1976.* Z = geometric altitude, T = temperature, P = pressure, g = acceleration of gravity, M = molecular weight, a = velocity of sound, μ = viscosity, k = thermal conductivity, λ = mean free path, ρ = density, and H = geopotential altitude. The notation 1.79.-5 signifies 1.79×10^{-5} .

TABLE 2-193 Thermodynamic Properties of Benzene

Temperature K	Pressure MPa	Density mol/dm ³	Volume dm ³ /mol	Int. energy kJ/mol	Enthalpy kJ/mol	Entropy kJ/(mol·K)	C _v kJ/(mol·K)	C _p kJ/(mol·K)	Sound speed m/s	Joule-Thomson K/MPa
Saturated Properties										
278.7	0.0047988	11.441	0.087404	-10.278	-10.278	-0.03257	0.095741	0.13301	1369.2	-0.45084
280	0.0051472	11.424	0.087532	-10.105	-10.105	-0.03196	0.095210	0.13274	1366.0	-0.45037
295	0.010954	11.227	0.089073	-8.1218	-8.1208	-0.02506	0.092757	0.13249	1316.2	-0.43580
310	0.021374	11.024	0.090715	-6.1160	-6.1140	-0.01842	0.094410	0.13531	1251.1	-0.41192
325	0.038777	10.816	0.092455	-4.0576	-4.0540	-0.01194	0.097865	0.13934	1180.0	-0.38479
340	0.066128	10.605	0.094297	-1.9360	-1.9297	-0.00556	0.10197	0.14373	1108.1	-0.35639
355	0.10696	10.389	0.096251	0.25114	0.26143	0.000737	0.10619	0.14815	1037.7	-0.32675
370	0.16531	10.170	0.098331	2.5029	2.5192	0.006950	0.11029	0.15251	969.46	-0.29499
385	0.24565	9.9444	0.10056	4.8180	4.8427	0.013084	0.11418	0.15684	903.49	-0.25976
400	0.35284	9.7123	0.10296	7.1959	7.2322	0.019144	0.11788	0.16124	839.45	-0.21937
415	0.49204	9.4716	0.10558	9.6372	9.6892	0.025138	0.12142	0.16581	776.89	-0.17166
430	0.66869	9.2204	0.10845	12.144	12.217	0.031076	0.12487	0.17070	715.33	-0.11372
445	0.88851	8.9560	0.11166	14.721	14.820	0.036970	0.12827	0.17609	654.26	-0.04137
460	1.1575	8.6747	0.11528	17.372	17.506	0.042839	0.13170	0.18223	593.15	0.03173
475	1.4820	8.3719	0.11945	20.108	20.285	0.048703	0.13524	0.18948	531.41	0.17604
490	1.8689	8.0406	0.12437	22.940	23.172	0.054589	0.13896	0.19847	468.41	0.35018
505	2.3256	7.6701	0.13038	25.887	26.190	0.060537	0.14300	0.21044	403.32	0.61096
520	2.8608	7.2419	0.13809	28.980	29.375	0.066611	0.14755	0.22839	335.01	1.0427
535	3.4853	6.7170	0.14888	32.284	32.802	0.072938	0.15298	0.26197	261.60	1.8878
550	4.2145	5.9774	0.16730	35.991	36.696	0.079902	0.16038	0.37221	179.15	4.2186
562.05	4.9012	3.9561	0.25278	41.513	42.752	0.090526			0	15.682
278.7	0.0047988	0.0020778	481.28	22.307	24.617	0.092630	0.067199	0.075641	182.14	69.790
280	0.0051472	0.0022187	450.72	22.394	24.714	0.092396	0.067633	0.076082	182.47	68.760
295	0.010954	0.0044939	222.52	23.427	25.864	0.090149	0.072601	0.081164	186.19	58.188
310	0.021374	0.0083797	119.34	24.522	27.073	0.088632	0.077506	0.086243	189.61	49.702
325	0.038777	0.014587	68.556	25.676	28.334	0.087716	0.082363	0.091352	192.67	42.885
340	0.066128	0.023968	41.723	26.881	29.640	0.087296	0.087187	0.096528	195.28	37.396
355	0.10696	0.037514	26.657	28.135	30.986	0.087285	0.091992	0.10181	197.37	32.960
370	0.16531	0.056356	17.744	29.431	32.365	0.087613	0.096792	0.10724	198.86	29.366
385	0.24565	0.081780	12.228	30.765	33.769	0.088218	0.10160	0.11287	199.67	26.447
400	0.35284	0.11526	8.6760	32.132	35.194	0.089048	0.10643	0.11877	199.73	24.076
415	0.49204	0.15852	6.3082	33.526	36.630	0.090056	0.11129	0.12502	198.94	22.158
430	0.66869	0.21364	4.6807	34.942	38.072	0.091203	0.11620	0.13176	197.20	20.623
445	0.88851	0.28321	3.5310	36.370	39.508	0.092449	0.12117	0.13918	194.42	19.421
460	1.1575	0.37058	2.6984	37.803	40.927	0.093754	0.12624	0.14759	190.45	18.522
475	1.4820	0.48038	2.0817	39.228	42.313	0.095076	0.13144	0.15753	185.11	17.915
490	1.8689	0.61931	1.6147	40.625	43.642	0.096364	0.13684	0.17002	178.19	17.610
505	2.3256	0.79794	1.2532	41.966	44.880	0.097548	0.14252	0.18715	169.36	17.642
520	2.8608	1.0349	0.96626	43.200	45.965	0.098514	0.14867	0.21415	158.20	18.090
535	3.4853	1.3697	0.73008	44.221	46.766	0.099038	0.15562	0.26827	144.00	19.073
550	4.2145	1.9242	0.51970	44.709	46.899	0.098452	0.16433	0.45840	125.56	20.568
562.05	4.9012	3.9561	0.25278	41.513	42.752	0.090526			0	15.682
Single-Phase Properties										
300.00	0.10000	11.161	0.089602	-7.4606	-7.4516	-0.022832	0.092996	0.13320	1296.2	-0.42861
350.00	0.10000	10.462	0.095585	-0.48554	-0.47598	-0.0013533	0.10479	0.14668	1061.0	-0.33684
352.81	0.10000	10.421	0.095958	-0.072586	-0.062991	-0.00017807	0.10558	0.14751	1047.8	-0.33119
352.81	0.10000	0.035232	28.383	27.949	30.787	0.087264	0.091290	0.10103	197.10	33.552
400.00	0.10000	0.030711	32.562	32.595	35.851	0.10072	0.10432	0.11349	210.66	20.922
450.00	0.10000	0.027110	36.887	38.153	41.842	0.11482	0.11715	0.12601	223.76	13.727
500.00	0.10000	0.024299	41.154	44.322	48.437	0.12870	0.12898	0.13766	235.93	9.5972
550.00	0.10000	0.022032	45.388	51.054	55.592	0.14233	0.13981	0.14838	247.41	7.0666
600.00	0.10000	0.020161	49.600	58.300	63.260	0.15567	0.14967	0.15817	258.31	5.4319

TABLE 2-193 Thermodynamic Properties of Benzene (Concluded)

Temperature K	Pressure MPa	Density mol/dm ³	Volume dm ³ /mol	Int. energy kJ/mol	Enthalpy kJ/mol	Entropy kJ/(mol·K)	C _v kJ/(mol·K)	C _p kJ/(mol·K)	Sound speed m/s	Joule-Thomson K/MPa
Single-Phase Properties										
300.00	1.0000	11.170	0.089523	-7.4897	-7.4002	-0.022929	0.092978	0.13308	1301.8	-0.43004
350.00	1.0000	10.476	0.095456	-0.52680	-0.43135	-0.0014714	0.10480	0.14651	1068.0	-0.33971
400.00	1.0000	9.7282	0.10279	7.1526	7.2554	0.019036	0.11785	0.16097	846.37	-0.22423
450.00	1.0000	8.8655	0.11280	15.593	15.706	0.038922	0.12940	0.17801	634.37	-0.013693
451.58	1.0000	8.8350	0.11319	15.873	15.987	0.039545	0.12977	0.17867	627.51	-0.0036091
451.58	1.0000	0.31908	3.1340	36.999	40.133	0.093016	0.12338	0.14272	192.83	18.991
500.00	1.0000	0.27026	3.7002	43.395	47.096	0.10766	0.13222	0.14607	214.43	11.641
550.00	1.0000	0.23728	4.2144	50.362	54.577	0.12192	0.14175	0.15344	231.44	7.9458
600.00	1.0000	0.21298	4.6952	57.755	62.450	0.13561	0.15089	0.16150	245.85	5.8511
300.00	5.0000	11.213	0.089185	-7.6160	-7.1700	-0.023353	0.092913	0.13259	1325.8	-0.43605
350.00	5.0000	10.537	0.094904	-0.70378	-0.22926	-0.0019818	0.10485	0.14581	1097.9	-0.35136
400.00	5.0000	9.8210	0.10182	6.8987	7.4078	0.018394	0.11775	0.15956	886.30	-0.25035
450.00	5.0000	9.0240	0.11082	15.189	15.743	0.038012	0.12877	0.17438	692.84	-0.088322
500.00	5.0000	8.0418	0.12435	24.331	24.953	0.057399	0.13990	0.19602	496.64	0.27193
550.00	5.0000	6.4075	0.15607	35.199	35.979	0.078369	0.15609	0.27120	246.43	2.1959
600.00	5.0000	1.5540	0.64348	53.945	57.162	0.11554	0.16178	0.21373	176.29	9.3898
300.00	10.000	11.263	0.088783	-7.7671	-6.8793	-0.023867	0.092869	0.13203	1354.1	-0.44280
350.00	10.000	10.608	0.094266	-0.91178	0.030879	-0.0025897	0.10497	0.14508	1132.3	-0.36378
400.00	10.000	9.9256	0.10075	6.6097	7.6172	0.017651	0.11774	0.15816	930.56	-0.27601
450.00	10.000	9.1886	0.10883	14.760	15.848	0.037025	0.12832	0.17132	752.83	-0.15003
500.00	10.000	8.3418	0.11988	23.600	24.799	0.055872	0.13831	0.18753	586.00	0.073722
550.00	10.000	7.2764	0.13743	33.351	34.726	0.074776	0.14918	0.21149	420.33	0.56941
600.00	10.000	5.7109	0.17510	44.567	46.318	0.094920	0.16240	0.25868	257.52	2.1761
350.00	50.000	11.061	0.090412	-2.2210	2.2996	-0.0066440	0.10685	0.14195	1337.7	-0.41928
400.00	50.000	10.527	0.094991	4.9365	9.6861	0.013066	0.11931	0.15301	1173.3	-0.37184
450.00	50.000	10.001	0.099985	12.570	17.570	0.031627	0.12871	0.16219	1041.8	-0.32474
500.00	50.000	9.4723	0.10557	20.624	25.902	0.049177	0.13669	0.17116	932.63	-0.26918
550.00	50.000	8.9322	0.11196	29.094	34.691	0.065924	0.14419	0.18047	839.96	-0.20274
600.00	50.000	8.3797	0.11934	37.984	43.951	0.082032	0.15154	0.18989	761.25	-0.12687
350.00	75.000	11.280	0.088652	-2.8344	3.8145	-0.0087087	0.10831	0.14116	1431.4	-0.43585
400.00	75.000	10.798	0.092613	4.2071	11.153	0.010874	0.12070	0.15181	1277.8	-0.39637
450.00	75.000	10.331	0.096793	11.699	18.958	0.029250	0.12977	0.16021	1157.1	-0.36122
500.00	75.000	9.8716	0.10130	19.570	27.167	0.046542	0.13730	0.16819	1058.5	-0.32227
550.00	75.000	9.4118	0.10625	27.813	35.782	0.062956	0.14435	0.17644	975.53	-0.27775
600.00	75.000	8.9496	0.11174	36.435	44.815	0.078670	0.15124	0.18489	905.02	-0.22901

The values in these tables were generated from the NIST REFPROP software (Lemmon, E. W., McLinden, M. O., and Huber, M. L., NIST Standard Reference Database 23: Reference Fluid Thermodynamic and Transport Properties—REFPROP, National Institute of Standards and Technology, Standard Reference Data Program, Gaithersburg, Md., 2002, Version 7.1). The primary source for the thermodynamic properties is Polt, A., Platzler, B., and Maurer, G., "Parameter der thermischen Zustandsgleichung von Bender fuer 14 mehratomige reine Stoffe," *Chem. Tech. (Leipzig)*, **44**(6):216–224, 1992. Validated equations for the viscosity and thermal conductivity are not currently available for this fluid.

Properties at the triple point and the critical point temperature are given in the first and last entries of the saturation tables, respectively. In the single-phase table, when the temperature range for a given isobar includes a vapor-liquid phase boundary, the temperature of phase equilibrium is noted, and properties for both the saturated liquid and saturated vapor are given (with liquid properties given in the upper line). Lines are omitted from the temperature-pressure grid of the single-phase table, when the system would be in the solid phase or if there are potential problems with the source property surface.

The uncertainties in density for benzene are 1% in the vapor phase, 0.3% in the liquid phase up to 400 K (with lower uncertainties at lower temperatures), 1% in the liquid phase between 400 and 500 K, and 2% and rising at temperatures above 500 K. Near the saturation line at temperatures below 350 K, the liquid-phase uncertainty decreases to 0.05%. The uncertainties in vapor pressures are 0.15% at temperatures below 380 K, and 0.5% at higher temperatures. The uncertainties in heat capacities and sound speeds are 2% in the vapor phase and 5% in the liquid phase.

TABLE 2-194 Saturated Bromine*

T , K	P , bar	v_f , m ³ /kg	v_g , m ³ /kg	h_f , kJ/kg	h_g , kJ/kg	s_f , kJ/(kg·K)	s_g , kJ/(kg·K)	$c_{p,f}$, kJ/(kg·K)	μ_f , 10 ⁻⁴ Pa·s	k_f , W/(m·K)
260	0.042	3.106-4	3.195	-147.2	51.8	0.903	1.669	0.486	13.4	0.131
280	0.124	3.168-4	1.169	-138.9	56.2	0.933	1.629	0.479	11.5	0.127
300	0.310	3.232-4	0.5002	-131.6	60.6	0.956	1.597	0.475	9.3	0.122
320	0.680	3.311-4	0.2425	-124.2	64.8	0.978	1.570	0.473	7.8	0.118
340	1.330	3.385-4	0.1309	-112.3	71.1	1.004	1.539	0.471	6.7	0.114
360	2.384	3.464-4	0.0767	-108.6	73.1	1.026	1.531	0.470	5.7	0.109
380	4.010	3.550-4	0.0477	-100.6	76.9	1.048	1.515	0.471	5.0	0.104
400	6.390	3.647-4	0.0311	-93.4	80.6	1.063	1.501	0.475	4.5	0.099
420	9.730	3.752-4	0.0211	-85.8	84.0	1.084	1.488	0.480	4.0	0.094
440	14.25	3.885-4	0.0148	-77.7	87.1	1.103	1.477	0.489	3.7	0.089
460	20.17	4.023-4	0.0107	-69.0	89.9	1.122	1.467	0.503	3.3	0.084
480	27.75	4.179-4	0.00786	-59.7	92.2	1.142	1.457	0.527	3.1	0.079
500	37.21	4.378-4	0.00589	-49.3	94.0	1.161	1.448	0.595	2.8	0.073
520	48.81	4.623-4	0.00445	-37.7	95.0	1.183	1.438	0.710	2.6	0.066
540	62.80	4.938-4	0.00337	-24.0	94.8	1.207	1.428	0.860	2.5	0.059
560	79.41	5.368-4	0.00251	-7.1	92.5	1.237	1.414	1.063	2.3	0.050
580	98.90	6.250-4	0.00167	18.8	82.5	1.280	1.390	2.31	2.2	0.035
584.2 ^c	103.4	8.475-4	0.00085	64.8	64.8	1.356	1.356	∞	2.1	∞

*Reproduced or converted from a tabulation by Seshadri, Viswanath, and Kuloor, *Ind. J. Technol.*, 6 (1970): 191-198. c = critical point.

TABLE 2-195 Thermodynamic Properties of Butane

Temperature K	Pressure MPa	Density mol/dm ³	Volume dm ³ /mol	Int. energy kJ/mol	Enthalpy kJ/mol	Entropy kJ/(mol·K)	C _v kJ/(mol·K)	C _p kJ/(mol·K)	Sound speed m/s	Joule-Thomson K/MPa	Therm. cond. mW/(m·K)	Viscosity μPa·s
Saturated Properties												
134.9	6.6566E-07	12.645	0.079082	-5.2207	-5.2207	-0.02703	0.083783	0.11467	1826.8	-0.57143	176.56	2304.3
140	1.6922E-06	12.563	0.079598	-4.6347	-4.6347	-0.02277	0.083802	0.11492	1793.1	-0.56883	174.84	1887.3
155	0.00001767	12.323	0.081151	-2.9051	-2.9051	-0.01103	0.083864	0.11573	1699.3	-0.55989	169.24	1195.3
170	0.00011616	12.082	0.082767	-1.1617	-1.1617	-0.00030	0.084118	0.11677	1610.1	-0.54850	163.00	844.68
185	0.00054113	11.840	0.084458	0.59963	0.59967	0.009630	0.084688	0.11813	1523.4	-0.53413	156.32	634.79
200	0.0019390	11.596	0.086236	2.3840	2.3842	0.018903	0.085627	0.11986	1438.2	-0.51637	149.36	496.50
215	0.0056671	11.349	0.088115	4.1972	4.1977	0.027645	0.086949	0.12199	1354.1	-0.49482	142.26	399.50
230	0.014106	11.097	0.090113	6.0455	6.0467	0.035954	0.088641	0.12455	1270.8	-0.46909	135.13	328.38
245	0.030885	10.840	0.092253	7.9351	7.9379	0.043912	0.090679	0.12755	1188.2	-0.43868	128.09	274.41
260	0.060978	10.575	0.094562	9.8722	9.8780	0.051585	0.093026	0.13098	1106.4	-0.40288	121.19	232.32
275	0.11065	10.301	0.097075	11.863	11.874	0.059030	0.095645	0.13488	1025.2	-0.36055	114.50	198.71
290	0.18734	10.016	0.099837	13.914	13.933	0.066292	0.098497	0.13925	944.51	-0.30993	108.06	171.28
305	0.29946	9.7171	0.10291	16.031	16.062	0.073412	0.10155	0.14418	864.09	-0.24825	101.92	148.46
320	0.45624	9.4002	0.10638	18.222	18.271	0.080426	0.10478	0.14976	783.62	-0.17103	96.103	129.09
335	0.66761	9.0607	0.11037	20.494	20.568	0.087371	0.10817	0.15620	702.63	-0.07074	90.627	112.34
350	0.94418	8.6916	0.11505	22.858	22.967	0.094284	0.11173	0.16389	620.37	0.066051	85.498	97.559
365	1.2974	8.2822	0.12074	25.328	25.485	0.10121	0.11552	0.17360	535.75	0.26565	80.706	84.220
380	1.7399	7.8141	0.12797	27.928	28.150	0.10822	0.11966	0.18719	447.13	0.58704	76.219	71.859
395	2.2868	7.2504	0.13792	30.703	31.018	0.11543	0.12445	0.21028	352.08	1.1936	71.976	59.958
410	2.9578	6.4885	0.15412	33.782	34.237	0.12318	0.13061	0.27186	246.50	2.7451	67.979	47.596
425.13	3.796	3.9228	0.25492	39.364	40.331	0.13735			0	15.851		
134.9	6.6566E-07	5.935E-07	1684900	22.482	23.604	0.18665	0.055993	0.064308	148.87	361.89	4.8545	3.3208
140	1.6922E-06	1.4538E-06	687860	22.771	23.935	0.18130	0.057048	0.065363	151.48	315.59	5.0913	3.4522
155	0.00001767	1.3712E-05	72930	23.648	24.937	0.16859	0.059941	0.068258	158.89	218.48	5.8353	3.8372
170	0.00011616	8.2203E-05	12165	24.567	25.980	0.15936	0.062670	0.070995	165.94	157.83	6.6513	4.2205
185	0.00054113	0.00035209	2840.2	25.525	27.062	0.15267	0.065393	0.073744	172.61	117.96	7.5389	4.6014
200	0.0019390	0.0011686	855.70	26.519	28.179	0.14788	0.068227	0.076640	178.87	90.683	8.4974	4.9792
215	0.0056671	0.0031862	313.85	27.550	29.328	0.14453	0.071254	0.079787	184.64	71.432	9.5258	5.3531
230	0.014106	0.0074503	134.22	28.614	30.507	0.14230	0.074521	0.083261	189.81	57.513	10.624	5.7226
245	0.030885	0.015434	64.792	29.709	31.711	0.14094	0.078047	0.087120	194.27	47.254	11.792	6.0877
260	0.060978	0.029042	34.433	30.834	32.934	0.14026	0.081835	0.091404	197.86	39.578	13.034	6.4502
275	0.11065	0.050611	19.759	31.984	34.170	0.14011	0.085872	0.096154	200.46	33.766	14.357	6.8133
290	0.18734	0.082943	12.056	33.156	35.414	0.14037	0.090138	0.10142	201.90	29.303	15.775	7.1826
305	0.29946	0.12941	7.7271	34.343	36.657	0.14094	0.094611	0.10730	202.04	25.936	17.311	7.5668
320	0.45624	0.19420	5.1494	35.541	37.890	0.14174	0.099274	0.11394	200.69	23.353	18.999	7.9782
335	0.66761	0.28270	3.5374	36.739	39.100	0.14269	0.10412	0.12161	197.62	21.423	20.889	8.4346
350	0.94418	0.40241	2.4850	37.923	40.270	0.14372	0.10910	0.13080	192.54	20.061	23.058	8.9610
365	1.2974	0.56471	1.7708	39.073	41.370	0.14473	0.11417	0.14259	185.07	19.268	25.626	9.5964
380	1.7399	0.78888	1.2676	40.147	42.353	0.14559	0.11962	0.16009	174.66	19.058	28.813	10.407
395	2.2868	1.1133	0.89820	41.076	43.130	0.14609	0.12600	0.19220	160.51	19.446	33.129	11.532
410	2.9578	1.6409	0.60943	41.673	43.475	0.14572	0.13401	0.28133	141.36	20.469	40.394	13.373
425.13	3.796	3.9228	0.25492	39.364	40.331	0.13735			0	15.851		
Single-Phase Properties												
150.00	0.10000	12.404	0.080622	-3.4846	-3.4765	-0.014834	0.083837	0.11544	1730.2	-0.56316	171.22	1370.9
200.00	0.10000	11.597	0.086227	2.3816	2.3902	0.018891	0.085632	0.11985	1438.8	-0.51649	149.40	496.90
250.00	0.10000	10.753	0.092993	8.5729	8.5822	0.046489	0.091432	0.12863	1161.4	-0.42760	125.81	259.42
272.31	0.10000	10.351	0.096608	11.502	11.512	0.057711	0.095158	0.13415	1039.7	-0.36868	115.68	204.22
272.31	0.10000	0.046045	21.718	31.776	33.948	0.14010	0.085131	0.095267	200.07	34.694	14.113	6.7480
300.00	0.10000	0.041289	24.220	34.241	36.663	0.14959	0.091498	0.10103	211.28	24.802	16.747	7.4522
350.00	0.10000	0.034963	28.601	39.149	42.009	0.16605	0.10399	0.11299	229.21	14.912	22.115	8.6907
400.00	0.10000	0.030400	32.894	44.681	47.970	0.18195	0.11669	0.12545	245.29	9.8194	28.275	9.8987
450.00	0.10000	0.026924	37.142	50.834	54.548	0.19743	0.12893	0.13755	260.14	6.9019	35.230	11.083
500.00	0.10000	0.024176	41.363	57.578	61.714	0.21252	0.14043	0.14897	274.06	5.0916	42.982	12.248
550.00	0.10000	0.021945	45.569	64.875	69.432	0.22723	0.15112	0.15960	287.25	3.8945	51.533	13.395
150.00	1.0000	12.411	0.080576	-3.4986	-3.4180	-0.014927	0.083887	0.11540	1733.9	-0.56354	171.48	1381.3
200.00	1.0000	11.608	0.086150	2.3598	2.4460	0.018782	0.085677	0.11977	1443.9	-0.51758	149.79	500.58

250.00	1.0000	10.770	0.092855	8.5389	8.6318	0.046353	0.091477	0.12845	1168.5	-0.43053	126.34	261.81
300.00	1.0000	9.8412	0.10161	15.271	15.373	0.070896	0.10054	0.14209	899.57	-0.27749	104.51	157.29
350.00	1.0000	8.6953	0.11500	22.851	22.966	0.094264	0.11173	0.16378	621.53	0.063603	85.560	97.696
352.62	1.0000	8.6234	0.11596	23.281	23.397	0.095491	0.11237	0.16540	605.80	0.095319	84.637	95.139
352.62	1.0000	0.42728	2.3404	38.127	40.468	0.14390	0.10997	0.13262	191.42	19.881	23.473	9.0627
400.00	1.0000	0.34181	2.9256	43.808	46.734	0.16057	0.11928	0.13410	221.49	11.545	29.230	10.156
450.00	1.0000	0.28958	3.4533	50.185	53.638	0.17683	0.13036	0.14250	244.24	7.5723	36.235	11.323
500.00	1.0000	0.25369	3.9418	57.063	61.005	0.19234	0.14132	0.15221	262.94	5.3868	44.067	12.475
550.00	1.0000	0.22679	4.4094	64.449	68.858	0.20730	0.15171	0.16189	279.30	4.0325	52.702	13.611
150.00	5.0000	12.442	0.080374	-3.5595	-3.1577	-0.015338	0.084107	0.11525	1749.9	-0.56513	172.63	1428.2
200.00	5.0000	11.653	0.085815	2.2656	2.6947	0.018306	0.085873	0.11943	1466.4	-0.52214	151.52	516.90
250.00	5.0000	10.838	0.092266	8.3942	8.8555	0.045767	0.091674	0.12773	1199.3	-0.44237	128.64	272.30
300.00	5.0000	9.9548	0.10045	15.037	15.539	0.070104	0.10072	0.14034	943.54	-0.31083	107.50	165.96
350.00	5.0000	8.9238	0.11206	22.411	22.971	0.092982	0.11170	0.15798	694.05	-0.067667	89.620	106.76
400.00	5.0000	7.5216	0.13295	30.873	31.537	0.11581	0.12435	0.18921	430.26	0.64313	75.035	65.426
450.00	5.0000	3.1209	0.32042	44.259	45.861	0.14921	0.14234	0.35080	147.05	11.475	55.862	19.322
500.00	5.0000	1.7051	0.58647	54.030	56.962	0.17272	0.14611	0.18483	208.77	6.6929	51.142	14.775
550.00	5.0000	1.3443	0.74389	62.232	65.951	0.18986	0.15448	0.17804	244.93	4.4692	57.838	14.928
150.00	10.000	12.480	0.080129	-3.6330	-2.8317	-0.015840	0.084373	0.11508	1769.4	-0.56694	174.03	1488.3
200.00	10.000	11.707	0.085415	2.1534	3.0075	0.017730	0.086111	0.11906	1493.4	-0.52718	153.61	537.30
250.00	10.000	10.919	0.091586	8.2254	9.1412	0.045071	0.091916	0.12697	1235.4	-0.45489	131.40	285.19
300.00	10.000	10.082	0.099189	14.776	15.768	0.069202	0.10096	0.13868	993.02	-0.34276	110.99	176.33
350.00	10.000	9.1484	0.10931	21.971	23.064	0.091668	0.11182	0.15374	766.31	-0.16435	94.017	116.79
400.00	10.000	8.0346	0.12446	29.964	31.209	0.11339	0.12357	0.17293	554.16	0.17567	81.081	77.782
450.00	10.000	6.5680	0.15225	38.976	40.499	0.13524	0.13606	0.20093	360.83	1.0509	71.907	48.326
500.00	10.000	4.6089	0.21697	49.153	51.323	0.15803	0.14784	0.22343	243.50	2.9827	65.910	27.075
550.00	10.000	3.2339	0.30923	58.940	62.032	0.17846	0.15662	0.20486	242.94	3.2916	65.615	19.386
150.00	30.000	12.622	0.079224	-3.9002	-1.5235	-0.017740	0.085345	0.11453	1842.9	-0.57242	179.28	1748.0
200.00	30.000	11.905	0.083996	1.7557	4.2756	0.015602	0.086999	0.11796	1591.7	-0.54200	161.37	619.22
250.00	30.000	11.197	0.089313	7.6534	10.333	0.042606	0.092823	0.12491	1361.4	-0.48867	141.44	335.06
300.00	30.000	10.483	0.095388	13.956	16.817	0.066223	0.10187	0.13486	1153.4	-0.41613	123.09	214.53
350.00	30.000	9.7548	0.10251	20.772	23.848	0.087875	0.11265	0.14654	971.05	-0.32840	108.07	150.45
400.00	30.000	9.0036	0.11107	28.147	31.479	0.10824	0.12399	0.15873	816.42	-0.22551	97.051	110.91
450.00	30.000	8.2322	0.12147	36.070	39.714	0.12762	0.13519	0.17053	691.11	-0.10687	90.031	83.811
500.00	30.000	7.4563	0.13411	44.490	48.514	0.14616	0.14590	0.18124	595.43	0.023732	86.541	64.099
550.00	30.000	6.7039	0.14917	53.337	57.812	0.16387	0.15594	0.19043	527.27	0.15444	85.903	49.561
150.00	65.000	12.844	0.077859	-4.2847	0.77614	-0.020732	0.086776	0.11392	1957.6	-0.57756	187.43	2300.4
200.00	65.000	12.196	0.081993	1.2046	6.5342	0.012378	0.088354	0.11690	1737.3	-0.55581	173.22	766.46
250.00	65.000	11.576	0.086384	6.9077	12.523	0.039078	0.094214	0.12318	1537.0	-0.51712	156.34	419.12
300.00	65.000	10.979	0.091087	12.978	18.898	0.062302	0.10329	0.13220	1359.9	-0.46758	140.34	275.14
350.00	65.000	10.399	0.096160	19.516	25.767	0.083456	0.11406	0.14267	1208.7	-0.41511	126.97	199.77
400.00	65.000	9.8373	0.10165	26.564	33.172	0.10322	0.12536	0.15351	1082.5	-0.36425	116.89	154.25
450.00	65.000	9.2935	0.10760	34.118	41.112	0.12191	0.13648	0.16402	979.42	-0.31694	110.18	123.77
500.00	65.000	8.7710	0.11401	42.152	49.563	0.13971	0.14709	0.17389	896.76	-0.27399	106.55	101.78
550.00	65.000	8.2737	0.12087	50.632	58.488	0.15671	0.15706	0.18299	831.73	-0.23593	105.59	85.075

The values in these tables were generated from the NIST REFPROP software (Lemmon, E. W., McLinden, M. O., and Huber, M. L., NIST Standard Reference Database 23: Reference Fluid Thermodynamic and Transport Properties—REFPROP, NIST Standard Reference Data Program, Gaithersburg, Md., 2002, Version 7.1). The primary source for the thermodynamic properties is Buecker, D., and Wagner, W., "Reference Equations of State for the Thermodynamic Properties of Fluid Phase *n*-Butane and Isobutane," *J. Phys. Chem. Ref. Data* **35**(2): 929–1019, 2006. The source for viscosity is Vogel, E., Kuechenmeister, C., and Bich, E., "Viscosity for *n*-Butane in the Fluid Region," *High Temp.—High Pressures* **31**(2):173–186, 1999. The source for thermal conductivity is Perkins, R. A., Ramires, M. L. V., Nieto de Castro, C. A., and Cusco, L., "Measurement and Correlation of the Thermal Conductivity of Butane from 135 K to 600 K at Pressures to 70 MPa," *J. Chem. Eng. Data* **47**(5):1263–1271, 2002.

Properties at the triple point temperature and the critical point temperature are given in the first and last entries of the saturation tables, respectively. In the single-phase table, when the temperature range for a given isobar includes a vapor-liquid phase boundary, the temperature of phase equilibrium is noted, and properties for both the saturated liquid and saturated vapor are given (with liquid properties given in the upper line). Lines are omitted from the temperature-pressure grid of the single-phase table, when the system would be in the solid phase or if there are potential problems with the source property surface.

The uncertainties in density are 0.02% at temperatures below 340 K and pressures below 12 MPa (both liquid and vapor states), 0.1% at temperatures below 270 K and pressures above 12 MPa, 0.2% between 340 and 515 K at pressures less than 0.6 MPa, and 0.4% elsewhere. In the critical region, deviations in pressure are 0.5%. At temperatures above 500 K, the uncertainties in density increase up to 1%. Uncertainties in heat capacities are typically 1%, rising to 5% in the critical region and at pressures above 30 MPa. Uncertainties in the speed of sound are typically 0.5%, rising to 1% at temperatures below 200 K and to 4% in a large area around the critical point.

The uncertainty in viscosity varies from 0.4% in the dilute gas between room temperature and 600 K, to 3.0% over the rest of the fluid surface.

Uncertainty in thermal conductivity is 3%, except in the critical region and dilute gas which have an uncertainty of 5%.

TABLE 2-196 Thermodynamic Properties of 1-Butene

Temperature K	Pressure MPa	Density mol/dm ³	Volume dm ³ /mol	Int. energy kJ/mol	Enthalpy kJ/mol	Entropy kJ/(mol·K)	C _v kJ/(mol·K)	C _p kJ/(mol·K)	Sound speed m/s	Joule-Thomson K/MPa
Saturated Properties										
87.800	5.95E-13	14.582	0.068578	-19.753	-19.753	-0.12145	0.080229	0.10913	2086.5	-0.55371
150.00	1.2730E-05	13.379	0.074746	-13.108	-13.108	-0.064173	0.071962	0.10631	1744.9	-0.55469
165.00	9.3335E-05	13.097	0.076351	-11.509	-11.509	-0.054011	0.072351	0.10701	1649.6	-0.54558
180.00	0.00046966	12.818	0.078017	-9.8961	-9.8961	-0.044655	0.073193	0.10813	1555.6	-0.53276
195.00	0.0017787	12.538	0.079756	-8.2633	-8.2632	-0.035943	0.074385	0.10964	1463.4	-0.51623
210.00	0.0054125	12.257	0.081585	-6.6054	-6.6050	-0.027753	0.075854	0.11149	1373.4	-0.49587
225.00	0.013876	11.973	0.083519	-4.9174	-4.9162	-0.019990	0.077551	0.11367	1285.6	-0.47138
240.00	0.031052	11.685	0.085582	-3.1944	-3.1918	-0.012577	0.079443	0.11619	1199.6	-0.44220
255.00	0.062301	11.390	0.087798	-1.4319	-1.4264	-0.0054542	0.081507	0.11904	1115.4	-0.40748
270.00	0.11440	11.086	0.090204	0.37503	0.38535	0.0014312	0.083732	0.12227	1032.5	-0.36587
285.00	0.19537	10.771	0.092841	2.2316	2.2497	0.0081238	0.086107	0.12593	950.65	-0.31542
300.00	0.31425	10.442	0.095769	4.1435	4.1736	0.014663	0.088628	0.13010	869.48	-0.25308
315.00	0.48093	10.094	0.099067	6.1173	6.1650	0.021087	0.091289	0.13492	788.58	-0.17406
330.00	0.70602	9.7227	0.10285	8.1613	8.2339	0.027432	0.094094	0.14061	707.49	-0.070421
345.00	1.0009	9.3197	0.10730	10.286	10.393	0.033738	0.097052	0.14758	625.58	0.071832
360.00	1.3777	8.8735	0.11269	12.507	12.662	0.040056	0.10019	0.15666	541.98	0.27973
375.00	1.8505	8.3641	0.11956	14.848	15.069	0.046456	0.10358	0.16976	455.28	0.61278
390.00	2.4356	7.7513	0.12901	17.357	17.672	0.053070	0.10741	0.19258	362.75	1.2326
405.00	3.1556	6.9234	0.14444	20.167	20.622	0.060243	0.11236	0.25490	258.01	2.7886
419.29	4.0057	4.2400	0.23585	25.194	26.139	0.073219			0	14.832
87.800	5.95E-13	8.1441E-13	1.2279E+12	10.763	11.493	0.23442	0.035901	0.044215	126.59	6453.8
150.00	1.2730E-05	1.0208E-05	97966.	13.339	14.586	0.12046	0.046819	0.055138	161.79	519.37
165.00	9.3335E-05	6.8053E-05	14694.	14.060	15.432	0.10927	0.049589	0.057921	168.95	334.05
180.00	0.00046966	0.00031411	3183.5	14.822	16.317	0.10097	0.052497	0.060867	175.70	224.29
195.00	0.0017787	0.0010999	909.21	15.621	17.238	0.094833	0.055552	0.064008	182.01	156.42
210.00	0.0054125	0.0031172	320.80	16.456	18.192	0.090329	0.058761	0.067378	187.84	112.91
225.00	0.013876	0.0074985	133.36	17.323	19.174	0.087076	0.062133	0.071013	193.09	84.169
240.00	0.031052	0.015861	63.049	18.219	20.177	0.084791	0.065668	0.074946	197.63	64.687
255.00	0.062301	0.030305	32.998	19.139	21.195	0.083257	0.069362	0.079208	201.32	51.184
270.00	0.11440	0.053404	18.725	20.081	22.223	0.082311	0.073208	0.083840	204.02	41.642
285.00	0.19537	0.088232	11.334	21.039	23.253	0.081820	0.077198	0.088901	205.56	34.789
300.00	0.31425	0.13847	7.2216	22.009	24.279	0.081681	0.081324	0.094492	205.77	29.808
315.00	0.48093	0.20868	4.7920	22.985	25.290	0.081801	0.085583	0.10078	204.47	26.172
330.00	0.70602	0.30478	3.2811	23.957	26.274	0.082098	0.089980	0.10808	201.43	23.538
345.00	1.0009	0.43505	2.2986	24.912	27.212	0.082489	0.094533	0.11696	196.37	21.690
360.00	1.3777	0.61215	1.6336	25.827	28.078	0.082878	0.099287	0.12863	188.91	20.504
375.00	1.8505	0.85778	1.1658	26.665	28.823	0.083133	0.10434	0.14599	178.55	19.927
390.00	2.4356	1.2160	0.82239	27.351	29.354	0.083025	0.10992	0.17800	164.58	19.957
405.00	3.1556	1.8085	0.55294	27.680	29.425	0.081979	0.11666	0.27163	145.93	20.477
419.29	4.0057	4.2400	0.23585	25.194	26.139	0.073219			0	14.832

Single-Phase Properties

100.00	0.10000	14.342	0.069727	-18.432	-18.425	-0.10737	0.076348	0.10761	2041.3	-0.55898
200.00	0.10000	12.446	0.080347	-7.7161	-7.7081	-0.033172	0.074849	0.11021	1433.8	-0.51000
266.51	0.10000	11.158	0.089625	-0.050006	-0.041044	-0.00015346	0.083200	0.12149	1051.7	-0.37627
266.51	0.10000	0.047098	21.232	19.860	21.983	0.082486	0.072300	0.082725	203.49	43.586
300.00	0.10000	0.041199	24.273	22.407	24.834	0.092558	0.078346	0.087850	217.19	27.387
400.00	0.10000	0.030377	32.920	31.321	34.613	0.12055	0.099614	0.10831	251.29	10.192
500.00	0.10000	0.024172	41.370	42.371	46.508	0.14700	0.12081	0.12931	280.25	5.2895
100.00	1.0000	14.347	0.069701	-18.441	-18.371	-0.10745	0.076343	0.10760	2045.4	-0.55906
200.00	1.0000	12.457	0.080273	-7.7377	-7.6574	-0.033280	0.074873	0.11013	1439.7	-0.51117
300.00	1.0000	10.465	0.095554	4.1009	4.1965	0.014521	0.088626	0.12974	878.06	-0.26069
344.96	1.0000	9.3208	0.10729	10.280	10.388	0.033722	0.097044	0.14756	625.79	0.071399
344.96	1.0000	0.43467	2.3006	24.909	27.210	0.082488	0.094521	0.11694	196.39	21.694
400.00	1.0000	0.33780	2.9603	30.561	33.521	0.099463	0.10210	0.11588	229.62	11.604
500.00	1.0000	0.25311	3.9508	41.920	45.871	0.12695	0.12152	0.13206	269.53	5.5503
100.00	5.0000	14.371	0.069585	-18.478	-18.131	-0.10783	0.076326	0.10752	2063.2	-0.55939
200.00	5.0000	12.507	0.079955	-7.8313	-7.4315	-0.033753	0.074982	0.10983	1464.8	-0.51602
300.00	5.0000	10.593	0.094404	3.8689	4.3409	0.013736	0.088648	0.12795	924.82	-0.29848
400.00	5.0000	7.924	0.12833	18.376	19.018	0.055643	0.10867	0.17944	398.89	0.92138
500.00	5.0000	1.6432	0.60858	39.334	42.377	0.10830	0.12539	0.15726	221.46	6.5598
100.00	10.000	14.400	0.069444	-18.524	-17.830	-0.10830	0.076316	0.10743	2084.7	-0.55976
200.00	10.000	12.566	0.079577	-7.9428	-7.1471	-0.034325	0.075127	0.10949	1494.9	-0.52136
300.00	10.000	10.734	0.093162	3.6108	4.5424	0.012845	0.088724	0.12625	976.91	-0.33426
400.00	10.000	8.4254	0.11869	17.389	18.576	0.053002	0.10763	0.15809	531.56	0.27589
500.00	10.000	4.4457	0.22494	35.004	37.254	0.094450	0.12805	0.20133	235.89	3.6822
100.00	30.000	14.511	0.068913	-18.695	-16.628	-0.11011	0.076383	0.10716	2164.7	-0.56070
200.00	30.000	12.781	0.078241	-8.3397	-5.9925	-0.036441	0.075766	0.10853	1602.5	-0.53694
300.00	30.000	11.176	0.089478	2.8019	5.4862	0.0099119	0.089276	0.12244	1142.6	-0.41541
400.00	30.000	9.5263	0.10497	15.547	18.696	0.047777	0.10751	0.14231	802.89	-0.21113
500.00	30.000	7.8006	0.12820	30.094	33.940	0.081710	0.12649	0.16189	578.80	0.077488
200.00	70.000	13.133	0.076142	-8.9642	-3.6342	-0.040078	0.077144	0.10763	1777.6	-0.55246
300.00	70.000	11.778	0.084903	1.7245	7.6677	0.0055841	0.090645	0.11961	1376.9	-0.47674
400.00	70.000	10.537	0.094902	13.811	20.454	0.042252	0.10876	0.13655	1099.3	-0.37969
500.00	70.000	9.3918	0.10648	27.536	34.989	0.074613	0.12760	0.15389	914.99	-0.28997

The values in these tables were generated from the NIST REFPROP software (Lemmon, E. W., McLinden, M. O., and Huber, M. L., NIST Standard Reference Database 23: Reference Fluid Thermodynamic and Transport Properties—REFPROP, National Institute of Standards and Technology, Standard Reference Data Program, Gaithersburg, Md., 2002, Version 7.1). The primary source for the thermodynamic properties is Lemmon, E. W., and Ihmel, E. C., "Thermodynamic Properties of the Butenes. Part II. Short Fundamental Equations of State," *Fluid Phase Equilibria* **228–229C**:173–187, 2005. Validated equations for the viscosity and thermal conductivity are not currently available for this fluid.

Properties at the triple point temperature and the critical point temperature are given in the first and last entries of the saturation tables, respectively. In the single-phase table, when the temperature range for a given isobar includes a vapor-liquid phase boundary, the temperature of phase equilibrium is noted, and properties for both the saturated liquid and saturated vapor are given (with liquid properties given in the upper line). Lines are omitted from the temperature-pressure grid of the single-phase table, when the system would be in the solid phase or if there are potential problems with the source property surface.

The uncertainties of densities calculated by the equation of state (based on a coverage factor of 2) are 0.1% in the liquid phase at temperatures above 270 K (rising to 0.5% in density at temperatures below 200 K), 0.2% at temperatures above the critical temperature and at pressures above 10 MPa, and 0.5% in the vapor phase, including supercritical conditions below 10 MPa. The uncertainty in vapor pressure is 0.25% above 200 K. The uncertainty in heat capacities is 0.5% at saturated liquid conditions, rising to 5% at much higher pressures and at temperatures above 350 K.

TABLE 2-197 Thermodynamic Properties of *cis*-2-Butene

Temperature K	Pressure MPa	Density mol/dm ³	Volume dm ³ /mol	Int. Energy kJ/mol	Enthalpy kJ/mol	Entropy kJ/(mol·K)	C _v kJ/(mol·K)	C _p kJ/(mol·K)	Sound speed m/s	Joule-Thomson K/MPa
Saturated Properties										
134.30	2.6365E-07	14.084	0.071002	-16.205	-16.205	-0.081920	0.079059	0.11421	1931.8	-0.50947
140.00	8.0149E-07	13.976	0.071549	-15.556	-15.556	-0.077189	0.078138	0.11344	1897.3	-0.51181
155.00	9.6316E-06	13.696	0.073014	-13.866	-13.866	-0.065723	0.076346	0.11195	1805.9	-0.51506
170.00	7.0502E-05	13.419	0.074523	-12.194	-12.194	-0.055424	0.075319	0.11114	1714.3	-0.51402
185.00	0.00035720	13.143	0.076087	-10.529	-10.529	-0.046038	0.074926	0.11096	1623.4	-0.50857
200.00	0.0013683	12.868	0.077715	-8.8626	-8.8625	-0.037376	0.075072	0.11135	1533.6	-0.49860
215.00	0.0042205	12.591	0.079421	-7.1860	-7.1857	-0.029294	0.075681	0.11228	1445.0	-0.48403
230.00	0.010977	12.312	0.081218	-5.4919	-5.4910	-0.021677	0.076690	0.11371	1357.7	-0.46470
245.00	0.024918	12.030	0.083127	-3.7731	-3.7710	-0.014438	0.078045	0.11560	1271.7	-0.44035
260.00	0.050686	11.742	0.085168	-2.0229	-2.0186	-0.0075050	0.079699	0.11795	1186.9	-0.41046
275.00	0.094280	11.446	0.087369	-0.23513	-0.22689	-0.00082003	0.081613	0.12075	1103.2	-0.37418
290.00	0.16294	11.140	0.089765	1.5965	1.6111	0.0056653	0.083753	0.12400	1020.4	-0.33016
305.00	0.26496	10.822	0.092403	3.4781	3.5026	0.011993	0.086090	0.12777	938.24	-0.27626
320.00	0.40952	10.488	0.095344	5.4164	5.4554	0.018199	0.088602	0.13211	856.41	-0.20906
335.00	0.60651	10.134	0.098675	7.4188	7.4786	0.024318	0.091273	0.13720	774.55	-0.12307
350.00	0.86653	9.7540	0.10252	9.4943	9.5831	0.030386	0.094094	0.14328	692.22	-0.0089736
365.00	1.2009	9.3387	0.10708	11.655	11.783	0.036443	0.097073	0.15087	608.84	0.14999
380.00	1.6221	8.8746	0.11268	13.918	14.101	0.042540	0.10024	0.16100	523.58	0.38688
395.00	2.1441	8.3381	0.11993	16.313	16.570	0.048756	0.10367	0.17620	435.01	0.77697
410.00	2.7840	7.6790	0.13023	18.901	19.263	0.055246	0.10763	0.20480	340.18	1.5369
425.00	3.5654	6.7389	0.14839	21.868	22.397	0.062490	0.11310	0.30217	231.16	3.6646
435.75	4.2360	4.2440	0.23563	26.307	27.305	0.073584			0	14.802
134.30	2.6365E-07	2.3611E-07	4235300.	13.340	14.457	0.14638	0.045782	0.054097	153.35	1022.9
140.00	8.0149E-07	6.8856E-07	1452300.	13.603	14.767	0.13940	0.046445	0.054760	156.40	846.64
155.00	9.6316E-06	7.4740E-06	133800.	14.312	15.601	0.12439	0.048209	0.056526	164.10	534.19
170.00	7.0502E-05	4.9890E-05	20044.	15.048	16.461	0.11314	0.050082	0.058410	171.37	352.76
185.00	0.00035720	0.00023239	4303.0	15.811	17.348	0.10465	0.052140	0.060499	178.22	241.97
200.00	0.0013683	0.00082449	1212.9	16.601	18.261	0.098239	0.054433	0.062862	184.64	171.51
215.00	0.0042205	0.0023717	421.65	17.417	19.197	0.093417	0.056990	0.065554	190.57	125.19
230.00	0.010977	0.0057914	172.67	18.259	20.154	0.089825	0.059826	0.068614	195.95	93.915
245.00	0.024918	0.012427	80.467	19.124	21.129	0.087196	0.062937	0.072067	200.67	72.325
260.00	0.050686	0.024061	41.562	20.011	22.117	0.085325	0.066305	0.075928	204.61	57.138
275.00	0.094280	0.042902	23.309	20.917	23.114	0.084057	0.069907	0.080211	207.65	46.280
290.00	0.16294	0.071600	13.966	21.839	24.115	0.083264	0.073716	0.084945	209.64	38.405
305.00	0.26496	0.11331	8.8256	22.775	25.113	0.082846	0.077706	0.090186	210.44	32.629
320.00	0.40952	0.17184	5.8195	23.718	26.101	0.082717	0.081857	0.096045	209.88	28.363
335.00	0.60651	0.25199	3.9684	24.662	27.069	0.082798	0.086156	0.10272	207.78	25.214
350.00	0.86653	0.36018	2.7764	25.597	28.003	0.083015	0.090605	0.11059	203.91	22.923
365.00	1.2009	0.50560	1.9779	26.506	28.882	0.083288	0.095223	0.12039	197.97	21.324
380.00	1.6221	0.70265	1.4232	27.364	29.673	0.083518	0.10007	0.13368	189.62	20.319
395.00	2.1441	0.97689	1.0237	28.124	30.319	0.083563	0.10526	0.15445	178.35	19.863
410.00	2.7840	1.3825	0.72331	28.692	30.706	0.083155	0.11109	0.19596	163.51	19.920
425.00	3.5654	2.0863	0.47931	28.785	30.494	0.081542	0.11843	0.34488	144.08	20.169
435.75	4.2360	4.2440	0.23563	26.307	27.305	0.073584			0	14.802

Single-Phase Properties

150.00	0.10000	13.790	0.072517	-14.429	-14.421	-0.069410	0.076853	0.11236	1836.9	-0.51448
250.00	0.10000	11.936	0.083783	-3.1958	-3.1874	-0.012105	0.078567	0.11633	1243.8	-0.43122
276.53	0.10000	11.415	0.087603	-0.050523	-0.041763	-0.00015051	0.081821	0.12106	1094.7	-0.37008
276.53	0.10000	0.045328	22.062	21.010	23.216	0.083956	0.070286	0.080672	207.90	45.358
350.00	0.10000	0.034963	28.602	26.707	29.567	0.10426	0.084207	0.093226	235.49	18.349
450.00	0.10000	0.026927	37.137	36.211	39.925	0.13019	0.10536	0.11396	266.57	8.0313
150.00	1.0000	13.797	0.072480	-14.442	-14.369	-0.069498	0.076879	0.11234	1840.9	-0.51475
250.00	1.0000	11.951	0.083676	-3.2258	-3.1421	-0.012226	0.078590	0.11619	1250.7	-0.43363
350.00	1.0000	9.7615	0.10244	9.4809	9.5833	0.030348	0.094087	0.14310	694.58	-0.013023
356.43	1.0000	9.5810	0.10437	10.409	10.513	0.032980	0.095350	0.14630	656.67	0.052242
356.43	1.0000	0.41725	2.3967	25.991	28.388	0.083130	0.092560	0.11449	201.64	22.160
450.00	1.0000	0.28985	3.4501	35.598	39.048	0.10966	0.10690	0.11882	250.49	8.7484
150.00	5.0000	13.827	0.072321	-14.500	-14.138	-0.069886	0.076995	0.11223	1858.7	-0.51590
250.00	5.0000	12.016	0.083219	-3.3549	-2.9388	-0.012747	0.078700	0.11561	1280.3	-0.44345
350.00	5.0000	9.9638	0.10036	9.1178	9.6196	0.029293	0.093949	0.13889	758.54	-0.10935
450.00	5.0000	3.4526	0.28964	29.287	30.736	0.080884	0.12364	0.49664	144.63	13.395
150.00	10.000	13.864	0.072127	-14.569	-13.848	-0.070362	0.077144	0.11212	1880.2	-0.51720
250.00	10.000	12.094	0.082686	-3.5069	-2.6800	-0.013371	0.078849	0.11500	1315.2	-0.45403
350.00	10.000	10.171	0.098318	8.7400	9.7232	0.028171	0.093912	0.13550	825.19	-0.18764
450.00	10.000	7.3847	0.13542	23.767	25.121	0.066644	0.11375	0.17964	387.53	1.0233
150.00	20.000	13.936	0.071757	-14.703	-13.268	-0.071287	0.077453	0.11192	1921.2	-0.51938
250.00	20.000	12.236	0.081725	-3.7846	-2.1501	-0.014539	0.079171	0.11403	1379.1	-0.47093
350.00	20.000	10.498	0.095255	8.1362	10.041	0.026317	0.094047	0.13149	932.72	-0.28055
450.00	20.000	8.4814	0.11791	22.018	24.376	0.062213	0.11264	0.15577	586.98	0.13495
250.00	50.000	12.592	0.079414	-4.4655	-0.49483	-0.017580	0.080215	0.11231	1538.7	-0.50151
350.00	50.000	11.161	0.089596	6.9055	11.385	0.022259	0.094937	0.12655	1160.5	-0.39521
450.00	50.000	9.7684	0.10237	19.807	24.926	0.056195	0.11311	0.14428	893.45	-0.26115

The values in these tables were generated from the NIST REFPROP software (Lemmon, E. W., McLinden, M. O., and Huber, M. L., NIST Standard Reference Database 23: Reference Fluid Thermodynamic and Transport Properties—REFPROP, National Institute of Standards and Technology, Standard Reference Data Program, Gaithersburg, Md., 2002, Version 7.1). The primary source for the thermodynamic properties is Lemmon, E. W., and Ihmels, E. C., "Thermodynamic Properties of the Butenes. Part II. Short Fundamental Equations of State," *Fluid Phase Equilibria* **228–229C**:173–187, 2005. Validated equations for the viscosity and thermal conductivity are not currently available for this fluid.

Properties at the triple point temperature and the critical point temperature are given in the first and last entries of the saturation tables, respectively. In the single-phase table, when the temperature range for a given isobar includes a vapor-liquid phase boundary, the temperature of phase equilibrium is noted, and properties for both the saturated liquid and saturated vapor are given (with liquid properties given in the upper line). Lines are omitted from the temperature-pressure grid of the single-phase table, when the system would be in the solid phase or if there are potential problems with the source property surface.

The uncertainties in densities calculated using the equation of state are 0.1% in the liquid phase at temperatures above 270 K (rising to 0.5% at temperatures below 200 K), 0.2% at temperatures above the critical temperature and at pressures above 10 MPa, and 0.5% in the vapor phase, including supercritical conditions below 10 MPa. The uncertainty in the vapor phase may be higher than 0.5% in some regions. The uncertainty in vapor pressure is 0.2% between 220 and 310 K and 0.5% above 310 K, and the uncertainty in heat capacities is 0.5% at saturated liquid conditions, rising to 5% at much higher pressures and at temperatures above 300 K.

TABLE 2-198 Thermodynamic Properties of *trans*-2-Butene

Temperature K	Pressure MPa	Density mol/dm ³	Volume dm ³ /mol	Int. energy kJ/mol	Enthalpy kJ/mol	Entropy kJ/(mol·K)	C _v kJ/(mol·K)	C _p kJ/(mol·K)	Sound speed m/s	Joule-Thomson K/MPa
Saturated Properties										
167.60	0.000074817	13.141	0.076099	-12.322	-12.322	-0.056582	0.075471	0.10906	1653.9	-0.53710
170.00	0.000098940	13.097	0.076351	-12.060	-12.060	-0.055030	0.075651	0.10931	1639.3	-0.53489
185.00	0.00047141	12.827	0.077960	-10.409	-10.409	-0.045722	0.076779	0.11086	1549.4	-0.52040
200.00	0.0017229	12.556	0.079642	-8.7337	-8.7336	-0.037018	0.077989	0.11250	1461.5	-0.50389
215.00	0.0051236	12.284	0.081408	-7.0328	-7.0324	-0.028818	0.079349	0.11434	1375.6	-0.48446
230.00	0.012948	12.008	0.083277	-5.3024	-5.3013	-0.021038	0.080901	0.11646	1291.2	-0.46138
245.00	0.028726	11.728	0.085267	-3.5381	-3.5357	-0.013608	0.082660	0.11890	1208.2	-0.43391
260.00	0.057367	11.441	0.087404	-1.7351	-1.7301	-0.0064657	0.084626	0.12171	1126.4	-0.40117
275.00	0.10513	11.146	0.089718	0.11181	0.12124	0.00044042	0.086786	0.12491	1045.4	-0.36199
290.00	0.17951	10.840	0.092251	2.0081	2.0247	0.0071551	0.089124	0.12854	965.18	-0.31463
305.00	0.28905	10.520	0.095056	3.9596	3.9871	0.013718	0.091618	0.13267	885.29	-0.25645
320.00	0.44317	10.183	0.098206	5.9728	6.0163	0.020164	0.094251	0.13740	805.47	-0.18323
335.00	0.65207	9.8227	0.10181	8.0553	8.1216	0.026529	0.097011	0.14294	725.30	-0.088064
350.00	0.92670	9.4330	0.10601	10.217	10.315	0.032849	0.099897	0.14962	644.30	0.041045
365.00	1.2790	9.0030	0.11107	12.471	12.613	0.039171	0.10292	0.15815	561.78	0.22658
380.00	1.7221	8.5154	0.11743	14.840	15.042	0.045556	0.10614	0.17004	476.68	0.51577
395.00	2.2718	7.9376	0.12598	17.363	17.650	0.052111	0.10969	0.18946	387.01	1.0273
410.00	2.9483	7.1898	0.13909	20.137	20.547	0.059086	0.11399	0.23383	288.25	2.1709
425.00	3.7851	5.8610	0.17062	23.657	24.303	0.067765	0.12174	0.63363	165.30	7.0491
428.61	4.0191	4.2130	0.23736	26.217	27.171	0.074373	0	0.63363	0	14.836
167.60	0.000074817	0.000053703	18.621.	13.917	15.310	0.10829	0.056121	0.064451	168.85	333.88
170.00	0.000098940	0.000070020	14.282.	14.051	15.465	0.10688	0.056517	0.064850	169.97	313.10
185.00	0.00047141	0.00030677	3259.8	14.913	16.450	0.099458	0.058961	0.067333	176.77	214.55
200.00	0.0017229	0.0010387	962.76	15.805	17.464	0.093969	0.061448	0.069906	183.16	152.47
215.00	0.0051236	0.0028818	347.00	16.724	18.502	0.089946	0.064084	0.072698	189.08	111.85
230.00	0.012948	0.0068419	146.16	17.667	19.560	0.087053	0.066934	0.075804	194.41	84.452
245.00	0.028726	0.014361	69.632	18.632	20.632	0.085037	0.070029	0.079283	199.05	65.512
260.00	0.057367	0.027327	36.594	19.616	21.716	0.083710	0.073369	0.083170	202.86	52.156
275.00	0.10513	0.048069	20.803	20.617	22.804	0.082924	0.076939	0.087492	205.70	42.578
290.00	0.17951	0.079385	12.597	21.632	23.893	0.082564	0.080711	0.092287	207.43	35.618
305.00	0.28905	0.12463	8.0236	22.656	24.976	0.082533	0.084658	0.097621	207.89	30.512
320.00	0.44317	0.18794	5.3209	23.685	26.043	0.082747	0.088756	0.10363	206.90	26.754
335.00	0.65207	0.27462	3.6414	24.709	27.083	0.083130	0.092992	0.11056	204.25	24.009
350.00	0.92670	0.39199	2.5511	25.716	28.080	0.083605	0.097368	0.11889	199.66	22.059
365.00	1.2790	0.55094	1.8151	26.685	29.006	0.084083	0.10191	0.12962	192.81	20.773
380.00	1.7221	0.76954	1.2995	27.583	29.821	0.084447	0.10670	0.14503	183.21	20.089
395.00	2.2718	1.0825	0.92378	28.347	30.445	0.084505	0.11191	0.17158	170.22	19.999
410.00	2.9483	1.5757	0.63463	28.822	30.693	0.083831	0.11800	0.23687	152.90	20.460
425.00	3.7851	2.6760	0.37369	28.287	29.702	0.080468	0.12690	0.83276	129.63	20.057
428.61	4.0191	4.2130	0.23736	26.217	27.171	0.074373	0	0.83276	0	14.836

Single-Phase Properties

200.00	0.10000	12.557	0.079634	-8.7360	-8.7280	-0.037029	0.077991	0.11249	1462.2	-0.50400
273.69	0.10000	11.172	0.089507	-0.051921	-0.042970	-0.00015647	0.086590	0.12461	1052.5	-0.36572
273.69	0.10000	0.045873	21.799	20.529	22.709	0.082975	0.076618	0.087096	205.49	43.299
300.00	0.10000	0.041314	24.205	22.623	25.044	0.091118	0.080917	0.090604	216.41	30.137
400.00	0.10000	0.030400	32.895	31.727	35.016	0.11968	0.10071	0.10946	251.03	11.036
500.00	0.10000	0.024180	41.357	42.796	46.932	0.14618	0.12004	0.12856	280.24	5.7119
200.00	1.0000	12.568	0.079566	-8.7565	-8.6769	-0.037132	0.078010	0.11242	1467.8	-0.50499
300.00	1.0000	10.652	0.093883	3.2597	3.3536	0.011401	0.090766	0.13089	920.75	-0.28393
353.43	1.0000	9.3386	0.10708	10.724	10.831	0.034294	0.10058	0.15138	625.59	0.077370
353.43	1.0000	0.42419	2.3574	25.942	28.299	0.083718	0.098392	0.12109	198.31	21.710
400.00	1.0000	0.34144	2.9288	30.880	33.808	0.098365	0.10374	0.11833	227.44	12.735
500.00	1.0000	0.25402	3.9367	42.308	46.245	0.12606	0.12089	0.13164	268.79	6.0235
200.00	5.0000	12.615	0.079271	-8.8455	-8.4492	-0.037581	0.078096	0.11215	1492.3	-0.50911
300.00	5.0000	10.766	0.092881	3.0452	3.5096	0.010676	0.090769	0.12936	964.95	-0.31451
400.00	5.0000	8.1724	0.12236	17.547	18.158	0.052539	0.10973	0.17328	451.39	0.61704
500.00	5.0000	1.7031	0.58716	39.420	42.355	0.10676	0.12565	0.16251	215.66	7.3063
200.00	10.000	12.671	0.078919	-8.9520	-8.1628	-0.038127	0.078213	0.11184	1521.6	-0.51368
300.00	10.000	10.895	0.091783	2.8039	3.7218	0.0098449	0.090820	0.12787	1014.7	-0.34416
400.00	10.000	8.6867	0.11512	16.708	17.859	0.050312	0.10892	0.15802	568.97	0.18397
500.00	10.000	4.7944	0.20858	34.462	36.547	0.091756	0.12831	0.21038	241.07	3.5123
200.00	25.000	12.827	0.077961	-9.2436	-7.2946	-0.039668	0.078610	0.11112	1602.1	-0.52436
300.00	25.000	11.215	0.089166	2.2040	4.4332	0.0076959	0.091136	0.12501	1139.2	-0.40118
400.00	25.000	9.5005	0.10526	15.305	17.937	0.046401	0.10862	0.14563	778.83	-0.17082
500.00	25.000	7.5935	0.13169	30.258	33.551	0.081157	0.12604	0.16587	531.13	0.22774
200.00	50.000	13.054	0.076608	-9.6567	-5.8263	-0.041984	0.079350	0.11038	1718.0	-0.53554
300.00	50.000	11.620	0.086061	1.4532	5.7562	0.0048127	0.091871	0.12263	1299.8	-0.44882
400.00	50.000	10.240	0.097652	13.991	18.873	0.042428	0.10919	0.13997	994.88	-0.32579
500.00	50.000	8.9015	0.11234	28.100	33.717	0.075482	0.12638	0.15648	788.67	-0.19336

The values in these tables were generated from the NIST REFPROP software (Lemmon, E. W., McLinden, M. O., and Huber, M. L., NIST Standard Reference Database 23: Reference Fluid Thermodynamic and Transport Properties—REFPROP, National Institute of Standards and Technology, Standard Reference Data Program, Gaithersburg, Md., 2002, Version 7.1). The primary source for the thermodynamic properties is Lemmon, E. W., and Ihmel, E. C., "Thermodynamic Properties of the Butenes. Part II. Short Fundamental Equations of State," *Fluid Phase Equilibria* **228–229C**:173–187, 2005. Validated equations for the viscosity and thermal conductivity are not currently available for this fluid.

Properties at the triple point temperature and the critical point temperature are given in the first and last entries of the saturation tables, respectively. In the single-phase table, when the temperature range for a given isobar includes a vapor-liquid phase boundary, the temperature of phase equilibrium is noted, and properties for both the saturated liquid and saturated vapor are given (with liquid properties given in the upper line). Lines are omitted from the temperature-pressure grid of the single-phase table, when the system would be in the solid phase or if there are potential problems with the source property surface.

The uncertainties in densities calculated using the equation of state are 0.1% in the liquid phase at temperatures above 270 K (rising to 0.5% at temperatures below 200 K), 0.2% at temperatures above the critical temperature and at pressures above 10 MPa, and 0.5% in the vapor phase, including supercritical conditions below 10 MPa. The uncertainty in the vapor phase may be higher than 0.5% in some regions. The uncertainty in vapor pressure is 0.3% above 200 K, and the uncertainty in heat capacities is 0.5% at saturated liquid conditions, rising to 5% at much higher pressures and at temperatures above 250 K.

TABLE 2-199 Thermodynamic Properties of Carbon Dioxide

Temperature K	Pressure MPa	Density mol/dm ³	Volume dm ³ /mol	Int. energy kJ/mol	Enthalpy kJ/mol	Entropy kJ/(mol·K)	C _v kJ/(mol·K)	C _p kJ/(mol·K)	Sound speed m/s	Joule-Thomson K/MPa	Therm. cond. mW/(m·K)	Viscosity μPa·s
Saturated Properties												
216.59	0.51796	26.777	0.037345	3.5030	3.5223	0.022943	0.042895	0.085960	975.85	-0.14430	180.63	256.70
220.00	0.59913	26.497	0.037740	3.7943	3.8169	0.024279	0.042682	0.086338	951.21	-0.13180	176.15	242.01
225.00	0.73509	26.078	0.038347	4.2235	4.2517	0.026209	0.042383	0.087024	915.16	-0.11104	169.67	222.19
230.00	0.89291	25.646	0.038992	4.6554	4.6902	0.028110	0.042103	0.087886	879.09	-0.086994	163.28	204.23
235.00	1.0747	25.201	0.039680	5.0908	5.1334	0.029986	0.041843	0.088954	842.88	-0.059053	156.98	187.88
240.00	1.2825	24.742	0.040418	5.5303	5.5821	0.031840	0.041605	0.090263	806.38	-0.026454	150.75	172.96
245.00	1.5185	24.264	0.041213	5.9749	6.0375	0.033678	0.041393	0.091866	769.44	0.011808	144.58	159.30
250.00	1.7850	23.767	0.042075	6.4256	6.5007	0.035505	0.041212	0.093831	731.78	0.057087	138.47	146.74
255.00	2.0843	23.246	0.043018	6.8836	6.9733	0.037326	0.041079	0.096251	693.01	0.11121	132.40	135.14
260.00	2.4188	22.697	0.044059	7.3505	7.4571	0.039148	0.041029	0.099258	652.58	0.17663	126.35	124.40
265.00	2.7909	22.114	0.045219	7.8282	7.9544	0.040979	0.041109	0.10306	610.07	0.25672	120.31	114.40
270.00	3.2033	21.491	0.046531	8.3190	8.4681	0.042829	0.041351	0.10798	565.46	0.35639	114.25	105.02
275.00	3.6589	20.817	0.048037	8.8266	9.0024	0.044711	0.041750	0.11457	519.14	0.48324	108.17	96.174
280.00	4.1607	20.077	0.049808	9.3560	9.5633	0.046643	0.042270	0.12385	471.54	0.64959	102.03	87.731
285.00	4.7123	19.247	0.051957	9.9154	10.160	0.048657	0.042900	0.13790	422.75	0.87650	95.810	79.548
290.00	5.3177	18.284	0.054693	10.519	10.810	0.050805	0.043734	0.16176	371.95	1.2037	89.546	71.409
295.00	5.9822	17.100	0.058480	11.197	11.547	0.053196	0.045175	0.21098	315.91	1.7218	83.558	62.936
300.00	6.7131	15.434	0.064793	12.036	12.471	0.056151	0.049288	0.38279	245.67	2.7258	80.593	53.107
304.13	7.3773	10.625	0.094118	13.928	14.622	0.063094			0	5.8665		
216.59	0.51796	0.31268	3.1982	17.286	18.943	0.094138	0.027691	0.039992	222.78	26.174	11.014	10.951
220.00	0.59913	0.35941	2.7824	17.329	18.996	0.093276	0.028120	0.040943	223.15	25.084	11.301	11.135
225.00	0.73509	0.43766	2.2849	17.387	19.067	0.092055	0.028782	0.042489	223.49	23.617	11.745	11.409
230.00	0.89291	0.52878	1.8912	17.438	19.127	0.090878	0.029488	0.044244	223.57	22.288	12.221	11.689
235.00	1.0747	0.63442	1.5762	17.481	19.175	0.089736	0.030241	0.046248	223.40	21.077	12.736	11.976
240.00	1.2825	0.75654	1.3218	17.515	19.210	0.088622	0.031042	0.048555	222.96	19.969	13.297	12.272
245.00	1.5185	0.89743	1.1143	17.538	19.230	0.087526	0.031899	0.051242	222.24	18.950	13.917	12.579
250.00	1.7850	1.0599	0.94353	17.550	19.234	0.086439	0.032827	0.054421	221.22	18.005	14.610	12.902
255.00	2.0843	1.2472	0.80180	17.549	19.220	0.085352	0.033844	0.058244	219.87	17.117	15.396	13.245
260.00	2.4188	1.4637	0.68320	17.532	19.185	0.084254	0.034955	0.062912	218.19	16.277	16.306	13.614
265.00	2.7909	1.7149	0.58314	17.498	19.125	0.083133	0.036164	0.068721	216.15	15.476	17.381	14.017
270.00	3.2033	2.0080	0.49800	17.441	19.037	0.081972	0.037482	0.076168	213.75	14.704	18.687	14.469
275.00	3.6589	2.3535	0.42490	17.359	18.913	0.080750	0.038949	0.086123	210.96	13.947	20.325	14.987
280.00	4.1607	2.7663	0.36150	17.241	18.746	0.079437	0.040628	0.10020	207.72	13.185	22.468	15.601
285.00	4.7123	3.2702	0.30579	17.078	18.519	0.077987	0.042629	0.12177	203.94	12.387	25.424	16.361
290.00	5.3177	3.9074	0.25593	16.848	18.209	0.076319	0.045155	0.15906	199.45	11.509	29.821	17.357
295.00	5.9822	4.7654	0.20985	16.509	17.764	0.074270	0.048677	0.23904	193.84	10.459	37.215	18.792
300.00	6.7131	6.1028	0.16386	15.935	17.035	0.071364	0.054908	0.52463	185.33	9.0093	53.689	21.306
304.13	7.3773	10.625	0.094118	13.928	14.622	0.063094			0	5.8665		

Single-Phase Properties

250.00	0.10000	0.048542	20.601	18.448	20.509	0.11415	0.026766	0.035428	247.79	17.399	12.950	12.565
450.00	0.10000	0.026758	37.372	24.664	28.401	0.13712	0.034775	0.043148	324.41	4.0212	29.346	21.901
650.00	0.10000	0.018506	54.037	32.199	37.602	0.15397	0.040192	0.048529	385.01	1.6551	45.466	29.873
850.00	0.10000	0.014148	70.683	40.636	47.705	0.16750	0.043944	0.052271	437.11	0.78058	60.295	36.707
1050.0	0.10000	0.011452	87.321	49.704	58.436	0.17883	0.046573	0.054895	483.65	0.34646	73.843	42.692
250.00	1.0000	0.53250	1.8779	18.023	19.901	0.093263	0.029361	0.042504	235.08	17.606	13.584	12.691
450.00	1.0000	0.27038	3.6985	24.546	28.244	0.11771	0.034954	0.043866	322.89	3.9880	29.620	21.954
650.00	1.0000	0.18527	5.3976	32.133	37.530	0.13473	0.040239	0.048779	385.36	1.6311	45.651	29.907
850.00	1.0000	0.14131	7.0767	40.591	47.668	0.14830	0.043965	0.052397	438.06	0.76632	60.435	36.732
1050.0	1.0000	0.11430	8.7487	49.671	58.419	0.15965	0.046585	0.054970	484.84	0.33777	73.956	42.712
250.00	5.0000	24.060	0.041563	6.2824	6.4902	0.034925	0.041321	0.090937	762.21	0.015208	142.22	153.15
287.43	5.0000	18.798	0.053196	10.202	10.468	0.049681	0.043268	0.14775	398.39	1.0195	92.760	75.598
287.43	5.0000	3.5600	0.28090	16.977	18.381	0.077209	0.043774	0.13705	201.86	11.974	27.323	16.808
450.00	5.0000	1.4155	0.70647	24.000	27.533	0.10313	0.035769	0.047478	317.50	3.8034	31.164	22.429
650.00	5.0000	0.92982	1.0755	31.842	37.219	0.12091	0.040445	0.049898	387.59	1.5263	46.589	30.157
850.00	5.0000	0.70241	1.4237	40.395	47.513	0.13469	0.044055	0.052945	442.64	0.70611	61.117	36.899
1050.0	5.0000	0.56658	1.7650	49.524	58.349	0.14613	0.046637	0.055297	490.31	0.30129	74.494	42.836
250.00	10.000	24.459	0.040885	6.0862	6.4950	0.034120	0.041488	0.087624	804.05	-0.034849	147.52	162.47
450.00	10.000	2.9910	0.33433	23.276	26.619	0.095787	0.036785	0.052935	314.60	3.4705	33.917	23.679
650.00	10.000	1.8632	0.53671	31.482	36.849	0.11461	0.040693	0.051293	391.91	1.3965	48.005	30.687
850.00	10.000	1.3930	0.71790	40.155	47.334	0.12866	0.044164	0.053603	449.04	0.63635	62.093	37.224
1050.0	10.000	1.1205	0.89248	49.347	58.271	0.14021	0.046701	0.055685	497.48	0.25964	75.242	43.066
250.00	100.00	28.075	0.035619	4.3002	7.8621	0.026023	0.043569	0.073521	1227.6	-0.27302	206.28	287.05
450.00	100.00	19.246	0.051959	16.560	21.756	0.067062	0.040841	0.066107	753.30	-0.11128	106.65	83.996
650.00	100.00	13.677	0.073117	27.132	34.444	0.090445	0.043108	0.061252	646.36	-0.054084	86.093	58.868
850.00	100.00	10.636	0.094022	37.076	46.478	0.10660	0.045620	0.059534	646.61	-0.13292	87.259	54.445
1050.0	100.00	8.7929	0.11373	46.995	58.368	0.11916	0.047676	0.059512	668.90	-0.21482	94.022	55.058
450.00	500.00	28.922	0.034576	13.014	30.302	0.050604	0.047702	0.063434	1576.4	-0.38514	239.59	303.64
650.00	500.00	25.661	0.038969	23.302	42.786	0.073576	0.048419	0.061885	1404.7	-0.40369	197.25	191.14
850.00	500.00	23.144	0.043208	33.551	55.155	0.090166	0.049676	0.061912	1320.1	-0.41098	177.31	145.07
1050.0	500.00	21.126	0.047334	43.903	67.570	0.10328	0.050818	0.062247	1278.7	-0.41674	168.50	123.33

The values in these tables were generated from the NIST REFPROP software (Lemmon, E. W., McLinden, M. O., and Huber, M. L., NIST Standard Reference Database 23: Reference Fluid Thermodynamic and Transport Properties—REFPROP, National Institute of Standards and Technology, Standard Reference Data Program, Gaithersburg, Md., 2002, Version 7.1). The primary source for the thermodynamic properties is Span, R., and Wagner, W., "A New Equation of State for Carbon Dioxide Covering the Fluid Region from the Triple-Point Temperature to 1100 K at Pressures up to 800 MPa," *J. Phys. Chem. Ref. Data* **25**(6):1509–1596, 1996. The source for viscosity is Fenghour, A., Wakeham, W. A., and Vesovic, V., "The Viscosity of Carbon Dioxide," *J. Phys. Chem. Ref. Data* **27**:31–44, 1998. The source for thermal conductivity is Vesovic, V., Wakeham, W. A., Olchowy, G. A., Sengers, J. V., Watson, J. T. R., and Millat, J., "The Transport Properties of Carbon Dioxide," *J. Phys. Chem. Ref. Data* **19**:763–808, 1990.

Properties at the triple point temperature and the critical point temperature are given in the first and last entries of the saturation tables, respectively. In the single-phase table, when the temperature range for a given isobar includes a vapor-liquid phase boundary, the temperature of phase equilibrium is noted, and properties for both the saturated liquid and saturated vapor are given (with liquid properties given in the upper line). Lines are omitted from the temperature-pressure grid of the single-phase table, when the system would be in the solid phase or if there are potential problems with the source property surface.

At pressures up to 30 MPa and temperatures up to 523 K, the estimated uncertainty ranges from 0.03% to 0.05% in density, 0.03% (in the vapor) to 1% in the speed of sound (0.5% in the liquid), and 0.15% (in the vapor) to 1.5% (in the liquid) in heat capacity. Special interest has been focused on the description of the critical region and the extrapolation behavior of the formulation (to the limits of chemical stability). The uncertainty in viscosity ranges from 0.3% in the dilute gas near room temperature to 5% at the highest pressures. The uncertainty in thermal conductivity is less than 5%.

TABLE 2-200 Thermodynamic Properties of Carbon Monoxide

Temperature K	Pressure MPa	Density mol/dm ³	Volume dm ³ /mol	Int. energy kJ/mol	Enthalpy kJ/mol	Entropy kJ/(mol·K)	C _v kJ/(mol·K)	C _p kJ/(mol·K)	Sound speed m/s	Joule-Thomson K/MPa	Therm. cond. mW/(m·K)	Viscosity μPa·s
Saturated Properties												
68.160	0.015537	30.330	0.032971	-0.81158	-0.81106	-0.010820	0.035351	0.060430	998.20	-0.36906	180.28	274.18
70.000	0.021053	30.064	0.033262	-0.70065	-0.69995	-0.0092140	0.034805	0.060226	980.50	-0.36553	175.49	252.15
72.000	0.028718	29.773	0.033588	-0.57950	-0.57950	-0.0075210	0.034248	0.060064	961.22	-0.36074	170.45	232.14
74.000	0.038447	29.478	0.033924	-0.46058	-0.45927	-0.0058785	0.033724	0.059961	941.89	-0.35489	165.55	215.32
76.000	0.050599	29.180	0.034270	-0.34088	-0.33915	-0.0042823	0.033232	0.059917	922.49	-0.34794	160.76	201.01
78.000	0.065559	28.878	0.034628	-0.22127	-0.21900	-0.0027285	0.032768	0.059930	903.01	-0.33981	156.06	188.69
80.000	0.083738	28.573	0.034999	-0.10165	-0.098716	-0.0012138	0.032329	0.060002	883.44	-0.33041	151.45	177.96
82.000	0.10556	28.262	0.035383	0.018099	0.021834	0.00026503	0.031915	0.060132	863.76	-0.31966	146.89	166.52
84.000	0.13148	27.947	0.035782	0.13806	0.14277	0.0017110	0.031522	0.060324	843.95	-0.30742	142.40	160.13
86.000	0.16196	27.626	0.036197	0.25835	0.26421	0.0031269	0.031150	0.060578	824.00	-0.29356	137.96	152.60
88.000	0.19748	27.300	0.036630	0.37906	0.38629	0.0045153	0.030798	0.060899	803.89	-0.27794	133.57	145.77
90.000	0.23852	26.967	0.037082	0.50030	0.50915	0.0058787	0.030463	0.061291	783.60	-0.26034	129.23	139.52
92.000	0.28559	26.627	0.037556	0.62218	0.63291	0.0072195	0.030146	0.061760	763.12	-0.24056	124.94	133.75
94.000	0.33919	26.280	0.038052	0.74482	0.75773	0.0085399	0.029846	0.062314	742.41	-0.21834	120.69	128.38
96.000	0.39983	25.924	0.038574	0.86835	0.88377	0.0098422	0.029562	0.062962	721.45	-0.19335	116.51	123.34
98.000	0.46805	25.559	0.039125	0.99289	1.0112	0.011129	0.029294	0.063716	700.22	-0.16523	112.38	118.57
100.000	0.54438	25.184	0.039708	1.1186	1.1402	0.012402	0.029043	0.064590	678.68	-0.13353	108.31	114.02
102.000	0.62934	24.798	0.040326	1.2457	1.2710	0.013663	0.028809	0.065604	656.78	-0.097704	104.30	109.66
104.000	0.72348	24.399	0.040985	1.3742	1.4039	0.014916	0.028592	0.066781	634.50	-0.057078	100.36	105.45
106.000	0.82736	23.987	0.041689	1.5045	1.5390	0.016162	0.028395	0.068153	611.77	-0.010824	96.482	101.35
108.000	0.94154	23.560	0.042446	1.6368	1.6768	0.017404	0.028218	0.069759	588.54	0.042104	92.679	97.342
110.000	1.0666	23.114	0.043263	1.7713	1.8175	0.018646	0.028066	0.071656	564.73	0.10304	88.948	93.404
112.000	1.2031	22.649	0.044151	1.9085	1.9616	0.019891	0.027941	0.073916	540.25	0.17371	85.290	89.510
114.000	1.3517	22.161	0.045124	2.0487	2.1097	0.021142	0.027850	0.076648	515.01	0.25641	81.702	85.641
116.000	1.5130	21.646	0.046197	2.1925	2.2624	0.022406	0.027800	0.080005	488.86	0.35427	78.180	81.774
118.000	1.6877	21.099	0.047395	2.3405	2.4205	0.023688	0.027803	0.084225	461.63	0.47167	74.716	77.888
120.000	1.8765	20.513	0.048749	2.4938	2.5853	0.024996	0.027874	0.089692	433.11	0.61495	71.296	73.954
122.000	2.0802	19.878	0.050307	2.6536	2.7583	0.026343	0.028038	0.097070	403.00	0.79382	67.896	69.940
124.000	2.2997	19.179	0.052141	2.8221	2.9420	0.027744	0.028333	0.10762	370.88	1.0239	64.476	65.797
126.000	2.5360	18.390	0.054377	3.0024	3.1403	0.029230	0.028826	0.12411	336.15	1.3325	60.972	61.448
128.000	2.7904	17.464	0.057259	3.2010	3.3608	0.030854	0.029646	0.15392	297.82	1.7728	57.261	56.748
130.000	3.0647	16.288	0.061393	3.4328	3.6210	0.032745	0.031097	0.22603	254.03	2.4703	53.107	51.348
132.86	3.4982	10.850	0.092166	4.2912	4.6137	0.040039			0	6.1475		
68.160	0.015537	0.027707	36.091	5.1252	5.6859	0.084499	0.021089	0.029785	167.25	40.804	6.6865	4.6366
70.000	0.021053	0.036656	27.281	5.1600	5.7343	0.082704	0.021155	0.029947	169.22	38.426	6.8845	4.7768
72.000	0.028718	0.048780	20.500	5.1971	5.7859	0.080887	0.021238	0.030153	171.27	36.126	7.1009	4.9329
74.000	0.038447	0.063796	15.675	5.2334	5.8361	0.079194	0.021333	0.030394	173.22	34.080	7.3188	5.0934
76.000	0.050599	0.082130	12.176	5.2688	5.8849	0.077613	0.021441	0.030672	175.07	32.250	7.5382	5.2589
78.000	0.065559	0.10424	9.5935	5.3031	5.9320	0.076131	0.021563	0.030993	176.80	30.604	7.7592	5.4300
80.000	0.083738	0.13059	7.6573	5.3363	5.9775	0.074739	0.021699	0.031360	178.42	29.116	7.9820	5.6076
82.000	0.10556	0.16171	6.1841	5.3682	6.0210	0.073426	0.021850	0.031777	179.92	27.763	8.2067	5.7922
84.000	0.13148	0.19810	5.0478	5.3988	6.0625	0.072185	0.022017	0.032250	181.29	26.527	8.4335	5.9847
86.000	0.16196	0.24036	4.1605	5.4280	6.1019	0.071007	0.022199	0.032783	182.54	25.392	8.6627	6.1860
88.000	0.19748	0.28906	3.4595	5.4556	6.1388	0.069885	0.022397	0.033383	183.66	24.345	8.8944	6.3968
90.000	0.23852	0.34486	2.8997	5.4816	6.1733	0.068813	0.022611	0.034057	184.65	23.377	9.1291	6.6182
92.000	0.28559	0.40845	2.4483	5.5058	6.2050	0.067785	0.022842	0.034813	185.51	22.477	9.3672	6.8512
94.000	0.33919	0.48058	2.0808	5.5280	6.2338	0.066796	0.023089	0.035661	186.22	21.638	9.6091	7.0969
96.000	0.39983	0.56209	1.7791	5.5482	6.2595	0.065840	0.023352	0.036615	186.80	20.853	9.8555	7.3566
98.000	0.46805	0.65388	1.5293	5.5661	6.2819	0.064912	0.023633	0.037690	187.23	20.118	10.107	7.6317
100.000	0.54438	0.75700	1.3210	5.5816	6.3007	0.064007	0.023931	0.038906	187.52	19.436	10.366	7.9239
102.000	0.62934	0.87260	1.1460	5.5945	6.3157	0.063120	0.024248	0.040288	187.67	18.773	10.632	8.2350
104.000	0.72348	1.0020	0.99799	5.6044	6.3265	0.062248	0.024586	0.041869	187.66	18.154	10.909	8.5675
106.000	0.82736	1.1468	0.87198	5.6112	6.3327	0.061385	0.024945	0.043694	187.51	17.569	11.198	8.9238
108.000	0.94154	1.3088	0.76404	5.6145	6.3339	0.060526	0.025329	0.045820	187.20	17.001	11.502	9.3073
110.000	1.0666	1.4903	0.67102	5.6138	6.3295	0.059665	0.025741	0.048326	186.73	16.458	11.828	9.7221
112.000	1.2031	1.6938	0.59039	5.6088	6.3191	0.058797	0.026186	0.051322	186.11	15.930	12.181	10.173

114.00	1.3517	1.9228	0.52008	5.5986	6.3016	0.057914	0.026671	0.054966	185.33	15.411	12.569	10.667
116.00	1.5130	2.1815	0.45841	5.5827	6.2762	0.057008	0.027203	0.059493	184.38	14.894	13.005	11.213
118.00	1.6877	2.4754	0.40397	5.5598	6.2416	0.056070	0.027794	0.065263	183.27	14.372	13.507	11.821
120.00	1.8765	2.8123	0.35558	5.5286	6.1959	0.055084	0.028462	0.072864	181.99	13.833	14.101	12.509
122.00	2.0802	3.2027	0.31224	5.4872	6.1367	0.054034	0.029229	0.083320	180.52	13.263	14.826	13.301
124.00	2.2997	3.6629	0.27301	5.4324	6.0602	0.052892	0.030133	0.098585	178.84	12.648	15.747	14.234
126.00	2.5360	4.2194	0.23700	5.3595	5.9605	0.051613	0.031233	0.12291	176.93	11.956	16.981	15.373
128.00	2.7904	4.9212	0.20320	5.2594	5.8264	0.050117	0.032636	0.16759	174.68	11.140	18.777	16.840
130.00	3.0647	5.8832	0.16998	5.1113	5.6322	0.048216	0.034579	0.27599	171.86	10.100	21.845	18.936
132.86	3.4982	10.850	0.092166	4.2912	4.6137	0.040039		0		6.1475		

Single-Phase Properties

100.00	0.10000	0.12298	8.1315	5.7653	6.5785	0.080014	0.021118	0.030153	201.29	17.820	10.075	6.9147
200.00	0.10000	0.060293	16.586	7.8674	9.5259	0.10048	0.020812	0.029239	288.05	5.3111	19.227	12.897
300.00	0.10000	0.040104	24.935	9.9522	12.446	0.11231	0.020833	0.029191	353.12	2.5186	26.605	17.731
400.00	0.10000	0.030062	33.265	12.045	15.371	0.12073	0.021028	0.029364	407.29	1.2653	33.106	21.870
500.00	0.10000	0.024045	41.588	14.169	18.328	0.12733	0.021479	0.029807	454.00	0.56244	39.272	25.540
100.00	1.0000	25.261	0.039586	1.1047	1.1443	0.012262	0.029062	0.064114	685.44	-0.14414	112.87	113.83
108.96	1.0000	23.349	0.042829	1.7009	1.7437	0.017998	0.028142	0.070627	577.22	0.070176	90.884	95.450
108.96	1.0000	1.3931	0.71782	5.6147	6.3325	0.060114	0.025522	0.046966	186.99	16.739	11.655	9.5017
200.00	1.0000	0.61727	1.6200	7.7647	9.3847	0.080819	0.020996	0.030510	286.20	5.1924	19.474	13.192
300.00	1.0000	0.40214	2.4867	9.8936	12.380	0.092976	0.020895	0.029646	354.42	2.4256	26.760	17.918
400.00	1.0000	0.29999	3.3334	12.005	15.338	0.10149	0.021064	0.029598	409.43	1.2088	33.222	22.024
500.00	1.0000	0.23962	4.1732	14.140	18.313	0.10812	0.021505	0.029948	456.39	0.52786	39.364	25.676
100.00	5.0000	25.864	0.038663	0.99666	1.1900	0.011154	0.029263	0.060925	737.92	-0.21740	152.30	112.19
200.00	5.0000	3.4130	0.29299	7.2656	8.7305	0.064994	0.021878	0.038000	285.27	4.3757	22.190	15.094
300.00	5.0000	2.0232	0.49426	9.6364	12.108	0.078767	0.021174	0.031673	362.95	2.0288	27.812	18.716
400.00	5.0000	1.4824	0.67458	11.834	15.207	0.087691	0.021224	0.030585	420.15	0.98413	33.871	22.588
500.00	5.0000	1.1786	0.84845	14.015	18.258	0.094498	0.021618	0.030535	467.56	0.39254	39.837	26.139
100.00	10.000	26.482	0.037761	0.88669	1.2643	0.0099878	0.029539	0.058409	792.04	-0.27800	200.46	110.33
200.00	10.000	7.4298	0.13459	6.5960	7.9419	0.056188	0.022832	0.048831	307.84	2.8854	34.772	19.114
300.00	10.000	4.0263	0.24837	9.3290	11.813	0.072068	0.021511	0.034036	379.01	1.5731	30.972	19.862
400.00	10.000	2.9079	0.34389	11.634	15.073	0.081462	0.021420	0.031689	435.68	0.74980	35.414	23.298
500.00	10.000	2.3052	0.43381	13.870	18.208	0.088461	0.021755	0.031188	482.48	0.25486	40.797	26.682
100.00	50.000	29.422	0.033988	0.39153	2.0910	0.0040257	0.031398	0.052094	1066.8	-0.43831	567.46	99.463
200.00	50.000	20.591	0.048566	4.5424	6.9707	0.038097	0.025036	0.045541	706.01	-0.28689	256.88	50.929
300.00	50.000	14.766	0.067725	7.7949	11.181	0.055259	0.023212	0.039083	609.73	-0.21242	139.18	34.086
400.00	50.000	11.439	0.087418	10.518	14.889	0.065951	0.022620	0.035519	604.51	-0.27153	94.476	31.319
500.00	50.000	9.3865	0.10654	13.024	18.350	0.073681	0.022659	0.033937	622.30	-0.36911	76.899	32.167
100.00	100.00	31.474	0.031772	0.095937	3.2732	-0.00053857	0.033037	0.050530	1282.4	-0.47725	1005.7	90.560
200.00	100.00	24.888	0.040181	3.9022	7.9203	0.031951	0.026437	0.043352	987.69	-0.50923	536.84	73.350
300.00	100.00	20.200	0.049505	7.0625	12.013	0.048608	0.024358	0.038799	866.60	-0.54516	331.69	54.648
400.00	100.00	16.970	0.058928	9.8487	15.741	0.059353	0.023555	0.036051	822.33	-0.59581	229.18	45.748
500.00	100.00	14.662	0.068206	12.449	19.269	0.067230	0.023434	0.034683	808.91	-0.64123	173.58	42.504

The values in these tables were generated from the NIST REFPROP software (Lemmon, E. W., McLinden, M. O., and Huber, M. L., NIST Standard Reference Database 23: Reference Fluid Thermodynamic and Transport Properties—REFPROP, National Institute of Standards and Technology, Standard Reference Data Program, Gaithersburg, Md., 2002, Version 7.1). The primary source for the thermodynamic properties is Lemmon, E. W., and Span, R., "Short Fundamental Equations of State for 20 Industrial Fluids," *J. Chem. Eng. Data*, **51**(3):785–850, 2006. The source for viscosity and thermal conductivity is Version 9.08 of the NIST14 database.

Properties at the triple point temperature and the critical point temperature are given in the first and last entries of the saturation tables, respectively. In the single-phase table, when the temperature range for a given isobar includes a vapor-liquid phase boundary, the temperature of phase equilibrium is noted, and properties for both the saturated liquid and saturated vapor are given (with liquid properties given in the upper line). Lines are omitted from the temperature-pressure grid of the single-phase table, when the system would be in the solid phase or if there are potential problems with the source property surface.

The equation of state is valid from the triple point to 500 K with pressures to 100 MPa. At higher pressures, the deviations from the equation increase rapidly, and it is not recommended to use the equation above 100 MPa. The uncertainties in the equation are 0.3% in density (approaching 1% near the critical point), 0.2% in vapor pressure, and 2% in heat capacities. For viscosity, estimated uncertainty is 2%. For thermal conductivity, estimated uncertainty, except near the critical region, is 4–6%.

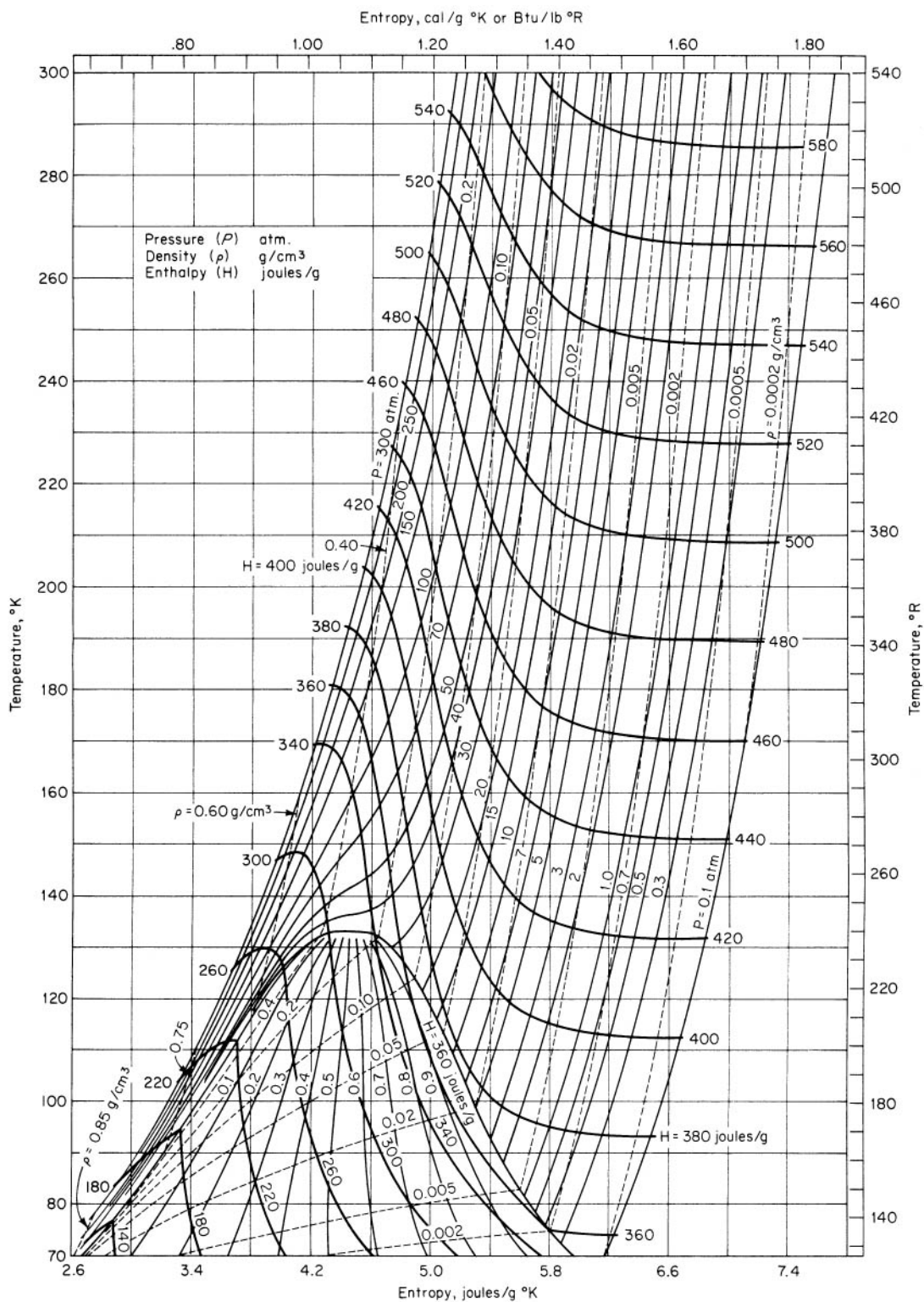


FIG. 2-8 Temperature-entropy diagram for carbon monoxide. Pressure P , in atmospheres; density ρ , in grams per cubic centimeter; enthalpy H , in joules per gram. (From Hust and Stewart, NBS Tech. Note 202, 1963.)

TABLE 2-201 Thermophysical Properties of Saturated Carbon Tetrachloride

T, K	P, bar	v_f , m ³ /kg	v_g , m ³ /kg	h_f , kJ/kg	h_g , kJ/kg	s_f , kJ/(kg·K)	s_g , kJ/(kg·K)	c_{pf} , kJ/(kg·K)	μ_f , 10 ⁻⁶ Pa·s	k_f , W/(m·K)	Pr
280	0.064	0.000 619	2.414	205.5	420.7	1.018	1.787	0.835	1042	0.1043	8.34
290	0.105	0.000 625	1.495	212.9	425.7	1.042	1.775	0.844	892	0.1020	7.38
300	0.165	0.000 633	0.971	220.9	430.9	1.068	1.768	0.853	774	0.0998	6.62
310	0.251	0.000 641	0.669	228.8	436.1	1.095	1.764	0.863	679	0.0975	6.01
320	0.370	0.000 649	0.463	236.9	441.3	1.121	1.760	0.874	603	0.0952	5.54
330	0.531	0.000 657	0.3306	246.0	446.4	1.149	1.756	0.885	539	0.0930	5.13
340	0.743	0.000 666	0.2407	254.5	451.5	1.174	1.754	0.897	486	0.0907	4.81
350	1.017	0.000 674	0.1802	263.1	456.6	1.199	1.752	0.910	441	0.0884	4.54
360	1.361	0.000 684	0.1370	271.8	461.7	1.224	1.751	0.924	402	0.0861	4.31
370	1.795	0.000 694	0.1053	280.8	466.6	1.248	1.751	0.939	368	0.0839	4.12
380	2.327	0.000 704	0.0820	289.7	471.5	1.272	1.750	0.954	338	0.0816	3.95
390	2.970	0.000 715	0.0651	298.1	475.8	1.295	1.751	0.970	311	0.0794	3.80
400	3.735	0.000 727	0.0525	307.9	481.2	1.319	1.752	0.987	287	0.0771	3.67
410	4.642	0.000 739	0.0426	317.1	485.8	1.341	1.753	1.010	265	0.0749	3.57
420	5.700	0.000 753	0.0350	326.0	490.4	1.363	1.754	1.034	246	0.0726	3.50
430	6.927	0.000 766	0.02899	335.2	494.9	1.384	1.756	1.060	227	0.0704	3.42
440	8.342	0.000 780	0.02413	344.3	499.2	1.405	1.757	1.094	211	0.0682	3.38
450	9.958	0.000 796	0.02020	353.6	503.4	1.426	1.759	1.141	195	0.0660	3.37
460	11.792	0.000 801	0.01692	363.1	507.3	1.446	1.760	1.207	180	0.0638	3.36
470	13.869	0.000 834	0.01425	372.8	511.1	1.467	1.761	1.240	167	0.0666	3.36
480	16.21	0.000 856	0.01205	382.6	514.6	1.487	1.762	1.278	156	0.0594	3.36
490	18.83	0.000 880	0.01011	392.0	517.5	1.507	1.763	1.320	145	0.0511	3.35
500	21.77	0.000 858	0.00858	402.5	520.2	1.526	1.762	1.375	133	0.0549	3.35
510	25.02	0.000 945	0.00722	412.9	522.6	1.546	1.761	1.44			
520	28.68	0.000 987	0.00607	424.3	524.2	1.568	1.760	1.52			
530	32.71	0.001 041	0.00500	436.4	524.5	1.590	1.756				
540	37.18	0.001 121	0.00400	448.3	522.7	1.614	1.749				
550	44.12	0.001 248	0.00309	463.4	518.2	1.638	1.738				
556.4 ^c	45.60	0.001 792	0.00179	494.4	494.4	1.692	1.692				

^c = critical point. Base points: $h_f = 200$ at 273.15 K = 0°C = $h_A - 300$ kJ/kg; $s_f = 1.000$ at 273.15 K = 0°C = $s_A - 4.000$ kJ/(kg·K). Values mostly rounded and converted from Altunin, V. V., V. Z. Geller, et al., *Thermophysical Properties of Freons*, vol. 9, Hemisphere, Washington, DC, 1987 (243 pp.). Some irregularities exist in these data.

TABLE 2-202 Saturated Carbon Tetrafluoride (R14)*

T, K	P, bar	v_f , m ³ /kg	v_g , m ³ /kg	h_f , kJ/kg	h_g , kJ/kg	s_f , kJ/(kg·K)	s_g , kJ/(kg·K)	c_{pf} , kJ/(kg·K)	μ_f , 10 ⁻⁴ Pa·s	k_f , W/(m·K)
100	0.0089	5.370.-4	10.77	495.8	648.4	5.487	7.003	0.887		0.136
110	0.0286	5.515.-4	3.648	502.7	652.9	5.556	6.919	0.887		0.128
120	0.0924	5.668.-4	1.228	510.4	657.1	5.624	6.847	0.890		0.119
130	0.2986	5.834.-4	0.4051	518.8	661.1	5.691	6.786	0.896		0.111
140	0.6901	6.018.-4	0.1855	527.7	664.8	5.757	6.736	0.904	3.56	0.104
150	1.4074	6.225.-4	0.0951	537.2	668.3	5.822	6.696	0.922	3.28	0.097
160	2.598	6.460.-4	0.0532	549.4	671.4	5.885	6.662	0.975	3.03	0.089
170	4.426	6.733.-4	0.0318	557.6	674.0	5.947	6.629	1.031	2.80	0.081
180	7.067	7.055.-4	0.0200	568.2	676.1	6.007	6.607	1.104	2.59	0.072
190	10.702	7.449.-4	0.0131	579.3	677.4	6.066	6.583	1.203	2.39	0.064
200	15.531	7.957.-4	0.0087	591.0	677.8	6.124	6.558	1.334	2.19	0.057
210	21.794	8.674.-4	0.0058	603.5	676.4	6.182	6.536	1.506	2.01	0.049
220	29.269	9.931.-4	0.0036	618.5	671.4	6.233	6.490	1.73	1.85	0.042
227.5 ^c	37.45	1.598.-3	0.0016	646.9	646.9	6.371	6.371	∞		∞

* P , v , h , and s values interpolated, extrapolated, and converted from Oguchi, *Reito*, 52 (1977): 869-889. c = critical point. The notation 5.370.-4 signifies 5.370×10^{-4} . Equations and constants approximated to ASHRAE tables are given by Mecaryk, K. and M. Masaryk, *Heat Recovery Systems and CHP*, 11, 2-3 (1991). The 1993 ASHRAE *Handbook—Fundamentals* (S.I. ed.) contains a saturation table from -140 to -45.65 °C and an enthalpy-log-pressure diagram from 0.1 to 300 bar, -140 to 300 °C. For properties to 1000 bar from 90 to 420 K, see Rublo, R. G., J. A. Zollweg, et al., *J. Chem. Eng. Data*, 36 (1991): 171-184. Saturation and superheat tables and a diagram to 80 bar, 600 K are given by Reynolds, W. C., *Thermodynamic Properties in S.I.*, Stanford Univ. publ., 1979 (173 pp.). Chari, Ph.D. thesis, University of Michigan, 1960, presents saturation-temperature tables in fps units for 1°F increments from -270 to -51°F. Thermodynamic and transport properties, equations, and computer code and tables at constant entropy from 89 to 845 K are given by Hunt, J. L. and Boney, L. R., NASA TN D-7181, 1973 (105 pp.), largely based upon the Chari data.

TABLE 2-203 Thermodynamic Properties of Carbonyl Sulfide

Temperature K	Pressure MPa	Density mol/dm ³	Volume dm ³ /mol	Int. energy kJ/mol	Enthalpy kJ/mol	Entropy kJ/(mol·K)	C _v kJ/(mol·K)	C _p kJ/(mol·K)	Sound speed m/s	Joule-Thomson K/MPa
Saturated Properties										
134.30	0.000064435	22.518	0.044409	-6.2965	-6.2965	-0.036049	0.050295	0.074835	1449.7	-0.47647
140.00	0.00014316	22.330	0.044783	-5.8733	-5.8733	-0.032962	0.049071	0.073691	1423.0	-0.48236
150.00	0.00049244	22.002	0.045451	-5.1446	-5.1446	-0.027934	0.047317	0.072140	1376.1	-0.48929
160.00	0.0014232	21.674	0.046138	-4.4289	-4.4289	-0.023315	0.045963	0.071067	1329.2	-0.49217
170.00	0.0035714	21.346	0.046847	-3.7220	-3.7219	-0.019029	0.044919	0.070377	1282.3	-0.49125
180.00	0.0079826	21.016	0.047583	-3.0204	-3.0201	-0.015019	0.044118	0.070000	1235.4	-0.48674
190.00	0.016210	20.683	0.048349	-2.3213	-2.3206	-0.011239	0.043507	0.069885	1188.5	-0.47875
200.00	0.030380	20.345	0.049151	-1.6224	-1.6209	-0.0076537	0.043047	0.069996	1141.6	-0.46727
210.00	0.053219	20.002	0.049994	-0.92144	-0.91878	-0.0042337	0.042708	0.070307	1094.7	-0.45221
220.00	0.088035	19.653	0.050884	-0.21676	-0.21228	-0.00095536	0.042464	0.070804	1047.8	-0.43335
230.00	0.13868	19.295	0.051827	0.49332	0.50050	0.0022014	0.042299	0.071479	1000.8	-0.41029
240.00	0.20947	18.927	0.052834	1.2104	1.2214	0.0052538	0.042198	0.072335	953.72	-0.38249
250.00	0.30513	18.548	0.053914	1.9359	1.9524	0.0082168	0.042150	0.073381	906.38	-0.34913
260.00	0.43069	18.155	0.055080	2.6716	2.6954	0.011104	0.042147	0.074640	858.76	-0.30911
270.00	0.59148	17.747	0.056348	3.4192	3.4525	0.013927	0.042186	0.076145	810.74	-0.26092
280.00	0.79300	17.320	0.057737	4.1805	4.2263	0.016699	0.042262	0.077949	762.21	-0.20244
290.00	1.0409	16.870	0.059276	4.9579	5.0196	0.019432	0.042376	0.080132	713.03	-0.13069
300.00	1.3412	16.394	0.060998	5.7542	5.8360	0.022138	0.042533	0.082812	663.05	-0.041371
310.00	1.6998	15.885	0.062953	6.5728	6.6798	0.024832	0.042738	0.086180	612.06	0.071920
320.00	2.1232	15.335	0.065210	7.4185	7.5570	0.027531	0.043007	0.090546	559.82	0.21913
330.00	2.6180	14.733	0.067877	8.2981	8.4758	0.030256	0.043365	0.096471	505.95	0.41667
340.00	3.1915	14.060	0.071123	9.2217	9.4487	0.033041	0.043857	0.10507	449.91	0.69379
350.00	3.8523	13.287	0.075261	10.207	10.497	0.035938	0.044569	0.11899	390.71	1.1092
360.00	4.6109	12.352	0.080962	11.289	11.662	0.039054	0.045699	0.14652	326.44	1.8033
370.00	5.4827	11.072	0.090320	12.572	13.067	0.042698	0.047851	0.23509	252.51	3.2373
378.77	6.3688	7.4100	0.13495	15.239	16.099	0.050522			0	8.9233
134.30	0.000064435	0.000057710	17.328	14.600	15.716	0.12786	0.022770	0.031089	159.29	230.42
140.00	0.00014316	0.00012301	8,129.4	14.730	15.894	0.12252	0.023105	0.031429	162.31	199.85
150.00	0.00049244	0.00039506	2,531.3	14.963	16.209	0.11442	0.023740	0.032079	167.40	158.07
160.00	0.0014232	0.0010711	933.62	15.201	16.529	0.10767	0.024427	0.032795	172.22	127.26
170.00	0.0035714	0.0025330	394.79	15.443	16.853	0.10200	0.025159	0.033580	176.77	104.13
180.00	0.0079826	0.0053579	186.64	15.689	17.179	0.097198	0.025933	0.034438	181.06	86.482
190.00	0.016210	0.010340	96.715	15.938	17.505	0.093108	0.026745	0.035375	185.07	72.846
200.00	0.030380	0.018492	54.078	16.187	17.830	0.089601	0.027592	0.036399	188.78	62.184
210.00	0.053219	0.031038	32.218	16.436	18.151	0.086575	0.028471	0.037521	192.15	53.756
220.00	0.088035	0.049400	20.243	16.684	18.466	0.083945	0.029382	0.038751	195.15	47.024
230.00	0.13868	0.075184	13.301	16.927	18.772	0.081643	0.030323	0.040105	197.76	41.595
240.00	0.20947	0.11018	9.0759	17.166	19.067	0.079610	0.031293	0.041602	199.92	37.175
250.00	0.30513	0.15639	6.3942	17.397	19.348	0.077800	0.032292	0.043268	201.62	33.545
260.00	0.43069	0.21605	4.6285	17.619	19.613	0.076171	0.033320	0.045137	202.81	30.541
270.00	0.59148	0.29173	3.4278	17.830	19.858	0.074687	0.034376	0.047258	203.46	28.040
280.00	0.79300	0.38642	2.5879	18.027	20.079	0.073316	0.035463	0.049700	203.53	25.945
290.00	1.0409	0.50374	1.9852	18.207	20.273	0.072030	0.036585	0.052570	202.98	24.185
300.00	1.3412	0.64823	1.5427	18.365	20.434	0.070799	0.037748	0.056029	201.77	22.698
310.00	1.6998	0.82581	1.2109	18.497	20.556	0.069593	0.038964	0.060340	199.84	21.437
320.00	2.1232	1.0446	0.95730	18.596	20.629	0.068379	0.040251	0.065951	197.14	20.357
330.00	2.6180	1.3165	0.75961	18.651	20.640	0.067117	0.041639	0.073691	193.61	19.412
340.00	3.1915	1.6600	0.60241	18.647	20.570	0.065750	0.043181	0.085260	189.17	18.546
350.00	3.8523	2.1078	0.47442	18.555	20.383	0.064185	0.044969	0.10478	183.76	17.674
360.00	4.6109	2.7278	0.36660	18.321	20.011	0.062245	0.047203	0.14532	177.26	16.625
370.00	5.4827	3.7183	0.26894	17.782	19.256	0.059425	0.050441	0.28170	169.47	14.934
378.77	6.3688	7.4100	0.13495	15.239	16.099	0.050522			0	8.9233

Single-Phase Properties

150.00	0.10000	22.003	0.045448	-5.1456	-5.1411	-0.027941	0.047320	0.072138	1376.4	-0.48934
200.00	0.10000	20.347	0.049148	-1.6235	-1.6186	-0.0076594	0.043049	0.069990	1141.9	-0.46739
222.70	0.10000	19.557	0.051133	-0.025288	-0.020175	-0.000090227	0.042413	0.070969	1035.1	-0.42755
222.70	0.10000	0.055571	17.995	16.750	18.550	0.083293	0.029634	0.039104	195.90	45.441
250.00	0.10000	0.049051	20.387	17.590	19.628	0.087860	0.030973	0.040014	207.32	32.301
300.00	0.10000	0.040528	24.674	19.215	21.683	0.095346	0.033493	0.042188	226.21	19.802
350.00	0.10000	0.034596	28.905	20.954	23.845	0.10201	0.035716	0.044263	243.37	13.574
150.00	1.0000	22.015	0.045423	-5.1547	-5.1093	-0.028002	0.047344	0.072112	1379.4	-0.48974
200.00	1.0000	20.365	0.049103	-1.6382	-1.5891	-0.0077331	0.043071	0.069917	1145.9	-0.46887
250.00	1.0000	18.572	0.053843	1.9164	1.9703	0.0081385	0.042163	0.073223	910.91	-0.35287
288.48	1.0000	16.940	0.059031	4.8385	4.8975	0.019018	0.042357	0.079771	720.56	-0.14261
288.48	1.0000	0.48426	2.0650	18.180	20.245	0.072221	0.036412	0.052100	203.11	24.434
300.00	1.0000	0.45571	2.1944	18.640	20.834	0.074222	0.036112	0.050249	209.62	21.627
350.00	1.0000	0.36985	2.7038	20.566	23.270	0.081735	0.036823	0.048032	233.01	14.214
150.00	5.0000	22.068	0.045315	-5.1945	-4.9679	-0.028269	0.047452	0.072006	1392.3	-0.49145
200.00	5.0000	20.446	0.048909	-1.7019	-1.4574	-0.0080546	0.043169	0.069609	1163.4	-0.47508
250.00	5.0000	18.707	0.053456	1.8087	2.0760	0.0077029	0.042245	0.072395	935.94	-0.37256
300.00	5.0000	16.644	0.060080	5.5592	5.8596	0.021479	0.042516	0.080087	701.33	-0.11429
350.00	5.0000	13.583	0.073622	10.000	10.369	0.035328	0.044139	0.10909	422.84	0.86866
150.00	10.000	22.132	0.045183	-5.2426	-4.7907	-0.028596	0.047587	0.071886	1408.1	-0.49341
200.00	10.000	20.543	0.048678	-1.7780	-1.2912	-0.0084436	0.043292	0.069265	1184.3	-0.48206
250.00	10.000	18.864	0.053012	1.6837	2.2138	0.0071898	0.042351	0.071522	965.13	-0.39347
300.00	10.000	16.938	0.059038	5.3293	5.9197	0.020687	0.042551	0.077434	746.52	-0.18740
350.00	10.000	14.430	0.069300	9.3887	10.082	0.033492	0.043442	0.091456	517.30	0.36632
150.00	20.000	22.256	0.044932	-5.3340	-4.4353	-0.029231	0.047854	0.071679	1438.4	-0.49677
200.00	20.000	20.726	0.048249	-1.9196	-0.95458	-0.0091833	0.043536	0.068683	1223.7	-0.49387
250.00	20.000	19.146	0.052230	1.4600	2.5046	0.0062486	0.042574	0.070163	1018.0	-0.42634
300.00	20.000	17.418	0.057411	4.9523	6.1005	0.019350	0.042705	0.074036	821.57	-0.28388
350.00	20.000	15.414	0.064877	8.6515	9.9491	0.031203	0.043268	0.080401	634.40	-0.00046299
200.00	50.000	21.201	0.047167	-2.2782	0.080117	-0.011163	0.044246	0.067514	1327.4	-0.51767
250.00	50.000	19.828	0.050433	0.93091	3.4526	0.0038870	0.043245	0.067745	1148.2	-0.48534
300.00	50.000	18.430	0.054259	4.1637	6.8767	0.016368	0.043321	0.069343	986.75	-0.42082
350.00	50.000	16.985	0.058876	7.4493	10.393	0.027205	0.043748	0.071325	844.44	-0.32515

The values in these tables were generated from the NIST REFPROP software (Lemmon, E. W., McLinden, M. O., and Huber, M. L., NIST Standard Reference Database 23: Reference Fluid Thermodynamic and Transport Properties—REFPROP, National Institute of Standards and Technology, Standard Reference Data Program, Gaithersburg, Md., 2002, Version 7.1). The primary source for the thermodynamic properties is Lemmon, E. W., and Span, R., "Short Fundamental Equations of State for 20 Industrial Fluids," *J. Chem. Eng. Data*, **51**(3):785–850, 2006. Validated equations for the viscosity and thermal conductivity are not currently available for this fluid.

Properties at the triple point temperature and the critical point temperature are given in the first and last entries of the saturation tables, respectively. In the single-phase table, when the temperature range for a given isobar includes a vapor-liquid phase boundary, the temperature of phase equilibrium is noted, and properties for both the saturated liquid and saturated vapor are given (with liquid properties given in the upper line). Lines are omitted from the temperature-pressure grid of the single-phase table, when the system would be in the solid phase or if there are potential problems with the source property surface.

The resulting equation has uncertainties of 0.1% in density in the liquid below 450 K, 1% in density at temperatures between 450 and 500 K, 3% in density at temperatures above 500 K, 0.5% in density in the vapor phase and at supercritical conditions below 10 MPa and 450 K, 0.5% in vapor pressure, and 2% in isobaric heat capacity.

2-248 PHYSICAL AND CHEMICAL DATA
TABLE 2-204 Saturated Cesium*

T, K	P, bar	v_f , m ³ /kg	v_g , m ³ /kg	h_f , kJ/kg	h_g , kJ/kg	s_f , kJ/(kg·K)	s_g , kJ/(kg·K)	c_{pf} , kJ/(kg·K)
301.6 ^m	2.66.-9	5.444.-4	7.01.+7	74.6	637.6	0.696	2.563	0.245
400	3.83.-6	5.615.-4	6.54.+4	98.5	651.9	0.765	2.148	0.240
500	3.11.-4	5.800.-4	1001	122.0	666.1	0.817	1.905	0.232
600	5.65.-3	5.999.-4	65.63	144.9	678.4	0.859	1.748	0.224
700	0.0440	6.215.-4	9.671	167.0	688.9	0.893	1.638	0.219
800	0.2029	6.443.-4	2.353	188.7	698.3	0.922	1.559	0.217
900	0.6620	6.689.-4	0.796	210.6	707.3	0.975	1.500	0.222
1000	1.693	6.954.-4	0.335	233.2	716.4	0.972	1.455	0.231
1200	6.790	7.628.-4	0.097	281.1	736.1	1.015	1.394	0.248
1500	27.6	8.84.-4	0.029	358.8	772.2	1.072	1.345	0.275

*Converted from tables in Vargaftik, *Tables of the Thermophysical Properties of Liquids and Gases*, Nauka, Moscow, 1972, and Hemisphere, Washington, 1975. m = melting point. The notation 2.66.-9 signifies 2.66×10^{-9} .

Many of the Vargaftik values also appear in Ohse, R. W., *Handbook of Thermodynamic and Transport Properties of Alkali Metals*, Blackwell Sci. Pubs., Oxford, 1985 (1020 pp.). This source contains superheat data.

Saturation and superheat tables and a diagram to 30 bar, 1550 K are given by Reynolds, W. C., *Thermodynamic Properties in S.I.*, Stanford Univ. publ., 1979 (173 pp.).

For a Mollier diagram from 0.1 to 327 psia, 1300–2700 °R, see Weatherford, W. D., J. C. Tyler, et al., WADD-TR-61-96, 1961.

An extensive review of properties of the solid and the saturated liquid was given by Alcock, C. B., M. W. Chase, et al., *J. Phys. Chem. Ref. Data*, **23**, 3 (1994): 385–497.

TABLE 2-205 Thermophysical Properties of Saturated Chlorine

$T, ^\circ\text{C}$	P, bar	$v_f, \text{m}^3/\text{kg}$	$v_g, \text{m}^3/\text{kg}$	$h_f, \text{kJ}/\text{kg}$	$h_g, \text{kJ}/\text{kg}$	$s_f, \text{kJ}/(\text{kg}\cdot\text{K})$	$s_g, \text{kJ}/(\text{kg}\cdot\text{K})$	$c_{pf}, \text{kJ}/(\text{kg}\cdot\text{K})$	$c_{pg}, \text{kJ}/(\text{kg}\cdot\text{K})$	$\mu_f, 10^{-6} \text{Pa}\cdot\text{s}$	$\mu_g, 10^{-6} \text{Pa}\cdot\text{s}$	$k_f, \text{W}/(\text{m}\cdot\text{K})$	$k_g, \text{W}/(\text{m}\cdot\text{K})$	Pr_f	Pr_g
-50	0.475	0.000 623	0.5448	221.5	518.2	1.7650	3.0946	0.9454	0.476	565	10.3	0.1684	0.0061	3.17	0.809
-40	0.773	0.000 634	0.3481	231.0	522.2	1.8074	3.0562	0.9474	0.484	520	10.8	0.1650	0.0065	2.99	0.815
-30	1.203	0.000 645	0.2314	240.6	526.1	1.8480	3.0223	0.9496	0.497	483	11.4	0.1613	0.0069	2.85	0.820
-20	1.802	0.000 656	0.1593	250.3	529.9	1.8869	2.9921	0.9520	0.513	452	11.9	0.1573	0.0074	2.74	0.826
-10	2.608	0.000 668	0.1134	260.0	533.9	1.9243	2.9649	0.9547	0.532	422	12.4	0.1527	0.0078	2.64	0.841
0	3.664	0.000 681	0.0829	269.7	537.4	1.9604	2.9402	0.9579	0.554	393	13.0	0.1478	0.0083	2.55	0.864
10	5.014	0.000 695	0.0619	279.4	540.5	1.9953	2.9177	0.9618	0.579	368	13.5	0.1427	0.0088	2.48	0.888
20	6.702	0.000 710	0.0471	289.2	543.3	2.0291	2.8924	0.9667	0.607	348	14.1	0.1378	0.0093	2.45	0.918
30	8.774	0.000 726	0.0364	299.0	545.7	2.0622	2.8777	0.9728	0.638	333	14.7	0.1327	0.0099	2.44	0.950
40	11.27	0.000 744	0.0286	308.8	548.0	2.0946	2.8593	0.9816	0.674	318	15.2	0.1282	0.0104	2.43	0.985
50	14.25	0.000 763	0.02276	318.6	549.8	2.1264	2.8417	0.9968	0.720	304	15.8	0.1230	0.0110	2.46	1.034
60	17.76	0.000 784	0.01827	329.1	551.2	2.1578	2.8245	1.022	0.786	290	16.4	0.1171	0.0117	2.53	1.107
70	21.85	0.000 808	0.01481	340.0	552.1	2.1892	2.8074	1.054	0.885	278	17.1	0.1122	0.0126	2.61	1.201
80	26.65	0.000 834	0.01202	351.4	552.5	2.2207	2.7900	1.124	1.017	267	17.9	0.1050	0.0137	2.85	1.331
90	32.17	0.000 865	0.00972	364.1	552.4	2.2528	2.7714	1.253	1.205	256	18.7	0.0986	0.0149	3.26	1.510
100	38.44	0.000 901	0.00789	377.8	551.0	2.2860	2.7502	1.418	1.434	247	19.5	0.0916	0.0163	3.82	1.700
110	45.54	0.000 956	0.00639	391.3	548.8	2.3207	2.7317	1.632	1.696	238	20.6	0.0850	0.0178	4.57	1.96
120	53.57	0.001 016	0.00508	407.1	543.7	2.3590	2.7064	1.891	1.960	230	22.2	0.0775	0.0195	5.61	2.23
130	62.68	0.001 121	0.00392	426.1	535.0	2.4032	2.6733								
140	72.84	0.001 335	0.00282	451.1	517.3	2.4595	2.6198								
144 ^c	77.10	0.001 77	0.00177	483.1	483.1	2.5365	2.5365								

^c = critical point.

Values interpolated and converted from Martin, J. J., 1977 (private communication), and from *Heat Exchanger Design Handbook*, vol. 5, Hemisphere, Washington, DC, 1983. Values of Ziegler, *Chem.-Ing.-Tech.*, **22** (1950): 229, apparently were also used in Landolt-Bornstein, **IVa**, (1967): 238–239, and in Ullmans *Enzyklopädie der technische Chemie*, 9, Verlag Chemie, Weinheim, 1975 (317–372).

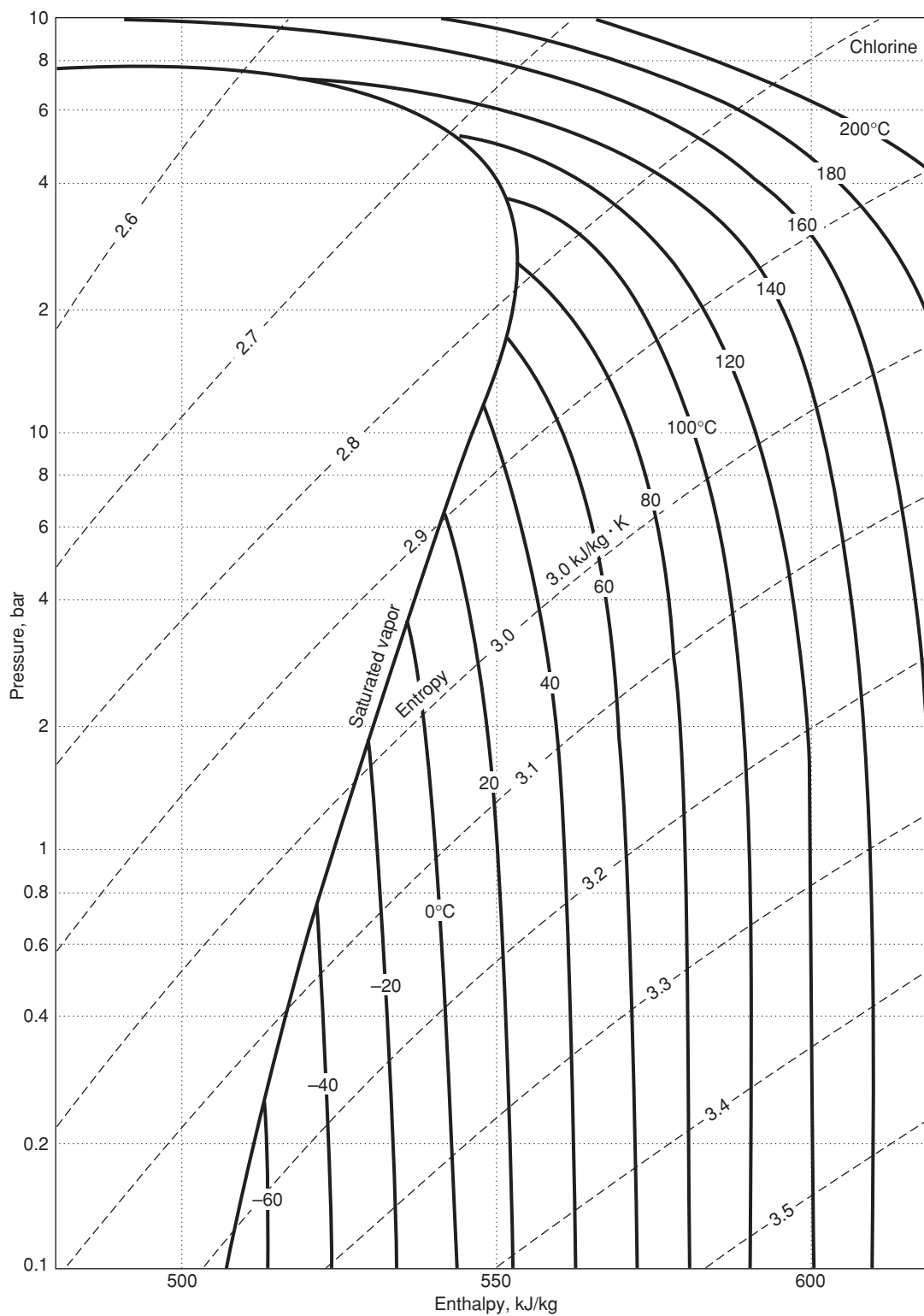


FIG. 2-9 Enthalpy-log-pressure diagram for chlorine.

TABLE 2-206 Saturated Chloroform (R20)

T , K	P , bar	v_f , m ³ /kg	v_g , m ³ /kg	h_f , kJ/kg	h_g , kJ/kg	s_f , kJ/(kg·K)	s_g , kJ/(kg·K)	c_{pf} , kJ/(kg·K)	μ_f , 10 ⁻⁶ Pa·s	k_f , W/(m·K)	Pr_f
280	0.115	0.000 660	1.689	-46.0	219.5	-0.165	0.798		748	0.120	
300	0.293	0.000 678	0.714	-32.6	230.6	-0.105	0.773		587	0.114	
320	0.620	0.000 695	0.358	-13.4	241.1	-0.041	0.754		468	0.109	
340	1.224	0.000 715	0.190	5.2	252.1	0.015	0.741		381	0.103	
360	2.255	0.000 739	0.107	23.3	263.0	0.065	0.731	1.03	319	0.095	3.35
380	3.830	0.000 765	0.0653	41.7	273.7	0.114	0.725	1.07	273	0.0921	3.17
400	6.039	0.000 795	0.0425	61.4	284.2	0.165	0.722	1.11	237	0.0863	3.04
420	9.058	0.000 822	0.0288	82.8	294.2	0.217	0.721	1.15	206	0.0808	2.93
440	13.39	0.000 871	0.0195	106.1	303.6	0.270	0.719	1.21	177	0.0750	2.86
460	18.80	0.000 921	0.0137	131.6	311.2	0.325	0.716	1.32	155	0.0694	2.95
480	26.00	0.000 980	0.00962	157.4	316.5	0.380	0.711	1.43	129.6	0.0641	2.89
500	34.66	0.001 059	0.00673	186.2	320.8	0.436	0.706	1.59	105.5	0.0584	2.87
520	44.68	0.001 193	0.00467	219.6	321.3	0.499	0.694		81.2	0.0518	
530	50.44	0.001 328	0.00359	242.7	315.7	0.540	0.678		67.7	0.0461	
536.6 ^c	54.72	0.002 00	0.00200	284.1	284.1	0.602	0.602				

c = critical point. $h_f = s_f = 0$ at n.b.p., 334.5 K.

P , v , h , and s interpolated from Altunin, V. V., V. Z. Geller, et al., *Thermophysical Properties of Freons*, U.S.S.R. N.S.R.D.S. series, vol. 9., Hemisphere, 1987.

TABLE 2-207 Thermodynamic Properties of Cyclohexane

Temperature K	Pressure MPa	Density mol/dm ³	Volume dm ³ /mol	Int. energy kJ/mol	Enthalpy kJ/mol	Entropy kJ/(mol·K)	C _v kJ/(mol·K)	C _p kJ/(mol·K)	Sound speed m/s	Joule-Thomson K/MPa
Saturated Properties										
279.47	0.0052538	9.4045	0.10633	-12.076	-12.075	-0.038084	0.094354	0.13918	1403.6	-0.50892
290.00	0.0089097	9.2862	0.10769	-10.567	-10.566	-0.032787	0.10358	0.14714	1314.7	-0.47482
300.00	0.014139	9.1736	0.10901	-9.0626	-9.0611	-0.027686	0.11089	0.15372	1245.3	-0.44719
310.00	0.021670	9.0604	0.11037	-7.4959	-7.4935	-0.022550	0.11715	0.15959	1185.7	-0.42239
320.00	0.032188	8.9462	0.11178	-5.8733	-5.8697	-0.017398	0.12261	0.16495	1132.8	-0.39928
330.00	0.046481	8.8309	0.11324	-4.1995	-4.1942	-0.012248	0.12749	0.16991	1084.4	-0.37708
340.00	0.065433	8.7142	0.11476	-2.4777	-2.4702	-0.0071081	0.13193	0.17461	1039.4	-0.35516
350.00	0.090023	8.5958	0.11634	-0.71047	-0.70000	-0.0019852	0.13604	0.17911	996.64	-0.33304
360.00	0.12131	8.4756	0.11799	1.1006	1.1149	0.0031169	0.13992	0.18349	955.45	-0.31028
370.00	0.16044	8.3533	0.11971	2.9544	2.9736	0.0081966	0.14362	0.18781	915.28	-0.28642
380.00	0.20862	8.2285	0.12153	4.8503	4.8756	0.013253	0.14720	0.19210	875.71	-0.26103
390.00	0.26711	8.1009	0.12344	6.7880	6.8210	0.018287	0.15069	0.19642	836.40	-0.23356
400.00	0.33727	7.9701	0.12547	8.7677	8.8100	0.023301	0.15412	0.20079	797.11	-0.20340
410.00	0.42046	7.8357	0.12762	10.790	10.843	0.028296	0.15751	0.20528	757.60	-0.16978
420.00	0.51814	7.6970	0.12992	12.855	12.922	0.033275	0.16088	0.20990	717.72	-0.13174
430.00	0.63180	7.5533	0.13239	14.964	15.048	0.038241	0.16425	0.21472	677.33	-0.087993
440.00	0.76300	7.4037	0.13507	17.119	17.222	0.043199	0.16762	0.21980	636.33	-0.036876
450.00	0.91333	7.2473	0.13798	19.321	19.447	0.048153	0.17101	0.22522	594.66	0.023882
460.00	1.0845	7.0828	0.14119	21.572	21.726	0.053108	0.17442	0.23106	552.32	0.097405
470.00	1.2781	6.9085	0.14475	23.876	24.061	0.058071	0.17788	0.23747	509.35	0.18807
480.00	1.4961	6.7225	0.14875	26.236	26.458	0.063050	0.18140	0.24464	465.88	0.30221
490.00	1.7402	6.5223	0.15332	28.655	28.922	0.068054	0.18499	0.25284	422.08	0.44929
500.00	2.0124	6.3048	0.15861	31.140	31.459	0.073094	0.18868	0.26259	378.12	0.64479
510.00	2.3150	6.0655	0.16487	33.699	34.081	0.078189	0.19249	0.27496	333.83	0.91793
520.00	2.6505	5.7961	0.17253	36.350	36.807	0.083372	0.19650	0.29284	287.99	1.3377
530.00	3.0222	5.4765	0.18260	39.135	39.687	0.088731	0.20083	0.32631	236.86	2.1175
540.00	3.4352	5.0307	0.19878	42.215	42.898	0.094586	0.20611	0.43566	171.37	4.2415
550.00	3.8928	4.1555	0.24065	46.176	47.113	0.10213	0.21549	0.97375	108.39	10.542
553.64	4.0750	3.2438	0.30828	48.978	50.235	0.10770			0	19.224
279.47	0.0052538	0.0022692	440.68	19.476	21.791	0.083095	0.088889	0.097282	173.20	37.820
290.00	0.0089097	0.0037161	269.10	20.430	22.828	0.082366	0.093915	0.10238	175.72	39.495
300.00	0.014139	0.0057156	174.96	21.380	23.854	0.082030	0.098579	0.10715	177.99	39.306
310.00	0.021670	0.0085063	117.56	22.370	24.917	0.082001	0.10318	0.11190	180.09	38.189
320.00	0.032188	0.012293	81.348	23.397	26.015	0.082241	0.10775	0.11667	182.00	36.613
330.00	0.046481	0.017306	57.785	24.459	27.145	0.082719	0.11233	0.12149	183.70	34.853
340.00	0.065433	0.023800	42.017	25.555	28.305	0.083406	0.11692	0.12641	185.14	33.070
350.00	0.090023	0.032056	31.195	26.684	29.492	0.084277	0.12155	0.13145	186.30	31.353
360.00	0.12131	0.042386	23.593	27.842	30.704	0.085309	0.12623	0.13663	187.14	29.750
370.00	0.16044	0.055130	18.139	29.029	31.939	0.086481	0.13097	0.14199	187.65	28.282
380.00	0.20862	0.070668	14.151	30.242	33.194	0.087775	0.13577	0.14756	187.78	26.956
390.00	0.26711	0.089425	11.183	31.480	34.467	0.089174	0.14063	0.15338	187.51	25.772
400.00	0.33727	0.11188	8.9379	32.739	35.754	0.090660	0.14557	0.15949	186.80	24.723
410.00	0.42046	0.13860	7.2152	34.019	37.053	0.092220	0.15059	0.16596	185.62	23.803
420.00	0.51814	0.17021	5.8751	35.315	38.359	0.093839	0.15569	0.17286	183.94	23.004
430.00	0.63180	0.20749	4.8195	36.625	39.670	0.095502	0.16088	0.18030	181.73	22.319
440.00	0.76300	0.25135	3.9785	37.945	40.980	0.097195	0.16615	0.18840	178.96	21.739
450.00	0.91333	0.30293	3.3011	39.270	42.285	0.098905	0.17153	0.19737	175.58	21.259
460.00	1.0845	0.36362	2.7501	40.597	43.579	0.10062	0.17701	0.20746	171.56	20.872
470.00	1.2781	0.43522	2.2977	41.918	44.855	0.10231	0.18259	0.21903	166.87	20.572
480.00	1.4961	0.52006	1.9228	43.228	46.105	0.10398	0.18828	0.23261	161.44	20.351
490.00	1.7402	0.62133	1.6095	44.519	47.319	0.10560	0.19406	0.24895	155.22	20.204
500.00	2.0124	0.74350	1.3450	45.779	48.486	0.10715	0.19990	0.26922	148.10	20.128
510.00	2.3150	0.89342	1.1193	46.995	49.586	0.10859	0.20573	0.29534	139.91	20.128
520.00	2.6505	1.0826	0.92368	48.145	50.593	0.10988	0.21142	0.33088	130.29	20.237
530.00	3.0222	1.3338	0.74972	49.186	51.452	0.11093	0.21669	0.38411	118.65	20.538
540.00	3.4352	1.7017	0.58765	50.020	52.039	0.11151	0.22086	0.48310	104.10	21.201
550.00	3.8928	2.3597	0.42378	50.334	51.984	0.11099	0.22221	0.96007	87.229	22.656
553.64	4.0750	3.2438	0.30828	48.978	50.235	0.10770			0	19.224

Single-Phase Properties

300.00	0.10000	9.1745	0.10900	-9.0661	-9.0552	-0.027698	0.11091	0.15371	1245.8	-0.44737
353.45	0.10000	8.5546	0.11690	-0.090837	-0.079147	-0.00022335	0.13740	0.18063	982.29	-0.32529
353.45	0.10000	0.035368	28.274	27.080	29.907	0.084616	0.12316	0.13322	186.62	30.786
400.00	0.10000	0.030817	32.450	33.301	36.546	0.10224	0.14262	0.15196	200.08	18.560
500.00	0.10000	0.024334	41.095	49.598	53.708	0.14037	0.18205	0.19081	224.91	8.2156
600.00	0.10000	0.020172	49.575	69.610	74.568	0.17831	0.21697	0.22554	246.67	4.7321
700.00	0.10000	0.017244	57.992	92.840	98.639	0.21535	0.24653	0.25502	266.50	3.1661
300.00	1.0000	9.1840	0.10888	-9.1021	-8.9932	-0.027818	0.11106	0.15360	1250.6	-0.44930
400.00	1.0000	7.9861	0.12522	8.7122	8.8374	0.023162	0.15416	0.20043	803.90	-0.20919
455.22	1.0000	7.1625	0.13962	20.490	20.630	0.050740	0.17279	0.22821	572.63	0.060445
455.22	1.0000	0.33339	2.9995	39.963	42.963	0.099799	0.17438	0.20248	173.56	21.046
500.00	1.0000	0.27733	3.6058	48.369	51.975	0.11868	0.18654	0.20332	198.76	11.678
600.00	1.0000	0.21435	4.6653	68.879	73.544	0.15793	0.21804	0.22955	233.28	5.2822
700.00	1.0000	0.17821	5.6112	92.287	97.898	0.19542	0.24682	0.25703	258.70	3.2649
300.00	5.0000	9.2252	0.10840	-9.2570	-8.7150	-0.028339	0.11167	0.15315	1272.4	-0.45730
400.00	5.0000	8.0768	0.12381	8.3977	9.0168	0.022365	0.15438	0.19856	843.04	-0.23916
500.00	5.0000	6.5774	0.15204	30.362	31.122	0.071493	0.18830	0.24756	459.37	0.29542
600.00	5.0000	1.8230	0.54855	63.154	65.897	0.13428	0.23018	0.32421	141.27	9.9456
700.00	5.0000	1.0620	0.94165	89.416	94.125	0.17787	0.24921	0.27380	220.29	3.9618
300.00	10.000	9.2742	0.10783	-9.4403	-8.3620	-0.028964	0.11229	0.15264	1300.3	-0.46622
400.00	10.000	8.1782	0.12228	8.0451	9.2679	0.021455	0.15456	0.19678	888.19	-0.26775
500.00	10.000	6.8741	0.14547	29.472	30.927	0.069619	0.18805	0.23749	554.89	0.059727
600.00	10.000	4.9059	0.20384	55.388	57.426	0.11776	0.22275	0.30052	265.77	1.5290
700.00	10.000	2.6733	0.37407	84.812	88.552	0.16576	0.25026	0.30095	217.61	2.8239
300.00	25.000	9.4073	0.10630	-9.9312	-7.2736	-0.030689	0.11356	0.15139	1386.2	-0.48739
400.00	25.000	8.4285	0.11864	7.1716	10.138	0.019116	0.15480	0.19342	1006.6	-0.32157
500.00	25.000	7.3968	0.13519	27.819	31.199	0.065971	0.18805	0.22750	739.78	-0.16655
600.00	25.000	6.2973	0.15880	51.613	55.583	0.11034	0.21982	0.25993	540.01	0.046982
700.00	25.000	5.1531	0.19406	78.272	83.123	0.15273	0.24808	0.28977	414.69	0.35809
400.00	75.000	8.9762	0.11141	5.2440	13.599	0.013443	0.15529	0.18906	1308.3	-0.39015
500.00	75.000	8.2410	0.12134	25.023	34.124	0.059111	0.18956	0.22091	1084.3	-0.31328
600.00	75.000	7.5637	0.13221	47.767	57.683	0.10198	0.22144	0.24976	931.19	-0.25806
700.00	75.000	6.9477	0.14393	73.174	83.969	0.14245	0.24950	0.27541	824.46	-0.21348

The values in these tables were generated from the NIST REFPROP software (Lemmon, E. W., McLinden, M. O., and Huber, M. L., NIST Standard Reference Database 23: Reference Fluid Thermodynamic and Transport Properties—REFPROP, National Institute of Standards and Technology, Standard Reference Data Program, Gaithersburg, Md., 2002, Version 7.1). The primary source for the thermodynamic properties is Penoncello, S. G., Goodwin, A. R. H., and Jacobsen, R. T., "A Thermodynamic Property Formulation for Cyclohexane," *Int. J. Thermophys.* **16**(2):519–531, 1995. Validated equations for the viscosity and thermal conductivity are not currently available for this fluid.

Properties at the triple point temperature and the critical point temperature are given in the first and last entries of the saturation tables, respectively. In the single-phase table, when the temperature range for a given isobar includes a vapor-liquid phase boundary, the temperature of phase equilibrium is noted, and properties for both the saturated liquid and saturated vapor are given (with liquid properties given in the upper line). Lines are omitted from the temperature-pressure grid of the single-phase table, when the system would be in the solid phase or if there are potential problems with the source property surface.

The uncertainties of the equation of state are 0.1% in density, 2% in heat capacity, and 1% in the speed of sound, except in the critical region.

TABLE 2-208 Thermodynamic Properties of Decane

Temperature K	Pressure MPa	Density mol/dm ³	Volume dm ³ /mol	Int. energy kJ/mol	Enthalpy kJ/mol	Entropy kJ/(mol·K)	C _v kJ/(mol·K)	C _p kJ/(mol·K)	Sound speed m/s	Joule-Thomson K/MPa	Therm. cond. mW/(m·K)	Viscosity μPa·s
Saturated Properties												
243.50	1.4042E-06	5.4064	0.18497	-69.252	-69.252	-0.20307	0.22393	0.28635	1468.5	-0.48339	144.08	2433.6
250.00	2.8673E-06	5.3702	0.18621	-67.383	-67.383	-0.19549	0.22704	0.28898	1438.4	-0.47764	142.30	2066.6
270.00	1.9993E-05	5.2597	0.19012	-61.516	-61.516	-0.17292	0.23712	0.29787	1349.4	-0.45826	136.88	1350.0
290.00	0.00010141	5.1502	0.19417	-55.461	-55.461	-0.15129	0.24780	0.30773	1265.6	-0.43680	131.57	957.69
310.00	0.00039985	5.0409	0.19838	-49.202	-49.202	-0.13043	0.25893	0.31832	1186.0	-0.41360	126.38	718.75
330.00	0.0012883	4.9312	0.20279	-42.725	-42.725	-0.11018	0.27034	0.32946	1109.9	-0.38881	121.32	561.90
350.00	0.0035240	4.8206	0.20744	-36.021	-36.020	-0.090462	0.28191	0.34100	1036.6	-0.36228	116.40	452.88
370.00	0.0084305	4.7082	0.21239	-29.084	-29.082	-0.071189	0.29354	0.35282	965.68	-0.33365	111.63	373.57
390.00	0.018060	4.5936	0.21770	-21.908	-21.905	-0.052306	0.30512	0.36483	896.48	-0.30225	107.04	313.65
410.00	0.035300	4.4757	0.22343	-14.493	-14.485	-0.033764	0.31659	0.37700	828.54	-0.26699	102.62	266.90
430.00	0.063919	4.3538	0.22968	-6.8339	-6.8192	-0.015527	0.32790	0.38931	761.40	-0.22626	98.409	229.40
450.00	0.10855	4.2266	0.23659	1.0694	1.0950	0.0024370	0.33901	0.40181	694.57	-0.17752	94.401	198.56
470.00	0.17465	4.0927	0.24434	9.2198	9.2624	0.020158	0.34991	0.41460	627.57	-0.11677	90.612	172.63
490.00	0.26846	3.9499	0.25317	17.622	17.690	0.037667	0.36059	0.42793	559.85	-0.037250	87.051	150.36
510.00	0.39696	3.7952	0.26349	26.283	26.388	0.054997	0.37108	0.44218	490.80	0.073195	83.726	130.83
530.00	0.56801	3.6240	0.27594	35.219	35.375	0.072193	0.38143	0.45818	419.70	0.23865	80.640	113.31
550.00	0.79054	3.4286	0.29166	44.457	44.687	0.089321	0.39176	0.47770	345.68	0.51353	77.794	97.183
570.00	1.0751	3.1943	0.31306	54.055	54.391	0.10649	0.40231	0.50540	267.65	1.0476	75.192	81.781
590.00	1.4353	2.8870	0.34638	64.149	64.646	0.12397	0.41372	0.55950	184.05	2.4223	72.934	66.154
610.00	1.8918	2.3754	0.42098	75.300	76.096	0.14276	0.42875	0.87382	91.074	9.9501	73.097	47.430
617.70	2.1014	1.6400	0.60976	82.386	83.668	0.15491			0	34.686		
243.50	1.4042E-06	6.9358E-07	1,441,800.	-15.410	-13.386	0.026360	0.19210	0.20042	121.84	320.14	6.4788	4.3408
250.00	2.8673E-06	1.3795E-06	724,920.	-14.150	-12.071	0.025751	0.19573	0.20405	123.41	287.01	6.7500	4.4520
270.00	1.9993E-05	8.9067E-06	112,280.	-10.121	-7.8760	0.025744	0.20739	0.21571	128.09	208.26	7.6856	4.7935
290.00	0.00010141	4.2071E-05	23,769.	-5.8536	-3.4432	0.028079	0.21963	0.22797	132.58	154.49	8.7681	5.1337
310.00	0.00039985	0.00015529	6,439.4	-1.3417	1.2331	0.032268	0.23228	0.24065	136.85	116.99	9.9889	5.4722
330.00	0.0012883	0.00047076	2,124.2	3.4167	6.1533	0.037934	0.24518	0.25363	140.87	90.369	11.339	5.8086
350.00	0.0035240	0.0012178	821.18	8.4178	11.312	0.044772	0.25823	0.26684	144.56	71.168	12.808	6.1419
370.00	0.0084305	0.0027701	361.00	13.654	16.697	0.052538	0.27134	0.28022	147.82	57.142	14.385	6.4713
390.00	0.018060	0.0056755	176.20	19.113	22.295	0.061027	0.28446	0.29376	150.52	46.790	16.056	6.7963
410.00	0.035300	0.010678	93.649	24.781	28.087	0.070070	0.29754	0.30748	152.52	39.094	17.808	7.1172
430.00	0.063919	0.018742	53.355	30.642	34.053	0.079524	0.31053	0.32142	153.66	33.355	19.629	7.4356
450.00	0.10855	0.031091	32.164	36.677	40.168	0.089267	0.32343	0.33567	153.78	29.089	21.506	7.7555
470.00	0.17465	0.049284	20.290	42.864	46.408	0.099191	0.33621	0.35042	152.66	25.969	23.438	8.0842
490.00	0.26846	0.075371	13.268	49.176	52.738	0.10919	0.34890	0.36600	150.07	23.781	25.431	8.4344
510.00	0.39696	0.11219	8.9134	55.580	59.118	0.11917	0.36154	0.38308	145.68	22.413	27.522	8.8280
530.00	0.56801	0.16399	6.0979	62.026	65.490	0.12901	0.37421	0.40300	139.04	21.855	29.799	9.3033
550.00	0.79054	0.23784	4.2045	68.438	71.762	0.13855	0.38707	0.42896	129.53	22.255	32.477	9.9327
570.00	1.0751	0.34741	2.8784	74.676	77.770	0.14751	0.40046	0.47018	116.14	24.065	36.104	10.874
590.00	1.4353	0.52650	1.8993	80.422	83.148	0.15533	0.41513	0.56612	97.344	28.492	42.347	12.566
610.00	1.8918	0.92143	1.0853	84.493	86.546	0.15989	0.43359	1.2127	71.032	37.614	59.648	17.240
617.70	2.1014	1.6400	0.60976	82.386	83.668	0.15491			0	34.686		

Single-Phase Properties

250.00	0.10000	5.3706	0.18620	-67.388	-67.369	-0.19551	0.22705	0.28898	1438.9	-0.47770	142.33	2069.3
350.00	0.10000	4.8213	0.20741	-36.029	-36.008	-0.090485	0.28192	0.34098	1037.4	-0.36251	116.44	453.43
446.75	0.10000	4.2477	0.23542	-0.23039	-0.20685	-0.00046204	0.33722	0.39976	705.42	-0.18612	95.037	203.20
446.75	0.10000	0.028735	34.801	35.686	39.166	0.087670	0.32134	0.33333	153.83	29.697	21.198	7.7032
450.00	0.10000	0.028470	35.125	36.739	40.251	0.090090	0.32313	0.33498	154.68	28.767	21.529	7.7604
550.00	0.10000	0.022477	44.491	71.828	76.277	0.16222	0.37514	0.38484	176.60	12.764	32.572	9.4815
650.00	0.10000	0.018766	53.287	111.67	117.00	0.23014	0.41928	0.42830	194.21	7.0015	44.613	11.158
250.00	1.0000	5.3745	0.18606	-67.431	-67.245	-0.19569	0.22712	0.28892	1443.8	-0.47822	142.62	2093.8
350.00	1.0000	4.8284	0.20711	-36.104	-35.897	-0.090699	0.28198	0.34075	1044.7	-0.36461	116.88	458.58
450.00	1.0000	4.2417	0.23575	0.92464	1.1604	0.0021144	0.33902	0.40097	706.99	-0.18764	95.062	201.71
550.00	1.0000	3.4433	0.29042	44.348	44.638	0.089120	0.39165	0.47560	353.85	0.47267	78.107	98.236
565.17	1.0000	3.2558	0.30715	51.697	52.004	0.10233	0.39972	0.49744	286.94	0.87812	75.797	85.478
565.17	1.0000	0.31644	3.1602	73.196	76.356	0.14542	0.39714	0.45776	119.81	23.453	35.085	10.603
650.00	1.0000	0.21839	4.5790	109.33	113.91	0.20734	0.42517	0.44558	167.63	8.8875	44.104	11.626
250.00	5.0000	5.3914	0.18548	-67.618	-66.691	-0.19644	0.22744	0.28869	1465.1	-0.48040	143.89	2204.8
350.00	5.0000	4.8586	0.20582	-36.424	-35.395	-0.091624	0.28223	0.33985	1075.7	-0.37303	118.77	481.47
450.00	5.0000	4.3034	0.23237	0.32894	1.4908	0.00076852	0.33912	0.39795	757.95	-0.22390	97.851	215.38
550.00	5.0000	3.6402	0.27471	42.808	44.181	0.086242	0.39052	0.45616	467.92	0.098466	82.872	114.20
650.00	5.0000	2.6391	0.37891	91.156	93.050	0.16772	0.43712	0.52513	213.89	1.6230	75.400	55.304
350.00	10.000	4.8938	0.20434	-36.797	-34.754	-0.092723	0.28255	0.33892	1112.2	-0.38180	121.04	510.17
450.00	10.000	4.3700	0.22883	-0.32038	1.9680	-0.00073280	0.33929	0.39532	813.41	-0.25552	101.03	231.67
550.00	10.000	3.7932	0.26363	41.527	44.163	0.083766	0.39008	0.44754	562.29	-0.060225	87.304	129.37
650.00	10.000	3.1242	0.32009	88.002	91.203	0.16225	0.43362	0.49145	369.51	0.31317	81.597	76.394
350.00	100.00	5.3085	0.18838	-41.033	-22.195	-0.10704	0.28785	0.33463	1562.8	-0.43121	152.54	1088.0
450.00	100.00	4.9747	0.20102	-6.2415	13.860	-0.016697	0.34377	0.38610	1360.6	-0.37226	139.48	498.37
550.00	100.00	4.6758	0.21387	33.447	54.834	0.065371	0.39337	0.43213	1216.3	-0.32986	130.26	308.65
650.00	100.00	4.4066	0.22693	77.332	100.03	0.14078	0.43497	0.47043	1111.9	-0.30079	124.76	219.90
550.00	300.00	5.3265	0.18774	28.160	84.482	0.047128	0.40016	0.43412	1858.1	-0.34462	192.00	698.31
650.00	300.00	5.1406	0.19453	71.521	129.88	0.12288	0.44112	0.47265	1766.6	-0.32003	188.95	480.95

The values in these tables were generated from the NIST REFPROP software (Lemmon, E. W., McLinden, M. O., and Huber, M. L., NIST Standard Reference Database 23: Reference Fluid Thermodynamic and Transport Properties—REFPROP, National Institute of Standards and Technology, Standard Reference Data Program, Gaithersburg, Md., 2002, Version 7.1). The primary source for the thermodynamic properties is Lemmon, E. W., and Span, R., "Short Fundamental Equations of State for 20 Industrial Fluids," *J. Chem. Eng. Data*, **51**(3):785–850, 2006. The source for viscosity is Huber, M. L., Laesecke, A., and Xiang, H. W., "Viscosity Correlations for Minor Constituent Fluids in Natural Gas: *n*-Octane, *n*-Nonane and *n*-Decane," *Fluid Phase Equilibria* **224**:263–270, 2004. The source for thermal conductivity is Huber, M. L., and Perkins, R. A., "Thermal Conductivity Correlations for Minor Constituent Fluids in Natural Gas: *n*-Octane, *n*-Nonane and *n*-Decane," *Fluid Phase Equilibria* **227**:47–55, 2004.

Properties at the triple point temperature and the critical point temperature are given in the first and last entries of the saturation tables, respectively. In the single-phase table, when the temperature range for a given isobar includes a vapor-liquid phase boundary, the temperature of phase equilibrium is noted, and properties for both the saturated liquid and saturated vapor are given (with liquid properties given in the upper line). Lines are omitted from the temperature-pressure grid of the single-phase table, when the system would be in the solid phase or if there are potential problems with the source property surface.

The uncertainties in density are 0.05% in the saturated liquid density between 290 and 320 K, 0.2% in the liquid phase at temperatures to 400 K (with somewhat higher uncertainties above 100 MPa, up to 0.5%), 1% in the liquid phase up to 500 MPa, and 2% at higher temperatures as well as in the vapor phase. Vapor pressures have an uncertainty of 0.2%, and the uncertainties in liquid heat capacities and liquid sound speeds are 1%. The uncertainty in heat capacities may be higher at pressures above 10 MPa. The estimated uncertainty in viscosity is 1% along the saturated liquid line, 2% in compressed liquid to 200 MPa, 5% in vapor and supercritical regions. Uncertainty in thermal conductivity is 3%, except in the supercritical region and dilute gas which have an uncertainty of 5%.

TABLE 2-209 Thermodynamic Properties of Deuterium Oxide (Heavy Water)

Temperature K	Pressure MPa	Density mol/dm ³	Volume dm ³ /mol	Int. energy kJ/mol	Enthalpy kJ/mol	Entropy kJ/(mol·K)	C _v kJ/(mol·K)	C _p kJ/(mol·K)	Sound speed m/s	Joule-Thomson K/MPa	Therm. cond. mW/(m·K)	Viscosity μPa·s
Saturated Properties												
276.97	0.00066103	55.198	0.018117	-8.2294	-8.2294	-0.025460	0.084185	0.084334	1324.3	-0.22218	564.56	2085.6
280.00	0.00082243	55.214	0.018111	-7.9735	-7.9735	-0.024541	0.084523	0.084574	1332.9	-0.21843	569.58	1868.6
300.00	0.0030641	55.126	0.018140	-6.2759	-6.2758	-0.018685	0.084432	0.084957	1394.9	-0.19991	596.96	1046.6
320.00	0.0094511	54.780	0.018255	-4.5798	-4.5796	-0.013212	0.082466	0.084598	1436.7	-0.18770	615.88	688.90
340.00	0.025012	54.254	0.018432	-2.8930	-2.8926	-0.0080990	0.079894	0.084075	1455.5	-0.17806	628.04	497.65
360.00	0.058391	53.593	0.018659	-1.2168	-1.2157	-0.0033082	0.077173	0.083580	1455.6	-0.16908	634.49	381.94
380.00	0.12292	52.817	0.018933	0.45077	0.45310	0.0011999	0.074503	0.083248	1440.4	-0.15944	635.99	306.06
400.00	0.23743	51.937	0.019254	2.1139	2.1185	0.0054654	0.071990	0.083196	1413.3	-0.14815	633.11	253.36
420.00	0.42676	50.957	0.019624	3.7786	3.7870	0.0095268	0.069689	0.083502	1376.7	-0.13444	626.31	215.11
440.00	0.72190	49.875	0.020050	5.4521	5.4666	0.013420	0.067622	0.084212	1331.9	-0.11766	616.01	186.33
460.00	1.1598	48.687	0.020539	7.1417	7.1655	0.017176	0.065790	0.085360	1279.7	-0.097022	602.53	164.01
480.00	1.7833	47.386	0.021103	8.8551	8.8927	0.020824	0.064181	0.087004	1219.9	-0.071339	586.08	146.23
500.00	2.6406	45.961	0.021758	10.601	10.658	0.024390	0.062780	0.089266	1152.3	-0.038642	566.82	131.71
520.00	3.7850	44.390	0.022528	12.390	12.475	0.027902	0.061580	0.092393	1076.5	0.0043364	544.81	119.53
540.00	5.2758	42.641	0.023452	14.236	14.360	0.031394	0.060585	0.096848	991.90	0.063056	520.11	109.01
560.00	7.1787	40.660	0.024594	16.162	16.339	0.034909	0.059829	0.10351	897.91	0.14707	492.75	99.548
580.00	9.5679	38.357	0.026071	18.203	18.453	0.038511	0.059403	0.11428	793.19	0.27477	462.70	90.597
600.00	12.530	35.563	0.028119	20.425	20.777	0.042313	0.059524	0.13431	674.99	0.48803	430.22	81.477
620.00	16.171	31.867	0.031381	22.980	23.487	0.046577	0.060792	0.18616	537.16	0.91327	396.40	70.992
640.00	20.654	24.976	0.040039	26.745	27.572	0.052801	0.066781	0.82671	359.72	2.2860	420.92	53.746
643.89	21.660	17.875	0.055943	29.926	31.137	0.058280			0	3.7063		
276.97	0.00066103	0.00028721	3481.8	36.006	38.307	0.14256	0.025895	0.034265	389.85	394.78	16.529	9.6017
280.00	0.00082242	0.00035350	2828.9	36.083	38.409	0.14111	0.025952	0.034329	391.88	363.66	16.753	9.6779
300.00	0.0030641	0.0012303	812.82	36.589	39.079	0.13250	0.026375	0.034822	404.89	220.57	18.277	10.228
320.00	0.0094511	0.0035636	280.61	37.091	39.743	0.12530	0.026887	0.035451	417.19	143.76	19.890	10.840
340.00	0.025012	0.0089021	112.33	37.585	40.394	0.11922	0.027487	0.036239	428.74	100.20	21.616	11.492
360.00	0.058391	0.019720	50.709	38.064	41.025	0.11403	0.028182	0.037225	439.47	74.063	23.487	12.169
380.00	0.12292	0.039608	25.247	38.521	41.624	0.10955	0.029002	0.038484	449.26	57.443	25.539	12.856
400.00	0.23743	0.073418	13.621	38.946	42.180	0.10562	0.030006	0.040139	457.95	46.206	27.812	13.544
420.00	0.42676	0.12741	7.8485	39.329	42.679	0.10213	0.031275	0.042357	465.33	38.108	30.356	14.226
440.00	0.72190	0.20947	4.7740	39.660	43.106	0.098964	0.032903	0.045350	471.15	31.903	33.231	14.897
460.00	1.1598	0.32939	3.0359	39.925	43.447	0.096048	0.034981	0.049371	475.13	26.904	36.529	15.558
480.00	1.7833	0.49953	2.0019	40.116	43.686	0.093309	0.037576	0.054720	476.97	22.747	40.398	16.213
500.00	2.6406	0.73576	1.3591	40.219	43.808	0.090658	0.040723	0.061780	476.36	19.244	45.081	16.871
520.00	3.7850	1.0594	0.94392	40.219	43.792	0.088127	0.044416	0.071116	472.96	16.294	50.974	17.547
540.00	5.2758	1.5008	0.66632	40.096	43.612	0.085564	0.048619	0.083703	466.44	13.819	58.649	18.267
560.00	7.1787	2.1062	0.47479	39.815	43.224	0.082917	0.053289	0.10149	456.44	11.743	68.218	19.071
580.00	9.5679	2.9537	0.33856	39.318	42.557	0.080069	0.058406	0.12892	442.43	9.9759	79.570	20.029
600.00	12.530	4.1942	0.23842	38.492	41.479	0.076817	0.064014	0.17822	423.35	8.4154	98.667	21.290
620.00	16.171	6.2033	0.16120	37.081	39.688	0.072707	0.070293	0.29956	395.96	6.9363	133.97	23.259
640.00	20.654	11.096	0.090120	33.747	35.608	0.065358	0.077762	1.5264	343.38	5.1241	285.74	28.595
643.89	21.660	17.875	0.055943	29.926	31.137	0.058280			0	3.7063		

Single-Phase Properties

300.00	0.10000	55.129	0.018139	-6.2760	-6.2742	-0.018686	0.084425	0.084951	1395.1	-0.19991	597.01	1046.5
374.20	0.10000	53.053	0.018849	-0.032221	-0.030336	-0.000080962	0.075265	0.083320	1446.2	-0.16237	636.03	325.15
374.20	0.10000	0.032646	30.631	38.391	41.454	0.11078	0.028748	0.038084	446.53	61.573	24.923	12.656
400.00	0.10000	0.030411	32.883	39.139	42.427	0.11330	0.028403	0.037410	462.35	46.430	27.024	13.658
500.00	0.10000	0.024157	41.395	42.023	46.162	0.12163	0.029147	0.037685	515.85	19.445	36.485	17.747
600.00	0.10000	0.020087	49.784	45.017	49.996	0.12861	0.030636	0.039048	562.30	10.077	47.629	21.980
700.00	0.10000	0.017202	58.134	48.166	53.980	0.13475	0.032285	0.040652	604.21	6.0901	60.182	26.224
800.00	0.10000	0.015045	66.469	51.481	58.128	0.14029	0.033959	0.042306	642.79	4.1486	73.869	30.405
300.00	1.0000	55.152	0.018132	-6.2770	-6.2589	-0.018689	0.084361	0.084894	1397.1	-0.19988	597.49	1046.3
400.00	1.0000	51.959	0.019246	2.1086	2.1279	0.0054522	0.071968	0.083157	1415.4	-0.14835	633.54	253.63
453.53	1.0000	49.083	0.020374	6.5927	6.6131	0.015974	0.066357	0.084938	1297.4	-0.10418	607.22	170.66
453.53	1.0000	0.28575	3.4996	39.847	43.347	0.096969	0.034254	0.047940	474.06	28.417	35.408	15.345
500.00	1.0000	0.25193	3.9693	41.482	45.451	0.10139	0.032240	0.043385	503.79	19.634	38.239	17.445
600.00	1.0000	0.20474	4.8843	44.748	49.632	0.10902	0.031708	0.041087	556.10	10.106	48.345	21.886
700.00	1.0000	0.17382	5.7529	48.001	53.754	0.11537	0.032710	0.041565	600.64	6.1060	60.651	26.233
800.00	1.0000	0.15139	6.6052	51.363	57.969	0.12100	0.034141	0.042787	640.67	4.1567	74.254	30.468
300.00	5.0000	55.254	0.018098	-6.2816	-6.1911	-0.018705	0.084079	0.084647	1405.7	-0.19974	599.61	1045.2
400.00	5.0000	52.073	0.019204	2.0813	2.1773	0.0053836	0.071858	0.082958	1426.2	-0.14937	635.76	255.02
500.00	5.0000	46.085	0.021699	10.558	10.667	0.024304	0.062722	0.088880	1163.3	-0.042258	568.91	132.48
536.66	5.0000	42.947	0.023284	13.923	14.039	0.030810	0.060736	0.095981	1006.7	0.051819	524.42	110.68
536.66	5.0000	1.4172	0.70563	40.127	43.655	0.085995	0.047884	0.081310	467.76	14.202	57.219	18.142
600.00	5.0000	1.1342	0.88170	43.329	47.738	0.093213	0.038071	0.054713	524.33	9.9010	53.862	21.508
700.00	5.0000	0.91389	1.0942	47.210	52.681	0.10085	0.034830	0.046443	584.32	6.1037	63.474	26.310
800.00	5.0000	0.77903	1.2836	50.818	57.237	0.10693	0.034981	0.045153	631.66	4.1656	76.389	30.769
300.00	10.000	55.380	0.018057	-6.2874	-6.1068	-0.018725	0.083735	0.084346	1415.9	-0.19956	602.23	1043.9
400.00	10.000	52.214	0.019152	2.0479	2.2394	0.0052992	0.071726	0.082718	1439.3	-0.15059	638.50	256.74
500.00	10.000	46.341	0.021579	10.471	10.687	0.024128	0.062611	0.088119	1185.7	-0.049352	573.22	134.06
583.19	10.000	37.950	0.026351	18.544	18.807	0.039101	0.059377	0.11663	775.32	0.30140	457.66	89.173
583.19	10.000	3.1198	0.32053	39.212	42.417	0.079584	0.059266	0.13479	439.77	9.7157	81.935	20.204
600.00	10.000	2.7732	0.36059	40.719	44.325	0.082812	0.051641	0.097980	468.72	9.0626	72.595	21.210
700.00	10.000	1.9660	0.50864	46.072	51.158	0.093421	0.038049	0.054970	562.64	5.9486	69.164	26.519
800.00	10.000	1.6183	0.61793	50.085	56.265	0.10025	0.036102	0.048671	621.09	4.1215	80.100	31.206
300.00	50.000	56.338	0.017750	-6.3323	-5.4448	-0.018905	0.081303	0.082295	1484.2	-0.19786	622.24	1038.3
400.00	50.000	53.254	0.018778	1.8073	2.7462	0.0046700	0.070872	0.081058	1527.2	-0.15849	659.16	269.56
500.00	50.000	48.076	0.020801	9.8899	10.930	0.022920	0.062103	0.083801	1327.9	-0.088396	603.54	145.01
600.00	50.000	40.498	0.024693	18.559	19.754	0.039048	0.057208	0.096053	997.60	0.10313	493.46	98.391
700.00	50.000	26.703	0.037449	29.678	31.551	0.057059	0.055751	0.15684	588.37	1.0407	331.10	62.248
800.00	50.000	12.014	0.083233	42.333	46.495	0.077124	0.045204	0.10482	569.23	2.4839	169.04	40.739
300.00	100.00	57.439	0.017410	-6.3859	-4.6449	-0.019168	0.078994	0.080433	1546.7	-0.19571	645.56	1041.5
700.00	100.00	35.855	0.027890	25.888	28.677	0.050728	0.052858	0.095839	944.96	0.21724	435.02	84.790
800.00	100.00	26.322	0.037991	34.906	38.706	0.064110	0.045160	0.10162	785.38	0.69848	323.29	66.016

The values in these tables were generated from the NIST REFPROP software (Lemmon, E. W., McLinden, M. O., and Huber, M. L., NIST Standard Reference Database 23: Reference Fluid Thermodynamic and Transport Properties—REFPROP, National Institute of Standards and Technology, Standard Reference Data Program, Gaithersburg, Md., 2002, Version 7.1). The primary source for the thermodynamic properties is Hill, P. G., MacMillan, R. D. C., and Lee, V., "A Fundamental Equation of State for Heavy Water," *J. Phys. Chem. Ref. Data*, **11**(1):1-14, 1982. The source for viscosity is International Association for the Properties of Water and Steam, "Viscosity and Thermal Conductivity of Heavy Water Substance," *Physical Chemistry of Aqueous Systems: Proceedings of the 12th International Conference on the Properties of Water and Steam*, Orlando, Fla., Sept. 11-16, 1994, A107-A138. The source for thermal conductivity is International Association for the Properties of Water and Steam, "Viscosity and Thermal Conductivity of Heavy Water Substance," *Physical Chemistry of Aqueous Systems: Proceedings of the 12th International Conference on the Properties of Water and Steam*, Orlando, Fla., Sept. 11-16, 1994, A107-A138.

Properties at the triple point temperature and the critical point temperature are given in the first and last entries of the saturation tables, respectively. In the single-phase table, when the temperature range for a given isobar includes a vapor-liquid phase boundary, the temperature of phase equilibrium is noted, and properties for both the saturated liquid and saturated vapor are given (with liquid properties given in the upper line). Lines are omitted from the temperature-pressure grid of the single-phase table, when the system would be in the solid phase or if there are potential problems with the source property surface.

For a discussion of the uncertainties associated with the equation of state and thermal conductivity entries of this table, please see the source references given above. The uncertainty in viscosity is 1% in the liquid below 474 K, 2% in the liquid at higher temperatures and in the vapor, and 5% between 623 and 723 K at pressures between 16 and 50 MPa. The uncertainty in viscosity is 2% in the liquid below 623 K and in the vapor below 573 K, 5% elsewhere in the liquid and vapor, and 10% in the critical region (623 to 723 K and 21.66 to 50 MPa).

TABLE 2-210 Thermodynamic Properties of 2,2-Dimethylpropane (Neopentane)

Temperature K	Pressure MPa	Density mol/dm ³	Volume dm ³ /mol	Int. energy kJ/mol	Enthalpy kJ/mol	Entropy kJ/(mol·K)	C _v kJ/(mol·K)	C _p kJ/(mol·K)	Sound speed m/s	Joule-Thomson K/MPa
Saturated Properties										
256.60	0.035401	8.7017	0.11492	-4.0448	-4.0407	-0.014961	0.11106	0.14987	1061.0	-0.45488
260.00	0.041178	8.6547	0.11554	-3.5333	-3.5286	-0.012981	0.11212	0.15116	1043.4	-0.44532
270.00	0.062611	8.5146	0.11745	-2.0036	-1.9963	-0.0072081	0.11525	0.15504	992.29	-0.41587
280.00	0.091973	8.3711	0.11946	-0.43520	-0.42422	-0.0015039	0.11839	0.15903	941.76	-0.38403
290.00	0.13106	8.2236	0.12160	1.1729	1.1889	0.0041396	0.12153	0.16315	891.68	-0.34919
300.00	0.18184	8.0715	0.12389	2.8218	2.8444	0.0097305	0.12467	0.16742	841.93	-0.31054
310.00	0.24636	7.9140	0.12636	4.5127	4.5439	0.015276	0.12781	0.17188	792.35	-0.26700
320.00	0.32680	7.7503	0.12903	6.2470	6.2892	0.020784	0.13096	0.17655	742.82	-0.21713
330.00	0.42545	7.5792	0.13194	8.0264	8.0826	0.026263	0.13411	0.18151	693.20	-0.15892
340.00	0.54466	7.3993	0.13515	9.8530	9.9266	0.031720	0.13728	0.18683	643.34	-0.089543
350.00	0.68688	7.2090	0.13872	11.729	11.825	0.037165	0.14047	0.19263	593.09	-0.0048767
360.00	0.85466	7.0060	0.14273	13.659	13.781	0.042610	0.14369	0.19910	542.29	0.10132
370.00	1.0507	6.7873	0.14733	15.647	15.802	0.048067	0.14696	0.20651	490.74	0.23893
380.00	1.2778	6.5488	0.15270	17.699	17.894	0.053555	0.15032	0.21536	438.21	0.42456
390.00	1.5390	6.2842	0.15913	19.824	20.069	0.059099	0.15380	0.22655	384.34	0.68847
400.00	1.8380	5.9837	0.16712	22.038	22.345	0.064738	0.15752	0.24199	328.55	1.0924
410.00	2.1788	5.6295	0.17764	24.368	24.755	0.070543	0.16164	0.26680	269.76	1.7855
420.00	2.5668	5.1798	0.19306	26.878	27.373	0.076679	0.16662	0.32099	205.53	3.2489
430.00	3.0111	4.4559	0.22442	29.850	30.525	0.083875	0.17440	0.65083	129.02	8.3551
433.74	3.1963	3.2700	0.30581	32.506	33.484	0.090610			0	19.128
256.60	0.035401	0.016951	58.993	18.019	20.107	0.079147	0.097392	0.10663	176.08	42.543
260.00	0.041178	0.019508	51.262	18.336	20.447	0.079232	0.098838	0.10818	176.77	40.673
270.00	0.062611	0.028804	34.717	19.288	21.461	0.079672	0.10307	0.11278	178.55	35.912
280.00	0.091973	0.041222	24.259	20.267	22.498	0.080361	0.10727	0.11744	179.94	32.069
290.00	0.13106	0.057423	17.415	21.271	23.554	0.081260	0.11146	0.12220	180.88	28.950
300.00	0.18184	0.078145	12.797	22.298	24.625	0.082334	0.11562	0.12709	181.34	26.412
310.00	0.24636	0.10423	9.5944	23.346	25.710	0.083553	0.11978	0.13214	181.26	24.346
320.00	0.32680	0.13664	7.3187	24.411	26.803	0.084890	0.12394	0.13741	180.58	22.672
330.00	0.42545	0.17651	5.6655	25.490	27.901	0.086318	0.12810	0.14299	179.24	21.330
340.00	0.54466	0.22521	4.4402	26.580	28.999	0.087815	0.13228	0.14898	177.18	20.277
350.00	0.68688	0.28448	3.5152	27.676	30.091	0.089355	0.13648	0.15554	174.30	19.485
360.00	0.85466	0.35651	2.8049	28.773	31.170	0.090912	0.14073	0.16293	170.51	18.940
370.00	1.0507	0.44433	2.2506	29.862	32.226	0.092458	0.14505	0.17158	165.68	18.642
380.00	1.2778	0.55219	1.8110	30.932	33.246	0.093957	0.14948	0.18223	159.65	18.607
390.00	1.5390	0.68654	1.4566	31.969	34.211	0.095360	0.15407	0.19633	152.23	18.876
400.00	1.8380	0.85798	1.1655	32.946	35.088	0.096596	0.15892	0.21707	143.15	19.520
410.00	2.1788	1.0863	0.92056	33.817	35.822	0.097537	0.16422	0.25302	132.06	20.655
420.00	2.5668	1.4175	0.70547	34.476	36.287	0.097901	0.17039	0.33783	118.40	22.431
430.00	3.0111	2.0429	0.48949	34.498	35.972	0.096542	0.17895	0.86590	100.88	24.389
433.74	3.1963	3.2700	0.30581	32.506	33.484	0.090610			0	19.128

Single-Phase Properties

300.00	0.10000	0.041573	24.054	22.482	24.888	0.087934	0.11446	0.12428	186.71	24.744
350.00	0.10000	0.035109	28.482	28.668	31.516	0.10834	0.13169	0.14083	203.23	14.420
400.00	0.10000	0.030488	32.800	35.683	38.963	0.12820	0.14811	0.15694	217.95	9.4234
450.00	0.10000	0.026981	37.063	43.493	47.199	0.14758	0.16371	0.17238	231.47	6.6348
500.00	0.10000	0.024215	41.296	52.060	56.190	0.16652	0.17858	0.18715	244.10	4.9220
550.00	0.10000	0.021973	45.510	61.352	65.903	0.18502	0.19273	0.20124	256.02	3.7932
300.00	1.0000	8.0927	0.12357	2.7638	2.8874	0.0095365	0.12470	0.16698	852.01	-0.31857
350.00	1.0000	7.2257	0.13839	11.687	11.825	0.037043	0.14045	0.19204	599.54	-0.017539
367.56	1.0000	6.8424	0.14615	15.155	15.301	0.046731	0.14616	0.20459	503.42	0.20165
367.56	1.0000	0.42120	2.3741	29.597	31.971	0.092083	0.14399	0.16932	166.96	18.691
400.00	1.0000	0.35635	2.8062	34.611	37.418	0.10628	0.15145	0.16863	188.60	12.099
450.00	1.0000	0.29713	3.3655	42.712	46.077	0.12667	0.16541	0.17859	211.98	7.6415
500.00	1.0000	0.25832	3.8712	51.444	55.315	0.14613	0.17958	0.19109	230.27	5.3700
550.00	1.0000	0.22988	4.3501	60.842	65.192	0.16494	0.19337	0.20397	245.89	4.0038
300.00	5.0000	8.1890	0.12211	2.4999	3.1104	0.0086423	0.12485	0.16516	897.98	-0.35167
350.00	5.0000	7.4104	0.13495	11.213	11.887	0.035660	0.14039	0.18654	671.51	-0.13585
400.00	5.0000	6.4044	0.15614	21.099	21.879	0.062302	0.15611	0.21533	444.29	0.37314
450.00	5.0000	4.6105	0.21690	33.057	34.142	0.091100	0.17461	0.30156	198.33	3.5214
500.00	5.0000	1.9914	0.50215	47.248	49.759	0.12411	0.18590	0.24909	166.16	7.2775
550.00	5.0000	1.4527	0.68839	57.986	61.428	0.14637	0.19664	0.22704	205.52	4.5988
300.00	10.000	8.2958	0.12054	2.2072	3.4126	0.0076277	0.12506	0.16345	949.31	-0.38267
350.00	10.000	7.5920	0.13172	10.739	12.056	0.034237	0.14048	0.18250	743.85	-0.22237
400.00	10.000	6.7750	0.14760	20.216	21.692	0.059940	0.15568	0.20328	555.11	0.041740
450.00	10.000	5.7764	0.17312	30.691	32.422	0.085190	0.17074	0.22624	391.52	0.55851
500.00	10.000	4.5715	0.21875	42.114	44.301	0.11020	0.18530	0.24770	276.41	1.5460
550.00	10.000	3.4249	0.29198	53.968	56.887	0.13419	0.19832	0.25208	234.55	2.4058
400.00	100.00	8.5990	0.11629	15.633	27.262	0.045388	0.15862	0.18487	1257.1	-0.42302
450.00	100.00	8.2554	0.12113	24.735	36.848	0.067954	0.17287	0.19848	1172.6	-0.38739
500.00	100.00	7.9290	0.12612	34.489	47.101	0.089546	0.18665	0.21152	1103.1	-0.35738
550.00	100.00	7.6203	0.13123	44.867	57.990	0.11029	0.19993	0.22395	1046.3	-0.33233
550.00	200.00	8.6161	0.11606	42.742	65.955	0.10250	0.20230	0.22337	1444.9	-0.36818

The values in these tables were generated from the NIST REFPROP software (Lemmon, E. W., McLinden, M. O., and Huber, M. L., NIST Standard Reference Database 23: Reference Fluid Thermodynamic and Transport Properties—REFPROP, National Institute of Standards and Technology, Standard Reference Data Program, Gaithersburg, Md., 2002, Version 7.1). The primary source for the thermodynamic properties is Lemmon, E. W., and Span, R., "Short Fundamental Equations of State for 20 Industrial Fluids," *J. Chem. Eng. Data*, **51**(3):785–850, 2006. Validated equations for the viscosity and thermal conductivity are not currently available for this fluid.

Properties at the triple point temperature and the critical point temperature are given in the first and last entries of the saturation tables, respectively. In the single-phase table, when the temperature range for a given isobar includes a vapor-liquid phase boundary, the temperature of phase equilibrium is noted, and properties for both the saturated liquid and saturated vapor are given (with liquid properties given in the upper line). Lines are omitted from the temperature-pressure grid of the single-phase table, when the system would be in the solid phase or if there are potential problems with the source property surface.

The uncertainties in density in the equation of state range from 0.2% in the liquid phase at pressures less than 10 MPa to 1% in the liquid phase at higher pressures (up to 200 MPa) and at temperatures above the critical point (up to 550 K). The uncertainty in density in the vapor phase is 0.5%. Uncertainties in other properties are 0.1% for the vapor pressure, 2% in liquid-phase heat capacities, 0.5% in vapor-phase heat capacities, 1% for liquid-phase sound speeds, and 0.02% for vapor-phase sound speeds.

2-260 PHYSICAL AND CHEMICAL DATA

TABLE 2-211 Saturated Diphenyl*

T, K	P, bar	v_f , m ³ /kg	v_g , m ³ /kg	h_f , kJ/kg	h_g , kJ/kg	s_f , kJ/(kg·K)	s_g , kJ/(kg·K)	c_{pf} , kJ/(kg·K)	μ_f , 10 ⁻⁴ Pa·s	k_f , W/(m·K)
343	0.0010	1.010.-3	252.5	0.0	444.2	0.000	1.298	1.760	15.0	0.139
350	0.0016	1.014.-3	156.1	13.0	444.2	0.036	1.266	1.782	13.5	0.138
360	0.0029	1.021.-3	85.0	30.0	446.7	0.084	1.236	1.813	11.7	0.136
370	0.0049	1.030.-3	49.9	47.2	449.7	0.130	1.213	1.844	10.3	0.135
380	0.0064	1.037.-3	29.9	65.0	454.5	0.178	1.200	1.875	9.1	0.133
390	0.0129	1.046.-3	18.3	82.7	462.7	0.224	1.194	1.906	8.1	0.132
400	0.0200	1.054.-3	11.7	99.3	461.2	0.273	1.202	1.936	7.3	0.130
420	0.0432	1.072.-3	5.84	139.9	499.0	0.358	1.228	1.998	6.0	0.127
440	0.0879	1.092.-3	3.021	180.3	532.4	0.451	1.267	2.060	5.0	0.125
460	0.1694	1.112.-3	1.652	222.7	569.7	0.545	1.378	2.122	4.3	0.122
480	0.3112	1.132.-3	0.9594	267.6	611.6	0.652	1.367	2.184	3.7	0.119
500	0.5218	1.154.-3	0.4452	314.9	651.8	0.746	1.424	2.246	3.3	0.116
520	0.8375	1.177.-3	0.3652	361.5	687.8	0.824	1.477	2.308	2.7	0.113
540	1.290	1.204.-3	0.2261	404.5	723.8	0.915	1.529	2.370	2.4	0.110
560	1.941	1.230.-3	0.1447	457.2	762.7	1.032	1.582	2.432	2.2	0.107
580	2.818	1.258.-3	0.0977	522.3	801.7	1.125	1.635	2.494	1.90	0.105
600	3.926	1.291.-3	0.0685	563.7	842.4	1.223	1.688	2.556	1.71	0.102
620	5.408	1.326.-3	0.0504	630.4	886.4	1.316	1.740	2.618	1.54	0.099
640	7.328	1.366.-3	0.0381	689.1	930.9	1.375	1.748	2.680	1.39	0.096
660	9.572	1.412.-3	0.0301	745.9	977.1	1.457	1.791	2.741	1.24	0.093
680	12.05	1.465.-3	0.0236	802.8	1024.9	1.585	1.856	2.803	1.10	0.090
700	15.21	1.529.-3	0.0186	860.1	1073.1	1.663	1.951	2.865	0.97	0.087
720	19.14	1.56.-3	0.0147	917.5	1116.7	1.746	2.003	2.93		
740	23.93	1.70.-3	0.0113	975.2	1152.8	1.822	2.058	3.00		
760	28.71	1.95.-3	0.0085	1033.1	1182.5	1.901	2.099			
780	34.83	2.16.-3	0.0058	1091.2	1163.0	1.977	2.107			
800	42.46	3.18.-3	0.0032	1148.4	1148.4	2.047	2.047			

*Interpolated by P. E. Liley from the Landolt-Börnstein band IVa, p. 557, 1967 tables based on *Technical Data on Fuel*, British National Committee, World Energy Conference, London.

TABLE 2-212 Thermodynamic Properties of Dodecane

Temperature K	Pressure MPa	Density mol/dm ³	Volume dm ³ /mol	Int. energy kJ/mol	Enthalpy kJ/mol	Entropy kJ/(mol·K)	C _v kJ/(mol·K)	C _p kJ/(mol·K)	Sound speed m/s	Joule-Thomson K/MPa	Therm. cond. mW/(m·K)	Viscosity μPa·s
Saturated Properties												
263.60	6.2621E-07	4.5291	0.22079	-96.621	-96.621	-0.26003	0.28923	0.35985	1427.2	-0.45503	143.93	2892.5
270.00	1.2617E-06	4.5008	0.22218	-94.309	-94.309	-0.25136	0.29275	0.36265	1398.7	-0.45038	142.27	2447.1
290.00	8.8545E-06	4.4131	0.22660	-86.960	-86.960	-0.22511	0.30440	0.37246	1313.5	-0.43398	137.24	1578.5
310.00	4.5799E-05	4.3261	0.23115	-79.402	-79.402	-0.19991	0.31679	0.38355	1233.4	-0.41526	132.45	1112.9
330.00	0.00018556	4.2393	0.23589	-71.612	-71.612	-0.17556	0.32968	0.39559	1157.5	-0.39464	127.86	832.98
350.00	0.00061679	4.1522	0.24084	-63.574	-63.574	-0.15192	0.34285	0.40831	1085.1	-0.37230	123.43	650.53
370.00	0.0017432	4.0641	0.24605	-55.276	-55.276	-0.12887	0.35616	0.42150	1015.6	-0.34817	119.12	524.02
390.00	0.0043088	3.9747	0.25159	-46.712	-46.711	-0.10633	0.36947	0.43503	948.42	-0.32197	114.92	431.83
410.00	0.0095271	3.8833	0.25751	-37.875	-37.872	-0.084231	0.38269	0.44878	883.07	-0.29316	110.81	361.82
430.00	0.019190	3.7893	0.26390	-28.762	-28.757	-0.062532	0.39574	0.46268	819.18	-0.26089	106.77	306.78
450.00	0.035739	3.6920	0.27085	-19.371	-19.361	-0.041187	0.40859	0.47672	756.37	-0.22391	102.79	262.21
470.00	0.062299	3.5907	0.27850	-9.6999	-9.6825	-0.020162	0.42118	0.49091	694.32	-0.18039	98.863	225.20
490.00	0.10268	3.4842	0.28701	0.25270	0.28217	0.00057539	0.43351	0.50530	632.70	-0.12755	94.976	193.79
510.00	0.16136	3.3713	0.29662	10.490	10.538	0.021053	0.44557	0.52003	571.20	-0.061022	91.129	166.63
530.00	0.24347	3.2503	0.30766	21.016	21.091	0.041300	0.45738	0.53534	509.51	0.026306	87.324	142.76
550.00	0.35486	3.1189	0.32063	31.839	31.953	0.061352	0.46897	0.55164	447.33	0.14688	83.568	121.46
570.00	0.50211	2.9736	0.33629	42.975	43.144	0.081249	0.48040	0.56974	384.30	0.32430	79.876	102.19
590.00	0.69279	2.8091	0.35598	54.448	54.695	0.10105	0.49179	0.59128	320.04	0.60884	76.283	84.516
610.00	0.93585	2.6161	0.38225	66.310	66.667	0.12086	0.50334	0.62041	253.82	1.1288	72.856	68.050
630.00	1.2426	2.3747	0.42111	78.676	79.199	0.14087	0.51558	0.67253	183.58	2.3418	69.764	52.302
650.00	1.6298	2.0078	0.49805	92.046	92.858	0.16193	0.53081	0.91317	100.02	8.0937	68.073	35.652
658.10	1.8176	1.3300	0.75188	101.36	102.72	0.17683			0	40.219		
263.60	6.2621E-07	2.8572E-07	3,499,900.	-33.699	-31.507	-0.013011	0.24443	0.25274	115.35	330.02	6.7106	3.8271
270.00	1.2617E-06	5.6205E-07	1,779,200.	-32.120	-29.875	-0.012718	0.24903	0.25734	116.70	296.37	7.0413	3.9297
290.00	8.8545E-06	3.6724E-06	272,300.	-26.993	-24.582	-0.010011	0.26382	0.27214	120.83	215.32	8.1425	4.2511
310.00	4.5799E-05	1.7772E-05	56,267.	-21.566	-18.989	-0.0050291	0.27906	0.28739	124.81	160.20	9.3434	4.5733
330.00	0.00018556	6.7670E-05	14,778.	-15.834	-13.092	0.0017708	0.29454	0.30288	128.63	121.85	10.640	4.8958
350.00	0.00061679	0.00021228	4,710.8	-9.7983	-6.8927	0.010028	0.31008	0.31848	132.26	94.623	12.030	5.2183
370.00	0.0017432	0.00056862	1,758.6	-3.4632	-0.39757	0.019454	0.32559	0.33408	135.66	74.946	13.512	5.5399
390.00	0.0043088	0.0013382	747.29	3.1615	6.3814	0.029808	0.34098	0.34965	138.74	60.510	15.090	5.8599
410.00	0.0095271	0.0028309	353.24	10.063	13.428	0.040891	0.35619	0.36515	141.40	49.785	16.769	6.1775
430.00	0.019190	0.0054855	182.30	17.224	20.723	0.052536	0.37119	0.38060	143.51	41.738	18.561	6.4920
450.00	0.035739	0.0098881	101.13	24.628	28.242	0.064598	0.38596	0.39603	144.95	35.662	20.479	6.8034
470.00	0.062299	0.016797	59.534	32.254	35.962	0.076955	0.40048	0.41151	145.55	31.061	22.543	7.1122
490.00	0.10268	0.027184	36.786	40.078	43.855	0.089500	0.41475	0.42715	145.16	27.591	24.775	7.4202
510.00	0.16136	0.042311	23.635	48.075	51.889	0.10213	0.42878	0.44316	143.58	25.017	27.206	7.7302
530.00	0.24347	0.063865	15.658	56.215	60.027	0.11477	0.44259	0.45987	140.61	23.184	29.871	8.0477
550.00	0.35486	0.094219	10.614	64.460	68.226	0.12730	0.45625	0.47792	135.98	22.013	32.819	8.3808
570.00	0.50211	0.13692	7.3034	72.758	76.425	0.13964	0.46984	0.49854	129.36	21.503	36.118	8.7440
590.00	0.69279	0.19777	5.0563	81.036	84.539	0.15163	0.48353	0.52443	120.31	21.771	39.870	9.1635
610.00	0.93585	0.28746	3.4787	89.170	92.425	0.16308	0.49764	0.56276	108.12	23.181	44.272	9.6956
630.00	1.2426	0.43012	2.3249	96.902	99.791	0.17355	0.51290	0.64061	91.557	26.817	49.828	10.493
650.00	1.6298	0.71569	1.3973	103.34	105.62	0.18156	0.53205	1.0334	67.007	37.545	60.081	12.293
658.10	1.8176	1.3300	0.75188	101.36	102.72	0.17683			49.653	0		

TABLE 2-212 Thermodynamic Properties of Dodecane (Concluded)

Temperature K	Pressure MPa	Density mol/dm ³	Volume dm ³ /mol	Int. energy kJ/mol	Enthalpy kJ/mol	Entropy kJ/(mol·K)	C _v kJ/(mol·K)	C _p kJ/(mol·K)	Sound speed m/s	Joule-Thomson K/MPa	Therm. cond. mW/(m·K)	Viscosity μPa·s
Single-Phase Properties												
300.00	0.10000	4.3700	0.22883	-83.216	-83.193	-0.21241	0.31053	0.37786	1273.5	-0.42497	134.86	1315.3
400.00	0.10000	3.9300	0.25445	-42.339	-42.313	-0.095254	0.37610	0.44184	916.43	-0.30827	112.91	395.13
488.89	0.10000	3.4902	0.28651	-0.30755	-0.27889	-0.00056937	0.43283	0.50449	636.11	-0.13079	95.191	195.41
488.89	0.10000	0.026496	37.741	39.638	43.413	0.088800	0.41397	0.42628	145.21	27.759	24.647	7.4030
500.00	0.10000	0.025735	38.857	44.299	48.185	0.098451	0.42081	0.43268	147.79	25.222	25.670	7.5935
600.00	0.10000	0.020711	48.284	89.425	94.254	0.18229	0.47769	0.48757	167.29	12.534	35.525	9.2766
700.00	0.10000	0.017494	57.163	139.71	145.42	0.26108	0.52517	0.53435	183.12	7.4958	46.039	10.929
300.00	1.0000	4.3739	0.22863	-83.277	-83.048	-0.21262	0.31061	0.37775	1279.2	-0.42580	135.18	1330.4
400.00	1.0000	3.9374	0.25398	-42.444	-42.190	-0.095518	0.37615	0.44147	924.90	-0.31138	113.40	400.40
500.00	1.0000	3.4447	0.29030	5.1293	5.4196	0.101431	0.43951	0.51125	616.23	-0.11178	93.839	183.76
600.00	1.0000	2.7332	0.36588	60.165	60.531	0.11067	0.49726	0.60093	296.10	0.75711	74.943	77.601
614.58	1.0000	2.5662	0.38968	69.090	69.480	0.12541	0.50605	0.62919	238.23	1.3130	72.109	64.404
614.58	1.0000	0.31406	3.1841	90.990	94.175	0.16559	0.50099	0.57515	104.78	23.748	45.410	9.8451
700.00	1.0000	0.21164	4.7249	136.66	141.39	0.23754	0.53113	0.55438	152.31	9.1496	51.144	11.188
300.00	5.0000	4.3910	0.22774	-83.541	-82.402	-0.21351	0.31099	0.37733	1303.7	-0.42924	136.59	1398.2
400.00	5.0000	3.9683	0.25200	-42.890	-41.630	-0.096648	0.37639	0.44002	960.72	-0.32355	115.50	423.55
500.00	5.0000	3.5099	0.28491	4.2808	5.7054	0.0087025	0.43938	0.50646	674.60	-0.16525	97.177	201.12
600.00	5.0000	2.9472	0.33930	57.896	59.593	0.10677	0.49475	0.57114	420.49	0.19333	81.179	99.888
700.00	5.0000	2.1498	0.46517	117.69	120.02	0.19979	0.54281	0.63863	215.10	1.5765	70.846	42.370
300.00	10.000	4.4115	0.22668	-83.856	-81.590	-0.21459	0.31147	0.37689	1333.1	-0.43298	138.29	1484.7
400.00	10.000	4.0039	0.24976	-43.403	-40.906	-0.097972	0.37674	0.43856	1001.9	-0.33581	117.98	452.04
500.00	10.000	3.5776	0.27952	3.3852	6.1804	0.0068314	0.43944	0.50252	735.90	-0.20845	100.85	221.12
600.00	10.000	3.0995	0.32263	56.144	59.370	0.10365	0.49390	0.55974	517.52	-0.0053841	86.682	119.96
700.00	10.000	2.5593	0.39074	113.82	117.72	0.19351	0.53945	0.60482	359.64	0.33979	77.506	65.788
400.00	100.00	4.3951	0.22753	-48.840	-26.088	-0.11422	0.38400	0.43214	1472.8	-0.39899	149.79	967.99
500.00	100.00	4.1426	0.24140	-4.0985	20.041	-0.011523	0.44564	0.48959	1297.7	-0.35002	140.67	510.30
600.00	100.00	3.9126	0.25559	46.019	71.578	0.082301	0.49884	0.53969	1169.1	-0.31375	134.18	334.45
700.00	100.00	3.7019	0.27013	100.67	127.69	0.16871	0.54304	0.58105	1073.9	-0.28792	129.56	242.80
600.00	300.00	4.4838	0.22302	40.123	107.03	0.062648	0.50752	0.54106	1807.8	-0.33126	190.55	737.48
700.00	300.00	4.3441	0.23020	94.208	163.27	0.14926	0.55080	0.58241	1725.5	-0.31036	190.65	531.88

The values in these tables were generated from the NIST REFPROP software (Lemmon, E. W., McLinden, M. O., and Huber, M. L., NIST Standard Reference Database 23: Reference Fluid Thermodynamic and Transport Properties—REFPROP, National Institute of Standards and Technology, Standard Reference Data Program, Gaithersburg, Md., 2002, Version 7.1). The primary source for the thermodynamic properties is Lemmon, E. W., and Huber, M. L., "Thermodynamic Properties of *n*-Dodecane," *Energy & Fuels*, **18**:960–967, 2004. The source for viscosity and thermal conductivity is Huber, M. L., Laesecke, A., and Perkins, R. A., "Transport Properties of *n*-Dodecane," *Energy & Fuels* **18**: 968–975, 2004.

Properties at the triple point temperature and the critical point temperature are given in the first and last entries of the saturation tables, respectively. In the single-phase table, when the temperature range for a given isobar includes a vapor-liquid phase boundary, the temperature of phase equilibrium is noted, and properties for both the saturated liquid and saturated vapor are given (with liquid properties given in the upper line). Lines are omitted from the temperature-pressure grid of the single-phase table, when the system would be in the solid phase or if there are potential problems with the source property surface.

The uncertainties (where the uncertainties can be considered as estimates of a combined expanded uncertainty with a coverage factor of 2) of density values calculated using the equation of state in the liquid phase (including at saturation) are 0.2% for pressures less than 200 MPa and 0.5% for higher pressures. The uncertainty for heat capacities is 1%, and that for sound speeds is 0.5%. The estimated uncertainties of vapor pressures calculated using the Maxwell criterion are 0.2% for temperatures above 350 K and approach 5% as the temperature decreases to the triple point temperature. These estimated uncertainties for calculated properties are consistent with the experimental accuracies of the various available experimental data. The estimated uncertainty in viscosity is 0.5% along the saturated-liquid line, 2% in compressed liquid to 200 MPa, 5% in vapor and supercritical regions. Uncertainty in thermal conductivity is 3%, except in the supercritical region and dilute gas which have an uncertainty of 5%.

TABLE 2-213 Thermodynamic Properties of Ethane

Temperature K	Pressure MPa	Density mol/dm ³	Volume dm ³ /mol	Int. energy kJ/mol	Enthalpy kJ/mol	Entropy kJ/(mol·K)	C _v kJ/(mol·K)	C _p kJ/(mol·K)	Sound speed m/s	Joule-Thomson K/MPa	Therm. cond. mW/(m·K)	Viscosity μPa·s
Saturated Properties												
90.368	1.1421E-06	21.668	0.046151	-6.5907	-6.5907	-0.04975	0.048264	0.069935	2008.7	-0.55899	255.62	1280.8
100	1.1081E-05	21.316	0.046913	-5.9245	-5.9245	-0.04275	0.046324	0.068639	1938.4	-0.56656	247.83	873.22
110	7.4287E-05	20.951	0.04773	-5.2401	-5.2401	-0.03623	0.045172	0.068351	1866.4	-0.56429	239.12	633.38
120	0.0003523	20.584	0.048581	-4.5559	-4.5559	-0.03027	0.044453	0.068544	1794.4	-0.55668	229.91	485.78
130	0.0012839	20.214	0.049469	-3.8686	-3.8685	-0.02477	0.043962	0.068959	1722.0	-0.54585	220.35	388.17
140	0.0038136	19.840	0.050402	-3.1764	-3.1762	-0.01964	0.043607	0.069499	1649.1	-0.53246	210.57	319.79
150	0.009638	19.461	0.051385	-2.4784	-2.4779	-0.01483	0.043351	0.070139	1575.5	-0.51640	200.71	269.55
160	0.021405	19.074	0.052426	-1.7736	-1.7724	-0.01028	0.043183	0.070888	1501.3	-0.49723	190.84	231.16
170	0.042819	18.680	0.053534	-1.0608	-1.0585	-0.00596	0.043100	0.071768	1426.3	-0.47424	181.03	200.83
180	0.078638	18.275	0.054720	-0.3389	-0.33459	-0.00183	0.043108	0.072812	1350.5	-0.44655	171.34	176.18
190	0.13459	17.858	0.055998	0.3938	0.40133	0.002133	0.043210	0.074056	1273.7	-0.41304	161.84	155.68
200	0.21723	17.426	0.057386	1.1391	1.1515	0.005957	0.043411	0.075548	1196.0	-0.37225	152.56	138.27
210	0.33380	16.976	0.058907	1.8991	1.9188	0.009667	0.043717	0.077345	1117.3	-0.32220	143.47	123.23
220	0.49205	16.504	0.060590	2.6766	2.7064	0.013287	0.044131	0.079529	1037.3	-0.26011	134.60	110.05
230	0.70018	16.006	0.062476	3.4747	3.5184	0.016839	0.044661	0.082221	956.09	-0.18185	125.95	98.339
240	0.96679	15.475	0.064622	4.2973	4.3598	0.020347	0.045314	0.085612	873.25	-0.08101	117.51	87.799
250	1.3008	14.901	0.067112	5.1501	5.2374	0.023839	0.046109	0.090024	788.33	0.05295	109.29	78.190
260	1.7118	14.270	0.070079	6.0406	6.1606	0.027349	0.047076	0.096059	700.52	0.23862	101.24	69.305
270	2.2100	13.559	0.073750	6.9809	7.1438	0.030924	0.048269	0.10496	608.92	0.51141	93.309	60.936
280	2.8067	12.728	0.078565	7.9919	8.2124	0.034644	0.049743	0.11989	512.38	0.94945	85.434	52.839
290	3.5159	11.684	0.085590	9.1194	9.4204	0.038677	0.051927	0.15219	405.70	1.7713	77.574	44.603
300	4.3573	10.094	0.099071	10.525	10.957	0.043620	0.057488	0.30137	274.91	3.9421	71.489	34.970
305.32	4.8722	6.8569	0.14584	12.490	13.200	0.050820			0	9.6957		
90.368	1.1421E-06	1.5201E-06	657,870	10.542	11.293	0.14815	0.026809	0.035124	180.93	249.88	2.9082	3.0427
100	1.1081E-05	1.3327E-05	75,033	10.803	11.634	0.13254	0.027384	0.035699	189.86	199.02	3.4563	3.3157
110	7.4287E-05	8.1234E-05	12,310	11.080	11.994	0.12045	0.027997	0.036318	198.61	177.19	4.0447	3.6034
120	0.0003523	0.00035326	2,830.8	11.362	12.359	0.11069	0.028651	0.036992	206.89	158.49	4.6568	3.8961
130	0.0012839	0.0011893	840.82	11.648	12.728	0.10289	0.029380	0.037770	214.69	129.38	5.2959	4.1937
140	0.0038136	0.0032857	304.35	11.938	13.099	0.096610	0.030154	0.038623	222.01	96.433	5.9661	4.4956
150	0.0096380	0.0077732	128.65	12.231	13.471	0.091501	0.030876	0.039449	228.84	70.230	6.6725	4.8011
160	0.021405	0.016263	61.489	12.525	13.841	0.087308	0.031513	0.040235	235.12	54.075	7.4216	5.1100
170	0.042819	0.030843	32.422	12.817	14.205	0.083831	0.032173	0.041138	240.73	45.339	8.2209	5.4223
180	0.078638	0.054053	18.500	13.104	14.559	0.080912	0.033015	0.042375	245.54	40.255	9.0790	5.7388
190	0.13459	0.088865	11.253	13.384	14.898	0.078433	0.034120	0.044070	249.41	36.410	10.005	6.0609
200	0.21723	0.13870	7.2100	13.654	15.221	0.076302	0.035457	0.046220	252.26	32.914	11.011	6.3908
210	0.33380	0.20749	4.8195	13.914	15.523	0.074447	0.036937	0.048771	254.02	29.687	12.109	6.7319
220	0.49205	0.29989	3.3346	14.160	15.801	0.072806	0.038486	0.051718	254.65	26.853	13.318	7.0889
230	0.70018	0.42157	2.3721	14.389	16.050	0.071324	0.040077	0.055176	254.05	24.485	14.662	7.4687
240	0.96679	0.57983	1.7246	14.597	16.264	0.069948	0.041742	0.059419	252.14	22.563	16.179	7.8514
250	1.3008	0.78456	1.2746	14.776	16.434	0.068624	0.043548	0.064956	248.79	21.017	17.930	8.3424
260	1.7118	1.0502	0.9522	14.915	16.545	0.067290	0.045586	0.072712	243.81	19.757	20.023	8.8764
270	2.2100	1.3998	0.71441	14.999	16.578	0.065865	0.047971	0.084634	237.02	18.700	22.667	9.5257
280	2.8067	1.8748	0.53338	14.998	16.495	0.064224	0.050986	0.10591	228.10	17.721	26.327	10.373
290	3.5159	2.5679	0.38943	14.846	16.215	0.062107	0.055181	0.15523	216.50	16.582	32.319	11.617
300	4.3573	3.8079	0.26261	14.314	15.458	0.058625	0.062820	0.39989	200.51	14.497	47.465	14.023
305.32	4.8722	6.8569	0.14584	12.490	13.200	0.050820			0	9.6957		

TABLE 2-213 Thermodynamic Properties of Ethane (Concluded)

Temperature K	Pressure MPa	Density mol/dm ³	Volume dm ³ /mol	Int. energy kJ/mol	Enthalpy kJ/mol	Entropy kJ/(mol·K)	C _v kJ/(mol·K)	C _p kJ/(mol·K)	Sound speed m/s	Joule-Thomson K/MPa	Therm. cond. mW/(m·K)	Viscosity μPa·s
Single-Phase Properties												
100.00	0.10000	21.317	0.046910	-5.9253	-5.9206	-0.042756	0.046328	0.068636	1938.8	-0.56660	247.88	873.92
200.00	0.10000	0.061716	16.203	13.768	15.388	0.083336	0.034553	0.043810	257.90	30.845	10.723	6.3683
300.00	0.10000	0.040388	24.760	17.702	20.178	0.10263	0.044475	0.053048	312.23	10.722	21.218	9.4081
400.00	0.10000	0.030155	33.162	22.785	26.102	0.11958	0.057153	0.065586	355.24	5.0759	35.965	12.213
500.00	0.10000	0.024084	41.521	29.137	33.289	0.13557	0.069620	0.078001	393.08	2.7932	53.769	14.778
600.00	0.10000	0.020056	49.861	36.675	41.661	0.15080	0.080870	0.089227	427.63	1.6883	73.338	17.135
100.00	1.0000	21.329	0.046885	-5.9325	-5.8856	-0.042828	0.046362	0.068612	1942.4	-0.56691	248.30	880.24
200.00	1.0000	17.457	0.057283	1.1164	1.1737	0.0058431	0.043441	0.075331	1204.0	-0.37737	153.30	139.33
241.10	1.0000	15.414	0.064876	4.3894	4.4543	0.020731	0.045394	0.086038	864.04	-0.068172	116.60	86.702
241.10	1.0000	0.59982	1.6672	14.618	16.285	0.069802	0.041932	0.059951	251.85	22.377	16.358	7.9293
300.00	1.0000	0.43455	2.3012	17.331	19.632	0.082230	0.045482	0.057061	296.92	11.381	22.177	9.6518
400.00	1.0000	0.30970	3.2290	22.568	25.797	0.099896	0.057476	0.067069	348.76	5.1250	36.459	12.417
500.00	1.0000	0.24355	4.1060	28.986	33.092	0.11613	0.069783	0.078784	390.24	2.7821	54.084	14.954
600.00	1.0000	0.20145	4.9639	36.562	41.526	0.13147	0.080969	0.089708	426.64	1.6715	73.562	17.289
100.00	5.0000	21.381	0.046771	-5.9638	-5.7300	-0.043144	0.046517	0.068510	1957.7	-0.56823	250.17	909.15
200.00	5.0000	17.610	0.056786	1.0063	1.2902	0.0052852	0.043595	0.074345	1242.5	-0.40076	156.99	144.70
300.00	5.0000	10.907	0.091680	10.087	10.546	0.042046	0.053743	0.17141	359.63	2.3430	73.067	39.648
400.00	5.0000	1.7653	0.56647	21.484	24.316	0.083790	0.059017	0.076481	322.27	5.2035	39.974	13.905
500.00	5.0000	1.2769	0.78316	28.293	32.209	0.10138	0.070476	0.082676	380.40	2.6757	55.976	15.995
600.00	5.0000	1.0245	0.97605	36.055	40.936	0.11726	0.081384	0.091919	424.37	1.5738	74.801	18.124
100.00	10.000	21.444	0.046634	-6.0016	-5.5352	-0.043532	0.046712	0.068393	1976.2	-0.56975	252.48	947.29
200.00	10.000	17.786	0.056225	0.88047	1.4427	0.0046352	0.043786	0.073343	1286.7	-0.42471	161.36	151.27
300.00	10.000	12.680	0.078863	9.0258	9.8145	0.038217	0.050799	0.10280	579.32	0.58968	86.388	52.867
400.00	10.000	4.1977	0.23822	19.826	22.208	0.073976	0.060880	0.096368	310.38	4.4129	48.699	17.942
500.00	10.000	2.6794	0.37322	27.390	31.122	0.093896	0.071226	0.088180	377.77	2.3866	59.523	17.954
600.00	10.000	2.0757	0.48177	35.421	40.239	0.11050	0.081836	0.094716	427.41	1.4041	76.885	19.504
100.00	30.000	21.682	0.046121	-6.1384	-4.7548	-0.045002	0.047466	0.068003	2044.8	-0.57447	261.51	1127.3
200.00	30.000	18.371	0.054434	0.46960	2.1026	0.0024068	0.044528	0.070795	1433.6	-0.48623	177.27	177.04
300.00	30.000	14.784	0.067640	7.6392	9.6684	0.032933	0.050618	0.081850	909.38	-0.18133	112.64	77.610
400.00	30.000	10.812	0.092490	15.788	18.563	0.058427	0.061395	0.094994	585.71	0.40872	81.974	42.216
500.00	30.000	7.6781	0.13024	24.381	28.288	0.080115	0.072527	0.098504	497.87	0.71195	78.720	30.510
600.00	30.000	5.8933	0.16968	33.201	38.291	0.098343	0.082911	0.10204	505.75	0.59060	88.635	27.539
200.00	70.000	19.230	0.052001	0.098974	3.5411	0.0010269	0.045892	0.068554	1648.3	-0.54018	204.45	230.70
300.00	70.000	16.537	0.060469	6.4673	10.700	0.027905	0.051766	0.075512	1238.5	-0.42067	145.70	113.52
400.00	70.000	14.033	0.071259	13.756	18.744	0.050977	0.062135	0.085472	970.70	-0.27243	115.84	71.766
500.00	70.000	11.869	0.084254	21.871	27.769	0.071077	0.073299	0.094785	827.80	-0.15903	107.39	53.331
600.00	70.000	10.144	0.098582	30.754	37.654	0.089078	0.083730	0.10274	764.56	-0.10326	111.32	44.741

The values in these tables were generated from the NIST REFPROP software (Lemmon, E. W., McLinden, M. O., and Huber, M. L., NIST Standard Reference Database 23: Reference Fluid Thermodynamic and Transport Properties—REFPROP, National Institute of Standards and Technology, Standard Reference Data Program, Gaithersburg, Md., 2002, Version 7.1). The primary source for the thermodynamic properties is Buecker, D., and Wagner, W., "A Reference Equation of State for the Thermodynamic Properties of Ethane for Temperatures from the Melting Line to 675 K and Pressures up to 900 MPa," *J. Phys. Chem. Ref. Data*, **35**(1):205–206, 2006. The source for viscosity and thermal conductivity is Friend, D. G., Ingham, H., and Ely, J. F., "Thermophysical Properties of Ethane," *J. Phys. Chem. Ref. Data*, **35**(1):205–266, 2006.

Properties at the triple point temperature and the critical point temperature are given in the first and last entries of the saturation tables, respectively. In the single-phase table, when the temperature range for a given isobar includes a vapor-liquid phase boundary, the temperature of phase equilibrium is noted, and properties for both the saturated liquid and saturated vapor are given (with liquid properties given in the upper line). Lines are omitted from the temperature-pressure grid of the single-phase table, when the system would be in the solid phase or if there are potential problems with the source property surface.

The uncertainties in the equation of state are 0.02% to 0.04% in density from the melting line up to temperatures of 520 K and pressures of 30 MPa. The uncertainties increase to 0.3% at higher temperatures and to 1% at higher pressures. The uncertainty in speed of sound ranges from 0.02% in the gaseous phase to 0.15% in the liquid phase. Above 450 K, the uncertainties increase to 0.3% at lower pressures and to 1% at higher pressures. At pressures above 40 MPa at all temperatures, the uncertainties are 1% up to 100 MPa, and 5% at higher pressures. The uncertainties in heat capacities range from 2% in the vapor and liquid regions below 450 K and 30 MPa to 5% at high pressures. The uncertainties in vapor pressure are 0.01% above 170 K and 10 MPa below 170 K. The uncertainty in viscosity is 2%. The uncertainty in thermal conductivity is 2%.

TABLE 2-214 Thermodynamic Properties of Ethanol

Temperature K	Pressure MPa	Density mol/dm ³	Volume dm ³ /mol	Int. energy kJ/mol	Enthalpy kJ/mol	Entropy kJ/(mol·K)	C _v kJ/(mol·K)	C _p kJ/(mol·K)	Sound speed m/s	Joule-Thomson K/MPa	Therm. cond. mW/(m·K)	Viscosity μPa·s
Saturated Properties												
250.00	0.00027007	17.911	0.055831	6.9274	6.9275	0.037330	0.076657	0.093612	1325.0	-0.44553	178.12	3140.9
265.00	0.00089527	17.642	0.056681	8.3792	8.3793	0.042968	0.083798	0.10028	1260.8	-0.41423	173.58	2182.0
280.00	0.0025823	17.376	0.057551	9.9424	9.9426	0.048704	0.091653	0.10829	1202.8	-0.37872	169.56	1564.4
295.00	0.0066146	17.106	0.058460	11.630	11.631	0.054574	0.099433	0.11678	1149.2	-0.34323	165.87	1152.5
310.00	0.015298	16.828	0.059426	13.445	13.446	0.060574	0.10670	0.12524	1098.1	-0.30910	162.38	869.40
325.00	0.032394	16.537	0.060469	15.385	15.387	0.066684	0.11322	0.13340	1048.0	-0.27615	159.01	669.49
340.00	0.063544	16.231	0.061610	17.444	17.448	0.072875	0.11893	0.14115	997.94	-0.24356	155.69	524.87
355.00	0.11663	15.905	0.062872	19.615	19.622	0.079123	0.12381	0.14847	947.31	-0.21011	152.39	417.88
370.00	0.20205	15.557	0.064281	21.892	21.905	0.085403	0.12792	0.15543	895.56	-0.17428	149.09	337.04
385.00	0.33279	15.181	0.065871	24.268	24.290	0.091699	0.13130	0.16215	842.31	-0.13410	145.78	274.76
400.00	0.52446	14.774	0.067684	26.740	26.775	0.098000	0.13405	0.16883	787.16	-0.086812	142.47	225.91
415.00	0.79509	14.331	0.069779	29.307	29.362	0.10430	0.13625	0.17576	729.67	-0.028333	139.18	186.93
430.00	1.1649	13.843	0.072241	31.970	32.054	0.11061	0.13798	0.18341	669.25	0.047976	135.93	155.35
445.00	1.6559	13.298	0.075202	34.737	34.862	0.11695	0.13934	0.19262	605.07	0.15384	132.78	129.37
460.00	2.2916	12.676	0.078889	37.629	37.810	0.12335	0.14041	0.20504	535.80	0.31228	129.85	107.62
475.00	3.0963	11.941	0.083745	40.684	40.943	0.12991	0.14134	0.22469	459.19	0.57597	127.41	88.972
490.00	4.0954	11.007	0.090848	44.002	44.374	0.13684	0.14234	0.26508	371.03	1.0976	126.33	72.213
505.00	5.3159	9.5842	0.10434	47.926	48.480	0.14485	0.14382	0.41790	264.74	2.5369	129.43	55.104
513.90	6.1480	5.9910	0.16692	53.880	54.906	0.15723			0	8.6373		
250.00	0.00027007	0.00012998	7693.7	49.039	51.116	0.21409	0.058885	0.067215	226.86	149.30	14.936	7.2715
265.00	0.00089527	0.00040670	2458.8	49.932	52.134	0.20808	0.060795	0.069146	233.03	111.11	15.737	7.7433
280.00	0.0025823	0.0011115	899.69	50.851	53.174	0.20310	0.062753	0.071149	238.89	87.283	16.612	8.2114
295.00	0.0066146	0.0027080	369.28	51.792	54.234	0.19899	0.064753	0.073238	244.41	71.858	17.566	8.6756
310.00	0.015298	0.0059814	167.18	52.749	55.307	0.19561	0.066816	0.075464	249.49	61.180	18.602	9.1353
325.00	0.032394	0.012150	82.305	53.717	56.383	0.19282	0.068988	0.077921	254.02	53.164	19.731	9.5902
340.00	0.063544	0.022975	43.525	54.684	57.450	0.19053	0.071336	0.080736	257.88	46.697	20.969	10.040
355.00	0.11663	0.040873	24.466	55.640	58.494	0.18862	0.073932	0.084059	260.92	41.226	22.341	10.486
370.00	0.20205	0.069039	14.485	56.573	59.500	0.18701	0.076838	0.088058	263.02	36.486	23.886	10.929
385.00	0.33279	0.11160	8.9606	57.469	60.451	0.18562	0.080106	0.092930	264.03	32.353	25.659	11.372
400.00	0.52446	0.17385	5.7521	58.312	61.329	0.18438	0.083774	0.098936	263.82	28.756	27.741	11.820
415.00	0.79509	0.26261	3.8080	59.087	62.115	0.18322	0.087876	0.10646	262.27	25.644	30.251	12.283
430.00	1.1649	0.38683	2.5851	59.774	62.785	0.18208	0.092450	0.11610	259.21	22.967	33.369	12.774
445.00	1.6559	0.55876	1.7897	60.348	63.312	0.18088	0.097544	0.12898	254.44	20.681	37.377	13.318
460.00	2.2916	0.79629	1.2558	60.777	63.654	0.17954	0.10323	0.14727	247.61	18.747	42.735	13.961
475.00	3.0963	1.1286	0.88602	61.004	63.747	0.17792	0.10966	0.17612	238.10	17.136	50.248	14.786
490.00	4.0954	1.6143	0.61945	60.916	63.453	0.17578	0.11709	0.23200	224.59	15.831	61.578	15.982
505.00	5.3159	2.4339	0.41086	60.144	62.328	0.17228	0.12644	0.42053	203.70	14.728	82.512	18.148
513.90	6.1480	5.9910	0.16692	53.880	54.906	0.15723			0	8.6373		

TABLE 2-214 Thermodynamic Properties of Ethanol (Concluded)

Temperature K	Pressure MPa	Density mol/dm ³	Volume dm ³ /mol	Int. energy kJ/mol	Enthalpy kJ/mol	Entropy kJ/(mol·K)	C _v kJ/(mol·K)	C _p kJ/(mol·K)	Sound speed m/s	Joule-Thomson K/MPa	Therm. cond. mW/(m·K)	Viscosity μPa·s
Single-Phase Properties												
300.00	0.10000	17.016	0.058768	12.219	12.225	0.056554	0.10193	0.11962	1132.5	-0.33179	164.74	1047.2
351.05	0.10000	15.993	0.062527	19.033	19.040	0.077475	0.12261	0.14658	960.72	-0.21908	153.26	443.11
351.05	0.10000	0.035314	28.317	55.390	58.222	0.18909	0.073221	0.083127	260.21	42.587	21.965	10.369
400.00	0.10000	0.030577	32.704	59.207	62.477	0.20043	0.080640	0.089997	279.09	28.685	26.374	11.853
500.00	0.10000	0.024191	41.338	67.925	72.058	0.22176	0.092910	0.10162	312.39	11.830	37.865	14.768
600.00	0.10000	0.020086	49.786	77.796	82.775	0.24127	0.10403	0.11252	341.55	5.6356	52.622	17.543
300.00	1.0000	17.034	0.058707	12.202	12.261	0.056497	0.10191	0.11954	1137.9	-0.33273	165.24	1053.2
400.00	1.0000	14.795	0.067589	26.715	26.783	0.097937	0.13400	0.16857	791.85	-0.089821	142.87	227.32
423.85	1.0000	14.049	0.071181	30.866	30.938	0.10802	0.13732	0.18015	694.41	0.013963	137.25	167.52
423.85	1.0000	0.33095	3.0216	59.504	62.526	0.18255	0.090516	0.11184	260.65	24.014	32.003	12.568
500.00	1.0000	0.25567	3.9114	67.014	70.925	0.20078	0.096953	0.11008	300.64	12.007	39.539	14.859
600.00	1.0000	0.20473	4.8846	77.311	82.195	0.22131	0.10581	0.11605	337.33	5.6301	53.583	17.678
300.00	5.0000	17.111	0.058443	12.129	12.421	0.056249	0.10185	0.11922	1161.4	-0.33665	167.43	1079.6
400.00	5.0000	14.961	0.066842	26.516	26.851	0.097435	0.13359	0.16658	829.44	-0.11211	146.07	238.82
500.00	5.0000	10.220	0.097846	46.419	46.908	0.14179	0.14311	0.32410	308.88	1.7596	127.42	61.882
501.39	5.0000	10.013	0.099875	46.876	47.375	0.14272	0.14340	0.35152	292.31	2.0063	128.00	59.510
501.39	5.0000	2.1809	0.45852	60.445	62.737	0.17336	0.12389	0.34099	209.80	15.000	75.676	17.454
600.00	5.0000	1.1372	0.87939	74.966	79.363	0.20395	0.11419	0.13659	314.06	5.6703	61.725	18.972
300.00	10.000	17.203	0.058131	12.041	12.623	0.055950	0.10179	0.11885	1189.5	-0.34096	170.07	1111.8
400.00	10.000	15.147	0.066020	26.293	26.953	0.096860	0.13313	0.16456	872.36	-0.13414	149.80	252.40
500.00	10.000	11.521	0.086800	44.752	45.620	0.13830	0.14031	0.22204	464.50	0.60618	130.15	80.680
600.00	10.000	2.8001	0.35713	71.266	74.837	0.19172	0.12599	0.18744	273.66	5.6926	84.190	23.411
300.00	100.00	18.389	0.054380	10.984	16.422	0.051802	0.10149	0.11571	1558.1	-0.37198	207.54	1611.3
400.00	100.00	17.030	0.058722	24.075	29.947	0.090466	0.12901	0.15081	1348.2	-0.25352	195.29	435.09
500.00	100.00	15.408	0.064899	39.356	45.846	0.12589	0.13221	0.16433	1166.1	-0.17199	188.35	192.15
600.00	100.00	13.601	0.073523	55.055	62.407	0.15608	0.12575	0.16553	1015.1	-0.082822	187.31	109.49
300.00	200.00	19.244	0.051963	10.349	20.742	0.048505	0.10196	0.11495	1830.4	-0.37578	238.67	2085.4
400.00	200.00	18.138	0.055134	22.905	33.931	0.086238	0.12678	0.14539	1660.3	-0.28090	228.57	591.02
500.00	200.00	16.878	0.059250	37.295	49.145	0.12014	0.12868	0.15623	1525.6	-0.22946	224.49	269.30
600.00	200.00	15.505	0.064494	51.902	64.801	0.14869	0.12066	0.15566	1422.7	-0.19099	226.40	148.43

The values in these tables were generated from the NIST REFPROP software (Lemmon, E.W., McLinden, M.O., and Huber, M.L., NIST Standard Reference Database 23: Reference Fluid Thermodynamic and Transport Properties—REFPROP, National Institute of Standards and Technology, Standard Reference Data Program, Gaithersburg, Md., 2002, Version 7.1). The primary source for the thermodynamic properties is Dillon, H.E., and Penoncello, S.G., "A Fundamental Equation for Calculation of the Thermodynamic Properties of Ethanol," *Int. J. Thermophys.*, **25**(2):321–335, 2004. The source for viscosity is Kiselev, S. B., Ely, J. F., Abdulagatov, I. M., and Huber, M. L., "Generalized SAFT-DFT/DMT Model for the Thermodynamic, Interfacial, and Transport Properties of Associating Fluids: Application for *n*-Alkanols," *Ind. Eng. Chem. Res.*, **44**:6916–6927, 2005. The source for thermal conductivity is unpublished, 2004; however, the fit uses functional form found in Marsh, K., Perkins, R., and Ramirez, M.L.V., "Measurement and Correlation of the Thermal Conductivity of Propane from 86 to 600 K at Pressures to 70 MPa," *J. Chem. Eng. Data*, **47**(4):932–940, 2002.

Properties at the critical point temperature are given in the last entry of the saturation tables. In the single-phase table, when the temperature range for a given isobar includes a vapor-liquid phase boundary, the temperature of phase equilibrium is noted, and properties for both the saturated liquid and saturated vapor are given (with liquid properties given in the upper line). Lines are omitted from the temperature-pressure grid of the single-phase table, when the system would be in the solid phase or if there are potential problems with the source property surface.

The uncertainties in the equation of state are 0.2% in density, 3% in heat capacities, 1% in speed of sound, and 0.5% in vapor pressure and saturation densities. The estimated uncertainty in the liquid phase along the saturation boundary is approximately 3%, increasing to 10% at pressures to 100 MPa, and is estimated at 10% in the vapor phase. The estimated uncertainty in the liquid phase is approximately 5% and is estimated as 10% in the vapor phase.

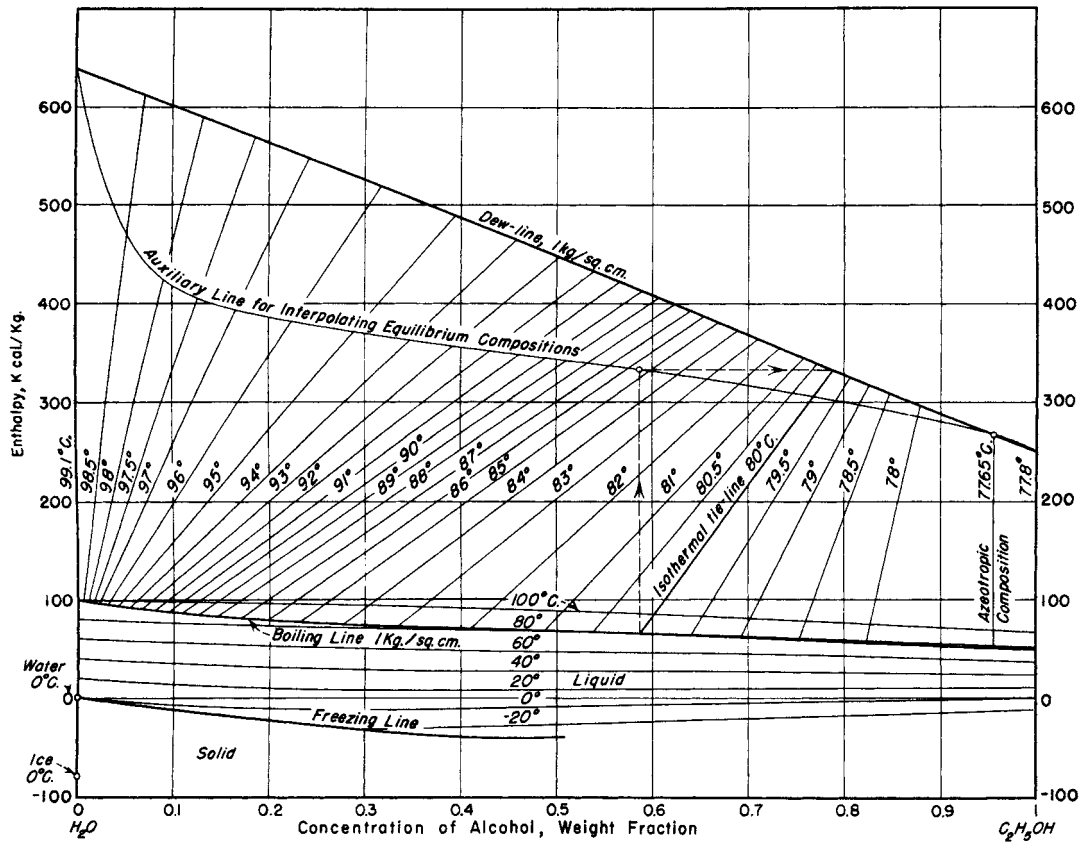


FIG. 2-10 Enthalpy-concentration diagram for aqueous ethyl alcohol. Reference states: Enthalpies of liquid water and ethyl alcohol at 0°C are zero. NOTE: In order to interpolate equilibrium compositions, a vertical may be erected from any liquid composition on the boiling line and its intersection with the auxiliary line determined. A horizontal from this intersection will establish the equilibrium vapor composition on the dew line. (Bosnjakovic, Technische Thermodynamik, T. Steinkopff, Leipzig, 1935.)

TABLE 2-215 Thermodynamic Properties of Ethylene

Temperature K	Pressure MPa	Density mol/dm ³	Volume dm ³ /mol	Int. energy kJ/mol	Enthalpy kJ/mol	Entropy kJ/(mol·K)	C _v kJ/(mol·K)	C _p kJ/(mol·K)	Sound speed m/s	Joule-Thomson K/MPa	Therm. cond. mW/(m·K)	Viscosity μPa·s
Saturated Properties												
103.99	0.00012196	23.334	0.042856	-4.4352	-4.4352	-0.033074	0.045503	0.068155	1766.6	-0.50257	270.65	685.73
105.00	0.00014568	23.288	0.042940	-4.3661	-4.3661	-0.032412	0.045394	0.068183	1760.2	-0.50171	269.25	662.48
115.00	0.00069745	22.834	0.043793	-3.6839	-3.6838	-0.026206	0.044202	0.068194	1694.4	-0.49455	255.56	488.07
125.00	0.0025267	22.375	0.044692	-3.0030	-3.0029	-0.020529	0.042929	0.067951	1626.0	-0.48779	242.07	378.67
135.00	0.0073921	21.909	0.045643	-2.3250	-2.3247	-0.015311	0.041693	0.067669	1556.2	-0.47928	228.83	305.49
145.00	0.018309	21.435	0.046652	-1.6496	-1.6488	-0.010484	0.040562	0.067475	1485.3	-0.46747	215.95	253.84
155.00	0.039755	20.952	0.047729	-0.97554	-0.97364	-0.0059884	0.039568	0.067448	1413.2	-0.45105	203.50	215.68
165.00	0.077693	20.456	0.048885	-0.30104	-0.29724	-0.0017710	0.038729	0.067649	1339.9	-0.42866	191.54	186.36
175.00	0.13944	19.945	0.050137	0.37612	0.38311	0.0022141	0.038051	0.068127	1265.0	-0.39877	180.09	163.03
185.00	0.23344	19.417	0.051502	1.0585	1.0706	0.0060075	0.037536	0.068937	1188.5	-0.35944	169.21	143.88
195.00	0.36901	18.865	0.053008	1.7492	1.7688	0.0096456	0.037184	0.070151	1110.0	-0.30804	158.78	127.73
205.00	0.55614	18.286	0.054687	2.4516	2.4820	0.013162	0.036995	0.071867	1029.3	-0.24081	148.78	113.76
215.00	0.80534	17.671	0.056589	3.1699	3.2155	0.016589	0.036970	0.074242	946.13	-0.15205	139.15	101.40
225.00	1.1276	17.011	0.058784	3.9095	3.9758	0.019960	0.037115	0.077537	860.08	-0.032706	129.81	90.217
235.00	1.5342	16.291	0.061382	4.6774	4.7715	0.023314	0.037446	0.082229	770.62	0.13270	120.64	79.891
245.00	2.0376	15.488	0.064566	5.4842	5.6157	0.026699	0.037996	0.089292	676.97	0.37286	111.48	70.142
255.00	2.6509	14.560	0.068682	6.3476	6.5297	0.030191	0.038851	0.10110	577.38	0.74844	102.11	60.685
265.00	3.3898	13.419	0.074519	7.3042	7.5568	0.033937	0.040322	0.12549	467.22	1.4173	92.171	51.112
275.00	4.2752	11.793	0.084795	8.4637	8.8262	0.038375	0.043922	0.21287	334.73	2.9732	81.576	40.397
282.35	5.0417	7.6368	0.13095	10.545	11.206	0.046609			0	8.7988		
103.99	0.00012196	0.00014109	7087.6	10.621	11.486	0.12003	0.024972	0.033295	202.67	154.90	6.8012	0.77270
105.00	0.00014568	0.00016690	5991.6	10.647	11.520	0.11888	0.024975	0.033300	203.65	150.43	6.7393	1.0011
115.00	0.00069745	0.00073000	1369.9	10.895	11.850	0.10888	0.025028	0.033376	213.03	114.92	6.6223	2.7342
125.00	0.0025267	0.0024363	410.46	11.142	12.179	0.10093	0.025131	0.033533	221.86	90.667	7.0116	3.8262
135.00	0.0073921	0.0066178	151.11	11.385	12.502	0.094519	0.025307	0.033814	230.09	73.502	7.5850	4.5578
145.00	0.018309	0.015333	65.217	11.624	12.818	0.089286	0.025577	0.034263	237.62	60.977	8.2013	5.0886
155.00	0.039755	0.031379	31.869	11.855	13.122	0.084954	0.025956	0.034922	244.36	51.588	8.8125	5.5112
165.00	0.077693	0.058231	17.173	12.078	13.412	0.081316	0.026454	0.035833	250.18	44.379	9.4170	5.8799
175.00	0.13944	0.099997	10.000	12.289	13.683	0.078216	0.027081	0.037045	254.99	38.733	10.036	6.2279
185.00	0.23344	0.16142	6.1950	12.486	13.933	0.075532	0.027844	0.038617	258.69	34.236	10.700	6.5765
195.00	0.36901	0.24802	4.0319	12.667	14.155	0.073165	0.028751	0.040637	261.18	30.602	11.446	6.9410
205.00	0.55614	0.36638	2.7294	12.829	14.346	0.071037	0.029816	0.043243	262.38	27.626	12.313	7.3341
215.00	0.80534	0.52471	1.9058	12.966	14.501	0.069079	0.031060	0.046651	262.18	25.155	13.346	7.7689
225.00	1.1276	0.73386	1.3627	13.074	14.610	0.067325	0.032511	0.051237	260.50	23.074	14.607	8.2612
235.00	1.5342	1.0092	0.99086	13.144	14.664	0.065409	0.034212	0.057696	257.19	21.287	16.186	8.8342
245.00	2.0376	1.3747	0.72745	13.162	14.645	0.063551	0.036243	0.067503	252.09	19.706	18.250	9.5251
255.00	2.6509	1.8719	0.53422	13.105	14.522	0.061532	0.038789	0.084393	244.94	18.213	21.166	10.404
265.00	3.3898	2.5886	0.38631	12.923	14.232	0.059128	0.042250	0.12086	235.28	16.604	26.045	11.632
275.00	4.2752	3.7947	0.26352	12.460	13.587	0.055687	0.048136	0.26071	221.57	14.315	39.168	13.765
282.35	5.0417	7.6368	0.13095	10.545	11.206	0.046609			0	8.7988		

Single-Phase Properties

150.00	0.10000	21.197	0.047176	-1.3137	-1.3090	-0.0082061	0.040048	0.067428	1449.9	-0.46008	209.74	233.39
169.16	0.10000	20.246	0.049393	-0.020110	-0.015171	-0.000089238	0.038427	0.067811	1309.0	-0.41725	186.72	176.06
169.16	0.10000	0.073519	13.602	12.167	13.527	0.079970	0.026699	0.036297	252.31	41.871	9.6709	6.0256
225.00	0.10000	0.054182	18.456	13.722	15.568	0.090386	0.028730	0.037508	291.07	20.438	12.903	7.8384
300.00	0.10000	0.040315	24.805	16.100	18.580	0.10190	0.034782	0.043294	330.82	10.015	20.558	10.381
375.00	0.10000	0.032159	31.096	18.990	22.099	0.11234	0.042202	0.050626	364.16	5.6845	31.002	12.827
450.00	0.10000	0.026764	37.364	22.436	26.173	0.12222	0.049547	0.057930	394.34	3.5485	42.200	15.092
150.00	1.0000	21.223	0.047119	-1.3281	-1.2810	-0.0083026	0.040075	0.067329	1456.3	-0.46205	210.67	232.98
221.33	1.0000	17.260	0.057938	3.6350	3.6929	0.018726	0.037041	0.076196	892.05	-0.080890	133.22	94.208
221.33	1.0000	0.65028	1.5378	13.038	14.576	0.067898	0.031952	0.049381	261.30	23.800	14.112	8.0724
225.00	1.0000	0.63206	1.5821	13.173	14.755	0.068701	0.031799	0.048297	265.10	22.637	14.323	8.1765
300.00	1.0000	0.42535	2.3510	15.822	18.173	0.081821	0.035459	0.046096	320.09	10.271	21.362	10.589
375.00	1.0000	0.32964	3.0336	18.803	21.836	0.092696	0.042478	0.051961	358.72	5.7053	31.533	13.017
450.00	1.0000	0.27097	3.6904	22.297	25.987	0.10277	0.049700	0.058724	391.57	3.5291	42.581	15.284
150.00	5.0000	21.333	0.046876	-1.3902	-1.1558	-0.0087214	0.040199	0.066921	1483.4	-0.47016	214.70	231.18
225.00	5.0000	17.364	0.057591	3.7130	4.0009	0.019071	0.037097	0.073970	926.49	-0.13327	135.08	93.288
281.98	5.0000	9.494	0.11050	9.9242	10.477	0.044044	0.061633	0.037041	189.76	3.7487	145.71	27.667
281.98	5.0000	6.2408	0.16024	11.247	12.048	0.049617	0.066988	5.9539	191.76	10.151	182.63	19.004
300.00	5.0000	3.1277	0.31972	13.977	15.576	0.061893	0.040822	0.089599	263.71	10.910	30.862	13.344
375.00	5.0000	1.8590	0.53792	17.877	20.567	0.076837	0.043817	0.060244	337.12	5.6244	35.453	14.287
450.00	5.0000	1.4297	0.69947	21.650	25.147	0.087965	0.050366	0.062753	381.96	3.3730	45.106	16.277
150.00	10.000	21.464	0.046589	-1.4634	-0.99754	-0.0092238	0.040364	0.066475	1515.1	-0.47905	219.60	229.03
225.00	10.000	17.739	0.056372	3.5022	4.0659	0.018094	0.037190	0.070996	996.58	-0.22081	140.93	96.609
300.00	10.000	11.510	0.086881	9.6517	10.521	0.042563	0.041889	0.11956	420.01	1.9372	79.635	37.621
375.00	10.000	4.3583	0.22945	16.483	18.778	0.067434	0.045508	0.077265	328.58	4.7029	45.198	17.402
450.00	10.000	3.0293	0.33011	20.798	24.099	0.080391	0.051131	0.068674	379.55	2.9790	50.075	18.014
150.00	100.00	23.148	0.043200	-2.3062	2.0139	-0.015964	0.043582	0.063328	1891.7	-0.54092	294.42	199.89
225.00	100.00	20.862	0.047935	1.8396	6.6331	0.0090426	0.040468	0.060888	1581.0	-0.54008	200.24	126.05
300.00	100.00	18.775	0.053261	5.9492	11.275	0.026831	0.043293	0.063490	1328.5	-0.48350	154.23	98.312
375.00	100.00	16.889	0.059210	10.287	16.208	0.041488	0.048765	0.068211	1143.7	-0.41039	131.89	81.449
450.00	100.00	15.219	0.065708	14.942	21.513	0.054370	0.054851	0.073224	1020.9	-0.34600	121.24	70.072
150.00	300.00	25.298	0.039530	-2.9624	8.8964	-0.024942	0.048504	0.062644	2343.7	-0.54689	432.13	161.49
225.00	300.00	23.718	0.042162	0.79998	13.448	-0.00029268	0.044752	0.059805	2151.3	-0.57336	275.32	155.50
300.00	300.00	22.336	0.044772	4.5667	17.998	0.017143	0.047124	0.062135	1984.6	-0.55352	209.21	157.18
375.00	300.00	21.120	0.047350	8.6213	22.826	0.031488	0.052222	0.066814	1847.1	-0.51701	178.33	156.74
450.00	300.00	20.042	0.049894	13.065	28.033	0.044131	0.057988	0.072043	1740.6	-0.48199	163.32	153.81

The values in these tables were generated from the NIST REFPROP software (Lemmon, E. W., McLinden, M. O., and Huber, M. L., NIST Standard Reference Database 23: Reference Fluid Thermodynamic and Transport Properties—REFPROP, National Institute of Standards and Technology, Standard Reference Data Program, Gaithersburg, Md., 2002, Version 7.1). The primary source for the thermodynamic properties is Smukala, J., Span, R., and Wagner, W., "A New Equation of State for Ethylene Covering the Fluid Region for Temperatures from the Melting Line to 450 K at Pressures up to 300 MPa," *J. Phys. Chem. Ref. Data*, **29**(5):1053–1122, 2000. The source for viscosity is Holland, P. M., Eaton, B. E., and Hanley, H. J. M., "A Correlation of the Viscosity and Thermal Conductivity Data of Gaseous and Liquid Ethylene," *J. Phys. Chem. Ref. Data*, **12**(4):917–932, 1983. The source for thermal conductivity is Holland, P. M., Eaton, B. E., and Hanley, H. J. M., "A Correlation of the Viscosity and Thermal Conductivity Data of Gaseous and Liquid Ethylene," *J. Phys. Chem. Ref. Data*, **12**(4):917–932, 1983.

Properties at the triple point temperature and the critical point temperature are given in the first and last entries of the saturation tables, respectively. In the single-phase table, when the temperature range for a given isobar includes a vapor-liquid phase boundary, the temperature of phase equilibrium is noted, and properties for both the saturated liquid and saturated vapor are given (with liquid properties given in the upper line). Lines are omitted from the temperature-pressure grid of the single-phase table, when the system would be in the solid phase or if there are potential problems with the source property surface.

The uncertainties in density of the equation of state range from 0.02% in the liquid and most of the vapor phase to 0.1% for supercritical states. At $p > 100$ MPa, the uncertainty in density is 0.5%. The uncertainty in heat capacity is 3% in the liquid phase, 0.2% in the vapor phase, and as high as 5% in the supercritical region at higher pressures. For the speed of sound, the uncertainty is 0.05 to 0.1% in the vapor phase, rising to 3% in the liquid phase. The uncertainty in vapor pressure is less than 0.05% above 140 K. The uncertainty in viscosity is 5%, increasing to 10% in the dense liquid. The uncertainty in thermal conductivity is 5%, increasing to 10% in the dense liquid.

TABLE 2-216 Thermodynamic Properties of Fluorine

Temperature K	Pressure MPa	Density mol/dm ³	Volume dm ³ /mol	Int. energy kJ/mol	Enthalpy kJ/mol	Entropy kJ/(mol·K)	C _v kJ/(mol·K)	C _p kJ/(mol·K)	Sound speed m/s	Joule-Thomson K/MPa
Saturated Properties										
53.481	0.00023881	44.917	0.022263	-1.7783	-1.7783	-0.026073	0.036802	0.057963	1041.6	-0.30422
55.000	0.00038159	44.657	0.022393	-1.6923	-1.6923	-0.024487	0.035214	0.055732	1040.8	-0.31810
60.000	0.0014872	43.829	0.022816	-1.4151	-1.4151	-0.019663	0.034254	0.055680	1043.5	-0.31768
65.000	0.0046126	43.005	0.023253	-1.1355	-1.1354	-0.015187	0.033385	0.056098	1019.2	-0.31059
70.000	0.011981	42.169	0.023714	-0.85459	-0.85430	-0.011024	0.032745	0.056274	973.15	-0.30322
75.000	0.027062	41.315	0.024204	-0.57283	-0.57217	-0.0071357	0.032241	0.056496	921.41	-0.29375
80.000	0.054668	40.437	0.024730	-0.28975	-0.28840	-0.0034817	0.031737	0.056860	871.16	-0.28123
85.000	0.10090	39.531	0.025296	-0.0046707	-0.0021183	-0.000024789	0.031196	0.057394	823.90	-0.26509
90.000	0.17296	38.590	0.025913	0.28316	0.28764	0.0032663	0.030634	0.058117	779.02	-0.24474
95.000	0.27894	37.609	0.026589	0.57448	0.58190	0.0064180	0.030073	0.059051	735.47	-0.21935
100.00	0.42751	36.582	0.027336	0.87013	0.88182	0.0094534	0.029532	0.060243	692.27	-0.18762
105.00	0.62778	35.499	0.028170	1.1711	1.1887	0.012394	0.029024	0.061773	648.60	-0.14746
110.00	0.88912	34.351	0.029112	1.4785	1.5044	0.015261	0.028561	0.063791	603.67	-0.095557
115.00	1.2212	33.119	0.030194	1.7943	1.8312	0.018078	0.028159	0.066559	556.65	-0.026510
120.00	1.6342	31.777	0.031470	2.1213	2.1728	0.020877	0.027847	0.070566	506.54	0.068825
125.00	2.1389	30.280	0.033025	2.4642	2.5349	0.023700	0.027681	0.076800	452.05	0.20691
130.00	2.7475	28.549	0.035027	2.8314	2.9276	0.026617	0.027791	0.085756	391.41	0.42042
135.00	3.4739	26.416	0.037855	3.2397	3.3712	0.029765	0.028512	0.10995	321.84	0.78572
140.00	4.3357	23.427	0.042685	3.7349	3.9200	0.033502	0.030963	0.18235	238.35	1.5459
144.41	5.2394	15.603	0.064090	4.7226	5.0584	0.041160			0	4.3227
53.481	0.00023881	0.00053725	1861.3	5.3412	5.7857	0.11536	0.020800	0.029129	127.97	76.144
55.000	0.00038159	0.00083488	1197.8	5.3726	5.8296	0.11228	0.020805	0.029139	129.76	71.404
60.000	0.0014872	0.0029857	334.92	5.4753	5.9734	0.10348	0.020831	0.029204	135.46	58.461
65.000	0.0046126	0.0085667	116.73	5.5765	6.1149	0.096356	0.020886	0.029341	140.83	48.604
70.000	0.011981	0.020743	48.208	5.6750	6.2526	0.090504	0.020984	0.029589	145.85	40.910
75.000	0.027062	0.044003	22.726	5.7697	6.3847	0.085622	0.021139	0.029984	150.47	34.772
80.000	0.054668	0.084093	11.892	5.8592	6.5093	0.081489	0.021361	0.030562	154.65	29.788
85.000	0.10090	0.14789	6.7617	5.9423	6.6246	0.077936	0.021653	0.031349	158.34	25.696
90.000	0.17296	0.24329	4.1103	6.0181	6.7290	0.074837	0.022013	0.032368	161.52	22.322
95.000	0.27894	0.37919	2.6372	6.0855	6.8212	0.072094	0.022432	0.033644	164.12	19.545
100.00	0.42751	0.56568	1.7678	6.1438	6.8995	0.069630	0.022900	0.035219	166.12	17.279
105.00	0.62778	0.81460	1.2276	6.1916	6.9623	0.067380	0.023406	0.037174	167.46	15.449
110.00	0.88912	1.1406	0.87675	6.2274	7.0070	0.065284	0.023951	0.039668	168.12	13.988
115.00	1.2212	1.5630	0.63979	6.2487	7.0300	0.063285	0.024547	0.043016	168.05	12.827
120.00	1.6342	2.1098	0.47398	6.2511	7.0256	0.061318	0.025234	0.047844	167.26	11.886
125.00	2.1389	2.8245	0.35404	6.2277	6.9850	0.059301	0.026096	0.055492	165.81	11.069
130.00	2.7475	3.7825	0.26438	6.1664	6.8928	0.057119	0.027303	0.069276	163.76	10.250
135.00	3.4739	5.1364	0.19469	6.0431	6.7195	0.054567	0.029246	0.099896	161.03	9.2577
140.00	4.3357	7.3237	0.13654	5.7921	6.3841	0.051103	0.033084	0.21077	156.46	7.8082
144.41	5.2394	15.603	0.064090	4.7226	5.0584	0.041160			0	4.3227
Single-Phase Properties										
84.922	0.10000	39.546	0.025287	-0.0091317	-0.0066030	-0.000077307	0.031205	0.057385	824.62	-0.26537
84.922	0.10000	0.14668	6.8177	5.9411	6.6228	0.077988	0.021648	0.031335	158.29	25.754
100.00	0.10000	0.12275	8.1468	6.2721	7.0868	0.083019	0.021268	0.030345	173.11	17.864
150.00	0.10000	0.080628	12.403	7.3358	8.5761	0.095107	0.021022	0.029539	213.56	7.4423
200.00	0.10000	0.060267	16.593	8.3977	10.057	0.10363	0.021401	0.029803	246.33	4.1219
250.00	0.10000	0.048155	20.766	9.4869	11.564	0.11035	0.022142	0.030505	274.27	2.6600
300.00	0.10000	0.040106	24.934	10.617	13.110	0.11598	0.023021	0.031368	298.96	1.8799
100.00	1.0000	36.645	0.027289	0.86105	0.88834	0.0093623	0.029558	0.060025	696.10	-0.19109
111.80	1.0000	33.918	0.029483	1.5911	1.6206	0.016279	0.028409	0.064682	587.03	-0.073051
111.80	1.0000	1.2803	0.78106	6.2369	7.0180	0.064557	0.024158	0.040751	168.18	13.540
150.00	1.0000	0.85139	1.1746	7.1946	8.3692	0.075007	0.021931	0.032606	207.71	7.3873

200.00	1.0000	0.61498	1.6261	8.3181	9.9441	0.084080	0.021681	0.030928	244.27	4.1390
250.00	1.0000	0.48577	2.0586	9.4313	11.490	0.090978	0.022225	0.031046	273.76	2.6581
300.00	1.0000	0.40251	2.4844	10.573	13.057	0.096691	0.023032	0.031678	299.28	1.8692
100.00	5.0000	37.065	0.026980	0.80142	0.93632	0.0087568	0.029727	0.058693	721.70	-0.21256
143.33	5.0000	19.879	0.050304	4.2229	4.4744	0.037196	0.036294	0.63033	169.23	2.8620
143.33	5.0000	10.490	0.095333	5.3751	5.8518	0.046806	0.039553	1.0196	148.40	6.0573
150.00	5.0000	6.5097	0.15362	6.2260	6.9941	0.054653	0.027354	0.084441	177.58	6.7256
200.00	5.0000	3.3899	0.29499	7.9204	9.3953	0.068706	0.022993	0.037593	237.67	3.8562
250.00	5.0000	2.5221	0.39650	9.1743	11.157	0.076582	0.022698	0.033813	273.06	2.4478
300.00	5.0000	2.0427	0.48954	10.377	12.824	0.082665	0.023148	0.033134	301.36	1.6957
100.00	10.000	37.536	0.026641	0.73479	1.0012	0.0080653	0.029857	0.057385	752.43	-0.23402
150.00	10.000	24.141	0.041423	3.9349	4.3491	0.034822	0.027090	0.094016	324.06	0.86131
200.00	10.000	7.6450	0.13080	7.3273	8.6354	0.060060	0.024489	0.050206	240.08	3.1116
250.00	10.000	5.2188	0.19162	8.8378	10.754	0.069563	0.023418	0.037864	278.39	2.0656
300.00	10.000	4.1242	0.24247	10.136	12.561	0.076160	0.023411	0.035025	307.87	1.4058
100.00	15.000	37.961	0.026343	0.67509	1.0702	0.0074311	0.029870	0.056345	783.34	-0.25114
150.00	15.000	27.008	0.037026	3.5725	4.1279	0.032052	0.026615	0.070563	415.88	0.33099
200.00	15.000	12.412	0.080569	6.7026	7.9111	0.053898	0.025220	0.060759	263.46	2.0529
250.00	15.000	7.9757	0.12538	8.4961	10.377	0.064977	0.024073	0.042125	289.64	1.7085
300.00	15.000	6.1790	0.16184	9.9020	12.330	0.072112	0.023725	0.036972	318.16	1.1770
100.00	20.000	38.348	0.026077	0.62089	1.1424	0.0068429	0.029763	0.055495	815.20	-0.26507
150.00	20.000	28.645	0.034910	3.3586	4.0568	0.030382	0.026518	0.062828	480.50	0.11826
200.00	20.000	16.458	0.060762	6.1944	7.4096	0.049659	0.025474	0.062710	304.19	1.2436
250.00	20.000	10.648	0.093913	8.1664	10.045	0.061490	0.024527	0.045421	307.96	1.3200
300.00	20.000	8.1626	0.12251	9.6749	12.125	0.069094	0.024015	0.038840	331.68	0.98352

The values in these tables were generated from the NIST REFPROP software (Lemmon, E. W., McLinden, M. O., and Huber, M. L., NIST Standard Reference Database 23: Reference Fluid Thermodynamic and Transport Properties—REFPROP, National Institute of Standards and Technology, Standard Reference Data Program, Gaithersburg, Md., 2002, Version 7.1). The primary source for the thermodynamic properties is de Reuck, K. M., "International Thermodynamic Tables of the Fluid State—11 Fluorine," *International Union of Pure and Applied Chemistry*, Pergamon Press, Oxford, 1990. Validated equations for the viscosity and thermal conductivity are not currently available for this fluid.

Properties at the triple point temperature and the critical point temperature are given in the first and last entries of the saturation tables, respectively. In the single-phase table, when the temperature range for a given isobar includes a vapor-liquid phase boundary, the temperature of phase equilibrium is noted, and properties for both the saturated liquid and saturated vapor are given (with liquid properties given in the upper line). Lines are omitted from the temperature-pressure grid of the single-phase table, when the system would be in the solid phase or if there are potential problems with the source property surface.

The uncertainties of the equation of state are 0.2% in density, 2% in heat capacity, and 1.5% in the speed of sound, except in the critical region.

TABLE 2-217 Flutec

Proprietary name for a series of fluorocarbons produced by the Imperial Smelting Corp., Avonmouth, Bristol, UK. Bulletins of thermodynamic properties include PP1 (C₆F₁₄), PP2 (C₇F₁₄), PP3 (C₈F₁₆), PP5 (C₁₀F₁₈), PP9 (C₁₁F₂₀), and PP50, usually for 0.1–100 kg/m³, 0–500°C. See also Green, S. W., *Chem. & Ind.* (1969): 63–67.

TABLE 2-218 Halon

A series of fire-extinguishing fluids. Halon 1211 is produced by ICI, and Halon 1301, by duPont, the latter issuing a bulletin with thermodynamic properties and a diagram for the range 0.6–600 psia, –160–460°F.

TABLE 2-219 Thermodynamic Properties of Helium

Temperature K	Pressure MPa	Density mol/dm ³	Volume dm ³ /mol	Int. energy kJ/mol	Enthalpy kJ/mol	Entropy kJ/(mol·K)	C_v kJ/(mol·K)	C_p kJ/(mol·K)	Sound speed m/s	Joule-Thomson K/MPa	Therm. cond. mW/(m·K)	Viscosity μPa·s
Saturated Properties												
2.1768	0.0048565	36.537	0.027370	-0.030158	-0.030025	-0.0087120	0.025164	0.025289	216.83	-1.0411	13.522	3.5963
2.2000	0.0051477	36.523	0.027380	-0.029596	-0.029455	-0.0084552	0.023062	0.023216	216.59	-1.1290	13.631	3.6153
2.3500	0.0073079	36.396	0.027475	-0.026858	-0.026658	-0.0072478	0.014101	0.014502	215.68	-1.7580	14.294	3.7039
2.5000	0.010001	36.217	0.027611	-0.025011	-0.024734	-0.0064839	0.010092	0.010808	216.03	-2.2958	14.894	3.7456
2.6500	0.013298	35.992	0.027784	-0.023514	-0.023145	-0.0059016	0.0085050	0.0095913	216.74	-2.5162	15.442	3.7541
2.8000	0.017270	35.727	0.027990	-0.022106	-0.021623	-0.0053835	0.0080743	0.0095802	216.57	-2.4447	15.946	3.7391
2.9500	0.021983	35.423	0.028230	-0.020660	-0.020040	-0.0048790	0.0081637	0.010142	215.08	-2.2326	16.408	3.7074
3.1000	0.027502	35.082	0.028504	-0.019120	-0.018336	-0.0043676	0.0084575	0.010969	212.50	-1.9844	16.829	3.6637
3.2500	0.033890	34.705	0.028814	-0.017461	-0.016485	-0.0038422	0.0088040	0.011921	209.15	-1.7406	17.209	3.6113
3.4000	0.041209	34.291	0.029162	-0.015675	-0.014473	-0.0033010	0.0091348	0.012944	205.24	-1.5095	17.548	3.5525
3.5500	0.049518	33.838	0.029553	-0.013757	-0.012294	-0.0027443	0.0094238	0.014037	200.91	-1.2873	17.844	3.4890
3.7000	0.058879	33.342	0.029993	-0.011706	-0.0099402	-0.0021719	0.0096652	0.015223	196.21	-1.0669	18.098	3.4218
3.8500	0.069351	32.799	0.030489	-0.0095155	-0.0074010	-0.0015832	0.0098629	0.016553	191.15	-0.84045	18.307	3.3516
4.0000	0.080998	32.203	0.031053	-0.0071756	-0.0046603	-0.00097628	0.010024	0.018104	185.70	-0.59987	18.474	3.2785
4.1500	0.093886	31.545	0.031700	-0.0046702	-0.0016940	-0.00034763	0.010158	0.019993	179.82	-0.33639	18.599	3.2025
4.3000	0.10809	30.813	0.032454	-0.0019735	0.0015343	0.00030858	0.010273	0.022416	173.44	-0.03948	18.688	3.1231
4.4500	0.12368	29.986	0.033349	0.0005551	0.0050800	0.0010017	0.010378	0.025720	166.48	0.30472	18.753	3.0392
4.6000	0.14075	29.032	0.034445	0.0041842	0.0090322	0.0017471	0.010481	0.030604	158.80	0.71637	18.811	2.9490
4.7500	0.15942	27.895	0.035849	0.0078334	0.013548	0.0025725	0.010592	0.038735	150.22	1.2278	18.892	2.8488
4.9000	0.17983	26.456	0.037798	0.012155	0.018953	0.0035365	0.010726	0.055286	140.44	1.8978	19.051	2.7312
5.0500	0.20225	24.384	0.041010	0.017863	0.026157	0.0048066	0.010920	0.10769	128.80	2.8635	19.490	2.5752
5.1953	0.22637	17.399	0.057475	0.034500	0.047510	0.0087388			0	5.6142		
2.1768	0.0048565	0.28619	3.4942	0.045977	0.062946	0.033998	0.013890	0.024259	83.225	27.717	3.9767	0.53761
2.2000	0.0051477	0.30076	3.3249	0.046200	0.063316	0.033714	0.013900	0.024319	83.564	27.045	4.0381	0.54487
2.3500	0.0073079	0.40515	2.4682	0.047628	0.065665	0.032039	0.013945	0.024692	85.668	23.375	4.4135	0.59162
2.5000	0.010001	0.52873	1.8913	0.049016	0.067931	0.030582	0.013954	0.025049	87.618	20.607	4.7651	0.63825
2.6500	0.013298	0.67363	1.4845	0.050355	0.070096	0.029283	0.013937	0.025413	89.415	18.480	5.1055	0.68502
2.8000	0.017270	0.84193	1.1878	0.051635	0.072147	0.028106	0.013897	0.025800	91.063	16.819	5.4423	0.73220
2.9500	0.021983	1.0357	0.96551	0.052848	0.074072	0.027023	0.013840	0.026230	92.568	15.504	5.7797	0.77999
3.1000	0.027502	1.2573	0.79536	0.053985	0.075859	0.026018	0.013767	0.026720	93.934	14.450	6.1203	0.82863
3.2500	0.033890	1.5091	0.66264	0.055037	0.077494	0.025074	0.013682	0.027292	95.167	13.597	6.4659	0.87831
3.4000	0.041209	1.7941	0.55738	0.055993	0.078962	0.024180	0.013588	0.027973	96.271	12.902	6.8180	0.92926
3.5500	0.049518	2.1157	0.47265	0.056842	0.080247	0.023324	0.013485	0.028799	97.250	12.329	7.1823	0.98171
3.7000	0.058879	2.4783	0.40351	0.057570	0.081328	0.022495	0.013376	0.029817	98.108	11.856	7.5561	1.0359
3.8500	0.069351	2.8871	0.34637	0.058158	0.082179	0.021684	0.013262	0.031095	98.847	11.460	7.9453	1.0922
4.0000	0.080998	3.3494	0.29856	0.058586	0.082769	0.020881	0.013144	0.032736	99.469	11.127	8.3558	1.1509
4.1500	0.093886	3.8747	0.25808	0.058825	0.083055	0.020074	0.013022	0.034897	99.978	10.841	8.7965	1.2125
4.3000	0.10809	4.4768	0.22337	0.058834	0.082977	0.019249	0.012898	0.037844	100.38	10.587	9.2815	1.2776
4.4500	0.12368	5.1759	0.19320	0.058554	0.082449	0.018388	0.012770	0.042056	100.67	10.349	9.8336	1.3473
4.6000	0.14075	6.0046	0.16654	0.057896	0.081335	0.017465	0.012637	0.048501	100.88	10.104	10.490	1.4230
4.7500	0.15942	7.0212	0.14243	0.056698	0.079403	0.016437	0.012496	0.059461	101.05	9.8116	11.319	1.5075
4.9000	0.17983	8.3467	0.11981	0.054637	0.076183	0.015216	0.012341	0.081908	101.28	9.3953	12.465	1.6065
5.0500	0.20225	10.326	0.096844	0.050816	0.070403	0.013568	0.012146	0.15172	101.95	8.6477	14.402	1.7364
5.1953	0.22637	17.399	0.057475	0.034500	0.047510	0.0087388			0	5.6142		

Single-Phase Properties

100.00	0.10000	0.12010	8.3265	1.2679	2.1006	0.089342	0.012475	0.020791	589.24	-0.54790	73.713	9.7778
350.00	0.10000	0.034351	29.111	4.3860	7.2972	0.11538	0.012472	0.020785	1101.2	-0.61403	173.53	22.154
600.00	0.10000	0.020042	49.896	7.5039	12.494	0.12659	0.012472	0.020785	1441.5	-0.57336	252.40	32.215
850.00	0.10000	0.014148	70.681	10.622	17.690	0.13383	0.012472	0.020786	1715.7	-0.54223	321.87	41.153
1100.0	0.10000	0.010933	91.467	13.740	22.886	0.13919	0.012472	0.020786	1951.7	-0.51882	385.47	49.382
1350.0	0.10000	0.0089085	112.25	16.857	28.083	0.14344	0.012472	0.020786	2162.0	-0.50057	444.91	57.105
100.00	1.0000	1.1854	0.84359	1.2672	2.1108	0.070191	0.012506	0.020837	596.88	-0.54470	74.600	9.8922
350.00	1.0000	0.34233	2.9212	4.3875	7.3086	0.096243	0.012477	0.020782	1104.7	-0.61441	174.19	22.180
600.00	1.0000	0.20005	4.9988	7.5054	12.504	0.10744	0.012474	0.020783	1444.0	-0.57410	253.00	32.231
850.00	1.0000	0.14131	7.0768	10.623	17.700	0.11468	0.012473	0.020784	1717.6	-0.54296	322.43	41.164
1100.0	1.0000	0.10923	9.1550	13.741	22.896	0.12004	0.012473	0.020784	1953.3	-0.51949	386.00	49.391
1350.0	1.0000	0.089021	11.233	16.859	28.092	0.12430	0.012472	0.020784	2163.5	-0.50117	445.41	57.112
100.00	5.0000	5.6058	0.17839	1.2641	2.1560	0.056777	0.012635	0.021029	630.65	-0.53640	79.465	10.374
350.00	5.0000	1.6858	0.59320	4.3938	7.3598	0.082880	0.012500	0.020769	1120.3	-0.61554	176.72	22.297
600.00	5.0000	0.99204	1.0080	7.5120	12.552	0.094074	0.012484	0.020771	1454.9	-0.57711	255.23	32.299
850.00	5.0000	0.70266	1.4232	10.630	17.745	0.10131	0.012479	0.020775	1726.3	-0.54605	324.52	41.212
1100.0	5.0000	0.54393	1.8385	13.747	22.939	0.10667	0.012477	0.020777	1960.6	-0.52237	387.99	49.428
1350.0	5.0000	0.44368	2.2539	16.864	28.134	0.11092	0.012475	0.020779	2169.9	-0.50380	447.32	57.143
100.00	10.000	10.505	0.095194	1.2606	2.2125	0.050975	0.012775	0.021226	672.30	-0.53355	85.417	10.926
350.00	10.000	3.3086	0.30224	4.4013	7.4237	0.077139	0.012527	0.020755	1140.1	-0.61584	179.43	22.435
600.00	10.000	1.9638	0.50921	7.5200	12.612	0.088326	0.012497	0.020756	1468.8	-0.58023	257.42	32.383
850.00	10.000	1.3957	0.71649	10.637	17.802	0.095556	0.012487	0.020763	1737.3	-0.54953	326.55	41.272
1100.0	10.000	1.0823	0.92394	13.754	22.994	0.10091	0.012482	0.020769	1969.9	-0.52572	389.94	49.475
1350.0	10.000	0.88379	1.1315	16.871	28.186	0.10516	0.012479	0.020772	2178.0	-0.50691	449.21	57.181
100.00	50.000	35.384	0.028261	1.2602	2.6732	0.037457	0.013484	0.021607	962.59	-0.53310	127.36	14.393
350.00	50.000	14.387	0.069507	4.4519	7.9272	0.063904	0.012710	0.020725	1299.0	-0.59388	197.39	23.353
600.00	50.000	9.0593	0.11038	7.5781	13.097	0.075052	0.012587	0.020666	1584.0	-0.58658	268.59	32.979
850.00	50.000	6.6048	0.15140	10.695	18.265	0.082253	0.012543	0.020682	1829.4	-0.56519	334.90	41.713
1100.0	50.000	5.1933	0.19256	13.811	23.438	0.087587	0.012521	0.020701	2047.7	-0.54419	397.07	49.825
1350.0	50.000	4.2772	0.23380	16.926	28.615	0.091828	0.012508	0.020716	2245.9	-0.52586	455.79	57.471
100.00	100.00	51.724	0.019333	1.3032	3.2366	0.031667	0.013965	0.021327	1228.1	-0.51530	197.79	18.001
350.00	100.00	24.886	0.040183	4.5034	8.5217	0.058239	0.012884	0.020817	1482.2	-0.55155	217.91	24.221
600.00	100.00	16.512	0.060563	7.6393	13.696	0.069398	0.012683	0.020630	1727.9	-0.57040	281.89	33.590
850.00	100.00	12.359	0.080910	10.759	18.850	0.076579	0.012605	0.020615	1948.4	-0.56473	342.93	42.188
1350.0	100.00	8.2113	0.12178	16.988	29.166	0.086124	0.012542	0.020653	2335.4	-0.53766	458.27	57.800

The values in these tables were generated from the NIST REFPROP software (Lemmon, E. W., McLinden, M. O., and Huber, M. L., NIST Standard Reference Database 23: Reference Fluid Thermodynamic and Transport Properties—REFPROP, National Institute of Standards and Technology, Standard Reference Data Program, Gaithersburg, Md., 2002, Version 7.1). The primary source for the thermodynamic properties is McCarty, R. D., and Arp, V. D., "A New Wide Range Equation of State for Helium," *Adv. Cryo. Eng.* **35**:1465–1475, 1990. The source for viscosity is Arp, V. D., McCarty, R. D., and Friend, D. G., "Thermophysical Properties of Helium-4 from 0.8 to 1500 K with Pressures to 2000 MPa," *NIST Technical Note* 1334, Boulder, Colo., 1998. The source for thermal conductivity is Hands, B. A., and Arp, V. D., "A Correlation of Thermal Conductivity Data for Helium," *Cryogenics*, **21**(12):697–703, 1981.

Properties at the triple point and the critical point temperature are given in the first and last entries of the saturation tables, respectively. In the single-phase table, when the temperature range for a given isobar includes a vapor-liquid phase boundary, the temperature of phase equilibrium is noted, and properties for both the saturated liquid and saturated vapor are given (with liquid properties given in the upper line). Lines are omitted from the temperature-pressure grid of the single-phase table, when the system would be in the solid phase or if there are potential problems with the source property surface.

The uncertainties of the equation of state range from 1% at low temperatures (<20 K) to 0.1% at temperatures between 200 and 400 K, and from 3% in the speed of sound in the liquid phase to 0.1% in the speed of sound between 100 and 500 K. The uncertainty in heat capacities is about 5%. The uncertainty in viscosity is 10%. The uncertainty in thermal conductivity is 5%, except at low temperatures where it increases to 10%.

TABLE 2-220 Thermodynamic Properties of Heptane

Temperature K	Pressure MPa	Density mol/dm ³	Volume dm ³ /mol	Int. energy kJ/mol	Enthalpy kJ/mol	Entropy kJ/(mol·K)	C _v kJ/(mol·K)	C _p kJ/(mol·K)	Sound speed m/s	Joule-Thomson K/MPa	Therm. cond. mW/(m·K)	Viscosity μPa·s
Saturated Properties												
182.55	1.7549E-07	7.7457	0.12910	-41.621	-41.621	-0.15398	0.14886	0.19662	1669.5	-0.52328	155.74	3857.1
185.00	2.5788E-07	7.7246	0.12946	-41.139	-41.139	-0.15136	0.14924	0.19687	1656.1	-0.52236	155.56	3523.8
205.00	4.0249E-06	7.5549	0.13236	-37.178	-37.178	-0.13103	0.15264	0.19936	1550.9	-0.51267	153.03	1889.1
225.00	3.5822E-05	7.3882	0.13535	-33.158	-33.158	-0.11232	0.15666	0.20287	1452.3	-0.49878	149.21	1175.0
245.00	0.00021055	7.2229	0.13845	-29.056	-29.056	-0.094861	0.16146	0.20746	1358.8	-0.48063	144.65	805.42
265.00	0.00090411	7.0579	0.14169	-24.852	-24.852	-0.078369	0.16706	0.21311	1269.3	-0.45837	139.70	589.93
285.00	0.0030469	6.8917	0.14510	-20.526	-20.525	-0.062631	0.17337	0.21972	1183.0	-0.43224	134.59	452.87
305.00	0.0084921	6.7233	0.14874	-16.058	-16.057	-0.047486	0.18029	0.22715	1099.5	-0.40232	129.47	359.75
325.00	0.020357	6.5515	0.15264	-11.436	-11.433	-0.032809	0.18765	0.23527	1018.0	-0.36834	124.41	293.16
345.00	0.043242	6.3747	0.15687	-6.6463	-6.6396	-0.018509	0.19534	0.24397	938.09	-0.32951	119.45	243.54
365.00	0.083287	6.1914	0.16151	-1.6791	-1.6656	-0.0045150	0.20321	0.25320	859.20	-0.28429	114.61	205.28
385.00	0.14809	5.9995	0.16668	3.4744	3.4991	0.0092301	0.21119	0.26293	780.76	-0.22999	109.90	174.90
405.00	0.24655	5.7965	0.17252	8.8226	8.8651	0.022774	0.21920	0.27327	702.10	-0.16200	105.28	150.12
425.00	0.38874	5.5785	0.17926	14.375	14.445	0.036160	0.22720	0.28444	622.51	-0.072112	100.73	129.39
445.00	0.58581	5.3401	0.18726	20.147	20.256	0.049436	0.23517	0.29693	541.08	0.055234	96.175	111.58
465.00	0.85019	5.0723	0.19715	26.159	26.327	0.062666	0.24315	0.31186	456.64	0.25318	91.522	95.804
485.00	1.1961	4.7587	0.21014	32.455	32.706	0.075947	0.25123	0.33203	367.46	0.60537	86.595	81.246
505.00	1.6406	4.3628	0.22921	39.129	39.506	0.089485	0.25971	0.36700	270.69	1.3922	81.058	66.925
525.00	2.2070	3.7651	0.26559	46.501	47.087	0.10393	0.26971	0.48246	161.32	4.2679	74.208	50.757
540.13	2.7311	2.3153	0.43191	55.157	56.336	0.12095			0	26.539		
182.55	1.7549E-07	1.1562E-07	8,649,000.	1.0688	2.5867	0.088185	0.11339	0.12171	127.51	478.91	4.8076	0.93944
185.00	2.5788E-07	1.6766E-07	5,964,600.	1.3477	2.8859	0.086612	0.11424	0.12255	128.33	454.07	4.9177	1.6197
205.00	4.0249E-06	2.3614E-06	423,480.	3.7004	5.4048	0.076690	0.12103	0.12935	134.83	301.84	5.8582	3.8170
225.00	3.5822E-05	1.9151E-05	52,218.	6.1891	8.0596	0.070867	0.12796	0.13628	140.99	208.67	6.8855	4.4411
245.00	0.00021055	0.00010342	9,669.6	8.8178	10.854	0.068037	0.13529	0.14363	146.83	148.90	8.0159	4.8725
265.00	0.00090411	0.00041102	2,433.0	11.592	13.792	0.067457	0.14313	0.15153	152.32	109.17	9.2615	5.2813
285.00	0.0030469	0.0012912	774.44	14.516	16.875	0.068598	0.15149	0.16002	157.38	82.064	10.631	5.6934
305.00	0.0084921	0.0033793	295.92	17.589	20.102	0.071069	0.16033	0.16910	161.89	63.190	12.128	6.1135
325.00	0.020357	0.0076646	130.47	20.809	23.465	0.074569	0.16957	0.17874	165.69	49.846	13.757	6.5434
345.00	0.043242	0.015529	64.395	24.169	26.954	0.078862	0.17912	0.18891	168.60	40.301	15.521	6.9849
365.00	0.083287	0.028777	34.750	27.660	30.555	0.083760	0.18889	0.19961	170.42	33.422	17.424	7.4417
385.00	0.14809	0.049694	20.123	31.271	34.251	0.089105	0.19880	0.21088	170.92	28.458	19.473	7.9194
405.00	0.24655	0.081188	12.317	34.984	38.021	0.094763	0.20878	0.22285	169.84	24.914	21.682	8.4272
425.00	0.38874	0.12711	7.8674	38.780	41.838	0.10061	0.21881	0.23587	166.88	22.470	24.071	8.9798
445.00	0.58581	0.19291	5.1838	42.627	45.663	0.10653	0.22889	0.25064	161.58	20.951	26.681	9.6020
465.00	0.85019	0.28714	3.4827	46.478	49.439	0.11237	0.23906	0.26877	153.35	20.312	29.592	10.339
485.00	1.1961	0.42516	2.3521	50.254	53.067	0.11793	0.24945	0.29447	141.27	20.689	32.980	11.280
505.00	1.6406	0.64076	1.5607	53.786	56.346	0.12283	0.26036	0.34231	123.97	22.542	37.355	12.649
525.00	2.2070	1.0396	0.96195	56.608	58.731	0.12611	0.27248	0.50359	99.655	26.764	45.104	15.245
540.13	2.7311	2.3153	0.43191	55.157	56.336	0.12095			0	26.539		

Single-Phase Properties

200.00	0.10000	7.5975	0.13162	-38.176	-38.163	-0.13596	0.15175	0.19864	1576.9	-0.51551	153.84	2174.6
300.00	0.10000	6.7666	0.14778	-17.194	-17.180	-0.051241	0.17852	0.22520	1120.8	-0.41037	130.79	380.51
371.09	0.10000	6.1340	0.16303	-0.13101	-0.11470	-0.00030834	0.20564	0.25610	835.31	-0.26890	113.16	195.32
371.09	0.10000	0.034210	29.231	28.747	31.670	0.085345	0.19189	0.20297	170.72	31.736	18.032	7.5845
400.00	0.10000	0.031296	31.953	34.506	37.702	0.10099	0.20404	0.21430	179.24	23.441	20.824	8.1460
500.00	0.10000	0.024471	40.864	57.027	61.114	0.15307	0.24438	0.25347	203.88	10.262	31.544	10.052
600.00	0.10000	0.020221	49.453	83.290	88.236	0.20242	0.27936	0.28808	224.61	5.6176	43.213	11.883
200.00	1.0000	7.6022	0.13154	-38.202	-38.071	-0.13609	0.15181	0.19861	1581.3	-0.51586	154.03	2203.0
300.00	1.0000	6.7756	0.14759	-17.244	-17.096	-0.051406	0.17857	0.22503	1127.5	-0.41229	131.16	385.02
400.00	1.0000	5.8668	0.17045	7.3729	7.5433	0.019169	0.21722	0.26994	732.61	-0.19065	107.01	158.14
474.30	1.0000	4.9336	0.20269	29.049	29.251	0.068829	0.24689	0.32029	415.88	0.38883	89.279	88.930
474.30	1.0000	0.34452	2.9026	48.251	51.154	0.11501	0.24385	0.27933	148.28	20.343	31.091	10.743
500.00	1.0000	0.30146	3.3172	54.943	58.260	0.12960	0.25108	0.27563	166.14	14.530	33.576	11.093
600.00	1.0000	0.22064	4.5322	82.131	86.663	0.18133	0.28189	0.29560	207.02	6.3945	44.625	12.599
200.00	5.0000	7.6229	0.13118	-38.316	-37.661	-0.13667	0.15208	0.19848	1600.2	-0.51732	154.89	2331.7
300.00	5.0000	6.8141	0.14675	-17.456	-16.722	-0.052121	0.17879	0.22435	1156.4	-0.42010	132.76	405.07
400.00	5.0000	5.9526	0.16799	6.9316	7.7715	0.018047	0.21734	0.26714	783.30	-0.23205	109.78	169.17
500.00	5.0000	4.8210	0.20743	35.998	37.035	0.083125	0.25622	0.32159	423.74	0.32892	89.492	84.960
600.00	5.0000	2.2376	0.44691	72.724	74.958	0.15188	0.29509	0.43674	134.50	7.5010	63.671	27.947
200.00	10.000	7.6479	0.13075	-38.454	-37.147	-0.13737	0.15241	0.19835	1623.3	-0.51893	155.94	2498.6
300.00	10.000	6.8595	0.14578	-17.705	-16.247	-0.052975	0.17908	0.22363	1190.5	-0.42839	134.68	430.15
400.00	10.000	6.0454	0.16542	6.4514	8.1056	0.016799	0.21753	0.26465	838.61	-0.26850	112.88	182.05
500.00	10.000	5.0885	0.19652	34.818	36.783	0.080607	0.25576	0.30908	532.87	0.040826	95.612	98.261
600.00	10.000	3.8337	0.26084	67.259	69.867	0.14081	0.29039	0.35093	303.32	0.87871	82.499	55.622
300.00	50.000	7.1493	0.13987	-19.254	-12.260	-0.058701	0.18121	0.22068	1412.7	-0.46360	147.62	635.00
400.00	50.000	6.5292	0.15316	3.9425	11.600	0.0096885	0.21935	0.25730	1139.8	-0.37509	130.89	269.35
500.00	50.000	5.9397	0.16836	30.741	39.159	0.071034	0.25677	0.29309	940.60	-0.29668	119.90	158.19
600.00	50.000	5.3846	0.18572	60.741	70.026	0.12723	0.28945	0.32327	800.70	-0.23327	114.54	109.31
300.00	100.00	7.4106	0.13494	-20.560	-7.0660	-0.064263	0.18354	0.21976	1622.2	-0.47764	160.40	909.65
400.00	100.00	6.8927	0.14508	2.1360	16.644	0.0037009	0.22143	0.25527	1385.0	-0.40643	146.71	364.81
500.00	100.00	6.4248	0.15565	28.397	43.961	0.064512	0.25865	0.29041	1216.1	-0.35005	137.75	209.24
600.00	100.00	6.0005	0.16665	57.894	74.559	0.12021	0.29113	0.32068	1095.6	-0.31028	133.53	143.14

The values in these tables were generated from the NIST REFPROP software (Lemmon, E. W., McLinden, M. O., and Huber, M. L., NIST Standard Reference Database 23: Reference Fluid Thermodynamic and Transport Properties—REFPROP, National Institute of Standards and Technology, Standard Reference Data Program, Gaithersburg, Md., 2002, Version 7.1). The primary source for the thermodynamic properties is Span, R., and Wagner, W., "Equations of State for Technical Applications. II. Results for Nonpolar Fluids," *Int. J. Thermophys.*, **24**(1):41–109, 2003. The source for viscosity is NIST14, Version 9.08. The source for thermal conductivity is NIST14, Version 9.08.

Properties at the triple point temperature and the critical point temperature are given in the first and last entries of the saturation tables, respectively. In the single-phase table, when the temperature range for a given isobar includes a vapor-liquid phase boundary, the temperature of phase equilibrium is noted, and properties for both the saturated liquid and saturated vapor are given (with liquid properties given in the upper line). Lines are omitted from the temperature-pressure grid of the single-phase table, when the system would be in the solid phase or if there are potential problems with the source property surface.

The uncertainties of the equation of state are approximately 0.2% (to 0.5% at high pressures) in density, 1% (in the vapor phase) to 2% in heat capacity, 1% (in the vapor phase) to 2% in the speed of sound, and 0.2% in vapor pressure, except in the critical region. For viscosity, estimated uncertainty is 2%. For thermal conductivity, estimated uncertainty, except near the critical region, is 4–6%.

TABLE 2-221 Thermodynamic Properties of Hexane

Temperature K	Pressure MPa	Density mol/dm ³	Volume dm ³ /mol	Int. energy kJ/mol	Enthalpy kJ/mol	Entropy kJ/(mol·K)	C_v kJ/(mol·K)	C_p kJ/(mol·K)	Sound speed m/s	Joule-Thomson K/MPa	Therm. cond. mW/(m·K)	Viscosity μPa·s
Saturated Properties												
177.83	1.2771E-06	8.8394	0.11313	-30.053	-30.053	-0.11799	0.11891	0.16166	1638.9	-0.55189	155.43	2392.6
180.00	1.7416E-06	8.8166	0.11342	-29.702	-29.702	-0.11602	0.11944	0.16212	1626.3	-0.54996	155.64	2235.0
195.00	1.2006E-05	8.6607	0.11546	-27.247	-27.247	-0.10292	0.12299	0.16527	1542.5	-0.53626	155.51	1474.2
210.00	6.0531E-05	8.5066	0.11756	-24.744	-24.744	-0.090556	0.12642	0.16850	1463.6	-0.52146	153.36	1048.0
225.00	0.00023840	8.3535	0.11971	-22.190	-22.190	-0.078815	0.12992	0.17196	1388.4	-0.50504	149.89	786.13
240.00	0.00077035	8.2006	0.12194	-19.583	-19.583	-0.067597	0.13361	0.17575	1316.2	-0.48667	145.59	613.59
255.00	0.0021200	8.0472	0.12427	-16.916	-16.916	-0.056819	0.13753	0.17992	1246.3	-0.46617	140.79	493.58
270.00	0.0051148	7.8927	0.12670	-14.184	-14.183	-0.046408	0.14172	0.18448	1178.5	-0.44339	135.74	406.45
285.00	0.011066	7.7363	0.12926	-11.380	-11.379	-0.036304	0.14616	0.18943	1112.3	-0.41819	130.60	340.96
300.00	0.021865	7.5774	0.13197	-8.4998	-8.4969	-0.026456	0.15084	0.19474	1047.6	-0.39031	125.50	290.31
315.00	0.040031	7.4151	0.13486	-5.5378	-5.5324	-0.016823	0.15571	0.20040	984.03	-0.35939	120.53	250.18
330.00	0.068721	7.2487	0.13796	-2.4895	-2.4800	-0.0073691	0.16074	0.20638	921.37	-0.32478	115.73	217.72
345.00	0.11169	7.0772	0.14130	0.64962	0.66541	0.0019333	0.16590	0.21269	859.40	-0.28553	111.15	190.99
360.00	0.17326	6.8995	0.14494	3.8834	3.9085	0.011109	0.17114	0.21932	797.86	-0.24020	106.82	168.61
375.00	0.25821	6.7141	0.14894	7.2160	7.2544	0.020180	0.17645	0.22633	736.47	-0.18658	102.74	149.58
390.00	0.37176	6.5194	0.15339	10.652	10.709	0.029166	0.18178	0.23378	674.93	-0.12130	98.910	133.16
405.00	0.51954	6.3129	0.15840	14.195	14.278	0.038087	0.18713	0.24184	612.85	-0.038945	95.319	118.78
420.00	0.70759	6.0916	0.16416	17.854	17.970	0.046965	0.19251	0.25078	549.78	0.069646	91.941	105.97
435.00	0.94243	5.8506	0.17092	21.638	21.799	0.055828	0.19791	0.26113	485.05	0.22117	88.736	94.348
450.00	1.2313	5.5825	0.17913	25.562	25.782	0.064717	0.20338	0.27400	417.67	0.44954	85.638	83.551
465.00	1.5827	5.2736	0.18963	29.656	29.956	0.073697	0.20902	0.29208	346.06	0.83549	82.537	73.177
480.00	2.0071	4.8943	0.20432	33.983	34.393	0.082910	0.21509	0.32426	267.23	1.6275	79.234	62.632
495.00	2.5196	4.3496	0.22990	38.752	39.331	0.092809	0.22251	0.42766	174.59	4.0963	75.402	50.415
507.82	3.0429	2.7059	0.36957	45.698	46.822	0.10743			0	21.950		
177.83	1.2771E-06	8.6377E-07	1,157,700.	6.5712	8.0497	0.096281	0.095572	0.10389	136.57	381.55	5.2567	3.0564
180.00	1.7416E-06	1.1637E-06	859,330.	6.7793	8.2759	0.094966	0.096248	0.10456	137.36	363.60	5.3651	3.2844
195.00	1.2006E-05	7.4054E-06	135,040.	8.2570	9.8783	0.087463	0.10079	0.10910	142.71	265.13	6.1371	4.1334
210.00	6.0531E-05	3.4674E-05	28,840.	9.8013	11.547	0.082256	0.10523	0.11356	147.84	198.42	6.9555	4.5617
225.00	0.00023840	0.00012750	7,842.9	11.411	13.281	0.078835	0.10975	0.11809	152.75	151.75	7.8286	4.9114
240.00	0.00077035	0.00038658	2,586.8	13.086	15.079	0.076827	0.11444	0.12282	157.43	118.24	8.7644	5.2472
255.00	0.0021200	0.0010029	997.06	14.827	16.941	0.075951	0.11936	0.12783	161.83	93.691	9.7697	5.5832
270.00	0.0051148	0.0022917	436.35	16.633	18.865	0.075993	0.12457	0.13317	165.91	75.403	10.851	5.9228
285.00	0.011066	0.0047185	211.93	18.505	20.850	0.076780	0.13005	0.13886	169.59	61.606	12.012	6.2669
300.00	0.021865	0.0089152	112.17	20.440	22.893	0.078177	0.13579	0.14492	172.79	51.090	13.258	6.6161
315.00	0.040031	0.015688	63.742	22.438	24.989	0.080072	0.14178	0.15136	175.43	43.011	14.592	6.9712
330.00	0.068721	0.026023	38.427	24.494	27.135	0.082372	0.14798	0.15817	177.42	36.767	16.018	7.3333
345.00	0.11169	0.041099	24.332	26.606	29.324	0.085000	0.15435	0.16537	178.64	31.926	17.540	7.7043
360.00	0.17326	0.062314	16.048	28.769	31.549	0.087889	0.16085	0.17297	179.01	28.172	19.162	8.0869
375.00	0.25821	0.091349	10.947	30.977	33.804	0.090978	0.16746	0.18106	178.39	25.277	20.892	8.4853
390.00	0.37176	0.13027	7.6763	33.223	36.077	0.094213	0.17415	0.18976	176.64	23.080	22.739	8.9054
405.00	0.51954	0.18173	5.5026	35.497	38.356	0.097538	0.18092	0.19931	173.59	21.471	24.719	9.3563
420.00	0.70759	0.24933	4.0108	37.783	40.621	0.10090	0.18775	0.21014	169.01	20.386	26.858	9.8524
435.00	0.94243	0.33826	2.9563	40.061	42.848	0.10422	0.19467	0.22312	162.60	19.809	29.203	10.417
450.00	1.2313	0.45679	2.1892	42.299	44.994	0.10741	0.20173	0.24003	153.94	19.784	31.843	11.090
465.00	1.5827	0.61964	1.6138	44.438	46.992	0.11033	0.20903	0.26537	142.42	20.448	34.979	11.951
480.00	2.0071	0.85826	1.1651	46.363	48.702	0.11272	0.21678	0.31367	127.17	22.098	39.160	13.186
495.00	2.5196	1.2664	0.78962	47.752	49.742	0.11384	0.22558	0.46871	106.85	25.172	46.755	15.416
507.82	3.0429	2.7059	0.36957	45.698	46.822	0.10743			0	21.950		

Single-Phase Properties

200.00	0.10000	8.6098	0.11615	-26.420	-26.409	-0.098737	0.12414	0.16632	1516.3	-0.53154	155.01	1308.5
300.00	0.10000	7.5784	0.13195	-8.5042	-8.4910	-0.026471	0.15084	0.19472	1048.3	-0.39056	125.55	290.66
341.45	0.10000	7.1184	0.14048	-0.10255	-0.088504	-0.00025850	0.16467	0.21117	874.04	-0.29532	112.22	196.89
341.45	0.10000	0.037028	27.006	26.101	28.801	0.084352	0.15282	0.16363	178.43	32.965	17.170	7.6155
400.00	0.10000	0.030895	32.368	35.725	38.962	0.11177	0.17421	0.18376	196.30	17.891	23.256	8.9061
500.00	0.10000	0.024344	41.078	54.980	59.088	0.15654	0.20940	0.21824	221.55	8.1885	35.216	11.054
600.00	0.10000	0.020168	49.583	77.506	82.464	0.19908	0.23990	0.24850	243.38	4.6052	48.247	13.104
200.00	1.0000	8.6159	0.11606	-26.445	-26.329	-0.098862	0.12419	0.16628	1521.0	-0.53204	155.38	1327.2
300.00	1.0000	7.5906	0.13174	-8.5541	-8.4223	-0.026637	0.15088	0.19451	1055.7	-0.39338	126.12	294.62
400.00	1.0000	6.4028	0.15618	12.928	13.084	0.034934	0.18534	0.23836	642.57	-0.081596	96.993	124.96
438.24	1.0000	5.7953	0.17255	22.473	22.645	0.057745	0.19908	0.26364	470.76	0.26228	88.060	91.958
438.24	1.0000	0.36099	2.7701	40.550	43.320	0.10492	0.19618	0.22634	160.93	19.754	29.744	10.551
500.00	1.0000	0.27702	3.6098	53.661	57.271	0.13470	0.21315	0.22970	196.29	10.036	36.713	11.711
600.00	1.0000	0.21383	4.6765	76.704	81.381	0.17859	0.24143	0.25320	230.76	5.0002	49.365	13.575
200.00	5.0000	8.6424	0.11571	-26.553	-25.975	-0.099407	0.12440	0.16610	1541.5	-0.53416	157.01	1411.9
300.00	5.0000	7.6426	0.13085	-8.7667	-8.1124	-0.027355	0.15106	0.19368	1087.5	-0.40464	128.58	312.23
400.00	5.0000	6.5335	0.15306	12.434	13.199	0.033675	0.18536	0.23424	702.66	-0.15548	100.50	136.08
500.00	5.0000	4.8882	0.20457	38.358	39.381	0.091842	0.22066	0.30042	311.48	1.0544	81.341	64.368
600.00	5.0000	1.5349	0.65149	71.648	74.906	0.15663	0.24956	0.30605	173.73	6.3809	59.195	20.153
200.00	10.000	8.6744	0.11528	-26.683	-25.530	-0.10007	0.12466	0.16591	1566.5	-0.53649	159.01	1521.9
300.00	10.000	7.7032	0.12982	-9.0138	-7.7156	-0.028204	0.15128	0.19280	1124.9	-0.41638	131.56	334.21
400.00	10.000	6.6684	0.14996	11.917	13.416	0.032326	0.18546	0.23093	765.76	-0.21470	104.41	148.74
500.00	10.000	5.3956	0.18533	36.755	38.608	0.088363	0.21933	0.27365	455.87	0.25439	88.518	80.764
600.00	10.000	3.6515	0.27386	65.462	68.201	0.14220	0.24998	0.31536	248.16	1.7834	79.582	43.840
300.00	50.000	8.0787	0.12378	-10.511	-4.3222	-0.033766	0.15301	0.18931	1362.7	-0.46412	152.57	513.27
400.00	50.000	7.3187	0.13664	9.3999	16.232	0.025137	0.18689	0.22225	1090.0	-0.36559	128.45	231.13
500.00	50.000	6.5956	0.15162	32.487	40.068	0.078194	0.21979	0.25371	895.54	-0.27952	115.10	140.55
600.00	50.000	5.9215	0.16888	58.351	66.794	0.12685	0.24844	0.27993	763.82	-0.21072	111.13	100.20
300.00	100.00	8.4063	0.11896	-11.737	0.15835	-0.039032	0.15494	0.18811	1582.2	-0.48273	175.12	753.68
400.00	100.00	7.7789	0.12855	7.6799	20.535	0.019368	0.18864	0.21997	1345.0	-0.40550	152.26	319.21
500.00	100.00	7.2120	0.13866	30.244	44.110	0.071845	0.22138	0.25089	1178.8	-0.34615	138.03	188.34
600.00	100.00	6.7006	0.14924	55.635	70.559	0.11999	0.24989	0.27732	1062.8	-0.30501	132.17	132.10

The values in these tables were generated from the NIST REFPROP software (Lemmon, E. W., McLinden, M. O., and Huber, M. L., NIST Standard Reference Database 23: Reference Fluid Thermodynamic and Transport Properties—REFPROP, National Institute of Standards and Technology, Standard Reference Data Program, Gaithersburg, Md., 2002, Version 7.1). The primary source for the thermodynamic properties is Span, R., and Wagner, W., "Equations of State for Technical Applications. II. Results for Nonpolar Fluids," *Int. J. Thermophys.* **24**(1):41–109, 2003. The source for viscosity and thermal conductivity is NIST14, Version 9.08.

Properties at the triple point temperature and the critical point temperature are given in the first and last entries of the saturation tables, respectively. In the single-phase table, when the temperature range for a given isobar includes a vapor-liquid phase boundary, the temperature of phase equilibrium is noted, and properties for both the saturated liquid and saturated vapor are given (with liquid properties given in the upper line). Lines are omitted from the temperature-pressure grid of the single-phase table, when the system would be in the solid phase or if there are potential problems with the source property surface.

The uncertainties of the equation of state are approximately 0.2% (to 0.5% at high pressures) in density, 1% (in the vapor phase) to 2% in heat capacity, 1% (in the vapor phase) to 2% in the speed of sound, and 0.2% in vapor pressure, except in the critical region. For viscosity, estimated uncertainty is 2%. For thermal conductivity, estimated uncertainty, except near the critical region, is 4–6 %.

2-278 PHYSICAL AND CHEMICAL DATA

TABLE 2-222 Saturated Hydrazine

Temperature, K	Pressure, bar	v_f , m ³ /kg	v_g , m ³ /kg	h_f , kJ/kg	h_g , kJ/kg	s_f , kJ/(kg·K)	s_g , kJ/(kg·K)
386.6	1.013	0.001 053	0.9833	-105.9	65.4	0.5994	1.0426
390	1.135	0.001 060	0.8850	-104.8	66.0	0.6029	1.0409
400	1.560	0.001 081	0.6579	-101.4	68.2	0.6120	1.0360
410	2.102	0.001 104	0.4994	-97.6	70.6	0.6211	1.0314
420	2.786	0.001 127	0.3850	-93.9	73.0	0.6300	1.0275
440	4.732	0.001 178	0.2355	-86.1	77.6	0.6492	1.0212
460	7.610	0.001 235	0.1500	-76.9	82.1	0.6707	1.0163
480	11.76	0.001 299	0.1005	-67.1	86.6	0.6916	1.0118
500	17.42	0.001 374	0.0690	-57.3	90.8	0.7124	1.0086
520	29.59	0.001 460	0.0407	-47.8	94.6	0.7320	1.0058
540	34.75	0.001 563	0.0353	-36.0	97.7	0.7566	1.0042
560	47.09	0.001 681	0.0263	-25.2	101.2	0.7762	1.0020
580	62.44	0.001 835	0.0196	-12.4	103.6	0.8002	1.0002
600	81.17	0.002 045	0.0142	5.2	104.2	0.8335	0.9988
620	102.7	0.002 320	0.0106	23.2	103.6	0.8671	0.9967
640	128.1	0.002 86	0.0074	45.9	98.1	0.9035	0.9906
653 ^c	146.9	0.004 33	0.0043	83.7	83.7	0.9715	0.9715

Converted from E. F. Fricke, Republic Aviation Co. rept. F-5028-101. c = critical point.

TABLE 2-223 Thermodynamic Properties of Normal Hydrogen

Temperature K	Pressure MPa	Density mol/dm ³	Volume dm ³ /mol	Int. energy kJ/mol	Enthalpy kJ/mol	Entropy kJ/(mol·K)	C _v kJ/(mol·K)	C _p kJ/(mol·K)	Sound speed m/s	Joule-Thomson K/MPa	Therm. cond. mW/(m·K)	Viscosity μPa·s
Saturated Properties												
13.957	0.0077031	38.148	0.026214	-0.10434	-0.10414	-0.0059480	0.011064	0.015654	1361.1	-1.4137	76.293	25.463
14.000	0.0078936	38.129	0.026226	-0.10367	-0.10346	-0.0059000	0.010957	0.015547	1359.6	-1.4230	76.650	25.310
15.000	0.013436	37.701	0.026524	-0.088896	-0.088539	-0.0048799	0.0096961	0.014420	1318.5	-1.5204	84.106	22.215
16.000	0.021534	37.261	0.026838	-0.074446	-0.073868	-0.0039471	0.0096482	0.014709	1271.6	-1.4695	90.079	19.784
17.000	0.032848	36.802	0.027172	-0.059414	-0.058521	-0.0030355	0.010003	0.015557	1226.6	-1.3623	94.784	17.815
18.000	0.048078	36.321	0.027533	-0.043440	-0.042116	-0.0021219	0.010462	0.016642	1185.5	-1.2409	98.405	16.182
19.000	0.067960	35.812	0.027923	-0.026375	-0.024477	-0.0011983	0.010915	0.017842	1147.3	-1.1194	101.10	14.799
20.000	0.093249	35.274	0.028350	-0.0081516	-0.0055080	-0.00026211	0.011323	0.019120	1110.7	-1.0003	103.01	13.607
21.000	0.12472	34.702	0.028817	0.011274	0.014868	0.00068790	0.011677	0.020476	1074.7	-0.88232	104.24	12.565
22.000	0.16314	34.092	0.029333	0.031947	0.036732	0.0016528	0.011978	0.021935	1038.2	-0.76268	104.87	11.641
23.000	0.20932	33.439	0.029905	0.053929	0.060188	0.0026344	0.012235	0.023539	1000.5	-0.63795	104.98	10.811
24.000	0.26406	32.738	0.030546	0.077308	0.085375	0.0036357	0.012457	0.025351	960.99	-0.50414	104.60	10.057
25.000	0.32818	31.979	0.031271	0.10222	0.11248	0.0046610	0.012655	0.027465	919.10	-0.35648	103.79	9.3625
26.000	0.40250	31.152	0.032101	0.12884	0.14176	0.0057167	0.012840	0.030024	874.29	-0.18882	102.53	8.7151
27.000	0.48788	30.242	0.033067	0.15744	0.17357	0.0068122	0.013025	0.033265	826.00	0.0073109	100.83	8.1034
28.000	0.58524	29.225	0.034217	0.18843	0.20846	0.0079614	0.013224	0.037610	773.58	0.24446	98.654	7.5160
29.000	0.69554	28.067	0.035629	0.22245	0.24723	0.0091865	0.013460	0.043909	716.22	0.54283	95.935	6.9409
30.000	0.81989	26.706	0.037444	0.26061	0.29132	0.010527	0.013764	0.054194	652.73	0.93827	92.547	6.3620
31.000	0.95964	25.017	0.039973	0.30524	0.34360	0.012063	0.014198	0.074872	581.16	1.5038	88.221	5.7518
32.000	1.1168	22.637	0.044175	0.36302	0.41236	0.014035	0.014926	0.14185	497.24	2.4292	82.176	5.0391
33.190	1.3301	14.940	0.066934	0.53004	0.61907	0.020012			0	5.3208		
13.957	0.0077031	0.067540	14.806	0.68715	0.80120	0.058918	0.013157	0.021964	304.61	31.943	10.375	0.66345
14.000	0.0078936	0.069018	14.489	0.68764	0.80201	0.058777	0.013129	0.021944	305.17	31.808	10.431	0.66695
15.000	0.013436	0.11050	9.0494	0.69864	0.82024	0.055705	0.012872	0.021898	316.15	28.572	11.624	0.74268
16.000	0.021534	0.16764	5.9651	0.70899	0.83745	0.053010	0.012907	0.022199	325.05	25.724	12.681	0.81064
17.000	0.032848	0.24349	4.1069	0.71875	0.85365	0.050622	0.012992	0.022618	333.00	23.407	13.681	0.87421
18.000	0.048078	0.34126	2.9303	0.72783	0.86871	0.048480	0.013083	0.023121	340.22	21.522	14.669	0.93555
19.000	0.067960	0.46437	2.1535	0.73614	0.88249	0.046537	0.013178	0.023724	346.75	19.961	15.675	0.99611
20.000	0.093249	0.61652	1.6220	0.74359	0.89484	0.044755	0.013280	0.024449	352.59	18.642	16.716	1.0569
21.000	0.12472	0.80187	1.2471	0.75005	0.90558	0.043103	0.013392	0.025329	357.75	17.507	17.806	1.1186
22.000	0.16314	1.0251	0.97549	0.75541	0.91455	0.041554	0.013514	0.026401	362.25	16.513	18.956	1.1819
23.000	0.20932	1.2919	0.77406	0.75951	0.92154	0.040085	0.013650	0.027724	366.11	15.629	20.180	1.2472
24.000	0.26406	1.6089	0.62153	0.76218	0.92630	0.038674	0.013802	0.029376	369.34	14.829	21.493	1.3151
25.000	0.32818	1.9848	0.50383	0.76318	0.92853	0.037303	0.013973	0.031482	371.95	14.091	22.916	1.3863
26.000	0.40250	2.4307	0.41141	0.76224	0.92783	0.035950	0.014167	0.034234	373.96	13.396	24.477	1.4619
27.000	0.48788	2.9618	0.33763	0.75895	0.92368	0.034594	0.014392	0.037960	375.38	12.726	26.218	1.5433
28.000	0.58524	3.6003	0.27775	0.75276	0.91531	0.033206	0.014655	0.043253	376.19	12.061	28.202	1.6331
29.000	0.69554	4.3810	0.22826	0.74277	0.90154	0.031749	0.014971	0.051322	376.39	11.374	30.535	1.7362
30.000	0.81989	5.3643	0.18642	0.72747	0.88031	0.030160	0.015358	0.065054	375.97	10.624	33.407	1.8628
31.000	0.95964	6.6763	0.14978	0.70374	0.84748	0.028317	0.015854	0.093486	374.91	9.7362	37.226	2.0375
32.000	1.1168	8.6823	0.11518	0.66274	0.79136	0.025879	0.016535	0.18606	373.31	8.5059	43.200	2.3378
33.190	1.3301	14.940	0.066934	0.53004	0.61907	0.020012			0	5.3208		

TABLE 2-223 Thermodynamic Properties of Normal Hydrogen (Concluded)

Temperature K	Pressure MPa	Density mol/dm ³	Volume dm ³ /mol	Int. energy kJ/mol	Enthalpy kJ/mol	Entropy kJ/(mol·K)	C _v kJ/(mol·K)	C _p kJ/(mol·K)	Sound speed m/s	Joule-Thomson K/MPa	Therm. cond. mW/(m·K)	Viscosity μPa·s
Single-Phase Properties												
25.000	0.10000	0.50823	1.9676	0.81207	1.0088	0.049309	0.012734	0.022519	403.66	12.894	20.761	1.3142
100.00	0.10000	0.12030	8.3127	1.7949	2.6261	0.079163	0.014263	0.022637	808.92	1.4058	68.334	4.1896
175.00	0.10000	0.068680	14.560	3.0224	4.4785	0.092882	0.018150	0.026480	1026.9	0.13575	117.11	6.1845
250.00	0.10000	0.048077	20.800	4.4642	6.5442	0.10269	0.020003	0.028323	1209.1	-0.22980	160.59	7.9025
325.00	0.10000	0.036986	27.037	5.9947	8.6984	0.11022	0.020681	0.028998	1371.7	-0.38965	197.72	9.4561
400.00	0.10000	0.030054	33.273	7.5545	10.882	0.11626	0.020865	0.029180	1519.7	-0.47650	234.06	10.892
25.000	1.0000	32.746	0.030538	0.089693	0.12023	0.0041410	0.012580	0.025394	985.14	-0.51115	106.80	9.9923
31.268	1.0000	24.474	0.040861	0.31894	0.35980	0.012531	0.014353	0.084709	560.14	1.7031	86.829	5.5759
31.268	1.0000	7.1182	0.14049	0.69511	0.83559	0.027747	0.016014	0.10713	374.52	9.4548	38.524	2.0997
100.00	1.0000	1.2044	0.83027	1.7679	2.5982	0.059751	0.014331	0.023244	817.03	1.3036	70.413	4.2550
175.00	1.0000	0.68243	1.4653	3.0101	4.4754	0.073667	0.018190	0.026659	1035.8	0.11718	118.31	6.2213
250.00	1.0000	0.47788	2.0926	4.4576	6.5501	0.083515	0.020028	0.028401	1217.3	-0.23428	161.46	7.9283
325.00	1.0000	0.36797	2.7176	5.9910	8.7086	0.091062	0.020699	0.029039	1379.1	-0.39039	198.43	9.4759
400.00	1.0000	0.29924	3.3418	7.5525	10.894	0.097113	0.020878	0.029204	1526.4	-0.47605	234.65	10.908
25.000	5.0000	35.661	0.028042	0.046611	0.18682	0.0021443	0.012376	0.020610	1223.4	-0.90198	119.36	13.101
100.00	5.0000	5.9683	0.16755	1.6549	2.4927	0.045314	0.014583	0.025613	865.94	0.86369	80.395	4.5875
175.00	5.0000	3.3132	0.30183	2.9582	4.4673	0.059998	0.018352	0.027370	1077.3	0.032971	123.58	6.3871
250.00	5.0000	2.3268	0.42978	4.4292	6.5781	0.070022	0.020136	0.028723	1254.0	-0.25678	165.19	8.0420
325.00	5.0000	1.7990	0.55587	5.9750	8.7543	0.077631	0.020776	0.029211	1412.0	-0.39563	201.36	9.5631
400.00	5.0000	1.4680	0.68120	7.5440	10.950	0.083710	0.020937	0.029304	1556.2	-0.47537	237.09	10.979
25.000	10.000	37.930	0.026364	0.020221	0.28386	0.00059913	0.012222	0.018499	1402.1	-1.0762	131.12	16.625
100.00	10.000	11.417	0.087588	1.5346	2.4105	0.038585	0.014838	0.027423	955.43	0.39679	94.196	5.1692
175.00	10.000	6.3697	0.15699	2.9000	4.4699	0.053931	0.018532	0.028063	1133.3	-0.068718	130.39	6.6199
250.00	10.000	4.5028	0.22209	4.3966	6.6175	0.064133	0.020260	0.029065	1300.6	-0.28786	169.92	8.1898
325.00	10.000	3.5006	0.28567	5.9563	8.8130	0.071811	0.020867	0.029402	1453.0	-0.40519	205.05	9.6733
400.00	10.000	2.8687	0.34859	7.5339	11.020	0.077921	0.021006	0.029419	1593.1	-0.47687	240.15	11.067
100.00	50.000	31.993	0.031257	1.1768	2.7397	0.023964	0.016349	0.026254	1710.1	-0.57213	192.47	10.534
175.00	50.000	22.700	0.044053	2.6415	4.8442	0.039587	0.019545	0.029321	1632.6	-0.46415	189.52	9.1377
250.00	50.000	17.524	0.057066	4.2297	7.0830	0.050225	0.020999	0.030163	1690.7	-0.46214	211.67	9.7772
325.00	50.000	14.304	0.069911	5.8539	9.3494	0.058153	0.021434	0.030202	1784.8	-0.48443	237.63	10.827
400.00	50.000	12.107	0.082595	7.4773	11.607	0.064404	0.021458	0.029985	1887.2	-0.51016	267.11	11.965
175.00	100.00	33.019	0.030286	2.5589	5.5875	0.033643	0.020316	0.029140	2128.4	-0.52750	282.17	13.079
250.00	100.00	27.257	0.036688	4.1604	7.8292	0.044291	0.021603	0.030346	2125.4	-0.50698	303.19	12.218
325.00	100.00	23.228	0.043051	5.8083	10.113	0.052281	0.021923	0.030469	2170.6	-0.51215	327.83	12.546
400.00	100.00	20.261	0.049356	7.4555	12.391	0.058588	0.021864	0.030246	2235.8	-0.52481	356.83	13.289

The values in these tables were generated from the NIST REFPROP software (Lemmon, E. W., McLinden, M. O., and Huber, M. L., NIST Standard Reference Database 23: Reference Fluid Thermodynamic and Transport Properties—REFPROP, National Institute of Standards and Technology, Standard Reference Data Program, Gaithersburg, Md., 2002, Version 7.1). The primary source for the thermodynamic properties is Younglove, B. A., "Thermophysical Properties of Fluids. I. Argon, Ethylene, Parahydrogen, Nitrogen, Nitrogen Trifluoride, and Oxygen," *J. Phys. Chem. Ref. Data*, Suppl. 1, **11**: 1-11, 1982. The source for viscosity is McCarty, R. D., and Weber, L. A., "Thermophysical Properties of Parahydrogen from the Freezing Liquid Line to 5000 R for Pressures to 10,000 psia," *N.B.S. Tech. Note 617*, 1972. The source for thermal conductivity is McCarty, R. D., and Weber, L. A., "Thermophysical Properties of Parahydrogen from the Freezing Liquid Line to 5000 R for Pressures to 10,000 psia," *N.B.S. Tech. Note 617*, 1972.

Properties at the triple point temperature and the critical point temperature are given in the first and last entries of the saturation tables, respectively. In the single-phase table, when the temperature range for a given isobar includes a vapor-liquid phase boundary, the temperature of phase equilibrium is noted, and properties for both the saturated liquid and saturated vapor are given (with liquid properties given in the upper line). Lines are omitted from the temperature-pressure grid of the single-phase table, when the system would be in the solid phase or if there are potential problems with the source property surface.

The uncertainties in density are 0.1% in the liquid phase, 0.25% in the vapor phase, and 0.2% in the supercritical region. The uncertainty in heat capacity is 3%, and the uncertainty in speed of sound is 2% in the liquid phase and 1% elsewhere. The uncertainty in viscosity ranges from 4% to 15%. The uncertainty in thermal conductivity below 100 K is estimated to be 3% below 150 atm and up to 10% below 700 atm. For temperatures around 100 K at low densities, the uncertainty is about 1%. Above 100 K, the uncertainty is estimated to be on the order of 10%.

TABLE 2-224 Thermodynamic Properties of para-Hydrogen

Temperature K	Pressure MPa	Density mol/dm ³	Volume dm ³ /mol	Int. energy kJ/mol	Enthalpy kJ/mol	Entropy kJ/(mol·K)	C _v kJ/(mol·K)	C _p kJ/(mol·K)	Sound speed m/s	Joule-Thomson K/MPa	Therm. cond. mW/(m·K)	Viscosity μPa·s
Saturated Properties												
13.800	0.0070373	38.214	0.026168	-0.10640	-0.10621	-0.0060986	0.010937	0.015530	1376.3	-1.4263	75.249	26.035
14.000	0.0078936	38.129	0.026226	-0.10334	-0.10313	-0.0058783	0.010548	0.015138	1367.4	-1.4615	76.869	25.310
15.000	0.013436	37.701	0.026524	-0.088758	-0.088401	-0.0048719	0.0096208	0.014345	1320.2	-1.5284	84.107	22.215
16.000	0.021534	37.261	0.026838	-0.074351	-0.073773	-0.0039418	0.0096210	0.014682	1272.2	-1.4722	90.003	19.784
17.000	0.032848	36.802	0.027172	-0.059344	-0.058452	-0.0030317	0.0099778	0.015532	1227.2	-1.3645	94.698	17.815
18.000	0.048078	36.321	0.027533	-0.043395	-0.042071	-0.0021196	0.010438	0.016618	1186.0	-1.2427	98.339	16.182
19.000	0.067960	35.812	0.027923	-0.026352	-0.024454	-0.0011972	0.010895	0.017822	1147.7	-1.1207	101.06	14.799
20.000	0.093249	35.274	0.028350	-0.0081471	-0.0055035	-0.00026188	0.011306	0.019103	1111.1	-1.0012	103.00	13.607
21.000	0.12472	34.702	0.028817	0.011263	0.014857	0.00068738	0.011663	0.020462	1075.0	-0.88292	104.25	12.565
22.000	0.16314	34.092	0.029333	0.031923	0.036709	0.0016517	0.011966	0.021923	1038.4	-0.76309	104.89	11.641
23.000	0.20932	33.439	0.029905	0.053894	0.060154	0.0026329	0.012226	0.023529	1000.7	-0.63820	105.01	10.811
24.000	0.26406	32.738	0.030546	0.077266	0.085332	0.0036338	0.012450	0.025344	961.13	-0.50428	104.64	10.057
25.000	0.32818	31.979	0.031271	0.10217	0.11243	0.0046588	0.012652	0.027461	919.17	-0.35652	103.82	9.3625
26.000	0.40250	31.152	0.032101	0.12879	0.14171	0.0057145	0.012841	0.030025	874.28	-0.18881	102.56	8.7151
27.000	0.48788	30.242	0.033067	0.15739	0.17353	0.0068101	0.013030	0.033270	825.90	0.0073097	100.85	8.1034
28.000	0.58524	29.225	0.034217	0.18839	0.20842	0.0079596	0.013235	0.037620	773.39	0.24439	98.669	7.5160
29.000	0.69554	28.067	0.035629	0.22242	0.24721	0.0091852	0.013476	0.043924	715.93	0.54264	95.941	6.9409
30.000	0.81989	26.706	0.037444	0.26061	0.29131	0.010526	0.013785	0.054215	652.36	0.93791	92.543	6.3620
31.000	0.95964	25.017	0.039973	0.30526	0.34362	0.012063	0.014225	0.074899	580.72	1.5033	88.209	5.7518
32.000	1.1168	22.637	0.044175	0.36307	0.41240	0.014036	0.014957	0.14188	496.76	2.4286	82.155	5.0391
32.938	1.2838	15.556	0.064284	0.51279	0.59532	0.019385			0	5.2019		
13.800	0.0070373	0.062340	16.041	0.68576	0.79865	0.059471	0.012705	0.021484	305.17	33.288	10.454	0.65046
14.000	0.0078936	0.069018	14.489	0.68798	0.80235	0.058799	0.012720	0.021535	307.13	32.412	10.649	0.66695
15.000	0.013436	0.11050	9.0494	0.69878	0.82037	0.055713	0.012797	0.021823	316.53	28.670	11.625	0.74268
16.000	0.021534	0.16764	5.9651	0.70909	0.83754	0.053015	0.012879	0.022172	325.20	25.755	12.604	0.81064
17.000	0.032848	0.24349	4.1069	0.71881	0.85372	0.050625	0.012967	0.022593	333.13	23.433	13.595	0.87421
18.000	0.048078	0.34126	2.9303	0.72787	0.86876	0.048482	0.013059	0.023097	340.35	21.544	14.603	0.93555
19.000	0.067960	0.46437	2.1535	0.73616	0.88251	0.046538	0.013158	0.023703	346.87	19.978	15.637	0.99611
20.000	0.093249	0.61652	1.6220	0.74359	0.89484	0.044755	0.013263	0.024433	352.69	18.654	16.705	1.0569
21.000	0.12472	0.80187	1.2471	0.75004	0.90557	0.043102	0.013378	0.025315	357.84	17.516	17.816	1.1186
22.000	0.16314	1.0251	0.97549	0.75539	0.91453	0.041553	0.013503	0.026390	362.33	16.521	18.981	1.1819
23.000	0.20932	1.2919	0.77406	0.75948	0.92151	0.040083	0.013641	0.027714	366.17	15.634	20.214	1.2472
24.000	0.26406	1.6089	0.62153	0.76213	0.92626	0.038672	0.013795	0.029369	369.39	14.832	21.529	1.3151
25.000	0.32818	1.9848	0.50383	0.76314	0.92848	0.037301	0.013969	0.031478	371.98	14.092	22.951	1.3863
26.000	0.40250	2.4307	0.41141	0.76219	0.92778	0.035948	0.014168	0.034235	373.96	13.396	24.507	1.4619
27.000	0.48788	2.9618	0.33763	0.75891	0.92363	0.034592	0.014397	0.037965	375.33	12.725	26.241	1.5433
28.000	0.58524	3.6003	0.27775	0.75272	0.91527	0.033204	0.014666	0.043264	376.10	12.058	28.217	1.6331
29.000	0.69554	4.3810	0.22826	0.74275	0.90151	0.031747	0.014986	0.051337	376.25	11.370	30.541	1.7362
30.000	0.81989	5.3643	0.18642	0.72747	0.88031	0.030159	0.015380	0.065075	375.77	10.621	33.404	1.8628
31.000	0.95964	6.6763	0.14978	0.70375	0.84749	0.028317	0.015881	0.093513	374.65	9.7335	37.214	2.0375
32.000	1.1168	8.6823	0.11518	0.66278	0.79141	0.025880	0.016566	0.18609	372.98	8.5044	43.179	2.3378
32.938	1.2838	15.556	0.064284	0.51279	0.59532	0.019385			0	5.2019		
Single-Phase Properties												
50.000	0.10000	0.24255	4.1229	1.1351	1.5474	0.064284	0.012710	0.021301	583.04	4.8322	38.576	2.4717
125.00	0.10000	0.096180	10.397	2.4062	3.4459	0.086764	0.022470	0.030820	841.25	0.59482	106.18	4.9004
200.00	0.10000	0.060094	16.641	4.2197	5.8837	0.10202	0.024087	0.032413	1054.3	-0.023305	155.64	6.7798
275.00	0.10000	0.043708	22.879	5.9434	8.2313	0.11200	0.022011	0.030330	1250.9	-0.27924	183.10	8.4358
350.00	0.10000	0.034345	29.116	7.5556	10.467	0.11919	0.021169	0.029486	1418.7	-0.41834	212.22	9.9461
50.000	1.0000	2.6201	0.38166	1.0703	1.4520	0.043845	0.012853	0.024464	575.43	4.4711	42.291	2.6080
125.00	1.0000	0.95806	1.0438	2.3861	3.4298	0.067460	0.022526	0.031195	848.73	0.55405	107.83	4.9523
200.00	1.0000	0.59708	1.6748	4.2097	5.8845	0.082821	0.024121	0.032545	1062.6	-0.032981	156.70	6.8120
275.00	1.0000	0.43458	2.3010	5.9379	8.2390	0.092837	0.022033	0.030392	1258.8	-0.28185	183.91	8.4592
350.00	1.0000	0.34179	2.9257	7.5525	10.478	0.10004	0.021186	0.029519	1425.9	-0.41854	212.88	9.9645

TABLE 2-224 Thermodynamic Properties of para-Hydrogen (Concluded)

Temperature K	Pressure MPa	Density mol/dm ³	Volume dm ³ /mol	Int. energy kJ/mol	Enthalpy kJ/mol	Entropy kJ/(mol·K)	C_v kJ/(mol·K)	C_p kJ/(mol·K)	Sound speed m/s	Joule-Thomson K/MPa	Therm. cond. mW/(m·K)	Viscosity μ Pa·s
Single-Phase Properties												
50.000	5.0000	16.715	0.059826	0.73484	1.0340	0.024551	0.013420	0.041376	692.39	1.6074	79.882	4.3382
125.00	5.0000	4.6789	0.21372	2.3021	3.3707	0.053441	0.022747	0.032653	888.35	0.37288	115.33	5.1978
200.00	5.0000	2.9000	0.34482	4.1677	5.8918	0.069234	0.024261	0.033076	1100.2	-0.078236	161.31	6.9555
275.00	5.0000	2.1189	0.47194	5.9145	8.2742	0.079371	0.022129	0.030649	1293.6	-0.29566	187.32	8.5624
350.00	5.0000	1.6731	0.59770	7.5394	10.528	0.086623	0.021255	0.029661	1457.5	-0.42110	215.63	10.045
50.000	10.000	26.141	0.038254	0.53828	0.92082	0.017729	0.013420	0.031369	1020.9	-0.00090690	109.43	6.6673
125.00	10.000	8.9624	0.11158	2.2107	3.3264	0.047053	0.022979	0.033916	952.54	0.16557	125.40	5.5904
200.00	10.000	5.5879	0.17896	4.1201	5.9097	0.063249	0.024419	0.033613	1149.8	-0.13543	167.23	7.1499
275.00	10.000	4.1087	0.24339	5.8874	8.3212	0.073512	0.022240	0.030928	1337.5	-0.31595	191.64	8.6948
350.00	10.000	3.2606	0.30669	7.5240	10.591	0.080815	0.021338	0.029822	1497.0	-0.42707	219.08	10.147
50.000	50.000	41.635	0.024018	0.33890	1.5398	0.0075571	0.014831	0.021072	1903.0	-0.85893	205.72	18.078
125.00	50.000	28.231	0.035422	1.8792	3.6503	0.032377	0.024288	0.034391	1571.6	-0.41268	207.03	9.5718
200.00	50.000	20.660	0.048403	3.8955	6.3157	0.049075	0.025325	0.034876	1590.0	-0.39075	219.10	9.2598
275.00	50.000	16.295	0.061368	5.7445	8.8129	0.059704	0.022913	0.031923	1701.1	-0.44355	229.75	10.106
350.00	50.000	13.485	0.074155	7.4386	11.146	0.067214	0.021862	0.030536	1813.9	-0.48674	249.51	11.203
125.00	100.00	38.364	0.026066	1.8103	4.4169	0.026596	0.025170	0.033554	2093.0	-0.46785	308.69	15.278
200.00	100.00	30.845	0.032420	3.8148	7.0568	0.043119	0.026034	0.034871	2056.2	-0.43974	320.11	12.564
275.00	100.00	25.763	0.038815	5.6828	9.5643	0.053790	0.023474	0.032151	2114.9	-0.48043	324.21	12.252
350.00	100.00	22.144	0.045159	7.4012	11.917	0.061362	0.022320	0.030806	2185.5	-0.50940	340.22	12.765

The values in these tables were generated from the NIST REFPROP software (Lemmon, E. W., McLinden, M. O., and Huber, M. L., NIST Standard Reference Database 23: Reference Fluid Thermodynamic and Transport Properties—REFPROP, National Institute of Standards and Technology, Standard Reference Data Program, Gaithersburg, Md., 2002, Version 7.1). The primary source for the thermodynamic properties is Younglove, B. A., "Thermophysical Properties of Fluids. I. Argon, Ethylene, Parahydrogen, Nitrogen, Nitrogen Trifluoride, and Oxygen," *J. Phys. Chem. Ref. Data*, Suppl. 1, **11**: 1-11, 1982. The source for viscosity is McCarty, R. D., and Weber, L. A., "Thermophysical Properties of Parahydrogen from the Freezing Liquid Line to 5000 R for Pressures to 10,000 psia," *N.B.S. Tech. Note* 617, 1972. The source for thermal conductivity is McCarty, R. D., and Weber, L. A., "Thermophysical Properties of Parahydrogen from the Freezing Liquid Line to 5000 R for Pressures to 10,000 psia," *N.B.S. Tech. Note* 617, 1972.

Properties at the triple point temperature and the critical point temperature are given in the first and last entries of the saturation tables, respectively. In the single-phase table, when the temperature range for a given isobar includes a vapor-liquid phase boundary, the temperature of phase equilibrium is noted, and properties for both the saturated liquid and saturated vapor are given (with liquid properties given in the upper line). Lines are omitted from the temperature-pressure grid of the single-phase table, when the system would be in the solid phase or if there are potential problems with the source property surface.

The uncertainties in density are 0.1% in the liquid phase, 0.25% in the vapor phase, and 0.2% in the supercritical region. The uncertainty in heat capacity is 3%, and the uncertainty in speed of sound is 2% in the liquid phase and 1% elsewhere. The uncertainty in viscosity ranges from 4% to 15%. The uncertainty in thermal conductivity below 100 K is estimated to be 3% below 150 atm and up to 10% below 700 atm. For temperatures around 100 K at low densities, the uncertainty is about 1%. Above 100 K, the uncertainty is estimated to be on the order of 10%.

TABLE 2-225 Saturated Hydrogen Peroxide*

T , K	P , bar	v_f , m ³ /kg	v_g , m ³ /kg	h_f , kJ/kg	h_g , kJ/kg	s_f , kJ/(kg·K)	s_g , kJ/(kg·K)	c_{pf} , kJ/(kg·K)	μ_f , 10 ⁻⁴ Pa·s	k_f , W/(m·K)
273	0.0004	0.00068	1672	-5577	-4027	2.990	8.662	1.45	18.0	0.483
300	0.0031	0.00069	235	-5510	-3995	3.224	8.269	1.48	11.3	0.481
350	0.0564	0.00072	15.1	-5376	-3933	3.631	7.758	1.54	4.3	0.474
400	0.4521	0.00076	2.12	-5238	-3878	4.032	7.440	1.61	2.2	0.464
450	2.143	0.00081	0.487	-5091	-3820	4.346	7.172	1.68	1.3	0.453
500	7.126	0.00088	0.155	-4945	-3777	4.656	6.992	1.75	0.89	0.443
550	18.56	0.00095	0.0605	-4794	-3745	4.941	6.846	1.82	0.65	0.431
600	40.75	0.00107	0.0268	-4635	-3731	5.209	6.720	1.90	0.50	0.416
650	79.27	0.00125	0.0125	-4463	-3746	5.485	6.582			
700	141.7	0.00171	0.0048	-4195	-3860	5.682	6.339			
708.5 ^c	155.3	0.00284	0.0028	-4012	-4012	5.732	5.732			

*Values reproduced or converted from a tabulation by Tsykalo and Tabachnikov in V. A. Rabinovich (ed.), *Thermophysical Properties of Gases and Liquids*, Standartov, Moscow, 1968; NBS-NSF transl. TT 69-55091, 1970. The reader may be reminded that very pure hydrogen peroxide is very difficult to obtain owing to its decomposition or instability. c = critical point. The FMC Corp., Philadelphia, PA tech. bull. 67, 1969 (100 pp.) contains an enthalpy-pressure diagram to 3000 psia, 1100 K.

TABLE 2-226 Thermodynamic Properties of Hydrogen Sulfide

Temperature K	Pressure MPa	Density mol/dm ³	Volume dm ³ /mol	Int. energy kJ/mol	Enthalpy kJ/mol	Entropy kJ/(mol·K)	C _v kJ/(mol·K)	C _p kJ/(mol·K)	Sound speed m/s	Joule-Thomson K/MPa	Therm. cond. mW/(m·K)	Viscosity μPa·s
Saturated Properties												
187.70	0.023259	29.116	0.034345	-1.7210	-1.7202	-0.0085877	0.044390	0.068835	1437.8	-0.34039	254.24	439.13
190.00	0.027106	29.003	0.034479	-1.5628	-1.5619	-0.0077504	0.044124	0.068707	1425.8	-0.33923	251.74	428.67
200.00	0.050340	28.505	0.035082	-0.87841	-0.87664	-0.0042394	0.043042	0.068273	1373.4	-0.33253	240.93	385.68
210.00	0.087474	27.998	0.035717	-0.19759	-0.19446	-0.00091743	0.042067	0.068029	1321.0	-0.32287	230.26	346.75
220.00	0.14366	27.480	0.036390	0.48138	0.48661	0.0022415	0.041188	0.067975	1268.4	-0.30988	219.81	311.74
230.00	0.22485	26.949	0.037107	1.1602	1.1686	0.0052596	0.040393	0.068115	1215.6	-0.29305	209.52	280.37
240.00	0.33767	26.403	0.037875	1.8406	1.8534	0.0081564	0.039677	0.068461	1162.3	-0.27174	199.43	252.29
250.00	0.48934	25.838	0.038702	2.5245	2.5434	0.010949	0.039030	0.069032	1108.5	-0.24509	189.56	227.14
260.00	0.68751	25.253	0.039599	3.2135	3.2408	0.013654	0.038449	0.069859	1053.9	-0.21197	179.91	204.60
270.00	0.94022	24.642	0.040580	3.9100	3.9481	0.016285	0.037930	0.070989	998.54	-0.17084	170.48	184.32
280.00	1.2558	24.002	0.041662	4.6161	4.6685	0.018857	0.037470	0.072490	942.08	-0.11959	161.26	166.02
290.00	1.6429	23.327	0.042868	5.3348	5.4053	0.021385	0.037070	0.074466	884.34	-0.055218	152.24	149.44
300.00	2.1103	22.609	0.044230	6.0696	6.1629	0.023885	0.036732	0.077082	825.04	0.026636	143.40	134.32
310.00	2.6672	21.838	0.045791	6.8248	6.9469	0.026373	0.036462	0.080603	763.84	0.13260	134.71	120.43
320.00	3.3233	21.000	0.047618	7.6068	7.7650	0.028873	0.036273	0.085498	700.23	0.27324	126.16	107.58
330.00	4.0889	20.073	0.049818	8.4246	8.6283	0.031414	0.036191	0.092666	633.51	0.46655	117.71	95.533
340.00	4.9755	19.021	0.052573	9.2932	9.5548	0.034044	0.036265	0.10410	562.59	0.74618	109.36	84.050
350.00	5.9969	17.776	0.056256	10.241	10.578	0.036848	0.036600	0.12534	485.59	1.1841	101.19	72.784
360.00	7.1713	16.172	0.061837	11.335	11.779	0.040035	0.037471	0.17963	398.86	1.9714	93.864	61.060
370.00	8.5294	13.436	0.074429	12.903	13.538	0.044599	0.040079	0.63367	292.76	3.9324	92.754	46.102
373.10	8.9987	10.190	0.098135	14.470	15.353	0.049374			0	6.3885		
187.70	0.023259	0.015024	66.559	16.328	17.876	0.095815	0.025347	0.034000	245.84	55.730	10.628	8.0025
190.00	0.027106	0.017314	57.758	16.382	17.947	0.094930	0.025386	0.034078	247.20	53.868	10.775	8.1053
200.00	0.050340	0.030704	32.569	16.611	18.250	0.091395	0.025586	0.034487	252.82	46.796	11.429	8.5566
210.00	0.087474	0.051165	19.545	16.832	18.541	0.088301	0.025837	0.035021	257.96	41.090	12.107	9.0159
220.00	0.14366	0.080932	12.356	17.043	18.818	0.085567	0.026142	0.035698	262.58	36.435	12.816	9.4844
230.00	0.22485	0.12253	8.1613	17.244	19.079	0.083129	0.026502	0.036537	266.64	32.601	13.566	9.9634
240.00	0.33767	0.17879	5.5933	17.431	19.320	0.080933	0.026917	0.037563	270.10	29.412	14.365	10.455
250.00	0.48934	0.25286	3.9547	17.604	19.539	0.078934	0.027388	0.038807	272.91	26.737	15.227	10.961
260.00	0.68751	0.34834	2.8707	17.761	19.735	0.077092	0.027914	0.040312	275.05	24.476	16.166	11.485
270.00	0.94022	0.46937	2.1305	17.899	19.902	0.075375	0.028496	0.042139	276.47	22.550	17.202	12.031
280.00	1.2558	0.62086	1.6107	18.016	20.039	0.073752	0.029136	0.044378	277.15	20.897	18.360	12.604
290.00	1.6429	0.80887	1.2363	18.108	20.139	0.072193	0.029838	0.047166	277.05	19.466	19.675	13.213
300.00	2.1103	1.0411	0.96050	18.171	20.198	0.070669	0.030608	0.050723	276.12	18.212	21.197	13.867
310.00	2.6672	1.3280	0.75300	18.199	20.207	0.069149	0.031458	0.055410	274.34	17.097	22.997	14.582
320.00	3.3233	1.6843	0.59373	18.183	20.156	0.067594	0.032407	0.061879	271.64	16.081	25.187	15.380
330.00	4.0889	2.1323	0.46898	18.109	20.027	0.065956	0.033485	0.071400	268.00	15.116	27.946	16.300
340.00	4.9755	2.7096	0.36906	17.957	19.793	0.064157	0.034746	0.086837	263.35	14.142	31.600	17.405
350.00	5.9969	3.4881	0.28669	17.684	19.403	0.062064	0.036293	0.11617	257.65	13.053	36.820	18.833
360.00	7.1713	4.6442	0.21532	17.192	18.736	0.059360	0.038364	0.19265	250.84	11.629	45.513	20.940
370.00	8.5294	6.9933	0.14299	16.046	17.266	0.054674	0.041755	0.80649	242.80	9.0701	70.939	25.604
373.10	8.9987	10.190	0.098135	14.470	15.353	0.049374			0	6.3885		

TABLE 2-226 Thermodynamic Properties of Hydrogen Sulfide (Concluded)

Temperature K	Pressure MPa	Density mol/dm ³	Volume dm ³ /mol	Int. energy kJ/mol	Enthalpy kJ/mol	Entropy kJ/(mol·K)	C _v kJ/(mol·K)	C _p kJ/(mol·K)	Sound speed m/s	Joule-Thomson K/MPa	Therm. cond. mW/(m·K)	Viscosity μPa·s
Single-Phase Properties												
200.00	0.10000	28.506	0.035080	-0.87902	-0.87551	-0.0042425	0.043042	0.068269	1373.6	-0.33258	240.95	385.79
212.60	0.10000	27.865	0.035888	-0.021243	-0.017654	-0.000082766	0.041830	0.067997	1307.4	-0.31984	227.54	337.30
212.60	0.10000	0.057900	17.271	16.888	18.615	0.087559	0.025911	0.035183	259.21	39.791	12.288	9.1366
300.00	0.10000	0.040389	24.759	19.164	21.640	0.099486	0.025979	0.034563	309.73	16.968	17.999	12.954
400.00	0.10000	0.030157	33.160	21.830	25.146	0.10956	0.027268	0.035693	356.35	8.9467	24.990	17.172
500.00	0.10000	0.024088	41.515	24.642	28.794	0.11770	0.028923	0.037297	396.06	5.5432	32.218	21.094
600.00	0.10000	0.020059	49.853	27.626	32.611	0.12465	0.030708	0.039059	431.20	3.7250	39.592	24.714
700.00	0.10000	0.017187	58.182	30.789	36.607	0.13081	0.032534	0.040873	463.05	2.6185	47.091	28.082
200.00	1.0000	28.528	0.035053	-0.89011	-0.85506	-0.0042980	0.043058	0.068210	1377.6	-0.33351	241.31	387.91
272.07	1.0000	24.513	0.040795	4.0550	4.0958	0.016821	0.037830	0.071266	986.97	-0.16116	168.56	180.39
272.07	1.0000	0.49800	2.0080	17.925	19.933	0.075033	0.028623	0.042564	276.67	22.188	17.430	12.147
300.00	1.0000	0.43539	2.2968	18.775	21.072	0.079019	0.027626	0.039427	296.60	17.369	19.015	13.337
400.00	1.0000	0.31003	3.2255	21.626	24.852	0.089907	0.027708	0.037234	351.09	9.0111	25.609	17.465
500.00	1.0000	0.24394	4.0993	24.507	28.606	0.098281	0.029100	0.038036	393.73	5.5366	32.691	21.319
600.00	1.0000	0.20183	4.9547	27.525	32.480	0.10534	0.030799	0.039492	430.30	3.7023	39.980	24.893
700.00	1.0000	0.17237	5.8015	30.710	36.511	0.11155	0.032589	0.041157	462.94	2.5947	47.423	28.227
200.00	5.0000	28.625	0.034935	-0.93837	-0.76369	-0.0045411	0.043127	0.067957	1394.7	-0.33745	242.90	397.26
300.00	5.0000	22.858	0.043749	5.9433	6.1620	0.023458	0.036740	0.075047	855.61	-0.017492	146.15	139.57
340.26	5.0000	18.992	0.052654	9.3164	9.5797	0.034113	0.036269	0.10449	560.70	0.75500	109.14	83.760
340.26	5.0000	2.7266	0.36675	17.952	19.786	0.064108	0.034782	0.087361	263.22	14.116	31.710	17.437
400.00	5.0000	1.8047	0.55412	20.549	23.319	0.073747	0.030043	0.048271	325.86	9.1749	29.786	19.070
500.00	5.0000	1.2939	0.77288	23.863	27.728	0.083609	0.029940	0.041996	384.33	5.4471	35.063	22.459
600.00	5.0000	1.0365	0.96476	27.065	31.889	0.091196	0.031216	0.041590	427.30	3.5816	41.773	25.773
700.00	5.0000	0.87211	1.1466	30.353	36.086	0.097665	0.032838	0.042472	463.26	2.4840	48.924	28.935
200.00	10.000	28.741	0.034793	-0.99643	-0.64850	-0.0048367	0.043212	0.067668	1415.5	-0.34197	244.82	408.90
300.00	10.000	23.238	0.043033	5.7496	6.1800	0.022795	0.036779	0.072377	902.78	-0.077399	150.49	148.08
400.00	10.000	5.0473	0.19812	18.370	20.351	0.062081	0.034651	0.10189	291.29	8.2243	44.719	23.639
500.00	10.000	2.8037	0.35667	22.959	26.526	0.076030	0.031080	0.048875	375.68	5.1487	38.963	24.438
600.00	10.000	2.1399	0.46730	26.466	31.139	0.084452	0.031755	0.044597	426.01	3.3812	44.210	27.165
700.00	10.000	1.7663	0.56617	29.903	35.564	0.091275	0.033155	0.044212	465.45	2.3347	50.878	30.013
300.00	75.000	26.050	0.038388	4.3332	7.2123	0.017506	0.037754	0.061705	1276.9	-0.33612	187.18	232.59
400.00	75.000	21.973	0.045510	9.9713	13.384	0.035260	0.035381	0.061962	983.51	-0.18247	134.39	124.22
500.00	75.000	17.947	0.055720	15.404	19.583	0.049092	0.034762	0.061649	786.35	0.057516	103.90	81.074
600.00	75.000	14.519	0.068874	20.474	25.640	0.060142	0.034994	0.059227	688.11	0.27314	87.712	62.531
700.00	75.000	11.974	0.083511	25.148	31.412	0.069045	0.035721	0.056291	654.55	0.36585	82.684	54.563
300.00	150.00	27.794	0.035979	3.5100	8.9069	0.013888	0.038777	0.058983	1538.4	-0.40376	214.24	311.25
400.00	150.00	24.751	0.040403	8.6429	14.703	0.030575	0.036402	0.057226	1302.6	-0.37006	165.64	174.85
500.00	150.00	21.937	0.045585	13.539	20.377	0.043238	0.035779	0.056273	1132.1	-0.31802	135.75	119.57
600.00	150.00	19.449	0.051416	18.248	25.960	0.053420	0.036044	0.055409	1019.1	-0.26874	118.38	93.323
700.00	150.00	17.335	0.057687	22.811	31.464	0.061906	0.036804	0.054711	949.06	-0.23292	110.03	79.581

The values in these tables were generated from the NIST REFPROP software (Lemmon, E. W., McLinden, M. O., and Huber, M. L., NIST Standard Reference Database 23: Reference Fluid Thermodynamic and Transport Properties—REFPROP National Institute of Standards and Technology, Standard Reference Data Program, Gaithersburg, Md., 2002, Version 7.1). The primary source for the thermodynamic properties is Lemmon, E. W., and Span, R., "Short Fundamental Equations of State for 20 Industrial Fluids," *J. Chem. Eng. Data* **51**(3): 785–850, 2006. The source for viscosity and thermal conductivity is NIST14, Version 9.08.

Properties at the triple point temperature and the critical point temperature are given in the first and last entries of the saturation tables, respectively. In the single-phase table, when the temperature range for a given isobar includes a vapor-liquid phase boundary, the temperature of phase equilibrium is noted, and properties for both the saturated liquid and saturated vapor are given (with liquid properties given in the upper line). Lines are omitted from the temperature-pressure grid of the single-phase table, when the system would be in the solid phase or if there are potential problems with the source property surface.

The uncertainties in density are 0.1% in the liquid phase below the critical temperature, 0.4% in the vapor phase, 1% at supercritical temperatures up to 500 K, and 2.5% at higher temperatures. Uncertainties will be higher near the critical point, and may be lower than 0.5% between 400 and 500 K. The uncertainty in vapor pressure is 0.25%, and the uncertainty in heat capacities is estimated to be 1%. For viscosity, estimated uncertainty is 2%. For thermal conductivity, estimated uncertainty, except near the critical region, is 4–6%.

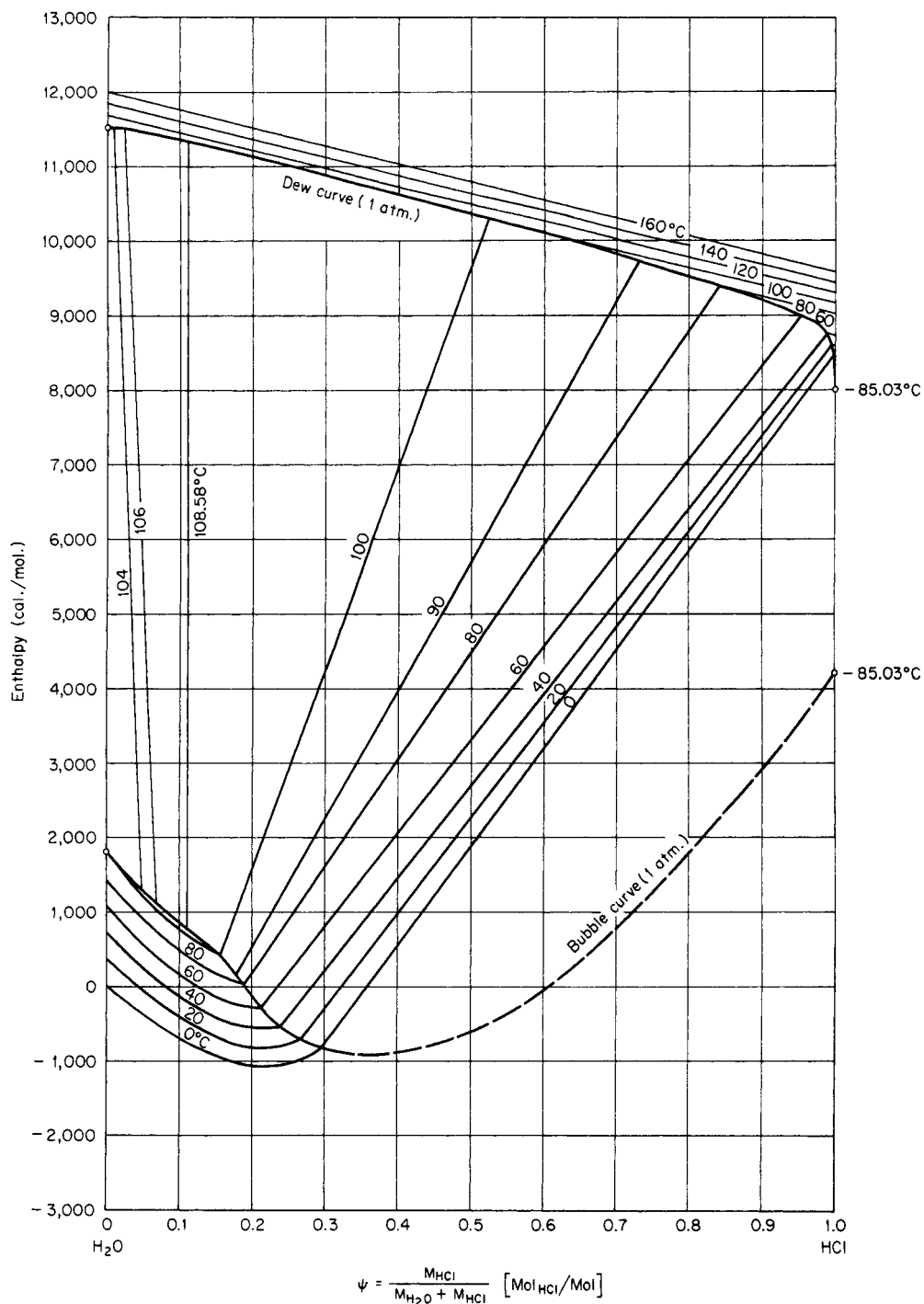


FIG. 2-11 Enthalpy-concentration diagram for aqueous hydrogen chloride at 1 atm. Reference states: enthalpy of liquid water at 0°C is zero; enthalpy of pure saturated HCl vapor at 1 atm (-85.03°C) is 8000 kcal/mol. NOTE: It should be observed that the weight basis includes the vapor, which is particularly important in the two-phase region. Saturation values may be read at the ends of the tie lines. [Van Nuys, Trans. Am. Inst. Chem. Eng., 39, 663 (1943).]

TABLE 2-227 Thermodynamic Properties of Isobutane

Temperature K	Pressure MPa	Density mol/dm ³	Volume dm ³ /mol	Int. energy kJ/mol	Enthalpy kJ/mol	Entropy kJ/(mol·K)	C _v kJ/(mol·K)	C _p kJ/(mol·K)	Sound speed m/s	Joule-Thomson K/MPa	Therm. cond. mW/(m·K)	Viscosity μPa·s
Saturated Properties												
113.73	2.2891E-08	12.738	0.078508	-6.5316	-6.5316	-0.03951	0.068243	0.098159	1999.8	-0.68375	157.92	8767.2
115	3.1711E-08	12.717	0.078635	-6.4068	-6.4068	-0.03842	0.068392	0.098388	1988.6	-0.68180	157.70	8096.1
130	8.8064E-07	12.473	0.080171	-4.9101	-4.9101	-0.02619	0.070255	0.10118	1863.4	-0.65814	154.39	3698.4
145	1.1510E-05	12.229	0.081772	-3.3714	-3.3714	-0.01499	0.072110	0.10397	1750.1	-0.63434	150.06	2060.1
160	8.8176E-05	11.984	0.083447	-1.7912	-1.7911	-0.00463	0.073940	0.10673	1645.3	-0.61032	144.95	1302.4
175	0.00045673	11.736	0.085209	-0.16946	-0.16942	0.005061	0.075811	0.10951	1546.1	-0.58545	139.28	897.76
190	0.0017628	11.485	0.087069	1.4945	1.4946	0.014182	0.077792	0.11237	1450.9	-0.55901	133.23	657.25
205	0.0054294	11.231	0.089043	3.2024	3.2029	0.022832	0.079933	0.11540	1358.6	-0.53024	126.94	502.16
220	0.014023	10.971	0.091150	4.9572	4.9585	0.031092	0.082269	0.11865	1268.6	-0.49839	120.56	395.73
235	0.031511	10.705	0.093415	6.7622	6.7652	0.039028	0.084817	0.12216	1180.3	-0.46255	114.21	319.15
250	0.06335	10.431	0.095866	8.6216	8.6277	0.046697	0.087581	0.12600	1093.4	-0.42158	107.94	262.04
265	0.11640	10.148	0.098544	10.540	10.551	0.054149	0.090556	0.13021	1007.7	-0.37389	101.85	218.23
280	0.19876	9.8523	0.10150	12.522	12.543	0.061427	0.093728	0.13486	922.77	-0.31712	95.986	183.83
295	0.31952	9.5416	0.10480	14.575	14.608	0.068569	0.097085	0.14006	838.36	-0.24757	90.398	156.24
310	0.48858	9.2114	0.10856	16.705	16.758	0.075615	0.10062	0.14598	753.97	-0.15928	85.118	133.64
325	0.71658	8.8560	0.11292	18.920	19.001	0.082601	0.10432	0.15290	669.03	-0.04193	80.169	114.69
340	1.0148	8.4662	0.11812	21.234	21.354	0.089574	0.10821	0.16139	582.74	0.12359	75.561	98.394
355	1.3957	8.0276	0.12457	23.665	23.839	0.096591	0.11234	0.17260	494.00	0.37690	71.293	83.919
370	1.8727	7.5139	0.13309	26.245	26.494	0.10375	0.11686	0.18958	401.01	0.81512	67.356	70.526
385	2.4620	6.8650	0.14567	29.045	29.404	0.11123	0.12220	0.22324	300.29	1.7502	63.794	57.352
400	3.1856	5.8674	0.17043	32.319	32.862	0.11975	0.13078	0.36901	184.38	4.9259	61.898	42.498
407.81	3.629	3.8798	0.25775	35.910	36.846	0.12937			0	16.282		
113.73	2.2891E-08	2.4207E-08	41,310,000	20.462	21.408	0.20615	0.042812	0.051127	139.39	577.37	2.2717	2.8476
115	3.1711E-08	3.3165E-08	30,152,000	20.517	21.473	0.20401	0.043157	0.051472	140.07	553.27	2.3426	2.8511
130	8.8064E-07	8.1474E-07	1,227,400	21.194	22.275	0.18292	0.047087	0.055402	147.92	348.08	3.2114	3.2763
145	1.1510E-05	9.5478E-06	104,740	21.928	23.133	0.16780	0.050787	0.059103	155.36	233.14	4.1386	3.6690
160	8.8176E-05	6.6294E-05	15,084	22.716	24.006	0.15686	0.054332	0.062655	162.43	164.07	5.1239	4.0588
175	0.00045673	0.0003141	3,183.6	23.555	25.009	0.14894	0.057806	0.066151	169.14	120.18	6.1666	4.4452
190	0.0017628	0.0011181	894.34	24.442	26.018	0.14325	0.061291	0.06969	175.44	91.024	7.2652	4.8275
205	0.0054294	0.0032007	312.43	25.374	27.070	0.13926	0.064859	0.07337	181.26	70.957	8.4173	5.2047
220	0.014023	0.0077418	129.17	26.348	28.159	0.13655	0.068567	0.077281	186.48	56.748	9.6201	5.5763
235	0.031511	0.016419	60.904	27.360	29.279	0.13483	0.072455	0.081501	190.96	46.450	10.872	5.9424
250	0.06335	0.031405	31.842	28.406	30.423	0.13388	0.076548	0.086099	194.52	38.843	12.174	6.3045
265	0.11640	0.055358	18.064	29.481	31.584	0.13352	0.080855	0.091145	197.02	33.140	13.532	6.6660
280	0.19876	0.091469	10.933	30.581	32.754	0.13361	0.085375	0.096722	198.29	28.823	14.961	7.0328
295	0.31952	0.14360	6.9638	31.700	33.925	0.13405	0.090101	0.10295	198.13	25.545	16.487	7.4136
310	0.48858	0.21659	4.6171	32.830	35.086	0.13474	0.09503	0.11003	196.37	23.074	18.151	7.8217
325	0.71658	0.31684	3.1561	33.960	36.222	0.13559	0.10017	0.11832	192.73	21.254	20.022	8.2772
340	1.0148	0.45354	2.2049	35.075	37.313	0.13651	0.10541	0.12842	186.90	20.032	22.207	8.8129
355	1.3957	0.64121	1.5596	36.146	38.323	0.13739	0.11078	0.14204	178.45	19.459	24.900	9.4859
370	1.8727	0.90588	1.1039	37.123	39.190	0.13806	0.11703	0.16455	166.77	19.526	28.498	10.409
385	2.4620	1.3046	0.76649	37.906	39.793	0.13822	0.12502	0.21348	150.88	20.215	34.050	11.844
400	3.1856	2.0369	0.49095	38.148	39.712	0.13688	0.13683	0.43911	128.90	21.293	46.452	14.761
407.81	3.629	3.8798	0.25775	35.910	36.846	0.12937			0	16.282		

Single-Phase Properties

200.00	0.10000	11.317	0.088361	2.6255	2.6343	0.019983	0.079206	0.11436	1389.7	-0.54030	129.10	547.68
261.07	0.10000	10.223	0.097817	10.031	10.040	0.052213	0.089756	0.12906	1030.1	-0.38717	103.43	228.69
261.07	0.10000	0.048038	20.817	29.197	31.278	0.13356	0.079705	0.089774	196.48	34.485	13.170	6.5710
300.00	0.10000	0.041143	24.305	32.513	34.944	0.14664	0.089474	0.098798	212.04	21.436	17.082	7.5436
400.00	0.10000	0.030372	32.925	42.834	46.127	0.17863	0.11631	0.12501	245.50	8.6878	28.880	9.9294
500.00	0.10000	0.024169	41.375	55.743	59.881	0.20922	0.14101	0.14952	274.09	4.5740	43.232	12.195
200.00	1.0000	11.329	0.088272	2.6017	2.6900	0.019864	0.079268	0.11426	1395.0	-0.54183	129.47	552.65
300.00	1.0000	9.4575	0.10574	15.229	15.335	0.070771	0.098270	0.14150	819.00	-0.23012	89.092	149.88
339.34	1.0000	8.4843	0.11786	21.129	21.247	0.089265	0.10803	0.16097	586.60	0.11482	75.758	99.071
339.34	1.0000	0.44655	2.2394	35.027	37.266	0.13647	0.10518	0.12792	187.21	20.073	22.102	8.7869
400.00	1.0000	0.33698	2.9675	42.086	45.054	0.15757	0.11833	0.13200	224.30	9.9934	29.559	10.129
500.00	1.0000	0.25270	3.9573	55.288	59.246	0.18916	0.14174	0.15229	263.78	4.7852	44.232	12.391
200.00	5.0000	11.379	0.087884	2.4992	2.9387	0.019346	0.079538	0.11385	1417.9	-0.54814	131.11	574.91
300.00	5.0000	9.5950	0.10422	14.958	15.479	0.069851	0.098458	0.13915	870.18	-0.28002	92.042	160.04
400.00	5.0000	6.7797	0.14750	31.029	31.767	0.11631	0.12520	0.20584	328.20	1.3689	64.364	56.352
500.00	5.0000	1.6118	0.62041	52.732	55.834	0.17060	0.14556	0.17644	219.06	5.5914	50.270	15.871
200.00	10.000	11.438	0.087424	2.3778	3.2521	0.018721	0.079860	0.11339	1445.4	-0.55506	133.10	603.11
300.00	10.000	9.7443	0.10262	14.662	15.689	0.068827	0.098710	0.13705	926.11	-0.32494	95.422	172.11
400.00	10.000	7.5550	0.13236	29.780	31.103	0.11292	0.12349	0.17456	486.23	0.34096	70.562	72.797
500.00	10.000	4.0999	0.24391	48.735	51.174	0.15751	0.14786	0.21137	239.25	3.1085	61.481	28.154
200.00	15.000	11.496	0.086989	2.2631	3.5679	0.018121	0.080166	0.11300	1471.7	-0.56110	135.03	631.76
300.00	15.000	9.8755	0.10126	14.403	15.922	0.067905	0.098964	0.13552	975.70	-0.35793	98.548	183.72
400.00	15.000	7.9692	0.12548	29.065	30.948	0.11092	0.12324	0.16619	583.15	0.062447	75.048	84.081
500.00	15.000	5.5655	0.17968	46.521	49.217	0.15156	0.14693	0.19670	343.01	1.1026	67.712	41.020
200.00	30.000	11.654	0.085807	1.9531	4.5274	0.016439	0.081000	0.11206	1544.8	-0.57512	140.47	720.69
300.00	30.000	10.198	0.098056	13.768	16.709	0.065552	0.099691	0.13266	1100.2	-0.41943	106.90	216.98
400.00	30.000	8.6989	0.11496	27.757	31.205	0.10708	0.12354	0.15745	775.70	-0.21676	85.299	109.96
500.00	30.000	7.1701	0.13947	43.945	48.129	0.14475	0.14649	0.18019	572.71	0.033041	78.479	66.356

The values in these tables were generated from the NIST REFPROP software (Lemmon, E. W., McLinden, M. O., and Huber, M. L., NIST Standard Reference Database 23: Reference Fluid Thermodynamic and Transport Properties—REFPROP, National Institute of Standards and Technology, Standard Reference Data Program, Gaithersburg, Md., 2002, Version 7.1). The primary source for the thermodynamic properties is Buecker, D., and Wagner, W., "Reference Equations of State for the Thermodynamic Properties of Fluid Phase *n*-Butane and Isobutane," *J. Phys. Chem. Ref. Data* **35**(2):929–1019, 2006. The source for viscosity is Vogel, E., Kuechenmeister, C., and Bich, E., "Viscosity Correlation for Isobutane over Wide Ranges of the Fluid Region," *Int. J. Thermophys.* **21**(2):343–356, 2000. The source for thermal conductivity is Perkins, R. A., "Measurement and Correlation of the Thermal Conductivity of Isobutane from 114 K to 600 K at Pressures to 70 MPa," *J. Chem. Eng. Data* **47**(5):1272–1279, 2002.

Properties at the triple point temperature and the critical point temperature are given in the first and last entries of the saturation tables, respectively. In the single-phase table, when the temperature range for a given isobar includes a vapor-liquid phase boundary, the temperature of phase equilibrium is noted, and properties for both the saturated liquid and saturated vapor are given (with liquid properties given in the upper line). Lines are omitted from the temperature-pressure grid of the single-phase table, when the system would be in the solid phase or if there are potential problems with the source property surface.

The uncertainties in density are 0.02% at temperatures below 340 K and pressures below 12 MPa (both liquid and vapor states), 0.3% at temperatures below 300 K and pressures above 12 MPa, 0.1% in the vapor phase between 340 and 450 K, and 0.5% elsewhere. In the critical region, deviations in pressure are 0.5%. Uncertainties in heat capacities are typically 1–2%, rising to 5% in the critical region and at temperatures below 200 K. Uncertainties in the speed of sound are typically 1–2%, rising to 5% at temperatures below 200 K and in the critical region. The uncertainty in viscosity varies from 0.4% in the dilute gas between room temperature and 600 K to 3.0% over the rest of the fluid surface. Uncertainty in thermal conductivity is 3%, except in the critical region and dilute gas which have an uncertainty of 5%.

TABLE 2-228 Thermodynamic Properties of Isobutene (2-Methyl 1-Propene)

Temperature K	Pressure MPa	Density mol/dm ³	Volume dm ³ /mol	Int. energy kJ/mol	Enthalpy kJ/mol	Entropy kJ/(mol·K)	C _v kJ/(mol·K)	C _p kJ/(mol·K)	Sound speed m/s	Joule-Thomson K/MPa
Saturated Properties										
132.40	6.7619E-07	13.667	0.073170	-15.196	-15.196	-0.078577	0.074156	0.10623	1842.9	-0.56574
135.00	1.1116E-06	13.619	0.073428	-14.919	-14.919	-0.076509	0.074179	0.10642	1827.0	-0.56403
150.00	1.3438E-05	13.343	0.074943	-13.315	-13.315	-0.065239	0.074543	0.10755	1734.4	-0.55349
165.00	9.7764E-05	13.070	0.076514	-11.692	-11.692	-0.054931	0.075233	0.10881	1641.6	-0.54130
180.00	0.00048920	12.796	0.078149	-10.049	-10.049	-0.045402	0.076215	0.11028	1549.8	-0.52677
195.00	0.0018451	12.522	0.079860	-8.3822	-8.3821	-0.036508	0.077475	0.11203	1459.4	-0.50932
210.00	0.0055971	12.246	0.081662	-6.6870	-6.6865	-0.028133	0.079001	0.11407	1370.6	-0.48847
225.00	0.014316	11.966	0.083571	-4.9587	-4.9575	-0.020185	0.080776	0.11645	1283.4	-0.46371
240.00	0.031980	11.681	0.085610	-3.1926	-3.1899	-0.012587	0.082776	0.11917	1197.6	-0.43442
255.00	0.064075	11.389	0.087805	-1.3838	-1.3782	-0.0052767	0.084977	0.12224	1113.1	-0.39974
270.00	0.11754	11.088	0.090191	0.47283	0.48343	0.0017979	0.087351	0.12570	1029.6	-0.35836
285.00	0.20057	10.774	0.092812	2.3824	2.4010	0.0086815	0.089877	0.12958	946.77	-0.30827
300.00	0.32243	10.446	0.095729	4.3506	4.3814	0.015413	0.092533	0.13397	864.37	-0.24634
315.00	0.49324	10.098	0.099027	6.3837	6.4326	0.022030	0.095306	0.13900	781.98	-0.16750
330.00	0.72386	9.7251	0.10283	8.4899	8.5643	0.028568	0.098189	0.14491	699.15	-0.063276
345.00	1.0259	9.3181	0.10732	10.680	10.790	0.035068	0.10119	0.15215	615.32	0.081482
360.00	1.4121	8.8642	0.11281	12.969	13.128	0.041581	0.10433	0.16163	529.74	0.29633
375.00	1.8963	8.3412	0.11989	15.383	15.611	0.048183	0.10770	0.17548	441.23	0.64712
390.00	2.4955	7.7041	0.12980	17.975	18.299	0.055015	0.11149	0.20028	347.41	1.3162
405.00	3.2319	6.8249	0.14652	20.892	21.365	0.062470	0.11647	0.27285	242.00	3.0714
418.09	4.0157	4.1700	0.23981	25.759	26.722	0.075104			0	15.166
132.40	6.7619E-07	6.1426E-07	1,628,000.	12.185	13.286	0.13654	0.045424	0.053739	152.35	932.58
135.00	1.1116E-06	9.9037E-07	1,009,700.	12.304	13.427	0.13346	0.046004	0.054319	153.69	849.42
150.00	1.3438E-05	1.0775E-05	92,803.	13.018	14.265	0.11863	0.049224	0.057543	161.19	514.47
165.00	9.7764E-05	7.1284E-05	14,028.	13.778	15.150	0.10775	0.052312	0.060645	168.31	329.24
180.00	0.00048920	0.00032720	3,056.2	14.581	16.076	0.099740	0.055381	0.063755	175.06	220.54
195.00	0.0018451	0.0011411	876.38	15.424	17.041	0.093867	0.058529	0.066994	181.39	153.60
210.00	0.0055971	0.0032245	310.13	16.303	18.039	0.089606	0.061825	0.070461	187.22	110.74
225.00	0.014316	0.0077400	129.20	17.214	19.064	0.086578	0.065309	0.074224	192.45	82.434
240.00	0.031980	0.016347	61.174	18.155	20.112	0.084503	0.068992	0.078326	196.96	63.248
255.00	0.064075	0.031202	32.049	19.122	21.176	0.083170	0.072865	0.082797	200.59	49.962
270.00	0.11754	0.054953	18.197	20.111	22.250	0.082415	0.076909	0.087668	203.21	40.590
285.00	0.20057	0.090771	11.017	21.118	23.328	0.082110	0.081099	0.092989	204.65	33.877
300.00	0.32243	0.14247	7.0191	22.138	24.401	0.082147	0.085414	0.098854	204.73	29.016
315.00	0.49324	0.21479	4.6557	23.164	25.460	0.082436	0.089840	0.10544	203.27	25.486
330.00	0.72386	0.31394	3.1853	24.185	26.491	0.082890	0.094375	0.11307	200.03	22.947
345.00	1.0259	0.44866	2.2289	25.186	27.473	0.083425	0.099036	0.12238	194.71	21.185
360.00	1.4121	0.63242	1.5812	26.144	28.377	0.083938	0.10387	0.13473	186.95	20.076
375.00	1.8963	0.88850	1.1255	27.018	29.152	0.084292	0.10900	0.15340	176.23	19.567
390.00	2.4955	1.2646	0.79073	27.725	29.699	0.084244	0.11468	0.18881	161.89	19.640
405.00	3.2319	1.8955	0.52758	28.046	29.751	0.083176	0.12162	0.29879	142.88	20.140
418.09	4.0157	4.1700	0.23981	25.759	26.722	0.075104			0	15.166

Single-Phase Properties

150.00	0.10000	13.344	0.074938	-13.316	-13.309	-0.065249	0.074545	0.10754	1734.9	-0.55354
250.00	0.10000	11.488	0.087047	-1.9936	-1.9849	-0.0076921	0.084223	0.12117	1141.5	-0.41214
265.81	0.10000	11.173	0.089503	-0.050895	-0.041944	-0.00015725	0.086672	0.12469	1052.8	-0.37070
265.81	0.10000	0.047251	21.164	19.833	21.949	0.082576	0.075763	0.086265	202.59	42.897
350.00	0.10000	0.034911	28.645	26.949	29.814	0.10818	0.092639	0.10158	234.72	15.195
450.00	0.10000	0.026911	37.160	37.274	40.990	0.13616	0.11313	0.12171	266.02	6.9323
550.00	0.10000	0.021943	45.572	49.523	54.081	0.16237	0.13123	0.13969	293.54	4.0208
150.00	1.0000	13.352	0.074895	-13.330	-13.255	-0.065342	0.074562	0.10751	1739.5	-0.55391
250.00	1.0000	11.506	0.086914	-2.0267	-1.9398	-0.0078249	0.084239	0.12099	1149.4	-0.41526
343.85	1.0000	9.3507	0.10694	10.509	10.616	0.034571	0.10096	0.15153	621.79	0.068431
343.85	1.0000	0.43682	2.2893	25.111	27.400	0.083383	0.098674	0.12159	195.20	21.295
350.00	1.0000	0.42121	2.3741	25.767	28.142	0.085521	0.098979	0.11981	199.99	19.480
450.00	1.0000	0.28769	3.4759	36.712	40.188	0.11575	0.11442	0.12599	251.31	7.4906
550.00	1.0000	0.22650	4.4150	49.150	53.565	0.14255	0.13168	0.14162	285.82	4.1331
150.00	5.0000	13.386	0.074707	-13.390	-13.017	-0.065747	0.074643	0.10737	1759.5	-0.55549
250.00	5.0000	11.581	0.086351	-2.1681	-1.7364	-0.0083971	0.084319	0.12027	1182.8	-0.42781
350.00	5.0000	9.4333	0.10601	10.992	11.522	0.035956	0.10188	0.14839	663.68	-0.014643
450.00	5.0000	2.4761	0.40387	32.462	34.481	0.092351	0.12422	0.22025	169.25	10.828
550.00	5.0000	1.3207	0.75720	47.230	51.016	0.12568	0.13385	0.15463	255.06	4.4151
150.00	10.000	13.426	0.074480	-13.463	-12.718	-0.066244	0.074751	0.10722	1783.6	-0.55725
250.00	10.000	11.668	0.085703	-2.3329	-1.4758	-0.0090755	0.084439	0.11952	1221.8	-0.44099
350.00	10.000	9.6916	0.10318	10.547	11.579	0.034624	0.10172	0.14363	741.89	-0.13006
450.00	10.000	6.6358	0.15070	26.495	28.002	0.075649	0.12143	0.19240	325.60	1.5013
550.00	10.000	3.1171	0.32081	44.413	47.621	0.11510	0.13595	0.17757	248.73	3.4960
150.00	20.000	13.504	0.074050	-13.601	-12.120	-0.067205	0.074987	0.10695	1829.3	-0.56021
250.00	20.000	11.827	0.084554	-2.6298	-0.93871	-0.010332	0.084720	0.11836	1292.1	-0.46137
350.00	20.000	10.075	0.099256	9.8719	11.857	0.032532	0.10175	0.13862	862.17	-0.25114
450.00	20.000	8.0205	0.12468	24.414	26.907	0.070229	0.11990	0.16238	539.83	0.19834
550.00	20.000	5.7872	0.17279	40.594	44.050	0.10458	0.13615	0.17749	377.20	0.90256
250.00	50.000	12.214	0.081874	-3.3402	0.75353	-0.013539	0.085706	0.11640	1463.7	-0.49631
350.00	50.000	10.805	0.092548	8.5711	13.199	0.028177	0.10258	0.13309	1105.6	-0.38284
450.00	50.000	9.4377	0.10596	22.086	27.384	0.063736	0.12031	0.15031	858.20	-0.25457
550.00	50.000	8.1524	0.12266	37.030	43.163	0.095351	0.13651	0.16471	704.72	-0.13437

The values in these tables were generated from the NIST REFPROP software (Lemmon, E. W., McLinden, M. O., and Huber, M. L., NIST Standard Reference Database 23: Reference Fluid Thermodynamic and Transport Properties—REFPROP, National Institute of Standards and Technology, Standard Reference Data Program, Gaithersburg, Md., 2002, Version 7.1). The primary source for the thermodynamic properties is Lemmon, E. W. and Ihmel, E. C., "Thermodynamic Properties of the Butenes. Part II. Short Fundamental Equations of State," *Fluid Phase Equilibria*, **228–229C**:173–187, 2005. Validated equations for the viscosity and thermal conductivity are not currently available for this fluid.

Properties at the triple point temperature and the critical point temperature are given in the first and last entries of the saturation tables, respectively. In the single-phase table, when the temperature range for a given isobar includes a vapor-liquid phase boundary, the temperature of phase equilibrium is noted, and properties for both the saturated liquid and saturated vapor are given (with liquid properties given in the upper line). Lines are omitted from the temperature-pressure grid of the single-phase table, when the system would be in the solid phase or if there are potential problems with the source property surface.

The uncertainties in densities calculated using the equation of state are 0.1% in the liquid phase at temperatures above 270 K (rising to 0.5% at temperatures below 200 K), 0.2% at temperatures above the critical temperature and at pressures above 10 MPa, and 0.5% in the vapor phase, including supercritical conditions below 10 MPa. The uncertainty in the vapor phase may be higher than 0.5% in some regions. The uncertainty in vapor pressure is 0.5% above 250 K, and the uncertainty in heat capacities is 0.5% at saturated liquid conditions, rising to 5% at much higher pressures and at temperatures above 250 K.

TABLE 2-229 Thermodynamic Properties of Krypton

Temperature K	Pressure MPa	Density mol/dm ³	Volume dm ³ /mol	Int. energy kJ/mol	Enthalpy kJ/mol	Entropy kJ/(mol·K)	C _v kJ/(mol·K)	C _p kJ/(mol·K)	Sound speed m/s	Joule-Thomson K/MPa
Saturated Properties										
115.77	0.073503	29.197	0.034250	-0.17537	-0.17285	-0.00146	0.021225	0.043334	698.97	-0.50800
120	0.10344	28.814	0.034705	0.008003	0.011593	9.61E-05	0.020889	0.043577	681.44	-0.49215
125	0.15007	28.353	0.035270	0.02606	0.23136	0.001877	0.020519	0.043953	660.52	-0.47002
130	0.21125	27.880	0.035867	0.44593	0.45351	0.003602	0.020175	0.044431	639.35	-0.44379
135	0.28957	27.396	0.036502	0.66802	0.67859	0.005280	0.019855	0.045022	617.89	-0.41290
140	0.38778	26.896	0.037180	0.89279	0.90720	0.006916	0.019558	0.045743	596.06	-0.37662
145	0.50867	26.381	0.037906	1.1207	1.1400	0.008518	0.019283	0.046614	573.82	-0.33403
150	0.65513	25.847	0.038689	1.3524	1.3778	0.010092	0.019030	0.047664	551.09	-0.28396
155	0.83007	25.291	0.039539	1.5885	1.6213	0.011644	0.018799	0.048934	527.76	-0.22485
160	1.0365	24.710	0.040469	1.8297	1.8716	0.013181	0.018594	0.050480	503.74	-0.15466
165	1.2774	24.100	0.041494	2.0770	2.1300	0.014711	0.018417	0.052386	478.86	-0.07060
170	1.5560	23.455	0.042636	2.3317	2.398	0.016241	0.018276	0.054776	452.95	0.03121
175	1.8754	22.766	0.043925	2.5952	2.6775	0.017781	0.018179	0.057846	425.75	0.15636
180	2.2390	22.024	0.045404	2.8697	2.9713	0.019345	0.018142	0.061924	396.95	0.31329
185	2.6505	21.213	0.047140	3.1584	3.2833	0.020950	0.018193	0.067602	366.08	0.51538
190	3.1140	20.309	0.049240	3.4661	3.6194	0.022623	0.018377	0.076087	332.48	0.78550
195	3.6340	19.267	0.051903	3.8015	3.9901	0.024412	0.018781	0.090283	295.17	1.1669
200	4.2163	17.995	0.055571	4.1824	4.4167	0.026413	0.019602	0.11946	252.47	1.7554
205	4.8690	16.222	0.061645	4.6620	4.9622	0.028917	0.021432	0.21813	200.85	2.8313
209.48	5.5255	10.850	0.092166	5.8827	6.3920	0.035568			0	6.4431
115.77	0.073503	0.078418	12.752	7.9735	8.9108	0.077003	0.013270	0.022596	136.12	49.758
120	0.10344	0.10724	9.3246	8.0103	8.9748	0.074790	0.013453	0.023062	138.00	45.644
125	0.15007	0.15089	6.6272	8.0498	9.0444	0.072381	0.013699	0.023713	140.03	41.448
130	0.21125	0.20670	4.8380	8.0846	9.1066	0.070164	0.013976	0.024485	141.85	37.834
135	0.28957	0.27668	3.6142	8.1140	9.1606	0.068109	0.014283	0.025395	143.45	34.693
140	0.38778	0.36308	2.7542	8.1375	9.2055	0.066190	0.014618	0.026463	144.82	31.940
145	0.50867	0.46836	2.1351	8.1544	9.2405	0.064384	0.014982	0.027716	145.98	29.510
150	0.65513	0.59537	1.6796	8.1640	9.2644	0.062670	0.015372	0.029193	146.92	27.351
155	0.83007	0.74740	1.3380	8.1655	9.2761	0.061030	0.015789	0.030948	147.64	25.418
160	1.0365	0.92843	1.0771	8.1578	9.2742	0.059447	0.016235	0.033060	148.13	23.675
165	1.2774	1.1433	0.87464	8.1395	9.2567	0.057903	0.016713	0.035646	148.39	22.088
170	1.5560	1.3983	0.71513	8.1089	9.2216	0.056379	0.017230	0.038887	148.42	20.627
175	1.8754	1.7017	0.58764	8.0637	9.1657	0.054856	0.017796	0.043072	148.21	19.260
180	2.2390	2.0649	0.48428	8.0007	9.0850	0.053310	0.018426	0.048693	147.75	17.955
185	2.6505	2.5046	0.39926	7.9154	8.9736	0.051708	0.019147	0.056647	147.01	16.679
190	3.1140	3.0471	0.32818	7.8004	8.8224	0.050007	0.019998	0.068771	145.97	15.388
195	3.6340	3.7380	0.26752	7.6434	8.6156	0.048132	0.021054	0.089467	144.56	14.023
200	4.2163	4.6709	0.21409	7.4192	8.3219	0.045939	0.022465	0.13256	142.62	12.486
205	4.8690	6.1126	0.16360	7.0576	7.8541	0.043024	0.024624	0.27498	139.66	10.545
209.48	5.5255	10.850	0.092166	5.8827	6.3920	0.035568			0	6.4431

Single-Phase Properties

200.00	0.10000	0.060557	16.513	9.0557	10.707	0.086165	0.012553	0.021091	181.32	15.987
300.00	0.10000	0.040171	24.893	10.313	12.803	0.094664	0.012488	0.020880	222.65	7.9817
400.00	0.10000	0.030088	33.236	11.564	14.888	0.10066	0.012478	0.020832	257.24	4.8486
500.00	0.10000	0.024059	41.565	12.813	16.970	0.10531	0.012475	0.020813	287.64	3.1571
600.00	0.10000	0.020044	49.889	14.062	19.051	0.10910	0.012474	0.020804	315.11	2.0967
700.00	0.10000	0.017179	58.210	15.310	21.131	0.11231	0.012474	0.020799	340.36	1.3720
200.00	1.0000	0.64884	1.5412	8.8431	10.384	0.065940	0.013359	0.024440	176.18	15.667
300.00	1.0000	0.40911	2.4443	10.207	12.651	0.075164	0.012634	0.021770	221.94	7.8257
400.00	1.0000	0.30268	3.3039	11.493	14.797	0.081341	0.012536	0.021250	257.69	4.7410
500.00	1.0000	0.24094	4.1505	12.761	16.911	0.086060	0.012509	0.021058	288.54	3.0825
600.00	1.0000	0.20035	4.9913	14.020	19.012	0.089890	0.012498	0.020965	316.19	2.0440
700.00	1.0000	0.17155	5.8291	15.276	21.105	0.093117	0.012492	0.020912	341.52	1.3340
200.00	5.0000	18.695	0.053490	4.0257	4.2932	0.025582	0.018694	0.092820	286.26	1.3105
205.94	5.0000	15.764	0.063436	4.7766	5.0938	0.029518	0.022035	0.27057	189.55	3.1528
205.94	5.0000	6.5051	0.15373	6.9575	7.7261	0.042300	0.025196	0.34754	138.88	10.086
300.00	5.0000	2.2268	0.44908	9.6909	11.936	0.060067	0.013335	0.026859	220.60	6.9488
400.00	5.0000	1.5501	0.64511	11.172	14.397	0.067171	0.012800	0.023237	260.80	4.2506
500.00	5.0000	1.2103	0.82624	12.528	16.659	0.072221	0.012660	0.022154	293.14	2.7636
600.00	5.0000	0.99847	1.0015	13.839	18.847	0.076212	0.012603	0.021667	321.36	1.8241
700.00	5.0000	0.85191	1.1738	15.130	20.999	0.079530	0.012572	0.021402	346.89	1.1768
200.00	10.000	20.764	0.048160	3.5349	4.0165	0.022941	0.017485	0.059683	386.03	0.41868
300.00	10.000	4.9580	0.20169	8.9533	10.970	0.051900	0.014221	0.035983	225.22	5.4452
400.00	10.000	3.1738	0.31508	10.764	13.915	0.060436	0.013132	0.025901	267.23	3.6190
500.00	10.000	2.4249	0.41238	12.241	16.365	0.065913	0.012848	0.023506	300.18	2.3913
600.00	10.000	1.9842	0.50399	13.620	18.660	0.070099	0.012733	0.022506	328.56	1.5769
700.00	10.000	1.6870	0.59277	14.954	20.881	0.073525	0.012672	0.021979	354.04	1.0028
200.00	100.00	27.903	0.035839	1.8128	5.3966	0.012020	0.019196	0.036607	779.27	-0.62535
300.00	100.00	23.193	0.043116	4.6453	8.9569	0.026484	0.016847	0.034479	643.59	-0.55209
400.00	100.00	19.351	0.051678	7.1023	12.270	0.036035	0.015591	0.031754	570.49	-0.49661
500.00	100.00	16.428	0.060871	9.2300	15.317	0.042844	0.014841	0.029280	537.49	-0.48427
600.00	100.00	14.234	0.070256	11.121	18.146	0.048008	0.014355	0.027397	525.89	-0.50576
700.00	100.00	12.558	0.079631	12.850	20.814	0.052122	0.014021	0.026021	525.42	-0.54812
200.00	200.00	30.673	0.032602	1.2743	7.7946	0.0070011	0.020666	0.035096	976.34	-0.69885
300.00	200.00	27.185	0.036785	3.8223	11.179	0.020757	0.018195	0.032708	867.80	-0.72858
400.00	200.00	24.274	0.041196	6.1068	14.346	0.029882	0.016813	0.030662	798.01	-0.75899
500.00	200.00	21.877	0.045709	8.1787	17.321	0.036526	0.015938	0.028881	754.77	-0.79823
600.00	200.00	19.905	0.050239	10.086	20.134	0.041659	0.015341	0.027435	728.59	-0.84213
700.00	200.00	18.266	0.054748	11.868	22.818	0.045799	0.014910	0.026300	713.29	-0.88605

The values in these tables were generated from the NIST REFPROP software (Lemmon, E. W., McLinden, M. O., and Huber, M. L., NIST Standard Reference Database 23: Reference Fluid Thermodynamic and Transport Properties—REFPROP, National Institute of Standards and Technology, Standard Reference Data Program, Gaithersburg, Md., 2002, Version 7.1). The primary source for the thermodynamic properties is Lemmon, E. W. and Span, R., "Short Fundamental Equations of State for 20 Industrial Fluids," *J. Chem. Eng. Data* **51**(3):785–850, 2006. Validated equations for the viscosity and thermal conductivity are not currently available for this fluid.

Properties at the triple point temperature and the critical point temperature are given in the first and last entries of the saturation tables, respectively. In the single-phase table, when the temperature range for a given isobar includes a vapor-liquid phase boundary, the temperature of phase equilibrium is noted, and properties for both the saturated liquid and saturated vapor are given (with liquid properties given in the upper line). Lines are omitted from the temperature-pressure grid of the single-phase table, when the system would be in the solid phase or if there are potential problems with the source property surface.

The equation of state is valid from the triple point to 750 K with pressures to 200 MPa, although the uncertainties increase substantially above 100 MPa. The uncertainties in density are typically 0.2% below 100 MPa, increasing to 1% at pressures up to 200 MPa. The uncertainty in vapor pressure is 0.2%, and the uncertainties in speed of sound are 0.01% in the vapor phase (including supercritical conditions) at low pressures, 1% below 20 MPa in the liquid phase, and 3% below 100 MPa at other state points. The limited amount of heat capacity data shows that the uncertainty is 1% near the triple point, and uncertainties in heat capacities at other states are probably within 2%, at least at pressures up to 20 MPa.

TABLE 2-230 Saturated Lithium*

T , K	P , bar	v_f , m ³ /kg	v_g , m ³ /kg	h_f , kJ/kg	h_g , kJ/kg	s_f , kJ/(kg·K)	s_g , kJ/(kg·K)	c_{pf} , kJ/(kg·K)
453.7 ^m	1.78.-13	1.912.-3		1703	24259	6.776	56.492	4.30
500	8.21.-12	1.946.-3		1905	24390	7.199	52.169	4.34
600	4.18.-9	1.988.-3		2334	24674	7.983	45.216	4.23
700	3.51.-7	2.028.-3	2.40.+7	2697	24869	8.633	40.307	4.19
800	9.57.-6	2.070.-3	9.94.+5	3174	25162	9.192	36.678	4.17
900	1.24.-4	2.114.-3	8.55.+4	3590	25341	9.682	33.850	4.16
1000	9.60.-4	2.160.-3	1.22.+4	4006	25477	10.120	31.591	4.16
1200	0.0204	2.262.-3	669.3	4835	25654	10.876	28.225	4.14
1400	0.1794	2.370.-3	86.06	5668	25778	11.518	25.882	4.19
1500	0.4269	2.433.-3	38.17	6088	25845	11.808	24.979	4.20

*Converted from tables in Vargaftik, *Tables of the Thermophysical Properties of Liquids and Gases*, Nauka, Moscow, 1972, and Hemisphere, Washington, 1975. m = melting point. The notation 1.78.-13 signifies 1.78×10^{-13} .

Many of the Vargaftik values also appear in Ohse, R. W., *Handbook of Thermodynamic and Transport Properties of Alkali Metals*, Blackwell Sci. Pubs., Oxford, 1985 (1020 pp.). This source contains superheat data.

Saturation and superheat tables and a diagram to 14 bar, 2200 K are given by Reynolds, W. C., *Thermodynamic properties in S.I.*, Stanford Univ. publ., 1979 (173 pp.). For a Mollier diagram from 0.1 to 140 psia, 2100–3600 °R, see Weatherford, P. M., J. C. Tyler, et al., WADD-TR-61-96, 1961.

An extensive review of properties of the solid and the saturated liquid was given by Alcock, C. B., M. W. Chase, et al., *J. Phys. Chem. Ref. Data*, **23**, 3 (1994): 385–497.

TABLE 2-231 Lithium Bromide—Water Solutions

Ruiter, J. P., *Rev. Int. Froid = Int. J. Refrig.*, **13** (1990): 223–236 gives subroutines for computer calculations. See also ASHRAE *Handbook—Fundamentals*.

TABLE 2-232 Saturated Mercury*

T, K	P, bar	$v_f \times 10^5, m^3/kg$	$v_g, m^3/kg$	$h_f, kJ/kg$	$h_g, kJ/kg$	$h_{fg}, kJ/kg$	$s_f, kJ/(kg \cdot K)$	$s_g, kJ/(kg \cdot K)$
203.15	$2.298 \cdot 10^{-11}$	7.26239	$3.665 \cdot 10^9$	33.131	342.637	309.506	0.32434	1.84787
213.15	$1.288 \cdot 10^{-10}$	7.27570	$6.862 \cdot 10^8$	34.567	343.674	309.107	0.33124	1.78142
223.15	$6.169 \cdot 10^{-10}$	7.28900	$1.499 \cdot 10^8$	35.997	344.710	308.713	0.33780	1.72123
233.15	$2.580 \cdot 10^{-9}$	7.30231	$3.746 \cdot 10^7$	37.422	345.746	308.324	0.34404	1.66647
243.15	$9.573 \cdot 10^{-9}$	7.31563	$1.053 \cdot 10^7$	38.842	346.782	307.940	0.35001	1.61647
253.15	$3.198 \cdot 10^{-8}$	7.32896	$3.281 \cdot 10^6$	40.258	347.819	307.561	0.35571	1.57065
263.15	$9.736 \cdot 10^{-8}$	7.34229	$1.120 \cdot 10^6$	41.668	348.855	307.187	0.36118	1.52852
273.15	$2.728 \cdot 10^{-7}$	7.35563	$4.150 \cdot 10^5$	43.074	349.891	306.817	0.36642	1.48967
283.15	$7.101 \cdot 10^{-7}$	7.36898	$1.653 \cdot 10^5$	44.476	350.927	306.451	0.37146	1.45375
293.15	$1.729 \cdot 10^{-6}$	7.38234	$7.026 \cdot 10^4$	45.874	351.964	306.090	0.37631	1.42045
303.15	$3.968 \cdot 10^{-6}$	7.39572	$3.167 \cdot 10^4$	47.268	353.000	305.732	0.38099	1.38951
313.15	$8.626 \cdot 10^{-6}$	7.40911	$1.505 \cdot 10^4$	48.659	354.036	305.377	0.38550	1.36068
323.15	$1.786 \cdot 10^{-5}$	7.42252	$7.501 \cdot 10^3$	50.046	355.072	305.026	0.38986	1.33378
333.15	$3.356 \cdot 10^{-5}$	7.43594	$3.905 \cdot 10^3$	51.430	356.108	304.678	0.39408	1.30862
343.15	$6.724 \cdot 10^{-5}$	7.44938	$2.115 \cdot 10^3$	52.810	357.145	304.335	0.39816	1.28505
353.15	$1.232 \cdot 10^{-4}$	7.46285	$1.188 \cdot 10^3$	54.188	358.181	303.993	0.40212	1.26292
363.15	$2.182 \cdot 10^{-4}$	7.47633	$6.899 \cdot 10^2$	55.563	359.217	303.654	0.40596	1.24213
373.15	$3.745 \cdot 10^{-4}$	7.48984	413.0	56.936	360.253	303.317	0.40969	1.22255
383.15	$6.247 \cdot 10^{-4}$	7.50337	254.2	58.306	361.289	302.983	0.41331	1.20408
393.15	$1.015 \cdot 10^{-3}$	7.51693	153.6	59.674	362.326	302.652	0.41684	1.18665
403.15	$1.608 \cdot 10^{-3}$	7.53052	103.9	61.039	363.362	302.323	0.42027	1.17017
413.15	$2.491 \cdot 10^{-3}$	7.55415	68.75	62.403	364.397	301.994	0.42361	1.15456
423.15	$3.778 \cdot 10^{-3}$	7.55780	46.43	63.765	365.433	301.668	0.42687	1.13978
433.15	$5.618 \cdot 10^{-3}$	7.57148	31.96	65.125	366.469	301.344	0.43004	1.12575
443.15	$8.204 \cdot 10^{-3}$	7.58520	22.39	66.484	367.504	301.020	0.43314	1.11242
453.15	$1.178 \cdot 10^{-2}$	7.59897	15.95	67.842	368.539	300.697	0.43617	1.09975
463.15	$1.664 \cdot 10^{-2}$	7.61277	11.54	69.198	369.574	300.376	0.43913	1.08768
473.15	$2.315 \cdot 10^{-2}$	7.62662	8.469	70.553	370.609	300.056	0.44203	1.07619
483.15	$3.177 \cdot 10^{-2}$	7.64051	6.301	71.908	371.642	299.734	0.44486	1.06524
493.15	$4.304 \cdot 10^{-2}$	7.65444	4.748	73.261	372.676	299.415	0.44763	1.05478
503.15	$5.758 \cdot 10^{-2}$	7.66843	3.621	74.614	373.708	299.094	0.45035	1.04479
513.15	$7.614 \cdot 10^{-2}$	7.68247	2.793	75.967	374.740	298.773	0.45301	1.03525
523.15	$9.959 \cdot 10^{-2}$	7.69656	2.176	77.319	375.771	298.452	0.45562	1.02611
533.15	0.12892	7.71071	1.7132	78.671	376.800	298.129	0.45818	1.01737
543.15	0.16527	7.72491	1.3613	80.023	377.829	297.806	0.46069	1.00899
553.15	0.20993	7.73918	1.0912	81.375	378.855	297.480	0.46316	1.00095
563.15	0.26435	7.75351	0.88213	82.728	379.880	297.152	0.46558	0.99324
573.15	0.33015	7.7679	0.71874	84.080	380.904	296.824	0.46796	0.98554
583.15	0.40910	7.7823	0.59002	85.434	381.925	296.491	0.47030	0.97893
593.15	0.50320	7.7969	0.48779	86.788	382.944	296.156	0.47260	0.97190
603.15	0.61460	7.8115	0.40600	88.143	383.960	295.817	0.47487	0.96532
613.15	0.74567	7.8262	0.34008	89.499	384.973	295.474	0.47709	0.95899
623.15	0.89896	7.8409	0.28660	90.856	385.984	295.128	0.47929	0.95289
633.15	1.0772	7.8558	0.24291	92.215	386.991	294.776	0.48145	0.94702
643.15	1.2834	7.8707	0.20702	93.575	387.994	294.419	0.48358	0.94135
653.15	1.5207	7.8858	0.17735	94.937	388.994	294.057	0.48568	0.93589
663.15	1.9725	7.9008	0.15269	96.300	389.989	293.689	0.48774	0.93061
673.15	2.1024	7.9160	0.13207	97.666	390.980	293.314	0.48978	0.92552
683.15	2.454	7.9313	0.11476	99.033	391.966	292.933	0.49180	0.92059
693.15	2.852	7.9467	0.10014	100.403	392.947	292.544	0.49378	0.91583
703.15	3.299	7.9622	0.08775	101.775	393.923	292.148	0.49574	0.91123
713.15	3.801	7.9778	0.07719	103.150	394.893	291.743	0.49768	0.90677
723.15	4.362	7.9935	0.06815	104.528	395.858	291.330	0.49959	0.90245
733.15	4.986	8.0094	0.06039	105.908	396.816	290.908	0.50148	0.89827
743.15	5.679	8.0252	0.05369	107.292	397.767	290.475	0.50335	0.89422
753.15	6.446	8.0413	0.04789	108.679	398.711	290.032	0.50519	0.89029
763.15	7.292	8.0574	0.04285	110.069	399.649	289.580	0.50702	0.88647
773.15	8.222	8.074	0.03846	111.463	400.579	289.116	0.50882	0.88277
783.15	9.242	8.090	0.03462	112.861	401.501	288.640	0.51061	0.87917
793.15	10.358	8.106	0.03124	114.262	402.415	288.153	0.51238	0.87568
803.15	11.576	8.123	0.02827	115.668	403.321	287.653	0.51412	0.87228
813.15	12.901	8.140	0.02565	117.078	404.218	287.140	0.51586	0.86898
823.15	14.340	8.157	0.02333	118.492	405.106	286.614	0.51757	0.86576
833.15	15.899	8.174	0.02126	119.911	405.985	286.074	0.51927	0.86263

*From Vukalovich, Ivanov, Fokin, and Yakovlev, *Thermophysical Properties of Mercury*, Standartov, Moscow, 1971. For the saturated liquid the specific volume at 203.15 K is $7.26239 \times 10^{-5} m^3/kg$, etc. All the tabular values for 203.15 K, 213.15 K, 223.15 K, and 233.15 K represent a metastable equilibrium between the subcooled liquid and the saturated vapor.

Saturation and superheat tables and a diagram to 100 bar, 1600 K are given by Reynolds, W. C., *Thermodynamic properties in S.I.*, Stanford Univ. publ., 1979 (173 pp.). For a Mollier diagram from 1 to 8200 psia and 2700°R, see Weatherford, W. D., J. C. Tyler, et al., WADD-TR-61-96, 1961.

2-294 PHYSICAL AND CHEMICAL DATA

TABLE 2-232 Saturated Mercury* (Concluded)

T, K	P, bar	$v_f \times 10^5, \text{m}^3/\text{kg}$	$v_g, \text{m}^3/\text{kg}$	$h_f, \text{kJ/kg}$	$h_g, \text{kJ/kg}$	$h_{fg}, \text{kJ/kg}$	$s_f, \text{kJ}/(\text{kg}\cdot\text{K})$	$s_g, \text{kJ}/(\text{kg}\cdot\text{K})$
843.15	17.584	8.191	0.019426	121.335	406.855	285.520	0.52095	0.85959
853.15	19.403	8.209	0.017785	122.763	407.715	284.952	0.52262	0.85662
863.15	21.36	8.226	0.016317	124.197	408.565	284.368	0.52427	0.85372
873.15	23.46	8.244	0.015000	125.636	409.405	283.769	0.52591	0.85090
883.15	25.72	8.262	0.013815	127.080	410.235	283.155	0.52753	0.84815
893.15	28.14	8.280	0.012748	128.530	411.054	282.524	0.52914	0.84546
903.15	30.72	8.298	0.011784	129.986	411.861	281.875	0.53074	0.84284
913.15	33.47	8.316	0.010911	131.448	412.658	281.210	0.53232	0.84028
923.15	36.41	8.335	0.010120	132.915	413.444	280.529	0.53389	0.83777
933.15	39.53	8.353	0.009401	134.389	414.218	279.829	0.53545	0.83533
943.15	42.85	8.372	0.008746	135.869	414.980	279.111	0.53700	0.83294
953.15	46.36	8.391	0.008150	137.356	415.731	278.375	0.53854	0.83060
963.15	50.09	8.410	0.007604	138.850	416.469	277.619	0.54006	0.82831
973.15	54.03	8.430	0.007105	140.350	417.195	276.845	0.54158	0.82606
983.15	58.20	8.450	0.006648	141.858	417.909	276.051	0.54308	0.82387
993.15	62.59	8.468	0.006228	143.372	418.610	275.238	0.54458	0.82172
1003.15	67.22	8.488	0.005842	144.894	419.298	274.404	0.54607	0.81961
1013.15	72.10	8.508	0.005487	146.424	419.974	273.550	0.54754	0.81754
1023.15	77.22	8.529	0.005159	147.961	420.636	272.675	0.54901	0.81552
1033.15	82.60	8.550	0.004856	149.506	421.286	271.780	0.55047	0.81353
1043.15	88.25	8.570	0.004576	151.059	421.923	270.864	0.55192	0.81158
1053.15	94.17	8.590	0.004317	152.619	422.546	269.927	0.55336	0.80966
1063.15	100.37	8.612	0.004077	154.188	423.156	268.968	0.55479	0.80778
1073.15	106.85	8.632	0.003854	155.766	423.752	267.986	0.55621	0.80593

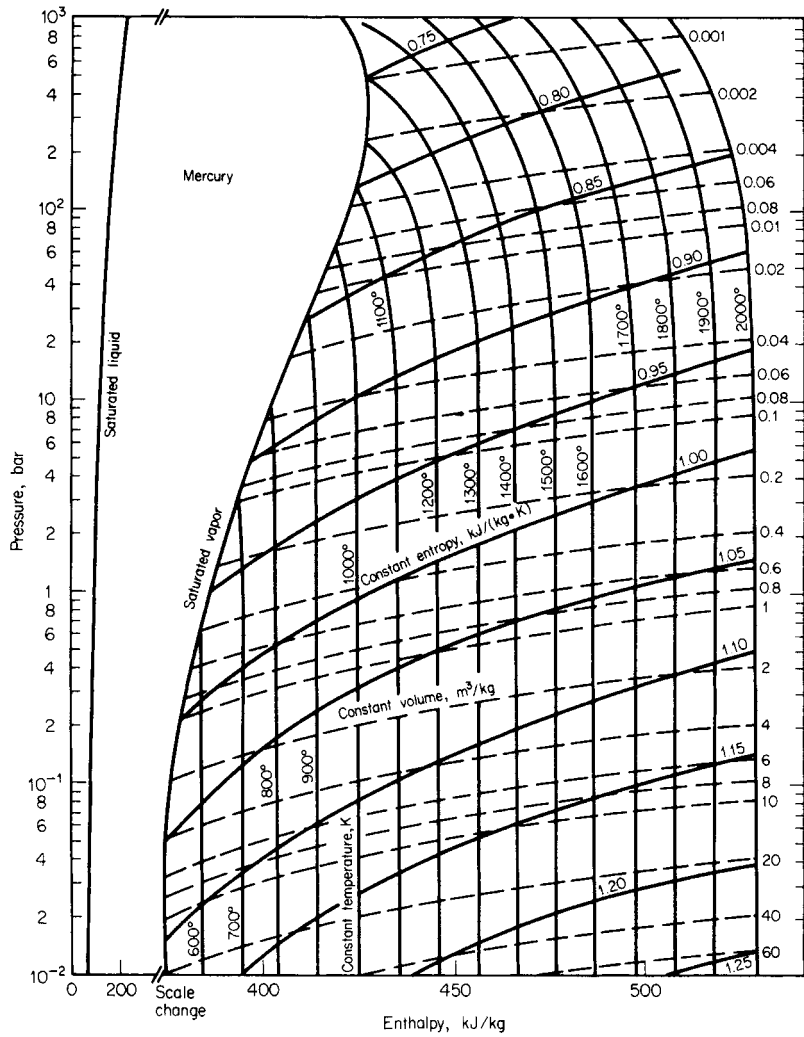


FIG. 2-12 Enthalpy-log-pressure diagram for mercury. (Drawn from tabular data in footnote reference to Table 2-232.)

TABLE 2-233 Thermodynamic Properties of Methane

Temperature K	Pressure MPa	Density mol/dm ³	Volume dm ³ /mol	Int. energy kJ/mol	Enthalpy kJ/mol	Entropy kJ/(mol·K)	C _v kJ/(mol·K)	C _p kJ/(mol·K)	Sound speed m/s	Joule-Thomson K/MPa	Therm. cond. mW/(m·K)	Viscosity μPa·s
Saturated Properties												
90.694	0.011696	28.142	0.035534	-1.1526	-1.1522	-0.011389	0.034776	0.054029	1538.6	-0.48191	211.24	204.52
100.00	0.034376	27.357	0.036554	-0.64728	-0.64602	-0.0060856	0.033908	0.054681	1452.0	-0.45812	199.67	155.78
105.00	0.056377	26.923	0.037143	-0.37306	-0.37097	-0.0034096	0.033500	0.055135	1403.9	-0.44202	193.03	136.86
110.00	0.088130	26.478	0.037768	-0.096585	-0.093257	-0.00083691	0.033115	0.055656	1354.7	-0.42328	186.18	121.34
115.00	0.13221	26.021	0.038431	0.18242	0.18750	0.0016441	0.032749	0.056253	1304.6	-0.40145	179.21	108.39
120.00	0.19143	25.551	0.039138	0.46425	0.47174	0.0040439	0.032400	0.056941	1253.5	-0.37589	172.15	97.432
125.00	0.26876	25.065	0.039896	0.74927	0.75999	0.0063722	0.032069	0.057741	1201.3	-0.34578	165.04	88.031
130.00	0.36732	24.562	0.040714	1.0379	1.0529	0.0086383	0.031757	0.058684	1148.1	-0.31006	157.91	79.868
135.00	0.49035	24.038	0.041600	1.3307	1.3511	0.010851	0.031469	0.059809	1093.6	-0.26735	150.78	72.699
140.00	0.64118	23.491	0.042569	1.6284	1.6557	0.013020	0.031206	0.061169	1037.7	-0.21579	143.65	66.333
145.00	0.82322	22.917	0.043636	1.9317	1.9676	0.015154	0.030974	0.062840	980.17	-0.15286	136.54	60.620
150.00	1.0400	22.309	0.044825	2.2418	2.2884	0.017264	0.030780	0.064932	920.85	-0.075032	129.43	55.437
155.00	1.2950	21.661	0.046165	2.5602	2.6199	0.019362	0.030631	0.067613	859.39	0.022798	122.32	50.682
160.00	1.5921	20.964	0.047702	2.8887	2.9647	0.021462	0.030541	0.071156	795.43	0.14836	115.19	46.266
165.00	1.9351	20.202	0.049500	3.2304	3.3262	0.023584	0.030531	0.076044	728.42	0.31398	108.01	42.105
170.00	2.3283	19.355	0.051667	3.5895	3.7098	0.025755	0.030634	0.083218	657.52	0.54087	100.73	38.115
175.00	2.7765	18.384	0.054394	3.9734	4.1244	0.028021	0.030920	0.094816	581.27	0.86918	93.324	34.196
180.00	3.2852	17.218	0.058078	4.3965	4.5873	0.030467	0.031554	0.11699	497.01	1.3866	85.799	30.193
185.00	3.8617	15.668	0.063825	4.8955	5.1420	0.033313	0.033085	0.17822	398.59	2.3397	78.733	25.773
190.00	4.5186	12.515	0.079902	5.7074	6.0685	0.038000	0.041746	1.5082	250.31	5.2488	96.970	18.982
190.56	4.5992	10.139	0.098628	6.2136	6.6672	0.041109			0	6.8877		
90.694	0.011696	0.015630	63.981	6.8310	7.5793	0.084885	0.025243	0.033851	249.13	47.921	8.8517	3.6388
100.00	0.034376	0.042048	23.782	7.0469	7.8644	0.079019	0.025487	0.034425	260.09	37.826	10.015	3.9976
105.00	0.056377	0.066154	15.116	7.1582	8.0104	0.076413	0.025652	0.034853	265.31	33.883	10.669	4.1951
110.00	0.088130	0.099622	10.038	7.2654	8.1501	0.074103	0.025842	0.035378	270.01	30.662	11.350	4.3964
115.00	0.13221	0.14457	6.9171	7.3680	8.2825	0.072036	0.026056	0.036016	274.17	28.004	12.062	4.6019
120.00	0.19143	0.20332	4.9183	7.4652	8.4067	0.070168	0.026295	0.036786	277.76	25.790	12.811	4.8123
125.00	0.26876	0.27844	3.5915	7.5562	8.5215	0.068464	0.026560	0.037714	280.76	23.928	13.604	5.0285
130.00	0.36732	0.37278	2.6825	7.6403	8.6257	0.066891	0.026854	0.038836	283.13	22.347	14.449	5.2517
135.00	0.49035	0.48962	2.0424	7.7165	8.7180	0.065421	0.027182	0.040203	284.86	20.993	15.355	5.4833
140.00	0.64118	0.63279	1.5803	7.7837	8.7970	0.064029	0.027549	0.041885	285.93	19.819	16.334	5.7254
145.00	0.82322	0.80691	1.2393	7.8406	8.8608	0.062694	0.027965	0.043985	286.31	18.789	17.402	5.9806
150.00	1.0400	1.0177	0.98256	7.8856	8.9074	0.061391	0.028439	0.046657	285.97	17.870	18.581	6.2526
155.00	1.2950	1.2728	0.78568	7.9166	8.9340	0.060098	0.028989	0.050144	284.88	17.035	19.904	6.5462
160.00	1.5921	1.5821	0.63206	7.9306	8.9369	0.058789	0.029636	0.054849	283.01	16.255	21.423	6.8688
165.00	1.9351	1.9603	0.51014	7.9238	8.9109	0.057431	0.030412	0.061496	280.30	15.500	23.225	7.2313
170.00	2.3283	2.4294	0.41163	7.8898	8.8482	0.055982	0.031374	0.071527	276.66	14.732	25.477	7.6515
175.00	2.7765	3.0268	0.33038	7.8184	8.7357	0.054371	0.032615	0.088273	271.99	13.896	28.545	8.1609
180.00	3.2852	3.8257	0.26139	7.6893	8.5480	0.052471	0.034338	0.12151	266.04	12.892	33.392	8.8251
185.00	3.8617	5.0137	0.19945	7.4515	8.2217	0.049961	0.037087	0.21701	258.03	11.492	43.706	9.8238
190.00	4.5186	7.8027	0.12816	6.7850	7.3641	0.044819	0.045796	2.2590	238.55	8.4951	119.40	12.455
190.56	4.5992	10.139	0.098628	6.2136	6.6672	0.041109			0	6.8877		

Single-Phase Properties

100.00	0.10000	27.360	0.036549	-0.64803	-0.64438	-0.0060931	0.033911	0.054672	1452.6	-0.45829	199.74	155.91
111.51	0.10000	26.341	0.037963	-0.012738	-0.0089413	-0.000079677	0.033003	0.055828	1339.7	-0.41705	184.09	117.20
111.51	0.10000	0.11186	8.9395	7.2969	8.1908	0.073456	0.025904	0.035558	271.33	29.808	11.561	4.4579
200.00	0.10000	0.060518	16.524	9.5570	11.209	0.093427	0.025259	0.033784	369.98	9.2893	21.941	7.8096
300.00	0.10000	0.040158	24.901	12.175	14.665	0.10741	0.027479	0.035869	449.74	4.3216	34.552	11.245
400.00	0.10000	0.030082	33.243	15.151	18.475	0.11834	0.032300	0.040652	510.56	2.2395	50.127	14.272
500.00	0.10000	0.024055	41.572	18.673	22.831	0.12803	0.038196	0.046533	561.86	1.2245	68.564	16.976
600.00	0.10000	0.020042	49.895	22.795	27.784	0.13705	0.044179	0.052509	608.04	0.68722	88.921	19.431
100.00	1.0000	27.403	0.036493	-0.65829	-0.62179	-0.0061960	0.033950	0.054562	1459.6	-0.46060	200.62	157.63
149.14	1.0000	22.416	0.044610	2.1878	2.2325	0.016902	0.030810	0.064535	931.21	-0.089695	130.66	56.297
149.14	1.0000	0.97852	1.0220	7.8788	8.9007	0.061614	0.028353	0.046147	286.08	18.022	18.368	6.2043
200.00	1.0000	0.64363	1.5537	9.3582	10.912	0.073276	0.025879	0.036730	357.81	9.5001	23.028	8.0145
300.00	1.0000	0.40776	2.4524	12.072	14.524	0.087922	0.027621	0.036721	447.04	4.2699	35.152	11.367
400.00	1.0000	0.30205	3.3108	15.083	18.393	0.099023	0.032360	0.041056	510.57	2.2001	50.558	14.357
500.00	1.0000	0.24058	4.1567	18.623	22.780	0.10879	0.038227	0.046766	562.99	1.1998	68.902	17.040
600.00	1.0000	0.20012	4.9971	22.755	27.752	0.11784	0.044198	0.052659	609.73	0.67124	89.200	19.483
100.00	5.0000	27.586	0.036250	-0.70190	-0.52065	-0.0066393	0.034116	0.054117	1490.0	-0.46993	204.45	165.25
200.00	5.0000	5.4706	0.18279	7.8197	8.7337	0.051495	0.032029	0.11667	291.29	8.9784	40.612	10.828
300.00	5.0000	2.1799	0.45874	11.590	13.884	0.072954	0.028262	0.041234	439.25	3.9428	38.480	12.194
400.00	5.0000	1.5333	0.65221	14.779	18.040	0.084897	0.032614	0.042903	513.11	2.0089	52.693	14.872
500.00	5.0000	1.2013	0.83240	18.401	22.563	0.094971	0.038361	0.047789	569.49	1.0870	70.509	17.410
600.00	5.0000	0.99281	1.0072	22.581	27.617	0.10417	0.044277	0.053309	618.13	0.60013	90.498	19.768
100.00	10.000	27.802	0.035969	-0.75239	-0.39270	-0.0071652	0.034314	0.053642	1525.7	-0.47979	209.07	174.83
200.00	10.000	16.593	0.060268	5.1551	5.7578	0.034542	0.030129	0.085085	567.92	1.0266	84.234	29.399
300.00	10.000	4.6859	0.21340	10.942	13.077	0.065137	0.028995	0.048165	444.53	3.2606	44.730	13.896
400.00	10.000	3.1002	0.32256	14.401	17.627	0.078246	0.032902	0.045220	522.58	1.7355	55.941	15.766
500.00	10.000	2.3887	0.41863	18.132	22.318	0.088698	0.038516	0.049007	580.99	0.94125	72.781	18.011
600.00	10.000	1.9619	0.50971	22.371	27.468	0.098073	0.044371	0.054070	630.63	0.51200	92.268	20.217
200.00	100.00	25.496	0.039222	3.0510	6.9732	0.020596	0.032058	0.048512	1541.0	-0.51619	188.05	80.392
300.00	100.00	21.266	0.047024	7.0865	11.789	0.040126	0.031823	0.048281	1267.5	-0.44889	137.68	47.835
400.00	100.00	17.881	0.055926	11.121	16.713	0.054276	0.035273	0.050523	1115.8	-0.37484	120.38	37.584
500.00	100.00	15.305	0.065340	15.405	21.939	0.065922	0.040312	0.054139	1044.8	-0.32811	120.87	33.590
600.00	100.00	13.357	0.074869	20.074	27.561	0.076160	0.045724	0.058364	1018.4	-0.30439	130.36	32.111
200.00	500.00	33.003	0.030301	2.3322	17.482	0.0061671	0.037832	0.047821	2664.2	-0.53926	429.60	205.24
300.00	500.00	30.786	0.032482	5.9505	22.192	0.025271	0.037006	0.047114	2500.0	-0.55416	358.93	106.90
400.00	500.00	28.929	0.034567	9.7401	27.024	0.039152	0.039890	0.049933	2360.3	-0.52806	312.36	78.768
500.00	500.00	27.331	0.036588	13.934	32.228	0.050747	0.044407	0.054280	2250.3	-0.49035	285.41	66.669
600.00	500.00	25.934	0.038559	18.612	37.892	0.061061	0.049344	0.059017	2168.1	-0.45514	272.14	60.413

The values in these tables were generated from the NIST REFPROP software (Lemmon, E. W., McLinden, M. O., and Huber, M. L., NIST Standard Reference Database 23: Reference Fluid Thermodynamic and Transport Properties—REFPROP, National Institute of Standards and Technology, Standard Reference Data Program, Gaithersburg, Md., 2002, Version 7.1). The primary source for the thermodynamic properties is Setzmann, U., and Wagner, W., "A New Equation of State and Tables of Thermodynamic Properties for Methane Covering the Range from the Melting Line to 625 K at Pressures up to 1000 MPa," *J. Phys. Chem. Ref. Data* **20**(6):1061–1151, 1991. The source for viscosity is Younglove, B. A., and Ely, J. F., "Thermophysical Properties of Fluids. II. Methane, Ethane, Propane, Isobutane and Normal Butane," *J. Phys. Chem. Ref. Data* **16**:577–798, 1987. The source for thermal conductivity is Friend, D. G., Ely, J. F., and Ingham, H., "Tables for the Thermophysical Properties of Methane," *NIST Tech. Note* 1325, 1989.

Properties at the triple point temperature and the critical point temperature are given in the first and last entries of the saturation tables, respectively. In the single-phase table, when the temperature range for a given isobar includes a vapor-liquid phase boundary, the temperature of phase equilibrium is noted, and properties for both the saturated liquid and saturated vapor are given (with liquid properties given in the upper line). Lines are omitted from the temperature-pressure grid of the single-phase table, when the system would be in the solid phase or if there are potential problems with the source property surface.

The uncertainties in density are 0.03% for pressures below 12 MPa and temperatures below 350 K and up to 0.07% for pressures less than 50 MPa. For the speed of sound, the uncertainty ranges from 0.03% (in the vapor phase) to 0.3% depending on temperature and pressure. Heat capacities may be generally calculated within an uncertainty of 1%. The uncertainty in viscosity is 2%, except in the critical region which is 5%. The uncertainty in thermal conductivity of the dilute gas between 130 and 625 K is 2.5%. For temperatures below 130 K, the uncertainty is less than 10%. Excluding the dilute gas, the uncertainty is 2% between 110 and 725 K at pressures up to 70 MPa, except near the critical point which has an uncertainty of 5% or greater. For the vapor at lower temperatures and the dense liquid near the triple point, an uncertainty of 10% is possible.

TABLE 2-234 Thermodynamic Properties of Methanol

Temperature K	Pressure MPa	Density mol/dm ³	Volume dm ³ /mol	Int. energy kJ/mol	Enthalpy kJ/mol	Entropy kJ/(mol·K)	C _v kJ/(mol·K)	C _p kJ/(mol·K)	Sound speed m/s	Joule-Thomson K/MPa
Saturated Properties										
175.61	1.8635E-07	28.230	0.035423	-12.440	-12.440	-0.049524	0.056728	0.070390	1625.1	-0.40884
180.00	3.7619E-07	28.096	0.035592	-12.130	-12.130	-0.047781	0.056689	0.070750	1590.2	-0.40373
195.00	3.2175E-06	27.629	0.036194	-11.067	-11.067	-0.042108	0.056604	0.070897	1496.4	-0.39791
210.00	1.9841E-05	27.163	0.036815	-10.001	-10.001	-0.036846	0.057072	0.071215	1425.3	-0.39361
225.00	9.4330E-05	26.703	0.037449	-8.9277	-8.9277	-0.031908	0.057992	0.072004	1363.2	-0.38674
240.00	0.00036348	26.250	0.038096	-7.8395	-7.8395	-0.027226	0.059275	0.073141	1304.6	-0.37793
255.00	0.0011791	25.802	0.038756	-6.7318	-6.7318	-0.022750	0.060916	0.074617	1248.2	-0.36733
270.00	0.0033166	25.360	0.039432	-5.5991	-5.5990	-0.018434	0.062917	0.076487	1194.1	-0.35457
285.00	0.0082787	24.922	0.040125	-4.4351	-4.4347	-0.014239	0.065250	0.078803	1142.6	-0.33915
300.00	0.018682	24.484	0.040844	-3.2329	-3.2322	-0.010129	0.067864	0.081584	1093.5	-0.32073
315.00	0.038692	24.041	0.041595	-1.9858	-1.9842	-0.0060725	0.070693	0.084823	1046.3	-0.29904
330.00	0.074453	23.590	0.042390	-0.68700	-0.68385	-0.0020451	0.073674	0.088505	1000.2	-0.27385
345.00	0.13447	23.124	0.043244	0.66961	0.67543	0.0019747	0.076752	0.092616	954.32	-0.24479
360.00	0.22992	22.638	0.044174	2.0901	2.1003	0.0060049	0.079881	0.097164	907.64	-0.21121
375.00	0.37483	22.123	0.045203	3.5806	3.5975	0.010061	0.083033	0.10219	859.31	-0.17199
390.00	0.58617	21.571	0.046358	5.1475	5.1746	0.014159	0.086189	0.10776	808.48	-0.12529
405.00	0.88399	20.973	0.047681	6.7983	6.8404	0.018314	0.089346	0.11405	754.41	-0.068163
420.00	1.2914	20.315	0.049226	8.5423	8.6058	0.022546	0.092514	0.12133	696.47	0.0042669
435.00	1.8349	19.579	0.051075	10.392	10.485	0.026879	0.095722	0.13007	634.17	0.10021
450.00	2.5433	18.741	0.053360	12.364	12.500	0.031347	0.099032	0.14120	567.09	0.23444
465.00	3.4456	17.759	0.056310	14.488	14.682	0.036009	0.10257	0.15679	494.36	0.43762
480.00	4.5713	16.553	0.060411	16.820	17.096	0.040977	0.10666	0.18345	412.12	0.79465
495.00	5.9794	14.880	0.067203	19.521	19.923	0.046590	0.11250	0.25717	308.94	1.6506
510.00	7.7496	11.689	0.085547	23.297	23.960	0.054351	0.12653	1.1088	192.83	4.6061
513.38	8.2159	8.7852	0.11383	25.917	26.852	0.059911			0	6.7425
175.61	1.8635E-07	1.2764E-07	7,834,400.	28.219	29.679	0.19032	0.031874	0.040287	239.95	1187400.
180.00	3.7619E-07	2.5140E-07	3,977,700.	28.353	29.850	0.18544	0.032397	0.040854	242.62	857090.
195.00	3.2175E-06	1.9855E-06	503,660.	28.810	30.430	0.17069	0.035224	0.043954	251.06	293110.
210.00	1.9841E-05	1.1378E-05	87,892.	29.259	31.003	0.15841	0.040104	0.049389	258.49	105090.
225.00	9.4330E-05	5.0556E-05	19,780.	29.698	31.564	0.14806	0.047248	0.057480	265.30	39363.
240.00	0.00036348	0.00018304	5,463.4	30.123	32.109	0.13923	0.056324	0.067973	271.89	15552.
255.00	0.0011791	0.00056065	1,783.7	30.534	32.637	0.13164	0.066572	0.080135	278.43	6557.5
270.00	0.0033166	0.0014959	668.48	30.932	33.149	0.12508	0.077055	0.093000	284.90	2971.8
285.00	0.0082787	0.0035581	281.05	31.321	33.648	0.11938	0.086920	0.10564	291.19	1449.9
300.00	0.018682	0.0076845	130.13	31.703	34.134	0.11442	0.095581	0.11740	297.15	759.96
315.00	0.038692	0.015300	65.359	32.077	34.606	0.11009	0.10279	0.12798	302.63	426.34
330.00	0.074453	0.028438	35.164	32.442	35.060	0.10627	0.10860	0.13749	307.47	254.84
345.00	0.13447	0.049870	20.052	32.789	35.485	0.10287	0.11331	0.14644	311.48	161.53
360.00	0.22992	0.083267	12.009	33.108	35.869	0.099808	0.11736	0.15559	314.48	108.02
375.00	0.37483	0.13344	7.4940	33.385	36.194	0.096984	0.12125	0.16605	316.20	75.802
390.00	0.58617	0.20674	4.8370	33.601	36.436	0.094317	0.12546	0.17917	316.34	55.467
405.00	0.88399	0.31179	3.2073	33.736	36.571	0.091723	0.13033	0.19663	314.53	42.002
420.00	1.2914	0.46071	2.1706	33.767	36.570	0.089128	0.13587	0.21986	310.36	32.587
435.00	1.8349	0.67055	1.4913	33.687	36.423	0.086505	0.14101	0.24709	303.71	25.532
450.00	2.5433	0.96219	1.0393	33.541	36.184	0.083978	0.14238	0.26502	295.26	19.860
465.00	3.4456	1.3555	0.73775	33.439	35.981	0.081813	0.13589	0.25879	285.25	15.568
480.00	4.5713	1.9102	0.52352	33.258	35.652	0.079634	0.12618	0.27959	267.83	13.904
495.00	5.9794	2.9050	0.34423	32.267	34.325	0.075685	0.12608	0.42448	247.46	12.099
510.00	7.7496	5.1706	0.19340	29.688	31.187	0.068520	0.13259	1.9096	212.65	9.5115
513.38	8.2159	8.7852	0.11383	25.917	26.852	0.059911			0	6.7425

Single-Phase Properties

200.00	0.10000	27.474	0.036398	-10.713	-10.709	-0.040317	0.056702	0.070943	1471.5	-0.39677
300.00	0.10000	24.486	0.040839	-3.2341	-3.2300	-0.010133	0.067862	0.081580	1094.1	-0.32081
337.30	0.10000	23.366	0.042798	-0.034546	-0.030266	-0.000089518	0.075163	0.090451	977.93	-0.26023
337.30	0.10000	0.037626	26.577	32.613	35.271	0.10457	0.11100	0.14187	309.54	202.71
400.00	0.10000	0.030452	32.839	36.075	39.359	0.11581	0.044972	0.054208	349.19	40.941
500.00	0.10000	0.024157	41.396	40.921	45.060	0.12851	0.051823	0.060380	387.15	12.933
600.00	0.10000	0.020089	49.779	46.476	51.454	0.14014	0.059065	0.067441	420.71	4.3382
200.00	1.0000	27.491	0.036376	-10.720	-10.684	-0.040354	0.056724	0.070932	1475.1	-0.39705
300.00	1.0000	24.514	0.040793	-3.2472	-3.2064	-0.010176	0.067848	0.081541	1100.0	-0.32177
400.00	1.0000	21.193	0.047185	6.2298	6.2770	0.016901	0.088257	0.11177	775.46	-0.090229
409.75	1.0000	20.772	0.048143	7.3401	7.3883	0.019645	0.090347	0.11623	736.51	-0.047179
409.75	1.0000	0.35352	2.8287	33.758	36.586	0.090904	0.13203	0.20333	313.48	38.678
500.00	1.0000	0.25202	3.9680	40.335	44.303	0.10818	0.056676	0.068069	376.08	13.330
600.00	1.0000	0.20501	4.8778	46.300	51.178	0.12070	0.061344	0.070369	413.09	4.5635
200.00	5.0000	27.561	0.036283	-10.752	-10.571	-0.040517	0.056820	0.070883	1490.9	-0.39825
300.00	5.0000	24.635	0.040592	-3.3039	-3.1010	-0.010367	0.067795	0.081377	1125.5	-0.32568
400.00	5.0000	21.441	0.046640	6.0896	6.3228	0.016546	0.087676	0.11029	818.58	-0.11504
484.95	5.0000	16.076	0.062203	17.655	17.966	0.042725	0.10826	0.19836	381.15	0.98684
484.95	5.0000	2.1711	0.46060	33.047	35.350	0.078574	0.12499	0.32263	260.06	13.826
500.00	5.0000	1.7679	0.56566	35.907	38.735	0.085457	0.098975	0.17315	301.43	12.155
600.00	5.0000	1.1389	0.87808	45.247	49.638	0.10553	0.072927	0.087489	379.21	5.1009
200.00	10.000	27.648	0.036169	-10.791	-10.430	-0.040716	0.056935	0.070820	1509.9	-0.39966
300.00	10.000	24.779	0.040357	-3.3713	-2.9677	-0.010598	0.067746	0.081196	1155.3	-0.32990
400.00	10.000	21.717	0.046048	5.9321	6.3925	0.016141	0.087087	0.10880	865.91	-0.13884
500.00	10.000	15.932	0.062765	19.374	20.002	0.046226	0.10760	0.18959	424.68	0.83939
600.00	10.000	2.6640	0.37537	43.262	47.015	0.096406	0.088868	0.12122	343.60	5.0965
200.00	100.00	28.911	0.034588	-11.305	-7.8460	-0.043691	0.057827	0.068992	1772.1	-0.41976
300.00	100.00	26.630	0.037552	-4.2043	-4.44914	-0.013840	0.067889	0.079818	1515.8	-0.35799
400.00	100.00	24.493	0.040827	4.3449	8.4277	0.011565	0.082823	0.098951	1334.7	-0.26099
500.00	100.00	22.020	0.045413	14.917	19.458	0.036085	0.095694	0.12152	1164.1	-0.14407
600.00	100.00	19.139	0.052250	27.300	32.525	0.059862	0.10406	0.13787	977.50	-0.023905
300.00	500.00	30.547	0.032736	-5.4195	10.949	-0.022106	0.070293	0.080627	2316.0	-0.34762
400.00	500.00	29.154	0.034300	2.2795	19.430	0.0022308	0.077541	0.089761	2194.8	-0.30897
500.00	500.00	27.670	0.036140	11.020	29.089	0.023726	0.084883	0.10419	2123.2	-0.24751
600.00	500.00	26.003	0.038457	21.094	40.322	0.044161	0.092281	0.12017	2074.1	-0.19279

The values in these tables were generated from the NIST REFPROP software (Lemmon, E. W., McLinden, M. O., and Huber, M. L., NIST Standard Reference Database 23: Reference Fluid Thermodynamic and Transport Properties—REFPROP, National Institute of Standards and Technology, Standard Reference Data Program, Gaithersburg, Md., 2002, Version 7.1). The primary source for the thermodynamic properties is de Reuck, K. M., and Craven, R. J. B., "Methanol, International Thermodynamic Tables of the Fluid State—12," *IUPAC*, Blackwell Scientific Publications, London, 1993. Validated equations for the viscosity and thermal conductivity are not currently available for this fluid.

Properties at the triple point temperature and the critical point temperature are given in the first and last entries of the saturation tables, respectively. In the single-phase table, when the temperature range for a given isobar includes a vapor-liquid phase boundary, the temperature of phase equilibrium is noted, and properties for both the saturated liquid and saturated vapor are given (with liquid properties given in the upper line). Lines are omitted from the temperature-pressure grid of the single-phase table, when the system would be in the solid phase or if there are potential problems with the source property surface.

The uncertainties of the equation of state are generally 0.1% in density and 2% in the speed of sound, except in the critical region and high pressures.

TABLE 2-235 Thermodynamic Properties of 2-Methyl Butane (Isopentane)

Temperature K	Pressure MPa	Density mol/dm ³	Volume dm ³ /mol	Int. energy kJ/mol	Enthalpy kJ/mol	Entropy kJ/(mol·K)	C _v kJ/(mol·K)	C _p kJ/(mol·K)	Sound speed m/s	Joule-Thomson K/MPa	Therm. Cond. mW/(m·K)	Viscosity μPa·s
Saturated Properties												
112.65	8.9347E-11	10.936	0.091442	-26.072	-26.072	-0.13287	0.088268	0.12675	2024.6	-0.61677	177.46	18091
115	1.9071E-10	10.903	0.091719	-25.774	-25.774	-0.13026	0.087968	0.12625	2007.2	-0.61938	177.30	15987
130	1.1761E-08	10.698	0.093478	-23.896	-23.896	-0.11491	0.087279	0.12456	1899.0	-0.62810	174.59	7701.7
145	2.8119E-07	10.500	0.095242	-22.028	-22.028	-0.10131	0.088069	0.12473	1796.0	-0.62623	169.97	4126.6
160	3.4585E-06	10.306	0.097028	-20.148	-20.148	-0.08897	0.089805	0.12613	1698.3	-0.61691	164.30	2438.0
175	2.6222E-05	10.116	0.09885	-18.240	-18.240	-0.07757	0.092192	0.12840	1605.5	-0.60215	158.07	1564.5
190	0.00013839	9.9281	0.10072	-16.293	-16.293	-0.06690	0.095056	0.13133	1517.0	-0.58328	151.59	1074.5
205	0.00055325	9.7405	0.10266	-14.298	-14.298	-0.05679	0.098282	0.13478	1432.2	-0.56116	145.02	779.51
220	0.0017804	9.5525	0.10468	-12.247	-12.247	-0.04714	0.10179	0.13865	1350.7	-0.53631	138.51	591.10
235	0.0048228	9.3629	0.10680	-10.136	-10.136	-0.03786	0.10553	0.14289	1271.9	-0.50892	132.11	464.45
250	0.011375	9.1708	0.10904	-7.9595	-7.9583	-0.02888	0.10944	0.14744	1195.4	-0.47898	125.89	375.48
265	0.023974	8.9750	0.11142	-5.7124	-5.7097	-0.02016	0.11351	0.15230	1120.7	-0.44620	119.87	310.55
280	0.046069	8.7745	0.11397	-3.3908	-3.3856	-0.01163	0.11771	0.15744	1047.6	-0.41003	114.07	261.53
295	0.082015	8.5679	0.11671	-0.99085	-0.98128	-0.00329	0.12200	0.16288	975.50	-0.36957	108.49	223.37
310	0.13700	8.3537	0.11971	1.4914	1.5078	0.004922	0.12638	0.16864	904.21	-0.32346	103.13	192.84
325	0.21693	8.1302	0.12300	4.0602	4.0869	0.013015	0.13084	0.17476	833.33	-0.26964	98.008	167.77
340	0.32835	7.8950	0.12666	6.7200	6.7616	0.021017	0.13535	0.18133	762.50	-0.20494	93.105	146.69
355	0.47831	7.6451	0.13080	9.4764	9.5389	0.028954	0.13992	0.18849	691.33	-0.12436	88.417	128.56
370	0.67436	7.3765	0.13557	12.336	12.428	0.036852	0.14455	0.19649	619.38	-0.01964	83.934	112.60
385	0.92461	7.0835	0.14117	15.310	15.440	0.044740	0.14926	0.20576	546.13	0.12385	79.645	98.258
400	1.2378	6.7572	0.14799	18.410	18.593	0.052658	0.15409	0.21716	470.92	0.33435	75.537	85.057
415	1.6238	6.3830	0.15667	21.662	21.916	0.060668	0.15915	0.23260	392.75	0.67407	71.596	72.595
430	2.0941	5.9327	0.16856	25.110	25.463	0.068880	0.16468	0.25764	309.77	1.3120	67.829	60.422
445	2.6640	5.3333	0.18750	28.871	29.370	0.077578	0.17145	0.31907	217.58	2.9280	64.403	47.740
460.35	3.3782	3.2710	0.30572	35.298	36.331	0.092549			0	18.924		
112.65	8.9527E-11	9.5585E-11	1.05E+10	7.8069	8.7435	0.17618	0.044856	0.053170	124.05		2.3120	2.775
115	1.9071E-10	1.9975E-10	5.01E+09	7.9134	8.8695	0.17099	0.045769	0.054083	125.14	1474.9	2.3996	2.827
130	1.1761E-08	1.0881E-08	91,905,000	8.6432	9.7241	0.14371	0.051515	0.059829	131.91	867.62	3.0011	3.1624
145	2.8119E-07	2.3324E-07	4,287,500	9.4580	10.664	0.12415	0.057098	0.065412	138.36	543.86	3.6746	3.5046
160	3.4585E-06	2.5998E-06	384,650	10.355	11.686	0.10999	0.062541	0.070856	144.53	358.94	4.4196	3.853
175	2.6222E-05	1.8023E-05	55,485	11.333	12.788	0.099732	0.067888	0.076206	150.45	247.17	5.2372	4.2074
190	0.00013839	8.7629E-05	11,412	12.390	13.969	0.092376	0.073180	0.081510	156.12	176.38	6.1289	4.5669
205	0.00055325	0.00032489	3,077.9	13.524	15.227	0.087227	0.078451	0.086811	161.53	129.80	7.0964	4.931
220	0.0017804	0.00097556	1,025.1	14.732	16.557	0.083784	0.083733	0.092156	166.66	98.138	8.1416	5.2989
235	0.0048228	0.0024804	403.15	16.011	17.955	0.081674	0.089051	0.09759	171.43	76.055	9.2673	5.6698
250	0.011375	0.0055234	181.05	17.357	19.416	0.080615	0.094425	0.10316	175.77	60.317	10.477	6.0432
265	0.023974	0.011056	90.449	18.766	20.935	0.080389	0.099871	0.10890	179.56	48.903	11.776	6.4187
280	0.046069	0.020302	49.256	20.234	22.503	0.080825	0.10539	0.11485	182.71	40.504	13.169	6.7963
295	0.082015	0.034759	28.769	21.756	24.115	0.081787	0.11100	0.12105	185.07	34.252	14.664	7.1769
310	0.13700	0.056212	17.790	23.326	25.763	0.083164	0.11669	0.12757	186.54	29.560	16.270	7.5619
325	0.21693	0.086783	11.523	24.939	27.438	0.084865	0.12246	0.13447	186.97	26.024	17.997	7.9543
340	0.32835	0.12904	7.7495	26.587	29.132	0.086812	0.12831	0.14187	186.20	23.372	19.860	8.3586
355	0.47831	0.18620	5.3705	28.263	30.831	0.088933	0.13425	0.14999	184.05	21.417	21.877	8.7821
370	0.67436	0.26252	3.8092	29.953	32.522	0.091161	0.14029	0.15916	180.31	20.043	24.077	9.2355
385	0.92461	0.36398	2.7474	31.643	34.183	0.093423	0.14648	0.17005	174.70	19.189	26.507	9.7357
400	1.2378	0.49975	2.0010	33.305	35.782	0.095630	0.15286	0.18403	166.85	18.851	29.248	10.311
415	1.6238	0.68534	1.4591	34.899	37.268	0.097660	0.15958	0.20431	156.26	19.092	32.469	11.011
430	2.0941	0.95152	1.0510	36.342	38.543	0.099299	0.16690	0.24064	142.23	20.076	36.596	11.947
445	2.6640	1.3789	0.72521	37.430	39.362	0.10003	0.17558	0.34061	123.63	22.072	43.254	13.438
460.35	3.3782	3.2710	0.30572	35.298	36.331	0.092549			0	18.924		

Single-Phase Properties

150.00	0.10000	10.435	0.095828	-21.406	-21.396	-0.097086	0.088566	0.12508	1763.3	-0.62386	168.19	3428.5
225.00	0.10000	9.4905	0.10537	-11.554	-11.543	-0.044025	0.10302	0.14001	1324.8	-0.52760	136.40	543.85
300.00	0.10000	8.4975	0.11768	-0.17289	-0.16112	-0.00053568	0.12345	0.16476	951.69	-0.35493	106.68	212.48
300.60	0.10000	8.4890	0.11780	-0.074609	-0.062829	-0.00020836	0.12363	0.16499	948.83	-0.35312	106.46	211.22
300.60	0.10000	0.041839	23.901	22.336	24.726	0.082257	0.11311	0.12344	185.73	32.344	15.250	7.3199
375.00	0.10000	0.032734	30.549	31.687	34.742	0.11194	0.13702	0.14615	210.31	14.520	23.271	9.1730
450.00	0.10000	0.027025	37.003	42.874	46.575	0.14064	0.16045	0.16919	231.26	8.0746	32.656	10.981
150.00	1.0000	10.441	0.095776	-21.422	-21.326	-0.097192	0.088617	0.12507	1767.4	-0.62411	168.39	3436.2
225.00	1.0000	9.5002	0.10526	-11.582	-11.477	-0.044150	0.10306	0.13992	1330.6	-0.52893	136.76	547.08
300.00	1.0000	8.5157	0.11743	-0.22558	-0.10815	-0.00071178	0.12349	0.16444	960.79	-0.36015	107.23	214.82
375.00	1.0000	7.2951	0.13708	13.279	13.417	0.039387	0.14609	0.19894	600.15	0.013112	82.749	108.44
388.92	1.0000	7.0019	0.14282	16.107	16.250	0.046804	0.15050	0.20848	526.70	0.17073	78.555	94.715
388.92	1.0000	0.39567	2.5273	32.081	34.609	0.094009	0.14812	0.17332	172.88	19.050	27.189	9.8772
450.00	1.0000	0.30367	3.2931	41.914	45.207	0.11931	0.16299	0.17764	207.91	9.5995	34.291	11.376
150.00	5.0000	10.466	0.095550	-21.491	-21.013	-0.097661	0.088840	0.12500	1785.1	-0.62511	169.25	3470.1
225.00	5.0000	9.5418	0.10480	-11.704	-11.180	-0.044697	0.10325	0.13954	1355.9	-0.53441	138.31	561.26
300.00	5.0000	8.5922	0.11638	-0.44721	0.13471	-0.0014609	0.12363	0.16321	999.20	-0.38047	109.58	224.97
375.00	5.0000	7.4791	0.13371	12.787	13.456	0.038048	0.14600	0.19336	670.90	-0.10299	86.612	119.86
450.00	5.0000	5.7922	0.17265	28.764	29.627	0.077218	0.16985	0.24769	327.62	1.0932	68.533	59.364
150.00	10.000	10.496	0.095275	-21.575	-20.622	-0.098235	0.089117	0.12494	1806.7	-0.62619	170.30	3511.8
225.00	10.000	9.5915	0.10426	-11.848	-10.805	-0.045356	0.10348	0.13913	1386.1	-0.54037	140.18	578.68
300.00	10.000	8.6795	0.11521	-0.69963	0.45251	-0.0023313	0.12382	0.16197	1043.2	-0.40072	112.31	237.18
375.00	10.000	7.6607	0.13054	12.293	13.598	0.036668	0.14603	0.18923	742.26	-0.18850	90.691	132.45
450.00	10.000	6.3848	0.15662	27.389	28.955	0.073910	0.16843	0.22130	471.81	0.27965	75.593	78.440
225.00	100.00	10.235	0.097700	-13.576	-3.8061	-0.054491	0.10727	0.13669	1787.0	-0.57796	165.84	860.73
300.00	100.00	9.6137	0.10402	-3.2651	7.1368	-0.012648	0.12720	0.15576	1539.5	-0.50239	145.78	420.70
375.00	100.00	9.0393	0.11063	8.5444	19.607	0.024366	0.14895	0.17686	1352.4	-0.43356	130.89	290.41
450.00	100.00	8.5029	0.11761	21.892	33.653	0.058454	0.17040	0.19748	1210.1	-0.37778	121.48	234.19
375.00	500.00	10.851	0.092161	5.2760	51.356	0.0033611	0.15705	0.17792	2411.2	-0.44269	211.59	864.12
450.00	500.00	10.550	0.094785	18.067	65.459	0.037589	0.17779	0.19805	2302.8	-0.40062	205.82	747.58

The values in these tables were generated from the NIST REFPROP software (Lemmon, E. W., McLinden, M. O., and Huber, M. L., NIST Standard Reference Database 23: Reference Fluid Thermodynamic and Transport Properties—REFPROP, National Institute of Standards and Technology, Standard Reference Data Program, Gaithersburg, Md., 2002, Version 7.1). The primary source for the thermodynamic properties is Lemmon, E. W., and Span, R., "Short Fundamental Equations of State for 20 Industrial Fluids," *J. Chem. Eng. Data* **51**(3):785–850, 2006. The source for viscosity and thermal conductivity is NIST14, Version 9.08.

Properties at the triple point temperature and the critical point temperature are given in the first and last entries of the saturation tables, respectively. In the single-phase table, when the temperature range for a given isobar includes a vapor-liquid phase boundary, the temperature of phase equilibrium is noted, and properties for both the saturated liquid and saturated vapor are given (with liquid properties given in the upper line). Lines are omitted from the temperature-pressure grid of the single-phase table, when the system would be in the solid phase or if there are potential problems with the source property surface.

The uncertainties are approximately 0.2% in density at temperatures up to 320 K, 0.5% in density at higher temperatures, 2% in heat capacity above 250 K, 4% in heat capacity at lower temperatures, 0.1% in the vapor phase speed of sound, 3% in the liquid-phase speed of sound, and 0.4% in vapor pressure at temperatures above 200 K. For viscosity, estimated uncertainty is 2%. For thermal conductivity, estimated uncertainty, except near the critical region, is 4–6%.

TABLE 2-236 Thermodynamic Properties of 2-Methyl Pentane (Isohexane)

Temperature K	Pressure MPa	Density mol/dm ³	Volume dm ³ /mol	Int. Energy kJ/mol	Enthalpy kJ/mol	Entropy kJ/(mol·K)	C _v kJ/(mol·K)	C _p kJ/(mol·K)	Sound speed m/s	Joule-Thomson K/MPa
Saturated Properties										
119.60	7.3432E-12	9.3708	0.10671	-36.470	-36.470	-0.17002	0.10838	0.15299	2019.9	-0.59545
120.00	8.6393E-12	9.3662	0.10677	-36.409	-36.409	-0.16951	0.10835	0.15291	2016.9	-0.59577
140.00	2.6628E-09	9.1438	0.10936	-33.376	-33.376	-0.14612	0.10816	0.15094	1877.8	-0.60440
160.00	1.6516E-07	8.9315	0.11196	-30.354	-30.354	-0.12595	0.10991	0.15162	1750.1	-0.60052
180.00	3.6662E-06	8.7257	0.11460	-27.297	-27.297	-0.10795	0.11321	0.15435	1631.2	-0.58671
200.00	4.0345E-05	8.5239	0.11732	-24.169	-24.169	-0.091478	0.11773	0.15866	1519.7	-0.56534
220.00	0.00026966	8.3237	0.12014	-20.943	-20.943	-0.076105	0.12318	0.16418	1414.3	-0.53846
240.00	0.0012504	8.1236	0.12310	-17.596	-17.596	-0.061550	0.12928	0.17061	1314.2	-0.50751
260.00	0.0044049	7.9216	0.12624	-14.114	-14.113	-0.047617	0.13582	0.17772	1218.4	-0.47322
280.00	0.012572	7.7163	0.12960	-10.484	-10.483	-0.034172	0.14266	0.18535	1126.1	-0.43565
300.00	0.030459	7.5058	0.13323	-6.6984	-6.6944	-0.021115	0.14969	0.19342	1036.6	-0.39411
320.00	0.064855	7.2881	0.13721	-2.7483	-2.7394	-0.0083705	0.15683	0.20190	948.94	-0.34721
340.00	0.12457	7.0608	0.14163	1.3732	1.3908	0.0041212	0.16404	0.21081	862.49	-0.29249
360.00	0.22023	6.8210	0.14661	5.6736	5.7059	0.016411	0.17128	0.22027	776.48	-0.22585
380.00	0.36396	6.5643	0.15234	10.162	10.218	0.028548	0.17854	0.23047	690.10	-0.14022
400.00	0.56922	6.2850	0.15911	14.852	14.942	0.040580	0.18581	0.24183	602.46	-0.022615
420.00	0.85081	5.9735	0.16740	19.761	19.903	0.052569	0.19312	0.25521	512.43	0.15352
440.00	1.2253	5.6136	0.17814	24.925	25.143	0.064603	0.20057	0.27266	418.45	0.45116
460.00	1.7125	5.1716	0.19337	30.414	30.745	0.076849	0.20838	0.30051	317.90	1.0612
480.00	2.3384	4.5506	0.21975	36.430	36.944	0.089761	0.21745	0.37420	204.95	2.9251
497.70	3.0426	2.7150	0.36832	44.813	45.934	0.10771			0	22.418
119.60	7.3432E-12	7.7171E-12	1.2958E+11	3.2114	4.2058	0.17008	0.062593	0.070908	114.33	1878.9
120.00	8.6393E-12	8.8145E-12	1.1345E+11	3.2365	4.2342	0.16919	0.062751	0.071065	114.51	1852.6
140.00	2.6628E-09	2.2870E-09	43,7250,000.	4.5677	5.7317	0.13321	0.070285	0.078600	122.90	971.14
160.00	1.6516E-07	1.2415E-07	8,054,900.	6.0465	7.3769	0.10987	0.077610	0.085925	130.73	557.20
180.00	3.6662E-06	2.4497E-06	4,08,210.	7.6734	9.1700	0.094644	0.085136	0.093451	138.07	341.59
200.00	4.0345E-05	2.4265E-05	41,212.	9.4535	11.116	0.084949	0.092992	0.10131	144.98	220.67
220.00	0.00026966	0.00014751	6,779.4	11.391	13.220	0.079177	0.10116	0.10950	151.49	148.98
240.00	0.0012504	0.00062783	1,592.8	13.489	15.480	0.076268	0.10956	0.11797	157.59	104.56
260.00	0.0044049	0.0020480	488.27	15.742	17.893	0.075483	0.11814	0.12670	163.19	76.030
280.00	0.012572	0.0054602	183.14	18.144	20.447	0.076291	0.12686	0.13570	168.11	57.168
300.00	0.030459	0.012471	80.187	20.686	23.128	0.078294	0.13569	0.14499	172.17	44.401
320.00	0.064855	0.025273	39.568	23.355	25.921	0.081194	0.14461	0.15463	175.13	35.601
340.00	0.12457	0.046680	21.422	26.139	28.807	0.084758	0.15360	0.16471	176.74	29.461
360.00	0.22023	0.080240	12.463	29.022	31.767	0.088803	0.16265	0.17537	176.73	25.167
380.00	0.36396	0.13054	7.6606	31.987	34.775	0.093173	0.17176	0.18690	174.77	22.214
400.00	0.56922	0.20388	4.9048	35.009	37.801	0.097727	0.18095	0.19986	170.42	20.301
420.00	0.85081	0.30983	3.2276	38.050	40.796	0.10231	0.19027	0.21550	163.11	19.294
440.00	1.2253	0.46493	2.1509	41.048	43.683	0.10674	0.19983	0.23692	151.97	19.227
460.00	1.7125	0.70383	1.4208	43.875	46.308	0.11068	0.20995	0.27434	135.67	20.404
480.00	2.3384	1.1281	0.88647	46.190	48.263	0.11334	0.22144	0.38625	112.14	23.602
497.70	3.0426	2.7150	0.36832	44.813	45.934	0.10771			0	22.418

Single-Phase Properties

150.00	0.10000	9.0371	0.11065	-31.868	-31.857	-0.13572	0.10883	0.15099	1813.1	-0.60387
250.00	0.10000	8.0239	0.12463	-15.876	-15.864	-0.054530	0.13251	0.17408	1266.4	-0.49091
332.95	0.10000	7.1422	0.14001	-0.099839	-0.085838	-0.00025709	0.16149	0.20761	892.88	-0.31289
332.95	0.10000	0.037947	26.353	25.145	27.780	0.083438	0.15042	0.16110	176.34	31.381
350.00	0.10000	0.035789	27.941	27.784	30.578	0.091632	0.15693	0.16712	181.93	25.747
450.00	0.10000	0.027168	36.808	45.429	49.110	0.13801	0.19438	0.20338	209.65	10.406
550.00	0.10000	0.022045	45.361	66.610	71.146	0.18212	0.22795	0.23660	232.80	5.5017
150.00	1.0000	9.0415	0.11060	-31.886	-31.775	-0.13584	0.10889	0.15098	1816.8	-0.60402
250.00	1.0000	8.0324	0.12450	-15.912	-15.787	-0.054671	0.13256	0.17397	1272.3	-0.49228
350.00	1.0000	6.9610	0.14366	3.4284	3.5720	0.010082	0.16769	0.21498	829.36	-0.26842
428.63	1.0000	5.8255	0.17166	21.956	22.127	0.057750	0.19631	0.26204	472.47	0.26084
428.63	1.0000	0.36934	2.7075	39.354	42.062	0.10426	0.19435	0.22372	158.83	19.140
450.00	1.0000	0.33044	3.0263	43.784	46.810	0.11507	0.19990	0.22188	173.64	14.396
550.00	1.0000	0.23887	4.1863	65.703	69.889	0.16131	0.22981	0.24260	216.16	6.1837
150.00	5.0000	9.0608	0.11037	-31.962	-31.410	-0.13635	0.10915	0.15096	1833.1	-0.60459
250.00	5.0000	8.0692	0.12393	-16.063	-15.443	-0.055282	0.13278	0.17352	1297.7	-0.49791
350.00	5.0000	7.0426	0.14199	3.1052	3.8152	0.0091444	0.16784	0.21301	873.72	-0.29846
450.00	5.0000	5.7124	0.17506	26.615	27.490	0.068380	0.20366	0.26396	476.76	0.22550
550.00	5.0000	2.3237	0.43035	58.312	60.464	0.13398	0.24134	0.37655	137.16	8.5257
150.00	10.000	9.0844	0.11008	-32.055	-30.954	-0.13698	0.10949	0.15093	1853.0	-0.60519
250.00	10.000	8.1131	0.12326	-16.241	-15.009	-0.056017	0.13305	0.17304	1328.1	-0.50401
350.00	10.000	7.1333	0.14019	2.7454	4.1473	0.0080780	0.16805	0.21116	923.39	-0.32667
450.00	10.000	5.9777	0.16729	25.695	27.368	0.066210	0.20340	0.25395	576.50	-0.0027791
550.00	10.000	4.3857	0.22801	52.778	55.059	0.12162	0.23673	0.29917	305.87	1.0063
250.00	100.00	8.6765	0.11525	-18.375	-6.8492	-0.066142	0.13735	0.17026	1729.6	-0.54229
350.00	100.00	8.0271	0.12458	-0.67131	11.787	-0.0037487	0.17182	0.20310	1445.5	-0.44895
450.00	100.00	7.4403	0.13440	20.331	33.771	0.051327	0.20635	0.23620	1247.4	-0.37634
550.00	100.00	6.9067	0.14479	44.426	58.905	0.10166	0.23764	0.26573	1108.2	-0.32474
450.00	500.00	9.0895	0.11002	16.069	71.078	0.028505	0.21492	0.23767	2315.0	-0.39042
550.00	500.00	8.7910	0.11375	39.474	96.350	0.079120	0.24537	0.26717	2204.0	-0.35059

The values in these tables were generated from the NIST REFPROP software (Lemmon, E. W., McLinden, M.O., and Huber, M. L., NIST Standard Reference Database 23: Reference Fluid Thermodynamic and Transport Properties—REFPROP, National Institute of Standards and Technology, Standard Reference Data Program, Gaithersburg, Md., 2002, Version 7.1). The primary source for the thermodynamic properties is Lemmon, E. W., and Span, R., "Short Fundamental Equations of State for 20 Industrial Fluids," *J. Chem. Eng. Data* **51**(3):785–850, 2006. Validated equations for the viscosity and thermal conductivity are not currently available for this fluid.

Properties at the triple point temperature and the critical point temperature are given in the first and last entries of the saturation tables, respectively. In the single-phase table, when the temperature range for a given isobar includes a vapor-liquid phase boundary, the temperature of phase equilibrium is noted, and properties for both the saturated liquid and saturated vapor are given (with liquid properties given in the upper line). Lines are omitted from the temperature-pressure grid of the single-phase table, when the system would be in the solid phase or if there are potential problems with the source property surface.

The uncertainties in the equation of state are 0.2% in density in the liquid phase, 0.5% in density in the vapor phase, 1% in density above the critical temperature, 0.2% in vapor pressure between 280 and 350 K, 0.5% in vapor pressure at higher temperatures, 2% in heat capacities, and 1% in the speed of sound.

2-304 PHYSICAL AND CHEMICAL DATA

TABLE 2-237 Saturated Methyl Chloride*

T, K	P, bar	v_f , m ³ /kg	v_g , m ³ /kg	h_f , kJ/kg	h_g , kJ/kg	s_f , kJ/(kg·K)	s_g , kJ/(kg·K)	c_{pf} , kJ/(kg·K)	μ_f , 10 ⁻⁴ Pa·s	k_f , W/(m·K)
175	0.0117	8.84-4	27.90	274.5	764.3	3.529	6.328	1.469		
180	0.0165	8.91-4	19.85	280.9	767.7	3.570	6.274	1.472		
185	0.0233	8.97-4	14.12	287.5	771.0	3.603	6.222	1.475		
190	0.0327	9.04-4	10.12	294.5	774.3	3.647	6.172	1.477		
195	0.0462	9.10-4	7.208	301.7	777.5	3.684	6.124	1.480		
200	0.0653	9.17-4	5.137	309.0	780.7	3.722	6.080	1.483	4.44	0.241
205	0.0919	9.25-4	3.835	316.3	783.9	3.756	6.038	1.486	4.27	0.236
210	0.1315	9.33-4	2.656	323.7	787.0	3.791	5.998	1.489	4.11	0.232
215	0.181	9.40-4	1.975	331.0	790.1	3.825	5.961	1.492	3.96	0.228
220	0.243	9.48-4	1.505	338.4	793.2	3.859	5.928	1.496	3.82	0.224
225	0.319	9.56-4	1.168	345.7	796.3	3.892	5.896	1.500	3.69	0.219
230	0.417	9.65-4	0.911	353.1	799.3	3.925	5.866	1.504	3.57	0.215
235	0.539	9.73-4	0.718	360.5	802.3	3.957	5.845	1.508	3.46	0.211
240	0.688	9.81-4	0.572	368.0	805.3	3.988	5.822	1.513	3.35	0.207
245	0.866	9.89-4	0.462	375.6	808.2	4.019	5.786	1.518	3.25	0.202
250	1.076	9.98-4	0.377	383.2	811.1	4.050	5.762	1.523	3.16	0.198
255	1.328	10.08-4	0.311	390.7	814.0	4.080	5.740	1.528	3.08	0.194
260	1.627	10.18-4	0.257	398.3	816.8	4.110	5.720	1.533	3.00	0.190
265	1.970	10.27-4	0.215	406.0	819.4	4.139	5.699	1.539	2.92	0.186
270	2.364	10.36-4	0.1807	413.7	822.0	4.168	5.680	1.546	2.85	0.182
275	2.830	10.46-4	0.1524	421.5	824.4	4.197	5.662	1.554	2.78	0.177
280	3.347	10.57-4	0.1301	429.4	826.8	4.225	5.644	1.565	2.72	0.173
285	3.936	10.68-4	0.1115	437.3	829.0	4.253	5.628	1.574	2.66	0.169
290	4.612	10.79-4	0.0960	445.2	831.2	4.280	5.612	1.583	2.61	0.165
295	5.361	10.91-4	0.0830	453.2	833.2	4.308	5.597	1.594	2.56	0.160
300	6.189	11.03-4	0.0723	461.2	835.2	4.334	5.581	1.605	2.51	0.156
305	7.110	11.15-4	0.0632	469.3	837.0	4.361	5.567	1.617	2.46	0.152
310	8.111	11.27-4	0.0556	477.4	838.8	4.388	5.553	1.631	2.42	0.148
315	9.243	11.40-4	0.0489	485.6	840.5	4.414	5.540	1.644	2.37	0.143
320	10.47	11.55-4	0.0433	493.8	841.9	4.440	5.527	1.658	2.33	0.139
325	11.78	11.70-4	0.0386	502.1	843.3	4.465	5.516		2.30	0.135
330	13.27	11.86-4	0.0343	510.4	844.5	4.491	5.504		2.27	0.131
340	16.52	12.17-4	0.0282	518.8	846.4	4.542	5.481		2.12	0.124
350	20.53	12.54-4	0.0228	538.3	847.5	4.592	5.457		1.99	0.117
360	25.29	12.97-4	0.0186	562.9	847.6	4.643	5.434		1.87	0.110
370	30.74	13.47-4	0.0151	581.6	845.9	4.694	5.398		1.77	0.103
380	36.99	14.11-4	0.0117	602.8	842.6	4.747	5.382		1.67	0.095
390	44.05	14.67-4	0.0096	622.9	837.4	4.805	5.358		1.59	0.086
400	52.29	15.66-4	0.0075	643.6	826.4	4.870	5.323		1.51	0.075
405	56.6	16.48-4	0.0063	663.2	819.1	4.904	5.289			
410	61.5	17.97-4	0.0052	677.3	807.1	4.954	5.256			
415	67.4	21.10-4	0.0038	714.1	778.6	5.025	5.200			
416 ^c	69.0	27.40-4	0.0027	749.3	749.3	5.116	5.116			

* Interpolated by P. E. Liley from the Landolt-Börnstein band IVa, p. 677, 1967 tables by Steinle/Dienemann. *c* = critical point. The notation 8.84-4 signifies 8.84 × 10⁻⁴.

TABLE 2-238 Thermodynamic Properties of Neon

Temperature K	Pressure MPa	Density mol/dm ³	Volume dm ³ /mol	Int. energy kJ/mol	Enthalpy kJ/mol	Entropy kJ/(mol·K)	C _v kJ/(mol·K)	C _p kJ/(mol·K)	Sound speed m/s	Joule-Thomson K/MPa
Saturated Properties										
24.562	0.043464	62.059	0.016114	-0.099873	-0.099172	-0.0038092	0.018679	0.043081	674.66	-0.22893
25.000	0.050920	61.645	0.016222	-0.081689	-0.080863	-0.0030751	0.018439	0.040416	652.08	-0.25101
26.000	0.071611	60.761	0.016458	-0.042983	-0.041805	-0.0015561	0.018193	0.037847	617.51	-0.27322
27.000	0.098173	59.903	0.016694	-0.0055930	-0.0039541	-0.00014422	0.018006	0.037540	596.00	-0.27053
28.000	0.13159	59.032	0.016940	0.031967	0.034196	0.0012227	0.017803	0.038200	579.65	-0.25492
29.000	0.17287	58.129	0.017203	0.070340	0.073314	0.0025706	0.017589	0.039303	564.56	-0.23297
30.000	0.22307	57.186	0.017487	0.10979	0.11370	0.0039099	0.017371	0.040595	548.99	-0.20788
31.000	0.28324	56.198	0.017794	0.15041	0.15545	0.0052441	0.017156	0.041956	532.26	-0.18090
32.000	0.35446	55.162	0.018128	0.19218	0.19860	0.0065735	0.016952	0.043347	514.19	-0.15212
33.000	0.43782	54.078	0.018492	0.23507	0.24317	0.0078977	0.016768	0.044788	494.83	-0.12096
34.000	0.53443	52.941	0.018889	0.27908	0.28917	0.0092172	0.016614	0.046343	474.28	-0.086349
35.000	0.64543	51.749	0.019324	0.32426	0.33673	0.010534	0.016498	0.048115	452.65	-0.046782
36.000	0.77202	50.493	0.019805	0.37073	0.38602	0.011853	0.016426	0.050251	429.96	-0.00027396
37.000	0.91543	49.162	0.020341	0.41874	0.43736	0.013181	0.016404	0.052967	406.17	0.055871
38.000	1.0770	47.736	0.020948	0.46869	0.49125	0.014529	0.016438	0.056597	381.08	0.12549
39.000	1.2581	46.187	0.021651	0.52120	0.54844	0.015914	0.016536	0.061719	354.35	0.21441
40.000	1.4603	44.462	0.022491	0.57729	0.61014	0.017363	0.016715	0.069475	325.39	0.33222
41.000	1.6855	42.471	0.023545	0.63879	0.67848	0.018922	0.017014	0.082509	293.27	0.49632
42.000	1.9355	40.021	0.024987	0.70940	0.75776	0.020686	0.017522	0.10852	256.54	0.74180
43.000	2.2121	36.640	0.027292	0.79805	0.85843	0.022883	0.018471	0.17680	213.78	1.1433
44.000	2.5168	31.327	0.031921	0.92402	1.0044	0.026030	0.020210	0.44810	170.57	1.8283
44.492	2.6786	23.882	0.041873	1.0877	1.1999	0.030313			0	2.9448
24.562	0.043464	0.22026	4.5402	1.4817	1.6790	0.068586	0.035186	0.047919	113.01	27.054
25.000	0.050920	0.25406	3.9361	1.4898	1.6902	0.067767	0.029819	0.041791	115.48	23.404
26.000	0.071611	0.34598	2.8903	1.5046	1.7116	0.065882	0.022043	0.033098	121.12	18.114
27.000	0.098173	0.46111	2.1687	1.5159	1.7288	0.064031	0.018031	0.028839	126.17	15.446
28.000	0.13159	0.60299	1.6584	1.5247	1.7430	0.062250	0.016001	0.026943	130.23	14.023
29.000	0.17287	0.77543	1.2896	1.5318	1.7547	0.060549	0.015021	0.026349	133.28	13.110
30.000	0.22307	0.98260	1.0177	1.5372	1.7642	0.058928	0.014604	0.026517	135.55	12.393
31.000	0.28324	1.2292	0.81356	1.5411	1.7716	0.057377	0.014497	0.027183	137.25	11.758
32.000	0.35446	1.5204	0.65772	1.5435	1.7767	0.055888	0.014566	0.028231	138.54	11.166
33.000	0.43782	1.8625	0.53690	1.5443	1.7794	0.054449	0.014745	0.029633	139.52	10.606
34.000	0.53443	2.2630	0.44190	1.5432	1.7794	0.053047	0.015000	0.031418	140.26	10.073
35.000	0.64543	2.7308	0.36619	1.5401	1.7765	0.051670	0.015316	0.033669	140.78	9.5602
36.000	0.77202	3.2778	0.30508	1.5347	1.7702	0.050303	0.015688	0.036531	141.11	9.0641
37.000	0.91543	3.9193	0.25515	1.5265	1.7601	0.048930	0.016118	0.040243	141.24	8.5780
38.000	1.0770	4.6762	0.21385	1.5150	1.7453	0.047531	0.016614	0.045207	141.18	8.0944
39.000	1.2581	5.5788	0.17925	1.4994	1.7249	0.046079	0.017189	0.052136	140.93	7.6033
40.000	1.4603	6.6734	0.14985	1.4784	1.6972	0.044539	0.017863	0.062405	140.49	7.0917
41.000	1.6855	8.0363	0.12443	1.4500	1.6597	0.042855	0.018664	0.079029	139.83	6.5404
42.000	1.9355	9.8091	0.10195	1.4107	1.6080	0.040930	0.019634	0.10997	138.95	5.9193
43.000	2.2121	12.303	0.081282	1.3530	1.5328	0.038566	0.020823	0.18428	137.87	5.1760
44.000	2.5168	16.541	0.060455	1.2537	1.4058	0.035154	0.022208	0.55080	136.83	4.1789
44.492	2.6786	23.882	0.041873	1.0877	1.1999	0.030313			0	2.9448

TABLE 2-238 Thermodynamic Properties of Neon (Concluded)

Temperature K	Pressure MPa	Density mol/dm ³	Volume dm ³ /mol	Int. energy kJ/mol	Enthalpy kJ/mol	Entropy kJ/(mol·K)	C _v kJ/(mol·K)	C _p kJ/(mol·K)	Sound speed m/s	Joule-Thomson K/MPa
Single-Phase Properties										
100.00	0.10000	0.12034	8.3098	2.4474	3.2784	0.091975	0.012479	0.020851	262.24	1.6033
200.00	0.10000	0.060106	16.637	3.6964	5.3601	0.10641	0.012475	0.020800	370.87	0.12447
300.00	0.10000	0.040072	24.955	4.9441	7.4396	0.11484	0.012473	0.020791	454.13	-0.30667
400.00	0.10000	0.030057	33.270	6.1915	9.5185	0.12082	0.012473	0.020789	524.31	-0.49467
500.00	0.10000	0.024047	41.585	7.4388	11.597	0.12546	0.012473	0.020787	586.15	-0.59137
600.00	0.10000	0.020040	49.899	8.6861	13.676	0.12925	0.012472	0.020787	642.06	-0.64538
700.00	0.10000	0.017178	58.214	9.9333	15.755	0.13245	0.012472	0.020786	693.47	-0.67670
100.00	1.0000	1.2090	0.82716	2.4215	3.2486	0.072572	0.012547	0.021444	264.06	1.5285
200.00	1.0000	0.59828	1.6715	3.6864	5.3579	0.087212	0.012502	0.020926	373.32	0.11185
300.00	1.0000	0.39903	2.5061	4.9392	7.4453	0.095677	0.012491	0.020841	456.29	-0.30952
400.00	1.0000	0.29952	3.3387	6.1891	9.5278	0.10167	0.012485	0.020813	526.19	-0.49518
500.00	1.0000	0.23978	4.1705	7.4379	11.608	0.10631	0.012482	0.020800	587.81	-0.59127
600.00	1.0000	0.19992	5.0020	8.6861	13.688	0.11010	0.012480	0.020794	643.54	-0.64516
700.00	1.0000	0.17143	5.8334	9.9339	15.767	0.11331	0.012478	0.020791	694.81	-0.67651
100.00	5.0000	6.1145	0.16355	2.3075	3.1252	0.058098	0.012814	0.024056	275.27	1.1885
200.00	5.0000	2.9287	0.34145	3.6436	5.3508	0.073620	0.012619	0.021453	384.50	0.054603
300.00	5.0000	1.9580	0.51074	4.9181	7.4718	0.082226	0.012565	0.021051	465.95	-0.32325
400.00	5.0000	1.4747	0.67810	6.1787	9.5693	0.088261	0.012539	0.020917	534.57	-0.49810
500.00	5.0000	1.1837	0.84478	7.4338	11.658	0.092921	0.012523	0.020858	595.18	-0.59116
600.00	5.0000	0.98897	1.0112	8.6860	13.742	0.096721	0.012513	0.020828	650.12	-0.64435
700.00	5.0000	0.84934	1.1774	9.9366	15.824	0.099930	0.012506	0.020810	700.76	-0.67575
100.00	10.000	12.113	0.082559	2.1736	2.9992	0.051158	0.013095	0.026878	296.54	0.80676
200.00	10.000	5.6967	0.17554	3.5933	5.3487	0.067620	0.012752	0.022026	399.17	-0.014628
300.00	10.000	3.8255	0.26141	4.8930	7.5070	0.076381	0.012653	0.021291	478.16	-0.34148
400.00	10.000	2.8938	0.34556	6.1661	9.6217	0.082467	0.012603	0.021040	545.08	-0.50266
500.00	10.000	2.3306	0.42908	7.4286	11.719	0.087148	0.012573	0.020927	604.43	-0.59158
600.00	10.000	1.9519	0.51231	8.6858	13.809	0.090958	0.012553	0.020868	658.38	-0.64363
700.00	10.000	1.6795	0.59540	9.9399	15.894	0.094172	0.012539	0.020835	708.23	-0.67492
100.00	100.00	50.564	0.019777	1.4006	3.3783	0.028294	0.016249	0.028809	728.18	-0.37331
200.00	100.00	34.632	0.028875	3.1327	6.0202	0.046773	0.014308	0.024694	673.52	-0.43751
300.00	100.00	26.457	0.037796	4.6205	8.4001	0.056445	0.013708	0.023102	694.50	-0.49312
400.00	100.00	21.512	0.046486	6.0160	10.665	0.062965	0.013422	0.022262	729.70	-0.54535
500.00	100.00	18.185	0.054990	7.3645	12.863	0.067874	0.013245	0.021756	767.75	-0.58985
600.00	100.00	15.781	0.063366	8.6852	15.022	0.071810	0.013121	0.021432	805.72	-0.62513
700.00	100.00	13.955	0.071657	9.9877	17.153	0.075096	0.013028	0.021216	842.83	-0.65210
300.00	500.00	59.131	0.016912	4.6368	13.093	0.042072	0.015948	0.024091	1306.5	-0.47221
400.00	500.00	53.366	0.018738	6.0941	15.463	0.048897	0.015200	0.023386	1293.9	-0.49185
500.00	500.00	48.708	0.020530	7.5120	17.777	0.054063	0.014770	0.022915	1294.1	-0.50859
600.00	500.00	44.864	0.022290	8.9046	20.049	0.058207	0.014481	0.022544	1301.3	-0.52455
700.00	500.00	41.633	0.024020	10.278	22.288	0.061658	0.014265	0.022235	1312.5	-0.53993

The values in these tables were generated from the NIST REFPROP software (Lemmon, E. W., McLinden, M. O., and Huber, M. L., NIST Standard Reference Database 23: Reference Fluid Thermodynamic and Transport Properties—REFPROP, National Institute of Standards and Technology, Standard Reference Data Program, Gaithersburg, Md., 2002, Version 7.1). The primary source for the thermodynamic properties is Katti, R. S., Jacobsen, R. T., Stewart, R. B., and Jahangiri, M., "Thermodynamic Properties for Neon for Temperatures from the Triple Point to 700 K at Pressures to 700 MPa," *Adv. Cryo. Eng.* **31**:1189-1197, 1986. Validated equations for the viscosity and thermal conductivity are not currently available for this fluid.

Properties at the triple point temperature and the critical point temperature are given in the first and last entries of the saturation tables, respectively. In the single-phase table, when the temperature range for a given isobar includes a vapor-liquid phase boundary, the temperature of phase equilibrium is noted, and properties for both the saturated liquid and saturated vapor are given (with liquid properties given in the upper line). Lines are omitted from the temperature-pressure grid of the single-phase table, when the system would be in the solid phase or if there are potential problems with the source property surface.

The uncertainties of the equation of state are 0.1% in density, 2% in heat capacity, and 1% in the speed of sound, except in the critical region. The uncertainty in vapor pressure is 0.2%.

TABLE 2-239 Thermodynamic Properties of Nitrogen

Temperature K	Pressure MPa	Density mol/dm ³	Volume dm ³ /mol	Int. energy kJ/mol	Enthalpy kJ/mol	Entropy kJ/(mol·K)	C _v kJ/(mol·K)	C _p kJ/(mol·K)	Sound speed m/s	Joule-Thomson K/MPa	Therm. cond. mW/(m·K)	Viscosity μPa·s
Saturated Properties												
63.151	0.012520	30.957	0.032303	-4.2230	-4.2226	0.067951	0.032951	0.056033	995.28	-0.40419	173.24	311.59
65.000	0.017404	30.685	0.032589	-4.1194	-4.1188	0.069569	0.032591	0.056121	976.36	-0.39833	169.51	282.07
67.000	0.024300	30.387	0.032909	-4.0071	-4.0063	0.071270	0.032207	0.056231	956.04	-0.39135	165.49	254.55
69.000	0.033213	30.085	0.033239	-3.8946	-3.8935	0.072924	0.031831	0.056360	935.83	-0.38364	161.47	230.85
71.000	0.044527	29.779	0.033581	-3.7819	-3.7804	0.074535	0.031463	0.056512	915.66	-0.37508	157.47	210.32
73.000	0.058656	29.468	0.033935	-3.6689	-3.6669	0.076105	0.031106	0.056690	895.49	-0.36560	153.46	192.43
75.000	0.076043	29.153	0.034302	-3.5556	-3.5530	0.077637	0.030760	0.056899	875.28	-0.35506	149.47	176.75
77.000	0.097152	28.832	0.034683	-3.4419	-3.4385	0.079133	0.030427	0.057142	855.00	-0.34334	145.48	162.94
79.000	0.12247	28.506	0.035080	-3.3278	-3.3235	0.080597	0.030105	0.057425	834.61	-0.33029	141.50	150.71
81.000	0.15251	28.175	0.035493	-3.2132	-3.2078	0.082030	0.029795	0.057752	814.07	-0.31574	137.55	139.82
83.000	0.18780	27.837	0.035924	-3.0980	-3.0913	0.083436	0.029499	0.058130	793.36	-0.29951	133.61	130.07
85.000	0.22886	27.492	0.036375	-2.9822	-2.9739	0.084815	0.029215	0.058566	772.44	-0.28135	129.66	121.31
87.000	0.27626	27.139	0.036847	-2.8657	-2.8555	0.086172	0.028944	0.059068	751.28	-0.26099	125.72	113.38
89.000	0.33055	26.779	0.037343	-2.7483	-2.7360	0.087507	0.028687	0.059647	729.84	-0.23813	121.77	106.18
91.000	0.39230	26.409	0.037865	-2.6301	-2.6152	0.088823	0.028444	0.060315	708.09	-0.21237	117.83	99.602
93.000	0.46210	26.030	0.038417	-2.5107	-2.4930	0.090123	0.028215	0.061088	685.99	-0.18326	113.89	93.568
95.000	0.54052	25.640	0.039002	-2.3902	-2.3691	0.091408	0.028001	0.061983	663.50	-0.15025	109.95	88.004
97.000	0.62817	25.238	0.039623	-2.2683	-2.2434	0.092682	0.027804	0.063026	640.57	-0.11264	106.02	82.847
99.000	0.72566	24.822	0.040288	-2.1449	-2.1156	0.093946	0.027624	0.064246	617.14	-0.069613	102.08	78.042
101.00	0.83358	24.390	0.041000	-2.0196	-1.9854	0.095204	0.027464	0.065684	593.17	-0.021010	98.144	73.543
103.00	0.95259	23.941	0.041769	-1.8923	-1.8525	0.096459	0.027327	0.067392	568.58	0.037239	94.208	69.306
105.00	1.0833	23.471	0.042605	-1.7625	-1.7163	0.097715	0.027214	0.069443	543.30	0.10414	90.272	65.292
107.00	1.2264	22.978	0.043520	-1.6298	-1.5765	0.098977	0.027133	0.071937	517.24	0.18288	86.337	61.464
109.00	1.3826	22.457	0.044530	-1.4938	-1.4323	0.10025	0.027088	0.075021	490.29	0.27654	82.404	57.786
111.00	1.5526	21.902	0.045658	-1.3537	-1.2828	0.10154	0.027089	0.078914	462.32	0.38936	78.472	54.224
113.00	1.7371	21.306	0.046935	-1.2086	-1.1271	0.10285	0.027149	0.083966	433.19	0.52741	74.544	50.740
115.00	1.9370	20.658	0.048407	-1.0571	-0.96336	0.10420	0.027290	0.090771	402.67	0.69974	70.626	47.290
117.00	2.1533	19.943	0.050144	-0.89741	-0.78944	0.10561	0.027545	0.10044	370.43	0.92076	66.728	43.824
119.00	2.3869	19.134	0.052262	-0.72635	-0.60161	0.10710	0.027981	0.11531	335.85	1.2154	62.883	40.270
121.00	2.6391	18.187	0.054985	-0.53833	-0.39322	0.10873	0.028755	0.14140	297.68	1.6317	59.196	36.509
123.00	2.9116	16.997	0.058834	-0.32093	-0.14962	0.11059	0.030317	0.20028	253.32	2.2811	56.121	32.310
125.00	3.2069	15.210	0.065747	-0.031475	0.17937	0.11310	0.034680	0.46831	195.48	3.5308	56.435	26.935
126.19	3.3958	11.184	0.089414	0.51527	0.81891	0.11807			0	6.0831		
63.151	0.012520	0.024070	41.546	1.2945	1.8147	0.16355	0.021007	0.029647	161.11	40.718	5.6209	4.3763
65.000	0.017404	0.032594	30.680	1.3299	1.8639	0.16161	0.021059	0.029788	163.20	38.268	5.8164	4.5123
67.000	0.024300	0.044300	22.573	1.3675	1.9160	0.15966	0.021123	0.029969	165.37	35.907	6.0298	4.6601
69.000	0.033213	0.059031	16.940	1.4042	1.9668	0.15786	0.021196	0.030180	167.43	33.803	6.2457	4.8088
71.000	0.044527	0.077273	12.941	1.4400	2.0162	0.15618	0.021278	0.030427	169.39	31.922	6.4645	4.9585
73.000	0.058656	0.099542	10.046	1.4747	2.0639	0.15461	0.021370	0.030712	171.23	30.231	6.6870	5.1096
75.000	0.076043	0.12638	7.9124	1.5082	2.1099	0.15314	0.021472	0.031039	172.95	28.707	6.9138	5.2621
77.000	0.097152	0.15838	6.3140	1.5404	2.1539	0.15176	0.021585	0.031413	174.55	27.328	7.1458	5.4164
79.000	0.12247	0.19613	5.0986	1.5713	2.1957	0.15046	0.021709	0.031839	176.03	26.074	7.3839	5.5727
81.000	0.15251	0.24030	4.1614	1.6007	2.2353	0.14923	0.021845	0.032323	177.38	24.931	7.6295	5.7313
83.000	0.18780	0.29157	3.4297	1.6284	2.2725	0.14806	0.021994	0.032873	178.60	23.884	7.8837	5.8924
85.000	0.22886	0.35069	2.8515	1.6544	2.3070	0.14694	0.022157	0.033496	179.68	22.923	8.1483	6.0565
87.000	0.27626	0.41846	2.3897	1.6784	2.3386	0.14587	0.022334	0.034204	180.63	22.035	8.4251	6.2238
89.000	0.33055	0.49576	2.0171	1.7005	2.3672	0.14485	0.022528	0.035008	181.43	21.212	8.7163	6.3948
91.000	0.39230	0.58355	1.7137	1.7203	2.3925	0.14385	0.022738	0.035925	182.10	20.446	9.0247	6.5700
93.000	0.46210	0.68291	1.4643	1.7377	2.4143	0.14289	0.022967	0.036973	182.62	19.730	9.3533	6.7499
95.000	0.54052	0.79504	1.2578	1.7525	2.4324	0.14195	0.023217	0.038177	182.99	19.057	9.7060	6.9353
97.000	0.62817	0.92134	1.0854	1.7645	2.4463	0.14103	0.023489	0.039568	183.21	18.421	10.087	7.1270
99.000	0.72566	1.0634	0.94038	1.7733	2.4557	0.14012	0.023787	0.041185	183.28	17.815	10.503	7.3260
101.00	0.83358	1.2231	0.81759	1.7788	2.4603	0.13922	0.024113	0.043081	183.18	17.236	10.960	7.5334
103.00	0.95259	1.4027	0.71291	1.7804	2.4595	0.13832	0.024471	0.045326	182.93	16.676	11.467	7.7509
105.00	1.0833	1.6049	0.62309	1.7778	2.4528	0.13742	0.024860	0.048012	182.51	16.132	12.035	7.9804
107.00	1.2264	1.8331	0.54553	1.7703	2.4394	0.13651	0.025284	0.051276	181.93	15.600	12.679	8.2245

TABLE 2-239 Thermodynamic Properties of Nitrogen (Concluded)

Temperature K	Pressure MPa	Density mol/dm ³	Volume dm ³ /mol	Int. energy kJ/mol	Enthalpy kJ/mol	Entropy kJ/(mol·K)	C _v kJ/(mol·K)	C _p kJ/(mol·K)	Sound speed m/s	Joule-Thomson K/MPa	Therm. cond. mW/(m·K)	Viscosity μPa·s
Saturated Properties												
109.00	1.3826	2.0916	0.47811	1.7573	2.4183	0.13557	0.025750	0.055332	181.19	15.075	13.419	8.4867
111.00	1.5526	2.3860	0.41911	1.7377	2.3884	0.13461	0.026284	0.060528	180.28	14.546	14.284	8.7716
113.00	1.7371	2.7240	0.36711	1.7102	2.3479	0.13360	0.026924	0.067435	179.15	13.996	15.315	9.0860
115.00	1.9370	3.1162	0.32091	1.6730	2.2946	0.13253	0.027721	0.077010	177.75	13.409	16.580	9.4395
117.00	2.1533	3.5786	0.27944	1.6234	2.2251	0.13138	0.028723	0.091003	176.01	12.767	18.186	9.8474
119.00	2.3869	4.1370	0.24172	1.5572	2.1341	0.13009	0.029997	0.11312	173.87	12.045	20.329	10.336
121.00	2.6391	4.8380	0.20670	1.4665	2.0119	0.12860	0.031683	0.15295	171.17	11.203	23.424	10.953
123.00	2.9116	5.7846	0.17287	1.3343	1.8376	0.12675	0.034185	0.24490	167.43	10.148	28.604	11.813
125.00	3.2069	7.3244	0.13653	1.1039	1.5417	0.12400	0.039278	0.66512	160.26	8.6030	41.535	13.326
126.19	3.3958	11.184	0.089414	0.51527	0.81891	0.11807			0	6.0831		
Single-Phase Properties												
100.00	0.10000	0.12268	8.1514	-2.0396	2.8547	0.15950	0.021049	0.030012	201.64	16.082	9.3806	6.9581
600.00	0.10000	0.020037	49.908	12.573	17.564	0.21217	0.021796	0.030118	496.27	0.021483	44.840	29.577
1100.0	0.10000	0.010930	91.489	24.284	33.433	0.23131	0.024932	0.032448	660.05	-0.65654	70.075	44.199
1600.0	0.10000	0.0075152	133.06	37.272	50.579	0.24414	0.026815	0.035130	788.94	-0.81543	92.344	56.398
100.00	1.0000	24.658	0.040554	-2.0907	-2.0501	0.094493	0.027546	0.064564	609.42	-0.054514	100.58	76.255
103.75	1.0000	23.768	0.042073	-1.8441	-1.8020	0.096928	0.027281	0.065113	559.22	0.060996	92.738	67.783
103.75	1.0000	1.4754	0.67778	1.7800	2.4577	0.13799	0.024612	0.046272	182.79	16.471	11.671	7.8351
600.00	1.0000	0.19960	5.0099	12.554	17.564	0.19300	0.021812	0.030198	498.66	0.0061465	44.992	29.626
1100.0	1.0000	0.10899	9.1755	24.277	33.452	0.21216	0.024938	0.032627	662.07	-0.65940	70.155	44.221
1600.0	1.0000	0.074993	13.335	37.270	50.605	0.22499	0.026820	0.035138	790.64	-0.81612	92.399	56.411
100.00	5.0000	25.436	0.039314	-2.2176	-2.0210	0.093188	0.027713	0.059868	673.24	-0.17096	108.13	84.510
600.00	5.0000	0.98084	1.0195	12.469	17.567	0.17948	0.021881	0.030539	509.60	-0.057679	45.797	29.882
1100.0	5.0000	0.53797	1.8588	24.247	33.541	0.19875	0.024969	0.033350	671.08	-0.67112	70.555	44.330
1600.0	5.0000	0.37146	2.6921	37.259	50.720	0.21161	0.026839	0.035170	798.18	-0.81886	92.663	56.476
100.00	10.000	26.188	0.038186	-2.3398	-1.9580	0.091882	0.028004	0.056646	734.22	-0.25658	115.90	93.648
600.00	10.000	1.9183	0.52130	12.368	17.581	0.17355	0.021965	0.030926	523.87	-0.12928	46.995	30.284
1100.0	10.000	1.0590	0.94433	24.211	33.654	0.19296	0.025006	0.033447	682.37	-0.68394	71.130	44.493
1600.0	10.000	0.73435	1.3618	37.246	50.864	0.20583	0.026863	0.035209	807.57	-0.82170	93.033	56.570
600.00	500.00	27.434	0.036451	10.778	29.003	0.13791	0.026493	0.035336	1574.4	-0.70223	177.40	103.10
1100.0	500.00	21.868	0.045729	23.840	46.705	0.15935	0.027586	0.035848	1501.4	-0.72394	149.37	79.801
1600.0	500.00	18.335	0.054541	37.584	64.855	0.17295	0.028647	0.036665	1506.6	-0.73166	147.47	79.226
600.00	1000.0	34.270	0.029180	11.714	40.894	0.13093	0.029169	0.036905	2107.2	-0.61888	278.97	208.00
1100.0	1000.0	29.362	0.034057	25.065	59.122	0.15303	0.029373	0.036577	1985.1	-0.65271	232.49	129.86
1600.0	1000.0	25.920	0.038580	38.999	77.579	0.16685	0.029977	0.037212	1942.0	-0.65439	214.36	110.35

The values in these tables were generated from the NIST REFPROP software (Lemmon, E. W., McLinden, M. O., and Huber, M. L., NIST Standard Reference Database 23: Reference Fluid Thermodynamic and Transport Properties—REFPROP, National Institute of Standards and Technology, Standard Reference Data Program, Gaithersburg, Md., 2002, Version 7.1). The primary source for the thermodynamic properties is Span, R., Lemmon, E. W., Jacobsen, R. T., Wagner, W., and Yokozeki, A., "A Reference Quality Thermodynamic Property Formulation for Nitrogen," *J. Phys. Chem. Ref. Data* **29**(6):1361–1433, 2000. See also *Int. J. Thermophys.* **14**(4):1121–1132, 1998. The source for viscosity is Lemmon, E. W., and Jacobsen, R. T., "Viscosity and Thermal Conductivity Equations for Nitrogen, Oxygen, Argon, and Air," *Int. J. Thermophys.* **25**:21–69, 2004. The source for thermal conductivity is Lemmon, E. W., and Jacobsen, R. T., "Viscosity and Thermal Conductivity Equations for Nitrogen, Oxygen, Argon, and Air," *Int. J. Thermophys.* **25**:21–69, 2004.

Properties at the triple point temperature and the critical point temperature are given in the first and last entries of the saturation tables, respectively. In the single-phase table, when the temperature range for a given isobar includes a vapor-liquid phase boundary, the temperature of phase equilibrium is noted, and properties for both the saturated liquid and saturated vapor are given (with liquid properties given in the upper line). Lines are omitted from the temperature-pressure grid of the single-phase table, when the system would be in the solid phase or if there are potential problems with the source property surface.

The uncertainty in density of the equation of state is 0.02% from the triple point up to temperatures of 523 K and pressures up to 12 MPa and from temperatures of 240 to 523 K at pressures less than 30 MPa. In the range from 270 to 350 K at pressures less than 12 MPa, the uncertainty in density is 0.01%. The uncertainty at very high pressures (>1 GPa) is 0.6% in density. The uncertainty in pressure in the critical region is estimated to be 0.02%. In the gaseous and supercritical region, the speed of sound can be calculated with a typical uncertainty of 0.005% to 0.1%. At liquid states and at high pressures, the uncertainty increases to 0.5% to 1.5%. For pressures up to 30 MPa, the estimated uncertainty for heat capacities ranges from 0.3% at gaseous and gaslike supercritical states up to 0.8% at liquid states and at certain gaseous and supercritical states at low temperatures. The uncertainty is 2% for pressures up to 200 MPa and larger at higher pressures. The estimated uncertainties of vapor pressure, saturated-liquid density, and saturated-vapor density are in general 0.02% for each property. The formulation yields a reasonable extrapolation behavior up to the limits of chemical stability of nitrogen.

For viscosity, the uncertainty is 0.5% in dilute gas. Away from the dilute gas (pressures greater than 1 MPa and in the liquid), the uncertainties are as low as 1% between 270 and 300 K at pressures less than 100 MPa, and increase outside that range. The uncertainties are around 2% at temperatures of 180 K and higher. Below this and away from the critical region, the uncertainties steadily increase to around 5% at the triple points of the fluids. The uncertainties in the critical region are higher.

For thermal conductivity, the uncertainty for the dilute gas is 2% with increasing uncertainties near the triple point. For the nondilute gas, the uncertainty is 2% for temperatures greater than 150 K. The uncertainty is 3% at temperatures less than the critical point and 5% in the critical region, except for states very near the critical point.

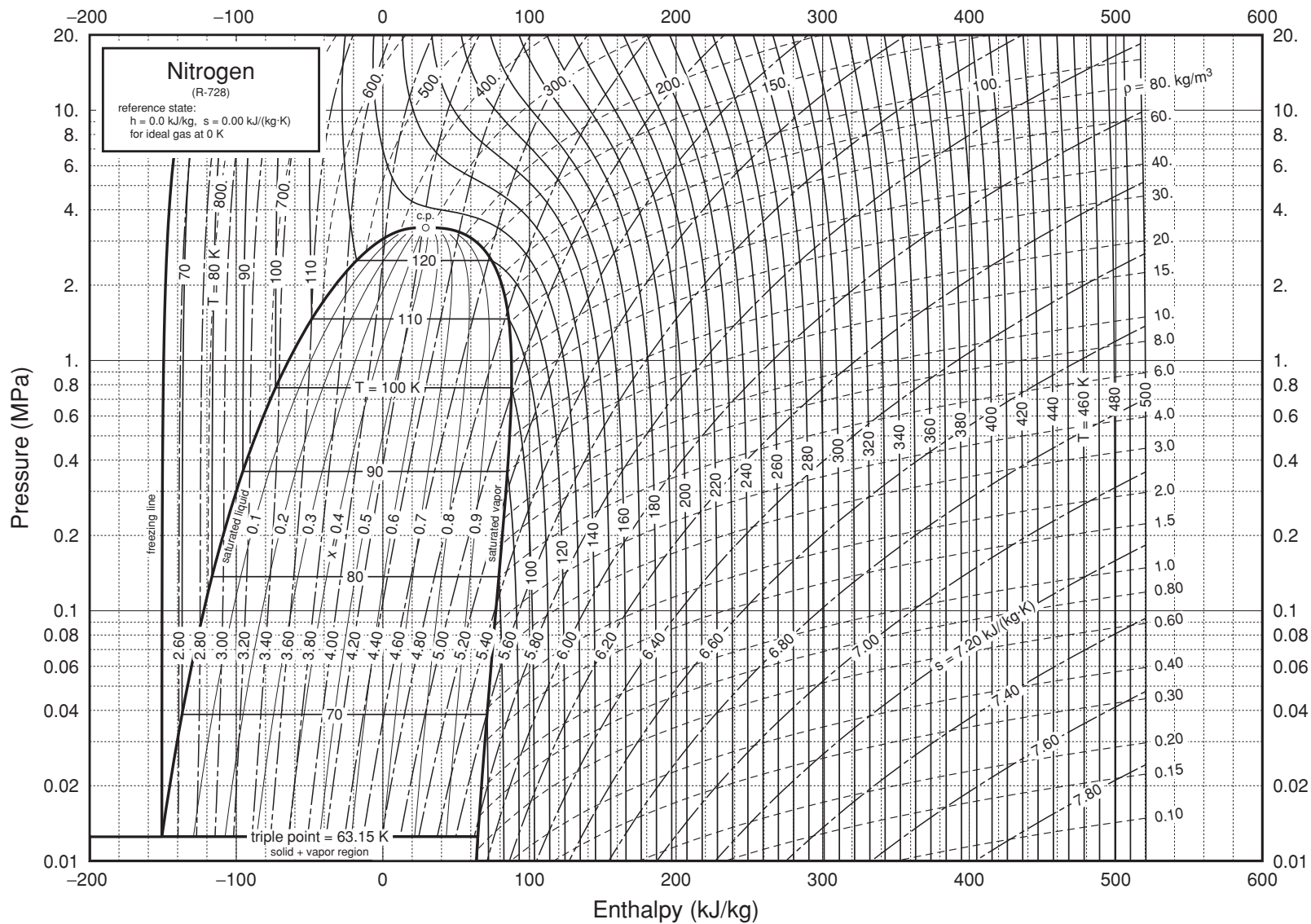


FIG. 2-13 Pressure-enthalpy diagram for nitrogen. Properties computed with the NIST REFPROP Database, Version 7.0 (Lemmon, E. W., McLinden, M. O., and Huber, M. L., 2002, NIST Standard Reference Database 23, NIST Reference Fluid Thermodynamic and Transport Properties—REFPROP, Version 7.0, Standard Reference Data Program, National Institute of Standards and Technology), based on the equation of state of Span, R., Lemmon, E. W., Jacobsen, R. T., Wagner, W., and Yokozeki, A., "A Reference Equation of State for the Thermodynamic Properties of Nitrogen for Temperatures from 63.151 to 1000 K and Pressures to 2200 MPa," *J. Phys. Chem. Ref. Data* **29**:1361–1433, 2000.

TABLE 2-240 Saturated Nitrogen Tetroxide

Pressure, bar	Temperature, K	v_f , m ³ /kg	v_g , m ³ /kg	M_f	M_g
1.0133	299.32	0.000 694	0.2996	91.857	79.157
2	309.57	0.000 711	0.1630	91.886	76.503
4	326.66	0.000 733	0.0876	91.766	73.538
6	337.43	0.000 749	0.0608	91.625	71.748
8	345.45	0.000 762	0.0469	91.488	70.480
10	351.88	0.000 774	0.0382	91.346	69.483
15	364.09	0.000 800	0.0262	90.979	67.742
20	373.17	0.000 822	0.0199	90.601	66.547
30	386.57	0.000 863	0.0133	89.823	64.997
40	396.52	0.000 903	0.0098	89.018	64.099
50	404.50	0.000 945	0.00761	88.191	63.532
60	411.20	0.000 993	0.00607	87.344	63.181
80	422.07	0.001 129	0.00394	85.602	62.959
100	430.76	0.001 577	0.00209	83.817	63.366

Condensed from McCarty, R. D., H-U. Steurer, et al., NBS IR 86 - 3054, 1986 (106 pp.). M = mol wt for the reaction $N_2O_4 \rightarrow 2NO_2 \rightarrow 2NO + O_2$. No derived thermodynamic functions were tabulated due to unduly large differences in literature values, but 92 references are given.

TABLE 2-241 Thermodynamic Properties of Nitrogen Trifluoride

Temperature K	Pressure MPa	Density mol/dm ³	Volume dm ³ /mol	Int. energy kJ/mol	Enthalpy kJ/mol	Entropy kJ/(mol·K)	C _v kJ/(mol·K)	C _p kJ/(mol·K)	Sound speed m/s	Joule-Thomson K/MPa
Saturated Properties										
90.000	0.00015612	25.006	0.039990	-3.8551	-3.8551	-0.033490	0.045791	0.070957	1081.4	-0.44772
95.000	0.00040547	24.719	0.040455	-3.4999	-3.4999	-0.029648	0.045221	0.071116	1049.3	-0.44233
100.00	0.00094625	24.427	0.040938	-3.1442	-3.1442	-0.026000	0.044514	0.071131	1018.1	-0.43718
105.00	0.0020164	24.132	0.041439	-2.7887	-2.7887	-0.022531	0.043768	0.071067	986.86	-0.43184
110.00	0.0039755	23.831	0.041962	-2.4336	-2.4336	-0.019227	0.043048	0.070980	955.57	-0.42594
115.00	0.0073310	23.526	0.042506	-2.0790	-2.0786	-0.016074	0.042394	0.070913	924.52	-0.41921
120.00	0.012759	23.217	0.043073	-1.7245	-1.7240	-0.013057	0.041825	0.070898	894.02	-0.41143
125.00	0.021119	22.902	0.043664	-1.3701	-1.3691	-0.010163	0.041346	0.070958	864.29	-0.40241
130.00	0.033457	22.583	0.044281	-1.0151	-1.0137	-0.0073784	0.040957	0.071113	835.40	-0.39193
135.00	0.051008	22.259	0.044925	-0.65928	-0.65699	-0.0046923	0.040653	0.071379	807.28	-0.37972
140.00	0.075184	21.931	0.045599	-0.30195	-0.29853	-0.0020929	0.040428	0.071771	779.79	-0.36549
145.00	0.10757	21.596	0.046304	0.057452	0.062433	0.00042986	0.040274	0.072303	752.68	-0.34889
150.00	0.14989	21.256	0.047046	0.41959	0.42664	0.0028558	0.040186	0.072988	725.72	-0.32951
155.00	0.20401	20.908	0.047829	0.78514	0.79490	0.0052840	0.040159	0.073841	698.67	-0.30688
160.00	0.27193	20.552	0.048658	1.1549	1.1681	0.0076328	0.040187	0.074876	671.28	-0.28044
165.00	0.35573	20.186	0.049539	1.5295	1.5472	0.0099402	0.040269	0.076114	643.36	-0.24950
170.00	0.45760	19.809	0.050483	1.9100	1.9331	0.012214	0.040404	0.077577	614.73	-0.21319
175.00	0.57979	19.418	0.051499	2.2972	2.3270	0.014461	0.040591	0.079300	585.25	-0.17042
180.00	0.72462	19.011	0.052602	2.6920	2.7301	0.016690	0.040834	0.081326	554.78	-0.11971
185.00	0.89450	18.584	0.053808	3.0957	3.1438	0.018907	0.041136	0.083719	523.23	-0.059078
190.00	1.0918	18.135	0.055141	3.5095	3.5697	0.021121	0.041505	0.086571	490.50	0.014249
195.00	1.3192	17.659	0.056630	3.9350	4.0097	0.023341	0.041953	0.090023	456.52	0.10427
200.00	1.5791	17.148	0.058316	4.3742	4.4663	0.025577	0.042494	0.094298	421.22	0.21696
205.00	1.8742	16.595	0.060260	4.8297	4.9426	0.027843	0.043150	0.099779	384.52	0.36170
210.00	2.2073	15.987	0.062552	5.3052	5.4433	0.030157	0.043953	0.10717	346.33	0.55413
215.00	2.5815	15.305	0.065340	5.8067	5.9754	0.032548	0.044950	0.11795	306.49	0.82239
220.00	3.0003	14.514	0.068899	6.3449	6.5516	0.035068	0.046220	0.13575	264.69	1.2231
225.00	3.4682	13.541	0.073850	6.9434	7.1995	0.037830	0.047920	0.17267	220.19	1.8903
230.00	3.9918	12.148	0.082320	7.6794	8.0080	0.041203	0.050506	0.30655	171.03	3.2539
234.00	4.4607	7.9200	0.12626	9.3687	9.9320	0.049280			0	8.0982
90.000	0.00015612	0.00020869	4791.8	9.0527	9.8008	0.11824	0.025384	0.033709	118.26	125.93
95.000	0.00040547	0.00051363	1946.9	9.1794	9.9688	0.11213	0.025553	0.033889	121.38	109.58
100.00	0.00094625	0.0011394	877.68	9.3064	10.137	0.10681	0.025759	0.034117	124.38	96.037
105.00	0.0020164	0.0023144	432.07	9.4337	10.305	0.10217	0.026007	0.034400	127.25	84.718
110.00	0.0039755	0.0043618	229.26	9.5609	10.472	0.098099	0.026301	0.034747	129.99	75.177
115.00	0.0073310	0.0077094	129.71	9.6879	10.639	0.094513	0.026641	0.035166	132.58	67.076
120.00	0.012759	0.012896	77.545	9.8143	10.804	0.091341	0.027032	0.035666	135.01	60.154
125.00	0.021119	0.020570	48.615	9.9397	10.966	0.088521	0.027474	0.036255	137.27	54.206
130.00	0.033457	0.031490	31.756	10.064	11.126	0.086004	0.027968	0.036942	139.35	49.068
135.00	0.051008	0.046520	21.496	10.186	11.282	0.083746	0.028515	0.037735	141.23	44.607
140.00	0.075184	0.066627	15.009	10.305	11.434	0.081709	0.029116	0.038644	142.91	40.717
145.00	0.10757	0.092885	10.766	10.422	11.580	0.079863	0.029770	0.039680	144.37	37.310
150.00	0.14989	0.12648	7.9063	10.536	11.721	0.078179	0.030477	0.040854	145.59	34.315
155.00	0.20401	0.16872	5.9269	10.645	11.854	0.076634	0.031236	0.042183	146.58	31.671
160.00	0.27193	0.22107	4.5236	10.750	11.980	0.075207	0.032049	0.043684	147.30	29.330
165.00	0.35573	0.28514	3.5071	10.850	12.097	0.073880	0.032913	0.045384	147.77	27.250
170.00	0.45760	0.36279	2.7564	10.943	12.205	0.072636	0.033831	0.047313	147.95	25.397
175.00	0.57979	0.45613	2.1923	11.031	12.302	0.071459	0.034801	0.049515	147.85	23.743
180.00	0.72462	0.56766	1.7616	11.110	12.386	0.070337	0.035825	0.052050	147.44	22.263
185.00	0.89450	0.70033	1.4279	11.181	12.458	0.069254	0.036905	0.055001	146.73	20.936
190.00	1.0918	0.85776	1.1658	11.241	12.514	0.068196	0.038044	0.058491	145.68	19.746
195.00	1.3192	1.0445	0.95740	11.289	12.552	0.067150	0.039245	0.062704	144.29	18.678
200.00	1.5791	1.2665	0.78960	11.323	12.570	0.066097	0.040516	0.067933	142.53	17.718
205.00	1.8742	1.5317	0.65287	11.340	12.563	0.065016	0.041867	0.074677	140.38	16.854
210.00	2.2073	1.8518	0.54001	11.333	12.525	0.063879	0.043315	0.083847	137.79	16.072
215.00	2.5815	2.2450	0.44543	11.296	12.446	0.062642	0.044890	0.097325	134.71	15.354

TABLE 2-241 Thermodynamic Properties of Nitrogen Trifluoride (Concluded)

Temperature K	Pressure MPa	Density mol/dm ³	Volume dm ³ /mol	Int. energy kJ/mol	Enthalpy kJ/mol	Entropy kJ/(mol·K)	C _v kJ/(mol·K)	C _p kJ/(mol·K)	Sound speed m/s	Joule-Thomson K/MPa
Saturated Properties										
220.00	3.0003	2.7432	0.36453	11.213	12.307	0.061229	0.046643	0.11971	131.07	14.662
225.00	3.4682	3.4146	0.29286	11.055	12.071	0.059479	0.048690	0.16599	126.78	13.900
230.00	3.9918	4.4712	0.22365	10.725	11.618	0.056898	0.051363	0.32814	121.80	12.709
234.00	4.4607	7.9200	0.12626	9.3687	9.9320	0.049280			0	8.0982
Single-Phase Properties										
100.00	0.10000	24.430	0.040934	-3.1452	-3.1411	-0.026009	0.044502	0.071124	1018.9	-0.43728
143.95	0.10000	21.667	0.046153	-0.018242	-0.013626	-0.000094174	0.040301	0.072179	758.35	-0.35259
143.95	0.10000	0.086803	11.520	10.398	11.550	0.080236	0.029628	0.039451	144.08	37.990
200.00	0.10000	0.060926	16.413	12.215	13.856	0.093729	0.034723	0.043508	169.06	15.650
300.00	0.10000	0.040232	24.856	16.237	18.723	0.11332	0.045284	0.053741	203.45	5.5743
400.00	0.10000	0.030102	33.220	21.208	24.530	0.12997	0.053558	0.061943	232.46	2.8668
500.00	0.10000	0.024060	41.562	26.869	31.025	0.14444	0.059251	0.067609	258.38	1.7661
100.00	1.0000	24.449	0.040901	-3.1540	-3.1131	-0.026098	0.044398	0.071055	1026.3	-0.43816
187.76	1.0000	18.339	0.054527	3.3230	3.3775	0.020131	0.041331	0.085231	505.29	-0.020346
187.76	1.0000	0.78400	1.2755	11.215	12.491	0.068667	0.037527	0.056853	146.19	20.263
200.00	1.0000	0.70199	1.4245	11.738	13.162	0.072132	0.037614	0.053386	154.62	16.645
300.00	1.0000	0.41548	2.4068	16.042	18.449	0.093526	0.045687	0.055540	199.37	5.5586
400.00	1.0000	0.30407	3.2887	21.082	24.371	0.11051	0.053632	0.062664	231.33	2.8289
500.00	1.0000	0.24110	4.1476	26.771	30.918	0.12510	0.059244	0.067998	258.62	1.7349
100.00	5.0000	24.532	0.040763	-3.1921	-2.9883	-0.026483	0.043955	0.070771	1057.9	-0.44174
200.00	5.0000	17.659	0.056627	4.1435	4.4266	0.024397	0.041665	0.087072	477.43	0.053822
300.00	5.0000	2.4334	0.41095	15.064	17.119	0.076882	0.047559	0.067409	183.97	5.3277
400.00	5.0000	1.5833	0.63161	20.512	23.670	0.095734	0.053907	0.066129	228.50	2.5958
500.00	5.0000	1.2132	0.82425	26.341	30.462	0.11087	0.059206	0.069735	260.85	1.5696
100.00	10.000	24.630	0.040600	-3.2377	-2.8317	-0.026951	0.043446	0.070455	1094.6	-0.44552
200.00	10.000	18.214	0.054902	3.8853	4.4343	0.023042	0.041251	0.081506	536.12	-0.078962
300.00	10.000	5.9501	0.16806	13.534	15.214	0.066202	0.049590	0.093780	185.51	3.9475
400.00	10.000	3.2770	0.30515	19.798	22.849	0.088300	0.054171	0.070777	231.76	2.1918
500.00	10.000	2.4256	0.41227	25.826	29.949	0.10414	0.059167	0.071809	266.86	1.3296
100.00	25.000	24.895	0.040168	-3.3631	-2.3589	-0.028280	0.042128	0.069766	1191.1	-0.45304
200.00	25.000	19.339	0.051709	3.3539	4.6466	0.020118	0.041959	0.074322	642.55	-0.26070
300.00	25.000	12.709	0.078686	10.815	12.782	0.052928	0.049110	0.086464	338.34	0.50765
400.00	25.000	7.8701	0.12706	17.964	21.141	0.077032	0.054897	0.079284	285.01	0.90188
500.00	25.000	5.7388	0.17425	24.506	28.863	0.094275	0.059344	0.076236	303.16	0.66132
100.00	50.000	25.271	0.039572	-3.5465	-1.5679	-0.030335	0.040341	0.069490	1322.6	-0.45498
200.00	50.000	20.560	0.048639	2.8054	5.2373	0.016816	0.044958	0.070043	734.96	-0.38097
300.00	50.000	15.995	0.062520	9.4909	12.617	0.046643	0.052084	0.076746	484.09	-0.15530
400.00	50.000	12.237	0.081722	16.326	20.412	0.069057	0.057087	0.078504	397.17	0.026532
500.00	50.000	9.6861	0.10324	23.086	28.248	0.086544	0.060630	0.078201	380.22	0.066751

The values in these tables were generated from the NIST REFPROP software (Lemmon, E. W., McLinden, M. O., and Huber, M. L., NIST Standard Reference Database 23: Reference Fluid Thermodynamic and Transport Properties—REFPROP, National Institute of Standards and Technology, Standard Reference Data Program, Gaithersburg, Md., 2002, Version 7.1). The primary source for the thermodynamic properties is Younglove, B. A., "Thermophysical Properties of Fluids. I. Argon, Ethylene, Parahydrogen, Nitrogen, Nitrogen Trifluoride, and Oxygen," *J. Phys. Chem. Ref. Data Suppl.* 1, **11**: 1–11, 1982. Validated equations for the viscosity and thermal conductivity are not currently available for this fluid.

Properties at the critical point temperature are given in the last entry of the saturation tables. In the single-phase table, when the temperature range for a given isobar includes a vapor-liquid phase boundary, the temperature of phase equilibrium is noted, and properties for both the saturated liquid and saturated vapor are given (with liquid properties given in the upper line). Lines are omitted from the temperature-pressure grid of the single-phase table, when the system would be in the solid phase or if there are potential problems with the source property surface.

The uncertainties in density are 0.25% in the liquid phase and 0.3% in the vapor and supercritical regions. The uncertainty in speed of sound and heat capacity is 5%.

TABLE 2-242 Thermodynamic Properties of Nitrous Oxide

Temperature K	Pressure MPa	Density mol/dm ³	Volume dm ³ /mol	Int. energy kJ/mol	Enthalpy kJ/mol	Entropy kJ/(mol·K)	C _v kJ/(mol·K)	C _p kJ/(mol·K)	Sound speed m/s	Joule-Thomson K/MPa
Saturated Properties										
182.33	0.087837	28.113	0.035570	-0.18142	-0.17830	-0.00096900	0.042295	0.075603	1149.6	-0.26723
185.00	0.10325	27.935	0.035797	0.020258	0.023954	0.00012922	0.042134	0.075669	1132.4	-0.26287
190.00	0.13782	27.599	0.036234	0.39840	0.40340	0.0021464	0.041852	0.075851	1100.2	-0.25377
195.00	0.18085	27.257	0.036688	0.77745	0.78408	0.0041159	0.041596	0.076111	1068.2	-0.24334
200.00	0.23367	26.910	0.037161	1.1577	1.1664	0.0060420	0.041365	0.076452	1036.3	-0.23146
205.00	0.29767	26.557	0.037656	1.5396	1.5508	0.0079284	0.041155	0.076875	1004.5	-0.21798
210.00	0.37431	26.197	0.038173	1.9234	1.9377	0.0097789	0.040967	0.077388	972.70	-0.20272
215.00	0.46509	25.829	0.038716	2.3094	2.3274	0.011597	0.040797	0.077995	940.94	-0.18545
220.00	0.57160	25.453	0.039288	2.6982	2.7206	0.013385	0.040645	0.078706	909.16	-0.16592
225.00	0.69544	25.069	0.039891	3.0899	3.1177	0.015148	0.040510	0.079533	877.35	-0.14379
230.00	0.83828	24.674	0.040529	3.4852	3.5192	0.016888	0.040392	0.080489	845.46	-0.11869
235.00	1.0018	24.268	0.041207	3.8844	3.9257	0.018607	0.040290	0.081595	813.47	-0.090113
240.00	1.1878	23.849	0.041930	4.2881	4.3379	0.020311	0.040203	0.082875	781.31	-0.057462
245.00	1.3979	23.417	0.042705	4.6969	4.7566	0.022000	0.040132	0.084362	748.95	-0.019968
250.00	1.6341	22.968	0.043538	5.1115	5.1826	0.023681	0.040078	0.086100	716.31	0.023355
255.00	1.8982	22.502	0.044440	5.5326	5.6170	0.025355	0.040041	0.088150	683.32	0.073794
260.00	2.1920	22.015	0.045423	5.9614	6.0609	0.027028	0.040025	0.090597	649.86	0.13307
265.00	2.5177	21.505	0.046501	6.3990	6.5161	0.028704	0.040030	0.093564	615.81	0.20351
270.00	2.8772	20.966	0.047697	6.8471	6.9843	0.030391	0.040064	0.097233	580.97	0.28843
275.00	3.2728	20.393	0.049037	7.3078	7.4682	0.032097	0.040134	0.10189	545.11	0.39261
280.00	3.7068	19.777	0.050564	7.7841	7.9715	0.033833	0.040251	0.10803	507.90	0.52333
285.00	4.1820	19.106	0.052339	8.2804	8.4993	0.035615	0.040437	0.11651	468.86	0.69225
290.00	4.7012	18.361	0.054464	8.8039	9.0600	0.037468	0.040727	0.12910	427.31	0.91943
295.00	5.2681	17.505	0.057125	9.3670	9.6680	0.039439	0.041190	0.14997	382.17	1.2430
300.00	5.8874	16.466	0.060732	9.9960	10.354	0.041620	0.041979	0.19222	331.57	1.7475
305.00	6.5663	15.022	0.066569	10.768	11.205	0.044293	0.043564	0.32907	271.24	2.6810
309.52	7.2447	10.270	0.097371	12.745	13.450	0.051414			0	6.2530
182.33	0.087837	0.059336	16.853	14.931	16.411	0.090017	0.025545	0.034993	211.93	44.590
185.00	0.10325	0.068951	14.503	14.984	16.481	0.089089	0.025844	0.035439	212.91	42.793
190.00	0.13782	0.090180	11.089	15.082	16.610	0.087443	0.026427	0.036334	214.62	39.645
195.00	0.18085	0.11615	8.6098	15.176	16.733	0.085908	0.027038	0.037309	216.14	36.768
200.00	0.23367	0.14754	6.7780	15.268	16.852	0.084469	0.027674	0.038365	217.48	34.146
205.00	0.29767	0.18508	5.4030	15.356	16.965	0.083117	0.028331	0.039506	218.62	31.765
210.00	0.37431	0.22958	4.3558	15.440	17.071	0.081842	0.029006	0.040736	219.56	29.606
215.00	0.46509	0.28190	3.5474	15.521	17.170	0.080634	0.029694	0.042062	220.30	27.653
220.00	0.57160	0.34298	2.9156	15.596	17.262	0.079485	0.030395	0.043494	220.82	25.888
225.00	0.69544	0.41387	2.4162	15.666	17.346	0.078387	0.031105	0.045048	221.13	24.295
230.00	0.83828	0.49575	2.0171	15.730	17.421	0.077332	0.031824	0.046741	221.20	22.858
235.00	1.0018	0.58993	1.6951	15.789	17.487	0.076314	0.032552	0.048600	221.04	21.560
240.00	1.1878	0.69791	1.4329	15.840	17.541	0.075325	0.033289	0.050660	220.64	20.387
245.00	1.3979	0.82145	1.2174	15.883	17.584	0.074359	0.034037	0.052967	219.98	19.325
250.00	1.6341	0.96261	1.0388	15.917	17.614	0.073408	0.034798	0.055585	219.07	18.361
255.00	1.8982	1.1239	0.88979	15.941	17.630	0.072464	0.035577	0.058600	217.88	17.483
260.00	2.1920	1.3082	0.76438	15.953	17.629	0.071519	0.036377	0.062136	216.41	16.679
265.00	2.5177	1.5196	0.65808	15.952	17.609	0.070564	0.037205	0.066370	214.64	15.939
270.00	2.8772	1.7627	0.56730	15.935	17.567	0.069588	0.038072	0.071572	212.56	15.251
275.00	3.2728	2.0443	0.48917	15.899	17.500	0.068575	0.038988	0.078164	210.15	14.603
280.00	3.7068	2.3734	0.42135	15.839	17.401	0.067508	0.039971	0.086856	207.39	13.981
285.00	4.1820	2.7632	0.36189	15.749	17.262	0.066361	0.041046	0.098934	204.24	13.366
290.00	4.7012	3.2349	0.30912	15.618	17.071	0.065093	0.042252	0.11700	200.67	12.734
295.00	5.2681	3.8252	0.26142	15.429	16.806	0.063636	0.043653	0.14723	196.63	12.043
300.00	5.8874	4.6102	0.21691	15.145	16.422	0.061848	0.045376	0.20883	192.02	11.210
305.00	6.5663	5.8106	0.17210	14.661	15.791	0.059328	0.047733	0.40691	186.66	10.014
309.52	7.2447	10.270	0.097371	12.745	13.450	0.051414			0	6.2530

TABLE 2-242 Thermodynamic Properties of Nitrous Oxide (Concluded)

Temperature K	Pressure MPa	Density mol/dm ³	Volume dm ³ /mol	Int. energy kJ/mol	Enthalpy kJ/mol	Entropy kJ/(mol·K)	C_v kJ/(mol·K)	C_p kJ/(mol·K)	Sound speed m/s	Joule-Thomson K/MPa
Single-Phase Properties										
200.00	0.10000	0.061319	16.308	15.382	17.013	0.092110	0.025918	0.035025	221.52	31.472
300.00	0.10000	0.040304	24.811	18.214	20.695	0.10698	0.030437	0.038943	267.85	10.733
400.00	0.10000	0.030129	33.190	21.467	24.786	0.11873	0.034363	0.042764	306.03	5.6159
500.00	0.10000	0.024075	41.537	25.072	29.226	0.12862	0.037563	0.045926	339.54	3.4059
200.00	1.0000	26.940	0.037120	1.1429	1.1800	0.0059677	0.041381	0.076317	1040.5	-0.23345
234.95	1.0000	24.272	0.041200	3.8803	3.9215	0.018590	0.040291	0.081583	813.80	-0.090429
234.95	1.0000	0.58888	1.6981	15.788	17.486	0.076324	0.032545	0.048580	221.04	21.573
300.00	1.0000	0.42412	2.3578	17.944	20.302	0.086931	0.031268	0.041833	260.01	10.924
400.00	1.0000	0.30696	3.2578	21.310	24.568	0.099190	0.034610	0.043833	303.02	5.5924
500.00	1.0000	0.24260	4.1220	24.963	29.085	0.10926	0.037680	0.046488	338.49	3.3701
200.00	5.0000	27.091	0.036913	1.0679	1.2525	0.0055897	0.041467	0.075665	1061.6	-0.24314
292.69	5.0000	17.918	0.055811	9.1008	9.3799	0.038510	0.040948	0.13883	403.56	1.0778
292.69	5.0000	3.5344	0.28294	15.525	16.940	0.064339	0.042976	0.13106	198.56	12.373
300.00	5.0000	3.1047	0.32209	16.114	17.725	0.066990	0.039518	0.091593	212.60	11.486
400.00	5.0000	1.6773	0.59621	20.558	23.539	0.083920	0.035787	0.049876	290.66	5.4199
500.00	5.0000	1.2538	0.79755	24.469	28.457	0.094897	0.038199	0.049186	334.89	3.1966
200.00	10.000	27.269	0.036672	0.97935	1.3461	0.0051379	0.041579	0.074951	1086.5	-0.25384
300.00	10.000	18.407	0.054327	9.1891	9.7324	0.038771	0.040304	0.11033	462.21	0.72534
400.00	10.000	3.7981	0.26329	19.470	22.102	0.075432	0.037387	0.061591	279.96	4.9171
500.00	10.000	2.6054	0.38381	23.835	27.673	0.087896	0.038831	0.052973	333.21	2.9341
200.00	25.000	27.751	0.036035	0.74199	1.6429	0.0038961	0.041933	0.073298	1154.2	-0.27902
300.00	25.000	20.902	0.047843	8.0747	9.2708	0.034710	0.039937	0.082004	654.64	0.10041
400.00	25.000	11.546	0.086610	16.070	18.235	0.060433	0.040060	0.087395	352.41	1.7332
500.00	25.000	6.9433	0.14402	21.962	25.563	0.076883	0.040346	0.063761	357.12	1.8422
300.00	50.000	22.869	0.043727	7.1665	9.3528	0.031190	0.040453	0.072893	828.55	-0.14288
400.00	50.000	17.051	0.058649	13.791	16.723	0.052389	0.040588	0.073379	568.05	0.23352
500.00	50.000	12.463	0.080236	19.764	23.776	0.068153	0.041531	0.067192	477.36	0.52378

The values in these tables were generated from the NIST REFPROP software (Lemmon, E. W., McLinden, M. O., and Huber, M. L., NIST Standard Reference Database 23: Reference Fluid Thermodynamic and Transport Properties—REFPROP, National Institute of Standards and Technology, Standard Reference Data Program, Gaithersburg, Md., 2002, Version 7.1). The primary source for the thermodynamic properties is Lemmon, E. W., and Span, R., "Short Fundamental Equations of State for 20 Industrial Fluids," *J. Chem. Eng. Data* **51**(3):785–850, 2006. Validated equations for the viscosity and thermal conductivity are not currently available for this fluid.

Properties at the triple point temperature and the critical point temperature are given in the first and last entries of the saturation tables, respectively. In the single-phase table, when the temperature range for a given isobar includes a vapor-liquid phase boundary, the temperature of phase equilibrium is noted, and properties for both the saturated liquid and saturated vapor are given (with liquid properties given in the upper line). Lines are omitted from the temperature-pressure grid of the single-phase table, when the system would be in the solid phase or if there are potential problems with the source property surface.

The uncertainties in the equation of state are 0.1% in density in the liquid and vapor phases between 220 and 300 K, 0.25% at temperatures above 300 K and at temperatures below 220 K, and 0.5% in the critical region, except very close to the critical point. The uncertainty in vapor pressure is 0.2%, that for heat capacities is 3%, and that for the speed of sound in the vapor phase is 0.05% above 220 K. The uncertainty in the liquid phase is not known but is estimated to be within 5%.

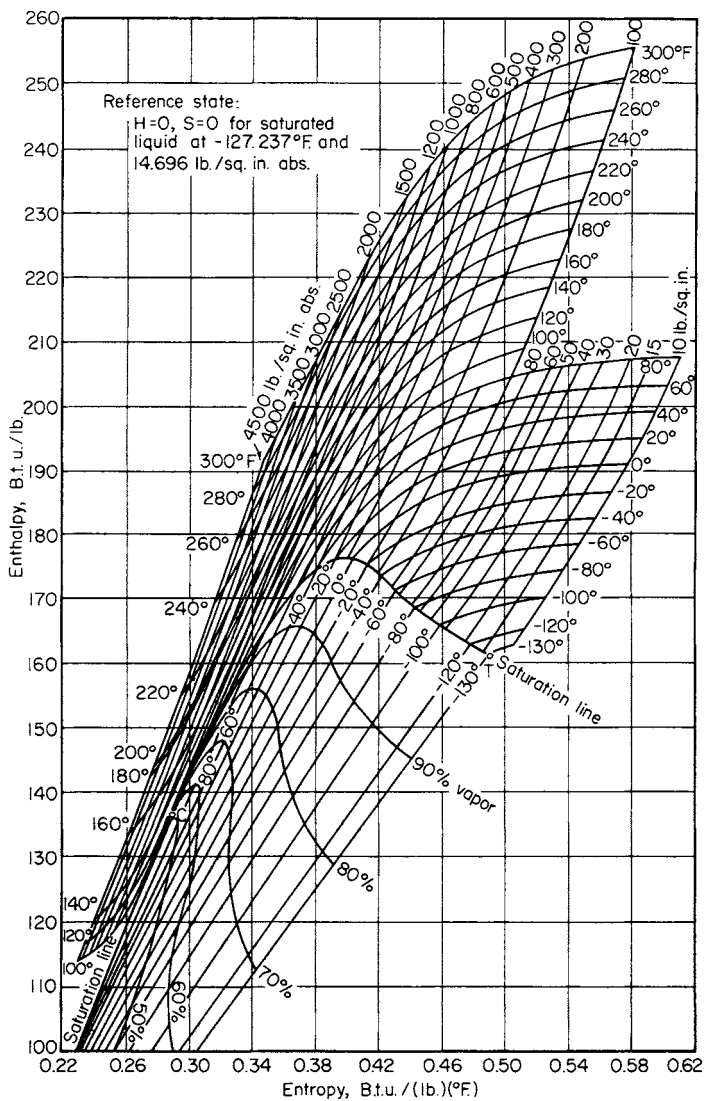


FIG. 2-14 Mollier diagram for nitrous oxide. (Fig. 9, *Univ. Texas Rep., Cont. DAI-23-072-ORD-685*, June 1, 1956, by Couch and Kobe. Reproduced by permission.) Some irregularity in the compressibility factors from 80 to 160 atm, 50 to 100°C exists (Couch, private communication, 1967). See Couch et al., *J. Chem. Eng. Data*, **6**, (1961) for PVT data.

TABLE 2-243 Thermodynamic Properties of Nonane

Temperature K	Pressure MPa	Density mol/dm ³	Volume dm ³ /mol	Int. energy kJ/mol	Enthalpy kJ/mol	Entropy kJ/(mol·K)	C _v kJ/(mol·K)	C _p kJ/(mol·K)	Sound speed m/s	Joule-Thomson K/MPa	Therm. cond. mW/(m·K)	Viscosity μPa·s
Saturated Properties												
219.70	4.4449E-07	6.0520	0.16524	-60.675	-60.675	-0.19174	0.19748	0.25433	1544.5	-0.50071	153.02	4037.3
220.00	4.6229E-07	6.0501	0.16529	-60.599	-60.599	-0.19139	0.19757	0.25440	1543.0	-0.50053	152.90	3978.4
240.00	4.8933E-06	5.9249	0.16878	-55.459	-55.459	-0.16904	0.20402	0.25984	1449.8	-0.48613	145.29	1914.0
260.00	3.3858E-05	5.8013	0.17237	-50.195	-50.195	-0.14797	0.21164	0.26681	1361.7	-0.46790	138.35	1194.3
280.00	0.00016888	5.6785	0.17610	-44.779	-44.779	-0.12791	0.22016	0.27497	1277.9	-0.44671	131.98	842.44
300.00	0.00065182	5.5557	0.18000	-39.190	-39.190	-0.10863	0.22932	0.28402	1197.9	-0.42315	126.11	638.13
320.00	0.0020515	5.4321	0.18409	-33.413	-33.413	-0.089996	0.23894	0.29376	1121.1	-0.39747	120.68	505.83
340.00	0.0054791	5.3071	0.18843	-27.437	-27.436	-0.071883	0.24886	0.30400	1046.8	-0.36960	115.63	413.37
360.00	0.012806	5.1799	0.19305	-21.252	-21.249	-0.054209	0.25894	0.31464	974.60	-0.33918	110.92	344.96
380.00	0.026830	5.0496	0.19803	-14.851	-14.846	-0.036909	0.26908	0.32557	903.98	-0.30546	106.50	292.08
400.00	0.051367	4.9154	0.20344	-8.2134	-8.2208	-0.019932	0.27921	0.33677	834.45	-0.26723	102.33	249.76
420.00	0.091247	4.7760	0.20938	-1.3870	-1.3679	-0.0032367	0.28927	0.34824	765.54	-0.22257	98.374	214.92
440.00	0.15227	4.6299	0.21599	5.6854	5.7183	0.013213	0.29920	0.36002	696.76	-0.16849	94.594	185.56
460.00	0.24110	4.4754	0.22345	12.991	13.045	0.029452	0.30899	0.37228	627.57	-0.10004	90.947	160.30
480.00	0.36527	4.3096	0.23204	20.537	20.622	0.045513	0.31863	0.38530	557.35	-0.0087139	87.384	138.18
500.00	0.53313	4.1286	0.24221	28.335	28.464	0.061438	0.32814	0.39965	485.36	0.12153	83.848	118.43
520.00	0.75413	3.9259	0.25472	36.408	36.600	0.077283	0.33756	0.41650	410.60	0.32444	80.262	100.46
540.00	1.0392	3.6898	0.27102	44.798	45.080	0.093141	0.34703	0.43881	331.60	0.68436	76.518	83.674
560.00	1.4023	3.3948	0.29457	53.602	54.015	0.10920	0.35685	0.47629	245.76	1.4810	72.450	67.309
594.55	2.2820	1.8100	0.55249	73.819	75.080	0.144498	—	—	—	31.599	—	—
219.70	4.4449E-07	2.4333E-07	4,109,700.	-9.8808	-8.0542	0.047770	0.16161	0.16993	122.37	363.94	6.2016	4.0513
220.00	4.6229E-07	2.5273E-07	3,956,800.	-9.8323	-8.0032	0.047676	0.16174	0.17006	122.45	361.95	6.2133	4.0567
240.00	4.8933E-06	2.4522E-06	407,790.	-6.5064	-4.5110	0.043246	0.17103	0.17935	127.73	254.36	7.0659	4.4125
260.00	3.3858E-05	1.5664E-05	63,840.	-2.9862	-0.82471	0.041911	0.18119	0.18951	132.76	183.36	8.0682	4.7673
280.00	0.00016888	7.2578E-05	13,778.	0.74180	3.0688	0.042975	0.19199	0.20033	137.56	135.32	9.2127	5.1206
300.00	0.00065182	0.00026168	3,821.5	4.6851	7.1760	0.045920	0.20323	0.21161	142.11	102.10	10.493	5.4722
320.00	0.0020515	0.00077364	1,292.6	8.8457	11.497	0.050349	0.21478	0.22326	146.36	78.695	11.902	5.8211
340.00	0.0054791	0.0019519	512.31	13.220	16.027	0.055950	0.22652	0.23519	150.21	61.932	13.436	6.1663
360.00	0.012806	0.0043356	230.65	17.802	20.756	0.062471	0.23839	0.24737	153.55	49.767	15.091	6.5069
380.00	0.026830	0.0086887	115.09	22.580	25.668	0.069707	0.25032	0.25979	156.23	40.846	16.864	6.8425
400.00	0.051367	0.016023	62.412	27.541	30.747	0.077488	0.26226	0.27245	158.10	34.258	18.757	7.1737
420.00	0.091247	0.027625	36.200	32.671	35.974	0.085673	0.27416	0.28541	158.99	29.384	20.773	7.5025
440.00	0.15227	0.045117	22.165	37.952	41.327	0.094142	0.28601	0.29878	158.70	25.803	22.918	7.8332
460.00	0.24110	0.070581	14.168	43.363	46.779	0.10279	0.29779	0.31276	157.00	23.233	25.205	8.1731
480.00	0.36527	0.10681	9.3627	48.876	52.296	0.11150	0.30950	0.32778	153.58	21.504	27.655	8.5341
500.00	0.53313	0.15781	6.3369	54.456	57.834	0.12018	0.32118	0.34467	148.05	20.545	30.306	8.9361
520.00	0.75413	0.22994	4.3490	60.045	63.325	0.12868	0.33293	0.36530	139.82	20.405	33.233	9.4142
540.00	1.0392	0.33476	2.9872	65.548	68.652	0.13679	0.34492	0.39454	127.99	21.346	36.613	10.039
560.00	1.4023	0.49815	2.0074	70.762	73.577	0.14413	0.35757	0.44973	111.07	24.126	40.989	10.990
594.55	2.2820	1.8100	0.55249	73.819	75.080	0.144498	—	—	—	31.599	—	—

Single-Phase Properties

250.00	0.10000	5.8635	0.17055	-52.849	-52.832	-0.15838	0.20771	0.26315	1405.7	-0.47750	141.78	1483.4
300.00	0.10000	5.5564	0.17997	-39.196	-39.178	-0.10865	0.22933	0.28401	1198.6	-0.42329	126.15	638.82
350.00	0.10000	5.2447	0.19067	-24.378	-24.359	-0.063016	0.25389	0.30925	1011.2	-0.35500	113.28	377.18
400.00	0.10000	4.9160	0.20342	-8.2368	-8.2164	-0.019946	0.27921	0.33675	834.97	-0.26752	102.36	249.91
423.42	0.10000	4.7515	0.21046	-0.19510	-0.17406	-0.00041018	0.29097	0.35022	753.80	-0.21411	97.717	209.56
423.42	0.10000	0.030145	33.173	33.563	36.880	0.087103	0.27619	0.28766	159.03	28.690	21.130	7.5587
450.00	0.10000	0.027993	35.724	41.125	44.697	0.10500	0.28978	0.30044	165.87	22.301	23.838	8.0448
500.00	0.10000	0.024798	40.326	56.284	60.317	0.13790	0.31440	0.32419	177.26	14.792	29.272	8.9428
250.00	1.0000	5.8679	0.17042	-52.889	-52.719	-0.15854	0.20778	0.26309	1410.5	-0.47809	142.11	1501.9
300.00	1.0000	5.5624	0.17978	-39.250	-39.070	-0.10883	0.22940	0.28387	1204.4	-0.42451	126.55	645.13
350.00	1.0000	5.2530	0.19037	-24.450	-24.260	-0.063223	0.25395	0.30900	1018.5	-0.35745	113.76	380.90
400.00	1.0000	4.9280	0.20292	-8.3375	-8.1346	-0.020199	0.27927	0.33627	844.45	-0.27280	102.96	252.79
450.00	1.0000	4.5708	0.21878	9.1743	9.3930	0.021057	0.30414	0.36516	674.11	-0.14850	93.482	174.91
500.00	1.0000	4.1469	0.24114	28.203	28.444	0.061172	0.32810	0.39811	496.26	0.096651	84.482	120.06
250.00	5.0000	5.8875	0.16985	-53.064	-52.214	-0.15925	0.20809	0.26282	1431.5	-0.48055	143.55	1587.0
300.00	5.0000	5.5884	0.17894	-39.480	-38.585	-0.10961	0.22969	0.28333	1229.8	-0.42952	128.25	673.50
350.00	5.0000	5.2884	0.18909	-24.758	-23.813	-0.064113	0.25422	0.30802	1049.7	-0.36725	115.82	397.43
400.00	5.0000	4.9781	0.20088	-8.7590	-7.7546	-0.021267	0.27950	0.33447	884.19	-0.29292	105.52	265.35
450.00	5.0000	4.6466	0.21521	8.5689	9.6450	0.019689	0.30429	0.36159	727.45	-0.19528	96.800	186.34
500.00	5.0000	4.2772	0.23380	27.246	28.415	0.059215	0.32797	0.38941	574.69	-0.043276	89.174	132.45
250.00	10.000	5.9111	0.16917	-53.273	-51.582	-0.16011	0.20848	0.26253	1456.9	-0.48327	145.29	1699.9
300.00	10.000	5.6194	0.17796	-39.753	-37.973	-0.11054	0.23005	0.28275	1260.0	-0.43494	130.31	709.84
350.00	10.000	5.3297	0.18763	-25.116	-23.240	-0.065168	0.25456	0.30700	1086.3	-0.37743	118.27	418.13
400.00	10.000	5.0347	0.19862	-9.2354	-7.2492	-0.022500	0.27981	0.33273	929.33	-0.31235	108.48	280.67
450.00	10.000	4.7272	0.21154	7.9189	10.034	0.018184	0.30452	0.35854	784.82	-0.23486	100.47	199.70
500.00	10.000	4.3995	0.22730	26.321	28.594	0.057270	0.32803	0.38371	650.34	-0.13338	93.894	145.66
300.00	100.00	6.0143	0.16627	-43.037	-26.410	-0.12342	0.23562	0.27987	1662.5	-0.46881	158.86	1638.6
350.00	100.00	5.8100	0.17212	-29.086	-11.875	-0.078654	0.25980	0.30194	1534.1	-0.43419	149.98	851.44
400.00	100.00	5.6178	0.17800	-13.998	3.8029	-0.036820	0.28476	0.32520	1426.4	-0.40174	143.57	557.39
450.00	100.00	5.4358	0.18396	2.2421	20.639	0.0028129	0.30915	0.34808	1335.5	-0.37331	139.19	406.92
500.00	100.00	5.2628	0.19001	19.589	38.590	0.040621	0.33224	0.36974	1258.2	-0.34915	136.49	316.22
500.00	300.00	5.9601	0.16778	15.017	65.352	0.023367	0.33895	0.37096	1885.2	-0.36365	184.31	733.45

The values in these tables were generated from the NIST REFPROP software (Lemmon, E. W., McLinden, M. O., and Huber, M. L., NIST Standard Reference Database 23: Reference Fluid Thermodynamic and Transport Properties—REFPROP, National Institute of Standards and Technology, Standard Reference Data Program, Gaithersburg, Md., 2002, Version 7.1). The primary source for the thermodynamic properties is Lemmon, E. W., and Span, R., "Short Fundamental Equations of State for 20 Industrial Fluids," *J. Chem. Eng. Data* **51**(3):785–850, 2006. The source for viscosity is Huber, M. L., Laesecke, A., and Xiang, H. W., "Viscosity Correlations for Minor Constituent Fluids in Natural Gas: *n*-Octane, *n*-Nonane and *n*-Decane," *Fluid Phase Equilibria* **224**:263–270, 2004. The source for thermal conductivity is Huber, M. L., and Perkins, R. A., "Thermal Conductivity Correlations for Minor Constituent Fluids in Natural Gas: *n*-Octane, *n*-Nonane and *n*-Decane," *Fluid Phase Equilibria* **227**:47–55, 2004.

Properties at the triple point temperature and the critical point temperature are given in the first and last entries of the saturation tables, respectively. In the single-phase table, when the temperature range for a given isobar includes a vapor-liquid phase boundary, the temperature of phase equilibrium is noted, and properties for both the saturated liquid and saturated vapor are given (with liquid properties given in the upper line). Lines are omitted from the temperature-pressure grid of the single-phase table, when the system would be in the solid phase or if there are potential problems with the source property surface.

The uncertainties in the equation are 0.05% in the saturated-liquid density between 280 and 335 K and 0.2% in density in the liquid phase below 430 K and 10 MPa. The uncertainty increases to 0.3% up to 100 MPa and 0.5% up to 800 MPa. In the vapor phase and at supercritical state points, the uncertainty in density is 1%, whereas in the liquid phase between 430 K and the critical point it is 0.5% in density. Other uncertainties are 0.2% in vapor pressure between 300 and 430 K, 0.5% in vapor pressure at higher temperatures, 2% in heat capacities below 550 K, 5% at higher temperatures, and 1% in the liquid-phase speed of sound below 430 K. The estimated uncertainty in viscosity is 1.0% along the saturated-liquid line, 5% elsewhere. Uncertainty in thermal conductivity is 3%, except in the supercritical region and dilute gas which have an uncertainty of 5%.

TABLE 2-244 Thermodynamic Properties of Octane

Temperature K	Pressure MPa	Density mol/dm ³	Volume dm ³ /mol	Int. energy kJ/mol	Enthalpy kJ/mol	Entropy kJ/(mol·K)	C _v kJ/(mol·K)	C _p kJ/(mol·K)	Sound speed m/s	Joule-Thomson K/MPa	Therm. cond. mW/(m·K)	Viscosity μPa·s
Saturated Properties												
216.37	1.9889E-06	6.6864	0.14956	-47.586	-47.586	-0.15718	0.18017	0.22965	1496.9	-0.50088	153.28	2275.3
220.00	3.0719E-06	6.6606	0.15014	-46.751	-46.751	-0.15335	0.18100	0.23031	1479.7	-0.49876	151.81	2055.6
240.00	2.5565E-05	6.5193	0.15339	-42.103	-42.103	-0.13313	0.18613	0.23473	1388.4	-0.48455	144.08	1275.2
260.00	0.00014507	6.3793	0.15676	-37.353	-37.353	-0.11412	0.19222	0.24044	1301.6	-0.46633	136.89	875.51
280.00	0.00061336	6.2396	0.16027	-32.477	-32.477	-0.096062	0.19917	0.24730	1218.5	-0.44452	130.16	644.21
300.00	0.0020600	6.0991	0.16396	-27.455	-27.454	-0.078739	0.20684	0.25511	1138.6	-0.41949	123.83	498.03
320.00	0.0057644	5.9569	0.16787	-22.268	-22.267	-0.062005	0.21505	0.26370	1061.2	-0.39136	117.86	399.06
340.00	0.013932	5.8120	0.17206	-16.904	-16.901	-0.045746	0.22363	0.27290	985.87	-0.35994	112.19	328.21
360.00	0.029907	5.6633	0.17657	-11.351	-11.345	-0.029879	0.23245	0.28260	912.09	-0.32455	106.78	275.06
380.00	0.058269	5.5097	0.18150	-5.6010	-5.5904	-0.014338	0.24139	0.29271	839.36	-0.28395	101.59	233.59
400.00	0.10483	5.3495	0.18693	0.35204	0.37164	0.00092888	0.25035	0.30321	767.20	-0.23602	96.614	200.14
420.00	0.17652	5.1809	0.19302	6.5150	6.5490	0.015963	0.25926	0.31416	695.05	-0.17723	91.804	172.37
440.00	0.28132	5.0012	0.19995	12.895	12.951	0.030805	0.26810	0.32572	622.34	-0.10167	87.139	148.75
460.00	0.42812	4.8068	0.20804	19.502	19.591	0.045494	0.27685	0.33823	548.39	0.0013050	82.591	128.19
480.00	0.62676	4.5922	0.21776	26.352	26.489	0.060080	0.28552	0.35240	472.36	0.15251	78.136	109.92
500.00	0.88820	4.3477	0.23000	33.473	33.677	0.074631	0.29419	0.36979	393.17	0.39829	73.755	93.322
520.00	1.2251	4.0556	0.24657	40.921	41.223	0.089269	0.30300	0.39457	309.23	0.86399	69.457	77.803
540.00	1.6533	3.6731	0.27225	48.832	49.282	0.10426	0.31238	0.44291	217.99	2.0228	65.431	62.572
560.00	2.1958	3.0341	0.32959	57.752	58.476	0.12068	0.32413	0.68855	115.40	7.6023	64.209	45.346
569.32	2.4978	2.0564	0.48629	64.527	65.741	0.13332			0	28.218		
216.37	1.9889E-06	1.1056E-06	904.510	-1.8491	-0.050104	0.062519	0.14278	0.15110	129.10	314.66	6.1594	4.2034
220.00	3.0719E-06	1.6794E-06	595.460	-1.3282	0.50093	0.061430	0.14422	0.15253	130.14	294.38	6.3194	4.2717
240.00	2.5565E-05	1.2813E-05	78.047	1.6370	3.6323	0.057431	0.15246	0.16078	135.72	207.62	7.2936	4.6468
260.00	0.00014507	6.7137E-05	14.895	4.7709	6.9318	0.056201	0.16128	0.16962	141.02	150.42	8.4195	5.0206
280.00	0.00061336	0.00026380	3,790.7	8.0822	10.407	0.057097	0.17068	0.17906	146.04	111.63	9.6907	5.3924
300.00	0.0020600	0.00082859	1,206.9	11.576	14.062	0.059649	0.18058	0.18906	150.71	84.719	11.102	5.7614
320.00	0.0057644	0.0021820	458.30	15.253	17.894	0.063500	0.19087	0.19955	154.94	65.728	12.651	6.1263
340.00	0.013932	0.0049961	200.15	19.108	21.897	0.068366	0.20147	0.21047	158.59	52.133	14.338	6.4865
360.00	0.029907	0.010232	97.731	23.136	26.058	0.074020	0.21227	0.22178	161.53	42.292	16.164	6.8419
380.00	0.058269	0.019165	52.177	27.323	30.363	0.080278	0.22318	0.23348	163.56	35.112	18.138	7.1948
400.00	0.10483	0.033420	29.922	31.658	34.794	0.086985	0.23415	0.24557	164.51	29.858	20.268	7.5505
420.00	0.17652	0.055042	18.168	36.123	39.330	0.094013	0.24512	0.25818	164.17	26.034	22.571	7.9191
440.00	0.28132	0.086662	11.539	40.698	43.945	0.10124	0.25607	0.27154	162.27	23.316	25.072	8.3171
460.00	0.42812	0.13183	7.5854	45.358	48.605	0.10857	0.26700	0.28610	158.49	21.503	27.811	8.7715
480.00	0.62676	0.19572	5.1093	50.064	53.266	0.11587	0.27795	0.30284	152.37	20.514	30.863	9.3258
500.00	0.88820	0.28672	3.4877	54.757	57.855	0.12299	0.28899	0.32404	143.24	20.401	34.377	10.056
520.00	1.2251	0.42068	2.3771	59.333	62.245	0.12970	0.30032	0.35598	130.05	21.459	38.702	11.113
540.00	1.6533	0.63573	1.5730	63.555	66.156	0.13551	0.31238	0.42387	111.06	24.546	44.855	12.885
560.00	2.1958	1.0851	0.92161	66.584	68.608	0.13877	0.32642	0.78365	83.717	31.412	57.602	17.102
569.32	2.4978	2.0564	0.48629	64.527	65.741	0.13332			0	28.218		

Single-Phase Properties

300.00	0.10000	6.0999	0.16394	-27.460	-27.444	-0.078758	0.20684	0.25509	1139.3	-0.41966	123.88	498.56
398.30	0.10000	5.3634	0.18645	-0.16168	-0.14303	-0.00035827	0.24959	0.30230	773.32	-0.24045	97.030	202.73
398.30	0.10000	0.031955	31.294	31.284	34.413	0.086401	0.23322	0.24453	164.48	30.243	20.080	7.5200
400.00	0.10000	0.031787	31.459	31.684	34.830	0.087444	0.23402	0.24527	164.97	29.707	20.249	7.5528
500.00	0.10000	0.024611	40.633	57.485	61.548	0.14688	0.27938	0.28878	189.53	12.431	31.224	9.4433
600.00	0.10000	0.020274	49.325	87.490	92.422	0.20307	0.31885	0.32771	209.46	6.6034	43.584	11.290
300.00	1.0000	6.1073	0.16374	-27.511	-27.347	-0.078927	0.20690	0.25495	1145.7	-0.42119	124.30	503.48
400.00	1.0000	5.3654	0.18638	0.25030	0.43668	0.00067378	0.25038	0.30262	778.09	-0.24368	97.295	202.65
500.00	1.0000	4.3556	0.22959	33.432	33.661	0.074548	0.29416	0.36900	396.85	0.38286	73.948	93.722
507.20	1.0000	4.2495	0.23532	36.111	36.346	0.079880	0.29733	0.37746	363.62	0.52889	72.196	87.646
507.20	1.0000	0.32874	3.0419	56.425	59.467	0.12547	0.29302	0.33370	139.04	20.620	35.810	10.386
600.00	1.0000	0.22849	4.3766	85.870	90.247	0.18117	0.32280	0.33940	186.79	8.0078	45.491	11.637
300.00	5.0000	6.1393	0.16288	-27.730	-26.915	-0.079664	0.20714	0.25435	1173.4	-0.42743	126.15	525.55
400.00	5.0000	5.4311	0.18413	-0.17211	0.74852	-0.00039889	0.25054	0.30044	823.37	-0.27213	100.17	213.73
500.00	5.0000	4.5686	0.21888	32.275	33.369	0.072174	0.29359	0.35339	499.49	0.076618	79.631	105.97
600.00	5.0000	3.0593	0.32688	70.832	72.466	0.14322	0.33497	0.44331	188.23	2.6621	64.841	42.657
300.00	10.000	6.1772	0.16188	-27.987	-26.368	-0.080546	0.20745	0.25373	1206.2	-0.43408	128.36	553.60
400.00	10.000	5.5037	0.18170	-0.64047	1.1765	-0.0016150	0.25077	0.29842	873.81	-0.29834	103.45	227.34
500.00	10.000	4.7443	0.21078	31.275	33.383	0.070056	0.29343	0.34556	588.81	-0.072942	84.985	118.55
600.00	10.000	3.7971	0.26336	67.577	70.211	0.13708	0.33156	0.38999	358.22	0.45738	73.121	61.952
300.00	50.000	6.4220	0.15572	-29.605	-21.819	-0.086527	0.20976	0.25121	1422.7	-0.46254	143.51	798.49
400.00	50.000	5.8987	0.16953	-3.1776	5.2989	-0.0087968	0.25276	0.29206	1159.5	-0.38084	123.35	335.22
500.00	50.000	5.4043	0.18504	27.307	36.559	0.060791	0.29481	0.33234	965.74	-0.30867	110.66	198.43
600.00	50.000	4.9374	0.20254	61.436	71.563	0.12452	0.33146	0.36666	826.07	-0.24994	103.74	134.83
300.00	100.00	6.6452	0.15048	-30.984	-15.936	-0.092407	0.21232	0.25061	1629.4	-0.47349	158.61	1163.7
400.00	100.00	6.2050	0.16116	-5.0534	11.063	-0.015013	0.25503	0.29032	1399.1	-0.40628	141.31	478.53
500.00	100.00	5.8059	0.17215	24.893	42.108	0.054099	0.29686	0.32988	1233.7	-0.35233	131.06	291.34
600.00	100.00	5.4489	0.18352	58.505	76.857	0.11736	0.33331	0.36412	1113.8	-0.31375	125.82	208.31

The values in these tables were generated from the NIST REFPROP software (Lemmon, E. W., McLinden, M. O., and Huber, M. L., NIST Standard Reference Database 23: Reference Fluid Thermodynamic and Transport Properties—REFPROP, National Institute of Standards and Technology, Standard Reference Data Program, Gaithersburg, Md., 2002, Version 7.1). The primary source for the thermodynamic properties is Span, R., and Wagner, W., "Equations of State for Technical Applications. II. Results for Nonpolar Fluids," *Int. J. Thermophys.* **24**(1):41–109, 2003. The source for viscosity is Huber, M. L., Laesecke, A., and Xiang, H. W., "Viscosity Correlations for Minor Constituent Fluids in Natural Gas: *n*-Octane, *n*-Nonane and *n*-Decane," *Fluid Phase Equilibria* **224**:263–270, 2004. The source for thermal conductivity is Huber, M. L., and Perkins, R. A., "Thermal Conductivity Correlations for Minor Constituent Fluids in Natural Gas: *n*-Octane, *n*-Nonane and *n*-Decane," *Fluid Phase Equilibria* **227**:47–55, 2004.

Properties at the triple point temperature and the critical point temperature are given in the first and last entries of the saturation tables, respectively. In the single-phase table, when the temperature range for a given isobar includes a vapor-liquid phase boundary, the temperature of phase equilibrium is noted, and properties for both the saturated liquid and saturated vapor are given (with liquid properties given in the upper line). Lines are omitted from the temperature-pressure grid of the single-phase table, when the system would be in the solid phase or if there are potential problems with the source property surface.

The uncertainties of the equation of state are approximately 0.2% (to 0.5% at high pressures) in density, 1% (in the vapor phase) to 2% in heat capacity, 1% (in the vapor phase) to 2% in the speed of sound, and 0.2% in vapor pressure, except in the critical region. The estimated uncertainty in viscosity is 0.5% along the saturated-liquid line, 2% in compressed liquid to 200 MPa, 5% in vapor and supercritical regions. Uncertainty in thermal conductivity is 3%, except in the supercritical region and dilute gas which have an uncertainty of 5%.

TABLE 2-245 Thermodynamic Properties of Oxygen

Temperature K	Pressure MPa	Density mol/dm ³	Volume dm ³ /mol	Int. energy kJ/mol	Enthalpy kJ/mol	Entropy kJ/(mol·K)	C _v kJ/(mol·K)	C _p kJ/(mol·K)	Sound speed m/s	Joule-Thomson K/MPa	Therm. cond. mW/(m·K)	Viscosity μPa·s
Saturated Properties												
54.361	0.00014628	40.816	0.024500	-6.1954	-6.1954	0.066946	0.038252	0.053541	1123.4	-0.37992	201.92	773.62
55.000	0.00017857	40.734	0.024549	-6.1613	-6.1612	0.067571	0.037651	0.053489	1126.9	-0.37886	201.02	747.53
60.000	0.00072582	40.064	0.024960	-5.8938	-5.8938	0.072225	0.034835	0.053548	1127.4	-0.37011	193.94	578.07
65.000	0.0023349	39.367	0.025402	-5.6258	-5.6257	0.076516	0.033469	0.053668	1101.7	-0.36312	186.82	457.94
70.000	0.0062623	38.656	0.025869	-5.3573	-5.3572	0.080495	0.032532	0.053697	1066.3	-0.35686	179.70	371.79
75.000	0.014547	37.936	0.026360	-5.0889	-5.0885	0.084199	0.031745	0.053719	1027.5	-0.34972	172.58	308.66
80.000	0.030123	37.203	0.026879	-4.8202	-4.8194	0.087667	0.031030	0.053808	987.43	-0.34056	165.44	261.22
85.000	0.056831	36.457	0.027430	-4.5510	-4.5495	0.090931	0.030365	0.054012	946.87	-0.32856	158.27	224.62
90.000	0.099350	35.692	0.028017	-4.2806	-4.2778	0.094023	0.029745	0.054361	905.90	-0.31302	151.05	195.64
95.000	0.16308	34.905	0.028649	-4.0084	-4.0038	0.096967	0.029169	0.054880	864.40	-0.29316	143.81	172.12
100.00	0.25400	34.092	0.029333	-3.7337	-3.7263	0.099787	0.028636	0.055599	822.19	-0.26804	136.55	152.56
105.00	0.37853	33.245	0.030079	-3.4556	-3.4442	0.10250	0.028146	0.056557	779.06	-0.23637	129.25	135.93
110.00	0.54340	32.360	0.030903	-3.1732	-3.1564	0.10513	0.027703	0.057816	734.77	-0.19639	121.92	121.52
115.00	0.75559	31.426	0.031820	-2.8853	-2.8612	0.10770	0.027311	0.059469	689.03	-0.14551	114.57	108.81
120.00	1.0223	30.434	0.032858	-2.5904	-2.5568	0.11022	0.026976	0.061666	641.52	-0.079899	107.23	97.426
125.00	1.3509	29.367	0.034051	-2.2867	-2.2407	0.11271	0.026712	0.064659	591.86	0.0063780	99.912	87.086
130.00	1.7491	28.203	0.035457	-1.9711	-1.9091	0.11520	0.026536	0.068905	539.50	0.12309	92.634	77.571
135.00	2.2250	26.907	0.037165	-1.6394	-1.5567	0.11773	0.026485	0.075327	483.69	0.28750	85.404	68.687
140.00	2.7878	25.415	0.039347	-1.2839	-1.1742	0.12035	0.026634	0.086099	423.10	0.53357	78.217	60.223
145.00	3.4477	23.599	0.042375	-0.88908	-0.74298	0.12319	0.027189	0.10778	355.20	0.93865	71.056	51.869
150.00	4.2186	21.110	0.047372	-0.41330	-0.21346	0.12654	0.028982	0.17484	273.80	1.7389	64.190	42.900
154.58	5.0428	13.630	0.073368	0.66752	1.0375	0.13442			0	5.0628		
54.361	0.00014628	0.00032370	3089.2	1.1195	1.5714	0.20982	0.021241	0.029631	140.32	507.90	4.4204	4.0962
55.000	0.00017857	0.00039060	2560.2	1.1327	1.5898	0.20850	0.021297	0.029698	141.11	480.26	4.4842	4.1481
60.000	0.00072582	0.0014561	686.75	1.2355	1.7339	0.19935	0.021815	0.030320	147.03	284.62	4.9840	4.5528
65.000	0.0023349	0.0043291	230.99	1.3377	1.8770	0.19194	0.022310	0.030934	152.65	156.71	5.4863	4.9555
70.000	0.0062623	0.010804	92.556	1.4393	2.0189	0.18587	0.022565	0.031294	158.07	87.254	5.9925	5.3557
75.000	0.014547	0.023509	42.536	1.5397	2.1584	0.18083	0.022513	0.031336	163.33	52.570	6.5051	5.7533
80.000	0.030123	0.045891	21.791	1.6377	2.2941	0.17659	0.022239	0.031177	168.36	35.817	7.0277	6.1486
85.000	0.056831	0.082138	12.175	1.7320	2.4239	0.17297	0.021896	0.031019	173.06	27.728	7.5654	6.5423
90.000	0.099350	0.13710	7.2938	1.8209	2.5455	0.16984	0.021624	0.031053	177.30	23.649	8.1241	6.9355
95.000	0.16308	0.21627	4.6239	1.9031	2.6571	0.16708	0.021515	0.031420	180.99	21.338	8.7113	7.3301
100.00	0.25400	0.32579	3.0695	1.9772	2.7569	0.16462	0.021605	0.032204	184.06	19.753	9.3362	7.7281
105.00	0.37853	0.47267	2.1156	2.0421	2.8430	0.16238	0.021894	0.033461	186.44	18.446	10.010	8.1324
110.00	0.54340	0.66506	1.5036	2.0966	2.9136	0.16032	0.022361	0.035245	188.14	17.250	10.748	8.5467
115.00	0.75559	0.91283	1.0955	2.1391	2.9668	0.15838	0.022978	0.037647	189.13	16.118	11.571	8.9760
120.00	1.0223	1.2284	0.81405	2.1678	3.0000	0.15652	0.023726	0.040839	189.41	15.045	12.509	9.4273
125.00	1.3509	1.6285	0.61407	2.1801	3.0097	0.15471	0.024597	0.045146	188.96	14.029	13.607	9.9112
130.00	1.7491	2.1366	0.46803	2.1722	2.9908	0.15289	0.025604	0.051204	187.75	13.062	14.940	10.445
135.00	2.2250	2.7893	0.35852	2.1380	2.9357	0.15100	0.026794	0.060349	185.74	12.120	16.641	11.061
140.00	2.7878	3.6487	0.27407	2.0670	2.8311	0.14896	0.028269	0.075824	182.82	11.155	18.977	11.823
145.00	3.4477	4.8412	0.20656	1.9383	2.6505	0.14659	0.030276	0.10781	178.78	10.071	22.582	12.881
150.00	4.2186	6.7170	0.14888	1.6938	2.3219	0.14345	0.033574	0.21201	172.82	8.6358	29.666	14.721
154.58	5.0428	13.630	0.073368	0.66752	1.0375	0.13442			0	5.0628		

Single-Phase Properties

100.00	0.10000	0.12316	8.1192	2.0355	2.8474	0.17297	0.020885	0.029925	188.37	18.479	9.0852	7.7121
300.00	0.10000	0.040116	24.928	6.2338	8.7265	0.20531	0.021078	0.029435	329.72	2.6530	26.485	20.652
500.00	0.10000	0.024050	41.579	10.604	14.762	0.22069	0.022781	0.031108	421.27	0.75388	41.046	30.486
700.00	0.10000	0.017177	58.216	15.357	21.179	0.23147	0.024672	0.032992	493.31	0.10517	53.966	38.653
900.00	0.10000	0.013360	74.849	20.438	27.923	0.23994	0.026045	0.034363	555.60	-0.18735	65.867	45.806
100.00	1.0000	34.158	0.029276	-3.7444	-3.7151	0.099680	0.028683	0.055399	826.85	-0.27181	137.23	153.89
119.62	1.0000	30.512	0.032774	-2.6131	-2.5803	0.11003	0.027000	0.061476	645.19	-0.085501	107.79	98.249
119.62	1.0000	1.2018	0.83209	2.1662	2.9983	0.15666	0.023665	0.040564	189.41	15.124	12.433	9.3921
300.00	1.0000	0.40337	2.4791	6.1772	8.6563	0.18598	0.021148	0.029887	329.90	2.6066	26.894	20.846
500.00	1.0000	0.24010	4.1649	10.576	14.741	0.20149	0.022802	0.031240	422.68	0.73726	41.288	30.630
700.00	1.0000	0.17135	5.8360	15.340	21.176	0.21230	0.024682	0.033052	494.87	0.098376	54.139	38.766
900.00	1.0000	0.13328	7.5029	20.426	27.929	0.22078	0.026051	0.034395	557.14	-0.19062	66.001	45.899
100.00	5.0000	34.497	0.028988	-3.7983	-3.6533	0.099132	0.028935	0.054458	850.39	-0.28978	140.71	160.92
154.36	5.0000	16.011	0.062457	0.35374	0.66602	0.13204	0.038878	3.5718	163.89	4.2044	75.954	29.668
154.36	5.0000	11.160	0.089610	1.0294	1.4774	0.13729	0.041906	4.2513	158.85	6.0016	72.313	20.574
300.00	5.0000	2.0616	0.48505	5.9227	8.3480	0.17177	0.021448	0.032003	332.25	2.3730	28.797	21.766
500.00	5.0000	1.1908	0.83975	10.454	14.653	0.18787	0.022894	0.031815	429.36	0.66261	42.362	31.267
700.00	5.0000	0.84728	1.1802	15.264	21.165	0.19881	0.024726	0.033309	501.98	0.068114	54.901	39.261
900.00	5.0000	0.65931	1.5167	20.373	27.956	0.20734	0.026076	0.034537	564.07	-0.20519	66.593	46.305
100.00	10.000	34.885	0.028665	-3.8593	-3.5726	0.098498	0.029235	0.053516	877.07	-0.30803	144.82	169.49
300.00	10.000	4.2056	0.23778	5.6024	7.9802	0.16499	0.021790	0.034749	339.35	2.0332	31.466	23.153
500.00	10.000	2.3538	0.42484	10.306	14.554	0.18182	0.022999	0.032491	438.67	0.56900	43.708	32.074
700.00	10.000	1.6705	0.59861	15.171	21.157	0.19292	0.024776	0.033613	511.24	0.030534	55.839	39.873
900.00	10.000	1.3010	0.76866	20.307	27.993	0.20150	0.026104	0.034706	572.92	-0.22339	67.321	46.804
100.00	25.000	35.884	0.027867	-4.0109	-3.3142	0.096845	0.030037	0.051627	945.24	-0.34532	155.97	194.38
300.00	25.000	10.393	0.096215	4.7194	7.1247	0.15490	0.022521	0.040917	390.80	1.0167	41.851	29.605
500.00	25.000	5.6243	0.17780	9.8920	14.337	0.17346	0.023256	0.034167	472.62	0.30658	47.943	34.705
700.00	25.000	3.9923	0.25048	14.907	21.169	0.18495	0.024901	0.034397	541.32	-0.076019	58.651	41.714
900.00	25.000	3.1222	0.32028	20.117	28.124	0.19369	0.026174	0.035155	600.66	-0.27597	69.464	48.271
100.00	75.000	38.263	0.026135	-4.3340	-2.3739	0.092788	0.031906	0.049123	1115.1	-0.39472	184.96	274.96
300.00	75.000	21.603	0.046289	3.1884	6.6601	0.14315	0.023601	0.041272	645.54	-0.18640	75.261	53.378
500.00	75.000	13.760	0.072675	8.8798	14.330	0.16284	0.023725	0.036534	619.75	-0.20732	64.149	45.084
700.00	75.000	10.201	0.098029	14.192	21.544	0.17498	0.025126	0.035903	657.04	-0.31840	68.835	48.269
900.00	75.000	8.1749	0.12233	19.571	28.745	0.18403	0.026293	0.036153	701.72	-0.40609	76.863	53.163

The values in these tables were generated from the NIST REFPROP software (Lemmon, E. W., McLinden, M. O., and Huber, M. L., NIST Standard Reference Database 23: Reference Fluid Thermodynamic and Transport Properties—REFPROP, National Institute of Standards and Technology, Standard Reference Data Program, Gaithersburg, Md., 2002, Version 7.1). The primary source for the thermodynamic properties is Schmidt, R., and Wagner, W., "A New Form of the Equation of State for Pure Substances and Its Application to Oxygen," *Fluid Phase Equilibria*, **19**:175–200, 1985. The source for viscosity and thermal conductivity is Lemmon, E. W., and Jacobsen, R. T., "Viscosity and Thermal Conductivity Equations for Nitrogen, Oxygen, Argon, and Air," *Int. J. Thermophys.* **25**:21–69, 2004.

Properties at the triple point temperature and the critical point temperature are given in the first and last entries of the saturation tables, respectively. In the single-phase table, when the temperature range for a given isobar includes a vapor-liquid phase boundary, the temperature of phase equilibrium is noted, and properties for both the saturated liquid and saturated vapor are given (with liquid properties given in the upper line). Lines are omitted from the temperature-pressure grid of the single-phase table, when the system would be in the solid phase or if there are potential problems with the source property surface.

The uncertainties of the equation of state are 0.1% in density, 2% in heat capacity, and 1% in the speed of sound, except in the critical region. For viscosity, the uncertainty is 1% in the dilute gas at temperatures above 200 K, and 5% in the dilute gas at lower temperatures. The uncertainty is around 2% between 270 and 300 K, and increases to 5% outside of this region. The uncertainty may be higher in the liquid near the triple point. The uncertainty for the dilute gas is 2% with increasing uncertainties near the triple point. For thermal conductivity, the uncertainties range from 3% between 270 and 300 K to 5% elsewhere. The uncertainties above 100 MPa are not known due to a lack of experimental data.

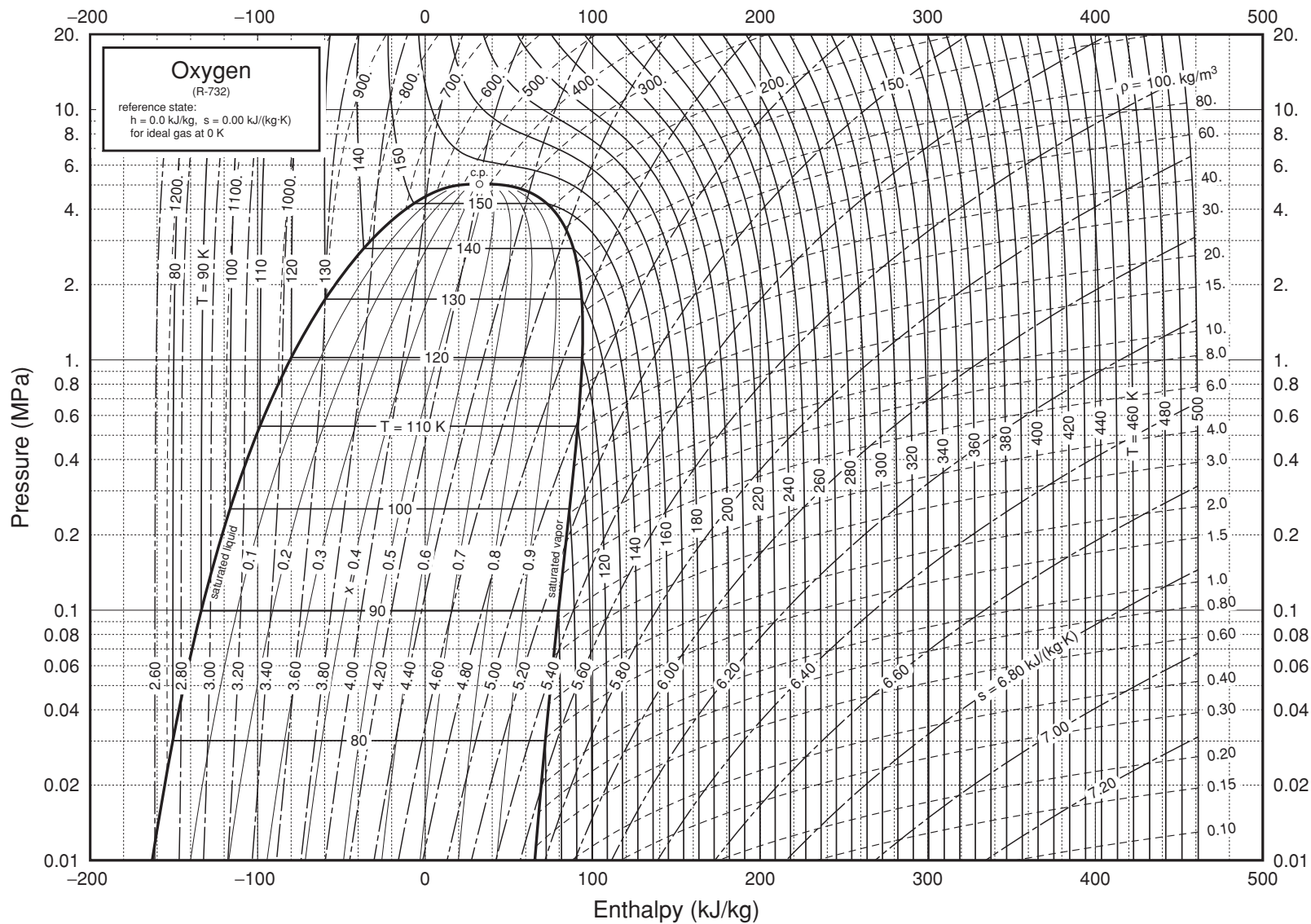


FIG. 2-15 Pressure-enthalpy diagram for oxygen. Properties computed with the NIST REFPROP Database, Version 7.0 (Lemmon, E. W., McLinden, M. O. and Huber, M. L., 2002, NIST Standard Reference Database 23, NIST Reference Fluid Thermodynamic and Transport Properties—REFPROP, Version 7.0, Standard Reference Data Program, National Institute of Standards and Technology), based on the equation of state of Schmidt, R., and Wagner, W., "A New Form of the Equation of State for Pure Substances and Its Application to Oxygen," *Fluid Phase Equilibria* **19**:175–200, 1985.

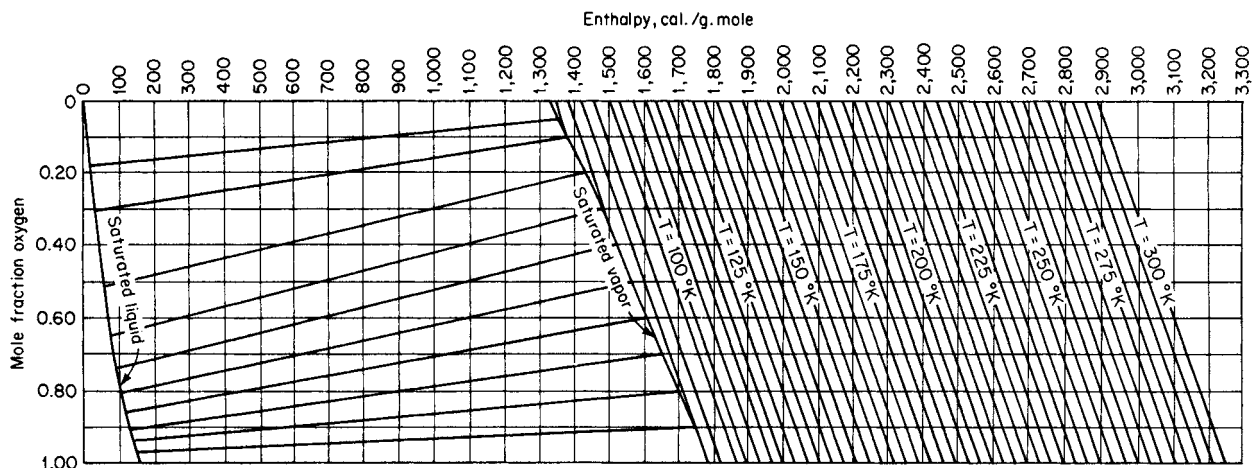


FIG. 2-16 Enthalpy-concentration diagram for oxygen-nitrogen mixture at 1 atm. Reference states: Enthalpies of liquid oxygen and liquid nitrogen at the normal boiling point of nitrogen are zero. (*Dodge*, *Chemical Engineering Thermodynamics*, *McGraw-Hill*, *New York*, *1944*.) *Wilson*, *Silverberg*, and *Zellner*, AFAPL TDR 64-64 (AD 603151), 1964, p. 314, present extensive vapor-liquid equilibrium data for the three-component system argon-nitrogen-oxygen as well as for binary systems including oxygen-nitrogen. Calculations for this mixture are also available with the NIST REFPROP software.

TABLE 2-246 Thermodynamic Properties of Pentane

Temperature K	Pressure MPa	Density mol/dm ³	Volume dm ³ /mol	Int. energy kJ/mol	Enthalpy kJ/mol	Entropy kJ/(mol·K)	C _v kJ/(mol·K)	C _p kJ/(mol·K)	Sound speed m/s	Joule-Thomson K/MPa	Therm. cond. mW/(m·K)	Viscosity μPa·s
Saturated Properties												
143.47	7.6322E-08	10.566	0.094640	-25.092	-25.092	-0.11487	0.10392	0.14205	1829.9	-0.54905	175.03	3709.1
150.00	2.6809E-07	10.482	0.095399	-24.164	-24.164	-0.10855	0.10408	0.14201	1788.3	-0.54859	172.92	2750.8
165.00	3.1471E-06	10.292	0.097163	-22.032	-22.032	-0.095008	0.10469	0.14231	1696.9	-0.54514	167.37	1587.7
180.00	2.3256E-05	10.105	0.098964	-19.892	-19.892	-0.082594	0.10558	0.14312	1610.3	-0.53850	161.20	1048.4
195.00	0.00012116	9.9190	0.10082	-17.737	-17.737	-0.071091	0.10680	0.14441	1527.4	-0.52866	154.70	757.19
210.00	0.00048191	9.7339	0.10273	-15.558	-15.557	-0.060326	0.10837	0.14621	1447.4	-0.51549	148.08	581.46
225.00	0.0015504	9.5483	0.10473	-13.348	-13.347	-0.050163	0.11032	0.14853	1369.7	-0.49891	141.47	466.22
240.00	0.0042112	9.3613	0.10682	-11.099	-11.099	-0.040489	0.11267	0.15137	1293.8	-0.47884	134.95	385.57
255.00	0.0099767	9.1719	0.10903	-8.8042	-8.8031	-0.031215	0.11539	0.15473	1219.4	-0.45516	128.57	326.15
270.00	0.021139	8.9791	0.11137	-6.4555	-6.4532	-0.022266	0.11847	0.15857	1146.3	-0.42770	122.40	280.49
285.00	0.040858	8.7818	0.11387	-4.0461	-4.0414	-0.013582	0.12186	0.16289	1074.0	-0.39609	116.43	244.17
300.00	0.073168	8.5788	0.11657	-1.5694	-1.5608	-0.0051134	0.12552	0.16766	1002.5	-0.35971	110.69	214.42
315.00	0.12293	8.3688	0.11949	0.98088	0.99557	0.0031816	0.12940	0.17288	931.46	-0.31748	105.17	189.45
330.00	0.19575	8.1499	0.12270	3.6106	3.6346	0.011338	0.13348	0.17857	860.59	-0.26769	99.882	168.04
345.00	0.29786	7.9200	0.12626	6.3259	6.3635	0.019386	0.13770	0.18478	789.61	-0.20766	94.813	149.32
360.00	0.43606	7.6765	0.13027	9.1332	9.1900	0.027354	0.14204	0.19161	718.18	-0.13303	89.958	132.67
375.00	0.61766	7.4155	0.13485	12.040	12.123	0.035271	0.14649	0.19928	645.89	-0.036610	85.304	117.61
390.00	0.85052	7.1319	0.14022	15.057	15.176	0.043168	0.15103	0.20814	572.27	0.094152	80.839	103.78
405.00	1.1432	6.8175	0.14668	18.197	18.364	0.051083	0.15570	0.21894	496.72	0.28299	76.544	90.837
420.00	1.5050	6.4595	0.15481	21.482	21.715	0.059073	0.16056	0.23325	418.39	0.58010	72.402	78.483
435.00	1.9472	6.0340	0.16573	24.952	25.275	0.067234	0.16578	0.25255	335.90	1.1123	68.402	66.354
450.00	2.4836	5.4866	0.18226	28.698	29.150	0.075780	0.17187	0.30145	246.17	2.3196	64.610	53.842
465.00	3.1355	4.5754	0.21856	33.125	33.811	0.085678	0.18139	0.60959	138.75	7.5108	63.369	38.530
469.70	3.3710	3.2156	0.31099	36.504	37.552	0.093548			0	19.135		
143.47	7.6322E-08	6.3981E-08	15.630,000.	8.3431	9.5360	0.12648	0.070619	0.078934	135.94	542.15	4.0211	3.2806
150.00	2.6809E-07	2.1496E-07	4,652,000.	8.8107	10.058	0.11959	0.072591	0.080906	138.80	453.68	4.3338	3.4236
165.00	3.1471E-06	2.2940E-06	435,920.	9.9311	11.303	0.10702	0.076717	0.085033	145.17	311.80	5.0759	3.7558
180.00	2.3256E-05	1.5540E-05	64,349.	11.110	12.607	0.097955	0.080473	0.088791	151.28	222.93	5.8544	4.0934
195.00	0.00012116	7.4749E-05	13,378.	12.343	13.964	0.091475	0.084066	0.092395	157.11	164.55	6.6764	4.4362
210.00	0.00048191	0.00027623	3,620.1	13.627	15.372	0.086957	0.087665	0.096021	162.67	124.69	7.5505	4.7837
225.00	0.0015504	0.00083048	1,204.1	14.962	16.829	0.083956	0.091392	0.099805	167.92	96.614	8.4862	5.1356
240.00	0.0042112	0.0021198	471.75	16.347	18.333	0.082144	0.095331	0.10385	172.81	76.365	9.4926	5.4918
255.00	0.0099767	0.0047454	210.73	17.780	19.882	0.081276	0.099526	0.10823	177.25	61.487	10.578	5.8525
270.00	0.021139	0.0095553	104.65	19.260	21.472	0.081162	0.10400	0.11297	181.16	50.401	11.752	6.2179
285.00	0.040858	0.017654	56.645	20.787	23.101	0.081654	0.10874	0.11811	184.42	42.052	13.022	6.5890
300.00	0.073168	0.030405	32.889	22.357	24.763	0.082633	0.11373	0.12367	186.93	35.715	14.394	6.9672
315.00	0.12293	0.049446	20.224	23.968	26.454	0.084003	0.11894	0.12966	188.56	30.879	15.879	7.3547
330.00	0.19575	0.076727	13.033	25.617	28.168	0.085681	0.12435	0.13613	189.17	27.184	17.484	7.7547
345.00	0.29786	0.11460	8.7259	27.297	29.896	0.087596	0.12993	0.14317	188.63	24.375	19.221	8.1719
360.00	0.43606	0.16601	6.0239	29.002	31.629	0.089654	0.13567	0.15092	186.76	22.275	21.106	8.6130
375.00	0.61766	0.23477	4.2594	30.721	33.352	0.091880	0.14155	0.15968	183.35	20.767	23.164	9.0883
390.00	0.85052	0.32623	3.0654	32.439	35.046	0.094117	0.14759	0.17000	178.13	19.785	25.433	9.6135
405.00	1.1432	0.44834	2.2305	34.133	36.682	0.096313	0.15383	0.18300	170.76	19.316	27.980	10.215
420.00	1.5050	0.61427	1.6279	35.764	38.214	0.098358	0.16037	0.20125	160.78	19.406	30.941	10.939
435.00	1.9472	0.84898	1.1779	37.264	39.557	0.10007	0.16742	0.23193	147.55	20.186	34.634	11.885
450.00	2.4836	1.2118	0.82522	38.471	40.520	0.10105	0.17552	0.30440	130.14	21.884	40.108	13.312
465.00	3.1355	1.9618	0.50974	38.730	40.328	0.099694	0.18671	0.82173	106.55	24.088	55.658	16.549
469.70	3.3710	3.2156	0.31099	36.504	37.552	0.093548			0	19.135		

Single-Phase Properties

200.00	0.10000	9.8581	0.10144	-17.016	-17.006	-0.067441	0.10728	0.14495	1501.0	-0.52472	152.53	690.14
300.00	0.10000	8.5793	0.11656	-1.5709	-1.5592	-0.0051184	0.12552	0.16765	1002.8	-0.35984	110.71	214.50
308.83	0.10000	8.4562	0.11826	-0.077672	-0.065846	-0.00021257	0.12778	0.17068	960.65	-0.33565	107.41	199.24
308.83	0.10000	0.040733	24.550	23.300	25.755	0.083398	0.11677	0.12714	188.00	32.712	15.254	7.1940
400.00	0.10000	0.030611	32.668	35.260	38.527	0.11949	0.14472	0.15376	217.34	12.986	24.749	9.3018
500.00	0.10000	0.024257	41.224	51.273	55.396	0.15700	0.17449	0.18314	243.86	6.4310	37.084	11.487
600.00	0.10000	0.020135	49.665	70.070	75.037	0.19274	0.20055	0.20906	267.28	3.8205	50.416	13.525
200.00	1.0000	9.8656	0.10136	-17.038	-16.937	-0.067555	0.10733	0.14489	1505.8	-0.52539	152.82	696.76
300.00	1.0000	8.5958	0.11634	-1.6210	-1.5046	-0.0052858	0.12555	0.16737	1011.2	-0.36413	111.23	217.09
398.07	1.0000	6.9671	0.14353	16.730	16.874	0.047422	0.15353	0.21364	531.90	0.18628	78.507	96.722
398.07	1.0000	0.38746	2.5809	33.355	35.936	0.095310	0.15092	0.17655	174.46	19.468	26.763	9.9253
400.00	1.0000	0.38317	2.6098	33.666	36.276	0.096162	0.15126	0.17612	175.97	18.915	26.951	9.9649
500.00	1.0000	0.26375	3.7914	50.465	54.257	0.13622	0.17624	0.18896	226.09	7.2197	38.498	12.017
600.00	1.0000	0.20980	4.7663	69.531	74.297	0.17270	0.20129	0.21181	257.70	3.9909	51.523	13.960
200.00	5.0000	9.8980	0.10103	-17.137	-16.632	-0.068053	0.10753	0.14467	1527.0	-0.52817	154.08	726.41
300.00	5.0000	8.6652	0.11540	-1.8329	-1.2559	-0.0060014	0.12571	0.16627	1047.2	-0.38106	113.46	228.42
400.00	5.0000	7.1612	0.13964	16.501	17.199	0.046820	0.15388	0.20601	606.55	0.017312	82.387	107.19
500.00	5.0000	3.2553	0.30719	42.207	43.743	0.10528	0.19073	0.42935	135.39	9.4810	59.214	26.017
600.00	5.0000	1.2834	0.77916	66.610	70.506	0.15448	0.20500	0.23291	220.81	4.4347	57.890	17.494
200.00	10.000	9.9373	0.10063	-17.255	-16.249	-0.068660	0.10778	0.14442	1552.6	-0.53127	155.61	763.99
300.00	10.000	8.7452	0.11435	-2.0763	-0.93280	-0.0068390	0.12592	0.16515	1088.8	-0.39826	116.08	242.27
400.00	10.000	7.3792	0.13552	15.896	17.251	0.045232	0.15383	0.20020	687.58	-0.10747	86.892	120.04
500.00	10.000	5.4581	0.18321	37.622	39.455	0.094589	0.18299	0.24567	349.25	0.88491	69.546	57.792
600.00	10.000	3.0774	0.32495	62.405	65.655	0.14230	0.20754	0.26294	229.05	2.8865	67.434	28.573
200.00	50.000	10.209	0.097953	-18.043	-13.146	-0.072988	0.10968	0.14331	1731.1	-0.54573	166.40	1086.9
300.00	50.000	9.2247	0.10840	-3.5039	1.9164	-0.012155	0.12755	0.16079	1343.9	-0.46478	132.95	346.81
400.00	50.000	8.2838	0.12072	13.310	19.346	0.037795	0.15501	0.18829	1056.0	-0.35370	109.81	195.02
500.00	50.000	7.3733	0.13562	32.748	39.529	0.082724	0.18248	0.21473	853.23	-0.25198	97.812	130.14
600.00	50.000	6.5265	0.15322	54.478	62.139	0.12389	0.20695	0.23672	723.60	-0.17131	94.951	95.489
200.00	100.00	10.479	0.095431	-18.760	-9.2168	-0.077502	0.11180	0.14305	1911.9	-0.55097	177.42	1550.8
300.00	100.00	9.6305	0.10384	-4.6330	5.7508	-0.017033	0.12937	0.15917	1570.5	-0.49017	148.83	473.34
400.00	100.00	8.8688	0.11275	11.680	22.955	0.032278	0.15665	0.18547	1325.1	-0.40837	128.55	270.23
500.00	100.00	8.1734	0.12235	30.587	42.822	0.076502	0.18394	0.21138	1153.2	-0.34418	117.64	187.06
600.00	100.00	7.5451	0.13254	51.860	65.113	0.11708	0.20826	0.23383	1035.8	-0.29936	114.07	142.50

The values in these tables were generated from the NIST REFPROP software (Lemmon, E. W., McLinden, M. O., and Huber, M. L., NIST Standard Reference Database 23: Reference Fluid Thermodynamic and Transport Properties—REFPROP, National Institute of Standards and Technology, Standard Reference Data Program, Gaithersburg, Md., 2002, Version 7.1). The primary source for the thermodynamic properties is Span, R., and Wagner, W., "Equations of State for Technical Applications. II. Results for Nonpolar Fluids," *Int. J. Thermophys.* **24**(1):41–109, 2003. The source for viscosity and thermal conductivity is NIST14, Version 9.08.

Properties at the triple point temperature and the critical point temperature are given in the first and last entries of the saturation tables, respectively. In the single-phase table, when the temperature range for a given isobar includes a vapor-liquid phase boundary, the temperature of phase equilibrium is noted, and properties for both the saturated liquid and saturated vapor are given (with liquid properties given in the upper line). Lines are omitted from the temperature-pressure grid of the single-phase table, when the system would be in the solid phase or if there are potential problems with the source property surface.

The uncertainties of the equation of state are approximately 0.2% (to 0.5% at high pressures) in density, 1% (in the vapor phase) to 2% in heat capacity, 1% (in the vapor phase) to 2% in the speed of sound, and 0.2% in vapor pressure, except in the critical region. For viscosity, estimated uncertainty is 2%. For thermal conductivity, estimated uncertainty, except near the critical region, is 4–6%.

TABLE 2-247 Saturated Potassium*

T, K	P, bar	v_f , m ³ /kg	v_g , m ³ /kg	h_f , kJ/kg	h_g , kJ/kg	s_f , kJ/(kg·K)	s_g , kJ/(kg·K)	c_{pf} , kJ/(kg·K)
336.4 ^m	1.37-9	0.001208		93.8	2327	1.928	8.567	0.822
400	1.84-7	0.001229	4.64+6	145.5	2342	2.068	7.559	0.805
500	3.13-5	0.001266	3.39+4	225.1	2390	2.246	6.576	0.785
600	9.26-4	0.001304	3164	302.7	2433	2.388	5.937	0.771
700	0.01022	0.001346	142.3	379.4	2468	2.506	5.490	0.762
800	0.06116	0.001389	26.75	455.5	2498	2.608	5.161	0.761
1000	0.7322	0.001488	2.691	609.7	2552	2.780	4.722	0.792
1200	3.913	0.001605	0.584	773.5	2610	2.929	4.459	0.846
1400	12.44	0.001742	0.207	948.0	2679	3.063	4.299	0.899
1500	20.0	0.001816	0.132	1040.0	2718	3.123	4.209	0.924

*Converted from tables in Vargaftik, *Tables of the Thermophysical Properties of Liquids and Gases*, Nauka, Moscow, 1972; and Hemisphere, Washington, 1975. m = melting point. The notation 1.37-9 signifies 1.37×10^{-9} .

Many of the Vargaftik values also appear in Ohse, R. W., *Handbook of Thermodynamic and Transport Properties of Alkali Metals*, Blackwell Sci. Pubs., Oxford, 1985 (1020 pp.). This source contains superheat data. Saturation and superheat tables and a diagram to 30 bar, 1650 K are given by Reynolds, W. C., *Thermodynamic Properties in S.I.*, Stanford Univ. publ., 1979 (173 pp.). For a Mollier diagram from 0.1 to 250 psia, 1300 to 2700°R, see Weatherford, W. D., J. C. Tyler, et al., WADD-TR-61-96, 1961. An extensive review of properties of the solid and the saturated liquid is given by Alcock, C. B., M. W. Chase, et al., *J. Phys. Chem. Ref. Data*, 23, 3 (1994):385-497.

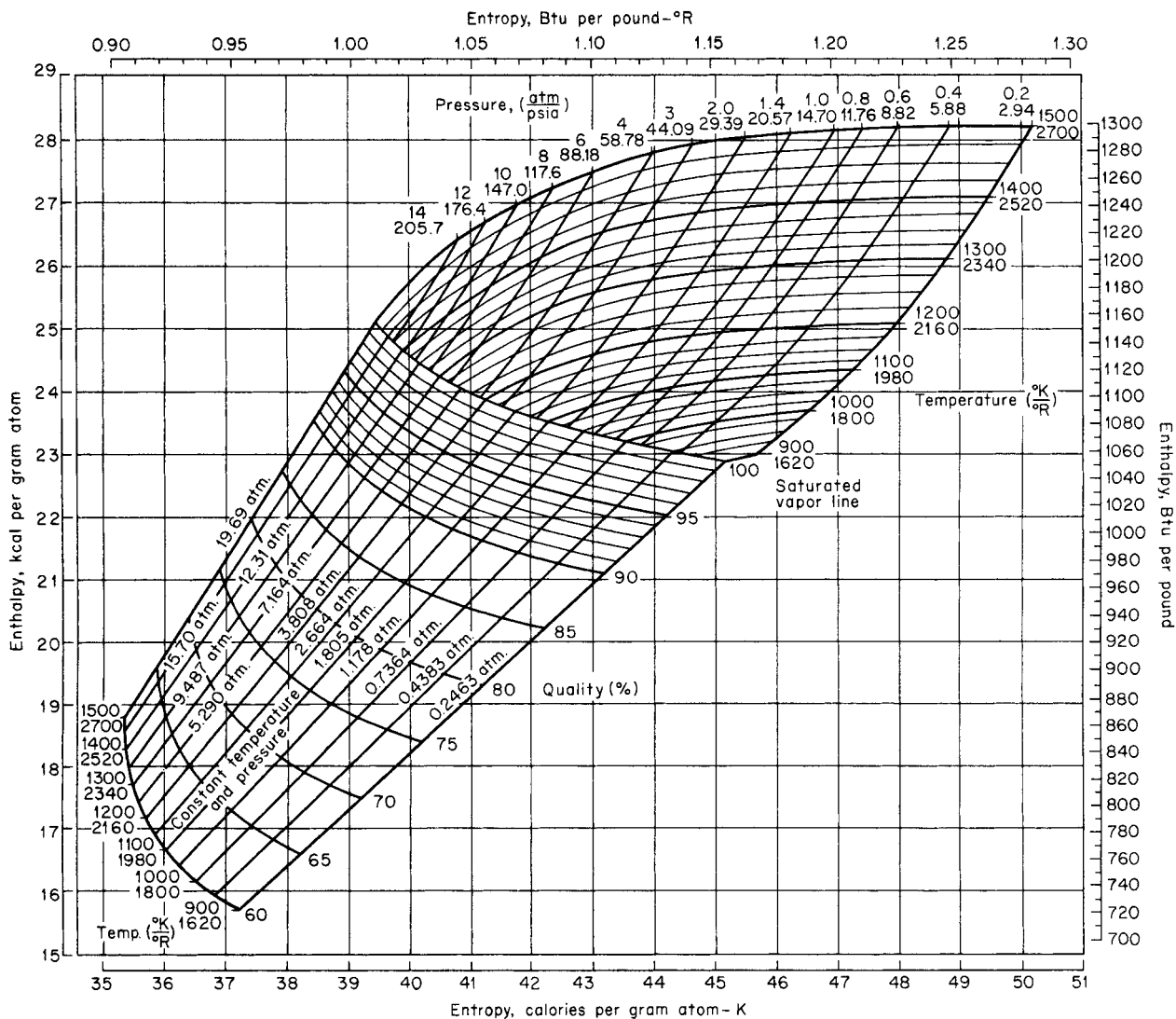


FIG. 2-17 Mollier diagram for potassium. Basis: enthalpy = 0.0 cal/g atom at 298 K; entropy = 15.8 cal/(g atom·K) at 298 K. (Aerojet-General Rep. AGN8194, vol. 2, 1967. Reproduced by permission.)

TABLE 2-248 Thermodynamic Properties of Propane

Temperature K	Pressure MPa	Density mol/dm ³	Volume dm ³ /mol	Int. energy kJ/mol	Enthalpy kJ/mol	Entropy kJ/(mol·K)	C _v kJ/(mol·K)	C _p kJ/(mol·K)	Sound speed m/s	Joule-Thomson K/MPa	Therm. cond. mW/(m·K)	Viscosity μPa·s
Saturated Properties												
100.00	2.5330E-08	16.287	0.061397	-7.4323	-7.4323	-0.048110	0.058376	0.083833	2030.4	-0.62852	203.23	3780.3
115.00	1.0677E-06	15.941	0.062730	-6.1638	-6.1638	-0.036293	0.058304	0.085262	1930.7	-0.61354	196.90	1822.7
130.00	1.7600E-05	15.596	0.064117	-4.8753	-4.8753	-0.025763	0.058442	0.086525	1827.2	-0.59904	189.40	1080.5
145.00	0.00015328	15.251	0.065568	-3.5682	-3.5682	-0.016249	0.058710	0.087764	1724.5	-0.58338	181.11	729.42
160.00	0.00084980	14.904	0.067094	-2.2418	-2.2418	-0.0075455	0.059141	0.089109	1623.4	-0.56521	172.30	534.62
175.00	0.0033874	14.554	0.068710	-0.89395	-0.89372	0.00050603	0.059774	0.090658	1523.6	-0.54342	163.19	412.89
190.00	0.010547	14.198	0.070434	0.47907	0.47981	0.0080327	0.060636	0.092484	1424.7	-0.51702	153.97	329.94
205.00	0.027195	13.834	0.072288	1.8816	1.8836	0.015137	0.061740	0.094646	1326.6	-0.48497	144.76	269.81
220.00	0.060583	13.459	0.074301	3.3189	3.3234	0.021903	0.063087	0.097193	1229.1	-0.44601	135.72	224.28
235.00	0.12030	13.070	0.076511	4.7964	4.8056	0.028399	0.064672	0.10018	1131.9	-0.39841	126.91	188.66
250.00	0.21798	12.663	0.078968	6.3203	6.3375	0.034686	0.066484	0.10368	1034.8	-0.33958	118.40	160.10
265.00	0.36693	12.234	0.081740	7.8975	7.9275	0.040815	0.068514	0.10780	937.63	-0.26538	110.26	136.69
280.00	0.58173	11.775	0.084925	9.5360	9.5854	0.046833	0.070755	0.11272	839.90	-0.16892	102.52	117.11
295.00	0.87805	11.277	0.088673	11.246	11.324	0.052790	0.073209	0.11880	741.08	-0.037850	95.209	100.38
310.00	1.2726	10.726	0.093229	13.041	13.159	0.058740	0.075898	0.12672	640.30	0.15178	88.324	85.735
325.00	1.7837	10.097	0.099036	14.943	15.120	0.064759	0.078882	0.13817	536.11	0.45297	81.819	72.510
340.00	2.4320	9.3403	0.10706	16.996	17.257	0.070985	0.082328	0.15818	425.33	1.0100	75.581	60.014
355.00	3.2432	8.3162	0.12025	19.317	19.707	0.077769	0.087215	0.21184	300.04	2.3857	69.491	47.137
369.83	4.2477	5.0000	0.20000	23.653	24.503	0.090537			0	12.890		
100.00	2.5330E-08	3.0465E-08	32,825,000.	15.887	16.718	0.19339	0.032981	0.041296	153.65	420.53	2.4171	2.9792
115.00	1.0677E-06	1.1166E-06	895,550.	16.399	17.356	0.16822	0.035381	0.043696	163.64	267.23	3.2182	3.3431
130.00	1.7600E-05	1.6284E-05	61,410.	16.947	18.028	0.15042	0.037630	0.045946	172.99	181.79	4.0849	3.7167
145.00	0.00015328	0.00012717	7,863.4	17.527	18.732	0.13755	0.039780	0.048104	181.78	130.32	5.0168	4.0976
160.00	0.00084980	0.00063940	1,564.0	18.137	19.466	0.12813	0.041911	0.050262	190.03	97.395	6.0131	4.4832
175.00	0.0033874	0.0023346	428.34	18.775	20.226	0.12119	0.044098	0.052519	197.68	75.331	7.0721	4.8708
190.00	0.010547	0.0067219	148.77	19.437	21.007	0.11607	0.046406	0.054975	204.61	59.995	8.1917	5.2578
205.00	0.027195	0.016180	61.804	20.120	21.801	0.11230	0.048888	0.057727	210.64	49.008	9.3706	5.6429
220.00	0.060583	0.033974	29.435	20.819	22.602	0.10953	0.051579	0.060867	215.59	40.931	10.611	6.0262
235.00	0.12030	0.064224	15.570	21.528	23.401	0.10753	0.054504	0.064488	219.25	34.865	11.922	6.4107
250.00	0.21798	0.11195	8.9325	22.242	24.189	0.10609	0.057677	0.068703	221.39	30.235	13.323	6.8027
265.00	0.36693	0.18328	5.4561	22.954	24.956	0.10507	0.061104	0.073667	221.82	26.669	14.845	7.2123
280.00	0.58173	0.28598	3.4968	23.656	25.690	0.10435	0.064794	0.079635	220.30	23.923	16.544	7.6551
295.00	0.87805	0.43050	2.3229	24.336	26.376	0.10381	0.068763	0.087064	216.53	21.832	18.503	8.1548
310.00	1.2726	0.63231	1.5815	24.977	26.989	0.10335	0.072895	0.096756	210.16	20.354	20.863	8.7494
325.00	1.7837	0.91726	1.0902	25.543	27.488	0.10282	0.077315	0.11131	200.74	19.511	23.881	9.5073
340.00	2.4320	1.3363	0.74835	25.971	27.791	0.10197	0.083072	0.13963	187.44	19.120	28.187	10.574
355.00	3.2432	2.0253	0.49375	26.098	27.699	0.10028	0.091334	0.22264	168.95	18.854	36.060	12.373
369.83	4.2477	5.0000	0.20000	23.653	24.503	0.090537			0	12.890		
Single-Phase Properties												
100.00	0.10000	16.288	0.061394	-7.4332	-7.4270	-0.048119	0.058377	0.083831	2030.8	-0.62854	203.26	3784.5
200.00	0.10000	13.958	0.071646	1.4085	1.4157	0.012800	0.061348	0.093874	1359.8	-0.49655	147.87	288.12
230.74	0.10000	13.182	0.075860	4.3719	4.3795	0.026576	0.064197	0.099283	1159.5	-0.41295	129.38	197.97
230.74	0.10000	0.054083	18.490	21.326	23.175	0.10803	0.053648	0.063403	218.35	36.423	11.542	6.3010
300.00	0.10000	0.040726	24.554	25.482	27.937	0.12602	0.065918	0.074796	249.37	16.357	18.513	8.1962
400.00	0.10000	0.030257	33.050	33.084	36.389	0.15020	0.085775	0.094327	286.19	7.1977	30.995	10.819
500.00	0.10000	0.024125	41.452	42.616	46.761	0.17327	0.10431	0.11276	318.30	3.9113	46.363	13.290
100.00	1.0000	16.295	0.061368	-7.4410	-7.3796	-0.048197	0.058391	0.083810	2034.6	-0.62871	203.49	3822.7
200.00	1.0000	13.974	0.071560	1.3862	1.4577	0.012688	0.061383	0.093756	1366.3	-0.49871	148.40	290.36
300.00	1.0000	11.101	0.090085	11.833	11.924	0.054770	0.074077	0.12118	707.81	0.017030	92.871	95.307
300.09	1.0000	11.097	0.090112	11.844	11.934	0.054806	0.074092	0.12123	707.18	0.018141	92.828	95.215

TABLE 2-248 Thermodynamic Properties of Propane (Continued)

Temperature K	Pressure MPa	Density mol/dm ³	Volume dm ³ /mol	Int. energy kJ/mol	Enthalpy kJ/mol	Entropy kJ/(mol·K)	C _v kJ/(mol·K)	C _p kJ/(mol·K)	Sound speed m/s	Joule-Thomson K/MPa	Therm. cond. mW/(m·K)	Viscosity μPa·s
Single-Phase Properties												
300.09	1.0000	0.49153	2.0344	24.559	26.593	0.10366	0.070157	0.090035	214.68	21.259	19.249	8.3433
400.00	1.0000	0.32145	3.1109	32.638	35.749	0.12993	0.086666	0.097825	272.57	7.6356	31.915	10.996
500.00	1.0000	0.24776	4.0362	42.322	46.359	0.15353	0.10468	0.11438	311.60	3.9684	47.555	13.477
100.00	5.0000	16.326	0.061251	-7.4751	-7.1688	-0.048542	0.058457	0.083721	2051.3	-0.62944	204.51	3995.6
200.00	5.0000	14.047	0.071191	1.2900	1.6459	0.012202	0.061542	0.093272	1394.2	-0.50758	150.70	300.33
300.00	5.0000	11.363	0.088002	11.506	11.946	0.053658	0.074005	0.11643	779.30	-0.10225	97.139	103.08
400.00	5.0000	2.5448	0.39296	29.499	31.463	0.10822	0.093912	0.16341	197.49	10.349	42.438	14.948
500.00	5.0000	1.4059	0.71129	40.868	44.425	0.13725	0.10638	0.12446	284.88	4.1092	52.411	15.207
100.00	10.000	16.365	0.061108	-7.5164	-6.9053	-0.048966	0.058554	0.083620	2071.2	-0.63025	205.77	4219.8
200.00	10.000	14.133	0.070758	1.1767	1.8843	0.011619	0.061744	0.092746	1427.0	-0.51720	153.49	312.82
300.00	10.000	11.627	0.086007	11.173	12.033	0.052499	0.074065	0.11280	851.72	-0.19531	101.80	111.73
400.00	10.000	7.5861	0.13182	24.108	25.426	0.090675	0.093138	0.16714	338.94	1.7653	68.250	41.091
500.00	10.000	3.2486	0.30783	38.754	41.832	0.12746	0.10818	0.14277	275.78	3.4683	58.851	19.828
100.00	50.000	16.644	0.060081	-7.8016	-4.7976	-0.052119	0.059685	0.083087	2203.4	-0.63391	214.99	6389.5
200.00	50.000	14.696	0.068047	0.46479	3.8672	0.0076714	0.063347	0.090345	1638.0	-0.56103	173.15	416.61
300.00	50.000	12.850	0.077822	9.6226	13.514	0.046601	0.075522	0.10376	1203.5	-0.42987	129.30	167.38
400.00	50.000	11.043	0.090552	20.208	24.735	0.078767	0.092492	0.12069	901.34	-0.26933	103.15	95.902
500.00	50.000	9.3527	0.10692	32.246	37.592	0.10739	0.10930	0.13596	721.97	-0.11844	94.269	63.347
100.00	100.00	16.946	0.059010	-8.0684	-2.1674	-0.055583	0.061388	0.082816	2328.3	-0.63418	225.01	10396.
200.00	100.00	15.221	0.065700	-0.13496	6.4350	0.0038087	0.065107	0.089250	1833.0	-0.58053	193.78	561.59
300.00	100.00	13.700	0.072994	8.6070	15.906	0.042047	0.077244	0.10131	1467.7	-0.49303	155.37	229.66
400.00	100.00	12.331	0.081095	18.712	26.822	0.073340	0.094108	0.11714	1214.6	-0.40159	129.74	138.80
500.00	100.00	11.114	0.089974	30.308	39.306	0.10113	0.11078	0.13224	1052.7	-0.33205	118.57	98.032

The values in these tables were generated from the NIST REFPROP software (Lemmon, E. W., McLinden, M. O., and Huber, M. L., NIST Standard Reference Database 23: Reference Fluid Thermodynamic and Transport Properties—REFPROP, National Institute of Standards and Technology, Standard Reference Data Program, Gaithersburg, Md., 2002, Version 7.1). The primary source for the thermodynamic properties is Buecker, D., and Wagner, W., "Reference Equations of State for the Thermodynamic Properties of Fluid Phase *n*-Butane and Isobutane," *J. Phys. Chem. Ref. Data* **35**(2):929–1019, 2006. The source for viscosity is Vogel, E., Kuechenmeister, C., Bich, E., and Laesecke, A., "Reference Correlation of the Viscosity of Propane," *J. Phys. Chem. Ref. Data* **27**(5):947–970, 1998. The source for thermal conductivity is Marsh, K., Perkins, R., and Ramires, M. L. V., "Measurement and Correlation of the Thermal Conductivity of Propane from 86 to 600 K at Pressures to 70 MPa," *J. Chem. Eng. Data* **47**(4):932–940, 2002.

Properties at the critical point temperature are given in the last entry of the saturation tables. In the single-phase table, when the temperature range for a given isobar includes a vapor-liquid phase boundary, the temperature of phase equilibrium is noted, and properties for both the saturated liquid and saturated vapor are given (with liquid properties given in the upper line). Lines are omitted from the temperature-pressure grid of the single-phase table, when the system would be in the solid phase or if there are potential problems with the source property surface.

Typical uncertainties in density are 0.02% in the liquid phase, 0.05% in the vapor phase and at supercritical temperatures, and 0.1% in the critical region, except very near the critical point, where the uncertainty in pressure is 0.1%. For vapor pressures, the uncertainty is 0.02% above 180 K, 0.05% above 1 Pa (115 K), and dropping to 0.001 mPa at the triple point. The uncertainty in heat capacity (isobaric, isochoric, and saturated) is 0.5% at temperatures above 125 K and 2% at temperatures below 125 K for the liquid, and is 0.5% for all vapor states. The uncertainty in the liquid-phase speed of sound is 0.5%, and that for the vapor phase is 0.05%. The uncertainties are higher for all properties very near the critical point except pressure (saturated vapor/liquid and single phase). The uncertainty in viscosity varies from 0.4% in the dilute gas between room temperature and 600 K, to about 2.5% from 100 to 475 K up to about 30 MPa, and to about 4% outside this range. Uncertainty in thermal conductivity is 3%, except in the critical region and dilute gas which have an uncertainty of 5%.

TABLE 2-249 Thermodynamic Properties of Propylene

Temperature K	Pressure MPa	Density mol/dm ³	Volume dm ³ /mol	Int. energy kJ/mol	Enthalpy kJ/mol	Entropy kJ/(mol·K)	C _v kJ/(mol·K)	C _p kJ/(mol·K)	Sound speed m/s	Joule-Thomson K/MPa
Saturated Properties										
105.00	1.8242E-07	17.799	0.056183	-6.2877	-6.2877	-0.039412	0.047146	0.074152	1984.2	-0.63335
120.00	4.8828E-06	17.383	0.057526	-5.1660	-5.1660	-0.029431	0.048479	0.076350	1860.6	-0.61019
135.00	5.9371E-05	16.973	0.058917	-3.9917	-3.9917	-0.020215	0.051603	0.080066	1740.6	-0.57672
150.00	0.00041697	16.567	0.060361	-2.7699	-2.7699	-0.011635	0.053564	0.082659	1637.2	-0.55180
165.00	0.0019723	16.162	0.061873	-1.5160	-1.5159	-0.0036693	0.054606	0.084443	1542.5	-0.53067
180.00	0.0069671	15.755	0.063470	-0.23811	-0.23766	0.0037429	0.055253	0.085952	1450.8	-0.50839
195.00	0.019747	15.343	0.065175	1.0625	1.0638	0.010683	0.055851	0.087538	1359.1	-0.48173
210.00	0.047272	14.922	0.067016	2.3884	2.3916	0.017233	0.056582	0.089404	1266.3	-0.44843
225.00	0.099223	14.487	0.069027	3.7442	3.7510	0.023468	0.057524	0.091663	1171.8	-0.40645
240.00	0.18775	14.035	0.071251	5.1356	5.1490	0.029455	0.058697	0.094401	1075.9	-0.35329
255.00	0.32701	13.559	0.073750	6.5692	6.5933	0.035251	0.060098	0.097711	978.69	-0.28530
270.00	0.53269	13.054	0.076607	8.0523	8.0931	0.040906	0.061715	0.10174	880.57	-0.19657
285.00	0.82165	12.509	0.079945	9.5938	9.6595	0.046469	0.063540	0.10676	781.63	-0.077005
300.00	1.2118	11.911	0.083956	11.205	11.307	0.051993	0.065577	0.11327	681.71	0.092061
315.00	1.7225	11.240	0.088971	12.904	13.057	0.057541	0.067855	0.12246	580.13	0.34911
330.00	2.3751	10.455	0.095644	14.722	14.949	0.063218	0.070450	0.13754	475.08	0.78805
345.00	3.1956	9.4631	0.10567	16.734	17.071	0.069261	0.073575	0.17154	362.18	1.7115
360.00	4.2202	7.8236	0.12782	19.290	19.829	0.076741	0.078178	0.39594	229.03	4.9073
365.57	4.6646	5.3086	0.18837	21.862	22.741	0.084569			0	12.042
105.00	1.8242E-07	2.0896E-07	4,785,700.	16.041	16.914	0.18156	0.031371	0.039685	162.00	260.32
120.00	4.8828E-06	4.8940E-06	204,330.	16.525	17.522	0.15964	0.033039	0.041354	172.27	186.64
135.00	5.9371E-05	5.2900E-05	18,904.	17.032	18.154	0.14383	0.034573	0.042891	181.89	139.37
150.00	0.00041697	0.00033450	2,989.5	17.560	18.807	0.13221	0.036090	0.044423	190.90	107.24
165.00	0.0019723	0.0014403	694.32	18.109	19.479	0.12357	0.037686	0.046064	199.27	84.470
180.00	0.0069671	0.0046776	213.78	18.676	20.166	0.11710	0.039423	0.047910	206.90	67.837
195.00	0.019747	0.012310	81.237	19.258	20.862	0.11221	0.041343	0.050046	213.67	55.441
210.00	0.047272	0.027633	36.188	19.850	21.560	0.10851	0.043468	0.052548	219.38	46.072
225.00	0.099223	0.054946	18.200	20.446	22.252	0.10570	0.045811	0.055492	223.85	38.921
240.00	0.18775	0.099531	10.047	21.042	22.928	0.10354	0.048376	0.058970	226.88	33.424
255.00	0.32701	0.16779	5.9598	21.630	23.579	0.10186	0.051168	0.063112	228.25	29.182
270.00	0.53269	0.26768	3.7358	22.202	24.192	0.10053	0.054191	0.068131	227.73	25.909
285.00	0.82165	0.40967	2.4410	22.749	24.754	0.099433	0.057457	0.074408	225.06	23.398
300.00	1.2118	0.60872	1.6428	23.254	25.245	0.098452	0.060989	0.082685	219.92	21.502
315.00	1.7225	0.88863	1.1253	23.693	25.632	0.097460	0.064833	0.094593	211.93	20.107
330.00	2.3751	1.2929	0.77343	24.022	25.859	0.096280	0.069077	0.11448	200.59	19.116
345.00	3.1956	1.9214	0.52045	24.137	25.801	0.094563	0.073899	0.15900	185.21	18.381
360.00	4.2202	3.1801	0.31446	23.631	24.958	0.090988	0.079791	0.42332	164.25	17.115
365.57	4.6646	5.3086	0.18837	21.862	22.741	0.084569			0	12.042
Single-Phase Properties										
100.00	0.10000	17.939	0.055745	-6.6629	-6.6573	-0.043075	0.049534	0.076050	2009.3	-0.61954
200.00	0.10000	15.206	0.065766	1.4997	1.5063	0.012896	0.056075	0.088113	1328.9	-0.47165
225.17	0.10000	14.482	0.069051	3.7598	3.7667	0.023538	0.057536	0.091692	1170.7	-0.40591
225.17	0.10000	0.055346	18.068	20.453	22.260	0.10567	0.045839	0.055529	223.89	38.850
300.00	0.10000	0.040648	24.601	24.309	26.769	0.12289	0.056666	0.065495	258.13	16.866
400.00	0.10000	0.030232	33.078	30.772	34.080	0.14382	0.072240	0.080757	295.63	7.2207
500.00	0.10000	0.024118	41.463	38.745	42.891	0.16342	0.086809	0.095223	328.33	3.7462
600.00	0.10000	0.020074	49.815	48.088	53.070	0.18194	0.099688	0.10806	357.96	2.2036
100.00	1.0000	17.947	0.055720	-6.6707	-6.6149	-0.043152	0.049534	0.076021	2014.7	-0.61988
200.00	1.0000	15.224	0.065684	1.4781	1.5437	0.012788	0.056080	0.087997	1335.9	-0.47384
292.39	1.0000	12.222	0.081820	10.378	10.460	0.049191	0.064516	0.10973	732.56	-0.0016360
292.39	1.0000	0.49938	2.0025	23.004	25.006	0.098942	0.059161	0.078164	222.86	22.395
300.00	1.0000	0.47670	2.0978	23.500	25.598	0.10094	0.059932	0.077330	228.89	20.287

TABLE 2-249 Thermodynamic Properties of Propylene (Concluded)

Temperature K	Pressure MPa	Density mol/dm ³	Volume dm ³ /mol	Int. energy kJ/mol	Enthalpy kJ/mol	Entropy kJ/(mol·K)	C _v kJ/(mol·K)	C _p kJ/(mol·K)	Sound speed m/s	Joule-Thomson K/MPa
Single-Phase Properties										
400.00	1.0000	0.31858	3.1389	30.390	33.529	0.12371	0.073331	0.084055	283.73	7.6465
500.00	1.0000	0.24704	4.0480	38.516	42.564	0.14381	0.087329	0.096722	322.07	3.8350
600.00	1.0000	0.20332	4.9183	47.935	52.854	0.16254	0.099980	0.10888	354.28	2.2229
200.00	5.0000	15.306	0.065334	1.3850	1.7117	0.012317	0.056114	0.087522	1365.9	-0.48279
300.00	5.0000	12.206	0.081924	10.889	11.299	0.050918	0.065369	0.10822	752.67	-0.041773
400.00	5.0000	2.2829	0.43803	27.896	30.087	0.10377	0.080080	0.12610	221.38	9.5490
500.00	5.0000	1.3832	0.72298	37.351	40.966	0.12811	0.089729	0.10566	297.48	4.0173
600.00	5.0000	1.0713	0.93348	47.197	51.865	0.14796	0.10124	0.11304	342.05	2.2088
200.00	10.000	15.402	0.064925	1.2752	1.9245	0.011753	0.056174	0.087009	1401.2	-0.49245
300.00	10.000	12.515	0.079905	10.553	11.352	0.049747	0.065258	0.10422	828.84	-0.15061
400.00	10.000	7.5283	0.13283	22.740	24.068	0.085918	0.081711	0.16868	302.55	2.6128
500.00	10.000	3.1462	0.31784	35.603	38.781	0.11902	0.092261	0.12166	287.51	3.5544
600.00	10.000	2.2419	0.44605	46.180	50.641	0.14065	0.10253	0.11891	340.40	1.9833
200.00	100.00	16.616	0.060184	-0.021002	5.9974	0.0040990	0.058338	0.083715	1815.4	-0.55416
300.00	100.00	14.839	0.067390	8.0040	14.743	0.039443	0.067573	0.092245	1457.4	-0.48492
400.00	100.00	13.274	0.075333	17.017	24.550	0.067574	0.081108	0.10402	1192.7	-0.40335
500.00	100.00	11.892	0.084087	27.127	35.536	0.092040	0.094320	0.11555	1020.4	-0.33132
600.00	100.00	10.680	0.093635	38.256	47.620	0.11404	0.10601	0.12591	913.65	-0.27115
200.00	200.00	17.488	0.057182	-0.77627	10.660	-0.0018754	0.060831	0.083362	2084.9	-0.55991
300.00	200.00	16.028	0.062389	6.8870	19.365	0.033304	0.070484	0.091727	1796.1	-0.51205
400.00	200.00	14.825	0.067452	15.619	29.110	0.061259	0.084735	0.10329	1568.7	-0.45996
500.00	200.00	13.819	0.072363	25.539	40.011	0.085539	0.098618	0.11458	1403.8	-0.42037
600.00	200.00	12.963	0.077142	36.558	51.987	0.10734	0.11085	0.12471	1282.8	-0.39117

The values in these tables were generated from the NIST REFPROP software (Lemmon, E. W., McLinden, M. O., and Huber, M. L., NIST Standard Reference Database 23: Reference Fluid Thermodynamic and Transport Properties—REFPROP, National Institute of Standards and Technology, Standard Reference Data Program, Gaithersburg, Md., 2002, Version 7.1). The primary source for the thermodynamic properties is Angus, S., Armstrong, B., and de Reuck, K. M., "International Thermodynamic Tables of the Fluid State—7 Propylene," *International Union of Pure and Applied Chemistry*, Pergamon Press, Oxford, 1980. Validated equations for the viscosity and thermal conductivity are not currently available for this fluid.

Properties at the triple point temperature and the critical point temperature are given in the first and last entries of the saturation tables, respectively. In the single-phase table, when the temperature range for a given isobar includes a vapor-liquid phase boundary, the temperature of phase equilibrium is noted, and properties for both the saturated liquid and saturated vapor are given (with liquid properties given in the upper line). Lines are omitted from the temperature-pressure grid of the single-phase table, when the system would be in the solid phase or if there are potential problems with the source property surface.

The uncertainties of the equation of state are generally 0.1% in density (except in the critical region), 1% in the heat capacity in the vapor phase, and 2–5% in the heat capacity in the liquid phase.

TABLE 2-250 Thermodynamic Properties of R-11, Trichlorofluoromethane

Temperature K	Pressure MPa	Density mol/dm ³	Volume dm ³ /mol	Int. energy kJ/mol	Enthalpy kJ/mol	Entropy kJ/(mol·K)	C _v kJ/(mol·K)	C _p kJ/(mol·K)	Sound speed m/s	Joule-Thomson K/MPa
Saturated Properties										
162.68	6.5101E-06	12.874	0.077673	15.035	15.035	0.079300	0.074722	0.10506	1224.2	-0.60355
165.00	9.0030E-06	12.841	0.077878	15.280	15.280	0.080791	0.074630	0.10557	1221.1	-0.59915
180.00	5.8433E-05	12.618	0.079249	16.886	16.886	0.090108	0.075084	0.10851	1178.8	-0.57445
195.00	0.00027433	12.392	0.080694	18.531	18.531	0.098885	0.076137	0.11069	1119.8	-0.55514
210.00	0.0010018	12.164	0.082210	20.204	20.204	0.10715	0.077185	0.11231	1057.5	-0.53850
225.00	0.0030014	11.933	0.083801	21.899	21.899	0.11494	0.078127	0.11364	996.42	-0.52214
240.00	0.0076770	11.699	0.085475	23.614	23.614	0.12232	0.078986	0.11489	937.75	-0.50429
255.00	0.017281	11.462	0.087246	25.346	25.347	0.12932	0.079799	0.11621	881.67	-0.48363
270.00	0.035048	11.219	0.089131	27.099	27.102	0.13600	0.080594	0.11767	827.91	-0.45904
285.00	0.065240	10.971	0.091150	28.875	28.881	0.14240	0.081391	0.11933	776.09	-0.42946
300.00	0.11311	10.715	0.093329	30.677	30.687	0.14856	0.082199	0.12124	725.77	-0.39364
315.00	0.18478	10.449	0.095702	32.508	32.525	0.15452	0.083025	0.12343	676.56	-0.34999
330.00	0.28718	10.172	0.098308	34.371	34.399	0.16030	0.083873	0.12595	628.04	-0.29629
345.00	0.42787	9.8812	0.10120	36.271	36.315	0.16594	0.084749	0.12888	579.81	-0.22926
360.00	0.61496	9.5733	0.10446	38.213	38.277	0.17145	0.085663	0.13232	531.47	-0.14389
375.00	0.85703	9.2442	0.10818	40.203	40.295	0.17687	0.086633	0.13648	482.57	-0.032121
390.00	1.1631	8.8882	0.11251	42.247	42.378	0.18223	0.087686	0.14171	432.58	0.11986
405.00	1.5427	8.4966	0.11769	44.359	44.541	0.18756	0.088870	0.14871	380.86	0.33760
420.00	2.0061	8.0545	0.12415	46.558	46.808	0.19292	0.090270	0.15899	326.51	0.67402
435.00	2.5648	7.5340	0.13273	48.882	49.223	0.19840	0.092058	0.17674	268.20	1.2582
450.00	3.2329	6.8663	0.14564	51.423	51.894	0.20422	0.094658	0.21832	203.77	2.4973
465.00	4.0318	5.7930	0.17262	54.535	55.231	0.21124	0.099494	0.43941	132.04	6.3140
471.11	4.4076	4.0330	0.24796	57.789	58.881	0.21886			0	15.427
162.68	6.5101E-06	4.8133E-06	207.760.	44.924	46.276	0.27134	0.049536	0.057858	107.23	1885.7
165.00	9.0030E-06	6.5631E-06	152.370.	45.039	46.411	0.26946	0.050011	0.058335	107.92	1701.5
180.00	5.8433E-05	3.9056E-05	25.605.	45.809	47.305	0.25910	0.052998	0.061344	112.26	905.28
195.00	0.00027433	0.00016934	5.905.3	46.618	48.238	0.25123	0.055869	0.064262	116.42	508.88
210.00	0.0010018	0.00057483	1.739.7	47.463	49.206	0.24525	0.058662	0.067140	120.39	301.60
225.00	0.0030014	0.0016103	621.01	48.339	50.203	0.24074	0.061395	0.070004	124.15	188.62
240.00	0.0076770	0.0038729	258.21	49.242	51.224	0.23736	0.064063	0.072855	127.67	124.75
255.00	0.017281	0.0082428	121.32	50.168	52.265	0.23488	0.066646	0.075684	130.89	87.418
270.00	0.035048	0.015895	62.911	51.115	53.320	0.23310	0.069122	0.078487	133.75	64.864
285.00	0.065240	0.028297	35.340	52.075	54.381	0.23188	0.071480	0.081281	136.17	50.774
300.00	0.11311	0.047202	21.186	53.045	55.441	0.23108	0.073723	0.084113	138.07	41.663
315.00	0.18478	0.074674	13.391	54.015	56.490	0.23060	0.075868	0.087058	139.37	35.564
330.00	0.28718	0.11315	8.8379	54.979	57.517	0.23036	0.077940	0.090222	140.01	31.344
345.00	0.42787	0.16555	6.0405	55.928	58.512	0.23028	0.079972	0.093753	139.89	28.342
360.00	0.61496	0.23549	4.2464	56.851	59.462	0.23030	0.081998	0.097861	138.95	26.165
375.00	0.85703	0.32766	3.0519	57.736	60.352	0.23035	0.084057	0.10286	137.09	24.577
390.00	1.1631	0.44843	2.2300	58.569	61.163	0.23039	0.086191	0.10929	134.19	23.443
405.00	1.5427	0.60714	1.6471	59.331	61.872	0.23035	0.088457	0.11813	130.10	22.687
420.00	2.0061	0.81886	1.2212	59.992	62.442	0.23014	0.090937	0.13148	124.58	22.277
435.00	2.5648	1.1115	0.89966	60.498	62.805	0.22962	0.093775	0.15496	117.29	22.202
450.00	3.2329	1.5503	0.64504	60.727	62.813	0.22849	0.097282	0.20995	107.74	22.379
465.00	4.0318	2.3952	0.41751	60.210	61.894	0.22557	0.10241	0.51972	95.245	21.779
471.11	4.4076	4.0330	0.24796	57.789	58.881	0.21886			0	15.427
Single-Phase Properties										
200.00	0.10000	12.317	0.081186	19.084	19.092	0.10168	0.076484	0.11128	1099.8	-0.54951
296.49	0.10000	10.776	0.092803	30.252	30.262	0.14714	0.082009	0.12077	737.44	-0.40266
296.49	0.10000	0.042088	23.760	52.817	55.193	0.23123	0.073207	0.083443	137.67	43.472
300.00	0.10000	0.041523	24.083	53.078	55.486	0.23221	0.073294	0.083384	138.61	41.094
400.00	0.10000	0.030462	32.827	60.756	64.039	0.25678	0.079843	0.088628	161.80	15.373
500.00	0.10000	0.024206	41.312	69.066	73.197	0.27719	0.085650	0.094219	181.31	9.4764
600.00	0.10000	0.020110	49.728	77.853	82.825	0.29474	0.089636	0.098111	198.74	6.5190

TABLE 2-250 Thermodynamic Properties of R-11, Trichlorofluoromethane (Concluded)

Temperature K	Pressure MPa	Density mol/dm ³	Volume dm ³ /mol	Int. energy kJ/mol	Enthalpy kJ/mol	Entropy kJ/(mol·K)	C _v kJ/(mol·K)	C _p kJ/(mol·K)	Sound speed m/s	Joule-Thomson K/MPa
Single-Phase Properties										
200.00	1.0000	12.325	0.081134	19.066	19.147	0.10159	0.076374	0.11122	1106.2	-0.55026
300.00	1.0000	10.733	0.093174	30.637	30.730	0.14843	0.082161	0.12101	731.85	-0.39806
382.43	1.0000	9.0718	0.11023	41.208	41.318	0.17953	0.087142	0.13891	457.99	0.036901
382.43	1.0000	0.38339	2.6083	58.156	60.765	0.23038	0.085101	0.10582	135.79	23.965
400.00	1.0000	0.35322	2.8311	59.743	62.574	0.23501	0.083835	0.10080	143.19	19.717
500.00	1.0000	0.25738	3.8853	68.469	72.354	0.25684	0.086291	0.097662	172.67	10.081
600.00	1.0000	0.20723	4.8256	77.413	82.239	0.27486	0.090004	0.10006	194.29	6.6365
200.00	5.0000	12.359	0.080912	18.988	19.393	0.10120	0.075954	0.11098	1133.5	-0.55346
300.00	5.0000	10.810	0.092509	30.464	30.926	0.14785	0.082048	0.12006	757.72	-0.41608
400.00	5.0000	8.8674	0.11277	43.167	43.731	0.18456	0.087727	0.13909	448.07	0.070413
500.00	5.0000	2.1555	0.46393	64.141	66.460	0.23416	0.094709	0.18205	120.07	14.043
600.00	5.0000	1.2189	0.82040	75.225	79.327	0.25776	0.091726	0.11326	173.08	7.0186
200.00	10.000	12.399	0.080649	18.894	19.700	0.10072	0.075562	0.11072	1164.8	-0.55716
300.00	10.000	10.899	0.091755	30.263	31.181	0.14716	0.082018	0.11907	787.03	-0.43502
400.00	10.000	9.1187	0.10966	42.641	43.737	0.18319	0.087335	0.13358	500.70	-0.076836
500.00	10.000	6.3465	0.15757	56.993	58.568	0.21613	0.093373	0.17100	231.94	1.9364
600.00	10.000	3.0124	0.33196	71.945	75.265	0.24670	0.093817	0.13897	167.77	5.3068
200.00	20.000	12.475	0.080163	18.716	20.320	0.099796	0.075119	0.11027	1220.3	-0.56373
300.00	20.000	11.057	0.090438	29.905	31.714	0.14590	0.082196	0.11753	838.26	-0.46461
400.00	20.000	9.4912	0.10536	41.844	43.951	0.18104	0.087334	0.12773	578.74	-0.23372
500.00	20.000	7.6205	0.13123	54.651	57.275	0.21072	0.091707	0.13823	378.80	0.31683
600.00	20.000	5.5967	0.17868	67.668	71.241	0.23619	0.094708	0.13794	265.18	1.2664
200.00	30.000	12.543	0.079723	18.552	20.943	0.098918	0.075012	0.10990	1268.1	-0.56938
300.00	30.000	11.197	0.089311	29.591	32.270	0.14476	0.082559	0.11638	882.50	-0.48678
400.00	30.000	9.7739	0.10231	41.235	44.304	0.17932	0.087676	0.12450	638.80	-0.31979
500.00	30.000	8.2190	0.12167	53.466	57.116	0.20788	0.091885	0.13097	464.35	-0.028029
600.00	30.000	6.6706	0.14991	65.781	70.278	0.23188	0.095040	0.13106	357.26	0.34752

The values in these tables were generated from the NIST REFPROP software (Lemmon, E. W., McLinden, M. O., and Huber, M. L., NIST Standard Reference Database 23: Reference Fluid Thermodynamic and Transport Properties—REFPROP, National Institute of Standards and Technology, Standard Reference Data Program, Gaithersburg, Md., 2002, Version 7.1). The primary source for the thermodynamic properties is Jacobsen, R. T., Penoncello, S. G., and Lemmon, E. W., "A Fundamental Equation for Trichlorofluoromethane (R-11)," *Fluid Phase Equilibria* **80**:45–56, 1992. Validated equations for the viscosity and thermal conductivity are not currently available for this fluid.

Properties at the triple point temperature and the critical point temperature are given in the first and last entries of the saturation tables, respectively. In the single-phase table, when the temperature range for a given isobar includes a vapor-liquid phase boundary, the temperature of phase equilibrium is noted, and properties for both the saturated liquid and saturated vapor are given (with liquid properties given in the upper line). Lines are omitted from the temperature-pressure grid of the single-phase table, when the system would be in the solid phase or if there are potential problems with the source property surface.

The uncertainties of the equation of state are 0.1% in density for the liquid, and 0.25% for the vapor, 2% in heat capacity, and 1% in the speed of sound, except in the critical region. The uncertainty in vapor pressure is 0.2%.

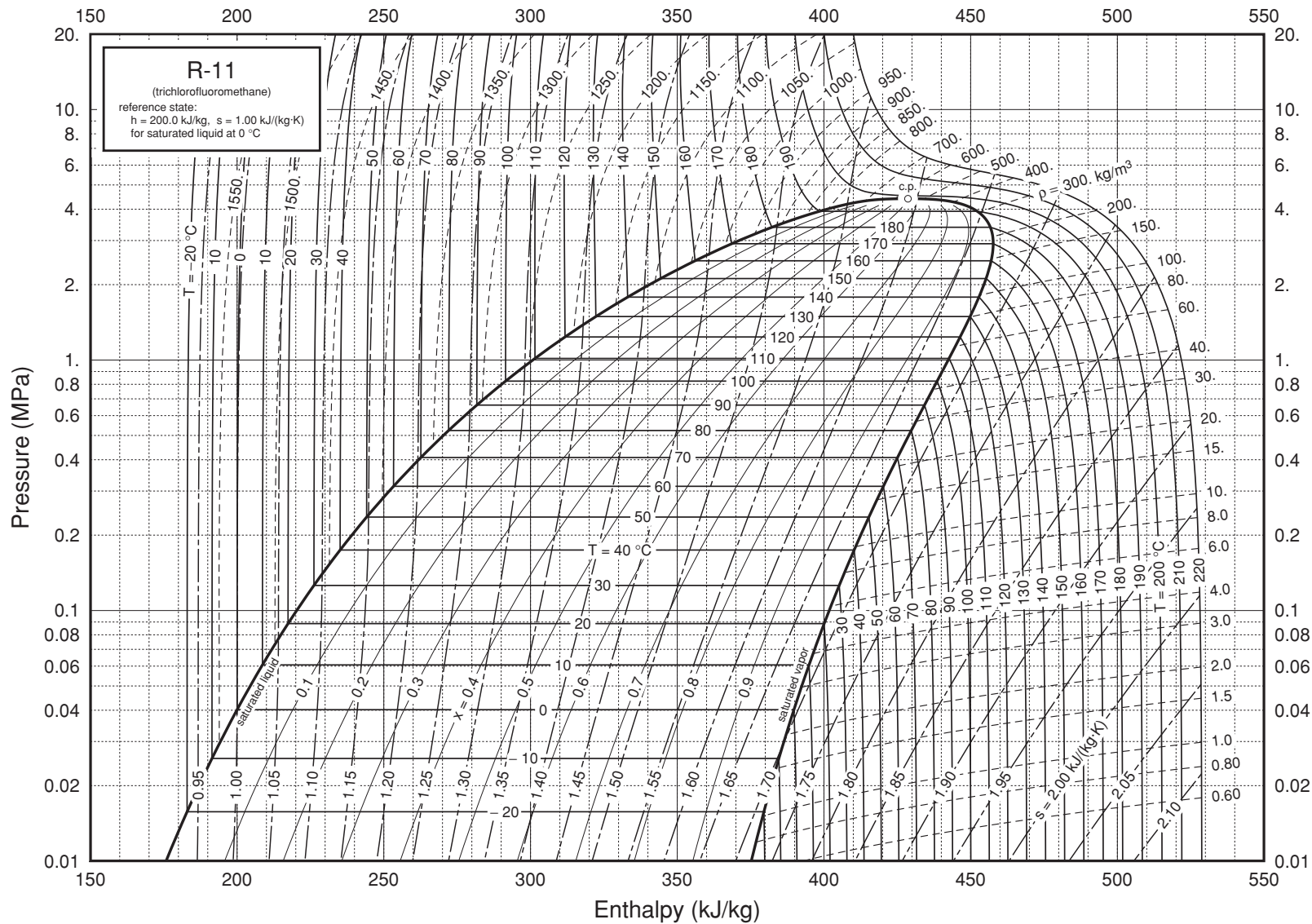


FIG. 2-18 Pressure-enthalpy diagram for Refrigerant 11. Properties computed with the NIST REFPROP Database, Version 7.0 (Lemmon, E. W., McLinden, M. O., and Huber, M. L., 2002, NIST Standard Reference Database 23, NIST Reference Fluid Thermodynamic and Transport Properties—REFPROP, Version 7.0, Standard Reference Data Program, National Institute of Standards and Technology), based on the equation of state of Jacobsen, R. T., Penoncello, S. G., and Lemmon, E. W., "A Fundamental Equation for Trichlorofluoromethane (R-11)," *Fluid Phase Equilibria* **80**:45–56, 1992.

TABLE 2-251 Thermodynamic Properties of R-12, Dichlorodifluoromethane

Temperature K	Pressure MPa	Density mol/dm ³	Volume dm ³ /mol	Int. energy kJ/mol	Enthalpy kJ/mol	Entropy kJ/(mol·K)	C _v kJ/(mol·K)	C _p kJ/(mol·K)	Sound speed m/s	Joule-Thomson K/MPa
Saturated Properties										
116.10	2.4255E-07	15.125	0.066114	8.0204	8.0204	0.033619	0.069219	0.10352	1310.0	-0.53048
120.00	5.8432E-07	15.039	0.066492	8.4220	8.4220	0.037021	0.068095	0.10239	1290.2	-0.53554
135.00	1.0092E-05	14.712	0.067972	9.9342	9.9342	0.048899	0.065219	0.099608	1215.7	-0.54646
150.00	9.1829E-05	14.387	0.069505	11.419	11.419	0.059328	0.063937	0.098564	1143.1	-0.54643
165.00	0.00053030	14.064	0.071106	12.897	12.897	0.068717	0.063633	0.098622	1072.5	-0.53813
180.00	0.0021945	13.738	0.072790	14.381	14.381	0.077328	0.063942	0.099406	1003.9	-0.52327
195.00	0.0070692	13.409	0.074574	15.881	15.882	0.085332	0.064638	0.10070	937.07	-0.50270
210.00	0.018793	13.075	0.076482	17.403	17.405	0.092852	0.065582	0.10237	872.00	-0.47654
225.00	0.043015	12.733	0.078538	18.953	18.956	0.099978	0.066683	0.10436	808.46	-0.44424
240.00	0.087479	12.380	0.080776	20.533	20.540	0.10678	0.067882	0.10664	746.23	-0.40455
255.00	0.16186	12.013	0.083241	22.149	22.162	0.11331	0.069143	0.10925	685.03	-0.35528
270.00	0.27747	11.629	0.085990	23.803	23.827	0.11961	0.070443	0.11226	624.56	-0.29292
285.00	0.44693	11.223	0.089104	25.502	25.541	0.12574	0.071775	0.11579	564.41	-0.21173
300.00	0.68394	10.787	0.092703	27.250	27.314	0.13172	0.073152	0.12012	504.07	-0.10203
315.00	1.0032	10.312	0.096973	29.059	29.157	0.13762	0.074611	0.12572	442.82	0.053692
330.00	1.4203	9.7818	0.10223	30.943	31.088	0.14348	0.076246	0.13360	379.59	0.29048
345.00	1.9528	9.1671	0.10909	32.930	33.143	0.14940	0.078279	0.14625	312.77	0.68965
360.00	2.6209	8.4050	0.11898	35.078	35.390	0.15556	0.081286	0.17199	239.96	1.4874
375.00	3.4527	7.3032	0.13693	37.570	38.042	0.16248	0.087150	0.26475	158.26	3.7100
385.12	4.1362	4.6728	0.21401	41.164	42.049	0.17270			0	13.369
116.10	2.4255E-07	2.5127E-07	3,979,800.	33.279	34.244	0.25949	0.034581	0.042896	99.513	532.61
120.00	5.8432E-07	5.8564E-07	1,707,500.	33.415	34.413	0.25361	0.035365	0.043680	100.95	464.92
135.00	1.0092E-05	8.9910E-06	111,220.	33.968	35.091	0.23524	0.038409	0.046725	106.27	288.39
150.00	9.1829E-05	7.3643E-05	13,579.	34.567	35.814	0.22196	0.041427	0.049750	111.28	190.47
165.00	0.00053030	0.00038683	2,585.1	35.208	36.579	0.21224	0.044365	0.052712	116.02	132.65
180.00	0.0021945	0.0014695	680.49	35.888	37.381	0.20511	0.047211	0.055621	120.49	96.659
195.00	0.0070692	0.0043835	228.13	36.602	38.214	0.19986	0.049977	0.058515	124.63	73.304
210.00	0.018793	0.010883	91.884	37.342	39.069	0.19601	0.052681	0.061451	128.34	57.635
225.00	0.043015	0.023468	42.611	38.102	39.935	0.19322	0.055348	0.064497	131.52	46.836
240.00	0.087479	0.045368	22.042	38.873	40.801	0.19120	0.058002	0.067735	134.05	39.210
255.00	0.16186	0.080547	12.415	39.647	41.657	0.18976	0.060669	0.071271	135.80	33.704
270.00	0.27747	0.13381	7.4735	40.415	42.488	0.18873	0.063373	0.075247	136.64	29.653
285.00	0.44693	0.21108	4.7376	41.165	43.283	0.18799	0.066138	0.079875	136.46	26.640
300.00	0.68394	0.32006	3.1244	41.887	44.024	0.18742	0.068991	0.085504	135.10	24.405
315.00	1.0032	0.47149	2.1209	42.562	44.689	0.18693	0.071972	0.092789	132.40	22.790
330.00	1.4203	0.68182	1.4667	43.166	45.249	0.18639	0.075158	0.10314	128.14	21.703
345.00	1.9528	0.97985	1.0206	43.655	45.648	0.18565	0.078715	0.12016	122.00	21.085
360.00	2.6209	1.4275	0.70055	43.941	45.777	0.18441	0.083065	0.15653	113.54	20.831
375.00	3.4527	2.2257	0.44930	43.738	45.289	0.18181	0.089754	0.30373	102.14	20.225
385.12	4.1362	4.6728	0.21401	41.164	42.049	0.17270			0	13.369

Single-Phase Properties

125.00	0.10000	14.931	0.066977	8.9296	8.9363	0.041166	0.066915	0.10121	1265.3	-0.54064
225.00	0.10000	12.734	0.078531	18.951	18.959	0.099970	0.066686	0.10435	808.74	-0.44443
243.09	0.10000	12.306	0.081264	20.863	20.871	0.10814	0.068138	0.10715	733.55	-0.39528
243.09	0.10000	0.051383	19.462	39.033	40.979	0.19086	0.058549	0.068435	134.48	37.929
325.00	0.10000	0.037543	26.636	44.257	46.920	0.21187	0.067874	0.076721	156.65	16.166
425.00	0.10000	0.028469	35.126	51.527	55.039	0.23360	0.076661	0.085212	179.16	8.3282
525.00	0.10000	0.022973	43.529	59.527	63.880	0.25225	0.082795	0.091242	198.90	5.1283
125.00	1.0000	14.938	0.066945	8.9186	8.9856	0.041078	0.066988	0.10119	1267.0	-0.54091
225.00	1.0000	12.752	0.078422	18.922	19.001	0.099842	0.066739	0.10418	813.10	-0.44741
314.87	1.0000	10.316	0.096933	29.043	29.140	0.13757	0.074598	0.12566	443.35	0.052069
314.87	1.0000	0.46996	2.1279	42.556	44.684	0.18693	0.071945	0.092716	132.43	22.802
325.00	1.0000	0.44273	2.2587	43.348	45.606	0.18982	0.071678	0.089701	137.48	19.919
425.00	1.0000	0.30150	3.1367	51.055	54.372	0.21333	0.077527	0.088660	171.39	8.7630
525.00	1.0000	0.23568	4.2430	59.210	63.453	0.23250	0.083185	0.092926	195.20	5.1839
125.00	5.0000	14.968	0.066807	8.8706	9.2046	0.040691	0.067308	0.10110	1274.3	-0.54205
225.00	5.0000	12.827	0.077958	18.799	19.189	0.099289	0.066963	0.10352	831.96	-0.45954
325.00	5.0000	10.252	0.097546	29.898	30.385	0.14025	0.075544	0.12368	450.15	0.017671
425.00	5.0000	2.2637	0.44176	47.937	50.146	0.19225	0.083408	0.14054	131.42	10.771
525.00	5.0000	1.3295	0.75217	57.642	61.402	0.21615	0.085038	0.10337	180.93	5.2339
125.00	10.000	15.006	0.066639	8.8124	9.4788	0.040215	0.067691	0.10099	1283.4	-0.54334
225.00	10.000	12.917	0.077418	18.655	19.429	0.098631	0.067222	0.10281	854.41	-0.47253
325.00	10.000	10.544	0.094842	29.472	30.420	0.13887	0.075613	0.11858	501.05	-0.12043
425.00	10.000	6.6383	0.15064	42.586	44.093	0.17528	0.084440	0.16445	204.25	2.4031
525.00	10.000	3.0541	0.32743	55.399	58.673	0.20629	0.087008	0.12146	177.27	4.2532
225.00	100.00	13.992	0.071470	17.017	24.164	0.090059	0.069779	0.098455	1155.1	-0.55347
325.00	100.00	12.599	0.079369	26.406	34.343	0.12742	0.077370	0.10504	937.26	-0.49945
425.00	100.00	11.358	0.088042	36.302	45.106	0.15626	0.084005	0.10984	788.21	-0.45110
525.00	100.00	10.262	0.097444	46.498	56.243	0.17978	0.088827	0.11260	690.80	-0.41225
225.00	200.00	14.702	0.068017	16.054	29.657	0.083541	0.070631	0.097995	1397.8	-0.56210
325.00	200.00	13.559	0.073751	25.016	39.766	0.12065	0.077764	0.10414	1220.9	-0.52944
425.00	200.00	12.582	0.079477	34.535	50.431	0.14923	0.084238	0.10881	1091.3	-0.50685
525.00	200.00	11.738	0.085195	44.429	61.468	0.17254	0.088994	0.11168	999.41	-0.49445

The values in these tables were generated from the NIST REFPROP software (Lemmon, E. W., McLinden, M. O., and Huber, M. L., NIST Standard Reference Database 23: Reference Fluid Thermodynamic and Transport Properties—REFPROP, National Institute of Standards and Technology, Standard Reference Data Program, Gaithersburg, Md., 2002, Version 7.1). The primary source for the thermodynamic properties is Marx, V., Pruss, A., and Wagner, W., "Neue Zustandsgleichungen fuer R 12, R 22, R 11 und R 113. Beschreibung des thermodynamischen Zustandsverhaltens bei Temperaturen bis 525 K und Druecken bis 200 MPa," Duesseldorf: *VDI Verlag*, Series 19 (Waermetechnik/Kaelte-technik), No. 57, 1992. Validated equations for the viscosity and thermal conductivity are not currently available for this fluid.

Properties at the triple point temperature and the critical point temperature are given in the first and last entries of the saturation tables, respectively. In the single-phase table, when the temperature range for a given isobar includes a vapor-liquid phase boundary, the temperature of phase equilibrium is noted, and properties for both the saturated liquid and saturated vapor are given (with liquid properties given in the upper line). Lines are omitted from the temperature-pressure grid of the single-phase table, when the system would be in the solid phase or if there are potential problems with the source property surface.

The uncertainties in density are 0.2% below the critical point temperature and increase to 1% in and above the critical region. The uncertainties for vapor pressures are 0.2% above 200 K and greater than 1% below 200 K. The uncertainties in heat capacities and sound speeds are 1% each.

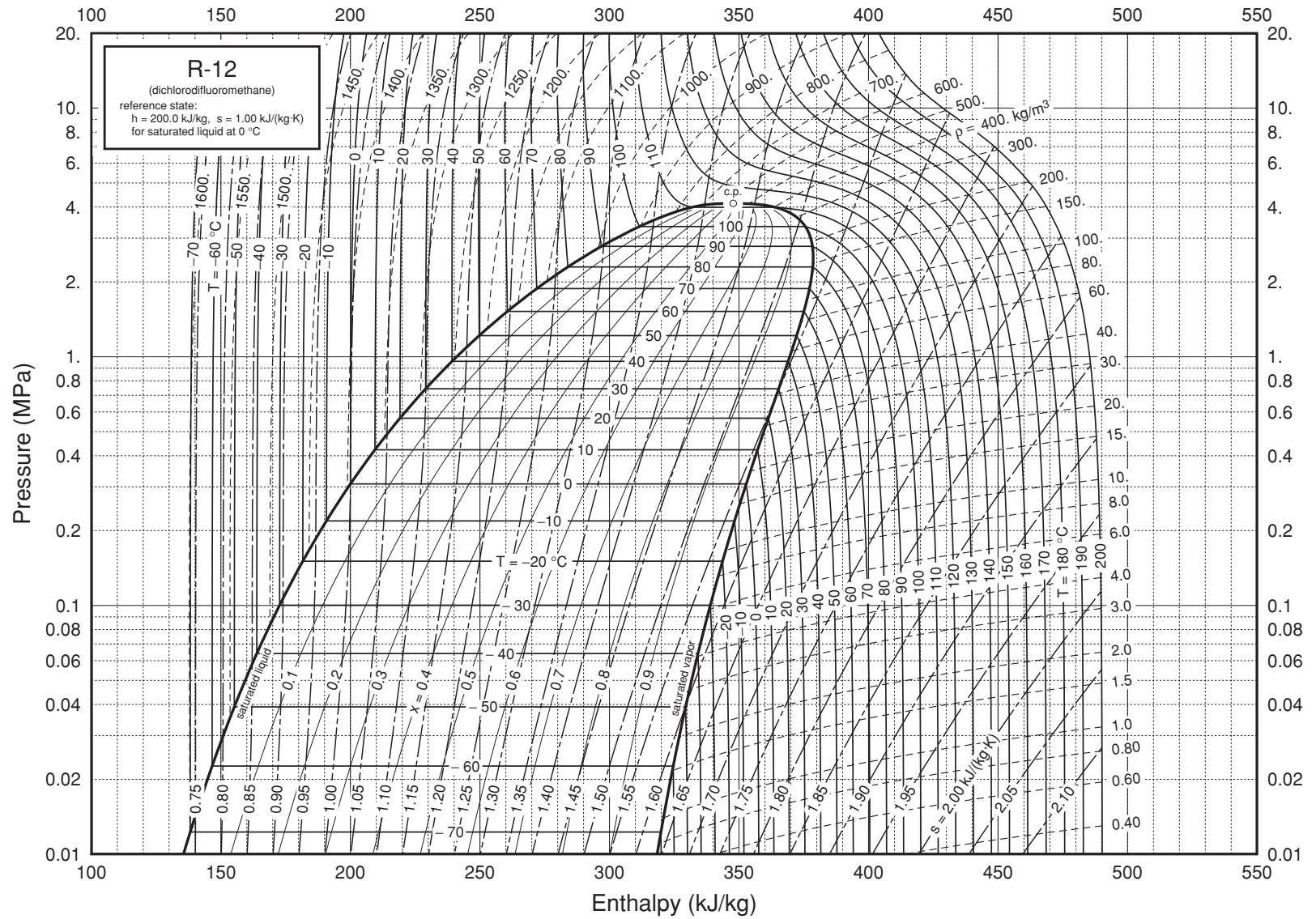


FIG. 2-19 Pressure-enthalpy diagram for Refrigerant 12. Properties computed with the NIST REFPROP Database, Version 7.0 (Lemmon, E. W., McLinden, M. O., and Huber, M. L., 2002, NIST Standard Reference Database 23, NIST Reference Fluid Thermodynamic and Transport Properties—REFPROP, Version 7.0, Standard Reference Data Program, National Institute of Standards and Technology), based on the equation of state of Marx, V., Prüß, A., and Wagner, W., "Neue Zustandsgleichungen für R 12, R 22, R 11 und R 113. Beschreibung des thermodynamischen Zustandsverhaltens bei Temperaturen bis 525 K und Drücken bis 200 MPa," VDI-Fortschritt-Ber. Series 19, No. 57, Düsseldorf: VDI Verlag, 1992.

TABLE 2-252 Thermodynamic Properties of R-13, Chlorotrifluoromethane

Temperature K	Pressure MPa	Density mol/dm ³	Volume dm ³ /mol	Int. energy kJ/mol	Enthalpy kJ/mol	Entropy kJ/(mol·K)	C _v kJ/(mol·K)	C _p kJ/(mol·K)	Sound speed m/s	Joule-Thomson K/MPa
Saturated Properties										
92.000	3.2889E-07	17.840	0.056054	3.4760	3.4760	0.0038039	0.059797	0.077526	918.05	-0.61098
100.00	2.6891E-06	17.596	0.056830	4.1217	4.1217	0.010530	0.059177	0.083231	1032.1	-0.56374
110.00	2.3101E-05	17.288	0.057844	4.9721	4.9721	0.018633	0.057632	0.086329	1078.3	-0.53784
120.00	0.00013272	16.976	0.058907	5.8413	5.8413	0.026196	0.055848	0.087308	1072.1	-0.52512
130.00	0.00056195	16.660	0.060023	6.7158	6.7159	0.033195	0.054335	0.087538	1039.3	-0.51544
140.00	0.0018797	16.339	0.061202	7.5918	7.5919	0.039687	0.053311	0.087670	992.15	-0.50447
150.00	0.0052264	16.012	0.062451	8.4698	8.4701	0.045744	0.052818	0.087987	937.71	-0.49023
160.00	0.012543	15.679	0.063780	9.3523	9.3531	0.051439	0.052815	0.088595	879.99	-0.47186
170.00	0.026741	15.337	0.065200	10.242	10.244	0.056835	0.053227	0.089527	821.49	-0.44883
180.00	0.051763	14.987	0.066725	11.143	11.146	0.061982	0.053972	0.090788	763.71	-0.42058
190.00	0.092557	14.626	0.068370	12.057	12.063	0.066925	0.054972	0.092386	707.45	-0.38628
200.00	0.15496	14.254	0.070158	12.988	12.999	0.071701	0.056159	0.094338	653.03	-0.34462
210.00	0.24553	13.866	0.072118	13.939	13.956	0.076341	0.057477	0.096688	600.48	-0.29355
220.00	0.37145	13.461	0.074289	14.913	14.940	0.080874	0.058882	0.099513	549.57	-0.22995
230.00	0.54033	13.033	0.076727	15.914	15.955	0.085328	0.060340	0.10294	499.97	-0.14899
240.00	0.76025	12.577	0.079511	16.947	17.007	0.089732	0.061829	0.10719	451.26	-0.043013
250.00	1.0397	12.083	0.082762	18.018	18.104	0.094118	0.063338	0.11266	402.91	0.10085
260.00	1.3878	11.537	0.086674	19.137	19.258	0.098526	0.064870	0.12009	354.31	0.30583
270.00	1.8145	10.919	0.091587	20.319	20.485	0.10301	0.066451	0.13115	304.57	0.61895
280.00	2.3316	10.183	0.098198	21.591	21.820	0.10769	0.068161	0.15049	252.29	1.1529
290.00	2.9538	9.2260	0.10839	23.021	23.341	0.11280	0.070241	0.19837	194.59	2.2680
300.00	3.7065	7.4440	0.13434	25.005	25.503	0.11981	0.074099	0.74301	122.38	6.3031
302.00	3.8790	5.5800	0.17921	26.462	27.158	0.12522			0	11.123
92.000	3.2889E-07	4.2996E-07	2,325,800.	22.976	23.741	0.22408	0.026152	0.034466	98.239	846.97
100.00	2.6891E-06	3.2343E-06	309,190.	23.192	24.023	0.20954	0.027668	0.035983	101.74	607.63
110.00	2.3101E-05	2.5261E-05	39,587.	23.477	24.392	0.19518	0.029536	0.037856	105.92	414.42
120.00	0.00013272	0.00013307	7,514.8	23.781	24.778	0.18400	0.031384	0.039718	109.91	291.57
130.00	0.00056195	0.00052045	1,921.4	24.101	25.181	0.17523	0.033228	0.041601	113.70	210.73
140.00	0.0018797	0.0016191	617.64	24.435	25.596	0.16829	0.035092	0.043546	117.29	155.99
150.00	0.0052264	0.0042135	237.33	24.782	26.022	0.16276	0.037002	0.045603	120.64	118.01
160.00	0.012543	0.0095248	104.99	25.137	26.454	0.15832	0.038978	0.047816	123.73	91.120
170.00	0.026741	0.019245	51.961	25.499	26.888	0.15474	0.041033	0.050218	126.48	71.760
180.00	0.051763	0.035532	28.144	25.864	27.321	0.15184	0.043168	0.052835	128.85	57.628
190.00	0.092557	0.060985	16.398	26.231	27.749	0.14948	0.045375	0.055688	130.77	47.196
200.00	0.15496	0.098644	10.137	26.597	28.168	0.14755	0.047639	0.058800	132.18	39.425
210.00	0.24553	0.15204	6.5771	26.959	28.574	0.14595	0.049946	0.062214	133.00	33.599
220.00	0.37145	0.22536	4.4373	27.315	28.963	0.14462	0.052282	0.066006	133.16	29.214
230.00	0.54033	0.32372	3.0891	27.659	29.329	0.14347	0.054636	0.070318	132.58	25.919
240.00	0.76025	0.45374	2.2039	27.987	29.663	0.14246	0.057009	0.075407	131.16	23.463
250.00	1.0397	0.62459	1.6010	28.289	29.954	0.14152	0.059411	0.081759	128.80	21.667
260.00	1.3878	0.84999	1.1765	28.552	30.185	0.14055	0.061872	0.090357	125.37	20.399
270.00	1.8145	1.1527	0.86755	28.753	30.327	0.13947	0.064450	0.10345	120.73	19.555
280.00	2.3316	1.5762	0.63445	28.850	30.329	0.13808	0.067265	0.12745	114.75	19.007
290.00	2.9538	2.2289	0.44866	28.740	30.066	0.13599	0.070591	0.19031	107.22	18.455
300.00	3.7065	3.7166	0.26906	27.886	28.884	0.13108	0.075537	0.91719	98.019	15.921
302.00	3.8790	5.5800	0.17921	26.462	27.158	0.12522			0	11.123
Single-Phase Properties										
100.00	0.10000	17.598	0.056826	4.1207	4.1264	0.010520	0.059127	0.083227	1033.2	-0.56370
175.00	0.10000	15.165	0.065942	10.689	10.696	0.059427	0.053557	0.090103	792.98	-0.43564
191.43	0.10000	14.574	0.068616	12.189	12.196	0.067617	0.055131	0.092642	699.56	-0.38082
191.43	0.10000	0.065539	15.258	26.284	27.809	0.14918	0.045695	0.056115	131.00	45.943
250.00	0.10000	0.048881	20.458	29.189	31.235	0.16476	0.052574	0.061514	150.16	17.864
325.00	0.10000	0.037259	26.839	33.487	36.171	0.18198	0.061422	0.069986	170.52	8.3711
400.00	0.10000	0.030170	33.145	38.384	41.699	0.19726	0.068694	0.077154	188.46	5.2121

TABLE 2-252 Thermodynamic Properties of R-13, Chlorotrifluoromethane (Concluded)

Temperature K	Pressure MPa	Density mol/dm ³	Volume dm ³ /mol	Int. energy kJ/mol	Enthalpy kJ/mol	Entropy kJ/(mol·K)	C _v kJ/(mol·K)	C _p kJ/(mol·K)	Sound speed m/s	Joule-Thomson K/MPa
Single-Phase Properties										
100.00	1.0000	17.609	0.056790	4.1118	4.1686	0.010431	0.058689	0.083187	1042.6	-0.56328
175.00	1.0000	15.188	0.065843	10.666	10.731	0.059291	0.053474	0.089928	800.56	-0.43907
248.71	1.0000	12.149	0.082311	17.878	17.960	0.093552	0.063142	0.11187	409.14	0.079502
248.71	1.0000	0.59985	1.6671	28.252	29.919	0.14164	0.059099	0.080842	129.16	21.866
250.00	1.0000	0.59355	1.6848	28.338	30.023	0.14205	0.059028	0.080216	129.97	21.418
325.00	1.0000	0.39827	2.5108	33.099	35.610	0.16162	0.062521	0.073958	162.24	8.9819
400.00	1.0000	0.31126	3.2128	38.116	41.329	0.17744	0.068870	0.078791	184.36	5.3350
100.00	5.0000	17.658	0.056633	4.0724	4.3555	0.010032	0.056929	0.083080	1081.6	-0.56120
175.00	5.0000	15.284	0.065427	10.564	10.891	0.058704	0.053220	0.089221	831.21	-0.45278
250.00	5.0000	12.436	0.080411	17.696	18.098	0.092801	0.062047	0.10644	461.89	-0.057256
325.00	5.0000	3.5611	0.28081	29.869	31.273	0.13759	0.071896	0.18862	120.24	10.597
400.00	5.0000	1.8042	0.55425	36.726	39.497	0.16061	0.070112	0.090875	170.26	5.4004
100.00	10.000	17.716	0.056446	4.0235	4.5880	0.0095294	0.055111	0.083086	1124.6	-0.55799
175.00	10.000	15.396	0.064954	10.446	11.096	0.058009	0.053119	0.088480	863.64	-0.46709
250.00	10.000	12.772	0.078295	17.377	18.160	0.091462	0.061300	0.10203	518.33	-0.17104
325.00	10.000	8.8242	0.11332	25.758	26.891	0.12181	0.069005	0.13617	240.23	1.3924
400.00	10.000	4.2213	0.23689	34.655	37.023	0.14997	0.071938	0.11434	173.36	3.9992
100.00	15.000	17.772	0.056268	3.9751	4.8192	0.0090235	0.053642	0.083232	1162.0	-0.55407
175.00	15.000	15.499	0.064521	10.336	11.304	0.057352	0.053200	0.087860	890.77	-0.47907
250.00	15.000	13.041	0.076680	17.115	18.265	0.090334	0.061058	0.099258	562.82	-0.24338
325.00	15.000	9.9265	0.10074	24.846	26.357	0.11854	0.068084	0.11665	322.91	0.49723
400.00	15.000	6.3827	0.15667	32.962	35.312	0.14333	0.072431	0.11694	213.68	1.9494
175.00	35.000	15.857	0.063065	9.9615	12.169	0.055005	0.054657	0.086150	962.40	-0.51269
250.00	35.000	13.811	0.072404	16.358	18.892	0.086896	0.062146	0.093881	679.17	-0.38660
325.00	35.000	11.718	0.085341	23.258	26.245	0.11257	0.069359	0.10153	492.75	-0.18758
400.00	35.000	9.7082	0.10301	30.364	33.969	0.13395	0.074599	0.10349	383.00	0.022671

The values in these tables were generated from the NIST REFPROP software (Lemmon, E. W., McLinden, M. O., and Huber, M. L., NIST Standard Reference Database 23: Reference Fluid Thermodynamic and Transport Properties—REFPROP, National Institute of Standards and Technology, Standard Reference Data Program, Gaithersburg, Md., 2002, Version 7.1). The primary source for the thermodynamic properties is Magee, J. W., Outcalt, S. L., and Ely, J. F., "Molar Heat Capacity $C(v)$, Vapor Pressure, and (p, ρ, T) Measurements from 92 to 350 K at Pressures to 35 MPa and a New Equation of State for Chlorotrifluoromethane (R13)," *Int. J. Thermophys.* **21**(5):1097–1121, 2000. Validated equations for the viscosity and thermal conductivity are not currently available for this fluid.

Properties at the triple point temperature and the critical point temperature are given in the first and last entries of the saturation tables, respectively. In the single-phase table, when the temperature range for a given isobar includes a vapor-liquid phase boundary, the temperature of phase equilibrium is noted, and properties for both the saturated liquid and saturated vapor are given (with liquid properties given in the upper line). Lines are omitted from the temperature-pressure grid of the single-phase table, when the system would be in the solid phase or if there are potential problems with the source property surface.

The uncertainties of the equation of state are 0.15% in density and 2% in heat capacity, except in the critical region. The uncertainty in vapor pressure is 0.1%.

TABLE 2-253 Saturated Refrigerant 13B1, Bromotrifluoromethane*

T, K	P, bar	v_f , m ³ /kg	v_g , m ³ /kg	h_f , kJ/kg	h_g , kJ/kg	s_f , kJ/(kg·K)	s_g , kJ/(kg·K)	c_{pf} , kJ/(kg·K)	μ_f , 10 ⁻⁴ Pa·s	k_f , W/(m·K)
170	0.059	4.594-4	1.6015	-40.90	90.95	-0.2033	0.5723	0.597	9.54	0.101
180	0.127	4.677-4	0.7840	-34.75	94.37	-0.1682	0.5491	0.618	7.60	0.096
190	0.250	4.765-4	0.4190	-28.51	97.83	-0.1345	0.5305	0.634	6.20	0.091
200	0.455	4.860-4	0.2407	-22.17	101.32	-0.1020	0.5154	0.648	5.13	0.086
210	0.777	4.961-4	0.1467	-15.68	104.82	-0.0704	0.5033	0.663	4.33	0.082
215.4	1.013	5.020-4	0.1147	-12.09	106.70	-0.0536	0.4978	0.670	3.97	0.079
220	1.254	5.071-4	0.0940	-9.02	108.28	-0.0396	0.4936	0.676	3.71	0.077
230	1.933	5.190-4	0.0628	-2.19	111.68	-0.0094	0.4857	0.690	3.22	0.073
240	2.863	5.321-4	0.0433	4.83	114.99	0.0202	0.4793	0.703	2.83	0.068
250	4.096	5.466-4	0.0308	12.03	118.16	0.0494	0.4739	0.721	2.51	0.063
260	5.690	5.627-4	0.0224	19.44	121.16	0.0781	0.4693	0.742	2.25	0.059
270	7.703	5.809-4	0.0166	27.06	123.93	0.1064	0.4652	0.767	2.04	0.054
280	10.20	6.018-4	0.0124	34.94	126.41	0.1345	0.4612	0.800	1.84	0.049
290	13.25	6.264-4	0.0094	43.11	128.51	0.1625	0.4570	0.842	1.69	0.045
300	16.91	6.562-4	0.0072	51.68	130.09	0.1908	0.4522	0.891	1.57	0.040
310	21.28	6.940-4	0.0055	60.81	130.97	0.2197	0.4460	0.951	1.45	0.035
320	26.44	7.458-4	0.0041	70.80	130.76	0.2503	0.4376	1.09	1.26	0.030
330	32.48	8.295-4	0.0030	82.42	128.59	0.2845	0.4245	1.29	0.99	0.026
340.2 ^c	39.64	1.344-3	0.0013	108.70	108.70	0.3605	0.3605	∞	0.35	∞

*Values reproduced or converted from Table 4, p. 17.83, *ASHRAE Handbook, 1981: Fundamentals*, American Society of Heating, Refrigerating and Air-Conditioning Engineers, Atlanta, 1981. Copyright material. Reproduced by permission of the copyright owner. c = critical point. The notation 4.594-4 signifies 4.594×10^{-4} .

The 1993 *ASHRAE Handbook—Fundamentals* (SI ed.) contains a table at closer temperature increments and also an enthalpy-log-pressure diagram from 0.1 to 35 bar, -80 to 220 °C. For tables and a chart to 500 psia, 480 °F, see Stewart, R. B., R. T. Jacobsen, et al., *Thermodynamic Properties of Refrigerants*, ASHRAE, Atlanta, GA, 1986 (521 pp.). For specific heat, thermal conductivity, and viscosity, see *Thermophysical Properties of Refrigerants*, ASHRAE, 1993.

Refrigerant 14 (tetrafluoromethane) See Carbon Tetrafluoride (Table 2-202).

Refrigerant 20 See Chloroform (Table 2-206).

TABLE 2-254 Saturated Refrigerant 21, Dichlorodifluoromethane

Temperature, K	Pressure, bar	v_f , m ³ /kg	v_g , m ³ /kg	h_f , kJ/kg	h_g , kJ/kg	s_f , kJ/(kg·K)	s_g , kJ/(kg·K)
250	0.2415	0.000 677	0.8292	16.6	274.8	0.0687	1.1015
260	0.3953	0.000 687	0.5247	26.5	279.9	0.1076	1.0820
270	0.6200	0.000 698	0.3455	36.6	284.9	0.1454	1.0653
280	0.9364	0.000 709	0.2355	46.7	290.0	0.1824	1.0511
290	1.3682	0.000 722	0.1654	57.1	295.0	0.2186	1.0389
300	1.9417	0.000 735	0.1192	67.7	300.0	0.2543	1.0286
310	2.6849	0.000 748	0.0879	78.4	304.8	0.2894	1.0196
320	3.6279	0.000 763	0.0661	89.5	309.5	0.3242	1.0119
330	4.8022	0.000 778	0.0505	100.7	314.1	0.3586	1.0051
340	6.2409	0.000 794	0.0391	112.3	318.4	0.3927	0.9989
350	7.978	0.000 812	0.0307	124.1	322.4	0.4266	0.9932
360	10.049	0.000 830	0.0243	136.2	326.1	0.4602	0.9877
370	12.489	0.000 850	0.0194	148.6	329.3	0.4935	0.9820
380	15.337	0.000 870	0.0155	161.2	331.9	0.5264	0.9758
390	18.630	0.000 893	0.0125	173.9	333.8	0.5587	0.9688
400	22.41	0.000 918	0.01011	186.4	334.8	0.5896	0.9605
410	26.72	0.000 944	0.00820	198.3	334.7	0.6180	0.9506
420	31.60	0.000 972	0.00672	208.7	333.7	0.6418	0.9394
430	37.10	0.001 002	0.00564	216.4	332.4	0.6587	0.9286
440	43.26	0.001 034	0.00491	221.1	332.3	0.6682	0.9208

Reproduced and rounded from unpublished Center for Applied Thermodynamic Studies, Moscow ID report, 1981. For a thermodynamic diagram to 350 bar, 370 °C, see Rombusch, U. K., *Allgem. Warme.*, **11**, 3 (1962).

TABLE 2-255 Thermodynamic Properties of R-22, Chlorodifluoromethane

Temperature K	Pressure MPa	Density mol/dm ³	Volume dm ³ /mol	Int. energy kJ/mol	Enthalpy kJ/mol	Entropy kJ/(mol·K)	C _v kJ/(mol·K)	C _p kJ/(mol·K)	Sound speed m/s	Joule-Thomson K/MPa
Saturated Properties										
115.73	3.7947E-07	19.907	0.050235	2.5595	2.5595	0.0065813	0.061918	0.092976	1410.9	-0.44463
120.00	9.9588E-07	19.777	0.050564	2.9559	2.9559	0.0099451	0.061567	0.092700	1388.4	-0.44526
135.00	1.7187E-05	19.325	0.051747	4.3400	4.3400	0.020814	0.060123	0.091960	1312.3	-0.44448
150.00	0.00015627	18.873	0.052985	5.7179	5.7179	0.030493	0.059099	0.091824	1239.0	-0.43872
165.00	0.00089946	18.420	0.054289	7.0951	7.0951	0.039243	0.058356	0.091789	1166.5	-0.43084
180.00	0.0037009	17.963	0.055670	8.4715	8.4717	0.047227	0.057679	0.091751	1095.0	-0.42063
195.00	0.011835	17.500	0.057141	9.8483	9.8490	0.054574	0.057097	0.091898	1024.5	-0.40608
210.00	0.031218	17.028	0.058726	11.230	11.232	0.061399	0.056707	0.092431	954.55	-0.38505
225.00	0.070909	16.542	0.060453	12.622	12.627	0.067804	0.056579	0.093482	884.79	-0.35555
240.00	0.14319	16.036	0.062359	14.034	14.043	0.073877	0.056737	0.095120	814.96	-0.31561
255.00	0.26329	15.506	0.064493	15.472	15.489	0.079692	0.057171	0.097391	744.97	-0.26226
270.00	0.44888	14.944	0.066919	16.945	16.975	0.085308	0.057856	0.10037	674.69	-0.19248
285.00	0.71966	14.341	0.069730	18.462	18.513	0.090782	0.058767	0.10424	603.91	-0.097827
300.00	1.0970	13.686	0.073070	20.034	20.114	0.096166	0.059887	0.10941	532.11	0.035333
315.00	1.6039	12.956	0.077181	21.676	21.800	0.10152	0.061218	0.11688	458.37	0.23608
330.00	2.2661	12.114	0.082547	23.418	23.605	0.10696	0.062814	0.12929	381.15	0.57205
345.00	3.1130	11.069	0.090340	25.325	25.606	0.11267	0.064858	0.15550	298.16	1.2334
360.00	4.1837	9.5229	0.10501	27.613	28.053	0.11931	0.068488	0.25950	201.90	3.0745
369.30	4.9900	6.0582	0.16506	30.901	31.725	0.12907			0	10.366
115.73	3.7947E-07	3.9436E-07	2,535,700.	27.807	28.769	0.23305	0.028465	0.036779	119.91	398.80
120.00	9.9588E-07	9.9813E-07	1,001,900.	27.929	28.927	0.22637	0.028872	0.037186	121.91	367.18
135.00	1.7187E-05	1.5313E-05	65,305.	28.373	29.495	0.20715	0.030386	0.038703	128.58	269.83
150.00	0.00015627	0.00012533	7,979.0	28.840	30.087	0.19295	0.031990	0.040316	134.79	197.57
165.00	0.00089946	0.00065634	1,523.6	29.329	30.699	0.18230	0.033655	0.042018	140.59	146.30
180.00	0.0037009	0.0024808	403.09	29.836	31.328	0.17421	0.035388	0.043849	145.98	110.28
195.00	0.011835	0.0073561	135.94	30.357	31.966	0.16800	0.037218	0.045881	150.87	84.902
210.00	0.031218	0.018161	55.062	30.885	32.603	0.16317	0.039177	0.048204	155.15	66.865
225.00	0.070909	0.038991	25.647	31.411	33.229	0.15937	0.041300	0.050920	158.70	53.872
240.00	0.14319	0.075182	13.301	31.928	33.833	0.15634	0.043615	0.054144	161.35	44.348
255.00	0.26329	0.13342	7.4950	32.428	34.401	0.15386	0.046138	0.058023	162.96	37.240
270.00	0.44888	0.22208	4.5029	32.900	34.922	0.15178	0.048881	0.062763	163.38	31.852
285.00	0.71966	0.35201	2.8409	33.335	35.380	0.14996	0.051851	0.068713	162.45	27.725
300.00	1.0970	0.53822	1.8580	33.717	35.755	0.14830	0.055064	0.076534	159.98	24.549
315.00	1.6039	0.80363	1.2443	34.021	36.017	0.14666	0.058574	0.087659	155.73	22.102
330.00	2.2661	1.1882	0.84159	34.207	36.114	0.14486	0.062516	0.10579	149.36	20.201
345.00	3.1130	1.7777	0.56253	34.184	35.935	0.14261	0.067254	0.14389	140.39	18.613
360.00	4.1837	2.8529	0.35052	33.661	35.127	0.13896	0.074178	0.29995	127.92	16.641
369.30	4.9900	6.0582	0.16506	30.901	31.725	0.12907			0	10.366

Single-Phase Properties

150.00	0.10000	18.874	0.052982	5.7167	5.7220	0.030484	0.059102	0.091820	1239.3	-0.43876
232.06	0.10000	16.306	0.061325	13.284	13.290	0.070699	0.056618	0.094177	851.94	-0.33819
232.06	0.10000	0.053734	18.610	31.656	33.517	0.15786	0.042364	0.052366	160.06	49.032
250.00	0.10000	0.049441	20.226	32.442	34.465	0.16180	0.043860	0.053391	166.39	38.154
350.00	0.10000	0.034652	28.859	37.325	40.211	0.18105	0.053191	0.061845	196.16	13.439
450.00	0.10000	0.026819	37.287	43.093	46.822	0.19762	0.061672	0.070141	221.08	6.7638
550.00	0.10000	0.021901	45.660	49.620	54.186	0.21238	0.068475	0.076877	243.30	4.0604
150.00	1.0000	18.885	0.052952	5.7053	5.7582	0.030408	0.059134	0.091780	1241.8	-0.43921
250.00	1.0000	15.711	0.063648	14.961	15.024	0.077665	0.057020	0.096318	773.25	-0.28642
296.57	1.0000	13.841	0.072248	19.669	19.741	0.094938	0.059612	0.10807	548.68	0.00029448
296.57	1.0000	0.48960	2.0425	33.635	35.677	0.14867	0.054305	0.074523	160.70	25.205
350.00	1.0000	0.37703	2.6523	36.754	39.407	0.16025	0.055369	0.068138	184.85	14.183
450.00	1.0000	0.27693	3.6110	42.774	46.385	0.17776	0.062289	0.072300	216.22	6.8582
550.00	1.0000	0.22209	4.5027	49.400	53.903	0.19283	0.068737	0.077971	241.16	4.0624
150.00	5.0000	18.931	0.052823	5.6555	5.9197	0.030074	0.059277	0.091614	1253.0	-0.44109
250.00	5.0000	15.837	0.063142	14.822	15.138	0.077105	0.057135	0.095206	797.37	-0.30700
350.00	5.0000	11.141	0.089759	25.585	26.034	0.11341	0.064765	0.143556	317.33	1.0314
450.00	5.0000	1.6422	0.60893	41.131	44.175	0.16067	0.065284	0.087278	194.56	7.0507
550.00	5.0000	1.1832	0.84520	48.377	52.603	0.17760	0.069855	0.083655	232.93	3.9600
150.00	10.000	18.987	0.052667	5.5953	6.1220	0.029665	0.059460	0.091420	1266.7	-0.44331
250.00	10.000	15.982	0.062569	14.663	15.289	0.076450	0.057274	0.094054	825.41	-0.32844
350.00	10.000	12.008	0.083275	24.782	25.615	0.11098	0.063647	0.11843	412.24	0.39255
450.00	10.000	4.2433	0.23566	38.423	40.780	0.14893	0.068870	0.12461	184.82	5.5220
550.00	10.000	2.5432	0.39321	47.019	50.951	0.16944	0.071068	0.092204	229.21	3.5059
150.00	30.000	19.198	0.052089	5.3741	6.9367	0.028113	0.060251	0.090769	1318.0	-0.45090
250.00	30.000	16.469	0.060719	14.132	15.953	0.074181	0.057799	0.091018	921.00	-0.38542
350.00	30.000	13.518	0.073976	23.279	25.499	0.10621	0.063170	0.10053	603.47	-0.13764
450.00	30.000	10.241	0.097648	33.086	36.016	0.13259	0.069234	0.10864	392.35	0.40072
550.00	30.000	7.3810	0.13548	42.738	46.802	0.15425	0.073417	0.10533	317.51	0.89994
150.00	60.000	19.480	0.051336	5.0916	8.1717	0.026007	0.061560	0.089983	1384.9	-0.45992
250.00	60.000	17.029	0.058724	13.533	17.056	0.071434	0.058519	0.088686	1034.6	-0.42947
350.00	60.000	14.650	0.068258	22.111	26.206	0.10216	0.063912	0.094730	764.59	-0.31532
450.00	60.000	12.381	0.080770	31.083	35.929	0.12657	0.070220	0.099099	589.21	-0.17799
550.00	60.000	10.405	0.096108	40.152	45.919	0.14662	0.075020	0.10030	492.11	-0.05349

The values in these tables were generated from the NIST REFPROP software (Lemmon, E. W., McLinden, M. O., and Huber, M. L., NIST Standard Reference Database 23: Reference Fluid Thermodynamic and Transport Properties—REFPROP, National Institute of Standards and Technology, Standard Reference Data Program, Gaithersburg, Md., 2002, Version 7.1). The primary source for the thermodynamic properties is Kamei, A., Beyerlein, S. W., and Jacobsen, R. T., "Application of Nonlinear Regression in the Development of a Wide Range Formulation for HCFC-22," *Int. J. Thermophys.* **16**:1155–1164, 1995. Validated equations for the viscosity and thermal conductivity are not currently available for this fluid.

Properties at the triple point temperature and the critical point temperature are given in the first and last entries of the saturation tables, respectively. In the single-phase table, when the temperature range for a given isobar includes a vapor-liquid phase boundary, the temperature of phase equilibrium is noted, and properties for both the saturated liquid and saturated vapor are given (with liquid properties given in the upper line). Lines are omitted from the temperature-pressure grid of the single-phase table, when the system would be in the solid phase or if there are potential problems with the source property surface.

The uncertainties of the equation of state are 0.1% in density, 1% in heat capacity, and 0.3% in the speed of sound, except in the critical region. The uncertainty in vapor pressure is 0.2%.

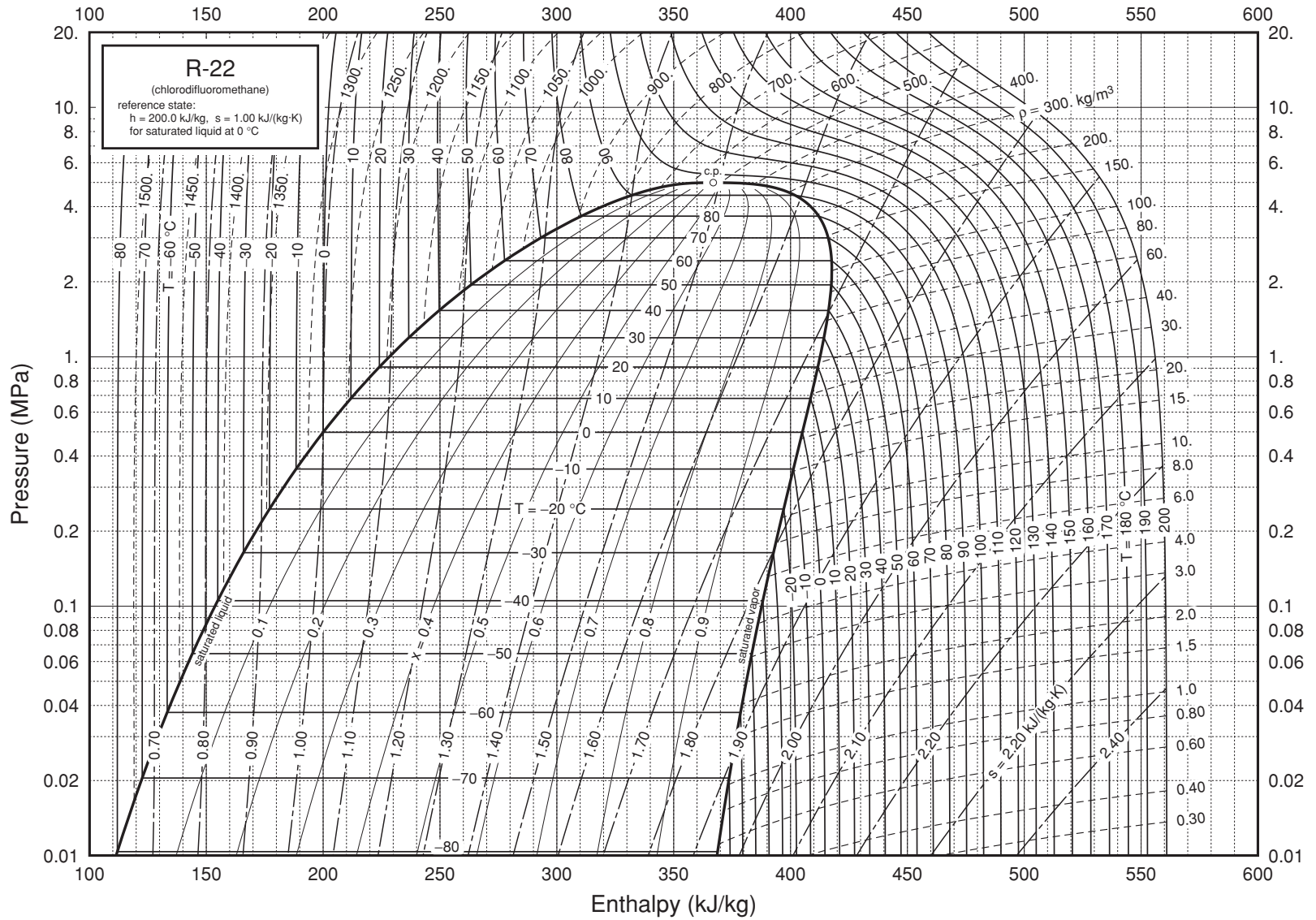


FIG. 2-20 Pressure-enthalpy diagram for Refrigerant 22. Properties computed with the NIST REFPROP Database, Version 7.0 (Lemmon, E. W., McLinden, M. O., and Huber, M. L., 2002, NIST Standard Reference Database 23, NIST Reference Fluid Thermodynamic and Transport Properties—REFPROP, Version 7.0, Standard Reference Data Program, National Institute of Standards and Technology), based on the equation of state of Kamei, A., Beylerlein, S. W., and Jacobsen, R. T., "Application of Nonlinear Regression in the Development of a Wide Range Formulation for HCFC-22," *Int. J. Thermophysics* **16**:1155–1164, 1995.

TABLE 2-256 Thermodynamic Properties of R-23, Trifluoromethane

Temperature K	Pressure MPa	Density mol/dm ³	Volume dm ³ /mol	Int. energy kJ/mol	Enthalpy kJ/mol	Entropy kJ/(mol·K)	C _v kJ/(mol·K)	C _p kJ/(mol·K)	Sound speed m/s	Joule-Thomson K/MPa	Therm. cond. mW/(m·K)	Viscosity μPa·s
Saturated Properties												
118.02	5.8041E-05	24.308	0.041139	-0.25719	-0.25719	-0.0049376	0.057095	0.085477	1211.2	-0.37494	268.59	2055.0
120.00	8.1883E-05	24.217	0.041293	-0.088512	-0.088509	-0.0035202	0.055755	0.084936	1208.8	-0.37515	261.17	1889.2
130.00	0.00038808	23.746	0.042112	0.75355	0.75356	0.0032204	0.052298	0.083783	1168.8	-0.37102	229.32	1285.4
140.00	0.0014276	23.263	0.042987	1.5903	1.5904	0.0094218	0.051128	0.083657	1111.2	-0.36298	204.76	927.74
150.00	0.0043019	22.771	0.043915	2.4276	2.4278	0.015198	0.050605	0.083836	1051.8	-0.35278	185.36	707.09
160.00	0.011055	22.272	0.044900	3.2675	3.2680	0.020619	0.050302	0.084188	994.03	-0.34018	169.64	551.48
170.00	0.024979	21.763	0.045950	4.1116	4.1127	0.025736	0.050114	0.084721	938.04	-0.32445	156.60	446.01
180.00	0.050823	21.243	0.047074	4.9618	4.9642	0.030596	0.050024	0.085477	883.23	-0.30465	145.55	369.03
190.00	0.094862	20.709	0.048258	5.8204	5.8250	0.035238	0.050032	0.086504	829.00	-0.27966	135.98	310.79
200.00	0.16485	20.158	0.049608	6.6899	6.6981	0.039699	0.050140	0.087863	774.87	-0.24798	127.54	265.32
210.00	0.26991	19.584	0.051061	7.5735	7.5873	0.044011	0.050350	0.089628	720.45	-0.20758	119.92	228.80
220.00	0.42035	18.982	0.052680	8.4748	8.4969	0.048206	0.050666	0.091906	665.40	-0.15554	112.91	198.71
230.00	0.62755	18.345	0.054512	9.3983	9.4325	0.052315	0.051093	0.094862	609.38	-0.087415	106.33	173.29
240.00	0.90390	17.660	0.056625	10.350	10.401	0.056370	0.051645	0.098763	552.02	0.0038879	100.01	151.31
250.00	1.2628	16.913	0.059125	11.336	11.411	0.060409	0.052347	0.10409	492.89	0.13049	93.771	131.85
260.00	1.7190	16.081	0.062186	12.370	12.477	0.064481	0.053248	0.11180	431.39	0.31494	87.445	114.17
270.00	2.2887	15.123	0.066126	13.469	13.621	0.068658	0.054447	0.12412	366.67	0.60438	80.778	97.624
280.00	2.9913	13.958	0.071643	14.670	14.885	0.073078	0.056175	0.14787	297.30	1.1166	73.344	81.444
290.00	3.8516	12.367	0.080863	16.074	16.386	0.078112	0.059136	0.21909	220.12	2.2579	64.064	64.222
299.29	4.8317	7.5200	0.13298	19.029	19.672	0.088893			0	8.4094		
118.02	5.8041E-05	5.9176E-05	16.899.	19.268	20.249	0.16881	0.026617	0.034991	135.67	1947.8	3.7962	5.3460
120.00	8.1883E-05	8.2116E-05	12.178.	19.320	20.317	0.16652	0.026770	0.035155	136.72	1684.9	3.9025	5.4612
130.00	0.00038808	0.00035955	2,781.2	19.581	20.661	0.15635	0.027678	0.036154	141.80	854.63	4.4400	6.0411
140.00	0.0014276	0.0012302	812.86	19.845	21.005	0.14810	0.028813	0.037439	146.52	472.27	4.9794	6.6166
150.00	0.0043019	0.0034701	288.17	20.109	21.348	0.14134	0.030153	0.039008	150.89	282.89	5.5230	7.1868
160.00	0.011055	0.0083994	119.06	20.372	21.688	0.13574	0.031671	0.040857	154.87	182.40	6.0746	7.7511
170.00	0.024979	0.017990	55.587	20.632	22.020	0.13107	0.033344	0.042992	158.43	125.40	6.6400	8.3091
180.00	0.050823	0.034921	28.636	20.886	22.342	0.12714	0.035155	0.045436	161.51	90.972	7.2268	8.8611
190.00	0.094862	0.062608	15.972	21.133	22.648	0.12378	0.037094	0.048225	164.02	68.962	7.8452	9.4081
200.00	0.16485	0.10526	9.5007	21.369	22.935	0.12088	0.039149	0.051416	165.89	54.182	8.5073	9.9521
210.00	0.26991	0.16798	5.9532	21.589	23.196	0.11834	0.041312	0.055095	167.03	43.846	9.2284	10.497
220.00	0.42035	0.25707	3.8900	21.791	23.426	0.11607	0.043578	0.059399	167.35	36.378	10.028	11.048
230.00	0.62755	0.38050	2.6281	21.968	23.617	0.11399	0.045950	0.064561	166.76	30.839	10.931	11.616
240.00	0.90390	0.54888	1.8219	22.112	23.759	0.11203	0.048442	0.070995	165.16	26.639	11.970	12.216
250.00	1.2628	0.77721	1.2866	22.214	23.839	0.11012	0.051088	0.079472	162.43	23.387	13.197	12.873
260.00	1.7190	1.0885	0.91866	22.256	23.835	0.10816	0.053955	0.091578	158.44	20.801	14.687	13.633
270.00	2.2887	1.5223	0.65691	22.209	23.712	0.10603	0.057163	0.11107	153.01	18.652	16.578	14.579
280.00	2.9913	2.1579	0.46341	22.017	23.403	0.10350	0.060947	0.14938	145.86	16.699	19.150	15.906
290.00	3.8516	3.2161	0.31093	21.529	22.727	0.099978	0.065857	0.26628	136.34	14.524	23.215	18.223
299.29	4.8317	7.5200	0.13298	19.029	19.672	0.088893			0	8.4094		
Single-Phase Properties												
150.00	0.10000	22.773	0.043911	2.4262	2.4306	0.015189	0.050608	0.083827	1052.1	-0.35289	185.41	702.64
190.90	0.10000	20.660	0.048402	5.8986	5.9034	0.035649	0.050037	0.086612	824.11	-0.27709	135.18	306.22
190.90	0.10000	0.065782	15.202	21.155	22.675	0.12350	0.037275	0.048496	164.22	67.381	7.9031	9.4574
250.00	0.10000	0.048799	20.492	23.373	25.422	0.13604	0.038440	0.047375	188.56	22.325	11.046	12.547
350.00	0.10000	0.034513	28.974	27.705	30.603	0.15338	0.048023	0.056526	220.23	8.0459	16.386	17.318
450.00	0.10000	0.026771	37.355	32.978	36.713	0.16869	0.057058	0.065464	247.21	4.0690	21.735	21.621
150.00	1.0000	22.792	0.043874	2.4134	2.4573	0.015103	0.050638	0.083752	1055.5	-0.35386	185.86	707.90
242.93	1.0000	17.448	0.057313	10.635	10.692	0.057555	0.051834	0.10015	534.88	0.036629	98.175	145.37
242.93	1.0000	0.60881	1.6425	22.147	23.790	0.11147	0.049200	0.073220	164.48	25.601	12.308	12.401
250.00	1.0000	0.57474	1.7399	22.544	24.284	0.11347	0.046933	0.067137	169.72	23.136	12.612	12.737
350.00	1.0000	0.35949	2.7818	27.401	30.182	0.13337	0.048882	0.059316	214.59	8.0837	17.536	17.376
450.00	1.0000	0.27164	3.6813	32.791	36.472	0.14914	0.057361	0.066629	245.15	4.0345	22.720	21.629

TABLE 2-256 Thermodynamic Properties of R-23, Trifluoromethane (Concluded)

Temperature K	Pressure MPa	Density mol/dm ³	Volume dm ³ /mol	Int. energy kJ/mol	Enthalpy kJ/mol	Entropy kJ/(mol·K)	C _v kJ/(mol·K)	C _p kJ/(mol·K)	Sound speed m/s	Joule-Thomson K/MPa	Therm. cond. mW/(m·K)	Viscosity μPa·s
Single-Phase Properties												
150.00	5.0000	22.876	0.043714	2.3577	2.5763	0.014729	0.050778	0.083431	1070.0	-0.35795	187.83	731.40
250.00	5.0000	17.302	0.057797	11.094	11.383	0.059422	0.051903	0.098833	539.89	0.027079	97.307	141.75
350.00	5.0000	2.2512	0.44420	25.765	27.986	0.11523	0.053415	0.081317	190.19	7.7729	23.888	19.400
450.00	5.0000	1.4480	0.69062	31.931	35.384	0.13386	0.058685	0.072566	237.91	3.7699	27.113	22.593
150.00	10.000	22.976	0.043523	2.2910	2.7262	0.014275	0.050969	0.083065	1086.9	-0.36259	190.23	761.17
250.00	10.000	17.719	0.056437	10.828	11.392	0.058319	0.051625	0.094482	590.19	-0.061719	101.24	153.45
350.00	10.000	6.4822	0.15427	22.835	24.378	0.10116	0.058836	0.14411	186.97	4.7798	39.852	30.808
450.00	10.000	3.1053	0.32203	30.818	34.039	0.12572	0.060182	0.081111	235.46	3.2093	33.390	25.446
150.00	50.000	23.670	0.042247	1.8477	3.9600	0.011072	0.052531	0.080990	1193.2	-0.38760	207.85	1020.9
250.00	50.000	19.633	0.050935	9.5803	12.127	0.052740	0.052051	0.083522	826.45	-0.29649	121.46	226.71
350.00	50.000	15.604	0.064086	17.587	20.792	0.081836	0.057678	0.089445	563.57	-0.085583	92.030	113.25
450.00	50.000	12.055	0.082953	25.724	29.871	0.10464	0.064073	0.091553	437.72	0.13382	77.100	73.803
250.00	100.00	20.957	0.047717	8.7360	13.508	0.048428	0.053244	0.080401	1002.1	-0.36685	137.85	307.24
350.00	100.00	17.954	0.055698	16.172	21.741	0.076094	0.059172	0.084434	778.97	-0.30018	111.99	167.69
450.00	100.00	15.405	0.064915	23.879	30.370	0.097761	0.065748	0.087934	652.70	-0.24430	100.34	119.14

The values in these tables were generated from the NIST REFPROP software (Lemmon, E. W., McLinden, M. O., and Huber, M. L., NIST Standard Reference Database 23: Reference Fluid Thermodynamic and Transport Properties—REFPROP, National Institute of Standards and Technology, Standard Reference Data Program, Gaithersburg, Md., 2002, Version 7.1). The primary source for the thermodynamic properties is Penoncello, S. G., Lemmon, E. W., Jacobsen, R. T., and Shan, Z., "A Fundamental Equation for Trifluoromethane (R-23)," *J. Phys. Chem. Ref. Data*, **32**(4):1473-1499, 2003. The source for viscosity and thermal conductivity is Shan, Z., Penoncello, S. G., and Jacobsen, R. T., "A Generalized Model for Viscosity and Thermal Conductivity of Trifluoromethane (R-23)," *ASHRAE Trans.* **106**:1-11, 2000.

Properties at the triple point temperature and the critical point temperature are given in the first and last entries of the saturation tables, respectively. In the single-phase table, when the temperature range for a given isobar includes a vapor-liquid phase boundary, the temperature of phase equilibrium is noted, and properties for both the saturated liquid and saturated vapor are given (with liquid properties given in the upper line). Lines are omitted from the temperature-pressure grid of the single-phase table, when the system would be in the solid phase or if there are potential problems with the source property surface.

The uncertainties of the equation of state are 0.1% in density, 0.5% in heat capacities and speed of sound, and 0.2% in vapor pressures. Uncertainties in the critical region will be higher. The uncertainty in viscosity is 1%. The uncertainty in thermal conductivity is 2%.

TABLE 2-257 Thermodynamic Properties of R-32, Difluoromethane

Temperature K	Pressure MPa	Density mol/dm ³	Volume dm ³ /mol	Int. energy kJ/mol	Enthalpy kJ/mol	Entropy kJ/(mol·K)	C _v kJ/(mol·K)	C _p kJ/(mol·K)	Sound speed m/s	Joule-Thomson K/MPa	Therm. cond. mW/(m·K)
Saturated Properties											
136.34	4.8000E-05	27.473	0.036399	-0.99220	-0.99220	-0.0054608	0.055447	0.082847	1414.4	-0.33760	242.91
140.00	8.3535E-05	27.302	0.036627	-0.68946	-0.68946	-0.0032696	0.054980	0.082588	1395.1	-0.33728	241.74
150.00	0.00032474	26.835	0.037265	0.13324	0.13325	0.0024067	0.053793	0.081975	1342.3	-0.33542	237.64
160.00	0.0010410	26.364	0.037930	0.95053	0.95057	0.0076815	0.052740	0.081513	1289.9	-0.33191	232.45
170.00	0.0028536	25.889	0.038626	1.7640	1.7641	0.012613	0.051818	0.081215	1237.6	-0.32650	226.39
180.00	0.0068782	25.409	0.039357	2.5753	2.5756	0.017251	0.051021	0.081087	1185.7	-0.31891	219.64
190.00	0.014904	24.921	0.040127	3.3862	3.3868	0.021635	0.050345	0.081137	1133.8	-0.30886	212.37
200.00	0.029545	24.424	0.040944	4.1983	4.1995	0.025800	0.049783	0.081373	1082.1	-0.29600	204.70
210.00	0.054344	23.916	0.041814	5.0135	5.0158	0.029778	0.049333	0.081803	1030.4	-0.27988	196.75
220.00	0.093819	23.394	0.042745	5.8337	5.8377	0.033594	0.048988	0.082443	978.59	-0.25996	188.62
230.00	0.15345	22.858	0.043749	6.6608	6.6675	0.037271	0.048747	0.083313	926.62	-0.23550	180.39
240.00	0.23965	22.303	0.044838	7.4969	7.5077	0.040830	0.048604	0.084442	874.35	-0.20551	172.14
250.00	0.35967	21.726	0.046028	8.3443	8.3609	0.044291	0.048559	0.085874	821.65	-0.16864	163.92
260.00	0.52157	21.124	0.047340	9.2056	9.2303	0.047671	0.048610	0.087676	768.33	-0.12292	155.78
270.00	0.73415	20.491	0.048802	10.084	10.120	0.050989	0.048761	0.089947	714.18	-0.065518	147.75
280.00	1.0069	19.820	0.050454	10.983	11.034	0.054264	0.049019	0.092852	658.88	0.0079177	139.86
290.00	1.3501	19.102	0.052350	11.908	11.979	0.057517	0.049399	0.096659	602.05	0.10428	132.11
300.00	1.7749	18.323	0.054577	12.866	12.963	0.060775	0.049934	0.10185	543.11	0.23517	124.48
310.00	2.2934	17.460	0.057273	13.867	13.998	0.064076	0.050685	0.10938	481.27	0.42163	116.94
320.00	2.9194	16.477	0.060691	14.930	15.107	0.067477	0.051776	0.12140	415.41	0.70602	109.42
330.00	3.6686	15.299	0.065364	16.088	16.328	0.071088	0.053487	0.14404	343.84	1.1876	101.80
340.00	4.5614	13.740	0.072779	17.428	17.760	0.075179	0.056594	0.20457	263.77	2.1660	94.166
350.00	5.6311	10.732	0.093180	19.453	19.977	0.081343	0.066340	1.2085	163.70	5.4955	97.067
351.26	5.7826	8.1501	0.12270	20.836	21.546	0.085769			0	8.0731	
136.34	4.8000E-05	4.2353E-05	23.611	21.981	23.115	0.17135	0.025987	0.034319	169.60	881.12	6.9492
140.00	8.3535E-05	7.1788E-05	13.930	22.076	23.239	0.16765	0.026110	0.034451	171.76	769.01	6.9554
150.00	0.00032474	0.00026061	3.837.2	22.335	23.581	0.15872	0.026507	0.034889	177.47	541.12	7.0006
160.00	0.0010410	0.00078411	1,275.3	22.593	23.921	0.15125	0.027014	0.035477	182.88	391.73	7.0875
170.00	0.0028536	0.0020270	493.35	22.850	24.258	0.14493	0.027667	0.036272	187.97	291.02	7.2166
180.00	0.0068782	0.0046295	216.01	23.103	24.589	0.13955	0.028505	0.037336	192.69	221.02	7.3887
190.00	0.014904	0.0095503	104.71	23.350	24.910	0.13492	0.029560	0.038728	197.00	170.81	7.6049
200.00	0.029545	0.018112	55.213	23.588	25.219	0.13090	0.030843	0.040483	200.85	133.79	7.8668
210.00	0.054344	0.032028	31.223	23.816	25.513	0.12738	0.032341	0.042613	204.20	106.00	8.1765
220.00	0.093819	0.053428	18.717	24.032	25.788	0.12428	0.034016	0.045105	206.99	84.924	8.5374
230.00	0.15345	0.084890	11.780	24.234	26.042	0.12151	0.035821	0.047943	209.19	68.870	8.9546
240.00	0.23965	0.12949	7.7224	24.421	26.272	0.11901	0.037709	0.051127	210.73	56.605	9.4365
250.00	0.35967	0.19093	5.2375	24.590	26.474	0.11674	0.039648	0.054696	211.57	47.194	9.9965
260.00	0.52157	0.27370	3.6537	24.738	26.643	0.11464	0.041621	0.058741	211.65	39.922	10.656
270.00	0.73415	0.38340	2.6083	24.860	26.775	0.11268	0.043631	0.063434	210.90	34.246	11.449
280.00	1.0069	0.52726	1.8966	24.952	26.862	0.11079	0.045693	0.069063	209.26	29.758	12.431
290.00	1.3501	0.71503	1.3985	25.006	26.894	0.10895	0.047840	0.076110	206.64	26.148	13.691
300.00	1.7749	0.96054	1.0411	25.011	26.858	0.10709	0.050119	0.085424	202.95	23.187	15.376
310.00	2.2934	1.2848	0.77830	24.950	26.735	0.10516	0.052598	0.098649	198.02	20.693	17.748
320.00	2.9194	1.7233	0.58029	24.797	26.491	0.10305	0.055390	0.11948	191.66	18.510	21.309
330.00	3.6686	2.3442	0.42658	24.503	26.068	0.10060	0.058707	0.15836	183.49	16.477	27.173
340.00	4.5614	3.3211	0.30111	23.943	25.316	0.097403	0.063103	0.26199	172.68	14.312	38.601
350.00	5.6311	5.7166	0.17433	22.380	23.365	0.091024	0.071998	1.9028	154.59	10.637	87.141
351.26	5.7826	8.1501	0.12270	20.836	21.546	0.085769			0	8.0731	
Single-Phase Properties											
150.00	0.10000	26.836	0.037263	0.13226	0.13599	0.0024002	0.053795	0.081971	1342.7	-0.33547	237.67
221.24	0.10000	23.329	0.042866	5.9359	5.9402	0.034057	0.048953	0.082538	972.15	-0.25719	187.60
221.24	0.10000	0.056727	17.628	24.058	25.821	0.12392	0.034234	0.045439	207.30	82.688	8.5859
225.00	0.10000	0.055592	17.988	24.191	25.989	0.12467	0.033681	0.044513	209.39	76.114	8.7199
300.00	0.10000	0.040576	24.645	26.760	29.224	0.13708	0.035327	0.044188	241.95	25.024	12.643
375.00	0.10000	0.032244	31.013	29.631	32.733	0.14749	0.041082	0.049630	267.64	12.117	18.907

TABLE 2-257 Thermodynamic Properties of R-32, Difluoromethane (Concluded)

Temperature K	Pressure MPa	Density mol/dm ³	Volume dm ³ /mol	Int. energy kJ/mol	Enthalpy kJ/mol	Entropy kJ/(mol·K)	C _v kJ/(mol·K)	C _p kJ/(mol·K)	Sound speed m/s	Joule-Thomson K/MPa	Therm. cond. mW/(m·K)
Single-Phase Properties											
150.00	1.0000	26.851	0.037243	0.12350	0.16075	0.0023417	0.053807	0.081935	1345.7	-0.33584	237.89
225.00	1.0000	23.159	0.043179	6.2265	6.2697	0.035360	0.048867	0.082690	957.47	-0.25084	185.10
279.77	1.0000	19.836	0.050414	10.962	11.013	0.054190	0.049012	0.092777	660.15	0.0060372	140.04
279.77	1.0000	0.52357	1.9100	24.951	26.861	0.11084	0.045646	0.068922	209.31	29.848	12.406
300.00	1.0000	0.46100	2.1692	25.950	28.120	0.11518	0.041298	0.057916	223.83	23.889	13.334
375.00	1.0000	0.33917	2.9484	29.227	32.175	0.12727	0.042549	0.053538	259.50	11.929	19.059
150.00	5.0000	26.915	0.037154	0.085198	0.27097	0.0020846	0.053863	0.081784	1358.9	-0.33741	238.83
225.00	5.0000	23.298	0.042923	6.1394	6.3541	0.034970	0.048922	0.082027	978.81	-0.26135	187.71
300.00	5.0000	18.710	0.053448	12.637	12.905	0.060001	0.049679	0.096911	586.17	0.13431	128.72
344.33	5.0000	12.808	0.078078	18.130	18.520	0.077304	0.059015	0.28240	224.84	2.9944	91.412
344.33	5.0000	3.9887	0.25071	23.524	24.777	0.095475	0.065786	0.39574	166.61	13.148	48.235
375.00	5.0000	2.3228	0.43051	26.928	29.080	0.10755	0.050835	0.090625	218.44	10.800	26.239
150.00	10.000	26.993	0.037047	0.038702	0.40917	0.0017692	0.053932	0.081608	1375.0	-0.33924	239.97
225.00	10.000	23.461	0.042625	6.0369	6.4632	0.034504	0.048996	0.081303	1004.1	-0.27287	190.81
300.00	10.000	19.196	0.052094	12.346	12.867	0.058997	0.049538	0.092105	639.69	0.031716	134.49
375.00	10.000	10.448	0.095714	21.112	22.069	0.085980	0.057265	0.21222	231.14	3.5190	77.284
150.00	30.000	27.285	0.036650	-0.13357	0.96593	0.00056834	0.054209	0.081027	1436.1	-0.34524	244.02
225.00	30.000	24.030	0.041614	5.6813	6.9297	0.032836	0.049307	0.079197	1094.1	-0.30661	201.89
300.00	30.000	20.517	0.048739	11.542	13.004	0.056105	0.049670	0.083697	789.57	-0.15824	152.78
375.00	30.000	16.472	0.060708	17.786	19.607	0.075712	0.052941	0.093069	536.98	0.21392	112.94
225.00	70.000	24.916	0.040135	5.1400	7.9495	0.030109	0.049916	0.076915	1240.7	-0.34341	219.54
300.00	70.000	22.090	0.045270	10.583	13.752	0.052355	0.050281	0.078370	986.17	-0.28333	179.29
375.00	70.000	19.309	0.051788	16.127	19.752	0.070195	0.053544	0.081767	788.81	-0.18583	147.00

The values in these tables were generated from the NIST REFPROP software (Lemmon, E. W., McLinden, M. O., and Huber, M. L., NIST Standard Reference Database 23: Reference Fluid Thermodynamic and Transport Properties—REFPROP, National Institute of Standards and Technology, Standard Reference Data Program, Gaithersburg, Md., 2002, Version 7.1). The primary source for the thermodynamic properties is Tillner-Roth, R., and Yokozeki, A., "An International Standard Equation of State for Difluoromethane (R-32) for Temperatures from the Triple Point at 136.34 K to 435 K and Pressures up to 70 MPa," *J. Phys. Chem. Ref. Data* **26**(6):1273–1328, 1997. Validated equations for the viscosity are not currently available for this fluid. The source for thermal conductivity is unpublished; however, the fit uses the functional form found in Marsh, K., Perkins, R., and Ramires, M. L. V., "Measurement and Correlation of the Thermal Conductivity of Propane from 86 to 600 K at Pressures to 70 MPa," *J. Chem. Eng. Data* **47**(4):932–940, 2002.

Properties at the triple point temperature and the critical point temperature are given in the first and last entries of the saturation tables, respectively. In the single-phase table, when the temperature range for a given isobar includes a vapor-liquid phase boundary, the temperature of phase equilibrium is noted, and properties for both the saturated liquid and saturated vapor are given (with liquid properties given in the upper line). Lines are omitted from the temperature-pressure grid of the single-phase table, when the system would be in the solid phase or if there are potential problems with the source property surface.

For the equation of state, typical uncertainties are 0.05% for density, 0.02% for the vapor pressure, and 0.5% to 1% for the heat capacity and speed of sound in the liquid phase. In the vapor phase, the uncertainty in the speed of sound is 0.02%. For thermal conductivity, the estimated uncertainty of the correlation is 5%, except for the dilute gas and points approaching critical where the uncertainty rises to 10%.

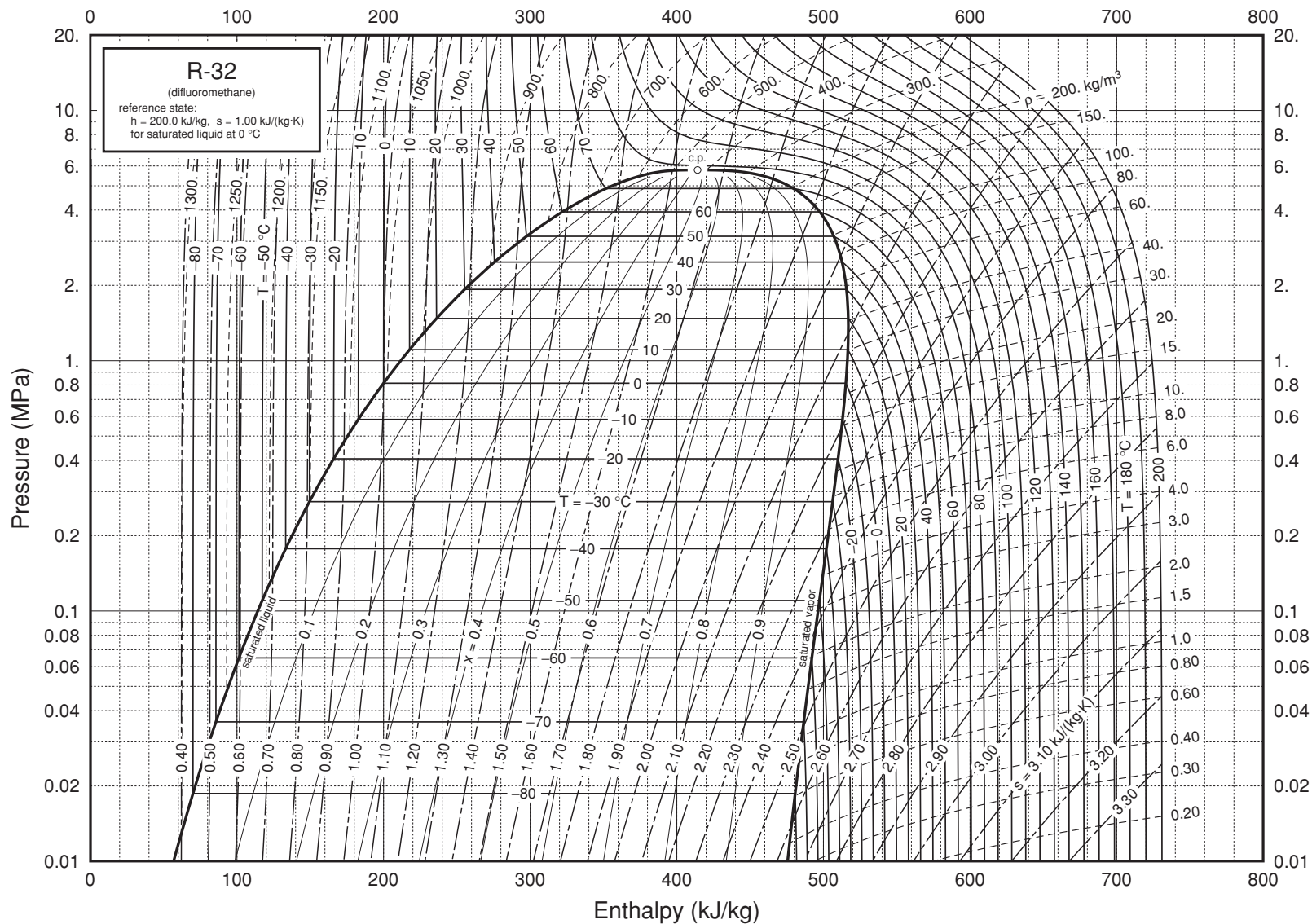


FIG. 2-21 Pressure-enthalpy diagram for Refrigerant 32. Properties computed with the NIST REFPROP Database, Version 7.0 (Lemmon, E. W., McLinden, M. O., and Huber, M. L., 2002, NIST Standard Reference Database 23, NIST Reference Fluid Thermodynamic and Transport Properties—REFPROP, Version 7.0, Standard Reference Data Program, National Institute of Standards and Technology), based on the equation of state of Tillner-Roth, R., and Yokozeki, A., “An International Standard Equation of State for Difluoromethane (R-32) for Temperatures from the Triple Point at 136.34 K to 435 K and Pressures up to 70 MPa,” *J. Phys. Chem. Ref. Data* **26**(6):1273–1328, 1997.

TABLE 2-258 Thermodynamic Properties of R-41, Fluoromethane

Temperature K	Pressure MPa	Density mol/dm ³	Volume dm ³ /mol	Int. energy kJ/mol	Enthalpy kJ/mol	Entropy kJ/(mol·K)	C _v kJ/(mol·K)	C _p kJ/(mol·K)	Sound speed m/s	Joule-Thomson K/MPa
Saturated Properties										
129.82	0.00034504	29.650	0.033727	-3.7550	-3.7549	-0.019920	0.050428	0.072206	1413.8	-0.35314
130.00	0.00035370	29.640	0.033738	-3.7420	-3.7420	-0.019820	0.050396	0.072196	1413.1	-0.35309
140.00	0.0012519	29.080	0.034388	-3.0231	-3.0230	-0.014492	0.048727	0.071584	1371.7	-0.35022
150.00	0.0036677	28.514	0.035070	-2.3102	-2.3100	-0.0095735	0.047265	0.071018	1325.5	-0.34606
160.00	0.0092373	27.942	0.035788	-1.6024	-1.6021	-0.0050057	0.045989	0.070568	1276.1	-0.33979
170.00	0.020585	27.362	0.036548	-0.89848	-0.89772	-0.00073794	0.044881	0.070278	1224.2	-0.33071
180.00	0.041505	26.770	0.037355	-0.19668	-0.19513	0.0032736	0.043923	0.070180	1170.6	-0.31808
190.00	0.077054	26.165	0.038218	0.50493	0.50787	0.0070672	0.043101	0.070303	1115.6	-0.30109
200.00	0.13355	25.544	0.039148	1.2085	1.2137	0.010676	0.042407	0.070678	1059.3	-0.27874
210.00	0.21852	24.901	0.040159	1.9164	1.9251	0.014131	0.041832	0.071342	1001.8	-0.24979
220.00	0.34056	24.233	0.041266	2.6312	2.6453	0.017458	0.041372	0.072345	943.19	-0.21256
230.00	0.50928	23.534	0.042492	3.3561	3.3778	0.020682	0.041022	0.073761	883.36	-0.16475
240.00	0.73518	22.796	0.043868	4.0946	4.1268	0.023828	0.040783	0.075695	822.19	-0.10306
250.00	1.0296	22.010	0.045434	4.8508	4.8976	0.026921	0.040657	0.078315	759.47	-0.022535
260.00	1.4048	21.164	0.047251	5.6304	5.6968	0.029987	0.040652	0.081902	694.85	0.084654
270.00	1.8740	20.239	0.049410	6.4408	6.5334	0.033058	0.040786	0.086969	627.81	0.23174
280.00	2.4519	19.207	0.052065	7.2930	7.4207	0.036178	0.041098	0.094564	557.39	0.44318
290.00	3.1548	18.018	0.055501	8.2059	8.3810	0.039414	0.041677	0.10725	481.85	0.77036
300.00	4.0027	16.564	0.060372	9.2189	9.4606	0.042906	0.042763	0.13357	397.63	1.3453
310.00	5.0232	14.501	0.068961	10.456	10.802	0.047088	0.045267	0.23071	295.99	2.6641
317.28	5.9062	9.3000	0.10753	12.765	13.400	0.055113			0	7.4905
129.82	0.00034504	0.00031992	3125.8	14.466	15.544	0.12874	0.025226	0.033592	205.35	365.81
130.00	0.00035370	0.00032749	3053.5	14.470	15.550	0.12858	0.025228	0.033595	205.49	363.97
140.00	0.0012519	0.0010777	927.93	14.716	15.878	0.12051	0.025399	0.033848	213.06	278.51
150.00	0.0036677	0.0029538	338.55	14.957	16.199	0.11382	0.025715	0.034322	220.17	217.09
160.00	0.0092373	0.0070026	142.80	15.190	16.509	0.10819	0.026225	0.035097	226.74	170.82
170.00	0.020585	0.014779	67.662	15.411	16.804	0.10339	0.026955	0.036230	232.71	135.12
180.00	0.041505	0.028398	35.214	15.620	17.081	0.099254	0.027900	0.037744	238.00	107.41
190.00	0.077054	0.050558	19.779	15.813	17.337	0.095640	0.029030	0.039636	242.53	85.993
200.00	0.13355	0.084573	11.824	15.988	17.567	0.092444	0.030304	0.041897	246.25	69.518
210.00	0.21852	0.13444	7.4384	16.144	17.769	0.089580	0.031684	0.044538	249.08	56.880
220.00	0.34056	0.20496	4.8791	16.278	17.940	0.086979	0.033143	0.047606	250.96	47.167
230.00	0.50928	0.30200	3.3112	16.388	18.075	0.084582	0.034668	0.051200	251.81	39.654
240.00	0.73518	0.43294	2.3098	16.470	18.168	0.082334	0.036262	0.055502	251.54	33.780
250.00	1.0296	0.60737	1.6464	16.519	18.214	0.080186	0.037939	0.060820	250.07	29.121
260.00	1.4048	0.83844	1.1927	16.527	18.203	0.078086	0.039727	0.067681	247.30	25.360
270.00	1.8740	1.1452	0.87319	16.484	18.121	0.075974	0.041668	0.077052	243.07	22.257
280.00	2.4519	1.5578	0.64192	16.374	17.948	0.073776	0.043822	0.090909	237.22	19.624
290.00	3.1548	2.1293	0.46963	16.167	17.649	0.071373	0.046290	0.11407	229.42	17.292
300.00	4.0027	2.9728	0.33638	15.803	17.149	0.068535	0.049264	0.16236	219.09	15.070
310.00	5.0232	4.4455	0.22495	15.090	16.220	0.064565	0.053237	0.33830	204.65	12.533
317.28	5.9062	9.3000	0.10753	12.765	13.400	0.055113			0	7.4905

Single-Phase Properties

150.00	0.10000	28.517	0.035067	-2.3112	-2.3077	-0.0095803	0.047264	0.071013	1326.0	-0.34613
194.60	0.10000	25.882	0.038637	0.82800	0.83187	0.0087476	0.042767	0.070442	1089.8	-0.29155
194.60	0.10000	0.064499	15.504	15.896	17.446	0.094125	0.029600	0.040629	244.34	77.876
225.00	0.10000	0.054701	18.281	16.776	18.604	0.099660	0.027396	0.036814	265.51	44.413
300.00	0.10000	0.040421	24.739	18.906	21.380	0.11030	0.029496	0.038140	305.33	18.192
375.00	0.10000	0.032197	31.059	21.292	24.398	0.11926	0.034142	0.042610	336.84	9.5450
150.00	1.0000	28.539	0.035039	-2.3206	-2.2855	-0.0096430	0.047252	0.070965	1330.7	-0.34675
225.00	1.0000	23.924	0.041800	2.9761	3.0179	0.019009	0.041178	0.072808	918.60	-0.19408
249.10	1.0000	22.083	0.045284	4.7819	4.8272	0.026644	0.040664	0.078045	765.18	-0.030727
249.10	1.0000	0.58959	1.6961	16.516	18.212	0.080377	0.037784	0.060289	250.26	29.499
300.00	1.0000	0.43831	2.2815	18.437	20.718	0.089572	0.032042	0.044524	291.25	17.553
375.00	1.0000	0.33366	2.9971	21.029	24.026	0.099411	0.034956	0.044943	329.85	9.3564
150.00	5.0000	28.637	0.034919	-2.3615	-2.1869	-0.0099181	0.047205	0.070762	1351.1	-0.34938
225.00	5.0000	24.159	0.041392	2.8706	3.0775	0.018535	0.041150	0.071655	952.55	-0.21829
300.00	5.0000	17.057	0.058628	9.0202	9.3133	0.042218	0.042199	0.11693	436.81	1.0494
309.79	5.0000	14.557	0.068696	10.426	10.769	0.046985	0.045181	0.22600	298.41	2.6188
309.79	5.0000	4.4014	0.22720	15.113	16.249	0.064673	0.053137	0.32991	205.02	12.597
375.00	5.0000	2.0056	0.49861	19.699	22.192	0.082450	0.038898	0.060151	299.64	8.3579
150.00	10.000	28.756	0.034776	-2.4107	-2.0629	-0.010253	0.047153	0.070531	1375.8	-0.35235
225.00	10.000	24.428	0.040937	2.7503	3.1596	0.017985	0.041136	0.070486	991.68	-0.24309
300.00	10.000	18.494	0.054071	8.4188	8.9595	0.040105	0.041153	0.090910	556.97	0.45639
375.00	10.000	5.4445	0.18367	17.496	19.333	0.070759	0.043934	0.10163	274.07	6.1896
150.00	30.000	29.189	0.034259	-2.5895	-1.5617	-0.011513	0.047004	0.069806	1467.3	-0.36156
225.00	30.000	25.306	0.039516	2.3574	3.5429	0.016117	0.041195	0.067503	1123.5	-0.30724
300.00	30.000	20.991	0.047639	7.3266	8.7557	0.036076	0.040629	0.072733	794.05	-0.067863
375.00	30.000	15.862	0.063045	12.699	14.590	0.053392	0.043123	0.082994	538.73	0.53694
225.00	70.000	26.558	0.037653	1.8062	4.4419	0.013266	0.041529	0.064822	1323.8	-0.36575
300.00	70.000	23.298	0.042923	6.3044	9.3090	0.031929	0.041001	0.065644	1056.2	-0.28880
375.00	70.000	20.079	0.049804	10.864	14.350	0.046913	0.043364	0.068927	851.76	-0.15494

The values in these tables were generated from the NIST REFPROP software (Lemmon, E. W., McLinden, M. O., and Huber, M. L., NIST Standard Reference Database 23: Reference Fluid Thermodynamic and Transport Properties—REFPROP, National Institute of Standards and Technology, Standard Reference Data Program, Gaithersburg, Md., 2002, Version 7.1). The primary source for the thermodynamic properties is Lemmon, E. W., and Span, R., "Short Fundamental Equations of State for 20 Industrial Fluids," *J. Chem. Eng. Data*, **51**(3):785–850, 2006. Validated equations for the viscosity and thermal conductivity are not currently available for this fluid.

Properties at the triple point temperature and the critical point temperature are given in the first and last entries of the saturation tables, respectively. In the single-phase table, when the temperature range for a given isobar includes a vapor-liquid phase boundary, the temperature of phase equilibrium is noted, and properties for both the saturated liquid and saturated vapor are given (with liquid properties given in the upper line). Lines are omitted from the temperature-pressure grid of the single-phase table, when the system would be in the solid phase or if there are potential problems with the source property surface.

The uncertainties in the equation of state are 0.1% in density (except near the critical point), 0.25% in vapor-pressure, 1% in heat capacities, 0.2% in the vapor-phase speed of sound, and 3% in the liquid speed of sound. The liquid speed of sound uncertainty is an estimate and cannot be verified without experimental information. The uncertainties above 290 K in vapor pressure may be as high as 0.5%.

2-350 PHYSICAL AND CHEMICAL DATA

TABLE 2-259 Saturated R-401A (SUVA MP 39)

Temp., °C	P_g , bar	P_s , bar	v_f , m ³ /kg	v_g , m ³ /kg	h_f , kJ/kg	h_g , kJ/kg	s_f , kJ/(kg·K)	s_g , kJ/(kg·K)	$c_{p,f}$, kJ/(kg·K)	μ_f , 10 ⁻⁶ Pa·s	k_f , W/(m·K)	Pr_f
-40	0.733	0.533	0.000 712	0.3778	154.0	385.0	0.8188	1.8244	1.078	351	0.1209	3.13
-30	1.155	0.871	0.000 728	0.2391	164.9	390.6	0.8647	1.8059	1.109	323	0.1154	3.06
-20	1.748	1.361	0.000 744	0.1576	176.2	396.3	0.9099	1.7907	1.137	291	0.1107	2.99
-10	2.553	2.043	0.000 762	0.1075	188.6	401.8	0.9577	1.7781	1.165	266	0.1057	2.93
0	3.615	2.965	0.000 781	0.0755	200.0	407.3	1.0000	1.7675	1.197	241	0.1012	2.85
10	4.984	4.177	0.000 803	0.0544	212.7	412.6	1.0454	1.7587	1.233	221	0.0967	2.82
20	6.712	5.733	0.000 826	0.0399	225.3	417.6	1.0884	1.7510	1.277	202	0.0922	2.80
30	8.857	7.697	0.000 851	0.0298	238.3	422.2	1.1316	1.7439	1.329	186	0.0877	2.83
40	11.475	10.133	0.000 878	0.0225	252.0	426.5	1.1752	1.7372	1.392	170	0.0830	2.85
50	14.628	13.112	0.000 909	0.0172	266.4	430.1	1.2194	1.7304	1.468	157	0.0781	2.95
60	18.378	16.711	0.000 944	0.01313	281.6	433.0	1.2647	1.7228	1.564	143	0.0737	3.04
70	22.79	21.01	0.000 988	0.01005	297.9	434.9	1.3118	1.7138	1.652	131	0.0684	3.16
80	27.92	26.12	0.001 028	0.00764	315.9	435.4	1.3616	1.7022	1.802	122	0.0631	3.48
90	33.83	32.13	0.001 084	0.00570	336.2	433.5	1.4163	1.6858	1.958	115	0.0577	3.90
100	40.53	39.22	0.001 140	0.00403	361.4	426.9	1.4820	1.6584	2.16	110	0.0533	4.46
108.0°	46.04	46.04	0.001 96	0.00196	397	397						

c = critical point. SUVA MP 39 = R401A = CHClF₂ (R22) 53% wt + CH₃CHF₂ (R 152a) 13% wt + CHClCF₃ (R124) 34% wt, near-azeotropic blend. Some values read from charts are approximate. Material used by permission of DuPont Fluoroproducts.

TABLE 2-260 R-401A (SUVA MP 39) at Atmospheric Pressure

Temp., °C	-27.01	-20	0	20	40	60	80	100	120	140
v (m ³ /kg)	0.2102	0.2167	0.2351	0.2534	0.2715	0.2896	0.3076	0.3256	0.3435	0.3613
h (kJ/kg)	351.7	396.9	410.4	424.5	439.2	454.4	470.3	486.6	503.5	521.2
s (kJ/kg·K)	1.8009	1.8193	1.8706	1.9204	1.9689	2.0161	2.0623	2.1073	2.1513	2.1943
c_p (kJ/kg·K)	0.648	0.669	0.698	0.727	0.757	0.787	0.811	0.836	0.859	0.883
μ (10 ⁻⁶ Pa·s)	10.17	10.43	11.18	11.93	12.68	13.42	14.17	14.89	15.61	16.32
k (W/m·K)	0.00878	0.00921	0.01041	0.01161	0.01282	0.01404	0.01536	0.01668	0.01796	0.01929
Pr	0.750	0.758	0.750	0.749	0.749	0.748	0.748	0.748	0.747	0.747
Z	0.9829	0.9852	0.9906	0.9949	0.9979	1.0005	1.0025	1.0043	1.0056	1.0060

For composition see footnote to Table 2-259. Some values read from charts are approximate. Material used by permission of DuPont Fluoroproducts.

TABLE 2-261 Thermodynamic Properties of Saturated R-407A (Klea 60)

Pressure, bar	T_f , K	T_g , K	v_f , m ³ /kg	v_g , m ³ /kg	h_f , kJ/kg	h_g , kJ/kg	s_f , kJ/(kg·K)	s_g , kJ/(kg·K)
1	227.3	234.0	0.000 7118	0.2097	-7.80	229.64		0.9965
1.5	236.1	242.5	0.000 7263	0.1433	3.92	235.02		0.9833
2	242.8	249.1	0.000 7381	0.1093	12.89	239.07		0.9744
2.5	248.3	254.5	0.000 7483	0.0885	20.27	242.35		0.9679
3	253.0	259.1	0.000 7573	0.0744	26.57	245.08		0.9629
4	260.7	266.8	0.000 7735	0.0564	37.23	249.54		0.9552
5	267.3	273.1	0.000 7880	0.0442	46.12	253.07		0.9496
6	272.9	278.5	0.000 8012	0.0384	53.84	255.24		0.9450
8	282.1	287.5	0.000 8254	0.0286	67.02	260.70		0.9378
10	289.8	295.0	0.000 8480	0.0228	78.23	263.86		0.9318
12.5	297.9	302.8	0.000 8750	0.01802	90.50	266.95		0.9257
15	304.8	309.5	0.000 9017	0.01481	101.51	269.12		0.9190
17.5	311.0	315.4	0.000 9290	0.01247	111.64	270.58		0.9128
20	316.5	320.7	0.000 9613	0.01069	121.18	271.46		0.9065
22.5	321.4	325.5	0.000 9884	0.00928	130.31	271.79		0.8999
25	326.1	329.8	0.001 023	0.00828	139.17	271.63		0.8927
27.5	330.4	333.9	0.001 063	0.00717	147.89	270.97		0.8850
30	334.5	337.6	0.001 115	0.00635	156.58	269.81		0.8765

$h_f = s_f = 0$ at 233.15 K = -40°C. Converted and interpolated from *Thermodynamic Properties of Klea 60* (British units, 20 pp.), copyright ICI Chemicals and Polymers Limited, 1993. Reproduced by permission. T_f = bubble point temperature; T_g = dew point temperature.

TABLE 2-262 Thermodynamic Properties of Saturated R-407B (Klea 61)

Pressure, bar	T_f , K	T_g , K	v_f , m ³ /kg	v_g , m ³ /kg	h_f , kJ/kg	h_g , kJ/kg	s_f , kJ/(kg·K)	s_g , kJ/(kg·K)
1	225.6	230.0	0.000 6852	0.1800	-9.45	191.64		0.8433
1.5	234.3	238.5	0.000 6994	0.1230	2.52	196.90		0.8341
2	241.8	245.0	0.000 7110	0.0937	9.72	200.88		0.8282
2.5	246.4	250.4	0.000 7211	0.0758	16.59	204.10		0.8245
3	251.1	254.9	0.000 7301	0.0637	22.47	206.80		0.8215
4	258.9	262.6	0.000 7463	0.04831	32.43	211.22		0.8172
5	265.4	269.0	0.000 7607	0.03888	40.76	214.74		0.8141
6	270.9	274.4	0.000 7740	0.03249	48.00	217.65		0.8123
8	280.2	283.4	0.000 7985	0.02435	59.82	222.21		0.8080
10	287.8	290.9	0.000 8214	0.01936	70.98	225.63		0.8048
12.5	295.8	298.7	0.000 8491	0.01528	82.59	228.80		0.8010
15	302.8	305.5	0.000 8768	0.01251	93.02	231.08		0.7971
17.5	308.8	311.4	0.000 9053	0.01049	102.67	232.64		0.7929
20	314.3	316.7	0.000 9353	0.00896	111.79	233.60		0.7882
22.5	319.3	321.5	0.000 9680	0.00774	120.55	233.99		0.7829
25	323.9	325.9	0.001 005	0.00674	129.11	233.85		0.7769
27.5	328.1	330.0	0.001 048	0.00590	137.62	233.16		0.7700
30	332.1	333.7	0.001 102	0.00518	146.21	231.84		0.7619

Converted and interpolated from *Thermodynamic Properties of Klea 61* (British units, 20 pp.), copyright ICI Chemicals and Polymers Limited, 1993. Reproduced by permission. T_f = bubble-point temperature; T_g = dew-point temperature. $h_f = s_f = 0$ at 233.15 K = -40°C.

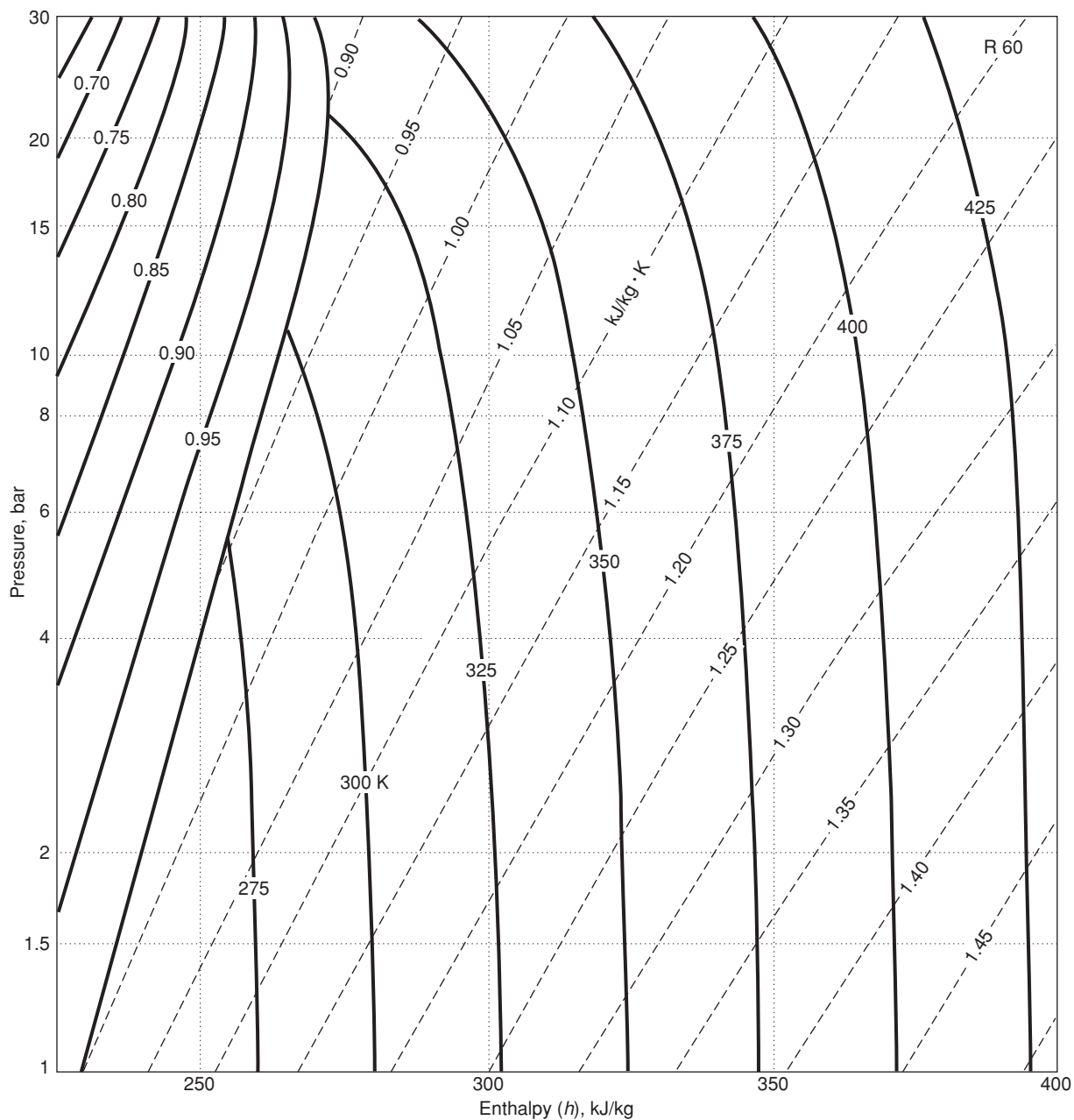


FIG. 2-22 Enthalpy-log-pressure diagram for R-407A (Klea 60).

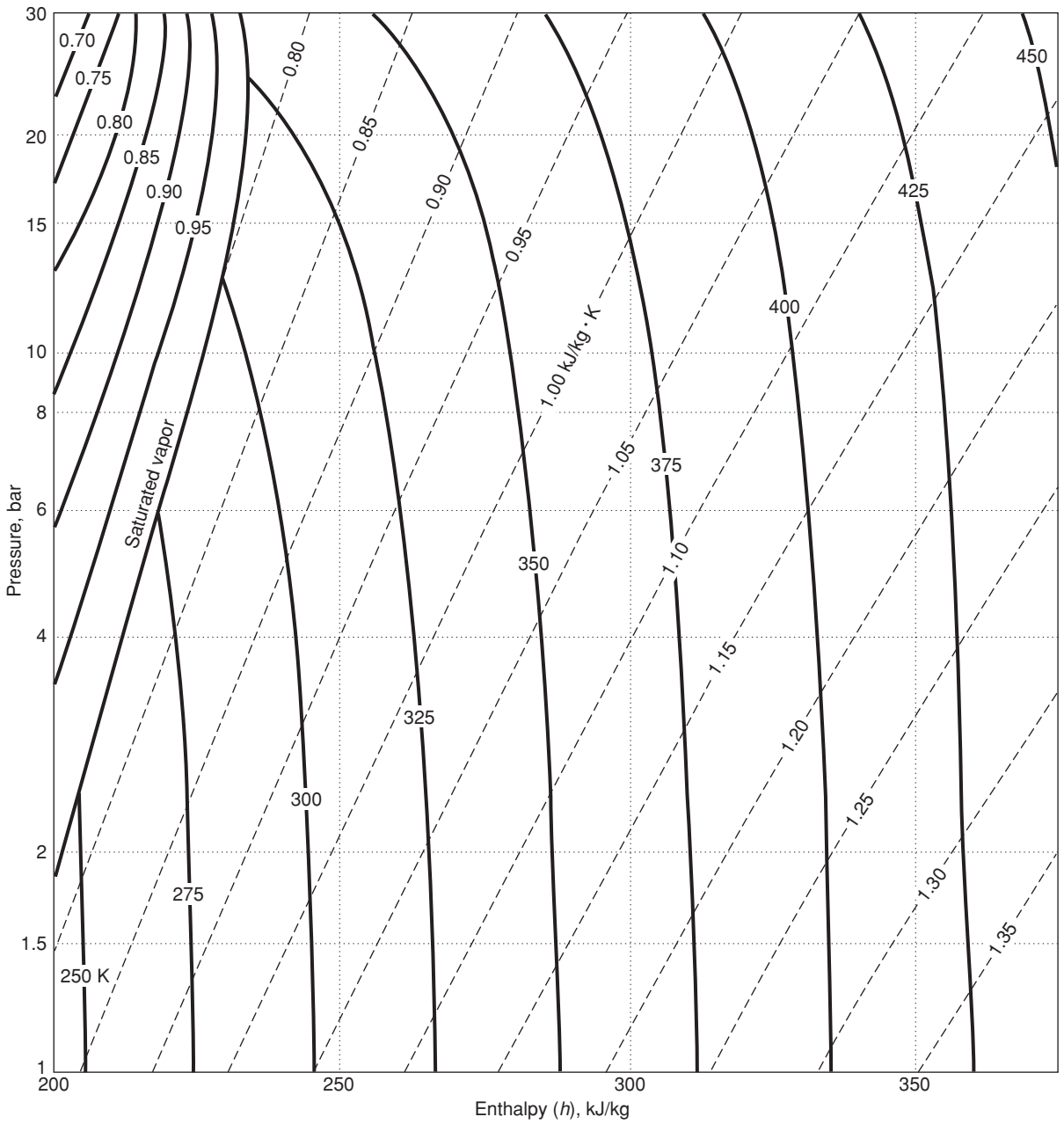


FIG. 2-23 Enthalpy-log-pressure diagram for R-407B (Klea 61).

2-354 PHYSICAL AND CHEMICAL DATA

TABLE 2-263 Saturated R-404A (SUVA HP 62)

Temp., °C	P_f , bar	P_g , bar	v_f , m ³ /kg	v_g , m ³ /kg	h_f , kJ/kg	h_g , kJ/kg	s_f , kJ/(kg·K)	s_g , kJ/(kg·K)	$c_{p,f}$, kJ/(kg·K)	μ_f , 10 ⁻⁶ Pa·s	k_f , W/(m·K)	Pr_f
-50	0.852	0.821	0.000 761	0.2244	133.1	337.3	0.7318	1.6487		370	0.0970	
-40	1.367	1.325	0.000 779	0.1434	145.6	343.8	0.7862	1.6380		318		
-30	2.095	2.041	0.000 799	0.0953	159.9	350.3	0.8460	1.6301	1.220	276	0.0868	3.88
-20	3.087	3.018	0.000 820	0.0656	172.8	356.5	0.8975	1.6245	1.260	238	0.0834	3.60
-10	4.404	4.321	0.000 843	0.0463	186.1	362.6	0.9487	1.6202	1.302	207	0.0801	3.37
0	6.111	6.013	0.000 868	0.03338	200.0	368.3	1.0000	1.6188	1.351	181	0.0767	3.19
10	8.278	8.165	0.000 898	0.02444	214.5	373.6	1.0515	1.6138	1.412	158	0.0733	3.04
20	10.977	10.851	0.000 933	0.01809	229.9	378.3	1.1038	1.6106	1.489	138	0.0698	2.94
30	14.287	14.150	0.000 977	0.01348	246.2	382.2	1.1574	1.6065	1.592	122	0.0663	2.93
40	18.292	18.148	0.001 037	0.01003	263.8	385.0	1.2130	1.6005	1.753	106	0.0624	2.98
50	23.08	22.94	0.001 122	0.00739	283.2	386.1	1.2723	1.5910	2.09	91	0.0583	3.26
60	28.75	28.63	0.001 261	0.00527	305.8	384.2	1.3389	1.5742		76	0.0535	
70	35.58			0.00285	339.8	375.9				61		
72.1°	37.32	37.32	0.002 06	0.00206	361	361						

c = critical point. SUVA HP 62 = CHF₂CF₃ (R125) 44% wt + CH₃CF₃ (R143a) 52% wt + CH₂FCF₃ (R134a) 4% wt, near-azeotropic blend. Material used by permission of DuPont Fluoroproducts. Some values read from charts may be approximate.

TABLE 2-264 R-404A (SUVA HP 62) at Atmospheric Pressure

Temp., °C	-45.63	-40	-20	0	20	40	60	80	100	120
v (m ³ /kg)	0.1866	0.1921	0.2100	0.2278	0.2455	0.2630	0.2805	0.2980	0.3153	0.3325
h (kJ/kg)	336.0	344.4	359.9	376.2	393.1	410.9	429.3	448.4	468.2	488.7
s (kJ/kg·K)	1.6599	1.6636	1.7274	1.7891	1.8491	1.9076	1.9646	2.0203	2.0747	2.1278
c_p (kJ/kg·K)	0.732	0.738	0.781	0.821	0.860	0.897	0.933	0.967	1.000	1.032
μ (10 ⁻⁶ Pa·s)	9.47	9.68	10.45	11.22	11.99	12.76	13.53	14.30	15.07	15.84
k (W/m·K)	0.00860	0.00932	0.01059	0.01186	0.01313	0.01440	0.01568	0.01695	0.01827	0.01949
Pr	0.806	0.767	0.771	0.777	0.785	0.795	0.805	0.816	0.827	0.839
Z	0.9755	0.9800	0.9867	0.9919	0.9961	0.9989	1.0014	1.0037	1.0050	1.0060

v , h , and s from DuPont bull. T—HP62—SI, June 1993 (17 pp.). c_p and k from DuPont bull. ART 18, June 1993 (37 pp.). Some values read from charts may be approximate. Material used by permission of DuPont Fluoroproducts.

TABLE 2-265 Saturated R-401B (SUVA MP 66)

Temp., °C	P_f , bar	P_g , bar	v_f , m ³ /kg	v_g , m ³ /kg	h_f , kJ/kg	h_g , kJ/kg	s_f , kJ/(kg·K)	s_g , kJ/(kg·K)	c_{pf} , kJ/(kg·K)	μ_f , 10 ⁻⁶ Pa·s	k_f , W/(m·K)	Pr_f
-40	0.788	0.585	0.000 710	0.3498	153.8	386.0	0.8184	1.8291	1.078	349	0.1209	3.11
-30	1.239	0.952	0.000 725	0.2224	164.8	391.6	0.8643	1.8100	1.109	313	0.1154	3.01
-20	1.872	1.479	0.000 740	0.1471	176.0	397.1	0.9095	1.7940	1.137	282	0.1106	2.90
-10	2.726	2.212	0.000 758	0.1008	188.6	402.6	0.9577	1.7807	1.165	257	0.1057	2.83
0	3.850	3.198	0.000 778	0.0710	200.0	407.8	1.0000	1.7694	1.197	236	0.1012	2.79
10	5.297	4.491	0.000 801	0.05124	212.6	412.9	1.0450	1.7598	1.233	217	0.0967	2.77
20	7.120	6.146	0.000 827	0.03771	225.1	417.7	1.0879	1.7512	1.277	198	0.0922	2.74
30	9.379	8.229	0.000 858	0.02818	238.2	422.1	1.1311	1.7433	1.329	181	0.0877	2.74
40	12.133	10.808	0.000 895	0.02131	251.9	426.1	1.1747	1.7357	1.392	168	0.0830	2.82
50	15.444	13.955	0.000 939	0.01625	266.3	429.4	1.2190	1.7278	1.468	151	0.0781	2.84
60	19.378	17.750	0.000 994	0.01244	281.6	431.9	1.2645	1.7191	1.564	139	0.0737	2.95
70	24.00	22.28	0.001 066	0.00951	298.1	433.4	1.3120	1.7088	1.652	127	0.0684	3.07
80	29.37	27.64	0.001 164	0.00721	316.3	433.2	1.3625	1.6956	1.802	116	0.0631	3.31
90	35.55	33.96	0.001 313	0.00534	337.2	430.4	1.4187	1.6768			0.0577	
100	42.30										0.0533	
106.1 ^c	46.82	46.82	0.001 95	0.00195	389	389						

c = critical point. SUVA MP 66 = R-401B = CHClF₂ (R22) 61% wt + CH₃CHF₂ (R152a) 11% wt + CHClFCF₃ (R124) 28% wt, near-azeotropic blend. Material used by permission of DuPont Fluoroproducts. Some values read from charts are approximate.

TABLE 2-266 R-401B (SUVA MP 66) at Atmospheric Pressure

Temp., °C	-28.63 ^b	-20	0	20	40	60	80	100	120	140
v (m ³ /kg)	0.2086	0.2177	0.2362	0.2545	0.2727	0.2908	0.3089	0.3269	0.3449	0.3629
h (kJ/kg)	392.2	397.9	411.2	425.1	439.6	454.6	470.1	486.2	502.7	519.4
s (kJ/kg·K)	1.8081	1.8299	1.8804	1.9295	1.9772	2.0237	2.0690	2.1132	2.1564	2.1986
c_p (kJ/kg·K)	0.641	0.652	0.688	0.716	0.744	0.771	0.796	0.822	0.844	0.866
μ (10 ⁻⁶ Pa·s)	9.78	10.43	11.18	11.93	12.68	13.42	14.17	14.89	15.61	16.32
k (W/m·K)	0.00817	0.00921	0.01041	0.01161	0.01282	0.01404	0.01536	0.01668	0.01796	0.01929
Pr	0.767	0.738	0.737	0.736	0.735	0.735	0.734	0.734	0.733	0.733
Z	0.9652	0.9730	0.9783	0.9822	0.9852	0.9876	0.9896	0.9912	0.9925	0.9937

v , h , and s from DuPont bull. T—MP 66—SI, Jan. 1993 (17 pp.). c_p , μ , and k from DuPont bull. ART 10, Jan. 1993 (27 pp.). Some values read from charts may be approximate. Material used by permission of DuPont Fluoroproducts. b = normal boiling point.

TABLE 2-267 Saturated R-402A (SUVA HP 80)

Temp., °C	P_f , bar	P_g , bar	v_f , m ³ /kg	v_g , m ³ /kg	h_f , kJ/kg	h_g , kJ/kg	s_f , kJ/(kg·K)	s_g , kJ/(kg·K)	c_{pf} , kJ/(kg·K)	μ_f , 10 ⁻⁶ Pa·s	k_f , W/(m·K)	Pr_f
-50	0.962	0.872	0.000 679	0.2033	139.6	334.1	0.7578	1.6327		377	0.0970	
-40	1.520	1.403	0.000 695	0.1303	150.8	339.9	0.8070	1.6206		317		
-30	2.305	2.156	0.000 713	0.0869	163.1	345.6	0.8584	1.6110	1.193	283	0.0880	3.84
-20	3.370	3.188	0.000 733	0.0598	174.9	351.1	0.9053	1.6034	1.217	247	0.0849	3.54
-10	4.776	4.560	0.000 757	0.0423	187.6	356.4	0.9541	1.5972	1.236	215	0.0813	3.27
0	6.588	6.336	0.000 785	0.03060	200.0	361.3	1.0000	1.5919	1.253	188	0.0778	3.03
10	8.877	8.592	0.000 819	0.02248	213.0	365.9	1.0461	1.5870	1.286	165	0.0743	2.86
20	11.720	11.404	0.000 860	0.01671	226.7	369.8	1.0927	1.5820	1.340	146	0.0708	2.76
30	15.195	14.855	0.000 911	0.01250	241.2	373.1	1.1403	1.5762	1.412	128	0.0672	2.69
40	19.388	19.034	0.000 977	0.00936	256.8	375.4	1.1897	1.5690	1.512	113	0.0634	2.70
50	24.39	24.04	0.001 070	0.00696	273.9	376.2	1.2420	1.5589	1.64	98	0.0593	2.71
60	30.30	29.97	0.001 212	0.00505	293.6	374.6	1.2998	1.5433	1.81	83	0.0551	2.79
70										68		
75.5 ^c	41.35	41.35	0.001 850	0.00185	340	340						

c = critical point. SUVA HP 80 = R-402A = CHF₂CF₃ (R125) 60% wt + CH₃CH₂CH₃ (R290) 2% wt + CHClF₂ (R22) 38% wt, near-azeotropic blend. Material used by permission of DuPont Fluoroproducts. Some values, read from charts, may be approximate.

2-356 PHYSICAL AND CHEMICAL DATA

TABLE 2-268 R-402A (SUVA HP 80) at Atmospheric Pressure

Temp., °C	-46.95 ^b	-40	-20	0	20	40	60	80	100	120
<i>v</i> (m ³ /kg)	0.1768	0.1827	0.1996	0.2164	0.2331	0.2497	0.2663	0.2828	0.2992	0.3155
<i>h</i> (kJ/kg)	335.9	340.5	354.3	368.6	383.5	398.7	414.9	431.4	448.5	466.1
<i>s</i> (kJ/kg·K)	1.6286	1.6490	1.7055	1.7599	1.8124	1.8633	1.9128	1.9610	2.0081	2.0541
<i>c_p</i> (kJ/kg·K)	0.648	0.654	0.687	0.721	0.749	0.779	0.807	0.836	0.863	0.890
<i>μ</i> (10 ⁻⁶ Pa·s)	9.42	9.69	10.45	11.22	11.99	12.75	13.52	14.29	15.06	15.82
<i>k</i> (W/m·K)	0.00888	0.00932	0.01059	0.01186	0.01313	0.01440	0.01568	0.01695	0.01822	0.01949
<i>Pr</i>	0.687	0.680	0.678	0.681	0.685	0.690	0.696	0.703	0.713	0.722
<i>Z</i>	0.9673	0.9697	0.9758	0.9804	0.9840	0.9868	0.9892	0.9910	0.9923	0.9932

b = normal boiling pt. *v*, *h*, and *s* from DuPont bull. T—HP 80—SI, Jan. 1993 (17 pp.). *c_p*, *μ*, and *k* from DuPont bull. ART 18, June 1993 (37 pp.). Some values read from charts may be approximate. Material used by permission of DuPont Fluoroproducts.

TABLE 2-269 Saturated R-402B (SUVA HP 81)

Temp., °C	<i>P_f</i> , bar	<i>P_g</i> , bar	<i>v_f</i> , m ³ /kg	<i>v_g</i> , m ³ /kg	<i>h_f</i> , kJ/kg	<i>h_g</i> , kJ/kg	<i>s_f</i> , kJ/(kg·K)	<i>s_g</i> , kJ/(kg·K)	<i>c_{pf}</i> , kJ/(kg·K)	<i>μ_f</i> , 10 ⁻⁶ Pa·s	<i>k_f</i> , W/(m·K)	<i>Pr_f</i>
-50	0.883	0.787	0.000 687	0.2425	140.3	351.7	0.7606	1.7122		383	0.1031	
-40	1.403	1.273	0.000 702	0.1548	151.4	357.2	0.8092	1.6957		333	0.0983	
-30	2.135	1.967	0.000 719	0.1028	163.3	362.7	0.8589	1.6820	1.178	290	0.0941	3.63
-20	3.132	2.923	0.000 739	0.0707	174.9	368.0	0.9054	1.6706	1.191	253	0.0900	3.35
-10	4.451	4.198	0.000 761	0.0499	187.8	373.0	0.9550	1.6611	1.204	223	0.0863	3.11
0	6.153	5.852	0.000 787	0.03610	200.0	377.8	1.0000	1.6528	1.221	195	0.0818	2.91
10	8.307	7.959	0.000 817	0.02656	212.7	382.2	1.0450	1.6451	1.288	173	0.0790	2.82
20	10.984	10.591	0.000 854	0.01980	226.0	386.0	1.0905	1.6376	1.313	151	0.0753	2.63
30	14.261	13.827	0.000 899	0.01490	240.1	389.3	1.1367	1.6299	1.37	137	0.0715	2.49
40	18.216	17.750	0.000 955	0.01125	255.1	391.5	1.1842	1.6211	1.75	122	0.0676	3.16
50	22.93	22.45	0.001 030	0.00848	271.4	392.8	1.2339	1.6104	2.07	106	0.0633	3.47
60	28.50	28.03	0.001 136	0.00632	289.5	392.2	1.2873	1.5961		91	0.0586	
70	35.01	34.60	0.001 307	0.00456	299.6	390.9	1.3164	1.5866		75	0.0544	
80												
82.6 ^c	44.45	44.45	0.001 88	0.00188	351	351						

c = critical point. SUVA HP 81 = R402B (38/2/60) = CHF₂CF₃ (R125) 38 wt + CH₃CH₂CH₃ (R290) 2% wt + CHClF₂ (R22) 60% wt, near-azeotropic blend. Material used by permission of DuPont Fluoroproducts. Some values read from charts may be approximate.

TABLE 2-270 R-402B (SUVA HP 81) at Atmospheric Pressure

Temp., °C	-44.87 ^b	-40	-20	0	20	40	60	80	100	120
<i>v</i> (m ³ /kg)	0.1903	0.1960	0.2142	0.2322	0.2500	0.2678	0.2856	0.3032	0.3209	0.3386
<i>h</i> (kJ/kg)	354.7	357.7	370.8	384.6	398.8	413.6	428.9	444.7	461.0	477.7
<i>s</i> (kJ/kg·K)	1.7032	1.7169	1.7711	1.8232	1.8735	1.9222	1.9696	2.0158	2.0607	2.1047
<i>c_p</i> (kJ/kg·K)	1.187	1.177	1.169	1.159	1.149	1.143	1.134	1.128	1.124	1.120
<i>μ</i> (10 ⁻⁶ Pa·s)	10.16	10.33	11.10	11.86	12.62	13.39	14.15	14.78	15.54	16.30
<i>k</i> (W/m·K)	0.00739	0.00768	0.00902	0.01036	0.01170	0.01304	0.01438	0.01572	0.01706	0.01840
<i>Pr</i>	1.632	1.583	1.439	1.327	1.239	1.174	1.124	1.061	1.024	0.992
<i>Z</i>	0.9622	0.9703	0.9766	0.9811	0.9843	0.9870	0.9894	0.9909	0.9926	0.9940

b = normal boiling point. *v*, *h*, and *s* from DuPont bull. T—HP 81—SI, Jan. 1993 (17 pp.). *c_p*, *μ*, and *k* from DuPont bull. ART 18, June 1993 (37 pp.). Some values, read from charts, may be approximate. Material used by permission of DuPont Fluoroproducts.

TABLE 2-271 Thermodynamic Properties of R-113, 1,1,2-Trichlorotrifluoroethane

Temperature K	Pressure MPa	Density mol/dm ³	Volume dm ³ /mol	Int. energy kJ/mol	Enthalpy kJ/mol	Entropy kJ/(mol·K)	C _v kJ/(mol·K)	C _p kJ/(mol·K)	Sound speed m/s	Joule-Thomson K/MPa
Saturated Properties										
236.93	0.0018714	9.0987	0.10991	31.483	31.484	0.16386	0.11672	0.16341	907.79	-0.45956
240.00	0.0022999	9.0614	0.11036	31.985	31.986	0.16596	0.11694	0.16366	897.63	-0.45692
250.00	0.0043168	8.9395	0.11186	33.627	33.627	0.17266	0.11797	0.16467	863.61	-0.44732
260.00	0.0076484	8.8172	0.11342	35.279	35.280	0.17914	0.11931	0.16593	828.94	-0.43622
270.00	0.012885	8.6941	0.11502	36.945	36.947	0.18543	0.12084	0.16735	794.26	-0.42364
280.00	0.020766	8.5702	0.11668	38.626	38.629	0.19154	0.12245	0.16891	759.92	-0.40951
290.00	0.032185	8.4450	0.11841	40.323	40.327	0.19750	0.12410	0.17056	726.09	-0.39367
300.00	0.048190	8.3183	0.12022	42.036	42.042	0.20331	0.12576	0.17231	692.84	-0.37590
310.00	0.069977	8.1897	0.12211	43.767	43.776	0.20898	0.12740	0.17414	660.17	-0.35588
320.00	0.098880	8.0588	0.12409	45.516	45.528	0.21453	0.12901	0.17606	628.04	-0.33321
330.00	0.13636	7.9252	0.12618	47.284	47.301	0.21998	0.13060	0.17807	596.38	-0.30739
340.00	0.18400	7.7884	0.12840	49.071	49.095	0.22531	0.13215	0.18020	565.13	-0.27774
350.00	0.24349	7.6479	0.13076	50.879	50.911	0.23055	0.13367	0.18247	534.20	-0.24340
360.00	0.31660	7.5029	0.13328	52.708	52.751	0.23571	0.13517	0.18491	503.50	-0.20323
370.00	0.40521	7.3529	0.13600	54.560	54.616	0.24079	0.13665	0.18755	472.94	-0.15569
380.00	0.51127	7.1968	0.13895	56.437	56.508	0.24579	0.13813	0.19047	442.41	-0.098686
390.00	0.63682	7.0336	0.14217	58.340	58.430	0.25074	0.13961	0.19374	411.80	-0.029233
400.00	0.78398	6.8619	0.14573	60.271	60.386	0.25564	0.14112	0.19749	380.97	0.057005
410.00	0.95499	6.6797	0.14971	62.235	62.378	0.26050	0.14266	0.20191	349.77	0.16660
420.00	1.1522	6.4845	0.15421	64.236	64.414	0.26533	0.14428	0.20730	317.99	0.31000
430.00	1.3781	6.2728	0.15942	66.280	66.500	0.27015	0.14601	0.21416	285.39	0.50481
440.00	1.6354	6.0390	0.16559	68.379	68.650	0.27500	0.14794	0.22344	251.65	0.78295
450.00	1.9271	5.7742	0.17318	70.548	70.881	0.27990	0.15016	0.23712	216.41	1.2078
460.00	2.2568	5.4624	0.18307	72.817	73.230	0.28494	0.15288	0.25998	179.46	1.9196
470.00	2.6288	5.0712	0.19719	75.247	75.765	0.29024	0.15638	0.30706	141.14	3.2778
480.00	3.0498	4.5104	0.22171	78.016	78.692	0.29621	0.16109	0.47179	101.80	6.5781
487.21	3.3923	2.9887	0.33460	82.401	83.536	0.30602			0	19.849
236.93	0.0018714	0.00095199	1050.4	61.277	63.243	0.29790	0.098915	0.10733	106.58	82.183
240.00	0.0022999	0.0011554	865.51	61.580	63.570	0.29756	0.099759	0.10819	107.21	77.881
250.00	0.0043168	0.0020850	479.61	62.580	64.650	0.29675	0.10244	0.11094	109.17	66.150
260.00	0.0076484	0.0035597	280.92	63.602	65.750	0.29634	0.10502	0.11361	111.03	57.141
270.00	0.012885	0.0057917	172.66	64.643	66.868	0.29625	0.10751	0.11623	112.77	50.111
280.00	0.020766	0.0090358	110.67	65.701	67.999	0.29644	0.10994	0.11883	114.38	44.541
290.00	0.032185	0.013590	73.586	66.774	69.143	0.29686	0.11231	0.12142	115.82	40.065
300.00	0.048190	0.019793	50.523	67.860	70.295	0.29748	0.11463	0.12402	117.08	36.421
310.00	0.069977	0.028029	35.677	68.957	71.453	0.29826	0.11691	0.12666	118.14	33.419
320.00	0.098880	0.038727	25.822	70.061	72.615	0.29918	0.11917	0.12935	118.97	30.923
330.00	0.13636	0.052364	19.097	71.172	73.776	0.30020	0.12140	0.13214	119.57	28.833
340.00	0.18400	0.069475	14.394	72.286	74.934	0.30131	0.12362	0.13503	119.89	27.074
350.00	0.24349	0.090662	11.030	73.400	76.086	0.30248	0.12583	0.13807	119.93	25.594
360.00	0.31660	0.11662	8.5752	74.513	77.228	0.30370	0.12804	0.14130	119.66	24.353
370.00	0.40521	0.14813	6.7508	75.621	78.356	0.30495	0.13024	0.14477	119.05	23.322
380.00	0.51127	0.18615	5.3719	76.720	79.467	0.30621	0.13246	0.14857	118.07	22.480
390.00	0.63682	0.23182	4.3136	77.808	80.555	0.30747	0.13469	0.15281	116.69	21.816
400.00	0.78398	0.28656	3.4897	78.878	81.614	0.30871	0.13695	0.15765	114.87	21.322
410.00	0.95499	0.35216	2.8396	79.926	82.638	0.30991	0.13926	0.16333	112.57	21.000
420.00	1.1522	0.43104	2.3200	80.944	83.617	0.31105	0.14165	0.17026	109.72	20.858
430.00	1.3781	0.52654	1.8992	81.922	84.539	0.31210	0.14414	0.17911	106.25	20.915
440.00	1.6354	0.64356	1.5539	82.844	85.386	0.31304	0.14679	0.19114	102.05	21.204
450.00	1.9271	0.78990	1.2660	83.689	86.129	0.31379	0.14969	0.20894	97.003	21.779
460.00	2.2568	0.97939	1.0210	84.417	86.721	0.31426	0.15299	0.23897	90.902	22.716
470.00	2.6288	1.2415	0.80548	84.942	87.059	0.31427	0.15703	0.30270	83.480	24.091
480.00	3.0498	1.6684	0.59937	85.005	86.833	0.31317	0.16277	0.54016	74.333	25.627
487.21	3.3923	2.9887	0.33460	82.401	83.536	0.30602			0	19.849

TABLE 2-271 Thermodynamic Properties of R-113, 1,1,2-Trichlorotrifluoroethane (Concluded)

Temperature K	Pressure MPa	Density mol/dm ³	Volume dm ³ /mol	Int. energy kJ/mol	Enthalpy kJ/mol	Entropy kJ/(mol·K)	C _v kJ/(mol·K)	C _p kJ/(mol·K)	Sound speed m/s	Joule-Thomson K/MPa
Single-Phase Properties										
250.00	0.10000	8.9405	0.11185	33.623	33.634	0.17265	0.11797	0.16466	864.02	-0.44747
320.34	0.10000	8.0543	0.12416	45.576	45.588	0.21472	0.12907	0.17612	626.96	-0.33239
320.34	0.10000	0.039138	25.551	70.099	72.654	0.29921	0.11925	0.12945	119.00	30.846
325.00	0.10000	0.038492	25.979	70.661	73.259	0.30109	0.11993	0.12998	120.05	29.068
400.00	0.10000	0.030653	32.623	80.120	83.382	0.32908	0.13100	0.14005	135.10	14.858
475.00	0.10000	0.025598	39.065	90.324	94.230	0.35391	0.14017	0.14891	148.01	9.5374
250.00	1.0000	8.9494	0.11174	33.589	33.701	0.17251	0.11802	0.16456	867.87	-0.44882
325.00	1.0000	8.0093	0.12485	46.338	46.463	0.21708	0.12985	0.17671	618.26	-0.32646
400.00	1.0000	6.8729	0.14550	60.238	60.383	0.25555	0.14107	0.19705	384.09	0.047064
412.41	1.0000	6.6340	0.15074	62.713	62.864	0.26166	0.14304	0.20311	342.18	0.19754
412.41	1.0000	0.36984	2.7039	80.174	82.878	0.31019	0.13983	0.16487	111.93	20.948
475.00	1.0000	0.28704	3.4839	89.325	92.809	0.33262	0.14241	0.15696	133.62	11.300
250.00	5.0000	8.9881	0.11126	33.441	33.998	0.17191	0.11826	0.16413	884.22	-0.45442
325.00	5.0000	8.0819	0.12373	46.082	46.701	0.21629	0.13008	0.17538	644.07	-0.34900
400.00	5.0000	7.0485	0.14187	59.694	60.403	0.25417	0.14058	0.19113	433.49	-0.086367
475.00	5.0000	5.5199	0.18116	74.959	75.865	0.28950	0.15167	0.23166	217.18	1.2219
250.00	10.000	9.0343	0.11069	33.266	34.373	0.17119	0.11861	0.16368	903.13	-0.46053
325.00	10.000	8.1644	0.12248	45.791	47.016	0.21536	0.13042	0.17407	672.87	-0.37126
400.00	10.000	7.2197	0.13851	59.149	60.534	0.25274	0.14040	0.18683	481.58	-0.18229
475.00	10.000	6.0609	0.16499	73.507	75.157	0.28621	0.14885	0.20446	313.71	0.32498
325.00	100.00	9.0570	0.11041	42.816	53.857	0.20444	0.13658	0.16811	970.17	-0.48114
400.00	100.00	8.5204	0.11737	54.955	66.691	0.23995	0.14351	0.17396	867.10	-0.45624
475.00	100.00	8.0191	0.12470	67.454	79.924	0.27026	0.14864	0.17872	788.68	-0.42986
475.00	200.00	8.7846	0.11384	65.196	87.963	0.26222	0.14928	0.17693	1035.9	-0.46436

The values in these tables were generated from the NIST REFPROP software (Lemmon, E. W., McLinden, M. O., and Huber, M. L., NIST Standard Reference Database 23: Reference Fluid Thermodynamic and Transport Properties—REFPROP, National Institute of Standards and Technology, Standard Reference Data Program, Gaithersburg, Md., 2002, Version 7.1). The primary source for the thermodynamic properties is Marx, V., Pruss, A., and Wagner, W., "Neue Zustandsgleichungen fuer R 12, R 22, R 11 und R 113. Beschreibung des thermodynamischen Zustandsverhaltens bei Temperaturen bis 525 K und Druucken bis 200 MPa," Duesseldorf: *VDI Verlag*, Series 19 (Waermeteknik/Kaeltetechnik), No. 57, 1992. Validated equations for the viscosity and thermal conductivity are not currently available for this fluid.

Properties at the triple point temperature and the critical point temperature are given in the first and last entries of the saturation tables, respectively. In the single-phase table, when the temperature range for a given isobar includes a vapor-liquid phase boundary, the temperature of phase equilibrium is noted, and properties for both the saturated liquid and saturated vapor are given (with liquid properties given in the upper line). Lines are omitted from the temperature-pressure grid of the single-phase table, when the system would be in the solid phase or if there are potential problems with the source property surface.

The uncertainty in density is 0.2%, that for vapor pressure is 0.3%, and that for the isobaric heat capacity is 2%. The uncertainties are higher in and above the critical region.

TABLE 2-272 Thermodynamic Properties of R-114, 1,2-Dichlorotetrafluoroethane

Temperature K	Pressure MPa	Density mol/dm ³	Volume dm ³ /mol	Int. energy kJ/mol	Enthalpy kJ/mol	Entropy kJ/(mol·K)	C _v kJ/(mol·K)	C _p kJ/(mol·K)	Sound speed m/s	Joule-Thomson K/MPa
Saturated Properties										
275.00	0.094764	8.9110	0.11222	34.479	34.490	0.17204	0.11622	0.16411	636.17	-0.32927
280.00	0.11455	8.8268	0.11329	35.301	35.314	0.17500	0.11691	0.16513	617.82	-0.31514
285.00	0.13740	8.7415	0.11440	36.128	36.143	0.17792	0.11763	0.16623	599.54	-0.29975
290.00	0.16362	8.6548	0.11554	36.960	36.979	0.18082	0.11838	0.16741	581.32	-0.28301
295.00	0.19353	8.5667	0.11673	37.798	37.820	0.18368	0.11917	0.16866	563.14	-0.26478
300.00	0.22746	8.4771	0.11796	38.641	38.668	0.18652	0.11997	0.16998	545.01	-0.24491
305.00	0.26574	8.3858	0.11925	39.491	39.523	0.18933	0.12079	0.17138	526.89	-0.22318
310.00	0.30872	8.2927	0.12059	40.348	40.385	0.19212	0.12162	0.17286	508.80	-0.19936
315.00	0.35677	8.1976	0.12199	41.211	41.255	0.19488	0.12247	0.17441	490.70	-0.17315
320.00	0.41024	8.1004	0.12345	42.082	42.133	0.19763	0.12333	0.17606	472.58	-0.14418
325.00	0.46953	8.0007	0.12499	42.960	43.019	0.20035	0.12419	0.17781	454.45	-0.11201
330.00	0.53501	7.8984	0.12661	43.846	43.913	0.20306	0.12507	0.17967	436.26	-0.076088
335.00	0.60708	7.7932	0.12832	44.739	44.817	0.20575	0.12595	0.18167	418.03	-0.035744
340.00	0.68615	7.6847	0.13013	45.642	45.731	0.20843	0.12684	0.18383	399.72	0.0098734
345.00	0.77265	7.5726	0.13205	46.553	46.655	0.21109	0.12775	0.18617	381.32	0.061838
350.00	0.86701	7.4565	0.13411	47.475	47.591	0.21375	0.12866	0.18875	362.81	0.12152
355.00	0.96967	7.3358	0.13632	48.407	48.539	0.21640	0.12959	0.19162	344.17	0.19072
360.00	1.0811	7.2098	0.13870	49.350	49.500	0.21904	0.13054	0.19485	325.38	0.27180
365.00	1.2018	7.0779	0.14129	50.306	50.476	0.22169	0.13152	0.19854	306.40	0.36794
370.00	1.3323	6.9389	0.14412	51.276	51.468	0.22434	0.13252	0.20284	287.21	0.48354
375.00	1.4730	6.7916	0.14724	52.261	52.478	0.22700	0.13356	0.20795	267.77	0.62482
380.00	1.6246	6.6345	0.15073	53.265	53.510	0.22967	0.13465	0.21417	248.03	0.80081
385.00	1.7878	6.4651	0.15468	54.291	54.567	0.23237	0.13581	0.22201	227.95	1.0252
390.00	1.9630	6.2804	0.15922	55.343	55.655	0.23511	0.13705	0.23227	207.45	1.3196
395.00	2.1511	6.0759	0.16459	56.428	56.782	0.23790	0.13842	0.24644	186.45	1.7200
400.00	2.3530	5.8442	0.17111	57.557	57.960	0.24078	0.13997	0.26750	164.86	2.2906
405.00	2.5694	5.5731	0.17943	58.749	59.211	0.24379	0.14180	0.30245	142.55	3.1570
410.00	2.8015	5.2381	0.19091	60.042	60.577	0.24704	0.14408	0.37230	119.37	4.5962
415.00	3.0507	4.7774	0.20932	61.532	62.171	0.25078	0.14726	0.57876	95.263	7.3420
418.83	3.2516	3.3932	0.29471	64.391	65.349	0.25828			0	18.568
275.00	0.094764	0.043032	23.239	55.626	57.828	0.25690	0.10567	0.11538	116.26	24.935
280.00	0.11455	0.051392	19.458	56.123	58.352	0.25728	0.10683	0.11680	116.64	24.301
285.00	0.13740	0.060964	16.403	56.622	58.875	0.25769	0.10799	0.11826	116.94	23.725
290.00	0.16362	0.071869	13.914	57.121	59.397	0.25812	0.10916	0.11977	117.15	23.203
295.00	0.19353	0.084238	11.871	57.620	59.917	0.25859	0.11032	0.12133	117.27	22.730
300.00	0.22746	0.098213	10.182	58.119	60.435	0.25908	0.11150	0.12295	117.29	22.303
305.00	0.26574	0.11395	8.7760	58.617	60.949	0.25958	0.11268	0.12465	117.20	21.919
310.00	0.30872	0.13161	7.5984	59.113	61.459	0.26010	0.11387	0.12643	117.00	21.576
315.00	0.35677	0.15138	6.6059	59.608	61.965	0.26063	0.11508	0.12831	116.68	21.272
320.00	0.41024	0.17347	5.7648	60.100	62.465	0.26117	0.11630	0.13031	116.25	21.005
325.00	0.46953	0.19810	5.0480	60.589	62.959	0.26171	0.11754	0.13245	115.69	20.776
330.00	0.53501	0.22553	4.4340	61.074	63.446	0.26225	0.11880	0.13475	115.00	20.582
335.00	0.60708	0.25605	3.9055	61.554	63.925	0.26279	0.12008	0.13725	114.17	20.423
340.00	0.68615	0.28999	3.4484	62.029	64.395	0.26332	0.12139	0.13998	113.19	20.301
345.00	0.77265	0.32774	3.0512	62.497	64.855	0.26384	0.12274	0.14299	112.05	20.216
350.00	0.86701	0.36975	2.7045	62.957	65.302	0.26435	0.12412	0.14634	110.75	20.169
355.00	0.96967	0.41655	2.4007	63.408	65.736	0.26484	0.12555	0.15013	109.28	20.160
360.00	1.0811	0.46878	2.1332	63.849	66.155	0.26531	0.12703	0.15444	107.63	20.193
365.00	1.2018	0.52722	1.8967	64.277	66.557	0.26575	0.12856	0.15945	105.77	20.269
370.00	1.3323	0.59285	1.6868	64.690	66.938	0.26615	0.13016	0.16534	103.71	20.392
375.00	1.4730	0.66690	1.4995	65.086	67.295	0.26651	0.13185	0.17244	101.42	20.565
380.00	1.6246	0.75097	1.3316	65.461	67.624	0.26681	0.13363	0.18118	98.885	20.790
385.00	1.7878	0.84722	1.1803	65.810	67.920	0.26705	0.13552	0.19228	96.087	21.072
390.00	1.9630	0.95861	1.0432	66.126	68.174	0.26720	0.13755	0.20692	92.999	21.411
395.00	2.1511	1.0895	0.91784	66.401	68.376	0.26725	0.13975	0.22720	89.593	21.805
400.00	2.3530	1.2467	0.80213	66.621	68.509	0.26715	0.14217	0.25728	85.834	22.243

TABLE 2-272 Thermodynamic Properties of R-114, 1,2-Dichlorotetrafluoroethane (Concluded)

Temperature K	Pressure MPa	Density mol/dm ³	Volume dm ³ /mol	Int. energy kJ/mol	Enthalpy kJ/mol	Entropy kJ/(mol·K)	C _v kJ/(mol·K)	C _p kJ/(mol·K)	Sound speed m/s	Joule-Thomson K/MPa
Saturated Properties										
405.00	2.5694	1.4416	0.69369	66.763	68.545	0.26684	0.14487	0.30666	81.678	22.687
410.00	2.8015	1.6966	0.58941	66.782	68.433	0.26620	0.14792	0.40278	77.066	23.035
415.00	3.0507	2.0686	0.48342	66.570	68.045	0.26493	0.15144	0.67085	71.914	22.963
418.83	3.2516	3.3932	0.29471	64.391	65.349	0.25828			0	18.568
Single-Phase Properties										
300.00	0.10000	0.041312	24.206	58.335	60.756	0.26666	0.11051	0.11990	122.03	19.386
350.00	0.10000	0.035003	28.569	64.107	66.964	0.28578	0.11931	0.12828	132.80	12.959
400.00	0.10000	0.030432	32.860	70.284	73.570	0.30341	0.12703	0.13580	142.49	9.4836
450.00	0.10000	0.026945	37.113	76.817	80.529	0.31980	0.13376	0.14241	151.42	7.3132
500.00	0.10000	0.024188	41.342	83.661	87.796	0.33510	0.13956	0.14813	159.78	5.8366
300.00	1.0000	8.4984	0.11767	38.583	38.701	0.18633	0.11994	0.16950	551.87	-0.25320
350.00	1.0000	7.4651	0.13396	47.454	47.588	0.21369	0.12863	0.18840	364.95	0.11384
356.40	1.0000	7.3010	0.13697	48.670	48.807	0.21714	0.12986	0.19249	338.92	0.21213
356.40	1.0000	0.43061	2.3223	63.533	65.855	0.26498	0.12596	0.15128	108.84	20.165
400.00	1.0000	0.34682	2.8833	69.357	72.240	0.28188	0.12912	0.14474	126.86	11.867
450.00	1.0000	0.29218	3.4226	76.104	79.526	0.29904	0.13466	0.14726	141.14	8.1166
500.00	1.0000	0.25510	3.9201	83.069	86.989	0.31477	0.14003	0.15132	152.73	6.1412
300.00	5.0000	8.6001	0.11628	38.303	38.884	0.18538	0.11983	0.16738	584.86	-0.28910
350.00	5.0000	7.6832	0.13015	46.919	47.570	0.21213	0.12793	0.18096	420.00	-0.048046
400.00	5.0000	6.4329	0.15545	56.400	57.177	0.23775	0.13659	0.20814	251.68	0.75207
450.00	5.0000	3.3217	0.30105	69.251	70.756	0.26953	0.14905	0.34888	94.479	9.2719
500.00	5.0000	1.7533	0.57034	79.658	82.509	0.29444	0.14423	0.18709	121.74	7.0501
300.00	10.000	8.7118	0.11479	37.991	39.139	0.18430	0.11975	0.16542	621.41	-0.32232
350.00	10.000	7.8877	0.12678	46.398	47.666	0.21057	0.12746	0.17597	473.47	-0.15701
400.00	10.000	6.9197	0.14452	55.329	56.774	0.23488	0.13488	0.18894	338.62	0.18601
450.00	10.000	5.6865	0.17586	64.892	66.650	0.25812	0.14158	0.20710	225.09	1.0459
500.00	10.000	4.2030	0.23793	74.962	77.341	0.28064	0.14594	0.21449	163.22	2.5802
300.00	15.000	8.8106	0.11350	37.713	39.415	0.18332	0.11973	0.16394	654.14	-0.34729
350.00	15.000	8.0508	0.12421	45.970	47.834	0.20926	0.12720	0.17290	517.56	-0.22334
400.00	15.000	7.2160	0.13858	54.628	56.707	0.23294	0.13421	0.18200	398.49	-0.017272
450.00	15.000	6.2819	0.15919	63.643	66.030	0.25489	0.14025	0.19084	301.49	0.34360
500.00	15.000	5.2683	0.18981	72.897	75.744	0.27536	0.14487	0.19667	235.39	0.89448
300.00	20.000	8.8998	0.11236	37.460	39.707	0.18241	0.11973	0.16278	683.99	-0.36679
350.00	20.000	8.1881	0.12213	45.603	48.046	0.20811	0.12704	0.17079	555.75	-0.26854
400.00	20.000	7.4361	0.13448	54.086	56.775	0.23141	0.13385	0.17821	446.47	-0.12632
450.00	20.000	6.6421	0.15056	62.835	65.846	0.25277	0.13972	0.18438	358.35	0.081032
500.00	20.000	5.8257	0.17165	71.746	75.179	0.27243	0.14442	0.18846	294.31	0.35805

The values in these tables were generated from the NIST REFPROP software (Lemmon, E. W., McLinden, M. O., and Huber, M. L., NIST Standard Reference Database 23: Reference Fluid Thermodynamic and Transport Properties—REFPROP, National Institute of Standards and Technology, Standard Reference Data Program, Gaithersburg, Md., 2002, Version 7.1). The primary source for the thermodynamic properties is Platzer, B., Polt, A., and Maurer, G., *Thermophysical Properties of Refrigerants*, Springer-Verlag, Berlin, 1990. Validated equations for the viscosity and thermal conductivity are not currently available for this fluid.

Properties at the critical point temperature are given in the last entry of the saturation tables. In the single-phase table, when the temperature range for a given isobar includes a vapor-liquid phase boundary, the temperature of phase equilibrium is noted, and properties for both the saturated liquid and saturated vapor are given (with liquid properties given in the upper line). Lines are omitted from the temperature-pressure grid of the single-phase table, when the system would be in the solid phase or if there are potential problems with the source property surface.

The uncertainty in density is 0.2% up to 400 K and 1% at higher temperatures. The vapor pressure uncertainty is 1.5%. In the liquid phase, the uncertainty in isobaric heat capacity is 3%.

TABLE 2-273 Saturated Refrigerant 115, Chloropentafluoroethane*

Temp., °F	Pressure, lb/in ² abs.	Volume, ft ³ /lb		Enthalpy, Btu/lb		Entropy, Btu/(lb)(°F)	
		Liquid	Vapor	Liquid	Vapor	Liquid	Vapor
-100	2.327	0.00966	10.57	-13.07	45.83	-0.0335	0.1302
-80	4.573	0.00986	5.624	-8.78	48.39	-0.0219	0.1286
-60	8.306	0.01009	3.218	-4.43	50.96	-0.0108	0.1278
-40	14.13	0.01033	1.953	0.00	53.53	0.0000	0.1275
-20	22.74	0.01060	1.245	4.50	56.07	0.0104	0.1277
0	34.94	0.01090	0.8257	9.09	58.56	0.0206	0.1282
20	51.59	0.01123	0.5657	13.76	61.00	0.0305	0.1290
40	73.65	0.01161	0.3979	18.54	63.35	0.0401	0.1298
60	102.1	0.01204	0.2857	23.45	65.60	0.0496	0.1308
80	138.1	0.01255	0.2081	28.54	67.71	0.0591	0.1317
100	182.7	0.01316	0.1530	33.85	69.63	0.0686	0.1325
120	237.3	0.01393	0.1125	39.50	71.24	0.0782	0.1330
140	303.2	0.01496	0.0817	45.67	72.36	0.0884	0.1329
160	382.0	0.01664	0.0567	52.76	72.42	0.0996	0.1314
170	427.0	0.01838	0.0444	56.56	71.33	0.1055	0.1290
175.89 ^c	457.6	0.0261	0.0261	64.30	64.30	0.1175	0.1175

* Unpublished data of General Chemicals Division, Allied Chemical Company. Used by permission. *c* = critical temperature.

No material in SI units appears in the 1993 ASHRAE *Handbook—Fundamentals* (SI ed.). Tables and a chart to 50 ata, 200 °C are given by Mathias, H. and H. J. Löffler, Techn. Univ. Berlin rept., 1966 (42 pp.). A chart to 1500 psia, 500 °F was given by Mears, W. H., E. Rosenthal, et al., *J. Chem. Eng. Data*, **11**, 3 (1966): 338–343.

TABLE 2-274 Thermodynamic Properties of R-116, Hexafluoroethane

Temperature K	Pressure MPa	Density mol/dm ³	Volume dm ³ /mol	Int. energy kJ/mol	Enthalpy kJ/mol	Entropy kJ/(mol·K)	C_v kJ/(mol·K)	C_p kJ/(mol·K)	Sound speed m/s	Joule-Thomson K/MPa
Saturated Properties										
173.10	0.026084	12.304	0.081274	13.031	13.033	0.073325	0.083104	0.12322	653.29	-0.38383
175.00	0.029802	12.247	0.081649	13.266	13.268	0.074672	0.083413	0.12375	645.09	-0.37807
180.00	0.041661	12.097	0.082664	13.887	13.891	0.078175	0.084236	0.12518	623.59	-0.36202
185.00	0.057021	11.945	0.083720	14.516	14.521	0.081622	0.085077	0.12670	602.22	-0.34452
190.00	0.076558	11.789	0.084824	15.153	15.159	0.085018	0.085933	0.12829	580.95	-0.32540
195.00	0.10101	11.631	0.085979	15.797	15.806	0.088366	0.086803	0.12996	559.75	-0.30443
200.00	0.13116	11.469	0.087192	16.450	16.461	0.091671	0.087686	0.13173	538.61	-0.28132
205.00	0.16784	11.303	0.088469	17.111	17.126	0.094937	0.088580	0.13361	517.48	-0.25573
210.00	0.21194	11.134	0.089818	17.781	17.800	0.098169	0.089485	0.13560	496.36	-0.22722
215.00	0.26438	10.959	0.091248	18.461	18.485	0.10137	0.090402	0.13773	475.20	-0.19525
220.00	0.32611	10.779	0.092769	19.151	19.181	0.10454	0.091330	0.14002	453.97	-0.15913
225.00	0.39814	10.594	0.094395	19.851	19.889	0.10769	0.092270	0.14249	432.64	-0.11798
230.00	0.48150	10.401	0.096140	20.563	20.609	0.11082	0.093224	0.14520	411.18	-0.070666
235.00	0.57725	10.201	0.098026	21.286	21.343	0.11394	0.094193	0.14818	389.53	-0.015673
240.00	0.68650	9.9926	0.10007	22.023	22.092	0.11705	0.095179	0.15152	367.64	0.049034
245.00	0.81042	9.7735	0.10232	22.774	22.857	0.12015	0.096188	0.15531	345.46	0.12626
250.00	0.95020	9.5423	0.10480	23.541	23.640	0.12326	0.097226	0.15970	322.91	0.21998
255.00	1.1071	9.2968	0.10756	24.325	24.444	0.12638	0.098301	0.16491	299.89	0.33604
260.00	1.2826	9.0336	0.11070	25.130	25.272	0.12952	0.099429	0.17129	276.28	0.48338
265.00	1.4781	8.7482	0.11431	25.959	26.128	0.13269	0.10063	0.17942	251.91	0.67638
270.00	1.6952	8.4341	0.11857	26.818	27.019	0.13593	0.10195	0.19040	226.54	0.93994
275.00	1.9360	8.0803	0.12376	27.715	27.955	0.13926	0.10345	0.20651	199.81	1.3211
280.00	2.2027	7.6671	0.13043	28.667	28.954	0.14274	0.10525	0.23354	171.13	1.9215
285.00	2.4983	7.1502	0.13986	29.710	30.059	0.14651	0.10768	0.29195	139.42	3.0109
290.00	2.8276	6.3727	0.15692	30.973	31.417	0.15106	0.11183	0.54643	102.12	5.6531
293.03	3.0477	4.4440	0.22502	33.029	33.715	0.15879			0	13.224
173.10	0.026084	0.018437	54.238	28.993	30.408	0.17370	0.067328	0.076383	106.90	43.932
175.00	0.029802	0.020874	47.907	29.113	30.541	0.17338	0.067932	0.077064	107.29	42.424
180.00	0.041661	0.028519	35.064	29.433	30.893	0.17263	0.069527	0.078887	108.24	38.839
185.00	0.057021	0.038215	26.168	29.755	31.247	0.17203	0.071130	0.080765	109.07	35.743
190.00	0.076558	0.050323	19.872	30.079	31.601	0.17155	0.072742	0.082706	109.78	33.062
195.00	0.10101	0.065236	15.329	30.406	31.954	0.17118	0.074365	0.084719	110.35	30.736
200.00	0.13116	0.083387	11.992	30.733	32.306	0.17090	0.076000	0.086816	110.78	28.716
205.00	0.16784	0.10525	9.5011	31.061	32.656	0.17069	0.077648	0.089011	111.05	26.960
210.00	0.21194	0.13135	7.6132	31.389	33.003	0.17056	0.079312	0.091322	111.15	25.435
215.00	0.26438	0.16228	6.1624	31.716	33.345	0.17049	0.080992	0.093772	111.07	24.112
220.00	0.32611	0.19868	5.0331	32.041	33.683	0.17046	0.082691	0.096389	110.80	22.967
225.00	0.39814	0.24133	4.1437	32.364	34.014	0.17047	0.084412	0.099211	110.33	21.983
230.00	0.48150	0.29110	3.4353	32.682	34.336	0.17051	0.086158	0.10229	109.63	21.143
235.00	0.57725	0.34902	2.8652	32.995	34.649	0.17056	0.087932	0.10569	108.69	20.435
240.00	0.68650	0.41636	2.4018	33.302	34.950	0.17063	0.089742	0.10951	107.50	19.850
245.00	0.81042	0.49465	2.0216	33.599	35.237	0.17068	0.091594	0.11388	106.02	19.381
250.00	0.95020	0.58587	1.7069	33.885	35.507	0.17072	0.093497	0.11901	104.24	19.024
255.00	1.1071	0.69256	1.4439	34.157	35.755	0.17073	0.095465	0.12520	102.13	18.777
260.00	1.2826	0.81820	1.2222	34.409	35.977	0.17069	0.097518	0.13296	99.661	18.637
265.00	1.4781	0.96766	1.0334	34.636	36.164	0.17056	0.099682	0.14316	96.789	18.605
270.00	1.6952	1.1482	0.87090	34.830	36.306	0.17033	0.10200	0.15741	93.477	18.677
275.00	1.9360	1.3717	0.72904	34.975	36.387	0.16992	0.10454	0.17918	89.681	18.837
280.00	2.2027	1.6592	0.60271	35.047	36.375	0.16924	0.10743	0.21720	85.354	19.040
285.00	2.4983	2.0572	0.48610	34.992	36.207	0.16807	0.11094	0.30201	80.445	19.127
290.00	2.8276	2.7232	0.36721	34.631	35.669	0.16572	0.11584	0.66697	74.869	18.438
293.03	3.0477	4.4440	0.22502	33.029	33.715	0.15879			0	13.224

Single-Phase Properties

175.00	0.10000	12.249	0.081637	13.263	13.271	0.074658	0.083417	0.12373	645.46	-0.37835
194.81	0.10000	11.637	0.085935	15.773	15.782	0.088242	0.086771	0.12990	560.54	-0.30525
194.81	0.10000	0.064625	15.474	30.394	31.941	0.17119	0.074304	0.084642	110.33	30.817
250.00	0.10000	0.049033	20.394	34.892	36.932	0.19368	0.087457	0.096533	126.48	13.742
325.00	0.10000	0.037293	26.815	42.103	44.784	0.22106	0.10389	0.11253	144.51	6.5149
400.00	0.10000	0.030174	33.141	50.430	53.744	0.24582	0.11740	0.12590	160.19	3.7890
175.00	1.0000	12.272	0.081484	13.232	13.314	0.074480	0.083472	0.12349	650.25	-0.38185
250.00	1.0000	9.5480	0.10473	23.534	23.638	0.12323	0.097224	0.15951	323.69	0.21614
251.65	1.0000	9.4631	0.10567	23.797	23.903	0.12428	0.097576	0.16132	315.37	0.25543
251.65	1.0000	0.61920	1.6150	33.976	35.591	0.17073	0.094138	0.12091	103.59	18.931
325.00	1.0000	0.40237	2.4853	41.594	44.080	0.20033	0.10529	0.11782	135.84	7.1157
400.00	1.0000	0.31155	3.2097	50.096	53.305	0.22584	0.11796	0.12829	156.26	3.8772
250.00	5.0000	9.9221	0.10078	23.073	23.577	0.12134	0.097206	0.14935	376.03	0.0088070
325.00	5.0000	3.7219	0.26868	37.500	38.843	0.17386	0.11497	0.24037	101.35	7.5484
400.00	5.0000	1.7961	0.55676	48.386	51.170	0.20825	0.12060	0.14444	144.06	3.8425
250.00	10.000	10.261	0.097459	22.648	23.622	0.11954	0.097376	0.14319	425.10	-0.12130
325.00	10.000	7.1151	0.14055	34.117	35.522	0.16098	0.11174	0.17544	207.64	1.0712
400.00	10.000	3.9471	0.25335	46.132	48.666	0.19742	0.12255	0.16440	156.43	2.4329
250.00	20.000	10.747	0.093053	22.031	23.892	0.11682	0.097852	0.13725	498.98	-0.24812
325.00	20.000	8.5892	0.11643	32.498	34.826	0.15497	0.11132	0.15339	328.94	0.093523
400.00	20.000	6.4948	0.15397	43.572	46.651	0.18769	0.12291	0.16013	246.48	0.50074
250.00	50.000	11.642	0.085893	20.902	25.197	0.11135	0.099289	0.13120	647.29	-0.37511
325.00	50.000	10.197	0.098067	30.607	35.511	0.14736	0.11250	0.14332	516.00	-0.28102
400.00	50.000	8.8968	0.11240	40.984	46.604	0.17805	0.12396	0.15192	437.11	-0.20643

The values in these tables were generated from the NIST REFPROP software (Lemmon, E. W., McLinden, M. O., and Huber, M. L., NIST Standard Reference Database 23: Reference Fluid Thermodynamic and Transport Properties—REFPROP, National Institute of Standards and Technology, Standard Reference Data Program, Gaithersburg, Md., 2002, Version 7.1). The primary source for the thermodynamic properties is Lemmon, E. W., and Span, R., "Short Fundamental Equations of State for 20 Industrial Fluids," *J. Chem. Eng. Data* **51**(3):785–850, 2006. Validated equations for the viscosity and thermal conductivity are not currently available for this fluid.

Properties at the triple point temperature and the critical point temperature are given in the first and last entries of the saturation tables, respectively. In the single-phase table, when the temperature range for a given isobar includes a vapor-liquid phase boundary, the temperature of phase equilibrium is noted, and properties for both the saturated liquid and saturated vapor are given (with liquid properties given in the upper line). Lines are omitted from the temperature-pressure grid of the single-phase table, when the system would be in the solid phase or if there are potential problems with the source property surface.

The uncertainties in the equation are 0.5% in density for liquid and vapor states and 1% in density or pressure for supercritical states. For vapor pressure, the uncertainty is 0.3%, that for vapor-phase speed of sounds is 0.2%, and the uncertainty for heat capacities is 5%.

TABLE 2-275 Thermodynamic Properties of R-123, 2,2-Dichloro-1,1,1-Trifluoroethane

Temperature K	Pressure MPa	Density mol/dm ³	Volume dm ³ /mol	Int. energy kJ/mol	Enthalpy kJ/mol	Entropy kJ/(mol·K)	C_v kJ/(mol·K)	C_p kJ/(mol·K)	Sound speed m/s	Joule-Thomson K/MPa	Therm. cond. mW/(m·K)	Viscosity μPa·s
Saturated Properties												
166.00	4.2021E-06	11.580	0.086355	15.111	15.111	0.081219	0.096271	0.14206	1243.8	-0.47555	115.89	4953.8
170.00	7.5115E-06	11.520	0.086807	15.678	15.678	0.084599	0.096537	0.14181	1227.9	-0.47661	114.18	4180.7
185.00	5.1172E-05	11.298	0.088511	17.800	17.800	0.096559	0.096881	0.14120	1167.0	-0.47672	109.51	2571.4
200.00	0.00024954	11.079	0.090257	19.919	19.919	0.10757	0.097283	0.14151	1104.3	-0.47027	105.59	1795.0
215.00	0.00093965	10.861	0.092076	22.050	22.050	0.11785	0.098162	0.14272	1040.9	-0.45811	101.48	1337.4
230.00	0.0028868	10.640	0.093989	24.204	24.204	0.12753	0.099479	0.14455	977.54	-0.44149	97.035	1036.8
245.00	0.0075380	10.415	0.096017	26.388	26.389	0.13673	0.10110	0.14676	914.89	-0.42124	92.395	825.41
260.00	0.017260	10.185	0.098182	28.607	28.609	0.14552	0.10291	0.14919	853.42	-0.39765	87.716	669.88
275.00	0.035500	9.9497	0.10051	30.863	30.867	0.15395	0.10483	0.15176	793.34	-0.37048	83.129	551.59
290.00	0.066848	9.7073	0.10302	33.158	33.165	0.16208	0.10680	0.15443	734.70	-0.33894	78.719	459.38
305.00	0.11700	9.4567	0.10575	35.492	35.504	0.16993	0.10879	0.15722	677.42	-0.30164	74.533	386.07
320.00	0.19264	9.1962	0.10874	37.867	37.888	0.17753	0.11080	0.16020	621.30	-0.25640	70.585	326.86
335.00	0.30136	8.9238	0.11206	40.286	40.319	0.18492	0.11283	0.16350	566.09	-0.19988	66.863	278.37
350.00	0.45147	8.6365	0.11579	42.751	42.804	0.19212	0.11491	0.16729	511.47	-0.12681	63.340	238.12
365.00	0.65201	8.3301	0.12005	45.270	45.349	0.19917	0.11704	0.17186	457.07	-0.028618	59.972	204.30
380.00	0.91268	7.9984	0.12502	47.853	47.967	0.20612	0.11927	0.17772	402.48	0.10963	56.709	175.46
395.00	1.2440	7.6316	0.13103	50.514	50.677	0.21300	0.12167	0.18579	347.23	0.31613	53.486	150.45
410.00	1.6577	7.2132	0.13863	53.281	53.510	0.21990	0.12433	0.19804	290.69	0.65103	50.222	128.23
425.00	2.1672	6.7113	0.14900	56.204	56.527	0.22695	0.12747	0.21999	231.85	1.2687	46.810	107.74
440.00	2.7898	6.0457	0.16541	59.412	59.873	0.23446	0.13159	0.27613	168.40	2.7240	43.102	87.306
455.00	3.5547	4.6936	0.21305	63.738	64.496	0.24446	0.13975	1.2865	90.823	10.053	39.324	58.622
456.83	3.6619	3.5964	0.27805	65.873	66.891	0.24965			0	16.566		
166.00	4.2021E-06	3.0446E-06	328.450	47.940	49.320	0.28730	0.064141	0.072457	100.97	335.67	1.6736	5.5300
170.00	7.5115E-06	5.3144E-06	188.170	48.198	49.612	0.28421	0.065216	0.073532	102.08	305.67	1.9014	5.7017
185.00	5.1172E-05	3.3272E-05	30.055	49.206	50.744	0.27463	0.069152	0.077473	106.14	219.47	2.7552	6.3386
200.00	0.00024954	0.00015013	6.660.7	50.269	51.931	0.26763	0.072951	0.081290	110.02	162.12	3.6080	6.9646
215.00	0.00093965	0.00052637	1.899.8	51.386	53.171	0.26259	0.076634	0.085017	113.72	122.83	4.4590	7.5791
230.00	0.0028868	0.0015145	660.29	52.550	54.456	0.25906	0.080226	0.088699	117.20	95.252	5.3073	8.1817
245.00	0.0075380	0.0037253	268.44	53.755	55.779	0.25669	0.083755	0.092390	120.41	75.497	6.1533	8.7712
260.00	0.017260	0.0080830	123.72	54.996	57.131	0.25522	0.087245	0.096144	123.27	61.102	6.9987	9.3465
275.00	0.035500	0.015852	63.083	56.264	58.504	0.25445	0.090715	0.10001	125.72	50.463	7.8477	9.9065
290.00	0.066848	0.028647	34.907	57.553	59.887	0.25242	0.094177	0.10405	127.66	42.504	8.7073	10.450
305.00	0.11700	0.048445	20.642	58.855	61.270	0.25440	0.097639	0.10832	129.01	36.493	9.5872	10.979
320.00	0.19264	0.077628	12.882	60.163	62.645	0.25489	0.10111	0.11290	129.68	31.923	10.500	11.494
335.00	0.30136	0.11908	8.3975	61.468	63.999	0.25560	0.10459	0.11790	129.58	28.442	11.463	12.002
350.00	0.45147	0.17640	5.6690	62.760	65.319	0.25645	0.10810	0.12353	128.62	25.804	12.497	12.515
365.00	0.65201	0.25423	3.9334	64.026	66.591	0.25737	0.11165	0.13011	126.67	23.846	13.627	13.054
380.00	0.91268	0.35900	2.7855	65.252	67.794	0.25829	0.11529	0.13821	123.57	22.466	14.889	13.656
395.00	1.2440	0.50026	1.9990	66.412	68.899	0.25913	0.11908	0.14902	119.13	21.617	16.332	14.390
410.00	1.6577	0.69385	1.4412	67.468	69.857	0.25977	0.12313	0.16522	113.03	21.309	18.039	15.384
425.00	2.1672	0.97042	1.0305	68.348	70.581	0.26002	0.12767	0.19466	104.85	21.605	20.168	16.913
440.00	2.7898	1.4081	0.71016	68.866	70.847	0.25940	0.13325	0.27310	93.850	22.561	23.176	19.744
455.00	3.5547	2.5178	0.39718	67.881	69.293	0.25500	0.14227	1.6671	78.287	21.950	30.870	29.346
456.83	3.6619	3.5964	0.27805	65.873	66.891	0.24965			0	16.566		

Single-Phase Properties

200.00	0.10000	11.080	0.090251	19.917	19.926	0.10756	0.097300	0.14151	1104.5	-0.47033	105.61	1797.1
300.00	0.10000	9.5412	0.10481	34.709	34.720	0.16734	0.10812	0.15627	696.38	-0.31484	75.903	408.75
300.61	0.10000	9.5309	0.10492	34.805	34.815	0.16766	0.10820	0.15639	694.05	-0.31326	75.734	405.88
300.61	0.10000	0.041795	23.926	58.473	60.866	0.25432	0.096626	0.10704	128.68	38.084	9.3269	10.826
400.00	0.10000	0.030530	32.754	68.902	72.178	0.28673	0.11170	0.12066	150.93	14.728	15.085	14.262
500.00	0.10000	0.024219	41.290	80.750	84.879	0.31502	0.12437	0.13300	169.33	7.9263	20.780	17.224
600.00	0.10000	0.020111	49.724	93.743	98.716	0.34022	0.13502	0.14352	185.60	5.0504	26.460	19.696
200.00	1.0000	11.087	0.090194	19.896	19.986	0.10745	0.097447	0.14145	1105.5	-0.47094	105.80	1815.8
300.00	1.0000	9.5586	0.10462	34.660	34.764	0.16717	0.10822	0.15597	701.57	-0.31949	76.273	413.78
384.30	1.0000	7.8974	0.12662	48.607	48.733	0.20809	0.11994	0.17975	386.73	0.16009	55.784	167.94
384.30	1.0000	0.39525	2.5301	65.592	68.122	0.25855	0.11636	0.14096	122.45	22.169	15.282	13.849
400.00	1.0000	0.36390	2.7480	67.553	70.301	0.26410	0.11698	0.13715	129.70	18.389	16.135	14.368
500.00	1.0000	0.25890	3.8625	80.024	83.887	0.29441	0.12571	0.13778	160.11	8.3865	21.585	17.431
600.00	1.0000	0.20738	4.8220	93.232	98.054	0.32022	0.13546	0.14581	181.06	5.1181	27.069	19.994
200.00	5.0000	11.118	0.089944	19.803	20.253	0.10699	0.098069	0.14121	1110.5	-0.47345	106.62	1902.1
300.00	5.0000	9.6324	0.10382	34.450	34.969	0.16646	0.10865	0.15478	723.64	-0.33792	77.874	436.12
400.00	5.0000	7.7754	0.12861	50.791	51.434	0.21368	0.12180	0.17810	388.06	0.14142	55.285	160.58
500.00	5.0000	2.1822	0.45826	74.934	77.225	0.27035	0.13698	0.23468	111.01	11.061	30.182	28.291
600.00	5.0000	1.2117	0.82529	90.757	94.883	0.32070	0.13749	0.16051	161.94	5.1664	30.009	24.445
200.00	10.000	11.156	0.089639	19.691	20.588	0.10642	0.098779	0.14095	1117.0	-0.47622	107.63	2017.3
300.00	10.000	9.7177	0.10290	34.208	35.237	0.16564	0.10912	0.15357	749.33	-0.35684	79.793	464.14
400.00	10.000	8.0432	0.12433	50.152	51.395	0.21200	0.12141	0.17093	447.83	-0.033773	58.469	181.18
500.00	10.000	5.5005	0.18180	68.419	70.237	0.25388	0.13402	0.21202	205.61	1.7914	41.785	78.103
600.00	10.000	2.8283	0.35357	87.359	90.895	0.29164	0.13939	0.18482	163.33	3.7808	35.942	39.777
200.00	20.000	11.229	0.089054	19.480	21.261	0.10532	0.099998	0.14055	1130.7	-0.48062	109.63	2276.1
300.00	20.000	9.8704	0.10131	33.778	35.804	0.16412	0.10993	0.15175	795.84	-0.38528	83.416	521.04
400.00	20.000	8.4163	0.11882	49.229	51.605	0.20949	0.12134	0.16430	534.29	-0.19523	63.653	217.09
500.00	20.000	6.7515	0.14812	65.791	68.753	0.24770	0.13081	0.17889	348.69	0.27303	49.919	115.74
600.00	20.000	4.9944	0.20022	83.034	87.039	0.28102	0.13822	0.18342	257.14	0.96765	41.677	74.025
200.00	40.000	11.368	0.087968	19.099	22.618	0.10325	0.10179	0.14011	1160.1	-0.48571	113.48	2947.0
300.00	40.000	10.125	0.098764	33.072	37.023	0.16152	0.11120	0.14952	875.49	-0.42067	90.039	640.89
400.00	40.000	8.9071	0.11227	47.981	52.472	0.20590	0.12199	0.15901	653.37	-0.32210	72.037	282.73
500.00	40.000	7.7025	0.12983	63.586	68.779	0.24225	0.13053	0.16697	503.02	-0.17413	60.777	165.05
600.00	40.000	6.5412	0.15288	79.686	85.801	0.27327	0.13791	0.17293	409.64	0.011715	52.389	115.87

The values in these tables were generated from the NIST REFPROP software (Lemmon, E. W., McLinden, M. O., and Huber, M. L., NIST Standard Reference Database 23: Reference Fluid Thermodynamic and Transport Properties—REFPROP, National Institute of Standards and Technology, Standard Reference Data Program, Gaithersburg, Md., 2002, Version 7.1). The primary source for the thermodynamic properties is Younglove, B. A., and McLinden, M. O., "An International Standard Equation of State for the Thermodynamic Properties of Refrigerant 123 (2,2-Dichloro-1,1,1-Trifluoroethane)," *J. Phys. Chem. Ref. Data* **23**:731–779, 1994. The source for viscosity is Tanaka, Y. and Sotani, T., "Transport Properties (Thermal Conductivity and Viscosity)," in McLinden, M. O., Ed., *R123—Thermodynamic and Physical Properties*, Paris: International Institute of Refrigeration, 1995. See also *Int. J. Thermophys.* **17**(2):293–328, 1996. The source for thermal conductivity is Laesecke, A., Perkins, R. A., and Howley, J. B., "An Improved Correlation for the Thermal Conductivity of HCFC123 (2,2-Dichloro-1,1,1-Trifluoroethane)," *Int. J. Refrigeration* **19**:231–238, 1996.

Properties at the triple point temperature and the critical point temperature are given in the first and last entries of the saturation tables, respectively. In the single-phase table, when the temperature range for a given isobar includes a vapor-liquid phase boundary, the temperature of phase equilibrium is noted, and properties for both the saturated liquid and saturated vapor are given (with liquid properties given in the upper line). Lines are omitted from the temperature-pressure grid of the single-phase table, when the system would be in the solid phase or if there are potential problems with the source property surface.

The uncertainties of the equation of state are 0.1% in density, 1.5% in heat capacity, and 2% in the speed of sound, except in the critical region. The uncertainty in vapor pressure is 0.1%. Uncertainties are greater below 180 K. The uncertainty in viscosity is 5%. The uncertainty in thermal conductivity is 2%.

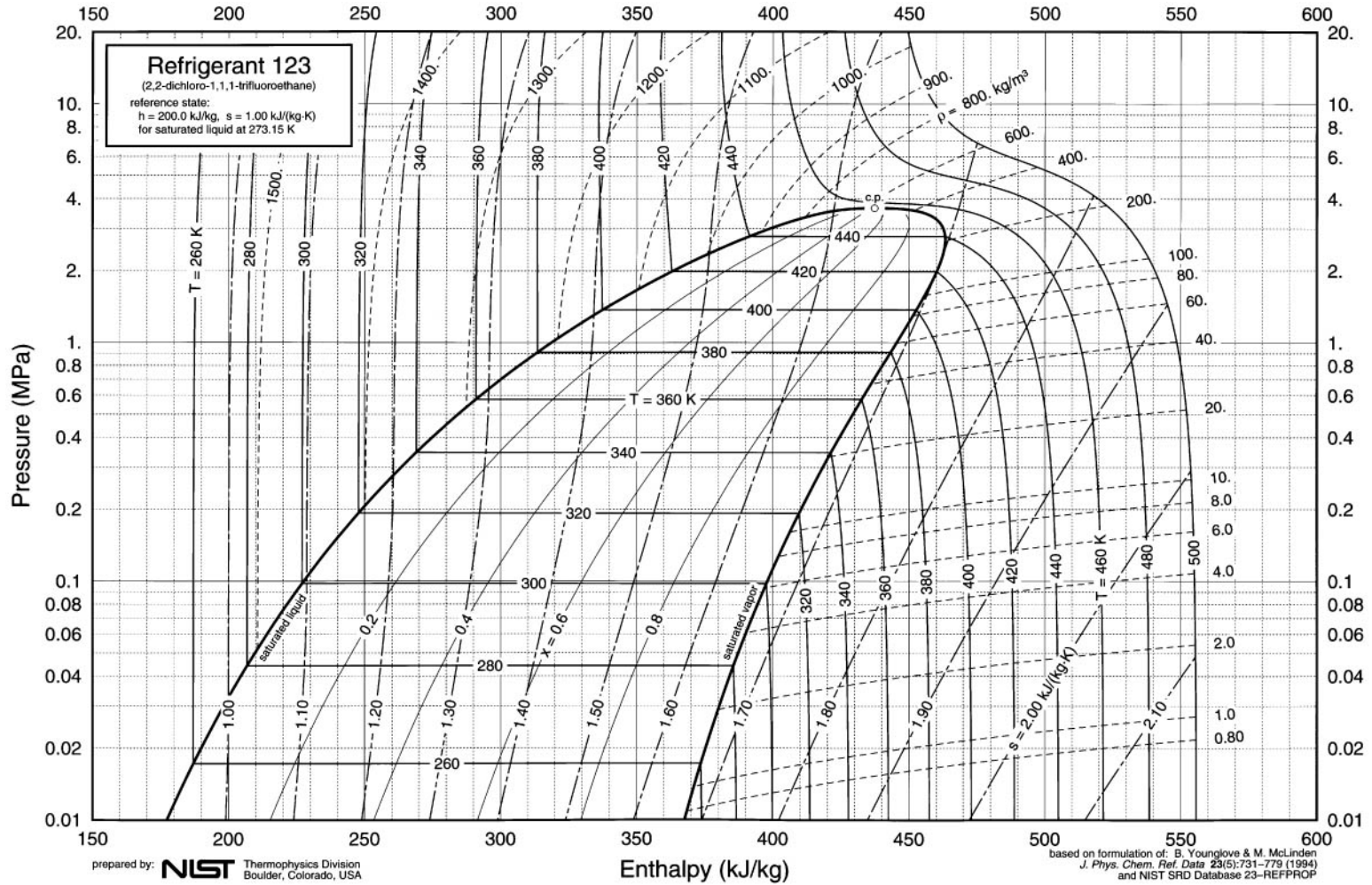


FIG. 2-24 Enthalpy-log-pressure diagram for Refrigerant 123.

TABLE 2-276 Thermodynamic Properties of R-124, 2-Chloro-1,1,1,2-Tetrafluoroethane

Temperature K	Pressure MPa	Density mol/dm ³	Volume dm ³ /mol	Int. energy kJ/mol	Enthalpy kJ/mol	Entropy kJ/(mol·K)	C _v kJ/(mol·K)	C _p kJ/(mol·K)	Sound speed m/s	Joule-Thomson K/MPa
Saturated Properties										
120.00	2.6739E-08	13.576	0.073661	6.7015	6.7015	0.027106	0.088123	0.12662	1293.6	-0.48257
135.00	8.0309E-07	13.288	0.075255	8.6014	8.6014	0.042024	0.087495	0.12684	1225.8	-0.47832
150.00	1.1223E-05	13.003	0.076906	10.510	10.510	0.055431	0.087696	0.12778	1157.4	-0.47012
165.00	9.0881E-05	12.718	0.078626	12.437	12.437	0.067673	0.088451	0.12919	1089.0	-0.45872
180.00	0.00049265	12.433	0.080432	14.388	14.388	0.078987	0.089589	0.13095	1021.3	-0.44440
195.00	0.0019732	12.145	0.082339	16.367	16.367	0.089547	0.091000	0.13299	954.41	-0.42707
210.00	0.0062626	11.853	0.084369	18.378	18.379	0.099484	0.092610	0.13527	888.65	-0.40640
225.00	0.016573	11.554	0.086547	20.426	20.427	0.10890	0.094368	0.13778	824.09	-0.38173
240.00	0.037986	11.248	0.088904	22.512	22.515	0.11787	0.096239	0.14055	760.75	-0.35205
255.00	0.077612	10.931	0.091481	24.641	24.648	0.12648	0.098199	0.14361	698.57	-0.31583
270.00	0.14453	10.601	0.094332	26.816	26.830	0.13477	0.10024	0.14702	637.46	-0.27079
285.00	0.24955	10.253	0.097528	29.043	29.067	0.14280	0.10235	0.15090	577.23	-0.21337
300.00	0.40500	9.8843	0.10117	31.327	31.368	0.15061	0.10454	0.15545	517.54	-0.13780
315.00	0.62447	9.4868	0.10541	33.677	33.743	0.15826	0.10685	0.16102	457.87	-0.034029
330.00	0.92279	9.0506	0.11049	36.106	36.208	0.16580	0.10933	0.16825	397.44	0.11699
345.00	1.3163	8.5590	0.11684	38.634	38.788	0.17332	0.11213	0.17860	335.05	0.35590
360.00	1.8234	7.9793	0.12532	41.302	41.531	0.18092	0.11553	0.19587	269.18	0.78492
375.00	2.4663	7.2348	0.13822	44.202	44.543	0.18889	0.12005	0.23450	198.17	1.7419
390.00	3.2770	6.0066	0.16648	47.714	48.259	0.19827	0.12812	0.46802	115.48	5.4469
395.43	3.6243	4.1033	0.24371	50.813	51.696	0.20684			0	14.607
120.00	2.6739E-08	2.6799E-08	37,314,000.	36.727	37.725	0.28563	0.051678	0.059992	92.125	997.50
135.00	8.0309E-07	7.1548E-07	1,397,700.	37.530	38.653	0.26462	0.055405	0.063720	97.256	558.90
150.00	1.1223E-05	8.9989E-06	111,120.	38.388	39.636	0.24960	0.059044	0.067361	102.10	338.42
165.00	9.0881E-05	6.6260E-05	15,092.	39.300	40.671	0.23879	0.062605	0.070933	106.70	218.53
180.00	0.00049265	0.00032946	3,035.3	40.262	41.757	0.23104	0.066113	0.074474	111.05	149.08
195.00	0.0019732	0.0012200	819.64	41.269	42.887	0.22555	0.069600	0.078043	115.13	106.83
210.00	0.0062626	0.0036077	277.19	42.318	44.054	0.22175	0.073111	0.081721	118.89	80.088
225.00	0.016573	0.0089652	111.54	43.400	45.248	0.21922	0.076698	0.085612	122.21	62.512
240.00	0.037986	0.019455	51.400	44.507	46.459	0.21764	0.080420	0.089837	124.99	50.458
255.00	0.077612	0.037965	26.340	45.631	47.675	0.21678	0.084321	0.094522	127.10	41.824
270.00	0.14453	0.068150	14.674	46.762	48.883	0.21645	0.088420	0.099789	128.40	35.421
285.00	0.24955	0.11457	8.7285	47.892	50.070	0.21649	0.092708	0.10578	128.75	30.583
300.00	0.40500	0.18300	5.4645	49.009	51.222	0.21679	0.097166	0.11271	128.00	26.921
315.00	0.62447	0.28114	3.5569	50.100	52.321	0.21724	0.10179	0.12102	125.97	24.195
330.00	0.92279	0.42003	2.3808	51.145	53.342	0.21772	0.10663	0.13162	122.47	22.252
345.00	1.3163	0.61719	1.6202	52.111	54.244	0.21811	0.11180	0.14664	117.17	21.001
360.00	1.8234	0.90480	1.1052	52.940	54.955	0.21821	0.11757	0.17189	109.67	20.405
375.00	2.4663	1.3577	0.73653	53.497	55.314	0.21761	0.12466	0.23071	99.240	20.431
390.00	3.2770	2.2903	0.43662	53.233	54.664	0.21470	0.13608	0.61311	84.410	20.196
395.43	3.6243	4.1033	0.24371	50.813	51.696	0.20684			0	14.607

TABLE 2-276 Thermodynamic Properties of R-124, 2-Chloro-1,1,1,2-Tetrafluoroethane (Concluded)

Temperature K	Pressure MPa	Density mol/dm ³	Volume dm ³ /mol	Int. energy kJ/mol	Enthalpy kJ/mol	Entropy kJ/(mol·K)	C _v kJ/(mol·K)	C _p kJ/(mol·K)	Sound speed m/s	Joule-Thomson K/MPa
Single-Phase Properties										
150.00	0.10000	13.004	0.076901	10.509	10.516	0.055420	0.087698	0.12777	1157.7	-0.47016
225.00	0.10000	11.556	0.086537	20.423	20.431	0.10889	0.094369	0.13777	824.54	-0.38192
260.87	0.10000	10.804	0.092562	25.487	25.496	0.12976	0.098988	0.14489	674.53	-0.29941
260.87	0.10000	0.048164	20.763	46.073	48.150	0.21660	0.085902	0.096509	127.71	39.096
300.00	0.10000	0.041129	24.314	49.579	52.011	0.23038	0.092039	0.10148	138.33	22.359
375.00	0.10000	0.032447	30.820	57.006	60.088	0.25436	0.10524	0.11403	155.52	10.936
450.00	0.10000	0.026891	37.187	65.395	69.114	0.27627	0.11804	0.12661	170.43	6.3680
150.00	1.0000	13.011	0.076859	10.494	10.570	0.055319	0.087712	0.12773	1160.8	-0.47053
225.00	1.0000	11.570	0.086432	20.392	20.479	0.10875	0.094382	0.13761	829.31	-0.38397
300.00	1.0000	9.9082	0.10093	31.280	31.381	0.15045	0.10452	0.15494	523.28	-0.14686
333.28	1.0000	8.9488	0.11175	36.649	36.760	0.16744	0.10991	0.17017	384.03	0.15954
333.28	1.0000	0.45731	2.1867	51.364	53.551	0.21782	0.10772	0.13441	121.47	21.922
375.00	1.0000	0.36697	2.7250	56.110	58.835	0.23277	0.10870	0.12428	140.23	12.660
450.00	1.0000	0.28511	3.5074	64.848	68.356	0.25590	0.11949	0.13091	162.32	6.7329
150.00	5.0000	13.042	0.076674	10.428	10.811	0.054877	0.087777	0.12756	1174.3	-0.47207
225.00	5.0000	11.630	0.085982	20.262	20.692	0.10817	0.094440	0.13696	849.95	-0.39231
300.00	5.0000	10.055	0.099451	30.991	31.488	0.14947	0.10448	0.15210	558.86	-0.19712
375.00	5.0000	7.8072	0.12809	43.322	43.963	0.18645	0.11692	0.19006	276.48	0.71939
450.00	5.0000	2.0764	0.48161	61.347	63.755	0.23451	0.12778	0.18398	124.73	8.2236
150.00	10.000	13.080	0.076452	10.348	11.113	0.054334	0.087856	0.12736	1190.9	-0.47382
225.00	10.000	11.702	0.085459	20.109	20.963	0.10747	0.094513	0.13626	874.54	-0.40129
300.00	10.000	10.213	0.097912	30.675	31.654	0.14838	0.10449	0.14957	597.87	-0.24225
375.00	10.000	8.3628	0.11958	42.388	43.584	0.18379	0.11566	0.17088	359.58	-0.22172
450.00	10.000	5.4895	0.18217	56.064	57.886	0.21844	0.12834	0.21040	179.08	2.3542
150.00	20.000	13.153	0.076029	10.197	11.717	0.053282	0.088011	0.12702	1222.7	-0.47677
225.00	20.000	11.832	0.084516	19.827	21.518	0.10615	0.094657	0.13514	920.41	-0.41563
300.00	20.000	10.473	0.095482	30.150	32.059	0.14651	0.10459	0.14630	664.60	-0.30098
375.00	20.000	8.9796	0.11136	41.285	43.513	0.18054	0.11536	0.15949	462.43	-0.080024
450.00	20.000	7.2897	0.13718	53.276	56.020	0.21090	0.12652	0.17382	319.21	0.35516
150.00	40.000	13.287	0.075260	9.9211	12.932	0.051293	0.088302	0.12653	1282.4	-0.48099
225.00	40.000	12.057	0.082941	19.345	22.662	0.10380	0.094922	0.13366	1002.2	-0.43482
300.00	40.000	10.865	0.092042	29.347	33.028	0.14350	0.10483	0.14289	772.84	-0.36270
375.00	40.000	9.6799	0.10331	39.971	44.103	0.17641	0.11550	0.15243	600.05	-0.26440
450.00	40.000	8.5132	0.11746	51.192	55.890	0.20504	0.12642	0.16186	479.46	-0.14030

The values in these tables were generated from the NIST REFPROP software (Lemmon, E. W., McLinden, M. O., and Huber, M. L., NIST Standard Reference Database 23: Reference Fluid Thermodynamic and Transport Properties—REFPROP, National Institute of Standards and Technology, Standard Reference Data Program, Gaithersburg, Md., 2002, Version 7.1). The primary source for the thermodynamic properties is de Vries, B., Tillner-Roth, R., and Baehr, H. D., "Thermodynamic Properties of HCFC 124," *19th Int. Congress of Refrigeration*, The Hague, The Netherlands, International Institute of Refrigeration, IVa:582–589, 1995. Validated equations for the viscosity and thermal conductivity are not currently available for this fluid.

Properties at the triple point temperature and the critical point temperature are given in the first and last entries of the saturation tables, respectively. In the single-phase table, when the temperature range for a given isobar includes a vapor-liquid phase boundary, the temperature of phase equilibrium is noted, and properties for both the saturated liquid and saturated vapor are given (with liquid properties given in the upper line). Lines are omitted from the temperature-pressure grid of the single-phase table, when the system would be in the solid phase or if there are potential problems with the source property surface.

The uncertainties of the equation of state are 0.05% in density, 1% in heat capacity, and 1% in the speed of sound, except in the critical region. The uncertainty in vapor pressure is 0.1%.

TABLE 2-277 Thermodynamic Properties of R-125, Pentafluoroethane

Temperature K	Pressure MPa	Density mol/dm ³	Volume dm ³ /mol	Int. energy kJ/mol	Enthalpy kJ/mol	Entropy kJ/(mol·K)	C _v kJ/(mol·K)	C _p kJ/(mol·K)	Sound speed m/s	Joule-Thomson K/MPa	Therm. cond. mW/(m·K)	Viscosity μPa·s
Saturated Properties												
172.52	0.0029140	14.086	0.070990	10.457	10.457	0.058837	0.081329	0.12417	932.57	-0.38374	116.02	1152.4
180.00	0.0056285	13.885	0.072020	11.389	11.389	0.064124	0.082012	0.12500	893.63	-0.37406	112.52	957.54
190.00	0.012328	13.613	0.073461	12.646	12.647	0.070919	0.083102	0.12647	843.11	-0.35818	107.79	768.40
200.00	0.024602	13.336	0.074988	13.919	13.921	0.077448	0.084327	0.12825	793.91	-0.33901	103.06	631.00
210.00	0.045417	13.052	0.076615	15.210	15.214	0.083750	0.085644	0.13028	745.67	-0.31627	98.331	527.00
220.00	0.078505	12.762	0.078360	16.523	16.529	0.089856	0.087029	0.13254	698.07	-0.28935	93.653	445.76
230.00	0.12833	12.461	0.080247	17.858	17.869	0.095792	0.088472	0.13505	650.89	-0.25723	89.019	380.67
240.00	0.20004	12.150	0.082305	19.219	19.235	0.10158	0.089971	0.13785	603.92	-0.21839	84.443	327.41
250.00	0.29934	11.824	0.084572	20.607	20.632	0.10725	0.091529	0.14102	556.99	-0.17062	79.940	283.01
260.00	0.43250	11.481	0.087098	22.025	22.063	0.11282	0.093153	0.14468	510.02	-0.11056	75.520	245.39
270.00	0.60624	11.117	0.089954	23.478	23.532	0.11830	0.094843	0.14903	462.91	-0.032921	71.187	213.02
280.00	0.82782	10.724	0.093245	24.971	25.048	0.12374	0.096594	0.15440	415.46	0.070972	66.940	184.73
290.00	1.1050	10.295	0.097130	26.511	26.619	0.12916	0.098430	0.16135	367.36	0.21606	62.772	159.60
300.00	1.4463	9.8162	0.10187	28.112	28.259	0.13461	0.10043	0.17099	318.17	0.43036	58.667	136.86
310.00	1.8610	9.2637	0.10795	29.793	29.994	0.14015	0.10274	0.18593	267.31	0.77370	54.597	115.81
320.00	2.3600	8.5923	0.11638	31.595	31.869	0.14593	0.10571	0.21395	213.55	1.4029	50.534	95.602
330.00	2.9579	7.6744	0.13030	33.632	34.017	0.15231	0.11043	0.29625	153.34	2.9184	46.661	74.602
339.17	3.6179	4.7790	0.20925	37.417	38.174	0.16438			0	12.361		
172.52	0.0029140	0.0020381	490.65	31.863	33.293	0.19120	0.059815	0.068285	116.43	90.257	5.2349	7.4339
180.00	0.0056285	0.0037809	264.49	32.307	33.795	0.18860	0.061648	0.070217	118.54	77.516	5.7185	7.7624
190.00	0.012328	0.0078784	126.93	32.913	34.477	0.18582	0.064126	0.072893	121.15	64.018	6.3724	8.1999
200.00	0.024602	0.015031	66.529	33.530	35.167	0.18368	0.066646	0.075712	123.47	53.589	7.0353	8.6344
210.00	0.045417	0.026661	37.508	34.157	35.860	0.18207	0.069223	0.078713	125.44	45.456	7.7081	9.0657
220.00	0.078505	0.044514	22.465	34.788	36.552	0.18087	0.071864	0.081939	127.01	39.066	8.3929	9.4944
230.00	0.12833	0.070679	14.148	35.421	37.237	0.18000	0.074575	0.085437	128.11	34.014	9.0929	9.9221
240.00	0.20004	0.10763	9.2907	36.052	37.911	0.17940	0.077362	0.089271	128.68	29.998	9.8136	10.353
250.00	0.29934	0.15835	6.3153	36.678	38.568	0.17900	0.080230	0.093526	128.64	26.787	10.563	10.791
260.00	0.43250	0.22645	4.4159	37.292	39.202	0.17874	0.083141	0.098283	127.93	24.232	11.356	11.246
270.00	0.60624	0.31661	3.1585	37.890	39.805	0.17857	0.086003	0.10368	126.44	22.293	12.213	11.732
280.00	0.82782	0.43510	2.2983	38.460	40.363	0.17844	0.088869	0.11025	124.10	20.938	13.169	12.266
290.00	1.1050	0.59084	1.6925	38.988	40.858	0.17826	0.092050	0.11918	120.81	20.043	14.286	12.884
300.00	1.4463	0.79742	1.2540	39.453	41.267	0.17797	0.095933	0.13255	116.42	19.438	15.680	13.638
310.00	1.8610	1.0777	0.92787	39.828	41.554	0.17744	0.10077	0.15449	110.71	19.016	17.586	14.635
320.00	2.3600	1.4778	0.67670	40.054	41.651	0.17649	0.10679	0.19725	103.29	18.738	20.574	16.104
330.00	2.9579	2.1269	0.47016	39.964	41.355	0.17454	0.11481	0.32843	93.550	18.404	26.607	18.766
339.17	3.6179	4.7790	0.20925	37.417	38.174	0.16438			0	12.361		

TABLE 2-277 Thermodynamic Properties of R-125, Pentafluoroethane (Concluded)

Temperature K	Pressure MPa	Density mol/dm ³	Volume dm ³ /mol	Int. energy kJ/mol	Enthalpy kJ/mol	Entropy kJ/(mol·K)	C _v kJ/(mol·K)	C _p kJ/(mol·K)	Sound speed m/s	Joule-Thomson K/MPa	Therm. cond. mW/(m·K)	Viscosity μPa·s
Single-Phase Properties												
200.00	0.10000	13.337	0.074979	13.916	13.924	0.077436	0.084327	0.12823	794.34	-0.33920	103.09	631.60
224.79	0.10000	12.619	0.079245	17.160	17.168	0.092721	0.087714	0.13371	675.42	-0.27468	91.425	412.85
224.79	0.10000	0.055877	17.897	35.092	36.881	0.18042	0.073155	0.083578	127.60	36.498	8.7263	9.6994
300.00	0.10000	0.040689	24.576	41.155	43.613	0.20616	0.086960	0.095910	149.16	13.603	14.156	13.041
400.00	0.10000	0.030228	33.082	50.746	54.054	0.23608	0.10398	0.11252	172.25	5.6807	22.115	17.070
500.00	0.10000	0.024108	41.479	61.864	66.012	0.26271	0.11764	0.12607	192.24	3.1093	30.917	20.691
200.00	1.0000	13.355	0.074878	13.888	13.963	0.077295	0.084329	0.12805	799.42	-0.34145	103.50	638.78
286.46	1.0000	10.452	0.095673	25.960	26.055	0.12724	0.097767	0.15865	384.49	0.15862	64.240	168.19
286.46	1.0000	0.53072	1.8842	38.807	40.691	0.17833	0.090862	0.11564	122.09	20.318	13.866	12.653
300.00	1.0000	0.48261	2.0720	40.159	42.231	0.18359	0.092286	0.11224	129.90	16.539	14.732	13.270
400.00	1.0000	0.31780	3.1466	50.310	53.456	0.21585	0.10520	0.11626	165.47	5.9354	22.513	17.404
500.00	1.0000	0.24593	4.0661	61.591	65.657	0.24302	0.11806	0.12764	189.33	3.1109	31.336	21.014
200.00	5.0000	13.432	0.074450	13.768	14.140	0.076686	0.084364	0.12732	820.94	-0.35061	105.29	671.00
300.00	5.0000	10.214	0.097901	27.606	28.095	0.13288	0.099404	0.15790	379.39	0.16755	62.727	155.81
400.00	5.0000	2.1222	0.47120	47.739	50.095	0.19593	0.11164	0.15240	136.55	6.6581	27.340	22.244
500.00	5.0000	1.3333	0.75004	60.288	64.038	0.22710	0.12001	0.13643	180.53	2.9952	33.551	23.530
200.00	10.000	13.522	0.073953	13.626	14.366	0.075959	0.084459	0.12655	845.71	-0.36040	107.42	712.07
300.00	10.000	10.597	0.094369	27.096	28.039	0.13109	0.098728	0.14971	441.85	-0.0032571	67.164	177.37
400.00	10.000	5.5436	0.18039	43.724	45.528	0.18103	0.11417	0.19389	165.42	2.8474	40.583	46.568
500.00	10.000	2.8438	0.35165	58.555	62.072	0.21813	0.12198	0.14925	183.47	2.4316	37.529	29.745
200.00	30.000	13.835	0.072281	13.138	15.306	0.073355	0.085197	0.12439	927.73	-0.38765	115.19	889.29
300.00	30.000	11.489	0.087039	25.838	28.449	0.12645	0.098551	0.13883	597.35	-0.23171	79.855	245.90
400.00	30.000	9.0272	0.11078	39.705	43.028	0.16830	0.11217	0.15193	391.05	0.060756	59.824	112.78
500.00	30.000	6.8239	0.14654	54.141	58.538	0.20288	0.12339	0.15662	307.14	0.34144	53.649	67.694
300.00	60.000	12.259	0.081575	24.732	29.626	0.12196	0.10001	0.13426	735.32	-0.32748	93.938	338.04
400.00	60.000	10.465	0.095559	37.854	43.587	0.16206	0.11339	0.14453	563.68	-0.23451	75.022	173.26
500.00	60.000	8.9121	0.11221	51.703	58.436	0.19516	0.12470	0.15193	471.23	-0.15582	67.810	113.08

The values in these tables were generated from the NIST REFPROP software (Lemmon, E. W., McLinden, M. O., and Huber, M. L., NIST Standard Reference Database 23: Reference Fluid Thermodynamic and Transport Properties—REFPROP, National Institute of Standards and Technology, Standard Reference Data Program, Gaithersburg, Md., 2002, Version 7.1). The primary source for the thermodynamic properties is Lemmon, E. W., and Jacobsen, R. T., "A New Functional Form and New Fitting Techniques for Equations of State with Application to Pentafluoroethane (HFC-125)," *J. Phys. Chem. Ref. Data* **34**(1):69–108, 2005. The source for viscosity is Huber, M. L., and Laesecke, A., "Correlation for the Viscosity of Pentafluoroethane (R125) from the Triple Point to 500 K at Pressures up to 60 MPa," *Ind. Eng. Chem. Res.*, **45**(12):4447–4453, 2006. The source for thermal conductivity is Perkins, R., and Huber, M. L., "Measurement and Correlation of the Thermal Conductivity of Pentafluoroethane (R125) from 190 K to 512 K at Pressures to 70 MPa," *J. Chem. Eng. Data* **51**(3):898–904, 2006.

Properties at the triple point temperature and the critical point temperature are given in the first and last entries of the saturation tables, respectively. In the single-phase table, when the temperature range for a given isobar includes a vapor-liquid phase boundary, the temperature of phase equilibrium is noted, and properties for both the saturated liquid and saturated vapor are given (with liquid properties given in the upper line). Lines are omitted from the temperature-pressure grid of the single-phase table, when the system would be in the solid phase or if there are potential problems with the source property surface.

The uncertainty in density is 0.1% at temperatures from the triple point to 400 K at pressures up to 60 MPa, except in the critical region, where an uncertainty of 0.2% in pressure is generally attained. In the limited region between 340 and 400 K and at pressures from 4 to 10 MPa, as well as for all states above 400 K, the uncertainty in density increases to 0.5%. At temperatures below 330 K and pressures below 30 MPa, the uncertainty in density in the liquid phase may be as low as 0.04%. In the vapor and supercritical region, speed of sound data are represented within 0.05% at pressures below 1 MPa. The estimated uncertainty for heat capacities is 0.5%, and the estimated uncertainty for the speed of sound in the liquid phase is 0.5% for $T > 250$ K. The estimated uncertainties of vapor pressures and saturated liquid densities calculated using the Maxwell criterion are 0.1% for each property, and the estimated uncertainty for saturated vapor densities is 0.2%. The uncertainty in density increases as the critical point is approached, while the accompanying uncertainty in calculated pressures is 0.2%. The viscosity correlation has an estimated uncertainty of 3.0% along the saturation boundary in the liquid phase, and 0.8% in the vapor. For thermal conductivity, the estimated uncertainty of the correlation is 3%, except for the dilute gas and points approaching critical, where the uncertainty rises to 5%.

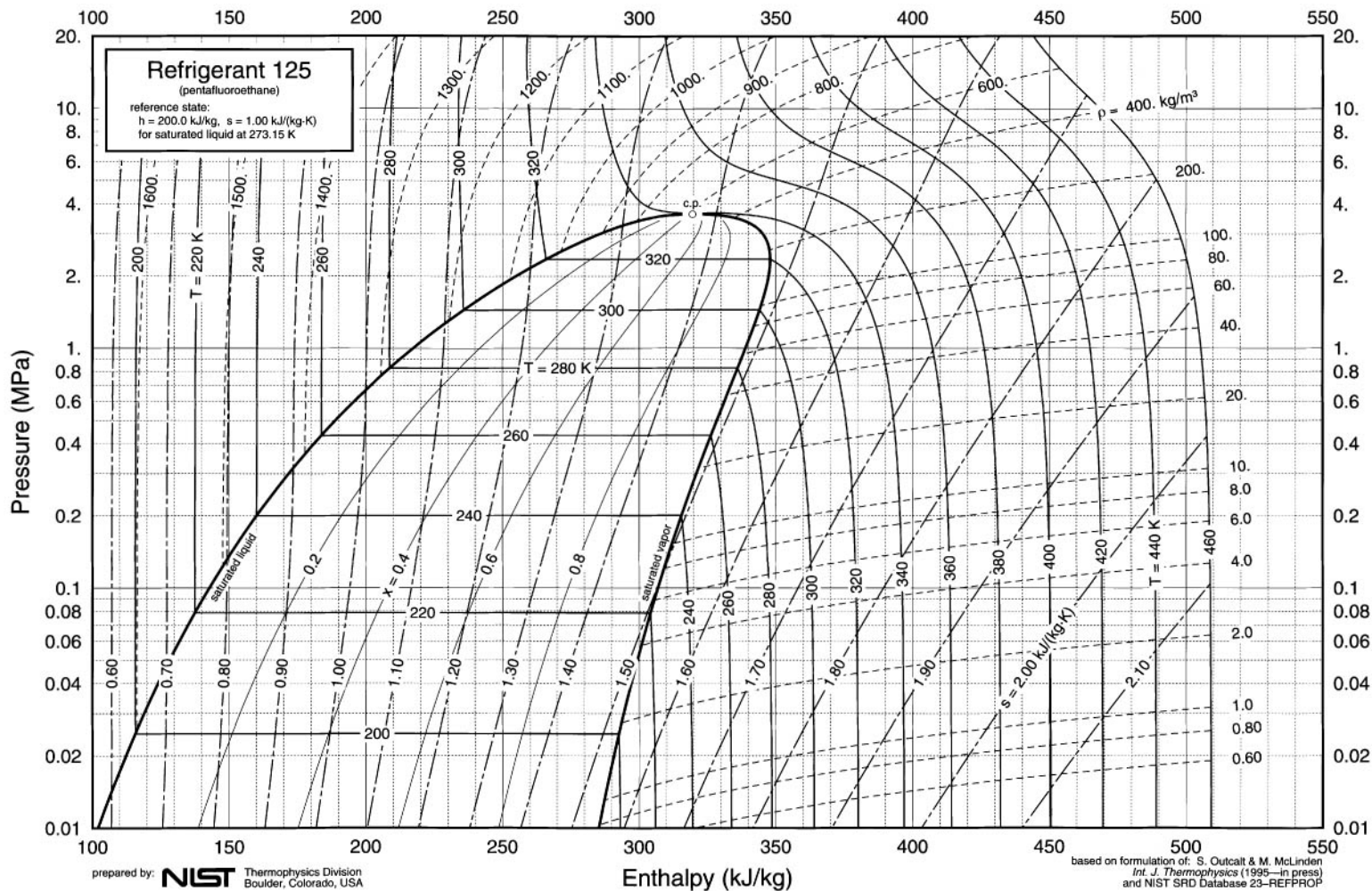


FIG. 2-25 Enthalpy–log-pressure diagram for Refrigerant 125.

TABLE 2-278 Thermodynamic Properties of R-134a, 1,1,1,2-Tetrafluoroethane

Temperature K	Pressure MPa	Density mol/dm ³	Volume dm ³ /mol	Int. energy kJ/mol	Enthalpy kJ/mol	Entropy kJ/(mol·K)	C _v kJ/(mol·K)	C _p kJ/(mol·K)	Sound speed m/s	Joule-Thomson K/MPa	Therm. cond. mW/(m·K)	Viscosity μPa·s
Saturated Properties												
169.85	0.00038956	15.594	0.064126	7.2907	7.2907	0.042100	0.080831	0.12079	1120.0	-0.38145	145.24	2153.6
170.00	0.00039617	15.590	0.064142	7.3088	7.3088	0.042207	0.080824	0.12079	1119.2	-0.38136	145.15	2139.7
180.00	0.0011275	15.331	0.065228	8.5179	8.5179	0.049117	0.080732	0.12112	1068.3	-0.37370	139.12	1479.1
190.00	0.0028170	15.069	0.066362	9.7328	9.7330	0.055686	0.081114	0.12193	1017.7	-0.36352	133.32	1106.2
200.00	0.0063130	14.804	0.067550	10.957	10.958	0.061966	0.081784	0.12303	967.61	-0.35119	127.74	867.31
210.00	0.012910	14.535	0.068798	12.194	12.195	0.067999	0.082633	0.12434	918.33	-0.33678	122.36	702.27
220.00	0.024433	14.262	0.070116	13.444	13.446	0.073815	0.083595	0.12582	869.85	-0.32011	117.17	582.15
230.00	0.043287	13.984	0.071512	14.710	14.713	0.079441	0.084636	0.12746	822.11	-0.30082	112.14	491.22
240.00	0.072481	13.699	0.072999	15.992	15.997	0.084899	0.085734	0.12927	775.00	-0.27839	107.27	420.20
250.00	0.11561	13.406	0.074593	17.293	17.301	0.090209	0.086879	0.13126	728.39	-0.25204	102.53	363.25
260.00	0.17684	13.104	0.076311	18.613	18.627	0.095389	0.088067	0.13348	682.14	-0.22073	97.922	316.57
270.00	0.26082	12.791	0.078179	19.956	19.976	0.10046	0.089298	0.13597	636.12	-0.18299	93.414	277.54
280.00	0.37271	12.465	0.080227	21.322	21.352	0.10543	0.090576	0.13883	590.17	-0.13675	88.995	244.34
290.00	0.51805	12.121	0.082499	22.716	22.759	0.11032	0.091908	0.14216	544.15	-0.079015	84.644	215.64
300.00	0.70282	11.758	0.085050	24.141	24.201	0.11516	0.093303	0.14615	497.89	-0.0052732	80.341	190.46
310.00	0.93340	11.368	0.087965	25.603	25.685	0.11996	0.094777	0.15108	451.23	0.091533	76.063	168.04
320.00	1.2166	10.945	0.091364	27.108	27.219	0.12475	0.096352	0.15740	404.00	0.22306	71.781	147.78
330.00	1.5599	10.478	0.095439	28.667	28.816	0.12956	0.098067	0.16598	355.90	0.41006	67.464	129.20
340.00	1.9715	9.9483	0.10052	30.297	30.495	0.13446	0.10001	0.17863	306.37	0.69376	63.075	111.81
350.00	2.4611	9.3237	0.10725	32.029	32.293	0.13952	0.10241	0.20012	254.06	1.1714	58.581	95.095
360.00	3.0405	8.5279	0.11726	33.932	34.289	0.14496	0.10601	0.24863	196.05	2.1419	54.062	78.146
370.00	3.7278	7.2558	0.13782	36.283	36.797	0.15159	0.11372	0.52085	127.23	5.1434	51.767	57.956
374.21	4.0591	5.0171	0.19932	38.947	39.756	0.15938			0	11.931		
169.85	0.00038956	0.00027611	3621.7	32.764	34.175	0.20038	0.051318	0.059719	126.79	373.57	3.0801	6.8294
170.00	0.00039617	0.00028055	3564.4	32.772	34.184	0.20029	0.051354	0.059756	126.84	370.78	3.0921	6.8353
180.00	0.0011275	0.00075481	1324.8	33.287	34.781	0.19502	0.053742	0.062208	130.05	234.43	3.8934	7.2319
190.00	0.0028170	0.0017896	558.79	33.821	35.395	0.19075	0.056118	0.064682	133.11	160.10	4.6952	7.6253
200.00	0.0063130	0.0038201	261.77	34.371	36.023	0.18729	0.058489	0.067201	135.98	116.94	5.4978	8.0147
210.00	0.012910	0.0074704	133.86	34.934	36.662	0.18451	0.060874	0.069802	138.63	90.215	6.3018	8.3993
220.00	0.024433	0.013574	73.669	35.508	37.308	0.18228	0.063296	0.072534	141.01	72.584	7.1080	8.7786
230.00	0.043287	0.023188	43.125	36.090	37.956	0.18050	0.065783	0.075455	143.06	60.236	7.9176	9.1524
240.00	0.072481	0.037603	26.593	36.675	38.602	0.17909	0.068357	0.078618	144.73	51.130	8.7324	9.5209
250.00	0.11561	0.058360	17.135	37.261	39.242	0.17797	0.071031	0.082078	145.98	44.137	9.5551	9.8853
260.00	0.17684	0.087278	11.458	37.844	39.870	0.17709	0.073812	0.085888	146.75	38.613	10.389	10.247
270.00	0.26082	0.12651	7.9043	38.420	40.482	0.17640	0.076698	0.090115	146.99	34.169	11.241	10.611
280.00	0.37271	0.17865	5.5976	38.986	41.073	0.17586	0.079686	0.094850	146.63	30.561	12.118	10.980
290.00	0.51805	0.24685	4.0511	39.538	41.636	0.17542	0.082776	0.10023	145.61	27.621	13.035	11.363
300.00	0.70282	0.33512	2.9840	40.069	42.166	0.17504	0.085974	0.10650	143.88	25.230	14.011	11.771
310.00	0.93340	0.44874	2.2285	40.573	42.653	0.17469	0.089297	0.11404	141.33	23.301	15.081	12.219
320.00	1.2166	0.59505	1.6805	41.038	43.083	0.17432	0.092780	0.12355	137.86	21.768	16.303	12.735
330.00	1.5599	0.78498	1.2739	41.451	43.438	0.17387	0.096484	0.13638	133.33	20.578	17.780	13.358
340.00	1.9715	1.0363	0.96498	41.785	43.687	0.17326	0.10052	0.15548	127.57	19.687	19.711	14.164
350.00	2.4611	1.3818	0.72368	41.994	43.775	0.17232	0.10510	0.18870	120.33	19.033	22.525	15.300
360.00	3.0405	1.8973	0.52707	41.973	43.576	0.17075	0.11074	0.26594	111.25	18.448	27.365	17.140
370.00	3.7278	2.8805	0.34717	41.323	42.617	0.16731	0.11928	0.70016	99.370	17.050	40.137	21.336
374.21	4.0591	5.0171	0.19932	38.947	39.756	0.15938			0	11.931		

Single-Phase Properties

200.00	0.10000	14.805	0.067543	10.955	10.962	0.061955	0.081787	0.12301	968.03	-0.35132	127.78	868.18
246.79	0.10000	13.501	0.074068	16.873	16.880	0.088519	0.086506	0.13060	743.31	-0.26099	104.04	380.27
246.79	0.10000	0.050898	19.647	37.073	39.037	0.17830	0.070161	0.080931	145.63	46.198	9.2899	9.7687
275.00	0.10000	0.044972	22.236	39.124	41.348	0.18716	0.073781	0.083445	154.76	29.047	11.540	10.906
350.00	0.10000	0.034753	28.775	45.154	48.032	0.20860	0.086248	0.095065	175.31	12.552	17.537	13.823
425.00	0.10000	0.028455	35.143	52.096	55.610	0.22818	0.098386	0.10695	192.97	6.7852	23.539	16.650
200.00	1.0000	14.819	0.067479	10.933	11.001	0.061846	0.081812	0.12291	972.08	-0.35256	128.11	876.60
275.00	1.0000	12.657	0.079009	20.597	20.676	0.10281	0.089915	0.13695	619.10	-0.16746	91.627	262.84
312.54	1.0000	11.264	0.088775	25.980	26.069	0.12117	0.095165	0.15252	439.31	0.12101	74.978	162.71
312.54	1.0000	0.48242	2.0729	40.695	42.768	0.17460	0.090164	0.11623	140.54	22.877	15.374	12.343
350.00	1.0000	0.39132	2.5555	44.290	46.846	0.18694	0.090315	0.10603	159.63	13.885	17.989	13.936
425.00	1.0000	0.29983	3.3352	51.597	54.933	0.20785	0.099891	0.11116	185.14	7.0297	23.806	16.917
200.00	5.0000	14.880	0.067202	10.839	11.175	0.061371	0.081929	0.12246	989.55	-0.35768	129.56	915.11
275.00	5.0000	12.804	0.078103	20.385	20.776	0.10203	0.089864	0.13495	651.41	-0.19924	94.015	277.35
350.00	5.0000	9.8674	0.10134	31.397	31.904	0.13765	0.10066	0.17178	320.01	0.59952	63.012	109.32
425.00	5.0000	2.0736	0.48225	48.647	51.058	0.18734	0.10791	0.15381	148.25	7.9048	28.574	20.974
200.00	10.000	14.954	0.066874	10.727	11.395	0.060796	0.082085	0.12196	1010.3	-0.36339	131.31	966.05
275.00	10.000	12.967	0.077121	20.149	20.920	0.10115	0.089868	0.13304	687.36	-0.22964	96.744	295.02
350.00	10.000	10.478	0.095440	30.642	31.597	0.13537	0.099573	0.15486	400.60	0.21924	68.919	128.79
425.00	10.000	6.1370	0.16295	43.563	45.193	0.17038	0.11141	0.20870	177.89	3.0434	44.888	46.711
200.00	30.000	15.216	0.065720	10.326	12.298	0.058683	0.082769	0.12047	1084.1	-0.38053	137.79	1211.0
275.00	30.000	13.479	0.074190	19.398	21.624	0.098210	0.090220	0.12865	801.47	-0.30014	105.87	364.87
350.00	30.000	11.662	0.085750	29.071	31.644	0.13038	0.098885	0.13885	582.52	-0.15240	82.955	183.26
425.00	30.000	9.7202	0.10288	39.385	42.471	0.15838	0.10808	0.14967	425.63	0.10364	67.154	107.03
275.00	70.000	14.181	0.070517	18.373	23.310	0.093839	0.091314	0.12519	962.41	-0.35619	119.84	521.91
350.00	70.000	12.797	0.078141	27.492	32.961	0.12484	0.099542	0.13226	787.10	-0.30093	99.868	277.09
425.00	70.000	11.494	0.087004	37.066	43.157	0.15121	0.10829	0.13963	661.39	-0.23655	86.640	181.77

The values in these tables were generated from the NIST REFPROP software (Lemmon, E. W., McLinden, M. O., and Huber, M. L., NIST Standard Reference Database 23: Reference Fluid Thermodynamic and Transport Properties—REFPROP, National Institute of Standards and Technology, Standard Reference Data Program, Gaithersburg, Md., 2002, Version 7.1). The primary source for the thermodynamic properties is Tillner-Roth, R., and Baehr, H. D., "An International Standard Formulation of the Thermodynamic Properties of 1,1,1,2-Tetrafluoroethane (HFC-134a) for temperatures from 170 K to 455 K at Pressures up to 70 MPa," *J. Phys. Chem. Ref. Data* **23**:657–729, 1994. The source for viscosity is Huber, M. L., Laesecke, A., and Perkins, R. A., "Model for the Viscosity and Thermal Conductivity of Refrigerants, Including a New Correlation for the Viscosity of R134a," *Ind. Eng. Chem. Res.* **42**:3163–3178, 2003. The source for thermal conductivity is Perkins, R. A., Laesecke, A., Howley, J., Ramires, M. L. V., Gurova, A. N., and Cusco, L., "Experimental Thermal Conductivity Values for the IUPAC Round-Robin Sample of 1,1,1,2-Tetrafluoroethane (R134a)," NISTIR, 2000.

Properties at the triple point temperature and the critical point temperature are given in the first and last entries of the saturation tables, respectively. In the single-phase table, when the temperature range for a given isobar includes a vapor-liquid phase boundary, the temperature of phase equilibrium is noted, and properties for both the saturated liquid and saturated vapor are given (with liquid properties given in the upper line). Lines are omitted from the temperature-pressure grid of the single-phase table, when the system would be in the solid phase or if there are potential problems with the source property surface.

Typical uncertainties are 0.05% for density, 0.02% for vapor pressure, 0.5% to 1% for heat capacity, 0.05% for vapor speed of sound, and 1% for liquid speed of sound, except in the critical region. The uncertainty in viscosity is 1.5% along the saturated-liquid line, 3% in the liquid phase, 0.5% in the dilute gas, 3% to 5% in the vapor phase, and 5% in the supercritical region, rising to 8% at pressures above 40 MPa. Below 200 K, the uncertainty is 8%. The uncertainty in thermal conductivity is 5%.

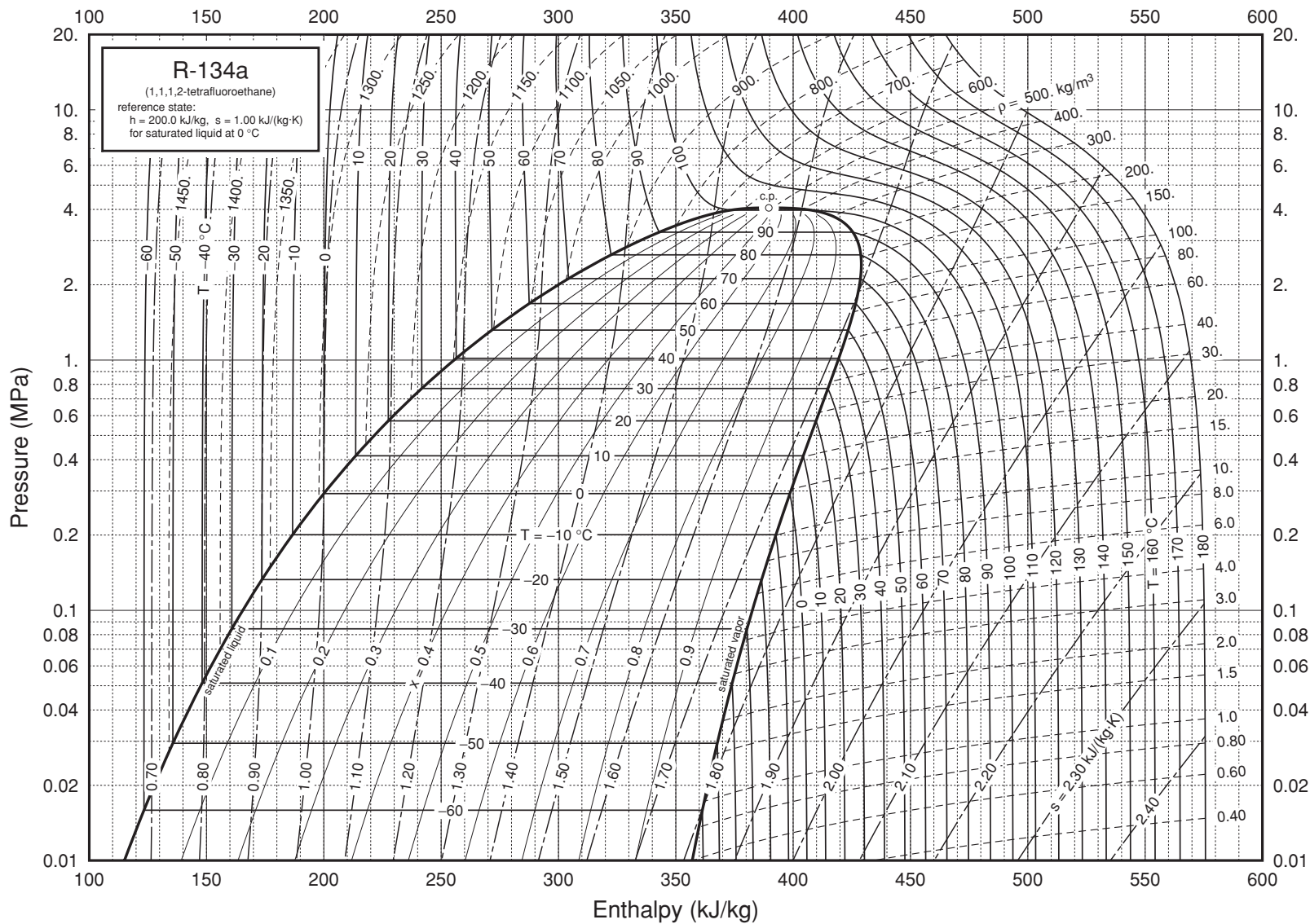


FIG. 2-26 Pressure-enthalpy diagram for Refrigerant 134a. Properties computed with the NIST REFPROP Database, Version 7.0 (Lemmon, E. W., McLinden, M. O., and Huber, M. L., 2002, NIST Standard Reference Database 23, NIST Reference Fluid Thermodynamic and Transport Properties—REFPROP, Version 7.0, Standard Reference Data Program, National Institute of Standards and Technology), based on the equation of state of Tillner-Roth, R., and Baehr, H. D., "An International Standard Formulation of the Thermodynamic Properties of 1,1,1,2-Tetrafluoroethane (HFC-134a) Covering Temperatures from 170 K to 455 K at Pressures up to 70 MPa," *J. Phys. Chem. Ref. Data* **23**(5):657–729, 1994.

TABLE 2-279 Thermodynamic Properties of R-141b, 1,1-Dichloro-1-Fluoroethane

Temperature K	Pressure MPa	Density mol/dm ³	Volume dm ³ /mol	Int. energy kJ/mol	Enthalpy kJ/mol	Entropy kJ/(mol·K)	C _v kJ/(mol·K)	C _p kJ/(mol·K)	Sound speed m/s	Joule-Thomson K/MPa
Saturated Properties										
169.68	6.4927E-06	12.560	0.079620	9.9164	9.9164	0.054895	0.094555	0.13580	1362.2	-0.46011
175.00	1.3392E-05	12.475	0.080158	10.635	10.635	0.059062	0.093422	0.13422	1336.2	-0.46486
190.00	7.9884E-05	12.241	0.081696	12.622	12.622	0.069959	0.091221	0.13103	1264.8	-0.47325
205.00	0.00035111	12.009	0.083271	14.573	14.573	0.079842	0.090109	0.12928	1196.3	-0.47511
220.00	0.0012182	11.779	0.084897	16.505	16.506	0.088942	0.089760	0.12859	1130.5	-0.47131
235.00	0.0035074	11.549	0.086588	18.434	18.434	0.097423	0.089963	0.12869	1067.1	-0.46244
250.00	0.0086986	11.318	0.088358	20.369	20.370	0.10540	0.090575	0.12943	1005.9	-0.44884
265.00	0.019117	11.083	0.090224	22.319	22.321	0.11298	0.091495	0.13069	946.56	-0.43061
280.00	0.038053	10.845	0.092205	24.291	24.294	0.12022	0.092648	0.13238	888.79	-0.40759
295.00	0.069799	10.602	0.094324	26.290	26.297	0.12717	0.093975	0.13446	832.34	-0.37931
310.00	0.11960	10.351	0.096609	28.323	28.334	0.13389	0.095432	0.13691	776.95	-0.34494
325.00	0.19353	10.092	0.099093	30.393	30.412	0.14041	0.096986	0.13972	722.38	-0.30314
340.00	0.29839	9.8211	0.10182	32.505	32.535	0.14677	0.098610	0.14292	668.39	-0.25184
355.00	0.44157	9.5371	0.10485	34.664	34.710	0.15299	0.10029	0.14659	614.74	-0.18789
370.00	0.63091	9.2365	0.10827	36.876	36.945	0.15909	0.10201	0.15085	561.17	-0.10633
385.00	0.87470	8.9148	0.11217	39.148	39.246	0.16512	0.10377	0.15592	507.38	0.00079658
400.00	1.1817	8.5660	0.11674	41.489	41.627	0.17110	0.10557	0.16222	452.97	0.14720
415.00	1.5611	8.1809	0.12224	43.912	44.103	0.17706	0.10745	0.17053	397.38	0.35834
430.00	2.0234	7.7444	0.12913	46.442	46.703	0.18308	0.10945	0.18264	339.70	0.68768
445.00	2.5805	7.2267	0.13838	49.122	49.480	0.18925	0.11171	0.20353	278.17	1.2701
460.00	3.2487	6.5517	0.15263	52.069	52.565	0.19586	0.11464	0.25500	208.92	2.5762
475.00	4.0574	5.2532	0.19036	55.987	56.760	0.20453	0.12111	0.92342	118.23	8.4848
477.50	4.2117	3.9210	0.25504	58.424	59.498	0.21020			0	15.683
169.68	6.4927E-06	4.6024E-06	217.280.	42.292	43.703	0.25401	0.054464	0.062782	117.92	881.00
175.00	1.3392E-05	9.2047E-06	108,640.	42.585	44.040	0.24995	0.055738	0.064059	119.57	725.60
190.00	7.9884E-05	5.0581E-05	19,770.	43.445	45.025	0.24050	0.059180	0.067515	124.11	439.35
205.00	0.00035111	0.00020615	4,850.8	44.353	46.056	0.23342	0.062459	0.070830	128.46	282.90
220.00	0.0012182	0.00066719	1,498.8	45.303	47.129	0.22814	0.065653	0.074095	132.61	192.43
235.00	0.0035074	0.0018021	554.92	46.291	48.237	0.22424	0.068824	0.077393	136.53	137.32
250.00	0.0086986	0.0042156	237.22	47.312	49.376	0.22143	0.072021	0.080793	140.16	102.08
265.00	0.019117	0.0087866	113.81	48.362	50.538	0.21946	0.075271	0.084345	143.44	78.530
280.00	0.038053	0.016681	59.949	49.437	51.718	0.21816	0.078582	0.088081	146.30	62.188
295.00	0.069799	0.029348	34.074	50.531	52.910	0.21739	0.081944	0.092019	148.66	50.500
310.00	0.11960	0.048516	20.612	51.641	54.106	0.21703	0.085336	0.096171	150.46	41.951
325.00	0.19353	0.076209	13.122	52.763	55.302	0.21700	0.088731	0.10056	151.61	35.598
340.00	0.29839	0.11480	8.7112	53.890	56.489	0.21722	0.092106	0.10521	152.02	30.835
355.00	0.44157	0.16710	5.9846	55.016	57.659	0.21763	0.095442	0.11023	151.61	27.254
370.00	0.63091	0.23659	4.2267	56.134	58.801	0.21817	0.098733	0.11578	150.27	24.582
385.00	0.87470	0.32780	3.0507	57.234	59.902	0.21877	0.10198	0.12213	147.85	22.633
400.00	1.1817	0.44696	2.2373	58.300	60.944	0.21939	0.10522	0.12983	144.19	21.289
415.00	1.5611	0.60344	1.6572	59.311	61.898	0.21994	0.10848	0.13996	139.04	20.490
430.00	2.0234	0.81289	1.2302	60.231	62.720	0.22033	0.11185	0.15495	132.06	20.229
445.00	2.5805	1.1059	0.90427	60.993	63.326	0.22037	0.11548	0.18176	122.74	20.562
460.00	3.2487	1.5609	0.64064	61.427	63.508	0.21965	0.11977	0.25134	110.25	21.544
475.00	4.0574	2.6472	0.37776	60.578	62.110	0.21579	0.12640	1.1603	93.316	21.336
477.50	4.2117	3.9210	0.25504	58.424	59.498	0.21020			0	15.683

TABLE 2-279 Thermodynamic Properties of R-141b, 1,1-Dichloro-1-Fluoroethane (Concluded)

Temperature K	Pressure MPa	Density mol/dm ³	Volume dm ³ /mol	Int. energy kJ/mol	Enthalpy kJ/mol	Entropy kJ/(mol·K)	C _v kJ/(mol·K)	C _p kJ/(mol·K)	Sound speed m/s	Joule-Thomson K/MPa
Single-Phase Properties										
200.00	0.10000	12.087	0.082735	13.923	13.931	0.076634	0.090387	0.12973	1219.1	-0.47521
300.00	0.10000	10.519	0.095063	26.963	26.973	0.12943	0.094448	0.13523	813.87	-0.36865
304.82	0.10000	10.438	0.095799	27.617	27.627	0.13160	0.094917	0.13602	795.96	-0.35757
304.82	0.10000	0.041044	24.364	51.257	53.693	0.21711	0.084163	0.094713	149.91	44.615
400.00	0.10000	0.030497	32.790	59.875	63.154	0.24405	0.096356	0.10524	173.74	15.111
500.00	0.10000	0.024216	41.296	70.152	74.282	0.26884	0.10833	0.11691	194.56	8.0045
200.00	1.0000	12.094	0.082685	13.904	13.987	0.076539	0.090431	0.12969	1222.5	-0.47573
300.00	1.0000	10.536	0.094914	26.923	27.018	0.12930	0.094476	0.13502	819.45	-0.37223
391.53	1.0000	8.7668	0.11407	40.158	40.272	0.16773	0.10455	0.15848	483.80	0.058567
391.53	1.0000	0.37577	2.6612	57.703	60.364	0.21904	0.10339	0.12527	146.42	21.978
400.00	1.0000	0.36041	2.7746	58.638	61.413	0.22169	0.10298	0.12252	150.55	19.770
500.00	1.0000	0.25865	3.8663	69.520	73.387	0.24841	0.10961	0.12123	184.02	8.7395
200.00	5.0000	12.127	0.082464	13.822	14.234	0.076124	0.090629	0.12954	1237.0	-0.47789
300.00	5.0000	10.606	0.094284	26.751	27.222	0.12872	0.094606	0.13416	843.29	-0.38665
400.00	5.0000	8.7814	0.11388	41.014	41.584	0.16989	0.10538	0.15604	502.40	0.0060632
500.00	5.0000	2.5394	0.39380	63.911	65.880	0.22278	0.12220	0.29767	113.94	14.372
200.00	10.000	12.166	0.082198	13.722	14.544	0.075616	0.090880	0.12937	1254.5	-0.48033
300.00	10.000	10.688	0.093559	26.550	27.486	0.12803	0.094784	0.13326	871.09	-0.40188
400.00	10.000	9.0042	0.11106	40.515	41.625	0.16859	0.10531	0.15122	554.81	-0.10586
500.00	10.000	6.4723	0.15451	56.831	58.376	0.20581	0.11637	0.19130	265.53	1.3996
300.00	100.00	11.645	0.085873	24.317	32.904	0.11935	0.098509	0.12788	1200.2	-0.49651
400.00	100.00	10.676	0.093670	36.738	46.105	0.15726	0.10834	0.13645	995.82	-0.44654
500.00	100.00	9.7763	0.10229	49.945	60.174	0.18863	0.11752	0.14460	852.98	-0.39437
400.00	400.00	12.505	0.079970	33.644	65.632	0.14209	0.11569	0.13564	1606.9	-0.48581
500.00	400.00	11.986	0.083429	46.201	79.572	0.17316	0.12401	0.14302	1498.0	-0.46416

The values in these tables were generated from the NIST REFPROP software (Lemmon, E. W., McLinden, M. O., and Huber, M. L., NIST Standard Reference Database 23: Reference Fluid Thermodynamic and Transport Properties—REFPROP, National Institute of Standards and Technology, Standard Reference Data Program, Gaithersburg, Md., 2002, Version 7.1). The primary source for the thermodynamic properties is Lemmon, E. W., and Span, R., "Short Fundamental Equations of State for 20 Industrial Fluids," *J. Chem. Eng. Data* **51**(3):785–850, 2006. Validated equations for the viscosity and thermal conductivity are not currently available for this fluid.

Properties at the triple point temperature and the critical point temperature are given in the first and last entries of the saturation tables, respectively. In the single-phase table, when the temperature range for a given isobar includes a vapor-liquid phase boundary, the temperature of phase equilibrium is noted, and properties for both the saturated liquid and saturated vapor are given (with liquid properties given in the upper line). Lines are omitted from the temperature-pressure grid of the single-phase table, when the system would be in the solid phase or if there are potential problems with the source property surface.

The equation has uncertainties of 0.2% in density between 180 and 400 K at pressures to 100 MPa, and 0.5% in density at higher pressures. The uncertainty in density may be higher as temperatures approach 400 K. Vapor pressures are represented with an uncertainty of 0.2% from 270 to 400 K. The uncertainty in speed of sound is 0.01% in the vapor phase and 0.5% in the liquid phase. There are no heat capacity data to verify the equation of state; however, the uncertainties are estimated to be within 2%.

TABLE 2-280 Thermodynamic Properties of R-142b, 1-Chloro-1,1-Difluoroethane

Temperature K	Pressure MPa	Density mol/dm ³	Volume dm ³ /mol	Int. energy kJ/mol	Enthalpy kJ/mol	Entropy kJ/(mol·K)	C _v kJ/(mol·K)	C _p kJ/(mol·K)	Sound speed m/s	Joule-Thomson K/MPa
Saturated Properties										
142.72	3.6327E-06	14.439	0.069257	5.0138	5.0138	0.026013	0.067327	0.11000	1457.9	-0.49370
150.00	1.1727E-05	14.281	0.070022	5.8147	5.8147	0.031486	0.068270	0.11005	1403.7	-0.49255
165.00	9.0545E-05	13.963	0.071619	7.4687	7.4687	0.041995	0.070168	0.11057	1301.7	-0.48684
180.00	0.00047371	13.650	0.073262	9.1343	9.1343	0.051656	0.072051	0.11158	1209.7	-0.47689
195.00	0.0018484	13.339	0.074968	10.818	10.818	0.060640	0.073955	0.11299	1125.1	-0.46285
210.00	0.0057557	13.028	0.076756	12.526	12.526	0.069077	0.075895	0.11477	1046.0	-0.44466
225.00	0.015025	12.715	0.078649	14.263	14.264	0.077064	0.077877	0.11689	971.28	-0.42204
240.00	0.034108	12.396	0.080672	16.033	16.036	0.084681	0.079897	0.11931	899.90	-0.39443
255.00	0.069220	12.069	0.082856	17.841	17.847	0.091990	0.081949	0.12205	831.11	-0.36085
270.00	0.12829	11.732	0.085239	19.692	19.703	0.099042	0.084027	0.12513	764.28	-0.31977
285.00	0.22078	11.380	0.087873	21.590	21.609	0.10588	0.086128	0.12859	698.87	-0.26876
300.00	0.35741	11.010	0.090824	23.538	23.571	0.11255	0.088252	0.13253	634.41	-0.20400
315.00	0.54995	10.617	0.094190	25.545	25.597	0.11908	0.090406	0.13714	570.43	-0.11928
330.00	0.81110	10.193	0.098109	27.617	27.696	0.12551	0.092605	0.14271	506.46	-0.0039877
345.00	1.1545	9.7272	0.10280	29.765	29.884	0.13189	0.094876	0.14984	441.95	0.16142
360.00	1.5950	9.2033	0.10866	32.009	32.182	0.13828	0.097271	0.15984	376.09	0.41716
375.00	2.1496	8.5896	0.11642	34.381	34.632	0.14477	0.099910	0.17613	307.44	0.86137
390.00	2.8397	7.8118	0.12801	36.963	37.327	0.15160	0.10313	0.21217	232.74	1.8155
405.00	3.6991	6.5381	0.15295	40.117	40.683	0.15973	0.10871	0.44141	141.73	5.3582
410.26	4.0548	4.4380	0.22533	43.151	44.065	0.16786			0	14.009
142.72	3.6327E-06	3.0614E-06	326.650.	32.685	33.872	0.22821	0.043630	0.051946	118.57	826.84
150.00	1.1727E-05	9.4031E-06	106.350.	33.008	34.256	0.22109	0.045288	0.053606	121.19	618.59
165.00	9.0545E-05	6.6018E-05	15.147.	33.711	35.083	0.20935	0.048631	0.056964	126.42	363.33
180.00	0.00047371	0.00031681	3,156.4	34.461	35.956	0.20067	0.051923	0.060296	131.39	230.77
195.00	0.0018484	0.0011428	875.03	35.253	36.870	0.19424	0.055225	0.063688	136.07	156.62
210.00	0.0057557	0.0033148	301.68	36.082	37.819	0.18952	0.058589	0.067227	140.40	112.18
225.00	0.015025	0.0081206	123.14	36.944	38.794	0.18609	0.062056	0.070991	144.30	83.865
240.00	0.034108	0.017432	57.365	37.831	39.787	0.18365	0.065643	0.075042	147.66	64.873
255.00	0.069220	0.033721	29.655	38.737	40.790	0.18196	0.069344	0.079422	150.35	51.637
270.00	0.12829	0.060064	16.649	39.657	41.793	0.18086	0.073133	0.084167	152.25	42.170
285.00	0.22078	0.10020	9.9797	40.582	42.786	0.18019	0.076978	0.089331	153.23	35.289
300.00	0.35741	0.15871	6.3006	41.506	43.758	0.17984	0.080851	0.095026	153.15	30.249
315.00	0.54995	0.24138	4.1428	42.419	44.697	0.17972	0.084737	0.10147	151.86	26.559
330.00	0.81110	0.35595	2.8094	43.306	45.585	0.17972	0.088646	0.10911	149.19	23.894
345.00	1.1545	0.51364	1.9469	44.149	46.397	0.17975	0.092615	0.11883	144.89	22.043
360.00	1.5950	0.73250	1.3652	44.916	47.094	0.17970	0.096730	0.13261	138.64	20.877
375.00	2.1496	1.0462	0.95585	45.551	47.605	0.17937	0.10116	0.15586	129.97	20.328
390.00	2.8397	1.5347	0.65159	45.920	47.771	0.17838	0.10632	0.21004	118.18	20.306
405.00	3.6991	2.5436	0.39314	45.483	46.938	0.17518	0.11368	0.55965	102.00	19.783
410.26	4.0548	4.4380	0.22533	43.151	44.065	0.16786			0	14.009

TABLE 2-280 Thermodynamic Properties of R-142b, 1-Chloro-1,1-Difluoroethane (Concluded)

Temperature K	Pressure MPa	Density mol/dm ³	Volume dm ³ /mol	Int. energy kJ/mol	Enthalpy kJ/mol	Entropy kJ/mol·K	C _v kJ/(mol·K)	C _p kJ/(mol·K)	Sound speed m/s	Joule-Thomson K/MPa
Single-Phase Properties										
150.00	0.10000	14.282	0.070018	5.8131	5.8201	0.031476	0.068275	0.11005	1404.1	-0.49259
225.00	0.10000	12.716	0.078641	14.260	14.268	0.077053	0.077880	0.11688	971.75	-0.42221
263.70	0.10000	11.875	0.084211	18.910	18.918	0.096110	0.083152	0.12379	792.14	-0.33806
263.70	0.10000	0.047556	21.028	39.269	41.372	0.18126	0.071534	0.082128	151.56	45.775
300.00	0.10000	0.041113	24.323	41.979	44.411	0.19205	0.076432	0.085864	162.77	26.250
375.00	0.10000	0.032446	30.820	48.175	51.257	0.21237	0.087964	0.096734	182.58	12.432
450.00	0.10000	0.026895	37.182	55.179	58.897	0.23092	0.098211	0.10678	199.94	7.4502
150.00	1.0000	14.289	0.069982	5.7989	5.8689	0.031381	0.068317	0.11003	1407.4	-0.49289
225.00	1.0000	12.730	0.078553	14.234	14.312	0.076937	0.077905	0.11676	976.69	-0.42404
300.00	1.0000	11.034	0.090630	23.498	23.589	0.11241	0.088238	0.13215	640.59	-0.21142
338.73	1.0000	9.9277	0.10073	28.857	28.957	0.12923	0.093915	0.14661	469.03	0.084297
338.73	1.0000	0.44153	2.2648	43.804	46.069	0.17974	0.090944	0.11443	146.90	22.728
375.00	1.0000	0.36746	2.7214	47.311	50.033	0.19087	0.091549	0.10695	164.80	14.567
450.00	1.0000	0.28570	3.5002	54.646	58.146	0.21058	0.099383	0.11074	190.29	7.9246
150.00	5.0000	14.321	0.069826	5.7370	6.0861	0.030965	0.068506	0.10997	1421.7	-0.49417
225.00	5.0000	12.791	0.078178	14.121	14.512	0.076430	0.078025	0.11629	997.91	-0.43157
300.00	5.0000	11.170	0.089523	23.263	23.710	0.11162	0.088194	0.13015	676.41	-0.25069
375.00	5.0000	8.9978	0.11114	33.787	34.343	0.14314	0.098897	0.15862	373.38	0.42121
450.00	5.0000	2.2231	0.44982	50.992	53.241	0.18867	0.10800	0.17517	139.23	10.314
150.00	10.000	14.360	0.069636	5.6618	6.3581	0.030454	0.068749	0.10991	1439.0	-0.49558
225.00	10.000	12.864	0.077739	13.987	14.765	0.075821	0.078190	0.11578	1023.0	-0.43976
300.00	10.000	11.321	0.088335	23.001	23.885	0.11072	0.088215	0.12826	716.03	-0.28769
375.00	10.000	9.4491	0.10583	33.097	34.155	0.14120	0.098194	0.14723	451.41	0.11527
450.00	10.000	6.5247	0.15326	45.004	46.536	0.17118	0.10853	0.18939	220.16	2.1126
225.00	30.000	13.119	0.076223	13.519	15.805	0.073606	0.078954	0.11435	1110.6	-0.46323
300.00	30.000	11.787	0.084836	22.183	24.728	0.10777	0.088691	0.12401	840.46	-0.37159
375.00	30.000	10.406	0.096097	31.547	34.430	0.13659	0.097974	0.13464	635.15	-0.22643
450.00	30.000	8.9530	0.11169	41.538	44.889	0.16199	0.10623	0.14384	484.32	-0.010974
225.00	60.000	13.434	0.074437	12.957	17.423	0.070756	0.080223	0.11326	1217.3	-0.48274
300.00	60.000	12.284	0.081409	21.322	26.207	0.10439	0.089774	0.12130	975.81	-0.42589
375.00	60.000	11.180	0.089443	30.259	35.626	0.13238	0.098881	0.12975	801.25	-0.35484
450.00	60.000	10.119	0.098828	39.706	45.636	0.15670	0.10699	0.13689	675.38	-0.27949

The values in these tables were generated from the NIST REFPROP software (Lemmon, E. W., McLinden, M. O., and Huber, M. L., NIST Standard Reference Database 23: Reference Fluid Thermodynamic and Transport Properties—REFPROP, National Institute of Standards and Technology, Standard Reference Data Program, Gaithersburg, Md., 2002, Version 7.1). The primary source for the thermodynamic properties is Lemmon, E. W., and Span, R., "Short Fundamental Equations of State for 20 Industrial Fluids," *J. Chem. Eng. Data* **51**(3):785–850, 2006. Validated equations for the viscosity and thermal conductivity are not currently available for this fluid.

Properties at the triple point temperature and the critical point temperature are given in the first and last entries of the saturation tables, respectively. In the single-phase table, when the temperature range for a given isobar includes a vapor-liquid phase boundary, the temperature of phase equilibrium is noted, and properties for both the saturated liquid and saturated vapor are given (with liquid properties given in the upper line). Lines are omitted from the temperature-pressure grid of the single-phase table, when the system would be in the solid phase or if there are potential problems with the source property surface.

The uncertainties in density are 0.3% in the liquid phase below 370 K, 1% at higher temperatures in the liquid and supercritical regions, and 0.5% in the vapor phase. Uncertainties for other properties are 0.5% for vapor pressure, 2% for heat capacities and liquid sound speeds, and 0.2% for vapor sound speeds.

TABLE 2-281 Thermodynamic Properties of R-143a, 1,1,1-Trifluoroethane

Temperature K	Pressure MPa	Density mol/dm ³	Volume dm ³ /mol	Int. energy kJ/mol	Enthalpy kJ/mol	Entropy kJ/(mol·K)	C _v kJ/(mol·K)	C _p kJ/(mol·K)	Sound speed m/s	Joule-Thomson K/MPa
Saturated Properties										
161.34	0.0010749	15.832	0.063163	4.4138	4.4138	0.026403	0.068393	0.10179	1058.1	-0.43936
170.00	0.0025084	15.583	0.064174	5.2969	5.2971	0.031735	0.068179	0.10225	1016.7	-0.42914
180.00	0.0059324	15.291	0.065399	6.3240	6.3244	0.037606	0.068405	0.10325	969.14	-0.41402
190.00	0.012629	14.994	0.066693	7.3629	7.3637	0.043223	0.068990	0.10460	921.61	-0.39585
200.00	0.024624	14.692	0.068062	8.4164	8.4181	0.048626	0.069825	0.10621	874.04	-0.37472
210.00	0.044602	14.384	0.069519	9.4869	9.4900	0.053849	0.070836	0.10803	826.46	-0.35034
220.00	0.075908	14.069	0.071077	10.576	10.581	0.058915	0.071969	0.11005	778.88	-0.32211
230.00	0.12252	13.745	0.072753	11.685	11.694	0.063848	0.073190	0.11227	731.28	-0.28906
240.00	0.18902	13.410	0.074570	12.817	12.831	0.068665	0.074475	0.11474	683.65	-0.24979
250.00	0.28049	13.062	0.076556	13.973	13.995	0.073385	0.075809	0.11750	635.90	-0.20231
260.00	0.40251	12.698	0.078751	15.156	15.188	0.078027	0.077186	0.12066	587.94	-0.14368
270.00	0.56112	12.314	0.081208	16.368	16.414	0.082607	0.078605	0.12435	539.61	-0.069548
280.00	0.76276	11.904	0.084004	17.615	17.680	0.087149	0.080078	0.12879	490.70	0.026895
290.00	1.0144	11.461	0.087249	18.903	18.991	0.091675	0.081625	0.13438	440.95	0.15683
300.00	1.3234	10.975	0.091119	20.239	20.360	0.096221	0.083293	0.14180	389.93	0.34002
310.00	1.6983	10.426	0.095914	21.638	21.801	0.10083	0.085172	0.15244	337.04	0.61491
320.00	2.1483	9.7846	0.10220	23.125	23.344	0.10559	0.087455	0.16980	281.21	1.0681
330.00	2.6850	8.9829	0.11132	24.750	25.048	0.11065	0.090641	0.20591	220.39	1.9469
340.00	3.3250	7.7913	0.12835	26.688	27.114	0.11659	0.096654	0.35704	149.32	4.3897
345.86	3.7618	5.1285	0.19499	29.429	30.163	0.12527			0	12.397
161.34	0.0010749	0.00080362	1244.4	25.521	26.859	0.16552	0.044397	0.052938	137.57	385.09
170.00	0.0025084	0.0017832	560.78	25.895	27.302	0.16118	0.046371	0.055037	140.62	262.77
180.00	0.0059324	0.0039967	250.20	26.340	27.824	0.15705	0.048691	0.057550	143.91	176.43
190.00	0.012629	0.0081006	123.45	26.796	28.355	0.15370	0.051040	0.060156	146.92	124.70
200.00	0.024624	0.015110	66.180	27.262	28.892	0.15100	0.053424	0.062886	149.60	92.835
210.00	0.044602	0.026311	38.007	27.736	29.431	0.14881	0.055867	0.065796	151.89	72.442
220.00	0.075908	0.043269	23.111	28.213	29.968	0.14704	0.058395	0.068954	153.71	58.764
230.00	0.12252	0.067850	14.738	28.693	30.498	0.14560	0.061026	0.072428	155.02	49.133
240.00	0.18902	0.10227	9.7783	29.170	31.018	0.14444	0.063766	0.076287	155.74	42.049
250.00	0.28049	0.14916	6.7041	29.641	31.521	0.14349	0.066612	0.080611	155.81	36.657
260.00	0.40251	0.21175	4.7225	30.102	32.003	0.14270	0.069560	0.085515	155.15	32.456
270.00	0.56112	0.29409	3.4004	30.548	32.456	0.14202	0.072606	0.091184	153.70	29.136
280.00	0.76276	0.40144	2.4910	30.972	32.872	0.14141	0.075756	0.097932	151.36	26.498
290.00	1.0144	0.54109	1.8481	31.366	33.240	0.14081	0.079035	0.10632	148.04	24.406
300.00	1.3234	0.72367	1.3818	31.715	33.544	0.14017	0.082489	0.11743	143.59	22.765
310.00	1.6983	0.96617	1.0350	32.000	33.758	0.13940	0.086214	0.13359	137.85	21.499
320.00	2.1483	1.2991	0.76974	32.183	33.837	0.13838	0.090400	0.16076	130.56	20.526
330.00	2.6850	1.7898	0.55871	32.184	33.684	0.13682	0.095488	0.22018	121.34	19.682
340.00	3.3250	2.6696	0.37458	31.732	32.977	0.13384	0.10298	0.47999	109.29	18.259
345.86	3.7618	5.1285	0.19499	29.429	30.163	0.12527			0	12.397

TABLE 2-281 Thermodynamic Properties of R-143a, 1,1,1-Trifluoroethane (Concluded)

Temperature K	Pressure MPa	Density mol/dm ³	Volume dm ³ /mol	Int. energy kJ/mol	Enthalpy kJ/mol	Entropy kJ/(mol·K)	C _v kJ/(mol·K)	C _p kJ/(mol·K)	Sound speed m/s	Joule-Thomson K/MPa
Single-Phase Properties										
200.00	0.10000	14.694	0.068054	8.4143	8.4211	0.048616	0.069829	0.10620	874.45	-0.37493
225.63	0.10000	13.888	0.072006	11.198	11.205	0.061709	0.072648	0.11128	752.07	-0.30416
225.63	0.10000	0.056043	17.843	28.483	30.268	0.14619	0.059863	0.070868	154.52	52.958
300.00	0.10000	0.040759	24.534	33.380	35.833	0.16745	0.070758	0.079793	179.93	18.414
400.00	0.10000	0.030247	33.061	41.260	44.566	0.19247	0.086121	0.094695	207.36	7.5341
500.00	0.10000	0.024114	41.469	50.551	54.698	0.21503	0.099065	0.10751	231.13	4.1010
600.00	0.10000	0.020066	49.836	61.004	65.987	0.23558	0.10950	0.11790	252.55	2.5191
200.00	1.0000	14.715	0.067956	8.3891	8.4570	0.048489	0.069866	0.10604	879.27	-0.37736
289.48	1.0000	11.485	0.087067	18.835	18.922	0.091441	0.081543	0.13406	443.55	0.14902
289.48	1.0000	0.53292	1.8765	31.346	33.223	0.14084	0.078861	0.10583	148.24	24.503
300.00	1.0000	0.49298	2.0285	32.269	34.298	0.14449	0.077834	0.099455	155.53	20.787
400.00	1.0000	0.32001	3.1249	40.778	43.903	0.17212	0.087343	0.098681	198.53	7.7199
500.00	1.0000	0.24665	4.0544	50.244	54.298	0.19527	0.099519	0.10927	227.30	4.0976
600.00	1.0000	0.20246	4.9391	60.781	65.720	0.21607	0.10975	0.11891	251.11	2.4913
200.00	5.0000	14.806	0.067539	8.2811	8.6188	0.047943	0.070021	0.10541	900.01	-0.38724
300.00	5.0000	11.380	0.087876	19.812	20.251	0.094764	0.082741	0.13222	452.11	0.11636
400.00	5.0000	2.2504	0.44436	38.004	40.225	0.15165	0.093496	0.13815	159.25	8.1026
500.00	5.0000	1.3639	0.73318	48.802	52.468	0.17903	0.10135	0.11872	213.49	3.8903
600.00	5.0000	1.0491	0.95318	59.789	64.554	0.20106	0.11075	0.12364	246.86	2.2996
200.00	10.000	14.913	0.067054	8.1545	8.8250	0.047292	0.070195	0.10473	924.61	-0.39776
300.00	10.000	11.776	0.084916	19.382	20.231	0.093258	0.082583	0.12585	514.06	-0.037998
400.00	10.000	6.3531	0.15740	33.679	35.253	0.13608	0.095653	0.17697	196.98	2.9315
500.00	10.000	3.0122	0.33199	46.933	50.252	0.16976	0.10303	0.13206	211.16	3.0876
600.00	10.000	2.1596	0.46305	58.580	63.211	0.19339	0.11178	0.12945	248.28	1.9304
200.00	50.000	15.598	0.064113	7.3673	10.573	0.042937	0.070934	0.10170	1089.7	-0.44295
300.00	50.000	13.358	0.074862	17.612	21.355	0.086486	0.083360	0.11389	794.12	-0.33796
400.00	50.000	11.268	0.088747	28.859	33.296	0.12077	0.096003	0.12454	590.09	-0.20571
500.00	50.000	9.4018	0.10636	40.839	46.157	0.14943	0.10668	0.13213	478.93	-0.077157
600.00	50.000	7.8978	0.12662	53.306	59.637	0.17399	0.11548	0.13720	431.69	-0.0052131
300.00	100.00	14.343	0.069721	16.500	23.472	0.081539	0.084059	0.11166	1008.9	-0.40055
400.00	100.00	12.767	0.078330	27.298	35.131	0.11502	0.097186	0.12126	833.69	-0.35302
500.00	100.00	11.435	0.087453	38.923	47.668	0.14296	0.10821	0.12921	723.22	-0.31534
600.00	100.00	10.314	0.096952	51.227	60.923	0.16711	0.11716	0.13566	656.57	-0.28902

The values in these tables were generated from the NIST REFPROP software (Lemmon, E. W., McLinden, M. O., and Huber, M. L., NIST Standard Reference Database 23: Reference Fluid Thermodynamic and Transport Properties—REFPROP, National Institute of Standards and Technology, Standard Reference Data Program, Gaithersburg, Md., 2002, Version 7.1). The primary source for the thermodynamic properties is Lemmon, E. W., and Jacobsen, R. T., "An International Standard Formulation for the Thermodynamic Properties of 1,1,1-Trifluoroethane (HFC-143a) for Temperatures from 161 to 450 K and Pressures to 50 MPa," *J. Phys. Chem. Ref. Data* **29**(4):521–552, 2000. Validated equations for the viscosity and thermal conductivity are not currently available for this fluid.

Properties at the triple point temperature and the critical point temperature are given in the first and last entries of the saturation tables, respectively. In the single-phase table, when the temperature range for a given isobar includes a vapor-liquid phase boundary, the temperature of phase equilibrium is noted, and properties for both the saturated liquid and saturated vapor are given (with liquid properties given in the upper line). Lines are omitted from the temperature-pressure grid of the single-phase table, when the system would be in the solid phase or if there are potential problems with the source property surface.

The estimated uncertainties of properties calculated using the equation of state are 0.1% in density, 0.5% in heat capacities, 0.02% in the speed of sound for the vapor at pressures less than 1 MPa, 0.5% in speed of sound elsewhere, and 0.1% in vapor pressure, except in the critical region.

TABLE 2-282 Thermodynamic Properties of R-152a, 1,1-Difluoroethane

Temperature K	Pressure MPa	Density mol/dm ³	Volume dm ³ /mol	Int. energy kJ/mol	Enthalpy kJ/mol	Entropy kJ/(mol·K)	C _v kJ/(mol·K)	C _p kJ/(mol·K)	Sound speed m/s	Joule-Thomson K/MPa
Saturated Properties										
154.56	6.4139E-05	18.061	0.055369	0.91117	0.91117	0.0073929	0.065711	0.097583	1400.9	-0.43262
160.00	0.00012983	17.910	0.055836	1.4460	1.4460	0.010794	0.066998	0.098932	1359.2	-0.42405
170.00	0.00041463	17.630	0.056720	2.4420	2.4421	0.016832	0.067926	0.10007	1293.7	-0.41381
180.00	0.0011411	17.350	0.057638	3.4453	3.4454	0.022566	0.068069	0.10053	1236.1	-0.40568
190.00	0.0027751	17.067	0.058594	4.4524	4.4525	0.028011	0.068043	0.10090	1182.6	-0.39686
200.00	0.0060859	16.781	0.059592	5.4638	5.4641	0.033199	0.068097	0.10143	1131.3	-0.38620
210.00	0.012233	16.491	0.060638	6.4814	6.4822	0.038164	0.068309	0.10218	1081.2	-0.37317
220.00	0.022836	16.198	0.061737	7.5077	7.5091	0.042938	0.068689	0.10317	1031.8	-0.35753
230.00	0.040024	15.899	0.062897	8.5448	8.5474	0.047548	0.069217	0.10439	982.80	-0.33902
240.00	0.066451	15.594	0.064128	9.5949	9.5992	0.052017	0.069868	0.10583	933.98	-0.31735
250.00	0.10530	15.281	0.065440	10.660	10.667	0.056365	0.070618	0.10747	885.23	-0.29203
260.00	0.16024	14.960	0.066846	11.741	11.752	0.060607	0.071447	0.10932	836.44	-0.26235
270.00	0.23541	14.628	0.068363	12.841	12.857	0.064759	0.072342	0.11140	787.50	-0.22731
280.00	0.33537	14.283	0.070011	13.962	13.985	0.068835	0.073294	0.11374	738.29	-0.18547
290.00	0.46506	13.924	0.071819	15.105	15.138	0.072848	0.074300	0.11641	688.71	-0.13478
300.00	0.62978	13.546	0.073821	16.273	16.319	0.076812	0.075363	0.11951	638.61	-0.07262
310.00	0.83519	13.147	0.076065	17.470	17.533	0.080741	0.076490	0.12318	587.86	0.0064939
320.00	1.0873	12.719	0.078621	18.699	18.785	0.084652	0.077694	0.12765	536.30	0.10833
330.00	1.3925	12.257	0.081587	19.968	20.081	0.088567	0.078997	0.13333	483.73	0.24433
340.00	1.7577	11.748	0.085118	21.284	21.434	0.092513	0.080433	0.14093	429.89	0.43380
350.00	2.1907	11.176	0.089475	22.662	22.858	0.096532	0.082059	0.15192	374.37	0.71349
360.00	2.7000	10.510	0.095147	24.126	24.383	0.10070	0.083973	0.16999	316.40	1.1636
370.00	3.2967	9.6829	0.10328	25.730	26.070	0.10515	0.086395	0.20774	254.38	2.0014
380.00	3.9966	8.4686	0.11808	27.655	27.655	0.11043	0.090038	0.35969	183.93	4.1151
386.41	4.5168	5.5715	0.17949	30.732	31.543	0.11914			0	11.292
154.56	6.4139E-05	4.9919E-05	20,032.	26.412	27.697	0.18069	0.037824	0.046148	154.04	336.54
160.00	1.2983E-04	9.7623E-05	10,244.	26.619	27.949	0.17644	0.038592	0.046923	156.44	294.63
170.00	0.00041463	0.00029357	3,406.3	27.009	28.422	0.16965	0.040032	0.048389	160.70	233.22
180.00	0.0011411	0.00076374	1,309.3	27.412	28.906	0.16401	0.041518	0.049922	164.78	186.99
190.00	0.0027751	0.0017625	567.37	27.825	29.399	0.15931	0.043061	0.051550	168.64	151.71
200.00	0.0060859	0.0036817	271.61	28.247	29.900	0.15538	0.044675	0.053297	172.27	124.45
210.00	0.012233	0.0070756	141.33	28.676	30.405	0.15208	0.046371	0.055192	175.63	103.17
220.00	0.022836	0.012679	78.873	29.110	30.911	0.14931	0.048158	0.057260	178.66	86.396
230.00	0.040024	0.021415	46.696	29.546	31.415	0.14697	0.050042	0.059528	181.32	73.068
240.00	0.066451	0.034408	29.063	29.984	31.915	0.14500	0.052027	0.062017	183.57	62.400
250.00	0.10530	0.052990	18.871	30.419	32.406	0.14332	0.054111	0.064754	185.35	53.805
260.00	0.16024	0.078721	12.703	30.851	32.887	0.14189	0.056291	0.067769	186.60	46.838
270.00	0.23541	0.11343	8.8162	31.277	33.352	0.14067	0.058564	0.071103	187.28	41.163
280.00	0.33537	0.15926	6.2791	31.694	33.800	0.13960	0.060926	0.074811	187.33	36.517
290.00	0.46506	0.21879	4.5705	32.099	34.224	0.13866	0.063373	0.078977	186.70	32.701
300.00	0.62978	0.29518	3.3877	32.488	34.622	0.13782	0.065904	0.083731	185.34	29.557
310.00	0.83519	0.39242	2.5483	32.857	34.985	0.13704	0.068522	0.089270	183.16	26.966
320.00	1.0873	0.51573	1.9390	33.199	35.308	0.13629	0.071233	0.095924	180.10	24.832
330.00	1.3925	0.67231	1.4874	33.506	35.577	0.13552	0.074054	0.10426	176.06	23.083
340.00	1.7577	0.87269	1.1459	33.764	35.779	0.13470	0.077013	0.11534	170.91	21.662
350.00	2.1907	1.1336	0.88218	33.953	35.886	0.13375	0.080160	0.13140	164.49	20.515
360.00	2.7000	1.4847	0.67352	34.036	35.855	0.13256	0.083590	0.15806	156.55	19.584
370.00	3.2967	1.9912	0.50220	33.933	35.589	0.13088	0.087501	0.21461	146.71	18.738
380.00	3.9966	2.8726	0.34812	33.381	34.772	0.12792	0.092461	0.44168	134.10	17.420
386.41	4.5168	5.5715	0.17949	30.732	31.543	0.11914			0	11.292

TABLE 2-282 Thermodynamic Properties of R-152a, 1,1-Difluoroethane (Concluded)

Temperature K	Pressure MPa	Density mol/dm ³	Volume dm ³ /mol	Int. energy kJ/mol	Enthalpy kJ/mol	Entropy kJ/(mol·K)	C _v kJ/(mol·K)	C _p kJ/(mol·K)	Sound speed m/s	Joule-Thomson K/MPa
Single-Phase Properties										
200.00	0.10000	16.782	0.059586	5.4618	5.4678	0.033189	0.068102	0.10142	1131.7	-0.38632
248.83	0.10000	15.318	0.065282	10.535	10.541	0.055862	0.070526	0.10726	890.93	-0.29520
248.83	0.10000	0.050481	19.809	30.369	32.350	0.14351	0.053862	0.064421	185.16	54.718
300.00	0.10000	0.040939	24.427	33.323	35.766	0.15598	0.060341	0.069611	204.37	27.531
400.00	0.10000	0.030290	33.014	40.103	43.405	0.17786	0.074770	0.083404	235.25	10.509
500.00	0.10000	0.024131	41.441	48.286	52.430	0.19794	0.088343	0.096818	261.80	5.4858
200.00	1.0000	16.798	0.059530	5.4436	5.5031	0.033097	0.068150	0.10133	1135.5	-0.38750
300.00	1.0000	13.568	0.073703	16.249	16.323	0.076732	0.075359	0.11920	642.81	-0.078450
316.76	1.0000	12.861	0.077752	18.296	18.374	0.083384	0.077294	0.12609	553.13	0.072197
316.76	1.0000	0.47247	2.1165	33.092	35.208	0.13653	0.070342	0.093615	181.20	25.479
400.00	1.0000	0.32539	3.0733	39.505	42.579	0.15720	0.076729	0.088940	222.89	10.836
500.00	1.0000	0.24847	4.0246	47.922	51.947	0.17807	0.088892	0.098930	256.19	5.4940
200.00	5.0000	16.867	0.059288	5.3645	5.6609	0.032698	0.068345	0.10098	1152.1	-0.39242
300.00	5.0000	13.783	0.072554	16.011	16.373	0.075926	0.075345	0.11645	684.64	-0.13417
400.00	5.0000	3.1526	0.31720	34.823	36.409	0.13126	0.092011	0.26333	148.13	12.808
500.00	5.0000	1.4336	0.69753	46.169	49.657	0.16117	0.091345	0.11166	232.93	5.3800
200.00	10.000	16.949	0.059000	5.2700	5.8600	0.032215	0.068554	0.10058	1172.7	-0.39792
300.00	10.000	14.014	0.071358	15.752	16.466	0.075036	0.075376	0.11401	729.99	-0.18420
400.00	10.000	9.5224	0.10502	28.480	29.530	0.11233	0.087211	0.16027	310.79	1.2458
500.00	10.000	3.4436	0.29039	43.674	46.578	0.15056	0.094041	0.13591	219.92	4.4385
200.00	30.000	17.248	0.057977	4.9338	6.6732	0.030434	0.069111	0.099355	1253.5	-0.41462
300.00	30.000	14.709	0.067986	14.971	17.010	0.072215	0.075740	0.10883	869.51	-0.29079
400.00	30.000	11.934	0.083794	26.048	28.561	0.10535	0.085262	0.12249	576.62	-0.0089214
500.00	30.000	8.9569	0.11165	38.069	41.418	0.13400	0.094199	0.13295	407.30	0.48690
200.00	60.000	17.625	0.056738	4.5216	7.9258	0.028097	0.069524	0.098187	1367.5	-0.42991
300.00	60.000	15.424	0.064836	14.174	18.064	0.069098	0.076558	0.10570	1020.4	-0.35644
400.00	60.000	13.309	0.075135	24.599	29.107	0.10080	0.086520	0.11507	770.60	-0.24663
500.00	60.000	11.312	0.088399	35.736	41.039	0.12739	0.095954	0.12324	613.84	-0.11541

The values in these tables were generated from the NIST REFPROP software (Lemmon, E. W., McLinden, M. O., and Huber, M. L., NIST Standard Reference Database 23: Reference Fluid Thermodynamic and Transport Properties—REFPROP, National Institute of Standards and Technology, Standard Reference Data Program, Gaithersburg, Md., 2002, Version 7.1). The primary source for the thermodynamic properties is Outcalt, S. L., and McLinden, M. O., "A Modified Benedict-Webb-Rubin Equation of State for the Thermodynamic Properties of R152a (1,1-Difluoroethane)," *J. Phys. Chem. Ref. Data* **25**(2):605–636, 1996. Validated equations for the viscosity and thermal conductivity are not currently available for this fluid.

Properties at the triple point temperature and the critical point temperature are given in the first and last entries of the saturation tables, respectively. In the single-phase table, when the temperature range for a given isobar includes a vapor-liquid phase boundary, the temperature of phase equilibrium is noted, and properties for both the saturated liquid and saturated vapor are given (with liquid properties given in the upper line). Lines are omitted from the temperature-pressure grid of the single-phase table, when the system would be in the solid phase or if there are potential problems with the source property surface.

The uncertainties of the equation of state are 0.1% in density, 2% in heat capacity, and 0.05% in the vapor speed of sound, except in the critical region. The uncertainty in vapor pressure is 0.1%.

TABLE 2-283 Saturated Refrigerant 216a, 1,3-Dichloro-1,1,2,2,3,3-Hexafluoropropane

Temp., °F	Pressure, lb/in ² abs.	Volume, ft ³ /lb		Enthalpy, Btu/lb		Entropy, Btu/(lb)(°F)	
		Liquid	Vapor	Liquid	Vapor	Liquid	Vapor
-40	0.339	0.00927	59.957	0.000	62.415	0.0000	0.1487
-20	0.713	0.00942	29.749	4.778	65.276	0.0111	0.1487
0	1.382	0.00958	15.986	9.541	68.208	0.0217	0.1493
20	2.497	0.00974	9.184	14.298	71.199	0.0318	0.1504
40	4.247	0.00992	5.582	19.056	74.239	0.0415	0.1520
60	6.862	0.01010	3.558	23.821	77.319	0.0509	0.1538
80	10.612	0.01030	2.361	28.598	80.429	0.0599	0.1559
100	15.797	0.01050	1.6215	33.391	83.559	0.0686	0.1582
120	22.753	0.01073	1.1462	38.205	86.701	0.0770	0.1607
140	31.845	0.01097	0.8304	43.049	89.845	0.0852	0.1632
160	43.468	0.01124	0.6142	47.930	92.981	0.0931	0.1658
180	58.046	0.01153	0.4623	52.861	96.099	0.1009	0.1685
200	76.033	0.01186	0.3529	57.857	99.186	0.1085	0.1712
220	97.913	0.01223	0.2725	62.939	102.225	0.1161	0.1739
240	124.21	0.01266	0.2121	68.132	105.196	0.1235	0.1765
260	155.50	0.01317	0.1660	73.474	108.066	0.1309	0.1790
280	192.40	0.01378	0.1300	79.015	110.789	0.1384	0.1813
300	235.63	0.01458	0.1013	84.835	113.282	0.1460	0.1834
320	286.03	0.01570	0.0776	91.089	115.373	0.1539	0.1851
340	344.81	0.01764	0.0565	98.234	116.538	0.1628	0.1856
355.98 ^c	399.45	0.02771	0.0277	110.248	110.248	0.1773	0.1773

^cFrom published data, Chemicals Division, Union Carbide Corporation. Used by permission. The paper describing these data is by Shank, *ASHRAE J.*, **1**(1965): 94-101. *c* = critical temperature.

The 1993 ASHRAE *Handbook—Fundamentals* (SI ed.) gives material for integral degrees Celsius with temperatures on the ITS 90 scale from -118.59 to 113.26 °C. The thermodynamic diagram from 0.1 to 30 bar extends to 180 °C. For tables and a diagram to 400 psia, 360 °F, see Stewart, R. B., R. T. Jacobsen, et al., *Thermodynamic Properties of Refrigerants*, ASHRAE, Atlanta, GA, 1986 (521 pp.). For specific heat and viscosity, see *Thermophysical Properties of Refrigerants*, ASHRAE, 1993. Thermal conductivity data as a function of pressure and temperature are reported by Krauss, R. and K. Stephan, *Proc. 12th Symp. Thermophys. Props.*, Boulder, CO, 1994.

TABLE 2-284 Thermodynamic Properties of R-218, Octafluoropropane

Temperature K	Pressure MPa	Density mol/dm ³	Volume dm ³ /mol	Int. energy kJ/mol	Enthalpy kJ/mol	Entropy kJ/(mol·K)	C _v kJ/(mol·K)	C _p kJ/(mol·K)	Sound speed m/s	Joule-Thomson K/MPa
Saturated Properties										
125.45	2.0186E-06	10.687	0.093572	12.346	12.346	0.057736	0.086723	0.14866	1157.7	-0.48474
130.00	4.8985E-06	10.598	0.094353	13.024	13.024	0.063044	0.088773	0.14939	1119.0	-0.48168
140.00	2.7215E-05	10.407	0.096088	14.528	14.528	0.074187	0.093214	0.15145	1041.4	-0.47276
150.00	0.00011605	10.219	0.097856	16.054	16.054	0.084719	0.097514	0.15392	972.09	-0.46146
160.00	0.00040065	10.033	0.099670	17.607	17.607	0.094739	0.10165	0.15668	909.32	-0.44819
170.00	0.0011659	9.8482	0.10154	19.189	19.189	0.10433	0.10561	0.15964	851.65	-0.43313
180.00	0.0029499	9.6632	0.10349	20.800	20.801	0.11354	0.10942	0.16276	797.99	-0.41623
190.00	0.0066482	9.4771	0.10552	22.444	22.445	0.12242	0.11310	0.16603	747.52	-0.39731
200.00	0.013606	9.2890	0.10765	24.121	24.122	0.13102	0.11667	0.16944	699.61	-0.37604
210.00	0.025681	9.0979	0.10992	25.832	25.835	0.13937	0.12014	0.17301	653.72	-0.35194
220.00	0.045264	8.9027	0.11233	27.580	27.585	0.14750	0.12355	0.17675	609.45	-0.32433
230.00	0.075274	8.7022	0.11491	29.365	29.374	0.15544	0.12690	0.18069	566.44	-0.29229
240.00	0.11911	8.4950	0.11772	31.190	31.204	0.16320	0.13022	0.18489	524.41	-0.25451
250.00	0.18060	8.2795	0.12078	33.056	33.077	0.17082	0.13351	0.18940	483.09	-0.20911
260.00	0.26395	8.0537	0.12417	34.966	34.998	0.17832	0.13680	0.19432	442.24	-0.15332
270.00	0.37369	7.8151	0.12796	36.923	36.971	0.18571	0.14010	0.19980	401.64	-0.082915
280.00	0.51466	7.5602	0.13227	38.933	39.001	0.19302	0.14343	0.20607	361.06	0.0089029
290.00	0.69206	7.2843	0.13728	41.000	41.095	0.20029	0.14683	0.21355	320.24	0.13369
300.00	0.91150	6.9802	0.14326	43.134	43.265	0.20754	0.15035	0.22299	278.86	0.31279
310.00	1.1793	6.6366	0.15068	45.351	45.528	0.21483	0.15405	0.23603	236.46	0.59020
320.00	1.5030	6.2324	0.16045	47.677	47.918	0.22226	0.15812	0.25690	192.26	1.0733
330.00	1.8924	5.7189	0.17486	50.177	50.508	0.23002	0.16294	0.30134	144.68	2.1079
340.00	2.3634	4.9092	0.20370	53.102	53.583	0.23893	0.17021	0.52335	89.750	5.6878
345.02	2.6402	3.3400	0.29940	56.252	57.042	0.24883			0	17.096
125.45	2.0186E-06	1.9353E-06	516.720.	37.874	38.917	0.26954	0.072287	0.080604	78.648	854.14
130.00	4.8985E-06	4.5321E-06	220.650.	38.208	39.289	0.26508	0.074826	0.083144	79.920	682.22
140.00	2.7215E-05	2.3384E-05	42.765.	38.983	40.147	0.25718	0.080190	0.088516	82.654	432.76
150.00	1.1605E-04	9.3093E-05	10.742.	39.808	41.055	0.25139	0.085274	0.093623	85.299	288.12
160.00	0.00040065	0.00030151	3,316.6	40.680	42.009	0.24725	0.090119	0.098514	87.846	200.28
170.00	0.0011659	0.00082688	1,209.4	41.595	43.005	0.24442	0.094776	0.10326	90.278	144.70
180.00	0.0029499	0.0019804	504.96	42.548	44.038	0.24263	0.099300	0.10792	92.569	108.17
190.00	0.0066482	0.0042437	235.65	43.536	45.102	0.24167	0.10374	0.11258	94.686	83.339
200.00	0.013606	0.0082953	120.55	44.553	46.193	0.24138	0.10814	0.11730	96.589	65.928
210.00	0.025681	0.015024	66.559	45.596	47.305	0.24161	0.11253	0.12213	98.233	53.394
220.00	0.045264	0.025536	39.161	46.661	48.433	0.24227	0.11693	0.12712	99.570	44.174
230.00	0.075274	0.041158	24.297	47.744	49.573	0.24326	0.12135	0.13232	100.55	37.278
240.00	0.11911	0.063461	15.758	48.843	50.720	0.24452	0.12577	0.13776	101.12	32.063
250.00	0.18060	0.094301	10.604	49.952	51.867	0.24598	0.13020	0.14351	101.22	28.095
260.00	0.26395	0.13591	7.3580	51.067	53.009	0.24759	0.13463	0.14970	100.79	25.083
270.00	0.37369	0.19105	5.2343	52.183	54.139	0.24929	0.13906	0.15649	99.737	22.826
280.00	0.51466	0.26332	3.7977	53.291	55.246	0.25104	0.14352	0.16420	97.968	21.188
290.00	0.69206	0.35768	2.7958	54.381	56.316	0.25277	0.14802	0.17340	95.356	20.088
300.00	0.91150	0.48153	2.0767	55.437	57.330	0.25442	0.15262	0.18521	91.730	19.493
310.00	1.1793	0.64702	1.5456	56.433	58.256	0.25589	0.15742	0.20207	86.859	19.423
320.00	1.5030	0.87704	1.1402	57.322	59.035	0.25700	0.16259	0.23055	80.422	19.958
330.00	1.8924	1.2252	0.81620	57.996	59.540	0.25739	0.16855	0.29532	72.007	21.201
340.00	2.3634	1.8924	0.52844	58.081	59.330	0.25584	0.17647	0.62247	61.241	22.532
345.02	2.6402	3.3400	0.29940	56.252	57.042	0.24883			0	17.096

Single-Phase Properties

150.00	0.10000	10.220	0.097848	16.052	16.061	0.084701	0.097521	0.15391	972.51	-0.46154
225.00	0.10000	8.8041	0.11358	28.465	28.477	0.15148	0.12523	0.17867	588.11	-0.30918
236.07	0.10000	8.5773	0.11659	30.468	30.479	0.16017	0.12892	0.18321	540.83	-0.27015
236.07	0.10000	0.053789	18.591	48.410	50.269	0.24400	0.12403	0.13558	100.95	33.943
300.00	0.10000	0.040933	24.430	56.919	59.362	0.27801	0.14104	0.15028	116.42	12.416
375.00	0.10000	0.032372	30.891	68.272	71.361	0.31363	0.16055	0.16927	131.00	6.1732
150.00	1.0000	10.228	0.097772	16.028	16.125	0.084540	0.097582	0.15385	976.23	-0.46230
225.00	1.0000	8.8236	0.11333	28.413	28.527	0.15125	0.12522	0.17828	594.72	-0.31433
300.00	1.0000	6.9891	0.14308	43.116	43.259	0.20748	0.15030	0.22248	280.68	0.30296
303.52	1.0000	6.8645	0.14568	43.905	44.051	0.21010	0.15163	0.22705	264.07	0.39586
303.52	1.0000	0.53424	1.8718	55.797	57.669	0.25497	0.15428	0.19038	90.170	19.406
375.00	1.0000	0.35613	2.8080	67.521	70.329	0.29246	0.16284	0.17689	120.35	7.1384
150.00	5.0000	10.262	0.097443	15.923	16.411	0.083839	0.097864	0.15361	992.31	-0.46544
225.00	5.0000	8.9050	0.11230	28.196	28.757	0.15027	0.12525	0.17677	622.21	-0.33410
300.00	5.0000	7.2996	0.13699	42.444	43.129	0.20518	0.14888	0.20895	346.02	0.039275
375.00	5.0000	4.0113	0.24930	60.519	61.765	0.26018	0.17483	0.31884	101.99	4.7668
150.00	10.000	10.304	0.097050	15.799	16.769	0.082988	0.098234	0.15336	1011.4	-0.46885
225.00	10.000	8.9969	0.11115	27.949	29.060	0.14913	0.12538	0.17531	653.07	-0.35341
300.00	10.000	7.5606	0.13227	41.847	43.170	0.20307	0.14819	0.20166	403.66	-0.10223
375.00	10.000	5.6952	0.17559	57.659	59.415	0.25128	0.16841	0.23156	219.93	0.67650
150.00	20.000	10.382	0.096321	15.565	17.492	0.081360	0.099023	0.15301	1046.6	-0.47434
225.00	20.000	9.1565	0.10921	27.517	29.701	0.14709	0.12580	0.17326	706.41	-0.38080
300.00	20.000	7.9189	0.12628	40.989	43.515	0.19992	0.14793	0.19500	486.73	-0.22897
375.00	20.000	6.5981	0.15156	55.836	58.867	0.24552	0.16668	0.21331	339.02	0.012472
150.00	30.000	10.454	0.095654	15.351	18.220	0.079818	0.099855	0.15280	1078.7	-0.47844
225.00	30.000	9.2933	0.10760	27.147	30.375	0.14527	0.12636	0.17191	751.98	-0.39925
300.00	30.000	8.1774	0.12229	40.353	44.022	0.19747	0.14819	0.19173	549.34	-0.28972
375.00	30.000	7.0690	0.14146	54.800	59.044	0.24210	0.16662	0.20796	416.45	-0.15627

The values in these tables were generated from the NIST REFPROP software (Lemmon, E. W., McLinden, M. O., and Huber, M. L., NIST Standard Reference Database 23: Reference Fluid Thermodynamic and Transport Properties—REFPROP, National Institute of Standards and Technology, Standard Reference Data Program, Gaithersburg, Md., 2002, Version 7.1). The primary source for the thermodynamic properties is Lemmon, E. W., and Span, R., "Short Fundamental Equations of State for 20 Industrial Fluids," *J. Chem. Eng. Data* **51**(3):785–850, 2006. Validated equations for the viscosity and thermal conductivity are not currently available for this fluid.

Properties at the triple point temperature and the critical point temperature are given in the first and last entries of the saturation tables, respectively. In the single-phase table, when the temperature range for a given isobar includes a vapor-liquid phase boundary, the temperature of phase equilibrium is noted, and properties for both the saturated liquid and saturated vapor are given (with liquid properties given in the upper line). Lines are omitted from the temperature-pressure grid of the single-phase table, when the system would be in the solid phase or if there are potential problems with the source property surface.

The uncertainty in density is 0.2% for the liquid phase and 0.5% for the vapor phase. Above the critical temperature, the uncertainties are estimated to be 1% in density and 0.5% in pressure. Calculated vapor pressures have an uncertainty of 0.5%. The uncertainties for heat capacities and sound speeds are 1%.

TABLE 2-285 Thermodynamic Properties of R-227ea, 1,1,1,2,3,3,3-Heptafluoropropane

Temperature K	Pressure MPa	Density mol/dm ³	Volume dm ³ /mol	Int. energy kJ/mol	Enthalpy kJ/mol	Entropy kJ/(mol·K)	C _v kJ/(mol·K)	C _p kJ/(mol·K)	Sound speed m/s	Joule-Thomson K/MPa
Saturated Properties										
146.35	7.0312E-06	11.086	0.090205	12.227	12.227	0.063811	0.11121	0.16308	1068.8	-0.42071
150.00	1.2811E-05	11.020	0.090746	12.821	12.821	0.067824	0.11136	0.16271	1048.3	-0.42085
160.00	5.6086E-05	10.841	0.092245	14.446	14.446	0.078309	0.11222	0.16238	994.14	-0.41876
170.00	0.00019958	10.663	0.093780	16.072	16.072	0.088164	0.11357	0.16286	942.81	-0.41349
180.00	0.00059967	10.487	0.095359	17.705	17.705	0.097501	0.11528	0.16396	893.95	-0.40546
190.00	0.0015672	10.310	0.096992	19.352	19.352	0.10641	0.11723	0.16554	847.26	-0.39497
200.00	0.0036466	10.133	0.098689	21.017	21.017	0.11495	0.11934	0.16750	802.44	-0.38217
210.00	0.0076967	9.9539	0.10046	22.703	22.704	0.12317	0.12157	0.16976	759.23	-0.36707
220.00	0.014961	9.7727	0.10233	24.413	24.414	0.13112	0.12386	0.17228	717.37	-0.34954
230.00	0.027114	9.5883	0.10429	26.148	26.151	0.13884	0.12618	0.17502	676.63	-0.32930
240.00	0.046286	9.3999	0.10638	27.912	27.917	0.14635	0.12851	0.17797	636.81	-0.30590
250.00	0.075058	9.2065	0.10862	29.706	29.714	0.15367	0.13085	0.18114	597.69	-0.27867
260.00	0.11644	9.0068	0.11103	31.531	31.544	0.16083	0.13318	0.18454	559.10	-0.24663
270.00	0.17384	8.7997	0.11364	33.390	33.410	0.16784	0.13549	0.18822	520.85	-0.20842
280.00	0.25102	8.5834	0.11650	35.286	35.315	0.17474	0.13781	0.19225	482.77	-0.16205
290.00	0.35208	8.3560	0.11967	37.220	37.262	0.18153	0.14011	0.19673	444.69	-0.10460
300.00	0.48145	8.1148	0.12323	39.197	39.256	0.18824	0.14243	0.20183	406.42	-0.031613
310.00	0.64388	7.8563	0.12729	41.221	41.303	0.19488	0.14477	0.20782	367.76	0.064014
320.00	0.84450	7.5756	0.13200	43.299	43.411	0.20149	0.14716	0.21515	328.49	0.19426
330.00	1.0889	7.2652	0.13764	45.442	45.592	0.20810	0.14964	0.22467	288.32	0.38093
340.00	1.3836	6.9135	0.14465	47.666	47.866	0.21476	0.15227	0.23817	246.84	0.66802
350.00	1.7358	6.4988	0.15387	50.002	50.269	0.22158	0.15517	0.26018	203.37	1.1593
360.00	2.1552	5.9733	0.16741	52.517	52.877	0.22873	0.15867	0.30696	156.53	2.1701
370.00	2.6553	5.1649	0.19361	55.458	55.972	0.23696	0.16399	0.51614	102.78	5.2930
375.95	2.9991	3.4100	0.29326	59.193	60.073	0.24773			0	16.489
146.35	7.0312E-06	5.7786E-06	173.050	41.158	42.374	0.26981	0.072002	0.080321	89.345	630.83
150.00	1.2811E-05	1.0273E-05	97.345	41.423	42.670	0.26682	0.073562	0.081883	90.352	540.51
160.00	5.6086E-05	4.2170E-05	23.714	42.179	43.509	0.25995	0.077861	0.086194	93.045	363.36
170.00	0.00019958	0.00014128	7.078.0	42.976	44.389	0.25474	0.082177	0.090535	95.643	253.26
180.00	0.00059967	0.00040123	2.492.3	43.814	45.308	0.25085	0.086488	0.094896	98.141	182.56
190.00	0.0015672	0.00099473	1.005.3	44.689	46.265	0.24805	0.090782	0.099275	100.53	135.75
200.00	0.0036466	0.0022037	453.78	45.600	47.255	0.24613	0.095053	0.10368	102.77	103.86
210.00	0.0076967	0.0044452	224.96	46.543	48.275	0.24494	0.099298	0.10813	104.85	81.549
220.00	0.014961	0.0082891	120.64	47.515	49.320	0.24433	0.10352	0.11263	106.73	65.553
230.00	0.027114	0.014469	69.111	48.513	50.387	0.24421	0.10771	0.11721	108.37	53.830
240.00	0.046286	0.023890	41.858	49.533	51.470	0.24448	0.11188	0.12189	109.71	45.075
250.00	0.075058	0.037635	26.571	50.570	52.565	0.24507	0.11601	0.12670	110.73	38.434
260.00	0.11644	0.056982	17.550	51.622	53.666	0.24591	0.12010	0.13166	111.36	33.337
270.00	0.17384	0.083437	11.985	52.684	54.768	0.24695	0.12416	0.13684	111.55	29.395
280.00	0.25102	0.11880	8.4176	53.752	55.864	0.24813	0.12818	0.14232	111.26	26.339
290.00	0.35208	0.16526	6.0510	54.818	56.949	0.24942	0.13216	0.14822	110.42	23.978
300.00	0.48145	0.22559	4.4328	55.878	58.012	0.25076	0.13612	0.15475	108.94	22.183
310.00	0.64388	0.30344	3.2956	56.922	59.044	0.25211	0.14009	0.16227	106.75	20.864
320.00	0.84450	0.40387	2.4761	57.938	60.029	0.25342	0.14409	0.17136	103.73	19.669
330.00	1.0889	0.53442	1.8712	58.909	60.946	0.25463	0.14817	0.18320	99.740	19.477
340.00	1.3836	0.70732	1.4138	59.808	61.764	0.25564	0.15244	0.20027	94.584	19.399
350.00	1.7358	0.94497	1.0582	60.587	62.424	0.25630	0.15704	0.22897	88.022	19.775
360.00	2.1552	1.2970	0.77102	61.146	62.807	0.25632	0.16228	0.29185	79.757	20.625
370.00	2.6553	1.9293	0.51831	61.164	62.540	0.25471	0.16893	0.56287	69.452	21.487
375.95	2.9991	3.4100	0.29326	59.193	60.073	0.24773			0	16.489

Single-Phase Properties

150.00	0.10000	11.021	0.090739	12.819	12.828	0.067809	0.11137	0.16271	1048.6	-0.42089
225.00	0.10000	9.6823	0.10328	25.274	25.284	0.13499	0.12502	0.17360	697.31	-0.34002
256.43	0.10000	9.0790	0.11014	30.875	30.886	0.15829	0.13235	0.18330	572.84	-0.25870
256.43	0.10000	0.049336	20.269	51.245	53.272	0.24559	0.11864	0.12987	111.18	35.009
300.00	0.10000	0.041177	24.286	56.684	59.112	0.26660	0.12925	0.13881	122.16	17.772
375.00	0.10000	0.032454	30.813	67.081	70.162	0.29941	0.14667	0.15550	137.79	8.4581
450.00	0.10000	0.026888	37.191	78.645	82.364	0.32903	0.16079	0.16939	151.34	5.1086
150.00	1.0000	11.028	0.090682	12.799	12.890	0.067676	0.11146	0.16267	1051.5	-0.42131
225.00	1.0000	9.6973	0.10312	25.234	25.337	0.13482	0.12507	0.17337	702.21	-0.34268
300.00	1.0000	8.1405	0.12284	39.137	39.260	0.18804	0.14240	0.20096	412.50	-0.045381
326.58	1.0000	7.3754	0.13559	44.701	44.837	0.20584	0.14878	0.22108	302.19	0.30867
326.58	1.0000	0.48574	2.0587	58.583	60.642	0.25423	0.14676	0.17873	101.23	19.600
375.00	1.0000	0.36801	2.7173	66.118	68.835	0.27764	0.15025	0.16647	123.32	10.030
450.00	1.0000	0.28468	3.5127	78.039	81.552	0.30854	0.16198	0.17375	144.14	5.4173
150.00	5.0000	11.058	0.090430	12.712	13.164	0.067092	0.11182	0.16253	1064.0	-0.42305
225.00	5.0000	9.7613	0.10245	25.066	25.578	0.13406	0.12533	0.17247	723.03	-0.35330
300.00	5.0000	8.3150	0.12026	38.729	39.330	0.18665	0.14230	0.19592	454.01	-0.12586
375.00	5.0000	6.0063	0.16649	54.845	55.677	0.23506	0.15968	0.25736	188.73	1.3729
450.00	5.0000	1.9568	0.51103	74.454	77.009	0.28716	0.16853	0.21820	117.53	5.8791
225.00	10.000	9.8358	0.10167	24.870	25.887	0.13316	0.12567	0.17153	747.22	-0.36439
300.00	10.000	8.4921	0.11776	38.308	39.485	0.18518	0.14237	0.19196	496.71	-0.18923
375.00	10.000	6.7736	0.14763	53.368	54.845	0.23077	0.15755	0.21921	286.63	0.34861
450.00	10.000	4.4095	0.22679	70.066	72.334	0.27322	0.17015	0.23938	162.15	2.0189
225.00	30.000	10.091	0.099103	24.209	27.182	0.13000	0.12709	0.16914	829.42	-0.39369
300.00	30.000	8.9874	0.11127	37.111	40.449	0.18079	0.14335	0.18477	619.36	-0.30379
375.00	30.000	7.8569	0.12728	51.038	54.856	0.22359	0.15736	0.19887	467.67	-0.17451
450.00	30.000	6.7284	0.14862	65.707	70.165	0.26078	0.16895	0.20846	368.25	-0.017558
225.00	60.000	10.391	0.096240	23.457	29.231	0.12610	0.12922	0.16752	926.46	-0.41551
300.00	60.000	9.4675	0.10562	35.965	42.302	0.17614	0.14519	0.18109	743.76	-0.36285
375.00	60.000	8.5978	0.11631	49.374	56.353	0.21789	0.15896	0.19315	617.08	-0.30676
450.00	60.000	7.7868	0.12842	63.495	71.201	0.25396	0.17036	0.20230	530.91	-0.25596

The values in these tables were generated from the NIST REFPROP software (Lemmon, E. W., McLinden, M. O., and Huber, M. L., NIST Standard Reference Database 23: Reference Fluid Thermodynamic and Transport Properties—REFPROP, National Institute of Standards and Technology, Standard Reference Data Program, Gaithersburg, Md., 2002, Version 7.1). The primary source for the thermodynamic properties is an interim equation from Lemmon, E. W., personal communication (NIST, Boulder, CO, 2006). Validated equations for the viscosity and thermal conductivity are not currently available for this fluid.

Properties at the triple point temperature and the critical point temperature are given in the first and last entries of the saturation tables, respectively. In the single-phase table, when the temperature range for a given isobar includes a vapor-liquid phase boundary, the temperature of phase equilibrium is noted, and properties for both the saturated liquid and saturated vapor are given (with liquid properties given in the upper line). Lines are omitted from the temperature-pressure grid of the single-phase table, when the system would be in the solid phase or if there are potential problems with the source property surface.

The uncertainties in the equation of state are 0.2% in density, except in a small region close to the critical point, 0.2% in vapor pressure between 250 and 360 K, 0.4% in vapor pressure outside this region, 1% in heat capacities (with increasing uncertainties in the critical region and at higher temperatures), 0.1% in the vapor-phase speed of sound, and 3% in the liquid-phase speed of sound.

TABLE 2-286 Saturated Refrigerant 245cb 1,1,1,2,2-Pentafluoropropane*

T, K	P, bar	v_f , m ³ /kg	v_g , m ³ /kg	h_f , kJ/kg	h_g , kJ/kg	s_f , kJ/(kg·K)	s_g , kJ/(kg·K)
172	0.0034	6.46-4	31.49	-63.4	133.8	-0.3131	0.8327
180	0.0076	6.57-4	14.63	-55.9	138.7	-0.2707	0.8099
190	0.0190	6.70-4	6.20	-46.2	145.1	-0.2182	0.7885
200	0.0425	6.83-4	2.91	-36.0	151.7	-0.1666	0.7725
210	0.0870	6.97-4	1.48	-25.7	158.5	-0.1157	0.7612
220	0.1654	7.11-4	0.822	-14.8	165.4	-0.0654	0.7539
230	0.2946	7.25-4	0.475	-3.6	172.5	-0.0156	0.7500
240	0.4958	7.40-4	0.292	8.0	179.6	0.0337	0.7487
250	0.7946	7.55-4	0.192	19.9	186.8	0.0824	0.7497
260	1.2204	7.72-4	0.125	32.3	194.0	0.1305	0.7525
270	1.806	7.89-4	0.0862	44.9	201.1	0.1781	0.7567
280	2.584	8.08-4	0.0611	57.9	208.3	0.2249	0.7621
290	3.600	8.30-4	0.0443	71.1	215.3	0.2711	0.7683
300	4.888	8.53-4	0.0327	84.6	222.2	0.3161	0.7751
310	6.491	8.80-4	0.0246	98.4	228.9	0.3614	0.7822
320	8.456	9.11-4	0.0186	112.6	235.3	0.4057	0.7893
330	10.83	9.48-4	0.0143	127.1	241.4	0.4497	0.7960
340	13.67	9.93-4	0.0111	142.1	246.9	0.4937	0.8018
350	17.04	0.00105	0.0084	157.2	251.5	0.5382	0.8060
360	21.02	0.00113	0.0063	174.7	254.8	0.5844	0.8071
370	25.71	0.00125	0.0045	193.6	255.2	0.6349	0.8013
375	28.46	0.00137	0.0036	205.2	252.5	0.6649	0.7953
380.1 ^c	31.37	0.00204	0.0020	231.8	231.8	0.7341	0.7341

*Values converted from tables of Shank, *Thermodynamic Properties of UCON 245 Refrigerant*, Union Carbide Corporation, New York, 1966. See also Shank, *J. Chem. Eng. Data*, **12**, 474-480 (1967). c = critical point. The notation 6.46-4 signifies 6.46×10^{-4} .

TABLE 2-287 Refrigerant RC 318, Octafluorocyclobutane*

T, K	P, bar	v_f , m ³ /kg	v_g , m ³ /kg	h_f , kJ/kg	h_g , kJ/kg	s_f , kJ/(kg·K)	s_g , kJ/(kg·K)	c_{pfs} , kJ/(kg·K)	μ_f , 10 ⁻⁴ Pa·s	k_f , W/(m·K)
200	0.0216	5.507-4	3.810	353.5	498.0	3.909	4.560			
210	0.0449	5.593-4	1.931	361.0	500.1	3.947	4.564			
220	0.0875	5.683-4	1.038	369.2	502.2	3.984	4.569			
230	0.1608	5.778-4	0.588	377.6	504.4	4.022	4.574	0.98	11.7	0.088
240	0.2810	5.879-4	0.349	386.4	510.9	4.060	4.578	1.00	9.55	0.085
250	0.466	5.988-4	0.2166	395.6	517.4	4.097	4.584	1.02	7.90	0.082
260	0.741	6.106-4	0.1401	405.2	524.0	4.133	4.592	1.03	6.63	0.078
270	1.133	6.234-4	0.0938	415.1	530.7	4.172	4.599	1.05	5.64	0.075
280	1.672	6.375-4	0.0647	425.8	537.3	4.210	4.609	1.07	4.85	0.071
290	2.392	6.529-4	0.0458	436.2	543.9	4.247	4.618	1.09	4.22	0.068
300	3.325	6.694-4	0.0332	447.3	550.4	4.284	4.626	1.12	3.70	0.065
310	4.522	6.893-4	0.0245	458.7	556.9	4.322	4.638	1.15	3.20	0.061
320	6.007	7.115-4	0.0184	470.5	563.3	4.359	4.648	1.18	2.94	0.058
330	7.826	7.365-4	0.0139	482.7	569.4	4.396	4.659	1.23	2.66	0.054
340	10.018	7.666-4	0.0106	495.2	575.4	4.433	4.669	1.27	2.33	0.051
350	12.632	8.034-4	0.0082	508.1	581.0	4.469	4.678	1.32	2.00	0.048
360	15.71	8.508-4	0.0062	521.5	585.8	4.507	4.685	1.39		
370	19.33	9.172-4	0.0047	535.6	589.9	4.544	4.691			
380	23.59	1.031-3	0.0033	551.4	591.5	4.585	4.691			
388.5 ^c	27.83	1.613-3	0.0016	577.2	577.2	4.651	4.651			

*Values of P , v , h , and s interpolated, extrapolated, and converted from tables of Oguchi, *Reito*, **52** (1977): 869-889. Values of c_p , μ , and k interpolated and converted from tables in *Thermophysical Properties of Refrigerants*, American Society of Heating, Refrigerating and Air-Conditioning Engineers, New York, 1976. c = critical point. Saturation and superheat tables and a diagram to 80 bar, 580 K are given by Reynolds, W. C., *Thermodynamic Properties in S.I.*, Stanford Univ. publ., 1979 (173 pp.). For equations, see Cipollone, R., *ASHRAE Trans.*, **97**, 2 (1991): 262-267.

TABLE 2-288 Thermodynamic Properties of R-404A

Temperature K	Pressure MPa	Density mol/dm ³	Volume dm ³ /mol	Int. energy kJ/mol	Enthalpy kJ/mol	Entropy kJ/(mol·K)	C _v kJ/(mol·K)	C _p kJ/(mol·K)	Sound speed m/s	Joule-Thomson K/MPa
Saturated Properties										
200.00	0.022649	14.209	0.070377	10.353	10.355	0.058867	0.076939	0.11881	859.89	-0.34161
205.00	0.030989	14.059	0.071131	10.948	10.950	0.061803	0.077522	0.11915	831.56	-0.33384
210.00	0.041658	13.907	0.071905	11.544	11.547	0.064678	0.078116	0.11965	804.42	-0.32460
215.00	0.055101	13.755	0.072703	12.144	12.148	0.067498	0.078719	0.12028	778.20	-0.31394
220.00	0.071804	13.600	0.073527	12.746	12.751	0.070269	0.079326	0.12103	752.69	-0.30185
225.00	0.092293	13.444	0.074380	13.353	13.359	0.072995	0.079940	0.12188	727.72	-0.28830
230.00	0.11713	13.286	0.075265	13.963	13.972	0.075679	0.080558	0.12282	703.16	-0.27318
235.00	0.14693	13.126	0.076185	14.578	14.590	0.078326	0.081183	0.12386	678.91	-0.25636
240.00	0.18232	12.963	0.077145	15.199	15.213	0.080939	0.081815	0.12499	654.88	-0.23766
245.00	0.22397	12.796	0.078147	15.824	15.842	0.083520	0.082456	0.12621	631.01	-0.21683
250.00	0.27258	12.627	0.079197	16.456	16.478	0.086073	0.083107	0.12754	607.23	-0.19356
255.00	0.32888	12.453	0.080301	17.094	17.120	0.088600	0.083770	0.12899	583.50	-0.16749
260.00	0.39363	12.275	0.081465	17.738	17.770	0.091104	0.084446	0.13057	559.77	-0.13814
265.00	0.46763	12.092	0.082697	18.390	18.429	0.093589	0.085137	0.13229	535.99	-0.10493
270.00	0.55168	11.904	0.084006	19.049	19.096	0.096056	0.085846	0.13419	512.13	-0.067104
275.00	0.64664	11.709	0.085402	19.717	19.772	0.098510	0.086574	0.13630	488.15	-0.023728
280.00	0.75338	11.508	0.086899	20.394	20.460	0.10095	0.087326	0.13866	464.02	0.026418
285.00	0.87280	11.298	0.088513	21.081	21.159	0.10339	0.088104	0.14133	439.69	0.084928
290.00	1.0059	11.078	0.090266	21.780	21.870	0.10583	0.088914	0.14438	415.13	0.15392
295.00	1.1536	10.848	0.092182	22.490	22.597	0.10826	0.089761	0.14793	390.28	0.23626
300.00	1.3169	10.605	0.094295	23.215	23.339	0.11071	0.090653	0.15211	365.11	0.33594
305.00	1.4970	10.346	0.096652	23.956	24.101	0.11317	0.091603	0.15715	339.56	0.45865
310.00	1.6950	10.069	0.099314	24.717	24.885	0.11566	0.092625	0.16339	313.56	0.61280
315.00	1.9122	9.7686	0.10237	25.500	25.695	0.11818	0.093744	0.17139	287.00	0.81141
320.00	2.1499	9.4384	0.10595	26.310	26.538	0.12075	0.094998	0.18212	259.73	1.0757
325.00	2.4096	9.0688	0.11027	27.157	27.423	0.12341	0.096455	0.19751	231.53	1.4433
330.00	2.6932	8.6431	0.11570	28.054	28.365	0.12619	0.098241	0.22197	201.95	1.9881
335.00	3.0027	8.1285	0.12302	29.026	29.396	0.12918	0.10064	0.26871	170.20	2.8807
340.00	3.3414	7.4362	0.13448	30.147	30.597	0.13261	0.10445	0.40392	134.59	4.6353
345.00	3.7150	5.7429	0.17413	32.108	32.755	0.13874	0.11650	8.2559	89.976	10.564
345.27	3.7348	4.9400	0.20243	32.875	33.631	0.14126			0	12.409
200.00	0.021264	0.013010	76.866	29.920	31.555	0.16521	0.058696	0.068032	138.13	88.073
205.00	0.029285	0.017550	56.979	30.185	31.853	0.16408	0.059968	0.069509	139.28	77.215
210.00	0.039592	0.023271	42.971	30.451	32.152	0.16307	0.061245	0.071021	140.34	68.305
215.00	0.052629	0.030378	32.919	30.718	32.451	0.16217	0.062526	0.072573	141.29	60.948
220.00	0.068883	0.039095	25.579	30.987	32.749	0.16138	0.063815	0.074172	142.12	54.835
225.00	0.088879	0.049667	20.134	31.256	33.046	0.16068	0.065113	0.075826	142.84	49.721
230.00	0.11318	0.062359	16.036	31.525	33.340	0.16006	0.066424	0.077546	143.43	45.413
235.00	0.14240	0.077463	12.909	31.795	33.633	0.15952	0.067750	0.079344	143.88	41.761
240.00	0.17718	0.095292	10.494	32.063	33.922	0.15903	0.069095	0.081232	144.18	38.642
245.00	0.21817	0.11619	8.6063	32.330	34.208	0.15861	0.070463	0.083226	144.33	35.962
250.00	0.26610	0.14055	7.1149	32.596	34.489	0.15823	0.071855	0.085343	144.32	33.645
255.00	0.32169	0.16879	5.9247	32.859	34.765	0.15789	0.073276	0.087604	144.14	31.630
260.00	0.38571	0.20137	4.9659	33.119	35.034	0.15759	0.074728	0.090033	143.77	29.871
265.00	0.45896	0.23885	4.1867	33.375	35.296	0.15732	0.076214	0.092660	143.22	28.327
270.00	0.54225	0.28183	3.5483	33.626	35.550	0.15707	0.077737	0.095524	142.46	26.970
275.00	0.63645	0.33102	3.0210	33.872	35.794	0.15684	0.079300	0.098671	141.49	25.773
280.00	0.74245	0.38725	2.5823	34.111	36.028	0.15661	0.080909	0.10217	140.29	24.718
285.00	0.86115	0.45152	2.2148	34.342	36.249	0.15639	0.082567	0.10609	138.85	23.789
290.00	0.99353	0.52501	1.9047	34.563	36.455	0.15616	0.084282	0.11056	137.16	22.972
295.00	1.1406	0.60922	1.6414	34.773	36.645	0.15592	0.086062	0.11574	135.19	22.256
300.00	1.3034	0.70599	1.4165	34.968	36.814	0.15566	0.087917	0.12186	132.92	21.633
305.00	1.4830	0.81772	1.2229	35.147	36.960	0.15536	0.089863	0.12929	130.34	21.094

TABLE 2-288 Thermodynamic Properties of R-404A (Concluded)

Temperature K	Pressure MPa	Density mol/dm ³	Volume dm ³ /mol	Int. energy kJ/mol	Enthalpy kJ/mol	Entropy kJ/(mol·K)	C _v kJ/(mol·K)	C _p kJ/(mol·K)	Sound speed m/s	Joule-Thomson K/MPa
Saturated Properties (Concluded)										
310.00	1.6806	0.94761	1.0553	35.304	37.078	0.15501	0.091922	0.13856	127.41	20.630
315.00	1.8975	1.1001	0.90903	35.435	37.159	0.15459	0.094123	0.15062	124.10	20.234
320.00	2.1351	1.2815	0.78032	35.530	37.196	0.15408	0.096513	0.16713	120.38	19.889
325.00	2.3950	1.5019	0.66583	35.578	37.173	0.15343	0.099162	0.19141	116.21	19.571
330.00	2.6789	1.7781	0.56239	35.558	37.065	0.15257	0.10220	0.23111	111.51	19.233
335.00	2.9893	2.1438	0.46645	35.429	36.824	0.15136	0.10585	0.30867	106.19	18.763
340.00	3.3299	2.6882	0.37199	35.084	36.323	0.14946	0.11074	0.53035	100.03	17.851
345.00	3.7109	4.2113	0.23746	33.615	34.496	0.14379	0.12022	8.6291	90.307	14.130
345.27	3.7348	4.9400	0.20243	32.875	33.631	0.14126			0	12.409
Single-Phase Properties										
226.65	0.10000	13.392	0.074669	13.554	13.561	0.073887	0.080143	0.12218	719.55	-0.28348
227.41	0.10000	0.055492	18.021	31.386	33.188	0.16038	0.065742	0.076645	143.14	47.558
300.00	0.10000	0.040750	24.540	36.596	39.050	0.18269	0.076875	0.085907	166.24	16.998
400.00	0.10000	0.030243	33.066	45.121	48.428	0.20956	0.092844	0.10141	191.81	6.9229
500.00	0.10000	0.024113	41.471	55.103	59.250	0.23365	0.10612	0.11456	213.92	3.7455
289.79	1.0000	11.088	0.090189	21.750	21.840	0.10572	0.088879	0.14425	416.16	0.15078
290.23	1.0000	0.52866	1.8916	34.573	36.464	0.15615	0.084363	0.11078	137.07	22.936
300.00	1.0000	0.49205	2.0323	35.486	37.518	0.15972	0.083854	0.10554	143.42	19.634
400.00	1.0000	0.31957	3.1292	44.644	47.773	0.18922	0.094142	0.10545	183.69	7.1401
500.00	1.0000	0.24648	4.0571	54.804	58.861	0.21391	0.10659	0.11631	210.41	3.7496
300.00	5.0000	10.994	0.090955	22.770	23.225	0.10919	0.089725	0.14193	427.56	0.11428
400.00	5.0000	2.2256	0.44932	41.867	44.113	0.16875	0.10069	0.14547	148.00	7.6582
500.00	5.0000	1.3561	0.73741	53.389	57.076	0.19774	0.10859	0.12579	198.35	3.5826
300.00	10.000	11.371	0.087944	22.323	23.203	0.10763	0.089307	0.13525	489.01	-0.035312
400.00	10.000	6.1241	0.16329	37.557	39.190	0.15323	0.10301	0.18569	184.17	2.8522
500.00	10.000	2.9622	0.33758	51.539	54.915	0.18852	0.11046	0.13925	198.11	2.8527
300.00	25.000	12.107	0.082594	21.419	23.484	0.10432	0.089393	0.12713	614.12	-0.22002
400.00	25.000	9.2730	0.10784	34.286	36.982	0.14304	0.10166	0.14227	381.56	0.20064
500.00	25.000	6.6326	0.15077	47.758	51.527	0.17548	0.11215	0.14633	292.53	0.65319
300.00	50.000	12.867	0.077719	20.472	24.358	0.10057	0.090168	0.12262	753.19	-0.32391
400.00	50.000	10.834	0.092300	32.538	37.153	0.13731	0.10251	0.13302	559.24	-0.19415
500.00	50.000	9.0225	0.11083	45.317	50.859	0.16786	0.11339	0.14051	455.37	-0.070101

The values in these tables were generated from the NIST REFPROP software (Lemmon, E. W., McLinden, M. O., and Huber, M. L., NIST Standard Reference Database 23: Reference Fluid Thermodynamic and Transport Properties—REFPROP, National Institute of Standards and Technology, Standard Reference Data Program, Gaithersburg, Md., 2002, Version 7.1). The primary source for the thermodynamic properties is Lemmon, E. W., "Pseudo Pure-Fluid Equations of State for the Refrigerant Blends R-410A, R-404A, R-507A, and R-407C," *Int. J. Thermophys.* **24**(4):991–1006, 2003. Validated equations for the viscosity and thermal conductivity are not currently available for this fluid.

Properties at the critical point temperature are given in the last entry of the saturation tables. In the single-phase table, when the temperature range for a given isobar includes a vapor-liquid phase boundary, the temperature of phase equilibrium is noted, and properties for both the saturated liquid and saturated vapor are given (with liquid properties given in the upper line). Lines are omitted from the temperature-pressure grid of the single-phase table, when the system would be in the solid phase or if there are potential problems with the source property surface.

The estimated uncertainty of density values calculated with the equation of state is 0.1%. The estimated uncertainty of calculated heat capacities and speed of sound values is 0.5%. Uncertainties of bubble and dew point pressures are 0.5%.

TABLE 2-289 Thermodynamic Properties of R-407C

Temperature K	Pressure MPa	Density mol/dm ³	Volume dm ³ /mol	Int. energy kJ/mol	Enthalpy kJ/mol	Entropy kJ/(mol·K)	C _v kJ/(mol·K)	C _p kJ/(mol·K)	Sound speed m/s	Joule-Thomson K/MPa
Saturated Properties										
200.00	0.019158	17.036	0.058698	8.8272	8.8283	0.050593	0.070988	0.11073	956.60	-0.31996
210.00	0.035795	16.697	0.059892	9.9359	9.9380	0.056002	0.071320	0.11118	903.06	-0.30662
220.00	0.062640	16.352	0.061156	11.051	11.055	0.061189	0.071817	0.11203	851.40	-0.28934
230.00	0.10366	15.999	0.062503	12.175	12.182	0.066188	0.072410	0.11319	801.12	-0.26790
240.00	0.16353	15.637	0.063949	13.312	13.323	0.071026	0.073074	0.11465	751.77	-0.24161
250.00	0.24755	15.264	0.065512	14.464	14.480	0.075728	0.073803	0.11641	703.01	-0.20937
260.00	0.36157	14.877	0.067218	15.632	15.657	0.080314	0.074597	0.11853	654.53	-0.16951
270.00	0.51193	14.472	0.069099	16.822	16.857	0.084805	0.075463	0.12111	606.09	-0.11964
280.00	0.70540	14.045	0.071198	18.035	18.085	0.089223	0.076412	0.12427	557.44	-0.056172
290.00	0.94916	13.591	0.073576	19.278	19.348	0.093590	0.077458	0.12822	508.32	0.026372
300.00	1.2507	13.102	0.076322	20.555	20.651	0.097931	0.078624	0.13331	458.46	0.13683
310.00	1.6182	12.567	0.079573	21.877	22.006	0.10228	0.079950	0.14013	407.51	0.29038
320.00	2.0599	11.969	0.083552	23.255	23.427	0.10668	0.081509	0.14989	354.98	0.51547
330.00	2.5851	11.278	0.088671	24.711	24.940	0.11119	0.083453	0.16541	300.07	0.87274
340.00	3.2038	10.435	0.095832	26.287	26.594	0.11596	0.086157	0.19551	241.20	1.5203
350.00	3.9255	9.2661	0.10792	28.110	28.534	0.12137	0.090943	0.28993	174.57	3.0499
359.35	4.6317	5.2600	0.19011	32.145	33.025	0.13372			0	10.947
200.00	0.011312	0.0068643	145.68	30.051	31.699	0.16726	0.048920	0.057805	149.59	109.12
210.00	0.022624	0.013151	76.041	30.504	32.224	0.16412	0.050967	0.060200	152.36	88.122
220.00	0.041929	0.023450	42.644	30.957	32.745	0.16151	0.053143	0.062854	154.78	72.006
230.00	0.072846	0.039384	25.391	31.409	33.259	0.15933	0.055439	0.065784	156.79	59.560
240.00	0.11979	0.062913	15.895	31.857	33.761	0.15749	0.057839	0.069010	158.33	49.904
250.00	0.18793	0.096374	10.376	32.298	34.248	0.15593	0.060328	0.072563	159.36	42.378
260.00	0.28317	0.14256	7.0147	32.728	34.715	0.15460	0.062897	0.076500	159.80	36.483
270.00	0.41203	0.20484	4.8820	33.145	35.157	0.15343	0.065542	0.080917	159.60	31.840
280.00	0.58173	0.28739	3.4796	33.544	35.568	0.15240	0.068266	0.085971	158.69	28.163
290.00	0.80008	0.39560	2.5278	33.918	35.940	0.15144	0.071085	0.091920	156.99	25.236
300.00	1.0757	0.53670	1.8632	34.259	36.263	0.15051	0.074027	0.099203	154.41	22.898
310.00	1.4179	0.72101	1.3869	34.556	36.523	0.14956	0.077140	0.10861	150.83	21.024
320.00	1.8375	0.96439	1.0369	34.790	36.696	0.14852	0.080507	0.12170	146.11	19.516
330.00	2.3470	1.2939	0.77283	34.931	36.745	0.14727	0.084283	0.14208	140.03	18.284
340.00	2.9627	1.7642	0.56682	34.916	36.595	0.14560	0.088801	0.18030	132.24	17.206
350.00	3.7100	2.5260	0.39588	34.578	36.047	0.14299	0.095065	0.28700	122.09	15.951
359.35	4.6317	5.2600	0.19011	32.145	33.025	0.13372			0	10.947

TABLE 2-289 Thermodynamic Properties of R-407C (Concluded)

Temperature K	Pressure MPa	Density mol/dm ³	Volume dm ³ /mol	Int. energy kJ/mol	Enthalpy kJ/mol	Entropy kJ/(mol·K)	C_v kJ/(mol·K)	C_p kJ/(mol·K)	Sound speed m/s	Joule-Thomson K/MPa
Single-Phase Properties										
200.00	0.10000	17.038	0.058692	8.8253	8.8312	0.050583	0.070990	0.11072	956.99	-0.32010
229.25	0.10000	16.026	0.062399	12.091	12.097	0.065819	0.072363	0.11310	804.85	-0.26966
236.25	0.10000	0.053062	18.846	31.690	33.574	0.15814	0.056928	0.067764	157.81	53.242
300.00	0.10000	0.040722	24.557	35.535	37.991	0.17467	0.063341	0.072378	179.00	20.041
400.00	0.10000	0.030231	33.079	42.554	45.862	0.19722	0.076588	0.085147	205.99	7.7925
500.00	0.10000	0.024109	41.479	50.849	54.997	0.21756	0.088895	0.097330	229.27	4.0471
291.84	1.0000	13.504	0.074050	19.510	19.584	0.094388	0.077662	0.12906	499.23	0.044233
297.47	1.0000	0.49738	2.0105	34.177	36.187	0.15075	0.073268	0.097199	155.15	23.442
300.00	1.0000	0.48865	2.0465	34.384	36.431	0.15156	0.072744	0.095419	156.77	22.566
400.00	1.0000	0.31821	3.1425	42.101	45.244	0.17694	0.078067	0.089213	198.26	7.9701
500.00	1.0000	0.24608	4.0637	50.576	54.639	0.19786	0.089416	0.099001	225.88	4.0390
300.00	5.0000	13.412	0.074559	20.240	20.613	0.096862	0.078093	0.12762	507.10	0.027202
400.00	5.0000	2.1880	0.45703	39.458	41.743	0.15675	0.086188	0.12964	161.10	8.5257
500.00	5.0000	1.3504	0.74050	49.289	52.992	0.18193	0.091753	0.10811	213.00	3.9036
300.00	10.000	13.740	0.072780	19.898	20.626	0.095679	0.077756	0.12301	558.94	-0.063246
400.00	10.000	7.1029	0.14079	34.426	35.834	0.13888	0.090433	0.20031	184.71	3.3408
500.00	10.000	2.9957	0.33381	47.547	50.885	0.17282	0.094263	0.12254	207.67	3.3327
300.00	25.000	14.443	0.069238	19.146	20.877	0.092972	0.077634	0.11624	672.43	-0.19834
400.00	25.000	10.899	0.091752	30.990	33.284	0.12855	0.087056	0.13223	399.92	0.28513
500.00	25.000	7.3363	0.13631	43.479	46.886	0.15889	0.096319	0.13592	289.22	0.97116
300.00	50.000	15.220	0.065703	18.302	21.587	0.089730	0.078160	0.11176	802.78	-0.28843
400.00	50.000	12.648	0.079064	29.255	33.209	0.12310	0.087179	0.12077	579.57	-0.12975
500.00	50.000	10.260	0.097468	40.787	45.660	0.15086	0.096753	0.12761	457.54	0.047330

The values in these tables were generated from the NIST REFPROP software (Lemmon, E. W., McLinden, M. O., and Huber, M. L., NIST Standard Reference Database 23: Reference Fluid Thermodynamic and Transport Properties—REFPROP, National Institute of Standards and Technology, Standard Reference Data Program, Gaithersburg, Md., 2002, Version 7.1). The primary source for the thermodynamic properties is Lemmon, E. W., "Pseudo Pure-Fluid Equations of State for the Refrigerant Blends R-410A, R-404A, R-507A, and R-407C," *Int. J. Thermophys.* **24**(4):991–1006, 2003. Validated equations for the viscosity and thermal conductivity are not currently available for this fluid.

Properties at the critical point temperature are given in the last entry of the saturation tables. In the single-phase table, when the temperature range for a given isobar includes a vapor-liquid phase boundary, the temperature of phase equilibrium is noted, and properties for both the saturated liquid and saturated vapor are given (with liquid properties given in the upper line). Lines are omitted from the temperature-pressure grid of the single-phase table, when the system would be in the solid phase or if there are potential problems with the source property surface.

The estimated uncertainty of density values calculated with the equation of state is 0.1%. The estimated uncertainty of calculated heat capacities and speed of sound values is 0.5%. Uncertainties of bubble and dew point pressures are 0.5%.

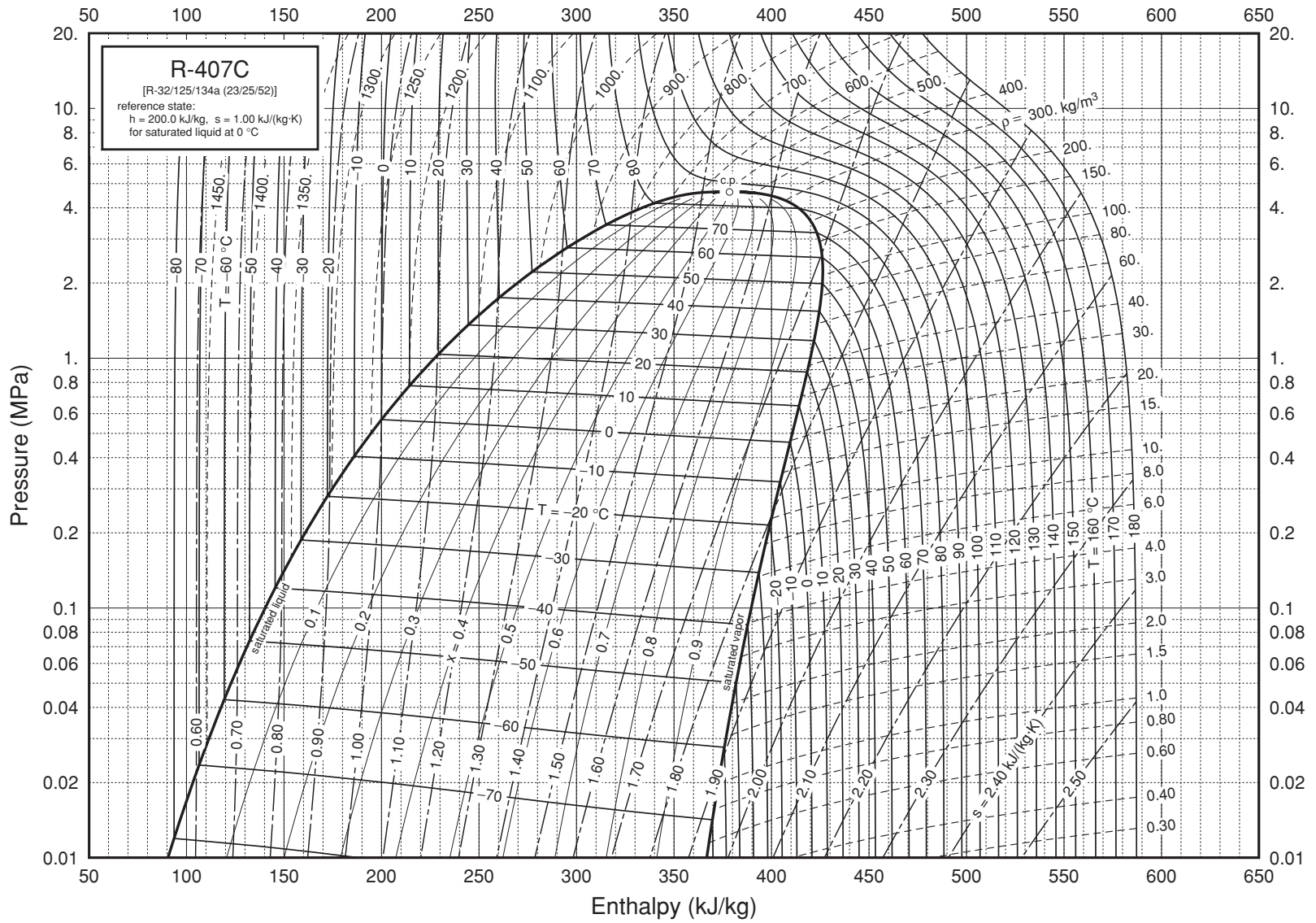


FIG. 2-27 Pressure-enthalpy diagram for Refrigerant 407C. Properties computed with the NIST REFPROP Database, Version 7.0 (Lemmon, E. W., McLinden, M. O., and Huber, M. L., 2002, NIST Standard Reference Database 23, NIST Reference Fluid Thermodynamic and Transport Properties—REFPROP, Version 7.0, Standard Reference Data Program, National Institute of Standards and Technology), based on the mixture model of Lemmon, E. W., and Jacobsen, R. T., "Equations of State for Mixtures of R-32, R-125, R-134a, R-143a, and R-152a," *J. Phys. Chem. Ref. Data* 33:593-620, 2004.

TABLE 2-290 Thermodynamic Properties of R-410A

Temperature K	Pressure MPa	Density mol/dm ³	Volume dm ³ /mol	Int. energy kJ/mol	Enthalpy kJ/mol	Entropy kJ/(mol·K)	C _v kJ/(mol·K)	C _p kJ/(mol·K)	Sound speed m/s	Joule-Thomson K/MPa
Saturated Properties										
200.00	0.029160	19.510	0.051256	7.0380	7.0395	0.040995	0.062260	0.097942	929.01	-0.30179
210.00	0.053727	19.093	0.052375	8.0188	8.0217	0.045781	0.062050	0.098396	879.84	-0.28524
215.00	0.071143	18.881	0.052962	8.5112	8.5149	0.048098	0.062014	0.098729	855.20	-0.27544
220.00	0.092819	18.667	0.053571	9.0052	9.0101	0.050370	0.062020	0.099138	830.52	-0.26446
225.00	0.11946	18.449	0.054202	9.5012	9.5077	0.052600	0.062066	0.099628	805.81	-0.25217
230.00	0.15182	18.229	0.054858	9.9997	10.008	0.054791	0.062151	0.10020	781.06	-0.23841
235.00	0.19070	18.005	0.055542	10.501	10.512	0.056948	0.062271	0.10088	756.26	-0.22300
240.00	0.23697	17.776	0.056255	11.006	11.019	0.059073	0.062426	0.10165	731.41	-0.20574
245.00	0.29152	17.543	0.057002	11.514	11.530	0.061169	0.062615	0.10253	706.48	-0.18637
250.00	0.35531	17.305	0.057786	12.026	12.047	0.063240	0.062837	0.10353	681.45	-0.16459
255.00	0.42933	17.062	0.058611	12.543	12.568	0.065289	0.063092	0.10466	656.31	-0.14006
260.00	0.51461	16.812	0.059482	13.065	13.096	0.067318	0.063380	0.10594	631.02	-0.11232
265.00	0.61223	16.555	0.060406	13.593	13.630	0.069331	0.063701	0.10738	605.55	-0.080861
270.00	0.72330	16.290	0.061388	14.127	14.172	0.071331	0.064057	0.10902	579.88	-0.045000
275.00	0.84899	16.016	0.062439	14.669	14.722	0.073321	0.064451	0.11088	553.95	-0.0039006
280.00	0.99048	15.732	0.063567	15.218	15.281	0.075304	0.064884	0.11300	527.72	0.043515
285.00	1.1490	15.436	0.064785	15.776	15.851	0.077284	0.065363	0.11543	501.14	0.098651
290.00	1.3260	15.127	0.066109	16.344	16.432	0.079266	0.065893	0.11825	474.14	0.16337
295.00	1.5226	14.802	0.067559	16.924	17.026	0.081254	0.066483	0.12156	446.66	0.24022
300.00	1.7404	14.459	0.069160	17.516	17.636	0.083253	0.067147	0.12550	418.60	0.33275
305.00	1.9809	14.095	0.070948	18.123	18.263	0.085270	0.067901	0.13029	389.87	0.44607
310.00	2.2456	13.704	0.072969	18.747	18.911	0.087314	0.068773	0.13630	360.33	0.58788
315.00	2.5364	13.282	0.075293	19.392	19.583	0.089398	0.069800	0.14413	329.82	0.77028
320.00	2.8550	12.816	0.078025	20.064	20.287	0.091537	0.071046	0.15493	298.10	1.0135
325.00	3.2037	12.294	0.081343	20.772	21.032	0.093762	0.072616	0.17109	264.83	1.3544
330.00	3.5848	11.685	0.085578	21.531	21.837	0.096123	0.074717	0.19853	229.46	1.8665
335.00	4.0009	10.930	0.091491	22.376	22.742	0.098732	0.077843	0.25685	190.98	2.7232
340.00	4.4556	9.8413	0.10161	23.414	23.867	0.10194	0.083650	0.46832	147.49	4.4554
344.49	4.9012	6.3240	0.15813	25.988	26.763	0.11022			0	9.7623
200.00	0.029010	0.017797	56.190	26.495	28.125	0.14644	0.042482	0.052236	164.41	113.67
210.00	0.053489	0.031567	31.678	26.835	28.530	0.14345	0.044604	0.055055	167.03	90.100
215.00	0.070844	0.041089	24.338	27.002	28.726	0.14212	0.045719	0.056590	168.16	80.508
220.00	0.092447	0.052763	18.953	27.167	28.919	0.14087	0.046862	0.058205	169.16	72.155
225.00	0.11900	0.066925	14.942	27.329	29.107	0.13972	0.048026	0.059899	170.03	64.889
230.00	0.15125	0.083936	11.914	27.488	29.290	0.13864	0.049206	0.061674	170.75	58.571
235.00	0.19000	0.10420	9.5972	27.645	29.468	0.13762	0.050400	0.063533	171.32	53.077
240.00	0.23611	0.12814	7.8039	27.798	29.640	0.13667	0.051603	0.065483	171.73	48.299
245.00	0.29049	0.15625	6.4000	27.947	29.806	0.13577	0.052814	0.067535	171.97	44.137
250.00	0.35407	0.18905	5.2895	28.092	29.965	0.13492	0.054033	0.069705	172.04	40.508
255.00	0.42786	0.22714	4.4026	28.232	30.116	0.13411	0.055260	0.072011	171.93	37.336
260.00	0.51287	0.27117	3.6877	28.367	30.258	0.13333	0.056497	0.074481	171.62	34.560
265.00	0.61019	0.32190	3.1066	28.496	30.392	0.13259	0.057747	0.077148	171.11	32.123
270.00	0.72092	0.38018	2.6303	28.619	30.515	0.13187	0.059014	0.080057	170.39	29.979
275.00	0.84622	0.44702	2.2371	28.733	30.626	0.13116	0.060302	0.083265	169.45	28.087
280.00	0.98729	0.52357	1.9100	28.839	30.725	0.13047	0.061618	0.086846	168.27	26.412
285.00	1.1454	0.61123	1.6360	28.935	30.809	0.12978	0.062969	0.090901	166.84	24.924
290.00	1.3218	0.71170	1.4051	29.019	30.876	0.12908	0.064364	0.095568	165.16	23.598
295.00	1.5179	0.82707	1.2091	29.090	30.925	0.12837	0.065814	0.10104	163.20	22.410
300.00	1.7351	0.95997	1.0417	29.144	30.951	0.12764	0.067335	0.10760	160.94	21.338

305.00	1.9749	1.1138	0.89779	29.178	30.951	0.12688	0.068945	0.11566	158.36	20.365
310.00	2.2390	1.2933	0.77322	29.189	30.920	0.12606	0.070671	0.12589	155.44	19.470
315.00	2.5291	1.5048	0.66456	29.170	30.850	0.12517	0.072551	0.13943	152.13	18.632
320.00	2.8472	1.7576	0.56894	29.112	30.732	0.12418	0.074643	0.15831	148.40	17.826
325.00	3.1955	2.0668	0.48384	29.002	30.548	0.12305	0.077041	0.18670	144.16	17.018
330.00	3.5766	2.4582	0.40681	28.817	30.272	0.12169	0.079915	0.23464	139.30	16.153
335.00	3.9935	2.9848	0.33503	28.510	29.848	0.11995	0.083629	0.33370	133.59	15.123
340.00	4.4504	3.7974	0.26334	27.951	29.123	0.11740	0.089197	0.65947	126.39	13.641
344.49	4.9012	6.3240	0.15813	25.988	26.763	0.11022			0	9.7623

Single-Phase Properties

221.45	0.10000	18.604	0.053751	9.1488	9.1541	0.051020	0.062030	0.099271	823.36	-0.26104
221.53	0.10000	0.056810	17.603	27.217	28.977	0.14051	0.047215	0.058714	169.44	69.827
300.00	0.10000	0.040605	24.628	31.028	33.491	0.15794	0.050980	0.059877	198.35	19.643
400.00	0.10000	0.030202	33.111	36.670	39.981	0.17654	0.061554	0.070067	227.37	7.7467
500.00	0.10000	0.024099	41.495	43.331	47.480	0.19323	0.071249	0.079663	252.59	4.0758
280.32	1.0000	15.713	0.063641	15.253	15.317	0.075429	0.064913	0.11314	526.05	0.046760
280.42	1.0000	0.53054	1.8849	28.848	30.733	0.13041	0.061731	0.087169	168.16	26.279
300.00	1.0000	0.46599	2.1460	30.151	32.297	0.13580	0.057548	0.075210	180.65	20.254
400.00	1.0000	0.31478	3.1769	36.304	39.481	0.15648	0.062713	0.073258	220.92	7.7768
500.00	1.0000	0.24505	4.0808	43.106	47.187	0.17364	0.071665	0.081012	249.79	4.0343
300.00	5.0000	14.870	0.067248	17.202	17.539	0.082188	0.066139	0.11773	472.56	0.17344
400.00	5.0000	1.9755	0.50621	34.349	36.880	0.13813	0.068570	0.097588	192.34	7.6786
500.00	5.0000	1.3185	0.75845	42.072	45.864	0.15821	0.073521	0.087959	239.51	3.7957
300.00	10.000	15.342	0.065180	16.830	17.482	0.080897	0.065435	0.11125	533.86	0.036775
400.00	10.000	5.7949	0.17257	30.845	32.570	0.12363	0.074099	0.16518	182.45	5.0121
500.00	10.000	2.8642	0.34914	40.710	44.202	0.14982	0.075667	0.098492	233.93	3.3106
300.00	25.000	16.289	0.061392	16.058	17.592	0.078110	0.065000	0.10273	658.09	-0.14678
400.00	25.000	11.685	0.085582	26.530	28.670	0.10987	0.072157	0.11830	379.59	0.50709
500.00	25.000	7.4115	0.13493	37.197	40.570	0.13644	0.078574	0.11515	291.31	1.2724
300.00	50.000	17.287	0.057845	15.231	18.123	0.074923	0.065499	0.097459	792.80	-0.26163
400.00	50.000	14.049	0.071182	24.722	28.281	0.10409	0.072480	0.10533	566.13	-0.063564
500.00	50.000	11.128	0.089864	34.526	39.019	0.12804	0.079657	0.10880	449.76	0.13566

The values in these tables were generated from the NIST REFPROP software (Lemmon, E. W., McLinden, M. O., and Huber, M. L., NIST Standard Reference Database 23: Reference Fluid Thermodynamic and Transport Properties—REFPROP, National Institute of Standards and Technology, Standard Reference Data Program, Gaithersburg, Md., 2002, Version 7.1). The primary source for the thermodynamic properties is Lemmon, E. W., "Pseudo Pure-Fluid Equations of State for the Refrigerant Blends R-410A, R-404A, R-507A, and R-407C," *Int. J. Thermophys.* **24**(4):991–1006, 2003. Validated equations for the viscosity and thermal conductivity are not currently available for this fluid.

Properties at the critical point temperature are given in the last entry of the saturation tables. In the single-phase table, when the temperature range for a given isobar includes a vapor-liquid phase boundary, the temperature of phase equilibrium is noted, and properties for both the saturated liquid and saturated vapor are given (with liquid properties given in the upper line). Lines are omitted from the temperature-pressure grid of the single-phase table, when the system would be in the solid phase or if there are potential problems with the source property surface.

The estimated uncertainty of density values calculated with the equation of state is 0.1%. The estimated uncertainty of calculated heat capacities and speed of sound values is 0.5%. Uncertainties of bubble and dew point pressures are 0.5%.

TABLE 2-291 Saturated Refrigerant 500*

T, K	P, bar	$v_f, m^3/kg$	$v_g, m^3/kg$	$h_f, kJ/kg$	$h_g, kJ/kg$	$s_f, kJ/(kg \cdot K)$	$s_g, kJ/(kg \cdot K)$	$c_{pf}, kJ/(kg \cdot K)$	$\mu_f, 10^{-4} Pa \cdot s$	$k_f, W/(m \cdot K)$
200	0.1219	6.966-4	1.360	-29.56	185.87	-0.1363	0.9408	1.044	6.11	0.113
210	0.2258	7.090-4	0.766	-21.03	191.25	-0.0948	0.9161	1.018	5.15	0.109
220	0.3936	7.222-4	0.457	-12.17	196.63	-0.0536	0.8955	0.997	4.42	0.106
230	0.6511	7.361-4	0.286	-2.97	201.96	-0.0130	0.8782	0.987	3.85	0.102
240	1.0291	7.509-4	0.187	6.58	207.23	0.0277	0.8638	0.987	3.42	0.098
250	1.5632	7.668-4	0.1261	16.50	212.40	0.0680	0.8517	0.997	3.04	0.094
260	2.2932	7.839-4	0.0879	26.78	217.45	0.1082	0.8415	1.017	2.74	0.090
270	3.2624	8.024-4	0.0628	37.44	222.35	0.1481	0.8329	1.048	2.48	0.086
280	4.5172	8.226-4	0.0459	48.48	227.06	0.1878	0.8257	1.089	2.26	0.082
290	6.1064	8.450-4	0.0342	59.91	231.56	0.2275	0.8194	1.140	2.08	0.078
300	8.0809	8.699-4	0.0259	71.76	235.79	0.2671	0.8139	1.201	1.92	0.074
310	10.49	8.981-4	0.0198	84.05	239.69	0.3067	0.8088	1.273	1.77	0.070
320	13.40	9.306-4	0.0154	96.83	243.19	0.3464	0.8038	1.355	1.63	0.066
330	16.86	9.690-4	0.0119	110.17	246.14	0.3864	0.7985	1.447	1.48	0.062
340	20.93	1.016-3	0.0093	124.20	248.36	0.4271	0.7922	1.550	1.34	0.058
350	25.70	1.077-3	0.0072	139.18	249.47	0.4689	0.7841	1.663		
360	31.25	1.162-3	0.0055	155.66	248.71	0.5135	0.7721	1.919		
370	37.72	1.307-3	0.0040	175.59	244.26	0.5650	0.7509	2.07		
378.6 ^c	44.26	2.012-3	0.0020	219.50	219.50	0.6729	0.6729	∞		

*Values reproduced and converted from Table 12, p. 17.99, ASHRAE Handbook, 1981: Fundamentals, American Society of Heating, Refrigerating and Air-Conditioning Engineers, Atlanta, 1981. Copyright material. Reproduced by permission of the copyright owner. c = critical point. The notation 6.966-4 signifies 6.966×10^{-4} .

The 1993 ASHRAE Handbook—Fundamentals (SI ed.) gives material for integral degrees Celsius with temperatures on the IPTS 68 scale from -70 to 105.60 °C. The thermodynamic diagram from 0.1 to 70 bar extends to 240 °C. Equations and constants approximated to the 1985 ASHRAE tables were given by Meczaryk, K. and M. Masaryk, Heat Recovery Systems and CHP, 11, 2/3 (1991): 193-197. Saturation and superheat tables and a diagram to 80 bar, 560 K are given by Reynolds, W. C., Thermodynamic Properties in S.I., Stanford Univ. publ., 1979 (173 pp.). Tables and a chart to 1000 psia, 480 °F are given by Stewart, R. B., R. T. Jacobsen, et al., Thermodynamic Properties of Refrigerants, ASHRAE, Atlanta, GA, 1986 (521 pp.). Specific heat and viscosity appear in Thermophysical Properties of Refrigerants, ASHRAE, 1993.

TABLE 2-292 Saturated Refrigerant 500*

T, K	P, bar	$v_f, m^3/kg$	$v_g, m^3/kg$	$h_f, kJ/kg$	$h_g, kJ/kg$	$s_f, kJ/(kg \cdot K)$	$s_g, kJ/(kg \cdot K)$	$c_{pf}, kJ/(kg \cdot K)$	$\mu_f, 10^{-4} Pa \cdot s$	$k_f, W/(m \cdot K)$
200	0.2274	6.381-4	0.646	-29.04	153.34	-0.1337	0.7782	1.018	5.72	0.103
210	0.4098	6.507-4	0.374	-20.83	158.42	-0.0937	0.7599	1.036	4.88	0.099
220	0.6965	6.640-4	0.228	-12.15	163.49	-0.0534	0.7449	1.055	4.23	0.095
230	1.1251	6.783-4	0.146	-2.99	168.50	-0.0128	0.7328	1.075	3.71	0.091
240	1.7392	6.938-4	0.0969	6.66	173.42	0.0280	0.7228	1.097	3.28	0.087
250	2.5867	7.105-4	0.0665	16.78	178.20	0.0691	0.7148	1.120	2.94	0.083
260	3.7188	7.289-4	0.0470	27.36	182.81	0.1102	0.7082	1.144	2.65	0.079
270	5.1893	7.492-4	0.0340	38.36	187.21	0.1514	0.7027	1.170	2.41	0.075
280	7.0530	7.720-4	0.0251	49.77	191.35	0.1923	0.6980	1.197	2.18	0.072
290	9.3660	7.979-4	0.0188	61.55	195.16	0.2330	0.6937	1.225	1.99	0.068
300	12.19	8.280-4	0.0143	73.68	198.56	0.2734	0.6896	1.254	1.79	0.064
310	15.57	8.637-4	0.0109	86.17	201.43	0.3134	0.6852	1.285	1.59	0.060
320	19.60	9.081-4	0.0084	99.06	203.57	0.3532	0.6798	1.317	1.40	0.056
330	24.35	9.666-4	0.0064	112.53	204.62	0.3933	0.6723	1.351	1.23	0.052
340	29.95	1.053-3	0.0048	127.13	203.71	0.4351	0.6604	1.386	1.07	0.048
350	36.62	1.220-3	0.0033	145.44	197.82	0.4859	0.6355	1.422	0.93	0.044
355.3 ^c	40.75	1.786-3	0.0018	174.00	174.00	0.5634	0.5634			

*Values reproduced and converted from Table 13, p. 17.101, ASHRAE Handbook, 1981: Fundamentals, American Society of Heating, Refrigerating and Air-Conditioning Engineers, Atlanta, 1981. Copyright material. Reproduced by permission of the copyright owner. c = critical point. The notation 6.381-4 signifies 6.381×10^{-4} .

The 1993 ASHRAE Handbook—Fundamentals (SI ed.) gives material for integral degrees Celsius with temperatures on the IPTS 68 scale from -70 to 82.2 °C. The thermodynamic diagram from 0.1 to 80 bar extends to 180 °C. Equations and constants approximated to 1985 ASHRAE tables are given by Meczaryk, K., and M. Masaryk, Heat Recovery Systems and CHP, 11, 2/3 (1991): 193-197. Saturation and superheat tables and a diagram to 20 bar, 515 K are given by Reynolds, W. C., Thermodynamic Properties in S.I., Stanford Univ. publ., 1979 (173 pp.). Tables and a chart to 1000 psia, 400 °F appear in Stewart, R. B., R. T. Jacobsen, et al., Thermodynamic Properties of Refrigerants, ASHRAE, Atlanta, GA, 1986 (521 pp.). For specific heat and viscosity, see Thermophysical Properties of Refrigerants, ASHRAE, 1993.

TABLE 2-293 Saturated Refrigerant 503*

T, K	P, bar	v_f , m ³ /kg	v_g , m ³ /kg	h_f , kJ/kg	h_g , kJ/kg	s_f , kJ/(kg·K)	s_g , kJ/(kg·K)	c_{pf} , kJ/(kg·K)	μ_f , 10 ⁻⁴ Pa·s	k_f , W/(m·K)
150	0.0750	6.384-4	1.894	-89.60	111.02	-0.4694	0.8681	0.482	6.12	0.128
160	0.1798	6.478-4	0.837	-79.73	115.40	-0.4057	0.8139	0.554	5.05	0.123
170	0.3828	6.585-4	0.414	-69.55	119.70	-0.3441	0.7691	0.620	4.16	0.116
180	0.7395	6.700-4	0.224	-59.08	123.84	-0.2844	0.7318	0.682	3.43	0.111
190	1.3187	6.850-4	0.130	-48.36	127.77	-0.2267	0.7003	0.747	2.94	0.105
200	2.1999	7.014-4	0.0803	-37.45	131.45	-0.1710	0.6735	0.817	2.56	0.099
210	3.4713	7.204-4	0.0520	-26.36	134.84	-0.1173	0.6503	0.896	2.25	0.094
220	5.2281	7.426-4	0.0350	-15.10	137.87	-0.0656	0.6298	0.988	1.98	0.088
230	7.5713	7.687-4	0.0242	-3.65	140.49	-0.0155	0.6112	1.017	1.73	0.082
240	10.61	8.001-4	0.0172	8.07	142.58	0.0334	0.5939	1.227	1.52	0.076
250	14.46	8.386-4	0.0124	20.22	143.98	0.0817	0.5767	1.382	1.33	0.070
260	19.25	8.874-4	0.0090	33.10	144.38	0.1305	0.5585	1.57	1.17	0.065
270	25.13	9.526-4	0.0064	47.22	143.23	0.1816	0.5373	1.79	1.03	0.059
280	32.27	1.050-3	0.0045	63.64	139.25	0.2354	0.5085	2.03	0.91	0.054
290	40.87	1.264-3	0.0028	86.41	127.51	0.3131	0.4548	2.35		
292.6 ^c	43.57	1.773-3	0.0018	110.20	110.20	0.3864	0.3864	∞		∞

*P, v, h, and s values reproduced and converted from Table 14, p. 17.103, ASHRAE Handbook, 1981: Fundamentals, American Society of Heating, Refrigerating and Air-Conditioning Engineers, Atlanta, 1981. Copyright material. Reproduced by permission of the copyright owner. c_p , μ , and k values interpolated and converted from Thermophysical Properties of Refrigerants, American Society of Heating, Refrigerating and Air-Conditioning Engineers, New York, 1976. c = critical point. The notation 6.384-4 signifies 6.384×10^{-4} .

Saturation and superheat tables and a diagram to 80 bar, 600 K are given by Reynolds, W. C., Thermodynamic Properties in S.I., Stanford Univ. publ., 1979 (173 pp.). Tables and a chart to 1000 psia, 460 °F are given by Stewart, R. B., R. T. Jacobsen, et al., Thermodynamic Properties of Refrigerants, ASHRAE, Atlanta, GA, 1986 (521 pp.). For specific heat and viscosity see Thermophysical Properties of Refrigerants, ASHRAE, 1993. The 1993 ASHRAE Handbook—Fundamentals (SI ed.) gives material for integral degrees Celsius with temperatures on the IPTS 68 scale for saturation conditions from -125 to 19.50 °C. The thermodynamic diagram from 0.1 to 80 bar extends to 220 °C.

TABLE 2-294 Saturated Refrigerant 504*

Temp., °F	Pressure, lb/in ² abs.	Volume, ft ³ /lb		Enthalpy, Btu/lb		Entropy, Btu/(lb)(°F)	
		Liquid	Vapor	Liquid	Vapor	Liquid	Vapor
-120	2.964	0.01095	15.31	-21.48	86.69	-0.0565	0.2609
-100	6.042	0.01119	7.874	-16.39	89.31	-0.0420	0.2519
-80	11.34	0.01146	4.372	-11.12	91.84	-0.0277	0.2435
-60	19.85	0.01175	2.585	-5.65	94.25	-0.0137	0.2362
-40	32.76	0.01206	1.609	0.00	96.50	0.0000	0.2299
-20	51.44	0.01242	1.045	5.85	98.58	0.0135	0.2244
0	77.41	0.01282	0.7029	11.91	100.45	0.0269	0.2195
20	112.3	0.01328	0.4859	18.22	102.09	0.0401	0.2150
40	158.0	0.01379	0.3431	24.81	103.44	0.0533	0.2107
60	216.2	0.01443	0.2458	31.78	104.41	0.0667	0.2065
80	289.2	0.01522	0.1773	39.25	104.85	0.0804	0.2020
100	379.1	0.01629	0.1274	47.43	104.49	0.0948	0.1968
120	488.3	0.01783	0.0893	56.78	102.72	0.1107	0.1899
140	618.1	0.02083	0.0578	69.97	97.70	0.1322	0.1784
150	692.2	0.02597	0.0394	76.96	89.76	0.1432	0.1642

*Unpublished data of Allied Chemical Company, 1970. Used by permission.

TABLE 2-295 Thermodynamic Properties of Refrigerant 507*

Temp., K	Pressure, bar	v_f , m ³ /kg	v_g , m ³ /kg	h_f , kJ/kg	h_g , kJ/kg	s_f , kJ/(kg·K)	s_g , kJ/(kg·K)
230.5	1.013	0.000 574	0.1280	-3.1	143.3	-0.015	0.620
240	1.59	0.000 602	0.0826	10.3	150.2	0.042	0.623
250	2.42	0.000 627	0.0546	22.6	154.5	0.092	0.619
260	3.54	0.000 658	0.0377	37.6	159.0	0.149	0.617
270	4.95	0.000 695	0.0270	51.6	163.8	0.202	0.618
280	6.70	0.000 738	0.0198	64.7	169.0	0.250	0.620
290	8.85	0.000 787	0.0148	77.2	174.6	0.295	0.634
300	11.52	0.000 839	0.0112	89.4	180.3	0.336	0.640
310	14.74	0.000 903	0.0084	101.6	185.4	0.378	0.648
320	18.76	0.001 006	0.0062	115.7	188.6	0.422	0.649
330	23.65	0.001 221	0.0042	135.5	189.3	0.481	0.641
340	29.57	0.001 618	0.0025	161.7	179.9	0.557	0.611
341.5 ^c	32.67	0.001 97	0.0020	172.7	172.7	0.590	0.590

*Azeotropic mixture of R152a and R218. $h_f = s_f = 0$ at 233.15 K = -40 °C. Interpolated, extrapolated and converted from Lavrenchenko, G. K., M. G. Khmelnuik, et al., Int. J. Refrig., 17, 7 (1994): 461. Some values are tentative. This source also gives a ln P-h diagram from 0.6 to 30 bar, -50 to 70 °C. Differences exist between the published diagram and tables. c = critical point.

TABLE 2-296 Thermodynamic Properties of R-507A

Temperature K	Pressure MPa	Density mol/dm ³	Volume dm ³ /mol	Int. energy kJ/mol	Enthalpy kJ/mol	Entropy kJ/(mol·K)	C _v kJ/(mol·K)	C _p kJ/(mol·K)	Sound speed m/s	Joule-Thomson K/MPa
Saturated Properties										
200.00	0.023233	14.130	0.070772	10.553	10.555	0.059915	0.077250	0.11931	851.53	-0.34068
210.00	0.042731	13.828	0.072318	11.749	11.752	0.065751	0.078412	0.12015	796.42	-0.32336
215.00	0.056515	13.675	0.073126	12.351	12.355	0.068583	0.079028	0.12081	770.28	-0.31246
220.00	0.073637	13.521	0.073961	12.956	12.962	0.071366	0.079658	0.12158	744.80	-0.30008
225.00	0.094634	13.365	0.074825	13.566	13.573	0.074104	0.080295	0.12247	719.84	-0.28620
230.00	0.12008	13.206	0.075722	14.179	14.188	0.076802	0.080939	0.12345	695.27	-0.27072
235.00	0.15060	13.045	0.076655	14.798	14.809	0.079463	0.081589	0.12453	671.01	-0.25349
240.00	0.18683	12.882	0.077628	15.421	15.436	0.082089	0.082245	0.12569	646.97	-0.23433
245.00	0.22945	12.715	0.078646	16.051	16.069	0.084685	0.082907	0.12696	623.07	-0.21297
250.00	0.27919	12.545	0.079714	16.686	16.708	0.087253	0.083579	0.12833	599.27	-0.18910
255.00	0.33679	12.371	0.080837	17.328	17.355	0.089796	0.084260	0.12982	575.51	-0.16232
260.00	0.40302	12.192	0.082022	17.976	18.009	0.092316	0.084954	0.13144	551.75	-0.13214
265.00	0.47868	12.008	0.083277	18.632	18.672	0.094817	0.085661	0.13321	527.94	-0.097937
270.00	0.56461	11.819	0.084612	19.296	19.344	0.097301	0.086385	0.13517	504.05	-0.058916
275.00	0.66165	11.623	0.086039	19.968	20.025	0.099772	0.087128	0.13735	480.04	-0.014071
280.00	0.77071	11.419	0.087571	20.650	20.718	0.10223	0.087895	0.13978	455.86	0.037902
285.00	0.89272	11.208	0.089225	21.343	21.422	0.10469	0.088688	0.14254	431.49	0.098716
290.00	1.0286	10.986	0.091024	22.046	22.140	0.10714	0.089513	0.14571	406.87	0.17067
295.00	1.1794	10.753	0.092996	22.763	22.873	0.10960	0.090377	0.14941	381.97	0.25689
300.00	1.3462	10.507	0.095177	23.495	23.623	0.11207	0.091290	0.15379	356.72	0.36179
305.00	1.5300	10.244	0.097618	24.243	24.392	0.11455	0.092263	0.15912	331.07	0.49171
310.00	1.7322	9.9616	0.10039	25.011	25.185	0.11707	0.093316	0.16577	304.91	0.65619
315.00	1.9539	9.6544	0.10358	25.803	26.006	0.11962	0.094477	0.17441	278.14	0.87027
320.00	2.1967	9.3151	0.10735	26.626	26.862	0.12224	0.095794	0.18622	250.55	1.1591
325.00	2.4622	8.9322	0.11195	27.487	27.763	0.12494	0.097351	0.20363	221.86	1.5687
330.00	2.7523	8.4856	0.11785	28.405	28.729	0.12779	0.099317	0.23262	191.54	2.1936
335.00	3.0697	7.9323	0.12607	29.412	29.799	0.13089	0.10208	0.29323	158.62	3.2672
340.00	3.4178	7.1361	0.14013	30.620	31.099	0.13460	0.10695	0.52176	121.00	5.5872
343.77	3.7049	4.9640	0.20145	32.908	33.654	0.14193			0	12.382
200.00	0.023222	0.014226	70.296	29.992	31.624	0.16527	0.059362	0.068766	137.04	85.105
210.00	0.042726	0.025154	39.755	30.526	32.225	0.16325	0.061910	0.071764	139.19	65.962
215.00	0.056512	0.032678	30.602	30.796	32.525	0.16240	0.063188	0.073318	140.11	58.876
220.00	0.073634	0.041875	23.881	31.067	32.825	0.16166	0.064473	0.074919	140.92	53.008
225.00	0.094628	0.052996	18.869	31.338	33.124	0.16100	0.065766	0.076576	141.60	48.113
230.00	0.12007	0.066313	15.080	31.610	33.420	0.16043	0.067072	0.078300	142.16	44.001
235.00	0.15057	0.082125	12.177	31.881	33.715	0.15992	0.068393	0.080105	142.57	40.521
240.00	0.18678	0.10075	9.9251	32.152	34.005	0.15947	0.069735	0.082005	142.84	37.557
245.00	0.22938	0.12256	8.1593	32.421	34.292	0.15907	0.071100	0.084017	142.95	35.013
250.00	0.27908	0.14794	6.7597	32.688	34.575	0.15872	0.072492	0.086159	142.90	32.816
255.00	0.33664	0.17732	5.6396	32.953	34.851	0.15841	0.073915	0.088453	142.67	30.909
260.00	0.40281	0.21120	4.7348	33.214	35.121	0.15814	0.075372	0.090927	142.26	29.244
265.00	0.47840	0.25014	3.9977	33.471	35.384	0.15788	0.076865	0.093613	141.66	27.785
270.00	0.56424	0.29478	3.3924	33.724	35.638	0.15765	0.078399	0.096551	140.85	26.502
275.00	0.66119	0.34585	2.8914	33.970	35.882	0.15744	0.079978	0.099795	139.83	25.372
280.00	0.77015	0.40424	2.4738	34.209	36.115	0.15723	0.081605	0.10341	138.57	24.376
285.00	0.89202	0.47097	2.1233	34.440	36.334	0.15702	0.083287	0.10750	137.08	23.500
290.00	1.0278	0.54731	1.8271	34.661	36.539	0.15680	0.085030	0.11218	135.32	22.730
295.00	1.1784	0.63483	1.5752	34.869	36.726	0.15656	0.086845	0.11764	133.29	22.057
300.00	1.3450	0.73552	1.3596	35.063	36.892	0.15630	0.088742	0.12415	130.95	21.472
305.00	1.5287	0.85197	1.1737	35.239	37.033	0.15600	0.090740	0.13211	128.30	20.967

310.00	1.7307	0.98768	1.0125	35.391	37.144	0.15565	0.092861	0.14217	125.29	20.534
315.00	1.9522	1.1475	0.87142	35.515	37.217	0.15521	0.095142	0.15545	121.90	20.163
320.00	2.1948	1.3389	0.74689	35.601	37.241	0.15467	0.097636	0.17401	118.07	19.838
325.00	2.4602	1.5733	0.63559	35.634	37.198	0.15397	0.10043	0.20216	113.77	19.531
330.00	2.7503	1.8717	0.53427	35.589	37.058	0.15303	0.10368	0.25052	108.90	19.179
335.00	3.0678	2.2784	0.43891	35.411	36.758	0.15166	0.10772	0.35438	103.35	18.634
340.00	3.4166	2.9318	0.34109	34.936	36.101	0.14932	0.11346	0.74186	96.734	17.407
343.77	3.7049	4.9640	0.20145	32.908	33.654	0.14193		0	0	12.382

Single-Phase Properties

226.14	0.10000	13.329	0.075025	13.705	13.712	0.074720	0.080441	0.12268	714.23	-0.28283
226.14	0.10000	0.055821	17.915	31.400	33.191	0.16087	0.066061	0.076961	141.74	47.115
300.00	0.10000	0.040743	24.544	36.736	39.190	0.18376	0.077477	0.086497	165.13	16.625
400.00	0.10000	0.030241	33.067	45.323	48.629	0.21080	0.093474	0.10204	190.54	6.8071
500.00	0.10000	0.024113	41.472	55.366	59.514	0.23504	0.10672	0.11516	212.51	3.6966
288.99	1.0000	11.032	0.090648	21.903	21.994	0.10665	0.089344	0.14503	411.87	0.15510
289.02	1.0000	0.53150	1.8815	34.618	36.500	0.15684	0.084683	0.11121	135.69	22.873
300.00	1.0000	0.49044	2.0390	35.647	37.686	0.16087	0.084205	0.10551	142.77	19.202
400.00	1.0000	0.31937	3.1312	44.851	47.983	0.19047	0.094741	0.10601	182.55	7.0158
500.00	1.0000	0.24643	4.0580	55.070	59.128	0.21530	0.10718	0.11688	209.06	3.6962
300.00	5.0000	10.905	0.091702	23.040	23.498	0.11052	0.090271	0.14306	420.12	0.12774
400.00	5.0000	2.2078	0.45293	42.120	44.385	0.17014	0.10115	0.14483	147.77	7.5193
500.00	5.0000	1.3533	0.73892	53.669	57.364	0.19916	0.10913	0.12621	197.37	3.5221
300.00	10.000	11.289	0.088585	22.583	23.469	0.10892	0.089813	0.13611	482.39	-0.028276
400.00	10.000	6.0317	0.16579	37.890	39.548	0.15478	0.10349	0.18529	182.13	2.8871
500.00	10.000	2.9478	0.33924	51.842	55.234	0.18999	0.11096	0.13942	197.45	2.8080
300.00	25.000	12.033	0.083106	21.667	23.744	0.10556	0.089890	0.12779	608.04	-0.21781
400.00	25.000	9.2040	0.10865	34.588	37.304	0.14446	0.10218	0.14278	377.87	0.20389
500.00	25.000	6.5873	0.15181	48.091	51.887	0.17699	0.11266	0.14661	290.93	0.64689
300.00	50.000	12.796	0.078149	20.711	24.618	0.10177	0.090684	0.12322	746.86	-0.32316
400.00	50.000	10.770	0.092847	32.830	37.472	0.13868	0.10306	0.13357	554.88	-0.19407
500.00	50.000	8.9711	0.11147	45.655	51.229	0.16935	0.11396	0.14097	452.46	-0.072291

The values in these tables were generated from the NIST REFPROP software (Lemmon, E. W., McLinden, M. O., and Huber, M. L., NIST Standard Reference Database 23: Reference Fluid Thermodynamic and Transport Properties—REFPROP, National Institute of Standards and Technology, Standard Reference Data Program, Gaithersburg, Md., 2002, Version 7.1). The primary source for the thermodynamic properties is Lemmon, E. W., "Pseudo Pure-Fluid Equations of State for the Refrigerant Blends R-410A, R-404A, R-507A, and R-407C," *Int. J. Thermophys.* **24**(4):991–1006, 2003. Validated equations for the viscosity and thermal conductivity are not currently available for this fluid.

Properties at the critical point temperature are given in the last entry of the saturation tables. In the single-phase table, when the temperature range for a given isobar includes a vapor-liquid phase boundary, the temperature of phase equilibrium is noted, and properties for both the saturated liquid and saturated vapor are given (with liquid properties given in the upper line). Lines are omitted from the temperature-pressure grid of the single-phase table, when the system would be in the solid phase or if there are potential problems with the source property surface.

The estimated uncertainty of density values calculated with the equation of state is 0.1%. The estimated uncertainty of calculated heat capacities and speed of sound values is 0.5%. Uncertainties of bubble and dew point pressures are 0.5%.

TABLE 2-297 Saturated Rubidium*

T, K	P, bar	v_f , m ³ /kg	v_g , m ³ /kg	h_f , kJ/kg	h_g , kJ/kg	s_f , kJ/(kg·K)	s_g , kJ/(kg·K)	c_{pf} , kJ/(kg·K)
312.7 ^m	2.46.-9	6.75.-4		118.7	1036	0.998	3.932	0.379
400	1.69.-6	6.98.-4	2.3.+5	151.6	1057	1.091	3.355	0.375
500	1.73.-4	7.22.-4	2790	188.8	1078	1.174	2.953	0.369
600	0.0037	7.46.-4	156.6	225.4	1096	1.241	2.692	0.362
700	0.0317	7.73.-4	20.75	261.3	1111	1.296	2.511	0.357
800	0.1584	8.10.-4	4.662	296.8	1124	1.343	2.378	0.353
1000	1.467	8.65.-4	0.605	367.6	1150	1.422	2.205	0.360
1200	6.466	9.40.-4	0.159	440.1	1179	1.490	2.104	0.385
1400	18.6	1.03.-3						
1500	28.5	1.08.-3						

*Converted from tables in Vargaftik, *Tables of the Thermophysical Properties of Liquids and Gases*, Nauka, Moscow, 1972, and Hemisphere, Washington, 1975. m = melting point. The notation 2.46.-9 signifies 2.46×10^{-9} .

Many of the Vargaftik values also appear in Ohse, R. W., *Handbook of Thermodynamic and Transport Properties of Alkali Metals*, Blackwell Sci. Pubs., Oxford, 1985 (1020 pp.). This source contains superheat data.

Saturation and superheat tables and a diagram to 40 bar, 1600 K are given by Reynolds, W. C., *Thermodynamic Properties in S.I.*, Stanford Univ. publ., 1979 (173 pp.).

For a Mollier diagram from 0.1 to 320 psia, 1200 to 2700 °R, see Weatherford, W. D., J. C. Tyler, et al., WADD-TR-61-96, 1961. An extensive review of properties of the solid and the saturated liquid was given by Alcock, C. B., M. W. Chase, et al., *J. Phys. Chem. Ref. Data*, **23**, 3 (1994): 385-497.

TABLE 2-298 Thermophysical Properties of Saturated Seawater

Temp., °C	Pressure, bar	v , (m ³ /kg)10 ³	c_p , kJ/(kg·K)	μ , Ns/m ²	k , W/(m·K)	N_{pr}	10 ⁵ κ , 1/bar
0	0.005993	1.000158	4.000	0.001884	0.560	13.46	5.06
1	0.006438	1.000099	4.000	0.001827	0.563	12.98	5.02
2	0.006916	1.000057	4.000	0.001772	0.565	12.55	4.98
3	0.007427	1.000033	4.000	0.001720	0.567	12.13	4.95
4	0.007970	1.000025	4.001	0.001669	0.569	11.74	4.92
5	0.008548	1.000033	4.001	0.001620	0.571	11.35	4.89
6	0.009163	1.000057	4.001	0.001574	0.574	10.97	4.86
7	0.009816	1.000096	4.002	0.001529	0.576	10.62	4.83
8	0.010511	1.000149	4.002	0.001486	0.578	10.29	4.80
9	0.011248	1.000261	4.002	0.001445	0.580	9.97	4.78
10	0.01203	1.000298	4.003	0.001405	0.582	9.70	4.76
11	0.01286	1.000392	4.003	0.001367	0.584	9.37	4.74
12	0.01374	1.000500	4.003	0.001330	0.586	9.09	4.72
13	0.01467	1.000620	4.004	0.001294	0.588	8.81	4.70
14	0.01566	1.000727	4.004	0.001259	0.590	8.54	4.68
15	0.01671	1.000899	4.005	0.001226	0.592	8.29	4.66
16	0.01781	1.001055	4.005	0.001195	0.594	8.06	4.65
17	0.01898	1.001224	4.006	0.001165	0.595	7.82	4.63
18	0.02022	1.001404	4.006	0.001136	0.597	7.62	4.62
19	0.02153	1.001595	4.007	0.001107	0.599	7.41	4.60
20	0.02291	1.001796	4.007	0.001080	0.600	7.21	4.59
21	0.02437	1.002009	4.007	0.001054	0.602	7.02	4.57
22	0.02591	1.002232	4.008	0.001029	0.604	6.82	4.56
23	0.02753	1.002465	4.008	0.001005	0.605	6.66	4.55
24	0.02924	1.002708	4.009	0.000981	0.607	6.48	4.54
25	0.03104	1.002961	4.009	0.000958	0.608	6.31	4.53
26	0.03294	1.003224	4.009	0.000936	0.609	6.16	4.52
27	0.03494	1.003496	4.010	0.000915	0.611	6.01	4.51
28	0.03705	1.003778	4.010	0.000895	0.612	5.86	4.50
29	0.03926	1.004069	4.011	0.000875	0.614	5.72	4.49
30	0.04159	1.004369	4.011	0.000855	0.615	5.58	4.48

$\kappa = (-1/V)(\partial v/\partial p)_T \cdot 10^5$. Thus, at 0 °C, the compressibility is 5.06×10^{-5} /bar.

For further information see, for instance, Bromley, LeR. A., *J. Chem. Eng. Data*, **12**, 2 (1967): 202-206; **13**, 1 (1968): 60-62 and **13**, 3: 399-402; **15**, 2 (1970): 246-253; and *A.I.Ch.E.J.*, **20**, 2 (1974): 326-335.

Thermal conductivity data sources include Castelli, V. J., E. M. Stanley, et al., *Deep Sea Res.*, **211** (1974): 311-318; Levy, F. L., *Int. J. Refrig.*, **5**, 3 (1982): 155-159.

For velocity of sound, see, for instance, U.S. Naval Oceanographic Office SP 58, 1962 (50 pp.). More recent information is contained in UNESCO technical papers. See *Marine Science* No. 38, 1981 (6 pp.) and No. 44, 1983 (53 pp.).

For sea ice properties, see Fukusako, S., *Int. J. Thermophys.*, **11**, 2 (1990): 353-372.

TABLE 2-299 Saturated Sodium

Temp., K	Pressure, bar	$v_f, \text{m}^3/\text{kg}$	$v_g, \text{m}^3/\text{kg}$	$h_f, \text{kJ}/\text{kg}$	$h_g, \text{kJ}/\text{kg}$	$s_f, \text{kJ}/(\text{kg}\cdot\text{K})$	$s_g, \text{kJ}/(\text{kg}\cdot\text{K})$	$c_{pf}, \text{kJ}/(\text{kg}\cdot\text{K})$	$c_{pg}, \text{kJ}/(\text{kg}\cdot\text{K})$	$\mu_f, 10^{-6} \text{ Pa}\cdot\text{s}$	$\mu_g, 10^{-6} \text{ Pa}\cdot\text{s}$	$k_f, \text{W}/(\text{m}\cdot\text{K})$	$k_g, \text{W}/(\text{m}\cdot\text{K})$	Pr_f	Pr_g
371	1.59,-10	0.001 078	8.54,+9	207	4739	2.259	14.475	1.383		688		89.4		0.0106	
400	1.80,-9	0.001 088	8.08,+8	247	4757	2.920	14.195	1.372	0.86	599		87.2		0.0094	
500	8.99,-7	0.001 115	1.99,+6	382	4817	3.222	12.092	1.334	1.25	415		80.1		0.0069	
600	5.57,-5	0.001 144	38022	514	4872	3.462	10.745	1.301	1.80	321		73.7		0.0057	
700	0.00105	0.001 174	2320	642	4921	3.661	10.631	1.277	2.28	264		68.0		0.0050	
800	0.00941	0.001 208	291.5	769	4966	3.830	9.076	1.260	2.59	227	19.6	62.9	0.0343	0.0045	1.48
900	0.05147	0.001 242	58.8	895	5007	3.978	8.547	1.252	2.72	201	20.6	58.3	0.0406	0.0043	1.38
1000	0.1995	0.001 280	16.6	1020	5044	4.110	8.134	1.252	2.70	181	23.0	54.2	0.0455	0.0042	1.36
1100	0.6016	0.001 323	5.95	1146	5079	4.230	7.805	1.261	2.62	166	25.3	50.5	0.0492	0.0042	1.35
1154.7	1.013	0.001 347	3.89	1215	5097	4.290	7.652	1.271	2.56	159	26.5	48.7	0.0522	0.0041	1.30
1200	1.50	0.001 366	2.54	1273	5111	4.340	7.538	1.279	2.51	153	27.5	47.2	0.0547	0.0041	1.26
1300	3.26	0.001 416	1.24	1402	5140	4.444	7.319	1.305	2.43	143	29.9	44.0	0.0570	0.0042	1.27
1400	6.30	0.001 471	0.676	1534	5168	4.542	7.138	1.340	2.39	135	32.2	41.1	0.0592	0.0044	1.30
1500	11.13	0.001 531	0.400	1671	5193	4.636	6.984	1.384	2.36	128	34.6	38.2		0.0046	
1600	18.28	0.001 597	0.253	1812	5217	4.727	6.855	1.437	2.34	122	37.1	35.4		0.0050	
1700	28.28	0.001 675	0.168	1959	5238	4.816	6.745	1.500	2.41	117		32.6		0.0054	
1800	41.61	0.001 761	0.117	2113	5256	4.904	6.650	1.574	2.46	112		29.7		0.0059	
1900	58.70	0.001 862	0.084	2274	5268	4.992	6.568	1.661	2.53	108		26.6		0.0067	
2000	79.91	0.001 984	0.063	2444	5273	5.079	6.494	1.764	2.66	104		23.2		0.0079	
2100	105.5	0.002 174	0.0472	2625	5265			1.926	2.91						
2200	135.7	0.002 320	0.0361	2822	5241			2.190	3.40						
2300	170.6	0.002 584	0.0275	3047	5188			2.690	4.47						
2400	210.3	0.002 985	0.0203	3331	5078			4.012	8.03						
2500	254.7	0.004 19	0.0098	3965	4617			39.3	417.						
2503.7 ^c	256.4	0.004 57	0.0046	4294	4294										

^c = critical point.

s_f values converted from Cordfunke, E. H. P. and R. J. M. Konings, *Thermochemical Data for Reactor Materials and Fission Products*, North Holland Elsevier, NY, 1990. s_g determined as $s_f + (h_g - h_f)/T$. μ_g and k_g values estimated by P. E. Liley. All other values are from Fink, J. K. and L. Leibowitz, Argonne Nat. Lab Rept. ANL/RE-95-2, 1995. The Fink and Leibowitz work also appeared in *High Temp. Materials Sci.*, **35**, 65-103, 1996. Saturation and superheat tables and a diagram to 14 bar; 1700 K are given by Reynolds, W. C., *Thermodynamic Properties in S.I.*, Stanford Univ. publ., 1979 (173 pp.). For a Mollier diagram for 0.1-150 psia, 1500-2700 °R, see Weatherford, P. M., J. C. Tyler, et al., WADD-TR-61-96, 1961.

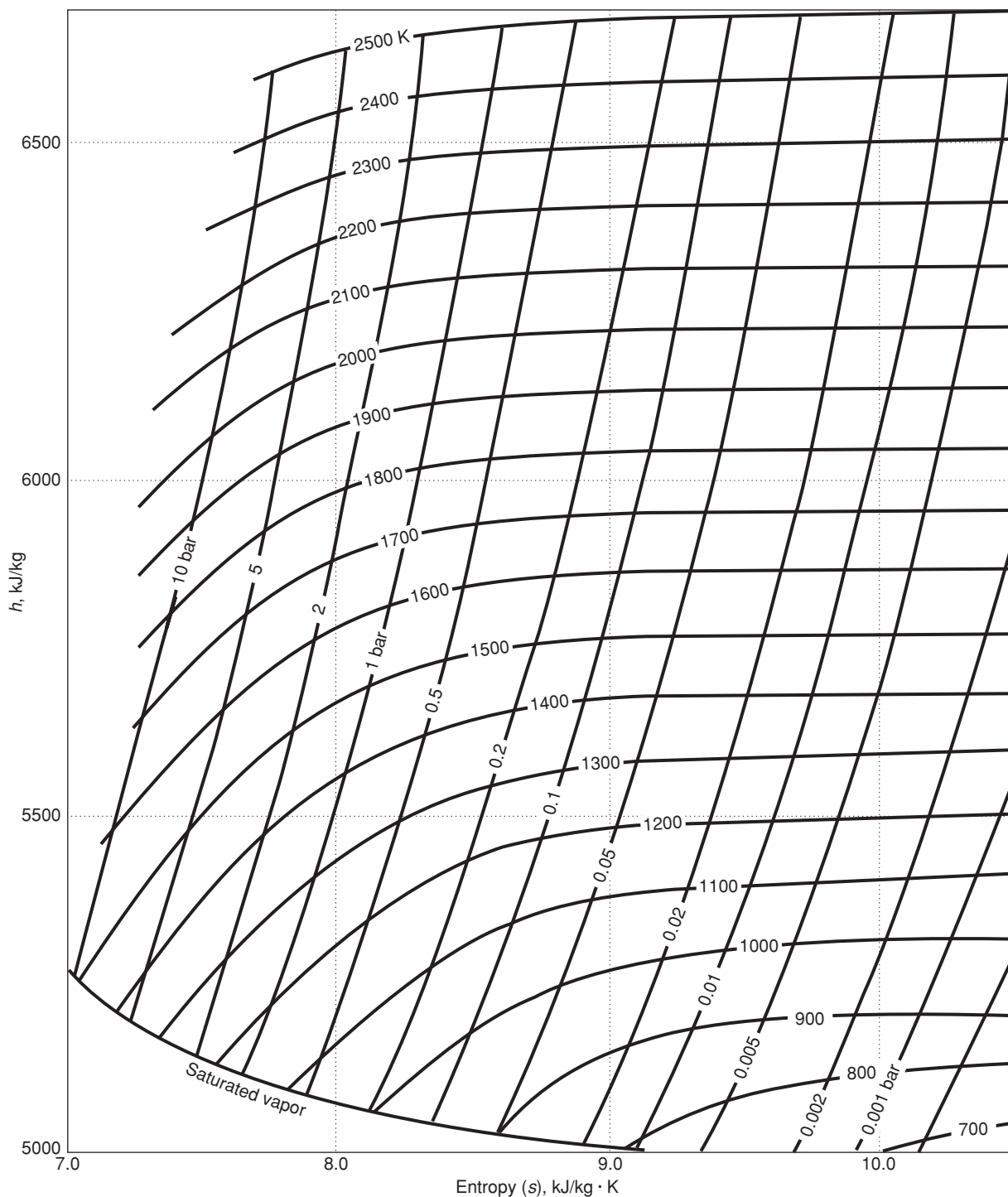


FIG. 2-28 Mollier Diagram for Sodium. Drawn from the Vargaftik et al. values in Ohse, R. W., *Handbook of Thermodynamic and Transport Properties of Alkali Metals*, Blackwell Sci. Pubs., Oxford, UK, 1985. These values are identical with those of Vargaftik, N. B., *Handbook of Thermophysical Properties of Gases and Liquids*, Moscow, 1972, and the Hemisphere translation, p. 19. An apparent discontinuity exists between the superheat values and the saturation values, not reproduced here. For a Mollier diagram in f.p.s. units from 0.1 to 150 psia, 1500 to 2700°R, see Fig. 3-36, p. 3-232 of the 6th edition of this handbook. An extensive review of properties of the solid and the saturated liquid was given by Alcock, C. B., Chase, M. W. et al., *J. Phys. Chem. Ref. Data*, **23**(3), 385–497, 1994.

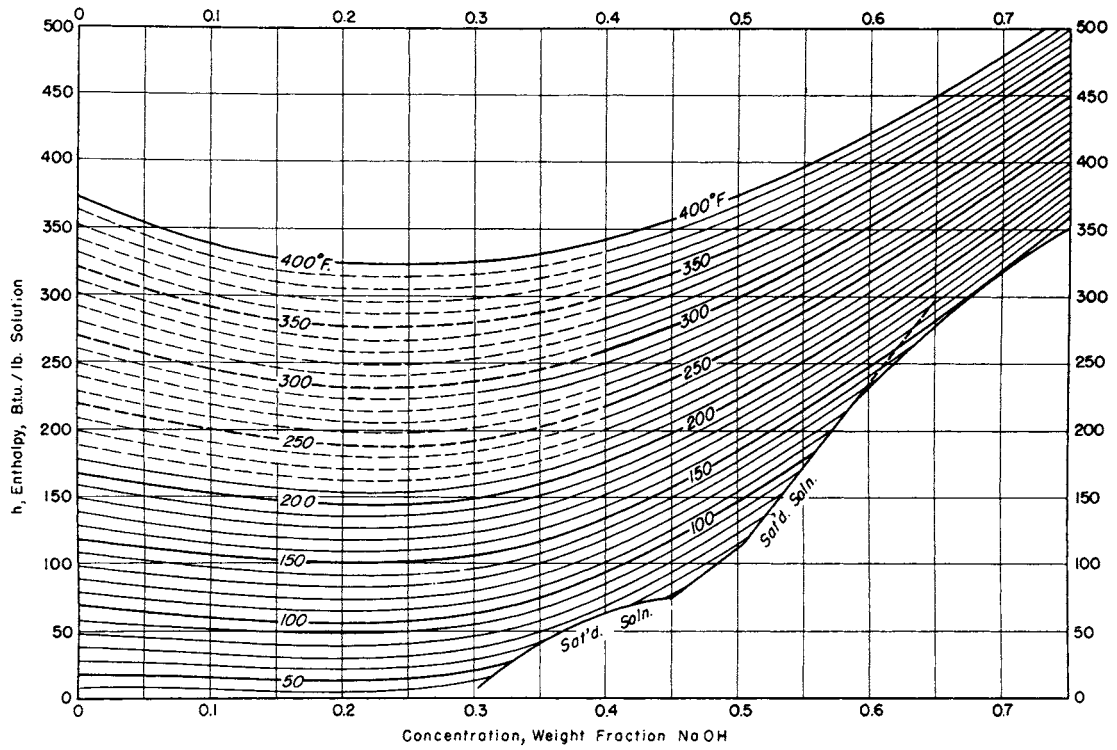


FIG. 2-29 Enthalpy-concentration diagram for aqueous sodium hydroxide at 1 atm. Reference states: enthalpy of liquid water at 32 °F and vapor pressure is zero; partial molal enthalpy of infinitely dilute NaOH solution at 64 °F and 1 atm is zero. [McCabe, *Trans. Am. Inst. Chem. Eng.*, **31**, 129 (1935).]

TABLE 2-300 Thermodynamic Properties of Sulfur Dioxide

Temperature K	Pressure MPa	Density mol/dm ³	Volume dm ³ /mol	Int. energy kJ/mol	Enthalpy kJ/mol	Entropy kJ/(mol·K)	C _v kJ/(mol·K)	C _p kJ/(mol·K)	Sound speed m/s	Joule-Thomson K/MPa
Saturated Properties										
197.70	0.0016602	25.290	0.039541	-5.7212	-5.7211	-0.024986	0.056222	0.088123	1361.6	-0.31925
200.00	0.0020260	25.205	0.039674	-5.5186	-5.5185	-0.023967	0.056094	0.088031	1350.1	-0.31864
210.00	0.0045390	24.835	0.040265	-4.6402	-4.6400	-0.019681	0.055527	0.087673	1301.1	-0.31528
220.00	0.0093340	24.463	0.040878	-3.7650	-3.7646	-0.015610	0.054955	0.087396	1253.3	-0.31064
230.00	0.017835	24.088	0.041514	-2.8921	-2.8914	-0.011730	0.054393	0.087214	1206.4	-0.30450
240.00	0.031988	23.709	0.042179	-2.0207	-2.0194	-0.0080208	0.053849	0.087137	1160.3	-0.29665
250.00	0.054309	23.324	0.042875	-1.1497	-1.1473	-0.0044649	0.053331	0.087177	1114.8	-0.28683
260.00	0.087910	22.932	0.043608	-0.27785	-0.27402	-0.0010454	0.052843	0.087344	1069.7	-0.27473
270.00	0.13649	22.532	0.044382	0.59591	0.60197	0.0022525	0.052388	0.087651	1024.9	-0.26000
280.00	0.20431	22.122	0.045204	1.4729	1.4821	0.0054424	0.051969	0.088112	980.26	-0.24217
290.00	0.29614	21.701	0.046081	2.3545	2.3682	0.0085368	0.051587	0.088748	935.65	-0.22070
300.00	0.41725	21.267	0.047021	3.2423	3.2619	0.011547	0.051243	0.089582	890.99	-0.19485
310.00	0.57327	20.818	0.048035	4.1378	4.1653	0.014485	0.050938	0.090647	846.15	-0.16370
320.00	0.77025	20.352	0.049136	5.0430	5.0809	0.017362	0.050675	0.091988	801.04	-0.12603
330.00	1.0145	19.865	0.050340	5.9601	6.0112	0.020187	0.050455	0.093668	755.54	-0.080167
340.00	1.3128	19.354	0.051670	6.8916	6.9594	0.022972	0.050281	0.095777	709.53	-0.023832
350.00	1.6720	18.814	0.053153	7.8408	7.9296	0.025730	0.050157	0.098448	662.87	0.046220
360.00	2.0994	18.239	0.054828	8.8116	8.9267	0.028473	0.050089	0.10189	615.37	0.13476
370.00	2.6028	17.621	0.056750	9.8095	9.9572	0.031220	0.050089	0.10644	566.77	0.24913
380.00	3.1904	16.949	0.059001	10.842	11.030	0.033991	0.050173	0.11271	516.72	0.40128
390.00	3.8713	16.204	0.061713	11.921	12.160	0.036818	0.050373	0.12189	464.59	0.61221
400.00	4.6557	15.355	0.065124	13.066	13.369	0.039753	0.050753	0.13673	409.36	0.92296
410.00	5.5562	14.340	0.069734	14.317	14.704	0.042899	0.051457	0.16539	349.05	1.4276
420.00	6.5903	12.987	0.077001	15.782	16.290	0.046536	0.052928	0.24772	279.41	2.4089
430.00	7.7908	9.8261	0.10177	18.415	19.207	0.053143	0.058931	3.7896	182.70	5.8716
430.64	7.8753	8.1950	0.12203	19.585	20.546	0.056233			0	7.4962
197.70	0.0016602	0.0010120	988.16	21.102	22.743	0.11899	0.028340	0.036808	182.19	299.66
200.00	0.0020260	0.0012211	818.93	21.164	22.824	0.11774	0.028464	0.036952	183.16	280.77
210.00	0.0045390	0.0026096	383.20	21.435	23.174	0.11277	0.029049	0.037650	187.23	214.32
220.00	0.0093340	0.0051346	194.76	21.702	23.520	0.10841	0.029713	0.038475	191.08	166.88
230.00	0.017835	0.0094158	106.20	21.967	23.861	0.10458	0.030462	0.039438	194.70	132.33
240.00	0.031988	0.016257	61.512	22.226	24.194	0.10120	0.031293	0.040551	198.07	106.70
250.00	0.054309	0.026653	37.519	22.480	24.518	0.098195	0.032204	0.041819	201.15	87.372
260.00	0.087910	0.041793	23.928	22.726	24.830	0.095507	0.033186	0.043246	203.92	72.572
270.00	0.13649	0.063061	15.858	22.964	25.128	0.093090	0.034230	0.044838	206.35	61.089
280.00	0.20431	0.092046	10.864	23.191	25.411	0.090902	0.035327	0.046602	208.42	52.073
290.00	0.29614	0.13055	7.6600	23.407	25.676	0.088908	0.036465	0.048552	210.09	44.917
300.00	0.41725	0.18062	5.5366	23.611	25.921	0.087077	0.037638	0.050709	211.33	39.185
310.00	0.57327	0.24460	4.0883	23.799	26.142	0.085379	0.038838	0.053111	212.12	34.550
320.00	0.77025	0.32522	3.0748	23.969	26.338	0.083789	0.040062	0.055813	212.43	30.772
330.00	1.0145	0.42570	2.3491	24.120	26.503	0.082284	0.041310	0.058901	212.22	27.666
340.00	1.3128	0.54995	1.8184	24.247	26.634	0.080838	0.042587	0.062502	211.47	25.092
350.00	1.6720	0.70287	1.4227	24.345	26.724	0.079427	0.043900	0.066814	210.13	22.939
360.00	2.0994	0.89084	1.1225	24.409	26.765	0.078025	0.045264	0.072150	208.17	21.118
370.00	2.6028	1.1225	0.89086	24.430	26.748	0.076601	0.046699	0.079031	205.54	19.558
380.00	3.1904	1.4103	0.70908	24.396	26.658	0.075116	0.048236	0.088395	202.18	18.192
390.00	3.8713	1.7733	0.56391	24.289	26.472	0.073516	0.049922	0.10210	198.02	16.958
400.00	4.6557	2.2444	0.44556	24.079	26.153	0.071714	0.051835	0.12442	192.95	15.777
410.00	5.5562	2.8887	0.34618	23.705	25.628	0.069543	0.054121	0.16795	186.81	14.529
420.00	6.5903	3.8804	0.25770	23.009	24.707	0.066577	0.057117	0.29279	179.31	12.934
430.00	7.7908	6.6270	0.15090	20.801	21.976	0.059582	0.062123	4.6423	168.96	9.1885
430.64	7.8753	8.1950	0.12203	19.585	20.546	0.056233			0	7.4962

Single-Phase Properties

200.00	0.10000	25.206	0.039672	-5.5197	-5.5158	-0.023973	0.056096	0.088028	1350.4	-0.31868
262.84	0.10000	22.819	0.043823	-0.030118	-0.025736	-0.000097639	0.052710	0.087416	1057.0	-0.27084
262.84	0.10000	0.047141	21.213	22.794	24.916	0.094795	0.033476	0.043681	204.65	69.019
300.00	0.10000	0.040764	24.532	24.043	26.497	0.10042	0.032826	0.041994	219.46	39.646
400.00	0.10000	0.030240	33.068	27.458	30.765	0.11269	0.035338	0.043891	252.48	15.140
500.00	0.10000	0.024117	41.465	31.151	35.297	0.12279	0.038292	0.046720	280.65	8.3690
200.00	1.0000	25.219	0.039653	-5.5302	-5.4905	-0.024025	0.056110	0.087995	1353.1	-0.31905
300.00	1.0000	21.287	0.046976	3.2251	3.2721	0.011490	0.051245	0.089444	894.23	-0.19703
329.46	1.0000	19.892	0.050272	5.9101	5.9604	0.020035	0.050466	0.093567	758.01	-0.082891
329.46	1.0000	0.41969	2.3827	24.112	26.495	0.082363	0.041242	0.058722	212.25	27.819
400.00	1.0000	0.31968	3.1281	27.007	30.135	0.092405	0.037220	0.048421	244.07	15.238
500.00	1.0000	0.24701	4.0483	30.891	34.939	0.10312	0.038821	0.048357	276.82	8.3664
200.00	5.0000	25.271	0.039570	-5.5759	-5.3780	-0.024255	0.056174	0.087853	1365.0	-0.32064
300.00	5.0000	21.420	0.046686	3.1113	3.3448	0.011108	0.051267	0.088566	915.79	-0.21095
400.00	5.0000	15.439	0.064770	13.003	13.327	0.039592	0.050649	0.13367	417.04	0.87444
403.99	5.0000	14.976	0.066773	13.548	13.882	0.040973	0.050981	0.14563	386.08	1.0922
403.99	5.0000	2.4748	0.40407	23.955	25.975	0.070906	0.052690	0.13790	190.64	15.297
500.00	5.0000	1.3950	0.71686	29.591	33.176	0.087109	0.041506	0.058653	259.84	8.2323
300.00	10.000	21.575	0.046350	2.9776	3.4411	0.010654	0.051308	0.087615	941.12	-0.22613
400.00	10.000	16.326	0.061251	12.327	12.940	0.037839	0.049804	0.11122	501.11	0.46626
500.00	10.000	3.4161	0.29273	27.477	30.404	0.076991	0.045669	0.085639	241.12	7.4245
300.00	20.000	21.859	0.045748	2.7336	3.6486	0.0098108	0.051422	0.086075	987.39	-0.25095
400.00	20.000	17.379	0.057542	11.494	12.644	0.035620	0.049297	0.096839	608.17	0.15187
500.00	20.000	9.7192	0.10289	22.208	24.266	0.061366	0.049635	0.13354	292.48	2.7261
300.00	35.000	22.232	0.044980	2.4136	3.9878	0.0086740	0.051645	0.084373	1048.5	-0.27869
400.00	35.000	18.377	0.054417	10.681	12.586	0.033379	0.049231	0.088711	717.32	-0.043488
500.00	35.000	13.607	0.073492	19.322	21.894	0.054113	0.048429	0.097089	462.83	0.67011

The values in these tables were generated from the NIST REFPROP software (Lemmon, E. W., McLinden, M. O., and Huber, M. L., NIST Standard Reference Database 23: Reference Fluid Thermodynamic and Transport Properties—REFPROP, National Institute of Standards and Technology, Standard Reference Data Program, Gaithersburg, Md., 2002, Version 7.1). The primary source for the thermodynamic properties is Lemmon, E. W., and Span, R., *J. Chem. Eng. Data*, **51**(3):785–850, 2006. Validated equations for the viscosity and thermal conductivity are not currently available for this fluid.

Properties at the triple point temperature and the critical point temperature are given in the first and last entries of the saturation tables, respectively. In the single-phase table, when the temperature range for a given isobar includes a vapor-liquid phase boundary, the temperature of phase equilibrium is noted, and properties for both the saturated liquid and saturated vapor are given (with liquid properties given in the upper line). Lines are omitted from the temperature-pressure grid of the single-phase table, when the system would be in the solid phase or if there are potential problems with the source property surface.

The uncertainty in density of the equation of state ranges from 0.1% at low temperatures in the liquid and vapor to 0.5% at the highest temperatures. The uncertainty in heat capacities is 2%, and the uncertainty in vapor pressure is 0.4% at temperatures above 270 K. The uncertainty in vapor pressure increases at lower temperatures due to the lack of experimental data. In the critical region, the uncertainties are higher for all properties except vapor pressure.

TABLE 2-301 Thermodynamic Properties of Sulfur Hexafluoride

Temperature K	Pressure MPa	Density mol/dm ³	Volume dm ³ /mol	Int. energy kJ/mol	Enthalpy kJ/mol	Entropy kJ/(mol·K)	C _v kJ/(mol·K)	C _p kJ/(mol·K)	Sound speed m/s	Joule-Thomson K/MPa
Saturated Properties										
222.38	0.22436	12.677	0.078884	22.560	22.578	0.11968	0.063933	0.10620	578.22	-0.32279
225.00	0.25012	12.592	0.079415	22.842	22.862	0.12094	0.066189	0.11001	565.05	-0.29395
230.00	0.30561	12.424	0.080489	23.405	23.430	0.12342	0.069989	0.11631	539.86	-0.24573
235.00	0.37011	12.249	0.081642	23.996	24.026	0.12596	0.073230	0.12154	514.71	-0.20297
240.00	0.44448	12.066	0.082875	24.610	24.647	0.12855	0.076028	0.12596	489.70	-0.16256
245.00	0.52962	11.878	0.084192	25.244	25.288	0.13117	0.078482	0.12981	464.88	-0.12208
250.00	0.62644	11.682	0.085600	25.894	25.948	0.13380	0.080672	0.13330	440.25	-0.079442
255.00	0.73591	11.480	0.087108	26.559	26.623	0.13643	0.082667	0.13661	415.80	-0.032633
260.00	0.85899	11.270	0.088731	27.238	27.315	0.13908	0.084519	0.13994	391.49	0.020496
265.00	0.99671	11.051	0.090487	27.932	28.022	0.14172	0.086274	0.14344	367.25	0.082465
270.00	1.1502	10.822	0.092400	28.640	28.746	0.14438	0.087968	0.14730	343.00	0.15646
275.00	1.3204	10.581	0.094507	29.363	29.488	0.14704	0.089631	0.15173	318.65	0.24678
280.00	1.5088	10.325	0.096852	30.105	30.251	0.14973	0.091292	0.15702	294.10	0.35955
285.00	1.7164	10.050	0.099503	30.867	31.037	0.15244	0.092978	0.16356	269.23	0.50392
290.00	1.9447	9.7505	0.10256	31.653	31.852	0.15519	0.094719	0.17202	243.92	0.69427
295.00	2.1952	9.4189	0.10617	32.470	32.703	0.15801	0.096558	0.18353	218.04	0.95460
300.00	2.4696	9.0428	0.11059	33.327	33.600	0.16093	0.098567	0.20035	191.41	1.3279
305.00	2.7698	8.6013	0.11626	34.240	34.562	0.16399	0.10090	0.22773	163.77	1.8996
310.00	3.0984	8.0537	0.12417	35.238	35.623	0.16732	0.10399	0.28254	134.40	2.8784
318.73	3.7539	5.0926	0.19636	38.575	39.312	0.17871			0	11.978
222.38	0.22436	0.13009	7.6872	36.790	38.515	0.19135	0.069340	0.080626	112.78	24.151
225.00	0.25012	0.14419	6.9355	36.943	38.678	0.19124	0.070316	0.081915	112.82	23.609
230.00	0.30561	0.17448	5.7314	37.235	38.987	0.19106	0.072196	0.084476	112.77	22.653
235.00	0.37011	0.20966	4.7696	37.528	39.293	0.19093	0.074101	0.087187	112.56	21.791
240.00	0.44448	0.25032	3.9949	37.820	39.595	0.19083	0.076031	0.090076	112.19	21.015
245.00	0.52962	0.29713	3.3655	38.110	39.892	0.19077	0.077991	0.093176	111.65	20.317
250.00	0.62644	0.35086	2.8502	38.397	40.183	0.19074	0.079983	0.096531	110.92	19.693
255.00	0.73591	0.41240	2.4248	38.681	40.465	0.19072	0.082010	0.10020	109.99	19.139
260.00	0.85899	0.48285	2.0711	38.960	40.739	0.19071	0.084077	0.10426	108.86	18.652
265.00	0.99671	0.56348	1.7747	39.232	41.001	0.19070	0.086191	0.10882	107.50	18.230
270.00	1.1502	0.65592	1.5246	39.496	41.249	0.19069	0.088360	0.11403	105.91	17.872
275.00	1.3204	0.76219	1.3120	39.749	41.481	0.19066	0.090597	0.12013	104.06	17.578
280.00	1.5088	0.88492	1.1301	39.988	41.693	0.19059	0.092917	0.12746	101.93	17.349
285.00	1.7164	1.0276	0.97310	40.209	41.879	0.19048	0.095345	0.13657	99.489	17.185
290.00	1.9447	1.1953	0.83661	40.407	42.034	0.19030	0.097913	0.14840	96.707	17.086
295.00	2.1952	1.3951	0.71677	40.573	42.147	0.19003	0.10068	0.16473	93.543	17.049
300.00	2.4696	1.6387	0.61023	40.695	42.202	0.18960	0.10372	0.18917	89.944	17.065
305.00	2.7698	1.9464	0.51377	40.751	42.174	0.18895	0.10722	0.23074	85.845	17.098
310.00	3.0984	2.3611	0.42353	40.693	42.006	0.18791	0.11155	0.31922	81.148	17.036
318.73	3.7539	5.0926	0.19636	38.575	39.312	0.17871			0	11.978

Single-Phase Properties

225.00	0.10000	0.054962	18.194	37.124	38.943	0.19969	0.069072	0.078403	117.21	20.832
300.00	0.10000	0.040537	24.669	43.122	45.589	0.22504	0.089337	0.098060	135.40	8.9939
375.00	0.10000	0.032243	31.015	50.424	53.525	0.24859	0.10425	0.11277	151.16	4.9674
450.00	0.10000	0.026801	37.312	58.668	62.399	0.27014	0.11482	0.12326	165.37	3.1241
525.00	0.10000	0.022943	43.585	67.581	71.940	0.28973	0.12235	0.13075	178.44	2.1242
225.00	1.0000	12.618	0.079249	22.807	22.886	0.12079	0.066092	0.10946	570.46	-0.30187
265.11	1.0000	11.046	0.090528	27.948	28.038	0.14178	0.086313	0.14352	366.71	0.083989
265.11	1.0000	0.56543	1.7686	39.238	41.007	0.19070	0.086239	0.10893	107.47	18.222
300.00	1.0000	0.45567	2.1946	42.504	44.699	0.20379	0.091458	0.10595	122.90	10.582
375.00	1.0000	0.33888	2.9509	50.051	53.002	0.22845	0.10508	0.11588	145.14	5.2070
450.00	1.0000	0.27473	3.6399	58.408	62.048	0.25042	0.11528	0.12496	162.15	3.1619
525.00	1.0000	0.23243	4.3024	67.387	71.689	0.27022	0.12264	0.13181	176.71	2.1142
300.00	5.0000	9.6705	0.10341	32.693	33.210	0.15873	0.096509	0.16433	257.24	0.56212
375.00	5.0000	2.2583	0.44281	47.826	50.040	0.20902	0.10970	0.14796	119.18	6.1481
450.00	5.0000	1.5252	0.65566	57.112	60.390	0.23421	0.11717	0.13497	151.89	3.1819
525.00	5.0000	1.2155	0.82269	66.464	70.578	0.25515	0.12378	0.13716	173.02	2.0030
300.00	10.000	10.303	0.097057	31.996	32.966	0.15625	0.095358	0.14728	332.30	0.14584
375.00	10.000	5.9487	0.16810	44.159	45.840	0.19435	0.11121	0.18759	145.44	2.6476
450.00	10.000	3.3384	0.29955	55.295	58.291	0.22473	0.11863	0.15056	154.01	2.5753
525.00	10.000	2.4910	0.40144	65.252	69.266	0.24729	0.12474	0.14433	177.25	1.6978
300.00	25.000	11.266	0.088766	30.853	33.072	0.15199	0.095576	0.13478	455.74	-0.17165
375.00	25.000	9.1060	0.10982	41.023	43.768	0.18375	0.10890	0.14958	314.62	0.14966
450.00	25.000	7.0706	0.14143	51.697	55.233	0.21161	0.11870	0.15437	248.92	0.47538
525.00	25.000	5.5874	0.17897	62.312	66.786	0.23536	0.12549	0.15348	234.29	0.57992
300.00	50.000	12.151	0.082298	29.792	33.906	0.14767	0.098484	0.12950	565.06	-0.30996
375.00	50.000	10.625	0.094118	39.323	44.029	0.17775	0.10946	0.14045	454.58	-0.19915
450.00	50.000	9.2093	0.10859	49.451	54.881	0.20410	0.11846	0.14799	394.01	-0.10589
525.00	50.000	8.0206	0.12468	59.888	66.122	0.22720	0.12538	0.15134	361.13	-0.058213

The values in these tables were generated from the NIST REFPROP software (Lemmon, E. W., McLinden, M. O., and Huber, M. L., NIST Standard Reference Database 23: Reference Fluid Thermodynamic and Transport Properties—REFPROP, National Institute of Standards and Technology, Standard Reference Data Program, Gaithersburg, Md., 2002, Version 7.1). The primary source for the thermodynamic properties is de Reuck, K. M., Craven, R. J. B., and Cole, W. A., "Report on the Development of an Equation of State for Sulphur Hexafluoride," IUPAC Thermodynamic Tables Project Centre, London, 1991. Validated equations for the viscosity and thermal conductivity are not currently available for this fluid.

Properties at the triple point temperature and the critical point temperature are given in the first and last entries of the saturation tables, respectively. In the single-phase table, when the temperature range for a given isobar includes a vapor-liquid phase boundary, the temperature of phase equilibrium is noted, and properties for both the saturated liquid and saturated vapor are given (with liquid properties given in the upper line). Lines are omitted from the temperature-pressure grid of the single-phase table, when the system would be in the solid phase or if there are potential problems with the source property surface.

The uncertainties of the equation of state are 0.1% in density, 2% in heat capacity, and 5% in the speed of sound, except in the critical region.

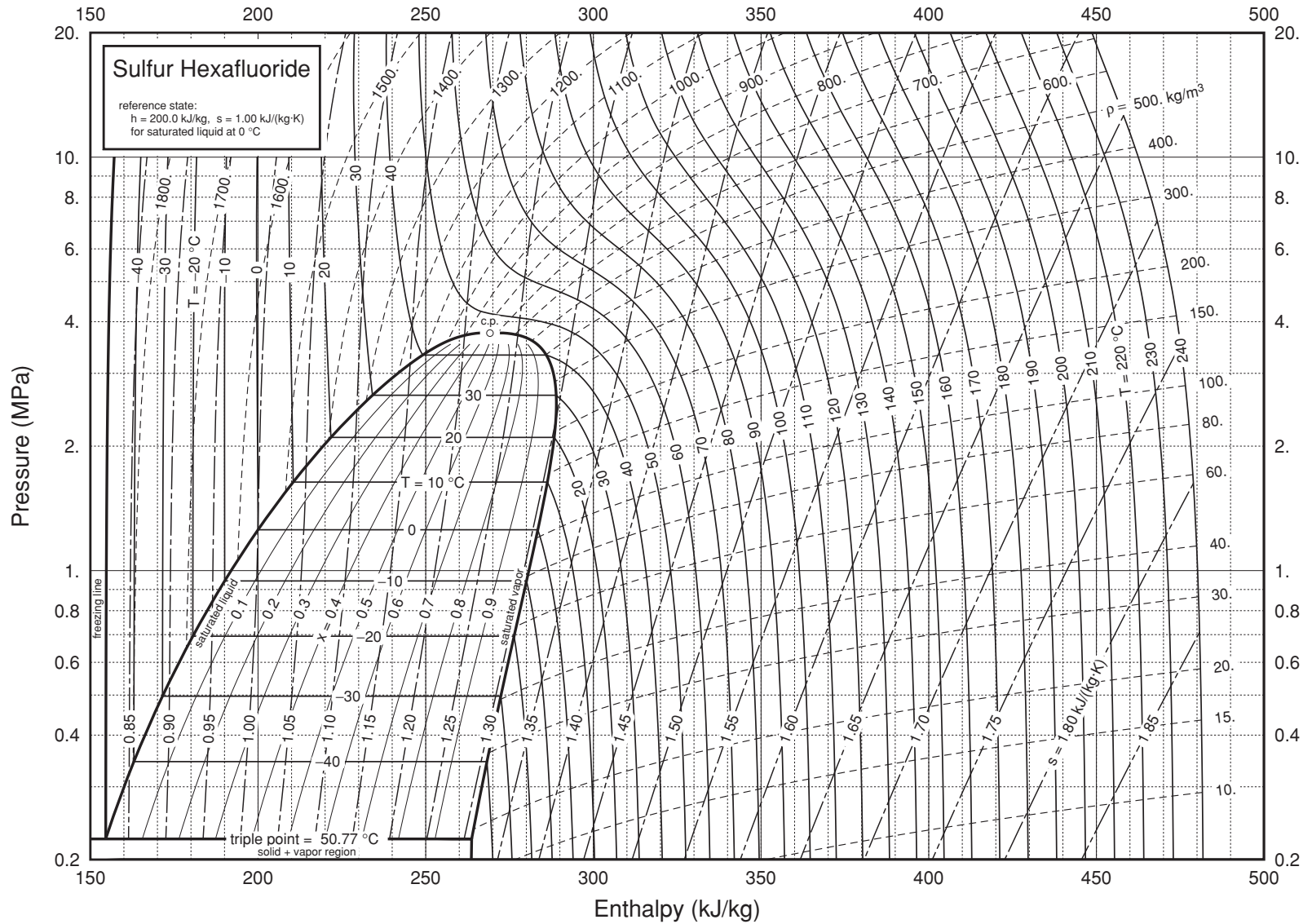


FIG. 2-30 Pressure-enthalpy diagram for sulfur hexafluoride (SF_6). Properties computed with the NIST REFPROP Database, Version 7.0 (Lemmon, E. W., McLinden, M. O., and Huber, M. L., 2002, NIST Standard Reference Database 23, NIST Reference Fluid Thermodynamic and Transport Properties—REFPROP, Version 7.0, Standard Reference Data Program, National Institute of Standards and Technology), based on the equation of state of de Reuck, K. M., Craven, R. J. B., and Cole, W. A., "Report on the Development of an Equation of State for Sulphur Hexafluoride," IUPAC Thermodynamic Tables Project Centre, London, 1991.

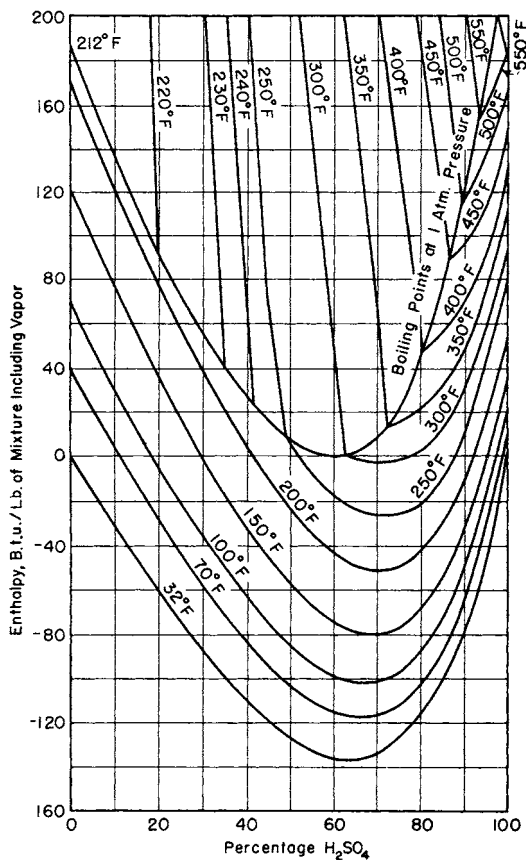


FIG. 2-31 Enthalpy-concentration diagram for aqueous sulfuric acid at 1 atm. Reference states: enthalpies of pure-liquid components at 32° F and vapor pressures are zero. NOTE: It should be observed that the weight basis includes the vapor, which is particularly important in the two-phase region. The upper ends of the tie lines in this region are assumed to be pure water. (*Hougen and Watson, Chemical Process Principles, part I, Wiley, New York, 1943.*)

TABLE 2-302 Saturated SUVA AC 9000

DuPont bulletin T-AC-9000-SI, 1994 (16 pp.) gives tables and a chart to 100 bar, 235°C. With a stated composition of 23% wt CH₂F₂ (R23), 25% wt CHF₂CF₃ (R125), and 52% wt CH₂FCH₃ (R134a) this is apparently identical to KLEA 66, to which the reader is referred.

TABLE 2-303 Thermodynamic Properties of Toluene

Temperature K	Pressure MPa	Density mol/dm ³	Volume dm ³ /mol	Int. energy kJ/mol	Enthalpy kJ/mol	Entropy kJ/(mol·K)	C _v kJ/(mol·K)	C _p kJ/(mol·K)	Sound speed m/s	Joule-Thomson K/MPa
Saturated Properties										
178.00	3.9393E-08	10.580	0.094517	-31.779	-31.779	-0.11617	0.094332	0.13565	1887.6	-0.57170
180.00	5.5336E-08	10.559	0.094708	-31.508	-31.508	-0.11466	0.094377	0.13561	1876.5	-0.57178
200.00	1.0833E-06	10.349	0.096627	-28.792	-28.792	-0.10035	0.095732	0.13627	1768.3	-0.56718
220.00	1.1479E-05	10.144	0.098582	-26.046	-26.046	-0.087266	0.098418	0.13855	1664.8	-0.55455
240.00	7.7542E-05	9.9416	0.10059	-23.242	-23.242	-0.075068	0.10209	0.14205	1565.9	-0.53604
260.00	0.00037312	9.7408	0.10266	-20.358	-20.358	-0.063529	0.10651	0.14648	1471.5	-0.51329
280.00	0.0013829	9.5402	0.10482	-17.378	-17.378	-0.052490	0.11147	0.15162	1381.2	-0.48747
300.00	0.0041774	9.3385	0.10708	-14.290	-14.289	-0.041839	0.11682	0.15729	1294.5	-0.45928
320.00	0.010727	9.1347	0.10947	-11.084	-11.083	-0.031496	0.12243	0.16337	1210.9	-0.42904
340.00	0.024170	8.9275	0.11201	-7.7538	-7.7511	-0.021403	0.12819	0.16976	1130.0	-0.39664
360.00	0.048980	8.7157	0.11474	-4.2939	-4.2882	-0.011516	0.13403	0.17640	1051.3	-0.36162
380.00	0.090988	8.4979	0.11768	-0.70017	-0.68946	-0.0018023	0.13988	0.18325	974.11	-0.32305
400.00	0.15731	8.2722	0.12089	3.0306	3.0496	0.0077653	0.14571	0.19032	898.08	-0.27947
420.00	0.25622	8.0367	0.12443	6.9017	6.9336	0.017209	0.15148	0.19764	822.67	-0.22860
440.00	0.39698	7.7887	0.12839	10.917	10.968	0.026551	0.15718	0.20531	747.37	-0.16688
460.00	0.58974	7.5246	0.13290	15.082	15.160	0.035811	0.16280	0.21350	671.66	-0.088509
480.00	0.84559	7.2394	0.13813	19.404	19.521	0.045015	0.16836	0.22253	594.94	0.016497
500.00	1.1766	6.9258	0.14439	23.896	24.066	0.054196	0.17388	0.23298	516.53	0.16681
520.00	1.5964	6.5719	0.15216	28.580	28.823	0.063400	0.17943	0.24610	435.57	0.40139
540.00	2.1207	6.1562	0.16244	33.494	33.839	0.072709	0.18518	0.26495	350.82	0.81616
560.00	2.7691	5.6334	0.17751	38.729	39.220	0.082291	0.19153	0.30025	260.06	1.7226
580.00	3.5688	4.8513	0.20613	44.585	45.321	0.092723	0.20008	0.44025	157.29	4.9610
591.75	4.1264	3.1690	0.31556	50.827	52.129	0.10409			0	19.734
178.00	3.9393E-08	2.6618E-08	37,569,000.	12.076	13.556	0.13852	0.054735	0.063049	136.02	821.69
180.00	5.5336E-08	3.6974E-08	27,046,000.	12.186	13.683	0.13640	0.055322	0.063636	136.69	783.08
200.00	1.0833E-06	6.5146E-07	1,535,000.	13.353	15.016	0.11869	0.061435	0.069750	143.14	496.50
220.00	1.1479E-05	6.2760E-06	159,340.	14.646	16.475	0.10601	0.067930	0.076246	149.27	328.33
240.00	7.7542E-05	3.8866E-05	25,729.	16.071	18.066	0.097048	0.074733	0.083057	155.12	225.22
260.00	0.00037312	0.00017271	5,790.1	17.632	19.793	0.090897	0.081779	0.090124	160.70	159.61
280.00	0.0013829	0.00059503	1,680.6	19.331	21.655	0.086914	0.089005	0.097403	166.00	116.50
300.00	0.0041774	0.0016815	594.71	21.165	23.649	0.084624	0.096358	0.10486	170.96	87.391
320.00	0.010727	0.0040644	246.04	23.130	25.769	0.083666	0.10379	0.11248	175.47	67.283
340.00	0.024170	0.0086767	115.25	25.218	28.003	0.083758	0.11127	0.12026	179.42	53.119
360.00	0.048980	0.016770	59.631	27.421	30.342	0.084678	0.11875	0.12819	182.67	42.979
380.00	0.090988	0.029922	33.420	29.730	32.770	0.086250	0.12622	0.13630	185.07	35.624
400.00	0.15731	0.050060	19.976	32.133	35.275	0.088329	0.13364	0.14463	186.44	30.237
420.00	0.25622	0.079525	12.575	34.618	37.840	0.090796	0.14100	0.15326	186.62	26.277
440.00	0.39698	0.12122	8.2496	37.172	40.447	0.093548	0.14832	0.16234	185.42	23.381
460.00	0.58974	0.17889	5.5901	39.776	43.073	0.096491	0.15558	0.17214	182.60	21.313
480.00	0.84559	0.25767	3.8810	42.408	45.690	0.099533	0.16283	0.18316	177.87	19.928
500.00	1.1766	0.36515	2.7386	45.035	48.257	0.10258	0.17013	0.19639	170.89	19.156
520.00	1.5964	0.51366	1.9468	47.606	50.713	0.10550	0.17758	0.21403	161.17	19.007
540.00	2.1207	0.72590	1.3776	50.033	52.955	0.10811	0.18540	0.24190	148.11	19.581
560.00	2.7691	1.0524	0.95020	52.136	54.768	0.11005	0.19407	0.30118	130.92	21.067
580.00	3.5688	1.6605	0.60222	53.371	55.520	0.11031	0.20499	0.55687	108.57	23.353
591.75	4.1264	3.1690	0.31556	50.827	52.129	0.10409			0	19.734

Single-Phase Properties

200.00	0.10000	10.350	0.096623	-28.794	-28.784	-0.10036	0.095737	0.13627	1768.7	-0.56720
325.00	0.10000	9.0842	0.11008	-10.267	-10.256	-0.028962	0.12386	0.16493	1191.0	-0.42130
383.28	0.10000	8.4614	0.11818	-0.097277	-0.085459	-0.00022242	0.14084	0.18440	961.57	-0.31629
383.28	0.10000	0.032692	30.589	30.118	33.177	0.086560	0.12744	0.13765	185.37	34.622
450.00	0.10000	0.027344	36.572	39.369	43.026	0.11021	0.14828	0.15755	202.98	18.656
575.00	0.10000	0.021125	47.338	60.145	64.879	0.15289	0.18229	0.19099	230.86	8.1724
700.00	0.10000	0.017270	57.904	84.697	90.487	0.19311	0.20915	0.21767	255.08	4.5991
200.00	1.0000	10.354	0.096581	-28.811	-28.715	-0.10045	0.095778	0.13625	1771.8	-0.56742
325.00	1.0000	9.0933	0.10997	-10.303	-10.193	-0.029074	0.12389	0.16482	1196.3	-0.42281
450.00	1.0000	7.6732	0.13032	12.928	13.058	0.031073	0.16000	0.20893	715.87	-0.13702
489.95	1.0000	7.0876	0.14109	21.616	21.757	0.049581	0.17110	0.22749	556.21	0.083851
489.95	1.0000	0.30691	3.2583	43.717	46.976	0.10105	0.16645	0.18937	174.71	19.469
575.00	1.0000	0.23372	4.2786	59.065	63.344	0.13184	0.18481	0.19848	210.35	9.4517
700.00	1.0000	0.18116	5.5199	84.035	89.555	0.17301	0.21011	0.22077	244.28	4.8519
200.00	5.0000	10.373	0.096400	-28.887	-28.405	-0.10083	0.095961	0.13619	1785.8	-0.56831
325.00	5.0000	9.1328	0.10950	-10.460	-9.9129	-0.029562	0.12404	0.16434	1219.1	-0.42907
450.00	5.0000	7.7765	0.12859	12.548	13.191	0.030217	0.16002	0.20635	761.15	-0.18092
575.00	5.0000	5.6051	0.17841	41.699	42.591	0.087531	0.19430	0.28257	285.95	1.3449
700.00	5.0000	1.1698	0.85487	80.250	84.524	0.15419	0.21547	0.24819	197.87	5.8706
200.00	10.000	10.397	0.096178	-28.980	-28.018	-0.10130	0.096187	0.13612	1802.9	-0.56932
325.00	10.000	9.1800	0.10893	-10.647	-9.5580	-0.030150	0.12422	0.16382	1246.4	-0.43597
450.00	10.000	7.8890	0.12676	12.131	13.398	0.029259	0.16009	0.20400	810.93	-0.22080
575.00	10.000	6.1856	0.16166	40.014	41.630	0.084396	0.19242	0.24975	425.25	0.38997
700.00	10.000	3.2697	0.30584	73.814	76.873	0.13965	0.21978	0.30359	189.44	3.9797
325.00	100.00	9.7930	0.10211	-12.967	-2.7551	-0.038333	0.12727	0.16019	1609.1	-0.48598
450.00	100.00	8.9423	0.11183	8.2140	19.397	0.019038	0.16256	0.19397	1308.6	-0.38806
575.00	100.00	8.1649	0.12248	33.274	45.521	0.070122	0.19323	0.22291	1104.9	-0.31962
700.00	100.00	7.4598	0.13405	61.439	74.845	0.11620	0.21782	0.24523	967.84	-0.27316
450.00	500.00	10.545	0.094835	3.6375	51.055	-0.00069710	0.17022	0.19432	2238.9	-0.40813
575.00	500.00	10.097	0.099035	27.662	77.179	0.050390	0.20000	0.22274	2087.2	-0.35992
700.00	500.00	9.7036	0.10305	54.974	106.50	0.096461	0.22392	0.24550	1977.5	-0.32978

The values in these tables were generated from the NIST REFPROP software (Lemmon, E. W., McLinden, M. O., and Huber, M. L., NIST Standard Reference Database 23: Reference Fluid Thermodynamic and Transport Properties—REFPROP, National Institute of Standards and Technology, Standard Reference Data Program, Gaithersburg, Md., 2002, Version 7.1). The primary source for the thermodynamic properties is Lemmon, E. W., and Span, R., "Short Fundamental Equations of State for 20 Industrial Fluids," *J. Chem. Eng. Data* **51**(3):785–850, 2006. Validated equations for the viscosity and thermal conductivity are not currently available for this fluid.

Properties at the triple point temperature and the critical point temperature are given in the first and last entries of the saturation tables, respectively. In the single-phase table, when the temperature range for a given isobar includes a vapor-liquid phase boundary, the temperature of phase equilibrium is noted, and properties for both the saturated liquid and saturated vapor are given (with liquid properties given in the upper line). Lines are omitted from the temperature-pressure grid of the single-phase table, when the system would be in the solid phase or if there are potential problems with the source property surface.

The uncertainties in density in the equation of state are 0.05% in the liquid phase up to 540 K, 0.5% up to the critical temperature, 1% at higher temperatures, 0.5% at pressures from 100 to 500 MPa, and 0.2% in the vapor phase. The uncertainty for the saturated-liquid density (and densities near atmospheric pressure) approaches 0.01% around 300 K. The uncertainties in vapor pressure are 0.3% from 270 to 305 K, 0.05% from 305 to 425 K, 0.1% up to 555 K, and 0.15% up to the critical temperature. The uncertainty in heat capacities is 0.5% and rises to 3% in the critical region. The uncertainty in the speed of sound is 1% up to 500 K and 100 MPa and rises to 2% at higher pressures and higher temperatures.

TABLE 2-304 Saturated Solid/Vapor Water*

Temp., °F	Pressure, lb/in ² abs.	Volume, ft ³ /lb		Enthalpy, Btu/lb		Entropy, Btu/(lb)(°F)	
		Solid	Vapor	Solid	Vapor	Solid	Vapor
-160	4.949.-8	0.01722	3.607.+9	-222.05	990.38	-0.4907	3.5549
-150	1.620.-7	0.01723	1.139.+9	-218.82	994.80	-0.4801	3.4387
-140	4.928.-7	0.01724	3.864.+8	-215.49	999.21	-0.4695	3.3301
-130	1.403.-6	0.01725	1.400.+8	-212.08	1003.63	-0.4590	3.2284
-120	3.757.-6	0.01726	5.386.+7	-208.58	1008.05	-0.4485	3.1330
-110	9.517.-6	0.01728	2.189.+7	-204.98	1012.47	-0.4381	3.0434
-100	2.291.-5	0.01729	9.352.+6	-201.28	1016.89	-0.4277	2.9591
-90	5.260.-5	0.01730	4.186.+6	-197.49	1021.31	-0.4173	2.8796
-80	1.157.-4	0.01731	1.955.+6	-193.60	1025.73	-0.4069	2.8045
-70	2.443.-4	0.01732	9.501.+5	-189.61	1030.15	-0.3965	2.7336
-60	4.972.-4	0.01734	4.788.+5	-185.52	1034.58	-0.3862	2.6664
-50	9.776.-4	0.01735	2.496.+5	-181.34	1039.00	-0.3758	2.6028
-45	1.354.-3	0.01736	1.824.+5	-179.21	1041.21	-0.3707	2.5723
-40	1.861.-3	0.01737	1.343.+5	-177.06	1043.42	-0.3655	2.5425
-35	2.540.-3	0.01737	9.961.+4	-174.88	1045.63	-0.3604	2.5135
-30	3.440.-3	0.01738	7.441.+4	-172.68	1047.84	-0.3552	2.4853
-25	4.627.-3	0.01739	5.596.+4	-170.46	1050.05	-0.3501	2.4577
-20	6.181.-3	0.01739	4.237.+4	-168.21	1052.26	-0.3449	2.4308
-15	8.204.-3	0.01740	3.228.+4	-165.94	1054.47	-0.3398	2.4046
-10	1.082.-2	0.01741	2.475.+4	-163.65	1056.67	-0.3347	2.3791
-5	1.419.-2	0.01741	1.909.+4	-161.33	1058.88	-0.3295	2.3541
0	1.849.-2	0.01742	1.481.+4	-158.98	1061.09	-0.3244	2.3297
5	2.396.-2	0.01743	1.155.+4	-156.61	1063.29	-0.3193	2.3039
10	3.087.-2	0.01744	9.060.+3	-154.22	1065.50	-0.3142	2.2827
15	3.957.-2	0.01744	7.144.+3	-151.80	1067.70	-0.3090	2.2600
16	4.156.-2	0.01745	6.817.+3	-151.32	1068.14	-0.3080	2.2555
18	4.581.-2	0.01745	6.210.+3	-150.34	1069.02	-0.3060	2.2466
20	5.045.-2	0.01745	5.662.+3	-149.36	1069.90	-0.3039	2.2378
22	5.552.-2	0.01746	5.166.+3	-148.38	1070.38	-0.3019	2.2291
24	6.105.-2	0.01746	4.717.+3	-147.39	1071.66	-0.2998	2.2205
26	6.708.-2	0.01746	4.311.+3	-146.40	1072.53	-0.2978	2.2119
28	7.365.-2	0.01746	3.943.+3	-145.40	1073.41	-0.2957	2.2034
30	8.080.-2	0.01747	3.608.+3	-144.40	1074.29	-0.2937	2.1950
31	8.461.-2	0.01747	3.453.+3	-143.90	1074.73	-0.2927	2.1908
32	8.858.-2	0.01747	3.305.+3	-143.40	1075.16	-0.2916	2.1867

*Condensed from *Fundamentals*, American Society of Heating, Refrigerating and Air-Conditioning Engineers, 1967 and 1972. Reproduced by permission. The validity of many standard reference tables has been critically reviewed by Janco, Papezin, and van Hook, *J. Phys. Chem.*, **74** (1970):2984. Current information on the properties of solid, vapor, and liquid water properties can be found at <http://www.iapws.org>. The notation 4.949.-8, 3.607.+9, etc., means 4.949×10^{-8} , 3.607×10^9 , etc.

TABLE 2-305 Thermodynamic Properties of Water

Temperature K	Pressure MPa	Density mol/dm ³	Volume dm ³ /mol	Int. energy kJ/mol	Enthalpy kJ/mol	Entropy kJ/(mol·K)	C _v kJ/(mol·K)	C _p kJ/(mol·K)	Sound speed m/s	Joule-Thomson K/MPa	Therm. cond. mW/(m·K)	Viscosity μPa·s
Saturated Properties												
273.16	0.000612	55.497	0.018019	0	1.1E-05	0	0.075978	0.076023	1402.3	-0.24142	561.04	1791.2
280	0.000992	55.501	0.018018	0.51875	0.51877	0.001876	0.075669	0.075668	1434.1	-0.23515	574.04	1433.7
290	0.001920	55.440	0.018038	1.2742	1.2742	0.004527	0.075095	0.075429	1472.1	-0.22720	592.73	1084.0
300	0.003537	55.315	0.018078	2.0278	2.0279	0.007082	0.074412	0.075320	1501.4	-0.22024	610.28	853.84
310	0.006231	55.139	0.018136	2.7808	2.7810	0.009551	0.073645	0.075294	1523.2	-0.21393	626.05	693.54
320	0.010546	54.919	0.018209	3.5339	3.5340	0.011941	0.072811	0.075317	1538.7	-0.20804	639.71	577.02
330	0.017213	54.662	0.018294	4.2873	4.2876	0.014260	0.071927	0.075373	1548.7	-0.20241	651.18	489.49
340	0.027188	54.371	0.018392	5.0414	5.0419	0.016511	0.071008	0.075456	1553.9	-0.19690	660.55	421.97
350	0.041682	54.049	0.018502	5.7964	5.7972	0.018700	0.070070	0.075567	1554.8	-0.19140	668.00	368.77
360	0.062194	53.698	0.018623	6.5526	6.5538	0.020830	0.069124	0.075708	1552.0	-0.18581	673.76	326.10
370	0.090535	53.321	0.018754	7.3104	7.3121	0.022906	0.068180	0.075883	1545.8	-0.18005	678.02	291.36
380	0.12885	52.918	0.018897	8.0701	8.0725	0.024932	0.067247	0.076098	1536.5	-0.17404	681.00	262.69
390	0.17964	52.490	0.019051	8.8320	8.8354	0.026911	0.066331	0.076357	1524.3	-0.16769	682.83	238.77
400	0.24577	52.038	0.019217	9.5966	9.6013	0.028847	0.065438	0.076664	1509.5	-0.16092	683.64	218.60
410	0.33045	51.563	0.019394	10.364	10.371	0.030743	0.064570	0.077026	1492.2	-0.15366	683.52	201.43
420	0.43730	51.064	0.019583	11.136	11.144	0.032602	0.063731	0.077447	1472.5	-0.14581	682.53	186.68
430	0.57026	50.541	0.019786	11.911	11.923	0.034427	0.062920	0.077934	1450.6	-0.13728	680.70	173.91
440	0.73367	49.994	0.020003	12.692	12.706	0.036222	0.062140	0.078495	1426.5	-0.12794	678.05	162.77
450	0.9322	49.421	0.020234	13.477	13.496	0.037988	0.061390	0.079136	1400.4	-0.11767	674.59	152.98
460	1.1709	48.824	0.020482	14.269	14.293	0.039729	0.060671	0.079869	1372.2	-0.10631	670.28	144.31
470	1.4551	48.199	0.020748	15.068	15.098	0.041448	0.059984	0.080706	1342.0	-0.09369	665.12	136.58
480	1.7905	47.545	0.021033	15.875	15.913	0.043147	0.059327	0.081662	1309.8	-0.07959	659.07	129.64
490	2.1831	46.861	0.021340	16.690	16.737	0.044830	0.058702	0.082757	1275.7	-0.06372	652.06	123.37
500	2.6392	46.145	0.021671	17.515	17.573	0.046498	0.058109	0.084013	1239.6	-0.04578	644.05	117.66
510	3.1655	45.393	0.022030	18.352	18.421	0.048156	0.057548	0.085464	1201.5	-0.02534	634.95	112.42
520	3.7690	44.603	0.022420	19.200	19.285	0.049807	0.057023	0.087149	1161.3	-0.00189	624.68	107.57
530	4.4569	43.770	0.022847	20.064	20.165	0.051454	0.056536	0.089124	1119.1	0.025264	613.15	103.05
540	5.2369	42.889	0.023316	20.943	21.065	0.053102	0.056089	0.091464	1074.6	0.057002	600.26	98.792
550	6.1172	41.954	0.023836	21.841	21.987	0.054756	0.055690	0.094275	1027.9	0.094527	585.95	94.746
560	7.1062	40.956	0.024417	22.762	22.935	0.056422	0.055347	0.097713	978.54	0.13949	570.21	90.857
570	8.2132	39.885	0.025072	23.709	23.915	0.058106	0.055071	0.10201	926.44	0.19425	553.08	87.074
580	9.448	38.725	0.025823	24.688	24.932	0.059821	0.054881	0.10754	871.23	0.26220	534.74	83.342
590	10.821	37.456	0.026698	25.707	25.996	0.061577	0.054808	0.11491	812.49	0.34857	515.43	79.600
600	12.345	36.048	0.027741	26.777	27.119	0.063396	0.054902	0.12526	749.57	0.46172	495.46	75.773
610	14.033	34.451	0.029026	27.917	28.324	0.065309	0.055258	0.14100	681.27	0.61660	475.03	71.759
620	15.901	32.577	0.030697	29.160	29.648	0.067371	0.056100	0.16852	604.73	0.84473	454.10	67.382
630	17.969	30.210	0.033101	30.585	31.180	0.069715	0.058152	0.23108	513.19	1.2251	432.51	62.244
640	20.265	26.729	0.037413	32.422	33.180	0.072737	0.064521	0.46736	400.66	1.9542	414.93	55.247
647.1	22.064	17.874	0.055948	36.314	37.548	0.079393			0	3.7410		
273.16	0.000612	0.000269	3711.0	42.785	45.055	0.16494	0.025553	0.033947	409.00	592.65	17.071	9.2163
280	0.000992	0.000426	2345.4	42.954	45.280	0.16174	0.025657	0.034073	413.92	477.26	17.442	9.3515
290	0.001920	0.000797	1254.3	43.201	45.609	0.15741	0.025816	0.034270	420.99	351.65	18.031	9.6414
300	0.003537	0.001420	704.01	43.446	45.936	0.15344	0.025982	0.034483	427.89	264.35	18.673	9.9195
310	0.006231	0.002424	412.60	43.690	46.261	0.14981	0.026158	0.034716	434.63	203.74	19.369	10.213
320	0.010546	0.003978	251.39	43.931	46.582	0.14647	0.026350	0.034980	441.18	161.25	20.117	10.518
330	0.017213	0.006304	158.62	44.169	46.900	0.14339	0.026568	0.035287	447.54	130.92	20.922	10.833
340	0.027188	0.009681	103.30	44.404	47.212	0.14054	0.026821	0.035653	453.68	108.77	21.784	11.157
350	0.041682	0.014448	69.213	44.634	47.519	0.13791	0.027118	0.036091	459.58	92.178	22.707	11.487
360	0.062194	0.021014	47.586	44.860	47.819	0.13546	0.027469	0.036617	465.22	79.440	23.695	11.823
370	0.090535	0.029859	33.491	45.079	48.111	0.13317	0.027883	0.037249	470.57	69.427	24.750	12.162
380	0.12885	0.041537	24.075	45.291	48.393	0.13104	0.028372	0.038004	475.61	61.373	25.875	12.504
390	0.17964	0.056683	17.642	45.496	48.665	0.12904	0.028944	0.038903	480.32	54.749	27.074	12.848
400	0.24577	0.076014	13.156	45.691	48.924	0.12715	0.029608	0.039963	484.67	49.181	28.347	13.192
410	0.33045	0.10034	9.9666	45.876	49.170	0.12537	0.030369	0.041203	488.65	44.405	29.699	13.538
420	0.43730	0.13055	7.6601	46.050	49.400	0.12369	0.031230	0.042634	492.22	40.237	31.128	13.883
430	0.57026	0.16765	5.9649	46.211	49.613	0.12208	0.032187	0.044269	495.39	36.550	32.638	14.228
440	0.73367	0.21276	4.7002	46.359	49.807	0.12054	0.033234	0.046114	498.12	33.259	34.230	14.573

TABLE 2-305 Thermodynamic Properties of Water (Continued)

Temperature K	Pressure MPa	Density mol/dm ³	Volume dm ³ /mol	Int. energy kJ/mol	Enthalpy kJ/mol	Entropy kJ/(mol·K)	C _v kJ/(mol·K)	C _p kJ/(mol·K)	Sound speed m/s	Joule-Thomson K/MPa	Therm. cond. mW/(m·K)	Viscosity μPa·s
Saturated Properties												
450	0.93220	0.26711	3.7438	46.492	49.982	0.11907	0.034362	0.048177	500.41	30.307	35.904	14.917
460	1.1709	0.33209	3.0113	46.609	50.134	0.11764	0.035561	0.050469	502.24	27.653	37.663	15.261
470	1.4551	0.40925	2.4435	46.708	50.263	0.11627	0.036821	0.053005	503.60	25.265	39.512	15.606
480	1.7905	0.50035	1.9986	46.788	50.367	0.11493	0.038137	0.055809	504.45	23.118	41.455	15.952
490	2.1831	0.60738	1.6464	46.848	50.442	0.11362	0.039503	0.058919	504.78	21.187	43.502	16.300
500	2.6392	0.73265	1.3649	46.885	50.487	0.11233	0.040920	0.062388	504.55	19.450	45.666	16.653
510	3.1655	0.87884	1.1379	46.898	50.500	0.11105	0.042391	0.066289	503.71	17.886	47.969	17.011
520	3.7690	1.0491	0.95318	46.883	50.475	0.10979	0.043920	0.070723	502.23	16.475	50.442	17.377
530	4.4569	1.2473	0.80174	46.838	50.411	0.10852	0.045519	0.075827	500.05	15.197	53.130	17.755
540	5.2369	1.4780	0.67659	46.758	50.302	0.10724	0.047197	0.081789	497.10	14.035	56.102	18.149
550	6.1172	1.7471	0.57238	46.641	50.142	0.10595	0.048968	0.088873	493.31	12.973	59.456	18.563
560	7.1062	2.0620	0.48497	46.478	49.925	0.10462	0.050848	0.097461	488.58	11.997	63.341	19.007
570	8.2132	2.4325	0.41110	46.264	49.641	0.10324	0.052856	0.10813	482.79	11.093	67.981	19.489
580	9.4480	2.8720	0.34819	45.988	49.278	0.10180	0.055017	0.12178	475.80	10.248	73.721	20.024
590	10.821	3.3994	0.29417	45.636	48.819	0.10026	0.057361	0.13994	467.41	9.4499	81.108	20.634
600	12.345	4.0434	0.24732	45.188	48.242	0.098600	0.059939	0.16540	457.33	8.6837	91.052	21.350
610	14.033	4.8497	0.20620	44.613	47.506	0.096755	0.062831	0.20384	445.11	7.9329	105.17	22.229
620	15.901	5.9009	0.16946	43.855	46.550	0.094631	0.066197	0.26923	429.99	7.1743	126.66	23.374
630	17.969	7.3737	0.13562	42.801	45.238	0.092029	0.070465	0.40819	410.21	6.3669	163.44	25.018
640	20.265	9.8331	0.10170	41.095	43.156	0.088324	0.077576	0.94736	379.64	5.3854	250.01	27.938
647.1	22.064	17.874	0.055948	36.314	37.548	0.079393			0	3.7410		
Single-Phase Properties												
300	0.1	55.317	0.018078	2.0277	2.0295	0.007081	0.074406	0.075315	1501.5	-0.22024	610.32	853.83
372.76	0.1	53.212	0.018793	7.5196	7.5214	0.02347	0.067921	0.075938	1543.5	-0.17843	678.97	282.91
372.76	0.1	0.032769	30.517	45.138	48.190	0.13257	0.02801	0.037444	471.99	67.038	25.053	12.256
400	0.1	0.030397	32.898	45.900	49.189	0.13516	0.02717	0.036170	490.31	47.254	27.008	13.285
500	0.1	0.024154	41.401	48.619	52.759	0.14313	0.02717	0.035693	548.31	19.298	35.861	17.270
600	0.1	0.020086	49.786	51.387	56.365	0.14970	0.028103	0.036513	598.61	10.567	46.367	21.407
700	0.1	0.017201	58.136	54.256	60.069	0.15541	0.029225	0.037592	643.92	6.6444	57.964	25.564
800	0.1	0.015044	66.471	57.240	63.887	0.16050	0.030431	0.038778	685.47	4.5167	70.385	29.669
900	0.1	0.013369	74.799	60.347	67.827	0.16514	0.031687	0.040024	724.03	3.2280	83.466	33.685
1000	0.1	0.012030	83.123	63.581	71.893	0.16943	0.032963	0.041293	760.17	2.3885	97.085	37.592
1100	0.1	0.010936	91.444	66.941	76.085	0.17342	0.034228	0.042554	794.33	1.8122	111.15	41.382
1200	0.1	0.010024	99.763	70.426	80.402	0.17718	0.035458	0.043781	826.85	1.4006	125.58	45.054
300	1	55.340	0.018070	2.0263	2.0444	0.007077	0.074353	0.075270	1503.0	-0.22022	610.73	853.67
400	1	52.060	0.019209	9.5914	9.6106	0.028834	0.065422	0.076628	1511.3	-0.16113	684.10	218.80
453.03	1	49.243	0.020307	13.717	13.737	0.038518	0.061169	0.079348	1392.0	-0.11435	673.37	150.24
453.03	1	0.28559	3.5015	46.529	50.030	0.11863	0.034718	0.048846	501.02	29.473	36.427	15.021
500	1	0.25158	3.9749	48.111	52.086	0.12295	0.030084	0.041065	535.74	19.741	38.799	17.051
600	1	0.20466	4.8861	51.123	56.009	0.13011	0.029002	0.038358	592.58	10.615	47.636	21.329
700	1	0.17377	5.7547	54.087	59.842	0.13602	0.029629	0.038495	640.55	6.6387	58.735	25.550
800	1	0.15134	6.6074	57.121	63.729	0.14121	0.030651	0.039301	683.48	4.5077	70.983	29.687
900	1	0.13418	7.4524	60.258	67.710	0.14590	0.031821	0.040358	722.85	3.2212	84.000	33.718
1000	1	0.12058	8.2932	63.511	71.804	0.15021	0.033051	0.041522	759.50	2.3837	97.573	37.630
1100	1	0.10951	9.1313	66.885	76.016	0.15422	0.034290	0.042790	794.01	1.8089	111.57	41.420
1200	1	0.10032	9.9677	70.380	80.347	0.15799	0.035504	0.043905	826.77	1.3982	125.89	45.088
300	5	55.439	0.018038	2.0204	2.1106	0.007057	0.074119	0.075070	1509.8	-0.22012	612.54	853.00
400	5	52.173	0.019167	9.5643	9.6601	0.028766	0.065337	0.076438	1520.9	-0.16222	686.54	219.84
500	5	46.267	0.021614	17.474	17.582	0.046415	0.058082	0.083643	1250.0	-0.04945	646.52	118.27
537.09	5	43.151	0.023175	20.685	20.801	0.052622	0.056215	0.090740	1087.8	0.047232	604.15	100.01
537.09	5	1.4072	0.71063	46.785	50.338	0.10762	0.046699	0.079952	498.04	14.362	55.203	18.032
600	5	1.1320	0.88340	49.734	54.151	0.11436	0.034611	0.051045	561.07	10.407	54.653	21.062
700	5	0.91269	1.0957	53.286	58.765	0.12148	0.031678	0.043318	624.59	6.5536	62.680	25.547

800	5	0.77805	1.2853	56.576	63.002	0.12714	0.031683	0.041848	674.39	4.4532	73.950	29.806
900	5	0.68224	1.4658	59.855	67.183	0.13207	0.032430	0.041922	717.57	3.1856	86.626	33.891
1000	5	0.60918	1.6416	63.197	71.405	0.13652	0.033447	0.042571	756.57	2.3599	99.971	37.821
1100	5	0.55109	1.8146	66.632	75.705	0.14061	0.034565	0.043465	792.63	1.7924	113.64	41.606
1200	5	0.50355	1.9859	70.172	80.101	0.14444	0.035704	0.044458	826.45	1.3865	127.51	45.257
300	10	55.561	0.017998	2.0131	2.1931	0.007031	0.073834	0.074829	1518.2	-0.21999	614.81	852.28
400	10	52.312	0.019116	9.5311	9.7222	0.028682	0.065233	0.076208	1532.7	-0.16351	689.57	221.13
500	10	46.517	0.021497	17.389	17.604	0.046244	0.058028	0.082910	1271.3	-0.05669	651.64	119.55
584.15	10	38.213	0.026169	25.105	25.367	0.060543	0.054835	0.11032	847.33	0.29540	526.83	81.795
584.15	10	3.0787	0.32482	45.852	49.100	0.10117	0.055964	0.128640	472.51	9.9124	76.543	20.267
600	10	2.7628	0.36195	47.183	50.802	0.10405	0.047271	0.092535	503.34	9.4382	71.110	21.036
700	10	1.9625	0.50956	52.145	57.241	0.11405	0.034838	0.051779	602.20	6.3228	69.301	25.704
800	10	1.6157	0.61893	55.851	62.040	0.12046	0.033089	0.045603	662.61	4.3529	78.476	30.054
900	10	1.3945	0.71709	59.334	66.505	0.12572	0.033219	0.044062	710.98	3.1289	90.516	34.176
1000	10	1.2345	0.81002	62.798	70.898	0.13035	0.033947	0.043952	753.03	2.3241	103.50	38.111
1100	10	1.1111	0.90002	66.314	75.314	0.13456	0.034908	0.044427	791.02	1.7683	116.73	41.882
1200	10	1.0119	0.98820	69.910	79.792	0.13846	0.035954	0.045164	826.16	1.3695	130.00	45.506
300	100	57.573	0.017369	1.8921	3.6290	0.006516	0.069812	0.071696	1667.9	-0.21618	654.50	856.88
400	100	54.500	0.018349	9.0423	10.877	0.027360	0.063582	0.073086	1717.3	-0.17905	741.80	243.50
500	100	49.914	0.020034	16.289	18.292	0.043895	0.057324	0.075607	1555.7	-0.12564	730.42	138.92
600	100	43.935	0.022761	23.820	26.097	0.058109	0.052776	0.081104	1300.4	-0.02079	645.83	101.51
700	100	36.179	0.027640	31.916	34.680	0.071320	0.049610	0.091576	1020.0	0.21155	510.14	79.363
800	100	26.768	0.037359	40.700	44.435	0.084331	0.047143	0.10108	813.97	0.65939	351.46	62.042
900	100	19.073	0.052429	48.805	54.048	0.095669	0.043932	0.088057	765.30	1.0399	257.03	53.250
1000	100	14.734	0.067868	55.188	61.975	0.10404	0.041345	0.071678	792.50	1.0944	232.07	51.518
1100	100	12.246	0.081656	60.470	68.635	0.11039	0.040131	0.062539	832.67	0.98401	223.70	52.497
1200	100	10.631	0.094062	65.222	74.628	0.11561	0.039810	0.057826	872.28	0.83544	219.07	54.415
300	500	63.750	0.015686	1.5247	9.3678	0.003746	0.063403	0.068296	2228.6	-0.19915	763.82	1089.4
400	500	60.862	0.016431	7.9635	16.179	0.023347	0.059634	0.067603	2258.7	-0.19486	929.09	320.18
500	500	57.695	0.017332	14.264	22.930	0.038412	0.055769	0.067522	2200.7	-0.18339	1096.6	189.08
600	500	54.316	0.018411	20.481	29.687	0.050731	0.052734	0.067584	2093.8	-0.16883	1097.9	141.83
700	500	50.847	0.019667	26.606	36.439	0.061141	0.050315	0.067436	1970.5	-0.15188	935.15	118.47
800	500	47.385	0.021104	32.615	43.167	0.070124	0.048442	0.067080	1850.1	-0.13256	738.72	104.70
900	500	44.018	0.022718	38.492	49.851	0.077998	0.047068	0.066596	1743.4	-0.11124	572.49	95.388
1000	500	40.814	0.024501	44.233	56.484	0.084987	0.046126	0.066041	1655.7	-0.08910	445.17	88.418
1100	500	37.834	0.026432	49.839	63.055	0.091251	0.045537	0.065356	1589.3	-0.06907	350.97	83.021
1200	500	35.124	0.028470	55.312	69.547	0.096900	0.045218	0.064451	1543.9	-0.05511	282.78	78.952
400	1000	65.942	0.015165	7.4792	22.644	0.019833	0.057934	0.065743	2718.6	-0.19303	1172.7	329.93
500	1000	63.253	0.015810	13.357	29.167	0.034391	0.055063	0.064967	2677.2	-0.19158	2199.5	190.55
600	1000	60.572	0.016509	19.141	35.650	0.046212	0.053055	0.064676	2602.3	-0.18789	3250.5	137.73
700	1000	57.937	0.017260	24.836	42.096	0.056150	0.051393	0.064219	2513.7	-0.18439	3202.2	108.98
800	1000	55.384	0.018056	30.435	48.491	0.064689	0.050059	0.063663	2423.7	-0.18105	2408.7	91.430
900	1000	52.937	0.018890	35.938	54.828	0.072155	0.049062	0.063101	2338.7	-0.17779	1610.7	80.198
1000	1000	50.611	0.019759	41.354	61.113	0.078776	0.048373	0.062594	2261.5	-0.17459	1052.9	72.716
1100	1000	48.415	0.020655	46.695	67.350	0.084722	0.047942	0.062176	2193.2	-0.17139	703.41	67.520
1200	1000	46.349	0.021575	51.976	73.551	0.090117	0.047713	0.061861	2133.6	-0.16808	487.61	63.774

The values in these tables were generated from the NIST REFPROP software (Lemmon, E. W., McLinden, M. O., and Huber, M. L., NIST Standard Reference Database 23: Reference Fluid Thermodynamic and Transport Properties—REFPROP, National Institute of Standards and Technology, Standard Reference Data Program, Gaithersburg, Md., 2002, Version 7.1). The primary source for the thermodynamic properties is Wagner, W., and Pruss, A., "The IAPWS Formulation 1995 for the Thermodynamic Properties of Ordinary Water Substance for General and Scientific Use," *J. Phys. Chem. Ref. Data* 31(2):387–535, 2002. The source for viscosity is International Association for the Properties of Water and Steam, *Revised Release on the IAPS Formulation 1985 for the Viscosity of Ordinary Water Substance*, IAPWS, 1997. The source for thermal conductivity is the International Association for the Properties of Water and Steam, *Revised Release on the IAPS Formulation 1985 for the Thermal Conductivity of Ordinary Water Substance*, IAPWS, 1998.

Properties at the triple point temperature and the critical point temperature are given in the first and last entries of the saturation tables, respectively. In the single-phase table, when the temperature range for a given isobar includes a vapor-liquid phase boundary, the temperature of phase equilibrium is noted, and properties for both the saturated liquid and saturated vapor are given (with liquid properties given in the upper line). Lines are omitted from the temperature-pressure grid of the single-phase table, when the system would be in the solid phase or if there are potential problems with the source property surface.

The uncertainty in density of the equation of state is 0.0001% at 1 atm in the liquid phase, and 0.001% at other liquid states at pressures up to 10 MPa and temperatures to 423 K. In the vapor phase, the uncertainty is 0.05% or less. The uncertainties rise at higher temperatures and/or pressures, but are generally less than 0.1% in density except at extreme conditions. The uncertainty in pressure in the critical region is 0.1%. The uncertainty of the speed of sound is 0.15% in the vapor and 0.1% or less in the liquid, and increases near the critical region and at high temperatures and pressures. The uncertainty in isobaric heat capacity is 0.2% in the vapor and 0.1% in the liquid, with increasing values in the critical region and at high pressures. The uncertainties of saturation conditions are 0.025% in vapor pressure, 0.0025% in saturated-liquid density, and 0.1% in saturated-vapor density. The uncertainties in the saturated densities increase substantially as the critical region is approached. For the uncertainties in the viscosity and thermal conductivity, see the IAPWS Release.

TABLE 2-306 Thermodynamic Properties of Water Substance along the Melting Line

P , bar	T , °C	$10^3 v_f$, m ³ /kg	h_f , kJ/kg	s_f , kJ/kg·K	c_{pf} , kJ/kg·K	c_{melt} , kJ/kg·K	$10^6 \alpha_f$, K ⁻¹	$10^6 K_{fT}$, bar ⁻¹
6.117×10^{-38}	0.0100	1.00021	0	0	4.219	3.969	-67.42	50.90
1.01325	0.0026	1.00016	0.0719	-0.0001	4.218	3.970	-67.17	50.88
50	-0.3618	0.99770	3.5140	-0.0054	4.196	3.997	-54.92	50.30
100	-0.7410	0.99523	6.9794	-0.0110	4.174	4.023	-42.52	49.73
150	-1.1249	0.99278	10.3964	-0.0167	4.152	4.047	-30.24	49.17
200	-1.5166	0.99037	13.7648	-0.0225	4.132	4.070	-18.05	48.63
250	-1.9151	0.98798	17.0843	-0.0285	4.112	4.092	-5.93	48.11
300	-2.3206	0.98562	20.3547	-0.0347	4.092	4.113	6.12	47.59
400	-3.1532	0.98098	26.7472	-0.0474	4.056	4.150	30.09	46.61
500	-4.0156	0.97643	32.9403	-0.0607	4.022	4.184	53.97	45.68
600	-4.909	0.97196	38.932	-0.0747	3.992	4.215	77.87	44.80
800	-6.790	0.96326	50.300	-0.1046	3.937	4.270	126.18	43.19
1000	-8.803	0.95493	60.836	-0.1371	3.893	4.320	175.98	41.74

Condensed from U. Grigull, Private communication, January 18, 1995.

Materials prepared at Technical University München, Germany by U. Grigull and S. Marek. For a table as a function of temperature, see Grigull, U. and S. Marek, *Wärme u. Stoff.*, **30** (1994): 1–8.

t = the triple point (at 6.117×10^{-3} bar, 0.01 °C); $v_f = 0.0010021$ m³/kg; $\alpha_f = -67.42 \times 10^{-6}$ /K.

Other equations for properties are given by Jones, F. E. and G. L. Harris, *J. Res. N.I.S.T.*, **97**, 3 (1992): 335–340, and by Wagner, W. and A. Pruss, *J. Phys. Chem. Ref. Data*, **22**, 3 (1993): 783–787. Steam tables include Walker, W. A., U.S. Naval Ordn. Lab. rept. NOLTR NOLTR-66-217 = AD 651105 (0–1000 bar, 0–150°C), 1967 (72 pp.); Grigull, U., J. Straub, et al., *Steam Tables in S.I. Units* (0.01–1000 bar, 0–1000 °C), Springer-Verlag, Berlin, 1990 (133 pp.); Tseng, C. M., T. A. Hamp, et al., Atomic Energy of Canada rept. (30 props, sat liq & vap., 1–220 bar), AECL-5910 1977 (90 pp.). For dissociation, see e.g., Knonicek, V., *Rozpr. Cesko Acad Ved., Rada techn ved* (0.01–100 bar, 1000–5000 K), **77**, 1 (1967). The proceedings of the 10th international conference on the properties of steam were edited by Sytchev, V. V. and A. A. Aleksandrov, Plenum, NY, 1984; and for the 11th conference by Fichal, M. and O. Sifner, Hemisphere, 1989 (550 pp.). Current information on the properties of solid, vapor, and liquid water properties can be found at <http://www.iapws.org>.

For electrical conductivity, see e.g., Marshall, W. L., *J. Chem. Eng. Data*, **32** (1987): 221–226.

TABLE 2-307 Thermodynamic Properties of Xenon

Temperature K	Pressure MPa	Density mol/dm ³	Volume dm ³ /mol	Int. energy kJ/mol	Enthalpy kJ/mol	Entropy kJ/(mol·K)	C _v kJ/(mol·K)	C _p kJ/(mol·K)	Sound speed m/s	Joule-Thomson K/MPa	Therm. cond. mW/(m·K)	Viscosity μPa·s
Saturated Properties												
161.40	0.081748	22.592	0.044263	-0.16663	-0.16301	-0.00099337	0.022064	0.044446	653.38	-0.63704	72.081	516.89
170.00	0.13343	22.155	0.045137	0.21574	0.22176	0.0013152	0.021486	0.044730	629.12	-0.60760	68.920	457.99
175.00	0.17325	21.855	0.045673	0.43915	0.44706	0.0026109	0.021176	0.044972	614.85	-0.58689	67.037	427.78
180.00	0.22153	21.630	0.046232	0.66366	0.67390	0.0038765	0.020884	0.045274	600.43	-0.56326	65.137	400.07
185.00	0.27933	21.361	0.046815	0.88953	0.90261	0.0051149	0.020609	0.045640	585.85	-0.53642	63.229	374.51
190.00	0.34774	21.085	0.047426	1.1170	1.1335	0.0063292	0.020349	0.046075	571.10	-0.50604	61.320	351.01
195.00	0.42789	20.804	0.048068	1.3464	1.3669	0.0075220	0.020104	0.046585	556.14	-0.47173	59.415	329.16
200.00	0.52091	20.516	0.048743	1.5779	1.6033	0.0086959	0.019873	0.047179	540.97	-0.43300	57.519	308.84
205.00	0.62797	20.220	0.049455	1.8119	1.8429	0.0098535	0.019656	0.047868	525.55	-0.38927	55.633	289.88
210.00	0.75025	19.916	0.050210	2.0487	2.0864	0.010997	0.019453	0.048666	509.85	-0.33987	53.759	272.13
215.00	0.88893	19.603	0.051013	2.2887	2.3341	0.012130	0.019264	0.049590	493.84	-0.28392	51.897	255.47
220.00	1.0452	19.279	0.051869	2.5324	2.5866	0.013254	0.019091	0.050663	477.47	-0.22039	50.048	239.78
225.00	1.2203	18.944	0.052787	2.7802	2.8446	0.014373	0.018933	0.051914	460.71	-0.14796	48.209	224.96
230.00	1.4155	18.596	0.053776	3.0328	3.1089	0.015488	0.018794	0.053385	443.49	-0.064982	46.379	210.92
235.00	1.6321	18.232	0.054847	3.2907	3.3802	0.016605	0.018675	0.055128	425.74	0.030670	44.554	197.57
240.00	1.8712	17.852	0.056017	3.5550	3.6598	0.017726	0.018580	0.057218	407.38	0.14178	42.730	184.83
245.00	2.1344	17.451	0.057304	3.8265	3.9488	0.018857	0.018515	0.059766	388.30	0.27205	40.903	172.63
250.00	2.4229	17.026	0.058735	4.1068	4.2491	0.020002	0.018487	0.062932	368.36	0.42662	39.071	160.90
255.00	2.7382	16.572	0.060344	4.3976	4.5628	0.021170	0.018507	0.066972	347.41	0.61272	37.238	149.54
260.00	3.0820	16.082	0.062183	4.7014	4.8930	0.022371	0.018591	0.072312	325.20	0.84107	35.418	138.48
265.00	3.4561	15.545	0.064330	5.0218	5.2441	0.023618	0.018767	0.079722	301.44	1.1284	33.653	127.61
270.00	3.8623	14.945	0.066910	5.3646	5.6230	0.024935	0.019077	0.090763	275.68	1.5023	32.016	116.78
275.00	4.3032	14.254	0.070156	5.7397	6.0416	0.026360	0.019604	0.10917	247.28	2.0135	30.622	105.75
280.00	4.7818	13.411	0.074566	6.1681	6.5247	0.027976	0.020521	0.14668	215.12	2.7688	29.654	94.067
285.00	5.3025	12.242	0.081686	6.7103	7.1435	0.030022	0.022329	0.26914	176.78	4.0593	29.742	80.469
289.73	5.8420	8.4000	0.11905	8.2423	8.9377	0.036074			0	8.3700		
161.40	0.081748	0.062613	15.971	11.189	12.495	0.077430	0.013321	0.022698	128.33	64.799	3.1160	13.386
170.00	0.13343	0.098131	10.190	11.261	12.621	0.074250	0.013615	0.023442	130.83	57.103	3.3040	14.014
175.00	0.17325	0.12476	8.0157	11.298	12.687	0.072554	0.013809	0.023957	132.15	53.274	3.4175	14.392
180.00	0.22153	0.15646	6.3913	11.332	12.748	0.070955	0.014020	0.024539	133.36	49.835	3.5348	14.781
185.00	0.27933	0.19385	5.1587	11.362	12.803	0.069442	0.014247	0.025194	134.47	46.729	3.6563	15.180
190.00	0.34774	0.23755	4.2096	11.388	12.852	0.068004	0.014491	0.025929	135.46	43.913	3.7826	15.592
195.00	0.42789	0.28826	3.4691	11.409	12.893	0.066633	0.014750	0.026755	136.35	41.350	3.9143	16.018
200.00	0.52091	0.34671	2.8842	11.426	12.928	0.065319	0.015025	0.027681	137.13	39.009	4.0523	16.460
205.00	0.62797	0.41374	2.4170	11.437	12.954	0.064056	0.015314	0.028722	137.79	36.862	4.1975	16.920
210.00	0.75025	0.49026	2.0397	11.442	12.973	0.062836	0.015618	0.029898	138.35	34.888	4.3511	17.399
215.00	0.88893	0.57731	1.7322	11.442	12.981	0.061653	0.015938	0.031232	138.80	33.066	4.5144	17.901
220.00	1.0452	0.67606	1.4791	11.434	12.980	0.060498	0.016273	0.032757	139.13	31.378	4.6894	18.429
225.00	1.2203	0.78791	1.2692	11.420	12.968	0.059367	0.016625	0.034515	139.35	29.805	4.8787	18.987
230.00	1.4155	0.91450	1.0935	11.397	12.945	0.058252	0.016996	0.036563	139.45	28.333	5.0855	19.579
235.00	1.6321	1.0578	0.94537	11.365	12.908	0.057147	0.017389	0.038982	139.43	26.946	5.3151	20.212
240.00	1.8712	1.2202	0.81952	11.322	12.856	0.056042	0.017808	0.041885	139.29	25.629	5.5745	20.892
245.00	2.1344	1.4049	0.71181	11.268	12.787	0.054930	0.018258	0.045436	139.02	24.367	5.8750	21.630
250.00	2.4229	1.6157	0.61892	11.199	12.699	0.053801	0.018748	0.049883	138.62	23.142	6.2336	22.437
255.00	2.7382	1.8581	0.53818	11.114	12.588	0.052641	0.019288	0.055621	138.07	21.938	6.6778	23.333
260.00	3.0820	2.1394	0.46742	11.009	12.450	0.051434	0.019894	0.063311	137.36	20.732	7.2524	24.341
265.00	3.4561	2.4705	0.40477	10.878	12.277	0.050157	0.020590	0.074154	136.47	19.500	8.0324	25.501
270.00	3.8623	2.8685	0.34861	10.713	12.059	0.048773	0.021413	0.090577	135.36	18.207	9.1495	26.874
275.00	4.3032	3.3629	0.29736	10.500	11.779	0.047224	0.022428	0.11833	133.95	16.800	10.852	28.575
280.00	4.7818	4.0140	0.24913	10.209	11.400	0.045388	0.023764	0.17512	132.11	15.185	13.688	30.845
285.00	5.3025	4.9911	0.20036	9.7610	10.823	0.042934	0.025741	0.35495	129.38	13.131	19.481	34.410
289.73	5.8420	8.4000	0.11905	8.2423	8.9377	0.036074			0	8.3700		
Single-Phase Properties												
200.00	0.10000	0.061174	16.347	11.693	13.328	0.080422	0.012825	0.021719	143.95	39.340	3.8225	16.051
300.00	0.10000	0.040297	24.816	12.971	15.453	0.089046	0.012529	0.021011	177.58	18.027	5.5664	23.114
400.00	0.10000	0.030132	33.188	14.227	17.546	0.095069	0.012489	0.020884	205.37	10.987	7.2216	30.061

TABLE 2-307 Thermodynamic Properties of Xenon (Concluded)

Temperature K	Pressure MPa	Density mol/dm ³	Volume dm ³ /mol	Int. energy kJ/mol	Enthalpy kJ/mol	Entropy kJ/(mol·K)	C _v kJ/(mol·K)	C _p kJ/(mol·K)	Sound speed m/s	Joule-Thomson K/MPa	Therm. cond. mW/(m·K)	Viscosity μPa·s
Single-Phase Properties (Concluded)												
500.00	0.10000	0.024077	41.533	15.479	19.632	0.099724	0.012480	0.020841	229.73	7.4876	8.7865	36.679
600.00	0.10000	0.020054	49.866	16.728	21.715	0.10352	0.012477	0.020822	251.71	5.3775	10.259	42.919
700.00	0.10000	0.017184	58.193	17.977	23.796	0.10673	0.012475	0.020811	271.90	3.9611	11.644	48.797
200.00	1.0000	20.545	0.048673	1.5644	1.6131	0.0086285	0.019883	0.047017	543.44	-0.43967	57.759	310.61
218.61	1.0000	19.370	0.051625	2.4644	2.5160	0.012943	0.019137	0.050348	482.05	-0.23885	50.560	244.05
218.61	1.0000	0.64740	1.5446	11.437	12.982	0.060816	0.016178	0.032313	139.05	31.834	4.6396	18.280
300.00	1.0000	0.42338	2.3619	12.735	15.097	0.069105	0.013071	0.023342	174.22	17.710	5.9066	23.825
400.00	1.0000	0.30719	3.2553	14.081	17.337	0.075560	0.012653	0.021812	204.53	10.799	7.4612	30.617
500.00	1.0000	0.24284	4.1179	15.373	19.491	0.080369	0.012555	0.021347	229.84	7.3466	8.9749	37.129
600.00	1.0000	0.20128	4.9682	16.646	21.614	0.084241	0.012521	0.021143	252.27	5.2698	10.414	43.291
700.00	1.0000	0.17205	5.8123	17.910	23.723	0.087491	0.012506	0.021033	272.69	3.8786	11.777	49.110
200.00	5.0000	20.777	0.048130	1.4588	1.6995	0.0080923	0.019975	0.045835	562.91	-0.48921	59.693	324.93
282.15	5.0000	12.969	0.077107	6.3800	6.7656	0.028774	0.021130	0.17857	199.64	3.2255	29.468	88.606
282.15	5.0000	4.3744	0.22860	10.045	11.188	0.044447	0.024500	0.22292	131.10	14.382	15.582	32.133
300.00	5.0000	3.0178	0.33137	11.189	12.846	0.050182	0.017212	0.057127	155.40	14.736	9.7191	29.671
400.00	5.0000	1.6846	0.59361	13.369	16.337	0.060390	0.013445	0.027264	202.15	9.6973	8.7332	33.661
500.00	5.0000	1.2596	0.79390	14.889	18.589	0.066031	0.012902	0.023853	231.38	6.6609	9.8856	39.357
600.00	5.0000	1.0212	0.97922	16.278	21.175	0.070256	0.012724	0.022627	255.44	4.7873	11.137	45.049
700.00	5.0000	0.86365	1.1579	17.615	23.404	0.073694	0.012645	0.022028	276.67	3.5219	12.377	50.547
200.00	10.000	21.038	0.047533	1.3406	1.8159	0.0074790	0.020097	0.044678	584.79	-0.53901	61.959	341.91
300.00	10.000	13.284	0.075281	6.0026	7.3554	0.029493	0.018200	0.088497	258.88	2.0533	29.649	94.113
400.00	10.000	3.8169	0.26199	12.321	14.941	0.052029	0.014472	0.037766	204.59	7.6552	11.158	39.566
500.00	10.000	2.6239	0.38111	14.257	18.068	0.059048	0.013339	0.027456	235.98	5.6862	11.280	42.848
600.00	10.000	2.0706	0.48294	15.817	20.646	0.063756	0.012977	0.024556	260.98	4.1777	12.172	47.602
700.00	10.000	1.7304	0.57792	17.251	23.030	0.067433	0.012819	0.023262	282.62	3.0965	13.210	52.559
200.00	100.00	23.707	0.042181	0.22766	4.4458	0.00066778	0.022077	0.038788	819.84	-0.80697	91.685	582.16
300.00	100.00	20.755	0.048181	3.3951	8.2132	0.015969	0.018781	0.036811	690.23	-0.77003	62.741	293.11
400.00	100.00	18.043	0.055422	6.2728	11.815	0.026343	0.017019	0.035156	597.21	-0.68464	46.987	188.96
500.00	100.00	15.689	0.063739	8.8555	15.229	0.033970	0.015937	0.033084	538.16	-0.60849	38.256	141.62
600.00	100.00	13.750	0.072728	11.158	18.431	0.039814	0.015222	0.030987	504.61	-0.56578	33.282	118.14
700.00	100.00	12.188	0.082045	13.232	21.437	0.044451	0.014724	0.029184	487.44	-0.55679	30.399	106.02
400.00	500.00	25.007	0.039989	4.1551	24.150	0.012220	0.020738	0.032768	1164.9	-0.96827	96.278	544.58
500.00	500.00	23.787	0.042040	6.3322	27.352	0.019372	0.019369	0.031337	1121.3	-1.0167	80.779	424.61
600.00	500.00	22.695	0.044062	8.3949	30.426	0.024980	0.018396	0.030178	1086.3	-1.0606	71.145	352.34
700.00	500.00	21.712	0.046058	10.364	33.393	0.029555	0.017664	0.029185	1058.1	-1.1030	64.734	304.58

The values in these tables were generated from the NIST REFPROP software (Lemmon, E. W., McLinden, M. O., and Huber, M. L., NIST Standard Reference Database 23: Reference Fluid Thermodynamic and Transport Properties—REFPROP, National Institute of Standards and Technology, Standard Reference Data Program, Gaithersburg, Md., 2002, Version 7.1). The primary source for the thermodynamic properties is Lemmon, E. W., and Span, R., "Short Fundamental Equations of State for 20 Industrial Fluids," *J. Chem. Eng. Data* **51**(3):785–850, 2006. The source for viscosity and thermal conductivity is McCarty, R. D., *Correlations for the Thermophysical Properties of Xenon*, National Institute of Standards and Technology, Boulder, Colo., 1989.

Properties at the triple point temperature and the critical point temperature are given in the first and last entries of the saturation tables, respectively. In the single-phase table, when the temperature range for a given isobar includes a vapor-liquid phase boundary, the temperature of phase equilibrium is noted, and properties for both the saturated liquid and saturated vapor are given (with liquid properties given in the upper line). Lines are omitted from the temperature-pressure grid of the single-phase table, when the system would be in the solid phase or if there are potential problems with the source property surface.

The uncertainties in the equation of state are 0.2% in density up to 100 MPa, rising to 1% at higher pressures, 0.2% in vapor pressure, 1% in the speed of sound, and 2% in heat capacities. For viscosity, estimated uncertainty is less than 5%. For thermal conductivity, estimated uncertainty is less than 6%.

TABLE 2-308 Surface Tension (N/m) of Saturated Liquid Refrigerants*

R no.	Temperature, °C								
	-50	-25	0	25	50	75	100	125	150
11	0.0279	0.0244	0.0210	0.0178	0.0146	0.0116	0.0087	0.0060	0.0036
12	0.0188	0.0152	0.0118	0.0085	0.0055	0.0029	0.0007	—	—
13	0.0092	0.0056	0.0025	0.0002	—	—	—	—	—
22	0.0197	0.0156	0.0117	0.0081	0.0047	0.0018	—	—	—
23	0.0115	0.0065	0.0025	—	—	—	—	—	—
32	—	—	—	0.0069	0.0032	0.0002	—	—	—
113	—	0.0231	0.0201	0.0172	0.0144	0.0118	0.0092	0.0067	0.0045
114	—	—	0.0138	0.0109	0.0082	0.0056	0.0033	0.0012	—
115	—	—	0.0075	0.0047	0.0022	—	—	—	—
134a	0.0192	0.0154	0.0117	0.0082	0.0050	0.0021	0.0000	—	—
142b	0.0213	0.0178	0.0145	0.0113	0.0083	0.0055	0.0029	—	—
152a	0.0201	0.0166	0.0132	0.0100	0.0068	0.0038	0.0011	—	—
170	0.0100	0.0051	0.0032	0.0005	—	—	—	—	—
290	—	—	0.0101	0.0082	0.0041	0.0016	—	—	—
C318	—	0.0143	0.0113	0.0085	0.0048	0.0033	0.0011	—	—
502	0.0159	0.0121	0.0086	0.0054	0.0026	—	—	—	—
503	0.0094	0.0053	0.0018	—	—	—	—	—	—
600	—	0.0180	0.0150	0.0122	0.0094	0.0068	0.0043	0.0020	0.0001
600a	—	—	0.0132	0.0101	0.0073	0.0047	0.0024	0.0005	—
718	—	—	0.0755	0.0720	0.0680	0.0636	0.0590	0.0540	0.0488
744	—	0.0096	0.0044	0.0005	—	—	—	—	—
1150	0.0100	0.0055	0.0013	—	—	—	—	—	—
1270	0.0171	0.0136	0.0102	0.0070	0.0041	0.0014	—	—	—

*Dashes indicate inaccessible states; blanks indicate no available data.

Values and equations were given by Srinivasan, K., *Can. J. Chem. Eng.* (27 liquids), **68** (1990): 493; Lielmezs, J. and T. A. Herrick, *Chem. Eng. J.* (34 liquids), **32** (1986): 165–169; Somayajulu, G. R., *Int. J. Thermophys.* (64 liquids), **9**, 4 (1988): 559–566; Ibrahim, N. and S. Murad, *Chem. Eng. Commun.* (29 polar liquids), **79** (1979): 165–174; Yaws, C. L.; Morachevsky, A. G. and I. B. Sladkov, *Physico-Chemical Properties of Molecular Inorganic Compounds* (200 compounds), Khimiya, Leningrad, 1987; Jasper, J., *J. Phys. Chem. Ref. Data* (2200 compounds), **1**, (1972): 841–1009; and Vargaftik, N. B., B. N. Volkov, et al., *J. Phys. Chem. Ref. Data* (water), **12**, 3 (1983): 817–820. See also Escobedo, J. and Mansoori, G. R., *AIChE J.*, **42**(5), May 1996: 1425–1433.

TABLE 2-309 Surface Tension σ (dyn/cm) of Various Liquids

Compound	T, K	σ	Compound	T, K	σ	Compound	T, K	σ
Acetic acid	293	27.59	<i>p</i> -Cresol	313	34.88	Isobutyric acid	293	25.04
	333	23.62		373	29.32		313	23.2
Acetone	298	24.02	Cyclohexane	293	25.24		333	21.36
	308	22.34		313	22.87		363	18.6
	318	21.22		333	20.49	Methyl formate	293	24.62
Aniline	293	42.67	Cyclopentane	293	22.61		323	20.05
	313	40.5		313	19.68		373	12.9
	333	38.33	Diethyl ether	288	17.56		423	6.3
	353	36.15		303	16.2		473	0.87
Benzene	293	28.88	2,3-Dimethylbutane	293	17.38	Methyl alcohol	293	22.56
	313	26.25		313	15.38		313	20.96
	333	23.67	Ethyl acetate	293	23.97		333	19.41
	353	21.2		313	21.65	Phenol	313	39.27
Benzonitrile	293	39.37		333	19.32		333	37.13
	323	35.89		353	17		373	32.96
	363	31.26		373	14.68	<i>n</i> -Propyl alcohol	293	23.71
Bromobenzene	293	35.82	Ethyl benzoate	293	35.04		313	22.15
	323	32.34		313	32.92		333	20.6
	373	26.54		333	30.81		363	18.27
<i>n</i> -Butane	203	23.31	Ethyl bromide	283	25.36	<i>n</i> -Propyl benzene	293	29.98
	233	19.69		303	23.04		313	26.83
	293	12.46	Ethyl mercaptan	288	23.87		333	24.68
Carbon disulfide	293	32.32		303	22.68		353	22.53
	313	29.35	Formamide	298	57.02		373	20.38
Carbon tetrachloride	288	27.65		338	53.66	Pyridine	293	37.21
	308	25.21		373	50.71		313	34.6
	328	22.76	<i>n</i> -Heptane	293	20.14		333	31.98
	348	20.31		313	18.18			
	368	17.86		333	16.22			
Chlorobenzene	293	33.59		353	14.26			
	323	30.01						
	373	24.06						

Methyl formate values from D. B. Macleod, *Trans. Faraday Soc.* **19**:38, 1923. All others from J. J. Jasper, *J. Phys. Chem. Ref. Data* **1**:841, 1972.

TABLE 2-310 Velocity of Sound (m/s) in Gaseous Refrigerants at Atmospheric Pressure*

R. no.	Temperature, °C								
	-50	-25	0	25	50	75	100	125	150
14	158	166	173	180	187	194	200	206	212
170	272	286	299	311	323	334	344	355	364
290	—	227	238	249	258	268	277	286	294
600	—	—	200	210	220	228	237	245	252
600a	—	—	201	211	221	229	237	246	253
718	—	—	—	—	—	—	473	490	505
744	—	248	258	269	279	288	297	307	316
1150	290	305	318	330	341	352	363	373	384
1270	—	235	246	257	267	277	286	295	303

*Dashes indicate inaccessible states; blanks indicate no available data. Values for the velocity of sound for all compounds listed in Table 2-184 are given in their respective tables earlier in this section.

TABLE 2-311 Velocity of Sound (m/s) in Saturated Liquid Refrigerants*

R. no.	Temperature, °C								
	-50	-25	0	25	50	75	100	125	150
14	182	—	—	—	—	—	—	—	—
290	1210	982	884	719	551	367	—	—	—
600	1290	1163	1031	896	759	609	477	325	142
600a	1205	1078	947	812	661	528	378	208	—
718	—	—	1402	1495	1542	1554	1543	1514	1468
744	—	751	525	272	—	—	—	—	—
1150	874	644	372	—	—	—	—	—	—
1270	1184	1022	859	694	524	335	—	—	—

*Dashes indicate inaccessible states; blanks indicate no available data. Values for the velocity of sound for all compounds listed in Table 2-184 are given in their respective tables earlier in this section.

TRANSPORT PROPERTIES

INTRODUCTION

Extensive tables of the viscosity and thermal conductivity of air and of water or steam for various pressures and temperatures are given with the thermodynamic-property tables. The thermal conductivity and the viscosity for the saturated-liquid state are also tabulated for many fluids along with the thermodynamic-property tables earlier in this section.

UNITS CONVERSIONS

For this subsection the following units conversions are applicable:

Diffusivity: to convert square centimeters per second to square feet per hour, multiply by 3.8750; to convert square meters per second to square feet per hour, multiply by 38,750.

Pressure: to convert bars to pounds-force per square inch, multiply by 14.504.

Temperature: °F = $\frac{9}{5}$ °C + 32; °R = $\frac{9}{5}$ K.

Thermal conductivity: to convert watts per meter-kelvin to British thermal unit–feet per hour–square foot–degree Fahrenheit, multiply by 0.57779; and to convert British thermal unit–feet per hour–square foot–degree Fahrenheit to watts per meter-kelvin, multiply by 1.7307.

Viscosity: to convert pascal-seconds to centipoises, multiply by 1000.

ADDITIONAL REFERENCES

An extensive coverage of the general pressure and temperature variation of thermal conductivity is given in the monograph by Vargaftik, Filippov, Tarzimanov, and Totksiy, *Thermal Conductivity of Liquids and Gases* (in Russian), Standartov, Moscow, 1978, now published in English translation by CRC Press, Miami, FL.

For a similar work on viscosity, see Stephan and Lucas, *Viscosity of Dense Fluids*, Plenum, New York and London, 1979. Tables and

polynomial fits for refrigerants in both the gaseous and the liquid state are contained in *ASHRAE Handbook—Fundamentals*, SI ed., ASHRAE, Atlanta, 2005. Other sources for viscosity include Fischer & Porter Co. catalog 10-A-94, "Fluid densities and viscosities," 1953 (200 industrial fluids in 48 pp.) and van Velzen, D., R. L. Cardozo et al., EURATOM Ispra, Italy rept. 4735 e, 1972 (160 pp.). Liquid viscosity, 314 cpds, is summarized in *I&EC Fundtls.*, 11 (1972): 20–26. Five hundred forty-nine binary and ternary systems are discussed in Skubla, P., *Coll. Czech. Chem. Commun.*, 46 (1981): 303–339.

See also Duhne, C. R., *Chem. Eng. (NY)*, 86, 15 (July 16, 1979): 83–91 (equations and 326 liquids); and Rao, K. V. K., *Chem. Eng. (NY)*, 90, 11 (May 30, 1983): 90–91 (nomograph, 87 liquids). For rheology, non-Newtonian behavior, and the like, see, for instance, Barnes, H., *The Chem. Engr. (UK)*, (June 24, 1993): 17–23; Hyman, W. A., *I&EC Fundtls.*, 16 (1976): 215–218; and Ferguson, J. and Z. Kemblowski, *Applied Fluid Rheology*, Elsevier, 1991 (325 pp.). Other sources for thermal conductivity include Ho, C. Y., R. W. Powell et al., *J. Phys. Chem. Ref. Data*, 1 (1972) and 3, suppl. 1 (1974); Childs, Ericks et al., N.B.S. Monogr. 131, 1973; Jamieson, D. T., J. B. Irving et al., *Liquid Thermal Conductivity*, H.M.S.O., Edinburgh, Scotland, 1975 (220 pp.).

Other references include Poling, Prausnitz, and O'Connell, *The Properties of Gases and Liquids*, 5th ed., McGraw-Hill, New York, 2000; Vargaftik, Vinogradov, and Yargin, *Handbook of Physical Properties of Liquids and Gases*, Begell House, New York, 1996; Yaws, *Chemical Properties Handbook: Physical, Thermodynamics, Environmental Transport, Safety & Health Related Properties for Organic & Inorganic Chemicals*, McGraw-Hill, New York, 1998; and Riazi, *Characterization and Properties of Petroleum Fractions*, ASTM, West Conshohocken, Pa., 2005. Free web resources include the NIST Webbook at <http://webbook.nist.gov> and the KDB (Korea thermo-physical properties) database at <http://www.cheric.org/research/kdb/>.

TABLE 2-312 Vapor Viscosity of Inorganic and Organic Substances (Pa-s)

Cmpd. no.	Name	Formula	CAS no.	Mol. wt.	C1	C2	C3	C4	T_{min} , K	Viscosity at T_{min}	T_{max} , K	Viscosity at T_{max}
1	Acetaldehyde	C ₂ H ₄ O	75-07-0	44.053	1.222E-07	0.787	77		150.15	4.171E-06	1000	2.605E-05
2	Acetamide	C ₂ H ₅ NO	60-35-5	59.067	1.423E-07	0.7574	272.14		353.33	6.842E-06	1000	2.094E-05
3	Acetic acid	C ₂ H ₄ O ₂	64-19-7	60.052	2.7449E-08	1.0123	7.4948		289.81	8.315E-06	1000	2.966E-05
4	Acetic anhydride	C ₄ H ₆ O ₃	108-24-7	102.089	1.20E-07	0.7915	105.3		200.15	5.213E-06	1000	2.572E-05
5	Acetone	C ₃ H ₆ O	67-64-1	58.079	3.1005E-08	0.9762	23.139		178.45	4.329E-06	1000	2.571E-05
6	Acetonitrile	C ₂ H ₃ N	75-05-8	41.052	5.1964E-08	0.8857	38.805		229.32	5.476E-06	1000	2.271E-05
7	Acetylene	C ₂ H ₂	74-86-2	26.037	1.2025E-06	0.4952	291.4		192.40	6.468E-06	600	1.923E-05
8	Acrolein	C ₃ H ₄ O	107-02-8	56.063	6.523E-07	0.579	410.8		185.45	4.174E-06	1000	2.523E-05
9	Acrylic acid	C ₃ H ₄ O ₂	79-10-7	72.063	1.7154E-07	0.7418	138.4		286.15	7.680E-06	1000	2.532E-05
10	Acrylonitrile	C ₃ H ₃ N	107-13-1	53.063	4.302E-08	0.9114	54.3		189.63	3.985E-06	1000	2.213E-05
11	Air	Mixture	132259-10-0	28.960	1.425E-06	0.5039	108.3		80.00	5.508E-06	2000	6.227E-05
12	Ammonia	H ₃ N	7664-41-7	17.031	4.1855E-08	0.9806	30.8		195.41	6.378E-06	1000	3.551E-05
13	Anisole	C ₇ H ₈ O	100-66-3	108.138	1.7531E-07	0.72	176.17		235.65	5.122E-06	1000	2.155E-05
14	Argon	Ar	7440-37-1	39.948	9.2121E-07	0.60529	83.24		83.78	6.742E-06	3273.1	1.001E-11
15	Benzamide	C ₇ H ₇ NO	55-21-0	121.137	2.5082E-08	0.96663			403.00	8.274E-06	1000	1.992E-05
16	Benzene	C ₆ H ₆	71-43-2	78.112	3.134E-08	0.9676	7.9		278.68	7.077E-06	1000	2.486E-05
17	Benzenethiol	C ₆ H ₆ S	108-98-5	110.177	1.1184E-07	0.8002	152.43		442.29	1.089E-05	1000	2.441E-05
18	Benzoic acid	C ₇ H ₆ O ₂	65-85-0	122.121	7.4266E-08	0.8289	91.197		395.45	8.578E-06	1000	2.087E-05
19	Benzonitrile	C ₇ H ₅ N	100-47-0	103.121	4.2137E-08	0.92271	45.387		260.40	6.079E-06	1000	2.363E-05
20	Benzophenone	C ₁₃ H ₁₀ O	119-61-9	182.218	3.779E-07	0.6005	409		321.35	5.324E-06	1000	1.698E-05
21	Benzyl alcohol	C ₇ H ₈ O	100-51-6	108.138	6.9022E-08	0.84014	74.746		257.85	5.680E-06	1000	2.129E-05
22	Benzyl ethyl ether	C ₉ H ₁₂ O	539-30-0	136.191	1.56E-07	0.7181	180		458.15	9.122E-06	1000	1.886E-05
23	Benzyl mercaptan	C ₇ H ₈ S	100-53-8	124.203	4.0138E-08	0.90735	34.714		243.95	5.151E-06	1000	2.045E-05
24	Biphenyl	C ₁₂ H ₁₀	92-52-4	154.208	1.3874E-06	0.4434	678.22		342.20	6.186E-06	1000	1.768E-05
25	Bromine	Br ₂	7726-95-6	159.808	7.3534E-08	0.93798			265.85	1.383E-05	600	2.967E-05
26	Bromobenzene	C ₆ H ₅ Br	108-86-1	157.008	2.232E-07	0.7146	184.9		429.24	1.187E-05	1000	2.623E-05
27	Bromoethane	C ₂ H ₅ Br	74-96-4	108.965	5.29E-07	0.632	226		154.55	5.195E-06	1000	3.396E-05
28	Bromomethane	CH ₃ Br	74-83-9	94.939	7.8796E-08	0.90476			179.47	8.626E-06	1000	4.081E-05
29	1,2-Butadiene	C ₄ H ₆	590-19-2	54.090	6.0259E-07	0.5309	199.64		136.95	3.340E-06	1000	1.966E-05
30	1,3-Butadiene	C ₄ H ₆	106-99-0	54.090	2.696E-07	0.6715	134.7		164.25	4.553E-06	1000	2.457E-05
31	Butane	C ₄ H ₁₀	106-97-8	58.122	3.4387E-08	0.94604			134.86	3.559E-06	1000	2.369E-05
32	1,2-Butanediol	C ₄ H ₁₀ O ₂	584-03-2	90.121	7.5626E-08	0.83521	71.798		220.00	5.157E-06	1000	2.260E-05
33	1,3-Butanediol	C ₄ H ₁₀ O ₂	107-88-0	90.121	7.0728E-08	0.84383	64.391		196.15	4.580E-06	1000	2.259E-05
34	1-Butanol	C ₄ H ₁₀ O	71-36-3	74.122	1.4031E-06	0.4611	537		183.85	3.961E-06	1000	2.207E-05
35	2-Butanol	C ₄ H ₁₀ O	78-92-2	74.122	1.2114E-07	0.76972	92.661		158.45	3.772E-06	1000	2.259E-05
36	1-Butene	C ₄ H ₈	106-98-9	56.106	6.9744E-07	0.5462	305.25		87.80	1.795E-06	1000	2.325E-05
37	cis-2-Butene	C ₄ H ₈	590-18-1	56.106	4.2898E-08	0.91349			134.26	3.770E-06	1000	2.360E-05
38	trans-2-Butene	C ₄ H ₈	624-64-6	56.106	1.05E-06	0.4867	358.7		167.62	4.044E-06	1000	2.229E-05
39	Butyl acetate	C ₆ H ₁₂ O ₂	123-86-4	116.158	1.006E-07	0.77881	95.108		199.65	4.216E-06	1000	1.993E-05
40	Butylbenzene	C ₁₀ H ₁₄	104-51-8	134.218	3.4205E-07	0.59764	234.21		185.30	3.425E-06	1000	1.720E-05
41	Butyl mercaptan	C ₄ H ₁₀ S	109-79-5	90.187	5.4539E-08	0.88896	43.687		157.46	3.833E-06	1000	2.427E-05
42	sec-Butyl mercaptan	C ₄ H ₁₀ S	513-53-1	90.187	3.1378E-08	0.96513			133.02	3.520E-06	1000	2.466E-05
43	1-Butyne	C ₄ H ₆	107-00-6	54.090	2.7856E-06	0.377	663.14		147.43	3.329E-06	800	1.893E-05
44	Butyraldehyde	C ₄ H ₈ O	123-72-8	72.106	8.0079E-08	0.8178	65.855		176.75	4.017E-06	1000	2.134E-05
45	Butyric acid	C ₄ H ₈ O ₂	107-92-6	88.105	2.128E-06	0.4273	886		267.95	6.220E-06	1000	2.208E-05
46	Butyronitrile	C ₄ H ₇ N	109-74-0	69.105	8.0223E-08	0.80561	75.207	-41,400	161.25	3.284E-06	1000	1.948E-05
47	Carbon dioxide	CO ₂	124-38-9	44.010	2.148E-06	0.46	290		194.67	9.749E-06	1500	5.203E-05
48	Carbon disulfide	CS ₂	75-15-0	76.141	5.8204E-08	0.9262	44.581		161.11	5.048E-06	800	2.693E-05
49	Carbon monoxide	CO	630-08-0	28.010	1.1127E-06	0.5338	94.7		68.15	4.434E-06	1250	4.654E-05
50	Carbon tetrachloride	CCl ₄	56-23-5	153.823	3.137E-06	0.3742	491.5		250.33	8.361E-06	1000	2.789E-05
51	Carbon tetrafluoride	CF ₄	75-73-0	88.004	2.1709E-06	0.45853	208		89.56	5.132E-06	1000	4.267E-05
52	Chlorine	Cl ₂	7782-50-5	70.906	2.60E-07	0.7423	98.3		200.00	8.900E-06	1000	3.992E-05
53	Chlorobenzene	C ₆ H ₅ Cl	108-90-7	112.557	1.065E-07	0.7942	94.7		227.95	5.611E-06	1000	2.348E-05
54	Chloroethane	C ₂ H ₅ Cl	75-00-3	64.514	3.12E-07	0.6711	139		134.80	4.127E-06	1000	2.824E-05
55	Chloroform	CHCl ₃	67-66-3	119.378	1.696E-07	0.7693	96.6		209.63	7.091E-06	1000	3.143E-05
56	Chloromethane	CH ₃ Cl	74-87-3	50.488	8.60E-08	0.8706	35.8		230.00	8.468E-06	700	2.454E-05
57	1-Chloropropane	C ₃ H ₇ Cl	540-54-5	78.541	3.638E-07	0.6417	208.3		150.35	3.805E-06	1000	2.534E-05
58	2-Chloropropane	C ₃ H ₇ Cl	75-29-6	78.541	3.8802E-07	0.6367	205.08		155.97	4.175E-06	1000	2.618E-05
59	m-Cresol	C ₇ H ₈ O	108-39-4	108.138	1.4427E-07	0.7438	166.15		285.39	6.113E-06	1000	2.108E-05

TABLE 2-312 Vapor Viscosity of Inorganic and Organic Substances (Pa-s) (Continued)

Cmpd. no.	Name	Formula	CAS no.	Mol. wt.	C1	C2	C3	C4	T_{min} , K	Viscosity at T_{min}	T_{max} , K	Viscosity at T_{max}
60	<i>o</i> -Cresol	C ₇ H ₈ O	95-48-7	108.138	8.7371E-08	0.80775	98.538		304.19	6.688E-06	1000	2.108E-05
61	<i>p</i> -Cresol	C ₇ H ₈ O	106-44-5	108.138	1.4305E-07	0.7451	159.8		307.93	6.731E-06	1000	2.120E-05
62	Cumene	C ₉ H ₁₂	98-82-8	120.192	3.3699E-07	0.60751	221.17		177.14	3.450E-06	1000	1.834E-05
63	Cyanogen	C ₂ N ₂	460-19-5	52.035	4.0854E-08	0.97182	6.6762		245.25	8.353E-06	600	2.024E-05
64	Cyclobutane	C ₄ H ₈	287-23-0	56.106	1.0881E-06	0.48359	330.86		182.48	4.797E-06	1000	2.308E-05
65	Cyclohexane	C ₆ H ₁₂	110-82-7	84.159	6.77E-08	0.8367	36.7		279.69	6.671E-06	900	1.928E-05
66	Cyclohexanol	C ₆ H ₁₂ O	108-93-0	100.159	7.9581E-08	0.8376	104.97		296.60	6.917E-06	1000	2.346E-05
67	Cyclohexanone	C ₆ H ₁₀ O	108-94-1	98.143	5.2312E-08	0.89422	58.008		242.00	5.714E-06	1000	2.381E-05
68	Cyclohexene	C ₆ H ₁₀	110-83-8	82.144	1.3326E-06	0.4537	445		169.67	3.778E-06	1000	2.118E-05
69	Cyclopentane	C ₅ H ₁₀	287-92-3	70.133	2.3619E-07	0.67465	139		179.28	4.409E-06	1000	2.191E-05
70	Cyclopentene	C ₅ H ₈	142-29-0	68.117	3.026E-07	0.64991	167.14		138.13	3.369E-06	1000	2.309E-05
71	Cyclopropane	C ₃ H ₆	75-19-4	42.080	1.7578E-06	0.4265	370.34		145.59	4.150E-06	1000	2.441E-05
72	Cyclohexyl mercaptan	C ₆ H ₁₂ S	1569-69-3	116.224	3.915E-08	0.91427	22.264		189.64	4.238E-06	1000	2.118E-05
73	Decanal	C ₁₀ H ₂₀ O	112-31-2	156.265	1.2638E-07	0.7248	176.88		267.15	4.365E-06	1000	1.605E-05
74	Decane	C ₁₀ H ₂₂	124-18-5	142.282	2.64E-08	0.9487	71		243.51	3.755E-06	1000	1.730E-05
75	Decanoic acid	C ₁₀ H ₂₀ O ₂	334-48-5	172.265	7.1748E-08	0.7982	109.38		304.55	5.070E-06	1000	1.605E-05
76	1-Decanol	C ₁₀ H ₂₂ O	112-30-1	158.281	5.5065E-08	0.8341	79.56		280.05	4.715E-06	1000	1.622E-05
77	1-Decene	C ₁₀ H ₂₀	872-05-9	140.266	6.1192E-08	0.82546	77.434		206.89	3.632E-06	1000	1.701E-05
78	Decyl mercaptan	C ₁₀ H ₂₂ S	143-10-2	174.347	3.272E-08	0.9302	39.13		247.56	4.761E-06	1000	1.944E-05
79	1-Decyne	C ₁₀ H ₁₈	764-93-2	138.250	5.6914E-07	0.50744	273.3		229.15	4.091E-06	1000	1.488E-05
80	Deuterium	D ₂	7782-39-0	4.032	2.4999E-07	0.6878	0.5962		60.00	4.137E-06	480	1.744E-05
81	1,1-Dibromoethane	C ₂ H ₄ Br ₂	557-91-5	187.861	1.4125E-07	0.8097	83.243		210.15	7.685E-06	1000	3.502E-05
82	1,2-Dibromoethane	C ₂ H ₄ Br ₂	106-93-4	187.861	1.1379E-07	0.8502	93.816		282.85	1.038E-05	1000	3.696E-05
83	Dibromomethane	CH ₂ Br ₂	74-95-3	173.835	2.9444E-07	0.728	154.74		370.10	1.538E-05	1000	3.895E-05
84	Dibutyl ether	C ₈ H ₁₈ O	142-96-1	130.228	7.7147E-08	0.79906	80.765		175.30	3.278E-06	1000	1.781E-05
85	<i>m</i> -Dichlorobenzene	C ₆ H ₄ Cl ₂	541-73-1	147.002	2.334E-07	0.714	260		248.39	5.850E-06	1000	2.569E-05
86	<i>o</i> -Dichlorobenzene	C ₆ H ₄ Cl ₂	95-50-1	147.002	1.603E-07	0.763	205		256.15	6.127E-06	1000	2.588E-05
87	<i>p</i> -Dichlorobenzene	C ₆ H ₄ Cl ₂	106-46-7	147.002	1.5913E-07	0.7639	193.14		326.14	8.313E-06	1000	2.611E-05
88	1,1-Dichloroethane	C ₂ H ₄ Cl ₂	75-34-3	98.959	2.0135E-07	0.73421	111.98		176.19	5.487E-06	1000	2.887E-05
89	1,2-Dichloroethane	C ₂ H ₄ Cl ₂	107-06-2	98.959	1.4321E-07	0.7785	98.159		237.49	7.164E-06	1000	2.824E-05
90	Dichloromethane	CH ₂ Cl ₂	75-09-2	84.933	7.6787E-07	0.5741	276.16		178.01	5.895E-06	1000	3.175E-05
91	1,1-Dichloropropane	C ₃ H ₆ Cl ₂	78-99-9	112.986	1.4906E-07	0.7617	105.9		200.00	5.515E-06	1000	2.599E-05
92	1,2-Dichloropropane	C ₃ H ₆ Cl ₂	78-87-5	112.986	1.1989E-07	0.79108	84.37		172.71	4.742E-06	1000	2.611E-05
93	Diethanol amine	C ₄ H ₁₁ NO ₂	111-42-2	105.136	3.3628E-08	0.9426	39.587		301.15	6.450E-06	1000	2.176E-05
94	Diethyl amine	C ₄ H ₁₁ N	109-89-7	73.137	4.3184E-07	0.6035	247		223.35	5.364E-06	1000	2.239E-05
95	Diethyl ether	C ₄ H ₁₀ O	60-29-7	74.122	1.948E-06	0.41	495.8		156.85	3.720E-06	1000	2.212E-05
96	Diethyl sulfide	C ₄ H ₁₀ S	352-93-2	90.187	6.5492E-08	0.86232	59.455		169.20	4.046E-06	1000	2.388E-05
97	1,1-Difluoroethane	C ₂ H ₄ F ₂	75-37-6	66.050	2.7228E-06	0.39531	445.07		154.56	5.148E-06	1000	2.891E-05
98	1,2-Difluoroethane	C ₂ H ₄ F ₂	624-72-6	66.050	4.3934E-07	0.64867	169.64		215.00	8.001E-06	1000	3.317E-05
99	Difluoromethane	CH ₂ F ₂	75-10-5	52.023	7.7484E-07	0.57978	198.7		136.95	5.478E-06	1000	1.172E-12
100	Di-isopropyl amine	C ₆ H ₁₅ N	108-18-9	101.190	4.138E-07	0.5999	269.5		357.05	8.016E-06	1000	2.055E-05
101	Di-isopropyl ether	C ₆ H ₁₄ O	108-20-3	102.175	1.691E-07	0.7114	124		187.65	4.218E-06	1000	2.049E-05
102	Di-isopropyl ketone	C ₇ H ₁₄ O	565-80-0	114.185	9.2797E-08	0.7819	93.399		204.81	4.089E-06	1000	1.881E-05
103	1,1-Dimethoxyethane	C ₄ H ₁₀ O ₂	534-15-6	90.121	4.4172E-08	0.91098			159.95	4.497E-06	1000	2.388E-05
104	1,2-Dimethoxypropane	C ₅ H ₁₂ O ₂	7778-85-0	104.148	3.9833E-08	0.91566			226.10	5.701E-06	1000	2.225E-05
105	Dimethyl acetylene	C ₄ H ₆	503-17-3	54.090	1.9377E-06	0.4093	492.69		240.91	6.006E-06	1000	2.194E-05
106	Dimethyl amine	C ₂ H ₇ N	124-40-3	45.084	2.757E-07	0.6841	133.2		180.96	5.563E-06	1000	2.744E-05
107	2,3-Dimethylbutane	C ₆ H ₁₄	79-29-8	86.175	6.8567E-07	0.52542	278.82		145.19	3.211E-06	1000	2.021E-05
108	1,1-Dimethylcyclohexane	C ₈ H ₁₆	590-66-9	112.213	7.822E-07	0.4994	371.6		392.70	7.936E-06	1000	1.796E-05
109	<i>cis</i> -1,2-Dimethylcyclohexane	C ₈ H ₁₆	2207-01-4	112.213	8.4576E-07	0.487	398		402.94	7.900E-06	1000	1.749E-05
110	<i>trans</i> -1,2-Dimethylcyclohexane	C ₈ H ₁₆	6876-23-9	112.213	9.9104E-07	0.4723	436.89		396.58	7.957E-06	1000	1.801E-05
111	Dimethyl disulfide	C ₂ H ₆ S ₂	624-92-0	94.199	3.2282E-08	0.97742			188.44	5.405E-06	1000	2.762E-05
112	Dimethyl ether	C ₂ H ₆ O	115-10-6	46.068	0.00000268	0.3975	534		131.65	3.688E-06	1000	2.722E-05
113	<i>N,N</i> -Dimethyl formamide	C ₃ H ₇ NO	68-12-2	73.094	3.5538E-06	0.3766	1176.1		212.72	4.097E-06	1000	2.202E-05
114	2,3-Dimethylpentane	C ₇ H ₁₆	565-59-3	100.202	5.0372E-07	0.54462	227.44		160.00	3.300E-06	1000	1.766E-05
115	Dimethyl phthalate	C ₁₀ H ₁₀ O ₄	131-11-3	194.184	5.2195E-08	0.85584	69.036		274.18	5.089E-06	1000	1.804E-05
116	Dimethylsilane	C ₂ H ₆ Si	1111-74-6	60.170	4.7238E-08	0.90849			122.93	3.739E-06	1000	2.511E-05
117	Dimethyl sulfide	C ₂ H ₆ S	75-18-3	62.134	5.2854E-07	0.6112	302.85		174.88	4.544E-06	1000	2.766E-05
118	Dimethyl sulfoxide	C ₂ H ₆ OS	67-68-5	78.133	8.6101E-08	0.8345	167.86		291.67	6.231E-06	1000	2.350E-05

119	Dimethyl terephthalate	C ₁₀ H ₁₀ O ₄	120-61-6	194.184	4.8739E-08	0.8749	51.885	413.80	8.433E-06	1000	1.953E-05
120	1,4-Dioxane	C ₄ H ₈ O ₂	123-91-1	88.105	2.7334E-07	0.7393	129.93	284.95	1.226E-05	1000	3.995E-05
121	Diphenyl ether	C ₁₂ H ₁₀ O	101-84-8	170.207	2.8451E-08	0.93622		300.03	5.933E-06	1000	1.831E-05
122	Dipropyl amine	C ₆ H ₁₅ N	142-84-7	101.190	1.29E-07	0.744	117.03	210.15	4.429E-06	1000	1.970E-05
123	Dodecane	C ₁₂ H ₂₆	112-40-3	170.335	6.344E-08	0.8287		263.57	3.511E-06	1000	1.593E-05
124	Eicosane	C ₂₀ H ₄₂	112-95-8	282.547	2.9236E-07	0.62458	702.84	309.58	3.214E-06	1000	1.284E-05
125	Ethane	C ₂ H ₆	74-84-0	30.069	2.5906E-07	0.67988	98.902	90.35	2.643E-06	1000	2.583E-05
126	Ethanol	C ₂ H ₆ O	64-17-5	46.068	1.0613E-07	0.8066	52.7	200.00	6.029E-06	1000	2.651E-05
127	Ethyl acetate	C ₄ H ₈ O ₂	141-78-6	88.105	3.214E-06	0.3572	667	189.60	4.632E-06	1000	2.274E-05
128	Ethyl amine	C ₂ H ₇ N	75-04-7	45.084	4.934E-07	0.5924	239.17	192.15	4.953E-06	1000	2.384E-05
129	Ethylbenzene	C ₈ H ₁₀	100-41-4	106.165	4.2231E-07	0.58154	239.21	178.20	3.673E-06	1000	1.893E-05
130	Ethyl benzoate	C ₉ H ₁₀ O ₂	93-89-0	150.175	6.3441E-08	0.8369	73.63	238.45	4.733E-06	1000	1.915E-05
131	2-Ethyl butanoic acid	C ₆ H ₁₂ O ₂	88-09-5	116.158	9.2371E-08	0.7908	102.32	258.15	5.344E-06	1000	1.975E-05
132	Ethyl butyrate	C ₆ H ₁₂ O ₂	105-54-4	116.158	1.6175E-07	0.7163	142.27	175.15	3.392E-06	1000	1.989E-05
133	Ethylcyclohexane	C ₈ H ₁₆	1678-91-7	112.213	4.107E-07	0.57143	230.06	161.84	3.103E-06	1000	1.729E-05
134	Ethylcyclopentane	C ₇ H ₁₄	1640-89-7	98.186	2.1696E-06	0.3812	577.77	134.71	2.659E-06	1000	1.914E-05
135	Ethylene	C ₂ H ₄	74-85-1	28.053	2.0789E-06	0.4163	352.7	169.41	5.714E-06	1000	2.726E-05
136	Ethylenediamine	C ₂ H ₈ N ₂	107-15-3	60.098	1.3744E-07	0.7557	122.8	284.29	6.863E-06	1000	2.264E-05
137	Ethylene glycol	C ₂ H ₆ O ₂	107-21-1	62.068	8.6706E-08	0.83923	75.512	260.15	7.150E-06	1000	2.655E-05
138	Ethyleneimine	C ₂ H ₅ N	151-56-4	43.068	2.8132E-07	0.6792	238.46	329.00	8.359E-06	1000	2.477E-05
139	Ethylene oxide	C ₂ H ₄ O	75-21-8	44.053	4.3403E-08	0.94806		160.65	5.356E-06	1000	3.032E-05
140	Ethyl formate	C ₃ H ₆ O ₂	109-94-4	74.079	6.761E-07	0.5804	354.9	193.55	5.069E-06	1000	2.750E-05
141	2-Ethyl hexanoic acid	C ₈ H ₁₆ O ₂	149-57-5	144.211	2.5704E-08	0.94738		235.00	4.532E-06	1000	1.787E-05
142	Ethylhexyl ether	C ₈ H ₁₈ O	5756-43-4	130.228	7.9129E-08	0.79565	83.193	180.00	3.371E-06	1000	1.781E-05
143	Ethylisopropyl ether	C ₅ H ₁₂ O	625-54-7	88.148	1.3974E-07	0.74266	98.58	140.00	3.219E-06	1000	2.150E-05
144	Ethylisopropyl ketone	C ₆ H ₁₂ O	565-69-5	100.159	1.0498E-07	0.76988	100.41	204.15	4.224E-06	1000	1.946E-05
145	Ethyl mercaptan	C ₂ H ₆ S	75-08-1	62.134	8.5992E-08	0.8427	58.148	125.26	3.441E-06	1000	2.742E-05
146	Ethyl propionate	C ₅ H ₁₀ O ₂	105-37-3	102.132	5.53E-07	0.6061	273.66	199.25	5.768E-06	1000	2.857E-05
147	Ethylpropyl ether	C ₅ H ₁₂ O	628-32-0	88.148	5.1539E-07	0.5726	288.76	145.65	2.994E-06	1000	2.088E-05
148	Ethyltrichlorosilane	C ₂ H ₅ Cl ₃ Si	115-21-9	163.506	3.2769E-08	0.9729		167.55	4.779E-06	1000	2.718E-05
149	Fluorine	F ₂	7782-41-4	37.997	6.36E-07	0.6638	61.6	53.48	4.148E-06	1000	5.874E-05
150	Fluorobenzene	C ₆ H ₅ F	462-06-6	96.102	2.1174E-07	0.7087	157.42	357.88	9.491E-06	1000	2.446E-05
151	Fluoroethane	C ₂ H ₅ F	353-36-6	48.060	8.8742E-07	0.5404	251.82	129.95	4.192E-06	1000	2.963E-05
152	Fluoromethane	CH ₃ F	593-53-3	34.033	1.2269E-07	0.82167		131.35	6.752E-06	1000	3.579E-05
153	Formaldehyde	CH ₂ O	50-00-0	30.026	4.758E-07	0.6405	161.7	181.15	7.025E-06	1000	3.419E-05
154	Formamide	CH ₃ NO	75-12-7	45.041	6.829E-08	0.8774	54.864	275.60	7.882E-06	1000	2.776E-05
155	Formic acid	CH ₂ O ₂	64-18-6	46.026	2.8608E-07	0.6958	184.25	281.45	8.751E-06	1000	2.954E-05
156	Furan	C ₄ H ₄ O	110-00-9	68.074	6.432E-07	0.5854	325.3	187.55	5.037E-06	1000	2.768E-05
157	Helium-4	He	7440-59-7	4.003	3.253E-07	0.7162	-9.6	20.00	3.531E-06	2000	7.561E-05
158	Heptadecane	C ₁₇ H ₃₆	629-78-7	240.468	3.1338E-07	0.6238	692.2	295.13	3.254E-06	1000	1.377E-05
159	Heptanal	C ₇ H ₁₄ O	111-71-7	114.185	8.4633E-08	0.79185	94.487	229.80	4.444E-06	1000	1.836E-05
160	Heptane	C ₇ H ₁₆	142-82-5	100.202	6.672E-08	0.82837	85.752	182.57	3.391E-06	1000	1.878E-05
161	Heptanoic acid	C ₇ H ₁₄ O ₂	111-14-8	130.185	7.2834E-08	0.81279	89.874	265.83	5.088E-06	1000	1.834E-05
162	1-Heptanol	C ₇ H ₁₆ O	111-70-6	116.201	2.572E-07	0.6502	248.6	239.15	4.440E-06	1000	1.838E-05
163	2-Heptanol	C ₇ H ₁₆ O	543-49-7	116.201	9.1526E-08	0.78346	100.28	230.00	4.516E-06	1000	1.864E-05
164	3-Heptanone	C ₇ H ₁₄ O	106-35-4	114.185	8.9656E-08	0.78236	100.14	234.15	4.485E-06	1000	1.812E-05
165	2-Heptanone	C ₇ H ₁₄ O	110-43-0	114.185	8.8629E-08	0.78376	100.18	238.15	4.550E-06	1000	1.809E-05
166	1-Heptene	C ₇ H ₁₄	592-76-7	98.186	7.7509E-08	0.81089	69.927	154.12	3.169E-06	1000	1.962E-05
167	Heptyl mercaptan	C ₇ H ₁₆ S	1639-09-4	132.267	4.697E-08	0.8932	57.6	229.92	4.832E-06	1000	2.124E-05
168	1-Heptyne	C ₇ H ₁₂	628-71-7	96.170	5.9501E-07	0.52758	274.02	192.22	3.932E-06	1000	1.787E-05
169	Hexadecane	C ₁₆ H ₃₄	544-76-3	226.441	1.2463E-07	0.7322	395	291.31	3.274E-06	1000	1.399E-05
170	Hexanal	C ₆ H ₁₂ O	66-25-1	100.159	9.6724E-08	0.78044	97.798	217.15	4.444E-06	1000	1.933E-05
171	Hexane	C ₆ H ₁₄	110-54-3	86.175	1.7514E-07	0.70737	157.14	177.83	3.631E-06	1000	2.005E-05
172	Hexanoic acid	C ₆ H ₁₂ O ₂	142-62-1	116.158	8.4032E-08	0.80073	96.779	269.25	5.457E-06	1000	1.934E-05
173	1-Hexanol	C ₆ H ₁₄ O	111-27-3	102.175	1.5773E-07	0.7189	163.3	228.55	4.567E-06	1000	1.945E-05
174	2-Hexanol	C ₆ H ₁₄ O	626-93-7	102.175	1.0652E-07	0.77022	105.85	223.00	4.650E-06	1000	1.970E-05
175	2-Hexanone	C ₆ H ₁₂ O	591-78-6	100.159	9.782E-08	0.7772	99.53	217.35	4.397E-06	1000	1.909E-05
176	3-Hexanone	C ₆ H ₁₂ O	589-38-8	100.159	9.8882E-08	0.7755	99.825	217.50	4.403E-06	1000	1.907E-05
177	1-Hexene	C ₆ H ₁₂	592-41-6	84.159	8.006E-08	0.81293	65.274	133.39	2.871E-06	1000	2.064E-05
178	3-Hexyne	C ₆ H ₁₀	928-49-4	82.144	5.2127E-07	0.5444	237.01	170.05	3.567E-06	1000	1.811E-05
179	Hexyl mercaptan	C ₆ H ₁₄ S	111-31-9	118.240	4.3636E-08	0.90747	42.32	192.62	4.235E-06	1000	2.209E-05
180	1-Hexyne	C ₆ H ₁₀	693-02-7	82.144	2.9986E-07	0.62647	178.17	141.25	2.947E-06	1000	3.758E-13
181	2-Hexyne	C ₆ H ₁₀	764-35-2	82.144	5.5562E-07	0.5337	244.38	183.65	3.851E-06	1000	1.782E-05

TABLE 2-312 Vapor Viscosity of Inorganic and Organic Substances (Pa-s) (Continued)

Cmpd. no.	Name	Formula	CAS no.	Mol. wt.	C1	C2	C3	C4	T_{min} , K	Viscosity at T_{min}	T_{max} , K	Viscosity at T_{max}
182	Hydrazine	H ₄ N ₂	302-01-2	32.045	2.3489E-07	0.7151	205.05		274.69	7.460E-06	1673.15	4.225E-05
183	Hydrogen	H ₂	1333-74-0	2.016	1.797E-07	0.685	-0.59	140	13.95	6.517E-07	3000	4.330E-05
184	Hydrogen bromide	HBr	10035-10-6	80.912	9.17E-08	0.9273			206.45	1.285E-05	800	4.512E-05
185	Hydrogen chloride	HCl	7647-01-0	36.461	4.924E-07	0.6702	157.7		200.00	9.594E-06	1000	4.358E-05
186	Hydrogen cyanide	CHN	74-90-8	27.025	1.278E-08	1.0631	340		300.00	2.576E-06	425	4.421E-06
187	Hydrogen fluoride	HF	7664-39-3	20.006	4.5101E-14	3.0005	-521.83	76,111	285.50	9.931E-06	472.68	2.019E-05
188	Hydrogen sulfide	H ₂ S	7783-06-4	34.081	3.9314E-08	1.0134			250.00	1.058E-05	480	2.050E-05
189	Isobutyric acid	C ₄ H ₈ O ₂	79-31-2	88.105	1.1202E-07	0.7822	100.3		227.15	5.415E-06	1000	2.261E-05
190	Isopropyl amine	C ₃ H ₉ N	75-31-0	59.110	5.2542E-08	0.88063			177.95	5.037E-06	1000	2.304E-05
191	Malonic acid	C ₃ H ₄ O ₄	141-82-2	104.061	8.4213E-08	0.82573	102.08		407.95	9.639E-06	1000	2.293E-05
192	Methacrylic acid	C ₄ H ₆ O ₂	79-41-4	86.089	9.113E-08	0.8222	93.57		288.15	7.242E-06	1000	2.440E-05
193	Methane	CH ₄	74-82-8	16.042	5.2546E-07	0.59006	105.67		90.69	3.468E-06	1000	2.800E-05
194	Methanol	CH ₃ O	67-56-1	32.042	3.0663E-07	0.69655	205		240.00	7.523E-06	1000	3.128E-05
195	N-Methyl acetamide	C ₃ H ₇ NO	79-16-3	73.094	8.0599E-08	0.8392	77.332		301.15	7.714E-06	1000	2.464E-05
196	Methyl acetate	C ₃ H ₆ O ₂	79-20-9	74.079	1.3226E-06	0.4885	504.3		250.00	6.505E-06	800	2.125E-05
197	Methyl acetylene	C ₃ H ₄	74-99-7	40.064	1.163E-06	0.4787	316		170.45	4.769E-06	800	2.045E-05
198	Methyl acrylate	C ₄ H ₆ O ₂	96-33-3	86.089	1.648E-06	0.4444	510.66		196.32	4.781E-06	1000	2.350E-05
199	Methyl amine	CH ₃ N	74-89-5	31.057	5.6409E-07	0.5863	231.9		179.69	5.167E-06	1000	2.628E-05
200	Methyl benzoate	C ₈ H ₈ O ₂	93-58-3	136.148	7.4106E-08	0.82436	83.086		260.75	5.515E-06	1000	2.034E-05
201	3-Methyl-1,2-butadiene	C ₅ H ₈	598-25-4	68.117	4.0824E-07	0.5923	208.22		159.53	3.572E-06	1000	2.022E-05
202	2-Methylbutane	C ₅ H ₁₂	78-78-4	72.149	2.4344E-08	0.97376	-91.597	18,720	150.00	2.621E-06	1000	2.191E-05
203	2-Methylbutanoic acid	C ₆ H ₁₀ O ₂	116-53-0	102.132	1.869E-07	0.7096	192		450.15	1.000E-05	1000	2.109E-05
204	3-Methyl-1-butanol	C ₅ H ₁₂ O	123-51-3	88.148	8.8783E-08	0.80279	77.075		155.95	3.423E-06	1000	2.111E-05
205	2-Methyl-1-butene	C ₅ H ₁₀	563-46-2	70.133	5.0602E-07	0.55258	199.82		135.58	3.083E-06	1000	1.918E-05
206	2-Methyl-2-butene	C ₅ H ₁₀	513-35-9	70.133	8.5423E-07	0.47389	239.34		139.39	3.263E-06	1000	1.820E-05
207	2-Methyl-1-butene-3-yne	C ₅ H ₆	78-80-8	66.101	5.6844E-07	0.553	227.18		160.15	3.893E-06	1000	2.112E-05
208	Methylbutyl ether	C ₈ H ₁₈ O	628-28-4	88.148	3.9342E-08	0.91086			157.48	3.947E-06	1000	2.125E-05
209	Methylbutyl sulfide	C ₈ H ₁₈ S	628-29-5	104.214	4.995E-08	0.89479	44.662		175.30	4.052E-06	1000	2.312E-05
210	3-Methyl-1-butene	C ₅ H ₈	598-23-2	68.117	4.0748E-08	0.92709			183.45	5.112E-06	1000	2.463E-05
211	Methyl butyrate	C ₆ H ₁₀ O ₂	623-42-7	102.132	3.733E-07	0.6177	256.5		187.35	3.993E-06	1000	2.118E-05
212	Methylchlorosilane	CH ₃ ClSi	993-00-0	80.589	4.8806E-08	0.92549			139.05	4.698E-06	1000	2.917E-05
213	Methylcyclohexane	C ₇ H ₁₄	108-87-2	98.186	6.5281E-07	0.5294	310.59		146.58	2.934E-06	1000	1.930E-05
214	1-Methylcyclohexanol	C ₇ H ₁₄ O	590-67-0	114.185	8.5736E-08	0.80277	100.77		299.15	6.232E-06	1000	1.994E-05
215	cis-2-Methylcyclohexanol	C ₇ H ₁₄ O	7443-70-1	114.185	2.40E-07	0.68	210		280.15	6.331E-06	1000	2.175E-05
216	trans-2-Methylcyclohexanol	C ₇ H ₁₄ O	7443-52-9	114.185	2.00E-07	0.704	187		269.15	6.062E-06	1000	2.181E-05
217	Methylcyclopentane	C ₆ H ₁₂	96-37-7	84.159	9.0798E-07	0.495	355.89		130.73	2.722E-06	1000	2.046E-05
218	1-Methylcyclopentene	C ₆ H ₁₀	693-89-0	82.144	3.7026E-08	0.92849			146.62	3.800E-06	1000	2.259E-05
219	3-Methylcyclopentene	C ₆ H ₁₀	1120-62-3	82.144	3.9771E-08	0.92242			115.00	3.165E-06	1000	2.327E-05
220	Methyldichlorosilane	CH ₂ Cl ₂ Si	75-54-7	115.034	1.977E-07	0.7453	131.22		182.55	5.574E-06	1000	3.009E-05
221	Methylethyl ether	C ₃ H ₈ O	540-67-0	60.095	2.6098E-07	0.68276	133.4		160.00	4.552E-06	1000	2.573E-05
222	Methylethyl ketone	C ₄ H ₈ O	78-93-3	72.106	2.6552E-08	0.98316			186.48	4.534E-06	1000	2.364E-05
223	Methylethyl sulfide	C ₃ H ₈ S	624-89-5	76.161	8.6219E-08	0.83591	72.564		167.23	4.341E-06	1000	2.588E-05
224	Methyl formate	C ₂ H ₄ O ₂	107-31-3	60.052	6.9755E-06	0.3154	1034.5		174.15	5.117E-06	1000	3.029E-05
225	Methylisobutyl ether	C ₅ H ₁₂ O	625-44-5	88.148	1.5035E-07	0.7338	108.5		150.00	3.448E-06	1000	2.157E-05
226	Methylisobutyl ketone	C ₆ H ₁₂ O	108-10-1	100.159	9.4257E-08	0.7845	90.183		189.15	3.901E-06	1000	1.951E-05
227	Methyl Isocyanate	C ₂ H ₃ NO	624-83-9	57.051	3.1573E-07	0.66404	173.59		256.15	7.481E-06	1000	2.642E-05
228	Methylisopropyl ether	C ₄ H ₁₀ O	598-53-8	74.122	1.925E-07	0.7091	109		127.93	3.242E-06	1000	2.327E-05
229	Methylisopropyl ketone	C ₅ H ₁₀ O	563-80-4	86.132	1.0826E-07	0.77382	93.349		180.15	3.968E-06	1000	2.076E-05
230	Methylisopropyl sulfide	C ₄ H ₁₀ S	1551-21-9	90.187	8.6077E-08	0.81669	71.294		171.64	4.065E-06	1000	2.265E-05
231	Methyl mercaptan	CH ₃ S	74-93-1	48.107	1.637E-07	0.76706	107.97		150.18	4.450E-06	1000	2.956E-05
232	Methyl methacrylate	C ₅ H ₈ O ₂	80-62-6	100.116	4.889E-07	0.6096	342.23		224.95	5.265E-06	1000	2.456E-05
233	2-Methyloctanoic acid	C ₉ H ₁₈ O ₂	3004-93-1	158.238	7.2131E-08	0.80319	99.437		240.00	4.162E-06	1000	1.685E-05
234	2-Methylpentane	C ₆ H ₁₄	107-83-5	86.175	1.1164E-06	0.4537	374.74		119.55	2.366E-06	1000	1.865E-05
235	Methyl pentyl ether	C ₆ H ₁₄ O	628-80-8	102.175	1.0546E-07	0.77106	93.745		176.00	3.707E-06	1000	1.983E-05
236	2-Methylpropane	C ₄ H ₁₀	75-28-5	58.122	1.0871E-07	0.78135	70.639		150.00	3.707E-06	1000	2.242E-05
237	2-Methyl-2-propanol	C ₄ H ₁₀ O	75-65-0	74.122	9.605E-07	0.4856	381		298.97	6.727E-06	600	1.312E-05
238	2-Methyl propene	C ₄ H ₈	115-11-7	56.106	9.0981E-07	0.49258	260.08		132.81	3.423E-06	1000	2.174E-05
239	Methyl propionate	C ₄ H ₈ O ₂	554-12-1	88.105	3.5642E-07	0.6327	232.2		185.65	4.316E-06	1000	2.288E-05
240	Methylpropyl ether	C ₄ H ₁₀ O	557-17-5	74.122	4.4941E-08	0.90199			133.97	3.725E-06	1000	2.284E-05

241	Methylpropyl sulfide	C ₆ H ₁₀ S	3877-15-4	90.187	5.8223E-08	0.88057	48.298	160.17	3.908E-06	1000	2.434E-05
242	Methylsilane	CH ₆ Si	992-94-9	46.144	3.8926E-07	0.63159	169.45	116.34	3.196E-06	1000	5.762E-13
243	alpha-Methyl styrene	C ₉ H ₁₀	98-83-9	118.176	7.1455E-07	0.49832	303.31	249.95	5.057E-06	1000	1.714E-05
244	Methyl <i>tert</i> -butyl ether	C ₇ H ₁₄ O	1634-04-4	88.148	1.571E-07	0.733	111.578	164.55	3.944E-06	1000	2.235E-05
245	Methyl vinyl ether	C ₄ H ₈ O	107-25-5	58.079	7.646E-07	0.5476	284	278.65	8.264E-06	1000	2.616E-05
246	Naphthalene	C ₁₀ H ₈	91-20-3	128.171	6.4318E-07	0.5389	400.16	353.43	7.125E-06	1000	1.900E-05
247	Neon	Ne	7440-01-9	20.180	7.19E-07	0.6659	5.3	30.00	5.884E-06	3273.1	1.573E-04
248	Nitroethane	C ₂ H ₅ NO ₂	79-24-3	75.067	2.4391E-07	0.702	280	183.63	3.752E-06	1000	2.432E-05
249	Nitrogen	N ₂	7727-37-9	28.013	6.5592E-07	0.6081	54.714	63.15	4.372E-06	1970	6.432E-05
250	Nitrogen trifluoride	F ₃ N	7783-54-2	71.002	8.2005E-07	0.61423	114.58	66.46	3.964E-06	1000	1.975E-12
251	Nitromethane	CH ₃ NO ₂	75-52-5	61.040	4.070E-07	0.6485	367.5	244.60	5.756E-06	1000	2.625E-05
252	Nitrous oxide	N ₂ O	10024-97-2	44.013	2.115E-06	0.4642	305.7	182.30	8.854E-06	1000	4.000E-05
253	Nitric oxide	NO	10102-43-9	30.006	1.467E-06	0.5123	125.4	110.00	7.618E-06	1500	5.737E-05
254	Nonadecane	C ₁₉ H ₄₀	629-92-5	268.521	3.0465E-07	0.62218	705.34	305.04	3.231E-06	1000	1.314E-05
255	Nonanal	C ₉ H ₁₈ O	124-19-6	142.239	7.1902E-08	0.8013	92.051	255.15	4.483E-06	1000	1.669E-05
256	Nonane	C ₉ H ₂₀	111-84-2	128.255	1.0344E-07	0.77301	220.47	219.66	3.335E-06	1000	1.767E-05
257	Nonanoic acid	C ₉ H ₁₈ O ₂	112-05-0	158.238	7.0165E-08	0.8062	100.36	285.65	4.957E-06	1000	1.672E-05
258	1-Nonanol	C ₉ H ₂₀ O	143-08-8	144.255	1.20E-07	0.74	180	268.15	4.499E-06	1000	1.688E-05
259	2-Nonanol	C ₉ H ₂₀ O	628-99-9	144.255	7.0111E-08	0.80701	89.582	238.15	4.219E-06	1000	1.697E-05
260	1-Nonene	C ₉ H ₁₈	124-11-8	126.239	6.6329E-08	0.82027	76.204	191.91	3.542E-06	1000	1.781E-05
261	Nonyl mercaptan	C ₉ H ₂₀ S	1455-21-6	160.320	3.8673E-08	0.91142	50.646	253.05	4.995E-06	1000	1.996E-05
262	1-Nonyne	C ₉ H ₁₆	3452-09-3	124.223	6.1447E-07	0.50705	287.19	223.15	4.170E-06	1000	1.585E-05
263	Octadecane	C ₁₈ H ₃₈	593-45-3	254.494	3.2095E-07	0.61839	709.09	301.31	3.266E-06	1000	1.345E-05
264	Octanal	C ₈ H ₁₆ O	124-13-0	128.212	1.0321E-07	0.7589	121.26	246.00	4.510E-06	1000	1.741E-05
265	Octane	C ₈ H ₁₈	111-65-9	114.229	3.1191E-08	0.92925	55.092	216.38	3.677E-06	1000	1.813E-05
266	Octanoic acid	C ₈ H ₁₆ O ₂	124-07-2	144.211	7.9611E-08	0.7948	106.6	289.65	5.267E-06	1000	1.743E-05
267	1-Octanol	C ₈ H ₁₈ O	111-87-5	130.228	1.752E-07	0.6941	206.8	257.65	4.583E-06	1000	1.755E-05
268	2-Octanol	C ₈ H ₁₈ O	123-96-6	130.228	8.1701E-08	0.79241	97.709	241.55	4.498E-06	1000	1.774E-05
269	2-Octanone	C ₈ H ₁₆ O	111-13-7	128.212	8.0901E-08	0.79062	99.338	252.85	4.611E-06	1000	1.733E-05
270	3-Octanone	C ₈ H ₁₆ O	106-68-3	128.212	6.1515E-11	1.8808		255.55	2.075E-06	1000	2.700E-05
271	1-Octene	C ₈ H ₁₆	111-66-0	112.213	5.0324E-05	0.077611	3604.6	171.45	3.406E-06	1000	1.868E-05
272	Octyl mercaptan	C ₈ H ₁₈ S	111-88-6	146.294	3.3253E-08	0.9351	32.426	223.95	4.579E-06	1000	2.057E-05
273	1-Octyne	C ₈ H ₁₄	629-05-0	110.197	5.7084E-07	0.52446	271.76	193.55	3.758E-06	1000	1.681E-05
274	Oxalic acid	C ₂ H ₂ O ₄	144-62-7	90.035	1.1453E-07	0.7968	126.34	462.65	1.196E-05	1000	2.498E-05
275	Oxygen	O ₂	7782-44-7	31.999	1.101E-06	0.5634	96.3	54.35	3.773E-06	1500	6.371E-05
276	Ozone	O ₃	10028-15-6	47.998	1.196E-07	0.84797		80.15	4.922E-06	1000	4.184E-05
277	Pentadecane	C ₁₅ H ₃₂	629-62-9	212.415	4.0828E-08	0.8766	212.68	283.07	3.288E-06	1000	1.436E-05
278	Pentanal	C ₅ H ₁₀ O	110-62-3	86.132	2.27E-07	0.6767	191.74	182.00	3.740E-06	1000	2.042E-05
279	Pentane	C ₅ H ₁₂	109-66-0	72.149	6.3412E-08	0.84758	41.718	143.42	3.305E-06	1000	2.124E-05
280	Pentanoic acid	C ₅ H ₁₀ O ₂	109-52-4	102.132	9.4314E-08	0.7932	98.279	239.15	5.150E-06	1000	2.058E-05
281	1-Pentanol	C ₅ H ₁₂ O	71-41-0	88.148	1.8903E-07	0.7031	175.9	410.95	9.111E-06	1000	2.068E-05
282	2-Pentanol	C ₅ H ₁₂ O	6032-29-7	88.148	1.1749E-07	0.7649	103.78	200.00	4.452E-06	1000	2.098E-05
283	2-Pentanone	C ₅ H ₁₀ O	107-87-9	86.132	2.463E-07	0.6653	208.7	196.29	4.003E-06	1000	2.019E-05
284	3-Pentanone	C ₅ H ₁₀ O	96-22-0	86.132	1.164E-07	0.7615	107.94	234.18	5.079E-06	1000	2.023E-05
285	1-Pentene	C ₅ H ₁₀	109-67-1	70.133	1.6378E-06	0.44337	636.11	108.02	2.813E-06	1000	2.176E-05
286	2-Pentyl mercaptan	C ₅ H ₁₂ S	2084-19-7	104.214	8.8646E-08	0.81492	85.198	160.75	3.638E-06	1000	2.275E-05
287	Pentyl mercaptan	C ₅ H ₁₂ S	110-66-7	104.214	2.7467E-08	0.97555		197.45	4.766E-06	1000	2.320E-05
288	1-Pentyne	C ₅ H ₈	627-19-0	68.117	4.1022E-08	0.90585		167.45	4.242E-06	1000	2.141E-05
289	2-Pentyne	C ₅ H ₈	627-21-4	68.117	5.765E-07	0.53498	235.2	163.83	3.621E-06	1000	1.879E-05
290	Phenanthrene	C ₁₄ H ₁₀	85-01-8	178.229	4.3478E-07	0.5272	238.27	372.38	6.010E-06	1000	1.340E-05
291	Phenol	C ₆ H ₆ O	108-95-2	94.111	1.0094E-07	0.799	103.1	314.06	7.514E-06	1000	2.283E-05
292	Phenyl isocyanate	C ₇ H ₅ NO	103-71-9	119.121	8.536E-08	0.80872	88.273	243.15	5.324E-06	1000	2.093E-05
293	Phthalic anhydride	C ₈ H ₄ O ₃	85-44-9	148.116	4.3511E-08	0.908	102.73	404.15	8.072E-06	1000	2.090E-05
294	Propadiene	C ₃ H ₄	463-49-0	40.064	6.0758E-07	0.53845	173.45	136.87	3.788E-06	1000	2.135E-05
295	Propane	C ₃ H ₈	74-98-6	44.096	4.9054E-08	0.90125		85.47	2.702E-06	1000	2.480E-05
296	1-Propanol	C ₃ H ₈ O	71-23-8	60.095	7.942E-07	0.5491	415.8	200.00	4.732E-06	1000	2.490E-05
297	2-Propanol	C ₃ H ₈ O	67-63-0	60.095	1.2003E-06	0.494	479.78	187.35	4.471E-06	1000	2.461E-05
298	Propenylcyclohexene	C ₉ H ₁₄	13511-13-2	122.207	5.4749E-07	0.53893	283.52	199.00	3.914E-06	1000	1.765E-05
299	Propionaldehyde	C ₃ H ₆ O	123-38-6	58.079	1.7526E-07	0.72691	119.93	170.00	4.297E-06	1000	2.373E-05
300	Propionic acid	C ₃ H ₆ O ₂	79-09-4	74.079	1.61E-07	0.7457	159.3	252.45	6.105E-06	1000	2.397E-05
301	Propionitrile	C ₃ H ₅ N	107-12-0	55.079	1.0111E-07	0.7821	89.5	180.26	3.927E-06	1000	2.060E-05
302	Propyl acetate	C ₅ H ₁₀ O ₂	109-60-4	102.132	2.1372E-07	0.6894	178.57	178.15	3.802E-06	1000	2.122E-05
303	Propyl amine	C ₃ H ₉ N	107-10-8	59.110	1.62E-07	0.7285	117	188.36	4.540E-06	1000	2.223E-05

-26,218

TABLE 2-312 Vapor Viscosity of Inorganic and Organic Substances (Pa-s) (Concluded)

Cmpd. no.	Name	Formula	CAS no.	Mol. wt.	C1	C2	C3	C4	T_{min} , K	Viscosity at T_{min}	T_{max} , K	Viscosity at T_{max}
304	Propylbenzene	C ₉ H ₁₂	103-65-1	120.192	3.0387E-07	0.61945	210.35		173.55	3.351E-06	1000	1.812E-05
305	Propylene	C ₃ H ₆	115-07-1	42.080	7.3919E-07	0.5423	263.73		87.89	2.093E-06	1000	2.477E-05
306	Propyl formate	C ₄ H ₈ O ₂	110-74-7	88.105	6.0741E-07	0.5863	367.29		180.25	4.203E-06	1000	2.550E-05
307	2-Propyl mercaptan	C ₃ H ₈ S	75-33-2	76.161	3.5532E-08	0.95654			142.61	4.085E-06	1000	2.632E-05
308	Propyl mercaptan	C ₃ H ₈ S	107-03-9	76.161	7.9457E-08	0.84656	65.878		159.95	4.132E-06	1000	2.583E-05
309	1,2-Propylene glycol	C ₃ H ₈ O ₂	57-55-6	76.094	4.543E-08	0.9173	61		213.15	4.832E-06	1000	2.418E-05
310	Quinone	C ₆ H ₄ O ₂	106-51-4	108.095	1.1085E-07	0.8008	152.51		388.85	9.439E-06	1000	2.429E-05
311	Silicon tetrafluoride	F ₄ Si	7783-61-1	104.079	2.1671E-07	0.76757	16.28		250.00	1.410E-05	500	2.475E-05
312	Styrene	C ₈ H ₈	100-42-5	104.149	6.3863E-07	0.5254	295.1		242.54	5.158E-06	1000	1.858E-05
313	Succinic acid	C ₄ H ₆ O ₄	110-15-6	118.088	2.273E-07	0.6845	229.8		460.65	1.009E-05	1000	2.091E-05
314	Sulfur dioxide	O ₂ S	7446-09-5	64.064	6.863E-07	0.6112	217		197.67	8.280E-06	1000	3.844E-05
315	Sulfur hexafluoride	F ₆ S	2551-62-4	146.055	5.3986E-07	0.6349	34.5	19,000	205.15	9.790E-06	5000	1.195E-04
316	Sulfur trioxide	O ₃ S	7446-11-9	80.063	3.9067E-06	0.3845	470.1		297.93	1.355E-05	694.19	2.883E-05
317	Terephthalic acid	C ₈ H ₆ O ₄	100-21-0	166.131	2.2452E-08	0.97631			700.15	1.346E-05	1000	1.906E-05
318	<i>o</i> -Terphenyl	C ₁₈ H ₁₄	84-15-1	230.304	7.0859E-07	0.51971	652.24		329.35	4.837E-06	1000	1.554E-05
319	Tetradecane	C ₁₄ H ₃₀	629-59-4	198.388	5.1567E-09	1.1561			279.01	3.465E-06	1000	1.516E-05
320	Tetrahydrofuran	C ₄ H ₈ O	109-99-9	72.106	3.778E-07	0.6533	271.01		164.65	4.006E-06	1000	2.710E-05
321	1,2,3,4-Tetrahydronaphthalene	C ₁₀ H ₁₂	119-64-2	132.202	5.0784E-07	0.5614	328.55		237.38	4.592E-06	1000	1.847E-05
322	Tetrahydrothiophene	C ₄ H ₈ S	110-01-0	88.171	8.5988E-08	0.82841	68.172		176.99	4.520E-06	1000	2.461E-05
323	2,2,3,3-Tetramethylbutane	C ₈ H ₁₈	594-82-1	114.229	8.1458E-07	0.50257	380.29		373.96	7.930E-06	1000	1.900E-05
324	Thiophene	C ₄ H ₄ S	110-02-1	84.140	1.03E-06	0.5497	569.4		234.94	6.049E-06	1000	2.926E-05
325	Toluene	C ₇ H ₈	108-88-3	92.138	8.7268E-07	0.49397	323.79		178.18	4.008E-06	1000	2.000E-05
326	1,1,2-Trichloroethane	C ₂ H ₃ Cl ₃	79-00-5	133.404	2.7081E-07	0.6955	187.93		236.50	6.756E-06	1000	2.782E-05
327	Tridecane	C ₁₃ H ₂₈	629-50-5	184.361	3.5585E-08	0.8987	165.3		267.76	3.344E-06	1000	1.517E-05
328	Triethyl amine	C ₆ H ₁₅ N	121-44-8	101.190	2.411E-07	0.6845	223		158.45	3.210E-06	1000	2.230E-05
329	Trimethyl amine	C ₃ H ₉ N	75-50-3	59.110	1.2434E-06	0.4832	447.7		156.08	3.689E-06	1000	2.418E-05
330	1,2,3-Trimethylbenzene	C ₉ H ₁₂	526-73-8	120.192	7.8498E-07	0.49855	362.79		247.79	4.975E-06	1000	1.803E-05
331	1,2,4-Trimethylbenzene	C ₉ H ₁₂	95-63-6	120.192	6.8812E-07	0.51063	330.88		229.33	4.520E-06	1000	1.760E-05
332	2,2,4-Trimethylpentane	C ₈ H ₁₈	540-84-1	114.229	1.107E-07	0.746	72.4		165.78	3.488E-06	1000	1.786E-05
333	2,3,3-Trimethylpentane	C ₈ H ₁₈	560-21-4	114.229	8.2418E-07	0.4931	371.44		387.91	7.958E-06	1000	1.812E-05
334	1,3,5-Trinitrobenzene	C ₆ H ₃ N ₃ O ₆	99-35-4	213.105	3.4066E-08	0.95252	43.528		398.40	9.208E-06	1000	2.352E-05
335	2,4,6-Trinitrotoluene	C ₇ H ₅ N ₃ O ₆	118-96-7	227.131	2.8471E-08	0.96571	30.83		354.00	7.581E-06	1000	2.179E-05
336	Undecane	C ₁₁ H ₂₄	1120-21-4	156.308	3.594E-08	0.9052	125		247.57	3.506E-06	1000	1.660E-05
337	1-Undecanol	C ₁₁ H ₂₄ O	112-42-5	172.308	5.9537E-08	0.81842	90.245		288.45	4.677E-06	1000	1.558E-05
338	Vinyl acetate	C ₄ H ₆ O ₂	108-05-4	86.089	1.388E-07	0.7599	98		180.35	4.660E-06	1000	2.407E-05
339	Vinyl acetylene	C ₄ H ₄	689-97-4	52.075	6.7484E-07	0.5304	230.17		173.15	4.459E-06	1000	2.140E-05
340	Vinyl chloride	C ₂ H ₃ Cl	75-01-4	62.498	2.379E-07	0.71517	102.84		119.36	3.907E-06	1000	1.263E-12
341	Vinyl trichlorosilane	C ₂ H ₃ Cl ₃ Si	75-94-5	161.490	3.6429E-08	0.95924			178.35	5.260E-06	1000	2.749E-05
342	Water	H ₂ O	7732-18-5	18.015	1.7096E-08	1.1146			273.16	8.882E-06	1073.15	4.082E-05
343	<i>m</i> -Xylene	C ₈ H ₁₀	108-38-3	106.165	6.8293E-07	0.52199	324.17		225.30	4.735E-06	1000	1.899E-05
344	<i>o</i> -Xylene	C ₈ H ₁₀	95-47-6	106.165	8.3436E-07	0.49713	365.86		247.98	5.225E-06	1000	1.894E-05
345	<i>p</i> -Xylene	C ₈ H ₁₀	106-42-3	106.165	9.3485E-07	0.47683	371.96		286.41	6.037E-06	1000	1.836E-05

The vapor viscosity is calculated by

$$\mu = \frac{C1T^{C2}}{1 + C3/T + C4/T^2}$$

where μ is the viscosity in Pa-s and T is the temperature in K. Viscosities are at either 1 atm or the vapor pressure, whichever is lower. All substances are listed by chemical family in Table 2-6 and by formula in Table 2-7.

Values in this table were taken from the Design Institute for Physical Properties (DIPPR) of the American Institute of Chemical Engineers (AIChE), copyright 2007 AIChE and reproduced with permission of AIChE and of the DIPPR Evaluated Process Design Data Project Steering Committee. Their source should be cited as R. L. Rowley, W. V. Wilding, J. L. Oscarson, Y. Yang, N. A. Zundel, T. E. Daubert, R. P. Danner, DIPPR® Data Compilation of Pure Chemical Properties, Design Institute for Physical Properties, AIChE, New York (2007).

The number of digits provided for values at T_{min} and T_{max} was chosen for uniformity of appearance and formatting; these do not represent the uncertainties of the physical quantities, but are the result of calculations from the standard thermophysical property formulations within a fixed format.

TABLE 2-313 Viscosity of Inorganic and Organic Liquids (Pa-s)

Cmpd. no.	Name	Formula	CAS no.	Mol. wt.	C1	C2	C3	C4	C5	T_{min} , K	Viscosity at T_{min}	T_{max} K	Viscosity at T_{max}
1	Acetaldehyde	C ₂ H ₄ O	75-07-0	44.053	-5.895	668.21	-0.84323			150.15	3.446E-03	294.00	2.216E-04
2	Acetamide	C ₂ H ₅ NO	60-35-5	59.067	1.5525	1376.4	-2.0126			353.33	1.728E-03	494.30	2.895E-04
3	Acetic acid	C ₂ H ₄ O ₂	64-19-7	60.052	-9.03	1212.3	-0.322			289.81	1.265E-03	391.05	3.890E-04
4	Acetic anhydride	C ₄ H ₆ O ₃	108-24-7	102.089	-14.164	1353.3	0.4492			210.00	4.834E-03	412.70	2.783E-04
5	Acetone	C ₃ H ₆ O	67-64-1	58.079	-14.918	1020.4	0.5961			190.00	1.655E-03	329.44	2.351E-04
6	Acetonitrile	C ₂ H ₃ N	75-05-8	41.052	-10.906	872.02				229.32	8.220E-04	436.40	1.350E-04
7	Acetylene	C ₂ H ₂	74-86-2	26.037	6.224	-151.8	-2.6554			193.15	1.958E-04	273.15	9.819E-05
8	Acrolein	C ₃ H ₄ O	107-02-8	56.063	-12.032	867.34	0.19534			185.45	1.773E-03	353.22	2.181E-04
9	Acrylic acid	C ₃ H ₄ O ₂	79-10-7	72.063	-28.12	2280.2	2.3956			286.15	1.359E-03	460.00	2.086E-04
10	Acrylonitrile	C ₃ H ₃ N	107-13-1	53.063	2.019	239.7	-1.8975			220.00	8.040E-04	350.50	2.215E-04
11	Air	Mixture	132259-10-0	28.960	-20.077	285.15	1.784	-6.2382E-22	10	59.15	3.430E-04	130.00	4.276E-05
12	Ammonia	H ₃ N	7664-41-7	17.031	-6.743	598.3	-0.7341	-3.69E-27	10	195.41	5.240E-04	393.15	4.858E-05
13	Anisole	C ₇ H ₈ O	100-66-3	108.138	-15.407	1518.7	0.60172			235.65	3.429E-03	426.73	2.736E-04
14	Argon	Ar	7440-37-1	39.948	-8.8685	204.29	-0.38305	-1.2937E-22	10	83.78	2.950E-04	150.00	3.823E-05
15	Benzamide	C ₇ H ₇ NO	55-21-0	121.137	-12.632	2668.2				403.00	2.451E-03	563.15	3.730E-04
16	Benzene	C ₆ H ₆	71-43-2	78.112	7.5117	294.68	-2.794			278.68	7.761E-04	545.00	7.106E-05
17	Benzenethiol	C ₆ H ₆ S	108-98-5	110.177	-8.4562	1024.4	-0.30635			258.27	2.047E-03	442.29	3.333E-04
18	Benzoic acid	C ₇ H ₆ O ₂	65-85-0	122.121	-12.947	2557.9	395.52			395.52	1.530E-03	600.80	1.680E-04
19	Benzonitrile	C ₇ H ₅ N	100-47-0	103.121	-20.236	1737.4	1.3531			270.00	1.977E-03	450.00	3.009E-04
20	Benzophenone	C ₁₃ H ₁₀ O	119-61-9	182.218	13.354	-232.91	-3.2685	1.7488E+20	-8.052	321.35	6.100E-03	664.00	2.660E-04
21	Benzyl alcohol	C ₇ H ₈ O	100-51-6	108.138	-14.152	2652				257.85	2.092E-02	478.60	1.821E-04
22	Benzyl ethyl ether	C ₉ H ₁₂ O	539-30-0	136.191	-11.46	1497	-0.043397			275.65	1.887E-03	458.15	2.121E-04
23	Benzyl mercaptan	C ₇ H ₈ S	100-53-8	124.203	-11.459	1334.4	0.00049694			243.95	2.513E-03	472.03	1.788E-04
24	Biphenyl	C ₁₂ H ₁₀	92-52-4	154.208	-9.9265	1576.3	-0.21119			342.20	1.427E-03	723.15	1.076E-04
25	Bromine	Br ₂	7726-95-6	159.808	16.775	-314	-3.9763			265.85	1.353E-03	350.00	6.021E-04
26	Bromobenzene	C ₆ H ₅ Br	108-86-1	157.008	-20.611	1656.5	1.4415			242.43	2.842E-03	429.24	3.310E-04
27	Bromoethane	C ₂ H ₅ Br	74-96-4	108.965	-10.015	823.43	-0.11122			154.55	5.260E-03	311.50	3.321E-04
28	Bromomethane	CH ₃ Br	74-83-9	94.939	-8.103	570.8	-0.32958			179.47	1.316E-03	276.71	3.732E-04
29	1,2-Butadiene	C ₄ H ₆	590-19-2	54.090	-10.143	472.79	-0.028241			136.95	1.081E-03	284.00	1.773E-04
30	1,3-Butadiene	C ₄ H ₆	106-99-0	54.090	17.844	-310.2	-4.5058			250.00	2.547E-04	400.00	4.880E-05
31	Butane	C ₄ H ₁₀	106-97-8	58.122	-7.2471	534.82	-0.57469	-4.6625E-27	10	134.86	2.243E-03	420.00	3.566E-05
32	1,2-Butanediol	C ₄ H ₁₀ O ₂	584-03-2	90.121	-393.86	19042	59.978	-0.049479	1	220.00	2.020E+02	544.00	3.440E-04
33	1,3-Butanediol	C ₄ H ₁₀ O ₂	107-88-0	90.121	-390.03	18609	60.014	-0.055844	1	196.15	4.410E+04	540.80	2.890E-04
34	1-Butanol	C ₄ H ₁₀ O	71-36-3	74.122	0.87669	1602.9	-2.1475	3.3866E+22	-9.9231	190.00	3.237E-01	391.90	3.877E-04
35	2-Butanol	C ₄ H ₁₀ O	78-92-2	74.122	-16.323	3141.7				158.45	3.327E+01	372.90	3.715E-04
36	1-Butene	C ₄ H ₈	106-98-9	56.106	-10.773	591.61				87.80	1.770E-02	335.60	1.220E-04
37	cis-2-Butene	C ₄ H ₈	590-18-1	56.106	-10.346	522.3	-0.011847			134.26	1.483E-03	276.87	1.982E-04
38	trans-2-Butene	C ₄ H ₈	624-64-6	56.106	-10.335	521.39	-0.013184			167.62	6.810E-04	274.03	2.022E-04
39	Butyl acetate	C ₆ H ₁₂ O ₂	123-86-4	116.158	-17.488	1478.2	0.91828			250.00	1.496E-03	399.26	2.521E-04
40	Butylbenzene	C ₁₀ H ₁₄	104-51-8	134.218	-23.802	1887.2	1.8479			200.00	1.030E-02	456.46	2.359E-04
41	Butyl mercaptan	C ₄ H ₁₀ S	109-79-5	90.187	-10.807	966.74	-0.014851			157.46	8.717E-03	373.15	2.475E-04
42	sec-Butyl mercaptan	C ₄ H ₁₀ S	513-53-1	90.187	-10.903	932.82	0.023034			133.02	2.288E-02	358.13	2.851E-04
43	1-Butyne	C ₄ H ₆	107-00-6	54.090	-3.4644	334.5	-1.0811			147.43	1.369E-03	373.15	1.271E-04
44	Butyraldehyde	C ₄ H ₈ O	123-72-8	72.106	-10.057	903.73	-0.13186			176.75	3.602E-03	348.05	2.660E-04
45	Butyric acid	C ₄ H ₈ O ₂	107-92-6	88.105	-9.817	1388	-0.238			267.95	2.561E-03	436.42	3.087E-04
46	Butyronitrile	C ₄ H ₇ N	109-74-0	69.105	-10.136	1006.4	-0.1337			161.25	1.031E-02	390.75	2.344E-04
47	Carbon dioxide	CO ₂	124-38-9	44.010	18.775	-402.92		-6.9171E-26	10	216.58	2.488E-04	303.15	5.652E-05
48	Carbon disulfide	CS ₂	75-15-0	76.141	-10.306	703.01				161.58	2.590E-03	441.60	1.640E-04
49	Carbon monoxide	CO	630-08-0	28.010	-4.9735	97.67	-1.1088			68.15	2.689E-04	131.37	6.515E-05
50	Carbon tetrachloride	CCl ₄	56-23-5	153.823	-8.0738	1121.1	-0.4726			250.00	2.032E-03	455.00	2.030E-04
51	Carbon tetrafluoride	CF ₄	75-73-0	88.004	-9.9212	300.5				89.56	1.408E-03	145.10	3.897E-04
52	Chlorine	Cl ₂	7782-50-5	70.906	-9.5412	456.62				172.12	1.020E-03	333.72	2.820E-04
53	Chlorobenzene	C ₆ H ₅ Cl	108-90-7	112.557	0.15772	540.5	-1.6075			250.00	1.422E-03	540.00	1.291E-04
54	Chloroethane	C ₂ H ₅ Cl	75-00-3	64.514	-10.216	702	-0.072			150.00	2.748E-03	373.15	1.567E-04
55	Chloroform	CHCl ₃	67-66-3	119.378	-14.109	1049.2	0.5377			209.63	1.970E-03	353.20	3.410E-04
56	Chloromethane	CH ₃ Cl	74-87-3	50.488	-25.132	1381.9	2.0811	-4.4999E-27	10	175.43	1.501E-03	403.15	5.951E-05
57	1-Chloropropane	C ₃ H ₇ Cl	540-54-5	78.541	-13.994	949.4	0.50223	-6.163E-17	6	150.35	5.728E-03	423.15	1.154E-04
58	2-Chloropropane	C ₃ H ₇ Cl	75-29-6	78.541	-15.458	1086	0.654			250.00	5.515E-04	308.85	2.767E-04
59	m-Cresol	C ₇ H ₈ O	108-39-4	108.138	59.686	-3517.9	-9.838	9.0312E+12	-5	273.15	8.670E-02	564.68	1.630E-04

TABLE 2-313 Viscosity of Inorganic and Organic Liquids (Pa-s) (Continued)

Cmpd. no.	Name	Formula	CAS no.	Mol. wt.	C1	C2	C3	C4	C5	T_{min} , K	Viscosity at T_{min}	T_{max} , K	Viscosity at T_{max}
60	<i>o</i> -Cresol	C ₇ H ₈ O	95-48-7	108.138	-0.033937	390.77	-1.4547	5.0187E+12	-5	293.15	9.600E-03	558.04	2.160E-04
61	<i>p</i> -Cresol	C ₇ H ₈ O	106-44-5	108.138	-1.6355	1052.9	-1.3891	3.6844E+17	-7	273.15	9.770E-02	563.72	1.940E-04
62	Cumene	C ₉ H ₁₂	98-82-8	120.192	-24.988	1807.9	2.0556			200.00	6.363E-03	400.00	2.881E-04
63	Cyanogen	C ₂ N ₂	460-19-5	52.035	-12.086	994.23				245.25	3.250E-04	320.12	1.260E-04
64	Cyclobutane	C ₄ H ₈	287-23-0	56.106	-3.4968	397.94	-1.1087			182.48	8.345E-04	367.94	1.278E-04
65	Cyclohexane	C ₆ H ₁₂	110-82-7	84.159	-33.763	2497.2	3.2236			279.69	1.260E-03	443.04	2.070E-04
66	Cyclohexanol	C ₆ H ₁₂ O	108-93-0	100.159	280.87	-31869	-38.837	3,994,500	-2.002	296.60	6.330E-02	520.08	1.650E-04
67	Cyclohexanone	C ₆ H ₁₀ O	108-94-1	98.143	-44.877	3227.7	4.887			242.00	8.960E-03	428.58	4.402E-04
68	Cyclohexene	C ₆ H ₁₀	110-83-8	82.144	-11.641	1154.3	0.066511			200.00	4.018E-03	373.15	2.877E-04
69	Cyclopentane	C ₅ H ₁₀	287-92-3	70.133	-3.2612	614.16	-1.156			225.00	1.122E-03	325.00	3.167E-04
70	Cyclopentene	C ₅ H ₈	142-29-0	68.117	-4.1508	599.77	-1.0308			138.13	7.531E-03	405.60	1.416E-04
71	Cyclopropane	C ₃ H ₆	75-19-4	42.080	-3.524	342.54	-1.1599			145.59	9.601E-04	318.40	1.080E-04
72	Cyclohexyl mercaptan	C ₆ H ₁₂ S	1569-69-3	116.224	-11.338	1304.1	0.000092396			189.64	1.155E-02	431.95	2.440E-04
73	Decanal	C ₁₀ H ₂₀ O	112-31-2	156.265	-10.115	1111.9	-0.015659			267.15	2.381E-03	488.15	3.583E-04
74	Decane	C ₁₀ H ₂₂	124-18-5	142.282	-9.6489	1181.1	-0.24367	9.0522E+34	-15	240.05	2.780E-03	494.16	1.550E-04
75	Decanoic acid	C ₁₀ H ₂₀ O ₂	334-48-5	172.265	-12.305	2324.1	-0.055494			304.55	6.798E-03	543.15	2.304E-04
76	1-Decanol	C ₁₀ H ₂₂ O	112-30-1	158.281	-69.985	5818.8	8.0715			285.00	1.937E-02	503.00	2.727E-04
77	1-Decene	C ₁₀ H ₂₀	872-05-9	140.266	-15.868	1434.8	0.68071			206.89	4.975E-03	443.75	2.064E-04
78	Decyl mercaptan	C ₁₀ H ₂₂ S	143-10-2	174.347	-11.464	1510.1	-0.012754			247.56	4.364E-03	512.35	1.848E-04
79	1-Decyne	C ₁₀ H ₁₈	764-93-2	138.250	-2.3633	791.93	-1.2272			229.15	3.786E-03	505.60	2.167E-04
80	Deuterium	D ₂	7782-39-0	4.032	0.000001348					20.35	1.348E-06	20.35	1.348E-06
81	1,1-Dibromoethane	C ₂ H ₄ Br ₂	557-91-5	187.861	-10.457	1101.1	-0.0031354			210.15	5.331E-03	381.15	5.071E-04
82	1,2-Dibromoethane	C ₂ H ₄ Br ₂	106-93-4	187.861	-17.582	1635.4	0.9932			282.85	2.042E-03	404.51	5.120E-04
83	Dibromomethane	CH ₂ Br ₂	74-95-3	173.835	-10.013	921.31				220.60	2.920E-03	488.80	2.950E-04
84	Dibutyl ether	C ₈ H ₁₈ O	142-96-1	130.228	10.027	206	-3.1607			175.30	5.931E-03	414.15	1.989E-04
85	<i>m</i> -Dichlorobenzene	C ₆ H ₄ Cl ₂	541-73-1	147.002	-1.9265	387.67	-1.1335	1.5037E+14	-6	248.39	2.540E-03	547.16	2.340E-04
86	<i>o</i> -Dichlorobenzene	C ₆ H ₄ Cl ₂	95-50-1	147.002	-30.6	2153.4	2.9371			256.15	2.727E-03	453.57	3.761E-04
87	<i>p</i> -Dichlorobenzene	C ₆ H ₄ Cl ₂	106-46-7	147.002	31.63	-1080	-6.114			326.14	8.543E-04	447.21	3.039E-04
88	1,1-Dichloroethane	C ₂ H ₄ Cl ₂	75-34-3	98.959	-8.991	870.2	-0.2805			176.19	4.076E-03	330.45	3.407E-04
89	1,2-Dichloroethane	C ₂ H ₄ Cl ₂	107-06-2	98.959	15.312	-41.12	-3.919			237.49	1.839E-03	400.00	2.557E-04
90	Dichloromethane	CH ₂ Cl ₂	75-09-2	84.933	-13.071	940.03	0.3733			208.38	1.407E-03	373.93	2.374E-04
91	1,1-Dichloropropane	C ₃ H ₆ Cl ₂	78-99-9	112.986	-10.872	1033.1	-0.00067435			200.00	3.312E-03	361.25	3.301E-04
92	1,2-Dichloropropane	C ₃ H ₆ Cl ₂	78-87-5	112.986	-11.269	1195.3	0.012736			172.71	1.381E-02	369.52	3.495E-04
93	Diethanol amine	C ₄ H ₁₁ NO ₂	111-42-2	105.136	-375.21	1717.7	66.66	-3.6367	0.5	293.15	8.130E-01	589.28	1.090E-04
94	Diethyl amine	C ₄ H ₁₁ N	109-89-7	73.137	-17.57	1385.7	0.85647			223.35	1.191E-03	329.10	2.260E-04
95	Diethyl ether	C ₄ H ₁₀ O	60-29-7	74.122	10.197	-63.8	-3.226			200.00	7.359E-04	373.15	1.141E-04
96	Diethyl sulfide	C ₄ H ₁₀ S	352-93-2	90.187	-5.135	667.5	-0.8553			225.00	1.113E-03	365.25	2.354E-04
97	1,1-Difluoroethane	C ₂ H ₄ F ₂	75-37-6	66.050	10.501	-52.181	-3.3459			154.56	1.229E-03	343.15	1.026E-04
98	1,2-Difluoroethane	C ₂ H ₄ F ₂	624-72-6	66.050	-10.072	710.48	-0.14677			215.00	5.231E-04	283.65	2.257E-04
99	Difluoromethane	CH ₂ F ₂	75-10-5	52.023	-17.723	850.2	1.0601	-1.1719E-18	7	137.00	1.830E-03	343.15	6.050E-05
100	Di-isopropyl amine	C ₆ H ₁₅ N	108-18-9	101.190	-1.7366	599.8	-1.4237			250.00	7.479E-04	357.05	2.193E-04
101	Di-isopropyl ether	C ₆ H ₁₄ O	108-20-3	102.175	-11.5	993	0.022			187.65	2.259E-03	341.45	2.110E-04
102	Di-isopropyl ketone	C ₇ H ₁₄ O	565-80-0	114.185	-15.097	1426.9	0.51512			204.81	4.569E-03	397.55	2.194E-04
103	1,1-Dimethoxyethane	C ₄ H ₁₀ O ₂	534-15-6	90.121	-10.968	885.49				159.95	4.375E-03	337.45	2.378E-04
104	1,2-Dimethoxypropane	C ₅ H ₁₂ O ₂	7778-85-0	104.148	-10.631	1086.4				226.10	2.950E-03	366.15	4.695E-04
105	Dimethyl acetylene	C ₄ H ₆	503-17-3	54.090	0.10842	300.2	-1.6831			240.91	3.796E-04	371.00	1.186E-04
106	Dimethyl amine	C ₂ H ₇ N	124-40-3	45.084	-10.93	699.5				200.00	5.917E-04	308.15	1.734E-04
107	2,3-Dimethylbutane	C ₆ H ₁₄	79-29-8	86.175	7.2565	221.4	-2.7946			220.00	1.103E-03	331.13	2.509E-04
108	1,1-Dimethylcyclohexane	C ₈ H ₁₆	590-66-9	112.213	-10.716	1140.5	-0.047736			239.66	1.992E-03	392.70	3.045E-04
109	<i>cis</i> -1,2-Dimethylcyclohexane	C ₈ H ₁₆	2207-01-4	112.213	-11.796	1463.5				223.16	5.310E-03	484.92	1.540E-04
110	<i>trans</i> -1,2-Dimethylcyclohexane	C ₈ H ₁₆	6876-23-9	112.213	-11.344	1168.9	0.04513			184.99	8.315E-03	396.58	2.956E-04
111	Dimethyl disulfide	C ₂ H ₆ S ₂	624-92-0	94.199	-10.577	1172.6	-0.14244			188.44	6.093E-03	382.90	2.336E-04
112	Dimethyl ether	C ₂ H ₆ O	115-10-6	46.068	-10.62	448.99	0.000083967			131.65	7.398E-04	248.31	1.490E-04
113	<i>N,N</i> -Dimethyl formamide	C ₃ H ₇ NO	68-12-2	73.094	-20.425	1515.5	1.4444			200.00	2.041E-03	425.15	2.981E-04
114	2,3-Dimethylpentane	C ₇ H ₁₆	565-59-3	100.202	-12.08	1112.2	0.09654			160.00	9.669E-03	362.93	2.147E-04
115	Dimethyl phthalate	C ₁₀ H ₁₀ O ₄	131-11-3	194.184	16.961	-423.16	-3.8178	1.362E+15	-6	274.18	6.030E-02	612.80	2.730E-04
116	Dimethylsilane	C ₂ H ₆ Si	1111-74-6	60.170									
117	Dimethyl sulfide	C ₂ H ₆ S	75-18-3	62.134	-17.641	1067.5	1.0317			225.00	6.696E-04	310.48	2.528E-04
118	Dimethyl sulfoxide	C ₂ H ₆ OS	67-68-5	78.133	-37.347	2835	3.7937			291.67	2.253E-03	464.00	3.547E-04

119	Dimethyl terephthalate	C ₁₀ H ₁₀ O ₄	120-61-6	194.184	-11.488	1922.6				413.80	1.068E-03	561.15	3.154E-04
120	1,4-Dioxane	C ₄ H ₈ O ₂	123-91-1	88.105	-46.166	3086.2				284.95	1.525E-03	374.65	4.610E-04
121	Diphenyl ether	C ₁₂ H ₁₀ O	101-84-8	170.207	-12.373	2017.5			5.104	293.15	4.120E-03	613.44	1.130E-04
122	Dipropyl amine	C ₆ H ₁₅ N	142-84-7	101.190	-15.404	1390			0.5564	260.00	9.454E-04	382.35	2.118E-04
123	Dodecane	C ₁₂ H ₂₆	112-40-3	170.335	-7.8244	1191.9		3.9572E+23	-10	262.15	3.020E-03	526.40	1.680E-04
124	Eicosane	C ₂₀ H ₄₂	112-95-8	282.547	-18.315	2283.5			0.95485	309.58	4.243E-03	616.93	2.078E-04
125	Ethane	C ₂ H ₆	74-84-0	30.069	-7.0046	276.38			-0.6087	90.35	1.247E-03	300.00	3.587E-05
126	Ethanol	C ₂ H ₆ O	64-17-5	46.068	7.875	781.98			-3.0418	200.00	1.315E-02	440.00	1.416E-04
127	Ethyl acetate	C ₄ H ₈ O ₂	141-78-6	88.105	14.354	-154.6			-3.7887	220.00	1.132E-03	473.15	9.061E-05
128	Ethyl amine	C ₂ H ₇ N	75-04-7	45.084	19.822	-0.12598			-4.9793	192.15	1.727E-03	289.73	2.236E-04
129	Ethylbenzene	C ₈ H ₁₀	100-41-4	106.165	-13.563	1208.6			0.377	178.20	8.012E-03	413.10	2.326E-04
130	Ethyl benzoate	C ₉ H ₁₀ O ₂	93-89-0	150.175	-40.706	3035			4.2655	250.00	6.643E-03	486.55	3.109E-04
131	2-Ethyl butanoic acid	C ₆ H ₁₂ O ₂	88-09-5	116.158	-12.24	1836.4			0.021868	258.15	6.705E-03	466.95	2.822E-04
132	Ethyl butyrate	C ₆ H ₁₂ O ₂	105-54-4	116.158	-15.485	1325.6			0.6432	250.00	1.319E-03	394.65	2.533E-04
133	Ethylcyclohexane	C ₈ H ₁₆	1678-91-7	112.213	-22.11	1673			1.641	200.00	6.406E-03	404.94	2.956E-04
134	Ethylcyclopentane	C ₇ H ₁₄	1640-89-7	98.186	-6.894	818.6			-0.5941	253.15	9.605E-04	378.15	2.599E-04
135	Ethylene	C ₂ H ₄	74-85-1	28.053	1.8878	78.865			-2.1554	104.00	6.334E-04	250.00	6.143E-05
136	Ethylenediamine	C ₂ H ₆ N ₂	107-15-3	60.098	-53.908	4030.8			5.9704	284.29	2.487E-03	483.15	1.723E-04
137	Ethylene glycol	C ₂ H ₆ O ₂	107-21-1	62.068	-20.515	2468.5			1.2435	260.15	1.340E-01	576.00	2.520E-04
138	Ethyleneimine	C ₂ H ₅ N	151-56-4	43.068	-11.012	967.4				250.00	7.909E-04	329.00	3.123E-04
139	Ethylene oxide	C ₂ H ₄ O	75-21-8	44.053	-8.521	634.2			-0.3314	160.65	1.918E-03	283.85	2.863E-04
140	Ethyl formate	C ₃ H ₆ O ₂	109-94-4	74.079	-9.8417	876.4			-0.1708	245.00	7.435E-04	345.00	2.486E-04
141	2-Ethyl hexanoic acid	C ₈ H ₁₆ O ₂	149-57-5	144.211	-13.037	2346				235.00	4.717E-02	510.10	2.165E-04
142	Ethylhexyl ether	C ₈ H ₁₈ O	5756-43-4	130.228	-11.311	1337.2			-0.02982	180.00	1.765E-02	417.15	2.522E-04
143	Ethylisopropyl ether	C ₅ H ₁₂ O	625-54-7	88.148	-11.331	908.46			0.00042478	140.00	7.908E-03	326.15	1.949E-04
144	Ethylisopropyl ketone	C ₆ H ₁₂ O	565-69-5	100.159	-11.452	1172.7			-0.00010095	204.15	3.319E-03	386.55	2.207E-04
145	Ethyl mercaptan	C ₂ H ₆ S	75-08-1	62.134	-9.7574	729.43			-0.14912	125.26	9.520E-03	308.15	2.626E-04
146	Ethyl propionate	C ₅ H ₁₀ O ₂	105-37-3	102.132	-8.9215	950.8			-0.32687	250.00	9.848E-04	372.25	2.480E-04
147	Ethylpropyl ether	C ₅ H ₁₂ O	628-32-0	88.148	0.7109	386.51			-1.7754	200.00	1.156E-03	337.01	2.086E-04
148	Ethyltrichlorosilane	C ₂ H ₅ Cl ₃ Si	115-21-9	163.506	7.8744	-106.34			-2.6884	167.55	1.010E-02	447.96	1.550E-04
149	Fluorine	F ₂	7782-41-4	37.997	8.18	-75.6			-3.5148	53.48	7.317E-04	140.00	5.954E-05
150	Fluorobenzene	C ₆ H ₅ F	462-06-6	96.102	-10.064	1058.7			-0.17162	232.15	1.599E-03	453.15	1.542E-04
151	Fluoroethane	C ₂ H ₅ F	353-36-6	48.060	-10.758	558.81			-0.016459	129.95	1.448E-03	235.45	2.087E-04
152	Fluoromethane	CH ₃ F	593-53-3	34.033	-10.501	427.78			0.0086309	131.35	7.450E-04	194.82	2.587E-04
153	Formaldehyde	CH ₂ O	50-00-0	30.026	-11.24	751.69			-0.024579	181.15	7.331E-04	254.05	2.210E-04
154	Formamide	CH ₃ NO	75-12-7	45.041	40.153	-912.39			-7.5664	273.15	7.408E-03	493.00	1.821E-04
155	Formic acid	CH ₂ O ₂	64-18-6	46.026	-48.529	3394.7			5.3903	281.45	2.319E-03	373.71	5.444E-04
156	Furan	C ₄ H ₄ O	110-00-9	68.074	-10.923	894.63			-0.00068418	200.00	1.575E-03	304.50	3.392E-04
157	Helium-4	He	7440-59-7	4.003	-9.6312	-3.841			-1.458	2.20	3.628E-06	5.10	2.532E-06
158	Heptadecane	C ₁₇ H ₃₆	629-78-7	240.468	-19.991	2245.1			1.1982	295.13	3.814E-03	575.30	2.088E-04
159	Heptanal	C ₇ H ₁₄ O	111-71-7	114.185	-10.443	1063.2			-0.031488	229.80	2.510E-03	425.95	2.924E-04
160	Heptane	C ₇ H ₁₆	142-82-5	100.202	-9.4622	877.07			-0.23445	180.15	4.420E-03	432.16	1.430E-04
161	Heptanoic acid	C ₇ H ₁₄ O ₂	111-14-8	130.185	-40.543	3328.3			4.1804	265.83	9.242E-03	496.15	3.754E-04
162	1-Heptanol	C ₇ H ₁₆ O	111-70-6	116.201	-66.654	5325.8			7.66	239.15	8.805E-02	448.60	3.190E-04
163	2-Heptanol	C ₇ H ₁₆ O	543-49-7	116.201	11.225	25.319			-3.2694	230.00	4.036E-01	432.90	2.723E-04
164	3-Heptanone	C ₇ H ₁₄ O	106-35-4	114.185	-9.3874	1204.9			-0.32618	234.15	2.427E-03	421.15	2.040E-04
165	2-Heptanone	C ₇ H ₁₄ O	110-43-0	114.185	-13.929	1321.9			0.40382	250.00	1.642E-03	424.18	2.318E-04
166	1-Heptene	C ₇ H ₁₄	592-76-7	98.186	-10.819	841.33				154.12	4.700E-03	429.92	1.420E-04
167	Heptyl mercaptan	C ₇ H ₁₆ S	1639-09-4	132.267	-11.812	1291.9			0.076469	229.92	3.097E-03	450.09	2.087E-04
168	1-Heptyne	C ₇ H ₁₂	628-71-7	96.170	-2.7947	563.86			-1.1636	192.22	2.528E-03	447.20	1.777E-04
169	Hexadecane	C ₁₆ H ₃₄	544-76-3	226.441	-20.182	2203.5			1.2289	291.31	3.536E-03	564.15	2.054E-04
170	Hexanal	C ₆ H ₁₂ O	66-25-1	100.159	-10.745	1021.4			-0.000055427	217.15	2.378E-03	401.45	2.744E-04
171	Hexane	C ₆ H ₁₄	110-54-3	86.175	-6.3276	640			-0.694	174.65	2.400E-03	406.08	1.340E-04
172	Hexanoic acid	C ₆ H ₁₂ O ₂	142-62-1	116.158	-46.402	3448.6			5.0849	269.25	5.854E-03	478.85	4.019E-04
173	1-Hexanol	C ₆ H ₁₄ O	111-27-3	102.175	-39.324	3841			3.6933	250.00	2.822E-02	429.90	3.343E-04
174	2-Hexanol	C ₆ H ₁₄ O	626-93-7	102.175	-82.705	7404.9			6.4721	223.00	4.919E-01	412.40	3.274E-04
175	2-Hexanone	C ₆ H ₁₂ O	591-78-6	100.159	-11.445	1187.2			0.0029076	117.35	2.561E-03	400.70	2.108E-04
176	3-Hexanone	C ₆ H ₁₂ O	589-38-8	100.159	-13.684	1283.4			0.33755	217.50	2.563E-03	396.65	2.185E-04
177	1-Hexene	C ₆ H ₁₂	592-41-6	84.159	-10.36	775.85			-0.082348	133.39	7.108E-03	336.63	1.966E-04
178	3-Hexyne	C ₆ H ₁₀	928-49-4	82.144	-4.2684	647.6			-1.0087	170.05	3.550E-03	432.00	1.377E-04
179	Hexyl mercaptan	C ₆ H ₁₄ S	111-31-9	118.240	-10.073	1123.3			-0.16515	192.62	6.035E-03	425.81	2.172E-04
180	1-Hexyne	C ₆ H ₁₀	693-02-7	82.144	-4.7263	594.43			-0.86247	141.25	8.332E-03	412.00	2.083E-04
181	2-Hexyne	C ₆ H ₁₀	764-35-2	82.144	-3.7464	624.2			-1.084	183.65	2.483E-03	435.00	1.368E-04

TABLE 2-313 Viscosity of Inorganic and Organic Liquids (Pa-s) (Continued)

Cmpd. no.	Name	Formula	CAS no.	Mol. wt.	C1	C2	C3	C4	C5	T_{\min} , K	Viscosity at T_{\min}	T_{\max} , K	Viscosity at T_{\max}
182	Hydrazine	H ₄ N ₂	302-01-2	32.045	-75.781	4175.4	9.6508	-7.27E-09	3	274.69	1.450E-03	522.52	2.190E-04
183	Hydrogen	H ₂	1333-74-0	2.016	-11.661	24.7	-0.261	-4.1E-16	10	13.95	2.546E-05	33.00	3.906E-06
184	Hydrogen bromide	HBr	10035-10-6	80.912	-11.633	316.38	0.56191			185.15	9.207E-04	206.45	8.206E-04
185	Hydrogen chloride	HCl	7647-01-0	36.461	-116.34	3834.6	16.864	-2.5875E-10	4	158.97	1.000E-03	318.15	5.780E-05
186	Hydrogen cyanide	HCN	74-90-8	27.025	-21.927	1266.5	1.5927			259.83	2.754E-04	298.85	1.821E-04
187	Hydrogen fluoride	HF	7664-39-3	20.006	353.99	13928	-41.717	-2,962	-0.5	189.79	1.550E-03	368.92	1.190E-04
188	Hydrogen sulfide	H ₂ S	7783-06-4	34.081	-10.905	762.11	-0.11863			187.68	5.726E-04	350.00	8.089E-05
189	Isobutyric acid	C ₄ H ₈ O ₂	79-31-2	88.105	-11.497	1365.7	0.036966			250.00	2.938E-03	450.00	2.649E-04
190	Isopropyl amine	C ₃ H ₉ N	75-31-0	59.110	-31.157	1926	2.925			250.00	6.737E-04	453.15	1.214E-04
191	Malonic acid	C ₃ H ₄ O ₄	141-82-2	104.061	-19.834	2784.5	1.1161			404.15	1.939E-03	580.00	3.593E-04
192	Methacrylic acid	C ₄ H ₆ O ₂	79-41-4	86.089	-14.527	1497.7	0.51747			288.15	1.664E-03	434.15	3.582E-04
193	Methane	CH ₄	74-82-8	16.042	-6.1572	178.15	-0.95239	-9.0606E-24	10	90.69	2.063E-04	188.00	2.263E-05
194	Methanol	CH ₃ O	67-56-1	32.042	-25.317	1789.2	2.069			175.47	1.193E-02	337.85	3.442E-04
195	N-Methyl acetamide	C ₃ H ₇ NO	79-16-3	73.094	-4.648	1832	-1.2191			301.15	3.995E-03	478.15	2.392E-04
196	Methyl acetate	C ₃ H ₆ O ₂	79-20-9	74.079	13.557	-187.3	-3.6592			250.00	6.135E-04	425.00	1.198E-04
197	Methyl acetylene	C ₃ H ₄	74-99-7	40.064	-2.8737	301.35	-1.2271			170.45	6.045E-04	373.15	8.846E-05
198	Methyl acrylate	C ₄ H ₆ O ₂	96-33-3	86.089	10.848	75	-3.297			275.00	6.126E-04	400.00	1.636E-04
199	Methyl amine	CH ₅ N	74-89-5	31.057	-17.044	1074	0.84203			179.69	1.236E-03	273.15	2.275E-04
200	Methyl benzoate	C ₈ H ₈ O ₂	93-58-3	136.148	-21.971	2267.4	1.4173			288.15	2.299E-03	472.65	2.149E-04
201	3-Methyl-1,2-butadiene	C ₅ H ₈	598-25-4	68.117	-10.481	648.37	-0.041947			159.53	1.321E-03	314.00	1.739E-04
202	2-Methylbutane	C ₅ H ₁₂	78-78-4	72.149	-12.596	889.11	0.20469			150.00	3.542E-03	310.00	1.928E-04
203	2-Methylbutanoic acid	C ₅ H ₁₀ O ₂	116-53-0	102.132	-1.035	1048.5	-1.5474			298.15	1.774E-03	450.15	2.859E-04
204	3-Methyl-1-butanol	C ₅ H ₁₂ O	123-51-3	88.148	-25.882	3359.4	1.5787			155.95	3.776E+01	404.15	3.051E-04
205	2-Methyl-1-butene	C ₅ H ₁₀	563-46-2	70.133	-10.755	705.48	-0.011113			135.58	3.675E-03	304.30	2.034E-04
206	2-Methyl-2-butene	C ₅ H ₁₀	513-35-9	70.133	-8.4453	639.21	-0.38409			139.39	3.164E-03	311.70	1.841E-04
207	2-Methyl-1-butene-3-yne	C ₅ H ₆	78-80-8	66.101	-3.6585	441.1	-1.0547			160.15	1.915E-03	390.15	1.476E-04
208	Methylbutyl ether	C ₅ H ₁₂ O	628-28-4	88.148	-11.278	949.12	-0.00012343			157.48	5.239E-03	343.31	2.006E-04
209	Methylbutyl sulfide	C ₅ H ₁₂ S	628-29-5	104.214	-10.97	1067.3	-0.017484			175.30	6.930E-03	396.58	2.286E-04
210	3-Methyl-1-butyne	C ₅ H ₈	598-23-2	68.117	-1.8842	433.58	-1.3238			183.45	1.628E-03	364.00	2.035E-04
211	Methyl butyrate	C ₅ H ₁₀ O ₂	623-42-7	102.132	-12.206	1141.7	0.15014			200.00	3.339E-03	375.90	2.539E-04
212	Methylchlorosilane	CH ₃ ClSi	993-00-0	80.589	-12.002	1009.7				139.05	8.730E-03	353.60	1.070E-04
213	Methylcyclohexane	C ₇ H ₁₄	108-87-2	98.186	-11.358	1213.1				146.58	4.590E-02	457.68	1.650E-04
214	1-Methylcyclohexanol	C ₇ H ₁₄ O	590-67-0	114.185	-6.1534	3219	-1.4494			299.15	2.584E-02	548.80	8.026E-05
215	cis-2-Methylcyclohexanol	C ₇ H ₁₄ O	7443-70-1	114.185	-6.6904	3150.5	-1.392			280.15	3.729E-02	491.20	1.360E-04
216	trans-2-Methylcyclohexanol	C ₇ H ₁₄ O	7443-52-9	114.185	-6.6915	3173.2	-1.3046			269.15	1.107E-01	493.60	2.356E-04
217	Methylcyclopentane	C ₆ H ₁₂	96-37-7	84.159	-1.8553	612.62	-1.3774			248.15	9.288E-04	353.15	2.742E-04
218	1-Methylcyclopentene	C ₆ H ₁₀	693-89-0	82.144	-4.8515	679.07	-0.93238			146.62	7.669E-03	433.60	1.301E-04
219	3-Methylcyclopentene	C ₆ H ₁₀	1120-62-3	82.144	-6.7424	788.86	-0.69862			115.00	4.086E-02	420.80	1.129E-04
220	Methyldichlorosilane	CH ₂ Cl ₂ Si	75-54-7	115.034	-10.517	745.32				275.00	4.070E-04	314.70	2.891E-04
221	Methylethyl ether	C ₃ H ₈ O	540-67-0	60.095	-11.104	627.18	0.036581			160.00	9.133E-04	280.50	1.731E-04
222	Methylethyl ketone	C ₄ H ₈ O	78-93-3	72.106	-1.0598	520.68	-1.4961			186.48	2.266E-03	535.50	7.577E-05
223	Methylethyl sulfide	C ₃ H ₆ S	624-89-5	76.161	-10.842	863.65	-0.00074603			167.23	3.409E-03	339.80	2.474E-04
224	Methyl formate	C ₂ H ₄ O ₂	107-31-3	60.052	-39.641	2113.3	4.308			250.00	6.104E-04	304.90	3.134E-04
225	Methylisobutyl ether	C ₅ H ₁₂ O	625-44-5	88.148	-11.27	888.42	0.024736			150.00	5.390E-03	331.70	2.143E-04
226	Methylisobutyl ketone	C ₆ H ₁₂ O	108-10-1	100.159	-11.394	1168.7	-0.007539			189.15	5.222E-03	389.15	2.170E-04
227	Methyl Isocyanate	C ₂ H ₃ NO	624-83-9	57.051									
228	Methylisopropyl ether	C ₄ H ₁₀ O	598-53-8	74.122	-11.216	737.75	0.019308			127.93	4.722E-03	303.92	1.703E-04
229	Methylisopropyl ketone	C ₅ H ₁₀ O	563-80-4	86.132	-11.272	1048.9	0.00030493			180.15	4.305E-03	367.55	2.212E-04
230	Methylisopropyl sulfide	C ₄ H ₁₀ S	1551-21-9	90.187	-11.075	990.72				171.64	4.977E-03	553.10	9.292E-05
231	Methyl mercaptan	CH ₃ S	74-93-1	48.107	-10.628	645	0.025885			150.18	2.023E-03	279.11	8.287E-04
232	Methyl methacrylate	C ₅ H ₈ O ₂	80-62-6	100.116	-0.099	496	-1.5939			260.00	8.635E-04	400.00	2.229E-04
233	2-Methyloctanoic acid	C ₉ H ₁₈ O ₂	3004-93-1	158.238	-12.579	2224.2				240.00	3.646E-02	518.15	2.519E-04
234	2-Methylpentane	C ₆ H ₁₄	107-83-5	86.175	-12.86	946.91	0.26191			119.55	2.506E-02	333.41	2.038E-04
235	Methyl pentyl ether	C ₆ H ₁₄ O	628-80-8	102.175	-11.391	1090.8	1.0752E-07			176.00	5.554E-03	372.00	2.120E-04
236	2-Methylpropane	C ₄ H ₁₀	75-28-5	58.122	-13.912	797.09	0.45308			110.00	1.072E-02	310.95	1.588E-04
237	2-Methyl-2-propanol	C ₄ H ₁₀ O	75-65-0	74.122	51.356	-1249.5	-9.4593	3.694E+24	-9.8759	295.56	5.440E-03	451.21	1.010E-04
238	2-Methyl propene	C ₄ H ₈	115-11-7	56.106	-10.385	599.59	-0.046088			132.81	2.253E-03	266.25	2.270E-04
239	Methyl propionate	C ₄ H ₈ O ₂	554-12-1	88.105	-4.841	696.7	-0.9194			250.00	8.002E-04	352.60	2.593E-04
240	Methylpropyl ether	C ₄ H ₁₀ O	557-17-5	74.122	-10.705	788.94	-0.048383			133.97	6.390E-03	312.20	2.127E-04

241	Methylpropyl sulfide	C ₄ H ₁₀ S	3877-15-4	90.187	-10.569	952.38	-0.063873			160.17	7.103E-03	368.69	2.333E-04
242	Methylsilane	CH ₆ Si	992-94-9	46.144									
243	alpha-Methyl styrene	C ₉ H ₁₀	98-83-9	118.176	-11.632	1251.6	0.071692			249.95	1.972E-03	438.65	2.382E-04
244	Methyl <i>tert</i> -butyl ether	C ₅ H ₁₂ O	1634-04-4	88.148	-6.921	790.773	-0.654			164.55	4.284E-03	450.00	1.052E-04
245	Methyl vinyl ether	C ₃ H ₆ O	107-25-5	58.079	-10.34	519.61	-0.013899			151.15	9.377E-04	278.65	1.929E-04
246	Naphthalene	C ₁₀ H ₈	91-20-3	128.171	-19.308	1822.5	1.218			353.43	9.077E-04	633.15	1.892E-04
247	Neon	Ne	7440-01-9	20.180	-17.945	115.57	1.428	-2.14E-17	10	25.09	1.602E-04	44.13	2.706E-05
248	Nitroethane	C ₂ H ₅ NO ₂	79-24-3	75.067	-4.438	746.5	-0.9385			200.00	3.421E-03	387.22	3.027E-04
249	Nitrogen	N ₂	7727-37-9	28.013	16.004	-181.61	-5.1551			63.15	2.633E-04	124.00	3.331E-05
250	Nitrogen trifluoride	F ₃ N	7783-54-2	71.002									
251	Nitromethane	CH ₃ NO ₂	75-52-5	61.040	-9.5556	981.64	-0.19453			244.60	1.344E-03	374.35	3.078E-04
252	Nitrous oxide	N ₂ O	10024-97-2	44.013	19.329	-381.68	-4.8618			210.00	2.065E-04	283.09	7.730E-05
253	Nitric oxide	NO	10102-43-9	30.006	-246.65	3150.3	49.98	-0.22541	1	109.50	3.858E-04	180.05	3.791E-05
254	Nonadecane	C ₁₉ H ₄₀	629-92-5	268.521	-16.403	2119.5	0.6881			305.04	4.012E-03	603.15	2.068E-04
255	Nonanal	C ₉ H ₁₈ O	124-19-6	142.239	-12.94	1257.6	0.37191			255.15	2.606E-03	468.15	3.468E-04
256	Nonane	C ₉ H ₂₀	111-84-2	128.255	-68.54	3165.3	9.0919	-0.000013519	2	218.15	3.310E-03	593.15	5.000E-05
257	Nonanoic acid	C ₉ H ₁₈ O ₂	112-05-0	158.238	-48.851	4095	5.294			285.55	1.030E-02	528.75	3.670E-04
258	1-Nonanol	C ₉ H ₂₀ O	143-08-8	144.255	-39.863	4089	3.7631			280.00	1.733E-02	485.20	2.852E-04
259	2-Nonanol	C ₉ H ₂₀ O	628-99-9	144.255	-98.854	7183.8	12.283			238.15	2.310E-01	471.70	3.334E-04
260	1-Nonene	C ₉ H ₁₈	124-11-8	126.239	-21.921	1603.9	1.5971			191.91	5.699E-03	420.02	2.127E-04
261	Nonyl mercaptan	C ₉ H ₂₀ S	1455-21-6	160.320	-11.319	1428	-0.022545			253.05	3.026E-03	492.95	1.913E-04
262	1-Nonyne	C ₉ H ₁₆	3452-09-3	124.223	-2.3409	715.52	-1.222			223.15	3.206E-03	487.20	2.172E-04
263	Octadecane	C ₁₈ H ₃₈	593-45-3	254.494	-22.688	2466	1.5703			301.31	3.926E-03	589.86	2.057E-04
264	Octanal	C ₈ H ₁₆ O	124-13-0	128.212	-10.191	1072.4	-0.030553			246.00	2.479E-03	447.15	3.425E-04
265	Octane	C ₈ H ₁₈	111-65-9	114.229	-7.556	881.09	-0.52502	4.6342E+22	-10	211.15	2.660E-03	454.96	1.460E-04
266	Octanoic acid	C ₈ H ₁₆ O ₂	124-07-2	144.211	-60.795	4617.8	7.028			289.65	6.652E-03	512.85	3.576E-04
267	1-Octanol	C ₈ H ₁₈ O	111-87-5	130.228	-19.907	2791.7	0.94296	2.3041E+24	-10.09	280.00	1.569E-02	468.35	2.901E-04
268	2-Octanol	C ₈ H ₁₈ O	123-96-6	130.228	16.792	1353.6	-4.6357	2.6663E+31	-13.039	241.55	4.576E-01	452.90	1.899E-04
269	2-Octanone	C ₈ H ₁₆ O	111-13-7	128.212	-11.736	1415.2	0.0003618			252.85	2.161E-03	446.15	1.913E-04
270	3-Octanone	C ₈ H ₁₆ O	106-68-3	128.212	-20.804	1834.6	1.3403			255.55	2.039E-03	440.65	2.075E-04
271	1-Octene	C ₈ H ₁₆	111-66-0	112.213	-11.19	1057.4				171.45	6.590E-03	453.52	1.420E-04
272	Octyl mercaptan	C ₈ H ₁₆ S	111-88-6	146.294	-11.498	1362.1	0.015575			223.95	4.837E-03	472.19	2.000E-04
273	1-Octyne	C ₈ H ₁₄	629-05-0	110.197	-3.8552	684.22	-1.0071			193.55	3.614E-03	468.00	1.868E-04
274	Oxalic acid	C ₂ H ₂ O ₄	144-62-7	90.035									
275	Oxygen	O ₂	7782-44-7	31.999	-4.1476	94.04	-1.207			54.36	7.170E-04	150.00	6.990E-05
276	Ozone	O ₃	10028-15-6	47.998	-10.94	415.96				77.55	3.790E-03	208.80	1.300E-04
277	Pentadecane	C ₁₅ H ₃₂	629-62-9	212.415	-19.299	2088.6	1.1091			283.07	3.486E-03	543.84	2.091E-04
278	Pentanal	C ₅ H ₁₀ O	110-62-3	86.132	-10.846	980.01	-0.0054565			182.00	4.129E-03	376.15	2.553E-04
279	Pentane	C ₅ H ₁₂	109-66-0	72.149	-53.509	1836.6	7.1409	-0.000019627	2	143.42	3.529E-03	465.15	4.796E-05
280	Pentanoic acid	C ₅ H ₁₀ O ₂	109-52-4	102.132	-37.067	2856.7	3.7344			270.00	3.773E-03	458.65	3.516E-04
281	1-Pentanol	C ₅ H ₁₂ O	71-41-0	88.148	-36.561	3542.2	3.3364	-8.0487E-37	12.84	253.15	1.649E-02	410.90	3.844E-04
282	2-Pentanol	C ₅ H ₁₂ O	6032-29-7	88.148	-410.49	18371	61.985	-0.0095612	1.2201	200.00	3.823E+01	392.20	5.828E-04
283	2-Pentanone	C ₅ H ₁₀ O	107-87-9	86.132	-11.055	1005.3	0.0039301			250.00	9.009E-04	375.46	2.354E-04
284	3-Pentanone	C ₅ H ₁₀ O	96-22-0	86.132	-2.8695	596.32	-1.2025			234.18	1.024E-03	375.14	2.232E-04
285	1-Pentene	C ₅ H ₁₀	109-67-1	70.133	-10.667	659.56				108.02	1.045E-02	303.22	2.051E-04
286	2-Pentyl mercaptan	C ₅ H ₁₂ S	2084-19-7	104.214	-6.9168	818.76	-0.59628			220.00	1.643E-03	385.15	2.385E-04
287	Pentyl mercaptan	C ₅ H ₁₂ S	110-66-7	104.214	-11.677	1091.2	0.10658			197.45	3.746E-03	399.79	2.463E-04
288	1-Pentyne	C ₅ H ₈	627-19-0	68.117	-1.7273	424.34	-1.342			167.45	2.323E-03	378.00	1.898E-04
289	2-Pentyne	C ₅ H ₈	627-21-4	68.117	-3.7241	516.54	-1.1167			163.83	1.902E-03	415.20	9.980E-05
290	Phenanthrene	C ₁₄ H ₁₀	85-01-8	178.229	-22.472	2566.9	1.5749			372.38	1.920E-03	610.03	2.849E-04
291	Phenol	C ₆ H ₆ O	108-95-2	94.111	-43.335	3881.7	4.3983	3.0548E+24	-10	291.45	1.270E-02	555.40	1.940E-04
292	Phenyl isocyanate	C ₇ H ₅ NO	103-71-9	119.121	-11.31	1280				243.15	2.370E-03	522.40	1.420E-04
293	Phthalic anhydride	C ₈ H ₆ O ₃	85-44-9	148.116	195.25	-11072	-29.084			404.15	1.229E-03	557.65	1.986E-04
294	Propadiene	C ₃ H ₄	463-49-0	40.064	-6.3528	240.85	-0.58229			136.87	5.772E-04	298.15	1.416E-04
295	Propane	C ₃ H ₈	74-98-6	44.096	-17.156	646.25	1.1101	-7.3439E-11	4	85.47	9.458E-03	360.00	4.275E-05
296	1-Propanol	C ₃ H ₈ O	71-23-8	60.095	23.467	116.07	-5.3372	2.8801E+09	-4.0267	146.95	2.069E+01	370.35	4.735E-04
297	2-Propanol	C ₃ H ₈ O	67-63-0	60.095	-8.8918	2357.6	-0.91376			185.26	3.917E-01	355.30	4.892E-04
298	Propenylcyclohexene	C ₉ H ₁₄	13511-13-2	122.207	-11.208	1079.8				199.00	3.080E-03	508.80	1.130E-04
299	Propionaldehyde	C ₃ H ₆ O	123-38-6	58.079	-9.9177	839.53	-0.16735			170.00	2.912E-03	321.15	2.562E-04
300	Propionic acid	C ₃ H ₆ O ₂	79-09-4	74.079	-23.931	1834.6	1.9124			252.45	2.275E-03	414.32	3.430E-04
301	Propionitrile	C ₃ H ₅ N	107-12-0	55.079	-5.7136	703.62	-0.78123			250.00	7.372E-04	370.50	2.171E-04
302	Propyl acetate	C ₅ H ₁₀ O ₂	109-60-4	102.132	17.797	-252.43	-4.291			250.00	1.002E-03	473.15	1.045E-04
303	Propyl amine	C ₃ H ₉ N	107-10-8	59.110	-9.8074	1010.4	-0.25697			188.36	3.060E-03	321.00	2.908E-04

TABLE 2-313 Viscosity of Inorganic and Organic Liquids (Pa·s) (Concluded)

Cmpd. no.	Name	Formula	CAS no.	Mol. wt.	C1	C2	C3	C4	C5	T_{min} , K	Viscosity at T_{min}	T_{max} , K	Viscosity at T_{max}
304	Propylbenzene	C ₉ H ₁₂	103-65-1	120.192	-18.282	1549.7	1.0454			200.00	6.774E-03	432.39	2.357E-04
305	Propylene	C ₃ H ₆	115-07-1	42.080	-92.082	1907.3	15.639	-0.043098	1	87.90	1.550E-02	333.15	5.150E-05
306	Propyl formate	C ₄ H ₈ O ₂	110-74-7	88.105	-73.735	2668.2	10.993	-0.018364	1	180.25	5.852E-03	353.97	2.810E-04
307	2-Propyl mercaptan	C ₃ H ₈ S	75-33-2	76.161	-5.7244	638.2	-0.76415			142.61	6.477E-03	325.71	2.784E-04
308	Propyl mercaptan	C ₃ H ₈ S	107-03-9	76.161	-10.153	840.71	-0.093763			159.95	4.641E-03	340.87	2.656E-04
309	1,2-Propylene glycol	C ₃ H ₈ O ₂	57-55-6	76.094	-804.54	30487	130.79	-0.15449	1	213.15	9.500E+02	500.80	3.310E-04
310	Quinone	C ₆ H ₄ O ₂	106-51-4	108.095	-14.846	1829.4	0.3729			388.85	3.643E-04	454.00	1.965E-04
311	Silicon tetrafluoride	F ₄ Si	7783-61-1	104.079									
312	Styrene	C ₈ H ₈	100-42-5	104.149	-22.675	1758	1.6701			242.54	1.919E-03	418.31	2.268E-04
313	Succinic acid	C ₄ H ₂ O ₄	110-15-6	118.088	-13.422	3431.8				460.65	2.550E-03	644.80	3.040E-04
314	Sulfur dioxide	O ₂ S	7446-09-5	64.064	46.223	-1378	-8.7475			225.00	6.900E-04	400.00	6.557E-05
315	Sulfur hexafluoride	F ₆ S	2551-62-4	146.055	3.8305	41.21	-2.1342			223.15	5.388E-04	318.69	2.383E-04
316	Sulfur trioxide	O ₃ S	7446-11-9	80.063	-88.793	6400.7	10.709			289.95	2.477E-03	318.15	9.456E-04
317	Terephthalic acid	C ₈ H ₆ O ₄	100-21-0	166.131									
318	<i>o</i> -Terphenyl	C ₁₈ H ₁₄	84-15-1	230.304	-215.09	11612	31.849	-0.026882	1	329.35	1.736E-02	723.15	1.522E-04
319	Tetradecane	C ₁₄ H ₃₀	629-59-4	198.388	-14.493	1710.8	0.4417	3.0895E+28	-12	277.65	3.350E-03	554.40	1.810E-04
320	Tetrahydrofuran	C ₄ H ₈ O	109-99-9	72.106	-10.321	900.92	-0.069128			164.65	5.505E-03	373.15	2.446E-04
321	1,2,3,4-Tetrahydronaphthalene	C ₁₀ H ₁₂	119-64-2	132.202	-11.167	1193.2	0.096226	9.5986E+11	-5	237.40	1.300E-02	576.00	2.100E-04
322	Tetrahydrothiophene	C ₄ H ₈ S	110-01-0	88.171	-10.843	1165.2				293.15	1.040E-03	303.15	9.125E-04
323	2,2,3,3-Tetramethylbutane	C ₈ H ₁₈	594-82-1	114.229	5.5351	632.38	-2.6576			373.96	1.999E-04	454.00	8.859E-05
324	Thiophene	C ₄ H ₄ S	110-02-1	84.140	-16.671	1342.5	0.8388			250.00	1.269E-03	393.15	2.625E-04
325	Toluene	C ₇ H ₈	108-88-3	92.138	-226.08	6805.7	37.542	-0.060853	1	178.18	1.569E-02	383.78	2.428E-04
326	1,1,2-Trichloroethane	C ₂ H ₃ Cl ₃	79-00-5	133.404	0.388	736.5	-1.7063			236.50	2.955E-03	387.00	3.798E-04
327	Tridecane	C ₁₃ H ₂₈	629-50-5	184.361	-4.1103	1005.3	-1.0188	1.0017E+19	-8	267.67	3.450E-03	540.00	1.740E-04
328	Triethyl amine	C ₆ H ₁₅ N	121-44-8	101.190	-3.7067	585.78	-1.0926			250.00	6.135E-04	359.05	2.028E-04
329	Trimethyl amine	C ₃ H ₉ N	75-50-3	59.110	10.142	-130.41	-3.2199			200.00	5.156E-04	308.15	1.612E-04
330	1,2,3-Trimethylbenzene	C ₉ H ₁₂	526-73-8	120.192	-11.756	1483.1	-0.040387			247.79	2.495E-03	449.27	1.663E-04
331	1,2,4-Trimethylbenzene	C ₉ H ₁₂	95-63-6	120.192	-9.6461	1281.2	-0.29478			229.33	3.477E-03	442.53	1.942E-04
332	2,2,4-Trimethylpentane	C ₈ H ₁₈	540-84-1	114.229	-12.928	1137.5	0.25725	-3.6929E-28	10	165.78	8.636E-03	541.15	4.530E-05
333	2,3,3-Trimethylpentane	C ₈ H ₁₈	560-21-4	114.229	-4.0309	990.76	-1.1771			172.22	1.305E-02	387.91	2.049E-04
334	1,3,5-Trinitrobenzene	C ₆ H ₃ N ₃ O ₆	99-35-4	213.105	-10.707	1818.5				398.40	2.150E-03	676.80	3.290E-04
335	2,4,6-Trinitrotoluene	C ₇ H ₅ N ₃ O ₆	118-96-7	227.131	-11.504	3301	-0.39102			353.15	1.167E-02	625.00	1.601E-04
336	Undecane	C ₁₁ H ₂₄	1120-21-4	156.308	52.176	-4951.9	-8.5676	570,980	-2	247.57	3.240E-03	511.20	1.570E-04
337	1-Undecanol	C ₁₁ H ₂₄ O	112-42-5	172.308	-69.778	5905.2	8.0214			288.45	2.089E-02	590.15	1.856E-04
338	Vinyl acetate	C ₄ H ₆ O ₂	108-05-4	86.089	-22.407	1462.8	1.7006			225.00	1.237E-03	345.65	2.654E-04
339	Vinyl acetylene	C ₄ H ₄	689-97-4	52.075	-2.2333	320.37	-1.2915			173.15	8.764E-04	364.00	1.273E-04
340	Vinyl chloride	C ₂ H ₃ Cl	75-01-4	62.498	0.26297	276.55	-1.7282			130.00	2.425E-03	400.00	8.272E-05
341	Vinyl trichlorosilane	C ₂ H ₃ Cl ₃ Si	75-94-5	161.490	-10.37	823.31				178.35	3.170E-03	434.52	2.090E-04
342	Water	H ₂ O	7732-18-5	18.015	-52.843	3703.6	5.866	-5.879E-29	10	273.16	1.702E-03	646.15	5.028E-05
343	<i>m</i> -Xylene	C ₈ H ₁₀	108-38-3	106.165	-11.91	1094.9	0.13825			225.30	1.834E-03	413.10	2.189E-04
344	<i>o</i> -Xylene	C ₈ H ₁₀	95-47-6	106.165	-15.489	1393.5	0.63711			247.98	1.735E-03	418.10	2.459E-04
345	<i>p</i> -Xylene	C ₈ H ₁₀	106-42-3	106.165	-7.381	911.7	-0.54152			286.41	7.021E-04	413.10	2.169E-04

The liquid viscosity is calculated by

$$\mu = \exp(C1 + C2/T + C3 \ln T + C4T^{0.5})$$

where μ is the viscosity in Pa·s and T is the temperature in K. Viscosities are at either 1 atm or the vapor pressure, whichever is higher. All substances are listed by chemical family in Table 2-6 and by formula in Table 2-7.

Values in this table were taken from the Design Institute for Physical Properties (DIPPR) of the American Institute of Chemical Engineers (AIChE), copyright 2007 AIChE and reproduced with permission of AIChE and of the DIPPR Evaluated Process Design Data Project Steering Committee. Their source should be cited as R. L. Rowley, W. V. Wilding, J. L. Oscarson, Y. Yang, N. A. Zundel, T. E. Daubert, R. P. Danner, DIPPR® Data Compilation of Pure Chemical Properties, Design Institute for Physical Properties, AIChE, New York (2007).

The number of digits provided for values at T_{min} and T_{max} was chosen for uniformity of appearance and formatting; these do not represent the uncertainties of the physical quantities, but are the result of calculations from the standard thermophysical property formulations within a fixed format.

TABLE 2-314 Vapor Thermal Conductivity of Inorganic and Organic Substances [W/(m·K)]

Cmpd. no.	Name	Formula	CAS no.	Mol. wt.	C1	C2	C3	C4	T_{min} , K	Thermal cond. at T_{min}	T_{max} , K	Thermal cond. at T_{max}
1	Acetaldehyde	C ₂ H ₄ O	75-07-0	44.05	3.7272E-07	1.8129			273.15	0.00973	994	0.10124
2	Acetamide	C ₂ H ₅ N/O	60-35-5	59.07	0.00013195	0.97	728.3		494.30	0.02189	1000	0.06206
3	Acetic acid	C ₂ H ₄ O ₂	64-19-7	60.05	0.000001691	1.6692		-95,400	294.70	0.01049	686.88	0.05236
4	Acetic anhydride	C ₄ H ₆ O ₃	108-24-7	102.09	0.00042004	0.8066	439.37	142,620	412.70	0.01864	1000	0.06981
5	Acetone	C ₃ H ₆ O	67-64-1	58.08	-26.8	0.9098	-126500000		329.44	0.01363	1000	0.11362
6	Acetonitrile	C ₂ H ₃ N	75-05-8	41.05	4.901E-08	2.1091			354.75	0.01170	994.75	0.10298
7	Acetylene	C ₂ H ₂	74-86-2	26.04	0.000075782	1.0327	-36.227	31,432	189.35	0.01011	1000	0.09545
8	Acrolein	C ₃ H ₄ O	107-02-8	56.06	0.024098	0.3285	1325.3	577,830	325.84	0.01534	1000	0.08028
9	Acrylic acid	C ₃ H ₄ O ₂	79-10-7	72.06	0.0009265	0.7035	627.58	112,460	414.15	0.02027	1000	0.06867
10	Acrylonitrile	C ₃ H ₃ N	107-13-1	53.06	0.0013784	1.2093	50594		350.50	0.01133	990.5	0.11107
11	Air	Mixture	132259-10-0	28.96	0.00031417	0.7786	-0.7116	2,121.7	70.00	0.00603	2000	0.11675
12	Ammonia	H ₃ N	7664-41-7	17.03	9.6608E-06	1.3799			200.00	0.01446	900	0.11523
13	Anisole	C ₇ H ₈ O	100-66-3	108.14	0.00059858	0.7527	354.04	241,830	426.73	0.01809	1000	0.06796
14	Argon	Ar	7440-37-1	39.95	0.000633	0.6221	70		90.00	0.00585	3273.1	0.09525
15	Benzamide	C ₇ H ₇ N/O	55-21-0	121.14	0.025389	0.28547	1018.3	1,228,600	563.15	0.02317	1000	0.05618
16	Benzene	C ₆ H ₆	71-43-2	78.11	0.00001652	1.3117	491		339.15	0.01407	1000	0.09542
17	Benzenethiol	C ₆ H ₆ S	108-98-5	110.18	0.00047951	0.7818	463.4	189,410	442.29	0.01861	1000	0.06427
18	Benzoic acid	C ₇ H ₆ O ₂	65-85-0	122.12	0.0001163	0.9705	740		522.40	0.02090	1000	0.05452
19	Benzonitrile	C ₇ H ₅ N	100-47-0	103.12	0.00015674	0.95503	711.32		464.15	0.02180	1000	0.06713
20	Benzophenone	C ₁₃ H ₁₀ O	119-61-9	182.22	0.0001235	0.9495	778.7		579.24	0.02213	1000	0.04899
21	Benzyl alcohol	C ₇ H ₈ O	100-51-6	108.14	0.00023476	0.8639	187.8	193,840	478.60	0.02167	1000	0.06636
22	Benzyl ethyl ether	C ₉ H ₁₂ O	539-30-0	136.19	0.00096451	0.69225	519.99	278,930	458.15	0.01936	1000	0.06398
23	Benzyl mercaptan	C ₇ H ₈ S	100-53-8	124.20	0.00015525	0.9446	715.78		472.03	0.02071	1000	0.06171
24	Biphenyl	C ₁₂ H ₁₀	92-52-4	154.21	2.8646E-06	1.4098	-391.35	156,820	373.15	0.01123	1000	0.06347
25	Bromine	Br ₂	7726-95-6	159.81	1.0404E-06	1.4685			300.00	0.00452	500	0.00956
26	Bromobenzene	C ₆ H ₅ Br	108-86-1	157.01	0.00027085	0.7932	278.33	165,880	429.24	0.01302	1000	0.04495
27	Bromoethane	C ₂ H ₅ Br	74-96-4	108.97	0.00019745	0.8824	647		311.50	0.01018	1000	0.05321
28	Bromomethane	CH ₃ Br	74-83-9	94.94	0.000038314	1.0484	287.38		273.00	0.00669	1000	0.04158
29	1,2-Butadiene	C ₄ H ₆	590-19-2	54.09	0.000088221	1.0273	75.316	99,063	284.00	0.01172	1000	0.09071
30	1,3-Butadiene	C ₄ H ₆	106-99-0	54.09	-20,890	0.9593	-9.382E+10		268.74	0.01281	1000	0.16809
31	Butane	C ₄ H ₁₀	106-97-8	58.12	0.051094	0.45253	5455.5	1,979,800	272.65	0.01357	1000	0.13799
32	1,2-Butanediol	C ₄ H ₁₀ O ₂	584-03-2	90.12	-295.44	-0.21463	91602	-7.6032E+08	469.57	0.02426	1000	0.10046
33	1,3-Butanediol	C ₄ H ₁₀ O ₂	107-88-0	90.12	-918.39	-0.21199	334420	-2.8842E+09	481.38	0.02110	1000	0.08332
34	1-Butanol	C ₄ H ₁₀ O	71-36-3	74.12	0.00111484	0.87647	3253.7		370.70	0.02097	712.94	0.06536
35	2-Butanol	C ₄ H ₁₀ O	78-92-2	74.12	4.5894E-06	1.4484			372.90	0.02435	1000	0.10161
36	1-Butene	C ₄ H ₈	106-98-9	56.11	0.000096809	1.1153	781.82		266.91	0.01252	1000	0.12049
37	cis-2-Butene	C ₄ H ₈	590-18-1	56.11	0.000067737	1.0709	-65.881	129,390	273.15	0.01105	1273.15	0.13926
38	trans-2-Butene	C ₄ H ₈	624-64-6	56.11	0.000078576	1.0565	14.63	105,920	274.03	0.01200	1257	0.13704
39	Butyl acetate	C ₈ H ₁₂ O ₂	123-86-4	116.16	5.86E-09	2.376	-401.32	69,280	273.00	0.00783	800	0.07634
40	Butylbenzene	C ₁₀ H ₁₄	104-51-8	134.22	0.1807	0.0082225	-129.42	1,691,500	456.46	0.02151	1000	0.07465
41	Butyl mercaptan	C ₄ H ₁₀ S	109-79-5	90.19	0.00097826	0.78643	1531.5		371.61	0.01832	1000	0.08610
42	sec-Butyl mercaptan	C ₄ H ₁₀ S	513-53-1	90.19	0.9719	-0.111	1167.2	3,163,200	358.13	0.01749	1000	0.08470
43	1-Butyne	C ₄ H ₆	107-00-6	54.09	0.000037269	1.1427	-43.844	79,421	281.22	0.01268	1000	0.09644
44	Butyraldehyde	C ₄ H ₈ O	123-72-8	72.11	1138.6	0.95596	7.5086E+09		347.95	0.01419	1000	0.11186
45	Butyric acid	C ₄ H ₈ O ₂	107-92-6	88.11	0.002751	0.2734	-314.55		436.40	0.05192	526.32	0.03792
46	Butyronitrile	C ₄ H ₇ N	109-74-0	69.11	5.2879E-07	1.6715	-381.9	95,650	273.00	0.00706	1000	0.07660
47	Carbon dioxide	CO ₂	124-38-9	44.01	3.69	-0.3538	964	1,860,000	194.67	0.00887	1500	0.09025
48	Carbon disulfide	CS ₂	75-15-0	76.14	0.0003467	0.7345	479		273.15	0.00776	1000	0.03745
49	Carbon monoxide	CO	630-08-0	28.01	0.00059882	0.6863	57.13	501.92	70.00	0.00576	1500	0.08724
50	Carbon tetrachloride	CCl ₄	56-23-5	153.82	0.00016599	0.94375	1449.6		349.79	0.00812	1000	0.04595
51	Carbon tetrafluoride	CF ₄	75-73-0	88.00	0.000092004	1.0164	270.83		145.10	0.00505	1000	0.08108
52	Chlorine	Cl ₂	7782-50-5	70.91	0.0009993	0.5472	458.6		200.00	0.00551	1000	0.03002
53	Chlorobenzene	C ₆ H ₅ Cl	108-90-7	112.56	0.0004783	0.8994	1845.5	163,000	400.00	0.01579	1000	0.07935
54	Chloroethane	C ₂ H ₅ Cl	75-00-3	64.51	-19.283	0.20238	-715050	-271,300,000	273.15	0.00960	1000	0.07920
55	Chloroform	CHCl ₃	67-66-3	119.38	0.00043073	0.83878	1874.5		334.33	0.00854	1000	0.04920
56	Chloromethane	CH ₃ Cl	74-87-3	50.49	-22136	0.7666	-4.8749E+10		213.15	0.00590	750	0.05448
57	1-Chloropropane	C ₃ H ₇ Cl	540-54-5	78.54	0.00004861	1.1407	593		319.67	0.01225	1000	0.08065
58	2-Chloropropane	C ₃ H ₇ Cl	75-29-6	78.54	0.00009154	1.0681	746.6		308.85	0.01222	1000	0.08389

TABLE 2-314 Vapor Thermal Conductivity of Inorganic and Organic Substances [W/(m·K)] (Continued)

Cmpd. no.	Name	Formula	CAS no.	Mol. wt.	C1	C2	C3	C4	T_{\min} , K	Thermal cond. at		Thermal cond. at T_{\max}
										T_{\min} , K	T_{\max} , K	
59	<i>m</i> -Cresol	C ₇ H ₈ O	108-39-4	108.14	0.00019307	0.9248	710		475.43	0.02316	1000	0.06716
60	<i>o</i> -Cresol	C ₇ H ₈ O	95-48-7	108.14	0.00018648	0.9302	709.37		464.15	0.02230	1000	0.06736
61	<i>p</i> -Cresol	C ₇ H ₈ O	106-44-5	108.14	0.00019063	0.9282	716.91		475.13	0.02319	1000	0.06762
62	Cumene	C ₉ H ₁₂	98-82-8	120.19	1.6743E-07	1.8369	-449.46	112,760	380.00	0.01534	1000	0.08181
63	Cyanogen	C ₂ N ₂	460-19-5	52.03	0.000026933	1.137	28.119		252.00	0.01302	1000	0.06749
64	Cyclobutane	C ₄ H ₈	287-23-0	56.11	-449.910	0.27364	-1.0001E+10		285.66	0.01356	1000	0.14994
65	Cyclohexane	C ₆ H ₁₂	110-82-7	84.16	0.000000859	1.7709	243		325.00	0.01380	1000	0.14198
66	Cyclohexanol	C ₆ H ₁₂ O	108-93-0	100.16	0.0032207	0.5991	608.69	509,290	434.00	0.02399	1000	0.09535
67	Cyclohexanone	C ₆ H ₁₀ O	108-94-1	98.14	-1.095.5	-0.023408	498,780		428.58	0.02291	1000	0.12704
68	Cyclohexene	C ₆ H ₁₀	110-83-8	82.14	0.0000901	1.0897	655		356.12	0.01914	1000	0.10116
69	Cyclopentane	C ₅ H ₁₀	287-92-3	70.13	9.5461E-06	1.4641	632.62		273.00	0.01061	1000	0.14429
70	Cyclopentene	C ₅ H ₈	142-29-0	68.12	0.0010949	0.71644	175.55	346,040	317.38	0.01360	1000	0.10148
71	Cyclopropane	C ₃ H ₆	75-19-4	42.08	-91.383	0.89718	-283,310,000		240.37	0.01061	1000	0.15854
72	Cyclohexyl mercaptan	C ₆ H ₁₂ S	1569-69-3	116.22	0.0000813	1.0674	697.6		431.95	0.02022	1000	0.07629
73	Decanal	C ₁₀ H ₂₀ O	112-31-2	156.27	-4.9825	0.04928	-1107	-67,349,000	488.15	0.02381	1000	0.10382
74	Decane	C ₁₀ H ₂₂	124-18-5	142.28	-668.4	0.9323	-4.071E+09		447.30	0.02173	1000	0.10286
75	Decanoic acid	C ₁₀ H ₂₀ O ₂	334-48-5	172.27	0.00017047	0.9313	757.67		543.15	0.02508	1000	0.06034
76	1-Decanol	C ₁₀ H ₂₂ O	112-30-1	158.28	-0.3072	0.489	-67,500	-29,400,000	504.07	0.02591	1000	0.09389
77	1-Decene	C ₁₀ H ₂₀	872-05-9	140.27	0.000027232	1.257	751.7		443.75	0.02149	1000	0.09175
78	Decyl mercaptan	C ₁₀ H ₂₂ S	143-10-2	174.35	0.00012058	1.0111	740		512.35	0.02709	1000	0.07482
79	1-Decyne	C ₁₀ H ₁₈	764-93-2	138.25	0.000016707	1.2128	-206.08	153,850	447.15	0.02092	1000	0.07667
80	Deuterium	D ₂	7782-39-0	4.03	0.00028527	0.9874	-200.51	21,807	233.15	0.011474	1500	0.44547
81	1,1-Dibromoethane	C ₂ H ₄ Br ₂	557-91-5	187.86	0.00021231	0.8052	649.51		381.15	0.00940	1000	0.03351
82	1,2-Dibromoethane	C ₂ H ₄ Br ₂	106-93-4	187.86	0.00015878	0.8636	659.5		404.51	0.01077	1000	0.03729
83	Dibromomethane	CH ₂ Br ₂	74-95-3	173.83	0.00021302	0.8719	1,620		370.10	0.00687	1000	0.03356
84	Dibutyl ether	C ₈ H ₁₈ O	142-96-1	130.23	0.0032694	0.58633	1259.9	300,890	323.15	0.01244	1000	0.07330
85	<i>m</i> -Dichlorobenzene	C ₆ H ₄ Cl ₂	541-73-1	147.00	-1.067.8	0.754	-3.0361E+09		446.23	0.01561	1000	0.06430
86	<i>o</i> -Dichlorobenzene	C ₆ H ₄ Cl ₂	95-50-1	147.00	-1.420	0.7614	-4.5040E+09		453.57	0.01507	1000	0.06066
87	<i>p</i> -Dichlorobenzene	C ₆ H ₄ Cl ₂	106-46-7	147.00	-1.520.8	0.754	-4.3328E+09		447.21	0.01564	1000	0.06417
88	1,1-Dichloroethane	C ₂ H ₄ Cl ₂	75-34-3	98.96	0.0001315	1.0113	1,023.8		330.45	0.01132	1000	0.07025
89	1,2-Dichloroethane	C ₂ H ₄ Cl ₂	107-06-2	98.96	0.00021054	0.9574	1,414		356.59	0.01177	1000	0.06498
90	Dichloromethane	CH ₂ Cl ₂	75-09-2	84.93	0.0014796	0.69531	2,657.4		312.90	0.00847	1000	0.04931
91	1,1-Dichloropropane	C ₃ H ₆ Cl ₂	78-99-9	112.99	0.000057603	1.1148	849.98		361.25	0.01220	1000	0.06881
92	1,2-Dichloropropane	C ₃ H ₆ Cl ₂	78-87-5	112.99	0.000062435	1.103	913.43		369.52	0.01222	1000	0.06647
93	Diethanol amine	C ₄ H ₁₁ NO ₂	111-42-2	105.14	-11,633	0.4621	-3.7939E+09		541.54	0.03044	1000	0.07463
94	Diethyl amine	C ₄ H ₁₁ N	109-89-7	73.14	0.00001706	1.248	-112.8	77,960	273.15	0.01148	1000	0.09804
95	Diethyl ether	C ₄ H ₁₀ O	60-29-7	74.12	-0.0044894	0.6155	-3266.3		200.00	0.00764	600	0.05181
96	Diethyl sulfide	C ₄ H ₁₀ S	352-93-2	90.19	0.0018097	0.67406	1179.7	174,850	365.25	0.01743	1000	0.08089
97	1,1-Difluoroethane	C ₂ H ₄ F ₂	75-37-6	66.05	0.000059249	1.0713	101.84	45,974	248.95	0.01016	1000	0.08447
98	1,2-Difluoroethane	C ₂ H ₄ F ₂	624-72-6	66.05	2.4194E-06	1.4456			303.65	0.00938	993.65	0.05206
99	Difluoromethane	CH ₂ F ₂	75-10-5	52.02	0.000013015	1.1897			221.50	0.00803	1000	0.04826
100	Di-isopropyl amine	C ₆ H ₁₃ N	108-18-9	101.19	0.00051305	0.8076	360.19	154,510	357.05	0.01836	1000	0.08967
101	Di-isopropyl ether	C ₆ H ₁₄ O	108-20-3	102.17	0.00019879	0.9423	306.8	106,230	328.05	0.01598	1000	0.09444
102	Di-isopropyl ketone	C ₉ H ₁₄ O	565-80-0	114.19	-8.5357	-0.0056423	1882.1	-65,622,000	397.55	0.02015	1000	0.13085
103	1,1-Dimethoxyethane	C ₄ H ₁₀ O ₂	534-15-6	90.12	0.00046265	0.81968	539.34	104,530	337.45	0.01554	1000	0.08099
104	1,2-Dimethoxypropane	C ₅ H ₁₂ O ₂	7778-85-0	104.15	3.7962E-06	1.4462			366.15	0.01936	1000	0.08279
105	Dimethyl acetylene	C ₄ H ₆	503-17-3	54.09	0.00021761	0.9187	217	132,070	300.13	0.01288	1000	0.09199
106	Dimethyl amine	C ₂ H ₇ N	124-40-3	45.08	1.6085	-0.1103	2160.3	2,989,300	280.03	0.01845	1000	0.12209
107	2,3-Dimethylbutane	C ₆ H ₁₄	79-29-8	86.18	0.000034741	1.1646	-99.956	130,820	331.13	0.01581	1000	0.10506
108	1,1-Dimethylcyclohexane	C ₈ H ₁₆	590-66-9	112.21	0.008856	0.4215	-50.645	764,580	392.70	0.01884	1000	0.09500
109	<i>cis</i> -1,2-Dimethylcyclohexane	C ₈ H ₁₆	2207-01-4	112.21	0.013298	0.3692	0.1027	852,540	402.94	0.01948	1000	0.09196
110	<i>trans</i> -1,2-Dimethylcyclohexane	C ₈ H ₁₆	6876-23-9	112.21	0.012144	0.3854	52.191	803,590	396.58	0.01952	1000	0.09376
111	Dimethyl disulfide	C ₂ H ₆ S ₂	624-92-0	94.20	0.00022578	0.892	697		382.90	0.01613	1000	0.06310
112	Dimethyl ether	C ₂ H ₆ O	115-10-6	46.07	0.059975	0.2667	1,018.6	1,098,800	248.31	0.01139	1500	0.19458
113	<i>N,N</i> -Dimethyl formamide	C ₃ H ₇ NO	68-12-2	73.09	0.014449	0.3612	595.22	728,130	425.15	0.02001	1000	0.07539
114	2,3-Dimethylpentane	C ₇ H ₁₆	565-59-3	100.20	0.000022421	1.2137	-146.91	131,830	362.93	0.01797	1000	0.09962
115	Dimethyl phthalate	C ₁₀ H ₁₀ O ₄	131-11-3	194.18	0.00012822	0.9324	752.5		556.85	0.01981	1000	0.04587
116	Dimethylsilane	C ₂ H ₆ Si	1111-74-6	60.17	0.0011808	0.742	1131	6,400	253.55	0.01291	1000	0.09296

117	Dimethyl sulfide	C ₂ H ₆ S	75-18-3	62.13	0.00023614	0.9204	638		310.48	0.01520	1000	0.08319
118	Dimethyl sulfoxide	C ₂ H ₆ OS	67-68-5	78.13	0.00064761	0.7716	1013.3		462.15	0.02059	1000	0.06379
119	Dimethyl terephthalate	C ₁₀ H ₁₀ O ₄	120-61-6	194.18	-25,190	0.3639	-8,669,000,000		561.15	0.02060	1000	0.04529
120	1,4-Dioxane	C ₄ H ₈ O ₂	123-91-1	88.11	6.4032E-07	1.7194			337.85	0.01427	768.01	0.05855
121	Diphenyl ether	C ₁₂ H ₁₀ O	101-84-8	170.21	0.00014629	0.9377		745.89	531.46	0.02188	1000	0.05449
122	Dipropyl amine	C ₆ H ₁₅ N	142-84-7	101.19	0.0001123	0.9958		183.2	279.65	0.01055	1000	0.08515
123	Dodecane	C ₁₂ H ₂₆	112-40-3	170.33	0.000005719	1.4699		579.4	489.47	0.02354	1000	0.09301
124	Eicosane	C ₂₀ H ₄₂	112-95-8	282.55	-375.32	1.0708	-8,783,600,000		616.93	0.02563	1000	0.06968
125	Ethane	C ₂ H ₆	74-84-0	30.07	0.000073869	1.1689		500.73	184.55	0.00886	1000	0.15807
126	Ethanol	C ₂ H ₆ O	64-17-5	46.07	-0.010109	0.6475		-7,332	293.15	0.01475	1000	0.13417
127	Ethyl acetate	C ₄ H ₈ O ₂	141-78-6	88.11	1.3575E-07	1.9681			273.15	0.00847	990.21	0.10682
128	Ethyl amine	C ₂ H ₇ N	75-04-7	45.08	0.3935	0.0131		1,380	289.73	0.01622	1000	0.10532
129	Ethylbenzene	C ₈ H ₁₀	100-41-4	106.17	0.000017537	1.3144		560.65	409.35	0.02007	1000	0.09859
130	Ethyl benzoate	C ₉ H ₁₀ O ₂	93-89-0	150.17	0.00002012	1.1513		-89.583	486.55	0.01855	1000	0.05524
131	2-Ethyl butanoic acid	C ₆ H ₁₂ O ₂	88-09-5	116.16	0.00017727	0.9428		712.4	466.95	0.02306	1000	0.06973
132	Ethyl butyrate	C ₈ H ₁₆ O ₂	105-54-4	116.16	829.29	1.0156	8,955,300,000		394.65	0.01583	1000	0.10314
133	Ethylcyclohexane	C ₈ H ₁₆	1678-91-7	112.21	0.0000748	1.1103		686	404.95	0.02180	1000	0.09505
134	Ethylcyclopentane	C ₇ H ₁₄	1640-89-7	98.19	0.0043244	0.5429		333.67	376.62	0.01832	1000	0.09659
135	Ethylene	C ₂ H ₄	74-85-1	28.05	6.6806E-06	1.4559		299.72	170.00	0.00879	590.92	0.06613
136	Ethylenediamine	C ₂ H ₆ N ₂	107-15-3	60.10	0.1655	0.1798		3,827.9	390.41	0.02272	1000	0.08915
137	Ethylene glycol	C ₂ H ₆ O ₂	107-21-1	62.07	-8,145,800	-0.30502	1,832,500,000		470.45	0.02513	1000	0.09896
138	Ethyleneimine	C ₂ H ₅ N	151-56-4	43.07	0.00077079	0.7713		446.16	329.00	0.01610	1000	0.09659
139	Ethylene oxide	C ₂ H ₄ O	75-21-8	44.05	-0.0003788	1.115		-5,641	273.15	0.01004	1000	0.18063
140	Ethyl formate	C ₃ H ₆ O ₂	109-94-4	74.08	508	0.9023	2,170,000,000		327.46	0.01426	1000	0.11921
141	2-Ethyl hexanoic acid	C ₈ H ₁₆ O ₂	149-57-5	144.21	2.5804E-06	1.4669		1,466.9	500.66	0.02353	1000	0.06492
142	Ethylhexyl ether	C ₈ H ₁₈ O	5756-43-4	130.23	0.0052833	0.52982		1,415.7	417.15	0.01967	1000	0.07348
143	Ethylisopropyl ether	C ₅ H ₁₂ O	625-54-7	88.15	0.00021652	0.94192		632.16	326.15	0.01717	1000	0.08882
144	Ethylisopropyl ketone	C ₆ H ₁₂ O	565-69-5	100.16	-152,400	-0.049106	80,955,000		386.55	0.01889	1000	0.12768
145	Ethyl mercaptan	C ₂ H ₆ S	75-08-1	62.13	0.0015251	0.70243		1,347.5	35,085	0.01487	1000	0.08195
146	Ethyl propionate	C ₅ H ₁₀ O ₂	105-37-3	102.13	1.0507E-07	1.9854			400.00	0.01540	1000	0.09499
147	Ethylpropyl ether	C ₅ H ₁₂ O	628-32-0	88.15	5.8174E-08	2.0116		-372.68	273.15	0.01133	550	0.03690
148	Ethyltrichlorosilane	C ₂ H ₅ Cl ₃ Si	115-21-9	163.51	2.9354E-06	1.4153			373.15	0.01281	573.15	0.02352
149	Fluorine	F ₂	7782-41-4	38.00	0.00012144	0.93831			70.00	0.00654	700	0.05675
150	Fluorobenzene	C ₆ H ₅ F	462-06-6	96.10	0.000053432	1.1576		760.75	357.88	0.01546	600	0.03874
151	Fluoroethane	C ₂ H ₅ F	353-36-6	48.06	0.0004104	0.8333		723	235.45	0.00955	1000	0.07531
152	Fluoromethane	CH ₃ F	593-53-3	34.03	0.003959	0.4834		997.4	194.82	0.00827	1000	0.05589
153	Formaldehyde	CH ₂ O	50-00-0	30.03	44.847	-0.7096		-3,493.5	254.05	0.01256	994.05	0.11532
154	Formamide	CH ₃ NO	75-12-7	45.04	0.00025893	0.9083		723.6	493.00	0.02930	1000	0.07973
155	Formic acid	CH ₂ O ₂	64-18-6	46.03	0.0003754	0.8459		674.4	373.71	0.02008	1000	0.07733
156	Furan	C ₄ H ₄ O	110-00-9	68.07	-644,950	0.2862		-1,6794E+10	304.50	0.01367	1000	0.13631
157	Helium-4	He	7440-59-7	4.00	0.00226	0.7305		-18.63	440	0.03124	2000	0.58820
158	Heptadecane	C ₁₇ H ₃₆	629-78-7	240.47	-114.41	1.0566	-2,211,400,000		575.30	0.02454	1000	0.07649
159	Heptanal	C ₇ H ₁₄ O	111-71-7	114.19	1,556.7	1.0284	17,049,000,000		425.95	0.01967	1000	0.11110
160	Heptane	C ₇ H ₁₆	142-82-5	100.20	-0.070028	0.38068		-7,049.9	339.15	0.01583	1000	0.11493
161	Heptanoic acid	C ₇ H ₁₄ O ₂	111-14-8	130.19	0.00019376	0.92344		739.56	496.15	0.02413	1000	0.06605
162	1-Heptanol	C ₇ H ₁₆ O	111-70-6	116.20	-0.061993	0.2792		-3,336	449.45	0.02345	1000	0.10722
163	2-Heptanol	C ₇ H ₁₆ O	543-49-7	116.20	0.00017569	0.97218		686.56	432.90	0.02484	1000	0.08596
164	3-Heptanone	C ₇ H ₁₄ O	106-35-4	114.19	1,348.6	1.0313	14,832,000,000		420.55	0.01943	1000	0.11287
165	2-Heptanone	C ₇ H ₁₄ O	110-43-0	114.19	2,049.3	1.0323	22,983,000,000		424.18	0.01951	1000	0.11145
166	1-Heptene	C ₇ H ₁₄	592-76-7	98.19	0.00002133	1.2885		487.8	366.79	0.01845	1000	0.10518
167	Heptyl mercaptan	C ₇ H ₁₆ S	1639-09-4	132.27	0.0083145	0.51862		2,253	532,590	0.02289	1000	0.07899
168	1-Heptyne	C ₇ H ₁₂	628-71-7	96.17	0.000060732	1.0586		-102.79	143,140	0.01827	1000	0.08751
169	Hexadecane	C ₁₆ H ₃₄	544-76-3	226.44	0.000004438	1.4949		682	560.01	0.02568	1000	0.08055
170	Hexanal	C ₆ H ₁₂ O	66-25-1	100.16	-7,157,100	-0.05819	4,089,000,000		401.45	0.01842	1000	0.11472
171	Hexane	C ₆ H ₁₄	110-54-3	86.18	-650.5	0.8053	-1,412,100,000		339.09	0.01704	1000	0.12003
172	Hexanoic acid	C ₆ H ₁₂ O ₂	142-62-1	116.16	0.00021014	0.91616		727.64	478.85	0.02381	1000	0.06816
173	1-Hexanol	C ₆ H ₁₄ O	111-27-3	102.17	-4,935,500	-0.1653	1,563,100,000		429.90	0.02220	1000	0.11104
174	2-Hexanol	C ₆ H ₁₄ O	626-93-7	102.18	0.00018361	0.97199		677.05	412.40	0.02421	1000	0.09022
175	2-Hexanone	C ₆ H ₁₂ O	591-78-6	100.16	-1,2158	0.026637		-1,711.6	273.00	0.00775	1000	0.10523
176	3-Hexanone	C ₆ H ₁₂ O	589-38-8	100.16	-0.33262	0.12054		-2,472.6	273.00	0.00800	1000	0.10980
177	1-Hexene	C ₆ H ₁₂	592-41-6	84.16	0.000064256	1.1355		445.15	64,810	0.01644	1000	0.10850
178	3-Hexyne	C ₆ H ₁₀	928-49-4	82.14	6.9682E-06	1.347		-214.35	354.35	0.01485	1000	0.08546
179	Hexyl mercaptan	C ₆ H ₁₄ S	111-31-9	118.24	0.074318	0.30035		4,470.1	1,775,800	0.02151	1000	0.08167

TABLE 2-314 Vapor Thermal Conductivity of Inorganic and Organic Substances [W/(m·K)] (Continued)

Cmpd. no.	Name	Formula	CAS no.	Mol. wt.	C1	C2	C3	C4	T_{\min} , K	Thermal cond. at		
										T_{\min}	T_{\max} , K	T_{\max}
180	1-Hexyne	C ₆ H ₁₀	693-02-7	82.14	0.000058116	1.0724	-77.165	123,900	344.48	0.01679	1000	0.09155
181	2-Hexyne	C ₆ H ₁₀	764-35-2	82.14	0.000011631	1.2753	-202.84	122,990	357.67	0.01506	1000	0.08466
182	Hydrazine	H ₄ N ₂	302-01-2	32.05	0.00043196	0.86603	641.48		386.65	0.02828	1000	0.10430
183	Hydrogen	H ₂	1333-74-0	2.02	0.002653	0.7452	12		22.00	0.01718	1600	0.64299
184	Hydrogen bromide	HBr	10035-10-6	80.91	0.00049725	0.63088	331.62		206.45	0.00551	600	0.01812
185	Hydrogen chloride	HCl	7647-01-0	36.46	0.001865	0.49755	358		190.00	0.00880	700	0.03213
186	Hydrogen cyanide	CHN	74-90-8	27.03	4.6496E-06	1.3669	-210.76	58,295	273.15	0.00985	673.15	0.04185
187	Hydrogen fluoride	HF	7664-39-3	20.01	0.000034629	1.1224	18.744		350.00	0.02356	450	0.03160
188	Hydrogen sulfide	H ₂ S	7783-06-4	34.08	1.381E-07	1.8379	-352.09	46,041	212.80	0.00724	600	0.03258
189	Isobutyric acid	C ₄ H ₈ O ₂	79-31-2	88.11	0.000214	0.9248	698		427.85	0.02206	1000	0.07497
190	Isopropyl amine	C ₃ H ₉ N	75-31-0	59.11	0.00028183	0.92094	619.17		304.92	0.01804	1000	0.10081
191	Malonic acid	C ₃ H ₄ O ₄	141-82-2	104.06	0.00033075	0.81895	777.75		580.00	0.02590	1000	0.05327
192	Methacrylic acid	C ₄ H ₆ O ₂	79-41-4	86.09	0.00019847	0.9284	678.69		434.15	0.02176	1000	0.07210
193	Methane	CH ₄	74-82-8	16.04	8.3983E-06	1.4268	-49.654		111.63	0.01263	600	0.08425
194	Methanol	CH ₃ O	67-56-1	32.04	5.7992E-07	1.7862			273.00	0.01303	684.37	0.06726
195	N-Methyl acetamide	C ₃ H ₇ NO	79-16-3	73.09	0.034177	0.3312	2,070	1,195,600	478.15	0.02498	1000	0.07895
196	Methyl acetate	C ₃ H ₆ O ₂	79-20-9	74.08	-25.343	-0.1934	11,164,000	-67,259,000,000	330.09	0.01415	1000	0.11878
197	Methyl acetylene	C ₃ H ₄	74-99-7	40.06	0.00026544	0.8921	222.19	79,869	249.94	0.01154	1000	0.09675
198	Methyl acrylate	C ₄ H ₆ O ₂	96-33-3	86.09	0.4734	-0.1111	533.57	1,649,600	353.35	0.01569	1000	0.06904
199	Methyl amine	CH ₃ N	74-89-5	31.06	-55.13	1.065	-448,200,000		266.82	0.01259	650	0.07917
200	Methyl benzoate	C ₈ H ₈ O ₂	93-58-3	136.15	0.000023963	1.1308	-67.272	125,720	472.65	0.01784	1000	0.05588
201	3-Methyl-1,2-butadiene	C ₅ H ₈	598-25-4	68.12	0.0002509	0.899	253.4	149,500	314.00	0.01326	1000	0.08902
202	2-Methylbutane	C ₅ H ₁₂	78-78-4	72.15	0.0008968	0.7742	456	230,640	273.15	0.01198	1000	0.11176
203	2-Methylbutanoic acid	C ₅ H ₁₀ O ₂	116-53-0	102.13	0.0001799	0.9457	704.6		450.15	0.02266	1000	0.07253
204	3-Methyl-1-butanol	C ₅ H ₁₂ O	123-51-3	88.15	2,053.4	0.90109	8,755,500,000		404.15	0.02116	1000	0.11843
205	2-Methyl-1-butene	C ₅ H ₁₀	563-46-2	70.13	0.00019098	0.9341	84.07	155,720	304.30	0.01348	1000	0.09771
206	2-Methyl-2-butene	C ₅ H ₁₀	513-35-9	70.13	0.00021736	0.9171	112.3	177,690	311.71	0.01320	1000	0.09504
207	2-Methyl-1-butene-3-yne	C ₅ H ₆	78-80-8	66.10	0.00015498	0.9364	15.366	137,400	305.40	0.01304	1000	0.08664
208	Methylbutyl ether	C ₆ H ₁₄ O	628-28-4	88.15	0.000023993	1.1976	58.59	35,667	273.15	0.01173	1000	0.08586
209	Methylbutyl sulfide	C ₆ H ₁₂ S	628-29-5	104.21	0.0079414	0.23442	2,671.9	1,366,100	396.58	0.01966	1000	0.07960
210	3-Methyl-1-butyne	C ₅ H ₈	598-23-2	68.12	0.000065855	1.072	-36.369	106,430	302.15	0.01468	1000	0.10120
211	Methyl butyrate	C ₆ H ₁₀ O ₂	623-42-7	102.13	1,333.1	0.9962	12,317,000,000		375.90	0.01495	1000	0.10543
212	Methylchlorosilane	CH ₃ ClSi	993-00-0	80.59	0.00037057	0.81367	609.17		281.85	0.01155	1000	0.06357
213	Methylcyclohexane	C ₇ H ₁₄	108-87-2	98.19	0.0000719	1.1274	667		374.08	0.02056	1000	0.10399
214	1-Methylcyclohexanol	C ₇ H ₁₄ O	590-67-0	114.19	0.00011359	1.0311	709.27		441.15	0.02322	1000	0.08238
215	cis-2-Methylcyclohexanol	C ₇ H ₁₄ O	7443-70-1	114.19	0.069565	0.1633	208.7	1,209,500	438.15	0.02415	1000	0.08888
216	trans-2-Methylcyclohexanol	C ₇ H ₁₄ O	7443-52-9	114.19	0.075448	0.155	218.44	1,252,500	440.15	0.02435	1000	0.08908
217	Methylcyclopentane	C ₆ H ₁₂	96-37-7	84.16	0.0024385	0.61774	223.01	477,570	344.96	0.01592	1000	0.10227
218	1-Methylcyclopentene	C ₆ H ₁₀	693-89-0	82.14	0.0040082	0.54462	242.12	559,040	348.64	0.01544	1000	0.09578
219	3-Methylcyclopentene	C ₆ H ₁₀	1120-62-3	82.14	0.0019845	0.6393	227.11	434,120	338.05	0.01501	1000	0.09888
220	Methyldichlorosilane	CH ₂ Cl ₂ Si	75-54-7	115.03	0.00041077	0.75688	591.5		314.70	0.01109	1000	0.04813
221	Methylethyl ether	C ₃ H ₈ O	540-67-0	60.10	0.00024036	0.93177	588.14		273.00	0.01419	1000	0.09447
222	Methylethyl ketone	C ₅ H ₁₀ O	78-93-3	72.11	-4,202,700	-0.1524	2,084,600,000	-1.4577E+13	352.79	0.01546	1000	0.11740
223	Methylethyl sulfide	C ₃ H ₈ S	624-89-5	76.16	0.0034805	0.61906	1,810.8	166,290	339.80	0.01653	1000	0.08415
224	Methyl formate	C ₂ H ₄ O ₂	107-31-3	60.05	-800,040	-0.2285	248,100,000	-1.5034E+12	300.00	0.01369	1000	0.13148
225	Methylisobutyl ether	C ₆ H ₁₂ O	625-44-5	88.15	0.00020053	0.95381	644.42		331.70	0.01729	1000	0.08863
226	Methylisobutyl ketone	C ₆ H ₁₂ O	108-10-1	100.16	-2,483,300	-0.046517	1,313,100,000	-1.5798E+13	389.65	0.01869	1000	0.12433
227	Methyl Isocyanate	C ₂ H ₃ NO	624-83-9	57.05	0.0026136	0.62	1,631.7	126,720	312.00	0.01221	1000	0.06864
228	Methylisopropyl ether	C ₅ H ₁₀ O	598-53-8	74.12	2.1191	-0.19015	1,453.4	3,575,500	303.92	0.01606	1000	0.09451
229	Methylisopropyl ketone	C ₅ H ₁₀ O	563-80-4	86.13	-5,935,000	-0.089497	3,098,800,000	-2.7994E+13	367.55	0.01760	1000	0.12847
230	Methylisopropyl sulfide	C ₅ H ₁₀ S	1551-21-9	90.19	0.0071536	0.53907	2,700.7	241,730	171.64	0.00459	1000	0.07516
231	Methyl mercaptan	CH ₃ S	74-93-1	48.11	0.00002653	1.1631	29,996	32,519	273.15	0.01171	1000	0.07704
232	Methyl methacrylate	C ₅ H ₈ O ₂	80-62-6	100.12	0.00072502	0.7395	365.68	204,360	373.45	0.01680	1000	0.07637
233	2-Methyloctanoic acid	C ₈ H ₁₆ O ₂	3004-93-1	158.24	0.0001813	0.92912	793.45		518.15	0.02383	1000	0.06195
234	2-Methylpentane	C ₆ H ₁₄	107-83-5	86.18	0.000661119	1.0861	-59.592	141,260	333.41	0.01606	1000	0.10242
235	Methyl pentyl ether	C ₆ H ₁₄ O	628-80-8	102.17	0.93312	-0.1172	1,154.3	2,961,700	372.00	0.01828	1000	0.08117
236	2-Methylpropane	C ₄ H ₁₀	75-28-5	58.12	0.089772	0.18501	639.23	1,114,700	261.43	0.01273	1000	0.11701
237	2-Methyl-2-propanol	C ₄ H ₁₀ O	75-65-0	74.12	1.1776E-06	1.6618			333.82	0.01839	766.87	0.07325

238	2-Methyl propene	C ₄ H ₈	115-11-7	56.11	-488.1	0.8877	-1,448,500,000	266.25	0.01276	1000	0.15513	
239	Methyl propionate	C ₅ H ₈ O ₂	554-12-1	88.11	-200.9	-0.1321	104,000	-846,000,000	350.00	0.01402	1000	0.10886
240	Methylpropyl ether	C ₅ H ₁₀ O	557-17-5	74.12	0.011136	0.4831	2,170.3	281.220	312.20	0.01648	1000	0.09079
241	Methylpropyl sulfide	C ₅ H ₁₀ S	3877-15-4	90.19	0.0023574	0.67434	1,804.1	155,660	368.69	0.01802	1000	0.08398
242	Methylsilane	CH ₃ Si	992-94-9	46.14	12.248	-0.5611	-1,067	2,715,200	216.25	0.01108	1000	0.09590
243	alpha-Methyl styrene	C ₉ H ₁₀	98-83-9	118.18	0.21276	-0.022299	-194.68	1,708,700	438.65	0.01969	1000	0.07255
244	Methyl tert-butyl ether	C ₇ H ₁₄ O	1634-04-4	88.15	0.0002084	0.93034	364.832	73,041	273.00	0.01161	1000	0.08958
245	Methyl vinyl ether	C ₅ H ₈ O	107-25-5	58.08	0.00032359	0.8892	623.22		278.65	0.01493	1000	0.09273
246	Naphthalene	C ₁₀ H ₈	91-20-3	128.17	0.000091828	1.0345	731.78		491.14	0.02243	1000	0.06730
247	Neon	Ne	7440-01-9	20.18	0.0011385	0.6646	8.7		30.00	0.00846	3273.1	0.24616
248	Nitroethane	C ₂ H ₅ NO ₂	79-24-3	75.07	0.0011282	0.6895	679.11	238,800	387.22	0.01580	1000	0.06887
249	Nitrogen	N ₂	7727-37-9	28.01	0.00033143	0.7722	16.323	373.72	63.15	0.00602	2000	0.11638
250	Nitrogen trifluoride	F ₃ N	7783-54-2	71.00	2.1443	-0.30545	1,860.3	1,216,700	144.09	0.00648	1000	0.06377
251	Nitromethane	CH ₃ NO ₂	75-52-5	61.04	0.00003135	1.1119	-91.6	128,000	374.35	0.01365	1000	0.06553
252	Nitrous oxide	N ₂ O	10024-97-2	44.01	0.001096	0.667	540		182.30	0.00891	1000	0.07133
253	Nitric oxide	NO	10102-43-9	30.01	0.0004096	0.7509	45.6		121.38	0.01094	750	0.05567
254	Nonadecane	C ₁₉ H ₄₀	629-92-5	268.52	0.000049571	1.2652	3,332.3		603.05	0.02502	1000	0.07147
255	Nonanal	C ₉ H ₁₈ O	124-19-6	142.24	-11.621	0.025653	2,248.3	-135,100,000	468.15	0.02228	1000	0.10522
256	Nonane	C ₉ H ₂₀	111-84-2	128.26	-0.065771	0.27198	-3,482.3	-1,580,300	423.97	0.02130	1000	0.10597
257	Nonanoic acid	C ₉ H ₁₈ O ₂	112-05-0	158.24	0.000178	0.9288	753		528.75	0.02484	1000	0.06209
258	1-Nonanol	C ₉ H ₂₀ O	143-08-8	144.25	-30.715	-0.1075	8,107	-156,830,000	485.20	0.02436	1000	0.09895
259	2-Nonanol	C ₉ H ₂₀ O	628-99-9	144.26	0.00016337	0.97256	709.74		471.70	0.02599	1000	0.07905
260	1-Nonene	C ₉ H ₁₈	124-11-8	126.24	0.000021269	1.2943	662.21		420.02	0.02051	1000	0.09771
261	Nonyl mercaptan	C ₉ H ₂₀ S	1455-21-6	160.32	0.047041	0.29733	2,460.6	1,367,200	492.95	0.02559	1000	0.07598
262	1-Nonyne	C ₉ H ₁₆	3452-09-3	124.22	0.000016681	1.218	-199.41	144,580	423.85	0.01981	1000	0.07956
263	Octadecane	C ₁₈ H ₃₈	593-45-3	254.49	-291.08	1.0615	-6,019,900,000	589.86	0.02491	1000	0.07395	
264	Octanal	C ₈ H ₁₆ O	124-13-0	128.21	-110.89	-0.00042988	51,384	-1.0701E+09	447.15	0.02117	1000	0.10893
265	Octane	C ₈ H ₁₈	111-65-9	114.23	-8,758	0.8448	-2,7121E+10	339.00	0.01503	1000	0.11053	
266	Octanoic acid	C ₈ H ₁₆ O ₂	124-07-2	144.21	0.00018263	0.9283	741.3		513.05	0.02450	1000	0.06391
267	1-Octanol	C ₈ H ₁₈ O	111-87-5	130.23	-0.0030238	0.8745	-13,352		468.35	0.02380	1000	0.10288
268	2-Octanol	C ₈ H ₁₈ O	123-96-6	130.23	0.00016915	0.97238	698.55		452.90	0.02545	1000	0.08229
269	2-Octanone	C ₈ H ₁₆ O	111-13-7	128.21	-0.0020184	1.0027	-20,406		446.15	0.02046	1000	0.10597
270	3-Octanone	C ₈ H ₁₆ O	106-68-3	128.21	8.1833E-08	2.0418			440.65	0.02050	1000	0.10923
271	1-Octene	C ₈ H ₁₆	111-66-0	112.21	0.00000133	1.3554	504.59		394.41	0.01926	1000	0.10295
272	Octyl mercaptan	C ₈ H ₁₈ S	111-88-6	146.29	-3,965.5	0.5213	-1,851,900,000		472.19	0.02505	1000	0.07845
273	1-Octyne	C ₈ H ₁₄	629-05-0	110.20	0.000060734	1.0516	-124.91	158,300	399.35	0.01967	1000	0.08394
274	Oxalic acid	C ₂ H ₂ O ₄	144-62-7	90.03	0.05881	0.278	14,815		569.00	0.01269	1000	0.02537
275	Oxygen	O ₂	7782-44-7	32.00	0.00044994	0.7456	56,699		80.00	0.00691	2000	0.12655
276	Ozone	O ₃	10028-15-6	48.00	0.0043147	0.47999	700.09		161.85	0.00931	1000	0.06990
277	Pentadecane	C ₁₅ H ₃₂	629-62-9	212.41	4.7796E-06	1.4851	643.13		543.84	0.02529	1000	0.08299
278	Pentanal	C ₅ H ₁₀ O	110-62-3	86.13	-4,918,700	-0.10297	2,691,100,000	-2.3179E+13	376.15	0.01705	1000	0.11788
279	Pentane	C ₅ H ₁₂	109-66-0	72.15	-684.4	0.764	-1,055,000,000		273.15	0.01288	1000	0.12707
280	Pentanoic acid	C ₅ H ₁₀ O ₂	109-52-4	102.13	0.00024601	0.8946	696.42		458.65	0.02349	1000	0.07002
281	1-Pentanol	C ₅ H ₁₂ O	71-41-0	88.15	2,896	0.8985	12,735,000,000		410.90	0.02084	990.95	0.11087
282	2-Pentanol	C ₅ H ₁₂ O	6032-29-7	88.15	0.00019575	0.9692	664.04		392.20	0.02372	1000	0.09509
283	2-Pentanone	C ₅ H ₁₀ O	107-87-9	86.13	-0.01719	0.4832	-3,798	-1,235,000	273.00	0.00877	1000	0.12002
284	3-Pentanone	C ₅ H ₁₀ O	96-22-0	86.13	22.775	1.0019	191,000,000		273.00	0.00898	1000	0.12082
285	1-Pentene	C ₅ H ₁₀	109-67-1	70.13	2.7081E-06	1.5493	41,075	8,301.3	303.22	0.01546	1000	0.11472
286	2-Pentyl mercaptan	C ₇ H ₁₄ S	2084-19-7	104.21	0.00022307	0.93358	794.16		385.15	0.01890	1000	0.07858
287	Pentyl mercaptan	C ₇ H ₁₄ S	110-66-7	104.21	0.00011261	1.034	693.05		399.79	0.02019	1000	0.08412
288	1-Pentyne	C ₅ H ₈	627-19-0	68.12	0.000052415	1.0948	-51.09	101,160	313.33	0.01517	1000	0.09608
289	2-Pentyne	C ₅ H ₈	627-21-4	68.12	0.00025623	1.0073	1,423.7		329.27	0.01653	1000	0.11119
290	Phenanthrene	C ₁₄ H ₁₀	85-01-8	178.23	0.00010167	0.988	797		610.03	0.02490	1000	0.05208
291	Phenol	C ₆ H ₆ O	108-95-2	94.11	0.038846	0.2392	985.81	937,170	454.99	0.02183	1000	0.06936
292	Phenyl isocyanate	C ₇ H ₇ NO	103-71-9	119.12	0.00016675	0.91777	730.1		439.43	0.01669	1000	0.05461
293	Phthalic anhydride	C ₈ H ₄ O ₃	85-44-9	148.12	0.0000593	1.046	765.5		557.65	0.01864	1000	0.04615
294	Propadiene	C ₃ H ₄	463-49-0	40.06	0.000061629	1.0731	1,8579	70,128	238.65	0.00980	1000	0.09526
295	Propane	C ₃ H ₈	74-98-6	44.10	-1.12	0.10972	-9,834.6	-7,535,800	231.10	0.01114	1000	0.14599
296	1-Propanol	C ₃ H ₈ O	71-23-8	60.10	-613.84	0.7927	-1,157,400,000		370.35	0.02135	720.25	0.07034
297	2-Propanol	C ₃ H ₈ O	67-63-0	60.10	7.3907E-07	1.7419			355.30	0.02049	1000	0.12428
298	Propenylcyclohexene	C ₉ H ₁₄	13511-13-2	122.21	0.00010242	1.0486	701.56		431.65	0.02262	1000	0.08421
299	Propionaldehyde	C ₃ H ₆ O	123-38-6	58.08	1,165.1	0.90419	5,472,900,000		321.15	0.01263	1000	0.10983
300	Propionic acid	C ₃ H ₆ O ₂	79-09-4	74.08	0.00022286	0.91704	678.21		414.32	0.02124	1000	0.07487

TABLE 2-314 Vapor Thermal Conductivity of Inorganic and Organic Substances [W/(m·K)] (Concluded)

Cmpd. no.	Name	Formula	CAS no.	Mol. wt.	C1	C2	C3	C4	T_{\min} , K	Thermal cond. at		T_{\max} , K	Thermal cond. at T_{\max}
										T_{\min}	T_{\max}		
301	Propionitrile	C ₃ H ₅ N	107-12-0	55.08	0.001321	1.2202	51,822		370.50	0.01278	990.5	0.11209	
302	Propyl acetate	C ₅ H ₁₀ O ₂	109-60-4	102.13	1,325.3	1	12,235,000,000		374.65	0.01520	1000	0.10832	
303	Propyl amine	C ₃ H ₉ N	107-10-8	59.11	0.2833	0.055046	1,325.9	1,817,600	321.00	0.01709	1000	0.10000	
304	Propylbenzene	C ₉ H ₁₂	103-65-1	120.19	0.16992	0.021258	-54.484	1,624,800	322.39	0.02022	1000	0.07658	
305	Propylene	C ₃ H ₆	115-07-1	42.08	0.0000449	1.2018	421		225.45	0.01054	1000	0.12737	
306	Propyl formate	C ₄ H ₈ O ₂	110-74-7	88.11	740.1	0.9732	5,646,000,000		353.97	0.01403	1000	0.10893	
307	2-Propyl mercaptan	C ₃ H ₈ S	75-33-2	76.16	0.00018367	0.9627	646.01		325.71	0.01616	1000	0.08624	
308	Propyl mercaptan	C ₃ H ₈ S	107-03-9	76.16	0.0087425	0.51733	2,358.1	334,590	340.87	0.01654	1000	0.08439	
309	1,2-Propylene glycol	C ₃ H ₈ O ₂	57-55-6	76.09	0.0001666	0.9765	706		460.75	0.02624	1000	0.08302	
310	Quinone	C ₆ H ₄ O ₂	106-51-4	108.09	-5,678,600	-0.045252	2,615,700,000	-3.5415E+13	454.00	0.02593	1000	0.12665	
311	Silicon tetrafluoride	F ₄ Si	7783-61-1	104.08	0.0000955	0.928	63.6		333.55	0.01761	702.45	0.03837	
312	Styrene	C ₈ H ₈	100-42-5	104.15	0.010048	0.4033	553.74	685,570	418.31	0.01837	1000	0.07276	
313	Succinic acid	C ₄ H ₆ O ₄	110-15-6	118.09	0.00032875	0.8172	740.97		591.00	0.02685	1000	0.05342	
314	Sulfur dioxide	O ₂ S	7446-09-5	64.06	10.527	-0.7732	-1,333	1,506,400	250.00	0.00745	900	0.03969	
315	Sulfur hexafluoride	F ₆ S	2551-62-4	146.06	0.00048883	0.6518	-117.08	78,863	273.15	0.01163	1000	0.04587	
316	Sulfur trioxide	O ₃ S	7446-11-9	80.06	1.0702	-0.2348	2,010.4	1,277,000	317.90	0.01386	1000	0.04930	
317	Terephthalic acid	C ₈ H ₆ O ₄	100-21-0	166.13	0.00017531	0.8901	909.56		832.00	0.03328	1000	0.04297	
318	<i>o</i> -Terphenyl	C ₁₈ H ₁₄	84-15-1	230.30	0.000078652	0.95174	-282.82	289,490	373.15	0.00950	1000	0.05598	
319	Tetradecane	C ₁₄ H ₃₀	629-59-4	198.39	-163.62	0.9193	-1.0876E+09		526.73	0.02517	1000	0.08615	
320	Tetrahydrofuran	C ₄ H ₈ O	109-99-9	72.11	9.5521E-06	1.4561	662.22		339.12	0.01564	1000	0.13419	
321	1,2,3,4-Tetrahydronaphthalene	C ₁₀ H ₁₂	119-64-2	132.20	0.00007754	1.0778	729		480.77	0.02395	1000	0.07676	
322	Tetrahydrothiophene	C ₄ H ₈ S	110-01-0	88.17	0.00085604	0.7297	531.99	213,840	394.27	0.01801	1000	0.07579	
323	2,2,3,3-Tetramethylbutane	C ₈ H ₁₈	594-82-1	114.23	0.000015235	1.2816	-111.88	124,120	379.44	0.01964	1000	0.10528	
324	Thiophene	C ₄ H ₄ S	110-02-1	84.14	0.00013384	0.98115	645.95		357.31	0.01525	1000	0.07139	
325	Toluene	C ₇ H ₈	108-88-3	92.14	0.00002392	1.2694	537		383.78	0.01901	1000	0.10007	
326	1,1,2-Trichloroethane	C ₂ H ₃ Cl ₃	79-00-5	133.40	0.0000952	1.0423	1,243.3		387.00	0.01125	1000	0.05684	
327	Tridecane	C ₁₃ H ₂₈	629-50-5	184.36	5.3701E-06	1.4751	599.09		508.62	0.02422	1000	0.08942	
328	Triethyl amine	C ₆ H ₁₅ N	121-44-8	101.19	0.000106	1.0161	91	132,900	273.15	0.01018	1000	0.09680	
329	Trimethyl amine	C ₃ H ₉ N	75-50-3	59.11	0.00027648	0.901	167.68	132,200	273.15	0.01280	1000	0.10734	
330	1,2,3-Trimethylbenzene	C ₉ H ₁₂	526-73-8	120.19	0.000098408	1.0452	720.49		449.27	0.02238	1000	0.07816	
331	1,2,4-Trimethylbenzene	C ₉ H ₁₂	95-63-6	120.19	0.00008498	1.061	708		442.53	0.02098	1000	0.07583	
332	2,2,4-Trimethylpentane	C ₈ H ₁₈	540-84-1	114.23	0.00001758	1.3114	392.9		355.15	0.01846	1000	0.10847	
333	2,3,3-Trimethylpentane	C ₈ H ₁₈	560-21-4	114.23	0.000020248	1.2284	-174.72	147,800	387.91	0.02001	1000	0.10079	
334	1,3,5-Trinitrobenzene	C ₆ H ₃ N ₃ O ₆	99-35-4	213.10	0.00020544	0.87137	807.3		629.60	0.02474	1000	0.04675	
335	2,4,6-Trinitrotoluene	C ₇ H ₅ N ₃ O ₆	118-96-7	227.13	0.00018189	0.88744	803.39		625.00	0.02410	1000	0.04635	
336	Undecane	C ₁₁ H ₂₄	1120-21-4	156.31	0.038012	0.68615	34,663	8,721,900	469.08	0.02259	1000	0.09798	
337	1-Undecanol	C ₁₁ H ₂₄ O	112-42-5	172.31	2,498.8	0.95209	2.0167E+10		520.30	0.02486	1000	0.08899	
338	Vinyl acetate	C ₄ H ₆ O ₂	108-05-4	86.09	-3,279,500	-0.12941	1.7104E+09		345.65	0.01515	1000	0.12177	
339	Vinyl acetylene	C ₄ H ₄	689-97-4	52.07	0.000054197	1.0632	-70.589	9,0617	278.25	0.01123	1000	0.08222	
340	Vinyl chloride	C ₂ H ₃ Cl	75-01-4	62.50	-229.41	0.59582	-169,430,000		259.25	0.00963	1000	0.08300	
341	Vinyl trichlorosilane	C ₂ H ₃ Cl ₃ Si	75-94-5	161.49	3510.8	0.225	401,720,000		363.85	0.01198	1000	0.04135	
342	Water	H ₂ O	7732-18-5	18.02	6.2041E-06	1.3973			273.16	0.01574	1073.15	0.10652	
343	<i>m</i> -Xylene	C ₈ H ₁₀	108-38-3	106.17	3.0593E-09	2.4182	-569.28	121,060	320	0.00867	1000	0.09965	
344	<i>o</i> -Xylene	C ₈ H ₁₀	95-47-6	106.17	4.9707E-06	1.3787	-225.64	66,786	320	0.01492	1000	0.08084	
345	<i>p</i> -Xylene	C ₈ H ₁₀	106-42-3	106.17	9.9305E-08	1.9229	-469.93	113,460	320	0.01019	1000	0.09060	

The vapor thermal conductivity is calculated by

$$k = \frac{C1T^{C2}}{1 + C3/T + C4/T^2}$$

where k is the thermal conductivity in W/(m·K) and T is the temperature in K. Thermal conductivities are at either 1 atm or the vapor pressure, whichever is lower. All substances are listed by chemical family in Table 2-6 and by formula in Table 2-7.

Values in this table were taken from the Design Institute for Physical Properties (DIPPR) of the American Institute of Chemical Engineers (AIChE), copyright 2007 AIChE and reproduced with permission of AIChE and of the DIPPR Evaluated Process Design Data Project Steering Committee. Their source should be cited as R. L. Rowley, W. V. Wilding, J. L. Oscarson, Y. Yang, N. A. Zundel, T. E. Daubert, R. P. Danner, DIPPR® Data Compilation of Pure Chemical Properties, Design Institute for Physical Properties, AIChE, New York (2007).

The number of digits provided for values at T_{\min} and T_{\max} was chosen for uniformity of appearance and formatting; these do not represent the uncertainties of the physical quantities, but are the result of calculations from the standard thermophysical property formulations within a fixed format.

TABLE 2-315 Thermal Conductivity of Inorganic and Organic Liquids [W/(m-K)]

Cmpd. no.	Name	Formula	CAS no.	Mol. wt.	C1	C2	C3	C4	C5	T_{min} , K	Thermal cond. at T_{min}	T_{max} , K	Thermal cond. at T_{max}
1	Acetaldehyde	C ₂ H ₄ O	75-07-0	44.05	0.311	-0.000436				150.15	0.2455	294.00	0.1828
2	Acetamide	C ₂ H ₅ NO	60-35-5	59.07	0.39363	-0.00037053				353.33	0.2627	494.30	0.2105
3	Acetic acid	C ₂ H ₄ O ₂	64-19-7	60.05	0.214	-0.0001834				289.81	0.1609	391.05	0.1423
4	Acetic anhydride	C ₄ H ₆ O ₃	108-24-7	102.09	0.23638	-0.00024263				200.15	0.1878	412.70	0.1363
5	Acetone	C ₃ H ₆ O	67-64-1	58.08	0.2878	-0.000427				178.45	0.2116	343.15	0.1413
6	Acetonitrile	C ₂ H ₃ N	75-05-8	41.05	0.33192	-0.00043243				229.32	0.2328	349.32	0.1809
7	Acetylene	C ₂ H ₂	74-86-2	26.04	0.33363	-0.00083655				192.40	0.1727	250.00	0.1245
8	Acrolein	C ₃ H ₄ O	107-02-8	56.06	0.2703	-0.0003764				185.45	0.2005	325.84	0.1477
9	Acrylic acid	C ₃ H ₄ O ₂	79-10-7	72.06	0.2441	-0.0002904				286.15	0.1610	484.50	0.1034
10	Acrylonitrile	C ₃ H _{3.5} N	107-13-1	53.06	0.28941	-0.00041691				189.63	0.2104	350.50	0.1433
11	Air	Mixture	132259-10-0	28.96	0.28472	-0.0017393				75.00	0.1543	125.00	0.0673
12	Ammonia	H ₃ N	7664-41-7	17.03	1.169	-0.002314				195.41	0.1768	400.05	0.2433
13	Anisole	C ₇ H ₈ O	100-66-3	108.14	0.23494	-0.00026477				235.65	0.1726	512.50	0.0992
14	Argon	Ar	7440-37-1	39.95	0.1819	-0.0003176	-0.00000411			83.78	0.1264	150.00	0.0418
15	Benzamide	C ₇ H ₇ NO	55-21-0	121.14	0.28485	-0.00025225				403.00	0.1832	563.15	0.1428
16	Benzene	C ₆ H ₆	71-43-2	78.11	0.23444	-0.00030572				278.68	0.1492	413.10	0.1082
17	Benzenethiol	C ₆ H ₆ S	108-98-5	110.18	0.20996	-0.0002146				258.27	0.1545	442.29	0.1150
18	Benzoic acid	C ₇ H ₆ O ₂	65-85-0	122.12	0.2391	-0.0002325				395.45	0.1472	596.00	0.1005
19	Benzonitrile	C ₇ H ₅ N	100-47-0	103.12	0.21284	-0.00021587				260.40	0.1566	464.15	0.1126
20	Benzophenone	C ₁₃ H ₁₀ O	119-61-9	182.22	0.25867	-0.00022516				321.35	0.1863	664.00	0.1092
21	Benzyl alcohol	C ₇ H ₈ O	100-51-6	108.14	0.17847	-0.000065843				257.85	0.1615	478.60	0.1470
22	Benzyl ethyl ether	C ₉ H ₁₂ O	539-30-0	136.19	0.2029	-0.0002226				275.65	0.1415	528.60	0.0852
23	Benzyl mercaptan	C ₇ H ₈ S	100-53-8	124.20	0.20316	-0.00019912				243.95	0.1546	472.03	0.1092
24	Biphenyl	C ₁₂ H ₁₀	92-52-4	154.21	0.19053	-0.00015145				342.20	0.1387	723.15	0.0810
25	Bromine	Br ₂	7726-95-6	159.81	-0.2185	0.0042143	-0.000017753	3.1041E-08	-2.0108E-11	266.00	0.1299	584.00	0.0316
26	Bromobenzene	C ₆ H ₅ Br	108-86-1	157.01	0.16983	-0.0001981				242.43	0.1218	429.24	0.0848
27	Bromoethane	C ₂ H ₅ Br	74-96-4	108.97	0.1799	-0.000262				154.55	0.1394	414.14	0.0714
28	Bromomethane	CH ₃ Br	74-83-9	94.94	0.1912	-0.000299				179.47	0.1375	370.10	0.0805
29	1,2-Butadiene	C ₄ H ₆	590-19-2	54.09	0.21966	-0.0003436				136.95	0.1726	284.00	0.1221
30	1,3-Butadiene	C ₄ H ₆	106-99-0	54.09	0.22231	-0.0003664				164.25	0.1621	268.74	0.1238
31	Butane	C ₄ H ₁₀	106-97-8	58.12	0.27349	-0.00071267	5.1555E-07			134.86	0.1868	400.00	0.0709
32	1,2-Butanediol	C ₄ H ₁₀ O ₂	584-03-2	90.12	0.064621	0.00067625	-1.0491E-06			220.00	0.1626	469.57	0.1509
33	1,3-Butanediol	C ₄ H ₁₀ O ₂	107-88-0	90.12	-0.0032865	0.0011463	-1.5525E-06			196.15	0.1618	481.38	0.1888
34	1-Butanol	C ₄ H ₁₀ O	71-36-3	74.12	0.2136	-0.0002034				183.85	0.1762	391.90	0.1339
35	2-Butanol	C ₄ H ₁₀ O	78-92-2	74.12	0.22787	-0.00030727				158.45	0.1792	372.90	0.1133
36	1-Butene	C ₄ H ₈	106-98-9	56.11	0.22153	-0.00035023				87.80	0.1908	266.91	0.1281
37	cis-2-Butene	C ₄ H ₈	590-18-1	56.11	0.21378	-0.00035445				134.26	0.1662	276.87	0.1156
38	trans-2-Butene	C ₄ H ₈	624-64-6	56.11	0.21153	-0.00035056				167.62	0.1528	274.03	0.1155
39	Butyl acetate	C ₆ H ₁₂ O ₂	123-86-4	116.16	0.21721	-0.00026563				199.65	0.1642	453.75	0.0967
40	Butylbenzene	C ₁₀ H ₁₄	104-51-8	134.22	0.18707	-0.00020037				185.30	0.1499	473.15	0.0923
41	Butyl mercaptan	C ₄ H ₉ S	109-79-5	90.19	0.21143	-0.000258				157.46	0.1708	371.61	0.1156
42	sec-Butyl mercaptan	C ₄ H ₁₀ S	513-53-1	90.19	0.2069	-0.0002568				133.02	0.1727	358.13	0.1149
43	1-Butyne	C ₄ H ₆	107-00-6	54.09	0.22334	-0.0003515				147.43	0.1715	281.22	0.1245
44	Butyraldehyde	C ₄ H ₈ O	123-72-8	72.11	0.21915	-0.00024846				176.75	0.1752	382.15	0.1242
45	Butyric acid	C ₄ H ₈ O ₂	107-92-6	88.11	0.1967	-0.000168				267.95	0.1517	573.15	0.1004
46	Butyronitrile	C ₄ H ₇ N	109-74-0	69.11	0.2597	-0.00031				161.25	0.2097	390.75	0.1386
47	Carbon dioxide	CO ₂	124-38-9	44.01	0.4406	-0.0012175				216.58	0.1769	300.00	0.0754
48	Carbon disulfide	CS ₂	75-15-0	76.14	0.2333	-0.000275				161.11	0.1890	319.37	0.1455
49	Carbon monoxide	CO	630-08-0	28.01	0.2855	-0.001784				68.15	0.1639	125.00	0.0625
50	Carbon tetrachloride	CCl ₄	56-23-5	153.82	0.1589	-0.0001987				250.33	0.1092	349.79	0.0894
51	Carbon tetrafluoride	CF ₄	75-73-0	88.00	0.20771	-0.00078883				89.56	0.1371	145.10	0.0933
52	Chlorine	Cl ₂	7782-50-5	70.91	0.2246	-0.000064	-0.000000788			172.12	0.1902	410.00	0.0659
53	Chlorobenzene	C ₆ H ₅ Cl	108-90-7	112.56	0.1841	-0.0001917				227.95	0.1404	404.87	0.1065
54	Chloroethane	C ₂ H ₅ Cl	75-00-3	64.51	0.2438	-0.000419				134.80	0.1873	373.15	0.0875
55	Chloroform	CHCl ₃	67-66-3	119.38	0.1778	-0.0002023				209.63	0.1354	400.00	0.0969
56	Chloromethane	CH ₃ Cl	74-87-3	50.49	0.41067	-0.0008478				175.43	0.2619	350.00	0.1139
57	1-Chloropropane	C ₃ H ₇ Cl	540-54-5	78.54	0.20143	-0.00028925				150.35	0.1579	400.95	0.0855
58	2-Chloropropane	C ₃ H ₇ Cl	75-29-6	78.54	0.21232	-0.0003149				155.97	0.1632	386.70	0.0905

TABLE 2-315 Thermal Conductivity of Inorganic and Organic Liquids [W/(m·K)] (Continued)

Cmpd. no.	Name	Formula	CAS no.	Mol. wt.	C1	C2	C3	C4	C5	T_{\min} , K	Thermal cond. at T_{\min}	T_{\max} , K	Thermal cond. at T_{\max}
59	<i>m</i> -Cresol	C ₇ H ₈ O	108-39-4	108.14	0.18241	-0.00011109				285.39	0.1507	475.43	0.1296
60	<i>o</i> -Cresol	C ₇ H ₈ O	95-48-7	108.14	0.19186	-0.0001303				304.19	0.1522	464.15	0.1314
61	<i>p</i> -Cresol	C ₇ H ₈ O	106-44-5	108.14	0.17971	-0.00012037				307.93	0.1426	475.13	0.1225
62	Cumene	C ₉ H ₁₂	98-82-8	120.19	0.1855	-0.00020895				177.14	0.1485	413.15	0.0992
63	Cyanogen	C ₂ N ₂	460-19-5	52.03	0.4685	-0.00086594				245.25	0.2561	252.00	0.2503
64	Cyclobutane	C ₄ H ₈	287-23-0	56.11	0.22262	-0.00034082				182.48	0.1604	285.66	0.1253
65	Cyclohexane	C ₆ H ₁₂	110-82-7	84.16	0.19813	-0.0002505				279.69	0.1281	353.87	0.1095
66	Cyclohexanol	C ₆ H ₁₂ O	108-93-0	100.16	0.1715	-0.0001255				296.60	0.1343	563.15	0.1008
67	Cyclohexanone	C ₆ H ₁₀ O	108-94-1	98.14	0.17557	-0.00012392				242.00	0.1456	428.58	0.1225
68	Cyclohexene	C ₆ H ₁₀	110-83-8	82.14	0.20926	-0.00026037				169.67	0.1651	356.12	0.1165
69	Cyclopentane	C ₅ H ₁₀	287-92-3	70.13	0.2066	-0.0002696				179.28	0.1583	322.40	0.1197
70	Cyclopentene	C ₅ H ₈	142-29-0	68.12	0.21776	-0.00027783				138.13	0.1794	333.15	0.1252
71	Cyclopropane	C ₃ H ₆	75-19-4	42.08	0.24348	-0.00042568				145.59	0.1815	240.37	0.1412
72	Cyclohexyl mercaptan	C ₆ H ₁₂ S	1569-69-3	116.22	0.18374	-0.0001925				189.64	0.1472	431.95	0.1006
73	Decanal	C ₁₀ H ₂₀ O	112-31-2	156.27	0.20383	-0.0002				267.15	0.1504	488.15	0.1062
74	Decane	C ₁₀ H ₂₂	124-18-5	142.28	0.2063	-0.00025				243.51	0.1454	447.30	0.0945
75	Decanoic acid	C ₁₀ H ₂₀ O ₂	334-48-5	172.27	0.206	-0.0002				304.75	0.1451	543.15	0.0974
76	1-Decanol	C ₁₀ H ₂₂ O	112-30-1	158.28	0.228	-0.000223				280.05	0.1656	503.00	0.1158
77	1-Decene	C ₁₀ H ₂₀	872-05-9	140.27	0.20237	-0.00024187				206.89	0.1523	443.75	0.0950
78	Decyl mercaptan	C ₁₀ H ₂₂ S	143-10-2	174.35	0.20134	-0.00020826				247.56	0.1498	512.35	0.0946
79	1-Decyne	C ₁₀ H ₁₈	764-93-2	138.25	0.20839	-0.00023622				229.15	0.1543	447.15	0.1028
80	Deuterium	D ₂	7782-39-0	4.03	1.264					20.40	1.2640	20.40	1.2640
81	1,1-Dibromoethane	C ₂ H ₄ Br ₂	557-91-5	187.86	0.1426	-0.00016402				210.15	0.1081	498.40	0.0609
82	1,2-Dibromoethane	C ₂ H ₄ Br ₂	106-93-4	187.86	0.13622	-0.0001179				282.85	0.1029	404.51	0.0885
83	Dibromomethane	CH ₂ Br ₂	74-95-3	173.83	0.17558	-0.00022499				220.60	0.1260	370.10	0.0923
84	Dibutyl ether	C ₈ H ₁₈ O	142-96-1	130.23	0.19418	-0.00022246				175.30	0.1552	523.15	0.0778
85	<i>m</i> -Dichlorobenzene	C ₆ H ₄ Cl ₂	541-73-1	147.00	0.16694	-0.0001667				248.39	0.1255	446.23	0.0926
86	<i>o</i> -Dichlorobenzene	C ₆ H ₄ Cl ₂	95-50-1	147.00	0.16994	-0.0001637				262.87	0.1269	351.71	0.1124
87	<i>p</i> -Dichlorobenzene	C ₆ H ₄ Cl ₂	106-46-7	147.00	0.16977	-0.0001799				326.14	0.1111	548.00	0.0712
88	1,1-Dichloroethane	C ₂ H ₄ Cl ₂	75-34-3	98.96	0.18881	-0.00026083				176.19	0.1429	416.90	0.0801
89	1,2-Dichloroethane	C ₂ H ₄ Cl ₂	107-06-2	98.96	0.214	-0.000266				253.15	0.1467	356.59	0.1192
90	Dichloromethane	CH ₂ Cl ₂	75-09-2	84.93	0.23847	-0.00033366				178.01	0.1791	325.00	0.1300
91	1,1-Dichloropropane	C ₃ H ₆ Cl ₂	78-99-9	112.99	0.18	-0.00023144				200.00	0.1337	438.00	0.0786
92	1,2-Dichloropropane	C ₃ H ₆ Cl ₂	78-87-5	112.99	0.19653	-0.00025012				172.71	0.1533	457.60	0.0821
93	Diethanol amine	C ₄ H ₁₁ NO ₂	111-42-2	105.14	0.0218	0.0010315	-0.000001355			301.15	0.2096	673.15	0.1022
94	Diethyl amine	C ₄ H ₁₁ N	109-89-7	73.14	0.2587	-0.00054343	4.2097E-07			223.35	0.1583	453.15	0.0989
95	Diethyl ether	C ₄ H ₁₀ O	60-29-7	74.12	0.2495	-0.000407				156.85	0.1857	433.15	0.0732
96	Diethyl sulfide	C ₄ H ₁₀ S	352-93-2	90.19	0.21065	-0.0002623				169.20	0.1663	365.25	0.1148
97	1,1-Difluoroethane	C ₂ H ₄ F ₂	75-37-6	66.05	0.27019	-0.000661	3.443E-07			154.56	0.1763	363.15	0.0756
98	1,2-Difluoroethane	C ₂ H ₄ F ₂	624-72-6	66.05	0.23171	-0.00038503				215.00	0.1489	372.80	0.0882
99	Difluoromethane	CH ₂ F ₂	75-10-5	52.02	0.37296	-0.00088707	2.5762E-07			136.95	0.2563	302.56	0.1282
100	Di-isopropyl amine	C ₆ H ₁₃ N	108-18-9	101.19	0.1844	-0.000239				176.85	0.1421	357.05	0.0991
101	Di-isopropyl ether	C ₆ H ₁₄ O	108-20-3	102.17	0.19162	-0.0002762				187.65	0.1398	400.10	0.0811
102	Di-isopropyl ketone	C ₇ H ₁₄ O	565-80-0	114.19	0.22076	-0.00027624				204.81	0.1642	460.00	0.0937
103	1,1-Dimethoxyethane	C ₄ H ₁₀ O ₂	534-15-6	90.12	0.22078	-0.00031271				159.95	0.1708	337.45	0.1153
104	1,2-Dimethoxypropane	C ₅ H ₁₂ O ₂	7778-85-0	104.15	0.22998	-0.00030372				226.10	0.1613	366.15	0.1188
105	Dimethyl acetylene	C ₄ H ₆	503-17-3	54.09	0.22773	-0.00034804				240.91	0.1439	300.13	0.1233
106	Dimethyl amine	C ₂ H ₇ N	124-40-3	45.08	0.2454	-0.000338				180.96	0.1842	403.15	0.1091
107	2,3-Dimethylbutane	C ₆ H ₁₄	79-29-8	86.18	0.1774	-0.0002436				145.19	0.1420	331.15	0.0967
108	1,1-Dimethylcyclohexane	C ₈ H ₁₆	590-66-9	112.21	0.1807	-0.0002177				239.66	0.1285	392.70	0.0952
109	<i>cis</i> -1,2-Dimethylcyclohexane	C ₈ H ₁₆	2207-01-4	112.21	0.18092	-0.0002108				223.16	0.1339	402.94	0.0960
110	<i>trans</i> -1,2-Dimethylcyclohexane	C ₈ H ₁₆	6876-23-9	112.21	0.17675	-0.0002077				184.99	0.1383	596.15	0.0529
111	Dimethyl disulfide	C ₂ H ₆ S ₂	624-92-0	94.20	0.21373	-0.0002447				188.44	0.1676	382.90	0.1200
112	Dimethyl ether	C ₂ H ₆ O	115-10-6	46.07	0.31174	-0.0005638				131.65	0.2375	320.03	0.1313
113	<i>N,N</i> -Dimethyl formamide	C ₃ H ₇ NO	68-12-2	73.09	0.26	-0.000255				250.00	0.1963	425.15	0.1516
114	2,3-Dimethylpentane	C ₇ H ₁₆	565-59-3	100.20	0.17964	-0.000246				160.00	0.1403	362.93	0.0904
115	Dimethyl phthalate	C ₁₀ H ₁₀ O ₄	131-11-3	194.18	0.13905	0.0001509	-3.978E-07			273.15	0.1506	556.85	0.0997

116	Dimethylsilane	C ₂ H ₆ Si	1111-74-6	60.17	0.25547	-0.0004411			122.93	0.2013	253.55	0.1436
117	Dimethyl sulfide	C ₂ H ₆ S	75-18-3	62.13	0.23942	-0.0003311			174.88	0.1815	310.48	0.1366
118	Dimethyl sulfoxide	C ₂ H ₆ OS	67-68-5	78.13	0.3142	-0.00030809			291.67	0.2243	464.00	0.1713
119	Dimethyl terephthalate	C ₁₀ H ₁₀ O ₄	120-61-6	194.18	0.21593	-0.00020805			413.80	0.1298	561.15	0.0992
120	1,4-Dioxane	C ₄ H ₈ O ₂	123-91-1	88.11	0.3027	-0.0004827			284.95	0.1652	374.47	0.1219
121	Diphenyl ether	C ₁₂ H ₁₀ O	101-84-8	170.21	0.18686	-0.00014953			300.03	0.1420	531.46	0.1074
122	Dipropyl amine	C ₆ H ₁₅ N	142-84-7	101.19	0.2224	-0.000314			210.15	0.1564	382.00	0.1025
123	Dodecane	C ₁₂ H ₂₆	112-40-3	170.33	0.2047	-0.0002326			263.57	0.1434	489.47	0.0908
124	Eicosane	C ₂₀ H ₄₂	112-95-8	282.55	0.2178	-0.0002233			309.58	0.1487	616.93	0.0800
125	Ethane	C ₂ H ₆	74-84-0	30.07	0.35758	-0.0011458	6.1866E-07		90.35	0.2591	300.00	0.0695
126	Ethanol	C ₂ H ₆ O	64-17-5	46.07	0.2468	-0.000264			159.05	0.2048	353.15	0.1536
127	Ethyl acetate	C ₄ H ₈ O ₂	141-78-6	88.11	0.2501	-0.0003563			189.60	0.1826	350.21	0.1253
128	Ethyl amine	C ₂ H ₇ N	75-04-7	45.08	0.30059	-0.000581	6.602E-07		192.15	0.2133	293.15	0.1870
129	Ethylbenzene	C ₈ H ₁₀	100-41-4	106.17	0.1999	-0.00023823			178.20	0.1575	413.10	0.1015
130	Ethyl benzoate	C ₉ H ₁₀ O ₂	93-89-0	150.17	0.20771	-0.00021265			238.45	0.1570	549.40	0.0909
131	2-Ethyl butanoic acid	C ₈ H ₁₆ O ₂	88-09-5	116.16	0.2175	-0.0002407			258.15	0.1554	516.50	0.0932
132	Ethyl butyrate	C ₈ H ₁₆ O ₂	105-54-4	116.16	0.21043	-0.00024903			175.15	0.1668	453.15	0.0976
133	Ethylcyclohexane	C ₈ H ₁₆	1678-91-7	112.21	0.17662	-0.0002014			161.84	0.1440	404.94	0.0951
134	Ethylcyclopentane	C ₇ H ₁₄	1640-89-7	98.19	0.18334	-0.0002228			134.71	0.1533	376.62	0.0994
135	Ethylene	C ₂ H ₄	74-85-1	28.05	0.4194	-0.001591	0.000001306		104.00	0.2681	280.00	0.0763
136	Ethylenediamine	C ₂ H ₈ N ₂	107-15-3	60.10	0.36434	-0.0004433			284.29	0.2383	390.41	0.1913
137	Ethylene glycol	C ₂ H ₆ O ₂	107-21-1	62.07	0.088067	0.00094712	-1.3114E-06		260.15	0.2457	470.45	0.2434
138	Ethyleneimine	C ₂ H ₅ N	151-56-4	43.07	0.3097	-0.0004023			195.20	0.2312	329.00	0.1773
139	Ethylene oxide	C ₂ H ₄ O	75-21-8	44.05	0.26957	-0.0003984			160.65	0.2056	283.85	0.1565
140	Ethyl formate	C ₃ H ₆ O ₂	109-94-4	74.08	0.2587	-0.00033			193.55	0.1948	433.15	0.1158
141	2-Ethyl hexanoic acid	C ₈ H ₁₆ O ₂	149-57-5	144.21	0.20954	-0.00022251			235.00	0.1573	500.66	0.0981
142	Ethylhexyl ether	C ₈ H ₁₈ O	5756-43-4	130.23	0.19356	-0.00024102			180.00	0.1502	466.40	0.0811
143	Ethylisopropyl ether	C ₆ H ₁₄ O	625-54-7	88.15	0.21928	-0.00032568			140.00	0.1737	391.20	0.0919
144	Ethylisopropyl ketone	C ₆ H ₁₂ O	565-69-5	100.16	0.22873	-0.0002913			204.15	0.1693	450.10	0.0976
145	Ethyl mercaptan	C ₂ H ₆ S	75-08-1	62.13	0.23392	-0.0003206			125.26	0.1938	308.15	0.1351
146	Ethyl propionate	C ₅ H ₁₀ O ₂	105-37-3	102.13	0.2137	-0.0002515			199.25	0.1636	495.00	0.0892
147	Ethylpropyl ether	C ₅ H ₁₂ O	628-32-0	88.15	0.22717	-0.0003298			145.65	0.1791	400.07	0.0952
148	Ethyltrichlorosilane	C ₂ H ₅ Cl ₃ Si	115-21-9	163.51	0.19769	-0.00017713	-1.5448E-07		167.55	0.1637	371.05	0.1107
149	Fluorine	F ₂	7782-41-4	38.00	0.2758	-0.0016297			53.48	0.1886	130.00	0.0639
150	Fluorobenzene	C ₆ H ₅ F	462-06-6	96.10	0.20962	-0.00025034			238.15	0.1429	353.15	0.1106
151	Fluoroethane	C ₂ H ₅ F	353-36-6	48.06	0.2595	-0.0005008			129.95	0.1944	292.59	0.1130
152	Fluoromethane	CH ₃ F	593-53-3	34.03	0.445	-0.001023			131.35	0.3106	283.15	0.1553
153	Formaldehyde	CH ₂ O	50-00-0	30.03	0.37329	-0.00065			204.00	0.2407	234.00	0.2212
154	Formamide	CH ₃ NO	75-12-7	45.04	0.3847	-0.0001065			275.70	0.3553	493.00	0.3322
155	Formic acid	CH ₂ O ₂	64-18-6	46.03	0.302	-0.000108			281.45	0.2716	373.71	0.2616
156	Furan	C ₄ H ₄ O	110-00-9	68.07	0.2198	-0.00031405			187.55	0.1609	304.50	0.1242
157	Helium-4	He	7440-59-7	4.00	-0.013833	0.022913	-0.0054872	0.0004585	2.20	0.0149	4.80	0.0204
158	Heptadecane	C ₁₇ H ₃₆	629-78-7	240.47	0.20926	-0.0002215			295.13	0.1439	575.30	0.0818
159	Heptanal	C ₇ H ₁₄ O	111-71-7	114.19	0.21816	-0.0003015	1.033E-07		229.80	0.1543	553.15	0.0830
160	Heptane	C ₇ H ₁₆	142-82-5	100.20	0.215	-0.000303			182.57	0.1597	371.58	0.1024
161	Heptanoic acid	C ₇ H ₁₄ O ₂	111-14-8	130.19	0.202	-0.0002			265.83	0.1488	496.15	0.1028
162	1-Heptanol	C ₇ H ₁₆ O	111-70-6	116.20	0.2239	-0.000226			239.15	0.1699	573.15	0.0944
163	2-Heptanol	C ₇ H ₁₆ O	543-49-7	116.20	0.21134	-0.00024776			230.00	0.1544	432.90	0.1041
164	3-Heptanone	C ₇ H ₁₄ O	106-35-4	114.19	0.2026	-0.0002234			234.15	0.1503	553.15	0.0790
165	2-Heptanone	C ₇ H ₁₄ O	110-43-0	114.19	0.2108	-0.000246			238.15	0.1522	424.05	0.1065
166	1-Heptene	C ₇ H ₁₄	592-76-7	98.19	0.19664	-0.00016623	-2.5241E-07		154.12	0.1650	366.79	0.1017
167	Heptyl mercaptan	C ₇ H ₁₆ S	1639-09-4	132.27	0.2037	-0.0002252			229.92	0.1519	450.09	0.1023
168	1-Heptyne	C ₇ H ₁₂	628-71-7	96.17	0.21098	-0.00026652			192.22	0.1598	372.93	0.1116
169	Hexadecane	C ₁₆ H ₃₄	544-76-3	226.44	0.20749	-0.00021917			291.31	0.1436	560.01	0.0848
170	Hexanal	C ₆ H ₁₂ O	66-25-1	100.16	0.22196	-0.00032053	1.1554E-07		217.15	0.1578	533.15	0.0839
171	Hexane	C ₆ H ₁₄	110-54-3	86.18	0.22492	-0.0003533			177.83	0.1621	370.00	0.0942
172	Hexanoic acid	C ₆ H ₁₂ O ₂	142-62-1	116.16	0.1855	-0.000146			269.25	0.1462	603.15	0.0974
173	1-Hexanol	C ₆ H ₁₄ O	111-27-3	102.17	0.2193	-0.00022			228.55	0.1690	575.00	0.0928
174	2-Hexanol	C ₆ H ₁₄ O	626-93-7	102.18	0.21391	-0.00026042			223.00	0.1558	412.40	0.1065
175	2-Hexanone	C ₆ H ₁₂ O	591-78-6	100.16	0.21076	-0.00024			217.35	0.1586	400.85	0.1146
176	3-Hexanone	C ₆ H ₁₂ O	589-38-8	100.16	0.23493	-0.0002912			217.50	0.1716	466.00	0.0992
177	1-Hexene	C ₆ H ₁₂	592-41-6	84.16	0.19112	-0.00083519	-5.1407E-07		133.39	0.1708	336.63	0.1048
178	3-Hexyne	C ₆ H ₁₀	928-49-4	82.14	0.20996	-0.0002692			170.05	0.1642	354.35	0.1146

TABLE 2-315 Thermal Conductivity of Inorganic and Organic Liquids [W/(m·K)] (Continued)

Cmpd. no.	Name	Formula	CAS no.	Mol. wt.	C1	C2	C3	C4	C5	T_{\min} K	Thermal cond. at T_{\min}	T_{\max} K	Thermal cond. at T_{\max}
179	Hexyl mercaptan	C ₆ H ₁₄ S	111-31-9	118.24	0.2058	-0.0002324				192.62	0.1610	425.81	0.1068
180	1-Hexyne	C ₆ H ₁₀	693-02-7	82.14	0.21492	-0.0002899				141.25	0.1740	344.48	0.1151
181	2-Hexyne	C ₆ H ₁₀	764-35-2	82.14	0.2119	-0.00027048				183.65	0.1622	357.67	0.1152
182	Hydrazine	H ₄ N ₂	302-01-2	32.05	1.3675	-0.0015895				274.69	0.9309	623.15	0.3770
183	Hydrogen	H ₂	1333-74-0	2.02	-0.0917	0.017678	-0.000382	-3.3324E-06	1.0266E-07	13.95	0.0754	31.00	0.0847
184	Hydrogen bromide	HBr	10035-10-6	80.91	0.234	-0.0004636				185.15	0.1482	290.62	0.0993
185	Hydrogen chloride	HCl	7647-01-0	36.46	0.8045	-0.002102				273.15	0.2303	323.15	0.1252
186	Hydrogen cyanide	CHN	74-90-8	27.03	0.43454	-0.0007008				259.83	0.2525	298.85	0.2251
187	Hydrogen fluoride	HF	7664-39-3	20.01	0.7516	-0.0010874				189.79	0.5452	394.45	0.3227
188	Hydrogen sulfide	H ₂ S	7783-06-4	34.08	0.4842	-0.001184				193.15	0.2555	292.42	0.1380
189	Isobutyric acid	C ₄ H ₈ O ₂	79-31-2	88.11	0.21668	-0.0002556				227.15	0.1586	482.75	0.0933
190	Isopropyl amine	C ₃ H ₉ N	75-31-0	59.11	0.237	-0.000332				177.95	0.1779	305.55	0.1356
191	Malonic acid	C ₃ H ₄ O ₄	141-82-2	104.06	0.28918	-0.0002614				407.95	0.1825	644.00	0.1208
192	Methacrylic acid	C ₄ H ₆ O ₂	79-41-4	86.09	0.2306	-0.00025201				288.15	0.1580	530.00	0.0970
193	Methane	CH ₄	74-82-8	16.04	0.41768	-0.0024528	3.5588E-06			90.69	0.2245	180.00	0.0915
194	Methanol	CH ₃ O	67-56-1	32.04	0.2837	-0.000281				175.47	0.2344	337.85	0.1888
195	N-Methyl acetamide	C ₃ H ₇ NO	79-16-3	73.09	0.23743	-0.0002362				301.15	0.1663	478.15	0.1245
196	Methyl acetate	C ₃ H ₆ O ₂	79-20-9	74.08	0.2777	-0.000417				175.15	0.2047	386.15	0.1167
197	Methyl acrylene	C ₃ H ₄	74-99-7	40.06	0.23648	-0.00041639				170.45	0.1655	249.94	0.1324
198	Methyl acrylate	C ₄ H ₆ O ₂	96-33-3	86.09	0.26082	-0.0003506				196.32	0.1920	421.00	0.1132
199	Methyl amine	CH ₃ N	74-89-5	31.06	0.33446	-0.00067427	8.033E-07			179.69	0.2392	283.15	0.2079
200	Methyl benzoate	C ₈ H ₈ O ₂	93-58-3	136.15	0.22142	-0.00022759				260.75	0.1621	547.90	0.0967
201	3-Methyl-1,2-butadiene	C ₅ H ₈	598-25-4	68.12	0.1983	-0.0002822				159.53	0.1533	314.00	0.1097
202	2-Methylbutane	C ₅ H ₁₂	78-78-4	72.15	0.21246	-0.00033581				113.25	0.1744	368.13	0.0888
203	2-Methylbutanoic acid	C ₅ H ₁₀ O ₂	116-53-0	102.13	0.22284	-0.0002516				357.15	0.1330	480.90	0.1019
204	3-Methyl-1-butanol	C ₅ H ₁₂ O	123-51-3	88.15	0.17471	-0.0001256				155.95	0.1551	404.15	0.1239
205	2-Methyl-1-butene	C ₅ H ₁₀	563-46-2	70.13	0.19447	-0.0002901				135.58	0.1551	304.30	0.1062
206	2-Methyl-2-butene	C ₅ H ₁₀	513-35-9	70.13	0.19636	-0.000291				139.39	0.1558	311.70	0.1057
207	2-Methyl-1-butene-3-yne	C ₅ H ₆	78-80-8	66.10	0.20385	-0.0002874				160.15	0.1578	305.40	0.1161
208	Methylbutyl ether	C ₅ H ₁₂ O	628-28-4	88.15	0.22235	-0.0003044				157.48	0.1744	463.15	0.0814
209	Methylbutyl sulfide	C ₅ H ₁₂ S	628-29-5	104.21	0.20698	-0.00024439				175.30	0.1641	396.58	0.1101
210	3-Methyl-1-butyne	C ₅ H ₈	598-23-2	68.12	0.20348	-0.0003106				183.45	0.1465	302.15	0.1096
211	Methyl butyrate	C ₅ H ₁₀ O ₂	623-42-7	102.13	0.21748	-0.00025913				187.35	0.1689	493.15	0.0897
212	Methylchlorosilane	CH ₃ ClSi	993-00-0	80.59	0.24683	-0.00038854				139.05	0.1928	281.85	0.1373
213	Methylcyclohexane	C ₇ H ₁₄	108-87-2	98.19	0.1791	-0.0002291				273.15	0.1165	374.08	0.0934
214	1-Methylcyclohexanol	C ₇ H ₁₄ O	590-67-0	114.19	0.21558	-0.00022728				299.15	0.1476	548.80	0.0908
215	cis-2-Methylcyclohexanol	C ₇ H ₁₄ O	7443-70-1	114.19	0.21839	-0.00025776				280.15	0.1462	484.20	0.0936
216	trans-2-Methylcyclohexanol	C ₇ H ₁₄ O	7443-52-9	114.19	0.21828	-0.0002557				269.15	0.1495	484.80	0.0943
217	Methylcyclopentane	C ₆ H ₁₂	96-37-7	84.16	0.1929	-0.0002492				130.73	0.1603	344.95	0.1069
218	1-Methylcyclopentene	C ₆ H ₁₀	693-89-0	82.14	0.20023	-0.00025551				146.62	0.1627	348.64	0.1110
219	3-Methylcyclopentene	C ₆ H ₁₀	1120-62-3	82.14	0.1994	-0.00026149				115.00	0.1693	338.05	0.1110
220	Methyldichlorosilane	CH ₂ Cl ₂ Si	75-54-7	115.03	0.21956	-0.00032153				182.55	0.1609	314.70	0.1184
221	Methylethyl ether	C ₃ H ₈ O	540-67-0	60.10	0.27304	-0.0004518				160.00	0.2008	341.34	0.1188
222	Methylethyl ketone	C ₄ H ₈ O	78-93-3	72.11	0.2197	-0.0002505				186.48	0.1730	352.79	0.1313
223	Methylethyl sulfide	C ₃ H ₈ S	624-89-5	76.16	0.22136	-0.00028938				167.23	0.1730	339.80	0.1230
224	Methyl formate	C ₂ H ₄ O ₂	107-31-3	60.05	0.3246	-0.000468				174.15	0.2431	373.15	0.1500
225	Methylisobutyl ether	C ₅ H ₁₂ O	625-44-5	88.15	0.222	-0.00032217				150.00	0.1737	390.00	0.0964
226	Methylisobutyl ketone	C ₆ H ₁₂ O	108-10-1	100.16	0.2301	-0.00028899				189.15	0.1754	451.42	0.0996
227	Methyl isocyanate	C ₂ H ₃ N	624-83-9	57.05	0.2822	-0.00042037				256.15	0.1745	312.00	0.1510
228	Methylisopropyl ether	C ₄ H ₁₀ O	598-53-8	74.12	0.24154	-0.0003774				127.93	0.1933	370.00	0.1019
229	Methylisopropyl ketone	C ₅ H ₁₀ O	563-80-4	86.13	0.2332	-0.0003044				180.15	0.1784	435.90	0.1005
230	Methylisopropyl sulfide	C ₅ H ₁₀ S	1551-21-9	90.19	0.20978	-0.00026468				171.64	0.1644	357.91	0.1151
231	Methyl mercaptan	CH ₃ S	74-93-1	48.11	0.26119	-0.00038345				150.18	0.2036	279.11	0.1542
232	Methyl methacrylate	C ₅ H ₈ O ₂	80-62-6	100.12	0.2583	-0.000379				290.15	0.1483	363.45	0.1206
233	2-Methyloctanoic acid	C ₉ H ₁₈ O ₂	3004-93-1	158.24	0.20911	-0.00021852				208.20	0.1636	555.20	0.0878
234	2-Methylpentane	C ₆ H ₁₄	107-83-5	86.18	0.19334	-0.00028038				119.55	0.1598	389.25	0.0842
235	Methyl pentyl ether	C ₆ H ₁₄ O	628-80-8	102.17	0.21698	-0.00028998				176.00	0.1659	432.30	0.0916
236	2-Methylpropane	C ₄ H ₁₀	75-28-5	58.12	0.20455	-0.00036589				113.54	0.1630	400.00	0.0582

237	2-Methyl-2-propanol	C ₄ H ₁₀ O	75-65-0	74.12	0.21258	-0.00029864				298.97	0.1233	404.96	0.0916
238	2-Methyl propene	C ₄ H ₈	115-11-7	56.11	0.2802	-0.000786	6.516E-07			132.81	0.1873	395.20	0.0713
239	Methyl propionate	C ₄ H ₈ O ₂	554-12-1	88.11	0.22534	-0.0002683				185.65	0.1755	475.00	0.0979
240	Methylpropyl ether	C ₄ H ₁₀ O	557-17-5	74.12	0.24817	-0.0003774				133.97	0.1976	373.00	0.1074
241	Methylpropyl sulfide	C ₄ H ₁₀ S	3877-15-4	90.19	0.21103	-0.00025985				160.17	0.1694	368.69	0.1152
242	Methylsilane	CH ₆ Si	992-94-9	46.14	0.2774	-0.00054608				116.34	0.2139	216.25	0.1593
243	α-Methyl styrene	C ₉ H ₁₀	98-83-9	118.18	0.19657	-0.0002118				249.95	0.1436	438.65	0.1037
244	Methyl <i>tert</i> -butyl ether	C ₆ H ₁₂ O	1634-04-4	88.15	0.2253	-0.00037273	1.1728E-07			164.55	0.1671	328.18	0.1156
245	Methyl vinyl ether	C ₃ H ₆ O	107-25-5	58.08	0.28035	-0.0004646				151.15	0.2101	341.10	0.1219
246	Naphthalene	C ₁₀ H ₈	91-20-3	128.17	0.17096	-0.00010059				353.43	0.1354	646.97	0.1059
247	Neon	Ne	7440-01-9	20.18	0.2971	-0.017356	0.0005911	-0.000007421		25.00	0.1167	44.00	0.0457
248	Nitroethane	C ₂ H ₅ NO ₂	79-24-3	75.07	0.247	-0.0002614				183.63	0.1953	387.22	0.1380
249	Nitrogen	N ₂	7727-37-9	28.01	0.2654	-0.001677				63.15	0.1595	124.00	0.0575
250	Nitrogen trifluoride	F ₃ N	7783-54-2	71.00									
251	Nitromethane	CH ₃ NO ₂	75-52-5	61.04	0.3276	-0.000405				244.60	0.2285	374.35	0.1760
252	Nitrous oxide	N ₂ O	10024-97-2	44.01	0.10112					277.59	0.1011	277.59	0.1011
253	Nitric oxide	NO	10102-43-9	30.01	0.1878	0.0010293	-0.00000943			110.00	0.1869	176.40	0.0759
254	Nonadecane	C ₁₉ H ₄₀	629-92-5	268.52	0.21229	-0.00022				305.04	0.1452	603.05	0.0796
255	Nonanal	C ₉ H ₁₈ O	124-19-6	142.24	0.21523	-0.0002799	9.572E-08			255.15	0.1501	593.15	0.0829
256	Nonane	C ₉ H ₂₀	111-84-2	128.26	0.209	-0.000264				219.66	0.1510	423.97	0.0971
257	Nonanoic acid	C ₉ H ₁₈ O ₂	112-05-0	158.24	0.204	-0.0002				285.55	0.1469	528.75	0.0983
258	1-Nonanol	C ₉ H ₂₀ O	143-08-8	144.25	0.2292	-0.00023				268.15	0.1675	578.65	0.0961
259	2-Nonanol	C ₉ H ₂₀ O	628-99-9	144.26	0.20829	-0.00022922				238.15	0.1537	471.70	0.1002
260	1-Nonene	C ₉ H ₁₈	124-11-8	126.24	0.20468	-0.00025738				191.91	0.1553	420.02	0.0966
261	Nonyl mercaptan	C ₉ H ₂₀ S	1455-21-6	160.32	0.20244	-0.00021343				253.05	0.1484	492.95	0.0972
262	1-Nonyne	C ₉ H ₁₆	3452-09-3	124.22	0.20954	-0.00024588				223.15	0.1547	423.85	0.1053
263	Octadecane	C ₁₈ H ₃₈	593-45-3	254.49	0.2137	-0.0002252				301.31	0.1458	589.86	0.0809
264	Octanal	C ₈ H ₁₆ O	124-13-0	128.21	0.20143	-0.00021102				246.00	0.1495	573.15	0.0805
265	Octane	C ₈ H ₁₈	111-65-9	114.23	0.2156	-0.00029483				216.38	0.1518	398.83	0.0980
266	Octanoic acid	C ₈ H ₁₆ O ₂	124-07-2	144.21	0.203	-0.0002				289.65	0.1451	512.85	0.1004
267	1-Octanol	C ₈ H ₁₈ O	111-87-5	130.23	0.2316	-0.0002407				257.65	0.1696	570.15	0.0944
268	2-Octanol	C ₈ H ₁₈ O	123-96-6	130.23	0.20955	-0.00023733				241.55	0.1522	452.90	0.1021
269	2-Octanone	C ₈ H ₁₆ O	111-13-7	128.21	0.2132	-0.0002494				252.85	0.1501	499.00	0.0887
270	3-Octanone	C ₈ H ₁₆ O	106-68-3	128.21	0.21732	-0.00024969				255.55	0.1535	440.65	0.1073
271	1-Octene	C ₈ H ₁₆	111-66-0	112.21	0.20467	-0.0002675				171.45	0.1588	394.41	0.0992
272	Octyl mercaptan	C ₈ H ₁₈ S	111-88-6	146.29	0.2012	-0.0002142				223.95	0.1532	472.19	0.1001
273	1-Octyne	C ₈ H ₁₄	629-05-0	110.20	0.2095	-0.00025334				193.55	0.1605	399.35	0.1083
274	Oxalic acid	C ₂ H ₂ O ₄	144-62-7	90.03	0.3074	-0.00028101				462.65	0.1774	643.20	0.1267
275	Oxygen	O ₂	7782-44-7	32.00	0.2741	-0.00138				60.00	0.1913	150.00	0.0671
276	Ozone	O ₃	10028-15-6	48.00	0.17483	0.00075288	-2.5228E-06			77.35	0.2180	161.85	0.2306
277	Pentadecane	C ₁₅ H ₃₂	629-62-9	212.41	0.20649	-0.00021911				283.07	0.1445	543.84	0.0873
278	Pentanal	C ₅ H ₁₀ O	110-62-3	86.13	0.22697	-0.00033227	1.177E-07			182.00	0.1704	513.15	0.0875
279	Pentane	C ₅ H ₁₂	109-66-0	72.15	0.2537	-0.000576	0.000000344			143.42	0.1782	445.00	0.0655
280	Pentanoic acid	C ₅ H ₁₀ O ₂	109-52-4	102.13	0.1848	-0.0001434				239.15	0.1505	458.65	0.1190
281	1-Pentanol	C ₅ H ₁₂ O	71-41-0	88.15	0.2006	-0.0001603				273.15	0.1568	353.15	0.1440
282	2-Pentanol	C ₅ H ₁₂ O	6032-29-7	88.15	0.21875	-0.00027849				200.00	0.1631	392.20	0.1095
283	2-Pentanone	C ₅ H ₁₀ O	107-87-9	86.13	0.2161	-0.00024866				196.29	0.1673	375.46	0.1227
284	3-Pentanone	C ₅ H ₁₀ O	96-22-0	86.13	0.21569	-0.00024081				234.18	0.1593	375.14	0.1254
285	1-Pentene	C ₅ H ₁₀	109-67-1	70.13	0.21361	-0.00030777				108.02	0.1804	303.22	0.1203
286	2-Pentyl mercaptan	C ₅ H ₁₂ S	2084-19-7	104.21	0.20597	-0.00024518				160.75	0.1666	385.15	0.1115
287	Pentyl mercaptan	C ₅ H ₁₂ S	110-66-7	104.21	0.2086	-0.00024536				197.45	0.1602	399.79	0.1105
288	1-Pentyne	C ₅ H ₈	627-19-0	68.12	0.22102	-0.000322				167.45	0.1671	313.33	0.1201
289	2-Pentyne	C ₅ H ₈	627-21-4	68.12	0.21282	-0.0002856				163.83	0.1660	329.27	0.1188
290	Phenanthrene	C ₁₄ H ₁₀	85-01-8	178.23	0.13753	-0.000025247				372.38	0.1281	610.03	0.1221
291	Phenol	C ₆ H ₆ O	108-95-2	94.11	0.18831	-0.0001				314.06	0.1569	454.99	0.1428
292	Phenyl isocyanate	C ₇ H ₅ NO	103-71-9	119.12	0.16326	-0.00017777				243.15	0.1200	439.43	0.0851
293	Phthalic anhydride	C ₈ H ₄ O ₃	85-44-9	148.12	0.22946	-0.00021345				404.15	0.1432	557.65	0.1104
294	Propadiene	C ₃ H ₄	463-49-0	40.06	0.23081	-0.0004078				136.87	0.1750	238.65	0.1335
295	Propane	C ₃ H ₈	74-98-6	44.10	0.26755	-0.00066457	2.774E-07			85.47	0.2128	350.00	0.0689
296	1-Propanol	C ₃ H ₈ O	71-23-8	60.10	0.2203	-0.0002155				200.00	0.1772	370.35	0.1405
297	2-Propanol	C ₃ H ₈ O	67-63-0	60.10	0.20161	-0.00021529				185.26	0.1617	425.00	0.1101
298	Propenylcyclohexene	C ₉ H ₁₄	13511-13-2	122.21	0.1831	-0.00020275				199.00	0.1428	431.65	0.0956
299	Propionaldehyde	C ₃ H ₆ O	123-38-6	58.08	0.2498	-0.00030075				170.00	0.1987	453.15	0.1135

TABLE 2-315 Thermal Conductivity of Inorganic and Organic Liquids [W/(m·K)] (Concluded)

Cmpd. no.	Name	Formula	CAS no.	Mol. wt.	C1	C2	C3	C4	C5	T_{\min} , K	Thermal cond. at T_{\min}	T_{\max} , K	Thermal cond. at T_{\max}
300	Propionic acid	C ₃ H ₆ O ₂	79-09-4	74.08	0.1954	-0.000164				252.45	0.1540	543.15	0.1063
301	Propionitrile	C ₃ H ₅ N	107-12-0	55.08	0.26626	-0.0003307				180.26	0.2067	370.50	0.1437
302	Propyl acetate	C ₅ H ₁₀ O ₂	109-60-4	102.13	0.2332	-0.0003096				178.15	0.1780	434.82	0.0986
303	Propyl amine	C ₃ H ₉ N	107-10-8	59.11	0.2632	-0.0004278	0.000000412			188.36	0.1972	333.15	0.1664
304	Propylbenzene	C ₉ H ₁₂	103-65-1	120.19	0.18707	-0.00019846				173.55	0.1526	583.15	0.0713
305	Propylene	C ₃ H ₆	115-07-1	42.08	0.24719	-0.00048824				87.89	0.2043	340.49	0.0809
306	Propyl formate	C ₄ H ₈ O ₂	110-74-7	88.11	0.2247	-0.000264				180.25	0.1771	483.15	0.0971
307	2-Propyl mercaptan	C ₃ H ₆ S	75-33-2	76.16	0.21706	-0.00028952				142.61	0.1758	325.71	0.1228
308	Propyl mercaptan	C ₃ H ₇ S	107-03-9	76.16	0.2202	-0.00028535				159.95	0.1746	340.87	0.1229
309	1,2-Propylene glycol	C ₃ H ₈ O ₂	57-55-6	76.09	0.2152	-0.0000497				213.15	0.2046	460.75	0.1923
310	Quinone	C ₆ H ₄ O ₂	106-51-4	108.09	0.26524	-0.00028676				388.85	0.1537	545.00	0.1090
311	Silicon tetrafluoride	F ₄ Si	7783-61-1	104.08									
312	Styrene	C ₈ H ₈	100-42-5	104.15	0.20215	-0.0002201				242.54	0.1488	418.31	0.1101
313	Succinic acid	C ₄ H ₆ O ₄	110-15-6	118.09	0.28215	-0.0002585				460.65	0.1631	642.00	0.1162
314	Sulfur dioxide	O ₂ S	7446-09-5	64.06	0.38218	-0.0006254				197.67	0.2586	400.00	0.1320
315	Sulfur hexafluoride	F ₆ S	2551-62-4	146.06	0.2544	-0.0006595				223.15	0.1072	318.69	0.0442
316	Sulfur trioxide	O ₃ S	7446-11-9	80.06	0.92882	-0.0030803	0.00000266			289.95	0.2593	481.47	0.0624
317	Terephthalic acid	C ₈ H ₆ O ₄	100-21-0	166.13									
318	<i>o</i> -Terphenyl	C ₁₈ H ₁₄	84-15-1	230.30	0.16853	-0.00010817				329.35	0.1329	723.15	0.0903
319	Tetradecane	C ₁₄ H ₃₀	629-59-4	198.39	0.20293	-0.00021798				279.01	0.1421	526.73	0.0881
320	Tetrahydrofuran	C ₄ H ₈ O	109-99-9	72.11	0.19428	-0.000249				164.65	0.1533	339.12	0.1098
321	1,2,3,4-Tetrahydronaphthalene	C ₁₀ H ₁₂	119-64-2	132.20	0.14563	-0.0000536				237.38	0.1329	480.77	0.1199
322	Tetrahydrothiophene	C ₄ H ₈ S	110-01-0	88.17	0.20414	-0.00021217				176.98	0.1666	394.27	0.1205
323	2,2,3,3-Tetramethylbutane	C ₈ H ₁₈	594-82-1	114.23	0.17835	-0.00023704				373.96	0.0897	426.00	0.0774
324	Thiophene	C ₄ H ₄ S	110-02-1	84.14	0.20571	-0.00020028				234.94	0.1587	357.31	0.1342
325	Toluene	C ₇ H ₈	108-88-3	92.14	0.20463	-0.00024252				178.18	0.1614	474.85	0.0895
326	1,1,2-Trichloroethane	C ₂ H ₃ Cl ₃	79-00-5	133.40	0.20731	-0.00024997				236.50	0.1482	482.00	0.0868
327	Tridecane	C ₁₃ H ₂₈	629-50-5	184.36	0.20447	-0.00022612				267.76	0.1439	508.62	0.0895
328	Triethyl amine	C ₆ H ₁₅ N	121-44-8	101.19	0.1918	-0.0002453				158.45	0.1529	483.15	0.0733
329	Trimethyl amine	C ₃ H ₉ N	75-50-3	59.11	0.23813	-0.00038397				156.08	0.1782	276.02	0.1322
330	1,2,3-Trimethylbenzene	C ₉ H ₁₂	526-73-8	120.19	0.18854	-0.0001963				247.79	0.1399	449.27	0.1004
331	1,2,4-Trimethylbenzene	C ₉ H ₁₂	95-63-6	120.19	0.19216	-0.0002105				229.33	0.1439	442.53	0.0990
332	2,2,4-Trimethylpentane	C ₈ H ₁₈	540-84-1	114.23	0.1659	-0.00022686				165.78	0.1283	372.39	0.0814
333	2,3,3-Trimethylpentane	C ₈ H ₁₈	560-21-4	114.23	0.16815	-0.00020535				172.22	0.1328	387.91	0.0885
334	1,3,5-Trinitrobenzene	C ₆ H ₃ N ₃ O ₆	99-35-4	213.10	0.18421	-0.00016097				398.40	0.1201	629.60	0.0829
335	2,4,6-Trinitrotoluene	C ₇ H ₅ N ₃ O ₆	118-96-7	227.13	-1.5128	0.0079553	-0.000010066			357.20	0.0445	393.20	0.0590
336	Undecane	C ₁₁ H ₂₄	1120-21-4	156.31	0.20515	-0.00023933				247.57	0.1459	469.08	0.0929
337	1-Undecanol	C ₁₁ H ₂₄ O	112-42-5	172.31	0.21211	-0.00021815				288.45	0.1492	561.20	0.0897
338	Vinyl acetate	C ₄ H ₆ O ₂	108-05-4	86.09	0.256	-0.0003542				180.35	0.1921	410.00	0.1108
339	Vinyl acetylene	C ₄ H ₄	689-97-4	52.07	0.22838	-0.00035173				173.15	0.1675	278.25	0.1305
340	Vinyl chloride	C ₂ H ₃ Cl	75-01-4	62.50	0.2333	-0.00039223				119.36	0.1865	345.60	0.0977
341	Vinyl trichlorosilane	C ₂ H ₃ Cl ₃ Si	75-94-5	161.49	0.21831	-0.00029122				178.35	0.1664	434.52	0.0918
342	Water	H ₂ O	7732-18-5	18.02	-0.432	0.0057255	-0.000008078	1.861E-09		273.16	0.5672	633.15	0.4272
343	<i>m</i> -Xylene	C ₈ H ₁₀	108-38-3	106.17	0.20044	-0.00023544				225.30	0.1474	413.10	0.1032
344	<i>o</i> -Xylene	C ₈ H ₁₀	95-47-6	106.17	0.19989	-0.0002299				247.98	0.1429	417.58	0.1039
345	<i>p</i> -Xylene	C ₈ H ₁₀	106-42-3	106.17	0.20003	-0.00023573				286.41	0.1325	413.10	0.1027

The liquid thermal conductivity is calculated by

$$k = C1 + C2T + C3T^2 + C4T^3 + C5T^4.$$

where k is the thermal conductivity in W/(m·K) and T is the temperature in K. Thermal conductivities are at either 1 atm or the vapor pressure, whichever is higher. All substances are listed by chemical family in Table 2-6 and by formula in Table 2-7.

Values in this table were taken from the Design Institute for Physical Properties (DIPPR) of the American Institute of Chemical Engineers (AIChE), copyright 2007 AIChE and reproduced with permission of AIChE and of the DIPPR Evaluated Process Design Data Project Steering Committee. Their source should be cited as R. L. Rowley, W. V. Wilding, J. L. Oscarson, Y. Yang, N. A. Zundel, T. E. Daubert, R. P. Danner, DIPPR® Data Compilation of Pure Chemical Properties, Design Institute for Physical Properties, AIChE, New York (2007).

The number of digits provided for values at T_{\min} and T_{\max} was chosen for uniformity of appearance and formatting; these do not represent the uncertainties of the physical quantities, but are the result of calculations from the standard thermophysical property formulations within a fixed format.

TABLE 2-316 Transport Properties of Selected Gases at Atmospheric Pressure*

Substance	Thermal conductivity, W/(m·K) Temperature, K					Viscosity, 10 ⁻⁴ Pa·s Temperature, K					Prandtl number, dimensionless Temperature, K			
	250	300	400	500	600	250	300	400	500	600	250	300	400	500
Acetone	0.0080	0.0115	0.0201	0.0310			0.077	0.101	0.128	0.156				
Acetylene	0.0162	0.0213	0.0332	0.0452	0.0561		0.104	0.135	0.164					
Benzene	0.0077	0.0104	0.0195	0.0335	0.0524		0.076	0.101	0.127	0.154				
Bromine	0.0038	0.0048	0.0067					0.203	0.260	0.291				
CCl ₄	0.0053	0.0067	0.0099	0.0126			0.101	0.131	0.162	0.191				
Chlorine	0.0071	0.0089	0.0124	0.0156	0.0190		0.136	0.178	0.218	0.259				
Deuterium	0.122	0.141	0.176			0.111	0.126	0.153	0.178	0.201				
Propylene	0.0114	0.0168	0.0226	0.0430	0.0580	0.073	0.087	0.115	0.141		0.860	0.797	0.762	
R 11		0.0078	0.0119			0.094	0.110	0.144				0.814	0.761	
R 12	0.0072	0.0097	0.0151	0.0208		0.108	0.126	0.162			0.827	0.781	0.745	0.708
R 13	0.0091	0.0121	0.0185	0.0248		0.123	0.145	0.190			0.796	0.766	0.759	0.757
R 21		0.0088	0.0135	0.0181		0.100	0.115	0.154				0.779	0.773	
R 22	0.0080	0.0109	0.0170	0.0230	0.0290	0.109	0.129	0.168			0.820	0.771	0.760	
SO ₂	0.0078	0.0096	0.0143	0.0200	0.0256		0.129	0.175	0.217	0.256				

*An approximate interpolation scheme is to plot the logarithm of the viscosity or the thermal conductivity versus the logarithm of the absolute temperature. At 250 K the viscosity of gaseous argon is to be read as 1.95×10^{-5} Pa·s = 0.0000195 N·s/m².

TABLE 2-317 Lower and Upper Flammability Limits, Flash Point, and Autoignition Temperature for Selected Hydrocarbons

Compound	CAS no.	Formula	LFL	LFL rating	UFL	UFL rating	Flash point °C	Flash point rating	Autoignition T °C	Autoignition rating
<i>Paraffin hydrocarbons</i>										
Methane	74828	CH ₄	5.00	12	15.00	12	-187.15	4	536.85	11
Ethane	74840	C ₂ H ₆	2.90	12	13.00	12	-130.15	4	471.85	11
Propane	74986	C ₃ H ₈	2.00	12	9.50	12	-104.00	4	449.85	11
Butane	106978	C ₄ H ₁₀	1.50	12	9.00	12	-69.00	6	287.55	11
Isobutane	75285	C ₄ H ₁₀	1.80	12	8.40	12	-82.59	5	460.00	11
Pentane	109660	C ₅ H ₁₂	1.30	14	8.00	14	-40.00	11	242.85	11
Isopentane	78784	C ₅ H ₁₂	1.30	12	8.00	12	-56.00	11	420.00	11
2,2-Dimethylpropane	463821	C ₅ H ₁₂	1.40	11	7.50	11	-72.15	4	450.00	11
Hexane	1100543	C ₆ H ₁₄	1.05	13	7.68	13	-21.65	11	224.85	11
Heptane	142825	C ₇ H ₁₆	1.00	14	7.00	14	-4.15	11	203.85	11
2,3-Dimethylpentane	565593	C ₇ H ₁₆	1.12	4	6.75	4	-6.00	4	335.00	11
Octane	111659	C ₈ H ₁₈	0.80	12	6.50	12	12.85	11	205.85	11
Isooctane	540841	C ₈ H ₁₈	0.95	11	6.00	11	-12.22	11	411.00	11
Nonane	111842	C ₉ H ₂₀	0.70	12	5.60	12	30.85	11	204.85	11
Decane	124185	C ₁₀ H ₂₂	0.70	12	5.40	12	45.85	11	200.85	11
<i>Olefins</i>										
Ethylene	74851	C ₂ H ₄	2.70	11	36.00	11	-146.15	4	450.00	11
Propylene	115071	C ₃ H ₆	2.00	11	11.00	11	-108.15	11	455.00	11
1-Butene	106989	C ₄ H ₈	1.60	11	9.30	11	-79.81	5	383.85	11
2-Butene	107017	C ₄ H ₈	1.70	8	9.70	8	<-34.00	1	325.00	8
1-Pentene	109671	C ₅ H ₁₀	1.50	11	8.70	11	-18.15	11	272.85	11
<i>Acetylenes</i>										
Acetylene	74862	C ₂ H ₂	2.50	12	80.00	12	-18.15	11	305.00	11
Vinylacetylene	689974	C ₄ H ₄	1.80	6	100.00	4	-66.15	4	310.00	6
Methylacetylene	613878	C ₃ H ₄	1.70	11	16.80	11	-86.15	4	340.00	11
<i>Aromatics</i>										
Benzene	71432	C ₆ H ₆	1.40	11	7.10	11	-11.15	11	561.85	11
Toluene	108583	C ₇ H ₈	1.20	11	7.10	11	4.85	11	535.85	11
o-Xylene	95476	C ₈ H ₁₀	1.00	11	6.00	11	16.85	11	463.85	11
Ethylbenzene	100414	C ₈ H ₁₀	1.00	11	6.70	11	15.00	11	431.85	11
Isopropylbenzene (Cumene)	98828	C ₈ H ₁₀	0.88	12	6.50	12	31.00	12	423.85	11
Anthracene	120127	C ₁₄ H ₁₀	0.65	8	5.46	4	120.85	4	540.00	8
<i>Cyclic hydrocarbons</i>										
Cyclopropane	75194	C ₃ H ₆	2.40	12	10.40	12	92.00	4	497.85	11
Furan	110009	C ₄ H ₄ O	2.30	11	14.30	11	-36.15	11	510.00	6
Cyclopentadiene	542927	C ₅ H ₆	1.62	4	7.70	4	-28.15	4	429.85	4
Cyclohexane	110827	C ₆ H ₁₂	1.30	8	7.80	8	-18.15	4	245.00	11
Methylcyclohexane	108872	C ₇ H ₁₄	1.10	11	6.70	11	-6.00	11	250.00	11
Phenol	108952	C ₆ H ₆ O	1.52	6	8.76	6	79.85	11	714.85	11
Dicyclopentadiene	77736	C ₁₀ H ₁₂	1.00	4	6.76	4	26.00	4	505.00	5
<i>Alcohols</i>										
Methyl alcohol	67561	CH ₃ O	7.30	11	36.00	11	10.85	11	463.85	11
Ethyl alcohol	64175	C ₂ H ₅ O	3.30	8	19.00	8	12.85	4	356.00	8
2-propen-1-ol	107186	C ₃ H ₆ O	2.50	11	18.00	11	20.85	11	377.85	11
n-Propyl alcohol	71238	C ₃ H ₇ O	2.10	8	13.50	8	24.63	5	440.00	8
Isopropyl alcohol	67630	C ₃ H ₇ O	2.20	8	12.00	8	21.85	4	399.00	5
n-Butyl alcohol	71363	C ₄ H ₁₀ O	1.40	8	11.20	8	37.19	5	359.00	5
2-Butanol	78922	C ₄ H ₁₀ O	1.68	4	9.80	4	23.85	4	405.00	8
2-Methyl-1-propanol	78831	C ₄ H ₁₀ O	1.70	11	10.90	11	27.85	11	408.00	11
2-Methyl-2-propanol	75650	C ₄ H ₁₀ O	1.90	4	9.00	4	10.85	4	480.00	8
Cyclohexanol	108930	C ₆ H ₁₂ O	1.20	11	9.30	10	67.85	11	300.00	11
<i>Aldehydes</i>										
Formaldehyde	50000	CH ₂ O	7.00	11	73.00	11	-52.96	3	430.00	11
Acetaldehyde	75070	C ₂ H ₄ O	4.00	11	60.00	11	-38.15	11	175.00	8
Acrolein	107028	C ₃ H ₄ O	2.80	11	31.00	11	-26.00	11	233.85	11
Propionaldehyde	123386	C ₃ H ₆ O	2.60	11	16.10	11	-30.00	11	206.85	11
Crönic aldehyde	123739	C ₄ H ₆ O	2.10	11	15.50	11	8.00	11	231.85	11
Crotonaldehyde	4170303	C ₄ H ₆ O	2.10	8	15.50	8	13.00	6	232.00	5
Isobutyraldehyde	78842	C ₄ H ₈ O	1.60	4	10.60	4	-18.15	4	204.85	11
Butyraldehyde	123728	C ₄ H ₈ O	2.50	8	12.50	4	-7.15	4	215.76	5
2-Furancarboxaldehyde	98011	C ₅ H ₄ O ₂	2.10	8	19.30	4	72.85	4	316.00	5
<i>Ethers</i>										
Dimethyl ether	115106	C ₂ H ₆ O	3.30	11	27.30	11	-41.15	11	350.00	11
Vinyl methyl ether	107255	C ₃ H ₆ O	2.60	11	39.00	11	-56.00	11	287.00	11
Diethyl ether	60297	C ₄ H ₁₀ O	1.90	11	48.00	11	-45.00	11	160.00	11
Diphenyl ether	101848	C ₁₂ H ₁₀ O	0.80	11	1.50	11	95.85	11	618.00	11
<i>Ketones</i>										
Acetone	67641	C ₃ H ₆ O	2.60	8	13.00	8	-18.15	4	465.00	8
Methylethyl ketone	78933	C ₄ H ₈ O	1.80	11	10.00	11	-6.15	11	515.85	11
Methyl phenyl ketone	98862	C ₈ H ₈ O	1.10	8	6.89	4	82.00	8	571.11	11
<i>Acids</i>										
Acetic acid	64197	C ₂ H ₄ O ₂	4.05	8	16.00	4	42.85	11	426.85	11
Hydrocyanic acid	74908	HCN	6.00	11	41.00	11	-18.00	6	537.85	11
Formic acid	64186	CH ₂ O ₂	15.70	10	38.00	11	48.00	12	480.00	11
<i>Esters</i>										
Methyl formate	107313	C ₂ H ₄ O ₂	5.90	11	20.00	11	-19.15	11	455.85	11
Ethyl formate	109944	C ₃ H ₆ O ₂	2.80	8	16.00	8	-19.50	6	455.00	8

Methyl acetate	79209	C ₄ H ₈ O ₂	3.20	8	16.00	8	-15.50	6	476.85	14
Vinyl acetate	108054	C ₄ H ₆ O ₂	2.60	11	13.40	11	-8.15	11	426.85	11
Ethyl acetate	141786	C ₄ H ₈ O ₂	2.20	11	11.40	11	-4.15	11	426.85	11
Propyl acetate	109604	C ₅ H ₁₀ O ₂	2.05	5	8.00	4	-	-	450.00	4
Isopropyl acetate	108214	C ₅ H ₁₀ O ₂	2.00	5	7.80	4	4.50	6	460.00	4
Butyl acetate	123864	C ₆ H ₁₂ O ₂	1.70	8	7.60	8	21.85	4	425.00	8
Isobutyl acetate	110190	C ₆ H ₁₂ O ₂	1.30	11	10.50	11	17.85	11	422.85	11
Anyl acetate	628637	C ₇ H ₁₄ O ₂	1.10	11	7.50	11	23.00	11	360.00	11
<i>Inorganic</i>										
Hydrogen	1333740	H ₂	4.00	11	75.00	11	-260.15	4	400.00	11
Ammonia	7664417	NH ₃	16.00	11	25.00	11	Gas	3	650.85	11
Cyanogen	460195	C ₂ N ₂	6.00	11	32.00	11	-62.15	4	661.85	4
<i>Oxides</i>										
Carbon monoxide	630380	CO	12.50	11	74.00	11	-206.15	4	608.85	11
Ethylene oxide	75218	C ₂ H ₄ O	3.00	11	100.00	8	-19.81	5	428.85	11
Propylene oxide	75569	C ₃ H ₆ O	2.10	11	21.50	11	-37.15	11	465.00	11
Dioxan	123911	C ₄ H ₈ O ₂	2.00	11	22.00	11	11.85	11	180.00	11
Mesityl oxide	141797	C ₈ H ₁₀ O	1.30	4	7.20	4	30.00	4	344.85	4
Styrene oxide	100425	C ₈ H ₈ O	1.10	11	-	-	31.85	11	463.00	11
<i>Peroxides</i>										
Di-tert-butyl peroxide	110054	C ₈ H ₁₈ O ₂	1.00	6	7.05	4	1.00	-	79.85	4
<i>Sulfur containing</i>										
Carbon disulfide	75150	CS ₂	1.30	11	50.00	11	-30.00	-	90.00	11
Hydrogen sulfide	7783064	H ₂ S	4.30	14	45.50	14	-107.15	-	260.00	11
Carbon oxysulfide	463581	COS	12.00	11	29.00	11	-88.15	-	250.00	6
Dimethyl sulfide	75183	C ₂ H ₆ S	2.20	8	19.70	8	-36.00	-	205.00	11
<i>Chlorine containing</i>										
Methyl chloride	74873	CH ₃ Cl	8.10	11	17.20	11	-70.15	4	631.85	11
Ethyl chloride	75003	C ₂ H ₅ Cl	3.80	11	15.40	11	-50.00	11	518.85	11
Isopropyl chloride	75296	C ₃ H ₇ Cl	2.80	11	10.70	11	-35.00	11	592.85	11
Ethylene dichloride	107062	C ₂ H ₄ Cl ₂	6.20	11	16.00	6	12.85	11	412.85	11
Propylene dichloride	75875	C ₃ H ₄ Cl ₂	3.40	11	14.50	11	13.00	11	556.85	11
Dichloromethane	75092	CH ₂ Cl ₂	14.00	6	22.00	4	-9.15	4	615.00	11
2-Chloroethanol	107073	C ₂ H ₅ ClO	4.90	11	15.90	11	40.55	12	425.00	11
Trichloroethylene	79016	C ₂ HCl ₃	8.00	11	40.00	5	32.22	11	410.00	11
Hexachlorobutadiene	87683	C ₄ Cl ₆	2.90	1	15.70	1	121.85	10	610.00	11
Vinyl chloride	75014	C ₂ H ₃ Cl	3.60	11	33.00	11	-78.15	11	471.85	11
Chlorobenzene	108907	C ₆ H ₅ Cl	1.30	11	7.10	11	31.85	11	637.85	11
Benzyl chloride	100447	C ₇ H ₇ Cl	1.10	11	8.00	4	60.00	11	585.00	11
<i>Bromides</i>										
Methyl bromide	74839	CH ₃ Br	10.00	11	15.00	11	-48.15	4	537.22	11
<i>Glycols</i>										
Ethylene glycol	107211	C ₂ H ₆ O ₂	3.20	11	33.00	10	110.85	11	395.85	11
Diethylene glycol	111466	C ₄ H ₁₀ O ₃	2.00	10	17.10	10	123.85	11	223.85	11
Triethylene glycol	112276	C ₆ H ₁₄ O ₄	0.90	11	9.20	11	156.00	11	370.85	11
<i>Amines</i>										
Methyl amine	74895	CH ₃ N	4.90	11	20.70	11	-62.00	7	430.00	11
Ethyl amine	75047	C ₂ H ₅ N	3.50	8	14.00	8	-39.00	6	383.85	7
Dimethyl amine	124403	C ₂ H ₇ N	2.80	11	14.40	11	-57.00	7	400.00	11
Isopropylamine	75310	C ₃ H ₇ N	2.00	11	10.40	11	-37.00	11	400.00	12
Trimethylamine	75503	C ₃ H ₉ N	2.00	11	11.60	11	-7.15	11	190.00	11
Isopropylamine	75310	C ₃ H ₉ N	2.00	11	10.40	11	-37.00	11	400.00	12
Allylamine	107119	C ₃ H ₇ N	2.20	11	22.00	11	-29.80	11	373.85	11
Diethylamine	109897	C ₄ H ₁₁ N	1.70	12	10.10	12	-30.00	11	310.00	12
tert-Butylamine	75349	C ₄ H ₁₁ N	1.70	11	8.90	11	-9.00	11	380.00	5
Triethylamine	121448	C ₆ H ₁₅ N	1.20	11	8.00	11	-12.15	12	231.85	10
Cyclohexylamine	108918	C ₆ H ₁₃ N	0.66	11	8.42	4	31.00	13	293.00	11
Monoethanolamine	141435	C ₂ H ₇ NO	3.02	4	24.06	4	85.00	11	410.00	5
Diethanolamine	111422	C ₄ H ₁₁ NO ₂	1.69	4	16.25	4	151.85	11	661.85	11
Dimethylethanolamine	108010	C ₄ H ₁₁ NO	1.67	4	11.36	4	41.00	11	295.00	11
<i>Miscellaneous</i>										
Acrylonitrile	107131	C ₃ H ₃ N	2.42	11	17.34	13	0.00	11	480.85	11
Aniline	62533	C ₆ H ₅ N	1.30	11	11.00	11	70.00	11	616.85	11
Diborane	19287457	B ₂ H ₆	0.90	11	98.00	11	-148.15	4	51.85	11
Methyl methacrylate	80626	C ₅ H ₈ O ₂	2.10	11	12.50	11	11.00	11	435.85	11
Naphia	8030306	-	0.80	8	5.00	8	-6.00	4	290.00	4
Styrene	100425	C ₈ H ₈	1.10	11	6.10	11	31.85	11	490.00	4
Biphenyl	92524	C ₁₂ H ₁₀	0.60	11	5.80	11	113.00	11	540.00	11
Methylacrylate	96333	C ₅ H ₈ O ₂	2.80	4	25.00	4	5.85	4	468.00	5
Phthalic anhydride	85449	C ₈ H ₆ O ₃	1.70	8	10.50	4	151.85	6	583.85	11

LFL and UFL are lower and upper flammability limits respectively in volume percent fuel in air. Values in this table were taken from the Design Institute for Physical Properties (DIPPR) of the American Institute of Chemical Engineers (AIChE), copyright 2007 AIChE and reproduced with permission of AIChE, the DIPPR Environmental Safety Property Data and Estimations Steering Committee and of the DIPPR Evaluated Process Design Data Project Steering Committee. Their source should be cited as T. N. Rogers, D. A. Zei, R. L. Rowley, W. V. Wilding, J. L. Oscarson, Y. Yang, N. A. Zundel, T. E. Daubert, T. E. P. Danner, DIPPR® Data Compilation of Pure Chemical Properties, Design Institute for Physical Properties, AIChE, New York (2007). Flammability limits are from B. Lewis and G. Von Elbe, *Combustion, Flames and Explosions of Gases*, New York: Harcourt Brace Jovanovich (1987). Flash point data are from N. I. Sax, *Dangerous Properties of Industrial Materials*, 6th ed., New York: Van Nostrand Reinhold (1984). Autoignition data are from I. Glassman, *Combustion*, 3d ed., New York: Academic Press (1996). The ratings reflect DIPPR® ESP's effort to provide a critical evaluation and quality assessment of each data point with 15 being the highest score possible. The rating is not directly correlated with the estimated experimental uncertainty.

2-448 PHYSICAL AND CHEMICAL DATA

TABLE 2-318 Viscosities of Liquids: Coordinates for Use with Fig. 2-32

Liquid	X	Y	Liquid	X	Y
Acetaldehyde	15.2	4.8	Freon-113	12.5	11.4
Acetic acid, 100%	12.1	14.2	Glycerol, 100%	2.0	30.0
Acetic acid, 70%	9.5	17.0	Glycerol, 50%	6.9	19.6
Acetic anhydride	12.7	12.8	Heptane	14.1	8.4
Acetone, 100%	14.5	7.2	Hexane	14.7	7.0
Acetone, 35%	7.9	15.0	Hydrochloric acid, 31.5%	13.0	16.6
Acetonitrile	14.4	7.4	Iodobenzene	12.8	15.9
Acrylic acid	12.3	13.9	Isobutyl alcohol	7.1	18.0
Allyl alcohol	10.2	14.3	Isobutyric acid	12.2	14.4
Allyl bromide	14.4	9.6	Isopropyl alcohol	8.2	16.0
Allyl iodide	14.0	11.7	Isopropyl bromide	14.1	9.2
Ammonia, 100%	12.6	2.0	Isopropyl chloride	13.9	7.1
Ammonia, 26%	10.1	13.9	Isopropyl iodide	13.7	11.2
Amyl acetate	11.8	12.5	Kerosene	10.2	16.9
Amyl alcohol	7.5	18.4	Linseed oil, raw	7.5	27.2
Aniline	8.1	18.7	Mercury	18.4	16.4
Anisole	12.3	13.5	Methanol, 100%	12.4	10.5
Arsenic trichloride	13.9	14.5	Methanol, 90%	12.3	11.8
Benzene	12.5	10.9	Methanol, 40%	7.8	15.5
Brine, CaCl ₂ , 25%	6.6	15.9	Methyl acetate	14.2	8.2
Brine, NaCl, 25%	10.2	16.6	Methyl acrylate	13.0	9.5
Bromine	14.2	13.2	Methyl <i>i</i> -butyrate	12.3	9.7
Bromotoluene	20.0	15.9	Methyl <i>n</i> -butyrate	13.2	10.3
Butyl acetate	12.3	11.0	Methyl chloride	15.0	3.8
Butyl acrylate	11.5	12.6	Methyl ethyl ketone	13.9	8.6
Butyl alcohol	8.6	17.2	Methyl formate	14.2	7.5
Butyric acid	12.1	15.3	Methyl iodide	14.3	9.3
Carbon dioxide	11.6	0.3	Methyl propionate	13.5	9.0
Carbon disulfide	16.1	7.5	Methyl propyl ketone	14.3	9.5
Carbon tetrachloride	12.7	13.1	Methyl sulfide	15.3	6.4
Chlorobenzene	12.3	12.4	Napthalene	7.9	18.1
Chloroform	14.4	10.2	Nitric acid, 95%	12.8	13.8
Chlorosulfonic acid	11.2	18.1	Nitric acid, 60%	10.8	17.0
Chlorotoluene, ortho	13.0	13.3	Nitrobenzene	10.6	16.2
Chlorotoluene, meta	13.3	12.5	Nitrogen dioxide	12.9	8.6
Chlorotoluene, para	13.3	12.5	Nitrotoluene	11.0	17.0
Cresol, meta	2.5	20.8	Octane	13.7	10.0
Cyclohexanol	2.9	24.3	Octyl alcohol	6.6	21.1
Cyclohexane	9.8	12.9	Pentachloroethane	10.9	17.3
Dibromomethane	12.7	15.8	Pentane	14.9	5.2
Dichloroethane	13.2	12.2	Phenol	6.9	20.8
Dichloromethane	14.6	8.9	Phosphorus tribromide	13.8	16.7
Diethyl ketone	13.5	9.2	Phosphorus trichloride	16.2	10.9
Diethyl oxalate	11.0	16.4	Propionic acid	12.8	13.8
Diethylene glycol	5.0	24.7	Propyl acetate	13.1	10.3
Diphenyl	12.0	18.3	Propyl alcohol	9.1	16.5
Dipropyl ether	13.2	8.6	Propyl bromide	14.5	9.6
Dipropyl oxalate	10.3	17.7	Propyl chloride	14.4	7.5
Ethyl acetate	13.7	9.1	Propyl formate	13.1	9.7
Ethyl acrylate	12.7	10.4	Propyl iodide	14.1	11.6
Ethyl alcohol, 100%	10.5	13.8	Sodium	16.4	13.9
Ethyl alcohol, 95%	9.8	14.3	Sodium hydroxide, 50%	3.2	25.8
Ethyl alcohol, 40%	6.5	16.6	Stannic chloride	13.5	12.8
Ethyl benzene	13.2	11.5	Succinonitrile	10.1	20.8
Ethyl bromide	14.5	8.1	Sulfur dioxide	15.2	7.1
2-Ethyl butyl acrylate	11.2	14.0	Sulfuric acid, 110%	7.2	27.4
Ethyl chloride	14.8	6.0	Sulfuric acid, 100%	8.0	25.1
Ethyl ether	14.5	5.3	Sulfuric acid, 98%	7.0	24.8
Ethyl formate	14.2	8.4	Sulfuric acid, 60%	10.2	21.3
2-Ethyl hexyl acrylate	9.0	15.0	Sulfuryl chloride	15.2	12.4
Ethyl iodide	14.7	10.3	Tetrachloroethane	11.9	15.7
Ethyl propionate	13.2	9.9	Thiophene	13.2	11.0
Ethyl propyl ether	14.0	7.0	Titanium tetrachloride	14.4	12.3
Ethyl sulfide	13.8	8.9	Toluene	13.7	10.4
Ethylene bromide	11.9	15.7	Trichloroethylene	14.8	10.5
Ethylene chloride	12.7	12.2	Triethylene glycol	4.7	24.8
Ethylene glycol	6.0	23.6	Turpentine	11.5	14.9
Ethylidene chloride	14.1	8.7	Vinyl acetate	14.0	8.8
Fluorobenzene	13.7	10.4	Vinyl toluene	13.4	12.0
Formic acid	10.7	15.8	Water	10.2	13.0
Freon-11	14.4	9.0	Xylene, ortho	13.5	12.1
Freon-12	16.8	5.6	Xylene, meta	13.9	10.6
Freon-21	15.7	7.5	Xylene, para	13.9	10.9
Freon-22	17.2	4.7			

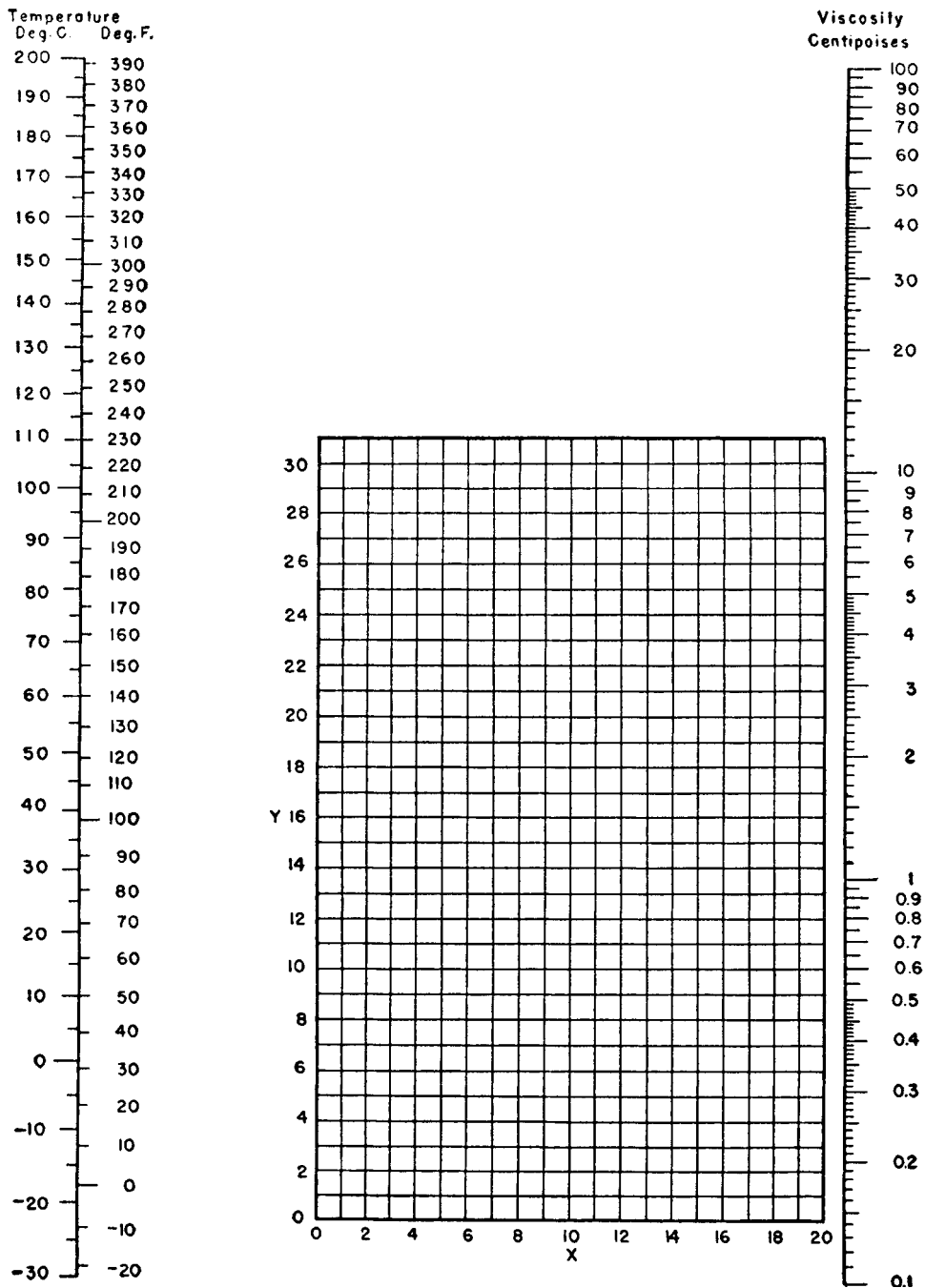


FIG. 2-32 Nomograph for viscosities of liquids at 1 atm. For coordinates see Table 2-318. To convert centipoises to pascal-seconds, multiply by 0.001.

TABLE 2-320

No.	Compound	Range, °C	Exp pt	% Avg abs devi
31	Acetaldehyde	0 - 30	2	0.4
40	Acetic acid	18 - 79	5	0.1
29	Acetone	0 - 40	3	0.4
20	Aniline	0 - 93	6	1.3
2	Benzaldehyde	16 - 68	4	0.7
13	Benzene	20 - 116	5	0.6
47	n-Butane	-21 - 0	2	0.2
16	n-Butanol	0 - 102	7	0.4
48	i-Butanol	0 - 20	2	0.6
49	s-Butanol	0 - 65	3	0.2
18	t-Butanol	20 - 77	3	2.5
28	Butyl acetate	0 - 38	4	1.1
23	Carbon tetrachloride	-20 - 25	4	1.1
25	Chlorobenzene	-40 - 80	6	0.5
42	Chloroform	0 - 40	3	1.3
19	m-Cresol	20 - 80	2	0.2
11	Cyclohexane	20 - 38	2	0.4
7	n-Decane	20 - 76	5	1.0
30	Diethyl ether	0 - 25	3	0.7
9	2,3-Dimethylbutane	32 - 49	2	0.3
38	n-Dodecane	0 - 63	6	1.1
15	Ethanol	17 - 77	7	0.5
27	Ethyl acetate	6 - 160	9	1.6
14	Ethylbenzene	0 - 80	3	0.7
24	Ethyl bromide	0 - 30	3	0.3
4	n-Heptane	0 - 60	3	0.3
3	n-Hexane	17 - 40	5	1.4
26	Iodobenzene	-20 - 80	4	0.7
41	Methanol	20 - 62	6	0.2
39	Methyl acetate	4 - 21	2	0.4
12	Methylcyclopentane	20 - 38	2	0.1
22	Methylene chloride	-20 - 20	3	0.9
8	2-Methylpentane	32 - 49	2	0.5
6	n-Nonane	16 - 77	5	2.0
5	n-Octane	0 - 77	3	0.3
10	i-Octane	20 - 77	4	1.6
17	n-Octanol	20 - 212	3	1.3
43	n-Pentanol	0 - 38	3	0.4
1	Propane	-60 - 50	4	1.6
32	n-Propanol	16 - 66	6	0.6
21	Propionic acid	12 - 30	3	1.7
44	n-Propyl acetate	0 - 38	2	0.1
33	i-Propylbenzene	0 - 38	4	0.2
45	Refrigerant-11, CFCl ₃	0 - 20	4	0.5
46	Refrigerant-12, CF ₂ Cl ₂	-42 - 70	4	1.8
50	Refrigerant-13, CF ₃ Cl	-20 - 20	4	1.7
51	Refrigerant-22, CHF ₂ Cl	-65 - 60	7	2.5
52	Refrigerant-113, C ₂ F ₃ Cl ₃	0 - 20	4	0.7
53	Refrigerant-114, C ₂ F ₂ Cl ₂	-25 - 20	4	0.8
54	Refrigerant-142, C ₂ F ₃ F ₂ Cl	0 - 90	2	0.9
34	Toluene	-70 - 200	5	1.8
55	n-Tridecane	20 - 228	5	2.4
36	m-Xylene	0 - 208	5	1.0
35	o-Xylene	0 - 208	5	0.7
37	p-Xylene	0 - 251	5	1.4

FIG. 2-33 and TABLE 2-320 Nomograph (right) for thermal conductivity of organic liquids. (From Mallu and Rao, *Hydroc. Proc.* 78, 1988.)

TABLE 2-319 Viscosity of Sucrose Solutions*

Viscosity in centipoises

Temp., °C	Percentage sucrose by weight			Temp., °C	Percentage sucrose by weight		
	20	40	60		20	40	60
0	3.818	14.82		50	0.974	2.506	14.06
5	3.166	11.60		55	0.887	2.227	11.71
10	2.662	9.830	113.9	60	0.811	1.989	9.87
15	2.275	7.496	74.9	65	0.745	1.785	8.37
20	1.967	6.223	56.7	70	0.688	1.614	7.18
25	1.710	5.206	44.02	75	0.637	1.467	6.22
30	1.510	4.398	34.01	80	0.592	1.339	5.42
35	1.336	3.776	26.62	85	0.552	1.226	4.75
40	1.197	3.261	21.30	90		1.127	4.17
45	1.074	2.858	17.24	95		1.041	3.73

*International Critical Tables, vol. 5, p. 23. Bingham and Jackson, *Bur. Standards Bull.* 14 (1919): 59.

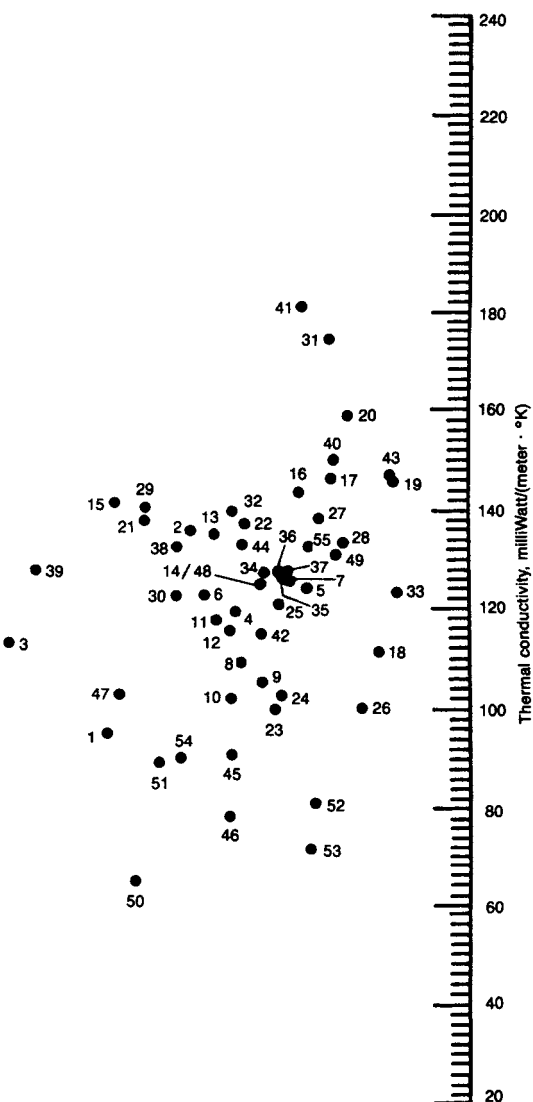


TABLE 2-321 Prandtl Number of Air*

Temperature, K	Pressure, bar											
	1	5	10	20	30	40	50	60	70	80	90	100
80	mix	2.31	2.32	2.35	2.37	2.40	2.42	2.45	2.48	2.51	2.54	2.57
90	0.796	1.76	1.77	1.78	1.79	1.81	1.82	1.83	1.85	1.87	1.89	1.91
100	0.786	0.872	1.54	1.53	1.53	1.53	1.53	1.53	1.53	1.54	1.54	1.55
120	0.773	0.813	0.89	1.44	1.65	1.54	1.48	1.43	1.40	1.38	1.36	1.34
140	0.763	0.782	0.82	0.94	1.20	1.59	2.14	2.43	2.07	1.78	1.62	1.52
160	0.754	0.765	0.78	0.84	0.92	1.03	1.13	1.25	1.37	1.65	1.83	1.72
180	0.745	0.754	0.763	0.792	0.830	0.876	0.932	1.00	1.07	1.14	1.20	1.25
200	0.738	0.743	0.749	0.766	0.788	0.812	0.841	0.87	0.90	0.95	0.97	1.00
240	0.724	0.727	0.729	0.737	0.746	0.756	0.767	0.78	0.80	0.81	0.81	0.82
280	0.710	0.711	0.713	0.717	0.721	0.726	0.731	0.737	0.742	0.75	0.75	0.76
300	0.705	0.707	0.708	0.712	0.715	0.717	0.721	0.725	0.728	0.732	0.737	0.742
350	0.699	0.699	0.699	0.701	0.703	0.705	0.707	0.709	0.711	0.712	0.714	0.716
400	0.694	0.694	0.694	0.695	0.696	0.697	0.698	0.699	0.700	0.701	0.703	0.704
450	0.691	0.691	0.691	0.691	0.692	0.692	0.693	0.693	0.694	0.695	0.695	0.696
500	0.689	0.689	0.689	0.689	0.689	0.690	0.690	0.690	0.690	0.691	0.691	0.691
600	0.690	0.690	0.690	0.689	0.689	0.689	0.689	0.689	0.689	0.690	0.690	0.690
700	0.696	0.696	0.695	0.695	0.695	0.695	0.695	0.695	0.695	0.695	0.695	0.695
800	0.705	0.704	0.704	0.704	0.704	0.703	0.703	0.703	0.703	0.702	0.702	0.702
900	0.709	0.709	0.708	0.708	0.708	0.708	0.708	0.708	0.708	0.708	0.708	0.708
1000	0.711	0.711	0.711	0.711	0.711	0.710	0.710	0.710	0.710	0.709	0.709	0.709

*Compiled by P. E. Liley from tables of specific heat at constant pressure, thermal conductivity, and viscosity given in SI units for integral kelvin temperatures and pressures in bars by Vasserman. *Thermophysical Properties of Air and Its Components and Thermophysical Properties of Liquid Air and Its Components*. Nauka, Moscow, and in translated form by the National Bureau of Standards, Washington. The number of significant figures given above reflects the similar numbers appearing for the constituent properties in the source references. While reasonable agreement occurs for atmospheric pressure with some other works, the fragmentary data available for the saturated, etc., states show large deviations.

TABLE 2-322 Prandtl Number of Liquid Refrigerants*

Refrigerant	No.	Temperature, K										
		180	200	220	240	260	280	300	320	340	360	380
Trichlorofluoromethane	11		11.9	8.64	6.73	5.33	4.74	4.18				
Dichlorodifluoromethane	12	7.00	5.25	4.27	3.65	3.27	3.08	3.04	3.19	3.44	4.00	
Chlorotrifluoromethane	13		2.96	2.67	2.69	3.05	3.57					
Bromotrifluoromethane	13B1	4.80	3.75	3.27	2.94	2.83	3.03	3.61	4.52			
Dichlorofluoromethane	21			5.72	4.50	3.87	3.48	3.25	3.16	3.17		
Chlorodifluoromethane	22	4.68	3.76	3.23	2.93	2.79	2.77	2.87	3.18	3.54		
Methyl chloride	40			2.53	2.42	2.40	2.45	2.60	2.85			
Trichlorotrifluoroethane	113								7.04	6.23	5.61	5.18
Dichlorotetrafluoroethane	114	25.7	15.13	11.18	8.59	6.94	5.77	5.06	4.78	4.82		
Chloropentafluoroethane	115		7.85	6.16	5.21	4.67	4.40	4.46	4.90			
Ethane	170	2.55	2.29	2.22	2.40	2.70						
Propane	290	5.28	4.46	3.88	3.44	3.16	3.02	3.16				
Octafluorocyclobutane	C318				11.2	8.74	7.35	6.37	5.87	5.96		
Dichlorodifluoromethane/difluoroethane	500		5.78	4.23	3.40	3.13	3.01	3.13	3.35	3.72		
Chlorodifluoromethane/chloropentafluoroethane	502		5.73	4.71	4.13	3.81						
Trifluoromethane/chlorotrifluoromethane	503	2.10	2.09	2.24	2.43	2.89						
Methylene fluoride/chloropentafluoroethane	504		4.90	3.60	3.04	2.79	2.69	2.85	3.30			
Butane	600	8.35	6.19	5.20	4.44	3.83	3.44	3.22	3.07	3.02		
Isobutane (2-methyl propane)	600a		8.26	6.36	5.18	4.49	3.93	3.66	3.53	3.53	3.77	4.68
Ammonia	717				1.97	1.76	1.54	1.40	1.29	1.24	1.25	1.34
Water	718						10.3	5.69	3.65	2.60	1.99	1.59
Ethylene	1150	1.85	1.74	1.78	2.07	2.70	4.4					
Propylene	1270	3.80	2.24	1.88	1.71	1.71	1.88	2.24	3.91	4.73		

*Dashes indicate inaccessible states. Average uncertainty is about 20 percent. Values derived from formulations for thermal conductivity, specific heat at constant pressure, and viscosity contained in *Thermophysical Properties of Refrigerants*. American Society of Heating, Refrigerating and Air-Conditioning Engineers, New York, 1976. For further details see M. W. Johnson, M.S.M.E. thesis, Purdue University, West Lafayette, Ind., 1976.

TABLE 2-323 Thermophysical Properties of Miscellaneous Saturated Liquids (Concluded)

Substance	Property	Temperature, °C															
		-50	-40	-30	-20	-10	0	10	20	30	40	50	60	70	80	90	100
Gasoline	ρ (kg/m ³)				784	775	767	759	751	743	735	721	717	708	699	690	681
	c_p (kJ/kg·K)				1.88	1.92	1.97	2.02	2.06	2.11	2.15	2.20	2.25	2.30	2.35	2.41	2.46
	μ (10 ⁻⁶ Pa·s)	1710	1400	1170	990	850	735	645	530	464	410	367	330	298	270	246	225
	k (W/m·K)	0.131	0.128	0.125	0.123	0.121	0.120	0.118	0.116	0.114	0.112	0.110	0.108	0.106	0.104	0.102	0.100
	Pr				15.1	13.5	12.1	11.0	9.41	8.59	7.87	7.34	6.88	6.47	6.10	5.81	5.54
Glycerol	ρ (kg/m ³)	—	—	—	—	—	1276	1270	1260	1254	1248	1242	1242	1242	1242	1242	1242
	c_p (kJ/kg·K)								2.393	2.406	2.457	2.504	2.548	2.588	2.625	2.657	2.686
	μ (10 ⁻⁶ Pa·s)						1.2+7	4.0+6	1.5+6	0.284	0.285	0.287	0.288	0.289	0.291	0.293	0.294
	k (W/m·K)																
	Pr																
Kerosene	ρ (kg/m ³)						781	774	767	760	754	748	742	742	742	742	742
	c_p (kJ/kg·K)						1.91	1.96	2.02	2.07	2.13	2.18	2.23	2.28	2.32	2.35	2.38
	μ (10 ⁻⁶ Pa·s)	1150	725	500	360	275	215	173	149	126	108	95	83	73	66	60	55
	k (W/m·K)						0.140	0.139	0.139	0.138	0.138	0.137	0.137	0.137	0.137	0.137	0.137
	Pr						2.93	2.44	2.17	1.89	1.67	1.51	1.35				
Methanol	ρ (kg/m ³)									783	774	766	756	746	736	725	711
	c_p (kJ/kg·K)	2.30	2.32	2.35	2.37	2.40	2.42	2.45	2.47	2.49	2.52	2.55	2.65	2.78	2.94	3.13	3.30
	μ (10 ⁻⁶ Pa·s)	2305	1800	1410	1170	975	820	692	590	510	455	400	355	315	271	240	218
	k (W/m·K)	0.225	0.222	0.219	0.216	0.212	0.209	0.206	0.203	0.199	0.195	0.192	0.189	0.187	0.184	0.182	0.180
	Pr	23.6	18.8	15.1	12.9	11.0	9.53	8.23	7.18	6.38	5.88	5.31	4.98	4.68	4.34	4.13	3.99
Methyl formate	ρ (kg/m ³)	1069	1056	1043	1030	1017	1003	989	975	960	944	929	913	897	880	863	845
	c_p (kJ/kg·K)	1.84	1.86	1.88	1.90	1.92	1.95	1.99	2.03	2.08							
	μ (10 ⁻⁶ Pa·s)	830	711	618	544	481	430	380	345	315							
	k (W/m·K)	0.217	0.213	0.209	0.205	0.200	0.195	0.191	0.186	0.180							
	Pr	7.04	6.21	5.56	5.04	4.62	4.30	3.96	3.77	3.64							
Oil, castor	ρ (kg/m ³)																
	c_p (kJ/kg·K)																
	μ (10 ⁻⁶ Pa·s)							2,420,000	986,000	451,000	231,000	125,000	74,000	43,000			
	k (W/m·K)							0.182	0.181	0.180	0.179	0.178	0.177	0.176	0.175	0.174	0.17
	Pr																
Oil, olive	ρ (kg/m ³)								914								
	c_p (kJ/kg·K)								1.633								
	μ (10 ⁻⁶ Pa·s)							138,000	84,000	52,000	36,300	24,500	17,000	12,400			
	k (W/m·K)							0.170	0.169	0.168	0.167	0.166	0.166	0.165	0.165	0.164	0.164
	Pr								810								
Pentane	ρ (kg/m ³)	693	684	674	665	656	646	636	626	616	606	596	585	574	562	550	538
	c_p (kJ/kg·K)	2.060	2.084	2.110	2.137	2.167	2.206	2.239	2.273								
	μ (10 ⁻⁶ Pa·s)	489	428	379	339	307	279	254	234	209	190	175	161	148	137	124	113
	k (W/m·K)	0.142	0.139	0.136	0.132	0.128	0.125	0.122	0.119	0.115	0.112	0.108	0.105	0.101	0.098	0.095	0.091
	Pr	7.14	6.42	5.88	5.49	5.20	4.92	4.66	4.47								
Propanol	ρ (kg/m ³)	849					819	811	814	796	788	779	770	761	752	747	743
	c_p (kJ/kg·K)	1.955					2.219										
	μ (10 ⁻⁶ Pa·s)	20,200	13,500	9500	6900	5110	3900	2900	2245	1720	1400	1130	921	760	630	508	447
	k (W/m·K)	0.167	0.166	0.165						0.171	0.169	0.168	0.167	0.165	0.164	0.163	0.162
	Pr	236															
Sulfuric acid	ρ (kg/m ³)								1834								
	c_p (kJ/kg·K)								1.382								
	μ (10 ⁻⁶ Pa·s)						48,400	35,200	25,400	15,700	11,500	8820	7220	6090	5190		
	k (W/m·K)						0.314										
	Pr																
Toluene	ρ (kg/m ³)	932	923	913	904	895	886	876	867	858	848	839	829	820	810	800	790
	c_p (kJ/kg·K)	1.514	1.535	1.556	1.579	1.602	1.633	1.652	1.675	1.701	1.73	1.76	1.80	1.83	1.87	1.92	1.97
	μ (10 ⁻⁶ Pa·s)	2120	1670	1345	1100	915	770	670	590	520	470	420	380	355	325	295	270
	k (W/m·K)	0.152	0.149	0.147	0.144	0.142	0.139	0.137	0.134	0.132	0.129	0.126	0.124	0.122	0.119	0.117	0.114
	Pr	21.1	17.8	14.2	12.1	10.3	9.0	8.1	7.4	6.7	6.3	5.9	5.5	5.3	5.1	4.8	4.7
Turpentine	ρ (kg/m ³)																
	c_p (kJ/kg·K)						1.72	1.76	1.80	1.80	1.80	1.80	1.80	1.80	1.80	1.80	1.80
	μ (10 ⁻⁶ Pa·s)						2250	1780	1490	1270	1070	925	820	730	675		
	k (W/m·K)						0.130	0.129	0.128	0.127	0.126	0.125	0.125	0.125	0.125	0.125	0.125
	Pr						29.8	24.3	20.9	18.4	16.1	14.3					

TABLE 2-324 Diffusivities of Pairs of Gases and Vapors (1 atm) (Concluded)
 D_c in cm^2/s

Substance	Temp., °C	Air	A	H ₂	O ₂	N ₂	CO ₂	N ₂ O	CH ₄	C ₂ H ₆	C ₂ H ₄	<i>n</i> -C ₄ H ₁₀	<i>i</i> -C ₄ H ₁₀	Ref.
Hydrogen cyanide	0	0.173												10
Hydrogen peroxide	60	.188												11
Iodine	0	.07				0.070								8, 12, 14
Mercury	0	.112		0.53		.13								8, 12, 13
Mesitylene	0	.056												8
Methane	500				1.1									18
Methyl acetate	0	.084		.333			0.0567							8
Methyl alcohol	0	.132		.506			.0879							8
Methyl butyrate	0	.0633		.242			.0446							8
Methyl <i>i</i> -butyrate	0	.0639		.257			.0451							8
Methyl cyclopentane	15		0.0731	.318	0.0742	0.0758								3
Methyl formate	0	.0872												8
Methyl propionate	0	.0735		.295			.0528							8
Methyl valerate	0	0.0569												8
Naphthalene	0	.0513												8
Nitrogen	0				0.181									8
Nitrous oxide	25						0.165			0.148	0.163	0.0960	0.0908	2
<i>n</i> -Octane	0	.0505		0.535			.096							8
Oxygen	30		0.0642	.271	0.0705	0.0710								8
Phosgene	0	.178		.697		0.181	.139							3
Propionic acid	0	.095												8
Propyl acetate	0	.0829		.330			.0588							8
<i>n</i> -Propyl alcohol	0	.067												8
<i>i</i> -Propyl alcohol	0	.085		.315			.0577							8
	30	.0818												8
<i>n</i> -Propyl benzene	0	.101												5
<i>i</i> -Propyl benzene	0	.0481												8
<i>n</i> -Propyl bromide	0	.0489												8
<i>i</i> -Propyl bromide	0	.085												8
Propyl butyrate	0	.0902												8
Propyl formate	0	.0530		.206			.0364							8
<i>n</i> -Propyl iodide	0	.0712		.281			.0490							8
<i>i</i> -Propyl iodide	0	.079												8
<i>n</i> -Propyl isobutyrate	0	.0802												8
<i>i</i> -Propyl isobutyrate	0	.0549		.212			.0388							8
Propyl propionate	0	.059												8
Propyl valerate	0	.057		.212			.0395							8
Safrol	0	.0466		.189			.0341							8
<i>i</i> -Safrol	0	.0434												8
Sulfur hexafluoride	0	.0455												8
Toluene	25			.418										2
Trimethyl carbinol	0	.076	0.071											4, 8
2,2,4-Trimethyl pentane	30	.088												5
2,2,3-Trimethyl heptane	0	.087												8
<i>n</i> -Valeric acid	30		0.0618	.288	0.0688	0.0705								3
<i>i</i> -Valeric acid	90	0.050		.270		0.0684								3
Water	0	0.0544		.212			.0376							8
	0	0.220		.75			.138							8, 20
	450				1.3									18

° 320 mmHg.

† 40 atm.

‡ Also at other temperatures.

§ Strong function of concentration.

References

- ¹ Amdur, Irvine, Mason, and Ross, *J. Chem. Phys.*, **20**, 436 (1952).
- ² Boyd, Stein, Steingrimsso, and Rumpel, *J. Chem. Phys.*, **19**, 548 (1951).
- ³ Cummings and Ubbelohde, *J. Chem. Soc. (London)*, 1953, p. 3751.
- ⁴ Fairbanks and Wilke, *Ind. Eng. Chem.*, **42**, 471 (1950).
- ⁵ Gilliland, *Ind. Eng. Chem.*, **26**, 681 (1934).
- ⁶ Gorynova and Kuvskinskii, *Zhur. Tekh. Fiz.*, **18**, 1421 (1948).
- ⁷ Hansen, Dissertation, Jena, 1907.
- ⁸ *International Critical Tables*, vol. 5, p. 62.
- ⁹ Jeffries and Drickamer, *J. Chem. Phys.*, **22**, 436 (1954).
- ¹⁰ Klotz and Miller, *J. Am. Chem. Soc.*, **69**, 2557 (1947).
- ¹¹ McMurtrie and Keyes, *J. Am. Chem. Soc.*, **70**, 3755 (1948).
- ¹² Mullaly and Jacques, *Phil. Mag.*, **48**, 6, 1105 (1924).
- ¹³ Spier, *Physica*, 6 (1939): 453; **7**, 381 (1940).
- ¹⁴ Topley and Whytlaw-Gray, *Phil. Mag.*, **4**, 873 (1927).
- ¹⁵ Trautz and Ludwig, *Ann. Physik*, **5**, 5, 887 (1930).
- ¹⁶ Trautz and Muller, *Ann. Physik*, **22**, 353 (1935).
- ¹⁷ Trautz and Ries, *Ann. Physik*, **8**, 163 (1931).
- ¹⁸ Walker and Westenberg, *J. Chem. Phys.*, **32**, 136 (1960).
- ¹⁹ Westenberg and Walker, *J. Chem. Phys.*, **26**, 1753 (1957).
- ²⁰ Winkelmann, *Wied. Ann.*, **22**, 152 (1884); **23**, 203 (1884); **26**, 105 (1885); **33**, 445 (1888); **36**, 92 (1889).

2-456 PHYSICAL AND CHEMICAL DATA

In this table are a representative selection of diffusion coefficients. The subsection "Prediction and Correlation of Physical Properties" should be consulted for estimation techniques. As general references, the works by Hirschfelder, Curtiss, and Bird, *Molecular Theory of Gases and Liquids*, Wiley, New York, 1964; Chapman and Cowling, *The Mathematical Theory of Non-Uniform Gases*, Cambridge, New York, 1970; Reid and Sherwood, *The Properties of Gases and Liquids*,

McGraw-Hill, New York, 1964; and Bretsznajder, *Prediction of Transport and Other Physical Properties of Fluids*, Pergamon, New York, 1971, may be found useful. The most exhaustive recent compilation for gases is by Mason and Marrero, *J. Phys. Chem. Ref. Data*, 1 (1972). Unfortunately, the Mason and Marrero work cites only equations and equation constants and not direct tabulations. For these, the Landolt-Börnstein series is suggested.

TABLE 2-325 Diffusivities in Liquids (25 °C)

Dilute solutions and 1 atm unless otherwise noted; use $D_i\mu/T = \text{constant}$ to estimate effect of temperature; ° indicates that reference gives effect of concentration.

Solute	Solvent	$D_i \times 10^5$, sq cm/sec	Estimated possible, error, ± %1	Ref.
Acetal°	Ethanol	1.25	5	11
Acetamide°	Ethanol	0.68	5	11
Acetamide°	Water	1.19	3	11
Acetic acid	Acetone	3.31		4
Acetic acid	Benzene	2.11		1, 4
Acetic acid	Carbon tetrachloride	1.49		4
Acetic acid	Ethylene glycol	0.13		4
Acetic acid	Toluene	2.26		4
Acetic acid°	Water	1.24	3	11
Acetonitrile	Water	1.66	5	11
Acetylene	Water	1.78, 2.11		1, 24
Allyl alcohol°	Ethanol	1.06	5	11
Allyl alcohol	Water	1.19	6	11
Ammonia°	Water	1.7, 2.0, 2.3		1, 11
<i>i</i> -Amyl alcohol°	Ethanol	0.87	5	11
<i>i</i> -Amyl alcohol	Water	1.0	8	11, 25
Benzene	Carbon tetrachloride	1.53		7
Benzene (50 mole %)	<i>n</i> -Decane	1.72		26
Benzene (50 mole %)	2,4-Dimethyl pentane	2.49		26
Benzene (50 mole %)	<i>n</i> -Dodecane	1.40		26
Benzene (50 mole %)	<i>n</i> -Heptane	2.47		26
Benzene (50 mole %)	<i>n</i> -Hexadecane	0.96		26
Benzene (50 mole %)	<i>n</i> -Octadecane	0.86		26
Benzoic acid	Acetone	2.62		4
Benzoic acid	Benzene	1.38		4
Benzoic acid	Carbon tetrachloride	0.91		4
Benzoic acid	Ethylene glycol	0.043		4
Benzoic acid	Toluene	1.49		4
Bromine	Benzene	2.7		11
Bromine	Carbon disulfide	4.1		11
Bromine	Water	1.3		11
Bromobenzene	Benzene	2.30		25
Bromoform°	Acetone	2.90		11
Bromoform	<i>i</i> -Amyl alcohol	0.53		11
Bromoform	Ethanol	1.08	5	11
Bromoform°	Ethyl ether	3.62		11
Bromoform	Methanol	2.20		23
Bromoform	<i>n</i> -Propanol	0.94		11
<i>n</i> -Butanol	Water	0.96	5	1, 11, 18, 25
Caffeine	Water	0.63	6	11
Carbon dioxide	Ethanol	4.0	6	11
Carbon dioxide	Water	1.96	1	1, 3, 5, 20, 24, 28
Carbon disulfide (50 mole %, 200 atm.)	<i>n</i> -Butanol	3.57		14
Carbon disulfide (50 mole %, 200 atm.)	<i>i</i> -Butanol	2.42		14
Carbon disulfide (50 mole %, 218 atm.)	Chlorobenzene	3.00		14
Carbon disulfide (50 mole %, 200 atm.)	2,4-Dimethyl pentane	3.63		14
Carbon disulfide (50 mole %, 100 atm.)	<i>n</i> -Heptane	3.0		14
Carbon disulfide (50 mole %, 50 atm.)	Methyl cyclohexane	3.5		14
Carbon disulfide (50 mole %, 200 atm.)	<i>n</i> -Octane	3.10		14
Carbon disulfide (50 mole %)	Toluene	2.06		14
Carbon tetrachloride	Benzene	2.04	3	7, 9
Carbon tetrachloride°	Cyclohexane	1.49	2	9, 10°
Carbon tetrachloride	Decalin	0.776	2	9
Carbon tetrachloride	Dioxane	1.02	2	9
Carbon tetrachloride°	Ethanol	1.50	2	9, 10°
Carbon tetrachloride	<i>n</i> -Heptane	3.17	2	9
Carbon tetrachloride	Kerosene	0.961	2	9
Carbon tetrachloride	Methanol	2.30	2	9
Carbon tetrachloride	<i>i</i> -Octane	2.57	2	9
Carbon tetrachloride	Tetralin	0.735	2	9
Chloral°	Ethanol	0.68	5	11
Chloral hydrate	Water	0.77	7	11

TABLE 2-325 Diffusivities in Liquids (25 °C) (Continued)

 Dilute solutions and 1 atm unless otherwise noted; use $D_L\mu/T = \text{constant}$ to estimate effect of temperature; ° indicates that reference gives effect of concentration.

Solute	Solvent	$D_L \times 10^5$, sq cm/sec	Estimated possible, error, \pm %1	Ref.
Chlorine	Water	1.44	4	1, 28
Chlorobenzene	Benzene	2.66		25
Chloroform	Benzene	2.50	6	1, 25
Chloroform	Ethanol	1.38	3	11
Cinnamic acid	Acetone	2.41		4
Cinnamic acid	Benzene	1.12		4
Cinnamic acid	Carbon tetrachloride	0.76		4
Cinnamic acid	Toluene	2.41		4
1,1'-Dichloropropanol	Water	1.0	6	11
Dicyanodiamide°	Water	1.18	4	11
Diethyl ether	Benzene	2.73		25
Diethyl ether	Water	0.85		2
2,4-Dimethyl pentane (50 mole %)	<i>n</i> -Dodecane	1.44		26
2,4-Dimethyl pentane (50 mole %)	<i>n</i> -Hexadecane	0.88		26
Ethanol°	Water	1.28	4	1, 7, 9, ° 11, ° 22
Ethyl acetate	Ethyl benzoate	0.94		6
Ethylene dichloride	Benzene	2.8		1, 25
Formic acid	Acetone	3.77		4
Formic acid	Benzene	2.28		4
Formic acid	Carbon tetrachloride	1.89		4
Formic acid	Ethylene glycol	0.094		4
Formic acid	Toluene	2.65		
Formic acid	Water	1.37	10	11
Glucose	Water	0.69	6	11
Glycerol	<i>i</i> -Amyl alcohol	0.12		11
Glycerol	Ethanol	0.56		11
Glycerol°	Water	0.94	6	1, 11°
<i>n</i> -Heptane (50 mole %)	<i>n</i> -Dodecane	1.58		26
<i>n</i> -Heptane (50 mole %)	<i>n</i> -Hexadecane	1.00		26
<i>n</i> -Heptane (50 mole %)	<i>n</i> -Octadecane	0.92		26
<i>n</i> -Heptane (50 mole %)	<i>n</i> -Tetradecane	1.29		26
Hexamethylene tetramine	Water	0.67		11
Hydrogen chloride°	Water	3.10	3	4, 11, ° 12°
Hydrogen	Water	5.85 (4.4)		1, 11, 24(?)
Hydrogen sulfide	Water	1.61		1
Hydroquinone°	Ethanol	0.53	5	11
Hydroquinone°	Water	0.88, 1.12		2, 11°
Iodine	Acetic acid	1.13		11
Iodine	Anisole	1.25		11
Iodine	Benzene	1.98		9, 19, 23
Iodine	Bromobenzene	1.25	10	4, 11, 19
Iodine	Carbon disulfide	3.2		11, 19, 23
Iodine	Carbon tetrachloride	1.45	8	9, 11, 19
Iodine	Chloroform	2.30	3	11, 23
Iodine	Cyclohexane	1.80		4
Iodine	Dioxane	1.07		9
Iodine°	Ethanol	1.30		4, 11°
Iodine	Ethyl acetate	2.2		11, 19
Iodine	Ethyl ether	3.61		11
Iodine	Ethylene bromide	0.93		11
Iodine	<i>n</i> -Heptane	3.4, 2.5		9, 11, 19
Iodine	<i>n</i> -Hexane	4.15		4, 9
Iodine	Mesitylene	1.49		9
Iodine	Methanol	1.74		19
Iodine	Methyl cyclohexane	2.1		4
Iodine	<i>n</i> -Octane	2.76		4
Iodine	Tetrabromoethane	2.0		11
Iodine	<i>n</i> -Tetradecane	0.96		4
Iodine	Toluene	2.1		11
Iodine	<i>m</i> -Xylene	1.82		9, 11
Iodobenzene	Ethanol	1.09	3	11
Lactose°	Water	0.49	5	11
Maltose°	Water	0.48	5	11
Mannitol°	Water	0.65	5	11
Methanol	Water	1.6		1, 7, 11
Nicotine°	Water	0.60	8	11
Nitric acid°	Water	2.98	2	11
Nitrobenzene	Carbon tetrachloride	1.00		7
Nitrogen	Water	1.9		1, 24
Nitrous oxide	Water	1.8		1, 11
Oxalic acid°	Water	1.61	2	11

TABLE 2-325 Diffusivities in Liquids (25 °C) (Concluded)

Dilute solutions and 1 atm unless otherwise noted; use $D_L\mu/T = \text{constant}$ to estimate effect of temperature; ° indicates that reference gives effect of concentration.

Solute	Solvent	$D_L \times 10^5$, sq cm/sec	Estimated possible, error, \pm %1	Ref.
Oxygen	Glycerol [°] -water (106 poise)	0.24		13
Oxygen	Sucrose [°] -water (125 poise)	0.25		13
Oxygen	Water	2.5	20	1, 3, 15, 21, 24
Pentaerythritol [°]	Water	0.77	4	11
Phenol	<i>i</i> -Amyl alcohol	0.2		11
Phenol	Benzene	1.68		1
Phenol	Carbon disulfide	3.7		11
Phenol	Chloroform	2.0		11
Phenol	Ethanol	0.89		11
Phenol	Ethyl ether	3.9		11
<i>n</i> -Propanol	Water	1.1		1, 7, 11
Pyridine [°]	Ethanol	1.24	3	11
Pyridine	Water	0.76	7	11
Pyrogallol	Water	0.74	7	11
Raffinose [°]	Water	0.41	4	11
Resorcinol [°]	Ethanol	0.46	5	11
Resorcinol [°]	Water	0.87	4	11
Saccharose [°]	Water	0.49	4	11
Stearic acid [°]	Ethanol	0.65	5	11
Succinic acid [°]	Water	0.94		11
Sucrose	Water	0.56	6	2, 27
Sulfur dioxide	Water	1.7		15, 17
Sulfuric acid [°]	Water	1.97	3	11
Tartaric acid [°]	Water	0.80	10	11
1,1,2,2-Tetrabromoethane	1,1,2,2-Tetra- chloroethane	0.61	4	11
Toluene	<i>n</i> -Decane	2.09		4
Toluene	<i>n</i> -Dodecane	1.38		4
Toluene	<i>n</i> -Heptane	3.72		4
Toluene	<i>n</i> -Hexane	4.21		4
Toluene	<i>n</i> -Tetradecane	1.02		4
Urea	Ethanol	0.73		11
Urea	Water	1.37	2	8, 11
Urethane	Water	1.06		11, 25
Water	Glycerol	0.021		16

References

- ¹Arnold, *J. Am. Chem. Soc.*, **52**, 3937 (1930).
- ²Calvet, *J. Chim. Phys.*, **44**, 47 (1947).
- ³Carlson, *J. Am. Chem. Soc.*, **33**, 1027 (1911).
- ⁴Chang and Wilke, *J. Phys. Chem.*, **59**, 592 (1955).
- ⁵Davidson and Cullen, *Trans. Inst. Chem. Eng.*, **35**, 51 (1957).
- ⁶Dummer, *Z. Anorg. Chem.*, **109**, 31 (1949).
- ⁷Gerlach, *Ann. Phys. (Leipzig)*, **10**, 437 (1931).
- ⁸Gosting and Akeley, *J. Am. Chem. Soc.*, **74**, 2058 (1952).
- ⁹Hammond and Stokes, *Trans. Faraday Soc.*, **49**, 890 (1953); **49**, 886 (1953).
- ¹⁰Hammond and Stokes, *Trans. Faraday Soc.*, **52**, 781 (1956).
- ¹¹*International Critical Tables*, vol. 5, p. 63.
- ¹²James, Hollingshead, and Gordon, *J. Chem. Phys.*, **7**, 89 (1939); **7**, 836 (1939).
- ¹³Jordon, Ackermann, and Berger, *J. Am. Chem. Soc.*, **78**, 2979 (1956).
- ¹⁴Koeller and Drickamer, *J. Chem. Phys.*, **21**, 575 (1953).
- ¹⁵Kolthoff and Miller, *J. Am. Chem. Soc.*, **63**, 1013 (1941).

TABLE 2-326 Thermal Conductivities of Some Building and Insulating Materials*

$$k = \text{Btu}/(\text{h}\cdot\text{ft}^2)(^\circ\text{F}/\text{ft})$$

Material	Apparent density ρ , lb/ft ³ at room temperature	t , °C	k	Material	Apparent density ρ , lb/ft ³ at room temperature	t , °C	k
Aerogel, silica, opacified	8.5	120	0.013	Cotton wool	5	30	0.024
		290	.026	Cork board	10	30	.025
Asbestos-cement boards	120	20	.43	Cork (regranulated)	8.1	30	.026
Asbestos sheets	55.5	51	.096	(ground)	9.4	30	.025
Asbestos slate	112	0	.087	Diatomaceous earth powder, coarse	20.0	38	.036
	112	60	.114	(Note 2)	20.0	871	.082
Asbestos	29.3	-200	.043	fine (Note 2)	17.2	204	.040
	29.3	0	.090		17.2	871	.074
	36	0	.087	molded pipe covering (Note 2)	26.0	204	.051
	36	100	.111		26.0	871	.088
	36	200	.120	4 vol. calcined earth and 1 vol. cement, poured and fired (Note 2)	61.8	204	.16
	36	400	.129		61.8	871	.23
	43.5	-200	.090	Dolomite	167	50	1.0
	43.5	0	.135	Ebonite			0.10
Aluminum foil (7 air spaces per 2.5 in.)	0.2	38	.025	Enamel, silicate	38		0.5-0.75
		177	.038	Felt, wool	20.6	30	0.03
Ashes, wood		0-100	.041	Fiber insulating board	14.8	21	.028
Asphalt	132	20	.43	Fiber, red	80.5	20	.27
Boiler scale (Note 1)				(with binder, baked)		20-97	.097
Bricks:				Gas carbon		0-100	2.0
Alumina (92-99% Al ₂ O ₃ by wt.) fused		427	1.8	Glass			0.2-0.73
Alumina (64-65% Al ₂ O ₃ by wt.)		1315	2.7	Borosilicate type	139	30-75	0.63
(See also Bricks, fire clay)	115	800	0.62	Window glass			0.3-0.61
	115	1100	.63	Soda glass			0.3-0.44
Building brick work		20	.4	Granite			1.0-2.3
Carbon	96.7		3.0	Graphite, longitudinal		20	95
Chrome brick (32% Cr ₂ O ₃ by wt.)	200	200	.67	powdered, through 100 mesh	30	40	0.104
	200	650	.85	Gypsum (molded and dry)	78	20	.25
	200	1315	1.0	Hair felt (perpendicular to fibers)	17	30	.021
Diatomaceous earth, natural, across strata (Note 2)	27.7	204	0.051	Ice	57.5	0	1.3
	27.7	871	.077	Infusorial earth, see diatomaceous earth			
Diatomaceous, natural, parallel to strata (Note 2)	27.7	204	.081	Kapok	0.88	20	0.020
	27.7	871	.106	Lampblack	10	40	.038
Diatomaceous earth, molded and fired (Note 2)	38	204	.14	Lava			.49
	38	871	.18	Leather, sole	62.4		.092
Diatomaceous earth and clay, molded and fired (Note 2)	42.3	204	.14	Limestone (15.3 vol. % H ₂ O)	103	24	.54
	42.3	871	.19	Linen		30	.05
Diatomaceous earth, high burn, large pores (Note 3)	37	200	.13	Magnesia (powdered)	49.7	47	.35
	37	1000	.34	Magnesia (light carbonate)	13	21	0.034
Fire clay (Missouri)		200	.58	Magnesium oxide (compressed)	49.9	20	.32
		600	.85	Marble			1.2-1.7
		1000	.95	Mica (perpendicular to planes)		50	0.25
		1400	1.02	Mill shavings			0.033-0.05
Kaolin insulating brick (Note 3)	27	500	0.15	Mineral wool	9.4	30	0.0225
	27	1150	.26		19.7	30	.024
Kaolin insulating firebrick (Note 4)	19	200	.050	Paper			.075
	19	760	.113	Paraffin wax		0	.14
Magnesite (86.8% MgO, 6.3% Fe ₂ O ₃ , 3% CaO, 2.6% SiO ₂ by wt.)	158	204	2.2	Petroleum coke		100	3.4
	158	650	1.6	Porcelain		500	2.9
	158	1200	1.1	Portland cement, see concrete		200	0.88
				Pumice stone		90	.17
Silicon carbide brick, recrystallized (Note 3)	129	600	10.7	Pyroxylin plastics		21-66	.14
	129	800	9.2	Rubber (hard)	74.8	0	.087
	129	1000	8.0	(para)		21	.109
	129	1200	7.0	(soft)		21	0.075-0.092
	129	1400	6.3	Sand (dry)	94.6	20	0.19
Calcium carbonate, natural	162	30	1.3	Sandstone	140	40	1.06
White marble			1.7	Sawdust	12	21	0.03
Chalk	96		0.4	Scale (Note 1)			
Calcium sulfate (4H ₂ O), artificial	84.6	40	.22	Silk	6.3		.026
plaster (artificial)	132	75	.43	varnished		38	.096
(building)	77.9	25	.25	Slag, blast furnace		24-127	.064
Cambic (varnished)		38	.091	Slag wool	12	30	.022
Carbon, gas		0-100	2.0	Slate		94	.86
Carbon stock	94	-184	0.55	Snow	34.7	0	.27
		0	3.6	Sulfur (monoclinic)		100	0.09-0.097
Cardboard, corrugated			0.037	(rhombic)		21	0.16
				Wall board, insulating type	14.8	21	.028
				Wall board, stiff paste board	43	30	.04
				Wood shavings	8.8	30	.034

2-460 PHYSICAL AND CHEMICAL DATA

TABLE 2-326 Thermal Conductivities of Some Building and Insulating Materials* (Concluded)

$$k = \text{Btu}/(\text{h}\cdot\text{ft}^2)(^\circ\text{F}/\text{ft})$$

Material	Apparent density ρ , lb/ft ³ at room temperature	t , °C	k	Material	Apparent density ρ , lb/ft ³ at room temperature	t , °C	k
Celluloid	87.3	30	.12	Wood (across grain):			
Charcoal flakes	11.9	80	.043	Balsa	7-8	30	0.025-0.03
	15	80	.051	Oak	51.5	15	0.12
Clinker (granular)		0-700	.27	Maple	44.7	50	.11
Coke, petroleum		100	3.4	Pine, white	34.0	15	.087
		500	2.9	Teak	40.0	15	.10
Coke, petroleum (20-100 mesh)	62	400	0.55	White fir	28.1	60	.062
Coke (powdered)		0-100	.11	Wood (parallel to grain):			
Concrete (cinder)			.20	Pine	34.4	21	.20
(stone)			.54	Wool, animal	6.9	30	.021
(1:4 dry)			.44				

*Marks, *Mechanical Engineers' Handbook*, 4th ed., McGraw-Hill, New York, 1941. *International Critical Tables*, McGraw-Hill, 1929, and other sources.

Note 1: B. Kamp [*Z. tech. Physik*, **12**, 30 (1931)] shows the effect of increased porosity in decreasing thermal conductivity of boiler scale. Partridge [University of Michigan, *Eng. Research Bull.*, **15**, 1930] has published a 170-page treatise on Formation and Properties of Boiler Scale.

Note 2: Townshend and Williams, *Chem. & Met.*, **39**, 219 (1932).

Note 3: Norton, *Refractories*, 2d ed., McGraw-Hill, New York, 1942.

Note 4: Norton, private communication.

TABLE 2-327 Thermal-Conductivity-Temperature Table for Metals*

Thermal conductivities tabulated in watts per meter-kelvin

Substance	Temperature, K														
	10	20	40	60	80	100	200	300	400	500	600	800	1000	1200	1400
Alumina	7	32	121	174	160	125	55	36	26	20	16	10	8	7	6
Aluminum	38,000	13,500	2,300	850	380	300	237	273	240	237	232	220	93	99	105
Antimony	470	230	110	80	60	48	32	26	22	20					
Beryllium oxide	47	196	810	1,400	1,650	1,490	480	272	196	146	111	70	47	33	25
Bismuth	240	100	45	31	24	22	18	16	14	12					
Boron	165	305	400	327	230	170	45	25	15	12					
Cadmium	900	250	150	120	110	110	105	104	101	99					
Chromium	400	570	450	250	180	158	111	90	87	85	81	71	65	62	61
Cobalt	250	450	380	250	190	160	120	100	85	70					
Constantan	4	9	16	18	19	20	23	25	27	30					
Copper	19,000	10,700	2,100	850	570	483	413	398	392	388	383	371	357	342	
Gallium	2,200	640	250	200	170	140	100	85							
Gold	2,800	1,500	520	380	350	345	327	315	312	309	304	292	278	262	
Graphite†	27	108	135	81	54	39	15	10	7	5	4	3	3	2	2
Graphite‡	81	420	1,630	2,980	4,290	4,980	3,250	2,000	1,460	1,140	930	680	530	440	370
Hastelloy	1	3	4	5	6	7	9	10	11	13					
Inconel	2	4	8	10	11	11	14	15							
Iridium	1,300	1,900	750	360	230	172	147	145	143	140					
Iron	710	1,000	560	270	170	132	94	80	69	61	55	43	33	28	31
Lead	175	57	43	42	41	40	37	35	34	33	31	19	22	24	26
Magnesium	1,200	1,300	620	290	190	169	159	156	153	151	149	146	84	98	112
Magnesium oxide	1,100	3,100	2,200	950	460	260	75	48	36	27	21	13	10	8	7
Manganese	2	2	4	5	5	6	7	8	9	9					
Manganin	2	4	9	11	13	13	17	22	28	34	40	12	13	14	
Mercury	54	40	35	33	32	32	8	10	11	12	13	14			
Molybdenum	150	280	350	250	210	179	143	138	134	130	126	118	112	105	100
Nickel	2,600	1,700	570	290	200	158	106	91	80	72	66	67	72	76	80
Nylon	0.04	0.10	0.17	0.20	0.23	0.25	0.28	0.30							
Palladium	1,200	610	160	100	88	80	78	78	78	80					
Platinum	1,200	490	130	92	82	79	75	73	72	72	72	73	78	78	81
PTFE§	0.94	1.43	1.94	2.1	2.15	2.16	2.20	2.25	2.3	2.5					
Pyrex	0.12	0.20	0.33	0.42	0.51	0.57	0.88	1.1	1.6	2.1					
Quartz	1,200	480	82	40	30										
Rhodium	2,900	3,900	1,000	370	250	190	160	150	145	140					
Rubber			0.13	0.15	0.16	0.17	0.20	0.22	0.24	0.25					
Selenium (axis)	140	57	25	15	10	8	6	4	3	2					
Silica								1.34	1.52	1.70	1.87	2.22	2.60		
Silver	16,500	5,200	1,100	630	500	430	425	424	420	413	405	389	374	358	
Tantalum	108	146	88	68	62	59	58	57	58	58	59	59	60	61	62
Tellurium	300	93	29	17	13	11	6	4	3	3					
Tin		320	130	101	90	84	72	67	62	60					
Titanium	14	28	39	37	33	31	26	21	20	20	19				
Tungsten			880	330	310	280	190	180	170	150	140				
Uranium				20	22	23	26	28	30	32					
Zinc			150	135	130	123	120	116	110	110					
Zirconium	100	110	59	42	38	34	25	23	22	21	21				

* Especially at low temperatures, the thermal conductivity can often be markedly reduced by even small traces of impurities. This table, for the highest-purity specimens available, should thus be used with caution in applications with commercial materials. From Perry, *Engineering Manual*, 3d ed., McGraw-Hill, New York, 1976. A more detailed table appears as Section 5.5.6 in the *Heat Exchanger Design Handbook*, Hemisphere Pub. Corp., Washington, DC, 1983.

† Parallel to basal plane.

‡ Perpendicular to basal plane.

§ Also known as Teflon, etc.

TABLE 2-328 Thermal Conductivity of Chromium Alloys*
 $k = \text{Btu}/(\text{h}\cdot\text{ft}^2)(^\circ\text{F}/\text{ft})$

American Iron and Steel Institute Type No.	k at 212 °F	k at 932 °F
301, 302, 302B, 303, 304, 316†	9.4	12.4
308	8.8	12.5
309, 310	8.0	10.8
321, 347	9.3	12.8
403, 406, 410, 414, 416†	14.4	16.6
430, 430F†	15.1	15.2
442	12.5	14.2
501, 502†	21.2	19.5

*Table 2-328 is based on information from manufacturers.

† Shelton and Swanger (National Bureau of Standards), *Trans. Am. Soc. Steel Treat.*, 21, 1061–1078 (1933).

TABLE 2-329 Thermal Conductivity of Some Alloys at High Temperature*

°R	Thermal conductivity, $\text{Btu}/(\text{ft})(\text{hr})(^\circ\text{R})$					
	Kovar	Advance	Monel	Hastelloy A	Inconel	Nichrome V
500	7.8		9.0	5.6	6.0	5.5
600	8.3	11.4	10.2	6.2	6.5	6.1
700	8.6	12.6	11.2	6.8	7.0	6.7
800	8.7	13.9	12.3	7.3	7.6	7.3
900	8.7	15.1	13.4	7.8	8.1	7.8
1000	8.9	16.4	14.4	8.4	8.6	8.4
1100	9.2	17.6	15.4	9.0	9.1	9.0
1200	9.5	18.8	16.5	9.5	9.7	9.5
1300	9.8	20.0	17.6	10.1	10.2	10.1
1400	10.2	21.2	18.7	10.7	10.8	10.7
1500	10.5	22.5	19.8	11.3	11.3	11.3
1600	10.8	23.8	20.8	11.8	11.8	11.9
1700	11.1	25.0	21.9	12.3	12.4	12.4
1800	11.3	26.2	23.0	12.9	13.0	13.0
1900	11.5	27.4	24.0	13.4	13.6	13.5
2000	11.8	28.7	25.1	14.0	14.0	14.1
2100	12.1	30.0	26.1	14.6	14.5	14.7
2200	12.3		27.2	15.1	15.0	15.3

*Silverman, *J. Metals*, 5, 631 (1953). Copyright American Institute of Mining, Metallurgical and Petroleum Engineers, Inc.

TABLE 2-330 Thermal Conductivities of Some Materials for Refrigeration and Building Insulation*
 $k = \text{Btu}/(\text{h}\cdot\text{ft}^2)(^\circ\text{F}/\text{ft})$ at approximately room temperature

Material	Apparent density, lb/cu ft room temp.	k
Soft flexible materials in sheet form:		
Chemically treated wood fiber	2.2	0.023
Eel grass between paper	3.4–4.6	0.021–0.022
Felted cattle hair	11–13	0.022
Flax fibers between paper	4.9	.023
Hair and asbestos fibers, felted	7.8	.023
Insulating hair, and jute	6.1–6.3	0.022–0.023
Jute and asbestos fibers, felted	10.0	0.031
Loose materials:		
Cork, regrulated, fine particles	8–9	.025
Charcoal, 6 mesh	15.2	.031
Diatomaceous earth, powdered	10.6	.026
Glass wool, curled	4–10	.024
Gypsum in powdered form	26–34	0.043–0.05
Mineral wool, fibrous	6	0.0217
	10	.0225
	14	.0233
	18	.0242
Sawdust	12	.034
Wood shavings, from planer	8.8	.034
Semiflexible materials in sheet form:		
Flax fiber	13.0	.026
Semirigid materials in board form:		
Corkboard	7.0	.0225
	10.6	.025
Mineral wool, block, with binder	16.7	.031
Stiff fibrous materials in sheet form:		
Wood pulp	16.2–16.9	.028
Sugar-cane fiber	13.2–14.8	.028
Cellular gypsum	8	.029
	12	.037
	18	.049
	24	.064
	30	.083

*Abstracted from *U.S. Bur. Standards Letter Circ.* 227, Apr. 19, 1927.

TABLE 2-331 Thermal Conductivities of Insulating Materials at High Temperatures*
 $k = \text{Btu}/(\text{h}\cdot\text{ft}^2)(^\circ\text{F}/\text{ft})$

Material	For temperatures, °F up to	Mean temperatures, °F										
		100	200	300	400	500	600	800	1000	1500	2000	
Laminated asbestos felt (approx. 40 laminations per in)	700	0.033	0.037	0.040	0.044	0.048						
Laminated asbestos felt (approx. 20 laminations per in)	500	.045	.050	.055	.060	.065						
Corrugated asbestos (4 plies per in)	300	.050	.058	.069								
85% magnesia (density, 13 lb/ft ³)	600	.034	.036	.038	.040							
Diatomaceous earth, asbestos and bonding material	1600	.045	.047	.049	.050	.053	0.055	0.060	0.065			
Diatomaceous earth brick	1600	.054	.056	.058	.060	.063	.065	.069	.073			
Diatomaceous earth brick	2000	.127	.130	.133	.137	.140	.143	.150	.158	0.176		
Diatomaceous earth brick	2500	.128	.131	.135	.139	.143	.148	.155	.163	.183	0.203	
Diatomaceous earth powder (density, 18 lb/ft ³)		.039	.042	.044	.048	.051	.054	.061	.068			
Rock wool		.030	.034	.039	.044	.050	.057					

Asbestos cement, 1.2; 85% magnesia cement, 0.05; asbestos and rock wool cement, 0.075 approx.

*Marks, *Mechanical Engineers Handbook*, 4th ed., McGraw-Hill, New York, 1941.

2-462 PHYSICAL AND CHEMICAL DATA

TABLE 2-332 Thermal Conductivities of Insulating Materials at Moderate Temperatures (Nusselt)*
 $k = \text{Btu}/(\text{h}\cdot\text{ft}^2)(^\circ\text{F}/\text{ft})$

Material	Weight, lb/cu ft	Temperatures, °F						
		32	100	200	300	400	600	800
Asbestos	36.0	0.087	0.097	0.110	0.117	0.121	0.125	0.130
Burned infusorial earth for pipe coverings	12.5	.043	.046	.052	.057	.062	.073	.085
Insulating composition (loose)	25.0	.040	.046	.050	.053	.055		
Cotton	5.0	.032	.035	.039				
Silk hair	9.1	.026	.030	.034				
Silk	6.3	.025	.028	.034				
Wool	8.5	.022	.027	.033				
Pulverized cork	10.0	.021	.026	.032				
Infusorial earth (loose)	22.0	.035	.039	.045	.047	.050	.053	

*Marks, *Mechanical Engineers' Handbook*, 4th ed., McGraw-Hill, New York, 1941.

TABLE 2-333 Thermal Conductivities of Insulating Materials at Low Temperatures (Gröber)*
 $k = \text{Btu}/(\text{h}\cdot\text{ft}^2)(^\circ\text{F}/\text{ft})$

Material	Weight, lb/cu ft	Temperatures, °F				
		32	-50	-100	-200	-300
Asbestos	44.0	0.135	0.132	0.130	0.125	0.100
Asbestos	29.0	.0894	.0860	.0820	.0720	.0545
Cotton	5.0	.0325	.0302	.0276	.0235	.0198
Silk	6.3	.0290	.0256	.0235	.0196	.0155

*Marks, *Mechanical Engineers' Handbook*, 4th ed., McGraw-Hill, New York, 1941.

TABLE 2-334 Thermal Diffusivity (m^2/s) of Selected Elements*

Element	Temperature, K									
	20	40	60	80	100	200	400	600	800	1000
Aluminum	0.50	0.012	0.0014	4.4. - 4	2.3. - 4	1.1. - 4	9.4. - 5	8.4. - 5	7.4. - 5	6.6. - 5
Beryllium					0.0036	1.5. - 4	4.0. - 5	2.6. - 5	2.1. - 5	1.7. - 5
Chromium	0.038	0.0037	5.9. - 4	2.0. - 4	1.2. - 4	4.1. - 5	2.6. - 5	2.0. - 5	1.7. - 5	1.4. - 5
Copper	0.16	0.0040	6.9. - 4	3.1. - 4	2.2. - 4	1.3. - 4	1.1. - 4	1.0. - 4	9.0. - 5	9.0. - 5
Gold	0.005	4.5. - 4	2.3. - 4	1.8. - 4	1.5. - 4	1.3. - 4	1.2. - 4	1.2. - 4	1.1. - 4	9.8. - 5
Iridium	0.046				8.4. - 5	5.6. - 5	4.8. - 5	4.4. - 5	4.1. - 5	3.5. - 5
Iron	0.043	3.2. - 3	4.9. - 4	1.6. - 4	8.2. - 5	3.1. - 5	1.8. - 5	1.3. - 5	1.1. - 5	1.0. - 5
Lead	9.3. - 5	3.9. - 5	3.3. - 5	3.1. - 5	2.9. - 5	2.6. - 5	2.3. - 5	2.0. - 5	1.3. - 5	1.5. - 5
Molybdenum	0.0095	0.0014	4.0. - 4	2.0. - 4	1.3. - 4	6.3. - 5	5.1. - 5	4.5. - 5	4.2. - 5	3.8. - 5
Nickel	0.033	0.0017	3.1. - 4	1.3. - 4	8.0. - 5	3.1. - 5	1.9. - 5	1.3. - 5	1.4. - 5	1.5. - 5
Platinum	0.0029	1.6. - 4	6.3. - 5	4.3. - 5	3.6. - 5	2.7. - 5	2.5. - 5	2.5. - 5	2.5. - 5	2.5. - 5
Silver	0.031	0.0013	4.5. - 4	2.8. - 4	2.3. - 4	1.8. - 4	1.7. - 4	1.6. - 4	1.5. - 4	1.4. - 4
Zinc	0.0046	3.1. - 4	1.0. - 4	7.0. - 5	5.5. - 5	4.7. - 5	3.9. - 5	3.4. - 5	1.8. - 5	2.2. - 5

*Tables for up to 24 temperatures for 47 elements appear in the *Handbook of Heat Transfer*, 2d ed., McGraw-Hill, New York, 1984. The notation 3.2. - 4 signifies 2.3×10^{-4} .

TABLE 2-335 Thermophysical Properties of Selected Nonmetallic Solid Substances

Material	Density, kg/m ³	Emissivity	Specific heat, kJ/(kg·K)	Thermal conductivity, W/(m·K)	Thermal diffusivity, m ² /s × 10 ⁶
Alumina	3975		0.765	36	11.9
Asphalt	2110		0.920	0.06	0.03
Bakelite	1300		1.465	1.4	0.74
Beryllia	3000	0.82	1.030	270	88
Brick	1925	0.93	0.835	0.72	0.45
Brick, fireclay	2640	0.93	0.960	1.0	0.39
Carbon, amorphous	1950	0.86	0.724	1.6	1.13
Clay	1460	0.91	0.880	1.3	1.01
Coal	1350	0.80	1.26	0.26	0.15
Cotton	80		1.30	0.06	0.58
Diamond	3500		0.509	2300	1290
Granite	2630		0.775	2.79	1.37
Hardboard	1000		1.38	0.15	0.11
Magnesite	3025	0.38	1.13	4.0	1.2
Magnesia	3635	0.72	0.943	48	14
Oak	770	0.90	2.38	0.18	0.10
Paper	930	0.83	1.34	0.011	0.01
Pine	525	0.84	2.75	0.12	0.54
Plaster board	800	0.91		0.17	
Plywood	540		1.22	0.12	0.18
Pyrex	2250	0.92	0.835	1.4	0.74
Rubber	1150	0.92	2.00	0.2	0.09
Rubber, foam	70	0.90		0.03	
Salt		0.34	0.854	7.1	
Sandstone	2150	0.59	0.745	2.9	1.8
Silica		0.79	0.743	1.3	
Sapphire	3975	0.48	0.765	46	15
Silicon carbide	3160	0.86	0.675	110	230
Soil	2050	0.38	1.84	0.52	0.14
Teflon	2200	0.92	0.35	0.26	0.34
Thoria	4160	0.28	0.71	14	4.7
Urethane foam	70		1.05	0.03	0.36
Vermiculite	120		0.84	0.06	0.60

NOTE: Difficulties of accurately characterizing many of the specimens mean that many of the values presented here must be regarded as being of order of magnitude only. For some materials, actual measurement may be the only way to obtain data of the required accuracy. To convert kilograms per cubic meter to pounds per cubic foot, multiply by 0.062428; to convert kilojoules per kilogram-kelvin to British thermal units per pound-degree Fahrenheit, multiply by 0.23885.

PREDICTION AND CORRELATION OF PHYSICAL PROPERTIES*

INTRODUCTION

Physical property values, sufficiently accurate for many engineering applications, can be estimated in the absence of reliable experimental data. The purpose of this subsection is to provide a set of recommended prediction methods for general engineering use; it is not a comprehensive review, and many alternative methods are available in the literature. Methods recommended were selected on the basis of accuracy, generality, and, in most cases, simplicity. They generally correspond to the methods tested and given priority in the DIPPR® 801 database project.†

Properties included in this subsection are divided into 10 categories: (1) physical constants: critical properties, normal melting and boiling points, acentric factor, radius of gyration, and dipole moment; (2) vapor

pressure: liquid and solid; (3) thermal properties: enthalpy and Gibbs' energy of formation and ideal gas entropy; (4) latent enthalpy: vaporization, fusion, and sublimation; (5) heat capacity: ideal gas, gas, liquid, and solid; (6) density: gas, liquid, and solid; (7) viscosity: gas and liquid; (8) thermal conductivity: gas and liquid; (9) surface tension; and (10) flammability properties: flash point, flammability limits, and autoignition temperature. Each of the 10 subsections provides a definition of the relevant properties and a description of one or more recommended prediction methods. Each description lists the type of method, its uncertainty, its limitations, and the expected uncertainty of the predicted value. A numerical example is also given to illustrate use of the method. For brevity, symbols used for physical properties and for variables and constants in the equations are defined under Nomenclature and are not generally defined after their use except where doing so clarifies usage. A list of equation and table numbers in which variables appear is included in the Nomenclature section for quick cross-referencing. Although emphasis is on pure-component properties, some mixture estimation techniques have been included for physical constants, density, viscosity, thermal conductivity, surface tension, and flammability. Correlation and estimation of properties that are inherently multicomponent (e.g., diffusion coefficients, mixture excess properties, activity coefficients, etc.) are treated elsewhere in the Handbook.

*Some material in this subsection has been retained from the corresponding subsection in the Seventh Edition, which was coauthored by Thomas E. Daubert and Evan Buck.

†The Design Institute for Physical Properties (DIPPR®) is an industrial consortium under the auspices of AIChE; Project 801, Evaluated Process Design Data, is a pure-component database of industrially important compounds.

UNITS

The International Metric System (SI) of units has been used throughout this subsection. Where possible, the estimation equations are set up in dimensionless groups. This makes transparent any conversion factors that should be applied to obtain the property in a desired set of units and eliminates the requirement of specific units for variables. For example, rather than use P_c as a variable with defined units, the dimensionless group P_c/P_a is used. When a value for P_c expressed in

any units (say, $P_c = 6.53$ MPa) is inserted into this group, the result is dimensionless with an explicit indication of conversion factors that must be included:

$$\frac{P_c}{P_a} = \frac{6.53 \text{ MPa}}{\text{Pa}} = \left(\frac{6.53 \text{ MPa}}{\text{Pa}} \right) \left(\frac{10^6 \text{ Pa}}{\text{MPa}} \right) = 6.53 \times 10^6$$

Section 1 of this handbook should be used for appropriate unit conversion factors.

Nomenclature

Physical constants	Definition	Value
h	Planck's constant	$6.626 \times 10^{-34} \text{ J}\cdot\text{s}$
k	Boltzmann's constant	$1.3806 \times 10^{-23} \text{ J}/(\text{molecule}\cdot\text{K})$
N_A	Avogadro's number	$6.022 \times 10^{26} \text{ molecule}/\text{kmol}$
R	Gas constant	$8.3143 \text{ Pa}\cdot\text{m}^3/(\text{kmol}\cdot\text{K})$
Properties	Definition	Typical units
A, B, C	Molecular principal moments of inertia	$\text{kg}\cdot\text{m}^2$
$B, B(T)$	Second virial coefficient	m^3/kmol
B_m	Second virial coefficient for a mixture	m^3/kmol
C_p	Constant-pressure molar heat capacity	$\text{J}/(\text{kmol}\cdot\text{K})$
$C_{p,i}$	Ideal gas constant-pressure molar heat capacity	$\text{J}/(\text{kmol}\cdot\text{K})$
C_v	Constant-volume molar heat capacity	$\text{J}/(\text{kmol}\cdot\text{K})$
H_i	Enthalpy of compound i	J/kmol
k	Thermal conductivity	$\text{W}/(\text{m}\cdot\text{K})$
k_b	Thermal conductivity at T_b	$\text{W}/(\text{m}\cdot\text{K})$
LFL	Lower flammability limit	%
M	Molecular weight	kg/kmol
P	Pressure	Pa
P	Parachor	unitless
P_c	Critical pressure	Pa
P_r	Reduced pressure; $P_r = P/P_c$	unitless
P^*	Vapor pressure	Pa
P^*_{meas}	Measured vapor pressure value	Pa
P_r^*	Reduced vapor pressure; $P_r^* = P^*/P_c$	unitless
P_t^*	Vapor pressure at triple point	Pa
R_g	Radius of gyration	m
S°	Ideal gas entropy	$\text{J}/(\text{kmol}\cdot\text{K})$
S°	Standard state entropy	$\text{J}/(\text{kmol}\cdot\text{K})$
S_r	Rotational contribution to entropy	$\text{J}/(\text{kmol}\cdot\text{K})$
S_{vib}	Vibrational contribution to entropy	$\text{J}/(\text{kmol}\cdot\text{K})$
T	Temperature	K
T_b	Normal boiling point temperature	K
T_{br}	Reduced temperature at T_b ; $T_{br} = T_b/T_c$	unitless
T_c	Critical temperature	K
T_m	Melting temperature	K
T_{meas}	T at which a dependent property was measured	K
T_r	Reduced temperature; $T_r = T/T_c$	unitless
T_t	Triple point temperature	K
UFL	Upper flammability limit	%
V	Molar volume	m^3/kmol
V_m	Mixture molar volume	m^3/kmol
V_r	Reduced volume; $V_r = ZT_r/P_r$	unitless
w_i	Mass fraction of component i	unitless
x_i	Mole fraction of component i	unitless
y_i	Mole fraction of component i in vapor phase	unitless
Z	Compressibility factor; $Z = PV/RT$	unitless
Z_c	Critical compressibility factor; $Z_c = P_c V_c / RT_c$	unitless
Z_i	Compressibility factor of reference fluid i	unitless
ΔG_f°	Ideal gas standard Gibbs energy of formation	J/kmol
ΔG_f°	Standard state Gibbs energy of formation	J/kmol
ΔH_f°	Ideal gas standard enthalpy of formation	J/kmol
ΔH_f°	Standard state enthalpy of formation	J/kmol
ΔH_{fus}	Enthalpy of fusion	J/kmol
ΔH_{rxn}	Enthalpy change per mole of reaction as written	J/kmol
ΔH_{sub}	Enthalpy of sublimation	J/kmol
ΔH_v	Enthalpy of vaporization	J/kmol
ΔS_f°	Standard state entropy of formation	$\text{J}/(\text{kmol}\cdot\text{K})$
ΔS_f°	Ideal gas entropy of formation	$\text{J}/(\text{kmol}\cdot\text{K})$
ΔS_{fus}	Latent entropy of fusion	$\text{J}/(\text{kmol}\cdot\text{K})$
ΔZ_v	Change in compressibility factor upon vaporization	unitless
ρ	Molar density; $\rho = V^{-1}$	kmol/m^3
ρ_c	Critical molar density; $\rho_c = V_c^{-1}$	kmol/m^3

Nomenclature (*Continued*)

Properties	Definition	Typical units
ρ_r	Reduced molar density; $\rho_r = \rho/\rho_c$	unitless
ω	Acentric factor	unitless
η	Viscosity	Pa·s
η^o	Viscosity at low pressure	Pa·s
σ	Surface tension	mN/m
σ_m	Surface tension of mixture	mN/m
τ	Complementary reduced temperature ($= 1 - T_r$)	unitless
τ_b	Complementary reduced normal boiling temperature ($= 1 - T_{br}$)	unitless
μ	Dipole moment	D
μ_r	Reduced dipole moment [defined in Eq. (2-62)]	unitless
Eq. variables	Definition	(Equations), [Tables]
a	EoS constant	(2-66), [2-354]
a, b, c, \dots	GC values for C_p and η	(2-51), (2-52), (2-53), (2-97), [2-356]
a, b, c	Correlation coefficients	(2-21), (2-23)
a_i	GC values	(2-43), (2-97), [2-346, 2-356]
a, b	Terms in second virial correlation	(2-61)
a, b	Chickos correlation parameters	(2-39), (2-40), (2-41)
a_i, b_i, d_i	GC values for liquid C_p	(2-51), [2-348]
$\bar{a}, \bar{\alpha}$	EoS constant for mixture	(2-76)
A, B, C, \dots	Correlation constants/parameters	(2-2), (2-20), (2-22), (2-34), (2-36), (2-50), (2-65), (2-68), (2-83), (2-85), (2-87), (2-88), (2-95), (2-96), (2-101), above (2-114)
A	Factor in liquid k correlation	(2-108), [2-358]
A_i	Constants in C_p^o correlation	(2-45), (2-46)
b	EoS constant	(2-66), [2-354]
b_b, c_b, \dots	Reference EoS constants	(2-65), [2-353]
\bar{b}_i	GC value for AIT	(2-124), [2-363, 2-364]
\bar{b}	EoS constant for mixture	(2-75)
$B^{(i)}$	Second virial expansion terms	(2-58), (2-59), (2-60), (2-61)
C	Number of components in mixture	(2-55), (2-72), (2-73), (2-74), (2-75), (2-76), (2-77), (2-80), (2-81), (2-82), (2-98), (2-113), (2-119)
C_i	GC values for T_b or η	(2-15), (2-87), [2-341, 2-355]
$C_{i,int}$	Sum of intramolecular group-group interactions	(2-16)
C_{ij}	Group-group intramolecular interaction pair	(2-16), [2-342]
$(C_p^o)_i$	GC values for ideal gas heat capacity	(2-49), [2-347]
C_{sj}	Chickos: GC value for C—H group	(2-41), [2-344]
C_{tj}	Chickos: GC value for functional group	(2-41), [2-345]
f_i	Halogen correction for ΔH_{sub} correlation	(2-43), [2-346]
$f^{(i)}$	Vapor pressure deviation function	(2-25)
F	Factor in surface tension equation	(2-116), (2-117)
G_{ij}	Adjustable mixture viscosity parameter	(2-98)
g_{sr}^E	UNIFAC combinatorial excess Gibbs energy	(2-99)
g_r^E	UNIFAC residual excess Gibbs energy	(2-99)
h	Parameter in Riedel vapor pressure equation	following (2-24)
K	Parameter in Riedel vapor pressure equation	following (2-24)
LFL_i	GC contribution	(2-122), [2-361, 2-362]
n	Number of nonhydrogen atoms	(2-15)
n_A	Number of atoms in molecule	(2-1), (2-30), (2-31), (2-48)
n_E	Number of occurrences of element E in compound	(2-54)
n_i	Number of occurrences of group i	(2-27), (2-43), (2-49), (2-51), (2-53), (2-87), (2-109), (2-115), (2-122), (2-123), (2-124)
n_f	Chickos: no. of different functional groups	(2-41)
n_s	Chickos: no. of different nonring or aromatic C—H groups bonded to functional groups	(2-41)
n_x	Total no. of halogen and H atoms attached to C and Si atoms for ΔH_{sub} correlation	(2-43)
N	Total number of groups in molecule	(2-12), (2-15) (2-16), (2-43), (2-49), (2-51), (2-53), (2-54), (2-87), (2-97), (2-109), (2-115)
N_C	Number of C atoms	(2-121)
N_f^i	Chickos: no. of functional groups of type i	(2-41)
N_g^i	Chickos: no. of C—H groups of type i bonded to other C atoms	(2-41)
N_H	Number of H atoms	(2-121)

Nomenclature (Continued)

Eq. variables	Definition	(Equations), [Tables]
N_{CR}	Chickos: no. of CH ₂ groups in nonaromatic ring to form cyclic paraffin of same ring size	(2-40)
N_O	Chickos: Number of O atoms	(2-121)
N_R	Chickos: no. of nonaromatic rings	(2-40)
N_S	Chickos: Number of S atoms	(2-121)
N_{S_i}	Chickos: no. of C—H groups of type i bonded to at least one functional group	(2-41)
N_X	Number of halogen atoms	(2-121)
\bar{P}_c	Pseudocritical pressure for mixture	(2-73)
$P_{c,ij}$	Cross term in mixing rule	(2-79)
q	Rackett equation power for Z_c	(2-69), (2-70), (2-81)
q_i	UNIFAC molecular surface area	following (2-100)
Q_k	UNIFAC group surface area	following (2-100)
r_i	UNIFAC molecular volume	following (2-100)
r°	Dimensionless separation distance	(2-4)
R_k	UNIFAC group volume	following (2-100)
$(S^\circ)_i$	GC value for entropy	(2-27), [2-343]
t	Chickos: total no. of functional groups	(2-41)
$t_{m1,i}$	First-order GC contribution for T_m	(2-13), [2-339]
$t_{m2,i}$	Second-order GC contribution for T_m	(2-13), [2-340]
\bar{T}_c	Pseudocritical temperature for mixture	(2-72), (2-73), (2-80)
$T_{c,ij}$	Cross term in mixing rule	(2-78), (2-80)
x_P	Term in Pailhes method = $\log(1 \text{ atm}/P)$	(2-14)
U°	Dimensionless intermolecular potential	(2-4)
UFL_i	GC contribution	(2-123), [2-361, 2-362]
$V_{c,ij}$	Cross term in mixing rule	(2-78), (2-79)
$Z^{(0)}$	Compressibility factor of simple fluid	(2-63), (2-64), [2-351]
$Z^{(1)}$	Acentric deviation term for Z	(2-63), (2-64), [2-352]
$Z_{c,ij}$	Cross term in mixing rule	(2-78), (2-79)
Z_{RA}	Modified Rackett correlation parameter	(2-70)
Z_{RA}	Modified Rackett parameter for mixture	(2-82)
$\alpha, \beta, \gamma, \dots$	Correlation parameters for k	(2-106), (2-107), (2-108), (2-109), [2-358]
$\alpha(T_r)$	EoS temperature-dependent function	(2-66), [2-354]
α_c	Parameter in Riedel vapor pressure equation	following (2-24)
α_{mn}	Viscosity group-group interactions	(2-100), [2-357]
β	Reference EoS constant	(2-65), [2-353]
β	Stoichiometric coefficient in FP correlation	(2-120), (2-121)
β_i	Nonlinear correction term in correlation	(2-43), (2-53), [2-346, 2-349]
γ	Reference EoS constant	(2-65), [2-353]
δ	= 0 for nonlinear molecules; = 1 for linear	(2-1), (2-48)
δ	EoS parameter	(2-66), [2-354]
Δ_E	Contribution of element E to heat capacity	(2-54), [2-350]
Δ_P	GC contribution to P_c	(2-7), (2-10), [2-336, 2-337]
Δ_T	GC contribution to T_c	(2-6), (2-9), [2-336, 2-337]
Δ_V	GC contribution to V_c	(2-8), (2-11), [2-336, 2-337]
$(\Delta H_f^\circ)_i$	GC value for enthalpy of formation	(2-27), [2-343]
Δk_i	GC for thermal conductivity at T_b	(2-109), [2-359]
ΔP_i	GC for parachor	(2-115), [2-360]
ΔS_i	Chickos: GC value for group i	(2-41), [2-344, 2-345]
ε	Lennard-Jones well depth parameter	following (2-4)
ε	EoS parameter	(2-66), [2-354]
ϕ	UNIFAC molecular volume fraction	following (2-100)
ϕ_i	Volume fraction of component i	(2-80), following (2-100), (2-113)
ν_i	Stoichiometric coefficient (+ for product and - for reactant) for compound i in reaction	(2-28), (2-29), (2-30)
ν_j	Frequency of vibrational mode j	(2-47)
θ	UNIFAC molecular surface fraction	following (2-100)
Θ	UNIFAC group surface fraction	following (2-100)
$\Theta_A, \Theta_B, \Theta_C$	Characteristic rotational T of molecule	before and following (2-31)
Θ_j	Characteristic vibrational T of mode j	(2-1), (2-31), (2-48)
σ	Lennard-Jones size parameter	(2-4)
σ	Rotational external symmetry number	following (2-31)
μ_r°	Modified reduced dipole moment	(2-85), (2-86)
ψ	Parameter in Riedel vapor pressure equation	following (2-24)
Ψ	Parameter in correlation of k for gases	(2-106)
Ψ_{mn}	UNIFAC interaction factor	(2-100)
ξ	Viscosity dedimensionalizing factor	(2-89), (2-90), (2-91), (2-92), (2-93), (2-94)
ω	Pseudoacentric factor for mixture	(2-74)
ω_j	Cross term in mixing rule	(2-79)

Acronyms and abbreviations

Definition

CC	Computational chemistry
CS	Corresponding states
DIPPR®	Design Institute for Physical Properties
EoS	Equation of state

Nomenclature (Concluded)

Acronyms and abbreviations	Definition
GC	Group contributions
LJ	Lennard-Jones
MC	Monte Carlo
MD	Molecular dynamics
QSPR	Quantitative structure-property relationships
TRC	Thermodynamics Research Center

GENERAL REFERENCES
(a) Prediction methods:

- [PGLA] Reid, R. C., J. M. Prausnitz, and B. E. Poling, *The Properties of Gases and Liquids*, 4th ed., McGraw-Hill, New York, 1987.
 [PGL5] Poling, B. E., J. M. Prausnitz, and J. P. O'Connell, *The Properties of Gases and Liquids*, 5th ed., McGraw-Hill, New York, 2001.

(b) Property databases:

- [DIPPR] Rowley, R. L., et al., *DIPPR® Data Compilation of Pure Chemicals Properties*, Design Institute for Physical Properties, AIChE, New York, 2007.
 [TRC] *TRC Thermodynamic Tables—Non-Hydrocarbons*, Thermodynamics Research Center, The Texas A&M University System, College Station, Tex., extant 2004; *TRC Thermodynamic Tables—Hydrocarbons*, Thermodynamics Research Center, The Texas A&M University System, College Station, Tex., extant 2004.
 [JANAF] Chase, M. W., Jr., et al., "JANAF Thermochemical Tables," *J. Phys. Chem. Ref. Data*, **14**, suppl. 1, 1985.
 [SWS] Stull, D. R., F. F. Westrum, Jr., and G. C. Sinke, *The Chemical Thermodynamics of Organic Compounds*, John Wiley & Sons, New York, 1969.

CLASSIFICATION OF ESTIMATION METHODS

Physical property estimation methods may be classified into six general areas: (1) theory and empirical extension of theory, (2) corresponding states, (3) group contributions, (4) computational chemistry, (5) empirical and quantitative structure property relations (QSPR) correlations, and (6) molecular simulation. A quick overview of each class is given below to provide context for the methods and to define the general assumptions, accuracies, and limitations inherent in each.

Theory and Empirical Extension of Theory Methods based on theory generally provide better extrapolation capability than empirical fits of experimental data. Assumptions required to simplify the theory to a manageable equation suggest accuracy limitations and possible improvements, if necessary. For example, the ideal gas isobaric heat capacity, rigorously obtained from statistical mechanics under the assumption of independent harmonic vibrational modes, is [Rowley, R. L., *Statistical Mechanics for Thermophysical Property Calculations*, Prentice-Hall, Englewood Cliffs, N.J., 1994]

$$\frac{C_p^\circ}{R} = \frac{8 - \delta}{2} + \sum_{j=1}^{3n_A - 6 + \delta} \left(\frac{\Theta_j}{T} \right)^2 \frac{e^{\Theta_j/T}}{(e^{\Theta_j/T} - 1)^2}$$

$$\delta = \begin{cases} 0 & \text{nonlinear molecules} \\ 1 & \text{linear molecules} \end{cases} \quad (2-1)$$

where Θ_j is the characteristic temperature for the j th vibrational frequency in a molecule of n_A atoms. The temperature dependence of this equation is exact to the extent that the frequencies are harmonic. Corrections for anharmonicity can be applied (albeit with difficulty) where warranted.

Extension of theory often requires introduction of empirical models and parameters in lieu of terms that cannot be rigorously calculated. Good accuracy is expected in the region where the model parameters were fitted to experimental data, but only limited accuracy when an empirical model is extrapolated to other conditions. For example, a simplified theory suggests that vapor pressure should have the form

$$\ln P^\circ = A - \frac{B}{T} \quad (2-2)$$

where the empirical parameter B is given by

$$B = \frac{\Delta H_v}{R\Delta Z_v} \quad (2-3)$$

and ΔH_v and ΔZ_v are differences between the vapor and liquid enthalpies and compressibility factors, respectively. Vapor pressures over a narrow temperature range can be effectively correlated using Eq. (2-2), but this equation should not be used to extrapolate vapor pressures over a wide range of temperatures.

Corresponding States (CS) The principle of CS applies to conformal fluids [Leland, T. L., Jr., and P. S. Chappelaar, *Ind. Eng. Chem.*, **60** (1968): 15]. Two fluids are conformal if their intermolecular interactions are equivalent when scaled in dimensionless form. For example, the Lennard-Jones (LJ) intermolecular pair potential energy U can be written in dimensionless form as

$$U^\circ = 4[(r^\circ)^{-12} - r^\circ^{-6}] \quad (2-4)$$

where $r^\circ = r/\sigma$, $U^\circ = U/\epsilon$, σ is the LJ size parameter, and ϵ is the LJ attractive well depth parameter. At equivalent scaled temperatures kT/ϵ (k is Boltzmann's constant) and pressures $P\sigma^3/\epsilon$, all LJ fluids will have identical dimensionless properties because the molecules interact through the identical scaled intermolecular potential given by Eq. (2-4). Generalization of this scaling principle is commonly done using critical temperature T_c and critical pressure P_c as scaling factors. At the same reduced coordinates ($T_r = T/T_c$ and $P_r = P/P_c$) all conformal fluids will have the same dimensionless properties; for example, $Z = Z(T_r, P_r)$ where the compressibility factor is defined as $Z = PV/RT$. A correlation of experimental data for one fluid can be used as the reference for the properties of all conformal fluids. Nonconformality is the main accuracy limitation. For instance, interactions between non-spherical or polar molecules may not be adequately represented by Eq. (2-4), and so the scaled properties of these fluids will not conform to those of a fluid with interactions well represented by Eq. (2-4). A correction for nonconformality is usually made by the addition of one or more reference fluids whose deviations from the first reference fluid are used to characterize the effect of nonconformality. For example, in the Lee-Kesler method [Lee, B. I., and M. G. Kesler, *AIChE J.*, **21** (1975): 510] n -octane is used as a second, nonspherical reference fluid, and deviations of n -octane scaled properties from those of the spherical reference fluid at equivalent reduced conditions are assumed to be a linear function of the acentric factor. An extended Lee-Kesler method [Wilding, W. V., and R. L. Rowley, *Int. J. Thermophys.*, **7** (1986): 525] uses three reference fluids: n -octane to correct for size-shape nonconformality relative to methane and water to correct for polar effects. Some CS methods [e.g., Teja, A., S. I. Sandler, and N. C. Patel, *Chem. Eng. J.*, **21** (1981): 21] utilize different reference fluids for different classes of fluids to maintain close conformality between the fluid whose properties are to be estimated and the reference fluids.

Group Contributions (GC) Chemical and physical properties generally correlate well with molecular structure. GC methods assume a summative behavior of the structural groups of the constituent molecules. For example, ethanol ($\text{CH}_3\text{—CH}_2\text{—OH}$) properties would be obtained as the sum of contributions from the —CH_3 , —CH_2 , and —OH groups. The contribution of each group is obtained by regression of experimental data that include as many different compounds containing that group as possible. Structural groups must be used exactly as defined in the original correlation. A general principle in deciding how to make the groupings is to give the more specific group priority. For example, although the structural piece —COOCH_3 is ambiguous in a methyl ester, a more specific group value available for an ester —COO— would take precedence over a combination the two smaller groups —(C=O)— and

—O— whose values were most likely regressed only from ketone and ether data, respectively. Excellent accuracy can usually be expected from GC methods when group values were regressed from large quantities of experimental data. However, if the ratio of number of groups to regressed experimental data is large, significant errors can result when the method is applied to new compounds (extrapolation). Such excessive specificity in the group definitions leads to poor extrapolation capabilities even though the fit of the regressed data may be excellent.

Computational Chemistry (CC) Commercial software is available that solves the Schrödinger equation for approximate forms of the wave function. Various levels of sophistication (termed *model chemistry*) for the wave function can be chosen at the expense of computational time. Results include structural information (bond lengths, bond angles, dihedral angles, etc.), electron/charge distribution information, internal vibrational modes (for ideal gas properties), and energy of the molecule, valid for the chosen model chemistry. Because calculations are performed on individual molecules, they are primarily suited for ideal gas properties. Relative energies for the same model chemistry are more accurately obtained than absolute energies, so enthalpies and entropies of reaction are common industrial uses of CC predictions in addition to individual structural and ideal gas properties.

Empirical QSPR Correlations In quantitative structure property relationship (QSPR) methods, physical properties are correlated with molecular descriptors that characterize the molecular and electronic structure of the molecule. Large amounts of experimental data are used to statistically determine the most significant descriptors to be used in the correlation and their contributions. The resultant correlations are simple to apply if the descriptors are available. Descriptors must generally be generated by the user with computational chemistry software, although the DIPPR® 801 database now contains a table of molecular descriptors for most of the compounds in it. QSPR methods are often very accurate for specific families of compounds for which the correlation was developed, but extrapolation problems are even more of an issue than with GC methods.

Molecular Simulations Molecular simulations are useful for predicting properties of bulk fluids and solids. Molecular dynamics (MD) simulations solve Newton's equations of motion for a small number (on the order of 10^3) of molecules to obtain the time evolution of the system. MD methods can be used for equilibrium and transport properties. Monte Carlo (MC) simulations use a model for the potential energy between molecules to simulate configurations of the molecules in proportion to their probability of occurrence. Statistical averages of MC configurations are useful for equilibrium properties, particularly for saturated densities, vapor pressures, etc. Property estimations using molecular simulation techniques are not illustrated in the remainder of this section as commercial software implementations are not generally available at this time.

PHYSICAL CONSTANTS

Critical Properties The critical temperature T_c , pressure P_c , and volume V_c of a compound are important, widely used constants. They are important in determining the phase boundaries of a compound and (particularly T_c and P_c) are required input parameters for most thermal and volumetric property calculations of the equilibrium phases using CS or analytical equations of state. Most estimation methods employ weighted group, atom, or bond contributions.

The critical temperature of a compound is the temperature above which a liquid phase cannot be formed, no matter the pressure of the system. The critical pressure is the vapor pressure of the compound at the critical temperature. The critical volume is the volume occupied by a set amount of a compound (typically 1 mol) at its critical temperature and pressure.

The critical compressibility factor Z_c is determined from the experimental or predicted values of the critical properties by the definition

$$Z_c = \frac{P_c V_c}{RT_c} \quad (2-5)$$

Recommended Methods

Organic molecules: The Ambrose method is recommended for all three critical properties of hydrocarbons and *n*-alcohols. The Joback method is recommended for T_c and P_c of all other organic molecules. Fedors' method is recommended for V_c of these compounds, but the Joback method can also be used.

Inorganic molecules: The simple correlation $T_c = 1.64T_b$ is recommended if the normal boiling point is known. Critical pressure P_c is best obtained by extrapolating vapor pressure data to T_c , and V_c is best obtained from a correlation of liquid density extrapolated to T_c .

Other recent methods including the Wilson-Jasperson (Wilson, G. M., and L.V. Jasperson, *Critical Constants T_c , P_c , Estimation Based on Zero, First and Second Order Methods*, AIChE Spring Meeting, New Orleans, La., 1996) and Marrero-Pardillo [Marrero-Morejon, J., and E. Pardillo-Fontdevila, *AIChE J.*, **45** (1999): 615] methods have proved to be as good as or better for some classes of compounds than the methods presented here; however, their application is more difficult.

Method: Ambrose method.

Reference: Ambrose, D., Correlation and Estimation of Vapour-Liquid Critical Properties. I. Critical Temperatures of Organic Compounds, *Natl. Phys. Lab. Report Chem.* **92** (1978); Correlation and Estimation of Vapour-Liquid Critical Properties. II. Critical Pressures and Volumes of Organic Compounds, *Natl. Phys. Lab Report Chem.* **98** (1979).

Classification: Group contributions.

Expected uncertainty: ~6 K for T_c (about 1 percent), ~2 bar for P_c (about 5 percent), ~8 cm³/mol for V_c (about 3 percent).

Applicability: Organic compounds.

Input data: T_b , M , group contributions Δ_T , Δ_P , and Δ_V from Table 2-336.

Description: A GC method with first-order contributions and corrections (delta Platt number) for branched alkanes. Variables T_c , P_c , and V_c are given by the following relations:

$$T_c = T_b \left[1 + \left(1.242 + \sum \Delta_T \right)^{-1} \right] \quad (2-6)$$

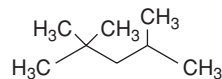
$$\frac{P_c}{\text{bar}} = \frac{M}{\text{kg/kmol}} \left(0.339 + \sum \Delta_P \right)^{-2} \quad (2-7)$$

$$\frac{V_c}{\text{cm}^3/\text{mol}} = 40 + \sum \Delta_V \quad (2-8)$$

Example Use the Ambrose method to estimate the critical constants of 2,2,4-trimethylpentane.

Required data: From the DIPPR® 801 database, $T_b = 372.39$ K and $M = 114.229$ kg/kmol.

Structure:



Group contributions from Table 2-336:

Group	n_i	Δ_T	Δ_P	Δ_V
Alkyl carbons	8	0.138	0.226	55.1
>CH— (correction)	1	-0.043	-0.006	-8
>C< (correction)	1	-0.120	-0.030	-17
Delta Platt no.	0	-0.023	-0.026	—

Calculations using Eqs. (2-6), (2-7), and (2-8):

$$\sum \Delta_T = (8)(0.138) + (1)(-0.043) + (1)(-0.120) = 0.941$$

$$T_c = T_b(1.4581) = (372.39 \text{ K})(1.4581) = 543.0 \text{ K}$$

$$\sum \Delta_P = (8)(0.226) + (1)(-0.006) + (1)(-0.030) = 1.772$$

$$\frac{P_c}{\text{bar}} = \frac{M}{\text{kg/kmol}} \left(0.339 + \sum \Delta_P \right)^{-2} = \frac{114.229}{(0.339 + 1.772)^2} = 25.63$$

$$P_c = 25.63 \text{ bar}$$

TABLE 2-336 Ambrose Group^a Contributions for Critical Constants

Group	Δ_T	Δ_P	Δ_V
Carbon atoms in alkyl groups	0.138	0.226	55.1
Corrections			
>CH— (each)	-0.043	-0.006	-8
>C< (each)	-0.120	-0.030	-17
Double bonds (nonaromatic)	-0.050	-0.065	-20
Triple bonds	-0.200	-0.170	-40
Delta Platt number, ^b multiply by	-0.023	-0.026	—
Aliphatic functional groups:			
—O—	0.138	0.160	20
>CO	0.220	0.282	60
—CHO	0.220	0.220	55
—COOH	0.578	0.450	80
—CO—O—OC—	1.156	0.900	160
—CO—O—	0.330	0.470	80
—NO ₂ —	0.370	0.420	78
—NH ₂	0.208	0.095	30
—NH—	0.208	0.135	30
>N—	0.088	0.170	30
—CN	0.423	0.360	80
—S—	0.105	0.270	55
—SH	0.090	0.270	55
—SiH ₃	0.200	0.460	119
—O—Si(CH ₃) ₂	0.496	—	—
—F	0.055	0.223	14
—Cl	0.055	0.318	45
—Br	0.055	0.500	67
—I	0.055	—	90
Halogen correction in aliphatic compounds:			
F is present	0.125		
F is absent, but Cl, Br, I are present	0.055		
Aliphatic alcohols ^c	<i>d</i>	<i>e</i>	15
Ring compound increments (listed only when different from aliphatic values):			
—CH ₂ —, >CH—, >C<	0.090	0.182	44.5
>CH— in fused ring	0.030	0.182	44.5
Double bond	-0.030	—	-15
—O—	0.090	—	10
—NH—	0.090	—	—
—S—	0.090	—	30
Aromatic compounds:			
Benzene	0.448	0.924	<i>f</i>
Pyridine	0.448	0.850	
C ₆ H ₄ (fused as in naphthalene)	0.220	0.515	
—F	0.080	0.183	
—Cl	0.080	0.318	
—Br	0.080	0.600	
—I	0.080	0.850	
—OH	0.198	-0.025	
Corrections for nonhalogenated substitutions:			
First	0.010	0	
Each subsequent	0.030	0.020	
Ortho pairs containing —OH	-0.080	-0.050	
Ortho pairs with no —OH	-0.040	-0.050	
Highly fluorinated aliphatic compounds:			
—CF ₃ —, —CF ₂ —, >CF—	0.200	0.550	
—CF ₂ —, >CF— (ring)	0.140	0.420	
>CF— (in fused ring)	0.030	—	
—H (monosubstitution)	-0.050	-0.350	
Double bond (nonring)	-0.150	-0.500	
Double bond (ring)	-0.030	—	
(other increments as in nonfluorinated compounds)			

^aAmbrose, D., Correlation and Estimation of Vapour-Liquid Critical Properties. I. Critical Temperatures of Organic Compounds, *Natl. Phys. Lab Report Chem.* **92** (1978); Correlation and Estimation of Vapour-Liquid Critical Properties. II. Critical Pressures and Volumes of Organic Compounds, *Natl. Phys. Lab Report Chem.* **98** (1979).

^bThe delta Platt number is defined as the Platt number of the isomer minus the Platt number of the corresponding alkane. (For *n*-alkanes the Platt number is *n* - 3.) The Platt number is the total number of groups of four carbon atoms three bonds apart [Platt, J. R., *J. Chem. Phys.*, **15**(1947): 419; **56**(1952): 328]. This correction is used only for branched alkanes.

^cIncludes naphthenic alcohols and glycols but not aromatic alcohols such as xylenol.

^dFirst determine the hydrocarbon homomorph, i.e., substitute —CH₃ for each —OH and calculate $\sum \Delta_T$ for this compound. Subtract 0.138 from $\sum \Delta_T$ for each —OH substituted. Next, add $0.87 - 0.11n + 0.003n^2$ where $n = [T_c/K(\text{alcohol}) - 314]/19.2$. Exceptions include methanol ($\sum \Delta_T = 0$), ethanol ($\sum \Delta_T = 0.939$), and any alcohol whose value of *n* exceeds 10.

^eDetermine the hydrocarbon homomorph as in footnote *d*. Calculate $\sum \Delta_P$ and subtract 0.226 for each —OH substituted. Add $0.100 - 0.013n$, where *n* is computed as in footnote *d*.

^fWhen estimating the critical volumes of aromatic substances, use ring compound values, if available, and correct for double bonds.

2-470 PHYSICAL AND CHEMICAL DATA

$$\sum \Delta_V = (8)(55.1) + (1)(-8) + (1)(-17) = 415.8$$

$$V_c = (40 + 415.8) \text{ cm}^3/\text{mol} = 455.8 \text{ cm}^3/\text{mol}$$

Results:

Property	DIPPR [®] recommended value	Ambrose estimation	% Difference
T_c/K	543.8	543.0	-0.15
P_c/bar	25.70	25.63	0.27
$V_c/(\text{cm}^3/\text{mol})$	468.0	455.8	-2.6

Method: Joback method.

Reference: Joback, K. G., M.S. Thesis in Chemical Engineering, Massachusetts Institute of Technology, Cambridge, Mass., June 1984.

Classification: Group contributions.

Expected uncertainty: 7 K (~1 percent) for T_c ; 2 bar (~5 percent) for P_c .

Applicability: Organic compounds.

Input data: T_b , group contributions Δ_T , Δ_P , Δ_V from Table 2-337, and the number of atoms in the molecule n_A .

Description: A GC method with first-order contributions. Variables T_c , P_c , and V_c are given by the following relations:

$$T_c = T_b \left[0.584 + 0.965 \sum \Delta_T - \left(\sum \Delta_T \right)^2 \right]^{-1} \quad (2-9)$$

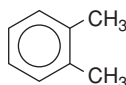
$$\frac{P_c}{\text{bar}} = \left(0.113 + 0.0032 n_A - \sum \Delta_P \right)^{-2} \quad (2-10)$$

$$\frac{V_c}{\text{cm}^3/\text{mol}} = 17.5 + \sum \Delta_V \quad (2-11)$$

where Δ_T , Δ_P , Δ_V are group contributions from Table 2-337 and n_A is the number of atoms in the molecule.

Example Estimate the critical constants of *o*-xylene by using the Joback method.

Structure:



Required input data: From the DIPPR[®] 801 database, $T_b = 417.58 \text{ K}$. From Table 2-337:

Group	n_i	Δ_T	Δ_P	Δ_V
—CH— (ring)	4	0.0082	0.0011	41
>C< (ring)	2	0.0143	0.0008	32
—CH_3	2	0.0141	-0.0012	65

From Eqs. (2-9), (2-10), and (2-11):

$$\sum \Delta_T = (4)(0.0082) + (2)(0.0143) + (2)(0.0141) = 0.0896$$

$$T_c = T_b [0.584 + 0.965 (0.896) - (0.896)^2]^{-1}$$

$$T_c = T_b (1.5096) = (417.58 \text{ K})(1.5096) = 630.37 \text{ K}$$

$$n_A = 18 \quad \sum \Delta_P = (4)(0.0011) + (2)(0.0008) + (2)(-0.0012) = 0.00360$$

$$\frac{P_c}{\text{bar}} = \left(0.113 + 0.0032 n_A - \sum \Delta_P \right)^{-2} = [0.113 + (0.0032)(18) - 0.0036]^{-2} = 35.86$$

$$P_c = 35.86 \text{ bar}$$

$$\sum \Delta_V = (4)(41) + (2)(32) + (2)(65) = 358$$

$$V_c = (17.5 + 358) \text{ cm}^3/\text{mol} = 375.5 \text{ cm}^3/\text{mol}$$

TABLE 2-337 Joback * Group Contributions for Critical Constants

Group	Δ_T	Δ_P	Δ_V
Nonring increments:			
—CH_3	0.0141	-0.0012	65
>CH_2	0.0189	0	56
>CH—	0.0164	0.0020	41
>C<	0.0067	0.0043	27
=CH_2	0.0113	-0.0028	56
=CH—	0.0129	-0.0006	46
=C<	0.0117	0.0011	38
=C=	0.0026	0.0028	36
≡CH	0.0027	-0.0008	46
≡C—	0.0020	0.0016	37
Ring increments:			
$\text{—CH}_2\text{—}$	0.0100	0.0025	48
>CH—	0.0122	0.0004	38
>C<	0.0042	0.0061	27
=CH—	0.0082	0.0011	41
=C<	0.0143	0.0008	32
Halogen increments:			
—F	0.0111	-0.0057	27
—Cl	0.0105	-0.0049	58
—Br	0.0133	0.0057	71
—I	0.0068	-0.0034	97
Oxygen increments:			
—OH (alcohol)	0.0741	0.0112	28
—OH (phenol)	0.0240	0.0184	-25
—O— (nonring)	0.0168	0.0015	18
—O— (ring)	0.0098	0.0048	13
>C=O (nonring)	0.0380	0.0031	62
>C=O (ring)	0.0284	0.0028	55
—CH=O (aldehyde)	0.0379	0.0030	82
—COOH (acid)	0.0791	0.0077	89
—COO— (ester)	0.0481	0.0005	82
$\text{=O (except as above)}$	0.0143	0.0101	36
Nitrogen increments:			
—NH_2	0.0243	0.0109	38
>NH (nonring)	0.0295	0.0077	35
>NH (ring)	0.0130	0.0114	29
>N— (nonring)	0.0169	0.0074	9
—N= (nonring)	0.0255	-0.0099	—
—N= (ring)	0.0085	0.0076	34
—CN	0.0496	-0.0101	91
—NO_2	0.0437	0.0064	91
Sulfur increments:			
—SH	0.0031	0.0084	63
—S— (nonring)	0.0119	0.0049	54
—S— (ring)	0.0019	0.0051	38

*Joback, K. G., M.S. thesis in chemical engineering, Massachusetts Institute of Technology, Cambridge, Mass., June 1984.

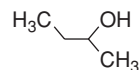
Results:

Property	DIPPR [®] 801 recommendation	Joback estimation	% Difference
T_c/K	630.3	630.37	0.00
P_c/bar	37.32	35.86	-3.92
$V_c/(\text{cm}^3/\text{mol})$	370	375.5	1.49

Example Estimate the critical constants of *sec*-butanol by using the Joback method.

Required input data: From DIPPR[®] 801 database, $T_b = 372.7 \text{ K}$, $M = 74.1216 \text{ kg/kmol}$.

Structure:



Group contributions from Table 2-337:

Group	n_i	Δ_T	Δ_P	Δ_V
—CH_3	2	0.0141	-0.0012	65
>CH_2	1	0.0189	0	56
>CH—	1	0.0164	0.0020	41
—OH (alcohol)	1	0.0741	0.0112	28

From Eqs. (2-9), (2-10), and (2-11):

TABLE 2-338 Fedors* Method Atomic and Structural Contributions

Atomic increments		Structural increments	
Atom	Δ_V	Feature	Δ_V
C	34.426	Three-member ring	-15.824
H	9.172	Four-member ring	-17.247
O	20.291	Five-member ring	-39.126
O (alcohols)	18.000	Six-member ring	-39.508
N	48.855	Double bond	5.028
N (amines)	47.422	Triple bond	0.797
F	22.242	Ring attached to another	35.524
Cl	52.801		
Br	71.774		
I	96.402		
S	50.866		

*Fedors, R. F., *AIChE J.*, **25** (1979): 202.

$$\sum \Delta_V = (2)(0.0141) + (1)(0.0189) + (1)(0.0164) + (1)(0.0741) = 0.1376$$

$$T_c = T_b(1.4330) = (372.7 \text{ K})(1.4330) = 534.1 \text{ K}$$

$$\sum \Delta_P = (2)(-0.0012) + (1)(0.0020) + (1)(0.0112) = 0.0108 \quad n_A = 15$$

$$\frac{P_c}{\text{bar}} = (0.1022 + 0.0032n_A)^{-2} = \left[\frac{1}{0.1022 + (0.0032)(15)} \right]^2 = 44.33$$

$$P_c = 44.33 \text{ bar}$$

$$\sum \Delta_V = (2)(65) + (1)(56) + (1)(41) + (1)(28) = 255$$

$$V_c = (17.5 + 255) \text{ cm}^3/\text{mol} = 272.5 \text{ cm}^3/\text{mol}$$

Results:

Property	DIPPR® 801 recommendation	Joback estimation	% Difference
T_c /K	536.2	534.1	-0.39
P_c /bar	42.02	44.33	5.50
V_c /(cm ³ /mol)	269	272.5	1.30

Method: Fedor method.

Reference: Fedors, R. F., *AIChE J.*, **25** (1979): 202.

Classification: Atom/structure contributions.

Expected uncertainty: ~8 cm³/mol (3 percent).

Applicability: Organic compounds.

Input data: Molecular structure, atom and structural increments, Δ_V in Table 2-238.

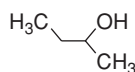
Description: An atom contribution method with structural increments for V_c , given by

$$\frac{V_c}{\text{cm}^3/\text{mol}} = 26.6 + \sum_{i=1}^N n_i \Delta_V \quad (2-12)$$

where Δ_V are structural contributions from Table 2-238.

Example Use Fedors' method to estimate the critical volume of *sec*-butanol.

Group contributions from Table 2-238:



Group	n_i	Δ_V
C	4	34.426
H	10	9.172
O (alcohol)	1	18.000

Calculation using Eq. (2-12):

$$\sum \Delta_V = (4)(34.426) + (10)(9.172) + (1)(18.000) = 247.4$$

$$V_c = (26.6 + 247.4) \text{ cm}^3/\text{mol} = 274.0 \text{ cm}^3/\text{mol}$$

This value differs from the DIPPR® 801 recommended value of 269 cm³/mol by 1.9 percent.

Mixtures Application of CS methods and analytical equations of state (EoS) to mixtures typically requires pseudocritical temperatures and pressures. These values are obtained from the pure-component critical properties by applying mixing rules specific to the method under consideration. While pseudocritical values should be used for mixture CS and EoS applications, the values are usually quite different from the mixture's true critical properties. A variety of methods are available for estimating true critical properties for mixtures (see PGLA), but only modest accuracy can be expected.

Normal Melting Point The *normal melting point* is defined as the temperature at which melting occurs at atmospheric pressure. Methods to estimate the melting point have not been particularly effective because the melting point depends strongly on solid crystal structure and that structure is not effectively correlated with standard GC or CS methods. If the triple point temperature is known, then the melting point is best estimated as being equal to the triple point temperature. However, rarely is the triple point temperature available if the melting point has not also been determined.

Recommended Method The method of Constantinou and Gani is recommended with caution.

Reference: Constantinou, L., and R. Gani, *AIChE J.*, **40** (1994): 1697.

Classification: Group contributions.

Expected uncertainty: 25 percent.

Applicability: Organic compounds.

Input data: First-order and second-order group contributions from molecular structure.

Description: A group contribution method given by

$$T_m = (102.425 \text{ K}) \cdot \ln \left(\sum_i N_i t_{m1,i} + \sum_j N_j t_{m2,j} \right) \quad (2-13)$$

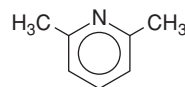
where N_i, N_j = number of first- and second-order groups, respectively

$t_{m1,i}$ = first-order group contributions from Table 2-339

$t_{m2,i}$ = second-order group contributions from Table 2-340

Example Estimate the melting point of 2,6-dimethylpyridine.

Structure and group contributions:



Group	N_i	$t_{m1,i}$	$t_{m2,i}$
-CH ₃	2	0.4640	
-C ₅ H ₃ (N)-	1	12.6275	
Six-member ring	1		1.5656

Calculation using Eq. (2-13):

$$T_m = (102.425 \text{ K}) \ln [(2)(0.4640) + 12.6275 + 1.5656] = 278 \text{ K}$$

The predicted value is 4 percent higher than the recommended experimental value of 267 K in the DIPPR® 801 database.

Normal Boiling Point The normal boiling temperature T_b is the temperature at which the vapor pressure of the liquid equals 101.325 kPa (1.0 atm). In some (usually older) literature sources, T_b values were reported at ambient pressures rather than at 101.325 kPa. If two or more such values are available, they can be used to obtain T_b by using Eq. (2-2) to linearly interpolate $\ln P'$ vs. $1/T$ values.

If there are sufficient vapor pressure data available, then T_b may be found from a regression of the data using an appropriate vapor pressure equation [e.g., Eqs. (2-21)–(2-26)]. If one or a few vapor pressure data at low pressure are available, a common occurrence, then the method of Pailhes can be used to estimate T_b . The most accurate method for prediction of normal boiling temperatures without experimental data is the Nannoolal method.

TABLE 2-339 First-Order Groups and Their Contributions for Melting Point*

Group	$t_{m1,i}$	Group	$t_{m1,i}$	Group	$t_{m1,i}$
—CH ₃	0.4640	—COOCH ₂ —	3.5572	—CCl ₃	10.2337
>CH ₂	0.9246	—OCH	4.2250	>ACCl	2.7336
>CH—	0.3557	—OCH ₃	2.9248	—CH ₂ NO ₂	5.5424
>C<	1.6479	—OCH ₂ —	2.0695	>CHNO ₂	4.9738
—CH=CH ₂	1.6472	—OCH<	4.0352	>ACNO ₂	8.4724
—CH=CH—	1.6322	—OCH ₂ F	4.5047	—CH ₂ SH	3.0044
>C=CH ₂	1.7899	—CH ₂ NH ₂	6.7684	—I	4.6089
>C=CH—	2.0018	>CHNH ₂	4.1187	—Br	3.7442
>C=C<	5.1175	—NHCH ₃	4.5341	—C≡CH	3.9106
—CH=C=CH ₂	3.3439	—CH ₂ NH—	6.0609	—C≡C—	9.5793
>ACH	1.4669	>CHNH—	3.4100	>C=CCl—	1.5598
>AC—	0.2098	>NCH ₃	4.0580	>ACF	2.5015
>ACCH ₃	1.8635	—NCH ₂ —	0.9544	—CF ₃	3.2411
>ACCH ₂ —	0.4177	>ACNH ₂	10.1031	—COO—	3.4448
>ACCH<	-1.7567	—C ₂ H ₅ (N)—	12.6275	—CCl ₂ F	7.4756
—OH	3.5979	—CH ₃ CN	4.1859	—CClF ₂	2.7523
>ACOH	13.7349	—COOH	11.5630	—F (other)	1.9623
—COCH ₃	4.8776	—CH ₂ Cl	3.3376	—CONH ₂	31.2786
—COCH ₂ —	5.6622	>CHCl	2.9933	—CON(CH ₃) ₂	11.3770
—CHO	4.2927	>Cl—	9.8409	—CH ₃ S	5.0506
—COOCH ₃	4.0823	—CHCl ₂	5.1638	>CH ₂ S	3.1468

*Constantinou, L., and R. Gani, *AIChE J.*, **40** (1994): 1697.**Recommended Method** Pailhes method.**Classification:** Group contributions.**Expected uncertainty:** 3 K (~1 to 2 percent).**Applicability:** Organic compounds.**Reference:** Pailhes, F., *Fluid Phase Equilib.*, **41** (1988): 97.

Input data: Molecular structure and one measured vapor pressure value P_{meas}^* (often at a low pressure). The method requires estimation of T_c and P_c using a group contribution method. The original Pailhes method used the Lydersen method [Lydersen, A. L., *AIChE J.*, **21** (1975): 510], but the Joback method is illustrated here for consistency with the previous examples on critical constant estimation.

Description: A simple group contribution method given by

$$T_b = T_{\text{meas}} \frac{\log(P_c/\text{bar}) + (1 - T_{br})x_p}{\log(P_c/\text{bar})} - 3x_p - 1.49x_p^2 \quad (2-14)$$

where T_b = estimate of normal boiling point P_c = critical pressure estimated from group contributions T_{br} = reduced normal boiling point estimated from Eq. (2-9) $x_p = \log(1 \text{ atm}/P_{\text{meas}}^*)$ T_{meas} = temperature at which experimental vapor pressure is known

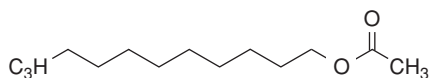
TABLE 2-340 Second-Order Groups and Their Contributions for Melting Point*

Group	$t_{m2,i}$	Group	$t_{m2,i}$
—CH(CH ₃) ₂	0.0381	CHCOOH; CCOOH	-3.1034
—C(CH ₃) ₃	-0.2355	ACCOOH	28.4324
—CH(CH ₃)CH(CH ₃)—	0.4401	CH ₃ COOCH; CH ₃ COOC	0.4838
—CH(CH ₃)C(CH ₃) ₂ —	-0.4923	COCH ₂ COO or COCHCOO or COCCOO	0.0127
—C(CH ₃) ₂ C(CH ₃) ₂ —	6.0650	CO—O—CO	-2.3598
Three-member ring	1.3772	ACCOO	-2.0198
Five-member ring	0.6824	CHOH	-0.5480
Six-member ring	1.5656	COH	0.3189
Seven-member ring	6.9709	CH _m (OH)CH _n (OH) [m, n = 0, 1, 2]	0.9124
CH _n =CH _m —CH _p =CH _k	1.9913	CH _{m cyclic} —OH [m = 0, 1]	9.5209
[k, n, m, p = 0, 1, 2]			
CH ₃ CH _m =CH _n [m, n = 0, 1, 2]	0.2476	CH _m (OH)CH _n (NH _p)	2.7826
CH ₂ CH _m =CH _n [m, n = 0, 1, 2]	-0.5870	[m, n, p = 0, 1, 2, 3]	
CHCH _m =CH _n or CCH _m =CH _n	-0.2361	CH _m (NH ₂)CH _n (NH ₂)	2.5114
[m, n = 0, 1, 2]		[m, n = 0, 1, 2]	
Alicyclic side chain: C _{cyclic} C _m	-2.8298	CH _{m cyclic} —NH _p —CH _{n cyclic}	1.0729
[m > 1]		[m, n, p = 0, 1, 2]	
CH ₃ CH ₃	1.4880	CH _m —O—CH _n =CH _p	0.2476
CHCHO; CCHO	2.0547	[m, n, p = 0, 1, 2]	
CH ₃ COCH ₂	-0.2951	AC—O—CH _m	0.1175
CH ₃ COCH; CH ₃ COC	-0.2986	[m = 0, 1, 2, 3]	
C _{cyclic} (=O)	0.7143	CH _{m cyclic} —S—CH _{n cyclic}	-0.2914
ACCHO	-0.6697	[m, n = 0, 1, 2]	
		CH _m =CH _n —F	-0.0514
		[m, n = 0, 1, 2]	
		CH _m =CH _n —Br	-1.6425
		[m, n = 0, 1, 2]	
		ACBr	2.5832
		ACl	-1.5511

*Constantinou, L., and R. Gani, *AIChE J.*, **40** (1994): 1697.

Example The vapor pressure of *n*-decylacetate at 348.65 K is 106.66 Pa. Estimate the normal boiling point of this compound.

Structure and group contributions from Table 2-337:



Group	n_i	Δ_r	Δ_p
—CH ₃	2	0.0141	-0.0012
>CH ₂	9	0.0189	0
—COO— (ester)	1	0.0481	0.0005

Group contribution calculations using Eqs. (2-9) and (2-10):

$$\sum \Delta_r = (2)(0.0141) + (9)(0.0189) + (1)(0.0481) = 0.2464$$

$$T_{br} = 0.584 + 0.965(0.2464) - (0.2464)^2 = 0.76106$$

$$\sum \Delta_p = (2)(-0.0012) + (1)(0.0005) = -0.0019$$

$$n_A = 38 \quad P_c = (0.113 + 0.0032n_A + 0.0019)^2 \text{ bar} = 17.88 \text{ bar} = 17.65 \text{ atm}$$

Calculation of auxiliary quantities:

$$x_p = \log \frac{1 \text{ atm}}{P'_{\text{meas}}} = \log \frac{101325 \text{ Pa}}{106.66 \text{ Pa}} = 2.9777$$

Calculation of normal boiling point using Eq. (2-14):

$$\frac{T_b}{K} = 348.65 \frac{\log 17.88 + (1 - 0.76016)(2.9777)}{\log 17.88} - 3(2.9777) - 1.49(2.9777)^2$$

$$T_b = 525.3 \text{ K}$$

The estimated value is 1.6 percent higher than the DIPPR® 801 recommended value of 517.15 K.

Recommended Method Nannoolal method.

Reference: Nannoolal, Y., et al., *Fluid Phase Equilib.*, **226** (2004): 45.

Classification: Group contributions.

Expected uncertainty: 7 K (on the order of 2 percent).

Applicability: Organic compounds for which group values are available.

Input data: GC values C_i in Table 2-341; intramolecular group-group interactions C_{ij} in Table 2-342.

Description: A GC method that includes second-order corrections for steric effects and intramolecular interactions. Variable T_b is found from

$$\frac{T_b}{K} = \frac{\sum_{i=1}^N n_i \cdot C_i}{n^{0.6583} + 1.6868} + 84.3395 \quad (2-15)$$

where n = number of nonhydrogen atoms

n_i = number of occurrences of group i

N = number of groups

C_i = group contribution from Table 2-341 or Eq. (2-16)

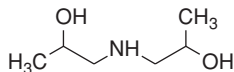
Corrections for intramolecular group-group interactions $C_{i,int}$ are made by dividing the sum of all unique group pairs within the molecule by n . This can be written as

$$C_{i,int} = \frac{1}{n} \sum_{i=1}^N \sum_{j>i}^N C_{ij} \quad (2-16)$$

or thought of as the sum of terms in the upper half (above and to the right of the diagonal) of the square matrix formed by listing each group in the molecule along the row and column. The values for the interactions are shown in this format in Table 2-342.

Example Estimate the normal boiling point of di-isopropanolamine by using the Nannoolal method.

Structure:



Group contributions and values:

Group	n_i	C_i	Group total
—CH ₃	2	177.3066	354.6132
>C(c)<(e)	4	266.8769	1067.508
—OH sec	2	390.2446	780.4892
—NH—	1	223.0992	223.0992
Corrections			
—OH::—OH	1/9	291.7985	32.42206
—OH::—NH—	2/9	286.9698	63.77107
Total			2521.902

Note that there are three interacting groups (—OH, —OH, —NH—) in the molecule which gives two —OH::—NH— interactions and one —OH::—OH interaction which are then divided by n ($=9$) as in Eq. (2-16) to give the frequency.

Calculation using Eq. (2-15):

$$\frac{T_b}{K} = \frac{2521.902}{9^{0.6583} + 1.6868} + 84.3395 = 509.3 \quad T_b = 509.3 \text{ K}$$

The calculated value differs by -2.4 percent from the DIPPR® 801 recommended value of 521.9 K.

Characterizing and Correlating Constants

Acentric Factor The acentric factor of a compound ω is defined in terms of the reduced vapor pressure evaluated at a reduced temperature of 0.7 as

$$\omega = -\log P_r \Big|_{T_r=0.7} - 1.0000 \quad (2-17)$$

It is primarily used as a third parameter (beyond T_c and P_c) in CS predictions as a measure of deviations from nonspherical molecular shape, hence the name, suggesting molecular interactions that are not between centers of molecules. However, as defined in Eq. (2-17), ω also contains polarity information, and ω increases slightly with increasing polarity for molecules of similar size and shape. The value of ω is close to zero for small, spherically shaped, nonpolar molecules (argon, methane, etc.). It increases in value with larger deviations of molecular shape from spherical (longer chain lengths, less chain branching, etc.) and with increasing molecular polarity. When possible, ω should be obtained from experimental vapor pressure correlations by using Eq. (2-17), but an accurate estimation of ω can be made by using the critical constants and a single vapor pressure point by application of CS vapor pressure equations.

Recommended Method Ambrose-Walton modification of Lee-Kesler vapor pressure equations.

References: Ambrose, D., and J. Walton, *Pure & Appl. Chem.*, **61** (1989): 1395; Lee, B. I., and M. G. Kesler, *AIChE J.*, **21** (1975): 510.

Classification: Corresponding states.

Expected uncertainty: Generally within 5 percent.

Applicability: Most organic compounds.

Input data: T_c , P_c , and a single vapor pressure point (e.g., the normal boiling point).

Description: See Eq. (2-25) for the equations used in this method. The vapor pressure equation is inverted to obtain the acentric factor from a single experimental vapor pressure point.

Example Calculate the acentric factor of chlorobenzene with a known value for T_b .

Input information: From the DIPPR® 801 database, $T_b = 404.87 \text{ K}$, $T_c = 632.35 \text{ K}$, and $P_c = 45.1911 \text{ bar}$.

Calculation of auxiliary quantities:

$$T_{br} = \frac{T_b}{T_c} = \frac{404.87}{632.35} = 0.64 \quad \tau = 1 - 0.64 = 0.36$$

$$f^{(0)} = \frac{(-5.97616)(0.36) + (1.29874)(0.36)^{1.5} - (0.60394)(0.36)^{2.5} - (1.06841)(0.36)^5}{0.64}$$

$$= -3.0034$$

$$f^{(1)} = \frac{(-5.03365)(0.36) + (1.11505)(0.36)^{1.5} - (5.41217)(0.36)^{2.5} - (7.46628)(0.36)^5}{0.64}$$

$$= -3.1788$$

2-474 PHYSICAL AND CHEMICAL DATA

TABLE 2-341 Group Contributions for the Nannoolal* Method for Normal Boiling Point

Table-specific nomenclature: (e) = connected to N, O, F, Cl; (ne) = not connected to N, O, F, Cl; (r) = in a ring; (c) = in a chain; (a) = aromatic, not necessarily carbon; (Ca) = aromatic carbon; b = any nonhydrogen atom

ID	Group	Description	Value
1	CH ₃ —(ne)	CH ₃ — not connected to N, O, F, or Cl	177.3066
2	CH ₃ —(e)	CH ₃ — connected to N, O, F, or Cl	251.8338
3	CH ₃ —(a)	CH ₃ — connected to an aromatic atom (not necessarily C)	157.9527
4	—C(e)H ₂ —	—CH ₂ — in a chain	239.4531
5	>C(e)H—	>CH— in a chain	240.6785
6	>C(e)<	>C< in a chain	249.5809
7	>C(e)<(e)	>C< in a chain connected to at least one F, Cl, N, or O	266.8769
8	>C(e)<(Ca)	>C< in a chain connected to at least one aromatic carbon	201.0115
9	—C(r)H ₂ —	—CH ₂ — in a ring	239.4957
10	>C(r)H—	>CH— in a ring	222.1163
11	>C(r)<	>C< in a ring	209.9749
12	>C(r)<(e, c)	>C< in a ring; connected to at least one N, O, Cl, or F which are not part of the ring	250.9584
13	>C(r)<(e, r)	>C< in a ring connected to at least one N or O which are part of the ring	291.2291
14	>C(r)<(Ca)	>C< in a ring connected to at least one aromatic carbon	244.3581
15	==C(a)H—	aromatic ==CH—	235.3462
16	==C(a)<(ne)	aromatic ==C< not connected to O, N, Cl, or F	315.4128
17	==C(a)<(e)	aromatic ==C< connected to O, N, Cl, or F	348.2779
18	(a) ==C(a)<2(a)	aromatic ==C< with three aromatic neighbors	367.9649
19	F—(C, Si)	F— connected to C or Si	106.5492
20	—CF==C<	F— on a C=C (vinylfluoride)	49.2701
21	F—(C, Si)(F)(2b)	F— connected to C or Si already substituted with at least one F and two other atoms	53.1871
22	F—(C, Si)([F, Cl])(b)	F— connected to a C or Si already substituted with one F or Cl and one other atom	78.7578
23	F—(C, Si)([F, Cl]2)	F— connected to C or Si already substituted with two F or Cl atoms	103.5672
24	F—(Ca)	F— connected to an aromatic carbon	-19.5575
25	Cl—(C, Si)	Cl— connected to C or Si not already substituted with F or Cl	330.9117
26	Cl—(C, Si)([F, Cl])	Cl— connected to C or Si already substituted with one F or Cl	287.1863
27	Cl—(C, Si)([F, Cl]2)	Cl— connected to C or Si already substituted with at least two F or Cl	267.4170
28	Cl—(Ca)	Cl— connected to aromatic C	205.7363
29	—C≡C—	Cl— on a C=C (vinylchloride)	292.5816
30	Br—(C, Si)	Br— connected to a nonaromatic C or Si	419.4959
31	Br—(Ca)	Br— connected to an aromatic C	377.6775
32	I—(C, Si)	I— connected to C or Si	556.3944
33	—OH <i>tert</i>	—OH connected to tertiary carbon	349.9409
34	HO—(C, Si) <i>sec</i>	—OH connected to secondary C or Si	390.2446
35	HO—(C, Si) <i>long</i>	—OH connected to primary C or Si; chain > 4 C or Si	443.8712
36	HO—(C, Si) <i>short</i>	—OH connected to primary C or Si; chain < 5 C or Si	488.0819
37	—OH (Ca)	—OH connected to an aromatic C (phenols)	361.4775
38	(C, Si)—O—(C, Si)	ether —O— connected to two C or Si	146.4836
39	>(OC ₂)<	>(OC ₂)< (epoxide)	820.7118
40	NH ₂ —(C, Si)	NH ₂ — connected to either C or Si	321.1759
41	NH ₂ —(Ca)	NH ₂ — connected to an aromatic C	441.4388
42	(C, Si)—NH—(C, Si)	—NH— connected to two C or Si (secondary amine)	223.0992
43	(C, Si)2>N—(C, Si)	>N— connected to three C or Si (tertiary amine)	126.2952
44	COOH—(C)	—COOH connected to C	1080.3139
45	(C)—COO—(C)	—COO— connected to two C (ester)	636.2020
46	HCOO—(C)	HCOO— connected to C (formic acid ester)	642.0427
47	—C(e)OO—	—COO— in ring, C is connected to C (lactone)	1142.6119
48	—CON<	—CON< disubstituted amide	1052.6072
49	—CONH—	—CONH— (monosubstituted amide)	1364.5333
50	—CONH ₂	—CONH ₂ (amide)	1487.4109
51	O=C<(Can)2	—CO— connected to two nonaromatic C (ketones)	618.9782
52	CHO—(Can)	CHO— connected to nonaromatic C (aldehydes)	553.8090
53	SH—(C)	—SH connected to C (thioles)	434.0811
54	(C)—S—(C)	—S— connected to two C	461.5784
55	(C)—S—S—(C)	—S—S— (disulfide) connected to two C	864.5074
56	—S(a)—	—S— in an aromatic ring	304.3321
57	(C)—C≡N	—C≡N (cyanide) connected to C	719.2462
58	>C(c)=C(c)<	>C=C< (both C have at least one non-H neighbor)	475.7958
59	>C(c)=C(c)<(Ca)	noncyclic >C=C< connected to at least one aromatic C	586.1413
60	—(e)C(c)=C(c)<	noncyclic >C=C< with at least one F, Cl, N, or O	500.2434
61	H ₂ C(c)=C<	H ₂ C=C< (1-ene)	412.6276
62	>C(r)=C(r)<	cyclic >C=C<	475.9623
63	—C=C—	—C=C—	512.2893
64	HC≡C—	HC≡C— (1-yne)	422.2307
65	(Ca)—O(a)—(Ca)	—O— in an aromatic ring with aromatic C neighbors	37.1936
66	==N(a)—(r5)	aromatic ==N— in a five-member ring, free electron pair	453.3397
67	==N(a)—(r6)	aromatic ==N— in a six-member ring	306.7139
68	NO ₂ —(C)	NO ₂ — connected to aliphatic C	866.5843
69	NO ₂ —(Ca)	NO ₂ — connected to aromatic C	821.4141
70	>Si<	>Si<	282.0181
71	>Si<(O)	>Si< connected to at least one O	207.9312
72	NO ₃ —	nitrate (esters of nitric acid)	920.3617
73	PO ₄ —	phosphates	1153.1344
74	O=N—O—(C)	nitrites (esters of nitrous acid)	494.2668

TABLE 2-341 Group Contributions for the Nannoolal* Method for Normal Boiling Point (Concluded)

Table-specific nomenclature: (e) = connected to N, O, F, Cl; (ne) = not connected to N, O, F, Cl; (r) = in a ring; (c) = in a chain; (a) = aromatic, not necessarily carbon; (Ca) = aromatic carbon; b = any nonhydrogen atom

ID	Group	Description	Value
75	ONC—	ONC— (oxime)	1041.0851
76	—C=O—O—C=O—	anhydride connected to two C	1251.2675
77	COCl—	COCl— connected to C (acid chloride)	778.9151
78	>Si<(F,Cl)	>Si< connected to at least one F or Cl	540.0895
79	O=C(—O—)2	noncyclic carbonate	879.7062
80	OCN—	OCN— connected to C or Si (cyanate)	660.4645
81	SCN—(C)	SCN— (thiocyanate) connected to C	1018.4865
82	(C)—SO2—(C)	noncyclic sulfone connected to two C (sulfones)	1559.9840
83	(C)2>Sn<(C)2	>Sn< connected to four carbons	510.4223
84	AsCl2—	AsCl2 connected to C	1149.9670
85	GeCl3—	GeCl3— connected to carbons	1209.2972
86	(C)2>Ge<(C)2	>Ge< connected to four carbons	347.7717
87	>C=C=C<	cumulated double bond	664.0903
88	>C=C—C=C<(r)	conjugated double bond in a ring	957.6388
89	>C=C—C=C<(c)	conjugated double bond in a chain	928.9954
90	CHO—(Ca)	CHO— connected to aromatic C (aldehydes)	560.1024
91	(C,Si)=N—	double-bonded amine connected to at least one C or Si	229.2258
92	(O=C<(C)2)a	—CO— connected to two C with at least one aromatic C (ketones)	606.1797
94	—O—O—	peroxide	273.1755
95	—C≡C—C≡C—	conjugated triple bond	1218.1878
96	(—C=O—O—C=O—)r	cyclic anhydride connected to two C	2082.3258
97	(C,Si)a—NH—(Ca,Si)a	—NH— connected to two C or Si with at least one aromatic (secondary amines)	201.3224
99	—OCON<	—CO connected to O and N (carbamate)	886.7613
100	>N—(C=O)—N<	—CO connected to two N (urea)	1045.0343
101	(C,Si)2>N<(C,Si)2	Quaternary amine connected to four C or Si	-109.6269
102	F—(C,Si)(Cl)(b)2	F— connected to C or Si already substituted with at least one Cl and two other atoms	111.0590
103	—OCOO—	—CO connected to two O (carbonates)	1573.3769
104	>SO2	S(=O)2 connected to two O (sulfates)	1483.1289
105	—SO2N<	—S(=O)2 connected to N	1506.8136
106	···=CNC=NC···	imidazole	484.6371
107	>S=O	sulfoxide	1379.4485
108	(S)—C≡N	—C≡N (cyanide) connected to S	659.7336
109	>N(C=O)	—CO connected to N	492.0707
111	(N)—C≡N	—C≡N (cyanide) connected to N	971.0365
113	>P<	phosphorus connected to at least 1 C or S (phosphine)	428.8911
115	—ON=(C,Si)	—ON= connected to C or Si (isoazole)	612.9506
116	>Se<	>Se< connected to at least one C or Si	562.1791
117	>Al<	>Al< connected to at least one C or Si	761.6006
Corrections			
118	C=C—C=O	—C=O connected to sp2 carbon	40.4205
119	(C=O)—C([F,Cl]2,3)	carbonyl connected to C with two or more halogens	-82.2328
120	(C=O)—C([F,Cl]2,3)2	carbonyl connected to two C, each with at least two halogens	-247.8893
121	C—[F,Cl]3	carbon with three halogens	-20.3996
122	(C)2—C—[F,Cl]2	secondary carbon with two halogens	15.4720
123	No hydrogen	component has no hydrogen	-172.4201
124	One-hydrogen	component has one hydrogen	-99.8035
125	(3,4) ring	a three- or four-member nonaromatic ring	-62.3740
126	5-ring	a five-member nonaromatic ring	-40.0058
127	Ortho pair(s)	Ortho- position counted only once and only if there are no meta or para pairs	-27.2705
128	Meta pair(s)	Meta- position counted only once and only if there are no para or ortho pairs	-3.5075
129	Para pair(s)	Para- position counted only once and only if there are no meta or ortho pairs	16.1061
130	((C=)(C)C—CC3)	carbon with four carbon neighbors and one double-bonded carbon neighbor	25.8348
131	C2C—CC2	carbon with four carbon neighbors, two on each side	35.8330
132	C3C—CC2	carbon with five carbon neighbors	51.9098
133	C3C—CC3	carbon with six carbon neighbors	111.8372

*Nannoolal, Y., et al., *Fluid Phase Equilib.* **226** (2004): 45.

$$f^{(2)} = \frac{(-0.64771)(0.36) + (2.41539)(0.36)^{1.5} - (4.26979)(0.36)^{2.5} + (3.25259)(0.36)^5}{0.64}$$

$$= -0.037$$

Calculation using Eq. (2-25) at the normal boiling point:

$$\ln \frac{1.01325}{45.1911} = -3.798 = f^{(0)} + \omega f^{(1)} + \omega f^{(2)} = 3.0034 + 3.1788\omega + 0.037\omega^2$$

$$\omega = 0.249$$

The value obtained from the Ambrose-Walton-Lee-Kesler method compares favorably with the value of 0.2499 recommended in the DIPPR® 801 database (obtained from the vapor pressure correlation).

Radius of Gyration The radius of gyration R_g is a measure of the mass distribution about the center of mass of a molecule. Radius R_g increases with molecular size. It is useful in CS applications to separate molecular size and shape effects from polar effects. It is defined in terms of the principal moments of inertia of a molecule (A, B, and C) as

$$R_g = \sqrt{\frac{(AB)^{1/2}N_A}{M}} \quad (2-18)$$

for planar molecules and as

$$R_g = \sqrt{\frac{2\pi(ABC)^{1/2}N_A}{M}} \quad (2-19)$$

TABLE 2-342 Intermolecular Interaction Corrections for the Nannoolal et al.* Method for Normal Boiling Point

	—OH	—OH(a)	—COOH	—O—	>(OC ₂)<	—COOC—	—CO—	—CHO
—OH	291.7985	0	146.7286	135.3991	226.4980	211.6814	46.3754	0
—OH(a)		288.6155	-1477.9671	130.3742	0	-1184.9784	0	43.9722
—COOH			117.2044	612.8821	0	-183.2986	-55.9871	0
—O—				91.4997	178.7845	322.5671	15.6980	17.0400
>(OC ₂)<					1006.388	0	22.5208	163.5475
—COOC—						431.0990	22.5208	0
—CO—							-303.9653	-391.3690
—CHO								582.1763

	—O(a)—	—S(na)—	—S(a)—	—SH	—NH ₂	>NH	—OCN	—CN
—OH	435.0923	-74.0193	0	38.6974	314.6126	286.9698	0	306.3979
—OH(a)	0	0	0	0	797.4327	0	0	0
—COOH	0	0	0	0	0	0	0	0
—O—	329.0050	394.5505	0	0	124.3549	101.8475	0	293.5974
>(OC ₂)<	0	0	0	0	0	0	0	0
—COOC—	707.9404	0	0	0	182.6291	317.0200	0	517.0677
—CO—	176.5481	0	381.0107	0	0	-215.3532	0	-574.2230
—CHO	674.6858	0	397.575	0	0	0	0	0
—O(a)—	0	0	0	0	395.4093	0	0	0
—S(na)—		-11.9406	0	0	-562.306	0	0	0
—S(a)—			0	0	0	0	0	-101.232
—SH				217.6360	0	0	0	0
—NH ₂					174.0258	510.3473	0	0
>NH						239.8076	0	0
—OCN							-356.5017	0
—CN								0

	Nitrate	≡N(a)—(r5)	≡N(a)—(r6)
—OH	0	0	1334.6747
—OH(a)	-1048.124	0	-614.3624
—COOH	0	0	0
—O—	963.6518	0	0
>(OC ₂)<	0	0	0
—COOC—	-205.6165	0	0
—CO—	-3628.903	0	124.1943
—CHO	140.9644	0	0
—O(a)—	0	-888.612	0
—S(na)—	0	0	0
—S(a)—	0	-348.740	0
—SH	0	0	0
—NH ₂	663.8009	0	27.2735
>NH	0	0	758.9855
—OCN	-263.0807	0	0
—CN	0	0	-370.9729
Nitrate	65.1432	0	0
≡N(a)—(r5)		0	0
≡N(a)—(r6)			-271.9449

*Nannoolal, Y., et al., *Fluid Phase Equilib.*, **226** (2004): 45.

for nonplanar molecules. Radii of gyration can be calculated from these defining equations and principal moments of inertia obtained from spectral data or from computational chemistry software.

Recommended Method Principal moments of inertia.

Classification: Computational chemistry.

Expected uncertainty: Less than 5 percent.

Applicability: All molecules.

Input data: *M* and molecular structure.

Description: Computational chemistry software is used to optimize the geometry of the molecule and obtain the principal moments of inertia to be used in Eqs. (2-18) and (2-19).

Example Calculate the radius of gyration for hydrazine.

Input information: From the DIPPR[®] 801 database, *M* = 32.0452 kg/kmol. The structure of hydrazine is



Calculation of the principal moments of inertia: Optimizing hydrazine with HF/6-31G model chemistry gives the following principal moments of inertia:

$$A = 12.24050 \text{ amu} \cdot \text{Bohr}^2 \quad B = 72.41081 \text{ amu} \cdot \text{Bohr}^2$$

$$C = 79.16893 \text{ amu} \cdot \text{Bohr}^2$$

Conversion from atomic units to SI gives

$$A = (12.24050 \text{ amu} \cdot \text{Bohr}^2) \left(\frac{5.29177 \times 10^{-11} \text{ m}}{\text{Bohr}} \right)^2 \left(\frac{1.66054 \times 10^{-27} \text{ kg}}{\text{amu}} \right) \\ = 5.692 \times 10^{-47} \text{ kg} \cdot \text{m}^2$$

$$B = (72.41081 \text{ amu} \cdot \text{Bohr}^2) \left(\frac{4.65010^{-48} \text{ kg} \cdot \text{m}^2}{\text{amu} \cdot \text{Bohr}^2} \right) = 3.367 \times 10^{-46} \text{ kg} \cdot \text{m}^2$$

$$C = (79.16893 \text{ amu} \cdot \text{Bohr}^2) \left(\frac{4.65010^{-48} \text{ kg} \cdot \text{m}^2}{\text{amu} \cdot \text{Bohr}^2} \right) = 3.681 \times 10^{-46} \text{ kg} \cdot \text{m}^2$$

Calculation using Eq. (2-19):

$$(\text{ABC})^{1/3} = [(5.692 \times 10^{-47})(3.367 \times 10^{-46})(3.681 \times 10^{-46})]^{1/3} \text{ kg} \cdot \text{m}^2 \\ = 1.918 \times 10^{-46} \text{ kg} \cdot \text{m}^2$$

$$R_g = \sqrt{\frac{2\pi(1.918 \times 10^{-46} \text{ kg}\cdot\text{m}^2)(6.022 \cdot 10^{26} \text{ kmol}^{-1})}{32.0452 \text{ kg/kmol}}} = 1.505 \times 10^{-10} \text{ m}$$

This is 3.8 percent below the DIPPR® 801 database value of 1.564×10^{-10} m which was obtained from spectral principal moments of inertia.

Dipole Moment The dipole moment of a molecule is the first moment of the electric charge density expansion. All normal paraffins have a value of zero. Charge separation within the molecule due to electronegativity differences between bonded atoms increases the dipole moment. Computational chemistry software uses the electron density distribution of the optimized molecule to calculate dipole moments.

Recommended Method Electron density distribution.

Classification: Computational chemistry.

Expected uncertainty: Uncertainty varies depending upon the model chemistry chosen, but it can be as large as 60 percent.

Applicability: All molecules.

Input data: Molecular structure.

Example Calculate the dipole moment for methanol.

Draw structure and optimize molecule using computational chemistry software: The dipole moment obtained from a geometry optimized with the HF/6-31G model chemistry for methanol is 2.288 D. This value is 35 percent larger than the experimental gas-phase value of 1.700 D in the DIPPR® 801 database.

VAPOR PRESSURE

Liquids Vapor pressure is the most important of the basic thermodynamic properties of fluids. It is the pressure of equilibrium, coexisting liquid and vapor phases at a specified temperature. The vapor pressure curve is a monotonic function of temperature from its minimum value (the triple point pressure) at the triple point temperature T_t to its maximum value (the critical pressure) at T_c .

Liquid vapor pressure data over a limited temperature range can be correlated with the Antoine [Antoine, C, *C.R.*, **107** (1888): 681, 836] equation

$$\ln \frac{P^*}{\text{Pa}} = A - \frac{B}{T/\text{K} + C} \quad (2-20)$$

Data from the triple point to the critical point can be correlated with either a modified form of the Wagner equation [Wagner, W., "A New Correlation Method for Thermodynamic Data Applied to the Vapor-Pressure Curve of Argon, Nitrogen, and Water," J.T.R. Watson (trans. and ed.), IUPAC Thermodynamic Tables Project Centre, London, 1977; Ambrose, D., *J. Chem. Thermodyn.*, **18** (1986): 45; Ambrose, D., and N. B. Ghiasse, *J. Chem. Thermodyn.*, **19** (1987): 903, 911]

$$\ln P_r^* = \frac{a\tau + b\tau^{1.5} + c\tau^{2.5} + d\tau^5}{1 - \tau} \quad \text{where } \tau \equiv 1 - T_r \quad (2-21)$$

or the Riedel [Riedel, L., *Chem. Ing. Tech.*, **26** (1954): 679] equation

$$\ln \frac{P^*}{\text{Pa}} = A + \frac{B}{T/\text{K}} + C \ln \frac{T}{\text{K}} + D \left(\frac{T}{\text{K}} \right)^E \quad (2-22)$$

Generally, E in Eq. (2-22) is assigned a value of 6, but values of 2 or 1 have also been used, particularly when correlating low-temperature data. While the Wagner equation can be used to correlate most fluids over the whole liquid range, a fifth term is often required for alcohols [Poling, B. E., *Fluid Phase Equil.*, **116** (1996): 102]:

$$\ln P_r^* = \frac{a\tau + b\tau^{1.5} + c\tau^{2.5} + d\tau^5 + e\tau^6}{1 - \tau} \quad (\text{for alcohols}) \quad (2-23)$$

Correlation of experimental data within a few tenths of a percent over the entire fluid range can usually be obtained with either the Wagner or Riedel equations.

Two prediction methods are recommended for liquid vapor pressure. The first method is based on the Riedel equation; the second is a CS method. Both methods require T_c and P_c as input, but these can

be estimated by the methods shown earlier if experimental values are unavailable.

Recommended Method 1 Riedel method.

Reference: Riedel, L., *Chem. Ing. Tech.*, **26** (1954): 679

Classification: Empirical extension of theory and corresponding states.

Expected uncertainty: Varies strongly depending upon relative T , but 1 percent or less above T_b is typical with uncertainties of 5 to 30 percent near the triple point.

Applicability: Most organic compounds.

Input data: T_b , T_c , P_c .

Description: Equation (2-22) in reduced form

$$\ln P_r = A + \frac{B}{T_r} + C \ln T_r + DT_r^6 \quad (2-24)$$

Constants for this equation are determined from the following set of relationships:

$$\psi = -35 + \frac{36}{T_{br}} + 42 \ln T_{br} - T_{br}^6 \quad \alpha_c = \frac{3.758K\psi + \ln(P_c/1.01325 \text{ bar})}{K\psi - \ln T_{br}}$$

$$h = T_{br} \frac{\ln(P_c/1.01325 \text{ bar})}{1 - T_{br}} \quad D = K(\alpha_c - 3.758)$$

$$C = \alpha_c - 42D \quad B = -36D \quad A = 35D$$

Values of the constant K [Vetere, A., *Ind. Eng. Chem Res.*, **30** (1991): 2487]:

Class	Value
Acids	$K = -0.120 + 0.025h$
Alcohols	$K = 0.373 - 0.030h$
All other organic compounds	$K = 0.0838$

Example Estimate the vapor pressure of chlorobenzene at 50 K intervals from 300 to 600 K.

Input information: From the DIPPR® 801 database, $T_b = 404.87$ K, $T_c = 632.35$ K, and $P_c = 45.1911$ bar.

Auxiliary Quantities:

$$K = 0.0838 \quad T_{br} = 404.87/632.35 = 0.640$$

$$\psi = -35 + \frac{36}{0.640} + 42 \ln 0.640 - (0.640)^6 = 2.431$$

$$\alpha_c = \frac{(3.758)(0.0838)(2.431) + \ln(45.191/1.01325)}{(0.0838)(2.431) - \ln(0.640)} = 7.0248$$

$$D = (0.0838)(7.0248 - 3.758) = 0.2738 \quad C = 7.0248 - (42)(0.2738) = -4.4729$$

$$B = -(36)(0.2738) = -9.8552 \quad A = -(35)(0.2738) = 9.5814$$

Calculation using Eq. (2-24) at each T (detailed calculation shown for $T = 500$ K):

$$T_r = 500/632.35 = 0.7907$$

$$\ln P_r = 9.5814 - \frac{9.8552}{0.7907} - 4.4729 \ln 0.7907 + (0.2738)(0.7907)^6 = -1.7651$$

$$P_r = \exp(-1.7651) = 0.1712 \quad P = P_r P_c = (0.1712)(45.1911 \text{ bar}) = 7.74 \text{ bar}$$

T/K	T_r	$\ln P_r$	P/bar	$P_{\text{DIPPR}}/\text{bar}$	% Error
300	0.4744	-7.8532	0.0176	0.0175	0.3
350	0.5535	-5.5704	0.172	0.172	0.1
400	0.6326	-3.9323	0.886	0.880	0.6
450	0.7116	-2.7101	3.01	2.98	0.9
500	0.7907	-1.7651	7.74	7.67	0.9
550	0.8698	-1.0067	16.51	16.39	0.8
600	0.9488	-0.3705	31.20	31.11	0.3

Recommended Method 2 Ambrose-Walton method.

References: Ambrose, D., and J. Walton, *Pure & Appl. Chem.*, **61** (1989): 1395; Lee, B. I., and M. G. Kesler, *AIChE J.*, **21** (1975): 510.

Classification: Corresponding states.

Expected uncertainty: Varies strongly with relative T , but less than 1 percent is typical above T_b if the acentric factor is known.

Applicability: Most organic compounds.

Input data: T_b , T_c , P_c , and ω .

Description: The acentric factor is used to linearly interpolate within the simple-fluid and deviation terms for the $\ln P^*$ values of the reference fluids, which themselves have been correlated with the Wagner vapor pressure equation.

$$\ln P_r^* = f^{(0)} + \omega f^{(1)} + \omega^2 f^{(2)}$$

$$\begin{aligned} f^{(0)} &= \frac{-5.97616\tau + 1.29874\tau^{1.5} - 0.60394\tau^{2.5} - 1.06841\tau^5}{1 - \tau} \\ f^{(1)} &= \frac{-5.03365\tau + 1.11505\tau^{1.5} - 5.41217\tau^{2.5} - 7.46628\tau^5}{1 - \tau} \\ f^{(2)} &= \frac{-0.64771\tau + 2.41539\tau^{1.5} - 4.26979\tau^{2.5} + 3.25259\tau^5}{1 - \tau} \end{aligned} \quad (2-25)$$

where $\tau = 1 - T_r$.

Example Repeat the calculation of the liquid vapor pressure of chlorobenzene at 50 K intervals from 300 to 600 K.

Input information: From the DIPPR® 801 database, $T_c = 632.35$ K, $P_c = 45.1911$ bar, and $\omega = 0.249857$.

Auxiliary quantities:

$$T_r = 500/632.35 = 0.7907 \quad \tau = 1 - 0.7907 = 0.2093$$

Simple-fluid and deviation vapor pressure terms at each T (shown for $T = 500$ K):

$$\begin{aligned} f^{(0)} &= \frac{(-5.97616)(0.2093) + (1.29874)(0.2093)^{1.5} - (0.60394)(0.2093)^{2.5} - (1.06841)(0.2093)^5}{0.7907} = -1.4405 \\ f^{(1)} &= \frac{(-5.03365)(0.2093) + (1.11505)(0.2093)^{1.5} - (5.41217)(0.2093)^{2.5} - (7.46628)(0.2093)^5}{0.7907} = -1.3383 \\ f^{(2)} &= \frac{(-0.64771)(0.2093) + (2.41539)(0.2093)^{1.5} - (4.26979)(0.2093)^{2.5} + (3.25259)(0.2093)^5}{0.7907} = 0.0145 \end{aligned}$$

Calculation using Eq. (2-25):

$$\begin{aligned} \ln P_r^* &= -1.4405 + (0.249857)(-1.3383) + (0.249857)^2(0.0145) = -1.774 \\ P^* &= (45.1911 \text{ bar})[\exp(-1.774)] = 7.667 \text{ bar} \end{aligned}$$

T	τ	$f^{(0)}$	$f^{(1)}$	$f^{(2)}$	$\ln P_r^*$	P^*/bar	$P^*_{\text{DIPPR}}/\text{bar}$	% Error
300	0.5256	-5.9228	-7.5966	-0.3050	-7.840	0.0178	0.0175	1.4
350	0.4465	-4.3006	-5.0017	-0.1439	-5.559	0.174	0.172	1.5
400	0.3674	-3.1036	-3.3106	-0.0437	-3.933	0.885	0.880	0.5
450	0.2884	-2.1800	-2.1576	0.0043	-2.719	2.98	2.98	0.0
500	0.2093	-1.4405	-1.3383	0.0145	-1.774	7.67	7.67	0.0
550	0.1302	-0.8289	-0.7318	0.0036	-1.012	16.43	16.39	0.3
600	0.0512	-0.3068	-0.2612	-0.0081	-0.373	31.14	31.11	0.1

Solids Below the triple point, the pressure at which the solid and vapor phases of a pure component are in equilibrium at any given temperature is the vapor pressure of the solid. It is a monotonic function of temperature with a maximum at the triple point. Solid vapor pressures can be correlated with the same equations used for liquids. Estimation of solid vapor pressure can be made from the integrated form of the Clausius-Clapeyron equation

$$\ln \frac{P^*}{P_t^*} = \frac{\Delta H_{\text{sub}}}{RT_t} \left(1 - \frac{T_t}{T} \right) \quad (2-26)$$

where T_t = triple point temperature

P_t^* = triple point pressure

ΔH_{sub} = enthalpy of sublimation

The liquid and solid vapor pressures are identical at the triple point. A good vapor pressure correlation that is valid at the triple point may be used to obtain the triple point pressure. Estimating solid vapor pressures by using Eq. (2-26) generally requires an estimation of ΔH_{sub} , and so the illustrative example is combined with the example on enthalpy of sublimation in the section on latent enthalpy.

THERMAL PROPERTIES

Enthalpy of Formation The standard enthalpy (heat) of formation is the enthalpy change upon formation of 1 mol of the compound in its standard state from its constituent elements in their standard states. Two different standard enthalpies of formation are commonly defined based on the chosen standard state. The standard state enthalpy of formation ΔH_f° uses the naturally occurring phase at 298.15 K and 1 bar as the standard state; the ideal gas standard enthalpy (heat) of formation ΔH_f° uses the compound in the ideal gas state at 298.15 K and 1 bar as the standard state. In both cases, the standard state for the elements is their naturally occurring state of aggregation at 298.15 K and 1 atm. Sources for data include DIPPR®, TRC, SWS, JANAF, and Daubert, T. E., and R. P. Danner, *Technical Data Book—Petroleum Refining*, 5th ed., American Petroleum Institute, Washington, extant 1994. The Domalski-Hearing method is the most accurate general method for estimating either ΔH_f° or ΔH_f° if the appropriate GC values are available, but a CC method is also as accurate for estimating ΔH_f° if an isodesmic reaction can be formulated and used. The Domalski-Hearing method also applies to entropies, and the entropy predictive equations are listed in this section for convenience because they are equivalent in form to the enthalpy equations. However, discussion and illustration of the estimation methods for entropy are delayed to the next subsection.

Recommended Method Domalski-Hearing method.

Reference: Domalski, E. S., and E. D. Hearing, *J. Phys. Chem. Ref. Data*, **22** (1993): 805.

Classification: Group contributions.

Expected uncertainty: 3 percent.

Applicability: Organic compounds for which group contributions have been regressed.

Input data: Molecular structure.

Description: GC values from Table 2-343 are directly additive for both enthalpy of formation and absolute third-law entropies:

$$\frac{\Delta H_f^\circ}{\text{kJ/mol}} = \sum_{i=1}^N n_i (\Delta H_f^\circ)_i \quad \frac{S^\circ}{\text{J}\cdot\text{mol}^{-1}\text{K}^{-1}} = \sum_{i=1}^N n_i (S^\circ)_i \quad (2-27)$$

where $(\Delta H_f^\circ)_i$ = enthalpy of formation GC value from Table 2-343 and $(S^\circ)_i$ = entropy GC value from Table 2-343.

Group values in Table 2-343 are defined by the central, nonhydrogen group and the atoms bonded to that group. Thus, C—(2H)(2C) represents a C atom to which 2 H and 2 C atoms are bonded. For example, propane (CH₃—CH₂—CH₃) is composed of three groups: two C—(3H)(C) and one C—(2H)(2C).

Example Estimate the standard and ideal gas enthalpies of formation of *o*-toluidine.

Input information: The melting point (256.8 K) and boiling point (473.49 K) given for *o*-toluidine in the DIPPR® 801 database bracket 298.15 K, and so the standard state phase at 298.15 K and 1 bar must be liquid.

Structure:

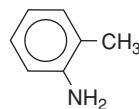


TABLE 2-343 Domalski-Hearing* Group Contribution Values for Standard State Thermal Properties

This table is a partial listing of GC values available from the original Domalski-Hearing tables. Table-specific nomenclature: Cd = carbon with double bond; Ct = carbon with triple bond; Cb = carbon in benzene ring; Ca = allenic carbon; corr = correction term; Cbf = fused benzene ring; N_A = azo nitrogen; N_I = imino nitrogen.

Group	ΔH_f°	S°	ΔH_f° liq.	S° liq.	ΔH_f° solid	S° solid
CH Groups						
C—(3H)(C)	-42.26	127.32	-47.61	83.30	-46.74	56.69
C—(2H)(2C)	-20.63	39.16	-25.73	32.38	-29.41	23.01
C—(H)(3C)	-1.17	-53.60	-4.77	-23.89	-5.98	-16.89
—CH ₃ _{corr} (tertiary)	-2.26	0.00	-2.18	0.00	-2.34	0.00
C—(4C)	19.20	-149.49	17.99	-98.65	12.47	-33.19
—CH ₃ _{corr} (quaternary)	-4.56	0.00	-4.39	0.00	-4.35	0.00
—CH ₃ _{corr} (tert/quat)	-1.80	0.00	-1.77	0.00	-2.70	0.00
—CH ₃ _{corr} (quat/quat)	-0.64	0.00	-0.64	0.00	-2.24	0.00
Cd—(2H)	-26.32	115.52	21.75	86.19	22.43	
Cd—(H)(C)	36.32	33.05	31.05	28.58	25.48	
Cd—(2C)	44.14	-50.84	39.16	-29.83	32.97	
Cd—(H)(Cd)	28.28	27.74	22.18	13.30	17.53	21.75
Cd—(C)(Cd)	36.78	-61.33	30.42	-41.92	27.91	
Cd—(Cd)(Cb)					56.07	
Cd—(H)(Cb)	28.28	27.74	22.18	13.30	17.53	21.75
Cd—(C)(Cb)	37.95	-51.97	38.58			
Cd—(H)(Ct)	28.28	27.74	22.18	13.30	17.53	21.75
C—(4H), Methane	-74.48	206.92				
Cd—(2Cb)	32.88		30.83		49.91	
C—(2H)(C)(Cd)	-20.88	38.20	-25.73	31.67	-24.35	
C—(H)(2C)(Cd)	-1.63	-50.38	-5.02	-28.07	-6.49	
—CH ₃ _{corr} (tertiary)	-2.26	0.00	-2.18	0.00	-2.34	0.00
C—(3C)(Cd)	22.13	-150.23	20.79	-108.20	12.51	
—CH ₃ _{corr} (quaternary)	-4.56	0.00	-4.39	0.00	-4.35	0.00
C—(H)(C)(2Cd)	-1.17	-53.60	-4.77	-23.89	-5.98	-16.89
C—(2H)(2Cd)	-18.92	42.08	-24.43	19.32	-21.60	
C—(2H)(Cd)(Cb)			-24.73			
C—(H)(C)(Cd)(Cb)			-6.90			
<i>cis</i> (unsat) _{corr}	4.85	5.06	5.27	0.00	5.73	0.00
tert—Butyl <i>cis</i> _{corr}	17.24	0.00	17.48	0.00	17.57	0.00
Ct—(H)	113.50	101.96	104.47	67.57	110.34	
Ct—(C)	115.10	26.32	107.15	14.25	101.66	
Ct—(Cd)	121.42	39.92	114.77			
Ct—(Cb)	120.76	17.77	119.00		103.28	
Ct—(Ct)	120.76	25.94	104.80		103.28	
C—(2H)(C)(Ct)	-19.70	42.80	-22.13	32.36	-29.41	
C—(H)(2C)(Ct)	-3.16	-45.69				
—CH ₃ _{corr} (tertiary)	-2.26	0.00	-2.18	0.00	-2.34	0.00
C—(3C)(Ct)			22.83		26.38	
—CH ₃ _{corr} (quaternary)	-4.56	0.00	-4.39	0.00	-4.35	0.00
C—(2H)(2Ct)	-41.14		-39.08			
C—(2C)(2Ct)			20.67			
Ca	142.67	26.28	134.68	14.39	131.08	
Cb—(H)(2Cb)	13.81	48.31	8.16	28.87	6.53	22.75
Cb—(C)(2Cb)	23.64	-35.61	19.16	-19.50	13.90	-5.50
Cb—(Cd)(2Cb)	24.17	-33.85	19.12	-9.04	20.27	-10.00
Cb—(Ct)(2Cb)	24.17	-33.85	19.12	-9.04	20.07	-10.00
Cb—(3Cb)	21.66	-36.57	17.21		17.03	-6.00
C—(2C)(2Cb)					52.81	
C—(2H)(C)(Cb)	-21.34	42.59	-24.81	47.40	-22.10	26.90
C—(H)(2C)(Cb)	-4.52	-48.00	-5.82	-13.90	-3.50	
C—(Cb)(3C)	18.28	-147.19	18.70	-96.10	21.57	
C—(2H)(2Cb)	-46.43		-26.50	51.97	-21.44	22.85
C—(H)(C)(2Cb)			-21.47	28.12	16.40	
C—(H)(3Cb)	-6.86				34.48	-12.62
C—(3Cb)(C)					116.25	
C—(4Cb)	27.04				64.89	
Cbf—(Cbf)(2Cb)	20.10	0.00	15.83	-5.54	14.10	-6.00
Cbf—(Cb)(2Cbf)	16.00		11.50		12.00	2.00
Cbf—(3Cbf)	3.59		-0.90		1.94	7.00
Cb—(2Cb)(Cbf)					-8.77	
Cb—(Cb)(2Cbf)	22.46				47.93	
<i>ortho</i> _{corr} hydrocarbons	1.26	-2.50	3.26	0.00	5.00	0.00
<i>meta</i> _{corr} hydrocarbons	-0.63	0.00	0.00	0.00	2.00	0.00
Cyclopropane rsc (unsub)	115.15	134.86	111.58			
Cyclobutane rsc	110.89	126.04	106.64	51.48	114.43	
Cyclopentane rsc (unsub)	26.75	116.22	22.84	42.24	34.00	
Cyclohexane rsc (unsub)	0.68	78.18	-1.77	10.07	10.94	
Cycloheptane rsc	26.34	73.97	23.50	15.89		
Cyclooctane rsc	40.65	70.78	38.10	2.96		
Cyclononane rsc	52.91		50.40			
Cyclodecane rsc	51.99		50.61			

2-480 PHYSICAL AND CHEMICAL DATA

TABLE 2-343 Domalski-Hearing* Group Contribution Values for Standard State Thermal Properties (Continued)

This table is a partial listing of GC values available from the original Domalski-Hearing tables. Table-specific nomenclature: Cd = carbon with double bond; Ct = carbon with triple bond; Cb = carbon in benzene ring; Ca = allenic carbon; corr = correction term; Cbf = fused benzene ring; N_A = azo nitrogen; N_I = imino nitrogen.

Group	ΔH_f°	S°	ΔH_f° liq.	S° liq.	ΔH_f° solid	S° solid
CHO Groups						
CO—(2H), formaldehyde	-108.60	224.54				
CO—(C)(CO)	-121.29		-135.04		-140.75	
CO—(H)(CO)	-105.98					
CO—(CO)(Cb)	-112.30				-117.75	
CO—(O)(CO)	-123.75		-123.30		-120.81	
CO—(Cd)(O)	-136.73	62.59	-155.56		-134.10	32.90
CO—(C)(O)	-137.24	62.59	-149.37	32.72	-153.60	32.13
CO—(H)(O)	-124.39	147.03	-142.42	94.68		
CO—(2O)	-111.88		-122.00		-123.00	-42.92
CO—(H)(Cd)	-126.96		-153.05			
CO—(2Cb)	-110.00		-119.00		-116.00	
CO—(C)(Cb)	-148.82		-145.22		-143.70	23.72
CO—(H)(Cb)	-121.35		-138.12		-160.18	
CO—(O)(Cb)	-125.00		-140.00		-145.00	32.13
CO—(2C)	-132.67	64.31	-152.76	33.81	-157.95	
CO—(H)(C)	-124.39	147.03	-142.42	93.55		
CO—(C)(Cd)						
O—(2CO), aliphatic	-214.50	34.16	-230.50		-235.00	
O—(2CO), aromatic	-238.30		-220.90		-207.00	
O—(Cd)(CO)	-198.03		-201.42			
O—(C)(CO)	-188.87	36.03	-196.02	38.28	-210.60	12.09
O—(H)(CO)	-254.30	101.71	-285.64	38.28	-282.15	21.78
O—(Cb)(CO)	-167.00		-165.50		-170.00	45.32
O—(C)(O)	-20.75		-23.50		-30.20	
O—(H)(O)	-72.26		-101.75		-105.30	
O—(2Cd)	-139.29		-137.32			
O—(H)(Cd)						
O—(C)(Cd)	-129.33		-133.72			
O—(2Cb)	-77.66		-85.27	23.31	-96.20	3.14
O—(C)(Cb)	-92.55		-104.85		-122.87	
O—(H)(Cb)	-160.30	121.50	-191.75	43.89	-199.25	28.62
O—(2C)	-101.42	29.33	-110.83	26.78	-119.00	
O—(H)(C)	-159.33	121.50	-191.50	43.89	-199.66	28.62
Cd—(H)(CO)	32.30	35.19	26.61		7.82	27.53
Cd—(C)(CO)						
Cd—(O)(Cd)	36.78	-61.34	30.42	-41.92	27.91	
Cd—(O)(C)	44.14	-50.84	39.08	-29.83	32.97	
Cd—(O)(H)	36.32	33.05	31.05	28.58	25.48	
Ct—(CO)					144.52	
Cb—(CO)(2Cb)	15.50		10.50		8.15	0.08
Cb—(O)(2Cb)	-4.75	-43.72	-5.61	-10.59	1.00	1.59
C—(2H)(2CO)	-30.74		-23.06		-19.10	
C—(CO)(3C)	23.93		26.15	-85.98	24.02	
C—(H)(CO)(2C)	-0.25		-3.89	-24.52	-9.83	
C—(2H)(CO)(C)	-21.84	39.58	-24.14	39.87	-27.90	24.73
C—(3H)(CO)	-42.26	127.32	-47.61	83.30	-46.74	56.69
C—(2H)(CO)(Cd)	-16.95		-19.62			
C—(2H)(CO)(Ct)	-25.48		-26.61			
C—(2H)(CO)(Cb)	-16.20		-11.67			
C—(H)(CO)(C)(Cb)					14.81	
C—(H)(O)(CO)(C)	126.63		123.43	-46.71	-14.39	8.08
C—(4O)	-152.46		-133.34			
C—(H)(3O)	-113.97		-107.74			
C—(3O)(C)	-114.39		-99.54			
C—(2O)(2C)	-53.56		-41.30			
C—(H)(2O)(C)	-57.78		-51.42			
C—(2H)(2O)	-62.22		-62.89	23.85		
C—(2H)(O)(Cb)	-33.76		-29.17			
C—(2H)(O)(Cd)	-27.49		-28.62			
C—(H)(CO)(C)(Cb)		37.49				
C—(H)(CO)(2Cb)					-14.39	
C—(O)(3Cb)					3.72	
C—(O)(3C) (ethers, esters)	9.50	-141.92	0.79	-94.68	60.46	
C—(H)(O)(2C) (ethers, esters)	-19.46	-52.80	-21.00	-25.31	-0.50	
C—(O)(3C) (alcohols, peroxides)	-13.50	-144.60	-11.13	-122.48	-20.08	
C—(H)(O)(2C) (alcohols, peroxides)	-26.10	-43.05	-27.60	-29.83	-12.25	-14.77
C—(2H)(O)(C)	-32.90	43.43	-35.80	32.59	-29.08	6.95
C—(3H)(O)	-42.26	127.32	-47.61	83.30	-33.00	24.73
O—(CO)(O)	-88.00		-90.00		-46.74	56.69
C—(2C)(O)(Cb)	15.30		25.80		-80.50	
C—(H)(C)(2O)					29.30	
					-52.50	

TABLE 2-343 Domalski-Hearing* Group Contribution Values for Standard State Thermal Properties (Continued)

This table is a partial listing of GC values available from the original Domalski-Hearing tables. Table-specific nomenclature: Cd = carbon with double bond; Ct = carbon with triple bond; Cb = carbon in benzene ring; Ca = allenic carbon; corr = correction term; Cbf = fused benzene ring; N_A = azo nitrogen; N_I = imino nitrogen.

Group	ΔH_f°	S°	ΔH_f° liq.	S° liq.	ΔH_f° solid	S° solid
CHN and CHNO Groups						
C—(3H)(N)	-42.26	127.32	-47.61	83.30	-46.74	56.69
C—(2H)(C)(N)	-28.30	42.26	-30.80	32.38	-34.00	23.01
C—(H)(2C)(N)	-16.70	-63.55	-14.65	-20.00	-13.90	
—CH ₃ corr (tertiary)	-2.26	0.00	-2.18	0.00	-2.34	0.00
C—(3C)(N)	0.29	-152.59	5.10	-87.99	1.00	
—CH ₃ corr (quaternary)	-4.56	0.00	-4.39	0.00	-4.35	0.00
C—(2H)(2N)	-30.00				-26.00	
C—(2H)(Cb)(N)	-24.14		-26.09		-33.31	
N—(2H)(C) (first, amino acids)	19.25	124.40	0.33	71.71	-6.30	39.00
N—(2H)(C) (second, amino acids)	19.25	126.90	0.33	71.71	-46.00	48.75
N—(H)(2C)	67.55	33.96	51.50	32.09	47.80	
N—(3C)	116.50	-61.71	112.00	-38.62	101.00	
N—(2H)(N)	47.70	122.18	25.30	60.58	18.97	
N—(H)(C)(N)	89.16		75.00	22.05		
N—(2C)(N)	120.71		119.00	-26.94		
N—(2Cb)(N)					137.35	
N—(H)(Cb)(N)	87.50		73.40		66.90	
N—(2CO)(N)					73.62	
N—(H)(2Cd)	83.55		50.50		45.40	
N—(C)(2Cd)	120.64		97.38		88.92	
N—(2H)(Cb)	19.25	126.90	-11.00	71.71	-21.60	70.00
N—(H)(C)(Cb)	59.00		26.25		36.55	
N—(2C)(Cb)	126.40		109.40		96.50	
N—(C)(2Cb)	120.44		97.38		89.30	
N—(H)(2Cb)	83.55		50.50		45.40	
N—(3Cb)	123.15		121.80		107.50	
N _I —(C)	81.46		73.68			
N _I —(Cb)	69.00	47.01	54.50	36.40	57.00	
N _A —(C)	109.50		104.85		103.00	
N _A —(Cb)	109.50		104.85		103.00	
N _A —(oxide)(C)	40.80		22.65			
C—(2H)(C)(N _A)	-20.70		-25.70		-29.41	
C—(H)(2C)(N _A)	-2.66		-5.42			
C—(3C)(N _A)	11.50		15.50		10.50	
Cd—(H)(N)	-16.00		-15.50		-13.00	
Cd—(C)(N)	-5.74		-5.62		-3.95	
Cb—(N)(2Cb)	-1.30	-43.53	1.50	-24.43	9.75	-37.57
Cb—(NO)(2Cb)	21.50				23.00	
Cb—(NO ₂)(2Cb)	-1.45		-28.30	79.95	-32.50	110.46
Cb—(CNO)(2Cb)	-177.63				155.69	
Cb—(CN)(2Cb)	151.00	85.25	122.38	64.75	121.20	50.45
Cb—(N _A)(2Cb)	22.55		20.08		18.65	
Cb—(H)(2N _I)	6.30				0.25	
CO—(H)(N)	-124.39	147.03	-188.00	93.55		
CO—(C)(N)	-133.26	56.70	-185.00		-194.60	40.00
CO—(Cb)(N) (amides)					-177.75	
CO—(Cb)(N) (amino acids)					-177.75	
CO—(Cd)(N)	-171.80					
CO—(2N)	-111.00	96.00	-190.50		-203.10	69.00
N—(2H)(CO) (amides, ureas)	-63.00	88.25	-63.90		-65.25	18.00
N—(2H)(CO) (amino acids)	-63.00		-63.90		-59.75	33.03
N—(H)(C)(CO) (amides, ureas)	-16.28		-17.10		-9.80	
N—(H)(C)(CO) (amino acids)	-16.28		-17.10		5.50	
N—(2C)(CO)	45.00		62.00		55.00	
N—(H)(Cb)(CO)	-20.84				-3.50	
N—(H)(2CO)	-91.00				-30.80	
N—(C)(2CO)	-11.64		56.20		64.00	
N—(Cb)(2CO)	9.12					
N—(2Cb)(CO)					60.85	
N—(C)(Cb)(CO)					72.00	
C—(3H)(CN), acetonitrile	74.04	252.60	40.56	149.62		
C—(2H)(C)(CN)	94.52	167.25	66.07	106.02	69.85	96.15
C—(H)(2C)(CN)	113.50	67.86	81.50		69.00	
C—(3C)(CN)	137.96		116.20	-17.91	102.07	
C—(2C)(2CN)						74.57
C—(2H)(Cd)(CN)	95.31		66.40			
Cd—(H)(CN)	146.65	158.41	117.28	92.72		
Ct—(CN)	264.60		250.20			
C—(3H)(NO ₂), nitromethane	-74.86	284.14	-112.60	171.75		
C—(2H)(2NO ₂), dinitromethane	-58.90		-104.90			
C—(H)(3NO ₂), trinitromethane	-0.30				-48.00	
C—(4NO ₂), tetranitromethane	82.30		38.30			
C—(2H)(C)(NO ₂)	-60.50	203.60	-93.50		-99.00	

2-482 PHYSICAL AND CHEMICAL DATA

TABLE 2-343 Domalski-Hearing* Group Contribution Values for Standard State Thermal Properties (Continued)

This table is a partial listing of GC values available from the original Domalski-Hearing tables. Table-specific nomenclature: Cd = carbon with double bond; Ct = carbon with triple bond; Cb = carbon in benzene ring; Ca = allenic carbon; corr = correction term; Cbf = fused benzene ring; N_A = azo nitrogen; N_I = imino nitrogen.

Group	ΔH_f°	S°	ΔH_f° liq.	S° liq.	ΔH_f° solid	S° solid
CHN and CHNO Groups						
C—(H)(2C)(NO ₂)	-53.00	115.32	-82.50		-89.00	
C—(3C)(NO ₂)	-36.65		-61.20		-76.55	
C—(2H)(Cb)(NO ₂)	-62.00		-82.76		-81.00	
C—(H)(C)(2NO ₂)	-36.80		-88.80		-91.50	
C—(2C)(2NO ₂)	-28.50		-77.20		-90.30	
C—(H)(C)(CO)(N)	-18.70				-11.65	-4.00
C—(2H)(CO)(N)	-3.10				-30.95	24.00
C—(H)(Cb)(CO)(N)						
O—(C)(NO)	-24.23	166.11	-46.50			
O—(C)(NO ₂)	-79.71	191.92	-108.96	127.50	-124.00	
N—(H)(C)(NO ₂)					16.50	
N—(H)(Cb)(NO ₂)						
N—(H)(CO)(NO ₂)					-14.00	
N—(C)(2NO ₂)	100.30		53.50			
N—(C)(Cb)(NO ₂)	183.00		167.00		150.50	
N—(2C)(NO)	90.00		59.00		55.00	
N—(2C)(NO ₂)	88.00		50.00		40.00	
C—(2H)(C)(N ₃)			321.70			
C—(H)(2C)(N ₃)	274.00		255.00			
C—(2H)(Cb)(N ₃)	347.00		327.40			
C—(3Cb)(N ₃)	328.60				346.50	
Cb—(N ₃)(2Cb)	320.00		303.50			
CHS and CHSO Groups						
C—(3H)(S)	-42.26	127.32	-47.61	83.30	-46.74	56.69
C—(2H)(C)(S)	-23.17	41.87	-26.77	41.09		
C—(H)(2C)(S)	-5.88	-47.36	-6.07	-16.61		
-CH ₃ corr (tertiary)	-2.26	0.00	-2.18	0.00	-2.34	0.00
C—(3C)(S)	13.52	-145.38	16.69	-86.86		
-CH ₃ corr (quaternary)	-4.56	0.00	-4.39	0.00	-4.35	0.00
-CH ₃ corr (tert/quat)	-1.80	0.00	-1.77	0.00	-2.70	0.00
-CH ₃ corr (quat/quat)	-0.64	0.00	-0.64	0.00	-2.24	0.00
C—(2H)(Cb)(S)	-18.53		-23.82			
C—(2H)(Cd)(S)	-25.93		-32.44			
C—(2H)(2S)	-25.10					
Cb—(S)(2Cb)	-4.75	43.72	-5.61	-10.59	1.00	1.59
Cd—(H)(S)	36.32	33.05	31.05	28.58	25.48	
Cd—(C)(S)	45.73	-51.92				
S—(C)(H)	18.64	137.67	0.06	85.95		
S—(Cb)(H)	48.10	57.34	28.51	89.04		
S—(2C)	46.99	55.19	29.82	29.80		
S—(H)(Cd)	25.52					
S—(C)(Cd)	54.39					
S—(2Cd)	102.60	68.59				
S—(Cb)(C)	76.21		58.20	35.44	42.00	
S—(C)(S)	27.62	50.50	14.36	30.84		
S—(Cb)(S)	57.45				40.60	
S—(2S)	12.59	56.07				
S—(2Cb)	102.60	68.59	93.02			
S—(H)(S)	7.95					
S—(H)(CO)	-5.90	130.54				
CO—(C)(S)	-132.67	64.31	-152.76	33.81		
C—(3H)(SO)	-42.26	127.32	-47.61	83.30	-46.74	56.69
C—(2H)(C)(SO)	-29.16		-36.88			
C—(H)(2C)(SO)						
-CH ₃ corr (tertiary)	-2.26	0.00	-2.18	0.00	-2.34	0.00
C—(3C)(SO)	4.56		0.97			
-CH ₃ corr (quaternary)	-4.56	0.00	-4.39	0.00	-4.35	0.00
C—(2H)(Cd)(SO)	-27.56		-32.63			
cis correction	4.11	5.06	5.27	0.00	5.73	0.00
Cb—(SO)(2Cb)	15.48		25.44		7.55	0.08
O—(SO)(H)	-158.60					
O—(C)(SO)	-92.60					
SO—(2C)	-66.78	75.73	-108.98	22.18		
SO—(2Cb)	-62.26					
SO—(2O)	-213.00					
SO—(C)(Cb)	-72.00					
C—(3H)(SO ₂)	-42.26	127.32	-47.61	83.30	-46.74	56.69
C—(2H)(C)(SO ₂)	-27.03		-33.76		-35.96	
C—(H)(2C)(SO ₂)	-14.00					
-CH ₃ corr (tertiary)	-2.26	0.00	-2.18	0.00	-2.34	0.00
C—(3C)(SO ₂)	1.52		2.00		3.78	
-CH ₃ corr (quaternary)	-4.56	0.00	-4.39	0.00	-4.35	0.00

TABLE 2-343 Domalski-Hearing* Group Contribution Values for Standard State Thermal Properties (Continued)

This table is a partial listing of GC values available from the original Domalski-Hearing tables. Table-specific nomenclature: Cd = carbon with double bond; Ct = carbon with triple bond; Cb = carbon in benzene ring; Ca = allenic carbon; corr = correction term; Cbf = fused benzene ring; N_A = azo nitrogen; N_I = imino nitrogen.

Group	ΔH_f°	S°	ΔH_f° liq.	S° liq.	ΔH_f° solid	S° solid
CHN and CHNO Groups						
-CH _{3,corr} (quat/quat)	-0.64		-0.64		-2.24	
C-(2H)(Cd)(SO ₂)	-29.49		-49.05			
C-(H)(C)(Cd)(SO ₂)	-71.99					
C-(2H)(Cb)(SO ₂)	-29.80					
C-(2H)(Ct)(SO ₂)	16.36					
Cb-(SO ₂)(2Cb)	15.48		25.44		7.55	0.08
Cd-(H)(SO ₂)	51.58					
Cd-(C)(SO ₂)	64.01					
Ct-(SO ₂)	177.10					
SO ₂ -(Cd)(Cb)	-291.55					
SO ₂ -(2Cd)	-306.70					
SO ₂ -(2C)	-288.58	87.37	-341.14		-356.62	32.10
SO ₂ -(C)(Cb)	-289.10					
SO ₂ -(2Cb)	-287.76				-305.40	
SO ₂ -(SO ₂)(Cb)	-325.18				-361.75	
SO ₂ -(2O)	-417.30					
SO ₂ -(C)(Cd)	-316.80					
SO ₂ -(Ct)(Cb)	-296.30					
O-(SO ₂)(H)	-158.60					
O-(C)(SO ₂)	-91.40					
CHX and CHXO Groups						
C-(3H)(F), methyl fluoride	-247.00	231.93				
C-(3H)(Cl), methyl chloride	-81.90	243.60				
C-(3H)(Br), methyl bromide	-37.66	254.94	-61.10			
C-(3H)(I), methyl iodide	14.30	263.14	-11.70			
C-(C)(3F)	-673.81	178.22	-709.07	135.56		
C-(2H)(C)(F)	-221.12	146.80				
C-(H)(2C)(F)	-204.46	55.76				
C-(3C)(F)	-202.92					
C-(H)(C)(2F)	-454.74	164.32	-487.23			
C-(2C)(2F)	-411.39	74.48	-400.37		-428.77	
C-(C)(Cl)(2F)	-462.70	169.45	-466.00			
C-(H)(C)(Cl)(F)	-271.14			138.31		
C-(C)(3Cl)	-81.98	202.14	-112.93	145.91		
C-(H)(C)(2Cl)	-79.10	183.28	-102.60	128.45		
C-(2H)(C)(Cl)	-69.45	159.24	-86.90	104.27	-85.65	
C-(2C)(2Cl)	-79.56	95.41	-101.80			
C-(H)(2C)(Cl)	-55.61	71.34	-71.17			
C-(3C)(Cl)	-43.70	-24.26	-56.78			
C-(C)(3Br)		233.05				
C-(H)(C)(2Br)						
C-(2H)(C)(Br)	-21.78	173.31	-42.65	113.00		
C-(2C)(2Br)						
C-(H)(2C)(Br)	-10.75	84.69	-27.31			
C-(3C)(Br)	7.26	-13.46	-7.40			
C-(C)(3I)						
C-(H)(C)(2I)	108.78	228.45				
C-(2H)(C)(I)	33.54	177.78	4.14		3.65	
C-(2C)(2I)						
C-(H)(2C)(I)	48.74	88.10	24.78			
C-(3C)(I)	68.46	-3.21	48.60			
C-(H)(C)(Br)(Cl)	-18.45	191.21				
N-(C)(2F)	-32.64					
C-(H)(C)(Cl)(O)	-90.37	66.53				
C-(2H)(I)(O)	15.90	170.29				
C-(C)(2Cl)(F)	-322.54		-343.87	141.71		
C-(C)(Br)(2F)	-394.55			149.70		
C-(C)(2Br)(F)						
C-(Br)(Cl)(F)						
Cd-(H)(F)	-165.12	137.24				
Cd-(H)(Cl)	4.37	147.85	-12.67			
Cd-(H)(Br)	50.94	159.91				
Cd-(H)(I)	102.36	169.45				
Cd-(C)(Cl)	-5.06	62.76	-2.23			
Cd-(2F)	-329.90	155.63				
Cd-(2Cl)	-11.51	175.41	-32.08	115.35		
Cd-(2Br)		199.16				
Cd-(2I)						
Cd-(Cl)(F)	-235.10	175.61				
Cd-(Br)(F)		177.82				
Cd-(Cl)(Br)		188.70				
Ct-(F)						

TABLE 2-343 Domalski-Hearing* Group Contribution Values for Standard State Thermal Properties (Concluded)

This table is a partial listing of GC values available from the original Domalski-Hearing tables. Table-specific nomenclature: Cd = carbon with double bond; Ct = carbon with triple bond; Cb = carbon in benzene ring; Ca = allenic carbon; corr = correction term; Cbf = fused benzene ring; N_A = azo nitrogen; N_I = imino nitrogen.

Group	ΔH_f°	S°	ΔH_f° liq.	S° liq.	ΔH_f° solid	S° solid
CHX and CHXO Groups						
Ct—(Cl)		140.00				
Ct—(Br)		151.30				
Ct—(I)	35.53					
Cb—(F)(2Cb)	-181.26	67.52	-191.20	54.19	-194.00	39.79
Cb—(Cl)(2Cb)	-17.03	77.08	-32.20	55.47	-32.00	43.37
Cb—(Br)(2Cb)	36.35	88.60	19.90	74.85	13.50	54.45
Cb—(I)(2Cb)	94.50	98.26	73.70	61.08	70.40	
cis _{corr} —(I)(I)	3.00	0.00	0.00	0.00	0.00	0.00
C—(2H)(CO)(Cl)	-44.26		-58.41		-74.75	
C—(H)(CO)(2Cl)	-40.40		-55.11			
CO—(C)(F)	-379.84		-419.59			
C—(Cb)(3F)	-691.79	179.08	-696.66			
C—(2H)(Cb)(Br)	-29.49		-44.06			
C—(2H)(Cb)(I)	7.31		-7.24			
C—(2H)(Cb)(Cl)	-73.79		-92.56			
CO—(C)(Cl)	-200.54	176.66	-225.29			
CO—(Cb)(Cl)			-216.67		-212.99	
CO—(C)(Br)	-148.54		-175.49			
CO—(C)(I)	-83.94		-117.09			
C—(H)(C)(CO)(Cl)	-39.88		-35.46			
C—(C)(CO)(2Cl)						
ortho _{corr} —(I)(I)	7.56	0.00	6.96	0.00	5.50	0.00
ortho _{corr} —(F)(F)	20.90	0.00	25.00	0.00	25.50	0.00
ortho _{corr} —(Cl)(Cl)	9.50	0.00	14.00	0.00	8.50	0.00
ortho _{corr} —(alkyl)(X)	2.51	0.00	6.30	0.00	0.00	0.00
cis _{corr} —(Cl)(Cl)	-4.00	0.00	0.00	0.00	0.00	0.00
cis _{corr} —(CH ₃)(Br)	-4.00	0.00	0.00	0.00	0.00	0.00
ortho _{corr} —(F)(Cl)	13.50	0.00	18.50	0.00	19.50	0.00
ortho _{corr} —(F)(Br)	37.25	0.00	40.60	0.00	42.50	0.00
ortho _{corr} —(F)(I)	85.40	0.00	83.55	0.00	85.20	0.00
meta _{corr} —(I)(I)	0.00	0.00	0.00	0.00	20.08	0.00
meta _{corr} —(COCl)(COCl)	0.00	0.00	0.00	0.00	16.06	0.00
ortho _{corr} —(COCl)(COCl)	0.00	0.00	0.00	0.00	0.00	0.00
ortho _{corr} —(F)(CF ₃)	111.00	0.00	112.00	0.00	0.00	0.00
meta _{corr} —(F)(CF ₃)	2.00	0.00	6.00	0.00	0.00	0.00
ortho _{corr} —(F)(CH ₃)	-3.30	0.00	-6.00	0.00	0.00	0.00
ortho _{corr} —(F)(F)	8.00	0.00	8.00	0.00	8.00	0.00
ortho _{corr} —(Cl)(Cl)	8.00	0.00	8.00	0.00	8.00	0.00
meta _{corr} —(F)(F)	0.00	0.00	6.00	0.00	8.50	0.00
meta _{corr} —(Cl)(Cl)	-5.00	0.00	10.00	0.00	4.00	0.00
ortho _{corr} —(Cl)(CHO)	-6.75	0.00	8.50	0.00	0.00	0.00
ortho _{corr} —(F)(COOH)	20.00	0.00	0.00	0.00	20.00	0.00
ortho _{corr} —(Cl)(COCl)	0.00	0.00	34.43	0.00	0.00	0.00
ortho _{corr} —(F)(OH)	25.50	0.00	23.00	0.00	20.00	0.00
ortho _{corr} —(Cl)(COOH)	0.00	0.00	0.00	0.00	20.00	0.00
ortho _{corr} —(Br)(COOH)	0.00	0.00	0.00	0.00	20.00	0.00
ortho _{corr} —(I)(COOH)	0.00	0.00	0.00	0.00	20.00	0.00
ortho _{corr} —(NH ₂)(NH ₂)	-10.00	0.00	0.00	0.00	0.00	0.00
meta _{corr} —(NH ₂)(NH ₂)	0.00	0.00	0.00	0.00	14.00	0.00
ortho _{corr} —(OH)(Cl)	7.50	0.00	0.00	0.00	11.00	0.00
cis _{corr} —(CH ₃)(I)	-4.00	0.00	0.00	0.00	0.00	0.00

*Domalski, E. S. and E. D. Hearing, *J. Phys. Chem. Ref. Data*, **22** (1993): 805

Group contributions:

Group	n _i	ΔH_f° gas	ΔH_f° liq.	S° gas	S° liq.
Cb—(H)(2Cb)	4	13.81	8.16	48.31	28.87
Cb—(C)(2Cb)	1	23.64	19.16	-35.61	-19.50
Cb—(N)(2Cb)	1	-1.30	1.50	-43.53	-24.43
C—(3H)(C)	1	-42.26	-47.61	127.32	83.30
N—(2H)(Cb)	1	19.25	-11.00	126.90	71.71
Total		54.57	-5.31	368.32	226.56

Calculation from Eq. (2-27):

$$\frac{\Delta H_f^\circ}{\text{kJ/mol}} = 54.57 \quad \frac{\Delta H_f^\circ}{\text{kJ/mol}} = -5.31$$

$$\frac{S^\circ}{\text{J/(mol}\cdot\text{K)}} = 368.32 \quad \frac{S^\circ}{\text{J/(mol}\cdot\text{K)}} = 226.56$$

The recommended DIPPR® 801 standard enthalpies of formation are $\Delta H_f^\circ = 53.20$ kJ/mol and $\Delta H_f^\circ = -4.72$ kJ/mol; the estimated values are higher than the recommended values by 2.6 and 12.5 percent, respectively. The recommended DIPPR® 801 standard entropies are $S^\circ = 355.5$ J/(mol·K) and $S^\circ = 231.2$ J/(mol·K). The estimated values differ from these by 3.5 and -2.0 percent, respectively.

Recommended Method Isodesmic reaction.

Reference: Foresman, J. B., and A. Frisch, *Exploring Chemistry with Electronic Structure Methods*, 2d ed., Gaussian Inc., Pittsburgh, Pa., 1996.

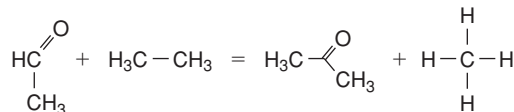
Classification: Computational chemistry.

Expected uncertainty: 5 to 10 percent depending upon the level of theory and basis set size used.

Applicability: Compounds for which an isodesmic reaction can be formulated.

Input data: Experimental ΔH_f° values for all *other* participants in the isodesmic reaction.

Description: While *ab initio* calculations of absolute enthalpies are not currently as accurate as GC methods, *relative* enthalpies of molecules calculated with the same level of theory and basis set can be very accurate, as in the case of isodesmic reactions. An isodesmic reaction is one in which the number and type of bonds are preserved during the reaction. For example, the reaction of acetaldehyde with ethane to form acetone and methane



is isodesmic with 12 single bonds and 1 double bond in both reactants and products. To use this method, one devises an isodesmic reaction involving the compound for which ΔH_f° is to be determined and other compounds for which experimental ΔH_f° values are available. *Ab initio* calculations are performed on all the participating compounds, all at the same level of theory and basis set size, to obtain the enthalpy for each at 298.15 K. The enthalpy of reaction is then calculated from

$$\Delta H_{\text{rxn}} = \sum v_i H_i \quad (2-28)$$

where v_i = stoichiometric coefficient of i (+ for products, - for reactants). The enthalpy of reaction is also related to ΔH_f° by

$$\Delta H_{\text{rxn}} = \sum v_i (\Delta H_f^\circ)_i \quad (2-29)$$

With experimental values available for all ΔH_f° except the desired compound, its value can be back-calculated from Eq. (2-29).

Example Estimate the standard ideal gas enthalpy of formation of acetaldehyde.

Input information: The isodesmic reaction shown above will be used. The recommended ΔH_f° values from DIPPR® 801 for the other three compounds are

Acetone	Methane	Ethane
-215.70 kJ/mol	-74.52 kJ/mol	-83.82 kJ/mol

Ab initio calculations of enthalpy: With structures optimized using HF/6-31G(d) model chemistry and energies calculated with B3LYP/6-311 + G(3df,2p), the following enthalpies are obtained (including the zero point energy):

Acetone	Methane	Ethane	Acetaldehyde
-5.071×10^5 kJ/mol	-1.063×10^5 kJ/mol	-2.095×10^5 kJ/mol	-4.039×10^5 kJ/mol

Calculation using Eq. (2-28):

$$\Delta H_{\text{rxn}} = (-1.063 - 5.071 + 2.095 + 4.039) \times 10^5 \text{ kJ/mol} = -41.67 \text{ kJ/mol}$$

Calculation using Eq. (2-29):

$$\Delta H_{f,\text{acetaldehyde}}^\circ = \Delta H_{f,\text{acetone}}^\circ + \Delta H_{f,\text{methane}}^\circ - \Delta H_{f,\text{ethane}}^\circ - \Delta H_{\text{rxn}}$$

$$\Delta H_{f,\text{acetaldehyde}}^\circ = (-215.70 - 74.52 + 83.82 + 41.67) \frac{\text{kJ}}{\text{mol}} = -164.73 \frac{\text{kJ}}{\text{mol}}$$

The estimated value is 1.0 percent above the DIPPR® 801 recommended value of -166.40 kJ/mol.

Entropy Absolute or third-law entropies (relative to a perfectly ordered crystal at 0 K) of a compound in its standard state S° or of an

ideal gas S° at 298.15 K and 1 bar can be found in various literature sources (DIPPR, JANAF, TRC, SWS, and Daubert, T. E., and R. P. Danner, *Technical Data Book-Petroleum Refining*, 5th ed., American Petroleum Institute, Washington, extant 1994). Very good estimates for S° or S° can be obtained by using the Domalski-Hearing method. Excellent S° values can also be obtained from statistical mechanics by using experimental vibrational frequencies or values of the frequencies generated from computational chemistry.

The standard state ΔS_f° and standard ideal gas ΔS_f° entropies of formation at 298.15 K and 1 bar are related to the standard entropies by

$$\Delta S_f^\circ = S_{\text{compound}}^\circ - \sum_{i=1}^{n_A} v_i S_{\text{element},i}^\circ \quad \Delta S_f^\circ = S_{\text{compound}}^\circ - \sum_{i=1}^{n_A} v_i S_{\text{element},i}^\circ \quad (2-30)$$

where $S_{\text{element},i}^\circ$ is the absolute entropy of element i in its standard state at 298.15 K and 1 bar.

Recommended Method Domalski-Hearing method.

Reference: Domalski, E. S., and E. D. Hearing, *J. Phys. Chem. Ref. Data*, **22** (1993): 805.

Classification: Group contributions.

Expected uncertainty: 3 percent.

Applicability: Organic compounds for which group contributions have been regressed.

Input data: Molecular structure.

Description: See description given under Enthalpy of Formation above.

Example Estimate the standard and ideal gas entropies of formation of *o*-toluidine.

Standard state entropies: Estimation of S° and S° using the Domalski-Hearing method was illustrated above in the Enthalpy of Formation section. The standard entropies of formation can be obtained from the values determined in that example.

Formula: C₇H₉N. The standard state entropies of the elements from the DIPPR® 801 database are as follows:

Compound:	N ₂	H ₂	C, graphite
v_i :	1/2	9/2	7
$S^\circ/[\text{J}(\text{kmol}\cdot\text{K})]$:	1.9151×10^5	1.3057×10^5	5740

Entropies of formation can be calculated from these values by using Eq. (2-30):

$$\Delta S_f^\circ = \left[0.22656 - \left(\frac{1}{2} \right) (1.9151) - \left(\frac{9}{2} \right) (1.3057) - (7)(0.0574) \right] \frac{10^5 \text{ J}}{\text{kmol}\cdot\text{K}}$$

$$= -7.008 \cdot 10^5 \frac{\text{J}}{\text{kmol}\cdot\text{K}}$$

$$\Delta S_f^\circ = \left[0.36832 - \left(\frac{1}{2} \right) (1.9151) - \left(\frac{9}{2} \right) (1.3057) - (7)(0.0574) \right] \frac{10^5 \text{ J}}{\text{kmol}\cdot\text{K}}$$

$$= -6.867 \cdot 10^5 \frac{\text{J}}{\text{kmol}\cdot\text{K}}$$

Recommended Method Statistical mechanics.

Classification: Theory and computational chemistry.

Expected uncertainty: 0.2 percent if vibrational frequencies (or their characteristic temperatures) are experimentally available; uncertainty depends upon model chemistry if frequencies are determined from computational chemistry, but generally within about 5 percent.

Applicability: Ideal gases.

Input data: M ; σ (external symmetry number); characteristic rotational temperature(s) (Θ_A for linear molecules; Θ_A , Θ_B , and Θ_C for nonlinear molecules); and $3n_A - 6 + \delta$ characteristic vibrational temperatures Θ_j .

Description: For harmonic frequencies, the rigorous temperature dependence of S° is given by

$$\frac{S^\circ}{R} = \frac{3}{2} \ln \left(6175 \frac{M}{\text{kg}/\text{kmol}} \right) + \frac{S_r}{R} + \sum_{j=1}^{3n_A - 6 + \delta} \left[\left(\frac{\Theta_j}{T} \right) (e^{\Theta_j/T} - 1)^{-1} - \ln (1 - e^{-\Theta_j/T}) \right] \quad (2-31)$$

where $\delta = \begin{cases} 0 & \text{nonlinear} \\ 1 & \text{linear} \end{cases}$

$$\frac{S_r}{R} = \begin{cases} \ln \left[\frac{1}{\sigma} \left(\frac{\pi T^3 e^3}{\Theta_A \Theta_B \Theta_C} \right)^{1/2} \right] & \text{nonlinear} \\ \ln \left[\left(\frac{T e}{\sigma \Theta_A} \right)^{1/2} \right] & \text{linear} \end{cases}$$

$$T = 298.15 \text{ K}$$

Example Calculate S° for ammonia.

Structure: NH_3 .

Input data: $M = 17 \text{ kg/kmol}$. McQuarrie [McQuarrie, D. A., *Statistical Mechanics*, Harper & Row, New York, 1976] gives the following $3m - 6 + \delta = 12 - 6 + 0 = 6$ characteristic vibrational temperatures (K): 1360, 2330, 2330, 4800, 4880, 4880. The characteristic rotational temperatures given by McQuarrie are $\Theta_A = 13.6 \text{ K}$, $\Theta_B = 13.6 \text{ K}$, and $\Theta_C = 8.92 \text{ K}$. For NH_3 , $\sigma = 3$.

Vibrational contribution: The table below shows a spreadsheet calculation of the vibrational terms inside the summation sign in Eq. (2-31).

Θ_j/K	Θ_j/T	S_{vib}
1207.91	4.051	0.08929
1850.16	6.205	0.01457
1850.16	6.205	0.01457
3688.19	12.370	0.00006
3821.36	12.817	0.00004
3821.36	12.817	0.00004
Sum		0.1186

Rotational contribution:

$$\frac{S_r}{R} = \ln \left\{ \frac{1}{3} \left[\frac{(298.15 \text{ K})^3 \pi c^3}{(13.6 \text{ K})(13.6 \text{ K})(8.92 \text{ K})} \right]^{1/2} \right\} = 5.81593$$

Calculation using Eq. (2-31):

$$\frac{S_{298}^\circ}{R} = \frac{3}{2} \ln(6175.17) + 5.81593 + 0.1186 = 23.277 \quad \Delta H_{\text{res}} = \sum \nu_i (\Delta H_f^\circ)_i$$

$$S_{298}^\circ = 1.935 \times 10^5 \frac{\text{J}}{\text{kmol} \cdot \text{K}}$$

The calculated value differs from the DIPPR® 801 recommended value of $1.9266 \times 10^5 \text{ J/(kmol} \cdot \text{K)}$ by 0.5 percent.

Gibbs' Energy of Formation The standard Gibbs energy of formation is the Gibbs energy change upon formation of 1 mol of the compound in its standard state from its constituent elements in their standard states. The standard state Gibbs energy of formation ΔG_f° uses the naturally occurring phase at 298.15 K and 1 bar as the standard state, while the ideal gas Gibbs energy of formation $\Delta G_f^{\circ\text{ig}}$ uses the compound in the ideal gas state at 298.15 K and 1 bar as the standard state. In both cases, the standard state for the elements is their naturally occurring state of aggregation at 298.15 K and 1 atm. Sources for data include DIPPR, TRC, JANAF, and Daubert and Danner, (Daubert, T. E., and R. P. Danner *Technical Data Book—Petroleum Refining*, 5th ed., American Petroleum Institute, Washington, extant 1994). The Gibbs energies of formation are related to the corresponding enthalpies and entropies of formation by

$$\Delta G_f^\circ = \Delta H_f^\circ - T \Delta S_f^\circ \quad \text{and} \quad \Delta G_f^{\circ\text{ig}} = \Delta H_f^{\circ\text{ig}} - T \Delta S_f^{\circ\text{ig}} \quad (2-32)$$

and predicted values of ΔG_f° and $\Delta G_f^{\circ\text{ig}}$ are obtained from Eq. (2-32) by estimating the enthalpies and entropies of formation as shown above.

LATENT ENTHALPY

Enthalpy of Vaporization The enthalpy (heat) of vaporization ΔH_v is the difference between the molar enthalpies of the saturated

vapor and saturated liquid at a temperature between the triple point and critical point (at the corresponding vapor pressure). Variable ΔH_v is related to the vapor pressure P° by the thermodynamically exact Clapeyron equation

$$\Delta H_v = -R \Delta Z_v \frac{d \ln P^\circ}{d(1/T)} = RT^2 \Delta Z_v \frac{d \ln P^\circ}{dT} \quad (2-33)$$

where $\Delta Z_v = Z_C - Z_L$
 $Z_C = Z$ of saturated vapor
 $Z_L = Z$ of saturated liquid

Experimental heats of vaporization can be effectively correlated with

$$\Delta H_v = A(1 - T_r)^{B+CT_r+DT_r^2+ET_r^3} \quad (2-34)$$

A simple method for obtaining ΔH_v at one temperature from a known value at a reference temperature, say, at the normal boiling point, is to truncate Eq. (2-34) after the B term, set $B = 0.38$, and take a ratio of the ΔH_v values at the two conditions to give the Watson [Thek, R. E., and L. I. Stiel, *AIChE J.*, **12** (1966): 599; 13(1967): 626] correlation

$$\Delta H_v = \Delta H_{v,\text{ref}} \left(\frac{1 - T_r}{1 - T_{r,\text{ref}}} \right)^{0.38} \quad (2-35)$$

If an accurate correlation for P° and accurate values for Z_C and Z_L are available, Eq. (2-33) is the preferred method for obtaining enthalpies of vaporization. Otherwise, the CS methods shown below should be used.

Recommended Method 1 Vapor pressure correlation.

Classification: Extension of theory.

Expected uncertainty: Varies significantly with temperature and with the quality and temperature range of the vapor pressure data used in the correlation.

Applicability: Organic compounds for which group contributions have been regressed.

Input data: Correlations for P° , Z_C , and Z_L . If $T_r < 0.8$, then Z_C can be set to 1.

Description: An expression for ΔH_v can be obtained from Eq. (2-33) by using an appropriate vapor pressure correlation. If one differentiates the Riedel vapor pressure correlation, Eq. (2-22), in accordance with Eq. (2-33), one obtains the heat of vaporization as

$$\Delta H_v = R \Delta Z_v (-B + CT + DET^{E+1}) \quad (2-36)$$

The Z_C and Z_L values can be evaluated by using the methods given in the subsection on densities below.

Example Calculate ΔH_v for anisole at 452 K.

Input data: The vapor pressure coefficients in the DIPPR® 801 database, based on Eq. (2-22), are

$$A = 128.06 \quad B = -9307.7 \quad C = -16.693 \quad D = 0.014919 \quad E = 1$$

The vapor pressure at 452 K is

$$\ln \frac{P_r}{\text{Pa}} = 128.06 - \frac{9307.7}{452} - 16.693 \ln 452 + 0.014919(452)^1 = 12.155$$

$$P_r = \exp(12.155) \cdot \text{Pa} = 1.901 \times 10^5 \text{ Pa}$$

Determine ΔZ : Required data from the DIPPR® 801 database for this calculation are $T_c = 645.6 \text{ K}$, $P_c = 4.25 \text{ MPa}$, and $\omega = 0.35017$. These values are used to determine the reduced conditions and the values of Z_C and Z_L from the Lee-Kesler corresponding states method as discussed in the subsection on density.

$$T_r = \frac{452}{645.6} = 0.7 \quad P_r = \frac{0.1901}{4.25} = 0.045$$

Interpolation of the P_r values in Tables 2-351 and 2-352 at a T_r of 0.7 gives

$$Z_C^{(0)} = 0.9904 + \frac{0.045 - 0.010}{0.050 - 0.010} (0.9504 - 0.9904) = 0.9554$$

$$Z_C^{(1)} = -0.0064 + \frac{0.045 - 0.010}{0.050 - 0.010} (-0.0507 + 0.0064) = -0.0452$$

$$Z_C = Z_C^{(0)} + \omega Z_C^{(1)} = 0.9554 + (0.35017)(-0.0452) = 0.94$$

At this low pressure, Z_L is very small compared to Z_C and may be neglected; so

$$\Delta Z_V = Z_C - Z_L = 0.94$$

Calculation using Eq. (2-36):

$$\begin{aligned} \Delta H_v &= \left(8.314 \frac{\text{J}}{\text{mol}\cdot\text{K}} \right) (0.94) [9307.7 - (16.693)(452) + (0.014919)(1)(452)^2] \\ &= 37.59 \frac{\text{kJ}}{\text{mol}\cdot\text{K}} \end{aligned}$$

This value is 0.2 percent higher than the value of 37.51 kJ/(mol·K) obtained from the DIPPR® 801 database.

Recommended Method 2 Corresponding states correlation.

Reference: PGL5, p. 7.18.

Classification: Corresponding states.

Expected uncertainty: Less than about 6 percent.

Applicability: Organic compounds.

Input data: T_c , P_c , and ω .

Description: The following correlation is used:

$$\frac{\Delta H_v}{RT_c} = 7.08\tau^{0.354} + 10.95\omega\tau^{0.456} \quad \text{where } \tau = 1 - T_r \quad (2-37)$$

Example Repeat the above calculation for anisole's ΔH_v at 452 K.

Input data: $T_c = 645.6$ K, $P_c = 4.25$ MPa, and $\omega = 0.35017$.

Auxiliary quantities: From the previous example, the reduced temperature is

$$T_r = 0.7 \quad \tau = 1 - 0.7 = 0.3$$

Calculation using Eq. (2-37):

$$\frac{\Delta H_v}{RT_c} = 7.08(0.3)^{0.354} + 10.95(0.35017)(0.3)^{0.456} = 6.838$$

$$\Delta H_v = (6.838) \left(8.314 \frac{\text{J}}{\text{mol}\cdot\text{K}} \right) (645.6 \text{ K}) = 36.70 \frac{\text{kJ}}{\text{mol}\cdot\text{K}}$$

This value is 2.2 percent below the DIPPR® 801 recommended value of 37.51 kJ/(mol·K).

Recommended Method 3 Vetere method for ΔH_v at T_b .

Reference: Vetere, A., *Fluid Phase Equilib.*, **106** (1995): 1.

Classification: Corresponding states.

Expected uncertainty: About 4 percent.

Applicability: Valid only at the normal boiling point.

Input data: T_c , P_c , and T_b .

Description: The following correlation is used:

$$\frac{\Delta H_v}{RT_b} = \frac{\tau_b^{0.38} \left[\ln(P_c/\text{bar}) - 0.513 + \frac{0.5066 \cdot \text{bar}}{P_c T_b^2} \right]}{\tau_b + F(1 - \tau_b^{0.38}) \ln T_{br}} \quad (2-38)$$

where $\tau_b = 1 - T_{br}$

For most compounds, $F = 1$; compounds that dimerize (e.g., SO_2 , NO , NO_2) and alcohols with more than two C atoms are assigned $F = 1.05$.

Example Calculate ΔH_v at the normal boiling point for acetaldehyde.

Input data: Recommended values from the DIPPR® 801 database are $T_c = 466.0$ K, $P_c = 5.55$ MPa, and $T_b = 294.0$ K.

Auxiliary quantities: From the previous example, the reduced temperature is

$$T_{br} = \frac{294}{466} = 0.631 \quad \tau_b = 1 - T_{br} = 0.369 \quad F = 1$$

Calculation using Eq. (2-38):

$$\frac{\Delta H_v}{RT_b} = \frac{(0.369)^{0.38} \left[\ln 55.5 - 0.513 + \frac{0.5066(55.5)(0.631)^2}{(0.369) + [1 - (0.369)^{0.38}] \ln 0.631} \right]}{(0.369) + [1 - (0.369)^{0.38}] \ln 0.631} = 10.785$$

$$\Delta H_v = (10.785) \left(8.314 \frac{\text{J}}{\text{mol}\cdot\text{K}} \right) (294 \text{ K}) = 26.36 \frac{\text{kJ}}{\text{mol}\cdot\text{K}}$$

This value is 2.4 percent above the DIPPR® 801 recommended value of 25.73 kJ/(mol·K).

Enthalpy of Fusion The enthalpy (heat) of fusion ΔH_{fus} is the difference between the molar enthalpies of the equilibrium liquid and solid at the melting temperature and 1.0 atm pressure. There is no generally applicable, high-accuracy estimation method for ΔH_{fus} , but the GC method of Chickos can be used to obtain approximate results if the melting temperature is known.

Recommended Method Chickos method.

Reference: Chickos, J. S., et al., *J. Org. Chem.*, **56** (1991): 927.

Classification: QSPR and group contributions.

Expected uncertainty: Considerable variation but generally less than 50 percent.

Applicability: Only valid at the melting temperature. The method is based on the ΔS_{fus} between a solid at 0 K and the liquid at the T_m so no solid-solid transitions are taken into account. Values of ΔH_{fus} will be overestimated if there are solid-solid transitions for the actual material.

Input data: T_m and molecular structure.

Description:

$$\frac{\Delta H_{\text{fus}}}{\text{J/mol}} = \frac{\Delta S_{\text{fus}}}{\text{J/(mol}\cdot\text{K)}} \left(\frac{T_m}{\text{K}} \right) = (T_m/\text{K})(a + b) \quad (2-39)$$

$$a = \begin{cases} 0 & \text{no nonaromatic rings} \\ 35.19N_R + 4.289(N_{CR} - 3N_R) & \text{nonaromatic rings} \end{cases} \quad (2-40)$$

$$b = \sum_{i=1}^{n_g} N_{g_i} \Delta s_i + \sum_{j=1}^{n_s} N_{s_j} C_{s_j} \Delta s_j + \sum_{k=1}^{n_f} N_{f_k} C_{t_k} \Delta s_k \quad (2-41)$$

where N_{g_i} = number of C—H groups of type i bonded to other carbon atoms

n_g = number of different nonring or aromatic C—H groups bonded to other carbon atoms

N_{s_j} = number of C—H groups of type j bonded to at least one functional group or atom

n_s = number of different nonring or aromatic C—H groups bonded to at least one functional group or atom

N_{f_k} = number of functional groups of type k

n_f = number of different functional groups or atoms

i = total number of functional groups or atoms with the exception that F atoms count as one regardless of number of occurrences

C_{s_j} = value from Table 2-344 for C—H group j bonded to at least one functional group or atom

C_{t_k} = value from Table 2-345 for functional group k

N_R = number of nonaromatic rings

N_{CR} = number of —CH₂— groups in nonaromatic ring(s) required to form cyclic paraffin of same ring size(s)

Δs_i = contribution from Table 2-344 for group i

Δs_k = contribution from Table 2-345 for group k

TABLE 2-344 C_s (C—H) Group Values for Chickos Estimation* of ΔH_{fus}

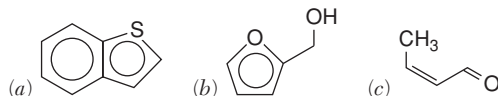
Group	Description	C _s	Δ_s	Group	Description	C _s	Δ_s
—CH ₃	methyl	1.0	18.33	—CH _{Ar}	aromatic C	1.0	6.44
>CH ₂	methylene	1.0	9.41	—C _{Ar} —	ar. C bonded to paraffinic C	1.0	-10.33
>CH—	secondary C	0.69	-16.91	—C _{Ar} —	ar. C bonded to olefinic C or non-C group	1.0	-4.27
>C<	tertiary C	0.67	-38.70	—C _{Ar} —	ar. C bonded to acetylinic C	1.0	-2.51
CH ₂ =	terminal alkene	1.0	14.56	>C _r H—	ring structure	0.76	-15.98
—CH=	alkene	3.23	4.85	>C _r <	ring structure	1.0	-32.97
>C=	subst. alkene	1.0	-11.38	—C _r H=	ring structure	0.62	-4.35
≡CH	term. alkyne	1.0	10.88	>C _r =	ring structure	0.86	-11.72
≡C—	alkyne	1.0	2.18	≡C _r — or =C _r =	ring structure	1.0	-5.36

*Chickos, J. S., et al., *J. Org. Chem.*, **56** (1991): 927.

Note that nonaromatic ring —CH₂ groups are accounted for in the *a* term and are *not* included in the *b* term.

Example Calculate ΔH_{fus} at the melting point for (a) benzothiophene, (b) furfuryl alcohol, and (c) *cis*-crotonaldehyde.

Structures:



(a) $t = 1$ (1 total “functional group”), so the C₁ column in Table 2-345 is used.

$$N_R = 1 \quad N_{CR} = 5 \quad a = 35.19 + (5 - 3)(4.289) = 43.77$$

Group	Description	N	C	Δ_s	Total
≡CH—	aromatic (Ng type)	4	1	6.44	25.76
≡C—	ring (Ng type)	1	1	-11.72	-11.72
≡C—	ring (Ns type)	1	0.86	-11.72	-10.08
≡CH—	ring (Ng type)	1	1	-4.35	-4.35
≡CH—	ring (Ns type)	1	0.62	-4.35	-2.70
—S—	ring	1	1	2.18	2.18
Total					-0.91

TABLE 2-345 C_t (Functional) Group Values for Chickos Estimation* of ΔH_{fus}

Group	Description	C ₁	C ₂	C ₃	C ₄	Δ_s
—OH	alcohol	1.0	12.6	18.9	26.4	1.13
—OH	phenol	1.0	1.0	1.0	1.0	16.57
—O—	nonring ether	1.0	1.0	1.0	1.0	1.09
—O—	ring ether	1.0	1.0	1.0	1.0	1.34
>C=O	nonring ketone	1.0	1.0			3.14
>C=O	ring ketone	1.0	1.0			-1.88
—CHO	aldehyde	1.0	1.0			19.66
—COOH	acid	1.0	1.83	1.88	1.72	14.90
—COO—	ester	1.0	1.0	1.0	1.0	3.68
—NH ₂	aliphatic	1.0	1.0			16.23
—NH ₂	aromatic	1.0	1.0			15.48
>NH	nonring	1.0	1.0			-2.18
>NH	ring	1.0	1.0			1.84
>N—	nonring	1.0	1.0			-15.90
>N—	ring	1.0	1.0			-17.07
—N—	ring	1.0	1.0			1.67
—N—	aromatic	1.0	1.0	1.0		7.32
—CN	nitrile	1.0	1.4			9.62
—NO ₂	nitro	1.0	1.0	1.0		17.36
—CONH ₂	primary amide	1.0	1.0			26.19
—CONH—	secondary amide	1.0	1.0			-0.42
—SH		1.0	1.0			17.99
—S—	nonring	1.0	1.0		0.36	7.20
—S—	ring	1.0	1.0			2.18
—SO ₂	nonring	1.0	1.0			3.26
—F	on aliph. C	1.0	1.0	1.0	1.0	14.73
—F	on olefinic C	1.0	1.0	1.0	1.0	13.01
—F	on ring C	1.0	1.0	1.0	1.0	15.90
—Cl		1.0	2.0	2.0	1.93	8.37
—Br		1.0	1.0	1.0	0.82	17.95
—I		1.0	1.0			16.95

*Chickos, J. S., et al., *J. Org. Chem.*, **56** (1991): 927.

$$T_m = 304.5 \text{ K} \quad \text{from DIPPR}^{\circ} \text{ 801 database}$$

$$\Delta H_{\text{fus}} = (T_m/K)(a + b) \text{ J/mol} = (304.5)(43.77 - 0.91) \text{ J/mol} = 13.05 \text{ kJ/mol}$$

This value is 10 percent higher than the DIPPR[®] 801 recommended value of 11.83 kJ/mol.

(b) $t = 2$ (2 total “functional groups”), so the C₂ column in Table 2-345 is used.

$$N_R = 1 \quad N_{CR} = 5 \quad a = 35.19 + (5 - 3)(4.289) = 43.77$$

Group	Description	N	C	Δ_s	Total
≡CH—	ring (Ng type)	2	1	-4.35	-8.70
≡CH—	ring (Ns type)	1	0.62	-4.35	-2.70
≡C<	ring (Ns type)	1	0.86	-11.72	-10.08
—O—	ring ether	1	1	1.34	1.34
—CH ₂ —	Ns type	1	1	9.41	9.41
—OH	alcohol	1	12.6	1.13	14.24
Total					3.51

$$T_m = 258.52 \text{ K} \quad \text{from DIPPR}^{\circ} \text{ 801 database}$$

$$\Delta H_{\text{fus}} = (T_m/K)(a + b) \text{ J/mol} = (258.52)(43.77 + 3.51) \text{ J/mol} = 12.22 \text{ kJ/mol}$$

This value is 7 percent lower than the DIPPR[®] 801 recommended value of 13.13 kJ/mol.

(c) $t = 1 \quad N_R = 0 \quad a = 0$

Group	Description	N	C	Δ_s	Total
—CH ₃	nonring (Ng type)	1	1	18.33	18.33
≡CH—	nonring (Ng type)	1	1	4.85	4.85
≡CH—	nonring (Ns type)	1	3.23	4.85	15.67
—CHO	aldehyde	1	1	19.66	19.66
Total					58.51

$$T_m = 158.38 \text{ K} \quad \text{from DIPPR}^{\circ} \text{ 801 database}$$

$$\Delta H_{\text{fus}} = (T_m/K)(a + b) \text{ J/mol} = (158.38)(0 + 58.51) \text{ J/mol} = 9.27 \text{ kJ/mol}$$

This value is 5 percent higher than the DIPPR[®] 801 recommended value of 8.86 kJ/mol.

Enthalpy of Sublimation The enthalpy (heat) of sublimation ΔH_{fus} is the difference between the molar enthalpies of the equilibrium vapor and solid along the sublimation curve below the triple point. The effects of pressure on ΔH_{fus} and melting temperature are very small so that T_i and the normal melting point are nearly equal and

$$\Delta H_{\text{sub}}(T_i) = \Delta H_v(T_i) + \Delta H_{\text{fus}}(T_i) \quad (2-42)$$

Equation (2-42) can be used to estimate ΔH_{sub} at the triple point if ΔH_v is accurately known at T_i . Because ΔH_v is usually obtained from Eq. (2-33), $\Delta H_v(T)$ correlations may be less accurate near T_i where $P^{\circ}(T_i)$ is very small and difficult to measure. In this case, it is better to estimate ΔH_{sub} directly by using the following recommended

method. Although Eqs. (2-33) and (2-34) apply to T_i , ΔH_{sub} is only a weak function of temperature and can generally be taken as a constant from the triple point temperature down to the first solid-solid phase transition.

Recommended Method Goodman method.

Reference: Goodman, B., et al., *Int. J. Thermophys.* **25** (2004): 337.

Classification: QSPR and group contributions.

Expected uncertainty: 6 percent.

Applicability: Organic compounds for which group contributions have been regressed.

Input data: Molecular structure and radius of gyration R_G .

Description:

$$\frac{\Delta H_{\text{sub}}(T_i)}{R K} = 698.04 + 3.83798 \times 10^{12} \left(\frac{R_G}{\text{m}} \right) + \sum_{i=1}^N n_i a_i + \sum_{i=1}^N n_i^2 \beta_i + \sum_{i=1}^N \frac{n_i}{n_x} f_i \quad (2-43)$$

where a_i = GC values from Table 2-346

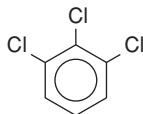
β_i = nonlinear corrections for $>\text{CH}_2$ and $\text{Ar}-\text{CH} =$ groups

f_i = halogen corrections

n_x = total number of all halogen and hydrogen atoms attached to C and Si atoms

Example Calculate ΔH_{sub} and the solid vapor pressure for 1,2,3-trichlorobenzene at 301.15 K.

Structure:



Group contributions:

Linear groups			Nonlinear and correction terms			
Group	n_i	a_i	Group	n_i	β_i	f_i
Ar—CH=	3	626.7621	Ar—CH=	3	-2.21614	
Ar >C=	3	348.8092	—Cl	3		-1543.66
—Cl	3	1243.445	n_x	6		
		$\sum_i n_i a_i$				
		6657.049				

Input data: The value of R_G from the DIPPR® 801 database is 4.455×10^{-10} m. *Calculation using Eq. (2-43):*

$$\frac{\Delta H_{\text{sub}}(T_i)}{R K} = 698.04 + (3.83798 \times 10^{12})(4.455 \times 10^{-10}) + 6657.049 + (3^2)(-2.21614) + \left(\frac{3}{6} \right)(-1543.66)$$

$$\Delta H_{\text{sub}}(T_i) = (8273.134 \text{ K}) \left(0.008314 \frac{\text{kJ}}{\text{mol}\cdot\text{K}} \right) = 68.78 \frac{\text{kJ}}{\text{mol}}$$

The estimated value is 5.6 percent above the DIPPR® 801 recommended value of 65.11 kJ/mol.

Estimate the solid vapor pressure from Eq. (2-26): The solid vapor pressure at 301.15 K can be calculated from Eq. (2-26) by using the estimated ΔH_{sub} . Recommended values for T_i and P_i^* from the DIPPR® 801 database are 325.65 K and 182.957 Pa, respectively.

$$\ln \frac{P^*}{182.957 \text{ Pa}} = \frac{68.78 \text{ kJ/mol}}{[0.008314 \text{ kJ}/(\text{mol}\cdot\text{K})](325.65 \text{ K})} \left(1 - \frac{325.65}{301.15} \right) = -2.067$$

$$P^* = (182.957 \text{ Pa})[\exp(-2.067)] = 23.16 \text{ Pa}$$

The estimated value is 0.3 percent above the DIPPR® 801 recommended value of 23.09 Pa.

HEAT CAPACITY

Heat capacity C_p is defined as the energy required to change the temperature of a unit mass (specific heat) or mole (molar heat capacity) of the material by one degree. Typical units are J/(kg·K).

Gases The heat capacity of a gas is related rigorously to the ideal gas heat capacity C_p^* by

$$C_p = C_p^* - T \int_0^P \left(\frac{\partial^2 V}{\partial T^2} \right)_P dP \quad (2-44)$$

The second term, giving the deviation of the real fluid heat capacity from the ideal gas value, can be neglected at low to moderate pressures, or it can be calculated directly from an appropriate EoS.

Ideal gas heat capacities are available from several sources (DIPPR, JANAF, TRC, and SWS). Two common correlating equations for C_p^* are the Aly-Lee [Aly, F. A., and L. L. Lee, *Fluid Phase Equilib.*, **6**

TABLE 2-346 Group Contributions and Corrections* for ΔH_{sub}

Group	Description	a_i	Group	Description	a_i
—CH ₃	methyl	736.5889	>C=O	ketone	1816.093
>CH ₂	methylene	561.3543	—COO—	ester	2674.525
>CH—	secondary C	111.0344	—COOH	acid	5006.188
>C<	tertiary C	-800.517	—NH ₂	primary amine	2219.148
CH ₂ =	terminal alkene	572.6245	—NH—	sec. amine	1561.222
—CH=	alkene	541.2918	>N—	tertiary amine	325.9442
>C=	substituted alkene	117.9504	—NO ₂	nitro	3661.233
Ar—CH=	aromatic C	626.7621	—SH	thiol/mercaptan	1921.097
Ar >C=	subst. aromatic C	348.8092	—S—	sulfide	1930.84
Ar—O—	furan O	763.284	—SS—	disulfide	2782.054
Ar—N=	pyridine N	1317.056	—F	fluoride	626.4494
Ar—S—	thiophene S	911.2903	—Cl	chloride	1243.445
—O—	ether	970.4474	—Br	bromide	669.9302
—OH	alcohol	3278.446	>Si<	silane	-83.7034
—COH	aldehyde	2402.093	>Si(O—)	siloxane	-16.0597
Nonlinear terms		β_i	Halogen correction terms		f_i
>CH ₂	methylene	9.5553	—F	F fraction	-1397.4
Ar—CH=	aromatic C	-2.21614	—Cl	Cl fraction	-1543.66
			—Br	Br fraction	5812.49

*Goodman, B., et al., *Int. J. Thermophys.*, **25** (2004): 337.

(1981): 169] equation

$$C_p^o = A_0 + A_1 \left[\frac{A_2/T}{\sinh(A_2/T)} \right]^2 + A_3 \left[\frac{A_4/T}{\cosh(A_4/T)} \right]^2 \quad (2-45)$$

and a polynomial form (generally fourth-order)

$$C_p^o = \sum_{i=0}^4 A_i T^i \quad (2-46)$$

Ideal gas heat capacities may also be estimated from several techniques, of which two of the most accurate and commonly used are recommended here.

Recommended Method 1 Statistical mechanics.

Reference: Rowley, R. L., *Statistical Mechanics for Thermophysical Property Calculations*, Prentice-Hall, Englewood Cliffs, N.J., 1994.

Classification: Theory and computational chemistry.

Expected uncertainty: 0.2 percent if vibrational frequencies (or their characteristic temperatures) are experimentally available; accuracy depends upon model chemistry if frequencies are determined from computational chemistry, but generally within 3 percent.

Applicability: Ideal gases.

Input data: $3n_A - 6 + \delta$ vibrational frequencies ν_j , or the corresponding characteristic vibrational temperatures Θ_j . The two are related by

$$\Theta_j = h\nu_j/k \quad (2-47)$$

where n_A = number of atoms in molecule and $\delta = 1$ for linear molecules and 0 for nonlinear molecules.

Description: For harmonic frequencies, the rigorous temperature dependence of C_p^o is given by

$$\frac{C_p^o}{R} = \frac{8 - \delta}{2} + \sum_{j=1}^{3n_A - 6 + \delta} \left(\frac{\Theta_j}{T} \right)^2 \left[\frac{e^{\Theta_j/T}}{(e^{\Theta_j/T} - 1)^2} \right] \quad \delta = \begin{cases} 0 & \text{nonlinear} \\ 1 & \text{linear} \end{cases} \quad (2-48)$$

Example Calculate the ideal gas heat capacity of ammonia at 300 K.

Structure:



Input data: McQuarrie (McQuarrie, D. A., *Statistical Mechanics*, Harper & Row, New York, 1976) gives the following $3m - 6 + \delta = 12 - 6 + 0 = 6$ characteristic vibrational temperatures (K): 1360, 2330, 2330, 4800, 4880, and 4880. Alternatively, a computational chemistry package gives the following *scaled* frequencies for HF/6-31G+ model chemistry (10^{13} Hz): 3.24, 4.97, 4.97, 9.90, 10.26, and 10.26.

Calculation: The table on the left uses the experimental Θ values to determine the individual terms in the summation of Eq. (2-48); the table on the right uses the scaled frequencies from computational chemistry software and Eq. (2-47) to obtain Θ values and the individual terms in Eq. (2-48).

Experimental frequencies		
Θ/K	$\Theta/(300\text{ K})$	Term
1360	4.533	0.2256
2330	7.767	0.0256
2330	7.767	0.0256
4800	16.000	0.0000
4880	16.267	0.0000
4880	16.267	0.0000
Sum		0.2769

From experimental frequencies:

$$C_p^o = \left(\frac{8}{2} + 0.2769 \right) R = (4.2769) \left(8.3143 \frac{\text{J}}{\text{mol}\cdot\text{K}} \right) = 35.56 \frac{\text{J}}{\text{mol}\cdot\text{K}}$$

From computational chemistry frequencies:

$$C_p^o = \left(\frac{8}{2} + 0.197 \right) R = (4.197) \left(8.3143 \frac{\text{J}}{\text{mol}\cdot\text{K}} \right) = 34.90 \frac{\text{J}}{\text{mol}\cdot\text{K}}$$

The value calculated from experimental frequencies is 0.1 percent lower than the DIPPR® 801 recommended value of 35.61 J/(mol·K); the value calculated from frequencies generated from computational chemistry software is 2.0 percent lower than the DIPPR® 801 value.

Recommended Method 2 Benson method as implemented in CHETAH program.

References: Benson, S. W., et al., *Chem. Rev.*, **69** (1969): 279; CHETAH Version 8.0: *The ASTM Computer Program for Chemical Thermodynamic and Energy Release Evaluation (NIST Special Database 16)*.

Classification: Group contributions.

Expected uncertainty: 4 percent.

Applicability: Ideal gases of organic compounds.

Input data: Table 2-347 group values at the seven specified temperatures.

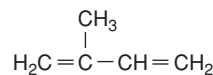
Description: Groups are summed at each individual temperature:

$$C_p^o = \sum_{i=1}^N n_i \cdot (C_p^o)_i \quad (2-49)$$

where n_i = number of occurrences of group i and $(C_p^o)_i$ = individual group contribution. Either Eq. (2-45) or Eq. (2-46) can be used to interpolate between the discrete temperatures.

Example Calculate the ideal gas heat capacity of isoprene (2-methyl-1,3-butadiene) at 400 K.

Structure:



Group identification and values:

Group	No.	Value, J/(mol·K)	Contribution, J/(mol·K)
=CH ₂	2	26.62	53.24
=C-(2C)	1	19.3	19.3
-CH ₂ -(=C)	1	32.82	32.82
=CH-(C)	1	21.05	21.05
Total			126.41

The value of 126.4 J/(mol·K) is 3.1 percent below the DIPPR® 801 recommended value of 130.4 J/(mol·K).

Liquids Liquid heat capacity increases with increasing temperature, although a minimum occurs near the triple point for many compounds. Usually liquid heat capacity is correlated as a function of temperature with a polynomial equation. A cubic equation is usually adequate.

Estimation of liquid heat capacity can be done by using a number of methods [Ruzicka, V., and E. S. Domalski, *J. Phys. Chem. Ref. Data*, **22** (1993): 597, 619; Chueh, C. F., and A. C. Swanson, *Chem. Eng.*

HF/6-31G + scaled frequencies			
$\nu_{\text{scaled}}/\text{Hz}$	Θ/K	$\Theta/(300\text{ K})$	Term
3.24	1555.0	5.183	0.1524
4.97	2385.3	7.951	0.0223
4.97	2385.3	7.951	0.0223
9.90	4751.4	15.838	0.0000
10.26	4924.2	16.414	0.0000
10.26	4924.2	16.414	0.0000
Sum			0.1970

NOTE: Empirical scaling factors have been developed for each model chemistry to help correct theoretical frequencies for anharmonic effects [Scott, A. P., and L. Radom, *J. Phys. Chem.*, **100** (1996): 16502].

TABLE 2-347 Benson* and CHETAH[†] Group Contributions for Ideal Gas Heat Capacity

Table-specific nomenclature: Cb = carbon in benzene ring; Ct = carbon with a triple bond, (=C) = carbon with a double bond; Cp = carbon in fused ring; Naz = azide; Nim = imino.

Group	298 K	400 K	500 K	600 K	800 K	1000 K	1500 K
CH ₃ Groups							
CH ₃ -(Cb)	25.91	32.82	39.35	45.17	54.5	61.83	73.59
CH ₃ -(CO)	25.91	32.82	39.35	45.17	54.5	61.83	73.59
CH ₃ -(Ct)	25.91	32.82	39.35	45.17	54.5	61.83	73.59
CH ₃ -(C)	25.91	32.82	39.35	45.17	54.5	61.83	73.59
CH ₃ -(N)	25.95	32.65	39.35	45.21	54.42	61.95	73.67
CH ₃ -(O)	25.91	32.82	39.35	45.17	54.54	61.83	73.59
CH ₃ -(PO)	25.91	32.82	39.35	45.17	54.54	61.83	73.59
CH ₃ -(P)	25.91	32.82	39.35	45.17	54.54	61.83	73.59
CH ₃ -(P=O)	25.91	32.82	39.35	45.17	54.54	61.83	73.59
CH ₃ -(Si)	25.91	32.82	39.35	45.17	54.5	61.83	73.59
CH ₃ -(SO ₂)	25.91	32.82	39.35	45.17	54.5	61.83	73.59
CH ₃ -(SO)	25.91	32.82	39.35	45.17	54.5	61.83	73.59
CH ₃ -(S)	25.91	32.82	39.35	45.17	54.5	61.83	73.59
CH ₃ -(=C)	25.91	32.82	39.35	45.17	54.5	61.83	73.59
Ct Groups							
Ct-(Cb)	10.76	14.82	14.65	20.59	22.35	23.02	24.28
Ct-(Ct)	14.82	16.99	18.42	19.42	20.93	21.89	23.32
Ct-(C)	13.1	14.57	15.95	17.12	19.25	20.59	26.58
Ct-(=C)	10.76	14.82	14.65	20.59	22.35	23.02	24.28
CtBr	34.74	36.42	37.67	38.51	39.77	40.6	
CtCl	33.07	35.16	36.42	37.67	39.35	40.18	
CtF	28.55	31.65	33.99	35.79	38.3	39.85	41.77
CtH	22.06	25.07	27.17	28.76	31.27	33.32	37.04
CtI	35.16	36.84	38.09	38.93	40.18	41.02	
Ct(CN)	43.11	47.3	50.65	53.16	56.93	59.86	64.04
CH ₂ Groups							
CH ₂ -(2CO)	16.03	26.66	32.15	37.8	45.46	51.74	
CH ₂ -(2C)	23.02	29.09	34.53	39.14	46.34	51.65	59.65
CH ₂ -(2O)	11.85	21.18	31.48	38.17	43.2	47.26	
CH ₂ -(2=C)	19.67	28.46	35.16	40.18	47.3	52.74	60.28
CH ₂ -(Cb,O)	15.53	26.26	34.66	40.98	49.35	55.25	
CH ₂ -(Cb,SO ₂)	15.53	27.5	34.66	40.98	49.77	55.25	
CH ₂ -(Cb,S)	38.09	49.02	57.43	63.71	72.58	78.82	
CH ₂ -(Cb,=C)	19.67	28.46	35.16	40.18	47.3	52.74	60.28
CH ₂ -(C,Cb)	24.45	31.85	37.59	41.9	48.1	52.49	57.6
CH ₂ -(C,CO)	25.95	32.23	36.42	39.77	46.46	51.07	
CH ₂ -(C,Ct)	20.72	27.46	33.19	38.01	45.46	51.03	59.44
CH ₂ -(C,N)	21.77	28.88	34.74	39.35	46.46	51.49	
CH ₂ -(C,O)	20.89	28.67	34.74	39.47	46.5	51.61	61.11
CH ₂ -(C,SO ₂)	17.12	24.99	31.56	36.84	44.58	49.94	
CH ₂ -(C,SO)	19.05	26.87	33.28	38.34	45.84	51.15	
CH ₂ -(C,S)	22.52	29.64	36	41.73	51.32	59.23	
CH ₂ -(C,=C)	21.43	28.71	34.83	39.72	46.97	52.24	60.11
CH ₂ -(=C,O)	19.51	29.18	36.21	41.36	48.3	53.29	
CH ₂ -(=C,SO ₂)	20.34	28.51	34.95	40.1	47.17	52.49	
CH ₂ -(=C,SO)	18.42	26.62	29.05	38.72	45.92	51.28	
CH ₂ -(=C,S)	22.23	28.59	34.45	40.85	50.98	59.48	
CH Groups							
CH-(2C,Cb)	20.43	27.88	33.07	36.63	40.73	42.9	44.7
CH-(2C,CO)	18.96	25.87	30.89	35.12	41.11	43.99	
CH-(2C,Ct)	16.7	23.48	28.67	32.57	38.09	41.44	46.55
CH-(2C,N)	19.67	26.37	31.81	35.16	40.18	42.7	
CH-(2C,O)	20.09	27.79	33.91	36.54	41.06	43.53	
CH-(2C,SO ₂)	18.5	26.16	31.65	35.5	40.35	43.11	
CH-(2C,S)	20.3	27.25	32.57	36.38	41.44	44.24	
CH-(2C,=C)	17.41	24.74	30.72	34.28	39.6	42.65	47.22
CH-(3C)	19	25.12	30.01	33.7	38.97	42.07	46.76
CH-(C,2O)	22.02	23.06	27.67	31.77	35.41	38.97	
C Groups							
C-(2C,2O)	19.25	19.25	23.02	25.53	27.63	28.46	
C-(3C,Cb)	19.72	28.42	33.86	36.75	38.47	37.51	31.94
C-(3C,CO)	9.71	18.33	23.86	27.17	30.43	31.69	
C-(3C,Ct)	0.33	7.33	14.36	19.97	25.2	26.71	
C-(3C,N)	18.42	25.95	30.56	33.07	35.58	35.58	
C-(3C,O)	18.12	25.91	30.35	32.23	34.32	34.49	
C-(3C,SO ₂)	9.71	18.33	23.86	27.17	30.43	31.23	
C-(3C,SO)	12.81	19.17	20.26	27.63	31.56	33.32	
C-(3C,S)	19.13	26.25	31.18	34.11	36.5	33.91	
C-(3C,=C)	16.7	25.28	31.1	34.58	37.34	37.51	34.45
C-(4C)	18.29	25.66	30.81	33.99	36.71	36.67	33.99

2-492 PHYSICAL AND CHEMICAL DATA

TABLE 2-347 Benson* and CHETAH† Group Contributions for Ideal Gas Heat Capacity (Continued)

Table-specific nomenclature: Cb = carbon in benzene ring; Ct = carbon with a triple bond, (=C) = carbon with a double bond; Cp = carbon in fused ring; Naz = azide; Nim = imino.

Group	298 K	400 K	500 K	600 K	800 K	1000 K	1500 K
Aromatic (Cb and Cp Groups)							
Cb—(Cb)	13.94	17.66	20.47	22.06	24.11	24.91	25.32
Cb—(CO)	11.18	13.14	15.4	17.37	20.76	22.77	
Cb—(Ct)	15.03	16.62	18.33	19.76	22.1	23.48	24.07
Cb—(C)	11.18	13.14	15.4	17.37	20.76	22.77	25.03
Cb—(N)	16.53	21.81	24.86	26.45	27.33	27.46	
Cb—(O)	16.32	22.19	25.95	27.63	28.88	28.88	
Cb—(Si)	11.18	13.14	15.4	17.37	20.76	22.77	25.03
Cb—(SO ₂)	11.18	13.14	15.4	17.37	20.76	22.77	
Cb—(SO)	11.18	13.14	15.4	17.37	20.76	22.77	
Cb—(S)	16.32	22.19	25.95	27.63	28.88	28.88	
Cb—(=C)	15.03	16.62	18.33	19.76	22.1	23.48	24.07
Cb—(=Nim)	16.53	21.81	24.86	26.45	27.33	27.46	
CbBr	32.65	36.42	39.35	41.44	43.11	43.95	
CbCl	30.98	35.16	38.51	40.6	42.7	43.53	
CbF	26.37	31.81	35.58	38.09	41.02	42.7	
CbH	13.56	18.59	22.85	26.37	31.56	35.2	40.73
CbI	33.49	37.25	40.18	41.44	43.11	43.95	
Cb(CHN ₂)	47.3						
Cb(CN)	41.86	48.14	52.74	55.67	59.86	62.79	
Cb(N ₃)	34.74						
Cb(NCO)	55.25	64.04	70.32	74.51	79.95	82.88	85.81
Cb(NCS)	32.23						
Cb(NO ₂)	38.93	50.23	59.44	66.56	76.18	80.37	
Cb(SO ₂ OH)	65.42	79.49	84.51	97.61	109.25	113.31	
Cp—(2Cb,Cp)	12.56	15.49	17.58	19.25	21.77	23.02	
Cp—(3Cp)	8.37	12.14	14.65	16.74	19.67	21.35	
Cp—(Cb,2Cp)	12.56	15.49	17.58	19.25	21.77	23.02	
=C=, =C-, =CH- Groups							
=C—(2C)	17.16	19.3	20.89	22.02	24.28	25.45	26.62
=C—(CO,O)	23.4	29.3	31.31	32.44	33.57	34.03	
=C—(C,Cb)	18.42	22.48	24.82	25.87	27.21	27.71	28.13
=C—(C,CO)	22.94	29.22	31.02	31.98	33.53	34.32	
=C—(C,O)	17.16	19.3	20.89	22.02	24.28	25.45	
=C—(C,SO ₂)	15.49	26.04	33.32	38.51	44.62	47.47	
=C—(C,S)	14.65	14.94	16.03	17.12	18.46	20.93	
=C—(C,=C)	18.42	22.48	24.82	25.87	27.21	27.71	28.13
=CC—(=C,O)	18.42	22.9	24.82	26.29	27.21	27.71	
=CH—(Cb)	18.67	24.24	28.25	31.06	34.95	37.63	41.77
=CH—(CO)	31.73	37.04	38.8	40.31	43.45	46.21	
=CH—(Ct)	18.67	24.24	28.25	31.06	34.95	37.63	41.77
=CH—(C)	17.41	21.05	24.32	27.21	32.02	35.37	40.27
=CH—(O)	17.41	21.05	24.32	27.21	32.02	35.37	40.27
=CH—(SO ₂)	12.72	19.55	24.82	28.63	32.94	36.29	
=CH—(S)	17.41	21.05	24.32	27.21	32.02	35.37	
=CH—(=C)	18.67	24.24	28.25	31.06	34.95	37.63	41.77
=CH ₂	21.35	26.62	31.44	35.58	42.15	47.17	55.21
=C=	16.32	18.42	19.67	20.93	22.19	23.02	23.86
Oxygen Groups							
O—(2C)	14.23	15.49	15.49	15.91	18.42	19.25	
O—(2O)	15.49	15.49	15.49	15.49	17.58	17.58	20.09
O—(2=C)	14.02	16.32	17.58	18.84	21.35	22.6	
O—(Cb,CO)	8.62	11.3	13.02	14.32	16.24	17.5	
O—(CO,O)	1.51	6.28	9.63	11.89	15.28	17.33	
O—(C,Cb)	2.6	3.01	4.94	7.45	11.89	14.99	
O—(C,CO)	11.64	15.86	18.33	19.8	20.55	21.05	
O—(C,O)	15.49	15.49	15.49	15.49	17.58	17.58	20.09
O—(C,=C)	12.72	13.9	14.65	15.49	17.54	18.96	
O—(=C,CO)	6.03	12.47	16.66	18.79	20.8	21.77	
OH—(Cb)	18	18.84	20.09	21.77	25.12	27.63	
OH—(CO)	15.95	20.85	24.28	26.54	30.01	32.44	37.34
OH—(C)	18.12	18.63	20.18	21.89	25.2	27.67	33.65
OH—(O)	21.64	24.24	26.29	27.88	29.93	31.44	34.2
O(CN)—(Cb)	34.74						
O(CN)—(C)	41.86						
O(CN)—(=C)	54.42						
O(NO ₂)—(C)	39.93				68.61	72.75	
O(NO)—(C)	38.09	43.11	46.88	50.23	55.67	58.18	60.69
(CO)Cl—(C)	42.28	46.04	49.39	51.9	55.67	57.76	
(CO)H—(Cb)	33.53	44.2	48.77	59.48	68.56	74.01	
(CO)H—(CO)	28.13	32.78	37.25	41.4	47.84	50.73	

TABLE 2-347 Benson* and CHETAH[†] Group Contributions for Ideal Gas Heat Capacity (Continued)

Table-specific nomenclature: Cb = carbon in benzene ring; Ct = carbon with a triple bond, (=C) = carbon with a double bond; Cp = carbon in fused ring; Naz = azide; Nim = imino.

Group	298 K	400 K	500 K	600 K	800 K	1000 K	1500 K
Oxygen Groups							
(CO)H—(C)	29.43	32.94	36.92	40.52	46.71	51.07	
(CO)H—(N)	29.43	32.94	36.92	40.52	46.71	51.07	
(CO)H—(O)	29.43	32.94	36.92	40.52	46.71	51.07	
(CO)H—(=C)	24.32	30.22	39.77	48.77	63.12	74.68	
CO—(Cb)(O)	9.12	11.51	16.65	21.05	26.32	29.54	
Halide Groups							
CBr—(3C)	39.35	47.72	52.74	55.25	56.93	56.09	
CBr ₃ —(C)	72.12	78.65	82.92	85.64	88.66	89.66	
CCl—(3C)	36.96	43.87	47.72	49.52	52.07	53.12	
CCl ₂ —(2C)	51.07	62.29	66.76	68.98	70.99	71.24	
CCl ₃ —(C)	68.23	75.35	79.95	82.88	86.23	87.9	
CClF ₂ —(C)	57.35	67.39	73.25	77.86	82.88	85.39	
CF—(3C)	28.46	37.09	42.7	46.71	52.03	53.24	
CF ₂ —(2C)	39.01	46.97	53.24	57.85	63.46	65.84	
CF ₃ —(Cb)	52.32	64.04	72	77.44	84.14	87.9	
CF ₃ —(C)	53.16	62.79	68.65	74.93	80.79	83.72	
CF ₃ —(S)	41.36	54.46	62.08	68.52	76.06	79.99	
CH ₂ Br—(Cb)	30.51	46.46	52.2	57.3	65.26	69.95	
CH ₂ Br—(C)	38.09	46.04	52.74	57.35	64.88	70.32	
CH ₂ Br—(=C)	40.6	47.72	54.42	59.86	67.81	73.67	
CH ₂ Cl—(C)	37.25	44.79	51.49	56.09	64.04	69.9	
CH ₂ F—(C)	33.91	41.86	50.23	54.42	63.62	69.49	
CH ₂ I—(Cb)	33.91	45.17	53.7	59.9	68.15	73.8	
CH ₂ I—(C)	38.51	46.04	54	58.18	66.14	72	
CH ₂ I—(O)	34.41	43.91	51.19	56.72	64.25	69.36	
CHBr—(2C)	37.38	44.62	50.06	53.75	58.81	61.62	
CHBrCl—(C)	51.9	58.6	63.3	68.23	74.93	79.53	
CHCl—(2C)	35.45	42.7	48.89	53.41	59.82	64.38	
CHCl—(C,O)	37.67	41.44	43.95	46.88			
CHCl ₂ —(C)	50.65	58.6	64.46	69.07	74.93	78.28	
CHF—(2C)	30.56	37.84	43.83	48.39	54.83	58.64	
CHF ₂ —(C)	41.44	50.23	57.35	63.21	69.9	74.51	
CHI—(2C)	38.64	45.67	50.9	54.42	59.31	61.95	
CHI ₂ —(C)	56.93	63.42	69.61	74.17	79.7	81.58	
CI—(3C)	41.15	49.18	54.08	56.3	57.72	56.93	
=CBr ₂	51.49	55.25	58.18	59.86	62.37	63.62	
=CBrCl	50.65	53.16	56.51	59.02	61.53	62.79	
=CBrF	45.21	50.23	53.58	56.51	59.86	61.53	
=CCl ₂	47.72	52.32	55.67	58.18	61.11	62.79	
=CClF	43.11	48.97	52.74	55.67	59.44	61.53	
=CF ₂	40.6	46.04	50.23	53.16	57.76	60.69	
=CHBr	33.91	39.77	44.37	47.72	51.9	55.25	
=CHCl	33.07	38.51	43.11	46.88	51.49	54.83	
=CHF	28.46	35.16	39.77	43.95	49.39	53.16	
=CHI	36.84	41.86	45.63	48.56	52.74	55.67	
Nitrogen Groups							
CH ₂ (N ₃)—(C)	64.46						
=CH(N ₃)	54.42						
N—(2C,Cb)	2.6	8.46	13.69	17.29	21.89	23.4	
N—(2C,CO)	13.02	19.17	23.52	26.16	28.42	28.76	
N—(2C,SO ₂)	25.2	26.58	31.56	34.45	37.8	38.47	
N—(2C,SO)	17.58	24.61	25.62	27.33	28.59	34.91	
N—(2C,S)	15.99	21.64	25.99	29.05	30.93	38.68	
N—(3C)	14.57	19.09	22.73	24.99	27.46	27.92	27.21
N—(Cb,2CO)	4.1	12.81	17.71	20.3	22.1	22.14	
N—(C,2CO)	4.48	12.99	18.04	20.93	22.94	27.08	
Nb pyrid—N	10.88	13.48	15.95	17.66	20.05	21.43	
NF ₂ —(C)	26.5	34.58	40.9	45.63	50.9	53.54	
NH—(2Cb)	9.04	13.06	17.29	21.35	28.3	32.98	
NH—(2CO)	15.03	23.19	28.05	30.93	33.28	34.28	
NH—(2C)	17.58	21.81	25.66	28.59	33.07	36.21	39.97
NH—(Cb,CO)	2.39	6.32	9.96	13.94	16.91	18.21	
NH—(C,Cb)	15.99	20.47	23.9	26.29	30.1	32.36	
NH—(C,CO)	2.76	6.49	10.3	14.57	17.75	18.96	
NH—(C,N)	20.09	24.28	27.21	29.3	32.65	34.74	37.67
NH ₂ —(Cb)	23.94	27.25	30.64	33.78	39.39	43.83	51.4
NH ₂ —(CO)	17.04	24.03	29.85	34.7	41.69	46.97	
NH ₂ —(C)	23.94	27.25	30.64	33.78	39.39	43.83	51.4
NH ₂ —N	25.53	30.98	35.16	38.93	43.95	48.14	55.25
=Naz—(C)	11.3	17.16	20.59	22.35	23.82	23.9	
=Naz—(N)	8.87	17.5	23.06	28.34	28.71	29.51	

2-494 PHYSICAL AND CHEMICAL DATA
TABLE 2-347 Benson* and CHETAH† Group Contributions for Ideal Gas Heat Capacity (Continued)

Table-specific nomenclature: Cb = carbon in benzene ring; Ct = carbon with a triple bond, (==C) = carbon with a double bond; Cp = carbon in fused ring; Naz = azide; Nim = imino.

Group	298 K	400 K	500 K	600 K	800 K	1000 K	1500 K
Nitrogen Groups							
==NazH	18.33	20.47	22.77	24.86	28.34	31.06	35.33
==Nim—(Cb)	12.56						
==Nim—(C)	10.38	13.98	16.53	17.96	19.21	19.25	
==NimH	12.35	19.17	27	32.27	38.22	41.52	
Sulfur Groups							
S—(2Cb)	8.37	8.41	9.38	11.47	15.91	19.72	
S—(2C)	20.89	20.76	21.01	21.22	22.65	23.98	
S—(2S)	19.67	20.93	21.35	21.77	22.19	22.6	
S—(2==C)	20.05	23.36	23.15	26.33	33.24	40.73	
S—(Cb,S)	12.1	14.19	15.57	17.37	20.01	21.35	
S—(C,Cb)	12.64	14.19	15.53	16.91	19.34	20.93	
S—(C,S)	21.89	22.69	23.06	23.06	22.52	21.43	
S—(C,==C)	17.66	21.26	23.27	24.15	24.57	24.57	
SH—(Cb)	21.43	22.02	23.32	25.24	29.26	32.82	
SH—(CO)	31.94	33.86	33.99	34.2	35.58	34.49	
SH—(C)	24.53	25.95	27.25	28.38	30.56	32.27	
SO—(2Cb)	23.94	38.05	40.6	47.93	47.97	47.09	
SO—(2C)	37.17	41.98	43.95	45.17	45.96	46.76	
SO ₂ —(2Cb)	34.99	46.17	56.72	62.54	66.39	66.81	
SO ₂ —(2C)	48.22	50.1	55.88	59.77	64.38	66.47	
SO ₂ —(2==C)	48.22	50.1	55.88	59.77	64.38	66.47	
SO ₂ —(Cb,SO ₂)	41.06	48.14	56.59	61.66	65.76	67.1	
SO ₂ —(Cb,==C)	41.4	48.14	55.88	61.16	65.8	66.64	
SO ₂ —(C,Cb)	41.61	48.14	56.3	60.74	65.38	66.64	
S(CN)—(Cb)	39.77						
S(CN)—(C)	46.88						
S(CN)—(==C)	59.44						
Boron and Silicon Groups							
Si—(4C)	113.23	134.95	154.5	171.2	198.62	219.72	252.91
SiH ₃ —(C)	-39.64						
Monovalent Ligands							
CH ₂ (CN)—(C)	47.72	56.93	64.04	70.74	80.79	85.81	
CH ₂ (NCS)—(C)	61.95						
CH ₂ (NO ₂)—(C)	52.7	66.22	77.52	86.48	99.58	108.41	
CH(CN)—(2C)	45.21	54	60.69	66.14	72	79.11	
CH(NO ₂)—(2C)	50.19	63.67	74.17	82.08	92.84	99.2	
CH(NO ₂) ₂ —(C)	80.79	101.3	117.2	129.76	146.09	156.13	
C(CN)—(3C)	36.21	46.71	53.96	58.81	64.92	67.77	
C(CN) ₂ —(2C)	61.62	74.47	83.72	90.46	99.54	104.48	
C(NO ₂)—(3C)	41.4	55.84	66.39	73.75	82.92	87.32	
==CH(CHN ₂)	72.42						
==CH(CN)	43.11	50.23	56.09	61.11	68.65	73.67	
==CH(NCS)	51.90						
==CH(NO ₂)	51.49	63.21	72.83	80.37	90.41	97.11	105.9
==C(CN) ₂	56.93	69.28	78.19	84.76	93.51	98.74	
3,4 Member Ring Corrections							
cyclobutane ring	-19.3	-16.28	-13.14	-11.05	-7.87	-5.78	-2.8
cyclobutene ring	-10.59	-9.17	-7.91	-7.03	-6.2	-5.57	-5.11
cyclopropane ring	-12.77	-10.59	-8.79	-7.95	-7.41	-6.78	-6.36
ethylene oxide ring	-8.37	-11.72	-12.56	-10.88	-9.63	-8.63	
ethylene sulfide ring	-11.93	-10.84	-11.13	-12.64	18.09	24.35	
thietane ring	-19.21	-17.5	-16.37	-16.37	-19.25	-23.86	
trimethylene oxide ring	-19.25	-20.93	-17.58	-14.56	-10.88	0.84	
5,6 Member Ring Corrections							
1,4 dioxane ring	-19.21	-20.8	-15.91	-10.97	-6.4	-1.8	
cyclohexane ring	-24.28	-17.16	-12.14	-5.44	4.6	9.21	13.81
cyclohexene ring	-17.92	-12.72	-8.29	-5.99	-1.21	0.33	3.39
cyclopentadiene ring	-14.44	-11.85	-8.96	-6.91	-5.36	-4.35	
cyclopentane ring	-27.21	-23.02	-18.84	-15.91	-11.72	-8.08	-1.55
cylopentene ring	-25.03	-22.39	-20.47	-17.33	-12.26	-9.46	-4.52
furan ring	-20.51	-18	-15.07	-12.56	-10.88	-10.05	
piperidine ring	-24.7	-19.67	-12.14	-3.77	9.21	17.58	
pyrrolidine ring	-25.83	-23.36	-20.09	-16.74	-12.01	-9.08	
tetrahydrofuran ring	-25.12	-24.28	-20.09	-15.91	-11.3	-7.53	
thiacyclohexane ring	-26.04	-17.83	-9.38	-2.89	3.6	5.4	
thiolane ring	-20.51	-19.55	-15.4	-15.32	-18.46	-23.32	
thiophene ring	-20.51	-19.55	-15.4	-15.32	-18.46	-23.32	

TABLE 2-347 Benson* and CHETAH† Group Contributions for Ideal Gas Heat Capacity (Concluded)

Table-specific nomenclature: Cb = carbon in benzene ring; Ct = carbon with a triple bond, (=C) = carbon with a double bond; Cp = carbon in fused ring; Naz = azide; Nim = imino.

Group	298 K	400 K	500 K	600 K	800 K	1000 K	1500 K
7 and 8 Member Ring Corrections							
cycloheptane ring	-38.01						
cyclooctane ring	-44.16						
Gauche and 1,5 Repulsion Corrections							
but-2-ene structure C—C=C—C	-5.61	-4.56	-3.39	-2.55	-1.63	-1.09	
but-3-ene structure C—C—C=C	-5.61	-4.56	-3.39	-2.55	-1.63	-1.09	
cis- between 2 t-butyl groups	-5.61	-4.56	-3.39	-2.55	-1.63	-1.09	
cis- involving 1 t-butyl group	-5.61	-4.56	-3.39	-2.55	-1.63	-1.09	
cis- (not with t-butyl group)	-5.61	-4.56	-3.39	-2.55	-1.63	-1.09	
ortho- between Cl atoms	-2.09	5.02	2.09	-2.51	-1.26		
ortho- between F atoms		-0.84	-0.42	1.26	2.93		
other ortho- (nonpolar-nonpolar)	4.69	5.65	5.44	4.9	3.68	2.76	-0.21

 *Benson, S. W., et al., *Chem. Rev.*, **69** (1969): 279.

 †CHETAH Version 8.0: *The ASTM Computer Program for Chemical Thermodynamic and Energy Release Evaluation (NIST Special Database 16)*.

Prog., **69**, 7 (1973): 83; Lee, B. I., and M. G. Kesler, *AIChE J.*, **21** (1975): 510; Tarakad, R. R., and R. P. Danner, *AIChE J.*, **23** (1977): 944] and thermodynamic differentiation. The most accurate and generally applicable method is that by Ruzicka and Domalski.

Recommended Method Ruzicka-Domalski.

References: Ruzicka, V., and E. S. Domalski, *J. Phys. Chem. Ref. Data*, **22** (1993): 597, 619.

Classification: Group contributions.

Expected Uncertainty: 4 percent.

Applicability: Organic compounds for which group values are available.

Input data: Molecular structure and Table 2-348 values.

Description: Groups are summed to find the temperature coefficients for a cubic polynomial correlation:

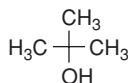
$$\frac{C_p}{R} = A + B\left(\frac{T}{100 \text{ K}}\right) + D\left(\frac{T}{100 \text{ K}}\right)^2 \quad (2-50)$$

$$A = \sum_{i=1}^N n_i a_i \quad B = \sum_{i=1}^N n_i b_i \quad D = \sum_{i=1}^N n_i d_i \quad (2-51)$$

where n_i = number of occurrences of group i and a_i , b_i , d_i = individual group contributions.

Example Estimate the liquid heat capacity for 2-methyl-2-propanol at 340 K.

Structure:



Group contributions:

Group	n_i	a_i	b_i	d_i
C—(3C,O) (alcohol)	1	-44.690	31.769	-4.8791
O—(H)(C)	1	12.952	-10.145	2.6261
C—(3H)(C)	3	3.8452	-0.33997	0.19489
Sum		-20.202	20.604	-1.668

$$\begin{aligned} C_p &= \left(8.3143 \frac{\text{J}}{\text{mol}\cdot\text{K}}\right) \left[-20.202 + 20.604 \left(\frac{340}{100}\right) - 1.668 \left(\frac{340}{100}\right)^2 \right] \\ &= 254.16 \frac{\text{J}}{\text{mol}\cdot\text{K}} \end{aligned}$$

This value is 0.7 percent higher than the DIPPR® 801 recommended value of 252.40 J/(mol·K).

Solids Solid heat capacity increases with increasing temperature and is proportional to T^3 near absolute zero. The heat capacity at a solid-solid phase transition becomes large, and there can be a substantial dif-

ference in the heat capacity of the two equilibrium solid phases that exist on either side of the transition temperature. The heat capacity generally rises steeply with increasing temperature near the triple point.

For a quick estimation of solid heat capacity specifically at 298.15 K, the very simple modification of Kopp's rule [Kopp, H., *Ann. Chem. Pharm. (Liebig)*, **126** (1863): 362] by Hurst and Harrison [Hurst, J. E., and B. K. Harrison, *Chem. Eng. Comm.*, **112** (1992): 21] can be used. At other temperatures and to obtain the temperature dependence of the solid heat capacity, the method given below by Goodman et al. should be used.

Recommended Method 1 Goodman method.

Reference: Goodman, B. T., et al., *J. Chem. Eng. Data*, **49** (2004): 24.

Classification: Group contributions.

Expected uncertainty: 10 percent.

Applicability: Organic compounds for which group values are available.

Input data: Molecular structure and Table 2-349 group values.

Description:

$$\frac{C_p}{\text{J}/(\text{mol}\cdot\text{K})} = \frac{A}{1000} \left(\frac{T}{\text{K}}\right)^{0.79267} \quad (2-52)$$

$$A = \exp\left(6.7796 + \sum_{i=1}^N n_i a_i + \sum_{i=1}^N n_i^2 \beta_i\right) \quad (2-53)$$

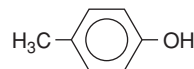
where n_i = number of occurrences of group i

a_i = individual group contribution

β_i = nonlinear correction terms for chain and aromatic carbons

Example Estimate the solid heat capacity for *p*-cresol at 307.93 K.

Structure:



Group contributions:

Group	n_i	a_i	β_i
—CH ₃	1	0.20184	0
Ar—CH=	4	0.082478	-0.00033
Ar >C=	2	0.012958	0
—OH	1	0.10341	0

From Eq. (2-53):

$$A = \exp[6.7796 + 0.20184 + (4)(0.082478) + (2)(0.012958) + 0.10341 + (4)^2(-0.00033)] = 1694.9$$

TABLE 2-348 Liquid Heat Capacity Group Parameters for Ruzicka-Domalski Method*

Table-specific nomenclature: Ct refers to a carbon atom with a triple bond; Cb refers to a carbon atom in benzene ring; =C refers to a carbon atom with a double bond; Cp refers to a carbon atom in a fused benzene ring; =C= refers to an allenic carbon atom.

Group Definition	<i>a</i>	<i>b</i>	<i>d</i>	<i>T</i> range (K)	Group Definition	<i>a</i>	<i>b</i>	<i>d</i>	<i>T</i> range (K)
Hydrocarbon Groups					Nitrogen Groups				
C—(3H,C)	3.8452	-0.33997	0.19489	80-490	N—(H,2C)	-0.10987	0.73024	0.89325	170-400
C—(2H,2C)	2.7972	-0.054967	0.10679	80-490	N—(3C)	4.5942	-2.2134	0.55316	160-360
C—(H,3C)	-0.42867	0.93805	0.0029498	85-385	N—(H,C,Cb)	0.49631	3.4617	-0.57161	240-380
C—(4C)	-2.9353	1.4255	-0.085271	145-395	N—(2C,Cb)	-0.23640	16.260	-2.5258	285-390
=C—(2H)	4.1763	-0.47392	0.099928	90-355	N—(C,2Cb)	4.5942	-2.2134	0.55316	160-360
=C—(H,C)	4.0749	-1.0735	0.21413	90-355	Cb—(N)	-0.78169	1.5059	-0.25287	240-455
=C—(2C)	1.9570	-0.31938	0.11911	140-315	N—(2H,N)	6.8050	-0.72563	0.15634	215-465
=C—(H,=C)	3.6968	-1.6037	0.55022	130-305	N—(H,C,N)	1.1411	3.5981	-0.69350	205-300
=C—(C,=C)	1.0679	-0.50952	0.33607	130-305	N—(2C,N)	-1.0570	4.0038	-0.71494	205-300
C—(3H,=C)	3.8452	-0.33997	0.19489	80-490	N—(H,Cb,N)	-0.74531	3.6258	-0.53306	295-385
C—(2H,C,=C)	2.0268	-0.20137	0.11624	90-355	C—(2H,C,CN)	11.976	-2.4886	0.52358	185-345
C—(H,2C,=C)	-0.87558	0.82109	0.18415	110-300	C—(3C,CN)	2.5774	3.5218	-0.58466	295-345
C—(3C,=C)	-4.8006	2.6004	-0.040688	165-295	=C—(H,CN)	9.0789	-0.86929	0.32986	195-345
C—(2H,2=C)	1.4973	-0.46017	0.52861	130-300	Cb—(CN)	1.9389	3.0269	-0.47276	265-480
Ct—(H)	9.1633	-4.6695	1.1400	150-275	C—(2H,C,NO ₂)	18.520	-5.4568	1.05080	190-300
Ct—(C)	1.4822	1.0770	-0.19489	150-285	O—(C,NO ₂)	-2.0181	10.505	-1.83980	180-350
=C=	3.0880	-0.62917	0.25779	140-315	Cb—(NO ₂)	15.277	-4.4049	0.71161	280-415
Ct—(Cb)	12.377	-7.5742	1.3760	230-550	N—(H,2Cb) (pyrrole)	-7.3662	6.3622	-0.68137	255-450
Cb—(H)	2.2609	-0.2500	0.12592	180-670	Nb—(2Cb)	0.84237	1.25560	-0.20336	210-395
Cb—(C)	1.5070	-0.13366	0.011799	180-670	Oxygen Groups				
Cb—(=C)	-5.7020	5.8271	-1.2013	230-550	O—(H,C)	12.952	-10.145	2.6261	155-505
Cb—(Cb)	5.8685	-0.86054	-0.063611	295-670	O—(H,C) (diol)	5.2302	-1.5124	0.54075	195-475
C—(2H,C,Ct)	2.0268	-0.20137	0.11624	90-355	O—(H,Cb) (diol)	5.2302	-1.5124	0.54075	195-475
C—(3H,Ct)	3.8452	-0.33997	0.19489	80-490	O—(H,Cb)	-7.9768	8.10450	-0.87263	285-400
C—(3H,Cb)	3.8452	-0.33997	0.19489	80-490	C—(3H,O)	3.8452	-0.33997	0.19489	80-490
C—(2H,C,Cb)	1.4142	0.56919	0.0053465	180-470	C—(2H,C,O)	1.4596	1.4657	-0.27140	135-505
C—(H,2C,Cb)	-0.10495	1.0141	-0.071918	180-670	C—(2H,Cb,O)	-35.127	28.409	-4.9593	260-460
C—(3C,Cb)	1.2367	-1.3997	0.41385	220-295	C—(2H,=C,O)	-35.127	28.409	-4.9593	260-460
C—(2H,2Cb)	-18.583	11.344	-1.4108	300-420	C—(H,2C,O) (alcohol)	2.2209	-1.4350	0.69508	185-460
C—(H,3Cb)	-46.611	24.987	-3.0249	375-595	C—(H,2C,O) (ether, ester)	0.98790	0.39403	-0.016124	130-170
=C—(H,Cb)	3.6968	-1.6037	0.55022	130-305	C—(3C,O) (alcohol)	-44.690	31.769	-4.8791	200-355
=C—(C,Cb)	1.0679	-0.50952	0.33607	130-305	C—(3C,O) (ether, ester)	-3.3182	2.6317	-0.44354	170-310
Cp—(Cp,2Cb)	-3.5572	2.8308	-0.39125	250-510	O—(2C)	5.0312	-1.5718	0.37860	130-350
Cp—(2Cp,Cb)	-11.635	6.4068	-0.78182	370-510	O—(C,Cb)	-22.5240	13.1150	-1.44210	320-350
Cp—(3Cp)	26.164	-11.353	1.2756	385-480	O—(2Cb)	-4.5788	0.94150	0.31655	300-535
Halogen Groups					C—(2H,2O)	1.0852	1.5402	-0.31693	170-310
C—(C,3F)	15.423	-9.2464	2.8647	125-345	C—(2C,2O)	-12.955	9.10270	-1.53670	275-335
C—(2C,2F)	-8.9527	10.550	-1.9986	125-345	Cb—(O)	-1.0686	3.52210	-0.79259	285-530
C—(C,3Cl)	8.5430	2.6966	-0.42564	245-310	C—(3H,CO)	3.8452	-0.33997	0.19489	80-490
C—(H,C,2Cl)	10.880	-0.35391	0.08488	180-355	C—(2H,C,CO)	6.6782	-2.44730	0.47121	180-465
C—(2H,C,Cl)	9.6663	-1.8601	0.41360	140-360	C—(H,2C,CO)	3.92380	-2.12100	0.49646	185-375
C—(2H,=C,Cl)	9.6663	-1.8601	0.41360	140-360	C—(3C,CO)	-2.2681	1.75580	-0.25674	225-360
C—(H,2C,Cl)	-2.0600	5.3281	-0.82721	275-360	CO—(H,C)	-3.82680	7.67190	-1.27110	180-430
C—(2H,C,Br)	6.3944	-0.10298	0.19403	168-360	CO—(H,=C)	-8.00240	3.63790	-0.15377	220-430
C—(H,2C,Br)	10.784	-2.4754	0.33288	190-420	CO—(H,Cb)	-8.00240	3.63790	-0.15377	220-430
C—(2H,C,I)	0.037620	5.6204	-0.92054	245-340	CO—(2C)	5.4375	0.72091	-0.18312	185-380
C—(C,2Cl,F)	13.532	-3.2794	0.80145	240-420	CO—(C,=C)	41.507	-32.632	6.0326	275-355
C—(C,Cl,2F)	7.2295	0.41759	0.15892	180-420	CO—(C,Cb)	-47.21100	24.36800	-2.82740	300-465
C—(C,Br,2F)	8.7956	-0.19165	0.24596	165-415	CO—(H,O)	13.11800	16.12000	-5.12730	280-340
=C—(H,Cl)	7.1564	-0.84442	0.27199	120-300	CO—(C,O)	29.24600	3.42610	-2.89620	180-445
=C—(2F)	7.6646	-2.0750	0.82003	120-240	CO—(=C,O)	41.61500	-12.78900	0.53631	195-350
=C—(2Cl)	9.3249	-1.2478	0.44241	155-300	CO—(O,O)	23.99000	6.25730	-3.24270	320-345
=C—(Cl,F)	7.8204	-0.69005	0.19165	120-240	O—(C,O)	-21.43400	-4.01640	3.05310	175-440
Cb—(F)	3.0794	0.46959	-0.0055745	210-365	O—(H,CO)	-27.58700	-0.16485	2.74830	230-500
Cb—(Cl)	4.5479	0.22250	-0.0097873	230-460	=C—(H,CO)	-9.01080	15.14800	-3.04360	195-355
Cb—(Br)	2.2857	2.2573	-0.40942	245-370	=C—(C,CO)	-12.81800	15.99700	-3.05670	195-430
Cb—(I)	2.9033	2.9763	-0.62960	250-320	Cb—(CO)	12.15100	-1.67050	-0.12758	175-500
C—(Cb,3F)	7.4477	-0.92230	0.39346	210-365	CO—(Cb,O)	16.58600	5.44910	-2.68490	175-500
C—(2H,Cb,Cl)	16.752	-6.7938	1.2520	245-345	Sulfur Groups				
Nitrogen Groups					C—(3H,S)	3.84520	-0.33997	0.19489	80-490
C—(3H,N)	3.8452	-0.33997	0.19489	80-490	C—(2H,C,S)	1.54560	0.85228	-0.08349	130-390
C—(2H,C,N)	2.4555	1.0431	-0.24054	190-375	C—(H,2C,S)	-1.64300	2.30700	-0.31234	150-390
C—(2H,Cb,N)	2.4555	1.0431	-0.24054	190-375	C—(3C,S)	-5.38250	4.50230	-0.72356	190-365
C—(H,2C,N)	2.6322	-2.0135	0.45109	240-370	Cb—(S)	-4.45070	4.43240	-0.75674	260-375
C—(3C,N)	1.9630	-1.7235	0.31086	255-375	S—(H,C)	10.99400	-3.21130	0.47368	130-380
N—(2H,C)	8.2758	-0.18365	0.035272	185-455	S—(H,Cb)	10.99400	-3.21130	0.47368	130-380
N—(2H,Cb)	8.2758	-0.18365	0.035272	185-455	S—(2C)	9.23060	-3.00870	0.45625	165-390
					S—(2Cb)	9.23060	-3.00870	0.45625	165-390
					S—(C,S)	6.65900	-1.35570	0.17938	170-350
					S—(Cb,S)	9.23060	-3.00870	0.45625	165-390
					S—(2Cb) (thiophene)	3.84610	0.36718	-0.06131	205-345

TABLE 2-348 Liquid Heat Capacity Group Parameters for Ruzicka-Domalski Method* (Concluded)

Table-specific nomenclature: Ct refers to a carbon atom with a triple bond; Cb refers to a carbon atom in benzene ring; =C refers to a carbon atom with a double bond; Cp refers to a carbon atom in a fused benzene ring; =C= refers to an allenic carbon atom.

Group Definition	<i>a</i>	<i>b</i>	<i>d</i>	<i>T</i> range (K)	Group Definition	<i>a</i>	<i>b</i>	<i>d</i>	<i>T</i> range (K)
Ring Strain Contributions									
Hydrocarbons (ring strain)									
cyclopropane	4.4297	-4.3392	1.0222	155-240	decahydronaphthalene	-6.8984	0.66846	-0.070012	235-485
cyclobutane	1.2313	-2.8988	0.75099	140-300	hexahydroindan	-3.9271	-0.29239	0.048561	210-425
cyclopentane (unsub)	-0.33642	-2.8663	0.70123	180-300	dodecahydrofluorene	-19.687	8.8265	-1.4031	315-485
cyclopentane (sub)	0.21983	-1.5118	0.28172	135-365	tetradecahydrophenanthrene	-0.67632	-1.4753	-0.13087	315-485
cyclohexane	-2.0097	-0.72656	0.14758	145-485	hexadecahydropyrene	61.213	-30.927	3.2269	310-485
cycloheptane	-11.460	4.9507	-0.74754	270-300	Nitrogen compounds				
cyclooctane	-4.1696	0.52991	-0.018423	295-320	ethyleneimine	15.281	-2.3360	-0.13720	195-330
spiro-pentane	5.9700	-3.7965	0.74612	175-310	pyrrolidine	12.703	1.3109	-1.18130	170-400
cyclopentene	0.21433	-2.5214	0.63136	140-300	piperidine	25.681	-7.0966	0.14304	265-370
cyclohexene	-1.2086	-1.5041	0.42863	160-320	Oxygen compounds				
cycloheptene	-5.6817	1.5073	-0.19810	220-300	ethylene oxide	6.8459	-5.8759	1.2408	135-325
cyclooctene	-14.885	7.4878	-1.0879	260-330	trimethylene oxide	-7.0148	7.3764	-2.1901	185-300
cyclohexadiene	-8.9683	6.4959	-1.5272	170-300	1, 3-dioxolane	-2.3985	-0.48585	0.10253	175-300
cyclooctadiene	-7.2890	3.1119	-0.43040	205-320	furan	9.6704	-2.8138	0.11376	190-305
cycloheptatriene	-8.7885	8.2530	-2.4573	200-310	tetrahydrofuran	3.2842	-5.8260	1.2681	160-320
cyclooctatetraene	-12.914	13.583	-4.0230	275-330	tetrahydropyran	-13.017	3.7416	-0.15622	295-325
indan	-6.1414	3.5709	-0.48620	170-395	Sulfur compounds				
1H-indene	-3.6501	2.4707	-0.60531	280-375	thiacyclobutane	-0.73127	-1.3426	0.40114	200-320
tetrahydronaphthalene	-6.3861	2.6257	-0.19578	250-320	thiacyclopentane	-3.2899	0.38399	0.089358	170-390
					thiacyclohexane	-12.766	5.2886	-0.59558	295-340

*Ruzicka, V., and E. S. Domalski, *J. Phys. Chem. Ref. Data*, **22** (1993): 597, 619.

From Eq. (2-52):

$$C_p = \frac{1694.9}{1000} (307.93)^{0.79267} \frac{\text{J}}{\text{mol}\cdot\text{K}} = 159.1 \frac{\text{J}}{\text{mol}\cdot\text{K}}$$

This value is 2.5 percent higher than the DIPPR® 801 recommended value of 155.2 J/(mol·K).

Recommended Method 2 Modified Kopp's rule.

Reference: Kopp, H., *Ann. Chem. Pharm. (Liebig)*, **126** (1863): 362; Hurst, J. E., and B. K. Harrison, *Chem. Eng. Comm.*, **112** (1992): 21.

Classification: Group contributions.

Expected uncertainty: 10 percent.

Applicability: 298.15 K; organic compounds that are solids at 298.15 K.

Input data: Compound chemical formula and element contributions of Table 2-350.

Description:

$$\frac{C_p}{\text{J}/(\text{mol}\cdot\text{K})} = \sum_{E=1}^N n_E \Delta_E \quad (2-54)$$

where N = number of different elements in compound
 n_E = number of occurrences of element E in compound
 Δ_E = contribution of element E from Table 2-350

Example Estimate the solid heat capacity at 298.15 K for dibenzothio-
 phene.

Structure: $\text{C}_{12}\text{H}_8\text{S}_2$.

Group values from Table 2-350:

$$\Delta_C = 10.89 \quad \Delta_H = 7.56 \quad \Delta_S = 12.36$$

Calculation using Eq. (2-54):

$$C_p = (12)(10.89) + (8)(7.56) + (1)(12.36) = 203.52 \text{ J}/(\text{mol}\cdot\text{K})$$

This value is 2.5 percent higher than the DIPPR® 801 recommended value of 198.45 J/(mol·K).

Mixtures The heat capacity of liquid and vapor mixtures can be estimated as mole fraction averages of the pure-component values

$$C_{p,m} = \sum_{i=1}^C x_i C_{p,i} \quad (2-55)$$

This neglects the excess heat capacity, which if available can be added to the mole fraction average to improve the estimated value.

DENSITY

Density is defined as the mass of a substance per unit volume. Density is given in kg/m³ in SI units, but lb_m/ft³ and g/cm³ are common AES and cgs units, respectively. Other commonly used forms of density include *molar density* (density divided by molecular weight) in kmol/m³, *relative density* (density relative to water at 15°C), and the older term *specific gravity* (density relative to water at 60°F). Often the inverse of *molar density*, *specific volume*, and the inverse of *molar density*, *molar volume*, are correlated and used to convey equivalent information.

Gases Gases/vapors are compressible and their densities are strong functions of both temperature and pressure. Equations of state (EoS) are commonly used to correlate molar densities or molar volumes. The most accurate EoS are those developed for specific fluids with parameters regressed from all available data for that fluid. Super EoS are available for some of the most industrially important gases and may contain 50 or more constants specific to that chemical. Different predictive methods may be used for gas densities depending upon the conditions:

1. At *very low densities* (high temperatures, generally above the critical, and very low pressures, generally below a few bar), the ideal gas EoS

$$Z \equiv \frac{PV}{RT} = 1 \quad (2-56)$$

may be applied.

2. At *moderate densities* (below 40 percent of the critical density), the virial equation truncated after the second virial coefficient

$$Z = 1 + \frac{B(T)}{V} \quad (2-57)$$

may be used. Second virial coefficients $B(T)$ are available in the DIPPR® 801 database for many chemicals and can be estimated for others by using the Tsionopoulos method.

TABLE 2-349 Group Values and Nonlinear Correction Terms for Estimation of Solid Heat Capacity with the Goodman et al.* Method

Group	Description	a_i	Group	Description	a_i
—CH ₃	methyl	0.20184	—CO ₃ —	carbonate	0.2517
>CH ₂	methylene	0.11644	—NH ₂	primary amine	0.056138
>CH—	secondary C	0.030492	>NH	secondary amine	-0.00717
>C<	tertiary C	-0.04064	>N—	tertiary amine	-0.01661
CH ₂ ==	terminal alkene	0.18511	==NH	double-bond NH	0.17689
—CH==	alkene	0.11224	#N	nitrile	0.015355
>C==	subst. alkene	0.028794	—N==N—	diazide	0.3687
==C==	allene	0.053464	—NO ₂	nitro	0.23327
#CH	terminal alkyne	-0.02914	—N=C=O	isocyanate	0.2698
#C—	alkyne	0.13298	—SH	thiol/mercaptan	0.21123
Ar—CH==	arom. C	0.082478	—S—	sulfide	0.14232
Ar>C==	subst. arom. C	0.012958	—SS—	disulfide	0.31457
Ar—O—	furan O	0.066027	==S	sulfur double bond	0.13753
Ar—N==	pyridine N	0.056641	>S=O	sulfoxide	0.040002
Ar>N—	subst. pyrrole N	0.008938	—F	fluoride	0.15511
Ar—NH—	pyrrole N	-0.05246	—Cl	chloride	0.16995
Ar—S—	thiophene S	0.090926	—Br	bromide	0.19112
—O—	ether	0.064068	—I	iodide	0.11318
—OH	alcohol	0.10341	>Si<	silane	0.12213
—COH	aldehyde	0.15699	>Si(O)—	linear siloxane	0.10125
>C=O	ketone	0.12939	cyc >Si(O)—	cyclic siloxane	0.063438
—COO—	ester	0.13686	P(=O)(O—) ₃	phosphate	0.15016
—COOH	acid	0.21019	>P—	phosphine	0.069602
—COOCO—	anhydride	0.33091	>P(=O)—	phosphine oxide	0.21875
Nonlinear Terms					
Groups	β_i		Usage		
>CH ₂	-0.00188		Methylene		
Ar==CH—	-0.00033		Aromatic carbon		

*Goodman, B. T., W. V. Wilding, J. L. Oscarson, and R. L. Rowley, *J. Chem. Eng. Data*, **49** (2004): 24**Recommended Method** Tsonopoulos method.Reference: Tsonopoulos, C., *AIChE J.*, **20** (1974): 263; **21** (1975): 827; **24** (1978): 1112.

Classification: Corresponding states.

Expected uncertainty: 8 percent for $B(T)$.

Applicability: Nonpolar organic compounds and some classes of polar compounds.

Input data: Class of fluid, ω , P_c , T_c , and μ .

Description:

$$\frac{BP_c}{RT_c} = B^{(0)} + \omega B^{(1)} + B^{(2)} \quad (2-58)$$

where ω = acentric factor P_c = critical pressure T_c = critical temperature

$$B^{(0)} = 0.1445 - \frac{0.330}{T_r} - \frac{0.1385}{T_r^2} - \frac{0.0121}{T_r^3} - \frac{0.000607}{T_r^6} \quad (2-59)$$

TABLE 2-350 Element Contributions to Solid Heat Capacity for the Modified Kopp's Rule*†

Element	Δ_E	Element	Δ_E	Element	Δ_E
C	10.89	Ba	32.37	Mo	29.44
H	7.56	Be	12.47	Na	26.19
O	13.42	Ca	28.25	Ni	25.46
N	18.74	Co	25.71	Pb	31.60
S	12.36	Cu	26.92	Si	17.00
F	26.16	Fe	29.08	Sr	28.41
Cl	24.69	Hg	27.87	Ti	27.24
Br	25.36	K	28.78	V	29.36
I	25.29	Li	23.25	W	30.87
Al	18.07	Mg	22.69	Zr	26.82
B	10.10	Mn	28.06	All others	26.63

*Kopp, H., *Ann. Chem. Pharm. (Liebig)*, **126** (1863): 362.†Hurst, J. E., and B. K. Harrison, *Chem. Eng. Comm.*, **112** (1992): 21.

$$B^{(1)} = 0.0637 + \frac{0.331}{T_r^2} - \frac{0.423}{T_r^3} - \frac{0.008}{T_r^6} \quad (2-60)$$

$$B^{(2)} = \frac{a}{T_r^6} - \frac{b}{T_r^8} \quad (2-61)$$

$$\mu_r = \left(\frac{\mu}{D} \right)^2 \left(\frac{P_c}{\text{bar}} \right) \left(\frac{T_c}{\text{K}} \right)^{-2} \quad (2-62)$$

where μ = dipole moment. The values of a and b used in Eq. (2-61) depend upon the class of fluid, as given in the table below:

Class	a	b
Nonpolar fluids	0	0
Ketones, aldehydes, nitriles, ethers, esters, NH ₃ , H ₂ S, HCN	$-21.4\mu_r - 4.308 \times 10^{19}\mu_r^8$	0
Monoalkylhalides, mercaptans, sulfides	$-2.188 \times 10^{16}\mu_r^4 - 7.831 \times 10^{19}\mu_r^8$	0
1-Alcohols except methanol	0.0878	$0.00908 + 69.57\mu_r$
Methanol	0.0878	0.0525

Example Estimate the molar volume of ammonia at 430 K and 2.82 MPa. Input properties: Recommended values from the DIPPR® S01 database are $T_c = 405.65$ K, $P_c = 11.28$ MPa, $\mu = 1.469$ D, and $\omega = 0.252608$.

Reduced conditions:

$$T_r = (430 \text{ K}) / (405.65 \text{ K}) = 1.06$$

$$P_r = (2.82 \text{ MPa}) / (11.28 \text{ MPa}) = 0.25$$

$$\mu_r = (1.469)^2 (112.8) / (405.65)^2 = 0.0014793$$

Second virial coefficient from Eqs. (2-59) to (2-61):

$$B^{(0)} = 0.1445 - 0.330/1.06 - 0.1385/(1.06)^2 - 0.0121/(1.06)^3$$

$$-0.000607/(1.06)^8 = -0.301$$

$$B^{(1)} = 0.0637 + 0.331/(1.06)^2 - 0.423/(1.06)^3 - 0.008/(1.06)^8 = -0.00189$$

$$a = (-21.4)(0.0014793) - (4.308 \times 10^{10})(0.0014793)^8 = -0.033$$

$$b = 0$$

$$B^{(2)} = (-0.033)/(1.06)^6 = -0.023$$

From Eq. (2-58):

$$BP_c/(RT_c) = -0.301 - (0.252608)(0.00189) - 0.023 = -0.324$$

$$B = (-0.324)[0.008314 \text{ m}^3 \cdot \text{MPa}/(\text{kmol} \cdot \text{K})](405.65 \text{ K})/(11.28 \text{ MPa}) \\ = -0.097 \text{ m}^3/\text{kmol}$$

Molar volume from Eq. (2-56):

$$V = \frac{RT}{P} \left(1 + \frac{B}{V} \right) = \frac{(0.0083143 \frac{\text{m}^3 \cdot \text{MPa}}{\text{kmol} \cdot \text{K}})(430 \text{ K})}{2.82 \text{ MPa}} \left(1 + \frac{-0.097 \frac{\text{m}^3}{\text{kmol}}}{V} \right) \\ = 1.162 \text{ m}^3/\text{kmol}$$

Note that the ideal gas value, $1.268 \text{ m}^3/\text{kmol}$, deviates by 9.1 percent from this more accurate value. The truncated virial EoS should be valid for this density since $\rho = V^{-1} = 0.86 \text{ kmol}/\text{m}^3$ is much less than 40 percent of the critical density (the DIPPR[®] 801 recommended value for the critical density is $13.8 \text{ kmol}/\text{m}^3$).

3. For higher gas densities, the Lee-Kesler method described below provides excellent predictions for nonpolar and slightly polar fluids. Extended four-parameter corresponding-states methods are available for polar and slightly associating compounds.

Recommended Method Lee-Kesler method.

Reference: Lee, B. I., and M. G. Kesler, *AIChE J.*, **21** (1975): 510.

Classification: Corresponding states.

Expected uncertainty: 1 percent except near the critical point where errors can be up to 30 percent.

Applicability: Nonpolar and moderately polar compounds. An extended Lee-Kesler method, not described here, may be used for polar and slightly associating compounds [Wilding, W. V., and R. L. Rowley, *Int. J. Thermophys.*, **8** (1986): 525].

Input data: T_c , P_c , ω , $Z^{(0)}$, $Z^{(1)}$.

Description:

$$Z = Z^{(0)} + \omega Z^{(1)} \quad (2-63)$$

where Z = compressibility factor

$Z^{(0)}$ = compressibility factor of simple fluid obtained from Table 2-351.

$Z^{(1)}$ = deviation from simple fluid obtained from Table 2-352.

Analytical expressions for $Z^{(0)}$ and $Z^{(1)}$ can also be generated by using

$$Z^{(0)} = Z_0 \quad Z^{(1)} = \frac{Z_1 - Z_0}{0.3978} \quad (2-64)$$

where Z_0 and Z_1 are determined from

$$Z_i = \frac{P_r V_r}{T_r} = 1 + \frac{B}{V_r} + \frac{C}{V_r^2} + \frac{D}{V_r^3} + \frac{c_4}{T_r^3 V_r^2} \left(\beta + \frac{\gamma}{V_r^2} \right) \exp \left(\frac{-\gamma}{V_r^2} \right) \quad (2-65)$$

$$B = b_1 - \frac{b_2}{T_r} - \frac{b_3}{T_r^2} - \frac{b_4}{T_r^3}$$

$$C = c_1 - \frac{c_2}{T_r} + \frac{c_3}{T_r^2}$$

$$D = d_1 + \frac{d_2}{T_r}$$

as applied to the simple reference fluid and to the acentric reference fluid (*n*-octane), respectively. The constants for Eq. (2-65) for the two reference fluids are given in Table 2-353.

Example Estimate the molar volume of saturated decane vapor at 540.5 K. Input properties: Recommended values from the DIPPR[®] 801 database are $T_c = 617.7 \text{ K}$, $P_c = 2.11 \text{ MPa}$, $P^s(540.5 \text{ K}) = 0.6799 \text{ MPa}$ (vapor pressure), and $\omega = 0.492328$.

Reduced conditions:

$$T_r = (540.5 \text{ K})/(617.7 \text{ K}) = 0.875$$

$$P_r = (0.6799 \text{ MPa})/(2.11 \text{ MPa}) = 0.322$$

LK compressibility factor: Since vapor phase values are needed, the appropriate values from Tables 2-351 and 2-352 that can be used to double-interpolate are

$Z^{(0)}$		
$T_r \backslash P_r$	0.2	0.4
0.85	0.8810	(0.7222)
0.90	0.9015	0.7800

$Z^{(1)}$		
$T_r \backslash P_r$	0.2	0.4
0.85	-0.0715	(-0.1503)
0.90	-0.0442	-0.1118

Double linear interpolation within these values gives $Z^{(0)} = 0.8058$ and $Z^{(1)} = -0.1025$.

From Eq. (2-63):

$$Z = 0.8058 + (0.492328)(-0.1025) = 0.7553$$

Note: If the analytical form available in Eq. (2-65) is used, the following more accurate values are obtained: $Z^{(0)} = 0.8131$, $Z^{(1)} = -0.1067$, and $Z = 0.7606$.

Molar volume:

$$V = \frac{ZRT}{P} = \frac{(0.7553) \left(0.0083143 \frac{\text{m}^3 \cdot \text{MPa}}{\text{kmol} \cdot \text{K}} \right) (540.5 \text{ K})}{0.6799 \text{ MPa}} = 4.992 \frac{\text{m}^3}{\text{kmol}}$$

4. Cubic EoS can be used to obtain both vapor and liquid densities as an alternative method to those mentioned above.

Recommended Method Cubic EoS.

Classification: Empirical extension of theory.

Expected uncertainty: Varies depending upon compound and conditions, but a general expectation is perhaps 10 to 20 percent.

Applicability: Nonpolar and moderately polar compounds.

Input data: T_c , P_c , ω .

Description: The more common cubic EoS can be written in the form

$$Z = \frac{V}{V-b} - \frac{V}{V^2 + \delta V + \epsilon} - \frac{a \alpha(T_r)}{RT} \quad (2-66)$$

where a , b , δ , and ϵ are constants that depend upon the model EoS chosen, as does the temperature dependence of the function $\alpha(T_r)$. Definitions of these constants and $\alpha(T_r)$ for some of the more commonly used EoS models are shown in Table 2-354. The corresponding relations for many other EoS models in this same form are available [Soave, G., *Chem. Eng. Sci.*, **27** (1972): 1197]. The independent parameters a and b in these models can be regressed from experimental data to correlate densities or obtained from known critical constants to predict density data. In the latter case, the relationships between a and b and the critical constants shown in Table 2-354 were obtained from the critical point requirements

$$\left(\frac{\partial P}{\partial V} \right)_{T=T_c} = 0 = \left(\frac{\partial^2 P}{\partial V^2} \right)_{T=T_c} \quad (2-67)$$

TABLE 2-351 Simple Fluid Compressibility Factors $Z^{(0)}$ Values in parentheses are for the opposite phase and may be used to interpolate to or near the phase boundary [PGL4; Wilding, W. V., J. K. Johnson, and R. L. Rowley, *Int. J. Thermophys.*, **8**(1987):717].

T/P_r	0.010	0.050	0.100	0.200	0.400	0.600	0.800	1.000	1.200	1.500	2.000	3.000	5.000	7.000	10.000
0.30	0.0029	0.0145	0.0290	0.0579	0.1158	0.1737	0.2315	0.2892	0.3470	0.4335	0.5775	0.8648	1.4366	2.0048	2.8507
0.35	0.0026	0.0130	0.0261	0.0522	0.1043	0.1564	0.2084	0.2604	0.3123	0.3901	0.5195	0.7775	1.2902	1.7987	2.5539
0.40	0.0024	0.0119	0.0239	0.0477	0.0953	0.1429	0.1904	0.2379	0.2853	0.3563	0.4744	0.7095	1.1758	1.6373	2.3211
0.45	0.0022	0.0110	0.0221	0.0442	0.0882	0.1322	0.1762	0.2200	0.2638	0.3294	0.4384	0.6551	1.0841	1.5077	2.1338
0.50	(0.9648) 0.0021	0.0103	0.0207	0.0413	0.0825	0.1236	0.1647	0.2056	0.2465	0.3077	0.4092	0.6110	1.0094	1.4017	1.9801
0.55	(0.9741) 0.9804	(0.8699) 0.0098	0.0195	0.0390	0.0778	0.1166	0.1553	0.1939	0.2323	0.2899	0.3853	0.5747	0.9475	1.3137	1.8520
0.60	(0.0020) 0.9849	(0.9000) 0.0093	(0.7995) 0.0186	0.0371	0.0741	0.1109	0.1476	0.1842	0.2207	0.2753	0.3657	0.5446	0.8959	1.2398	1.7440
0.65	(0.0019) 0.9881	(0.9211) 0.9377	(0.8405) 0.0178	0.0356	0.0710	0.1063	0.1415	0.1765	0.2113	0.2634	0.3495	0.5197	0.8526	1.1773	1.6519
0.70	(0.0018) 0.9904	(0.0089) 0.9504	(0.8570) 0.8958	(0.7367) 0.0344	0.0687	0.1027	0.1366	0.1703	0.2038	0.2538	0.3364	0.4991	0.8161	1.1241	1.5729
0.75	0.9922	0.9598	0.9165	0.8336	0.0670	0.1001	0.1330	0.1656	0.1981	0.2464	0.3260	0.4823	0.7854	1.0787	1.5047
0.80	0.9935	0.9669	0.9319	0.8539	0.0661	0.0985	0.1307	0.1626	0.1942	0.2411	0.3182	0.4690	0.7598	1.0400	1.4456
0.85	0.9946	0.9725	0.9436	0.8810	0.0661	0.0983	0.1301	0.1614	0.1924	0.2382	0.3132	0.4591	0.7388	1.0071	1.3943
0.90	0.9954	0.9768	0.9528	0.9015	0.0655	0.1006	0.1321	0.1630	0.1935	0.2383	0.3114	0.4527	0.7220	0.9793	1.3496
0.93	0.9959	0.9790	0.9573	0.9115	0.0659	0.1359	0.1359	0.1664	0.1963	0.2405	0.3122	0.4507	0.7138	0.9648	1.3257
0.95	0.9961	0.9803	0.9600	0.9174	0.8206	0.6967	0.1410	0.1705	0.1998	0.2432	0.3138	0.4501	0.7092	0.9561	1.3108
0.97	0.9963	0.9815	0.9625	0.9227	0.8338	0.7240	0.5580	0.1779	0.2055	0.2474	0.3164	0.4504	0.7052	0.9480	1.2968
0.98	0.9965	0.9821	0.9637	0.9253	0.8398	0.7360	0.5887	0.1844	0.2097	0.2503	0.3182	0.4508	0.7035	0.9442	1.2901
0.99	0.9966	0.9826	0.9648	0.9277	0.8455	0.7471	0.6138	0.1959	0.2154	0.2538	0.3204	0.4514	0.7018	0.9406	1.2835
1.00	0.9967	0.9832	0.9659	0.9300	0.8509	0.7574	0.6353	0.2901	0.2237	0.2583	0.3229	0.4522	0.7004	0.9372	1.2772
1.01	0.9968	0.9837	0.9669	0.9322	0.8561	0.7671	0.6542	0.4648	0.2370	0.2640	0.3260	0.4533	0.6991	0.9339	1.2710
1.02	0.9969	0.9842	0.9679	0.9343	0.8610	0.7761	0.6710	0.5146	0.2629	0.2715	0.3297	0.4547	0.6980	0.9307	1.2650
1.05	0.9971	0.9855	0.9707	0.9401	0.8743	0.8002	0.7130	0.6026	0.4437	0.3131	0.3452	0.4604	0.6956	0.9222	1.2481
1.10	0.9975	0.9874	0.9747	0.9485	0.8930	0.8323	0.7649	0.6880	0.5984	0.4580	0.3953	0.4770	0.6950	0.9110	1.2232
1.15	0.9978	0.9891	0.9780	0.9554	0.9081	0.8576	0.8032	0.7443	0.6803	0.5798	0.4760	0.5042	0.6987	0.9033	1.2021
1.20	0.9981	0.9904	0.9808	0.9611	0.9205	0.8779	0.8330	0.7858	0.7363	0.6605	0.5605	0.5425	0.7069	0.8990	1.1844
1.30	0.9985	0.9926	0.9852	0.9702	0.9396	0.9083	0.8764	0.8438	0.8111	0.7624	0.6908	0.6344	0.7358	0.8998	1.1580
1.40	0.9988	0.9942	0.9884	0.9768	0.9534	0.9298	0.9062	0.8827	0.8595	0.8256	0.7753	0.7202	0.7761	0.9112	1.1419
1.50	0.9991	0.9954	0.9909	0.9818	0.9636	0.9456	0.9278	0.9103	0.8933	0.8689	0.8328	0.7887	0.8200	0.9297	1.1339
1.60	0.9993	0.9964	0.9928	0.9856	0.9714	0.9575	0.9439	0.9308	0.9180	0.9000	0.8738	0.8410	0.8617	0.9518	1.1320
1.70	0.9994	0.9971	0.9943	0.9886	0.9775	0.9667	0.9563	0.9463	0.9367	0.9234	0.9043	0.8809	0.8984	0.9745	1.1343
1.80	0.9995	0.9977	0.9955	0.9910	0.9823	0.9739	0.9659	0.9583	0.9511	0.9413	0.9275	0.9118	0.9297	0.9961	1.1391
1.90	0.9996	0.9982	0.9964	0.9929	0.9861	0.9796	0.9735	0.9678	0.9624	0.9552	0.9456	0.9359	0.9557	1.0157	1.1452
2.00	0.9997	0.9986	0.9972	0.9944	0.9892	0.9842	0.9796	0.9754	0.9715	0.9664	0.9599	0.9550	0.9772	1.0328	1.1516
2.20	0.9998	0.9992	0.9983	0.9967	0.9937	0.9910	0.9886	0.9865	0.9847	0.9826	0.9806	0.9827	1.0094	1.0600	1.1635
2.40	0.9999	0.9996	0.9991	0.9983	0.9969	0.9957	0.9948	0.9941	0.9936	0.9935	0.9945	1.0011	1.0313	1.0793	1.1728
2.60	1.0000	0.9998	0.9997	0.9994	0.9991	0.9990	0.9990	0.9993	0.9998	1.0010	1.0040	1.0137	1.0463	1.0926	1.1792
2.80	1.0000	1.0000	1.0001	1.0002	1.0007	1.0013	1.0021	1.0031	1.0042	1.0063	1.0106	1.0223	1.0565	1.1016	1.1830
3.00	1.0000	1.0002	1.0004	1.0008	1.0018	1.0030	1.0043	1.0057	1.0074	1.0101	1.0153	1.0284	1.0635	1.1075	1.1848
3.50	1.0001	1.0004	1.0008	1.0017	1.0035	1.0055	1.0075	1.0097	1.0120	1.0156	1.0221	1.0368	1.0723	1.1138	1.1834
4.00	1.0001	1.0005	1.0010	1.0021	1.0043	1.0066	1.0090	1.0115	1.0140	1.0179	1.0249	1.0401	1.0741	1.1136	1.1773

Table 2-352 Acentric Deviations $Z^{(1)}$ from the Simple Fluid Compressibility Factor

Values in parentheses are for the opposite phase and may be used to interpolate to or near the phase boundary [PGL4; Wilding, W. V., J. K. Johnson, and R. L. Rowley, *Int. J. Thermophys.*, 8(1987):717].

$TrPr$	0.010	0.050	0.100	0.200	0.400	0.600	0.800	1.000	1.200	1.500	2.000	3.000	5.000	7.000	10.000
0.30	-0.0008	-0.0040	-0.0081	-0.0161	-0.0323	-0.0484	-0.0645	-0.0806	-0.0966	-0.1207	-0.1608	-0.2407	-0.3996	-0.5572	-0.7915
0.35	-0.0009	-0.0046	-0.0093	-0.0185	-0.0370	-0.0554	-0.0738	-0.0921	-0.1105	-0.1379	-0.1834	-0.2738	-0.4523	-0.6279	-0.8863
0.40	-0.0010	-0.0048	-0.0095	-0.0190	-0.0380	-0.0570	-0.0758	-0.0946	-0.1134	-0.1414	-0.1879	-0.2799	-0.4603	-0.6365	-0.8936
0.45	-0.0009 (-0.0740)	-0.0047	-0.0094	-0.0187	-0.0374	-0.0560	-0.0745	-0.0929	-0.1113	-0.1387	-0.1840	-0.2734	-0.4475	-0.6162	-0.8606
0.50	-0.0009 (-0.0457)	-0.0045 (-0.2270)	-0.0090	-0.0181	-0.0360	-0.0539	-0.0716	-0.0893	-0.1069	-0.1330	-0.1762	-0.2611	-0.4253	-0.5831	-0.8099
0.55	-0.0314 (-0.0009)	-0.0043 (-0.1438)	-0.0086 (-0.2864)	-0.0172	-0.0343	-0.0513	-0.0682	-0.0849	-0.1015	-0.1263	-0.1669	-0.2465	-0.3991	-0.5446	-0.7521
0.60	-0.0205 (0.0008)	-0.0041 (0.0949)	-0.0082 (-0.1857)	-0.0164	-0.0326	-0.0487	-0.0646	-0.0803	-0.0960	-0.1192	-0.1572	-0.2312	-0.3718	-0.5047	-0.6928
0.65	-0.0137 (-0.0008)	-0.0772 (0.0039)	-0.0078 (-0.1262)	-0.0156 (-0.2424)	-0.0309	-0.0461	-0.0611	-0.0759	-0.0906	-0.1122	-0.1476	-0.2160	-0.3447	-0.4653	-0.6346
0.70	-0.0093	-0.0507 (-0.0038)	-0.01161 (-0.0075)	-0.0148 (-0.1685)	-0.0294	-0.0438	-0.0579	-0.0718	-0.0855	-0.1057	-0.1385	-0.2013	-0.3184	-0.4270	-0.5785
0.75	-0.0064	-0.0339 (-0.0037)	-0.0744 (-0.0072)	-0.0143 (-0.1298)	-0.0282 (-0.2203)	-0.0417	-0.0550	-0.0681	-0.0808	-0.0996	-0.1298	-0.1872	-0.2929	-0.3901	-0.5250
0.80	-0.0044	-0.0228 (-0.0073)	-0.0487 (-0.0139)	-0.1160 (-0.0144)	-0.0272 (-0.1503)	-0.0401 (-0.1692)	-0.0526	-0.0648	-0.0767	-0.0940	-0.1217	-0.1736	-0.2682	-0.3545	-0.4740
0.85	-0.0029	-0.0152	-0.0319	-0.0715 (-0.0144)	-0.0268 (-0.1503)	-0.0391 (-0.1692)	-0.0509	-0.0622	-0.0731	-0.0888	-0.1138	-0.1602	-0.2439	-0.3201	-0.4254
0.90	-0.0019	-0.0099	-0.0205	-0.0442 (-0.0179)	-0.1118 (-0.0286)	-0.0396 (-0.1580)	-0.0503 (-0.1464)	-0.0604	-0.0701	-0.0840	-0.1059	-0.1463	-0.2195	-0.2862	-0.3788
0.93	-0.0015	-0.0075	-0.0154	-0.0326	-0.0763 (-0.0340)	-0.1662 (-0.0424)	-0.0514 (-0.1418)	-0.0602	-0.0687	-0.0810	-0.1007	-0.1374	-0.2045	-0.2661	-0.3516
0.95	-0.0012	-0.0062	-0.0126	-0.0262	-0.0589 (-0.0444)	-0.1110 (-0.0490)	-0.0540 (-0.1532)	-0.0607	-0.0678	-0.0788	-0.0967	-0.1310	-0.1943	-0.2526	-0.3339
0.97	-0.0010	-0.0050	-0.0101	-0.0208	-0.0450	-0.0770 (-0.0714)	-0.1647 (-0.0643)	-0.0623	-0.0669	-0.0759	-0.0921	-0.1240	-0.1837	-0.2391	-0.3163
0.98	-0.0009	-0.0044	-0.0090	-0.0184	-0.0390	-0.0641	-0.1100 (-0.0828)	-0.0641	-0.0661	-0.0740	-0.0893	-0.1202	-0.1783	-0.2322	-0.3075
0.99	-0.0008	-0.0039	-0.0079	-0.0161	-0.0335	-0.0531	-0.0796 (-0.1621)	-0.0680	-0.0646	-0.0715	-0.0861	-0.1162	-0.1728	-0.2254	-0.2989
1.00	-0.0007	-0.0034	-0.0069	-0.0140	-0.0285	-0.0435	-0.0588	-0.0879	-0.0609	-0.0678	-0.0824	-0.1118	-0.1672	-0.2185	-0.2902
1.01	-0.0006	-0.0030	-0.0060	-0.0120	-0.0240	-0.0351	-0.0429	-0.0223	-0.0473	-0.0621	-0.0778	-0.1072	-0.1615	-0.2116	-0.2816
1.02	-0.0005	-0.0026	-0.0051	-0.0102	-0.0198	-0.0277	-0.0303	-0.0062	0.0227	-0.0524	-0.0722	-0.1021	-0.1556	-0.2047	-0.2731
1.05	-0.0003	-0.0015	-0.0029	-0.0054	-0.0092	-0.0097	-0.0032	0.0220	0.1059	0.0451	-0.0432	-0.0838	-0.1370	-0.1835	-0.2476
1.10	0.0000	0.0000	0.0001	0.0007	0.0038	0.0106	0.0236	0.0476	0.0897	0.1630	0.0698	-0.0373	-0.1021	-0.1469	-0.2056
1.15	0.0002	0.0011	0.0023	0.0052	0.0127	0.0237	0.0396	0.0625	0.0943	0.1548	0.1667	0.0332	-0.0611	-0.1084	-0.1642
1.20	0.0004	0.0019	0.0039	0.0084	0.0190	0.0326	0.0499	0.0719	0.0991	0.1477	0.1990	0.1095	-0.0141	-0.0678	-0.1231
1.30	0.0006	0.0030	0.0061	0.0125	0.0267	0.0429	0.0612	0.0819	0.1048	0.1420	0.1991	0.2079	0.0875	0.0176	-0.0423
1.40	0.0007	0.0036	0.0072	0.0147	0.0306	0.0477	0.0661	0.0857	0.1063	0.1383	0.1894	0.2397	0.1737	0.1008	0.0350
1.50	0.0008	0.0039	0.0078	0.0158	0.0323	0.0497	0.0677	0.0864	0.1055	0.1345	0.1806	0.2433	0.2309	0.1717	0.1058
1.60	0.0008	0.0040	0.0080	0.0162	0.0330	0.0501	0.0677	0.0855	0.1035	0.1303	0.1729	0.2381	0.2631	0.2255	0.1673
1.70	0.0008	0.0040	0.0081	0.0163	0.0329	0.0497	0.0667	0.0838	0.1008	0.1259	0.1658	0.2305	0.2788	0.2628	0.2179
1.80	0.0008	0.0040	0.0081	0.0162	0.0325	0.0488	0.0652	0.0816	0.0978	0.1216	0.1593	0.2224	0.2846	0.2871	0.2576
1.90	0.0008	0.0040	0.0079	0.0159	0.0318	0.0477	0.0635	0.0792	0.0947	0.1173	0.1532	0.2144	0.2848	0.3017	0.2876
2.00	0.0008	0.0039	0.0078	0.0155	0.0310	0.0464	0.0617	0.0767	0.0916	0.1133	0.1476	0.2069	0.2819	0.3097	0.3096
2.20	0.0007	0.0037	0.0074	0.0147	0.0293	0.0437	0.0579	0.0719	0.0857	0.1057	0.1374	0.1932	0.2720	0.3135	0.3355
2.40	0.0007	0.0035	0.0070	0.0139	0.0276	0.0411	0.0544	0.0675	0.0803	0.0989	0.1285	0.1812	0.2602	0.3089	0.3459
2.60	0.0007	0.0033	0.0066	0.0131	0.0260	0.0387	0.0512	0.0634	0.0754	0.0929	0.1207	0.1706	0.2484	0.3009	0.3475
2.80	0.0006	0.0031	0.0062	0.0124	0.0245	0.0365	0.0483	0.0598	0.0711	0.0876	0.1138	0.1613	0.2372	0.2915	0.3443
3.00	0.0006	0.0029	0.0059	0.0117	0.0232	0.0345	0.0456	0.0565	0.0672	0.0828	0.1076	0.1529	0.2268	0.2817	0.3385
3.50	0.0005	0.0026	0.0052	0.0103	0.0204	0.0303	0.0401	0.0497	0.0591	0.0728	0.0949	0.1356	0.2042	0.2584	0.3194
4.00	0.0005	0.0023	0.0046	0.0091	0.0182	0.0270	0.0357	0.0443	0.0527	0.0651	0.0849	0.1219	0.1857	0.2378	0.2994

2-502 PHYSICAL AND CHEMICAL DATA

TABLE 2-353 Constants for the Two Reference Fluids Used in Lee-Kesler Method*

Constant	Simple reference fluid	Acentric reference fluid
b_1	0.1181193	0.2026579
b_2	0.265728	0.331511
b_3	0.154790	0.027655
b_4	0.030323	0.203488
c_1	0.0236744	0.0313385
c_2	0.0186984	0.0503618
c_3	0.0	0.016901
c_4	0.042724	0.041577
$d_1 \times 10^4$	0.155488	0.48736
$d_2 \times 10^4$	0.623689	0.0740336
β	0.65392	1.226
γ	0.060167	0.03754

*Lee, B. I., and M. G. Kesler, *AIChE J.*, **21** (1975): 510.

Of the cubic EoS given in Table 2-354, the Soave and Peng-Robinson are the most accurate, but there is no general rule for which EoS produces the best estimated volumes for specific fluids or conditions. The Peng-Robinson equation has been better tuned to liquid densities, while the Soave equation has been better tuned to vapor-liquid equilibrium and vapor densities. In solving the cubic equation for volume, a convenient initial guess to find the vapor root is the ideal gas value, while an initial value of $1.05b$ is convenient to locate the liquid root.

Example Estimate the molar density of liquid and vapor saturated ammonia at 353.15 K, using the Soave and Peng-Robinson EoS.

Required properties: Recommended values in the DIPPR® 801 database are

$$T_c = 405.65 \text{ K} \quad P_c = 112.8 \text{ bar} \quad \omega = 0.252608$$

$$P^* (353.15 \text{ K}) = 41.352 \text{ bar (vapor pressure at 353.15 K)}$$

EoS parameters (shown for Soave EoS):

$$a = \frac{0.42748(RT_c)^2}{P_c} = \frac{0.42748 \left[\left(83.145 \frac{\text{bar}\cdot\text{cm}^3}{\text{mol}\cdot\text{K}} \right) (405.65 \text{ K}) \right]^2}{112.8 \text{ bar}}$$

$$= 4.311 \times 10^6 \frac{\text{cm}^6\cdot\text{bar}}{\text{mol}^2}$$

$$b = \frac{0.08664(RT_c)}{P_c} = \frac{0.08664 \left(83.145 \frac{\text{bar}\cdot\text{cm}^3}{\text{mol}\cdot\text{K}} \right) (405.65 \text{ K})}{112.8 \text{ bar}}$$

$$= 25.906 \frac{\text{cm}^3}{\text{mol}}$$

$$T_r = (353.15 \text{ K}) / (405.65 \text{ K}) = 0.871$$

$$\alpha = [1 + [0.48 + (1.574)(0.252608) - (0.176)(0.252608)^2][1 - (0.871)^{0.5}]^2 = 1.119$$

Rearrange and solve Eq. (2-66) for V :

$$P = \frac{RT}{V-b} - \frac{a\alpha}{V(V+b)} \quad \text{or} \quad PV^3 - RTV^2 + (a\alpha - bRT - Pb^2)V - ab\alpha = 0$$

$$41.352 \left(\frac{V}{\text{m}^3/\text{mol}} \right)^3 - \left(0.029 \frac{\text{m}^3}{\text{mol}} \right) \left(\frac{V}{\text{m}^3/\text{mol}} \right)^2 + \left(4.037 \times 10^{-6} \frac{\text{m}^6}{\text{mol}^2} \right)$$

$$\times \left(\frac{V}{\text{m}^3/\text{mol}} \right) - 1.25 \times 10^{-10} = 0$$

Vapor root (initial guess of $V = 7.1 \times 10^{-7} \text{ m}^3/\text{mol}$ from ideal gas equation):

$$V_{\text{vap}} = 5.395 \times 10^{-4} \text{ m}^3/\text{mol} \quad \text{and} \quad \rho_{\text{vap}} = 1/V_{\text{vap}} = 1.854 \text{ kmol/m}^3$$

Liquid root (initial guess of $V = 2.72 \times 10^{-5} \text{ m}^3/\text{mol}$ from 1.05b):

$$V_{\text{liq}} = 4.441 \times 10^{-5} \text{ m}^3/\text{mol} \quad \text{and} \quad \rho_{\text{liq}} = 1/V_{\text{liq}} = 22.516 \text{ kmol/m}^3$$

The corresponding values and equation for the Peng-Robinson EoS are

$$a = 4.611 \times 10^6 \text{ cm}^6\cdot\text{bar/mol}^2 \quad b = 23.262 \text{ cm}^3/\text{mol}$$

$$\alpha = 1.103$$

$$P = \frac{RT}{V-b} - \frac{a\alpha}{V^2 + 2bV - b^2}$$

or

$$PV^3 + (bP - RT)V^2 + (a\alpha - 2bRT - 3Pb^2)V + (bP^3 + RTb^2 - ab\alpha) = 0$$

$$41.352 \left(\frac{V}{\text{m}^3/\text{mol}} \right)^3 - \left(0.0284 \frac{\text{m}^3}{\text{mol}} \right) \left(\frac{V}{\text{m}^3/\text{mol}} \right)^2 + \left(3.651 \times 10^{-6} \frac{\text{m}^6}{\text{mol}^2} \right)$$

$$\times \left(\frac{V}{\text{m}^3/\text{mol}} \right) - 1.018 \times 10^{-10} = 0$$

$$V_{\text{vap}} = 5.286 \times 10^{-4} \text{ m}^3/\text{mol} \quad \text{and} \quad \rho_{\text{vap}} = 1.892 \text{ kmol/m}^3$$

$$V_{\text{liq}} = 3.914 \times 10^{-5} \text{ m}^3/\text{mol} \quad \text{and} \quad \rho_{\text{liq}} = 25.55 \text{ kmol/m}^3$$

The liquid density calculated from the Soave EoS is 24.2 percent below the DIPPR® 801 recommended value of 29.69 kmol/m³, while that calculated from the Peng-Robinson EoS is 13.9 percent below the recommended value.

TABLE 2-354 Relationships for Eq. (2-66) for Common Cubic EoS

EoS	δ	ϵ	$\alpha(T_r)$	$aP_c/(RT_c)^2$	$bP_c/(RT_c)$
van der Waals*	0	0	1	0.42188	0.125
Rellich-Kwong†	0	0	$T_r^{-0.5}$	0.42748	0.08664
Soave‡	b	0	$[1 + (0.48 + 1.574\omega - 0.176\omega^2)(1 - T_r^{0.5})]^2$	0.42748	0.08664
Peng-Robinson§	$2b$	$-b^2$	$[1 + (0.37464 + 1.54226\omega - 0.2699\omega^2)(1 - T_r^{0.5})]^2$	0.45724	0.0778

*van der Waal, J. H., *Z. Phys. Chem.*, **5** (1890): 133.

†Redlich, O., and J. N. S. Kwong, *Chem. Rev.*, **44** (1949): 233.

‡Soave, G., *Chem. Eng. Sci.*, **27** (1972): 1197.

§Peng, D. Y., and D. B. Robinson, *Ind. Eng. Chem. Fundam.*, **15** (1976): 59.

Liquids For most liquids, the saturated molar liquid density ρ can be effectively correlated with

$$\rho = \frac{A}{B^{[1+(1-T/C)^D]}} \quad (2-68)$$

adapted from the Rackett prediction equation [Rackett, H. G., *J. Chem. Eng. Data*, **15** (1970): 514]. The regression constants A , B , and D are determined from the nonlinear regression of available data, while C is usually taken as the critical temperature. The liquid density decreases approximately linearly from the triple point to the normal boiling point and then nonlinearly to the critical density (the reciprocal of the critical volume). A few compounds such as water cannot be fit with this equation over the entire range of temperature.

The recommended method for estimation of saturated liquid density for pure organic compounds is the Rackett prediction method.

Recommended Method Rackett method.

Reference: Rackett, H. G., *J. Chem. Eng. Data*, **15** (1970): 514.

Classification: Corresponding states.

Expected uncertainty: 8 percent as purely predictive equation; 2 percent if Z_{RA} (see Description below) or some liquid density data are available.

Applicability: Saturated liquid densities of organic compounds.

Input data: T_c , P_c , and Z_c (or, equivalently, V_c).

Description: A predictive form of the equation is given by

$$\frac{1}{\rho} = V = \left(\frac{RT_c}{P_c} \right) Z_c^q \quad \text{where } q = 1.0 + (1.0 - T_r)^{2.7} \quad (2-69)$$

A modification of the Rackett method by Spencer and Danner [Spencer, C. F., and R. P. Danner, *J. Chem. Eng. Data*, **17** (1972): 236] replaces Z_c with an adjustable parameter Z_{RA}

$$\frac{1}{\rho} = V = \left(\frac{RT_c}{P_c} \right) Z_{RA}^q \quad (2-70)$$

to provide better estimations of liquid density away from the critical point [Eq. (2-70) gives the correct critical density only when $Z_{RA} = Z_c$]. An alternative to this modification when several liquid density data points are available is to replace the 2/7 power in q of Eq. (2-69) with an adjustable parameter. This generally provides good agreement with the experimental values and permits accurate extrapolation of the densities all the way to the critical point.

Example Estimate the saturated liquid density of acetonitrile at 376.69 K.

Required properties: The recommended values from the DIPPR® 801 database are

$$T_c = 545.5 \text{ K} \quad P_c = 4.83 \text{ MPa} \quad Z_c = 0.184$$

Calculate supporting quantities:

$$T_r = (376.69 \text{ K}) / (545.5 \text{ K}) = 0.691$$

$$q = 1 + (1 - 0.691)^{2.7} = 1.715$$

Calculate saturated liquid density from Eq. (2-69):

$$\rho = \left[\frac{4.83 \times 10^6 \text{ Pa}}{\left(8.314 \frac{\text{Pa}\cdot\text{m}^3}{\text{mol}\cdot\text{K}} \right) (545.5 \text{ K})} \right] (0.184)^{-1.715} = 19.42 \frac{\text{kmol}}{\text{m}^3}$$

This estimated value is 16.1 percent above the DIPPR® 801 recommended value of 16.726 kmol/m³.

Calculate ρ_{sat} from Eq. (2-70): Kratzke [Kratzke, H., and S. Muller, *J. Chem. Thermo.*, **17** (1985): 151] reported an experimental density of 18.919 kmol/m³ at 298.08 K. Use of this experimental value in Eq. (2-70) to calculate Z_{RA} gives

$$T_r = (298.08 \text{ K}) / (545.5 \text{ K}) = 0.546 \quad q = 1 + (1 - 0.546)^{2.7} = 1.798$$

$$Z_{RA} = \left[\frac{4.83 \times 10^6 \text{ Pa}}{\left(8.314 \frac{\text{Pa}\cdot\text{m}^3}{\text{mol}\cdot\text{K}} \right) (545.5 \text{ K}) \left(18.919 \frac{\text{kmol}}{\text{m}^3} \right)} \right]^{1/1.798} = 0.202$$

$$\rho = \left[\frac{4.83 \times 10^6 \text{ Pa}}{\left(8.314 \frac{\text{Pa}\cdot\text{m}^3}{\text{mol}\cdot\text{K}} \right) (545.5 \text{ K})} \right] (0.202)^{-1.715} = 16.577 \frac{\text{kmol}}{\text{m}^3}$$

The value obtained by the modified Rackett method is 0.9 percent below the DIPPR® 801 recommended value. Note, however, that with $Z_{RA} = 0.202$, Eq. (2-70) gives $\rho_c = 5.28$ kmol/m³ as opposed to the DIPPR® 801 recommended value of 5.79 kmol/m³. If the power is regressed from the Kratzke density, one obtains $q_1 = 0.452$ and $\rho = 15.68$ kmol/m³ (4 percent below the experimental value), while still retaining $\rho_c = 5.79$ kmol/m³.

Solids Solid density data are sparse and usually available only within a narrow temperature range. For most solids, density decreases approximately linearly with increasing temperature. Prediction of solid densities is an inexact science, but reasonable correlation has been found between the density of the liquid phase at the triple point and the solid that is stable at the triple point conditions.

Recommended Method Goodman method.

Reference: Goodman, B. T., et al., *J. Chem. Eng. Data*, **49** (2004): 1512.

Classification: Empirical correlation.

Expected uncertainty: 6 percent.

Applicability: Organic compounds; applicable to the stable solid phase at the triple point temperature T_i , to either the next solid-phase transition temperature or to approximately $0.3T_i$.

Input data: Liquid density at the triple point.

Description: The density for the solid phase that is stable at the triple point has been correlated as a function of temperature and the liquid density at T_i :

$$\rho_s = \left(1.28 - 0.16 \frac{T}{T_i} \right) \rho_L(T_i) \quad (2-71)$$

Example Estimate the density of solid naphthalene at 281.46 K.

Required properties: The recommended values from the DIPPR® 801 database for T_i and the liquid density at T_i are

$$T_i = 353.43 \text{ K} \quad \rho_L(T_i) = 7.6326 \text{ kmol/m}^3$$

From Eq. (2-71):

$$\rho_s = \left(1.28 - 0.16 \frac{281.46 \text{ K}}{353.43 \text{ K}} \right) \left(7.6326 \frac{\text{kmol}}{\text{m}^3} \right) = 8.797 \frac{\text{kmol}}{\text{m}^3}$$

The estimated value is 4.3 percent lower than the DIPPR® 801 recommended value of 9.1905 kmol/m³.

Mixtures Both liquid and vapor densities can be estimated using pure-component CS and EoS methods by treating the fluid as a pseudo-pure component with effective parameters calculated from the pure-component parameters and using ad hoc mixing rules.

To apply the Lee-Kesler CS method to mixtures, pseudo-pure fluid constants are required. One of the simplest set of mixing rules for these quantities is [Prausnitz, J. M., and R. D. Gunn, *AIChE J.*, **4** (1958): 430, 494; Joffe, J., *Ind. Eng. Chem. Fundam.*, **10** (1971): 532]:

$$\bar{T}_c = \sum_{i=1}^C x_i T_{c,i} \quad (2-72)$$

$$\bar{P}_c = \frac{\sum_{i=1}^C x_i Z_{c,i}}{\sum_{i=1}^C x_i V_{c,i}} \bar{RT}_c \quad (2-73)$$

$$\bar{\omega} = \sum_{i=1}^C x_i \omega_i \quad (2-74)$$

The procedures are identical to those for pure components with the replacement of T_c , P_c , and ω with the effective mixture values calculated by using these equations.

To use a cubic EoS for a mixture, mixing rules are used to calculate effective mixture parameters in terms of the pure-component values. Although there are more complex mixing rules available that may improve prediction accuracy, the simplest forms are recommended here for their simplicity and reasonable accuracy without adjustable parameters:

$$\bar{b} = \sum_{i=1}^C x_i b_i \quad (2-75)$$

$$\bar{a}\bar{\alpha} = \left[\sum_{i=1}^C x_i (a_i \alpha_i)^{1/2} \right]^2 \quad (2-76)$$

Mixture calculations are then identical to the pure-component calculations using these effective mixture parameters for the pure-component $a\alpha$ and b values.

The actual mixture second virial coefficient B_m is related to the pure-component values by

$$B_m = \sum_{i=1}^C \sum_{j=1}^C x_i x_j B_{ij} \quad \text{where} \quad B_{ii} = B_i \quad (2-77)$$

This requires calculation of all possible binary pair interaction virials (B_{ij} , $i \neq j$) for the mixture. Again the pure-component methods can be used to provide estimates of these values by using the following combining rules:

$$T_{c,ij} = \sqrt{T_{c,i} T_{c,j}} \quad V_{c,ij} = \left(\frac{V_{c,i}^{1/3} + V_{c,j}^{1/3}}{2} \right)^3 \quad Z_{c,ij} = \frac{Z_{c,i} + Z_{c,j}}{2} \quad (2-78)$$

$$\omega_{ij} = \frac{\omega_i + \omega_j}{2} \quad P_{c,ij} = \frac{Z_{c,ij} RT_{c,ij}}{V_{c,ij}} \quad (2-79)$$

These interaction parameters are used in place of the corresponding pure-component parameters to determine the B_{ij} values.

The modified Rackett method has also been extended to liquid mixtures [Spencer, C. F., and R. P. Danner, *J. Chem. Eng. Data*, **17** (1972): 236; Li, C. C., *Can. J. Chem. Eng.*, **19** (1971): 709]:

$$T_{c,ij} = \sqrt{T_{c,i} T_{c,j}} \quad \phi_i = \frac{x_i V_{c,i}}{\sum_{j=1}^C x_j V_{c,j}} \quad \bar{T}_c = \sum_{i=1}^C \sum_{j=1}^C \phi_i \phi_j T_{c,ij} \quad (2-80)$$

Recommended Method Spencer-Danner-Li mixing rules with Rackett equation.

References: Spencer, C. F., and R. P. Danner, *J. Chem. Eng. Data*, **17** (1972): 236; Li, C. C., *Can. J. Chem. Eng.*, **19** (1971): 709.

Classification: Corresponding states.

Expected uncertainty: About 7 percent on average; higher near the T_c of any of the components.

Applicability: Saturated (at the bubble point) liquid mixtures.

Input data: T_c , V_c , and x_i .

Description: The predictive form of the equation is given by

$$\frac{1}{\rho} = V = R \left(\sum_{i=1}^C \frac{x_i T_{c,i}}{P_{c,i}} \right) \bar{Z}_{RA}^q \quad q = 1.0 + (1.0 - T_r)^{2/7} \quad (2-81)$$

where

$$\bar{Z}_{RA} = 0.29056 - 0.08775 \sum_{i=1}^C x_i \omega_i \quad \text{and} \quad T_r = \frac{T}{T_c} \quad (2-82)$$

Example Estimate the saturated liquid density of a liquid mixture of 50 mol % ethane(1) and 50 mol % *n*-decane(2) at 377.6 K.

Required properties: The recommended values from the DIPPR® 801 database for the required properties are as follows:

	T_c /K	V_c /(m ³ ·kmol ⁻¹)	P_c /bar	ω
Ethane	305.32	0.1455	48.72	0.0995
Decane	617.7	0.617	21.1	0.4923

Auxiliary quantities from Eq. (2-80):

$$\phi_1 = \frac{(0.5)(0.1455)}{(0.5)(0.1455) + (0.5)(0.617)} = 0.191; \quad \phi_2 = 0.809$$

$$T_{c,12} = \sqrt{(305.32 \text{ K})(617.7 \text{ K})} = 434.3 \text{ K}$$

$$\begin{aligned} \frac{\bar{T}_c}{\text{K}} &= \phi_1^2 T_{c,1} + 2\phi_1 \phi_2 T_{c,12} + \phi_2^2 T_{c,2} \\ &= (0.191)^2 (305.32) + (2)(0.191)(0.809)(434.3) + (0.809)^2 (617.7) \end{aligned}$$

$$\bar{T}_c = 549.68 \text{ K}$$

Calculations from Eqs. (2-81) and (2-82):

$$T_r = (377.6 \text{ K}) / (549.68 \text{ K}) = 0.687$$

$$q = 1 + (1 - 0.687)^{2/7} = 1.718$$

$$\bar{Z}_{RA} = 0.29056 - 0.08775[(0.5)(0.0995) + (0.5)(0.4923)] = 0.2646$$

$$\begin{aligned} V &= \left(0.08314 \frac{\text{m}^3 \cdot \text{bar}}{\text{K} \cdot \text{kmol}} \right) \left[\frac{(0.5)(305.32 \text{ K})}{48.72 \text{ bar}} + \frac{(0.5)(617.7 \text{ K})}{21.1 \text{ bar}} \right] (0.2646)^{1.718} \\ &= 0.151 \frac{\text{m}^3}{\text{kmol}} \end{aligned}$$

The experimental value [Reamer, H. H., and B. H. Sage, *J. Chem. Eng. Data*, **7** (1962): 161] is 0.149 m³/kmol, and the error in the estimated value is 1.3 percent.

VISCOSITY

Viscosity is defined as the shear stress per unit area at any point in a confined fluid, divided by the velocity gradient in the direction perpendicular to the direction of flow. The *absolute viscosity* η is the shear stress at a point, divided by the velocity gradient at that point. The SI unit of viscosity is Pa·s [1 kg/(m·s)], but the cgs unit of poise (P) [1 g/(cm·s)] is also commonly used. Because many common fluids have viscosities on the order of 0.01 P, the unit of centipoise (cP) is also frequently used (1 cP = 1 mPa·s). The *kinematic viscosity* ν is defined as the ratio of the absolute viscosity to density at the same temperature and pressure. The SI unit for ν is m²/s, but again cgs units are very common and ν is often given in stokes (St) (1 cm²/s) or centistokes (cSt) (0.01 cm²/s).

Gases Experimental data for gases and vapors at low density are often correlated with

$$\eta^0 = \frac{AT^B}{1 + C/T + D/T^2} \quad (2-83)$$

Over smaller temperature ranges, parameters C and D may not be necessary as $\ln \eta$ is often reasonably linear with $\ln T$. Care should be taken in extrapolating using Eq. (2-83) as there can be unintended mathematical poles where the denominator approaches zero.

Numerous methods have been developed for estimation of vapor viscosity. For nonpolar vapors, the Yoon-Thodos CS method works well, but for polar fluids the Reichenberg method is preferred. Both methods are illustrated below.

Recommended Method Yoon-Thodos method.

Reference: Yoon, P., and G. Thodos, *AIChE J.*, **16** (1970): 300.

Classification: Corresponding states.

Expected uncertainty: 5 percent.

Applicability: Nonpolar and slightly polar organic vapors.

Input data: T_c , P_c , and M .

Description: The correlation for viscosity as a function of reduced temperature is

$$\frac{\eta^o}{\text{Pa}\cdot\text{s}} = \frac{46.1T_r^{0.618} - 20.4 \exp(-0.449T_r) + 19.4 \exp(-4.058T_r) + 1}{2.173424 \times 10^{11}(T_c/K)^{1/6}(M/\text{g}\cdot\text{mol})^{-1}(P_c/\text{Pa})^{-2/3}} \quad (2-84)$$

Example Estimate the low-pressure vapor viscosity of propane at 353 K.

Required constants: The DIPPR® 801 database recommends the following values:

$$T_c = 369.83 \text{ K} \quad P_c = 4.248 \text{ MPa} \quad M = 44.0956 \text{ g/mol}$$

Reduced temperature:

$$T_r = (353 \text{ K})/(369.83 \text{ K}) = 0.9545$$

Calculation using Eq. (2-84):

$$\frac{\eta^o}{\text{Pa}\cdot\text{s}} = \frac{(46.1)(0.9545)^{0.618} - 20.4 \exp[-0.449(0.9545)] + 19.4 \exp[-4.058(0.9545)] + 1}{(2.173424 \times 10^{11})(369.83)^{-1/2}(44.0956)^{-1/2}(4.248 \times 10^6)^{-2/3}}$$

$$= 9.84 \times 10^{-6}$$

The estimated value is 1.5 percent higher than the DIPPR® 801 recommended value of 9.70×10^{-6} Pa·s.

Recommended Method Reichenberg method.

Reference: Reichenberg, D., *AIChE J.*, **21** (1975): 181.

Classification: Group contributions and corresponding states.

Expected uncertainty: 5 percent.

Applicability: Nonpolar and polar organic and inorganic vapors.

Input data: T_c , P_c , M , μ , and molecular structure.

Description: The temperature dependence of the viscosity is given by

$$\frac{\eta^o}{\text{Pa}\cdot\text{s}} = \frac{AT_r^2}{[1 + 0.36T_r(T_r - 1)]^{1/6}} \left[\frac{1 + 270(\mu_r^*)^4}{T_r + 270(\mu_r^*)^4} \right] \quad (2-85)$$

where the parameter A is determined from group contributions and the modified reduced dipole μ_r^* is found from

$$\mu_r^* = 52.46\mu_r \quad (2-86)$$

and Eq. (2.62).

For organic compounds, A is found from the group values C_i , listed in Table 2-355, using

$$A = 10^{-7} \frac{\left[\frac{M}{(\text{kg}/\text{kmol})} \right]^{1/2} (T_c/K)}{\sum_{i=1}^N n_i C_i} \quad (2-87)$$

For inorganic gases, A is obtained from

$$A = 1.6104 \times 10^{-10} \left[\left(\frac{M}{\text{g/mol}} \right)^{1/2} \left(\frac{P_c}{\text{Pa}} \right)^{2/3} \left(\frac{T_c}{\text{K}} \right)^{-1/6} \right] \quad (2-88)$$

TABLE 2-355 Reichenberg* Group Contribution Values

Group	C_i	Group	C_i
—CH ₃	9.04	—F	4.46
>CH ₂	6.47	—Cl	10.06
>CH—	2.67	—Br	12.83
>C<	-1.53	—OH alcohol	7.96
═CH ₂	7.68	>O	3.59
═CH—	5.53	>C═O	12.02
>C═	1.78	—CHO	14.02
≡CH	7.41	—COOH	18.65
≡C—	5.24	—COO— or HCOO—	13.41
>CH ₂ ring	6.91	—NH ₂	9.71
>CH— ring	1.16	>NH	3.68
>C< ring	0.23	—N— ring	4.97
═CH— ring	5.90	—CN	18.13
>C═ ring	3.59	>S ring	8.86

*Reichenberg, D., *AIChE J.*, **21** (1975): 181.

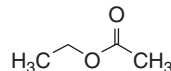
Example Estimate the low-pressure vapor viscosity of ethyl acetate at 401.25 K.

Required constants: The DIPPR® 801 database recommends the following values:

$$M = 88.1051 \text{ g/mol} \quad T_c = 523.3 \text{ K} \quad P_c = 3.88 \text{ MPa} \quad \mu = 1.78 \text{ D}$$

Supporting quantities:

Structural groups:



Group	n_i	C_i	Contribution
—CH ₃	2	9.04	18.08
>CH ₂	1	6.47	6.47
—COO—	1	13.41	13.41
Total			37.96

$$T_r = (401.25 \text{ K})/(523.3 \text{ K}) = 0.767$$

From Eqs. (2-62) and (2-86):

$$\mu_r^* = 52.46 \frac{(1.78)^2(38.8)}{(523.3)^2} = 0.024$$

From Eq. (2-87):

$$A = 10^{-7} \frac{(88.1051)^{1/2}(523.3)}{37.96} = 1.294 \times 10^{-5}$$

Calculation using Eq. (2-84):

$$\frac{\eta^o}{\text{Pa}\cdot\text{s}} = \frac{(1.294 \times 10^{-5})(0.767)^2}{[1 + (0.36)(0.767)(0.767 - 1)]^{1/6}} \frac{1 + (270)(0.024)^4}{0.767 + (270)(0.024)^4} = 1.003 \times 10^{-5}$$

The estimated value is 1.5 percent lower than the DIPPR® 801 recommended value of 1.018×10^{-5} Pa·s.

The dependence of viscosity upon pressure is principally a density effect. Estimation of vapor viscosity at elevated pressures is commonly done by correlating density deviations from the low-pressure values, which are in turn estimated by using the procedures mentioned above. Several methods are available, but the method developed by Jossi et al. and extended to polar fluids by Stiel and Thodos is relatively accurate and easy to apply.

Recommended Method Jossi-Stiel-Thodos Method.

References: Stiel, L. I., and G. Thodos, *AIChE J.*, **10** (1964): 26;

Jossi, J. A., L. I. Stiel, and G. Thodos, *AIChE J.*, **8** (1962): 59.

Classification: Empirical correlation and corresponding states.

Expected uncertainty: 9 percent—often less for nonpolar gases, larger for polar gases.

Applicability: Nonassociating gases; $\rho_r < 2.6$.

Input data: M , T_c , P_c , Z_c , μ_r^* , η^o (low-pressure viscosity at same T may be estimated by using methods given above), and ρ (may be calculated from T and P by using density methods given above).

2-506 PHYSICAL AND CHEMICAL DATA

Description: Deviation of η from the low-pressure value η^o is given by one of the following correlations depending upon its polarity and reduced density range:

For nonpolar gases, $0.1 < \rho_r < 3.0$:

$$\left[\left(\frac{\eta - \eta^o}{\text{mPa}\cdot\text{s}} \right) \xi + 1 \right]^{1/4} = 1.0230 + 0.23364\rho_r - 0.58533\rho_r^2 - 0.40758\rho_r^3 + 0.093324\rho_r^4 \quad (2-89)$$

For polar gases, $\rho_r \leq 0.1$:

$$\left(\frac{\eta - \eta^o}{\text{mPa}\cdot\text{s}} \right) \xi = 1.656\rho_r^{1.111} \quad (2-90)$$

For polar gases, $0.1 < \rho_r \leq 0.9$:

$$\left(\frac{\eta - \eta^o}{\text{mPa}\cdot\text{s}} \right) \xi = 0.0607(9.045\rho_r + 0.63)^{1.739} \quad (2-91)$$

For polar gases, $0.9 < \rho_r \leq 2.2$:

$$\log \left\{ 4 - \log \left[\left(\frac{\eta - \eta^o}{\text{mPa}\cdot\text{s}} \right) \xi \right] \right\} = 0.6439 - 0.1005\rho_r \quad (2-92)$$

For polar gases, $2.2 < \rho_r \leq 2.6$:

$$\log \left\{ 4 - \log \left[\left(\frac{\eta - \eta^o}{\text{mPa}\cdot\text{s}} \right) \xi \right] \right\} = 0.6439 - 0.1005\rho_r - 0.000475(\rho_r^3 - 10.65)^2 \quad (2-93)$$

where $\rho_r = P_c/(Z_cRT_c)$ and

$$\xi = 2173.4 \left(\frac{T_c}{\text{K}} \right)^{1/6} \left(\frac{M}{\text{kg/kmol}} \right)^{-1/2} \left(\frac{P_c}{\text{MPa}} \right)^{-2/3} \quad (2-94)$$

Example Estimate the vapor viscosity of CO_2 at 350 K and 20 MPa if $\eta^o = 0.0174$ mPa·s and $Z = 0.4983$ (estimated from Lee-Kesler method, see section on density).

Required properties: From the DIPPR® 801 database,

$$M = 44.01 \text{ kg/kmol} \quad T_c = 304.21 \text{ K} \quad P_c = 7.383 \text{ MPa} \\ Z_c = 0.274 \quad \mu = 0 \text{ D (nonpolar)}$$

Auxiliary quantities:

$$\xi = 2173.4(304.21)^{1/6}(44.01)^{-1/2}(7.383)^{-2/3} = 224.1$$

$$\rho_r = \frac{7.383 \text{ MPa}}{0.274[8.314 \text{ m}^3\text{Pa}/(\text{K}\cdot\text{mol})](304.21 \text{ K})} = 10.654 \frac{\text{kmol}}{\text{m}^3}$$

$$\rho_r = \frac{\rho}{\rho_c} = \frac{P}{ZRT\rho_c} = \frac{20 \text{ MPa}}{0.4983[8.314 \text{ m}^3\text{Pa}/(\text{K}\cdot\text{mol})](350 \text{ K})(10.654 \text{ m}^3\cdot\text{kmol})} \\ = 1.295$$

Calculation using Eq. (2-89) for nonpolar fluids:

$$\left[224.1 \left(\frac{\eta - \eta^o}{\text{mPa}\cdot\text{s}} \right) + 1 \right]^{1/4} = 1.0230 + 0.23364(1.295) + 0.58533(1.295)^2 \\ - 0.40758(1.295)^3 + 0.093324(1.295)^4 = 1.684 \\ \eta = \frac{1.684^4 - 1}{224.1} \text{ mPa}\cdot\text{s} + 0.0174 \text{ mPa}\cdot\text{s} = 0.0489 \text{ mPa}\cdot\text{s}$$

This differs from the experimental value of 0.0473 mPa·s by 3.4 percent.

Liquids Liquid viscosity can be correlated as a function of temperature for low pressures. Usually the correlation is based on the Andrade equation [Andrade, E. N. da C., *Nature*, **125** (1930): 309]

$$\ln \eta = A + \frac{B}{T} \quad (2-95)$$

or an extension of it. For example, the DIPPR® 801 database uses the equation

$$\ln \eta = A + \frac{B}{T} + C \ln T + DT^E \quad (2-96)$$

which is analogous to the Riedel [Riedel, L., *Chem. Ing. Tech.*, **26** (1954): 83] vapor pressure equation.

Currently the most accurate method for predicting pure liquid viscosity is the following GC method.

Recommended Method Hsu method.

Reference: Hsu, H.-C., Y.-W. Sheu, and C.-H. Tu, *Chem. Eng. J.*, **88** (2002): 27.

Classification: Group contributions.

Expected uncertainty: 20 percent.

Applicability: Organic liquids; $T_r < 0.75$.

Input data: P_c and molecular structure.

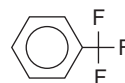
Description: The temperature dependence of the liquid viscosity is given by

$$\ln \left(\frac{\eta}{\text{mPa}\cdot\text{s}} \right) = \sum_{i=1}^N a_i + T \sum_{i=1}^N b_i + \frac{\sum_{i=1}^N c_i}{T^2} + \left(\sum_{i=1}^N d_i \right) \ln \left(\frac{P_c}{\text{bar}} \right) \quad (2-97)$$

where P_c is critical pressure and the coefficients a , b , c , and d are the sum of the group contributions obtained from Table 2-356.

Example Estimate the liquid viscosity of benzotrifluoride at 303.15 K.

Structural information:



Group	Number	a	$100b$	$0.0001c$	d
>C<	1	1.0031	-0.3677	-6.0316	1.1972
(=CH—) _A	5	-0.8570	-0.0098	2.4376	0.1311
(=C<) _A	1	0.7896	-0.0231	-0.9222	0.1928
(—F) ₃	1	1.5394	0.8465	17.8121	-2.9915
Total		-0.9529	0.4067	23.0463	-0.9460

Supporting values:

$$P_c = 32.1 \text{ MPa}$$

Calculation using Eq. (2-97):

$$\frac{\eta}{\text{mPa}\cdot\text{s}} = \exp \left[-0.9529 + (0.004067)(303.15) + \frac{230463}{(303.15)^2} - 0.9460 \ln 32.1 \right] \\ = 0.610$$

The estimated value is 20 percent higher than the DIPPR® 801 recommended value of 0.509 mPa·s.

Liquid Mixtures Almost all methods for estimating liquid mixture viscosity interpolate between the pure-component values at the same temperature. The Grunberg-Nissan [Grunberg, L., and A. H. Nissan, *Nature*, **164** (1949): 799] equation

$$\ln \eta = \sum_i^C x_i \ln \eta_i + \frac{1}{2} \sum_{i=1}^C \sum_{j=1}^C x_i x_j G_{ij} \quad (2-98)$$

is commonly used for nonaqueous mixtures. The parameter G_{ij} generally must be regressed from an experimental mixture viscosity. However, in the case of hydrocarbon mixtures G_{ij} can be set to zero with expected errors in the mixture viscosity of about 15 percent.

TABLE 2-356 Group Contributions for the Hsu et al. Method*

Table-specific nomenclature: R = in nonaromatic ring, A = in aromatic ring, RC = attached to nonaromatic ring, AC = attached to aromatic ring, X = halogen, (-X)_n = n X atoms attached to same C atom

Group	a	100b	0.0001c	d
C, H Groups				
CH ₄	-1.7296	-1.0563	0.8928	-0.0019
-CH ₃	0.0570	-0.2382	0.7556	-0.1765
-CH ₂ -	-0.1497	0.0060	1.4157	0.0751
>CH-	-2.2942	0.4028	4.5094	0.6679
>C<	1.0031	-0.3677	-6.0316	1.1972
=CH ₂	0.9256	-0.2656	0.9860	-0.4417
=CH-	1.3365	0.1612	1.9408	0.2507
=C<	-3.5020	0.4305	3.1287	1.0465
≡CH	87.6040	-0.1106	4.4245	-24.1836
≡C-	-91.6154	-0.0111	0.3265	25.0542
(-CH ₂) _R	6.0416	-0.1778	0.8437	-1.5184
(>CH-) _R	-33.8745	0.7637	7.2433	8.5951
(=CH-) _R cycloalkene	1.2028	-0.0120	2.0143	-0.3677
(>C<) _R spirocycloane	-56.2158	1.7694	19.0452	13.3885
(=CH-) _A	-0.8570	-0.0098	2.4376	0.1311
(=C<) _A cycloalkene	0.7896	-0.0231	-0.9222	0.1928
(=C<) _A bi/terphenyl	2.0973	0.0444	8.1690	-0.4351
(=C<) _A naphthalene	0.4392	0.0683	8.8426	-0.1685
(=C<) _A turpentine	27.3350	1.2165	34.2857	-11.6500
(=C<) _A tetralin	14.2586	-0.8665	-14.7474	-2.7574
O, S Groups				
-OH primary for C<3	5.7852	-0.5310	9.5499	-1.0300
-OH primary for C>2	1.4351	-1.0010	13.8366	0.3418
-OH secondary	-2.6895	-0.3645	29.8404	0.4246
-OH tertiary	-18.5630	2.4275	78.5417	0.9650
(-OH) _{RC}	16.7808	0.8509	77.1759	-6.9285
-OH polyhydric	-0.0125	-0.3634	23.2329	-0.0172
(-OH) _{AC}	-2.0856	0.6362	50.0840	-1.0539
-OH alkoxyalcohol	-2.6991	-0.4377	17.2243	0.7139
-O-	-0.7185	0.0985	2.9405	0.1149
(-O-) _R	-29.8045	-0.2847	-4.3145	8.3131
(-O-) _{AC}	-2.3454	0.0872	6.4296	0.5389
-CHO	-0.8288	-0.2612	3.7241	0.2386
>CO	-2.6622	0.1142	6.7008	0.7348
(>CO) _R	45.9143	-0.2405	3.8828	-12.4994
HCOOH	-2.7291	0.0413	27.4079	0.0002
-COOH for C<7	-4.0451	-0.1841	12.6878	1.1139
-COOH for C>6	-0.6721	-0.1693	20.0309	0.0279
HCOO-	-3.3731	-0.0113	9.4694	0.6071
-COO- for C<8	-0.0635	-0.2162	1.9325	0.4686
-COO- for C>7	-2.5390	0.0006	5.4231	0.8717
>CHO-	-5.4872	1.5834	34.5474	-0.4244
-(CO)-O-(CO)- anhydride	-11.8236	0.0111	7.2831	3.6587
-O-(CO)-O- carbonate	-8.0314	0.2848	9.3746	2.1486
(>NO) _R	-16.9531	1.0614	49.1049	2.8583
-NO ₂	-13.0333	0.1801	12.9392	2.8987
=CHNO ₂	-1.9653	0.1322	15.8672	-0.0701
(-NO ₂) _{AC}	-1.2954	0.0427	12.1837	-0.0948
-S-	-3.2767	0.0779	4.4123	0.9549
-SH primary	-2.1030	-0.0965	6.0066	0.3464
-SH secondary	-0.2481	-0.3285	1.9387	0.1148
-SH tertiary	-12.3498	1.2621	23.1473	1.3950
-CSO- for C<13	-15.2678	0.5248	14.2694	3.7646
-CSO- for C>12	3.7475	-1.2592	-23.9353	0.8329
>SO	-32.8607	0.6232	27.5184	7.7525
N, X Groups				
-NH ₂	-1.1345	-0.2126	7.0544	0.1336
-NH-	-6.9489	-0.1723	5.7804	1.6467
-N<	-2.1403	0.4842	6.1893	0.4718
(-NH ₂) _{AC}	-6.3646	-0.0180	23.2752	1.0653
(-NH-) _{AC}	-1.7592	0.2208	14.9707	0.1171
(-N<) _{AC}	-1.2982	0.5975	14.0415	-0.0031
HCONH ₂	-1.5435	-0.2774	31.8007	0.0001
HCONH-	-8.1097	0.0432	20.9135	1.8795
HCON<	-122.3280	26.4615	394.1670	0.3530
-CONH ₂	-6.7363	0.1316	45.5193	1.2172
-CONH-	8.9977	1.5664	60.8742	-4.6399
-COONH ₂	17.8400	-4.5188	-62.0987	1.2353
-COONH-	-10.1316	0.6712	37.9465	1.9199
(>NH) _R	-0.1589	0.1910	12.0578	-0.0276

TABLE 2-356 Group Contributions for the Hsu et al. Method* (Concluded)

Table-specific nomenclature: R = in nonaromatic ring, A = in aromatic ring, RC = attached to nonaromatic ring, AC = attached to aromatic ring, X = halogen, $(-X)_n = n$ X atoms attached to same C atom

Group	<i>a</i>	100 <i>b</i>	0.0001 <i>c</i>	<i>d</i>
N, X Groups				
(=N→) _R	-4.7601	0.1120	6.98437	0.9719
-C≡N	-2.7194	-0.1324	7.7955	0.6293
(-C≡N) _{AC}	0.9435	-0.0086	8.6310	-0.6443
-Cl primary	-1.7997	-0.3851	3.0118	0.5524
=CHCl	1.5851	-0.1934	3.7798	-0.4748
(-Cl) ₂	-3.0561	-1.0770	0.1882	1.2223
(-Cl) ₃	-1.3357	-0.3220	8.8683	0.1702
(-Cl) ₄	4.2070	-0.4130	13.3194	-1.1972
(-Cl) _{AC}	-0.3083	-0.0623	4.1382	-0.2644
-F primary	-9.4982	0.2607	11.3406	1.8461
(-F) ₂	-10.3980	-1.1189	1.3134	2.6681
(-F) ₃	1.5394	0.8465	17.8121	-2.9915
(-F) _{AC}	0.4079	-0.2352	-0.1505	-0.2893
(-F)(-Cl)	-0.8565	-0.3682	4.6451	-0.0751
(-F)(-Cl) ₂	-3.4552	-0.5629	3.6831	0.3613
(-F) ₂ (-Cl)	54.2824	0.0109	5.9474	-14.5771
(-F) ₂ (-Cl) ₂	-2.1710	0.1403	10.3743	-1.1972
-Br primary	-0.7586	-0.6623	-2.4228	0.7385
-Br secondary	-279.0030	-0.3420	1.4253	73.6293
(-Br) _{AC}	-8.1919	-0.1635	3.0150	0.0621
-I primary	-1.4672	-0.2787	4.3362	0.5635
(-I) _{AC}	70.9918	-0.0245	7.2061	-18.9106
-(CO)-Cl	-2.3300	-0.0470	8.2815	0.4485

*Hsu, H.-C., Y.-W. Sheu, and C.-H. Tu, *Chem. Eng. J.*, **88** (2002): 27

Estimation of liquid mixture viscosity without any mixture data is difficult because the viscosity is strongly affected by large molecular size differences and strong cross interactions between the different types of molecules. Viscosity-composition plots for aqueous mixtures can have maxima or minima, and viscosities for these mixtures are particularly difficult to estimate. The UNIFAC-VISCO method described below can be used to predict liquid viscosity of organic mixtures without any mixture data. It is relatively successful even for large differences in molecular size, but it is currently limited in scope by the small number of group contributions available.

Recommended Method UNIFAC-VISCO method.

Reference: Chevalier, J. L., P. Petrino, and Y. Gaston-Bonhomme, *Chem. Eng. Sci.*, **43** (1988): 1303; Gaston-Bonhomme, Y., P. Petrino, and J. L. Chevalier, *Chem. Eng. Sci.*, **49** (1994): 1799.

Classification: Group contributions.

Expected uncertainty: 20 percent.

Applicability: Organic liquids.

Input data: Molecular structure; pure-component molar volumes and viscosities at the mixture temperature.

Description: The equations for this method are

$$\ln\left(\frac{\eta}{\text{mPa}\cdot\text{s}}\right) = \sum_{i=1}^{\text{comp}} x_i \ln\left(\frac{\eta_i}{\text{mPa}\cdot\text{s}} \cdot \frac{V_i}{V_m}\right) + \frac{g^E}{RT} - \frac{g^E}{RT} \quad (2-99)$$

where V_m is the mixture molar volume and V_i is the pure-component molar volume of component i . The combinatorial and residual excess Gibbs energies are calculated exactly as in the UNIFAC method (see Sec. 13) with the exception that the group interactions Ψ_{mn} are calculated by using

$$\Psi_{mn} = \exp\left(-\frac{\alpha_{mn}}{298.15}\right) \quad (2-100)$$

The interaction parameters α_{mn} are obtained from Table 2-357.

Example Estimate the viscosity of a mixture of 51.13 mol % ethanol(1) and 48.87 mol % benzene(2) at 298.15 K.

Required input: Values from the DIPPR® 801 database for the pure components at 298.15 K are $\eta_1 = 1.0774$ mPa·s, $\eta_2 = 0.5997$ mPa·s, $V_1 = 0.05862$ m³/kmol, and $V_2 = 0.08948$ m³/kmol.

Groups, area fractions, volume fractions:

Group	R	Q	N ₁	N ₂
CH ₃	0.9011	0.8480	1	0
CH ₂	0.6744	0.5400	1	0
CH _{ar}	0.5313	0.4000	0	6
OH	1.0000	1.2000	1	0

Group	r ₁	q ₁	r ₂	q ₂
CH ₃	0.9011	0.848	0	0
CH ₂	0.6744	0.54	0	0
CH _{ar}	0	0	3.1878	2.4
OH	1	1.2	0	0
Total	2.5755	2.588	3.1878	2.4

where in the above table

$$q_i = \sum_{k=1}^N N_{i,k} Q_k \quad \text{and} \quad r_i = \sum_{k=1}^N N_{i,k} R_k$$

$$\theta_1 = \frac{x_1 q_1}{\sum_{i=1}^4 x_i q_i} = \frac{(0.5113)(2.588)}{(0.5113)(2.588) + (0.4887)(2.4)} = 0.53 \quad \theta_2 = 0.47$$

$$\phi_1 = \frac{x_1 r_1}{\sum_{i=1}^4 x_i r_i} = \frac{(0.5113)(2.5755)}{(0.5113)(2.5755) + (0.4887)(3.1878)} = 0.458 \quad \phi_2 = 0.542$$

UNIFAC combinatorial term:

$$\frac{g^E}{RT} = \sum_{i=1}^2 x_i \ln \frac{\phi_i}{x_i} + 5 \sum_{i=1}^2 x_i q_i \ln \frac{\theta_i}{\phi_i} = 0.124$$

TABLE 2-357 UNIFAC-VISCO* Group Interaction Parameters α_{mn}

<i>m/n</i>	CH ₂	CH ₃	CH _{2cy}	CH _{ar}	Cl	CO	COO	OH	CH ₃ OH
CH ₂	0	66.53	224.9	406.7	60.30	859.5	1172.0	498.6	-219.7
CH ₃	-709.5	0	-130.7	-119.5	82.41	11.86	-172.4	594.4	-228.7
CH _{2cy}	-538.1	187.3	0	8.958	251.4	-125.4	-165.7	694.4	-381.53
CH _{ar}	-623.7	237.2	50.89	0	177.2	128.4	-49.85	419.3	-88.81
Cl	-710.3	375.3	-163.3	-139.8	0	-404.3	-525.4	960.2	-165.4
CO	586.2	-21.56	740.6	-117.9	-4.145	0	29.20	221.5	55.52
COO	541.6	-44.25	416.2	-36.17	240.5	22.92	0	186.8	69.62
OH	-634.5	1209.0	-138	197.7	195.7	664.1	68.35	0	416.4
CH ₃ OH	-526.1	653.1	751.3	51.31	-140.9	-22.59	-286.2	-23.91	0

*Chevalier, J. L., P. Petrino, and Y. Gaston-Bonhomme, *Chem. Eng. Sci.*, **43** (1988): 1303; Gaston-Bonhomme, Y., P. Petrino, and J. L. Chevalier, *Chem. Eng. Sci.*, **49** (1994): 1799.

Group interactions:

<i>m/n</i>	α_{mn}			
group	CH ₃	CH ₂	CH _{ar}	OH
CH ₃	0	-709.5	-119.5	594.4
CH ₂	66.53	0	406.7	498.6
CH _{ar}	237.2	-623.7	0	419.3
OH	1209	-634.5	197.7	0

<i>m/n</i>	Ψ_{mn}			
group	CH ₃	CH ₂	CH _{ar}	OH
CH ₃	1.000	10.801	1.493	0.136
CH ₂	0.800	1.000	0.256	0.188
CH _{ar}	0.451	8.100	1.000	0.245
OH	0.017	8.399	0.515	1.000

The α_{mn} values were obtained from Table 2-357, and Ψ_{mn} values were calculated from Eq. (2-100).

Group fractions in the mixture:

Group	<i>N</i>	<i>X</i>	<i>XQ</i>	Θ	$\ln \gamma$
CH ₃	0.5113	0.1145	0.097083	0.17370	0.293
CH ₂	0.5113	0.1145	0.061822	0.11061	-0.873
CH _{ar}	2.9322	0.6565	0.262618	0.46988	0.066
OH	0.5113	0.1145	0.137382	0.24581	1.077
Sum	4.4661		0.558905		

$$\text{Here } \Theta_m = \frac{X_m Q_m}{\sum_{i=1}^4 X_i Q_i}$$

and

$$\ln \gamma_m = Q_m \left[1 - \ln \left(\sum_{i=1}^4 \Theta_i \Psi_{i,m} \right) - \sum_{j=1}^4 \frac{\Theta_j \Psi_{m,j}}{\sum_{j=1}^4 \Theta_j \Psi_{j,j}} \right]$$

Group fractions in pure components:

Ethanol					
Group	<i>N</i>	<i>X</i>	<i>XQ</i>	Θ	$\ln \gamma$
CH ₃	1	0.3333	0.283	0.3277	0.5306
CH ₂	1	0.3333	0.180	0.2087	-0.9405
CH _{ar}	0	0.0000	0.000	0.0000	0.2095
OH	1	0.3333	0.400	0.4637	0.6179
Sum	3		0.863		

Benzene					
Group	<i>N</i>	<i>X</i>	<i>XQ</i>	Θ	$\ln \gamma$
CH ₃	0	0	0	0	0.257
CH ₂	0	0	0	0	-0.728
CH _{ar}	6	1	0.4	1	0.000
OH	0	0	0	0	2.270
Sum	6		0.4		

Here Θ and $\ln \gamma$ are defined by the same equations shown above for the mixture groups.

UNIFAC residual term:

$$\frac{g^E}{RT} = \sum_{i=1}^2 x_i \left[\sum_{m=1}^4 N_{m,i} (\ln \gamma_m - \ln \gamma_{m,i}) \right] = 0.3425$$

where N_m and $\ln \gamma_m$ refer to the mixture and $N_{m,i}$ and $\ln \gamma_{m,i}$ refer to the pure-component values.

Mixture volume:

$$V_m = \sum_{i=1}^2 x_i V_i = 0.5113 \left(\frac{0.05862 \text{ m}^3}{\text{kmol}} \right) + 0.4887 \left(\frac{0.08948 \text{ m}^3}{\text{kmol}} \right) = 0.07370 \frac{\text{m}^3}{\text{kmol}}$$

Using Eq. (2-99):

$$\ln \left(\frac{\eta}{\text{mPa}\cdot\text{s}} \right) = 0.5113 \ln \left[1.0774 \left(\frac{0.05862}{0.07370} \right) \right] + 0.4887$$

$$\ln \left[0.5997 \left(\frac{0.08948}{0.07370} \right) \right] + 0.124 - 0.3425 = -0.4523$$

$$\eta = \exp(-0.4523) \text{ mPa}\cdot\text{s} = 0.636 \text{ mPa}\cdot\text{s}$$

The estimated value is 6.6 percent below the reported experimental value of 0.681 mPa·s [Kouris, S., and C. Panayiotou, *J. Chem. Eng. Data*, **34** (1989): 200].

THERMAL CONDUCTIVITY

Thermal conductivity k is a measure of the rate at which heat conducts through the material and is defined as the proportionality constant in Fourier's law of heat conduction that relates the gradient of temperature to the heat flux or flow per unit area. In SI units, it has the units of W/(m·K). The conduction mechanism in low-density media, gases,

2-510 PHYSICAL AND CHEMICAL DATA

is primarily via molecular collisions, and k increases with increasing temperature (increasing molecular velocity). In dense media such as liquids, the energy transfer by conduction occurs more efficiently through the attractive intermolecular potential wells between the molecules than through collisions. As a result, liquid thermal conductivity generally decreases with increasing temperature (except for water, aqueous solutions, and a few multihydroxy and multiamine compounds), corresponding to the decrease in density with increased temperature. Below or near the normal boiling point, the temperature dependence of liquid thermal conductivity is nearly linear for modest temperature ranges and can be represented by

$$k = A - BT \quad (2-101)$$

where B is generally in the range of 1×10^{-4} to 3×10^{-4} W/(m·K²).

Gases Methods for estimating low-pressure gas thermal conductivities are based on kinetic theory and generally correlate the dimensionless group $kM/\eta C_v$ (M = molecular weight, η = viscosity, C_v = isochoric heat capacity) known as the Eucken factor. The method of Stiel and Thodos is recommended for pure nonpolar compounds, and the method of Chung is recommended for pure polar compounds.

Recommended Method Stiel-Thodos method.

Reference: Stiel, L. I., and G. Thodos, *AIChE J.*, **10** (1964): 26.

Classification: Empirical extension of theory.

Expected uncertainty: 15 percent.

Applicability: Pure nonpolar gases at low pressure.

Input data: M , T_c , η , and C_v .

Description: The following equations may be used depending upon the molecular shape:

$$\frac{kM}{\eta C_v} = 2.5 \quad \text{monatomic} \quad (2-102)$$

$$\frac{kM}{\eta C_v} = 1.30 + \left(\frac{R}{C_v}\right) \left(1.7614 - \frac{0.3523}{T_r}\right) \quad \text{linear molecules} \quad (2-103)$$

$$\frac{kM}{\eta C_v} = 1.15 + 2.033 \left(\frac{R}{C_v}\right) \quad \text{nonlinear molecules} \quad (2-104)$$

where η = viscosity at same conditions as desired for k . *Note:* Because this method is only applicable at low pressures, C_v may be calculated as $C_p - R$, where C_p is the ideal gas isobaric heat capacity.

Example Estimate the low-pressure thermal conductivity of toluene vapor at 500 K.

Required properties from the DIPPR® 801 database:

$$T_c = 591.75 \text{ K} \quad M = 92.138 \text{ g/mol} \quad \eta(500 \text{ K}) = 1.1408 \times 10^{-5} \text{ Pa}\cdot\text{s}$$

$$C_v = C_p - R = (170.78 - 8.314) \text{ J/(mol}\cdot\text{K)} = 162.47 \text{ J/(mol}\cdot\text{K)}$$

Auxiliary quantities:

$$T_r = 500/591.75 = 0.845 \quad R/C_v = (8.314)/(162.47) = 0.0512$$

From Eq. (2-104):

$$k = [1.15 + (2.033)(0.0512)] \left[\frac{(1.1408 \times 10^{-5} \text{ Pa}\cdot\text{s}) \left(\frac{162.47 \text{ J}}{\text{mol}\cdot\text{K}} \right)}{92.138 \frac{\text{g}}{\text{mol}}} \right] = 25.2 \frac{\text{mW}}{\text{m}\cdot\text{K}}$$

The estimated value is 18 percent below the DIPPR® 801 recommended value of 30.76 mW/(m·K).

Recommended Method Chung-Lee-Starling method.

Reference: Chung, T.-H., L. L. Lee, and K. E. Starling, *Ind. Eng. Chem. Fundam.*, **23** (1984): 8.

Classification: Corresponding states.

Expected uncertainty: 15 percent.

Applicability: Pure organic gases at low pressure.

Input data: C_v , ω , T_c , M , and η .

Description: The following equations apply:

$$\frac{kM}{\eta C_v} = 3.75 \Psi \left(\frac{R}{C_v} \right) \quad (2-105)$$

$$\Psi = 1 + \alpha \left(\frac{0.215 + 0.28288\alpha - 1.061\beta + 0.26665\gamma}{0.6366 + \beta\gamma + 1.061\alpha\beta} \right) \quad (2-106)$$

$$\alpha = \frac{C_v}{R} - 1.5 \quad \beta = 0.7862 - 0.7109\omega + 1.3168\omega^2$$

$$\gamma = 2.0 + 10.5T_r^2 \quad (2-107)$$

Example Estimate the low-pressure thermal conductivity of naphthalene vapor at 500 K.

Required properties from the DIPPR® 801 database:

$$T_c = 748.4 \text{ K} \quad M = 128.17 \text{ g/mol} \quad \omega = 0.30203$$

$$\eta(500 \text{ K}) = 1.0173 \times 10^{-5} \text{ Pa}\cdot\text{s}$$

$$C_v = C_p - R = (219.82 - 8.314) \text{ J/(mol}\cdot\text{K)} = 211.51 \text{ J/(mol}\cdot\text{K)}$$

Auxiliary quantities [Eqs. (2-106) and (2-107)]:

$$T_r = 500/748.4 = 0.6681 \quad R/C_v = (8.314)/(211.51) = 0.0393$$

$$\gamma = 2.0 + (10.5)(0.6681)^2 = 6.6866 \quad \alpha = (0.0393)^{-1} - 1.5 = 23.9388$$

$$\beta = 0.7862 - (0.7109)(0.30203) + (1.3168)(0.30203)^2 = 0.6916$$

$$\Psi = 1 + 23.9388$$

$$\times \left[\frac{0.215 + 0.28288(23.9388) - 1.061(0.6916) + 0.26665(6.6866)}{0.6366 + 0.6916(6.6866) + 1.061(23.9388)(0.6916)} \right]$$

$$= 9.4273$$

From Eq. (2-105):

$$k = (3.75)(9.4273) \left[\frac{(1.1408 \times 10^{-5} \text{ Pa}\cdot\text{s}) \left(\frac{8.314 \text{ J}}{\text{mol}\cdot\text{K}} \right)}{128.17 \frac{\text{g}}{\text{mol}}} \right] = 23.33 \frac{\text{mW}}{\text{m}\cdot\text{K}}$$

The estimated value is 1.0 percent above the DIPPR® 801 recommended value of 23.09 mW/(m·K).

Liquids The Baroncini method provides accurate liquid thermal conductivity estimates if the compound clearly belongs to one of the specific families designated by the correlation. The Sastri-Rao method is recommended for other specific families as listed in the discussion of the method given below. As a general method for estimating thermal conductivity of pure liquids at ambient pressure for all other compounds, the Missenard method is recommended.

Recommended Method Baroncini method.

Reference: Baroncini, C., et al., *Int. J. Thermophys.*, **2** (1981): 21.

Classification: Empirical correlation.

Expected uncertainty: 10 percent.

Applicability: Particularly accurate for the following families: acetates, aliphatic ethers, halogenated compounds, dicarboxylic acids, ketones, aliphatic alcohols, aliphatic acids, propionates and butyrates, and unsaturated aliphatic esters.

Input data: M , T_b (normal boiling point), T_c .

Description:

$$\frac{k}{\text{W/(m}\cdot\text{K)}} = A \left(\frac{T_b}{K} \right)^\alpha \left(\frac{M}{\text{g/mol}} \right)^\beta \left(\frac{T_c}{K} \right)^{-\gamma} \frac{(1 - T_r)^{0.38}}{T_r^{1/6}} \quad (2-108)$$

where A , α , β , and γ are obtained from Table 2-358.

TABLE 2-358 Correlation Parameters for Baroncini et al. Method^a for Estimation of Thermal Conductivity

Family	A	α	β	γ
Saturated hydrocarbons	0.00350	1.2	0.5	0.167
Olefins	0.0361	1.2	1	0.167
Cycloparaffins	0.0310	1.2	1	0.167
Aromatics	0.0346	1.2	1	0.167
Alcohols	0.00339	1.2	0.5	0.167
Organic acids	0.00319	1.2	0.5	0.167
Ketones	0.00383	1.2	0.5	0.167
Esters	0.0415	1.2	1	0.167
Ethers	0.0385	1.2	1	0.167
Refrigerants				
R20, R21, R22, R23	0.562	0	0.5	-0.167
Others	0.494	0	0.5	-0.167

^aBaroncini, C., et al., *Int. J. Thermophys.*, **2** (1981): 21.

Example Estimate the thermal conductivity of liquid *p*-cresol at 400 K. Required properties from DIPPR[®] 801 database:

$$M = 108.1378 \text{ g/mol} \quad T_c = 704.65 \text{ K} \quad T_b = 475.133 \text{ K}$$

Auxiliary properties:

$$T_r = T/T_c = (400 \text{ K})/(704.65 \text{ K}) = 0.5677$$

From Table 2-358 for alcohols:

$$A = 0.00339 \quad \alpha = 1.2 \quad \beta = \frac{1}{2} \quad \gamma = 0.167$$

From Eq. (2-108):

$$\frac{k}{W/(m \cdot K)} = (0.00339)(475.13)^{1.2}(108.1378)^{-1/2}(704.65)^{-0.167}$$

$$\frac{(1 - 0.5677)^{0.38}}{0.5677^{1/6}} = 0.142$$

The estimated value is 7.6 percent higher than the DIPPR[®] 801 recommended value of 0.132 W/(m·K).

Recommended Method Sastri-Rao method.

Reference: Sastri, S. R. S., and K. K. Rao, *Chem. Eng. J.*, **74** (1999): 161.

Classification: Group contributions and corresponding states.

Expected uncertainty: 10 percent.

Applicability: Particularly accurate for the following families: alkanes, alkenes, aromatic alcohols, cycloalkanes, epoxides, aliphatic acids, condensed rings.

Input data: T_c , T_b (normal boiling point), and molecular structure.

Description: The thermal conductivity at the normal boiling point k_b is calculated from the sum of the group contributions given in Table 2-359. This value is then scaled to the desired reduced temperature by using a factor α^β in which the power β is related to the fractional reduced temperature distance between the normal boiling point and the critical point as shown in the following equations:

$$k_b = \sum_{i=1}^N n_i \Delta k_i \quad \beta = 1 - \left(\frac{1 - T_r}{1 - T_{br}} \right)^\gamma \quad k = k_b \alpha^\beta \quad (2-109)$$

where $\gamma = 1.23$ for alcohols and 0.2 for all other compounds and $\alpha = 0.856$ for alcohols and 0.16 for all other compounds.

TABLE 2-359 Sastri-Rao^a Group Contributions for Liquid Thermal Conductivity at the Normal Boiling Point

Group	Δk_i (W/m·K)	Group	Δk_i (W/m·K)
Hydrocarbons		—COOH	0.0650
—CH ₃	0.0545	—NH ₂	0.0880
—CH ₂ —	-0.0008	—NH—	0.0065
>CH—	-0.0600	—NH— ring	0.0450
>C<	-0.1230	>N—	-0.0605
==CH ₂	0.0545	>N— ring	0.0135
==CH—	0.0020	—CN	0.0645
==C<	-0.0630	—NO ₂	0.0700
==C==	0.1200	—S	0.0100
ring ^c	0.1130	—F perfluoro	0.0568
Nonhydrocarbons		—F other	0.0510
—O—	0.0100	—Cl	0.0550
—OH primary ^b	0.0830	—Br	0.0415
—OH other	0.0680	—I	0.0245
>CO	0.0175	—H ^c	0.0675
>CHO	0.0730	3-ring	0.1500
—COO—	0.0070	other ring ^d	0.1100

Corrections for multigroup interactions

Hydrocarbons with 4 or fewer carbon atoms	^e 0.0150(5 - nC)
Single CH ₃ group + nonhydrocarbon groups other than COOH, Br, I ^f	0.0600
Two hydrocarbon + nonhydrocarbon groups other than COOH, Br, I ^f	0.0285
Unsaturated aliphatic compounds with three hydrocarbon groups	0.0285
Special groups Cl(CH ₂) _n Cl	0.0350
More than one nonhydrocarbon group with hydrocarbon groups	0.0095
Nonhydrocarbon groups but no hydrocarbon groups	0.1165

^aAll rings are treated as separate rings in polycyclic compounds.

^bUsed only for aliphatic primary alcohols and phenols having no branch chains.

^cUsed in methane, formic acid, formates, etc.

^dUsed for all rings in polycyclic compounds with at least one nonhydrocarbon ring.

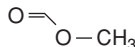
^eThe number of carbon atoms is nC.

^fAliphatic nonhydrocarbon liquids such as methylformate, acetanhydride, and ethylformate, having more than one type of nonhydrocarbon group and (1) one or two methyl groups or (2) one ethyl group only, require two correction factors. One is due to the hydrocarbon groups, and one is due to the presence of more than one type of nonhydrocarbon group.

^gSOURCE: Sastri, S. R. S., and K. K. Rao, *Chem. Eng. J.*, **74** (1999): 161.

2-512 PHYSICAL AND CHEMICAL DATA

Example Estimate the thermal conductivity of liquid methyl formate at 323 K.
Molecular structure:



Group contributions from Table 2-359:

Group	n_i	Δk_i	$n_i \Delta k_i$
—CH ₃	1	0.0545	0.0545
—COO—	1	0.0070	0.0070
—H	1	0.0675	0.0675
Corrections for multigroup interactions			
Single CH ₃ group + nonhydrocarbon groups			0.0600
More than one nonhydrocarbon with hydrocarbon groups			0.0095
Total			0.1985

Required input properties from DIPPR[®] 801 recommended values:

$$T_c = 487.2 \text{ K} \quad T_b = 304.9 \text{ K}$$

$$T_r = T/T_c = 323/487.2 = 0.6630 \quad T_{br} = 304.9/487.2 = 0.6258$$

From Eq. (2-109):

$$\alpha = 0.16 \quad \gamma = 0.2 \quad (\text{nonalcohol values})$$

$$\beta = 1 - \left(\frac{1 - 0.633}{1 - 0.6257} \right)^{0.2} = 0.0207 \quad k_b = 0.1985 \text{ W/(m}\cdot\text{K)}$$

$$k = [0.1985 \text{ W/(m}\cdot\text{K)}] (0.16)^{0.0207} = 0.1911 \text{ W/(m}\cdot\text{K)}$$

The estimated value is 10.2 percent above the DIPPR[®] 801 recommended value of 0.1734 W/(m·K).

Recommended Method Missenard method.

Reference: Missenard, A., *Comptes Rendus*, **260** (1965): 5521.

Classification: Corresponding states.

Expected uncertainty: 20 percent.

Applicability: Organic compounds; nonassociating.

Input data: T_c , m (number of atoms in molecule), ρ_{273} (liquid density at 273.15 K), T_b , M , $C_{p,273}$ (liquid heat capacity at 273.15 K).

Description:

$$\frac{k_{273}}{\text{mW/(m}\cdot\text{K)}} = \frac{8.4}{m^{1/4}} \cdot \left(\frac{T_b}{\text{K}} \right)^{1/2} \left(\frac{\rho_{273}}{\text{g/m}^3} \right)^{1/2} \left(\frac{M}{\text{g/mol}} \right)^{-1/2} \times \left[\frac{C_{p,273}}{\text{J/(mol}\cdot\text{K)}} \right] \quad (2-110)$$

$$k = \frac{k_{273} [3 + 20(1 - T_r)^{2/3}]}{3 + 20(1 - T_{r,273})^{2/3}} \quad (2-111)$$

where $T_{r,273} = (273 \text{ K})/T_c$.

Example Estimate the thermal conductivity of *m*-xylene at 350 K.

Required properties from DIPPR[®] 801 database:

$$T_c = 617 \text{ K} \quad m = 18 \quad \rho_{273} = 7.6812 \text{ kmol/m}^3$$

$$T_b = 412.27 \text{ K} \quad M = 106.165 \text{ kg/kmol} \quad C_{p,273} = 200.64 \text{ kJ/(kmol}\cdot\text{K)}$$

Auxiliary properties:

$$T_r = 350/617 = 0.5673 \quad T_{br} = 412.27/617 = 0.6682$$

$$T_{r,273} = 273/617 = 0.4425$$

From Eq. (2-110):

$$\left(\frac{k_{273}}{\text{mW/(m}\cdot\text{K)}} \right) = (8.4)(412.27)^{1/2} (0.007681)^{1/2} (106.165)^{-1/2} (200.64)(18)^{-0.25} = 141.3$$

From Eq. (2-111):

$$k = \frac{k_{273} [3 + 20(1 - T_r)^{2/3}]}{3 + 20(1 - T_{r,273})^{2/3}} = \frac{\left(\frac{141.3 \text{ mW}}{\text{m}\cdot\text{K}} \right) [3 + 20(1 - 0.5673)^{2/3}]}{3 + 20(1 - 0.4425)^{2/3}} = 123.3 \frac{\text{mW}}{\text{m}\cdot\text{K}}$$

The estimated value is 4.5 percent above the DIPPR[®] 801 recommended value of 118.0 mW/(m·K).

Liquid Mixtures The thermal conductivity of liquid mixtures generally shows a modest negative deviation from a linear mass-fraction-weighted average of the pure-component values. Although more complex methods with some improved accuracy are available, two simple methods are recommended here that require very little additional information. The first method applies only to binary mixtures while the second can be used for multiple components.

Recommended Method Filippov correlation.

References: Filippov, L. P., *Vest. Mosk. Univ., Ser. Fiz. Mat. Estestv. Nauk*, **10** (1955): 67; Filippov, L. P., and N. S. Novoselova, *Sugden, Vest. Mosk. Univ., Ser. Fiz. Mat. Estestv. Nauk*, **10** (1955): 37.

Classification: Empirical correlation.

Expected uncertainty: 4 to 8 percent.

Applicability: Binary liquid mixtures.

Input data: Pure-component thermal conductivities k_i at mixture conditions; w_i .

Description: The mixture thermal conductivity is calculated from the pure-component values using

$$k = w_1 k_1 + w_2 k_2 - 0.72 w_1 w_2 |k_2 - k_1| \quad (2-112)$$

where w_i is the mass fraction of pure fluid i .

Recommended Method Li correlation.

References: Li, C. C., *AIChE J.*, **22** (1976): 927.

Classification: Empirical correlation.

Expected uncertainty: 4 to 8 percent.

Applicability: Liquid mixtures.

Input data: Pure-component thermal conductivities k_i at mixture conditions; $\rho_{L,i}$

Description: The mixture thermal conductivity is correlated as a function of the mixture volume fractions ϕ_i :

$$k = \sum_{i=1}^C \sum_{j=1}^C \phi_i \phi_j \frac{2k_i k_j}{k_i + k_j} \quad (2-113)$$

$$\text{where } \phi_i = \frac{x_i \rho_{L,i}^{-1}}{\sum_{j=1}^C x_j \rho_{L,j}^{-1}}$$

Example Estimate the thermal conductivity of a mixture containing 30.2 mol % diethyl ether(1) and 69.8 mol % methanol(2) at 273.15 K and 0.1 MPa, using the Filippov and Li correlations.

Auxiliary data: The pure-component thermal conductivities and molar densities at 273.15 K recommended in the DIPPR[®] 801 database are

$$k_1 = 0.1383 \text{ W/(m}\cdot\text{K)} \quad \rho_1 = 9.9335 \text{ kmol/m}^3 \quad M_1 = 74.1216 \text{ kg/kmol}$$

$$k_2 = 0.2069 \text{ W/(m}\cdot\text{K)} \quad \rho_2 = 25.371 \text{ kmol/m}^3 \quad M_2 = 32.0419 \text{ kg/kmol}$$

The mass fractions corresponding to the mole fractions given above are

$$w_1 = 0.5 \quad w_2 = 0.5$$

The volume fractions are

$$\phi_1 = \frac{(0.302)(9.9335)^{-1}}{(0.302)(9.9335)^{-1} + (0.698)(25.371)^{-1}} = 0.525 \quad \phi_2 = 0.475$$

Calculation using Eq. (2-112):

$$k = [(0.5)(0.1383) + (0.5)(0.2069) - (0.72)(0.5)(0.5)(0.2069 - 0.1383)] \frac{W}{m \cdot K}$$

$$= 0.160 \text{ W/(m}\cdot\text{K)}$$

Calculation using Eq. (2-113):

$$k = \left[(0.525)^2(0.1383) + 2 \cdot \frac{(0.525)(0.475)(2)(0.1383)(0.2069)}{0.1383 + 0.2069} + (0.475)^2(0.2069) \right] \frac{W}{m \cdot K}$$

$$= 0.167 \text{ W/(m}\cdot\text{K)}$$

The Filippov value is 7.5 percent lower than the experimental value of 0.173 W/(m·K) [Jamieson, D. T., and B. K. Hastings, *Thermal Conductivity, Proceedings of the Eighth Conference*, C. Y. Ho and R. E. Taylor, eds., Plenum Press, New York, 1969]; the Li value is 3.5 percent lower than the experimental value.

Solids There is no reliable method for estimating solid thermal conductivity at this time.

SURFACE TENSION

The surface layer at a vapor-liquid interface is in tension and will contract to minimize the surface area. Qualitatively, the surface tension is due to the larger attractive forces that molecules at the interface experience from molecules in the dense liquid phase than from those in the low-density gas phase. Quantitatively, *surface tension* is defined as the force in the surface plane per unit length. Jasper [Jasper, J. J., *J. Phys. Chem. Ref. Data*, **1** (1972): 841] has made a critical evaluation of experimental surface tension data for approximately 2200 pure chemicals and correlated surface tension σ (mN/m = dyn/cm) with temperature as

$$\sigma = A - BT$$

Jasper's evaluation also includes values of A and B for most of the tabulated chemicals. Surface tension decreases with increasing temperature and increasing pressure.

Pure Liquids An approach suggested by Macleod [Macleod, D. B., *Trans. Faraday Soc.*, **19** (1923): 38] and modified by Sugden [Sugden, S. J., *Chem. Soc.*, **125** (1924): 32] relates σ to the liquid and vapor molar densities and a temperature-independent parameter called the parachor P

$$\frac{\sigma}{\text{mN/m}} = \left[P \cdot \left(\frac{\rho_L - \rho_V}{10^3 \text{ kmol/m}^3} \right) \right]^4 \quad (2-114)$$

where ρ_L and ρ_V are the saturated molar liquid and vapor densities, respectively. At low temperatures, where $\rho_L \gg \rho_V$, the vapor density can be neglected, but at higher temperatures the density of both phases must be calculated. At the critical point the surface tension is zero as $\rho_L = \rho_V$. Quayle [Quayle, O. R., *Chem. Rev.*, **53** (1953): 439] proposed a group contribution method for estimating P that has been improved in recent years by Knotts et al. [Knotts, T. A., et al., *J. Chem. Eng. Data*, **46** (2001): 1007]. This method using P is recommended when groups are available; otherwise, the Brock-Bird [Brock, J. R., and R. B. Bird, *AIChE J.*, **1** (1955): 174] corresponding-states method as modified by Miller [Miller, D. G., *Ind. Eng. Chem. Fundam.*, **2** (1963): 78] may be used to estimate surface tension for compounds that are not strongly polar or associating.

Recommended Method Parachor method.

References: Macleod, D. B., *Trans. Faraday Soc.*, **19** (1923): 38; Sugden, S. J., *Chem. Soc.*, **125** (1924): 32; Knotts, T. A., et al., *J. Chem. Eng. Data*, **46** (2001): 1007.

Classification: Group contributions and QSPR.

Expected uncertainty: 4 percent.

Applicability: Organic compounds for which group values are available.

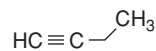
Input Data: ρ_L , molecular structure, and Table 2-360.

Description: Equation (2-114) is used with P calculated from

$$P = \sum_{i=1}^N n_i \Delta P_i \quad (2-115)$$

Group values for the parachor are given in Table 2-360.

Example Estimate the surface tension of ethylacetylene at 237.45 K.
Structure:



Group	n_i	ΔP_i	$n_i \Delta P_i$
$\equiv \text{CH}$	1	43.64	43.64
$\equiv \text{C}-$	1	28.64	28.64
$>\text{CH}_2$ ($n = 1-11$)	1	39.92	39.92
CH_3	1	55.25	55.25
Total			167.45

Required properties: The DIPPR® 801 database gives $\rho_L = 13.2573 \text{ kmol/m}^3$ at 237.45 K.

Calculation using Eq. (2-114):

$$\sigma = \left[(167.45) \left(\frac{13.2573}{1000} \right) \right]^4 \frac{\text{mN}}{\text{m}} = 0.02429 \frac{\text{N}}{\text{m}}$$

The estimated value is 0.9 percent above the DIPPR® 801 recommended value of 0.02407 N/m.

Recommended Method Brock-Bird method.

Reference: Brock, J. R., and R. B. Bird, *AIChE J.*, **1** (1955): 174; Miller, D. G., *Ind. Eng. Chem. Fundam.*, **2** (1963): 78.

Classification: Corresponding states.

Expected uncertainty: 5 percent.

Applicability: Nonpolar and moderately polar organic compounds.

Input data: T_c , P_c , and T_b .

Description:

$$\frac{\sigma}{\text{mN/m}} = (5.553 \times 10^{-5}) \left(\frac{P_c}{\text{Pa}} \right)^{2/3} \left(\frac{T_c}{\text{K}} \right)^{1/3} F(1 - T_r)^{11/9} \quad (2-116)$$

where

$$F = \frac{T_{br} [\ln(P_c/\text{Pa}) - 11.5261]}{1 - T_{br}} - 1.3281 \quad (2-117)$$

Example Estimate the surface tension for ethyl mercaptan at 303.15 K.

Required properties from DIPPR® 801:

$$T_c = 499.15 \text{ K} \quad P_c = 5.49 \times 10^6 \text{ Pa} \quad T_b = 308.15 \text{ K}$$

Supporting quantities:

$$T_r = (303.15 \text{ K}) / (499.15 \text{ K}) = 0.6073$$

$$T_{br} = (308.15 \text{ K}) / (499.15 \text{ K}) = 0.6173$$

$$F = [0.6173 [\ln(5.49 \times 10^6) - 11.5261] / (1 - 0.6173)] - 1.3281 = 5.113$$

[from Eq. (2-117)]

From Eq. (2-116):

$$\sigma = (5.553 \times 10^{-5}) (5.49 \times 10^6)^{2/3} (499.15)^{1/3} (5.113) (1 - 0.6073)^{11/9} \text{ mN/m}$$

$$= 22.36 \text{ mN/m}$$

The estimated value is 1.4 percent lower than the DIPPR® 801 recommended value of 22.68 mN/m.

TABLE 2-360 Knotts* Group Contributions for the Parachor in Estimating Surface Tension

Group	ΔP_i	Group	ΔP_i
(a) Nonring C		(e) Nitrogen groups	
—CH ₃	55.25	R—NH ₂ (primary R)	44.98
>CH ₂ (n = 1–11)	39.92	R—NH ₂ (sec R)	44.63
>CH ₂ (n = 12–20)	40.11	R—NH ₂ (tert R)	46.44
>CH ₂ (n > 20)	40.51	A—NH ₂ (attached to arom ring)	46.53
>CH—	28.90	>NH (nonring)	29.04
>C<	15.76	>NH (ring)	31.97
==CH ₂	49.76	>NH (in arom ring)	33.92
==CH—	34.57	>N- (nonring)	10.77
==C<	24.50	>N- (ring)	15.71
==C==	24.76	—N= (nonring)	23.24
==CH	43.64	>N (aromatic)	26.49
==C—	28.64	HC≡N (hyd cyanide)	80.94
Branch corrections		—C≡N	65.23
Per branch	−6.02	—C≡N (aromatic)	67.54
sec-sec adjacency	−2.73	(f) Nitrogen and oxygen groups	
sec-tert adjacency	−3.61	—C=ONH ₂ (amides)	93.43
tert-tert adjacency	−6.10	—C=ONH- (amides)	73.64
(b) Nonaromatic ring C		—C=ON< (amides)	57.05
—CH ₂ —	39.21	—NHCHO	91.69
>CH—	23.94	>NCHO	77.12
>C<	7.19	—N=O	64.32
==CH—	34.07	—NO ₂	73.86
==C<	18.85	—NO ₂ (aromatic)	75.05
>CH— (fused ring)	22.05	(g) Sulfur groups	
Ring corrections		R-SH (primary R)	66.89
Three-member ring	12.67	R-SH (sec R)	63.34
Four-member ring	15.76	R-SH (tert R)	65.33
Five-member ring	7.04	—SH (aromatic)	68.30
Six-member ring	5.19	—S— (nonring)	51.37
Seven-member ring	3.00	—S— (ring)	51.75
(c) Aromatic ring C		—S— (aromatic)	51.47
>CH	34.36	>S=O (nonring)	72.21
>C—	16.07	>SO ₂ (nonring)	93.20
—C— (fused arom/arom)	19.73	>SO ₂ (ring)	90.13
—C— (fused arom/aliph)	14.41	(h) Halogen groups	
Arom ring corr		—F	21.81
ortho	−0.60	—Cl	26.24
para	3.40	—Br	51.16
meta	2.24	—I	54.56
subst. naphthalene corr	−7.07	—F (aromatic)	66.30
(d) Oxygen groups		—Cl (aromatic)	70.39
—OH (alc, primary)	31.42	—Br (aromatic)	90.84
—OH (alc, sec)	22.68	—I (aromatic)	92.04
—OH (alc, tertiary)	20.66	(i) Si groups	
—OH (phenol)	30.32	SiH ₄	105.11
—O— (nonring)	20.61	>SiH—	54.50
—O— (ring)	21.67	>Si<	44.93
—O— (aromatic)	23.54	>Si< (ring)	28.64
>C=O (nonring)	47.02	(j) Other inorganic groups	
>C=O (ring)	50.04	—PO ₄	115.59
O=CH— (aldehyde)	66.06	>P—	48.84
CHOOH (formic)	94.01	>B—	22.65
—COOH (acid)	74.57	>Al—	25.06
—OCHO (formate)	82.29	—ClO ₃	106.03
—COO— (ester)	64.97		
—COOCO— (acid anhyd)	115.07		
—OC(=O)O— (ring)	84.05		

*Knotts, T. A., et al., *J. Chem. Eng. Data*, **46** (2001): 1007.

Liquid Mixtures Compositions at the liquid-vapor interface are not the same as in the bulk liquid, and so simple (bulk) composition-weighted averages of the pure-fluid values do not provide quantitative estimates of the surface tension at the vapor-liquid interface of a mixture. The behavior of aqueous mixtures is more difficult to correlate and estimate than that of nonpolar mixtures because small amounts of organic material can have a pronounced effect upon the surface concentrations and the resultant surface tension. These effects are usually modeled with thermodynamic methods that account for the activity coefficients. For example, a UNIFAC method [Suarez, J. T. C. Torres-Marchal, and P. Rasmussen, *Chem. Eng. Sci.*, **44** (1989): 782] is recommended and illustrated in PGL5. For nonaqueous systems the extension of the parachor method, used above for pure fluids, is a simple and reasonably effective method for estimating σ for mixtures.

Recommended Method Parachor correlation.

Reference: Huggill, J. A., and A. J. van Welsenes, *Fluid Phase Equil.*, **29** (1986): 383; Macleod, D. B., *Trans. Faraday Soc.*, **19** (1923): 38; Sugden, S. J., *Chem. Soc.*, **125** (1924).

Classification: Corresponding states.

Expected uncertainty: 3 to 10 percent.

Applicability: Nonaqueous mixtures.

Input data: Liquid and vapor ρ at mixture T ; parachors of pure components; x_i .

Description:

$$\frac{\sigma_m}{\text{mN/m}} = \left(P_{L,m} \frac{\rho_{L,m}}{10^3 \text{ kmol/m}^3} - P_{V,m} \frac{\rho_{V,m}}{10^3 \text{ kmol/m}^3} \right)^4 \quad (2-118)$$

where σ_m = surface tension of the mixture

$P_{L,m}$ = parachor of liquid mixture

$P_{V,m}$ = parachor of vapor mixture

$\rho_{L,m}$ = liquid mixture molar density

$\rho_{V,m}$ = vapor mixture molar density

The following definitions are used for the liquid and vapor mixture parachors:

$$P_{L,m} = \frac{1}{2} \sum_{i=1}^C \sum_{j=1}^C x_i x_j (P_i + P_j) \quad P_{V,m} = \frac{1}{2} \sum_{i=1}^C \sum_{j=1}^C y_i y_j (P_i + P_j) \quad (2-119)$$

where x_i is the mole fraction of component i in the liquid and y_i is the mole fraction of component i in the vapor.

Note that ρ_V is generally very small compared to ρ_L at temperatures substantially lower than T_c and can often be neglected.

Example Estimate the surface tension for a 16.06 mol % *n*-pentane(1) + 83.94 mol % dichloromethane(2) mixture at 298.15 K.

Required properties from DIPPR® 801:

	P	ρ_L /(kmol·m ⁻³) at 298.15 K
<i>n</i> -Pentane	231.1	8.6173
Dichloromethane	146.6	15.5211

Mixture parachor from Eq. (2-119) and mixture density:

$$P_{L,m} = (0.1606)^2(231.1) + (0.1606)(0.8394)(231.1 + 146.6) + (0.8394)^2(146.6) = 160.17$$

$$\rho_{L,m} = \left(\sum_{i=1}^C \frac{x_i}{\rho_i} \right)^{-1} = \left(\frac{0.1606}{8.6173} + \frac{0.8394}{15.5211} \right)^{-1} \frac{\text{kmol}}{\text{m}^3} = 13.752 \frac{\text{kmol}}{\text{m}^3}$$

Calculation using Eq. (2-118): Because the temperature is low, the density of the vapor can be neglected, and

$$\frac{\sigma_m}{\text{mN/m}} = [(160.17)(0.013752)]^4 = 23.54 \frac{\text{mN}}{\text{m}}$$

The estimated value is 2.9 percent below the experimental value of 24.24 mN/m reported by De Soria et al. [De Soria, M. L. G., et al., *J. Colloid Interface Sci.*, **103** (1985): 354].

FLAMMABILITY PROPERTIES

Flash points, lower and upper flammability limits, and autoignition temperature are important properties for determining safe operating limits when processing organic compounds. As with any property, experimental values are preferable to predicted values, and prediction techniques for these properties are only modestly accurate.

The flash point is the lowest temperature at which a liquid gives off sufficient vapor to form an ignitable mixture with air near the surface of the liquid or within the vessel used. ASTM test methods include procedures using a closed-cup apparatus (ASTM D 56, ASTM D 93, and ASTM D 3828), which is preferred, and an open-cup apparatus (ASTM D 92 and ASTM D 1310). Closed-cup values are typically lower than open-cup values. When several values are available, the lowest reasonable temperature is usually accepted in order to ensure safe operations.

The lower and upper flammability limits are the boundary-line equilibrium mixtures of vapor or gas with air, which if ignited will just propagate a flame away from the ignition source. Each of these limits has a temperature at which the flammability limits are reached. The lower flammability limit temperature corresponds approximately to the flash point, but since the flash point is determined with downward flame propagation and nonuniform mixtures and the lower flammability temperature is determined with upward flame propagation and uniform vapor mixtures, the measured lower flammability temperature is often somewhat lower than the flash point.

The autoignition temperature is the minimum temperature for a substance to initiate self-combustion in air in the absence of an ignition source.

Recommended Methods Flash point: Thornton method.

Reference: As described by N. Y. Shebeko, A. V. Ivanov, and E. N. Alekhina, "Calculation of Flash Points and Ignition Temperatures of Organic Compounds," *Soviet Chem. Ind.* **16**(1984):1371.

Classification: Atomic contributions.

Expected uncertainty: 5 K.

Applicability: Organic compounds.

Input data: Number of carbon, hydrogen, sulfur, halogen, and oxygen atoms; vapor pressure correlation.

Description: A simple atom contribution method is given by

$$P^* - \frac{P_{\text{sys}}}{1 + 4.76(2\beta - 1)} = 0 \quad (2-120)$$

where P^* = vapor pressure at flash point temperature

P_{sys} = total system pressure, typically 1.01325×10^5 Pa

β = stoichiometric coefficient, defined by

$$\beta = N_C + N_S + \frac{N_H - N_X}{4} - \frac{N_O}{2} \quad (2-121)$$

where N_C = number of carbon atoms in compound

N_S = number of sulfur atoms in compound

N_H = number of hydrogen atoms in compound

N_X = number of halogen atoms in compound

N_O = number of oxygen atoms in compound

Procedure:

Step 1. Determine the number of carbon, sulfur, hydrogen, halogen, and oxygen atoms in the compound.

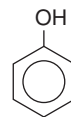
Step 2. Calculate β from Eq. (2-121).

Step 3. Substitute a temperature-dependent expression for vapor pressure in Eq. (2-120) for P^* .

Step 4. Solve Eq. (2-120) for temperature. This temperature is the flash point estimate.

Example Estimate the flash point of phenol.

Structure:



Atomic contributions:

Atom type	Number
C	6
H	6
O	1

$$\beta = 6 + \frac{6}{4} - \frac{1}{2} = 7$$

The DIPPR® 801 correlation for the vapor pressure of phenol is

$$P^* = \exp(95.444 - \frac{10,113}{T} - 10.09 \ln T + 6.7603 \times 10^{-18} T^6)$$

When this expression is used in Eq. (2-120) and solved for temperature, one obtains $T_{\text{FP}} = 348.7$ K, which is 1.2 percent below the DIPPR recommended value of 353 K.

Recommended Method Flammability limits: Pintar method.

Reference: Pintar, A. J., Technical Support Document DIPPR Project 912, Michigan Technological University, Houghton, 1996.

Classification: Group contributions.

Expected uncertainty: 25 percent.

TABLE 2-361 Group Contributions for Pintar* Flammability Limits Method for Organic Compounds

Group	LFL _i	UFL _i	Group	LFL _i	UFL _i
—CH ₃	17.2750	3.8461	>NH	3.2709	-1.9112
>CH ₂	13.7022	1.4959	—N≡	-7.2149	-2.3309
>CH—	10.0000	0.2183	—CN	8.0990	3.6918
>C<	5.5291	-0.8422	≡C=N—	2.5963	-1.1463
—H	2.7250	2.8206	≡N—NH ₂	-3.5071	-0.29897
—OH	2.1797	0.5856	>N—NH ₂	0.5861	2.4811
—O—	-3.0156	-2.2427	—NO ₂	-3.1507	0.8011
—O—O—	-6.0312	-4.4854	—SH	7.9424	0.5344
≡C=O	4.6752	0.6009	—S—	11.0079	-1.9832
—CHO	10.3801	-1.2148	—SO—	3.9115	-4.1834
—COOH	4.8890	1.6121	—SO ₂ —	5.5400	—
—COO—	1.2955	-1.1840	—SO ₃ —	2.8600	—
—CO—O—CO—	4.6740	2.4751	—SO ₄ —	0.1800	—
—C ₆ H ₅	73.8338	9.6661	—CO ₃ —	2.4103	-3.4894
<i>m</i> -C ₆ H ₄	57.4447	7.6126	—OPO ₂ —	7.1419	—
<i>o</i> -C ₆ H ₄	57.4447	7.2450	—P≡	47.6909	—
<i>p</i> -C ₆ H ₄	57.4447	7.9291	—PO—	7.1515	—
Arom. ring	45.0633	-5.9925	—PO ₄ ≡	-11.5096	-6.0260
≡	4.2821	2.0269	Si—C†	-2.2855	-3.0576
≡≡	17.5470	0.7842	Si—O†	2.5034	1.4282
—Cl	-2.9697	1.4008	Si—H†	8.3130	-24.4160
—Cl ₂	-5.9764	3.1943	Si—Cl†	4.1010	9.7131
—Cl ₃	-8.0982	4.2024	Si—N†	15.8960	1.6577
—F	-1.2615	0.3984	Si—Si	—	—
—F ₂	-2.1224	0.6847	Al	—	—
—F ₃	-5.1300	1.1952	B	47.3806	—
—Br	-8.0405	4.0018	Cr	—	—
—Br ₂	-16.0809	8.0036	Na	—	—
—Br ₃	-21.9000	12.0054	<i>cis</i>	-6.8350	1.8040
—I	-22.0000	11.4300	<i>trans</i>	0.5821	0.9183
—I ₂	-44.0000	22.8600	Nonarom. ring	2.9082	3.7760
—I ₃	-60.0000	34.2900	Add'l. ring	14.2712	3.1127
—NH ₂	3.7078	1.8802			

*Pintar, A. J., Technical Support Document DIPPR Project 912, Michigan Technological University, Houghton, 1996.

†Does not include contribution of atoms attached to silicon.

TABLE 2-362 Group Contributions for Pintar* Flammability Limits Method for Inorganic Compounds

Group	LFL _i	UFL _i	Group	LFL _i	UFL _i
B	24.5190	-1.3818	>N—NH ₂	0.5861	-0.2990
Br	—	—	O	-24.3242	2.2990
C	32.0745	-0.6259	P	24.8302	—
Cl	14.2658	-1.4231	S	26.6776	1.3171
F	—	—	Si—C†	-2.2855	-3.0576
Fe	—	—	Si—O†	2.5034	1.4282
H	10.3452	0.6500	Si—H†	8.3130	-24.4160
N	-24.5487	1.8453	Si—Cl†	4.1010	9.7131
Na	—	—	Si—N†	15.8960	1.6577
Ni	—	—	Si—Si	—	—

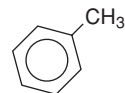
*Pintar, A. J., Technical Support Document DIPPR Project 912, Michigan Technological University, Houghton, 1996.

†Does not include contribution of atoms attached to silicon.

Applicability: Organic and inorganic compounds.**Input data:** Group contributions from Tables 2-361 and 2-362.**Description:** A simple GC method with first-order contributions with lower flammability limit (LFL) and upper flammability limit (UFL) in volume % given by

$$\text{LFL} = \frac{100\%}{\sum n_i \text{LFL}_i} \quad (2-122)$$

$$\text{UFL} = \frac{100\%}{\sum n_i \text{UFL}_i} \quad (2-123)$$

where n_i = number of groups of type i in moleculeLFL_{*i*} = contribution of group i to LFLUFL_{*i*} = contribution of group i to UFL**Example** Estimate the lower and upper flammability limits of toluene.**Structure:****Group contributions:**

Group	LFL	UFL
—CH ₃	17.2750	3.8461
—C ₆ H ₅	73.8338	9.6661

Calculations using Eqs. (2-122) and (2-123):

$$\text{LFL} = \frac{100\%}{17.2750 + 73.8338} = 1.10\%$$

$$\text{UFL} = \frac{100\%}{3.8461 + 9.6661} = 7.40\%$$

TABLE 2-363 Group Contributions for Pintar* Autoignition Temperature Method for Organic Compounds

Group	b_i	Group	b_i	Group	b_i
—CH ₃	301.91	—Cl ₃	1073.47	—SO ₃ —	—
>CH ₂	-10.86	—F	360.60	—SO ₄ —	-31.71
>CH—	-275.17	—F ₂	753.54	—CO ₃ —	442.26
>C<	-570.43	—F ₃	1082.00	—P=	-334.91
—H	391.48	—Br	420.96	—PO—	-549.59
—OH	324.10	—Br ₂	607.69	—OPO ₂ —	—
—O—	-18.60	—Br ₃	1260.00	—PO ₄ =	-329.45
—O—O—	-397.61	—I	310.53	Si—C†	-147.69
=C=O	57.65	—I ₂	—	Si—O†	-136.99
—CHO	195.20	—I ₃	—	Si—H†	-310.52
—COOH	370.75	—NH ₂	354.11	Si—Cl†	-200.88
—CO—	43.90	>NH	9.88	Si—N†	—
—CO—O—CO—	46.11	—N=	-249.91	Si—Si	—
—C ₆ H ₅	380.27	—CN	469.67	Al	—
<i>m</i> -C ₆ H ₄	153.15	=C=N—	-273.70	B	—
<i>o</i> -C ₆ H ₄	77.48	=N—NH ₂	378.27	Cr	—
<i>p</i> -C ₆ H ₄	99.87	>N—NH ₂	-215.02	Na	534.29
Aromatic ring	-1339.65	—NO ₂	292.57	<i>cis</i>	-29.19
≡	578.72	—SH	273.84	<i>trans</i>	-38.31
≡	1116.50	—S—	-60.75	Nonarom. ring	605.97
—Cl	347.39	—SO—	-91.10	Add'l. ring	565.11
—Cl ₂	726.03	—SO ₂ —	—	Zn	349.02

*Pintar, A. J., *Estimation of Autoignition Temperature*, Technical Support Document DIPPR Project 912, Michigan Technological University, Houghton, 1996.

†Does not include contribution of atoms attached to silicon.

TABLE 2-364 Group Contributions for Pintar* Autoignition Temperature Method for Inorganic Compounds

Group	b_i	Group	b_i	Group	b_i
B	-457.14	N	0.71	Si—C†	-147.69
Br	—	Na	—	Si—O†	-136.99
C	489.19	Ni	-1595.10	Si—H†	-310.52
Cl	395.42	>N—NH ₂	-215.02	Si—Cl†	-200.88
F	—	O	-13.39	Si—N†	—
Fe	-2050.90	P	108.45	Si—Si	—
H	204.55	S	-3.57		

*Pintar, A. J., *Estimation of Autoignition Temperature*, Technical Support Document DIPPR Project 912, Michigan Technological University, Houghton, 1996.

†Does not include contribution of atoms attached to silicon.

The values recommended in the DIPPR® 801 database are 1.2 and 7.1 percent, respectively.

Flammability temperatures are found by determining the temperature at which the vapor pressure equals the partial pressure corresponding to the LFL or UFL.

Recommended Methods Autoignition temperature: Pintar method.

Reference: Pintar, A. J., *Estimation of Autoignition Temperature*, Technical Support Document DIPPR Project 912, Michigan Technological University, Houghton, 1996.

Classification: Group contributions.

Expected uncertainty: 25 percent.

Applicability: Organic and inorganic compounds.

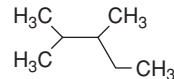
Input data: Group contributions from Tables 2-363 and 2-364.

Description: A simple GC method with first-order contributions is given by

$$\text{AIT} = \sum n_i b_i \quad (2-124)$$

where n_i is the number of groups of type i in the molecule and b_i is the contribution of group i to the autoignition temperature. A more accurate but somewhat more complicated logarithmic GC method was also developed by Pintar in the same reference cited here.

Example Estimate the autoignition temperature of 2,3-dimethylpentane. *Structure and group information:*



Group	n_i	b_i
—CH ₃	4	301.91
>CH ₂	1	-10.86
>CH—	2	-275.17

Calculation using Eq. (2-124):

$$\text{AIT} = 4(301.91) - 10.86 + 2(-275.17) = 646.4 \text{ K}$$

The estimated value is 6.3 percent above the DIPPR® 801 recommended value of 608.15 K.

SECTION 3

Mathematics

PERRY'S CHEMICAL ENGINEERS' HANDBOOK

8TH EDITION



BRUCE A. FINLAYSON
LORENZ T. BIEGLER

Copyright © 2008, 1997, 1984, 1973, 1963, 1950, 1941, 1934 by The McGraw-Hill Companies, Inc. All rights reserved. Manufactured in the United States of America. Except as permitted under the United States Copyright Act of 1976, no part of this publication may be reproduced or distributed in any form or by any means, or stored in a database or retrieval system, without the prior written permission of the publisher.

0-07-154210-8

The material in this eBook also appears in the print version of this title: 0-07-151126-1.

All trademarks are trademarks of their respective owners. Rather than put a trademark symbol after every occurrence of a trademarked name, we use names in an editorial fashion only, and to the benefit of the trademark owner, with no intention of infringement of the trademark. Where such designations appear in this book, they have been printed with initial caps.

McGraw-Hill eBooks are available at special quantity discounts to use as premiums and sales promotions, or for use in corporate training programs. For more information, please contact George Hoare, Special Sales, at george_hoare@mcgraw-hill.com or (212) 904-4069.

TERMS OF USE

This is a copyrighted work and The McGraw-Hill Companies, Inc. (“McGraw-Hill”) and its licensors reserve all rights in and to the work. Use of this work is subject to these terms. Except as permitted under the Copyright Act of 1976 and the right to store and retrieve one copy of the work, you may not decompile, disassemble, reverse engineer, reproduce, modify, create derivative works based upon, transmit, distribute, disseminate, sell, publish or sublicense the work or any part of it without McGraw-Hill’s prior consent. You may use the work for your own noncommercial and personal use; any other use of the work is strictly prohibited. Your right to use the work may be terminated if you fail to comply with these terms.

THE WORK IS PROVIDED “AS IS.” MCGRAW-HILL AND ITS LICENSORS MAKE NO GUARANTEES OR WARRANTIES AS TO THE ACCURACY, ADEQUACY OR COMPLETENESS OF OR RESULTS TO BE OBTAINED FROM USING THE WORK, INCLUDING ANY INFORMATION THAT CAN BE ACCESSED THROUGH THE WORK VIA HYPERLINK OR OTHERWISE, AND EXPRESSLY DISCLAIM ANY WARRANTY, EXPRESS OR IMPLIED, INCLUDING BUT NOT LIMITED TO IMPLIED WARRANTIES OF MERCHANTABILITY OR FITNESS FOR A PARTICULAR PURPOSE. McGraw-Hill and its licensors do not warrant or guarantee that the functions contained in the work will meet your requirements or that its operation will be uninterrupted or error free. Neither McGraw-Hill nor its licensors shall be liable to you or anyone else for any inaccuracy, error or omission, regardless of cause, in the work or for any damages resulting therefrom. McGraw-Hill has no responsibility for the content of any information accessed through the work. Under no circumstances shall McGraw-Hill and/or its licensors be liable for any indirect, incidental, special, punitive, consequential or similar damages that result from the use of or inability to use the work, even if any of them has been advised of the possibility of such damages. This limitation of liability shall apply to any claim or cause whatsoever whether such claim or cause arises in contract, tort or otherwise.

DOI: 10.1036/0071511261

Mathematics

Bruce A. Finlayson, Ph.D. *Rehnberg Professor, Department of Chemical Engineering, University of Washington; Member, National Academy of Engineering (Section Editor, numerical methods and all general material)*

Lorenz T. Biegler, Ph.D. *Bayer Professor of Chemical Engineering, Carnegie Mellon University (Optimization)*

MATHEMATICS

General	3-3
Miscellaneous Mathematical Constants	3-4
The Real-Number System	3-4
Algebraic Inequalities	3-5

MENSURATION FORMULAS

Plane Geometric Figures with Straight Boundaries	3-6
Plane Geometric Figures with Curved Boundaries	3-6
Solid Geometric Figures with Plane Boundaries	3-7
Solids Bounded by Curved Surfaces	3-7
Miscellaneous Formulas	3-8
Irregular Areas and Volumes	3-8

ELEMENTARY ALGEBRA

Operations on Algebraic Expressions	3-8
The Binomial Theorem	3-9
Progressions	3-9
Permutations, Combinations, and Probability	3-10
Theory of Equations	3-10

ANALYTIC GEOMETRY

Plane Analytic Geometry	3-11
Solid Analytic Geometry	3-13

PLANE TRIGONOMETRY

Angles	3-16
Functions of Circular Trigonometry	3-16
Inverse Trigonometric Functions	3-17
Relations between Angles and Sides of Triangles	3-17
Hyperbolic Trigonometry	3-18
Approximations for Trigonometric Functions	3-18

DIFFERENTIAL AND INTEGRAL CALCULUS

Differential Calculus	3-18
Multivariable Calculus Applied to Thermodynamics	3-21
Integral Calculus	3-22

INFINITE SERIES

Definitions	3-25
Operations with Infinite Series	3-25
Tests for Convergence and Divergence	3-26
Series Summation and Identities	3-26

COMPLEX VARIABLES

Algebra	3-27
Special Operations	3-27
Trigonometric Representation	3-27
Powers and Roots	3-27
Elementary Complex Functions	3-27
Complex Functions (Analytic)	3-28

DIFFERENTIAL EQUATIONS

Ordinary Differential Equations	3-29
Ordinary Differential Equations of the First Order	3-30
Ordinary Differential Equations of Higher Order	3-30
Special Differential Equations	3-31
Partial Differential Equations	3-32

DIFFERENCE EQUATIONS

Elements of the Calculus of Finite Differences	3-34
Difference Equations	3-34

INTEGRAL EQUATIONS

Classification of Integral Equations	3-36
Relation to Differential Equations	3-36
Methods of Solution	3-37

INTEGRAL TRANSFORMS (OPERATIONAL METHODS)

Laplace Transform	3-37
Convolution Integral	3-39
z -Transform	3-39
Fourier Transform	3-39
Fourier Cosine Transform	3-39

3-2 MATHEMATICS

MATRIX ALGEBRA AND MATRIX COMPUTATIONS

Matrix Algebra	3-40
Matrix Computations	3-41

NUMERICAL APPROXIMATIONS TO SOME EXPRESSIONS

Approximation Identities	3-43
--------------------------------	------

NUMERICAL ANALYSIS AND APPROXIMATE METHODS

Introduction	3-43
Numerical Solution of Linear Equations	3-44
Numerical Solution of Nonlinear Equations in One Variable	3-44
Methods for Multiple Nonlinear Equations	3-44
Interpolation and Finite Differences	3-45
Numerical Differentiation	3-47
Numerical Integration (Quadrature)	3-47
Numerical Solution of Ordinary Differential Equations as Initial Value Problems	3-48
Ordinary Differential Equations-Boundary Value Problems	3-51
Numerical Solution of Integral Equations	3-54
Monte Carlo Simulations	3-54
Numerical Solution of Partial Differential Equations	3-54
Fast Fourier Transform	3-59

OPTIMIZATION

Introduction	3-60
Gradient-Based Nonlinear Programming	3-60
Optimization Methods without Derivatives	3-65
Global Optimization	3-66
Mixed Integer Programming	3-67
Development of Optimization Models	3-70

STATISTICS

Introduction	3-70
Enumeration Data and Probability Distributions	3-72
Measurement Data and Sampling Densities	3-73
Tests of Hypothesis	3-78
Least Squares	3-84
Error Analysis of Experiments	3-86
Factorial Design of Experiments and Analysis of Variance	3-86

DIMENSIONAL ANALYSIS

PROCESS SIMULATION

Classification	3-89
Thermodynamics	3-89
Process Modules or Blocks	3-89
Process Topology	3-90
Commercial Packages	3-90

GENERAL REFERENCES: Abramowitz, M., and I. A. Stegun, *Handbook of Mathematical Functions*, National Bureau of Standards, Washington, D.C. (1972); Finlayson, B.A., *Nonlinear Analysis in Chemical Engineering*, McGraw-Hill, New York (1980), Ravenna Park, Seattle (2003); Jeffrey, A., *Mathematics for Engineers and Scientists*, Chapman & Hall/CRC, New York (2004); Jeffrey, A., *Essentials of Engineering Mathematics*, 2d ed., Chapman &

Hall/CRC, New York (2004); Weisstein, E. W., *CRC Concise Encyclopedia of Mathematics*, 2d ed., CRC Press, New York (2002); Wrede, R. C., and Murray R. Spiegel, *Schaum's Outline of Theory and Problems of Advanced Calculus*, 2d ed., McGraw-Hill, New York (2006); Zwillinger, D., *CRC Standard Mathematical Tables and Formulae*, 1st ed., CRC Press, New York (2002); <http://eqworld.ipmnet.ru/>.

MATHEMATICS

GENERAL

The basic problems of the sciences and engineering fall broadly into three categories:

1. *Steady state problems.* In such problems the configuration of the system is to be determined. This solution does not change with time but continues indefinitely in the same pattern, hence the name "steady state." Typical chemical engineering examples include steady temperature distributions in heat conduction, equilibrium in chemical reactions, and steady diffusion problems.

2. *Eigenvalue problems.* These are extensions of equilibrium problems in which critical values of certain parameters are to be determined in addition to the corresponding steady-state configurations. The determination of eigenvalues may also arise in propagation problems and stability problems. Typical chemical engineering problems include those in heat transfer and resonance in which certain boundary conditions are prescribed.

3. *Propagation problems.* These problems are concerned with predicting the subsequent behavior of a system from a knowledge of the initial state. For this reason they are often called the transient (time-varying) or unsteady-state phenomena. Chemical engineering examples include the transient state of chemical reactions (kinetics), the propagation of pressure waves in a fluid, transient behavior of an adsorption column, and the rate of approach to equilibrium of a packed distillation column.

The mathematical treatment of engineering problems involves four basic steps:

1. *Formulation.* The expression of the problem in mathematical language. That translation is based on the appropriate physical laws governing the process.

2. *Solution.* Appropriate mathematical and numerical operations are accomplished so that logical deductions may be drawn from the mathematical model.

3. *Interpretation.* Development of relations between the mathematical results and their meaning in the physical world.

4. *Refinement.* The recycling of the procedure to obtain better predictions as indicated by experimental checks.

Steps 1 and 2 are of primary interest here. The actual details are left to the various subsections, and only general approaches will be discussed.

The formulation step may result in algebraic equations, difference equations, differential equations, integral equations, or combinations of these. In any event these mathematical models usually arise from statements of physical laws such as the laws of mass and energy conservation in the form

$$\text{Input of } x - \text{output of } x + \text{production of } x = \text{accumulation of } x$$

or

$$\text{Rate of input of } x - \text{rate of output of } x + \text{rate of production of } x = \text{rate of accumulation of } x$$

where x = mass, energy, etc. These statements may be abbreviated by the statement

$$\text{Input} - \text{output} + \text{production} = \text{accumulation}$$

Many general laws of the physical universe are expressible by differential equations. Specific phenomena are then singled out from the infinity of solutions of these equations by assigning the individual initial or boundary conditions which characterize the given problem. For steady state or boundary-value problems (Fig. 3-1) the solution must

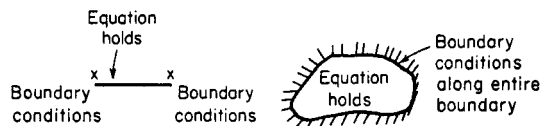


FIG. 3-1 Boundary conditions.

satisfy the differential equation inside the region and the prescribed conditions on the boundary.

In mathematical language, the propagation problem is known as an initial-value problem (Fig. 3-2). Schematically, the problem is characterized by a differential equation plus an open region in which the equation holds. The solution of the differential equation must satisfy the initial conditions plus any "side" boundary conditions.

The description of phenomena in a "continuous" medium such as a gas or a fluid often leads to partial differential equations. In particular, phenomena of "wave" propagation are described by a class of partial differential equations called "hyperbolic," and these are essentially different in their properties from other classes such as those that describe equilibrium ("elliptic") or diffusion and heat transfer ("parabolic"). Prototypes are:

1. *Elliptic.* Laplace's equation

$$\frac{\partial^2 u}{\partial x^2} + \frac{\partial^2 u}{\partial y^2} = 0$$

Poisson's equation

$$\frac{\partial^2 u}{\partial x^2} + \frac{\partial^2 u}{\partial y^2} = g(x, y)$$

These do not contain the variable t (time) explicitly; accordingly, their solutions represent equilibrium configurations. Laplace's equation corresponds to a "natural" equilibrium, while Poisson's equation corresponds to an equilibrium under the influence of $g(x, y)$. Steady heat-transfer and mass-transfer problems are elliptic.

2. *Parabolic.* The heat equation

$$\frac{\partial u}{\partial t} = \frac{\partial^2 u}{\partial x^2} + \frac{\partial^2 u}{\partial y^2}$$

describes unsteady or propagation states of diffusion as well as heat transfer.

3. *Hyperbolic.* The wave equation

$$\frac{\partial^2 u}{\partial t^2} = \frac{\partial^2 u}{\partial x^2} + \frac{\partial^2 u}{\partial y^2}$$

describes wave propagation of all types when the assumption is made that the wave amplitude is small and that interactions are linear.

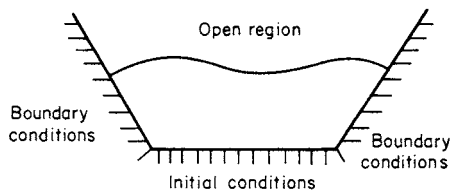


FIG. 3-2 Propagation problem.

3-4 MATHEMATICS

The solution phase has been characterized in the past by a concentration on methods to obtain analytic solutions to the mathematical equations. These efforts have been most fruitful in the area of the linear equations such as those just given. However, many natural phenomena are nonlinear. While there are a few nonlinear problems that can be solved analytically, most cannot. In those cases, numerical methods are used. Due to the widespread availability of software for computers, the engineer has quite good tools available.

Numerical methods almost never fail to provide an answer to any particular situation, but they can never furnish a general solution of any problem.

The mathematical details outlined here include both analytic and numerical techniques useful in obtaining solutions to problems.

Our discussion to this point has been confined to those areas in which the governing laws are well known. However, in many areas, information on the governing laws is lacking and statistical methods are reused. Broadly speaking, statistical methods may be of use whenever conclusions are to be drawn or decisions made on the basis of experimental evidence. Since statistics could be defined as the technology of the scientific method, it is primarily concerned with the first two aspects of the method, namely, the performance of experiments and the drawing of conclusions from experiments. Traditionally the field is divided into two areas:

1. *Design of experiments.* When conclusions are to be drawn or decisions made on the basis of experimental evidence, statistical techniques are most useful when experimental data are subject to errors. The design of experiments may then often be carried out in such a fashion as to avoid some of the sources of experimental error and make the necessary allowances for that portion which is unavoidable. Second, the results can be presented in terms of probability statements which express the reliability of the results. Third, a statistical approach frequently forces a more thorough evaluation of the experimental aims and leads to a more definitive experiment than would otherwise have been performed.

2. *Statistical inference.* The broad problem of statistical inference is to provide measures of the uncertainty of conclusions drawn from experimental data. This area uses the theory of probability, enabling scientists to assess the reliability of their conclusions in terms of probability statements.

Both of these areas, the mathematical and the statistical, are intimately intertwined when applied to any given situation. The methods of one are often combined with the other. And both in order to be successfully used must result in the numerical answer to a problem—that is, they constitute the means to an end. Increasingly the numerical answer is being obtained from the mathematics with the aid of computers. The mathematical notation is given in Table 3-1.

MISCELLANEOUS MATHEMATICAL CONSTANTS

Numerical values of the constants that follow are approximate to the number of significant digits given.

$\pi = 3.1415926536$	Pi
$e = 2.7182818285$	Napierian (natural) logarithm base
$\gamma = 0.5772156649$	Euler's constant
$\ln \pi = 1.1447298858$	Napierian (natural) logarithm of pi, base e
$\log \pi = 0.4971498727$	Briggsian (common logarithm of pi, base 10)
Radian = 57.2957795131°	
Degree = 0.0174532925 rad	
Minute = 0.0002908882 rad	
Second = 0.0000048481 rad	

$$\gamma = \lim_{n \rightarrow \infty} \left(\sum_{m=1}^n \frac{1}{m} - \ln n \right) = 0.577215$$

THE REAL-NUMBER SYSTEM

The natural numbers, or counting numbers, are the positive integers: 1, 2, 3, 4, 5, The negative integers are -1, -2, -3,

A number in the form a/b , where a and b are integers, $b \neq 0$, is a rational number. A real number that cannot be written as the quotient of two integers is called an irrational number, e.g., $\sqrt{2}$, $\sqrt{3}$, $\sqrt{5}$, π , e , $\sqrt[3]{2}$.

TABLE 3-1 Mathematical Signs, Symbols, and Abbreviations

\pm (\mp)	plus or minus (minus or plus)
:	divided by, ratio sign
::	proportional sign
<	less than
\ll	not less than
>	greater than
\gg	not greater than
\cong	approximately equals, congruent
\sim	similar to
\simeq	equivalent to
\neq	not equal to
\doteq	approaches, is approximately equal to
∞	varies as
∞	infinity
\therefore	therefore
$\sqrt{\quad}$	square root
$\sqrt[3]{\quad}$	cube root
$\sqrt[n]{\quad}$	n th root
\angle	angle
\perp	perpendicular to
\parallel	parallel to
$ x $	numerical value of x
\log or \log_{10}	common logarithm or Briggsian logarithm
\log_e or \ln	natural logarithm or hyperbolic logarithm or Napierian logarithm
e	base (2.718) of natural system of logarithms
a°	an angle a degrees
$a' a$	prime, an angle a minutes
$a'' a$	double prime, an angle a seconds, a second
\sin	sine
\cos	cosine
\tan	tangent
ctn or cot	cotangent
\sec	secant
\csc	cosecant
vers	versed sine
covers	covered sine
exsec	exsecant
\sin^{-1}	anti sine or angle whose sine is
\sinh	hyperbolic sine
\cosh	hyperbolic cosine
\tanh	hyperbolic tangent
\sinh^{-1}	anti hyperbolic sine or angle whose hyperbolic sine is
$f(x)$ or $\phi(x)$	function of x
Δx	increment of x
Σ	summation of
dx	differential of x
dy/dx or y'	derivative of y with respect to x
d^2y/dx^2 or y''	second derivative of y with respect to x
$d^n y/dx^n$	n th derivative of y with respect to x
$\partial y/\partial x$	partial derivative of y with respect to x
$\partial^n y/\partial x^n$	n th partial derivative of y with respect to x
$\frac{\partial^n z}{\partial x \partial y}$	n th partial derivative with respect to x and y
\int	integral of
\int_a^b	integral between the limits a and b
\dot{y}	first derivative of y with respect to time
\ddot{y}	second derivative of y with respect to time
Δ or ∇^2	the "Laplacian"
	$\left(\frac{\partial^2}{\partial x^2} + \frac{\partial^2}{\partial y^2} + \frac{\partial^2}{\partial z^2} \right)$
δ	sign of a variation
\oint	sign for integration around a closed path

There is a one-to-one correspondence between the set of real numbers and the set of points on an infinite line (coordinate line).

Order among Real Numbers; Inequalities

- $a > b$ means that $a - b$ is a positive real number.
- If $a < b$ and $b < c$, then $a < c$.
- If $a < b$, then $a \pm c < b \pm c$ for any real number c .
- If $a < b$ and $c > 0$, then $ac < bc$.
- If $a < b$ and $c < 0$, then $ac > bc$.
- If $a < b$ and $c < d$, then $a + c < b + d$.
- If $0 < a < b$ and $0 < c < d$, then $ac < bd$.
- If $a < b$ and $ab > 0$, then $1/a > 1/b$.
- If $a < b$ and $ab < 0$, then $1/a < 1/b$.

Absolute Value For any real number x , $|x| = \begin{cases} x & \text{if } x \geq 0 \\ -x & \text{if } x < 0 \end{cases}$

Properties

- If $|x| = a$, where $a > 0$, then $x = a$ or $x = -a$.
- $|x| = |-x|$; $-|x| \leq x \leq |x|$; $|xy| = |x| |y|$.
- If $|x| < c$, then $-c < x < c$, where $c > 0$.
- $||x| - |y|| \leq |x + y| \leq |x| + |y|$.
- $\sqrt{x^2} = |x|$.

Proportions If $\frac{a}{b} = \frac{c}{d}$, then $\frac{a+b}{b} = \frac{c+d}{d}$, $\frac{a-b}{b} = \frac{c-d}{d}$,

$$\frac{a-b}{a+b} = \frac{c-d}{c+d}$$

Indeterminants

Form	Example	
$(\infty)(0)$	xe^{-x}	$x \rightarrow \infty$
0^0	x^x	$x \rightarrow 0^+$
∞^0	$(\tan x)^{\cos x}$	$x \rightarrow \frac{1}{2}\pi^-$
1^∞	$(1+x)^{1/x}$	$x \rightarrow 0^+$
$\infty - \infty$	$\sqrt{x+1} - \sqrt{x-1}$	$x \rightarrow \infty$
$\frac{0}{0}$	$\frac{\sin x}{x}$	$x \rightarrow 0$
$\frac{\infty}{\infty}$	$\frac{e^x}{x}$	$x \rightarrow \infty$

Integral Exponents (Powers and Roots) If m and n are positive integers and a, b are numbers or functions, then the following properties hold:

$$\begin{aligned}
 a^{-n} &= 1/a^n & a \neq 0 \\
 (ab)^n &= a^n b^n \\
 (a^n)^m &= a^{nm}, & a^n a^m &= a^{n+m} \\
 \sqrt[n]{a} &= a^{1/n} & \text{if } a > 0 \\
 \sqrt[m]{\sqrt[n]{a}} &= \sqrt[mn]{a}, a > 0 \\
 a^{m/n} &= (a^m)^{1/n} = \sqrt[n]{a^m}, a > 0 \\
 a^0 &= 1 (a \neq 0) \\
 0^a &= 0 (a \neq 0)
 \end{aligned}$$

Logarithms $\log ab = \log a + \log b, a > 0, b > 0$

$$\begin{aligned}
 \log a^n &= n \log a \\
 \log (a/b) &= \log a - \log b \\
 \log \sqrt[n]{a} &= (1/n) \log a
 \end{aligned}$$

The common logarithm (base 10) is denoted $\log a$ or $\log_{10} a$. The natural logarithm (base e) is denoted $\ln a$ (or in some texts $\log_e a$). If the text is ambiguous (perhaps using $\log x$ for $\ln x$), test the formula by evaluating it.

Roots If a is a real number, n is a positive integer, then x is called the n th root of a if $x^n = a$. The number of n th roots is n , but not all of them are necessarily real. The principal n th root means the following: (1) if $a > 0$ the principal n th root is the unique positive root, (2) if

$a < 0$, and n odd, it is the unique negative root, and (3) if $a < 0$ and n even, it is any of the complex roots. In cases (1) and (2), the root can be found on a calculator by taking $y = \ln a/n$ and then $x = e^y$. In case (3), see the section on complex variables.

ALGEBRAIC INEQUALITIES

Arithmetic-Geometric Inequality Let A_n and G_n denote respectively the arithmetic and the geometric means of a set of positive numbers a_1, a_2, \dots, a_n . The $A_n \geq G_n$, i.e.,

$$\frac{a_1 + a_2 + \dots + a_n}{n} \geq (a_1 a_2 \dots a_n)^{1/n}$$

The equality holds only if all of the numbers a_i are equal.

Carleman's Inequality The arithmetic and geometric means just defined satisfy the inequality

$$\sum_{r=1}^n (a_1 a_2 \dots a_r)^{1/r} \leq n e A_n$$

where e is the best possible constant in this inequality.

Cauchy-Schwarz Inequality Let $a = (a_1, a_2, \dots, a_n)$, $b = (b_1, b_2, \dots, b_n)$, where the a_i 's and b_i 's are real or complex numbers. Then

$$\left| \sum_{k=1}^n a_k \bar{b}_k \right|^2 \leq \left(\sum_{k=1}^n |a_k|^2 \right) \left(\sum_{k=1}^n |b_k|^2 \right)$$

The equality holds if, and only if, the vectors a, b are linearly dependent (i.e., one vector is scalar times the other vector).

Minkowski's Inequality Let a_1, a_2, \dots, a_n and b_1, b_2, \dots, b_n be any two sets of complex numbers. Then for any real number $p > 1$,

$$\left(\sum_{k=1}^n |a_k + b_k|^p \right)^{1/p} \leq \left(\sum_{k=1}^n |a_k|^p \right)^{1/p} + \left(\sum_{k=1}^n |b_k|^p \right)^{1/p}$$

Hölder's Inequality Let a_1, a_2, \dots, a_n and b_1, b_2, \dots, b_n be any two sets of complex numbers, and let p and q be positive numbers with $1/p + 1/q = 1$. Then

$$\left| \sum_{k=1}^n a_k \bar{b}_k \right| \leq \left(\sum_{k=1}^n |a_k|^p \right)^{1/p} \left(\sum_{k=1}^n |b_k|^q \right)^{1/q}$$

The equality holds if, and only if, the sequences $|a_1|^p, |a_2|^p, \dots, |a_n|^p$ and $|b_1|^q, |b_2|^q, \dots, |b_n|^q$ are proportional and the argument (angle) of the complex numbers $a_k \bar{b}_k$ is independent of k . This last condition is of course automatically satisfied if a_1, \dots, a_n and b_1, \dots, b_n are positive numbers.

Lagrange's Inequality Let a_1, a_2, \dots, a_n and b_1, b_2, \dots, b_n be real numbers. Then

$$\left(\sum_{k=1}^n a_k b_k \right)^2 \leq \left(\sum_{k=1}^n a_k^2 \right) \left(\sum_{k=1}^n b_k^2 \right) - \sum_{1 \leq k < j \leq n} (a_k b_j - a_j b_k)^2$$

Example Two chemical engineers, John and Mary, purchase stock in the same company at times t_1, t_2, \dots, t_n when the price per share is respectively p_1, p_2, \dots, p_n . Their methods of investment are different, however: John purchases x shares each time, whereas Mary invests P dollars each time (fractional shares can be purchased). Who is doing better?

While one can argue intuitively that the average cost per share for Mary does not exceed that for John, we illustrate a mathematical proof using inequalities. The average cost per share for John is equal to

$$\frac{\text{Total money invested}}{\text{Number of shares purchased}} = \frac{x \sum_{i=1}^n p_i}{nx} = \frac{1}{n} \sum_{i=1}^n p_i$$

The average cost per share for Mary is

$$\frac{nP}{\sum_{i=1}^n \frac{P}{p_i}} = \frac{n}{\sum_{i=1}^n \frac{1}{p_i}}$$

3-6 MATHEMATICS

Thus the average cost per share for John is the arithmetic mean of p_1, p_2, \dots, p_n , whereas that for Mary is the harmonic mean of these n numbers. Since the harmonic mean is less than or equal to the arithmetic mean for any set of positive numbers and the two means are equal only if $p_1 = p_2 = \dots = p_n$, we conclude that the average cost per share for Mary is less than that for John if two of the prices p_i are distinct. One can also give a proof based on the Cauchy-Schwarz inequality. To this end, define the vectors

$$a = (p_1^{-1/2}, p_2^{-1/2}, \dots, p_n^{-1/2}) \quad b = (p_1^{1/2}, p_2^{1/2}, \dots, p_n^{1/2})$$

Then $a \cdot b = 1 + \dots + 1 = n$, and so by the Cauchy-Schwarz inequality

$$(a \cdot b)^2 = n^2 \leq \sum_{i=1}^n \frac{1}{p_i} \sum_{i=1}^n p_i$$

with the equality holding only if $p_1 = p_2 = \dots = p_n$. Therefore

$$\frac{n}{\sum_{i=1}^n \frac{1}{p_i}} \leq \frac{\sum_{i=1}^n p_i}{n}$$

MENSURATION FORMULAS

REFERENCES: Liu, J., *Mathematical Handbook of Formulas and Tables*, McGraw-Hill, New York (1999); <http://mathworld.wolfram.com/SphericalSector.html>, etc.

Let A denote areas and V volumes in the following.

PLANE GEOMETRIC FIGURES WITH STRAIGHT BOUNDARIES

Triangles (see also "Plane Trigonometry") $A = \frac{1}{2}bh$ where b = base, h = altitude.

Rectangle $A = ab$ where a and b are the lengths of the sides.

Parallelogram (opposite sides parallel) $A = ah = ab \sin \alpha$ where a, b are the lengths of the sides, h the height, and α the angle between the sides. See Fig. 3-3.

Rhombus (equilateral parallelogram) $A = \frac{1}{2}ab$ where a, b are the lengths of the diagonals.

Trapezoid (four sides, two parallel) $A = \frac{1}{2}(a + b)h$ where the lengths of the parallel sides are a and b , and h = height.

Quadrilateral (four-sided) $A = \frac{1}{2}ab \sin \theta$ where a, b are the lengths of the diagonals and the acute angle between them is θ .

Regular Polygon of n Sides See Fig. 3-4.

$$A = \frac{1}{4}nl^2 \cot \frac{180^\circ}{n} \quad \text{where } l = \text{length of each side}$$

$$R = \frac{l}{2} \csc \frac{180^\circ}{n} \quad \text{where } R \text{ is the radius of the circumscribed circle}$$

$$r = \frac{l}{2} \cot \frac{180^\circ}{n} \quad \text{where } r \text{ is the radius of the inscribed circle}$$

Radius r of Circle Inscribed in Triangle with Sides a, b, c

$$r = \sqrt{\frac{(s-a)(s-b)(s-c)}{s}} \quad \text{where } s = \frac{1}{2}(a+b+c)$$

Radius R of Circumscribed Circle

$$R = \frac{abc}{4\sqrt{s(s-a)(s-b)(s-c)}}$$

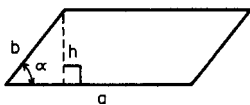


FIG. 3-3 Parallelogram.

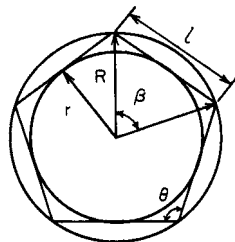


FIG. 3-4 Regular polygon.

Area of Regular Polygon of n Sides Inscribed in a Circle of Radius r

$$A = (nr^2/2) \sin (360^\circ/n)$$

Perimeter of Inscribed Regular Polygon

$$P = 2nr \sin (180^\circ/n)$$

Area of Regular Polygon Circumscribed about a Circle of Radius r

$$A = nr^2 \tan (180^\circ/n)$$

Perimeter of Circumscribed Regular Polygon

$$P = 2nr \tan \frac{180^\circ}{n}$$

PLANE GEOMETRIC FIGURES WITH CURVED BOUNDARIES

Circle (Fig. 3-5) Let

C = circumference

r = radius

D = diameter

A = area

S = arc length subtended by θ

l = chord length subtended by θ

H = maximum rise of arc above chord, $r - H = d$

θ = central angle (rad) subtended by arc S

$$C = 2\pi r = \pi D \quad (\pi = 3.14159 \dots)$$

$$S = r\theta = \frac{1}{2}D\theta$$

$$l = 2\sqrt{r^2 - d^2} = 2r \sin (\theta/2) = 2d \tan (\theta/2)$$

$$d = \frac{1}{2} \sqrt{4r^2 - l^2} = \frac{1}{2} l \cot \frac{\theta}{2}$$

$$\theta = \frac{S}{r} = 2 \cos^{-1} \frac{d}{r} = 2 \sin^{-1} \frac{l}{D}$$

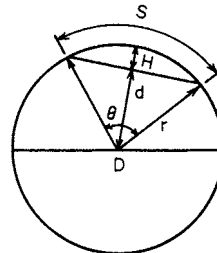


FIG. 3-5 Circle.

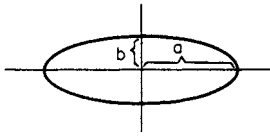


FIG. 3-6 Ellipse.

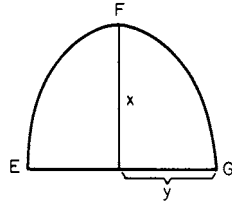


FIG. 3-7 Parabola.

A (circle) = $\pi r^2 = \frac{1}{4}\pi D^2$
 A (sector) = $\frac{1}{2}rS = \frac{1}{2}r^2\theta$
 A (segment) = A (sector) - A (triangle) = $\frac{1}{2}r^2(\theta - \sin \theta)$

Ring (area between two circles of radii r_1 and r_2) The circles need not be concentric, but one of the circles must enclose the other.

$A = \pi(r_1 + r_2)(r_1 - r_2) \quad r_1 > r_2$

Ellipse (Fig. 3-6) Let the semi-axes of the ellipse be a and b

$A = \pi ab$
 $C = 4aE(e)$

where $e^2 = 1 - b^2/a^2$ and $E(e)$ is the complete elliptic integral of the second kind,

$$E(e) = \frac{\pi}{2} \left[1 - \left(\frac{1}{2}\right)^2 e^2 + \dots \right]$$

[an approximation for the circumference $C = 2\pi \sqrt{(a^2 + b^2)/2}$].

Parabola (Fig. 3-7)

Length of arc $EFG = \sqrt{4x^2 + y^2} + \frac{y^2}{2x} \ln \frac{2x + \sqrt{4x^2 + y^2}}{y}$

Area of section $EFG = \frac{4}{3}xy$

Catenary (the curve formed by a cord of uniform weight suspended freely between two points A, B ; Fig. 3-8)

$y = a \cosh (x/a)$

Length of arc between points A and B is equal to $2a \sinh (L/a)$. Sag of the cord is $D = a \cosh (L/a) - a$.

SOLID GEOMETRIC FIGURES WITH PLANE BOUNDARIES

Cube Volume = a^3 ; total surface area = $6a^2$; diagonal = $a\sqrt{3}$, where a = length of one side of the cube.

Rectangular Parallelepiped Volume = abc ; surface area = $2(ab + ac + bc)$; diagonal = $\sqrt{a^2 + b^2 + c^2}$, where a, b, c are the lengths of the sides.

Prism Volume = (area of base) \times (altitude); lateral surface area = (perimeter of right section) \times (lateral edge).

Pyramid Volume = $\frac{1}{3}$ (area of base) \times (altitude); lateral area of regular pyramid = $\frac{1}{2}$ (perimeter of base) \times (slant height) = $\frac{1}{2}$ (number of sides) (length of one side) (slant height).

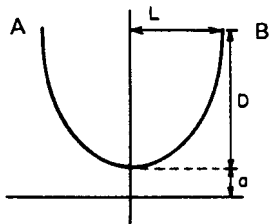


FIG. 3-8 Catenary.

Frustum of Pyramid (formed from the pyramid by cutting off the top with a plane

$V = \frac{1}{3} (A_1 + A_2 + \sqrt{A_1 \cdot A_2})h$

where h = altitude and A_1, A_2 are the areas of the base; lateral area of a regular figure = $\frac{1}{2}$ (sum of the perimeters of base) \times (slant height).

Volume and Surface Area of Regular Polyhedra with Edge l

Type of surface	Name	Volume	Surface area
4 equilateral triangles	Tetrahedron	$0.1179 l^3$	$1.7321 l^2$
6 squares	Hexahedron (cube)	$1.0000 l^3$	$6.0000 l^2$
8 equilateral triangles	Octahedron	$0.4714 l^3$	$3.4641 l^2$
12 pentagons	Dodecahedron	$7.6631 l^3$	$20.6458 l^2$
20 equilateral triangles	Icosahedron	$2.1817 l^3$	$8.6603 l^2$

SOLIDS BOUNDED BY CURVED SURFACES

Cylinders (Fig. 3-9) V = (area of base) \times (altitude); lateral surface area = (perimeter of right section) \times (lateral edge).

Right Circular Cylinder $V = \pi$ (radius)² \times (altitude); lateral surface area = 2π (radius) \times (altitude).

Truncated Right Circular Cylinder

$V = \pi r^2 h$; lateral area = $2\pi r h$

$h = \frac{1}{2} (h_1 + h_2)$

Hollow Cylinders Volume = $\pi h (R^2 - r^2)$, where r and R are the internal and external radii and h is the height of the cylinder.

Sphere (Fig. 3-10)

V (sphere) = $\frac{4}{3}\pi R^3$, $\frac{1}{6}\pi D^3$

V (spherical sector) = $\frac{2}{3}\pi R^2 h_i = 2$ (open spherical sector), $i = 1$ (spherical cone)

V (spherical segment of one base) = $\frac{1}{6}\pi h_1 (3r_2^2 + h_1^2)$

V (spherical segment of two bases) = $\frac{1}{6}\pi h_2 (3r_1^2 + 3r_2^2 + h_2^2)$

A (sphere) = $4\pi R^2 = \pi D^2$

A (zone) = $2\pi R h = \pi D h$

A (lune on the surface included between two great circles, the inclination of which is θ radians) = $2R^2\theta$.

Cone $V = \frac{1}{3}$ (area of base) \times (altitude).

Right Circular Cone $V = (\pi/3) r^2 h$, where h is the altitude and r is the radius of the base; curved surface area = $\pi r \sqrt{r^2 + h^2}$, curved surface of the frustum of a right cone = $\pi(r_1 + r_2) \sqrt{h^2 + (r_1 - r_2)^2}$, where r_1, r_2 are the radii of the base and top, respectively, and h is the altitude; volume of the frustum of a right cone = $\pi(h/3)(r_1^2 + r_1 r_2 + r_2^2) = h/3(A_1 + A_2 + \sqrt{A_1 A_2})$, where A_1 = area of base and A_2 = area of top.

Ellipsoid $V = (\frac{4}{3})\pi abc$, where a, b, c are the lengths of the semi-axes.

Torus (obtained by rotating a circle of radius r about a line whose distance is $R > r$ from the center of the circle)

$V = 2\pi^2 R r^2$ Surface area = $4\pi^2 R r$

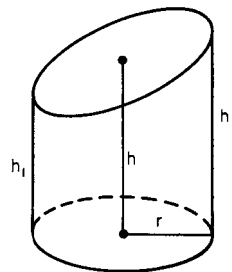


FIG. 3-9 Cylinder.

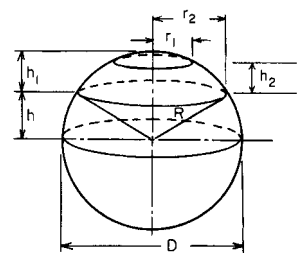


FIG. 3-10 Sphere.

3-8 MATHEMATICS

Prolate Spheroid (formed by rotating an ellipse about its major axis [2a])

$$\text{Surface area} = 2\pi b^2 + 2\pi(ab/e) \sin^{-1} e \quad V = \frac{4}{3}\pi ab^2$$

where a , b are the major and minor axes and e = eccentricity ($e < 1$).

Oblate Spheroid (formed by the rotation of an ellipse about its minor axis [2b]) Data as given previously.

$$\text{Surface area} = 2\pi a^2 + \pi \frac{b^2}{e} \ln \frac{1+e}{1-e} \quad V = \frac{4}{3}\pi a^2 b$$

For process vessels, the formulas reduce to the following:

Hemisphere

$$V = \frac{\pi}{12} D^3, \quad A = \frac{\pi}{2} D^2$$

For a hemisphere (concave up) partially filled to a depth h_1 , use the formulas for spherical segment with one base, which simplify to

$$V = \pi h_1^2 (R - h_1/3) = \pi h_1^2 (D/2 - h_1/3)$$

$$A = 2\pi R h_1 = \pi D h_1$$

For a hemisphere (concave down) partially filled from the bottom, use the formulas for a spherical segment of two bases, one of which is a plane through the center, where h = distance from the center plane to the surface of the partially filled hemisphere.

$$V = \pi h (R^2 - h^2/3) = \pi h (D^2/4 - h^2/3)$$

$$A = 2\pi R h = \pi D h$$

Cone For a cone partially filled, use the same formulas as for right circular cones, but use r and h for the region filled.

Ellipsoid If the base of a vessel is one-half of an oblate spheroid (the cross section fitting to a cylinder is a circle with radius of $D/2$ and the minor axis is smaller), then use the formulas for one-half of an oblate spheroid.

$$V = 0.1745D^3, \quad S = 1.236D^2, \quad \text{minor axis} = D/3$$

$$V = 0.1309D^3, \quad S = 1.084D^2, \quad \text{minor axis} = D/4$$

MISCELLANEOUS FORMULAS

See also "Differential and Integral Calculus."

Volume of a Solid Revolution (the solid generated by rotating a plane area about the x axis)

$$V = \pi \int_a^b [f(x)]^2 dx$$

where $y = f(x)$ is the equation of the plane curve and $a \leq x \leq b$.

Area of a Surface of Revolution

$$S = 2\pi \int_a^b y ds$$

where $ds = \sqrt{1 + (dy/dx)^2} dx$ and $y = f(x)$ is the equation of the plane curve rotated about the x axis to generate the surface.

Area Bounded by $f(x)$, the x Axis, and the Lines $x = a$, $x = b$

$$A = \int_a^b f(x) dx \quad [f(x) \geq 0]$$

Length of Arc of a Plane Curve

If $y = f(x)$,

$$\text{Length of arc } s = \int_a^b \sqrt{1 + \left(\frac{dy}{dx}\right)^2} dx$$

If $x = g(y)$,

$$\text{Length of arc } s = \int_c^d \sqrt{1 + \left(\frac{dx}{dy}\right)^2} dy$$

If $x = f(t)$, $y = g(t)$,

$$\text{Length of arc } s = \int_{t_0}^{t_1} \sqrt{\left(\frac{dx}{dt}\right)^2 + \left(\frac{dy}{dt}\right)^2} dt$$

In general, $(ds)^2 = (dx)^2 + (dy)^2$.

IRREGULAR AREAS AND VOLUMES

Irregular Areas Let y_0, y_1, \dots, y_n be the lengths of a series of equally spaced parallel chords and h be their distance apart (Fig. 3-11). The area of the figure is given approximately by any of the following:

$$A_T = (h/2)[(y_0 + y_n) + 2(y_1 + y_2 + \dots + y_{n-1})] \quad (\text{trapezoidal rule})$$

$$A_S = (h/3)[(y_0 + y_n) + 4(y_1 + y_3 + y_5 + \dots + y_{n-1}) + 2(y_2 + y_4 + \dots + y_{n-2})] \quad (n \text{ even, Simpson's rule})$$

The greater the value of n , the greater the accuracy of approximation.

Irregular Volumes To find the volume, replace the y 's by cross-sectional areas A_j and use the results in the preceding equations.

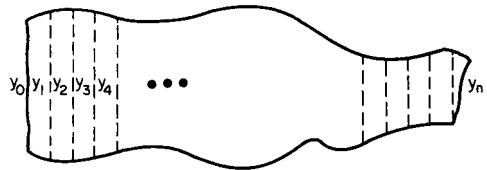


FIG. 3-11 Irregular area.

ELEMENTARY ALGEBRA

REFERENCES: Stillwell, J. C., *Elements of Algebra*, CRC Press, New York (1994); Rich, B., and P. Schmidt, *Schaum's Outline of Elementary Algebra*, McGraw-Hill, New York (2004).

OPERATIONS ON ALGEBRAIC EXPRESSIONS

An algebraic expression will here be denoted as a combination of letters and numbers such as

$$3ax - 3xy + 7x^2 + 7x^{3/2} - 2.8xy$$

Addition and Subtraction Only like terms can be added or subtracted in two algebraic expressions.

Example $(3x + 4xy - x^2) + (3x^2 + 2x - 8xy) = 5x - 4xy + 2x^2$.

Example $(2^x + 3xy - 4x^{1/2}) + (3^x + 6x - 8xy) = 2^x + 3^x + 6x - 5xy - 4x^{1/2}$.

Multiplication Multiplication of algebraic expressions is term by term, and corresponding terms are combined.

Example $(2x + 3y - 2xy)(3 + 3y) = 6x + 9y + 9y^2 - 6xy^2$.

Division This operation is analogous to that in arithmetic.

Example Divide $3e^{2x} + e^x + 1$ by $e^x + 1$.

$$\begin{array}{r}
 \text{Dividend} \\
 \text{Divisor } e^x + 1 \mid 3e^{2x} + e^x + 1 \quad \text{quotient } 3e^{2x} + 3e^x \\
 \underline{-2e^x + 1} \\
 \underline{-2e^x - 2} \\
 + 3 \text{ (remainder)}
 \end{array}$$

Therefore, $3e^{2x} + e^x + 1 = (e^x + 1)(3e^x - 2) + 3$.

Operations with Zero All numerical computations (except division) can be done with zero: $a + 0 = 0 + a = a$; $a - 0 = a$; $0 - a = -a$; $(a)(0) = 0$; $a^0 = 1$ if $a \neq 0$; $0/a = 0$, $a \neq 0$. $a/0$ and $0/0$ have no meaning.

Fractional Operations

$$-\frac{x}{y} = -\left(\frac{-x}{-y}\right) = \frac{x}{-y} = \frac{-x}{y}; \quad \frac{x}{y} = \frac{-x}{-y}; \quad \frac{x}{y} = \frac{ax}{ay}, \text{ if } a \neq 0.$$

$$\frac{x}{y} \pm \frac{z}{y} = \frac{x \pm z}{y}; \quad \left(\frac{x}{y}\right)\left(\frac{z}{t}\right) = \frac{xz}{yt}; \quad \frac{x/y}{z/t} = \left(\frac{x}{y}\right)\left(\frac{t}{z}\right) = \frac{xt}{yz}$$

Factoring That process of analysis consisting of reducing a given expression into the product of two or more simpler expressions called *factors*. Some of the more common expressions are factored here:

- (1) $(x^2 - y^2) = (x - y)(x + y)$
- (2) $x^2 + 2xy + y^2 = (x + y)^2$
- (3) $x^3 - y^3 = (x - y)(x^2 + xy + y^2)$
- (4) $(x^3 + y^3) = (x + y)(x^2 - xy + y^2)$
- (5) $(x^4 - y^4) = (x - y)(x + y)(x^2 + y^2)$
- (6) $x^5 + y^5 = (x + y)(x^4 - x^3y + x^2y^2 - xy^3 + y^4)$
- (7) $x^n - y^n = (x - y)(x^{n-1} + x^{n-2}y + x^{n-3}y^2 + \dots + y^{n-1})$

Laws of Exponents

$(a^n)^m = a^{nm}$; $a^{n+m} = a^n \cdot a^m$; $a^{n/m} = (a^n)^{1/m}$; $a^{-n} = a^n/a^m$; $a^{1/m} = \sqrt[m]{a}$; $a^{1/2} = \sqrt{a}$; $\sqrt{x^2} = |x|$ (absolute value of x). For $x > 0$, $y > 0$, $\sqrt{xy} = \sqrt{x}\sqrt{y}$; for $x > 0$, $\sqrt[n]{x^m} = x^{m/n}$; $\sqrt[n]{1/x} = 1/\sqrt[n]{x}$

THE BINOMIAL THEOREM

If n is a positive integer,

$$\begin{aligned}
 (a + b)^n &= a^n + na^{n-1}b + \frac{n(n-1)}{2!} a^{n-2}b^2 \\
 &\quad + \frac{n(n-1)(n-2)}{3!} a^{n-3}b^3 + \dots + b^n = \sum_{j=0}^n \binom{n}{j} a^{n-j}b^j
 \end{aligned}$$

where $\binom{n}{j} = \frac{n!}{j!(n-j)!}$ = number of combinations of n things taken j at a time. $n! = 1 \cdot 2 \cdot 3 \cdot 4 \cdot \dots \cdot n$, $0! = 1$.

Example Find the sixth term of $(x + 2y)^{12}$. The sixth term is obtained by setting $j = 5$. It is

$$\binom{12}{5} x^{12-5}(2y)^5 = 792x^7(2y)^5$$

Example $\sum_{j=0}^{14} \binom{14}{j} = (1 + 1)^{14} = 2^{14}$.

If n is not a positive integer, the sum formula no longer applies and an infinite series results for $(a + b)^n$. The coefficients are obtained from the first formulas in this case.

Example $(1 + x)^{1/2} = 1 + \frac{1}{2}x - \frac{1}{2} \cdot \frac{1}{4}x^2 + \frac{1}{2} \cdot \frac{1}{4} \cdot \frac{3}{6}x^3 \dots$ (convergent for $x^2 < 1$).

Additional discussion is under "Infinite Series."

PROGRESSIONS

An arithmetic progression is a succession of terms such that each term, except the first, is derivable from the preceding by the addition of a quantity d called the common difference. All arithmetic progressions have the form $a, a + d, a + 2d, a + 3d, \dots$. With a = first term, l = last term, d = common difference, n = number of terms, and s = sum of the terms, the following relations hold:

$$\begin{aligned}
 l &= a + (n - 1)d = \frac{s}{n} + \frac{(n - 1)}{2} d \\
 s &= \frac{n}{2} [2a + (n - 1)d] = \frac{n}{2} (a + l) = \frac{n}{2} [2l - (n - 1)d] \\
 a &= l - (n - 1)d = \frac{s}{n} - \frac{(n - 1)d}{2} = \frac{2s}{n} - l \\
 d &= \frac{l - a}{n - 1} = \frac{2(s - an)}{n(n - 1)} = \frac{2(nl - s)}{n(n - 1)} \\
 n &= \frac{l - a}{d} + 1 = \frac{2s}{l + a}
 \end{aligned}$$

The **arithmetic mean or average** of two numbers a, b is $(a + b)/2$; of n numbers a_1, \dots, a_n is $(a_1 + a_2 + \dots + a_n)/n$.

A **geometric progression** is a succession of terms such that each term, except the first, is derivable from the preceding by the multiplication of a quantity r called the common ratio. All such progressions have the form $a, ar, ar^2, \dots, ar^{n-1}$. With a = first term, l = last term, r = ratio, n = number of terms, s = sum of the terms, the following relations hold:

$$\begin{aligned}
 l &= ar^{n-1} = \frac{[a + (r - 1)s]}{r} = \frac{(r - 1)sr^{n-1}}{r^n - 1} \\
 s &= \frac{a(r^n - 1)}{r - 1} = \frac{a(1 - r^n)}{1 - r} = \frac{rl - a}{r - 1} = \frac{lr^n - l}{r^n - r^{n-1}} \\
 a &= \frac{l}{r^{n-1}} = \frac{(r - 1)s}{r^n - 1}, \quad r = \frac{s - a}{s - l}, \quad \log r = \frac{\log l - \log a}{n - 1} \\
 n &= \frac{\log l - \log a}{\log r} + 1 = \frac{\log[a + (r - 1)s] - \log a}{\log r}
 \end{aligned}$$

The geometric mean of two nonnegative numbers a, b is \sqrt{ab} ; of n numbers is $(a_1 a_2 \dots a_n)^{1/n}$. The geometric mean of a set of positive numbers is less than or equal to the arithmetic mean.

Example Find the sum of $1 + \frac{1}{2} + \frac{1}{4} + \dots + \frac{1}{64}$. Here $a = 1$, $r = \frac{1}{2}$, $n = 7$. Thus

$$\begin{aligned}
 s &= \frac{\frac{1}{2}(\frac{1}{64}) - 1}{\frac{1}{2} - 1} = 127/64 \\
 s &= a + ar + ar^2 + \dots + ar^{n-1} = \frac{a}{1 - r} - \frac{ar^n}{1 - r}
 \end{aligned}$$

If $|r| < 1$, then $\lim_{n \rightarrow \infty} s = \frac{a}{1 - r}$

which is called the sum of the infinite geometric progression.

Example The present worth (PW) of a series of cash flows C_k at the end of year k is

$$PW = \sum_{k=1}^n \frac{C_k}{(1 + i)^k}$$

where i is an assumed interest rate. (Thus the present worth always requires specification of an interest rate.) If all the payments are the same, $C_k = R$, the present worth is

$$PW = R \sum_{k=1}^n \frac{1}{(1 + i)^k}$$

This can be rewritten as

$$PW = \frac{R}{1 + i} \sum_{k=1}^n \frac{1}{(1 + i)^{k-1}} = \frac{R}{1 + i} \sum_{j=0}^{n-1} \frac{1}{(1 + i)^j}$$

3-10 MATHEMATICS

This is a geometric series with $r = 1/(1+i)$ and $a = R/(1+i)$. The formulas above give

$$PW (=s) = \frac{R}{i} \frac{(1+i)^n - 1}{(1+i)^n}$$

The same formula applies to the value of an annuity (PW) now, to provide for equal payments R at the end of each of n years, with interest rate i .

A progression of the form $a, (a+d)r, (a+2d)r^2, (a+3d)r^3$, etc., is a combined arithmetic and geometric progression. The sum of n such terms is

$$s = \frac{a - [a + (n-1)d]r^n}{1-r} + \frac{rd(1-r^{n-1})}{(1-r)^2}$$

If $|r| < 1$, $\lim_{n \rightarrow \infty} s = \frac{a}{1-r} + \frac{rd}{(1-r)^2}$.

The non-zero numbers a, b, c , etc., form a harmonic progression if their reciprocals $1/a, 1/b, 1/c$, etc., form an arithmetic progression.

Example The progression $1, \frac{1}{3}, \frac{1}{6}, \frac{1}{9}, \dots, \frac{1}{31}$ is harmonic since $1, 3, 5, 7, \dots, 31$ form an arithmetic progression.

The **harmonic mean** of two numbers a, b is $2ab/(a+b)$.

PERMUTATIONS, COMBINATIONS, AND PROBABILITY

Each separate arrangement of all or a part of a set of things is called a **permutation**. The number of permutations of n things taken r at a time, written

$$P(n, r) = \frac{n!}{(n-r)!} = n(n-1)(n-2) \cdots (n-r+1)$$

Each separate selection of objects that is possible irrespective of the order in which they are arranged is called a combination. The number of combinations of n things taken r at a time, written $C(n, r) = n!/[r!(n-r)!]$.

An important relation is $r! C(n, r) = P(n, r)$.

If an event can occur in p ways and fail to occur in q ways, all ways being equally likely, the **probability** of its occurrence is $p/(p+q)$, and that of its failure $q/(p+q)$.

Example Two dice may be thrown in 36 separate ways. What is the probability of throwing such that their sum is 7? Seven may arise in 6 ways: 1 and 6, 2 and 5, 3 and 4, 4 and 3, 5 and 2, 6 and 1. The probability of shooting 7 is $1/6$.

THEORY OF EQUATIONS

Linear Equations A linear equation is one of the first degree (i.e., only the first powers of the variables are involved), and the process of obtaining definite values for the unknown is called solving the equation. Every linear equation in one variable is written $Ax + B = 0$ or $x = -B/A$. Linear equations in n variables have the form

$$\begin{aligned} a_{11}x_1 + a_{12}x_2 + \cdots + a_{1n}x_n &= b_1 \\ a_{21}x_1 + a_{22}x_2 + \cdots + a_{2n}x_n &= b_2 \\ \vdots \\ a_{m1}x_1 + a_{m2}x_2 + \cdots + a_{mn}x_n &= b_m \end{aligned}$$

The solution of the system may then be found by elimination or matrix methods if a solution exists (see "Matrix Algebra and Matrix Computations").

Quadratic Equations Every quadratic equation in one variable is expressible in the form $ax^2 + bx + c = 0$, $a \neq 0$. This equation has two solutions, say, x_1, x_2 , given by

$$\left. \begin{aligned} x_1 \\ x_2 \end{aligned} \right\} = \frac{-b \pm \sqrt{b^2 - 4ac}}{2a}$$

If a, b, c are real, the discriminant $b^2 - 4ac$ gives the character of the roots. If $b^2 - 4ac > 0$, the roots are real and unequal. If $b^2 - 4ac < 0$, the roots are complex conjugates. If $b^2 - 4ac = 0$ the roots are **real and equal**. Two quadratic equations in two variables can in general be solved only by numerical methods (see "Numerical Analysis and Approximate Methods").

Cubic Equations A cubic equation, in one variable, has the form $x^3 + bx^2 + cx + d = 0$. Every cubic equation having complex coefficients has three complex roots. If the coefficients are real numbers, then at least one of the roots must be real. The cubic equation $x^3 + bx^2 + cx + d = 0$ may be reduced by the substitution $x = y - (b/3)$ to the form $y^3 + py + q = 0$, where $p = \frac{1}{3}(3c - b^2)$, $q = \frac{1}{27}(27d - 9bc + 2b^3)$. This equation has the solutions $y_1 = A + B$, $y_2 = -\frac{1}{2}(A + B) + (i\sqrt{3}/2)(A - B)$, $y_3 = -\frac{1}{2}(A + B) - (i\sqrt{3}/2)(A - B)$, where $i^2 = -1$, $A = \sqrt[3]{-q/2 + \sqrt{R}}$, $B = \sqrt[3]{-q/2 - \sqrt{R}}$, and $R = (p/3)^3 + (q/2)^2$. If b, c, d are all real and if $R > 0$, there are one real root and two conjugate complex roots; if $R = 0$, there are three real roots, of which at least two are equal; if $R < 0$, there are three real unequal roots. If $R < 0$, these formulas are impractical. In this case, the roots are given by $y_k = \sqrt[3]{2} \sqrt{-p/3} \cos[(\phi/3) + 120k]$, $k = 0, 1, 2$ where

$$\phi = \cos^{-1} \sqrt{\frac{q^2/4}{-p^3/27}}$$

and the upper sign applies if $q > 0$, the lower if $q < 0$.

Example $y^3 - 7y + 7 = 0$, $p = -7$, $q = 7$, $R < 0$. Hence

$$y_k = -\sqrt{\frac{28}{3}} \cos\left(\frac{\phi}{3} + 120k\right)$$

where $\phi = \cos^{-1} \sqrt{\frac{27}{28}}$, $\frac{\phi}{3} = 3.6311315 \text{ rad} = 3^\circ 37' 52''$

The roots are approximately -3.048917 , 1.692021 , and 1.356896 .

Example Many equations of state involve solving cubic equations for the compressibility factor Z . For example, the Redlich-Kwong-Soave equation of state requires solving

$$Z^3 - Z^2 + cZ + d = 0, \quad d < 0$$

where c and d depend on critical constants of the chemical species. In this case, only positive solutions, $Z > 0$, are desired.

Quartic Equations See Abramowitz and Stegun (1972, p. 17).

General Polynomials of the n th Degree Denote the general polynomial equation of degree n by

$$P(x) = a_0x^n + a_1x^{n-1} + \cdots + a_{n-1}x + a_n = 0$$

If $n > 4$, there is no formula which gives the roots of the general equation. For fourth and higher order (even third order), the roots can be found numerically (see "Numerical Analysis and Approximate Methods"). However, there are some general theorems that may prove useful.

Remainder Theorems When $P(x)$ is a polynomial and $P(x)$ is divided by $x - a$ until a remainder independent of x is obtained, this remainder is equal to $P(a)$.

Example $P(x) = 2x^4 - 3x^2 + 7x - 2$ when divided by $x + 1$ (here $a = -1$) results in $P(x) = (x + 1)(2x^3 - 2x^2 - x + 8) - 10$ where -10 is the remainder. It is easy to see that $P(-1) = -10$.

Factor Theorem If $P(a)$ is zero, the polynomial $P(x)$ has the factor $x - a$. In other words, if a is a root of $P(x) = 0$, then $x - a$ is a factor of $P(x)$.

If a number a is found to be a root of $P(x) = 0$, the division of $P(x)$ by $(x - a)$ leaves a polynomial of degree one less than that of the original equation, i.e., $P(x) = Q(x)(x - a)$. Roots of $Q(x) = 0$ are clearly roots of $P(x) = 0$.

Example $P(x) = x^3 - 6x^2 + 11x - 6 = 0$ has the root $+3$. Then $P(x) = (x - 3)(x^2 - 3x + 2)$. The roots of $x^2 - 3x + 2 = 0$ are 1 and 2. The roots of $P(x)$ are therefore 1, 2, 3.

Fundamental Theorem of Algebra Every polynomial of degree n has exactly n real or complex roots, counting multiplicities.

Every polynomial equation $a_0x^n + a_1x^{n-1} + \cdots + a_n = 0$ with **rational coefficients** may be rewritten as a polynomial, of the same degree, with **integral coefficients** by multiplying each coefficient by the least common multiple of the denominators of the coefficients.

Example The coefficients of $\frac{1}{2}x^4 + \frac{7}{3}x^3 - \frac{5}{6}x^2 + 2x - \frac{1}{6} = 0$ are rational numbers. The least common multiple of the denominators is $2 \times 3 \times 6 = 6$. Therefore, the equation is equivalent to $9x^4 + 14x^3 - 5x^2 + 12x - 1 = 0$.

Determinants Consider the system of two linear equations

$$\begin{aligned} a_{11}x_1 + a_{12}x_2 &= b_1 \\ a_{21}x_1 + a_{22}x_2 &= b_2 \end{aligned}$$

If the first equation is multiplied by a_{22} and the second by $-a_{12}$ and the results added, we obtain

$$(a_{11}a_{22} - a_{21}a_{12})x_1 = b_1a_{22} - b_2a_{12}$$

The expression $a_{11}a_{22} - a_{21}a_{12}$ may be represented by the symbol

$$\begin{vmatrix} a_{11} & a_{12} \\ a_{21} & a_{22} \end{vmatrix} = a_{11}a_{22} - a_{21}a_{12}$$

This symbol is called a determinant of second order. The value of the square array of n^2 quantities a_{ij} , where $i = 1, \dots, n$ is the row index, $j = 1, \dots, n$ the column index, written in the form

$$|A| = \begin{vmatrix} a_{11} & a_{12} & \dots & a_{1n} \\ a_{21} & a_{22} & \dots & a_{2n} \\ \vdots & \vdots & \ddots & \vdots \\ a_{n1} & a_{n2} & \dots & a_{nn} \end{vmatrix}$$

is called a determinant. The n^2 quantities a_{ij} are called the elements of the determinant. In the determinant $|A|$ let the i th row and j th column be deleted and a new determinant be formed having $n - 1$ rows and columns. This new determinant is called the minor of a_{ij} denoted M_{ij} .

Example $\begin{vmatrix} a_{11} & a_{12} & a_{13} \\ a_{21} & a_{22} & a_{23} \\ a_{31} & a_{32} & a_{33} \end{vmatrix}$ The minor of a_{23} is $M_{23} = \begin{vmatrix} a_{11} & a_{12} \\ a_{31} & a_{32} \end{vmatrix}$

The cofactor A_{ij} of the element a_{ij} is the signed minor of a_{ij} determined by the rule $A_{ij} = (-1)^{i+j}M_{ij}$. The value of $|A|$ is obtained by forming any of the equivalent expressions $\sum_{j=1}^n a_{ij}A_{ij}$, $\sum_{i=1}^n a_{ij}A_{ij}$, where the elements a_{ij} must be taken from a single row or a single column of A .

Example

$$\begin{vmatrix} a_{11} & a_{12} & a_{13} \\ a_{21} & a_{22} & a_{23} \\ a_{31} & a_{32} & a_{33} \end{vmatrix} = a_{31}A_{31} + a_{32}A_{32} + a_{33}A_{33}$$

$$= a_{31} \begin{vmatrix} a_{12} & a_{13} \\ a_{22} & a_{23} \end{vmatrix} - a_{32} \begin{vmatrix} a_{11} & a_{13} \\ a_{21} & a_{23} \end{vmatrix} + a_{33} \begin{vmatrix} a_{11} & a_{12} \\ a_{21} & a_{22} \end{vmatrix}$$

In general, A_{ij} will be determinants of order $n - 1$, but they may in turn be expanded by the rule. Also,

$$\sum_{j=1}^n a_{ji}A_{jk} = \sum_{j=1}^n a_{ij}A_{jk} = \begin{cases} |A| & i = k \\ 0 & i \neq k \end{cases}$$

Fundamental Properties of Determinants

1. The value of a determinant $|A|$ is not changed if the rows and columns are interchanged.
2. If the elements of one row (or one column) of a determinant are all zero, the value of $|A|$ is zero.
3. If the elements of one row (or column) of a determinant are multiplied by the same constant factor, the value of the determinant is multiplied by this factor.
4. If one determinant is obtained from another by interchanging any two rows (or columns), the value of either is the negative of the value of the other.
5. If two rows (or columns) of a determinant are identical, the value of the determinant is zero.
6. If two determinants are identical except for one row (or column), the sum of their values is given by a single determinant obtained by adding corresponding elements of dissimilar rows (or columns) and leaving unchanged the remaining elements.
7. The value of a determinant is not changed if one row (or column) is multiplied by a constant and added to another row (or column).

ANALYTIC GEOMETRY

REFERENCES: Fuller, G., *Analytic Geometry*, 7th ed., Addison Wesley Longman (1994); Larson, R., R. P. Hostetler, and B. H. Edwards, *Calculus with Analytic Geometry*, 7th ed., Houghton Mifflin (2001); Riddle, D. F., *Analytic Geometry*, 6th ed., Thompson Learning (1996); Spiegel, M. R., and J. Liu, *Mathematical Handbook of Formulas and Tables*, 2d ed., McGraw-Hill (1999); Thomas, G. B., Jr., and R. L. Finney, *Calculus and Analytic Geometry*, 9th ed., Addison-Wesley (1996).

Analytic geometry uses algebraic equations and methods to study geometric problems. It also permits one to visualize algebraic equations in terms of geometric curves, which frequently clarifies abstract concepts.

PLANE ANALYTIC GEOMETRY

Coordinate Systems The basic concept of analytic geometry is the establishment of a one-to-one correspondence between the points of the plane and number pairs (x, y) . This correspondence may be done in a number of ways. The rectangular or cartesian coordinate system consists of two straight lines intersecting at right angles (Fig. 3-12). A point is designated by (x, y) , where x (the abscissa) is the distance of the point from the y axis measured parallel to the x axis,

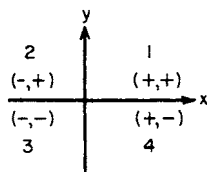


FIG. 3-12 Rectangular coordinates.

positive if to the right, negative to the left. y (ordinate) is the distance of the point from the x axis, measured parallel to the y axis, positive if above, negative if below the x axis. The **quadrants** are labeled 1, 2, 3, 4 in the drawing, the coordinates of points in the various quadrants having the depicted signs. Another common coordinate system is the polar coordinate system (Fig. 3-13). In this system the position of a point is designated by the pair (r, θ) , $r = \sqrt{x^2 + y^2}$ being the distance to the origin $(0,0)$ and θ being the angle the line r makes with the positive x axis (polar axis). To change from polar to rectangular coordinates, use $x = r \cos \theta$ and $y = r \sin \theta$. To change from rectangular to polar coordinates, use $r = \sqrt{x^2 + y^2}$ and $\theta = \tan^{-1}(y/x)$ if $x \neq 0$; $\theta = \pi/2$ if $x = 0$. The distance between two points (x_1, y_1) , (x_2, y_2) is defined by $d = \sqrt{(x_1 - x_2)^2 + (y_1 - y_2)^2}$ in rectangular coordinates or by $d = \sqrt{r_1^2 + r_2^2 - 2r_1r_2 \cos(\theta_1 - \theta_2)}$ in polar coordinates. Other coordinate systems are sometimes used. For example, on the surface of a sphere latitude and longitude prove useful.

The Straight Line (Fig. 3-14) The slope m of a straight line is the tangent of the inclination angle θ made with the positive x axis. If

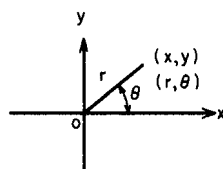


FIG. 3-13 Polar coordinates.

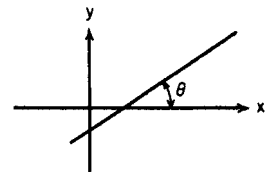


FIG. 3-14 Straight line.

3-12 MATHEMATICS

(x_1, y_1) and (x_2, y_2) are any two points on the line, slope $m = (y_2 - y_1)/(x_2 - x_1)$. The slope of a line parallel to the x axis is zero; parallel to the y axis, it is undefined. Two lines are parallel if and only if they have the same slope. Two lines are perpendicular if and only if the product of their slopes is -1 (the exception being that case when the lines are parallel to the coordinate axes). Every equation of the type $Ax + By + C = 0$ represents a straight line, and every straight line has an equation of this form. A straight line is determined by a variety of conditions:

Given conditions	Equation of line
(1) Parallel to x axis	$y = \text{constant}$
(2) Parallel y axis	$x = \text{constant}$
(3) Point (x_1, y_1) and slope m	$y - y_1 = m(x - x_1)$
(4) Intercept on y axis $(0, b)$, m	$y = mx + b$
(5) Intercept on x axis $(a, 0)$, m	$y = m(x - a)$
(6) Two points (x_1, y_1) , (x_2, y_2)	$y - y_1 = \frac{y_2 - y_1}{x_2 - x_1}(x - x_1)$
(7) Two intercepts $(a, 0)$, $(0, b)$	$x/a + y/b = 1$

The angle β a line with slope m_1 makes with a line having slope m_2 is given by $\tan \beta = (m_2 - m_1)/(m_1 m_2 + 1)$. A line is determined if the length and direction of the perpendicular to it (the normal) from the origin are given (see Fig. 3-15). Let p = length of the perpendicular and α the angle that the perpendicular makes with the positive x axis. The equation of the line is $x \cos \alpha + y \sin \alpha = p$. The equation of a line perpendicular to a given line of slope m and passing through a point (x_1, y_1) is $y - y_1 = -(1/m)(x - x_1)$. The distance from a point (x_1, y_1) to a line with equation $Ax + By + C = 0$ is

$$d = \frac{|Ax_1 + By_1 + C|}{\sqrt{A^2 + B^2}}$$

Occasionally some nonlinear algebraic equations can be reduced to linear equations under suitable substitutions or changes of variables. In other words, certain curves become the graphs of lines if the scales or coordinate axes are appropriately transformed.

Example Consider $y = bx^n$. $B = \log b$. Taking logarithms $\log y = n \log x + \log b$. Let $Y = \log y$, $X = \log x$, $B = \log b$. The equation then has the form $Y = nX + B$, which is a linear equation. Consider $k = k_0 \exp(-E/RT)$, taking logarithms $\log_e k = \log_e k_0 - E/(RT)$. Let $Y = \log_e k$, $B = \log_e k_0$, and $m = -E/R$, $X = 1/T$, and the result is $Y = mX + B$. Next consider $y = a + bx^n$. If the substitution $t = x^n$ is made, then the graph of y is a straight line versus t .

Asymptotes The limiting position of the tangent to a curve as the point of contact tends to an infinite distance from the origin is called an **asymptote**. If the equation of a given curve can be expanded in a Laurent power series such that

$$f(x) = \sum_{k=0}^n a_k x^k + \sum_{k=1}^n \frac{b_k}{x^k}$$

and

$$\lim_{x \rightarrow \infty} f(x) = \sum_{k=0}^n a_k x^k$$

then the equation of the asymptote is $y = \sum_{k=0}^n a_k x^k$. If $n = 1$, then the asymptote is (in general oblique) a line. In this case, the equation of the asymptote may be written as

$$y = mx + b \quad m = \lim_{x \rightarrow \infty} f'(x)$$

$$b = \lim_{x \rightarrow \infty} [f(x) - xf'(x)]$$

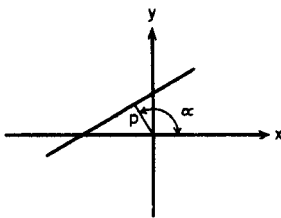


FIG. 3-15 Determination of line.

Geometric Properties of a Curve When the Equation Is Given The analysis of the properties of an equation is facilitated by the investigation of the equation by using the following techniques:

1. *Points of maximum, minimum, and inflection.* These may be investigated by means of the calculus.
2. *Symmetry.* Let $F(x, y) = 0$ be the equation of the curve.

Condition on $F(x, y)$	Symmetry
$F(x, y) = F(-x, y)$	With respect to y axis
$F(x, y) = F(x, -y)$	With respect to x axis
$F(x, y) = F(-x, -y)$	With respect to origin
$F(x, y) = F(y, x)$	With respect to the line $y = x$

3. *Extent.* Only real values of x and y are considered in obtaining the points (x, y) whose coordinates satisfy the equation. The extent of them may be limited by the condition that negative numbers do not have real square roots.

4. *Intercepts.* Find those points where the curves of the function cross the coordinate axes.

5. *Asymptotes.* See preceding discussion.

6. *Direction at a point.* This may be found from the derivative of the function at a point. This concept is useful for distinguishing among a family of similar curves.

Example $y^2 = (x^2 + 1)/(x^2 - 1)$ is symmetric with respect to the x and y axis, the origin, and the line $y = x$. It has the vertical asymptotes $x = \pm 1$. When $x = 0$, $y^2 = -1$; so there are no y intercepts. If $y = 0$, $(x^2 + 1)/(x^2 - 1) = 0$; so there are no x intercepts. If $|x| < 1$, y^2 is negative; so $|x| > 1$. From $x^2 = (y^2 + 1)/(y^2 - 1)$, $y = \pm 1$ are horizontal asymptotes and $|y| > 1$. As $x \rightarrow 1^+$, $y \rightarrow +\infty$; as $x \rightarrow +\infty$, $y \rightarrow +1$. The graph is given in Fig. 3-16.

Conic Sections The curves included in this group are obtained from plane sections of the cone. They include the circle, ellipse, parabola, hyperbola, and degeneratively the point and straight line. A **conic** is the locus of a point whose distance from a fixed point called the **focus** is in a constant ratio to its distance from a fixed line, called the **directrix**. This ratio is the eccentricity e . If $e = 0$, the conic is a circle; if $0 < e < 1$, the conic is an ellipse; if $e = 1$, the conic is a parabola; if $e > 1$, the conic is a hyperbola. Every conic section is representable by an equation of second degree. Conversely, every equation of second degree in two variables represents a conic. The general equation of the second degree is $Ax^2 + Bxy + Cy^2 + Dx + Ey + F = 0$. Let Δ be defined as the determinant

$$\Delta = \begin{vmatrix} 2A & B & D \\ B & 2C & E \\ D & E & 2F \end{vmatrix}$$

The table characterizes the curve represented by the equation.

	$B^2 - 4AC < 0$	$B^2 - 4AC = 0$	$B^2 - 4AC > 0$
$\Delta \neq 0$	$A\Delta < 0$ $A \neq C$, an ellipse $A\Delta < 0$ $A = C$, a circle $A\Delta > 0$, no locus	Parabola	Hyperbola
$\Delta = 0$	Point	2 parallel lines if $Q = D^2 + E^2 - 4(A + C)F > 0$ 1 straight line if $Q = 0$, no locus if $Q < 0$	2 intersecting straight lines

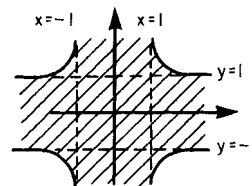


FIG. 3-16 Graph of $y^2 = (x^2 + 1)/(x^2 - 1)$.

Some common equations in parametric form are given below.

(1) $(x - h)^2 + (y - k)^2 = a^2$	$x = h + a \cos \theta$ $y = k + a \sin \theta$	Circle (Fig. 3-23) Parameter is angle θ .
(2) $\frac{(x - h)^2}{a^2} + \frac{(y - k)^2}{b^2} = 1$	$x = h + a \cos \phi$ $y = k + a \sin \phi$	Ellipse (Fig. 3-20) Parameter is angle ϕ .
(3) $x^2 + y^2 = a^2$	$x = \frac{-at}{\sqrt{t^2 + 1}}$ $y = \frac{a}{\sqrt{t^2 + 1}}$	Circle Parameter is $t = \frac{dy}{dx}$ = slope of tangent at (x, y) .
(4) $x^2 = y + k$		Parabola (Fig. 3-22)
(5) $\frac{x^2}{a^2} - \frac{y^2}{b^2} = 1$		Hyperbola with the origin at the center (Fig. 3-21)
(6) $y = a \cosh \frac{x}{a}$	$x = a \sinh^{-1} \frac{s}{a}$ $y^2 = a^2 + s^2$	Catenary (such as hanging cable under gravity) Parameter s = arc length from $(0, a)$ to (x, y) .
(7) Cycloid	$x = a(\phi - \sin \phi)$ $y = a(1 - \cos \phi)$	Fig. 3.24

Example $3x^2 + 4xy - 2y^2 + 3x - 2y + 7 = 0$.

$$\Delta = \begin{vmatrix} 6 & 4 & 3 \\ 4 & -4 & -2 \\ 3 & -2 & 14 \end{vmatrix} = -596 \neq 0, B^2 - 4AC = 40 > 0$$

The curve is therefore a hyperbola.

The following tabulation gives the form of the more common equations.

Polar equation	Type of curve
(1) $r = a$	Circle, Fig. 3-17
(2) $r = 2a \cos \theta$	Circle, Fig. 3-18
(3) $r = 2a \sin \theta$	Circle, Fig. 3-19
(4) $r^2 - 2br \cos(\theta - \beta) + b^2 - a^2 = 0$	Circle at (b, β) , radius a
(5) $r = \frac{ke}{1 - e \cos \theta}$	$e = 1$ parabola, Fig. 3-22 $0 < e < 1$ ellipse, Fig. 3-20 $e > 1$ hyperbola, Fig. 3-21

Parametric Equations It is frequently useful to write the equations of a curve in terms of an auxiliary variable called a parameter. For example, a circle of radius a , center at $(0, 0)$, can be written in the equivalent form $x = a \cos \phi, y = a \sin \phi$ where ϕ is the parameter.

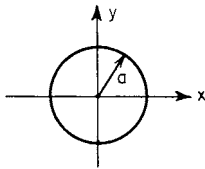


FIG. 3-17 Circle center $(0,0)$ $r = a$.

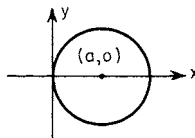


FIG. 3-18 Circle center $(a,0)$ $r = 2a \cos \theta$.

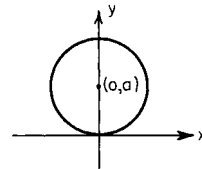


FIG. 3-19 Circle center $(0,a)$ $r = 2a \sin \theta$.

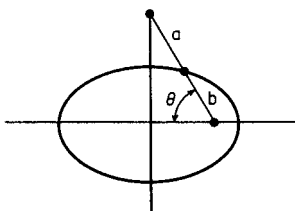


FIG. 3-20 Ellipse, $0 < e < 1$.

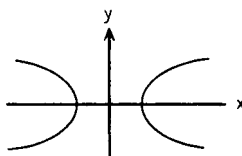


FIG. 3-21 Hyperbola, $e > 1$.

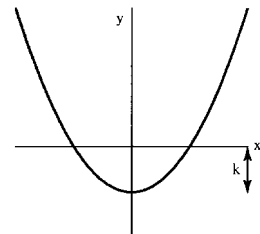


FIG. 3-22 Parabola, $e = 1$.

Similarly, $x = a \cos \phi, y = b \sin \phi$ are the parametric equations of the ellipse $x^2/a^2 + y^2/b^2 = 1$ with parameter ϕ .

SOLID ANALYTIC GEOMETRY

Coordinate Systems The commonly used coordinate systems are three in number. Others may be used in specific problems [see Morse, P. M., and H. Feshbach, *Methods of Theoretical Physics*, vols. I and II, McGraw-Hill, New York (1953)]. The **rectangular** (cartesian) system (Fig. 3-25) consists of mutually orthogonal axes x, y, z . A triple of numbers (x, y, z) is used to represent each point. The **cylindrical** coordinate system (r, θ, z) ; Fig. 3-26) is frequently used to locate a point in space. These are essentially the polar coordinates (r, θ) coupled with the z coordinate. As before, $x = r \cos \theta, y = r \sin \theta, z = z$ and $r^2 = x^2 + y^2, y/x = \tan \theta$. If r is held constant and θ and z are allowed to vary, the locus of (r, θ, z) is a right circular cylinder of radius r along the z axis. The locus of $r = C$ is a circle, and $\theta = \text{constant}$ is a plane containing the z axis and making an angle θ with the xz plane. Cylindrical coordinates are convenient to use when the problem has an axis of symmetry.

The **spherical** coordinate system is convenient if there is a point of symmetry in the system. This point is taken as the origin and the coordinates (ρ, ϕ, θ) illustrated in Fig. 3-27. The relations are $x =$

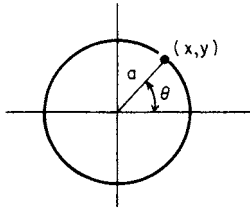


FIG. 3-23 Circle.

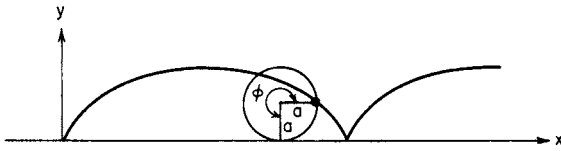


FIG. 3-24 Cycloid.

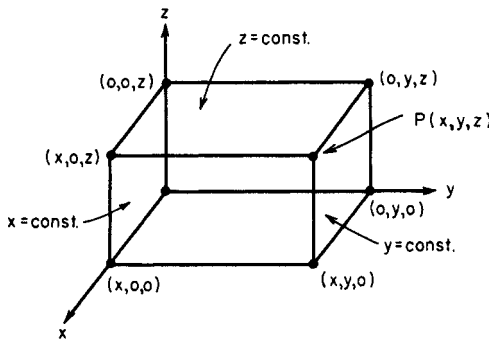


FIG. 3-25 Cartesian coordinates.

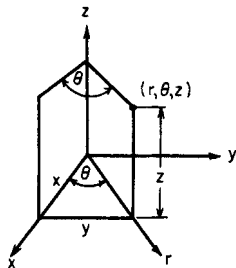


FIG. 3-26 Cylindrical coordinates.

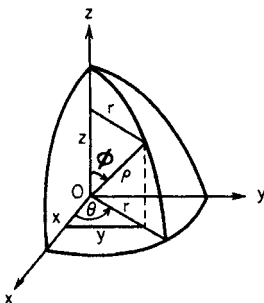


FIG. 3-27 Spherical coordinates.

$\rho \sin \phi \cos \theta$, $y = \rho \sin \phi \sin \theta$, $z = \rho \cos \phi$, and $r = \rho \sin \phi$. $\theta = \text{constant}$ is a plane containing the z axis and making an angle θ with the xz plane. $\phi = \text{constant}$ is a cone with vertex at 0. $\rho = \text{constant}$ is the surface of a sphere of radius ρ , center at the origin 0. Every point in the space may be given spherical coordinates restricted to the ranges $0 \leq \phi \leq \pi$, $\rho \geq 0$, $0 \leq \theta < 2\pi$.

Lines and Planes The distance between two points (x_1, y_1, z_1) , (x_2, y_2, z_2) is $d = \sqrt{(x_1 - x_2)^2 + (y_1 - y_2)^2 + (z_1 - z_2)^2}$. There is nothing in the geometry of three dimensions quite analogous to the slope of a line in the plane case. Instead of specifying the direction of a line by a trigonometric function evaluated for one angle, a trigonometric function evaluated for three angles is used. The angles α , β , γ that a line segment makes with the positive x , y , and z axes, respectively, are called the **direction angles** of the line, and $\cos \alpha$, $\cos \beta$, $\cos \gamma$ are called the **direction cosines**. Let (x_1, y_1, z_1) , (x_2, y_2, z_2) be on the line. Then $\cos \alpha = (x_2 - x_1)/d$, $\cos \beta = (y_2 - y_1)/d$, $\cos \gamma = (z_2 - z_1)/d$, where d is the distance between the two points. Clearly $\cos^2 \alpha + \cos^2 \beta + \cos^2 \gamma = 1$. If two lines are specified by the direction cosines $(\cos \alpha_1, \cos \beta_1, \cos \gamma_1)$, $(\cos \alpha_2, \cos \beta_2, \cos \gamma_2)$, then the angle θ between the lines is $\cos \theta = \cos \alpha_1 \cos \alpha_2 + \cos \beta_1 \cos \beta_2 + \cos \gamma_1 \cos \gamma_2$. Thus the lines are perpendicular if and only if $\theta = 90^\circ$ or $\cos \alpha_1 \cos \alpha_2 + \cos \beta_1 \cos \beta_2 + \cos \gamma_1 \cos \gamma_2 = 0$. The equation of a line with direction cosines $(\cos \alpha, \cos \beta, \cos \gamma)$ passing through (x_1, y_1, z_1) is $(x - x_1)/\cos \alpha = (y - y_1)/\cos \beta = (z - z_1)/\cos \gamma$.

The equation of every plane is of the form $Ax + By + Cz + D = 0$. The numbers

$$\frac{A}{\sqrt{A^2 + B^2 + C^2}}, \frac{B}{\sqrt{A^2 + B^2 + C^2}}, \frac{C}{\sqrt{A^2 + B^2 + C^2}}$$

are direction cosines of the normal lines to the plane. The plane through the point (x_1, y_1, z_1) whose normals have these as direction cosines is $A(x - x_1) + B(y - y_1) + C(z - z_1) = 0$.

Example Find the equation of the plane through $(1, 5, -2)$ perpendicular to the line $(x + 9)/7 = (y - 3)/-1 = z/8$. The numbers $(7, -1, 8)$ are called **direction numbers**. They are a constant multiple of the direction cosines. $\cos \alpha = 7/114$, $\cos \beta = -1/114$, $\cos \gamma = 8/114$. The plane has the equation $7(x - 1) - 1(y - 5) + 8(z + 2) = 0$ or $7x - y + 8z + 14 = 0$.

The distance from the point (x_1, y_1, z_1) to the plane $Ax + By + Cz + D = 0$ is

$$d = \frac{|Ax_1 + By_1 + Cz_1 + D|}{\sqrt{A^2 + B^2 + C^2}}$$

Space Curves Space curves are usually specified as the set of points whose coordinates are given parametrically by a system of equations $x = f(t)$, $y = g(t)$, $z = h(t)$ in the parameter t .

Example The equation of a straight line in space is $(x - x_1)/a = (y - y_1)/b = (z - z_1)/c$. Since all these quantities must be equal (say, to t), we may write $x = x_1 + at$, $y = y_1 + bt$, $z = z_1 + ct$, which represent the parametric equations of the line.

Example The equations $z = a \cos bt$, $y = a \sin bt$, $x = bt$, a, β , b positive constants, represent a circular helix.

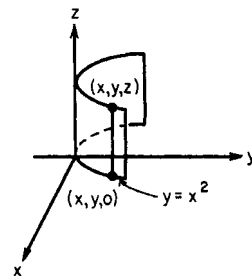


FIG. 3-28 Parabolic cylinder.

Surfaces The locus of points (x, y, z) satisfying $f(x, y, z) = 0$, broadly speaking, may be interpreted as a surface. The simplest surface is the **plane**. The next simplest is a **cylinder**, which is a surface generated by a straight line moving parallel to a given line and passing through a given curve.

Example The parabolic cylinder $y = x^2$ (Fig. 3-28) is generated by a straight line parallel to the z axis passing through $y = x^2$ in the plane $z = 0$.

A surface whose equation is a quadratic in the variables $x, y,$ and z is called a **quadric surface**. Some of the more common such surfaces are tabulated and pictured in Figs. 3-28 to 3-36.

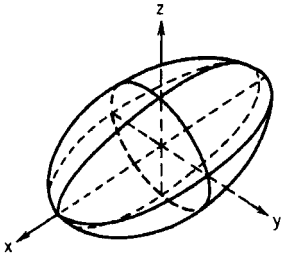


FIG. 3-29 Ellipsoid. $\frac{x^2}{a^2} + \frac{y^2}{b^2} + \frac{z^2}{c^2} = 1$ (sphere if $a = b = c$)

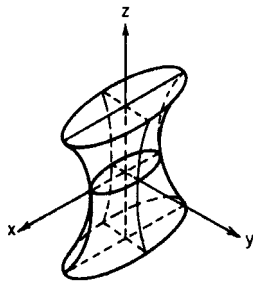


FIG. 3-30 Hyperboloid of one sheet. $\frac{x^2}{a^2} + \frac{y^2}{b^2} - \frac{z^2}{c^2} = 1$

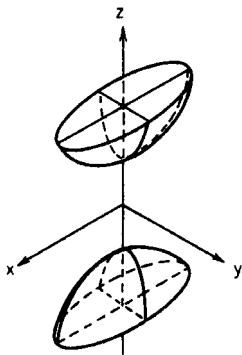


FIG. 3-31 Hyperboloid of two sheets. $\frac{x^2}{a^2} + \frac{y^2}{b^2} - \frac{z^2}{c^2} = -1$

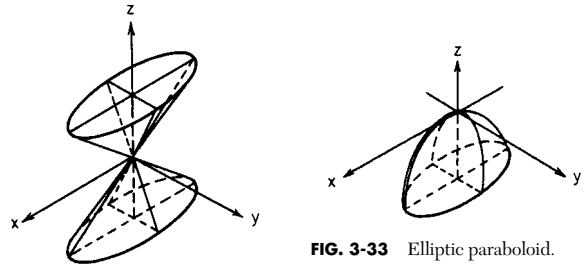


FIG. 3-32 Cone. $\frac{x^2}{a^2} + \frac{y^2}{b^2} + \frac{z^2}{c^2} = 0$

FIG. 3-33 Elliptic paraboloid.

$$\frac{x^2}{a^2} + \frac{y^2}{b^2} + cz = 0$$

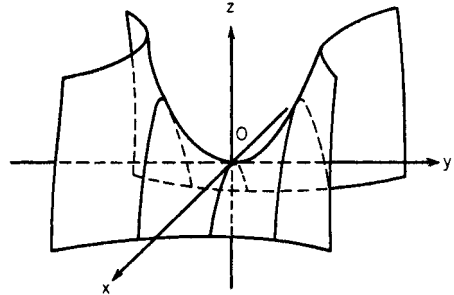


FIG. 3-34 Hyperbolic paraboloid. $\frac{x^2}{a^2} - \frac{y^2}{b^2} + cz = 0$

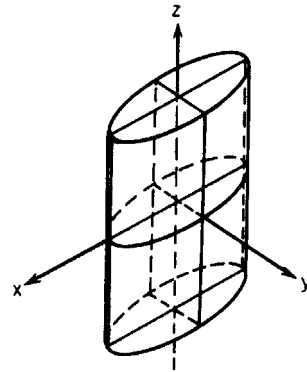


FIG. 3-35 Elliptic cylinder. $\frac{x^2}{a^2} + \frac{y^2}{b^2} = 1$

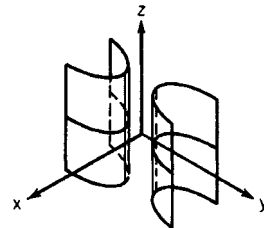


FIG. 3-36 Hyperbolic cylinder.

$$\frac{x^2}{a^2} - \frac{y^2}{b^2} = 1$$

PLANE TRIGONOMETRY

REFERENCES: Gelfand, I. M., and M. Saul, *Trigonometry*, Birkhäuser, Boston (2001); Heineman, E. Richard, and J. Dalton Tarwater, *Plane Trigonometry*, 7th ed., McGraw-Hill (1993).

ANGLES

An angle is generated by the rotation of a line about a fixed center from some initial position to some terminal position. If the rotation is clockwise, the angle is negative; if it is counterclockwise, the angle is positive. Angle size is unlimited. If α, β are two angles such that $\alpha + \beta = 90^\circ$, they are complementary; they are supplementary if $\alpha + \beta = 180^\circ$. Angles are most commonly measured in the sexagesimal system or by radian measure. In the first system there are 360 degrees in one complete revolution; one degree = $\frac{1}{90}$ of a right angle. The degree is subdivided into 60 minutes; the minute is subdivided into 60 seconds. In the radian system one radian is the angle at the center of a circle subtended by an arc whose length is equal to the radius of the circle. Thus $2\pi \text{ rad} = 360^\circ$; $1 \text{ rad} = 57.29578^\circ$; $1^\circ = 0.01745 \text{ rad}$; $1 \text{ min} = 0.00029089 \text{ rad}$. The advantage of radian measure is that it is *dimensionless*. The quadrants are conventionally labeled as Fig. 3-37 shows.

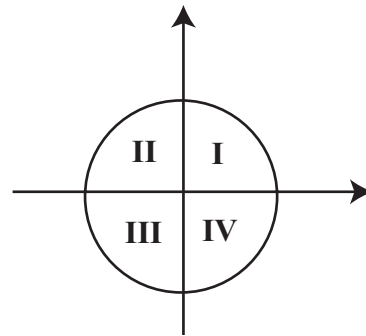


FIG. 3-37 Quadrants.

FUNCTIONS OF CIRCULAR TRIGONOMETRY

The trigonometric functions of angles are the ratios between the various sides of the reference triangles shown in Fig. 3-38 for the various quadrants. Clearly $r = \sqrt{x^2 + y^2} \geq 0$. The fundamental functions (see Figs. 3-39, 3-40, 3-41) are

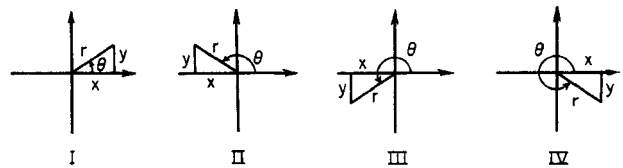


FIG. 3-38 Triangles.

Plane Trigonometry

- | | |
|-----------------------------------------|-------------------------------------------|
| Sine of $\theta = \sin \theta = y/r$ | Secant of $\theta = \sec \theta = r/x$ |
| Cosine of $\theta = \cos \theta = x/r$ | Cosecant of $\theta = \csc \theta = r/y$ |
| Tangent of $\theta = \tan \theta = y/x$ | Cotangent of $\theta = \cot \theta = x/y$ |

Values of the Trigonometric Functions for Common Angles

θ°	θ, rad	$\sin \theta$	$\cos \theta$	$\tan \theta$
0	0	0	1	0
30	$\pi/6$	$1/2$	$\sqrt{3}/2$	$\sqrt{3}/3$
45	$\pi/4$	$\sqrt{2}/2$	$\sqrt{2}/2$	1
60	$\pi/3$	$\sqrt{3}/2$	$1/2$	$\sqrt{3}$
90	$\pi/2$	1	0	$+\infty$

If $90^\circ \leq \theta \leq 180^\circ$, $\sin \theta = \sin (180^\circ - \theta)$; $\cos \theta = -\cos (180^\circ - \theta)$; $\tan \theta = -\tan (180^\circ - \theta)$. If $180^\circ \leq \theta \leq 270^\circ$, $\sin \theta = -\sin (270^\circ - \theta)$; $\cos \theta = -\cos (270^\circ - \theta)$; $\tan \theta = \tan (270^\circ - \theta)$. If $270^\circ \leq \theta \leq 360^\circ$, $\sin \theta = -\sin (360^\circ - \theta)$; $\cos \theta = \cos (360^\circ - \theta)$; $\tan \theta = -\tan (360^\circ - \theta)$. The reciprocal properties may be used to find the values of the other functions.

If it is desired to find the angle when a function of it is given, the procedure is as follows: There will in general be two angles between 0° and 360° corresponding to the given value of the function.

Given ($a > 0$)	Find an acute angle θ_0 such that	Required angles are
$\sin \theta = +a$	$\sin \theta_0 = a$	θ_0 and $(180^\circ - \theta_0)$
$\cos \theta = +a$	$\cos \theta_0 = a$	θ_0 and $(360^\circ - \theta_0)$
$\tan \theta = +a$	$\tan \theta_0 = a$	θ_0 and $(180^\circ + \theta_0)$
$\sin \theta = -a$	$\sin \theta_0 = a$	$180^\circ + \theta_0$ and $360^\circ - \theta_0$
$\cos \theta = -a$	$\cos \theta_0 = a$	$180^\circ - \theta_0$ and $180^\circ + \theta_0$
$\tan \theta = -a$	$\tan \theta_0 = a$	$180^\circ - \theta_0$ and $360^\circ - \theta_0$

Relations between Functions of a Single Angle $\sec \theta = 1/\cos \theta$; $\csc \theta = 1/\sin \theta$, $\tan \theta = \sin \theta/\cos \theta = \sec \theta/\csc \theta = 1/\cot \theta$; $\sin^2 \theta + \cos^2 \theta = 1$; $1 + \tan^2 \theta = \sec^2 \theta$; $1 + \cot^2 \theta = \csc^2 \theta$. For $0 \leq \theta \leq 90^\circ$ the following results hold:

$$\sin \theta = 2 \sin \left(\frac{\theta}{2} \right) \cos \left(\frac{\theta}{2} \right)$$

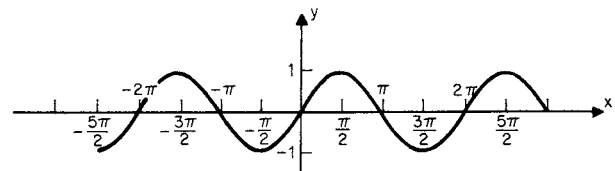


FIG. 3-39 Graph of $y = \sin x$.

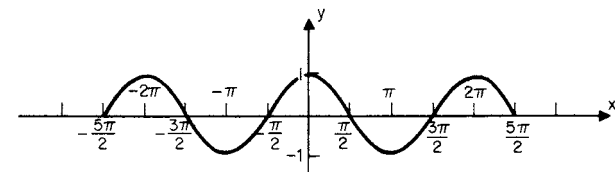


FIG. 3-40 Graph of $y = \cos x$.

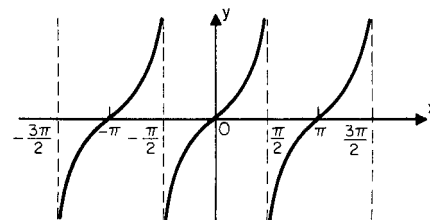


FIG. 3-41 Graph of $y = \tan x$.

$$\text{and } \cos \theta = \cos^2\left(\frac{\theta}{2}\right) - \sin^2\left(\frac{\theta}{2}\right)$$

The cofunction property is very important. $\cos \theta = \sin(90^\circ - \theta)$, $\sin \theta = \cos(90^\circ - \theta)$, $\tan \theta = \cot(90^\circ - \theta)$, $\cot \theta = \tan(90^\circ - \theta)$, etc.

Functions of Negative Angles $\sin(-\theta) = -\sin \theta$, $\cos(-\theta) = \cos \theta$, $\tan(-\theta) = -\tan \theta$, $\sec(-\theta) = \sec \theta$, $\csc(-\theta) = -\csc \theta$, $\cot(-\theta) = -\cot \theta$.

Identities

Sum and Difference Formulas Let x, y be two angles. $\sin(x \pm y) = \sin x \cos y \pm \cos x \sin y$; $\cos(x \pm y) = \cos x \cos y \mp \sin x \sin y$; $\tan(x \pm y) = \frac{\tan x \pm \tan y}{1 \mp \tan x \tan y}$; $\sin x \pm \sin y = 2 \sin \frac{1}{2}(x \pm y) \cos \frac{1}{2}(x \mp y)$; $\cos x + \cos y = 2 \cos \frac{1}{2}(x + y) \cos \frac{1}{2}(x - y)$; $\cos x - \cos y = -2 \sin \frac{1}{2}(x + y) \sin \frac{1}{2}(x - y)$; $\tan x \pm \tan y = \frac{\sin(x \pm y)}{\cos x \cos y}$; $\sin^2 x - \sin^2 y = \cos^2 y - \cos^2 x = \sin(x + y) \sin(x - y)$; $\cos^2 x - \sin^2 y = \cos^2 y - \sin^2 x = \cos(x + y) \cos(x - y)$; $\sin(45^\circ + x) = \cos(45^\circ - x)$; $\sin(45^\circ - x) = \cos(45^\circ + x)$; $\tan(45^\circ \pm x) = \cot(45^\circ \mp x)$.

Multiple and Half Angle Identities Let $x = \text{angle}$, $\sin 2x = 2 \sin x \cos x$; $\sin x = 2 \sin \frac{1}{2}x \cos \frac{1}{2}x$; $\cos 2x = \cos^2 x - \sin^2 x = 1 - 2 \sin^2 x = 2 \cos^2 x - 1$. $\tan 2x = \frac{2 \tan x}{1 - \tan^2 x}$; $\sin 3x = 3 \sin x - 4 \sin^3 x$; $\cos 3x = 4 \cos^3 x - 3 \cos x$. $\tan 3x = \frac{3 \tan x - \tan^3 x}{1 - 3 \tan^2 x}$; $\sin 4x = 4 \sin x \cos x - 8 \sin^3 x \cos x$; $\cos 4x = 8 \cos^4 x - 8 \cos^2 x + 1$.

$$\sin\left(\frac{x}{2}\right) = \sqrt{\frac{1 - \cos x}{2}}$$

$$\cos\left(\frac{x}{2}\right) = \sqrt{\frac{1 + \cos x}{2}}$$

$$\tan\left(\frac{x}{2}\right) = \sqrt{\frac{1 - \cos x}{1 + \cos x}} = \frac{\sin x}{1 + \cos x} = \frac{1 - \cos x}{\sin x}$$

INVERSE TRIGONOMETRIC FUNCTIONS

$y = \sin^{-1} x = \arcsin x$ is the angle y whose sine is x .

Example $y = \sin^{-1} \frac{1}{2}$, y is 30° .

The complete solution of the equation $x = \sin y$ is $y = (-1)^n \sin^{-1} x + n(180^\circ)$, $-\pi/2 \leq \sin^{-1} x \leq \pi/2$ where $\sin^{-1} x$ is the principal value of the angle whose sine is x . The range of principal values of the $\cos^{-1} x$ is $0 \leq \cos^{-1} x \leq \pi$ and $-\pi/2 \leq \tan^{-1} x \leq \pi/2$. If these restrictions are allowed to hold, the following formulas result:

$$\sin^{-1} x = \cos^{-1} \sqrt{1 - x^2} = \tan^{-1} \frac{x}{\sqrt{1 - x^2}} = \cot^{-1} \frac{\sqrt{1 - x^2}}{x}$$

$$= \sec^{-1} \frac{1}{\sqrt{1 - x^2}} = \csc^{-1} \frac{1}{x} = \frac{\pi}{2} - \cos^{-1} x$$

$$\cos^{-1} x = \sin^{-1} \sqrt{1 - x^2} = \tan^{-1} \frac{\sqrt{1 - x^2}}{x}$$

$$= \cot^{-1} \frac{x}{\sqrt{1 - x^2}} = \sec^{-1} \frac{1}{x}$$

$$= \csc^{-1} \frac{1}{\sqrt{1 - x^2}} = \frac{\pi}{2} - \sin^{-1} x$$

$$\tan^{-1} x = \sin^{-1} \frac{x}{\sqrt{1 + x^2}} = \cos^{-1} \frac{1}{\sqrt{1 + x^2}}$$

$$= \cot^{-1} \frac{1}{x} = \sec^{-1} \sqrt{1 + x^2} = \csc^{-1} \frac{\sqrt{1 + x^2}}{x}$$

RELATIONS BETWEEN ANGLES AND SIDES OF TRIANGLES

Solutions of Triangles (Fig. 3-42) Let a, b, c denote the sides and α, β, γ the angles opposite the sides in the triangle. Let $2s = a +$

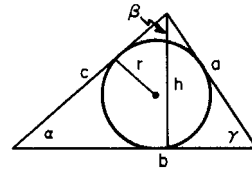


FIG. 3-42 Triangle.

$b + c$, $A = \text{area}$, $r = \text{radius of the inscribed circle}$, $R = \text{radius of the circumscribed circle}$, and $h = \text{altitude}$. In any triangle $\alpha + \beta + \gamma = 180^\circ$.

Law of Sines $\sin \alpha/a = \sin \beta/b = \sin \gamma/c = 1/(2R)$.

Law of Tangents

$$\frac{a + b}{a - b} = \frac{\tan \frac{1}{2}(\alpha + \beta)}{\tan \frac{1}{2}(\alpha - \beta)}; \frac{b + c}{b - c} = \frac{\tan \frac{1}{2}(\beta + \gamma)}{\tan \frac{1}{2}(\beta - \gamma)}; \frac{a + c}{a - c} = \frac{\tan \frac{1}{2}(\alpha + \gamma)}{\tan \frac{1}{2}(\alpha - \gamma)}$$

Law of Cosines $a^2 = b^2 + c^2 - 2bc \cos \alpha$; $b^2 = a^2 + c^2 - 2ac \cos \beta$; $c^2 = a^2 + b^2 - 2ab \cos \gamma$.

Other Relations In this subsection, where appropriate, two more formulas can be generated by replacing a by b , b by c , c by a , α by β , β by γ , and γ by α . $\cos \alpha = \frac{b^2 + c^2 - a^2}{2bc}$; $a = b \cos \gamma + c \cos \beta$; $\sin \alpha = \frac{(2/bc) \sqrt{s(s-a)(s-b)(s-c)}}$;

$$\sin\left(\frac{\alpha}{2}\right) = \sqrt{\frac{(s-b)(s-c)}{bc}}; \cos\left(\frac{\alpha}{2}\right) = \sqrt{\frac{s(s-a)}{bc}}$$

$$A = \frac{1}{2} bh = \frac{1}{2} ab \sin \gamma = \frac{a^2 \sin \beta \sin \gamma}{2 \sin \alpha} = \sqrt{s(s-a)(s-b)(s-c)} = rs$$

where $r = \sqrt{\frac{(s-a)(s-b)(s-c)}{s}}$

$$R = a/(2 \sin \alpha) = abc/4A; h = c \sin a = a \sin \gamma = 2rs/b.$$

Right Triangle (Fig. 3-43) Given one side and any acute angle α or any two sides, the remaining parts can be obtained from the following formulas:

$$a = \sqrt{(c+b)(c-b)} = c \sin \alpha = b \tan \alpha$$

$$b = \sqrt{(c+a)(c-a)} = c \cos \alpha = a \cot \alpha$$

$$c = \sqrt{a^2 + b^2}, \sin \alpha = \frac{a}{c}, \cos \alpha = \frac{b}{c}, \tan \alpha = \frac{a}{b}, \beta = 90^\circ - \alpha$$

$$A = \frac{1}{2} ab = \frac{a^2}{2 \tan \alpha} = \frac{b^2 \tan \alpha}{2} = \frac{c^2 \sin 2\alpha}{4}$$

Oblique Triangles (Fig. 3-44) There are four possible cases.

1. Given b, c and the included angles α ,

$$\frac{1}{2}(\beta + \gamma) = 90^\circ - \frac{1}{2}\alpha; \tan \frac{1}{2}(\beta - \gamma) = \frac{b - c}{b + c} \tan \frac{1}{2}(\beta + \gamma)$$

$$\beta = \frac{1}{2}(\beta + \gamma) + \frac{1}{2}(\beta - \gamma); \gamma = \frac{1}{2}(\beta + \gamma) - \frac{1}{2}(\beta - \gamma); a = \frac{b \sin \alpha}{\sin \beta}$$

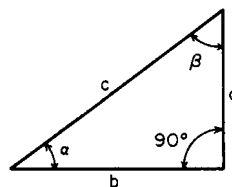


FIG. 3-43 Right triangle.

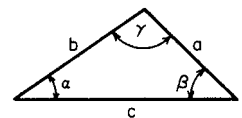


FIG. 3-44 Oblique triangle.

3-18 MATHEMATICS

2. Given the three sides $a, b, c, s = \frac{1}{2}(a + b + c)$;

$$r = \sqrt{\frac{(s-a)(s-b)(s-c)}{s}}$$

$$\tan \frac{1}{2} \alpha = \frac{r}{s-a}; \quad \tan \frac{1}{2} \beta = \frac{r}{s-b}; \quad \tan \frac{1}{2} \gamma = \frac{r}{s-c}$$

3. Given any two sides a, c and an angle opposite one of them $\alpha, \sin \gamma = (c \sin \alpha)/a; \beta = 180^\circ - a - \gamma; b = (a \sin \beta)/(\sin \alpha)$. There may be two solutions here. γ may have two values $\gamma_1, \gamma_2; \gamma_1 < 90^\circ, \gamma_2 = 180^\circ - \gamma_1 > 90^\circ$. If $\alpha + \gamma_2 > 180^\circ$, use only γ_1 . This case may be *impossible* if $\sin \gamma > 1$.

4. Given any side c and two angles α and $\beta, \gamma = 180^\circ - \alpha - \beta; a = (c \sin \alpha)/(\sin \gamma); b = (c \sin \beta)/(\sin \gamma)$.

HYPERBOLIC TRIGONOMETRY

The hyperbolic functions are certain combinations of exponentials e^x and e^{-x} .

$$\cosh x = \frac{e^x + e^{-x}}{2}; \quad \sinh x = \frac{e^x - e^{-x}}{2}; \quad \tanh x = \frac{\sinh x}{\cosh x} = \frac{e^x - e^{-x}}{e^x + e^{-x}}$$

$$\coth x = \frac{e^x + e^{-x}}{e^x - e^{-x}} = \frac{1}{\tanh x} = \frac{\cosh x}{\sinh x}; \quad \operatorname{sech} x = \frac{1}{\cosh x} = \frac{2}{e^x + e^{-x}};$$

$$\operatorname{csch} x = \frac{1}{\sinh x} = \frac{2}{e^x - e^{-x}}$$

Fundamental Relationships $\sinh x + \cosh x = e^x; \cosh x - \sinh x = e^{-x}; \cosh^2 x - \sinh^2 x = 1; \operatorname{sech}^2 x + \tanh^2 x = 1; \coth^2 x - \operatorname{csch}^2 x = 1; \sinh 2x = 2 \sinh x \cosh x; \cosh 2x = \cosh^2 x + \sinh^2 x = 1 + 2 \sinh^2 x = 2 \cosh^2 x - 1. \tanh 2x = (2 \tanh x)/(1 + \tanh^2 x); \sinh(x \pm y) = \sinh x \cosh y \pm \cosh x \sinh y; \cosh(x \pm y) = \cosh x \cosh y \pm \sinh x \sinh y; \cosh(-x) = \cosh x; \tanh(-x) = -\tanh x.$

$\cosh y \pm \cosh x \sinh y; \cosh(x \pm y) = \cosh x \cosh y \pm \sinh x \sinh y; 2 \sinh^2 x/2 = \cosh x - 1; 2 \cosh^2 x/2 = \cosh x + 1; \sinh(-x) = -\sinh x; \cosh(-x) = \cosh x; \tanh(-x) = -\tanh x.$

When $u = a \cosh x, v = a \sinh x$, then $u^2 - v^2 = a^2$; which is the equation for a hyperbola. In other words, the hyperbolic functions in the parametric equations $u = a \cosh x, v = a \sinh x$ have the same relation to the hyperbola $u^2 - v^2 = a^2$ that the equations $u = a \cos \theta, v = a \sin \theta$ have to the circle $u^2 + v^2 = a^2$.

Inverse Hyperbolic Functions If $x = \sinh y$, then y is the inverse hyperbolic sine of x written $y = \sinh^{-1} x$ or $\operatorname{arsinh} x. \sinh^{-1} x = \log_e(x + \sqrt{x^2 + 1})$

$$\cosh^{-1} x = \log_e(x + \sqrt{x^2 - 1}); \quad \tanh^{-1} x = \frac{1}{2} \log_e \frac{1+x}{1-x};$$

$$\coth^{-1} x = \frac{1}{2} \log_e \frac{x+1}{x-1}; \quad \operatorname{sech}^{-1} x = \log_e \left(\frac{1 + \sqrt{1-x^2}}{x} \right);$$

$$\operatorname{csch}^{-1} x = \log_e \left(\frac{1 + \sqrt{1+x^2}}{x} \right)$$

Magnitude of the Hyperbolic Functions $\cosh x \geq 1$ with equality only for $x = 0; -\infty < \sinh x < \infty; -1 < \tanh x < 1. \cosh x \sim e^{x/2}$ as $x \rightarrow \infty; \sinh x \rightarrow e^{x/2}$ as $x \rightarrow \infty.$

APPROXIMATIONS FOR TRIGONOMETRIC FUNCTIONS

For small values of θ (θ measured in radians) $\sin \theta \approx \theta, \tan \theta \approx \theta; \cos \theta \approx 1 - (\theta^2/2)$. The behavior ratio of the functions as $\theta \rightarrow 0$ is given by the following:

$$\lim_{\theta \rightarrow 0} \sin \theta / \theta = 1; \quad \sin \theta / \tan \theta = 1.$$

DIFFERENTIAL AND INTEGRAL CALCULUS

REFERENCES: Char, B. W., et al., *Maple V Language Reference Manual*, Springer-Verlag, New York (1991); Wolfram, S., *The Mathematics Book*, 5th ed., Wolfram Media (2003).

DIFFERENTIAL CALCULUS

An Example of Functional Notation Suppose that a storage warehouse of $16,000 \text{ ft}^3$ is required. The construction costs per square foot are \$10, \$3, and \$2 for walls, roof, and floor respectively. What are the minimum cost dimensions? Thus, with $h =$ height, $x =$ width, and $y =$ length, the respective costs are

$$\text{Walls} = 2 \times 10hy + 2 \times 10hx = 20h(y + x)$$

$$\text{Roof} = 3xy$$

$$\text{Floor} = 2xy$$

$$\text{Total cost} = 2xy + 3xy + 20h(x + y) = 5xy + 20h(x + y) \quad (3-1)$$

and the restriction

$$\text{Total volume} = xyh \quad (3-2)$$

Solving for h from Eq. (3-2),

$$h = \text{volume}/xy = 16,000/xy \quad (3-3)$$

$$\text{Cost} = 5xy + \frac{320,000}{xy}(y + x) = 5xy + 320,000 \left(\frac{1}{x} + \frac{1}{y} \right) \quad (3-4)$$

In this form it can be shown that the minimum cost will occur for $x = y$; therefore

$$\text{Cost} = 5x^2 + 640,000(1/x)$$

By evaluation, the smallest cost will occur when $x = 40$.

$$\text{Cost} = 5(1600) + 640,000/40 = \$24,000$$

The dimensions are then $x = 40 \text{ ft}, y = 40 \text{ ft}, h = 16,000/(40 \times 40) = 10 \text{ ft}$. Symbolically, the original cost relationship is written

$$\text{Cost} = f(x, y, h) = 5xy + 20h(y + x)$$

and the volume relation

$$\text{Volume} = g(x, y, h) = xyh = 16,000$$

In terms of the derived general relationships (3-1) and (3-2), $x, y,$ and h are **independent variables**—cost and volume, **dependent variables**. That is, the cost and volume become fixed with the specification of dimensions. However, corresponding to the given restriction of the problem, relative to volume, the function $g(x, y, z) = xyh$ becomes a constraint function. In place of three independent and two dependent variables the problem reduces to two independent (volume has been constrained) and two dependent as in functions (3-3) and (3-4). Further, the requirement of minimum cost reduces the problem to three dependent variables (x, y, h) and no **degrees of freedom**, that is, freedom of independent selection.

Limits The limit of function $f(x)$ as x approaches a (a is finite or else x is said to increase without bound) is the number N .

$$\lim_{x \rightarrow a} f(x) = N$$

This states that $f(x)$ can be calculated as close to N as desirable by making x sufficiently close to a . This does not put any restriction on $f(x)$ when $x = a$. Alternatively, for any given positive number ϵ , a number δ can be found such that $0 < |a - x| < \delta$ implies that $|N - f(x)| < \epsilon$.

The following operations with limits (when they exist) are valid:

$$\lim_{x \rightarrow a} bf(x) = b \lim_{x \rightarrow a} f(x)$$

$$\lim_{x \rightarrow a} [f(x) + g(x)] = \lim_{x \rightarrow a} f(x) + \lim_{x \rightarrow a} g(x)$$

$$\lim_{x \rightarrow a} [f(x)g(x)] = \lim_{x \rightarrow a} f(x) \cdot \lim_{x \rightarrow a} g(x)$$

$$\lim_{x \rightarrow a} \frac{f(x)}{g(x)} = \frac{\lim_{x \rightarrow a} f(x)}{\lim_{x \rightarrow a} g(x)} \quad \text{if } \lim_{x \rightarrow a} g(x) \neq 0$$

See "Indeterminant Forms" below when $g(a) = 0$.
Continuity A function $f(x)$ is continuous at the point $x = a$ if

$$\lim_{h \rightarrow 0} [f(a+h) - f(a)] = 0$$

Rigorously, it is stated $f(x)$ is continuous at $x = a$ if for any positive ϵ there exists a $\delta > 0$ such that $|f(a+h) - f(a)| < \epsilon$ for all x with $|x - a| < \delta$. For example, the function $(\sin x)/x$ is not continuous at $x = 0$ and therefore is said to be discontinuous. Discontinuities are classified into three types:

1. Removable $y = \sin x/x$ at $x = 0$
2. Infinite $y = 1/x$ at $x = 0$
3. Jump $y = 10/(1 + e^{1/x})$ at $x = 0^+$ $y = 0^+$
 $x = 0$ $y = 0$
 $x = 0^-$ $y = 10$

Derivative The function $f(x)$ has a derivative at $x = a$, which can be denoted as $f'(a)$, if

$$\lim_{h \rightarrow 0} \frac{f(a+h) - f(a)}{h}$$

exists. This implies continuity at $x = a$. Conversely, a function may be continuous but not have a derivative. The derivative function is

$$f'(x) = \frac{df}{dx} = \lim_{h \rightarrow 0} \frac{f(x+h) - f(x)}{h}$$

Differentiation Define $\Delta y = f(x + \Delta x) - f(x)$. Then dividing by Δx

$$\frac{\Delta y}{\Delta x} = \frac{f(x + \Delta x) - f(x)}{\Delta x}$$

Call $\lim_{\Delta x \rightarrow 0} \frac{\Delta y}{\Delta x} = \frac{dy}{dx}$

then $\frac{dy}{dx} = \lim_{\Delta x \rightarrow 0} \frac{f(x + \Delta x) - f(x)}{\Delta x}$

Example Find the derivative of $y = \sin x$.

$$\begin{aligned} \frac{dy}{dx} &= \lim_{\Delta x \rightarrow 0} \frac{\sin(x + \Delta x) - \sin(x)}{\Delta x} \\ &= \lim_{\Delta x \rightarrow 0} \frac{\sin x \cos \Delta x + \sin \Delta x \cos x - \sin x}{\Delta x} \\ &= \lim_{\Delta x \rightarrow 0} \frac{\sin x(\cos \Delta x - 1)}{\Delta x} + \lim_{\Delta x \rightarrow 0} \frac{\sin \Delta x \cos x}{\Delta x} \\ &= \cos x \text{ since } \lim_{\Delta x \rightarrow 0} \frac{\sin \Delta x}{\Delta x} = 1 \end{aligned}$$

Differential Operations The following differential operations are valid: f, g, \dots are differentiable functions of x , c and n are constants; e is the base of the natural logarithms.

$$\frac{dc}{dx} = 0 \tag{3-5}$$

$$\frac{dx}{dx} = 1 \tag{3-6}$$

$$\frac{d}{dx}(f + g) = \frac{df}{dx} + \frac{dg}{dx} \tag{3-7}$$

$$\frac{d}{dx}(f \times g) = f \frac{dg}{dx} + g \frac{df}{dx} \tag{3-8}$$

$$\frac{dy}{dx} = \frac{1}{dx/dy} \quad \text{if } \frac{dx}{dy} \neq 0 \tag{3-9}$$

$$\frac{d}{dx} f^n = n f^{n-1} \frac{df}{dx} \tag{3-10}$$

$$\frac{d}{dx} \left(\frac{f}{g} \right) = \frac{g(df/dx) - f(dg/dx)}{g^2} \tag{3-11}$$

$$\frac{df}{dx} = \frac{df}{dv} \times \frac{dv}{dx} \quad (\text{chain rule}) \tag{3-12}$$

$$\frac{df^g}{dx} = g f^{g-1} \frac{df}{dx} + f^g \ln f \frac{dg}{dx} \tag{3-13}$$

$$\frac{da^x}{dx} = (\ln a) a^x \tag{3-14}$$

Example Derive dy/dx for $x^2 + y^3 = x + xy + A$.

Here $\frac{d}{dx} x^2 + \frac{d}{dx} y^3 = \frac{d}{dx} x + \frac{d}{dx} xy + \frac{d}{dx} A$

$$2x + 3y^2 \frac{dy}{dx} = 1 + y + x \frac{dy}{dx} + 0$$

by rules (3-10), (3-10), (3-6), (3-8), and (3-5) respectively.

Thus $\frac{dy}{dx} = \frac{2x - 1 - y}{x - 3y^2}$

Differentials

$$de^x = e^x dx \tag{3-15a}$$

$$d(a^x) = a^x \log a dx \tag{3-15b}$$

$$d \ln x = (1/x) dx \tag{3-16}$$

$$d \log x = (\log e/x) dx \tag{3-17}$$

$$d \sin x = \cos x dx \tag{3-18}$$

$$d \cos x = -\sin x dx \tag{3-19}$$

$$d \tan x = \sec^2 x dx \tag{3-20}$$

$$d \cot x = -\csc^2 x dx \tag{3-21}$$

$$d \sec x = \tan x \sec x dx \tag{3-22}$$

$$d \csc x = -\cot x \csc x dx \tag{3-23}$$

$$d \sin^{-1} x = (1 - x^2)^{-1/2} dx \tag{3-24}$$

$$d \cos^{-1} x = -(1 - x^2)^{-1/2} dx \tag{3-25}$$

$$d \tan^{-1} x = (1 + x^2)^{-1} dx \tag{3-26}$$

$$d \cot^{-1} x = -(1 + x^2)^{-1} dx \tag{3-27}$$

$$d \sec^{-1} x = x^{-1}(x^2 - 1)^{-1/2} dx \tag{3-28}$$

$$d \csc^{-1} x = -x^{-1}(x^2 - 1)^{-1/2} dx \tag{3-29}$$

$$d \sinh x = \cosh x dx \tag{3-30}$$

$$d \cosh x = \sinh x dx \tag{3-31}$$

$$d \tanh x = \text{sech}^2 x dx \tag{3-32}$$

$$d \coth x = -\text{csch}^2 x dx \tag{3-33}$$

$$d \text{sech } x = -\text{sech } x \tanh x dx \tag{3-34}$$

$$d \text{csch } x = -\text{csch } x \coth x dx \tag{3-35}$$

$$d \sinh^{-1} x = (x^2 + 1)^{-1/2} dx \tag{3-36}$$

$$d \cosh^{-1} x = (x^2 - 1)^{-1/2} dx \tag{3-37}$$

$$d \tanh^{-1} x = (1 - x^2)^{-1} dx \tag{3-38}$$

$$d \coth^{-1} x = -(x^2 - 1)^{-1} dx \tag{3-39}$$

$$d \text{sech}^{-1} x = -(1/x)(1 - x^2)^{-1/2} dx \tag{3-40}$$

$$d \text{csch}^{-1} x = -x^{-1}(x^2 + 1)^{-1/2} dx \tag{3-41}$$

3-20 MATHEMATICS

Example Find dy/dx for $y = \sqrt{x} \cos(1-x^2)$. Using

$$\frac{dy}{dx} = \sqrt{x} \frac{d}{dx} \cos(1-x^2) + \cos(1-x^2) \frac{d}{dx} \sqrt{x} \quad (3-8)$$

$$\begin{aligned} \frac{d}{dx} \cos(1-x^2) &= -\sin(1-x^2) \frac{d}{dx} (1-x^2) & (3-19) \\ &= -\sin(1-x^2)(0-2x) & (3-5), (3-10) \end{aligned}$$

$$\frac{d\sqrt{x}}{dx} = \frac{1}{2} x^{-1/2} \quad (3-10)$$

$$\frac{dy}{dx} = 2x^{3/2} \sin(1-x^2) + \frac{1}{2} x^{-1/2} \cos(1-x^2)$$

Example Find the derivative of $\tan x$ with respect to $\sin x$.

$$\begin{aligned} v &= \sin x \\ y &= \tan x & \text{Using} \\ \frac{d \tan x}{d \sin x} &= \frac{dy}{dv} = \frac{dy}{dx} \frac{dx}{dv} & (3-12) \\ &= \frac{d \tan x}{dx} \frac{1}{\frac{d \sin x}{dx}} & (3-9) \\ &= \sec^2 x / \cos x & (3-18), (3-20) \end{aligned}$$

Very often in experimental sciences and engineering functions and their derivatives are available only through their numerical values. In particular, through measurements we may know the values of a function and its derivative only at certain points. In such cases the preceding operational rules for derivatives, including the chain rule, can be applied numerically.

Example Given the following table of values for differentiable functions f and g ; evaluate the following quantities:

x	$f(x)$	$f'(x)$	$g(x)$	$g'(x)$
1	3	1	4	-4
3	0	2	4	7
4	-2	10	3	6

$$\begin{aligned} \frac{d}{dx} [f(x) + g(x)]_{x=4} &= f'(4) + g'(4) = 10 + 6 = 16 \\ \left(\frac{f}{g}\right)'(1) &= \frac{f'(1)g(1) - f(1)g'(1)}{[g(1)]^2} = \frac{1 \cdot 4 - 3(-4)}{(4)^2} = \frac{16}{16} = 1 \end{aligned}$$

Higher Differentials The first derivative of $f(x)$ with respect to x is denoted by f' or df/dx . The derivative of the first derivative is called the second derivative of $f(x)$ with respect to x and is denoted by f'' , $f^{(2)}$, or d^2f/dx^2 ; and similarly for the higher-order derivatives.

Example Given $f(x) = 3x^3 + 2x + 1$, calculate all derivative values at $x = 3$.

$$\begin{aligned} \frac{df(x)}{dx} &= 9x^2 + 2 & x = 3, f'(3) = 9(9) + 2 = 83 \\ \frac{d^2f(x)}{dx^2} &= 18x & x = 3, f''(3) = 18(3) = 54 \\ \frac{d^3f(x)}{dx^3} &= 18 & x = 3, f'''(3) = 18 \\ \frac{d^nf(x)}{dx^n} &= 0 & \text{for } n \geq 4 \end{aligned}$$

If $f'(x) > 0$ on (a, b) , then f is increasing on (a, b) . If $f'(x) < 0$ on (a, b) , then f is decreasing on (a, b) .

The graph of a function $y = f(x)$ is concave up if f' is increasing on (a, b) ; it is concave down if f' is decreasing on (a, b) .

If $f''(x)$ exists on (a, b) and if $f''(x) > 0$, then f is concave up on (a, b) . If $f''(x) < 0$, then f is concave down on (a, b) .

An inflection point is a point at which a function changes the direction of its concavity.

Indeterminate Forms: L'Hospital's Theorem Forms of the type $0/0$, ∞/∞ , $0 \times \infty$, etc., are called indeterminates. To find the limiting values that the corresponding functions approach, L'Hospital's theorem is useful: If two functions $f(x)$ and $g(x)$ both become zero at $x = a$, then the limit of their quotient is equal to the limit of the quotient of their separate derivatives, if the limit exists, or is $+\infty$ or $-\infty$.

Example Find $\lim_{x \rightarrow 0} \frac{\sin x}{x}$.

Here
$$\lim_{x \rightarrow 0} \frac{\sin x}{x} = \lim_{x \rightarrow 0} \frac{d \sin x}{dx} = \lim_{x \rightarrow 0} \frac{\cos x}{1} = 1$$

Example Find $\lim_{x \rightarrow \infty} \frac{(1.1)^x}{x^{1000}}$.

$$\lim_{x \rightarrow \infty} \frac{(1.1)^x}{x^{1000}} = \lim_{x \rightarrow \infty} \frac{d(1.1)^x}{dx^{1000}} = \lim_{x \rightarrow \infty} \frac{(\ln 1.1)(1.1)^x}{1000x^{999}}$$

Obviously $\lim_{x \rightarrow \infty} \frac{1.1^x}{x^{1000}} = \infty$ since repeated application of the rule will reduce the denominator to a finite number 1000! while the numerator remains infinitely large.

Example Find $\lim_{x \rightarrow \infty} x^3 e^{-x}$.

$$\lim_{x \rightarrow \infty} x^3 e^{-x} = \lim_{x \rightarrow \infty} \frac{x^3}{e^x} = \lim_{x \rightarrow \infty} \frac{6}{e^x} = 0$$

Example Find $\lim_{x \rightarrow 0} (1-x)^{1/x}$.

Let
$$y = (1-x)^{1/x}$$

$$\ln y = (1/x) \ln(1-x)$$

$$\lim_{x \rightarrow 0} (\ln y) = \lim_{x \rightarrow 0} \frac{\ln(1-x)}{x} = -1$$

Therefore,
$$\lim_{x \rightarrow 0} y = e^{-1}$$

Partial Derivative The abbreviation $z = f(x, y)$ means that z is a function of the two variables x and y . The derivative of z with respect to x , treating y as a constant, is called the partial derivative with respect to x and is usually denoted as $\partial z/\partial x$ or $\partial f(x, y)/\partial x$ or simply f_x . Partial differentiation, like full differentiation, is quite simple to apply. Conversely, the solution of partial differential equations is appreciably more difficult than that of differential equations.

Example Find $\partial z/\partial x$ and $\partial z/\partial y$ for $z = ye^{x^2} + xe^y$.

$$\begin{aligned} \frac{\partial z}{\partial x} &= y \frac{\partial e^{x^2}}{\partial x} + e^y \frac{\partial x}{\partial x} & \frac{\partial z}{\partial y} &= e^{x^2} \frac{\partial y}{\partial y} + x \frac{\partial e^y}{\partial y} \\ &= 2xye^{x^2} + e^y & &= e^{x^2} + xe^y \end{aligned}$$

Order of Differentiation It is generally true that the order of differentiation is immaterial for any number of differentiations or variables provided the function and the appropriate derivatives are continuous. For $z = f(x, y)$ it follows:

$$\frac{\partial^2 f}{\partial y^2 \partial x} = \frac{\partial^2 f}{\partial y \partial x \partial y} = \frac{\partial^2 f}{\partial x \partial y^2}$$

General Form for Partial Differentiation

1. Given $f(x, y) = 0$ and $x = g(t)$, $y = h(t)$.

Then
$$\frac{df}{dt} = \frac{\partial f}{\partial x} \frac{dx}{dt} + \frac{\partial f}{\partial y} \frac{dy}{dt}$$

$$\begin{aligned} \frac{d^2f}{dt^2} &= \frac{\partial^2 f}{\partial x^2} \left(\frac{dx}{dt}\right)^2 + 2 \frac{\partial^2 f}{\partial x \partial y} \frac{dx}{dt} \frac{dy}{dt} + \frac{\partial^2 f}{\partial y^2} \left(\frac{dy}{dt}\right)^2 + \frac{\partial f}{\partial x} \frac{d^2x}{dt^2} \\ &\quad + \frac{\partial f}{\partial y} \frac{d^2y}{dt^2} \end{aligned}$$

Example Find df/dt for $f = xy$, $x = \rho \sin t$, $y = \rho \cos t$.

$$\begin{aligned} \frac{df}{dt} &= \frac{\partial(xy)}{\partial x} \left(\frac{d\rho \sin t}{dt} \right) + \frac{\partial(xy)}{\partial y} \left(\frac{d\rho \cos t}{dt} \right) \\ &= y(\rho \cos t) + x(-\rho \sin t) \\ &= \rho^2 \cos^2 t - \rho^2 \sin^2 t \end{aligned}$$

2. Given $f(x, y) = 0$ and $x = g(t, s)$, $y = h(t, s)$.

Then

$$\begin{aligned} \frac{\partial f}{\partial t} &= \frac{\partial f}{\partial x} \frac{\partial x}{\partial t} + \frac{\partial f}{\partial y} \frac{\partial y}{\partial t} \\ \frac{\partial f}{\partial s} &= \frac{\partial f}{\partial x} \frac{\partial x}{\partial s} + \frac{\partial f}{\partial y} \frac{\partial y}{\partial s} \end{aligned}$$

Differentiation of Composite Function

Rule 1. Given $f(x, y) = 0$, then $\frac{dy}{dx} = -\frac{\partial f/\partial x}{\partial f/\partial y}$ ($\frac{\partial f}{\partial y} \neq 0$).

Rule 2. Given $f(u) = 0$ where $u = g(x)$, then

$$\begin{aligned} \frac{df}{dx} &= f'(u) \frac{du}{dx} \\ \frac{d^2f}{dx^2} &= f''(u) \left(\frac{du}{dx} \right)^2 + f'(u) \frac{d^2u}{dx^2} \end{aligned}$$

Example Find df/dx for $f = \sin^2 u$ and $u = \sqrt{1-x^2}$

$$\begin{aligned} \frac{df}{dx} &= \frac{d \sin^2 u}{du} \frac{d\sqrt{1-x^2}}{dx} \\ &= 2 \sin u \cos u \left(\frac{1}{2} \right) (-2x)(1-x^2)^{-1/2} \\ &= -2 \frac{\sqrt{1-u^2}}{u} \sin u \cos u \end{aligned}$$

Rule 3. Given $f(u) = 0$ where $u = g(x, y)$, then

$$\begin{aligned} \frac{\partial f}{\partial x} &= f'(u) \frac{\partial u}{\partial x} \quad \frac{\partial f}{\partial y} = f'(u) \frac{\partial u}{\partial y} \\ \frac{\partial^2 f}{\partial x^2} &= f'' \left(\frac{\partial u}{\partial x} \right)^2 + f' \frac{\partial^2 u}{\partial x^2} \\ \frac{\partial^2 f}{\partial x \partial y} &= f'' \frac{\partial u}{\partial x} \frac{\partial u}{\partial y} + f' \frac{\partial^2 u}{\partial x \partial y} \\ \frac{\partial^2 f}{\partial y^2} &= f'' \left(\frac{\partial u}{\partial y} \right)^2 + f' \frac{\partial^2 u}{\partial y^2} \end{aligned}$$

MULTIVARIABLE CALCULUS APPLIED TO THERMODYNAMICS

Many of the functional relationships needed in thermodynamics are direct applications of the rules of multivariable calculus. This section reviews those rules in the context of the needs of thermodynamics. These ideas were expounded in one of the classic books on chemical engineering thermodynamics [see Hougén, O. A., et al., Part II, "Thermodynamics," in *Chemical Process Principles*, 2d ed., Wiley, New York (1959)].

State Functions State functions depend only on the state of the system, not on past history or how one got there. If z is a function of two variables, x and y , then $z(x, y)$ is a state function, since z is known once x and y are specified. The differential of z is

$$dz = M dx + N dy$$

The line integral

$$\int_C (M dx + N dy)$$

is independent of the path in x - y space if and only if

$$\frac{\partial M}{\partial y} = \frac{\partial N}{\partial x} \tag{3-42}$$

The total differential can be written as

$$dz = \left(\frac{\partial z}{\partial x} \right)_y dx + \left(\frac{\partial z}{\partial y} \right)_x dy \tag{3-43}$$

and the following condition guarantees path independence.

$$\frac{\partial}{\partial y} \left(\frac{\partial z}{\partial x} \right)_y = \frac{\partial}{\partial x} \left(\frac{\partial z}{\partial y} \right)_x$$

or

$$\frac{\partial^2 z}{\partial y \partial x} = \frac{\partial^2 z}{\partial x \partial y} \tag{3-44}$$

Example Suppose z is constant and apply Eq. (3-43).

$$\left[0 = \left(\frac{\partial z}{\partial x} \right)_y dx + \left(\frac{\partial z}{\partial y} \right)_x dy \right]_z$$

Rearrangement gives

$$\left(\frac{\partial z}{\partial x} \right)_y = - \left(\frac{\partial y}{\partial x} \right)_z \left(\frac{\partial z}{\partial y} \right)_x = - \frac{(\partial y/\partial x)_z}{(\partial y/\partial z)_x} \tag{3-45}$$

Alternatively, divide Eq. (3-43) by dy when holding some other variable w constant to obtain

$$\left(\frac{\partial z}{\partial x} \right)_w = \left(\frac{\partial z}{\partial x} \right)_y \left(\frac{\partial x}{\partial y} \right)_w + \left(\frac{\partial z}{\partial y} \right)_x \tag{3-46}$$

Also divide both numerator and denominator of a partial derivative by dw while holding a variable y constant to get

$$\left(\frac{\partial z}{\partial x} \right)_y = \frac{(\partial z/\partial w)_y}{(\partial x/\partial w)_y} = \left(\frac{\partial z}{\partial w} \right)_y \left(\frac{\partial w}{\partial x} \right)_y \tag{3-47}$$

Thermodynamic State Functions In thermodynamics, the state functions include the internal energy, U ; enthalpy, H ; and Helmholtz and Gibbs free energies, A and G , respectively, defined as follows:

$$\begin{aligned} H &= U + pV \\ A &= U - TS \\ G &= H - TS = U + pV - TS = A + pV \end{aligned}$$

S is the entropy, T the absolute temperature, p the pressure, and V the volume. These are also state functions, in that the entropy is specified once two variables (like T and p) are specified, for example. Likewise, V is specified once T and p are specified; it is therefore a state function.

All applications are for closed systems with constant mass. If a process is reversible and only p - V work is done, the first law and differentials can be expressed as follows.

$$\begin{aligned} dU &= T dS - p dV \\ dH &= T dS + V dp \\ dA &= -S dT - p dV \\ dG &= -S dT + V dp \end{aligned}$$

Alternatively, if the internal energy is considered a function of S and V , then the differential is:

$$dU = \left(\frac{\partial U}{\partial S} \right)_V dS + \left(\frac{\partial U}{\partial V} \right)_S dV$$

This is the equivalent of Eq. (3-43) and gives the following definitions.

$$T = \left(\frac{\partial U}{\partial S} \right)_V, \quad p = - \left(\frac{\partial U}{\partial V} \right)_S$$

Since the internal energy is a state function, then Eq. (3-44) must be satisfied.

$$\frac{\partial^2 U}{\partial V \partial S} = \frac{\partial^2 U}{\partial S \partial V}$$

This is

$$\left(\frac{\partial T}{\partial V} \right)_S = - \left(\frac{\partial p}{\partial S} \right)_V$$

This is one of the Maxwell relations, and the other Maxwell relations can be derived in a similar fashion by applying Eq. (3-44).

See Sec. 4, Thermodynamics, "Constant-Composition Systems."

3-22 MATHEMATICS

Partial Derivatives of All Thermodynamic Functions The various partial derivatives of the thermodynamic functions can be classified into six groups. In the general formulas below, the variables U, H, A, G or S are denoted by Greek letters, while the variables V, T, p or p are denoted by Latin letters.

Type I (3 possibilities plus reciprocals)

$$\text{General: } \left(\frac{\partial a}{\partial b}\right)_c; \text{ Specific: } \left(\frac{\partial p}{\partial T}\right)_V$$

Eq. (3-45) gives

$$\left(\frac{\partial p}{\partial T}\right)_V = -\left(\frac{\partial V}{\partial T}\right)_p \left(\frac{\partial p}{\partial V}\right)_T = -\frac{(\partial V/\partial T)_p}{(\partial V/\partial p)_T}$$

Type II (30 possibilities plus reciprocals)

$$\text{General: } \left(\frac{\partial \alpha}{\partial b}\right)_c; \text{ Specific: } \left(\frac{\partial G}{\partial T}\right)_V$$

The differential for G gives

$$\left(\frac{\partial G}{\partial T}\right)_V = -S + V \left(\frac{\partial p}{\partial T}\right)_V$$

Using the other equations for U, H, A , or S gives the other possibilities.

Type III (15 possibilities plus reciprocals)

$$\text{General: } \left(\frac{\partial a}{\partial b}\right)_\alpha; \text{ Specific: } \left(\frac{\partial V}{\partial T}\right)_S$$

First expand the derivative using Eq. (3-45).

$$\left(\frac{\partial V}{\partial T}\right)_S = -\left(\frac{\partial S}{\partial T}\right)_V \left(\frac{\partial V}{\partial S}\right)_T = -\frac{(\partial S/\partial T)_V}{(\partial S/\partial V)_T}$$

Then evaluate the numerator and denominator as type II derivatives.

$$\left(\frac{\partial V}{\partial T}\right)_S = -\frac{\frac{C_V}{T}}{-\left(\frac{\partial V}{\partial T}\right)_p \left(\frac{\partial p}{\partial V}\right)_T} = \frac{C_V}{T} \left(\frac{\partial p}{\partial V}\right)_T$$

These derivatives are of importance for reversible, adiabatic processes (such as in an ideal turbine or compressor), since then the entropy is constant. An example is the Joule-Thomson coefficient for constant H .

$$\left(\frac{\partial T}{\partial p}\right)_H = \frac{1}{C_p} \left[-V + T \left(\frac{\partial V}{\partial T}\right)_p \right]$$

Type IV (30 possibilities plus reciprocals)

$$\text{General: } \left(\frac{\partial \alpha}{\partial \beta}\right)_c; \text{ Specific: } \left(\frac{\partial G}{\partial A}\right)_p$$

Use Eq. (3-47) to introduce a new variable.

$$\left(\frac{\partial G}{\partial A}\right)_p = \left(\frac{\partial G}{\partial T}\right)_p \left(\frac{\partial T}{\partial A}\right)_p = \frac{(\partial G/\partial T)_p}{(\partial A/\partial T)_p}$$

This operation has created two type II derivatives; by substitution we obtain

$$\left(\frac{\partial G}{\partial A}\right)_p = \frac{S}{S + p (\partial V/\partial T)_p}$$

Type V (60 possibilities plus reciprocals)

$$\text{General: } \left(\frac{\partial \alpha}{\partial b}\right)_\beta; \text{ Specific: } \left(\frac{\partial G}{\partial p}\right)_A$$

Start from the differential for dG . Then we get

$$\left(\frac{\partial G}{\partial p}\right)_A = -S \left(\frac{\partial T}{\partial p}\right)_A + V$$

The derivative is type III and can be evaluated by using Eq. (3-45).

$$\left(\frac{\partial G}{\partial p}\right)_A = S \frac{(\partial A/\partial p)_T}{(\partial A/\partial T)_p} + V$$

The two type II derivatives are then evaluated.

$$\left(\frac{\partial G}{\partial p}\right)_A = \frac{Sp (\partial V/\partial p)_T}{S + p (\partial V/\partial T)_p} + V$$

These derivatives are also of interest for free expansions or isentropic changes.

Type VI (30 possibilities plus reciprocals)

$$\text{General: } \left(\frac{\partial \alpha}{\partial \beta}\right)_\gamma; \text{ Specific: } \left(\frac{\partial G}{\partial A}\right)_H$$

We use Eq. (3-47) to obtain two type V derivatives.

$$\left(\frac{\partial G}{\partial A}\right)_H = \frac{(\partial G/\partial T)_H}{(\partial A/\partial T)_H}$$

These can then be evaluated using the procedures for Type V derivatives.

INTEGRAL CALCULUS

Indefinite Integral If $f'(x)$ is the derivative of $f(x)$, an antiderivative of $f'(x)$ is $f(x)$. Symbolically, the indefinite integral of $f'(x)$ is

$$\int f'(x) dx = f(x) + c$$

where c is an arbitrary constant to be determined by the problem. By virtue of the known formulas for differentiation the following relationships hold (a is a constant):

$$\int (du + dv + dw) = \int du + \int dv + \int dw \quad (3-48)$$

$$\int a dv = a \int dv \quad (3-49)$$

$$\int v^n dv = \frac{v^{n+1}}{n+1} + c \quad (n \neq -1) \quad (3-50)$$

$$\int \frac{dv}{v} = \ln |v| + c \quad (3-51)$$

$$\int a^v dv = \frac{a^v}{\ln a} + c \quad (3-52)$$

$$\int e^v dv = e^v + c \quad (3-53)$$

$$\int \sin v dv = -\cos v + c \quad (3-54)$$

$$\int \cos v dv = \sin v + c \quad (3-55)$$

$$\int \sec^2 v dv = \tan v + c \quad (3-56)$$

$$\int \csc^2 v dv = -\cot v + c \quad (3-57)$$

$$\int \sec v \tan v dv = \sec v + c \quad (3-58)$$

$$\int \csc v \cot v dv = -\csc v + c \quad (3-59)$$

$$\int \frac{dv}{v^2 + a^2} = \frac{1}{a} \tan^{-1} \frac{v}{a} + c \quad (3-60)$$

$$\int \frac{dv}{\sqrt{a^2 - v^2}} = \sin^{-1} \frac{v}{a} + c \quad (3-61)$$

$$\int \frac{dv}{v^2 - a^2} = \frac{1}{2a} \ln \left| \frac{v-a}{v+a} \right| + c \quad (3-62)$$

$$\int \frac{dv}{\sqrt{v^2 \pm a^2}} = \ln |v + \sqrt{v^2 \pm a^2}| + c \quad (3-63)$$

$$\int \sec v dv = \ln |\sec v + \tan v| + c \quad (3-64)$$

$$\int \csc v \, dv = \ln |\csc v - \cot v| + c \quad (3-65)$$

Example Find $\int (3x^2 + e^x - 10) \, dx$ using Eq. (3-48). $\int (3x^2 + e^x - 10) \, dx = 3 \int x^2 \, dx + \int e^x \, dx - 10 \int dx = x^3 + e^x - 10x + c$ (by Eqs. 3-50, 3-53).

Example Find $\int \frac{7x \, dx}{2 - 3x^2}$. Let $v = 2 - 3x^2$; $dv = -6x \, dx$

Thus
$$\begin{aligned} \int \frac{7x \, dx}{2 - 3x^2} &= 7 \int \frac{x \, dx}{2 - 3x^2} = -\frac{7}{6} \int \frac{-6x \, dx}{2 - 3x^2} \\ &= -\frac{7}{6} \int \frac{dv}{v}, \text{ with } v = 2 - 3x^2 \text{ and } dv = -6x \, dx \\ &= -\frac{7}{6} \ln |v| + c = -\frac{7}{6} \ln |2 - 3x^2| + c \end{aligned}$$

Example—Constant of Integration By definition the derivative of x^3 is $3x^2$, and x^3 is therefore the integral of $3x^2$. However, if $f = x^3 + 10$, it follows that $f' = 3x^2$, and $x^3 + 10$ is therefore also the integral of $3x^2$. For this reason the constant c in $\int 3x^2 \, dx = x^3 + c$ must be determined by the problem conditions, i.e., the value of f for a specified x .

Methods of Integration In practice it is rare when generally encountered functions can be directly integrated. For example, the integrand in $\int \sqrt{\sin x} \, dx$ which appears quite simple has no elementary function whose derivative is $\sqrt{\sin x}$. In general, there is no explicit way of determining whether a particular function can be integrated into an elementary form. As a whole, integration is a trial-and-error proposition which depends on the effort and ingenuity of the practitioner. The following are general procedures which can be used to find the elementary forms of the integral when they exist. When they do not exist or cannot be found either from tabled integration formulas or directly, the only recourse is series expansion as illustrated later. Indefinite integrals cannot be solved numerically unless they are redefined as definite integrals (see "Definite Integral"), i.e., $F(x) = \int f(x) \, dx$, indefinite, whereas $F(x) = \int_a^x f(t) \, dt$, definite.

Direct Formula Many integrals can be solved by transformation in the integrand to one of the forms given previously.

Example Find $\int x^2 \sqrt{3x^3 + 10} \, dx$. Let $v = 3x^3 + 10$ for which $dv = 9x^2 \, dx$. Thus

$$\begin{aligned} \int x^2 \sqrt{3x^3 + 10} \, dx &= \int (3x^3 + 10)^{1/2} (x^2 \, dx) \\ &= \frac{1}{9} \int (3x^3 + 10)^{1/2} (9x^2 \, dx) = \frac{1}{9} \int v^{1/2} \, dv \\ &= \frac{1}{9} \frac{v^{3/2}}{3/2} + c \quad [\text{by Eq. (3-50)}] \\ &= \frac{2}{27} (3x^3 + 10)^{3/2} + c \end{aligned}$$

Trigonometric Substitution This technique is particularly well adapted to integrands in the form of radicals. For these the function is transformed into a trigonometric form. In the latter form they may be more easily recognizable relative to the identity formulas. These functions and their transformations are

$$\begin{aligned} \sqrt{x^2 - a^2} \quad &\text{Let } x = a \sec \theta \\ \sqrt{x^2 + a^2} \quad &\text{Let } x = a \tan \theta \\ \sqrt{a^2 - x^2} \quad &\text{Let } x = a \sin \theta \end{aligned}$$

Example Find $\int \frac{\sqrt{4-9x^2}}{x^2} \, dx$. Let $x = \frac{2}{3} \sin \theta$; then $dx = \frac{2}{3} \cos \theta \, d\theta$.

$$3 \int \frac{\sqrt{(2/3)^2 - x^2}}{x^2} \, dx = 3 \int \frac{2/3 \sqrt{1 - \sin^2 \theta}}{(2/3)^2 \sin^2 \theta} \left(\frac{2}{3} \cos \theta \, d\theta \right)$$

$$\begin{aligned} &= 3 \int \frac{\cos^2 \theta}{\sin^2 \theta} \, d\theta = 3 \int \cot^2 \theta \, d\theta \\ &= -3 \cot \theta - 3\theta + c \text{ by trigonometric transform} \\ &= -\frac{\sqrt{4-9x^2}}{x} - 3 \sin^{-1} \frac{3}{2} x + c \text{ in terms of } x \end{aligned}$$

Algebraic Substitution Functions containing elements of the type $(a + bx)^{1/n}$ are best handled by the algebraic transformation $y^n = a + bx$.

Example Find $\int \frac{x \, dx}{(3 + 4x)^{1/4}}$. Let $3 + 4x = y^4$; then $4dx = 4y^3 \, dy$ and

$$\begin{aligned} \int \frac{x \, dx}{(3 + 4x)^{1/4}} &= \int \frac{y^4 - 3}{4} \frac{y^3 \, dy}{y} = \frac{1}{4} \int y^2(y^4 - 3) \, dy \\ &= \frac{1}{4} \frac{y^7}{7} - \frac{3}{4} \frac{y^3}{3} + c = \frac{1}{28} (3 + 4x)^{7/4} - \frac{1}{4} (3 + 4x)^{3/4} + c \end{aligned}$$

General The number of possible transformations one might use are unlimited. No specific overall rules can be given. Success in handling integration problems depends primarily upon experience and ingenuity. The following example illustrates the extent to which alternative approaches are possible.

Example Find $\int \frac{dx}{e^x - 1}$. Let $e^x = y$; then $e^x \, dx = dy$ or $dx = 1/y \, dy$.

$$\int \frac{dx}{e^x - 1} = \int \frac{(1/y) \, dy}{y - 1} = \int \frac{dy}{y^2 - y} = \ln \frac{y - 1}{y} = \ln \frac{e^x - 1}{e^x}$$

Partial Fractions Rational functions are of the type $f(x)/g(x)$ where $f(x)$ and $g(x)$ are polynomial expressions of degrees m and n respectively. If the degree of f is higher than g , perform the algebraic division—the remainder will then be at least one degree less than the denominator. Consider the following types:

Type 1 Reducible denominator to linear unequal factors. For example,

$$\begin{aligned} \frac{1}{x^3 - x^2 - 4x + 4} &= \frac{1}{(x + 2)(x - 2)(x - 1)} \\ &= \frac{A}{x + 2} + \frac{B}{x - 2} + \frac{C}{x - 1} \\ &= \frac{A(x - 2)(x - 1) + B(x + 2)(x - 1) + C(x + 2)(x - 2)}{(x + 2)(x - 2)(x - 1)} \\ &= \frac{x^2(A + B + C) + x(-3A + B) + (2A - 2B - 4C)}{(x + 2)(x - 2)(x - 1)} \end{aligned}$$

Equate coefficients and solve for A , B , and C .

$$\begin{aligned} A + B + C &= 0 \\ -3A + B &= 0 \\ 2A - 2B - 4C &= 1 \\ A = 1/2, B = 1/4, C = -1/4 \end{aligned}$$

$$\frac{1}{x^3 - x^2 - 4x + 4} = \frac{1}{12(x + 2)} + \frac{1}{4(x - 2)} - \frac{1}{3(x - 1)}$$

Hence

$$\int \frac{dx}{x^3 - x^2 - 4x + 4} = \int \frac{dx}{12(x + 2)} + \int \frac{dx}{4(x - 2)} - \int \frac{dx}{3(x - 1)}$$

Parts An extremely useful formula for integration is the relation

$$d(uv) = u \, dv + v \, du$$

and $uv = \int u \, dv + \int v \, du$

or $\int u \, dv = uv - \int v \, du$

3-24 MATHEMATICS

No general rule for breaking an integrand can be given. Experience alone limits the use of this technique. It is particularly useful for trigonometric and exponential functions.

Example Find $\int xe^x dx$. Let

$$\begin{aligned} u &= x & \text{and} & & dv &= e^x dx \\ du &= dx & & & v &= e^x \end{aligned}$$

Therefore
$$\begin{aligned} \int xe^x dx &= xe^x - \int e^x dx \\ &= xe^x - e^x + c \end{aligned}$$

Example Find $\int e^x \sin x dx$. Let

$$\begin{aligned} u &= e^x & dv &= \sin x dx \\ du &= e^x dx & v &= -\cos x \end{aligned}$$

$$\int e^x \sin x dx = -e^x \cos x + \int e^x \cos x dx$$

Again
$$\begin{aligned} u &= e^x & dv &= \cos x dx \\ du &= e^x dx & v &= \sin x \end{aligned}$$

$$\begin{aligned} \int e^x \sin x dx &= -e^x \cos x + e^x \sin x - \int e^x \sin x dx + c \\ &= (e^x/2)(\sin x - \cos x) + \frac{c}{2} \end{aligned}$$

Series Expansion When an explicit function cannot be found, the integration can sometimes be carried out by a series expansion.

Example Find $\int e^{-x^2} dx$. Since

$$e^{-x^2} = 1 - x^2 + \frac{x^4}{2!} - \frac{x^6}{3!} + \dots$$

$$\begin{aligned} \int e^{-x^2} dx &= \int dx - \int x^2 dx + \int \frac{x^4}{2!} dx - \int \frac{x^6}{3!} dx + \dots \\ &= x - \frac{x^3}{3} + \frac{x^5}{5 \cdot 2!} - \frac{x^7}{7 \cdot 3!} + \dots \quad \text{for all } x \end{aligned}$$

Definite Integral The concept and derivation of the definite integral are completely different from those for the indefinite integral. These are by definition different types of operations. However, the formal operation \int as it turns out treats the integrand in the same way for both.

Consider the function $f(x) = 10 - 10e^{-2x}$. Define $x_1 = a$ and $x_n = b$, and suppose it is desirable to compute the area between the curve and the coordinate axis $y = 0$ and bounded by $x_1 = a$, $x_n = b$. Obviously, by a sufficiently large number of rectangles this area could be approximated as closely as desired by the formula

$$\begin{aligned} \sum_{i=1}^{n-1} f(\xi_i)(x_{i+1} - x_i) &= f(\xi_1)(x_2 - a) + f(\xi_2)(x_3 - x_2) \\ &\quad + \dots + f(\xi_{n-1})(b - x_{n-1}) \quad x_{i-1} \leq \xi_i \leq x_i \end{aligned}$$

The definite integral of $f(x)$ is defined as

$$\int_a^b f(x) dx = \lim_{n \rightarrow \infty} \sum_{i=1}^n f(\xi_i)(x_{i+1} - x_i)$$

where the points x_1, x_2, \dots, x_n are equally spaced.

Thus, the value of a definite integral depends on the limits a, b , and any selected variable coefficients in the function but not on the dummy variable of integration x . Symbolically

$$F(x) = \int f(x) dx \quad \text{indefinite integral where } dF/dx = f(x)$$

or
$$F(a, b) = \int_a^b f(x) dx \quad \text{definite integral}$$

$$F(\alpha) = \int_a^b f(x, \alpha) dx$$

There are certain restrictions of the integration definition. "The function $f(x)$ must be continuous in the finite interval (a, b) with at most a finite number of finite discontinuities," which must be observed before integration formulas can be generally applied. Relaxing two of

these restrictions gives rise to so-called **improper integrals** and requires special handling. These occur when

1. The limits of integration are not both finite, i.e., $\int_0^\infty e^{-x} dx$.
2. The function becomes infinite within the interval of integration, i.e.,

$$\int_0^1 \frac{1}{\sqrt{x}} dx$$

Techniques for determining when integration is valid under these conditions are available in the references.

Properties The fundamental theorem of calculus states

$$\int_a^b f(x) dx = F(b) - F(a)$$

where
$$dF(x)/dx = f(x)$$

Other properties of the definite integral are

$$\int_a^b c[f(x) dx] = c \int_a^b f(x) dx$$

$$\int_a^b [f_1(x) + f_2(x)] dx = \int_a^b f_1(x) dx + \int_a^b f_2(x) dx$$

$$\int_a^b f(x) dx = -\int_b^a f(x) dx$$

$$\int_a^b f(x) dx = \int_a^c f(x) dx + \int_c^b f(x) dx$$

$$\int_a^b f(x) dx = (b - a)f(\xi) \quad \text{for some } \xi \text{ in } (a, b)$$

$$\frac{\partial}{\partial b} \int_a^b f(x) dx = f(b)$$

$$\frac{\partial}{\partial a} \int_a^b f(x) dx = -f(a)$$

$$\frac{dF(\alpha)}{d\alpha} = \int_a^b \frac{\partial f(x, \alpha)}{\partial \alpha} dx \quad \text{if } a \text{ and } b \text{ are constant}$$

$$\int_a^b dx \int_c^d f(x, \alpha) d\alpha = \int_c^d d\alpha \int_a^b f(x, \alpha) dx \quad (3-66)$$

When $F(x) = \int_{a(x)}^{b(x)} f(x, y) dy$, the Leibniz rule gives

$$\frac{dF}{dx} = \frac{db}{dx} f[x, b(x)] - \frac{da}{dx} f[x, a(x)] + \int_{a(x)}^{b(x)} \frac{\partial f}{\partial x} dy$$

Example Find $\int_0^2 \frac{dx}{(x-1)^2}$. Direct application of the formula would yield the incorrect value

$$\int_0^2 \frac{dx}{(x-1)^2} = \left[-\frac{1}{x-1} \right]_0^2 = -2$$

It should be noted that $f(x) = 1/(x-1)^2$ becomes unbounded as $x \rightarrow 1$ and by Rule 2 the integral diverges and hence is said not to exist.

Methods of Integration All the methods of integration available for the indefinite integral can be used for definite integrals. In addition, several others are available for the latter integrals and are indicated below.

Change of Variable This substitution is basically the same as previously indicated for indefinite integrals. However, for definite integrals, the limits of integration must also be changed: i.e., for $x = \phi(t)$,

$$\int_a^b f(x) dx = \int_{t_0}^{t_1} f[\phi(t)]\phi'(t) dt$$

where
$$\begin{aligned} t &= t_0 \text{ when } x = a \\ t &= t_1 \text{ when } x = b \end{aligned}$$

Example Find $\int_0^4 \sqrt{16-x^2} dx$. Let
 $x = 4 \sin \theta$ ($x = 0, \theta = 0$)
 $dx = 4 \cos \theta d\theta$ ($x = 4, \theta = \pi/2$)

Then $\int_0^4 \sqrt{16-x^2} dx = 16 \int_0^{\pi/2} \cos^2 \theta d\theta = 16[\frac{1}{2}\theta + \frac{1}{4} \sin 2\theta]_0^{\pi/2} = 4\pi$

Integration It is sometimes useful to generate a double integral to solve a problem. By this approach, the fundamental theorem indicated by Eq. (3-66) can be used.

Example Find $\int_0^1 \frac{x^b - x^a}{\ln x} dx$

Consider $\int_0^1 x^\alpha dx = \frac{1}{\alpha+1} (\alpha > -1)$

Then multiplying both sides by $d\alpha$ and integrating between a and b ,

$$\int_a^b d\alpha \int_0^1 x^\alpha dx = \int_a^b \frac{d\alpha}{\alpha+1} = \ln \left| \frac{b+1}{a+1} \right|$$

But also

$$\int_a^b d\alpha \int_0^1 x^\alpha dx = \int_0^1 dx \int_a^b x^\alpha d\alpha = \int_0^1 \frac{x^b - x^a}{\ln x} dx$$

Therefore $\int_0^1 \frac{x^b - x^a}{\ln x} dx = \ln \left| \frac{b+1}{a+1} \right|$

INFINITE SERIES

REFERENCES: de Bruijn, N. G., *Asymptotic Methods in Analysis*, Dover, New York (1981); Folland, G. B., *Advanced Calculus*, Prentice-Hall, Saddle River, N.J. (2002); Gradshteyn, I. S., and I. M. Ryzhik, *Tables of Integrals, Series, and Products*, Academic, New York (2000); Kaplan, W., *Advanced Calculus*, 5th ed., Addison-Wesley, Redwood City, Calif. (2003).

DEFINITIONS

A succession of numbers or terms that are formed according to some definite rule is called a sequence. The indicated sum of the terms of a sequence is called a series. A series of the form $a_0 + a_1(x-c) + a_2(x-c)^2 + \dots + a_n(x-c)^n + \dots$ is called a power series.

Consider the sum of a finite number of terms in the geometric series (a special case of a power series).

$$S_n = a + ar + ar^2 + ar^3 + \dots + ar^{n-1} \quad (3-67)$$

For any number of terms n , the sum equals

$$S_n = a \frac{1-r^n}{1-r}$$

In this form, the geometric series is assumed finite.

In the form of Eq. (3-67), it can further be defined that the terms in the series be nonending and therefore an infinite series.

$$S = a + ar + ar^2 + \dots + ar^n + \dots \quad (3-68)$$

However, the defined sum of the terms [Eq. (3-67)]

$$S_n = a \frac{1-r^n}{1-r} \quad r \neq 1$$

while valid for any finite value of r and n now takes on a different interpretation. In this sense it is necessary to consider the limit of S_n as n increases indefinitely:

$$\begin{aligned} S &= \lim_{n \rightarrow \infty} S_n \\ &= a \lim_{n \rightarrow \infty} \frac{1-r^n}{1-r} \end{aligned}$$

For this, it is stated the infinite series converges if the limit of S_n approaches a fixed finite value as n approaches infinity. Otherwise, the series is **divergent**.

On this basis an analysis of

$$S = a \lim_{n \rightarrow \infty} \frac{1-r^n}{1-r}$$

shows that if r is less than 1 but greater than -1 , the infinite series is convergent. For values outside of the range $-1 < r < 1$, the series is divergent because the sum is not defined. The range $-1 < r < 1$ is called the **region of convergence**. (We assume $a \neq 0$.)

There are also two types of convergent series. Consider the new series

$$S = 1 - \frac{1}{2} + \frac{1}{3} - \frac{1}{4} + \dots + (-1)^{n+1} \frac{1}{n} + \dots \quad (3-69)$$

It can be shown that the series (3-69) does converge to the value $S = \log 2$. However, if each term is replaced by its absolute value, the series becomes unbounded and therefore divergent (unbounded divergent):

$$S = 1 + \frac{1}{2} + \frac{1}{3} + \frac{1}{4} + \frac{1}{5} + \dots \quad (3-70)$$

In this case the series (3-69) is defined as a conditionally convergent series. If the replacement series of absolute values also converges, the series is defined to converge absolutely.

Series (3-69) is further defined as an alternating series, while series (3-70) is referred to as a positive series.

OPERATIONS WITH INFINITE SERIES

1. The convergence or divergence of an infinite series is unaffected by the removal of a finite number of finite terms. This is a trivial theorem but useful to remember, especially when using the comparison test to be described in the subsection "Tests for Convergence and Divergence."

2. If a series is conditionally convergent, its sums can be made to have any arbitrary value by a suitable rearrangement of the series; it can in fact be made divergent or oscillatory (Riemann's theorem).

3. A series of positive terms; if convergent, has a sum independent of the order of its terms; but if divergent, it remains divergent however its terms are rearranged.

4. An oscillatory series can always be made to converge by grouping terms.

5. A power series can be inverted, provided the first-degree term is not zero. Given

$$y = b_1x + b_2x^2 + b_3x^3 + b_4x^4 + b_5x^5 + b_6x^6 + b_7x^7 + \dots$$

then $x = B_1y + B_2y^2 + B_3y^3 + B_4y^4 + B_5y^5 + B_6y^6 + B_7y^7 + \dots$

where $B_1 = 1/b_1$

$$B_2 = -b_2/b_1^3$$

$$B_3 = (1/b_1^5)(2b_2^2 - b_1b_3)$$

$$B_4 = (1/b_1^7)(5b_1b_2b_3 - b_1^2b_4 - 5b_2^3)$$

Additional coefficients are available in the references.

6. Two series may be added or subtracted term by term provided each is a convergent series. The joint sum is equal to the sum (or difference) of the individuals.

3-26 MATHEMATICS

7. The sum of two divergent series can be convergent. Similarly, the sum of a convergent series and a divergent series must be divergent.

8. A power series may be integrated term by term to represent the integral of the function within an interval of the region of convergence. If $f(x) = a_0 + a_1x + a_2x^2 + \dots$, then

$$\int_{x_1}^{x_2} f(x) dx = \int_{x_1}^{x_2} a_0 dx + \int_{x_1}^{x_2} a_1x dx + \int_{x_1}^{x_2} a_2x^2 dx + \dots$$

9. A power series may be differentiated term by term and represents the function $df(x)/dx$ within the same region of convergence as $f(x)$.

TESTS FOR CONVERGENCE AND DIVERGENCE

In general, the problem of determining whether a given series will converge or not can require a great deal of ingenuity and resourcefulness. There is no all-inclusive test which can be applied to all series. As the only alternative, it is necessary to apply one or more of the developed theorems in an attempt to ascertain the convergence or divergence of the series under study. The following defined tests are given in relative order of effectiveness. For examples, see references on advanced calculus.

1. **Comparison Test.** A series will converge if the absolute value of each term (with or without a finite number of terms) is less than the corresponding term of a known convergent series. Similarly, a positive series is divergent if it is termwise larger than a known divergent series of positive terms.

2. **n th-Term Test.** A series is divergent if the n th term of the series does not approach zero as n becomes increasingly large.

3. **Ratio Test.** If the absolute ratio of the $(n + 1)$ term divided by the n th term as n becomes unbounded approaches

- a. A number less than 1, the series is absolutely convergent
- b. A number greater than 1, the series is divergent
- c. A number equal to 1, the test is inconclusive

4. **Alternating-Series Leibniz Test.** If the terms of a series are alternately positive and negative and never increase in value, the absolute series will converge, provided that the terms tend to zero as a limit.

5. **Cauchy's Root Test.** If the n th root of the absolute value of the n th term, as n becomes unbounded, approaches

- a. A number less than 1, the series is absolutely convergent
- b. A number greater than 1, the series is divergent
- c. A number equal to 1, the test is inconclusive

6. **Maclaurin's Integral Test.** Suppose $\sum a_n$ is a series of positive terms and f is a continuous decreasing function such that $f(x) \geq 0$ for $1 \leq x < \infty$ and $f(n) = a_n$. Then the series and the improper integral $\int_1^\infty f(x) dx$ either both converge or both diverge.

SERIES SUMMATION AND IDENTITIES

Sums for the First n Numbers to Integer Powers

$$\sum_{j=1}^n j = \frac{n(n+1)}{2} = 1 + 2 + 3 + 4 + \dots + n$$

$$\sum_{j=1}^n j^2 = \frac{n(n+1)(2n+1)}{6} = 1^2 + 2^2 + 3^2 + 4^2 + \dots + n^2$$

$$\sum_{j=1}^n j^3 = \frac{n^2(n+1)^2}{4} = 1^3 + 2^3 + 3^3 + \dots + n^3$$

Arithmetic Progression

$$\begin{aligned} \sum_{k=1}^n [a + (k-1)d] &= a + (a+d) + (a+2d) \\ &\quad + (a+3d) + \dots + [a + (n-1)d] \\ &= na + \frac{1}{2}n(n-1)d \end{aligned}$$

Geometric Progression

$$\sum_{j=1}^n ar^{j-1} = a + ar + ar^2 + ar^3 + \dots + ar^{n-1} = a \frac{1-r^n}{1-r} \quad r \neq 1$$

Harmonic Progression

$$\sum_{k=0}^n \frac{1}{a+kd} = \frac{1}{a} + \frac{1}{a+d} + \frac{1}{a+2d} + \frac{1}{a+3d} + \frac{1}{a+4d} + \dots + \frac{1}{a+nd}$$

The reciprocals of the terms of the arithmetic-progression series are called harmonic progression. No general summation formulas are available for this series.

Binomial Series (see also Elementary Algebra)

$$(1 \pm x)^n = 1 \pm nx + \frac{n(n-1)}{2!}x^2 \pm \frac{n(n-1)(n-2)}{3!}x^3 + \dots \quad (x^2 < 1)$$

Taylor's Series

$$f(h+x) = f(h) + xf'(h) + \frac{x^2}{2!}f''(h) + \frac{x^3}{3!}f'''(h) + \dots$$

$$\text{or } f(x) = f(x_0) + f'(x_0)(x-x_0) + \frac{f''(x_0)}{2!}(x-x_0)^2 + \frac{f'''(x_0)}{3!}(x-x_0)^3 + \dots$$

Example Find a series expansion for $f(x) = \ln(1+x)$ about $x_0 = 0$.

$$f(x) = (1+x)^{-1}, \quad f'(x) = -(1+x)^{-2}, \quad f''(x) = 2(1+x)^{-3}, \text{ etc.}$$

thus $f(0) = 0, \quad f'(0) = 1, \quad f''(0) = -1, \quad f'''(0) = 2, \text{ etc.}$

$$\ln(1+x) = x - \frac{x^2}{2} + \frac{x^3}{3} - \frac{x^4}{4} + \dots + (-1)^{n+1} \frac{x^n}{n} + \dots$$

which converges for $-1 < x \leq 1$.

Maclaurin's Series

$$f(x) = f(0) + xf'(0) + \frac{x^2}{2!}f''(0) + \frac{x^3}{3!}f'''(0) + \dots$$

This is simply a special case of Taylor's series when h is set to zero.

Exponential Series

$$e^x = 1 + x + \frac{x^2}{2!} + \frac{x^3}{3!} + \dots + \frac{x^n}{n!} + \dots \quad -\infty < x < \infty$$

Logarithmic Series

$$\ln x = \frac{x-1}{x} + \frac{1}{2} \left(\frac{x-1}{x} \right)^2 + \frac{1}{3} \left(\frac{x-1}{x} \right)^3 + \dots \quad (x > 1/2)$$

$$\ln x = 2 \left[\frac{x-1}{x+1} \right] + \frac{1}{3} \left(\frac{x-1}{x+1} \right)^3 + \dots \quad (x > 0)$$

Trigonometric Series*

$$\sin x = x - \frac{x^3}{3!} + \frac{x^5}{5!} - \frac{x^7}{7!} + \dots \quad -\infty < x < \infty$$

$$\cos x = 1 - \frac{x^2}{2!} + \frac{x^4}{4!} - \frac{x^6}{6!} + \dots \quad -\infty < x < \infty$$

$$\sin^{-1} x = x + \frac{x^3}{6} + \frac{1}{2} \cdot \frac{3}{4} \cdot \frac{x^5}{5} + \frac{1}{2} \cdot \frac{3}{4} \cdot \frac{5}{6} \cdot \frac{x^7}{7} + \dots \quad (x^2 < 1)$$

$$\tan^{-1} x = x - \frac{1}{3}x^3 + \frac{1}{5}x^5 - \frac{1}{7}x^7 + \dots \quad (x^2 < 1)$$

Taylor Series The Taylor series for a function of two variables, expanded about the point (x_0, y_0) , is

* $\tan x$ series has awkward coefficients and should be computed as $\left[(\text{sign}) \frac{\sin x}{\sqrt{1-\sin^2 x}} \right]$.

$$f(x, y) = f(x_0, y_0) + \left. \frac{\partial f}{\partial x} \right|_{x_0, y_0} (x - x_0) + \left. \frac{\partial f}{\partial y} \right|_{x_0, y_0} (y - y_0) + \frac{1}{2!} \left[\left. \frac{\partial^2 f}{\partial x^2} \right|_{x_0, y_0} (x - x_0)^2 + 2 \left. \frac{\partial^2 f}{\partial x \partial y} \right|_{x_0, y_0} (x - x_0)(y - y_0) + \left. \frac{\partial^2 f}{\partial y^2} \right|_{x_0, y_0} (y - y_0)^2 \right] + \dots$$

Partial Sums of Infinite Series, and How They Grow Calculus textbooks devote much space to tests for convergence and divergence of series that are of little practical value, since a convergent series either converges rapidly, in which case almost any test (among those presented in the preceding subsections) will do; or it converges slowly, in which case it is not going to be of much use unless there is some way to get at its sum without adding up an unreasonable number of terms. To find out, as accurately as possible, how fast a convergent series converges and how fast a divergent series diverges, see Boas, R. P., Jr., *Am. Math. Mon.* **84**: 237–258 (1977).

COMPLEX VARIABLES

REFERENCES: Ablowitz, M. J., and A. S. Fokas, *Complex Variables: Introduction and Applications*, Cambridge University Press, New York (2003); Asmar, N., and G. C. Jones, *Applied Complex Analysis with Partial Differential Equations*, Prentice-Hall, Upper Saddle River, N.J. (2002); Brown, J. W., and R. V. Churchill, *Complex Variables and Applications*, 7th ed., McGraw-Hill, New York (2003); Kaplan, W., *Advanced Calculus*, 5th ed., Addison-Wesley, Redwood City, Calif. (2003); Kwok, Y. K., *Applied Complex Variables for Scientists and Engineers*, Cambridge University Press, New York (2002); McGehee, O. C., *An Introduction to Complex Analysis*, Wiley, New York (2000); Priestley, H. A., *Introduction to Complex Analysis*, Oxford University Press, New York (2003).

Numbers of the form $z = x + iy$, where x and y are real, $i^2 = -1$, are called complex numbers. The numbers $z = x + iy$ are representable in the plane as shown in Fig. 3-45. The following definitions and terminology are used:

1. Distance $OP = r$ = modulus of z written $|z|$. $|z| = \sqrt{x^2 + y^2}$.
2. x is the real part of z .
3. y is the imaginary part of z .
4. The angle θ , $0 \leq \theta < 2\pi$, measured counterclockwise from the positive x axis to OP is the argument of z . $\theta = \arctan y/x = \arcsin y/r = \arccos x/r$ if $x \neq 0$, $\theta = \pi/2$ if $x = 0$ and $y > 0$.
5. The numbers r, θ are the polar coordinates of z .
6. $\bar{z} = x - iy$ is the complex conjugate of z .

ALGEBRA

Let $z_1 = x_1 + iy_1, z_2 = x_2 + iy_2$.

Equality $z_1 = z_2$ if and only if $x_1 = x_2$ and $y_1 = y_2$.

Addition $z_1 + z_2 = (x_1 + x_2) + i(y_1 + y_2)$.

Subtraction $z_1 - z_2 = (x_1 - x_2) + i(y_1 - y_2)$.

Multiplication $z_1 \cdot z_2 = (x_1x_2 - y_1y_2) + i(x_1y_2 + x_2y_1)$.

Division $z_1/z_2 = \frac{x_1x_2 + y_1y_2}{x_2^2 + y_2^2} + i \frac{x_2y_1 - x_1y_2}{x_2^2 + y_2^2}, z_2 \neq 0$.

SPECIAL OPERATIONS

$\bar{z}\bar{z} = x^2 + y^2 = |z|^2; \overline{z_1 \pm z_2} = \bar{z}_1 \pm \bar{z}_2; \overline{\bar{z}_1} = z_1; \overline{z_1 z_2} = \bar{z}_1 \bar{z}_2; |z_1 \cdot z_2| = |z_1| \cdot |z_2|; \arg(z_1 \cdot z_2) = \arg z_1 + \arg z_2; \arg(\bar{z}_1/z_2) = \arg z_1 - \arg z_2; i^{4n} = 1$ for n any integer; $i^{2n} = -1$ where n is any odd integer; $z + \bar{z} = 2x; z - \bar{z} = 2iy$.

Every complex quantity can be expressed in the form $x + iy$.

TRIGONOMETRIC REPRESENTATION

By referring to Fig. 3-45, there results $x = r \cos \theta, y = r \sin \theta$ so that $z = x + iy = r(\cos \theta + i \sin \theta)$, which is called the polar form of the

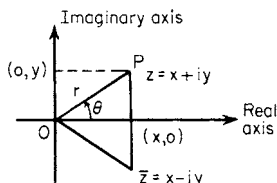


FIG. 3-45 Complex plane.

complex number. $\cos \theta + i \sin \theta = e^{i\theta}$. Hence $z = x + iy = re^{i\theta}, \bar{z} = x - iy = re^{-i\theta}$. Two important results from this are $\cos \theta = (e^{i\theta} + e^{-i\theta})/2$ and $\sin \theta = (e^{i\theta} - e^{-i\theta})/2i$. Let $z_1 = r_1 e^{i\theta_1}, z_2 = r_2 e^{i\theta_2}$. This form is convenient for multiplication for $z_1 z_2 = r_1 r_2 e^{i(\theta_1 + \theta_2)}$ and for division for $z_1/z_2 = (r_1/r_2)e^{i(\theta_1 - \theta_2)}, z_2 \neq 0$.

POWERS AND ROOTS

If n is a positive integer, $z^n = (re^{i\theta})^n = r^n e^{in\theta} = r^n(\cos n\theta + i \sin n\theta)$.

If n is a positive integer,

$$z^{1/n} = r^{1/n} e^{i[(\theta + 2k\pi)/n]} = r^{1/n} \left[\cos \left(\frac{\theta + 2k\pi}{n} \right) + i \sin \left(\frac{\theta + 2k\pi}{n} \right) \right]$$

and selecting values of $k = 0, 1, 2, 3, \dots, n - 1$ give the n distinct values of $z^{1/n}$. The n roots of a complex quantity are uniformly spaced around a circle, with radius $r^{1/n}$, in the complex plane in a symmetric fashion.

Example Find the three cube roots of -8 . Here $r = 8, \theta = \pi$. The roots are $z_0 = 2(\cos \pi/3 + i \sin \pi/3) = 1 + i\sqrt{3}, z_1 = 2(\cos \pi + i \sin \pi) = -2, z_2 = 2(\cos 5\pi/3 + i \sin 5\pi/3) = 1 - i\sqrt{3}$.

ELEMENTARY COMPLEX FUNCTIONS

Polynomials A polynomial in $z, a_n z^n + a_{n-1} z^{n-1} + \dots + a_0$, where n is a positive integer, is simply a sum of complex numbers times integral powers of z which have already been defined. Every polynomial of degree n has precisely n complex roots provided each multiple root of multiplicity m is counted m times.

Exponential Functions The exponential function e^z is defined by the equation $e^z = e^{x+iy} = e^x \cdot e^{iy} = e^x(\cos y + i \sin y)$. Properties: $e^0 = 1; e^{z_1} \cdot e^{z_2} = e^{z_1+z_2}; e^{z_1}/e^{z_2} = e^{z_1-z_2}; e^{z+2k\pi i} = e^z$.

Trigonometric Functions $\sin z = (e^{iz} - e^{-iz})/2i; \cos z = (e^{iz} + e^{-iz})/2; \tan z = \sin z/\cos z; \cot z = \cos z/\sin z; \sec z = 1/\cos z; \csc z = 1/\sin z$. Fundamental identities for these functions are the same as their real counterparts. Thus $\cos^2 z + \sin^2 z = 1, \cos(z_1 \pm z_2) = \cos z_1 \cos z_2 \mp \sin z_1 \sin z_2, \sin(z_1 \pm z_2) = \sin z_1 \cos z_2 \pm \cos z_1 \sin z_2$. The sine and cosine of z are periodic functions of period 2π ; thus $\sin(z + 2\pi) = \sin z$. For computation purposes $\sin z = \sin(x + iy) = \sin x \cosh y + i \cos x \sinh y$, where $\sin x, \cosh y$, etc., are the real trigonometric and hyperbolic functions. Similarly, $\cos z = \cos x \cosh y - i \sin x \sinh y$. If $x = 0$ in the results given, $\cos iy = \cosh y, \sin iy = i \sinh y$.

Example Find all solutions of $\sin z = 3$. From previous data $\sin z = \sin x \cosh y + i \cos x \sinh y = 3$. Equating real and imaginary parts $\sin x \cosh y = 3, \cos x \sinh y = 0$. The second equation can hold for $y = 0$ or for $x = \pi/2, 3\pi/2, \dots$. If $y = 0, \cosh 0 = 1$ and $\sin x = 3$ is impossible for real x . Therefore, $x = \pm \pi/2, \pm 3\pi/2, \dots, \pm(2n + 1)\pi/2, n = 0, \pm 1, \pm 2, \dots$. However, $\sin 3\pi/2 = -1$ and $\cosh y \geq 1$. Hence $x = \pi/2, 5\pi/2, \dots$. The solution is $z = [(4n + 1)\pi]/2 + i \cosh^{-1} 3, n = 0, 1, 2, 3, \dots$.

Example Find all solutions of $e^z = -i$. $e^z = e^x(\cos y + i \sin y) = -i$. Equating real and imaginary parts gives $e^x \cos y = 0, e^x \sin y = -1$. From the first $y = \pm \pi/2, \pm 3\pi/2, \dots$. But $e^x > 0$. Therefore, $y = 3\pi/2, 7\pi/2, -\pi/2, \dots$. Then $x = 0$. The solution is $z = i[(4n + 3)\pi]/2$.

Two important facets of these functions should be recognized. First, the $\sin z$ is unbounded; and, second, e^z takes all complex values except 0.

Hyperbolic Functions $\sinh z = (e^z - e^{-z})/2$; $\cosh z = (e^z + e^{-z})/2$; $\tanh z = \sinh z/\cosh z$; $\coth z = \cosh z/\sinh z$; $\operatorname{csch} z = 1/\sinh z$; $\operatorname{sech} z = 1/\cosh z$. Identities are: $\cosh^2 z - \sinh^2 z = 1$; $\sinh(z_1 + z_2) = \sinh z_1 \cosh z_2 + \cosh z_1 \sinh z_2$; $\cosh(z_1 + z_2) = \cosh z_1 \cosh z_2 + \sinh z_1 \sinh z_2$; $\cosh z + \sinh z = e^z$; $\cosh z - \sinh z = e^{-z}$. The hyperbolic sine and hyperbolic cosine are periodic functions with the imaginary period $2\pi i$. That is, $\sinh(z + 2\pi i) = \sinh z$.

Logarithms The logarithm of z , $\log z = \log |z| + i(\theta + 2n\pi)$, where $\log |z|$ is taken to the base e and θ is the principal argument of z , that is, the particular argument lying in the interval $0 \leq \theta < 2\pi$. The logarithm of z is infinitely many valued. If $n = 0$, the resulting logarithm is called the principal value. The familiar laws $\log z_1 z_2 = \log z_1 + \log z_2$, $\log z_1/z_2 = \log z_1 - \log z_2$, $\log z^n = n \log z$ hold for the principal value.

General powers of z are defined by $z^\alpha = e^{\alpha \log z}$. Since $\log z$ is infinitely many valued, so too is z^α unless α is a rational number.

DeMoivre's formula can be derived from properties of e^z .

$$z^n = r^n (\cos \theta + i \sin \theta)^n = r^n (\cos n\theta + i \sin n\theta)$$

Thus $(\cos \theta + i \sin \theta)^n = \cos n\theta + i \sin n\theta$

COMPLEX FUNCTIONS (ANALYTIC)

In the real-number system a greater than b ($a > b$) and b less than c ($b < c$) define an order relation. These relations have no meaning for complex numbers. The absolute value is used for ordering. Some important relations follow: $|z| \geq x$; $|z| \geq y$; $|z_1 \pm z_2| \leq |z_1| + |z_2|$; $|z_1 - z_2| \geq ||z_1| - |z_2||$; $|z| \geq (|x| + |y|)/\sqrt{2}$. Parts of the complex plane, commonly called **regions** or **domains**, are described by using inequalities.

Example $|z - 3| \leq 5$. This is equivalent to $\sqrt{(x - 3)^2 + y^2} \leq 5$, which is the set of all points within and on the circle, centered at $x = 3, y = 0$ of radius 5.

Example $|z - 1| \leq x$ represents the set of all points inside and on the parabola $2x = y^2 + 1$ or, equivalently, $2x \geq y^2 + 1$.

Functions of a Complex Variable If $z = x + iy, w = u + iv$ and if for each value of z in some region of the complex plane one or more values of w are defined, then w is said to be a function of $z, w = f(z)$. Some of these functions have already been discussed, e.g., $\sin z, \log z$. All functions are reducible to the form $w = u(x, y) + iv(x, y)$, where u, v are real functions of the real variables x and y .

Example $z^3 = (x + iy)^3 = x^3 + 3x^2(iy) + 3x(iy)^2 + (iy)^3 = (x^3 - 3xy^2) + i(3x^2y - y^3)$.

Differentiation The derivative of $w = f(z)$ is

$$\frac{dw}{dz} = \lim_{\Delta z \rightarrow 0} \frac{f(z + \Delta z) - f(z)}{\Delta z}$$

and for the derivative to exist the limit must be the same no matter how Δz approaches zero. If w_1, w_2 are differentiable functions of z , the following rules apply:

$$\frac{d(w_1 \pm w_2)}{dz} = \frac{dw_1}{dz} \pm \frac{dw_2}{dz} \quad \frac{d(w_1 w_2)}{dz} = w_2 \frac{dw_1}{dz} + w_1 \frac{dw_2}{dz}$$

$$\frac{d(w_1/w_2)}{dz} = \frac{w_2(dw_1/dz) - w_1(dw_2/dz)}{w_2^2}$$

and $\frac{dw_1^n}{dz} = n w_1^{n-1} \frac{dw_1}{dz}$

For $w = f(z)$ to be differentiable, it is necessary that $\partial u/\partial x = \partial v/\partial y$ and $\partial v/\partial x = -\partial u/\partial y$. The last two equations are called the Cauchy-Riemann equations. The derivative

$$\frac{dw}{dz} = \frac{\partial u}{\partial x} + i \frac{\partial v}{\partial x} = \frac{\partial v}{\partial y} - i \frac{\partial u}{\partial y}$$

If $f(z)$ possesses a derivative at z_0 and at every point in some neighborhood of z_0 , then $f(z)$ is said to be analytic or homomorphic at z_0 . If the

Cauchy-Riemann equations are satisfied and

$$u, v, \frac{\partial u}{\partial x}, \frac{\partial u}{\partial y}, \frac{\partial v}{\partial x}, \frac{\partial v}{\partial y}$$

are continuous in a region of the complex plane, then $f(z)$ is analytic in that region.

Example $w = z\bar{z} = x^2 + y^2$. Here $u = x^2 + y^2, v = 0, \partial u/\partial x = 2x, \partial u/\partial y = 2y, \partial v/\partial x = \partial v/\partial y = 0$. These are continuous everywhere, but the Cauchy-Riemann equations hold only at the origin. Therefore, w is nowhere analytic, but it is differentiable at $z = 0$ only.

Example $w = e^z = e^x \cos y + i e^x \sin y, u = e^x \cos y, v = e^x \sin y, \partial u/\partial x = e^x \cos y, \partial u/\partial y = -e^x \sin y, \partial v/\partial x = e^x \sin y, \partial v/\partial y = e^x \cos y$. The continuity and Cauchy-Riemann requirements are satisfied for all finite z . Hence e^z is analytic (except at ∞) and $dw/dz = \partial u/\partial x + i(\partial v/\partial x) = e^z$.

Example $w = \frac{1}{z} = \frac{x - iy}{x^2 + y^2} = \frac{x}{x^2 + y^2} - i \frac{y}{x^2 + y^2}$

It is easy to see that dw/dz exists except at $z = 0$. Thus $1/z$ is analytic except at $z = 0$.

Singular Points If $f(z)$ is analytic in a region except at certain points, those points are called singular points.

Example $1/z$ has a singular point at zero.

Example $\tan z$ has singular points at $z = \pm(2n + 1)(\pi/2), n = 0, 1, 2, \dots$

The derivatives of the common functions, given earlier, are the same as their real counterparts.

Example $(d/dz)(\log z) = 1/z, (d/dz)(\sin z) = \cos z$.

Harmonic Functions Both the real and the imaginary parts of any analytic function $f = u + iv$ satisfy Laplace's equation $\partial^2 \phi/\partial x^2 + \partial^2 \phi/\partial y^2 = 0$. A function which possesses continuous second partial derivatives and satisfies Laplace's equation is called a harmonic function.

Example $e^z = e^x \cos y + i e^x \sin y, u = e^x \cos y, \partial u/\partial x = e^x \cos y, \partial^2 u/\partial x^2 = e^x \cos y, \partial u/\partial y = -e^x \sin y, \partial^2 u/\partial y^2 = -e^x \cos y$. Clearly $\partial^2 u/\partial x^2 + \partial^2 u/\partial y^2 = 0$. Similarly, $v = e^x \sin y$ is also harmonic.

If $w = u + iv$ is analytic, the curves $u(x, y) = c$ and $v(x, y) = k$ intersect at right angles, if $w'(z) \neq 0$.

Integration In much of the work with complex variables a simple extension of integration called line or curvilinear integration is of fundamental importance. Since any complex line integral can be expressed in terms of real line integrals, we define only real line integrals. Let $F(x, y)$ be a real, continuous function of x and y and c be any continuous curve of finite length joining the points A and B (Fig. 3-46). $F(x, y)$ is not related to the curve c . Divide c up into n segments, Δs_i whose projection on the x axis is Δx_i and on the y axis is Δy_i . Let (ϵ_i, η_i) be the coordinates of an arbitrary point on Δs_i . The limits of the sums

$$\lim_{\Delta s_i \rightarrow 0} \sum_{i=1}^n F(\epsilon_i, \eta_i) \Delta s_i = \int_c F(x, y) ds$$

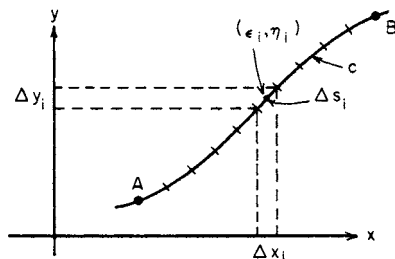


FIG. 3-46 Line integral.

$$\lim_{\Delta x_i \rightarrow 0} \sum_{i=1}^n F(\epsilon_i, \eta_i) \Delta x_i = \int_c F(x, y) dx$$

$$\lim_{\Delta y_i \rightarrow 0} \sum_{i=1}^n F(\epsilon_i, \eta_i) \Delta y_i = \int_c F(x, y) dy$$

are known as line integrals. Much of the initial strangeness of these integrals will vanish if it be observed that the ordinary definite integral $\int_a^b f(x) dx$ is just a line integral in which the curve c is a line segment on the x axis and $F(x, y)$ is a function of x alone. The evaluation of line integrals can be reduced to evaluation of ordinary integrals.

Example $\int_c y(1+x) dy$, where $c: y = 1 - x^2$ from $(-1, 0)$ to $(1, 0)$. Clearly $y = 1 - x^2, dy = -2x dx$. Thus $\int_c y(1+x) dy = -2 \int_{-1}^1 (1-x^2)(1+x) dx = -9/5$.

Example $\int_c x^2 y ds$, c is the square whose vertices are $(0, 0), (1, 0), (1, 1), (0, 1)$. $ds = \sqrt{dx^2 + dy^2}$. When $dx = 0, ds = dy$. From $(0, 0)$ to $(1, 0), y = 0, dy = 0$. Similar arguments for the other sides give

$$\int_c x^2 y ds = \int_0^1 0 \cdot x^2 dx + \int_0^1 y dy + \int_1^0 x^2 dx + \int_1^0 0 \cdot y dy = 1/2 - 1/3 = 1/6$$

Let $f(z)$ be any function of z , analytic or not, and c any curve as above. The complex integral is calculated as $\int_c f(z) dz = \int_c (u dx - v dy) + i \int_c (v dx + u dy)$, where $f(z) = u(x, y) + iv(x, y)$. Properties of line integrals are the same as those for ordinary integrals. That is, $\int_c [f(z) \pm g(z)] dz = \int_c f(z) dz \pm \int_c g(z) dz$; $\int_c kf(z) dz = k \int_c f(z) dz$ for any constant k , etc.

Example $\int_c (x^2 + iy) dz$ along $c: y = x, 0$ to $1 + i$. This becomes

$$\int_c (x^2 + iy) dz = \int_c (x^2 dx - y dy) + i \int_c (y dx + x^2 dy) = \int_0^1 x^2 dx - \int_0^1 x dx + i \int_0^1 x dx + i \int_0^1 x^2 dx = -1/6 + 5i/6$$

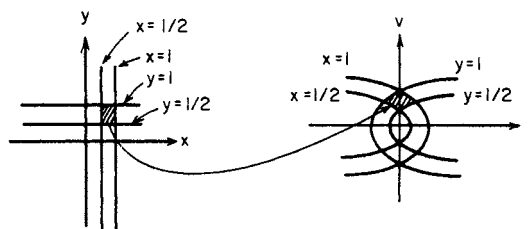


FIG. 3-47 Conformal transformation.

Conformal Mapping Every function of a complex variable $w = f(z) = u(x, y) + iv(x, y)$ transforms the x, y plane into the u, v plane in some manner. A conformal transformation is one in which angles between curves are preserved in *magnitude* and *sense*. Every analytic function, except at those points where $f'(z) = 0$, is a conformal transformation. See Fig. 3-47.

Example $w = z^2. u + iv = (x^2 - y^2) + 2ixy$ or $u = x^2 - y^2, v = 2xy$. These are the transformation equations between the (x, y) and (u, v) planes. Lines parallel to the x axis, $y = c_1$ map into curves in the u, v plane with parametric equations $u = x^2 - c_1^2, v = 2c_1x$. Eliminating $x, u = (v^2/4c_1^2) - c_1^2$, which represents a family of parabolas with the origin of the v plane as focus, the line $v = 0$ as axis and opening to the right. Similar arguments apply to $x = c_2$.

The principles of complex variables are useful in the solution of a variety of applied problems, including Laplace transforms and process control (Sec. 8).

DIFFERENTIAL EQUATIONS

REFERENCES: Ames, W. F., *Nonlinear Partial Differential Equations in Engineering*, Academic Press, New York (1965); Aris, R., and N. R. Amundson, *Mathematical Methods in Chemical Engineering*, vol. 2, *First-Order Partial Differential Equations with Applications*, Prentice-Hall, Englewood Cliffs, N.J. (1973); Asmar, N., and G. C. Jones, *Applied Complex Analysis with Partial Differential Equations*, Prentice-Hall, Upper Saddle River, N.J. (2002); Boyce, W. E., and R. C. Di Prima, *Elementary Differential Equations and Boundary Value Problems*, 7th ed., Wiley, New York (2004); Braun, M., *Differential Equations and Their Applications: An Introduction to Applied Mathematics*, 4th ed., Springer-Verlag, New York (1993); Bronson, R., and G. Costa, *Schaum's Outline of Differential Equations*, 3d ed., McGraw-Hill, New York (2007); Brown, J. W., and R. V. Churchill, *Fourier Series and Boundary Value Problems*, 6th ed., McGraw-Hill, New York (2000); Courant, R., and D. Hilbert, *Methods of Mathematical Physics*, vols. I and II, Interscience, New York (1953, 1962); Duffy, D., *Green's Functions with Applications*, Chapman and Hall/CRC (2001); Kreyszig, E., *Advanced Engineering Mathematics*, 8th ed., Wiley, New York (1999); Morse, P. M., and H. Feshbach, *Methods of Theoretical Physics*, vols. I and II, McGraw-Hill, New York (1953); Polyanin, A. D., *Handbook of Linear Partial Differential Equations for Engineers and Scientists*, Chapman and Hall/CRC (2002); Polyanin, A. D., and V. F. Zaitsev, *Handbook of Exact Solutions for Ordinary Differential Equations*, 2d ed., Chapman and Hall/CRC (2002); Ramkrishna, D., and N. R. Amundson, *Linear Operator Methods in Chemical Engineering with Applications to Transport and Chemical Reaction Systems*, Prentice-Hall, Englewood Cliffs, N.J. (1985).

The natural laws in any scientific or technological field are not regarded as precise and definitive until they have been expressed in mathematical form. Such a form, often an equation, is a relation between the quantity of interest, say, product yield, and independent variables such as time and temperature upon which yield depends. When it happens that this equation involves, besides the function itself, one or more of its derivatives it is called a differential equation.

Example The rate of the homogeneous bimolecular reaction $A + B \xrightarrow{k} C$ is characterized by the differential equation $dx/dt = k(a-x)(b-x)$, where $a =$ initial

concentration of $A, b =$ initial concentration of B , and $x = x(t) =$ concentration of C as a function of time t .

Example The differential equation of heat conduction in a moving fluid with velocity components v_x, v_y is

$$\frac{\partial u}{\partial t} + v_x \frac{\partial u}{\partial x} + v_y \frac{\partial u}{\partial y} = \frac{K}{\rho c_p} \left(\frac{\partial^2 u}{\partial x^2} + \frac{\partial^2 u}{\partial y^2} \right)$$

where $u = u(x, y, t) =$ temperature, $K =$ thermal conductivity, $\rho =$ density, and $c_p =$ specific heat at constant pressure.

ORDINARY DIFFERENTIAL EQUATIONS

When the function involved in the equation depends upon only one variable, its derivatives are ordinary derivatives and the differential equation is called an ordinary differential equation. When the function depends upon several independent variables, then the equation is called a partial differential equation. The theories of ordinary and partial differential equations are quite different. In almost every respect the latter is more difficult.

Whichever the type, a differential equation is said to be of n th order if it involves derivatives of order n but no higher. The equation in the first example is of first order and that in the second example of second order. The degree of a differential equation is the power to which the derivative of the highest order is raised after the equation has been cleared of fractions and radicals in the dependent variable and its derivatives.

A relation between the variables, involving no derivatives, is called a solution of the differential equation if this relation, when substituted in the equation, satisfies the equation. A solution of an ordinary differential equation which includes the maximum possible number of "arbitrary" constants is called the **general solution**. The maximum number of "arbitrary" constants is exactly equal to the order of the

3-30 MATHEMATICS

differential equation. If any set of specific values of the constants is chosen, the result is called a **particular solution**.

Example The general solution of $(d^2x/dt^2) + k^2x = 0$ is $x = A \cos kt + B \sin kt$, where A, B are arbitrary constants. A particular solution is $x = \frac{1}{2} \cos kt + 3 \sin kt$.

In the case of some equations still other solutions exist called singular solutions. A **singular solution** is any solution of the differential equation which is not included in the general solution.

Example $y = x(dy/dx) - \sqrt{4(dy/dx)^2}$ has the general solution $y = cx - \frac{1}{4}c^2$, where c is an arbitrary constant; $y = x^2$ is a singular solution, as is easily verified.

ORDINARY DIFFERENTIAL EQUATIONS OF THE FIRST ORDER

Equations with Separable Variables Every differential equation of the first order and of the first degree can be written in the form $M(x, y) dx + N(x, y) dy = 0$. If the equation can be transformed so that M does not involve y and N does not involve x , then the variables are said to be separated. The solution can then be obtained by **quadrature**, which means that $y = \int f(x) dx + c$, which may or may not be expressible in simpler form.

Example Two liquids A and B are boiling together in a vessel. Experimentally it is found that the ratio of the rates at which A and B are evaporating at any time is proportional to the ratio of the amount of A (say, x) to the amount of B (say, y) still in the liquid state. This physical law is expressible as $(dy/dt)/(dx/dt) = ky/x$ or $dy/dx = ky/x$, where k is a proportionality constant. This equation may be written $dy/y = k(dx/x)$, in which the variables are separated. The solution is $\ln y = k \ln x + \ln c$ or $y = cx^k$.

Exact Equations The equation $M(x, y) dx + N(x, y) dy = 0$ is exact if and only if $\partial M/\partial y = \partial N/\partial x$. In this case there exists a function $w = f(x, y)$ such that $\partial f/\partial x = M$, $\partial f/\partial y = N$, and $f(x, y) = C$ is the required solution. $f(x, y)$ is found as follows: treat y as though it were constant and evaluate $\int M(x, y) dx$. Then treat x as though it were constant and evaluate $\int N(x, y) dy$. The sum of all unlike terms in these two integrals (including no repetitions) is $f(x, y)$.

Example $(2xy - \cos x) dx + (x^2 - 1) dy = 0$ is exact for $\partial M/\partial y = 2x$, $\partial N/\partial x = 2x$. $\int M dx = \int (2xy - \cos x) dx = x^2y - \sin x$; $\int N dy = \int (x^2 - 1) dy = x^2y - y$. The solution is $x^2y - \sin x - y = C$, as may easily be verified.

Linear Equations A differential equation is said to be linear when it is of first degree in the dependent variable and its derivatives. The general linear first-order differential equation has the form $dy/dx + P(x)y = Q(x)$. Its general solution is

$$y = e^{-\int P dx} \left[\int Q e^{\int P dx} dx + C \right]$$

Example A tank initially holds 200 gal of a salt solution in which 100 lb is dissolved. Six gallons of brine containing 4 lb of salt run into the tank per minute. If mixing is perfect and the output rate is 4 gal/min, what is the amount A of salt in the tank at time t ? The differential equation of A is $dA/dt = [2/(100 + t)]A = 4$. Its general solution is $A = (4/3)(100 + t) + C/(100 + t)^2$. At $t = 0$, $A = 100$; so the particular solution is $A = (4/3)(100 + t) - (1/3)10^6/(100 + t)^2$.

ORDINARY DIFFERENTIAL EQUATIONS OF HIGHER ORDER

The higher-order differential equations, especially those of order 2, are of great importance because of physical situations describable by them.

Equation $y^{(n)} = f(x)$ Such a differential equation can be solved by n integrations. The solution will contain n arbitrary constants.

Linear Differential Equations with Constant Coefficients and Right-Hand Member Zero (Homogeneous) The solution of $y'' + ay' + by = 0$ depends upon the nature of the roots of the characteristic equation $m^2 + am + b = 0$ obtained by substituting the trial solution $y = e^{mx}$ in the equation.

Distinct Real Roots If the roots of the characteristic equation are distinct real roots, r_1 and r_2 , say, the solution is $y = Ae^{r_1x} + Be^{r_2x}$, where A and B are arbitrary constants.

Example $y'' + 4y' + 3 = 0$. The characteristic equation is $m^2 + 4m + 3 = 0$. The roots are -3 and -1 , and the general solution is $y = Ae^{-3x} + Be^{-x}$.

Multiple Real Roots If $r_1 = r_2$, the solution of the differential equation is $y = e^{r_1x}(A + Bx)$.

Example $y'' + 4y' + 4 = 0$. The characteristic equation is $m^2 + 4m + 4 = 0$ with roots -2 and -2 . The solution is $y = e^{-2x}(A + Bx)$.

Complex Roots If the characteristic roots are $p \pm iq$, then the solution is $y = e^{px}(A \cos qx + B \sin qx)$.

Example The differential equation $My'' + Ay' + ky = 0$ represents the vibration of a linear system of mass M , spring constant k , and damping constant A . If $A < 2\sqrt{kM}$, the roots of the characteristic equation

$$Mm^2 + Am + k = 0 \text{ are complex } -\frac{A}{2M} \pm i \sqrt{\frac{k}{M} - \left(\frac{A}{2M}\right)^2}$$

and the solution is

$$y = e^{-(A/2M)t}$$

$$\left\{ c_1 \cos \left(\sqrt{\frac{k}{M} - \left(\frac{A}{2M}\right)^2} t \right) + c_2 \sin \left(\sqrt{\frac{k}{M} - \left(\frac{A}{2M}\right)^2} t \right) \right\}$$

This solution is oscillatory, representing undercritical damping.

All these results generalize to homogeneous linear differential equations with constant coefficients of order higher than 2. These equations (especially of order 2) have been much used because of the ease of solution. Oscillations, electric circuits, diffusion processes, and heat-flow problems are a few examples for which such equations are useful.

Second-Order Equations: Dependent Variable Missing Such an equation is of the form

$$F \left(x, \frac{dy}{dx}, \frac{d^2y}{dx^2} \right) = 0$$

It can be reduced to a first-order equation by substituting $p = dy/dx$ and $dp/dx = d^2y/dx^2$.

Second-Order Equations: Independent Variable Missing Such an equation is of the form

$$F \left(y, \frac{dy}{dx}, \frac{d^2y}{dx^2} \right) = 0$$

Set $\frac{dy}{dx} = p$, $\frac{d^2y}{dx^2} = p \frac{dp}{dy}$

The result is a first-order equation in p ,

$$F \left(y, p, p \frac{dp}{dy} \right) = 0$$

Example The capillary curve for one vertical plate is given by

$$\frac{d^2y}{dx^2} = \frac{4y}{c^2} \left[1 + \left(\frac{dy}{dx} \right)^2 \right]^{3/2}$$

Its solution by this technique is

$$x + \sqrt{c^2 - y^2} - \sqrt{c^2 - h_0^2} = \frac{c}{2} \left(\cosh^{-1} \frac{c}{y} - \cosh^{-1} \frac{c}{h_0} \right)$$

where c, h_0 are physical constants.

Example The equation governing chemical reaction in a porous catalyst in plane geometry of thickness L is

$$D \frac{d^2c}{dx^2} = k f(c), \quad \frac{dc}{dx}(0) = 0, \quad c(L) = c_0$$

where D is a diffusion coefficient, k is a reaction rate parameter, c is the concentration, $k f(c)$ is the rate of reaction, and c_0 is the concentration at the

*The superscript (n) means n derivatives.

boundary. Making the substitution $p = \frac{dc}{ds}$ gives (Finlayson, 1980, p. 92)

$$p \frac{dp}{dc} = \frac{k}{D} f(c)$$

Integrating gives

$$\frac{p^2}{2} = \frac{k}{D} \int_{c(0)}^c f(c) dc$$

If the reaction is very fast, $c(0) = 0$ and the average reaction rate is related to $p(L)$. This variable is given by

$$p(L) = \left[\frac{2k}{D} \int_0^{c_0} f(c) dc \right]^{1/2}$$

Thus, the average reaction rate can be calculated without solving the complete problem.

Linear Nonhomogeneous Differential Equations

Linear Differential Equations Right-Hand Member $f(x) \neq 0$
 Again the specific remarks for $y'' + ay' + by = f(x)$ apply to differential equations of similar type but higher order. We shall discuss two general methods.

Method of Undetermined Coefficients Use of this method is limited to equations exhibiting both constant coefficients and particular forms of the function $f(x)$. In most cases $f(x)$ will be a sum or product of functions of the type constant, x^n (n a positive integer), e^{mx} , $\cos kx$, $\sin kx$. When this is the case, the solution of the equation is $y = H(x) + P(x)$, where $H(x)$ is a solution of the homogeneous equations found by the method of the preceding subsection and $P(x)$ is a particular integral found by using the following table subject to these conditions: (1) When $f(x)$ consists of the sum of several terms, the appropriate form of $P(x)$ is the sum of the particular integrals corresponding to these terms individually. (2) When a term in any of the trial integrals listed is already a part of the homogeneous solution, the indicated form of the particular integral is multiplied by x .

Form of Particular Integral

If $f(x)$ is	Then $P(x)$ is
a (constant)	A (constant)
ax^n	$A_n x^n + A_{n-1} x^{n-1} + \dots + A_1 x + A_0$
ae^{rx}	Be^{rx}
$\left. \begin{matrix} c \cos kx \\ d \sin kx \end{matrix} \right\}$	$A \cos kx + B \sin kx$
$\left. \begin{matrix} g x^n e^{rx} \cos kx \\ h x^n e^{rx} \sin kx \end{matrix} \right\}$	$(A_n x^n + \dots + A_0) e^{rx} \cos kx + (B_n x^n + \dots + B_0) e^{rx} \sin kx$

Since the form of the particular integral is known, the constants may be evaluated by substitution in the differential equation.

Example $y'' + 2y' + y = 3e^{2x} - \cos x + x^3$. The characteristic equation is $(m + 1)^2 = 0$ so that the homogeneous solution is $y = (c_1 + c_2 x)e^{-x}$. To find a particular solution we use the trial solution from the table, $y = a_1 e^{2x} + a_2 \cos x + a_3 \sin x + a_4 x^3 + a_5 x^2 + a_6 x + a_7$. Substituting this in the differential equation collecting and equating like terms, there results $a_1 = 1/3$, $a_2 = 0$, $a_3 = -1/2$, $a_4 = 1$, $a_5 = -6$, $a_6 = 18$, and $a_7 = -24$. The solution is $y = (c_1 + c_2 x)e^{-x} + 1/3 e^{2x} - 1/2 \sin x + x^3 - 6x^2 + 18x - 24$.

Method of Variation of Parameters This method is applicable to any linear equation. The technique is developed for a second-order equation but immediately extends to higher order. Let the equation be $y'' + a(x)y' + b(x)y = R(x)$ and let the solution of the homogeneous equation, found by some method, be $y = c_1 f_1(x) + c_2 f_2(x)$. It is now assumed that a particular integral of the differential equation is of the form $P(x) = u f_1 + v f_2$ where u, v are functions of x to be determined by two equations. One equation results from the requirement that $u f_1 + v f_2$ satisfy the differential equation, and the other is a degree of freedom open to the analyst. The best choice proves to be

$$u' f_1 + v' f_2 = 0 \quad \text{and} \quad u' f_1' + v' f_2' = R(x)$$

Then
$$u' = \frac{du}{dx} = - \frac{f_2}{f_1 f_2' - f_2' f_1} R(x)$$

$$v' = \frac{dv}{dx} = \frac{f_1}{f_1 f_2' - f_2' f_1} R(x)$$

and since f_1, f_2 , and R are known u, v may be found by direct integration.

Perturbation Methods If the ordinary differential equation has a parameter that is small and is not multiplying the highest derivative, perturbation methods can give solutions for small values of the parameter.

Example Consider the differential equation for reaction and diffusion in a catalyst; the reaction is second order: $c'' = ac^2$, $c'(0) = 0$, $c(1) = 1$. The solution is expanded in the following Taylor series in a .

$$c(x, a) = c_0(x) + ac_1(x) + a^2 c_2(x) + \dots$$

The goal is to find equations governing the functions $\{c_i(x)\}$ and solve them. Substitution into the equations gives the following equations:

$$\begin{aligned} c_0''(x) + a c_0'(x) + a^2 c_0^2(x) + \dots &= a[c_0(x) + ac_1(x) + a^2 c_2(x) + \dots]^2 \\ c_0'(0) + ac_1'(0) + a^2 c_2'(0) + \dots &= 0 \\ c_0(1) + ac_1(1) + a^2 c_2(1) + \dots &= 1 \end{aligned}$$

Like terms in powers of a are collected to form the individual problems.

$$\begin{aligned} c_0'' &= 0, \quad c_0'(0) = 0, \quad c_0(1) = 1 \\ c_1'' &= c_0^2, \quad c_1'(0) = 0, \quad c_1(1) = 0 \\ c_2'' &= 2c_0 c_1, \quad c_2'(0) = 0, \quad c_2(1) = 0 \end{aligned}$$

The solution proceeds in turn.

$$c_0(x) = 1, \quad c_1(x) = \frac{(x^2 - 1)}{2}, \quad c_2(x) = \frac{5 - 6x^2 + x^4}{12}$$

SPECIAL DIFFERENTIAL EQUATIONS [SEE ABRAMOWITZ AND STEGUN (1972)]

Euler's Equation The linear equation $x^n y^{(n)} + a_n x^{n-1} y^{(n-1)} + \dots + a_{n-1} x y' + a_n y = R(x)$ can be reduced to a linear equation with constant coefficients by the change of variable $x = e^r$. To solve the homogeneous equation substitute $y = x^r$ into it, cancel the powers of x , which are the same for all terms, and solve the resulting polynomial for r . In case of multiple or complex roots there results the form $y = x^r (\log x)^r$ and $y = x^{i\alpha} [\cos(\beta \log x) + i \sin(\beta \log x)]$.

Bessel's Equation The linear equation $x^2(d^2y/dx^2) + (1 - 2\alpha)x(dy/dx) + [\beta^2 \gamma^2 x^{2\gamma} + (\alpha^2 - p^2 \gamma^2)]y = 0$ is the general Bessel equation. By series methods, not to be discussed here, this equation can be shown to have the solution

$$\begin{aligned} y &= Ax^\alpha J_p(\beta x^\gamma) + Bx^\alpha J_{-p}(\beta x^\gamma) \quad p \text{ not an integer or zero} \\ y &= Ax^\alpha J_p(\beta x^\gamma) + Bx^\alpha Y_p(\beta x^\gamma) \quad p \text{ an integer} \end{aligned}$$

where
$$J_p(x) = \left(\frac{x}{2}\right)^p \sum_{k=0}^{\infty} \frac{(-1)^k (x/2)^{2k}}{k! \Gamma(p+k+1)}$$

$$J_{-p}(x) = \left(\frac{x}{2}\right)^{-p} \sum_{k=0}^{\infty} \frac{(-1)^k (x/2)^{2k}}{k! \Gamma(k+1-p)} \quad p \text{ not an integer}$$

$$\Gamma(n) = \int_0^{\infty} x^{n-1} e^{-x} dx \quad n > 0$$

is the gamma function. For p an integer

$$J_p(x) = \left(\frac{x}{2}\right)^p \sum_{k=0}^{\infty} \frac{(-1)^k (x/2)^{2k}}{k! (p+k)!}$$

(Bessel function of the first kind of order p)

$$Y_p(x) = \frac{[J_p(x) \cos(p\pi) - J_{-p}(x)]}{\sin(p\pi)}$$

(replace right-hand side by limiting value if p is an integer or zero).

The series converge for all x . Much of the importance of Bessel's equation and Bessel functions lies in the fact that the solutions of numerous linear differential equations can be expressed in terms of them.

Legendre's Equation The Legendre equation $(1 - x^2)y'' - 2xy' + n(n + 1)y = 0$, $n \geq 0$, has the solution P_n for n an integer.

The polynomials P_n are the so-called Legendre polynomials, $P_0(x) = 1$, $P_1(x) = x$, $P_2(x) = \frac{1}{2}(3x^2 - 1)$, $P_3(x) = \frac{1}{2}(5x^3 - 3x)$, . . .

For n positive and not an integer, see Abramowitz and Stegun (1972).

Laguerre's Equation The Laguerre equation $x(d^2y/dx^2) + (c - x)(dy/dx) - ay = 0$ is satisfied by the confluent hypergeometric function. See Abramowitz and Stegun (1972) and Kreszig (1999).

Hermite's Equation The Hermite equation $y'' - 2xy' + 2ny = 0$ is satisfied by the Hermite polynomial of degree n , $y = AH_n(x)$ if n is a positive integer or zero. $H_0(x) = 1$, $H_1(x) = 2x$, $H_2(x) = 4x^2 - 2$, $H_3(x) = 8x^3 - 12x$, $H_4(x) = 16x^4 - 48x^2 + 12$, $H_{r+1}(x) = 2xH_r(x) - 2rH_{r-1}(x)$.

Chebyshev's Equation The equation $(1 - x^2)y'' - xy' + n^2y = 0$ for n a positive integer or zero is satisfied by the n th Chebyshev polynomial $y = AT_n(x)$. $T_0(x) = 1$, $T_1(x) = x$, $T_2(x) = 2x^2 - 1$, $T_3(x) = 4x^3 - 3x$, $T_4(x) = 8x^4 - 8x^2 + 1$; $T_{r+1}(x) = 2xT_r(x) - T_{r-1}(x)$.

PARTIAL DIFFERENTIAL EQUATIONS

The analysis of situations involving two or more independent variables frequently results in a partial differential equation.

Example The equation $\partial T/\partial t = K(\partial^2 T/\partial x^2)$ represents the unsteady one-dimensional conduction of heat.

Example The equation for the unsteady transverse motion of a uniform beam clamped at the ends is

$$\frac{\partial^4 y}{\partial x^4} + \frac{\rho}{EI} \frac{\partial^2 y}{\partial t^2} = 0$$

Example The expansion of a gas behind a piston is characterized by the simultaneous equations

$$\frac{\partial u}{\partial t} + u \frac{\partial u}{\partial x} + \frac{c^2}{\rho} \frac{\partial \rho}{\partial x} = 0 \quad \text{and} \quad \frac{\partial \rho}{\partial t} + u \frac{\partial \rho}{\partial x} + \rho \frac{\partial u}{\partial x} = 0$$

The partial differential equation $\partial^2 f/\partial x \partial y = 0$ can be solved by two integrations yielding the solution $f = g(x) + h(y)$, where $g(x)$ and $h(y)$ are arbitrary differentiable functions. This result is an example of the fact that the general solution of partial differential equations involves arbitrary functions in contrast to the solution of ordinary differential equations, which involve only arbitrary constants. A number of methods are available for finding the general solution of a partial differential equation. In most applications of partial differential equations the general solution is of limited use. In such applications the solution of a partial differential equation must satisfy both the equation and certain auxiliary conditions called **initial** and/or **boundary** conditions, which are dictated by the problem. Examples of these include those in which the wall temperature is a fixed constant $T(x_0) = T_0$, there is no diffusion across a nonpermeable wall, and the like. In ordinary differential equations these auxiliary conditions allow definite numbers to be assigned to the constants of integration.

Partial Differential Equations of Second and Higher Order Many of the applications to scientific problems fall naturally into partial differential equations of second order, although there are important exceptions in elasticity, vibration theory, and elsewhere.

A second-order differential equation can be written as

$$a \frac{\partial^2 u}{\partial x^2} + b \frac{\partial^2 u}{\partial x \partial y} + c \frac{\partial^2 u}{\partial y^2} = f$$

where a , b , c , and f depend upon x , y , u , $\partial u/\partial x$, and $\partial u/\partial y$. This equation is hyperbolic, parabolic, or elliptic, depending on whether the discriminant $b^2 - 4ac$ is >0 , $=0$, or <0 , respectively. Since a , b , c , and f depend on the solution, the type of equation can be different at different x and y locations. If the equation is hyperbolic, discontinuities can be propagated. See Courant and Hilbert (1953, 1962) and LeVeque, R. J., *Numerical Methods for Conservation Laws*, Birkhäuser, Basel (1992).

Phenomena of **propagation** such as vibrations are characterized by equations of "hyperbolic" type which are essentially different in their

properties from other classes such as those which describe equilibrium (elliptic) or unsteady diffusion and heat transfer (parabolic). Prototypes are as follows:

Elliptic Laplace's equation $\partial^2 u/\partial x^2 + \partial^2 u/\partial y^2 = 0$ and Poisson's equation $\partial^2 u/\partial x^2 + \partial^2 u/\partial y^2 = g(x, y)$ do not contain the variable time explicitly and consequently represent equilibrium configurations. Laplace's equation is satisfied by static electric or magnetic potential at points free from electric charges or magnetic poles. Other important functions satisfying Laplace's equation are the velocity potential of the irrotational motion of an incompressible fluid, used in hydrodynamics; the steady temperature at points in a homogeneous solid, and the steady state of diffusion through a homogeneous body.

Parabolic The heat equation $\partial T/\partial t = \partial^2 T/\partial x^2 + \partial^2 T/\partial y^2$ represents nonequilibrium or unsteady states of heat conduction and diffusion.

Hyperbolic The wave equation $\partial^2 u/\partial t^2 = c^2(\partial^2 u/\partial x^2 + \partial^2 u/\partial y^2)$ represents wave propagation of many varied types.

Quasilinear first-order differential equations are like

$$a \frac{\partial u}{\partial x} + b \frac{\partial u}{\partial y} = f$$

where a , b , and f depend on x , y , and u , with $a^2 + b^2 \neq 0$. This equation can be solved using the method of characteristics, which writes the solution in terms of a parameter s , which defines a path for the characteristic.

$$\frac{dx}{ds} = a, \quad \frac{dy}{ds} = b, \quad \frac{du}{ds} = f$$

These equations are integrated from some initial conditions. For a specified value of s , the value of x and y shows the location where the solution is u . The equation is semilinear if a and b depend just on x and y (and not u), and the equation is linear if a , b , and f all depend on x and y , but not u . Such equations give rise to shock propagation, and conditions have been derived to deduce the presence of shocks. Courant and Hilbert (1953, 1962); Rhee, H. K., R. Aris, and N. R. Amundson, *First-Order Partial Differential Equations*, vol. I, *Theory and Applications of Single Equations*, Prentice-Hall, Englewood Cliffs, N.J. (1986); and LeVeque (1992), *ibid*.

An example of a linear hyperbolic equation is the advection equation for flow of contaminants when the x and y velocity components are u and v , respectively.

$$\frac{\partial c}{\partial t} + u \frac{\partial c}{\partial x} + v \frac{\partial c}{\partial y} = 0$$

The equations for flow and adsorption in a packed bed or chromatography column give a quasilinear equation.

$$\phi \frac{\partial c}{\partial t} + \phi u \frac{\partial c}{\partial x} + (1 - \phi) \frac{df}{dc} \frac{\partial c}{\partial t} = 0$$

Here $n = f(c)$ is the relation between concentration on the adsorbent and fluid concentration.

The solution of problems involving partial differential equations often revolves about an attempt to reduce the partial differential equation to one or more ordinary differential equations. The solutions of the ordinary differential equations are then combined (if possible) so that the boundary conditions as well as the original partial differential equation are simultaneously satisfied. Three of these techniques are illustrated.

Similarity Variables The physical meaning of the term "similarity" relates to internal similitude, or self-similitude. Thus, similar solutions in boundary-layer flow over a horizontal flat plate are those for which the horizontal component of velocity u has the property that two velocity profiles located at different coordinates x differ only by a scale factor. The mathematical interpretation of the term similarity is a transformation of variables carried out so that a reduction in the number of independent variables is achieved. There are essentially two methods for finding similarity variables, "separation of variables" (not the classical concept) and the use of "continuous transformation groups." The basic theory is available in Ames (1965).

Example The equation $\partial\theta/\partial x = (A/y)(\partial^2\theta/\partial y^2)$ with the boundary conditions $\theta = 0$ at $x = 0, y > 0; \theta = 0$ at $y = \infty, x > 0; \theta = 1$ at $y = 0, x > 0$ represents the nondimensional temperature θ of a fluid moving past an infinitely wide flat plate immersed in the fluid. Turbulent transfer is neglected, as is molecular transport except in the y direction. It is now assumed that the equation and the boundary conditions can be satisfied by a solution of the form $\theta = f(y/x^n) = f(u)$, where $\theta = 0$ at $x = \infty$ and $\theta = 1$ at $u = 0$. The purpose here is to replace the independent variables x and y by the single variable u when it is hoped that a value of n exists which will allow x and y to be completely eliminated in the equation. In this case since $u = y/x^n$, there results after some calculation $\partial\theta/\partial x = -(nu/x)(d\theta/du)$, $\partial^2\theta/\partial y^2 = (1/x^{2n})(d^2\theta/du^2)$, and when these are substituted in the equation, $-(1/x)nu(d\theta/du) = (1/x^{2n})(A/u)(d^2\theta/du^2)$. For this to be a function of u only, choose $n = 1/2$. There results $(d^2\theta/du^2) + (u^2/3A)(d\theta/du) = 0$. Two integrations and use of the boundary conditions for this ordinary differential equation give the solution

$$\theta = \int_u^\infty \exp(-u^2/9A) du \Big/ \int_0^\infty \exp(-u^2/9A) du$$

Group Method The type of transformation can be deduced using group theory. For a complete exposition, see Ames (1965) and Hill, J. M., *Differential Equations and Group Methods for Scientists and Engineers*, CRC Press, New York (1992); a shortened version is in Finlayson (1980, 2003). Basically, a similarity transformation should be considered when one of the independent variables has no physical scale (perhaps it goes to infinity). The boundary conditions must also simplify (and combine) since each transformation leads to a differential equation with one fewer independent variable.

Example A similarity variable is found for the problem

$$\frac{\partial c}{\partial t} = \frac{\partial}{\partial x} \left(\frac{D(c)}{D} \frac{\partial c}{\partial x} \right), \quad c(0, t) = 1, \quad c(\infty, t) = 0, \quad c(x, 0) = 0$$

Note that the length dimension goes to infinity, so that there is no length scale in the problem statement; this is a clue to try a similarity transformation. The transformation examined here is

$$\bar{t} = a^\alpha t, \quad \bar{x} = a^\beta x, \quad \bar{c} = a^\gamma c$$

With this substitution, the equation becomes

$$a^{\alpha-\gamma} \frac{\partial \bar{c}}{\partial \bar{t}} = a^{2\beta-\gamma} \frac{\partial}{\partial \bar{x}} \left[D(a^{-\gamma} \bar{c}) \frac{\partial \bar{c}}{\partial \bar{x}} \right]$$

Group theory says a system is conformally invariant if it has the same form in the new variables; here, that is

$$\gamma = 0, \quad \alpha - \gamma = 2\beta - \gamma, \quad \text{or } \alpha = 2\beta$$

The invariants are

$$\eta = \frac{x}{t^\beta}, \quad \delta = \frac{\beta}{\alpha}$$

and the solution is

$$c(x, t) = f(\eta)t^{\gamma/\alpha}$$

We can take $\gamma = 0$ and $\delta = \beta/\alpha = 1/2$. Note that the boundary conditions combine because the point $x = \infty$ and $t = 0$ give the same value of η and the conditions on c at $x = \infty$ and $t = 0$ are the same. We thus make the transformation

$$\eta = \frac{x}{\sqrt{4D_0t}}, \quad c(x, t) = f(\eta)$$

The use of the 4 and D_0 makes the analysis below simpler. The result is

$$\frac{d}{d\eta} \left[\frac{D(c)}{D_0} \frac{df}{d\eta} \right] + 2\eta \frac{df}{d\eta} = 0, \quad f(0) = 1, \quad f(\infty) = 0$$

Thus, we solve a two-point boundary value problem instead of a partial differential equation. When the diffusivity is constant, the solution is the error function, a tabulated function.

$$c(x, t) = 1 - \operatorname{erf} \eta = \operatorname{erfc} \eta \\ \operatorname{erf} \eta = \int_0^\eta e^{-\xi^2} d\xi \Big/ \int_0^\infty e^{-\xi^2} d\xi$$

Separation of Variables This is a powerful, well-utilized method which is applicable in certain circumstances. It consists of assuming that the solution for a partial differential equation has the form $U = f(x)g(y)$. If it is then possible to obtain an ordinary differential equation on one side of the equation depending only on x and on the other side only on y , the partial differential equation is said to be

separable in the variables x, y . If this is the case, one side of the equation is a function of x alone and the other of y alone. The two can be equal only if each is a constant, say λ . Thus the problem has again been reduced to the solution of ordinary differential equations.

Example Laplace's equation $\partial^2 V/\partial x^2 + \partial^2 V/\partial y^2 = 0$ plus the boundary conditions $V(0, y) = 0, V(l, y) = 0, V(x, \infty) = 0, V(x, 0) = f(x)$ represents the steady-state potential in a thin plate (in z direction) of infinite extent in the y direction and of width l in the x direction. A potential $f(x)$ is impressed (at $y = 0$) from $x = 0$ to $x = l$, and the sides are grounded. To obtain a solution of this boundary-value problem assume $V(x, y) = f(x)g(y)$. Substitution in the differential equation yields $f''(x)g(y) + f(x)g''(y) = 0$, or $g''(y)/g(y) = -f''(x)/f(x) = \lambda^2$ (say). This system becomes $g''(y) - \lambda^2 g(y) = 0$ and $f''(x) + \lambda^2 f(x) = 0$. The solutions of these ordinary differential equations are respectively $g(y) = Ae^{\lambda y} + Be^{-\lambda y}, f(x) = C \sin \lambda x + D \cos \lambda x$. Then $f(0)g(y) = (Ae^{\lambda y} + Be^{-\lambda y})(C \sin \lambda x + D \cos \lambda x)$. Now $V(0, y) = 0$ so that $f(0)g(y) = (Ae^{\lambda y} + Be^{-\lambda y})D = 0$ for all y . Hence $D = 0$. The solution then has the form $\sin \lambda x (Ae^{\lambda y} + Be^{-\lambda y})$ where the multiplicative constant C has been eliminated. Since $V(l, y) = 0, \sin \lambda l (Ae^{\lambda y} + Be^{-\lambda y}) = 0$. Clearly the bracketed function of y is not zero, for the solution would then be the identically zero solution. Hence $\sin \lambda l = 0$ or $\lambda_n = n\pi/l, n = 1, 2, \dots$ where $\lambda_n = n$ th eigenvalue.

The solution now has the form $\sin(n\pi x/l)(Ae^{n\pi y/l} + Be^{-n\pi y/l})$. Since $V(x, \infty) = 0, A$ must be taken to be zero because e^y becomes arbitrarily large as $y \rightarrow \infty$. The solution then reads $B_n \sin(n\pi x/l)e^{-n\pi y/l}$, where B_n is the multiplicative constant. The differential equation is linear and homogeneous so that $\sum_{n=1}^\infty B_n e^{-n\pi y/l} \sin(n\pi x/l)$ is also a solution. Satisfaction of the last boundary condition is ensured by taking

$$B_n = \frac{2}{l} \int_0^l f(x) \sin(n\pi x/l) dx = \text{Fourier sine coefficients of } f(x)$$

Further, convergence and differentiability of this series are established quite easily. Thus the solution is

$$V(x, y) = \sum_{n=1}^\infty B_n e^{-n\pi y/l} \sin \frac{n\pi x}{l}$$

Example The diffusion problem in a slab of thickness L

$$\frac{\partial c}{\partial t} = D \frac{\partial^2 c}{\partial x^2}, \quad c(0, t) = 1, \quad c(L, t) = 0, \quad c(x, 0) = 0$$

can be solved by separation of variables. First transform the problem so that the boundary conditions are homogeneous (having zeros on the right-hand side). Let

$$c(x, t) = 1 - \frac{x}{L} + u(x, t)$$

Then $u(x, t)$ satisfies

$$\frac{\partial u}{\partial t} = D \frac{\partial^2 u}{\partial x^2}, \quad u(x, 0) = \frac{x}{L} - 1, \quad u(0, t) = 0, \quad u(L, t) = 0$$

Assume a solution of the form $u(x, t) = X(x)T(t)$, which gives

$$\frac{1}{DT} \frac{dT}{dt} = \frac{1}{X} \frac{d^2 X}{dx^2}$$

Since both sides are constant, this gives the following ordinary differential equations to solve.

$$\frac{1}{DT} \frac{dT}{dt} = -\lambda, \quad \frac{1}{X} \frac{d^2 X}{dx^2} = -\lambda$$

The solution of these is

$$T = A e^{-\lambda Dt}, \quad X = B \cos \sqrt{\lambda} x + E \sin \sqrt{\lambda} x$$

The combined solution for $u(x, t)$ is

$$u = A (B \cos \sqrt{\lambda} x + E \sin \sqrt{\lambda} x) e^{-\lambda Dt}$$

Apply the boundary condition that $u(0, t) = 0$ to give $B = 0$. Then the solution is

$$u = A (\sin \sqrt{\lambda} x) e^{-\lambda Dt}$$

where the multiplicative constant E has been eliminated. Apply the boundary condition at $x = L$.

$$0 = A (\sin \sqrt{\lambda} L) e^{-\lambda Dt}$$

This can be satisfied by choosing $A = 0$, which gives no solution. However, it can also be satisfied by choosing λ such that

$$\sin \sqrt{\lambda} L = 0, \quad \sqrt{\lambda} L = n\pi$$

Thus

$$\lambda = \frac{n^2 \pi^2}{L^2}$$

3-34 MATHEMATICS

The combined solution can now be written as

$$u = A \left(\frac{\sin n\pi x}{L} \right) e^{-n^2\pi^2 D t / L^2}$$

Since the initial condition must be satisfied, we use an infinite series of these functions.

$$u = \sum_{n=1}^{\infty} A_n \left(\frac{\sin n\pi x}{L} \right) e^{-n^2\pi^2 D t / L^2}$$

At $t = 0$, we satisfy the initial condition.

$$\frac{x}{L} - 1 = \sum_{n=1}^{\infty} A_n \left(\frac{\sin n\pi x}{L} \right)$$

This is done by multiplying the equation by

$$\frac{\sin m\pi x}{L}$$

and integrating over $x: 0 \rightarrow L$. (This is the same as minimizing the mean-square error of the initial condition.) This gives

$$\frac{A_m L}{2} = \int_0^L \left(\frac{x}{L} - 1 \right) \sin \frac{m\pi x}{L} dx$$

which completes the solution.

Integral-Transform Method A number of integral transforms are used in the solution of differential equations. Only one, the Laplace transform, will be discussed here [for others, see "Integral Transforms (Operational Methods)"]. The one-sided Laplace transform indicated by $L[f(t)]$ is defined by the equation $L[f(t)] = \int_0^{\infty} f(t)e^{-st} dt$. It has numerous important properties. The ones of interest here are $L[f'(t)] = sL[f(t)] - f(0)$; $L[f''(t)] = s^2L[f(t)] - sf(0) - f'(0)$; $L[f^{(n)}(t)] = s^nL[f(t)] - s^{n-1}f(0) - s^{n-2}f'(0) - \dots - f^{(n-1)}(0)$ for ordinary derivatives. For partial derivatives an indication of which variable is being transformed avoids confusion. Thus, if

$$y = y(x, t), \quad L_t \left[\frac{\partial y}{\partial t} \right] = sL[y(x, t)] - y(x, 0)$$

whereas

$$L_x \left[\frac{\partial y}{\partial x} \right] = \frac{dL_x[y(x, t)]}{dx}$$

since $L[y(x, t)]$ is "really" only a function of x . Otherwise the results are similar. These facts coupled with the linearity of the transform, i.e., $L[af(t) + bg(t)] = aL[f(t)] + bL[g(t)]$, make it a useful device in solving some linear differential equations. Its use reduces the solution of ordinary differential equations to the solution of algebraic equations for $L[y]$. The inverse transform must be obtained either from tables or by use of complex inversion methods.

Example The equation $\partial c / \partial t = D(\partial^2 c / \partial x^2)$ represents the diffusion in a semi-infinite medium, $x \geq 0$. Under the boundary conditions $c(0, t) = c_0$, $c(x, 0) = 0$ find a solution of the diffusion equation. By taking the Laplace transform of both sides with respect to t ,

$$\int_0^{\infty} e^{-st} \frac{\partial^2 c}{\partial x^2} dt = \frac{1}{D} \int_0^{\infty} e^{-st} \frac{\partial c}{\partial t} dt$$

$$\text{or} \quad \frac{d^2 F}{dx^2} = (1/D)sF - c(x, 0) = \frac{sF}{D}$$

where $F(x, s) = L_t[c(x, t)]$. Hence

$$\frac{d^2 F}{dx^2} - \left(\frac{s}{D} \right) F = 0$$

The other boundary condition transforms into $F(0, s) = c_0/s$. Finally the solution of the ordinary differential equation for F subject to $F(0, s) = c_0/s$ and F remains finite as $x \rightarrow \infty$ is $F(x, s) = (c_0/s)e^{-\sqrt{s/D}x}$. Reference to a table shows that the function having this as its Laplace transform is

$$c(x, t) = c_0 \left[1 - \frac{2}{\sqrt{\pi}} \int_0^{x/2\sqrt{Dt}} e^{-u^2} du \right] = C_0 \operatorname{erfc} \left(\frac{x}{\sqrt{4Dt}} \right)$$

Matched-Asymptotic Expansions Sometimes the coefficient in front of the highest derivative is a small number. Special perturbation techniques can then be used, provided the proper scaling laws are found. See Kevorkian, J., and J. D. Cole, *Perturbation Methods in Applied Mathematics*, Springer-Verlag, New York (1981); and Lagerstrom, P. A., *Matched Asymptotic Expansions: Ideas and Techniques*, Springer-Verlag, New York (1988).

DIFFERENCE EQUATIONS

REFERENCES: Elaydi, Saber, and S. N. Elaydi, *An Introduction to Difference Equations*, Springer-Verlag, New York (1999); Fulford, G., P. Forrester, and A. Jones, *Modelling with Differential and Difference Equations*, Cambridge University Press, New York (1997); Goldberg, S., *Introduction to Difference Equations*, Dover (1986); Kelley, W. G., and A. C. Peterson, *Difference Equations: An Introduction with Applications*, 2d ed., Harcourt/Academic Press, San Diego (2001).

Certain situations are such that the independent variable does not vary continuously but has meaning only for discrete values. Typical illustrations occur in the stagewise processes found in chemical engineering such as distillation, staged extraction systems, and absorption columns. In each of these the operation is characterized by a finite between-stage change of the dependent variable in which the independent variable is the integral number of the stage. The importance of difference equations is twofold: (1) to analyze problems of the type described and (2) to obtain approximate solutions of problems which lead, in their formulation, to differential equations. In this subsection only problems of analysis are considered; the application to approximate solutions is considered under "Numerical Analysis and Approximate Methods."

ELEMENTS OF THE CALCULUS OF FINITE DIFFERENCES

Let $y = f(x)$ be defined for discrete equidistant values of x , which will be denoted by x_n . The corresponding value of y will be written $y_n = f(x_n)$. The first forward difference of $f(x)$ denoted by $\Delta f(x) = f(x+h) - f(x)$ where $h = x_n - x_{n-1} =$ interval length.

Example Let $f(x) = x^2$. Then $\Delta f(x) = (x+h)^2 - x^2 = 2hx + h^2$.

The second forward difference is obtained by taking the difference of the first; thus $\Delta^2 f(x) = \Delta^2 f(x) = \Delta f(x+h) - \Delta f(x) = f(x+2h) - 2f(x+h) + f(x)$.

Example $f(x) = x^2$, $\Delta^2 f(x) = \Delta[\Delta f(x)] = \Delta 2hx + \Delta h^2 = 2h(x+h) - 2hx + h^2 - h^2 = 2h^2$.

Similarly the n th forward difference is defined by the relation $\Delta^n f(x) = \Delta[\Delta^{n-1} f(x)]$. Other difference relations are also quite useful. Some of these are $\nabla f(x) = f(x) - f(x-h)$, which is called the backward difference, and $\delta f(x) = f[x+(h/2)] - f[x-(h/2)]$, called the central difference. Some properties of the operator Δ are quite important. If C is any constant, $\Delta C = 0$; if $f(x)$ is any function of period h , $\Delta f(x) = 0$ (in fact, periodic functions of period h play the same role here as constants do in the differential calculus); $\Delta[f(x) + g(x)] = \Delta f(x) + \Delta g(x)$; $\Delta^n[\Delta^m f(x)] = \Delta^{m+n} f(x)$; $\Delta[f(x)g(x)] = f(x)\Delta g(x) + g(x+h)\Delta f(x)$

$$\Delta \left[\frac{f(x)}{g(x)} \right] = \frac{g(x)\Delta f(x) - f(x)\Delta g(x)}{g(x)g(x+h)}$$

Example $\Delta(x \sin x) = x\Delta \sin x + \sin(x+h)\Delta x = 2x \sin(h/2) \cos[x+(h/2)] + h \sin(x+h)$.

DIFFERENCE EQUATIONS

A difference equation is a relation between the differences and the independent variable, $\phi(\Delta^n y, \Delta^{n-1} y, \dots, \Delta y, y, x) = 0$, where ϕ is some

given function. The general case in which the interval between the successive points is any real number h , instead of 1, can be reduced to that with interval size 1 by the substitution $x = hx'$. Hence all further difference-equation work will assume the interval size between successive points is 1.

Example $f(x+1) - (\alpha + 1)f(x) + \alpha f(x-1) = 0$. Common notation usually is $y_x = f(x)$. This equation is then written $y_{x+1} - (\alpha + 1)y_x + \alpha y_{x-1} = 0$.

Example $y_{x+2} + 2y_x y_{x+1} + y_x = x^2$.

Example $y_{x+1} - y_x = 2^x$.

The order of the difference equation is the difference between the largest and smallest arguments when written in the form of the second example. The first and second examples are both of order 2, while the third example is of order 1. A linear difference equation involves no products or other nonlinear functions of the dependent variable and its differences. The first and third examples are linear, while the second example is nonlinear.

A solution of a difference equation is a relation between the variables which satisfies the equation. If the difference equation is of order n , the general solution involves n arbitrary constants. The techniques for solving difference equations resemble techniques used for differential equations.

Equation $\Delta^n y = a$ The solution of $\Delta^n y = a$, where a is a constant, is a polynomial of degree n plus an arbitrary periodic function of period 1. That is, $y = (a^n n! / \Gamma(n)) + c_1 x^{n-1} + c_2 x^{n-2} + \dots + c_n + f(x)$, where $f(x+1) = f(x)$.

Example $\Delta^3 y = 6$. The solution is $y = x^3 + c_1 x^2 + c_2 x + c_3 + f(x)$; c_1, c_2, c_3 are arbitrary constants, and $f(x)$ is an arbitrary periodic function of period 1.

Equation $y_{x+1} - y_x = \phi(x)$ This equation states that the first difference of the unknown function is equal to the given function $\phi(x)$. The solution by analogy with solving the differential equation $dy/dx = \phi(x)$ by integration is obtained by "finite integration" or summation. When there are only a finite number of data points, this is easily accomplished by writing $y_x = y_0 + \sum_{t=1}^x \phi(t-1)$, where the data points are numbered from 1 to x . This is the only situation considered here.

Examples If $\phi(x) = 1, y_x = x$. If $\phi(x) = x, y_x = [x(x-1)]/2$. If $\phi(x) = a^x, a \neq 0, y_x = a^x/(a-1)$. In all cases $y_0 = 0$.

Other examples may be evaluated by using summation, that is, $y_2 = y_1 + \phi(1), y_3 = y_2 + \phi(2) = y_1 + \phi(1) + \phi(2), y_4 = y_3 + \phi(3) = y_1 + \phi(1) + \phi(2) + \phi(3), \dots, y_x = y_1 + \sum_{t=1}^{x-1} \phi(t)$.

Example $y_{x+1} - r y_x = 1, r$ constant, $x > 0$ and $y_0 = 1, y_1 = 1 + r, y_2 = 1 + r + r^2, \dots, y_x = 1 + r + \dots + r^x = (1 - r^{x+1})/(1 - r)$ for $r \neq 1$ and $y_x = 1 + x$ for $r = 1$.

Linear Difference Equations The linear difference equation of order n has the form $P_n y_{x+n} + P_{n-1} y_{x+n-1} + \dots + P_1 y_{x+1} + P_0 y_x = Q(x)$ with $P_n \neq 0$ and $P_0 \neq 0$ and $P_j, j = 0, \dots, n$ are functions of x .

Constant Coefficient and $Q(x) = 0$ (Homogeneous) The solution is obtained by trying a solution of the form $y_x = c\beta^x$. When this trial solution is substituted in the difference equation, a polynomial of degree n results for β . If the solutions of this polynomial are denoted by $\beta_1, \beta_2, \dots, \beta_n$ then the following cases result: (1) if all the β_j 's are real and unequal, the solution is $y_x = \sum_{j=1}^n c_j \beta_j^x$, where the c_1, \dots, c_n are arbitrary constants; (2) if the roots are real and repeated, say, β_1 has multiplicity m , then the partial solution corresponding to β_1 is $\beta_1^x (c_1 + c_2 x + \dots + c_m x^{m-1})$; (3) if the roots are complex conjugates, say, $a + ib = p e^{i\theta}$ and $a - ib = p e^{-i\theta}$, the partial solution corresponding to this pair is $p^x (c_1 \cos \theta x + i c_2 \sin \theta x)$; and (4) if the roots are multiple complex conjugates, say, $a + ib = p e^{i\theta}$ and $a - ib = p e^{-i\theta}$ are m -fold, then the partial solution corresponding to these is $p^x [(c_1 + c_2 x + \dots + c_m x^{m-1}) \cos \theta x + i (d_1 + d_2 x + \dots + d_m x^{m-1}) \sin \theta x]$.

Example The equation $y_{x+1} - (\alpha + 1)y_x + \alpha y_{x-1} = 0, y_0 = c_0$ and $y_{m+1} = x_{m+1}/k$ represents the steady-state composition of transferable material in the raffinate stream of a staged countercurrent liquid-liquid extraction system.

Clearly y is a function of the stage number x . α is a combination of system constants. By using the trial solution $y_x = c\beta^x$, there results $\beta^2 - (\alpha + 1)\beta + \alpha = 0$, so that $\beta_1 = 1, \beta_2 = \alpha$. The general solution is $y_x = c_1 + c_2 \alpha^x$. By using the side conditions, $c_1 = c_0 - c_2, c_2 = (y_{m+1} - c_0)/(\alpha^{m+1} - 1)$. The desired solution is $(y_x - c_0)/(y_{m+1} - c_0) = (\alpha^x - 1)/(\alpha^{m+1} - 1)$.

Example $y_{x+3} - 3y_{x+2} + 4y_x = 0$. By setting $y_x = c\beta^x$, there results $\beta^3 - 3\beta^2 + 4 = 0$ or $\beta_1 = -1, \beta_2 = 2, \beta_3 = 2$. The general solution is $y_x = c_1(-1)^x + 2^x(c_2 + c_3 x)$.

Example $y_{x+1} - 2y_x + 2y_{x-1} = 0, \beta_1 = 1 + i, \beta_2 = 1 - i, p = \sqrt{1+1} = \sqrt{2}, \theta = \pi/4$. The solution is $y_x = 2^{x/2} [c_1 \cos(x\pi/4) + i c_2 \sin(x\pi/4)]$.

Constant Coefficients and $Q(x) \neq 0$ (Nonhomogeneous) In this case the general solution is found by first obtaining the homogeneous solution, say, y_x^h and adding to it any particular solution with $Q(x) \neq 0$, say, y_x^p . There are several means of obtaining the particular solution.

Method of Undetermined Coefficients If $Q(x)$ is a product or linear combination of products of the functions e^{bx}, a^x, x^p (p a positive integer or zero) $\cos cx$ and $\sin cx$, this method may be used. The "families" $[a^x], [e^{bx}], [\sin cx, \cos cx]$ and $[x^p, x^{p-1}, \dots, x, 1]$ are defined for each of the above functions in the following way: The family of a term f_x is the set of all functions of which f_x and all operations of the form $a^{x+y}, \cos c(x+y), \sin c(x+y), (x+y)^p$ on f_x and their linear combinations result in. The technique involves the following steps: (1) Solve the homogeneous system. (2) Construct the family of each term. (3) If the family has no representative in the homogeneous solution, assume y_x^p is a linear combination of the families of each term and determine the constants so that the equation is satisfied. (4) If a family has a representative in the homogeneous solution, multiply each member of the family by the smallest integral power of x for which all such representatives are removed and revert to step 3.

Example $y_{x+1} - 3y_x + 2y_{x-1} = 1 + a^x, a \neq 0$. The homogeneous solution is $y_x^h = c_1 + c_2 2^x$. The family of 1 is 1 and of a^x is a^x . However, 1 is a solution of the homogeneous system. Therefore, try $y_x^p = Ax + Ba^x$. Substituting in the equation there results

$$y_x = c_1 + c_2 2^x - x + \frac{a}{(a-1)(a-2)} a^x, a \neq 1, a \neq 2$$

If $a = 1, y_x = c_1 + c_2 2^x - 2x$. If $a = 2, y_x = c_1 + c_2 2^x - x + x 2^x$.

Example The family of $x^2 3^x$ is $[x^2 3^x, x 3^x, 3^x]$.

Method of Variation of Parameters This technique is applicable to general linear difference equations. It is illustrated for the second-order system $y_{x+2} + A y_{x+1} + B y_x = \phi(x)$. Assume that the homogeneous solution has been found by some technique and write $y_x^h = c_1 u_x + c_2 v_x$. Assume that a particular solution $y_x^p = D_x u_x + E_x v_x$. E_x and D_x can be found by solving the equations:

$$E_{x+1} - E_x = \frac{u_{x+1} \phi(x)}{u_{x+1} v_{x+2} - u_{x+2} v_{x+1}}$$

$$D_{x+1} - D_x = \frac{v_{x+1} \phi(x)}{v_{x+1} u_{x+2} - v_{x+2} u_{x+1}}$$

by summation. The general solution is then $y_x = y_x^p + y_x^h$.

Variable Coefficients The method of variation of parameters applies equally well to the linear difference equation with variable coefficients. Techniques are therefore needed to solve the homogeneous system with variable coefficients.

Equation $y_{x+1} - a_x y_x = 0$ By assuming that this equation is valid for $x \geq 0$ and $y_0 = c$, the solution is $y_x = c \prod_{n=1}^x a_{n-1}$.

Example $y_{x+1} + \frac{x+2}{x+1} y_x = 0$. The solution is

$$y_x = c \prod_{n=1}^x \left(-\frac{n+1}{n} \right) = c(-1)^x \frac{2}{1} \cdot \frac{3}{2} \cdot \dots \cdot \frac{x+1}{x} = (-1)^x c(x+1)$$

Example $y_{x+1} - x y_x = 0$. The solution is $y_x = c(x-1)!$

Reduction of Order If one homogeneous solution, say, u_x , can be found by inspection or otherwise, an equation of lower order can be obtained by the substitution $v_x = y_x/u_x$. The resultant equation must be satisfied by $v_x = \text{constant}$ or $\Delta v_x = 0$. Thus the equation will be of reduced order if the new variable $U_x = \Delta(y_x/u_x)$ is introduced.

Example $(x + 2)y_{x+2} - (x + 3)y_{x+1} + y_x = 0$. By observation $u_x = 1$ is a solution. Set $U_x = \Delta y_x = y_{x+1} - y_x$. There results $(x + 2)U_{x+1} - U_x = 0$, which is of degree one lower than the original equation. The complete solution for y_x is finally

$$y_x = c_0 \sum_{n=0}^x \frac{1}{n!} + c_1$$

Factorization If the difference equation can be factored, then the general solution can be obtained by solving two or more successive equations of lower order. Consider $y_{x+2} + A_x y_{x+1} + B_x y_x = \phi(x)$. If there exists a_x, b_x such that $a_x + b_x = -A_x$ and $a_x b_x = B_x$, then the difference equation may be written $y_{x+2} - (a_x + b_x)y_{x+1} + a_x b_x y_x = \phi(x)$. First solve $U_{x+1} - b_x U_x = \phi(x)$ and then $y_{x+1} - a_x y_x = U_x$.

Example $y_{x+2} - (2x + 1)y_{x+1} + (x^2 + x)y_x = 0$. Set $a_x = x, b_x = x + 1$. Solve $u_{x+1} - (x + 1)u_x = 0$ and then $y_{x+1} - x y_x = u_x$.

Substitution If it is possible to rearrange a difference equation so that it takes the form $a_x y_{x+2} + b_x y_{x+1} + c_x y_x = \phi(x)$ with a, b, c constants, then the substitution $u_x = f_x y_x$ reduces the equation to one with constant coefficients.

Example $(x + 2)^2 y_{x+2} - 3(x + 1)^2 y_{x+1} + 2x^2 y_x = 0$. Set $u_x = x^2 y_x$. The equation becomes $u_{x+2} - 3u_{x+1} + 2u_x = 0$, which is linear and easily solved by previous methods.

The substitution $u_x = y_x/f_x$ reduces $a_x f_x y_{x+2} + b_x f_x y_{x+1} + c_x f_x y_x = \phi(x)$ to an equation with constant coefficients.

Example $x(x + 1)y_{x+2} + 3x(x + 2)y_{x+1} - 4(x + 1)(x + 2)y_x = x$. Set $u_x = y_x/f_x = y_x/x$. Then $y_x = x u_x, y_{x+1} = (x + 1)u_{x+1}$ and $y_{x+2} = (x + 2)u_{x+2}$. Substitution in the equation yields $x(x + 1)(x + 2)u_{x+2} + 3x(x + 2)(x + 1)u_{x+1} - 4x(x + 1)(x + 2)u_x = x$ or $u_{x+2} + 3u_{x+1} - 4u_x = 1/(x + 1)(x + 2)$, which is a linear equation with constant coefficients.

Nonlinear Difference Equations: Riccati Difference Equation The Riccati equation $y_{x+1}y_x + a y_{x+1} + b y_x + c = 0$ is a nonlinear difference equation which can be solved by reduction to linear form. Set $y = z + h$. The equation becomes $z_{x+1}z_x + (h + a)z_{x+1} + (h + b)z_x + h^2 + (a + b)h + c = 0$. If h is selected as a root of $h^2 + (a + b)h + c = 0$ and the equation is divided by $z_{x+1}z_x$ there results $[(h + b)/z_{x+1}] + [(h + a)/z_x] + 1 = 0$. This is a linear equation with constant coefficients. The solution is

$$y_x = h + \frac{1}{c \left[\frac{a+h}{b+h} \right]^x - \frac{1}{(a+h) + (b+h)}}$$

Example This equation is obtained in distillation problems, among others, in which the number of theoretical plates is required. If the relative volatility is assumed to be constant, the plates are theoretically perfect, and the molal liquid and vapor rates are constant, then a material balance around the n th plate of the enriching section yields a Riccati difference equation.

INTEGRAL EQUATIONS

REFERENCES: Courant, R., and D. Hilbert, *Methods of Mathematical Physics*, vol. I, Interscience, New York (1953); Linz, P., *Analytical and Numerical Methods for Volterra Equations*, SIAM Publications, Philadelphia (1985); Porter, D., and D. S. G. Stirling, *Integral Equations: A Practical Treatment from Spectral Theory to Applications*, Cambridge University Press (1990); Stogdole, I., *Green's Functions and Boundary Value Problems*, 2d ed., Interscience, New York (1997).

An integral equation is any equation in which the unknown function appears under the sign of integration and possibly outside the sign of integration. If derivatives of the dependent variable appear elsewhere in the equation, the equation is said to be integrodifferential.

CLASSIFICATION OF INTEGRAL EQUATIONS

Volterra integral equations have an integral with a variable limit. The Volterra equation of the second kind is

$$u(x) = f(x) + \lambda \int_a^x K(x, t)u(t) dt$$

whereas a Volterra equation of the first kind is

$$u(x) = \lambda \int_a^x K(x, t)u(t) dt$$

Equations of the first kind are very sensitive to solution errors so that they present severe numerical problems. Volterra equations are similar to initial value problems.

A Fredholm equation of the second kind is

$$u(x) = f(x) + \lambda \int_a^b K(x, t)u(t) dt$$

whereas a Fredholm equation of the first kind is

$$u(x) = \int_a^b K(x, t)u(t) dt$$

The limits of integration are fixed, and these problems are analogous to boundary value problems.

An eigenvalue problem is a homogeneous equation of the second kind, and solutions exist only for certain λ .

$$u(x) = \lambda \int_a^b K(x, t)u(t) dt$$

See Linz (1985) for further information and existence proofs.

If the unknown function u appears in the equation in any way except to the first power, the integral equation is said to be nonlinear. The equation $u(x) = f(x) + \int_a^b K(x, t)[u(t)]^{3/2} dt$ is nonlinear. The differential equation $du/dx = g(x, u)$ is equivalent to the nonlinear integral equation $u(x) = c + \int_a^x g[t, u(t)] dt$.

An integral equation is said to be singular when either one or both of the limits of integration become infinite or if $K(x, t)$ becomes infinite for one or more points of the interval under discussion.

Example $u(x) = x + \int_0^\infty \cos(xt)u(t) dt$ and $f(x) = \int_0^x \frac{u(t)}{x-t} dt$ are both singular. The kernel of the first equation is $\cos(xt)$, and that of the second is $(x-t)^{-1}$.

RELATION TO DIFFERENTIAL EQUATIONS

The Leibniz rule (see "Integral Calculus") can be used to show the equivalence of the initial-value problem consisting of the second-order differential equation $d^2y/dx^2 + A(x)(dy/dx) + B(x)y = f(x)$ together with the prescribed initial conditions $y(a) = y_0, y'(a) = y'_0$ to the integral equation.

$$y(x) = \int_a^x K(x, t)y(t) dt + F(x)$$

where $K(x, t) = (t-x)[B(t) - A'(t)] - A(t)$

and
$$F(x) = \int_a^x (x-t)f(t) dt + [A(a)y_0 + y_0'](x-a) + y_0$$

This integral equation is a **Volterra equation** of the second kind. Thus the initial-value problem is equivalent to a Volterra integral equation of the second kind.

Example $d^2y/dx^2 + x^2(dy/dx) + xy = x$, $y(0) = 1$, $y'(0) = 0$. Here $A(x) = x^2$, $B(x) = x$, $f(x) = x$. The equivalent integral equation is $y(x) = \int_0^x K(x, t)y(t) dt + F(x)$ where $K(x, t) = t(x-t) - t^2$ and $F(x) = \int_0^x (x-t)t dt + 1 = x^3/6 + 1$. Combining these $y(x) = \int_0^x t[x - 2t]y(t) dt + x^3/6 + 1$.

Eigenvalue problems can also be related. For example, the problem $(d^2y/dx^2) + \lambda y = 0$ with $y(0) = 0$, $y(a) = 0$ is equivalent to the integral equation $y(x) = \lambda \int_0^a K(x, t)y(t) dt$, where $K(x, t) = (t/a)(a-x)$ when $t < x$ and $K(x, t) = (x/a)(a-t)$ when $t > x$. The differential equation may be recovered from the integral equation by differentiating the integral equation by using the Leibniz rule.

METHODS OF SOLUTION

In general, the solution of integral equations is not easy, and a few exact and approximate methods are given here. Often numerical methods must be employed, as discussed in "Numerical Solution of Integral Equations."

Equations of Convolution Type The equation $u(x) = f(x) + \lambda \int_0^x K(x-t)u(t) dt$ is a special case of the linear integral equation of the second kind of Volterra type. The integral part is the convolution integral discussed under "Integral Transforms (Operational Methods)"; so the solution can be accomplished by Laplace transforms; $L[u(x)] = L[f(x)] + \lambda L[u(x)]L[K(x)]$ or

$$L[u(x)] = \frac{L[f(x)]}{1 - \lambda L[K(x)]}, \quad u(x) = L^{-1} \left[\frac{L[f(x)]}{1 - \lambda L[K(x)]} \right]$$

INTEGRAL TRANSFORMS (OPERATIONAL METHODS)

REFERENCES: Brown, J. W., and R. V. Churchill, *Fourier Series and Boundary Value Problems*, 6th ed., McGraw-Hill, New York (2000); Churchill, R. V., *Operational Mathematics*, 3d ed., McGraw-Hill, New York (1972); Davies, B., *Integral Transforms and Their Applications*, 3d ed., Springer (2002); Duffy, D. G., *Transform Methods for Solving Partial Differential Equations*, Chapman & Hall/CRC, New York (2004); Varma, A., and M. Morbidelli, *Mathematical Methods in Chemical Engineering*, Oxford, New York (1997).

The term "operational method" implies a procedure of solving differential and difference equations by which the boundary or initial conditions are automatically satisfied in the course of the solution. The technique offers a very powerful tool in the applications of mathematics, but it is limited to linear problems.

Most integral transforms are special cases of the equation $g(s) = \int_a^b f(t)K(s, t) dt$ in which $g(s)$ is said to be the transform of $f(t)$ and $K(s, t)$ is called the kernel of the transform. A tabulation of the more important kernels and the interval (a, b) of applicability follows. The first three transforms are considered here.

Name of transform	(a, b)	$K(s, t)$
Laplace	$(0, \infty)$	e^{-st}
Fourier	$(-\infty, \infty)$	$\frac{1}{\sqrt{2\pi}} e^{-ist}$
Fourier cosine	$(0, \infty)$	$\sqrt{\frac{2}{\pi}} \cos st$
Fourier sine	$(0, \infty)$	$\sqrt{\frac{2}{\pi}} \sin st$
Mellin	$(0, \infty)$	t^{s-1}
Hankel	$(0, \infty)$	$tJ_\nu(st), \nu \geq -1/2$

Equations of the type considered here occur quite frequently in practice in what can be called "cause-and-effect" systems.

Example In a certain linear system, the effect $E(t)$ due to a cause $C = \lambda E$ at time τ is a function only of the elapsed time $t - \tau$. If the system has the activity level 1 at time $t < 0$, the cause λE and effect (E) relation is given by the integral equation $E(t) = 1 + \lambda \int_0^t K(t - \tau)E(\tau) d\tau$. Let $K(t - \tau) = t - \tau$. Then $E(t) = 1 + \lambda \int_0^t (t - \tau)E(\tau) d\tau$. By using the transform method

$$E(t) = L^{-1} \left[\frac{L[1]}{1 - \lambda L[K(t)]} \right] = L^{-1} \left[\frac{1/p}{1 - \lambda/p^2} \right] = L^{-1} \left[\frac{p}{p^2 - \lambda} \right] = \cosh \sqrt{\lambda} t$$

Method of Successive Approximations Consider the equation $y(x) = f(x) + \lambda \int_a^b K(x, t)y(t) dt$. In this method a unique solution is obtained in sequence form as follows: Substitute in the right-hand member of the equation $y_0(t)$ for $y(t)$. Upon integration there results $y_1(t) = f(x) + \lambda \int_a^b K(x, t)y_0(t) dt$. Continue in like manner by replacing y_0 by y_1 , y_1 by y_2 , etc. A series of functions $y_0(x)$, $y_1(x)$, $y_2(x)$, ... are obtained which satisfy the equations

$$y_n(x) = f(x) + \lambda \int_a^b K(x, t)y_{n-1}(t) dt$$

Then $y_n(x) = f(x) + \lambda \int_a^b K(x, t)f(t) dt + \lambda^2 \int_a^b K(x, t) \int_a^b K(t, t_1)f(t_1) dt_1 dt + \lambda^3 \int_a^b K(x, t) \int_a^b K(t, t_1) \int_a^b K(t_1, t_2)f(t_2) dt_2 dt_1 dt + \dots + R_n$, where R_n is the remainder, and

$$|R_n| \leq |\lambda|^n \left(\max_{a \leq x \leq b} y_0 \right) M^n (b-a)^n$$

where M = maximum value of $|K|$ in the rectangle $a \leq t \leq b$, $a \leq x \leq b$. If $|\lambda|M(b-a) < 1$, $\lim_{n \rightarrow \infty} R_n = 0$. Then $y_n(x) \rightarrow y(x)$, which is the unique solution.

LAPLACE TRANSFORM

The Laplace transform of a function $f(t)$ is defined by $F(s) = L\{f(t)\} = \int_0^\infty e^{-st}f(t) dt$, where s is a complex variable. Note that the transform is an improper integral and therefore may not exist for all continuous functions and all values of s . We restrict consideration to those values of s and those functions f for which this improper integral converges. The Laplace transform is used in process control (see Sec. 8).

The function $L\{f(t)\} = g(s)$ is called the direct transform, and $L^{-1}\{g(s)\} = f(t)$ is called the inverse transform. Both the direct and the inverse transforms are tabulated for many often-occurring functions. In general,

$$L^{-1}\{g(s)\} = \frac{1}{2\pi i} \int_{\alpha - i\infty}^{\alpha + i\infty} e^{st}g(s) ds$$

and to evaluate this integral requires a knowledge of complex variables, the theory of residues, and contour integration.

A function is said to be piecewise continuous on an interval if it has only a finite number of finite (or jump) discontinuities. A function f on $0 < t < \infty$ is said to be of exponential growth at infinity if there exist constants M and α such that $|f(t)| \leq Me^{\alpha t}$ for sufficiently large t .

Sufficient Conditions for the Existence of Laplace Transform Suppose f is a function which is (1) piecewise continuous on every finite interval $0 < t < T$, (2) of exponential growth at infinity, and (3) $\int_0^\delta |f(t)| dt$ exist (finite) for every finite $\delta > 0$. Then the Laplace transform of f exists for all complex numbers s with sufficiently large real part.

Note that condition 3 is automatically satisfied if f is assumed to be piecewise continuous on every finite interval $0 \leq t < T$. The function $f(t) = t^{-1/2}$ is not piecewise continuous on $0 \leq t \leq T$ but satisfies conditions 1 to 3.

Let Λ denote the class of all functions on $0 < t < \infty$ which satisfy conditions 1 to 3.

Example Let $f(t)$ be the Heaviside step function at $t = t_0$; i.e., $f(t) = 0$ for $t \leq t_0$, and $f(t) = 1$ for $t > t_0$. Then

$$L\{f(t)\} = \int_0^\infty e^{-st} dt = \lim_{T \rightarrow \infty} \int_0^T e^{-st} dt = \lim_{T \rightarrow \infty} \frac{1}{s} (e^{-st_0} - e^{-sT}) = \frac{e^{-st_0}}{s}$$

provided $s > 0$.

Example Let $f(t) = e^{at}$, $t \geq 0$, where a is a real number. Then $L\{e^{at}\} = \int_0^\infty e^{-(s-a)t} dt = 1/(s-a)$, provided $\text{Re } s > a$.

Properties of the Laplace Transform

1. The Laplace transform is a linear operator: $L\{af(t) + bg(t)\} = aL\{f(t)\} + bL\{g(t)\}$ for any constants a, b and any two functions f and g whose Laplace transforms exist.

2. The Laplace transform of a real-valued function is real for real s . If $f(t)$ is a complex-valued function, $f(t) = u(t) + iv(t)$, where u and v are real, then $L\{f(t)\} = L\{u(t)\} + iL\{v(t)\}$. Thus $L\{u(t)\}$ is the real part of $L\{f(t)\}$, and $L\{v(t)\}$ is the imaginary part of $L\{f(t)\}$.

3. The Laplace transform of a function in the class Λ has derivatives of all orders, and $L\{t^k f(t)\} = (-1)^k d^k F(s)/ds^k$, $k = 1, 2, 3, \dots$

Example $\int_0^\infty e^{-st} \sin at dt = \frac{a}{s^2 + a^2}$, $s > 0$. By property 3, $\frac{2as}{(s^2 + a^2)^2} = \int_0^\infty e^{-st} t \sin at dt = L\{t \sin at\}$.

Example By applying property 3 with $f(t) = 1$ and using the preceding results, we obtain

$$L\{t^k\} = (-1)^k \frac{d^k}{ds^k} \left(\frac{1}{s} \right) = \frac{k!}{s^{k+1}}$$

provided $\text{Re } s > 0$; $k = 1, 2, \dots$. Similarly, we obtain

$$L\{t^k e^{at}\} = (-1)^k \frac{d^k}{ds^k} \left(\frac{1}{s-a} \right) = \frac{k!}{(s-a)^{k+1}}$$

4. Frequency-shift property (or, equivalently, the transform of an exponentially modulated function). If $F(s)$ is the Laplace transform of a function $f(t)$ in the class Λ , then for any constant a , $L\{e^{at} f(t)\} = F(s-a)$.

Example $L\{te^{-at}\} = \frac{1}{(s+a)^2}$, $s > 0$.

5. Time-shift property. Let $u(t-a)$ be the unit step function at $t = a$. Then $L\{f(t-a)u(t-a)\} = e^{-as}F(s)$.

6. Transform of a derivative. Let f be a differentiable function such that both f and f' belong to the class Λ . Then $L\{f'(t)\} = sF(s) - f(0)$.

7. Transform of a higher-order derivative. Let f be a function which has continuous derivatives up to order n on $(0, \infty)$, and suppose that f and its derivatives up to order n belong to the class Λ . Then $L\{f^{(j)}(t)\} = s^j F(s) - s^{j-1} f(0) - s^{j-2} f'(0) - \dots - f^{(j-2)}(0) - f^{(j-1)}(0)$ for $j = 1, 2, \dots, k$.

Example $L\{f''(t)\} = s^2 L\{f(t)\} - sf(0) - f'(0)$

$$L\{f'''(t)\} = s^3 L\{f(t)\} - s^2 f(0) - sf'(0) - f''(0)$$

Example Solve $y'' + y = 2e^t$, $y(0) = y'(0) = 2$. $L[y''] = -y'(0) - sy(0) + s^2 L[y] = -2 - 2s + s^2 L[y]$. Thus

$$-2 - 2s + s^2 L[y] + L[y] = 2L\{e^t\} = \frac{2}{s-1}$$

$$L[y] = \frac{2s^2}{(s-1)(s^2+1)} = \frac{1}{s-1} + \frac{s}{s^2+1} + \frac{1}{s^2+1}$$

Hence $y = e^t + \cos t + \sin t$.

A short table (Table 3-2) of very common Laplace transforms and inverse transforms follows. The references include more detailed tables. NOTE: $\Gamma(n+1) = \int_0^\infty x^n e^{-x} dx$ (gamma function); $J_n(t)$ = Bessel function of the first kind of order n .

$$8. L\left[\int_a^t f(t) dt\right] = \frac{1}{s} L\{f(t)\} + \frac{1}{s} \int_a^0 f(t) dt$$

TABLE 3-2 Laplace Transforms

$f(t)$	$g(s)$	$f(t)$	$g(s)$
1	$1/s$	$e^{-at}(1-at)$	$\frac{s}{(s+a)^2}$
t^n , ($n+1$ integer)	$\frac{n!}{s^{n+1}}$	$\frac{t \sin at}{2a}$	$\frac{s}{(s^2+a^2)^2}$
t^n , $n \neq$ integer	$\frac{\Gamma(n+1)}{s^{n+1}}$	$\frac{1}{2a^2} \sin at \sinh at$	$\frac{s}{s^4+4a^4}$
$\cos at$	$\frac{s}{s^2+a^2}$	$\cos at \cosh at$	$\frac{s^2}{s^4+4a^4}$
$\sin at$	$\frac{a}{s^2+a^2}$	$\frac{1}{2a} (\sinh at + \sin at)$	$\frac{s^2}{s^4-a^4}$
$\cosh at$	$\frac{s}{s^2-a^2}$	$\frac{1}{2} (\cosh at + \cos at)$	$\frac{s^3}{s^4-a^4}$
$\sinh at$	$\frac{a}{s^2-a^2}$	$\frac{\sin at}{t}$	$\tan^{-1} \frac{a}{s}$
e^{-at}	$\frac{1}{s+a}$	$J_0(at)$	$\frac{1}{\sqrt{s^2+a^2}}$
$e^{-bt} \cos at$	$\frac{s+b}{(s+b)^2+a^2}$	$na^n \frac{J_n(at)}{t}$	$(\sqrt{s^2+a^2}-s)^n (n > 0)$
$e^{-bt} \sin at$	$\frac{a}{(s+b)^2+a^2}$	$J_0(2\sqrt{at})$	$\frac{1}{s} e^{-a/s}$
$\text{erfc} \frac{k}{2\sqrt{t}}$	$\frac{1}{s} e^{-k\sqrt{s}}$		

Example Find $f(t)$ if $L\{f(t)\} = \frac{1}{s^2} \left[\frac{1}{s^2-a^2} \right]$. $L\left[\frac{1}{a} \sinh at\right] = \frac{1}{s^2-a^2}$.

Therefore $f(t) = \int_0^t \left[\int_0^t \frac{1}{a} \sinh at dt \right] dt = \frac{1}{a^2} \left[\frac{\sinh at}{a} - t \right]$.

9. $L\left[\frac{f(t)}{t}\right] = \int_s^\infty g(s) ds$ $L\left[\frac{f(t)}{t^k}\right] = \underbrace{\int_s^\infty \dots \int_s^\infty}_{k \text{ integrals}} g(s)(ds)^k$

Example $L\left[\frac{\sin at}{t}\right] = \int_s^\infty L\{\sin at\} ds = \int_s^\infty \frac{a ds}{s^2+a^2} = \cot^{-1} \frac{s}{a}$

10. The unit step function

$$u(t-a) = \begin{cases} 0 & t < a \\ 1 & t > a \end{cases} \quad L\{u(t-a)\} = e^{-as}/s$$

11. The unit impulse function is

$$\delta(a) = u'(t-a) = \begin{cases} \infty & \text{at } t = a \\ 0 & \text{elsewhere} \end{cases} \quad L\{u'(t-a)\} = e^{-as}$$

12. $L^{-1}[e^{-as}g(s)] = f(t-a)u(t-a)$ (second shift theorem).

13. If $f(t)$ is periodic of period b , i.e., $f(t+b) = f(t)$, then

$$L\{f(t)\} = \left[\frac{1}{1-e^{-bs}} \right] \int_0^b e^{-st} f(t) dt$$

Example The partial differential equations relating gas composition to position and time in a gas chromatograph are $\partial y/\partial n + \partial x/\partial \theta = 0$, $\partial y/\partial n = x - y$, where $x = mx'$, $n = (k_C a P/C_m)h$, $\theta = (mk_C a P/\rho_b)t$ and C_M = molar velocity, y = mole fraction of the component in the gas phase, ρ_b = bulk density, h = distance from the entrance, P = pressure, k_C = mass-transfer coefficient, and m = slope of the equilibrium line. These equations are equivalent to $\partial^2 y/\partial n \partial \theta + \partial y/\partial n + \partial y/\partial \theta = 0$, where the boundary conditions considered here are $y(0, \theta) = 0$ and $x(n, 0) = y(n, 0) + (\partial y/\partial n)(n, 0) = \delta(0)$ (see property 11). The problem is conveniently

solved by using the Laplace transform of y with respect to n ; write $g(s, \theta) = \int_0^\infty e^{-sn} y(n, \theta) dn$. Operating on the partial differential equation gives $s(dg/d\theta) - (\partial y/\partial \theta)(0, \theta) + sg - y(0, \theta) + dg/d\theta = 0$ or $(s+1)(dg/d\theta) + sg = (\partial y/\partial \theta)(0, \theta) + y(0, \theta) = 0$. The second boundary condition gives $g(s, 0) + sg(s, 0) - y(0, 0) = 1$ or $g(s, 0) + sg(s, 0) = 1$ ($L[\delta(0)] = 1$). A solution of the ordinary differential equation for g consistent with this second condition is

$$g(s, \theta) = \frac{1}{s+1} e^{-\theta/(s+1)}$$

Inversion of this transform gives the solution $y(n, \theta) = e^{-(n+\theta)} I_0(2\sqrt{n\theta})$ where I_0 = zero-order Bessel function of an imaginary argument. For large u , $I_n(u) \sim e^u/\sqrt{2\pi u}$. Hence for large n ,

$$y(n, \theta) \sim \frac{\exp[-(\sqrt{\theta} - \sqrt{n})^2]}{2\pi^{1/2}(n\theta)^{1/4}}$$

or for sufficiently large n , the peak concentration occurs near $\theta = n$.

Other applications of Laplace transforms are given under "Difference Equations."

CONVOLUTION INTEGRAL

The convolution integral (faltung) of two functions $f(t)$, $r(t)$ is $x(t) = f(t) \circ r(t) = \int_0^t f(\tau)r(t-\tau) d\tau$.

Example $t^\circ \sin t = \int_0^t \tau \sin(t-\tau) d\tau = t - \sin t$

$$L[f(t)]L[h(t)] = L[f(t) \circ h(t)]$$

z-TRANSFORM

See Ogunnaike, Babatunde A., and W. Harmon Ray, *Process Dynamics, Modeling, and Control*, Oxford University Press (1994); Seborg, D., T. F. Edgar, and D. A. Mellichamp, *Process Dynamics and Control*, 2d ed., Wiley, New York (2003). The z -transform is useful when data is available at only discrete points. Let

$$f^\circ(t) = f(t_k)$$

be the value of f at the sample points

$$t_k = k \Delta t, \quad k = 0, 1, 2, \dots$$

Then the function $f^\circ(t)$ is

$$f^\circ(t) = \sum_{k=0}^\infty f(t_k) \delta(t - t_k)$$

Take the Laplace transform of this.

$$g^\circ(s) = L[f^\circ(t)] = \sum_{k=0}^\infty f(t_k) e^{-st_k} = \sum_{k=0}^\infty f(t_k) e^{-s\Delta t k}$$

For convenience, replace $e^{s\Delta t}$ by z and call $g^\circ(z)$ the z -transform of $f^\circ(t)$.

$$g^\circ(z) = \sum_{k=0}^\infty f(t_k) z^{-k}$$

The z -transform is used in process control when the signals are at intervals of Δt . A brief table (Table 3-3) is provided here.

The z -transform can also be used to solve difference equations, just like the Laplace transform can be used to solve differential equations.

Example The difference equation for $y(k)$ is

$$y(k) + a_1 y(k-1) + a_2 y(k-2) = b_1 u(k)$$

Take the z -transform

$$(1 + a_1 z^{-1} + a_2 z^{-2}) y^\circ(z) = b_1 u^\circ(z)$$

Then

$$y^\circ(z) = \frac{u^\circ(z)}{1 + a_1 z^{-1} + a_2 z^{-2}}$$

The inverse transform must be found, usually from a table of inverse transforms.

FOURIER TRANSFORM

REFERENCES: Bateman, H., *Tables of Integral Transforms*, vol. I, McGraw-Hill, New York (1954); Varma, A., and M. Morbidelli, *Mathematical Methods in Chemical Engineering*, Oxford, New York (1997).

TABLE 3-3 z-Transforms

$f(k)$	$g^\circ(z)$
1(k)	$\frac{1}{1-z^{-1}}$
$k \Delta t$	$\frac{\Delta t z^{-1}}{(1-z^{-1})^2}$
$(k \Delta t)^{n-1}$	$\lim_{a \rightarrow 0} (-1)^{n-1} \frac{\partial^{n-1}}{\partial a^{n-1}} \left(\frac{1}{1 - e^{-a\Delta t} z^{-1}} \right)$
$\sin a k \Delta t$	$\frac{z^{-1} \sin a \Delta t}{(1 - 2z^{-1} \cos a \Delta t + z^{-2})}$
$\cos a k \Delta t$	$\frac{1 - z^{-1} \cos a \Delta t}{(1 - 2z^{-1} \cos a \Delta t + z^{-2})}$
$e^{-ak\Delta t}$	$\frac{1}{1 - e^{-a\Delta t} z^{-1}}$
$e^{-bk\Delta t} \cos a k \Delta t$	$\frac{1 - z^{-1} e^{-b\Delta t} \cos a \Delta t}{1 - 2z^{-1} e^{-b\Delta t} \cos a \Delta t + z^{-2} e^{-2b\Delta t}}$
$\frac{1}{b} e^{-bk\Delta t} \sin a k \Delta t$	$\frac{1}{b} \frac{z^{-1} e^{-b\Delta t} \sin a \Delta t}{1 - 2z^{-1} e^{-b\Delta t} \cos a \Delta t + z^{-2} e^{-2b\Delta t}}$

The Fourier transform is given by

$$F[f(t)] = \frac{1}{\sqrt{2\pi}} \int_{-\infty}^\infty f(t) e^{-ist} dt = g(s)$$

and its inverse by

$$F^{-1}[g(s)] = \frac{1}{\sqrt{2\pi}} \int_{-\infty}^\infty g(s) e^{ist} dt = f(t)$$

In brief, the condition for the Fourier transform to exist is that $\int_{-\infty}^\infty |f(t)| dt < \infty$, although certain functions may have a Fourier transform even if this is violated.

Example The function $f(t) = \begin{cases} 1 - a \leq t \leq a \\ 0 \text{ elsewhere} \end{cases}$ has $F[f(t)] = \int_{-a}^a e^{-ist} dt =$

$$\int_0^a e^{ist} dt + \int_0^a e^{-ist} dt = 2 \int_0^a \cos st dt = \frac{2 \sin sa}{s}$$

Properties of the Fourier Transform Let $F[f(t)] = g(s)$; $F^{-1}[g(s)] = f(t)$.

- $F[f^{(n)}(t)] = (is)^n F[f(t)]$.
- $F[af(t) + bh(t)] = aF[f(t)] + bF[h(t)]$.
- $F[f(-t)] = g(-s)$.
- $F[f(at)] = \frac{1}{a} g\left(\frac{s}{a}\right), a > 0$.
- $F[e^{-iwt} f(t)] = g(s + w)$.
- $F[f(t + t_1)] = e^{ist_1} g(s)$.
- $F[f(t)] = G(is) + G(-is)$ if $f(t) = f(-t)$ (f even)
 $F[f(t)] = G(is) - G(-is)$ if $f(t) = -f(-t)$ (f odd)

where $G(s) = L[f(t)]$. This result allows the use of the Laplace-transform tables to obtain the Fourier transforms.

Example Find $F[e^{-at|t|}]$ by property 7. $e^{-at|t|}$ is even. So $L[e^{-at}] = 1/(s+a)$. Therefore, $F[e^{-at|t|}] = 1/(is+a) + 1/(-is+a) = 2a/(s^2 + a^2)$.

FOURIER COSINE TRANSFORM

The Fourier cosine transform is given by

$$F_c[f(t)] = g(s) = \sqrt{\frac{2}{\pi}} \int_0^\infty f(t) \cos st dt$$

and its inverse by

$$F_c^{-1}[g(s)] = f(t) = \sqrt{\frac{2}{\pi}} \int_0^{\infty} g(s) \cos st \, ds$$

The Fourier sine transform F_s is obtainable by replacing the cosine by the sine in these integrals. They can be used to solve linear differential equations; see the transform references.

MATRIX ALGEBRA AND MATRIX COMPUTATIONS

REFERENCES: Anton, H., and C. Rorres, *Elementary Linear Algebra with Applications*, 9th ed., Wiley (2004); Bernstein, D. S., *Matrix Mathematics: Theory, Facts, and Formulas with Application to Linear Systems Theory*, Princeton University Press, Princeton, N.J. (2005); Kolman, B., and D. R. Hill, *Introductory Linear Algebra: An Applied First Course*, 8th ed., Prentice-Hall, Englewood Cliffs, N.J. (2004); Lay, D. C., *Linear Algebra and Its Applications*, 3d ed., Addison Wesley (2002); Lipschutz, S., and M. Lipson, *Schaum's Outline of Linear Algebra*, McGraw-Hill, New York (2000); Noble, B., and J. W. Daniel, *Applied Linear Algebra*, 3d ed., Prentice-Hall, Englewood Cliffs, N.J. (1987); Press, W. H., et al., *Numerical Recipes*, Cambridge University Press, Cambridge (1986).

MATRIX ALGEBRA

Matrices A rectangular array of mn quantities, arranged in m rows and n columns

$$A = (a_{ij}) = \begin{bmatrix} a_{11} & \cdots & a_{1n} \\ a_{21} & \cdots & a_{2n} \\ \vdots & & \vdots \\ a_{m1} & \cdots & a_{mn} \end{bmatrix}$$

is called a matrix. The elements a_{ij} may be real or complex. The notation a_{ij} means the element in the i th row and j th column, i is called the row index, j the column index. If $m = n$ the matrix is said to be square and of order n . A matrix, even if it is square, does not have a numerical value, as a determinant does. However, if the matrix A is square, a determinant can be formed which has the same elements as the matrix A . This is called the determinant of the matrix and is written $\det(A)$ or $|A|$. If A is square and $\det(A) \neq 0$, A is said to be nonsingular; if $\det(A) = 0$, A is said to be singular. A matrix A has rank r if and only if it has a nonvanishing determinant of order r and no nonvanishing determinant of order $> r$.

Equality of Matrices Let $A = (a_{ij})$, $B = (b_{ij})$. Two matrices A and B are equal ($=$) if and only if they are identical; that is, they have the same number of rows and the same number of columns and equal corresponding elements ($a_{ij} = b_{ij}$ for all i and j).

Addition and Subtraction The operations of addition (+) and subtraction (-) of two or more matrices are possible if and only if they have the same number of rows and columns. Thus $A \pm B = (a_{ij} \pm b_{ij})$; i.e., addition and subtraction are of corresponding elements.

Transposition The matrix obtained from A by interchanging the rows and columns of A is called the transpose of A , written A^T or A^T .

Example $A = \begin{bmatrix} 1 & 3 & 4 \\ 2 & 1 & 6 \end{bmatrix}$, $A^T = \begin{bmatrix} 1 & 2 \\ 3 & 1 \\ 4 & 6 \end{bmatrix}$

Note that $(A^T)^T = A$.

Multiplication Let $A = (a_{ij})$, $i = 1, \dots, m_1; j = 1, \dots, m_2$. $B = (b_{ij})$, $i = 1, \dots, n_1, j = 1, \dots, n_2$. The product AB is defined if and only if the number of columns of A (m_2) equals the number of rows of B (n_1), i.e., $n_1 = m_2$. For two such matrices the product $P = AB$ is defined by summing the element by element products of a row of A by a column of B . This is the row by column rule. Thus

$$p_{ij} = \sum_{k=1}^{n_1} a_{ik} b_{kj}$$

The resulting matrix has m_1 rows and n_2 columns.

Example $\begin{bmatrix} 3 & 2 \\ 1 & 1 \\ 5 & 4 \end{bmatrix} \begin{bmatrix} 0 & 1 & 5 & 6 \\ -2 & 0 & 1 & 3 \end{bmatrix} = \begin{bmatrix} -4 & 3 & 17 & 24 \\ -2 & 1 & 6 & 9 \\ -8 & 5 & 29 & 42 \end{bmatrix}$

It is helpful to remember that the element p_{ij} is formed from the i th row of the first matrix and the j th column of the second matrix. The matrix product is not commutative. That is, $AB \neq BA$ in general.

Inverse of a Matrix A square matrix A is said to have an inverse if there exists a matrix B such that $AB = BA = I$, where I is the identity matrix of order n .

$$\begin{bmatrix} 1 & 0 & \cdots & 0 \\ & 1 & & \\ & & \ddots & \\ 0 & \cdots & 0 & 1 \end{bmatrix}$$

The inverse B is a square matrix of the order of A , designated by A^{-1} . Thus $AA^{-1} = A^{-1}A = I$. A square matrix A has an inverse if and only if A is nonsingular.

Certain relations are important:

- (1) $(AB)^{-1} = B^{-1}A^{-1}$
- (2) $(AB)^T = B^T A^T$
- (3) $(A^{-1})^T = (A^T)^{-1}$
- (4) $(ABC)^{-1} = C^{-1}B^{-1}A^{-1}$

Scalar Multiplication Let c be any real or complex number. Then $cA = (ca_{ij})$.

Adjugate Matrix of a Matrix Let A_{ij} denote the cofactor of the element a_{ij} in the determinant of the matrix A . The matrix B^T where $B = (A_{ij})$ is called the adjugate matrix of A written $\text{adj } A = B^T$. The elements b_{ij} are calculated by taking the matrix A , deleting the i th row and j th column, and calculating the determinant of the remaining matrix times $(-1)^{i+j}$. Then $A^{-1} = \text{adj } A / |A|$. This definition may be used to calculate A^{-1} . However, it is very laborious and the inversion is usually accomplished by numerical techniques shown under "Numerical Analysis and Approximate Methods."

Linear Equations in Matrix Form Every set of n nonhomogeneous linear equations in n unknowns

$$\begin{aligned} a_{11}x_1 + a_{12}x_2 + \cdots + a_{1n}x_n &= b_1 \\ a_{21}x_1 + a_{22}x_2 + \cdots + a_{2n}x_n &= b_2 \\ \vdots & \vdots \\ a_{n1}x_1 + a_{n2}x_2 + \cdots + a_{nn}x_n &= b_n \end{aligned}$$

can be written in matrix form as $AX = B$, where $A = (a_{ij})$, $X^T = [x_1 \cdots x_n]$, and $B^T = [b_1 \cdots b_n]$. The solution for the unknowns is $X = A^{-1}B$.

Special Square Matrices

1. A triangular matrix is a matrix all of whose elements above or below the main diagonal (set of elements a_{11}, \dots, a_{nn}) are zero.

If A is triangular, $\det(A) = a_{11} a_{22} \cdots a_{nn}$.

2. A diagonal matrix is one such that all elements both above and below the main diagonal are zero (i.e., $a_{ij} = 0$ for all $i \neq j$). If all diagonal elements are equal, the matrix is called scalar. If A is diagonal, $A = (a_{ij})$, $A^{-1} = (1/a_{ij})$.

3. If $a_{ij} = a_{ji}$ for all i and j (i.e., $A = A^T$), the matrix is symmetric.

4. If $a_{ij} = -a_{ji}$ for $i \neq j$ but the a_{ij} are not all zero, the matrix is skew.

5. If $a_{ij} = -a_{ji}$ for all i and j (i.e., $a_{ii} = 0$), the matrix is skew symmetric.

6. If $A^T = A^{-1}$, the matrix A is orthogonal.

7. If the matrix $A^{\circ} = (\bar{a}_{ij})^T$, \bar{a}_{ij} = complex conjugate of a_{ij} , A° is the hermitian transpose of A .

8. If $A = A^{-1}$, A is involutory.

9. If $A = A^{\circ}$, A is hermitian.

10. If $A = -A^{\circ}$, A is skew hermitian.

11. If $A^{-1} = A^{\circ}$, A is unitary.

If A is any matrix, then AA^T and $A^T A$ are square symmetric matrices, usually of different order.

Example Let $A = \begin{bmatrix} 5 & 1 & 3 & 0 \\ 3 & 4 & 1 & 5 \\ 2 & -2 & 0 & 1 \end{bmatrix}$, $A^T = \begin{bmatrix} 5 & 3 & 2 \\ 1 & 4 & -2 \\ 3 & 1 & 0 \\ 0 & 5 & 1 \end{bmatrix}$

$AA^T = \begin{bmatrix} 35 & 22 & 8 \\ 22 & 51 & 3 \\ 8 & 3 & 9 \end{bmatrix}$, $A^T A = \begin{bmatrix} 38 & 13 & 18 & 17 \\ 13 & 21 & 7 & 18 \\ 18 & 7 & 10 & 5 \\ 17 & 18 & 5 & 26 \end{bmatrix}$

Using a program such as MATLAB, these are easily calculated.

Matrix Calculus

Differentiation Let the elements of $A = [a_{ij}(t)]$ be differentiable functions of t . Then $\frac{dA}{dt} = \left[\frac{da_{ij}(t)}{dt} \right]$.

Example $A = \begin{bmatrix} \sin t & \cos t \\ -\cos t & \sin t \end{bmatrix}$, $\frac{dA}{dt} = \begin{bmatrix} \cos t & -\sin t \\ \sin t & \cos t \end{bmatrix}$.

Integration The integral $\int A dt = [\int a_{ij}(t) dt]$.

Example $A = \begin{bmatrix} t & 2 \\ t^2 & e^t \end{bmatrix}$, $\int A dt = \begin{bmatrix} t^2/2 & 2t \\ t^3/3 & e^t \end{bmatrix}$.

The matrix $B = A - \lambda I$ is called the characteristic (eigen) matrix of A . Here A is square of order n , λ is a scalar parameter, and I is the $n \times n$ identity. $\det B = \det (A - \lambda I) = 0$ is the characteristic (eigen) equation for A . The characteristic equation is always of the same degree as the order of A . The roots of the characteristic equation are called the eigenvalues of A .

Example $A = \begin{bmatrix} 1 & 2 \\ 3 & 8 \end{bmatrix}$, $B = \begin{bmatrix} 1-\lambda & 2 \\ 3 & 8-\lambda \end{bmatrix} = \begin{bmatrix} 1-\lambda & 2 \\ 3 & 8-\lambda \end{bmatrix}$

is the characteristic matrix and $f(\lambda) = \det (B) = \det (A - \lambda I) = (1 - \lambda)(8 - \lambda) - 6 = 2 - 9\lambda + \lambda^2 = 0$ is the characteristic equation. The eigenvalues of A are the roots of $\lambda^2 - 9\lambda + 2 = 0$, which are $(9 \pm \sqrt{73})/2$.

A nonzero matrix X_i , which has one column and n rows, called a column vector satisfying the equation

$(A - \lambda I)X_i = 0$

and associated with the i th characteristic root λ_i is called an eigenvector.

Vector and Matrix Norms To carry out error analysis for approximate and iterative methods for the solutions of linear systems, one needs notions for vectors in R^n and for matrices that are analogous to the notion of length of a geometric vector. Let R^n denote the set of all vectors with n components, $x = (x_1, \dots, x_n)$. In dealing with matrices it is convenient to treat vectors in R^n as columns, and so $x = (x_1, \dots, x_n)^T$; however, we shall here write them simply as row vectors. A norm on R^n is a real-valued function f defined on R^n with the following properties:

1. $f(x) \geq 0$ for all $x \in R^n$.
2. $f(x) = 0$ if and only if $x = (0, 0, \dots, 0)$.
3. $f(ax) = |a|f(x)$ for all real numbers a and $x \in R^n$.
4. $f(x + y) \leq f(x) + f(y)$ for all $x, y \in R^n$.

The usual notation for a norm is $f(x) = \|x\|$.

The norm of a matrix is

$\kappa(A) \equiv \|A\| \|A^{-1}\|$

where $\|A\| = \sup_{x \neq 0} \frac{\|Ax\|}{\|x\|} = \max_k \sum_{j=1}^n |a_{jk}|$

The norm is useful when doing numerical calculations. If the computer's floating-point precision is 10^{-6} , then $\kappa = 10^6$ indicates an ill-conditioned matrix. If the floating-point precision is 10^{-12} (double precision), then a matrix with $\kappa = 10^{12}$ may be ill-conditioned. Two other measures are useful and are more easily calculated:

Ratio = $\frac{\max_k |a_{kk}^{(k)}|}{\min_k |a_{kk}^{(k)}|}$, $V = \frac{|\det A|}{\alpha_1 \alpha_2 \dots \alpha_n}$, $\alpha_i = (a_{i1}^2 + a_{i2}^2 + \dots + a_{in}^2)^{1/2}$

where $a_{kk}^{(k)}$ are the diagonal elements of the LU decomposition.

MATRIX COMPUTATIONS

The principal topics in linear algebra involve systems of linear equations, matrices, vector spaces, linear transformations, eigenvalues and eigenvectors, and least-squares problems. The calculations are routinely done on a computer.

LU Factorization of a Matrix To every $m \times n$ matrix A there exists a permutation matrix P , a lower triangular matrix L with unit diagonal elements, and an $m \times n$ (upper triangular) echelon matrix U such that $PA = LU$. The Gauss elimination is in essence an algorithm to determine U , P , and L . The permutation matrix P may be needed since it may be necessary in carrying out the Gauss elimination to interchange two rows of A to produce a (nonzero) pivot, such as if we start with

$A = \begin{bmatrix} 0 & 2 \\ 1 & 6 \end{bmatrix}$

If A is a square matrix and if principal submatrices of A are all nonsingular, then we may choose P as the identity in the preceding factorization and obtain $A = LU$. This factorization is unique if L is normalized (as assumed previously), so that it has unit elements on the main diagonal.

Solution of $Ax = b$ by Using LU Factorization Suppose that the indicated system is compatible and that $A = LU$ (the case $PA = LU$ is similarly handled and amounts to rearranging the equations). Let $z = Ux$. Then $Ax = LUx = b$ implies that $Lz = b$. Thus to solve $Ax = b$ we first solve $Lz = b$ for z and then solve $Ux = z$ for x . This procedure does not require that A be invertible and can be used to determine all solutions of a compatible system $Ax = b$. Note that the systems $Lz = b$ and $Ux = z$ are both in triangular forms and thus can be easily solved.

The LU decomposition is essentially a Gaussian elimination, arranged for maximum efficiency. The chief reason for doing an LU decomposition is that it takes fewer multiplications than would be needed to find an inverse. Also, once the LU decomposition has been found, it is possible to solve for multiple right-hand sides with little increase in work. The multiplication count for an $n \times n$ matrix and m right-hand sides is

operation count = $\frac{1}{3} n^3 - \frac{1}{3} n + mn^2$

If an inverse is desired, it can be calculated by solving for the LU decomposition and then solving n problems with right-hand sides consisting of all zeros except one entry. Thus $4n^2/3 - n/3$ multiplications are required for the inverse. The determinant is given by

$\text{Det } A = \prod_{i=1}^n a_{ii}^{(i)}$

where $a_{ii}^{(i)}$ are the diagonal elements obtained in the LU decomposition.

A tridiagonal matrix is one in which the only nonzero entries lie on the main diagonal and the diagonal just above and just below the main diagonal. The set of equations can be written as

$a_i x_{i-1} + b_i x_i + c_i x_{i+1} = d_i$

The LU decomposition is

$b_1 = b_1$

for $k=2, n$ do

$a'_k = \frac{a_k}{b'_{k-1}}$, $b'_k = b_k - \frac{a_k}{b'_{k-1}} c_{k-1}$

enddo

$d'_1 = d_1$

for $k=2, n$ do

$d'_k = d_k - a'_k d'_{k-1}$

enddo

$x_n = d'_n / b'_n$

for $k=n-1, 1$ do

$x_k = \frac{d'_k - c_k x_{k+1}}{b'_k}$

enddo

3-42 MATHEMATICS

The operation count for an $n \times n$ matrix with m right-hand sides is

$$2(n-1) + m(3n-2)$$

If $|b_i| > |a_i| + |c_i|$

no pivoting is necessary, and this is true for many boundary-value problems and partial-differential equations.

Sparse matrices are ones in which the majority of the elements are zero. If the structure of the matrix is exploited, the solution time on a computer is greatly reduced. See Duff, I. S., J. K. Reid, and A. M. Erisman (eds.), *Direct Methods for Sparse Matrices*, Clarendon Press, Oxford (1986); Saad, Y., *Iterative Methods for Sparse Linear Systems*, 2d ed., Society for Industrial and Applied Mathematics, Philadelphia (2003). The conjugate gradient method is one method for solving sparse matrix problems, since it only involves multiplication of a matrix times a vector. Thus the sparseness of the matrix is easy to exploit. The conjugate gradient method is an iterative method that converges for sure in n iterations where the matrix is an $n \times n$ matrix.

Matrix methods, in particular finding the rank of the matrix, can be used to find the number of independent reactions in a reaction set. If the stoichiometric numbers for the reactions and molecules are put in the form of a matrix, the rank of the matrix gives the number of independent reactions. See Amundson, N. R., *Mathematical Methods in Chemical Engineering*, Prentice-Hall, Englewood Cliffs, N.J. (1966, p. 50).

QR Factorization of a Matrix If A is an $m \times n$ matrix with $m \geq n$, there exists an $m \times m$ unitary matrix $Q = [q_1, q_2, \dots, q_m]$ and an $m \times n$ right triangular matrix R such that $A = QR$. The QR factorization is frequently used in the actual computations when the other transformations are unstable.

Singular-Value Decomposition If A is an $m \times n$ matrix with $m \geq n$ and rank $k \leq n$, consider the two following matrices.

$$AA^{\circ} \text{ and } A^{\circ}A$$

An $m \times m$ unitary matrix U is formed from the eigenvectors \mathbf{u}_i of the first matrix.

$$U = [\mathbf{u}_1, \mathbf{u}_2, \dots, \mathbf{u}_m]$$

An $n \times n$ unitary matrix V is formed from the eigenvectors \mathbf{v}_i of the second matrix.

$$V = [\mathbf{v}_1, \mathbf{v}_2, \dots, \mathbf{v}_n]$$

Then matrix A can be decomposed into

$$A = U\Sigma V^{\circ}$$

where Σ is a $k \times k$ diagonal matrix with diagonal elements $d_{ii} = \sigma_i > 0$ for $1 \leq i \leq k$. The eigenvalues of $\Sigma^{\circ}\Sigma$ are σ_i^2 . The vectors \mathbf{u}_i for $k+1 \leq i \leq m$ and \mathbf{v}_i for $k+1 \leq i \leq n$ are eigenvectors associated with the eigenvalue zero; the eigenvalues for $1 \leq i \leq k$ are σ_i^2 . The values of σ_i are called the singular values of matrix A . If A is real, then U and V are real and hence orthogonal matrices. The value of the singular-value decomposition comes when a process is represented by a linear transformation and the elements of A , a_{ij} , are the contribution to an output i for a particular variable as input variable j . The input may be the size of a disturbance, and the output is the gain [Seborg, D. E., T. F. Edgar, and D. A. Mellichamp, *Process Dynamics and Control*, 2d ed., Wiley, New York (2004)]. If the rank is less than n , not all the variables are independent and they cannot all be controlled. Furthermore, if the singular values are widely separated, the process is sensitive to small changes in the elements of the matrix, and the process will be difficult to control.

Example Consider the following example from Noble and Daniel [*Applied Linear Algebra*, Prentice-Hall (1987)] with the MATLAB commands to do the analysis. Define the following real matrix with $m = 3$ and $n = 2$ (whose rank $k = 1$).

```
>> a = [ 1 1
        2 2
        2 2]
```

```
>> a1 = a^{\circ}a
a1 = 9 9 % (n \times n or 2 \times 2)
     9 9
>> a2 = a^{\circ}a^{\circ}
a2 = 2 4 4 % (m \times m or 3 \times 3)
     4 8 8
     4 8 8
>> [v,d1]=eig(a1)
v = -0.7071 0.7071 % (n \times n or 2 \times 2)
     0.7071 0.7071
d1 = 0 0
     0 18
>> [u,d2]=eig(a2)
u = 0.8944 0.2981 0.3333 % (m \times m or 3 \times 3)
     -0.4472 0.5963 0.6667
     0 -0.7454 0.6667
d2 = 0 0 0
     0 0 0
     0 0 18
```

Thus, $\sigma_1^2 = 18$ and the eigenfunctions are the rows of v and u . The second column of v is associated with the eigenvalue $\sigma_1^2 = 18$, and the third column of u is associated with the eigenvalue $\sigma_1^2 = 18$.

If A is square and nonsingular, the vector \mathbf{x} that minimizes

$$\|A\mathbf{x} - \mathbf{b}\| \quad (3-71)$$

is obtained by solving the linear equations

$$\mathbf{x} = A^{-1}\mathbf{b}$$

When A is not square, then the solution to

$$A\mathbf{x} = \mathbf{b}$$

is

$$\mathbf{x} = V\mathbf{y}$$

where $y_i = b'_i/\sigma_i$ for $i = 1, \dots, k$, $\mathbf{b}' = U^{\circ}\mathbf{b}$, and $y_{k+1}, y_{k+2}, \dots, y_m$ are arbitrary. The matrices U and V are those obtained in the singular-value decomposition. The solution which minimizes the norm, Eq. (3-71), is \mathbf{x} with $y_{k+1}, y_{k+2}, \dots, y_m$ zero. These techniques can be used to monitor process variables. See Montgomery, D. C., *Introduction to Statistical Quality Control*, 4th ed., Wiley, New York (2001); Piovos, M. J., and K. A. Hoo, "Multivariate Statistics for Process Control," *IEEE Control Systems* **22**(5):8 (2002).

Principal Component Analysis (PCA) PCA is used to recognize patterns in data and reduce the dimensionality of the problem. Let the matrix A now represent data with the columns of A representing different samples and the rows representing different variables. The covariance matrix is defined as

$$\text{cov}(A) = \frac{A^{\circ}A}{m-1}$$

This is just the same matrix discussed with singular value decomposition. For data analysis, though, it is necessary to adjust the columns to have zero mean by subtracting from each entry in the column the average of the column entries. Once this is done, the *loadings* are the \mathbf{v}_i and satisfy

$$\text{cov}(A) \mathbf{v}_i = \sigma_i^2 \mathbf{v}_i$$

and the *score* vector \mathbf{u}_i is given by

$$A\mathbf{v}_i = \sigma_i \mathbf{u}_i$$

In process analysis, the columns of A represent different measurement techniques (temperatures, pressures, etc.) and the rows represent the measurement output at different times. In that case

the columns of A are adjusted to have a zero mean and a variance of 1.0 (by dividing each entry in the column by the variance of the column). The goal is to represent the essential variation of the process with as few variables as possible. The $\mathbf{u}_i, \mathbf{v}_i$ pairs are arranged in descending order according to the associated σ_i . The σ_i can be thought of as the variance, and the $\mathbf{u}_i, \mathbf{v}_i$ pair captures the greatest amount of variation in the data. Instead of having to deal with n variables, one can capture most of the variation of the

data by using only the first few pairs. An excellent example of this is given by Wise, B. M., and B. R. Kowalski, "Process Chemometrics," Chap. 8 in *Process Analytical Chemistry*, F. McLennan and B. Kowalski (eds.), Blackie Academic & Professional, London (1995). When modeling a slurry-fed ceramic melter, they were able to capture 97 percent of the variation by using only four eigenvalues and eigenvectors, even though there were 16 variables (columns) measured.

NUMERICAL APPROXIMATIONS TO SOME EXPRESSIONS

APPROXIMATION IDENTITIES

For the following relationships the sign \cong means approximately equal to, when X is small. These equations are derived by using a Taylor's series (see "Series Summation and Identities").

Approximation	Approximation
$\frac{1}{1 \pm X} \cong 1 \mp X$	$\sqrt{1 \pm X} \cong 1 \pm \frac{X}{2}$

Approximation	Approximation
$(1 \pm X)^n \cong 1 \pm nX$	$(1 \pm X)^{-n} \cong 1 \mp nX$
$(a \pm X)^2 \cong a^2 \pm 2aX$	$e^x \cong 1 + X$
$\sin X \cong X(X \text{ rad})$	$\tan X \cong X$
$\sqrt{Y(Y + X)} \cong \frac{2Y + X}{2}$	$\sqrt{Y^2 + X^2} \cong Y + \frac{X^2}{2Y} \left(\frac{X}{Y} \text{ small}\right)$

NUMERICAL ANALYSIS AND APPROXIMATE METHODS

REFERENCES: Buchanan, G. R., *Schaum's Outline of Finite Element Analysis*, McGraw-Hill, New York (1995); Burden, R. L., J. D. Faires, and A. C. Reynolds, *Numerical Analysis*, 8th ed., Brookes Cole (2004); Chapra, S. C., and R. P. Canal, *Numerical Methods for Engineers*, 5th ed., McGraw-Hill, New York (2006); Finlayson, B. A., *Nonlinear Analysis in Chemical Engineering*, McGraw-Hill (1980), Ravenna Park (2003); Finlayson, B. A., and L. T. Biegler, "Mathematics in Chemical Engineering," *Ullmann's Encyclopedia of Industrial Chemistry*, vol. 20, VCH, Weinheim (2006); Gunzburger, M. D., *Finite Element Methods for Viscous Incompressible Flows*, Academic Press (1989); Kardestuncer, H., and D. H. Norrie (eds.), *Finite Element Handbook*, McGraw-Hill, New York (1987); Lau, H. T., *A Numerical Library in C for Scientists and Engineers*, CRC Press (1994); Lau, H. T., *A Numerical Library in Java for Scientists and Engineers*, CRC Press (2004); Morton, K. W., and D. F. Mayers, *Numerical Solution of Partial Differential Equations*, Cambridge University Press (1994); Press, W. H., et al., *Numerical Recipes*, Cambridge University Press, Cambridge (1986); Quarteroni, A., and A. Valli, *Numerical Approximation of Partial Differential Equations*, Springer (1997); Reddy, J. N., and D. K. Gartling, *The Finite Element Method in Heat Transfer and Fluid Dynamics*, 2d ed., CRC Press (2000); Scheid, F., *Schaum's Outline of Numerical Analysis*, 2d ed., McGraw-Hill, New York (1989); Schiesser, W. E., *The Numerical Method of Lines*, Academic Press (1991); Shampine, L., *Numerical Solution of Ordinary Differential Equations*, Chapman & Hall (1994); Zienkiewicz, O. C., R. L. Taylor, and J. Z. Zhu, *The Finite Element Method: Its Basis and Fundamentals*, vol. 1, 6th ed., Elsevier Butterworth-Heinemann (2005); Zienkiewicz, O. C., and R. L. Taylor, *The Finite Element Method: Solid Mechanics*, vol. 2, 5th ed., Butterworth-Heinemann (2000); Zienkiewicz, O. C., and R. L. Taylor, *The Finite Element Method: Fluid Mechanics*, vol. 2, 5th ed., Butterworth-Heinemann (2000).

INTRODUCTION

The goal of approximate and numerical methods is to provide convenient techniques for obtaining useful information from mathematical formulations of physical problems. Often this mathematical statement is not solvable by analytical means. Or perhaps analytic solutions are available but in a form that is inconvenient for direct interpretation. In the first case it is necessary either to attempt to approximate the problem satisfactorily by one which will be amenable to analysis, to obtain an approximate solution to the original problem by numerical means, or to use the two techniques in combination.

Numerical techniques therefore do not yield exact results in the sense of the mathematician. Since most numerical calculations are inexact, the concept of error is an important feature. The error associated with an approximate value is defined as

$$\text{True value} = \text{approximate value} + \text{error}$$

The four sources of error are as follows:

1. *Gross errors.* These result from unpredictable human, mechanical, or electrical mistakes.
2. *Round-off errors.* These are the consequence of using a number specified by m correct digits to approximate a number which requires more than m digits for its exact specification. For example, approximate the irrational number $\sqrt{2}$ by 1.414. Such errors are often present in experimental data, in which case they may be called inherent errors, due either to empiricism or to the fact that the computer dictates the number of digits. Such errors may be especially damaging in areas such as matrix inversion or the numerical solution of partial differential equations when the number of algebraic operations is extremely large.
3. *Truncation errors.* These errors arise from the substitution of a finite number of steps for an infinite sequence of steps which would yield the exact result. To illustrate this error consider the infinite series for e^{-x} : $e^{-x} = 1 - x + x^2/2 - x^3/6 + E_T(x)$, where E_T is the truncation error, $E_T = (1/24)e^{-\epsilon}x^4$, $0 < \epsilon < x$. If x is positive, ϵ is also positive. Hence $e^{-\epsilon} < 1$. The approximation $e^{-x} \approx 1 - x + x^2/2 - x^3/6$ is in error by a positive amount smaller than $(1/24)x^4$.
4. *Inherited errors.* These arise as a result of errors occurring in the previous steps of the computational algorithm.

The study of errors in a computation is related to the theory of probability. In what follows a relation for the error will be given in certain instances.

A variety of general-purpose computer programs are available commercially. Mathematica (<http://www.wolfram.com/>), Maple (<http://www.maplesoft.com/>), and Mathcad (<http://www.mathcad.com/>) all have the capability of doing symbolic manipulation so that algebraic solutions can be obtained. For example, Mathematica can solve some ordinary and partial differential equations analytically; Maple can make simple graphs and do linear algebra and simple computations; and Mathcad can do simple calculations. In this section, examples are given for the use of Matlab (<http://www.mathworks.com/>), which is a package of numerical analysis tools, some of which are accessed by simple commands and others of which are accessed by writing programs in C. Spreadsheets can also be used to solve certain problems, and these are described below too. A popular program used in chemical engineering education is Polymath (<http://www.polymath-software.com/>), which can numerically solve sets of linear or nonlinear equations, ordinary differential equations as initial-value problems, and perform data analysis and regression.

NUMERICAL SOLUTION OF LINEAR EQUATIONS

See the section entitled “Matrix Algebra and Matrix Computation.”

NUMERICAL SOLUTION OF NONLINEAR EQUATIONS IN ONE VARIABLE

Special Methods for Polynomials Consider a polynomial equation of degree n :

$$P(x) = a_0x^n + a_1x^{n-1} + a_2x^{n-2} + \dots + a_{n-1}x + a_n = 0 \quad (3-72)$$

with real coefficients. $P(x)$ has exactly n roots, which may be real or complex. If the roots are complex, they occur in pairs with their complex conjugates.

One can obtain an upper and lower bound for the real roots by the following device: If $a_0 > 0$ in Eq. (3-72) and if in Eq. (3-72) the first negative coefficient is preceded by k coefficients which are positive or zero, and if G is the greatest of the absolute values of the negative coefficients, then each real root is less than $1 + \sqrt[k]{G/a_0}$.

Example $P(x) = x^5 + 3x^4 - 7x^3 - 40x + 2 = 0$. Here $a_0 = 1$, $G = 40$, and $k = 3$ since we must supply 0 as the coefficient for x^3 . Thus $1 + \sqrt[3]{40} \approx 4.42$ is an upper bound for the real roots. The largest real root is 2.19.

A lower bound to the real roots may be found by applying the criterion to the equation $P(-x)$.

Example $P(-x) = -x^5 + 3x^4 - 7x^3 + 40x + 2 = 0$, which is equivalent to $x^5 - 3x^4 + 7x^3 - 40x - 2 = 0$ since a_0 must be +. Then $a_0 = 1$, $G = 40$, and $k = 1$. Hence $-(1 + 40) = -41$ is a lower bound. The smallest real root is -3.41 . Thus all real roots are between -41 and 4.42.

One last result is helpful in getting an estimate of how many positive and negative real roots there are.

Descartes Rule The number of positive real roots of a polynomial with real coefficients is either equal to the number of changes in sign v or is less than v by a positive even integer. The number of negative roots of $P(x)$ is either equal to the number of variations of sign of $P(-x)$ or is less than this by a positive even integer.

Example $f(x) = x^4 - 13x^2 + 4x - 2 = 0$ has three changes in sign; therefore, there are either three or one positive root. $f(-x) = x^4 - 13x^2 - 4x - 2$ has one change in sign. Therefore, there is one negative root. Using MATLAB, one defines the vector

$$C(i) = a_{i-1}$$

and uses the command roots(c) to find all the roots.

Methods for Nonlinear Equations in One Variable

Successive Substitutions Let $f(x) = 0$ be the nonlinear equation to be solved. If this is rewritten as $x = F(x)$, then an iterative scheme can be set up in the form $x_{k+1} = F(x_k)$. To start the iteration an initial guess must be obtained graphically or otherwise. The convergence or divergence of the procedure depends upon the method of writing $x = F(x)$, of which there will usually be several forms. However, if a is a root of $f(x) = 0$, and if $|F'(a)| < 1$, then for any initial approximation sufficiently close to a , the method converges to a . This process is called first order because the error in x_{k+1} is proportional to the first power of the error in x_k for large k .

One way of writing the equation is $x_{k+1} = x_k + \beta f(x_k)$. The choice of β is made such that $|1 + \beta df/dx(a)| < 1$. Convergence is guaranteed by the theorem given for simultaneous equations.

Methods of Perturbation Let $f(x) = 0$ be the equation. In general, the iterative relation is

$$x_{k+1} = x_k - [f(x_k)/\alpha_k]$$

where the iteration begins with x_0 as an initial approximation and α_k as some functional, derived below.

Newton-Raphson Procedure This variant chooses $\alpha_k = f'(x_k)$ where $f' = df/dx$ and geometrically consists of replacing the graph of

$f(x)$ by the tangent line at $x = x_k$ in each successive step. If $f'(x)$ and $f''(x)$ have the same sign throughout an interval $a \leq x \leq b$ containing the solution, with $f(a), f(b)$ of opposite signs, then the process converges starting from any x_0 in the interval $a \leq x \leq b$. The process is second order.

Example $f(x) = x - 1 + \frac{(0.5)^x - 0.5}{0.3}$

$$f'(x) = 1 - 2.3105[0.5]^x$$

An approximate root (obtained graphically) is 2.

Step k	x_k	$f(x_k)$	$f'(x_k)$
0	2	0.1667	0.4224
1	1.6054	0.0342	0.2407
2	1.4632	0.0055	0.1620

Method of False Position This variant is commenced by finding x_0 and x_1 such that $f(x_0), f(x_1)$ are of opposite signs. Then $\alpha_1 =$ slope of secant line joining $[x_0, f(x_0)]$ and $[x_1, f(x_1)]$ so that

$$x_2 = x_1 - \frac{x_1 - x_0}{f(x_1) - f(x_0)} f(x_1)$$

In each of the following steps α_k is the slope of the line joining $[x_k, f(x_k)]$ to the most recently determined point where $f(x_i)$ has the opposite sign from that of $f(x_k)$. This method is of first order. If one uses the most recently determined point (regardless of sign), the method is a secant method.

Method of Wegstein This is a variant of the method of successive substitutions which forces and/or accelerates convergence. The iterative procedure $x_{k+1} = F(x_k)$ is revised by setting $\hat{x}_{k+1} = F(x_k)$ and then taking $x_{k+1} = qx_k + (1 - q)\hat{x}_{k+1}$, where q is a suitably chosen number which may be taken as constant throughout or may be adjusted at each step. Wegstein found that suitable q 's are:

Behavior of successive substitution process		Range of optimum q
Oscillatory convergence		$0 < q < 1/2$
Oscillatory divergence	without Wegstein	$1/2 < q < 1$
Monotonic convergence		$q < 0$
Monotonic divergence	without Wegstein	$1 < q$

At each step q may be calculated to give a locally optimum value by setting

$$q = \frac{\hat{x}_{k+1} - \hat{x}_k}{\hat{x}_{k+1} - 2\hat{x}_k + \hat{x}_{k-1}}$$

The Wegstein method is a secant method applied to $g(x) \equiv x - F(x)$. In Microsoft Excel, roots are found by using Goal Seek or Solver. Assign one cell to be x , put the equation for $f(x)$ in another cell, and let Goal Seek or Solver find the value of x that makes the equation cell zero. In MATLAB, the process is similar except that a function (m-file) is defined and the command fzero('f',x0) provides the solution x , starting from the initial guess x_0 .

METHODS FOR MULTIPLE NONLINEAR EQUATIONS

Method of Successive Substitutions Write a system of equations as

$$\alpha_i = f_i(\alpha), \quad \text{or } \alpha = f(\alpha)$$

The following theorem guarantees convergence. Let α be the solution to $\alpha_i = f_i(\alpha)$. Assume that given $h > 0$, there exists a number $0 < \mu < 1$ such that

$$\sum_{j=1}^n \left| \frac{\partial f_i}{\partial x_j} \right| \leq \mu \quad \text{for } |x_i - \alpha_i| < h, \quad i = 1, \dots, n$$

$$x_i^{k+1} = f_i(x_i^k)$$

Then $x_i^k \rightarrow \alpha_i$

as k increases [see Finlayson (2003)].

Newton-Raphson Method To solve the set of equations

$$F_i(x_1, x_2, \dots, x_n) = 0, \text{ or } F_i(\{x_j\}) = 0, \text{ or } F_i(\mathbf{x}) = 0$$

one uses a truncated Taylor series to give

$$0 = F_i(\{x^k\}) + \sum_{j=1}^n \frac{\partial F_i}{\partial x_j} \Big|_{x^k} (x_j^{k+1} - x_j^k)$$

Thus one solves iteratively from one point to another.

$$\sum_{j=1}^n A_{ij}^k (x_j^{k+1} - x_j^k) = -F_i(\{x^k\})$$

where

$$A_{ij}^k = \frac{\partial F_i}{\partial x_j} \Big|_{x^k}$$

This method requires solution of sets of linear equations until the functions are zero to some tolerance or the changes of the solution between iterations is small enough. Convergence is guaranteed provided the norm of the matrix **A** is bounded, **F(x)** is bounded for the initial guess, and the second derivative of **F(x)** with respect to all variables is bounded. See Finlayson (2003).

Method of Continuity (Homotopy) In the case of *n* equations in *n* unknowns, when *n* is large, determining the approximate solution may involve considerable effort. In such a case the method of continuity is admirably suited for use on digital computers. It consists basically of the introduction of an extra variable into the *n* equations

$$f_i(x_1, x_2, \dots, x_n) = 0 \quad i = 1, \dots, n \quad (3-73)$$

and replacing them by

$$f_i(x_1, x_2, \dots, x_n, \lambda) = 0 \quad i = 1, \dots, n \quad (3-74)$$

where λ is introduced in such a way that the functions (3-74) depend in a simple way upon λ and reduce to an easily solvable system for $\lambda = 0$ and to the original equations (3-73) for $\lambda = 1$. A system of ordinary differential equations, with independent variable λ , is then constructed by differentiating Eqs. (3-74) with respect to λ . There results

$$\sum_{j=1}^n \frac{\partial f_i}{\partial x_j} \frac{dx_j}{d\lambda} + \frac{\partial f_i}{\partial \lambda} = 0 \quad (3-75)$$

where x_1, \dots, x_n are considered as functions of λ . Equations (3-75) are integrated, with initial conditions obtained from Eqs. (3-74) with $\lambda = 0$, from $\lambda = 0$ to $\lambda = 1$. If the solution can be continued to $\lambda = 1$, the values of x_1, \dots, x_n for $\lambda = 1$ will be a solution of the original equations. If the integration becomes infinite, the parameter λ must be introduced in a different fashion. Integration of the differential equations (which are usually nonlinear in λ) may be accomplished by using techniques described under "Numerical Solution of Ordinary Differential Equations."

Other Methods Other methods can be found in the literature. See Chan, T. F. C., and H. B. Keller, *SIAM J. Sci. Stat. Comput.* **3**:173-194 (1982); Seader, J. D., "Computer Modeling of Chemical Processes," *AIChE Monograph Series* **81**(15) (1986).

INTERPOLATION AND FINITE DIFFERENCES

Linear Interpolation If a function $f(x)$ is approximately linear in a certain range, then the ratio

$$\frac{f(x_1) - f(x_0)}{x_1 - x_0} = f[x_0, x_1]$$

is approximately independent of x_0, x_1 in the range. The linear approximation to the function $f(x), x_0 < x < x_1$ then leads to the interpolation formula

$$\begin{aligned} f(x) &\approx f(x_0) + (x - x_0)f[x_0, x_1] \\ &\approx f(x_0) + \frac{x - x_0}{x_1 - x_0} [f(x_1) - f(x_0)] \\ &\approx \frac{1}{x_1 - x_0} [(x_1 - x)f(x_0) - (x_0 - x)f(x_1)] \end{aligned}$$

Divided Differences of Higher Order and Higher-Order Interpolation The first-order divided difference $f[x_0, x_1]$ was defined previously. Divided differences of second and higher order are defined iteratively by

$$\begin{aligned} f[x_0, x_1, x_2] &= \frac{f[x_1, x_2] - f[x_0, x_1]}{x_2 - x_0} \\ &\vdots \\ f[x_0, x_1, \dots, x_k] &= \frac{f[x_1, \dots, x_k] - f[x_0, x_1, \dots, x_{k-1}]}{x_k - x_0} \end{aligned}$$

and a convenient form for computational purposes is

$$f[x_0, x_1, \dots, x_k] = \sum_{j=0}^k \frac{f(x_j)}{(x_j - x_0)(x_j - x_1) \dots (x_j - x_k)}$$

for any $k \geq 0$, where the ' means that the term $(x_j - x_j)$ is omitted in the denominator. For example,

$$f[x_0, x_1, x_2] = \frac{f(x_0)}{(x_0 - x_1)(x_0 - x_2)} + \frac{f(x_1)}{(x_1 - x_0)(x_1 - x_2)} + \frac{f(x_2)}{(x_2 - x_0)(x_2 - x_1)}$$

If the accuracy afforded by a linear approximation is inadequate, a generally more accurate result may be based upon the assumption that $f(x)$ may be approximated by a polynomial of degree 2 or higher over certain ranges. This assumption leads to Newton's fundamental interpolation formula with divided differences

$$\begin{aligned} f(x) \approx &f(x_0) + (x - x_0)f[x_0, x_1] + (x - x_0)(x - x_1)f[x_0, x_1, x_2] \\ &+ \dots + (x - x_0)(x - x_1) \dots (x - x_{n-1})f[x_0, x_1, \dots, x_n] + E_n(x) \end{aligned}$$

where $E_n(x) = \text{error} = \frac{1}{(n + 1)!} f^{n+1}(\epsilon)\pi(x)$

where minimum $(x_0, \dots, x) < \epsilon < \text{maximum } (x_0, x_1, \dots, x_n, x)$ and $\pi(x) = (x - x_0)(x - x_1) \dots (x - x_n)$. In order to use the previous equation most effectively one may first form a divided-difference table. For example, for third-order interpolation the difference table is

x_0	$f(x_0)$	>	$f[x_0, x_1]$	>	$f[x_0, x_1, x_2]$	>	$f[x_0, x_1, x_2, x_3]$
x_1	$f(x_1)$	>	$f[x_1, x_2]$	>	$f[x_1, x_2, x_3]$	>	$f[x_1, x_2, x_3]$
x_2	$f(x_2)$	>	$f[x_2, x_3]$	>	$f[x_2, x_3]$	>	$f[x_2, x_3]$
x_3	$f(x_3)$	>	$f[x_3]$	>	$f[x_3]$	>	$f[x_3]$

where each entry is given by taking the difference between diagonally adjacent entries to the left, divided by the abscissas corresponding to the ordinates intercepted by the diagonals passing through the calculated entry.

Equally Spaced Forward Differences If the ordinates are equally spaced, i.e., $x_j - x_{j-1} = \Delta x$ for all *j*, then the first differences are denoted by $\Delta f(x_0) = f(x_1) - f(x_0)$ or $\Delta y_0 = y_1 - y_0$, where $y = f(x)$. The differences of these first differences, called second differences, are denoted by $\Delta^2 y_0, \Delta^2 y_1, \dots, \Delta^2 y_n$. Thus

$$\Delta^2 y_0 = \Delta y_1 - \Delta y_0 = y_2 - y_1 - y_1 + y_0 = y_2 - 2y_1 + y_0$$

And in general

$$\Delta^j y_0 = \sum_{n=0}^j (-1)^n \binom{j}{n} y_{j-n}$$

where $\binom{j}{n} = \frac{j!}{n!(j-n)!} = \text{binomial coefficients}$.

If the ordinates are equally spaced,

$$\begin{aligned} x_{n+1} - x_n &= \Delta x \\ y_n &= y(x_n) \end{aligned}$$

then the first and second differences are denoted by

$$\begin{aligned} \Delta y_n &= y_{n+1} - y_n \\ \Delta^2 y_n &= \Delta y_{n+1} - \Delta y_n = y_{n+2} - 2y_{n+1} + y_n \end{aligned}$$

A new variable is defined

$$\alpha = \frac{x - x_0}{\Delta x}$$

and the finite interpolation formula through the points y_0, y_1, \dots, y_n is written as follows:

$$y_\alpha = y_0 + \alpha \Delta y_0 + \frac{\alpha(\alpha-1)}{2!} \Delta^2 y_0 + \dots + \frac{\alpha(\alpha-1) \dots (\alpha-n+1)}{n!} \Delta^n y_0 \tag{3-76}$$

Keeping only the first two terms gives a straight line through (x_0, y_0) – (x_1, y_1) ; keeping the first three terms gives a quadratic function of position going through those points plus (x_2, y_2) . The value $\alpha = 0$ gives $x = x_0$; $\alpha = 1$ gives $x = x_1$, and so on.

Equally Spaced Backward Differences Backward differences are defined by

$$\begin{aligned} \nabla y_n &= y_n - y_{n-1} \\ \nabla^2 y_n &= \nabla y_n - \nabla y_{n-1} = y_n - 2y_{n-1} + y_{n-2} \end{aligned}$$

The interpolation polynomial of order n through the points $y_0, y_{-1}, \dots, y_{-n}$ is

$$y_\alpha = y_0 + \alpha \nabla y_0 + \frac{\alpha(\alpha+1)}{2!} \nabla^2 y_0 + \dots + \frac{\alpha(\alpha+1) \dots (\alpha+n-1)}{n!} \nabla^n y_0$$

The value of $\alpha = 0$ gives $x = x_0$; $\alpha = -1$ gives $x = x_{-1}$, and so on. Alternatively, the interpolation polynomial of order n through the points $y_1, y_0, y_{-1}, \dots, y_{-n}$ is

$$y_\alpha = y_1 + (\alpha-1) \nabla y_1 + \frac{\alpha(\alpha-1)}{2!} \nabla^2 y_1 + \dots + \frac{(\alpha-1) \alpha (\alpha+1) \dots (\alpha+n-2)}{n!} \nabla^n y_1 \tag{3-77}$$

Now $\alpha = 1$ gives $x = x_1$; $\alpha = 0$ gives $x = x_0$.

Central Differences The central difference denoted by

$$\begin{aligned} \delta f(x) &= f\left(x + \frac{h}{2}\right) - f\left(x - \frac{h}{2}\right) \\ \delta^2 f(x) &= \delta f\left(x + \frac{h}{2}\right) - \delta f\left(x - \frac{h}{2}\right) = f(x+h) - 2f(x) + f(x-h) \\ \delta^n f(x) &= \delta^{n-1} f\left(x + \frac{h}{2}\right) - \delta^{n-1} f\left(x - \frac{h}{2}\right) \end{aligned}$$

is useful for calculating at the interior points of tabulated data.

Lagrange Interpolation Formulas A global polynomial is defined over the entire region of space

$$P_m(x) = \sum_{j=0}^m c_j x^j$$

This polynomial is of degree m (highest power is x^m) and order $m + 1$ ($m + 1$ parameters $\{c_j\}$). If we are given a set of $m + 1$ points

$$y_1 = f(x_1), y_2 = f(x_2), \dots, y_{m+1} = f(x_{m+1})$$

then Lagrange's formula gives a polynomial of degree m that goes through the $m + 1$ points:

$$\begin{aligned} P_m(x) &= \frac{(x-x_2)(x-x_3) \dots (x-x_{m+1})}{(x_1-x_2)(x_1-x_3) \dots (x_1-x_{m+1})} y_1 \\ &+ \frac{(x-x_1)(x-x_3) \dots (x-x_{m+1})}{(x_2-x_1)(x_2-x_3) \dots (x_2-x_{m+1})} y_2 + \dots \\ &+ \frac{(x-x_1)(x-x_2) \dots (x-x_{m+1})}{(x_{m+1}-x_1)(x_{m+1}-x_2) \dots (x_{m+1}-x_m)} y_{m+1} \end{aligned}$$

Note that each coefficient of y_j is a polynomial of degree m that vanishes at the points $\{x_j\}$ (except for one value of j) and takes the value of

1.0 at that point:

$$P_m(x_j) = y_j, \quad j = 1, 2, \dots, m + 1$$

If the function $f(x)$ is known, the error in the approximation is, per Anderson, E., et al., LAPACK Users' Guide, SIAM(1992),

$$|\text{error}(x)| \leq \frac{|x_{m+1} - x_1|^{m+1}}{(m+2)!} \max_{x_1 \leq x \leq x_{m+1}} |f^{(m+2)}(x)|$$

The evaluation of $P_m(x)$ at a point other than at the defining points can be made with Neville's algorithm [Press et al. (1986)]. Let P_1 be the value at x of the unique function passing through the point (x_1, y_1) ; or $P_1 = y_1$. Let P_{12} be the value at x of the unique polynomial passing through the points x_1 and x_2 . Likewise, $P_{jk \dots r}$ is the unique polynomial passing through the points x_j, x_k, \dots, x_r . Then use the table

x_1	$y_1 = P_1$			
x_2	$y_2 = P_2$	P_{12}		
x_3	$y_3 = P_3$	P_{23}	P_{123}	
x_4	$y_4 = P_4$	P_{34}	P_{234}	P_{1234}

These entries are defined using

$$P_{i(i+1) \dots (i+m)} = \frac{(x - x_{i+m}) P_{i(i+1) \dots (i+m-1)} + (x_i - x) P_{(i+1)(i+2) \dots (i+m)}}{x_i - x_{i+m}}$$

For example, consider P_{1234} . The terms on the right-hand side involve P_{123} and P_{234} . The "parents," P_{123} and P_{234} , already agree at points 2 and 3. Here $i = 1, m = 3$; thus, the parents agree at $x_{i+1}, \dots, x_{i+m-1}$ already. The formula makes $P_{i(i+1) \dots (i+m)}$ agree with the function at the additional points x_{i+m} and x_i . Thus, $P_{i(i+1) \dots (i+m)}$ agrees with the function at all the points $\{x_i, x_{i+1}, \dots, x_{i+m}\}$.

Spline Functions Splines are functions that match given values at the points x_1, \dots, x_{NT} and have continuous derivatives up to some order at the knots, or the points x_2, \dots, x_{NT-1} . Cubic splines are most common; see de Boor, C., *A Practical Guide to Splines*, Springer (1978). The function is represented by a cubic polynomial within each interval (x_i, x_{i+1}) and has continuous first and second derivatives at the knots. Two more conditions can be specified arbitrarily. These are usually the second derivatives at the two end points, which are commonly taken as zero; this gives the natural cubic splines.

Take $y_i = y(x_i)$ at each of the points x_i , and let $\Delta x_i = x_{i+1} - x_i$. Then, in the interval (x_i, x_{i+1}) , the function is represented as a cubic polynomial.

$$C_i(x) = a_{0i} + a_{1i}x + a_{2i}x^2 + a_{3i}x^3$$

The interpolating function takes on specified values at the knots and has continuous first and second derivatives at the knots. Within the i th interval, the function is

$$\begin{aligned} C_i(x) &= C_i(x_i) + C'_i(x_i)(x - x_i) + C''_i(x_i) \frac{(x - x_i)^2}{2\Delta x_i} \\ &+ [C''_i(x_{i+1}) - C''_i(x_i)] \frac{(x - x_i)^3}{6\Delta x_i} \end{aligned}$$

where $C_i(x_i) = y_i$. The second derivative $C''_i(x_i) = y''_i$ is found by solving the following tridiagonal system of equations:

$$y''_{i-1} \Delta x_{i-1} + y''_i 2(\Delta x_{i-1} + \Delta x_i) + y''_{i+1} \Delta x_i = -6 \left(\frac{y_i - y_{i-1}}{\Delta x_{i-1}} - \frac{y_{i+1} - y_i}{\Delta x_i} \right)$$

Since the continuity conditions apply only for $i = 2, \dots, NT - 1$, we have only $NT - 2$ conditions for the NT values of y''_i . Two additional conditions are needed, and these are usually taken as the value of the second derivative at each end of the domain, y''_1, y''_{NT} . If these values are zero, we get the natural cubic splines; they can also be set to achieve some other purpose, such as making the first derivative match some desired condition at the two ends. With these values taken as zero in the natural cubic spline, we have a $NT - 2$ system of tridiagonal equations, which is easily solved. Once the second derivatives are

known at each of the knots, the first derivatives are given by

$$y'_i = \frac{y_{i+1} - y_i}{\Delta x_i} - y''_i \frac{\Delta x_i}{3} - y''_{i+1} \frac{\Delta x_i}{6}$$

The function itself is then known within each element.

NUMERICAL DIFFERENTIATION

Numerical differentiation should be avoided whenever possible, particularly when data are empirical and subject to appreciable observation errors. Errors in data can affect numerical derivatives quite strongly; i.e., differentiation is a roughening process. When such a calculation must be made, it is usually desirable first to smooth the data to a certain extent.

Use of Interpolation Formula If the data are given over equidistant values of the independent variable x , an interpolation formula such as the Newton formula [Eq. (3-76) or (3-77)] may be used and the resulting formula differentiated analytically. If the independent variable is not at equidistant values, then Lagrange's formulas must be used. By differentiating three-point Lagrange interpolation formulas the following differentiation formulas result for equally spaced tabular points:

Three-Point Formulas Let x_0, x_1, x_2 be the three points.

$$\begin{aligned} f'(x_0) &= \frac{1}{2h} [-3f(x_0) + 4f(x_1) - f(x_2)] + \frac{h^2}{3} f'''(\epsilon) \\ f'(x_1) &= \frac{1}{2h} [-f(x_0) + f(x_2)] - \frac{h^2}{6} f'''(\epsilon) \\ f'(x_2) &= \frac{1}{2h} [f(x_0) - 4f(x_1) + 3f(x_2)] + \frac{h^2}{3} f'''(\epsilon) \end{aligned}$$

where the last term is an error term $\min_j x_j < \epsilon < \max_j x_j$.

Smoothing Techniques These techniques involve the approximation of the tabular data by a least-squares fit of the data by using some known functional form, usually a polynomial (for the concept of least squares see "Statistics"). In place of approximating $f(x)$ by a single least-squares polynomial of degree n over the entire range of the tabulation, it is often desirable to replace each tabulated value by the value taken on by a least-squares polynomial of degree n relevant to a subrange of $2M + 1$ points centered, when possible, at the point for which the entry is to be modified. Thus each smoothed value replaces a tabulated value. Let $f_j = f(x_j)$ be the tabular points and $y_j =$ smoothed values.

First-Degree Least Squares with Three Points

$$\begin{aligned} y_0 &= 1/6[5f_0 + 2f_1 - f_2] \\ y_1 &= 1/3[f_0 + f_1 + f_2] \\ y_2 &= 1/6[-f_0 + 2f_1 + 5f_2] \end{aligned}$$

The derivatives at all the points are

$$f'_0 = f'_1 = f'_2 = \frac{1}{2}h [y_2 - y_1]$$

Second-Degree Least Squares with Five Points For five evenly spaced points $x_{-2}, x_{-1}, x_0, x_1,$ and x_2 (separated by distance h) and their ordinates $f_{-2}, f_{-1}, f_0, f_1,$ and f_2 , assume a parabola is fit by least squares. Then the derivative at the center point is

$$f'_0 = 1/10h [-2f_{-2} - f_{-1} + f_1 + 2f_2]$$

The derivatives at the other points are

$$\begin{aligned} f'_{-2} &= 1/70h [-54f_{-2} + 13f_{-1} + 40f_0 + 27f_1 - 26f_2] \\ f'_{-1} &= 1/70h [-34f_{-2} + 3f_{-1} + 20f_0 + 17f_1 - 6f_2] \\ f'_1 &= 1/70h [6f_{-2} - 17f_{-1} - 20f_0 - 3f_1 + 34f_2] \\ f'_2 &= 1/70h [26f_{-2} - 27f_{-1} - 40f_0 - 13f_1 + 54f_2] \end{aligned}$$

Numerical Derivatives The results given above can be used to obtain numerical derivatives when solving problems on the computer,

in particular for the Newton-Raphson method and homotopy methods. Suppose one has a program, subroutine, or other function evaluation device that will calculate f given x . One can estimate the value of the first derivative at x_0 using

$$\left. \frac{df}{dx} \right|_{x_0} \approx \frac{f[x_0(1 + \epsilon)] - f[x_0]}{\epsilon x_0}$$

(a first-order formula) or

$$\left. \frac{df}{dx} \right|_{x_0} \approx \frac{f[x_0(1 + \epsilon)] - f[x_0(1 - \epsilon)]}{2\epsilon x_0}$$

(a second-order formula). The value of ϵ is important; a value of 10^{-6} is typical, but smaller or larger values may be necessary depending on the computer precision and the application. One must also be sure that the value of x_0 is not zero and use a different increment in that case.

NUMERICAL INTEGRATION (QUADRATURE)

A multitude of formulas have been developed to accomplish numerical integration, which consists of computing the value of a definite integral from a set of numerical values of the integrand.

Newton-Cotes Integration Formulas (Equally Spaced Ordinates) for Functions of One Variable The definite integral $\int_a^b f(x) dx$ is to be evaluated.

Trapezoidal Rule This formula consists of subdividing the interval $a \leq x \leq b$ into n subintervals a to $a + h$, $a + h$ to $a + 2h$, . . . and replacing the graph of $f(x)$ by the result of joining the ends of adjacent ordinates by line segments. If $f_j = f(x_j) = f(a + jh), f_0 = f(a), f_n = f(b)$, the integration formula is

$$\int_a^b f(x) dx = \frac{h}{2} [f_0 + 2f_1 + 2f_2 + \dots + 2f_{n-1} + f_n] + E_n$$

where $|E_n| = \frac{nh^3}{12} |f'''(\epsilon)| = \frac{(b-a)^3}{12n^2} |f'''(\epsilon)| \quad a < \epsilon < b$

This procedure is not of high accuracy. However, if $f'''(x)$ is continuous in $a < x < b$, the error goes to zero as $1/n^2, n \rightarrow \infty$.

Parabolic Rule (Simpson's Rule) This procedure consists of subdividing the interval $a < x < b$ into $n/2$ subintervals, each of length $2h$, where n is an even integer. By using the notation as above the integration formula is

$$\int_a^b f(x) dx = \frac{h}{3} [f_0 + 4f_1 + 2f_2 + 4f_3 + \dots + 4f_{n-3} + 2f_{n-2} + 4f_{n-1} + f_n] + E_n$$

where $|E_n| = \frac{nh^5}{180} |f^{(IV)}(\epsilon)| = \frac{(b-a)^5}{180n^4} |f^{(IV)}(\epsilon)| \quad a < \epsilon < b$

This method approximates $f(x)$ by a parabola on each subinterval. This rule is generally more accurate than the trapezoidal rule. It is the most widely used integration formula.

Gaussian Quadrature Gaussian quadrature provides a highly accurate formula based on irregularly spaced points, but the integral needs to be transformed onto the interval 0 to 1.

$$x = a + (b - a)u, \quad dx = (b - a)du$$

$$\int_a^b f(x) dx = (b - a) \int_0^1 f(u) du$$

$$\int_0^1 f(u) du = \sum_{i=1}^m W_i f(u_i)$$

The quadrature is exact when f is a polynomial of degree $2m - 1$ in x . Because there are m weights and m Gauss points, we have $2m$ parameters that are chosen to exactly represent a polynomial of degree

$2m - 1$, which has $2m$ parameters. The Gauss points and weights are given in the table.

Gaussian Quadrature Points and Weights

m	u_i	W_i
2	0.21132 48654	0.50000 00000
	0.78867 51346	0.50000 00000
3	0.11270 16654	0.27777 77778
	0.50000 00000	0.44444 44445
	0.88729 83346	0.27777 77778
4	0.06943 18442	0.17392 74226
	0.33000 94783	0.32607 25774
	0.66999 05218	0.32607 25774
	0.93056 81558	0.17392 74226
5	0.04691 00771	0.11846 34425
	0.23076 53450	0.23931 43353
	0.50000 00000	0.28444 44444
	0.76923 46551	0.23931 43353
	0.95308 99230	0.11846 34425

Example Calculate the value of the following integral.

$$I = \int_0^1 e^{-x} \sin x \, dx \tag{3-78}$$

Using the Gaussian quadrature formulas gives the following values for various values of m . Clearly, three internal points, requiring evaluation of the integrand at only three points, gives excellent results.

m	I
2	0.24609643062368
3	0.24583487736505
4	0.24583700444293
5	0.24583700700700

Romberg's Method Romberg's method uses extrapolation techniques to improve the answer [Press et al. (1986)]. If we let I_1 be the value of the integral obtained using interval size $h = \Delta x$, and I_2 be the value of I obtained when using interval size $h/2$, and I_0 the true value of I , then the error in a method is approximately h^m , or

$$I_1 \approx I_0 + ch^m$$

$$I_2 \approx I_0 + c\left(\frac{h}{2}\right)^m$$

Replacing the \approx by an equality (an approximation) and solving for c and I_0 gives

$$I_0 = \frac{2^m I_2 - I_1}{2^m - 1}$$

This process can also be used to obtain I_1, I_2, \dots , by halving h each time, and then calculating new estimates from each pair, calling them J_1, J_2, \dots ; that is, in the formula above, replace I_0 with J_1 . The formulas are reapplied for each pair of J to obtain K_1, K_2, \dots . The process continues until the required tolerance is obtained.

$$\begin{matrix} I_1 & I_2 & I_3 & I_4 \\ J_1 & J_2 & J_3 & \\ & K_1 & K_2 & \\ & & L_1 & \end{matrix}$$

Romberg's method is most useful for a low-order method (small m) because significant improvement is then possible.

Example Evaluate the same integral (3-78) by using the trapezoid rule and then apply the Romberg method. Use 11, 21, 41, and 81 points with $m = 2$. To achieve six-digit accuracy, any result from J_2 through L_1 is suitable, even though the base results (I_1 through I_4) are not that accurate.

$I_1 = 0.24491148225216$	$I_2 = 0.24560560017077$	$I_3 = 0.24577915369183$	$I_4 = 0.24582254357310$
$J_1 = 0.24583697281030$	$J_2 = 0.24583700486552$	$J_3 = 0.24583700686685$	
	$K_1 = 0.24583701555059$	$K_2 = 0.24583700753396$	
		$L_1 = 0.24583700486175$	

Computer Methods These methods are easily programmed in a spreadsheet program such as Microsoft Excel. In MATLAB, the trapezoid rule can be calculated by using the command `trapz(x,y)`, where x is a vector of x values x_i and y is a vector of values $y(x_i)$. Alternatively, use the commands

$$F = @(x) \exp(-x) .* \sin(x)$$

$$Q = \text{quad}(F,0,1)$$

$I_1 = 0.24491148225216$	$I_2 = 0.24560560017077$	$I_3 = 0.24577915369183$	$I_4 = 0.24582254357310$
	$J_1 = 0.24583697281030$	$J_2 = 0.24583700486552$	$J_3 = 0.24583700686685$
		$K_1 = 0.24583701555059$	$K_2 = 0.24583700753396$
			$L_1 = 0.24583700486175$

Singularities When the integrand has singularities, a variety of techniques can be tried. The integral may be divided into one part that can be integrated analytically near the singularity and another part that is integrated numerically. Sometimes a change of argument allows analytical integration. Series expansion might be helpful, too. When the domain is infinite, it is possible to use Gauss-Legendre or Gauss-Hermite quadrature. Also a transformation can be made. For example, let $u = 1/x$ and then

$$\int_a^b f(x) \, dx = \int_{1/b}^{1/a} \frac{1}{u^2} f\left(\frac{1}{u}\right) \, du \quad ab > 0$$

Two-Dimensional Formula Two-dimensional integrals can be calculated by breaking down the integral into one-dimensional integrals.

$$\int_a^b \int_{g_1(x)}^{g_2(x)} f(x, y) \, dx \, dy = \int_a^b G(x) \, dx$$

$$G(x) = \int_{g_1(x)}^{g_2(x)} f(x, y) \, dy$$

Gaussian quadrature can also be used in two dimensions, provided the integration is on a square or can be transformed to one. (Domain transformations might be used to convert the domain to a square.)

$$\int_0^1 \int_0^1 f(x, y) \, dx \, dy = \sum_{i=1}^{m_x} W_{xi} \sum_{j=1}^{m_y} W_{yj} f(x_i, y_j)$$

NUMERICAL SOLUTION OF ORDINARY DIFFERENTIAL EQUATIONS AS INITIAL VALUE PROBLEMS

A differential equation for a function that depends on only one variable, often time, is called an ordinary differential equation. The general solution to the differential equation includes many possibilities; the boundary or initial conditions are needed to specify which of those are desired. If all conditions are at one point, then the problem is an initial value problem and can be integrated from that point on. If some of the conditions are available at one point and others at another point, then the ordinary differential equations become two-point boundary value problems, which are treated in the next section. Initial value problems as ordinary differential equations arise in control of lumped parameter models, transient models of stirred tank reactors, and in all models where there are no spatial gradients in the unknowns.

A higher-order differential equation

$$y^{(n)} + F(y^{(n-1)}, y^{(n-2)}, \dots, y', y) = 0$$

with initial conditions

$$G_i(y^{(n-1)}(0), y^{(n-2)}(0), \dots, y(0), y'(0)) = 0, \quad i = 1, \dots, n$$

can be converted into a set of first-order equations using

$$y_i \equiv y^{(i-1)} = \frac{d^{(i-1)}y}{dt^{(i-1)}} = \frac{d}{dt} y^{(i-2)} = \frac{dy_{i-1}}{dt}$$

The higher-order equation can be written as a set of first-order equations.

$$\frac{dy_1}{dt} = y_2$$

$$\begin{aligned} \frac{dy_2}{dt} &= y_3 \\ \frac{dy_3}{dt} &= y_4 \\ &\dots \\ \frac{dy_n}{dt} &= -F(y_{n-1}, y_{n-2}, \dots, y_2, y_1) \end{aligned}$$

The initial conditions would have to be specified for variables $y_1(0), \dots, y_n(0)$, or equivalently $y(0), \dots, y^{(n-1)}(0)$. The set of equations is then written as

$$\frac{dy}{dt} = \mathbf{f}(\mathbf{y}, t)$$

All the methods in this section are described for a single equation; the methods apply to multiple equations.

Euler's method is first-order.

$$y^{n+1} = y^n + \Delta t f(y^n)$$

and errors are proportional to Δt . The second-order Adams-Bashforth method is

$$y^{n+1} = y^n + \frac{\Delta t}{2} [3f(y^n) - f(y^{n-1})]$$

Errors are proportional to Δt^2 , and high-order methods are available. Notice that the higher-order explicit methods require knowing the solution (or the right-hand side) evaluated at times in the past. Since these were calculated to get to the current time, this presents no problem except for starting the problem. Then it may be necessary to use Euler's method with a very small step size for several steps in order to generate starting values at a succession of time points. The error terms, order of the method, function evaluations per step, and stability limitations are listed in Finlayson (2003). The advantage of the high-order Adams-Bashforth method is that it uses only one function evaluation per step yet achieves high-order accuracy. The disadvantage is the necessity of using another method to start.

Runge-Kutta methods are explicit methods that use several function evaluations for each time step. Runge-Kutta methods are traditionally written for $f(t, y)$. The first-order Runge-Kutta method is Euler's method. A second-order Runge-Kutta method is

$$y^{n+1} = y^n + \frac{\Delta t}{2} [f^n + f(t^n + \Delta t, y^n + \Delta t f^n)]$$

while the midpoint scheme is also a second-order Runge-Kutta method.

$$y^{n+1} = y^n + \Delta t f\left(t^n + \frac{\Delta t}{2}, y^n + \frac{\Delta t}{2} f^n\right)$$

A popular fourth-order Runge-Kutta method is the Runge-Kutta-Feldberg formulas, which have the property that the method is fourth-order but achieves fifth-order accuracy. The popular integration package RKF45 is based on this method.

$$\begin{aligned} k_1 &= \Delta t f(t^n, y^n) \\ k_2 &= \Delta t f\left(t^n + \frac{\Delta t}{4}, y^n + \frac{k_1}{4}\right) \\ k_3 &= \Delta t f\left(t^n + \frac{3}{8}\Delta t, y^n + \frac{3}{32}k_1 + \frac{9}{32}k_2\right) \\ k_4 &= \Delta t f\left(t^n + \frac{12}{13}\Delta t, y^n + \frac{1932}{2197}k_1 - \frac{7200}{2197}k_2 + \frac{7296}{2197}k_3\right) \\ k_5 &= \Delta t f\left(t^n + \Delta t, y^n + \frac{439}{216}k_1 - 8k_2 + \frac{3680}{513}k_3 - \frac{845}{4104}k_4\right) \\ k_6 &= \Delta t f\left(t^n + \frac{\Delta t}{2}, y^n - \frac{8}{27}k_1 + 2k_2 - \frac{3544}{2565}k_3 + \frac{1859}{4104}k_4 - \frac{11}{40}k_5\right) \end{aligned}$$

$$\begin{aligned} y^{n+1} &= y^n + \frac{25}{216}k_1 + \frac{1408}{2565}k_3 + \frac{2197}{4104}k_4 - \frac{1}{5}k_5 \\ z^{n+1} &= y^n + \frac{16}{135}k_1 + \frac{6656}{12825}k_3 + \frac{28561}{56430}k_4 - \frac{9}{50}k_5 + \frac{2}{55}k_6 \end{aligned}$$

The value of $y^{n+1} - z^{n+1}$ is an estimate of the error in y^{n+1} and can be used in step-size control schemes.

Usually one would use a high-order method to achieve high accuracy. The Runge-Kutta-Feldberg method is popular because it is high order and does not require a starting method (as does an Adams-Bashforth method). However, it does require four function evaluations per time step, or four times as many as a fourth-order Adams-Bashforth method. For problems in which the function evaluations are a significant portion of the calculation time, this might be important. Given the speed and availability of desktop computers, the efficiency of the methods is most important only for very large problems that are going to be solved many times. For other problems, the most important criterion for choosing a method is probably the time the user spends setting up the problem.

The stability limits for the explicit methods are based on the largest eigenvalue of the linearized system of equations

$$\frac{dy_i}{dt} = \sum_{j=1}^n A_{ij} y_j, \quad A_{ij} = \left. \frac{\delta f_i}{\delta y_j} \right|_y$$

For linear problems, the eigenvalues do not change, so that the stability and oscillation limits must be satisfied for every eigenvalue of the matrix \mathbf{A} . When solving nonlinear problems, the equations are linearized about the solution at the local time, and the analysis applies for small changes in time, after which a new analysis about the new solution must be made. Thus, for nonlinear problems, the eigenvalues keep changing, and the largest stable time step changes, too. The stability limits are:

- Euler method, $\lambda \Delta t \leq 2$
- Runge-Kutta, 2nd order, $\lambda \Delta t < 2$
- Runge-Kutta-Feldberg, $\lambda \Delta t < 3.0$

Richardson extrapolation can be used to improve the accuracy of a method. Suppose we step forward one step Δt with a p th-order method. Then redo the problem, this time stepping forward from the same initial point, but in two steps of length $\Delta t/2$, thus ending at the same point. Call the solution of the one-step calculation y_1 and the solution of the two-step calculation y_2 . Then an improved solution at the new time is given by

$$y = \frac{2^p y_2 - y_1}{2^p - 1}$$

This gives a good estimate provided Δt is small enough that the method is truly convergent with order p . This process can also be repeated in the same way Romberg's method was used for quadrature.

The error term in the various methods can be used to deduce a step size that will give a user-specified accuracy. Most packages today are based on a user-specified tolerance; the step-size is changed during the calculation to achieve that accuracy. The accuracy itself is not guaranteed, but it improves as the tolerance is decreased.

Implicit Methods By using different interpolation formulas involving y^{n+1} , it is possible to derive implicit integration methods. Implicit methods result in a nonlinear equation to be solved for y^{n+1} so that iterative methods must be used. The backward Euler method is a first-order method.

$$y^{n+1} = y^n + \Delta t f(y^{n+1})$$

Errors are proportional to Δt for small Δt . The trapezoid rule is a second-order method.

$$y^{n+1} = y^n + \frac{\Delta t}{2} [f(y^n) + f(y^{n+1})]$$

Errors are proportional to Δt^2 for small Δt . When the trapezoid rule is used with the finite difference method for solving partial differential equations, it is called the Crank-Nicolson method. The implicit methods are stable for any step size but do require the solution of a set of nonlinear equations, which must be solved iteratively. The set of equations can be solved using the successive substitution method

or Newton-Raphson method. See Bogacki, M. B., K. Alejski, and J. Szymanski, *Comp. Chem. Eng.* **13**: 1081–1085 (1989) for an application to dynamic distillation problems.

The best packages for stiff equations (see below) use Gear's backward difference formulas. The formulas of various orders are [Gear, G. W., *Numerical Initial Value Problems in Ordinary Differential Equations*, Prentice-Hall, Englewood Cliffs, N.J. (1971)]

$$(1) y^{n+1} = y^n + \Delta t f(y^{n+1})$$

$$(2) y^{n+1} = \frac{4}{3} y^n - \frac{1}{3} y^{n-1} + \frac{2}{3} \Delta t f(y^{n+1})$$

$$(3) y^{n+1} = \frac{18}{11} y^n - \frac{9}{11} y^{n-1} + \frac{2}{11} y^{n-2} + \frac{6}{11} \Delta t f(y^{n+1})$$

$$(4) y^{n+1} = \frac{48}{25} y^n - \frac{36}{25} y^{n-1} + \frac{16}{25} y^{n-2} - \frac{3}{25} y^{n-3} + \frac{12}{25} \Delta t f(y^{n+1})$$

$$(5) y^{n+1} = \frac{300}{137} y^n - \frac{300}{137} y^{n-1} + \frac{200}{137} y^{n-2} - \frac{75}{137} y^{n-3} + \frac{12}{137} y^{n-4} + \frac{60}{137} \Delta t f(y^{n+1})$$

Stiffness The concept of stiffness is described for a system of linear equations.

$$\frac{dy}{dt} = \mathbf{A}y$$

Let λ_i be the eigenvalues of the matrix \mathbf{A} . The stiffness ratio is defined as

$$\text{SR} = \frac{\max_i |\text{Re}(\lambda_i)|}{\min_i |\text{Re}(\lambda_i)|} \quad (3-79)$$

SR = 20 is not stiff, SR = 10^3 is stiff, and SR = 10^6 is very stiff. If the problem is nonlinear, then the solution is expanded about the current state.

$$\frac{dy_i}{dt} = f_i[y(t^n)] + \sum_{j=1}^n \frac{\partial f_i}{\partial y_j} [y_j - y_j(t^n)]$$

The question of stiffness then depends on the solution at the current time. Consequently nonlinear problems can be stiff during one time period and not stiff during another. While the chemical engineer may not actually calculate the eigenvalues, it is useful to know that they determine the stability and accuracy of the numerical scheme and the step size used.

Problems are stiff when the time constants for different phenomena have very different magnitudes. Consider flow through a packed bed reactor. The time constants for different phenomena are:

1. Time for device flow-through

$$t_{\text{flow}} = \frac{L}{u} = \frac{\phi AL}{Q}$$

where Q is the volumetric flow rate, A is the cross sectional area, L is the length of the packed bed, and ϕ is the void fraction;

2. Time for reaction

$$t_{r \times n} = \frac{1}{k}$$

where k is a rate constant (time^{-1});

3. Time for diffusion inside the catalyst

$$t_{\text{internal diffusion}} = \frac{\epsilon R^2}{D_e}$$

where ϵ is the porosity of the catalyst, R is the catalyst radius, and D_e is the effective diffusion coefficient inside the catalyst;

4. Time for heat transfer is

$$t_{\text{internal heat transfer}} = \frac{R^2}{\alpha} = \frac{\rho_s C_s R^2}{k_c}$$

where ρ_s is the catalyst density, C_s is the catalyst heat capacity per unit mass, k_c is the effective thermal conductivity of the catalyst, and

α is the thermal diffusivity. For example, in the model of a catalytic converter for an automobile [Ferguson, N. B., and B. A. Finlayson, *AIChE J.* **20**:539–550 (1974)], the time constants for internal diffusion was 0.3 seconds; internal heat transfer, 21 seconds; and device flow-through, 0.003 seconds. The device flow-through is so fast that it might as well be instantaneous. The stiffness is approximately 7000. Implicit methods must be used to integrate the equations. Alternatively, a quasistate model can be developed [Ramirez, W. F., *Computational Methods for Process Simulations*, 2d ed., Butterworth-Heinemann, Boston (1997)].

Differential-Algebraic Systems Sometimes models involve ordinary differential equations subject to some algebraic constraints. For example, the equations governing one equilibrium stage (as in a distillation column) are

$$M \frac{dx^n}{dt} = V^{n+1} y^{n+1} - L^n x^n - V^n y^n + L^{n-1} x^{n-1}$$

$$x^{n-1} - x^n = E^n (x^{n-1} - x^{*n})$$

$$\sum_{i=1}^N x_i = 1$$

where x and y are the mole fraction in the liquid and vapor, respectively; L and V are liquid and vapor flow rates, respectively; M is the holdup; and the superscript is the stage number. The efficiency is E , and the concentration in equilibrium with the vapor is x^* . The first equation is an ordinary differential equation for the mass of one component on the stage, while the third equation represents a constraint that the mass fractions add to one. This is a differential-algebraic system of equations.

Differential-algebraic equations can be written in the general notation

$$F\left(t, y, \frac{dy}{dt}\right) = 0$$

To solve the general problem using the backward Euler method, replace the nonlinear differential equation with the nonlinear algebraic equation for one step.

$$F\left(t, y^{n+1}, \frac{y^{n+1} - y^n}{\Delta t}\right) = 0$$

This equation must be solved for y^{n+1} . The Newton-Raphson method can be used, and if convergence is not achieved within a few iterations, the time step can be reduced and the step repeated. In actuality, the higher-order backward-difference Gear methods are used in DASSL [Ascher, U. M., and L. R. Petzold, *Computer Methods for Ordinary Differential Equations and Differential-Algebraic Equations*, SIAM, Philadelphia (1998); and Brenan, K. E., S. L. Campbell, and L. R. Petzold, *Numerical Solution of Initial-Value Problems in Differential-Algebraic Equations*, North Holland: Elsevier (1989)].

Differential-algebraic systems are more complicated than differential systems because the solution may not always be defined. Pontelides et al. [*Comp. Chem. Eng.* **12**: 449–454 (1988)] introduced the term *index* to identify the possible problems. The index is defined as the minimum number of times the equations need to be differentiated with respect to time to convert the system to a set of ordinary differential equations. These higher derivatives may not exist, and the process places limits on which variables can be given initial values. Sometimes the initial values must be constrained by the algebraic equations. For a differential-algebraic system modeling a distillation tower, Pontelides et al. show that the index depends on the specification of pressure for the column. Byrne and Ponzi [*Comp. Chem. Eng.* **12**: 377–382 (1988)]; also Chan, T. F. C., and H. B. Keller, *SIAM J. Sci. Stat. Comput.* **3**: 173–194 (1982)] also list several chemical engineering examples of differential-algebraic systems and solve one involving two-phase flow.

Computer Software Efficient computer packages are available for solving ordinary differential equations as initial value problems. The packages are widely available and good enough that most chemical engineers use them and do not write their own. Here we discuss three of them: RKF45, LSODE, and EPISODE. In each of the packages, the user specifies the differential equation to be solved and a

desired error criterion. The package then integrates in time and adjusts the step size to achieve the error criterion within the limitations imposed by stability.

A popular explicit, Runge-Kutta package is RKF45. Notice there that an estimate of the truncation error at each step is available. Then the step size can be reduced until this estimate is below the user-specified tolerance. The method is thus automatic, and the user is assured of the results. Note, however, that the tolerance is set on the local truncation error, namely from one step to another, whereas the user is usually interested in the global truncation error, or the error after several steps. The global error is generally made smaller by making the tolerance smaller, but the absolute accuracy is not the same as the tolerance. If the problem is stiff, then very small step sizes are used; the computation becomes very lengthy. The RKF45 code discovers this and returns control to the user with a message indicating the problem is too hard to solve with RKF45.

A popular implicit package is LSODE, a version of Gear's method (Gear, *ibid.*) written by Alan Hindmarsh at Lawrence Livermore Laboratory. In this package, the user specifies the differential equation to be solved and the tolerance desired. Now the method is implicit and therefore stable for any step size. The accuracy may not be acceptable, however, and sets of nonlinear equations must be solved. Thus, in practice the step size is limited but not nearly so much as in the Runge-Kutta methods. In these packages, both the step size and order of the method are adjusted by the package. Suppose we are calculating with a k th order method. The truncation error is determined by the $(k+1)$ th order derivative. This is estimated using difference formulas and the values of the right-hand sides at previous times. An estimate is also made for the k th and $(k+2)$ th derivative. Then it is possible to estimate the error in a $(k-1)$ th order method, a k th order method, and a $(k+1)$ th order method. Furthermore, the step size needed to satisfy the tolerance with each of these methods can be determined. Then we can choose the method and step size for the next step that achieves the biggest step, with appropriate adjustments due to the different work required for each order. The package generally starts with a very small step size and a first-order method, the backward Euler method. Then it integrates along, adjusting the order up (and later down) depending on the error estimates. The user is thus assured that the local truncation error meets the tolerance. There is a further difficulty, since the set of nonlinear equations must be solved. Usually a good guess of the solution is available, since the solution is evolving in time and past history can be extrapolated. Thus, the Newton-Raphson method will usually converge. The package protects itself, though, by only doing a few iterations. If convergence is not reached within this many iterations, then the step size is reduced and the calculation is redone for that time step. The convergence theorem for the Newton-Raphson method (p. 3-50) indicates that the method will converge if the step size is small enough. Thus the method is guaranteed to work. Further economies are possible. The Jacobian needed in the Newton-Raphson method can be fixed over several time steps. Then, if the iteration does not converge, the Jacobian can be reevaluated at the current time-step. If the iteration still does not converge, then the step-size is reduced and a new Jacobian is evaluated. Also the successive substitution method can be used, which is even faster, except that it may not converge. However, it, too, will converge if the time step is small enough.

The Runge-Kutta methods give extremely good accuracy, especially when the step size is kept small for stability reasons. If the problem is stiff, though, backward difference implicit methods must be used. Many chemical reactor problems are stiff, necessitating the use of implicit methods. In the MATLAB suite of ODE solvers, the `ode45` uses a revision of the RKF45 program, while the `ode15s` program uses an improved backward difference method. Shampine and Reichelt [SIAM J. Sci. Comp. 18:1-22 (1997)] give details of the programs in MATLAB. Fortunately, many packages are available. On the NIST web page <http://gams.nist.gov/>, choose "problem decision tree" and then "differential and integral equations" to find packages that can be downloaded. On the Netlib web site <http://www.netlib.org/>, choose "ode" to find packages that can be downloaded. Using Microsoft Excel to solve ordinary differential equations is cumbersome, except for the simplest problems.

Stability, Bifurcations, Limit Cycles Some aspects of this subject involve the solution of nonlinear equations; other aspects involve

the integration of ordinary differential equations; applications include chaos and fractals as well as unusual operation of some chemical engineering equipment. Kubicek, M., and M. Marek, *Computational Methods in Bifurcation Theory and Dissipative Structures*, Springer-Verlag, Berlin (1983), give an excellent introduction to the subject and the details needed to apply the methods. Chan, T. F. C., and H. B. Keller, *SIAM J. Sci. Stat. Comput.* 3:173-194 (1982), give more details of the algorithms. A concise survey with some chemical engineering examples is given in Doherty, M. F., and J. M. Ottino, *Chem. Eng. Sci.* 43:139-183 (1988). Bifurcation results are closely connected with stability of the steady states, which is essentially a transient phenomenon.

Sensitivity Analysis When solving differential equations, it is frequently necessary to know the solution as well as the sensitivity of the solution to the value of a parameter. Such information is useful when doing parameter estimation (to find the best set of parameters for a model) and for deciding if a parameter needs to be measured accurately. See Finlayson, et al. (2006).

Molecular Dynamics Special integration methods have been developed for molecular dynamics calculations due to the structure of the equations. A very large number of equations are to be integrated, with the following form based on molecular interactions between molecules.

$$m_i \frac{d^2 \mathbf{r}_i}{dt^2} = \mathbf{F}_i(\{\mathbf{r}\}) \quad \mathbf{F}_i(\{\mathbf{r}\}) = -\nabla V$$

The symbol m_i is the mass of the i th particle, \mathbf{r}_i is the position of the i th particle, \mathbf{F}_i is the force acting on the i th particle, and V is the potential energy that depends upon the location of all the particles (but not their velocities). Since the major part of the calculation lies in the evaluation of the forces, or potentials, a method must be used that minimizes the number of times the forces are calculated to move from one time to another time. Rewrite this equation in the form of an acceleration as

$$\frac{d^2 \mathbf{r}_i}{dt^2} = \frac{1}{m_i} \mathbf{F}_i(\{\mathbf{r}\}) \equiv \mathbf{a}_i$$

In the Verlet method, this equation is written by using central finite differences (see "Interpolation and Finite Differences"). Note that the accelerations do not depend upon the velocities.

$$\mathbf{r}_i(t + \Delta t) = 2\mathbf{r}_i(t) - \mathbf{r}_i(t - \Delta t) + \mathbf{a}_i(t)\Delta t^2$$

The calculations are straightforward, and no explicit velocity is needed. The storage requirement is modest, and the precision is modest (it is a second-order method). Note that one must start the calculation with values of $\{\mathbf{r}\}$ at times t and $t - \Delta t$.

In the Verlet velocity method, an equation is written for the velocity, too.

$$\frac{d\mathbf{v}_i}{dt} = \mathbf{a}_i$$

The trapezoid rule [see "Numerical Integration (Quadrature)"] is applied to obtain

$$\mathbf{v}_i(t + \Delta t) = \mathbf{v}_i(t) + \frac{1}{2} [\mathbf{a}_i(t) + \mathbf{a}_i(t + \Delta t)] \Delta t$$

The position of the particles is expanded in a Taylor series.

$$\mathbf{r}_i(t + \Delta t) = \mathbf{r}_i(t) + \mathbf{v}_i \Delta t + \frac{1}{2} \mathbf{a}_i(t) \Delta t^2$$

Beginning with values of $\{\mathbf{r}\}$ and $\{\mathbf{v}\}$ at time 0, one calculates the new positions and then the new velocities. This method is second-order in Δt , too. For additional details, see Allen, M. P., and D. J. Tildesley, *Computer Simulation of Liquids*, Clarendon Press, Oxford (1989); Frenkel, D., and B. Smit, *Understanding Molecular Simulation*, Academic Press (2002); Haile, J. M., *Molecular Dynamics Simulation*, Wiley (1992); Leach, A. R., *Molecular Modelling: Principles and Applications*, Prentice-Hall (2001); Schlick, T., *Molecular Modeling and Simulations*, Springer, New York (2002).

ORDINARY DIFFERENTIAL EQUATIONS-BOUNDARY VALUE PROBLEMS

Diffusion problems in one dimension lead to boundary value problems. The boundary conditions are applied at two different spatial

locations: at one side the concentration may be fixed and at the other side the flux may be fixed. Because the conditions are specified at two different locations, the problems are not initial value in character. It is not possible to begin at one position and integrate directly because at least one of the conditions is specified somewhere else and there are not enough conditions to begin the calculation. Thus, methods have been developed especially for boundary value problems.

Boundary value methods provide a description of the solution either by providing values at specific locations or by an expansion in a series of functions. Thus, the key issues are the method of representing the solution, the number of points or terms in the series, and how the approximation converges to the exact answer, i.e., how the error changes with the number of points or number of terms in the series. These issues are discussed for each of the methods: finite difference, orthogonal collocation, and Galerkin finite element methods.

Finite Difference Method To apply the finite difference method, we first spread grid points through the domain. Figure 3-48 shows a uniform mesh of n points (nonuniform meshes are possible, too). The unknown, here $c(x)$, at a grid point x_i is assigned the symbol $c_i = c(x_i)$. The finite difference method can be derived easily by using a Taylor expansion of the solution about this point. Expressions for the derivatives are:

$$\frac{dc}{dx}\bigg|_i = \frac{c_{i+1} - c_i}{\Delta x} - \frac{d^2c}{dx^2}\bigg|_i \frac{\Delta x}{2} + \dots, \quad \frac{dc}{dx}\bigg|_i = \frac{c_i - c_{i-1}}{\Delta x} + \frac{d^2c}{dx^2}\bigg|_i \frac{\Delta x}{2} + \dots$$

$$\frac{d^2c}{dx^2}\bigg|_i = \frac{c_{i+1} - 2c_i + c_{i-1}}{\Delta x^2} - \frac{d^3c}{dx^3}\bigg|_i \frac{\Delta x^2}{3!} + \dots$$

The truncation error in the first two expressions is proportional to Δx , and the methods are said to be first-order. The truncation error in the third expression is proportional to Δx^2 , and the method is said to be second-order. Usually the last equation is used to insure the best accuracy. The finite difference representation of the second derivative is:

$$\frac{d^2c}{dx^2}\bigg|_i = \frac{c_{i+1} - 2c_i + c_{i-1}}{\Delta x^2} - \frac{d^4c}{dx^4}\bigg|_i \frac{2\Delta x^2}{4!} + \dots$$

The truncation error is proportional to Δx^2 . To solve a differential equation, it is evaluated at a point i and then these expressions are inserted for the derivatives.

Example Consider the equation for convection, diffusion, and reaction in a tubular reactor.

$$\frac{1}{Pe} \frac{d^2c}{dx^2} - \frac{dc}{dx} = Da R(c)$$

The finite difference representation is

$$\frac{1}{Pe} \frac{c_{i+1} - 2c_i + c_{i-1}}{\Delta x^2} - \frac{c_{i+1} - c_{i-1}}{2\Delta x} = Da R(c_i)$$

This equation is written for $i = 2$ to $n - 1$, or the internal points. The equations would then be coupled but would also involve the values of c_1 and c_n , as well. These are determined from the boundary conditions.

If the boundary condition involves a derivative, it is important that the derivatives be evaluated using points that exist. Three possibilities exist:

$$\frac{dc}{dx}\bigg|_1 = \frac{c_2 - c_1}{\Delta x}$$

$$\frac{dc}{dx}\bigg|_1 = \frac{-3c_1 + 4c_2 - c_3}{2\Delta x}$$

The third alternative is to add a false point, outside the domain, as $c_0 = c(x = -\Delta x)$.

$$\frac{dc}{dx}\bigg|_1 = \frac{c_2 - c_0}{2\Delta x}$$

Since this equation introduces a new variable, c_0 , another equation is needed and is obtained by writing the finite difference equation for $i = 1$, too.

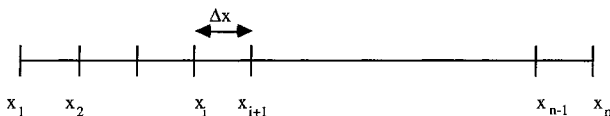


FIG. 3-48 Finite difference mesh; Δx uniform.

The sets of equations can be solved using the Newton-Raphson method. The first form of the derivative gives a tridiagonal system of equations, and the standard routines for solving tridiagonal equations suffice. For the other two options, some manipulation is necessary to put them into a tridiagonal form.

Frequently, the transport coefficients, such as diffusion coefficient or thermal conductivity, depend on the dependent variable, concentration, or temperature, respectively. Then the differential equation might look like

$$\frac{d}{dx} \left(D(c) \frac{dc}{dx} \right) = 0$$

This could be written as two equations.

$$-\frac{dJ}{dx} = 0 \quad J = -D(c) \frac{dc}{dx}$$

Because the coefficient depends on c , the equations are more complicated. A finite difference method can be written in terms of the fluxes at the midpoints, $i + 1/2$.

$$-\frac{J_{i+1/2} - J_{i-1/2}}{\Delta x} = 0 \quad J_{i+1/2} = -D(c_{i+1/2}) \frac{c_{i+1} - c_i}{\Delta x}$$

These are combined to give the complete equation.

$$\frac{D(c_{i+1/2})(c_{i+1} - c_i) - D(c_{i-1/2})(c_i - c_{i-1})}{\Delta x^2} = 0$$

This represents a set of nonlinear algebraic equations that can be solved with the Newton-Raphson method. However, in this case, a viable iterative strategy is to evaluate the transport coefficients at the last value and then solve

$$\frac{D(c_{i+1/2}^k)(c_{i+1}^{k+1} - c_i^{k+1}) - D(c_{i-1/2}^k)(c_i^{k+1} - c_{i-1}^{k+1})}{\Delta x^2} = 0$$

The advantage of this approach is that it is easier to program than a full Newton-Raphson method. If the transport coefficients do not vary radically, then the method converges. If the method does not converge, then it may be necessary to use the full Newton-Raphson method.

There are two common ways to evaluate the transport coefficient at the midpoint: Use the average value of the solution on each side to evaluate the diffusivity, or use the average value of the diffusivity on each side. Both methods have truncation error Δx^2 (Finlayson, 2003). The spacing of the grid points need not be uniform; see Finlayson (2003) and Finlayson et al. (2006) for the formulas in that case.

Example A reaction diffusion problem is solved with the finite difference method.

$$\frac{d^2c}{dx^2} = \phi^2 c, \quad \frac{dc}{dx}(0) = 0, \quad c(1) = 1$$

The solution is derived for $\phi = 2$. It is solved several times, first with two intervals and three points (at $x = 0, 0.5, 1$), then with four intervals, then with eight intervals. The reason is that when an exact solution is not known, one must use several Δx and see that the solution converges as Δx approaches zero. With two intervals, the equations are as follows. The points are $x_1 = 0$, $x_2 = 0.5$, and $x_3 = 1.0$; and the solution at those points are c_1, c_2 , and c_3 , respectively. A false boundary is used at $x_0 = -0.5$.

$$\frac{c_0 - c_2}{2\Delta x} = 0, \quad \frac{c_0 - 2c_1 + c_2}{\Delta x^2} - \phi^2 c_1 = 0, \quad \frac{c_1 - 2c_2 + c_3}{\Delta x^2} - \phi^2 c_2 = 0, \quad c_3 = 1$$

The solution is $c_1 = 0.2857$, $c_2 = 0.4286$, and $c_3 = 1.0$. The problem is solved again with four and then eight intervals. The value of concentration at $x = 0$ takes the following values for different Δx . These values are extrapolated using the Richardson extrapolation technique to give $c(0) = 0.265718$. Using this value as the best estimate of the exact solution, the errors in the solution are tabulated versus Δx . Clearly the errors go as Δx^2 (decreasing by a factor of 4 when Δx decreases by a factor of 2), thus validating the solution. The exact solution is 0.265802.

$n - 1$	Δx	$c(0)$
2	0.5	0.285714
4	0.25	0.271043
8	0.125	0.267131

$n - 1$	Δx	Error in $c(0)$
2	0.5	0.02000
4	0.25	0.00532
8	0.125	0.00141

Finite Difference Methods Solved with Spreadsheets A convenient way to solve the finite difference equations for simple problems is to use a computer spreadsheet. The equations for the problem solved in the example can be cast into the following form

$$c_i = \frac{2c_2}{2 + \phi^2 \Delta x^2}$$

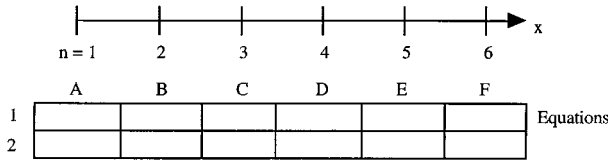


FIG. 3-49 Finite difference method using spreadsheets.

$$c_i = \frac{c_{i+1} + c_{i-1}}{2 + \phi^2 \Delta x^2}$$

$$c_{n+1} = 1$$

Let us solve the problem using 6 nodes, or 5 intervals. Then the connection between the cell in the spreadsheet and the nodal value is shown in Fig. 3-49. The following equations are placed into the various cells.

```
A1: = 2*B1/(2.+(phi*dx)**2)
B1: = (A1 + C1)/(2.+(phi*dx)**2)
F1: = 1.
```

The equation in cell B1 is copied into cells C1 though E1. Then turn on the iteration scheme in the spreadsheet and watch the solution converge. Whether or not convergence is achieved can depend on how you write the equations, so some experimentation may be necessary. Theorems for convergence of the successive substitution method are useful in this regard.

Orthogonal Collocation The orthogonal collocation method has found widespread application in chemical engineering, particularly for chemical reaction engineering. In the collocation method, the dependent variable is expanded in a series of orthogonal polynomials. See “Interpolation and Finite Differences: Lagrange Interpolation Formulas.”

$$c(x) = \sum_{m=0}^N a_m P_m(x)$$

The differential equation is evaluated at certain collocation points. The collocation points are the roots to an orthogonal polynomial, as first used by Lanczos [Lanczos, C., *J. Math. Phys.* **17**:123–199 (1938); and Lanczos, C., *Applied Analysis*, Prentice-Hall (1956)]. A major improvement was proposed by Villadsen and Stewart [Villadsen, J. V., and W. E. Stewart, *Chem. Eng. Sci.* **22**:1483–1501 (1967)], who proposed that the entire solution process be done in terms of the solution at the collocation points rather than the coefficients in the expansion. This method is especially useful for reaction-diffusion problems that frequently arise when modeling chemical reactors. It is highly efficient when the solution is smooth, but the finite difference method is preferred when the solution changes steeply in some region of space. The error decreases very rapidly as N is increased since it is proportional to $[1/(1 - N)]^{N-1}$. See Finlayson (2003) and Villadsen, J. V., and M. Michelsen, *Solution of Differential Equation Models by Polynomial Approximations*, Prentice-Hall (1978).

Galerkin Finite Element Method In the finite element method, the domain is divided into elements and an expansion is made for the solution on each finite element. In the Galerkin finite element method an additional idea is introduced: the Galerkin method is used to solve the equation. The Galerkin method is explained before the finite element basis set is introduced, using the equations for reaction and diffusion in a porous catalyst pellet.

$$\frac{d^2c}{dx^2} = \phi^2 R(c)$$

$$\frac{dc}{dx}(0) = 0, \quad c(1) = 1$$

The unknown solution is expanded in a series of known functions $\{b_i(x)\}$ with unknown coefficients $\{a_i\}$.

$$c(x) = \sum_{i=1}^{NT} a_i b_i(x)$$

The trial solution is substituted into the differential equation to obtain

the residual.

$$\text{Residual} = \sum_{i=1}^{NT} a_i \frac{d^2 b_i}{dx^2} - \phi^2 R \left[\sum_{i=1}^{NT} a_i b_i(x) \right]$$

The residual is then made orthogonal to the set of basis functions.

$$\int_0^1 b_j(x) \left\{ \sum_{i=1}^{NT} a_i \frac{d^2 b_i}{dx^2} - \phi^2 R \left[\sum_{i=1}^{NT} a_i b_i(x) \right] \right\} dx = 0 \quad j = 1, \dots, NT$$

This is the process that makes the method a Galerkin method. The basis for the orthogonality condition is that a function that is made orthogonal to each member of a complete set is then zero. The residual is being made orthogonal, and if the basis functions are complete and you use infinitely many of them, then the residual is zero. Once the residual is zero, the problem is solved.

This equation is integrated by parts to give the following equation

$$-\sum_{i=1}^{NT} \int_0^1 \frac{db_i}{dx} \frac{db_i}{dx} dx a_i = \phi^2 \int_0^1 b_j(x) R \left[\sum_{i=1}^{NT} a_i b_i(x) \right] dx \quad j = 1, \dots, NT - 1 \quad (3-80)$$

This equation defines the Galerkin method and a solution that satisfies this equation (for all $j = 1, \dots, \infty$) is called a weak solution. For an approximate solution, the equation is written once for each member of the trial function, $j = 1, \dots, NT - 1$, and the boundary condition is applied.

$$\sum_{i=1}^{NT} a_i b_i(1) = c_B$$

The Galerkin finite element method results when the Galerkin method is combined with a finite element trial function. The domain is divided into elements separated by nodes, as in the finite difference method. The solution is approximated by a linear (or sometimes quadratic) function of position within the element. These approximations are substituted into Eq. (3-80) to provide the Galerkin finite element equations. For example, with the grid shown in Fig. 3-48, a linear interpolation would be used between points x_i and x_{i+1} .

$$c(x) = c_i(1 - u) + c_{i+1}u \quad u \equiv \frac{x - x_i}{x_{i+1} - x_i}$$

A finite element method based on these functions would have an error proportional to Δx^2 . The finite element representations for the first derivative and second derivative are the same as in the finite difference method, but this is not true for other functions or derivatives. With quadratic finite elements, take the region from x_{i-1} and x_{i+1} as one element. Then the interpolation would be

$$c(x) = c_{i-1}N_1(u) + c_iN_2(u) + c_{i+1}N_3(u)$$

$$N_1(u) = 2(u-1)\left(u - \frac{1}{2}\right) \quad N_2(u) = 4u(1-u)$$

$$N_3(u) = 2u\left(u - \frac{1}{2}\right)$$

A finite element method based on these functions would have an error proportional to Δx^3 . Thus, it would converge faster than one based on linear interpolation. A variety of other finite element functions can be used as well, including B splines (see “Interpolation and Finite Differences: Spline Functions”).

Adaptive Meshes In many two-point boundary value problems, the difficulty in the problem is the formation of a boundary layer region, or a region in which the solution changes very dramatically. In such cases, it is prudent to use small mesh spacing there, either with the finite difference method or the finite element method. If the region is known *a priori*, small mesh spacings can be assumed at the boundary layer. If the region is not known, though, other techniques must be used. These techniques are known as adaptive mesh techniques. The mesh size is made small where some property of the solution is large. For example, if the truncation error of the method is n th order, then the n th-order derivative of the solution is evaluated and a small mesh is used where it is large. Alternatively, the residual (the differential equation with the numerical

solution substituted into it) can be used as a criterion. It is also possible to define the error that is expected from a method one order higher and one order lower. Then a decision about whether to increase or decrease the order of the method can be made, taking into account the relative work of the different orders. This provides a method of adjusting both the mesh spacing (Δx , or sometimes called h) and the degree of polynomial (p). Such methods are called h - p methods. Many finite element programs have the capability to do this mesh refinement automatically.

Singular Problems and Infinite Domains If the solution being sought has a singularity, it may be difficult to find a good numerical solution. Sometimes even the location of the singularity may not be known. One method of solving such problems is to refine the mesh near the singularity, relying on the better approximation due to a smaller Δx . Another approach is to incorporate the singular trial function into the approximation. Thus, if the solution approaches $f(x)$ as x goes to zero and $f(x)$ becomes infinite, one may define a new variable $u(x) = y(x) - f(x)$ and derive an equation for u . The differential equation is more complicated, but the solution is better near the singularity. Press et al. (1986).

Sometimes the domain is semi-infinite, as in boundary layer flow. The domain can be transformed from the x domain $(0 - \infty)$ to the η domain $(1 - 0)$ using the transformation $\eta = \exp(-x)$. Another approach is to use a variable mesh, perhaps with the same transformation. For example, use $\eta = \exp(-\beta x)$ and a constant mesh size in η ; the value of β is found experimentally. Still another approach is to solve on a finite mesh in which the last point is far enough away that its location does not influence the solution. A location that is far enough away must be found by trial and error.

Packages to solve boundary value problems are available on the Internet. On the NIST web page <http://gams.nist.gov/>, choose "problem decision tree" and then "differential and integral equations" and then "ordinary differential equations" and "multipoint boundary value problems." On the Netlib web site <http://www.netlib.org/>, search on "boundary value problem." Any spreadsheet that has an iteration capability can be used with the finite difference method. Some packages for partial differential equations also have a capability for solving one-dimensional boundary value problems [e.g. Comsol Multiphysics (formerly FEMLAB)].

NUMERICAL SOLUTION OF INTEGRAL EQUATIONS

In this subsection is considered a method of solving numerically the Fredholm integral equation of the second kind:

$$u(x) = f(x) + \lambda \int_a^b k(x, t)u(t) dt \quad \text{for } u(x) \quad (3-81)$$

The method discussed arises because a definite integral can be closely approximated by any of several numerical integration formulas (each of which arises by approximating the function by some polynomial over an interval). Thus the definite integral in Eq. (3-81) can be replaced by an integration formula, and Eq. (3-81) may be written

$$u(x) = f(x) + \lambda(b - a) \left[\sum_{i=1}^n c_i k(x, t_i)u(t_i) \right] \quad (3-82)$$

where t_1, \dots, t_n are points of subdivision of the t axis, $a \leq t \leq b$, and the c 's are coefficients whose values depend upon the type of numerical integration formula used. Now Eq. (3-82) must hold for all values of x , $a \leq x \leq b$; so it must hold for $x = t_1, x = t_2, \dots, x = t_n$. Substituting for x successively t_1, t_2, \dots, t_n and setting $u(t_i) = u_i, f(t_i) = f_i$, we get n linear algebraic equations for the n unknowns u_1, \dots, u_n . That is,

$$u_i = f_i + \lambda(b - a) [c_1 k(t_i, t_1)u_1 + c_2 k(t_i, t_2)u_2 + \dots + c_n k(t_i, t_n)u_n] \quad i = 1, 2, \dots, n$$

These u_i may be solved for by the methods under "Numerical Solution of Linear Equations and Associated Problems" and substituted into Eq. (3-82) to yield an approximate solution for Eq. (3-81).

Because of the work involved in solving large systems of simultaneous linear equations it is desirable that only a small number of u 's be computed. Thus the gaussian integration formulas are useful because of the economy they offer.

Solutions for Volterra equations are done in a similar fashion, except that the solution can proceed point by point, or in small groups of points depending on the quadrature scheme. See Linz, P., *Analytical and Numerical Methods for Volterra Equations*, SIAM, Philadelphia (1985). There are methods that are analogous to the usual methods for

integrating differential equations (Runge-Kutta, predictor-corrector, Adams methods, etc.). Explicit methods are fast and efficient until the time step is very small to meet the stability requirements. Then implicit methods are used, even though sets of simultaneous algebraic equations must be solved. The major part of the calculation is the evaluation of integrals, however, so that the added time to solve the algebraic equations is not excessive. Thus, implicit methods tend to be preferred. Volterra equations of the first kind are not well posed, and small errors in the solution can have disastrous consequences. The boundary element method uses Green's functions and integral equations to solve differential equations. See Brebbia, C. A., and J. Dominguez, *Boundary Elements—An Introductory Course*, 2d ed., Computational Mechanics Publications, Southampton (1992); and Mackerle, J., and C. A. Brebbia (eds.), *Boundary Element Reference Book*, Springer-Verlag (1988).

MONTE CARLO SIMULATIONS

Some physical problems, such as those involving interaction of molecules, are usually formulated as integral equations. Monte Carlo methods are especially well-suited to their solution. This section cannot give a comprehensive treatment of such methods, but their use in calculating the value of an integral will be illustrated. Suppose we wish to calculate the integral

$$G = \int_{\Omega_0} g(x)f(x) dx$$

where the distribution function $f(x)$ satisfies:

$$f(x) \geq 0, \quad \int_{\Omega_0} f(x) dx = 1$$

The distribution function $f(x)$ can be taken as constant; for example, $1/\Omega_0$. We choose variables x_1, x_2, \dots, x_N randomly from $f(x)$ and form the arithmetic mean

$$G_N = \frac{1}{N} \sum_i g(x_i)$$

The quantity G_N is an estimation of G , and the fundamental theorem of Monte Carlo guarantees that the expected value of G_N is G , if G exists [Kalos, M. H., and P. A. Whitlock, *Monte Carlo Methods*, vol. 1, Wiley, New York (1986)]. The error in the calculation is given by

$$\epsilon = \frac{\sigma_1}{N^{1/2}}$$

where σ_1^2 is calculated from

$$\sigma_1^2 = \int_{\Omega_0} g^2(x)f(x) dx - G^2$$

Thus the number of terms needed to achieve a specified accuracy ϵ can be calculated once an estimate of σ_1^2 is known.

$$N = \frac{\sigma_1^2}{\epsilon^2}$$

Various methods, such as influence sampling, can be used to reduce the number of calculations needed. See also Lapeyre, B., *Introduction to Monte-Carlo Methods for Transport and Diffusion Equations*, Oxford University Press (2003), and Liu, J. S., *Monte Carlo Strategies in Scientific Computing*, Springer (2001). Some computer programs are available that perform simple Monte Carlo calculations using Microsoft Excel.

NUMERICAL SOLUTION OF PARTIAL DIFFERENTIAL EQUATIONS

The numerical methods for partial differential equations can be classified according to the type of equation (see "Partial Differential Equations"); parabolic, elliptic, and hyperbolic. This section uses the finite difference method to illustrate the ideas, and these results can be programmed for simple problems. For more complicated problems, though, it is common to rely on computer packages. Thus, some discussion is given to the issues that arise when using computer packages.

Parabolic Equations in One Dimension By combining the techniques applied to initial value problems and boundary value problems it

is possible to easily solve parabolic equations in one dimension. The method is often called the method of lines. It is illustrated here using the finite difference method, but the Galerkin finite element method and the orthogonal collocation method can also be combined with initial value methods in similar ways. The analysis is done by example. The finite volume method is described under Hyperbolic Equations.

Example Consider the diffusion equation, with boundary and initial conditions.

$$\begin{aligned} \frac{\partial c}{\partial t} &= D \frac{\partial^2 c}{\partial x^2} \\ c(x, 0) &= 0 \\ c(0, t) &= 1, \quad c(1, t) = 0 \end{aligned}$$

We denote by c_i the value of $c(x_i, t)$ at any time. Thus, c_i is a function of time, and differential equations in c_i are ordinary differential equations. By evaluating the diffusion equation at the i th node and replacing the derivative with a finite difference equation, the following working equation is derived for each node $i, i = 2, \dots, n$ (see Fig. 3-50).

$$\frac{dc_i}{dt} = D \frac{c_{i+1} - 2c_i + c_{i-1}}{\Delta x^2}$$

This can be written in the general form of a set of ordinary differential equations by defining the matrix \mathbf{AA} .

$$\frac{dc}{dt} = \mathbf{AA}c$$

This set of ordinary differential equations can be solved using any of the standard methods, and the stability of the integration of these equations is governed by the largest eigenvalue of \mathbf{AA} . When Euler's method is used to integrate in time, the equations become

$$\frac{c_i^{n+1} - c_i^n}{\Delta t} = D \frac{c_{i+1}^n - 2c_i^n + c_{i-1}^n}{\Delta x^2}$$

where $c_i^n = c(x_i, t^n)$. Notice that if the solution is known at every point at one time n , then it is a straightforward calculation to find the solution at every point at the new time $n+1$.

If Euler's method is used for integration, the time step is limited by

$$\Delta t \leq \frac{2}{|\lambda|_{\max}}$$

whereas if the Runge-Kutta-Feldberg method is used, the 2 in the numerator is replaced by 3.0. The largest eigenvalue of \mathbf{AA} is bounded by Gerschgorin's Theorem.

$$|\lambda|_{\max} \leq \max_{2 < j < n} \sum_{i=2}^n |\mathbf{AA}_{ji}| = \frac{4D}{\Delta x^2}$$

This gives the well-known stability limit

$$\Delta t \frac{D}{\Delta x^2} \leq \frac{1}{2}$$

The smallest eigenvalue is independent of Δx (it is $D\pi^2/L^2$) so that the ratio of largest to smallest eigenvalue is proportional to $1/\Delta x^2$. Thus, the problem becomes stiff as Δx approaches zero. See Eq. (3-79).

The effect of the increased stiffness is that a smaller and smaller time step (Δt) must be taken as the mesh is refined ($\Delta x^2 \rightarrow 0$). At the same time, the number of points is increasing, so that the computation becomes very lengthy. Implicit methods are used to overcome this problem.

Write a finite difference form for the time derivative and average the right-hand sides, evaluated at the old and new time.

$$\frac{c_i^{n+1} - c_i^n}{\Delta t} = D(1 - \theta) \frac{c_{i+1}^n - 2c_i^n + c_{i-1}^n}{\Delta x^2} + D\theta \frac{c_{i+1}^{n+1} - 2c_i^{n+1} + c_{i-1}^{n+1}}{\Delta x^2}$$

Now the equations are of the form

$$\begin{aligned} -\frac{D\Delta t\theta}{\Delta x^2} c_{i+1}^{n+1} + \left[1 + 2\frac{D\Delta t\theta}{\Delta x^2} \right] c_i^{n+1} - \frac{D\Delta t\theta}{\Delta x^2} c_{i-1}^{n+1} \\ = c_i^n + \frac{D\Delta t(1 - \theta)}{\Delta x^2} (c_{i+1}^n - 2c_i^n + c_{i-1}^n) \end{aligned}$$

and require solving a set of simultaneous equations, which have a tridiagonal structure. Using $\theta = 0$ gives the Euler method (as above),

$$\frac{du}{dx} \Big|_{i,j} = \frac{1}{2h} \left\{ \begin{array}{c} (-1) \text{---} (0) \text{---} (1) \\ \text{\scriptsize } i-1,j \quad i,j \quad i+1,j \end{array} \right\} + O(h^2)$$

$$\frac{du}{dy} \Big|_{i,j} = \frac{1}{2k} \left\{ \begin{array}{c} (1) \\ \text{\scriptsize } i, j+1 \\ (0) \\ \text{\scriptsize } i, j \\ (-1) \\ \text{\scriptsize } i, j-1 \end{array} \right\} + O(k^2)$$

$$\frac{d^2u}{dx^2} \Big|_{i,j} = \frac{1}{h^2} \left\{ \begin{array}{c} (1) \text{---} (-2) \text{---} (1) \\ \text{\scriptsize } i-1,j \quad i,j \quad i+1,j \end{array} \right\} + O(h^2)$$

$$= \frac{1}{4h^2} \left\{ \begin{array}{ccc} (-1) & (0) & (1) \\ | & | & | \\ (0) & (0) & (0) \\ | & | & | \\ (1) & (0) & (-1) \end{array} \right\} + O(h^2)$$

$$\nabla^2 u \Big|_{i,j} = \frac{1}{h^2} \left\{ \begin{array}{c} (1) \\ | \\ (1) \text{---} (-4) \text{---} (1) \\ | \\ (1) \end{array} \right\} + O(h^2)$$

$$\nabla^4 u \Big|_{i,j} = \frac{1}{h^4} \left\{ \begin{array}{ccccc} & & (1) & & \\ & & | & & \\ & (2) & (-8) & (2) & \\ | & | & | & | & | \\ (1) & (-8) & (20) & (-8) & (1) \\ | & | & | & | & | \\ & (2) & (-8) & (2) & \\ & & | & & \\ & & (1) & & \end{array} \right\} + O(h^2)$$

$$\int_{\boxplus} u \, d\boxplus = \frac{h^2}{9} \left\{ \begin{array}{ccc} (1) & (4) & (1) \\ | & | & | \\ (4) & (16) & (4) \\ | & | & | \\ (1) & (4) & (1) \end{array} \right\} + O(h^6)$$

FIG. 3-50 Computational molecules. $h = \Delta x = \Delta y$.

$\theta = 0.5$ gives the Crank-Nicolson method, and $\theta = 1$ gives the backward Euler method. The Crank-Nicolson method is also the same as applying the trapezoid rule to do the integration. The stability limit is given by

$$\frac{D\Delta t}{\Delta x^2} \leq \frac{0.5}{1 - 2\theta}$$

The price of using implicit methods is that one now has a system of equations to solve at each time step, and the solution methods are more complicated (particularly for nonlinear problems) than the straightforward explicit methods. Phenomena that happen quickly can also be obliterated or smoothed over by using a large time step, so implicit methods are not suitable in all cases. The engineer must decide if he or she wants to track those fast phenomena, and choose an appropriate method that handles the time scales that are important in the problem.

Other methods can be used in space, such as the finite element method, the orthogonal collocation method, or the method of orthogonal collocation on finite elements. One simply combines the methods for ordinary differential equations (see “Ordinary Differential Equations—Boundary Value Problems”) with the methods for initial-value problems (see “Numerical Solution of Ordinary Differential Equations as Initial Value Problems”). Fast Fourier transforms can also be used on regular grids (see “Fast Fourier Transform”).

Elliptic Equations Elliptic equations can be solved with both finite difference and finite element methods. One-dimensional elliptic problems are two-point boundary value problems. Two- and three-dimensional elliptic problems are often solved with iterative methods when the finite difference method is used and direct methods when the finite element method is used. So there are two aspects to consider: how the equations are discretized to form sets of algebraic equations and how the algebraic equations are then solved.

The prototype elliptic problem is steady-state heat conduction or diffusion,

$$k \left(\frac{\partial^2 T}{\partial x^2} + \frac{\partial^2 T}{\partial y^2} \right) = Q$$

possibly with a heat generation term per unit volume, Q . The boundary conditions taken here are $T = f(x, y)$ on the boundary (S) with f a known function. Illustrations are given for constant thermal conductivity k while Q is a known function of position. The finite difference formulation is given using the following nomenclature:

$$T_{i,j} = T(i\Delta x, j\Delta y)$$

The finite difference formulation is then (see Fig. 3-50)

$$\frac{T_{i+1,j} - 2T_{i,j} + T_{i-1,j}}{\Delta x^2} + \frac{T_{i,j+1} - 2T_{i,j} + T_{i,j-1}}{\Delta y^2} = Q_{i,j} \quad (3-83)$$

$$T_{i,j} = f(x_i, y_j) \text{ on } S$$

If the boundary is parallel to a coordinate axis any derivative is evaluated as in the section on boundary value problems, using either a one-sided, centered difference or a false boundary. If the boundary is more irregular and not parallel to a coordinate line then more complicated expressions are needed and the finite element method may be the better method.

Equation (3-83) provides a set of linear equations that must be solved. These equations and their boundary conditions may be written in matrix form as

$$\mathbf{A}\mathbf{t} = \mathbf{f}$$

where \mathbf{t} is the set of temperatures at all the points, \mathbf{f} is the set of heat generation terms at all points, and \mathbf{A} is formed from the coefficients of T_{ij} in Eq. (3-83). The solution can be obtained simply by solving the set of linear equations. For three-dimensional problems, the matrix \mathbf{A} is sparse, and iterative methods are used. These include Gauss-Seidel, alternating direction, overrelaxation methods, conjugate gradient, and multigrid methods. In Gauss-Seidel methods, one writes the equation for T_{ij} in terms of the other temperatures and cycles through all the points over and over. In the alternating direction method, one solves along one line (that is, $x = \text{constant}$), keeping the side values fixed, and then repeats this for all lines, and then repeats the process. Multigrid methods solve the problem on successively refined grids, which has advantages for both convergence and error estimation. Conjugate gradient methods frequently use a preconditioned matrix. The equation is multiplied by another matrix, which is chosen so that the resulting problem is easier to solve than the original one. Finding such matrices

is an art, but it can speed convergence. The generalized minimal residual method is described in <http://mathworld.wolfram.com/GeneralizedMinimalResidualMethod.html>. Additional resources can be found at http://www.netlib.org/linalg/html_templates/Templates.html. When the problem is nonlinear, the iterative methods may not converge, or the mesh may have to be refined before they converge, so some experimentation is sometimes necessary.

Spreadsheets can be used to solve two-dimensional problems on rectangular grids. The equation for T_{ij} is obtained by rearranging Eq. (3-83).

$$2 \left(1 + \frac{\Delta x^2}{\Delta y^2} \right) T_{i,j} = T_{i+1,j} + T_{i-1,j} + \frac{\Delta x^2}{\Delta y^2} (T_{i,j+1} + T_{i,j-1}) - \Delta x^2 \frac{Q_{i,j}}{k}$$

This equation is inserted into a cell and copied throughout the space represented by all the cells; when the iteration feature is turned on, the solution is obtained.

The Galerkin finite element method (FEM) is useful for solving elliptic problems and is particularly effective when the domain or geometry is irregular. As an example, cover the domain with triangles and define a trial function on each triangle. The trial function takes the value 1.0 at one corner and 0.0 at the other corners and is linear in between. See Fig. 3-51. These trial functions on each triangle are pieced together to give a trial function on the whole domain. General treatments of the finite element method are available (see references). The steps in the solution method are similar to those described for boundary value problems, except now the problems are much bigger so that the numerical analysis must be done very carefully to be efficient. Most engineers, though, just use a finite element program without generating it. There are three major caveats that must be addressed. The first one is that the solution is dependent on the mesh laid down, and the only way to assess the accuracy of the solution is to solve the problem with a more refined mesh. The second concern is that the solution obeys the shape of the trial function inside the element. Thus, if linear functions are used on triangles, a three-dimensional view of the solution, plotting the solution versus x and y , consists of a series of triangular planes joined together at the edges, as in a geodesic dome. The third caveat is that the Galerkin finite element method is applied to both the differential equations and the boundary conditions. Computer programs are usually quite general and may allow the user to specify boundary conditions that are not realistic. Also, natural boundary conditions are satisfied if no other boundary condition (ones involving derivatives) is set at a node. Thus, the user of finite element codes must be very clear what boundary conditions and differential equations are built into the computer code. When the problem is nonlinear, the Newton-Raphson method is used to iterate from an initial guess. Nonlinear problems lead to complicated integrals to evaluate, and they are usually evaluated using Gaussian quadrature.

One nice feature of the finite element method is the use of natural boundary conditions. It may be possible to solve the problem on a domain that is shorter than needed to reach some limiting condition (such as at an outflow boundary). The externally applied flux is still applied at the shorter domain, and the solution *inside* the truncated domain is still valid. Examples are given in Chang, M. W., and B. A. Finlayson, *Int. J. Num. Methods Eng.* **15**, 935–942 (1980), and Finlayson, B. A. (1992). The effect of this is to allow solutions in domains that are smaller, thus saving computation time and permitting the solution in semi-infinite domains.

The trial functions in the finite element method are not limited to linear ones. Quadratic functions and even higher-order functions are frequently used. The same considerations hold as for boundary value problems: The higher-order trial functions converge faster, but require more work. It is possible to refine both the mesh h and the power of polynomial in the trial function p in an hp method. Some problems have constraints on some of the variables. For flow problems, the pressure must usually be approximated by using a trial function that is one order lower than the polynomial used to approximate the velocity.

Hyperbolic Equations The most common situation yielding hyperbolic equations involves unsteady phenomena with convection. Two typical equations are the convective diffusive equation

$$\frac{\partial c}{\partial t} + u \frac{\partial c}{\partial x} = D \frac{\partial^2 c}{\partial x^2}$$

and the chromatography equation.

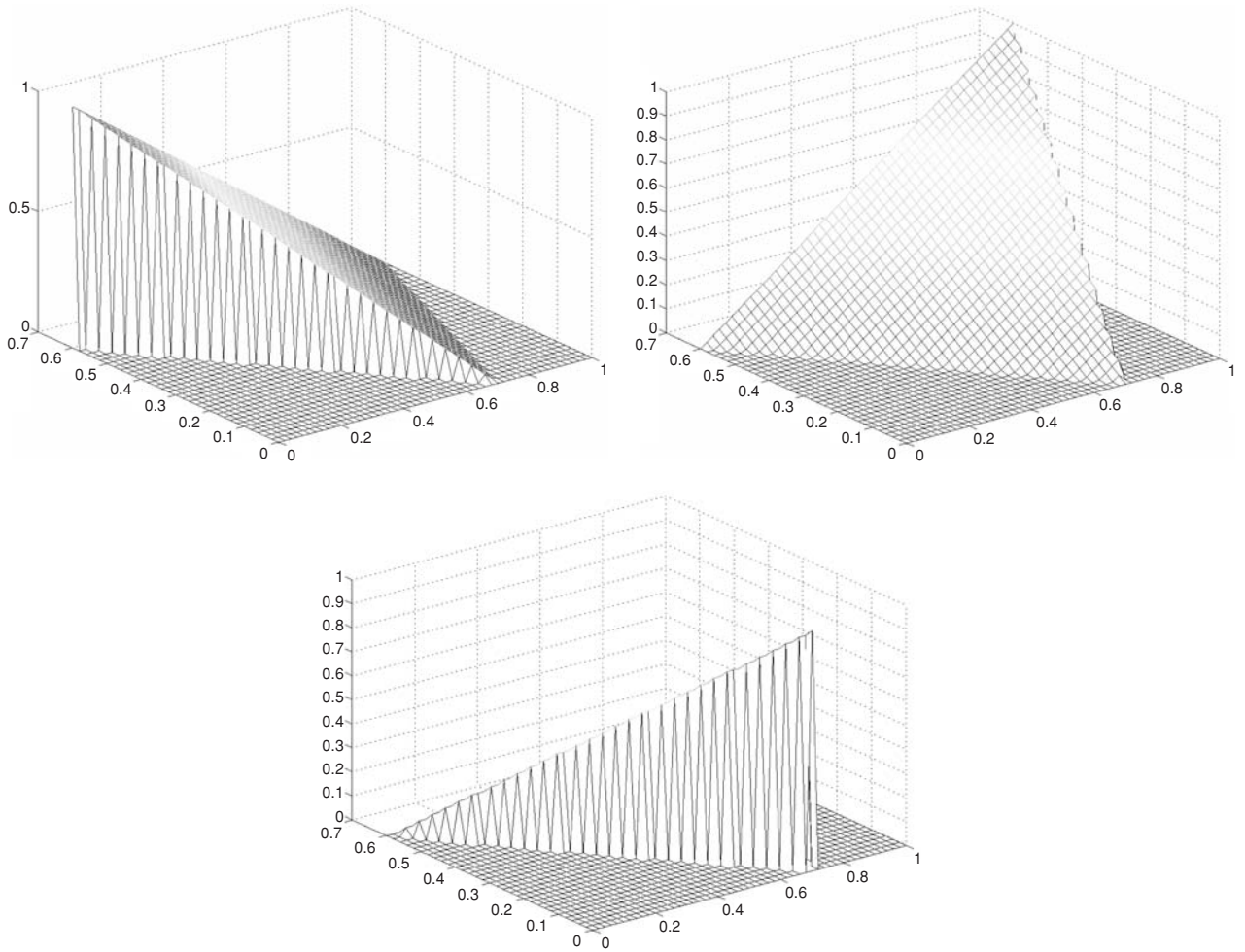


FIG. 3-51 Trial functions for Galerkin finite element method: linear polynomial on triangle.

(See “Partial Differential Equations.”) If the diffusion coefficient is zero, the convective diffusion equation is hyperbolic. If D is small, the phenomenon may be essentially hyperbolic, even though the equations are parabolic. Thus the numerical methods for hyperbolic equations may be useful even for parabolic equations.

Equations for several methods are given here, as taken from the book by Finlayson [Finlayson, B. A. (1992)]. If the convective term is treated with a centered difference expression, the solution exhibits oscillations from node to node, and these only go away if a very fine grid is used. The simplest way to avoid the oscillations with a hyperbolic equation is to use upstream derivatives. If the flow is from left to right, this would give

$$\frac{dc_i}{dt} + u \frac{c_i - c_{i-1}}{\Delta x} = D \frac{c_{i+1} - 2c_i + c_{i-1}}{\Delta x^2}$$

The effect of using upstream derivatives is to add artificial or numerical diffusion to the model. This can be ascertained by rearranging the finite difference form of the convective diffusion equation

$$\frac{dc_i}{dt} + u \frac{c_{i+1} - c_{i-1}}{2\Delta x} = \left(D + \frac{u\Delta x}{2} \right) \frac{c_{i+1} - 2c_i + c_{i-1}}{\Delta x^2}$$

Thus the diffusion coefficient has been changed from

$$D \text{ to } D + \frac{u\Delta x}{2}$$

Alternatively, the diffusion coefficient has been multiplied by the factor

$$D' = D \left(1 + \frac{u\Delta x}{2D} \right) = D \left(1 + \frac{Pe_{cell}}{2} \right)$$

where $Pe_{cell} = \frac{u\Delta x}{D} = \frac{uL}{D} \frac{\Delta x}{L} = Pe \frac{\Delta x}{L}$ is called the cell Peclet number.

When the diffusion coefficient is very small (or diffusion is slow compared with convection), the Peclet number will be large. In that case, extraneous diffusion will be included in the solution unless the mesh size (denoted by Δx) is small compared with the characteristic length of the problem. To avoid this problem (by keeping the factor small), very fine meshes must be used, and the smaller the diffusion coefficient, the smaller the required mesh size.

A variety of other methods are used to obtain a good solution without using extremely fine meshes. The flux correction methods keep track of the flux of material into and out of a cell (from one node to another) and put limits on the flux to make sure that no more material

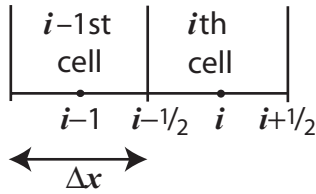


FIG. 3-52 Nomenclature for finite volume method.

leaves the cell than is there originally plus the input amount. See Finlayson, *ibid.*, for many examples.

All the methods have a limit to the time step that is set by the convection term. Essentially, the time step should not be so big as to take the material farther than it can go at its velocity. This is usually expressed as a Courant number limitation.

$$Co = \frac{u\Delta t}{\Delta x} \leq 1$$

Some methods require a smaller limit, depending upon the amount of diffusion present (see Finlayson, *ibid.*, Appendix).

In the finite element method, Petrov-Galerkin methods are used to minimize the unphysical oscillations. The Petrov-Galerkin method essentially adds a small amount of diffusion in the flow direction to smooth the unphysical oscillations. The amount of diffusion is usually proportional to Δx so that it becomes negligible as the mesh size is reduced. The value of the Petrov-Galerkin method lies in being able to obtain a smooth solution when the mesh size is large, so that the computation is feasible. This is not so crucial in one-dimensional problems, but it is essential in two- and three-dimensional problems and purely hyperbolic problems.

Finite Volume Methods Finite volume methods are utilized extensively in computational fluid dynamics. In this method, a mass balance is made over a cell, accounting for the change in what is in the cell, and the flow in and out. Figure 3-52 illustrates the geometry of the i th cell. A mass balance made on this cell (with area A perpendicular to the paper) is

$$A \Delta x (c_i^{n+1} - c_i^n) = \Delta t A (J_{i-1/2} - J_{i+1/2})$$

where J is the flux due to convection and diffusion, positive in the $+x$ direction.

$$J = uc - D \frac{\partial c}{\partial x}, \quad J_{i-1/2} = u_{i-1/2} c_{i-1/2} - D \frac{c_i - c_{i-1}}{\Delta x}$$

The concentration at the edge of the cell is taken as

$$c_{i-1/2} = \frac{1}{2}(c_i + c_{i-1})$$

Rearrangement for the case when the velocity u is the same for all nodes gives

$$\frac{c_i^{n+1} - c_i^n}{\Delta t} + \frac{u(c_{i+1} - c_{i-1})}{2\Delta x} = \frac{D}{\Delta x^2} (c_{i+1} - 2c_i + c_{i-1})$$

This is the same equation obtained by using the finite difference method. This isn't always true, and the finite volume equations are easy to derive. In two and three dimensions, the mesh need not be rectangular, as long as it is possible to compute the velocity normal to an edge of the cell. The finite volume method is useful for applications involving filling, such as injection molding, when only part of the cell is filled with fluid. Such applications do involve some approximations, since the interface is not tracked precisely, but they are useful engineering approximations.

Parabolic Equations in Two or Three Dimensions Computations become much more lengthy when there are two or more spatial dimensions. For example, we may have the unsteady heat conduction equation

$$\rho C_p \frac{\partial T}{\partial t} = k \left(\frac{\partial^2 T}{\partial x^2} + \frac{\partial^2 T}{\partial y^2} \right) - Q$$

Most engineers use computer packages to solve such problems. If there is both convection and diffusion in the problem, the same considerations apply: A fine mesh is needed when the Peclet number is large. The upstream weighting and Petrov-Galerkin methods can be used, but it is important to apply the smoothing only in the direction of flow, since smoothing in the direction transverse to the flow direction would be incorrect. Some transverse smoothing is unavoidable, but the engineer needs to be sure that the smoothing is just enough to allow a good solution without creating large errors.

Computer Software When you are choosing computer software to solve your problem, there are a number of important considerations. The first decision is whether to use an approximate, engineering flow model, developed from correlations, or to solve the partial differential equations that govern the problem. Correlations are quick and easy to apply, but they may not be appropriate to your problem or give the needed detail. When you are using a computer package to solve partial differential equations, the first task is always to generate a mesh covering the problem domain. This is not a trivial task, and special methods have been developed to permit importation of a geometry from a computer-aided design (CAD) program. Then the mesh must be created automatically. If the boundary is irregular, the finite element method is especially well suited, although special embedding techniques can be used in finite difference methods (which are designed to be solved on rectangular meshes). Another capability to consider is the ability to track free surfaces that move during the computation. This phenomenon introduces the same complexity that occurs in problems with a large Peclet number, with the added difficulty that the free surface moves between mesh points and improper representation can lead to unphysical oscillations. The method used to solve the equations is important, and both explicit and implicit methods (as described above) can be used. Implicit methods may introduce unacceptable extra diffusion, so the engineer needs to examine the solution carefully. The methods used to smooth unphysical oscillations from node to node are also important, and the engineer needs to verify that the added diffusion or smoothing does not give inaccurate solutions. Since current-day problems are mostly nonlinear, convergence is always an issue since the problems are solved iteratively. Robust programs provide several methods for convergence, each of which is best in some circumstance or other. It is wise to have a program that includes many iterative methods. If the iterative solver is not very robust, the only recourse to solving a steady-state problem may be to integrate the time-dependent problem to steady state. The solution time may be long, and the final result may be further from convergence than would be the case if a robust iterative solver were used.

A variety of computer programs are available on the Internet, some free. First consider general-purpose programs. On the NIST web page <http://gams.nist.gov/>, choose "problem decision tree" then "differential and integral equations" and then "partial differential equations." The programs are organized by type of problem (elliptic, parabolic, and hyperbolic) and by the number of spatial dimensions (one or more than one). On the Netlib web site <http://www.netlib.org/>, search on "partial differential equation." Lau (1994, 2004) provides many programs in C++ (also see <http://www.nr.com/>). The multiphysics program Comsol Multiphysics (formerly FEMLAB) (<http://www.comsol.com/>), and ANSYS (<http://www.ansys.com/>). Of these, Comsol Multiphysics is particularly useful because it has a convenient graphical-user interface, permits easy mesh generation and refinement (including adaptive mesh refinement), allows the user to add phenomena and equations easily, permits solution by continuation methods (thus enhancing

Computational fluid dynamics (CFD) programs are more specialized, and most have been designed to solve sets of equations that are appropriate to specific industries. They can then include approximations and correlations for some features that would be difficult to solve for directly. Four major packages widely used are Fluent (<http://www.fluent.com/>), CFX (now part of ANSYS), Comsol Multiphysics (formerly FEMLAB) (<http://www.comsol.com/>), and ANSYS (<http://www.ansys.com/>). Of these, Comsol Multiphysics is particularly useful because it has a convenient graphical-user interface, permits easy mesh generation and refinement (including adaptive mesh refinement), allows the user to add phenomena and equations easily, permits solution by continuation methods (thus enhancing

convergence), and has extensive graphical output capabilities. Other packages are also available (see <http://cfd-online.com/>), and these may contain features and correlations specific to the engineer's industry. One important point to note is that for turbulent flow, all the programs contain approximations, using the k -epsilon models of turbulence, or large eddy simulations; the direct numerical simulation of turbulence is too slow to apply to very big problems, although it does give insight (independent of any approximations) that is useful for interpreting turbulent phenomena. Thus, the method used to include those turbulent correlations is important, and the method also may affect convergence or accuracy.

FAST FOURIER TRANSFORM

The Fourier transform and inverse transform are

$$Y(\omega) = \int_{-\infty}^{\infty} y(t)e^{i\omega t} dt$$

$$y(t) = \frac{1}{2\pi} \int_{-\infty}^{\infty} Y(\omega)e^{-i\omega t} d\omega$$

Suppose a signal $y(t)$ is sampled at equal intervals

$$y_n = y(n\Delta), \quad n = \dots, -2, -1, 0, 1, 2, \dots$$

$\Delta =$ sampling interval (e.g., time between samples)

The Nyquist critical frequency or critical angular frequency is

$$f_c = \frac{1}{2\Delta}, \quad \omega_c = \frac{\pi}{\Delta}$$

If a function $y(t)$ is bandwidth-limited to frequencies smaller than f_c , such as

$$Y(\omega) = 0 \quad \text{for } \omega > \omega_c$$

then the function is completely determined by its samples y_n . Thus, the entire information content of a signal can be recorded by sampling at a rate $\Delta^{-1} = 2f_c$. If the function is *not* bandwidth-limited, then aliasing occurs. Once a sample rate Δ is chosen, information corresponding to frequencies greater than f_c is simply aliased into that range. The way to detect this in a Fourier transform is to see if the transform approaches zero at $\pm f_c$; if not, aliasing has occurred, and a higher sampling rate is needed.

Next, suppose we have N samples, where N is even

$$y_k = y(t_k) \quad t_k = k\Delta \quad k = 0, 1, 2, \dots, N-1$$

and the sampling interval is Δ . With only N values $\{y_k\}$, it is not possible to determine the complete Fourier transform $Y(\omega)$. We calculate the value $Y(\omega_n)$ at the discrete points

$$\omega_n = \frac{2\pi n}{N\Delta}, \quad n = -\frac{N}{2}, \dots, 0, \dots, \frac{N}{2}$$

$$Y_n = \sum_{k=0}^{N-1} y_k e^{2\pi i k n / N}$$

$$Y(\omega_n) = \Delta Y_n$$

The discrete inverse Fourier transform is

$$y_k = \frac{1}{N} \sum_{n=0}^{N-1} Y_n e^{-2\pi i k n / N}$$

The fast Fourier transform (FFT) is used to calculate the Fourier transform as well as the inverse Fourier transform. A discrete Fourier transform of length N can be written as the sum of two discrete Fourier transforms, each of length $N/2$.

$$Y_k = Y_k^e + W^k Y_k^o$$

Here Y_k is the k th component of the Fourier transform of y , and Y_k^e is the k th component of the Fourier transform of the even components

of $\{y_j\}$ and is of length $N/2$. Similarly, Y_k^o is the k th component of the Fourier transform of the odd components of $\{y_j\}$ and is of length $N/2$. W is a constant, which is taken to the k th power.

$$W = e^{2\pi i / N}$$

Since Y_k has N components, while Y_k^e and Y_k^o have $N/2$ components, Y_k^e and Y_k^o are repeated once to give N components in the calculation of Y_k . This decomposition can be used recursively. Thus, Y_k^e is split into even and odd terms of length $N/4$.

$$Y_k^e = Y_k^{ee} + W^k Y_k^{eo}$$

$$Y_k^o = Y_k^{oe} + W^k Y_k^{oo}$$

This process is continued until there is only one component. For this reason, the number N is taken as a power of 2. The vector $\{y_j\}$ is filled with zeroes, if need be, to make $N = 2^p$ for some p . The standard Fourier transform takes N^2 operations to calculate, whereas the fast Fourier transform takes only $N \log_2 N$. For large N , the difference is significant; at $N = 100$ it is a factor of 15, but for $N = 1000$ it is a factor of 100.

The discrete Fourier transform can also be used for differentiating a function, and this is used in the spectral method for solving differential equations [Gottlieb, D., and S. A. Orszag, *Numerical Analysis of Spectral Methods: Theory and Applications*, SIAM, Philadelphia (1977); Trefethen, L. N., *Spectral Methods in Matlab*, SIAM, Philadelphia (2000)]. Suppose we have a grid of equidistant points

$$x_n = n\Delta x, \quad n = 0, 1, 2, \dots, 2N-1, \quad \Delta x = \frac{L}{2N}$$

The solution is known at each of these grid points $\{y(x_n)\}$. First the discrete Fourier transform is taken:

$$Y_k = \frac{1}{2N} \sum_{n=0}^{2N-1} y(x_n) e^{-2ik\pi x_n / L}, \quad k = -N, -N+1, \dots, 0, \dots, N-1, N$$

The inverse transformation is

$$y(x) = \frac{1}{L} \sum_{k=-N}^N Y_k e^{2ik\pi x / L}$$

Differentiate this to get

$$\frac{dy}{dx} = \frac{1}{L} \sum_{k=-N}^N Y_k \frac{2\pi i k}{L} e^{2ik\pi x / L}$$

Thus at the grid points

$$\left. \frac{dy}{dx} \right|_n = \sum_{k=-N}^N Y_k \frac{2\pi i k}{L} e^{2ik\pi x_n / L}$$

The process works as follows. From the solution at all grid points the Fourier transform is obtained using FFT, $\{Y_k\}$. Then this is multiplied by $2\pi i k / L$ to obtain the Fourier transform of the derivative.

$$Y'_k = Y_k \frac{2\pi i k}{L}$$

Then the inverse Fourier transform is taken using FFT, giving the value of the derivative at each of the grid points.

$$\left. \frac{dy}{dx} \right|_n = \frac{1}{L} \sum_{k=-N}^N Y'_k e^{2ik\pi x_n / L}$$

The spectral method is used for direct numerical simulation (DNS) of turbulence. The Fourier transform is taken of the differential equation, and the resulting equation is solved. Then the inverse transformation gives the solution. When there are nonlinear terms, they are calculated at each node in physical space, and the Fourier transform is taken of the result. This technique is especially suited to time-dependent problems, and the major computational effort is in the fast Fourier transform.

OPTIMIZATION

REFERENCES: General references include the following textbooks. For nonlinear programming, Fletcher, R., *Practical Methods of Optimization*, Wiley (1987); Nocedal, J., and S. J. Wright, *Numerical Optimization*, Springer, New York (1999); Conn, A. R., N. Gould, and P. Toint, *Trust Region Methods*, SIAM, Philadelphia (2000); Edgar, T. F., D. M. Himmelblau, and L. S. Lasdon, *Optimization of Chemical Processes*, McGraw-Hill (2002). For linear programming, Dantzig, G. B., *Linear Programming and Extensions*, Princeton, N.J.: Princeton University Press, (1963); Hillier, F., and G. J. Lieberman, *Introduction to Operations Research*, Holden-Day, San Francisco (1974). For mixed integer programming, Biegler, L. T., I. E. Grossmann, and A. W. Westerberg, *Systematic Methods for Chemical Process Design*, Prentice-Hall, Englewood Cliffs, N.J. (1997); Nemhauser, G. L., and L. A. Wolsey, *Integer and Combinatorial Optimization*, Wiley-Interscience, New York (1988). For global optimization, Floudas, C. A., *Deterministic Global Optimization: Theory, Algorithms and Applications*, Kluwer Academic Publishers (2000); Horst, R., and H. Tuy, *Global Optimization: Deterministic Approaches*, Springer-Verlag, Berlin (1993); Tawarmalani, M., and N. Sahinidis, *Convexification and Global Optimization in Continuous and Mixed-Integer Nonlinear Programming: Theory, Algorithms, Software, and Applications*, Kluwer Academic Publishers (2002). Many useful resources including descriptions, trial software, and examples can be found on the NEOS server (<http://www-neos.mcs.anl.gov>) maintained at Argonne National Laboratory. Background material for this section includes the two previous sections on matrix algebra and numerical analysis.

INTRODUCTION

Optimization is a key enabling tool for decision making in chemical engineering. It has evolved from a methodology of academic interest into a technology that continues to have a significant impact on engineering research and practice. Optimization algorithms form the core tools for (1) experimental design, parameter estimation, model development, and statistical analysis; (2) process synthesis analysis, design, and retrofit; (3) model predictive control and real-time optimization; and (4) planning, scheduling, and the integration of process operations into the supply chain.

As shown in Fig. 3-53, optimization problems that arise in chemical engineering can be classified in terms of continuous and discrete variables. For the former, nonlinear programming (NLP) problems form the most general case, and widely applied specializations include linear programming (LP) and quadratic programming (QP). An important distinction for NLP is whether the optimization problem is convex or nonconvex. The latter NLP problem may have multiple local optima, and an important question is whether a global solution is required for the NLP. Another important distinction is whether the problem is assumed to be differentiable or not.

Mixed integer problems also include discrete variables. These can be written as mixed integer nonlinear programs (MINLP), or as mixed integer linear programs (MILP), if all variables appear linearly in the constraint and objective functions. For the latter an important case occurs when all the variables are integer; this gives rise to an integer programming (IP) problem. IP problems can be further classified into many special problems (e.g., assignment, traveling salesperson, etc.), which are not shown in Fig. 3-53. Similarly, the MINLP problem also gives rise to special problem classes, although here the main distinction is whether its relaxation is convex or nonconvex.

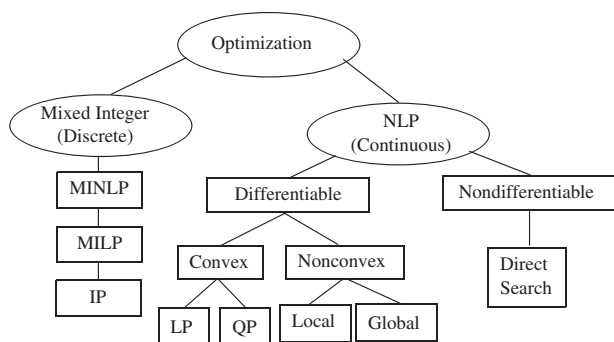


FIG. 3-53 Classes of optimization problems and algorithms.

The ingredients of formulating optimization problems include a mathematical model of the system, an objective function that quantifies a criterion to be extremized, variables that can serve as decisions, and, optionally, inequality constraints on the system. When represented in algebraic form, the general formulation of discrete/continuous optimization problems can be written as the following mixed integer optimization problem:

$$\begin{aligned} \text{Min } & f(x, y) \\ \text{subject to } & h(x, y) = 0 \\ & g(x, y) \leq 0 \\ & x \in \mathfrak{R}_n, y \in \{0, 1\} \end{aligned} \quad (3-84)$$

where $f(x, y)$ is the objective function (e.g., cost, energy consumption, etc.), $h(x, y) = 0$ are the equations that describe the performance of the system (e.g., material balances, production rates), and the inequality constraints $g(x, y) \leq 0$ can define process specifications or constraints for feasible plans and schedules. Note that the operator $\max f(x)$ is equivalent to $\min [-f(x)]$. We define the real n vector x to represent the continuous variables while the t vector y represents the discrete variables, which, without loss of generality, are often restricted to take values of 0 or 1 to define logical or discrete decisions, such as assignment of equipment and sequencing of tasks. (These variables can also be formulated to take on other integer values as well.) Problem (3-84) corresponds to a mixed integer nonlinear program when any of the functions involved are nonlinear. If all functions are linear, it corresponds to a mixed integer linear program. If there are no 0–1 variables, then problem (3-84) reduces to a nonlinear program (3-85) or linear program (3-97) depending on whether the functions are linear.

We start with continuous variable optimization and consider in the next section the solution of NLP problems with differentiable objective and constraint functions. If only local solutions are required for the NLP problem, then very efficient large-scale methods can be considered. This is followed by methods that are not based on local optimality criteria; we consider direct search optimization methods that do not require derivatives as well as deterministic global optimization methods. Following this, we consider the solution of mixed integer problems and outline the main characteristics of algorithms for their solution. Finally, we conclude with a discussion of optimization modeling software and its implementation on engineering models.

GRADIENT-BASED NONLINEAR PROGRAMMING

For continuous variable optimization we consider (3-84) without discrete variable y . The general NLP problem (3-85) is presented here:

$$\begin{aligned} \text{Min } & f(x) \\ \text{subject to } & h(x) = 0 \\ & g(x) \leq 0 \end{aligned} \quad (3-85)$$

and we assume that the functions $f(x)$, $h(x)$, and $g(x)$ have continuous first and second derivatives. A key characteristic of (3-85) is whether the problem is convex or not, i.e., whether it has a convex objective function and a convex feasible region. A function $\phi(x)$ of x in some domain X is convex if and only if for all points $x_1, x_2 \in X$

$$\phi[\alpha x_1 + (1 - \alpha)x_2] \leq \alpha\phi[x_1] + (1 - \alpha)\phi[x_2] \quad (3-86)$$

holds for all $\alpha \in (0, 1)$. [Strict convexity requires that the inequality (3-86) be strict.] Convex feasible regions require $g(x)$ to be a convex function and $h(x)$ to be linear. If (3-85) is a convex problem, then any local solution is guaranteed to be a global solution to (3-85). Moreover, if the objective function is strictly convex, then this solution x^* is unique. On the other hand, nonconvex problems may have multiple local solutions, i.e., feasible solutions that minimize the objective function within some neighborhood about the solution.

We consider first methods that find only local solutions to nonconvex problems, as more difficult (and expensive) search procedures are required to find a global solution. Local methods are currently very

efficient and have been developed to deal with very large NLP problems. Moreover, by considering the structure of convex NLP problems (including LP and QP problems), even more powerful methods can be applied. To study these methods, we first consider conditions for local optimality.

Local Optimality Conditions: A Kinematic Interpretation
 Instead of a formal development of conditions that define a local optimum, we present a more intuitive kinematic illustration. Consider the contour plot of the objective function $f(x)$, given in Fig. 3-54, as a smooth valley in space of the variables x_1 and x_2 . For the contour plot of this unconstrained problem $\text{Min } f(x)$, consider a ball rolling in this valley to the lowest point of $f(x)$, denoted by x^* . This point is at least a local minimum and is defined by a point with a zero gradient and at least nonnegative curvature in all (nonzero) directions p . We use the first-derivative (*gradient*) vector $\nabla f(x)$ and second-derivative (*Hessian*) matrix $\nabla_{xx} f(x)$ to state the necessary first- and second-order conditions for unconstrained optimality:

$$\nabla_x f(x^*) = 0 \quad p^T \nabla_{xx} f(x^*) p \geq 0 \quad \text{for all } p \neq 0 \quad (3-87)$$

These necessary conditions for local optimality can be strengthened to sufficient conditions by making the inequality in (3-87) strict (i.e., positive curvature in all directions). Equivalently, the sufficient (necessary) curvature conditions can be stated as follows: $\nabla_{xx} f(x^*)$ has all positive (nonnegative) eigenvalues and is therefore defined as a positive (semidefinite) definite matrix.

Now consider the imposition of inequality [$g(x) \leq 0$] and equality constraints [$h(x) = 0$] in Fig. 3-55. Continuing the kinematic interpretation, the inequality constraints $g(x) \leq 0$ act as “fences” in the valley, and equality constraints $h(x) = 0$ act as “rails.” Consider now a ball, constrained on a rail and within fences, to roll to its lowest point. This stationary point occurs when the normal forces exerted by the fences [$-\nabla g(x^*)$] and rails [$-\nabla h(x^*)$] on the ball are balanced by the force of gravity [$-\nabla f(x^*)$]. This condition can be stated by the following *Karush-Kuhn-Tucker (KKT) necessary conditions* for constrained optimality:

Balance of Forces It is convenient to define the L function $L(x, \lambda, \nu) = f(x) + g(x)^T \lambda + h(x)^T \nu$, along with “weights” or multipliers λ and ν for the constraints. The stationarity condition (balance of forces acting on the ball) is then given by

$$\nabla L(x, \lambda, \nu) = \nabla f(x) + \nabla h(x)\lambda + \nabla g(x)\nu = 0 \quad (3-88)$$

Feasibility Both inequality and equality constraints must be satisfied (ball must lie on the rail and within the fences):

$$h(x) = 0, \quad g(x) \leq 0 \quad (3-89)$$

Complementarity Inequality constraints are either strictly satisfied (active) or inactive, in which case they are irrelevant to the solu-

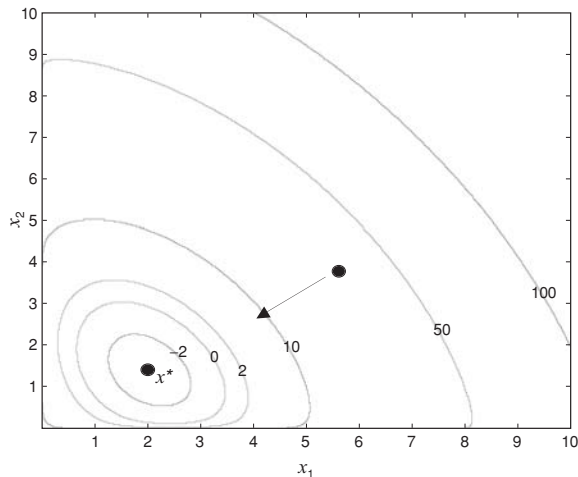


FIG. 3-54 Unconstrained minimum.

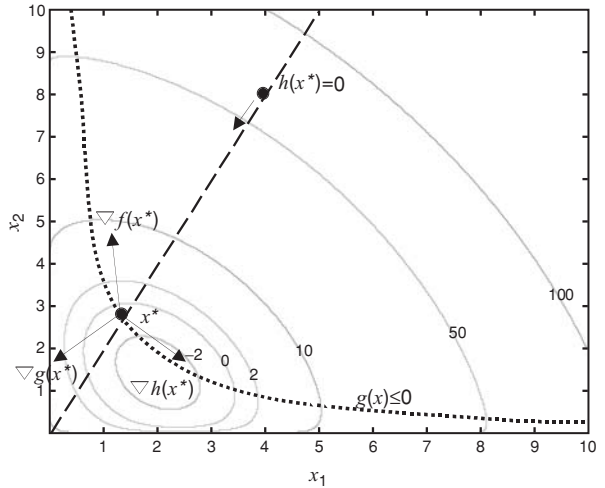


FIG. 3-55 Constrained minimum.

tion. In the latter case the corresponding KKT multiplier must be zero. This is written as

$$\nu^T g(x) = 0, \quad \nu \geq 0 \quad (3-90)$$

Constraint Qualification For a local optimum to satisfy the KKT conditions, an additional regularity condition is required on the constraints. This can be defined in several ways. A typical condition is that the active constraints at x^* be linearly independent; i.e., the matrix: $[\nabla h(x^*) | \nabla g_A(x^*)]$ is full column rank, where g_A is the vector of inequality constraints with elements that satisfy $g_{A,i}(x^*) = 0$. With this constraint qualification, the KKT multipliers (λ, ν) are guaranteed to be unique at the optimal solution.

Second-Order Conditions As with unconstrained optimization, nonnegative (positive) curvature is necessary (sufficient) in all the allowable (i.e., constrained) nonzero directions p . The necessary second-order conditions can be stated as

$$p^T \nabla_{xx} L(x^*) p \geq 0 \quad \text{for all } p \neq 0, \nabla h(x^*)^T p = 0, \nabla g(x^*)^T p \geq 0, \nabla g_A(x^*)^T p = 0 \quad (3-91)$$

and the corresponding sufficient conditions require first the inequality in (3-91) to be strict. Note that for the example in Fig. 3-54, the allowable directions p span the entire space for x while in Fig. 3-55 there are *no* allowable directions p .

Example To illustrate the KKT conditions, consider the following unconstrained NLP problem:

$$\text{Min } (x_1)^2 - 4x_1 + 3/2 (x_2)^2 - 7x_2 + x_1 x_2 + 9 - \ln x_1 - \ln x_2 \quad (3-92)$$

corresponding to the contour plot in Fig. 3-54. The optimal solution can be found by solving for the first-order conditions (3-87):

$$\nabla f(x) = \begin{bmatrix} 2x_1 - 4 + x_2 - 1/x_1 \\ 3x_2 - 7 + x_1 - 1/x_2 \end{bmatrix} = 0 \Rightarrow x^* = \begin{bmatrix} 1.3475 \\ 2.0470 \end{bmatrix} \quad (3-93)$$

and $f(x^*) = -2.8742$. Checking the second-order conditions leads to

$$\begin{aligned} \nabla_{xx} f(x^*) &= \begin{bmatrix} 2 + 1/(x_1^*)^2 & 1 \\ 1 & 3 + 1/(x_2^*)^2 \end{bmatrix} \\ \Rightarrow \nabla_{xx} f(x^*) &= \begin{bmatrix} 2.5507 & 1 \\ 1 & 3.2387 \end{bmatrix} \quad (\text{positive definite}) \end{aligned} \quad (3-94)$$

Now consider the constrained NLP problems

$$\begin{aligned} \text{Min } (x_1)^2 - 4x_1 + 3/2(x_2)^2 - 7x_2 + x_1 x_2 + 9 - \ln x_1 - \ln x_2 \\ \text{subject to } 4 - x_1 x_2 \leq 0 \\ 2x_1 - x_2 = 0 \end{aligned} \quad (3-95)$$

that correspond to the plot in Fig. 3-54. The optimal solution can be found by

applying the first-order KKT conditions (3-88) to (3-90):

$$\begin{aligned} \nabla L(x, \lambda, v) &= \nabla f(x) + \nabla h(x)\lambda + \nabla g(x)v = \begin{bmatrix} 2x_1 - 4 + x_2 - 1/x_1 \\ 3x_2 - 7 + x_1 - 1/x_2 \end{bmatrix} \\ &\quad + \begin{bmatrix} 2 \\ -1 \end{bmatrix} \lambda + \begin{bmatrix} -x_2 \\ -x_1 \end{bmatrix} v = 0 \\ g(x) &= 4 - x_1x_2 \leq 0, \quad h(x) = 2x_1 - x_2 = 0 \\ g(x)v &= (4 - x_1x_2)v, \quad v \geq 0 \end{aligned} \tag{3-96}$$

$$\Downarrow$$

$$x^* = \begin{bmatrix} 1.4142 \\ 2.8284 \end{bmatrix}, \quad \lambda^* = 1.036, \quad v^* = 1.068$$

and $f(x^*) = -1.8421$. Checking the second-order conditions (3-91) leads to

$$\begin{aligned} \nabla_{xx}L(x^*, \lambda^*, v^*) &= \nabla_{xx}[f(x^*) + h(x^*)\lambda^* + g(x^*)v^*] = \begin{bmatrix} 2 + 1/(x_1)^2 & 1 - v \\ 1 - v & 3 + 1/(x_2)^2 \end{bmatrix} \\ &= \begin{bmatrix} 2.5 & 0.068 \\ 0.068 & 3.125 \end{bmatrix} \\ [\nabla h(x^*) \mid \nabla g_A(x^*)]^T p &= \begin{bmatrix} 2 & -2.8284 \\ -1 & -1.4142 \end{bmatrix}^T p = 0, \quad p \neq 0 \end{aligned}$$

However, note that because $[\nabla h(x^*) \mid \nabla g_A(x^*)]$ is nonsingular, there are no nonzero vectors p that satisfy the allowable directions. Hence, the sufficient second-order conditions $[p^T \nabla_{xx}L(x^*, \lambda^*, v^*)p > 0, \text{ for all allowable } p]$ are *vacuously satisfied* for this problem.

Convex Cases of NLP Problems Linear programs and quadratic programs are special cases of (3-85) that allow for more efficient solution, based on application of KKT conditions (3-88) through (3-91). Because these are convex problems, any locally optimal solution is a global solution. In particular, if the objective and constraint functions in (3-85) are linear, then the following linear program (LP)

$$\begin{aligned} \text{Min } & c^T x \\ \text{subject to } & Ax = b \\ & Cx \leq d \end{aligned} \tag{3-97}$$

can be solved in a finite number of steps, and the optimal solution lies at a vertex of the polyhedron described by the linear constraints. This is shown in Fig. 3-56, and in so-called primal degenerate cases, multiple vertices can be alternate optimal solutions, with the same values of the objective function. The standard method to solve (3-97) is the simplex method, developed in the late 1940s (see Dantzig, 1963) although, starting from Karmarkar's discovery in 1984, interior point methods have become quite advanced and competitive for highly constrained problems [Wright, S. J., *Primal-Dual Interior Point Methods*,

SIAM, Philadelphia (1996)]. The simplex method proceeds by moving successively from vertex to vertex with improved objective function values. Methods to solve (3-97) are well implemented and widely used, especially in planning and logistical applications. They also form the basis for MILP methods discussed later. Currently, state-of-the-art LP solvers can handle millions of variables and constraints, and the application of further decomposition methods leads to the solution of problems that are two or three orders of magnitude larger than this. See the general references of Hillier and Lieberman (1974) and Edgar et al. (2002) for more details. Also, the interior point method is described below from the perspective of more general NLP problems.

Quadratic programs (QPs) represent a slight modification of (3-97) and can be stated as

$$\begin{aligned} \text{Min } & c^T x + 1/2 x^T Q x \\ \text{subject to } & Ax = b \\ & Cx \leq d \end{aligned} \tag{3-98}$$

If the matrix Q is positive semidefinite (positive definite) when projected into the null space of the active constraints, then (3-98) is (strictly) convex and the QP is a global (and unique) minimum. Otherwise, local solutions exist for (3-98), and more extensive global optimization methods are needed to obtain the global solution. Like LPs, convex QPs can be solved in a finite number of steps. However, as seen in Fig. 3-57, these optimal solutions can lie on a vertex, on a constraint boundary, or in the interior. A number of active set strategies have been created that solve the KKT conditions of the QP and incorporate efficient updates of active constraints. Popular methods include null space algorithms, range space methods, and Schur complement methods. As with LPs, QP problems can also be solved with interior point methods [see Wright (1996)].

Solving the General NLP Problem Solution techniques for (3-85) deal with satisfaction of the KKT conditions (3-88) through (3-91). Many NLP solvers are based on successive quadratic programming (SQP) as it allows the construction of a number of NLP algorithms based on the Newton-Raphson method for equation solving (see "Numerical Analysis" section). SQP solvers have been shown to require the fewest function evaluations to solve NLP problems [Schittkowski, K., *Lecture Notes in Economics and Mathematical Systems*, no. 282, Springer-Verlag, Berlin (1987)], and they can be tailored to a broad range of process engineering problems with different structure.

The SQP strategy applies the equivalent of a Newton step to the KKT conditions of the nonlinear programming problem, and this leads to a fast rate of convergence. By adding slack variables s , the first-order KKT conditions can be rewritten as

$$\begin{aligned} \nabla f(x) + \nabla h(x)\lambda + \nabla g(x)v &= 0 & (3-99a) \\ h(x) &= 0 & (3-99b) \end{aligned}$$

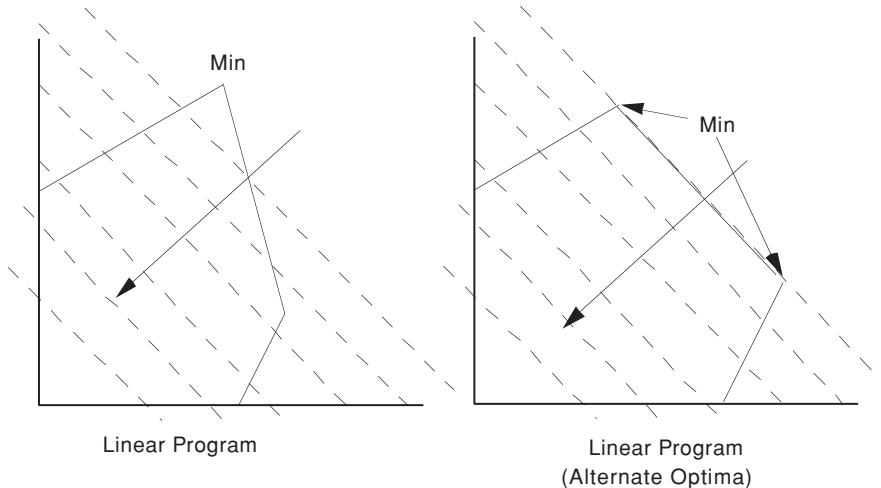


FIG. 3-56 Contour plots of linear programs.

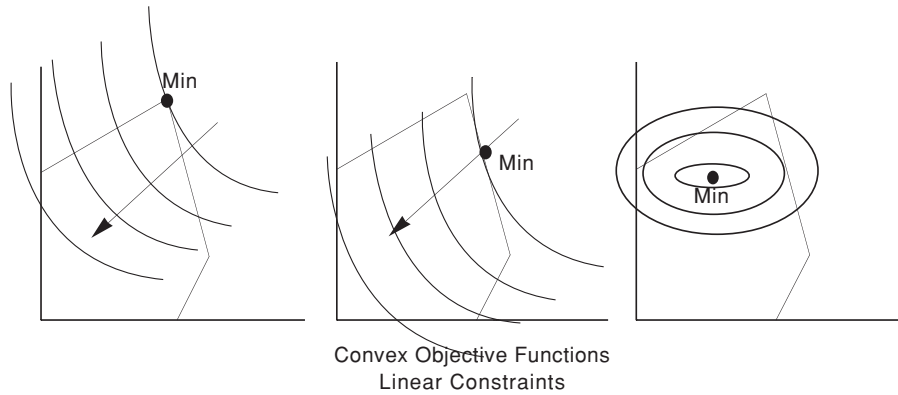


FIG. 3-57 Contour plots of convex quadratic programs.

$$g(x) + s = 0 \quad (3-99c)$$

$$Sve = 0 \quad (3-99d)$$

$$(s, v) \geq 0 \quad (3-99e)$$

where $e = [1, 1, \dots, 1]^T$, $S = \text{diag}\{s\}$, and $V = \text{diag}\{v\}$. SQP methods find solutions that satisfy (3-99) by generating Newton-like search directions at iteration k . However, Eqs. (3-99d) and active bounds (3-99e) are dependent at the solution and serve to make the KKT system ill-conditioned near the solution. SQP algorithms treat these conditions in two ways. In the *active set strategy*, discrete decisions are made regarding the active constraint set $i \in I = \{i | g_i(x^*) = 0\}$ and (3-99d) is replaced by $s_i = 0$, $i \in I$, and $v_i = 0$, $i \notin I$. Determining the active set is a combinatorial problem, and a straightforward way to determine an estimate of the active set [and to satisfy (3-99e)] is to formulate and solve, at a point x^k , the following QP at iteration k :

$$\begin{aligned} \text{Min } & \nabla f(x^k)^T p + 1/2 p^T \nabla_{xx} L(x^k, \lambda^k, v^k) p \\ \text{subject to } & h(x^k) + \nabla h(x^k)^T p = 0 \\ & g(x^k) + \nabla g(x^k)^T p + s = 0, \quad s \geq 0 \end{aligned} \quad (3-100)$$

The KKT conditions of (3-100) are given by

$$\nabla f(x^k) + \nabla^2 L(x^k, \lambda^k, v^k) p + \nabla h(x^k) \lambda + \nabla g(x^k) v = 0 \quad (3-101a)$$

$$h(x^k) + \nabla h(x^k)^T p = 0 \quad (3-101b)$$

$$g(x^k) + \nabla g(x^k)^T p + s = 0 \quad (3-101c)$$

$$Sve = 0 \quad (3-101d)$$

$$(s, v) \geq 0 \quad (3-101e)$$

where the Hessian of the Lagrange function $\nabla_{xx} L(x, \lambda, v) = \nabla_{xx} [f(x) + h(x)^T \lambda + g(x)^T v]$ is calculated directly or through a quasi-Newton approximation (created by differences of gradient vectors). It is easy to show that (3-101a) through (3-101c) correspond to a Newton-Raphson step for (3-99a) through (3-99c) applied at iteration k . Also, selection of the active set is now handled at the QP level by satisfying the conditions (3-101d) and (3-101e). To evaluate and change candidate active sets, QP algorithms apply inexpensive matrix updating strategies to the KKT matrix associated with (3-100). Details of this approach can be found in Nocedal and Wright (1999) and Fletcher (1987).

As alternatives that avoid the combinatorial problem of selecting the active set, interior point (or barrier) methods modify the NLP problem (3-85) to form

$$\begin{aligned} \text{Min } & f(x^k) - \mu \sum_i \ln s_i \\ \text{subject to } & h(x^k) = 0 \\ & g(x^k) + s = 0 \end{aligned} \quad (3-102)$$

where the solution to (3-103) has $s > 0$ for the penalty parameter $\mu > 0$, and decreasing μ to 0 leads to solution of problem (3-85). The KKT conditions for this problem can be written as

$$\nabla f(x^*) + \nabla h(x^*) \lambda + \nabla g(x^*) v = 0$$

$$\begin{aligned} h(x^*) &= 0 \\ g(x^*) + s &= 0 \\ Sve &= \mu e \end{aligned} \quad (3-103)$$

and for $\mu > 0$, $s > 0$, and $v > 0$, Newton steps generated to solve (3-103) are well behaved and analogous to (3-101), with a modification on the right-hand side of (3-101d). A detailed description of this algorithm, called IPOPT, can be found in Wächter and Biegler [*Math. Prog.* **106**(1), 25–57 (2006)].

Both active set and interior point methods possess clear tradeoffs. Interior point methods may require more iterations to solve (3-102) for various values of μ , while active set methods require the solution of the more expensive QP subproblem (3-100). Thus, if there are few inequality constraints or an active set is known (say from a good starting guess, or a known QP solution from a previous iteration), then solving (3-100) is not expensive and the active set method is favored. On the other hand, for problems with many inequality constraints, interior point methods are often faster, as they avoid the combinatorial problem of selecting the active set. This is especially true for large-scale problems and when a large number of bounds are active. Examples that demonstrate the performance of these approaches include the solution of model predictive control (MPC) problems [Rao et al., *J. Optim. Theory Appl.* **99**:723 (1998); Albuquerque et al., *Comp. Chem. Eng.* **23**:283 (1997)] and the solution of large optimal control problems using barrier NLP solvers. For instance, IPOPT allows the solution of problems with more than 1,000,000 variables and up to 50,000 degrees of freedom [see Biegler et al., *Chem. Eng. Sci.* **57**(4):575–593 (2002); Laird et al., *ASCE J. Water Resource Management and Planning* **131**(2):125 (2005)].

Other Gradient-Based NLP Solvers In addition to SQP methods, a number of NLP solvers have been developed and adapted for large-scale problems. Generally these methods require more function evaluations than of SQP methods, but they perform very well when interfaced to optimization modeling platforms, where function evaluations are cheap. All these can be derived from the perspective of applying Newton steps to portions of the KKT conditions.

LANCELOT (Conn et al., 2000) is based on the solution of bound-constrained subproblems. Here an augmented Lagrangian is formed from (3-85) and the following subproblem is solved:

$$\begin{aligned} \text{Min } & f(x) + \lambda^T h(x) + v^T [g(x) + s] + 1/2 \rho \|h(x), g(x) + s\|^2 \\ \text{subject to } & s \geq 0 \end{aligned} \quad (3-104)$$

The above subproblem can be solved very efficiently for fixed values of the multipliers λ and v and penalty parameter ρ . Here a gradient projection trust region method is applied. Once subproblem (3-104) is solved, the multipliers and penalty parameter are updated in an outer loop and the cycle repeats until the KKT conditions for (3-85) are satisfied. LANCELOT works best when exact second derivatives are available. This promotes a fast convergence rate in solving each

subproblem and allows a bound-constrained trust region method to exploit directions of negative curvature in the Hessian matrix.

Reduced gradient methods are active set strategies that rely on partitioning the variables and solving (3-99) in a nested manner. Without loss of generality, problem (3-85) can be rewritten as $\text{Min } f(z)$ subject to $c(z) = 0$, $a \leq z \leq b$. Variables are partitioned as nonbasic variables (those fixed to their bounds), basic variables (those that can be solved from the equality constraints), and superbasic variables (those remaining variables between bounds that serve to drive the optimization); this leads to $z^T = [z_N^T, z_B^T, z_S^T]$. This partition is derived from local information and may change over the course of the optimization iterations. The corresponding KKT conditions can be written as

$$\nabla_N f(z) + \nabla_N c(z)\gamma = \beta_a - \beta_b \quad (3-105a)$$

$$\nabla_B f(z) + \nabla_B c(z)\gamma = 0 \quad (3-105b)$$

$$\nabla_S f(z) + \nabla_S c(z)\gamma = 0 \quad (3-105c)$$

$$c(z) = 0 \quad (3-105d)$$

$$z_{N,j} = a_j \text{ or } b_j, \quad \beta_{a,j} \geq 0, \quad \beta_{b,j} = 0 \text{ or } \beta_{b,j} \geq 0, \quad \beta_{a,j} = 0 \quad (3-105e)$$

where γ and β are the KKT multipliers for the equality and bound constraints, respectively, and (3-105e) replaces the complementarity conditions (3-90). Reduced gradient methods work by nesting equations (3-105b,d) within (3-105a,c). At iteration k , for fixed values of z_N^k and z_S^k , we can solve for z_B by using (3-105d) and for γ by using (3-105b). Moreover, linearization of these equations leads to sensitivity information (i.e., constrained derivatives or reduced gradients) that indicates how z_B changes with respect to z_S and z_N . The algorithm then proceeds by updating z_S by using reduced gradients in a Newton-type iteration to solve Eq. (3-105c). Following this, bound multipliers β are calculated from (3-105a). Over the course of the iterations, if the variables z_B or z_S exceed their bounds or if some bound multipliers β become negative, then the variable partition needs to be changed and Eqs. (3-105) are reconstructed. These reduced gradient methods are embodied in the popular GRG2, CONOPT, and SOLVER codes (Edgar et al., 2002). The SOLVER code has been incorporated into Microsoft Excel. CONOPT [Drud, A., *ORSA J. Computing* **6**: 207–216 (1994)] is an efficient and widely used code in several optimization modelling environments.

MINOS (Murtagh and Saunders, Technical Report SOL 83-20R, Stanford University, 1987) is a well-implemented package that offers a variation on reduced gradient strategies. At iteration k , Eq. (3-105d) is replaced by its linearization

$$c(z_N^k, z_B^k, z_S^k) + \nabla_B c(z^k)^T (z_B - z_B^k) + \nabla_S c(z^k)^T (z_S - z_S^k) = 0 \quad (3-106)$$

and Eqs. (3-105a–c, e) are solved with (3-106) as a subproblem by using concepts from the reduced gradient method. At the solution of this subproblem, constraints (3-105d) are relinearized and the cycle repeats until the KKT conditions of (3-105) are satisfied. The augmented lagrangian function from (3-104) is used to penalize movement away from the feasible region. For problems with few degrees of freedom, the resulting approach leads to an extremely efficient method even for very large problems. MINOS has been interfaced to a number of modelling systems and enjoys widespread use. It performs especially well on large problems with few nonlinear constraints. However, on highly nonlinear problems it is usually less reliable than other reduced gradient methods.

Algorithmic Details for NLP Methods All the above NLP methods incorporate concepts from the Newton-Raphson method for equation solving. Essential features of these methods are that they provide (1) accurate derivative information to solve for the KKT conditions, (2) stabilization strategies to promote convergence of the Newton-like method from poor starting points, and (3) regularization of the Jacobian matrix in Newton's method (the so-called KKT matrix) if it becomes singular or ill-conditioned.

1. *NLP methods provide first and second derivatives.* The KKT conditions require first derivatives to define stationary points, so accurate first derivatives are essential to determine locally optimal solutions for differentiable NLPs. Moreover, Newton-Raphson methods that are applied to the KKT conditions, as well as the task of checking second-order KKT conditions, necessarily require second-

derivative information. (Note that second-order conditions are not checked by methods that do not use second derivatives.) With the recent development of automatic differentiation tools, many modeling and simulation platforms can provide exact first and second derivatives for optimization. When second derivatives are available for the objective or constraint functions, they can be used directly in LANCELOT as well as SQP and reduced gradient methods. Otherwise, on problems with few superbasic variables, both reduced gradient methods and SQP methods [with reduced gradient methods applied to the QP subproblem (3-100)] can benefit from positive definite quasi-Newton approximations [Nocedal and Wright (1999)] applied to reduced second-derivative quantities (the so-called reduced Hessian). Finally, for problems with least squares functions (see “Statistics” subsection), as in data reconciliation, parameter estimation, and model predictive control, one can often assume that the values of the objective function and its gradient at the solution are vanishingly small. Under these conditions, one can show that the multipliers (λ, v) also vanish and $\nabla_{xx} L(x, \lambda, v)$ can be substituted by $\nabla_{xx} f(x^*)$. This *Gauss-Newton approximation* has been shown to be very efficient for the solution of least squares problems [see Nocedal and Wright (1999)].

2. *Line search and trust region methods promote convergence from poor starting points.* These are commonly used with the search directions calculated from NLP subproblems such as (3-100). In a *trust region approach*, the constraint $\|p\| \leq \Delta$ is added and the iteration step is taken if there is sufficient reduction of some merit function (e.g., the objective function weighted with some measure of the constraint violations). The size of the trust region Δ is adjusted based on the agreement of the reduction of the actual merit function compared to its predicted reduction from the subproblem (see Conn et al., 2000, for details). Such methods have strong global convergence properties and are especially appropriate for ill-conditioned NLPs. This approach has been applied in the KNITRO code [Byrd, Hribar, and Nocedal, *SIAM J. Optimization* **9**(4):877 (1999)]. *Line search methods* can be more efficient on problems with reasonably good starting points and well-conditioned subproblems, as in real-time optimization. Typically, once a search direction is calculated from (3-100), or other related subproblem, a step size $\alpha \in (0, 1)$ is chosen so that $x^k + \alpha p$ leads to a sufficient decrease of a merit function. As a recent alternative, a novel *filter* stabilization strategy (for both line search and trust region approaches) has been developed based on a bicriterion minimization, with the objective function and constraint infeasibility as competing objectives [Fletcher et al., *SIAM J. Optimization* **13**(3):635 (2002)]. This method often leads to better performance than that based on merit functions.

3. *Regularization of the KKT matrix for the NLP subproblem is essential for good performance of general-purpose algorithms.* For instance, to obtain a unique solution to (3-100), active constraint gradients must be full rank and the Hessian matrix, when projected into the null space of the active constraint gradients, must be positive definite. These properties may not hold far from the solution, and corrections to the Hessian in SQP may be necessary (see Fletcher, 1987). Regularization methods ensure that subproblems such as (3-100) remain well-conditioned; they include addition of positive constants to the diagonal of the Hessian matrix to ensure its positive definiteness, judicious selection of active constraint gradients to ensure that they are linearly independent, and scaling the subproblem to reduce the propagation of numerical errors. Often these strategies are heuristics built into particular NLP codes. While quite effective, most of these heuristics do not provide convergence guarantees for general NLPs.

From the conceptual descriptions as well as algorithmic details given above, it is clear that NLP solvers are complex algorithms that have required considerable research and development to turn them into reliable and efficient software tools. Practitioners who are confronted with engineering optimization problems should therefore leverage these efforts, rather than write their own codes. Table 3-4 presents a sampling of available NLP codes that represent the above classifications. Much more information on these and other codes can be found on the NEOS server (www-neos.mcs.anl.gov) and the NEOS Software Guide: <http://www-fp.mcs.anl.gov/otc/Guide/SoftwareGuide>.

TABLE 3-4 Representative NLP Solvers

Method	Algorithm type	Stabilization	Second-order information
CONOPT (Drud, 1994)	Reduced gradient	Line search	Exact and quasi-Newton
GRC2 (Edgar et al., 2002)	Reduced gradient	Line search	Quasi-Newton
IPOPT	SQP, barrier	Line search	Exact
KNITRO (Byrd et al., 1997)	SQP, barrier	Trust region	Exact and quasi-Newton
LANCELOT	Augmented lagrangian, bound constrained	Trust region	Exact and quasi-Newton
LOQO	SQP, barrier	Line search	Exact
MINOS	Reduced gradient, augmented lagrangian	Line search	Quasi-Newton
NPSOL	SQP, active set	Line search	Quasi-Newton
SNOPT	Reduced space SQP, active set	Line search	Quasi-Newton
SOCS	SQP, active set	Line search	Exact
SOLVER	Reduced gradient	Line search	Quasi-Newton
SRQP	Reduced space SQP, active set	Line search	Quasi-Newton

OPTIMIZATION METHODS WITHOUT DERIVATIVES

A broad class of optimization strategies does not require derivative information. These methods have the advantage of easy implementation and little prior knowledge of the optimization problem. In particular, such methods are well suited for "quick and dirty" optimization studies that explore the scope of optimization for new problems, prior to investing effort for more sophisticated modeling and solution strategies. Most of these methods are derived from heuristics that naturally spawn numerous variations. As a result, a very broad literature describes these methods. Here we discuss only a few important trends in this area.

Classical Direct Search Methods Developed in the 1960s and 1970s, these methods include one-at-a-time search and methods based on experimental designs (EVOP). At that time, these direct search methods were the most popular optimization methods in chemical engineering. Methods that fall into this class include the pattern search of Hooke and Jeeves [*J. ACM* **8**:212 (1961)], the conjugate direction method of Powell (1964), simplex and complex searches, in particular Nelder-Mead [*Comput. J.* **7**: 308 (1965)], and the adaptive random search methods of Luus-Jaakola [*AIChE J.* **19**: 760 (1973)], Goulcher and Cesares Long [*Comp. Chem. Engr.* **2**: 23 (1978)] and

Banga et al. [in *State of the Art in Global Optimization*, C. Floudas and P. Pardalos (eds.), Kluwer, Dordrecht, p. 563 (1996)]. All these methods require only objective function values for unconstrained minimization. Associated with these methods are numerous studies on a wide range of process problems. Moreover, many of these methods include heuristics that prevent premature termination (e.g., directional flexibility in the complex search as well as random restarts and direction generation). To illustrate these methods, Fig. 3-58 illustrates the performance of a pattern search method as well as a random search method on an unconstrained problem.

Simulated Annealing This strategy is related to random search methods and derives from a class of heuristics with analogies to the motion of molecules in the cooling and solidification of metals [Laarhoven and Aarts, *Simulated Annealing: Theory and Applications*, Reidel Publishing, Dordrecht (1987)]. Here a temperature parameter θ can be raised or lowered to influence the probability of accepting points that do not improve the objective function. The method starts with a base point x and objective value $f(x)$. The next point x' is chosen at random from a distribution. If $f(x') < f(x)$, the move is accepted with x' as the new point. Otherwise, x' is accepted with probability $p(\theta, x', x) = \exp\{-[f(x') - f(x)]/\theta\}$ and the Glauber distribution, $p(\theta, x, x') = \exp\{-[f(x') - f(x)]/\theta\} / (1 + \exp\{-[f(x') - f(x)]/\theta\})$. The θ parameter is then reduced, and the method continues until no further progress is made.

Genetic Algorithms This approach, first proposed in Holland, J. H., *Adaptations in Natural and Artificial Systems* [University of Michigan Press, Ann Arbor (1975)], is based on the analogy of improving a population of solutions through modifying their gene pool. It also has similar performance characteristics as random search methods and simulated annealing. Two forms of genetic modification, crossover or mutation, are used and the elements of the optimization vector \mathbf{x} are represented as binary strings. Crossover deals with random swapping of vector elements (among parents with highest objective function values or other rankings of population) or any linear combinations of two parents. Mutation deals with the addition of a random variable to elements of the vector. Genetic algorithms (GAs) have seen widespread use in process engineering, and a number of codes are available. Edgar et al. (2002) describe a related GA that is available in MS Excel.

Derivative-free Optimization (DFO) In the past decade, the availability of parallel computers and faster computing hardware and the need to incorporate complex simulation models within optimization studies have led a number of optimization researchers to reconsider classical direct search approaches. In particular, Dennis and Torczon [*SIAM J. Optim.* **1**: 448 (1991)] developed a multidimensional search algorithm that extends the simplex approach of Nelder

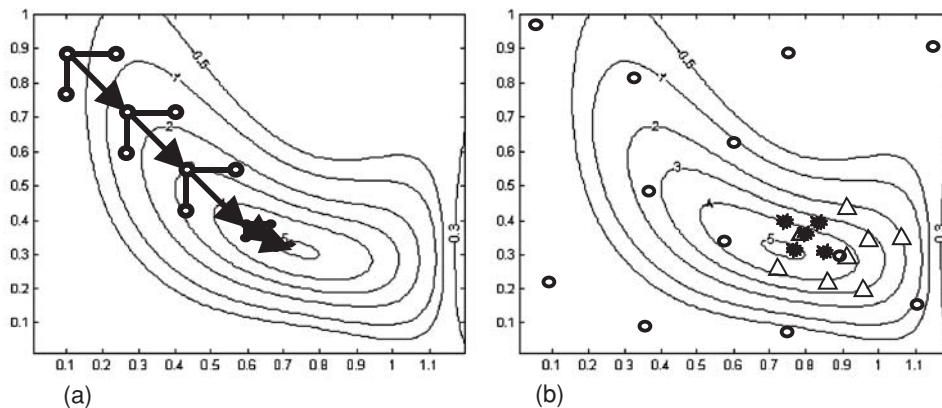


FIG. 3-58 Examples of optimization methods without derivatives. (a) Pattern search method. (b) Random search method. \circ , first phase; Δ , second phase; \square , third phase.

and Mead (1965). They note that the Nelder-Mead algorithm fails as the number of variables increases, even for very simple problems. To overcome this, their multidimensional pattern search approach combines reflection, expansion, and contraction steps that act as line search algorithms for a number of linear independent search directions. This approach is easily adapted to parallel computation, and the method can be tailored to the number of processors available. Moreover, this approach converges to locally optimal solutions for unconstrained problems and observes an unexpected performance synergy when multiple processors are used. The work of Dennis and Torczon (1991) has spawned considerable research on the analysis and code development for DFO methods. For instance, Conn et al. [*Math. Programming*, Series B, **79**(3): 397 (1997)] constructed a multivariable DFO algorithm that uses a surrogate model for the objective function within a trust region method. Here points are sampled to obtain a well-defined quadratic interpolation model, and descent conditions from trust region methods enforce convergence properties. A number of trust region methods that rely on this approach are reviewed in Conn et al. (1997). Moreover, a number of DFO codes have been developed that lead to black box optimization implementations for large, complex simulation models [see Audet and Dennis, *SIAM J. Optim.* **13**: 889 (2003); Kolda et al., *SIAM Rev.* **45**(3): 385 (2003)]. These include the DAKOTA package at Sandia National Lab (Eldred, 2002; <http://endo.sandia.gov/DAKOTA/software.html>) and FOCUS developed at Boeing Corporation (Booker et al., CRPC Technical Report 98739, Rice University, February 1998).

Direct search methods are easy to apply to a wide variety of problem types and optimization models. Moreover, because their termination criteria are not based on gradient information and stationary points, they are more likely to favor the search for globally optimal rather than locally optimal solutions. These methods can also be adapted easily to include integer variables. However, no rigorous convergence properties to globally optimal solutions have yet been discovered. Also, these methods are best suited for unconstrained problems or for problems with simple bounds. Otherwise, they may have difficulties with constraints, as the only options open for handling constraints are equality constraint elimination and addition of penalty functions for inequality constraints. Both approaches can be unreliable and may lead to failure of the optimization algorithm. Finally, the performance of direct search methods scales poorly (and often exponentially) with the number of decision variables. While performance can be improved with the use of parallel computing, these methods are rarely applied to problems with more than a few dozen decision variables.

GLOBAL OPTIMIZATION

Deterministic optimization methods are available for nonconvex nonlinear programming problems of the form (3-85) that guarantee convergence to the global optimum. More specifically, one can show under mild conditions that they converge to an ϵ distance to the global optimum in a finite number of steps. These methods are generally more expensive than local NLP methods, and they require the exploitation of the structure of the nonlinear program.

Because there are no optimality conditions like the KKT conditions for global optimization, these methods work by first partitioning the problem domain (i.e., containing the feasible region) into subregions. Upper bounds on the objective function are computed over all subregions of the problem. In addition, lower bounds can be derived from convex relaxations of the objective function and constraints for each subregion. The algorithm then proceeds to eliminate all subregions that have infeasible constraint relaxations or lower bounds that are greater than the least upper bound. After this, the remaining regions are further partitioned to create new subregions, and the cycle continues until the upper and lower bounds converge.

This basic concept leads to a wide variety of global algorithms, with the following features that can exploit different problem classes. *Bounding* strategies relate to the calculation of upper and lower bounds. For the former, any feasible point or, preferably, a locally optimal point in the subregion can be used. For the lower bound, convex relaxations of the objective and constraint functions are derived.

The *refining* step deals with the construction of partitions in the domain and further partitioning them during the search process. Finally, the *selection* step decides on the order of exploring the open subregions.

For simplicity, consider the problem $\text{Min } f(x)$ subject to $g(x) \leq 0$ where each function can be defined by additive terms. Convex relaxations for $f(x)$ and $g(x)$ can be derived in the following ways:

- Convex additive terms remain unmodified in these functions.
- Concave additive unary terms are replaced by a linear underestimating function that matches the term at the bounds of the subregion.
- Nonconvex polynomial terms can be replaced by a set of binary terms, with new variables introduced to define the higher-order polynomials.
- Binary terms can be relaxed by using the McCormick underestimator; e.g., the binary term xz is replaced by a new variable w and linear inequality constraints

$$\begin{aligned} w &\geq x_l z + z_l x - x_l z_l \\ w &\geq x_u z + z_u x - x_u z_u \\ w &\leq x_l z + z_l x - x_l z_l \\ w &\leq x_u z + z_u x - x_u z_u \end{aligned} \tag{3-107}$$

where the subregions are defined by $x_l \leq x \leq x_u$ and $z_l \leq z \leq z_u$. Thus the feasible region and the objective function are replaced by convex envelopes to form relaxed problems.

Solving these convex relaxed problems leads to global solutions that are lower bounds to the NLP in the particular subregion. Finally, we see that gradient-based NLP solvers play an important role in global optimization algorithms, as they often yield the lower and upper bounds for the subregions. The *spatial branch and bound* global optimization algorithm can therefore be given by the following steps:

0. Initialize algorithm: calculate upper and lower bounds over the entire (relaxed) feasible region.

For iteration k with a set of partitions M_{kj} and bounds in each subregion f_{lj} and f_{uj} :

1. *Bound*. Define best upper bound: $f_U = \min_j f_{Uj}$ and delete (fathom) all subregions j with lower bounds $f_{lj} \geq f_U - \epsilon$. If the remaining subregions satisfy $f_{lj} \geq f_U - \epsilon$, stop.

2. *Refine*. Divide the remaining active subregions into partitions $M_{k,j1}$ and $M_{k,j2}$. (Many branching rules are available for this step.)

3. *Select*. Solve the convex relaxed NLP in the new partitions to obtain $f_{l,j1}$ and $f_{l,j2}$. Delete the partition if there is no feasible solution.

4. *Update*. Obtain upper bounds f_{Uj1} and f_{Uj2} to new partitions, if present. Set $k = k+1$, update partition sets, and go to step 1.

Example To illustrate the spatial branch and bound algorithm, consider the global solution of

$$\text{Min } f(x) = \frac{5}{2} x^4 - 20x^3 + 55x^2 - 57x, \quad \text{subject to } 0.5 \leq x \leq 2.5 \tag{3-108}$$

As seen in Fig. 3-59, this problem has local solutions at $x^* = 2.5$ and at $x^* = 0.8749$. The latter is also the global solution with $f(x^*) = -19.7$. To find the global solution, we note that all but the $-20x^3$ term in (3-108) are convex, so we replace this term by a new variable and a linear underestimator within a particular subregion, i.e.,

$$\begin{aligned} \text{Min } f_L(x) &= \frac{5}{2} x^4 - 20w + 55x^2 - 57x \\ \text{subject to } x_l &\leq x \leq x_u \\ w &= x_l^3 \frac{x_u - x}{x_u - x_l} + x_u^3 \frac{x - x_l}{x_u - x_l} \end{aligned} \tag{3-109}$$

In Fig. 3-59 we also propose subregions that are created by simple bisection partitioning rules, and we use a “loose” bounding tolerance of $\epsilon = 0.2$. In each partition the lower bound f_L is determined by (3-109) and the upper bound f_U is determined by the local solution of the original problem in the subregion. Figure 3-60 shows the progress of the spatial branch and bound algorithm as the partitions are refined and the bounds are updated. In Fig. 3-60, note the definitions of the partitions for the nodes, and the sequence numbers in each node that show the order in which the partitions are

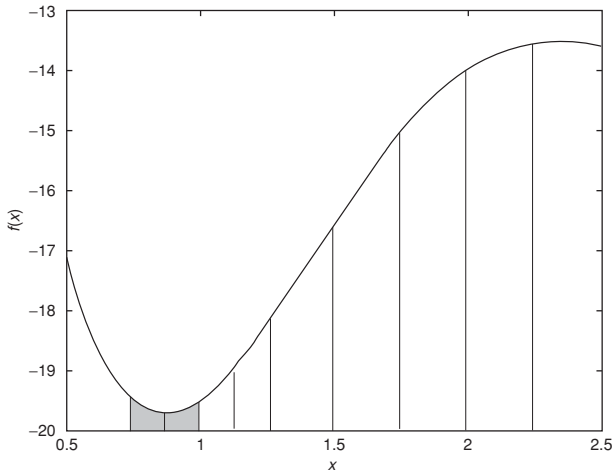


FIG. 3-59 Global optimization example with partitions.

processed. The grayed partitions correspond to the deleted subregions, and at termination of the algorithm we see that $f_U \geq f_U - \epsilon$ (that is, $-19.85 \geq -19.7 - 0.2$), with the gray subregions in Fig. 3-59 still active. Further partitioning in these subregions will allow the lower and upper bounds to converge to a tighter tolerance.

Note that a number of improvements can be made to the bounding, refinement, and selection strategies in the algorithm that accelerate the convergence of this method. A comprehensive discussion of all these options can be found in Floudas (2000), Tawarlamani and Sahinidis (2002), and Horst and Tuy (1993). Also, a number of efficient global optimization codes have recently been developed, including α BB, BARON, LGO, and OQNLP. An interesting numerical comparison of these and other codes can be found in Neumaier et al., *Math. Prog. B* 103(2): 335 (2005).

MIXED INTEGER PROGRAMMING

Mixed integer programming deals with both discrete and continuous decision variables. For the purpose of illustration we consider discrete decisions as binary variables, that is, $y_i = 0$ or 1 , and we consider the mixed integer problem (3-84). Unlike in local optimization methods, there are no optimality conditions, such as the KKT conditions, that can be applied directly. Instead, as in the global optimization methods, a systematic search of the solution space, coupled with upper and lower bounding information, is applied. As with global optimization problems, large mixed integer programs can be expensive to solve, and some care is needed in the problem formulation.

Mixed Integer Linear Programming If the objective and constraint functions are all linear, then (3-84) becomes a mixed integer linear programming problem given by

$$\begin{aligned} \text{Min } Z &= a^T x + c^T y \\ \text{subject to } Ax + By &\leq b \\ x &\geq 0, y \in \{0, 1\}^l \end{aligned} \tag{3-110}$$

Note that if we relax the t binary variables by the inequalities $0 \leq y \leq 1$, then (3-110) becomes a linear program with a (global) solution that is a lower bound to the MILP (3-110). There are specific MILP classes where the LP relaxation of (3-110) has the same solution as the MILP. Among these problems is the well-known *assignment problem*. Other MILPs that can be solved with efficient special-purpose methods are the *knapsack problem*, the *set covering* and *set partitioning* problems, and the *traveling salesperson* problem. See Nemhauser and Wolsey (1988) for a detailed treatment of these problems.

More generally, MILPs are solved with branch and bound algorithms, similar to the spatial branch and bound method of the previous section, that explore the search space. As seen in Fig. 3-61, binary variables are used to define the search tree, and a number of bounding properties can be noted from the structure of (3-110).

Upper bounds on the objective function can be found from any feasible solution to (3-110), with y set to integer values. These can be found at the bottom or “leaf” nodes of a branch and bound tree (and sometimes at intermediate nodes as well). The top, or root, node in

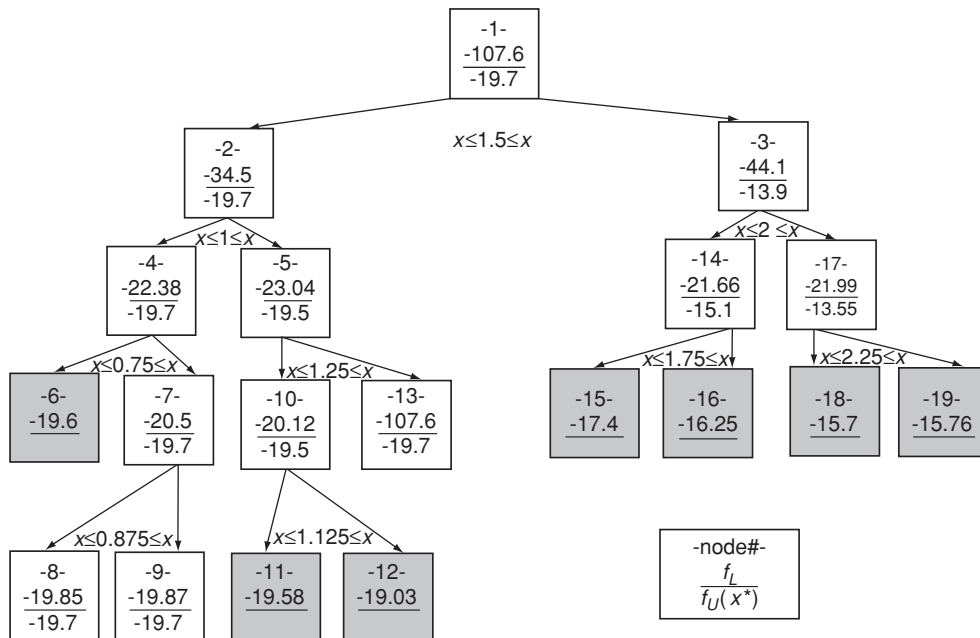


FIG. 3-60 Spatial branch and bound sequence for global optimization example.

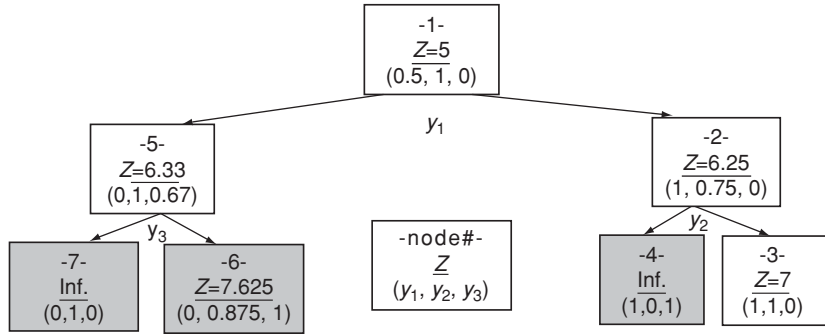


FIG. 3-61 Branch and bound sequence for MILP example.

the tree is the solution to the linear programming relaxation of (3-110); this is a lower bound to (3-110). On the other hand, as one proceeds down the tree with a partial assignment of the binary variables, a lower bound for any leaf node in that branch can be found from solution of the linear program at this intermediate node with the remaining binary variables relaxed. This leads to the following properties:

- Any intermediate node with an infeasible LP relaxation has infeasible leaf nodes and can be fathomed (i.e., all remaining children of this node can be eliminated).
- If the LP solution at an intermediate node is not less than an existing integer solution, then the node can be fathomed.

These properties lead to pruning of the search tree. Branching then continues in the tree until the upper and lower bounds converge.

This basic concept leads to a wide variety of MILP algorithms with the following features. LP solutions at intermediate nodes are relatively easy to calculate with the simplex method. If the solution of the parent node is known, multiplier information from this solution can be used to calculate (via a very efficient pivoting operation) the LP solution at the child node. Branching strategies to navigate the tree take a number of forms. More common *depth-first strategies* expand the most recent node to a leaf node or infeasible node and then backtrack to other branches in the tree. These strategies are simple to program and require little storage of past nodes. On the other hand, *breadth-first strategies* expand all the nodes at each level of the tree, select the node with the lowest objective function, and then proceed until the leaf nodes are reached. Here, more storage is required but generally fewer nodes are evaluated than in depth-first search. In addition, *selection of binary variable for branching* is based on a number of criteria, including choosing the variable with the relaxed value closest to 0 or 1, or the one leading to the largest change in the objective. Additional description of these strategies can be found in Biegler et al. (1997) and Nemhauser and Wolsey (1988).

Example To illustrate the branch and bound approach, we consider the MILP:

$$\begin{aligned} \text{Min } Z &= x + y_1 + 2y_2 + 3y_3 \\ \text{subject to } &-x + 3y_1 + y_2 + 2y_3 \leq 0 \\ &-4y_1 - 8y_2 - 3y_3 \leq -10 \\ &x \geq 0, y_1, y_2, y_3 = \{0, 1\} \end{aligned} \tag{3-111}$$

The solution to (3-111) is given by $x = 4, y_1 = 1, y_2 = 1, y_3 = 0$, and $Z = 7$. Here we use a depth-first strategy and branch on the variables closest to 0 or 1. Fig. 3-61 shows the progress of the branch and bound algorithm as the binary variables are selected and the bounds are updated. The sequence numbers for each node in Fig. 3-61 show the order in which they are processed. The grayed partitions correspond to the deleted nodes, and at termination of the algorithm we see that $Z = 7$ and an integer solution is obtained at an intermediate node where coincidentally $y_3 = 0$.

A number of improvements that can be made to the branching rules will accelerate the convergence of this method. A comprehensive discussion of all these options can be found in Nemhauser and Wolsey (1988). Also, a number of efficient MILP codes have recently been developed, including CPLEX, OSL, XPRESS, and ZOOM. All these serve as excellent large-scale optimization codes as well. A detailed description and availability of these and other MILP solvers

can be found in the NEOS Software Guide: <http://www-fp.mcs.anl.gov/otc/Guide/SoftwareGuide>.

Mixed Integer Nonlinear Programming Without loss of generality, we can rewrite the MINLP in (3-84) as:

$$\begin{aligned} \text{Min } Z &= f(x) + c^T y \\ \text{subject to } &g(x) + B y \leq b \\ &x \geq 0, y \in \{0, 1\}^l \end{aligned} \tag{3-112}$$

where the binary variables are kept as separate linear terms. We develop several MINLP solution strategies by drawing from the material in the preceding sections. MINLP strategies can be classified into two types. The first deals with nonlinear extensions of the branch and bound method discussed above for MILPs. The second deals with outer approximation decomposition strategies that provide lower and upper bounding information for convergence.

Nonlinear Branch and Bound The MINLP (3-112) can be solved in a similar manner to (3-110). If the functions $f(x)$ and $g(x)$ in (3-112) are convex, then direct extensions to the branch and bound method can be made. A relaxed NLP can be solved at the root node, upper bounds to the solution of (3-112) can be found at the leaf nodes, and the bounding properties due to NLP solutions at intermediate nodes still hold. However, this approach is more expensive than the corresponding MILP method. First, NLPs are more expensive than LPs to solve. Second, unlike with relaxed LP solutions, NLP solutions at child nodes cannot be updated directly from solutions at parent nodes. Instead, the NLP needs to be solved again (but one hopes with a better starting guess). The NLP branch and bound method is used in the SBB code interfaced to GAMS. In addition, Leyffer, [*Comput. Optim. Appl.* 18: 295 (2001)] proposed a hybrid MINLP strategy nested within an SQP algorithm. At each iteration, a mixed integer quadratic program is formed, and a branch and bound algorithm is executed to solve it.

If $f(x)$ and $g(x)$ are nonconvex, additional difficulties can occur. In this case, nonunique, local solutions can be obtained at intermediate nodes, and consequently lower bounding properties would be lost. In addition, the nonconvexity in $g(x)$ can lead to locally infeasible problems at intermediate nodes, even if feasible solutions can be found in the corresponding leaf node. To overcome problems with nonconvexities, global solutions to relaxed NLPs can be solved at the intermediate nodes. This preserves the lower bounding information and allows nonlinear branch and bound to inherit the convergence properties from the linear case. However, as noted above, this leads to much more expensive solution strategies.

Outer Approximation Decomposition Methods Again, we consider the MINLP (3-112) with convex $f(x)$ and $g(x)$. Note that the NLP with binary variables fixed at \bar{y}

$$\begin{aligned} \text{Min } Z &= f(x) + c^T \bar{y} \\ \text{subject to } &g(x) + B \bar{y} \leq b \\ &x \geq 0 \end{aligned} \tag{3-113}$$

if feasible, leads to a solution that is an upper bound on the MINLP

solution. In addition, linearizations of convex functions lead to underestimation of the function itself:

$$\phi(x) \geq \phi(x^k) + \nabla\phi(x^k)^T(x - x^k) \quad (3-114)$$

Consequently, linearization of (3-112) at a point x^k , to form the problem

$$\begin{aligned} \text{Min } Z &= f(x^k) + \nabla f(x^k)^T(x - x^k) + c^T y \\ \text{subject to } &g(x^k) + \nabla g(x^k)^T(x - x^k) + B y \leq b \\ &x \geq 0, y \in \{0, 1\}^l \end{aligned} \quad (3-115)$$

leads to overapproximation of the feasible region and underapproximation of the objective function in (3-112). Consequently, solution of (3-115) is a lower bound to the solution of (3-112). Adding more linearizations from other points does not change the bounding property, so for a set of points $x^l, l = 1, \dots, k$, the problem

$$\begin{aligned} \text{Min } Z &= \alpha \\ \text{subject to } &\alpha \geq f(x^l) + \nabla f(x^l)^T(x - x^l) + c^T y \\ &g(x^l) + \nabla g(x^l)^T(x - x^l) + B y \leq b \\ &x \geq 0, y \in \{0, 1\}^l \end{aligned} \quad l = 1, \dots, k \quad (3-116)$$

where α is a scalar variable, still has a solution that is a lower bound to (3-112). The outer approximation strategy is depicted in Fig. 3-62.

The outer approximation algorithm [Duran, M., and I. E. Grossmann, *Math. Programming* **36**: 307 (1986)] begins by initializing the problem, either with a predetermined starting guess or by solving a relaxed NLP based on (3-112). An upper bound to the solution is then generated by fixing the binary variables to their current values y^k and solving the NLP (3-113). This solution determines the continuous variable values x^k for the MILP (3-116). [If (3-113) is an infeasible problem, any point may be chosen for x^k , or the linearizations could be omitted.] Note that this MILP also contains linearizations from previous solutions of (3-113). Finally, the integer cut $\sum |y_i - y_i^k| \geq 1$ is added to (3-116) to avoid revisiting previously encountered values of binary variables. (In convex problems the integer cut is not needed, but it helps to accelerate solution of the MILP.) Solution of (3-116) yields new values of y and (without the integer cut) must lead to a lower bound to the solution of (3-112). Consequently, if the objective function of the lower bounding MILP is greater than the least upper bound determined in solutions of (3-113), then the algorithm terminates. Otherwise, the new values of y are used to solve the next NLP (3-113).

Compared to nonlinear branch and bound, the outer approximation algorithm usually requires very few solutions of the MILP and NLP subproblems. This is especially advantageous on problems where the NLPs are large and expensive to solve. Moreover, there are two variations of outer approximation that may be suitable for particular problem types:

In *Generalized Benders Decomposition* (GBD) [see Sahinidis and Grossmann, *Computers and Chem. Eng.* **15**: 481 (1991)], the lower

bounding problem in Fig. 3-62 is replaced by the following MILP:

$$\begin{aligned} \text{Min } &\alpha \\ \text{subject to } &\alpha \geq f(x^l) + c^T y + v^{lT} [g(x^l) + B y] \\ &\sum |y_i - y_i^l| \geq 1 \end{aligned} \quad l = 1, \dots, k \quad (3-117)$$

where v^l is the vector of KKT multipliers from the solution of (3-113) at iteration l . This MILP can be derived through a reformulation of the MILP used in Fig. 3-62 with the *inactive constraints* from (3-113) dropped. Solution of (3-117) leads to a weaker lower bound than (3-116), and consequently, more solutions of the NLP and MILP subproblems are needed to converge to the solution. However, (3-117) contains only a single continuous variable and far fewer inequality constraints and is much less expensive to solve than (3-116). Thus, GBD is favored over outer approximation if (3-113) is relatively inexpensive to solve or solution of (3-116) is too expensive.

The *extended cutting plane* (ECP) algorithm [Westerlund and Pettersson, *Computers and Chem. Engng.* **19**: S131 (1995)] is complementary to GBD. While the lower bounding problem in Fig. 3-62 remains essentially the same, the continuous variables x^k are chosen from the MILP solution and the NLP (3-113) is replaced by a simple evaluation of the objective and constraint functions. As a result, only MILP problems [(3-116) plus integer cuts] need be solved. Consequently, the ECP approach has weaker upper bounds than outer approximation and requires more MILP solutions. It has advantages over outer approximation when the NLP (3-113) is expensive to solve.

Additional difficulties arise for the outer approximation algorithm and its GBD and ECP extensions when neither $f(x)$ nor $g(x)$ is convex. Under these circumstances, the lower bounding properties resulting from the linearization and formulation of the MILP subproblem are lost, and the MILP solution may actually exclude the solution of (3-112). Hence, these algorithms need to be applied with care to nonconvex problems. To deal with nonconvexities, one can relax the linearizations in (3-116) through the introduction of additional *deviation variables* that can be penalized in the objective function. Alternately, the linearizations in (3-116) can be replaced by valid underestimating functions, such as those derived for global optimization [e.g., (3-107)]. However, this requires knowledge of structural information for (3-112) and may lead to weak lower bounds in the resulting MILP.

Finally, the performance of both MILP and MINLP algorithms is strongly dependent on the problem formulations (3-110) and (3-112). In particular, the efficiency of the approach is impacted by the lower bounds produced by the relaxation of the binary variables and subsequent solution of the linear program in the branch and bound tree. A number of approaches have been proposed to improve the quality of the lower bounds, including these:

- Logic-based methods such as *generalized disjunctive programming* (GDP) can be used to formulate MINLPs with fewer discrete variables that have tighter relaxations. Moreover, the imposition of logic-based constraints prevents the generation of unsuitable alternatives, leading to a less expensive search. In addition, constrained logic programming (CLP) methods offer an efficient search alternative to MILP solvers for highly combinatorial problems. See Raman and Grossmann, *Computers and Chem. Engng.* **18**(7): 563 (1994) for more details.
- Convex hull formulations of MILPs and MINLPs lead to relaxed problems that have much tighter lower bounds. This leads to the examination of far fewer nodes in the branch and bound tree. See Grossmann and Lee, *Comput. Optim. Appl.* **26**: 83 (2003) for more details.
- *Reformulation and preprocessing* strategies including bound tightening of the variables, coefficient reduction, lifting facets, and special ordered set constraints frequently lead to improved lower bounds and significant performance improvements in mixed integer programming algorithms.

A number of efficient codes are available for the solution of MINLPs. These include the AlphaECP, BARON, DICOPT, MINLP, and SBB solvers; descriptions of these can be found on the <http://www.gamsworld.org/minlp/solvers.htm> web site.

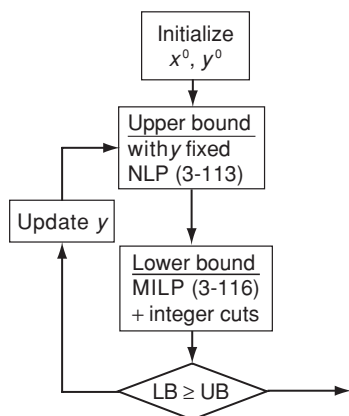


FIG. 3-62 Outer approximation MINLP algorithm.

DEVELOPMENT OF OPTIMIZATION MODELS

The most important aspect to a successful optimization study is the formulation of the optimization model. These models must reflect the real-world problem so that meaningful optimization results are obtained; they also must satisfy the properties of the problem class. For instance, NLPs addressed by gradient-based methods need to have functions that are defined in the variable domain and have bounded and continuous first and second derivatives. In mixed integer problems, proper formulations are also needed to yield good lower bounds for efficient search. With increased understanding of optimization methods and the development of efficient and reliable optimization codes, optimization practitioners now focus on the *formulation* of optimization models that are realistic, well posed, and inexpensive to solve. Finally, convergence properties of NLP, MILP, and MINLP solvers require accurate first (and often second) derivatives from the optimization model. If these contain numerical errors (say, through finite difference approximations), then the performance of these solvers can deteriorate considerably. As a result of these characteristics, modeling platforms are essential for the formulation task. These are classified into two broad areas: optimization modeling platforms and simulation platforms with optimization.

Optimization modeling platforms provide general-purpose interfaces for optimization algorithms and remove the need for the user to interface to the solver directly. These platforms allow the general formulation for all problem classes discussed above with direct interfaces to state-of-the-art optimization codes. Three representative platforms are the GAMS (General Algebraic Modeling Systems), AMPL (A Mathematical Programming Language), and AIMMS (Advanced Integrated Multidimensional Modeling Software). All three require problem model input via a declarative modeling language and provide exact gradient and Hessian information through automatic differentiation strategies. Although it is possible, these platforms were not designed to handle externally added procedural models. As a result, these platforms are best applied on optimization models that can be developed entirely within their modeling framework. Nevertheless, these platforms are widely used for large-scale research and industrial applications. In addition, the MATLAB platform allows the flexible formulation of optimization models as well, although it currently has only limited capabilities for automatic differentiation and limited optimization solvers. More information on these and other modeling platforms can be found at <http://www-fp.mcs.anl.gov/otc/Guide/SoftwareGuide>.

Simulation platforms with optimization are often dedicated, application-specific modeling tools to which optimization solvers have been interfaced. These lead to very useful optimization studies, but because they were not originally designed for optimization models, they need to be used with some caution. In particular, most of these platforms do not provide exact derivatives to the optimization solver; often they are approximated through finite differences. In addition, the models themselves are constructed and calculated through numerical procedures, instead of through an open declarative language. Examples of these include widely used process simulators such as Aspen/Plus, PRO/II, and Hysys. Also note that more recent platforms such as Aspen Custom Modeler and gPROMS include declarative models and exact derivatives.

For optimization tools linked to procedural models, note that reliable and efficient automatic differentiation tools are available that link to models written, say, in FORTRAN and C, and calculate exact first (and often second) derivatives. Examples of these include ADIFOR, ADOL-C, GRESS, Odyssey, and PADRE. When used with care, these can be applied to existing procedural models and, when linked to modern NLP and MINLP algorithms, can lead to powerful optimization capabilities. More information on these and other automatic differentiation tools can be found at http://www-unix.mcs.anl.gov/autodiff/AD_Tools/.

For optimization problems that are derived from (ordinary or partial) differential equation models, a number of advanced optimization strategies can be applied. Most of these problems are posed as NLPs, although recent work has also extended these models to MINLPs and global optimization formulations. For the optimization of profiles in time and space, *indirect methods* can be applied based on the optimality conditions of the infinite-dimensional problem using, for instance, the calculus of variations. However, these methods become difficult to apply if inequality constraints and discrete decisions are part of the optimization problem. Instead, current methods are based on NLP and MINLP formulations and can be divided into two classes:

- *Simultaneous formulations* are based on converting the differential equation model to algebraic constraints via discretization (say, with a Runge-Kutta method) and solving a large-scale NLP or MINLP. This approach requires efficient large-scale optimization solvers but also leads to very flexible and efficient problem formulations, particularly for optimal control and state-constrained problems. It also allows the treatment of unstable dynamics. A review of these strategies can be found in Biegler et al. [*Chem. Engng. Sci.* **57**(4): 575 (2002)] and Betts [*Practical Methods for Optimal Control Using Nonlinear Programming*, SIAM, Philadelphia (2001)].
- *Sequential formulations* require the linkage of NLP or MINLP solvers to embedded ODE or PDE solvers. This leads to smaller optimization problems only in the decision (or control) variables. However, an important aspect to this formulation is the need to recover accurate gradient information from the differential equation solver. Here, methods based on the solution of *direct* and *adjoint sensitivity* equations have been derived and automated [see Cao et al., *SIAM J. Sci. Comp.* **24**(3): 1076 (2003) for a description of these sensitivity methods]. For the former, commercial tools such as Aspen Custom Modeler and gPROMS have been developed.

Finally, the availability of automatic differentiation and related sensitivity tools for differential equation models allows for considerable flexibility in the formulation of optimization models. In van Bloemen Waanders et al. (Sandia Technical Report SAND2002-3198, October 2002), a seven-level modeling hierarchy is proposed that matches optimization algorithms with models that range from completely open (fully declarative model) to fully closed (entirely procedural without sensitivities). At the lowest, fully procedural level, only derivative-free optimization methods are applied, while the highest, declarative level allows the application of an efficient large-scale solver that uses first and second derivatives. This report notes that, based on the modeling level, optimization solver performance can vary by several orders of magnitude.

STATISTICS

REFERENCES: Baird, D. C., *Experimentation: An Introduction to Measurement Theory and Experiment Design*, 3d ed., Prentice-Hall, Englewood Cliffs, N.J. (1995); Box, G. P., J. S. Hunter, and W. G. Hunter, *Statistics for Experimenters: Design, Innovation, and Discovery*, 2d ed., Wiley, New York (2005); Cropley, J. B., "Heuristic Approach to Complex Kinetics," pp. 292–302 in *Chemical Reaction Engineering—Houston*, ACS Symposium Series 65, American Chemical Society, Washington (1978); Lipschutz, S., and J. J. Schiller, Jr., *Schaum's Outline of Theory and Problems of Introduction to Probability and Statistics*, McGraw-Hill, New York (1988); Moore, D. S., and G. P. McCabe, *Introduction to the Practice of Statistics*, 4th ed., Freeman, San Francisco (2003); Montgomery, D. C., and G. C. Runger, *Applied Statistics and Probability for Engineers*, 3d ed., Wiley, New York

(2002); and Montgomery, D. C., G. C. Runger, and N. F. Hubele, *Engineering Statistics*, 3d ed., Wiley, New York (2004).

INTRODUCTION

Statistics represents a body of knowledge which enables one to deal with quantitative data reflecting any degree of uncertainty. There are six basic aspects of applied statistics. These are:

1. Type of data
2. Random variables

3. Models
4. Parameters
5. Sample statistics
6. Characterization of chance occurrences

From these can be developed strategies and procedures for dealing with (1) estimation and (2) inferential statistics. The following has been directed more toward inferential statistics because of its broader utility.

Detailed illustrations and examples are used throughout to develop basic statistical methodology for dealing with a broad area of applications. However, in addition to this material, there are many specialized topics as well as some very subtle areas which have not been discussed. The references should be used for more detailed information. Section 8 discusses the use of statistics in statistical process control (SPC).

Type of Data In general, statistics deals with two types of data: counts and measurements. Counts represent the number of discrete outcomes, such as the number of defective parts in a shipment, the number of lost-time accidents, and so forth. Measurement data are treated as a continuum. For example, the tensile strength of a synthetic yarn theoretically could be measured to any degree of precision. A subtle aspect associated with count and measurement data is that some types of count data can be dealt with through the application of techniques which have been developed for measurement data alone. This ability is due to the fact that some simplified measurement statistics serve as an excellent approximation for the more tedious count statistics.

Random Variables Applied statistics deals with quantitative data. In tossing a fair coin the successive outcomes would tend to be different, with heads and tails occurring randomly over a period of time. Given a long strand of synthetic fiber, the tensile strength of successive samples would tend to vary significantly from sample to sample.

Counts and measurements are characterized as random variables, that is, observations which are susceptible to chance. Virtually all quantitative data are susceptible to chance in one way or another.

Models Part of the foundation of statistics consists of the mathematical models which characterize an experiment. The models themselves are mathematical ways of describing the probability, or relative likelihood, of observing specified values of random variables. For example, in tossing a coin once, a random variable x could be defined by assigning to x the value 1 for a head and 0 for a tail. Given a fair coin, the probability of observing a head on a toss would be a .5, and similarly for a tail. Therefore, the mathematical model governing this experiment can be written as

x	$P(x)$
0	.5
1	.5

where $P(x)$ stands for what is called a probability function. This term is reserved for count data, in that probabilities can be defined for particular outcomes.

The probability function that has been displayed is a very special case of the more general case, which is called the binomial probability distribution.

For measurement data which are considered continuous, the term *probability density* is used. For example, consider a spinner wheel which conceptually can be thought of as being marked off on the circumference infinitely precisely from 0 up to, but not including, 1. In spinning the wheel, the probability of the wheel's stopping at a specified marking point at any particular x value, where $0 \leq x < 1$, is zero, for example, stopping at the value $x = \sqrt{.5}$. For the spinning wheel, the probability density function would be defined by $f(x) = 1$ for $0 \leq x < 1$. Graphically, this is shown in Fig. 3-63. The relative-probability concept refers to the fact that density reflects the relative likelihood of occurrence; in this case, each number between 0 and 1 is equally likely. For measurement data, probability is defined by the area under the curve between specified limits. A density function always must have a total area of 1.

Example For the density of Fig. 3-63 the

$$P[0 \leq x \leq .4] = .4$$

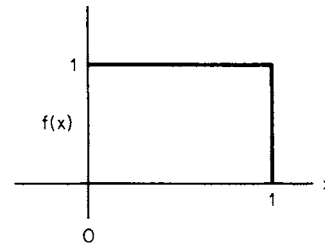


FIG. 3-63 Density function.

$$P[.2 \leq x \leq .9] = .7$$

$$P[.6 \leq x < 1] = .4$$

and so forth. Since the probability associated with any particular point value is zero, it makes no difference whether the limit point is defined by a closed interval (\leq or \geq) or an open interval ($<$ or $>$).

Many different types of models are used as the foundation for statistical analysis. These models are also referred to as **populations**.

Parameters As a way of characterizing probability functions and densities, certain types of quantities called parameters can be defined. For example, the center of gravity of the distribution is defined to be the population mean, which is designated as μ . For the coin toss $\mu = .5$, which corresponds to the average value of x ; i.e., for half of the time x will take on a value 0 and for the other half a value 1. The average would be .5. For the spinning wheel, the average value would also be .5.

Another parameter is called the **standard deviation**, which is designated as σ . The square of the standard deviation is used frequently and is called the popular **variance**, σ^2 . Basically, the standard deviation is a quantity which measures the spread or dispersion of the distribution from its mean μ . If the spread is broad, then the standard deviation will be larger than if it were more constrained.

For specified probability and density functions, the respective means and variances are defined by the following:

Probability functions	Probability density functions
$E(x) = \mu = \sum_x x P(x)$	$E(x) = \mu = \int_x x f(x) dx$
$\text{Var}(x) = \sigma^2 = \sum_x (x - \mu)^2 P(x)$	$\text{Var}(x) = \sigma^2 = \int_x (x - \mu)^2 f(x) dx$

where $E(x)$ is defined to be the expected or average value of x .

Sample Statistics Many types of sample statistics will be defined. Two very special types are the **sample mean**, designated as \bar{x} , and the sample standard deviation, designated as s . These are, by definition, random variables. Parameters like μ and σ are not random variables; they are fixed constants.

Example In an experiment, six random numbers (rounded to four decimal places) were observed from the uniform distribution $f(x) = 1$ for $0 \leq x < 1$:

- .1009
- .3754
- .0842
- .9901
- .1280
- .6606

The sample mean corresponds to the arithmetic average of the observations, which will be designated as x_1 through x_6 , where

$$\bar{x} = \frac{1}{n} \sum_{i=1}^n x_i \text{ with } n = 6, \quad \bar{x} = 0.3899$$

The sample standard deviation s is defined by the computation

$$s = \sqrt{\frac{\sum (x_i - \bar{x})^2}{n - 1}}$$

$$= \sqrt{\frac{n \sum x_i^2 - (\sum x_i)^2}{n(n-1)}} \quad (3-118)$$

In effect, this represents the root of a statistical average of the squares. The divisor quantity $(n - 1)$ will be referred to as the degrees of freedom. The sample value of the standard deviation for the data given is .3686.

The value of $n - 1$ is used in the denominator because the deviations from the sample average must total zero, or

$$\sum(x_i - \bar{x}) = 0$$

Thus knowing $n - 1$ values of $x_i - \bar{x}$ permits calculation of the n th value of $x_i - \bar{x}$.

The sample mean and sample standard deviation are obtained by using Microsoft Excel with the commands AVERAGE(B2:B7) and STDEV(B2:B7) when the observations are in cells B2 to B7.

In effect, the standard deviation quantifies the relative magnitude of the deviation numbers, i.e., a special type of “average” of the distance of points from their center. In statistical theory, it turns out that the corresponding variance quantities s^2 have remarkable properties which make possible broad generalities for sample statistics and therefore also their counterparts, the standard deviations.

For the corresponding population, the parameter values are $\mu = .50$ and $\sigma = .2887$, which are obtained by calculating the integrals defined above with $f(x) = 1$ and $0 \leq x \leq 1$. If, instead of using individual observations only, averages of six were reported, then the corresponding population parameter values would be $\mu = .50$ and $\sigma_{\bar{x}} = \sigma/\sqrt{6} = .1179$. The corresponding variance for an average will be written occasionally as $\text{Var}(\bar{x}) = \text{var}(x)/n$. In effect, the variance of an average is inversely proportional to the sample size n , which reflects the fact that sample averages will tend to cluster about μ much more closely than individual observations. This is illustrated in greater detail under “Measurement Data and Sampling Densities.”

Characterization of Chance Occurrences To deal with a broad area of statistical applications, it is necessary to characterize the way in which random variables will vary by chance alone. The basic foundation for this characteristic is laid through a density called the gaussian, or normal, distribution.

Determining the area under the normal curve is a very tedious procedure. However, by standardizing a random variable that is normally distributed, it is possible to relate all normally distributed random variables to one table. The standardization is defined by the identity $z = (x - \mu)/\sigma$, where z is called the unit normal. Further, it is possible to standardize the sampling distribution of averages \bar{x} by the identity $z = (\bar{x} - \mu)/(\sigma/\sqrt{n})$.

A remarkable property of the normal distribution is that, almost regardless of the distribution of x , sample averages \bar{x} will approach the gaussian distribution as n gets large. Even for relatively small values of n , of about 10, the approximation in most cases is quite close. For example, sample averages of size 10 from the uniform distribution will have essentially a gaussian distribution.

Also, in many applications involving count data, the normal distribution can be used as a close approximation. In particular, the approximation is quite close for the binomial distribution within certain guidelines.

The normal probability distribution function can be obtained in Microsoft Excel by using the NORMDIST function and supplying the desired mean and standard deviation. The cumulative value can also be determined. In MATLAB, the corresponding command is randn.

ENUMERATION DATA AND PROBABILITY DISTRIBUTIONS

Introduction Many types of statistical applications are characterized by enumeration data in the form of counts. Examples are the number of lost-time accidents in a plant, the number of defective items in a sample, and the number of items in a sample that fall within several specified categories.

The sampling distribution of count data can be characterized through probability distributions. In many cases, count data are appropriately

interpreted through their corresponding distributions. However, in other situations analysis is greatly facilitated through distributions which have been developed for measurement data. Examples of each will be illustrated in the following subsections.

Binomial Probability Distribution

Nature Consider an experiment in which each outcome is classified into one of two categories, one of which will be defined as a success and the other as a failure. Given that the probability of success p is constant from trial to trial, then the probability of observing a specified number of successes x in n trials is defined by the binomial distribution. The sequence of outcomes is called a **Bernoulli process**,

Nomenclature

n = total number of trials

x = number of successes in n trials

p = probability of observing a success on any one trial

$\hat{p} = x/n$, the proportion of successes in n trials

Probability Law

$$P(x) = P\left(\frac{x}{n}\right) = \binom{n}{x} p^x (1-p)^{n-x} \quad x = 0, 1, 2, \dots, n$$

where $\binom{n}{x} = \frac{n!}{x!(n-x)!}$

Properties $E(x) = np$

$\text{Var}(x) = np(1-p)$

$E(\hat{p}) = p$

$\text{Var}(\hat{p}) = p(1-p)/n$

Geometric Probability Distribution

Nature Consider an experiment in which each outcome is classified into one of two categories, one of which will be defined as a success and the other as a failure. Given that the probability of success p is constant from trial to trial, then the probability of observing the first success on the x th trial is defined by the geometric distribution.

Nomenclature

p = probability of observing a success on any one trial

x = the number of trials to obtain the first success

Probability Law

$$P(x) = p(1-p)^{x-1} \quad x = 1, 2, 3, \dots$$

Properties

$E(x) = 1/p$ $\text{Var}(x) = (1-p)/p^2$

Poisson Probability Distribution

Nature In monitoring a moving threadline, one criterion of quality would be the frequency of broken filaments. These can be identified as they occur through the threadline by a broken-filament detector mounted adjacent to the threadline. In this context, the random occurrences of broken filaments can be modeled by the Poisson distribution. This is called a Poisson process and corresponds to a probabilistic description of the frequency of defects or, in general, what are called arrivals at points on a continuous line or in time. Other examples include:

1. The number of cars (arrivals) that pass a point on a high-speed highway between 10:00 and 11:00 A.M. on Wednesdays
2. The number of customers arriving at a bank between 10:00 and 10:10 A.M.
3. The number of telephone calls received through a switchboard between 9:00 and 10:00 A.M.
4. The number of insurance claims that are filed each week
5. The number of spinning machines that break down during 1 day at a large plant.

Nomenclature

x = total number of arrivals in a total length L or total period T

a = average rate of arrivals for a unit length or unit time

$\lambda = aL =$ expected or average number of arrivals for the total length L

$\lambda = aT =$ expected or average number of arrivals for the total time T

Probability Law Given that a is constant for the total length L or period T , the probability of observing x arrivals in some period L or T

is given by

$$P(x) = \frac{\lambda^x}{x!} e^{-\lambda} \quad x = 0, 1, 2, \dots$$

Properties $E(x) = \lambda \quad \text{Var}(x) = \lambda$

Example The number of broken filaments in a threadline has been averaging .015 per yard. What is the probability of observing exactly two broken filaments in the next 100 yd? In this example, $a = .015/\text{yd}$ and $L = 100$ yd; therefore $\lambda = (.015)(100) = 1.5$:

$$P(x = 2) = \frac{(1.5)^2}{2!} e^{-1.5} = .2510$$

Example A commercial item is sold in a retail outlet as a unit product. In the past, sales have averaged 10 units per month with no seasonal variation. The retail outlet must order replacement items 2 months in advance. If the outlet starts the next 2-month period with 25 items on hand, what is the probability that it will stock out before the end of the second month?

Given $a = 10/\text{month}$, then $\lambda = 10 \times 2 = 20$ for the total period of 2 months:

$$P(x \geq 26) = \sum_{x=26}^{\infty} P(x) = 1 - \sum_{x=0}^{25} P(x)$$

$$\sum_{x=0}^{25} \frac{20^x}{x!} e^{-20} = e^{-20} \left[1 + \frac{20}{1} + \frac{20^2}{2!} + \dots + \frac{20^{25}}{25!} \right]$$

$$= .887815$$

Therefore $P(x \geq 26) = .112185$ or roughly an 11 percent chance of a stockout.

Hypergeometric Probability Distribution

Nature In an experiment in which one samples from a relatively small group of items, each of which is classified in one of two categories, A or B , the hypergeometric distribution can be defined. One example is the probability of drawing two red and two black cards from a deck of cards. The hypergeometric distribution is the analog of the binomial distribution when successive trials are not independent, i.e., when the total group of items is not infinite. This happens when the drawn items are not replaced.

Nomenclature

- N = total group size
- n = sample group size
- X = number of items in the total group with a specified attribute A
- $N - X$ = number of items in the total group with the other attribute B
- x = number of items in the sample with a specified attribute A
- $n - x$ = number of items in the sample with the other attribute B

	Population	Sample
Category A	X	x
Category B	$N - X$	$n - x$
Total	N	n

Probability Law

$$P(x) = \frac{\binom{N-X}{n-x} \binom{X}{x}}{\binom{N}{n}}$$

$$E(x) = \frac{nX}{N}$$

$$\text{var}(x) = nP(1-P) \frac{N-n}{N-1}$$

Example What is the probability that an appointed special committee of 4 has no female members when the members are randomly selected from a candidate group of 10 males and 7 females?

$$P(x = 0) = \frac{\binom{10}{4} \binom{7}{0}}{\binom{17}{4}} = .0882$$

Example A bin contains 300 items, of which 240 are good and 60 are defective. In a sample of 6 what is the probability of selecting 4 good and 2 defective items by chance?

$$P(x) = \frac{\binom{240}{4} \binom{60}{2}}{\binom{300}{6}} = .2478$$

Multinomial Distribution

Nature For an experiment in which successive outcomes can be classified into two or more categories and the probabilities associated with the respective outcomes remain constant, then the experiment can be characterized through the multinomial distribution.

Nomenclature

- n = total number of trials
- k = total number of distinct categories
- p_j = probability of observing category j on any one trial, $j = 1, 2, \dots, k$
- x_j = total number of occurrences in category j in n trials

Probability Law

$$P(x_1, x_2, \dots, x_k) = \frac{n!}{x_1! x_2! \dots x_k!} p_1^{x_1} p_2^{x_2} \dots p_k^{x_k}$$

Example In tossing a die 12 times, what is the probability that each face value will occur exactly twice?

$$p(2, 2, 2, 2, 2, 2) = \frac{12!}{2!2!2!2!2!2!} \left(\frac{1}{6}\right)^2 \left(\frac{1}{6}\right)^2 \left(\frac{1}{6}\right)^2 \left(\frac{1}{6}\right)^2 \left(\frac{1}{6}\right)^2 \left(\frac{1}{6}\right)^2 = .003438$$

To compute these probabilities in Microsoft Excel, put the value of x in cell B2, say, and use the functions

- Binomial distribution: = BINOMDIST(B2, n , p , 0)
- Poisson distribution: = POISSON(B2, λ , 0)
- Hypergeometric distribution: = HYPGEOMDIST(B2, n , X , N)

To generate a table of values with these probability distributions, in Microsoft Excel use the following functions:

- Bernoulli random values: = CRITBINOM(1, p , RAND())
- Binomial random values: = CRITBINOM(n , p , RAND())

The factorial function is FACT(n) in Microsoft Excel and factorial(n) in MATLAB. Be sure that x is an integer.

MEASUREMENT DATA AND SAMPLING DENSITIES

Introduction The following example data are used throughout this subsection to illustrate concepts. Consider, for the purpose of illustration, that five synthetic-yarn samples have been selected randomly from a production line and tested for tensile strength on each of 20 production days. For this, assume that each group of five corresponds to a day, Monday through Friday, for a period of 4 weeks:

Monday 1	Tuesday 2	Wednesday 3	Thursday 4	Friday 5	Groups of 25 pooled
36.48	38.06	35.28	36.34	36.73	
35.33	31.86	36.58	36.25	37.17	
35.92	33.81	38.81	30.46	33.07	
32.28	30.30	33.31	37.37	34.27	
31.61	35.27	33.88	37.52	36.94	
$\bar{x} = 34.32$	33.86	35.57	35.59	35.64	35.00
$s = 2.22$	3.01	2.22	2.92	1.85	2.40
6	7	8	9	10	
38.67	36.62	35.03	35.80	36.82	
32.08	33.05	36.22	33.16	36.49	
33.79	35.43	32.71	35.19	32.83	
32.85	36.63	32.52	32.91	32.43	
35.22	31.46	27.23	35.44	34.16	
$\bar{x} = 34.52$	34.64	32.74	34.50	34.54	34.19
$s = 2.60$	2.30	3.46	1.36	2.03	2.35

11	12	13	14	15	
39.63	34.52	36.05	36.64	31.57	
34.38	37.39	35.36	31.18	36.21	
36.51	34.16	35.00	36.13	33.84	
30.00	35.76	33.61	37.51	35.01	
39.64	37.63	36.98	39.05	34.95	
$\bar{x} = 36.03$	35.89	35.40	36.10	34.32	35.55
$s = 4.04$	1.59	1.25	2.96	1.75	2.42
Monday 16	Tuesday 17	Wednesday 18	Thursday 19	Friday 20	Groups of 25 pooled
37.68	35.97	33.71	35.61	36.65	
36.38	35.92	32.34	37.13	37.91	
38.43	36.51	33.29	31.37	42.18	
39.07	33.89	32.81	35.89	39.25	
33.06	36.01	37.13	36.33	33.32	
$\bar{x} = 36.92$	35.66	33.86	35.27	37.86	35.91
$s = 2.38$	1.02	1.90	2.25	3.27	2.52

Pooled sample of 100: $\bar{x} = 35.16$ $s = 2.47$

Even if the process were at steady state, tensile strength, a key property would still reflect some variation. Steady state, or stable operation of any process, has associated with it a characteristic variation. Superimposed on this is the testing method, which is itself a process with its own characteristic variation. The observed variation is a composite of these two variations.

Assume that the table represents "typical" production-line performance. The numbers themselves have been generated on a computer and represent random observations from a population with $\mu = 35$ and a population standard deviation $\sigma = 2.45$. The sample values reflect the way in which tensile strength can vary by chance alone. In practice, a production supervisor unschooled in statistics but interested in high tensile performance would be despondent on the eighth day and exuberant on the twentieth day. If the supervisor were more concerned with uniformity, the lowest and highest points would have been on the eleventh and seventeenth days.

An objective of statistical analysis is to serve as a guide in decision making in the context of normal variation. In the case of the production supervisor, it is to make a decision, with a high probability of being correct, that something has in fact changed the operation.

Suppose that an engineering change has been made in the process and five new tensile samples have been tested with the results:

36.81	
38.34	$\bar{x} = 37.14$
34.87	$s = 1.85$
39.58	
36.12	

In this situation, management would inquire whether the product has been improved by increased tensile strength. To answer this question, in addition to a variety of analogous questions, it is necessary to have some type of scientific basis upon which to draw a conclusion.

A scientific basis for the evaluation and interpretation of data is contained in the accompanying table descriptions. These tables characterize the way in which sample values will vary by chance alone in the context of individual observations, averages, and variances.

Table number	Designated symbol	Variable	Sampling distribution of
3-5	z	$\frac{x - \mu}{\sigma}$	Observations*
3-5	z	$\frac{\bar{x} - \mu}{\sigma/\sqrt{n}}$	Averages
3-6	t	$\frac{\bar{x} - \mu}{s/\sqrt{n}}$	Averages when σ is unknown*
3-7	χ^2	$(s^2/\sigma^2)(df)$	Variances*
3-8	F	s_1^2/s_2^2	Ratio of two independent sample variances*

*When sampling from a gaussian distribution.

Normal Distribution of Observations Many types of data follow what is called the gaussian, or bell-shaped, curve; this is especially true of averages. Basically, the gaussian curve is a purely mathematical function which has very special properties. However, owing to some mathematically intractable aspects primary use of the function is restricted to tabulated values.

Basically, the tabled values represent area (proportions or probability) associated with a scaling variable designated by Z in Fig. 3-64. The normal curve is centered at 0, and for particular values of Z , designated as z , the tabulated numbers represent the corresponding area under the curve between 0 and z . For example, between 0 and 1 the area is .3413. (Get this number from Table 3-5. The value of A includes the area on both sides of zero. Thus we want $A/2$. For $z = 1$, $A = 0.6827$, $A/2 = 0.3413$. For $z = 2$, $A/2 = 0.4772$.) The area between 0 and 2 is .4772; therefore, the area between 1 and 2 is $.4772 - .3413 = .1359$.

Also, since the normal curve is symmetric, areas to the left can be determined in exactly the same way. For example, the area between -2 and $+1$ would include the area between -2 and 0, $.4772$ (the same as 0 to 2), plus the area between 0 and 1, $.3413$, or a total area of $.8185$.

Any types of observation which are applicable to the normal curve can be transformed to Z values by the relationship $z = (x - \mu)/\sigma$ and, conversely, Z values to x values by $x = \mu + \sigma z$, as shown in Fig. 3-64. For example, for tensile strength, with $\mu = 35$ and $\sigma = 2.45$, this would dictate $z = (x - 35)/2.45$ and $x = 35 + 2.45z$.

Example What proportion of tensile values will fall between 34 and 36?

$$z_1 = (34 - 35)/2.45 = -.41 \quad z_2 = (36 - 35)/2.45 = .41$$

$$P[-.41 \leq z \leq .41] = .3182, \text{ or roughly } 32 \text{ percent}$$

The value 0.3182 is interpolated from Table 3-4 using $z = \pm 0.40$, $A = 0.3108$, and $z = \pm 0.45$, $A = 0.3473$.

Example What midrange of tensile values will include 95 percent of the sample values? Since $P[-1.96 \leq z \leq 1.96] = .95$, the corresponding values of x are

$$x_1 = 35 - 1.96(2.45) = 30.2$$

$$x_2 = 35 + 1.96(2.45) = 39.8$$

or

$$P[30.2 \leq x \leq 39.8] = .95$$

Normal Distribution of Averages An examination of the tensile-strength data previously tabulated would show that the range (largest minus the smallest) of tensile strength within days averages 5.12. The average range in \bar{x} values within each week is 2.37, while the range in the four weekly averages is 1.72. This reflects the fact that averages tend to be less variable in a predictable way. Given that the variance of x is $\text{var}(x) = \sigma^2$, then the variance of \bar{x} based on n observations is $\text{var}(\bar{x}) = \sigma^2/n$.

For averages of n observations, the corresponding relationship for the Z -scale relationship is

$$z = (\bar{x} - \mu) / \sigma / \sqrt{n} \quad \text{or} \quad \bar{x} = \mu + \frac{\sigma}{\sqrt{n}} z$$

The Microsoft Excel function NORMDIST($X, \mu, \sigma, 1$) gives the probability that $x \leq \mu$.

The command CONFIDENCE(α, σ, n) gives the confidence interval about the mean for a sample size n . To obtain 95 percent confidence limits, use $\alpha = .025$; $2\alpha = 1 - A$.

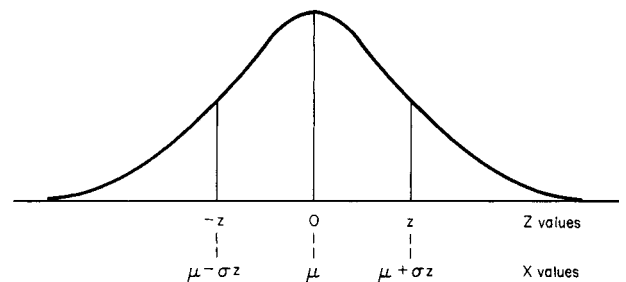


FIG. 3-64 Transformation of z values.

TABLE 3-5 Ordinates and Areas between Abscissa Values $-z$ and $+z$ of the Normal Distribution Curve

A = area between $\mu - \sigma_z$ and $\mu + \sigma_z$

z	X	Y	A	$1 - A$	z	X	Y	A	$1 - A$
0	μ	0.399	0.0000	1.0000	± 1.50	$\mu \pm 1.50\sigma$	0.1295	0.8664	0.1336
$\pm .10$	$\mu \pm .10\sigma$.397	.0797	.9203	± 1.60	$\mu \pm 1.60\sigma$.1109	.8904	.1096
$\pm .20$	$\mu \pm .20\sigma$.391	.1585	.8415	± 1.70	$\mu \pm 1.70\sigma$.0940	.9109	.0891
$\pm .30$	$\mu \pm .30\sigma$.381	.2358	.7642	± 1.80	$\mu \pm 1.80\sigma$.0790	.9281	.0719
$\pm .40$	$\mu \pm .40\sigma$.368	.3108	.6892	± 1.90	$\mu \pm 1.90\sigma$.0656	.9446	.0574
$\pm .50$	$\mu \pm .50\sigma$.352	.3829	.6171	± 2.00	$\mu \pm 2.00\sigma$.0540	.9545	.0455
$\pm .60$	$\mu \pm .60\sigma$.333	.4515	.5485	± 2.10	$\mu \pm 2.10\sigma$.0440	.9643	.0357
$\pm .70$	$\mu \pm .70\sigma$.312	.5161	.4839	± 2.20	$\mu \pm 2.20\sigma$.0335	.9722	.0278
$\pm .80$	$\mu \pm .80\sigma$.290	.5763	.4237	± 2.30	$\mu \pm 2.30\sigma$.0283	.9786	.0214
$\pm .90$	$\mu \pm .90\sigma$.266	.6319	.3681	± 2.40	$\mu \pm 2.40\sigma$.0224	.9836	.0164
± 1.00	$\mu \pm 1.00\sigma$.242	.6827	.3173	± 2.50	$\mu \pm 2.50\sigma$.0175	.9876	.0124
± 1.10	$\mu \pm 1.10\sigma$.218	.7287	.2713	± 2.60	$\mu \pm 2.60\sigma$.0136	.9907	.0093
± 1.20	$\mu \pm 1.20\sigma$.194	.7699	.2301	± 2.70	$\mu \pm 2.70\sigma$.0104	.9931	.0069
± 1.30	$\mu \pm 1.30\sigma$.171	.8064	.1936	± 2.80	$\mu \pm 2.80\sigma$.0079	.9949	.0051
± 1.40	$\mu \pm 1.40\sigma$.150	.8385	.1615	± 2.90	$\mu \pm 2.90\sigma$.0060	.9963	.0037
± 1.50	$\mu \pm 1.50\sigma$.130	.8664	.1336	± 3.00	$\mu \pm 3.00\sigma$.0044	.9973	.0027
					± 4.00	$\mu \pm 4.00\sigma$.0001	.99994	.00006
					± 5.00	$\mu \pm 5.00\sigma$.000001	.9999994	.0000006
± 0.000	μ	0.3989	.0000	1.0000	± 1.036	$\mu \pm 1.036\sigma$	0.2331	0.7000	0.3000
$\pm .126$	$\mu \pm 0.126\sigma$.3958	.1000	0.9000	± 1.282	$\mu \pm 1.282\sigma$.1755	.8000	.2000
$\pm .253$	$\mu \pm .253\sigma$.3863	.2000	.8000	± 1.645	$\mu \pm 1.645\sigma$.1031	.9000	.1000
$\pm .385$	$\mu \pm .385\sigma$.3704	.3000	.7000	± 1.960	$\mu \pm 1.960\sigma$.0584	.9500	.0500
$\pm .524$	$\mu \pm .524\sigma$.3477	.4000	.6000	± 2.576	$\mu \pm 2.576\sigma$.0145	.9900	.0100
$\pm .674$	$\mu \pm .674\sigma$.3178	.5000	.5000	± 3.291	$\mu \pm 3.291\sigma$.0018	.9990	.0010
$\pm .842$	$\mu \pm .842\sigma$.2800	.6000	.4000	± 3.891	$\mu \pm 3.891\sigma$.0002	.9999	.0001

This table is obtained in Microsoft Excel with the function $Y = \text{NORMDIST}(X, \mu, \sigma, 0)$.
 If $X > \mu$, $A = 2 \text{ NORMDIST}(X, \mu, \sigma, 1) - 1$. If $X < \mu$, $A = 1 - 2 \text{ NORMDIST}(X, \mu, \sigma, 1)$

Example What proportion of daily tensile averages will fall between 34 and 36? Using Table 3-5

$$z_1 = (34 - 35)/(2.45/\sqrt{5}) = -.91 \quad z_2 = (36 - 35)/(2.45/\sqrt{5}) = .91$$

$$P[-.91 \leq z \leq .91] = .637, \text{ or roughly } 64 \text{ percent}$$

Using Microsoft Excel, the more precise answer is

$$P[34 \leq \bar{x} \leq 36] = 2 \text{ NORMDIST}(36, 35, 2.45/\sqrt{5}, 1) - 1$$

$$= 1 - 2 \text{ NORMDIST}(34, 35, 2.45/\sqrt{5}, 1) = .6386$$

Example What midrange of daily tensile averages will include 95 percent of the sample values? Using Table 3-5

$$x_1 = 35 - 1.96(2.45/\sqrt{5}) = 32.85$$

$$x_2 = 35 + 1.96(2.45/\sqrt{5}) = 37.15$$

$$P[32.85 \leq \bar{x} \leq 37.15] = .95$$

or using Microsoft Excel,

$$35 \pm \text{CONFIDENCE}(.05, 2.45, 5) = 35 \pm 2.15$$

t Distribution of Averages The normal curve relies on a knowledge of σ , or in special cases, when it is unknown, s can be used with the normal curve as an approximation when $n > 30$. For example, with $n > 30$ the intervals $\bar{x} \pm s$ and $\bar{x} \pm 2s$ will include roughly 68 and 95 percent of the sample values respectively when the distribution is normal.

In applications sample sizes are usually small and σ unknown. In these cases, the t distribution can be used where

$$t = (\bar{x} - \mu)/(s/\sqrt{n}) \quad \text{or} \quad \bar{x} = \mu + ts/\sqrt{n}$$

The t distribution is also symmetric and centered at zero. It is said to be robust in the sense that even when the individual observations x are not normally distributed, sample averages of x have distributions which tend toward normality as n gets large. Even for small n of 5

through 10, the approximation is usually relatively accurate. It is sometimes called the Student's t distribution.

In reference to the tensile-strength table, consider the summary statistics \bar{x} and s by days. For each day, the t statistic could be computed. If this were repeated over an extensive simulation and the resultant t quantities plotted in a frequency distribution, they would match the corresponding distribution of t values summarized in Table 3-6.

Since the t distribution relies on the sample standard deviation s , the resultant distribution will differ according to the sample size n . To designate this difference, the respective distributions are classified according to what are called the degrees of freedom and abbreviated as df . In simple problems, the df are just the sample size minus 1. In more complicated applications the df can be different. In general, degrees of freedom are the number of quantities minus the number of constraints. For example, four numbers in a square which must have row and column sums equal to zero have only one df , i.e., four numbers minus three constraints (the fourth constraint is redundant). The Microsoft Excel function $\text{TDIST}(X, df, 1)$ gives the right-tail probability, and $\text{TDIST}(X, df, 2)$ gives twice that. The probability that $t \leq X$ is $1 - \text{TDIST}(X, df, 1)$ when $X \geq 0$ and $\text{TDIST}(\text{abs}(X), df, 1)$ when $X < 0$. The probability that $-X \leq t \leq +X$ is $1 - 2\text{TDIST}(X, df, 2)$.

Example For a sample size $n = 5$, what values of t define a midarea of 90 percent? For 4 df the tabled value of t corresponding to a midarea of 90 percent is 2.132; i.e., $P[-2.132 \leq t \leq 2.132] = .90$.

Using Microsoft Excel, $\text{TINV}(.1, 4) = 2.132$.

Example For a sample size $n = 25$, what values of t define a midarea of 95 percent? For 24 df the tabled value of t corresponding to a midarea of 95 percent is 2.064; i.e., $P[-2.064 \leq t \leq 2.064] = .95$.

Example Also, $1 - \text{TDIST}(2.064, 24, 2) = .9500$.

Using Microsoft Excel, $\text{TINV}(.05, 24) = 2.064$.

TABLE 3-6 Values of *t*

df	<i>t</i> _{.40}	<i>t</i> _{.30}	<i>t</i> _{.20}	<i>t</i> _{.10}	<i>t</i> _{.05}	<i>t</i> _{.025}	<i>t</i> _{.01}	<i>t</i> _{.005}
1	0.325	0.727	1.376	3.078	6.314	12.706	31.821	63.657
2	.289	.617	1.061	1.886	2.920	4.303	6.965	9.925
3	.277	.584	0.978	1.638	2.353	3.182	4.541	5.841
4	.271	.569	.941	1.533	2.132	2.776	3.747	4.604
5	.267	.559	.920	1.476	2.015	2.571	3.365	4.032
6	.265	.553	.906	1.440	1.943	2.447	3.143	3.707
7	.263	.549	.896	1.415	1.895	2.365	2.998	3.499
8	.262	.546	.889	1.397	1.860	2.306	2.896	3.355
9	.261	.543	.883	1.383	1.833	2.262	2.821	3.250
10	.260	.542	.879	1.372	1.812	2.228	2.764	3.169
11	.260	.540	.876	1.363	1.796	2.201	2.718	3.106
12	.259	.539	.873	1.356	1.782	2.179	2.681	3.055
13	.259	.538	.870	1.350	1.771	2.160	2.650	3.012
14	.258	.537	.868	1.345	1.761	2.145	2.624	2.977
15	.258	.536	.866	1.341	1.753	2.131	2.602	2.947
16	.258	.535	.865	1.337	1.746	2.120	2.583	2.921
17	.257	.534	.863	1.333	1.740	2.110	2.567	2.898
18	.257	.534	.862	1.330	1.734	2.101	2.552	2.878
19	.257	.533	.861	1.328	1.729	2.093	2.539	2.861
20	.257	.533	.860	1.325	1.725	2.086	2.528	2.845
21	.257	.532	.859	1.323	1.721	2.080	2.518	2.831
22	.256	.532	.858	1.321	1.717	2.074	2.508	2.819
23	.256	.532	.858	1.319	1.714	2.069	2.500	2.807
24	.256	.531	.857	1.318	1.711	2.064	2.492	2.797
25	.256	.531	.856	1.316	1.708	2.060	2.485	2.787
26	.256	.531	.856	1.315	1.706	2.056	2.479	2.779
27	.256	.531	.855	1.314	1.703	2.052	2.473	2.771
28	.256	.530	.855	1.313	1.701	2.048	2.467	2.763
29	.256	.530	.854	1.311	1.699	2.045	2.462	2.756
30	.256	.530	.854	1.310	1.697	2.042	2.457	2.750
40	.255	.529	.851	1.303	1.684	2.021	2.423	2.704
60	.254	.527	.848	1.296	1.671	2.000	2.390	2.660
120	.254	.526	.845	1.289	1.658	1.980	2.358	2.617
∞	.253	.524	.842	1.282	1.645	1.960	2.326	2.576

Above values refer to a single tail outside the indicated limit of *t*. For example, for 95 percent of the area to be between $-t$ and $+t$ in a two-tailed *t* distribution, use the values for *t*_{.025} or 2.5 percent for each tail. This table is obtained in Microsoft Excel using the function TINV(α ,*df*), where α is .05.

Example What is the sample value of *t* for the first day of tensile data?
 Sample $t = (34.32 - 35)/(2.22/\sqrt{5}) = -6.8$

Note that on the average 90 percent of all such sample values would be expected to fall within the interval ± 2.132 .

***t* Distribution for the Difference in Two Sample Means with Equal Variances** The *t* distribution can be readily extended to the difference in two sample means when the respective populations have the same variance σ :

$$t = \frac{(\bar{x}_1 - \bar{x}_2) - (\mu_1 - \mu_2)}{s_p \sqrt{1/n_1 + 1/n_2}} \tag{3-119}$$

where s_p^2 is a pooled variance defined by

$$s_p^2 = \frac{(n_1 - 1)s_1^2 + (n_2 - 1)s_2^2}{(n_1 - 1) + (n_2 - 1)} \tag{3-120}$$

In this application, the *t* distribution has $(n_1 + n_2 - 2)$ df.

***t* Distribution for the Difference in Two Sample Means with Unequal Variances** When population variances are unequal, an approximate *t* quantity can be used:

$$t = \frac{(\bar{x}_1 - \bar{x}_2) - (\mu_1 - \mu_2)}{\sqrt{a + b}}$$

with $a = s_1^2/n_1$ $b = s_2^2/n_2$

and
$$df = \frac{(a + b)^2}{a^2/(n_1 - 1) + b^2/(n_2 - 1)}$$

Chi-Square Distribution For some industrial applications, product uniformity is of primary importance. The sample standard deviation *s* is most often used to characterize uniformity. In dealing with this problem, the chi-square distribution can be used where $\chi^2 = (s^2/\sigma^2)(df)$. The chi-square distribution is a family of distributions which are defined by the degrees of freedom associated with the sample variance. For most applications, df is equal to the sample size minus 1.

The probability distribution function is

$$p(y) = y_0 y^{df-2} \exp \left[\frac{-(df)y^2}{2} \right]$$

where y_0 is chosen such that the integral of $p(y)$ over all y is one.

In terms of the tensile-strength table previously given, the respective chi-square sample values for the daily, weekly, and monthly figures could be computed. The corresponding df would be 4, 24, and 99 respectively. These numbers would represent sample values from the respective distributions which are summarized in Table 3-7.

In a manner similar to the use of the *t* distribution, chi square can be interpreted in a direct probabilistic sense corresponding to a midarea of $(1 - \alpha)$:

$$P[\chi_1^2 \leq (s^2/\sigma^2)(df) \leq \chi_2^2] = 1 - \alpha$$

where χ_1^2 corresponds to a lower-tail area of $\alpha/2$ and χ_2^2 an upper-tail area of $\alpha/2$.

The basic underlying assumption for the mathematical derivation of chi square is that a random sample was selected from a normal distribution with variance σ^2 . When the population is not normal but skewed, chi-square probabilities could be substantially in error.

Example On the basis of a sample size $n = 5$, what midrange of values will include the sample ratio s/σ with a probability of 95 percent?

Use Table 3-7 for 4 df and read $\chi_1^2 = 0.484$ for a lower tail area of 0.05/2, 2.5 percent, and read $\chi_2^2 = 11.1$ for an upper tail area of 97.5 percent.

$$P[.484 \leq (s^2/\sigma^2)(4) \leq 11.1] = .95$$

or

$$P[.35 \leq s/\sigma \leq 1.66] = .95$$

The Microsoft Excel functions CHIINV(.025, 4) and CHIINV(.975, 4) give the same values.

Example On the basis of a sample size $n = 25$, what midrange of values will include the sample ratio s/σ with a probability of 95 percent?

$$P[12.4 \leq (s^2/\sigma^2)(24) \leq 39.4] = .95$$

or

$$P[.72 \leq s/\sigma \leq 1.28] = .95$$

This states that the sample standard deviation will be at least 72 percent and not more than 128 percent of the population variance 95 percent of the time. Conversely, 10 percent of the time the standard deviation will underestimate or overestimate the population standard deviation by the corresponding amount. Even for samples as large as 25, the relative reliability of a sample standard deviation is poor.

The chi-square distribution can be applied to other types of application which are of an entirely different nature. These include applications which are discussed under "Goodness-of-Fit Test" and "Two-Way Test for Independence of Count Data." In these applications, the mathematical formulation and context are entirely different, but they do result in the same table of values.

F Distribution In reference to the tensile-strength table, the successive pairs of daily standard deviations could be ratioed and squared. These ratios of variance would represent a sample from a distribution called the *F* distribution or *F* ratio. In general, the *F* ratio is defined by the identity

$$F(\gamma_1, \gamma_2) = s_1^2/s_2^2$$

where γ_1 and γ_2 correspond to the respective df's for the sample variances. In statistical applications, it turns out that the primary area of interest is found when the ratios are greater than 1. For this reason, most tabled values are defined for an upper-tail area. However,

TABLE 3-7 Percentiles of the χ^2 Distribution

df	Percent									
	0.5	1	2.5	5	10	90	95	97.5	99	99.5
1	0.000039	0.00016	0.00098	0.0039	0.0158	2.71	3.84	5.02	6.63	7.88
2	.0100	.0201	.0506	.1026	.2107	4.61	5.99	7.38	9.21	10.60
3	.0717	.115	.216	.352	.584	6.25	7.81	9.35	11.34	12.84
4	.207	.297	.484	.711	1.064	7.78	9.49	11.14	13.28	14.86
5	.412	.554	.831	1.15	1.61	9.24	11.07	12.83	15.09	16.75
6	.676	.872	1.24	1.64	2.20	10.64	12.59	14.45	16.81	18.55
7	.989	1.24	1.69	2.17	2.83	12.02	14.07	16.01	18.48	20.28
8	1.34	1.65	2.18	2.73	3.49	13.36	15.51	17.53	20.09	21.96
9	1.73	2.09	2.70	3.33	4.17	14.68	16.92	19.02	21.67	23.59
10	2.16	2.56	3.25	3.94	4.87	15.99	18.31	20.48	23.21	25.19
11	2.60	3.05	3.82	4.57	5.58	17.28	19.68	21.92	24.73	26.76
12	3.07	3.57	4.40	5.23	6.30	18.55	21.03	23.34	26.22	28.30
13	3.57	4.11	5.01	5.89	7.04	19.81	22.36	24.74	27.69	29.82
14	4.07	4.66	5.63	6.57	7.79	21.06	23.68	26.12	29.14	31.32
15	4.60	5.23	6.26	7.26	8.55	22.31	25.00	27.49	30.58	32.80
16	5.14	5.81	6.91	7.96	9.31	23.54	26.30	28.85	32.00	34.27
18	6.26	7.01	8.23	9.39	10.86	25.99	28.87	31.53	34.81	37.16
20	7.43	8.26	9.59	10.85	12.44	28.41	31.41	34.17	37.57	40.00
24	9.89	10.86	12.40	13.85	15.66	33.20	36.42	39.36	42.98	45.56
30	13.79	14.95	16.79	18.49	20.60	40.26	43.77	46.98	50.89	53.67
40	20.71	22.16	24.43	26.51	29.05	51.81	55.76	59.34	63.69	66.77
60	35.53	37.48	40.48	43.19	46.46	74.40	79.08	83.30	88.38	91.95
120	83.85	86.92	91.58	95.70	100.62	140.23	146.57	152.21	158.95	163.64

For large values of degrees of freedom the approximate formula

$$\chi^2_\alpha = n \left(1 - \frac{2}{9n} + z_\alpha \sqrt{\frac{2}{9n}} \right)^3$$

where z_α is the normal deviate and n is the number of degrees of freedom, may be used. For example, $\chi^2_{.99} = 60[1 - 0.00370 + 2.326(0.06086)]^3 = 60(1.1379)^3 = 88.4$ for the 99th percentile for 60 degrees of freedom. The Microsoft Excel function CHIDIST(X , df), where X is the table value, gives 1 - Percent. The function CHIINV(1 - Percent, df) gives the table value.

defining F_2 to be that value corresponding to an upper-tail area of $\alpha/2$, then F_1 for a lower-tail area of $\alpha/2$ can be determined through the identity

$$F_1(\gamma_1, \gamma_2) = 1/F_2(\gamma_2, \gamma_1)$$

The F distribution, similar to the chi square, is sensitive to the basic assumption that sample values were selected randomly from a normal distribution. The Microsoft Excel function FDIST(X , df_1 , df_2) gives the upper percent points of Table 3-8, where X is the tabular value. The function FINV(Percent, df_1 , df_2) gives the table value.

Example For two sample variances with 4 df each, what limits will bracket their ratio with a midarea probability of 90 percent?

Use Table 3-8 with 4 df in the numerator and denominator and upper 5 percent points (to get both sides totaling 10 percent). The entry is 6.39. Thus:

$$P[1/6.39 \leq s_1^2/s_2^2 \leq 6.39] = .90$$

or
$$P[.40 \leq s_1/s_2 \leq 2.53] = .90$$

The Microsoft Excel function FINV(.05, 4, 4) gives 6.39, too.

Confidence Interval for a Mean For the daily sample tensile-strength data with 4 df it is known that $P[-2.132 \leq t \leq 2.132] = .90$. This states that 90 percent of all samples will have sample t values which fall within the specified limits. In fact, for the 20 daily samples exactly 16 do fall within the specified limits (note that the binomial with $n = 20$ and $p = .90$ would describe the likelihood of exactly none through 20 falling within the prescribed limits—the sample of 20 is only a sample).

Consider the new daily sample (with $n = 5$, $\bar{x} = 37.14$, and $s = 1.85$) which was observed after a process change. In this case, the same probability holds. However, in this instance the sample value of t cannot be computed, since the new μ , under the process change, is not known. Therefore $P[-2.132 \leq (37.14 - \mu)/(1.85/\sqrt{5}) \leq 2.132] = .90$. In effect, this identity limits the magnitude of possible values for

μ . The magnitude of μ can be only large enough to retain the t quantity above -2.132 and small enough to retain the t quantity below $+2.132$. This can be found by rearranging the quantities within the bracket; i.e., $P[35.38 \leq \mu \leq 38.90] = .90$. This states that we are 90 percent sure that the interval from 35.38 to 38.90 includes the unknown parameter μ .

In general,

$$P\left[\bar{x} - t \frac{s}{\sqrt{n}} \leq \mu \leq \bar{x} + t \frac{s}{\sqrt{n}}\right] = 1 - \alpha$$

where t is defined for an upper-tail area of $\alpha/2$ with $(n - 1)$ df. In this application, the interval limits $(\bar{x} \pm t s/\sqrt{n})$ are random variables which will cover the unknown parameter μ with probability $(1 - \alpha)$. The converse, that we are $100(1 - \alpha)$ percent sure that the parameter value is within the interval, is not correct. This statement defines a probability for the parameter rather than the probability for the interval.

Example What values of t define the midarea of 95 percent for weekly samples of size 25, and what is the sample value of t for the second week?

$$P[-2.064 \leq t \leq 2.064] = .95$$

and
$$(34.19 - 35)/(2.35/\sqrt{25}) = 1.72.$$

Example For the composite sample of 100 tensile strengths, what is the 90 percent confidence interval for μ ?

Use Table 3-6 for $t_{.05}$ with $df = \infty$.

$$P\left[35.16 - 1.645 \frac{2.47}{\sqrt{100}} < \mu < 35.16 + 1.645 \frac{2.47}{\sqrt{100}}\right] = .90$$

or
$$P[34.75 \leq \mu \leq 35.57] = .90$$

Confidence Interval for the Difference in Two Population Means The confidence interval for a mean can be extended to

TABLE 3-8 F Distribution

		Upper 5% Points ($F_{.95}$)																			
		Degrees of freedom for numerator																			
		1	2	3	4	5	6	7	8	9	10	12	15	20	24	30	40	60	120	∞	
Degrees of freedom for denominator	1	161	200	216	225	230	234	237	239	241	242	244	246	248	249	250	251	252	253	254	
	2	18.5	19.0	19.2	19.2	19.3	19.3	19.4	19.4	19.4	19.4	19.4	19.4	19.4	19.4	19.5	19.5	19.5	19.5	19.5	19.5
	3	10.1	9.55	9.28	9.12	9.01	8.94	8.89	8.85	8.81	8.79	8.74	8.70	8.66	8.64	8.62	8.59	8.57	8.55	8.53	8.53
	4	7.71	6.94	6.59	6.39	6.26	6.16	6.09	6.04	6.00	5.96	5.91	5.86	5.80	5.77	5.75	5.72	5.69	5.66	5.63	5.63
	5	6.61	5.79	5.41	5.19	5.05	4.95	4.88	4.82	4.77	4.74	4.68	4.62	4.56	4.53	4.50	4.46	4.43	4.40	4.37	4.37
	6	5.99	5.14	4.76	4.53	4.39	4.28	4.21	4.15	4.10	4.06	4.00	3.94	3.87	3.84	3.81	3.77	3.74	3.70	3.67	3.67
	7	5.59	4.74	4.35	4.12	3.97	3.87	3.79	3.73	3.68	3.64	3.57	3.51	3.44	3.41	3.38	3.34	3.30	3.27	3.23	3.23
	8	5.32	4.46	4.07	3.84	3.69	3.58	3.50	3.44	3.39	3.35	3.28	3.22	3.15	3.12	3.08	3.04	3.01	2.97	2.93	2.93
	9	5.12	4.26	3.86	3.63	3.48	3.37	3.29	3.23	3.18	3.14	3.07	3.01	2.94	2.90	2.86	2.83	2.79	2.75	2.71	2.71
	10	4.96	4.10	3.71	3.48	3.33	3.22	3.14	3.07	3.02	2.98	2.91	2.85	2.77	2.74	2.70	2.66	2.62	2.58	2.54	2.54
	11	4.84	3.98	3.59	3.36	3.20	3.09	3.01	2.95	2.90	2.85	2.79	2.72	2.65	2.61	2.57	2.53	2.49	2.45	2.40	2.40
	12	4.75	3.89	3.49	3.26	3.11	3.00	2.91	2.85	2.80	2.75	2.69	2.62	2.54	2.51	2.47	2.43	2.38	2.34	2.30	2.30
	13	4.67	3.81	3.41	3.18	3.03	2.92	2.83	2.77	2.71	2.67	2.60	2.53	2.46	2.42	2.38	2.34	2.30	2.25	2.21	2.21
	14	4.60	3.74	3.34	3.11	2.96	2.85	2.76	2.70	2.65	2.60	2.53	2.46	2.39	2.35	2.31	2.27	2.22	2.18	2.13	2.13
	15	4.54	3.68	3.29	3.06	2.90	2.79	2.71	2.64	2.59	2.54	2.48	2.40	2.33	2.29	2.25	2.20	2.16	2.11	2.07	2.07
	16	4.49	3.63	3.24	3.01	2.85	2.74	2.66	2.59	2.54	2.49	2.42	2.35	2.28	2.24	2.19	2.15	2.11	2.06	2.01	2.01
	17	4.45	3.59	3.20	2.96	2.81	2.70	2.61	2.55	2.49	2.45	2.38	2.31	2.23	2.19	2.15	2.10	2.06	2.01	1.96	1.96
	18	4.41	3.55	3.16	2.93	2.77	2.66	2.58	2.51	2.46	2.41	2.34	2.27	2.19	2.15	2.11	2.06	2.02	1.97	1.92	1.92
	19	4.38	3.52	3.13	2.90	2.74	2.63	2.54	2.48	2.42	2.38	2.31	2.23	2.16	2.11	2.07	2.03	1.98	1.93	1.88	1.88
	20	4.35	3.49	3.10	2.87	2.71	2.60	2.51	2.45	2.39	2.35	2.28	2.20	2.12	2.08	2.04	1.99	1.95	1.90	1.84	1.84
	21	4.32	3.47	3.07	2.84	2.68	2.57	2.49	2.42	2.37	2.32	2.25	2.18	2.10	2.05	2.01	1.96	1.92	1.87	1.81	1.81
	22	4.30	3.44	3.05	2.82	2.66	2.55	2.46	2.40	2.34	2.30	2.23	2.15	2.07	2.03	1.98	1.94	1.89	1.84	1.78	1.78
	23	4.28	3.42	3.03	2.80	2.64	2.53	2.44	2.37	2.32	2.27	2.20	2.13	2.05	2.01	1.96	1.91	1.86	1.81	1.76	1.76
	24	4.26	3.40	3.01	2.78	2.62	2.51	2.42	2.36	2.30	2.25	2.18	2.11	2.03	1.98	1.94	1.89	1.84	1.79	1.73	1.73
	25	4.24	3.39	2.99	2.76	2.60	2.49	2.40	2.34	2.28	2.24	2.16	2.09	2.01	1.96	1.92	1.87	1.82	1.77	1.71	1.71
30	4.17	3.32	2.92	2.69	2.53	2.42	2.33	2.27	2.21	2.16	2.09	2.01	1.93	1.89	1.84	1.79	1.74	1.68	1.62	1.62	
40	4.08	3.23	2.84	2.61	2.45	2.34	2.25	2.18	2.12	2.08	2.00	1.92	1.84	1.79	1.74	1.69	1.64	1.58	1.51	1.51	
60	4.00	3.15	2.76	2.53	2.37	2.25	2.17	2.10	2.04	1.99	1.92	1.84	1.75	1.70	1.65	1.59	1.53	1.47	1.39	1.39	
120	3.92	3.07	2.68	2.45	2.29	2.18	2.09	2.02	1.96	1.91	1.83	1.75	1.66	1.61	1.55	1.50	1.43	1.35	1.25	1.25	
∞	3.84	3.00	2.60	2.37	2.21	2.10	2.01	1.94	1.88	1.83	1.75	1.67	1.57	1.52	1.46	1.39	1.32	1.22	1.00	1.00	

Interpolation should be performed using reciprocals of the degrees of freedom.

include the difference between two population means. This interval is based on the assumption that the respective populations have the same variance σ^2 :

$$(\bar{x}_1 - \bar{x}_2) - t_{s_p} \sqrt{1/n_1 + 1/n_2} \leq \mu_1 - \mu_2 \leq (\bar{x}_1 - \bar{x}_2) + t_{s_p} \sqrt{1/n_1 + 1/n_2}$$

Example Compute the 95 percent confidence interval based on the original 100-point sample and the subsequent 5-point sample:

$$s_p^2 = \frac{99(2.47)^2 + 4(1.85)^2}{103} = 5.997$$

or $s_p = 2.45$

With 103 df and $\alpha = .05$, $t = \pm 1.96$ using $t_{.025}$ in Table 3-6. Therefore

$$(35.16 - 37.14) \pm 1.96(2.45) \sqrt{1/100 + 1/5} = -1.98 \pm 2.20$$

or $-4.18 \leq (\mu_1 - \mu_2) \leq .22$

Note that if the respective samples had been based on 52 observations each rather than 100 and 5, the uncertainty factor would have been $\pm .94$ rather than the observed ± 2.20 . The interval width tends to be minimum when $n_1 = n_2$.

Confidence Interval for a Variance The chi-square distribution can be used to derive a confidence interval for a population variance σ^2 when the parent population is normally distributed. For a $100(1 - \alpha)$ percent confidence interval

$$\frac{(df)s^2}{\chi^2_2} \leq \sigma^2 \leq \frac{(df)s^2}{\chi^2_1}$$

where χ^2_1 corresponds to a lower-tail area of $\alpha/2$ and χ^2_2 to an upper-tail area of $\alpha/2$.

Example For the first week of tensile-strength samples compute the 90 percent confidence interval for σ^2 (df = 24, corresponding to $n = 25$, using 5 percent and 95 percent in Table 3-7):

$$\frac{24(2.40)^2}{36.4} \leq \sigma^2 \leq \frac{24(2.40)^2}{13.8}$$

$$3.80 \leq \sigma^2 \leq 10.02$$

or

$$1.95 \leq \sigma \leq 3.17$$

TESTS OF HYPOTHESIS

General Nature of Tests The general nature of tests can be illustrated with a simple example. In a court of law, when a defendant is charged with a crime, the judge instructs the jury initially to presume that the defendant is innocent of the crime. The jurors are then presented with evidence and counterargument as to the defendant's guilt or innocence. If the evidence suggests beyond a reasonable doubt that the defendant did, in fact, commit the crime, they have been instructed to find the defendant guilty; otherwise, not guilty. The burden of proof is on the prosecution.

Jury trials represent a form of decision making. In statistics, an analogous procedure for making decisions falls into an area of statistical inference called **hypothesis testing**.

Suppose that a company has been using a certain supplier of raw materials in one of its chemical processes. A new supplier approaches the company and states that its material, at the same cost, will increase the process yield. If the new supplier has a good reputation, the company might be willing to run a limited test. On the basis of the test results it would then make a decision to change suppliers or not. Good management would dictate that an improvement must be demonstrated

(beyond a reasonable doubt) for the new material. That is, the burden of proof is tied to the new material. In setting up a test of hypothesis for this application, the initial assumption would be defined as a null hypothesis and symbolized as H_0 . The null hypothesis would state that yield for the new material is no greater than for the conventional material. The symbol μ_0 would be used to designate the known current level of yield for the standard material and μ for the unknown population yield for the new material. Thus, the null hypothesis can be symbolized as $H_0: \mu \leq \mu_0$.

The alternative to H_0 is called the alternative hypothesis and is symbolized as $H_1: \mu > \mu_0$.

Given a series of tests with the new material, the average yield \bar{x} would be compared with μ_0 . If $\bar{x} < \mu_0$, the new supplier would be dismissed. If $\bar{x} > \mu_0$, the question would be: Is it sufficiently greater in the light of its corresponding reliability, i.e., beyond a reasonable doubt? If the confidence interval for μ included μ_0 , the answer would be no, but if it did not include μ_0 , the answer would be yes. In this simple application, the formal test of hypothesis would result in the same conclusion as that derived from the confidence interval. However, the utility of tests of hypothesis lies in their generality, whereas confidence intervals are restricted to a few special cases.

Test of Hypothesis for a Mean Procedure

Nomenclature

- μ = mean of the population from which the sample has been drawn
- σ = standard deviation of the population from which the sample has been drawn
- μ_0 = base or reference level
- H_0 = null hypothesis
- H_1 = alternative hypothesis
- α = significance level, usually set at .10, .05, or .01
- t = tabled t value corresponding to the significance level α . For a two-tailed test, each corresponding tail would have an area of $\alpha/2$, and for a one-tailed test, one tail area would be equal to α . If σ^2 is known, then z would be used rather than the t .
- $t = (\bar{x} - \mu_0)/(s/\sqrt{n})$ = sample value of the test statistic.

Assumptions

1. The n observations x_1, x_2, \dots, x_n have been selected randomly.
2. The population from which the observations were obtained is normally distributed with an unknown mean μ and standard deviation σ . In actual practice, this is a robust test, in the sense that in most types of problems it is not sensitive to the normality assumption when the sample size is 10 or greater.

Test of Hypothesis

1. Under the null hypothesis, it is assumed that the sample came from a population whose mean μ is equivalent to some base or reference designated by μ_0 . This can take one of three forms:

Form 1	Form 2	Form 3
$H_0: \mu = \mu_0$	$H_0: \mu \leq \mu_0$	$H_0: \mu \geq \mu_0$
$H_1: \mu \neq \mu_0$	$H_1: \mu > \mu_0$	$H_1: \mu < \mu_0$
Two-tailed test	Upper-tailed test	Lower-tailed test

2. If the null hypothesis is assumed to be true, say, in the case of a two-sided test, form 1, then the distribution of the test statistic t is known. Given a random sample, one can predict how far its sample value of t might be expected to deviate from zero (the midvalue of t) by chance alone. If the sample value of t does, in fact, deviate too far from zero, then this is defined to be sufficient evidence to refute the assumption of the null hypothesis. It is consequently rejected, and the converse or alternative hypothesis is accepted.

3. The rule for accepting H_0 is specified by selection of the α level as indicated in Fig. 3-65. For forms 2 and 3 the α area is defined to be in the upper or the lower tail respectively. The parameter α is the probability of rejecting the null hypothesis when it is actually true.

4. The decision rules for each of the three forms are defined as follows: If the sample t falls within the acceptance region, accept H_0 for lack of contrary evidence. If the sample t falls in the critical region, reject H_0 at a significance level of 100α percent.

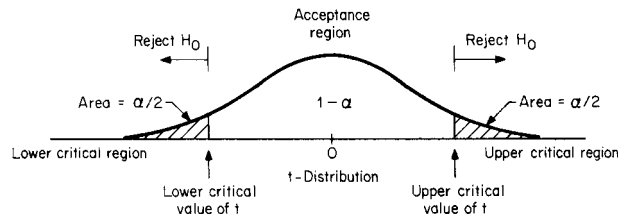


FIG. 3-65 Acceptance region for two-tailed test. For a one-tailed test, area = α on one side only.

Example

Application. In the past, the yield for a chemical process has been established at 89.6 percent with a standard deviation of 3.4 percent. A new supplier of raw materials will be used and tested for 7 days.

Procedure

1. The standard of reference is $\mu_0 = 89.6$ with a known $\sigma = 3.4$.
2. It is of interest to demonstrate whether an increase in yield is achieved with the new material; H_0 says it has not; therefore,

$$H_0: \mu \leq 89.6 \quad H_1: \mu > 89.6$$

3. Select $\alpha = .05$, and since σ is known (the new material would not affect the day-to-day variability in yield), the test statistic would be z with a corresponding critical value $cv(z) = 1.645$ (Table 3-6, $df = \infty$).
4. The decision rule:

Accept H_0 if sample $z < 1.645$
 Reject H_0 if sample $z > 1.645$

5. A 7-day test was carried out, and daily yields averaged 91.6 percent with a sample standard deviation $s = 3.6$ (this is not needed for the test of hypothesis).
6. For the data sample $z = (91.6 - 89.6)/(3.4/\sqrt{7}) = 1.56$.
7. Since the sample $z < cv(z)$, accept the null hypothesis for lack of contrary evidence; i.e., an improvement has not been demonstrated beyond a reasonable doubt.

Example

Application. In the past, the break strength of a synthetic yarn has averaged 34.6 lb. The first-stage draw ratio of the spinning machines has been increased. Production management wants to determine whether the break strength has changed under the new condition.

Procedure

1. The standard of reference is $\mu_0 = 34.6$.
2. It is of interest to demonstrate whether a change has occurred; therefore,

$$H_0: \mu = 34.6 \quad H_1: \mu \neq 34.6$$

3. Select $\alpha = .05$, and since with the change in draw ratio the uniformity might change, the sample standard deviation would be used, and therefore t would be the appropriate test statistic.
4. A sample of 21 ends was selected randomly and tested on an Instron with the results $\bar{x} = 35.55$ and $s = 2.041$.
5. For 20 df and a two-tailed α level of 5 percent, the critical values of $t_{0.025}$ (two tailed) are given by ± 2.086 with a decision rule (Table 3-6, $t_{0.025}$, $df = 20$):

Accept H_0 if $-2.086 < \text{sample } t < 2.086$
 Reject H_0 if sample $t < -2.086$ or > 2.086

6. For the data sample $t = (35.55 - 34.6)/(2.041/\sqrt{21}) = 2.133$.
7. Since $2.133 > 2.086$, reject H_0 and accept H_1 . It has been demonstrated that an improvement in break strength has been achieved.

Two-Population Test of Hypothesis for Means

Nature Two samples were selected from different locations in a plastic-film sheet and measured for thickness. The thickness of the respective samples was measured at 10 close but equally spaced points in each of the samples. It was of interest to compare the average thickness of the respective samples to detect whether they were significantly different. That is, was there a significant variation in thickness between locations?

From a modeling standpoint statisticians would define this problem as a two-population test of hypothesis. They would define the respective sample sheets as two populations from which 10 sample thickness determinations were measured for each.

In order to compare populations based on their respective samples, it is necessary to have some basis of comparison. This basis is predicated on the distribution of the t statistic. In effect, the t statistic characterizes

the way in which two sample means from two separate populations will tend to vary by chance alone when the population means and variances are equal. Consider the following:

Population 1		Population 2	
Normal	Sample 1	Normal	Sample 2
μ_1	n_1	μ_2	n_2
σ_1^2	\bar{x}_1	σ_2^2	\bar{x}_2
	s_1^2		s_2^2

Consider the hypothesis $\mu_1 = \mu_2$. If, in fact, the hypothesis is correct, i.e., $\mu_1 = \mu_2$ (under the condition $\sigma_1^2 = \sigma_2^2$), then the sampling distribution of $(\bar{x}_1 - \bar{x}_2)$ is predictable through the t distribution. The observed sample values then can be compared with the corresponding t distribution. If the sample values are reasonably close (as reflected through the α level), that is, \bar{x}_1 and \bar{x}_2 are not "too different" from each other on the basis of the t distribution, the null hypothesis would be accepted. Conversely, if they deviate from each other "too much" and the deviation is therefore not ascribable to chance, the conjecture would be questioned and the null hypothesis rejected.

Example

Application. Two samples were selected from different locations in a plastic-film sheet. The thickness of the respective samples was measured at 10 close but equally spaced points.

Procedure

1. Demonstrate whether the thicknesses of the respective sample locations are significantly different from each other; therefore,

$$H_0: \mu_1 = \mu_2 \quad H_1: \mu_1 \neq \mu_2$$

2. Select $\alpha = .05$.

3. Summarize the statistics for the respective samples:

Sample 1		Sample 2	
1.473	1.367	1.474	1.417
1.484	1.276	1.501	1.448
1.484	1.485	1.485	1.469
1.425	1.462	1.435	1.474
1.448	1.439	1.348	1.452
$\bar{x}_1 = 1.434$	$s_1 = .0664$	$\bar{x}_2 = 1.450$	$s_2 = .0435$

4. As a first step, the assumption for the standard t test, that $\sigma_1^2 = \sigma_2^2$, can be tested through the F distribution. For this hypothesis, $H_0: \sigma_1^2 = \sigma_2^2$ would be tested against $H_1: \sigma_1^2 \neq \sigma_2^2$. Since this is a two-tailed test and conventionally only the upper tail for F is published, the procedure is to use the largest ratio and the corresponding ordered degrees of freedom. This achieves the same end result through one table. However, since the largest ratio is arbitrary, it is necessary to define the true α level as twice the value of the tabled value. Therefore, by using Table 3-8 with $\alpha = .05$ the corresponding critical value for $F(9,9) = 3.18$ would be for a true $\alpha = .10$. For the sample,

$$\text{Sample } F = (.0664/.0435)^2 = 2.33$$

Therefore, the ratio of sample variances is no larger than one might expect to observe when in fact $\sigma_1^2 = \sigma_2^2$. There is not sufficient evidence to reject the null hypothesis that $\sigma_1^2 = \sigma_2^2$.

5. For 18 df and a two-tailed α level of 5 percent the critical values of t are given by ± 2.101 (Table 3-6, $t_{0.025}, df = 18$).

6. The decision rule:

Accept H_0 if $-2.101 \leq \text{sample } t \leq 2.101$

Reject H_0 otherwise

7. For the sample the pooled variance estimate is given by Eq. (3-120).

$$s_p^2 = \frac{9(.0664)^2 + 9(.0435)^2}{9 + 9} = \frac{(.0664)^2 + (.0435)^2}{2} = .00315$$

or $s_p = .056$

8. The sample statistic value of t is given by Eq. (3-119).

$$\text{Sample } t = \frac{1.434 - 1.450}{.056\sqrt{1/10 + 1/10}} = -.64$$

9. Since the sample value of t falls within the acceptance region, accept H_0 for lack of contrary evidence; i.e., there is insufficient evidence to demonstrate that thickness differs between the two selected locations.

Test of Hypothesis for Paired Observations

Nature In some types of applications, associated pairs of observations are defined. For example, (1) pairs of samples from two populations are treated in the same way, or (2) two types of measurements are made on the same unit. For applications of this type, it is not only more effective but necessary to define the random variable as the difference between the pairs of observations. The difference numbers can then be tested by the standard t distribution.

Examples of the two types of applications are as follows:

1. *Sample treatment*

- a. Two types of metal specimens buried in the ground together in a variety of soil types to determine corrosion resistance
- b. Wear-rate test with two different types of tractor tires mounted in pairs on n tractors for a defined period of time

2. *Same unit*

- a. Blood-pressure measurements made on the same individual before and after the administration of a stimulus
- b. Smoothness determinations on the same film samples at two different testing laboratories

Test of Hypothesis for Matched Pairs: Procedure

Nomenclature

d_i = sample difference between the i th pair of observations

s = sample standard deviation of differences

μ = population mean of differences

σ = population standard deviation of differences

μ_0 = base or reference level of comparison

H_0 = null hypothesis

H_1 = alternative hypothesis

α = significance level

t = tabled value with $(n - 1)$ df

$t = (\bar{d} - \mu_0)/(s/\sqrt{n})$, the sample value of t

Assumptions

1. The n pairs of samples have been selected and assigned for testing in a random way.

2. The population of differences is normally distributed with a mean μ and variance σ^2 . As in the previous application of the t distribution, this is a robust procedure, i.e., not sensitive to the normality assumption if the sample size is 10 or greater in most situations.

Test of Hypothesis

1. Under the null hypothesis, it is assumed that the sample came from a population whose mean μ is equivalent to some base or reference level designated by μ_0 . For most applications of this type, the value of μ_0 is defined to be zero; that is, it is of interest generally to demonstrate a difference not equal to zero. The hypothesis can take one of three forms:

Form 1	Form 2	Form 3
$H_0: \mu = \mu_0$	$H_0: \mu \leq \mu_0$	$H_0: \mu \geq \mu_0$
$H_1: \mu \neq \mu_0$	$H_1: \mu > \mu_0$	$H_1: \mu < \mu_0$
Two-tailed test	Upper-tailed test	Lower-tailed test

2. If the null hypothesis is assumed to be true, say, in the case of a lower-tailed test, form 3, then the distribution of the test statistic t is known under the null hypothesis that limits $\mu = \mu_0$. Given a random sample, one can predict how far its sample value of t might be expected to deviate from zero by chance alone when $\mu = \mu_0$. If the sample value of t is too small, as in the case of a negative value, then this would be defined as sufficient evidence to reject the null hypothesis.

3. Select α .

4. The critical values or value of t would be defined by the tabled value of t with $(n - 1)$ df corresponding to a tail area of α . For a two-tailed test, each tail area would be $\alpha/2$, and for a one-tailed test there would be an upper-tail or a lower-tail area of α corresponding to forms 2 and 3 respectively.

5. The decision rule for each of the three forms would be to reject the null hypothesis if the sample value of t fell in that area of the t distribution defined by α , which is called the critical region.

Otherwise, the alternative hypothesis would be accepted for lack of contrary evidence.

Example

Application. Pairs of pipes have been buried in 11 different locations to determine corrosion on nonbituminous pipe coatings for underground use. One type includes a lead-coated steel pipe and the other a bare steel pipe.

Procedure

1. The standard of reference is taken as $\mu_0 = 0$, corresponding to no difference in the two types.
2. It is of interest to demonstrate whether either type of pipe has a greater corrosion resistance than the other. Therefore,

$$H_0: \mu = 0 \quad H_1: \mu \neq 0$$

3. Select $\alpha = .05$. Therefore, with $n = 11$ the critical values of t with 10 df are defined by $t = \pm 2.228$ (Table 3.5, $t_{.025}$).

4. The decision rule:

Accept H_0 if $-2.228 \leq \text{sample } t \leq 2.228$

Reject H_0 otherwise

5. The sample of 11 pairs of corrosion determinations and their differences are as follows:

Soil type	Lead-coated steel pipe	Bare steel pipe	$d = \text{difference}$
A	27.3	41.4	-14.1
B	18.4	18.9	-0.5
C	11.9	21.7	-9.8
D	11.3	16.8	-5.5
E	14.8	9.0	5.8
F	20.8	19.3	1.5
G	17.9	32.1	-14.2
H	7.8	7.4	0.4
I	14.7	20.7	-6.0
J	19.0	34.4	-15.4
K	65.3	76.2	-10.9

6. The sample statistics, Eq. (3-118)

$$\bar{d} = -6.245 \quad s^2 = \frac{11 \sum d^2 - (\sum d)^2}{11 \times 10} = 52.59$$

or

$$s = 7.25$$

$$\text{Sample } t = \frac{(-6.245 - 0)/(7.25/\sqrt{11})}{1} = -2.86$$

7. Since the sample t of $-2.86 < \text{tabled } t$ of -2.228 , reject H_0 and accept H_1 ; that is, it has been demonstrated that, on the basis of the evidence, lead-coated steel pipe has a greater corrosion resistance than bare steel pipe.

Example

Application. A stimulus was tested for its effect on blood pressure. Ten men were selected randomly, and their blood pressure was measured before and after the stimulus was administered. It was of interest to determine whether the stimulus had caused a significant increase in the blood pressure.

Procedure

1. The standard of reference was taken as $\mu_0 \leq 0$, corresponding to no increase.
2. It was of interest to demonstrate an increase in blood pressure if in fact an increase did occur. Therefore,

$$H_0: \mu_0 \leq 0 \quad H_1: \mu_0 > 0$$

3. Select $\alpha = .05$. Therefore, with $n = 10$ the critical value of t with 9 df is defined by $t = 1.833$ (Table 3-6, $t_{.05}$, one-sided).

4. The decision rule:

Accept H_0 if sample $t < 1.833$

Reject H_0 if sample $t > 1.833$

5. The sample of 10 pairs of blood pressure and their differences were as follows:

Individual	Before	After	$d = \text{difference}$
1	138	146	8
2	116	118	2
3	124	120	-4
4	128	136	8

5	155	174	19
6	129	133	4
7	130	129	-1
8	148	155	7
9	143	148	5
10	159	155	-4

6. The sample statistics:

$$\bar{d} = 4.4 \quad s = 6.85$$

$$\text{Sample } t = (4.4 - 0)/(6.85/\sqrt{10}) = 2.03$$

7. Since the sample $t = 2.03 > \text{critical } t = 1.833$, reject the null hypothesis. It has been demonstrated that the population of men from which the sample was drawn tend, as a whole, to have an increase in blood pressure after the stimulus has been given. The distribution of differences d seems to indicate that the degree of response varies by individuals.

Test of Hypothesis for a Proportion

Nature Some types of statistical applications deal with counts and proportions rather than measurements. Examples are (1) the proportion of workers in a plant who are out sick, (2) lost-time worker accidents per month, (3) defective items in a shipment lot, and (4) preference in consumer surveys.

The procedure for testing the significance of a sample proportion follows that for a sample mean. In this case, however, owing to the nature of the problem the appropriate test statistic is Z . This follows from the fact that the null hypothesis requires the specification of the goal or reference quantity p_0 , and since the distribution is a binomial proportion, the associated variance is $[p_0(1 - p_0)]n$ under the null hypothesis. The primary requirement is that the sample size n satisfy normal approximation criteria for a binomial proportion, roughly $np > 5$ and $n(1 - p) > 5$.

Test of Hypothesis for a Proportion: Procedure

Nomenclature

p = mean proportion of the population from which the sample has been drawn

p_0 = base or reference proportion

$[p_0(1 - p_0)]/n$ = base or reference variance

$\hat{p} = x/n$ = sample proportion, where x refers to the number of observations out of n which have the specified attribute

H_0 = assumption or null hypothesis regarding the population proportion

H_1 = alternative hypothesis

α = significance level, usually set at .10, .05, or .01

z = tabled Z value corresponding to the significance level α . The sample sizes required for the z approximation according to the magnitude of p_0 are given in Table 3-6.

$z = (\hat{p} - p_0)/\sqrt{p_0(1 - p_0)/n}$, the sample value of the test statistic

Assumptions

1. The n observations have been selected randomly.
2. The sample size n is sufficiently large to meet the requirement for the Z approximation.

Test of Hypothesis

1. Under the null hypothesis, it is assumed that the sample came from a population with a proportion p_0 of items having the specified attribute. For example, in tossing a coin the population could be thought of as having an unbounded number of potential tosses. If it is assumed that the coin is fair, this would dictate $p_0 = 1/2$ for the proportional number of heads in the population. The null hypothesis can take one of three forms:

Form 1	Form 2	Form 3
$H_0: p = p_0$	$H_0: p \leq p_0$	$H_0: p \geq p_0$
$H_1: p \neq p_0$	$H_1: p > p_0$	$H_1: p < p_0$
Two-tailed test	Upper-tailed test	Lower-tailed test

2. If the null hypothesis is assumed to be true, then the sampling distribution of the test statistic Z is known. Given a random sample, it is possible to predict how far the sample proportion x/n might deviate from its assumed population proportion p_0 through the Z distribution. When the sample proportion deviates too far, as defined by the significance level α , this serves as the justification for rejecting the assumption, that is, rejecting the null hypothesis.

3. The decision rule is given by
 Form 1: Accept H_0 if lower critical $z < \text{sample } z < \text{upper critical } z$
 Reject H_0 otherwise
 Form 2: Accept H_0 if sample $z < \text{upper critical } z$
 Reject H_0 otherwise
 Form 3: Accept H_0 if lower critical $z < \text{sample } z$
 Reject H_0 otherwise

Example

Application. A company has received a very large shipment of rivets. One product specification required that no more than 2 percent of the rivets have diameters greater than 14.28 mm. Any rivet with a diameter greater than this would be classified as defective. A random sample of 600 was selected and tested with a go-no-go gauge. Of these, 16 rivets were found to be defective. Is this sufficient evidence to conclude that the shipment contains more than 2 percent defective rivets?

Procedure

- The quality goal is $p \leq .02$. It would be assumed initially that the shipment meets this standard; i.e., $H_0: p \leq .02$.
- The assumption in step 1 would first be tested by obtaining a random sample. Under the assumption that $p \leq .02$, the distribution for a sample proportion would be defined by the z distribution. This distribution would define an upper bound corresponding to the upper critical value for the sample proportion. It would be unlikely that the sample proportion would rise above that value if, in fact, $p \leq .02$. If the observed sample proportion exceeds that limit, corresponding to what would be a very unlikely chance outcome, this would lead one to question the assumption that $p \leq .02$. That is, one would conclude that the null hypothesis is false. To test, set

$$H_0: p \leq .02 \quad H_1: p > .02$$

- Select $\alpha = .05$.
- With $\alpha = .05$, the upper critical value of $Z = 1.645$ (Table 3-6, $t_{.05}$, $df = \infty$, one-sided).
- The decision rule:

$$\begin{aligned} &\text{Accept } H_0 \text{ if sample } z < 1.645 \\ &\text{Reject } H_0 \text{ if sample } z > 1.645 \end{aligned}$$

6. The sample z is given by

$$\begin{aligned} \text{Sample } z &= \frac{(16/600) - .02}{\sqrt{(.02)(.98)/600}} \\ &= 1.17 \end{aligned}$$

7. Since the sample $z < 1.645$, accept H_0 for lack of contrary evidence; there is not sufficient evidence to demonstrate that the defect proportion in the shipment is greater than 2 percent.

Test of Hypothesis for Two Proportions

Nature In some types of engineering and management-science problems, we may be concerned with a random variable which represents a proportion, for example, the proportional number of defective items per day. The method described previously relates to a single proportion. In this subsection two proportions will be considered.

A certain change in a manufacturing procedure for producing component parts is being considered. Samples are taken by using both the existing and the new procedures in order to determine whether the new procedure results in an improvement. In this application, it is of interest to demonstrate statistically whether the population proportion p_2 for the new procedure is less than the population proportion p_1 for the old procedure on the basis of a sample of data.

Test of Hypothesis for Two Proportions: Procedure

Nomenclature

- p_1 = population 1 proportion
- p_2 = population 2 proportion
- n_1 = sample size from population 1
- n_2 = sample size from population 2

- x_1 = number of observations out of n_1 that have the designated attribute
- x_2 = number of observations out of n_2 that have the designated attribute

- $\hat{p}_1 = x_1/n_1$, the sample proportion from population 1
- $\hat{p}_2 = x_2/n_2$, the sample proportion from population 2
- α = significance level

- H_0 = null hypothesis
- H_1 = alternative hypothesis
- z = tabled Z value corresponding to the stated significance level α
- $z = \frac{\hat{p}_1 - \hat{p}_2}{\sqrt{\hat{p}_1(1 - \hat{p}_1)/n_1 + \hat{p}_2(1 - \hat{p}_2)/n_2}}$, the sample value of Z

Assumptions

- The respective two samples of n_1 and n_2 observations have been selected randomly.
- The sample sizes n_1 and n_2 are sufficiently large to meet the requirement for the Z approximation; i.e., $x_1 > 5$, $x_2 > 5$.

Test of Hypothesis

1. Under the null hypothesis, it is assumed that the respective two samples have come from populations with equal proportions $p_1 = p_2$. Under this hypothesis, the sampling distribution of the corresponding Z statistic is known. On the basis of the observed data, if the resultant sample value of Z represents an unusual outcome, that is, if it falls within the critical region, this would cast doubt on the assumption of equal proportions. Therefore, it will have been demonstrated statistically that the population proportions are in fact not equal. The various hypotheses can be stated:

Form 1	Form 2	Form 3
$H_0: p_1 = p_2$	$H_0: p_1 \leq p_2$	$H_0: p_1 \geq p_2$
$H_1: p_1 \neq p_2$	$H_1: p_1 > p_2$	$H_1: p_1 < p_2$
Two-tailed test	Upper-tailed test	Lower-tailed test

2. The decision rule for form 1 is given by
 Accept H_0 if lower critical $z < \text{sample } z < \text{upper critical } z$
 Reject H_0 otherwise

Example

Application. A change was made in a manufacturing procedure for component parts. Samples were taken during the last week of operations with the old procedure and during the first week of operations with the new procedure. Determine whether the proportional numbers of defects for the respective populations differ on the basis of the sample information.

Procedure

- The hypotheses are

$$H_0: p_1 = p_2 \quad H_1: p_1 \neq p_2$$
- Select $\alpha = .05$. Therefore, the critical values of z are ± 1.96 (Table 3-5, $A = 0.9500$).
- For the samples, 75 out of 1720 parts from the previous procedure and 80 out of 2780 parts under the new procedure were found to be defective; therefore,

$$\hat{p}_1 = 75/1720 = .0436 \quad \hat{p}_2 = 80/2780 = .0288$$

4. The decision rule:
 Accept H_0 if $-1.96 \leq \text{sample } z \leq 1.96$
 Reject H_0 otherwise

5. The sample statistic:

$$\begin{aligned} \text{Sample } z &= \frac{.0436 - .0288}{\sqrt{(.0436)(.9564)/1720 + (.0288)(.9712)/2780}} \\ &= 2.53 \end{aligned}$$

6. Since the sample z of 2.53 $>$ tabled z of 1.96, reject H_0 and conclude that the new procedure has resulted in a reduced defect rate.

Goodness-of-Fit Test

Nature A standard die has six sides numbered from 1 to 6. If one were really interested in determining whether a particular die was well balanced, one would have to carry out an experiment. To do this, it might be decided to count the frequencies of outcomes, 1 through 6, in tossing the die N times. On the assumption that the die is perfectly balanced,

one would expect to observe $N/6$ occurrences each for 1, 2, 3, 4, 5, and 6. However, chance dictates that exactly $N/6$ occurrences each will not be observed. For example, given a perfectly balanced die, the probability is only 1 chance in 65 that one will observe 1 outcome each, for 1 through 6, in tossing the die 6 times. Therefore, an outcome different from 1 occurrence each can be expected. Conversely, an outcome of six 3s would seem to be too unusual to have occurred by chance alone.

Some industrial applications involve the concept outlined here. The basic idea is to test whether or not a group of observations follows a pre-conceived distribution. In the case cited, the distribution is uniform; i.e., each face value should tend to occur with the same frequency.

Goodness-of-Fit Test: Procedure

Nomenclature Each experimental observation can be classified into one of r possible categories or cells.

- r = total number of cells
- O_j = number of observations occurring in cell j
- E_j = expected number of observations for cell j based on the pre-conceived distribution
- N = total number of observations
- f = degrees of freedom for the test. In general, this will be equal to $(r - 1)$ minus the number of statistical quantities on which the E_j s are based (see the examples which follow for details).

Assumptions

1. The observations represent a sample selected randomly from a population which has been specified.
2. The number of expectation counts E_j within each category should be roughly 5 or more. If an E_j count is significantly less than 5, that cell should be pooled with an adjacent cell.

Computation for E_j On the basis of the specified population, the probability of observing a count in cell j is defined by p_j . For a sample of size N , corresponding to N total counts, the expected frequency is given by $E_j = Np_j$.

Test Statistics: Chi Square

$$\chi^2 = \sum_{j=1}^r \frac{(O_j - E_j)^2}{E_j} \quad \text{with } f \text{ df}$$

Test of Hypothesis

1. H_0 : The sample came from the specified theoretical distribution
 H_1 : The sample did not come from the specified theoretical distribution
2. For a stated level of α ,
 Reject H_0 if sample $\chi^2 >$ tabled χ^2
 Accept H_0 if sample $\chi^2 <$ tabled χ^2

Example

Application A production-line product is rejected if one of its characteristics does not fall within specified limits. The standard goal is that no more than 2 percent of the production should be rejected.

Computation

1. Of 950 units produced during the day, 28 units were rejected.
2. The hypotheses:
 H_0 : the process is in control
 H_1 : the process is not in control
3. Assume that $\alpha = .05$; therefore, the critical value of $\chi^2(1) = 3.84$ (Table 3-7, 95 percent, $df = 1$). One degree of freedom is defined since $(r - 1) = 1$, and no statistical quantities have been computed for the data.
4. The decision rule:

Reject H_0 if sample $\chi^2 > 3.84$
 Accept H_0 otherwise

5. Since it is assumed that $p = .02$, this would dictate that in a sample of 950 there would be on the average $(.02)(950) = 19$ defective items and 931 acceptable items:

Category	Observed O_j	Expectation $E_j = 950p_j$
Acceptable	922	931
Not acceptable	28	19
Total	950	950

$$\begin{aligned} \text{Sample } \chi^2 &= \frac{(922 - 931)^2}{931} + \frac{(28 - 19)^2}{19} \\ &= 4.35 \text{ with critical } \chi^2 = 3.84 \end{aligned}$$

6. Conclusion. Since the sample value exceeds the critical value, it would be concluded that the process is not in control.

Example

Application A frequency count of workers was tabulated according to the number of defective items that they produced. An unresolved question is whether the observed distribution is a Poisson distribution. That is, do observed and expected frequencies agree within chance variation?

Computation

1. The hypotheses:
 H_0 : there are no significant differences, in number of defective units, between workers
 H_1 : there are significant differences
2. Assume that $\alpha = .05$.
3. Test statistic:

No. of defective units	O_j	E_j
0	3	2.06
1	7	6.64
2	9	10.73
3	12	11.55
4	9	9.33
5	6	6.03
6	3	3.24
7	2	1.50
8	0	.60
9	1	.22
≥ 10	0	.10
Sum	52	52

The expectation numbers E_j were computed as follows: For the Poisson distribution, $\lambda = E(x)$; therefore, an estimate of λ is the average number of defective units per worker, i.e., $\lambda = (1/52)(0 \times 3 + 1 \times 7 + \dots + 9 \times 1) = 3.23$. Given this approximation, the probability of no defective units for a worker would be $(3.23)^0(0!)e^{-3.23} = .0396$. For the 52 workers, the number of workers producing no defective units would have an expectation $E = 52(0.0396) = 2.06$, and so forth.

The sample chi-square value is computed from

$$\begin{aligned} \chi^2 &= \frac{(10 - 8.70)^2}{8.70} + \frac{(9 - 10.73)^2}{10.73} + \dots + \frac{(6 - 5.66)^2}{5.66} \\ &= .522 \end{aligned}$$

4. The critical value of χ^2 would be based on four degrees of freedom. This corresponds to $(r - 1) - 1$, since one statistical quantity λ was computed from the sample and used to derive the expectation numbers.
5. The critical value of $\chi^2(4) = 9.49$ (Table 3-7) with $\alpha = .05$; therefore, accept H_0 .

Two-Way Test for Independence for Count Data

Nature When individuals or items are observed and classified according to two different criteria, the resultant counts can be statistically analyzed. For example, a market survey may examine whether a new product is preferred and if it is preferred due to a particular characteristic.

Count data, based on a random selection of individuals or items which are classified according to two different criteria, can be statistically analyzed through the χ^2 distribution. The purpose of this analysis is to determine whether the respective criteria are dependent. That is, is the product preferred because of a particular characteristic?

Two-Way Test for Independence for Count Data: Procedure

Nomenclature

1. Each observation is classified according to two categories:
 - a. The first one into 2, 3, . . . , or r categories
 - b. The second one into 2, 3, . . . , or c categories
2. O_{ij} = number of observations (observed counts) in cell (i, j) with

$$i = 1, 2, \dots, r$$

$$j = 1, 2, \dots, c$$

3. N = total number of observations
4. E_{ij} = computed number for cell (i,j) which is an expectation based on the assumption that the two characteristics are independent
5. R_i = subtotal of counts in row i
6. C_j = subtotal of counts in column j
7. α = significance level
8. H_0 = null hypothesis
9. H_1 = alternative hypothesis
10. χ^2 = critical value of χ^2 corresponding to the significance level α and $(r-1)(c-1)$ df
11. Sample $\chi^2 = \sum_{i,j} \frac{(O_{ij} - E_{ij})^2}{E_{ij}}$

Assumptions

1. The observations represent a sample selected randomly from a large total population.
2. The number of expectation counts E_{ij} within each cell should be approximately 2 or more for arrays 3×3 or larger. If any cell contains a number smaller than 2, appropriate rows or columns should be combined to increase the magnitude of the expectation count. For arrays 2×2 , approximately 4 or more are required. If the number is less than 4, the exact Fisher test should be used.

Test of Hypothesis Under the null hypothesis, the classification criteria are assumed to be independent, i.e.,

- H_0 : the criteria are independent
- H_1 : the criteria are not independent

For the stated level of α ,

- Reject H_0 if sample $\chi^2 >$ tabled χ^2
- Accept H_0 otherwise

Computation for E_{ij} Compute E_{ij} across rows or down columns by using either of the following identities:

$$E_{ij} = C_j \left(\frac{R_i}{N} \right) \text{ across rows}$$

$$E_{ij} = R_i \left(\frac{C_j}{N} \right) \text{ down columns}$$

Sample χ^2 Value

$$\chi^2 = \sum_{i,j} \frac{(O_{ij} - E_{ij})^2}{E_{ij}}$$

In the special case of $r = 2$ and $c = 2$, a more accurate and simplified formula which does not require the direct computation of E_{ij} can be used:

$$\chi^2 = \frac{[O_{11}O_{22} - O_{12}O_{21} - \frac{1}{2}N]^2 N}{R_1 R_2 C_1 C_2}$$

Example

Application A market research study was carried out to relate the subjective "feel" of a consumer product to consumer preference. In other words, is the consumer's preference for the product associated with the feel of the product, or is the preference independent of the product feel?

Procedure

1. It was of interest to demonstrate whether an association exists between feel and preference; therefore, assume
 - H_0 : feel and preference are independent
 - H_1 : they are not independent
2. A sample of 200 people was asked to classify the product according to two criteria:
 - a. Liking for this product
 - b. Liking for the feel of the product

		Like feel		R_i
		Yes	No	
Like product	Yes	114	13	= 127
	No	55	18	= 73
		C_j	169	31
				200

3. Select $\alpha = .05$; therefore, with $(r-1)(c-1) = 1$ df, the critical value of χ^2 is 3.84 (Table 3-7, 95 percent).
4. The decision rule:
 - Accept H_0 if sample $\chi^2 < 3.84$
 - Reject H_0 otherwise

5. The sample value of χ^2 by using the special formula is

$$\text{Sample } \chi^2 = \frac{[114 \times 18 - 13 \times 55 - 100]^2 200}{(169)(31)(127)(73)} = 6.30$$

6. Since the sample χ^2 of 6.30 > tabled χ^2 of 3.84, reject H_0 and accept H_1 . The relative proportionality of $E_{11} = 169(127/200) = 107.3$ to the observed 114 compared with $E_{22} = 31(73/200) = 11.3$ to the observed 18 suggests that when the consumer likes the feel, the consumer tends to like the product, and conversely for not liking the feel. The proportions $169/200 = 84.5$ percent and $127/200 = 63.5$ percent suggest further that there are other attributes of the product which tend to nullify the beneficial feel of the product.

LEAST SQUARES

When experimental data is to be fit with a mathematical model, it is necessary to allow for the fact that the data has errors. The engineer is interested in finding the parameters in the model as well as the uncertainty in their determination. In the simplest case, the model is a linear equation with only two parameters, and they are found by a least-squares minimization of the errors in fitting the data. Multiple regression is just linear least squares applied with more terms. Non-linear regression allows the parameters of the model to enter in a non-linear fashion. See Press et al. (1986); for a description of maximum likelihood as it applies to both linear and nonlinear least squares.

In a least squares parameter estimation, it is desired to find parameters that minimize the sum of squares of the deviation between the experimental data and the theoretical equation.

$$\chi^2 = \sum_{i=1}^N [y_i - y(x_i; a_1, a_2, \dots, a_M)]^2$$

where y_i is the i th experimental data point for the value x_i , $y(x_i; a_1, a_2, \dots, a_M)$ is the theoretical equation at x_i , and the parameters $\{a_1, a_2, \dots, a_M\}$ are to be determined to minimize χ^2 . This will also minimize the variance of the curve fit

$$\sigma^2 = \sum_{i=1}^N \frac{[y_i - y(x_i; a_1, a_2, \dots, a_M)]^2}{N}$$

Linear Least Squares When the model is a straight line, one is minimizing

$$\chi^2 = \sum_{i=1}^N (y_i - a - bx_i)^2$$

The linear correlation coefficient r is defined by

$$r = \frac{\sum_{i=1}^N (x_i - \bar{x})(y_i - \bar{y})}{\sqrt{\sum_{i=1}^N (x_i - \bar{x})^2} \sqrt{\sum_{i=1}^N (y_i - \bar{y})^2}}$$

and

$$\chi^2 = (1 - r^2) \sum_{i=1}^N (y_i - \bar{y})^2$$

where \bar{y} is the average of the y_i values. Values of r near 1 indicate a positive correlation; r near -1 means a negative correlation, and r near 0 means no correlation. These parameters are easily found by using standard programs, such as Microsoft Excel.

Example

Application. Brenner (*Magnetic Method for Measuring the Thickness of Non-magnetic Coatings on Iron and Steel*, National Bureau of Standards, RP1081, March 1938) suggests an alternative way of measuring the thickness of nonmagnetic coatings of galvanized zinc on iron and steel. This procedure is based on a nondestructive magnetic method as a substitute for the standard

destructive stripping method. A random sample of 11 pieces was selected and measured by both methods.

Nomenclature. The calibration between the magnetic and the stripping methods can be determined through the model

$$y = a + bx + \epsilon$$

where x = strip-method determination

y = magnetic-method determination

Sample data

Thickness, 10 ⁻⁵ in	
Stripping method, x	Magnetic method, y
104	85
114	115
116	105
129	127
132	120
139	121
174	155
312	250
338	310
465	443
720	630

This example is solved by using Microsoft Excel. Put the data into columns A and B as shown, using rows 1 through 11. Then the commands

SLOPE(B1:B11, A1:A11), INTERCEPT(B1:B11, A1:A11),
RSQ(B1:B11, A1:A11)

give the slope b , the intercept a , and the value of r^2 . Here they are 3.20, 0.884, and 0.9928, respectively, so that $r = 0.9964$. By choosing Insert/Chart and Scatter Plot, the data are plotted. Once that is done, place the cursor on a data point and right-click; choose Format trendline with options selected to display the equation and r^2 , and you get Fig. 3-66. On the Macintosh, use CTRL-click.

Polynomial Regression In polynomial regression, one expands the function in a polynomial in x .

$$y(x) = \sum_{j=1}^M a_j x^{j-1}$$

Example

Application. Merriman ("The Method of Least Squares Applied to a Hydraulic Problem," *J. Franklin Inst.*, 233-241, October 1877) reported on a

study of stream velocity as a function of relative depth of the stream.

Sample data

Depth ^a	Velocity, y , ft/s
0	3.1950
.1	3.2299
.2	3.2532
.3	3.2611
.4	3.2516
.5	3.2282
.6	3.1807
.7	3.1266
.8	3.0594
.9	2.9759

^aAs a fraction of total depth.

The model is taken as a quadratic function of position:

$$\text{Velocity} = a + bx + cx^2$$

The parameters are easily determined by using computer software. In Microsoft Excel, the data are put into columns A and B and the graph is created as for a linear curve fit. This time, though, when adding the trendline, choose the polynomial icon and use 2 (which gives powers up to and including x^2). The result is

$$\text{Velocity} = 3.195 + 0.4425x - 0.7653x^2$$

The value of r^2 is .9993.

Multiple Regression In multiple regression, any set of functions can be used, not just polynomials, such as

$$y(x) = \sum_{j=1}^M a_j f_j(x)$$

where the set of functions $\{f_j(x)\}$ is known and specified. Note that the unknown parameters $\{a_j\}$ enter the equation linearly. In this case, the spreadsheet can be expanded to have a column for x and then successive columns for $f_j(x)$. In Microsoft Excel, you choose Regression under Tools/Data Analysis, and complete the form. In addition to the actual correlation, you get the expected variance of the unknowns, which allows you to assess how accurately they were determined. In the example above, by creating a column for x and x^2 , one obtains an intercept of 3.195 with a standard error of .0039, $b = .4416$ with a standard error of .018, and $c = -.7645$ with a standard error of .018.

Nonlinear Least Squares There are no analytic methods for determining the most appropriate model for a particular set of data.

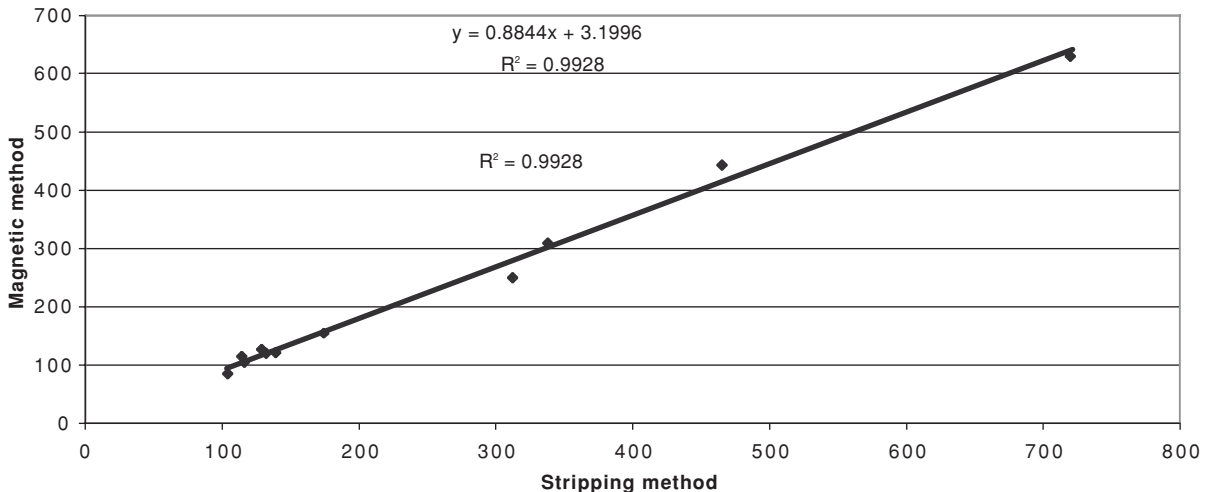


FIG. 3-66 Plot of data and correlating line.

In many cases, however, the engineer has some basis for a model. If the parameters occur in a nonlinear fashion, then the analysis becomes more difficult. For example, in relating the temperature to the elapsed time of a fluid cooling in the atmosphere, a model that has an asymptotic property would be the appropriate model ($\text{temp} = a + b \exp(-c \text{ time})$), where a represents the asymptotic temperature corresponding to $t \rightarrow \infty$. In this case, the parameter c appears nonlinearly. The usual practice is to concentrate on model development and computation rather than on statistical aspects. In general, nonlinear regression should be applied only to problems in which there is a well-defined, clear association between the two variables; therefore, a test of hypothesis on the significance of the fit would be somewhat ludicrous. In addition, the generalization of the theory for the associate confidence intervals for nonlinear coefficients is not well developed.

Example

Application. Data were collected on the cooling of water in the atmosphere as a function of time.

Sample data

Time x	Temperature y
0	92.0
1	85.5
2	79.5
3	74.5
5	67.0
7	60.5
10	53.5
15	45.0
20	39.5

Model. MATLAB can be used to find the best fit of the data to the formula $y = a + be^{cx}$: $a = 33.54$, $b = 57.89$, $c = 0.11$. The value of χ^2 is 1.83. Using an alternative form, $y = a + b/(c + x)$, gives $a = 9.872$, $b = 925.7$, $c = 11.27$, and $\chi = 0.19$. Since this model had a smaller value of χ^2 it might be the chosen one, but it is only a fit of the specified data and may not be generalized beyond that. Both forms give equivalent plots.

ERROR ANALYSIS OF EXPERIMENTS

Consider the problem of assessing the accuracy of a series of measurements. If measurements are for independent, identically distributed observations, then the errors are independent and uncorrelated. Then \bar{y} , the experimentally determined mean, varies about $E(y)$, the true mean, with variance σ^2/n , where n is the number of observations in \bar{y} . Thus, if one measures something several times today, and each day, and the measurements have the same distribution, then the variance of the means decreases with the number of samples in each day's measurement, n . Of course, other factors (weather, weekends) may make the observations on different days *not* distributed identically.

Consider next the problem of estimating the error in a variable that cannot be measured directly but must be calculated based on results of other measurements. Suppose the computed value Y is a linear combination of the measured variables $\{y_i\}$, $Y = \alpha_1 y_1 + \alpha_2 y_2 + \dots$. Let the random variables y_1, y_2, \dots have means $E(y_1), E(y_2), \dots$ and variances $\sigma^2(y_1), \sigma^2(y_2), \dots$. The variable Y has mean

$$E(Y) = \alpha_1 E(y_1) + \alpha_2 E(y_2) + \dots$$

and variance (Cropley, 1978)

$$\sigma^2(Y) = \sum_{i=1}^n \alpha_i^2 \sigma^2(y_i) + 2 \sum_{i=1}^n \sum_{j=i+1}^n \alpha_i \alpha_j \text{Cov}(y_i, y_j)$$

If the variables are uncorrelated and have the same variance, then

$$\sigma^2(Y) = \left(\sum_{i=1}^n \alpha_i^2 \right) \sigma^2$$

Next suppose the model relating Y to $\{y_i\}$ is nonlinear, but the errors are small and independent of one another. Then a change in Y is related to changes in y_i by

$$dY = \frac{\partial Y}{\partial y_1} dy_1 + \frac{\partial Y}{\partial y_2} dy_2 + \dots$$

If the changes are indeed small, then the partial derivatives are constant among all the samples. Then the expected value of the change, $E(dY)$, is zero. The variances are given by the following equation (Baird, 1995; Box et al., 2005):

$$\sigma^2(dY) = \sum_{i=1}^N \left(\frac{\partial Y}{\partial y_i} \right)^2 \sigma_i^2$$

Thus, the variance of the desired quantity Y can be found. This gives an independent estimate of the errors in measuring the quantity Y from the errors in measuring each variable it depends upon.

Example Suppose one wants to measure the thermal conductivity of a solid (k). To do this, one needs to measure the heat flux (q), the thickness of the sample (d), and the temperature difference across the sample (ΔT). Each measurement has some error. The heat flux (q) may be the rate of electrical heat input (\dot{Q}) divided by the area (A), and both quantities are measured to some tolerance. The thickness of the sample is measured with some accuracy, and the temperatures are probably measured with a thermocouple to some accuracy. These measurements are combined, however, to obtain the thermal conductivity, and it is desired to know the error in the thermal conductivity. The formula is

$$k = \frac{d}{\Delta T} \dot{Q}$$

The variance in the thermal conductivity is then

$$\sigma_k^2 = \left(\frac{k}{d} \right)^2 \sigma_d^2 + \left(\frac{k}{\dot{Q}} \right)^2 \sigma_{\dot{Q}}^2 + \left(\frac{k}{A} \right)^2 \sigma_A^2 + \left(\frac{k}{\Delta T} \right)^2 \sigma_{\Delta T}^2$$

FACTORIAL DESIGN OF EXPERIMENTS AND ANALYSIS OF VARIANCE

Statistically designed experiments consider, of course, the effect of primary variables, but they also consider the effect of extraneous variables and the interactions between variables, and they include a measure of the random error. Primary variables are those whose effect you wish to determine. These variables can be quantitative or qualitative. The quantitative variables are ones you may fit to a model in order to determine the model parameters (see the section "Least Squares"). Qualitative variables are ones you wish to know the effect of, but you do not try to quantify that effect other than to assign possible errors or magnitudes. Qualitative variables can be further subdivided into Type I variables, whose effect you wish to determine directly, and Type II variables, which contribute to the performance variability and whose effect you wish to average out. For example, if you are studying the effect of several catalysts on yield in a chemical reactor, each different type of catalyst would be a Type I variable because you would like to know the effect of each. However, each time the catalyst is prepared, the results are slightly different due to random variations; thus, you may have several batches of what purports to be the same catalyst. The variability between batches is a Type II variable. Since the ultimate use will require using different batches, you would like to know the overall effect including that variation, since knowing precisely the results from one batch of one catalyst might not be representative of the results obtained from all batches of the same catalyst. A randomized block design, incomplete block design, or Latin square design (Box et al., *ibid.*), for example, all keep the effect of experimental error in the blocked variables from influencing the effect of the primary variables. Other uncontrolled variables are accounted for by introducing randomization in parts of the experimental design. To study all variables and their interaction requires a factorial design, involving all possible combinations of each variable, or a fractional factorial design, involving only a selected set. Statistical techniques are then used to determine which are the important variables, what are the important interactions, and what the error is in estimating these effects. The discussion here is only a brief overview of the excellent book by Box et al. (2005).

Suppose we have two methods of preparing some product and we wish to see which treatment is best. When there are only two treatments, then the sampling analysis discussed in the section "Two-Population Test of Hypothesis for Means" can be used to deduce if the means of the two treatments differ significantly. When there are more treatments, the analysis is more detailed. Suppose the experimental results are arranged

as shown in the table: several measurements for each treatment. The goal is to see if the treatments differ significantly from each other; that is, whether their means are different when the samples have the same variance. The hypothesis is that the treatments are all the same, and the null hypothesis is that they are different. The statistical validity of the hypothesis is determined by an analysis of variance.

Estimating the Effect of Four Treatments

	Treatment			
	1	2	3	4
	—	—	—	—
	—	—	—	—
	—	—	—	—
	—	—	—	—
Treatment average	—	—	—	—
Grand average	—	—	—	—

The data for $k = 4$ treatments is arranged in the table. For each treatment, there are n_t experiments and the outcome of the i th experiment with treatment t is called y_{it} . Compute the treatment average

$$\bar{y}_t = \frac{\sum_{i=1}^{n_t} y_{it}}{n_t}$$

Also compute the grand average

$$\bar{y} = \frac{\sum_{t=1}^k n_t \bar{y}_t}{N}, \quad N = \sum_{t=1}^k n_t$$

Next compute the sum of squares of deviations from the average within the t th treatment

$$S_t = \sum_{i=1}^{n_t} (y_{it} - \bar{y}_t)^2$$

Since each treatment has n_t experiments, the number of degrees of freedom is $n_t - 1$. Then the sample variances are

$$s_t^2 = \frac{S_t}{n_t - 1}$$

The within-treatment sum of squares is

$$S_R = \sum_{t=1}^k S_t$$

and the within-treatment sample variance is

$$s_R^2 = \frac{S_R}{N - k}$$

Now, if there is no difference between treatments, a second estimate of σ^2 could be obtained by calculating the variation of the treatment averages about the grand average. Thus compute the between-treatment mean square

$$s_T^2 = \frac{S_T}{k - 1}, \quad S_T = \sum_{t=1}^k n_t (\bar{y}_t - \bar{y})^2$$

Basically the test for whether the hypothesis is true or not hinges on a comparison of the within-treatment estimate s_R^2 (with $v_R = N - k$ degrees of freedom) with the between-treatment estimate s_T^2 (with $v_T = k - 1$ degrees of freedom). The test is made based on the F distribution for v_R and v_T degrees of freedom (Table 3-8).

Next consider the case that uses randomized blocking to eliminate the effect of some variable whose effect is of no interest, such as the batch-to-batch variation of the catalysts in the chemical reactor example. Suppose there are k treatments and n experiments in each treatment. The results from nk experiments can be arranged as shown in the block design table; within each block, the various treatments are applied in a random order. Compute the block average, the treatment average, as well as the grand average as before.

Block Design with Four Treatments and Five Blocks

Treatment	1	2	3	4	Block average
Block 1	—	—	—	—	—
Block 2	—	—	—	—	—
Block 3	—	—	—	—	—
Block 4	—	—	—	—	—
Block 5	—	—	—	—	—

The following quantities are needed for the analysis of variance table.

Name	Formula	dof
average	$S_A = nk\bar{y}^2$	1
blocks	$S_B = k \sum_{i=1}^n (\bar{y}_i - \bar{y})^2$	$n - 1$
treatments	$S_T = n \sum_{t=1}^k (\bar{y}_t - \bar{y})^2$	$k - 1$
residuals	$S_R = \sum_{t=1}^k \sum_{i=1}^{n_t} (y_{it} - \bar{y}_t - \bar{y}_t + \bar{y})^2$	$(n - 1)(k - 1)$
total	$S = \sum_{t=1}^k \sum_{i=1}^{n_t} y_{it}^2$	$N = nk$

The key test is again a statistical one, based on the value of

$$\frac{s_T^2}{s_R^2}, \quad s_T^2 = \frac{S_T}{k - 1}, \quad s_R^2 = \frac{S_R}{(n - 1)(k - 1)}$$

and the F distribution for v_R and v_T degrees of freedom (Table 3-8). The assumption behind the analysis is that the variations are linear. See Box et al. (2005). There are ways to test this assumption as well as transformations to make if it is not true. Box et al. also give an excellent example of how the observations are broken down into a grand average, a block deviation, a treatment deviation, and a residual. For two-way factorial design in which the second variable is a real one rather than one you would like to block out, see Box et al.

To measure the effects of variables on a single outcome a factorial design is appropriate. In a two-level factorial design, each variable is considered at two levels only, a high and low value, often designated as a + and -. The two-level factorial design is useful for indicating trends, showing interactions, and it is also the basis for a fractional factorial design. As an example, consider a 2^3 factorial design with 3 variables and 2 levels for each. The experiments are indicated in the factorial design table.

Two-Level Factorial Design with Three Variables

Run	Variable		
	1	2	3
1	-	-	-
2	+	-	-
3	-	+	-
4	+	+	-
5	-	-	+
6	+	-	+
7	-	+	+
8	+	+	+

The main effects are calculated by calculating the difference between results from all high values of a variable and all low values of a variable; the result is divided by the number of experiments at each level. For example, for the first variable:

$$\text{Effect of variable 1} = \frac{(y_2 + y_4 + y_6 + y_8) - (y_1 + y_3 + y_5 + y_7)}{4}$$

Note that all observations are being used to supply information on each of the main effects and each effect is determined with the precision of a fourfold replicated difference. The advantage of a one-at-a-time experiment is the gain in precision if the variables are additive and the measure of nonadditivity if it occurs (Box et al., 2005).

Interaction effects between variables 1 and 2 are obtained by calculating the difference between the results obtained with the high and low value of 1 at the low value of 2 compared with the results obtained

with the high and low value 1 at the high value of 2. The 12-interaction is

$$12\text{-interaction} = \frac{[(y_4 - y_3 + y_8 - y_7) - (y_2 - y_1 + y_6 - y_5)]}{2}$$

The key step is to determine the errors associated with the effect of each variable and each interaction so that the significance can be determined. Thus, standard errors need to be assigned. This can be done by repeating the experiments, but it can also be done by using higher-order interactions (such as 123 interactions in a 2⁴ factorial design). These are assumed negligible in their effect on the mean but can be used to estimate the standard error. Then, calculated

effects that are large compared with the standard error are considered important, while those that are small compared with the standard error are considered to be due to random variations and are unimportant.

In a fractional factorial design one does only part of the possible experiments. When there are *k* variables, a factorial design requires 2^{*k*} experiments. When *k* is large, the number of experiments can be large; for *k* = 5, 2⁵ = 32. For a *k* this large, Box et al. (2005) do a fractional factorial design. In the fractional factorial design with *k* = 5, only 16 experiments are done. Cropley (1978) gives an example of how to combine heuristics and statistical arguments in application to kinetics mechanisms in chemical engineering.

DIMENSIONAL ANALYSIS

Dimensional analysis allows the engineer to reduce the number of variables that must be considered to model experiments or correlate data. Consider a simple example in which two variables *F*₁ and *F*₂ have the units of force and two additional variables *L*₁ and *L*₂ have the units of length. Rather than having to deduce the relation of one variable on the other three, *F*₁ = fn (*F*₂, *L*₁, *L*₂), dimensional analysis can be used to show that the relation must be of the form *F*₁/*F*₂ = fn (*L*₁/*L*₂). Thus considerable experimentation is saved. Historically, dimensional analysis can be done using the Rayleigh method or the Buckingham pi method. This brief discussion is equivalent to the Buckingham pi method but uses concepts from linear algebra; see Amundson, N. R., *Mathematical Methods in Chemical Engineering*, Prentice-Hall, Englewood Cliffs, N.J. (1966), p. 54, for further information.

The general problem is posed as finding the minimum number of variables necessary to define the relationship between *n* variables. Let {*Q*_{*i*}} represent a set of fundamental units, like length, time, force, and so on. Let [*P*_{*i*}] represent the dimensions of a physical quantity *P*_{*i*}; there are *n* physical quantities. Then form the matrix α_{*ij*}

	[<i>P</i> ₁]	[<i>P</i> ₂]	...	[<i>P</i> _{<i>n</i>}]
<i>Q</i> ₁	α ₁₁	α ₁₂	...	α _{1<i>n</i>}
<i>Q</i> ₂	α ₂₁	α ₂₂	...	α _{2<i>n</i>}
...				
<i>Q</i> _{<i>m</i>}	α _{<i>m</i>1}	α _{<i>m</i>2}	...	α _{<i>m</i><i>n</i>}

in which the entries are the number of times each fundamental unit appears in the dimensions [*P*_{*i*}]. The dimensions can then be expressed as follows.

$$[P_i] = Q_1^{\alpha_{i1}} Q_2^{\alpha_{i2}} \dots Q_m^{\alpha_{im}}$$

Let *m* be the rank of the α matrix. Then *p* = *n* - *m* is the number of dimensionless groups that can be formed. One can choose *m* variables {*P*_{*i*}} to be the basis and express the other *p* variables in terms of them, giving *p* dimensionless quantities.

Example: Buckingham Pi Method—Heat-Transfer Film Coefficient

It is desired to determine a complete set of dimensionless groups with which to correlate experimental data on the film coefficient of heat transfer between the walls of a straight conduit with circular cross section and a fluid flowing in that conduit. The variables and the dimensional constant believed to be involved and their dimensions in the engineering system are given below:

- Film coefficient = *h* = (*F*/*LθT*)
- Conduit internal diameter = *D* = (*L*)
- Fluid linear velocity = *V* = (*L*/*θ*)
- Fluid density = ρ = (*M*/*L*³)
- Fluid absolute viscosity = μ = (*M*/*Lθ*)
- Fluid thermal conductivity = *k* = (*F*/*θT*)
- Fluid specific heat = *c_p* = (*FL*/*MT*)
- Dimensional constant = *g_c* = (*ML*/*Fθ*²)

The matrix α in this case is as follows.

	[<i>P</i> _{<i>i</i>}]							
	<i>h</i>	<i>D</i>	<i>V</i>	ρ	μ	<i>k</i>	<i>C_p</i>	<i>g_c</i>
<i>F</i>	1	0	0	0	0	1	1	-1
<i>M</i>	0	0	0	1	1	0	-1	1
<i>L</i>	-1	1	1	-3	-1	0	1	1
θ	-1	0	-1	0	-1	-1	0	-2
<i>T</i>	-1	0	0	0	0	-1	-1	0

Here *m* ≤ 5, *n* = 8, *p* ≥ 3. Choose *D*, *V*, μ, *k*, and *g_c* as the primary variables. By examining the 5 × 5 matrix associated with those variables, we can see that its determinant is not zero, so the rank of the matrix is *m* = 5; thus, *p* = 3. These variables are thus a possible basis set. The dimensions of the other three variables *h*, ρ, and *C_p* must be defined in terms of the primary variables. This can be done by inspection, although linear algebra can be used, too.

$$[h] = D^{-1}k^{-1}; \text{ thus } \frac{h}{D^{-1}k^{-1}} = \frac{hD}{k} \text{ is a dimensionless group}$$

$$[\rho] = \mu^1 V^{-1} D^{-1}; \text{ thus } \frac{\rho}{\mu^1 V^{-1} D^{-1}} = \frac{\rho VD}{\mu} \text{ is a dimensionless group}$$

$$[C_p] = k^{-1} \mu^{-1}; \text{ thus } \frac{C_p}{k^{-1} \mu^{-1}} = \frac{C_p \mu}{k} \text{ is a dimensionless group}$$

Thus, the dimensionless groups are

$$\frac{[P_i]}{Q_1^{\alpha_{i1}} Q_2^{\alpha_{i2}} \dots Q_m^{\alpha_{im}}}; \frac{hD}{k}, \frac{\rho VD}{\mu}, \frac{C_p \mu}{k}$$

The dimensionless group *hD*/*k* is called the Nusselt number, *N_{Nu}*, and the group *C_p*μ/*k* is the Prandtl number, *N_{Pr}*. The group *DVρ*/*μ* is the familiar Reynolds number, *N_{Re}*, encountered in fluid-friction problems. These three dimensionless groups are frequently used in heat-transfer-film-coefficient correlations. Functionally, their relation may be expressed as

$$\Phi(N_{Nu}, N_{Pr}, N_{Re}) = 0 \tag{3-121}$$

or as

$$N_{Nu} = \Phi_1(N_{Pr}, N_{Re})$$

TABLE 3-9 Dimensionless Groups in the Engineering System of Dimensions

Biot number	<i>N_{Bi}</i>	<i>hL</i> / <i>k</i>
Condensation number	<i>N_{Co}</i>	(<i>h</i> / <i>k</i>)(μ ² /ρ ² <i>g</i>) ^{1/3}
Number used in condensation of vapors	<i>N_{Cv}</i>	<i>L</i> ³ ρ ² <i>g</i> λ/ <i>k</i> μΔ <i>t</i>
Euler number	<i>N_{Eu}</i>	<i>g_c</i> (-Δ <i>p</i>)/ρ <i>V</i> ²
Fourier number	<i>N_{Fo}</i>	<i>kθ</i> /ρ <i>cL</i> ²
Froude number	<i>N_{Fr}</i>	<i>V</i> ² / <i>Lg</i>
Graetz number	<i>N_{Gz}</i>	<i>wc</i> / <i>kL</i>
Grashof number	<i>N_{Gr}</i>	<i>L</i> ³ ρ ² β <i>g</i> Δ <i>t</i> /μ ²
Mach number	<i>N_{Ma}</i>	<i>V</i> / <i>V_a</i>
Nusselt number	<i>N_{Nu}</i>	<i>hD</i> / <i>k</i>
Peclet number	<i>N_{Pe}</i>	<i>DVρc</i> / <i>k</i>
Prandtl number	<i>N_{Pr}</i>	<i>cμ</i> / <i>k</i>
Reynolds number	<i>N_{Re}</i>	<i>DVρ</i> / <i>μ</i>
Schmidt number	<i>N_{Sc}</i>	μ/ρ <i>D_v</i>
Stanton number	<i>N_{St}</i>	<i>h</i> / <i>cVρ</i>
Weber number	<i>N_{We}</i>	<i>LV</i> ² /σ <i>g_c</i>

It has been found that these dimensionless groups may be correlated well by an equation of the type

$$hD/k = K(c_p \mu/k)^a (DV\rho/\mu)^b$$

in which K , a , and b are experimentally determined dimensionless constants. However, any other type of algebraic expression or perhaps simply a graphical relation among these three groups that accurately fits the experimental data would be an equally valid manner of expressing Eq. (3-121).

Naturally, other dimensionless groups might have been obtained in the example by employing a different set of five repeating quantities

that would not form a dimensionless group among themselves. Some of these groups may be found among those presented in Table 3-9. Such a complete set of three dimensionless groups might consist of Stanton, Reynolds, and Prandtl numbers or of Stanton, Peclet, and Prandtl numbers. Also, such a complete set different from that obtained in the preceding example will result from a multiplication of appropriate powers of the Nusselt, Prandtl, and Reynolds numbers. For such a set to be complete, however, it must satisfy the condition that each of the three dimensionless groups be independent of the other two.

PROCESS SIMULATION

REFERENCES: Dimian, A., *Chem. Eng. Prog.* **90**: 58–66 (Sept. 1994); Kister, H. Z., “Can We Believe the Simulation Results?” *Chem. Eng. Prog.*, pp. 52–58 (Oct. 2002); Krieger, J. H., *Chem. Eng. News* **73**: 50–61 (Mar. 27, 1995); Mah, R. S. H., *Chemical Process Structure and Information Flows*, Butterworths (1990); Seader, J. D., *Computer Modeling of Chemical Processes*, AIChE Monograph Series no. 15 (1985); Seider, W. D., J. D. Seader, and D. R. Lewin, *Product and Process Design Principles: Synthesis, Analysis, and Evaluation*, 2d ed., Wiley, New York (2004).

CLASSIFICATION

Process simulation refers to the activity in which mathematical systems of chemical processes and refineries are modeled with equations, usually on the computer. The usual distinction must be made between steady-state models and transient models, following the ideas presented in the introduction to this section. In a chemical process, of course, the process is nearly always in a transient mode, at some level of precision, but when the time-dependent fluctuations are below some value, a steady-state model can be formulated. This subsection presents briefly the ideas behind steady-state process simulation (also called flowsheeting), which are embodied in commercial codes. The transient simulations are important for designing the start-up of plants and are especially useful for the operation of chemical plants.

THERMODYNAMICS

The most important aspect of the simulation is that the thermodynamic data of the chemicals be modeled correctly. It is necessary to decide what equation of state to use for the vapor phase (ideal gas, Redlich-Kwong-Soave, Peng-Robinson, etc.) and what model to use for liquid activity coefficients [ideal solutions, solubility parameters, Wilson equation, nonrandom two liquid (NRTL), UNIFAC, etc.]. See Sec. 4, “Thermodynamics.” It is necessary to consider mixtures of chemicals, and the interaction parameters must be predictable. The best case is to determine them from data, and the next-best case is to use correlations based on the molecular weight, structure, and normal boiling point. To validate the model, the computer results of vapor-liquid equilibria could be checked against experimental data to ensure their validity before the data are used in more complicated computer calculations.

PROCESS MODULES OR BLOCKS

At the first level of detail, it is not necessary to know the internal parameters for all the units, since what is desired is just the overall performance. For example, in a heat exchanger design, it suffices to know the heat duty, the total area, and the temperatures of the output streams; the details such as the percentage baffle cut, tube layout, or baffle spacing can be specified later when the details of the proposed plant are better defined. It is important to realize the level of detail modeled by a commercial computer program. For example, a chemical reactor could be modeled as an equilibrium reactor, in which the input stream is brought to a new temperature and pressure and the

output stream is in chemical equilibrium at those new conditions. Or, it may suffice to simply specify the conversion, and the computer program will calculate the outlet compositions. In these cases, the model equations are algebraic ones, and you do not learn the volume of the reactor. A more complicated reactor might be a stirred tank reactor, and then you would have to specify kinetic information so that the simulation can be made, and one output would be either the volume of the reactor or the conversion possible in a volume you specify. Such models are also composed of sets of algebraic equations. A plug flow reactor is modeled as a set of ordinary differential equations as initial-value problems, and the computer program must use numerical methods to integrate them. See “Numerical Solution of Ordinary Differential Equations as Initial Value Problems.” Kinetic information must be specified, and one learns the conversion possible in a given reactor volume, or, in some cases, the volume reactor that will achieve a given conversion. The simulation engineer determines what a reactor of a given volume will do for the specified kinetics and reactor volume. The design engineer, though, wants to achieve a certain result and wants to know the volume necessary. Simulation packages are best suited for the simulation engineer, and the design engineer must vary specifications to achieve the desired output.

Distillation simulations can be based on shortcut methods, using correlations based on experience, but more rigorous methods involve solving for the vapor-liquid equilibrium on each tray. The shortcut method uses relatively simple equations, and the rigorous method requires solution of huge sets of nonlinear equations. The computation time of the latter is significant, but the rigorous method may be necessary when the chemicals you wish to distill are not well represented in the correlations. Then the designer must specify the number of trays and determine the separation that is possible. This, of course, is not what he or she wants: the number of trays needed to achieve a specified objective. Thus, again, some adjustment of parameters is necessary in a design situation.

Absorption columns can be modeled in a plate-to-plate fashion (even if it is a packed bed) or as a packed bed. The former model is a set of nonlinear algebraic equations, and the latter model is an ordinary differential equation. Since streams enter at both ends, the differential equation is a two-point boundary value problem, and numerical methods are used (see “Numerical Solution of Ordinary Differential Equations as Initial-Value Problems”).

If one wants to model a process unit that has significant flow variation, and possibly some concentration distributions as well, one can consider using computational fluid dynamics (CFD) to do so. These calculations are very time-consuming, though, so that they are often left until the mechanical design of the unit. The exception would occur when the flow variation and concentration distribution had a significant effect on the output of the unit so that mass and energy balances couldn't be made without it.

The process units are described in greater detail in other sections of the Handbook. In each case, parameters of the unit are specified (size, temperature, pressure, area, and so forth). In addition, in a computer simulation, the computer program must be able to take any input to the unit and calculate the output for those parameters. Since the entire calculation is done iteratively, there is no assurance that the

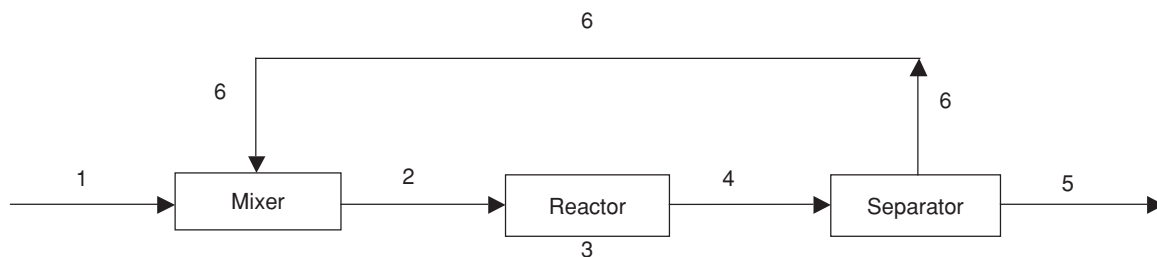


FIG. 3-67 Prototype flowsheet.

input stream is a “reasonable” one, so that the computer codes must be written to give some sort of output even when the input stream is unreasonable. This difficulty makes the iterative process even more complicated.

PROCESS TOPOLOGY

A chemical process usually consists of a series of units, such as distillation towers, reactors, and so forth (see Fig. 3-67). If the feed to the process is known and the operating parameters of the units are specified by the user, then one can begin with the first unit, take the process input, calculate the unit output, carry that output to the input of the next unit, and continue the process. However, if the process involves a recycle stream, as nearly all chemical processes do, then when the calculation is begun, it is discovered that the recycle stream is unknown. This situation leads to an iterative process: the flow rates, temperature, and pressure of the unknown recycle stream are guessed, and the calculations proceed as before. When one reaches the end of the process, where the recycle stream is formed to return to the first unit, it is necessary to check to see if the recycle stream is the same as assumed. If not, an iterative procedure must be used to cause convergence. Possible techniques are described in “Numerical Solutions of Nonlinear Equations in One Variable” and “Numerical Solution of Simultaneous Equations.” The direct method (or successive substitution method) just involves calculating around the process over and over. The Wegstein method accelerates convergence for a single variable, and Broyden’s method does the same for multiple variables. The Newton method can be used provided there is some way to calculate the derivatives (possibly by using a numerical derivative). Optimization methods can also be used (see “Optimization” in this section). In the description given here, the recycle stream is called the tear stream: this is the stream that must be guessed to begin the calculation. When there are multiple recycle streams, convergence is even more difficult, since more guesses are necessary, and what happens in one recycle stream may cause difficulties for the guesses in other recycle streams. See Seader (1985) and Mah (1990).

It is sometimes desired to control some stream by varying an operating parameter. For example, in a reaction/separation system, if there is an impurity that must be purged, a common objective is to set the purge fraction so that the impurity concentration into the reactor is kept at some moderate value. Commercial packages contain procedures for

doing this using what are often called control blocks. However, this can also make the solution more difficult to find.

An alternative method of solving the equations is to solve them as simultaneous equations. In that case, one can specify the design variables and the desired specifications and let the computer figure out the process parameters that will achieve those objectives. It is possible to overspecify the system or to give impossible conditions. However, the biggest drawback to this method of simulation is that large sets (tens of thousands) of nonlinear algebraic equations must be solved simultaneously. As computers become faster, this is less of an impediment, provided efficient software is available.

Dynamic simulations are also possible, and these require solving differential equations, sometimes with algebraic constraints. If some parts of the process change extremely quickly when there is a disturbance, that part of the process may be modeled in the steady state for the disturbance at any instant. Such situations are called stiff, and the methods for them are discussed in “Numerical Solution of Ordinary Differential Equations as Initial-Value Problems.” It must be realized, though, that a dynamic calculation can also be time-consuming, and sometimes the allowable units are lumped-parameter models that are simplifications of the equations used for the steady-state analysis. Thus, as always, the assumptions need to be examined critically before accepting the computer results.

COMMERCIAL PACKAGES

Computer programs are provided by many companies, and the models range from empirical models to deterministic models. For example, if one wanted to know the pressure drop in a piping network, one would normally use a correlation for friction factor as a function of Reynolds number to calculate the pressure drop in each segment. A sophisticated turbulence model of fluid flow is not needed in that case. As computers become faster, however, more and more models are deterministic. Since the commercial codes have been used by many customers, the data in them have been verified, but possibly not for the case you want to solve. Thus, you must test the thermodynamics correlations carefully. In 2005, there were a number of computer codes, but the company names change constantly. Here are a few of them for process simulation: Aspen Tech (Aspen Plus), Chemstations (CHEMCAD), Honeywell (UniSim Design), ProSim (ProSimPlus), and SimSci-Esseor (Pro II). The CAPE-OPEN project is working to make details as transferable as possible.

SECTION 4

Thermodynamics

PERRY'S CHEMICAL ENGINEERS' HANDBOOK

8TH EDITION



HENDRICK C. VAN NESS
MICHAEL M. ABBOTT

Copyright © 2008, 1997, 1984, 1973, 1963, 1950, 1941, 1934 by The McGraw-Hill Companies, Inc. All rights reserved. Manufactured in the United States of America. Except as permitted under the United States Copyright Act of 1976, no part of this publication may be reproduced or distributed in any form or by any means, or stored in a database or retrieval system, without the prior written permission of the publisher.

0-07-154211-6

The material in this eBook also appears in the print version of this title: 0-07-151127-X.

All trademarks are trademarks of their respective owners. Rather than put a trademark symbol after every occurrence of a trademarked name, we use names in an editorial fashion only, and to the benefit of the trademark owner, with no intention of infringement of the trademark. Where such designations appear in this book, they have been printed with initial caps.

McGraw-Hill eBooks are available at special quantity discounts to use as premiums and sales promotions, or for use in corporate training programs. For more information, please contact George Hoare, Special Sales, at george_hoare@mcgraw-hill.com or (212) 904-4069.

TERMS OF USE

This is a copyrighted work and The McGraw-Hill Companies, Inc. (“McGraw-Hill”) and its licensors reserve all rights in and to the work. Use of this work is subject to these terms. Except as permitted under the Copyright Act of 1976 and the right to store and retrieve one copy of the work, you may not decompile, disassemble, reverse engineer, reproduce, modify, create derivative works based upon, transmit, distribute, disseminate, sell, publish or sublicense the work or any part of it without McGraw-Hill’s prior consent. You may use the work for your own noncommercial and personal use; any other use of the work is strictly prohibited. Your right to use the work may be terminated if you fail to comply with these terms.

THE WORK IS PROVIDED “AS IS.” MCGRAW-HILL AND ITS LICENSORS MAKE NO GUARANTEES OR WARRANTIES AS TO THE ACCURACY, ADEQUACY OR COMPLETENESS OF OR RESULTS TO BE OBTAINED FROM USING THE WORK, INCLUDING ANY INFORMATION THAT CAN BE ACCESSED THROUGH THE WORK VIA HYPERLINK OR OTHERWISE, AND EXPRESSLY DISCLAIM ANY WARRANTY, EXPRESS OR IMPLIED, INCLUDING BUT NOT LIMITED TO IMPLIED WARRANTIES OF MERCHANTABILITY OR FITNESS FOR A PARTICULAR PURPOSE. McGraw-Hill and its licensors do not warrant or guarantee that the functions contained in the work will meet your requirements or that its operation will be uninterrupted or error free. Neither McGraw-Hill nor its licensors shall be liable to you or anyone else for any inaccuracy, error or omission, regardless of cause, in the work or for any damages resulting therefrom. McGraw-Hill has no responsibility for the content of any information accessed through the work. Under no circumstances shall McGraw-Hill and/or its licensors be liable for any indirect, incidental, special, punitive, consequential or similar damages that result from the use of or inability to use the work, even if any of them has been advised of the possibility of such damages. This limitation of liability shall apply to any claim or cause whatsoever whether such claim or cause arises in contract, tort or otherwise.

DOI: 10.1036/007151127X

Thermodynamics

Hendrick C. Van Ness, D.Eng. *Howard P. Isermann Department of Chemical and Biological Engineering, Rensselaer Polytechnic Institute; Fellow, American Institute of Chemical Engineers; Member, American Chemical Society (Section Coeditor)*

Michael M. Abbott, Ph.D. *Deceased; Professor Emeritus, Howard P. Isermann Department of Chemical and Biological Engineering, Rensselaer Polytechnic Institute (Section Coeditor)**

INTRODUCTION		
Postulate 1	4-4	
Postulate 2 (First Law of Thermodynamics)	4-4	
Postulate 3	4-5	
Postulate 4 (Second Law of Thermodynamics)	4-5	
Postulate 5	4-5	
VARIABLES, DEFINITIONS, AND RELATIONSHIPS		
Constant-Composition Systems	4-6	
U , H , and S as Functions of T and P or T and V	4-6	
The Ideal Gas Model	4-7	
Residual Properties	4-7	
PROPERTY CALCULATIONS FOR GASES AND VAPORS		
Evaluation of Enthalpy and Entropy in the Ideal Gas State	4-8	
Residual Enthalpy and Entropy from PVT Correlations	4-9	
Virial Equations of State	4-9	
Cubic Equations of State	4-11	
Pitzer's Generalized Correlations	4-12	
OTHER PROPERTY FORMULATIONS		
Liquid Phase	4-13	
Liquid/Vapor Phase Transition	4-13	
THERMODYNAMICS OF FLOW PROCESSES		
Mass, Energy, and Entropy Balances for Open Systems	4-14	
Mass Balance for Open Systems	4-14	
General Energy Balance	4-14	
Energy Balances for Steady-State Flow Processes	4-14	
Entropy Balance for Open Systems	4-14	
Summary of Equations of Balance for Open Systems	4-15	
Applications to Flow Processes	4-15	
Duct Flow of Compressible Fluids	4-15	
Pipe Flow	4-15	
Nozzles	4-15	
Throttling Process	4-16	
Turbines (Expanders)	4-16	
Compression Processes	4-16	
Example 1: LNG Vaporization and Compression	4-17	
SYSTEMS OF VARIABLE COMPOSITION		
Partial Molar Properties	4-17	
Gibbs-Duhem Equation	4-18	
Partial Molar Equation-of-State Parameters	4-18	
Partial Molar Gibbs Energy	4-19	
Solution Thermodynamics	4-19	
Ideal Gas Mixture Model	4-19	
Fugacity and Fugacity Coefficient	4-19	
Evaluation of Fugacity Coefficients	4-20	
Ideal Solution Model	4-20	
Excess Properties	4-21	
Property Changes of Mixing	4-21	
Fundamental Property Relations Based on the Gibbs Energy	4-21	
Fundamental Residual-Property Relation	4-21	
Fundamental Excess-Property Relation	4-22	
Models for the Excess Gibbs Energy	4-23	
Behavior of Binary Liquid Solutions	4-26	
EQUILIBRIUM		
Criteria	4-26	
Phase Rule	4-27	
Example 2: Application of the Phase Rule	4-27	
Duhem's Theorem	4-27	
Vapor/Liquid Equilibrium	4-28	
Gamma/Phi Approach	4-28	
Modified Raoult's Law	4-28	
Example 3: Dew and Bubble Point Calculations	4-29	

*Dr. Abbott died on May 31, 2006. This, his final contribution to the literature of chemical engineering, is deeply appreciated, as are his earlier contributions to the handbook.

Nomenclature and Units

Correlation- and application-specific symbols are not shown.

Symbol	Definition	SI units	U.S. Customary System units	Symbol	Definition	SI units	U.S. Customary System units
A	Molar (or unit-mass) Helmholtz energy	J/mol [J/kg]	Btu/lb mol [Btu/lbm]	P_i^{sat}	Saturation or vapor pressure of species i	kPa	psi
A	Cross-sectional area in flow	m ²	ft ²	Q	Heat	J	Btu
\hat{a}_i	Activity of species i in solution	Dimensionless	Dimensionless	q	Volumetric flow rate	m ³ /s	ft ³ /s
\bar{a}_i	Partial parameter, cubic equation of state			\dot{Q}	Rate of heat transfer	J/s	Btu/s
B	2d virial coefficient, density expansion	cm ³ /mol	cm ³ /mol	\bar{R}	Universal gas constant	J/(mol-K)	Btu/(lb-mol-R)
\bar{B}_i	Partial molar second virial coefficient	cm ³ /mol	cm ³ /mol	S	Molar (or unit-mass) entropy	J/(mol-K)	Btu/(lb-mol-R)
\hat{B}	Reduced second virial coefficient			\dot{S}_G	Rate of entropy generation, Eq. (4-151)	J/(kg-K)	[Btu/(lbm-R)] Btu/(R-s)
C	3d virial coefficient, density expansion	cm ⁶ /mol ²	cm ⁶ /mol ²	T	Absolute temperature	K	R
\hat{C}	Reduced third virial coefficient			T_c	Critical temperature	K	R
D	4th virial coefficient, density expansion	cm ⁹ /mol ³	cm ⁹ /mol ³	U	Molar (or unit-mass) internal energy	J/mol [J/kg]	Btu/(lb-mol) [Btu/lbm]
B'	2d virial coefficient, pressure expansion	kPa ⁻¹	kPa ⁻¹	u	Fluid velocity	m/s	ft/s
C'	3d virial coefficient, pressure expansion	kPa ⁻²	kPa ⁻²	V	Molar (or unit-mass) volume	m ³ /mol [m ³ /kg]	ft ³ /lb-mol [ft ³ /lbm]
D'	4th virial coefficient, pressure expansion	kPa ⁻³	kPa ⁻³	W	Work	J	Btu
B_{ij}	Interaction 2d virial coefficient	cm ³ /mol	cm ³ /mol	W_s	Shaft work for flow process	J	Btu
C_{ijk}	Interaction 3d virial coefficient	cm ⁶ /mol ²	cm ⁶ /mol ²	\dot{W}_s	Shaft power for flow process	J/s	Btu/s
C_p	Heat capacity at constant pressure	J/(mol-K)	Btu/(lb-mol-R)	x_i	Mole fraction in general		
C_v	Heat capacity at constant volume	J/(mol-K)	Btu/(lb-mol-R)	x_i	Mole fraction of species i in liquid phase		
f_i	Fugacity of pure species i	kPa	psi	y_i	Mole fraction of species i in vapor phase		
f_i^s	Fugacity of species i in solution	kPa	psi	Z	Compressibility factor	Dimensionless	Dimensionless
\bar{G}	Molar (or unit-mass) Gibbs energy	J/mol [J/kg]	Btu/(lb-mol) [Btu/lbm]	z	Elevation above a datum level	m	ft
g	Acceleration of gravity	m/s ²	ft/s ²	Superscripts			
$\frac{g}{RT}$		Dimensionless	Dimensionless	E	Denotes excess thermodynamic property		
\bar{H}	Molar (or unit-mass) enthalpy	J/mol [J/kg]	Btu/(lb-mol) [Btu/lbm]	id	Denotes value for an ideal solution		
K_i	Equilibrium K value, y_i/x_i	Dimensionless	Dimensionless	ig	Denotes value for an ideal gas		
K_j	Equilibrium constant for chemical reaction j	Dimensionless	Dimensionless	l	Denotes liquid phase		
k_1	Henry's constant for solute species 1	kPa	psi	lv	Denotes phase transition, liquid to vapor		
M	Molar or unit-mass solution property (A, G, H, S, U, V)			R	Denotes residual thermodynamic property		
\mathbf{M}	Mach number	Dimensionless	Dimensionless	t	Denotes total value of property		
M_i	Molar or unit-mass pure-species property ($A_i, G_i, H_i, S_i, U_i, V_i$)			v	Denotes vapor phase		
\bar{M}_i	Partial property of species i in solution ($\bar{A}_i, \bar{G}_i, \bar{H}_i, \bar{S}_i, \bar{U}_i, \bar{V}_i$)			∞	Denotes value at infinite dilution		
M^R	Residual thermodynamic property ($A^R, C^R, H^R, S^R, U^R, V^R$)			Subscripts			
M^E	Excess thermodynamic property ($A^E, C^E, H^E, S^E, U^E, V^E$)			c	Denotes value for the critical state		
\bar{M}_i^E	Partial molar excess thermodynamic property			cv	Denotes the control volume		
ΔM	Property change of mixing ($\Delta A, \Delta G, \Delta H, \Delta S, \Delta U, \Delta V$)			fs	Denotes flowing streams		
ΔM_j°	Standard property change of reaction j ($\Delta C_j^\circ, \Delta H_j^\circ, \Delta C_p^\circ$)			n	Denotes the normal boiling point		
m	Mass	kg	lbm	r	Denotes a reduced value		
\dot{m}	Mass flow rate	kg/s	lbm/s	rev	Denotes a reversible process		
n	Number of moles			Greek Letters			
\dot{n}	Molar flow rate			α, β	As superscripts, identify phases		
n_i	Number of moles of species i			β	Volume expansivity	K ⁻¹	°R ⁻¹
P	Absolute pressure	kPa	psi	ϵ_j	Reaction coordinate for reaction j	mol	lb-mol
				$\Gamma_i(T)$	Defined by Eq. (4-196)	J/mol	Btu/(lb-mol)
				γ	Heat capacity ratio C_p/C_v	Dimensionless	Dimensionless
				γ_i	Activity coefficient of species i in solution	Dimensionless	Dimensionless
				κ	Isothermal compressibility	kPa ⁻¹	psi ⁻¹
				μ_i	Chemical potential of species i	J/mol	Btu/(lb-mol)
				ν_{ij}	Stoichiometric number of species i in reaction j	Dimensionless	Dimensionless
				ρ	Molar density	mol/m ³	lb-mol/ft ³
				σ	As subscript, denotes a heat reservoir		
				Φ_i	Defined by Eq. (4-304)	Dimensionless	Dimensionless
				ϕ_i	Fugacity coefficient of pure species i	Dimensionless	Dimensionless
				$\hat{\phi}_i$	Fugacity coefficient of species i in solution	Dimensionless	Dimensionless
				ω	Acentric factor	Dimensionless	Dimensionless

GENERAL REFERENCES: Abbott, M. M., and H. C. Van Ness, *Schaum's Outline of Theory and Problems of Thermodynamics*, 2d ed., McGraw-Hill, New York, 1989. Poling, B. E., J. M. Prausnitz, and J. P. O'Connell, *The Properties of Gases and Liquids*, 5th ed., McGraw-Hill, New York, 2001. Prausnitz, J. M., R. N. Lichtenthaler, and E. G. de Azevedo, *Molecular Thermodynamics of Fluid-Phase Equilibria*, 3d ed., Prentice-Hall PTR, Upper Saddle River, N.J., 1999. Sandler, S. I., *Chemical and Engineering Thermodynamics*, 3d ed.,

Wiley, New York, 1999. Smith, J. M., H. C. Van Ness, and M. M. Abbott, *Introduction to Chemical Engineering Thermodynamics*, 7th ed., McGraw-Hill, New York, 2005. Tester, J. W., and M. Modell, *Thermodynamics and Its Applications*, 3d ed., Prentice-Hall PTR, Upper Saddle River, N.J., 1997. Van Ness, H. C., and M. M. Abbott, *Classical Thermodynamics of Nonelectrolyte Solutions: With Applications to Phase Equilibria*, McGraw-Hill, New York, 1982.

INTRODUCTION

Thermodynamics is the branch of science that lends substance to the principles of energy transformation in macroscopic systems. The general restrictions shown by experience to apply to all such transformations are known as the laws of thermodynamics. These laws are primitive; they cannot be derived from anything more basic.

The first law of thermodynamics states that energy is conserved, that although it can be altered in form and transferred from one place to another, the total quantity remains constant. Thus the first law of thermodynamics depends on the concept of energy, but conversely energy is an *essential* thermodynamic function because it allows the first law to be formulated. This coupling is characteristic of the primitive concepts of thermodynamics.

The words *system* and *surroundings* are similarly coupled. A system can be an object, a quantity of matter, or a region of space, selected for study and set apart (mentally) from everything else, which is called the surroundings. An envelope, imagined to enclose the system and to separate it from its surroundings, is called the *boundary* of the system.

Attributed to this boundary are special properties which may serve either to *isolate* the system from its surroundings or to provide for *interaction* in specific ways between the system and surroundings. An isolated system exchanges neither matter nor energy with its surroundings. If a system is not isolated, its boundaries may permit exchange of matter or energy or both with its surroundings. If the exchange of matter is allowed, the system is said to be *open*; if only energy and not matter may be exchanged, the system is *closed* (but not isolated), and its mass is constant.

When a system is isolated, it cannot be affected by its surroundings. Nevertheless, changes may occur within the system that are detectable with measuring instruments such as thermometers and pressure gauges. However, such changes cannot continue indefinitely, and the system must eventually reach a final static condition of *internal equilibrium*.

For a closed system which interacts with its surroundings, a final static condition may likewise be reached such that the system is not only internally at equilibrium but also in *external equilibrium* with its surroundings.

The concept of equilibrium is central in thermodynamics, for associated with the condition of internal equilibrium is the concept of *state*. A system has an identifiable, reproducible state when all its *properties*, such as temperature T , pressure P , and molar volume V , are fixed. The concepts of *state* and *property* are again coupled. One can equally well say that the properties of a system are fixed by its state. Although the properties T , P , and V may be detected with measuring instruments, the existence of the *primitive* thermodynamic properties (see postulates 1 and 3 following) is recognized much more indirectly. The number of properties for which values must be specified in order to fix the state of a system depends on the nature of the system, and is ultimately determined from experience.

When a system is displaced from an equilibrium state, it undergoes a *process*, a change of state, which continues until its properties attain new equilibrium values. During such a process, the system may be caused to interact with its surroundings so as to interchange energy in the forms of heat and work and so to produce in the system changes considered desirable for one reason or another. A process that proceeds so that the system is never displaced more than differentially from an equilibrium state is said to be *reversible*, because such a process can be reversed at any point by an infinitesimal change in external conditions, causing it to retrace the initial path in the opposite direction.

Thermodynamics finds its origin in experience and experiment, from which are formulated a few postulates that form the foundation of the subject. The first two deal with energy.

POSTULATE 1

*There exists a form of energy, known as **internal energy**, which for systems at internal equilibrium is an intrinsic property of the system, functionally related to the measurable coordinates that characterize the system.*

POSTULATE 2 (FIRST LAW OF THERMODYNAMICS)

*The **total energy** of any system and its surroundings is conserved.*

Internal energy is quite distinct from such external forms as the kinetic and potential energies of macroscopic bodies. Although it is a macroscopic property, characterized by the macroscopic coordinates T and P , internal energy finds its origin in the kinetic and potential energies of molecules and submolecular particles. In applications of the first law of thermodynamics, all forms of energy must be considered, including the internal energy. It is therefore clear that postulate 2 depends on postulate 1. For an isolated system the first law requires that its energy be constant. For a closed (but not isolated) system, the first law requires that energy changes of the system be exactly compensated by energy changes in the surroundings. For such systems energy is exchanged between a system and its surroundings in two forms: heat and work.

Heat is energy crossing the system boundary under the influence of a temperature difference or gradient. A quantity of heat Q represents an amount of energy in transit between a system and its surroundings, and is not a property of the system. The convention with respect to sign makes numerical values of Q positive when heat is added to the system and negative when heat leaves the system.

Work is again energy in transit between a system and its surroundings, but resulting from the displacement of an external force acting on the system. Like heat, a quantity of work W represents an amount of energy, and is not a property of the system. The sign convention, analogous to that for heat, makes numerical values of W positive when work is done on the system by the surroundings and negative when work is done on the surroundings by the system.

When applied to closed (constant-mass) systems in which only internal-energy changes occur, the first law of thermodynamics is expressed mathematically as

$$dU^i = dQ + dW \quad (4-1)$$

where U^i is the total internal energy of the system. Note that dQ and dW , differential *quantities* representing energy exchanges between the system and its surroundings, serve to account for the energy change of the surroundings. On the other hand, dU^i is directly the differential *change* in internal energy of the system. Integration of Eq. (4-1) gives for a finite process

$$\Delta U^i = Q + W \quad (4-2)$$

where ΔU^i is the finite change given by the difference between the final and initial values of U^i . The heat Q and work W are finite quantities of heat and work; they are not properties of the system or functions of the thermodynamic coordinates that characterize the system.

POSTULATE 3

There exists a property called **entropy**, which for systems at internal equilibrium is an intrinsic property of the system, functionally related to the measurable coordinates that characterize the system. For reversible processes, changes in this property may be calculated by the equation

$$dS' = \frac{dQ_{\text{rev}}}{T} \quad (4-3)$$

where S' is the total entropy of the system and T is the absolute temperature of the system.

POSTULATE 4 (SECOND LAW OF THERMODYNAMICS)

The entropy change of any system and its surroundings, considered together, resulting from any real process is positive, approaching zero when the process approaches reversibility.

In the same way that the first law of thermodynamics cannot be formulated without the prior recognition of internal energy as a property, so also the second law can have no complete and quantitative expression without a prior assertion of the existence of entropy as a property.

The second law requires that the entropy of an isolated system either increase or, in the limit where the system has reached an equilibrium state, remain constant. For a closed (but not isolated) system it requires that any entropy decrease in either the system or its surroundings be more than compensated by an entropy increase in the other part, or that in the limit where the process is reversible, the total entropy of the system plus its surroundings be constant.

The fundamental thermodynamic properties that arise in connection with the first and second laws of thermodynamics are internal energy and entropy. These properties together with the two laws for which they are essential apply to all types of systems. However, different types of systems are characterized by different sets of measurable coordinates or variables. The type of system most commonly encountered in chemical technology is one for which the primary characteristic variables are temperature T , pressure P , molar volume V , and composition, not all of which are necessarily independent. Such systems are usually made up of fluids (liquid or gas) and are called *PVT* systems.

For closed systems of this kind the work of a reversible process may always be calculated from

$$dW_{\text{rev}} = -PdV^t \quad (4-4)$$

where P is the absolute pressure and V^t is the total volume of the system. This equation follows directly from the definition of mechanical work.

POSTULATE 5

The macroscopic properties of homogeneous *PVT* systems at internal equilibrium can be expressed as functions of temperature, pressure, and composition only.

This postulate imposes an idealization, and is the basis for all subsequent property relations for *PVT* systems. The *PVT* system serves as a satisfactory model in an enormous number of practical applications. In accepting this model one assumes that the effects of fields (e.g., electric, magnetic, or gravitational) are negligible and that surface and viscous shear effects are unimportant.

Temperature, pressure, and composition are thermodynamic coordinates representing conditions imposed upon or exhibited by the system, and the functional dependence of the thermodynamic properties on these conditions is determined by experiment. This is quite direct for molar or specific volume V , which can be measured, and leads immediately to the conclusion that there exists an *equation of state* relating molar volume to temperature, pressure, and composition for any particular homogeneous *PVT* system. The equation of state is a primary tool in applications of thermodynamics.

Postulate 5 affirms that the other molar or specific thermodynamic properties of *PVT* systems, such as internal energy U and entropy S , are also functions of temperature, pressure, and composition. These molar or unit-mass properties, represented by the plain symbols V , U , and S , are independent of system size and are called *intensive*. Temperature, pressure, and the composition variables, such as mole fraction, are also intensive. Total-system properties (V^t , U^t , S^t) do depend on system size and are *extensive*. For a system containing n mol of fluid, $M^t = nM$, where M is a molar property.

Applications of the thermodynamic postulates necessarily involve the abstract quantities of internal energy and entropy. The solution of any problem in applied thermodynamics is therefore found through these quantities.

VARIABLES, DEFINITIONS, AND RELATIONSHIPS

Consider a single-phase closed system in which there are no chemical reactions. Under these restrictions the composition is fixed. If such a system undergoes a differential, reversible process, then by Eq. (4-1)

$$dU^t = dQ_{\text{rev}} + dW_{\text{rev}}$$

Substitution for dQ_{rev} and dW_{rev} by Eqs. (4-3) and (4-4) gives

$$dU^t = T dS' - P dV^t$$

Although derived for a reversible process, this equation relates properties only and is valid for any change between equilibrium states in a closed system. It is equally well written as

$$d(nU) = T d(nS) - P d(nV) \quad (4-5)$$

where n is the number of moles of fluid in the system and is constant for the special case of a closed, nonreacting system. Note that

$$n \equiv n_1 + n_2 + n_3 + \cdots = \sum_i n_i$$

where i is an index identifying the chemical species present. When U , S , and V represent *specific* (unit-mass) properties, n is replaced by m .

Equation (4-5) shows that for a single-phase, nonreacting, closed system, $nU = u(nS, nV)$.

$$\text{Then} \quad d(nU) = \left[\frac{\partial(nU)}{\partial(nS)} \right]_{nV,n} d(nS) + \left[\frac{\partial(nU)}{\partial(nV)} \right]_{nS,n} d(nV)$$

where subscript n indicates that all mole numbers n_i (and hence n) are held constant. Comparison with Eq. (4-5) shows that

$$\left[\frac{\partial(nU)}{\partial(nS)} \right]_{nV,n} = T \quad \text{and} \quad \left[\frac{\partial(nU)}{\partial(nV)} \right]_{nS,n} = -P$$

For an **open** single-phase system, we assume that $nU = \mathcal{U}(nS, nV, n_1, n_2, n_3, \dots)$. In consequence,

$$d(nU) = \left[\frac{\partial(nU)}{\partial(nS)} \right]_{nV,n} d(nS) + \left[\frac{\partial(nU)}{\partial(nV)} \right]_{nS,n} d(nV) + \sum_i \left[\frac{\partial(nU)}{\partial n_i} \right]_{nS,nV,n_j} dn_i$$

where the summation is over all species present in the system and subscript n_j indicates that all mole numbers are held constant except the i th. Define

$$\mu_i \equiv \left[\frac{\partial(nU)}{\partial n_i} \right]_{nS,nV,n_j}$$

The expressions for T and $-P$ of the preceding paragraph and the definition of μ_i allow replacement of the partial differential coefficients in the preceding equation by T , $-P$, and μ_i . The result is Eq. (4-6) of Table 4-1, where important equations of this section are collected. Equation (4-6) is the **fundamental property relation** for single-phase *PVT* systems, from which all other equations connecting properties of

4-6 THERMODYNAMICS

TABLE 4-1 Mathematical Structure of Thermodynamic Property Relations

Primary thermodynamic functions	Fundamental property relations	For homogeneous systems of constant composition	Maxwell equations
$U = TS - PV + \sum_i x_i \mu_i$ (4-7)	$d(nU) = T d(nS) - P d(nV) + \sum_i \mu_i dn_i$ (4-6)	$dU = T dS - P dV$ (4-14)	$\left(\frac{\partial T}{\partial V}\right)_S = -\left(\frac{\partial P}{\partial S}\right)_V$ (4-18)
$H \equiv U + PV$ (4-8)	$d(nH) = T d(nS) + nV dP + \sum_i \mu_i dn_i$ (4-11)	$dH = T dS + V dP$ (4-15)	$\left(\frac{\partial T}{\partial P}\right)_S = \left(\frac{\partial V}{\partial S}\right)_P$ (4-19)
$A \equiv U - TS$ (4-9)	$d(nA) = -nS dT - P d(nV) + \sum_i \mu_i dn_i$ (4-12)	$dA = -S dT - P dV$ (4-16)	$\left(\frac{\partial P}{\partial T}\right)_V = \left(\frac{\partial S}{\partial V}\right)_T$ (4-20)
$G \equiv H - TS$ (4-10)	$d(nG) = -nS dT + nV dP + \sum_i \mu_i dn_i$ (4-13)	$dG = -S dT + V dP$ (4-17)	$\left(\frac{\partial V}{\partial T}\right)_P = -\left(\frac{\partial S}{\partial P}\right)_T$ (4-21)
$U, H,$ and S as functions of T and P or T and V		Partial derivatives	Total derivatives
$dH = \left(\frac{\partial H}{\partial T}\right)_P dT + \left(\frac{\partial H}{\partial P}\right)_T dP$ (4-22)	$\left(\frac{\partial H}{\partial T}\right)_P = T \left(\frac{\partial S}{\partial T}\right)_P = C_P$ (4-28)	$dH = C_P dT + \left[V - T \left(\frac{\partial V}{\partial T}\right)_P\right] dP$ (4-32)	
$dS = \left(\frac{\partial S}{\partial T}\right)_P dT + \left(\frac{\partial S}{\partial P}\right)_T dP$ (4-23)	$\left(\frac{\partial H}{\partial P}\right)_T = T \left(\frac{\partial S}{\partial P}\right)_T + V = V - T \left(\frac{\partial V}{\partial T}\right)_P$ (4-29)	$dS = \frac{C_P}{T} dT - \left(\frac{\partial V}{\partial T}\right)_P dP$ (4-33)	
$dU = \left(\frac{\partial U}{\partial T}\right)_V dT + \left(\frac{\partial U}{\partial V}\right)_T dV$ (4-24)	$\left(\frac{\partial U}{\partial T}\right)_V = T \left(\frac{\partial S}{\partial T}\right)_V = C_V$ (4-30)	$dU = C_V dT + \left[T \left(\frac{\partial P}{\partial T}\right)_V - P\right] dV$ (4-34)	
$dS = \left(\frac{\partial S}{\partial T}\right)_V dT + \left(\frac{\partial S}{\partial V}\right)_T dV$ (4-25)	$\left(\frac{\partial U}{\partial V}\right)_T = T \left(\frac{\partial S}{\partial V}\right)_T - P = T \left(\frac{\partial P}{\partial T}\right)_V - P$ (4-31)	$dS = \frac{C_V}{T} dT + \left(\frac{\partial P}{\partial T}\right)_V dV$ (4-35)	

$U \equiv$ Internal energy; $H \equiv$ enthalpy; $A \equiv$ Helmholtz energy; $G \equiv$ Gibbs energy.

such systems are derived. The quantity μ_i is called the *chemical potential* of species i , and it plays a vital role in the thermodynamics of phase and chemical equilibria.

Additional property relations follow directly from Eq. (4-6). Because $n_i = x_i n$, where x_i is the mole fraction of species i , this equation may be rewritten as

$$d(nU) - T d(nS) + P d(nV) - \sum_i \mu_i d(x_i n) = 0$$

Expansion of the differentials and collection of like terms yield

$$\left[dU - T dS + P dV - \sum_i \mu_i dx_i \right] n + \left[U - TS + PV - \sum_i x_i \mu_i \right] dn = 0$$

Because n and dn are independent and arbitrary, the terms in brackets must separately be zero. This provides two useful equations:

$$dU = T dS - P dV + \sum_i \mu_i dx_i \quad U = TS - PV + \sum_i x_i \mu_i$$

The first is similar to Eq. (4-6). However, Eq. (4-6) applies to a system of n mol where n may vary. Here, however, n is unity and invariant. It is therefore subject to the constraints $\sum_i x_i = 1$ and $\sum_i dx_i = 0$. Mole fractions are not independent of one another, whereas the mole numbers in Eq. (4-6) are.

The second of the preceding equations dictates the possible combinations of terms that may be defined as additional primary functions. Those in common use are shown in Table 4-1 as Eqs. (4-7) through (4-10). Additional thermodynamic properties are related to these and arise by arbitrary definition.

Multiplication of Eq. (4-8) of Table 4-1 by n and differentiation yield the general expression

$$d(nH) = d(nU) + P d(nV) + nV dP$$

Substitution for $d(nU)$ by Eq. (4-6) reduces this result to Eq. (4-11). The total differentials of nA and nG are obtained similarly and are expressed by Eqs. (4-12) and (4-13). These equations and Eq. (4-6) are equivalent forms of the fundamental property relation, and appear under that heading in Table 4-1. Each expresses a total property— nU , nH , nA , and nG —as a function of a particular set of independent

variables, called the *canonical variables* for the property. The choice of which equation to use in a particular application is dictated by convenience. However, the Gibbs energy G is special, because of its relation to the canonical variables T , P , and $\{n_i\}$, the variables of primary interest in chemical processing. Another set of equations results from the substitutions $n = 1$ and $n_i = x_i$. The resulting equations are of course less general than their parents. Moreover, because the mole fractions are not independent, mathematical operations requiring their independence are invalid.

CONSTANT-COMPOSITION SYSTEMS

For 1 mol of a homogeneous fluid of constant composition, Eqs. (4-6) and (4-11) through (4-13) simplify to Eqs. (4-14) through (4-17) of Table 4-1. Because these equations are *exact differential expressions*, application of the reciprocity relation for such expressions produces the common Maxwell relations as described in the subsection “Multi-variable Calculus Applied to Thermodynamics” in Sec. 3. These are Eqs. (4-18) through (4-21) of Table 4-1, in which the partial derivatives are taken with composition held constant.

$U, H,$ and S as Functions of T and P or T and V At constant composition, molar thermodynamic properties can be considered functions of T and P (postulate 5). Alternatively, because V is related to T and P through an equation of state, V can serve rather than P as the second independent variable. The useful equations for the total differentials of $U, H,$ and S that result are given in Table 4-1 by Eqs. (4-22) through (4-25). The obvious next step is substitution for the partial differential coefficients in favor of measurable quantities. This purpose is served by definition of two *heat capacities*, one at constant pressure and the other at constant volume:

$$C_P \equiv \left(\frac{\partial H}{\partial T}\right)_P \quad (4-26)$$

$$C_V \equiv \left(\frac{\partial U}{\partial T}\right)_V \quad (4-27)$$

Both are properties of the material and functions of temperature, pressure, and composition.

Equation (4-15) of Table 4-1 may be divided by dT and restricted to constant P , yielding $(\partial H/\partial T)_P$ as given by the first equality of Eq. (4-28). Division of Eq. (4-15) by dP and restriction to constant T yield $(\partial H/\partial P)_T$ as given by the first equality of Eq. (4-29). Equation (4-28) is completed by Eq. (4-26), and Eq. (4-29) is completed by Eq. (4-21). Similarly, equations for $(\partial U/\partial T)_V$ and $(\partial U/\partial V)_T$ derive from Eq. (4-14), and these with Eqs. (4-27) and (4-20) yield Eqs. (4-30) and (4-31) of Table 4-1.

Equations (4-22), (4-26), and (4-29) combine to yield Eq. (4-32); Eqs. (4-23), (4-28), and (4-21) to yield Eq. (4-33); Eqs. (4-24), (4-27), and (4-31) to yield Eq. (4-34); and Eqs. (4-25), (4-30), and (4-20) to yield Eq. (4-35).

Equations (4-32) and (4-33) are general expressions for the enthalpy and entropy of homogeneous fluids at constant composition as functions of T and P . Equations (4-34) and (4-35) are general expressions for the internal energy and entropy of homogeneous fluids at constant composition as functions of temperature and molar volume. The coefficients of dT , dP , and dV are all composed of measurable quantities.

The Ideal Gas Model An ideal gas is a model gas comprising imaginary molecules of zero volume that do not interact. Its PVT behavior is represented by the simplest of equations of state $PV^{ig} = RT$, where R is a universal constant, values of which are given in Table 1-9. The following partial derivatives, all taken at constant composition, are obtained from this equation:

$$\left(\frac{\partial P}{\partial T}\right)_V = \frac{R}{V^{ig}} = \frac{P}{T} \quad \left(\frac{\partial V^{ig}}{\partial T}\right)_P = \frac{R}{P} = \frac{V^{ig}}{T} \quad \left(\frac{\partial P}{\partial V}\right)_T = -\frac{P}{V^{ig}}$$

The first two of these relations when substituted appropriately into Eqs. (4-29) and (4-31) of Table 4-1 lead to very simple expressions for ideal gases:

$$\left(\frac{\partial U^{ig}}{\partial V}\right)_T = \left(\frac{\partial H^{ig}}{\partial P}\right)_T = 0 \quad \left(\frac{\partial S^{ig}}{\partial P}\right)_T = -\frac{R}{P} \quad \left(\frac{\partial S^{ig}}{\partial V}\right)_T = \frac{R}{V^{ig}}$$

Moreover, Eqs. (4-32) through (4-35) become

$$dH^{ig} = C_P^{ig} dT \quad dS^{ig} = \frac{C_P^{ig}}{T} dT - \frac{R}{P} dP$$

$$dU^{ig} = C_V^{ig} dT \quad dS^{ig} = \frac{C_V^{ig}}{T} dT + \frac{R}{V^{ig}} dV$$

In these equations V^{ig} , U^{ig} , C_V^{ig} , H^{ig} , C_P^{ig} , and S^{ig} are ideal gas state values—the values that a PVT system would have were the ideal gas equation the true equation of state. They apply equally to pure species and to constant-composition mixtures, and they show that U^{ig} , C_V^{ig} , H^{ig} , and C_P^{ig} are functions of temperature only, independent of P and V . The entropy, however, is a function of both T and P or of both T and V . Regardless of composition, the ideal gas volume is given by $V^{ig} = RT/P$, and it provides the basis for comparison with true molar volumes through the *compressibility factor* Z . By definition,

$$Z \equiv \frac{V}{V^{ig}} = \frac{V}{RT/P} = \frac{PV}{RT} \quad (4-36)$$

The ideal gas state properties of mixtures are directly related to the ideal gas state properties of the constituent pure species. For those properties that are independent of P — U^{ig} , H^{ig} , C_V^{ig} , and C_P^{ig} —the mixture property is the sum of the properties of the pure constituent species, each weighted by its mole fraction:

$$M^{ig} = \sum_i y_i M_i^{ig} \quad (4-37)$$

where M^{ig} can represent any of the properties listed. For the entropy, which is a function of both T and P , an additional term is required to account for the difference in partial pressure of a species between its pure state and its state in a mixture:

$$S^{ig} = \sum_i y_i S_i^{ig} - R \sum_i y_i \ln y_i \quad (4-38)$$

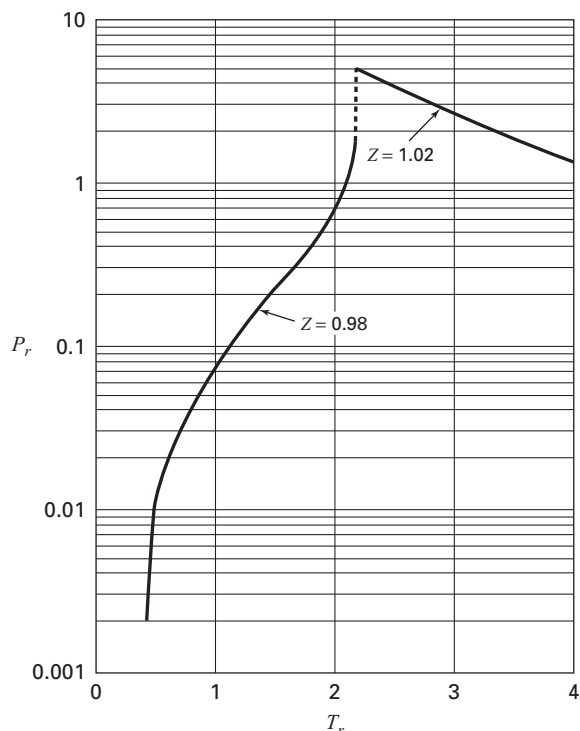


FIG. 4-1 Region where Z lies between 0.98 and 1.02, and the ideal-gas equation is a reasonable approximation. [Smith, Van Ness, and Abbott, Introduction to Chemical Engineering Thermodynamics, 7th ed., p. 104, McGraw-Hill, New York (2005).]

For the Gibbs energy, $G^{ig} = H^{ig} - TS^{ig}$; whence by Eqs. (4-37) and (4-38):

$$G^{ig} = \sum_i y_i G_i^{ig} + RT \sum_i y_i \ln y_i \quad (4-39)$$

The ideal gas model may serve as a reasonable approximation to reality under conditions indicated by Fig. 4-1.

Residual Properties The differences between true and ideal gas state properties are defined as residual properties M^R :

$$M^R \equiv M - M^{ig} \quad (4-40)$$

where M is the molar value of an extensive thermodynamic property of a fluid in its actual state and M^{ig} is its corresponding ideal gas state value at the same T , P , and composition. Residual properties depend on interactions *between* molecules and not on characteristics of individual molecules. Because the ideal gas state presumes the absence of molecular interactions, residual properties reflect deviations from ideality. The most commonly used residual properties are as follows:

$$\begin{aligned} \text{Residual volume } V^R &\equiv V - V^{ig} & \text{Residual enthalpy } H^R &\equiv H - H^{ig} \\ \text{Residual entropy } S^R &\equiv S - S^{ig} & \text{Residual Gibbs energy } G^R &\equiv G - G^{ig} \end{aligned}$$

Useful relations connecting these residual properties derive from Eq. (4-17), an alternative form of which follows from the mathematical identity:

$$d\left(\frac{G}{RT}\right) \equiv \frac{1}{RT} dG - \frac{G}{RT^2} dT$$

4-8 THERMODYNAMICS

Substitution for dG by Eq. (4-17) and for G by Eq. (4-10) gives, after algebraic reduction,

$$d\left(\frac{G}{RT}\right) = \frac{V}{RT} dP - \frac{H}{RT^2} dT \quad (4-41)$$

This equation may be written for the special case of an ideal gas and subtracted from Eq. (4-41) itself, yielding

$$d\left(\frac{G^R}{RT}\right) = \frac{V^R}{RT} dP - \frac{H^R}{RT^2} dT \quad (4-42)$$

As a consequence,
$$\frac{V^R}{RT} = \left[\frac{\partial(G^R/RT)}{\partial P} \right]_T \quad (4-43)$$

and
$$\frac{H^R}{RT} = -T \left[\frac{\partial(G^R/RT)}{\partial T} \right]_P \quad (4-44)$$

Equation (4-43) provides a direct link to PVT correlations through the compressibility factor Z as given by Eq. (4-36). Thus, with $V = ZRT/P$,

$$V^R \equiv V - V^{ig} = \frac{ZRT}{P} - \frac{RT}{P} = \frac{RT}{P} (Z - 1)$$

This equation in combination with a rearrangement of Eq. (4-43) yields

$$d\left(\frac{G^R}{RT}\right) = \frac{V^R}{RT} dP = (Z - 1) \frac{dP}{P} \quad (\text{constant } T)$$

Integration from $P = 0$ to arbitrary pressure P gives

$$\frac{G^R}{RT} = \int_0^P (Z - 1) \frac{dP}{P} \quad (\text{constant } T) \quad (4-45)$$

Smith, Van Ness, and Abbott [*Introduction to Chemical Engineering Thermodynamics*, 7th ed., pp. 210–211, McGraw-Hill, New York (2005)] show that it is permissible here to set the lower limit of integration $(G^R/RT)_{P=0}$ equal to zero. Note also that the integrand $(Z - 1)/P$ remains finite as $P \rightarrow 0$. Differentiation of Eq. (4-45) with respect to T in accord with Eq. (4-44) gives

$$\frac{H^R}{RT} = -T \int_0^P \left(\frac{\partial Z}{\partial T} \right)_P \frac{dP}{P} \quad (\text{constant } T) \quad (4-46)$$

Because $G = H - TS$ and $G^{ig} = H^{ig} - TS^{ig}$, then by difference, $G^R = H^R - TS^R$, and

$$\frac{S^R}{R} = \frac{H^R}{RT} - \frac{G^R}{RT} \quad (4-47)$$

Equations (4-45) through (4-47) provide the basis for calculation of residual properties from PVT correlations. They may be put into *generalized* form by substitution of the relationships

$$P = P_c P_r \quad T = T_c T_r \\ dP = P_c dP_r \quad dT = T_c dT_r$$

The resulting equations are

$$\frac{G^R}{RT} = \int_0^{P_r} (Z - 1) \frac{dP_r}{P_r} \quad (4-48)$$

$$\frac{H^R}{RT_c} = -T_c^2 \int_0^{P_r} \left(\frac{\partial Z}{\partial T_r} \right) \frac{dP_r}{P_r} \quad (4-49)$$

The terms on the right sides of these equations depend only on the upper limit P_r of the integrals and on the reduced temperature at which they are evaluated. Thus, values of G^R/RT and H^R/RT_c may be determined once and for all at any reduced temperature and pressure from generalized compressibility factor data.

PROPERTY CALCULATIONS FOR GASES AND VAPORS

The most satisfactory calculation procedure for the thermodynamic properties of gases and vapors is based on ideal gas state heat capacities and residual properties. Of primary interest are the enthalpy and entropy; these are given by rearrangement of the residual property definitions:

$$H = H^{ig} + H^R \quad \text{and} \quad S = S^{ig} + S^R$$

These are simple sums of the ideal gas and residual properties, evaluated separately.

EVALUATION OF ENTHALPY AND ENTROPY IN THE IDEAL GAS STATE

For the ideal gas state at constant composition:

$$dH^{ig} = C_P^{ig} dT \quad \text{and} \quad dS^{ig} = C_P^{ig} \frac{dT}{T} - R \frac{dP}{P}$$

Integration from an initial ideal gas *reference state* at conditions T_0 and P_0 to the ideal gas state at T and P gives

$$H^{ig} = H_0^{ig} + \int_{T_0}^T C_P^{ig} dT \\ S^{ig} = S_0^{ig} + \int_{T_0}^T C_P^{ig} \frac{dT}{T} - R \ln \frac{P}{P_0}$$

Substitution into the equations for H and S yields

$$H = H_0^{ig} + \int_{T_0}^T C_P^{ig} dT + H^R \quad (4-50)$$

$$S = S_0^{ig} + \int_{T_0}^T C_P^{ig} \frac{dT}{T} - R \ln \frac{P}{P_0} + S^R \quad (4-51)$$

The reference state at T_0 and P_0 is arbitrarily selected, and the values assigned to H_0^{ig} and S_0^{ig} are also arbitrary. In practice, only *changes* in H and S are of interest, and fixed reference state values ultimately cancel in their calculation.

The ideal gas state heat capacity C_P^{ig} is a function of T but not of P . For a mixture the heat capacity is simply the molar average $\sum_i y_i C_{P,i}^{ig}$. Empirical equations relating C_P^{ig} to T are available for many pure gases; a common form is

$$\frac{C_P^{ig}}{R} = A + BT + CT^2 + DT^{-2} \quad (4-52)$$

where A , B , C , and D are constants characteristic of the particular gas, and either C or D is zero. The ratio C_P^{ig}/R is dimensionless; thus the units of C_P^{ig} are those of R . Data for ideal gas state heat capacities are given for many substances in Table 2-155.

Evaluation of the integrals $\int C_P^{ig} dT$ and $\int (C_P^{ig}/T) dT$ is accomplished by substitution for C_P^{ig} , followed by integration. For temperature limits of T_0 and T and with $\tau \equiv T/T_0$, the equations that follow from Eq. (4-52) are

$$\int_{T_0}^T \frac{C_P^{ig}}{R} dT = AT_0(\tau - 1) + \frac{B}{2} T_0^2(\tau^2 - 1) + \frac{C}{3} T_0^3(\tau^3 - 1) + \frac{D}{T_0} \left(\frac{\tau - 1}{\tau} \right) \quad (4-53)$$

$$\int_{T_0}^T \frac{C_P^{ig}}{RT} dT = A \ln \tau + \left[BT_0 + \left(CT_0^2 + \frac{D}{\tau^2 T_0^2} \right) \left(\frac{\tau + 1}{2} \right) \right] (\tau - 1) \quad (4-54)$$

Equations (4-50) and (4-51) may sometimes be advantageously expressed in alternative form through use of mean heat capacities:

$$H = H_0^{ig} + \langle C_P^{ig} \rangle_H (T - T_0) + H^R \quad (4-55)$$

$$S = S_0^{ig} + \langle C_P^{ig} \rangle_S \ln \frac{T}{T_0} - R \ln \frac{P}{P_0} + S^R \quad (4-56)$$

where $\langle C_P^{ig} \rangle_H$ and $\langle C_P^{ig} \rangle_S$ are mean heat capacities specific, respectively, for enthalpy and entropy calculations. They are given by the following equations:

$$\frac{\langle C_P^{ig} \rangle_H}{R} = A + \frac{B}{2} T_0 (\tau + 1) + \frac{C}{3} T_0^2 (\tau^2 + \tau + 1) + \frac{D}{\tau T_0^2} \quad (4-57)$$

$$\frac{\langle C_P^{ig} \rangle_S}{R} = A + \left[B T_0 + \left(C T_0^2 + \frac{D}{\tau^2 T_0^2} \right) \left(\frac{\tau + 1}{2} \right) \right] \frac{\tau - 1}{\ln \tau} \quad (4-58)$$

RESIDUAL ENTHALPY AND ENTROPY FROM PVT CORRELATIONS

The residual properties of gases and vapors depend on their *PVT* behavior. This is often expressed through correlations for the compressibility factor Z , defined by Eq. (4-36). Analytical expressions for Z as functions of T and P or T and V are known as *equations of state*. They may also be reformulated to give P as a function of T and V or V as a function of T and P .

Virial Equations of State The virial equation in *density* is an infinite series expansion of the compressibility factor Z in powers of molar density ρ (or reciprocal molar volume V^{-1}) about the real gas state at zero density (zero pressure):

$$Z = 1 + B\rho + C\rho^2 + D\rho^3 + \dots \quad (4-59)$$

The density series virial coefficients B , C , D , \dots depend on temperature and composition only. In practice, truncation is to two or three terms. The composition dependencies of B and C are given by the exact *mixing rules*

$$B = \sum_i \sum_j y_i y_j B_{ij} \quad (4-60)$$

$$C = \sum_i \sum_j \sum_k y_i y_j y_k C_{ijk} \quad (4-61)$$

where y_i , y_j , and y_k are mole fractions for a gas mixture and i , j , and k identify species.

The coefficient B_{ij} characterizes a bimolecular interaction between molecules i and j , and therefore $B_{ij} = B_{ji}$. Two kinds of second virial coefficient arise: B_{ii} and B_{jj} , wherein the subscripts are the same ($i = j$), and B_{ij} , wherein they are different ($i \neq j$). The first is a virial coefficient for a pure species; the second is a mixture property, called a *cross coefficient*. Similarly for the third virial coefficients: C_{iii} , C_{jjj} , and C_{kkk} are for the pure species, and $C_{ijj} = C_{jii} = C_{jij} = \dots$ are cross coefficients.

Although the virial equation itself is easily rationalized on empirical grounds, the mixing rules of Eqs. (4-60) and (4-61) follow rigorously from the methods of statistical mechanics. The temperature derivatives of B and C are given exactly by

$$\frac{dB}{dT} = \sum_i \sum_j y_i y_j \frac{dB_{ij}}{dT} \quad (4-62)$$

$$\frac{dC}{dT} = \sum_i \sum_j \sum_k y_i y_j y_k \frac{dC_{ijk}}{dT} \quad (4-63)$$

An alternative form of the virial equation expresses Z as an expansion in powers of pressure about the real gas state at zero pressure (zero density):

$$Z = 1 + B'P + C'P^2 + D'P^3 + \dots \quad (4-64)$$

Equation (4-64) is the virial equation in *pressure*, and B' , C' , D' , \dots are the pressure series virial coefficients. Again, truncation is to two

or three terms, with B' and C' depending on temperature and composition only. Moreover, the two sets of coefficients are related:

$$B' = B/RT \quad (4-65)$$

$$C' = (C - B^2)/(RT)^2 \quad (4-66)$$

Values can often be found for B , but not so often for C . Generalized correlations for both B and C are given by Meng, Duan, and Li [*Fluid Phase Equilibria* **226**: 109–120 (2004)].

For pressures up to several bars, the two-term expansion in pressure, with B' given by Eq. (4-65), is usually preferred:

$$Z = 1 + B'P = 1 + BP/RT \quad (4-67)$$

For supercritical temperatures, it is satisfactory to ever higher pressures as the temperature increases. For pressures above the range where Eq. (4-67) is useful, but below the critical pressure, the virial expansion in density truncated to three terms is usually suitable:

$$Z = 1 + B\rho + C\rho^2 \quad (4-68)$$

Equations for residual enthalpy and entropy may be developed from each of these expressions. Consider first Eq. (4-67), which is explicit in volume. Equations (4-45) and (4-46) are therefore applicable. Direct substitution for Z in Eq. (4-45) gives

$$\frac{G^R}{RT} = \frac{BP}{RT} \quad (4-69)$$

Differentiation of Eq. (4-67) yields

$$\left(\frac{\partial Z}{\partial T} \right)_P = \left(\frac{dB}{dT} - \frac{B}{T} \right) \frac{P}{RT}$$

By Eq. (4-46),

$$\frac{H^R}{RT} = \frac{P}{R} \left(\frac{B}{T} - \frac{dB}{dT} \right) \quad (4-70)$$

and by Eq. (4-47),

$$\frac{S^R}{R} = - \frac{P}{R} \frac{dB}{dT} \quad (4-71)$$

An extensive set of three-parameter corresponding-states correlations has been developed by Pitzer and coworkers [Pitzer, *Thermodynamics*, 3d ed., App. 3, McGraw-Hill, New York (1995)]. Particularly useful is the one for the second virial coefficient. The basic equation is

$$\frac{BP_c}{RT_c} = B^0 + \omega B^1 \quad (4-72)$$

with the *acentric factor* defined by Eq. (2-17). For pure chemical species B^0 and B^1 are functions of reduced temperature only. Substitution for B in Eq. (4-67) by this expression gives

$$Z = 1 + (B^0 + \omega B^1) \frac{P_r}{T_r} \quad (4-73)$$

By differentiation,

$$\left(\frac{\partial Z}{\partial T_r} \right)_{P_r} = P_r \left(\frac{dB^0/dT_r}{T_r} - \frac{B^0}{T_r^2} \right) + \omega P_r \left(\frac{dB^1/dT_r}{T_r} - \frac{B^1}{T_r^2} \right)$$

Upon substitution of these equations into Eqs. (4-48) and (4-49), integration yields

$$\frac{G^R}{RT} = (B^0 + \omega B^1) \frac{P_r}{T_r} \quad (4-74)$$

$$\frac{H^R}{RT_c} = P_r \left[B^0 - T_r \frac{dB^0}{dT_r} + \omega \left(B^1 - T_r \frac{dB^1}{dT_r} \right) \right] \quad (4-75)$$

The residual entropy follows from Eq. (4-47):

$$\frac{S^R}{R} = - P_r \left(\frac{dB^0}{dT_r} + \omega \frac{dB^1}{dT_r} \right) \quad (4-76)$$

4-10 THERMODYNAMICS

In these equations, B^0 and B^1 and their derivatives are well represented by Abbott's correlations [Smith and Van Ness, *Introduction to Chemical Engineering Thermodynamics*, 3d ed., p. 87, McGraw-Hill, New York (1975)]:

$$B^0 = 0.083 - \frac{0.422}{T_r^{1.6}} \quad (4-77)$$

$$B^1 = 0.139 - \frac{0.172}{T_r^{4.2}} \quad (4-78)$$

$$\frac{dB^0}{dT_r} = \frac{0.675}{T_r^{2.6}} \quad (4-79)$$

$$\frac{dB^1}{dT_r} = \frac{0.722}{T_r^{5.2}} \quad (4-80)$$

Although limited to pressures where the two-term virial equation in pressure has approximate validity, these correlations are applicable for most chemical processing conditions. As with all generalized correlations, they are least accurate for polar and associating molecules.

Although developed for pure materials, these correlations can be extended to gas or vapor mixtures. Basic to this extension are the mixing rules for the second virial coefficient and its temperature derivative as given by Eqs. (4-60) and (4-62). Values for the cross coefficients B_{ij} , with $i \neq j$, and their derivatives are provided by Eq. (4-72) written in extended form:

$$B_{ij} = \frac{RT_{cij}}{P_{cij}} (B^0 + \omega_{ij} B^1) \quad (4-81)$$

where B^0 , B^1 , dB^0/dT_r , and dB^1/dT_r are the same functions of T_r as given by Eqs. (4-77) through (4-80). Differentiation produces

$$\begin{aligned} \frac{dB_{ij}}{dT} &= \frac{RT_{cij}}{P_{cij}} \left(\frac{dB^0}{dT} + \omega_{ij} \frac{dB^1}{dT} \right) \\ \frac{dB_{ij}}{dT} &= \frac{R}{P_{cij}} \left(\frac{dB^0}{dT_{rij}} + \omega_{ij} \frac{dB^1}{dT_{rij}} \right) \end{aligned} \quad (4-82)$$

where $T_{rij} = T/T_{cij}$. The following combining rules for ω_{ij} , T_{cij} , and P_{cij} are given by Prausnitz, Lichtenthaler, and de Azevedo [*Molecular Thermodynamics of Fluid-Phase Equilibria*, 2d ed., pp. 132 and 162, Prentice-Hall, Englewood Cliffs, N.J. (1986)]:

$$\omega_{ij} = \frac{\omega_i + \omega_j}{2} \quad (4-83)$$

$$T_{cij} = (T_{ci} T_{cj})^{1/2} (1 - k_{ij}) \quad (4-84)$$

$$P_{cij} = \frac{Z_{cij} RT_{cij}}{V_{cij}} \quad (4-85)$$

with
$$Z_{cij} = \frac{Z_{ci} + Z_{cj}}{2} \quad (4-86)$$

and
$$V_{cij} = \left(\frac{V_{ci}^{1/3} + V_{cj}^{1/3}}{2} \right)^3 \quad (4-87)$$

In Eq. (4-84), k_{ij} is an empirical interaction parameter specific to an $i-j$ molecular pair. When $i=j$ and for chemically similar species, $k_{ij}=0$. Otherwise, it is a small (usually) positive number evaluated from minimal PVT data or, absence data, set equal to zero.

When $i=j$, all equations reduce to the appropriate values for a pure species. When $i \neq j$, these equations define a set of interaction parameters without physical significance. For a mixture, values of B_{ij} and dB_{ij}/dT from Eqs. (4-81) and (4-82) are substituted into Eqs. (4-60) and (4-62) to provide values of the mixture second virial coefficient

B and its temperature derivative. Values of H^R and S^R are then given by Eqs. (4-70) and (4-71).

A primary virtue of Abbott's correlations for second virial coefficients is simplicity. More complex correlations of somewhat wider applicability include those by Tsionopoulos [*AIChE J.* **20**: 263–272 (1974); *ibid.*, **21**: 827–829 (1975); *ibid.*, **24**: 1112–1115 (1978); *Adv. in Chemistry Series 182*, pp. 143–162 (1979)] and Hayden and O'Connell [*Ind. Eng. Chem. Proc. Des. Dev.* **14**: 209–216 (1975)]. For aqueous systems see Bishop and O'Connell [*Ind. Eng. Chem. Res.*, **44**: 630–633 (2005)].

Because Eq. (4-68) is explicit in P , it is incompatible with Eqs. (4-45) and (4-46), and they must be transformed to make V (or molar density ρ) the variable of integration. The resulting equations are given by Smith, Van Ness, and Abbott [*Introduction to Chemical Engineering Thermodynamics*, 7th ed., pp. 216–217, McGraw-Hill, New York (2005)]:

$$\frac{G^R}{RT} = Z - 1 - \ln Z + \int_0^{\rho} (Z - 1) \frac{d\rho}{\rho} \quad (4-88)$$

$$\frac{H^R}{RT} = Z - 1 - T \int_0^{\rho} \left(\frac{\partial Z}{\partial T} \right)_{\rho} \frac{d\rho}{\rho} \quad (4-89)$$

By differentiation of Eq. (4-68),

$$\left(\frac{\partial Z}{\partial T} \right)_{\rho} = \frac{dB}{dT} \rho + \frac{dC}{dT} \rho^2$$

Substituting in Eqs. (4-88) and (4-89) for Z by Eq. (4-68) and in Eq. (4-89) for the derivative yields, upon integration and reduction,

$$\frac{G^R}{RT} = 2B\rho + \frac{3}{2}C\rho^2 - \ln Z \quad (4-90)$$

$$\frac{H^R}{RT} = \left(B - T \frac{dB}{dT} \right) \rho + \left(C - \frac{T}{2} \frac{dC}{dT} \right) \rho^2 \quad (4-91)$$

The residual entropy is given by Eq. (4-47).

In a process calculation, T and P , rather than T and ρ (or T and V), are usually the favored independent variables. Applications of Eqs. (4-90) and (4-91) therefore require prior solution of Eq. (4-68) for Z or ρ . With $Z = P/\rho RT$, Eq. (4-68) may be written in two equivalent forms:

$$Z^3 - Z^2 - \left(\frac{BP}{RT} \right) Z - \frac{CP^2}{(RT)^2} = 0 \quad (4-92)$$

$$\rho^3 + \left(\frac{B}{C} \right) \rho^2 + \left(\frac{1}{C} \right) \rho - \frac{P}{CRT} = 0 \quad (4-93)$$

In the event that three real roots obtain for these equations, only the largest Z (smallest ρ), appropriate for the vapor phase, has physical significance, because the virial equations are suitable only for vapors and gases.

Data for third virial coefficients are often lacking, but generalized correlations are available. Equation (4-68) may be rewritten in reduced form as

$$Z = 1 + \hat{B} \frac{P_r}{T_r Z} + \hat{C} \left(\frac{P_r}{T_r Z} \right)^2 \quad (4-94)$$

where \hat{B} is the reduced second virial coefficient given by Eq. (4-72). Thus by definition,

$$\hat{B} \equiv \frac{BP_c}{RT_c} = B^0 + \omega B^1 \quad (4-95)$$

The reduced third virial coefficient \hat{C} is defined as

$$\hat{C} \equiv \frac{CP_c^2}{R^2 T_c^2} \quad (4-96)$$

A Pitzer-type correlation for \hat{C} is then written as

$$\hat{C} = C^0 + \omega C^1 \quad (4-97)$$

Correlations for C^0 and C^1 with reduced temperature are

$$C^0 = 0.01407 + \frac{0.02432}{T_r} - \frac{0.00313}{T_r^{10.5}} \quad (4-98)$$

$$C^1 = -0.02676 + \frac{0.05539}{T_r^{2.7}} - \frac{0.00242}{T_r^{10.5}} \quad (4-99)$$

The first is given by, and the second is inspired by, Orbey and Vera [AIChE J. **29**: 107–113 (1983)].

Equation (4-94) is cubic in Z , with T_r and P_r specified, solution for Z is by iteration. An initial guess of $Z = 1$ on the right side usually leads to rapid convergence.

Another class of equations, known as *extended virial equations*, was introduced by Benedict, Webb, and Rubin [J. Chem. Phys. **8**: 334–345 (1940); **10**: 747–758 (1942)]. This equation contains eight parameters, all functions of composition. It and its modifications, despite their complexity, find application in the petroleum and natural gas industries for light hydrocarbons and a few other commonly encountered gases [see Lee and Kesler, AIChE J., **21**: 510–527 (1975)].

Cubic Equations of State The modern development of cubic equations of state started in 1949 with publication of the Redlich-Kwong (RK) equation [Chem. Rev., **44**: 233–244 (1949)], and many others have since been proposed. An extensive review is given by Valderrama [Ind. Eng. Chem. Res. **42**: 1603–1618 (2003)]. Of the equations published more recently, the two most popular are the Soave-Redlich-Kwong (SRK) equation, a modification of the RK equation [Chem. Eng. Sci. **27**: 1197–1203 (1972)] and the Peng-Robinson (PR) equation [Ind. Eng. Chem. Fundam. **15**: 59–64 (1976)]. All are encompassed by a *generic* cubic equation of state, written as

$$P = \frac{RT}{V-b} - \frac{a(T)}{(V+\epsilon b)(V+\sigma b)} \quad (4-100)$$

For a specific form of this equation, ϵ and σ are pure numbers, the same for all substances, whereas parameters $a(T)$ and b are substance-dependent. Suitable estimates of the parameters in cubic equations of state are usually found from values for the critical constants T_c and P_c . The procedure is discussed by Smith, Van Ness, and Abbott [Introduction to Chemical Engineering Thermodynamics, 7th ed., pp. 93–94, McGraw-Hill, New York (2005)], and for Eq. (4-100) the appropriate equations are given as

$$a(T) = \psi \frac{\alpha(T_r) R^2 T_c^2}{P_c} \quad (4-101)$$

$$b = \Omega \frac{RT_c}{P_c} \quad (4-102)$$

Function $\alpha(T_r)$ is an empirical expression, specific to a particular form of the equation of state. In these equations ψ and Ω are pure numbers, independent of substance and determined for a particular equation of state from the values assigned to ϵ and σ .

As an equation cubic in V , Eq. (4-100) has three volume roots, of which two may be complex. Physically meaningful values of V are always real, positive, and greater than parameter b . When $T > T_c$, solution for V at any positive value of P yields only one real positive root. When $T = T_c$, this is also true, except at the critical pressure, where three roots exist, all equal to V_c . For $T < T_c$, only one real positive (liquidlike) root exists at high pressures, but for a range of lower pressures there are three. Here, the middle root is of no significance; the smallest root is a liquid or liquidlike volume, and the largest root is a vapor or vaporlike volume.

Equation (4-100) may be rearranged to facilitate its solution either for a vapor or vaporlike volume or for a liquid or liquidlike volume.

$$\text{Vapor:} \quad V = \frac{RT}{P} + b - \frac{a(T)}{P} \frac{V-b}{(V+\epsilon b)(V+\sigma b)} \quad (4-103a)$$

$$\text{Liquid:} \quad V = b + (V+\epsilon b)(V+\sigma b) \left[\frac{RT - bP - VP}{a(T)} \right] \quad (4-103b)$$

Solution for V is most convenient with the solve routine of a software package. An initial estimate for V in Eq. (4-103a) is the ideal gas value RT/P ; for Eq. (4-103b) it is $V = b$. In either case, iteration is initiated by substituting the estimate on the right side. The resulting value of V on the left is returned to the right side, and the process continues until the change in V is suitably small.

Equations for Z equivalent to Eqs. (4-103) are obtained by substituting $V = ZRT/P$.

$$\text{Vapor:} \quad Z = 1 + \beta - q\beta \frac{Z - \beta}{(Z + \epsilon\beta)(Z + \sigma\beta)} \quad (4-104a)$$

$$\text{Liquid:} \quad Z = \beta + (Z + \epsilon b)(Z + \sigma b) \left(\frac{1 + \beta - Z}{q\beta} \right) \quad (4-104b)$$

$$\text{where by definition} \quad \beta \equiv \frac{bP}{RT} \quad (4-105)$$

$$\text{and} \quad q \equiv \frac{a(T)}{bRT} \quad (4-106)$$

These dimensionless quantities provide simplification, and when combined with Eqs. (4-101) and (4-102), they yield

$$\beta = \Omega \frac{P_r}{T_r} \quad (4-107)$$

$$q = \frac{\Psi\alpha(T_r)}{\Omega T_r} \quad (4-108)$$

In Eq. (4-104a) the initial estimate is $Z = 1$; in Eq. (4-104b) it is $Z = \beta$. Iteration follows the same pattern as for Eqs. (4-103). The final value of Z yields the volume root through $V = ZRT/P$.

Equations of state, such as the Redlich-Kwong (RK) equation, which expresses Z as a function of T_r and P_r only, yield two-parameter corresponding-states correlations. The SRK equation and the PR equation, in which the acentric factor ω enters through function $\alpha(T_r; \omega)$ as an additional parameter, yield three-parameter corresponding-states correlations. The numerical assignments for parameters ϵ , σ , Ω , and Ψ are given in Table 4-2. Expressions are also given for $\alpha(T_r; \omega)$ for the SRK and PR equations.

As shown by Smith, Van Ness, and Abbott [Introduction to Chemical Engineering Thermodynamics, 7th ed., pp. 218–219, McGraw-Hill, New York (2005)], Eqs. (4-104) in conjunction with Eqs. (4-88), (4-89), and (4-47) lead to

$$\frac{G^R}{RT} = Z - 1 - \ln(Z - \beta) - qI \quad (4-109)$$

$$\frac{H^R}{RT} = Z - 1 + \left[\frac{d \ln \alpha(T_r)}{d \ln T_r} - 1 \right] qI \quad (4-110)$$

TABLE 4-2 Parameter Assignments for Cubic Equations of State*

For use with Eqs. (4-104) through (4-106)

Eq. of state	$\alpha(T_r)$	σ	ϵ	Ω	Ψ
RK (1949)	$T_r^{-1/2}$	1	0	0.08664	0.42748
SRK (1972)	$\alpha_{\text{SRK}}(T_r; \omega)^{\dagger}$	1	0	0.08664	0.42748
PR (1976)	$\alpha_{\text{PR}}(T_r; \omega)^{\ddagger}$	$1 + \sqrt{2}$	$1 - \sqrt{2}$	0.07780	0.45724

*Smith, Van Ness, and Abbott, *Introduction to Chemical Engineering Thermodynamics*, 7th ed., p. 98, McGraw-Hill, New York (2005).

$\dagger \alpha_{\text{SRK}}(T_r; \omega) = [1 + (0.480 + 1.574\omega - 0.176\omega^2)(1 - T_r^{1/2})]^2$

$\ddagger \alpha_{\text{PR}}(T_r; \omega) = [1 + (0.37464 + 1.54226\omega - 0.26992\omega^2)(1 - T_r^{1/2})]^2$

4-12 THERMODYNAMICS

$$\frac{S^R}{R} = \ln(Z - \beta) + \frac{d \ln \alpha(T_r)}{d \ln T_r} qI \quad (4-111)$$

$$\text{where} \quad I = \frac{1}{\sigma - \epsilon} \ln \left(\frac{Z + \sigma\beta}{Z + \epsilon\beta} \right) \quad (4-112)$$

Preliminary to application of these equations Z is found by solution of either Eq. (4-104a) or (4-104b).

Cubic equations of state may be applied to mixtures through expressions that give the parameters as functions of composition. No established theory prescribes the form of this dependence, and empirical *mixing rules* are often used to relate mixture parameters to pure-species parameters. The simplest realistic expressions are a linear mixing rule for parameter b and a quadratic mixing rule for parameter a

$$b = \sum_i x_i b_i \quad (4-113)$$

$$a = \sum_i \sum_j x_i x_j a_{ij} \quad (4-114)$$

with $a_{ij} = a_{ji}$. The a_{ij} are of two types: pure-species parameters (like subscripts) and interaction parameters (unlike subscripts). Parameter b_i is for pure species i . The interaction parameter a_{ij} is often evaluated from pure-species parameters by a geometric mean *combining rule*

$$a_{ij} = (a_i a_j)^{1/2} \quad (4-115)$$

These traditional equations yield mixture parameters solely from parameters for the pure constituent species. They are most likely to be satisfactory for mixtures comprised of simple and chemically similar molecules.

Pitzer's Generalized Correlations In addition to the corresponding-states correlation for the second virial coefficient, Pitzer and coworkers [*Thermodynamics*, 3d ed., App. 3, McGraw-Hill, New York (1995)] developed a full set of generalized correlations. They have as their basis an equation for the compressibility factor, as given by Eq. (2-63):

$$Z = Z^0 + \omega Z^1 \quad (2-63)$$

where Z^0 and Z^1 are each functions of reduced temperature T_r and reduced pressure P_r . Acentric factor ω is defined by Eq. (2-17). Correlations for Z appear in Sec. 2.

Generalized correlations are developed here for the residual enthalpy and residual entropy from Eqs. (4-48) and (4-49). Substitution for Z by Eq. (2-63) puts Eq. (4-48) into generalized form:

$$\frac{G^R}{RT} = \int_0^{P_r} (Z^0 - 1) \frac{dP_r}{P_r} + \omega \int_0^{P_r} Z^1 \frac{dP_r}{P_r} \quad (4-116)$$

Differentiation of Eq. (2-63) yields

$$\left(\frac{\partial Z}{\partial T_r} \right)_{P_r} = \left(\frac{\partial Z^0}{\partial T_r} \right)_{P_r} + \omega \left(\frac{\partial Z^1}{\partial T_r} \right)_{P_r}$$

Substitution for $(\partial Z / \partial T_r)_{P_r}$ in Eq. (4-49) gives

$$\frac{H^R}{RT_c} = -T_r^2 \int_0^{P_r} \left(\frac{\partial Z^0}{\partial T_r} \right)_{P_r} \frac{dP_r}{P_r} - \omega T_r^2 \int_0^{P_r} \left(\frac{\partial Z^1}{\partial T_r} \right)_{P_r} \frac{dP_r}{P_r} \quad (4-117)$$

$$\text{By Eq. (4-47),} \quad \frac{S^R}{R} = \frac{1}{T_r} \left(\frac{H^R}{RT_c} \right) - \frac{G^R}{RT}$$

Combination of Eqs. (4-116) and (4-117) leads to

$$\frac{S^R}{R} = - \int_0^{P_r} \left[T_r \left(\frac{\partial Z^0}{\partial T_r} \right)_{P_r} + Z^0 - 1 \right] \frac{dP_r}{P_r} - \omega \int_0^{P_r} \left[T_r \left(\frac{\partial Z^1}{\partial T_r} \right)_{P_r} + Z^1 \right] \frac{dP_r}{P_r}$$

If the first terms on the right sides of Eq. (4-117) and of this equation (including the minus signs) are represented by $(H^R)^0/RT_c$ and $(S^R)^0/R$ and if the second terms, excluding ω but including the minus signs, are represented by $(H^R)^1/RT_c$ and $(S^R)^1/R$, then

$$\frac{H^R}{RT_c} = \frac{(H^R)^0}{RT_c} + \omega \frac{(H^R)^1}{RT_c} \quad (4-118)$$

$$\frac{S^R}{R} = \frac{(S^R)^0}{R} + \omega \frac{(S^R)^1}{R} \quad (4-119)$$

Pitzer's original correlations for Z and the derived quantities were determined graphically and presented in tabular form. Since then, analytical refinements to the tables have been developed, with extended range and accuracy. The most popular Pitzer-type correlation is that of Lee and Kesler [*AIChE J.* **21**: 510–527 (1975); see also Smith, Van Ness, and Abbott, *Introduction to Chemical Engineering Thermodynamics*, 5th, 6th, and 7th eds., App. E, McGraw-Hill, New York (1996, 2001, 2005)]. These tables cover both the liquid and gas phases and span the ranges $0.3 \leq T_r \leq 4.0$ and $0.01 \leq P_r \leq 10.0$. They list values of Z^0 , Z^1 , $(H^R)^0/RT_c$, $(H^R)^1/RT_c$, $(S^R)^0/R$, and $(S^R)^1/R$.

Lee and Kesler also included a Pitzer-type correlation for vapor pressures:

$$\ln P_r^{\text{sat}}(T_r) = \ln P_r^0(T_r) + \omega \ln P_r^1(T_r) \quad (4-120)$$

$$\text{where} \quad \ln P_r^0(T_r) = 5.92714 - \frac{6.09648}{T_r} - 1.28862 \ln T_r + 0.1693477 T_r^6 \quad (4-121)$$

$$\text{and} \quad \ln P_r^1(T_r) = 15.2518 - \frac{15.6875}{T_r} - 13.4721 \ln T_r + 0.435777 T_r^6 \quad (4-122)$$

The value of ω to be used with Eq. (4-120) is found from the correlation by requiring that it reproduce the normal boiling point; that is, ω for a particular substance is determined from

$$\omega = \frac{\ln P_{r_s}^{\text{sat}} - \ln P_r^0(T_{r_s})}{\ln P_r^1(T_{r_s})} \quad (4-123)$$

where T_{r_s} is the reduced normal boiling point and $P_{r_s}^{\text{sat}}$ is the reduced vapor pressure corresponding to 1 standard atmosphere (1.01325 bar).

Although the tables representing the Pitzer correlations are based on data for pure materials, they may also be used for the calculation of mixture properties. A set of recipes is required relating the parameters T_c , P_c , and ω for a mixture to the pure-species values and to composition. One such set is given by Eqs. (2-80) through (2-82) in the Seventh Edition of *Perry's Chemical Engineers' Handbook* (1997). These equations define *pseudoparameters*, so called because the defined values of T_{pc} , P_{pc} , and ω have no physical significance for the mixture.

The Lee-Kesler correlations provide reliable data for nonpolar and slightly polar gases; errors of less than 3 percent are likely. Larger errors can be expected in applications to highly polar and associating gases.

The quantum gases (e.g., hydrogen, helium, and neon) do not conform to the same corresponding-states behavior as do normal fluids. Prausnitz, Lichtenthaler, and de Azevedo [*Molecular Thermodynamics of Fluid-Phase Equilibria*, 3d ed., pp. 172–173, Prentice-Hall PTR, Upper Saddle River, N.J. (1999)] propose the use of temperature-dependent *effective* critical parameters. For hydrogen, the quantum gas most commonly found in chemical processing, the recommended equations are

$$\frac{T_c}{\text{K}} = \frac{43.6}{1 + 21.8/2.016T} \quad (\text{for H}_2) \quad (4-124)$$

$$\frac{P_c}{\text{bar}} = \frac{20.5}{1 + 44.2/2.016T} \quad (\text{for H}_2) \quad (4-125)$$

$$\frac{V_c}{\text{cm}^3 \text{mol}^{-1}} = \frac{51.5}{1 - 9.91/2.016T} \quad (\text{for H}_2) \quad (4-126)$$

where T is absolute temperature in kelvins. Use of these *effective* critical parameters for hydrogen requires the further specification that $\omega = 0$.

OTHER PROPERTY FORMULATIONS

LIQUID PHASE

Although residual properties have formal reality for liquids as well as for gases, their advantageous use as *small* corrections to ideal gas state properties is lost. Calculation of property changes for the liquid state are usually based on alternative forms of Eqs. (4-32) through (4-35), shown in Table 4-1. Useful here are the definitions of two liquid-phase properties—the volume expansivity β and the isothermal compressibility κ :

$$\beta \equiv \frac{1}{V} \left(\frac{\partial V}{\partial T} \right)_P \quad (4-127)$$

$$\kappa \equiv - \frac{1}{V} \left(\frac{\partial V}{\partial P} \right)_T \quad (4-128)$$

$$\text{For } V = f(T, P), \quad dV = \left(\frac{\partial V}{\partial T} \right)_P dT + \left(\frac{\partial V}{\partial P} \right)_T dP$$

This equation in combination with Eqs. (4-127) and (4-128) becomes

$$\frac{dV}{V} = \beta dT - \kappa dP \quad (4-129)$$

$$\text{If } V \text{ is constant,} \quad \left(\frac{\partial P}{\partial T} \right)_V = \frac{\beta}{\kappa} \quad (4-130)$$

Because liquid-phase isotherms of P versus V are very steep and closely spaced, both β and κ are small. Moreover (outside the critical region), they are weak functions of T and P and are often assumed constant at average values. Integration of Eq. (4-129) then gives

$$\ln \frac{V_2}{V_1} = \beta(T_2 - T_1) - \kappa(P_2 - P_1) \quad (4-131)$$

Substitution for the partial derivatives in Eqs. (4-32) through (4-35) by Eqs. (4-127) and (4-130) yields

$$dH = C_p dT + (1 - \beta T) V dP \quad (4-132)$$

$$dS = C_p \frac{dT}{T} - \beta V dP \quad (4-133)$$

$$dU = C_v dT + \left(\frac{\beta}{\kappa} T - P \right) dV \quad (4-134)$$

$$dS = \frac{C_v}{T} dT + \frac{\beta}{\kappa} dV \quad (4-135)$$

Integration of these equations is most common from the saturated-liquid state to the state of compressed liquid at constant T . For example, Eqs. (4-132) and (4-133) in integral form become

$$H = H^{\text{sat}} + \int_{P^{\text{sat}}}^P (1 - \beta T) V dP \quad (4-136)$$

$$S = S^{\text{sat}} - \int_{P^{\text{sat}}}^P \beta V dP \quad (4-137)$$

Again, β and V are weak functions of pressure for liquids, and are often assumed constant at the values for the saturated liquid at temperature T . An alternative treatment of V comes from Eq. (4-131), which for this application can be written

$$V = V^{\text{sat}} \exp[-\kappa(P - P^{\text{sat}})]$$

LIQUID/VAPOR PHASE TRANSITION

The isothermal vaporization of a pure liquid results in a phase change from saturated liquid to saturated vapor at vapor pressure P^{sat} . The

treatment of this transition is facilitated by definition of property changes of vaporization ΔM^{lv} :

$$\Delta M^{\text{lv}} \equiv M^v - M^l \quad (4-138)$$

where M^l and M^v are molar properties for states of saturated liquid and saturated vapor. Some experimental values of the enthalpy change of vaporization ΔH^{lv} , usually called the latent heat of vaporization, are listed in Table 2-150.

The enthalpy change and entropy change of vaporization are directly related:

$$\Delta H^{\text{lv}} = T \Delta S^{\text{lv}} \quad (4-139)$$

This equation follows from Eq. (4-15), because vaporization at the vapor pressure P^{sat} occurs at constant T .

As shown by Smith, Van Ness, and Abbott [*Introduction to Chemical Engineering Thermodynamics*, 7th ed., p. 221, McGraw-Hill, New York (2005)] the heat of vaporization is directly related to the slope of the vapor-pressure curve.

$$\Delta H^{\text{lv}} = T \Delta V^{\text{lv}} \frac{dP^{\text{sat}}}{dT} \quad (4-140)$$

Known as the Clapeyron equation, this exact thermodynamic relation provides the connection between the properties of the liquid and vapor phases.

In application an empirical vapor pressure versus temperature relation is required. The simplest such equation is

$$\ln P^{\text{sat}} = A - \frac{B}{T} \quad (4-141)$$

where A and B are constants for a given chemical species. This equation approximates P^{sat} over its entire temperature range from triple point to critical point. It is also a sound basis for interpolation between reasonably spaced values of T . More satisfactory for general use is the Antoine equation

$$\ln P^{\text{sat}} = A - \frac{B}{T + C} \quad (4-142)$$

The Wagner equation is useful for accurate representation of vapor pressure data over a wide temperature range. It expresses the reduced vapor pressure as a function of reduced temperature

$$\ln P_r^{\text{sat}} = \frac{A\tau + B\tau^{1.5} + C\tau^3 + D\tau^6}{1 - \tau} \quad (4-143)$$

where

$$\tau \equiv 1 - T_r$$

and A , B , C , and D are constants. Values of the constants for either the Wagner equation or the Antoine equation are given for many species by Poling, Prausnitz, and O'Connell [*The Properties of Gases and Liquids*, 5th ed., App. A, McGraw-Hill, New York (2001)].

Latent heats of vaporization are functions of temperature, and experimental values at a particular temperature are often not available. Recourse is then made to approximate methods. *Trouton's rule* of 1884 provides a simple check on whether values calculated by other methods are reasonable:

$$\frac{\Delta H_n^{\text{lv}}}{RT_n} \sim 10$$

Here, T_n is the absolute temperature of the normal boiling point, and ΔH_n^{lv} is the latent heat at this temperature. The units of ΔH_n^{lv} , R , and T_n must be chosen so that $\Delta H_n^{\text{lv}}/RT_n$ is dimensionless.

A much more accurate equation is that of Riedel [*Chem. Ing. Tech.* **26**: 679-683 (1954)]:

$$\frac{\Delta H_n^{\text{lv}}}{RT_n} = \frac{1.092(\ln P_c - 1.013)}{0.930 - T_{r_c}} \quad (4-144)$$

4-14 THERMODYNAMICS

where P_c is the critical pressure in bars and T_r is the reduced temperature at T_r . This equation provides reasonable approximations; errors rarely exceed 5 percent.

Estimates of the latent heat of vaporization of a pure liquid at any temperature from the known value at a single temperature may be based on an experimental value or on a value estimated by Eq. (4-144).

Watson's equation [*Ind. Eng. Chem.* **35**: 398–406 (1943)] has found wide acceptance:

$$\frac{\Delta H_{12}^{lg}}{\Delta H_1^{lg}} = \left(\frac{1 - T_{r2}}{1 - T_{r1}} \right)^{0.38} \quad (4-145)$$

This equation is simple and fairly accurate.

THERMODYNAMICS OF FLOW PROCESSES

The thermodynamics of flow encompasses mass, energy, and entropy balances for open systems, i.e., for systems whose boundaries allow the inflow and outflow of fluids. The common measures of flow are as follows:

Mass flow rate \dot{m} molar flow rate \dot{n} volumetric flow rate q velocity u
Also $\dot{m} = M\dot{n}$ and $q = uA$

where M is molar mass. Mass flow rate is related to velocity by

$$\dot{m} = uA\rho \quad (4-146)$$

where A is the cross-sectional area of a conduit and ρ is mass density. If ρ is molar density, then this equation yields molar flow rate. Flow rates \dot{m} , \dot{n} , and q measure quantity per unit of time. Although velocity u does not represent quantity of flow, it is an important design parameter.

MASS, ENERGY, AND ENTROPY BALANCES FOR OPEN SYSTEMS

Mass and energy balances for an open system are written with respect to a region of space known as a *control volume*, bounded by an imaginary *control surface* that separates it from the surroundings. This surface may follow fixed walls or be arbitrarily placed; it may be rigid or flexible.

Mass Balance for Open Systems Because mass is conserved, the time rate of change of mass within the control volume equals the net rate of flow of mass into the control volume. The flow is positive when directed into the control volume and negative when directed out. The mass balance is expressed mathematically by

$$\frac{dm_{cv}}{dt} + \Delta(\dot{m})_{fs} = 0 \quad (4-147)$$

The operator Δ signifies the difference between exit and entrance flows, and the subscript fs indicates that the term encompasses all flowing streams. When the mass flow rate \dot{m} is given by Eq. (4-146),

$$\frac{dm_{cv}}{dt} + \Delta(\rho uA)_{fs} = 0 \quad (4-148)$$

This form of the mass balance equation is often called the *continuity equation*. For the special case of *steady-state* flow, the control volume contains a constant mass of fluid, and the first term of Eq. (4-148) is zero.

General Energy Balance Because energy, like mass, is conserved, the time rate of change of energy within the control volume equals the net rate of energy transfer into the control volume. Streams flowing into and out of the control volume have associated with them energy in its internal, potential, and kinetic forms, and all contribute to the energy change of the system. Energy may also flow across the control surface as heat and work. Smith, Van Ness, and Abbott [*Introduction to Chemical Engineering Thermodynamics*, 7th ed., pp. 47–48, McGraw-Hill, New York (2005)] show that the general energy balance for flow processes is

$$\frac{d(mU)_{cv}}{dt} + \Delta \left[\left(H + \frac{1}{2}u^2 + zg \right) \dot{m} \right]_{fs} = \dot{Q} + \dot{W} \quad (4-149)$$

The work rate \dot{W} may be of several forms. Most commonly there is shaft work \dot{W}_s . Work may be associated with expansion or contraction of the control volume, and there may be stirring work. The velocity u in the kinetic energy term is the bulk mean velocity as defined by the

equation $u = \dot{m}/\rho A$; z is elevation above a datum level, and g is the local acceleration of gravity.

Energy Balances for Steady-State Flow Processes Flow processes for which the first term of Eq. (4-149) is zero are said to occur at *steady state*. As discussed with respect to the mass balance, this means that the mass of the system within the control volume is constant; it also means that no changes occur with time in the properties of the fluid within the control volume or at its entrances and exits. No expansion of the control volume is possible under these circumstances. The only work of the process is shaft work, and the general energy balance, Eq. (4-149), becomes

$$\Delta \left[\left(H + \frac{1}{2}u^2 + zg \right) \dot{m} \right]_{fs} = \dot{Q} + \dot{W}_s \quad (4-150)$$

Entropy Balance for Open Systems An entropy balance differs from an energy balance in a very important way—*entropy is not conserved*. According to the second law, the entropy changes in the system and surroundings as the result of any process must be positive, with a limiting value of zero for a reversible process. Thus, the entropy changes resulting from the process sum not to zero, but to a positive quantity called the *entropy generation* term. The statement of balance, expressed as rates, is therefore

$$\left\{ \begin{array}{l} \text{Net rate of} \\ \text{change in} \\ \text{entropy of} \\ \text{flowing streams} \end{array} \right\} + \left\{ \begin{array}{l} \text{Time rate of} \\ \text{change of} \\ \text{entropy} \\ \text{in control} \\ \text{volume} \end{array} \right\} + \left\{ \begin{array}{l} \text{Time rate of} \\ \text{change of} \\ \text{entropy in} \\ \text{surroundings} \end{array} \right\} = \left\{ \begin{array}{l} \text{Total rate} \\ \text{of entropy} \\ \text{generation} \end{array} \right\}$$

The equivalent *equation of entropy balance* is

$$\Delta(S\dot{m})_{fs} + \frac{d(mS)_{cv}}{dt} + \frac{dS_{surr}}{dt} = \dot{S}_C \geq 0 \quad (4-151)$$

where \dot{S}_C is the entropy generation term. In accord with the second law, it must be positive, with zero as a limiting value. This equation is the general *rate* form of the entropy balance, applicable at any instant. The three terms on the left are the net rate of gain in entropy of the flowing streams, the time rate of change of the entropy of the fluid contained within the control volume, and the time rate of change of the entropy of the surroundings.

The entropy change of the surroundings results from heat transfer between system and surroundings. Let \dot{Q}_j represent the heat-transfer rate at a particular location on the control surface associated with a surroundings temperature $T_{\sigma,j}$. In accord with Eq. (4-3), the rate of entropy change in the surroundings as a result of this transfer is $-\dot{Q}_j/T_{\sigma,j}$. The minus sign converts \dot{Q}_j , defined with respect to the system, to a heat rate with respect to the surroundings. The third term in Eq. (4-151) is therefore the sum of all such quantities, and Eq. (4-151) can be written

$$\Delta(S\dot{m})_{fs} + \frac{d(mS)_{cv}}{dt} - \sum_j \frac{\dot{Q}_j}{T_{\sigma,j}} = \dot{S}_C \geq 0 \quad (4-152)$$

For any process, the two kinds of irreversibility are (1) those *internal* to the control volume and (2) those resulting from heat transfer across finite temperature differences that may exist between the

TABLE 4-3 Equations of Balance

General equations of balance	Balance equations for steady-flow processes	Balance equations for single-stream steady-flow processes
$\frac{dm_{cv}}{dt} + \Delta(\dot{m})_s = 0$ (4-147)	$\Delta(\dot{m})_s = 0$ (4-153)	$\dot{m}_1 = \dot{m}_2 = \dot{m}$ (4-154)
$\frac{d(mU)_{cv}}{dt} + \Delta\left[\left(H + \frac{1}{2}u^2 + zg\right)\dot{m}\right] = \dot{Q} + \dot{W}$ (4-149)	$\Delta\left[\left(H + \frac{1}{2}u^2 + zg\right)\dot{m}\right] = \dot{Q} + \dot{W}_s$ (4-150)	$\Delta H + \frac{\Delta u^2}{2} + g\Delta z = Q + W_s$ (4-155)
$\frac{d(mS)_{cv}}{dt} + \Delta(S\dot{m})_s - \sum_j \frac{\dot{Q}_j}{T_{\sigma,j}} = \dot{S}_G \geq 0$ (4-152)	$\Delta(S\dot{m})_s - \sum_j \frac{\dot{Q}_j}{T_{\sigma,j}} = \dot{S}_G \geq 0$ (4-156)	$\Delta S - \sum_j \frac{Q_j}{T_{\sigma,j}} = S_G \geq 0$ (4-157)

system and surroundings. In the limiting case where $\dot{S}_G = 0$, the process is *completely reversible*, implying that

- The process is internally reversible within the control volume.
- Heat transfer between the control volume and its surroundings is reversible.

Summary of Equations of Balance for Open Systems Only the most general equations of mass, energy, and entropy balance appear in the preceding sections. In each case important applications require less general versions. The most common restricted case is for steady flow processes, wherein the mass and thermodynamic properties of the fluid within the control volume are not time-dependent. A further simplification results when there is but one entrance and one exit to the control volume. In this event, \dot{m} is the same for both streams, and the equations may be divided through by this rate to put them on the basis of a unit amount of fluid flowing through the control volume. Summarized in Table 4-3 are the basic equations of balance and their important restricted forms.

APPLICATIONS TO FLOW PROCESSES

Duct Flow of Compressible Fluids Thermodynamics provides equations interrelating pressure changes, velocity, duct cross-sectional area, enthalpy, entropy, and specific volume within a flowing stream. Considered here is the adiabatic, steady-state, one-dimensional flow of a compressible fluid in the absence of shaft work and changes in potential energy. The appropriate energy balance is Eq. (4-155). With $Q, W_s,$ and Δz all set equal to zero,

$$\Delta H + \frac{\Delta u^2}{2} = 0$$

In differential form, $dH = -u du$ (4-158)

The continuity equation given by Eq. (4-148) here becomes $d(\rho uA) = d(uA/V) = 0$, whence

$$\frac{dV}{V} - \frac{du}{u} - \frac{dA}{A} = 0$$
 (4-159)

Smith, Abbott, and Van Ness [*Introduction to Chemical Engineering Thermodynamics*, 7th ed., pp. 255–258, McGraw-Hill, New York (2005)] show that these basic equations in combination with Eq. (4-15) and other property relations yield two very general equations

$$V(1 - M^2) \frac{dP}{dx} + T\left(1 + \frac{\beta u^2}{C_p}\right) \frac{dS}{dx} - \frac{u^2}{A} \frac{dA}{dx} = 0$$
 (4-160)

$$u \frac{du}{dx} - T\left(\frac{\beta u^2/C_p + M^2}{1 - M^2}\right) \frac{dS}{dx} + \left(\frac{1}{1 - M^2}\right) \frac{u^2}{A} \frac{dA}{dx} = 0$$
 (4-161)

Mach number M is the ratio of the speed of fluid in the duct to the speed of sound in the fluid. The derivatives in these equations are rates of change with length as the fluid passes through a duct. Equation (4-160) relates the pressure derivative, and Eq. (4-161), the velocity derivative, to the entropy and area derivatives. According to

the second law, the irreversibilities of fluid friction in adiabatic flow cause an entropy increase in the fluid in the direction of flow. In the limit as the flow approaches reversibility, this increase approaches zero. In general, then, $dS/dx \geq 0$.

Pipe Flow For a pipe of constant cross-sectional area, $dA/dx = 0$, and Eqs. (4-160) and (4-161) reduce to

$$\frac{dp}{dx} = -\frac{T}{V} \left(\frac{1 + \beta u^2/C_p}{1 - M^2}\right) \frac{ds}{dx} \quad u \frac{du}{dx} = T \left(\frac{\beta u^2/C_p + M^2}{1 - M^2}\right) \frac{ds}{dx}$$

When flow is subsonic, $M^2 < 1$; all terms on the right in these equations are then positive, and $dP/dx < 0$ and $du/dx > 0$. Pressure therefore decreases and velocity increases in the direction of flow. The velocity increase is, however, limited, because these inequalities would reverse if the velocity were to become supersonic. This is not possible in a pipe of constant cross-sectional area, and the maximum fluid velocity obtainable is the speed of sound, reached at the *exit* of the pipe. Here, dS/dx reaches its limiting value of zero. For a discharge pressure low enough, the flow becomes sonic and lengthening the pipe does not alter this result; the mass rate of flow decreases so that the sonic velocity is still obtained at the outlet of the lengthened pipe.

According to the equations for supersonic pipe flow, pressure increases and velocity decreases in the direction of flow. However, this flow regime is unstable, and a supersonic stream entering a pipe of constant cross section undergoes a compression shock, the result of which is an abrupt and finite increase in pressure and decrease in velocity to a subsonic value.

Nozzles Nozzle flow is quite different from pipe flow. In a properly designed nozzle, its cross-sectional area changes with length in such a way as to make the flow nearly frictionless. The limit is reversible flow, for which the rate of entropy increase is zero. In this event $dS/dx = 0$, and Eqs. (4-160) and (4-161) become

$$\frac{dP}{dx} = \frac{u^2}{VA} \left(\frac{1}{1 - M^2}\right) \frac{dA}{dx} \quad \frac{du}{dx} = -\frac{u}{A} \left(\frac{1}{1 - M^2}\right) \frac{dA}{dx}$$

The characteristics of flow depend on whether the flow is subsonic ($M < 1$) or supersonic ($M > 1$). The possibilities are summarized in Table 4-4. Thus, for subsonic flow in a converging nozzle, the velocity increases and the pressure decreases as the cross-sectional area

TABLE 4-4 Nozzle Characteristics

	Subsonic: $M < 1$		Supersonic: $M > 1$	
	Converging	Diverging	Converging	Diverging
$\frac{dA}{dx}$	-	+	-	+
$\frac{dP}{dx}$	-	+	+	-
$\frac{du}{dx}$	+	-	-	+

4-16 THERMODYNAMICS

diminishes. The maximum possible fluid velocity is the speed of sound, reached at the exit. A converging subsonic nozzle can therefore deliver a constant flow rate into a region of variable pressure.

Supersonic velocities characterize the diverging section of a properly designed converging/diverging nozzle. Sonic velocity is reached at the throat, where $dA/dx = 0$, and a further increase in velocity and decrease in pressure require a diverging cross-sectional area to accommodate the increasing volume of flow. The pressure at the throat must be low enough for the velocity to become sonic. If this is not the case, the diverging section acts as a diffuser—the pressure rises and the velocity decreases in the conventional behavior of subsonic flow in a diverging section.

An analytical expression relating velocity to pressure in an isentropic nozzle is readily derived for an ideal gas with constant heat capacities. Combination of Eqs. (4-15) and (4-159) for isentropic flow gives

$$u du = -V dP$$

Integration, with nozzle entrance and exit conditions denoted by 1 and 2, yields

$$u_2^2 - u_1^2 = -2 \int_{P_1}^{P_2} V dP = \frac{2\gamma P_1 V_1}{\gamma - 1} \left[1 - \left(\frac{P_2}{P_1} \right)^{(\gamma-1)/\gamma} \right] \quad (4-162)$$

where the final term is obtained upon elimination of V by $PV^\gamma = \text{const}$, an equation valid for ideal gases with constant heat capacities. Here, $\gamma \equiv C_p/C_v$.

Throttling Process Fluid flowing through a restriction, such as an orifice, without appreciable change in kinetic or potential energy undergoes a finite pressure drop. This *throttling process* produces no shaft work, and in the absence of heat transfer, Eq. (4-155) reduces to $\Delta H = 0$ or $H_2 = H_1$. The process therefore occurs at constant enthalpy.

The temperature of an ideal gas is not changed by a throttling process, because its enthalpy depends on temperature only. For most real gases at moderate conditions of T and P , a reduction in pressure at constant enthalpy results in a decrease in temperature, although the effect is usually small. Throttling of a wet vapor to a sufficiently low pressure causes the liquid to evaporate and the vapor to become superheated. This results in a considerable temperature drop because of the evaporation of liquid.

If a saturated liquid is throttled to a lower pressure, some of the liquid vaporizes or *flashes*, producing a mixture of saturated liquid and saturated vapor at the lower pressure. Again, the large temperature drop results from evaporation of liquid.

Turbines (Expanders) High-velocity streams from nozzles impinging on blades attached to a rotating shaft form a turbine (or expander) through which vapor or gas flows in a steady-state expansion process which converts internal energy of a high-pressure stream into shaft work. The motive force may be provided by steam (turbine) or by a high-pressure gas (expander).

In any properly designed turbine, heat transfer and changes in potential and kinetic energy are negligible. Equation (4-155) therefore reduces to

$$W_s = \Delta H = H_2 - H_1 \quad (4-163)$$

The rate form of this equation is

$$\dot{W}_s = \dot{m} \Delta H = \dot{m}(H_2 - H_1) \quad (4-164)$$

When inlet conditions T_1 and P_1 and discharge pressure P_2 are known, the value of H_1 is fixed. In Eq. (4-163) both H_2 and W_s are unknown, and the energy balance alone does not allow their calculation. However, if the fluid expands *reversibly and adiabatically*, i.e., isentropically, in the turbine, then $S_2 = S_1$. This second equation establishes the final state of the fluid and allows calculation of H_2 . Equation (4-164) then gives the isentropic work:

$$W_s(\text{isentropic}) = (\Delta H)_s \quad (4-165)$$

The absolute value $|W_s(\text{isentropic})|$ is the *maximum* work that can be produced by an adiabatic turbine with given inlet conditions and given

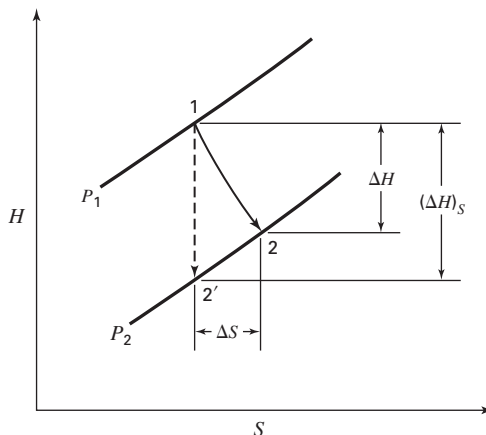


FIG. 4-2 Adiabatic expansion process in a turbine or expander. [Smith, Van Ness, and Abbott, *Introduction to Chemical Engineering Thermodynamics*, 7th ed., p. 269, McGraw-Hill, New York (2005).]

discharge pressure. Because the actual expansion process is irreversible, *turbine efficiency* is defined as

$$\eta \equiv \frac{W_s}{W_s(\text{isentropic})}$$

where W_s is the actual shaft work. By Eqs. (4-163) and (4-165),

$$\eta = \frac{\Delta H}{(\Delta H)_s} \quad (4-166)$$

Values of η usually range from 0.7 to 0.8.

The HS diagram of Fig. 4-2 compares the path of an actual expansion in a turbine with that of an isentropic expansion for the same intake conditions and the same discharge pressure. The isentropic path is the dashed vertical line from point 1 at intake pressure P_1 to point 2' at P_2 . The irreversible path (solid line) starts at point 1 and terminates at point 2 on the isobar for P_2 . The process is adiabatic, and irreversibilities cause the path to be directed toward increasing entropy. The greater the irreversibility, the farther point 2 lies to the right on the P_2 isobar, and the lower the value of η .

Compression Processes Compressors, pumps, fans, blowers, and vacuum pumps are all devices designed to bring about pressure increases. Their energy requirements for steady-state operation are of interest here. Compression of gases may be accomplished in rotating equipment (high-volume flow) or for high pressures in cylinders with reciprocating pistons. The energy equations are the same; indeed, based on the same assumptions, they are the same as for turbines or expanders. Thus, Eqs. (4-159) through (4-161) apply to adiabatic compression.

The isentropic work of compression, as given by Eq. (4-165), is the *minimum* shaft work required for compression of a gas from a given initial state to a given discharge pressure. A compressor efficiency is defined as

$$\eta \equiv \frac{W_s(\text{isentropic})}{W_s}$$

In view of Eqs. (4-163) and (4-165), this becomes

$$\eta \equiv \frac{(\Delta H)_s}{\Delta H} \quad (4-167)$$

Compressor efficiencies are usually in the range of 0.7 to 0.8.

The compression process is shown on an HS diagram in Fig. 4-3. The vertical dashed line rising from point 1 to point 2' represents the reversible adiabatic (isentropic) compression process from P_1 to P_2 .

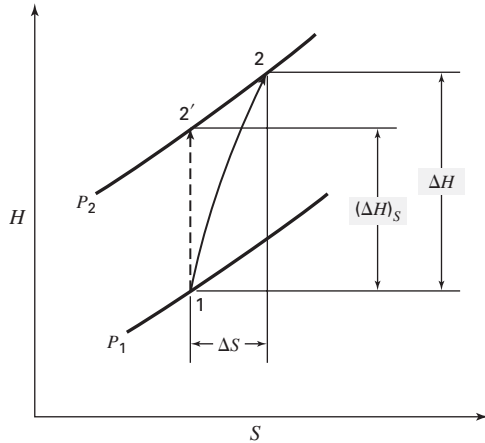


FIG. 4-3 Adiabatic compression process. [Smith, Van Ness, and Abbott, Introduction to Chemical Engineering Thermodynamics, 7th ed., p. 274, McGraw-Hill, New York (2005).]

The actual irreversible compression process follows the solid line from point 1 upward and to the right in the direction of increasing entropy, terminating at point 2. The more irreversible the process, the farther this point lies to the right on the P_2 isobar, and the lower the efficiency η of the process.

Liquids are moved by pumps, usually by rotating equipment. The same equations apply to adiabatic pumps as to adiabatic compressors. Thus, Eqs. (4-163) through (4-165) and Eq. (4-167) are valid. However, application of Eq. (4-163) requires values of the enthalpy of compressed (subcooled) liquids, and these are seldom available. The fundamental property relation, Eq. (4-15), provides an alternative. For an isentropic process,

$$dH = V dP \quad (\text{constant } S)$$

Combining this with Eq. (4-165) yields

$$W_s(\text{isentropic}) = (\Delta H)_S = \int_{P_1}^{P_2} V dP$$

The usual assumption for liquids (at conditions well removed from the critical point) is that V is independent of P . Integration then gives

$$W_s(\text{isentropic}) = (\Delta H)_S = V(P_2 - P_1) \quad (4-168)$$

Also useful are Eqs. (4-132) and (4-133). Because temperature changes in the pumped fluid are very small and because the properties of liquids are insensitive to pressure (again at conditions not close to the critical point), these equations are usually integrated on the assumption that C_p , V , and β are constant, usually at initial values. Thus, to a good approximation

$$\Delta H = C_p \Delta T + V(1 - \beta T) \Delta P \quad (4-169)$$

$$\Delta S = C_p \ln \frac{T_2}{T_1} - \beta V \Delta P \quad (4-170)$$

Example 1: LNG Vaporization and Compression A port facility for unloading liquefied natural gas (LNG) is under consideration. The LNG arrives by ship, stored as saturated liquid at 115 K and 1.325 bar, and is unloaded at the rate of 450 kg s⁻¹. It is proposed to vaporize the LNG with heat discarded from a heat engine operating between 300 K, the temperature of atmospheric air, and 115 K, the temperature of the vaporizing LNG. The saturated-vapor LNG so produced is compressed adiabatically to 20 bar, using the work produced by the heat engine to supply part of the compression work. Estimate the work to be supplied from an external source.

For estimation purposes we need not be concerned with the design of the heat engine, but assume that a suitable engine can be built to deliver 30 percent of the work of a Carnot engine operating between the temperatures of 300 and 115 K. The equations that apply to Carnot engines can be found in any thermodynamics text.

$$\text{By the first law:} \quad |W| = |Q_H| - |Q_C|$$

$$\text{By the second law:} \quad \frac{|Q_H|}{|Q_C|} = \frac{T_H}{T_C}$$

$$\text{In combination:} \quad |W| = |Q_C| \left(\frac{T_H}{T_C} - 1 \right)$$

Here, $|W|$ is the work produced by the Carnot engine; $|Q_C|$ is the heat transferred at the cold temperature, i.e., to vaporize the LNG; T_H and T_C are the hot and cold temperatures of the heat reservoirs between which the heat engine operates, or 300 and 115 K, respectively. LNG is essentially pure methane, and enthalpy values from Table 2-281 of the Seventh Edition of *Perry's Chemical Engineers' Handbook* provide its heat of vaporization:

$$\Delta H^{lv} = H^v - H^l = 802.5 - 297.7 = 504.8 \text{ kJ kg}^{-1}$$

For a flow rate of 450 kg s⁻¹,

$$|Q_C| = (450)(504.8) = 227,160 \text{ kJ s}^{-1}$$

The equation for work gives

$$|W| = (227,160) \left(\frac{300}{115} - 1 \right) = 3.654 \times 10^5 \text{ kJ s}^{-1} = 3.654 \times 10^5 \text{ kW}$$

This is the reversible work of a Carnot engine. The assumption is that the actual power produced is 30 percent of this, or 1.096 × 10⁵ kW.

The enthalpy and entropy of saturated vapor at 115 K and 1.325 bar are given in Table 2-281 of the Seventh Edition of *Perry's* as

$$H^v = 802.5 \text{ kJ kg}^{-1} \quad \text{and} \quad S^v = 9.436 \text{ kJ kg}^{-1} \text{ K}^{-1}$$

Isentropic compression of saturated vapor at 1.325 to 20 bar produces superheated vapor with an entropy of 9.436 kJ kg⁻¹ K⁻¹. Interpolation in Table 2-282 at 20 bar yields an enthalpy of $H = 1026.2$ kJ kg⁻¹ at 234.65 K. The enthalpy change of isentropic compression is then

$$\Delta H_S = 1026.2 - 802.5 = 223.7 \text{ kJ kg}^{-1}$$

For a compressor efficiency of 75 percent, the actual enthalpy change of compression is

$$\Delta H = \frac{\Delta H_S}{\eta} = \frac{223.7}{0.75} = 298.3 \text{ kJ kg}^{-1}$$

The actual enthalpy of superheated LNG at 20 bar is then

$$H = 802.5 + 298.3 = 1100.8 \text{ kJ kg}^{-1}$$

Interpolation in Table 2-282 of the Seventh Edition of *Perry's* indicates an actual temperature of 265.9 K for the compressed LNG, which is quite suitable for its entry into the distribution system.

The work of compression is

$$|W| = m \Delta H = (450 \text{ kg s}^{-1})(298.3 \text{ kJ kg}^{-1}) = 1.342 \times 10^5 \text{ kJ s}^{-1} = 1.342 \times 10^5 \text{ kW}$$

The estimated power which must be supplied from an external source is

$$\dot{W} = 1.342 \times 10^5 - 1.096 \times 10^5 = 24,600 \text{ kW}$$

SYSTEMS OF VARIABLE COMPOSITION

The composition of a system may vary because the system is open or because of chemical reactions even in a closed system. The equations developed here apply regardless of the cause of composition changes.

PARTIAL MOLAR PROPERTIES

For a homogeneous PVT system comprised of any number of chemical species, let symbol M represent the molar (or unit-mass) value of an

extensive thermodynamic property, say, U , H , S , A , or G . A total-system property is then nM , where $n = \sum_i n_i$ and i is the index identifying chemical species. One might expect the solution property M to be related solely to the properties M_i of the pure chemical species which comprise the solution. However, no such generally valid relation is known, and the connection must be established experimentally for every specific system.

Although the chemical species which make up a solution do not have their own individual properties, a solution property may be arbitrarily

4-18 THERMODYNAMICS

apportioned among the individual species. Once an apportioning recipe is adopted, the assigned property values are quite logically treated as though they were indeed properties of the individual species in solution, and reasoning on this basis leads to valid conclusions.

For a homogeneous PVT system, postulate 5 requires that

$$nM = \mathcal{M}(T, P, n_1, n_2, n_3, \dots)$$

The total differential of nM is therefore

$$d(nM) = \left[\frac{\partial(nM)}{\partial T} \right]_{P,n} dT + \left[\frac{\partial(nM)}{\partial P} \right]_{T,n} dP + \sum_i \left[\frac{\partial(nM)}{\partial n_i} \right]_{T,P,n_j} dn_i$$

where subscript n indicates that all mole numbers n_i are held constant, and subscript n_j signifies that all mole numbers are held constant except the i th. This equation may also be written

$$d(nM) = n \left(\frac{\partial M}{\partial T} \right)_{P,x} dT + n \left(\frac{\partial M}{\partial P} \right)_{T,x} dP + \sum_i \left[\frac{\partial(nM)}{\partial n_i} \right]_{T,P,n_j} dn_i$$

where subscript x indicates that all mole fractions are held constant. The derivatives in the summation are called *partial molar properties*. They are given the generic symbol \bar{M}_i and are defined by

$$\bar{M}_i \equiv \left[\frac{\partial(nM)}{\partial n_i} \right]_{T,P,n_j} \quad (4-171)$$

The basis for calculation of partial properties from solution properties is provided by this equation. Moreover,

$$d(nM) = n \left(\frac{\partial M}{\partial T} \right)_{P,x} dT + n \left(\frac{\partial M}{\partial P} \right)_{T,x} dP + \sum_i \bar{M}_i dn_i \quad (4-172)$$

This equation, valid for any equilibrium phase, either closed or open, attributes changes in total property nM to changes in T and P and to mole-number changes resulting from mass transfer or chemical reaction.

The following are mathematical identities:

$$d(nM) = n dM + M dn \quad dn_i = d(x_i n) = x_i dn + n dx_i$$

Combining these expressions with Eq. (4-172) and collecting like terms give

$$\left[dM - \left(\frac{\partial M}{\partial T} \right)_{P,x} dT - \left(\frac{\partial M}{\partial P} \right)_{T,x} dP - \sum_i \bar{M}_i dx_i \right] n + \left[M - \sum_i \bar{M}_i x_i \right] dn = 0$$

Because n and dn are independent and arbitrary, the terms in brackets must separately be zero, whence

$$dM = \left(\frac{\partial M}{\partial T} \right)_{P,x} dT + \left(\frac{\partial M}{\partial P} \right)_{T,x} dP + \sum_i \bar{M}_i dx_i \quad (4-173)$$

and

$$M = \sum_i x_i \bar{M}_i \quad (4-174)$$

The first of these equations is merely a special case of Eq. (4-172); however, Eq. (4-174) is a vital new relation. Known as the *summability equation*, it provides for the calculation of solution properties from partial properties, a purpose opposite to that of Eq. (4-171). Thus a solution property apportioned according to the recipe of Eq. (4-171) may be recovered simply by adding the properties attributed to the individual species, each weighted by its mole fraction in solution. The equations for partial molar properties are valid also for partial specific properties, in which case m replaces n and $\{x_i\}$ are mass fractions. Equation (4-171) applied to the definitions of Eqs. (4-8) through (4-10) yields the partial-property relations

$$\bar{H}_i = \bar{U}_i + P\bar{V}_i \quad \bar{A}_i = \bar{U}_i - T\bar{S}_i \quad \bar{G}_i = \bar{H}_i - T\bar{S}_i$$

These equations illustrate the parallelism that exists between the equations for a constant-composition solution and those for the corresponding partial properties. This parallelism exists whenever the

solution properties in the parent equation are related linearly (in the algebraic sense).

Gibbs-Duhem Equation Differentiation of Eq. (4-174) yields

$$dM = \sum_i x_i d\bar{M}_i + \sum_i \bar{M}_i dx_i$$

Because this equation and Eq. (4-173) are both valid in general, their right sides can be equated, yielding

$$\left(\frac{\partial M}{\partial T} \right)_{P,x} dT + \left(\frac{\partial M}{\partial P} \right)_{T,x} dP - \sum_i x_i d\bar{M}_i = 0 \quad (4-175)$$

This general result, the Gibbs-Duhem equation, imposes a constraint on how the partial properties of any phase may vary with temperature, pressure, and composition. For the special case where T and P are constant,

$$\sum_i x_i d\bar{M}_i = 0 \quad (\text{constant } T, P) \quad (4-176)$$

Symbol M may represent the molar value of any extensive thermodynamic property, say, V , U , H , S , or G . When $M \equiv H$, the derivatives $(\partial H/\partial H)_P$ and $(\partial H/\partial P)_T$ are given by Eqs. (4-28) and (4-29), and Eqs. (4-173), (4-174), and (4-175) specialize to

$$dH = C_P dT + \left[V - T \left(\frac{\partial V}{\partial T} \right)_{P,x} \right] dP + \sum_i \bar{H}_i dx_i \quad (4-177)$$

$$H = \sum_i x_i \bar{H}_i \quad (4-178)$$

$$C_P dT + \left[V - T \left(\frac{\partial V}{\partial T} \right)_{P,x} \right] dP - \sum_i x_i d\bar{H}_i = 0 \quad (4-179)$$

Similar equations are readily derived when M takes on other identities.

Equation (4-171), which defines a partial molar property, provides a general means by which partial-property values may be determined. However, for a *binary* solution an alternative method is useful. Equation (4-174) for a binary solution is

$$M = x_1 \bar{M}_1 + x_2 \bar{M}_2$$

Moreover, the Gibbs-Duhem equation for a solution at given T and P , Eq. (4-176), becomes

$$x_1 d\bar{M}_1 + x_2 d\bar{M}_2 = 0$$

These two equations combine to yield

$$\bar{M}_1 = M + x_2 \frac{dM}{dx_1} \quad (4-180a)$$

$$\bar{M}_2 = M - x_1 \frac{dM}{dx_1} \quad (4-180b)$$

Thus for a binary solution, the partial properties are given directly as functions of composition for given T and P . For multicomponent solutions such calculations are complex, and direct use of Eq. (4-171) is appropriate.

Partial Molar Equation-of-State Parameters The parameters in equations of state as applied to mixtures are related to composition by mixing rules. For the second virial coefficient

$$B = \sum_i \sum_j y_i y_j B_{ij} \quad (4-60)$$

The partial molar second virial coefficient is by definition

$$\bar{B}_i \equiv \left[\frac{\partial(nB)}{\partial n_i} \right]_{T,n_j} \quad (4-181)$$

Because B is independent of P , this is in accord with Eq. (4-171). These two equations lead through derivation to useful expressions for \bar{B}_i , as shown in detail by Van Ness and Abbott [*Classical Thermodynamics of Nonelectrolyte Solutions: With Applications to Phase*

Equilibria, pp. 137–140, McGraw-Hill, New York (1982)]. The simplest result is

$$\bar{B} = 2 \sum_k y_k B_{ki} - B \quad (4-182)$$

An analogous expression follows from Eq. (4-114) for parameter a in the generic cubic equation of state given by Eqs. (4-100), (4-103), and (4-104):

$$\bar{a}_i = 2 \sum_k y_k a_{ki} - a \quad (4-183)$$

This expression is independent of the combining rule [e.g., Eq. (4-114)] used for a_{ki} . For the *linear* mixing rule of Eq. (4-113) for b , the result of derivation is simply $b_i = b_i$.

Partial Molar Gibbs Energy Implicit in Eq. (4-13) is the relation

$$\mu_i = \left[\frac{\partial(nG)}{\partial n_i} \right]_{T,P,n_j}$$

Comparison with Eq. (4-171) indicates the following identity:

$$\mu_i = \bar{G}_i \quad (4-184)$$

The reciprocity relation for an exact differential applied to Eq. (4-13) produces not only the Maxwell relation, Eq. (4-21), but also two other useful equations:

$$\left(\frac{\partial \mu_i}{\partial P} \right)_{T,n} = \left[\frac{\partial(nV)}{\partial n_i} \right]_{T,P,n_j} = \bar{V}_i \quad (4-185)$$

$$\left(\frac{\partial \mu_i}{\partial T} \right)_{P,n} = - \left[\frac{\partial(nS)}{\partial n_i} \right]_{T,P,n_j} = -\bar{S}_i \quad (4-186)$$

Because $\mu = f(T, P)$,

$$d\mu_i = d\bar{G}_i = \left(\frac{\partial \mu_i}{\partial T} \right)_{P,n} dT + \left(\frac{\partial \mu_i}{\partial P} \right)_{T,n} dP$$

$$\text{and} \quad d\bar{G}_i = -\bar{S}_i dT + \bar{V}_i dP \quad (4-187)$$

Similarly, in view of Eqs. (4-14), (4-15), and (4-16),

$$d\bar{U}_i = T d\bar{S}_i - P d\bar{V}_i \quad (4-188)$$

$$d\bar{H}_i = T d\bar{S}_i + \bar{V}_i dP \quad (4-189)$$

$$d\bar{A}_i = -\bar{S}_i dT - P d\bar{V}_i \quad (4-190)$$

These equations again illustrate the fact that for every equation providing a *linear* relation among the thermodynamic properties of a *constant-composition* solution there exists a parallel relationship for the partial properties of the species in solution.

The following equation is a mathematical identity:

$$d \left(\frac{nG}{RT} \right) \equiv \frac{1}{RT} d(nG) - \frac{nG}{RT^2} dT$$

Substitution for $d(nG)$ by Eq. (4-13), with $\mu_i = \bar{G}_i$, and for G by Eq. (4-10) gives, after algebraic reduction,

$$d \left(\frac{nG}{RT} \right) = \frac{nV}{RT} dP - \frac{nH}{RT^2} dT + \sum_i \frac{\bar{G}_i}{RT} dn_i \quad (4-191)$$

This result is a useful alternative to the fundamental property relation given by Eq. (4-13). All terms in this equation have units of moles; moreover, the enthalpy rather than the entropy appears on the right side.

SOLUTION THERMODYNAMICS

Ideal Gas Mixture Model The ideal gas mixture model is useful because it is molecularly based, is analytically simple, is realistic in the

limit of zero pressure, and provides a conceptual basis upon which to build the structure of solution thermodynamics. Smith, Van Ness, and Abbott [*Introduction to Chemical Engineering Thermodynamics*, 7th ed., pp. 391–394, McGraw-Hill, New York (2005)] develop the following property relations for the ideal gas model.

$$\bar{V}_i^{ig} = V_i^{ig} = \frac{RT}{P} \quad (4-192)$$

Because the enthalpy is independent of pressure,

$$\bar{H}_i^{ig} = H_i^{ig} \quad (4-193)$$

where S_i^{ig} is evaluated at the *mixture* T and P . The entropy of an ideal gas *does* depend on pressure, and here

$$\bar{S}_i^{ig} = S_i^{ig} - R \ln y_i \quad (4-194)$$

where S_i^{ig} is evaluated at the mixture T and P .

From the definition of the Gibbs energy, $\bar{G}_i^{ig} = \bar{H}_i^{ig} - T\bar{S}_i^{ig}$. In combination with Eqs. (4-193) and (4-194), this becomes

$$\bar{G}_i^{ig} = H_i^{ig} - TS_i^{ig} + RT \ln y_i$$

$$\text{or} \quad \mu_i^{ig} \equiv \bar{G}_i^{ig} = G_i^{ig} + RT \ln y_i \quad (4-195)$$

Elimination of G_i^{ig} from this equation is accomplished through Eq. (4-17), written for pure species i as an ideal gas:

$$dG_i^{ig} = V_i^{ig} dP = \frac{RT}{P} dP = RT d \ln P \quad (\text{constant } T)$$

$$\text{Integration gives} \quad G_i^{ig} = \Gamma_i(T) + RT \ln P \quad (4-196)$$

where integration constant $\Gamma_i(T)$ is a function of temperature only. Equation (4-195) now becomes

$$\mu_i^{ig} = \bar{G}_i^{ig} = \Gamma_i(T) + RT \ln(y_i P) \quad (4-197)$$

$$\text{By Eq. (4-172)} \quad G^{id} = \sum_i y_i \Gamma_i(T) + RT \sum_i \ln(y_i P) \quad (4-198)$$

A dimensional ambiguity is apparent with Eqs. (4-196) through (4-198) in that P has units, whereas $\ln P$ must be dimensionless. In practice this is of no consequence, because only *differences* in Gibbs energy appear, along with *ratios* of the quantities with units of pressure in the arguments of the logarithm. Consistency in the units of pressure is, of course, required.

Fugacity and Fugacity Coefficient The chemical potential μ_i plays a vital role in both phase and chemical reaction equilibria. However, the chemical potential exhibits certain unfortunate characteristics that discourage its use in the solution of practical problems. The Gibbs energy, and hence μ_i , is defined in relation to the internal energy and entropy, both primitive quantities for which absolute values are unknown. Moreover, μ_i approaches negative infinity when either P or y_i approaches zero. While these characteristics do not preclude the use of chemical potentials, the application of equilibrium criteria is facilitated by introduction of the *fugacity*, a quantity that takes the place of μ_i but that does not exhibit its less desirable characteristics.

The origin of the fugacity concept resides in Eq. (4-196), an equation valid only for pure species i in the ideal gas state. For a *real* fluid, an analogous equation is written as

$$G_i \equiv \Gamma_i(T) + RT \ln f_i \quad (4-199)$$

in which a new property f_i replaces the pressure P . This equation serves as a partial definition of the *fugacity* f_i .

Subtraction of Eq. (4-196) from Eq. (4-199), both written for the same temperature and pressure, gives

$$G_i - G_i^{ig} = RT \ln \frac{f_i}{P}$$

4-20 THERMODYNAMICS

According to the definition of Eq. (4-40), $G_i - G_i^{ig}$ is the residual Gibbs energy G_i^R . The dimensionless ratio f_i/P is another new property called the *fugacity coefficient* ϕ_i . Thus,

$$G_i^R = RT \ln \phi_i \quad (4-200)$$

where

$$\phi_i \equiv \frac{f_i}{P} \quad (4-201)$$

The definition of fugacity is completed by setting the ideal gas state fugacity of pure species i equal to its pressure, $f_i^{ig} = P$. Thus for the special case of an ideal gas, $G_i^R = 0$, $\phi_i = 1$, and Eq. (4-196) is recovered from Eq. (4-199).

The definition of the fugacity of a species in solution is parallel to the definition of the pure-species fugacity. An equation analogous to the ideal gas expression, Eq. (4-197), is written for species i in a fluid mixture

$$\mu_i \equiv \Gamma_i(T) + RT \ln \hat{f}_i \quad (4-202)$$

where the partial pressure $y_i P$ is replaced by \hat{f}_i , the fugacity of species i in solution. Because it is not a partial property, it is identified by a circumflex rather than an overbar.

Subtracting Eq. (4-197) from Eq. (4-202), both written for the same temperature, pressure, and composition, yields

$$\mu_i - \mu_i^{ig} = RT \ln \frac{\hat{f}_i}{y_i P}$$

The residual Gibbs energy of a mixture is defined by $G^R \equiv G - G^{ig}$, and the analogous definition of a partial molar residual Gibbs energy is $G_i^R \equiv G_i - G_i^{ig} = \mu_i - \mu_i^{ig}$. Therefore

$$\overline{G}_i^R = RT \ln \hat{\phi}_i \quad (4-203)$$

where by definition

$$\hat{\phi}_i \equiv \frac{\hat{f}_i}{y_i P} \quad (4-204)$$

The dimensionless ratio $\hat{\phi}_i$ is called the *fugacity coefficient of species i in solution*.

Equation (4-203) is the analog of Eq. (4-200), which relates ϕ_i to G_i^R . For an ideal gas, G_i^R is necessarily zero; therefore $\hat{\phi}_i^{ig} = 1$ and $\hat{f}_i^{ig} = y_i P$. Thus the fugacity of species i in an ideal gas mixture is equal to its partial pressure.

Evaluation of Fugacity Coefficients Combining Eq. (4-200) with Eq. (4-45) gives

$$\ln \phi = \frac{G^R}{RT} = \int_0^P (Z - 1) \frac{dP}{P} \quad (4-205)$$

Subscript i is omitted, with the understanding that ϕ here is for a pure species. Clearly, all correlations for G^R/RT are also correlations for $\ln \phi$.

Equation (4-200) with Eqs. (4-48) and (4-73) yields

$$\ln \phi = \int_0^{P_r} (Z - 1) \frac{dP_r}{P_r} = (B^0 + \omega B^1) \frac{P_r}{T_r} \quad (4-206)$$

This equation, used in conjunction with Eqs. (4-77) and (4-78), provides a useful generalized correlation for the fugacity coefficients of pure species.

A more comprehensive generalized correlation results from Eqs. (4-200) and (4-116):

$$\ln \phi = \int_0^{P_r} (Z^0 - 1) \frac{dP_r}{P_r} + \omega \int_0^{P_r} Z^1 \frac{dP_r}{P_r}$$

An alternative form is $\ln \phi = \ln \phi^0 + \omega \ln \phi^1$ (4-207)

where $\ln \phi^0 \equiv \int_0^{P_r} (Z^0 - 1) \frac{dP_r}{P_r}$ and $\ln \phi^1 \equiv \int_0^{P_r} Z^1 \frac{dP_r}{P_r}$

By Eq. (4-207), $\phi = (\phi^0)(\phi^1)^\omega$ (4-208)

Correlations may therefore be presented for ϕ^0 and ϕ^1 , as was done by Lee and Kesler [AIChE J. 21: 510-527 (1975)].

Ideal Solution Model The ideal gas model is useful as a standard of comparison for real gas behavior. This is formalized through residual properties. The *ideal solution* is similarly useful as a standard to which real solution behavior may be compared.

The partial molar Gibbs energy or chemical potential of species i in an ideal gas mixture is given by Eq. (4-195), written as

$$\mu_i^{ig} = \overline{G}_i^{ig} = G_i^{ig}(T, P) + RT \ln y_i$$

This equation takes on new meaning when $G_i^{ig}(T, P)$ is replaced by $G_i(T, P)$, the Gibbs energy of pure species i in its *real physical state* of gas, liquid, or solid at the mixture T and P . The ideal solution is therefore *defined* as one for which

$$\mu_i^{id} = \overline{G}_i^{id} \equiv G_i(T, P) + RT \ln x_i \quad (4-209)$$

where superscript *id* denotes an ideal solution property and x_i represents the mole fraction because application is usually to liquids.

This equation is the basis for development of expressions for all other thermodynamic properties of an ideal solution. Equations (4-185) and (4-186), applied to an ideal solution with μ_i replaced by \overline{G}_i , are written as

$$\overline{V}_i^{id} = \left(\frac{\partial \overline{G}_i^{id}}{\partial P} \right)_{T,x} \quad \text{and} \quad \overline{S}_i^{id} = - \left(\frac{\partial \overline{G}_i^{id}}{\partial T} \right)_{P,x}$$

Differentiation of Eq. (4-209) yields

$$\left(\frac{\partial \overline{G}_i^{id}}{\partial P} \right)_{T,x} = \left(\frac{\partial G_i}{\partial P} \right)_T \quad \text{and} \quad \left(\frac{\partial \overline{G}_i^{id}}{\partial T} \right)_{P,x} = \left(\frac{\partial G_i}{\partial T} \right)_P + R \ln x_i$$

Equation (4-17) implies that

$$\left(\frac{\partial G_i}{\partial P} \right)_T = V_i \quad \text{and} \quad \left(\frac{\partial G_i}{\partial T} \right)_P = -S_i$$

In combination these sets of equations provide

$$\overline{V}_i^{id} = V_i \quad (4-210)$$

and $\overline{S}_i^{id} = S_i - R \ln x_i$ (4-211)

Because $\overline{H}_i^{id} = \overline{G}_i^{id} + T \overline{S}_i^{id}$, substitutions by Eqs. (4-209) and (4-211) yield

$$\overline{H}_i^{id} = H_i \quad (4-212)$$

The summability relation, Eq. (4-174), written for the special case of an ideal solution, may be applied to Eqs. (4-209) through (4-212):

$$G^{id} = \sum_i x_i G_i + RT \sum_i x_i \ln x_i \quad (4-213)$$

$$V^{id} = \sum_i x_i V_i \quad (4-214)$$

$$S^{id} = \sum_i x_i S_i - R \sum_i x_i \ln x_i \quad (4-215)$$

$$H^{id} = \sum_i x_i H_i \quad (4-216)$$

A simple equation for the fugacity of a species in an ideal solution follows from Eq. (4-209). For the special case of species i in an ideal solution, Eq. (4-202) becomes

$$\mu_i^{id} = \overline{G}_i^{id} = \Gamma_i(T) + RT \ln \hat{f}_i^{id}$$

When this equation and Eq. (4-199) are combined with Eq. (4-209), $\Gamma_i(T)$ is eliminated, and the resulting expression reduces to

$$\hat{f}_i^{id} = x_i f_i \quad (4-217)$$

This equation, known as the *Lewis-Randall rule*, shows that the fugacity of each species in an ideal solution is proportional to its mole fraction; the proportionality constant is the fugacity of pure species i in the same physical state as the solution and at the same T and P . Division of both sides of Eq. (4-217) by $x_i P$ and substitution of $\hat{\phi}_i^{id}$ for $\hat{f}_i^{id}/x_i P$ [Eq. (4-204)] and of ϕ_i for f_i/P [Eq. (4-201)] give the alternative form

$$\hat{\phi}_i^{id} = \phi_i \quad (4-218)$$

Thus the fugacity coefficient of species i in an ideal solution equals the fugacity coefficient of *pure* species i in the same physical state as the solution and at the same T and P .

Ideal solution behavior is often approximated by solutions comprised of molecules not too different in size and of the same chemical nature. Thus, a mixture of isomers conforms very closely to ideal solution behavior. So do mixtures of adjacent members of a homologous series.

Excess Properties An excess property M^E is defined as the difference between the actual property value of a solution and the value it would have as an ideal solution at the same T , P , and composition. Thus,

$$M^E \equiv M - M^{id} \quad (4-219)$$

where M represents the molar (or unit-mass) value of any extensive thermodynamic property (say, V , U , H , S , G). This definition is analogous to the definition of a residual property as given by Eq. (4-40). However, excess properties have no meaning for pure species, whereas residual properties exist for pure species as well as for mixtures. Partial molar excess properties \bar{M}_i^E are defined analogously:

$$\bar{M}_i^E \equiv \bar{M}_i - \bar{M}_i^{id} \quad (4-220)$$

Of particular interest is the partial molar excess Gibbs energy. Equation (4-202) may be written as

$$\bar{G}_i = \Gamma_i(T) + RT \ln \hat{f}_i$$

In accord with Eq. (4-217) for an ideal solution, this becomes

$$\bar{G}_i^{id} = \Gamma_i(T) + RT \ln x_i f_i$$

By difference

$$\bar{G}_i - \bar{G}_i^{id} = RT \ln \frac{\hat{f}_i}{x_i f_i}$$

The left side is the partial excess Gibbs energy \bar{G}_i^E ; the dimensionless ratio $\hat{f}_i/x_i f_i$ on the right is the *activity coefficient of species i in solution*, given the symbol γ_i and *by definition*,

$$\gamma_i \equiv \frac{\hat{f}_i}{x_i f_i} \quad (4-221)$$

Thus,

$$\bar{G}_i^E = RT \ln \gamma_i \quad (4-222)$$

Comparison with Eq. (4-203) shows that Eq. (4-222) relates γ_i to \bar{G}_i^E exactly as Eq. (4-203) relates $\hat{\phi}_i$ to \bar{G}_i^R . For an ideal solution, $\bar{G}_i^E = 0$, and therefore $\gamma_i = 1$.

Property Changes of Mixing A property change of mixing is defined by

$$\Delta M \equiv M - \sum_i x_i M_i \quad (4-223)$$

where M represents a molar thermodynamic property of a homogeneous solution and M_i is the molar property of pure species i at the T and P of the solution and in the same physical state. Applications are usually to liquids.

Each of Eqs. (4-213) through (4-216) is an expression for an ideal solution property, and each may be combined with the defining equation for an excess property [Eq. (4-219)], yielding the equations of the first column of Table 4-5. In view of Eq. (4-223) these may be written as shown in the second column of Table 4-5, where ΔG , ΔV ,

ΔS , and ΔH are the Gibbs energy change of mixing, the volume change of mixing, the entropy change of mixing, and the enthalpy change of mixing. For an ideal solution, each excess property is zero, and for this special case the equations reduce to those shown in the third column of Table 4-5.

Property changes of mixing and excess properties are easily calculated one from the other. The most common property changes of mixing are the volume change of mixing ΔV and the enthalpy change of mixing ΔH , commonly called the *heat of mixing*. These properties are identical to the corresponding excess properties. Moreover, they are directly measurable, providing an experimental entry into the network of equations of solution thermodynamics.

FUNDAMENTAL PROPERTY RELATIONS BASED ON THE GIBBS ENERGY

Of the four fundamental property relations shown in the second column of Table 4-1, only Eq. (4-13) has as its special or canonical variables T , P , and $\{n_i\}$. It is therefore the basis for extension to several useful supplementary thermodynamic properties. Indeed an alternative form has been developed as Eq. (4-191). These equations are the first two entries in the upper left quadrant of Table 4-6, which is now to be filled out with important derived relationships.

Fundamental Residual-Property Relation Equation (4-191) is general and may be written for the special case of an ideal gas

$$d\left(\frac{nG^{ig}}{RT}\right) = \frac{nV^{ig}}{RT} dP - \frac{nH^{ig}}{RT^2} dT + \sum_i \frac{\bar{G}_i^{ig}}{RT} dn_i$$

Subtraction of this equation from Eq. (4-191) gives

$$d\left(\frac{nG^R}{RT}\right) = \frac{nV^R}{RT} dP - \frac{nH^R}{RT^2} dT + \sum_i \frac{\bar{G}_i^R}{RT} dn_i \quad (4-236)$$

where the definitions $G^R \equiv G - G^{ig}$ and $\bar{G}_i^R \equiv \bar{G}_i - \bar{G}_i^{ig}$ have been imposed. Equation (4-236) is the *fundamental residual-property relation*. An alternative form follows by introduction of the fugacity coefficient given by Eq. (4-203). The result is listed as Eq. (4-237) in the upper left quadrant of Table 4-6.

Limited forms of this equation are particularly useful. Division by dP and restriction to constant T and composition lead to

$$\frac{V^R}{RT} = \left[\frac{\partial(G^R/RT)}{\partial P} \right]_{T,x} \quad (4-238)$$

Similarly, the result of division by dT and restriction to constant P and composition is

$$\frac{H^R}{RT} = -T \left[\frac{\partial(G^R/RT)}{\partial T} \right]_{P,x} \quad (4-239)$$

Also implicit in Eq. (4-237) is the relation

$$\ln \hat{\phi}_i = \left[\frac{\partial(nG^R/RT)}{\partial n_i} \right]_{T,P,n_j} \quad (4-240)$$

This equation demonstrates that $\ln \hat{\phi}_i$ is a partial property with respect to G^R/RT . The summability relation therefore applies, and

$$\frac{G^R}{RT} = \sum_i x_i \ln \hat{\phi}_i \quad (4-241)$$

TABLE 4-5 Relations Connecting Property Changes of Mixing and Excess Properties

M^E in relation to M	M^E in relation to ΔM	Expressions for ΔM^{id}
$G^E = G - \sum_i x_i G_i - RT \sum_i x_i \ln x_i$ (4-224)	$G^E = \Delta G - RT \sum_i x_i \ln x_i$ (4-228)	$\Delta G^{id} = RT \sum_i x_i \ln x_i$ (4-232)
$V^E = V - \sum_i x_i V_i$ (4-225)	$V^E = \Delta V$ (4-229)	$\Delta V^{id} = 0$ (4-233)
$S^E = S - \sum_i x_i S_i + R \sum_i x_i \ln x_i$ (4-226)	$S^E = \Delta S + R \sum_i x_i \ln x_i$ (4-230)	$\Delta S^{id} = -R \sum_i x_i \ln x_i$ (4-234)
$H^E = H - \sum_i x_i H_i$ (4-227)	$H^E = \Delta H$ (4-231)	$\Delta H^{id} = 0$ (4-235)

TABLE 4-6 Fundamental Property Relations for the Gibbs Energy and Related Properties

General equations for an open system	Equations for 1 mol (constant composition)
$d(nG) = nV dP - nS dT + \sum_i \mu_i dn_i$ (4-13)	$dG = V dP - S dT$ (4-17)
$d\left(\frac{nG}{RT}\right) = \frac{nV}{RT} dP - \frac{nH}{RT^2} dT + \sum_i \frac{\bar{G}_i}{RT} dn_i$ (4-191)	$d\left(\frac{G}{RT}\right) = \frac{V}{RT} dP - \frac{H}{RT^2} dT$ (4-253)
$d\left(\frac{nG^R}{RT}\right) = \frac{nV^R}{RT} dP - \frac{nH^R}{RT^2} dT + \sum_i \ln \hat{\phi}_i dn_i$ (4-237)	$d\left(\frac{G^R}{RT}\right) = \frac{V^R}{RT} dP - \frac{H^R}{RT^2} dT$ (4-254)
$d\left(\frac{nG^E}{RT}\right) = \frac{nV^E}{RT} dP - \frac{nH^E}{RT^2} dT + \sum_i \ln \gamma_i dn_i$ (4-248)	$d\left(\frac{G^E}{RT}\right) = \frac{V^E}{RT} dP - \frac{H^E}{RT^2} dT$ (4-255)
Equations for partial molar properties (constant composition)	Gibbs-Duhem equations
$d\bar{G}_i = d\mu_i = \bar{V}_i dP - \bar{S}_i dT$ (4-256)	$V dP - S dT = \sum_i x_i d\mu_i$ (4-260)
$d\left(\frac{\bar{G}_i}{RT}\right) = d\left(\frac{\mu_i}{RT}\right) = \frac{\bar{V}_i}{RT} dP - \frac{\bar{H}_i}{RT^2} dT$ (4-257)	$\frac{V}{RT} dP - \frac{H}{RT^2} dT = \sum_i x_i d\left(\frac{\bar{G}_i}{RT}\right)$ (4-261)
$d\left(\frac{\bar{G}_i^R}{RT}\right) = d \ln \hat{\phi}_i = \frac{\bar{V}_i^R}{RT} dP - \frac{\bar{H}_i^R}{RT^2} dT$ (4-258)	$\frac{V^R}{RT} dP - \frac{H^R}{RT^2} dT = \sum_i x_i d \ln \hat{\phi}_i$ (4-262)
$d\left(\frac{\bar{G}_i^E}{RT}\right) = d \ln \gamma_i = \frac{\bar{V}_i^E}{RT} dP - \frac{\bar{H}_i^E}{RT^2} dT$ (4-259)	$\frac{V^E}{RT} dP - \frac{H^E}{RT^2} dT = \sum_i x_i d \ln \gamma_i$ (4-263)

Application of Eq. (4-240) to an expression giving G^R as a function of composition yields an equation for $\ln \hat{\phi}_i$. In the simplest case of a gas mixture for which the virial equation [Eq. (4-67)] is appropriate, Eq. (4-69) provides the relation

$$\frac{nG^R}{RT} = \frac{P}{RT} (nB)$$

Differentiation in accord with Eqs. (4-240) and (4-181) yields

$$\ln \hat{\phi}_i = \frac{P}{RT} \bar{B}_i \quad (4-242)$$

where \bar{B}_i is given by Eq. (4-182). For a binary system these equations reduce to

$$\ln \hat{\phi}_1 = \frac{P}{RT} (B_{11} + y_2^2 \delta_{12}) \quad (4-243a)$$

$$\ln \hat{\phi}_2 = \frac{P}{RT} (B_{22} + y_1^2 \delta_{12}) \quad (4-243b)$$

where $\delta_{12} \equiv 2B_{12} - B_{11} - B_{22}$

For the special case of pure species i , these equations reduce to

$$\ln \phi_i = \frac{P}{RT} B_{ii} \quad (4-244)$$

For the generic cubic equation of state [Eqs. (4-104)], G^R/RT is given by Eq. (4-109), which in view of Eq. (4-200) for a pure species becomes

$$\ln \phi_i = Z_i - 1 - \ln(Z_i - \beta_i) - q_i I_i \quad (4-245)$$

For species i in solution Smith, Van Ness, and Abbott [*Introduction to Chemical Engineering Thermodynamics*, 7th ed., pp. 562–563, McGraw-Hill, New York (2005)] show that

$$\ln \hat{\phi}_i = \frac{\bar{b}_i}{b} (Z - 1) - \ln(Z - \beta) - \bar{q}_i I \quad (4-246)$$

Symbols without subscripts represent mixture properties, and I is given by Eq. (4-112).

Fundamental Excess-Property Relation Equations for excess properties are developed in much the same way as those for residual properties. For the special case of an ideal solution, Eq. (4-191) becomes

$$d\left(\frac{nG^{id}}{RT}\right) = \frac{nV^{id}}{RT} dP - \frac{nH^{id}}{RT^2} dT + \sum_i \frac{\bar{G}_i^{id}}{RT} dn_i$$

Subtraction of this equation from Eq. (4-191) yields

$$d\left(\frac{nG^E}{RT}\right) = \frac{nV^E}{RT} dP - \frac{nH^E}{RT^2} dT + \sum_i \frac{\bar{G}_i^E}{RT} dn_i \quad (4-247)$$

where the definitions $G^E \equiv G - G^{id}$ and $\bar{G}_i^E \equiv \bar{G}_i - \bar{G}_i^{id}$ have been imposed. Equation (4-247) is the *fundamental excess-property relation*. An alternative form follows by introduction of the activity coefficient as given by Eq. (4-222). This result is listed as Eq. (4-248) in the upper left quadrant of Table 4-6.

The following equations are in complete analogy to those for residual properties.

$$\frac{V^E}{RT} = \left[\frac{\partial(G^E/RT)}{\partial P} \right]_{T,x} \quad (4-249)$$

$$\frac{H^E}{RT} = -T \left[\frac{\partial(G^E/RT)}{\partial T} \right]_{P,x} \quad (4-250)$$

$$\ln \gamma_i = \left[\frac{\partial(nG^E/RT)}{\partial n_i} \right]_{T,P,n_j} \quad (4-251)$$

This last equation demonstrates that $\ln \gamma_i$ is a partial property with respect to G^E/RT , implying also the validity of the summability relation

$$\frac{G^E}{RT} = \sum_i x_i \ln \gamma_i \quad (4-252)$$

The equations of the upper left quadrant of Table 4-6 reduce to those of the upper right quadrant for $n = 1$ and $dn_i = 0$. Each equation in the upper left quadrant has a partial-property analog, as shown in the lower left quadrant. Each equation of the upper left quadrant is a special case of Eq. (4-172) and therefore has associated with it a Gibbs-Duhem equation of the form of Eq. (4-173). These are shown in the lower right quadrant. The equations of Table 4-6 store an enormous amount of information, but they are so general that their direct

application is seldom appropriate. However, by inspection one can write a vast array of relations valid for particular applications. For example, one sees immediately from Eqs. (4-258) and (4-259) that

$$\left(\frac{\partial \ln \hat{\phi}_i}{\partial P}\right)_{T,x} = \frac{\bar{V}_i^R}{RT} \quad (4-264)$$

$$\left(\frac{\partial \ln \hat{\phi}_i}{\partial T}\right)_{P,x} = -\frac{\bar{H}_i^R}{RT^2} \quad (4-265)$$

$$\left(\frac{\partial \ln \gamma_i}{\partial P}\right)_{T,x} = \frac{\bar{V}_i^E}{RT} \quad (4-266)$$

$$\left(\frac{\partial \ln \gamma_i}{\partial T}\right)_{P,x} = -\frac{\bar{H}_i^E}{RT^2} \quad (4-267)$$

MODELS FOR THE EXCESS GIBBS ENERGY

Excess properties find application in the treatment of liquid solutions. Of primary importance for engineering calculations is the excess Gibbs energy G^E , because its canonical variables are T , P , and composition, the variables usually specified or sought in design calculations. Knowing G^E as a function of T , P , and composition, one can in principle compute from it all other excess properties.

The excess volume for liquid mixtures is usually small, and in accord with Eq. (4-249) the pressure dependence of G^E is usually ignored. Thus, engineering efforts to model G^E center on representing its composition and temperature dependence. For binary systems at constant T , G^E becomes a function of just x_1 , and the quantity most conveniently represented by an equation is G^E/x_1x_2RT . The simplest procedure is to express this quantity as a power series in x_1 :

$$\frac{G^E}{x_1x_2RT} = a + bx_1 + cx_1^2 + \dots \quad (\text{constant } T)$$

An equivalent power series with certain advantages is the *Redlich-Kister expansion* [Redlich, Kister, and Turnquist, *Chem. Eng. Progr. Symp. Ser. No. 2*, **48**: 49–61 (1952)]:

$$\frac{G^E}{x_1x_2RT} = A + B(x_1 - x_2) + C(x_1 - x_2)^2 + \dots$$

In application, different truncations of this expansion are appropriate, and for each truncation specific expressions for $\ln \gamma_1$ and $\ln \gamma_2$ result from application of Eq. (4-251). When all parameters are zero, $G^E/RT = 0$, and the solution is ideal. If $B = C = \dots = 0$, then

$$\frac{G^E}{x_1x_2RT} = A$$

where A is a constant for a given temperature. The corresponding equations for $\ln \gamma_1$ and $\ln \gamma_2$ are

$$\ln \gamma_1 = Ax_2^2 \quad (4-268a)$$

$$\ln \gamma_2 = Ax_1^2 \quad (4-268b)$$

The symmetric nature of these relations is evident. The infinite dilution values of the activity coefficients are $\ln \gamma_1^\infty = \ln \gamma_2^\infty = A$.

If $C = \dots = 0$, then

$$\frac{G^E}{x_1x_2RT} = A + B(x_1 - x_2) = A + B(2x_1 - 1)$$

and in this case G^E/x_1x_2RT is linear in x_1 . The substitutions $A + B = A_{21}$ and $A - B = A_{12}$ transform this expression to the *Margules equation*:

$$\frac{G^E}{x_1x_2RT} = A_{21}x_1 + A_{12}x_2 \quad (4-269)$$

Application of Eq. (4-251) yields

$$\ln \gamma_1 = x_2^2 [A_{12} + 2(A_{21} - A_{12})x_1] \quad (4-270a)$$

$$\ln \gamma_2 = x_1^2 [A_{21} + 2(A_{12} - A_{21})x_2] \quad (4-270b)$$

When $x_1 = 0$, $\ln \gamma_1^\infty = A_{12}$; when $x_2 = 0$, $\ln \gamma_2^\infty = A_{21}$.

An alternative equation is obtained when the reciprocal quantity x_1x_2RT/G^E is expressed as a linear function of x_1 :

$$\frac{x_1x_2}{G^E/RT} = A' + B'(x_1 - x_2) = A' + B'(2x_1 - 1)$$

This may also be written as

$$\frac{x_1x_2}{G^E/RT} = A'(x_1 + x_2) + B'(x_1 - x_2) = (A' + B')x_1 + (A' - B')x_2$$

The substitutions $A' + B' = 1/A'_{21}$ and $A' - B' = 1/A'_{12}$ ultimately produce

$$\frac{G^E}{x_1x_2RT} = \frac{A'_{12}A'_{21}}{A'_{21}x_1 + A'_{12}x_2} \quad (4-271)$$

The activity coefficients implied by this equation are given by

$$\ln \gamma_1 = A'_{12} \left(1 + \frac{A'_{12}x_1}{A'_{21}x_2}\right)^{-2} \quad (4-272a)$$

$$\ln \gamma_2 = A'_{21} \left(1 + \frac{A'_{21}x_2}{A'_{12}x_1}\right)^{-2} \quad (4-272b)$$

These are the *van Laar equations*. When $x_1 = 0$, $\ln \gamma_1^\infty = A'_{12}$; when $x_2 = 0$, $\ln \gamma_2^\infty = A'_{21}$.

The Redlich-Kister expansion, the Margules equations, and the van Laar equations are all special cases of a very general treatment based on rational functions, i.e., on equations for G^E given by ratios of polynomials [Van Ness and Abbott, *Classical Thermodynamics of Nonelectrolyte Solutions: With Applications to Phase Equilibria*, Sec. 5-7, McGraw-Hill, New York (1982)]. Although providing great flexibility in the fitting of VLE data for binary systems, they are without theoretical foundation, with no basis in theory for their extension to multi-component systems. Nor do they incorporate an explicit temperature dependence for the parameters.

Theoretical developments in the molecular thermodynamics of liquid solution behavior are often based on the concept of *local composition*, presumed to account for the short-range order and nonrandom molecular orientations resulting from differences in molecular size and intermolecular forces. Introduced by G. M. Wilson [*J. Am. Chem. Soc.* **86**: 127–130 (1964)] with the publication of a model for G^E , this concept prompted the development of alternative local composition models, most notably the NRTL (Non-Random Two-Liquid) equation of Renon and Prausnitz [*AIChE J.* **14**: 135–144 (1968)] and the UNIQUAC (UNIversal QUAsi-Chemical) equation of Abrams and Prausnitz [*AIChE J.* **21**: 116–128 (1975)].

The Wilson equation, like the Margules and van Laar equations, contains just two parameters for a binary system (Λ_{12} and Λ_{21}) and is written as

$$\frac{G^E}{RT} = -x_1 \ln(x_1 + x_2\Lambda_{12}) - x_2 \ln(x_2 + x_1\Lambda_{21}) \quad (4-273)$$

$$\ln \gamma_1 = -\ln(x_1 + x_2\Lambda_{12}) + x_2 \left(\frac{\Lambda_{12}}{x_1 + x_2\Lambda_{12}} - \frac{\Lambda_{21}}{x_2 + x_1\Lambda_{21}} \right) \quad (4-274a)$$

$$\ln \gamma_2 = -\ln(x_2 + x_1\Lambda_{21}) - x_1 \left(\frac{\Lambda_{12}}{x_1 + x_2\Lambda_{12}} - \frac{\Lambda_{21}}{x_2 + x_1\Lambda_{21}} \right) \quad (4-274b)$$

At infinite dilution,

$$\ln \gamma_1^\infty = -\ln \Lambda_{12} + 1 - \Lambda_{21} \quad \ln \gamma_2^\infty = -\ln \Lambda_{21} + 1 - \Lambda_{12}$$

Both Λ_{12} and Λ_{21} must be positive numbers.

4-24 THERMODYNAMICS

The NRTL equation contains three parameters for a binary system and is written as

$$\frac{G^E}{x_1 x_2 RT} = \frac{G_{21} \tau_{21}}{x_1 + x_2 G_{21}} + \frac{G_{12} \tau_{12}}{x_2 + x_1 G_{12}} \quad (4-275)$$

$$\ln \gamma_1 = x_2^2 \left[\tau_{21} \left(\frac{G_{21}}{x_1 + x_2 G_{21}} \right)^2 + \frac{G_{12} \tau_{12}}{(x_2 + x_1 G_{12})^2} \right] \quad (4-276a)$$

$$\ln \gamma_2 = x_1^2 \left[\tau_{12} \left(\frac{G_{12}}{x_2 + x_1 G_{12}} \right)^2 + \frac{G_{21} \tau_{21}}{(x_1 + x_2 G_{21})^2} \right] \quad (4-276b)$$

Here $G_{12} = \exp(-\alpha \tau_{12})$ $G_{21} = \exp(-\alpha \tau_{21})$

and $\tau_{12} = \frac{b_{12}}{RT}$ $\tau_{21} = \frac{b_{21}}{RT}$

where α , b_{12} , and b_{21} , parameters specific to a particular pair of species, are independent of composition and temperature. The infinite dilution values of the activity coefficients are

$$\ln \gamma_1^\infty = \tau_{21} + \tau_{12} \exp(-\alpha \tau_{12}) \quad \ln \gamma_2^\infty = \tau_{12} + \tau_{21} \exp(-\alpha \tau_{21})$$

The local composition models have limited flexibility in the fitting of data, but they are adequate for most engineering purposes. Moreover, they are implicitly generalizable to multicomponent systems without the introduction of any parameters beyond those required to describe the constituent binary systems. For example, the Wilson equation for multicomponent systems is written as

$$\frac{G^E}{RT} = -\sum_i x_i \ln \left(\sum_j x_j \Lambda_{ij} \right) \quad (4-277)$$

and
$$\ln \gamma_i = 1 - \ln \left(\sum_j x_j \Lambda_{ij} \right) - \sum_k \frac{x_k \Lambda_{ki}}{\sum_j x_j \Lambda_{kj}} \quad (4-278)$$

where $\Lambda_{ij} = 1$ for $i = j$, etc. All indices in these equations refer to the same species, and all summations are over *all* species. For each ij pair there are two parameters, because $\Lambda_{ij} \neq \Lambda_{ji}$. For example, in a ternary system the three possible ij pairs are associated with the parameters $\Lambda_{12}, \Lambda_{21}$; $\Lambda_{13}, \Lambda_{31}$; and $\Lambda_{23}, \Lambda_{32}$.

The temperature dependence of the parameters is given by

$$\Lambda_{ij} = \frac{V_j}{V_i} \exp \frac{-a_{ij}}{RT} \quad i \neq j \quad (4-279)$$

where V_j and V_i are the molar volumes of pure liquids j and i and a_{ij} is a constant independent of composition and temperature. Molar volumes V_j and V_i , themselves weak functions of temperature, form ratios that in practice may be taken as independent of T , and are usually evaluated at or near 25°C.

The Wilson parameters Λ_{ij} and NRTL parameters G_{ij} inherit a Boltzmann-type T dependence from the origins of the expressions for G^E , but it is only approximate. Computations of properties sensitive to this dependence (e.g., heats of mixing and liquid/liquid solubility) are in general only qualitatively correct. However, all parameters are found from data for binary (in contrast to multicomponent) systems, and this makes parameter determination for the local composition models a task of manageable proportions.

The UNIQUAC equation treats $g \equiv G^E/RT$ as made up of two additive parts, a *combinatorial* term g^C , accounting for molecular size and shape differences, and a *residual* term g^R (not a residual property), accounting for molecular interactions:

$$g = g^C + g^R \quad (4-280)$$

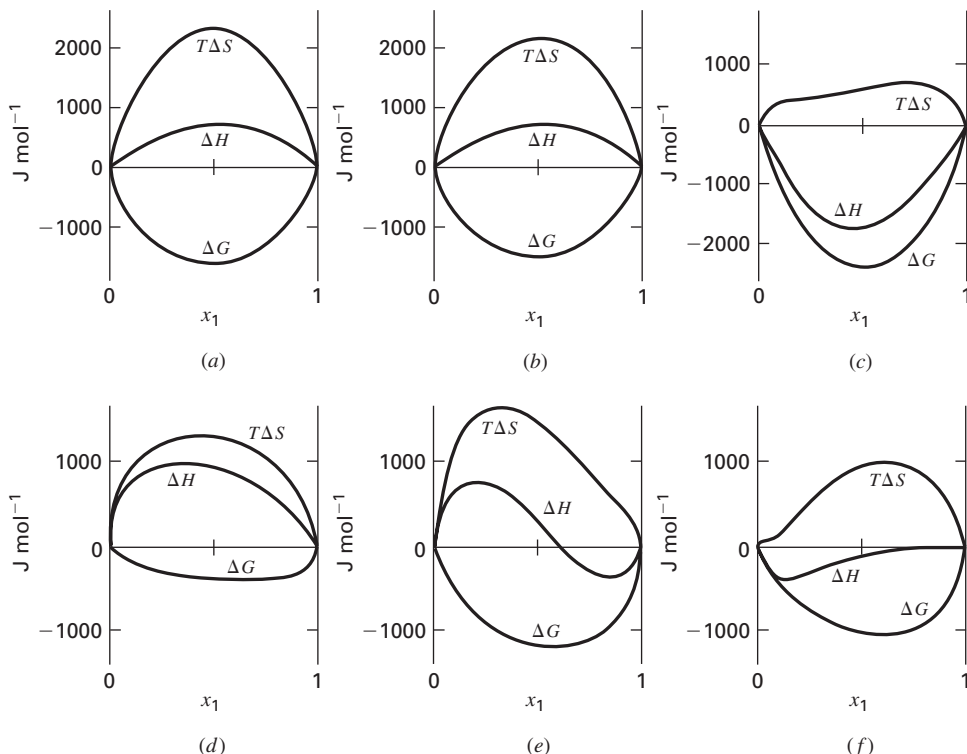


FIG. 4-4 Property changes of mixing at 50°C for six binary liquid systems: (a) chloroform(1)/n-heptane(2); (b) acetone(1)/methanol(2); (c) acetone(1)/chloroform(2); (d) ethanol(1)/n-heptane(2); (e) ethanol(1)/chloroform(2); (f) ethanol(1)/water(2). [Smith, Van Ness, and Abbott, Introduction to Chemical Engineering Thermodynamics, 7th ed., p. 455, McGraw-Hill, New York (2005).]

Function g^C contains pure-species parameters only, whereas function g^R incorporates two *binary* parameters for each pair of molecules. For a multicomponent system,

$$g^C = \sum_i x_i \ln \frac{\Phi_i}{x_i} + 5 \sum_i q_i x_i \ln \frac{\theta_i}{\Phi_i} \quad (4-281)$$

$$g^R = - \sum_i q_i x_i \ln \left(\sum_j \theta_j \tau_{ji} \right) \quad (4-282)$$

where

$$\Phi_i \equiv \frac{x_i r_i}{\sum_j x_j r_j} \quad (4-283)$$

and

$$\theta_i \equiv \frac{x_i q_i}{\sum_j x_j q_j} \quad (4-284)$$

Subscript i identifies species, and j is a dummy index; all summations are over all species. Note that $\tau_{ii} \neq \tau_{ij}$; however, when $i=j$, then $\tau_{ii} = \tau_{ij} = 1$. In these equations r_i (a relative molecular volume) and q_i (a relative molecular surface area) are pure-species parameters. The influence of temperature on g enters through the interaction parameters τ_{ji} of Eq. (4-282), which are temperature-dependent:

$$\tau_{ji} = \exp \frac{-(u_{ji} - u_{ii})}{RT} \quad (4-285)$$

Parameters for the UNIQUAC equation are therefore values of $u_{ji} - u_{ii}$.

An expression for $\ln \gamma_i$ is found by application of Eq. (4-251) to the UNIQUAC equation for g [Eqs. (4-280) through (4-282)]. The result is given by the following equations:

$$\ln \gamma_i = \ln \gamma_i^C + \ln \gamma_i^R \quad (4-286)$$

$$\ln \gamma_i^C = 1 - J_i + \ln J_i - 5q_i \left(1 - \frac{J_i}{L_i} + \ln \frac{J_i}{L_i} \right) \quad (4-287)$$

$$\ln \gamma_i^R = q_i \left(1 - \ln s_i - \sum_j \theta_j \frac{\tau_{ij}}{s_j} \right) \quad (4-288)$$

where in addition to Eqs. (4-284) and (4-285),

$$J_i = \frac{r_i}{\sum_j r_j x_j} \quad (4-289)$$

$$L_i = \frac{q_i}{\sum_j q_j x_j} \quad (4-290)$$

$$s_i = \sum_l \theta_l \tau_{li} \quad (4-291)$$

Again subscript i identifies species, and j and l are dummy indices.

Values for the parameters of the commonly used models for the excess Gibbs energy are given by Gmehling, Onken, and Arlt [*Vapor-Liquid Equilibrium Data Collection*, Chemistry Data Series, vol. 1, parts 1-8, DECHEMA, Frankfurt/Main (1974-1990)].

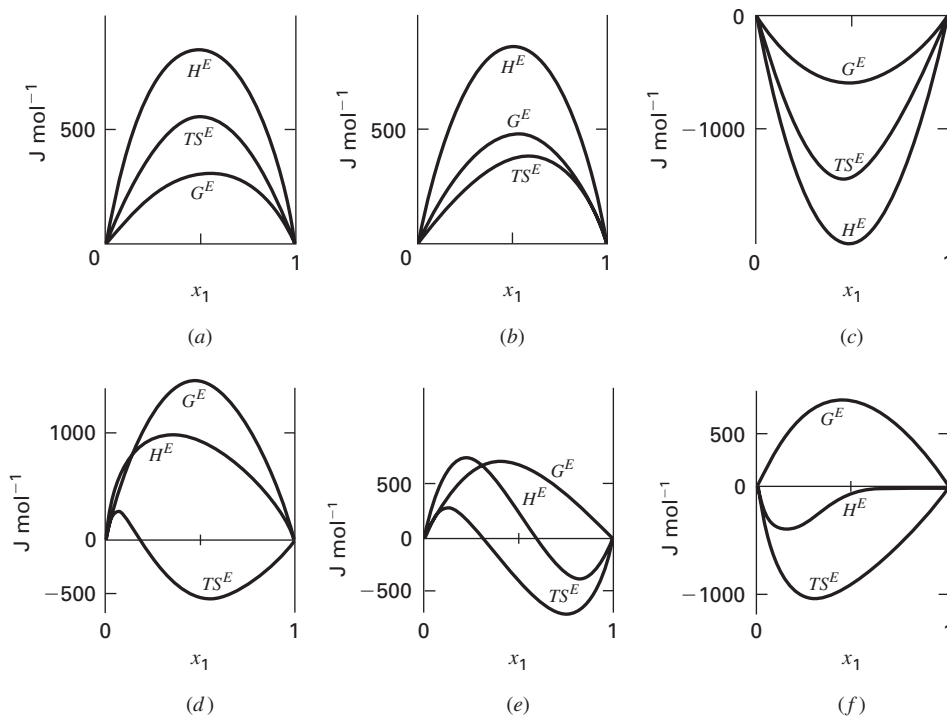


FIG. 4-5 Excess properties at 50°C for six binary liquid systems: (a) chloroform(1)/n-heptane(2); (b) acetone(1)/methanol(2); (c) acetone(1)/chloroform(2); (d) ethanol(1)/n-heptane(2); (e) ethanol(1)/chloroform(2); (f) ethanol(1)/water(2). [Smith, Van Ness, and Abbott, *Introduction to Chemical Engineering Thermodynamics*, 7th ed., p. 420, McGraw-Hill, New York (2005).]

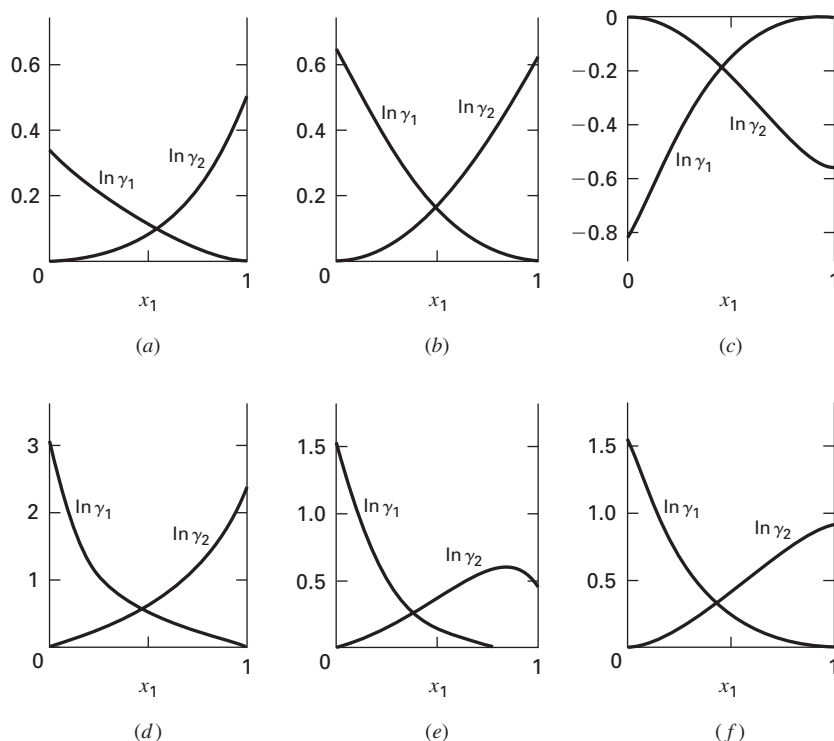


FIG. 4-6 Activity coefficients at 50°C for six binary liquid systems: (a) chloroform(1)/n-heptane(2); (b) acetone(1)/methanol(2); (c) acetone(1)/chloroform(2); (d) ethanol(1)/n-heptane(2); (e) ethanol(1)/chloroform(2); (f) ethanol(1)/water(2). [Smith, Van Ness, and Abbott, Introduction to Chemical Engineering Thermodynamics, 7th ed., p. 445, McGraw-Hill, New York (2005).]

Behavior of Binary Liquid Solutions Property changes of mixing and excess properties find greatest application in the description of liquid mixtures at low reduced temperatures, i.e., at temperatures well below the critical temperature of each constituent species. The properties of interest to the chemical engineer are V^E ($\equiv \Delta V$), H^E ($\equiv \Delta H$), S^E , ΔS , G^E , and ΔG . The activity coefficient is also of special importance because of its application in phase equilibrium calculations.

The volume change of mixing ($V^E = \Delta V$), the heat of mixing ($H^E = \Delta H$), and the excess Gibbs energy G^E are experimentally accessible, ΔV and ΔH by direct measurement and G^E (or $\ln \gamma_i$) indirectly by reduction of vapor/liquid equilibrium data. Knowledge of H^E and

G^E allows calculation of S^E by Eq. (4-10), written for excess properties as

$$S^E = \frac{H^E - G^E}{T} \quad (4-292)$$

with ΔS then given by Eq. (4-230).

Figure 4-4 displays plots of ΔH , ΔS , and ΔG as functions of composition for six binary solutions at 50°C. The corresponding excess properties are shown in Fig. 4-5; the activity coefficients, derived from Eq. (4-251), appear in Fig. 4-6. The properties shown here are insensitive to pressure and for practical purposes represent solution properties at 50°C and low pressure ($P \approx 1$ bar).

EQUILIBRIUM

CRITERIA

The equations developed in preceding sections are for *PVT* systems in states of internal equilibrium. The criteria for internal thermal and mechanical equilibrium simply require uniformity of temperature and pressure throughout the system. The criteria for phase and chemical reaction equilibria are less obvious.

If a closed *PVT* system of uniform T and P , either homogeneous or heterogeneous, is in thermal and mechanical equilibrium with its surroundings, but is not at internal equilibrium with respect to mass transfer or chemical reaction, then changes in the system are irreversible and necessarily bring the system closer to an equilibrium state. The first and second laws written for the entire system are

$$dU^t = dQ + dW \quad dS^t \geq \frac{dQ}{T}$$

$$\text{Combination gives} \quad dU^t - dW - TdS^t \leq 0$$

Because mechanical equilibrium is assumed, $dW = -PdV^t$, whence

$$dU^t + PdV^t - TdS^t \leq 0$$

The inequality applies to all incremental changes toward the equilibrium state, whereas the equality holds at the equilibrium state where change is reversible.

Constraints put on this expression produce alternative criteria for the directions of irreversible processes and for the condition of equilibrium. For example, $dU_{S^t, V^t} \leq 0$. Particularly important is fixing T and P ; this produces

$$d(U^t + PV^t - TS^t)_{T,P} \leq 0 \quad \text{or} \quad dG_{T,P}^t \leq 0$$

This expression shows that all irreversible processes occurring at constant T and P proceed in a direction such that the total Gibbs energy of the system decreases. Thus the equilibrium state of a closed system is the state with the minimum total Gibbs energy attainable at the given T and P . At the equilibrium state, differential variations may occur in the system at constant T and P without producing a change in G^t . This is the meaning of the equilibrium criterion

$$dG_{T,P}^t = 0 \quad (4-293)$$

This equation may be applied to a closed, nonreactive, two-phase system. Each phase taken separately is an *open* system, capable of exchanging mass with the other; Eq. (4-13) is written for each phase:

$$d(nG)' = -(nS)' dT + (nV)' dP + \sum_i \mu_i' dn_i'$$

$$d(nG)'' = -(nS)'' dT + (nV)'' dP + \sum_i \mu_i'' dn_i''$$

where the primes and double primes denote the two phases; the presumption is that T and P are uniform throughout the two phases. The change in the Gibbs energy of the two-phase system is the sum of these equations. When each total-system property is expressed by an equation of the form $nM = (nM)' + (nM)''$, this sum is given by

$$d(nG) = (nV)dP - (nS)dT + \sum_i \mu_i' dn_i' + \sum_i \mu_i'' dn_i''$$

If the two-phase system is at equilibrium, then application of Eq. (4-293) yields

$$dG_{T,P}^t = d(nG)_{T,P} = \sum_i \mu_i' dn_i' + \sum_i \mu_i'' dn_i'' = 0$$

The system is closed and without chemical reaction; material balances therefore require that $dn_i'' = -dn_i'$, reducing the preceding equation to

$$\sum_i (\mu_i' - \mu_i'') dn_i' = 0$$

Because the dn_i' are independent and arbitrary, it follows that $\mu_i' = \mu_i''$. This is the criterion of two-phase equilibrium. It is readily generalized to multiple phases by successive application to pairs of phases. The general result is

$$\mu_i' = \mu_i'' = \mu_i''' = \dots \quad (4-294)$$

Substitution for each μ_i by Eq. (4-202) produces the equivalent result:

$$\hat{f}_i' = \hat{f}_i'' = \hat{f}_i''' = \dots \quad (4-295)$$

These are the criteria of phase equilibrium applied in the solution of practical problems.

For the case of equilibrium with respect to chemical reaction within a single-phase closed system, combination of Eqs. (4-13) and (4-293) leads immediately to

$$\sum_i \mu_i dn_i = 0 \quad (4-296)$$

For a system in which both phase and chemical reaction equilibrium prevail, the criteria of Eqs. (4-295) and (4-296) are superimposed.

PHASE RULE

The *intensive* state of a *PVT* system is established when its temperature and pressure and the compositions of all phases are fixed. However, for equilibrium states not all these variables are independent, and fixing a limited number of them automatically establishes the others. This number of independent variables is given by the phase rule, and it is called the *number of degrees of freedom* of the system. It is the number of variables that may be arbitrarily specified and that must be so specified in order to fix the *intensive* state of a system at equilibrium. This number is the difference between the number of variables needed to characterize the system and the number of equations that may be written connecting these variables.

For a system containing N chemical species distributed at equilibrium among π phases, the phase rule variables are T and P , presumed uniform throughout the system, and $N - 1$ mole fractions in each

phase. The number of these variables is $2 + (N - 1)\pi$. The masses of the phases are not phase rule variables, because they have nothing to do with the intensive state of the system.

The equilibrium equations that may be written express chemical potentials or fugacities as functions of T , P , and the phase compositions, the phase rule variables:

1. Equation (4-295) for each species, giving $(\pi - 1)N$ phase equilibrium equations

2. Equation (4-296) for each independent chemical reaction, giving r equations

The total number of independent equations is therefore $(\pi - 1)N + r$. Because the degrees of freedom of the system F is the difference between the number of variables and the number of equations,

$$F = 2 + (N - 1)\pi - (\pi - 1)N - r$$

$$\text{or} \quad F = 2 - \pi + N - r \quad (4-297)$$

The number of independent chemical reactions r can be determined as follows:

1. Write *formation* reactions from the elements for each chemical compound present in the system.

2. Combine these reaction equations so as to eliminate from the set all elements not present as elements in the system. A systematic procedure is to select one equation and combine it with each of the other equations of the set so as to eliminate a particular element. This usually reduces the set by one equation for each element eliminated, although two or more elements may be simultaneously eliminated.

The resulting set of r equations is a complete set of independent reactions. More than one such set is often possible, but all sets number r and are equivalent.

Example 2: Application of the Phase Rule

a. For a system of two miscible nonreacting species in vapor/liquid equilibrium,

$$F = 2 - \pi + N - r = 2 - 2 + 2 - 0 = 2$$

The 2 degrees of freedom for this system may be satisfied by setting T and P , or T and y_1 , or P and x_1 , or x_1 and y_1 , etc., at fixed values. Thus for equilibrium at a particular T and P , this state (if possible at all) exists only at one liquid and one vapor composition. Once the 2 degrees of freedom are used up, no further specification is possible that would restrict the phase rule variables. For example, one cannot *in addition* require that the system form an azeotrope (assuming this is possible), for this requires $x_1 = y_1$, an equation not taken into account in the derivation of the phase rule. Thus the requirement that the system form an azeotrope imposes a special constraint, making $F = 1$.

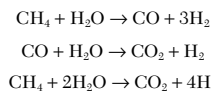
b. For a gaseous system consisting of CO, CO₂, H₂, H₂O, and CH₄ in chemical reaction equilibrium,

$$F = 2 - \pi + N - r = 2 - 1 + 5 - 2 = 4$$

The value of $r = 2$ is found from the formation reactions:



Systematic elimination of C and O₂ from this set of chemical equations reduces the set to two. Three possible pairs of equations may result, depending on how the combination of equations is effected. Any *pair* of the following three equations represents a complete set of independent reactions, and all pairs are equivalent.



The result, $F = 4$, means that one is free to specify, for example, T , P , and two mole fractions in an equilibrium mixture of these five chemical species, provided nothing else is arbitrarily set. Thus it cannot simultaneously be required that the system be prepared from specified amounts of particular constituent species.

Duhem's Theorem Because the phase rule treats only the intensive state of a system, it applies to both closed and open systems. Duhem's theorem, on the other hand, is a rule relating to closed systems only: *For any closed system formed initially from given masses of prescribed chemical species, the equilibrium state is completely*

determined by any two properties of the system, provided only that the two properties are independently variable at the equilibrium state. The meaning of completely determined is that both the intensive and extensive states of the system are fixed; not only are T , P , and the phase compositions established, but so also are the masses of the phases.

VAPOR/LIQUID EQUILIBRIUM

Vapor/liquid equilibrium (VLE) relationships (as well as other inter-phase equilibrium relationships) are needed in the solution of many engineering problems. The required data can be found by experiment, but measurements are seldom easy, even for binary systems, and they become ever more difficult as the number of species increases. This is the incentive for application of thermodynamics to the calculation of phase equilibrium relationships.

The general VLE problem treats a multicomponent system of N constituent species for which the independent variables are T , P , $N - 1$ liquid-phase mole fractions, and $N - 1$ vapor-phase mole fractions. (Note that $\sum x_i = 1$ and $\sum y_i = 1$, where x_i and y_i represent liquid and vapor mole fractions, respectively.) Thus there are $2N$ independent variables, and application of the phase rule shows that exactly N of these variables must be fixed to establish the intensive state of the system. This means that once N variables have been specified, the remaining N variables can be determined by simultaneous solution of the N equilibrium relations

$$f_i^l = f_i^v \quad i = 1, 2, \dots, N \quad (4-298)$$

where superscripts l and v denote the liquid and vapor phases, respectively.

In practice, either T or P and either the liquid-phase or vapor-phase composition are specified, thus fixing $1 + (N - 1) = N$ independent variables. The remaining N variables are then subject to calculation, provided that sufficient information is available to allow determination of all necessary thermodynamic properties.

Gamma/Phi Approach For many VLE systems of interest, the pressure is low enough that a relatively simple equation of state, such as the two-term virial equation, is satisfactory for the vapor phase. Liquid-phase behavior, on the other hand, is described by an equation for the excess Gibbs energy, from which activity coefficients are derived. The fugacity of species i in the liquid phase is given by Eq. (4-221), and the vapor-phase fugacity is given by Eq. (4-204). These are here written as

$$\hat{f}_i^l = \gamma_i x_i f_i \quad \text{and} \quad \hat{f}_i^v = \hat{\phi}_i^v y_i P$$

By Eq. (4-298), $\gamma_i x_i f_i = \hat{\phi}_i^v y_i P \quad i = 1, 2, \dots, N \quad (4-299)$

Identifying superscripts l and v are omitted here with the understanding that γ_i and f_i are liquid-phase properties, whereas $\hat{\phi}_i$ is a vapor-phase property. Applications of Eq. (4-299) represent what is known as the *gamma/phi* approach to VLE calculations.

Evaluation of $\hat{\phi}_i$ is usually by Eq. (4-243), based on the two-term virial equation of state. The activity coefficient γ_i is ultimately based on Eq. (4-251) applied to an expression for G^E/RT , as described in the section "Models for the Excess Gibbs Energy."

The fugacity f_i of pure compressed liquid i must be evaluated at the T and P of the equilibrium mixture. This is done in two steps. First, one calculates the fugacity coefficient of saturated vapor $\hat{\phi}_i^v = \hat{\phi}_i^{\text{sat}}$ by an integrated form of Eq. (4-205), most commonly by Eq. (4-242) evaluated for pure species i at temperature T and the corresponding vapor pressure $P = P_i^{\text{sat}}$. Equation (4-298) written for pure species i becomes

$$f_i^v = f_i^l = f_i^{\text{sat}} \quad (4-300)$$

where f_i^{sat} indicates the value both for saturated liquid and for saturated vapor. Division by P_i^{sat} yields corresponding fugacity coefficients:

$$\frac{f_i^{\text{sat}}}{P_i^{\text{sat}}} = \frac{f_i^v}{P_i^{\text{sat}}} = \frac{f_i^l}{P_i^{\text{sat}}}$$

or $\hat{\phi}_i^v = \hat{\phi}_i^l = \hat{\phi}_i^{\text{sat}} \quad (4-301)$

The second step is the evaluation of the change in fugacity of the liquid with a change in pressure to a value above or below P_i^{sat} . For this isothermal change of state from saturated liquid at P_i^{sat} to liquid at pressure P , Eq. (4-17) is integrated to give

$$G_i - G_i^{\text{sat}} = \int_{P_i^{\text{sat}}}^P V_i dP$$

Equation (4-199) is then written twice: for G_i and for G_i^{sat} . Subtraction provides another expression for $G_i - G_i^{\text{sat}}$:

$$G_i - G_i^{\text{sat}} = RT \ln \frac{f_i}{f_i^{\text{sat}}}$$

Equating the two expressions for $G_i - G_i^{\text{sat}}$ yields

$$\ln \frac{f_i}{f_i^{\text{sat}}} = \frac{1}{RT} \int_{P_i^{\text{sat}}}^P V_i dP$$

Because V_i , the liquid-phase molar volume, is a very weak function of P at temperatures well below T_c , an excellent approximation is usually obtained when evaluation of the integral is based on the assumption that V_i is constant at the value for saturated liquid V_i^l :

$$\ln \frac{f_i}{f_i^{\text{sat}}} = \frac{V_i^l(P - P_i^{\text{sat}})}{RT}$$

Substituting $f_i^{\text{sat}} = \hat{\phi}_i^{\text{sat}} P_i^{\text{sat}}$ and solving for f_i give

$$f_i = \hat{\phi}_i^{\text{sat}} P_i^{\text{sat}} \exp \frac{V_i^l(P - P_i^{\text{sat}})}{RT} \quad (4-302)$$

The exponential is known as the Poynting factor.

Equation (4-299) may now be written as

$$y_i P \Phi_i = x_i \gamma_i P_i^{\text{sat}} \quad i = 1, 2, \dots, N \quad (4-303)$$

where

$$\Phi_i = \frac{\hat{\phi}_i}{\hat{\phi}_i^{\text{sat}}} \exp \frac{-V_i^l(P - P_i^{\text{sat}})}{RT} \quad (4-304)$$

If evaluation of $\hat{\phi}_i^{\text{sat}}$ and $\hat{\phi}_i$ is by Eqs. (4-244) and (4-243), this reduces to

$$\Phi_i = \exp \frac{\overline{P} B_i - P_i^{\text{sat}} B_{ii} - V_i^l(P - P_i^{\text{sat}})}{RT} \quad (4-305)$$

where \overline{B}_i is given by Eq. (4-182).

The N equations represented by Eq. (4-303) in conjunction with Eq. (4-305) may be solved for N unknown phase equilibrium variables. For a multicomponent system the calculation is formidable, but well suited to computer solution.

When Eq. (4-303) is applied to VLE for which the vapor phase is an ideal gas and the liquid phase is an ideal solution, it reduces to a very simple expression. For ideal gases, fugacity coefficients $\hat{\phi}_i$ and $\hat{\phi}_i^{\text{sat}}$ are unity, and the right side of Eq. (4-304) reduces to the Poynting factor. For the systems of interest here, this factor is always very close to unity, and for practical purposes $\Phi_i = 1$. For ideal solutions, the activity coefficients γ_i are also unity, and Eq. (4-303) reduces to

$$y_i P = x_i P_i^{\text{sat}} \quad i = 1, 2, \dots, N \quad (4-306)$$

an equation which expresses *Raoult's law*. It is the simplest possible equation for VLE and as such fails to provide a realistic representation of real behavior for most systems. Nevertheless, it is useful as a standard of comparison.

Modified Raoult's Law Of the qualifications that lead to Raoult's law, the one least often reasonable is the supposition of solution ideality for the liquid phase. Real solution behavior is reflected by values of activity coefficients that differ from unity. When γ_i of Eq. (4-303) is retained in the equilibrium equation, the result is the *modified Raoult's law*:

$$y_i P = x_i \gamma_i P_i^{\text{sat}} \quad i = 1, 2, \dots, N \quad (4-307)$$

This equation is often adequate when applied to systems at low to moderate pressures and is therefore widely used. Bubble point and dew point calculations are only a bit more complex than the same calculations with Raoult's law.

Activity coefficients are functions of temperature and liquid-phase composition and are correlated through equations for the excess Gibbs energy. When an appropriate correlating equation for C^E is not available, suitable estimates of activity coefficients may often be obtained from a group contribution correlation. This is the "solution of groups" approach, wherein activity coefficients are found as sums of contributions from the structural groups that make up the molecules of a solution. The most widely applied such correlations are based on the UNIQUAC equation, and they have their origin in the UNIFAC method (UNIQUAC Functional-group Activity Coefficients), proposed by Fredenslund, Jones, and Prausnitz [*AIChE J.* **21**: 1086–1099 (1975)], and given detailed treatment by Fredenslund, Gmehling, and Rasmussen [*Vapor-Liquid Equilibrium Using UNIFAC*, Elsevier, Amsterdam (1977)].

Subsequent development has led to a variety of applications, including liquid/liquid equilibria [Magnussen, Rasmussen, and Fredenslund, *Ind. Eng. Chem. Process Des. Dev.* **20**: 331–339 (1981)], solid/liquid equilibria [Anderson and Prausnitz, *Ind. Eng. Chem. Fundam.* **17**: 269–273 (1978)], solvent activities in polymer solutions [Oishi and Prausnitz, *Ind. Eng. Chem. Process Des. Dev.* **17**: 333–339 (1978)], vapor pressures of pure species [Jensen, Fredenslund, and Rasmussen, *Ind. Eng. Chem. Fundam.* **20**: 239–246 (1981)], gas solubilities [Sander, Skjold-Jørgensen, and Rasmussen, *Fluid Phase Equilib.* **11**: 105–126 (1983)], and excess enthalpies [Dang and Tassios, *Ind. Eng. Chem. Process Des. Dev.* **25**: 22–31 (1986)].

The range of applicability of the original UNIFAC model has been greatly extended and its reliability enhanced. Its most recent revision and extension is treated by Wittig, Lohmann, and Gmehling [*Ind. Eng. Chem. Res.* **42**: 183–188 (2003)], wherein are cited earlier pertinent papers. Because it is based on temperature-independent parameters, its application is largely restricted to 0 to 150°C.

Two modified versions of the UNIFAC model, based on temperature-dependent parameters, have come into use. Not only do they provide a wide temperature range of applicability, but also they allow correlation of various kinds of property data, including phase equilibria, infinite dilution activity coefficients, and excess properties. The most recent revision and extension of the modified UNIFAC (Dortmund) model is provided by Gmehling et al. [*Ind. Eng. Chem. Res.* **41**: 1678–1688 (2002)]. An extended UNIFAC model called KT-UNIFAC is described in detail by Kang et al. [*Ind. Eng. Chem. Res.* **41**: 3260–3273 (2003)]. Both papers contain extensive literature citations.

The UNIFAC model has also been combined with the predictive Soave-Redlich-Kwong (PSRK) equation of state. The procedure is most completely described (with background literature citations) by Horstmann et al. [*Fluid Phase Equilibria* **227**: 157–164 (2005)].

Because $\sum y_i = 1$, Eq. (4-307) may be summed over all species to yield

$$P = \sum_i x_i \gamma_i P_i^{\text{sat}} \quad (4-308)$$

Alternatively, Eq. (4-307) may be solved for x_i , in which case summing over all species yields

$$P = \frac{1}{\sum_i y_i / \gamma_i P_i^{\text{sat}}} \quad (4-309)$$

Example 3: Dew and Bubble Point Calculations As indicated by Example 2a, a binary system in vapor/liquid equilibrium has 2 degrees of freedom. Thus of the four phase rule variables T , P , x_1 , and y_1 , two must be fixed to allow calculation of the other two, regardless of the formulation of the equilibrium equations. Modified Raoult's law [Eq. (4-307)] may therefore be applied to the calculation of any pair of phase rule variables, given the other two.

The necessary vapor pressures and activity coefficients are supplied by data correlations. For the system acetone(1)/*n*-hexane(2), vapor pressures are given by Eq. (4-142), the Antoine equation:

$$\ln P_i^{\text{sat}}/\text{kPa} = A_i - \frac{B_i}{T/\text{K} + C_i} \quad i = 1, 2 \quad (A)$$

with parameters

i	A_i	B_i	C_i
1	14.3145	2756.22	-45.090
2	13.8193	2696.04	-48.833

Activity coefficients are given by Eq. (4-274), the Wilson equation:

$$\ln \gamma_1 = -\ln(x_1 + x_2 \Lambda_{12}) + x_2 \lambda \quad (B)$$

$$\ln \gamma_2 = -\ln(x_2 + x_1 \Lambda_{21}) - x_1 \lambda \quad (C)$$

where

$$\lambda = \frac{\Lambda_{12}}{x_1 + x_2 \Lambda_{12}} - \frac{\Lambda_{21}}{x_2 + x_1 \Lambda_{21}}$$

$$\text{By Eq. (4-279)} \quad \Lambda_{ij} = \frac{V_j}{V_i} \exp \frac{-a_{ij}}{RT} \quad i \neq j$$

with parameters [Gmehling et al., *Vapor-Liquid Data Collection*, Chemistry Data Series, vol. 1, part 3, DECHEMA, Frankfurt/Main (1983)]

a_{12} cal mol ⁻¹	a_{21} cal mol ⁻¹	V_1 cm ³ mol ⁻¹	V_2 cm ³ mol ⁻¹
985.05	453.57	74.05	131.61

When T and x_1 are given, the calculation is direct, with final values for vapor pressures and activity coefficients given immediately by Eqs. (A), (B), and (C). In all other cases either T or x_1 or both are initially unknown, and calculations require trial or iteration.

a. BUBL P calculation: Find y_1 and P , given x_1 and T . Calculation here is direct. For $x_1 = 0.40$ and $T = 325.15$ K (52°C), Eqs. (A), (B), and (C) yield the values listed in the table on the following page. Equations (4-308) and (4-307) then become

$$P = x_1 \gamma_1 P_1^{\text{sat}} + x_2 \gamma_2 P_2^{\text{sat}} = (0.40)(1.8053)(87.616) + (0.60)(1.2569)(58.105) = 108.134 \text{ kPa}$$

$$y_1 = \frac{x_1 \gamma_1 P_1^{\text{sat}}}{P} = \frac{(0.40)(1.8053)(87.616)}{108.134} = 0.5851$$

b. DEW P calculation: Find x_1 and P , given y_1 and T . With x_1 an unknown, the activity coefficients cannot be immediately calculated. However, an iteration scheme based on Eqs. (4-309) and (4-307) is readily devised, and is part of any solve routine of a software package. Starting values result from setting each $\gamma_i = 1$. For $y_1 = 0.4$ and $T = 325.15$ K (52°C), results are listed in the accompanying table.

c. BUBL T calculation: Find y_1 and T , given x_1 and P . With T unknown, neither the vapor pressures nor the activity coefficients can be initially calculated. An iteration scheme or a solve routine with starting values for the unknowns is required. Results for $x_1 = 0.32$ and $P = 80$ kPa are listed in the accompanying table.

d. DEW T calculation: Find x_1 and T , given y_1 and P . Again, an iteration scheme or a solve routine with starting values for the unknowns is required. For $y_1 = 0.60$ and $P = 101.33$ kPa, results are listed in the accompanying table.

e. Azeotrope calculations: As noted in Example 1a, only a single degree of freedom exists for this special case. The most sensitive quantity for identifying the azeotropic state is the *relative volatility*, defined as

$$\alpha_{12} = \frac{y_1/x_1}{y_2/x_2}$$

Because $y_i = x_i$ for the azeotropic state, $\alpha_{12} = 1$. Substitution for the two ratios by Eq. (4-307) provides an equation for calculation of α_{12} from the thermodynamic functions:

$$\alpha_{12} = \frac{\gamma_1 P_1^{\text{sat}}}{\gamma_2 P_2^{\text{sat}}}$$

Because α_{12} is a monotonic function of x_1 , the test of whether an azeotrope exists at a given T or P is provided by values of α_{12} in the limits of $x_1 = 0$ and $x_1 = 1$. If *both* values are either > 1 or < 1 , no azeotrope exists. But if one value is < 1 and the other > 1 , an azeotrope necessarily exists at the given T or P . Given T , the azeotropic composition and pressure is found by seeking the value of P that makes $x_1 = y_1$ or that makes $\alpha_{12} = 1$. Similarly, given P , one finds the azeotropic composition and temperature. Shown in the accompanying table are calculated azeotropic states for a temperature of 46°C and for a pressure of 101.33 kPa. At 46°C, the limiting values of α_{12} are 8.289 at $x_1 = 0$ and 0.223 at $x_1 = 1$.

4-30 THERMODYNAMICS

	<i>T</i> /K	<i>P</i> ^{sat} /kPa	<i>P</i> ₂ ^{sat} /kPa	γ_1	γ_2	<i>x</i> ₁	<i>y</i> ₁	<i>P</i> /kPa
a.	325.15	87.616	58.105	1.8053	1.2869	0.4000	0.5851	108.134
b.	325.15	87.616	58.105	3.5535	1.0237	0.1130	0.4000	87.939
c.	317.24	65.830	43.591	2.1286	1.1861	0.3200	0.5605	80.000
d.	322.98	81.125	53.779	1.6473	1.3828	0.4550	0.6000	101.330
e.	319.15	70.634	46.790	1.2700	1.9172	0.6445 = 0.6445	0.6445	89.707
f.	322.58	79.986	53.021	1.2669	1.9111	0.6454 = 0.6454	0.6454	101.330

Given values are italic; calculated results are boldface.

Data Reduction Correlations for G^E and the activity coefficients are based on VLE data taken at low to moderate pressures. Group-contribution methods, such as UNIFAC, depend for validity on parameters evaluated from a large base of such data. The process of finding a suitable analytic relation for g ($\equiv G^E/RT$) as a function of its independent variables T and x_1 , thus producing a correlation of VLE data, is known as data reduction. Although g is in principle also a function of P , the dependence is so weak as to be universally and properly neglected. Given here is a brief description of the treatment of data taken for binary systems under *isothermal* conditions. A more comprehensive development is given by Van Ness [J. Chem. Thermodyn. 27: 113–134 (1995); Pure & Appl. Chem. 67: 859–872 (1995)].

Presumed in all that follows is the existence of an equation inherently capable of correlating values of G^E for the liquid phase as a function of x_1 :

$$g \equiv G^E/RT = \mathcal{G}(x_1; \alpha, \beta, \dots) \quad (4-310)$$

where α, β, \dots , represent adjustable parameters.

The measured variables of binary VLE are x_1, y_1, T , and P . Experimental values of the activity coefficient of species i in the liquid are related to these variables by Eq. (4-303), written as

$$\gamma_i^\circ = \frac{y_i P^\circ}{x_i P^{\text{sat}}} \Phi_i \quad i = 1, 2 \quad (4-311)$$

where Φ_i is given by Eq. (4-305) and the asterisks denote experimental values. A simple summability relation analogous to Eq. (4-252) defines an experimental value of g° :

$$g^\circ \equiv x_1 \ln \gamma_1^\circ + x_2 \ln \gamma_2^\circ \quad (4-312)$$

Moreover, Eq. (4-263), the Gibbs-Duhem equation, may be written for experimental values in a binary system at constant T and P as

$$x_1 \frac{d \ln \gamma_1^\circ}{dx_1} + x_2 \frac{d \ln \gamma_2^\circ}{dx_1} = 0 \quad (4-313)$$

Because experimental measurements are subject to systematic error, sets of values of $\ln \gamma_1^\circ$ and $\ln \gamma_2^\circ$ may not satisfy, i.e., may not be *consistent* with, the Gibbs-Duhem equation. Thus Eq. (4-313) applied to sets of experimental values becomes a test of the thermodynamic consistency of the data, rather than a valid general relationship.

Values of g provided by the equation used to correlate the data, as represented by Eq. (4-310), are called *derived* values, and produce derived values of the activity coefficients by Eqs. (4-180) with $M \equiv g$:

$$\ln \gamma_1 = g + x_2 \frac{dg}{dx_1} \quad (4-314a)$$

$$\ln \gamma_2 = g - x_1 \frac{dg}{dx_1} \quad (4-314b)$$

These two equations combine to yield

$$\frac{dg}{dx_1} = \ln \frac{\gamma_1}{\gamma_2} \quad (4-315)$$

This equation is valid for *derived* property values. The corresponding *experimental* values are given by differentiation of Eq. (4-312):

$$\frac{dg^\circ}{dx_1} = x_1 \frac{d \ln \gamma_1^\circ}{dx_1} + \ln \gamma_1^\circ + x_2 \frac{d \ln \gamma_2^\circ}{dx_1} - \ln \gamma_2^\circ$$

$$\text{or} \quad \frac{dg^\circ}{dx_1} = \ln \frac{\gamma_1^\circ}{\gamma_2^\circ} + x_1 \frac{d \ln \gamma_1^\circ}{dx_1} + x_2 \frac{d \ln \gamma_2^\circ}{dx_1} \quad (4-316)$$

Subtraction of Eq. (4-316) from Eq. (4-315) gives

$$\frac{dg}{dx_1} - \frac{dg^\circ}{dx_1} = \ln \frac{\gamma_1}{\gamma_2} - \ln \frac{\gamma_1^\circ}{\gamma_2^\circ} - \left(x_1 \frac{d \ln \gamma_1^\circ}{dx_1} + x_2 \frac{d \ln \gamma_2^\circ}{dx_1} \right)$$

The differences between like terms represent *residuals* between derived and experimental values. Defining these residuals as

$$\delta g \equiv g - g^\circ \quad \text{and} \quad \delta \ln \frac{\gamma_i}{\gamma_j} \equiv \ln \frac{\gamma_i}{\gamma_j} - \ln \frac{\gamma_i^\circ}{\gamma_j^\circ}$$

puts this equation into the form

$$\frac{d \delta g}{dx_1} = \delta \ln \frac{\gamma_1}{\gamma_2} - \left(x_1 \frac{d \ln \gamma_1^\circ}{dx_1} + x_2 \frac{d \ln \gamma_2^\circ}{dx_1} \right)$$

If a data set is reduced so as to yield parameters— α, β , etc.—that make the δg residuals scatter about zero, then the derivative on the left is effectively zero, and the preceding equation becomes

$$\delta \ln \frac{\gamma_1}{\gamma_2} = x_1 \frac{d \ln \gamma_1^\circ}{dx_1} + x_2 \frac{d \ln \gamma_2^\circ}{dx_1} \quad (4-317)$$

The right side of this equation is the quantity required by Eq. (4-313), the Gibbs-Duhem equation, to be zero for consistent data. The residual on the left is therefore a direct measure of deviations from the Gibbs-Duhem equation. The extent to which values of this residual fail to scatter about zero measures the departure of the data from consistency with respect to this equation.

The data reduction procedure just described provides parameters in the correlating equation for g that make the δg residuals scatter about zero. This is usually accomplished by finding the parameters that minimize the sum of squares of the residuals. Once these parameters are found, they can be used for the calculation of derived values of both the pressure P and the vapor composition y_1 . Equation (4-303) is solved for $y_1 P$ and written for species 1 and for species 2. Adding the two equations gives

$$P = \frac{x_1 \gamma_1 P_1^{\text{sat}}}{\Phi_1} + \frac{x_2 \gamma_2 P_2^{\text{sat}}}{\Phi_2} \quad (4-318)$$

$$\text{whence by Eq. (4-303),} \quad y_1 = \frac{x_1 \gamma_1 P_1^{\text{sat}}}{\Phi_1 P} \quad (4-319)$$

These equations allow calculation of the *primary* residuals:

$$\delta P \equiv P - P^\circ \quad \text{and} \quad \delta y_1 \equiv y_1 - y_1^\circ$$

If the experimental values P° and y_1° are closely reproduced by the correlating equation for g , then these residuals, evaluated at the experimental values of x_1 , scatter about zero. This is the result obtained when the data approach thermodynamic consistency. When they do not, these residuals fail to scatter about zero and the correlation for g does not properly reproduce the experimental values P° and y_1° .

Such a correlation is unnecessarily divergent. An alternative is to base data reduction on just the P - x_1 data subset; this is possible because the full P - x_1 - y_1 data set includes redundant information. Assuming that the correlating equation is appropriate to the data, one merely searches for values of the parameters α, β , etc., that yield pressures by Eq. (4-318) that are as close as possible to the measured values. The usual procedure is to minimize the sum of squares of the residuals δP . Known as *Barker's method* [Austral. J. Chem. 6: 207–210 (1953)], it provides the best possible fit of the experimental pressures. When experimental y_1° values are not consistent with the P - x_1 data, Barker's method cannot lead to calculated y_1 values that closely match the experimental y_1° values. With experimental error usually concentrated in the y_1° values, the calculated y_1 values are likely to be more nearly correct. Because Barker's method requires only the P - x_1 data subset, the measurement of y_1° values is not usually worth the extra effort, and the correlating parameters α, β , etc., are usually best determined without them. Hence, many P - x_1 data subsets appear in the literature; they are of course not subject to a test for consistency by the Gibbs-Duhem equation.

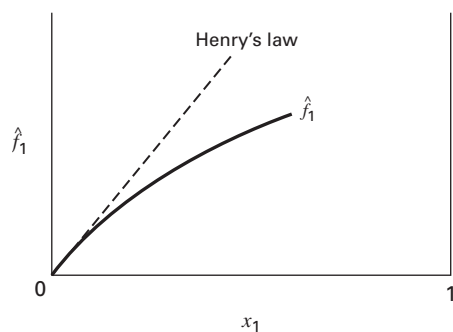


FIG. 4-7 Plot of solute fugacity \hat{f}_1 versus solute mole fraction. [Smith, Van Ness, and Abbott, *Introduction to Chemical Engineering Thermodynamics*, 7th ed., p. 555, McGraw-Hill, New York (2005).]

The world's store of VLE data has been compiled by Gmehling et al. [*Vapor-Liquid Equilibrium Data Collection*, Chemistry Data Series, vol. 1, parts 1–8, DECHEMA, Frankfurt am Main (1979–1990)].

Solute/Solvent Systems The gamma/phi approach to VLE calculations presumes knowledge of the vapor pressure of each species at the temperature of interest. For certain binary systems species 1, designated the solute, is either unstable at the system temperature or is *supercritical* ($T > T_c$). Its vapor pressure cannot be measured, and its fugacity as a pure liquid at the system temperature f_1 cannot be calculated by Eq. (4-302).

Equations (4-303) and (4-304) are applicable to species 2, designated the solvent, but not to the solute, for which an alternative approach is required. Figure 4-7 shows a typical plot of the liquid-phase fugacity of the solute \hat{f}_1 versus its mole fraction x_1 at constant temperature. Since the curve representing \hat{f}_1 does not extend all the way to $x_1 = 1$, the location of f_1 , the liquid-phase fugacity of pure species 1, is not established. The tangent line at the origin, representing *Henry's law*, provides alternative information. The slope of the tangent line is *Henry's constant*, defined as

$$k_1 \equiv \lim_{x_1 \rightarrow 0} \frac{\hat{f}_1}{x_1} \quad (4-320)$$

This is the definition of k_1 for temperature T and for a pressure equal to the vapor pressure of the pure solvent P_2^{sat} .

The activity coefficient of the solute at infinite dilution is

$$\lim_{x_1 \rightarrow 0} \gamma_1 = \lim_{x_1 \rightarrow 0} \frac{\hat{f}_1}{x_1 f_1} = \frac{1}{f_1} \lim_{x_1 \rightarrow 0} \frac{\hat{f}_1}{x_1}$$

In view of Eq. (4-320), this becomes $\gamma_1^\infty = k_1/f_1$, or

$$f_1 = \frac{k_1}{\gamma_1^\infty} \quad (4-321)$$

where γ_1^∞ represents the infinite dilution value of the activity coefficient of the solute. Because both k_1 and γ_1^∞ are evaluated at P_2^{sat} , this pressure also applies to f_1 . However, the effect of P on a liquid-phase fugacity, given by a Poynting factor, is very small and for practical purposes may usually be neglected. The activity coefficient of the solute then becomes

$$\gamma_1 \equiv \frac{\hat{f}_1}{x_1 f_1} = \frac{y_1 P \hat{\phi}_1}{x_1 f_1} = \frac{y_1 P \hat{\phi}_1 \gamma_1^\infty}{x_1 k_1}$$

For the solute, this equation takes the place of Eqs. (4-303) and (4-304). Solution for y_1 gives

$$y_1 = \frac{x_1 (\gamma_1 / \gamma_1^\infty) k_1}{\hat{\phi}_1 P} \quad (4-322)$$

For the solvent, species 2, the analog of Eq. (4-319) is

$$y_2 = \frac{x_2 \gamma_2 P_2^{\text{sat}}}{\hat{\Phi}_2 P} \quad (4-323)$$

$$\text{Because } y_1 + y_2 = 1, \quad P = \frac{x_1 (\gamma_1 / \gamma_1^\infty) k_1}{\hat{\phi}_1} + \frac{x_2 \gamma_2 P_2^{\text{sat}}}{\hat{\Phi}_2} \quad (4-324)$$

The same correlation that provides for the evaluation of γ_1 also allows evaluation of γ_1^∞ .

There remains the problem of finding Henry's constant from the available VLE data.

For equilibrium $\hat{f}_1 \equiv \hat{f}_1^l = \hat{f}_1^v = y_1 P \hat{\phi}_1$

$$\text{Division by } x_1 \text{ gives} \quad \frac{\hat{f}_1}{x_1} = P \hat{\phi}_1 \frac{y_1}{x_1}$$

Henry's constant is defined as the limit as $x_1 \rightarrow 0$ of the ratio on the left; therefore

$$k_1 = P_2^{\text{sat}} \hat{\phi}_1^\infty \lim_{x_1 \rightarrow 0} \frac{y_1}{x_1}$$

The limiting value of y_1/x_1 can be found by plotting y_1/x_1 versus x_1 and extrapolating to zero.

K Values, VLE, and Flash Calculations A measure of the distribution of a chemical species between liquid and vapor phases is the K value, defined as the equilibrium ratio:

$$K_i \equiv \frac{y_i}{x_i} \quad (4-325)$$

It has no thermodynamic content, but may make for computational convenience through elimination of one set of mole fractions in favor of the other. It does characterize "lightness" of a constituent species. A "light" species, with $K > 1$, tends to concentrate in the vapor phase whereas a "heavy" species, with $K < 1$, tends to concentrate in the liquid phase.

The rigorous evaluation of a K value follows from Eq. (4-299):

$$K_i \equiv \frac{y_i}{x_i} = \frac{\gamma_i f_i^l}{\hat{\phi}_i P} \quad (4-326)$$

When Raoult's law applies, Eq. (4-326) reduces to $K_i = P_i^{\text{sat}}/P$. For modified Raoult's law, $K_i = \gamma_i P_i^{\text{sat}}/P$. With $K_i = y_i/x_i$, these are alternative expressions of Raoult's law and modified Raoult's law. Were Raoult's valid, K values could be correlated as functions of just T and P . However, Eq. (4-326) shows that they are in general functions of T , P , $\{x_i\}$, and $\{y_i\}$, making convenient and accurate correlation impossible. Those correlations that do exist are approximate and severely limited in application. The nomographs for K values of light hydrocarbons as functions of T and P , prepared by DePriester [*Chem. Eng. Progr. Symp. Ser. No. 7*, **49**: 1–43 (1953)], do allow for an *average* effect of composition, but their essential basis is Raoult's law.

The defining equation for K can be rearranged as $y_i = K_i x_i$. The sum $\sum_i y_i = 1$ then yields

$$\sum_i K_i x_i = 1 \quad (4-327)$$

With the alternative rearrangement $x_i = y_i/K_i$, the sum $\sum_i x_i = 1$ yields

$$\sum_i \frac{y_i}{K_i} = 1 \quad (4-328)$$

Thus for bubble point calculations, where the x_i are known, the problem is to find the set of K values that satisfies Eq. (4-327), whereas for dew point calculations, where the y_i are known, the problem is to find the set of K values that satisfies Eq. (4-328).

The *flash calculation* is a very common application of VLE. Considered here is the P, T flash, in which are calculated the quantities and compositions of the vapor and liquid phases in equilibrium at known T, P , and *overall* composition. This problem is determinate on the basis of Duhem's theorem: *For any closed system formed initially from*

4-32 THERMODYNAMICS

given masses of prescribed chemical species, the equilibrium state is completely determined when any two independent variables are fixed. The independent variables are here T and P , and systems are formed from given masses of nonreacting chemical species.

For 1 mol of a system with overall composition represented by the set of mole fractions $\{z_i\}$, let \mathcal{L} represent the molar fraction of the system that is liquid (mole fractions $\{x_i\}$) and let \mathcal{V} represent the molar fraction that is vapor (mole fractions $\{y_i\}$). The material balance equations are

$$\mathcal{L} + \mathcal{V} = 1 \quad \text{and} \quad z_i = x_i \mathcal{L} + y_i \mathcal{V} \quad i = 1, 2, \dots, N$$

Combining these equations to eliminate \mathcal{L} gives

$$z_i = x_i(1 - \mathcal{V}) + y_i \mathcal{V} \quad i = 1, 2, \dots, N \quad (4-329)$$

Substitute $x_i = y_i/K_i$ and solve for y_i :

$$y_i = \frac{z_i K_i}{1 + \mathcal{V}(K_i - 1)} \quad i = 1, 2, \dots, N$$

Because $\sum y_i = 1$, this equation, summed over all species, yields

$$\sum_i \frac{z_i K_i}{1 + \mathcal{V}(K_i - 1)} = 1 \quad (4-330)$$

The initial step in solving a P, T flash problem is to find the value of \mathcal{V} which satisfies this equation. Note that $\mathcal{V} = 1$ is always a *trivial* solution.

Example 4: Flash Calculation The system of Example 3 has the overall composition $z_1 = 0.4000$ at $T = 325.15$ K and $P = 101.33$ kPa. Determine \mathcal{V} , x_1 , and y_1 .

The *BUBL P* and *DEW P* calculations at $T = 325.15$ K of Example 3a and 3b show that for $x_1 = z_1$, $P_{\text{bubl}} = 108.134$ kPa, and for $y_1 = z_1$, $P_{\text{dew}} = 87.939$ kPa. Because P here lies between these values, the system is in two-phase equilibrium, and a flash calculation is appropriate.

The modified Raoult's law K values are given by

$$K_1 = \frac{(\gamma_1)(P_1^{\text{sat}})}{P} \quad \text{and} \quad K_2 = \frac{(\gamma_2)(P_2^{\text{sat}})}{P}$$

Equation (4-329) may be solved for \mathcal{V} : $\mathcal{V} = \frac{z_1 - x_1}{y_1 - x_1}$

Equation (4-330) here becomes

$$\frac{(z_1)(K_1)}{1 + \mathcal{V}(K_1 - 1)} + \frac{(z_2)(K_2)}{1 + \mathcal{V}(K_2 - 1)} = 1$$

A trial calculation illustrates the nature of the solution. Vapor pressures are taken from Example 3a or 3b; a trial value of x_1 then allows calculation of γ_1 and γ_2 by Eqs. (B) and (C) of Example 3. The values of K_1 , K_2 , and \mathcal{V} that result are substituted into the summation equation. In the unlikely event that the sum is indeed unity, the chosen value of x_1 is correct. If not, then successive trials easily lead to this value. Note that the trivial solution giving $\mathcal{V} = 1$ must be avoided. More elegant solution procedures can of course be employed. The answers are

$$x_1 = 0.2373 \quad y_1 = 0.5190 \quad \mathcal{V} = 0.5775$$

with $\gamma_1 = 2.5297 \quad \gamma_2 = 1.0997 \quad K_1 = 2.1873 \quad K_2 = 0.6306$

Equation-of-State Approach Although the gamma/phi approach to VLE is in principle generally applicable to systems comprised of subcritical species, in practice it has found use primarily where pressures are no more than a few bars. Moreover, it is most satisfactory for correlation of constant-temperature data. A temperature dependence for the parameters in expressions for G^E is included only for the local composition equations, and it is at best approximate.

A generally applicable alternative to the gamma/phi approach results when both the liquid and vapor phases are described by the same equation of state. The defining equation for the fugacity coefficient, Eq. (4-204), may be applied to each phase:

$$\text{Liquid: } \hat{f}_i^l = \hat{\phi}_i^l x_i P \quad \text{Vapor: } \hat{f}_i^v = \hat{\phi}_i^v y_i P$$

By Eq. (4-298), $x_i \hat{\phi}_i^l = y_i \hat{\phi}_i^v \quad i = 1, 2, \dots, N \quad (4-331)$

This introduces compositions x_i and y_i into the equilibrium equations, but neither is explicit, because the $\hat{\phi}_i$ are functions, not only of T and

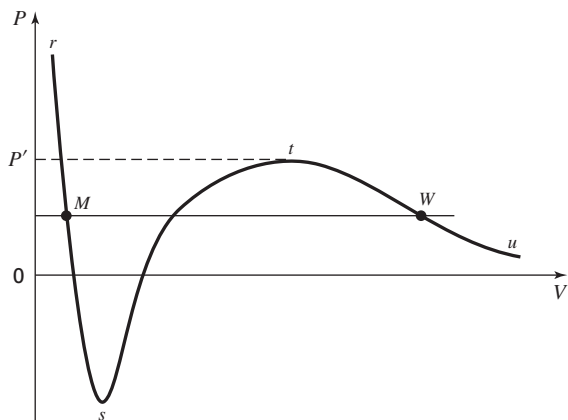


FIG. 4-8 A subcritical isotherm on a PV diagram for a pure fluid. [Smith, Van Ness, and Abbott, *Introduction to Chemical Engineering Thermodynamics*, 7th ed., p. 557, McGraw-Hill, New York (2005).]

P , but of composition. Thus, Eq. (4-331) represents N complex relationships connecting T , P , $\{x_i\}$, and $\{y_i\}$.

Two widely used cubic equations of state appropriate for VLE calculations, both special cases of Eq. (4-100) [with Eqs. (4-101) and (4-102)], are the Soave-Redlich-Kwong (SRK) equation and the Peng-Robinson (PR) equation. The present treatment is applicable to both. The pure numbers ϵ , σ , Ψ , and Ω and expressions for $\alpha(T_i)$ specific to these equations are listed in Table 4-2. The associated expression for ϕ_i is given by Eq. (4-246).

The simplest application of equations of state in vapor/liquid equilibrium is to the calculation of vapor pressures P_i^{sat} of pure liquids. Vapor pressures can of course be measured, but values are also implicit in cubic equations of state.

A subcritical PV isotherm, generated by a cubic equation of state, is shown in Fig. 4-8. Three segments are evident. The very steep one on the left (rs) is characteristic of liquids. Note that as $P \rightarrow \infty, V \rightarrow b$, where b is a constant in the cubic equation. The gently sloping segment on the right (tu) is characteristic of vapors; here $\dot{P} \rightarrow 0$ as $V \rightarrow \infty$. The middle segment (st), with both a minimum (note $P < 0$) and a maximum, provides a transition from liquid to vapor, but has no physical meaning. The actual transition occurs along a horizontal line, such as connects points M and W .

For pure species i , Eq. (4-331) reduces to $\phi_i^v = \phi_i^l$, which may be written as

$$\ln \phi_i^v = \ln \phi_i^l \quad (4-332)$$

For given T , line MW lies at the vapor pressure P_i^{sat} if and only if the fugacity coefficients for points M and W satisfy Eq. (4-332). These points then represent *saturated* liquid and vapor phases in equilibrium at temperature T .

The fugacity coefficients in Eq. (4-332) are given by Eq. (4-245):

$$\ln \phi_i^p = Z_i^p - 1 - \ln(Z_i^p - \beta_i) - q_i I_i^p \quad p = l, v \quad (4-333)$$

Expressions for Z_i^v and Z_i^l come from Eqs. (4-104):

$$Z_i^v = 1 + \beta_i - q_i \beta_i \frac{Z_i^v - \beta_i}{(Z_i^v + \epsilon \beta_i)(Z_i^v + \sigma \beta_i)} \quad (4-334)$$

$$Z_i^l = \beta_i + (Z_i^l + \epsilon \beta_i)(Z_i^l + \sigma \beta_i) \left(\frac{1 + \beta_i - Z_i^l}{q_i \beta_i} \right) \quad (4-335)$$

and I_i^p comes from Eq. (4-112):

$$I_i^p = \frac{1}{\sigma - \epsilon} \ln \frac{Z_i^p + \sigma \beta_i}{Z_i^p + \epsilon \beta_i} \quad p = l, v \quad (4-336)$$

The equation-of-state parameters are independent of phase. As defined by Eq. (4-105), β_i is a function of P and here becomes

$$\beta_i \equiv \frac{b_i P_i^{\text{sat}}}{RT} \quad (4-337)$$

The remaining equation-of-state parameters, given by Eqs. (4-101), (4-102), and (4-106), are functions of T only and are written here as

$$a_i(T) = \psi \frac{\alpha(T_r) R^2 T_c^2}{P_c} \quad (4-338)$$

$$b_i = \Omega \frac{RT_c}{P_c} \quad (4-339)$$

$$q_i \equiv \frac{a_i(T)}{b_i RT} \quad (4-340)$$

The eight equations (4-332) through (4-337) may be solved for the eight unknowns P_i^{sat} , β_i , Z_i^l , Z_i^v , I_i^l , I_i^v , $\ln \phi_i^l$, and $\ln \phi_i^v$.

Perhaps more useful is the reverse calculation whereby an equation-of-state parameter is evaluated from a known vapor pressure. Thus, Eqs. (4-332) and (4-333) may be combined and solved for q_i , yielding

$$q_i = \frac{Z_i^v - Z_i^l + \ln [(Z_i^l - \beta_i)/(Z_i^v - \beta_i)]}{I_i^v - I_i^l} \quad (4-341)$$

Expressions for Z_i^l , Z_i^v , I_i^l , I_i^v , and β_i are given by Eqs. (4-334) through (4-337). Because Z_i^l and Z_i^v depend on q_i , an iterative procedure is indicated, with a starting value for q_i from a generalized correlation as given by Eqs. (4-338), (4-339), and (4-340).

For mixtures the presumption is that the equation of state has exactly the same form as when written for pure species. Equations (4-104) are therefore applicable, with parameters β and q given by Eqs. (4-105) and (4-106). Here, these parameters, and therefore b and $a(T)$, are *functions of composition*. Liquid and vapor mixtures in equilibrium in general have different compositions. The PV isotherms generated by an equation of state for these different compositions are represented in Fig. 4-9 by two similar lines: the solid line for the liquid-phase composition and the dashed line for the vapor-phase composition. They are displaced from each other because the equation-of-state parameters are different for the two compositions.

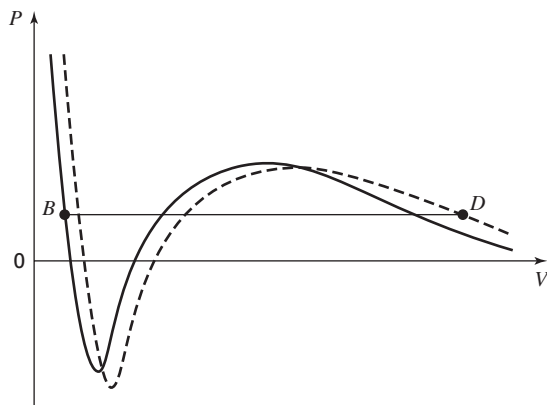


FIG. 4-9 Two PV isotherms at the same T for mixtures. The solid line is for a liquid-phase composition; the dashed line is for a vapor-phase composition. Point B represents a bubble point with the liquid-phase composition; point D represents a dew point with the vapor-phase composition. When these points lie at the same P (as shown), they represent phases in equilibrium. [Smith, Van Ness, and Abbott, Introduction to Chemical Engineering Thermodynamics, 7th ed., p. 560, McGraw-Hill, New York (2005).]

Each line includes three *segments* as described for the isotherm of Fig. 4-8: the leftmost segment representing a liquid phase and the rightmost segment, a vapor phase, *both with the same composition*. Each left segment contains a bubble point (saturated liquid), and each right segment contains a dew point (saturated vapor). Because these points for a given line are for the same composition, they do not represent phases in equilibrium and do not lie at the same pressure. Shown in Fig. 4-9 is a bubble point B on the solid line and a dew point D on the dashed line. Because they lie at the same P , they represent phases in equilibrium, and the lines are characterized by the liquid and vapor compositions.

For a *BUBL P* calculation, the temperature and the liquid composition are known, and this fixes the location of the PV isotherm for the composition of the liquid phase (solid line). The problem then is to locate a second (dashed) line for a vapor composition such that the line contains a dew point D on its vapor segment that lies at the pressure of the bubble point B on the liquid segment of the solid line. This pressure is the phase equilibrium pressure, and the composition for the dashed line is that of the equilibrium vapor. This equilibrium condition is shown by Fig. 4-9.

In the absence of a theory to prescribe the composition dependence of parameters for cubic equations of state, empirical *mixing rules* are used to relate mixture parameters to pure-species parameters. The simplest realistic expressions are a linear mixing rule for parameter b and a quadratic mixing rule for parameter a , as shown by Eqs. (4-113) and (4-114). A common combining rule is given by Eq. (4-115). The general mole fraction variable x_i is used here because application is to both liquid and vapor mixtures. These equations, known as van der Waals prescriptions, provide for the evaluation of mixture parameters solely for parameters for the pure constituent species. They find application primarily for mixtures comprised of simple and chemically similar molecules.

Useful in the application of cubic equations of state to mixtures are *partial* equation-of-state parameters. For the parameters of the generic cubic, represented by Eqs. (4-104), (4-105), and (4-106), the definitions are

$$\bar{a}_i \equiv \left[\frac{\partial(na)}{\partial n_i} \right]_{T,n_j} \quad (4-342)$$

$$\bar{b}_i \equiv \left[\frac{\partial(nb)}{\partial n_i} \right]_{T,n_j} \quad (4-343)$$

$$\bar{q}_i \equiv \left[\frac{\partial(nq)}{\partial n_i} \right]_{T,n_j} \quad (4-344)$$

These are general equations, valid regardless of the particular mixing or combining rules adopted for the composition dependence of mixture parameters.

Parameter q is defined in relation to parameters a and b by Eq. (4-106). Thus,

$$nq = \frac{n(na)}{RT(nb)}$$

$$\text{whence} \quad \bar{q}_i \equiv \left[\frac{\partial(nq)}{\partial n_i} \right]_{T,n_j} = q \left(1 + \frac{\bar{a}_i}{a} - \frac{\bar{b}_i}{b} \right) \quad (4-345)$$

Any two of the three partial parameters form an independent pair, and any one of them can be found from the other two. Because q , a , and b are not linearly related, $\bar{q}_i \neq \bar{a}_i/\bar{b}_i/RT$.

Values of $\hat{\phi}_i^l$ and $\hat{\phi}_i^v$ as given by Eq. (4-246) are implicit in an equation of state and with Eq. (4-331) allow calculation of *mixture VLE*. Although more complex, the same basic principle applies as for pure-species VLE. With $\hat{\phi}_i^l$ a function of T , P , and $\{x_i\}$, and $\hat{\phi}_i^v$ a function of T , P , and $\{y_i\}$, Eq. (4-331) represents N relations among the $2N$ variables: T , P , $(N-1)$ x 's, and $(N-1)$ y 's. Thus, specification of N of these variables, usually either T or P and either the liquid- or vapor-phase composition, allows solution for the remaining N variables by *BUBL P*, *DEW P*, *BUBL T*, and *DEW T* calculations.

Because of limitations inherent in empirical mixing and combining rules, such as those given by Eqs. (4-113) through (4-115), the equation-of-state approach has found primary application to systems exhibiting modest deviations from ideal solution behavior in the liquid phase, e.g., to systems containing hydrocarbons and cryogenic fluids. However, since 1990, extensive research has been devoted to developing mixing rules that incorporate the excess Gibbs energy or activity coefficient data available for many systems. The extensive literature on this subject is reviewed by Valderrama [*Ind. Eng. Chem. Res.* **42**: 1603–1618 (2003)] and by Twu, Sim, and Tassone [*Chem. Eng. Progress* **98**(11): 58–65 (Nov. 2002)].

The idea here is to exploit the connection between fugacity coefficients and activity coefficients provided by their definitions:

$$\gamma_i \equiv \frac{\hat{f}_i}{x_i f_i} = \frac{\hat{f}_i/x_i P}{f_i/P} = \frac{\hat{\phi}_i}{\phi_i}$$

Therefore, $\ln \gamma_i = \ln \hat{\phi}_i - \ln \phi_i$ (4-346)

Because γ_i is a liquid-phase property, this equation is written for the liquid phase. Substituting for $\ln \hat{\phi}_i$ and $\ln \phi_i$ by Eqs. (4-245) and Eq. (4-246) gives

$$\ln \gamma_i = \frac{b_i}{b} (Z-1) - Z_i + 1 - \ln \frac{Z-\beta}{Z_i-\beta_i} - \bar{q}_i I + q_i I_i$$

Symbols without subscripts are mixture properties. Solution for \bar{q}_i yields

$$\bar{q}_i = \frac{1}{I} \left[1 - Z_i + \frac{b_i}{b} (Z-1) - \ln \frac{Z-\beta}{Z_i-\beta_i} + q_i I_i - \ln \gamma_i \right] \quad (4-347)$$

Because \bar{q}_i is a partial property, the summability equation provides an exact mixing rule:

$$q = \sum_i x_i \bar{q}_i \quad (4-348)$$

Application of this equation in the solution of VLE problems is illustrated by Smith, Van Ness, and Abbott [*Introduction to Chemical Engineering Thermodynamics*, 7th ed., pp. 569–572, McGraw-Hill, New York (2005)].

Extrapolation of Data with Temperature Liquid-phase excess-property data for binary systems at near-ambient temperatures appear in the literature. They provide for the extrapolation of G^E correlations with temperature. The key relations are Eq. (4-250), written as

$$d\left(\frac{G^E}{RT}\right) = -\frac{H^E}{RT^2} dT \quad \text{constant } P, x$$

and the excess-property analog of Eq. (4-26):

$$dH^E = C_P^E dT \quad \text{constant } P, x$$

Integration of the first equation from T_0 to T gives

$$\frac{G^E}{RT} = \left(\frac{G^E}{RT}\right)_{T_0} - \int_{T_0}^T \frac{H^E}{RT^2} dT \quad (4-349)$$

Integration of the second equation from T_1 to T yields

$$H^E = H_1^E + \int_{T_1}^T C_P^E dT \quad (4-350)$$

In addition,

$$dC_P^E = \left(\frac{\partial C_P^E}{\partial T}\right)_{P,x} dT$$

Integrate from T_2 to T :

$$C_P^E = C_{P_2}^E + \int_{T_2}^T \left(\frac{\partial C_P^E}{\partial T}\right)_{P,x} dT$$

Combining this equation with Eqs. (4-349) and (4-350) leads to

$$\begin{aligned} \frac{G^E}{RT} = & \left(\frac{G^E}{RT}\right)_{T_0} - \left(\frac{H^E}{RT}\right)_{T_1} \left(\frac{T}{T_0} - 1\right) \frac{T_1}{T} \\ & - \frac{C_{P_2}^E}{R} \left[\ln \frac{T}{T_0} - \left(\frac{T}{T_0} - 1\right) \frac{T_1}{T} \right] - I \quad (4-351) \end{aligned}$$

where

$$I \equiv \int_{T_0}^T \frac{1}{RT^2} \int_{T_1}^T \left(\frac{\partial C_P^E}{\partial T}\right)_{P,x} dT dT dT$$

This general equation employs excess Gibbs energy data at temperature T_0 , excess enthalpy (heat-of-mixing) data at T_1 , and excess heat capacity data at T_2 . Integral I depends on the temperature dependence of C_P^E . Excess heat capacity data are uncommon, and the T dependence is rarely known. Assuming C_P^E independent of T makes the integral zero, and the closer T_0 and T_1 are to T , the less the influence of this assumption. When no information is available for C_P^E and excess enthalpy data are available at only a single temperature, C_P^E must be assumed zero. In this case only the first two terms on the right side of Eq. (4-351) are retained, and it more rapidly becomes imprecise as T increases.

For application of Eq. (4-351) to binary systems at *infinite dilution* of one of the constituent species, it is divided by the product $x_1 x_2$.

$$\begin{aligned} \frac{G^E}{x_1 x_2 RT} = & \left(\frac{G^E}{x_1 x_2 RT}\right)_{T_0} - \left(\frac{H^E}{x_1 x_2 RT}\right)_{T_1} \left(\frac{T}{T_0} - 1\right) \frac{T_1}{T} \\ & - \frac{C_{P_2}^E}{x_1 x_2 R} \left[\ln \frac{T}{T_0} - \left(\frac{T}{T_0} - 1\right) \frac{T_1}{T} \right] \end{aligned}$$

The assumption here is that C_P^E is independent of T , making $I = 0$. As shown by Smith, Van Ness and Abbott [*Introduction to Chemical Engineering Thermodynamics*, 7th ed., p. 437, McGraw-Hill, New York (2005)],

$$\left(\frac{G^E}{x_1 x_2 RT}\right)_{x_i=0} \equiv \ln \gamma_i^\infty$$

The preceding equation may therefore be written as

$$\begin{aligned} \ln \gamma_i^\infty = & (\ln \gamma_i^\infty)_{T_0} - \left(\frac{H^E}{x_1 x_2 RT}\right)_{T_1, x_i=0} \left(\frac{T}{T_0} - 1\right) \frac{T_1}{T} \\ & - \left(\frac{C_{P_2}^E}{x_1 x_2 R}\right)_{x_i=0} \left[\ln \frac{T}{T_0} - \left(\frac{T}{T_0} - 1\right) \frac{T_1}{T} \right] \quad (4-352) \end{aligned}$$

Example 5: VLE at Several Temperatures For the methanol(1)/acetone(2) system at a base temperature of $T_0 = 323.15$ K (50°C), both VLE data [Van Ness and Abbott, *Int. DATA Ser., Ser. A, Sel. Data Mixtures*, **1978**: 67 (1978)] and excess enthalpy data [Morris et al., *J. Chem. Eng. Data* **20**: 403–405 (1975)] are available. The VLE data are well correlated by the Margules equations. As noted in connection with Eq. (4-270), parameters A_{12} and A_{21} relate directly to infinite dilution values of the activity coefficients. Thus, we have from the VLE data at 323.15 K:

$$A_{12} = \ln \gamma_1^\infty = 0.6281 \quad \text{and} \quad A_{21} = \ln \gamma_2^\infty = 0.6557$$

These values allow calculation of equilibrium pressures through Eqs. (4-270) and (4-308) for comparison with the measured pressures of the data set. Values of P_i^{sat} required in Eq. (4-308) are the measured values reported with the data set. The root-mean-square (rms) value of the pressure differences is given in Table 4-7 as 0.08 kPa, thus confirming the suitability of the Margules equation for this system. Vapor-phase mole fractions were not reported; hence no value can be given for rms δy_1 .

Experimental VLE data at 372.8 and 397.7 K are given by Wilsak et al. [*Fluid Phase Equilib.* **28**: 13–37 (1986)]. Values of $\ln \gamma_i^\infty$ and hence of the Margules parameters for these higher temperatures are found from Eq. (4-352) with $C_P^E = 0$. The required excess enthalpy values at T_0 are

$$\left(\frac{H^E}{x_1 x_2 RT}\right)_{T_0, x_i=0} = 1.3636 \quad \text{and} \quad \left(\frac{H^E}{x_1 x_2 RT}\right)_{T_0, x_2=0} = 1.0362$$

TABLE 4-7 VLE Results for Methanol(1)/Acetone(2)

T, K	$A_{12} = \ln \gamma_1^\infty$	$A_{21} = \ln \gamma_2^\infty$	RMS $\delta P/kPa$	RMS % δP	RMS δy_1
323.15	0.6281	0.6557	0.08	0.12	
372.8	0.4465 (0.4607)	0.5177 (0.5271)	0.85 (0.83)	0.22	0.004 (0.006)
397.7	0.3725 (0.3764)	0.4615 (0.4640)	2.46 (1.39)	0.32	0.014 (0.013)

Results of calculations with the Margules equations are displayed as the primary entries at each temperature in Table 4-7. The values in parentheses are from the gamma/phi approach as reported in the papers cited.

Results for the higher temperatures indicate the quality of predictions based only on vapor-pressure data for the pure species and on mixture data at 323.15 K. Extrapolations based on the same data to still higher temperatures can be expected to become progressively less accurate.

Only the Wilson, NRTL, and UNIQUAC equations are suited to the treatment of multicomponent systems. For such systems, the parameters are determined for pairs of species exactly as for a binary system.

LIQUID/LIQUID AND VAPOR/LIQUID/LIQUID EQUILIBRIA

Equation (4-295) is the basis for both liquid/liquid equilibria (LLE) and vapor/liquid/liquid equilibria (VLLE). Thus for LLE with supercritical α and β denoting the two phases, Eq. (4-295) is written as

$$\hat{f}_i^\alpha = \hat{f}_i^\beta \quad i = 1, 2, \dots, N \quad (4-353)$$

Eliminating fugacities in favor of activity coefficients gives

$$x_i^\alpha \gamma_i^\alpha = x_i^\beta \gamma_i^\beta \quad i = 1, 2, \dots, N \quad (4-354)$$

For most LLE applications, the effect of pressure on the γ_i can be ignored, and Eq. (4-354) then constitutes a set of N equations relating equilibrium compositions to one another and to temperature. For a given temperature, solution of these equations requires a single expression for the composition dependence of G^E suitable for both liquid phases. Not all expressions for G^E suffice, even in principle, because some cannot represent liquid/liquid phase splitting. The UNIQUAC equation is suitable, and therefore prediction is possible by UNIFAC models. A special table of parameters for LLE calculations is given by Magnussen et al. [*Ind. Eng. Chem. Process Des. Dev.* **20**: 331–339 (1981)].

A comprehensive treatment of LLE is given by Sorensen et al. [*Fluid Phase Equilib.* **2**: 297–309 (1979); **3**: 47–82 (1979); **4**: 151–163 (1980)]. Data for LLE are collected in a three-part set compiled by Sorensen and Arlt [*Liquid-Liquid Equilibrium Data Collection*, Chemistry Data Series, vol. 5, parts 1–3, DECHEMA, Frankfurt am Main (1979–1980)].

For vapor/liquid/liquid equilibria, Eq. (4-295) becomes

$$\hat{f}_i^\alpha = \hat{f}_i^\beta = \hat{f}_i^v \quad i = 1, 2, \dots, N \quad (4-355)$$

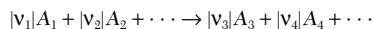
where α and β designate the two liquid phases. With activity coefficients applied to the liquid phases and fugacity coefficients to the vapor phase, the $2N$ equilibrium equations for subcritical VLLE are

$$\left. \begin{aligned} x_i^\alpha \gamma_i^\alpha \hat{f}_i^\alpha &= y_i \hat{\phi}_i P \\ x_i^\beta \gamma_i^\beta \hat{f}_i^\beta &= y_i \hat{\phi}_i P \end{aligned} \right\} \quad \text{all } i \quad (4-356)$$

As for LLE, an expression for C^E capable of representing liquid/liquid phase splitting is required; as for VLE, a vapor-phase equation of state for computing the $\hat{\phi}_i$ is also needed.

CHEMICAL REACTION STOICHIOMETRY

For a phase in which a chemical reaction occurs according to the equation



the $|v_i|$ are stoichiometric coefficients and the A_i stand for chemical formulas. The v_i themselves are called stoichiometric numbers, and associated with them is a sign convention such that the value is positive for a product and negative for a reactant. More generally, for a system containing N chemical species, any or all of which can participate in r chemical reactions, the reactions are represented by the equations

$$0 = \sum_i v_{ij} A_i \quad j = \text{I, II, } \dots, r \quad (4-357)$$

where $\text{sign}(v_{i,j}) = \begin{cases} - & \text{for a reactant species} \\ + & \text{for a product species} \end{cases}$

If species i does not participate in reaction j , then $v_{ij} = 0$.

The stoichiometric numbers provide relations among the changes in mole numbers of chemical species which occur as the result of chemical reaction. Thus, for reaction j

$$\frac{\Delta n_{1,j}}{v_{1,j}} = \frac{\Delta n_{2,j}}{v_{2,j}} = \dots = \frac{\Delta n_{N,j}}{v_{N,j}} \quad (4-358)$$

All these terms are equal, and they can be equated to the change in a single quantity ϵ_j , called the *reaction coordinate* for reaction j , thereby giving

$$\Delta n_{i,j} = v_{i,j} \Delta \epsilon_j \quad \begin{aligned} i &= 1, 2, \dots, N \\ j &= \text{I, II, } \dots, r \end{aligned} \quad (4-359)$$

Because the total change in mole number Δn_i is just the sum of the changes $\Delta n_{i,j}$ resulting from the various reactions,

$$\Delta n_i = \sum_j \Delta n_{i,j} = \sum_j v_{i,j} \Delta \epsilon_j \quad i = 1, 2, \dots, N \quad (4-360)$$

If the initial number of moles of species i is n_{i_0} and if the convention is adopted that $\epsilon_j = 0$ for each reaction in this initial state, then

$$n_i = n_{i_0} + \sum_j v_{i,j} \epsilon_j \quad i = 1, 2, \dots, N \quad (4-361)$$

Equation (4-361) is the basic expression of material balance for a closed system in which r chemical reactions occur. It shows for a reacting system that at most r mole-number-related quantities ϵ_j are capable of independent variation. It is not an equilibrium relation, but merely an accounting scheme, valid for tracking the progress of the reactions to arbitrary levels of conversion. The reaction coordinate has units of moles. A change in ϵ_j of 1 mol signifies a *mole of reaction*, meaning that reaction j has proceeded to such an extent that the change in mole number of each reactant and product is equal to its stoichiometric number.

CHEMICAL REACTION EQUILIBRIA

The general criterion of chemical reaction equilibria is given by Eq. (4-296). For a system in which just a single reaction occurs, Eq. (4-361) becomes

$$n_i = n_{i_0} + v_i \epsilon \quad \text{whence} \quad dn_i = v_i d\epsilon$$

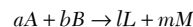
Substitution for dn_i in Eq. (4-296) leads to

$$\sum_i v_i \mu_i = 0 \quad (4-362)$$

Generalization of this result to multiple reactions produces

$$\sum_i v_{i,j} \mu_i = 0 \quad j = \text{I, II, } \dots, r \quad (4-363)$$

Standard Property Changes of Reaction For the reaction



a *standard* property change is defined as the property change resulting when a mol of A and b mol of B in their *standard states at temperature*

4-36 THERMODYNAMICS

T react to form l mol of L and m mol of M in their *standard states also at temperature T* . A *standard state* of species i is its real or hypothetical state as a pure species *at temperature T* and at a standard state pressure P° . The standard property change of reaction j is given the symbol ΔM_j° and its general mathematical definition is

$$\Delta M_j^\circ \equiv \sum_i \nu_{i,j} M_i^\circ \quad (4-364)$$

For species present as gases in the actual reactive system, the standard state is the pure *ideal gas* at pressure P° . For liquids and solids, it is usually the state of pure real liquid or solid at P° . The standard state pressure P° is fixed at 100 kPa. Note that the standard states may represent different physical states for different species; any or all the species may be gases, liquids, or solids.

The most commonly used standard property changes of reaction are

$$\Delta G_j^\circ \equiv \sum_i \nu_{i,j} G_i^\circ = \sum_i \nu_{i,j} \mu_i^\circ \quad (4-365)$$

$$\Delta H_j^\circ \equiv \sum_i \nu_{i,j} H_i^\circ \quad (4-366)$$

$$\Delta C_{p,j}^\circ \equiv \sum_i \nu_{i,j} C_{p,i}^\circ \quad (4-367)$$

The standard Gibbs energy change of reaction ΔG_j° is used in the calculation of equilibrium compositions. The standard heat of reaction ΔH_j° is used in the calculation of the heat effects of chemical reaction, and the standard heat capacity change of reaction is used for extrapolating ΔH_j° and ΔG_j° with T . Numerical values for ΔH_j° and ΔG_j° are computed from tabulated formation data, and $\Delta C_{p,j}^\circ$ is determined from empirical expressions for the T dependence of the $C_{p,i}^\circ$ [see, e.g., Eq. (4-52)].

Equilibrium Constants For practical application, Eq. (4-363) must be reformulated. The initial step is elimination of the μ_i in favor of fugacities. Equation (4-199) for species i in its standard state is subtracted from Eq. (4-202) for species i in the equilibrium mixture, giving

$$\mu_i = G_i^\circ + RT \ln \hat{a}_i \quad (4-368)$$

where by definition $\hat{a}_i \equiv f_i/f_i^\circ$ and is called an *activity*. Substitution of this equation into Eq. (4-364) yields, upon rearrangement,

$$\sum_i [\nu_{i,j} (G_i^\circ + RT \ln \hat{a}_i)] = 0$$

$$\text{or} \quad \sum_i \nu_{i,j} G_i^\circ + RT \sum_i \ln \hat{a}_i^{\nu_{i,j}} = 0$$

$$\text{or} \quad \ln \prod_i \hat{a}_i^{\nu_{i,j}} = \frac{-\sum_i \nu_{i,j} G_i^\circ}{RT}$$

The right side of this equation is a function of temperature only for given reactions and given standard states. Convenience suggests setting it equal to $\ln K_j$, whence

$$\prod_i \hat{a}_i^{\nu_{i,j}} = K_j \quad \text{all } j \quad (4-369)$$

$$\text{where, by definition,} \quad K_j \equiv \exp\left(\frac{-\Delta G_j^\circ}{RT}\right) \quad (4-370)$$

Quantity K_j is the chemical reaction equilibrium constant for reaction j , and ΔG_j° is the corresponding standard Gibbs energy change of reaction [see Eq. (4-365)]. Although called a "constant," K_j is a function of T , but only of T .

The activities in Eq. (4-369) provide the connection between the *equilibrium* states of interest and the *standard* states of the constituent species, for which data are presumed available. The standard states are always at the equilibrium temperature. Although the standard state need not be the same for all species, for a *particular* species it must be the state represented by both G_i° and the f_i° upon which activity \hat{a}_i is based.

The application of Eq. (4-369) requires explicit introduction of composition variables. For gas-phase reactions this is accomplished through the fugacity coefficient

$$\hat{a}_i \equiv \frac{\hat{f}_i}{f_i^\circ} = \frac{y_i \hat{\phi}_i P}{f_i^\circ}$$

However, the standard state for gases is the ideal gas state at the standard state pressure, for which $f_i^\circ = P^\circ$. Therefore,

$$\hat{a}_i = \frac{y_i \hat{\phi}_i P}{P^\circ}$$

and Eq. (4-369) becomes

$$\prod_i (y_i \hat{\phi}_i)^{\nu_{i,j}} \left(\frac{P}{P^\circ}\right)^{\sum_i \nu_{i,j}} = K_j \quad \text{all } j \quad (4-371)$$

where $\nu_j \equiv \sum_i \nu_{i,j}$ and P° is the standard state pressure of 100 kPa, expressed in the same units used for P . The y_i 's may be eliminated in favor of equilibrium values of the reaction coordinates ϵ_j (see Example 6). Then, for fixed temperature Eqs. (4-371) relate the ϵ_j to P . In principle, specification of the pressure allows solution for the ϵ_j . However, the problem may be complicated by the dependence of the $\hat{\phi}_i$ on composition, i.e., on the ϵ_j . If the equilibrium mixture is assumed an ideal solution, then [Eq. (4-218)] each $\hat{\phi}_i$ becomes ϕ_i , the fugacity coefficient of pure species i at the mixture T and P . This quantity does not depend on composition and may be determined from experimental data, from a generalized correlation, or from an equation of state.

An important special case of Eq. (4-371) results for gas-phase reactions when the phase is assumed an ideal gas. In this event $\hat{\phi}_i = 1$, and

$$\prod_i (y_i)^{\nu_{i,j}} \left(\frac{P}{P^\circ}\right)^{\nu_j} = K_j \quad \text{all } j \quad (4-372)$$

In the general case the evaluation of the $\hat{\phi}_i$ requires an iterative process. An initial step is to set each $\hat{\phi}_i$ equal to unity and to solve the problem by Eq. (4-372). This provides a set of y_i values, allowing evaluation of the $\hat{\phi}_i$ by, for example, Eq. (4-243) or (4-246). Equation (4-371) can then be solved for a new set of y_i values, with the process continued to convergence.

For liquid-phase reactions, Eq. (4-369) is modified by introduction of the activity coefficient $\gamma_i = \hat{f}_i/x_i f_i^\circ$, where x_i is the liquid-phase mole fraction. The activity is then

$$\hat{a}_i \equiv \frac{\hat{f}_i}{f_i^\circ} = \gamma_i x_i \left(\frac{f_i}{f_i^\circ}\right)$$

Both f_i and f_i° represent fugacity of pure liquid i at temperature T , but at pressures P and P° , respectively. Except in the critical region, pressure has little effect on the properties of liquids, and the ratio f_i/f_i° is often taken as unity. When this is not acceptable, this ratio is evaluated by the equation

$$\ln \frac{f_i}{f_i^\circ} = \frac{1}{RT} \int_{P^\circ}^P V_i dP \approx \frac{V_i(P - P^\circ)}{RT}$$

When the ratio f_i/f_i° is taken as unity, $\hat{a}_i = \gamma_i x_i$, and Eq. (4-369) becomes

$$\prod_i (\gamma_i x_i)^{\nu_{i,j}} = K_j \quad \text{all } j \quad (4-373)$$

Here the difficulty is to determine the γ_i 's, which depend on the x_i 's. This problem has not been solved for the general case. Two courses are open: the first is experiment; the second, assumption of solution ideality. In the latter case, $\gamma_i = 1$, and Eq. (4-373) reduces to

$$\prod_i (x_i)^{\nu_{i,j}} = K_j \quad \text{all } j \quad (4-374)$$

the "law of mass action." The significant feature of Eqs. (4-372) and (4-374), the simplest expressions for gas- and liquid-phase reaction

equilibrium, is that the temperature-, pressure-, and composition-dependent terms are distinct and separate.

The effect of temperature on the equilibrium constant follows from Eq. (4-41) written for pure species j in its standard state (wherein the pressure P° is fixed):

$$\frac{d(G_j^\circ/RT)}{dT} = \frac{-H_j^\circ}{RT^2}$$

With Eqs. (4-365) and (4-366) this equation easily extends to relate standard property changes of reaction:

$$\frac{d(\Delta G_j^\circ/RT)}{dT} = \frac{-\Delta H_j^\circ}{RT^2} \quad (4-375)$$

In view of Eq. (4-370) this may also be written as

$$\frac{d \ln K_j}{dT} = \frac{\Delta H_j^\circ}{RT^2} \quad (4-376)$$

For an endothermic reaction, ΔH_j° is positive and K_j increases with increasing T ; for an exothermic reaction, it is negative and K_j decreases with increasing T .

Because the standard state pressure is constant, Eq. (4-28) may be extended to relate standard properties of reaction, yielding

$$d\Delta H_j^\circ = \Delta C_{P_j}^\circ dT \quad \text{and} \quad d\Delta S_j^\circ = \Delta C_{P_j}^\circ \frac{dT}{T}$$

Integration of these equations from reference temperature T_0 (usually 298.15 K) to temperature T gives

$$\Delta H^\circ = \Delta H_0^\circ + R \int_{T_0}^T \frac{\Delta C_P^\circ}{R} dT \quad (4-377)$$

$$\Delta S^\circ = \Delta S_0^\circ + R \int_{T_0}^T \frac{\Delta C_P^\circ}{R} \frac{dT}{T} \quad (4-378)$$

where for simplicity subscript j has been suppressed. The definition of G leads directly to $\Delta G^\circ = \Delta H^\circ - T\Delta S^\circ$. Combining this equation with Eqs. (4-370), (4-377), and (4-378) yields

$$\ln K = \frac{-\Delta G^\circ}{RT} = \frac{-\Delta H_0^\circ}{RT} - \frac{1}{T} \int_{T_0}^T \frac{\Delta C_P^\circ}{R} dT + \frac{\Delta S_0^\circ}{R} + \int_{T_0}^T \frac{\Delta C_P^\circ}{R} \frac{dT}{T}$$

Substituting $\Delta S_0^\circ = (\Delta G_0^\circ - \Delta H_0^\circ)/T_0$, rearranging, and defining $\tau \equiv T/T_0$ give finally

$$\ln K = \frac{-\Delta G_0^\circ}{RT_0} + \frac{\Delta H_0^\circ}{RT_0} \left(\frac{\tau - 1}{\tau} \right) - \frac{1}{T} \int_{T_0}^T \frac{\Delta C_P^\circ}{R} dT + \int_{T_0}^T \frac{\Delta C_P^\circ}{R} \frac{dT}{T} \quad (4-379)$$

When heat capacity equations have the form of Eq. (4-52), the integrals are evaluated by equations of exactly the form of Eqs. (4-53) and (4-54), but with parameters A , B , C , and D replaced by ΔA , ΔB , ΔC , and ΔD , in accord with Eq. (4-364). Thus for the ideal gas standard state

$$\int_{T_0}^T \frac{\Delta C_P^\circ}{R} dT = \Delta A T_0(\tau - 1) + \frac{\Delta B}{2} T_0^2(\tau^2 - 1) + \frac{\Delta C}{3} T_0^3(\tau^3 - 1) + \frac{\Delta D}{T_0} \left(\frac{\tau - 1}{\tau} \right) \quad (4-380)$$

$$\int_{T_0}^T \frac{\Delta C_P^\circ}{R} \frac{dT}{T} = \Delta A \ln \tau + \left[\Delta B T_0 + \left(\Delta C T_0^2 + \frac{\Delta D}{\tau^2 T_0^2} \right) \left(\frac{\tau + 1}{2} \right) \right] (\tau - 1) \quad (4-381)$$

Equations (4-379) through (4-381) together allow an equation to be written for $\ln K$ as a function of T for any reaction for which appropriate data are available.

In the more extensive compilations of data, values of ΔG° and ΔH° for formation reactions are given for a wide range of temperatures, rather than just at the reference temperature $T_0 = 298.15$ K. [See in particular *TRC Thermodynamic Tables—Hydrocarbons* and *TRC Thermodynamic Tables—Non-hydrocarbons*, serial publications of the Thermodynamics Research Center, Texas A & M Univ. System, College Station, Tex.; "The NBS Tables of Chemical Thermodynamic Properties," *J. Phys. Chem. Ref. Data* **11**, supp. 2 (1982).] Where data are lacking, methods of estimation are available; these are reviewed by Poling, Prausnitz, and O'Connell, *The Properties of Gases and Liquids*, 5th ed., chap. 6, McGraw-Hill, New York, 2000. For an estimation procedure based on molecular structure, see Constantinou and Gani, *Fluid Phase Equilib.* **103**: 11–22 (1995). See also Sec. 2.

Example 6: Single-Reaction Equilibrium The hydrogenation of benzene to produce cyclohexane by the reaction



is carried out over a catalyst formulated to repress side reactions. Operating conditions cover a pressure range from 10 to 35 bar and a temperature range from 450 to 670 K. Reaction rate increases with increasing T , but because the reaction is exothermic the equilibrium conversion decreases with increasing T . A comprehensive study of the effect of operating variables on the chemical equilibrium of this reaction has been published by J. Carrero-Mantilla and M. Llano-Restrepo, *Fluid Phase Equilib.* **219**: 181–193 (2004). Presented here are calculations for a single set of operating conditions, namely, $T = 600$ K, $P = 15$ bar, and a molar feed ratio $\text{H}_2/\text{C}_6\text{H}_6 = 3$, the stoichiometric value. For these conditions we determine the fractional conversion of benzene to cyclohexane. Carrero-Mantilla and Llano-Restrepo express $\ln K$ as a function of T by an equation which for 600 K yields the value $K = 0.02874$.

A feed stream containing 3 mol H_2 for each 1 mol C_6H_6 is the basis of calculation, and for this single reaction, Eq. (4-361) becomes $n_i = n_{i0} + \nu_{ie}$, yielding

$$\begin{aligned} n_B &= 1 - \epsilon && \text{benzene} \\ n_{\text{H}_2} &= 3 - 3\epsilon && \text{hydrogen} \\ n_C &= \epsilon && \text{cyclohexane} \\ \sum_i n_i &= 4 - 3\epsilon \end{aligned}$$

Each mole fraction is therefore given by $y_i = n_i/(4 - 3\epsilon)$.

Assume first that the equilibrium mixture is an ideal gas, and apply Eq. (4-372), written for a single reaction, with subscript j omitted and $\nu = -3$:

$$\prod_i y_i^{\nu_i} \left(\frac{P}{P^\circ} \right)^\nu = \frac{\epsilon}{4 - 3\epsilon} = \left(\frac{1 - \epsilon}{4 - 3\epsilon} \right)^3 \left(\frac{15}{1} \right)^{-3} = K = 0.02874$$

$$\text{whence} \quad \frac{\epsilon}{1 - \epsilon} \left(\frac{4 - 3\epsilon}{3 - 3\epsilon} \right)^3 (15)^{-3} = 0.02874 \quad \text{and} \quad \epsilon = 0.815$$

Thus, the assumption of ideal gases leads to a calculated conversion of 81.5 percent.

An alternative assumption is that the equilibrium mixture is an ideal solution. This requires application of Eq. (4-371). However, in the case of an ideal solution Eq. (4-218) indicates that $\hat{\phi}_i^s = \phi_i$, in which case Eq. (4-371) for a single reaction becomes

$$\prod_i (y_i \phi_i)^{\nu_i} \left(\frac{P}{P^\circ} \right)^\nu = K$$

For purposes of illustration we evaluate the pure-species fugacity coefficients by Eq. (4-206), written here as

$$\phi_i = \exp(B_i^0 + \omega B_i^1) \frac{P_i}{T_i}$$

The following table shows values for the various quantities in this equation. Note that T_i and P_i for hydrogen are effective values as calculated by Eqs. (4-124) and (4-125) and used with $\omega = 0$.

	T_c	T_r	P_c	P_r	ω	B^0	B^1	ϕ
C_6H_6	562.2	1.067	48.98	0.306	0.21	-0.2972	0.008	0.919
H_2	42.8	14.009	19.78	0.758	0.00	0.0768	0.139	1.004
C_6H_{12}	553.6	1.084	40.73	0.368	0.21	-0.2880	0.016	0.908

4-38 THERMODYNAMICS

The equilibrium equation now becomes:

$$\prod_i (y_i \phi_i)^{\nu_i} \left(\frac{P}{P^\circ} \right)^{\sum \nu_i} = \frac{\frac{\varepsilon}{4-3\varepsilon} 0.919}{\left(\frac{1-\varepsilon}{4-3\varepsilon} 0.908 \right) \left(\frac{3-3\varepsilon}{4-3\varepsilon} 1.004 \right)^3} \left(\frac{15}{1} \right)^{-3} = K = 0.02874$$

Solution yields $\varepsilon = 0.816$

This result is hardly different from that based on the ideal gas assumption. The fugacity coefficients in the equilibrium equation clearly cancel one another. This is not uncommon in reaction equilibrium calculations, as there are always products and reactions, making the ideal gas assumption far more useful than might be expected.

Carrero-Mantilla and Llano-Restrep present results for a wide range of conditions, both for the ideal gas assumption and for calculations wherein ϕ_i values are determined from the Soave-Redlich-Kwong equation of state. In no case are these calculated conversions significantly divergent.

Complex Chemical Reaction Equilibria When the composition of an equilibrium mixture is determined by a number of simultaneous reactions, calculations based on equilibrium constants become complex and tedious. A more direct procedure (and one suitable for general computer solution) is based on minimization of the total Gibbs energy G^t in accord with Eq. (4-293). The treatment here is limited to gas-phase reactions for which the problem is to find the equilibrium composition for given T and P and for a given initial feed.

1. Formulate the constraining material-balance equations, based on conservation of the total number of atoms of each *element* in a system comprised of w elements. Let subscript k identify a particular atom, and define A_k as the total number of atomic masses of the k th element in the feed. Further, let a_{ik} be the number of atoms of the k th element present in each molecule of chemical species i . The material balance for element k is then

$$\sum_i n_i a_{ik} = A_k \quad k = 1, 2, \dots, w \quad (4-382)$$

or
$$\sum_i n_i a_{ik} - A_k = 0 \quad k = 1, 2, \dots, w$$

2. Multiply each element balance by λ_k , a Lagrange multiplier:

$$\lambda_k \left(\sum_i n_i a_{ik} - A_k \right) = 0 \quad k = 1, 2, \dots, w$$

Summed over k , these equations give

$$\sum_k \lambda_k \left(\sum_i n_i a_{ik} - A_k \right) = 0$$

3. Form a function F by addition of this sum to G^t :

$$F = G^t + \sum_k \lambda_k \left(\sum_i n_i a_{ik} - A_k \right)$$

Function F is identical with G^t , because the summation term is zero. However, the partial derivatives of F and G^t with respect to n_i are different, because function F incorporates the constraints of the material balances.

4. The minimum value of both F and G^t is found when the partial derivatives of F with respect to n_i are set equal to zero:

$$\left(\frac{\partial F}{\partial n_i} \right)_{T,P,n_j} = \left(\frac{\partial G^t}{\partial n_i} \right)_{T,P,n_j} + \sum_k \lambda_k a_{ik} = 0$$

The first term on the right is the definition of the chemical potential; therefore,

$$\mu_i + \sum_k \lambda_k a_{ik} = 0 \quad i = 1, 2, \dots, N \quad (4-383)$$

However, the chemical potential is given by Eq. (4-368); for gas-phase reactions and standard states as the pure ideal gases at P° , this equation becomes

$$\mu_i = G_i^\circ + RT \ln \frac{\hat{f}_i}{P^\circ}$$

If G_i° is arbitrarily set equal to zero for all *elements* in their standard states, then for compounds $G_i^\circ = \Delta G_{f,i}^\circ$, the standard Gibbs energy change of formation of species i . In addition, the fugacity is eliminated—in favor of the fugacity coefficient by Eq. (4-204), $\hat{f}_i = y_i \hat{\phi}_i P$. With these substitutions, the equation for μ_i becomes

$$\mu_i = \Delta G_{f,i}^\circ + RT \ln \frac{y_i \hat{\phi}_i P}{P^\circ}$$

Combination with Eq. (4-383) gives

$$\Delta G_{f,i}^\circ + RT \ln \frac{y_i \hat{\phi}_i P}{P^\circ} + \sum_k \lambda_k a_{ik} = 0 \quad i = 1, 2, \dots, N \quad (4-384)$$

If species i is an element, $\Delta G_{f,i}^\circ$ is zero. There are N equilibrium equations [Eqs. (4-384)], one for each chemical species, and there are w material balance equations [Eqs. (4-382)], one for each element—a total of $N + w$ equations. The unknowns in these equations are the n_i 's (note that $y_i = n_i / \sum n_i$), of which there are N , and the λ_i 's, of which there are w —a total of $N + w$ unknowns. Thus the number of equations is sufficient for the determination of all unknowns.

Equation (4-384) is derived on the presumption that the set $\{\hat{\phi}_i\}$ is known. If the phase is an ideal gas, then each $\hat{\phi}_i$ is unity. If the phase is an ideal solution, each $\hat{\phi}_i$ becomes ϕ_i and can at least be estimated. For real gases, each $\hat{\phi}_i$ is a function of the set $\{y_i\}$, the quantities being calculated. Thus an iterative procedure is indicated, initiated with each $\hat{\phi}_i$ set equal to unity. Solution of the equations then provides a preliminary set $\{y_i\}$. For low pressures or high temperatures this result is usually adequate. Where it is not satisfactory, an equation of state with the preliminary set $\{y_i\}$ gives a new and more nearly correct set $\{\hat{\phi}_i\}$ for use in Eq. (4-384). Then a new set $\{y_i\}$ is determined. The process is repeated to convergence. All calculations are well suited to computer solution.

In this procedure, the question of what chemical reactions are involved never enters directly into any of the equations. However, the choice of a set of species is entirely equivalent to the choice of a set of independent reactions among the species. In any event, a set of species or an equivalent set of independent reactions must always be assumed, and different assumptions produce different results.

A detailed example of a complex gas-phase equilibrium calculation is given by Smith, Van Ness, and Abbott [*Introduction to Chemical Engineering Thermodynamics*, 5th ed., Example 15.13, pp. 602–604; 6th ed., Example 13.14, pp. 511–513; 7th ed., Example 13.14, pp. 527–528, McGraw-Hill, New York (1996, 2001, 2005)]. General application of the method to multicomponent, multiphase systems is treated by Iglesias-Silva et al. [*Fluid Phase Equilib.* **210**: 229–245 (2003)] and by Sotyan, Ghajar, and Gasem [*Ind. Eng. Chem. Res.* **42**: 3786–3801 (2003)].

THERMODYNAMIC ANALYSIS OF PROCESSES

Real irreversible processes can be subjected to thermodynamic analysis. The goal is to calculate the efficiency of energy use or production and to show how wasted energy is apportioned among the steps of a process. The treatment here is limited to steady-state steady-flow processes, because of their predominance in chemical technology.

CALCULATION OF IDEAL WORK

In any steady-state steady-flow process *requiring* work, a minimum amount must be expended to bring about a specific change of state in the flowing fluid. In a process *producing* work, a maximum amount is

attainable for a specific change of state in the flowing fluid. In either case, the limiting value obtains when the specific change of state is accomplished *completely reversibly*. The implications of this requirement are that

1. The process is internally reversible within the control volume.
2. Heat transfer external to the control volume is reversible.

The second item means that heat exchange between system and surroundings must occur at the temperature of the surroundings, presumed to constitute a heat reservoir at a constant and uniform temperature T_σ . This may require Carnot engines or heat pumps internal to the system that provide for the reversible transfer of heat from the temperatures of the flowing fluid to that of the surroundings. Because Carnot engines and heat pumps are cyclic, they undergo no net change of state.

These conditions are implicit in the entropy balance of Eq. (4-156) when $\dot{S}_C = 0$. If in addition there is but a single surroundings temperature T_σ , this equation becomes

$$\Delta(S\dot{m})_{fs} - \frac{\dot{Q}}{T_\sigma} = 0 \quad (4-385)$$

The energy balance for a steady-state steady-flow process as given by Eq. (4-150) is

$$\Delta\left[\left(H + \frac{1}{2}u^2 + zg\right)\dot{m}\right]_{fs} = \dot{Q} + \dot{W}_s \quad (4-150)$$

Combining this equation with Eq. (4-385) to eliminate \dot{Q} yields

$$\Delta\left[\left(H + \frac{1}{2}u^2 + zg\right)\dot{m}\right]_{fs} = T_\sigma \Delta(S\dot{m})_{fs} + \dot{W}_s(\text{rev})$$

where $\dot{W}_s(\text{rev})$ indicates that the shaft work is for a completely reversible process. This work is called the *ideal work* \dot{W}_{ideal} . Thus

$$\dot{W}_{\text{ideal}} = \Delta\left[\left(H + \frac{1}{2}u^2 + zg\right)\dot{m}\right]_{fs} - T_\sigma \Delta(S\dot{m})_{fs} \quad (4-386)$$

In most applications to chemical processes, the kinetic and potential energy terms are negligible compared with the others; in this event Eq. (4-386) is written as

$$\dot{W}_{\text{ideal}} = \Delta(H\dot{m})_{fs} - T_\sigma \Delta(S\dot{m})_{fs} \quad (4-387)$$

For the special case of a single stream flowing through the system, Eq. (4-387) becomes

$$\dot{W}_{\text{ideal}} = \dot{m}(\Delta H - T_\sigma \Delta S) \quad (4-388)$$

Division by \dot{m} puts this equation on a unit-mass basis:

$$w_{\text{ideal}} = \Delta H - T_\sigma \Delta S \quad (4-389)$$

A completely reversible process is hypothetical, devised solely to find the ideal work associated with a given change of state. Its only connection with an actual process is that it brings about the same change of state as the actual process, allowing comparison of the actual work of a process with the work of the hypothetical reversible process.

Equations (4-386) through (4-389) give the work of a completely reversible process associated with given property changes in the flowing streams. When the same property changes occur in an actual process, the actual work \dot{W}_s (or W_s) is given by an energy balance, and comparison can be made of the actual work with the ideal work. When \dot{W}_{ideal} (or W_{ideal}) is positive, it is the *minimum work required* to bring about a given change in the properties of the flowing streams, and it is smaller than \dot{W}_s . In this case a thermodynamic efficiency η_r is defined as the ratio of the ideal work to the actual work:

$$\eta_r(\text{work required}) = \frac{\dot{W}_{\text{ideal}}}{\dot{W}_s} \quad (4-390)$$

When \dot{W}_{ideal} (or W_{ideal}) is negative, $|\dot{W}_{\text{ideal}}|$ is the *maximum work obtainable* from a given change in the properties of the flowing streams, and it is larger than $|\dot{W}_s|$. In this case, the thermodynamic efficiency is defined as the ratio of the actual work to the ideal work:

$$\eta_r(\text{work produced}) = \frac{\dot{W}_s}{\dot{W}_{\text{ideal}}} \quad (4-391)$$

LOST WORK

Work that is wasted as the result of irreversibilities in a process is called *lost work* \dot{W}_{lost} , and it is defined as the difference between the actual work of a process and the ideal work for the process. Thus by definition,

$$W_{\text{lost}} \equiv W_s - W_{\text{ideal}} \quad (4-392)$$

The rate form is

$$\dot{W}_{\text{lost}} \equiv \dot{W}_s - \dot{W}_{\text{ideal}} \quad (4-393)$$

The actual work rate comes from Eq. (4-150):

$$\dot{W}_s = \Delta\left[\left(H + \frac{1}{2}u^2 + zg\right)\dot{m}\right]_{fs} - \dot{Q}$$

Subtracting the ideal work rate as given by Eq. (4-386) yields

$$\dot{W}_{\text{lost}} = T_\sigma \Delta(S\dot{m})_{fs} - \dot{Q} \quad (4-394)$$

For the special case of a single stream flowing through the control volume,

$$\dot{W}_{\text{lost}} = \dot{m}T_\sigma \Delta S - \dot{Q} \quad (4-395)$$

Division of this equation by \dot{m} gives

$$w_{\text{lost}} = T_\sigma \Delta S - Q \quad (4-396)$$

where the basis is now a unit amount of fluid flowing through the control volume.

The total rate of entropy generation (in both system and surroundings) as a result of a process is

$$\dot{S}_C = \Delta(S\dot{m})_{fs} - \frac{\dot{Q}}{T_\sigma} \quad (4-397)$$

Division by \dot{m} provides an equation based on a unit amount of fluid flowing through the control volume:

$$s_C = \Delta S - \frac{Q}{T_\sigma} \quad (4-398)$$

Equations (4-397) and (4-398) are special cases of Eqs. (4-156) and (4-157).

Multiplication of Eq. (4-397) by T_σ gives

$$T_\sigma \dot{S}_C = T_\sigma \Delta(S\dot{m})_{fs} - \dot{Q}$$

Because the right sides of this equation and of Eq. (4-394) are identical, it follows that

$$\dot{W}_{\text{lost}} = T_\sigma \dot{S}_C \quad (4-399)$$

For flow on the basis of a unit amount of fluid, this becomes

$$w_{\text{lost}} = T_\sigma s_C \quad (4-400)$$

Because the second law of thermodynamics requires

$$\dot{S}_C \geq 0 \quad \text{and} \quad s_C \geq 0$$

therefore

$$\dot{W}_{\text{lost}} \geq 0 \quad \text{and} \quad w_{\text{lost}} \geq 0$$

When a process is completely reversible, the equality holds and the lost work is zero. For irreversible processes the inequality holds, and the lost work, i.e., the energy that becomes unavailable for work, is positive. The engineering significance of this result is clear: The greater the irreversibility of a process, the greater the rate of entropy generation and the greater the amount of energy that becomes unavailable for work. Thus every irreversibility carries with it a price.

ANALYSIS OF STEADY-STATE STEADY-FLOW PROCESSES

Many processes consist of a number of steps, and lost-work calculations are then made for each step separately. Writing Eq. (4-399) for each step of the process and summing give

$$\sum \dot{W}_{\text{lost}} = T_\sigma \sum \dot{S}_C$$

4-40 THERMODYNAMICS

Dividing Eq. (4-399) by this result yields

$$\frac{\dot{W}_{\text{lost}}}{\sum \dot{W}_{\text{lost}}} = \frac{\dot{S}_G}{\sum \dot{S}_G}$$

Thus an analysis of the lost work, made by calculation of the fraction that each individual lost-work term represents of the total lost work, is the same as an analysis of the rate of entropy generation, made by expressing each individual entropy generation term as a fraction of the sum of all entropy generation terms.

An alternative to the lost-work or entropy generation analysis is a work analysis. This is based on Eq. (4-393), written as

$$\sum \dot{W}_{\text{lost}} = \dot{W}_s - \dot{W}_{\text{ideal}} \quad (4-401)$$

For a work-requiring process, all these work quantities are positive and $\dot{W}_s > \dot{W}_{\text{ideal}}$. The preceding equation is then expressed as

$$\dot{W}_s = \dot{W}_{\text{ideal}} + \sum \dot{W}_{\text{lost}} \quad (4-402)$$

A work analysis then gives each of the individual work terms in the summation on the right as a fraction of \dot{W}_s .

For a work-producing process, \dot{W}_s and \dot{W}_{ideal} are negative, and $|\dot{W}_{\text{ideal}}| > |\dot{W}_s|$. Equation (4-401) in this case is best written as

$$|\dot{W}_{\text{ideal}}| = |\dot{W}_s| + \sum \dot{W}_{\text{lost}} \quad (4-403)$$

A work analysis here expresses each of the individual work terms on the right as a fraction of $|\dot{W}_{\text{ideal}}|$. A work analysis cannot be carried out in the case where a process is so inefficient that \dot{W}_{ideal} is negative, indicating that the process should produce work; but \dot{W}_s is positive, indicating that the process in fact requires work. A lost-work or entropy generation analysis is always possible.

Example 7: Lost-Work Analysis A work analysis follows for a simple Linde system for the separation of air into gaseous oxygen and nitrogen, as depicted in Fig. 4-10. Table 4-8 lists a set of operating conditions for the numbered points of the diagram. Heat leaks into the column of 147 J/mol of entering air and into the exchanger of 70 J/mol of entering air have been assumed. Take $T_a = 300$ K.

The basis for analysis is 1 mol of entering air, assumed to contain 79 mol % N₂ and 21 mol % O₂. By a material balance on the nitrogen, 0.79 = 0.9148 x, whence

$$\begin{aligned} x &= 0.8636 \text{ mol of nitrogen product} \\ 1 - x &= 0.1364 \text{ mol of oxygen product} \end{aligned}$$

Calculation of ideal work: If changes in kinetic and potential energies are neglected, Eq. (4-387) is applicable. From the tabulated data,

$$\begin{aligned} \Delta(H\dot{m})_{\text{is}} &= (13,460)(0.1364) + (12,074)(0.8636) - (12,407)(1) = -144 \text{ J} \\ \Delta(S\dot{m})_{\text{is}} &= (118.48)(0.1364) + (114.34)(0.8636) - (117.35)(1) = -2.4453 \text{ J/K} \end{aligned}$$

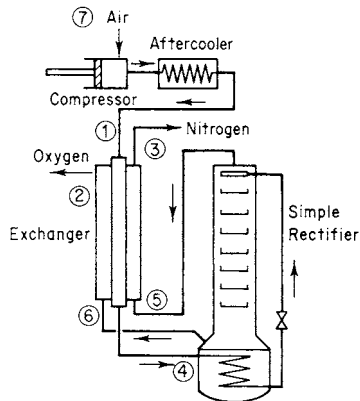


FIG. 4-10 Diagram of simple Linde system for air separation.

TABLE 4-8 States and Values of Properties for the Process of Fig. 4-10*

Point	P, bar	T, K	Composition	State	H, J/mol	S, J/(mol·K)
1	55.22	300	Air	Superheated	12,046	82.98
2	1.01	295	Pure O ₂	Superheated	13,460	118.48
3	1.01	295	91.48% N ₂	Superheated	12,074	114.34
4	55.22	147.2	Air	Superheated	5,850	52.08
5	1.01	79.4	91.48% N ₂	Saturated vapor	5,773	75.82
6	1.01	90	Pure O ₂	Saturated vapor	7,485	83.69
7	1.01	300	Air	Superheated	12,407	117.35

*Properties on the basis of Miller and Sullivan, U.S. Bur. Mines Tech. Pap. 424 (1928).

Thus, by Eq. (4-387),

$$\dot{W}_{\text{ideal}} = -144 - (300)(-2.4453) = 589.6 \text{ J}$$

Calculation of actual work of compression: For simplicity, the work of compression is calculated by the equation for an ideal gas in a three-stage reciprocating machine with complete intercooling and with isentropic compression in each stage. The work so calculated is assumed to represent 80 percent of the actual work. The following equation may be found in any number of textbooks on thermodynamics:

$$\dot{W}_s = \frac{n\gamma RT_1}{0.8(\gamma - 1)} \left[\left(\frac{P_2}{P_1} \right)^{(\gamma - 1)/n\gamma} - 1 \right]$$

where n = number of stages, here taken as 3

γ = ratio of heat capacities, here taken as 1.4

T_1 = initial absolute temperature, equal to 300 K

P_2/P_1 = overall pressure ratio, equal to 54.5

R = universal gas constant, equal to 8.314 J/(mol·K)

The efficiency factor of 0.8 is already included in the equation. Substitution of the remaining values gives

$$\dot{W}_s = \frac{(3)(1.4)(8.314)(300)}{(0.8)(0.4)} \left[(54.5)^{0.4/(3)(1.4)} - 1 \right] = 15,171 \text{ J}$$

The heat transferred to the surroundings during compression as a result of intercooling and aftercooling to 300 K is found from the first law:

$$\dot{Q} = \dot{m}(\Delta H) - \dot{W}_s = (12,046 - 12,407) - 15,171 = -15,532 \text{ J}$$

Calculation of lost work: Equation (4-394) may be applied to each of the major units of the process. For the compressor/cooler,

$$\begin{aligned} \dot{W}_{\text{lost}} &= (300)[(82.98)(1) - (117.35)(1)] - (-15,532) \\ &= 5221.0 \text{ J} \end{aligned}$$

For the exchanger,

$$\begin{aligned} \dot{W}_{\text{lost}} &= (300)[(118.48)(0.1364) + (114.34)(0.8636) + (52.08)(1) \\ &\quad - (75.82)(0.8636) - (83.69)(0.1364) - (82.98)(1)] - 70 \\ &= 2063.4 \text{ J} \end{aligned}$$

Finally, for the rectifier,

$$\dot{W}_{\text{lost}} = (300)[(75.82)(0.8636) + (83.69)(0.1364) - (52.08)(1)] - 147 = 7297.0 \text{ J}$$

Work analysis: Because the process requires work, Eq. (4-402) is appropriate for a work analysis. The various terms of this equation appear as entries in the following table and are on the basis of 1 mol of entering air.

			% of \dot{W}_s
\dot{W}_{ideal}		589.6 J	3.9
\dot{W}_{lost}	Compressor/cooler	5,221.0 J	34.4
\dot{W}_{lost}	Exchanger	2,063.4 J	13.6
\dot{W}_{lost}	Rectifier	7,297.0 J	48.1
\dot{W}_s		15,171.0 J	100.0

The thermodynamic efficiency of this process as given by Eq. (4-390) is only 3.9 percent. Significant inefficiencies reside with each of the primary units of the process.

SECTION 5

Heat and Mass
Transfer

PERRY'S CHEMICAL ENGINEERS' HANDBOOK

8TH EDITION



HOYT C. HOTTEL, JAMES J. NOBLE
ADEL F. SAROFIM, GEOFFREY D. SILCOX
PHILLIP C. WANKAT, KENT S. KNAEBEL

Copyright © 2008, 1997, 1984, 1973, 1963, 1950, 1941, 1934 by The McGraw-Hill Companies, Inc. All rights reserved. Manufactured in the United States of America. Except as permitted under the United States Copyright Act of 1976, no part of this publication may be reproduced or distributed in any form or by any means, or stored in a database or retrieval system, without the prior written permission of the publisher.

0-07-154212-4

The material in this eBook also appears in the print version of this title: 0-07-151128-8.

All trademarks are trademarks of their respective owners. Rather than put a trademark symbol after every occurrence of a trademarked name, we use names in an editorial fashion only, and to the benefit of the trademark owner, with no intention of infringement of the trademark. Where such designations appear in this book, they have been printed with initial caps.

McGraw-Hill eBooks are available at special quantity discounts to use as premiums and sales promotions, or for use in corporate training programs. For more information, please contact George Hoare, Special Sales, at george_hoare@mcgraw-hill.com or (212) 904-4069.

TERMS OF USE

This is a copyrighted work and The McGraw-Hill Companies, Inc. (“McGraw-Hill”) and its licensors reserve all rights in and to the work. Use of this work is subject to these terms. Except as permitted under the Copyright Act of 1976 and the right to store and retrieve one copy of the work, you may not decompile, disassemble, reverse engineer, reproduce, modify, create derivative works based upon, transmit, distribute, disseminate, sell, publish or sublicense the work or any part of it without McGraw-Hill’s prior consent. You may use the work for your own noncommercial and personal use; any other use of the work is strictly prohibited. Your right to use the work may be terminated if you fail to comply with these terms.

THE WORK IS PROVIDED “AS IS.” McGRAW-HILL AND ITS LICENSORS MAKE NO GUARANTEES OR WARRANTIES AS TO THE ACCURACY, ADEQUACY OR COMPLETENESS OF OR RESULTS TO BE OBTAINED FROM USING THE WORK, INCLUDING ANY INFORMATION THAT CAN BE ACCESSED THROUGH THE WORK VIA HYPERLINK OR OTHERWISE, AND EXPRESSLY DISCLAIM ANY WARRANTY, EXPRESS OR IMPLIED, INCLUDING BUT NOT LIMITED TO IMPLIED WARRANTIES OF MERCHANTABILITY OR FITNESS FOR A PARTICULAR PURPOSE. McGraw-Hill and its licensors do not warrant or guarantee that the functions contained in the work will meet your requirements or that its operation will be uninterrupted or error free. Neither McGraw-Hill nor its licensors shall be liable to you or anyone else for any inaccuracy, error or omission, regardless of cause, in the work or for any damages resulting therefrom. McGraw-Hill has no responsibility for the content of any information accessed through the work. Under no circumstances shall McGraw-Hill and/or its licensors be liable for any indirect, incidental, special, punitive, consequential or similar damages that result from the use of or inability to use the work, even if any of them has been advised of the possibility of such damages. This limitation of liability shall apply to any claim or cause whatsoever whether such claim or cause arises in contract, tort or otherwise.

DOI: 10.1036/0071511288

Heat and Mass Transfer*

Hoyt C. Hottel, S.M. *Deceased; Professor Emeritus of Chemical Engineering, Massachusetts Institute of Technology; Member, National Academy of Sciences, National Academy of Arts and Sciences, American Academy of Arts and Sciences, American Institute of Chemical Engineers, American Chemical Society, Combustion Institute (Radiation)*[†]

James J. Noble, Ph.D., P.E., CE [UK] *Research Affiliate, Department of Chemical Engineering, Massachusetts Institute of Technology; Fellow, American Institute of Chemical Engineers; Member, New York Academy of Sciences (Radiation Section Coeditor)*

Adel F. Sarofim, Sc.D. *Presidential Professor of Chemical Engineering, Combustion, and Reactors, University of Utah; Member, American Institute of Chemical Engineers, American Chemical Society, Combustion Institute (Radiation Section Coeditor)*

Geoffrey D. Silcox, Ph.D. *Professor of Chemical Engineering, Combustion, and Reactors, University of Utah; Member, American Institute of Chemical Engineers, American Chemical Society, American Society for Engineering Education (Conduction, Convection, Heat Transfer with Phase Change, Section Coeditor)*

Phillip C. Wankat, Ph.D. *Clifton L. Lovell Distinguished Professor of Chemical Engineering, Purdue University; Member, American Institute of Chemical Engineers, American Chemical Society, International Adsorption Society (Mass Transfer Section Coeditor)*

Kent S. Knaebel, Ph.D. *President, Adsorption Research, Inc.; Member, American Institute of Chemical Engineers, American Chemical Society, International Adsorption Society; Professional Engineer (Ohio) (Mass Transfer Section Coeditor)*

HEAT TRANSFER			
Modes of Heat Transfer	5-3	Unsteady-State Conduction	5-6
HEAT TRANSFER BY CONDUCTION		One-Dimensional Conduction: Lumped and Distributed Analysis	5-6
Fourier's Law	5-3	Example 2: Correlation of First Eigenvalues by Eq. (5-22)	5-6
Thermal Conductivity	5-3	Example 3: One-Dimensional, Unsteady Conduction Calculation ..	5-6
Steady-State Conduction	5-3	Example 4: Rule of Thumb for Time Required to Diffuse a Distance R	5-6
One-Dimensional Conduction	5-3	One-Dimensional Conduction: Semi-infinite Plate	5-7
Conduction with Resistances in Series	5-5	HEAT TRANSFER BY CONVECTION	
Example 1: Conduction with Resistances in Series and Parallel	5-5	Convective Heat-Transfer Coefficient	5-7
Conduction with Heat Source	5-5	Individual Heat-Transfer Coefficient	5-7
Two- and Three-Dimensional Conduction	5-5		

*The contribution of James G. Knudsen, Ph.D., coeditor of this section in the seventh edition, is acknowledged.

[†]Professor H. C. Hottel was the principal author of the radiation section in this *Handbook*, from the first edition in 1934 through the seventh edition in 1997. His classic zone method remains the basis for the current revision.

5-2 HEAT AND MASS TRANSFER

Overall Heat-Transfer Coefficient and Heat Exchangers	5-7
Representation of Heat-Transfer Coefficients	5-7
Natural Convection	5-8
External Natural Flow for Various Geometries	5-8
Simultaneous Heat Transfer by Radiation and Convection	5-8
Mixed Forced and Natural Convection	5-8
Enclosed Spaces	5-8
Example 5: Comparison of the Relative Importance of Natural Convection and Radiation at Room Temperature	5-8
Forced Convection	5-9
Flow in Round Tubes	5-9
Flow in Noncircular Ducts	5-9
Example 6: Turbulent Internal Flow	5-10
Coiled Tubes	5-10
External Flows	5-10
Flow-through Tube Banks	5-10
Jackets and Coils of Agitated Vessels	5-12
Nonnewtonian Fluids	5-12

HEAT TRANSFER WITH CHANGE OF PHASE

Condensation	5-12
Condensation Mechanisms	5-12
Condensation Coefficients	5-12
Boiling (Vaporization) of Liquids	5-14
Boiling Mechanisms	5-14
Boiling Coefficients	5-15

HEAT TRANSFER BY RADIATION

Introduction	5-16
Thermal Radiation Fundamentals	5-16
Introduction to Radiation Geometry	5-16
Blackbody Radiation	5-16
Blackbody Displacement Laws	5-18
Radiative Properties of Opaque Surfaces	5-19
Emissance and Absorptance	5-19
View Factors and Direct Exchange Areas	5-20
Example 7: The Crossed-Strings Method	5-23
Example 8: Illustration of Exchange Area Algebra	5-24
Radiative Exchange in Enclosures—The Zone Method	5-24
Total Exchange Areas	5-24
General Matrix Formulation	5-24
Explicit Matrix Solution for Total Exchange Areas	5-25
Zone Methodology and Conventions	5-25
The Limiting Case of a Transparent Medium	5-26
The Two-Zone Enclosure	5-26
Multizone Enclosures	5-27
Some Examples from Furnace Design	5-28
Example 9: Radiation Pyrometry	5-28
Example 10: Furnace Simulation via Zoning	5-29
Allowance for Specular Reflection	5-30
An Exact Solution to the Integral Equations—The Hohlraum	5-30
Radiation from Gases and Suspended Particulate Matter	5-30
Introduction	5-30
Emissivities of Combustion Products	5-31
Example 11: Calculations of Gas Emissivity and Absorptivity	5-32
Flames and Particle Clouds	5-34
Radiative Exchange with Participating Media	5-35
Energy Balances for Volume Zones—The Radiation Source Term	5-35

Weighted Sum of Gray Gas (WSGG) Spectral Model	5-35
The Zone Method and Directed Exchange Areas	5-36
Algebraic Formulas for a Single Gas Zone	5-37
Engineering Approximations for Directed Exchange Areas	5-38
Example 12: WSGG Clear plus Gray Gas Emissivity Calculations	5-38
Engineering Models for Fuel-Fired Furnaces	5-39
Input/Output Performance Parameters for Furnace Operation	5-39
The Long Plug Flow Furnace (LPFF) Model	5-39
The Well-Stirred Combustion Chamber (WSCC) Model	5-40
Example 13: WSCC Furnace Model Calculations	5-41
WSCC Model Utility and More Complex Zoning Models	5-43

MASS TRANSFER

Introduction	5-45
Fick's First Law	5-45
Mutual Diffusivity, Mass Diffusivity, Interdiffusion Coefficient	5-45
Self-Diffusivity	5-45
Tracer Diffusivity	5-45
Mass-Transfer Coefficient	5-45
Problem Solving Methods	5-45
Continuity and Flux Expressions	5-49
Material Balances	5-49
Flux Expressions: Simple Integrated Forms of Fick's First Law	5-49
Stefan-Maxwell Equations	5-50
Diffusivity Estimation—Gases	5-50
Binary Mixtures—Low Pressure—Nonpolar Components	5-50
Binary Mixtures—Low Pressure—Polar Components	5-52
Binary Mixtures—High Pressure	5-52
Self-Diffusivity	5-52
Supercritical Mixtures	5-52
Low-Pressure/Multicomponent Mixtures	5-53
Diffusivity Estimation—Liquids	5-53
Stokes-Einstein and Free-Volume Theories	5-53
Dilute Binary Nonelectrolytes: General Mixtures	5-54
Binary Mixtures of Gases in Low-Viscosity, Nonelectrolyte Liquids	5-55
Dilute Binary Mixtures of a Nonelectrolyte in Water	5-55
Dilute Binary Hydrocarbon Mixtures	5-55
Dilute Binary Mixtures of Nonelectrolytes with Water as the Solute	5-55
Dilute Dispersions of Macromolecules in Nonelectrolytes	5-55
Concentrated, Binary Mixtures of Nonelectrolytes	5-55
Binary Electrolyte Mixtures	5-57
Multicomponent Mixtures	5-57
Diffusion of Fluids in Porous Solids	5-58
Interphase Mass Transfer	5-59
Mass-Transfer Principles: Dilute Systems	5-59
Mass-Transfer Principles: Concentrated Systems	5-60
HTU (Height Equivalent to One Transfer Unit)	5-61
NTU (Number of Transfer Units)	5-61
Definitions of Mass-Transfer Coefficients \hat{k}_G and \hat{k}_L	5-61
Simplified Mass-Transfer Theories	5-61
Mass-Transfer Correlations	5-62
Effects of Total Pressure on \hat{k}_G and \hat{k}_L	5-68
Effects of Temperature on \hat{k}_G and \hat{k}_L	5-68
Effects of System Physical Properties on \hat{k}_G and \hat{k}_L	5-74
Effects of High Solute Concentrations on \hat{k}_G and \hat{k}_L	5-74
Influence of Chemical Reactions on \hat{k}_G and \hat{k}_L	5-74
Effective Interfacial Mass-Transfer Area a	5-83
Volumetric Mass-Transfer Coefficients \hat{k}_{cA} and \hat{k}_{lA}	5-83
Chilton-Colburn Analogy	5-83

HEAT TRANSFER

GENERAL REFERENCES: Arpaci, *Conduction Heat Transfer*, Addison-Wesley, 1966. Arpaci, *Convection Heat Transfer*, Prentice-Hall, 1984. Arpaci, *Introduction to Heat Transfer*, Prentice-Hall, 1999. Baehr and Stephan, *Heat and Mass Transfer*, Springer, Berlin, 1998. Bejan, *Convection Heat Transfer*, Wiley, 1995. Carslaw and Jaeger, *Conduction of Heat in Solids*, Oxford University Press, 1959. Edwards, *Radiation Heat Transfer Notes*, Hemisphere Publishing, 1981. Hottel and Sarofim, *Radiative Transfer*, McGraw-Hill, 1967. Incropera and DeWitt, *Fundamentals of Heat and Mass Transfer*, 5th ed., Wiley, 2002. Kays and Crawford, *Convective Heat and Mass Transfer*, 3d ed., McGraw-Hill, 1993. Mills, *Heat Transfer*, 2d ed., Prentice-Hall, 1999. Modest, *Radiative Heat Transfer*, McGraw-Hill, 1993. Patankar, *Numerical Heat Transfer and Fluid Flow*, Taylor and Francis, London, 1980. Pletcher, Anderson, and Tannehill, *Computational Fluid Mechanics and Heat Transfer*, 2d ed., Taylor and Francis, London, 1997. Rohsenow, Hartnett, and Cho, *Handbook of Heat Transfer*, 3d ed., McGraw-Hill, 1998. Siegel and Howell, *Thermal Radiation Heat Transfer*, 4th ed., Taylor and Francis, London, 2001.

MODES OF HEAT TRANSFER

Heat is energy transferred due to a difference in temperature. There are three modes of heat transfer: conduction, convection, and radiation. All three may act at the same time. Conduction is the transfer of energy between adjacent particles of matter. It is a local phenomenon and can only occur through matter. Radiation is the transfer of energy from a point of higher temperature to a point of lower energy by electromagnetic radiation. Radiation can act at a distance through transparent media and vacuum. Convection is the transfer of energy by conduction and radiation in moving, fluid media. The motion of the fluid is an essential part of convective heat transfer.

HEAT TRANSFER BY CONDUCTION

FOURIER'S LAW

The heat flux due to conduction in the x direction is given by Fourier's law

$$\dot{Q} = -kA \frac{dT}{dx} \quad (5-1)$$

where \dot{Q} is the rate of heat transfer (W), k is the thermal conductivity [W/(m·K)], A is the area perpendicular to the x direction, and T is temperature (K). For the homogeneous, one-dimensional plane shown in Fig. 5-1a, with constant k , the integrated form of (5-1) is

$$\dot{Q} = kA \frac{T_1 - T_2}{\Delta x} \quad (5-2)$$

where Δx is the thickness of the plane. Using the thermal circuit shown in Fig. 5-1b, Eq. (5-2) can be written in the form

$$\dot{Q} = \frac{T_1 - T_2}{\Delta x/kA} = \frac{T_1 - T_2}{R} \quad (5-3)$$

where R is the thermal resistance (K/W).

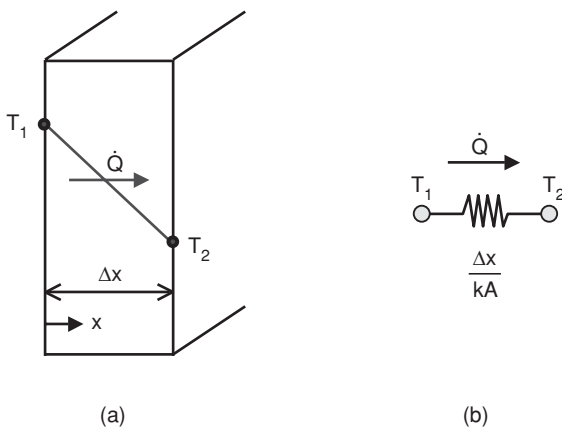


FIG. 5-1 Steady, one-dimensional conduction in a homogeneous planar wall with constant k . The thermal circuit is shown in (b) with thermal resistance $\Delta x/(kA)$.

THERMAL CONDUCTIVITY

The thermal conductivity k is a transport property whose value for a variety of gases, liquids, and solids is tabulated in Sec. 2. Section 2 also provides methods for predicting and correlating vapor and liquid thermal conductivities. The thermal conductivity is a function of temperature, but the use of constant or averaged values is frequently sufficient. Room temperature values for air, water, concrete, and copper are 0.026, 0.61, 1.4, and 400 W/(m·K). Methods for estimating contact resistances and the thermal conductivities of composites and insulation are summarized by Gebhart, *Heat Conduction and Mass Diffusion*, McGraw-Hill, 1993, p. 399.

STEADY-STATE CONDUCTION

One-Dimensional Conduction In the absence of energy source terms, \dot{Q} is constant with distance, as shown in Fig. 5-1a. For steady conduction, the integrated form of (5-1) for a planar system with constant k and A is Eq. (5-2) or (5-3). For the general case of variables k (k is a function of temperature) and A (cylindrical and spherical systems with radial coordinate r , as sketched in Fig. 5-2), the average heat-transfer area and thermal conductivity are defined such that

$$\dot{Q} = \overline{kA} \frac{T_1 - T_2}{\Delta x} = \frac{T_1 - T_2}{R} \quad (5-4)$$

For a thermal conductivity that depends linearly on T ,

$$k = k_0(1 + \gamma T) \quad (5-5)$$

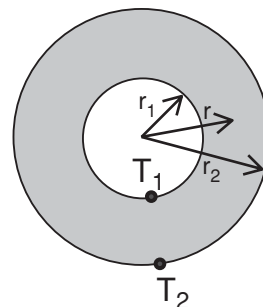


FIG. 5-2 The hollow sphere or cylinder.

5-4 HEAT AND MASS TRANSFER

Nomenclature and Units—Heat Transfer by Conduction, by Convection, and with Phase Change

Symbol	Definition	SI units	Symbol	Definition	SI units
A	Area for heat transfer	m^2	Ra_x	Rayleigh number, $\beta \Delta T g x^3 / \nu \alpha$	
A_c	Cross-sectional area	m^2	Re_D	Reynolds number, GD/μ	
A_f	Area for heat transfer for finned portion of tube	m^2	S	Volumetric source term	W/m^3
A_i	Inside area of tube		S	Cross-sectional area	m^2
A_o	External area of bare, unfinned tube	m^2	S_1	Fourier spatial function	
A_{of}	External area of tube before tubes are attached = A_o		t	Time	s
A_T	Total external area of finned tube	m^2	t_{sv}	Saturated-vapor temperature	K
A_{uf}	Area for heat transfer for unfinned portion of finned tube	m^2	t_s	Surface temperature	K
A_1	First Fourier coefficient		T	Temperature	K or °C
a_c	Cross-sectional area of fin	m^2	T_b	Bulk or mean temperature at a given cross section	K
b	Geometry; $b = 1$, plane; $b = 2$, cylinder; $b = 3$, sphere		\bar{T}_b	Bulk mean temperature, $(T_{b,in} + T_{b,out})/2$	K
b_f	Height of fin	m	T_C	Temperature of cold surface in enclosure	K
B_1	First Fourier coefficient		T_f	Film temperature, $(T_s + T_\infty)/2$	K
Bi	Biot number, hR/k		T_H	Temperature of hot surface in enclosure	K
c	Specific heat	J/(kg·K)	T_i	Initial temperature	K
c_p	Specific heat, constant pressure	J/(kg·K)	T_e	Temperature of free stream	K
D	Diameter	m	T_s	Temperature of surface	K
D_i	Inner diameter	m	T_∞	Temperature of fluid in contact with a solid surface	K
D_o	Outer diameter	m	U	Overall heat-transfer coefficient	$W/(m^2 \cdot K)$
f	Fanning friction factor		V	Volume	m^3
Fo	Dimensionless time or Fourier number, $\alpha t/R^2$		V_F	Velocity of fluid approaching a bank of finned tubes	m/s
g_c	Conversion factor	1.0 kg·m/(N·s ²)	V_∞	Velocity upstream of tube bank	m/s
g	Acceleration of gravity, 9.81 m/s ²	m^2/s	W_F	Total rate of vapor condensation on one tube	kg/s
G	Mass velocity, \dot{m}/A_c ; G_e for vapor mass velocity	kg/(m ² ·s)	x	Cartesian coordinate direction, characteristic dimension of a surface, or distance from entrance	m
G_{max}	Mass velocity through minimum free area between rows of tubes normal to the fluid stream	kg/(m ² ·s)	x	Vapor quality, x_i for inlet and x_o for outlet	
Gz	Graetz number = Re Pr		\tilde{z}_p	Distance (perimeter) traveled by fluid across fin	m
\bar{h}	Heat-transfer coefficient	$W/(m^2 \cdot K)$	Greek Symbols		
h	Average heat-transfer coefficient	$W/(m^2 \cdot K)$	α	Thermal diffusivity, $k/(\rho c)$	m^2/s
h_f	Heat-transfer coefficient for finned-tube exchangers based on total external surface	$W/(m^2 \cdot K)$	β	Volumetric coefficient of expansion	K^{-1}
h_f	Outside heat-transfer coefficient calculated for a bare tube for use with Eq. (5-73)	$W/(m^2 \cdot K)$	β'	Contact angle between a bubble and a surface	°
h_{fi}	Effective outside heat-transfer coefficient based on inside area of a finned tube	$W/(m^2 \cdot K)$	Γ	Mass flow rate per unit length perpendicular to flow	kg/(m·s)
h_i	Heat-transfer coefficient at inside tube surface	$W/(m^2 \cdot K)$	ΔP	Pressure drop	Pa
h_o	Heat-transfer coefficient at outside tube surface	$W/(m^2 \cdot K)$	Δt	Temperature difference	K
h_{am}	Heat-transfer coefficient for use with ΔT_{am} ; see Eq. (5-33)	$W/(m^2 \cdot K)$	ΔT	Temperature difference	K
h_{im}	Heat-transfer coefficient for use with ΔT_{im} ; see Eq. (5-32)	$W/(m^2 \cdot K)$	ΔT_{am}	Arithmetic mean temperature difference, see Eq. (5-32)	K
\bar{k}	Thermal conductivity	$W/(m \cdot K)$	ΔT_{lm}	Logarithmic mean temperature difference, see Eq. (5-33)	K
k	Average thermal conductivity	$W/(m \cdot K)$	Δx	Thickness of plane wall for conduction	m
L	Length of cylinder or length of flat plate in direction of flow or downstream distance. Length of heat-transfer surface	m	δ_1	First dimensionless eigenvalue	
m	Fin parameter defined by Eq. (5-75).		$\delta_{1,0}$	First dimensionless eigenvalue as Bi approaches 0	
\dot{m}	Mass flow rate	kg/s	$\delta_{1,\infty}$	First dimensionless eigenvalue as Bi approaches ∞	
Nu_D	Nusselt number based on diameter D , hD/k		δ_s	Correction factor, ratio of nonnewtonian to newtonian shear rates	
\bar{Nu}_D	Average Nusselt number based on diameter D , $\bar{h}D/k$		ϵ	Emissivity of a surface	
Nu_{im}	Nusselt number based on h_{im}		ζ	Dimensionless distance, r/R	
n'	Flow behavior index for nonnewtonian fluids		$\hat{\theta}/\theta_1$	Dimensionless temperature, $(T - T_\infty)/(T_i - T_\infty)$	
p	Perimeter	m	λ	Latent heat (enthalpy) of vaporization (condensation)	J/kg
p_f	Fin perimeter	m	μ	Viscosity; μ_L , viscosity of liquid; μ_g , μ_v , viscosity of gas or vapor	kg/(m·s)
p'	Center-to-center spacing of tubes in a bundle	m	ν	Kinematic viscosity, μ/ρ	m^2/s
P	Absolute pressure; P_c for critical pressure	kPa	ρ	Density; ρ_L , ρ_f for density of liquid; ρ_G , ρ_v for density of vapor	kg/m ³
Pr	Prandtl number, ν/α		σ	Stefan-Boltzmann constant, 5.67×10^{-8}	$W/(m^2 \cdot K^4)$
q	Rate of heat transfer	W	σ	Surface tension between and liquid and its vapor	N/m
Q	Amount of heat transfer	J	τ	Time constant, time scale	s
\dot{Q}	Rate of heat transfer	W	Ω	Efficiency of fin	
\dot{Q}/Q_i	Heat loss fraction, $Q/[\rho c V(T_i - T_\infty)]$				
r	Distance from center in plate, cylinder, or sphere	m			
R	Thermal resistance or radius	K/W or m			

and the average heat thermal conductivity is

$$\bar{k} = k_0(1 + \gamma\bar{T}) \quad (5-6)$$

where $\bar{T} = 0.5(T_1 + T_2)$.

For cylinders and spheres, A is a function of radial position (see Fig. 5-2): $2\pi rL$ and $4\pi r^2$, where L is the length of the cylinder. For constant k , Eq. (5-4) becomes

$$\dot{Q} = \frac{T_1 - T_2}{[\ln(r_2/r_1)]/(2\pi kL)} \quad \text{cylinder} \quad (5-7)$$

and

$$\dot{Q} = \frac{T_1 - T_2}{(r_2 - r_1)/(4\pi k r_1 r_2)} \quad \text{sphere} \quad (5-8)$$

Conduction with Resistances in Series A steady-state temperature profile in a planar composite wall, with three constant thermal conductivities and no source terms, is shown in Fig. 5-3a. The corresponding thermal circuit is given in Fig. 5-3b. The rate of heat transfer through each of the layers is the same. The total resistance is the sum of the individual resistances shown in Fig. 5-3b:

$$Q = \frac{T_1 - T_2}{\frac{\Delta X_A}{k_A A} + \frac{\Delta X_B}{k_B A} + \frac{\Delta X_C}{k_C A}} = \frac{T_1 - T_2}{R_A + R_B + R_C} \quad (5-9)$$

Additional resistances in the series may occur at the surfaces of the solid if they are in contact with a fluid. The rate of convective heat transfer, between a surface of area A and a fluid, is represented by Newton's law of cooling as

$$\dot{Q} = hA(T_{\text{surface}} - T_{\text{fluid}}) = \frac{T_{\text{surface}} - T_{\text{fluid}}}{1/(hA)} \quad (5-10)$$

where $1/(hA)$ is the resistance due to convection (K/W) and the heat-transfer coefficient is h [W/(m²·K)]. For the cylindrical geometry shown in Fig. 5-2, with convection to inner and outer fluids at temperatures T_i and T_o , with heat-transfer coefficients h_i and h_o , the steady-state rate of heat transfer is

$$\dot{Q} = \frac{T_i - T_o}{\frac{1}{2\pi r_1 L h_i} + \frac{\ln(r_2/r_1)}{2\pi k L} + \frac{1}{2\pi r_2 L h_o}} = \frac{T_i - T_o}{R_i + R_1 + R_o} \quad (5-11)$$

where resistances R_i and R_o are the convective resistances at the inner and outer surfaces. The total resistance is again the sum of the resistances in series.

Example 1: Conduction with Resistances in Series and Parallel Figure 5-4 shows the thermal circuit for a furnace wall. The outside surface has a known temperature $T_2 = 625$ K. The temperature of the surroundings

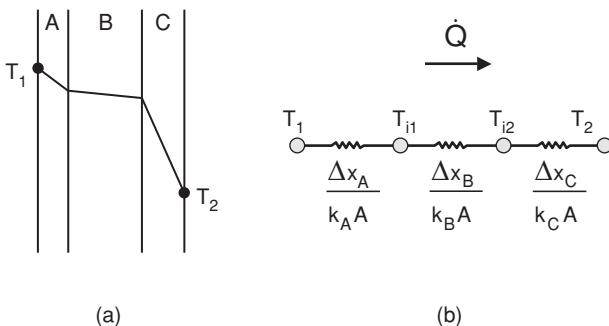


FIG. 5-3 Steady-state temperature profile in a composite wall with constant thermal conductivities k_A , k_B , and k_C and no energy sources in the wall. The thermal circuit is shown in (b). The total resistance is the sum of the three resistances shown.

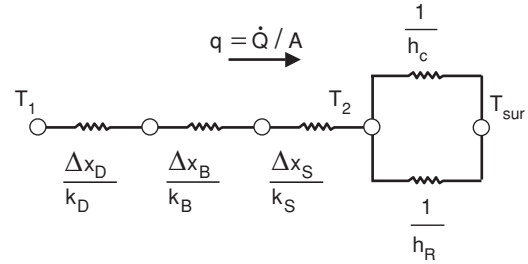


FIG. 5-4 Thermal circuit for Example 1. Steady-state conduction in a furnace wall with heat losses from the outside surface by convection (h_c) and radiation (h_R) to the surroundings at temperature T_{sur} . The thermal conductivities k_D , k_B , and k_S are constant, and there are no sources in the wall. The heat flux q has units of W/m².

T_{sur} is 290 K. We want to estimate the temperature of the inside wall T_1 . The wall consists of three layers: deposit [$k_D = 1.6$ W/(m·K), $\Delta x_D = 0.080$ m], brick [$k_B = 1.7$ W/(m·K), $\Delta x_B = 0.15$ m], and steel [$k_S = 45$ W/(m·K), $\Delta x_S = 0.00254$ m]. The outside surface loses heat by two parallel mechanisms—convection and radiation. The convective heat-transfer coefficient $h_c = 5.0$ W/(m²·K). The radiative heat-transfer coefficient $h_R = 16.3$ W/(m²·K). The latter is calculated from

$$h_R = \epsilon_2 \sigma (T_2^2 + T_{\text{sur}}^2)(T_2 + T_{\text{sur}}) \quad (5-12)$$

where the emissivity of surface 2 is $\epsilon_2 = 0.76$ and the Stefan-Boltzmann constant $\sigma = 5.67 \times 10^{-8}$ W/(m²·K⁴).

Referring to Fig. 5-4, the steady-state heat flux q (W/m²) through the wall is

$$q = \frac{\dot{Q}}{A} = \frac{T_1 - T_2}{\frac{\Delta x_D}{k_D} + \frac{\Delta x_B}{k_B} + \frac{\Delta x_S}{k_S}} = (h_c + h_R)(T_2 - T_{\text{sur}})$$

Solving for T_1 gives

$$T_1 = T_2 + \left(\frac{\Delta x_D}{k_D} + \frac{\Delta x_B}{k_B} + \frac{\Delta x_S}{k_S} \right) (h_c + h_R)(T_2 - T_{\text{sur}})$$

and

$$T_1 = 625 + \left(\frac{0.080}{1.6} + \frac{0.15}{1.7} + \frac{0.00254}{45} \right) (5.0 + 16.3)(625 - 290) = 1610 \text{ K}$$

Conduction with Heat Source Application of the law of conservation of energy to a one-dimensional solid, with the heat flux given by (5-1) and volumetric source term S (W/m³), results in the following equations for steady-state conduction in a flat plate of thickness $2R$ ($b = 1$), a cylinder of diameter $2R$ ($b = 2$), and a sphere of diameter $2R$ ($b = 3$). The parameter b is a measure of the curvature. The thermal conductivity is constant, and there is convection at the surface, with heat-transfer coefficient h and fluid temperature T_∞ .

$$\frac{d}{dr} \left(r^{b-1} \frac{dT}{dr} \right) + \frac{S}{k} r^{b-1} = 0$$

$$\frac{dT(0)}{dr} = 0 \quad (\text{symmetry condition}) \quad (5-13)$$

$$-k \frac{dT}{dr} = h[T(R) - T_\infty]$$

The solutions to (5-13), for uniform S , are

$$\frac{T(r) - T_\infty}{SR^2/k} = \frac{1}{2b} \left[1 - \left(\frac{r}{R} \right)^2 \right] + \frac{1}{b\text{Bi}} \begin{cases} b = 1, \text{ plate, thickness } 2R \\ b = 2, \text{ cylinder, diameter } 2R \\ b = 3, \text{ sphere, diameter } 2R \end{cases} \quad (5-14)$$

where $\text{Bi} = hR/k$ is the Biot number. For $\text{Bi} \ll 1$, the temperature in the solid is uniform. For $\text{Bi} \gg 1$, the surface temperature $T(R) = T_\infty$.

Two- and Three-Dimensional Conduction Application of the law of conservation of energy to a three-dimensional solid, with the

5-6 HEAT AND MASS TRANSFER

heat flux given by (5-1) and volumetric source term S (W/m^3), results in the following equation for steady-state conduction in rectangular coordinates.

$$\frac{\partial}{\partial x} \left(k \frac{\partial T}{\partial x} \right) + \frac{\partial}{\partial y} \left(k \frac{\partial T}{\partial y} \right) + \frac{\partial}{\partial z} \left(k \frac{\partial T}{\partial z} \right) + S = 0 \quad (5-15)$$

Similar equations apply to cylindrical and spherical coordinate systems. Finite difference, finite volume, or finite element methods are generally necessary to solve (5-15). Useful introductions to these numerical techniques are given in the General References and Sec. 3. Simple forms of (5-15) (constant k , uniform S) can be solved analytically. See Arpaci, *Conduction Heat Transfer*, Addison-Wesley, 1966, p. 180, and Carslaw and Jaeger, *Conduction of Heat in Solids*, Oxford University Press, 1959. For problems involving heat flow between two surfaces, each isothermal, with all other surfaces being adiabatic, the shape factor approach is useful (Mills, *Heat Transfer*, 2d ed., Prentice-Hall, 1999, p. 164).

UNSTEADY-STATE CONDUCTION

Application of the law of conservation of energy to a three-dimensional solid, with the heat flux given by (5-1) and volumetric source term S (W/m^3), results in the following equation for unsteady-state conduction in rectangular coordinates.

$$\rho c \frac{\partial T}{\partial t} = \frac{\partial}{\partial x} \left(k \frac{\partial T}{\partial x} \right) + \frac{\partial}{\partial y} \left(k \frac{\partial T}{\partial y} \right) + \frac{\partial}{\partial z} \left(k \frac{\partial T}{\partial z} \right) + S \quad (5-16)$$

The energy storage term is on the left-hand side, and ρ and c are the density (kg/m^3) and specific heat [$J/(kg \cdot K)$]. Solutions to (5-16) are generally obtained numerically (see General References and Sec. 3). The one-dimensional form of (5-16), with constant k and no source term, is

$$\frac{\partial T}{\partial t} = \alpha \frac{\partial^2 T}{\partial x^2} \quad (5-17)$$

where $\alpha = k/(\rho c)$ is the thermal diffusivity (m^2/s).

One-Dimensional Conduction: Lumped and Distributed Analysis The one-dimensional transient conduction equations in rectangular ($b = 1$), cylindrical ($b = 2$), and spherical ($b = 3$) coordinates, with constant k , initial uniform temperature T_i , $S = 0$, and convection at the surface with heat-transfer coefficient h and fluid temperature T_∞ , are

$$\frac{\partial T}{\partial t} = \frac{\alpha}{r^{b-1}} \frac{\partial}{\partial r} \left(r^{b-1} \frac{\partial T}{\partial r} \right) \quad \begin{cases} b = 1, \text{ plate, thickness } 2R \\ b = 2, \text{ cylinder, diameter } 2R \\ b = 3, \text{ sphere, diameter } 2R \end{cases}$$

$$\text{for } t < 0, \quad T = T_i \quad (\text{initial temperature}) \quad (5-18)$$

$$\text{at } r = 0, \quad \frac{\partial T}{\partial r} = 0 \quad (\text{symmetry condition})$$

$$\text{at } r = R, \quad -k \frac{\partial T}{\partial r} = h(T - T_\infty)$$

The solutions to (5-18) can be compactly expressed by using dimensionless variables: (1) temperature $\theta/\theta_i = [T(r,t) - T_\infty]/(T_i - T_\infty)$; (2) heat loss fraction $Q/Q_i = Q/[\rho c V (T_i - T_\infty)]$, where V is volume; (3) distance from center $\zeta = r/R$; (4) time $Fo = \alpha t/R^2$, and (5) Biot number $Bi = hR/k$. The temperature and heat loss are functions of ζ , Fo , and Bi .

When the Biot number is small, $Bi < 0.2$, the temperature of the solid is nearly uniform and a lumped analysis is acceptable. The solution to the lumped analysis of (5-18) is

$$\frac{\theta}{\theta_i} = \exp\left(-\frac{hA}{\rho c V} t\right) \quad \text{and} \quad \frac{Q}{Q_i} = 1 - \exp\left(-\frac{hA}{\rho c V} t\right) \quad (5-19)$$

where A is the active surface area and V is the volume. The time scale for the lumped problem is

$$\tau = \frac{\rho c V}{hA} \quad (5-20)$$

TABLE 5-1 Fourier Coefficients and Spatial Functions for Use in Eqs. (5-21)

Geometry	A_1	B_1	S_1
Plate	$\frac{2\sin\delta_1}{\delta_1 + \sin\delta_1\cos\delta_1}$	$\frac{2Bi^2}{\delta_1^2(Bi^2 + Bi + \delta_1^2)}$	$\cos(\delta_1\zeta)$
Cylinder	$\frac{2J_1(\delta_1)}{\delta_1[J_0'(\delta_1) + J_1'(\delta_1)]}$	$\frac{4Bi^2}{\delta_1^2(\delta_1^2 + Bi^2)}$	$J_0(\delta_1\zeta)$
Sphere	$\frac{2Bi[\delta_1^2 + (Bi - 1)^2]^{1/2}}{\delta_1^2 + Bi^2 - Bi}$	$\frac{6Bi^2}{\delta_1^2(\delta_1^2 + Bi^2 - Bi)}$	$\frac{\sin\delta_1\zeta}{\delta_1\zeta}$

The time scale is the time required for most of the change in θ/θ_i or Q/Q_i to occur. When $t = \tau$, $\theta/\theta_i = \exp(-1) = 0.368$ and roughly two-thirds of the possible change has occurred.

When a lumped analysis is not valid ($Bi > 0.2$), the single-term solutions to (5-18) are convenient:

$$\frac{\theta}{\theta_i} = A_1 \exp(-\delta_1^2 Fo) S_1(\delta_1\zeta) \quad \text{and} \quad \frac{Q}{Q_i} = 1 - B_1 \exp(-\delta_1^2 Fo) \quad (5-21)$$

where the first Fourier coefficients A_1 and B_1 and the spatial functions S_1 are given in Table 5-1. The first eigenvalue δ_1 is given by (5-22) in conjunction with Table 5-2. The one-term solutions are accurate to within 2 percent when $Fo > Fo_c$. The values of the critical Fourier number Fo_c are given in Table 5-2.

The first eigenvalue is accurately correlated by (Yovanovich, Chap. 3 of Rohsenow, Hartnett, and Cho, *Handbook of Heat Transfer*, 3d ed., McGraw-Hill, 1998, p. 3.25)

$$\delta_1 = \frac{\delta_{1,\infty}}{[1 + (\delta_{1,\infty}/\delta_{1,0})^n]^{1/n}} \quad (5-22)$$

Equation (5-22) gives values of δ_1 that differ from the exact values by less than 0.4 percent, and it is valid for all values of Bi . The values of $\delta_{1,\infty}$, $\delta_{1,0}$, n , and Fo_c are given in Table 5-2.

Example 2: Correlation of First Eigenvalues by Eq. (5-22) As an example of the use of Eq. (5-22), suppose that we want δ_1 for the flat plate with $Bi = 5$. From Table 5-2, $\delta_{1,\infty} = \pi/2$, $\delta_{1,0} = \sqrt{Bi} = \sqrt{5}$, and $n = 2.139$. Equation (5-22) gives

$$\delta_1 = \frac{\pi/2}{[1 + (\pi/2/\sqrt{5})^{2.139}]^{1/2.139}} = 1.312$$

The tabulated value is 1.3138.

Example 3: One-Dimensional, Unsteady Conduction Calculation As an example of the use of Eq. (5-21), Table 5-1, and Table 5-2, consider the cooking time required to raise the center of a spherical, 8-cm-diameter dumpling from 20 to 80°C. The initial temperature is uniform. The dumpling is heated with saturated steam at 95°C. The heat capacity, density, and thermal conductivity are estimated to be $c = 3500$ J/(kg·K), $\rho = 1000$ kg/m³, and $k = 0.5$ W/(m·K), respectively.

Because the heat-transfer coefficient for condensing steam is of order 10^4 , the $Bi \rightarrow \infty$ limit in Table 5-2 is a good choice and $\delta_1 = \pi$. Because we know the desired temperature at the center, we can calculate θ/θ_i and then solve (5-21) for the time.

$$\frac{\theta}{\theta_i} = \frac{T(0,t) - T_\infty}{T_i - T_\infty} = \frac{80 - 95}{20 - 95} = 0.200$$

For $Bi \rightarrow \infty$, A_1 in Table 5-1 is 2 and for $\zeta = 0$, S_1 in Table 5-1 is 1. Equation (5-21) becomes

$$\frac{\theta}{\theta_i} = 2 \exp(-\pi^2 Fo) = 2 \exp\left(-\frac{\pi^2 \alpha t}{R^2}\right)$$

TABLE 5-2 First Eigenvalues for $Bi \rightarrow 0$ and $Bi \rightarrow \infty$ and Correlation Parameter n

The single-term approximations apply only if $Fo \geq Fo_c$.

Geometry	$Bi \rightarrow 0$	$Bi \rightarrow \infty$	n	Fo_c
Plate	$\delta_1 \rightarrow \sqrt{Bi}$	$\delta_1 \rightarrow \pi/2$	2.139	0.24
Cylinder	$\delta_1 \rightarrow \sqrt{2Bi}$	$\delta_1 \rightarrow 2.4048255$	2.238	0.21
Sphere	$\delta_1 \rightarrow \sqrt{3Bi}$	$\delta_1 \rightarrow \pi$	2.314	0.18

Solving for t gives the desired cooking time.

$$t = -\frac{R^2}{\alpha\pi^2} \ln \frac{\theta}{2\theta_1} = -\frac{(0.04 \text{ m})^2}{1.43 \times 10^{-7} (\text{m}^2/\text{s})\pi^2} \ln \frac{0.2}{2} = 43.5 \text{ min}$$

Example 4: Rule of Thumb for Time Required to Diffuse a Distance R A general rule of thumb for estimating the time required to diffuse a distance R is obtained from the one-term approximations. Consider the equation for the temperature of a flat plate of thickness $2R$ in the limit as $\text{Bi} \rightarrow \infty$. From Table 5-2, the first eigenvalue is $\delta_1 = \pi/2$, and from Table 5-1,

$$\frac{\theta}{\theta_1} = A_1 \exp\left[-\left(\frac{\pi}{2}\right)^2 \frac{\alpha t}{R^2}\right] \cos \delta_1 \zeta$$

When $t = R^2/\alpha$, the temperature ratio at the center of the plate ($\zeta = 0$) has decayed to $\exp(-\pi^2/4)$, or 8 percent of its initial value. We conclude that *diffusion through a distance R takes roughly R^2/α units of time, or alternatively, the distance diffused in time t is about $(\alpha t)^{1/2}$.*

One-Dimensional Conduction: Semi-infinite Plate Consider a semi-infinite plate with an initial uniform temperature T_i . Suppose that the temperature of the surface is suddenly raised to T_∞ ; that is, the heat-transfer coefficient is infinite. The unsteady temperature of the plate is

$$\frac{T(x,t) - T_\infty}{T_i - T_\infty} = \text{erfc}\left(\frac{x}{2\sqrt{\alpha t}}\right) \quad (5-23)$$

where $\text{erf}(z)$ is the error function. The depth to which the heat penetrates in time t is approximately $(12\alpha t)^{1/2}$.

If the heat-transfer coefficient is finite,

$$\frac{T(x,t) - T_\infty}{T_i - T_\infty} = \text{erfc}\left(\frac{x}{2\sqrt{\alpha t}}\right) - \exp\left(\frac{hx}{k} + \frac{h^2\alpha t}{k^2}\right) \text{erfc}\left(\frac{x}{2\sqrt{\alpha t}} + \frac{h\sqrt{\alpha t}}{k}\right) \quad (5-24)$$

where $\text{erfc}(z)$ is the complementary error function. Equations (5-23) and (5-24) are both applicable to finite plates provided that their half-thickness is greater than $(12\alpha t)^{1/2}$.

Two- and Three-Dimensional Conduction The one-dimensional solutions discussed above can be used to construct solutions to multidimensional problems. The unsteady temperature of a rectangular, solid box of height, length, and width $2H$, $2L$, and $2W$, respectively, with governing equations in each direction as in (5-18), is

$$\left(\frac{\theta}{\theta_1}\right)_{2H \times 2L \times 2W} = \left(\frac{\theta}{\theta_1}\right)_{2H} \left(\frac{\theta}{\theta_1}\right)_{2L} \left(\frac{\theta}{\theta_1}\right)_{2W} \quad (5-25)$$

Similar products apply for solids with other geometries, e.g., semi-infinite, cylindrical rods.

HEAT TRANSFER BY CONVECTION

CONVECTIVE HEAT-TRANSFER COEFFICIENT

Convection is the transfer of energy by conduction and radiation in moving, fluid media. The motion of the fluid is an essential part of convective heat transfer. A key step in calculating the rate of heat transfer by convection is the calculation of the heat-transfer coefficient. This section focuses on the estimation of heat-transfer coefficients for natural and forced convection. The conservation equations for mass, momentum, and energy, as presented in Sec. 6, can be used to calculate the rate of convective heat transfer. Our approach in this section is to rely on correlations.

In many cases of industrial importance, heat is transferred from one fluid, through a solid wall, to another fluid. The transfer occurs in a heat exchanger. Section 11 introduces several types of heat exchangers, design procedures, overall heat-transfer coefficients, and mean temperature differences. Section 3 introduces dimensional analysis and the dimensionless groups associated with the heat-transfer coefficient.

Individual Heat-Transfer Coefficient The local rate of convective heat transfer between a surface and a fluid is given by Newton's law of cooling

$$q = h(T_{\text{surface}} - T_{\text{fluid}}) \quad (5-26)$$

where h [$\text{W}/(\text{m}^2 \cdot \text{K})$] is the local heat-transfer coefficient and q is the energy flux (W/m^2). The definition of h is arbitrary, depending on whether the bulk fluid, centerline, free stream, or some other temperature is used for T_{fluid} . The heat-transfer coefficient may be defined on an average basis as noted below.

Consider a fluid with bulk temperature T , flowing in a cylindrical tube of diameter D , with constant wall temperature T_s . An energy balance on a short section of the tube yields

$$c_p \dot{m} \frac{dT}{dx} = \pi D h (T_s - T) \quad (5-27)$$

where c_p is the specific heat at constant pressure [$\text{J}/(\text{kg} \cdot \text{K})$], \dot{m} is the mass flow rate (kg/s), and x is the distance from the inlet. If the temperature of the fluid at the inlet is T_{in} , the temperature of the fluid at a downstream distance L is

$$\frac{T(L) - T_s}{T_{\text{in}} - T_s} = \exp\left(-\frac{\bar{h}\pi DL}{\dot{m}c_p}\right) \quad (5-28)$$

The average heat-transfer coefficient \bar{h} is defined by

$$\bar{h} = \frac{1}{L} \int_0^L h \, dx \quad (5-29)$$

Overall Heat-Transfer Coefficient and Heat Exchangers A local, overall heat-transfer coefficient U for the cylindrical geometry shown in Fig. 5-2 is defined by using Eq. (5-11) as

$$\frac{\dot{Q}}{\Delta x} = \frac{T_i - T_o}{\frac{1}{2\pi r_1 h_i} + \frac{\ln(r_2/r_1)}{2\pi k} + \frac{1}{2\pi r_2 h_o}} = 2\pi r_1 U (T_i - T_o) \quad (5-30)$$

where Δx is a short length of tube in the axial direction. Equation (5-30) defines U by using the inside perimeter $2\pi r_1$. The outer perimeter can also be used. Equation (5-30) applies to clean tubes. Additional resistances are present in the denominator for dirty tubes (see Sec. 11).

For counterflow and parallel flow heat exchanges, with high- and low-temperature fluids (T_H and T_C) and flow directions as defined in Fig. 5-5, the total heat transfer for the exchanger is given by

$$\dot{Q} = UA \Delta T_{\text{lm}} \quad (5-31)$$

where A is the area for heat exchange and the log mean temperature difference ΔT_{lm} is defined as

$$\Delta T_{\text{lm}} = \frac{(T_H - T_C)_L - (T_H - T_C)_0}{\ln[(T_H - T_C)_L / (T_H - T_C)_0]} \quad (5-32)$$

Equation (5-32) applies to both counterflow and parallel flow exchangers with the nomenclature defined in Fig. 5-5. Correction factors to ΔT_{lm} for various heat exchanger configurations are given in Sec. 11.

In certain applications, the log mean temperature difference is replaced with an arithmetic mean difference:

$$\Delta T_{\text{am}} = \frac{(T_H - T_C)_L + (T_H - T_C)_0}{2} \quad (5-33)$$

Average heat-transfer coefficients are occasionally reported based on Eqs. (5-32) and (5-33) and are written as h_{lm} and h_{am} .

Representation of Heat-Transfer Coefficients Heat-transfer coefficients are usually expressed in two ways: (1) dimensionless relations and (2) dimensional equations. Both approaches are used below. The dimensionless form of the heat-transfer coefficient is the Nusselt

5-8 HEAT AND MASS TRANSFER

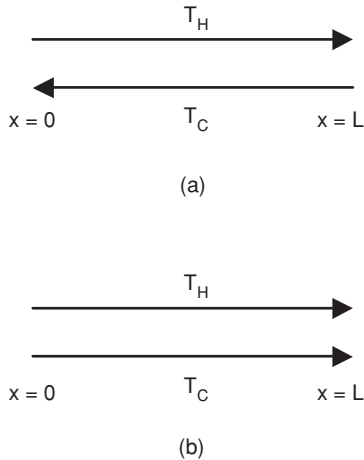


FIG. 5-5 Nomenclature for (a) counterflow and (b) parallel flow heat exchangers for use with Eq. (5-32).

number. For example, with a cylinder of diameter D in cross flow, the local Nusselt number is defined as $Nu_D = hD/k$, where k is the thermal conductivity of the fluid. The subscript D is important because different characteristic lengths can be used to define Nu . The average Nusselt number is written $\overline{Nu}_D = \overline{h}D/k$.

NATURAL CONVECTION

Natural convection occurs when a fluid is in contact with a solid surface of different temperature. Temperature differences create the density gradients that drive natural or free convection. In addition to the Nusselt number mentioned above, the key dimensionless parameters for natural convection include the Rayleigh number $Ra_s = \beta \Delta T g x^3 / \nu \alpha$ and the Prandtl number $Pr = \nu / \alpha$. The properties appearing in Ra and Pr include the volumetric coefficient of expansion β (K^{-1}); the difference ΔT between the surface (T_s) and free stream (T_∞) temperatures (K or $^\circ C$); the acceleration of gravity g (m/s^2); a characteristic dimension x of the surface (m); the kinematic viscosity ν (m^2/s); and the thermal diffusivity α (m^2/s). The volumetric coefficient of expansion for an ideal gas is $\beta = 1/T$, where T is absolute temperature. For a given geometry,

$$\overline{Nu}_x = f(Ra_x, Pr) \quad (5-34)$$

External Natural Flow for Various Geometries For vertical walls, Churchill and Chu [*Int. J. Heat Mass Transfer*, **18**, 1323 (1975)] recommend, for laminar and turbulent flow on isothermal, vertical walls with height L ,

$$\overline{Nu}_L = \left\{ 0.825 + \frac{0.387 Ra_L^{1/6}}{[1 + (0.492/Pr)^{9/16}]^{8/27}} \right\}^2 \quad (5-35)$$

where the fluid properties for Eq. (5-35) and $\overline{Nu}_L = \overline{h}L/k$ are evaluated at the film temperature $T_f = (T_s + T_\infty)/2$. This correlation is valid for all Pr and Ra_L . For vertical cylinders with boundary layer thickness much less than their diameter, Eq. (5-35) is applicable. An expression for uniform heating is available from the same reference.

For laminar and turbulent flow on isothermal, horizontal cylinders of diameter D , Churchill and Chu [*Int. J. Heat Mass Transfer*, **18**, 1049 (1975)] recommend

$$\overline{Nu}_L = \left\{ 0.60 + \frac{0.387 Ra_D^{1/6}}{[1 + (0.559/Pr)^{9/16}]^{8/27}} \right\}^2 \quad (5-36)$$

Fluid properties for (5-36) should be evaluated at the film temperature $T_f = (T_s + T_\infty)/2$. This correlation is valid for all Pr and Ra_D .

For horizontal flat surfaces, the characteristic dimension for the correlations is [Goldstein, Sparrow, and Jones, *Int. J. Heat Mass Transfer*, **16**, 1025–1035 (1973)]

$$L = \frac{A}{p} \quad (5-37)$$

where A is the area of the surface and p is the perimeter. With hot surfaces facing upward, or cold surfaces facing downward [Lloyd and Moran, ASME Paper 74-WA/HT-66 (1974)],

$$\overline{Nu}_L = \begin{cases} 0.54 Ra_L^{1/4} & 10^4 < Ra_L < 10^7 \\ 0.15 Ra_L^{1/3} & 10^7 < Ra_L < 10^{10} \end{cases} \quad (5-38)$$

and for hot surfaces facing downward, or cold surfaces facing upward,

$$\overline{Nu}_L = 0.27 Ra_L^{1/4} \quad 10^5 < Ra_L < 10^{10} \quad (5-40)$$

Fluid properties for Eqs. (5-38) to (5-40) should be evaluated at the film temperature $T_f = (T_s + T_\infty)/2$.

Simultaneous Heat Transfer by Radiation and Convection Simultaneous heat transfer by radiation and convection is treated per the procedure outlined in Examples 1 and 5. A radiative heat-transfer coefficient h_R is defined by (5-12).

Mixed Forced and Natural Convection Natural convection is commonly assisted or opposed by forced flow. These situations are discussed, e.g., by Mills (*Heat Transfer*, 2d ed., Prentice-Hall, 1999, p. 340) and Raithby and Hollands (Chap. 4 of Rohsenow, Hartnett, and Cho, *Handbook of Heat Transfer*, 3d ed., McGraw-Hill, 1998, p. 4.73).

Enclosed Spaces The rate of heat transfer across an enclosed space is described in terms of a heat-transfer coefficient based on the temperature difference between two surfaces:

$$\overline{h} = \frac{\dot{Q}/A}{T_H - T_C} \quad (5-41)$$

For rectangular cavities, the plate spacing between the two surfaces L is the characteristic dimension that defines the Nusselt and Rayleigh numbers. The temperature difference in the Rayleigh number, $Ra_L = \beta \Delta T g L^3 / \nu \alpha$ is $\Delta T = T_H - T_C$.

For a horizontal rectangular cavity heated from below, the onset of advection requires $Ra_L > 1708$. Globe and Dropkin [*J. Heat Transfer*, **81**, 24–28 (1959)] propose the correlation

$$\overline{Nu}_L = 0.069 Ra_L^{1/3} Pr^{0.074} \quad 3 \times 10^5 < Ra_L < 7 \times 10^9 \quad (5-42)$$

All properties in (5-42) are calculated at the average temperature $(T_H + T_C)/2$.

For vertical rectangular cavities of height H and spacing L , with $Pr \approx 0.7$ (gases) and $40 < H/L < 110$, the equation of Shewen et al. [*J. Heat Transfer*, **118**, 993–995 (1996)] is recommended:

$$\overline{Nu}_L = \left\{ 1 + \left[\frac{0.0665 Ra_L^{1/3}}{1 + (9000/Ra_L)^{1.4}} \right]^2 \right\}^{1/2} \quad Ra_L < 10^6 \quad (5-43)$$

All properties in (5-43) are calculated at the average temperature $(T_H + T_C)/2$.

Example 5: Comparison of the Relative Importance of Natural Convection and Radiation at Room Temperature

Estimate the heat losses by natural convection and radiation for an undraped person standing in still air. The temperatures of the air, surrounding surfaces, and skin are 19, 15, and 35 $^\circ C$, respectively. The height and surface area of the person are 1.8 m and 1.8 m 2 . The emissivity of the skin is 0.95.

We can estimate the Nusselt number by using (5-35) for a vertical, flat plate of height $L = 1.8$ m. The film temperature is $(19 + 35)/2 = 27^\circ C$. The Rayleigh number, evaluated at the film temperature, is

$$Ra_L = \frac{\beta \Delta T g L^3}{\nu \alpha} = \frac{(1/300)(35 - 19)9.81(1.8)^3}{1.589 \times 10^{-5}(2.25 \times 10^{-5})} = 8.53 \times 10^9$$

From (5-35) with $Pr = 0.707$, the Nusselt number is 240 and the average heat-transfer coefficient due to natural convection is

$$\overline{h} = \frac{k}{L} \overline{Nu}_L = \frac{0.0263}{1.8} (240) = 3.50 \frac{W}{m^2 \cdot K}$$

The radiative heat-transfer coefficient is given by (5-12):

$$h_R = \epsilon_{\text{skin}} \sigma (T_{\text{skin}}^2 + T_{\text{sur}}^2)(T_{\text{skin}} + T_{\text{sur}}) \\ = 0.95(5.67 \times 10^{-8})(308^2 + 288^2)(308 + 288) = 5.71 \frac{\text{W}}{\text{m}^2 \cdot \text{K}}$$

The total rate of heat loss is

$$\dot{Q} = \bar{h}A(T_{\text{skin}} - T_{\text{sur}}) + \bar{h}_R A(T_{\text{skin}} - T_{\text{sur}}) \\ = 3.50(1.8)(35 - 19) + 5.71(1.8)(35 - 15) = 306 \text{ W}$$

At these conditions, radiation is nearly twice as important as natural convection.

FORCED CONVECTION

Forced convection heat transfer is probably the most common mode in the process industries. Forced flows may be internal or external. This subsection briefly introduces correlations for estimating heat-transfer coefficients for flows in tubes and ducts; flows across plates, cylinders, and spheres; flows through tube banks and packed beds; heat transfer to nonevaporating falling films; and rotating surfaces. Section 11 introduces several types of heat exchangers, design procedures, overall heat-transfer coefficients, and mean temperature differences.

Flow in Round Tubes In addition to the Nusselt ($\text{Nu}_D = hD/k$) and Prandtl ($\text{Pr} = \nu/\alpha$) numbers introduced above, the key dimensionless parameter for forced convection in round tubes of diameter D is the Reynolds number $\text{Re} = GD/\mu$, where G is the mass velocity $G = \dot{m}/A_c$ and A_c is the cross-sectional area $A_c = \pi D^2/4$. For internal flow in a tube or duct, the heat-transfer coefficient is defined as

$$q = h(T_s - T_b) \quad (5-44)$$

where T_b is the bulk or mean temperature at a given cross section and T_s is the corresponding surface temperature.

For laminar flow ($\text{Re}_D < 2100$) that is fully developed, both hydrodynamically and thermally, the Nusselt number has a constant value. For a uniform wall temperature, $\text{Nu}_D = 3.66$. For a uniform heat flux through the tube wall, $\text{Nu}_D = 4.36$. In both cases, the thermal conductivity of the fluid in Nu_D is evaluated at T_b . The distance x required for a fully developed laminar velocity profile is given by $[(x/D)/\text{Re}_D] \approx 0.05$. The distance x required for fully developed velocity and thermal profiles is obtained from $[(x/D)/(\text{Re}_D \text{Pr})] \approx 0.05$.

For a constant wall temperature, a fully developed laminar velocity profile, and a developing thermal profile, the average Nusselt number is estimated by [Hausen, *Allg. Waermetech.*, **9**, 75 (1959)]

$$\bar{\text{Nu}}_D = 3.66 + \frac{0.0668(D/L) \text{Re}_D \text{Pr}}{1 + 0.04[(D/L) \text{Re}_D \text{Pr}]^{2/3}} \quad (5-45)$$

For large values of L , Eq. (5-45) approaches $\text{Nu}_D = 3.66$. Equation (5-45) also applies to developing velocity and thermal profiles conditions if $\text{Pr} \gg 1$. The properties in (5-45) are evaluated at the bulk mean temperature

$$\bar{T}_b = (T_{b,\text{in}} + T_{b,\text{out}})/2 \quad (5-46)$$

For a constant wall temperature with developing laminar velocity and thermal profiles, the average Nusselt number is approximated by [Sieder and Tate, *Ind. Eng. Chem.*, **28**, 1429 (1936)]

$$\bar{\text{Nu}}_D = 1.86 \left(\frac{D}{L} \text{Re}_D \text{Pr} \right)^{1/3} \left(\frac{\mu_b}{\mu_s} \right)^{0.14} \quad (5-47)$$

The properties, except for μ_s , are evaluated at the bulk mean temperature per (5-46) and $0.48 < \text{Pr} < 16,700$ and $0.0044 < \mu_b/\mu_s < 9.75$.

For fully developed flow in the transition region between laminar and turbulent flow, and for fully developed turbulent flow, Gnielinski's [Int. Chem. Eng., **16**, 359 (1976)] equation is recommended:

$$\text{Nu}_D = \frac{(f/2)(\text{Re}_D - 1000)(\text{Pr})}{1 + 12.7(f/2)^{1/2}(\text{Pr}^{2/3} - 1)} K \quad (5-48)$$

where $0.5 < \text{Pr} < 10^5$, $2300 < \text{Re}_D < 10^6$, $K = (\text{Pr}_b/\text{Pr}_s)^{0.11}$ for liquids ($0.05 < \text{Pr}_b/\text{Pr}_s < 20$), and $K = (T_b/T_s)^{0.45}$ for gases ($0.5 < T_b/T_s < 1.5$). The factor K corrects for variable property effects. For smooth tubes, the Fanning friction factor f is given by

$$f = 0.25(0.790 \ln \text{Re}_D - 1.64)^{-2} \quad 2300 < \text{Re}_D < 10^6 \quad (5-49)$$

TABLE 5-3 Effect of Entrance Configuration on Values of C and n in Eq. (5-53) for $\text{Pr} \approx 1$ (Gases and Other Fluids with Pr about 1)

Entrance configuration	C	n
Long calming section	0.9756	0.760
Open end, 90° edge	2.4254	0.676
180° return bend	0.9759	0.700
90° round bend	1.0517	0.629
90° elbow	2.0152	0.614

For rough pipes, approximate values of Nu_D are obtained if f is estimated by the Moody diagram of Sec. 6. Equation (5-48) is corrected for entrance effects per (5-53) and Table 5-3. Sieder and Tate [Ind. Eng. Chem., **28**, 1429 (1936)] recommend a simpler but less accurate equation for fully developed turbulent flow

$$\text{Nu}_D = 0.027 \text{Re}_D^{4/5} \text{Pr}^{1/3} \left(\frac{\mu_b}{\mu_s} \right)^{0.14} \quad (5-50)$$

where $0.7 < \text{Pr} < 16,700$, $\text{Re}_D < 10,000$, and $L/D > 10$. Equations (5-48) and (5-50) apply to both constant temperature and uniform heat flux along the tube. The properties are evaluated at the bulk temperature T_b , except for μ_s , which is at the temperature of the tube. For L/D greater than about 10, Eqs. (5-48) and (5-50) provide an estimate of Nu_D . In this case, the properties are evaluated at the bulk mean temperature per (5-46). More complicated and comprehensive predictions of fully developed turbulent convection are available in Churchill and Žajic [AIChE J., **48**, 927 (2002)] and Yu, Ozoe, and Churchill [Chem. Eng. Science, **56**, 1781 (2001)].

For fully developed turbulent flow of liquid metals, the Nusselt number depends on the wall boundary condition. For a constant wall temperature [Notter and Sleicher, Chem. Eng. Science, **27**, 2073 (1972)],

$$\text{Nu}_D = 4.8 + 0.0156 \text{Re}_D^{0.85} \text{Pr}^{0.93} \quad (5-51)$$

while for a uniform wall heat flux,

$$\text{Nu}_D = 6.3 + 0.0167 \text{Re}_D^{0.85} \text{Pr}^{0.93} \quad (5-52)$$

In both cases the properties are evaluated at T_b and $0.004 < \text{Pr} < 0.01$ and $10^4 < \text{Re}_D < 10^6$.

Entrance effects for turbulent flow with simultaneously developing velocity and thermal profiles can be significant when $L/D < 10$. Shah and Bhatti correlated entrance effects for gases ($\text{Pr} \approx 1$) to give an equation for the average Nusselt number in the entrance region (in Kaka, Shah, and Aung, eds., *Handbook of Single-Phase Convective Heat Transfer*, Chap. 3, Wiley-Interscience, 1987).

$$\frac{\bar{\text{Nu}}_D}{\text{Nu}_D} = 1 + \frac{C}{(x/D)^n} \quad (5-53)$$

where Nu_D is the fully developed Nusselt number and the constants C and n are given in Table 5-3 (Ebadian and Dong, Chap. 5 of Rohsenow, Hartnett, and Cho, *Handbook of Heat Transfer*, 3d ed., McGraw-Hill, 1998, p. 5.31). The tube entrance configuration determines the values of C and n as shown in Table 5-3.

Flow in Noncircular Ducts The length scale in the Nusselt and Reynolds numbers for noncircular ducts is the hydraulic diameter, $D_h = 4A_c/p$, where A_c is the cross-sectional area for flow and p is the wetted perimeter. Nusselt numbers for fully developed laminar flow in a variety of noncircular ducts are given by Mills (*Heat Transfer*, 2d ed., Prentice-Hall, 1999, p. 307). For turbulent flows, correlations for round tubes can be used with D replaced by D_h .

For annular ducts, the accuracy of the Nusselt number given by (5-48) is improved by the following multiplicative factors [Petukhov and Roizen, *High Temp.*, **2**, 65 (1964)].

$$\text{Inner tube heated} \quad 0.86 \left(\frac{D_i}{D_o} \right)^{-0.16}$$

$$\text{Outer tube heated} \quad 1 - 0.14 \left(\frac{D_i}{D_o} \right)^{0.6}$$

where D_i and D_o are the inner and outer diameters, respectively.

Example 6: Turbulent Internal Flow Air at 300 K, 1 bar, and 0.05 kg/s enters a channel of a plate-type heat exchanger (Mills, *Heat Transfer*, 2d ed., Prentice-Hall, 1999) that measures 1 cm wide, 0.5 m high, and 0.8 m long. The walls are at 600 K, and the mass flow rate is 0.05 kg/s. The entrance has a 90° edge. We want to estimate the exit temperature of the air.

Our approach will use (5-48) to estimate the average heat-transfer coefficient, followed by application of (5-28) to calculate the exit temperature. We assume ideal gas behavior and an exit temperature of 500 K. The estimated bulk mean temperature of the air is, by (5-46), 400 K. At this temperature, the properties of the air are $Pr = 0.690$, $\mu = 2.301 \times 10^{-5}$ kg/(m·s), $k = 0.0338$ W/(m·K), and $c_p = 1014$ J/(kg·K).

We start by calculating the hydraulic diameter $D_h = 4A_c/p$. The cross-sectional area for flow A_c is 0.005 m², and the wetted perimeter p is 1.02 m. The hydraulic diameter $D_h = 0.01961$ m. The Reynolds number is

$$Re_D = \frac{\dot{m} D_h}{A_c \mu} = \frac{0.05(0.01961)}{0.005(2.301 \times 10^{-5})} = 8521$$

The flow is in the transition region, and Eqs. (5-49) and (5-48) apply:

$$f = 0.25(0.790 \ln Re_D - 1.64)^{-2} = 0.25(0.790 \ln 8521 - 1.64)^{-2} = 0.008235$$

$$Nu_D = \frac{(f/2)(Re_D - 1000)(Pr)}{1 + 12.7(f/2)^{1/2}(Pr^{2/3} - 1)} K$$

$$= \frac{(0.008235/2)(8521 - 1000)(0.690)}{1 + 12.7(0.008235/2)^{1/2}(0.690^{2/3} - 1)} \left(\frac{400}{600}\right)^{0.45} = 21.68$$

Entrance effects are included by using (5-53) for an open end, 90° edge:

$$\overline{Nu}_D = \left[1 + \frac{C}{(x/D)^n}\right] Nu_D = \left[1 + \frac{2.4254}{(0.8/0.01961)^{0.676}}\right] (21.68) = 25.96$$

The average heat-transfer coefficient becomes

$$\bar{h} = \frac{k}{D_h} \overline{Nu}_D = \frac{0.0338}{0.01961} (25.96) = 44.75 \frac{W}{m^2 \cdot K}$$

The exit temperature is calculated from (5-28):

$$T(L) = T_s - (T_s - T_m) \exp\left(-\frac{\bar{h} p L}{\dot{m} c_p}\right)$$

$$= 600 - (600 - 300) \exp\left[-\frac{44.75(1.02)0.8}{0.05(1014)}\right] = 450 \text{ K}$$

We conclude that our estimated exit temperature of 500 K is too high. We could repeat the calculations, using fluid properties evaluated at a revised bulk mean temperature of 375 K.

Coiled Tubes For turbulent flow inside helical coils, with tube inside radius a and coil radius R , the Nusselt number for a straight tube Nu_s is related to that for a coiled tube Nu_c , by (Rohsenow, Hartnett, and Cho, *Handbook of Heat Transfer*, 3d ed., McGraw-Hill, 1998, p. 5.90)

$$\frac{Nu_c}{Nu_s} = 1.0 + 3.6 \left(1 - \frac{a}{R}\right) \left(\frac{a}{R}\right)^{0.5} \quad (5-54)$$

where $2 \times 10^4 < Re_D < 1.5 \times 10^5$ and $5 < R/a < 84$. For lower Reynolds numbers ($1.5 \times 10^3 < Re_D < 2 \times 10^4$), the same source recommends

$$\frac{Nu_c}{Nu_s} = 1.0 + 3.4 \frac{a}{R} \quad (5-55)$$

External Flows For a single cylinder in cross flow, Churchill and Bernstein recommend [*J. Heat Transfer*, **99**, 300 (1977)]

$$\overline{Nu}_D = 0.3 + \frac{0.62 Re_D^{1/2} Pr^{1/3}}{[1 + (0.4/Pr)^{2/3}]^{1/4}} \left[1 + \left(\frac{Re_D}{282,000}\right)^{5/8}\right]^{4/5} \quad (5-56)$$

where $\overline{Nu}_D = \bar{h}D/k$. Equation (5-56) is for all values of Re_D and Pr , provided that $Re_D Pr > 0.4$. The fluid properties are evaluated at the film temperature $(T_e + T_s)/2$, where T_e is the free-stream temperature and T_s is the surface temperature. Equation (5-56) also applies to the uniform heat flux boundary condition provided \bar{h} is based on the perimeter-averaged temperature difference between T_s and T_e .

For an isothermal spherical surface, Whitaker recommends [*AIChE*, **18**, 361 (1972)]

$$\overline{Nu}_D = 2 + (0.4 Re_D^{1/2} + 0.06 Re_D^{2/3}) Pr^{0.4} \left(\frac{\mu_e}{\mu_s}\right)^{1/4} \quad (5-57)$$

This equation is based on data for $0.7 < Pr < 380$, $3.5 < Re_D < 8 \times 10^4$, and $1 < (\mu_e/\mu_s) < 3.2$. The properties are evaluated at the free-stream temperature T_e , with the exception of μ_s , which is evaluated at the surface temperature T_s .

The average Nusselt number for laminar flow over an isothermal flat plate of length x is estimated from [Churchill and Ozoe, *J. Heat Transfer*, **95**, 416 (1973)]

$$\overline{Nu}_x = \frac{1.128 Pr^{1/2} Re_x^{1/2}}{[1 + (0.0468/Pr)^{2/3}]^{1/4}} \quad (5-58)$$

This equation is valid for all values of Pr as long as $Re_x Pr > 100$ and $Re_x < 5 \times 10^5$. The fluid properties are evaluated at the film temperature $(T_e + T_s)/2$, where T_e is the free-stream temperature and T_s is the surface temperature. For a uniformly heated flat plate, the local Nusselt number is given by [Churchill and Ozoe, *J. Heat Transfer*, **95**, 78 (1973)]

$$Nu_x = \frac{0.886 Pr^{1/2} Re_x^{1/2}}{[1 + (0.0207/Pr)^{2/3}]^{1/4}} \quad (5-59)$$

where again the properties are evaluated at the film temperature.

The average Nusselt number for turbulent flow over a smooth, isothermal flat plate of length x is given by (Mills, *Heat Transfer*, 2d ed., Prentice-Hall, 1999, p. 315)

$$\overline{Nu}_x = 0.664 Re_{cr}^{1/2} Pr^{1/3} + 0.036 Re_x^{0.8} Pr^{0.43} \left[1 - \left(\frac{Re_{cr}}{Re_x}\right)^{0.5}\right] \quad (5-60)$$

The critical Reynolds number Re_{cr} is typically taken as 5×10^5 , $Re_{cr} < Re_x < 3 \times 10^7$, and $0.7 < Pr < 400$. The fluid properties are evaluated at the film temperature $(T_e + T_s)/2$, where T_e is the free-stream temperature and T_s is the surface temperature. Equation (5-60) also applies to the uniform heat flux boundary condition provided \bar{h} is based on the average temperature difference between T_s and T_e .

Flow-through Tube Banks Aligned and staggered tube banks are sketched in Fig. 5-6. The tube diameter is D , and the transverse and longitudinal pitches are S_T and S_L , respectively. The fluid velocity upstream of the tubes is V_∞ .

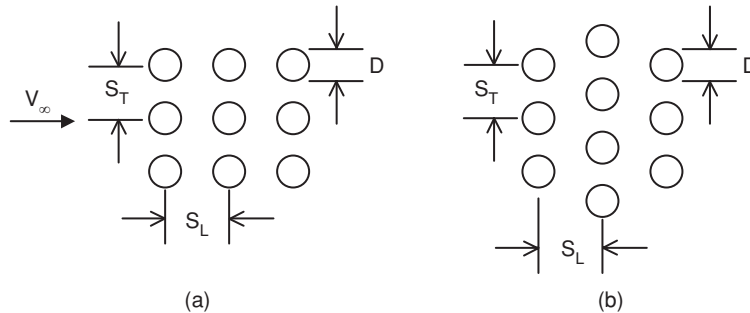


FIG. 5-6 (a) Aligned and (b) staggered tube bank configurations. The fluid velocity upstream of the tubes is V_∞ .

of the tubes is V_∞ . To estimate the overall heat-transfer coefficient for the tube bank, Mills proceeds as follows (*Heat Transfer*, 2d ed., Prentice-Hall, 1999, p. 348). The Reynolds number for use in (5-56) is recalculated with an effective average velocity in the space between adjacent tubes:

$$\frac{\bar{V}}{V_\infty} = \frac{S_T}{S_T - (\pi/4)D} \quad (5-61)$$

The heat-transfer coefficient increases from row 1 to about row 5 of the tube bank. The average Nusselt number for a tube bank with 10 or more rows is

$$\overline{Nu}_D^{10+} = \Phi \overline{Nu}_D \quad (5-62)$$

where Φ is an arrangement factor and \overline{Nu}_D is the Nusselt number for the first row, calculated by using the velocity in (5-61). The arrangement factor is calculated as follows. Define dimensionless pitches as $P_T = S_T/D$ and P_L/D and calculate a factor ψ as follows.

$$\psi = \begin{cases} 1 - \frac{\pi}{4P_T} & \text{if } P_L \geq 1 \\ 1 - \frac{\pi}{4P_T P_L} & \text{if } P_L < 1 \end{cases} \quad (5-63)$$

The arrangement factors are

$$\Phi_{\text{aligned}} = 1 + \frac{0.7}{\psi^{1.5}} \frac{S_T/S_T - 0.3}{(S_T/S_T + 0.7)^2} \quad (5-64)$$

$$\Phi_{\text{staggered}} = 1 + \frac{2}{3P_L} \quad (5-65)$$

If there are fewer than 10 rows,

$$\overline{Nu}_D = \frac{1 + (N-1)\Phi}{N} \overline{Nu}_D \quad (5-66)$$

where N is the number of rows.

The fluid properties for gases are evaluated at the average mean film temperature $[(T_{in} + T_{out})/2 + T_s]/2$. For liquids, properties are evaluated at the bulk mean temperature $(T_{in} + T_{out})/2$, with a Prandtl number correction $(Pr_b/Pr_s)^{0.11}$ for cooling and $(Pr_b/Pr_s)^{0.25}$ for heating.

Falling Films When a liquid is distributed uniformly around the periphery at the top of a vertical tube (either inside or outside) and allowed to fall down the tube wall by the influence of gravity, the fluid does not fill the tube but rather flows as a thin layer. Similarly, when a liquid is applied uniformly to the outside and top of a horizontal tube, it flows in layer form around the periphery and falls off the bottom. In both these cases the mechanism is called gravity flow of liquid layers or falling films.

For the turbulent flow of **water** in layer form down the walls of **vertical tubes** the dimensional equation of McAdams, Drew, and Bays [*Trans. Am. Soc. Mech. Eng.*, **62**, 627 (1940)] is recommended:

$$h_{lm} = b\Gamma^{1/3} \quad (5-67)$$

where $b = 9150$ (SI) or 120 (U.S. Customary) and is based on values of $\Gamma = W_F = \dot{M}/\pi D$ ranging from 0.25 to 6.2 kg/(m·s) [600 to 15,000 lb/(h·ft)] of wetted perimeter. This type of water flow is used in vertical vapor-in-shell ammonia condensers, acid coolers, cycle water coolers, and other process-fluid coolers.

The following dimensional equations may be used for **any liquid** flowing in layer form down **vertical surfaces**:

$$\text{For } \frac{4\Gamma}{\mu} > 2100 \quad h_{lm} = 0.01 \left(\frac{k^3 \rho^2 g}{\mu^2} \right)^{1/3} \left(\frac{c\mu}{k} \right)^{1/3} \left(\frac{4\Gamma}{\mu} \right)^{1/3} \quad (5-68a)$$

$$\text{For } \frac{4\Gamma}{\mu} < 2100 \quad h_{am} = 0.50 \left(\frac{k^3 \rho^{4/3} c g^{2/3}}{L\mu^{1/3}} \right)^{1/3} \left(\frac{\mu}{\mu_w} \right)^{1/4} \left(\frac{4\Gamma}{\mu} \right)^{1/9} \quad (5-68b)$$

Equation (5-68b) is based on the work of Bays and McAdams [*Ind. Eng. Chem.*, **29**, 1240 (1937)]. The significance of the term L is not clear. When $L = 0$, the coefficient is definitely not infinite. When L is large and the fluid temperature has not yet closely approached the wall temperature, it does not appear that the coefficient should

necessarily decrease. Within the finite limits of 0.12 to 1.8 m (0.4 to 6 ft), this equation should give results of the proper order of magnitude.

For falling films applied to the **outside of horizontal tubes**, the Reynolds number rarely exceeds 2100. Equations may be used for falling films on the outside of the tubes by substituting $\pi D/2$ for L .

For **water** flowing over a **horizontal tube**, data for several sizes of pipe are roughly correlated by the dimensional equation of McAdams, Drew, and Bays [*Trans. Am. Soc. Mech. Eng.*, **62**, 627 (1940)].

$$h_{am} = b(\Gamma/D_0)^{1/3} \quad (5-69)$$

where $b = 3360$ (SI) or 65.6 (U.S. Customary) and Γ ranges from 0.94 to 4 kg/(m·s) [100 to 1000 lb/(h·ft)].

Falling films are also used for evaporation in which the film is both entirely or partially evaporated (juice concentration). This principle is also used in crystallization (freezing).

The advantage of high coefficient in falling-film exchangers is partially offset by the difficulties involved in distribution of the film, maintaining complete wettability of the tube, and pumping costs required to lift the liquid to the top of the exchanger.

Finned Tubes (Extended Surface) When the heat-transfer coefficient on the outside of a metal tube is much lower than that on the inside, as when steam condensing in a pipe is being used to heat air, externally finned (or extended) heating surfaces are of value in increasing substantially the rate of heat transfer per unit length of tube. The data on extended heating surfaces, for the case of air flowing outside and at right angles to the axes of a bank of finned pipes, can be represented approximately by the dimensional equation derived from

$$h_f = b \frac{V_F^{0.6}}{D_0^{0.4}} \left(\frac{p'}{p' - D_0} \right)^{0.6} \quad (5-70)$$

where $b = 5.29$ (SI) or (5.39)(10⁻³) (U.S. Customary); h_f is the coefficient of heat transfer on the air side; V_F is the face velocity of the air; p' is the center-to-center spacing, m, of the tubes in a row; and D_0 is the outside diameter, m, of the bare tube (diameter at the root of the fins).

In atmospheric air-cooled finned tube exchangers, the air-film coefficient from Eq. (5-70) is sometimes converted to a value based on outside bare surface as follows:

$$h_{fo} = h_f \frac{A_f + A_{uf}}{A_{of}} = h_f \frac{A_T}{A_o} \quad (5-71)$$

in which h_{fo} is the air-film coefficient based on external bare surface; h_f is the air-film coefficient based on total external surface; A_T is total external surface, and A_o is external bare surface of the unfinned tube; A_f is the area of the fins; A_{uf} is the external area of the unfinned portion of the tube; and A_{of} is area of tube before fins are attached.

Fin efficiency is defined as the ratio of the mean temperature difference from surface to fluid divided by the temperature difference from fin to fluid at the base or root of the fin. Graphs of fin efficiency for extended surfaces of various types are given by Gardner [*Trans. Am. Soc. Mech. Eng.*, **67**, 621 (1945)].

Heat-transfer coefficients for finned tubes of various types are given in a series of papers [*Trans. Am. Soc. Mech. Eng.*, **67**, 601 (1945)].

For flow of air normal to fins in the form of **short strips or pins**, Norris and Spofford [*Trans. Am. Soc. Mech. Eng.*, **64**, 489 (1942)] correlate their results for air by the dimensionless equation of Pohlhausen:

$$\frac{h_m}{c_p G_{\max}} \left(\frac{c_p \mu}{k} \right)^{2/3} = 1.0 \left(\frac{z_p G_{\max}}{\mu} \right)^{-0.5} \quad (5-72)$$

for values of $z_p G_{\max}/\mu$ ranging from 2700 to 10,000.

For the general case, the treatment suggested by Kern (*Process Heat Transfer*, McGraw-Hill, New York, 1950, p. 512) is recommended. Because of the wide variations in fin-tube construction, it is convenient to convert all coefficients to values based on the inside bare surface of the tube. Thus to convert the coefficient based on outside area (finned side) to a value based on inside area Kern gives the following relationship:

$$h_{fi} = (\Omega A_f + A_o)(h_f/A_o) \quad (5-73)$$

5-12 HEAT AND MASS TRANSFER

in which h_f is the effective outside coefficient based on the inside area, h_f is the outside coefficient calculated from the applicable equation for bare tubes, A_f is the surface area of the fins, A_o is the surface area on the outside of the tube which is not finned, A_i is the inside area of the tube, and Ω is the fin efficiency defined as

$$\Omega = (\tanh mb_f)/mb_f \quad (5-74)$$

in which

$$m = (h_f p_f / ka_f)^{1/2} \quad \text{m}^{-1} \text{ (ft}^{-1}\text{)} \quad (5-75)$$

and b_f = height of fin. The other symbols are defined as follows: p_f is the perimeter of the fin, a_f is the cross-sectional area of the fin, and k is the thermal conductivity of the material from which the fin is made.

Fin efficiencies and fin dimensions are available from manufacturers. Ratios of finned to inside surface are usually available so that the terms A_f , A_o , and A_i may be obtained from these ratios rather than from the total surface areas of the heat exchangers.

JACKETS AND COILS OF AGITATED VESSELS

See Secs. 11 and 18.

NONNEWTONIAN FLUIDS

A wide variety of nonnewtonian fluids are encountered industrially. They may exhibit Bingham-plastic, pseudoplastic, or dilatant behavior

and may or may not be thixotropic. For design of equipment to handle or process nonnewtonian fluids, the properties must usually be measured experimentally, since no generalized relationships exist to predict the properties or behavior of the fluids. Details of handling nonnewtonian fluids are described completely by Skelland (*Non-Newtonian Flow and Heat Transfer*, Wiley, New York, 1967). The generalized shear-stress rate-of-strain relationship for nonnewtonian fluids is given as

$$n' = \frac{d \ln (D \Delta P / 4L)}{d \ln (8V/D)} \quad (5-76)$$

as determined from a plot of shear stress versus velocity gradient.

For **circular tubes**, $Gz > 100$, $n' > 0.1$, and laminar flow

$$Nu_m = 1.75 \delta_s^{1/3} Gz^{1/3} \quad (5-77)$$

where $\delta_s = (3n' + 1)/4n'$. When natural convection effects are considered, Metzner and Gluck [*Chem. Eng. Sci.*, **12**, 185 (1960)] obtained the following for **horizontal tubes**:

$$Nu_m = 1.75 \delta_s^{1/3} \left[Gz + 12.6 \left(\frac{\text{Pr Gr} D}{L} \right)^{0.4} \right]^{1/3} \left(\frac{\gamma_b}{\gamma_w} \right)^{0.14} \quad (5-78)$$

where properties are evaluated at the wall temperature, i.e., $\gamma = g_r K' 8^{n'-3}$ and $\tau_w = K' (8V/D)^{n'}$.

Metzner and Friend [*Ind. Eng. Chem.*, **51**, 879 (1959)] present relationships for turbulent heat transfer with nonnewtonian fluids. Relationships for heat transfer by natural convection and through laminar boundary layers are available in Skelland's book (op. cit.).

HEAT TRANSFER WITH CHANGE OF PHASE

In any operation in which a material undergoes a change of phase, provision must be made for the addition or removal of heat to provide for the latent heat of the change of phase plus any other sensible heating or cooling that occurs in the process. Heat may be transferred by any one or a combination of the three modes—conduction, convection, and radiation. The process involving change of phase involves mass transfer simultaneous with heat transfer.

CONDENSATION

Condensation Mechanisms Condensation occurs when a saturated vapor comes in contact with a surface whose temperature is below the saturation temperature. Normally a film of condensate is formed on the surface, and the thickness of this film, per unit of breadth, increases with increase in extent of the surface. This is called **film-type condensation**.

Another type of condensation, called **dropwise**, occurs when the wall is not uniformly wetted by the condensate, with the result that the condensate appears in many small droplets at various points on the surface. There is a growth of individual droplets, a coalescence of adjacent droplets, and finally a formation of a rivulet. Adhesive force is overcome by gravitational force, and the rivulet flows quickly to the bottom of the surface, capturing and absorbing all droplets in its path and leaving dry surface in its wake.

Film-type condensation is more common and more dependable. Dropwise condensation normally needs to be promoted by introducing an impurity into the vapor stream. Substantially higher (6 to 18 times) coefficients are obtained for dropwise condensation of steam, but design methods are not available. Therefore, the development of equations for condensation will be for the film type only.

The physical properties of the liquid, rather than those of the vapor, are used for determining the coefficient for condensation. Nusselt [*Z. Ver. Dtsch. Ing.*, **60**, 541, 569 (1916)] derived theoretical relationships for predicting the coefficient of heat transfer for condensation of a pure saturated vapor. A number of simplifying assumptions were used in the derivation.

The **Reynolds number** of the condensate film (falling film) is $4\Gamma/\mu$, where Γ is the weight rate of flow (loading rate) of condensate per unit perimeter $\text{kg}/(\text{s}\cdot\text{m})$ [$\text{lb}/(\text{h}\cdot\text{ft})$]. The thickness of the condensate film for Reynolds number less than 2100 is $(3\mu\Gamma/\rho^2g)^{1/3}$.

Condensation Coefficients

Vertical Tubes For the following cases Reynolds number < 2100 and is calculated by using $\Gamma = W_F/\pi D$. The **Nusselt equation** for the heat-transfer coefficient for condensate films may be written in the following ways (using liquid physical properties and where L is the cooled length and Δt is $t_{sv} - t_s$):

Nusselt type:

$$\frac{hL}{k} = 0.943 \left(\frac{L^3 \rho^2 g \lambda}{k \mu \Delta t} \right)^{1/4} = 0.925 \left(\frac{L^3 \rho^2 g}{\mu \Gamma} \right)^{1/3} \quad (5-79)^{\circ}$$

Dimensional:

$$h = b(k^3 \rho^2 D / \mu_b W_F)^{1/3} \quad (5-80)^{\circ}$$

where $b = 127$ (SI) or 756 (U.S. Customary). For steam at atmospheric pressure, $k = 0.682 \text{ J}/(\text{m}\cdot\text{s}\cdot\text{K})$ [$0.394 \text{ Btu}/(\text{h}\cdot\text{ft}\cdot^{\circ}\text{F})$], $\rho = 960 \text{ kg}/\text{m}^3$ ($60 \text{ lb}/\text{ft}^3$), $\mu_b = (0.28)(10^{-3}) \text{ Pa}\cdot\text{s}$ (0.28 cP),

$$h = b(D/W_F)^{1/3} \quad (5-81)$$

where $b = 2954$ (SI) or 6978 (U.S. Customary). For organic vapors at normal boiling point, $k = 0.138 \text{ J}/(\text{m}\cdot\text{s}\cdot\text{K})$ [$0.08 \text{ Btu}/(\text{h}\cdot\text{ft}\cdot^{\circ}\text{F})$], $\rho = 720 \text{ kg}/\text{m}^3$ ($45 \text{ lb}/\text{ft}^3$), $\mu_b = (0.35)(10^{-3}) \text{ Pa}\cdot\text{s}$ (0.35 cP),

$$h = b(D/W_F)^{1/3} \quad (5-82)$$

where $b = 457$ (SI) or 1080 (U.S. Customary).

Horizontal Tubes For the following cases Reynolds number < 2100 and is calculated by using $\Gamma = W_F/2L$.

^o If the vapor density is significant, replace ρ^2 with $\rho(\rho_l - \rho_v)$.

No.	Substance
10	Acetic Acid
6	Acetone
1	Ammonia
5	Aniline
12	Benzene
8	Carbon Disulfide
14	Carbon Tetrachloride
9	Ethyl Acetate
4	Ethyl Alcohol
13	Ethyl Ether
3	Methyl Alcohol
11	Nitrobenzene
7	n-Propyl Alcohol
2	Water

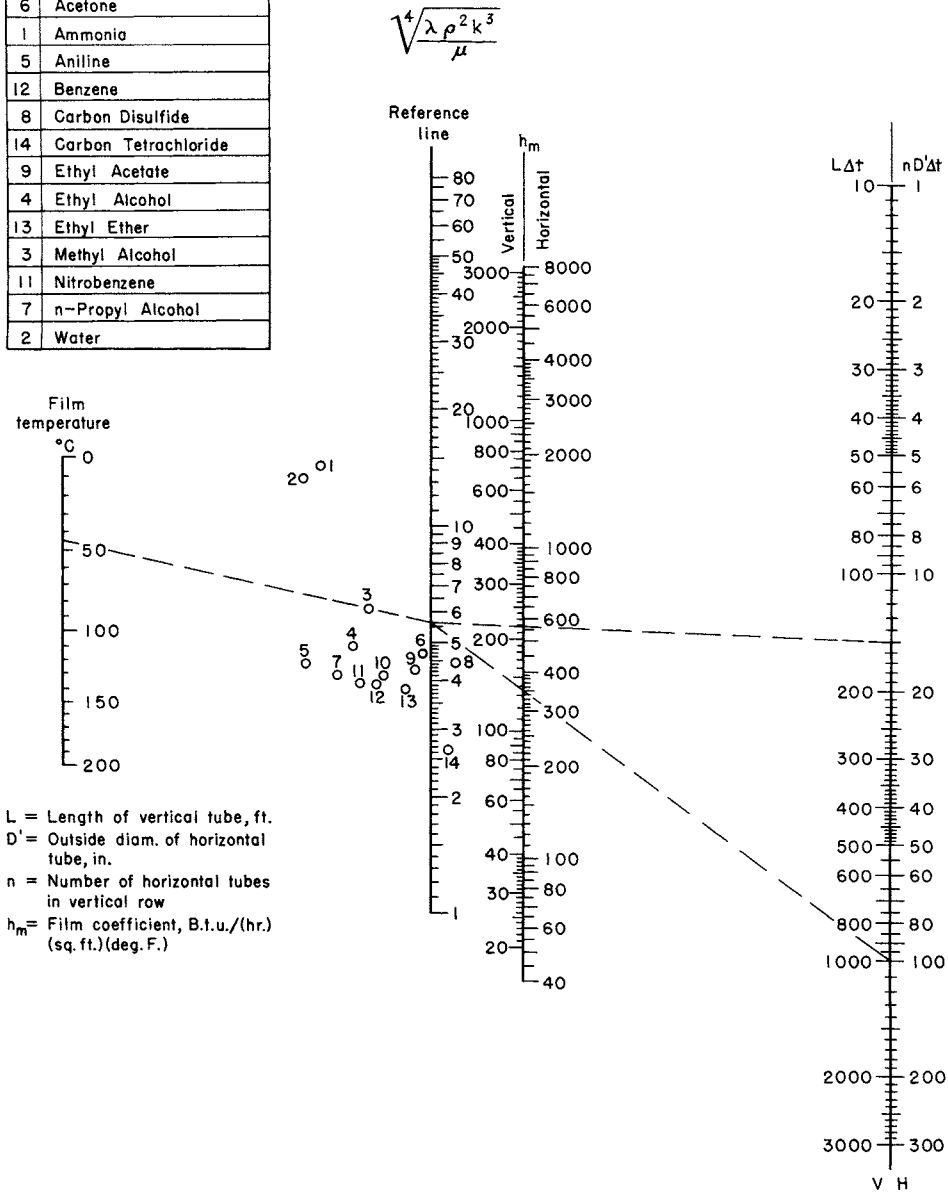


FIG. 5-7 Chart for determining heat-transfer coefficient h_m for film-type condensation of pure vapor, based on Eqs. (5-79) and (5-83). For vertical tubes multiply h_m by 1.2. If $4\Gamma/\mu$ exceeds 2100, use Fig. 5-8. $\sqrt[4]{\lambda \rho^2 k^3 / \mu}$ is in U.S. Customary units; to convert feet to meters, multiply by 0.3048; to convert inches to centimeters, multiply by 2.54; and to convert British thermal units per hour-square foot-degrees Fahrenheit to watts per square meter-kelvins, multiply by 5.6780.

Nusselt type:

$$\frac{hD}{k} = 0.73 \left(\frac{D^3 \rho^2 g \lambda}{k \mu \Delta t} \right)^{1/4} = 0.76 \left(\frac{D^3 \rho^2 g}{\mu \Gamma} \right)^{1/3} \quad (5-83)^\circ$$

Dimensional:

$$h = b(k^3 \rho^2 L / \mu_b W_F)^{1/3} \quad (5-84)^\circ$$

where $b = 205.4$ (SI) or 534 (U.S. Customary). For steam at atmospheric pressure

[°] If the vapor density is significant, replace ρ^2 with $\rho_1(\rho_1 - \rho_c)$.

$$h = b(L/W_F)^{1/3} \quad (5-85)$$

where $b = 2080$ (SI) or 4920 (U.S. Customary). For organic vapors at normal boiling point

$$h = b(L/W_F)^{1/3} \quad (5-86)$$

where $b = 324$ (SI) or 766 (U.S. Customary).

Figure 5-7 is a nomograph for determining coefficients of heat transfer for condensation of pure vapors.

Banks of Horizontal Tubes ($Re < 2100$) In the idealized case of N tubes in a vertical row where the total condensate flows smoothly from one tube to the one beneath it, without splashing, and still in laminar flow on the tube, the mean condensing coefficient h_N for the entire row of N tubes is related to the condensing coefficient for the top tube h_1 by

$$h_N = h_1 N^{-1/4} \quad (5-87)$$

Dukler Theory The preceding expressions for condensation are based on the classical Nusselt theory. It is generally known and conceded that the film coefficients for steam and organic vapors calculated by the Nusselt theory are conservatively low. Dukler [*Chem. Eng. Prog.*, **55**, 62 (1959)] developed equations for velocity and temperature distribution in thin films on vertical walls based on expressions of Deissler (NACA Tech. Notes 2129, 1950; 2138, 1952; 3145, 1959) for the eddy viscosity and thermal conductivity near the solid boundary. According to the Dukler theory, three fixed factors must be known to establish the value of the average film coefficient: the terminal Reynolds number, the Prandtl number of the condensed phase, and a dimensionless group N_d defined as follows:

$$N_d = (0.250\mu_L^{1.173} \mu_G^{0.16}) / (g^{2/3} D^2 \rho_L^{0.553} \rho_G^{0.78}) \quad (5-88)$$

Graphical relationships of these variables are available in Document 6058, ADI Auxiliary Publications Project, Library of Congress, Washington. If rigorous values for condensing-film coefficients are desired, especially if the value of N_d in Eq. (5-88) exceeds $(1)(10^{-5})$, it is suggested that these graphs be used. For the case in which interfacial shear is zero, Fig. 5-8 may be used. It is interesting to note that, according to the Dukler development, there is no definite transition Reynolds number; deviation from Nusselt theory is less at low Reynolds numbers; and when the Prandtl number of a fluid is less than 0.4 (at Reynolds number above 1000), the predicted values for film coefficient are lower than those predicted by the Nusselt theory.

The Dukler theory is applicable for condensate films on horizontal tubes and also for falling films, in general, i.e., those not associated with condensation or vaporization processes.

Vapor Shear Controlling For vertical in-tube condensation with vapor and liquid flowing concurrently downward, if gravity controls, Figs. 5-7 and 5-8 may be used. If vapor shear controls, the Carpenter-Colburn correlation (*General Discussion on Heat Transfer*, London, 1951, ASME, New York, p. 20) is applicable:

$$h\mu_i/k_i\rho_i^{1/2} = 0.065(Pr)^{1/2} F_{vc}^{1/2} \quad (5-89a)$$

$$\text{where } F_{vc} = fG_{vm}^2/2\rho_v \quad (5-89b)$$

$$G_{vm} = \left(\frac{G_{vi}^2 + G_{vi}G_{vo} + G_{vo}^2}{3} \right)^{1/2} \quad (5-89c)$$

and f is the Fanning friction factor evaluated at

$$(Re)_{vm} = D_i G_{vm} / \mu_v \quad (5-89d)$$

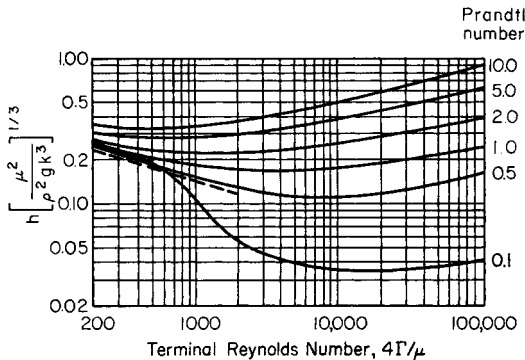


FIG. 5-8 Dukler plot showing average condensing-film coefficient as a function of physical properties of the condensate film and the terminal Reynolds number. (Dotted line indicates Nusselt theory for Reynolds number < 2100 .) [Reproduced by permission from *Chem. Eng. Prog.*, **55**, 64 (1959).]

and the subscripts vi and vo refer to the vapor inlet and outlet, respectively. An alternative formulation, directly in terms of the friction factor, is

$$h = 0.065 (c\rho k_f/2\mu_v)^{1/2} G_{vm} \quad (5-89e)$$

expressed in consistent units.

Another correlation for vapor-shear-controlled condensation is the Boyko-Kruzhilin correlation [*Int. J. Heat Mass Transfer*, **10**, 361 (1967)], which gives the mean condensing coefficient for a stream between inlet quality x_i and outlet quality x_o :

$$\frac{hD_i}{k_l} = 0.024 \left(\frac{D_i G_T}{\mu_l} \right)^{0.8} (Pr)_l^{0.43} \frac{\sqrt{(\rho/\rho_m)_i} + \sqrt{(\rho/\rho_m)_o}}{2} \quad (5-90a)$$

where G_T = total mass velocity in consistent units

$$\left(\frac{\rho}{\rho_m} \right)_i = 1 + \frac{\rho_l - \rho_v}{\rho_v} x_i \quad (5-90b)$$

$$\left(\frac{\rho}{\rho_m} \right)_o = 1 + \frac{\rho_l - \rho_v}{\rho_v} x_o \quad (5-90c)$$

For horizontal in-tube condensation at low flow rates Kern's modification (*Process Heat Transfer*, McGraw-Hill, New York, 1950) of the Nusselt equation is valid:

$$h_m = 0.761 \left[\frac{Lk_l^3 \rho_l (\rho_l - \rho_v) g}{W_F \mu_l} \right]^{1/3} = 0.815 \left[\frac{k_l^3 \rho_l (\rho_l - \rho_v) g \lambda}{\pi \mu_l D_i \Delta t} \right]^{1/4} \quad (5-91)$$

where W_F is the total vapor condensed in one tube and Δt is $t_{sc} - t_s$. A more rigorous correlation has been proposed by Chaddock [*Refrig. Eng.*, **65**(4), 36 (1957)]. Use consistent units.

At high condensing loads, with vapor shear dominating, tube orientation has no effect, and Eq. (5-90a) may also be used for horizontal tubes.

Condensation of pure vapors under laminar conditions in the presence of noncondensable gases, interfacial resistance, superheating, variable properties, and diffusion has been analyzed by Minkowycz and Sparrow [*Int. J. Heat Mass Transfer*, **9**, 1125 (1966)].

BOILING (VAPORIZATION) OF LIQUIDS

Boiling Mechanisms Vaporization of liquids may result from various mechanisms of heat transfer, singly or combinations thereof. For example, vaporization may occur as a result of heat absorbed, by radiation and convection, at the surface of a pool of liquid; or as a result of heat absorbed by natural convection from a hot wall beneath the disengaging surface, in which case the vaporization takes place when the superheated liquid reaches the pool surface. Vaporization also occurs from falling films (the reverse of condensation) or from the flashing of liquids superheated by forced convection under pressure.

Pool boiling refers to the type of boiling experienced when the heating surface is surrounded by a relatively large body of fluid which is not flowing at any appreciable velocity and is agitated only by the motion of the bubbles and by natural-convection currents. Two types of pool boiling are possible: subcooled pool boiling, in which the bulk fluid temperature is below the saturation temperature, resulting in collapse of the bubbles before they reach the surface, and saturated pool boiling, with bulk temperature equal to saturation temperature, resulting in net vapor generation.

The general shape of the curve relating the heat-transfer coefficient to Δt_b , the temperature driving force (difference between the wall temperature and the bulk fluid temperature) is one of the few parametric relations that are reasonably well understood. The familiar boiling curve was originally demonstrated experimentally by Nukiyama [*J. Soc. Mech. Eng. (Japan)*, **37**, 367 (1934)]. This curve points out one of the great dilemmas for boiling-equipment designers. They are faced with at least six heat-transfer regimes in pool boiling: natural convection (+), incipient nucleate boiling (+), nucleate boiling (+), transition to film boiling (-), stable film boiling (+), and film boiling with increasing radiation (+). The signs indicate the sign of the derivative $d(q/A)/d \Delta t_b$. In the transition to film boiling, heat-transfer rate decreases with driving force. The regimes of greatest commercial interest are the nucleate-boiling and stable-film-boiling regimes.

Heat transfer by nucleate boiling is an important mechanism in the vaporization of liquids. It occurs in the vaporization of liquids in

kettle-type and natural-circulation reboilers commonly used in the process industries. High rates of heat transfer per unit of area (heat flux) are obtained as a result of bubble formation at the liquid-solid interface rather than from mechanical devices external to the heat exchanger. There are available several expressions from which reasonable values of the film coefficients may be obtained.

The boiling curve, particularly in the nucleate-boiling region, is significantly affected by the temperature driving force, the total system pressure, the nature of the boiling surface, the geometry of the system, and the properties of the boiling material. In the nucleate-boiling regime, heat flux is approximately proportional to the cube of the temperature driving force. Designers in addition must know the minimum Δt (the point at which nucleate boiling begins), the critical Δt (the Δt above which transition boiling begins), and the maximum heat flux (the heat flux corresponding to the critical Δt). For designers who do not have experimental data available, the following equations may be used.

Boiling Coefficients For the nucleate-boiling coefficient the Mostinski equation [*Teplenergetika*, **4**, 66 (1963)] may be used:

$$h = b P_c^{0.69} \left(\frac{q}{A} \right)^{0.7} \left[1.8 \left(\frac{P}{P_c} \right)^{0.17} + 4 \left(\frac{P}{P_c} \right)^{1.2} + 10 \left(\frac{P}{P_c} \right)^{10} \right] \quad (5-92)$$

where $b = (3.75)(10^{-5})$ (SI) or $(2.13)(10^{-4})$ (U.S. Customary), P_c is the critical pressure and P the system pressure, q/A is the heat flux, and h is the nucleate-boiling coefficient. The McNelly equation [*J. Imp. Coll. Chem. Eng. Soc.*, 7(18), (1953)] may also be used:

$$h = 0.225 \left(\frac{q c_l}{A \lambda} \right)^{0.69} \left(\frac{P k_l}{\sigma} \right)^{0.31} \left(\frac{p_l}{p_c} - 1 \right)^{0.33} \quad (5-93)$$

where c_l is the liquid heat capacity, λ is the latent heat, P is the system pressure, k_l is the thermal conductivity of the liquid, and σ is the surface tension.

An equation of the Nusselt type has been suggested by Rohsenow [*Trans. Am. Soc. Mech. Eng.*, **74**, 969 (1952)].

$$h D/k = C_r (D G/\mu)^{2/3} (c\mu/k)^{-0.7} \quad (5-94a)$$

in which the variables assume the following form:

$$\frac{h \beta'}{k} \left[\frac{g_c \sigma}{g(\rho_L - \rho_v)} \right]^{1/2} = C_r \left[\frac{\beta'}{\mu} \left(\frac{g_c \sigma}{g(\rho_L - \rho_v)} \right)^{1/2} \frac{W}{A} \right]^{2/3} \left(\frac{c\mu}{k} \right)^{-0.7} \quad (5-94b)$$

The coefficient C_r is not truly constant but varies from 0.006 to 0.015.* It is possible that the nature of the surface is partly responsible for the variation in the constant. The only factor in Eq. (5-94b) not readily available is the value of the contact angle β' .

Another Nusselt-type equation has been proposed by Forster and Zuber:†

$$Nu = 0.0015 Re^{0.62} Pr^{1/3} \quad (5-95)$$

which takes the following form:

$$\frac{c \rho_L \sqrt{\pi \alpha}}{k \rho_v} \frac{W}{A} \left(\frac{2\sigma}{\Delta p} \right)^{1/2} \left(\frac{\rho_L}{\Delta p g_c} \right)^{1/4} = 0.0015 \left[\frac{\rho_L}{\mu} \left(\frac{c \rho_L \Delta T \sqrt{\pi \alpha}}{\lambda \rho_v} \right)^2 \right]^{0.62} \left(\frac{c\mu}{k} \right)^{1/2} \quad (5-96)$$

where $\alpha = k/\rho c$ (all liquid properties)

Δp = pressure of the vapor in a bubble minus saturation pressure of a flat liquid surface

Equations (5-94b) and (5-96) have been arranged in dimensional form by Westwater.

The numerical constant may be adjusted to suit any particular set of data if one desires to use a certain criterion. However, surface conditions vary so greatly that deviations may be as large as ± 25 percent from results obtained.

The **maximum heat flux** may be predicted by the Kutateladse-Zuber [*Trans. Am. Soc. Mech. Eng.*, **80**, 711 (1958)] relationship, using consistent units:

$$\left(\frac{q}{A} \right)_{\max} = 0.18 g_c^{1/4} \rho_v \lambda \left[\frac{(\rho_l - \rho_v) \sigma g_c}{\rho_v^2} \right]^{1/4} \quad (5-97)$$

Alternatively, Mostinski presented an equation which approximately represents the Cichelli-Bonilla [*Trans. Am. Inst. Chem. Eng.*, **41**, 755 (1945)] correlation:

$$\frac{(q/A)_{\max}}{P_c} = b \left(\frac{P}{P_c} \right)^{0.35} \left(1 - \frac{P}{P_c} \right)^{0.9} \quad (5-98)$$

where $b = 0.368$ (SI) or 5.58 (U.S. Customary); P_c is the critical pressure, P absolute; P is the system pressure; and $(q/A)_{\max}$ is the maximum heat flux.

The lower limit of applicability of the nucleate-boiling equations is from 0.1 to 0.2 of the maximum limit and depends upon the magnitude of natural-convection heat transfer for the liquid. The best method of determining the lower limit is to plot two curves: one of h versus Δt for natural convection, the other of h versus Δt for nucleate boiling. The intersection of these two curves may be considered the lower limit of applicability of the equations.

These equations apply to single tubes or to flat surfaces in a large pool. In tube bundles the equations are only approximate, and designers must rely upon experiment. Palen and Small [*Hydrocarbon Process.*, **43**(11), 199 (1964)] have shown the effect of tube-bundle size on maximum heat flux.

$$\left(\frac{q}{A} \right)_{\max} = b \frac{P}{D_o \sqrt{N_T}} \rho_v \lambda \left[\frac{g \sigma (\rho_l - \rho_v)}{\rho_v^2} \right]^{1/4} \quad (5-99)$$

where $b = 0.43$ (SI) or 61.6 (U.S. Customary), p is the tube pitch, D_o is the tube outside diameter, and N_T is the number of tubes (twice the number of complete tubes for U-tube bundles).

For **film boiling**, Bromley's [*Chem. Eng. Prog.*, **46**, 221 (1950)] correlation may be used:

$$h = b \left[\frac{k_v^3 (\rho_l - \rho_v) \rho_v g}{\mu_v D_o \Delta t_b} \right]^{1/4} \quad (5-100)$$

where $b = 4.306$ (SI) or 0.620 (U.S. Customary). Katz, Myers, and Balekjian [*Pet. Refiner*, **34**(2), 113 (1955)] report boiling heat-transfer coefficients on finned tubes.

HEAT TRANSFER BY RADIATION

GENERAL REFERENCES: Baukal, C. E., ed., *The John Zink Combustion Handbook*, CRC Press, Boca Raton, Fla., 2001. Blokh, A. G., *Heat Transfer in Steam Boiler Furnaces*, 3d ed., Taylor & Francis, New York, 1987. Brewster, M. Quinn, *Thermal Radiation Heat Transfer and Properties*, Wiley, New York, 1992. Goody, R. M., and Y. L. Yung, *Atmospheric Radiation—Theoretical Basis*, 2d ed., Oxford University Press, 1995. Hottel, H. C., and A. F. Sarofim, *Radiative Transfer*, McGraw-Hill, New York, 1967. Modest, Michael F., *Radiative Heat Transfer*, 2d ed., Academic Press, New York, 2003. Noble, James J., "The Zone

Method: Explicit Matrix Relations for Total Exchange Areas," *Int. J. Heat Mass Transfer*, **18**, 261–269 (1975). Rhine, J. M., and R. J. Tucker, *Modeling of Gas-Fired Furnaces and Boilers*, British Gas Association with McGraw-Hill, 1991. Siegel, Robert, and John R. Howell, *Thermal Radiative Heat Transfer*, 4th ed., Taylor & Francis, New York, 2001. Sparrow, E. M., and R. D. Cess, *Radiation Heat Transfer*, 3d ed., Taylor & Francis, New York, 1988. Stultz, S. C., and J. B. Kitto, *Steam: Its Generation and Use*, 40th ed., Babcock and Wilcox, Barkington, Ohio, 1992.

* Reported by Westwater in Drew and Hoopes, *Advances in Chemical Engineering*, vol. I, Academic, New York, 1956, p. 15.

† Forster, *J. Appl. Phys.*, **25**, 1067 (1954); Forster and Zuber, *J. Appl. Phys.*, **25**, 474 (1954); Forster and Zuber, Conference on Nuclear Engineering, University of California, Los Angeles, 1955; excellent treatise on boiling of liquids by Westwater in Drew and Hoopes, *Advances in Chemical Engineering*, vol. I, Academic, New York, 1956.

INTRODUCTION

Heat transfer by thermal radiation involves the transport of electromagnetic (EM) energy from a source to a sink. In contrast to other modes of heat transfer, radiation does not require the presence of an intervening medium, e.g., as in the irradiation of the earth by the sun. Most industrially important applications of radiative heat transfer occur in the *near infrared* portion of the EM spectrum (0.7 through 25 μm) and may extend into the *far infrared* region (25 to 1000 μm). For very high temperature sources, such as solar radiation, relevant wavelengths encompass the entire *visible region* (0.4 to 0.7 μm) and may extend down to 0.2 μm in the *ultraviolet* (0.01- to 0.4-μm) portion of the EM spectrum. Radiative transfer can also exhibit unique *action-at-a-distance* phenomena which do not occur in other modes of heat transfer. Radiation differs from conduction and convection not only with regard to mathematical characterization but also with regard to its fourth power dependence on temperature. Thus it is usually dominant in high-temperature combustion applications. The temperature at which radiative transfer accounts for roughly one-half of the total heat loss from a surface in air depends on such factors as surface **emissivity** and the convection coefficient. For pipes in free convection, radiation is important at ambient temperatures. For fine wires of low emissivity it becomes important at temperatures associated with bright red heat (1300 K). Combustion gases at furnace temperatures typically lose more than 90 percent of their energy by radiative emission from constituent carbon dioxide, water vapor, and particulate matter. Radiative transfer methodologies are important in myriad engineering applications. These include semiconductor processing, illumination theory, and gas turbines and rocket nozzles, as well as furnace design.

THERMAL RADIATION FUNDAMENTALS

In a vacuum, the wavelength λ, frequency, ν and wavenumber η for electromagnetic radiation are interrelated by λ = c/ν = 1/η, where c is the speed of light. Frequency is independent of the index of refraction of a medium n, but both the speed of light and the wavelength in the medium vary according to c_m = c/n and λ_m = λ/n. When a radiation beam passes into a medium of different refractive index, not only does its wavelength change but so does its direction (Snell's law) as well as the magnitude of its intensity. In most engineering heat-transfer calculations, wavelength is usually employed to characterize radiation while wave number is often used in gas spectroscopy. For a vacuum, air at ambient conditions, and most gases, n ≈ 1.0. For this reason this presentation sometimes does not distinguish between λ and λ_m. *Dielectric materials* exhibit 1.4 < n < 4, and the speed of light decreases considerably in such media.

In radiation heat transfer, the **monochromatic intensity** I_λ ≡ I_λ(\vec{r} , $\vec{\Omega}$, λ), is a *fundamental* (scalar) *field variable* which characterizes EM energy transport. Intensity defines the radiant energy flux passing through an infinitesimal area dA, oriented *normal* to a radiation beam of arbitrary direction $\vec{\Omega}$. At steady state, the monochromatic intensity is a function of position \vec{r} , direction $\vec{\Omega}$, and wavelength and has units of W/(m²·sr·μm). In the general case of an *absorbing-emitting* and *scattering* medium, characterized by some absorption coefficient K(m⁻¹), intensity in the direction $\vec{\Omega}$ will be modified by attenuation and by *scattering* of radiation into and out of the beam. For the special case of a nonabsorbing (transparent), nonscattering, medium of constant refractive index, the radiation intensity is *constant and independent of position in a given direction* $\vec{\Omega}$. This circumstance arises in *illumination theory* where the light intensity in a room is constant in a *given direction* but may vary with respect to *all other directions*. The basic conservation law for radiation intensity is termed the *equation of transfer* or *radiative transfer equation*. The equation of transfer is a *directional* energy balance and mathematically is an *integrodifferential equation*. The relevance of the transport equation to radiation heat transfer is discussed in many sources; see, e.g., Modest, M. F., *Radiative Heat Transfer*, 2d ed., Academic Press, 2003, or Siegel, R., and J. R. Howell, *Thermal Radiative Heat Transfer*, 4th ed., Taylor & Francis, New York, 2001.

Introduction to Radiation Geometry Consider a homogeneous medium of constant refractive index n. A pencil of radiation

originates at differential area element dA_i and is incident on differential area element dA_j. Designate \vec{n}_i and \vec{n}_j as the unit vectors normal to dA_i and dA_j, and let r_{ij} with unit direction vector $\vec{\Omega}$, define the distance of separation between the area elements. Moreover, φ_i and φ_j denote the *confined angles* between $\vec{\Omega}$ and \vec{n}_i and \vec{n}_j , respectively [i.e., cosφ_i ≡ cos($\vec{\Omega}$, \vec{r}_{ij}) and cosφ_j ≡ cos($\vec{\Omega}$, \vec{r}_{ji})]. As the beam travels toward dA_j, it will *diverge* and subtend a solid angle

$$d\Omega_j = \frac{\cos\phi_j}{r^2} dA_j \text{ sr}$$

at dA_j. Moreover, the projected area of dA_i in the direction of $\vec{\Omega}$ is given by cos($\vec{\Omega}$, \vec{r}_i) dA_i = cosφ_i dA_i. Multiplication of the intensity I_λ ≡ I_λ(\vec{r} , $\vec{\Omega}$, λ) by dΩ_j and the apparent area of dA_i then yields an expression for the (*differential*) *net monochromatic radiant energy flux* dQ_{ij} originating at dA_i and intercepted by dA_j.

$$dQ_{ij} \equiv I_{\lambda}(\vec{\Omega}, \lambda) \cos\phi_i \cos\phi_j dA_i dA_j / r^2 \quad (5-101)$$

The **hemispherical emissive power**^{*} E is defined as the radiant flux density (W/m²) associated with emission from an element of surface area dA into a surrounding unit hemisphere whose base is coplanar with dA. If the monochromatic intensity I_λ($\vec{\Omega}$, λ) of emission from the surface is *isotropic* (independent of the angle of emission, $\vec{\Omega}$), Eq. (5-101) may be integrated over the 2π sr of the surrounding unit hemisphere to yield the simple relation E_λ = πI_λ, where E_λ ≡ E_λ(λ) is defined as the monochromatic or *spectral* hemispherical emissive power.

Blackbody Radiation Engineering calculations involving thermal radiation normally employ the **hemispherical blackbody emissive power** as the thermal driving force analogous to temperature in the cases of conduction and convection. A **blackbody** is a theoretical idealization for a *perfect theoretical radiator*; i.e., it absorbs all incident radiation without reflection and emits isotropically. In practice, soot-covered surfaces sometimes approximate blackbody behavior. Let E_{b,λ} = E_{b,λ}(T, λ) denote the monochromatic blackbody hemispherical emissive power *frequency function* defined such that E_{b,λ}(T, λ)dλ represents the fraction of blackbody energy lying in the wavelength region from λ to λ + dλ. The function E_{b,λ} = E_{b,λ}(T, λ) is given by **Planck's law**

$$\frac{E_{b,\lambda}(T,\lambda)}{n^2 T^5} = \frac{c_1 (\lambda T)^{-5}}{e^{c_2/\lambda T} - 1} \quad (5-102)$$

where c₁ = 2πhc² and c₂ = hc/k are defined as Planck's first and second constants, respectively.

Integration of Eq. (5-102) over all wavelengths yields the **Stefan-Boltzman law** for the hemispherical blackbody emissive power

$$E_b(T) = \int_{\lambda=0}^{\infty} E_{b,\lambda}(T, \lambda) d\lambda = n^2 \sigma T^4 \quad (5-103)$$

where σ = c₁(π/c₂)⁴/15 is the Stephan-Boltzman constant. Since a blackbody is an *isotropic emitter*, it follows that the intensity of blackbody emission is given by the simple formula I_b = E_b/π = n²σT⁴/π. The intensity of radiation emitted over all wavelengths by a blackbody is thus uniquely determined by its temperature. In this presentation, all references to hemispherical emissive power shall be to the *blackbody* emissive power, and the subscript b may be suppressed for expediency.

For short wavelengths λT → 0, the asymptotic form of Eq. (5-102) is known as the **Wien equation**

$$\frac{E_{b,\lambda}(T, \lambda)}{n^2 T^5} \equiv c_1 (\lambda T)^{-5} e^{-c_2/\lambda T} \quad (5-104)$$

The error introduced by use of the Wien equation is less than 1 percent when λT < 3000 μm·K. The Wien equation has significant practical value in optical pyrometry for T < 4600 K when a red filter (λ = 0.65 μm) is employed. The long-wavelength asymptotic approximation for Eq. (5-102) is known as the **Rayleigh-Jeans formula**, which is accurate to within 1 percent for λT > 778,000 μm·K. The Rayleigh-Jeans formula is of limited engineering utility since a blackbody emits over 99.9 percent of its total energy below the value of λT = 53,000 μm·K.

^{*} In the literature the emissive power is variously called the emittance, total hemispherical intensity, or radiant flux density.

Nomenclature and Units—Radiative Transfer

$a, a_g, a_{g,1}$	WSGG spectral model clear plus gray weighting constants
$\bar{C}_p, \bar{C}_{p,prod}$	Heat capacity per unit mass, $J \cdot kg^{-1} \cdot K^{-1}$
$ij = s_i s_j$	Shorthand notation for direct exchange area
A, A_i	Area of enclosure or zone i , m^2
c	Speed of light in vacuum, m/s
c_1, c_2	Planck's first and second constants, $W \cdot m^2$ and $m \cdot K$
d_p, r_p	Particle diameter and radius, μm
$E_{b,\lambda} = E_{b,\lambda}(T, \lambda)$	Monochromatic, blackbody emissive power, $W/(m^2 \cdot \mu m)$
$E_n(x)$	Exponential integral of order n , where $n = 1, 2, 3, \dots$
E	Hemispherical emissive power, W/m^2
$E_b = n^2 \sigma T^4$	Hemispherical blackbody emissive power, W/m^2
f_v	Volumetric fraction of soot
$F_b(\lambda T)$	Blackbody fractional energy distribution
F_{ij}	Direct view factor from surface zone i to surface zone j
\bar{F}_{ij}	Refractory augmented black view factor; F -bar
$F_{i,j}$	Total view factor from surface zone i to surface zone j
h	Planck's constant, $J \cdot s$
h_i	Heat-transfer coefficient, $W/(m^2 \cdot K)$
H_i	Incident flux density for surface zone i , W/m^2
H	Enthalpy rate, W
\dot{H}_f	Enthalpy feed rate, W
$\dot{I}_\lambda \equiv I_\lambda(\vec{r}, \vec{\Omega}, \lambda)$	Monochromatic radiation intensity, $W/(m^2 \cdot \mu m \cdot sr)$
k	Boltzmann's constant, J/K
$k_{\lambda,p}$	Monochromatic line absorption coefficient, $(atm \cdot m)^{-1}$
K	Gas absorption coefficient, m^{-1}
L_M, L_{M0}	Average and optically thin mean beam lengths, m
\dot{m}	Mass flow rate, kg/h^{-1}
n	Index of refraction
M, N	Number of surface and volume zones in enclosure
p_k	Partial pressure of species k , atm
P	Number of WSGG gray gas spectral windows
Q_i	Total radiative flux originating at surface zone i , W
Q_{ij}	Net radiative flux between zone i and zone j , W
T	Temperature, K
U	Overall heat-transfer coefficient in WSCC model
V	Enclosure volume, m^3
W	Leaving flux density (radiosity), W/m^2

Greek Characters

$\alpha, \alpha_{1,2}$	Surface absorptivity or absorptance; subscript 1 refers to the surface temperature while subscript 2 refers to the radiation source
$\alpha_{g,1}, \epsilon_g, \tau_{g,1}$	Gas absorptivity, emissivity, and transmissivity
β	Dimensionless constant in mean beam length equation, $L_M = \beta \cdot L_{M0}$
$\Delta T_{fit} \equiv T_g - T_e$	Adjustable temperature fitting parameter for WSCC model, K
ϵ	Gray diffuse surface emissivity
$\epsilon_g(T, r)$	Gas emissivity with path length r
$\epsilon'_g(T, \Omega, \lambda)$	Monochromatic, unidirectional, surface emissivity
$\eta = 1/\lambda$	Wave number in vacuum, cm^{-1}
$\lambda = c/\nu$	Wavelength in vacuum, μm
ν	Frequency, Hz
$\rho = 1 - \epsilon$	Diffuse reflectivity
σ	Stefan-Boltzmann constant, $W/(m^2 \cdot K^4)$
Σ	Number of unique direct surface-to-surface direct exchange areas
$\tau_g = 1 - \epsilon_g$	Gas transmissivity
Ω	Solid angle, sr (steradians)
Φ	Equivalence ratio of fuel and oxidant
$\Psi^{(3)}(x)$	Pentagramma function of x
ω	Albedo for single scatter

Dimensionless Quantities

$D_{eff} = \frac{N_{FD}}{(S_i G_R/A_1) + N_{CR}}$	Effective firing density
$N_{CR} = \frac{h}{4\sigma T_{g,1}^3}$	Convection-radiation number
$N_{FD} = \dot{H}_f / \sigma T_{ref}^4 \cdot A_1$	Dimensionless firing density
η_g	Gas-side furnace efficiency
$\eta'_g = \eta_g(1 - \Theta_0)$	Reduced furnace efficiency
$\Theta_1 = T/T_{ref}$	Dimensionless temperature

Vector Notation

\vec{n}_1 and \vec{n}_2	Unit vectors normal to differential area elements dA_1 and dA_2
\vec{r}	Position vector
$\vec{\Omega}$	Arbitrary unit direction vector

Matrix Notation

\mathbf{I}_M	Column vector; all of whose elements are unity, $[M \times 1]$
$\mathbf{I} = [\delta_{ij}]$	Identity matrix, where δ_{ij} is the Kronecker delta; i.e., $\delta_{ij} = 1$ for $i = j$ and $\delta_{ij} = 0$ for $i \neq j$.
\mathbf{aI}	Diagonal matrix of WSGG gray gas surface zone a -weighting factors $[M \times M]$
$\mathbf{a}_g \mathbf{I}$	Diagonal matrix of gray gas WSGG volume zone a -weighting factors $[N \times N]$
$\mathbf{A} = [A_{ij}]$	Arbitrary nonsingular square matrix
$\mathbf{A}^T = [A_{ji}]$	Transpose of \mathbf{A}
$\mathbf{A}^{-1} = [A_{ij}]^{-1}$	Inverse of \mathbf{A}
$\mathbf{DI} = [D_i \cdot \delta_{ij}]$	Arbitrary diagonal matrix
$\mathbf{DI}^{-1} = [\delta_{ij}/D_i]$	Inverse of diagonal matrix
\mathbf{CDI}	$\mathbf{CI} \cdot \mathbf{DI} = [C_i \cdot D_i \cdot \delta_{ij}]$, product of two diagonal matrices
$\mathbf{AI} = [A_i \cdot \delta_{ij}]$	Diagonal matrix of surface zone areas, $m^2 [M \times M]$
$\epsilon \mathbf{I} = [\epsilon_i \cdot \delta_{ij}]$	Diagonal matrix of diffuse zone emissivities $[M \times M]$
$\rho \mathbf{I} = [\rho_i \cdot \delta_{ij}]$	Diagonal matrix of diffuse zone reflectivities $[M \times M]$
$\mathbf{E} = [E_i] = [\sigma T_i^4]$	Column vector of surface blackbody hemispherical emissive powers, $W/m^2 [M \times 1]$
$\mathbf{EI} = [E_i \cdot \delta_{ij}] = [\sigma T_i^4 \cdot \delta_{ij}]$	Diagonal matrix of surface blackbody emissive powers, $W/m^2 [M \times M]$
$\mathbf{E}_g = [E_{g,i}] = [\sigma T_{g,i}^4]$	Column vector of gas blackbody hemispherical emissive powers, $W/m^2 [N \times 1]$
$\mathbf{E}_g \mathbf{I} = [E_{g,i} \cdot \delta_{ij}] = [\sigma T_{g,i}^4 \cdot \delta_{ij}]$	Diagonal matrix of gas blackbody emissive powers, $W/m^2 [N \times N]$
$\mathbf{H} = [H_i]$	Column vector of surface zone incident flux densities, $W/m^2 [M \times 1]$
$\mathbf{W} = [W_i]$	Column vector of surface zone leaving flux densities, $W/m^2 [M \times 1]$
$\mathbf{Q} = [Q_i]$	Column vector of surface zone fluxes, $W [M \times 1]$
$\mathbf{R} = [\mathbf{AI} - \mathbf{ss} \cdot \rho \mathbf{I}]^{-1}$	Inverse multiple-reflection matrix, $m^{-2} [M \times M]$
$\mathbf{KI}_p = [\delta_{ij} \cdot K_{p,i}]$	Diagonal matrix of WSGG $K_{p,i}$ values for the i th zone and p th gray gas component, $m^{-1} [N \times N]$
$\bar{\mathbf{K}}\mathbf{I}$	Diagonal matrix of WSGG-weighted gray gas absorption coefficients, $m^{-1} [N \times N]$
\mathbf{S}'	Column vector for net volume absorption, $W [N \times 1]$
$\bar{\mathbf{ss}} = [\bar{s}_i \bar{s}_j]$	Array of direct surface-to-surface exchange areas, $m^2 [M \times M]$
$\bar{\mathbf{sg}} = [\bar{s}_i \bar{g}_j] = \bar{\mathbf{gs}}^T$	Array of direct gas-to-surface exchange areas, $m^2 [M \times N]$
$\bar{\mathbf{gg}} = [\bar{g}_i \bar{g}_j]$	Array of direct gas-to-gas exchange areas, $m^2 [N \times N]$
$\bar{\mathbf{SS}} = [\bar{S}_i \bar{S}_j]$	Array of total surface-to-surface exchange areas, $m^2 [M \times M]$
$\bar{\mathbf{SG}} = [\bar{S}_i \bar{G}_j]$	Array of total gas-to-surface exchange areas, $m^2 [M \times N]$
$\bar{\mathbf{GS}} = \bar{\mathbf{GS}}^T$	Array of total surface-to-gas exchange areas, $m^2 [N \times M]$
$\bar{\mathbf{GG}} = [\bar{G}_i \bar{G}_j]$	Array of total gas-to-gas exchange areas, $m^2 [N \times N]$
$\bar{\mathbf{SS}} = [\bar{S}_i \bar{S}_i]$	Array of directed surface-to-surface exchange areas, $m^2 [M \times M]$
$\bar{\mathbf{SG}} = [\bar{S}_i \bar{G}_i]$	Array of directed gas-to-surface exchange areas, $m^2 [M \times N]$
$\bar{\mathbf{GS}} \neq \bar{\mathbf{SG}}^T$	Array of directed surface-to-gas exchange areas, $m^2 [N \times M]$
$\bar{\mathbf{GG}} = [\bar{G}_i \bar{G}_i]$	Array of directed gas-to-gas exchange areas, $m^2 [N \times N]$
$\mathbf{VI} = [V_i \cdot \delta_{ij}]$	Diagonal matrix of zone volumes, $m^3 [N \times N]$

Subscripts

b	Blackbody or denotes a black surface zone
f	Denotes flux surface zone
h	Denotes hemispherical surface emissivity
i, j	Zone number indices
n	Denotes normal component of surface emissivity
p	Index for p th gray gas window
r	Denotes refractory surface zone
s	Denotes source-sink surface zone
λ	Denotes monochromatic variable
Ref	Denotes reference quantity

Abbreviations

CFD	Computational fluid dynamics
DO, FV	Discrete ordinate and finite volume methods
EM	Electromagnetic
RTE	Radiative transfer equation; equation of transfer
LPFF	Long plug flow furnace model
SSR	Source-sink refractory model
WSCC	Well-stirred combustion chamber model
WSGG	Weighted sum of gray gases spectral model

The blackbody fractional energy *distribution function* is defined by

$$F_b(\lambda T) = \frac{\int_0^\lambda E_{b,\lambda}(T, \lambda) d\lambda}{\int_0^\infty E_{b,\lambda}(T, \lambda) d\lambda} \quad (5-105)$$

The function $F_b(\lambda T)$ defines the fraction of total energy in the blackbody spectrum which lies below λT and is a unique function of λT . For purposes of digital computation, the following series expansion for $F_b(\lambda T)$ proves especially useful.

$$F_b(\lambda T) = \frac{15}{\pi^4} \sum_{k=1}^{\infty} \frac{e^{-k\xi}}{k} \left(\xi^3 + \frac{3\xi^2}{k} + \frac{6\xi}{k^2} + \frac{6}{k^3} \right) \text{ where } \xi = \frac{c_2}{\lambda T} \quad (5-106)$$

Equation (5-106) converges rapidly and is due to Lowan [1941] as referenced in Chang and Rhee [*Int. Comm. Heat Mass Transfer*, **11**, 451-455 (1984)].

Numerically, in the preceding, $h = 6.6260693 \times 10^{-34}$ J-s is the Planck constant; $c = 2.99792458 \times 10^8$ m/s is the velocity of light in vacuum; and $k = 1.3806505 \times 10^{-23}$ J/K is the Boltzmann constant. These data lead to the following values of Planck's first and second constants: $c_1 = 3.741771 \times 10^{-16}$ W·m² and $c_2 = 1.438775 \times 10^{-2}$ m·K, respectively. Numerical values of the Stephan-Boltzmann constant σ in several systems of units are as follows: 5.67040×10^{-8} W/(m²·K⁴); 1.3544×10^{-12} cal/(cm²·s·K⁴); 4.8757×10^{-8} kcal/(m²·h·K⁴); 9.9862×10^{-9} CHU/(ft²·h·K⁴); and 0.17123×10^{-5} Btu/(ft²·h·°R⁴) (CHU = centigrade heat unit; 1.0 CHU = 1.8 Btu.)

Blackbody Displacement Laws The blackbody energy spectrum

is plotted *logarithmically* in Fig. 5-9 as $\frac{E_{b,\lambda}(\lambda T)}{n^2 T^5} \times 10^{13} \frac{\text{W}}{\text{m}^2 \cdot \mu\text{m} \cdot \text{K}^5}$

versus λT $\mu\text{m} \cdot \text{K}$. For comparison a companion inset is provided in Cartesian coordinates. The upper abscissa of Fig. 5-9 also shows the blackbody energy distribution function $F_b(\lambda T)$. Figure 5-9 indicates that the wavelength-temperature product for which the maximum intensity occurs is $\lambda_{\text{max}} T = 2898 \mu\text{m} \cdot \text{K}$. This relationship is known as **Wien's displacement law**, which indicates that the wavelength for maximum intensity is *inversely* proportional to the absolute temperature. Blackbody displacement laws are useful in engineering practice to estimate wavelength intervals appropriate to relevant system temperatures. The Wien displacement law can be misleading, however, because the wavelength for maximum intensity depends on whether the intensity is defined in terms of frequency or wavelength interval. Two additional useful displacement laws are defined in terms of either the value of λT corresponding to the maximum energy per unit *fractional change* in wavelength or frequency, that is, $\lambda T = 3670 \mu\text{m} \cdot \text{K}$, or to the value of λT corresponding to one-half the blackbody energy, that is, $\lambda T = 4107 \mu\text{m} \cdot \text{K}$. Approximately one-half of the blackbody energy lies within the twofold λT range *geometrically centered* on $\lambda T = 3670 \mu\text{m} \cdot \text{K}$, that is, $3670/\sqrt{2} < \lambda T < 3670\sqrt{2} \mu\text{m} \cdot \text{K}$. Some 95 percent of the blackbody energy lies in the interval $1662.6 < \lambda T < 16,295 \mu\text{m} \cdot \text{K}$. It thus follows that for the temperature range between ambient (300 K) and flame temperatures (2000 K or

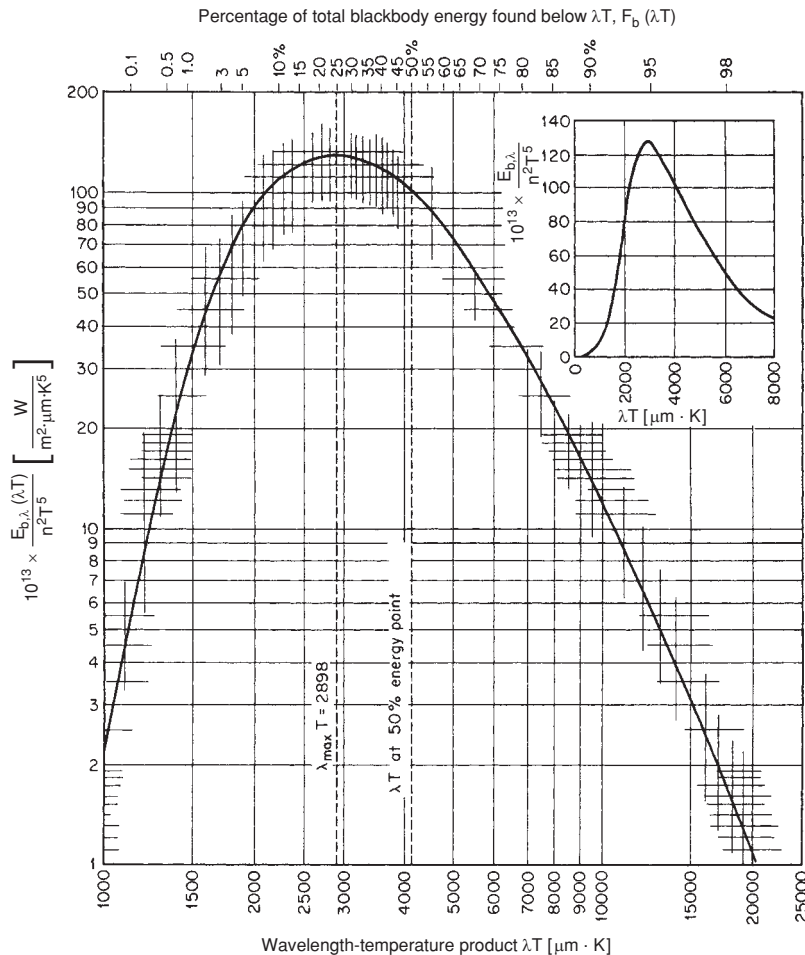


FIG. 5-9 Spectral dependence of monochromatic blackbody hemispherical emissive power.

3140°F), wavelengths of engineering heat-transfer importance are bounded between 0.83 and 54.3 μm.

RADIATIVE PROPERTIES OF OPAQUE SURFACES

Emittance and Absorptance The ratio of the total radiating power of any surface to that of a black surface at the same temperature is called the **emittance** or **emissivity**, ϵ of the surface.^o In general, the monochromatic emissivity is a function of temperature, direction, and wavelength, that is, $\epsilon_\lambda = \epsilon_\lambda(T, \Omega, \lambda)$. The subscripts n and h are sometimes used to denote the normal and hemispherical values, respectively, of the emittance or emissivity. If radiation is incident on a surface, the fraction absorbed is called the **absorptance** (**absorptivity**). Two subscripts are usually appended to the absorptance $\alpha_{1,2}$ to distinguish between the temperature of the absorbing surface T_1 and the spectral energy distribution of the emitting surface T_2 . According to **Kirchhoff's law**, the emissivity and absorptivity of a surface exposed to surroundings at its own temperature are the same for both monochromatic and total radiation. When the temperatures of the surface and its surroundings differ, the total emissivity and absorptivity of the surface are often found to be unequal; but because the absorptivity is substantially independent of irradiation density, the monochromatic emissivity and absorptivity of surfaces are equal for all practical purposes. The difference between *total* emissivity and absorptivity depends on the variation of ϵ_λ with wavelength and on the difference between the temperature of the surface and the effective temperature of the surroundings.

Consider radiative exchange between a real surface of area A_1 at temperature T_1 with black surroundings at temperature T_2 . The *net* radiant interchange is given by

$$Q_{1,2} = A_1 \int_{\lambda=0}^{\infty} [\epsilon_\lambda(T_1, \lambda) \cdot E_{b,\lambda}(T_1, \lambda) - \alpha_\lambda(T_1, \lambda) \cdot E_{b,\lambda}(T_2, \lambda)] d\lambda \quad (5-107a)$$

$$\text{or} \quad Q_{1,2} = A_1 (\epsilon_1 \sigma T_1^4 - \alpha_{1,2} \sigma T_2^4) \quad (5-107b)$$

$$\text{where} \quad \epsilon_1(T_1) = \int_{\lambda=0}^{\infty} \epsilon_\lambda(T_1, \lambda) \cdot \frac{E_{b,\lambda}(T_1, \lambda)}{E_b(T_1)} d\lambda \quad (5-108)$$

$$\text{and since} \quad \alpha_\lambda(T, \lambda) = \epsilon_\lambda(T, \lambda),$$

$$\alpha_{1,2}(T_1, T_2) = \int_{\lambda=0}^{\infty} \epsilon_\lambda(T_1, \lambda) \cdot \frac{E_{b,\lambda}(T_2, \lambda)}{E_b(T_2)} d\lambda \quad (5-109)$$

For a *gray surface* $\epsilon_1 = \alpha_{1,2} = \epsilon_\lambda$. A *selective surface* is one for which $\epsilon_\lambda(T, \lambda)$ exhibits a strong dependence on wavelength. If the wavelength dependence is *monotonic*, it follows from Eqs. (5-107) to (5-109) that ϵ_1 and $\alpha_{1,2}$ can differ markedly when T_1 and T_2 are widely separated. For example, in solar energy applications, the nominal temperature of the earth is $T_1 = 294$ K, and the sun may be represented as a blackbody with radiation temperature $T_2 = 5800$ K. For these temperature conditions, a *white paint* can exhibit $\epsilon_1 = 0.9$ and $\alpha_{1,2} = 0.1$ to 0.2. In contrast, a *thin layer of copper oxide on bright aluminum* can exhibit ϵ_1 as low as 0.12 and $\alpha_{1,2}$ greater than 0.9.

The effect of radiation source temperature on low-temperature absorptivity for a number of representative materials is shown in Fig. 5-10. Polished aluminum (curve 15) and anodized (surface-oxidized) aluminum (curve 13) are representative of metals and nonmetals, respectively. Figure 5-10 thus demonstrates the generalization that metals and nonmetals respond in *opposite directions* with regard to changes in the radiation source temperature. Since the effective solar temperature is 5800 K (10,440°R), the extreme right-hand side of Fig. 5-10 provides surface absorptivity data relevant to solar energy applications. The dependence of emittance and absorptance on the real and imaginary components of the refractive index and on the geometric

structure of the surface layer is quite complex. However, a number of generalizations concerning the radiative properties of opaque surfaces are possible. These are summarized in the following discussion.

Polished Metals

1. In the infrared region, the magnitude of the monochromatic emissivity ϵ_λ is small and is dependent on free-electron contributions. Emissivity is also a function of the ratio of resistivity to wavelength r/λ , as depicted in Fig. 5-11. At shorter wavelengths, bound-electron contributions become significant, ϵ_λ is larger in magnitude, and it sometimes exhibits a maximum value. In the visible spectrum, common values for ϵ_λ are 0.4 to 0.8 and ϵ_λ decreases slightly as temperature increases. For $0.7 < \lambda < 1.5$ μm, ϵ_λ is approximately independent of temperature. For $\lambda > 8$ μm, ϵ_λ is approximately proportional to the square root of temperature since $\epsilon_\lambda \propto \sqrt{r}$ and $r \propto T$. Here the Drude or Hagen-Rubens relation applies, that is, $\epsilon_{\lambda,n} \approx 0.0365 \sqrt{r/\lambda}$, where r has units of ohm-meters and λ is measured in micrometers.

2. Total emittance is substantially proportional to absolute temperature, and at moderate temperatures $\epsilon_n = 0.058T \sqrt{rT}$, where T is measured in kelvins.

3. The total absorptance of a metal at temperature T_1 with respect to radiation from a black or gray source at temperature T_2 is equal to the emissivity evaluated at the geometric mean of T_1 and T_2 . Figure 5-11 gives values of ϵ_λ and $\epsilon_{\lambda,n}$, and their ratio, as a function of the product rT (solid lines). Although Fig. 5-11 is based on free-electron

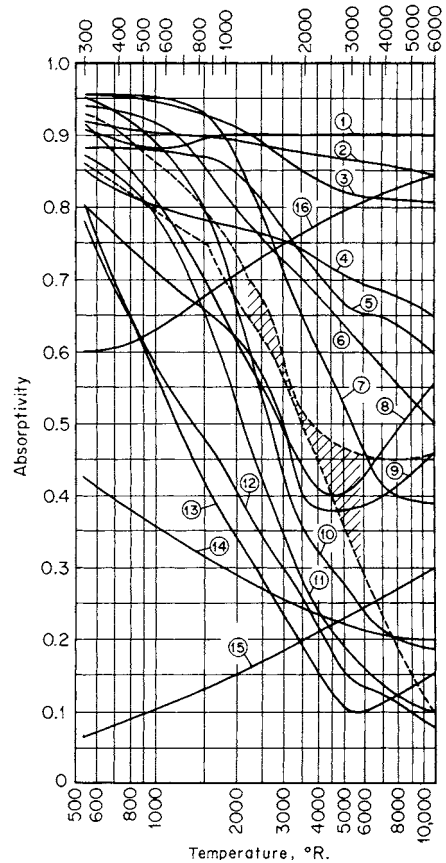


FIG. 5-10 Variation of absorptivity with temperature of radiation source. (1) Slate composition roofing. (2) Linoleum, red brown. (3) Asbestos slate. (4) Soft rubber, gray. (5) Concrete. (6) Porcelain. (7) Vitreous enamel, white. (8) Red brick. (9) Cork. (10) White dutch tile. (11) White chamotte. (12) MgO, evaporated. (13) Anodized aluminum. (14) Aluminum paint. (15) Polished aluminum. (16) Graphite. The two dashed lines bound the limits of data on gray paving brick, asbestos paper, wood, various cloths, plaster of paris, lithopone, and paper. To convert degrees Rankine to kelvins, multiply by (5.556)(10⁻³).

^oIn the literature, *emittance* and *emissivity* are often used interchangeably. NIST (the National Institute of Standards and Technology) recommends use of the suffix *-ivity* for pure materials with optically smooth surfaces, and *-ance* for rough and contaminated surfaces. Most real engineering materials fall into the latter category.

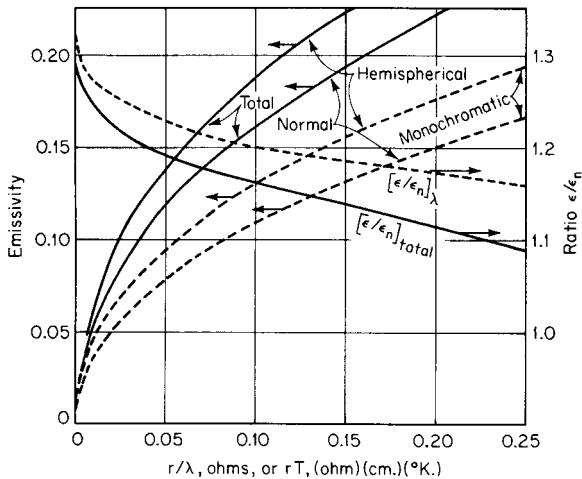


FIG. 5-11 Hemispherical and normal emissivities of metals and their ratio. Dashed lines: monochromatic (spectral) values versus r/λ . Solid lines: total values versus rT . To convert ohm-centimeter-kelvins to ohm-meter-kelvins, multiply by 10^{-2} .

contributions to emissivity in the far infrared, the relations for total emissivity are remarkably good even at high temperatures. Unless extraordinary efforts are taken to prevent oxidation, a metallic surface may exhibit an emissance or absorptance which may be several times that of a polished specimen. For example, the emissance of iron and steel depends strongly on the degree of oxidation and roughness. Clean iron and steel surfaces have an emissance from 0.05 to 0.45 at ambient temperatures and 0.4 to 0.7 at high temperatures. Oxidized and/or roughened iron and steel surfaces have values of emissance ranging from 0.6 to 0.95 at low temperatures to 0.9 to 0.95 at high temperatures.

Refractory Materials For refractory materials, the dependence of emissance and absorptance on grain size and impurity concentrations is quite important.

1. Most refractory materials are characterized by $0.8 < \epsilon_\lambda < 1.0$ for the wavelength region $2 < \lambda < 4 \mu\text{m}$. The monochromatic emissivity ϵ_λ decreases rapidly toward shorter wavelengths for materials that are white in the visible range but demonstrates high values for black materials such as FeO and Cr_2O_3 . Small concentrations of FeO and Cr_2O_3 or other colored oxides, can cause marked increases in the emissance of materials that are normally white. The sensitivity of the emissance of refractory oxides to small additions of absorbing materials is demonstrated by the results of calculations presented in Fig. 5-12. Figure 5-12 shows the emissance of a semi-infinite absorbing-scattering medium as a function of its *albedo* $\omega \equiv K_s/(K_a + K_s)$, where K_a and K_s are the scatter and absorption coefficients, respectively. These results are relevant to the radiative properties of fibrous materials, paints, oxide coatings, refractory materials, and other *particulate* media. They demonstrate that over the relatively small range $1 - \omega = 0.005$ to 0.1 , the hemispherical emissance ϵ_h increases from approximately 0.15 to 1.0. For refractory materials, ϵ_λ varies little with temperature, with the exception of some white oxides which at high temperatures become good emitters in the visible spectrum as a consequence of the induced electronic transitions.

2. For refractory materials at ambient temperatures, the total emissance ϵ is generally high (0.7 to 1.0). Total refractory emissance decreases with increasing temperature, such that a temperature increase from 1000 to 1570°C may result in a 20 to 30 percent reduction in ϵ .

3. Emissance and absorptance increase with increase in grain size over a grain size range of 1 to 200 μm .

4. The ratio ϵ_h/ϵ_n of hemispherical to normal emissivity of polished surfaces varies with refractive index n ; e.g., the ratio decreases from a value of 1.0 when $n = 1.0$ to a value of 0.93 when $n = 1.5$ (common glass) and increases back to 0.96 at $n = 3.0$.

5. As shown in Fig. 5-12, for a surface composed of particulate

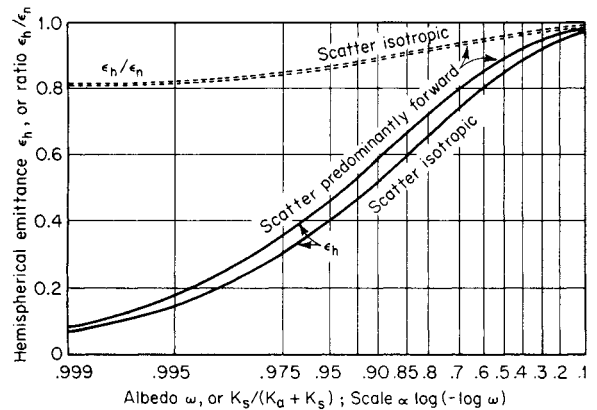


FIG. 5-12 Hemispherical emissance ϵ_h and the ratio of hemispherical to normal emissance ϵ_h/ϵ_n for a semi-infinite absorbing-scattering medium.

matter which scatters isotropically, the ratio ϵ_h/ϵ_n varies from 1.0 when $\omega < 0.1$ to about 0.8 when $\omega = 0.999$.

6. The total absorptance exhibits a decrease with an increase in temperature of the radiation source similar to the decrease in emissance with an increase in the emitter temperature.

Figure 5-10 shows a regular variation of $\alpha_{1,2}$ with T_2 . When T_2 is not very different from T_1 , $\alpha_{1,2} = \epsilon_1(T_2/T_1)^m$. It may be shown that Eq. (5-107b) is then approximated by

$$Q_{1,2} = (1 + m/4)\epsilon_{av} A_1 \sigma(T_1^4 - T_2^4) \quad (5-110)$$

where ϵ_{av} is evaluated at the arithmetic mean of T_1 and T_2 . For metals $m \approx 0.5$ while for nonmetals m is small and negative.

Table 5-4 illustrates values of emissance for materials encountered in engineering practice. It is based on a critical evaluation of early emissivity data. Table 5-4 demonstrates the wide variation possible in the emissivity of a particular material due to variations in surface roughness and thermal pretreatment. With few exceptions the data in Table 5-4 refer to emissances ϵ_n normal to the surface. The hemispherical emissance ϵ_h is usually slightly smaller, as demonstrated by the ratio ϵ_h/ϵ_n depicted in Fig. 5-12. More recent data support the range of emissance values given in Table 5-4 and their dependence on surface conditions. An extensive compilation is provided by Goldsmith, Waterman, and Hirschorn (*Thermophysical Properties of Matter*, Purdue University, Touloukian, ed., Plenum, 1970-1979).

For opaque materials the reflectance ρ is the complement of the absorptance. The directional distribution of the reflected radiation depends on the material, its degree of roughness or grain size, and, if a metal, its state of oxidation. Polished surfaces of homogeneous materials are specular reflectors. In contrast, the intensity of the radiation reflected from a perfectly diffuse or *Lambert surface* is independent of direction. The directional distribution of reflectance of many oxidized metals, refractory materials, and natural products approximates that of a perfectly diffuse reflector. A better model, adequate for many calculation purposes, is achieved by assuming that the total reflectance is the sum of diffuse and specular components ρ_D and ρ_S , as discussed in a subsequent section.

VIEW FACTORS AND DIRECT EXCHANGE AREAS

Consider radiative interchange between two *finite* black surface area elements A_1 and A_2 separated by a transparent medium. Since they are black, the surfaces emit isotropically and totally absorb all incident radiant energy. It is desired to compute the fraction of radiant energy, per unit emissive power E_1 , leaving A_1 in all directions which is intercepted and absorbed by A_2 . The required quantity is defined as the **direct view factor** and is assigned the notation $F_{1,2}$. Since the *net radiant energy interchange* $Q_{1,2} \equiv A_1 F_{1,2} E_1 - A_2 F_{2,1} E_2$ between surfaces A_1 and A_2 must be zero when their temperatures are equal, it follows

TABLE 5-4 Normal Total Emissivity of Various Surfaces

A. Metals and Their Oxides					
Surface	$t, ^\circ\text{F}^\circ$	Emissivity*	Surface	$t, ^\circ\text{F}^\circ$	Emissivity*
Aluminum			Sheet steel, strong rough oxide layer	75	0.80
Highly polished plate, 98.3% pure	440–1070	0.039–0.057	Dense shiny oxide layer	75	0.82
Polished plate	73	0.040	Cast plate:		
Rough plate	78	0.055	Smooth	73	0.80
Oxidized at 1110°F	390–1110	0.11–0.19	Rough	73	0.82
Aluminum-surfaced roofing	100	0.216	Cast iron, rough, strongly oxidized	100–480	0.95
Calorized surfaces, heated at 1110°F.			Wrought iron, dull oxidized	70–680	0.94
Copper	390–1110	0.18–0.19	Steel plate, rough	100–700	0.94–0.97
Steel	390–1110	0.52–0.57	High temperature alloy steels (see Nickel Alloys).		
Brass			Molten metal		
Highly polished:			Cast iron	2370–2550	0.29
73.2% Cu, 26.7% Zn	476–674	0.028–0.031	Mild steel	2910–3270	0.28
62.4% Cu, 36.8% Zn, 0.4% Pb, 0.3% Al	494–710	0.033–0.037	Lead		
82.9% Cu, 17.0% Zn	530	0.030	Pure (99.96%), unoxidized	260–440	0.057–0.075
Hard rolled, polished:			Gray oxidized	75	0.281
But direction of polishing visible	70	0.038	Oxidized at 390°F.	390	0.63
But somewhat attacked	73	0.043	Mercury	32–212	0.09–0.12
But traces of stearin from polish left on	75	0.053	Molybdenum filament	1340–4700	0.096–0.292
Polished	100–600	0.096	Monel metal, oxidized at 1110°F	390–1110	0.41–0.46
Rolled plate, natural surface	72	0.06	Nickel		
Rubbed with coarse emery	72	0.20	Electroplated on polished iron, then polished	74	0.045
Dull plate	120–660	0.22	Technically pure (98.9% Ni, + Mn), polished	440–710	0.07–0.087
Oxidized by heating at 1110°F	390–1110	0.61–0.59	Electroplated on pickled iron, not polished	68	0.11
Chromium; see Nickel Alloys for Ni-Cr steels	100–1000	0.08–0.26	Wire	368–1844	0.096–0.186
Copper			Plate, oxidized by heating at 1110°F	390–1110	0.37–0.48
Carefully polished electrolytic copper	176	0.018	Nickel oxide	1200–2290	0.59–0.86
Commercial, emiered, polished, but pits remaining	66	0.030	Nickel alloys		
Commercial, scraped shiny but not mirror-like	72	0.072	Chromnickel	125–1894	0.64–0.76
Polished	242	0.023	Nickelin (18–32 Ni; 55–68 Cu; 20 Zn), gray oxidized	70	0.262
Plate, heated long time, covered with thick oxide layer	77	0.78	KA-2S alloy steel (8% Ni; 18% Cr), light silvery, rough, brown, after heating After 42 hr. heating at 980°F.	420–914	0.44–0.36
Plate heated at 1110°F	390–1110	0.57	NCT-3 alloy (20% Ni; 25% Cr.), brown, splotted, oxidized from service	420–980	0.62–0.73
Cuprous oxide	1470–2010	0.66–0.54	NCT-6 alloy (60% Ni; 12% Cr), smooth, black, firm adhesive oxide coat from service	420–980	0.90–0.97
Molten copper	1970–2330	0.16–0.13	Platinum		
Gold			Pure, polished plate	440–1160	0.054–0.104
Pure, highly polished	440–1160	0.018–0.035	Strip	1700–2960	0.12–0.17
Iron and steel			Filament	80–2240	0.036–0.192
Metallic surfaces (or very thin oxide layer):			Wire	440–2510	0.073–0.182
Electrolytic iron, highly polished	350–440	0.052–0.064	Silver		
Polished iron	800–1880	0.144–0.377	Polished, pure	440–1160	0.0198–0.0324
Iron freshly emiered	68	0.242	Polished	100–700	0.0221–0.0312
Cast iron, polished	392	0.21	Steel, see Iron.		
Wrought iron, highly polished	100–480	0.28	Tantalum filament	2420–5430	0.194–0.31
Cast iron, newly turned	72	0.435	Tin—bright tinned iron sheet	76	0.043 and 0.064
Polished steel casting	1420–1900	0.52–0.56	Tungsten		
Ground sheet steel	1720–2010	0.55–0.61	Filament, aged	80–6000	0.032–0.35
Smooth sheet iron	1650–1900	0.55–0.60	Filament	6000	0.39
Cast iron, turned on lathe	1620–1810	0.60–0.70	Zinc		
Oxidized surfaces:			Commercial, 99.1% pure, polished	440–620	0.045–0.053
Iron plate, pickled, then rusted red	68	0.612	Oxidized by heating at 750°F.	750	0.11
Completely rusted	67	0.685	Galvanized sheet iron, fairly bright	82	0.228
Rolled sheet steel	70	0.657	Galvanized sheet iron, gray oxidized	75	0.276
Oxidized iron	212	0.736			
Cast iron, oxidized at 1100°F	390–1110	0.64–0.78			
Steel, oxidized at 1100°F	390–1110	0.79			
Smooth oxidized electrolytic iron	260–980	0.78–0.82			
Iron oxide	930–2190	0.85–0.89			
Rough ingot iron	1700–2040	0.87–0.95			
B. Refractories, Building Materials, Paints, and Miscellaneous					
Asbestos			Carbon		
Board	74	0.96	T-carbon (Gebr. Siemens) 0.9% ash (this started with emissivity at 260°F. of 0.72, but on heating changed to values given)	260–1160	0.81–0.79
Paper	100–700	0.93–0.945	Carbon filament	1900–2560	0.526
Brick			Candle soot	206–520	0.952
Red, rough, but no gross irregularities	70	0.93	Lampblack-waterglass coating	209–362	0.959–0.947
Silica, unglazed, rough	1832	0.80			
Silica, glazed, rough	2012	0.85			
Grog brick, glazed	2012	0.75			
See Refractory Materials below.					

TABLE 5-4 Normal Total Emissivity of Various Surfaces (Concluded)

B. Refractories, Building Materials, Paints, and Miscellaneous					
Surface	$t, ^\circ\text{F}^\circ$	Emissivity ^o	Surface	$t, ^\circ\text{F}^\circ$	Emissivity ^o
Same	260-440	0.957-0.952	Oil paints, sixteen different, all colors	212	0.92-0.96
Thin layer on iron plate	69	0.927	Aluminum paints and lacquers		
Thick coat	68	0.967	10% Al, 22% lacquer body, on rough or smooth surface	212	0.52
Lampblack, 0.003 in. or thicker	100-700	0.945	26% Al, 27% lacquer body, on rough or smooth surface	212	0.3
Enamel, white fused, on iron	66	0.897	Other Al paints, varying age and Al content	212	0.27-0.67
Glass, smooth	72	0.937	Al lacquer, varnish binder, on rough plate	70	0.39
Gypsum, 0.02 in. thick on smooth or blackened plate	70	0.903	Al paint, after heating to 620°F.	300-600	0.35
Marble, light gray, polished	72	0.931	Paper, thin		
Oak, planed	70	0.895	Pasted on tinned iron plate	66	0.924
Oil layers on polished nickel (lube oil)	68		On rough iron plate	66	0.929
Polished surface, alone		0.045	On black lacquered plate	66	0.944
+0.001-in. oil		0.27	Plaster, rough lime	50-190	0.91
+0.002-in. oil		0.46	Porcelain, glazed	72	0.924
+0.005-in. oil		0.72	Quartz, rough, fused	70	0.932
Infinitely thick oil layer		0.82	Refractory materials, 40 different poor radiators	1110-1830	$\left[\begin{matrix} 0.65 \\ 0.70 \\ 0.80 \\ 0.85 \end{matrix} \right] - \left[\begin{matrix} 0.75 \\ 0.85 \\ 0.90 \end{matrix} \right]$
Oil layers on aluminum foil (linseed oil)			good radiators		
Al foil	212	0.087†	Roofing paper	69	
+1 coat oil	212	0.561	Rubber		
+2 coats oil	212	0.574	Hard, glossy plate	74	0.945
Paints, lacquers, varnishes			Soft, gray, rough (reclaimed)	76	0.859
Snowwhite enamel varnish or rough iron plate	73	0.906	Serpentine, polished	74	0.900
Black shiny lacquer, sprayed on iron	76	0.875	Water	32-212	0.95-0.963
Black shiny shellac on tinned iron sheet	70	0.821			
Black matte shellac	170-295	0.91			
Black lacquer	100-200	0.80-0.95			
Flat black lacquer	100-200	0.96-0.98			
White lacquer	100-200	0.80-0.95			

^oWhen two temperatures and two emissivities are given, they correspond, first to first and second to second, and linear interpolation is permissible. °C = (°F - 32)/1.8.

†Although this value is probably high, it is given for comparison with the data by the same investigator to show the effect of oil layers. See Aluminum, Part A of this table.

thermodynamically that $A_1F_{1,2} = A_2F_{2,1}$. The product of area and view factor $\overline{s_1s_2} \equiv A_1F_{1,2}$, which has the dimensions of area, is termed the **direct surface-to-surface exchange area** for finite black surfaces. Clearly, direct exchange areas are symmetric with respect to their subscripts, that is, $\overline{s_1s_2} = \overline{s_2s_1}$, but view factors are not symmetric unless the associated surface areas are equal. This property is referred to as the **symmetry or reciprocity relation** for direct exchange areas. The shorthand notation $\overline{s_1s_2} \equiv 12 = 21$ for direct exchange areas is often found useful in mathematical developments.

Equation (5-101) may also be restated as

$$\frac{\partial^2 \overline{s_1s_2}}{\partial A_i \partial A_j} = \frac{\cos \phi_i \cos \phi_j}{\pi r^2} \quad (5-111)$$

which leads directly to the required definition of the direct exchange area as a double surface integral

$$\overline{s_1s_2} = \iint_{A_i} \iint_{A_j} \frac{\cos \phi_i \cos \phi_j}{\pi r^2} dA_j dA_i \quad (5-112)$$

All terms in Eq. (5-112) have been previously defined.

Suppose now that Eq. (5-112) is integrated over the entire confining surface of an **enclosure** which has been subdivided into M finite area elements. Each of the M surface **zones** must then satisfy certain **conservation relations** involving *all* the direct exchange areas in the enclosure

$$\sum_{j=1}^M \overline{s_1s_j} = A_1 \quad \text{for } 1 \leq i \leq M \quad (5-113a)$$

or in terms of view factors

$$\sum_{j=1}^M F_{1j} = 1 \quad \text{for } 1 \leq i \leq M \quad (5-113b)$$

Contour integration is commonly used to simplify the evaluation of Eq. (5-112) for specific geometries; see Modest (op. cit., Chap. 4)

or Siegel and Howell (op. cit., Chap. 5). The formulas for two particularly useful view factors involving perpendicular rectangles of area xz and yz with common edge z and equal parallel rectangles of area xy and distance of separation z are given for **perpendicular rectangles** with common dimension z

$$\begin{aligned} (\pi \cdot X) \cdot F_{XY} = & X \tan^{-1} \frac{1}{X} + Y \tan^{-1} \frac{1}{Y} - \sqrt{X^2 + Y^2} \tan^{-1} \sqrt{\frac{1}{X^2 + Y^2}} \\ & + \frac{1}{4} \ln \left\{ \frac{(1+X^2)(1+Y^2)}{1+X^2+Y^2} \left[\frac{X^2(1+X^2+Y^2)}{(1+X^2)(X^2+Y^2)} \right]^{X^2} \left[\frac{Y^2(1+X^2+Y^2)}{(1+Y^2)(X^2+Y^2)} \right]^{Y^2} \right\} \end{aligned} \quad (5-114a)$$

and for **parallel rectangles**, separated by distance z ,

$$\begin{aligned} \left(\frac{\pi \cdot X \cdot Y}{2} \right) \cdot F_{XY} = & \ln \left[\frac{(1+X^2)(1+Y^2)}{1+X^2+Y^2} \right]^{1/2} + X\sqrt{1+Y^2} \tan^{-1} \frac{X}{\sqrt{1+Y^2}} \\ & + Y\sqrt{1+X^2} \tan^{-1} \frac{Y}{\sqrt{1+X^2}} - X \tan^{-1} X - Y \tan^{-1} Y \end{aligned} \quad (5-114b)$$

In Eqs. (5-114) X and Y are normalized whereby $X = x/z$ and $Y = y/z$ and the corresponding **dimensional** direct surface areas are given by $\overline{s_1s_2} = xzF_{XY}$ and $\overline{s_1s_2} = xyF_{XY}$, respectively.

The exchange area between any two area elements of a sphere is independent of their relative shape and position and is simply the product of the areas, divided by the area of the entire sphere; i.e., any spot on a sphere has equal views of all other spots.

Figure 5-13, curves 1 through 4, shows view factors for selected parallel opposed disks, squares, and 2:1 rectangles and parallel rectangles with one infinite dimension as a function of the ratio of the

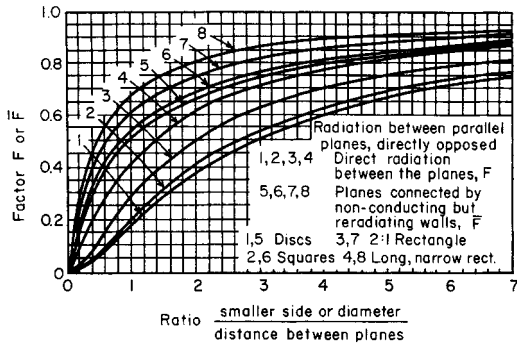


FIG. 5-13 Radiation between parallel planes, directly opposed.

smaller diameter or side to the distance of separation. Curves 2 through 4 of Fig. 5-13, for opposed rectangles, can be computed with Eq. (5-114b). The view factors for two finite coaxial coextensive cylinders of radii $r \leq R$ and height L are shown in Fig. 5-14. The direct view factors for an infinite plane parallel to a system of rows of parallel tubes (see Fig. 5-16) are given as curves 1 and 3 of Fig. 5-15. The view factors for this two-dimensional geometry can be readily calculated by using the **crossed-strings method**.

The crossed-strings method, due to Hottel (*Radiative Transfer*, McGraw-Hill, New York, 1967), is stated as follows: "The exchange area for two-dimensional surfaces, A_1 and A_2 , per unit length (in the infinite dimension) is given by the sum of the lengths of crossed strings from the ends of A_1 to the ends of A_2 less the sum of the uncrossed strings from and to the same points all divided by 2." The strings must be drawn so that all the flux from one surface to the other must cross each of a pair of crossed strings and neither of the pair of uncrossed strings. If one surface can see the other around both sides of an obstruction, two more pairs of strings are involved. The calculation procedure is demonstrated by evaluation of the tube-to-tube view factor for one row of a tube bank, as illustrated in Example 7.

Example 7: The Crossed-Strings Method Figure 5-16 depicts the transverse cross section of two infinitely long, parallel circular tubes of diameter D and center-to-center distance of separation C . Use the crossed-strings method to formulate the tube-to-tube direct exchange area and view factor $\overline{s_1s_2}$ and F_{12} , respectively.

Solution: The circumferential area of each tube is $A_i = \pi D$ per unit length in the infinite dimension for this two-dimensional geometry. Application of the crossed-strings procedure then yields simply

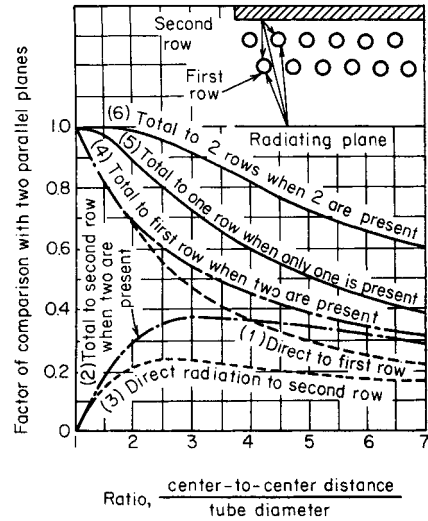


FIG. 5-15 Distribution of radiation to rows of tubes irradiated from one side. Dashed lines: direct view factor F from plane to tubes. Solid lines: total view factor F for black tubes backed by a refractory surface.

$$\overline{s_1s_2} = \frac{2(EFGH - HJ)}{2} = D[\sin^{-1}(1/R) + \sqrt{R^2 - 1} - R]$$

and

$$F_{12} = \overline{s_1s_2}/A_1 = [\sin^{-1}(1/R) + \sqrt{R^2 - 1} - R]/\pi$$

where $EFGH$ and $HJ = C$ are the indicated line segments and $R \equiv C/D \geq 1$. Curve 1 of Fig. 5-15, denoted by $F_{p,1}$, is a function of F_{12} , that is, $F_{p,1} = (\pi/R)(\frac{1}{2} - F_{12})$.

The **Yamauti principle** [Yamauti, *Res. Electrotech Lab. (Tokyo)*, 148 (1924); 194 (1927); 250 (1929)] is stated as follows: *The exchange areas between two pairs of surfaces are equal when there is a one-to-one correspondence for all sets of symmetrically positioned pairs of differential elements in the two surface combinations.* Figure 5-17 illustrates the Yamauti principle applied to surfaces in perpendicular planes having a common edge. With reference to Fig. 5-17, the Yamauti principle states that the diagonally opposed exchange areas are equal, that is, $(1)(4) = (2)(3)$. Figure 5-17 also shows a more complex geometric construction for displaced cylinders for which the Yamauti principle also applies. Collectively the three terms *reciprocity* or *symmetry principle*, *conservation*

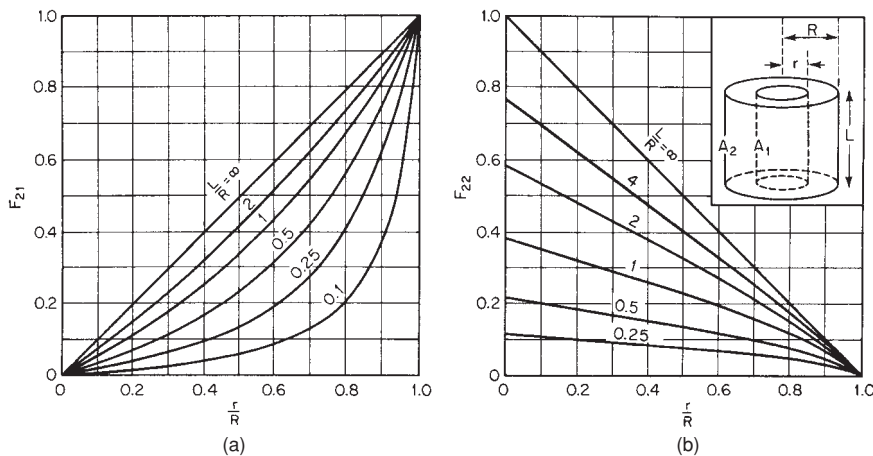


FIG. 5-14 View factors for a system of two concentric coaxial cylinders of equal length. (a) Inner surface of outer cylinder to inner cylinder. (b) Inner surface of outer cylinder to itself.

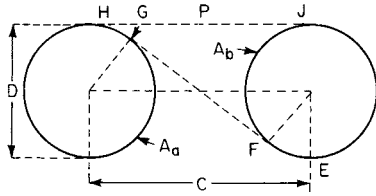


FIG. 5-16 Direct exchange between parallel circular tubes.

principle, and Yamauti principle are referred to as **view factor or exchange area algebra**.

Example 8: Illustration of Exchange Area Algebra Figure 5-17 shows a graphical construction depicting four perpendicular opposed rectangles with a common edge. Numerically evaluate the direct exchange areas and view factors for the diagonally opposed (shaded) rectangles A_1 and A_4 , that is, $\overline{(1)(4)}$, as well as $\overline{(1)(3+4)}$. The dimensions of the rectangular construction are shown in Fig. 5-17 as $x=3$, $y=2$, and $z=1$.

Solution: Using shorthand notation for direct exchange areas, the conservation principle yields

$$\overline{(1+2)(3+4)} = \overline{(1+2)(3)} + \overline{(1+2)(4)} = \overline{(1)(3)} + \overline{(2)(3)} + \overline{(1)(4)} + \overline{(2)(4)}$$

Now by the Yamauti principle we have $\overline{(1)(4)} \equiv \overline{(2)(3)}$. Combination of these two relations yields the first result $\overline{(1)(4)} = [\overline{(1+2)(3+4)} - \overline{(1)(3)} - \overline{(2)(4)}]/2$. For $\overline{(1)(3+4)}$, again conservation yields $\overline{(1)(3+4)} = \overline{(1)(3)} + \overline{(1)(4)}$, and substitution of the expression for $\overline{(1)(4)}$ just obtained yields the second result, that is, $\overline{(1)(3+4)} = [\overline{(1+2)(3+4)} + \overline{(1)(3)} - \overline{(2)(4)}]/2.0$. All three required direct exchange areas in these two relations are readily evaluated from Eq. (5-114a). Moreover, these equations apply to opposed parallel rectangles as well as rectangles with a common edge oriented at any angle. Numerically it follows from Eq. (5-114a) that for $X = \frac{1}{3}$, $Y = \frac{2}{3}$, and $z = 3$ that $\overline{(1+2)(3+4)} = 0.95990$; for $X = 1$, $Y = 2$, and $z = 1$ that $\overline{(1)(3)} = 0.23285$; and for $X = \frac{1}{2}$, $Y = 1$, and $z = 2$ that $\overline{(2)(4)} = 0.585747$. Since $A_1 = 1.0$, this leads to $s_{134} = F_{1,4} = (0.95990 - 0.23285 - 0.584747)/2.0 = 0.07115$ and $s_{13+4} = F_{1,3+4} = (0.95990 + 0.23285 - 0.584747)/2.0 = 0.30400$.

Many literature sources document closed-form algebraic expressions for view factors. Particularly comprehensive references include the compendia by Modest (op. cit., App. D) and Siegel and Howell (op. cit., App. C). The appendices for both of these textbooks also provide a wealth of resource information for radiative transfer. Appendix F of Modest, e.g., references an extensive listing of Fortran computer codes for a variety of radiation calculations which include view factors. These codes are archived in the dedicated Internet web site maintained by the publisher. The textbook by Siegel and Howell also includes an extensive database of view factors archived on a CD-ROM and includes a reference to an author-maintained Internet web site. Other historical sources for view factors include Hottel and Sarofim (op. cit., Chap. 2) and Hamilton and Morgan (NACA-TN 2836, December 1952).

RADIATIVE EXCHANGE IN ENCLOSURES—THE ZONE METHOD

Total Exchange Areas When an enclosure contains reflective surface zones, allowance must be made for not only the radiant energy transferred directly between any two zones but also the additional transfer attendant to however many multiple reflections which occur among the intervening reflective surfaces. Under such circumstances,

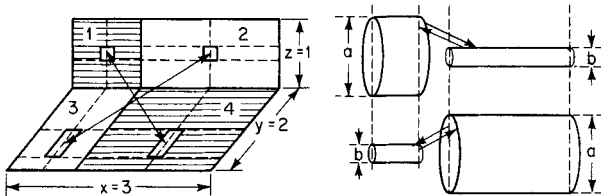


FIG. 5-17 Illustration of the Yamauti principle.

it can be shown that the net radiative flux Q_{ij} between all such surface zone pairs A_i and A_j , making full allowance for all multiple reflections, may be computed from

$$Q_{ij} = \sigma(A_i F_{ij} T_i^4 - A_j F_{ji} T_j^4) \tag{5-115}$$

Here, F_{ij} is defined as the **total surface-to-surface view factor** from A_i to A_j , and the quantity $S_i S_j \equiv A_i F_{ij}$ is defined as the corresponding **total surface-to-surface exchange area**. In analogy with the direct exchange areas, the total surface-to-surface exchange areas are also symmetric and thus obey reciprocity, that is, $A_i F_{ij} = A_j F_{ji}$ or $S_i S_j = S_j S_i$. When applied to an enclosure, total exchange areas and view factors also must satisfy appropriate conservation relations. Total exchange areas are functions of the geometry and radiative properties of the entire enclosure. They are also independent of temperature if all surfaces and any radiatively participating media are gray. The following subsection presents a general matrix method for the explicit evaluation of total exchange areas from direct exchange areas and other enclosure parameters.

In what follows, conventional matrix notation is strictly employed as in $\mathbf{A} = [a_{ij}]$ wherein the scalar subscripts always denote the row and column indices, respectively, and all matrix entities defined here are denoted by boldface notation. Section 3 of this handbook, "Mathematics," provides an especially convenient reference for introductory matrix algebra and matrix computations.

General Matrix Formulation The zone method is perhaps the simplest numerical quadrature of the governing integral equations for radiative transfer. It may be derived from first principles by starting with the equation of transfer for radiation intensity. The zone method always conserves radiant energy since the spatial discretization utilizes macroscopic energy balances involving spatially averaged radiative flux quantities. Because large sets of linear algebraic equations can arise in this process, matrix algebra provides the most compact notation and the most expeditious methods of solution. The mathematical approach presented here is a matrix generalization of the original (scalar) development of the zone method due to Hottel and Sarofim (op. cit.). The present matrix development is abstracted from that introduced by Noble [Noble, J. J., Int. J. Heat Mass Transfer, 18, 261–269 (1975)].

Consider an arbitrary three-dimensional enclosure of total volume V and surface area A which confines an absorbing-emitting medium (gas). Let the enclosure be subdivided (zoned) into M finite surface area and N finite volume elements, each small enough that all such zones are substantially isothermal. The mathematical development in this section is restricted by the following conditions and/or assumptions:

1. The gas temperatures are given a priori.
2. Allowance is made for gas-to-surface radiative transfer.
3. Radiative transfer with respect to the confined gas is either monochromatic or gray. The gray gas absorption coefficient is denoted here by $K(m^{-1})$. In subsequent sections the monochromatic absorption coefficient is denoted by $K_r(\lambda)$.
4. All surface emissivities are assumed to be gray and thus independent of temperature.
5. Surface emission and reflection are isotropic or diffuse.
6. The gas does not scatter.

Noble (op. cit.) has extended the present matrix methodology to the case where the gaseous absorbing-emitting medium also scatters isotropically.

In matrix notation the blackbody emissive powers for all surface and volume zones comprising the zoned enclosure are designated as $\mathbf{E} = [E_i] = [\sigma T_i^4]$, an $M \times 1$ vector, and $\mathbf{E}_g = [E_{g,i}] = [\sigma T_{g,i}^4]$, an $N \times 1$ vector, respectively. Moreover, all surface zones are characterized by three $M \times M$ diagonal matrices for zone area $\mathbf{AI} = [A_i \delta_{ij}]$, diffuse emissivity $\mathbf{eI} = [e_i \delta_{ij}]$, and diffuse reflectivity, $\rho\mathbf{I} = [(1 - e_i) \delta_{ij}]$, respectively. Here δ_{ij} is the **Kronecker delta** (that is, $\delta_{ij} = 1$ for $i = j$ and $\delta_{ij} = 0$ for $i \neq j$).

Two arrays of direct exchange areas are now defined; i.e., the matrix $\mathbf{ss} = [s_{ij}]$ is the $M \times M$ array of **direct surface-to-surface exchange areas**, and the matrix $\mathbf{sg} = [s_{ij}^g]$ is the $M \times N$ array of **direct gas-to-surface exchange areas**. Here the scalar elements of \mathbf{ss} and \mathbf{sg} are computed from the integrals

$$s_{ij} = \iint_{A_i} \iint_{A_j} \frac{e^{-Kr}}{\pi r^2} \cos \phi_i \cos \phi_j dA_i dA_j \tag{5-116a}$$

$$\overline{s_i g_j} = \iint_{A_i} \iint_{A_j} K \frac{e^{-Kr}}{\pi r^2} \cos \phi_i dV_j dA_i \quad (5-116b)$$

Equation (5-116a) is a generalization of Eq. (5-112) for the case $K \neq 0$ while $\overline{s_i g_j}$ is a new quantity, which arises *only* for the case $K \neq 0$.

Matrix characterization of the radiative energy balance at each surface zone is facilitated via definition of three $M \times 1$ vectors; the radiative surface fluxes $\mathbf{Q} = [Q_i]$, with units of watts; and the vectors $\mathbf{H} = [H_i]$ and $\mathbf{W} = [W_i]$ both having units of W/m^2 . The arrays \mathbf{H} and \mathbf{W} define the *incident* and *leaving* flux densities, respectively, at each surface zone. The variable \mathbf{W} is also referred to in the literature as the **radiosity** or **exitance**. Since $\mathbf{W} \equiv \epsilon \mathbf{I} \cdot \mathbf{E} + \rho \mathbf{I} \cdot \mathbf{H}$, the radiative flux at each surface zone is also defined in terms of \mathbf{E} , \mathbf{H} , and \mathbf{W} by three equivalent matrix relations, namely,

$$\mathbf{Q} = \mathbf{AI} \cdot [\mathbf{W} - \mathbf{H}] = \epsilon \mathbf{AI} \cdot [\mathbf{E} - \mathbf{H}] = \rho \mathbf{I}^{-1} \cdot \epsilon \mathbf{AI} \cdot [\mathbf{E} - \mathbf{W}] \quad (5-117)$$

where the third form is valid *if and only if the matrix inverse* $\rho \mathbf{I}^{-1}$ *exists*. Two other ancillary matrix expressions are

$$\epsilon \mathbf{AI} \cdot \mathbf{E} = \rho \mathbf{I} \cdot \mathbf{Q} + \epsilon \mathbf{AI} \cdot \mathbf{W} \quad \text{and} \quad \mathbf{AI} \cdot \mathbf{H} = \overline{\mathbf{SS}} \cdot \mathbf{W} + \overline{\mathbf{SG}} \cdot \mathbf{E}_g \quad (5-117a,b)$$

which lead to

$$\epsilon \mathbf{I} \cdot \mathbf{E} = [\mathbf{I} - \rho \mathbf{I} \cdot \mathbf{AI}^{-1} \cdot \overline{\mathbf{SS}}] \cdot \mathbf{W} - \rho \mathbf{I} \cdot \mathbf{AI}^{-1} \cdot \overline{\mathbf{SG}} \cdot \mathbf{E}_g \quad (5-117c)$$

The latter relation is especially useful in radiation pyrometry where true wall temperatures must be computed from wall radiositivities.

Explicit Matrix Solution for Total Exchange Areas For gray or monochromatic transfer, the **primary working relation** for zoning calculations via the matrix method is

$$\mathbf{Q} = \epsilon \mathbf{I} \cdot \mathbf{AI} \cdot \mathbf{E} - \overline{\mathbf{SS}} \cdot \mathbf{E} - \overline{\mathbf{SG}} \cdot \mathbf{E}_g \quad [M \times 1] \quad (5-118)$$

Equation (5-118) makes full allowance for multiple reflections in an enclosure of any degree of complexity. To apply Eq. (5-118) for design or simulation purposes, the gas temperatures must be known and surface boundary conditions must be specified for each and every surface zone in the form of *either* E_i or Q_i . In application of Eq. (5-118), *physically impossible values* of E_i may well result if *physically unrealistic values* of Q_i are specified.

In Eq. (5-118), $\overline{\mathbf{SS}}$ and $\overline{\mathbf{SG}}$ are defined as the *required* arrays of **total surface-to-surface exchange areas** and **total gas-to-surface exchange areas**, respectively. The matrices for total exchange areas are calculated *explicitly* from the corresponding arrays of direct exchange areas and the other enclosure parameters by the following matrix formulas:

$$\text{Surface-to-surface exchange} \quad \overline{\mathbf{SS}} = \epsilon \mathbf{I} \cdot \mathbf{AI} \cdot \mathbf{R} \cdot \overline{\mathbf{ss}} \cdot \epsilon \mathbf{I} \quad [M \times M] \quad (5-118a)$$

$$\text{Gas-to-surface exchange} \quad \overline{\mathbf{SG}} = \epsilon \mathbf{I} \cdot \mathbf{AI} \cdot \mathbf{R} \cdot \overline{\mathbf{sg}} \quad [M \times N] \quad (5-118b)$$

where in Eqs. (5-118), \mathbf{R} is the explicit **inverse reflectivity matrix**, defined as

$$\mathbf{R} = [\mathbf{AI} - \overline{\mathbf{ss}} \cdot \rho \mathbf{I}]^{-1} \quad [M \times M] \quad (5-118c)$$

While the \mathbf{R} matrix is generally not symmetric, the matrix product $\rho \mathbf{I} \cdot \mathbf{R}$ is *always* symmetric. This fact proves useful for error checking.

The most computationally significant aspect of the matrix method is that the inverse reflectivity matrix \mathbf{R} *always exists* for any physically meaningful enclosure problem. More precisely, \mathbf{R} always exists provided that $K \neq 0$. For a transparent medium, \mathbf{R} exists provided that there *formally* exists at least one surface zone A_i such that $\epsilon_i \neq 0$. An important computational corollary of this statement for *transparent media* is that the matrix $[\mathbf{AI} - \overline{\mathbf{ss}}]$ is *always singular* and demonstrates *matrix rank* $M - 1$ (Noble, op. cit.).

Finally, the four matrix arrays $\overline{\mathbf{ss}}$, $\overline{\mathbf{gs}}$, $\overline{\mathbf{SS}}$, and $\overline{\mathbf{SG}}$ of direct and total exchange areas must satisfy **matrix conservation relations**, i.e.,

$$\text{Direct exchange areas} \quad \mathbf{AI} \cdot \mathbf{I}_M = \overline{\mathbf{ss}} \cdot \mathbf{I}_M + \overline{\mathbf{sg}} \cdot \mathbf{I}_N \quad (5-119a)$$

$$\text{Total exchange areas} \quad \epsilon \mathbf{I} \cdot \mathbf{AI} \cdot \mathbf{I}_M = \overline{\mathbf{SS}} \cdot \mathbf{I}_M + \overline{\mathbf{SG}} \cdot \mathbf{I}_N \quad (5-119b)$$

Here \mathbf{I}_M is an $M \times 1$ column vector all of whose elements are unity. If $\epsilon \mathbf{I} = \mathbf{I}$ or equivalently, $\rho \mathbf{I} = \mathbf{0}$, Eq. (5-118c) reduces to $\mathbf{R} = \mathbf{AI}^{-1}$ with

the result that Eqs. (5-118a) and (5-118b) degenerate to simply $\overline{\mathbf{SS}} = \overline{\mathbf{ss}}$ and $\overline{\mathbf{SG}} = \overline{\mathbf{sg}}$. Further, while the array $\overline{\mathbf{SS}}$ is always symmetric, the array $\overline{\mathbf{SG}}$ is generally not square.

For purposes of digital computation, it is good practice to enter all data for direct exchange surface-to-surface areas $\overline{\mathbf{ss}}$ with a precision of *at least five significant figures*. This need arises because all the scalar elements of $\overline{\mathbf{sg}}$ can be calculated *arithmetically* from appropriate direct surface-to-surface exchange areas by using view factor algebra rather than via the definition of the defining integral, Eq. (5-116b). This process often involves small arithmetic differences between two numbers of nearly equal magnitude, and numerical significance is easily lost.

Computer implementation of the matrix method proves straightforward, given the availability of modern software applications. In particular, several especially user-friendly GUI mathematical utilities are available that perform matrix computations using *essentially algebraic notation*. Many simple zoning problems may be solved with spreadsheets. For large M and N , the matrix method can involve management of a large amount of data. Error checks based on symmetry and conservation by calculation of the row sums of the four arrays of direct and total exchange areas then prove indispensable.

Zone Methodology and Conventions For a transparent medium, no more than $\Sigma = M(M - 1)/2$ of the M^2 elements of the $\overline{\mathbf{ss}}$ array are *unique*. Further, surface zones are characterized into two generic types. **Source-sink zones** are defined as those for which temperature is specified and whose radiative flux Q_i is to be determined. For **flux zones**, conversely, these conditions are reversed. When both types of zones are present in an enclosure, Eq. (5-118) may be *partitioned* to produce a more efficient computational algorithm. Let $M = M_s + M_f$ represent the total number of surface zones where M_s is the number of source-sink zones and M_f is the number of flux zones. The flux zones are the *last to be numbered*. Equation (5-118) is then partitioned as follows:

$$\begin{bmatrix} \mathbf{Q}_1 \\ \mathbf{Q}_2 \end{bmatrix} = \begin{bmatrix} \epsilon \mathbf{AI}_{1,1} & \mathbf{0} \\ \mathbf{0} & \epsilon \mathbf{AI}_{2,2} \end{bmatrix} \cdot \begin{bmatrix} \mathbf{E}_1 \\ \mathbf{E}_2 \end{bmatrix} - \begin{bmatrix} \overline{\mathbf{SS}}_{1,1} & \overline{\mathbf{SS}}_{1,2} \\ \overline{\mathbf{SS}}_{2,1} & \overline{\mathbf{SS}}_{2,2} \end{bmatrix} \cdot \begin{bmatrix} \mathbf{E}_1 \\ \mathbf{E}_2 \end{bmatrix} - \begin{bmatrix} \overline{\mathbf{SG}}_1 \\ \overline{\mathbf{SG}}_2 \end{bmatrix} \cdot \mathbf{E}_g \quad (5-120)$$

Here the dimensions of the submatrices $\epsilon \mathbf{AI}_{1,1}$ and $\overline{\mathbf{SS}}_{1,1}$ are both $M_s \times M_s$ and $\overline{\mathbf{SG}}_1$ has dimensions $M_s \times N$. Partition algebra then yields the following two matrix equations for \mathbf{Q}_1 , the $M_s \times 1$ vector of unknown source-sink fluxes and \mathbf{E}_2 , the $M_f \times 1$ vector of unknown emissive powers for the flux zones, i.e.,

$$\mathbf{E}_2 = [\epsilon \mathbf{AI}_{2,2} - \overline{\mathbf{SS}}_{2,2}]^{-1} \cdot [\mathbf{Q}_2 + \overline{\mathbf{SS}}_{2,1} \cdot \mathbf{E}_1 + \overline{\mathbf{SG}}_2 \cdot \mathbf{E}_g] \quad (5-120a)$$

$$\mathbf{Q}_1 = \epsilon \mathbf{AI}_{1,1} \cdot \mathbf{E}_1 - \overline{\mathbf{SS}}_{1,1} \cdot \mathbf{E}_1 - \overline{\mathbf{SS}}_{1,2} \cdot \mathbf{E}_2 - \overline{\mathbf{SG}}_1 \cdot \mathbf{E}_g \quad (5-120b)$$

The inverse matrix in Eq. (5-120a) formally does not exist if there is at least one flux zone such that $\epsilon_i = 0$. However, well-behaved results are usually obtained with Eq. (5-120a) by utilizing a *notional zero*, say, $\epsilon_i \approx 10^{-5}$, to simulate $\epsilon_i = 0$. Computationally, \mathbf{E}_2 is first obtained from Eq. (5-120a) and then substituted into either Eq. (5-120b) or Eq. (5-118).

Surface zones need not be *contiguous*. For example, in a symmetric enclosure, zones on opposite sides of the plane of symmetry may be "lumped" into a single zone for computational purposes. Lumping nonsymmetrical zones is also possible as long as the zone temperatures and emissivities are equal.

An **adiabatic refractory surface** of area A_i and emissivity ϵ_r , for which $Q_r = 0$, proves quite important in practice. A nearly radiatively adiabatic refractory surface occurs when differences between internal conduction and convection and external heat losses through the refractory wall are small compared with the *magnitude* of the *incident* and *leaving* radiation fluxes. For *any* surface zone, the radiant flux is given by $Q = A(W - H) = \epsilon A(E - H)$ and $Q = \epsilon A/\rho(E - W)$ (if $\rho \neq 0$). These equations then lead to the result that if $Q_r = 0$, $E_r = H_r = W_r$, for all $0 \leq \epsilon_r \leq 1$. *Sufficient conditions* for modeling an adiabatic refractory zone are thus *either* to put $\epsilon_r = 0$ or to specify *directly* that $Q_r = 0$ with $\epsilon_r \neq 0$. If $\epsilon_r = 0$, $S_r S_j = 0$ for all $1 \leq j \leq M$ which leads *directly by definition* to $Q_r = 0$. For $\epsilon_r = 0$, the refractory emissive power E_r *never enters the zoning calculations*. For the special case of $K = 0$ and $M_r = 1$, a single (lumped) refractory, with $Q_r = 0$ and $\epsilon_r \neq 0$, $S_r S_j \neq 0$ and the refractory emissive power may be calculated from Eq. (5-120a) as a weighted sum of all *other known blackbody emissive powers* which

characterize the enclosure, i.e.,

$$E_r = \frac{\sum_{j=1}^{M_s} \overline{S_r S_j} E_j}{\sum_{j=1}^{M_s} \overline{S_r S_j}} \quad \text{with } j \neq r \quad (5-121)$$

Equation (5-121) specifically includes those zones which may not have a direct view of the refractory. When $Q_r = 0$, the refractory surface is said to be in **radiative equilibrium** with the entire enclosure. Equation (5-121) is indeterminate if $\epsilon_r = 0$. If $\epsilon_r = 0$, E_r does indeed exist and may be evaluated with use of the statement $E_r = H_r = W_r$. It transpires, however, that E_r is independent of ϵ_r for all $0 \leq \epsilon_r \leq 1$. Moreover, since $W_r = H_r$ when $Q_r = 0$, for all $0 \leq \epsilon_r \leq 1$, the value specified for ϵ_r is irrelevant to radiative transfer in the entire enclosure. In particular it follows that if $Q_r = 0$, then the vectors \mathbf{W} , \mathbf{H} , and \mathbf{Q} for the entire enclosure are also independent of all $0 \leq \epsilon_r \leq 1.0$. A surface zone for which $\epsilon_i = 0$ is termed a **perfect diffuse mirror**. A perfect diffuse mirror is thus also an adiabatic surface zone. The matrix method automatically deals with all options for flux and adiabatic refractory surfaces.

The Limiting Case of a Transparent Medium For the special case of a transparent medium, $K = 0$, many practical engineering applications can be modeled with the zone method. These include combustion-fired muffle furnaces and electrical resistance furnaces. When $K \rightarrow 0$, $\overline{\mathbf{sg}} \rightarrow \mathbf{0}$ and $\overline{\mathbf{SC}} \rightarrow \mathbf{0}$. Equations (5-118) through (5-119) then reduce to three simple matrix relations

$$\mathbf{Q} = \epsilon \mathbf{I} \mathbf{A} \mathbf{I} \mathbf{E} - \overline{\mathbf{SS}} \mathbf{E} \quad (5-122a)$$

$$\overline{\mathbf{SS}} = \epsilon \mathbf{I} \mathbf{A} \mathbf{I} \mathbf{R} \overline{\mathbf{SS}} \epsilon \mathbf{I} \quad (5-122b)$$

with again

$$\mathbf{R} \equiv [\mathbf{A} \mathbf{I} - \overline{\mathbf{SS}} \rho \mathbf{I}]^{-1} \quad (5-122c)$$

The radiant surface flux vector \mathbf{Q} , as computed from Eq. (5-122a), always satisfies the (scalar) conservation condition $\mathbf{1}_M^T \mathbf{Q} = \mathbf{0}$ or $\sum_{i=1}^M Q_i = 0$, which is a statement of the overall radiant energy balance.

The matrix conservation relations also simplify to

$$\mathbf{A} \mathbf{I} \mathbf{1}_M = \overline{\mathbf{SS}} \mathbf{1}_M \quad (5-123a)$$

$$\epsilon \mathbf{I} \mathbf{A} \mathbf{I} \mathbf{1}_M = \overline{\mathbf{SS}} \mathbf{1}_M \quad (5-123b)$$

And the $M \times M$ arrays for all the direct and total view factors can be readily computed from

$$\mathbf{F} = \mathbf{A} \mathbf{I}^{-1} \overline{\mathbf{SS}} \quad (5-124a)$$

and

$$\mathcal{F} = \mathbf{A} \mathbf{I}^{-1} \overline{\mathbf{SS}} \quad (5-124b)$$

where the following matrix conservation relations must also be satisfied,

$$\mathbf{F} \mathbf{1}_M = \mathbf{1}_M \quad (5-125a)$$

and

$$\mathcal{F} \mathbf{1}_M = \epsilon \mathbf{I} \mathbf{1}_M \quad (5-125b)$$

The Two-Zone Enclosure Figure 5-18 depicts four simple enclosure geometries which are particularly useful for engineering calculations characterized by only two surface zones. For $M = 2$, the reflectivity matrix \mathbf{R} is readily evaluated in closed form since an explicit algebraic inversion formula is available for a 2×2 matrix. In this case knowledge of only $\Sigma = 1$ direct exchange area is required. Direct evaluation of Eqs. (5-122) then leads to

$$\overline{\mathbf{SS}} = \begin{bmatrix} \epsilon_1 A_1 - S_1 S_2 & S_1 S_2 \\ S_1 S_2 & \epsilon_2 A_2 - S_1 S_2 \end{bmatrix} \quad (5-126)$$

where

$$\overline{S_1 S_2} = \frac{1}{\left(\frac{1}{s_1 s_2} + \frac{\rho_1}{\epsilon_1 A_1} + \frac{\rho_2}{\epsilon_2 A_2} \right)} \quad (5-127)$$

Equation (5-127) is of general utility for any two-zone system for which $\epsilon_i \neq 0$.

The total exchange areas for the four geometries shown in Fig. 5-18 follow directly from Eqs. (5-126) and (5-127).

1. A planar surface A_1 completely surrounded by a second surface $A_2 > A_1$. Here $F_{1,1} = 0$, $F_{1,2} = 1$, and $\overline{S_1 S_2} = A_1$, resulting in

$$\overline{\mathbf{SS}} = \begin{bmatrix} \epsilon_1 \rho_2 A_1^2 + \epsilon_2 \rho_1 A_1 A_2 & \epsilon_1 \epsilon_2 A_1 A_2 \\ \epsilon_1 \epsilon_2 A_1 A_2 & \epsilon_2 A_2^2 + \epsilon_1 (\rho_2 - \epsilon_2) A_1 A_2 \end{bmatrix} / [\epsilon_1 \rho_2 A_1 + \epsilon_2 A_2]$$

and in particular $\overline{S_1 S_2} = \frac{A_1}{1/\epsilon_1 + (A_1/A_2)(\rho_2/\epsilon_2)}$ (5-127a)

In the limiting case, where A_1 has no negative curvature and is completely surrounded by a very much larger surface A_2 such that $A_1 \ll A_2$, Eq. (5-127a) leads to the even simpler result that $\overline{S_1 S_2} = \epsilon_1 A_1$.

2. Two parallel plates of equal area which are large compared to their distance of separation (infinite parallel plates). Case 2 is a limiting form of case 1 with $A_1 = A_2$. Algebraic manipulation then results in

$$\overline{\mathbf{SS}} = \begin{bmatrix} (\epsilon_1 + \epsilon_2 - 2\epsilon_1 \epsilon_2) A_1 & \epsilon_1 \epsilon_2 A_1 \\ \epsilon_1 \epsilon_2 A_1 & (\epsilon_1 + \epsilon_2 - 2\epsilon_1 \epsilon_2) A_1 \end{bmatrix} / [\epsilon_1 + \epsilon_2 - \epsilon_1 \epsilon_2]$$

and in particular

$$\overline{S_1 S_2} = \frac{A_1}{1/\epsilon_1 + 1/\epsilon_2 - 1} \quad (5-127b)$$

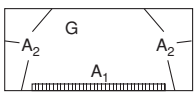

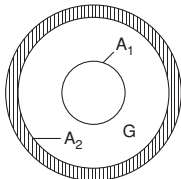
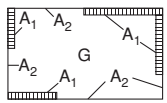
Case 1	Case 2	Case 3	Case 4
			
A planar surface A_1 completely surrounded by a second surface $A_2 > A_1$.	Two infinite parallel plates where $A_1 = A_2$.	Concentric spheres or infinite cylinders where $A_1 < A_2$. Identical to Case 1.	A speckled enclosure with two surface zones.
$\mathbf{F} = \begin{bmatrix} 0 & 1 \\ A_1/A_2 & 1 - A_1/A_2 \end{bmatrix}$	$\mathbf{F} = \begin{bmatrix} 0 & 1 \\ 1 & 0 \end{bmatrix}$	$\mathbf{F} = \begin{bmatrix} 0 & 1 \\ A_1/A_2 & 1 - A_1/A_2 \end{bmatrix}$	$\mathbf{F} = \frac{1}{(A_1 + A_2)} \begin{bmatrix} A_1 & A_2 \\ A_1 & A_2 \end{bmatrix}$

FIG. 5-18 Four enclosure geometries characterized by two surface zones and one volume zone. (Marks' Standard Handbook for Mechanical Engineers, McGraw-Hill, New York, 1999, p. 4-73, Table 4.3.5.)

3. Concentric spheres or cylinders where $A_2 > A_1$. Case 3 is mathematically identical to case 1.

4. A **speckled enclosure** with two surface zones. Here $\mathbf{F} = \frac{1}{A_1 + A_2} \begin{bmatrix} A_1 & A_2 \\ A_1 & A_2 \end{bmatrix}$ such that $\overline{\mathbf{SS}} = \frac{1}{A_1 + A_2} \begin{bmatrix} A_1^2 & A_1 A_2 \\ A_1 A_2 & A_2^2 \end{bmatrix}$ and Eqs.

(5-126) and (5-127) then produce

$$\overline{\mathbf{SS}} = \begin{bmatrix} \epsilon_1^2 A_1^2 & \epsilon_1 \epsilon_2 A_1 A_2 \\ \epsilon_1 \epsilon_2 A_1 A_2 & \epsilon_2^2 A_2^2 \end{bmatrix} / (\epsilon_1 A_1 + \epsilon_2 A_2)$$

with the particular result

$$\overline{S_1 S_2} = \frac{1}{1/(\epsilon_1 A_1) + 1/(\epsilon_2 A_2)} \quad (5-127c)$$

Physically, a two-zone speckled enclosure is characterized by the fact that the view factor from any point on the enclosure surface to the sink zone is identical to that from any other point on the bounding surface. This is only possible when the two zones are "intimately mixed." The seemingly simplistic concept of a speckled enclosure provides a surprisingly useful *default option* in engineering calculations when the *actual* enclosure geometries are quite complex.

Multizone Enclosures [$M \geq 3$] Again assume $K = 0$. The major numerical effort involved in implementation of the zone method is the evaluation of the inverse reflection matrix \mathbf{R} . For $M = 3$, explicit closed-form algebraic formulas *do indeed exist* for the nine scalar elements of the inverse of any arbitrary nonsingular matrix. These formulas are so algebraically complex, however, that it proves impractical to present universal closed-form expressions for the total exchange areas, as has been done for the case $M = 2$. Fortunately, many practical furnace configurations can be idealized with zoning such that only relatively simple *hand calculation procedures are required*. Here the enclosure is modeled with only $M = 3$ surface zones, e.g., a single source, a single sink, and a lumped adiabatic refractory zone. This approach is sometimes termed the **SSR model**. The SSR model assumes that all adiabatic refractory surfaces are *perfect diffuse mirrors*. To implement the SSR procedure, it is necessary to develop *specialized algebraic formulas* and to define a *third black view factor* F_{ij} with an *overbar* as follows.

Refractory Augmented Black View Factors \overline{F}_{ij} Let $M = M_r + M_b$, where M_b is the number of black surface zones and M_r is the number of adiabatic refractory zones. Assume $\epsilon_r = 0$ or $\rho_r = 1$ or, equivalently, that all adiabatic refractory surfaces are *perfect diffuse mirrors*. The view factor \overline{F}_{ij} is then defined as the **refractory augmented black view factor**, i.e., the direct view factor between *any two* black source-sink zones, A_i and A_j , with *full allowance for reflections from all intervening refractory surfaces*. The quantity \overline{F}_{ij} shall be referred to as **F-bar**, for expediency.

Consider the special situation where $M_b = 2$, with any number of refractory zones $M_r \geq 1$. By use of appropriate row and column reduction of the reflectivity matrix \mathbf{R} , an especially useful relation can be derived that allows computation of the conventional total exchange area $S_i S_j$ from the *corresponding refractory augmented black view factor* \overline{F}_{ij}

$$\overline{S_1 S_2} = \frac{1}{\left(\frac{\rho_1}{\epsilon_1 A_1} + \frac{\rho_2}{\epsilon_2 A_2} + \frac{1}{A_1 \overline{F}_{1,2}} \right)} \quad (5-128a)$$

or

$$\overline{F}_{1,2} = \frac{1}{\left(\frac{\rho_1}{\epsilon_1} + \left(\frac{A_1}{A_2} \right) \cdot \frac{\rho_2}{\epsilon_2} + \frac{1}{\overline{F}_{1,2}} \right)} \quad (5-128b)$$

where $\epsilon_i \neq 0$. Notice that Eq. (5-128a) appears *deceptively similar* to Eq. (5-127). Collectively, Eqs. (5-128) along with various formulas to compute \overline{F}_{ij} (*F-bar*) are sometimes called the three-zone source/sink/refractory **SSR model**.

The following formulas permit the calculation of \overline{F}_{ij} from requisite *direct* exchange areas. For the special case where the enclosure is divided into *any number of* black source-sink zones, $M_b \geq 2$, and the remainder of the enclosure is lumped together into a single refractory

zone ($M_r = 1$) with total area A_r and uniform average temperature T_r , then the direct refractory augmented exchange area for the black zone pairs is given by

$$A_i \overline{F}_{ij} = A_j \overline{F}_{ji} = \overline{s_i s_j} + \frac{\overline{s_i s_r} \overline{s_r s_j}}{A_r - \overline{s_r s_r}} \quad \text{for } 1 \leq i, j \leq M_b \quad (5-129)$$

For the special case $M_b = 2$ and $M_r = 1$, Eq. (5-129) then simplifies to

$$A_1 \overline{F}_{1,2} = A_2 \overline{F}_{2,1} = \overline{s_1 s_2} + \frac{1}{1/\overline{s_1 s_r} + 1/\overline{s_2 s_r}} \quad (5-130)$$

and if $\overline{s_1 s_r} = \overline{s_2 s_r} = 0$, Eq. (5-130) further reduces to

$$A_1 \overline{F}_{1,2} = \overline{s_1 s_2} + \frac{1}{1/(A_1 - \overline{s_1 s_2}) + 1/(A_2 - \overline{s_2 s_1})} = \frac{A_1 A_2 - (\overline{s_1 s_2})^2}{A_1 + A_2 - 2\overline{s_1 s_2}} \quad (5-131)$$

which necessitates the evaluation of only one direct exchange area. Let the M_r refractory zones be numbered *last*. Then the $M_b \times M_b$ array of refractory augmented direct exchange areas $[A_i \overline{F}_{ij}]$ is symmetric and satisfies and the conservation relation

$$[A_i \overline{F}_{ij}] \cdot \mathbf{1}_{M_b} = \mathbf{A} \cdot \mathbf{1}_{M_b} \quad (5-132a)$$

with

$$\overline{\mathbf{F}} \cdot \mathbf{1}_{M_b} = \mathbf{1}_{M_b} \quad (5-132b)$$

Temporarily denote $\overline{S_1 S_2}_R$ as the value of $\overline{S_1 S_2}$ computed from Eq. (5-128a) which assumes $\epsilon_r = 0$. It remains to demonstrate the relationship between $\overline{S_1 S_2}_R$ and the total exchange area $S_1 S_2$ computed from the matrix method for $M = 3$ when zone 3 is an adiabatic refractory for which $Q_3 = 0$ and $\epsilon_3 \neq 0$. Let $\Theta_i = (E_i - E_2)/(E_1 - E_2)$ denote the dimensionless emissive power where $E_1 > E_2$ such that $\Theta_1 = 1$ and $\Theta_2 = 0$. The dimensionless refractory emissive power may then be calculated from Eq. (5-121) as $\Theta_3 = S_3 S_1 / [S_3 S_1 + S_3 S_2]$, which when substituted into Eq. (5-122a) leads to $S_1 S_2}_R = \overline{S_1 S_2} + \overline{S_2 S_3} \Theta_3 = \overline{S_1 S_2} + \overline{S_1 S_3} \cdot S_3 S_2 / [S_3 S_1 + S_3 S_2]$. Thus $\overline{S_1 S_2}_R$ is clearly the *refractory-aided* total exchange area between zone 1 and zone 2 and *not* $\overline{S_1 S_2}$ as calculated by the matrix method in general. That is, $\overline{S_1 S_2}_R$ includes not only the radiant energy originating at zone 1 and arriving at zone 2 directly and by reflection from zones 2 and 3, but also radiation originating at zone 1 that is *absorbed* by zone 3 and then wholly reemitted to zone 2; that is, $H_3 = W_3 = E_3$.

Evaluation of any total view factor \mathcal{F}_{ij} using the requisite refractory augmented black view factor \overline{F}_{ij} obviously requires that the latter be readily available and/or capable of calculation. The refractory augmented view factor \overline{F}_{ij} is documented for a few geometrically simple cases and can be calculated or approximated for others. If A_1 and A_2 are equal parallel disks, squares, or rectangles, connected by nonconducting but reradiating refractory surfaces, then \overline{F}_{ij} is given by Fig. 5-13 in curves 5 to 8. Let A_1 represent an infinite plane and A_2 represent one or two rows of infinite parallel tubes. If the only other surface is an adiabatic refractory surface located behind the tubes, $\overline{F}_{2,1}$ is then given by curve 5 or 6 of Fig. 5-15.

Experience has shown that the simple SSR model can yield quite useful results for a host of practical engineering applications without resorting to digital computation. The error due to representation of the source and sink by single zones is often small, even if the views of the enclosure from different parts of the same zone are dissimilar, provided the surface emissivities are near unity. The error is also small if the temperature variation of the refractory is small. Any degree of accuracy can, of course, be obtained via the matrix method for arbitrarily large M and N by using a digital computer. From a computational viewpoint, when $M \geq 4$, the matrix method *must be used*. The matrix method must also be used for finer-scale calculations such as more detailed wall temperature and flux density profiles.

The Electrical Network Analog At each surface zone the *total* radiant flux is proportional to the difference between E_i and W_i , as indicated by the equation $Q_i = (\epsilon_i A_i \rho_i)(E_i - W_i)$. The *net* flux between zones i and j is also given by $Q_{ij} = s_i s_j (W_i - W_j)$, where $Q_i = \sum_{j=1}^M Q_{ij}$, for all $1 \leq i \leq M$, is the *total* heat flux leaving each zone. These relations

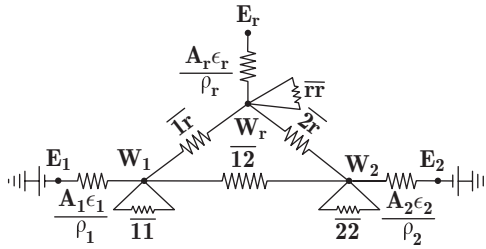


FIG. 5-19 Generalized electrical network analog for a three-zone enclosure. Here A_1 and A_2 are gray surfaces and A_r is a radiatively adiabatic surface. (Hottel, H. C., and A. F. Sarofim, Radiative Transfer, McGraw-Hill, New York, 1967, p. 91.)

suggest a *visual* electrical analog in which E_i and W_i are analogous to voltage potentials. The quantities $\epsilon_r A_r / \rho_r$ and $s_i s_j$ are analogous to conductances (reciprocal impedances), and Q_i or Q_{ij} is analogous to electric currents. Such an electrical analog has been developed by Oppenheim [Oppenheim, A. K., *Trans. ASME*, **78**, 725–735 (1956)].

Figure 5-19 illustrates a generalized electrical network analog for a three-zone enclosure consisting of one refractory zone and two gray zones A_1 and A_2 . The potential points E_i and W_i are separated by conductances $\epsilon_r A_r / \rho_r$. The emissive powers E_1 , E_2 represent potential sources or sinks, while W_1 , W_2 , and W_r are internal node points. In this construction the nodal point representing each surface is connected to that of every other surface it can see *directly*. Figure 5-19 can be used to formulate the total exchange area $S_1 S_2$ for the SSR model virtually by inspection. The refractory zone is first characterized by a floating potential such that $E_r = W_r$. Next, the resistance for the parallel “current paths” between the internal nodes W_1 and W_2 is defined by $\frac{1}{A_1 F_{1,2}} \equiv \frac{1}{s_1 s_2 + 1/(1/s_1 s_r + 1/s_2 s_r)}$ which is identical to Eq. (5-130).

Finally, the overall impedance between the source E_1 and the sink E_2 is represented simply by three resistors in series and is thus given by

$$\frac{1}{S_1 S_2} = \frac{\rho_1}{\epsilon_1 A_1} + \frac{1}{A_1 F_{1,2}} + \frac{\rho_2}{\epsilon_2 A_2}$$

or

$$\frac{1}{S_1 S_2} = \frac{1}{\frac{\rho_1}{\epsilon_1 A_1} + \frac{\rho_2}{\epsilon_2 A_2} + \frac{1}{A_1 F_{1,2}}} \quad (5-133)$$

This result is identically that for the SSR model as obtained previously in Eq. (5-128a). This equation is also valid for $M_r \geq 1$ as long as $M_b = 2$. The electrical network analog methodology can be generalized for enclosures having $M > 3$.

Some Examples from Furnace Design The theory of the past several subsections is best understood in the context of two engineering examples involving furnace modeling. The engineering idealization of the **equivalent gray plane concept** is introduced first. Figure 5-20 depicts a common furnace configuration in which the

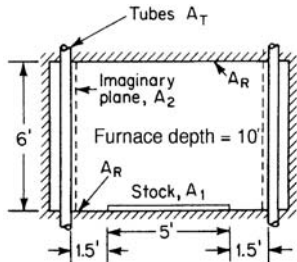


FIG. 5-20 Furnace chamber cross section. To convert feet to meters, multiply by 0.3048.

heating source is two refractory-backed, internally fired tube banks. Clearly the overall geometry for even this common furnace configuration is too complex to be modeled in an expeditious manner by anything other than a *simple engineering idealization*. Thus the furnace shown in Fig. 5-20 is modeled in Example 10, by *partitioning* the entire enclosure into two subordinate furnace compartments. The approach first defines an imaginary gray plane A_2 , located on the inward-facing side of the tube assemblies. Second, the total exchange area between the tubes to this *equivalent* gray plane is calculated, making full allowance for the reflection from the refractory tube backing. The plane-to-tube view factor is then *defined* to be the emissivity of the required equivalent gray plane whose temperature is further assumed to be that of the tubes. This procedure guarantees continuity of the radiant flux *into* the interior radiant portion of the furnace arising from a moderately complicated *external* source.

Example 9 demonstrates classical zoning calculations for radiation pyrometry in furnace applications. Example 10 is a classical furnace design calculation via zoning an enclosure with a *diathermanous* atmosphere and $M = 4$. The latter calculation can only be addressed with the matrix method. The results of Example 10 demonstrate the relative insensitivity of zoning to $M > 3$ and the engineering utility of the SSR model.

Example 9: Radiation Pyrometry A long tunnel furnace is heated by electrical resistance coils embedded in the ceiling. The stock travels on a floor-mounted conveyor belt and has an estimated emissivity of 0.7. The sidewalls are unheated refractories with emissivity 0.55, and the ceiling emissivity is 0.8. The furnace cross section is rectangular with height 1 m and width 2 m. A total radiation pyrometer is sighted on the walls and indicates the following apparent temperatures: ceiling, 1340°C; sidewall readings average about 1145°C; and the load indicates about 900°C. (a) What are the true temperatures of the furnace walls and stock? (b) What is the net heat flux at each surface? (c) How do the matrix method and SSR models compare?

Three-zone model, $M = 3$:

Zone 1: Source (top)

Zone 2: Sink (bottom)

Zone 3: Refractory (lumped sides)

Physical constants:

$$T_0 \equiv 273.15 \text{ K} \quad \sigma \equiv 5.670400 \times 10^{-8} \frac{\text{W}}{\text{m}^2 \cdot \text{K}^4}$$

Enclosure input parameters:

$$H_c := 1 \text{ m} \quad W_c := 2 \text{ m} \quad L_c := 1 \text{ m} \quad A_1 := W_c L_c \quad A_2 := A_1 \quad A_3 := 2H_c L_c$$

$$\epsilon_1 := .8 \quad \epsilon_2 := .7 \quad \epsilon_3 := .55 \quad \rho_1 := 1 - \epsilon_1 \quad \rho_2 := 1 - \epsilon_2 \quad \rho_3 := 1 - \epsilon_3$$

$$\mathbf{AI} := \begin{bmatrix} A_1 & 0 & 0 \\ 0 & A_2 & 0 \\ 0 & 0 & A_3 \end{bmatrix} \quad \mathbf{eI} := \begin{bmatrix} \epsilon_1 & 0 & 0 \\ 0 & \epsilon_2 & 0 \\ 0 & 0 & \epsilon_3 \end{bmatrix} \quad \mathbf{\rho I} := \begin{bmatrix} \rho_1 & 0 & 0 \\ 0 & \rho_2 & 0 \\ 0 & 0 & \rho_3 \end{bmatrix}$$

$$\mathbf{AI} := \begin{bmatrix} 2 & 0 & 0 \\ 0 & 2 & 0 \\ 0 & 0 & 2 \end{bmatrix} \text{m}^2 \quad \mathbf{eI} := \begin{bmatrix} 0.8 & 0 & 0 \\ 0 & 0.7 & 0 \\ 0 & 0 & 0.55 \end{bmatrix} \quad \mathbf{\rho I} := \begin{bmatrix} 0.2 & 0 & 0 \\ 0 & 0.3 & 0 \\ 0 & 0 & 0.45 \end{bmatrix}$$

Compute direct exchange areas by using crossed strings ($\Sigma = 3$):

$$ss_{11} := 0 \quad ss_{22} := 0 \quad ss_{33} := 2(\sqrt{H_c^2 + W_c^2} - W_c)L_c \quad ss_{33} := 0.4721 \text{ m}^2$$

From symmetry and conservation, there are three linear simultaneous results for the off-diagonal elements of \mathbf{ss} :

$$\begin{bmatrix} 12 \\ 13 \\ 23 \end{bmatrix} = \begin{bmatrix} 1 & 1 & 0 \\ 1 & 0 & 1 \\ 0 & 1 & 1 \end{bmatrix}^{-1} \begin{bmatrix} A_1 - 11 \\ A_2 - 22 \\ A_3 - 33 \end{bmatrix} = \frac{1}{2} \begin{bmatrix} 1 & 1 & -1 \\ 1 & -1 & 1 \\ -1 & 1 & 1 \end{bmatrix}$$

$$\times \begin{bmatrix} A_1 - 11 \\ A_2 - 22 \\ A_3 - 33 \end{bmatrix} = \frac{1}{2} \begin{bmatrix} +A_1 + A_2 - A_3 - 11 - 22 + 33 \\ +A_1 - A_2 + A_3 - 11 + 22 - 33 \\ -A_1 + A_2 + A_3 + 11 - 22 - 33 \end{bmatrix}$$

Thus

$$ss_{12} := 0.5 (A_1 + A_2 - A_3 + ss_{33})$$

$$ss_{13} := 0.5 (A_1 - A_2 + A_3 - ss_{33}) \quad ss_{23} := 0.5 (-A_1 + A_2 + A_3 - ss_{33})$$

$$\mathbf{ss} := \begin{bmatrix} ss_{11} & ss_{12} & ss_{13} \\ ss_{12} & ss_{22} & ss_{23} \\ ss_{13} & ss_{23} & ss_{33} \end{bmatrix} \quad \mathbf{ss} := \begin{bmatrix} 0 & 1.2361 & 0.7639 \\ 1.2361 & 0 & 0.7639 \\ 0.7639 & 0.7639 & 0.4721 \end{bmatrix} \text{m}^2 \quad (\mathbf{AI} - \mathbf{ss}) \begin{bmatrix} 1 \\ 1 \\ 1 \end{bmatrix} = \begin{bmatrix} 0 \\ 0 \\ 0 \end{bmatrix} \text{m}^2$$

Compute radiosities W from pyrometer temperature readings:

$$\mathbf{T}_{wc} := \begin{bmatrix} 1340.0 \\ 900.0 \\ 1145.0 \end{bmatrix} C \quad \mathbf{W} := \sigma \left(\mathbf{T}_{wc} \frac{K}{C} + T_0 \right)^4 \quad \mathbf{W} := \begin{bmatrix} 384.0 \\ 107.4 \\ 229.4 \end{bmatrix} \frac{kW}{m^2}$$

Matrix wall flux density relations and heat flux calculations based on W:

$$\mathbf{H} := \mathbf{AI}^{-1}\mathbf{ss}\mathbf{W} \quad \mathbf{Q} := \mathbf{AI}(\mathbf{W} - \mathbf{H}) \quad \mathbf{E} := (\mathbf{eI} - \mathbf{AI})^{-1} \cdot \mathbf{Q} + \mathbf{H}$$

$$\mathbf{H} := \begin{bmatrix} 154.0 \\ 324.9 \\ 241.8 \end{bmatrix} \frac{kW}{m^2} \quad \mathbf{Q} := \begin{bmatrix} 460.0 \\ -435.0 \\ -25.0 \end{bmatrix} kW \quad \mathbf{E} := \begin{bmatrix} 441.5 \\ 14.2 \\ 219.1 \end{bmatrix} \frac{kW}{m^2}$$

The sidewalls act as near-adiabatic surfaces since the heat loss through each sidewall is only about 2.7 percent of the total heat flux originating at the source.

Actual temperatures versus pyrometer readings:

$$\mathbf{T} := \left[\left(\frac{E}{\sigma} \right)^{0.25} - T_0 \right] \frac{C}{K} \quad \mathbf{T} = \begin{bmatrix} 1397.3 \\ 434.1 \\ 1128.9 \end{bmatrix} C \quad \text{versus} \quad \mathbf{T}_{wc} = \begin{bmatrix} 1340.0 \\ 900.0 \\ 1145.0 \end{bmatrix} C$$

Compare SSR model versus matrix method [use Eqs. (5-128a) and (5-130)]: From Eq. (5-130)

$$ssbar_{12} := ss_{1,2} + \frac{1}{\frac{1}{ss_{1,3}} + \frac{1}{ss_{2,3}}} \quad ssbar_{12} = 1.6180 m^2$$

And from Eq. (5-128a)

$$SSR_{12} := \frac{1}{\frac{\rho_1}{\epsilon_1 A_1} + \frac{\rho_2}{\epsilon_2 A_2} + \frac{1}{ssbar_{12}}} \quad SSR_{12} = 1.0446 m^2$$

With the numerical result $Q_{12} := SSR_{12}(E_1 - E_2) \quad Q_{12} = 446.3 kW$

Thus the SSR model produces $Q_{12} = 446.3 kW$ versus the measured value $Q_1 = 460.0 kW$ or a discrepancy of about 3.0 percent. Mathematically the SSR model assumes a value of $\epsilon_3 = 0.0$, which precludes the sidewall heat loss of $Q_3 = -25.0 kW$. This assumption accounts for all of the difference between the two values. It remains to compare SSR_{12} and $SS_{1,2}$ computed by the matrix method.

Compute total exchange areas ($\epsilon_3 = 0.55$):

$$\mathbf{R} := (\mathbf{AI} - \overline{ss} \cdot \mathbf{\rho I})^{-1}$$

$$\overline{SS} := \mathbf{eI} - \mathbf{AI} - \mathbf{R} \cdot \overline{ss} \cdot \mathbf{eI} \quad \overline{SS} = \begin{bmatrix} 0.2948 & 0.8284 & 0.4769 \\ 0.8284 & 0.1761 & 0.3955 \\ 0.4769 & 0.3955 & 0.2277 \end{bmatrix} m^2 \quad (\mathbf{eI} - \mathbf{AI} - \overline{SS}) \begin{bmatrix} 1 \\ 1 \\ 1 \end{bmatrix} = \begin{bmatrix} 0 \\ 0 \\ 0 \end{bmatrix} m^2$$

Clearly SSR_{21} and $SS_{1,2}$ are unequal. But if

$$\Theta_3 := \frac{SS_{3,1}}{SS_{3,1} + SS_{3,2}}$$

define

$$SSA_{12} := SS_{1,2} + SS_{2,3} \cdot \Theta_3$$

and

$$\Theta_3 := 0.5466 \quad SSA_{12} = 1.0446 m^2 \quad E_r := E_2 + (E_1 - E_2) \cdot \Theta_3 \quad E_r = 247.8 \frac{kW}{m^2}$$

Numerically the matrix method predicts $SSA_{12} = 1.0446 m^2$ for $Q_3 = 0$ and $\epsilon_3 = 0.55$, which is identical to $SSR_{1,2}$ for the SSR model. Thus $SSR_{1,2} = SSA_{12}$ is the refractory-aided total exchange area between zone 1 and zone 2. The SSR model also predicts $E_r = 247.8 kW/m^2$ versus the experimental value $E_3 = 219.1 kW/m^2$ (1172.6C vs. 1128.9C), which is also a consequence of the actual 25.0-kW refractory heat loss.

(This example was developed as a MATHCAD 14® worksheet. Mathcad is a registered trademark of Parametric Technology Corporation.)

Example 10: Furnace Simulation via Zoning The furnace chamber depicted in Fig. 5-20 is heated by combustion gases passing through 20 vertical radiant tubes which are backed by refractory sidewalls. The tubes have an outside diameter of $D = 5$ in (12.7 cm) mounted on $C = 12$ in (4.72 cm) centers and a gray body emissivity of 0.8. The interior (radiant) portion of the furnace is a $6 \times 8 \times 10$ ft rectangular parallelepiped with a total surface area of $376 ft^2$ ($34.932 m^2$). A $50-ft^2$ ($4.645-m^2$) sink is positioned centrally on the floor of the furnace. The tube and sink temperatures are measured with embedded thermocouples as 1500 and 1200°F, respectively. The gray refractory emissivity may be taken as 0.5. While all other refractories are assumed to be radiatively adia-

batic, the roof of the furnace is estimated to lose heat to the surroundings with a flux density (W/m^2) equal to 5 percent of the source and sink emissive power difference. An estimate of the radiant flux arriving at the sink is required, as well as estimates for the roof and average refractory temperatures in consideration of refractory service life.

Part (a): Equivalent Gray Plane Emissivity Algebraically compute the equivalent gray plane emissivity for the refractory-backed tube bank idealized by the imaginary plane A_2 , depicted in Fig. 5-15.

Solution: Let zone 1 represent one tube and zone 2 represent the effective plane 2, that is, the unit cell for the tube bank. Thus $A_1 = \pi D$ and $A_2 = C$ are the corresponding zone areas, respectively (per unit vertical dimension). This notation is consistent with Example 3. Also put $\epsilon_1 = 0.8$ with $\epsilon_2 = 1.0$ and define $R = C/D = 12/5 = 2.4$. The gray plane effective emissivity is then calculated as the total view factor for the effective plane to tubes, that is, $\mathcal{F}_{2,1} \equiv \bar{\epsilon}_2$. For $R = 2.4$, Fig. 5-15, curve 5, yields the refractory augmented view factor $\bar{\mathcal{F}}_{2,1} \approx 0.81$. Then $\mathcal{F}_{2,1}$ is calculated from Eq. (5-128b) as $\mathcal{F}_{2,1} = \frac{1}{0/1 + (2.4/\pi) \cdot 0.2/0.8 + 1/0.81} \approx 0.702$.

A more accurate value is obtained via the matrix method as $\mathcal{F}_{2,1} = 0.70295$.

Part (b): Radiant Furnace Chamber with Heat Loss

Four-zone model, $M = 4$: Use matrix method.

Zone 1: Sink (floor)

Zone 2: Source (lumped sides)

Zone 3: Refractory (roof)

Zone 4: Refractory (ends and floor strips)

Physical constants:

$$T_0 \equiv 273.15 K \quad \sigma \equiv 5.6704 \times 10^{-8} \frac{W}{m^2 \cdot K^4}$$

Enclosure input parameters:

$A_1 := 50 ft^2 \quad A_2 := 120 ft^2 \quad A_3 := 80 ft^2 \quad A_4 := 126 ft^2 \quad D := 5$ in $H := 6$ ft

$\epsilon_1 := .9 \quad \epsilon_2 := .70295 \quad \epsilon_3 := .5 \quad \epsilon_4 := .5 \quad \mathbf{I}_4 := \text{identity}(4)$

$$\mathbf{eI} = \begin{bmatrix} 0.9 & 0 & 0 & 0 \\ 0 & 0.7029 & 0 & 0 \\ 0 & 0 & 0.5 & 0 \\ 0 & 0 & 0 & 0.5 \end{bmatrix} \quad \mathbf{\rho I} := \mathbf{I}_4 - \mathbf{eI} \quad \mathbf{\rho I} = \begin{bmatrix} 0.1 & 0 & 0 & 0 \\ 0 & 0.2971 & 0 & 0 \\ 0 & 0 & 0.5 & 0 \\ 0 & 0 & 0 & 0.5 \end{bmatrix}$$

Compute direct exchange areas: There are $\Sigma = 6$ unique direct exchange areas. These are obtained from Eqs. (5-114) and view factor algebra. The final array of direct exchange areas is:

$$\overline{ss} = \begin{bmatrix} 0 & 1.559 & 1.575 & 1.511 \\ 1.559 & 2.078 & 2.839 & 4.673 \\ 1.575 & 2.839 & 0 & 3.018 \\ 1.511 & 4.673 & 3.018 & 2.503 \end{bmatrix} m^2 \quad \mathbf{AI} = \begin{bmatrix} 4.645 & 0 & 0 & 0 \\ 0 & 11.148 & 0 & 0 \\ 0 & 0 & 7.432 & 0 \\ 0 & 0 & 0 & 11.706 \end{bmatrix} m^2$$

Compute total exchange areas:

$$\mathbf{R} := (\mathbf{AI} - \overline{ss} \cdot \mathbf{\rho I})^{-1}$$

$$\overline{SS} := \mathbf{eI} - \mathbf{AI} - \mathbf{R} \cdot \overline{ss} \cdot \mathbf{eI} \quad \overline{SS} = \begin{bmatrix} 0.405 & 1.669 & 0.955 & 1.152 \\ 1.669 & 2.272 & 1.465 & 2.431 \\ 0.955 & 1.465 & 0.234 & 1.063 \\ 1.152 & 2.431 & 1.063 & 1.207 \end{bmatrix} m^2$$

Check matrix conservation via row-sums:

$$(\mathbf{AI} - \overline{ss}) \begin{bmatrix} 1 \\ 1 \\ 1 \\ 1 \end{bmatrix} = \begin{bmatrix} 0 \\ 0 \\ 0 \\ 0 \end{bmatrix} m^2 \quad (\mathbf{eI} - \mathbf{AI} - \overline{SS}) \begin{bmatrix} 1 \\ 1 \\ 1 \\ 1 \end{bmatrix} = \begin{bmatrix} 0 \\ 0 \\ 0 \\ 0 \end{bmatrix} m^2$$

Emissive power and wall flux input data:

$$\mathbf{T}_F := \begin{bmatrix} 1200 \\ 1500 \\ 32 \\ 32 \end{bmatrix} F \quad \mathbf{T} := \frac{5}{9} (\mathbf{T}_F - 32 F) \frac{C}{F} \quad \mathbf{E} := \sigma \left(\mathbf{T} \frac{K}{C} + T_0 \right)^4$$

$$\mathbf{T} = \begin{bmatrix} 648.9 \\ 815.6 \\ 0.0 \\ 0.0 \end{bmatrix} C \quad \mathbf{E} = \begin{bmatrix} 40.98 \\ 79.66 \\ 0.32 \\ 0.32 \end{bmatrix} \frac{kW}{m^2}$$

$$Q_3 := -0.05 \cdot A_3 (E_2 - E_1) \quad Q_3 = -14.37 kW \quad Q_4 := 0$$

5-30 HEAT AND MASS TRANSFER

Compute refractory emissive powers from known flux inputs Q_3 and Q_4 using partitioned matrix equations [Eq. (5-120b)]:

$$\mathbf{E}_R := \begin{bmatrix} \epsilon_3 A_3 - SS_{3,3} & -SS_{3,4} \\ -SS_{4,3} & \epsilon_4 A_4 - SS_{4,4} \end{bmatrix}^{-1} \cdot \begin{bmatrix} Q_3 + SS_{3,1} E_1 + SS_{3,2} E_2 \\ Q_4 + SS_{4,1} E_1 + SS_{4,2} E_2 \end{bmatrix}$$

$$\mathbf{E}_R = \begin{bmatrix} 60.68 \\ 65.73 \end{bmatrix} \frac{\text{kW}}{\text{m}^2} \quad \mathbf{E} := \begin{bmatrix} E_1 \\ E_2 \\ E_{R1} \\ E_{R2} \end{bmatrix} \quad \mathbf{E} = \begin{bmatrix} 40.98 \\ 79.66 \\ 60.68 \\ 65.73 \end{bmatrix} \frac{\text{kW}}{\text{m}^2}$$

Compute flux values and final zone temperatures:

$$\mathbf{Q} := \epsilon \mathbf{I} \cdot \mathbf{A} \cdot \mathbf{E} - \overline{SS} \cdot \mathbf{E} \quad \mathbf{T} := \left[\left(\frac{\mathbf{E}}{\sigma} \right)^{0.25} - T_0 \right] \frac{\text{C}}{\text{K}}$$

$$\mathbf{Q} = \begin{bmatrix} -111.87 \\ 126.24 \\ -14.37 \\ 0.00 \end{bmatrix} \text{kW} \quad \mathbf{T} = \begin{bmatrix} 648.9 \\ 815.6 \\ 743.9 \\ 764.5 \end{bmatrix} \text{C}$$

Auxiliary calculations for tube area and effective tube emissivity:

$$A_{\text{Tubes}} := 20\pi \cdot D \cdot H \quad \epsilon_{\text{Tubes}} := \frac{Q_2}{A_{\text{Tubes}}(E_2 - E_1)} \quad A_{\text{Tubes}} = 14.59 \text{ m}^2 \quad \epsilon_{\text{Tubes}} = 0.2237$$

Notes: (1) Results for Q and T here are independent of ϵ_3 and ϵ_4 with the exception of T_3 , which is indeed a function of ϵ_3 . (2) The total surface area of the tubes is $A_{\text{Tubes}} = 14.59 \text{ m}^2$. Suppose the tubes were totally surrounded by a black enclosure at the temperature of the sink. The hypothetical emissivity of the tubes would then be $\epsilon_{\text{Tubes}} = 0.224$. (3) A 5 percent roof heat loss is consistent with practical measurement errors. A sensitivity test was performed with $M = 3, 4, \text{ and } 5$ with and without roof heat loss. The SSR model corresponds to $M = 3$ with zero heat loss. For $M = 5$, zone 4 corresponded to the furnace ends and zone 5 corresponded to the floor strips. The results are summarized in the following table. With the exception of the temperature of the floor strips, the computed results are seen to be remarkably insensitive to M .

Effect of Zone Number M on Computed Results

	Zero roof heat loss			5 percent roof heat loss		
	$M = 3$	$M = 4$	$M = 5$	$M = 3$	$M = 4$	$M = 5$
Temperature, °C						
T_3	765.8	762.0	762.4	756.2	743.9	744.3
T_4	NA	765.4	765.0	NA	764.5	761.1
T_5	NA	NA	780.9	NA	NA	776.7
Heat flux, kW						
Q_1	-117.657	-117.275	-116.251	-112.601	-111.870	-110.877
Q_2	117.657	117.275	116.251	126.975	126.244	125.251
Q_3	0.000	0.000	0.000	-14.374	-14.374	-14.374
Q_4	NA	0.000	0.000	NA	0.00	0.00
Q_5	NA	NA	0.000	NA	NA	0.00

(This example was developed as a MATHCAD 14® worksheet. Mathcad is a registered trademark of Parametric Technology Corporation.)

Allowance for Specular Reflection If the assumption that all surface zones are diffuse emitters and reflectors is relaxed, the zoning equations become much more complex. Here, all surface parameters become functions of the *angles of incidence and reflection* of the radiation beams at each surface. In practice, such details of reflectance and emission are seldom known. When they are, the Monte Carlo method of tracing a large number of beams emitted from random positions and in random initial directions is probably the best method of obtaining a solution. Siegel and Howell (op. cit., Chap. 10) and Modest (op. cit., Chap. 20) review the utilization of the Monte Carlo approach to a variety of radiant transfer applications. Among these is the Monte Carlo calculation of direct exchange areas for very complex geometries. Monte Carlo techniques are generally *not used* in practice for simpler engineering applications.

A simple *engineering* approach to specular reflection is the so-called **diffuse plus specular reflection model**. Here the total reflectivity $\rho_i = 1 - \epsilon_i = \rho_{Si} + \rho_{Di}$ is represented as the sum of a *diffuse component*

ρ_{Si} and a *specular component* ρ_{Di} . The method yields analytical results for a number of two surface zone geometries. In particular, the following equation is obtained for exchange between concentric spheres or infinitely long coaxial cylinders for which $A_1 < A_2$:

$$\overline{S_1 S_2} = \frac{A_1}{\left(\frac{1}{\epsilon_1} + \frac{\rho_2}{\epsilon_2} \frac{A_1}{A_2} + \frac{\rho_{S2}}{(1 - \rho_{S2})} [1 - A_1/A_2] \right)} \quad (5-134)$$

For $\rho_{D1} = \rho_{D2} = 0$ (or equivalently $\rho_1 = \rho_{S1}$ with $\rho_2 = \rho_{S2}$), Eq. (5-134) yields the limiting case for wholly specular reflection, i.e.

$$\text{Specular limit} \quad \overline{S_1 S_2} = \frac{A_1}{\left(\frac{1}{\epsilon_1} + \frac{1}{\epsilon_2} - 1 \right)} \quad (5-134a)$$

which is independent of the area ratio, A_1/A_2 . It is important to notice that Eq. (5-124a) is *similar* to Eq. (5-127b) but the emissivities here are defined as $\epsilon_1 \equiv 1 - \rho_{S1}$ and $\epsilon_2 \equiv 1 - \rho_{S2}$. When surface reflection is wholly diffuse [$\rho_{S1} = \rho_{S2} = 0$ or $\rho_1 = \rho_{D1}$ with $\rho_2 = \rho_{D2}$], Eq. (5-134) results in a formula *identical* to Eq. (5-127a), viz.

$$\text{Diffuse limit} \quad \overline{S_1 S_2} = \frac{A_1}{\left[\frac{1}{\epsilon_1} + \left(\frac{A_1}{A_2} \right) \frac{\rho_2}{\epsilon_2} \right]} \quad (5-134b, 5-127a)$$

For the case of (infinite) parallel flat plates where $A_1 = A_2$, Eq. (5-134) leads to a general formula *similar* to Eq. (5-134a) but with the stipulation here that $\epsilon_1 \equiv 1 - \rho_{D1} - \rho_{S1}$ and $\epsilon_2 \equiv 1 - \rho_{D2} - \rho_{S2}$.

Another particularly interesting limit of Eq. (5-134) occurs when $A_2 \gg A_1$, which might represent a small sphere irradiated by an infinite surroundings which can reflect radiation originating at A_1 back to A_1 . That is to say, even though $A_2 \rightarrow \infty$, the "self" total exchange area does not necessarily vanish, to wit

$$\overline{S_1 S_1} = \frac{\epsilon_1^2 \rho_{S2} \cdot A_1}{[1 - \rho_1 \cdot \rho_{S2}]} \quad \text{and} \quad \overline{S_1 S_2} = \frac{\epsilon_1 (1 - \rho_{S2}) \cdot A_1}{[1 - \rho_1 \cdot \rho_{S2}]} \quad (5-134c,d)$$

which again exhibit diffuse and specular limits. The diffuse plus specular reflection model becomes significantly more complex for geometries with $M \geq 3$ where digital computation is usually required.

An Exact Solution to the Integral Equations—The Hohlraum Exact solutions of the fundamental *integral equations* for radiative transfer are available for only a few simple cases. One of these is the evaluation of the emittance from a small aperture, of area A_1 , in the surface of an isothermal spherical cavity of radius R . In German, this geometry is termed a *hohlraum* or hollow space. For this special case the radiosity W is constant over the inner surface of the cavity. It then follows that the ratio W/E is given by

$$W/E = \frac{\epsilon}{1 - \rho [1 - A_1/(4\pi R^2)]} \quad (5-135)$$

where ϵ and $\rho = 1 - \epsilon$ are the diffuse emissivity and reflectivity of the interior cavity surface, respectively. The ratio W/E is the effective emittance of the aperture as sensed by an external narrow-angle receiver (radiometer) viewing the cavity interior. Assume that the cavity is constructed of a rough material whose (diffuse) emissivity is $\epsilon = 0.5$. As a point of reference, if the cavity is to simulate a blackbody emitter to better than 98 percent of an ideal theoretical blackbody, Eq. (5-135) then predicts that the ratio of the aperture to sphere areas $A_1/(4\pi R^2)$ must be less than 2 percent. Equation (5-135) has practical utility in the experimental design of calibration standards for laboratory radiometers.

RADIATION FROM GASES AND SUSPENDED PARTICULATE MATTER

Introduction Flame radiation originates as a result of emission from water vapor and carbon dioxide in the hot gaseous combustion

products and from the presence of particulate matter. The latter includes emission from burning of microscopic and submicroscopic soot particles, and from large suspended particles of coal, coke, or ash. Thermal radiation owing to the presence of water vapor and carbon dioxide is not visible. The characteristic blue color of clean natural gas flames is due to chemiluminescence of the excited intermediates in the flame which contribute negligibly to the radiation from combustion products.

Gas Emissivities Radiant transfer in a gaseous medium is characterized by three quantities; the gas emissivity, gas absorptivity, and gas transmissivity. Gas emissivity refers to radiation originating within a gas volume which is incident on some reference surface. Gas absorptivity and transmissivity, however, refer to the absorption and transmission of radiation from some *external* surface radiation source characterized by some radiation temperature T_1 . The sum of the gas absorptivity and transmissivity must, by definition, be unity. Gas absorptivity may be calculated from an appropriate gas emissivity. The gas emissivity is a function only of the gas temperature T_g while the absorptivity and transmissivity are functions of *both* T_g and T_1 .

The **standard hemispherical monochromatic gas emissivity** is defined as the direct volume-to-surface exchange area for a hemispherical gas volume to an infinitesimal area element located at the center of the planar base. Consider monochromatic transfer in a *black* hemispherical enclosure of radius R that confines an isothermal volume of gas at temperature T_g . The temperature of the bounding surfaces is T_1 . Let A_2 denote the area of the finite hemispherical surface and dA_1 denote an infinitesimal element of area located at the center of the planar base. The (dimensionless) monochromatic direct exchange area for exchange between the finite hemispherical surface A_2 and dA_1 then follows from direct integration of Eq. (5-116a) as

$$\frac{\partial(\overline{s_1 s_2})_\lambda}{\partial A_1} = \int_{\phi_1=0}^{\pi/2} \frac{e^{-K_\lambda R}}{\pi R^2} \cos\phi_1 2\pi R^2 \sin\phi_1 d\phi_1 = e^{-K_\lambda R} \quad (5-136a)$$

and from conservation there results

$$\frac{\partial(\overline{s_1 \overline{g}})_\lambda}{\partial A_1} = 1 - e^{-K_\lambda R} \quad (5-136b)$$

Note that Eq. (5-136b) is identical to the expression for the gas emissivity for a column of path length R . In Eqs. (5-136) the gas absorption coefficient is a function of gas temperature, composition, and wavelength, that is, $K_\lambda = K_\lambda(T, \lambda)$. The net monochromatic radiant flux density at dA_1 due to irradiation from the gas volume is then given by

$$q_{1g,\lambda} = \frac{\partial(\overline{s_1 \overline{g}})_\lambda}{\partial A_1} (E_{1,\lambda} - E_{g,\lambda}) \equiv \alpha_{g,1,\lambda} E_{1,\lambda} - \epsilon_{g,\lambda} E_{g,\lambda} \quad (5-137)$$

In Eq. (5-137), $\epsilon_{g,\lambda}(T, \lambda) = 1 - \exp(-K_\lambda R)$ is defined as the monochromatic or *spectral gas emissivity* and $\alpha_{g,\lambda}(T, \lambda) = \epsilon_{g,\lambda}(T, \lambda)$.

If Eq. (5-137) is integrated with respect to wavelength over the entire EM spectrum, an expression for the *total* flux density is obtained

$$q_{1g} = \alpha_{g,1} E_1 - \epsilon_g E_g \quad (5-138)$$

where
$$\epsilon_g(T_g) = \int_{\lambda=0}^{\infty} \epsilon_\lambda(T_g, \lambda) \cdot \frac{E_{b,\lambda}(T_g, \lambda)}{E_b(T_g)} d\lambda \quad (5-138a)$$

and
$$\alpha_{g,1}(T_1, T_g) = \int_{\lambda=0}^{\infty} \alpha_{g,\lambda}(T_g, \lambda) \cdot \frac{E_{b,\lambda}(T_1, \lambda)}{E_b(T_1)} d\lambda \quad (5-138b)$$

define the *total* gas emissivity and absorptivity, respectively. The notation used here is analogous to that used for surface emissivity and absorptivity as previously defined. For a *real* gas $\epsilon_g = \alpha_{g,1}$ only if $T_1 = T_g$, while for a *gray* gas mass of arbitrarily shaped volume $\epsilon_g = \alpha_{g,1} = \partial(\overline{s_1 \overline{g}})/\partial A_1$ is independent of temperature. Because $K_\lambda(T, \lambda)$ is also a function of the composition of the radiating species, it is necessary in what follows to define a second absorption coefficient $k_{p,\lambda}$, where $K_\lambda = k_{p,\lambda} p$. Here p is the partial pressure of the radiating species, and $k_{p,\lambda}$, with units of $(\text{atm}\cdot\text{m})^{-1}$, is referred to as the *monochromatic line absorption coefficient*.

Mean Beam Lengths It is always possible to represent the emissivity of an arbitrarily shaped volume of gray gas (and thus the corre-

sponding direct gas-to-surface exchange area) with an equivalent sphere of radius $\overline{R} = L_M$. In this context the hemispherical radius $R = L_M$ is referred to as the **mean beam length** of the arbitrary gas volume. Consider, e.g., an isothermal gas layer at temperature T_g confined by two infinite parallel plates separated by distance L . Direct integration of Eq. (5-116a) and use of conservation yield a closed-form expression for the requisite surface-gas direct exchange area

$$\frac{\partial(\overline{s_1 \overline{g}})}{\partial A_1} = [1 - 2E_3(KL)] \quad (5-139a)$$

where $E_n(z) = \int_{t=1}^{\infty} \frac{e^{-zt}}{t^n} dt$ is defined as the ***n*th-order exponential**

integral which is readily available. Employing the definition of gas emissivity, the **mean beam length** between the plates L_M is then defined by the expression

$$\epsilon_g = [1 - 2E_3(KL)] \equiv 1 - e^{-KL_M} \quad (5-139b)$$

Solution of Eq. (5-139b) yields $KL_M = -\ln[2E_3(KL)]$, and it is apparent that KL_M is a function of KL . Since $E_n(0) = 1/(n-1)$ for $n > 1$, the mean beam length approximation also correctly predicts the gas emissivity as zero when $K = 0$ and $K \rightarrow \infty$.

In the limit $K \rightarrow 0$, power series expansion of both sides of the Eq. (5-139b) leads to $KL_M \rightarrow 2KL \equiv KL_{M0}$, where $L_M \equiv L_{M0} = 2L$. Here L_{M0} is defined as the **optically thin mean beam length** for radiant transfer from the entire *infinite* planar gas layer to a differential element of surface area on one of the plates. The optically thin mean beam length for two infinite parallel plates is thus simply *twice* the plate spacing L . In a similar manner it may be shown that for a sphere of diameter D , $L_{M0} = \frac{2}{3}D$, and for an infinitely long cylinder $L_{M0} = D$. A useful default formula for an arbitrary enclosure of volume V and area A is given by $L_{M0} = 4V/A$. This expression predicts $L_{M0} = \frac{2}{3}R$ for the standard hemisphere of radius R because the optically thin mean beam length is averaged over the *entire* hemispherical enclosure.

Use of the optically thin value of the mean beam length yields values of gas emissivities or exchange areas that are too high. It is thus necessary to introduce a dimensionless constant $\beta \leq 1$ and define some new **average mean beam length** such that $KL_M \equiv \beta KL_{M0}$. For the case of parallel plates, we now require that the mean beam length exactly predict the gas emissivity for a *third* value of KL . In this example we find $\beta = -\ln[2E_3(KL)]/2KL$ and for $KL = 0.193095$ there results $\beta = 0.880$. The value $\beta = 0.880$ is not wholly arbitrary. It also happens to minimize the error defined by the so-called shape correction factor $\phi = [\partial(\overline{s_1 \overline{g}})/\partial A_1]/(1 - e^{-KL_M})$ for all $KL > 0$. The required *average* mean beam length for all $KL > 0$ is then taken simply as $L_M = 0.88L_{M0} = 1.76L$. The error in this approximation is less than 5 percent.

For an arbitrary geometry, the average mean beam length is defined as the radius of a hemisphere of gas which predicts values of the direct exchange area $\overline{s_1 \overline{g}}/A_1 = [1 - \exp(-KL_M)]$, subject to the optimization condition indicated above. It has been found that the error introduced by using average mean beam lengths to approximate direct exchange areas is sufficiently small to be appropriate for many engineering calculations. When $\beta = L_M/L_{M0}$ is evaluated for a large number of geometries, it is found that $0.8 < \beta < 0.95$. It is recommended here that $\beta = 0.88$ be employed in lieu of any further geometric information. For a single-gas zone, all the requisite direct exchange areas can be approximated for engineering purposes in terms of a *single* appropriately defined average mean beam length.

Emissivities of Combustion Products Absorption or emission of radiation by the constituents of gaseous combustion products is determined primarily by vibrational and rotational transitions between the energy levels of the gaseous molecules. Changes in both vibrational and rotational energy states gives rise to *discrete* spectral lines. Rotational lines accompanying vibrational transitions usually overlap, forming a so-called vibration-rotation band. These bands are thus associated with the major vibrational frequencies of the molecules.

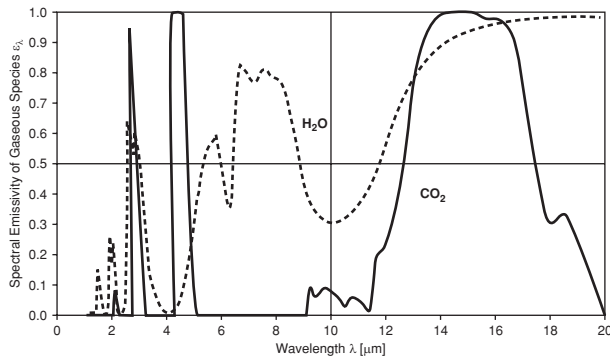


FIG. 5-21 Spectral emittances for carbon dioxide and water vapor after RADCAL. $p_c L = p_w L = 0.36 \text{ atm}\cdot\text{m}$, $T_g = 1500 \text{ K}$.

Each spectral line is characterized by an absorption coefficient $k_{p,\lambda}$ which exhibits a maximum at some central characteristic wavelength or wave number $\eta_0 = 1/\lambda_0$ and is described by a Lorentz² probability distribution. Since the widths of spectral lines are dependent on collisions with other molecules, the absorption coefficient will also depend upon the composition of the combustion gases and the total system pressure. This brief discussion of gas spectroscopy is intended as an introduction to the factors controlling absorption coefficients and thus the factors which govern the empirical correlations to be presented for gas emissivities and absorptivities.

Figure 5-21 shows computed values of the spectral emissivity $\epsilon_{g,\lambda} \equiv \epsilon_{g,\lambda}(T,pL,\lambda)$ as a function of wavelength for an equimolar mixture of carbon dioxide and water vapor for a gas temperature of 1500 K, partial pressure of 0.18 atm, and a path length $L = 2 \text{ m}$. Three principal absorption-emission bands for CO_2 are seen to be centered on 2.7, 4.3, and 15 μm . Two weaker bands at 2 and 9.7 μm are also evident. Three principal absorption-emission bands for water vapor are also identified near 2.7, 6.6, and 20 μm with lesser bands at 1.17, 1.36, and 1.87 μm . The total emissivity ϵ_g and absorptivity $\alpha_{g,1}$ are calculated by integration with respect to wavelength of the spectral emissivities, using Eqs. (5-138) in a manner similar to the development of total surface properties.

Spectral Emissivities Highly resolved spectral emissivities can be generated at ambient temperatures from the HITRAN database (high-resolution transmission molecular absorption) that has been developed for atmospheric models [Rothman, L. S., Chance, K., and Goldman, A., eds., *J. Quant. Spectroscopy & Radiative Trans.*, **82** (1-4), 2003]. This database includes the chemical species: H_2O , CO_2 , O_3 , N_2O , CO , CH_4 , O_2 , NO , SO_2 , NO_2 , NH_3 , HNO_3 , OH , HF , HCl , HBr , ClO , OCS , H_2CO , HOCl , N_2 , HCN , CH_3C , HCl , H_2O_2 , C_2H_2 , C_2H_6 , PH_3 , COF_2 , SF_6 , H_2S , and HCO_2H . These data have been extended to high temperature for CO_2 and H_2O , allowing for the changes in the population of different energy levels and in the line half width [Denison, M. K., and Webb, B. W., *Heat Transfer*, **2**, 19-24 (1994)]. The resolution in the single-line models of emissivities is far greater than that needed in engineering calculations. A number of models are available that average the emissivities over narrow-wavelength regimes or over the entire band. An extensive set of measurements of narrowband parameters performed at NASA (Ludwig, C., et al., *Handbook of Infrared Radiation from Combustion Gases*, NASA SP-3080, 1973) has been used to develop the RADCAL computer code to obtain spectral emissivities for CO_2 , H_2O , CH_4 , CO , and soot (Grosshandler,

²Spectral lines are conventionally described in terms of wave number $\eta = 1/\lambda$, with each line having a peak absorption at wave number η_0 . The Lorentz distribution is defined as $k_{\eta}/S = \frac{b_c}{\pi[b_c^2 + (\eta - \eta_0)^2]}$ where S is the integral of k_{η} over all

wave numbers. The parameter S is known as the integrated line intensity, and b_c is defined as the collision line half-width, i.e., the half-width of the line is one-half of its peak centerline value. The units of k_{η} are $\text{m}^{-1} \text{ atm}^{-1}$.

W. L., "RADCAL," NIST Technical Note 1402, 1993). The exponential wideband model is available for emissions averaged over a band for H_2O , CO_2 , CO , CH_4 , NO , SO_2 , N_2O , NH_3 , and C_2H_2 [Edwards, D. K., and Menard, W. A., *Appl. Optics*, **3**, 621-625 (1964)]. The line and band models have the advantages of being able to account for complexities in determining emissivities of line broadening due to changes in composition and pressure, exchange with spectrally selective walls, and greater accuracy in formulating fluxes in gases with temperature gradients. These models can be used to generate the total emissivities and absorptivities that will be used in this chapter. RADCAL is a command-line FORTRAN code which is available in the public domain on the Internet.

Total Emissivities and Absorptivities Total emissivities and absorptivities for water vapor and carbon dioxide at present are still based on data embodied in the classical **Hottel emissivity charts**. These data have been adjusted with the more recent measurements in RADCAL and used to develop the correlations of emissivities given in Table 5-5. Two empirical correlations which permit hand calculation of emissivities for water vapor, carbon dioxide, and four mixtures of the two gases are presented in Table 5-5. The first section of Table 5-5 provides data for the two constants b and n in the empirical relation

$$\overline{\epsilon_g T_g} = b[pL - 0.015]^n \quad (5-140a)$$

while the second section of Table 5-5 utilizes the four constants in the empirical correlation

$$\log(\overline{\epsilon_g T_g}) = a_0 + a_1 \log(pL) + a_2 \log^2(pL) + a_3 \log^3(pL) \quad (5-140b)$$

In both cases the empirical constants are given for the three temperatures of 1000, 1500, and 2000 K. Table 5-5 also includes some six values for the partial pressure ratios p_w/p_c of water vapor to carbon dioxide, namely, 0, 0.5, 1.0, 2.0, 3.0, and ∞ . These ratios correspond to composition values of $p_c/(p_c + p_w) = 1/(1 + p_w/p_c)$ of 0, 1/3, 1/2, 2/3, 3/4, and unity. For emissivity calculations at other temperatures and mixture compositions, linear interpolation of the constants is recommended.

The absorptivity can be obtained from the emissivity with aid of Table 5-5 by using the following functional equivalence.

$$\overline{\alpha_{g,1} T_1} = [\overline{\epsilon_g T_1}(pL \cdot T_1/T_g)] \left(\frac{T_g}{T_1} \right)^{0.5} \quad (5-141)$$

Verbally, the absorptivity computed from Eq. (5-141) by using the correlations in Table 5-5 is based on a value for gas emissivity ϵ_g calculated at a temperature T_1 and at a partial-pressure path-length product of $(p_c + p_w)LT_1/T_g$. The absorptivity is then equal to this value of gas emissivity multiplied by $(T_g/T_1)^{0.5}$. It is recommended that spectrally based models such as RADCAL (loc. cit.) be used particularly when extrapolating beyond the temperature, pressure, or partial-pressure-length product ranges presented in Table 5-5.

A comparison of the results of the predictions of Table 5-5 with values obtained via the integration of the spectral results calculated from the narrowband model in RADCAL is provided in Fig. 5-22. Here calculations are shown for $p_c L = p_w L = 0.12 \text{ atm}\cdot\text{m}$ and a gas temperature of 1500 K. The RADCAL predictions are 20 percent higher than the measurements at low values of pL and are 5 percent higher at the large values of pL . An extensive comparison of different sources of emissivity data shows that disparities up to 20 percent are to be expected at the current time [Lallemant, N., Sayre, A., and Weber, R., *Prog. Energy Combust. Sci.*, **22**, 543-574, (1996)]. However, smaller errors result for the range of the total emissivity measurements presented in the Hottel emissivity tables. This is demonstrated in Example 11.

Example 11: Calculations of Gas Emissivity and Absorptivity Consider a slab of gas confined between two infinite parallel plates with a distance of separation of $L = 1 \text{ m}$. The gas pressure is 101.325 kPa (1 atm), and the gas temperature is 1500 K (2240°F). The gas is an equimolar mixture of CO_2 and H_2O , each with a partial pressure of 12 kPa ($p_c = p_w = 0.12 \text{ atm}$). The radiative flux to one of its bounding surfaces has been calculated by using RADCAL for two cases. For case (a) the flux to the bounding surface is 68.3 kW/m^2 when the emitting gas is backed by a black surface at an ambient temperature of 300 K (80°F). This (cold) back surface contributes less than 1 percent to the flux. In case (b), the flux is calculated as 106.2 kW/m^2 when the gas is backed by a black surface at a temperature of 1000 K (1340°F). In this example, gas emissivity and

TABLE 5-5 Emissivity-Temperature Product for CO₂-H₂O Mixtures, $\overline{\epsilon_g T_g}$

Limited range for furnaces, valid over 25-fold range of $p_w + p_c L$, 0.046–1.15 m-atm (0.15–3.75 ft-atm)

p_w/p_c	0	1/2	1	2	3	∞
$\frac{p_w}{p_w + p_c}$	0	1/2(0.3–0.42)	1/2(0.42–0.5)	2/3(0.6–0.7)	3/4(0.7–0.8)	1
	CO ₂ only	Corresponding to (CH ₂) _x , covering coal, heavy oils, pitch	Corresponding to (CH ₂) _x , covering distillate oils, paraffins, olefines	Corresponding to CH ₄ , covering natural gas and refinery gas	Corresponding to (CH ₆) _x , covering future high H ₂ fuels	H ₂ O only

Section 1 Constants b and n of $\overline{\epsilon_g T_g} = b(pL - 0.015)^n$, $pL = \text{m-atm}$, $T = \text{K}$

T, K	b	n	b	n	b	n	b	n	b	n	b	n
1000	188	0.209	384	0.33	416	0.34	444	0.34	455	0.35	416	0.400
1500	252	0.256	448	0.38	495	0.40	540	0.42	548	0.42	548	0.523
2000	267	0.316	451	0.45	509	0.48	572	0.51	594	0.52	632	0.640

Constants b and n of $\overline{\epsilon_g T_g} = b(pL - 0.05)^n$, $pL = \text{ft-atm}$, $T = \text{°R}$

$T, \text{°R}$	b	n	b	n	b	n	b	n	b	n	b	n
1800	264	0.209	467	0.33	501	0.34	534	0.34	541	0.35	466	0.400
2700	335	0.256	514	0.38	555	0.40	591	0.42	600	0.42	530	0.523
3600	330	0.316	476	0.45	519	0.48	563	0.51	577	0.52	532	0.640

Section 2 Full range, valid over 2000-fold range of $p_w + p_c L$, 0.005–10.0 m-atm (0.016–32.0 ft-atm)
Constants of $\log_{10} \overline{\epsilon_g T_g} = a_0 + a_1 \log pL + a_2 \log^2 pL + a_3 \log^3 pL$

$\frac{p_w}{p_c}$	$\frac{p_w}{p_w + p_c}$	$pL = \text{m-atm}$, $T = \text{K}$				$pL = \text{ft-atm}$, $T = \text{°R}$					
		T, K	a_0	a_1	a_2	a_3	$T, \text{°R}$	a_0	a_1	a_2	a_3
0	0	1000	2.2661	0.1742	-0.0390	0.0040	1800	2.4206	0.2176	-0.0452	0.0040
		1500	2.3954	0.2203	-0.0433	0.00562	2700	2.5248	0.2695	-0.0521	0.00562
		2000	2.4104	0.2602	-0.0651	-0.00155	3600	2.5143	0.3621	-0.0627	-0.00155
1/2	1/2	1000	2.5754	0.2792	-0.0648	0.0017	1800	2.6691	0.3474	-0.0674	0.0017
		1500	2.6451	0.3418	-0.0685	-0.0043	2700	2.7074	0.4091	-0.0618	-0.0043
		2000	2.6504	0.4279	-0.0674	-0.0120	3600	2.6686	0.4879	-0.0489	-0.0120
1	1/2	1000	2.6090	0.2799	-0.0745	-0.0006	1800	2.7001	0.3563	-0.0736	-0.0006
		1500	2.6862	0.3450	-0.0816	-0.0039	2700	2.7423	0.4561	-0.0756	-0.0039
		2000	2.7029	0.4440	-0.0859	-0.0135	3600	2.7081	0.5210	-0.0650	-0.0135
2	2/3	1000	2.6367	0.2723	-0.0804	0.0030	1800	2.7296	0.3577	-0.0850	0.0030
		1500	2.7178	0.3386	-0.0990	-0.0030	2700	2.7724	0.4384	-0.0944	-0.0030
		2000	2.7482	0.4464	-0.1086	-0.0139	3600	2.7461	0.5474	-0.0871	-0.0139
3	3/4	1000	2.6432	0.2715	-0.0816	0.0052	1800	2.7359	0.3599	-0.0896	0.0052
		1500	2.7257	0.3355	-0.0981	0.0045	2700	2.7811	0.4403	-0.1051	0.0045
		2000	2.7592	0.4372	-0.1122	-0.0065	3600	2.7599	0.5478	-0.1021	-0.0065
∞	1	1000	2.5995	0.3015	-0.0961	0.0119	1800	2.6720	0.4102	-0.1145	0.0119
		1500	2.7083	0.3969	-0.1309	0.0123	2700	2.7238	0.5330	-0.1328	0.0123
		2000	2.7709	0.5099	-0.1646	-0.0165	3600	2.7215	0.6666	-0.1391	-0.0165

NOTE: $p_w/(p_w + p_c)$ of 1/2, 2/3, 3/4, and 3/4 may be used to cover the ranges 0.2–0.4, 0.4–0.6, 0.6–0.7, and 0.7–0.8, respectively, with a maximum error in ϵ_g of 5 percent at $pL = 6.5$ m-atm, less at lower pL 's. Linear interpolation reduces the error generally to less than 1 percent. Linear interpolation or extrapolation on T introduces an error generally below 2 percent, less than the accuracy of the original data.

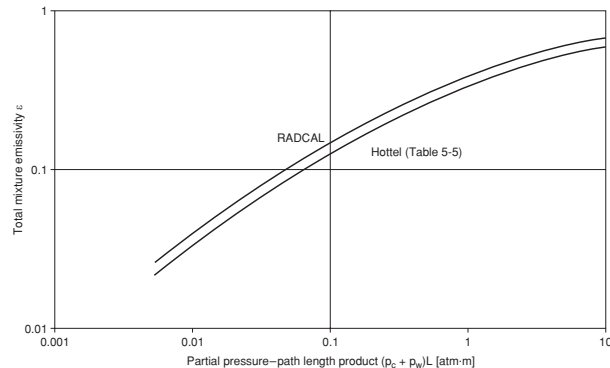


FIG. 5-22 Comparison of Hottel and RADCAL total gas emissivities. Equimolar gas mixture of CO₂ and H₂O with $p_c = p_w = 0.12$ atm and $T_g = 1500$ K.

absorptivity are to be computed from these flux values and compared with values obtained by using Table 5-5.

Case (a): The flux incident on the surface is equal to $\epsilon_g \sigma T_g^4 = 68.3 \text{ kW/m}^2$; therefore, $\epsilon_g = 68,300 / (5.6704 \times 10^{-8} \cdot 1500^4) = 0.238$. To utilize Table 5-5, the mean beam length for the gas is calculated from the relation $L_M = 0.88 L_{M0} = 0.88 \cdot 2L = 1.76$ m. For $T_g = 1500$ K and $(p_c + p_w)L_M = 0.24(1.76) = 0.422$ atm-m, the two-constant correlation in Table 5-5 yields $\epsilon_g = 0.230$ and the four-constant correlation yields $\epsilon_g = 0.234$. These results are clearly in excellent agreement with the predicted value of $\epsilon_g = 0.238$ obtained from RADCAL.

Case (b): The flux incident on the surface (106.2 kW/m^2) is the sum of that contributed by (1) gas emission $\epsilon_g \sigma T_g^4 = 68.3 \text{ kW/m}^2$ and (2) emission from the opposing surface corrected for absorption by the intervening gas using the gas transmissivity, that is, $\tau_{g,1} \sigma T_1^4$ where $\tau_{g,1} = 1 - \alpha_{g,1}$. Therefore $\alpha_{g,1} = [1 - (106,200 - 68,300) / (5.6704 \times 10^{-8} \cdot 1000^4)] = 0.332$. Using Table 5-5, the two-constant and four-constant gas emissivities evaluated at $T_1 = 1000$ K and $pL = 0.4224(1000/1500) = 0.282$ atm-m are $\epsilon_g = 0.2654$ and $\epsilon_g = 0.2707$, respectively. Multiplication by the factor $(T_g/T_1)^{0.5} = (1500/1000)^{0.5} = 1.225$ produces the final values of the two corresponding gas absorptivities $\alpha_{g,1} = 0.325$ and $\alpha_{g,1} = 0.332$, respectively. Again the agreement with RADCAL is excellent.

Other Gases The most extensive available data for gas emissivity are those for carbon dioxide and water vapor because of their importance in the radiation from the products of fossil fuel combustion. Selected data for other species present in combustion gases are provided in Table 5-6.

TABLE 5-6 Total Emissivities of Some Gases

Temperature $P_r L$, atm-ft	1000°R			1600°R			2200°R			2800°R		
	0.01	0.1	1.0	0.01	0.1	1.0	0.01	0.1	1.0	0.01	0.1	1.0
NH ₃ ^a	0.047	0.20	0.61	0.020	0.120	0.44	0.0057	0.051	0.25	(0.001)	(0.015)	(0.14)
SO ₂ ^b	0.020	0.13	0.28	0.013	0.090	0.32	0.0085	0.051	0.27	0.0058	0.043	0.20
CH ₄ ^c	0.0116	0.0518	0.1296	0.0111	0.0615	0.1880	0.0087	0.0608	0.2004	0.00622	0.04702	0.1525
CO ^d	0.0052	0.0167	0.0403	0.0055	0.0196	0.0517	0.0036	0.0145	0.0418	0.00224	0.00986	0.02855
NO ^d	0.0046	0.018	0.060	0.0046	0.021	0.070	0.0019	0.010	0.040	0.0078	0.004	0.025
HCl ^e	0.00022	0.00079	0.0020	0.00036	0.0013	0.0033	0.00037	0.0014	0.0036	0.00029	0.0010	0.0027

NOTE: Figures in this table are taken from plots in Hottel and Sarofim, *Radiative Transfer*, McGraw-Hill, New York, 1967, chap. 6. Values in parentheses are extrapolated. To convert degrees Rankine to kelvins, multiply by (5.556)(10⁻¹). To convert atmosphere-feet to kilopascal-meters, multiply by 30.89.

^aTotal-radiation measurements of Port (Sc.D. thesis in chemical engineering, MIT, 1940) at 1-atm total pressure, $L = 1.68$ ft, T to 2000°R.
^bCalculations of Guerrieri (S.M. thesis in chemical engineering, MIT, 1932) from room-temperature absorption measurements of Coblentz (*Investigations of Infrared Spectra*, Carnegie Institution, Washington, 1905) with poor allowance for temperature.
^cEstimated using Grosshandler, W.L., "RADCAL: A Narrow-Band Model for Radial Calculations in a Combustion Environment," NIST Technical Note 1402, 1993.
^dCalculations of Malkmus and Thompson [*J. Quant. Spectros. Radiat. Transfer*, **2**, 16 (1962)], to $T = 5400$ °R and $PL = 30$ atm-ft.
^eCalculations of Malkmus and Thompson [*J. Quant. Spectros. Radiat. Transfer*, **2**, 16 (1962)], to $T = 5400$ °R and $PL = 300$ atm-ft.

Flames and Particle Clouds

Luminous Flames Luminosity conventionally refers to soot radiation. At atmospheric pressure, soot is formed in locally fuel-rich portions of flames in amounts that usually correspond to less than 1 percent of the carbon in the fuel. Because soot particles are small relative to the wavelength of the radiation of interest in flames (primary particle diameters of soot are of the order of 20 nm compared to wavelengths of interest of 500 to 8000 nm), the incident radiation permeates the particles, and the absorption is proportional to the volume of the particles. In the limit of $r_p/\lambda \ll 1$, the Rayleigh limit, the monochromatic emissivity ϵ_λ is given by

$$\epsilon_\lambda = 1 - \exp(-K \cdot f_v \cdot L/\lambda) \tag{5-142}$$

where f_v is the volumetric soot concentration, L is the path length in the same units as the wavelength λ , and K is dimensionless. The value K will vary with fuel type, experimental conditions, and the temperature history of the soot. The values of K for a wide range of systems are within a factor of about 2 of one another. The single most important variable governing the value of K is the hydrogen/carbon ratio of the soot, and the value of K increases as the H/C ratio decreases. A value of $K = 9.9$ is recommended on the basis of seven studies involving 29 fuels [Mulholland, G. W., and Croarkin, C., *Fire and Materials*, **24**, 227–230 (2000)].

The total emissivity of soot ϵ_s can be obtained by substituting ϵ_λ from Eq. (5-142) for ϵ_λ in Eq. (5-138a) to yield

$$\epsilon_s = \int_{\lambda=0}^{\infty} \epsilon_\lambda \frac{E_{b,\lambda}(T_g, \lambda)}{E_b(T_g)} d\lambda = 1 - \frac{15}{4} [\Psi^{(3)}(1 + K \cdot f_v \cdot L \cdot T/c_2)] \tag{5-143}$$

$$\cong (1 + K \cdot f_v \cdot L \cdot T/c_2)^{-4}$$

Here $\Psi^{(3)}(x)$ is defined as the pentagamma function of x and c_2 (m·K) is again Planck's second constant. The approximate relation in Eq. (5-143) is accurate to better than 1 percent for arguments yielding values of $\epsilon_s < 0.7$. At present, the largest uncertainty in estimating total soot emissivities is in the estimation of the soot volume fraction f_v . Soot forms in the fuel-rich zones of flames. Soot formation rates are a function of fuel type, mixing rate, local equivalence ratio Φ , temperature, and pressure. The equivalence ratio is defined as the quotient of the actual to stoichiometric fuel-to-oxidant ratio $\Phi = [F/O]_{Act}/[F/O]_{Stoich}$. Soot formation increases with the aromaticity or C/H ratio of fuels with benzene, α -methyl naphthalene, and acetylene having a high propensity to form soot and methane having a low soot formation propensity. Oxygenated fuels, such as alcohols, emit little soot. In practical turbulent diffusion flames, soot forms on the fuel side of the flame front. In premixed flames, at a given temperature, the rate of soot formation increases rapidly for $\Phi > 2$. For temperatures above

1500 K, soot burns out rapidly (in less than 0.1s) under fuel-lean conditions, $\Phi < 1$. Because of this rapid soot burnout, soot is usually localized in a relatively small fraction of a furnace or combustor volume. Long, poorly mixed diffusion flames promote soot formation while highly backmixed combustors can burn soot-free. In a typical flame at atmospheric pressure, maximum volumetric soot concentrations are found to be in the range $10^{-7} < f_v < 10^{-6}$. This corresponds to a soot formation of about 1.5 to 15 percent of the carbon in the fuel. When f_v is to be calculated at high pressures, allowance must be made for the significant increase in soot formation with pressure and for the inverse proportionality of f_v with respect to pressure. Great progress is being made in the ability to calculate soot in premixed flames. For example, predicted and measured soot concentration have been compared in a well-stirred reactor operated over a wide range of temperatures and equivalence ratios [Brown, N.J., Revzan, K. L., Frenklach, M., *Twenty-seventh Symposium (International) on Combustion*, pp. 1573–1580, 1998]. Moreover, CFD (computational fluid dynamics) and population dynamics modeling have been used to simulate soot formation in a turbulent non-premixed ethylene-air flame [Zucca, A., Marchisio, D. L., Barresi, A. A., Fox, R. O., *Chem. Eng. Sci.*, 2005]. The importance of soot radiation varies widely between combustors. In large boilers the soot is confined to small volumes and is of only local importance. In gas turbines, cooling the combustor liner is of primary importance so that only small incremental soot radiation is of concern. In high-temperature glass tanks, the presence of soot adds 0.1 to 0.2 to emissivities of oil-fired flames. In natural gas-fired flames, efforts to augment flame emissivities with soot generation have generally been unsuccessful. The contributions of soot to the radiation from pool fires often dominates, and thus the presence of soot in such flames directly impacts the safe separation distances from dikes around oil tanks and the location of flares with respect to oil rigs.

Clouds of Large Black Particles The emissivity ϵ_M of a cloud of black particles with a large perimeter-to-wavelength ratio is

$$\epsilon_M = 1 - \exp[-(a/v)L] \tag{5-144}$$

where a/v is the projected area of the particles per unit volume of space. If the particles have no negative curvature (the particle does not "see" any of itself) and are randomly oriented, $a = a'/4$, where a' is the actual surface area. If the particles are uniform, $a/v = cA = cA'/4$, where A and A' are the projected and total areas of each particle and c is the number concentration of particles. For spherical particles this leads to

$$\epsilon_M = 1 - \exp[-(\pi/4)cd_p^2L] = 1 - \exp(-1.5f_vL/d_p) \tag{5-145}$$

As an example, consider a heavy fuel oil (CH_{1.5}, specific gravity, 0.95) atomized to a mean surface particle diameter of d_p burned with

20 percent excess air to produce coke-residue particles having the original drop diameter and suspended in combustion products at 1204°C (2200°F). The flame emissivity due to the particles along a path of L m, with d_p measured in micrometers, is

$$\epsilon_M = 1 - \exp(-24.3L/d_p) \quad (5-146)$$

For 200- μm particles and $L = 3.05$ m, the particle contribution to emissivity is calculated as 0.31.

Clouds of Nonblack Particles For nonblack particles, emissivity calculations are complicated by multiple scatter of the radiation reflected by each particle. The emissivity ϵ_M of a cloud of gray particles of individual emissivity ϵ_1 can be estimated by the use of a simple modification Eq. (5-144), i.e.,

$$\epsilon_M = 1 - \exp[-\epsilon_1(a/v)L] \quad (5-147)$$

Equation (5-147) predicts that $\epsilon_M \rightarrow 1$ as $L \rightarrow \infty$. This is *impossible* in a scattering system, and use of Eq. (5-147) is restricted to values of the optical thickness $(a/v)L < 2$. Instead, the asymptotic value of ϵ_M is obtained from Fig. 5-12 as $\epsilon_M = \epsilon_b$ ($\lim L \rightarrow \infty$), where the albedo ω is replaced by the particle-surface reflectance $\omega = 1 - \epsilon_1$. Particles with perimeter-to-wavelength ratios of 0.5 to 5.0 can be analyzed, with significant mathematical complexity, by use of the *Mie equations* (Bohren, C. F., and Huffman, D. R., *Absorption and Scattering of Light by Small Particles*, Wiley, 1998).

Combined Gas, Soot, and Particulate Emission In a mixture of emitting species, the emission of each constituent is attenuated on its way to the system boundary by absorption by all other constituents. The transmissivity of a mixture is the product of the transmissivities of its component parts. This statement is a corollary of Beer's law. For present purposes, the transmissivity of "species k " is defined as $\tau_k = 1 - \epsilon_k$. For a mixture of combustion products consisting of carbon dioxide, water vapor, soot, and oil coke or char particles, the total emissivity ϵ_T at any wavelength can therefore be obtained from

$$(1 - \epsilon_T)_\lambda = (1 - \epsilon_C)_\lambda(1 - \epsilon_W)_\lambda(1 - \epsilon_S)_\lambda(1 - \epsilon_M)_\lambda \quad (5-148)$$

where the subscripts denote the four flame species. The total emissivity is then obtained by integrating Eq. (5-148) over the entire EM energy spectrum, taking into account the variability of ϵ_C , ϵ_W , and ϵ_S with respect to wavelength. In Eq. (5-148), ϵ_M is independent of wavelength because absorbing char or coke particles are effectively black-body absorbers. Computer programs for spectral emissivity, such as RADCAL (loc. cit.), perform the integration with respect to wavelength for obtaining total emissivity. Corrections for the overlap of vibration-rotation bands of CO_2 and H_2O are automatically included in the correlations for ϵ_g for mixtures of these gases. The monochromatic soot emissivity is higher at shorter wavelengths, resulting in higher attenuations of the bands at 2.7 μm for CO_2 and H_2O than at longer wavelengths. The following equation is recommended for calculating the emissivity ϵ_{g+s} of a mixture of CO_2 , H_2O , and soot

$$\epsilon_{g+s} = \epsilon_g + \epsilon_s - M \cdot \epsilon_g \epsilon_s \quad (5-149)$$

where M can be represented with acceptable error by the dimensionless function

$$M = 1.12 - 0.27 \cdot (T/1000) + 2.7 \times 10^{-5} f_p \cdot L \quad (5-150)$$

In Eq. (5-150), T has units of kelvins and L is measured in meters. Since coke or char emissivities are gray, their addition to those of the CO_2 , H_2O , and soot follows simply from Eq. (5-148) as

$$\epsilon_T = \epsilon_{g+s} + \epsilon_M - \epsilon_{g+s} \epsilon_M \quad (5-151)$$

with the definition $1 - \epsilon_{g+s} \equiv (1 - \epsilon_C)(1 - \epsilon_W)(1 - \epsilon_S)$.

RADIATIVE EXCHANGE WITH PARTICIPATING MEDIA

Energy Balances for Volume Zones—The Radiation Source Term Reconsider a generalized enclosure with N volume zones confining a gray gas. When the N gas temperatures are *unknown*, an *additional* set of N equations is required in the form of radiant energy

balances for each volume zone. These N equations are given by the *definition* of the N -vector for the **net radiant volume absorption** $\mathbf{S}' = [S'_j]$ for each volume zone

$$\mathbf{S}' = \overline{\mathbf{GS}} \cdot \mathbf{E} + \overline{\mathbf{GG}} \cdot \mathbf{E}_g - 4K\mathbf{VI} \cdot \mathbf{E}_g \quad [N \times 1] \quad (5-152)$$

The radiative source term is a discretized formulation of the *net radiant absorption* for each volume zone which may be incorporated as a *source term* into numerical approximations for the generalized *energy equation*. As such, it permits formulation of energy balances on each zone that may include conductive and convective heat transfer. For $K \rightarrow 0$, $\overline{\mathbf{GS}} \rightarrow 0$, and $\overline{\mathbf{GG}} \rightarrow 0$ leading to $\mathbf{S}' \rightarrow \mathbf{0}_N$. When $K \neq 0$ and $\mathbf{S}' = \mathbf{0}_N$, the gas is said to be in a state of *radiative equilibrium*. In the notation usually associated with the discrete ordinate (DO) and finite volume (FV) methods, see Modest (op. cit., Chap. 16), one would write $S'_j/V_j = K[G - 4E_g] = -\nabla \cdot \vec{q}_r$. Here $H_g = G/4$ is the average flux density incident on a given volume zone from all other surface and volume zones. The DO and FV methods are currently available options as "RTE-solvers" in complex simulations of combustion systems using *computational fluid dynamics* (CFD).^{*}

Implementation of Eq. (5-152) necessitates the definition of two additional *symmetric* $N \times N$ arrays of exchange areas, namely, $\overline{\mathbf{gg}} = [\overline{g_i g_j}]$ and $\overline{\mathbf{GG}} = [\overline{G_i G_j}]$. In Eq. (5-152) $\mathbf{VI} = [V_j \delta_{ij}]$ is an $N \times N$ diagonal matrix of zone volumes. The total exchange areas in Eq. (5-151) are *explicit* functions of the direct exchange areas as follows:

$$\text{Surface-to-gas exchange} \quad \overline{\mathbf{GS}} = \overline{\mathbf{SG}}^T \quad [N \times M] \quad (5-153a)$$

$$\text{Gas-to-gas exchange} \quad \overline{\mathbf{GG}} = \overline{\mathbf{gg}} + \overline{\mathbf{sg}} \cdot \rho \mathbf{I} \cdot \overline{\mathbf{Rg}} \quad [N \times M] \quad (5-153b)$$

The matrices $\overline{\mathbf{gg}} = [\overline{g_i g_j}]$ and $\overline{\mathbf{GG}} = [\overline{G_i G_j}]$ must also satisfy the following **matrix conservation relations**:

$$\text{Direct exchange areas:} \quad 4K\mathbf{VI} \cdot \mathbf{1}_N = \overline{\mathbf{gs}} \cdot \mathbf{1}_M + \overline{\mathbf{gg}} \cdot \mathbf{1}_N \quad (5-154a)$$

$$\text{Total exchange areas:} \quad 4K\mathbf{VI} \cdot \mathbf{1}_N = \overline{\mathbf{GS}} \cdot \mathbf{1}_M + \overline{\mathbf{GG}} \cdot \mathbf{1}_N \quad (5-154b)$$

The formal integral definition of the direct gas-gas exchange area is

$$\overline{g_i g_j} = \iiint_{V_i} \iiint_{V_j} K^2 \frac{e^{-K_r}}{\pi^2} dV_j dV_i \quad (5-155)$$

Clearly, when $K = 0$, the two direct exchange areas involving a gas zone $\overline{\mathbf{gs}}_i$ and $\overline{\mathbf{g}_i \mathbf{g}_j}$ vanish. Computationally it is *never* necessary to make resort to Eq. (5-155) for calculation of $\overline{g_i g_j}$. This is so because $\overline{s_i g_j}$, $\overline{g_i s_j}$, and $\overline{g_i g_j}$ may *all* be calculated *arithmetically* from appropriate values of $\overline{s_i s_j}$ by using associated conservation relations and view factor algebra.

Weighted Sum of Gray Gas (WSGG) Spectral Model Even in simple engineering calculations, the assumption of a gray gas is almost never a good one. The zone method is now further generalized to make allowance for nongray radiative transfer via incorporation of the **weighted sum of gray gas** (WSGG) spectral model. Hottel has shown that the emissivity $\epsilon_g(T, L)$ of an absorbing-emitting gas mixture containing CO_2 and H_2O of known composition can be approximated by a *weighted sum of P gray gases*

$$\epsilon_g(T, L) \approx \sum_{p=1}^P a_p(T)(1 - e^{-K_p L}) \quad (5-156a)$$

where

$$\sum_{p=1}^P a_p(T) = 1.0 \quad (5-156b)$$

In Eqs. (5-156), K_p is some gray gas absorption coefficient and L is some appropriate path length. In practice, Eqs. (5-156) usually yield acceptable accuracy for $P \leq 3$. For $P = 1$, Eqs. (5-156) degenerate to the case of a single gray gas.

^{*}To further clarify the mathematical differences between zoning and the DO and FV methods recognize that (neglecting scatter) the matrix expressions $\mathbf{H} = \mathbf{AI}^{-1} \cdot \overline{\mathbf{ss}} \cdot \mathbf{W} + \mathbf{AI}^{-1} \cdot \overline{\mathbf{sg}} \cdot \mathbf{E}_g$ and $4K\mathbf{VI} \cdot \mathbf{E}_g = \mathbf{VI}^{-1} \cdot \overline{\mathbf{gs}} \cdot \mathbf{W} + \mathbf{VI}^{-1} \cdot \overline{\mathbf{gg}} \cdot \mathbf{E}_g$ represent spatial discretizations of the integral form(s) of the RTE applied at any point (zone) on the boundary or interior of an enclosure, respectively, for a gray gas.

The Clear plus Gray Gas WSGG Spectral Model In principle, the emissivity of all gases approaches unity for infinite path length L . In practice, however, the gas emissivity may fall considerably short of unity for representative values of pL . This behavior results because of the *band* nature of real gas spectral absorption and emission whereby there is usually no significant overlap between dominant absorption bands. Mathematically, this physical phenomenon is modeled by defining one of the gray gas components in the WSGG spectral model to be *transparent*.

For $P = 2$ and path length L_M , Eqs. (5-156) yield the following expression for the gas emissivity

$$\epsilon_g = a_1(1 - e^{-K_1 L_M}) + a_2(1 - e^{-K_2 L_M}) \quad (5-157)$$

In Eq. (5-157) if $K_1 = 0$ and $a_2 \neq 0$, the limiting value of gas emissivity is $\epsilon_g(T, \infty) \rightarrow a_2$. Put $K_1 = 0$ in Eq. (5-157), $a_g = a_2$, and define $\tau_g = e^{-K_2 L_M}$ as the gray gas transmissivity. Equation (5-157) then simplifies to

$$\epsilon_g = a_g(1 - \tau_g) \quad (5-158)$$

It is important to note in Eq. (5-158) that $0 \leq a_g, \tau_g \leq 1.0$ while $0 \leq \epsilon_g \leq a_g$.

Equation (5-158) constitutes a two-parameter model which may be fitted with only *two* empirical emissivity data points. To obtain the constants a_g and τ_g in Eq. (5-158) at fixed composition and temperature, denote the two emissivity data points as $\epsilon_{g,2} = \epsilon_g(2pL) > \epsilon_{g,1} = \epsilon_g(pL)$ and recognize that $\epsilon_{g,1} = a_g(1 - \tau_g)$ and $\epsilon_{g,2} = a_g(1 - \tau_g^2) = a_g(1 - \tau_g)(1 + \tau_g) = \epsilon_{g,1}(1 + \tau_g)$. These relations lead directly to the final emissivity fitting equations

$$\tau_g = \frac{\epsilon_{g,2}}{\epsilon_{g,1}} - 1 \quad (5-159a)$$

and

$$a_g = \frac{\epsilon_{g,1}}{2 - \epsilon_{g,2}/\epsilon_{g,1}} \quad (5-159b)$$

The clear plus gray WSGG spectral model also readily leads to values for gas *absorptivity* and *transmissivity*, with respect to some appropriate surface radiation source at temperature T_1 , for example,

$$\alpha_{g,1} = a_{g,1}(1 - \tau_g) \quad (5-160a)$$

and

$$\tau_{g,1} = a_{g,1} \tau_g \quad (5-160b)$$

In Eqs. (5-160) the *gray* gas transmissivity τ_g is taken to be identical to that obtained for the gas emissivity ϵ_g . The constant $a_{g,1}$ in Eq. (5-160a) is then obtained with knowledge of *one additional empirical value* for $\alpha_{g,1}$ which may also be obtained from the correlations in Table 5-5. Notice further in the definitions of the three parameters ϵ_g , $\alpha_{g,1}$, and $\tau_{g,1}$ that *all* the temperature dependence is forced into the *two* WSGG constants a_g and $a_{g,1}$.

The *three* clear plus gray WSGG constants a_g , $a_{g,1}$, and τ_g are functions of total pressure, temperature, and mixture composition. It is not necessary to ascribe any particular physical significance to them. Rather, they may simply be visualized as three constants that happen to fit the gas emissivity data. It is noteworthy that *three* constants are far fewer than the number required to calculate gas emissivity data from fundamental spectroscopic data. The two constants a_g and $a_{g,1}$ defined in Eqs. (5-158) and (5-160) can, however, be interpreted *physically* in a particularly simple manner. Suppose the gas absorption spectrum is idealized by *many* absorption bands (boxes), *all* of which are characterized by the *identical* absorption coefficient K . The a 's might then be calculated from the total blackbody energy fraction $F_b(\lambda T)$ defined in Eqs. (5-105) and (5-106). That is, a_g simply represents the total *energy fraction* of the blackbody energy distribution in which the gas *absorbs*. This concept may be further generalized to real gas absorption spectra via the *wideband stepwise gray spectral box model* (Modest, op. cit., Chap. 14).

When $P \geq 3$, exponential curve-fitting procedures for the WSGG spectral model become significantly more difficult for hand computation but are quite routine with the aid of a variety of readily available

mathematical software utilities. The clear plus gray WSGG fitting procedure is demonstrated in Example 8.

The Zone Method and Directed Exchange Areas Spectral dependence of real gas spectral properties is now introduced into the zone method via the WSGG spectral model. It is still assumed, however, that all surface zones are gray isotropic emitters and absorbers.

General Matrix Representation We first define a new set of four **directed exchange areas** $\overleftarrow{\mathbf{SS}}$, $\overleftarrow{\mathbf{SG}}$, $\overleftarrow{\mathbf{GS}}$, and $\overleftarrow{\mathbf{GG}}$ which are denoted by an overarrow. The directed exchange areas are obtained from the total exchange areas for gray gases by simple matrix multiplication using weighting factors derived from the WSGG spectral model. The directed exchange areas are denoted by an overarrow to indicate the "sending" and "receiving" zone. The a -weighting factors for transfer originating at a gas zone $a_{g,i}$ are derived from WSGG gas *emissivity* calculations, while those for transfers originating at a surface zone, a_i are derived from appropriate WSGG gas *absorptivity* calculations. Let $\mathbf{agI}_p = [a_{p,g} \delta_{ij}]$ and $\mathbf{aI}_p = [a_{p,i} \delta_{ij}]$ represent the P [$M \times M$] and [$N \times N$] *diagonal* matrices comprised of the appropriate WSGG a constants. The *directed* exchange areas are then computed from the associated *total* gray gas exchange areas via simple *diagonal* matrix multiplication.

$$\overleftarrow{\mathbf{SS}} = \sum_{p=1}^P \overleftarrow{\mathbf{SS}}_p \cdot \mathbf{aI}_p \quad [M \times M] \quad (5-161a)$$

$$\overleftarrow{\mathbf{SG}} = \sum_{p=1}^P \overleftarrow{\mathbf{SG}}_p \cdot \mathbf{agI}_p \quad [M \times N] \quad (5-161b)$$

$$\overleftarrow{\mathbf{GS}} = \sum_{p=1}^P \overleftarrow{\mathbf{GS}}_p \cdot \mathbf{aI}_p \quad [M \times N] \quad (5-161c)$$

$$\overleftarrow{\mathbf{GG}} = \sum_{p=1}^P \overleftarrow{\mathbf{GG}}_p \cdot \mathbf{agI}_p \quad [N \times N] \quad (5-161d)$$

$$\text{with } \overleftarrow{\mathbf{KI}} = \sum_{p=1}^P \overleftarrow{\mathbf{KI}}_p \cdot \mathbf{agI}_p \quad [N \times N] \quad (5-161e)$$

In contrast to the *total* exchange areas which are always independent of temperature, the four *directed* arrays $\overleftarrow{\mathbf{SS}}$, $\overleftarrow{\mathbf{SG}}$, $\overleftarrow{\mathbf{GS}}$, and $\overleftarrow{\mathbf{GG}}$ are dependent on the temperatures of each and every zone, i.e., as in $a_{p,i} = a_p(T_i)$. Moreover, in contrast to *total* exchange areas, the *directed* arrays $\overleftarrow{\mathbf{SS}}$ and $\overleftarrow{\mathbf{GG}}$ are generally not symmetric and $\overleftarrow{\mathbf{GS}} \neq \overleftarrow{\mathbf{SG}}^T$. Finally, since the directed exchange areas are temperature-*dependent*, iteration may be required to update the \mathbf{aI}_p and \mathbf{agI}_p arrays during the course of a calculation. There is a great deal of latitude with regard to fitting the WSGG a constants in these matrix equations, especially if $N > 1$ and composition variations are to be allowed for in the gas. An extensive discussion of a fitting for $N > 1$ is beyond the scope of this presentation. Details of the fitting procedure, however, are presented in Example 12 in the context of a single-gas zone.

Having formulated the directed exchange areas, the governing matrix equations for the radiative flux equations at each surface zone and the radiant source term are then given as follows:

$$\mathbf{Q} = \epsilon \mathbf{AI} \cdot \mathbf{E} - \overleftarrow{\mathbf{SS}} \cdot \mathbf{E} - \overleftarrow{\mathbf{SG}} \cdot \mathbf{E}_g \quad (5-162a)$$

$$\mathbf{S}' = \overleftarrow{\mathbf{GG}} \cdot \mathbf{E}_g + \overleftarrow{\mathbf{GS}} \cdot \mathbf{E} - 4 \overleftarrow{\mathbf{KI}} \cdot \mathbf{VI} \cdot \mathbf{E}_g \quad (5-162b)$$

or the alternative forms

$$\mathbf{Q} = [\mathbf{EI} \cdot \overleftarrow{\mathbf{SS}} - \overleftarrow{\mathbf{SS}} \cdot \mathbf{EI}] \cdot \mathbf{I}_M + [\mathbf{EI} \cdot \overleftarrow{\mathbf{SG}} - \overleftarrow{\mathbf{SG}} \cdot \mathbf{E}_g \mathbf{I}] \cdot \mathbf{I}_N \quad (5-163a)$$

$$\mathbf{S}' = -[\mathbf{E}_g \mathbf{I} \cdot \overleftarrow{\mathbf{GS}} - \overleftarrow{\mathbf{GS}} \cdot \mathbf{EI}] \cdot \mathbf{I}_M - [\mathbf{E}_g \mathbf{I} \cdot \overleftarrow{\mathbf{GG}} - \overleftarrow{\mathbf{GG}} \cdot \mathbf{E}_g \mathbf{I}] \cdot \mathbf{I}_N \quad (5-163b)$$

It may be *proved* that the \mathbf{Q} and \mathbf{S}' vectors computed from Eqs. (5-162) and (5-163) always *exactly* satisfy the overall (scalar) *radiant* energy balance $\mathbf{I}_M^T \cdot \mathbf{Q} = \mathbf{I}_N^T \cdot \mathbf{S}'$. In words, the total radiant gas emission for all gas zones in the enclosure must always exactly equal the total radiant energy received at all surface zones which comprise the enclosure. In Eqs. (5-162) and (5-163), the following definitions are employed for the *four forward-directed* exchange areas

$$\overleftarrow{\mathbf{SS}} = \overleftarrow{\mathbf{SS}}^T \quad \overleftarrow{\mathbf{SG}} = \overleftarrow{\mathbf{GS}}^T \quad \overleftarrow{\mathbf{GS}} = \overleftarrow{\mathbf{SG}}^T \quad \overleftarrow{\mathbf{GG}} = \overleftarrow{\mathbf{GG}}^T \quad (5-64a,b,c,d)$$

such that formally there are some *eight* matrices of directed exchange areas. The four *backward-directed* arrays of directed exchange areas must satisfy the following conservation relations

$$\overleftarrow{\mathbf{SS}} \cdot \mathbf{I}_M + \overleftarrow{\mathbf{SG}} \cdot \mathbf{I}_N = \varepsilon \mathbf{I} \cdot \mathbf{AI} \cdot \mathbf{I}_M \quad (5-165a)$$

$$4\overleftarrow{\mathbf{KI}} \cdot \mathbf{VI} \cdot \mathbf{I}_N = \overleftarrow{\mathbf{GS}} \cdot \mathbf{I}_M + \overleftarrow{\mathbf{GG}} \cdot \mathbf{I}_N \quad (5-165b)$$

Subject to the restrictions of no scatter and diffuse surface emission and reflection, the above equations are the most general matrix statement possible for the zone method. When $P = 1$, the *directed* exchange areas all reduce to the *total* exchange areas for a single gray gas. If, in addition, $K = 0$, the much simpler case of radiative transfer in a transparent medium results. If, in addition, all surface zones are *black*, the direct, total, and directed exchange areas are all identical.

Allowance for Flux Zones As in the case of a transparent medium, we now distinguish between source and flux surface zones. Let $M = M_s + M_f$ represent the total number of surface zones where M_s is the number of source-sink zones and M_f is the number of flux zones. The flux zones are the *last to be numbered*. To accomplish this, partition the

surface emissive power and flux vectors as $\mathbf{E} = \begin{bmatrix} \mathbf{E}_1 \\ \mathbf{E}_2 \end{bmatrix}$ and $\mathbf{Q} = \begin{bmatrix} \mathbf{Q}_1 \\ \mathbf{Q}_2 \end{bmatrix}$,

where the subscript 1 denotes surface source/sink zones whose emissive power \mathbf{E}_1 is specified a priori, and subscript 2 denotes surface flux zones of unknown emissive power vector \mathbf{E}_2 and known radiative flux vector \mathbf{Q}_2 . Suppose the radiative source vector \mathbf{S}' is *known*. Appropriate partitioning of Eqs. (5-162) then produces

$$\begin{bmatrix} \mathbf{Q}_1 \\ \mathbf{Q}_2 \end{bmatrix} = \begin{bmatrix} \varepsilon \mathbf{AI}_{1,1} & \mathbf{0} \\ \mathbf{0} & \varepsilon \mathbf{AI}_{2,2} \end{bmatrix} \cdot \begin{bmatrix} \mathbf{E}_1 \\ \mathbf{E}_2 \end{bmatrix} + \begin{bmatrix} \overleftarrow{\mathbf{SS}}_{1,2} & \overleftarrow{\mathbf{SS}}_{1,2} \\ \overleftarrow{\mathbf{SS}}_{2,1} & \overleftarrow{\mathbf{SS}}_{2,2} \end{bmatrix} \cdot \begin{bmatrix} \mathbf{E}_1 \\ \mathbf{E}_2 \end{bmatrix} - \begin{bmatrix} \overleftarrow{\mathbf{SG}} \\ \overleftarrow{\mathbf{SG}} \end{bmatrix} \cdot \mathbf{E}_g \quad (5-166a)$$

and

$$\mathbf{S}' = \overleftarrow{\mathbf{GG}} \cdot \mathbf{E}_g + \begin{bmatrix} \overleftarrow{\mathbf{GS}}_1 & \overleftarrow{\mathbf{GS}}_2 \end{bmatrix} \begin{bmatrix} \mathbf{E}_1 \\ \mathbf{E}_2 \end{bmatrix} - 4\overleftarrow{\mathbf{KI}} \cdot \mathbf{VI} \cdot \mathbf{E}_g \quad (5-166b)$$

where the definitions of the matrix partitions follow the conventions with respect to Eq. (5-120). Simultaneous solution of the *two* unknown vectors in Eqs. (5-166) then yields

$$\mathbf{E}_2 = \mathbf{RP} \cdot \begin{bmatrix} \overleftarrow{\mathbf{SS}}_{2,1} + \overleftarrow{\mathbf{SG}}_2 \cdot \mathbf{PP} \cdot \overleftarrow{\mathbf{GS}}_1 \\ \overleftarrow{\mathbf{SS}}_{2,2} + \overleftarrow{\mathbf{SG}}_2 \cdot \mathbf{PP} \cdot \mathbf{S}' \end{bmatrix} \cdot \mathbf{E}_1 + \mathbf{RP} \cdot \begin{bmatrix} \mathbf{Q}_2 - \overleftarrow{\mathbf{SG}}_2 \cdot \mathbf{PP} \cdot \mathbf{S}' \end{bmatrix} \quad (5-167a)$$

and

$$\mathbf{E}_g = \mathbf{PP} \cdot \begin{bmatrix} \overleftarrow{\mathbf{GS}}_1 & \overleftarrow{\mathbf{GS}}_2 \end{bmatrix} \begin{bmatrix} \mathbf{E}_1 \\ \mathbf{E}_2 \end{bmatrix} - \mathbf{PP} \cdot \mathbf{S}' \quad (5-167b)$$

where two auxiliary inverse matrices \mathbf{RP} and \mathbf{PP} are defined as

$$\mathbf{PP} = [4\overleftarrow{\mathbf{KI}} \cdot \mathbf{VI} - \overleftarrow{\mathbf{GG}}]^{-1} \quad (5-168a)$$

$$\mathbf{RP} = [\varepsilon \mathbf{AI}_{2,2} - \overleftarrow{\mathbf{SS}}_{2,2} - \overleftarrow{\mathbf{SG}}_2 \cdot \mathbf{PP} \cdot \overleftarrow{\mathbf{GS}}_2]^{-1} \quad (5-168b)$$

The emissive power vectors \mathbf{E} and \mathbf{E}_g are then both *known* quantities for purposes of subsequent calculation.

Algebraic Formulas for a Single Gas Zone As shown in Fig. 5-10, the three-zone system with $M = 2$ and $N = 1$ can be employed to simulate a surprisingly large number of useful engineering geometries. These include two infinite parallel plates confining an absorbing-emitting medium; *any* two-surface zone system where a nonconvex surface zone is completely surrounded by a second zone (this includes concentric spheres and cylinders), and the speckled two-surface enclosure. As in the case of a transparent medium, the inverse reflectivity matrix \mathbf{R} is capable of explicit matrix inversion for $M = 2$. This allows derivation of *explicit* algebraic equations for all the required *directed* exchange areas for the clear plus gray WSGG spectral model with $M = 1$ and 2 and $N = 1$.

The Limiting Case $M = 1$ and $N = 1$ The directed exchange areas for this special case correspond to a single well-mixed gas zone completely surrounded by a single surface zone A_1 . Here the reflectivity matrix is a 1×1 scalar quantity which follows directly from the

general matrix equations as $\mathbf{R} = [1/(A_1 - \overleftarrow{s_1 s_1} \cdot \rho_1)]$. There are *two* WSGG clear plus gray constants a_1 and a_g , and only *one* unique directed exchange area which satisfies the conservation relation $\overleftarrow{s_1 s_1} + \overleftarrow{s_1 g} = A_1$. The only two physically meaningful directed exchange areas are those between the surface zone A_1 and the gas zone

$$\overleftarrow{S_1 G} = \frac{a_g \cdot \varepsilon_1 A_1 \cdot \overleftarrow{s_1 g}}{\varepsilon_1 \cdot A_1 + \rho_1 \cdot \overleftarrow{s_1 g}} \quad (5-169a)$$

$$\overleftarrow{G S_1} = \frac{a_1 \cdot \varepsilon_1 A_1 \cdot \overleftarrow{s_1 g}}{\varepsilon_1 \cdot A_1 + \rho_1 \cdot \overleftarrow{s_1 g}} \quad (5-169b)$$

The total radiative flux Q_1 at surface A_1 and the radiative source term $Q_1 = S$ are given by

$$Q_1 = \overleftarrow{G S_1} \cdot E_1 - \overleftarrow{S_1 G} \cdot E_g \quad (5-169)$$

Directed Exchange Areas for $M = 2$ and $N = 1$ For this case there are *four* WSGG constants, i.e., a_1 , a_2 , a_g , and τ_g . There is one required value of K that is readily obtained from the equation $K = -\ln(\tau_g)/L_{0g}$, where $\tau_g = \exp(-KL_{0g})$. For an enclosure with $M = 2$, $N = 1$, and $K \neq 0$, only *three* unique direct exchange areas are required because conservation stipulates $A_1 = \overleftarrow{s_1 s_2} + \overleftarrow{s_1 s_2} + \overleftarrow{s_1 g}$ and $A_2 = \overleftarrow{s_1 s_2} + \overleftarrow{s_2 s_2} + \overleftarrow{s_2 g}$. For $M = 2$ and $N = 1$, the matrix Eqs. (5-118) readily lead to the *general* gray gas matrix solution for $\overleftarrow{\mathbf{SS}}$ and $\overleftarrow{\mathbf{SG}}$ with $K \neq 0$ as

$$\overleftarrow{\mathbf{SS}} = \begin{bmatrix} \varepsilon_1 A_1 - \overleftarrow{S_1 S_2} - \overleftarrow{S_1 G} & \overleftarrow{S_1 S_2} \\ \overleftarrow{S_1 S_1} & \varepsilon_2 A_2 - \overleftarrow{S_1 S_2} - \overleftarrow{S_2 G} \end{bmatrix} \quad (5-170a)$$

where

$$\overleftarrow{S_1 S_2} = \varepsilon_1 \varepsilon_2 A_1 A_2 \overleftarrow{s_1 s_2} / \det \mathbf{R}^{-1} \quad (5-170b)$$

$$\text{and } \overleftarrow{\mathbf{SG}} = \begin{bmatrix} \varepsilon_1 A_1 [(A_2 - \rho_2 \cdot \overleftarrow{s_2 s_2}) \cdot \overleftarrow{s_1 g} + \rho_2 \cdot \overleftarrow{s_1 s_2} \cdot \overleftarrow{s_2 g}] \\ \varepsilon_2 A_2 [(A_1 - \rho_1 \cdot \overleftarrow{s_1 s_1}) \cdot \overleftarrow{s_2 g} + \rho_1 \cdot \overleftarrow{s_1 s_2} \cdot \overleftarrow{s_1 g}] \end{bmatrix} / \det \mathbf{R}^{-1} \quad (5-170c)$$

with $\overleftarrow{\mathbf{GS}} = \overleftarrow{\mathbf{SG}}^T$ and the indicated determinate of \mathbf{R}^{-1} is evaluated algebraically as

$$\det \mathbf{R}^{-1} = (A_1 - \overleftarrow{s_1 s_1} \cdot \rho_1) \cdot (A_2 - \overleftarrow{s_2 s_2} \cdot \rho_2) - \rho_1 \cdot \rho_2 \cdot \overleftarrow{s_1 s_2}^2 \quad (5-170d)$$

For the WSGG clear gas components we denote $\overleftarrow{\mathbf{SS}} \Big|_{K=0} \equiv \overleftarrow{\mathbf{SS}}_0$ and $\overleftarrow{\mathbf{SG}} \Big|_{K=0} \equiv \overleftarrow{\mathbf{SG}}_0 = \mathbf{0}$. Finally the WSGG arrays of directed exchange areas are computed simply from a -weighted sums of the gray gas total exchange areas as

$$\overleftarrow{\mathbf{SS}} = \overleftarrow{\mathbf{SS}}_0 \cdot \begin{bmatrix} 1 - a_1 & 0 \\ 0 & 1 - a_2 \end{bmatrix} + \overleftarrow{\mathbf{SS}} \cdot \begin{bmatrix} a_1 & 0 \\ 0 & a_2 \end{bmatrix} \quad (5-171a,b,c)$$

$$\overleftarrow{\mathbf{SG}} = \overleftarrow{\mathbf{SG}} \cdot a_g$$

$$\overleftarrow{\mathbf{GS}} = \overleftarrow{\mathbf{GS}} \cdot \begin{bmatrix} a_1 & 0 \\ 0 & a_2 \end{bmatrix} \neq \overleftarrow{\mathbf{SG}}^T$$

and finally

$$\overleftarrow{\mathbf{GG}} = a_g \cdot 4KV - \overleftarrow{\mathbf{GS}} \cdot \begin{bmatrix} 1 \\ 1 \end{bmatrix} \quad (5-171d)$$

The results of this development may be further expanded into algebraic form with the aid of Eq. (5-127) to yield the following

$$\overleftarrow{S_2 S_1} = \frac{\varepsilon_1 \varepsilon_2 A_1 A_2 \overleftarrow{s_2 s_1} (1 - a_1)}{\varepsilon_1 \varepsilon_1 A_1 A_2 + (\varepsilon_1 A_1 \rho_2 + \varepsilon_2 A_2 \rho_1) \overleftarrow{s_2 s_1} + \rho_1 \rho_2 \overleftarrow{s_1 s_2}^2} + \frac{\varepsilon_1 \varepsilon_2 A_1 A_2 \overleftarrow{s_2 s_1} a_1}{\det \mathbf{R}^{-1}} \quad (5-171e)$$

$$\overleftarrow{\mathbf{SG}} = \begin{bmatrix} \varepsilon_1 A_1 [(A_2 - \rho_2 \cdot \overleftarrow{s_2 s_2}) \cdot \overleftarrow{s_1 g} + \rho_2 \cdot \overleftarrow{s_1 s_2} \cdot \overleftarrow{s_2 g}] a_g \\ \varepsilon_2 A_2 [(A_1 - \rho_1 \cdot \overleftarrow{s_1 s_1}) \cdot \overleftarrow{s_2 g} + \rho_1 \cdot \overleftarrow{s_1 s_2} \cdot \overleftarrow{s_1 g}] a_g \end{bmatrix} / \det \mathbf{R}^{-1} \quad (5-171f)$$

$$\text{and } \overleftarrow{\mathbf{GS}} = \begin{bmatrix} \overleftarrow{G S_1} & \overleftarrow{G S_2} \end{bmatrix} \quad (5-171g)$$

whose matrix elements are given by $\overleftarrow{GS}_1 \equiv \epsilon_1 A_1 [(A_2 - \rho_2 \overleftarrow{s}_1 \overleftarrow{s}_1) \cdot \overleftarrow{s}_1 \overleftarrow{g} + \rho_2 \overleftarrow{s}_1 \overleftarrow{s}_2 \cdot \overleftarrow{s}_2 \overleftarrow{g}] / \det \mathbf{R}^{-1}$ and $\overleftarrow{GS}_2 \equiv \epsilon_2 A_2 [(A_1 - \rho_1 \overleftarrow{s}_1 \overleftarrow{s}_1) \cdot \overleftarrow{s}_2 \overleftarrow{g} + \rho_1 \overleftarrow{s}_1 \overleftarrow{s}_2 \cdot \overleftarrow{s}_1 \overleftarrow{g}] / \det \mathbf{R}^{-1}$. Derivation of the scalar (algebraic) forms for the directed exchange areas here is done primarily for pedagogical purposes. Computationally, the only advantage is to obviate the need for a digital computer to evaluate a $[2 \times 2]$ matrix inverse.

Allowance for an Adiabatic Refractory with $N = 1$ and $M = 2$
 Put $N = 1$ and $M = 2$, and let zone 2 represent the refractory surface. Let $Q_2 = 0$ and $\epsilon_2 \neq 0$, and it then follows that we may define a refractory-aided directed exchange area $\overleftarrow{S}_1 \overleftarrow{G}_R$ by

$$\overleftarrow{S}_1 \overleftarrow{G}_R = \overleftarrow{S}_1 \overleftarrow{G} + \frac{\overleftarrow{S}_1 \overleftarrow{S}_2 \cdot \overleftarrow{S}_2 \overleftarrow{G}}{\overleftarrow{S}_1 \overleftarrow{S}_2 + \overleftarrow{S}_2 \overleftarrow{G}} \quad (5-172a)$$

Assuming radiative equilibrium, the emissive power of the refractory may also be calculated from the companion equation

$$E_2 = \frac{\overleftarrow{S}_2 \overleftarrow{S}_1 \cdot E_1 + \overleftarrow{S}_2 \overleftarrow{G} \cdot E_g}{\overleftarrow{S}_2 \overleftarrow{S}_1 + \overleftarrow{S}_2 \overleftarrow{G}} \quad (5-172b)$$

In this circumstance, *all* the radiant energy originating in the gas volume is transferred to the *sole* sink zone A_1 . Equation (5-172a) is thus tantamount to the statement that $Q_1 = S'$ or that the net emission from the source ultimately must arrive at the sink. Notice that if $\epsilon_1 = 0$, Eq. (5-172a) leads to a physically incongruous statement since *all* the directed exchange areas would vanish and *no sink* would exist. Even for the simple case of $M = 2, N = 1$, the algebraic complexity of Eqs. (5-171) suggests that *numerical matrix manipulation* of directed exchange areas is to be preferred rather than calculations using algebraic formulas.

Engineering Approximations for Directed Exchange Areas
 Use of the preceding equations for directed exchange areas with $M = 2, N = 1$ and the WSGG clear plus gray gas spectral approximation requires knowledge of three independent direct exchange areas. It also formally requires evaluation of three WSGG weighting constants $a_1, a_2,$ and a_g with respect to the three temperatures $T_1, T_2,$ and T_g . Further simplifications may be made by assuming that radiant transfer for the *entire* enclosure is characterized by the *single* mean beam length $L_M = 0.88 \cdot 4 \cdot V/A$. The requisite direct exchange areas are then approximated by

$$\overleftarrow{SS} = \tau_g \begin{bmatrix} A_1 \cdot F_{1,1} & A_1 \cdot F_{1,2} \\ A_2 \cdot F_{2,1} & A_2 \cdot F_{2,2} \end{bmatrix} \quad (5-173a)$$

with
$$\overleftarrow{sg} = (1 - \tau_g) \begin{bmatrix} A_1 \\ A_2 \end{bmatrix} \quad (5-173b)$$

and for the particular case of a speckled enclosure

$$\overleftarrow{SS} = \frac{\tau_g}{A_1 + A_2} \begin{bmatrix} A_1^2 & A_1 \cdot A_2 \\ A_1 \cdot A_2 & A_2^2 \end{bmatrix} \quad (5-174a)$$

also with
$$\overleftarrow{sg} = (1 - \tau_g) \begin{bmatrix} A_1 \\ A_2 \end{bmatrix} \quad (5-174b)$$

where again τ_g is obtained from the WSGG fit of gas emissivity. These approximate formulas clearly obviate the need for *exact* values of the direct exchange areas and may be used in conjunction with Eqs. (5-171).

For engineering calculations, an additional simplification is sometimes warranted. Again characterize the system by a single mean beam length $L_M = 0.88 \cdot 4 \cdot V/A$ and employ the *identical* value of $\tau_g = KL_M$ for all surface-gas transfers. The three a constants *might* then be obtained by a WSGG data-fitting procedure for gas emissivity and gas absorptivity which utilizes the three different temperatures $T_g, T_1,$ and T_2 . For engineering purposes we choose a simpler method, however. First calculate values of ϵ_g and $\alpha_{g,1}$ for gas temperature T_g with respect to the *dominant* (sink) temperature T_1 . The *net* radiative flux between an isothermal gas mass at temperature T_g and a black isothermal bounding surface A_1 at temperature T_1 (the sink) is given by Eq. (5-138) as

$$Q_{1,g} = A_1 \sigma (\alpha_{g,1} T_1^4 - \epsilon_g T_g^4) \quad (5-175)$$

It is clear that transfer from the gas to the surface and transfer from the surface into the gas are characterized by two different constants of proportionality, ϵ_g and $\alpha_{g,1}$. To allow for the difference between gas emissivity and absorptivity, it proves convenient to introduce a single *mean gas emissivity* defined by

$$\sigma [\epsilon_g T_g^4 - \alpha_{g,1} T_1^4] = \epsilon_m \sigma (T_g^4 - T_1^4) \quad (5-176a)$$

or
$$\epsilon_m \equiv \frac{\epsilon_g - \alpha_{g,1} (T_1/T_g)^4}{1 - (T_1/T_g)^4} \quad (5-176b)$$

The calculation then proceeds by computing *two* values of ϵ_m at the given T_g and T_1 temperature pair and the two values of pL_M and $2pL_M$. We thereby obtain the expression $\epsilon_m = a_m (1 - \tau_m)$. It is then assumed that $a_1 = a_2 = a_g = a_m$ for use in Eqs. (5-171). This simplification may be used for $M > 2$ as long as $N = 1$. This simplification is illustrated in Example 12.

Example 12: WSGG Clear plus Gray Gas Emissivity Calculations
 Methane is burned to completion with 20 percent excess air (50 percent relative humidity at 298 K or 0.0088 mol water/mol dry air) in a furnace chamber of floor dimensions 3×10 m and height 5 m. The entire surface area of the enclosure is a gray sink with emissivity of 0.8 at temperature 1000 K. The confined gas is well stirred at a temperature of 1500 K. Evaluate the clear plus gray WSGG constants and the mean effective gas emissivity, and calculate the average radiative flux density to the enclosure surface.

Two-zone model, $M = 1, N = 1$: A single volume zone completely surrounded by a single sink surface zone.

Function definitions:

Gas emissivity: $\epsilon_g F(T_g, pL, b, n) := b \cdot (pL - 0.015)^n + T_g$
 Eq. (5-140a)

Gas absorptivity: $\alpha_g 1F(T_g, T_1, pL, b, n)$
 Eq. (5-141)

$$:= \frac{\epsilon_g F(T_1, pL \cdot T_1 + T_g, b, n) \cdot T_1 \cdot (T_g + T_1)^{0.5}}{T_1}$$

Mean effective gas emissivity: $\epsilon_{gm}(\epsilon_g, \alpha_g, T_g, T_1) := \frac{\epsilon_g - \alpha_g (T_1 + T_g)^4}{1 - (T_1 + T_g)^4}$
 Eq. (5-176a)

Physical constants: $\sigma \equiv 5.670400 \times 10^{-8} \frac{W}{m^2 \cdot K^4}$

Enclosure input parameters:

$T_g := 1500 \text{ K} \quad T_1 := 1000 \text{ K} \quad A_1 := 190 \text{ m}^2 \quad V := 150 \text{ m}^3$

$\epsilon_1 := 0.8 \quad \rho_1 := 1 - \epsilon_1 \quad \rho_1 = 0.2$

$E_1 := \sigma T_1^4 \quad E_g := \sigma T_g^4 \quad E_1 = 56.70 \frac{kW}{m^2} \quad E_g = 287.06 \frac{kW}{m^2}$

Stoichiometry yields the following mole table:

Mole Table: Basis 1.0 mol Methane

Species	MW	Moles in	Mass in	Moles out	Y out
CH ₄	16.04	1.00000	16.04	0.00000	0.00000
O ₂	32.00	2.40000	76.80	0.40000	0.03193
N ₂	28.01	9.02857	252.93	9.02857	0.72061
CO ₂	44.01	0.00000	0.00	1.00000	0.07981
H ₂ O	18.02	0.10057	1.81	2.10057	0.16765
Totals	27.742	12.52914	347.58	1.52914	1.00000

$p_W := .16765 \text{ atm} \quad p_C := 0.07981 \text{ atm} \quad p := p_W + p_C \quad p = 0.2475 \text{ atm}$
 $p_W + p_C = 2.101$

The mean beam length is approximated by

$$L_M := 0.88 \cdot 4 \cdot V \div A_1 \quad L_M = 2.7789 \text{ m}$$

and $pL_M := p \cdot L_M \quad pL_M = 0.6877 \text{ atm} \cdot \text{m} \quad 2pL_M := 0.6877$

The gas emissivities and absorptivities are then calculated from the two constant correlation in Table 5-5 (column 5 with $p_w/p_c = 2.0$) as follows:

$\epsilon_{g1} := \epsilon_g F(1500, pL_M, 540, .42) \quad \epsilon_{g1} = 0.3048$

$$\begin{aligned}\varepsilon_{g2} &:= \varepsilon_{gF}(1500, 2pL_M, 540, .42) & \varepsilon_{g2} &= 0.4097 \\ \alpha_{g11} &:= \alpha_{g1F}(1500, 1000, pL_M, 444, .34) & \alpha_{g11} &= 0.4124 \\ \alpha_{g12} &:= \alpha_{g1F}(1500, 1000, 2pL_M, 444, .34) & \alpha_{g12} &= 0.5250\end{aligned}$$

Case (a): Compute Flux Density Using Exact Values of the WSGG Constants

$$\begin{aligned}\tau_g &:= \frac{\varepsilon_{g2}}{\varepsilon_{g1}} - 1 & a_g &:= \frac{\varepsilon_{g1}}{1 - \tau_g} & \varepsilon_g &:= a_g \cdot (1 - \tau_g) & a_{g1} &:= \frac{\alpha_{g11}}{1 - \tau_g} \\ \tau_g &= 0.3442 & a_g &= 0.4647 & \varepsilon_g &= 0.3048 & a_{g1} &= 0.6289\end{aligned}$$

and the WSGG gas absorption coefficient (which is necessary for calculation of direct exchange areas) is calculated as $K_1 := \frac{-\ln \tau_g}{L_M}$ or $K_1 = 0.3838 \frac{1}{m}$

Compute directed exchange areas:
Eqs. (5-169)

$$\begin{aligned}s1g &:= (1 - \tau_g) \cdot A_1 & s1g &= 124.61 \text{ m}^2 \\ DS1G &:= \frac{a_g \cdot \varepsilon_1 \cdot A_1 \cdot s1g}{\varepsilon_1 \cdot A_1 + \rho_1 \cdot s1g} & DGS1 &:= \frac{a_{g1} \cdot \varepsilon_1 \cdot A_1 \cdot s1g}{\varepsilon_1 \cdot A_1 + \rho_1 \cdot s1g} \\ DS1G &= 49.75 \text{ m}^2 & DGS1 &= 67.32 \text{ m}^2\end{aligned}$$

And finally the gas to sink flux density is computed as

$$Q_1 := DGS1 \cdot E_1 - DS1G \cdot E_g \quad Q_1 = -10464.0 \text{ kW} \quad \frac{Q_1}{A_1} = -55.07 \frac{\text{kW}}{\text{m}^2}$$

Case (b): Compute the Flux Density Using Mean Effective Gas Emissivity Approximation

$$\begin{aligned}\varepsilon_{gm1} &:= \varepsilon_{gm}(\varepsilon_{g1}, \alpha_{g11}, T_g, T_1) & \varepsilon_{gm1} &= 0.2783 \\ \varepsilon_{gm2} &:= \varepsilon_{gm}(\varepsilon_{g2}, \alpha_{g12}, T_g, T_1) & \varepsilon_{gm2} &= 0.3813 \\ \tau_m &:= \frac{\varepsilon_{gm2}}{\varepsilon_{gm1}} - 1 & a_m &:= \frac{\varepsilon_{gm1}}{1 - \tau_m} & \varepsilon_{gm} &:= a_m \cdot (1 - \tau_m) \\ \tau_m &= 0.3701 & a_m &= 0.4418 & \varepsilon_{gm} &= 0.2783 & s1g_m &:= (1 - \tau_m) \cdot A_1 \\ S1G_m &:= \frac{\varepsilon_1 \cdot a_m \cdot s1g_m \cdot A_1}{\varepsilon_1 \cdot A_1 + \rho_1 \cdot s1g_m} & S1G_m &= 45.68 \text{ m}^2 & s1g_m &= 119.67 \text{ m}^2 \\ q_{1m} &:= \frac{S1G_m \cdot (E_1 - E_g)}{A_1} & q_{1m} &= -55.38 \frac{\text{kW}}{\text{m}^2} \\ \text{compared with } \frac{Q_1}{A_1} &= -55.07 \frac{\text{kW}}{\text{m}^2}\end{aligned}$$

The computed flux densities are nearly equal because there is a *single* sink zone A_1 . (This example was developed as a MATHCAD 14[®] worksheet. Mathcad is a registered trademark of Parametric Technology Corporation.)

ENGINEERING MODELS FOR FUEL-FIRED FURNACES

Modern digital computation has evolved methodologies for the design and simulation of fuel-fired combustion chambers and furnaces which incorporate virtually *all* the transport phenomena, chemical kinetics, and thermodynamics studied by chemical engineers. Nonetheless, there still exist many furnace design circumstances where such computational sophistication is not always appropriate. Indeed, a practical need still exists for simple engineering models for purposes of conceptual process design, cost estimation, and the correlation of test performance data. In this section, the zone method is used to develop perhaps the simplest **computational template** available to address some of these practical engineering needs.

Input/Output Performance Parameters for Furnace Operation The term **firing density** is typically used to define the basic *operational input parameter* for fuel-fired furnaces. In practice, firing density is often defined as the input fuel feed rate per unit area (or volume) of furnace heat-transfer surface. Thus defined, the firing density is a *dimensional quantity*. Since the feed enthalpy rate H_f is

proportional to the feed rate, we employ the sink area A_1 to define a **dimensionless firing density** as $\bar{N}_{FD} = H_f / \sigma T_{Ref}^4 A_1$ where T_{Ref} is some characteristic reference temperature. In practice, gross furnace *output performance* is often described by using one of several *furnace efficiencies*. The most common is the **gas or gas-side furnace efficiency** η_g , defined as the total enthalpy transferred to furnace internals divided by the total available feed enthalpy. Here the total available feed enthalpy is defined to include the lower heating value (LHV) of the fuel plus any air preheat above an arbitrary ambient datum temperature. Under certain conditions the definition of furnace efficiency reduces to some variant of the simple equation $\eta_g = (T_{Ref} - T_{out}) / (T_{Ref} - T_0)$ where again T_{Ref} is some reference temperature appropriate to the system in question.

The Long Plug Flow Furnace (LPFF) Model If a combustion chamber of cross-sectional area A_{Duct} and perimeter P_{Duct} is sufficiently long in the direction of flow, compared to its mean hydraulic radius, $L \gg R_h = A_{Duct} / P_{Duct}$, the radiative flux from the gas to the bounding surfaces can sometimes be adequately characterized by the *local* gas temperature. The physical rationale for this is that the *magnitudes* of the opposed upstream and downstream radiative fluxes through a cross section transverse to the direction of flow are sufficiently large as to substantially balance each other. Such a situation is not unusual in engineering practice and is referred to as the *long furnace approximation*. As a result, the radiative flux from the gas to the bounding surface may then be approximated using *two-dimensional* directed exchange areas, $\overleftarrow{S_1G} / A_1 \equiv \frac{\partial(S_1G)}{\partial A_1}$, calculated using methods as described previously.

Consider a duct of length L and perimeter P , and assume plug flow in the direction of flow z . Further assume high-intensity mixing at the entrance end of the chamber such that combustion is *complete* as the combustion products enter the duct. The duct then acts as a long heat exchanger in which heat is transferred to the walls at constant temperature T_1 by the combined effects of radiation and convection. Subject to the long furnace approximation, a differential energy balance on the duct then yields

$$\dot{m} \bar{C}_p \frac{dT_g}{dz} = P \left[\frac{\overleftarrow{S_1G}}{A_1} \sigma (T_g^4 - T_1^4) + h(T_g - T_1) \right] \quad (5-177)$$

where \dot{m} is the mass flow rate and \bar{C}_p is the heat capacity per unit mass. Equation (5-177) is nonlinear with respect to temperature. To solve Eq. (5-177), first linearize the convective heat-transfer term in the right-hand side with the approximation $\Delta T = T_2 - T_1 \approx (T_2^3 - T_1^3) / 4T_{1,2}^2$ where $T_{1,2} = (T_1 + T_2) / 2$. This linearization underestimates ΔT by no more than 5 percent when $T_2 / T_1 < 1.59$. Integration of Eq. (5-177) then leads to the solution

$$\ln \left[\frac{(T_{g,out} - T_1)(T_{g,in} + T_1)}{(T_{g,out} + T_1)(T_{g,in} - T_1)} \right] + 2.0 \tan^{-1} \left[\frac{(T_{g,in} - T_{g,out}) \cdot T_1}{(T_1^2 + T_{g,in} \cdot T_{g,out})} \right] = - \frac{4}{D_{eff}} \quad (5-178)$$

The LPFF model is described by only two dimensionless parameters, namely an *effective* firing density and a dimensionless sink temperature, viz.,

$$D_{eff} = \frac{N_{FD}}{\left(\frac{\overleftarrow{S_1G}}{A_1} \right) + N_{CR}} \quad \text{and} \quad \Theta_1 = T_1 / T_{g,in} \quad (5-178a,b)$$

Here the dimensionless firing density, N_{FD} , and a dimensionless convection-radiation number N_{CR} are defined as

$$N_{FD} = \frac{\dot{m} \bar{C}_p}{\sigma T_1^3 A_1} \quad \text{and} \quad N_{CR} = \frac{h}{4\sigma T_{g,1}^3} \quad (5-178c,d)$$

where $A_1 = PL$ is the duct surface area (the sink area), and $\bar{T}_{g,1} = (T_g + T_1) / 2$ is treated as a constant. This definition of the effective dimensionless firing density, D_{eff} , clearly delineates the relative

roles of radiation and convective heat transfer since radiation and convection are identified as *parallel (electrical) conductances*.

In analogy with a conventional heat exchanger, Eq. (5-178) displays two asymptotic limits. First define

$$\eta_f = \frac{T_{g,\text{in}} - T_{g,\text{out}}}{T_{g,\text{in}} - T_1} = 1 - \frac{T_{g,\text{out}} - T_1}{T_{g,\text{in}} - T_1} \quad (5-179)$$

as the efficiency of the long furnace. The two asymptotic limits with respect to firing density are then given by

$$D_{\text{eff}} \ll 1, \quad T_{g,\text{out}} \rightarrow T_1 \quad \eta_f \rightarrow 1 \quad (5-179a)$$

and

$$D_{\text{eff}} \gg 1, \quad T_{g,\text{out}} \rightarrow T_{g,\text{in}}$$

$$\eta_f \rightarrow \frac{4}{D_{\text{eff}} \left[1 - \frac{R-1}{R+1} - 2 \frac{R-1}{R^2+1} \right]} \quad (5-179b)$$

where $R \equiv T_{g,\text{in}}/T_1 = 1/\Theta_1$.

For low firing rates, the exit temperature of the furnace gases approaches that of the sink, i.e., sufficient residence time is provided for nearly complete heat removal from the gases. When the combustion chamber is overfired, only a small fraction of the available feed enthalpy heat is removed within the furnace. The exit gas temperature then remains essentially that of the inlet temperature, and the furnace efficiency tends asymptotically to zero.

It is important to recognize that the two-dimensional exchange area $\frac{\overline{S_1 G}}{A_1} \equiv \frac{\partial(\overline{S_1 G})}{\partial A_1}$ in the definition of D_{eff} can represent a *lumped* two-

dimensional exchange area of somewhat arbitrary complexity. This quantity also contains *all* the information concerning furnace geometry and gas and surface emissivities. To compare the relative importance of radiation with respect to convection, suppose $h = 10 \text{ Btu}/(\text{hr-ft}^2 \cdot ^\circ\text{R}) = 0.057 \text{ kW}/(\text{K} \cdot \text{m}^2)$ and $T_{g,1} = 1250 \text{ K}$, which leads to the numerical value $N_{\text{CR}} = 0.128$; or, in general, N_{CR} is of order 0.1 or less. The importance of the radiation contribution is estimated by bounding the magnitude of the dimensionless directed exchange area. For the case of a single gas zone completely surrounded by a black enclosure, Eq. (5-169) reduces to simply $\overline{S_1 G}/A_1 = \epsilon_g \leq 1.0$, and it is evident that the magnitude of the radiation contribution never exceeds unity. At high temperatures, radiative effects can easily dominate other modes of heat transfer by an order of magnitude or more. When mean beam length calculations are employed, use $L_M/D = 0.94$ for a cylindrical cross section of diameter D , and

$$L_{M0} = \frac{2H \cdot W}{H + W}$$

for a rectangular duct of height H and width W .

The Well-Stirred Combustion Chamber (WSCC) Model
Many combustion chambers utilize high-momentum feed conditions with associated high-intensity mixing. The **well-stirred combustion chamber (WSCC) model** assumes a single gas zone and high-intensity mixing. Moreover, combustion and heat transfer are visualized to occur *simultaneously* within the combustion chamber. The WSCC model is characterized by some *six* temperatures which are listed in rank order as T_0 , T_{air} , T_1 , T_e , T_g , and T_f . Even though the combustion chamber is well mixed, it is *arbitrarily* assumed that the gas temperature within the enclosure T_g is *not necessarily equal* to the gas exit temperature T_e . Rather the two temperatures are related by the simple relation $\Delta T_{ge} \equiv T_g - T_e$, where $\Delta T_{ge} \approx 170 \text{ K}$ (as a representative value) is introduced as an *adjustable parameter* for purposes of data fitting and to make allowance for nonideal mixing. In addition, T_0 is the ambient temperature, T_{air} is the air preheat temperature, and T_f is a *pseudoadiabatic flame temperature*, as shall be explained in the following development. The condition $\Delta T_{ge} \equiv 0$ is intended to simulate a perfect continuous well-stirred reactor (CSTR).

Dimensional WSCC Approach A macroscopic enthalpy balance on the well-stirred combustion chamber is written as

$$-\Delta H = H_{\text{in}} - H_{\text{out}} = Q_{\text{Rad}} + Q_{\text{Con}} + Q_{\text{Ref}} \quad (5-180)$$

Here $Q_{\text{Rad}} = \overline{S_1 G_R} \sigma (T_g^4 - T_1^4)$ represents radiative heat transfer to the sink (with due allowance for the presence of any refractory surfaces). And the two terms $Q_{\text{Con}} = h_1 A_1 (T_g - T_1)$ and $Q_{\text{Ref}} = U A_R (T_g - T_0)$ formulate the convective heat transfer to the sink and *through* the refractory, respectively.

Formulation of the left-hand side of Eq. (5-180) requires representative thermodynamic data and information on the combustion stoichiometry. In particular, the former includes the lower heating value of the fuel, the temperature-dependent molal heat capacity of the inlet and outlet streams, and the air preheat temperature T_{air} . It proves especially convenient now to introduce the definition of a pseudoadiabatic flame temperature T_f , which is *not* the true adiabatic flame temperature, but rather is an adiabatic flame temperature based on the average heat capacity of the combustion products over the temperature interval $T_0 < T < T_e$. The calculation of T_f does not allow for dissociation of chemical species and is a surrogate for the total enthalpy content of the input fuel-air mixture. It also proves to be an especially convenient system *reference temperature*. Details for the calculation of T_f are illustrated in Example 13.

In terms of this particular definition of the pseudoadiabatic flame temperature T_f , the total enthalpy change and gas efficiency are given simply as

$$\Delta H = \dot{H}_f - \dot{m} \cdot \overline{C}_{P,\text{Prod}} (T_e - T_0) = \dot{m} \overline{C}_{P,\text{Prod}} (T_f - T_e) \quad (5-181a,b)$$

where $\dot{H}_f \equiv \dot{m} \cdot \overline{C}_{P,\text{Prod}} (T_f - T_0)$ and $T_e = T_g - \Delta T_{ge}$. This particular definition of T_f leads to an especially convenient formulation of furnace efficiency

$$\eta_g = Q/\dot{H}_f = \frac{\dot{m} \cdot \overline{C}_{P,\text{Prod}} (T_f - T_e)}{\dot{m} \cdot \overline{C}_{P,\text{Prod}} (T_f - T_0)} = \frac{T_f - T_e}{T_f - T_0} \quad (5-182)$$

In Eq. (5-182), \dot{m} is the total mass flow rate and $\overline{C}_{P,\text{Prod}}$ [J/(kg·K)] is defined as the average heat capacity of the product stream over the temperature interval $T_0 < T < T_e$.

The final overall enthalpy balance is then written as

$$\dot{m} \cdot \overline{C}_{P,\text{Prod}} (T_f - T_e) = \overline{S_1 G_R} \sigma (T_g^4 - T_1^4) + h_1 A_1 (T_g - T_1) + U A_R (T_g - T_0) \quad (5-183)$$

with $T_e = T_g - \Delta T_{ge}$.

Equation (5-183) is a nonlinear algebraic equation which may be solved by a variety of iterative methods. The *sole* unknown quantity, however, in Eq. (5-183) is the *gas* temperature T_g . It should be recognized, in particular, that T_f , T_e , $\overline{C}_{P,\text{Prod}}$, and the directed exchange area are all explicit functions of T_g . The method of solution of Eq. (5-183) is demonstrated in some detail in Example 13.

Dimensionless WSCC Approach In Eq. (5-183), assume the convective heat loss through the refractory is negligible, and linearize the convective heat transfer to the sink. These approximations lead to the result

$$\dot{m} \cdot \overline{C}_{P,\text{Prod}} (T_f - T_g + \Delta T_{ge}) = \overline{S_1 G_R} \sigma (T_g^4 - T_1^4) + h_1 A_1 (T_g - T_1) / 4 \overline{T}_{g,1}^3 \quad (5-184)$$

where $\overline{T}_{g,1} = (T_g + T_1)/2$ is some characteristic average temperature which is taken as constant. Now normalize all temperatures based on the pseudoadiabatic temperature as in $\Theta_i = T_i/T_f$. Equation (5-184) then leads to the dimensionless equation

$$D_{\text{eff}} (1 - \Theta_g + \Delta^\circ) = (\Theta_g^4 - \Theta_1^4) \quad (5-185)$$

where again $D_{\text{eff}} = N_{\text{FD}} / (\overline{S_1 G}/A_1 + N_{\text{CR}})$ is defined *exactly* as in the case of the LPFF model, with the proviso that the WSCC dimensionless firing density is defined here as $N_{\text{FD}} = \dot{m} \overline{C}_{P,\text{Prod}} / (\sigma T_f^3 A_1)$. The dimensionless furnace efficiency follows directly from Eq. (5-182) as

$$\eta_g = \frac{1 - \Theta_e}{1 - \Theta_0} = \frac{1 - \Theta_g + \Delta^\circ}{1 - \Theta_0} \quad (5-186a)$$

We also define a **reduced furnace efficiency** η'_g

$$\eta'_g \equiv (1 - \Theta_0)\eta_g = 1 - \Theta_g + \Delta^\circ \tag{5-186b}$$

Since Eq. (5-186b) may be rewritten as $\Theta_g = (1 + \Delta^\circ - \eta'_g)$, combination of Eqs. (5-185) and (5-186b) then yields the final result

$$D_{\text{eff}}\eta'_g = (1 + \Delta^\circ - \eta'_g)^4 - \Theta_1^4 \tag{5-187}$$

Equation (5-187) provides an *explicit* relation between the modified furnace efficiency and the effective firing density directly in which the gas temperature is eliminated.

Equation (5-187) has two asymptotic limits

$$\begin{aligned} D_{\text{eff}} \ll 1 \quad \Theta_g &\rightarrow \Theta_1 \\ \eta'_g &\rightarrow 1 - \Theta_1 + \Delta^\circ \end{aligned} \tag{5-188a}$$

and

$$\begin{aligned} D_{\text{eff}} \gg 1 \quad \Theta_g &\rightarrow 1 + \Delta^\circ \quad \text{and} \quad \Theta_e \rightarrow 1 \\ \eta'_g &\rightarrow \frac{(1 + \Delta^\circ)^4 - \Theta_1^4}{D_{\text{eff}} + 4(1 + \Delta^\circ)^3} \end{aligned} \tag{5-188b}$$

Figure 5-23 is a plot of η'_g versus D_{eff} computed from Eq. (5-187) for the case $\Delta^\circ = 0$.

The asymptotic behavior of Eq. (5-189) mirrors that of the LPPF model. Here, however, for low firing densities, the exit temperature of the furnace exit gases approaches $\Theta_e = \Theta_1 - \Delta^\circ$ rather than the sink temperature. Moreover, for $D_{\text{eff}} \ll 1$ the reduced furnace efficiency adopts the constant value $\eta'_g = 1 - \Theta_e = 1 + \Delta^\circ - \Theta_1$. Again at very high firing rates, only a very small fraction of the available feed enthalpy heat is recovered within the furnace. Thus the exit gas temperature remains nearly unchanged from the pseudoadiabatic flame temperature $[T_e \approx T_f]$ and the gas-side efficiency necessarily approaches zero.

Example 13: WSCC Furnace Model Calculations Consider the furnace geometry and combustion stoichiometry described in Example 12. The end-fired furnace is 3 m wide, 5 m tall, and 10 m long. Methane at a firing rate of 2500 kg/h is burned to completion with 20 percent excess air which is preheated to 600°C. The speckled furnace model is to be used. The sink (zone 1)

occupies 60 percent of the total interior furnace area and is covered with two rows of 5-in (0.127-m) tubes mounted on equilateral centers with a center-to-center distance of twice the tube diameter. The sink temperature is 1000 K, and the tube emissivity is 0.7. Combustion products discharge from a 10-m² duct in the roof which is also tube-screen covered and is to be considered part of the sink. The refractory (zone 2) with emissivity 0.6 is radiatively adiabatic but demonstrates a small convective heat loss to be calculated with an overall heat transfer coefficient U . Compute all unknown furnace temperatures, the gas-side furnace efficiency, and the mean heat flux density through the tube surface. Use the *dimensional* solution approach for the well-stirred combustor model and compare computed results with the *dimensionless* WSCC and LPPF models. Computed values for mean equivalent gas emissivity obtained from Eq. (5-174b) and Table 5-5 for $T_g = 2000$ K for $L_M = 2.7789$ m and $T_1 = 1000$ K are found to be

$T_g = 1500$ K	$a_m = 0.44181$	$\tau_m = 0.37014$	$\epsilon_m = 0.27828$
$T_g = 2000$ K	$a_m = 0.38435$	$\tau_m = 0.41844$	$\epsilon_m = 0.22352$

Over this temperature range the gas emissivity may be calculated by linear interpolation. Additional heat-transfer and thermodynamic data are supplied in context.

Three-zone speckled furnace model, M = 2, N = 1:

Zone 1: Sink (60 percent of total furnace area)

Zone 2: Refractory surface (40 percent of total furnace area)

Physical constants:

$$\sigma = 5.670400 \times 10^{-8} \frac{\text{W}}{\text{m}^2 \cdot \text{K}^4}$$

Linear interpolation function for mean effective gas emissivity constants:

$$\text{LINTF}(T, Y_2, Y_1) := \frac{Y_1 \cdot (2000 \text{ K} - T) + Y_2 \cdot (T - 1500 \text{ K})}{500 \text{ K}} \quad (1500 \text{ K} < T < 2000 \text{ K})$$

Enclosure input parameters:

$$V_{\text{tot}} := 150 \text{ m}^3 \quad A_{\text{tot}} := 190 \text{ m}^2 \quad C_1 := 0.6 \quad C_2 := 1 - C_1$$

$$A_1 := C_1 \cdot A_{\text{tot}} \quad A_2 := C_2 \cdot A_{\text{tot}} \quad D_{\text{tube}} := .127 \text{ m}$$

Direct exchange areas for WSCC clear gas component (temperature independent):

$$F := \begin{pmatrix} C_1 & C_2 \\ C_1 & C_2 \end{pmatrix} \quad AI := \begin{pmatrix} A_1 & 0 \\ 0 & A_2 \end{pmatrix} \quad ss1 := AI \cdot F \quad ss1 = \begin{pmatrix} 68.40 & 45.60 \\ 45.60 & 30.40 \end{pmatrix} \text{m}^2$$

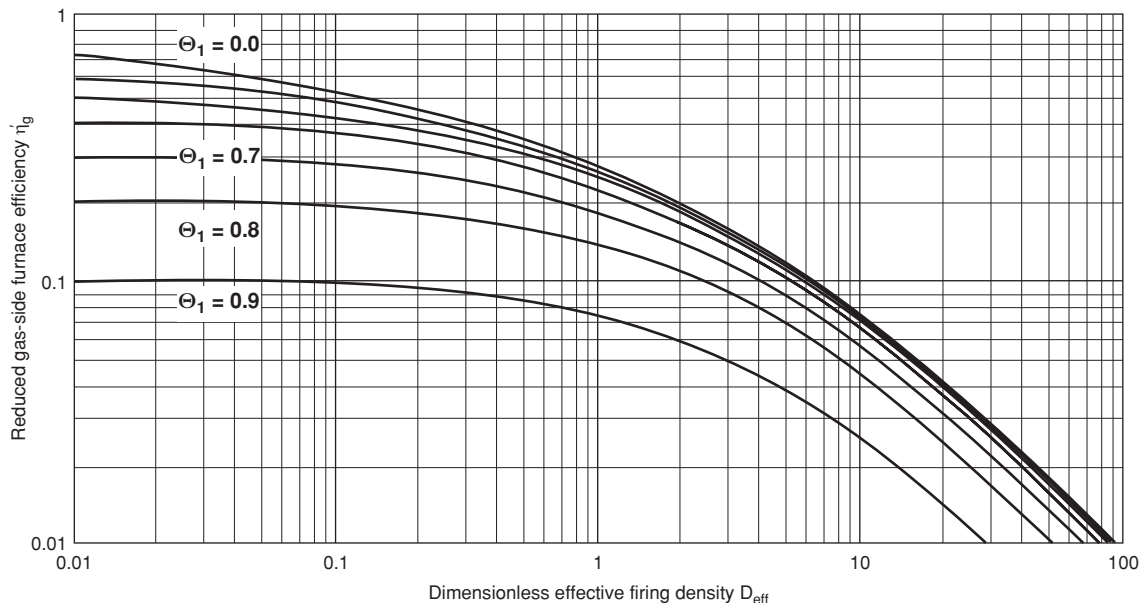


FIG. 5-23 Reduced gas-side furnace efficiency versus effective firing density for well-stirred combustion chamber model. $\Delta^\circ = 0$, $\Theta_1 = 0.0, 0.4, 0.5, 0.6, 0.7, 0.8, 0.9$.

5-42 HEAT AND MASS TRANSFER

Equivalent gray plane emissivity calculations for sink:

$$\epsilon_{\text{tube}} := 0.7 \quad F_{\text{bar}} := 0.987 \quad (\text{from Fig. 5-13, curve 6 with ratio} = 2.0)$$

$$\epsilon_{1,\text{eq}} := \frac{1}{\left(\frac{1}{\epsilon_1} - 1\right) + 2 \cdot \frac{D_{\text{tube}}}{2 \cdot \pi \cdot D_{\text{tube}}} \cdot \left(\frac{1}{\epsilon_{\text{tube}}} - 1\right) + \frac{1}{F_{\text{bar}}}} \quad \epsilon_{1,\text{eq}} = 0.86988$$

$$\epsilon_1 := \epsilon_{1,\text{eq}} \quad \epsilon_2 := 0.6 \quad \epsilon I := \begin{pmatrix} \epsilon_1 & 0 \\ 0 & \epsilon_2 \end{pmatrix} \quad \rho I := \text{identity}(2) - \epsilon I$$

Total exchange areas for WSGG clear gas component:

$$R1 := (AI - ss1 \cdot \rho I)^{-1} \quad SS1 := \epsilon I \cdot AI \cdot R1 \cdot ss1 \cdot \epsilon I \quad SS1 = \begin{pmatrix} 67.93 & 31.24 \\ 31.24 & 14.36 \end{pmatrix} \text{m}^2$$

Temperature and emissive power input data:

$$T_1 := 1000.0 \text{ K} \quad T_{\text{air}} := 873.15 \text{ K}$$

$$T_0 := 298.15 \text{ K} \quad \Delta T_{\text{gr}} := 170 \text{ K} \quad E_1 := \sigma \cdot T_1^4 \quad E_1 = 56.704 \frac{\text{kW}}{\text{m}^2}$$

Mean beam length calculations:

$$L_{M0} := 4 \cdot \frac{V_{\text{tot}}}{A_{\text{tot}}} \quad L_{M0} = 3.1579 \text{ m} \quad L_M := 0.88 L_{M0} \quad L_M = 2.7789 \text{ m}$$

Stoichiometric and thermodynamic input data:

$$\text{MCH}_{4,\text{dot}} := 2500 \frac{\text{kg}}{\text{h}} \quad \text{MW}_{\text{CH}_4} := 16.04 \frac{\text{g}}{\text{mol}} \quad \text{MW}_{\text{in}} := 27.742 \frac{\text{g}}{\text{mol}}$$

$$\Sigma \text{Mols} := 12.52914 \quad \text{LHV} := 191760 \frac{\text{cal}}{\text{mol}} \quad \text{MCP}_{\text{air}} := 7.31 \frac{\text{cal}}{\text{mol} \cdot \text{K}}$$

$$\text{MCP}(T) := \left[7.01 + 0.875 \left(\frac{T}{1000 \text{ K}} \right) \right] \frac{\text{cal}}{\text{mol} \cdot \text{K}} \quad (800 \text{ K} < T < 1200 \text{ K})$$

M_{dot} is the total mass flowrate and $\text{NCH}_{4,\text{dot}}$ is the molal flowrate of CH_4 .

$$M_{\text{dot}} := \frac{\text{MCH}_{4,\text{dot}} \cdot \text{MW}_{\text{in}} \cdot \Sigma \text{Mols}}{\text{MW}_{\text{CH}_4}} \quad \text{NCH}_{4,\text{dot}} := \frac{\text{MCH}_{4,\text{dot}}}{\text{MW}_{\text{CH}_4}}$$

$$M_{\text{dot}} = 54174.5 \frac{\text{kg}}{\text{h}} \quad \text{NCH}_{4,\text{dot}} = 155860.3 \frac{\text{mol}}{\text{h}}$$

Overall refractory heat-transfer coefficient:

$$D_r := 0.343 \text{ m} \quad k_r := 0.00050 \frac{\text{kW}}{\text{m} \cdot \text{K}}$$

$$h_0 := 0.0114 \frac{\text{kW}}{\text{m}^2 \cdot \text{K}} \quad h_0 = 2.0077 \frac{\text{Btu}}{\text{h} \cdot \text{ft}^2 \cdot \text{R}} \quad h_1 := 0.0170 \frac{\text{kW}}{\text{m}^2 \cdot \text{K}}$$

$$h_1 = 2.9939 \frac{\text{Btu}}{\text{h} \cdot \text{ft}^2 \cdot \text{R}} \quad U := \frac{1}{\frac{1}{h_0} + \frac{1}{h_1} + \frac{D_r}{k_r}}$$

$$U = 0.001201 \frac{\text{kW}}{\text{m}^2 \cdot \text{K}} \quad U = 0.2115 \frac{\text{Btu}}{\text{h} \cdot \text{ft}^2 \cdot \text{R}}$$

START OF ITERATION LOOP: Successive Substitution with T_g as the Trial Variable

$$\text{Assume } T_g := 1759.1633222447 \text{ K} \quad T_r := T_g - \Delta T_{\text{gr}} \quad T_e = 1589.2 \text{ K}$$

$$E_g := \sigma \cdot T_g^4 \quad E_g = 543.05 \frac{\text{kW}}{\text{m}^2}$$

Compute temperature-dependent mean effective gas emissivity via linear interpolation:

$$\tau_m := \text{LINTF}(T_g, 0.37014, 0.418442) \quad a_m := \text{LINTF}(T_g, 0.44181, 0.38435)$$

$$\tau_m = 0.3934 \quad a_m = 0.4141 \quad \epsilon_m := a_m \cdot (1 - \tau_m) \quad \epsilon_m = 0.2512$$

Compare interpolated value:

$$\epsilon_{\text{com}} := \text{LINTF}(T_g, 0.27828, 0.22352) \quad \epsilon_{\text{com}} = 0.2519$$

Direct and total exchange areas for WSGG gray gas component:

$$ss2 := \tau_m \cdot ss1 \quad sg2 := (AI - ss2) \begin{bmatrix} 1 \\ 1 \end{bmatrix} \quad R2 := (AI - ss2 \cdot \rho I)^{-1}$$

$$ss2 = \begin{pmatrix} 26.91 & 17.94 \\ 17.94 & 11.96 \end{pmatrix} \text{m}^2 \quad sg2 = \begin{pmatrix} 69.15 \\ 46.10 \end{pmatrix} \text{m}^2 \quad SS2 := \epsilon I \cdot AI \cdot R2 \cdot ss2 \cdot \epsilon I$$

Compute directed exchange areas:

$$DSS := (1 - a_m) \cdot SS1 + a_m \cdot SS2 \quad DSG := a_m \cdot \epsilon I \cdot AI \cdot R2 \cdot sg2$$

Refractory augmented directed gas-sink exchange area:

$$\text{DS1GR} := \text{DSG}_1 + \frac{\text{DSS}_{1,2} \cdot \text{DSG}_2}{\text{DSS}_{1,2} + \text{DSG}_2} \quad \text{DS1GR} = 35.59 \text{ m}^2 \quad \text{Eq. (5-172a)}$$

Compute refractory temperature (T_2); assume radiative equilibrium:

$$\text{Equation (5-172b): } E_2 := \frac{\text{DSS}_{2,1} \cdot E_1 + \text{DSG}_{2,1} \cdot E_g}{\text{DSS}_{2,1} + \text{DSG}_{2,1}}$$

$$E_2 = 231.24 \frac{\text{kW}}{\text{m}^2}$$

$$T_2 := \left(\frac{E_2}{\sigma} \right)^{0.25} \quad T_2 = 1421.1 \text{ K}$$

Enthalpy balance: Basis: 1 mole CH_4 :

$$h_{\text{in}} := \text{LHV} + (\Sigma \text{Mols} - 1) \cdot \text{MCP}_{\text{air}} \cdot (T_{\text{air}} - T_0) \quad h_{\text{in}} = 240219.9 \frac{\text{cal}}{\text{mol}}$$

Compute pseudoadiabatic flame temperature T_f :

$$T_f := T_0 + \frac{h_{\text{in}}}{\Sigma \text{Mols} \cdot \text{MCP}(T_e)} \quad h_{\text{out}} := \Sigma \text{Mols} \cdot \text{MCP}(T_e) \cdot (T_e - T_0)$$

$$T_f = 2580.5 \text{ K} \quad h_{\text{out}} = 135880.8 \frac{\text{cal}}{\text{mol}}$$

$$H_{\text{in}} := \text{NCH}_{4,\text{dot}} \cdot h_{\text{in}} \quad H_{\text{out}} := \text{NCH}_{4,\text{dot}} \cdot h_{\text{out}} \quad \Delta H := H_{\text{out}} - H_{\text{in}}$$

$$H_{\text{in}} = 43543.59 \text{ kW} \quad H_{\text{out}} = 24630.51 \text{ kW} \quad \Delta H = -18913.08 \text{ kW}$$

Overall enthalpy balance:

$$Q1_g := \text{DS1GR} \cdot (E_g - E_1) \quad Q1_g = 17308.45 \text{ kW}$$

$$Q1_{\text{Con}} := h_1 \cdot A_1 \cdot (T_g - T_1) \quad Q1_{\text{Con}} = 1471.26 \text{ kW}$$

$$Q2_{\text{Con}} := U \cdot A_2 \cdot (T_g - T_0) \quad Q2_{\text{Con}} = 133.37 \text{ kW}$$

$$\text{ERROR} := Q1_g + Q1_{\text{Con}} + Q2_{\text{Con}} + \Delta H \quad \% \text{ERROR}1 := 100 \frac{\text{ERROR}}{\Delta H}$$

$$\text{ERROR} = -0.0000 \text{ kW} \quad \% \text{ERROR}1 = 0.00000$$

$$T_{\text{gcalc}} := \left[\frac{\text{DS1GR} \cdot E_1 - (\Delta H + Q1_{\text{Con}} + Q2_{\text{Con}})}{\text{DS1GR} \cdot \sigma} \right]^{0.25} \quad T_{\text{gcalc}} = 1759.16332 \text{ K}$$

Average assumed and calculated temperatures for next iteration

$$T_{\text{gnew}} := \frac{T_g + T_{\text{gcalc}}}{2} \quad T_{\text{gnew}} = 1759.1633222935 \text{ K} \quad \text{Go to Start}$$

END OF ITERATION LOOP: Final Gas Temperature $T_g = 1759.16 \text{ K}$

$$\eta_g := \frac{H_{\text{in}} - H_{\text{out}}}{H_{\text{in}}} \quad \text{or} \quad \eta_{1g} := \frac{T_f - T_e}{T_f - T_0} \quad \eta_g = 0.43435 \quad \eta_{1g} = 0.43435$$

Heat flux density calculations:

$$q_1 := \frac{Q1_g + Q1_{\text{Con}}}{A_1} \quad q_{\text{tube}} := q_1 \cdot \left(2 \cdot \frac{D_{\text{tube}}}{2 \cdot \pi \cdot D_{\text{tube}}} \right)$$

$$q_1 = 164.7 \frac{\text{kW}}{\text{m}^2} \quad q_{\text{tube}} = 52.44 \frac{\text{kW}}{\text{m}^2}$$

Note: This example was also solved with $\Delta T_{\text{gr}} = 0$. The results were as follows: $T_f = 2552.8 \text{ K}$, $T_e = T_r = 1707.1 \text{ K}$, $T_2 = 1381.1 \text{ K}$, $\eta_g = 37.51$ percent, $D_{\text{eff}} = 0.53371$, and $\Delta H = 16332.7 \text{ kW}$. The WSCC model with $\Delta T_{\text{gr}} = 0$ predicts a lower performance bound.

Compare dimensionless WSCC model:

$$\Theta_0 := \frac{T_0}{T_f} \quad \Theta_1 := \frac{T_1}{T_f} \quad \Delta T_{\text{star}} := \frac{\Delta T_{\text{gr}}}{T_f}$$

$$T_{\text{gl}} := \frac{T_1 + T_g}{2}$$

$$\Theta_0 = 0.1155 \quad \Theta_1 = 0.3875 \quad \Delta T_{star} = 0.06588 \quad T_{g1} = 1379.58 \text{ K}$$

$$C_{P_{prod}} := \frac{MCp(T_c)}{MW_{in}} \quad C_{P_{prod}} = 0.000352 \text{ kW} \cdot \frac{\text{h}}{\text{kg} \cdot \text{K}}$$

$$N_{FD} := M_{dot} \frac{C_{P_{prod}}}{\sigma T_g^3 A_1} \quad N_{CR} := \frac{h_1}{4 \sigma T_{g1}^3} \quad D_{eff} := \frac{N_{FD}}{\frac{DSIGR}{A_1} + N_{CR}}$$

$$N_{FD} = 0.17176 \quad N_{CR} = 0.02855 \quad D_{eff} = 0.50409 \quad \frac{DSIGR}{A_1} = 0.31218$$

$$\eta_{prime} := \eta_g (1 - \Theta_0) \quad D1_{eff} := \frac{(1 + \Delta T_{star} - \eta_{prime})^4 - \Theta_1^4}{\eta_{prime}}$$

$$D1_{eff} = 0.50350 \quad \text{versus} \quad D_{eff} = 0.50409$$

This small discrepancy is due to linearization and neglect of convective refractory heat losses in the dimensionless WSCC model.

Compare dimensionless LPFF model:

$$R_{in} := \frac{1}{\Theta_1} \quad R_{in} = 2.58050$$

Trial and error calculation to match effective firing densities:

Assume:

$$T_{out} := 1000.13763 \text{ K} \quad R_{out} := \frac{T_{out}}{T_1} \quad R_{out} = 1.00014 \quad \frac{4}{D_{eff}} = 7.93513$$

$$CLong := -\ln \left[\frac{(R_{out} - 1)(R_{in} + 1)}{(R_{in} - 1)(R_{out} + 1)} \right] - 2 \cdot \text{atan} \left(\frac{R_{in} - R_{out}}{1 + R_{in} R_{out}} \right) \quad CLong = 7.93514$$

$$\eta_{L_f} := \frac{R_{in} - R_{out}}{R_{in} - 1} \quad \eta_{L_f} = 0.99991292 \quad \text{versus} \quad \eta_g = 0.43435$$

Note: The long plug flow furnace Model is so efficient that it would be grossly underfired using the computed WSCC effective firing density. Of the two models, the LPFF model always predicts an upper theoretical performance limit.

(This example was developed as a MATHCAD 14® worksheet. Mathcad is registered trademark of Parametric Technology Corporation.)

WSCC Model Utility and More Complex Zoning Models

Despite its simplicity, the WSCC construct has a wide variety of practical uses and is of significant pedagogical value. Here an engineering situation of inordinate complexity is described by the definition of only eight dimensionless quantities D_{eff} , N_{FD} , $\hat{S}_i G_R/A_1$, N_{CR} , η_g , Δ^* , Θ_0 , and Θ_1 . The first three are related by the simple algebraic definition $D_{eff} = N_{FD}/(\hat{S}_i G_R/A_1 + N_{CR})$. These dimensionless quantities con-

tain all the physical input information for the model, namely, furnace parameters and geometry, radiative properties of the combustion products, and the stoichiometry and thermodynamics of the combustion process. The WSCC model leads to a dimensionless two-dimensional plot of *reduced* effective furnace efficiency versus dimensionless effective firing density (Fig. 5-23), which is characterized by only two additional parameters, namely, Δ^* and Θ_1 .

Of the models presented here, the WSCC model with $\Delta T_{ge} = 0$ produces the lowest furnace efficiencies. The long furnace model usually produces the highest furnace efficiency. This is really not a fair statement because two distinctly different pieces of process equipment are compared. In this regard, a more appropriate definition of the dimensionless firing density for the LPFF model might be $N'_{FD} = \dot{m} \bar{C}_p / (\sigma T_{g,in}^3 A_1)$. It may be counterintuitive, but the WSCC and LPFF models *generally do not* characterize the extreme conditions for the performance of combustors as in the case of chemical reactors.

Figure 5-23 has been used to correlate furnace performance data for a multitude of industrial furnaces and combustors. Typical operational domains for a variety of fuel-fired industrial furnaces are summarized in Table 5-7. The WSCC approach (or "speckled" furnace model) is a classic contribution to furnace design methodology which was first due to Hottel [op. cit.]. The WSCC model provides a simple *furnace design template* which leads to a host of more complex furnace models. These models include an obvious extension to a tanks-in-series model as well as multizone models utilizing empirical cold-flow velocity patterns. For more information on practical furnace design models, reference is made to Hottel and Sarofim (op. cit., Chap. 14). Qualitative aspects of process equipment have been treated in some detail elsewhere (Baukal, C. E., ed., *The John Zink Combustion Handbook*, CRC Press, Boca Raton, Fla., 2001).

TABLE 5-7 Operational Domains for Representative Process Furnaces and Combustors

Domain	Furnace or combustor type	Dimensionless sink temperature	Dimensionless firing density
A	Oil processing furnaces; radiant section of oil tube stills and cracking coils	$\Theta_1 \approx 0.4$	$0.1 < D_{eff} < 1.0$
B	Domestic boiler combustion chambers	$\Theta_1 \approx 0.2$	$0.5 < D_{eff} < 1.1$
C	Glass furnaces	$0.7 < \Theta_1 < 0.8$	$0.035 < D_{eff} < 0.8$
D	Soaking pits	$\Theta_1 \approx 0.6$	$0.7 < D_{eff} < 1.1$
E	Gas-turbine combustors	$0.4 < \Theta_1 < 0.7$	$4.0 < D_{eff} < 25.0$

MASS TRANSFER

GENERAL REFERENCES: Bird, Stewart, and Lightfoot, *Transport Phenomena*, 2d ed., Wiley, New York, 2002. Cussler, *Diffusion: Mass Transfer in Fluid Systems*, 2d ed., Cambridge University Press, Cambridge, 1997. Danner and Daubert, *Manual for Predicting Chemical Process Design Data*, AIChE, New York, 1983. Daubert and Danner, *Physical and Thermodynamic Properties of Pure Chemicals*, Taylor and Francis, Bristol, Pa., 1989–1995. Gammon, Marsh, and Dewan, *Transport Properties and Related Thermodynamic Data of Binary Mixtures*, AIChE, New York, Part 1, 1993; Part 2, 1994. Geankoplis, *Transport Processes and Separation Process Principles*, 5th ed., Prentice-Hall PTR, Upper Saddle River, N.J., 2003. Kirwan, "Mass Transfer Principles," Chap. 2 in Rousseau, R. W. (ed.), *Handbook of Separation Process Technology*, Wiley, New York, 1987. McCabe, Smith, and Harriott, *Unit Operations of Chemical Engineering*, 7th ed., McGraw-Hill, New York, 2006. Middleman, *An Introduction to Mass and Heat Transfer*, Wiley, New York, 1997. Poling, Prausnitz, and O'Connell, *The Properties of Gases and Liquids*, 5th ed., McGraw-Hill, New York, 2001. Schwartzberg and Chao, *Food Technol.*, **36**(2), 73 (1982). Sherwood, Pigford, and Wilke, *Mass Transfer*, McGraw-Hill, New York, 1975. Skelland, *Diffusional Mass Transfer*, Wiley, New York, 1974. Taylor and Krishna, *Multicomponent Mass Transfer*, Wiley, New York, 1993. Thompson, *Introduction to Transport Phenomena*, Prentice-Hall PTR, Upper Saddle River, N.J., 1999. Treybal, *Mass-Transfer Operations*, 3d ed., McGraw-Hill, New York, 1980.

REFERENCES FOR DIFFUSIVITIES, TABLES 5-10, 5-13 TO 5-15

- Asfour and Dullien, *Chem. Eng. Sci.*, **41**, 1891 (1986).
- Blanc, *J. Phys.*, **7**, 825 (1908).
- Bosse and Bart, *Ind. Eng. Chem. Res.*, **45**, 1822 (2006).
- Brokaw, *Ind. Eng. Chem. Process Des. and Dev.*, **8**, 2, 240 (1969).
- Caldwell and Babb, *J. Phys. Chem.*, **60**, 51 (1956).
- Catchpole and King, *Ind. Eng. Chem. Res.*, **33**, 1828 (1994).
- Chen and Chen, *Chem. Eng. Sci.*, **40**, 1735 (1985).
- Cullinan, *AIChE J.*, **31**, 1740–1741 (1985).
- Cussler, *AIChE J.*, **26**, 1 (1980).
- Fuller, Schettler, and Giddings, *Ind. Eng. Chem.*, **58**, 18 (1966).
- Hayduk and Laudie, *AIChE J.*, **20**, 3, 611 (1974).
- Hayduk and Minhas, *Can. J. Chem. Eng.*, **60**, 195 (1982).
- He and Yu, *Ind. Eng. Chem. Res.*, **36**, 4430 (1997).
- Lee and Thodos, *Ind. Eng. Chem. Fundam.*, **22**, 17–26 (1983).
- Lee and Thodos, *Ind. Eng. Chem. Res.*, **27**, 992–997 (1988).
- Leffler and Cullinan, *Ind. Eng. Chem. Fundam.*, **9**, 84, 88 (1970).
- Liu and Ruckenstein, *Ind. Eng. Chem. Res.*, **36**, 888 (1997) and corrections **37**, 3524 (1998).
- Mathur and Thodos, *AIChE J.*, **11**, 613 (1965).
- Matthews and Akgerman, *AIChE J.*, **33**, 881 (1987).

20. Rathbun and Babb, *Ind. Eng. Chem. Proc. Des. Dev.*, **5**, 273 (1966).
 21. Riazi and Whitson, *Ind. Eng. Chem. Res.*, **32**, 3081 (1993).
 22. Siddiqi and Lucas, *Can. J. Chem. Eng.*, **64**, 839 (1986).
 23. Smith and Taylor, *Ind. Eng. Chem. Fundam.*, **22**, 97 (1983).
 24. Sridhar and Potter, *AIChE J.*, **23**, 4, 590 (1977).
 25. Sun and Chen, *Ind. Eng. Chem. Res.*, **26**, 815 (1987).
 26. Tyn and Calus, *J. Chem. Eng. Data*, **20**, 310 (1975).
 27. Úmesi and Danner, *Ind. Eng. Chem. Process Des. Dev.*, **20**, 662 (1981).
 28. Vignes, *Ind. Eng. Chem. Fundam.*, **5**, 184 (1966).
 29. Wilke, *Chem. Eng. Prog.*, **46**, 2, 95 (1950).
 30. Wilke and Chang, *AIChE J.*, **1**, 164 (1955).
 31. Wilke and Lee, *Ind. Eng. Chem.*, **47**, 1253 (1955).
- REFERENCES FOR DIFFUSIVITIES IN POROUS SOLIDS, TABLE 5-16**
32. Ruthven, *Principles of Adsorption and Adsorption Processes*, Wiley, 1984.
 33. Satterfield, *Mass Transfer in Heterogeneous Catalysis*, MIT Press, 1970.
 34. Suzuki, *Adsorption Engineering*, Kodansha—Elsevier, 1990.
 35. Yang, *Gas Separation by Adsorption Processes*, Butterworths, 1987.
- REFERENCES FOR TABLES 5-17 TO 5-24**
36. Bahmanyar, et al., *Chem. Eng. Rsch. Des.*, **68**, 74 (1990).
 37. Baier et al., *Chem. Eng. Sci.*, **54**, 343 (1999).
 38. Beenackers and van Swaij, *Chem. Eng. Sci.*, **48**, 3109 (1993).
 39. Bird, Stewart, and Lightfoot, *Transport Phenomena*, Wiley, 1960.
 40. Blatt et al. (eds.), (ed.), *Membrane Science and Technology*, **47**, Plenum, 1970.
 41. Bocquet et al., *AIChE J.*, **51**, 1067 (2005).
 42. Bolles and Fair, *Institution Chem. Eng. Symp. Ser.*, **56**, 3/35 (1979).
 43. Bolles and Fair, *Chem. Eng.*, **89**(14), 109 (July 12, 1982).
 44. Bravo and Fair, *Ind. Eng. Chem. Process Des. Dev.*, **21**, 162 (1982).
 45. Bravo, Rocha and Fair, *Hydrocarbon Processing*, 91 (Jan. 1985).
 46. Brian and Hales, *AIChE J.*, **15**, 419 (1969).
 47. Calderbank and Moo-Young, *Chem. Eng. Sci.*, **16**, 39 (1961).
 48. Cavatorta, Bohm, and Chiappori de del Giorgio, *AIChE J.*, **45**, 938 (1999).
 49. Chaumat et al., *Chem. Eng. Sci.*, **60**, 5930 (2005).
 50. Chen, Lin, and Liu, *Ind. Eng. Chem. Res.*, **44**, 7868 (2005).
 51. Chilton and Colburn, *Ind. Eng. Chem.*, **26**, 1183 (1934).
 52. Chowdhia, Foutch, and Lee, *Ind. Eng. Chem. Res.*, **42**, 1485 (2003).
 53. Colburn, *Trans. AIChE*, **29**, 174 (1933).
 54. Cornell, Knapp, and Fair, *Chem. Eng. Prog.*, **56**(7), 68 (1960).
 55. Cornet and Kaloo, *Proc. 3rd Int'l. Congr. Metallic Corrosion—Moscow*, **3**, 83 (1966).
 56. Crause and Nieuwoudt, *Ind. Eng. Chem. Res.*, **38**, 4928 (1999).
 57. Deckwer et al., *Biotech. Bioeng.* (1981).
 58. Dudukovic, Milosevic, and Pjanovic, *AIChE J.*, **42**, 269 (1996).
 59. Dwivedi and Upadhyay, *Ind. Eng. Chem. Process Des. Develop.*, **16**, 1657 (1977).
 60. Eisenberg, Tobias, and Wilke, *Chem. Eng. Prog. Symp. Sec.*, **51**(16), 1 (1955).
 61. El-Shazly et al., *Ind. Eng. Chem. Res.*, **41**, 5516 (2002).
 62. Elzinga and Banchemo, *Chem. Eng. Progr. Symp. Ser.*, **55**(29), 149 (1959).
 63. Fair, "Distillation" in Rousseau (ed.), *Handbook of Separation Process Technology*, Wiley, 1987.
 64. Fan, Yang, and Wen, *AIChE J.*, **6**, 482 (1960).
 65. Garner and Suckling, *AIChE J.*, **4**, 114 (1958).
 66. Geankoplis, *Transport Processes and Unit Operations*, 4th ed., Prentice Hall, 2003.
 67. Gibilaro et al., *Chem. Eng. Sci.*, **40**, 1811 (1985).
 68. Gilliland and Sherwood, *Ind. Eng. Chem.*, **26**, 516 (1934).
 69. Costick et al., *Ind. Eng. Chem. Res.*, **42**, 3626 (2003).
 70. Griffith, *Chem. Eng. Sci.*, **12**, 198 (1960).
 71. Guedes de Carvalho and Alves, *AIChE J.*, **45**, 2495 (1999).
 72. Gupta and Thodos, *AIChE J.*, **9**, 751 (1963).
 73. Gupta and Thodos, *Ind. Eng. Chem. Fundam.*, **3**, 218 (1964).
 74. Harriott, *AIChE J.*, **8**, 93 (1962).
 75. Hassan et al., *Ind. Eng. Chem. Res.*, **44**, 5761 (2005).
 76. Heertjes, Holve, and Talsma, *Chem. Eng. Sci.*, **3**, 122 (1954).
 77. Hines and Maddox, *Mass Transfer: Fundamentals and Applications*, Prentice-Hall, 1985.
 78. Hoffer et al., *Chem. Eng. Sci.*, **59**, 259 (2004).
 79. Houwing, Billiet, and van der Wielin, *AIChE J.*, **49**, 1158 (2003).
 80. Hsiung and Thodos, *Int. J. Heat Mass Transfer*, **20**, 331 (1977).
 81. Hsu, Sato, and Sage, *Ind. Eng. Chem.*, **46**, 870 (1954).
 82. Hughmark, *Ind. Eng. Chem. Fundam.*, **6**, 408 (1967).
 83. Johnson, Besic, and Hamielec, *Can. J. Chem. Eng.*, **47**, 559 (1969).
 84. Johnstone and Pigford, *Trans. AIChE*, **38**, 25 (1942).
 85. Kafesjian, Plank, and Gerhard, *AIChE J.*, **7**, 463 (1961).
 86. Kelly and Swenson, *Chem. Eng. Prog.*, **52**, 263 (1956).
 87. King, *Separation Processes*, 2d ed., McGraw-Hill (1980).
 88. Kirwan, "Mass Transfer Principles" in Rousseau, *Handbook of Separation Process Technology*, Wiley, 1987.
 89. Klein, Ward, and Lacey, "Membrane Processes—Dialysis and Electro-Dialysis" in Rousseau, *Handbook of Separation Process Technology*, Wiley, 1987.
 90. Kohl, "Absorption and Stripping" in Rousseau, *Handbook of Separation Process Technology*, Wiley, 1987.
 91. Kojima et al., *J. Chem. Engng. Japan*, **20**, 104 (1987).
 92. Koloini, Sopic, and Zumer, *Chem. Eng. Sci.*, **32**, 637 (1977).
 93. Kreutzer et al., *Ind. Eng. Chem. Res.*, **44**, 9646 (2005).
 94. Lancia, Musmarra, and Pepe, *Ind. Eng. Chem. Res.*, **36**, 3859 (1997).
 95. Larachi et al., *Ind. Eng. Chem. Res.*, **42**, 222 (2003).
 96. Lau et al., *Ind. Eng. Chem. Res.*, **43**, 1302 (2004).
 97. Lee, *Biochemical Engineering*, Prentice-Hall, 1992.
 98. Lee and Foster, *Appl. Catal.*, **63**, 1 (1990).
 99. Lee and Holder, *Ind. Eng. Chem. Res.*, **34**, 906 (1995).
 100. Lee and Lueptow, *Separ. Sci. Technol.*, **39**, 539 (2004).
 101. Levich, *Physicochemical Hydrodynamics*, Prentice-Hall, 1962.
 102. Levins and Gastonbury, *Trans. Inst. Chem. Eng.*, **50**, 32, 132 (1972).
 103. Linton and Sherwood, *Chem. Eng. Prog.*, **46**, 258 (1950).
 104. Ludwig, *Applied Process Design for Chemical and Petrochemical Plants*, 2d ed., vol. 2, Gulf Pub. Co., 1977.
 105. McCabe, Smith, and Harriott, *Unit Operations of Chemical Engineering*, 7th ed., McGraw-Hill, 2005.
 106. Nelson and Galloway, *Chem. Eng. Sci.*, **30**, 7 (1975).
 107. Notter and Sleicher, *Chem. Eng. Sci.*, **26**, 161 (1971).
 108. Ohashi et al., *J. Chem. Eng. Japan*, **14**, 433 (1981).
 109. Onda, Takeuchi, and Okumoto, *J. Chem. Eng. Japan*, **1**, 56 (1968).
 110. Pangarkar et al., *Ind. Eng. Chem. Res.*, **41**, 4141 (2002).
 111. Pasternak and Gauvin, *AIChE J.*, **7**, 254 (1961).
 112. Pasternak and Gauvin, *Can. J. Chem. Eng.*, **38**, 35 (April 1960).
 113. Patil, Deshmukh, and Joshi, *Ind. Eng. Chem. Res.*, **43**, 2765 (2004).
 114. Pekdemir, Davies, and Sara, *Ind. Eng. Chem. Res.*, **37**, 1560 (1998).
 115. Perez and Sandall, *AIChE J.*, **20**, 770 (1974).
 116. Petrovic and Thodos, *Ind. Eng. Chem. Fundam.*, **7**, 274 (1968).
 117. Pinczewski and Sideman, *Chem. Eng. Sci.*, **29**, 1969 (1974).
 118. Prasad and Sirkar, *AIChE J.*, **34**, 177 (1988).
 119. Rahman and Streat, *Chem. Eng. Sci.*, **36**, 293 (1981).
 120. Ramirez and Davis, *AIChE J.*, **45**, 1355 (1999).
 121. Ranz and Marshall, *Chem. Eng. Prog.*, **48**, 141, 173 (1952).
 122. Reiss, *Ind. Eng. Chem. Process Des. Develop.*, **6**, 486 (1967).
 123. Riet, *Ind. Eng. Chem. Process Des. Dev.*, **18**, 357 (1979).
 124. Rocha, Bravo, and Fair, *Ind. Eng. Chem. Res.*, **35**, 1660 (1996).
 125. Rowe, *Chem. Eng. Sci.*, **30**, 7 (1975).
 126. Rowe, Claxton, and Lewis, *Trans. Inst. Chem. Eng. London*, **43**, 14 (1965).
 127. Ruckenstein and Rajagopalan, *Chem. Eng. Commun.*, **4**, 15 (1980).
 128. Ruthven, *Principles of Adsorption and Adsorption Processes*, Wiley, 1984.
 129. Sanger and Deckwer, *Chem. Eng. J.*, **22**, 179 (1981).
 130. Satterfield, *AIChE J.*, **21**, 209 (1975).
 131. Schluter and Deckwer, *Chem. Eng. Sci.*, **47**, 2357 (1992).
 132. Schmitz, Steiff, and Weinspach, *Chem. Engng. Technol.*, **10**, 204 (1987).
 133. Schugerl et al., *Adv. Biochem. Eng.*, **8**, 63 (1978).
 134. Scott and Lobato, *Ind. Eng. Chem. Res.*, **42**, 5697 (2003).
 135. Sedahmed, Zatout, and Zewail, *Ind. Eng. Chem. Res.*, **37**, 3481 (1998).
 136. Shah et al., *AIChE J.*, **28**, 353 (1982).
 137. Sherwood et al., *Ind. Eng. Chem. Fundam.*, **4**, 113 (1965).
 138. Sherwood, Pigford, and Wilke, *Mass Transfer*, McGraw-Hill, 1975.
 139. Siegel, Sparrow, and Hallman, *Appl. Sci. Res. Sec. A*, **7**, 386 (1958).
 140. Sissom and Pitts, *Elements of Transport Phenomena*, McGraw-Hill, 1972.
 141. Skelland, *Diffusional Mass Transfer*, Wiley (1974).
 142. Skelland and Cornish, *AIChE J.*, **9**, 73 (1963).
 143. Skelland and Moeti, *Ind. Eng. Chem. Res.*, **29**, 2258 (1990).
 144. Skelland and Tedder, "Extraction—Organic Chemicals Processing" in Rousseau, *Handbook of Separation Process Technology*, Wiley, 1987, pp. 405–466.
 145. Skelland and Wellek, *AIChE J.*, **10**, 491, 789 (1964).
 146. Slater, "Rate Coefficients in Liquid-Liquid Extraction Systems" in Godfrey and Slater, *Liquid-Liquid Extraction Equipment*, Wiley, 1994, pp. 45–94.
 147. Steinberger and Treybal, *AIChE J.*, **6**, 227 (1960).
 148. Taniguchi and Kimura, *AIChE J.*, **47**, 1967 (2000).
 149. Taylor and Krishna, *Multicomponent Mass Transfer*, Wiley, 1993.
 150. Tokarz, Millies, and Mewes, *AIChE J.*, **47**, 799 (2001).
 151. Tournie, Laguerie, and Couderc, *Chem. Eng. Sci.*, **34**, 1247 (1979).
 152. Treybal, *Mass Transfer Operations*, 3d ed., McGraw-Hill, 1980.

153. Vandu, Liu, and Krishna, *Chem. Eng. Sci.*, **60**, 6430 (2005).
154. Von Karman, *Trans. ASME*, **61**, 705 (1939).
155. Wakao and Funazkri, *Chem. Eng. Sci.*, **33**, 1375 (1978).
156. Wang, Yuan, and Yu, *Ind. Eng. Chem. Res.*, **44**, 8715 (2005).
157. Wankat, *Separation Process Engineering*, 2d ed., Prentice-Hall, 2007.
158. Wilson and Geankoplis, *Ind. Eng. Chem. Fundam.*, **5**, 9 (1966).
159. Wright and Glasser, *AIChE J.*, **47**, 474 (2001).
160. Yagi and Yoshida, *Ind. Eng. Chem. Process Des. Dev.*, **14**, 488 (1975).
161. Yapici and Ozbahar, *Ind. Eng. Chem. Res.*, **37**, 643 (1998).
162. Zaki, Nirdosh, and Sedahmed, *Ind. Eng. Chem. Res.*, **41**, 3307 (2002).

INTRODUCTION

This part of Sec. 5 provides a concise guide to solving problems in situations commonly encountered by chemical engineers. It deals with diffusivity and mass-transfer coefficient estimation and common flux equations, although material balances are also presented in typical coordinate systems to permit a wide range of problems to be formulated and solved.

Mass-transfer calculations involve transport properties, such as diffusivities, and other empirical factors that have been found to relate mass-transfer rates to measured “driving forces” in myriad geometries and conditions. The context of the problem dictates whether the fundamental or more applied coefficient should be used. One key distinction is that, whenever there is flow parallel to an interface through which mass transfer occurs, the relevant coefficient is an empirical combination of properties and conditions. Conversely, when diffusion occurs in stagnant media or in creeping flow without transverse velocity gradients, ordinary diffusivities may be suitable for solving the problem. In either case, it is strongly suggested to employ data, whenever available, instead of relying on correlations.

Units employed in diffusivity correlations commonly followed the cgs system. Similarly, correlations for mass transfer correlations used the cgs or English system. In both cases, only the most recent correlations employ SI units. Since most correlations involve other properties and physical parameters, often with mixed units, they are repeated here as originally stated. Common conversion factors are listed in Table 1-4.

Fick's First Law This law relates flux of a component to its composition gradient, employing a constant of proportionality called a diffusivity. It can be written in several forms, depending on the units and frame of reference. Three that are related but not identical are

$$vJ_A = -D_{AB} \frac{dc_A}{dz} \approx mJ_A = -cD_{AB} \frac{dx_A}{dz} \approx mJ_A = -\rho D_{AB} \frac{dw_A}{dz} \quad (5-189)$$

The first equality (on the left-hand side) corresponds to the molar flux with respect to the volume average velocity, while the equality in the center represents the molar flux with respect to the molar average velocity and the one on the right is the mass flux with respect to the mass average velocity. These must be used with consistent flux expressions for fixed coordinates and for N_C components, such as:

$$N_A = vJ_A + c_A \sum_{i=1}^{N_C} N_i \bar{V}_i = mJ_A + x_A \sum_{i=1}^{N_C} N_i = \frac{mJ_A + w_A \sum_{i=1}^{N_C} n_i}{M_A} \quad (5-190)$$

In each case, the term containing the summation accounts for *conveyance*, which is the amount of component A carried by the net flow in the direction of diffusion. Its impact on the total flux can be as much as 10 percent. In most cases it is much less, and it is frequently ignored. Some people refer to this as the “convective” term, but that conflicts with the other sense of convection which is promoted by flow perpendicular to the direction of flux.

Mutual Diffusivity, Mass Diffusivity, Interdiffusion Coefficient Diffusivity is denoted by D_{AB} and is defined by Fick's first law as the ratio of the flux to the concentration gradient, as in Eq. (5-189). It is analogous to the thermal diffusivity in Fourier's law and to the kinematic viscosity in Newton's law. These analogies are flawed because both heat and momentum are conveniently defined with respect to fixed coordinates, irrespective of the direction of transfer or its magnitude, while mass diffusivity most commonly requires infor-

mation about bulk motion of the medium in which diffusion occurs. For liquids, it is common to refer to the limit of infinite dilution of A in B using the symbol, D_{AB}° .

When the flux expressions are consistent, as in Eq. (5-190), the diffusivities in Eq. (5-189) are identical. As a result, experimental diffusivities are often measured under constant volume conditions but may be used for applications involving open systems. It turns out that the two versions are very nearly equivalent for gas-phase systems because there is negligible volume change on mixing. That is not usually true for liquids, however.

Self-Diffusivity Self-diffusivity is denoted by D_{AA} and is the measure of mobility of a species in itself; for instance, using a small concentration of molecules tagged with a radioactive isotope so they can be detected. Tagged and untagged molecules presumably do not have significantly different properties. Hence, the solution is ideal, and there are practically no gradients to “force” or “drive” diffusion. This kind of diffusion is presumed to be purely statistical in nature.

In the special case that A and B are similar in molecular weight, polarity, and so on, the self-diffusion coefficients of pure A and B will be approximately equal to the mutual diffusivity, D_{AB} . Second, when A and B are the less mobile and more mobile components, respectively, their self-diffusion coefficients can be used as rough lower and upper bounds of the mutual diffusion coefficient. That is, $D_{AA} \leq D_{AB} \leq D_{BB}$. Third, it is a common means for evaluating diffusion for gases at high pressure. Self-diffusion in liquids has been studied by many [Easteal, *AIChE J.* **30**, 641 (1984), Ertl and Dullien, *AIChE J.* **19**, 1215 (1973), and Vadovic and Colver, *AIChE J.* **18**, 1264 (1972)].

Tracer Diffusivity Tracer diffusivity, denoted by $D_{A'B}$ is related to both mutual and self-diffusivity. It is evaluated in the presence of a second component B , again using a tagged isotope of the first component. In the dilute range, tagging A merely provides a convenient method for indirect composition analysis. As concentration varies, tracer diffusivities approach mutual diffusivities at the dilute limit, and they approach self-diffusivities at the pure component limit. That is, at the limit of dilute A in B , $D_{A'B} \rightarrow D_{AB}^\circ$ and $D_{B'A} \rightarrow D_{B'B}^\circ$; likewise at the limit of dilute B in A , $D_{B'A} \rightarrow D_{BA}^\circ$ and $D_{A'B} \rightarrow D_{A'A}^\circ$.

Neither the tracer diffusivity nor the self-diffusivity has much practical value except as a means to understand ordinary diffusion and as order-of-magnitude estimates of mutual diffusivities. Darken's equation [Eq. (5-230)] was derived for tracer diffusivities but is often used to relate mutual diffusivities at moderate concentrations as opposed to infinite dilution.

Mass-Transfer Coefficient Denoted by k_c , k_x , K_c , and so on, the mass-transfer coefficient is the ratio of the flux to a concentration (or composition) difference. These coefficients generally represent rates of transfer that are much greater than those that occur by diffusion alone, as a result of convection or turbulence at the interface where mass transfer occurs. There exist several principles that relate that coefficient to the diffusivity and other fluid properties and to the intensity of motion and geometry. Examples that are outlined later are the film theory, the surface renewal theory, and the penetration theory, all of which pertain to idealized cases. For many situations of practical interest like investigating the flow inside tubes and over flat surfaces as well as measuring external flow through banks of tubes, in fixed beds of particles, and the like, correlations have been developed that follow the same forms as the above theories. Examples of these are provided in the subsequent section on mass-transfer coefficient correlations.

Problem Solving Methods Most, if not all, problems or applications that involve mass transfer can be approached by a systematic course of action. In the simplest cases, the unknown quantities are obvious. In more complex (e.g., multicomponent, multiphase, multi-dimensional, nonisothermal, and/or transient) systems, it is more subtle to resolve the known and unknown quantities. For example, in multicomponent systems, one must know the fluxes of the components before predicting their effective diffusivities and vice versa. More will be said about that dilemma later. Once the known and unknown quantities are resolved, however, a combination of conservation equations, definitions, empirical relations, and properties are

Nomenclature and Units—Mass Transfer

Symbols	Definition	SI units	U.S. Customary units
a	Effective interfacial mass transfer area per unit volume	m^2/m^3	ft^2/ft^3
A_s	Cross-sectional area of vessel	m^2 or cm^2	ft^2
A'	Constant (see Table 5-24-K)		
a_p	See a		
c	Concentration = P/RT for an ideal gas	mol/m^3 or mol/l or $gequiv/l$	$lbmol/ft^3$
c_i	Concentration of component $i = x, c$ at gas-liquid interface	mol/m^3 or mol/l or $gequiv/l$	$lbmol/ft^3$
c_p	Specific heat	$kJ/(kg \cdot K)$	$Btu/(lb \cdot ^\circ F)$
d	Characteristic length	m or cm	ft
d_b	Bubble diameter	m	ft
d_c	Column diameter	m or cm	ft
d_{drop}	Sauter mean diameter	m	ft
d_{imp}	Impeller diameter	m	ft
d_{pore}	Pore diameter	m or cm	ft
$D_{A,A}$	Self-diffusivity ($= D_A$ at $x_A = 1$)	m^2/s or cm^2/s	ft^2/h
D_{AB}	Mutual diffusivity	m^2/s or cm^2/s	ft^2/h
D_{AB}^∞	Mutual diffusivity at infinite dilution of A in B	m^2/s or cm^2/s	ft^2/h
D_{eff}	Effective diffusivity within a porous solid $= \epsilon_p D/\tau$	m^2/s	ft^2/h
D_K	Knudson diffusivity for gases in small pores	m^2/s or cm^2/s	ft^2/h
D_L	Liquid phase diffusion coefficient	m^2/s	ft^2/h
D_s	Surface diffusivity	m^2/s or cm^2/s	ft^2/h
E	Energy dissipation rate/mass		
E_s	Activation energy for surface diffusion	J/mol or cal/mol	
f	Friction factor for fluid flow	Dimensionless	Dimensionless
F	Faraday's constant	$96,487$ Coulomb/gequiv	
g	Acceleration due to gravity	m/s^2	ft/h^2
g_c	Conversion factor	1.0	4.17×10^8 lb ft/(lbf-h ²)
G	Gas-phase mass flux	$kg/(s \cdot m^2)$	$lb/(h \cdot ft^2)$
G_a	Dry air flux	$kg/(s \cdot m^2)$	$lb/(h \cdot ft^2)$
G_M	Molar gas-phase mass flux	$kmol/(s \cdot m^2)$	$(lbmol)/(h \cdot ft^2)$
h'	Heat transfer coefficient	$W/(m^2 \cdot K) = J/(s \cdot m^2 \cdot K)$	$Btu/(h \cdot ft^2 \cdot ^\circ F)$
h_T	Total height of tower packing	m	ft
H	Compartment height	m	ft
H	Henry's law constant	$kPa/(mole-fraction solute in liquid phase)$	$(lbf/in^2)/(mole-fraction solute in liquid phase)$
H'	Henry's law constant	$kPa/[kmol/(m^3 \text{ solute in liquid phase})]$	$(lbf/in^2)/[(lbmol)/(ft^3 \text{ solute in liquid phase})]$ or $atm/[(lbmole)/(ft^3 \text{ solute in liquid phase})]$
H_G	Height of one transfer unit based on gas-phase resistance	m	ft
H_{OG}	Height of one overall gas-phase mass-transfer unit	m	ft
H_L	Height of one transfer unit based on liquid-phase resistance	m	ft
H_{OL}	Height of one overall liquid-phase mass-transfer unit	m	ft
HTU	Height of one transfer unit (general)	m	ft
j_D	Chilton-Colburn factor for mass transfer, Eq. (5-289)	Dimensionless	Dimensionless
j_H	Chilton-Colburn factor for heat transfer	Dimensionless	Dimensionless
j_M	See j_D		
m_{JA}	Mass flux of A by diffusion with respect to the mean mass velocity	$kmol/(m^2 \cdot s)$ or $mol/(cm^2 \cdot s)$	$lbmol/(ft^2 \cdot h)$
M_{JA}	Molar flux of A by diffusion with respect to mean molar velocity	$kmol/(m^2 \cdot s)$ or $mol/(cm^2 \cdot s)$	$lbmol/(ft^2 \cdot h)$
v_{JA}	Molar flux of A with respect to mean volume velocity	$kmol/(m^2 \cdot s)$	$lbmol/(ft^2 \cdot h)$
J_{si}	Molar flux by surface diffusion	$kmol/(m^2 \cdot s)$ or $gmol/(cm^2 \cdot s)$	$lbmol/(ft^2 \cdot h)$
k	Boltzmann's constant	8.9308×10^{-10} gequiv ohm/s	
k	Film mass transfer coefficient	m/s or cm/s	ft/hr
k	Thermal conductivity	$(J \cdot m)/(s \cdot m^2 \cdot K)$	$Btu/(h \cdot ft \cdot ^\circ F)$
k'	Mass-transfer coefficient for dilute systems	$kmol/[(s \cdot m^2)(kmol/m^3)]$ or m/s	$lbmol/[(h \cdot ft^2)(lbmol/ft^3)]$ or ft/hr
k_G	Gas-phase mass-transfer coefficient for dilute systems	$kmol/[(s \cdot m^2)(kPa \text{ solute partial pressure})]$	$lbmol/[(h \cdot ft^2)lbf/in^2 \text{ solute partial pressure}]$
K_G	Gas-phase mass-transfer coefficient for dilute systems	$kmol/[(s \cdot m^2)(mole fraction in gas)]$	$lbmol/[(h \cdot ft^2)(mole fraction in gas)]$
k_{GA}	Volumetric gas-phase mass-transfer coefficient for concentrated systems	$kmol/[(s \cdot m^3)(mole fraction)]$	$(lbmol)/[(h \cdot ft^3)(mole fraction)]$
\tilde{k}_{GA}	Overall volumetric gas-phase mass-transfer coefficient for concentrated systems	$kmol/(s \cdot m^3)$	$lbmol/(h \cdot ft^3)$
\tilde{k}_L'	Liquid phase mass transfer coefficient for pure absorption (no reaction)	$kmol/(s \cdot m^2)$	$lbmol/(h \cdot ft^2)$
k_L	Liquid-phase mass-transfer coefficient for dilute systems	$kmol/[(s \cdot m^2)(mole-fraction solution in liquid)]$	$(lbmol)/[(h \cdot ft^2)(mole-fraction solute in liquid)]$
k_L'	Liquid-phase mass-transfer coefficient for dilute systems	$kmol/[(s \cdot m^2)(kmol/m^3)]$ or m/s	$(lbmol)/[(h \cdot ft^2)(lbmol/ft^3)]$ or ft/h
\tilde{k}_L	Liquid-phase mass-transfer coefficient for concentrated systems	$kmol/(s \cdot m^2)$	$lbmol/(h \cdot ft^2)$
k_{LA}	Volumetric liquid-phase mass-transfer coefficient for dilute systems	$kmol/[(s \cdot m^3)(mole fraction)]$	$(lbmol)/[(h \cdot ft^3)(mole fraction)]$
K	Overall mass transfer coefficient	m/s or cm/s	ft/h
K	α/R = specific conductance	ohm/cm	
K_G	Overall gas-phase mass-transfer coefficient for dilute systems	$kmol/[(s \cdot m^2)(mole fraction)]$	$(lbmol)/[(h \cdot ft^2)(mole fraction)]$

Nomenclature and Units—Mass Transfer (Continued)

Symbols	Definition	SI units	U.S. Customary units
\hat{K}_G	Overall gas-phase mass-transfer coefficient for concentrated systems	kmol/(s·m ²)	lbmol/(h·ft ²)
$K_{G,a}$	Overall volumetric gas-phase mass-transfer dilute systems	kmol/[(s·m ³)(mole-fraction solute in gas)]	(lbmol)/[(h·ft ³)(mole-fraction solute in gas)]
$K'_{G,a}$	Overall volumetric gas-phase mass-transfer dilute systems	kmol/[(s·m ³)(kPa solute partial pressure)]	(lbmol)/[(h·ft ³)(lbf/in ² solute partial pressure)]
$(Ka)_H$	Overall enthalpy mass-transfer coefficient	kmol/[(s·m ²)(mole fraction)]	lb/[(h·ft ²)(lb water/lb dry air)]
K_L	Overall liquid-phase mass-transfer coefficient	kmol/[(s·m ²)(mole fraction)]	(lbmol)/[(h·ft ²)(mole fraction)]
\hat{K}_L	Liquid-phase mass-transfer coefficient for concentrated systems	kmol/(s·m ²)	(lbmol)/(h·ft ²)
$K_{L,a}$	Overall volumetric liquid-phase mass-transfer coefficient for dilute systems	kmol/[(s·m ³)(mole-fraction solute in liquid)]	(lbmol)/[(h·ft ³)(mole-fraction solute in liquid)]
$\hat{K}_{L,a}$	Overall volumetric liquid-phase mass-transfer coefficient for concentrated systems	kmol/(s·m ³)	(lbmol)/(h·ft ³)
L	Liquid-phase mass flux	kg/(s·m ²)	lb/(h·ft ²)
L_M	Molar liquid-phase mass flux	kmol/(s·m ²)	(lbmol)/(h·ft ²)
m	Slope of equilibrium curve = dy/dx (mole-fraction solute in gas)/(mole-fraction solute in liquid)	Dimensionless	Dimensionless
m	Molality of solute	mol/1000 g solvent	
M_i	Molecular weight of species i	kg/kmol or g/mol	lb/lbmol
M	Mass in a control volume V	kg or g	lb
$ n_+ , n_- $	Valences of cationic and anionic species	Dimensionless	Dimensionless
n'	See Table 5-24-K	Dimensionless	Dimensionless
n_A	Mass flux of A with respect to fixed coordinates	kg/(s·m ²)	lb/(h·ft ²)
N	Impeller speed	Revolution/s	Revolution/min
N'	Number deck levels	Dimensionless	Dimensionless
N_A	Interphase mass-transfer rate of solute A per interfacial area with respect to fixed coordinates	kmol/(s·m ²)	(lbmol)/(h·ft ²)
N_c	Number of components	Dimensionless	Dimensionless
N_{Fr}	Froude Number ($d_{imp} N^2/g$)	Dimensionless	Dimensionless
N_{Gr}	Grashof number ($\frac{g x^3}{(\mu/\rho)^2} \left(\frac{\rho_\infty}{\rho_s} - 1 \right)$)	Dimensionless	Dimensionless
N_{OG}	Number of overall gas-phase mass-transfer units	Dimensionless	Dimensionless
N_{OL}	Number of overall liquid-phase mass-transfer units	Dimensionless	Dimensionless
NTU	Number of transfer units (general)	Dimensionless	Dimensionless
N_{Kn}	Knudson number = l/d_{pore}	Dimensionless	Dimensionless
N_{Pr}	Prandtl number ($c_p \mu/k$)	Dimensionless	Dimensionless
N_{Re}	Reynolds number (Gd/μ_G)	Dimensionless	Dimensionless
N_{Sc}	Schmidt number ($\mu_G/\rho_G D_{AB}$) or ($\mu_L/\rho_L D_L$)	Dimensionless	Dimensionless
N_{Sh}	Sherwood number ($k_c R T d / D_{AB} p_T$), see also Tables 5-17 to 5-24	Dimensionless	Dimensionless
N_{St}	Stanton number (k_c / G_M) or (k_L / L_M)	Dimensionless	Dimensionless
N_{We}	Weber number ($\rho N^2 d_{imp}^3 / \sigma$)	Dimensionless	Dimensionless
p	Solute partial pressure in bulk gas	kPa	lbf/in ²
$p_{B,M}$	Log mean partial pressure difference of stagnant gas B	Dimensionless	Dimensionless
p_i	Solute partial pressure at gas-liquid interface	kPa	lbf/in ²
p_T	Total system pressure	kPa	lbf/in ²
P	Pressure	Pa	lbf/in ² or atm
P	Power	Watts	
P_c	Critical pressure	Pa	lbf/in ² or atm
Per	Perimeter/area	m ⁻¹	ft ⁻¹
Q	Volumetric flow rate	m ³ /s	ft ³ /h
r_A	Radius of dilute spherical solute	Å	
R	Gas constant	8.314 J/mol K = 8.314 Pa m ³ /(mol K) = 82.057 atm cm ³ /mol K	10.73 ft ³ psia/lbmol·h
R	Solution electrical resistance	ohm	
R_i	Radius of gyration of the component i molecule	Å	
s	Fractional surface-renewal rate	s ⁻¹	h ⁻¹
S	Tower cross-sectional area = $\pi d^2/4$	m ²	ft ²
t	Contact time	s	h
t_f	Formation time of drop	s	h
T	Temperature	K	°R
T_b	Normal boiling point	K	°R
T_c	Critical temperature	K	°R
T_r	Reduced temperature = T/T_c	Dimensionless	Dimensionless
u, v	Fluid velocity	m/s or cm/s	ft/h
u_o	Blowing or suction velocity	m/s	ft/h
u_∞	Velocity away from object	m/s	ft/h
u_L	Superficial liquid velocity in vertical direction	m/s	ft/h
v_s	Slip velocity	m/s	ft/h
v_T	Terminal velocity	m/s	ft/h
v_{TS}	Stokes law terminal velocity	m/s	ft/h
V	Packed volume in tower	m ³	ft ³
V	Control volume	m ³ or cm ³	ft ³
V_b	Volume at normal boiling point	m ³ /kmol or cm ³ /mol	ft ³ /lbmol
V_i	Molar volume of i at its normal boiling point	m ³ /kmol or cm ³ /mol	ft ³ /lbmol
\bar{v}_i	Partial molar volume of i	m ³ /kmol or cm ³ /mol	ft ³ /lbmol

5-48 HEAT AND MASS TRANSFER

Nomenclature and Units—Mass Transfer (Concluded)

Symbols	Definition	SI units	U.S. Customary units
V_{mli}	Molar volume of the liquid-phase component i at the melting point	m^3/kmol or cm^3/mol	ft^3/lbmol
V_{tower}	Tower volume per area	m^3/m^2	ft^3/ft^2
w	Width of film	m	ft
x	Length along plate	m	ft
x	Mole-fraction solute in bulk-liquid phase	$(\text{kmol solute})/(\text{kmol liquid})$	$(\text{lbmol solute})/(\text{lb mol liquid})$
x_A	Mole fraction of component A	$\text{kmole A}/\text{kmole fluid}$	$\text{lbmol A}/\text{lb mol fluid}$
x^o	Mole-fraction solute in bulk liquid in equilibrium with bulk-gas solute concentration y	$(\text{kmol solute})/(\text{kmol liquid})$	$(\text{lbmol solute})/(\text{lbmol liquid})$
x_{BM}	Logarithmic-mean solvent concentration between bulk liquid and interface values	$(\text{kmol solvent})/(\text{kmol liquid})$	$(\text{lbmol solvent})/(\text{lbmol liquid})$
x_{BM}^o	Logarithmic-mean inert-solvent concentration between bulk-liquid value and value in equilibrium with bulk gas	$(\text{kmol solvent})/(\text{kmol liquid})$	$(\text{lbmol solvent})/(\text{lbmol liquid})$
x_i	Mole-fraction solute in liquid at gas-liquid interface	$(\text{kmol solute})/(\text{kmol liquid})$	$(\text{lbmol solute})/(\text{lbmol liquid})$
y	Mole-fraction solute in bulk-gas phase	$(\text{kmol solute})/(\text{kmol gas})$	$(\text{lbmol solute})/(\text{lbmol gas})$
y_{BM}	Logarithmic-mean inert-gas concentration [Eq. (5-275)]	$(\text{kmol inert gas})/(\text{kmol gas})$	$(\text{lbmol inert gas})/(\text{lbmol gas})$
y_{BM}^o	Logarithmic-mean inert-gas concentration	$(\text{kmol inert gas})/(\text{kmol gas})$	$(\text{lbmol inert gas})/(\text{lbmol gas})$
y_i	Mole fraction solute in gas at interface	$(\text{kmol solute})/(\text{kmol gas})$	$(\text{lbmol solute})/(\text{lbmol gas})$
y_i^o	Mole-fraction solute in gas at interface in equilibrium with the liquid-phase interfacial solute concentration x_i	$(\text{kmol solute})/(\text{kmol gas})$	$(\text{lbmol solute})/(\text{lbmol gas})$
z	Direction of unidimensional diffusion	m	ft
Greek Symbols			
α	$1 + N_B/N_A$	Dimensionless	Dimensionless
α	Conductance cell constant (measured)	cm^{-1}	
β	$M_A^{1/2} p_c^{1/3}/T_c^{5/6}$	Dimensionless	Dimensionless
δ	Effective thickness of stagnant-film layer	m	ft
ϵ	Fraction of discontinuous phase in continuous phase for two-phase flow	Dimensionless	Dimensionless
ϵ	Void fraction available for gas flow or fractional gas holdup	m^3/m^3	ft^3/ft^3
ϵ_A	Characteristic Lennard-Jones energy	Dimensionless	Dimensionless
ϵ_{AB}	$(\epsilon_A \epsilon_B)^{1/2}$	Dimensionless	Dimensionless
γ_i	Activity coefficient of solute i	Dimensionless	Dimensionless
γ_{\pm}	Mean ionic activity coefficient of solute	Dimensionless	Dimensionless
$\lambda_+ \lambda_-$	Infinite dilution conductance of cation and anion	$\text{cm}^2/(\text{equiv-ohm})$	
Λ	$1000 \text{ K}/C = \lambda_+ + \lambda_- = \Lambda_o + f(C)$	$\text{cm}^2/\text{ohm gequiv}$	
Λ_o	Infinite dilution conductance	$\text{cm}^2/\text{equiv ohm}$	
μ_i	Dipole moment of i	Debeyes	
μ_i	Viscosity of pure i	cP or Pa s	$\text{lb}/(\text{h-ft})$
μ_G	Gas-phase viscosity	$\text{kg}/(\text{s-m})$	$\text{lb}/(\text{h-ft})$
μ_L	Liquid-phase viscosity	$\text{kg}/(\text{s-m})$	$\text{lb}/(\text{h-ft})$
ν	Kinematic viscosity = ρ/μ	m^2/s	ft^2/h
ρ	Density of A	kg/m^3 or g/cm^3	lb/ft^3
ρ_c	Critical density of A	kg/m^3 or g/cm^3	lb/ft^3
ρ_c	Density continuous phase	kg/m^3	lb/ft^3
ρ_G	Gas-phase density	kg/m^3	lb/ft^3
$\bar{\rho}_L$	Average molar density of liquid phase	kmol/m^3	$(\text{lbmol})/\text{ft}^3$
ρ_p	Particle density	kg/m^3 or g/cm^3	lb/ft^3
ρ_r	Reduced density = ρ/ρ_c	Dimensionless	Dimensionless
ψ_i	Parachor of component $i = V_i \sigma^{1/4}$		
ψ	Parameter, Table 5-24-G	Dimensionless	Dimensionless
σ	Interfacial tension	dyn/cm	lb/ft
σ_i	Characteristic length	\AA	
σ_i	Surface tension of component i	dyn/cm	
σ_{AB}	Binary pair characteristic length = $(\sigma_A + \sigma_B)/2$	\AA	
τ	Intraparticle tortuosity	Dimensionless	Dimensionless
ω	Pitzer's acentric factor = $-[1.0 + \log_{10}(P^o/P_c)]$	Dimensionless	
ω	Rotational velocity	Radians/s	
Ω	Diffusion collision integral = $f(kT/\epsilon_{AB})$	Dimensionless	Dimensionless
Subscripts			
A	Solute component in liquid or gas phase		
B	Inert-gas or inert-solvent component		
G	Gas phase		
m	Mean value		
L	Liquid phase		
super	Superficial velocity		
Superscript			
°	At equilibrium		

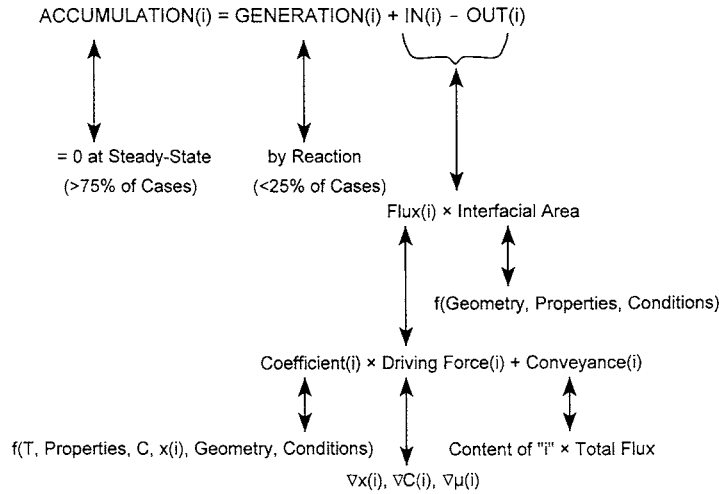


FIG. 5-24 Flowchart illustrating problem solving approach using mass-transfer rate expressions in the context of mass conservation.

applied to arrive at an answer. Figure 5-24 is a flowchart that illustrates the primary types of information and their relationships, and it applies to many mass-transfer problems.

CONTINUITY AND FLUX EXPRESSIONS

Material Balances Whenever mass-transfer applications involve equipment of specific dimensions, flux equations alone are inadequate to assess results. A material balance or continuity equation must also be used. When the geometry is simple, macroscopic balances suffice. The following equation is an overall mass balance for such a unit having N_m bulk-flow ports and N_n ports or interfaces through which diffusive flux can occur:

$$\frac{dM}{dt} = \sum_{i=1}^{N_m} m_i + \sum_{i=1}^{N_n} n_i A_{cs_i} \tag{5-191}$$

where M represents the mass in the unit volume V at any time t ; m_i is the mass flow rate through the i th port; and n_i is the mass flux through the i th port, which has a cross-sectional area of A_{cs_i} . The corresponding balance equation for individual components includes a reaction term:

$$\frac{dM_j}{dt} = \sum_{i=1}^{N_m} m_{ij} + \sum_{i=1}^{N_n} n_{ij} A_{cs_i} + r_j V \tag{5-192}$$

For the j th component, $m_{ij} = m_i w_{ij}$ is the component mass flow rate in stream i ; w_{ij} is the mass fraction of component j in stream i ; and r_j is the net reaction rate (mass generation minus consumption) per unit volume V that contains mass M . If it is inconvenient to measure mass flow rates, the product of density and volumetric flow rate is used instead.

In addition, most situations that involve mass transfer require material balances, but the pertinent area is ambiguous. Examples are packed columns for absorption, distillation, or extraction. In such

cases, flow rates through the discrete ports (nozzles) must be related to the mass-transfer rate in the packing. As a result, the mass-transfer rate is determined via flux equations, and the overall material balance incorporates the stream flow rates m_i and integrated fluxes. In such instances, it is common to begin with the most general, differential material balance equations. Then, by eliminating terms that are negligible, the simplest applicable set of equations remains to be solved. Table 5-8 provides material balances for Cartesian, cylindrical, and spherical coordinates. The generic form applies over a unit cross-sectional area and constant volume:

$$\frac{\partial \rho_j}{\partial t} = -\nabla \cdot n_j + r_j \tag{5-193a}$$

where $n_j = \rho v_j$. Applying Fick's law and expressing composition as concentration gives

$$\frac{\partial c_j}{\partial t} = -v \cdot \nabla c_j + D_j \nabla^2 c_j + r_j \tag{5-193b}$$

Flux Expressions: Simple Integrated Forms of Fick's First Law Simplified flux equations that arise from Eqs. (5-189) and (5-190) can be used for unidimensional, steady-state problems with binary mixtures. The boundary conditions represent the compositions x_{A_L} and x_{A_R} at the left-hand and right-hand sides of a hypothetical layer having thickness Δz . The principal restriction of the following equations is that the concentration and diffusivity are assumed to be constant. As written, the flux is positive from left to right, as depicted in Fig. 5-25.

1. Equimolar counterdiffusion ($N_A = -N_B$)

$$N_A = M J_A = -D_{AB} c \frac{dx_A}{dz} = \frac{D_{AB}}{\Delta z} c (x_{A_L} - x_{A_R}) \tag{5-197}$$

TABLE 5-8 Continuity Equation in Various Coordinate Systems

Coordinate System	Equation
Cartesian	$\frac{\partial \rho_j}{\partial t} = -\left(\frac{\partial n_{x_j}}{\partial x} + \frac{\partial n_{y_j}}{\partial y} + \frac{\partial n_{z_j}}{\partial z}\right) + r_j$ (5-194)
Cylindrical	$\frac{\partial \rho_j}{\partial t} = -\left(\frac{1}{r} \frac{\partial m_{r_j}}{\partial r} + \frac{1}{r} \frac{\partial n_{\theta_j}}{\partial \theta} + \frac{\partial n_{z_j}}{\partial z}\right) + r_j$ (5-195)
Spherical	$\frac{\partial \rho_j}{\partial t} = -\left(\frac{1}{r^2} \frac{\partial r^2 n_{r_j}}{\partial r} + \frac{1}{r \sin \theta} \frac{\partial n_{\theta_j} \sin \theta}{\partial \theta} + \frac{1}{r \sin \theta} \frac{\partial n_{\phi_j}}{\partial \phi}\right) + r_j$ (5-196)

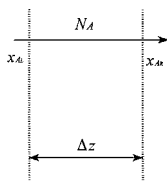


FIG. 5-25 Hypothetical film and boundary conditions.

2. Unimolar diffusion ($N_A \neq 0, N_B = 0$)

$$N_A = M J_A + x_A N_A = \frac{D_{AB}}{\Delta z} c \ln \frac{1 - x_{A_R}}{1 - x_{A_L}} \quad (5-198)$$

3. Steady state diffusion ($N_A \neq -N_B \neq 0$)

$$N_A = M J_A + x_A (N_A + N_B) = \frac{N_A}{N_A + N_B} \frac{D_{AB}}{\Delta z} c \ln \frac{\frac{N_A}{N_A + N_B} - x_{A_R}}{\frac{N_A}{N_A + N_B} - x_{A_L}} \quad (5-199)$$

The unfortunate aspect of the last relationship is that one must know a priori the ratio of the fluxes to determine the magnitudes. It is not possible to solve simultaneously the pair of equations that apply for components *A* and *B* because the equations are not independent.

Stefan-Maxwell Equations Following Eq. (5-190), a simple and intuitively appealing flux equation for applications involving N_c components is

$$N_i = -c D_{im} \nabla x_i + x_i \sum_{j=1}^{N_c} N_j \quad (5-200)$$

In the late 1800s, the development of the kinetic theory of gases led to a method for calculating multicomponent gas diffusion (e.g., the flux of each species in a mixture). The methods were developed simultaneously by Stefan and Maxwell. The problem is to determine the diffusion coefficient D_{im} . The Stefan-Maxwell equations are simpler in principle since they employ binary diffusivities:

$$\nabla x_i = \sum_{j=1}^{N_c} \frac{1}{c D_{ij}} (x_i N_j - x_j N_i) \quad (5-201)$$

If Eqs. (5-200) and (5-201) are combined, the multicomponent diffusion coefficient may be assessed in terms of binary diffusion coefficients [see Eq. (5-214)]. For gases, the values D_{ij} of this equation are approximately equal to the binary diffusivities for the *ij* pairs. The Stefan-Maxwell diffusion coefficients may be negative, and the method may be applied to liquids, even for electrolyte diffusion [Kraaijeveld, Wesselingh, and Kuiken, *Ind. Eng. Chem. Res.*, **33**, 750 (1994)]. Approximate solutions have been developed by linearization [Toor, H.L., *AIChE J.*, **10**, 448 and 460 (1964); Stewart and Prober, *Ind. Eng. Chem. Fundam.*, **3**, 224 (1964)]. Those differ in details but yield about the same accuracy. More recently, efficient algorithms for solving the equations exactly have been developed (see Taylor and Krishna, Krishnamurthy and Taylor [*Chem. Eng. J.*, **25**, 47 (1982)], and Taylor and Webb [*Comput. Chem. Eng.*, **5**, 61 (1981)]).

Useful studies of multicomponent diffusion were presented by Vrentas and Vrentas [*Ind. Eng. Chem. Res.*, **44**, 1112 (2005)], Curtis

and Bird [*Ind. Eng. Chem. Res.*, **38**, 2515 (1999)], and Amundson, Pan, and Paulson [*AIChE J.*, **48**, 813 (2003)]. Vrentas and Vrentas treated only ternary mixtures, such as restrictions due to the entropy inequality, application of the Onsager reciprocal relations, and stability. Curtis and Bird reconciled the multicomponent Fick's law approach with the more elegant Stefan-Maxwell theory. They also provided interrelationships of multicomponent diffusivities devised for various situations, i.e., binary, ternary, and quaternary mixtures. Amundson et al. presented numerical methods for coping with mixtures having four or more components, which are nearly intractable via the analytical S-M method, due to the difficult inversion. Related studies were performed by Ghorayeb and Firoozabadi [*AIChE J.*, **46**, 883 (2000)] and Firoozabadi, Ghorayeb, and Saukla [*AIChE J.*, **46**, 892 (2000)]. The former covered ordinary molecular diffusion as well as pressure and thermal diffusion for multicomponent mixtures. The latter covered thermal diffusion in multicomponent mixtures.

DIFFUSIVITY ESTIMATION—GASES

Whenever measured values of diffusivities are available, they should be used. Typically, measurement errors are less than those associated with predictions by empirical or even semitheoretical equations. A few general sources of data are Sec. 2 of this handbook; e.g., experimental values for gas mixtures are listed in Table 2-371. Estimation methods for some gaseous applications appear in Eqs. (2-150) through (2-154). Other pertinent references are Schwartzberg and Chao; Poling et al.; Gammon et al.; and Daubert and Danner. Many other more restricted sources are listed under specific topics later in this subsection.

Before using diffusivities from either data or correlations, it is a good idea to check their reasonableness with respect to values that have been commonly observed in similar situations. Table 5-9 is a compilation of several rules of thumb. These values are not authoritative; they simply represent guidelines based on experience.

Diffusivity correlations for gases are outlined in Table 5-10. Specific parameters for individual equations are defined in the specific text regarding each equation. References are given at the beginning of the "Mass Transfer" subsection. The errors reported for Eqs. (5-202) through (5-205) were compiled by Poling et al., who compared the predictions with 68 experimental values of D_{AB} . Errors cited for Eqs. (5-206) to (5-212) were reported by the authors.

Binary Mixtures—Low Pressure—Nonpolar Components Many evaluations of correlations are available [Elliott and Watts, *Can. J. Chem.*, **50**, 31 (1972); Lugg, *Anal. Chem.*, **40**, 1072 (1968); Marrero and Mason, *AIChE J.*, **19**, 498 (1973)]. The differences in accuracy of the correlations are minor, and thus the major concern is ease of calculation. The Fuller-Schettler-Giddings equation is usually the simplest correlation to use and is recommended by Poling et al.

Chapman-Enskog (Bird et al.) and Wilke and Lee [31] The inherent assumptions of these equations are quite restrictive (i.e., low density, spherical atoms), and the intrinsic potential function is empirical. Despite that, they provide good estimates of D_{AB} for many polyatomic gases and gas mixtures, up to about 1000 K and a maximum of 70 atm. The latter constraint is because observations for many gases indicate that $D_{AB}P$ is constant up to 70 atm.

The characteristic length is $\sigma_{AB} = (\sigma_A + \sigma_B)/2$ in Å. In order to estimate Ω_D for Eq. (5-202) or (5-203), two empirical equations are

TABLE 5-9 Rules of Thumb for Diffusivities (See Cussler, Poling et al., Schwartzberg and Chao)

Continuous phase	D_i magnitude		D_i range		Comments
	m ² /s	cm ² /s	m ² /s	cm ² /s	
Gas at atmospheric pressure	10 ⁻⁵	0.1	10 ⁻⁴ –10 ⁻⁶	1–10 ⁻²	Accurate theories exist, generally within ±10%; $D_i P \cong \text{constant}$; $D_i \propto T^{1.66 \text{ to } 2.0}$
Liquid	10 ⁻⁹	10 ⁻⁵	10 ⁻⁸ –10 ⁻¹⁰	10 ⁻⁴ –10 ⁻⁶	Approximate correlations exist, generally within ±25%
Liquid occluded in solid matrix	10 ⁻¹⁰	10 ⁻⁶	10 ⁻⁸ –10 ⁻¹²	10 ⁻⁴ –10 ⁻⁸	Hard cell walls: $D_{\text{eff}}/D_i = 0.1$ to 0.2. Soft cell walls: $D_{\text{eff}}/D_i = 0.3$ to 0.9
Polymers and glasses	10 ⁻¹²	10 ⁻⁸	10 ⁻¹⁰ –10 ⁻¹⁴	10 ⁻⁶ –10 ⁻¹⁰	Approximate theories exist for dilute and concentrated limits; strong composition dependence
Solid	10 ⁻¹⁴	10 ⁻¹⁰	10 ⁻¹⁰ –10 ⁻³⁴	10 ⁻⁶ –10 ⁻³⁰	Approximate theories exist; strong temperature dependence

TABLE 5-10 Correlations of Diffusivities for Gases

Authors*	Equation	Error, %
1. Binary Mixtures—Low Pressure—Nonpolar		
Chapman-Enskog	$D_{AB} = \frac{0.001858T^{3/2} M_{AB}^{1/2}}{P\sigma_{AB}^2 \Omega_D}$ (5-202)	7.3
Wilke-Lee [31]	$D_{AB} = \frac{(0.00217 - 0.0005M_{AB}^{1/2}) T^{3/2} M_{AB}^{1/2}}{P\sigma_{AB}^2 \Omega_D}$ (5-203)	7.0
Fuller-Schettler-Giddings [10]	$D_{AB} = \frac{0.001T^{1.75} M_{AB}^{1/2}}{P[(\sum v)_A^{1/3} + (\sum v)_B^{1/3}]^2}$ (5-204)	5.4
2. Binary Mixtures—Low Pressure—Polar		
Brokaw [4]	$D_{AB} = \frac{0.001858T^{3/2} M_{AB}^{1/2}}{P\sigma_{AB}^2 \Omega_D}$ (5-205)	9.0
3. Self-Diffusivity		
Mathur-Thodos [18]	$D_{AA} = \frac{10.7 \times 10^{-5} T_r}{\beta \rho_r} \{ \rho_r \leq 1.5 \}$ (5-206)	5
Lee-Thodos [14]	$D_{AA} = \frac{0.77 \times 10^{-5} T_r}{\rho \delta} \{ \rho_r \leq 1 \}$ (5-207)	0.5
Lee-Thodos [15]	$D_{AA} = \frac{(0.007094G + 0.001916)^{2.5} T_r}{\delta}, [\rho_r > 1, G < 1]$ (5-208)	17
4. Supercritical Mixtures		
Sun and Chen [25]	$D_{AB} = \frac{1.23 \times 10^{-10} T}{\mu^{0.799} V_{CA}^{0.49}}$ (5-209)	5
Catchpole and King [6]	$D_{AB} = 5.152 D_c T_r \frac{(\rho_r^{-0.667} - 0.4510)(1 + M_A/M_B)R}{(1 + (V_{cB}/V_{cA})^{0.333})^2}$ (5-210)	10
Liu and Ruckenstein [17]	$D_{AB} = \frac{kT}{f\pi\mu_A\sigma_{AB}} \left[\frac{1}{1 + \frac{2}{3} \left(1 - \frac{1}{2} \theta_{AB}^{\infty}\right)^{1/2}} + \frac{\sigma_{AB}}{3\sigma_A} \right]$ (5-211)	5.7
	$D_{AB} = \alpha(V_A^k - \beta) \sqrt{\frac{T}{M_B}}, \alpha = 10^{-5} \left[0.56392 + 2.1417 \exp\left(\frac{-0.95088 \sqrt{M_A V_{CA}}}{P_{CA}}\right) \right]$ (5-212)	6.9
	$\beta = 8.9061 + 0.93858 \frac{\sqrt{M_A V_{CA}}}{P_{CA}}$	
	$k = \frac{2}{3} [1 - 0.28 \exp(-0.3 \sqrt{M_A} \rho_{v,1})]$	

*References are listed at the beginning of the "Mass Transfer" subsection.

available. The first is:

$$\Omega_D = (44.54T^{0-4.909} + 1.911T^{0-1.575})^{0.10} \quad (5-213a)$$

where $T^{\circ} = kT/\epsilon_{AB}$ and $\epsilon_{AB} = (\epsilon_A \epsilon_B)^{1/2}$. Estimates for σ_i and ϵ_i are given in Table 5-11. This expression shows that Ω_D is proportional to temperature roughly to the -0.49 power at low temperatures and to the

-0.16 power at high temperature. Thus, gas diffusivities are proportional to temperatures to the 2.0 power and 1.66 power, respectively, at low and high temperatures. The second is:

$$\Omega_D = \frac{A}{T^{\circ B}} + \frac{C}{\exp(DT^{\circ})} + \frac{E}{\exp(FT^{\circ})} + \frac{G}{\exp(HT^{\circ})} \quad (5-213b)$$

TABLE 5-11 Estimates for ϵ_i and σ_i (K, Å, atm, cm³, mol)

Critical point	$\epsilon/k = 0.75 T_c$	$\sigma = 0.841 V_c^{1/3}$ or $2.44 (T_c/P_c)^{1/3}$
Critical point	$\epsilon/k = 65.3 T_c \rho_c^{-3.6}$	$\sigma = \frac{1.866 V_c^{1/3}}{\rho_c^{1.2}}$
Normal boiling point	$\epsilon/k = 1.15 T_b$	$\sigma = 1.18 V_b^{1/3}$
Melting point	$\epsilon/k = 1.92 T_m$	$\sigma = 1.222 V_m^{1/3}$
Acentric factor	$\epsilon/k = (0.7915 + 0.1693 \omega) T_c$	$\sigma = (2.3551 - 0.087 \omega) \left(\frac{T_c}{P_c}\right)^{1/3}$

NOTE: These values may not agree closely, so usage of a consistent basis is suggested (e.g., data at the normal boiling point).

TABLE 5-12 Atomic Diffusion Volumes for Use in Estimating D_{AB} by the Method of Fuller, Schettler, and Giddings [10]

Atomic and Structural Diffusion-Volume Increments, v_i (cm ³ /mol)			
C	16.5	(Cl)	19.5
H	1.98	(S)	17.0
O	5.48	Aromatic ring	-20.2
(N)	5.69	Heterocyclic ring	-20.2
Diffusion Volumes for Simple Molecules, Σv_i (cm ³ /mol)			
H ₂	7.07	CO	18.9
D ₂	6.70	CO ₂	26.9
He	2.88	N ₂ O	35.9
N ₂	17.9	NH ₃	14.9
O ₂	16.6	H ₂ O	12.7
Air	20.1	(CCl ₂ F ₂)	114.8
Ar	16.1	(SF ₆)	69.7
Kr	22.8	(Cl ₂)	37.7
(Xe)	37.9	(Br ₂)	67.2
Ne	5.59	(SO ₂)	41.1

Parentheses indicate that the value listed is based on only a few data points.

where $A = 1.06036$, $B = 0.15610$, $C = 0.1930$, $D = 0.47635$, $E = 1.03587$, $F = 1.52996$, $G = 1.76474$, and $H = 3.89411$.

Fuller, Schettler, and Giddings [10] The parameters and constants for this correlation were determined by regression analysis of 340 experimental diffusion coefficient values of 153 binary systems. Values of Σv_i used in this equation are in Table 5-12.

Binary Mixtures—Low Pressure—Polar Components The Brokaw [4] correlation was based on the Chapman-Enskog equation, but σ_{AB}^* and Ω_D^* were evaluated with a modified Stockmayer potential for polar molecules. Hence, slightly different symbols are used. That potential model reduces to the Lennard-Jones 6-12 potential for interactions between nonpolar molecules. As a result, the method should yield accurate predictions for polar as well as nonpolar gas mixtures. Brokaw presented data for 9 relatively polar pairs along with the prediction. The agreement was good: an average absolute error of 6.4 percent, considering the complexity of some of the gas pairs [e.g., (CH₃)₂O and CH₃Cl]. Despite that, Poling, (op. cit.) found the average error was 9.0 percent for combinations of mixtures (including several polar-nonpolar gas pairs), temperatures and pressures. In this equation, Ω_D is calculated as described previously, and other terms are:

$$\begin{aligned}\Omega_{D^*} &= \Omega_D + 0.19 \delta_{AB}^2/T^\circ & T^\circ &= kT/\epsilon_{AB} \\ \sigma_{AB}^* &= (\sigma_A \sigma_B)^{1/2} & \sigma_i^* &= [1.585 V_{bi}/(1 + 1.3 \delta_i^2)]^{1/3} \\ \delta_{AB} &= (\delta_A \delta_B)^{1/2} & \delta_i &= 1.94 \times 10^3 \mu_i^2/V_{bi} T_{bi} \\ \epsilon_{AB} &= (\epsilon_A \epsilon_B)^{1/2} & \epsilon_i/k &= 1.18 (1 + 1.3 \delta_i^2) T_{bi}\end{aligned}$$

Binary Mixtures—High Pressure Of the various categories of gas-phase diffusion, this is the least studied. This is so because of the effects of diffusion being easily distorted by even a slight pressure gradient, which is difficult to avoid at high pressure. Harstad and Bellan [Ind. Eng. Chem. Res. 43, 645 (2004)] developed a corresponding-states expression that extends the Chapman-Enskog method, covered earlier. They express the diffusivity at high pressure by accounting for the reduced temperature, and they suggest employing an equation of state and shifting from $D_{AB}^o = f(T, P)$ to $D_{AB} = g(T, V)$.

Self-Diffusivity Self-diffusivity is a property that has little intrinsic value, e.g., for solving separation problems. Despite that, it reveals quite a lot about the inherent nature of molecular transport, because the effects of discrepancies of other physical properties are eliminated, except for those that constitute isotopic differences, which are necessary to ascertain composition differences. Self-diffusivity has been studied extensively under high pressures, e.g., greater than 70 atm. There are few accurate estimation methods for mutual diffusivities at such high pressures, because composition measurements are difficult.

The general observation for gas-phase diffusion $D_{AB} P = \text{constant}$, which holds at low pressure, is not valid at high pressure. Rather, $D_{AB} P$ decreases as pressure increases. In addition, composition effects, which frequently are negligible at low pressure, are very significant at high pressure.

Liu and Ruckenstein [Ind. Eng. Chem. Res. 36, 3937 (1997)] studied self-diffusion for both liquids and gases. They proposed a semiempirical equation, based on hard-sphere theory, to estimate self-diffusivities. They extended it to Lennard-Jones fluids. The necessary energy parameter is estimated from viscosity data, but the molecular collision diameter is estimated from diffusion data. They compared their estimates to 26 pairs, with a total of 1822 data points, and achieved a relative deviation of 7.3 percent.

Zielinski and Hanley [AIChE J. 45, 1 (1999)] developed a model to predict multicomponent diffusivities from self-diffusion coefficients and thermodynamic information. Their model was tested by estimated experimental diffusivity values for ternary systems, predicting drying behavior of ternary systems, and reconciling ternary self-diffusion data measured by pulsed-field gradient NMR.

Mathur and Thodos [18] showed that for reduced densities less than unity, the product $D_{AB} \rho$ is approximately constant at a given temperature. Thus, by knowing the value of the product at low pressure, it is possible to estimate its value at a higher pressure. They found at higher pressures the density increases, but the product $D_{AB} \rho$ decreases rapidly. In their correlation, $\beta = M_A^{1/2} P_C^{1/3} / T_C^{5/6}$.

Lee and Thodos [14] presented a generalized treatment of self-diffusivity for gases (and liquids). These correlations have been tested for more than 500 data points each. The average deviation of the first is 0.51 percent, and that of the second is 17.2 percent. $\delta = M_A^{1/2} / P_C^{1/2} V_C^{5/6}$, s/cm^2 , and where $G = (X^\circ - X)/(X^\circ - 1)$, $X = \rho_r / T_r^{0.1}$, and $X^\circ = \rho_r / T_r^{0.1}$ evaluated at the solid melting point.

Lee and Thodos [15] expanded their earlier treatment of self-diffusivity to cover 58 substances and 975 data points, with an average absolute deviation of 5.26 percent. Their correlation is too involved to repeat here, but those interested should refer to the original paper.

Liu, Silva, and Macedo [Chem. Eng. Sci. 53, 2403 (1998)] present a theoretical approach incorporating hard-sphere, square-well, and Lennard-Jones models. They compared their resulting estimates to estimates generated via the Lee-Thodos equation. For 2047 data points with nonpolar species, the Lee-Thodos equation was slightly superior to the Lennard-Jones fluid-based model, that is, 5.2 percent average deviation versus 5.5 percent, and much better than the square-well fluid-based model (10.6 percent deviation). For over 467 data points with polar species, the Lee-Thodos equation yielded 36 percent average deviation, compared with 25 percent for the Lennard-Jones fluid-based model, and 19 percent for the square-well fluid-based model.

Silva, Liu, and Macedo [Chem. Eng. Sci. 53, 2423 (1998)] present an improved theoretical approach incorporating slightly different Lennard-Jones models. For 2047 data points with nonpolar species, their best model yielded 4.5 percent average deviation, while the Lee-Thodos equation yielded 5.2 percent, and the prior Lennard-Jones fluid-based model produced 5.5 percent. The new model was much better than all the other models for over 424 data points with polar species, yielding 4.3 percent deviation, while the Lee-Thodos equation yielded 34 percent and the Lennard-Jones fluid-based model yielded 23 percent.

Supercritical Mixtures Debenedetti and Reid [AIChE J., 32, 2034 (1986) and 33, 496 (1987)] showed that conventional correlations based on the Stokes-Einstein relation (for liquid phase) tend to overpredict diffusivities in the supercritical state. Nevertheless, they observed that the Stokes-Einstein group $D_{AB} \mu / T$ was constant. Thus, although no general correlation applies, only one data point is necessary to examine variations of fluid viscosity and/or temperature effects. They explored certain combinations of aromatic solids in SF₆ and CO₂.

Sun and Chen [25] examined tracer diffusion data of aromatic solutes in alcohols up to the supercritical range and found their data correlated with average deviations of 5 percent and a maximum deviation of 17 percent for their rather limited set of data.

Catchpole and King [6] examined binary diffusion data of near-critical fluids in the reduced density range of 1 to 2.5 and found that their data correlated with average deviations of 10 percent and a maximum deviation of 60 percent. They observed two classes of behavior. For the first, no correction factor was required ($R = 1$). That class was comprised of alcohols as solvents with aromatic or aliphatic solutes, or

carbon dioxide as a solvent with aliphatics except ketones as solutes, or ethylene as a solvent with aliphatics except ketones and naphthalene as solutes. For the second class, the correction factor was $R = X^{0.17}$. The class was comprised of carbon dioxide with aromatics; ketones and carbon tetrachloride as solutes; and aliphatics (propane, hexane, dimethyl butane), sulfur hexafluoride, and chlorotrifluoromethane as solvents with aromatics as solutes. In addition, sulfur hexafluoride combined with carbon tetrachloride, and chlorotrifluoromethane combined with 2-propanone were included in that class. In all cases, $X = (1 + (V_{CS}/V_{CA})^{1/3})^2 / (1 + M_A/M_B)$ was in the range of 1 to 10.

Liu and Ruckenstein [17] presented a semiempirical equation to estimate diffusivities under supercritical conditions that is based on the Stokes-Einstein relation and the long-range correlation, respectively. The parameter $2\theta_{AB}^*$ was estimated from the Peng-Robinson equation of state. In addition, $f = 2.72 - 0.3445 T_{cB}/T_{cA}$ for most solutes, but for C_5 through C_{14} linear alkanes, $f = 3.046 - 0.786 T_{cB}/T_{cA}$. In both cases T_{ci} is the species critical temperature. They compared their estimates to 33 pairs, with a total of 598 data points, and achieved lower deviations (5.7 percent) than the Sun-Chen correlation (13.3 percent) and the Catchpole-King equation (11.0 percent).

He and Yu [13] presented a semiempirical equation to estimate diffusivities under supercritical conditions that is based on hard-sphere theory. It is limited to $\rho_r \geq 0.21$, where the reduced density is $\rho_r = \rho_A(T, P)/\rho_{cA}$. They compared their estimates to 107 pairs, with a total of 1167 data points, and achieved lower deviations (7.8 percent) than the Catchpole-King equation (9.7 percent), which was restricted to $\rho_r \geq 1$.

Silva and Macedo [Ind. Eng. Chem. Res. 37, 1490 (1998)] measured diffusivities of ethers in CO_2 under supercritical conditions and compared them to the Wilke-Chang [Eq. (5-218)], Tyn-Calus [Eq. (5-219)], Catchpole-King [Eq. (5-210)], and their own equations. They found that the Wilke-Chang equation provided the best fit.

Gonzalez, Bueno, and Medina [Ind. Eng. Chem. Res. 40, 3711 (2001)] measured diffusivities of aromatic compounds in CO_2 under supercritical conditions and compared them to the Wilke-Chang [Eq. (5-218)], Hayduk-Minhas [Eq. (5-226)], and other equations. They recommended the Wilke-Chang equation (which yielded a relative error of 10.1 percent) but noted that the He-Yu equation provided the best fit (5.5 percent).

Low-Pressure/Multicomponent Mixtures These methods are outlined in Table 5-13. Stefan-Maxwell equations were discussed earlier. Smith and Taylor [23] compared various methods for predicting multicomponent diffusion rates and found that Eq. (5-214) was superior among the effective diffusivity approaches, though none is very good. They also found that linearized and exact solutions are roughly equivalent and accurate.

Blanc [3] provided a simple limiting case for dilute component i diffusing in a stagnant medium (i.e., $N \approx 0$), and the result, Eq. (5-215), is known as Blanc's law. The restriction basically means that the compositions of all the components, besides component i , are relatively large and uniform.

Wilke [29] obtained solutions to the Stefan-Maxwell equations. The first, Eq. (5-216), is simple and reliable under the same conditions as Blanc's law. This equation applies when component i diffuses through

a stagnant mixture. It has been tested and verified for diffusion of toluene in hydrogen + air + argon mixtures and for diffusion of ethyl propionate in hydrogen + air mixtures [Fairbanks and Wilke *Ind. Eng. Chem.*, 42, 471 (1950)]. When the compositions vary from one boundary to the other, Wilke recommends that the arithmetic average mole fractions be used. Wilke also suggested using the Stefan-Maxwell equation, which applies when the fluxes of two or more components are significant. In this situation, the mole fractions are arithmetic averages of the boundary conditions, and the solution requires iteration because the ratio of fluxes is not known a priori.

DIFFUSIVITY ESTIMATION—LIQUIDS

Many more correlations are available for diffusion coefficients in the liquid phase than for the gas phase. Most, however, are restricted to binary diffusion at infinite dilution D_{AB}^* or to self-diffusivity D_{AA} . This reflects the much greater complexity of liquids on a molecular level. For example, gas-phase diffusion exhibits negligible composition effects and deviations from thermodynamic ideality. Conversely, liquid-phase diffusion almost always involves volumetric and thermodynamic effects due to composition variations. For concentrations greater than a few mole percent of A and B , corrections are needed to obtain the true diffusivity. Furthermore, there are many conditions that do not fit any of the correlations presented here. Thus, careful consideration is needed to produce a reasonable estimate. Again, if diffusivity data are available at the conditions of interest, then they are strongly preferred over the predictions of any correlations. Experimental values for liquid mixtures are listed in Table 2-325.

Stokes-Einstein and Free-Volume Theories The starting point for many correlations is the Stokes-Einstein equation. This equation is derived from continuum fluid mechanics and classical thermodynamics for the motion of large spherical particles in a liquid. For this case, the need for a molecular theory is cleverly avoided. The Stokes-Einstein equation is (Bird et al.)

$$D_{AB} = \frac{kT}{6\pi r_A \mu_B} \quad (5-217)$$

where A refers to the solute and B refers to the solvent. This equation is applicable to very large unhydrated molecules ($M > 1000$) in low-molecular-weight solvents or where the molar volume of the solute is greater than $500 \text{ cm}^3/\text{mol}$ (Reddy and Doraiswamy, *Ind. Eng. Chem. Fundam.*, 6, 77 (1967); Wilke and Chang [30]). Despite its intellectual appeal, this equation is seldom used "as is." Rather, the following principles have been identified: (1) The diffusion coefficient is inversely proportional to the size $r_A \approx V_A^{1/3}$ of the solute molecules. Experimental observations, however, generally indicate that the exponent of the solute molar volume is larger than one-third. (2) The term $D_{AB}\mu_B/T$ is approximately constant only over a 10-to-15 K interval. Thus, the dependence of liquid diffusivity on properties and conditions does not generally obey the interactions implied by that grouping. For example, Robinson, Edmister, and Dullien [*Ind. Eng. Chem. Fundam.*, 5, 75 (1966)] found that $\ln D_{AB} \propto -1/T$. (3) Finally, pressure does not affect liquid-phase diffusivity much, since μ_B and V_A are only weakly pressure-dependent. Pressure does have an impact at very high levels.

TABLE 5-13 Relationships for Diffusivities of Multicomponent Gas Mixtures at Low Pressure

Authors*	Equation
Stefan-Maxwell, Smith and Taylor [23]	$D_{im} = \left[1 - x_i \left(\sum_{j=1}^{NC} N_j \right) / N_i \right] \sum_{j=1}^{NC} \left[\left(x_j - \frac{x_i N_i}{N_i} \right) / D_{ij} \right] \quad (5-214)$
Blanc [2]	$D_{im} = \left(\sum_{j=1}^{NC} \frac{x_j}{D_{ij}} \right)^{-1} \quad (5-215)$
Wilke [29]	$D_{im} = \left(\sum_{j=1, j \neq i}^{NC} \frac{x_j}{D_{ij}} \right)^{-1} \quad (5-216)$

*References are listed at the beginning of the "Mass Transfer" subsection.

Another advance in the concepts of liquid-phase diffusion was provided by Hildebrand [*Science*, **174**, 490 (1971)] who adapted a theory of viscosity to self-diffusivity. He postulated that $D_{A'A}^{\circ} = B(V - V_{ms})/V_{ms}$, where $D_{A'A}^{\circ}$ is the self-diffusion coefficient, V is the molar volume, and V_{ms} is the molar volume at which fluidity is zero (i.e., the molar volume of the solid phase at the melting temperature). The difference ($V - V_{ms}$) can be thought of as the free volume, which increases with temperature; and B is a proportionality constant.

Ertl and Dullien (ibid.) found that Hildebrand's equation could not fit their data with B as a constant. They modified it by applying an empirical exponent n (a constant greater than unity) to the volumetric ratio. The new equation is not generally useful, however, since there is no means for predicting n . The theory does identify the free volume as an important physical variable, since $n > 1$ for most liquids implies that diffusion is more strongly dependent on free volume than is viscosity.

Dilute Binary Nonelectrolytes: General Mixtures These correlations are outlined in Table 5-14.

Wilke-Chang [30] This correlation for D_{AB}° is one of the most widely used, and it is an empirical modification of the Stokes-Einstein equation. It is not very accurate, however, for water as the solute. Otherwise, it applies to diffusion of very dilute A in B . The average absolute error for 251 different systems is about 10 percent. Φ_B is an association factor of solvent B that accounts for hydrogen bonding.

Component B	Φ_B
Water	2.26
Methanol	1.9
Ethanol	1.5
Propanol	1.2
Others	1.0

The value of Φ_B for water was originally stated as 2.6, although when the original data were reanalyzed, the empirical best fit was 2.26. Random comparisons of predictions with 2.26 versus 2.6 show no consistent advantage for either value, however. Kooijman [*Ind. Eng. Chem. Res.* **41**, 3326 (2002)] suggests replacing V_A with $\theta_A V_{A^*}$, in which $\theta_A = 1$ except when $A = \text{water}$, $\theta_A = 4.5$. This modification leads to an overall error of 8.7 percent for 41 cases he compared. He suggests retaining $\Phi_B = 2.6$ when $B = \text{water}$. It has been suggested to replace the exponent of 0.6 with 0.7 and to use an association factor of 0.7 for systems containing aromatic hydrocarbons. These modifications, however, are not recommended by Umesi and Danner [27]. Lees and Sarram [*J. Chem. Eng. Data*, **16**, 41 (1971)] present a comparison of the association parameters. The average absolute error for 87 different solutes in water is 5.9 percent.

Tyn-Calus [26] This correlation requires data in the form of molar volumes and parachors $\psi_i = V_i \sigma_i^{1/4}$ (a property which, over moderate temperature ranges, is nearly constant), measured at the same temperature (not necessarily the temperature of interest). The parachors for the components may also be evaluated at different temperatures from each other. Quale [*Chem. Rev.* **53**, 439 (1953)] has compiled values of ψ_i for many chemicals. Group contribution methods are available for estimation purposes (Poling et al.). The following suggestions were made by Poling et al.: The correlation is constrained to cases in which $\mu_B < 30$ cP. If the solute is water or if the solute is an organic acid and the solvent is not water or a short-chain alcohol, dimerization of the solute A should be assumed for purposes of estimating its volume and parachor. For example, the appropriate values for water as solute at 25°C are $V_W = 37.4$ cm³/mol and $\psi_W = 105.2$ cm³g^{1/4}/s^{1/2}/mol. Finally, if the solute is nonpolar, the solvent volume and parachor should be multiplied by $\delta\mu_B$. According to Kooijman (ibid.), if the Brock-Bird method (described in Poling et al.) is used to

TABLE 5-14 Correlations for Diffusivities of Dilute, Binary Mixtures of Nonelectrolytes in Liquids

Authors ^a	Equation	Error
1. General Mixtures		
Wilke-Chang [30]	$D_{AB}^{\circ} = \frac{7.4 \times 10^{-8} (\Phi_B M_B)^{1/2} T}{\mu_B V_A^{0.6}} \quad (5-218)$	20%
Tyn-Calus [26]	$D_{AB}^{\circ} = \frac{8.93 \times 10^{-8} (V_A/V_B^2)^{1/6} (\psi_B/\psi_A)^{0.6} T}{\mu_B} \quad (5-219)$	10%
Umesi-Danner [27]	$D_{AB}^{\circ} = \frac{2.75 \times 10^{-8} (R_B/R_A^{2/3}) T}{\mu_B} \quad (5-220)$	16%
Siddiqi-Lucas [22]	$D_{AB}^{\circ} = \frac{9.89 \times 10^{-8} V_B^{0.265} T}{V_A^{0.45} \mu_B^{0.907}} \quad (5-221)$	13%
2. Gases in Low Viscosity Liquids		
Sridhar-Potter [24]	$D_{AB}^{\circ} = D_{BB} \left(\frac{V_{cB}}{V_{cA}} \right)^{2/3} \left(\frac{V_B}{V_{mB}} \right) \quad (5-222)$	18%
Chen-Chen [7]	$D_{AB}^{\circ} = 2.018 \times 10^{-9} \frac{(\beta V_{cB})^{2/3} (RT_{cB})^{1/2}}{M_A^{1/6} (M_B V_{cA})^{1/3}} (V_f - 1) \left(\frac{T}{T_{cA}} \right)^{1/2} \quad (5-223)$	6%
3. Aqueous Solutions		
Hayduk-Laudie [11]	$D_{AW}^{\circ} = \frac{13.16 \times 10^{-5}}{\mu_w^{1.14} V_A^{0.589}} \quad (5-224)$	18%
Siddiqi-Lucas [22]	$D_{AW}^{\circ} = 2.98 \times 10^{-7} V_A^{-0.5473} \mu_w^{-1.026} T \quad (5-225)$	13%
4. Hydrocarbon Mixtures		
Hayduk-Minhas [12]	$D_{AB}^{\circ} = 13.3 \times 10^{-8} T^{1.47} \mu_B^{(10.2/V_A - 0.791)} V_A^{-0.71} \quad (5-226)$	5%
Matthews-Akgerman [19]	$D_{AB}^{\circ} = 32.88 M_A^{-0.61} V_D^{1.04} T^{0.5} (V_B - V_D) \quad (5-227)$	5%
Riazi-Whitson [21]	$D_{AB} = 1.07 \frac{(\rho D_{AB})^{\circ}}{\rho} \left(\frac{\mu}{\mu^{\circ}} \right)^{-0.27 - 0.38 \omega + (-0.05 + 0.1 \omega) P} \quad (5-228)$	15%

^aReferences are listed at the beginning of the "Mass Transfer" subsection.

estimate the surface tension, the error is only increased by about 2 percent, relative to employing experimentally measured values.

Umesi-Danner [27] They developed an equation for nonaqueous solvents with nonpolar and polar solutes. In all, 258 points were involved in the regression. R_i is the radius of gyration in Å of the component molecule, which has been tabulated by Passut and Danner [*Chem. Eng. Progress Symp. Ser.*, **140**, 30 (1974)] for 250 compounds. The average absolute deviation was 16 percent, compared with 26 percent for the Wilke-Chang equation.

Siddiqi-Lucas [22] In an impressive empirical study, these authors examined 1275 organic liquid mixtures. Their equation yielded an average absolute deviation of 13.1 percent, which was less than that for the Wilke-Chang equation (17.8 percent). Note that this correlation does not encompass aqueous solutions; those were examined and a separate correlation was proposed, which is discussed later.

Binary Mixtures of Gases in Low-Viscosity, Nonelectrolyte Liquids **Sridhar and Potter [24]** derived an equation for predicting gas diffusion through liquid by combining existing correlations. Hildebrand had postulated the following dependence of the diffusivity for a gas in a liquid: $D_{AB}^o = D_{B'B}(V_{cB}/V_{cA})^{2/3}$, where $D_{B'B}$ is the solvent self-diffusion coefficient and V_{cA} is the critical volume of component i , respectively. To correct for minor changes in volumetric expansion, Sridhar and Potter multiplied the resulting equation by V_B/V_{mB} , where V_{mB} is the molar volume of the liquid B at its melting point and $D_{B'B}$ can be estimated by the equation of Ertl and Dullien (see p. 5-54). Sridhar and Potter compared experimentally measured diffusion coefficients for twenty-seven data points of eleven binary mixtures. Their average absolute error was 13.5 percent, but Chen and Chen [7] analyzed about 50 combinations of conditions and 3 to 4 replicates each and found an average error of 18 percent. This correlation does not apply to hydrogen and helium as solutes. However, it demonstrates the usefulness of self-diffusion as a means to assess mutual diffusivities and the value of observable physical property changes, such as molar expansion, to account for changes in conditions.

Chen-Chen [7] Their correlation was based on diffusion measurements of 50 combinations of conditions with 3 to 4 replicates each and exhibited an average error of 6 percent. In this correlation, $V_r = V_B/[0.9724(V_{mB} + 0.04765)]$ and V_{mB} is the liquid molar volume at the melting point, as discussed previously. Their association parameter β [which is different from the definition of that symbol in Eq. (5-229)] accounts for hydrogen bonding of the solvent. Values for acetonitrile and methanol are: $\beta = 1.58$ and 2.31, respectively.

Dilute Binary Mixtures of a Nonelectrolyte in Water The correlations that were suggested previously for general mixtures, unless specified otherwise, may also be applied to diffusion of miscellaneous solutes in water. The following correlations are restricted to the present case, however.

Hayduk and Laudie [11] They presented a simple correlation for the infinite dilution diffusion coefficients of nonelectrolytes in water. It has about the same accuracy as the Wilke-Chang equation (about 5.9 percent). There is no explicit temperature dependence, but the 1.14 exponent on μ_w compensates for the absence of T in the numerator. That exponent was misprinted (as 1.4) in the original article and has been reproduced elsewhere erroneously.

Siddiqi and Lucas [227] These authors examined 658 aqueous liquid mixtures in an empirical study. They found an average absolute deviation of 19.7 percent. In contrast, the Wilke-Chang equation gave 35.0 percent and the Hayduk-Laudie correlation gave 30.4 percent.

Dilute Binary Hydrocarbon Mixtures **Hayduk and Minhas [12]** presented an accurate correlation for normal paraffin mixtures that was developed from 58 data points consisting of solutes from C_5 to C_{32} and solvents from C_5 to C_{16} . The average error was 3.4 percent for the 58 mixtures.

Matthews and Akgerman [19] The free-volume approach of Hildebrand was shown to be valid for binary, dilute liquid paraffin mixtures (as well as self-diffusion), consisting of solutes from C_8 to C_{16} and solvents of C_6 and C_{12} . The term they referred to as the "diffusion volume" was simply correlated with the critical volume, as $V_D = 0.308 V_c$. We can infer from Table 5-11 that this is approximately related to the volume at the melting point as $V_D = 0.945 V_m$. Their correlation was valid for diffusion of linear alkanes at temperatures

up to 300°C and pressures up to 3.45 MPa. Matthews, Rodden, and Akgerman [*J. Chem. Eng. Data*, **32**, 317 (1987)] and Erkey and Akgerman [*AIChE J.*, **35**, 443 (1989)] completed similar studies of diffusion of alkanes, restricted to n -hexadecane and n -octane, respectively, as the solvents.

Riasi and Whitson [21] They presented a generalized correlation in terms of viscosity and molar density that was applicable to both gases and liquids. The average absolute deviation for gases was only about 8 percent, while for liquids it was 15 percent. Their expression relies on the Chapman-Enskog correlation [Eq. (5-202)] for the low-pressure diffusivity and the Stiel-Thodos [*AIChE J.*, **7**, 234 (1961)] correlation for low-pressure viscosity:

$$\mu^o = \frac{x_A \mu_A^o M_A^{1/2} + x_B \mu_B^o M_B^{1/2}}{x_A M_A^{1/2} + x_B M_B^{1/2}}$$

where $\mu_i^o \xi_i = 3.4 \times 10^{-4} T_{r,i}^{0.94}$ for $T_{r,i} < 1.5$ or $\mu_i^o \xi_i = 1.778 \times 10^{-4} (4.58 T_{r,i} - 1.67)^{0.58}$ for $T_{r,i} > 1.5$. In these equations, $\xi_i = T_{c,i}^{1/6} P_{c,i}^{2/3} M_i^{1/2}$, and units are in cP, atm, K, and mol. For dense gases or liquids, the Chung et al. [*Ind. Eng. Chem. Res.*, **27**, 671 (1988)] or Jossi-Stiel-Thodos [*AIChE J.*, **8**, 59 (1962)] correlation may be used to estimate viscosity. The latter is:

$$(\mu - \mu^o) \xi + 10^{-4} = (0.1023 + 0.023364 \rho_r + 0.058533 \rho_r^2 - 0.040758 \rho_r^3 + 0.093324 \rho_r^4)$$

$$\text{where } \xi = \frac{(x_A T_{cA} + x_B T_{cB})^{1/6}}{(x_A M_A + x_B M_B)^{1/2} (x_A P_{cA} + x_B P_{cB})}$$

$$\text{and } \rho_r = (x_A V_{cA} + x_B V_{cB}) \rho$$

Dilute Binary Mixtures of Nonelectrolytes with Water as the Solute **Olander [AIChE J., **7**, 175 (1961)] modified the Wilke-Chang equation to adapt it to the infinite dilution diffusivity of water as the solute. The modification he recommended is simply the division of the right-hand side of the Wilke-Chang equation by 2.3. Unfortunately, neither the Wilke-Chang equation nor that equation divided by 2.3 fit the data very well. A reasonably valid generalization is that the Wilke-Chang equation is accurate if water is very insoluble in the solvent, such as pure hydrocarbons, halogenated hydrocarbons, and nitro-hydrocarbons. On the other hand, the Wilke-Chang equation divided by 2.3 is accurate for solvents in which water is very soluble, as well as those that have low viscosities. Such solvents include alcohols, ketones, carboxylic acids, and aldehydes. Neither equation is accurate for higher-viscosity liquids, especially diols.**

Dilute Dispersions of Macromolecules in Nonelectrolytes The Stokes-Einstein equation has already been presented. It was noted that its validity was restricted to large solutes, such as spherical macromolecules and particles in a continuum solvent. The equation has also been found to predict accurately the diffusion coefficient of spherical latex particles and globular proteins. Corrections to Stokes-Einstein for molecules approximating spheroids is given by Tanford *Physical Chemistry of Macromolecules*, Wiley, New York, (1961). Since solute-solute interactions are ignored in this theory, it applies in the dilute range only.

Hiss and Cussler [AIChE J., **19, 698 (1973)] Their basis is the diffusion of a small solute in a fairly viscous solvent of relatively large molecules, which is the opposite of the Stokes-Einstein assumptions. The large solvent molecules investigated were not polymers or gels but were of moderate molecular weight so that the macroscopic and microscopic viscosities were the same. The major conclusion is that $D_{AB}^o \mu^{2/3} = \text{constant}$ at a given temperature and for a solvent viscosity from 5×10^{-3} to 5 Pa·s or greater (5 to 5×10^3 cP). This observation is useful if D_{AB}^o is known in a given high-viscosity liquid (oils, tars, etc.). Use of the usual relation of $D_{AB}^o \propto 1/\mu$ for such an estimate could lead to large errors.**

Concentrated, Binary Mixtures of Nonelectrolytes Several correlations that predict the composition dependence of D_{AB} are summarized in Table 5-15. Most are based on known values of D_{AB}^o and D_{BA}^o . In fact, a rule of thumb states that, for many binary systems, D_{AB}^o and D_{BA}^o bound the D_{AB} vs. x_A curve. Cullinan's [8] equation predicts diffusivities even in lieu of values at infinite dilution, but requires accurate density, viscosity, and activity coefficient data.

TABLE 5-15 Correlations of Diffusivities for Concentrated, Binary Mixtures of Nonelectrolyte Liquids

Authors*	Equation
Caldwell-Babb [5]	$D_{AB} = (x_A D_{BA}^{\circ} + x_B D_{AB}^{\circ}) \beta_A$ (5-231)
Rathbun-Babb [20]	$D_{AB} = (x_A D_{BA}^{\circ} + x_B D_{AB}^{\circ}) \beta_A^n$ (5-232)
Vignes [28]	$D_{AB} = D_{AB}^{\circ} D_{BA}^{\circ} \beta_A$ (5-233)
Leffler-Cullinan [16]	$D_{AB} \mu_{mix} = (D_{AB}^{\circ} \mu_B)^{x_B} (D_{BA}^{\circ} \mu_A)^{x_A} \beta_A$ (5-234)
Cussler [9]	$D_{AB} = D_0 \left[1 + \frac{K}{x_A x_B} \left(\frac{\partial \ln x_A}{\partial \ln a_A} - 1 \right) \right]^{-1/2}$ (5-235)
Cullinan [8]	$D_{AB} = \frac{kT}{2\pi \mu_{mix} (V/A)^{1/3}} \left[\frac{2\pi x_A x_B \beta_A}{1 + \beta_A (2\pi x_A x_B - 1)} \right]^{1/2}$ (5-236)
Asfour-Dullien [1]	$D_{AB} = \left(\frac{D_{AB}^{\circ}}{\mu_B} \right)^{x_B} \left(\frac{D_{BA}^{\circ}}{\mu_A} \right)^{x_A} \zeta \mu \beta_A$ (5-237)
Siddiqi-Lucas [22]	$D_{AB} = (C_B \bar{V}_B D_{AB}^{\circ} + C_A \bar{V}_A D_{BA}^{\circ}) \beta_A$ (5-238)
Bosse and Bart no. 1 [3]	$D_{AB} = (D_{AB}^{\circ})^{x_B} (D_{BA}^{\circ})^{x_A} \exp \left(-\frac{g^E}{RT} \right)$ (5-239)
Bosse and Bart no. 2 [3]	$\mu D_{AB} = (\mu_B D_{AB}^{\circ})^{x_B} (\mu_A D_{BA}^{\circ})^{x_A} \exp \left(-\frac{g^E}{RT} \right)$ (5-240)

Relative errors for the correlations in this table are very dependent on the components of interest and are cited in the text. *See the beginning of the "Mass Transfer" subsection for references.

Since the infinite dilution values D_{AB}° and D_{BA}° are generally unequal, even a thermodynamically ideal solution like $\gamma_A = \gamma_B = 1$ will exhibit concentration dependence of the diffusivity. In addition, non-ideal solutions require a thermodynamic correction factor to retain the true "driving force" for molecular diffusion, or the gradient of the chemical potential rather than the composition gradient. That correction factor is:

$$\beta_A = 1 + \frac{\partial \ln \gamma_A}{\partial \ln x_A} \quad (5-229)$$

Caldwell and Babb [5] Darken [*Trans. Am. Inst. Mining Met. Eng.*, **175**, 184 (1948)] observed that solid-state diffusion in metallurgical applications followed a simple relation. His equation related the tracer diffusivities and mole fractions to the mutual diffusivity:

$$D_{AB} = (x_A D_B + x_B D_A) \beta_A \quad (5-230)$$

Caldwell and Babb used virtually the same equation to evaluate the mutual diffusivity for concentrated mixtures of common liquids.

Van Geet and Adamson [*J. Phys. Chem.*, **68**, 238 (1964)] tested that equation for the *n*-dodecane (*A*) and *n*-octane (*B*) system and found the average deviation of D_{AB} from experimental values to be -0.68 percent. In addition, that equation was tested for benzene + bromobenzene, *n*-hexane + *n*-dodecane, benzene + CCl_4 , octane + decane, heptane + cetane, benzene + diphenyl, and benzene + nitromethane with success. For systems that depart significantly from thermodynamic ideality, it breaks down, sometimes by a factor of eight. For example, in the binary systems acetone + CCl_4 , acetone + chloroform, and ethanol + CCl_4 , it is not accurate. Thus, it can be expected to be fairly accurate for nonpolar hydrocarbons of similar molecular weight but not for polar-polar mixtures. Siddiqi, Krahn, and Lucas [*J. Chem. Eng. Data*, **32**, 48 (1987)] found that this relation was superior to those of Vignes and Leffler and Cullinan for a variety of mixtures. Umesi and Danner [27] found an average absolute deviation of 13.9 percent for 198 data points.

Rathbun and Babb [20] suggested that Darken's equation could be improved by raising the thermodynamic correction factor β_A to a power, *n*, less than unity. They looked at systems exhibiting negative deviations from Raoult's law and found $n = 0.3$. Furthermore, for polar-nonpolar mixtures, they found $n = 0.6$. In a separate study, Siddiqi and Lucas [22] followed those suggestions and found an average absolute error of 3.3 percent for nonpolar-nonpolar mixtures, 11.0 percent for polar-nonpolar mixtures, and 14.6 percent for polar-polar mixtures. Siddiqi, Krahn, and Lucas (ibid.) examined a few other mixtures and

found that $n = 1$ was probably best. Thus, this approach is, at best, highly dependent on the type of components being considered.

Vignes [28] empirically correlated mixture diffusivity data for 12 binary mixtures. Later Ertl, Ghai, and Dollon [*AIChE J.*, **20**, 1 (1974)] evaluated 122 binary systems, which showed an average absolute deviation of only 7 percent. None of the latter systems, however, was very nonideal.

Leffler and Cullinan [16] modified Vignes' equation using some theoretical arguments to arrive at Eq. (5-234), which the authors compared to Eq. (5-233) for the 12 systems mentioned above. The average absolute maximum deviation was only 6 percent. Umesi and Danner [27], however, found an average absolute deviation of 11.4 percent for 198 data points. For normal paraffins, it is not very accurate. In general, the accuracies of Eqs. (5-233) and (5-234) are not much different, and since Vignes' is simpler to use, it is suggested. The application of either should be limited to nonassociating systems that do not deviate much from ideality ($0.95 < \beta_A < 1.05$).

Cussler [9] studied diffusion in concentrated associating systems and has shown that, in associating systems, it is the size of diffusing clusters rather than diffusing solutes that controls diffusion. D_0 is a reference diffusion coefficient discussed hereafter; a_A is the activity of component A; and K is a constant. By assuming that D_0 could be predicted by Eq. (5-233) with $\beta = 1$, K was found to be equal to 0.5 based on five binary systems and validated with a sixth binary mixture. The limitations of Eq. (5-235) using D_0 and K defined previously have not been explored, so caution is warranted. Gurkan [*AIChE J.*, **33**, 175 (1987)] showed that K should actually be closer to 0.3 (rather than 0.5) and discussed the overall results.

Cullinan [8] presented an extension of Cussler's cluster diffusion theory. His method accurately accounts for composition and temperature dependence of diffusivity. It is novel in that it contains no adjustable constants, and it relates transport properties and solution thermodynamics. This equation has been tested for six very different mixtures by Rollins and Knaebel [*AIChE J.*, **37**, 470 (1991)], and it was found to agree remarkably well with data for most conditions, considering the absence of adjustable parameters. In the dilute region (of either A or B), there are systematic errors probably caused by the breakdown of certain implicit assumptions (that nevertheless appear to be generally valid at higher concentrations).

Asfour and Dullien [1] developed a relation for predicting alkane diffusivities at moderate concentrations that employs:

$$\zeta = \left(\frac{V_{fm}}{V_{fxA} V_{fxB}} \right)^{2/3} \frac{M_{xA} M_{xB}}{M_m} \quad (5-241)$$

where $V_{f_i} = V_{\beta_i}^0$; the fluid free volume is $V_{f_i} = V_i - V_{m_i}$ for $i = A, B$, and m , in which V_{m_i} is the molar volume of the liquid at the melting point and

$$V_{m,m} = \left(\frac{x_A^2}{V_{m,A}} + \frac{2x_A x_B}{V_{m,AB}} + \frac{x_B^2}{V_{m,B}} \right)^{-1}$$

and

$$V_{m,AB} = \left[\frac{V_{m,A}^{1/3} + V_{m,B}^{1/3}}{2} \right]^3$$

and μ is the mixture viscosity; M_m is the mixture mean molecular weight; and β_A is defined by Eq. (5-229). The average absolute error of this equation is 1.4 percent, while the Vignes equation and the Lefler-Cullinan equation give 3.3 percent and 6.2 percent, respectively.

Siddiqi and Lucas [22] suggested that component volume fractions might be used to correlate the effects of concentration dependence. They found an average absolute deviation of 4.5 percent for nonpolar-nonpolar mixtures, 16.5 percent for polar-nonpolar mixtures, and 10.8 percent for polar-polar mixtures.

Bosse and Bart added a term to account for excess Gibbs free energy, involved in the activation energy for diffusion, which was previously omitted. Doing so yielded minor modifications of the Vignes and Lefler-Cullinan equations [Eqs. (5-233) and (5-234), respectively]. The UNIFAC method was used to assess the excess Gibbs free energy. Comparing predictions of the new equations with data for 36 pairs and 326 data points yielded relative deviations of 7.8 percent and 8.9 percent, respectively, but which were better than the closely related Vignes (12.8 percent) and Lefler-Cullinan (10.4 percent) equations.

Binary Electrolyte Mixtures When electrolytes are added to a solvent, they dissociate to a certain degree. It would appear that the solution contains at least three components: solvent, anions, and cations. If the solution is to remain neutral in charge at each point (assuming the absence of any applied electric potential field), the anions and cations diffuse effectively as a single component, as for molecular diffusion. The diffusion of the anionic and cationic species in the solvent can thus be treated as a binary mixture.

Nernst-Haskell The theory of dilute diffusion of salts is well developed and has been experimentally verified. For dilute solutions of a single salt, the well-known Nernst-Haskell equation (Poling et al.) is applicable:

$$D_{AB}^0 = \frac{RT}{F^2} \frac{\left| \frac{1}{n_+} + \frac{1}{n_-} \right|}{\frac{1}{\lambda_+^0} + \frac{1}{\lambda_-^0}} = 8.9304 \times 10^{-10} T \frac{\left| \frac{1}{n_+} + \frac{1}{n_-} \right|}{\frac{1}{\lambda_+^0} + \frac{1}{\lambda_-^0}} \quad (5-242)$$

where D_{AB}^0 = diffusivity based on molarity rather than normality of dilute salt A in solvent B, cm^2/s .

The previous definitions can be interpreted in terms of ionic-species diffusivities and conductivities. The latter are easily measured and depend on temperature and composition. For example, the equivalent conductance Λ is commonly tabulated in chemistry handbooks as the limiting (infinite dilution) conductance Λ_0 , and at standard concentrations, typically at 25°C. $\Lambda = 1000K/C = \lambda_+ + \lambda_- = \Lambda_0 + f(C)$, ($\text{cm}^2/\text{ohm gequiv}$); $K = \alpha/R$ = specific conductance, (ohm cm^{-1}); C = solution concentration, (gequiv/ℓ); α = conductance cell constant (measured), (cm^{-1}); R = solution electrical resistance, which is measured (ohm); and $f(C)$ = a complicated function of concentration. The resulting equation of the electrolyte diffusivity is

$$D_{AB} = \frac{|\lambda_{+}| + |\lambda_{-}|}{(|\lambda_{-}|/D_{+}) + (|\lambda_{+}|/D_{-})} \quad (5-243)$$

where $|\lambda_{\pm}|$ represents the magnitude of the ionic charge and where the cationic or anionic diffusivities are $D_{\pm} = 8.9304 \times 10^{-10} T \lambda_{\pm} / |\lambda_{\pm}| \text{ cm}^2/\text{s}$. The coefficient is $kN_0/F^2 = R/F^2$. In practice, the equivalent conductance of the ion pair of interest would be obtained and supplemented with conductances of permutations of those ions and one independent cation and anion. This would allow determination of all the ionic conductances and hence the diffusivity of the electrolyte solution.

Gordon [J. Phys. Chem. **5**, 522 (1937)] Typically, as the concentration of a salt increases from infinite dilution, the diffusion coefficient

decreases rapidly from D_{AB}^0 . As concentration is increased further, however, D_{AB} rises steadily, often becoming greater than D_{AB}^0 . Gordon proposed the following empirical equation, which is applicable up to concentrations of $2N$:

$$D_{AB} = D_{AB}^0 \frac{1}{C_B \bar{V}_B} \frac{\mu_B}{\mu} \left(1 + \frac{\ln \gamma_{\pm}}{\ln m} \right) \quad (5-244)$$

where D_{AB}^0 is given by the Nernst-Haskell equation. References that tabulate γ_{\pm} as a function of m , as well as other equations for D_{AB} , are given by Poling et al.

Morgan, Ferguson, and Scovazzo [Ind. Eng. Chem. Res. **44**, 4815 (2005)] They studied diffusion of gases in ionic liquids having moderate to high viscosity (up to about 1000 cP) at 30°C. Their range was limited, and the empirical equation they found was

$$D_{AB} = 3.7 \times 10^{-3} \left(\frac{1}{\mu_B^{0.59} V_{A0} \rho_B^2} \right) \quad (5-245)$$

which yielded a correlation coefficient of 0.975. Of the estimated diffusivities 90 percent were within ± 20 percent of the experimental values. The exponent for viscosity approximately confirmed the observation of Hiss and Cussler (ibid).

Multicomponent Mixtures No simple, practical estimation methods have been developed for predicting multicomponent liquid-diffusion coefficients. Several theories have been developed, but the necessity for extensive activity data, pure component and mixture volumes, mixture viscosity data, and tracer and binary diffusion coefficients have significantly limited the utility of the theories (see Poling et al.).

The generalized Stefan-Maxwell equations using binary diffusion coefficients are not easily applicable to liquids since the coefficients are so dependent on conditions. That is, in liquids, each D_{ij} can be strongly composition dependent in binary mixtures and, moreover, the binary D_{ij} is strongly affected in a multicomponent mixture. Thus, the convenience of writing multicomponent flux equations in terms of binary coefficients is lost. Conversely, they apply to gas mixtures because each D_{ij} is practically independent of composition by itself and in a multicomponent mixture (see Taylor and Krishna for details).

One particular case of multicomponent diffusion that has been examined is the dilute diffusion of a solute in a homogeneous mixture (e.g., of A in B + C). Umesi and Danner [27] compared the three equations given below for 49 ternary systems. All three equations were equivalent, giving average absolute deviations of 25 percent.

Perkins and Geankoplis [Chem. Eng. Sci., **24**, 1035 (1969)]

$$D_{am} \mu_m^{0.8} = \sum_{\substack{j=1 \\ j \neq A}}^n x_j D_{Aj}^0 \mu_j^{0.8} \quad (5-246)$$

Cullinan [Can. J. Chem. Eng. **45**, 377 (1967)] This is an extension of Vignes' equation to multicomponent systems:

$$D_{am} = \prod_{\substack{j=1 \\ j \neq A}}^n (D_{Aj}^0)^{x_j} \quad (5-247)$$

Lefler and Cullinan [16] They extended their binary relation to an arbitrary multicomponent mixture, as follows:

$$D_{am} \mu_m = \prod_{\substack{j=1 \\ j \neq A}}^n (D_{Aj}^0 \mu_j)^{x_j} \quad (5-248)$$

where D_{Aj} is the dilute binary diffusion coefficient of A in j; D_{am} is the dilute diffusion of A through m; x_j is the mole fraction; μ_j is the viscosity of component j; and μ_m is the mixture viscosity.

Akita [Ind. Eng. Chem. Fundam., **10**, 89 (1981)] Another case of multicomponent dilute diffusion of significant practical interest is that of gases in aqueous electrolyte solutions. Many gas-absorption processes use electrolyte solutions. Akita presents experimentally tested equations for this case.

Graham and Dranoff [Ind. Eng. Chem. Fundam., **21**, 360 and 365 (1982)] They studied multicomponent diffusion of electrolytes in ion exchangers. They found that the Stefan-Maxwell interaction coefficients reduce to limiting ion tracer diffusivities of each ion.

Pinto and Graham [AIChE J. **32**, 291 (1986) and **33**, 436 (1987)] They studied multicomponent diffusion in electrolyte solutions. They focused on the Stefan-Maxwell equations and corrected for solvation effects. They achieved excellent results for 1-1 electrolytes in water at 25°C up to concentrations of 4M.

Anderko and Lencka [Ind. Eng. Chem. Res. **37**, 2878 (1998)] These authors present an analysis of self-diffusion in multicomponent aqueous electrolyte systems. Their model includes contributions of long-range (Coulombic) and short-range (hard-sphere) interactions. Their mixing rule was based on equations of nonequilibrium thermodynamics. The model accurately predicts self-diffusivities of ions and gases in aqueous solutions from dilute to about 30 mol/kg water. It makes it possible to take single-solute data and extend them to multicomponent mixtures.

DIFFUSION OF FLUIDS IN POROUS SOLIDS

Diffusion in porous solids is usually the most important factor controlling mass transfer in adsorption, ion exchange, drying, heterogeneous catalysis, leaching, and many other applications. Some of the applications of interest are outlined in Table 5-16. Applications of these equations are found in Secs. 16, 22, and 23.

Diffusion within the largest cavities of a porous medium is assumed to be similar to ordinary or bulk diffusion except that it is hindered by the pore walls (see Eq. 5-249). The tortuosity τ that expresses this hindrance has been estimated from geometric arguments. Unfortunately,

measured values are often an order of magnitude greater than those estimates. Thus, the effective diffusivity D_{eff} (and hence τ) is normally determined by comparing a diffusion model to experimental measurements. The normal range of tortuosities for silica gel, alumina, and other porous solids is $2 \leq \tau \leq 6$, but for activated carbon, $5 \leq \tau \leq 65$.

In small pores and at low pressures, the mean free path ℓ of the gas molecule (or atom) is significantly greater than the pore diameter d_{pore} . Its magnitude may be estimated from

$$\ell = \frac{3.2 \mu}{P} \left(\frac{RT}{2\pi M} \right)^{1/2} \text{ m}$$

As a result, collisions with the wall occur more frequently than with other molecules. This is referred to as the Knudsen mode of diffusion and is contrasted with ordinary or bulk diffusion, which occurs by intermolecular collisions. At intermediate pressures, both ordinary diffusion and Knudsen diffusion may be important [see Eqs. (5-252) and (5-253)].

For gases and vapors that adsorb on the porous solid, surface diffusion may be important, particularly at high surface coverage [see Eqs. (5-254) and (5-257)]. The mechanism of surface diffusion may be viewed as molecules hopping from one surface site to another. Thus, if adsorption is too strong, surface diffusion is impeded, while if adsorption is too weak, surface diffusion contributes insignificantly to the overall rate. Surface diffusion and bulk diffusion usually occur in parallel [see Eqs. (5-258) and (5-259)]. Although D_s is expected to be less than D_{eff} , the solute flux due to surface diffusion may be larger

TABLE 5-16 Relations for Diffusion in Porous Solids

Mechanism	Equation	Applies to	References°
Bulk diffusion in pores	$D_{eff} = \frac{\epsilon_p D}{\tau}$ (5-249)	Gases or liquids in large pores. $N_{Kn} = \ell/d_{pore} < 0.01$	[33]
Knudsen diffusion	$D_K = 48.5 d_{pore} \left(\frac{T}{M} \right)^{1/2}$ in m^2/s (5-250) $D_{K,eff} = \frac{\epsilon_p D_K}{\tau}$	Dilute (low pressure) gases in small pores. $N_{Kn} = \ell/d_{pore} > 10$	Geankoplis, [34, 35]
	$N_i = -D_K \frac{dC_i}{dz}$ (5-251)	" " " "	
Combined bulk and Knudsen diffusion	$D_{eff} = \left(\frac{1 - \alpha X_A}{D_{eff}} + \frac{1}{D_{K,eff}} \right)^{-1}$ (5-252) $\alpha = 1 + \frac{N_B}{N_A}$	" " " " $N_A \neq N_B$	Geankoplis, [32, 35]
	$D_{eff} = \left(\frac{1}{D_{eff}} + \frac{1}{D_{K,eff}} \right)^{-1}$ (5-253)	$N_A = N_B$	
Surface diffusion	$J_{si} = -D_{s,eff} \rho_p \left(\frac{dq_i}{dz} \right)$ (5-254) $D_{s,eff} = \frac{\epsilon_p D_s}{\tau}$ (5-255)	Adsorbed gases or vapors " " " "	[32, 34, 35]
	$D_{s\theta} = \frac{D_{s\theta=0}}{(1 - \theta)}$ (5-256)	θ = fractional surface coverage ≤ 0.6	
	$D_s = D'_s(q) \exp\left(\frac{-E_s}{RT}\right)$ (5-257)	" " " "	
Parallel bulk and surface diffusion	$J = -\left[D_{eff} \left(\frac{dp_i}{dz} \right) + D_{s,eff} \rho_p \left(\frac{dq_i}{dz} \right) \right]$ (5-258) $J = -D_{app} \left(\frac{dp_i}{dz} \right)$ (5-259) $D_{app} = D_{eff} + D_{s,eff} \rho_p \left(\frac{dq_i}{dp_i} \right)$ (5-260)	" " " " " " " " " " " "	[34]

°See the beginning of the "Mass Transfer" subsection for references.

than that due to bulk diffusion if $\partial q_i/\partial z \gg \partial C_i/\partial z$. This can occur when a component is strongly adsorbed and the surface coverage is high. For all that, surface diffusion is not well understood. The references in Table 5-16 should be consulted for further details.

INTERPHASE MASS TRANSFER

Transfer of material between phases is important in most separation processes in which two phases are involved. When one phase is pure, mass transfer in the pure phase is not involved. For example, when a pure liquid is being evaporated into a gas, only the gas-phase mass transfer need be calculated. Occasionally, mass transfer in one of the two phases may be neglected even though pure components are not involved. This will be the case when the resistance to mass transfer is much larger in one phase than in the other. Understanding the nature and magnitudes of these resistances is one of the keys to performing reliable mass transfer. In this section, mass transfer between gas and liquid phases will be discussed. The principles are easily applied to the other phases.

Mass-Transfer Principles: Dilute Systems When material is transferred from one phase to another across an interface that separates the two, the resistance to mass transfer in each phase causes a concentration gradient in each, as shown in Fig. 5-26 for a gas-liquid interface. The concentrations of the diffusing material in the two phases immediately adjacent to the interface generally are unequal, even if expressed in the same units, but usually are assumed to be related to each other by the laws of thermodynamic equilibrium. Thus, it is assumed that the thermodynamic equilibrium is reached at the gas-liquid interface almost immediately when a gas and a liquid are brought into contact.

For systems in which the solute concentrations in the gas and liquid phases are dilute, the rate of transfer may be expressed by equations which predict that the rate of mass transfer is proportional to the difference between the bulk concentration and the concentration at the gas-liquid interface. Thus

$$N_A = k'_G(p - p_i) = k'_L(c_i - c) \tag{5-261}$$

where N_A = mass-transfer rate, k'_G = gas-phase mass-transfer coefficient, k'_L = liquid-phase mass-transfer coefficient, p = solute partial pressure in bulk gas, p_i = solute partial pressure at interface, c = solute concentration in bulk liquid, and c_i = solute concentration in liquid at interface.

The mass-transfer coefficients k'_G and k'_L by definition are equal to the ratios of the molar mass flux N_A to the concentration driving forces $(p - p_i)$ and $(c_i - c)$ respectively. An alternative expression for the rate of transfer in dilute systems is given by

$$N_A = k_C(y - y_i) = k_L(x_i - x) \tag{5-262}$$

where N_A = mass-transfer rate, k_C = gas-phase mass-transfer coefficient, k_L = liquid-phase mass-transfer coefficient, y = mole-fraction

solute in bulk-gas phase, y_i = mole-fraction solute in gas at interface, x = mole-fraction solute in bulk-liquid phase, and x_i = mole-fraction solute in liquid at interface.

The mass-transfer coefficients defined by Eqs. (5-261) and (5-262) are related to each other as follows:

$$k_C = k'_G p_T \tag{5-263}$$

$$k_L = k'_L \bar{\rho}_L \tag{5-264}$$

where p_T = total system pressure employed during the experimental determinations of k'_G values and $\bar{\rho}_L$ = average molar density of the liquid phase. The coefficient k_C is relatively independent of the total system pressure and therefore is more convenient to use than k'_G , which is inversely proportional to the total system pressure.

The above equations may be used for finding the interfacial concentrations corresponding to any set of values of x and y provided the ratio of the individual coefficients is known. Thus

$$(y - y_i)/(x_i - x) = k_L/k_C = k'_L \bar{\rho}_L / k'_G p_T = L_M H_C / G_M H_L \tag{5-265}$$

where L_M = molar liquid mass velocity, G_M = molar gas mass velocity, H_L = height of one transfer unit based on liquid-phase resistance, and H_C = height of one transfer unit based on gas-phase resistance. The last term in Eq. (5-265) is derived from Eqs. (5-284) and (5-286).

Equation (5-265) may be solved graphically if a plot is made of the equilibrium vapor and liquid compositions and a point representing the bulk concentrations x and y is located on this diagram. A construction of this type is shown in Fig. 5-27, which represents a gas-absorption situation.

The interfacial mole fractions y_i and x_i can be determined by solving Eq. (5-265) simultaneously with the equilibrium relation $y_i^\circ = F(x_i)$ to obtain y_i and x_i . The rate of transfer may then be calculated from Eq. (5-262).

If the equilibrium relation $y_i^\circ = F(x_i)$ is sufficiently simple, e.g., if a plot of y_i° versus x_i is a straight line, not necessarily through the origin, the rate of transfer is proportional to the difference between the bulk concentration in one phase and the concentration (in that same phase) which would be in equilibrium with the bulk concentration in the second phase. One such difference is $y - y^\circ$, and another is $x^\circ - x$. In this case, there is no need to solve for the interfacial compositions, as may be seen from the following derivation.

The rate of mass transfer may be defined by the equation

$$N_A = K_C(y - y^\circ) = k_C(y - y_i) = k_L(x_i - x) = K_L(x^\circ - x) \tag{5-266}$$

where K_C = overall gas-phase mass-transfer coefficient, K_L = overall liquid-phase mass-transfer coefficient, y° = vapor composition in equilibrium with x , and x° = liquid composition in equilibrium with vapor of composition y . This equation can be rearranged to the formula

$$\frac{1}{K_C} = \frac{1}{k_C} \left(\frac{y - y^\circ}{y - y_i} \right) = \frac{1}{k_C} + \frac{1}{k_C} \left(\frac{y_i - y^\circ}{y - y_i} \right) = \frac{1}{k_C} + \frac{1}{k_L} \left(\frac{y_i - y^\circ}{x_i - x} \right) \tag{5-267}$$

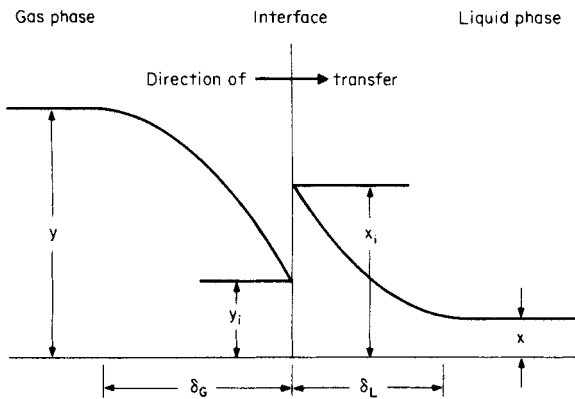


FIG. 5-26 Concentration gradients near a gas-liquid interface.

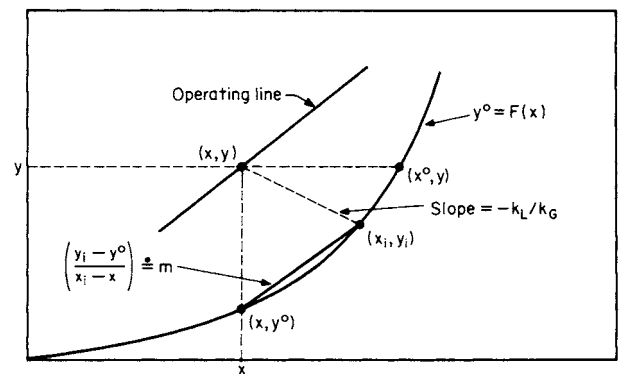


FIG. 5-27 Identification of concentrations at a point in a countercurrent absorption tower.

in view of Eq. (5-265). Comparison of the last term in parentheses with the diagram of Fig. 5-27 shows that it is equal to the slope of the chord connecting the points (x, y°) and (x_i, y_i) . If the equilibrium curve is a straight line, then this term is the slope m . Thus

$$1/K_G = (1/k_G + m/k_L) \quad (5-268)$$

When Henry's law is valid ($p_A = Hx_A$ or $p_A = H'C_A$), the slope m can be computed according to the relationship

$$m = H/p_T = H'\bar{p}_L/p_T \quad (5-269)$$

where m is defined in terms of mole-fraction driving forces compatible with Eqs. (5-262) through (5-268), i.e., with the definitions of k_L , k_G , and K_G .

If it is desired to calculate the rate of transfer from the overall concentration difference based on bulk-liquid compositions ($x^\circ - x$), the appropriate overall coefficient K_L is related to the individual coefficients by the equation

$$1/K_L = [1/k_L + 1/(mk_G)] \quad (5-270)$$

Conversion of these equations to a k'_G, k'_L basis can be accomplished readily by direct substitution of Eqs. (5-263) and (5-264).

Occasionally one will find k'_L or K'_L values reported in units (SI) of meters per second. The correct units for these values are $\text{kmol}/[(s \cdot \text{m}^2)(\text{kmol}/\text{m}^3)]$, and Eq. (5-264) is the correct equation for converting them to a mole-fraction basis.

When k'_G and K'_G values are reported in units (SI) of $\text{kmol}/[(s \cdot \text{m}^2)(\text{kPa})]$, one must be careful in converting them to a mole-fraction basis to multiply by the total pressure actually employed in the original experiments and *not* by the total pressure of the system to be designed. This conversion is valid for systems in which Dalton's law of partial pressures ($p = yp_T$) is valid.

Comparison of Eqs. (5-268) and (5-270) shows that for systems in which the equilibrium line is straight, the overall mass transfer coefficients are related to each other by the equation

$$K_L = mK_G \quad (5-271)$$

When the equilibrium curve is not straight, there is no strictly logical basis for the use of an overall transfer coefficient, since the value of m will be a function of position in the apparatus, as can be seen from Fig. 5-27. In such cases the rate of transfer must be calculated by solving for the interfacial compositions as described above.

Experimentally observed rates of mass transfer often are expressed in terms of overall transfer coefficients even when the equilibrium lines are curved. This procedure is empirical, since the theory indicates that in such cases the rates of transfer may not vary in direct proportion to the overall bulk concentration differences $(y - y^\circ)$ and $(x^\circ - x)$ at all concentration levels even though the rates may be proportional to the concentration difference in each phase taken separately, i.e., $(x_i - x)$ and $(y - y_i)$.

In most types of separation equipment such as packed or spray towers, the interfacial area that is effective for mass transfer cannot be accurately determined. For this reason it is customary to report experimentally observed rates of transfer in terms of transfer coefficients based on a unit volume of the apparatus rather than on a unit of interfacial area. Such volumetric coefficients are designated as K_{Ca} , k_{La} , etc., where a represents the interfacial area per unit volume of the apparatus. Experimentally observed variations in the values of these volumetric coefficients with variations in flow rates, type of packing, etc., may be due as much to changes in the effective value of a as to changes in k . Calculation of the overall coefficients from the individual volumetric coefficients is made by means of the equations

$$1/K_{Ca} = (1/k_{Ca} + m/k_{La}) \quad (5-272)$$

$$1/K_{La} = (1/k_{La} + 1/mk_{Ca}) \quad (5-273)$$

Because of the wide variation in equilibrium, the variation in the values of m from one system to another can have an important effect on the overall coefficient and on the selection of the type of equipment to use. For example, if m is large, the liquid-phase part of the overall resistance might be extremely large where k_L might be relatively small. This kind of reasoning must be applied with caution, however, since species with different equilibrium characteristics are separated under different

operating conditions. Thus, the effect of changes in m on the overall resistance to mass transfer may partly be counterbalanced by changes in the individual specific resistances as the flow rates are changed.

Mass-Transfer Principles: Concentrated Systems When solute concentrations in the gas and/or liquid phases are large, the equations derived above for dilute systems no longer are applicable. The correct equations to use for concentrated systems are as follows:

$$N_A = \hat{k}_G(y - y_i)/y_{BM} = \hat{k}_L(x_i - x)/x_{BM} \\ = \hat{K}_G(y - y^\circ)/y_{BM}^\circ = \hat{K}_L(x^\circ - x)/x_{BM}^\circ \quad (5-274)$$

where ($N_B = 0$)

$$y_{BM} = \frac{(1 - y) - (1 - y_i)}{\ln [(1 - y)/(1 - y_i)]} \quad (5-275)$$

$$y_{BM}^\circ = \frac{(1 - y) - (1 - y^\circ)}{\ln [(1 - y)/(1 - y^\circ)]} \quad (5-276)$$

$$x_{BM} = \frac{(1 - x) - (1 - x_i)}{\ln [(1 - x)/(1 - x_i)]} \quad (5-277)$$

$$x_{BM}^\circ = \frac{(1 - x) - (1 - x^\circ)}{\ln [(1 - x)/(1 - x^\circ)]} \quad (5-278)$$

and where \hat{k}_G and \hat{k}_L are the gas-phase and liquid-phase mass-transfer coefficients for concentrated systems and \hat{K}_G and \hat{K}_L are the overall gas-phase and liquid-phase mass-transfer coefficients for concentrated systems. These coefficients are defined later in Eqs. (5-281) to (5-283).

The factors y_{BM} and x_{BM} arise from the fact that, in the diffusion of a solute through a second stationary layer of insoluble fluid, the resistance to diffusion varies in proportion to the concentration of the insoluble stationary fluid, approaching zero as the concentration of the insoluble fluid approaches zero. See Eq. (5-198).

The factors y_{BM}° and x_{BM}° cannot be justified on the basis of mass-transfer theory since they are based on overall resistances. These factors therefore are included in the equations by analogy with the corresponding film equations.

In dilute systems the logarithmic-mean insoluble-gas and nonvolatile-liquid concentrations approach unity, and Eq. (5-274) reduces to the dilute-system formula. For equimolar counter diffusion (e.g., binary distillation), these log-mean factors should be omitted. See Eq. (5-197).

Substitution of Eqs. (5-275) through (5-278) into Eq. (5-274) results in the following simplified formula:

$$N_A = \hat{k}_G \ln [(1 - y_i)/(1 - y)] \\ = \hat{K}_G \ln [(1 - y^\circ)/(1 - y)] \\ = \hat{k}_L \ln [(1 - x)/(1 - x_i)] \\ = \hat{K}_L \ln [(1 - x^\circ)/(1 - x^\circ)] \quad (5-279)$$

Note that the units of \hat{k}_G , \hat{K}_G , \hat{k}_L , and \hat{K}_L are all identical to each other, i.e., $\text{kmol}/(s \cdot \text{m}^2)$ in SI units.

The equation for computing the interfacial gas and liquid compositions in concentrated systems is

$$(y - y_i)/(x_i - x) = \hat{k}_L y_{BM} / \hat{k}_G x_{BM} \\ = L_M H_C y_{BM} / G_M H_L x_{BM} = k_L / k_G \quad (5-280)$$

This equation is identical to the one for dilute systems since $\hat{k}_G = k_G y_{BM}$ and $\hat{k}_L = k_L x_{BM}$. Note, however, that when \hat{k}_G and \hat{k}_L are given, the equation must be solved by trial and error, since x_{BM} contains x_i and y_{BM} contains y_i .

The overall gas-phase and liquid-phase mass-transfer coefficients for concentrated systems are computed according to the following equations:

$$\frac{1}{\hat{K}_G} = \frac{y_{BM}}{y_{BM}^\circ} \frac{1}{\hat{k}_G} + \frac{x_{BM}}{y_{BM}^\circ} \frac{1}{\hat{k}_L} \left(\frac{y_i - y^\circ}{x_i - x} \right) \quad (5-281)$$

$$\frac{1}{\hat{K}_L} = \frac{x_{BM}}{x_{BM}^\circ} \frac{1}{\hat{k}_L} + \frac{y_{BM}}{x_{BM}^\circ} \frac{1}{\hat{k}_G} \left(\frac{x^\circ - x_i}{y - y_i} \right) \quad (5-282)$$

When the equilibrium curve is a straight line, the terms in parentheses can be replaced by the slope m or $1/m$ as before. In this case the

overall mass-transfer coefficients for concentrated systems are related to each other by the equation

$$\hat{K}_L = m \hat{K}_G (x_{BM}^{\circ} / y_{BM}^{\circ}) \quad (5-283)$$

All these equations reduce to their dilute-system equivalents as the inert concentrations approach unity in terms of mole fractions of inert concentrations in the fluids.

HTU (Height Equivalent to One Transfer Unit) Frequently the values of the individual coefficients of mass transfer are so strongly dependent on flow rates that the quantity obtained by dividing each coefficient by the flow rate of the phase to which it applies is more nearly constant than the coefficient itself. The quantity obtained by this procedure is called the height equivalent to one transfer unit, since it expresses in terms of a single length dimension the height of apparatus required to accomplish a separation of standard difficulty.

The following relations between the transfer coefficients and the values of HTU apply:

$$H_G = G_M / k_G a y_{BM} = G_M / \hat{K}_G a \quad (5-284)$$

$$H_{OG} = G_M / K_G a y_{BM}^{\circ} = G_M / \hat{K}_G a \quad (5-285)$$

$$H_L = L_M / k_L a x_{BM} = L_M / \hat{K}_L a \quad (5-286)$$

$$H_{OL} = L_M / K_L a x_{BM}^{\circ} = L_M / \hat{K}_L a \quad (5-287)$$

The equations that express the addition of individual resistances in terms of HTUs, applicable to either dilute or concentrated systems, are

$$H_{OG} = \frac{y_{BM}}{y_{BM}^{\circ}} H_G + \frac{m G_M}{L_M} \frac{x_{BM}}{y_{BM}^{\circ}} H_L \quad (5-288)$$

$$H_{OL} = \frac{x_{BM}}{x_{BM}^{\circ}} H_L + \frac{L_M}{m G_M} \frac{y_{BM}}{x_{BM}^{\circ}} H_G \quad (5-289)$$

These equations are strictly valid only when m , the slope of the equilibrium curve, is constant, as noted previously.

NTU (Number of Transfer Units) The NTU required for a given separation is closely related to the number of theoretical stages or plates required to carry out the same separation in a stagewise or plate-type apparatus. For equimolar counterdiffusion, such as in a binary distillation, the number of overall gas-phase transfer units N_{OG} required for changing the composition of the vapor stream from y_1 to y_2 is

$$N_{OG} = \int_{y_2}^{y_1} \frac{dy}{y - y^{\circ}} \quad (5-290)$$

When diffusion is in one direction only, as in the absorption of a soluble component from an insoluble gas,

$$N_{OG} = \int_{y_2}^{y_1} \frac{y_{BM}^{\circ} dy}{(1 - y)(y - y^{\circ})} \quad (5-291)$$

The total height of packing required is then

$$h_T = H_{OG} N_{OG} \quad (5-292)$$

When it is known that H_{OG} varies appreciably within the tower, this term must be placed inside the integral in Eqs. (5-290) and (5-291) for accurate calculations of h_T . For example, the packed-tower design equation in terms of the overall gas-phase mass-transfer coefficient for absorption would be expressed as follows:

$$h_T = \int_{y_2}^{y_1} \left[\frac{G_M}{K_G a y_{BM}^{\circ}} \right] \frac{y_{BM}^{\circ} dy}{(1 - y)(y - y^{\circ})} \quad (5-293)$$

where the first term under the integral can be recognized as the HTU term. Convenient solutions of these equations for special cases are discussed later.

Definitions of Mass-Transfer Coefficients \hat{K}_G and \hat{K}_L The mass-transfer coefficient is defined as the ratio of the molar mass flux N_A to the concentration driving force. This leads to many different ways of defining these coefficients. For example, gas-phase mass-transfer rates may be defined as

$$N_A = k_G (y - y_i) = k'_G (p - p_i) = \hat{k}_G (y - y_i) / y_{BM} \quad (5-294)$$

where the units (SI) of k_G are $\text{kmol}/[(\text{s}\cdot\text{m}^2)(\text{mole fraction})]$, the units of

k'_G are $\text{kmol}/[(\text{s}\cdot\text{m}^2)(\text{kPa})]$, and the units of \hat{k}_G are $\text{kmol}/(\text{s}\cdot\text{m}^2)$. These coefficients are related to each other as follows:

$$k_G = k_C y_{BM} = k'_G p_T y_{BM} \quad (5-295)$$

where p_T is the total system pressure (it is assumed here that Dalton's law of partial pressures is valid).

In a similar way, liquid-phase mass-transfer rates may be defined by the relations

$$N_A = k_L (x_i - x) = k'_L (c_i - c) = \hat{k}_L (x_i - x) / x_{BM} \quad (5-296)$$

where the units (SI) of k_L are $\text{kmol}/[(\text{s}\cdot\text{m}^2)(\text{mole fraction})]$, the units of k'_L are $\text{kmol}/[(\text{s}\cdot\text{m}^2)(\text{kmol}/\text{m}^3)]$ or meters per second, and the units of \hat{k}_L are $\text{kmol}/(\text{s}\cdot\text{m}^2)$. These coefficients are related as follows:

$$\hat{k}_L = k_L x_{BM} = k'_L \bar{\rho}_L x_{BM} \quad (5-297)$$

where $\bar{\rho}_L$ is the molar density of the liquid phase in units (SI) of kilomoles per cubic meter. Note that, for dilute solutions where $x_{BM} \doteq 1$, k_L and \hat{k}_L will have identical numerical values. Similarly, for dilute gases $\hat{k}_G \doteq k_G$.

Simplified Mass-Transfer Theories In certain simple situations, the mass-transfer coefficients can be calculated from first principles. The film, penetration, and surface-renewal theories are attempts to extend these theoretical calculations to more complex situations. Although these theories are often not accurate, they are useful to provide a physical picture for variations in the mass-transfer coefficient.

For the special case of steady-state unidirectional diffusion of a component through an inert-gas film in an ideal-gas system, the rate of mass transfer is derived as

$$N_A = \frac{D_{AB} p_T}{RT \delta_C} \frac{(y - y_i)}{y_{BM}} = \frac{D_{AB} p_T}{RT \delta_C} \ln \frac{1 - y_i}{1 - y} \quad (5-298)$$

where D_{AB} is the diffusion coefficient or "diffusivity," δ_C is the "effective" thickness of a stagnant-gas layer which would offer a resistance to molecular diffusion equal to the experimentally observed resistance, and R is the gas constant. [Nernst, *Z. Phys. Chem.*, **47**, 52 (1904); Whitman, *Chem. Mat. Eng.*, **29**, 149 (1923), and Lewis and Whitman, *Ind. Eng. Chem.*, **16**, 1215 (1924)].

The film thickness δ_C depends primarily on the hydrodynamics of the system and hence on the Reynolds number and the Schmidt number. Thus, various correlations have been developed for different geometries in terms of the following dimensionless variables:

$$N_{Sh} = \hat{k}_G R T d / D_{AB} p_T = f(N_{Re}, N_{Sc}) \quad (5-299)$$

where N_{Sh} is the Sherwood number, $N_{Re} (= Gd/\mu_C)$ is the Reynolds number based on the characteristic length d appropriate to the geometry of the particular system; and $N_{Sc} (= \mu_C/\rho_C D_{AB})$ is the Schmidt number.

According to this analysis one can see that for gas-absorption problems, which often exhibit unidirectional diffusion, the most appropriate driving-force expression is of the form $(y - y_i)/y_{BM}$, and the most appropriate mass-transfer coefficient is therefore \hat{k}_G . This concept is to be found in all the key equations for the design of mass-transfer equipment.

The Sherwood-number relation for gas-phase mass-transfer coefficients as represented by the film diffusion model in Eq. (5-299) can be rearranged as follows:

$$N_{Sh} = (\hat{k}_G / G_M) N_{Re} N_{Sc} = N_{St} N_{Re} N_{Sc} = f(N_{Re}, N_{Sc}) \quad (5-300)$$

where $N_{St} = \hat{k}_G / G_M = k'_G p_{BM} / G_M$ is known as the Stanton number. This equation can now be stated in the alternative functional forms

$$N_{St} = \hat{k}_G / G_M = g(N_{Re}, N_{Sc}) \quad (5-301)$$

$$j_D = N_{St} \cdot N_{Sc}^{2/3} \quad (5-302)$$

where j is the Chilton-Colburn "j factor" for mass transfer (discussed later).

The important point to note here is that the gas-phase mass-transfer coefficient \hat{k}_G depends principally upon the transport properties of the fluid (N_{Sc}) and the hydrodynamics of the particular system involved (N_{Re}). It also is important to recognize that specific mass-transfer correlations can be derived only in conjunction with the

investigator's particular assumptions concerning the numerical values of the effective interfacial area a of the packing.

The stagnant-film model discussed previously assumes a steady state in which the local flux across each element of area is constant; i.e., there is no accumulation of the diffusing species within the film. Higbie [*Trans. Am. Inst. Chem. Eng.*, **31**, 365 (1935)] pointed out that industrial contactors often operate with repeated brief contacts between phases in which the contact times are too short for the steady state to be achieved. For example, Higbie advanced the theory that in a packed tower the liquid flows across each packing piece in laminar flow and is remixed at the points of discontinuity between the packing elements. Thus, a fresh liquid surface is formed at the top of each piece, and as it moves downward, it absorbs gas at a decreasing rate until it is mixed at the next discontinuity. This is the basis of penetration theory.

If the velocity of the flowing stream is uniform over a very deep region of liquid (total thickness, $\delta_T \gg \sqrt{Dt}$), the time-averaged mass-transfer coefficient according to penetration theory is given by

$$k'_L = 2\sqrt{D_L/\pi t} \quad (5-303)$$

where k'_L = liquid-phase mass-transfer coefficient, D_L = liquid-phase diffusion coefficient, and t = contact time.

In practice, the contact time t is not known except in special cases in which the hydrodynamics are clearly defined. This is somewhat similar to the case of the stagnant-film theory in which the unknown quantity is the thickness of the stagnant layer δ (in film theory, the liquid-phase mass-transfer coefficient is given by $k'_L = D_L/\delta$).

The penetration theory predicts that k'_L should vary by the square root of the molecular diffusivity, as compared with film theory, which predicts a first-power dependency on D . Various investigators have reported experimental powers of D ranging from 0.5 to 0.75, and the Chilton-Colburn analogy suggests a $2/3$ power.

Penetration theory often is used in analyzing absorption with chemical reaction because it makes no assumption about the depths of penetration of the various reacting species, and it gives a more accurate result when the diffusion coefficients of the reacting species are not equal. When the reaction process is very complex, however, penetration theory is more difficult to use than film theory, and the latter method normally is preferred.

Danckwerts [*Ind. Eng. Chem.*, **42**, 1460 (1951)] proposed an extension of the penetration theory, called the surface renewal theory, which allows for the eddy motion in the liquid to bring masses of fresh liquid continually from the interior to the surface, where they are exposed to the gas for finite lengths of time before being replaced. In his development, Danckwerts assumed that every element of fluid has an equal chance of being replaced regardless of its age. The Danckwerts model gives

$$k'_L = \sqrt{Ds} \quad (5-304)$$

where s = fractional rate of surface renewal.

Note that both the penetration and the surface-renewal theories predict a square-root dependency on D . Also, it should be recognized that values of the surface-renewal rate s generally are not available, which presents the same problems as do δ and t in the film and penetration models.

The predictions of correlations based on the film model often are nearly identical to predictions based on the penetration and surface-renewal models. Thus, in view of its relative simplicity, the film model normally is preferred for purposes of discussion or calculation. It should be noted that none of these theoretical models has proved adequate for making a priori predictions of mass-transfer rates in packed towers, and therefore empirical correlations such as those outlined later in Table 5-24 must be employed.

Mass-Transfer Correlations Because of the tremendous importance of mass transfer in chemical engineering, a very large number of studies have determined mass-transfer coefficients both empirically and theoretically. Some of these studies are summarized in Tables 5-17 to 5-24. Each table is for a specific geometry or type of contactor, starting with flat plates, which have the simplest geometry (Table 5-17); then wetted wall columns (Table 5-18); flow in pipes and ducts (Table 5-19); submerged objects (Table 5-20); drops and

bubbles (Table 5-21); agitated systems (Table 5-22); packed beds of particles for adsorption, ion exchange, and chemical reaction (Table 5-23); and finishing with packed bed two-phase contactors for distillation, absorption and other unit operations (Table 5-24). Although extensive, these tables are not meant to be encyclopedic, but a variety of different configurations are shown to provide a flavor of the range of correlations available. These correlations include transfer to or from one fluid and either a second fluid or a solid. Many of the correlations are for k_L and k_G values obtained from dilute systems where $x_{BM} \approx 1.0$ and $y_{BM} \approx 1.0$. The most extensive source for older mass-transfer correlations in a variety of geometries is Skelland (*Diffusional Mass Transfer*, 1974). The extensive review of bubble column systems (see Table 5-21) by Shah et al. [*AIChE J.*, **28**, 353 (1982)] includes estimation of bubble size, gas holdup, interfacial area $k_L a$, and liquid dispersion coefficient. For correlations for particle-liquid mass transfer in stirred tanks (part of Table 5-22) see the review by Pangarkar et al. [*Ind. Eng. Chem. Res.*, **41**, 4141 (2002)]. For mass transfer in distillation, absorption, and extraction in packed beds (Table 5-24), see also the appropriate sections in this handbook and the review by Wang, Yuan, and Yu [*Ind. Eng. Chem. Res.*, **44**, 8715 (2005)]. For simple geometries, one may be able to determine a theoretical (T) form of the mass-transfer correlation. For very complex geometries, only an empirical (E) form can be found. In systems of intermediate complexity, semiempirical (S) correlations where the form is determined from theory and the coefficients from experiment are often useful. Although the major limitations and constraints in use are usually included in the tables, obviously many details cannot be included in this summary form. Readers are strongly encouraged to check the references before using the correlations in important situations. Note that even authoritative sources occasionally have typographical errors in the fairly complex correlation equations. Thus, it is a good idea to check several sources, including the original paper. The references will often include figures comparing the correlations with data. These figures are very useful since they provide a visual picture of the scatter in the data.

Since there are often several correlations that are applicable, how does one choose the correlation to use? First, the engineer must determine which correlations are closest to the current situation. This involves recognizing the similarity of geometries, which is often challenging, and checking that the range of parameters in the correlation is appropriate. For example, the Bravo, Rocha, and Fair correlation for distillation with structured packings with triangular cross-sectional channels (Table 5-24-H) uses the Johnstone and Pigford correlation for rectification in vertical wetted wall columns (Table 5-18-F). Recognizing that this latter correlation pertains to a rather different application and geometry was a nontrivial step in the process of developing a correlation. If several correlations appear to be applicable, check to see if the correlations have been compared to each other and to the data. When a detailed comparison of correlations is not available, the following heuristics may be useful:

1. Mass-transfer coefficients are derived from models. They must be employed in a similar model. For example, if an arithmetic concentration difference was used to determine k , that k should only be used in a mass-transfer expression with an arithmetic concentration difference.
2. Semiempirical correlations are often preferred to purely empirical or purely theoretical correlations. Purely empirical correlations are dangerous to use for extrapolation. Purely theoretical correlations may predict trends accurately, but they can be several orders of magnitude off in the value of k .
3. Correlations with broader data bases are often preferred.
4. The analogy between heat and mass transfer holds over wider ranges than the analogy between mass and momentum transfer. Good heat transfer data (without radiation) can often be used to predict mass-transfer coefficients.
5. More recent data is often preferred to older data, since end effects are better understood, the new correlation often builds on earlier data and analysis, and better measurement techniques are often available.
6. With complicated geometries, the product of the interfacial area per volume and the mass-transfer coefficient is required. Correlations of ka_p or of HTU are more accurate than individual correlations of k and

TABLE 5-17 Mass-Transfer Correlations for a Single Flat Plate or Disk—Transfer to or from Plate to Fluid

Situation	Correlation	Comments E = Empirical, S = Semiempirical, T = Theoretical	References°
A. Laminar, local, flat plate, forced flow	$N_{Sh,x} = \frac{k'x}{D} = 0.323(N_{Re,x})^{1/2}(N_{Sc})^{1/3}$ Coefficient 0.323 is a better fit.	[T] Low M.T. rates. Low mass-flux, constant property systems. $N_{Sh,x}$ is local k . Use with arithmetic difference in concentration. Coefficient 0.323 is Blasius' approximate solution. $N_{Re,x} = \frac{xu_\infty\rho}{\mu}$, x = length along plate	[77] p. 183 [87] p. 526 [138] p. 79 [140] p. 518 [141] p. 110
Laminar, average, flat plate, forced flow	$N_{Sh,avg} = \frac{k'_m L}{D} = 0.664(N_{Re,L})^{1/2}(N_{Sc})^{1/3}$ Coefficient 0.664 is a better fit. k'_m is mean mass-transfer coefficient for dilute systems.	$N_{Re,L} = \frac{Lu_\infty\rho}{\mu}$, 0.664 (Polhausen) is a better fit for $N_{Sc} > 0.6$, $N_{Re,x} < 3 \times 10^5$.	[91] p. 480
j_D -factors	$j_D = j_H = \frac{f}{2} = 0.664(N_{Re,L})^{-1/2}$	[S] Analogy. $N_{Sc} = 1.0$, f = drag coefficient. j_D is defined in terms of k'_m .	[141] p. 271
B. Laminar, local, flat plate, blowing or suction and forced flow	$N_{Sh,x} = \frac{k'x}{D} = (\text{Slope})_{y=0} (N_{Re,x})^{1/2}(N_{Sc})^{1/3}$	[T] Blowing is positive. Other conditions as above. $\frac{u_o}{u_\infty} \sqrt{N_{Re,x}}$ $\frac{u_\infty}{(\text{Slope})_{y=0}}$ 0.6 0.5 0.25 0.0 -2.5 0.01 0.06 0.17 0.332 1.64	[77] p. 185 [140] p. 271
C. Laminar, local, flat plate, natural convection vertical plate	$N_{Sh,x} = \frac{k'x}{D} = 0.508N_{Sc}^{1/2}(0.952 + N_{Sc})^{-1/4}N_{Gr}^{1/4}$ $N_{Gr} = \frac{gx^3}{(\mu/\rho)^2} \left(\frac{\rho_\infty}{\rho_0} - 1 \right)$	[T] Low MT rates. Dilute systems, $\Delta\rho/\rho \ll 1$. $N_{Gr}, N_{Sc} < 10^9$. Use with arithmetic concentration difference. x = length from plate bottom.	[141] p. 120
D. Laminar, stationary disk	$N_{Sh} = \frac{k'd_{\text{disk}}}{D} = \frac{8}{\pi}$	[T] Stagnant fluid. Use arithmetic concentration difference.	[138] p. 240
Laminar, spinning disk	$N_{Sh} = \frac{k'd_{\text{disk}}}{D} = 0.879N_{Re}^{1/2}N_{Sc}^{1/3}$ $N_{Re} < \sim 10^4$	[T] Asymptotic solution for large N_{Sc} . $u = \omega d_{\text{disk}}/2$, ω = rotational speed, rad/s. Rotating disks are often used in electrochemical research.	[101] p. 60 [138] p. 240
E. Laminar, inclined, plate	$N_{Sh,avg} = 0.783N_{Re,\text{film}}^{1/3}N_{Sc}^{1/3} \left(\frac{x^3\rho^2g\sin\alpha}{\mu^2} \right)^{2/9}$ $N_{Re,\text{film}} = \frac{4Q\rho}{\mu^2} < 2000$ $N_{Sh,avg} = \frac{k'_m x}{D}$ $\delta_{\text{film}} = \left(\frac{3\mu Q}{w\rho g \sin\alpha} \right)^{1/3}$ = film thickness	[T] Constant-property liquid film with low mass-transfer rates. Use arithmetic concentration difference. Newtonian fluid. Solute does not penetrate past region of linear velocity profile. Differences between theory and experiment. w = width of plate, δ_j = film thickness, α = angle of inclination, x = distance from start soluble surface.	[141] p. 130 [138] p. 209
F. Turbulent, local flat plate, forced flow	$N_{Sh,x} = \frac{k'x}{D} = 0.0292N_{Re,x}^{0.8}$	[S] Low mass-flux with constant property system. Use with arithmetic concentration difference. $N_{Sc} = 1.0$, $N_{Re,x} > 10^5$	[77] p. 191 [138] p. 201 [141] p. 221
Turbulent, average, flat plate, forced flow	$N_{Sh,avg} = \frac{k'L}{D} = 0.0365N_{Re,L}^{0.8}$	Based on Prandtl's 1/7-power velocity law, $\frac{u}{u_\infty} = \left(\frac{y}{\delta} \right)^{1/7}$	
G. Laminar and turbulent, flat plate, forced flow	$j_D = j_H = \frac{f}{2} = 0.037N_{Re,L}^{0.2}$ $j_D = (k_C/G_M)N_{Sc}^{2/3}$ $j_H = (h'/C_p G)N_{Pr}^{2/3}$	[E] Chilton-Colburn analogies, $N_{Sc} = 1.0$, (gases), f = drag coefficient. Corresponds to item 5-17-F and refers to same conditions. $8000 < N_{Re} < 300,000$. Can apply analogy, $j_D = f/2$, to entire plate (including laminar portion) if average values are used.	[77] p. 193 [88] p. 112 [138] p. 201 [141] p. 271 [80] [53]

5-64 HEAT AND MASS TRANSFER

TABLE 5-17 Mass-Transfer Correlations for a Single Flat Plate or Disk—Transfer to or from Plate to Fluid (Concluded)

Situation	Correlation	Comments E = Empirical, S = Semiempirical, T = Theoretical	References*
H. Laminar and turbulent, flat plate, forced flow	$N_{Sh,avg} = 0.037N_{Sc}^{1/3}(N_{Re,L}^{0.8} - 15,500)$ to $N_{Re,L} = 320,000$ $N_{Sh,avg} = 0.037N_{Sc}^{1/3} \times \left(N_{Re,L}^{0.8} - N_{Re,Cr}^{0.8} + \frac{0.664}{0.037} N_{Re,Cr}^{1/2} \right)$ in range 3×10^5 to 3×10^6 .	[E] Use arithmetic concentration difference. $N_{Sh,avg} = \frac{k_m L}{D}$, $N_{Sc} > 0.5$ Entrance effects are ignored. $N_{Re,Cr}$ is transition laminar to turbulent.	[88] p. 112 [138] p. 201
I. Turbulent, local flat plate, natural convection, vertical plate Turbulent, average, flat plate, natural convection, vertical plate	$N_{Sh,x} = \frac{k'x}{D} = 0.0299N_{Gr}^{2/5}N_{Sc}^{7/15} \times (1 + 0.494N_{Sc}^{2/3})^{-2/5}$ $N_{Sh,avg} = 0.0249N_{Gr}^{2/5}N_{Sc}^{7/15} \times (1 + 0.494N_{Sc}^{2/3})^{-2/5}$ $N_{Cr} = \frac{gx^3}{(\mu/\rho)^2} \left(\frac{\rho_\infty}{\rho_0} - 1 \right), \quad N_{Sh,avg} = \frac{k_m L}{D}$	[S] Low solute concentration and low transfer rates. Use arithmetic concentration difference. $N_{Gr} > 10^{10}$ Assumes laminar boundary layer is small fraction of total.	[141] p. 225
J. Perforated flat disk Perforated vertical plate. Natural convection.	$N_{Sh} = 0.059N_{Sc}^{0.35}N_{Gr}^{0.35} \left(\frac{d_h}{d} \right)^{0.04}$ Characteristic length = disk diameter d $N_{Sh} = 0.1N_{Sc}^{1/3}N_{Gr}^{1/3}$ Characteristic length = L , electrode height	[E] $6 \times 10^9 < N_{Sc}N_{Gr} < 10^{12}$ and $1943 < N_{Sc} < 2168$ d_h = hole diameter [E] $1 \times 10^{10} < N_{Sc}N_{Gr} < 5 \times 10^{13}$ and $1939 < N_{Sc} < 2186$ Average deviation $\pm 10\%$	[162]
K. Turbulent, vertical plate	$N_{Sh,avg} = \frac{k'_m x}{D} = 0.327N_{Re, \text{film}}^{2/9}N_{Sc}^{1/3} \left(\frac{x^3 \rho^2 g}{\mu^2} \right)^{2/9}$ $\delta_{\text{film}} = 0.172 \left(\frac{Q^2}{w^2 g} \right)^{1/3}$	[E] See 5-17-E for terms. $N_{Re, \text{film}} = \frac{4Q\rho}{w\mu^2} > 2360$ Solute remains in laminar sublayer.	[141] p. 229
L. Cross-corrugated plate (turbulence promoter for membrane systems)	$N_{Sh} = cN_{Re}^a N_{Sc}^c$	[E] Entrance turbulent channel For parallel flow and corrugations: $N_{Sc} = 1483$, $a = 0.56$, $c = 0.268$ $N_{Sc} = 4997$, $a = 0.50$, $c = 0.395$ Corrugations perpendicular to flow: $N_{Sc} = 1483$, $a = 0.57$, $c = 0.368$ $N_{Sc} = 4997$, $a = 0.52$, $c = 0.487$	[134]
M. Turbulent, spinning disk	$N_{Sh} = \frac{k'd_{\text{disk}}}{D} = 5.6N_{Re}^{1.1}N_{Sc}^{1/3}$ $6 \times 10^5 < N_{Re} < 2 \times 10^6$ $120 < N_{Sc} < 1200$	[E] Use arithmetic concentration difference. $u = \omega d_{\text{disk}}/2$ where ω = rotational speed, radians/s. $N_{Re} = \rho \omega d^2 / 2\mu$.	[55] [138] p. 241
N. Mass transfer to a flat plate membrane in a stirred vessel	$N_{Sh} = \frac{k'd_{\text{tank}}}{D} = aN_{Re}^b N_{Sc}^c$ a depends on system. $a = 0.0443$ [40]; b is often 0.65–0.70 [89]. If $N_{Re} = \frac{\omega d_{\text{tank}}^2 \rho}{\mu}$	[E] Use arithmetic concentration difference. ω = stirrer speed, radians/s. Useful for laboratory dialysis, R.O., U.F., and microfiltration systems. $b = 0.785$ [40]. c is often 0.33 but other values have been reported [89].	[40] [89] p. 965
O. Spiral type RO (seawater desalination)	$N_{Sh} = 0.210 N_{Re}^{2/3} N_{Sc}^{1/4}$ Or with slightly larger error, $N_{Sh} = 0.080 N_{Re}^{0.875} N_{Sc}^{1/4}$	[E] Polyamide membrane. $p = 6.5$ MPa and TDS rejection = 99.8%. Recovery ratio 40%.	[148]

*See the beginning of the "Mass Transfer" subsection for references.

TABLE 5-18 Mass-Transfer Correlations for Falling Films with a Free Surface in Wetted Wall Columns—Transfer between Gas and Liquid

Situation	Correlation	Comments E = Empirical, S = Semiempirical, T = Theoretical	References*
A. Laminar, vertical wetted wall column	$N_{Sh,avg} = \frac{K'_m x}{D} \approx 3.41 \frac{x}{\delta_{film}}$ (first term of infinite series) $\delta_{film} = \left(\frac{3\mu Q}{w\rho g} \right)^{1/3} = \text{film thickness}$ $N_{Re, film} = \frac{4Q\rho}{w\mu} < 20$	[T] Low rates M.T. Use with log mean concentration difference. Parabolic velocity distribution in films. w = film width (circumference in column) Derived for flat plates, used for tubes if $r_{tube} \left(\frac{\rho g}{2\sigma} \right)^{1/2} > 3.0$. σ = surface tension If $N_{Re, film} > 20$, surface waves and rates increase. An approximate solution $D_{apparent}$ can be used. Ripples are suppressed with a wetting agent good to $N_{Re} = 1200$.	[138] p. 78 [141] p. 137 [152] p. 50
B. Turbulent, vertical wetted wall column	$N_{Sh,avg} = \frac{K'_m d_t}{D} = 0.023 N_{Re}^{0.83} N_{Sc}^{0.44}$ A coefficient 0.0163 has also been reported using $N_{Re'}$, where $v = v$ of gas relative to liquid film.	[E] Use with log mean concentration difference for correlations in B and D. N_{Re} is for gas. N_{Sc} for vapor in gas. $2000 < N_{Re} \leq 35,000$, $0.6 \leq N_{Sc} \leq 2.5$. Use for gases, d_t = tube diameter.	[68] [77] p. 181 [138] p. 211 [141] p. 265 [149] p. 212 [152] p. 71 [58]
Better fit	$N_{Sh,avg} = 0.0318 N_{Re}^{0.790} N_{Sc}^{0.5}$	[S] Reevaluated data	
C. Turbulent, very short column	$N_{Sh} = 0.00283 N_{Re,g}^{0.5} N_{Sc,g}^{0.06} N_{Re,liq}$ $N_{Sh} = k_g(d_{tube} - 2\delta)/D$ $N_{Re,g} = \rho_g u_g (d_{tube} - 2\delta)/\mu_g$ $N_{Re,liq} = \rho_{liq} Q_{liq} / [\pi \mu (d_{tube} - 2\delta)]$	[E] Evaporation data $N_{Sh,g} = 11$ to 65 , $N_{Re,g} = 2400$ to 9100 $N_{Re,liq} = 110$ to 480 , $N_{Sc,g} = 0.62$ to 1.93 δ = film thickness	[56]
D. Turbulent, vertical wetted wall column with ripples	$N_{Sh,avg} = \frac{K'_m d_t}{D} = 0.00814 N_{Re}^{0.83} N_{Sc}^{0.44} \left(\frac{4Q\rho}{w\mu} \right)^{0.15}$ $30 \leq \left(\frac{4Q\rho}{w\mu} \right) < 1200$ $N_{Sh,avg} = \frac{K'_m d_t}{D} = 0.023 N_{Re}^{0.8} N_{Sc}^{1/3}$	[E] For gas systems with rippling. Fits 5-18-B for $\left(\frac{4Q\rho}{w\mu} \right) = 1000$ [E] "Rounded" approximation to include ripples. Includes solid-liquid mass-transfer data to find $1/3$ coefficient on N_{Sc} . May use $N_{Re}^{0.83}$. Use for liquids. See also Table 5-19.	[85] [138] p. 213
E. Turbulent, with ripples	$N_{Sh} = \left(\frac{2}{\pi} \right)^{0.5} N_{Re,\dot{\epsilon}}^{0.5} N_{Sc}^{0.5}$ $N_{Re,\dot{\epsilon}} = \dot{\epsilon} L^2 / \nu$	[E] $\dot{\epsilon}$ = dilation rate of surface = $\frac{\partial v_x^c}{\partial x} + \frac{\partial v_y^c}{\partial y}$	[150]
F. Rectification in vertical wetted wall column with turbulent vapor flow, Johnstone and Pigford correlation	$N_{Sh,avg} = \frac{k'_c d_{col} p_{BM}}{D_c p} = 0.0328 (N_{Re}')^{0.77} N_{Sc}^{0.33}$ $3000 < N_{Re}' < 40,000, 0.5 < N_{Sc} < 3$ $N_{Re}' = \frac{d_{col} v_{rel} \rho_v}{\mu_v}, v_{rel} = \text{gas velocity relative to liquid film} = \frac{3}{2} u_{avg} \text{ in film}$	[E] Use logarithmic mean driving force at two ends of column. Based on four systems with gas-side resistance only. p_{BM} = logarithmic mean partial pressure of nondiffusing species B in binary mixture. p = total pressure Modified form is used for structured packings (See Table 5-24-H).	[84] [138] p. 214 [156]

*See the beginning of the "Mass Transfer" subsection for references.

a_p since the measurements are simpler to determine the product ka_p or HTU.

7. Finally, if a mass-transfer coefficient looks too good to be true, it probably is incorrect.

To determine the mass-transfer rate, one needs the interfacial area in addition to the mass-transfer coefficient. For the simpler geometries, determining the interfacial area is straightforward. For packed beds of particles a , the interfacial area per volume can be estimated as shown in Table 5-23-A. For packed beds in distillation, absorption, and so on in Table 5-24, the interfacial area per volume is included with the mass-transfer coefficient in the correlations for HTU. For agitated liquid-liquid systems, the interfacial area can be estimated

from the dispersed phase holdup and mean drop size correlations. Godfrey, Obi, and Reeve [*Chem. Engr. Prog.* **85**, 61 (Dec. 1989)] summarize these correlations. For many systems, $\bar{d}_{drop}/d_{imp} = (\text{const})N_{We}^{-0.6}$ where $N_{We} = \rho_c N^2 d_{imp}^3 / \sigma$. Piché, Grandjean, and Larachi [*Ind. Eng. Chem. Res.* **41**, 4911 (2002)] developed two correlations for reconciling the gas-liquid mass-transfer coefficient and interfacial area in randomly packed towers. The correlation for the interfacial area was a function of five dimensionless groups, and yielded a relative error of 22.5 percent for 325 data points. That equation, when combined with a correlation for N_{Sh} as a function of four dimensionless groups, achieved a relative error of 24.4 percent, for 3455 data points for the product $k'_c a$.

TABLE 5-19 Mass-Transfer Correlations for Flow in Pipes and Ducts—Transfer Is from Wall to Fluid

Situation	Correlation	Comments E = Empirical, S = Semiempirical, T = Theoretical	References°																		
A. Tubes, laminar, fully developed parabolic velocity profile, developing concentration profile, constant wall concentration	$N_{Sh} = \frac{k'd_t}{D} = 3.66 + \frac{0.0668(d_t/x)N_{Re}N_{Sc}}{1 + 0.04[(d_t/x)N_{Re}N_{Sc}]^{2/3}}$	[T] Use log mean concentration difference. For $\frac{x/d_t}{N_{Re}N_{Sc}} < 0.10$, $N_{Re} < 2100$. x = distance from tube entrance. Good agreement with experiment at values $10^4 > \frac{\pi}{4} \frac{d_t}{x} N_{Re}N_{Sc} > 10$	[77] p. 176 [87] p. 525 [141] p. 159																		
Fully developed concentration profile	$N_{Sh} = \frac{k'd_t}{D} = 3.66$	[T] $\frac{x/d_t}{N_{Re}N_{Sc}} > 0.1$	[141] p. 165																		
B. Tubes, approximate solution	$N_{Sh,x} = \frac{k'd_t}{D} = 1.077 \left(\frac{d_t}{x}\right)^{1/3} (N_{Re}N_{Sc})^{1/3}$ $N_{Sh,avg} = \frac{k'd_t}{D} = 1.615 \left(\frac{d_t}{L}\right)^{1/3} (N_{Re}N_{Sc})^{1/3}$	[T] For arithmetic concentration difference. $\frac{W}{\rho D x} > 400$ Leveque's approximation: Concentration BL is thin. Assume velocity profile is linear. High mass velocity. Fits liquid data well.	[141] p. 166																		
C. Tubes, laminar, uniform plug velocity, developing concentration profile, constant wall concentration	$N_{Sh,avg} = \frac{1}{2} \frac{d_t}{L} N_{Re}N_{Sc} \left[\frac{1 - 4 \sum_{j=1}^{\infty} a_j^{-2} \exp\left(\frac{-2a_j^2(x/r_t)}{N_{Re}N_{Sc}}\right)}{1 + 4 \sum_{j=1}^{\infty} a_j^{-2} \exp\left(\frac{-2a_j^2(x/r_t)}{N_{Re}N_{Sc}}\right)} \right]$ Graetz solution for heat transfer written for M.T.	[T] Use arithmetic concentration difference. Fits gas data well, for $\frac{W}{D \rho x} < 50$ (fit is fortuitous). $N_{Sh,avg} = (k'_m d_t)/D$. $a_1 = 2.405$, $a_2 = 5.520$, $a_3 = 8.654$, $a_4 = 11.792$, $a_5 = 14.931$. Graphical solutions are in references.	[103] [141] p. 150																		
D. Laminar, fully developed parabolic velocity profile, constant mass flux at wall	$N_{Sh,x} = \left[\frac{11}{48} - \frac{1}{2} \sum_{j=1}^{\infty} \frac{\exp[-\lambda_j^2(x/r_t)/(N_{Re}N_{Sc})]}{C_j \lambda_j^4} \right]^{-1}$ <table style="margin-left: auto; margin-right: auto;"> <tr> <td>j</td> <td>λ_j^2</td> <td>C_j</td> </tr> <tr> <td>1</td> <td>25.68</td> <td>7.630×10^{-3}</td> </tr> <tr> <td>2</td> <td>83.86</td> <td>2.058×10^{-3}</td> </tr> <tr> <td>3</td> <td>174.2</td> <td>0.901×10^{-3}</td> </tr> <tr> <td>4</td> <td>296.5</td> <td>0.487×10^{-3}</td> </tr> <tr> <td>5</td> <td>450.9</td> <td>0.297×10^{-3}</td> </tr> </table>	j	λ_j^2	C_j	1	25.68	7.630×10^{-3}	2	83.86	2.058×10^{-3}	3	174.2	0.901×10^{-3}	4	296.5	0.487×10^{-3}	5	450.9	0.297×10^{-3}	[T] Use log mean concentration difference. $N_{Re} < 2100$ $N_{Sh,x} = \frac{k'd_t}{D}$ $N_{Re} = \frac{vd_t \rho}{\mu}$	[139] [141] p. 167
j	λ_j^2	C_j																			
1	25.68	7.630×10^{-3}																			
2	83.86	2.058×10^{-3}																			
3	174.2	0.901×10^{-3}																			
4	296.5	0.487×10^{-3}																			
5	450.9	0.297×10^{-3}																			
E. Laminar, alternate	$N_{Sh} = 4.36 + \frac{0.023(d_t/L)N_{Re}N_{Sc}}{1 + 0.0012(d_t/L)N_{Re}N_{Sc}}$	[T] $N_{Sh} = \frac{k'd_t}{D}$, Use log mean concentration difference. $N_{Re} < 2100$	[77] p. 176																		
F. Laminar, fully developed concentration and velocity profile	$N_{Sh} = \frac{k'd_t}{D} = \frac{48}{11} = 4.3636$	[T] Use log mean concentration difference. $N_{Re} < 2100$	[141] p. 167																		
G. Vertical tubes, laminar flow, forced and natural convection	$N_{Sh,avg} = 1.62N_{Gz}^{1/3} \left[1 \pm 0.0742 \frac{(N_{Gr}N_{Sc}d/L)^{3/4}}{N_{Gz}} \right]^{1/3}$	[T] Approximate solution. Use minus sign if forced and natural convection oppose each other. Good agreement with experiment. $N_{Gz} = \frac{N_{Re}N_{Sc}d}{L}$, $N_{Gr} = \frac{g\Delta\rho d^3}{\rho\nu^2}$	[127]																		
H. Hollow-fiber extraction inside fibers	$N_{Sh} = 0.5N_{Gz}$, $N_{Gz} < 6$ $N_{Sh} = 1.62N_{Gz}^{0.5}$, $N_{Gz} \geq 6$	[E] Use arithmetic concentration difference.	[41]																		
I. Tubes, laminar, RO systems	$N_{Sh,avg} = \frac{k'_m d_t}{D} = 1.632 \left(\frac{ud_t^2}{DL} \right)^{1/3}$	Use arithmetic concentration difference. Thin concentration polarization layer, not fully developed. $N_{Re} < 2000$, L = length tube.	[40]																		
J. Tubes and parallel plates, laminar RO	Graphical solutions for concentration polarization. Uniform velocity through walls.	[T]	[137]																		
K. Rotating annulus for reverse osmosis	For nonvortical flow: $N_{Sh} = 2.15 \left[N_{Tb} \left(\frac{d}{r_i} \right)^{0.5} \right]^{0.18} N_{Sc}^{1/3}$ For vortical flow: $N_{Sh} = 1.05 \left[N_{Tb} \left(\frac{d}{r_i} \right)^{0.5} \right]^{1/3} N_{Sc}^{1/3}$	[E,S] N_{Tb} = Taylor number = $r_i \omega d / \nu$ r_i = inner cylinder radius ω = rotational speed, rad/s d = gap width between cylinders	[100]																		

TABLE 5-19 Mass-Transfer Correlations for Flow in Pipes and Ducts—Transfer Is from Wall to Fluid (Continued)

Situation	Correlation	Comments E = Empirical, S = Semiempirical, T = Theoretical	References°
L. Parallel plates, laminar, parabolic velocity, developing concentration profile, constant wall concentration	Graphical solution	[T] Low transfer rates.	[141] p. 176
L'. 5-19-L, fully developed	$N_{Sh} = \frac{k'(2h)}{D} = 7.6$	[T] h = distance between plates. Use log mean concentration difference. $\frac{N_{Re} N_{Sc}}{x/(2h)} < 20$	[141] p. 177
M. Parallel plates, laminar, parabolic velocity, developing concentration profile, constant mass flux at wall	Graphical solution	[T] Low transfer rates.	[141] p. 176
N. 5-19-M, fully developed	$N_{Sh} = \frac{k'(2h)}{D} = 8.23$	[T] Use log mean concentration difference. $\frac{N_{Re} N_{Sc}}{x/(2h)} < 20$	[141] p. 177
O. Laminar flow, vertical parallel plates, forced and natural convection	$N_{Sh,avg} = 1.47 N_{Gz}^{1/3} \left[1 \pm 0.0989 \frac{(N_{Gr} N_{Sc} h/L)^{3/4}}{N_{Gz}} \right]^{1/3}$	[T] Approximate solution. Use minus sign if forced and natural convection oppose each other. Good agreement with experiment. $N_{Gz} = \frac{N_{Re} N_{Sc} h}{L}, N_{Gr} = \frac{g \Delta \rho h^3}{\rho \nu^2}$	[127]
P. Parallel plates, laminar, RO systems	$N_{Sh,avg} = \frac{k'(2H_p)}{D} = 2.354 \left(\frac{u H_p^2}{DL} \right)^{1/3}$	Thin concentration polarization layer. Short tubes, concentration profile not fully developed. Use arithmetic concentration difference.	[40]
Q. Tubes, turbulent	$N_{Sh,avg} = \frac{k'_m d_t}{D} = 0.023 N_{Re}^{0.83} N_{Sc}^{1/3}$ $2100 < N_{Re} < 35,000$ $0.6 < N_{Sc} < 3000$ $N_{Sh,avg} = \frac{k'_m d_t}{D} = 0.023 N_{Re}^{0.83} N_{Sc}^{0.44}$ $2000 < N_{Re} < 35,000$ $0.6 < N_{Sc} < 2.5$	[E] Use with log mean concentration difference at two ends of tube. Good fit for liquids. From wetted wall column and dissolution data—see Table 5-18-B. [E] Evaporation of liquids. Use with log mean concentration difference. Better fit for gases.	[77] p. 181 [103] [152] p. 72 [68][77] p. 181 [88] p. 112 [138] p. 211
R. Tubes, turbulent	$N_{Sh} = \frac{k' d_t}{D} = 0.0096 N_{Re}^{0.913} N_{Sc}^{0.346}$	[E] $430 < N_{Sc} < 100,000$. Dissolution data. Use for high N_{Sc} .	[105] p. 668
S. Tubes, turbulent, smooth tubes, Reynolds analogy	$N_{Sh} = \frac{k' d_t}{D} = \left(\frac{f}{2} \right) N_{Re} N_{Sc}$ f = Fanning friction factor	[T] Use arithmetic concentration difference. N_{Sc} near 1.0 Turbulent core extends to wall. Of limited utility.	[66] p. 474 [77] p. 171 [141] p. 239 [149] p. 250
T. Tubes, turbulent, smooth tubes, Chilton-Colburn analogy	$j_D = j_H \leq \frac{f}{2}$ If $\frac{f}{2} = 0.023 N_{Re}^{-0.2}, j_D = \frac{N_{Sh}}{N_{Re} N_{Sc}^{1/3}} = 0.023 N_{Re}^{-0.2}$ $N_{Sh} = \frac{k' d_t}{D}$, Sec. 5-17-G $j_D = j_H = f(N_{Re}, \text{geometry and B.C.})$	[E] Use log-mean concentration difference. Relating j_D to $f/2$ approximate. N_{Re} and N_{Sc} near 1.0. Low concentration. Results about 20% lower than experiment. $3 \times 10^4 < N_{Re} < 10^6$ [E] Good over wide ranges.	[39] pp. 400, 647 [51][53] [141] p. 264 [149] p. 251 [66] p. 475 [39] p. 647 [51]
U. Tubes, turbulent, smooth tubes, constant surface concentration, Prandtl analogy	$N_{Sh} = \frac{k' d_t}{D} = \frac{(f/2) N_{Re} N_{Sc}}{1 + 5\sqrt{f/2}(N_{Sc} - 1)}$ $\frac{f}{2} = 0.04 N_{Re}^{-0.25}$	[T] Use arithmetic concentration difference. Improvement over Reynolds analogy. Best for N_{Sc} near 1.0.	[77] p. 173 [141] p. 241

TABLE 5-19 Mass-Transfer Correlations for Flow in Pipes and Ducts—Transfer Is from Wall to Fluid (Concluded)

Situation	Correlation	Comments E = Empirical, S = Semiempirical, T = Theoretical	References ^o
V. Tubes, turbulent, smooth tubes, Constant surface concentration, Von Karman analogy	$N_{Sh} = \frac{(f/2)N_{Re}N_{Sc}}{1 + 5\sqrt{f/2} \left\{ (N_{Sc} - 1) + \ln \left[1 + \frac{5}{6}(N_{Sc} - 1) \right] \right\}}$ $\frac{f}{2} = 0.04 N_{Re}^{-0.25}$	[T] Use arithmetic concentration difference. $N_{Sh} = k'd_t/D$. Improvement over Prandtl, $N_{Sc} < 25$.	[77] p. 173 [141] p. 243 [149] p. 250 [154]
W. Tubes, turbulent, smooth tubes, constant surface concentration	For $0.5 < N_{Sc} < 10$: $N_{Sh,avg} = 0.0097 N_{Re}^{9/10} N_{Sc}^{1/2} \times (1.10 + 0.44 N_{Sc}^{-1/3} - 0.70 N_{Sc}^{-1/6})$ For $10 < N_{Sc} < 1000$: $N_{Sh,avg}$ $= \frac{0.0097 N_{Re}^{9/10} N_{Sc}^{1/2} (1.10 + 0.44 N_{Sc}^{-1/3} - 0.70 N_{Sc}^{-1/6})}{1 + 0.064 N_{Sc}^{1/2} (1.10 + 0.44 N_{Sc}^{-1/3} - 0.70 N_{Sc}^{-1/6})}$ For $N_{Sc} > 1000$: $N_{Sh,avg} = 0.0102 N_{Re}^{9/10} N_{Sc}^{1/3}$	[S] Use arithmetic concentration difference. Based on partial fluid renewal and an infrequently replenished thin fluid layer for high N_{Sc} . Good fit to available data. $N_{Re} = \frac{u_{bulk} d_t}{\nu}$ $N_{Sh,avg} = \frac{k'_{avg} d_t}{D}$	[77] p. 179 [117]
X. Turbulent flow, tubes	$N_{St} = \frac{N_{Sh}}{N_{Pe}} = \frac{N_{Sh}}{N_{Re} N_{Sc}} = 0.0149 N_{Re}^{-0.12} N_{Sc}^{-2/3}$	[E] Smooth pipe data. Data fits within 4% except at $N_{Sc} > 20,000$, where experimental data is underpredicted. $N_{Sc} > 100$, $10^5 > N_{Re} > 2100$	[107]
Y. Turbulent flow, noncircular ducts	Use correlations with $d_{eq} = \frac{4 \text{ cross-sectional area}}{\text{wetted perimeter}}$	Can be suspect for systems with sharp corners. Parallel plates: $d_{eq} = 4 \frac{2hw}{2w + 2h}$	[141] p. 289
Z. Decaying swirling flow in pipe	$N_{Sh,avg} = 0.3508 N_{Sc}^{1/2} N_{Re}^{0.759} (x/d)^{-0.400} \times (1 + \tan\theta)^{0.271}$ $N_{Re} = 1730 \text{ to } 8650, N_{Sc} = 1692$	[E,S] x = axial distance, d = diameter, θ = vane angle (15° to 60°) Regression coefficient = 0.9793. Swirling increases mass transfer.	[161]

^oSee the beginning of the "Mass Transfer" subsection for references.

Effects of Total Pressure on k_C and k_L . The influence of total system pressure on the rate of mass transfer from a gas to a liquid or to a solid has been shown to be the same as would be predicted from stagnant-film theory as defined in Eq. (5-298), where

$$\hat{k}_C = D_{AB} p_T / RT \delta_C \quad (5-305)$$

Since the quantity $D_{AB} p_T$ is known to be relatively independent of the pressure, it follows that the rate coefficients \hat{k}_C , $k_C y_{BM}$, and $K_C p_T y_{BM}$ ($= k_C p_{BM}$) do not depend on the total pressure of the system, subject to the limitations discussed later.

Investigators of tower packings normally report $k'_C a$ values measured at very low inlet-gas concentrations, so that $y_{BM} = 1$, and at total pressures close to 100 kPa (1 atm). Thus, the correct rate coefficient for use in packed-tower designs involving the use of the driving force $(y - y_i)/y_{BM}$ is obtained by multiplying the reported $k'_C a$ values by the value of p_T employed in the actual test unit (e.g., 100 kPa) and *not* the total pressure of the system to be designed.

From another point of view one can correct the reported values of $k'_C a$ in $\text{kmol}/[(s \cdot \text{m}^3)(\text{kPa})]$, valid for a pressure of 101.3 kPa (1 atm), to some other pressure by dividing the quoted values of $k'_C a$ by the design pressure and multiplying by 101.3 kPa, i.e., $(k'_C a \text{ at design pressure } p_T) = (k'_C a \text{ at } 1 \text{ atm}) \times 101.3/p_T$.

One way to avoid a lot of confusion on this point is to convert the experimentally measured $k'_C a$ values to values of $\hat{k}_C a$ straightaway, before beginning the design calculations. A design based on the rate coefficient $\hat{k}_C a$ and the driving force $(y - y_i)/y_{BM}$ will be independent of the total system pressure with the following limitations: caution should be employed in assuming that $\hat{k}_C a$ is independent of total pressure for systems having significant vapor-phase non-idealities, for systems that operate in the vicinity of the critical

point, or for total pressures higher than about 3040 to 4050 kPa (30 to 40 atm).

Experimental confirmations of the relative independence of \hat{k}_C with respect to total pressure have been widely reported. Deviations do occur at extreme conditions. For example, Bretsznajder (*Prediction of Transport and Other Physical Properties of Fluids*, Pergamon Press, Oxford, 1971, p. 343) discusses the effects of pressure on the $D_{AB} p_T$ product and presents experimental data on the self-diffusion of CO_2 which show that the D - p product begins to decrease at a pressure of approximately 8100 kPa (80 atm). For reduced temperatures higher than about 1.5, the deviations are relatively modest for pressures up to the critical pressure. However, deviations are large near the critical point (see also p. 5-52). The effect of pressure on the gas-phase viscosity is also negligible for pressures below about 5060 kPa (50 atm).

For the liquid-phase mass-transfer coefficient k_L , the effects of total system pressure can be ignored for all practical purposes. Thus, when using \hat{k}_C and \hat{k}_L for the design of gas absorbers or strippers, the primary pressure effects to consider will be those which affect the equilibrium curves and the values of m . If the pressure changes affect the hydrodynamics, then \hat{k}_C , \hat{k}_L , and a can all change significantly.

Effects of Temperature on k_C and k_L . The Stanton-number relationship for gas-phase mass transfer in packed beds, Eq. (5-301), indicates that for a given system geometry the rate coefficient \hat{k}_C depends only on the Reynolds number and the Schmidt number. Since the Schmidt number for a gas is approximately independent of temperature, the principal effect of temperature upon \hat{k}_C arises from changes in the gas viscosity with changes in temperature. For normally encountered temperature ranges, these effects will be small owing to the fractional powers involved in Reynolds-number terms (see Tables 5-17 to 5-24). It thus can be concluded that for all

TABLE 5-20 Mass-Transfer Correlations for Flow Past Submerged Objects

Situation	Correlation	Comments E = Empirical, S = Semiempirical, T = Theoretical	References ^a												
A. Single sphere	$N_{Sh} = \frac{k'_C p_{BLM} R T d_s}{PD} = \frac{2r}{r - r_s}$ <table border="1" style="margin-left: auto; margin-right: auto;"> <tr> <td>r/r_s</td> <td>2</td> <td>5</td> <td>10</td> <td>50</td> <td>∞ (asymptotic limit)</td> </tr> <tr> <td>N_{Sh}</td> <td>4.0</td> <td>2.5</td> <td>2.22</td> <td>2.04</td> <td>2.0</td> </tr> </table>	r/r_s	2	5	10	50	∞ (asymptotic limit)	N_{Sh}	4.0	2.5	2.22	2.04	2.0	[T] Use with log mean concentration difference. r = distance from sphere, r_s , d_s = radius and diameter of sphere. No convection.	[141] p. 18
r/r_s	2	5	10	50	∞ (asymptotic limit)										
N_{Sh}	4.0	2.5	2.22	2.04	2.0										
B. Single sphere, creeping flow with forced convection	$N_{Sh} = \frac{k'd}{D} = [4.0 + 1.21(N_{Re} N_{Sc})^{2/3}]^{1/2}$ $N_{Sh} = \frac{k'd}{D} = a(N_{Re} N_{Sc})^{1/3}$ $a = 1.00 \pm 0.01$	[T] Use with log mean concentration difference. Average over sphere. Numerical calculations. ($N_{Re} N_{Sc}$) < 10,000 N_{Re} < 1.0. Constant sphere diameter. Low mass-transfer rates. [T] Fit to above ignoring molecular diffusion. 1000 < ($N_{Re} N_{Sc}$) < 10,000.	[46][88] p. 114 [105] [138] p. 214 [101] p. 80 [138] p. 215												
C. Single spheres, molecular diffusion, and forced convection, low flow rates	$N_{Sh} = 2.0 + AN_{Re}^{1/2} N_{Sc}^{1/3}$ $A = 0.5 \text{ to } 0.62$ $A = 0.60.$ $A = 0.95.$ $A = 0.95.$ $A = 0.544.$	[E] Use with log mean concentration difference. Average over sphere. Frössling Eq. ($A = 0.552$), $2 \leq N_{Re} \leq 800$, $0.6 \leq N_{Sc} \leq 2.7$. N_{Sh} lower than experimental at high N_{Re} . [E] Ranz and Marshall $2 \leq N_{Re} \leq 200$, $0.6 \leq N_{Sc} \leq 2.5$. Modifications recommended [110] See also Table 5-23-O. [E] Liquids $2 \leq N_{Re} \leq 2,000$. Graph in Ref. 138, p. 217–218. [E] $100 \leq N_{Re} \leq 700$; $1,200 \leq N_{Sc} \leq 1525$. [E] Use with arithmetic concentration difference. $N_{Sc} = 1$; $50 \leq N_{Re} \leq 350$.	[39] [77], p. 194 [88] p. 114 [141] p. 276 [39] p. 409, 647 [121] [110] [138] p. 217 [141] p. 276 [65][66] p. 482 [138] p. 217 [126][141] p. 276 [81][141] p. 276												
D. Same as 5-20-C	$N_{Sh} = \frac{k'd_s}{D} = 2.0 + 0.575 N_{Re}^{1/2} N_{Sc}^{0.35}$	[E] Use with log mean concentration difference. $N_{Sc} \leq 1$, $N_{Re} < 1$.	[70][141] p. 276												
E. Same as 5-20-C	$N_{Sh} = \frac{k'd_s}{D} = 2.0 + 0.552 N_{Re}^{0.53} N_{Sc}^{1/3}$	[E] Use with log mean concentration difference. $1.0 < N_{Re} \leq 48,000$ Gases: $0.6 \leq N_{Sc} \leq 2.7$.	[66] p. 482												
F. Single spheres, forced concentration, any flow rate	$N_{Sh} = \frac{k'_L d_s}{D} = 2.0 + 0.59 \left[\frac{E^{1/3} d_p^{4/3} \rho}{\mu} \right]^{0.57} N_{Sc}^{1/3}$ <p>Energy dissipation rate per unit mass of fluid (ranges $570 < N_{Sc} < 1420$):</p> $E = \left(\frac{C_{Dr}}{2} \right) \left(\frac{v_r^3}{d_p} \right) \frac{m^2}{s^3}$	[S] Correlates large amount of data and compares to published data. v_r = relative velocity between fluid and sphere, m/s. C_{Dr} = drag coefficient for single particle fixed in fluid at velocity v_r . See 5-23-F for calculation details and applications. $2 < \left(\frac{E^{1/3} d_p^{4/3} \rho}{\mu} \right) < 63,000$	[108]												
G. Single spheres, forced convection, high flow rates, ignoring molecular diffusion	$N_{Sh} = \frac{k'd_s}{D} = 0.347 N_{Re}^{0.62} N_{Sc}^{1/3}$ $N_{Sh} = \frac{k'd_s}{D} = 0.33 N_{Re}^{0.6} N_{Sc}^{1/3}$ $N_{Sh} = \frac{k'd_s}{D} = 0.43 N_{Re}^{0.56} N_{Sc}^{1/3}$ $N_{Sh} = \frac{k'd_s}{D} = 0.692 N_{Re}^{0.514} N_{Sc}^{1/3}$	[E] Use with arithmetic concentration difference. Liquids, $2000 < N_{Re} < 17,000$. High N_{Sc} , graph in Ref. 138, p. 217–218. [E] $1500 \leq N_{Re} \leq 12,000$. [E] $200 \leq N_{Re} \leq 4 \times 10^4$, “air” $\leq N_{Sc} \leq$ “water.” [E] $500 \leq N_{Re} \leq 5000$.	[66] p. 482 [147] [138] p. 217 [141] p. 276 [141] p. 276 [112] [141] p. 276												
H. Single sphere immersed in bed of smaller particles. For gases.	$N_{Sh,avg} = \frac{k d_1}{D'} = \epsilon \left[4 + \frac{4}{5} N_{Pe'}^{2/3} + \frac{4}{\pi} N_{Pe'} \right] \left(1 + \frac{1}{9} N_{Pe'} \right)^{1/2}$ <p>Limit $N_{Pe'} \rightarrow 0, N_{Sh,avg} = 2\epsilon$</p>	[T] Compared to experiment. $N_{Pe'} = \frac{u_c d_1}{D'}$, $D' = D/\tau$, D = molecular diffusivity, d_1 = diameter large particle, τ = tortuosity. Arithmetic conc. difference fluid flow in inert bed follows Darcy's law.	[71]												
I. Single cylinders, perpendicular flow	$N_{Sh} = \frac{k'd_s}{D} = AN_{Re}^{1/2} N_{Sc}^{1/3}, A = 0.82$ $A = 0.74$ $A = 0.582$ $\hat{j}_D = 0.600(N_{Re})^{-0.487}$ $N_{Sh} = \frac{k'd_{cyl}}{D}$	[E] $100 < N_{Re} \leq 3500$, $N_{Sc} = 1560$. [E] $120 \leq N_{Re} \leq 6000$, $N_{Sc} = 2.44$. [E] $300 \leq N_{Re} \leq 7600$, $N_{Sc} = 1200$. [E] Use with arithmetic concentration difference. $50 \leq N_{Re} \leq 50,000$; gases, $0.6 \leq N_{Sc} \leq 2.6$; liquids; $1000 \leq N_{Sc} \leq 3000$. Data scatter $\pm 30\%$.	[141] p. 276 [141] p. 276 [142] [141] p. 276 [66] p. 486												

5-70 HEAT AND MASS TRANSFER

TABLE 5-20 Mass-Transfer Correlations for Flow Past Submerged Objects (Concluded)

Situation	Correlation	Comments E = Empirical, S = Semiempirical, T = Theoretical	References°
J. Rotating cylinder in an infinite liquid, no forced flow	$j_D = \frac{k'}{v} N_{Sc}^{0.644} = 0.0791 N_{Re}^{-0.30}$ <p>Results presented graphically to $N_{Re} = 241,000$.</p> $N_{Re} = \frac{v d_{cyl} \rho}{\mu} \text{ where } v = \frac{\omega d_{cyl}}{2} = \text{peripheral velocity}$	<p>[E] Used with arithmetic concentration difference. Useful geometry in electrochemical studies.</p> <p>$112 < N_{Re} \leq 100,000$. $835 < N_{Sc} < 11490$</p> <p>k' = mass-transfer coefficient, cm/s; ω = rotational speed, radian/s.</p>	<p>[60]</p> <p>[138] p. 238</p>
K. Stationary or rotating cylinder for air	<p>Stationary:</p> $N_{Sh,avg} = AN_{Re}^c Sc^{1/3}$ <p>$2.0 \times 10^4 \leq N_{Re} \leq 2.5 \times 10^5$; $d/H = 0.3$, $Tu = 0.6\%$</p> <p>$A = 0.0539$, $c = 0.771$ [114]</p> <p>A and c depend on geometry [37]</p> <p>Rotating in still air:</p> $N_{Sh,avg} = 0.169 N_{Re, \omega}^{2/3}$ <p>$1.0E4 \leq N_{Re, \omega} \leq 1.0E5$; $N_{Sc} \approx 2.0$; $N_{Gr} \approx 2.0 \times 10^6$</p>	<p>[E] Reasonable agreement with data of other investigators. d = diameter of cylinder; H = height of wind tunnel, Tu of = turbulence level, $N_{Re, \omega}$ = rotational Reynold's number = $u_{\omega} d \rho / \mu$, u_{ω} = cylinder surface velocity. Also correlations for two-dimensional slot jet flow [114]. For references to other correlations see [37].</p>	<p>[37]</p> <p>[114]</p>
L. Oblate spheroid, forced convection	$j_D = \frac{N_{Sh}}{N_{Re} N_{Sc}^{1/3}} = 0.74 N_{Re}^{-0.5}$ $N_{Re} = \frac{d_{ch} v \rho}{\mu}, d_{ch} = \frac{\text{total surface area}}{\text{perimeter normal to flow}}$ <p>e.g., for cube with side length a, $d_{ch} = 1.27a$.</p> $N_{Sh} = \frac{k' d_{ch}}{D}$	<p>[E] Used with arithmetic concentration difference.</p> <p>$120 \leq N_{Re} \leq 6000$; standard deviation 2.1%.</p> <p>Eccentricities between 1:1 (spheres) and 3:1. Oblate spheroid is often approximated by drops.</p>	<p>[141] p. 284</p> <p>[142]</p>
M. Other objects, including prisms, cubes, hemispheres, spheres, and cylinders; forced convection	$j_D = 0.692 N_{Re,p}^{-0.486}, N_{Re,p} = \frac{v d_{ch} \rho}{\mu}$ <p>Terms same as in 5-20-J.</p>	<p>[E] Used with arithmetic concentration difference. Agrees with cylinder and oblate spheroid results, $\pm 15\%$. Assumes molecular diffusion and natural convection are negligible.</p> <p>$500 \leq N_{Re,p} \leq 5000$. Turbulent.</p>	<p>[88] p. 115</p> <p>[141] p. 285</p> <p>[111] [112]</p>
N. Other objects, molecular diffusion limits	$N_{Sh} = \frac{k' d_{ch}}{D} = A$	<p>[T] Use with arithmetic concentration difference. Hard to reach limits in experiments. Spheres and cubes $A = 2$, tetrahedrons $A = 2\sqrt{6}$ octahedrons $2\sqrt{2}$.</p>	<p>[88] p. 114</p>
O. Shell side of microporous hollow fiber module for solvent extraction	$N_{Sh} = \beta [d_h (1 - \phi) / L] N_{Re}^{0.6} N_{Sc}^{0.33}$ $N_{Sh} = \frac{\bar{K} d_h}{D}$ $N_{Re} = \frac{d_h v \rho}{\mu}, \bar{K} = \text{overall mass-transfer coefficient}$ <p>$\beta = 5.8$ for hydrophobic membrane.</p> <p>$\beta = 6.1$ for hydrophilic membrane.</p>	<p>[E] Use with logarithmic mean concentration difference.</p> <p>d_h = hydraulic diameter</p> $= \frac{4 \times \text{cross-sectional area of flow}}{\text{wetted perimeter}}$ <p>ϕ = packing fraction of shell side.</p> <p>L = module length.</p> <p>Based on area of contact according to inside or outside diameter of tubes depending on location of interface between aqueous and organic phases. Can also be applied to gas-liquid systems with liquid on shell side.</p>	<p>[118]</p>

See Table 5-23 for flow in packed beds.

°See the beginning of the "Mass Transfer" subsection for references.

TABLE 5-21 Mass-Transfer Correlations for Drops, Bubbles, and Bubble Columns

Conditions	Correlations	Comments E = Empirical, S = Semiempirical, T = Theoretical	References*																																																								
A. Single liquid drop in immiscible liquid, drop formation, discontinuous (drop) phase coefficient	$\hat{k}_{df} = A \left(\frac{\rho_d}{M_d} \right)_{av} \left(\frac{D_d}{\pi t_f} \right)^{1/2}$ $A = \frac{24}{7} \text{ (penetration theory)}$ $A = 1.31 \text{ (semiempirical value)}$ $A = \left[\frac{24}{7} (0.8624) \right] \text{ (extension by fresh surface elements)}$	<p>[T,S] Use arithmetic mole fraction difference.</p> <p>Fits some, but not all, data. Low mass transfer rate. M_d = mean molecular weight of dispersed phase; t_f = formation time of drop. $k_{L,d}$ = mean dispersed liquid phase M.T. coefficient kmole/[s·m² (mole fraction)].</p>	[141] p. 399																																																								
B. Same as 5-21-A	$\hat{k}_{df} = 0.0432$ $\times \frac{d_p}{t_f} \left(\frac{\rho_d}{M_d} \right)_{av} \left(\frac{u_o}{d_p g} \right)^{0.089} \left(\frac{d_p^2}{t_f D_d} \right)^{-0.334} \left(\frac{\mu_d}{\sqrt{\rho_d d_p \sigma g_c}} \right)^{-0.601}$	<p>[E] Use arithmetic mole fraction difference. Based on 23 data points for 3 systems. Average absolute deviation 26%. Use with surface area of drop after detachment occurs. u_o = velocity through nozzle; σ = interfacial tension.</p>	[141] p. 401 [144] p. 434																																																								
C. Single liquid drop in immiscible liquid, drop formation, continuous phase coefficient	$\hat{k}_{cf} = 4.6 \left(\frac{\rho_c}{M_c} \right)_{av} \sqrt{\frac{D_c}{\pi t_f}}$	<p>[T] Use arithmetic mole fraction difference. Based on rate of bubble growth away from fixed orifice. Approximately three times too high compared to experiments.</p>	[141] p. 402																																																								
D. Same as 5-21-C	$k_{L,c} = 0.386$ $\times \left(\frac{\rho_c}{M_c} \right)_{av} \left(\frac{D_c}{t_f} \right)^{0.5} \left(\frac{\rho_c \sigma g_c}{\Delta \rho g t_f \mu_c} \right)^{0.407} \left(\frac{g t_f^2}{d_p} \right)^{0.148}$	<p>[E] Average absolute deviation 11% for 20 data points for 3 systems.</p>	[141] p. 402 [144] p. 434																																																								
E. Single liquid drop in immiscible liquid, free rise or fall, discontinuous phase coefficient, stagnant drops	$k_{L,d,m} = \frac{-d_p}{6t} \left(\frac{\rho_d}{M_d} \right)_{av} \ln \left[\frac{6}{\pi^2} \sum_{j=1}^{\infty} \frac{1}{j^2} \exp \left[\left(\frac{-D_d j^2 \pi^2 t}{(d_p/2)^2} \right) \right] \right]$	<p>[T] Use with log mean mole fraction differences based on ends of column. t = rise time. No continuous phase resistance. Stagnant drops are likely if drop is very viscous, quite small, or is coated with surface active agent. $k_{L,d,m}$ = mean dispersed liquid M.T. coefficient.</p>	[141] p. 404 [144] p. 435																																																								
F. Same as 5-21-E	$\hat{k}_{L,d,m} = \frac{-d_p}{6t} \left(\frac{\rho_d}{M_d} \right)_{av} \ln \left[1 - \frac{\pi D_d^{1/2} t^{1/2}}{d_p/2} \right]$	<p>[S] See 5-21-E. Approximation for fractional extractions less than 50%.</p>	[141] p. 404 [144] p. 435																																																								
G. Same as 5-21-E, continuous phase coefficient, stagnant drops, spherical	$N_{Sh} = \frac{k_{L,c,m} d_c}{D_c} = 0.74 \left(\frac{\rho_c}{M_c} \right)_{av} N_{Re}^{1/2} (N_{Sc,c})^{1/3}$	<p>[E] $N_{Re} = \frac{v_s d_p \rho_c}{\mu_c}$, v_s = slip velocity between drop and continuous phase.</p>	[141] p. 407 [142][144] p. 436																																																								
H. Single bubble or drop with surfactant. Stokes flow.	$N_{Sh} = 2.0 + \alpha N_{Pe,s}^{\beta}, N_{Sh} = 2r\kappa/D$ $\alpha = \frac{5.49}{A + 6.10} + \frac{A}{A + 28.64}$ $\beta = \frac{0.35A + 17.21}{A + 34.14}$ <p>$2r = 2$ to $50 \mu\text{m}$, $A = 2.8\text{E}4$ to $7.0\text{E}5$ $0.0026 < N_{Pe,s} < 340$, $2.1 < N_{Ma} < 1.3\text{E}6$ $N_{Pe} = 1.0$ to 2.5×10^4, $N_{Re} = 2.2 \times 10^{-6}$ to 0.034</p>	<p>[T] A = surface retardation parameter $A = B\Gamma_o r / \mu D_s = N_{Ma} N_{Pe,s}$ $N_{Ma} = B\Gamma_o / \mu u$ = Marangoni no. Γ = surfactant surface conc. $N_{Pe,s}$ = surface Peclet number = ur/D_s, D_s = surface diffusivity N_{Pe} = bulk Peclet number For $A \gg 1$ acts like rigid sphere: $\beta \rightarrow 0.35$, $\alpha \rightarrow 1/2864 = 0.035$</p>	[120]																																																								
I. 5-21-E, oblate spheroid	$N_{Sh} = \frac{k_{L,c,m} d_3}{D_c} = 0.74 \left(\frac{\rho_c}{M_c} \right)_{av} (N_{Re,3})^{1/2} (N_{Sc,c})^{1/3}$ $N_{Re,3} = \frac{v_s d_3 \rho_c}{\mu_c}$	<p>[E] Used with log mean mole fraction. Differences based on ends of extraction column; 100 measured values $\pm 2\%$ deviation. Based on area oblate spheroid. v_s = slip velocity, $d_3 = \frac{\text{total drop surface area}}{\text{perimeter normal to flow}}$</p>	[141] p. 285, 406, 407																																																								
J. Single liquid drop in immiscible liquid, Free rise or fall, discontinuous phase coefficient, circulating drops	$k_{d,circ} = -\frac{d_p}{6\theta} \ln \left[\frac{3}{8} \sum_{j=1}^{\infty} B_j^2 \exp \left(-\frac{\lambda_j 64 D_d \theta}{d_p^2} \right) \right]$ <table border="1" style="width: 100%; border-collapse: collapse; text-align: center;"> <thead> <tr> <th colspan="7">Eigenvalues for Circulating Drop</th> </tr> <tr> <th>$k_d d_p / D_d$</th> <th>λ_1</th> <th>λ_2</th> <th>λ_3</th> <th>B_1</th> <th>B_2</th> <th>B_3</th> </tr> </thead> <tbody> <tr> <td>3.20</td> <td>0.262</td> <td>0.424</td> <td></td> <td>1.49</td> <td>0.107</td> <td></td> </tr> <tr> <td>10.7</td> <td>0.680</td> <td>4.92</td> <td></td> <td>1.49</td> <td>0.300</td> <td></td> </tr> <tr> <td>26.7</td> <td>1.082</td> <td>5.90</td> <td>15.7</td> <td>1.49</td> <td>0.495</td> <td>0.205</td> </tr> <tr> <td>107</td> <td>1.484</td> <td>7.88</td> <td>19.5</td> <td>1.39</td> <td>0.603</td> <td>0.384</td> </tr> <tr> <td>320</td> <td>1.60</td> <td>8.62</td> <td>21.3</td> <td>1.31</td> <td>0.583</td> <td>0.391</td> </tr> <tr> <td>∞</td> <td>1.656</td> <td>9.08</td> <td>22.2</td> <td>1.29</td> <td>0.596</td> <td>0.386</td> </tr> </tbody> </table>	Eigenvalues for Circulating Drop							$k_d d_p / D_d$	λ_1	λ_2	λ_3	B_1	B_2	B_3	3.20	0.262	0.424		1.49	0.107		10.7	0.680	4.92		1.49	0.300		26.7	1.082	5.90	15.7	1.49	0.495	0.205	107	1.484	7.88	19.5	1.39	0.603	0.384	320	1.60	8.62	21.3	1.31	0.583	0.391	∞	1.656	9.08	22.2	1.29	0.596	0.386	<p>[T] Use with arithmetic concentration difference.</p> <p>θ = drop residence time. A more complete listing of eigenvalues is given by Refs. 62 and 76.</p> <p>$k_{L,d,circ}$ is m/s.</p>	[62][76][141] p. 405 [152] p. 523
Eigenvalues for Circulating Drop																																																											
$k_d d_p / D_d$	λ_1	λ_2	λ_3	B_1	B_2	B_3																																																					
3.20	0.262	0.424		1.49	0.107																																																						
10.7	0.680	4.92		1.49	0.300																																																						
26.7	1.082	5.90	15.7	1.49	0.495	0.205																																																					
107	1.484	7.88	19.5	1.39	0.603	0.384																																																					
320	1.60	8.62	21.3	1.31	0.583	0.391																																																					
∞	1.656	9.08	22.2	1.29	0.596	0.386																																																					

5-72 HEAT AND MASS TRANSFER

TABLE 5-21 Mass-Transfer Correlations for Drops, Bubbles, and Bubble Columns (Continued)

Conditions	Correlations	Comments E = Empirical, S = Semiempirical, T = Theoretical	References°
K. Same as 5-21-J	$\hat{k}_{L,d,circ} = -\frac{d_p}{6\theta} \left(\frac{\rho_d}{M_d}\right)_{av} \ln \left[1 - \frac{R^{1/2} \pi D_d^2 \theta^{1/2}}{d_p/2} \right]$	[E] Used with mole fractions for extraction less than 50%, $R \approx 2.25$.	[141] p. 405
L. Same as 5-21-J	$N_{Sh} = \frac{\hat{k}_{L,d,circ} d_p}{D_d}$ $= 31.4 \left(\frac{\rho_d}{M_d}\right)_{av} \left(\frac{4D_d t}{d_p^2}\right)^{-0.34} N_{Sc,d}^{-0.125} \left(\frac{d_p v_s^2 \rho_c}{\sigma g_c}\right)^{-0.37}$	[E] Used with log mean mole fraction difference. d_p = diameter of sphere with same volume as drop. $856 \leq N_{Sc} \leq 79,800$, $2.34 \leq \sigma \leq 4.8$ dynes/cm.	[144] p. 435 [145]
M. Liquid drop in immiscible liquid, free rise or fall, continuous phase coefficient, circulating single drops	$N_{Sh,c} = \frac{k'_{L,c} d_p}{D_c}$ $= \left[2 + 0.463 N_{Re,drop}^{0.484} N_{Sc,c}^{0.330} \left(\frac{d_p g^{1/3}}{D_c^2}\right)^{0.072} \right] F$ $F = 0.281 + 1.615K + 3.73K^2 - 1.874K$ $K = N_{Re,drop}^{1/8} \left(\frac{\mu_c}{\mu_d}\right)^{1/4} \left(\frac{\mu_c v_s}{\sigma g_c}\right)^{1/6}$	[E] Used as an arithmetic concentration difference. $N_{Re,drop} = \frac{d_p v_s \rho_c}{\mu_c}$ Solid sphere form with correction factor F .	[82]
N. Same as 5-21-M, circulating, single drop	$N_{Sh} = \frac{k_{L,c} d_p}{D_c} = 0.6 \left(\frac{\rho_c}{M_c}\right)_{av} N_{Re,drop}^{1/2} N_{Sc,c}^{1/2}$	[E] Used as an arithmetic concentration difference. Low σ .	[141] p. 407
O. Same as 5-21-M, circulating swarm of drops	$k_{L,c} = 0.725 \left(\frac{\rho_c}{M_c}\right)_{av} N_{Re,drop}^{-0.43} N_{Sc,c}^{-0.58} v_s (1 - \phi_d)$	[E] Used as an arithmetic concentration difference. Low σ , disperse-phase holdup of drop swarm. ϕ_d = volume fraction dispersed phase.	[141] p. 407 [144] p. 436
P. Liquid drops in immiscible liquid, free rise or fall, discontinuous phase coefficient, oscillating drops	$N_{Sh} = \frac{k_{L,d,osc} d_p}{D_d}$ $= 0.32 \left(\frac{\rho_d}{M_d}\right)_{av} \left(\frac{4D_d t}{d_p^2}\right)^{-0.14} N_{Re,drop}^{0.68} \left(\frac{\sigma^3 g_c^2 \rho_c^2}{g \mu_c^4 \Delta \rho}\right)^{0.10}$	[E] Used with a log mean mole fraction difference. Based on ends of extraction column. $N_{Re,drop} = \frac{d_p v_s \rho_c}{\mu_c}$, $411 \leq N_{Re} \leq 3114$ d_p = diameter of sphere with volume of drop. Average absolute deviation from data, 10.5%. Low interfacial tension (3.5–5.8 dyn), $\mu_c < 1.35$ centipoise.	[141] p. 406 [144] p. 435 [145]
Q. Same as 5-21-P	$k_{L,d,osc} = \frac{0.00375 v_s}{1 + \mu_d / \mu_c}$	[T] Use with log mean concentration difference. Based on end of extraction column. No continuous phase resistance. $k_{L,d,osc}$ in cm/s, v_s = drop velocity relative to continuous phase.	[138] p. 228 [141] p. 405
R. Single liquid drop in immiscible liquid, range rigid to fully circulating	$N_{Sh,c,rigid} = \frac{k_c d_p}{D_c} = 2.43 + 0.774 N_{Re}^{0.5} N_{Sc}^{0.33} + 0.0103 N_{Re} N_{Sc}^{0.33}$ $N_{Sh,c,fully\ circular} = \left[\frac{2}{\pi^{0.5}} \right] N_{Pe,c}^{0.5}$ Drops in intermediate range: $\frac{N_{Sh,c} - N_{Sh,c,rigid}}{N_{Sh,c,fully\ circular} - N_{Sh,c,rigid}} = 1 - \exp [-(4.18 \times 10^{-3}) N_{Pe,c}^{0.42}]$	[E] Allows for slight effect of wake. Rigid drops: $10^4 < N_{Pe,c} < 10^6$ Circulating drops: $10 < N_{Re} < 1200$, $190 < N_{Sc} < 241,000$, $10^3 < N_{Pe,c} < 10^6$	[146] p. 58
S. Coalescing drops in immiscible liquid, discontinuous phase coefficient	$\hat{k}_{d,coal} = 0.173 \frac{d_p}{t_f} \left(\frac{\rho_d}{M_d}\right)_{av} \left(\frac{\mu_d}{\rho_d D_d}\right)^{-1.115} \times \left(\frac{\Delta \rho g d_p^2}{\sigma g_c}\right)^{1.302} \left(\frac{v_s^2 t_f}{D_d}\right)^{0.146}$	[E] Used with log mean mole fraction difference. 23 data points. Average absolute deviation 25%. t_f = formation time.	[141] p. 408
T. Same as 5-21-S, continuous phase coefficient	$\hat{k}_{c,coal} = 5.959 \times 10^{-4} \left(\frac{\rho}{M}\right)_{av} \times \left(\frac{D_c}{t_f}\right)^{0.5} \left(\frac{\rho_d u_s^3}{g \mu_c}\right)^{0.332} \left(\frac{d_p^2 \rho_c \rho_d v_s^3}{\mu_d \sigma g_c}\right)^{0.525}$	[E] Used with log mean mole fraction difference. 20 data points. Average absolute deviation 22%.	[141] p. 409

TABLE 5-21 Mass-Transfer Correlations for Drops, Bubbles, and Bubble Columns (Continued)

Conditions	Correlations	Comments E = Empirical, S = Semiempirical, T = Theoretical	References°
U. Single liquid drops in gas, gas side coefficient	$\frac{\hat{k}_g M_g d_p P}{D_{\text{gas}} \rho_g} = 2 + AN_{Re,g}^{1/2} N_{Sc,g}^{1/3}$ $A = 0.552 \text{ or } 0.60.$ $N_{Re,g} = \frac{d_p \rho_g v_s}{\mu_g}$	[E] Used for spray drying (arithmetic partial pressure difference). v_s = slip velocity between drop and gas stream. Sometimes written with $M_g P / \rho_g = RT$.	[90] p. 388 [121]
V. Single water drop in air, liquid side coefficient	$k_L = 2 \left(\frac{D_L}{\pi t} \right)^{1/2}$, short contact times $k_L = 10 \frac{D_L}{d_p}$, long contact times	[T] Use arithmetic concentration difference. Penetration theory. t = contact time of drop. Gives plot for $k_C a$ also. Air-water system.	[90] p. 389
W. Single bubbles of gas in liquid, continuous phase coefficient, very small bubbles	$N_{Sh} = \frac{k'_c d_b}{D_c} = 1.0(N_{Re} N_{Sc})^{1/3}$	[T] Solid-sphere Eq. (see Table 5-20-B). $d_b < 0.1$ cm, k'_c is average over entire surface of bubble.	[105] [138] p. 214
X. Same as 5-21-W, medium to large bubbles	$N_{Sh} = \frac{k'_c d_b}{D_c} = 1.13(N_{Re} N_{Sc})^{1/2}$	[T] Use arithmetic concentration difference. Droplet equation: $d_b > 0.5$ cm.	[138] p. 231
Y. Same as 5-21-X	$N_{Sh} = \frac{k'_c d_b}{D_c} = 1.13(N_{Re} N_{Sc})^{1/2} \left[\frac{d_b}{0.45 + 0.2d_b} \right]$ $500 \leq N_{Re} \leq 8000$	[S] Use arithmetic concentration difference. Modification of above (X), $d_b > 0.5$ cm. No effect SAA for $d_p > 0.6$ cm.	[83][138] p. 231
Z. Taylor bubbles in single capillaries (square or circular)	$k_L a = 4.5 \left(\frac{Du_C}{L_{uc}} \right)^{1/2} \frac{1}{d_c}$ Applicable $\left(\frac{u_C + u_L}{L_{slug}} \right)^{0.5} > 3s^{-0.5}$	[E] Air-water L_{uc} = unit cell length, L_{slug} = slug length, d_c = capillary i.d. For most data $k_L a \pm 20\%$.	[153]
AA. Gas-liquid mass transfer in monoliths	$k_L a \approx 0.1 \left(\frac{P}{V} \right)^{1/4}$ P/V = power/volume (kW/m ³), range = 100 to 10,000	[E] Each channel in monolith is a capillary. Results are in expected order of magnitude for capillaries based on 5-21-Z. k_L is larger than in stirred tanks.	[93]
AB. Rising small bubbles of gas in liquid, continuous phase. Calderbank and Moo-Young correlation	$N_{Sh} = \frac{k'_c d_b}{D_c} = 2 + 0.31(N_{Gr})^{1/3} N_{Sc}^{1/3}$, $d_b < 0.25$ cm $N_{Re} = \frac{d_b^3 \rho_C - \rho_L g}{\mu_L D_L} = \text{Raleigh number}$	[E] Use with arithmetic concentration difference. Valid for single bubbles or swarms. Independent of agitation as long as bubble size is constant. Recommended by [136]. Note that $N_{Re} = N_{Gr} N_{Sc}$.	[47][66] p. 451 [88] p. 119 [152] p. 156 [136]
AC. Same as 5-21-AB, large bubbles	$N_{Sh} = \frac{k'_c d_b}{D_c} = 0.42(N_{Gr})^{1/3} N_{Sc}^{1/2}$, $d_b > 0.25$ cm $\frac{\text{Interfacial area}}{\text{volume}} = a = \frac{6 H_g}{d_b}$	[E] Use with arithmetic concentration difference. For large bubbles, k'_c is independent of bubble size and independent of agitation or liquid velocity. Resistance is entirely in liquid phase for most gas-liquid mass transfer. H_g = fractional gas holdup, volume gas/total volume.	[47][66] p. 452 [88] p. 119 [97] p. 249 [136]
AD. Bubbles in bubble columns. Hughmark correlation	$N_{Sh} = \frac{k_L d}{D} = 2 + b N_{Sc}^{0.546} N_{Re}^{0.779} \left(\frac{d_g^{1/3}}{D^{2/3}} \right)^{0.116}$ $b = 0.061$ single gas bubbles; $b = 0.0187$ swarms of bubbles, $V_s = \frac{V_g}{\phi_C} - \frac{V_L}{1 - \phi_C}$	[E] d = bubble diameter Air-liquid. Recommended by [136, 152]. For swarms, calculate N_{Re} with slip velocity V_s . ϕ_C = gas holdup V_G = superficial gas velocity Col. diameter = 0.025 to 1.1 m ρ_L = 776 to 1696 kg/m ³ μ_L = 0.0009 to 0.152 Pa·s	[55] [82] [152] p. 144
AE. Bubbles in bubble column	$k_L a = 0.00315 a_C^{0.59} \mu_{\text{eff}}^{-0.84}$	[E] Recommended by [136].	[57]

TABLE 5-21 Mass-Transfer Correlations for Drops, Bubbles, and Bubble Columns (Concluded)

Conditions	Correlations	Comments E = Empirical, S = Semiempirical, T = Theoretical	References*
AF. Bubbles in bubble column	$k_L = \frac{0.15D}{d_{Vs}} \left(\frac{v}{D} \right)^{1/2} N_{Re}^{3/4}$	[E] d_{Vs} = Sauter mean bubble diameter, $N_{Re} = d_{Vs} u_G \rho_L / \mu_L$. Recommended by [49] based on experiments in industrial system.	[49] [133]
AG. High-pressure bubble column	$k_L a = 1.77 \sigma^{-0.22} \exp(1.65 u_L - 65.3 \mu_L) \epsilon_g^{1.2}$ $790 < \rho_L < 1580 \text{ kg/m}^3$ $0.00036 < \mu_L < 0.0383 \text{ Pa}\cdot\text{s}$ $0.0232 < \sigma_L < 0.0726 \text{ N/m}$ $0.028 < u_g < 0.678 \text{ m/s}$ $0 < u_L < 0.00089 \text{ m/s}$	[E] Pressure up to 4.24 MPa. T up to 92°C. ϵ_g = gas holdup. Correlation to estimate ϵ_g is given. $0.045 < d_{col} < 0.45 \text{ m}$, $d_{col}/H_{col} > 5$ $0.97 < \rho_g < 33.4 \text{ kg/m}^3$	[96]
AH. Three phase (gas-liquid-solid) bubble column to solid spheres	$N_{sh} = \frac{k_L d_p}{D} = 2.0 + 0.545 N_{Sc}^{1/3} \left(\frac{e d_p^4}{\nu^3} \right)^{0.264}$ $N_{Sc} = 137$ to 50,000 (very wide range) d_p = particle diameter (solids)	[E] e = local energy dissipation rate/unit mass, $e = u_{gg}$ $N_{Sc} = \mu_L / (\rho_L D)$ Recommended by [136].	[129] [136]

See Table 5-22 for agitated systems.

*See the beginning of the "Mass Transfer" subsection for references.

practical purposes \hat{k}_C is independent of temperature and pressure in the normal ranges of these variables.

For modest changes in temperature the influence of temperature upon the interfacial area a may be neglected. For example, in experiments on the absorption of SO₂ in water, Whitney and Vivian [*Chem. Eng. Prog.*, **45**, 323 (1949)] found no appreciable effect of temperature upon $k'_C a$ over the range from 10 to 50°C.

With regard to the liquid-phase mass-transfer coefficient, Whitney and Vivian found that the effect of temperature upon $k_L a$ could be explained entirely by variations in the liquid-phase viscosity and diffusion coefficient with temperature. Similarly, the oxygen-desorption data of Sherwood and Holloway [*Trans. Am. Inst. Chem. Eng.*, **36**, 39 (1940)] show that the influence of temperature upon H_L can be explained by the effects of temperature upon the liquid-phase viscosity and diffusion coefficients (see Table 5-24-A).

It is important to recognize that the effects of temperature on the liquid-phase diffusion coefficients and viscosities can be very large and therefore must be carefully accounted for when using k_L or H_L data. For liquids the mass-transfer coefficient k_L is correlated as either the Sherwood number or the Stanton number as a function of the Reynolds and Schmidt numbers (see Table 5-24). Typically, the general form of the correlation for H_L is (Table 5-24)

$$H_L = b N_{Re}^a N_{Sc}^{1/2} \quad (5-306)$$

where b is a proportionality constant and the exponent a may range from about 0.2 to 0.5 for different packings and systems. The liquid-phase diffusion coefficients may be corrected from a base temperature T_1 to another temperature T_2 by using the Einstein relation as recommended by Wilke [*Chem. Eng. Prog.*, **45**, 218 (1949)]:

$$D_2 = D_1 (T_2/T_1) (\mu_1/\mu_2) \quad (5-307)$$

The Einstein relation can be rearranged to the following equation for relating Schmidt numbers at two temperatures:

$$N_{Sc2} = N_{Sc1} (T_1/T_2) (\rho_1/\rho_2) (\mu_2/\mu_1)^2 \quad (5-308)$$

Substitution of this relation into Eq. (5-306) shows that for a given geometry the effect of temperature on H_L can be estimated as

$$H_{L2} = H_{L1} (T_1/T_2)^{1/2} (\rho_1/\rho_2)^{1/2} (\mu_2/\mu_1)^{1-a} \quad (5-309)$$

In using these relations it should be noted that for equal liquid flow rates

$$H_{L2}/H_{L1} = (\hat{k}_{L1} a)_1 / (\hat{k}_{L1} a)_2 \quad (5-310)$$

Effects of System Physical Properties on \hat{k}_C and \hat{k}_L . When designing packed towers for nonreacting gas-absorption systems for which no experimental data are available, it is necessary to make corrections for differences in composition between the existing test data and the system in question. The ammonia-water test data (see Table 5-24-B) can be used to estimate H_C , and the oxygen desorption data (see Table 5-24-A) can be used to estimate H_L . The method for doing this is illustrated in Table 5-24-E. There is some conflict on whether the value of the exponent for the Schmidt number is 0.5 or 2/3 [Yadav and Sharma, *Chem. Eng. Sci.* **34**, 1423 (1979)]. Despite this disagreement, this method is extremely useful, especially for absorption and stripping systems.

It should be noted that the influence of substituting solvents of widely differing viscosities upon the interfacial area a can be very large. One therefore should be cautious about extrapolating $k_L a$ data to account for viscosity effects between different solvent systems.

Effects of High Solute Concentrations on k_C and k_L . As discussed previously, the stagnant-film model indicates that k_C should be independent of y_{BM} and k_C should be inversely proportional to y_{BM} . The data of Vivian and Behrman [*Am. Inst. Chem. Eng. J.*, **11**, 656 (1965)] for the absorption of ammonia from an inert gas strongly suggest that the film model's predicted trend is correct. This is another indication that the most appropriate rate coefficient to use in concentrated systems is k_C and the proper driving-force term is of the form $(y - y_i)/y_{BM}$.

The use of the rate coefficient \hat{k}_L and the driving force $(x_i - x)/x_{BM}$ is believed to be appropriate. For many practical situations the liquid-phase solute concentrations are low, thus making this assumption unimportant.

Influence of Chemical Reactions on k_C and k_L . When a chemical reaction occurs, the transfer rate may be influenced by the chemical reaction as well as by the purely physical processes of diffusion and convection within the two phases. Since this situation is common in gas absorption, gas absorption will be the focus of this discussion. One must consider the impacts of chemical equilibrium and reaction kinetics on the absorption rate in addition to accounting for the effects of gas solubility, diffusivity, and system hydrodynamics.

There is no sharp dividing line between pure physical absorption and absorption controlled by the rate of a chemical reaction. Most cases fall in an intermediate range in which the rate of absorption is limited both by the resistance to diffusion and by the finite velocity of the reaction. Even in these intermediate cases the equilibria between the various diffusing species involved in the reaction may affect the rate of absorption.

TABLE 5-22 Mass-Transfer Correlations for Particles, Drops, and Bubbles in Agitated Systems

Situation	Correlation	Comments E = Empirical, S = Semiempirical, T = Theoretical	References*														
<p>A. Solid particles suspended in agitated vessel containing vertical baffles, continuous phase coefficient</p>	$\frac{k'_{LT} d_p}{D} = 2 + 0.6 N_{Re,T}^{1/2} N_{Sc}^{1/3}$ <p>Replace v_{slip} with v_T = terminal velocity. Calculate Stokes' law terminal velocity</p> $v_{Ts} = \frac{d_p^2 \rho_p - \rho_c g}{18 \mu_c}$ <p>and correct:</p> <table border="1" data-bbox="400 447 808 495"> <tr> <td>$\frac{N_{Re,T}}{v_T/v_{Ts}}$</td> <td>1</td> <td>10</td> <td>100</td> <td>1,000</td> <td>10,000</td> <td>100,000</td> </tr> <tr> <td></td> <td>0.9</td> <td>0.65</td> <td>0.37</td> <td>0.17</td> <td>0.07</td> <td>0.023</td> </tr> </table> <p>Approximate: $k'_{LT} = 2k'_{LT}$</p>	$\frac{N_{Re,T}}{v_T/v_{Ts}}$	1	10	100	1,000	10,000	100,000		0.9	0.65	0.37	0.17	0.07	0.023	<p>[S] Use log mean concentration difference.</p> <p>Modified Frossling equation: $N_{Re,T} = \frac{v_{Ts} d_p \rho_c}{\mu_c}$</p> <p>(Reynolds number based on Stokes' law.)</p> $N_{Re,T} = \frac{v_T d_p \rho_c}{\mu_c}$ <p>(terminal velocity Reynolds number.)</p> <p>k'_{LT} almost independent of d_p.</p> <p>Harriott suggests different correction procedures. Range k'_{LT}/k'_{LT} is 1.5 to 8.0.</p>	<p>[74][138] p. 220-222 [110]</p> <p>[74]</p>
$\frac{N_{Re,T}}{v_T/v_{Ts}}$	1	10	100	1,000	10,000	100,000											
	0.9	0.65	0.37	0.17	0.07	0.023											
<p>B. Solid, neutrally buoyant particles, continuous phase coefficient</p>	$N_{Sh} = \frac{k'_L d_p}{D} = 2 + 0.47 N_{Re,p}^{0.62} N_{Sc}^{0.36} \left(\frac{d_{imp}}{d_{tank}}\right)^{0.17}$ <p>Graphical comparisons are in Ref. 88, p. 116.</p>	<p>[E] Use log mean concentration difference. Density unimportant if particles are close to neutrally buoyant. Also used for drops. Geometric effect (d_{imp}/d_{tank}) is usually unimportant. Ref. 102 gives a variety of references on correlations.</p> <p>[E] E = energy dissipation rate per unit mass fluid</p> $= \frac{Pg_c}{V_{tank} \rho_c}, P = \text{power}, N_{Re,p} = \frac{E^{1/3} d_p^{4/3}}{v}$	<p>[88] p. 115 [102] p. 132 [152] p. 523</p>														
<p>C. Same as 22-B, small particles</p>	$N_{Sh} = 2 + 0.52 N_{Re,p}^{0.52} N_{Sc}^{1/3}, N_{Re,p} < 1.0$	<p>[E] Terms same as above.</p>	<p>[88] p. 116</p>														
<p>D. Solid particles with significant density difference</p>	$N_{Sh} = \frac{k'_L d_p}{D} = 2 + 0.44 \left(\frac{d_p v_{slip}}{v}\right)^{1/2} N_{Sc}^{0.38}$	<p>[E] Use log mean concentration difference. N_{Sh} standard deviation 11.1%. v_{slip} calculated by methods given in reference.</p>	<p>[102] [110]</p>														
<p>E. Small solid particles, gas bubbles or liquid drops, $d_p < 2.5$ mm. Aerated mixing vessels</p>	$N_{Sh} = \frac{k'_L d_p}{D} = 2 + 0.31 \left[\frac{d_p^3 \rho_p - \rho_c }{\mu_c D}\right]^{1/3}$	<p>[E] Use log mean concentration difference. $g = 9.80665$ m/s². Second term RHS is free-fall or rise term. For large bubbles, see Table 5-21-AC.</p>	<p>[46][67] p. 487 [97] p. 249</p>														
<p>F. Highly agitated systems; solid particles, drops, and bubbles; continuous phase coefficient</p>	$k'_L N_{Sc}^{2/3} = 0.13 \left[\frac{(PN_{tank}) \mu_c g_c}{\rho_c^2}\right]^{1/4}$	<p>[E] Use arithmetic concentration difference. Use when gravitational forces overcome by agitation. Up to 60% deviation. Correlation prediction is low (Ref. 102). (PN_{tank}) = power dissipated by agitator per unit volume liquid.</p>	<p>[47] [66] p. 489 [110]</p>														
<p>G. Liquid drops in baffled tank with flat six-blade turbine</p>	$k'_L a = 2.621 \times 10^{-3} \frac{(ND)^{1/2}}{d_{imp}}$ $\times \phi^{0.304} \left(\frac{d_{imp}}{d_{tank}}\right)^{1.582} N_{Re}^{1.929} N_{Oh}^{1.025}$	<p>[E] Use arithmetic concentration difference. Studied for five systems.</p> $N_{Re} = d_{imp}^2 N_{\rho_c} / \mu_c, N_{Oh} = \mu_c / (\rho_c d_{imp} \sigma)^{1/2}$ <p>ϕ = volume fraction dispersed phase. N = impeller speed (revolutions/time). For $d_{tank} = h_{tank}$, average absolute deviation 23.8%.</p>	<p>[144] p. 437</p>														
<p>H. Liquid drops in baffled tank, low volume fraction dispersed phase</p>	$N_{Sh} = \frac{k'_L d_p}{D} = 1.237 \times 10^{-5} N_{Sc}^{1/3} N^{2/3}$ $\times N_{Fr}^{5/12} \left(\frac{d_{imp}}{d_p}\right) \left(\frac{d_p}{D_{tank}}\right)^{1/2} \left(\frac{\rho_a d_p^2}{\sigma}\right)^{5/4} \phi^{-1/2}$ <p>Stainless steel flat six-blade turbine. Tank had four baffles. Correlation recommended for $\phi \leq 0.06$ [Ref. 146] $a = 6\phi/d_{32}$, where d_{32} is Sauter mean diameter when 33% mass transfer has occurred.</p>	<p>[E] 180 runs, 9 systems, $\phi = 0.01$. k_c is time-averaged. Use arithmetic concentration difference.</p> $N_{Re} = \left(\frac{d_{imp}^2 N_{Sc}}{\mu_c}\right), N_{Fr} = \left(\frac{d_{imp} N^2}{g}\right)$ <p>d_p = particle or drop diameter; σ = interfacial tension, N/m; ϕ = volume fraction dispersed phase; a = interfacial volume, 1/m; and $k_c \alpha D^{2/3}$ implies rigid drops. Negligible drop coalescence. Average absolute deviation—19.71%. Graphical comparison given by Ref. 143.</p>	<p>[143] [146] p. 78</p>														

5-76 HEAT AND MASS TRANSFER

TABLE 5-22 Mass-Transfer Correlations for Particles, Drops, and Bubbles in Agitated Systems (Concluded)

Situation	Correlation	Comments E = Empirical, S = Semiempirical, T = Theoretical	References*
I. Gas bubble swarms in sparged tank reactors	$k_L' a \left(\frac{v}{g^2} \right)^{1/3} = C \left[\frac{P/V_L}{\rho(vg^4)^{1/3}} \right]^a \left[\frac{q_G}{V_L} \left(\frac{v}{g^2} \right)^{1/3} \right]^b$ Rushton turbines: $C = 7.94 \times 10^{-4}$, $a = 0.62$, $b = 0.23$. Intermig impellers: $C = 5.89 \times 10^{-4}$, $a = 0.62$, $b = 0.19$.	[E] Use arithmetic concentration difference. Done for biological system. O ₂ transfer. $h_{\text{tank}}/D_{\text{tank}} = 2.1$; P = power, kW. V_L = liquid volume, m ³ . q_G = gassing rate, m ³ /s. $k_L' a = \text{s}^{-1}$. Since $a = \text{m}^2/\text{m}^3$, v = kinematic viscosity, m ² /s. Low viscosity system. Better fit claimed with q_G/V_L than with u_G (see 5-22-J to N).	[131]
J. Same as 5-22-I	$k_L' a = 2.6 \times 10^{-2} \left(\frac{P}{V_L} \right)^{0.4} u_G^{0.5}$	[E] Use arithmetic concentration difference. Ion free water $V_L < 2.6$, u_G = superficial gas velocity in m/s. $500 < P/V_L < 10,000$. P/V_L = watts/m ³ , V_L = liquid volume, m ³ .	[98] [123]
K. Same as 5-22-J	$k_L' a = 2.0 \times 10^{-3} \left(\frac{P}{V_L} \right)^{0.7} u_G^{0.2}$	[E] Use arithmetic concentration difference. Water with ions. $0.002 < V_L < 4.4$, $500 < P/V_L < 10,000$. Same definitions as 5-22-I.	[98] [101]
L. Same as 5-22-I, baffled tank with standard blade Rushton impeller	$k_L' a = 93.37 \left(\frac{P}{V_L} \right)^{0.76} u_G^{0.45}$	[E] Air-water. Same definitions as 5-22-I. $0.005 < u_G < 0.025$, $3.83 < N < 8.33$, $400 < P/V_L < 7000$. $h = D_{\text{tank}} = 0.305$ or 0.610 m. V_G = gas volume, m ³ , N = stirrer speed, rpm. Method assumes perfect liquid mixing.	[67] [98]
M. Same as 5-22-L	$k_L' a \frac{d_{\text{imp}}^2}{D} = 7.57 \left[\frac{\mu_{\text{eff}}}{\rho D} \right]^{0.57} \left[\frac{\mu_C}{\mu_{\text{eff}}} \right]^{0.694} \times \left[\frac{d_{\text{imp}}^2 N \rho_L}{\mu_{\text{eff}}} \right]^{1.11} \left(\frac{u_G d}{\sigma} \right)^{0.447}$ d_{imp} = impeller diameter, m; D = diffusivity, m ² /s	[E] Use arithmetic concentration difference. CO ₂ into aqueous carboxyl polymethylene. Same definitions as 5-22-L. μ_{eff} = effective viscosity from power law model, Pa·s. σ = surface tension liquid, N/m.	[98] [115]
N. Same as 5-22-L, bubbles	$\frac{k_L' a d_{\text{imp}}^2}{D} = 0.060 \left(\frac{d_{\text{imp}}^2 N \rho}{\mu_{\text{eff}}} \right) \left(\frac{d_{\text{imp}}^2 N^2}{g} \right)^{0.19} \left(\frac{\mu_{\text{eff}} u_G}{\sigma} \right)^{0.6}$	[E] Use arithmetic concentration difference. O ₂ into aqueous glycerol solutions. O ₂ into aqueous millet jelly solutions. Same definitions as 5-22-L.	[98] [160]
O. Gas bubble swarm in sparged stirred tank reactor with solids present	$\frac{k_L' a}{(k_L' a)_0} = 1 - 3.54(\epsilon_s - 0.03)$ $300 \leq P/V_{rx} < 10,000 \text{ W/m}^3$, $0.03 \leq \epsilon_s \leq 0.12$ $0.34 \leq u_G \leq 4.2 \text{ cm/s}$, $5 < \mu_L < 75 \text{ Pa}\cdot\text{s}$	[E] Use arithmetic concentration difference. Solids are glass beads, $d_p = 320 \mu\text{m}$. ϵ_s = solids holdup m ³ /m ³ liquid. $(k_L' a)_0$ = mass transfer in absence of solids. Ionic salt solution—noncoalescing.	[38] [132]
P. Surface aerators for air-water contact	$\frac{k_L a}{N} = b N_p^{0.71} N_{Fr}^{0.48} N_{Re}^{0.82} \left(\frac{H}{d} \right)^{-0.54} \left(\frac{V}{d^3} \right)^{-1.08}$ $b = 7 \times 10^{-6}$, $N_p = P/(\rho N^3 d^5)$ $N_{Re} = Nd^2 \rho_{\text{liq}}/\mu_{\text{liq}}$ $N_{Fr} = N^2 d/g$, $P/V = 90$ to 400 W/m^3	[E] Three impellers: Pitched blade downflow turbine, pitched blade upflow turbine, standard disk turbine. Baffled cylindrical tanks 1.0- and 1.5-m ID and 8.2 × 8.2-m square tank. Submergence optimized all cases. Good agreement with data. N = impeller speed, s ⁻¹ ; d = impeller diameter, m; H = liquid height, m; V = liquid volume, m ³ ; $k_L a = \text{s}^{-1}$, g = acceleration gravity = 9.81 m/s ²	[113]
Q. Gas-inducing impeller for air-water contact	$k_L a V (v/g^2)^{1/3} d^3 = AN_{Fr}^B \left(\frac{V_A}{V} \right)^C$ Single impeller: $A = 0.00497$, $B = 0.56$, $C = 0.32$ Multiple impeller: $A = 0.00746$, $B = 0.54$, $C = 0.38$	[E] Same tanks and same definitions as in 5-22-P. V_A = active volume = $p/(\pi \rho g N d)$.	[113]
R. Gas-inducing impeller with dense solids	$Sh_{GL} = \frac{k_L a d_{st}^2}{D} = (1.26 \times 10^{-5}) N_{Re}^{1.8} N_{Sc}^{0.9} N_{We}^{-0.1}$ $N_{Re} = \rho N d_{st}^2 \mu$, $N_{Sc} = \mu/(\rho D)$, $N_{We} = \rho N^2 d_{st}^3 / \sigma$	[E] Hydrogenation with Raney-type nickel catalyst in stirred autoclave. Used varying T , p , solvents. d_{st} = stirrer diameter.	[78]

See also Table 5-21.

*See the beginning of the "Mass Transfer" subsection for references.

TABLE 5-23 Mass-Transfer Correlations for Fixed and Fluidized Beds

Transfer is to or from particles

Situation	Correlation	Comments E = Empirical, S = Semiempirical, T = Theoretical	References ^o												
A. For gases, fixed and fluidized beds, Gupta and Thodos correlation	$j_H = j_D = \frac{2.06}{\epsilon N_{Re}^{0.575}}, 90 \leq N_{Re} \leq A$ <p>Equivalent:</p> $N_{Sh} = \frac{2.06}{\epsilon} N_{Re}^{0.425} N_{Sc}^{1/3}$ <p>For other shapes:</p> $\frac{\epsilon j_D}{(\epsilon j_D)_{\text{sphere}}} = 0.79 \text{ (cylinder) or } 0.71 \text{ (cube)}$	<p>[E] For spheres. $N_{Re} = \frac{v_{\text{super}} d_p \rho}{\mu}$</p> <p>A = 2453 [Ref. 141], A = 4000 [Ref. 77]. For $N_{Re} > 1900$, $j_H = 1.05 j_D$. Heat transfer result is in absence of radiation.</p> $N_{Sh} = \frac{k' d_s}{D}$ <p>Graphical results are available for N_{Re} from 1900 to 10,300.</p> $a = \frac{\text{surface area}}{\text{volume}} = 6(1 - \epsilon)/d_p$ <p>For spheres, $d_p = \text{diameter}$. For nonspherical: $d_p = 0.567 \sqrt{\text{Part. Surf. Area}}$</p>	<p>[72][73]</p> <p>[77] p. 195 [141]</p>												
B. For gases, for fixed beds, Petrovic and Thodos correlation	$N_{Sh} = \frac{0.357}{\epsilon} N_{Re}^{0.641} N_{Sc}^{1/3}$ <p>$3 < N_{Re} < 900$ can be extrapolated to $N_{Re} < 2000$.</p>	<p>[E] Packed spheres, deep beds. Corrected for axial dispersion with axial Peclet number = 2.0. Prediction is low at low N_{Re}. N_{Re} defined as in 5-23-A.</p>	<p>[116][128] p. 214 [155]</p>												
C. For gases and liquids, fixed and fluidized beds	$j_D = \frac{0.4548}{\epsilon N_{Re}^{0.4069}}, 10 \leq N_{Re} \leq 2000$ $j_D = \frac{N_{Sh}}{N_{Re} N_{Sc}^{1/3}}, N_{Sh} = \frac{k' d_s}{D}$	<p>[E] Packed spheres, deep bed. Average deviation $\pm 20\%$. $N_{Re} = d_p v_{\text{super}} \rho / \mu$. Can use for fluidized beds. $10 \leq N_{Re} \leq 4000$.</p>	<p>[60][66] p. 484</p>												
D. For gases, fixed beds	$j_D = \frac{0.499}{\epsilon N_{Re}^{0.382}}$	<p>[E] Data on sublimation of naphthalene spheres dispersed in inert beds. $0.1 < N_{Re} < 100$, $N_{Sc} = 2.57$. Correlation coefficient = 0.978.</p>	<p>[80]</p>												
E. For liquids, fixed bed, Wilson and Geankoplis correlation	$j_D = \frac{1.09}{\epsilon N_{Re}^{2/3}}, 0.0016 < N_{Re} < 55$ <p>$165 \leq N_{Sc} \leq 70,600$, $0.35 < \epsilon < 0.75$</p> <p>Equivalent:</p> $N_{Sh} = \frac{1.09}{\epsilon} N_{Re}^{1/3} N_{Sc}^{1/3}$ $j_D = \frac{0.25}{\epsilon N_{Re}^{0.31}}, 55 < N_{Re} < 1500, 165 \leq N_{Sc} \leq 10,690$ <p>Equivalent: $N_{Sh} = \frac{0.25}{\epsilon} N_{Re}^{0.60} N_{Sc}^{1/3}$</p>	<p>[E] Beds of spheres,</p> $N_{Re} = \frac{d_p v_{\text{super}} \rho}{\mu}$ <p>Deep beds.</p> $N_{Sh} = \frac{k' d_s}{D}$	<p>[66] p. 484</p> <p>[77] p. 195</p> <p>[141] p. 287 [158]</p>												
F. For liquids, fixed beds, Ohashi et al. correlation	$N_{Sh} = \frac{k' d_s}{D} = 2 + 0.51 \left(\frac{E^{1/3} d_p^{4/3} \rho}{\mu} \right)^{0.60} N_{Sc}^{1/3}$ <p>E = Energy dissipation rate per unit mass of fluid</p> $= 50(1 - \epsilon) \epsilon^2 C_{D0} \left(\frac{v_r^3}{d_p} \right), \text{ m}^2/\text{s}^3$ $= \left[\frac{50(1 - \epsilon) C_D}{\epsilon} \right] \left(\frac{v_{\text{super}}^3}{d_p} \right)$ <p>General form:</p> $N_{Sh} = 2 + K \left(\frac{E^{1/3} D_p^{4/3} \rho}{\mu} \right)^\alpha N_{Sc}^\beta$ <p>applies to single particles, packed beds, two-phase tube flow, suspended bubble columns, and stirred tanks with different definitions of E.</p>	<p>[S] Correlates large amount of published data. Compares number of correlations, $v_r = \text{relative velocity, m/s}$. In packed bed, $v_r = v_{\text{super}}/\epsilon$.</p> <p>$C_{D0} = \text{single particle drag coefficient at } v_{\text{super}}$ calculated from $C_{D0} = AN_{Re}^{-m}$.</p> <table border="1" data-bbox="870 1433 1202 1519"> <thead> <tr> <th>N_{Re}</th> <th>A</th> <th>m</th> </tr> </thead> <tbody> <tr> <td>0 to 5.8</td> <td>24</td> <td>1.0</td> </tr> <tr> <td>5.8 to 500</td> <td>10</td> <td>0.5</td> </tr> <tr> <td>>500</td> <td>0.44</td> <td>0</td> </tr> </tbody> </table> <p>Ranges for packed bed:</p> <p>$0.001 < N_{Re} < 1000$, $505 < N_{Sc} < 70,600$,</p> $0.2 < \frac{E^{1/3} d_p^{4/3} \rho}{\mu} < 4600$ <p>Compares different situations versus general correlation. See also 5-20-F.</p>	N_{Re}	A	m	0 to 5.8	24	1.0	5.8 to 500	10	0.5	>500	0.44	0	<p>[108]</p>
N_{Re}	A	m													
0 to 5.8	24	1.0													
5.8 to 500	10	0.5													
>500	0.44	0													

TABLE 5-23 Mass Transfer Correlations for Fixed and Fluidized Beds (Continued)

Situation	Correlation	Comments E = Empirical, S = Semiempirical, T = Theoretical	References°
G. Electrolytic system. Pall rings. Transfer from fluid to rings.	Full liquid upflow: $N_{sh} = k_L d_p / D = 4.1 N_{Re}^{0.39} N_{Sc}^{1/3}$ $N_{Re} d_p u / \nu = 80$ to 550 Irrigated liquid downflow (no gas flow): $N_{Sh} = 5.1 N_{Re}^{0.44} N_{Sc}^{1/3}$	[E] d_c = diameter of sphere with same surface area as Pall ring. Full liquid upflow agreed with literature values. Schmidt number dependence was assumed from literature values. In downflow, N_{Re} used superficial fluid velocity.	[69]
H. For liquids, fixed and fluidized beds	$\epsilon j_D = \frac{1.1068}{N_{Re}^{0.72}}, 1.0 < N_{Re} \leq 10$ $\epsilon j_D = \frac{N_{Sh}}{N_{Re} N_{Sc}^{1/3}}, N_{Sh} = \frac{k' d_s}{D}$	[E] Spheres: $N_{Re} = \frac{d_p v_{super} \rho}{\mu}$	[59][66] p. 484
I. For gases and liquids, fixed and fluidized beds, Dwivedi and Upadhyay correlation	$\epsilon j_D = \frac{0.765}{N_{Re}^{0.82}} + \frac{0.365}{N_{Re}^{0.386}}$ Gases: $10 \leq N_{Re} \leq 15,000$. Liquids: $0.01 \leq N_{Re} \leq 15,000$. $N_{Re} = \frac{d_p v_{super} \rho}{\mu}, N_{Sh} = \frac{k' d_s}{D}$	[E] Deep beds of spheres, $j_D = \frac{N_{Sh}}{N_{Re} N_{Sc}^{1/3}}$ Best fit correlation at low conc. [52] Based on 20 gas studies and 17 liquid studies. Recommended instead of 5-23-C or E.	[59] [77] p. 196 [52]
J. For gases and liquids, fixed bed	$j_D = 1.17 N_{Re}^{-0.415}, 10 \leq N_{Re} \leq 2500$ $j_D = \frac{k'}{v_{av}} \frac{p_{BM}}{P} N_{Sc}^{2/3}$	[E] Spheres: Variation in packing that changes ϵ not allowed for. Extensive data referenced. $0.5 < N_{Sc} < 15,000$. Comparison with other results are shown. $N_{Re} = \frac{d_p v_{super} \rho}{\mu}$	[138] p. 241
K. For liquids, fixed and fluidized beds, Rahman and Streat correlation	$N_{Sh} = \frac{0.86}{\epsilon} N_{Re}^{1/3} N_{Sc}^{1/3}, 2 \leq N_{Re} \leq 25$	[E] Can be extrapolated to $N_{Re} = 2000$. $N_{Re} = d_p v_{super} \rho / \mu$. Done for neutralization of ion exchange resin.	[119]
L. Size exclusion chromatography of proteins	$N_{Sh} = \frac{k_L d}{D} = \frac{1.903}{\epsilon} N_{Re}^{1/3} N_{Sc}^{1/3}$	[E] Slow mass transfer with large molecules. Aqueous solutions. Modest increase in N_{Sh} with increasing velocity.	[79]
M. Liquid-free convection with fixed bed Raschig rings. Electrochemical.	$N_{Sh} = kd/D = 0.15 (N_{Sc} N_{Gr})^{0.32}$ $N_{Gr} = \text{Grashof no.} = gd^3 \Delta \rho / (\nu^2 \rho)$ If forced convection superimposed, $N_{Sh, overall} = (N_{Sh, forced}^3 + N_{Sh, free}^3)^{1/3}$	[E] d = Raschig ring diameter, h = bed height $1810 < N_{Sc} < 2532, 0.17 < d/h < 1.0$ $10.6 \times 10^6 < N_{Sc} N_{Gr} < 21 \times 10^7$	[135]
N. Oscillating bed packed with Raschig rings. Dissolution of copper rings.	Batch (no net solution flow): $N_{Sh} = 0.76 N_{Sc}^{0.33} N_{Re, v}^{0.7} (d_c/h)^{0.35}$ $503 < N_{Re, v} < 2892$ $960 < N_{Sc} < 1364, 2.3 < d_c/h < 7.6$	[E] $N_{Sh} = kd/D, N_{Re, v} = \text{vibrational } Re = \rho v_c d_c / \mu$ $v_c = \text{vibrational velocity (intensity)}$ $d_c = \text{col. diameter, } h = \text{column height}$ Average deviation is $\pm 12\%$.	[61]
O. For liquids and gases, Ranz and Marshall correlation	$N_{Sh} = \frac{k' d}{D} = 2.0 + 0.6 N_{Sc}^{1/3} N_{Re}^{1/2}$ $N_{Re} = \frac{d_p v_{super} \rho}{\mu}$	[E] Based on freely falling, evaporating spheres (see 5-20-C). Has been applied to packed beds, prediction is low compared to experimental data. Limit of 2.0 at low N_{Re} is too high. Not corrected for axial dispersion.	[121][128] p. 214 [155] [110]
P. For liquids and gases, Wakao and Funazkri correlation	$N_{Sh} = 2.0 + 1.1 N_{Sc}^{1/3} N_{Re}^{0.6}, 3 < N_{Re} < 10,000$ $N_{Sh} = \frac{k'_{lim} d_p}{D}, N_{Re} = \frac{\rho r v_{super} \rho}{\mu}$ $\frac{\epsilon D_{axial}}{D} = 10 + 0.5 N_{Sc} N_{Re}$	[E] Correlate 20 gas studies and 16 liquid studies. Corrected for axial dispersion with: Graphical comparison with data shown [128], p. 215, and [155]. D_{axial} is axial dispersion coefficient.	[128] p. 214 [155]
Q. Acid dissolution of limestone in fixed bed	$N_{Sh} = 1.77 N_{Re}^{0.56} N_{Sc}^{1/3} (1 - \epsilon)^{0.44}$ $20 < N_{Re} < 6000$	[E] Best fit was to correlation of Chu et al., <i>Chem. Eng. Prog.</i> , 49 (3), 141(1953), even though no reaction in original.	[94]
R. Semifluidized or expanded bed. Liquid-solid transfer.	$N_{Sh} = \frac{k'_{lim} d_p}{D} = 2 + 1.5 (1 - \epsilon_L) N_{Re}^{1/3} N_{Sc}^{1/3}$ $N_{Re} = \rho_p d_p u / \mu \epsilon_L, N_{Sc} = \mu / \rho D$	[E] ϵ_L = liquid-phase void fraction, ρ_p = particle density, ρ = fluid density, d_p = particle diameter. Fits expanded bed chromatography in viscous liquids.	[64] [159]

TABLE 5-23 Mass Transfer Correlations for Fixed and Fluidized Beds (Concluded)

Situation	Correlation	Comments E = Empirical, S = Semiempirical, T = Theoretical	References ^o
S. Mass-transfer structured packing and static mixers. Liquid with or without fluidized particles. Electrochemical	Fixed bed: $j' = 0.927N_{Re}^{0.572}$, $N'_{Re} < 219$ $j' = 0.443N_{Re}^{0.435}$, $219 < N'_{Re} < 1360$ Fluidized bed with particles: $j = 6.02N_{Re}^{0.885}$, or $j' = 16.40N_{Re}^{0.950}$ Natural convection: $N_{Sh} = 0.252(N_{Sc}N_{Gr})^{0.299}$ Bubble columns: Structured packing: $N_{St} = 0.105(N_{Re}N_{Fr}N_{Sc}^2)^{-0.268}$ Static mixer: $N_{St} = 0.157(N_{Re}N_{Fr}N_{Sc}^2)^{-0.298}$	[E] Sulzer packings, $j' = \frac{k \cos \beta}{v} N_{Sc}^{2/3}$, $\beta =$ corrugation incline angle. $N_{Re} = v' d_h \rho / \mu$, $v' = v_{super} / (\epsilon \cos \beta)$, $d_h =$ channel side width. Particles enhance mass transfer in laminar flow for natural convection. Good fit with correlation of Ray et al., <i>Intl. J. Heat Mass Transfer</i> , 41 , 1693 (1998). $N_{Gr} = g \Delta \rho Z' / \rho \mu^2$, $Z =$ corrugated plate length. Bubble column results fit correlation of Neme et al., <i>Chem. Eng. Technol.</i> , 20 , 297 (1997) for structured packing. $N_{St} =$ Stanton number = kZ/D $N_{Fr} =$ Froude number = v_{super}^2 / gz	[48]
T. Liquid fluidized beds	$N_{Sh} = \frac{2\xi/\epsilon^m + \left[\frac{(2\xi/\epsilon^m)(1-\epsilon)^{1/2}}{1-(1-\epsilon)^{1/3}} - 2 \right] \tan h(\xi/\epsilon^m)}{\frac{\xi/\epsilon^m}{1-(1-\epsilon)^{1/2}} - \tan h(\xi/\epsilon^m)}$ where $\xi = \left[\frac{1}{(1-\epsilon)^{1/3}} - 1 \right] \frac{\alpha}{2} N_{Sc}^{1/3} N_{Re}^{1/2}$ This simplifies to: $N_{Sh} = \frac{\epsilon^{1-2m}}{(1-\epsilon)^{1/3}} \left[\frac{1}{(1-\epsilon)^{1/3}} - 1 \right] \frac{\alpha^2}{2} N_{Re} N_{Sc}^{2/3} \quad (N_{Re} < 0.1)$	[S] Modification of theory to fit experimental data. For spheres, $m = 1$, $N_{Re} > 2$. $N_{Sh} = \frac{k_L d_p}{D}, \quad N_{Re} = \frac{V_{super} d_p \xi}{\mu}$ $m = 1$ for $N_{Re} > 2$; $m = 0.5$ for $N_{Re} < 1.0$; $\epsilon =$ voidage; $\alpha =$ const. Best fit data is $\alpha = 0.7$. Comparison of theory and experimental ion exchange results in Ref. 92.	[92] [106] [125]
U. Liquid fluidized beds	$N_{Sh} = 0.250 N_{Re}^{0.023} N_{Ga}^{0.306} \left(\frac{\rho_s - \rho}{\rho} \right)^{0.282} N_{Sc}^{0.410} \quad (\epsilon < 0.85)$ $N_{Sh} = 0.304 N_{Re}^{-0.057} N_{Ga}^{0.332} \left(\frac{\rho_s - \rho}{\rho} \right)^{0.297} N_{Sc}^{0.404} \quad (\epsilon > 0.85)$ This can be simplified (with slight loss in accuracy at high ϵ) to $N_{Sh} = 0.245 N_{Ga}^{0.323} \left(\frac{\rho_s - \rho}{\rho} \right)^{0.300} N_{Sc}^{0.400}$	[E] Correlate amount of data from literature. Predicts very little dependence of N_{Sh} on velocity. Compare large number of published correlations. $N_{Sh} = \frac{k_L d_p}{D}, \quad N_{Re} = \frac{d_p \rho v_{super}}{\mu}, \quad N_{Ga} = \frac{d_p^3 \rho^2 g}{\mu^2},$ $N_{Sc} = \frac{\mu}{\rho D}$ $1.6 < N_{Re} < 1320, 2470 < N_{Ga} < 4.42 \times 10^6$ $0.27 < \frac{\rho_s - \rho}{\rho} < 1.114, 305 < N_{Sc} < 1595$	[151]
V. Liquid film flowing over solid particles with air present, trickle bed reactors, fixed bed	$N_{Sh} = \frac{k_L}{aD} = 1.8 N_{Re}^{1/2} N_{Sc}^{1/3}, 0.013 < N_{Re} < 12.6$ two-phases, liquid trickle, no forced flow of gas. $N_{Sh} = 0.8 N_{Re}^{1/2} N_{Sc}^{1/3}$, one-phase, liquid only.	[E] $N_{Re} = \frac{L}{a\mu}$, irregular granules of benzoic acid, $0.29 \leq d_p \leq 1.45$ cm. $L =$ superficial liquid flow rate, kg/m ² s. $a =$ surface area/col. volume, m ² /m ³ .	[130]
W. Supercritical fluids in packed bed	$\frac{N_{Sh}}{(N_{Sc} N_{Gr})^{1/4}} = 0.5265 \left(\frac{N_{Re}^{1/2} N_{Sc}^{1/3}}{(N_{Sc} N_{Gr})^{1/4}} \right)^{1.6808} + 2.48 \left \left(\frac{N_{Re}^2 N_{Sc}^{1/3}}{N_{Gr}} \right)^{0.6439} - 0.8768 \right ^{1.553}$	[E] Natural and forced convection. $0.3 < N_{Re} < 135$.	[99]
X. Cocurrent gas-liquid flow in fixed beds	Downflow in trickle bed and upflow in bubble columns.	Literature review and meta-analysis. Analyzed both downflow and upflow. Recommendations for best mass- and heat-transfer correlations (see reference).	[95]
Y. Liquid-solid transfer. Electrochemical reaction. Lessing rings. Transfer from liquid to solid	Liquid only: $N_{Sh} = kd/D = 1.57 N_{Sc}^{1/3} N_{Re}^{0.46}$ $1390 < N_{Sc} < 4760, 166 < N_{Re} < 722$ Cocurrent two-phase (liquid and gas) in packed bubble column: $N_{Sh} = 1.93 N_{Sc}^{1/3} N_{Re}^{0.34} N_{Re, gas}^{0.11}$ $60 < N_{Re, gas} < 818, 144 < N_{Re} < 748$	[E] Electrochemical reactors only. $d =$ Lessing ring diameter, $1 < d < 1.4$ cm, $N_{Re} = \rho v_{super} d / \mu$, Deviation $\pm 7\%$ for both cases. $N_{Re, gas} = \rho_{gas} V_{super, gas} d / \mu_{gas}$ Presence of gas enhances mass transfer.	[75]

NOTE: For $N_{Re} < 3$ convective contributions which are not included may become important. Use with logarithmic concentration difference (integrated form) or with arithmetic concentration difference (differential form).

^oSee the beginning of the "Mass Transfer" subsection for references.

TABLE 5-24 Mass-Transfer Correlations for Packed Two-Phase Contactors—Absorption, Distillation, Cooling Towers, and Extractors (Packing Is Inert)

Situation	Correlations	Comments E = Empirical, S = Semiempirical, T = Theoretical	References*																																																																																								
A. Absorption, counter-current, liquid-phase coefficient H_L , Sherwood and Holloway correlation for random packings	$H_L = a_L \left(\frac{L}{\mu_L} \right)^n N_{Sc,L}^{0.5}, L = \text{lb/hr ft}^2$ <hr/> <p style="text-align: center;">Ranges for 5-24-B (G and L)</p> <table border="1" style="width: 100%; border-collapse: collapse;"> <thead> <tr> <th>Packing</th> <th>a_C</th> <th>b</th> <th>c</th> <th>G</th> <th>L</th> <th>a_L</th> <th>n</th> </tr> </thead> <tbody> <tr> <td colspan="8" style="text-align: center;">Raschig rings</td> </tr> <tr> <td>3/8 inch</td> <td>2.32</td> <td>0.45</td> <td>0.47</td> <td>200–500</td> <td>500–1500</td> <td>0.00182</td> <td>0.46</td> </tr> <tr> <td>1</td> <td>7.00</td> <td>0.39</td> <td>0.58</td> <td>200–800</td> <td>400–500</td> <td>0.010</td> <td>0.22</td> </tr> <tr> <td>1</td> <td>6.41</td> <td>0.32</td> <td>0.51</td> <td>200–600</td> <td>500–4500</td> <td>—</td> <td>—</td> </tr> <tr> <td>2</td> <td>3.82</td> <td>0.41</td> <td>0.45</td> <td>200–800</td> <td>500–4500</td> <td>0.0125</td> <td>0.22</td> </tr> <tr> <td colspan="8" style="text-align: center;">Bert saddles</td> </tr> <tr> <td>1/2 inch</td> <td>32.4</td> <td>0.30</td> <td>0.74</td> <td>200–700</td> <td>500–1500</td> <td>0.0067</td> <td>0.28</td> </tr> <tr> <td>1/2</td> <td>0.811</td> <td>0.30</td> <td>0.24</td> <td>200–800</td> <td>400–4500</td> <td>—</td> <td>—</td> </tr> <tr> <td>1</td> <td>1.97</td> <td>0.36</td> <td>0.40</td> <td>200–800</td> <td>400–4500</td> <td>0.0059</td> <td>0.28</td> </tr> <tr> <td>1.5</td> <td>5.05</td> <td>0.32</td> <td>0.45</td> <td>200–1000</td> <td>400–4500</td> <td>0.0062</td> <td>0.28</td> </tr> </tbody> </table>	Packing	a_C	b	c	G	L	a_L	n	Raschig rings								3/8 inch	2.32	0.45	0.47	200–500	500–1500	0.00182	0.46	1	7.00	0.39	0.58	200–800	400–500	0.010	0.22	1	6.41	0.32	0.51	200–600	500–4500	—	—	2	3.82	0.41	0.45	200–800	500–4500	0.0125	0.22	Bert saddles								1/2 inch	32.4	0.30	0.74	200–700	500–1500	0.0067	0.28	1/2	0.811	0.30	0.24	200–800	400–4500	—	—	1	1.97	0.36	0.40	200–800	400–4500	0.0059	0.28	1.5	5.05	0.32	0.45	200–1000	400–4500	0.0062	0.28	<p>[E] From experiments on desorption of sparingly soluble gases from water. Graphs [Ref. 138], p. 606. Equation is dimensional. A typical value of n is 0.3 [Ref. 66] has constants in kg, m, and s units for use in 5-24-A and B with \hat{k}_G in kgmole/s m² and \hat{k}_L in kgmole/s m² (kgmol/m³). Constants for other packings are given by Refs. 104, p. 187 and 152, p. 239.</p> $H_L = \frac{L_M}{\hat{k}_L a}$ <p>$L_M = \text{lbmol/hr ft}^2, \hat{k}_L = \text{lbmol/hr ft}^2, a = \text{ft}^2/\text{ft}^3, \mu_L$ in lb/(hr ft). Range for 5-24-A is $400 < L < 15,000 \text{ lb/hr ft}^2$</p>	<p>[104] p. 187 [105] [138] p. 606 [157] [156]</p>
Packing	a_C	b	c	G	L	a_L	n																																																																																				
Raschig rings																																																																																											
3/8 inch	2.32	0.45	0.47	200–500	500–1500	0.00182	0.46																																																																																				
1	7.00	0.39	0.58	200–800	400–500	0.010	0.22																																																																																				
1	6.41	0.32	0.51	200–600	500–4500	—	—																																																																																				
2	3.82	0.41	0.45	200–800	500–4500	0.0125	0.22																																																																																				
Bert saddles																																																																																											
1/2 inch	32.4	0.30	0.74	200–700	500–1500	0.0067	0.28																																																																																				
1/2	0.811	0.30	0.24	200–800	400–4500	—	—																																																																																				
1	1.97	0.36	0.40	200–800	400–4500	0.0059	0.28																																																																																				
1.5	5.05	0.32	0.45	200–1000	400–4500	0.0062	0.28																																																																																				
B. Absorption counter-current, gas-phase coefficient H_G , for random packing	$H_G = \frac{G_M}{\hat{k}_G a} = \frac{a_G(G)^b N_{Sc,G}^{0.5}}{(L)^c}$	<p>[E] Based on ammonia-water-air data in Fellingner's 1941 MIT thesis. Curves: Refs. 104, p. 186 and 138, p. 607. Constants given in 5-24-A. The equation is dimensional. $G = \text{lb/hr ft}^2, G_M = \text{lbmol/hr ft}^2, \hat{k}_G = \text{lbmol/hr ft}^2$.</p>	<p>[104] p. 189 [138] p. 607 [157]</p>																																																																																								
C. Absorption and distillation, counter-current, gas and liquid individual coefficients and wetted surface area, Onda et al. correlation for random packings	$\frac{k'_G RT}{a_p D_G} = A \left(\frac{G}{a_p \mu_G} \right)^{0.7} N_{Sc,G}^{1/3} (a_p d_p')^{-2.0}$ $k'_L \left(\frac{\rho_L}{\mu_L} \right)^{1/3} = 0.0051 \left(\frac{L}{a_w \mu_L} \right)^{2/3} N_{Sc,L}^{-1/2} (a_p d_p')^{0.4}$ <p>$k'_L = \text{lbmol/hr ft}^2 \text{ (lbmol/ft}^3 \text{) [kgmol/s m}^2 \text{ (kgmol/m}^3 \text{)]}$</p> $\frac{a_w}{a_p} = 1 - \exp \left\{ \begin{array}{l} -1.45 \left(\frac{\sigma_c}{\sigma} \right)^{0.75} \left(\frac{L}{a_p \mu_L} \right)^{0.1} \\ \times \left(\frac{L^2 a_p}{\rho_L^2 g} \right)^{-0.05} \left(\frac{L}{\rho_L \sigma a_p} \right)^{0.2} \end{array} \right\}$	<p>[E] Gas absorption and desorption from water and organics plus vaporization of pure liquids for Raschig rings, saddles, spheres, and rods. d_p' = nominal packing size, a_p = dry packing surface area/volume, a_w = wetted packing surface area/volume. Equations are dimensionally consistent, so any set of consistent units can be used. σ = surface tension, dynes/cm. $A = 5.23$ for packing $\geq 1/2$ inch (0.012 m) $A = 2.0$ for packing $< 1/2$ inch (0.012 m) $k'_G = \text{lbmol/hr ft}^2 \text{ atm [kg mol/s m}^2 \text{ (N/m}^2 \text{)]}$</p> <p>Critical surface tensions, $\sigma_c = 61$ (ceramic), 75 (steel), 33 (polyethylene), 40 (PVC), 56 (carbon) dynes/cm.</p> $4 < \frac{L}{a_w \mu_L} < 400$ $5 < \frac{G}{a_p \mu_G} < 1000$ <p>Most data $\pm 20\%$ of correlation, some $\pm 50\%$. Graphical comparison with data in Ref. 109.</p>	<p>[44] [90] p. 380 [109][149] p. 355 [156]</p>																																																																																								
D. Distillation and absorption, counter-current, random packings, modification of Onda correlation, Bravo and Fair correlation to determine interfacial area	<p>Use Onda's correlations (5-24-C) for k'_G and k'_L. Calculate:</p> $H_G = \frac{G}{k'_G a_p P M_G}, H_L = \frac{L}{k'_L a_p \rho_L}, H_{OG} = H_G + \lambda H_L$ $\lambda = \frac{m}{L_M / G_M}$ $a_e = 0.498 a_p \left(\frac{\sigma^{0.5}}{Z^{0.4}} \right) (N_{Ca,L} N_{Re,G})^{0.392}$ $N_{Re,G} = \frac{6G}{a_p \mu_G}, N_{Ca,L} = \frac{L \mu_L}{\rho_L \sigma g_c} \text{ (dimensionless)}$	<p>[E] Use Bolles & Fair (Ref. 43) database to determine new effective area a_e to use with Onda et al. (Ref. 109) correlation. Same definitions as 5-24-C. P = total pressure, atm; M_G = gas, molecular weight; m = local slope of equilibrium curve; L_M / G_M = slope operating line; Z = height of packing in feet. Equation for a_e is dimensional. Fit to data for effective area quite good for distillation. Good for absorption at low values of $(N_{Ca,L} \times N_{Re,G})$, but correlation is too high at higher values of $(N_{Ca,L} \times N_{Re,G})$.</p>	<p>[44]</p>																																																																																								

TABLE 5-24 Mass-Transfer Correlations for Packed Two-Phase Contactors—Absorption, Distillation, Cooling Towers, and Extractors (Packing Is Inert) (Continued)

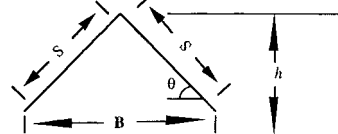
Situation	Correlations	Comments E = Empirical, S = Semiempirical, T = Theoretical	References ^o																														
<p>E. Absorption and distillation, countercurrent gas-liquid flow, random and structured packing. Determine H_L and H_C</p>	$H_C = \left(\frac{0.226}{f_p} \right) \left(\frac{N_{Sc}}{0.660} \right)^b \left(\frac{G_x}{6.782} \right)^{-0.5} \left(\frac{G_y}{0.678} \right)^{0.35}$ $H_L = \left(\frac{0.357}{f_p} \right) \left(\frac{N_{Sc}}{372} \right)^{0.5} \left(\frac{G_x/\mu}{6.782/0.0008937} \right)^{0.3}$ <p>Relative transfer coefficients [91], f_p values are in table:</p> <table border="1" data-bbox="412 434 805 576"> <thead> <tr> <th>Size, in.</th> <th>Ceramic Raschig rings</th> <th>Ceramic Berl saddles</th> <th>Metal Pall rings</th> <th>Metal Intalox</th> <th>Metal Hypac</th> </tr> </thead> <tbody> <tr> <td>0.5</td> <td>1.52</td> <td>1.58</td> <td>—</td> <td>—</td> <td>—</td> </tr> <tr> <td>1.0</td> <td>1.20</td> <td>1.36</td> <td>1.61</td> <td>1.78</td> <td>1.51</td> </tr> <tr> <td>1.5</td> <td>1.00</td> <td>—</td> <td>1.34</td> <td>—</td> <td>—</td> </tr> <tr> <td>2.0</td> <td>0.85</td> <td>—</td> <td>1.14</td> <td>1.27</td> <td>1.07</td> </tr> </tbody> </table> <p>Norton Intalox structured: 2T, $f_p = 1.98$; 3T, $f_p = 1.94$.</p>	Size, in.	Ceramic Raschig rings	Ceramic Berl saddles	Metal Pall rings	Metal Intalox	Metal Hypac	0.5	1.52	1.58	—	—	—	1.0	1.20	1.36	1.61	1.78	1.51	1.5	1.00	—	1.34	—	—	2.0	0.85	—	1.14	1.27	1.07	<p>[S] H_C based on NH_3 absorption data (5-28B) for which $H_{C, \text{base}} = 0.226$ m with $N_{Sc, \text{base}} = 0.660$ at $G_{x, \text{base}} = 6.782$ kg/(sm²) and $G_{y, \text{base}} = 0.678$ kg/(sm²) with 1/2 in. ceramic Raschig rings. The exponent b on N_{Sc} is reported as either 0.5 or as 2/3.</p> $f_p = \frac{H_C \text{ for } \text{NH}_3 \text{ with } 1/2 \text{ Raschig rings}}{H_C \text{ for } \text{NH}_3 \text{ with desired packing}}$ <p>H_L based on O_2 desorption data (5-24-A). Base viscosity, $\mu_{\text{base}} = 0.0008937$ kg/(ms). H_L in m. $G_y < 0.949$ kg/(sm²), $0.678 < G_x < 6.782$ kg/(sm²). Best use is for absorption and stripping. Limited use for organic distillation [156].</p>	<p>[66] p. 686, 659 [138] [156]</p>
Size, in.	Ceramic Raschig rings	Ceramic Berl saddles	Metal Pall rings	Metal Intalox	Metal Hypac																												
0.5	1.52	1.58	—	—	—																												
1.0	1.20	1.36	1.61	1.78	1.51																												
1.5	1.00	—	1.34	—	—																												
2.0	0.85	—	1.14	1.27	1.07																												
<p>F. Absorption, cocurrent downward flow, random packings, Reiss correlation</p>	<p>Air-oxygen-water results correlated by $k'_L a = 0.12E_L^{0.5}$. Extended to other systems.</p> $k'_L a = 0.12E_L^{0.5} \left(\frac{D_L}{2.4 \times 10^5} \right)^{0.5}$ $E_L = \left(\frac{\Delta p}{\Delta L} \right)_{2\text{-phase}} v_L$ <p>$\frac{\Delta p}{\Delta L}$ = pressure loss in two-phase flow = lbf/ft² ft</p> $k'_C a = 2.0 + 0.91E_C^{2/3} \text{ for } \text{NH}_3$ $E_g = \left(\frac{\Delta p}{\Delta L} \right)_{2\text{-phase}} v_g$ <p>v_g = superficial gas velocity, ft/s</p>	<p>[E] Based on oxygen transfer from water to air 77°F. Liquid film resistance controls. ($D_{\text{water}} @ 77^\circ\text{F} = 2.4 \times 10^{-5}$). Equation is dimensional. Data was for thin-walled polyethylene Raschig rings. Correlation also fit data for spheres. Fit $\pm 25\%$. See [122] for graph.</p> $k'_L a = s^{-1}$ <p>$D_L = \text{cm/s}$ $E_L = \text{ft, lbf/s ft}^3$ $v_L = \text{superficial liquid velocity, ft/s}$</p> <p>[E] Ammonia absorption into water from air at 70°F. Gas-film resistance controls. Thin-walled polyethylene Raschig rings and 1-inch Intalox saddles. Fit $\pm 25\%$. See [122] for fit. Terms defined as above.</p>	<p>[122] [130] p. 217</p> <p>[122]</p>																														
<p>G. Absorption, stripping, distillation, counter-current, H_L, and H_C, random packings, Bolles and Fair correlation</p>	<p>For Raschig rings, Berl saddles, and spiral tile:</p> $H_L = \frac{\phi C_{\text{flood}}}{3.28} N_{Sc,L}^{0.5} \left(\frac{Z}{3.05} \right)^{0.15}$ <p>$C_{\text{flood}} = 1.0$ if below 40% flood—otherwise, use figure in [54] and [157].</p> $H_C = \frac{A\psi(d'_{\text{col}})^{mZ^{0.33}N_{Sc,G}^{0.5}}}{\left[L \left(\frac{\mu_L}{\mu_{\text{water}}} \right)^{0.16} \left(\frac{\rho_{\text{water}}}{\rho_L} \right)^{1.25} \left(\frac{\sigma_{\text{water}}}{\sigma_L} \right)^{0.8} \right]^n}$ <p>Figures for ϕ and ψ in [42 and 43] Ranges: $0.02 < \phi > 0.300$; $25 < \psi < 190$ m.</p>	<p>[E] Z = packed height, m of each section with its own liquid distribution. The original work is reported in English units. Cornell et al. (Ref. 54) review early literature. Improved fit of Cornell's ϕ values given by Bolles and Fair (Refs. [42], [43]) and [157].</p> <p>$A = 0.017$ (rings) or 0.029 (saddles) d'_{col} = column diameter in m (if diameter > 0.6 m, use $d'_{\text{col}} = 0.6$) $m = 1.24$ (rings) or 1.11 (saddles) $n = 0.6$ (rings) or 0.5 (saddles)</p> <p>L = liquid rate, kg/(sm²), $\mu_{\text{water}} = 1.0$ Pa·s, $\rho_{\text{water}} = 1000$ kg/m³, $\sigma_{\text{water}} = 72.8$ mN/m (72.8 dyn/cm). H_C and H_L will vary from location to location. Design each section of packing separately.</p>	<p>[42, 43, 54] [77] p. 428 [90] p. 381 [141] p. 353 [157] [156]</p>																														
<p>H. Distillation and absorption. Counter-current flow. Structured packings. Gauze-type with triangular flow channels, Bravo, Rocha, and Fair correlation</p>	<p>Equivalent channel:</p>  <p>Use modified correlation for wetted wall column (See 5-18-F)</p> $N_{Sh,v} = \frac{k'_L d_{\text{eq}}}{D_v} = 0.0338 N_{Re,v}^{0.8} N_{Sc,v}^{0.333}$ $N_{Re,v} = \frac{d_{\text{eq}} \rho_v (U_{v,\text{eff}} + U_{L,\text{eff}})}{\mu_v}$ <p>Calculate k'_L from penetration model (use time for liquid to flow distance s). $k'_L = 2(D_L U_{L,\text{eff}}/\pi S)^{1/2}$.</p>	<p>[T] Check of 132 data points showed average deviation 14.6% from theory. Johnstone and Figford [Ref. 84] correlation (5-18-F) has exponent on N_{Re} rounded to 0.8. Assume gauze packing is completely wet. Thus, $a_{\text{eff}} = a_p$ to calculate H_C and H_L. Same approach may be used generally applicable to sheet-metal packings, but they will not be completely wet and need to estimate transfer area.</p> <p>L = liquid flux, kg/s m², G = vapor flux, kg/s m². Fit to data shown in Ref. [45].</p> $H_C = \frac{G}{k'_L a_p \rho_v}, H_L = \frac{L}{k'_L a_p \rho_L}$ <p>effective velocities</p> $U_{v,\text{eff}} = \frac{U_{L,\text{super}}}{\epsilon \sin \theta}, U_{L,\text{eff}} = \frac{3\Gamma}{2\rho_L} \left(\frac{\rho_L g}{3\mu_L \Gamma} \right)^{0.333}, \Gamma = \frac{L}{\text{Per}}$ $\text{Per} = \frac{\text{Perimeter}}{\text{Area}} = \frac{4S + 2B}{Bh}$	<p>[45] [63] p. 310, 326 [149] p. 356, 362 [156]</p>																														

TABLE 5-24 Mass-Transfer Correlations for Packed Two-Phase Contactors—Absorption, Distillation, Cooling Towers, and Extractors (Packing Is Inert) (Concluded)

Situation	Correlations	Comments E = Empirical, S = Semiempirical, T = Theoretical	References°																									
I. Distillation and absorption, counter-current flow. Structured packing with corrugations. Rocha, Bravo, and Fair correlation.	$N_{Sh,G} = \frac{k_g S}{D_g} = 0.054 N_{Re}^{0.8} N_{Sc}^{0.33}$ $u_{e,eff} = \frac{u_{g,super}}{\epsilon(1-h_L)\sin\theta}, \quad u_{L,eff} = \frac{u_{liq,super}}{\epsilon h_L \sin\theta}$ $k_L = 2 \left(\frac{D_L C_E u_{L,eff}}{\pi S} \right)$ $H_{OC} = H_G + \lambda H_L = \frac{u_{g,super}}{k_g a_e} + \frac{\lambda u_{L,super}}{k_L a_e}$ <p>Interfacial area:</p> $\frac{a_e}{a_p} = F_{SE} \frac{29.12 (N_{We} N_{Fr})^{0.15} S^{0.359}}{N_{Re,L}^{0.2} \epsilon^{0.6} (1 - 0.93 \cos \gamma) (\sin \theta)^{0.3}}$ <p>Packing factors:</p> <table border="1" data-bbox="407 609 808 714"> <thead> <tr> <th></th> <th>a_p</th> <th>ϵ</th> <th>F_{SE}</th> <th>θ</th> </tr> </thead> <tbody> <tr> <td>Flexi-pac 2</td> <td>233</td> <td>0.95</td> <td>0.350</td> <td>45°</td> </tr> <tr> <td>Gempak 2A</td> <td>233</td> <td>0.95</td> <td>0.344</td> <td>45°</td> </tr> <tr> <td>Intalox 2T</td> <td>213</td> <td>0.95</td> <td>0.415</td> <td>45°</td> </tr> <tr> <td>Mellapak 350Y</td> <td>350</td> <td>0.93</td> <td>0.350</td> <td>45°</td> </tr> </tbody> </table>		a_p	ϵ	F_{SE}	θ	Flexi-pac 2	233	0.95	0.350	45°	Gempak 2A	233	0.95	0.344	45°	Intalox 2T	213	0.95	0.415	45°	Mellapak 350Y	350	0.93	0.350	45°	<p>[E, T] Modification of Bravo, Rocha, and Fair (5-24-H). Same definitions as in (5-24-H) unless defined differently here. Recommended [156].</p> <p>h_L = fractional hold-up of liquid</p> <p>C_E = factor for slow surface renewal</p> <p>$C_E \sim 0.9$</p> <p>a_e = effective area/volume (1/m)</p> <p>a_p = packing surface area/volume (1/m)</p> <p>F_{SE} = surface enhancement factor</p> <p>γ = contact angle; for sheet metal, $\cos \gamma = 0.9$ for $\sigma < 0.055$ N/m</p> <p>$\cos \gamma = 5.211 \times 10^{-16.8336}$, $\sigma > 0.055$ N/m</p> <p>$\lambda = \frac{m}{L/V}$, $m = \frac{dy}{dx}$ from equilibrium</p>	[124], [156]
	a_p	ϵ	F_{SE}	θ																								
Flexi-pac 2	233	0.95	0.350	45°																								
Gempak 2A	233	0.95	0.344	45°																								
Intalox 2T	213	0.95	0.415	45°																								
Mellapak 350Y	350	0.93	0.350	45°																								
J. Rotating packed bed (Higee)	$\frac{k_L a d_p}{D a_p} \left(1 - 0.93 \frac{V_o}{V_i} - 1.13 \frac{V_t}{V_i} \right) = 0.65 N_{Sc}^{0.5}$ $\times \left(\frac{L}{a_p \mu} \right)^{0.17} \left(\frac{d_p^3 \rho^2 a_c}{\mu^2} \right)^{0.3} \left(\frac{L^2}{\rho a_p \sigma} \right)^{0.3}$ <p>500 $\leq N_{Sc} \leq 1.2$ E5; 0.0023 $\leq L/(a_p \mu) \leq 8.7$</p> <p>120 $\leq (d_p^3 \rho^2 a_c)/\mu^2 \leq 7.0$ E7; 3.7 E - 6 $\leq L^2/(\rho a_p \sigma) \leq 9.4$ E - 4</p> <p>9.12 $\leq \frac{k_L a d_p}{D a_p} \leq 2540$</p>	<p>[E] Studied oxygen desorption from water into N₂. Packing 0.22-mm-diameter stainless-steel mesh.</p> <p>$\epsilon = 0.954$, $a_p = 829$ (1/m), $h_{bed} = 2$ cm.</p> <p>a = gas-liquid area/vol (1/m)</p> <p>L = liquid mass flux, kg/(m²S)</p> <p>a_c = centrifugal accel, m²/S</p> <p>V_o, V_t, V_i = volumes inside inner radius, between outer radius and housing, and total, respectively, m³. Coefficient (0.3) on centrifugal acceleration agrees with literature values (0.3–0.38).</p>	[50]																									
K. High-voidage packings, cooling towers, splash-grid packings	$\frac{(Ka)_H V_{tower}}{L} = 0.07 + A' N'^{n'}$ <p>A' and n' depend on deck type (Ref. 86), 0.060 $\leq A' \leq 0.135$, 0.46 $\leq n' \leq 0.62$.</p> <p>General form fits the graphical comparisons (Ref. 138).</p>	<p>[E] General form. $G_a = \text{lb dry air/hr ft}^2$.</p> <p>$L = \text{lb/h ft}^2$, N' = number of deck levels.</p> <p>$(Ka)_H$ = overall enthalpy transfer coefficient =</p> $\text{lb}/(\text{h}/(\text{ft}^3) \left(\frac{\text{lb water}}{\text{lb dry air}} \right))$ <p>V_{tower} = tower volume, ft³/ft².</p> <p>If normal packings are used, use absorption mass-transfer correlations.</p>	[86][104] p. 220 [138] p. 286																									
L. Liquid-liquid extraction, packed towers	Use k values for drops (Table 5-21). Enhancement due to packing is at most 20%.	[E] Packing decreases drop size and increases interfacial area.	[146] p. 79																									
M. Liquid-liquid extraction in rotating-disc contactor (RDC)	$\frac{k_{e,RDC}}{k_c} = 1.0 + 2.44 \left(\frac{N}{N_{Cr}} \right)^{2.5}$ $N_{Cr} = 7.6 \times 10^{-4} \left(\frac{\sigma}{d_{drop} \mu_c} \right) \left(\frac{H}{D_{tank}} \right)$ $\frac{k_{d,RDC}}{k_d} = 1.0 + 1.825 \left(\frac{N}{N_{Cr}} \right) \frac{H}{D_{tank}}$	<p>k_c, k_d are for drops (Table 5-21) Breakage occurs when $N > N_{Cr}$. Maximum enhancement before breakage was factor of 2.0.</p> <p>N = impeller speed</p> <p>H = compartment height, D_{tank} = tank diameter,</p> <p>σ = interfacial tension, N/m.</p> <p>Done in 0.152 and 0.600 m RDC.</p>	[36][146] p. 79																									
N. Liquid-liquid extraction, stirred tanks	See Table 5-22-E, F, G, and H.	[E]																										

See also Sec. 14.

°See the beginning of the "Mass Transfer" subsection for references.

The gas-phase rate coefficient \hat{k}_C is not affected by the fact that a chemical reaction is taking place in the liquid phase. If the liquid-phase chemical reaction is extremely fast and irreversible, the rate of absorption may be governed completely by the resistance to diffusion in the gas phase. In this case the absorption rate may be estimated by

knowing only the gas-phase rate coefficient \hat{k}_C or else the height of one gas-phase transfer unit $H_G = G_M/(\hat{k}_C a)$.

It should be noted that the highest possible absorption rates will occur under conditions in which the liquid-phase resistance is negligible and the equilibrium back pressure of the gas over the solvent is zero.

Such situations would exist, for instance, for NH_3 absorption into an acid solution, for SO_2 absorption into an alkali solution, for vaporization of water into air, and for H_2S absorption from a dilute-gas stream into a strong alkali solution, provided there is a large excess of reagent in solution to consume all the dissolved gas. This is known as the gas-phase mass-transfer limited condition, when both the liquid-phase resistance and the back pressure of the gas equal zero. Even when the reaction is sufficiently reversible to allow a small back pressure, the absorption may be gas-phase-controlled, and the values of \hat{k}_G and H_G that would apply to a physical-absorption process will govern the rate.

The liquid-phase rate coefficient k_L is strongly affected by fast chemical reactions and generally increases with increasing reaction rate. Indeed, the condition for zero liquid-phase resistance ($m\hat{k}_L$) implies that either the equilibrium back pressure is negligible, or that \hat{k}_L is very large, or both. Frequently, even though reaction consumes the solute as it is dissolving, thereby enhancing both the mass-transfer coefficient and the driving force for absorption, the reaction rate is slow enough that the liquid-phase resistance must be taken into account. This may be due either to an insufficient supply of a second reagent or to an inherently slow chemical reaction.

In any event the value of \hat{k}_L in the presence of a chemical reaction normally is larger than the value found when only physical absorption occurs, \hat{k}_L^0 . This has led to the presentation of data on the effects of chemical reaction in terms of the "reaction factor" or "enhancement factor" defined as

$$\phi = \hat{k}_L / \hat{k}_L^0 \geq 1 \quad (5-311)$$

where \hat{k}_L = mass-transfer coefficient with reaction and \hat{k}_L^0 = mass-transfer coefficient for pure physical absorption.

It is important to understand that when chemical reactions are involved, this definition of \hat{k}_L is based on the driving force defined as the difference between the concentration of *unreacted* solute gas at the interface and in the bulk of the liquid. A coefficient based on the total of both unreacted and reacted gas could have values *smaller* than the physical-absorption mass-transfer coefficient \hat{k}_L^0 .

When liquid-phase resistance is important, particular care should be taken in employing any given set of experimental data to ensure that the equilibrium data used conform with those employed by the original author in calculating values of \hat{k}_L or H_L . Extrapolation to widely different concentration ranges or operating conditions should be made with caution, since the mass-transfer coefficient \hat{k}_L may vary in an unexpected fashion, owing to changes in the apparent chemical-reaction mechanism.

Generalized prediction methods for \hat{k}_L and H_L do not apply when chemical reaction occurs in the liquid phase, and therefore one must use actual operating data for the particular system in question. A discussion of the various factors to consider in designing gas absorbers and strippers when chemical reactions are involved is presented by Astarita, Savage, and Bisio, *Gas Treating with Chemical Solvents*, Wiley (1983) and by Kohl and Nielsen, *Gas Purification*, 5th ed., Gulf (1997).

Effective Interfacial Mass-Transfer Area a In a packed tower of constant cross-sectional area S the differential change in solute flow per unit time is given by

$$-d(G_M S y) = N_A a dV = N_A a S dh \quad (5-312)$$

where a = interfacial area effective for mass transfer per unit of packed volume and V = packed volume. Owing to incomplete wetting of the packing surfaces and to the formation of areas of stagnation in the liquid film, the effective area normally is significantly less than the total external area of the packing pieces.

The effective interfacial area depends on a number of factors, as discussed in a review by Charpentier [*Chem. Eng. J.*, **11**, 161 (1976)]. Among these factors are (1) the shape and size of packing, (2) the packing material (for example, plastic generally gives smaller interfacial areas than either metal or ceramic), (3) the liquid mass velocity, and (4), for small-diameter towers, the column diameter.

Whereas the interfacial area generally increases with increasing liquid rate, it apparently is relatively independent of the superficial gas mass velocity below the flooding point. According to Charpentier's review, it appears valid to assume that the interfacial area is independent of the column height when specified in terms of unit packed volume (i.e., as a). Also, the existing data for chemically reacting gas-liquid systems (mostly aqueous electrolyte solutions) indicate that

the interfacial area is independent of the chemical system. However, this situation may not hold true for systems involving large heats of reaction.

Rizzuti et al. [*Chem. Eng. Sci.*, **36**, 973 (1981)] examined the influence of solvent viscosity upon the effective interfacial area in packed columns and concluded that for the systems studied the effective interfacial area a was proportional to the kinematic viscosity raised to the 0.7 power. Thus, the hydrodynamic behavior of a packed absorber is strongly affected by viscosity effects. Surface-tension effects also are important, as expressed in the work of Onda et al. (see Table 5-24-C).

In developing correlations for the mass-transfer coefficients \hat{k}_G and \hat{k}_L , the various authors have assumed different but internally compatible correlations for the effective interfacial area a . It therefore would be inappropriate to mix the correlations of different authors unless it has been demonstrated that there is a valid area of overlap between them.

Volumetric Mass-Transfer Coefficients $\hat{K}_G a$ and $\hat{K}_L a$ Experimental determinations of the individual mass-transfer coefficients \hat{k}_G and \hat{k}_L and of the effective interfacial area a involve the use of extremely difficult techniques, and therefore such data are not plentiful. More often, column experimental data are reported in terms of overall volumetric coefficients, which normally are defined as follows:

$$K'_{G a} = n_A / (h_T S p_T \Delta y_{1m}^0) \quad (5-313)$$

$$\text{and} \quad K_{L a} = n_A / (h_T S \Delta x_{1m}^0) \quad (5-314)$$

where $K'_{G a}$ = overall volumetric gas-phase mass-transfer coefficient, $K_{L a}$ = overall volumetric liquid-phase mass-transfer coefficient, n_A = overall rate of transfer of solute A , h_T = total packed depth in tower, S = tower cross-sectional area, p_T = total system pressure employed during the experiment, and Δx_{1m}^0 and Δy_{1m}^0 are defined as

$$\Delta y_{1m}^0 = \frac{(y - y^0)_1 - (y - y^0)_2}{\ln [(y - y^0)_1 / (y - y^0)_2]} \quad (5-315)$$

$$\text{and} \quad \Delta x_{1m}^0 = \frac{(x^0 - x)_2 - (x^0 - x)_1}{\ln [(x^0 - x)_2 / (x^0 - x)_1]} \quad (5-316)$$

where subscripts 1 and 2 refer to the bottom and top of the tower respectively.

Experimental $K'_{G a}$ and $K_{L a}$ data are available for most absorption and stripping operations of commercial interest (see Sec. 14). The solute concentrations employed in these experiments normally are very low, so that $K_{L a} \approx \hat{K}_{L a}$ and $K'_{G a} p_T \approx \hat{K}'_{G a}$, where p_T is the total pressure employed in the actual experimental-test system. Unlike the individual gas-film coefficient $\hat{k}_G a$, the overall coefficient $\hat{K}'_{G a}$ will vary with the total system pressure except when the liquid-phase resistance is negligible (i.e., when either $m = 0$, or $\hat{k}_L a$ is very large, or both).

Extrapolation of $K'_{G a}$ data for absorption and stripping to conditions other than those for which the original measurements were made can be extremely risky, especially in systems involving chemical reactions in the liquid phase. One therefore would be wise to restrict the use of overall volumetric mass-transfer-coefficient data to conditions not too far removed from those employed in the actual tests. The most reliable data for this purpose would be those obtained from an operating commercial unit of similar design.

Experimental values of H_{OG} and H_{OL} for a number of distillation systems of commercial interest are also readily available. Extrapolation of the data or the correlations to conditions that differ significantly from those used for the original experiments is risky. For example, pressure has a major effect on vapor density and thus can affect the hydrodynamics significantly. Changes in flow patterns affect both mass-transfer coefficients and interfacial area.

Chilton-Colburn Analogy On occasion one will find that heat-transfer-rate data are available for a system in which mass-transfer-rate data are not readily available. The Chilton-Colburn analogy [90, 53] (see Tables 5-17-G and 5-19-T) provides a procedure for developing estimates of the mass-transfer rates based on heat-transfer data. Extrapolation of experimental j_M or j_H data obtained with gases to predict liquid systems (and vice versa) should be approached with caution, however. When pressure-drop or friction-factor data are available, one may be able to place an upper bound on the rates of heat and mass transfer of $f/2$. The Chilton-Colburn analogy can be used for simultaneous heat and mass transfer as long as the concentration and temperature fields are independent [Venkatesan and Fogler, *AIChE J.*, **50**, 1623 (2004)].

SECTION 6

Fluid and
Particle
Dynamics

PERRY'S CHEMICAL ENGINEERS' HANDBOOK

8TH EDITION



JAMES N. TILTON

Copyright © 2008, 1997, 1984, 1973, 1963, 1950, 1941, 1934 by The McGraw-Hill Companies, Inc. All rights reserved. Manufactured in the United States of America. Except as permitted under the United States Copyright Act of 1976, no part of this publication may be reproduced or distributed in any form or by any means, or stored in a database or retrieval system, without the prior written permission of the publisher.

0-07-154213-2

The material in this eBook also appears in the print version of this title: 0-07-151129-6.

All trademarks are trademarks of their respective owners. Rather than put a trademark symbol after every occurrence of a trademarked name, we use names in an editorial fashion only, and to the benefit of the trademark owner, with no intention of infringement of the trademark. Where such designations appear in this book, they have been printed with initial caps.

McGraw-Hill eBooks are available at special quantity discounts to use as premiums and sales promotions, or for use in corporate training programs. For more information, please contact George Hoare, Special Sales, at george_hoare@mcgraw-hill.com or (212) 904-4069.

TERMS OF USE

This is a copyrighted work and The McGraw-Hill Companies, Inc. (“McGraw-Hill”) and its licensors reserve all rights in and to the work. Use of this work is subject to these terms. Except as permitted under the Copyright Act of 1976 and the right to store and retrieve one copy of the work, you may not decompile, disassemble, reverse engineer, reproduce, modify, create derivative works based upon, transmit, distribute, disseminate, sell, publish or sublicense the work or any part of it without McGraw-Hill’s prior consent. You may use the work for your own noncommercial and personal use; any other use of the work is strictly prohibited. Your right to use the work may be terminated if you fail to comply with these terms.

THE WORK IS PROVIDED “AS IS.” McGRAW-HILL AND ITS LICENSORS MAKE NO GUARANTEES OR WARRANTIES AS TO THE ACCURACY, ADEQUACY OR COMPLETENESS OF OR RESULTS TO BE OBTAINED FROM USING THE WORK, INCLUDING ANY INFORMATION THAT CAN BE ACCESSED THROUGH THE WORK VIA HYPERLINK OR OTHERWISE, AND EXPRESSLY DISCLAIM ANY WARRANTY, EXPRESS OR IMPLIED, INCLUDING BUT NOT LIMITED TO IMPLIED WARRANTIES OF MERCHANTABILITY OR FITNESS FOR A PARTICULAR PURPOSE. McGraw-Hill and its licensors do not warrant or guarantee that the functions contained in the work will meet your requirements or that its operation will be uninterrupted or error free. Neither McGraw-Hill nor its licensors shall be liable to you or anyone else for any inaccuracy, error or omission, regardless of cause, in the work or for any damages resulting therefrom. McGraw-Hill has no responsibility for the content of any information accessed through the work. Under no circumstances shall McGraw-Hill and/or its licensors be liable for any indirect, incidental, special, punitive, consequential or similar damages that result from the use of or inability to use the work, even if any of them has been advised of the possibility of such damages. This limitation of liability shall apply to any claim or cause whatsoever whether such claim or cause arises in contract, tort or otherwise.

DOI: 10.1036/0071511296

Fluid and Particle Dynamics

James N. Tilton, Ph.D., P.E. *Principal Consultant, Process Engineering, E. I. du Pont de Nemours & Co.; Member, American Institute of Chemical Engineers; Registered Professional Engineer (Delaware)*

FLUID DYNAMICS

Nature of Fluids	6-4	Slip Flow	6-15
Deformation and Stress	6-4	Frictional Losses in Pipeline Elements	6-16
Viscosity	6-4	Equivalent Length and Velocity Head Methods	6-16
Rheology	6-4	Contraction and Entrance Losses	6-16
Kinematics of Fluid Flow	6-5	Example 5: Entrance Loss	6-16
Velocity	6-5	Expansion and Exit Losses	6-17
Compressible and Incompressible Flow	6-5	Fittings and Valves	6-17
Streamlines, Pathlines, and Streaklines	6-5	Example 6: Losses with Fittings and Valves	6-18
One-dimensional Flow	6-5	Curved Pipes and Coils	6-19
Rate of Deformation Tensor	6-5	Screens	6-20
Vorticity	6-5	Jet Behavior	6-20
Laminar and Turbulent Flow, Reynolds Number	6-6	Flow through Orifices	6-22
Conservation Equations	6-6	Compressible Flow	6-22
Macroscopic and Microscopic Balances	6-6	Mach Number and Speed of Sound	6-22
Macroscopic Equations	6-6	Isothermal Gas Flow in Pipes and Channels	6-22
Mass Balance	6-6	Adiabatic Frictionless Nozzle Flow	6-23
Momentum Balance	6-6	Example 7: Flow through Frictionless Nozzle	6-23
Total Energy Balance	6-7	Adiabatic Flow with Friction in a Duct of Constant	
Mechanical Energy Balance, Bernoulli Equation	6-7	Cross Section	6-24
Microscopic Balance Equations	6-7	Example 8: Compressible Flow with Friction Losses	6-24
Mass Balance, Continuity Equation	6-7	Convergent/Divergent Nozzles (De Laval Nozzles)	6-24
Stress Tensor	6-7	Multiphase Flow	6-26
Cauchy Momentum and Navier-Stokes Equations	6-8	Liquids and Gases	6-26
Examples	6-8	Gases and Solids	6-30
Example 1: Force Exerted on a Reducing Bend	6-8	Solids and Liquids	6-30
Example 2: Simplified Ejector	6-9	Fluid Distribution	6-32
Example 3: Venturi Flowmeter	6-9	Perforated-Pipe Distributors	6-32
Example 4: Plane Poiseuille Flow	6-9	Example 9: Pipe Distributor	6-33
Incompressible Flow in Pipes and Channels	6-9	Slot Distributors	6-33
Mechanical Energy Balance	6-9	Turning Vanes	6-33
Friction Factor and Reynolds Number	6-10	Perforated Plates and Screens	6-34
Laminar and Turbulent Flow	6-10	Beds of Solids	6-34
Velocity Profiles	6-11	Other Flow Straightening Devices	6-34
Entrance and Exit Effects	6-11	Fluid Mixing	6-34
Residence Time Distribution	6-11	Stirred Tank Agitation	6-35
Noncircular Channels	6-12	Pipeline Mixing	6-36
Nonisothermal Flow	6-12	Tube Banks	6-36
Open Channel Flow	6-13	Turbulent Flow	6-36
Non-Newtonian Flow	6-13	Transition Region	6-37
Economic Pipe Diameter, Turbulent Flow	6-14	Laminar Region	6-37
Economic Pipe Diameter, Laminar Flow	6-15	Beds of Solids	6-39
Vacuum Flow	6-15	Fixed Beds of Granular Solids	6-39
Molecular Flow	6-15	Porous Media	6-39

6-2 FLUID AND PARTICLE DYNAMICS

Tower Packings	6-40	Cavitation	6-45
Fluidized Beds	6-40	Turbulence	6-46
Boundary Layer Flows	6-40	Time Averaging	6-46
Flat Plate, Zero Angle of Incidence	6-40	Closure Models	6-46
Cylindrical Boundary Layer	6-41	Eddy Spectrum	6-47
Continuous Flat Surface	6-41	Computational Fluid Dynamics	6-47
Continuous Cylindrical Surface	6-41	Dimensionless Groups	6-49
Vortex Shedding	6-41		
Coating Flows	6-42	PARTICLE DYNAMICS	
Falling Films	6-43	Drag Coefficient	6-51
Minimum Wetting Rate	6-43	Terminal Settling Velocity	6-51
Laminar Flow	6-43	Spherical Particles	6-51
Turbulent Flow	6-43	Nonspherical Rigid Particles	6-52
Effect of Surface Traction	6-44	Hindered Settling	6-53
Flooding	6-44	Time-dependent Motion	6-53
Hydraulic Transients	6-44	Gas Bubbles	6-54
Water Hammer	6-44	Liquid Drops in Liquids	6-55
Example 10: Response to Instantaneous Valve Closing	6-44	Liquid Drops in Cases	6-55
Pulsating Flow	6-45	Wall Effects	6-56

Nomenclature and Units*

In this listing, symbols used in this section are defined in a general way and appropriate SI units are given. Specific definitions, as denoted by subscripts, are stated at the place of application in the section. Some specialized symbols used in the section are defined only at the place of application. Some symbols have more than one definition; the appropriate one is identified at the place of application.

Symbol	Definition	SI units	U.S. customary units	Symbol	Definition	SI units	U.S. customary units
a	Pressure wave velocity	m/s	ft/s	s	Entropy per unit mass	J/(kg · K)	Btu/(lbm · R)
A	Area	m ²	ft ²	S	Slope	Dimensionless	Dimensionless
b	Wall thickness	m	in	S	Pumping speed	m ³ /s	ft ³ /s
b	Channel width	m	ft	S	Surface area per unit volume	1/m	1/ft
c	Acoustic velocity	m/s	ft/s	St	Strouhal number	Dimensionless	Dimensionless
c_f	Friction coefficient	Dimensionless	Dimensionless	t	Time	s	s
C	Conductance	m ³ /s	ft ³ /s	t	Force per unit area	Pa	lbf/in ²
Ca	Capillary number	Dimensionless	Dimensionless	T	Absolute temperature	K	R
C_0	Discharge coefficient	Dimensionless	Dimensionless	u	Internal energy per unit mass	J/kg	Btu/lbm
C_D	Drag coefficient	Dimensionless	Dimensionless	u	Velocity	m/s	ft/s
d	Diameter	m	ft	U	Velocity	m/s	ft/s
D	Diameter	m	ft	v	Velocity	m/s	ft/s
De	Dean number	Dimensionless	Dimensionless	V	Velocity	m/s	ft/s
D_{ij}	Deformation rate tensor components	1/s	1/s	V	Volume	m ³	ft ³
E	Elastic modulus	Pa	lbf/in ²	We	Weber number	Dimensionless	Dimensionless
\dot{E}_v	Energy dissipation rate	J/s	ft · lbf/s	\dot{W}_s	Rate of shaft work	J/s	Btu/s
Eo	Eotvos number	Dimensionless	Dimensionless	δW_s	Shaft work per unit mass	J/kg	Btu/lbm
f	Fanning friction factor	Dimensionless	Dimensionless	x	Cartesian coordinate	m	ft
f	Vortex shedding frequency	1/s	1/s	y	Cartesian coordinate	m	ft
F	Force	N	lbf	z	Cartesian coordinate	m	ft
F	Cumulative residence time distribution	Dimensionless	Dimensionless	z	Elevation	m	ft
Fr	Froude number	Dimensionless	Dimensionless	Greek Symbols			
g	Acceleration of gravity	m/s ²	ft/s ²	α	Velocity profile factor	Dimensionless	Dimensionless
G	Mass flux	kg/(m ² · s)	lbm/(ft ² · s)	α	Included angle	Radians	Radians
h	Enthalpy per unit mass	J/kg	Btu/lbm	β	Velocity profile factor	Dimensionless	Dimensionless
h	Liquid depth	m	ft	β	Bulk modulus of elasticity	Pa	lbf/in ²
k	Ratio of specific heats	Dimensionless	Dimensionless	$\dot{\gamma}$	Shear rate	1/s	1/s
k	Kinetic energy of turbulence	J/kg	ft · lbf/lbm	Γ	Mass flow rate per unit width	kg/(m · s)	lbm/(ft · s)
K	Power law coefficient	kg/(m · s ²⁻ⁿ)	lbm/(ft · s ²⁻ⁿ)	δ	Boundary layer or film thickness	m	ft
l_c	Viscous losses per unit mass	J/kg	ft · lbf/lbm	δ_{ij}	Kronecker delta	Dimensionless	Dimensionless
L	Length	m	ft	ϵ	Pipe roughness	m	ft
\dot{m}	Mass flow rate	kg/s	lbm/s	ϵ	Void fraction	Dimensionless	Dimensionless
M	Mass	kg	lbm	ϵ	Turbulent dissipation rate	J/(kg · s)	ft · lbf/(lbm · s)
M	Mach number	Dimensionless	Dimensionless	θ	Residence time	s	s
M	Morton number	Dimensionless	Dimensionless	θ	Angle	Radians	Radians
M_w	Molecular weight	kg/kgmole	lbm/lbmole	λ	Mean free path	m	ft
n	Power law exponent	Dimensionless	Dimensionless	μ	Viscosity	Pa · s	lbm/(ft · s)
N_b	Blend time number	Dimensionless	Dimensionless	ν	Kinematic viscosity	m ² /s	ft ² /s
N_D	Best number	Dimensionless	Dimensionless	ρ	Density	kg/m ³	lbm/ft ³
N_P	Power number	Dimensionless	Dimensionless	σ	Surface tension	N/m	lbf/ft
N_Q	Pumping number	Dimensionless	Dimensionless	σ	Cavitation number	Dimensionless	Dimensionless
p	Pressure	Pa	lbf/in ²	σ_{ij}	Components of total stress tensor	Pa	lbf/in ²
q	Entrained flow rate	m ³ /s	ft ³ /s	τ	Shear stress	Pa	lbf/in ²
Q	Volumetric flow rate	m ³ /s	ft ³ /s	τ	Time period	s	s
Q	Throughput (vacuum flow)	Pa · m ³ /s	lbf · ft ³ /s	τ_{ij}	Components of deviatoric stress tensor	Pa	lbf/in ²
δQ	Heat input per unit mass	J/kg	Btu/lbm	Φ	Energy dissipation rate per unit volume	J/(m ³ · s)	ft · lbf/(ft ³ · s)
r	Radial coordinate	m	ft	ϕ	Angle of inclination	Radians	Radians
R	Radius	m	ft	ω	Vorticity	1/s	1/s
R	Ideal gas universal constant	J/(kgmole · K)	Btu/(lbmole · R)				
R_i	Volume fraction of phase i	Dimensionless	Dimensionless				
Re	Reynolds number	Dimensionless	Dimensionless				
s	Density ratio	Dimensionless	Dimensionless				

* Note that with U.S. Customary units, the conversion factor g_c may be required to make equations in this section dimensionally consistent; $g_c = 32.17$ (lbm-ft)/(lbf-s²).

FLUID DYNAMICS

GENERAL REFERENCES: Batchelor, *An Introduction to Fluid Dynamics*, Cambridge University, Cambridge, 1967; Bird, Stewart, and Lightfoot, *Transport Phenomena*, 2d ed., Wiley, New York, 2002; Brodkey, *The Phenomena of Fluid Motions*, Addison-Wesley, Reading, Mass., 1967; Denn, *Process Fluid Mechanics*, Prentice-Hall, Englewood Cliffs, N.J., 1980; Landau and Lifshitz, *Fluid Mechanics*, 2d ed., Pergamon, 1987; Govier and Aziz, *The Flow of Complex Mixtures in Pipes*, Van Nostrand Reinhold, New York, 1972; Krieger, Huntington, N.Y., 1977; Panton, *Incompressible Flow*, Wiley, New York, 1984; Schlichting, *Boundary Layer Theory*, 8th ed., McGraw-Hill, New York, 1987; Shames, *Mechanics of Fluids*, 3d ed., McGraw-Hill, New York, 1992; Streeter, *Handbook of Fluid Dynamics*, McGraw-Hill, New York, 1971; Streeter and Wylie, *Fluid Mechanics*, 8th ed., McGraw-Hill, New York, 1985; Vennard and Street, *Elementary Fluid Mechanics*, 5th ed., Wiley, New York, 1975; Whitaker, *Introduction to Fluid Mechanics*, Prentice-Hall, Englewood Cliffs, N.J., 1968; Krieger, Huntington, N.Y., 1981.

NATURE OF FLUIDS

Deformation and Stress A fluid is a substance which undergoes continuous deformation when subjected to a shear stress. Figure 6-1 illustrates this concept. A fluid is bounded by two large parallel plates, of area A , separated by a small distance H . The bottom plate is held fixed. Application of a force F to the upper plate causes it to move at a velocity U . The fluid continues to deform as long as the force is applied, unlike a solid, which would undergo only a finite deformation.

The force is directly proportional to the area of the plate; the shear stress is $\tau = F/A$. Within the fluid, a linear velocity profile $u = Uy/H$ is established; due to the **no-slip condition**, the fluid bounding the lower plate has zero velocity and the fluid bounding the upper plate moves at the plate velocity U . The velocity gradient $\dot{\gamma} = du/dy$ is called the **shear rate** for this flow. Shear rates are usually reported in units of reciprocal seconds. The flow in Fig. 6-1 is a **simple shear flow**.

Viscosity The ratio of shear stress to shear rate is the viscosity, μ .

$$\mu = \frac{\tau}{\dot{\gamma}} \quad (6-1)$$

The SI units of viscosity are $\text{kg}/(\text{m} \cdot \text{s})$ or $\text{Pa} \cdot \text{s}$ (pascal second). The cgs unit for viscosity is the poise; $1 \text{ Pa} \cdot \text{s}$ equals 10 poise or 1000 centipoise (cP) or 0.672 $\text{lbm}/(\text{ft} \cdot \text{s})$. The terms *absolute viscosity* and *shear viscosity* are synonymous with the viscosity as used in Eq. (6-1).

Kinematic viscosity $\nu \equiv \mu/\rho$ is the ratio of viscosity to density. The SI units of kinematic viscosity are m^2/s . The cgs stoke is $1 \text{ cm}^2/\text{s}$.

Rheology In general, fluid flow patterns are more complex than the one shown in Fig. 6-1, as is the relationship between fluid deformation and stress. Rheology is the discipline of fluid mechanics which studies this relationship. One goal of rheology is to obtain **constitutive equations** by which stresses may be computed from deformation rates. For simplicity, fluids may be classified into rheological types in reference to the simple shear flow of Fig. 6-1. Complete definitions require extension to multidimensional flow. For more information, several good references are available, including Bird, Armstrong, and Hassager (*Dynamics of Polymeric Liquids*, vol. 1: *Fluid Mechanics*, Wiley, New York, 1977); Metzner ("Flow of Non-Newtonian Fluids" in Streeter, *Handbook of Fluid Dynamics*, McGraw-Hill, New York, 1971); and Skelland (*Non-Newtonian Flow and Heat Transfer*, Wiley, New York, 1967).

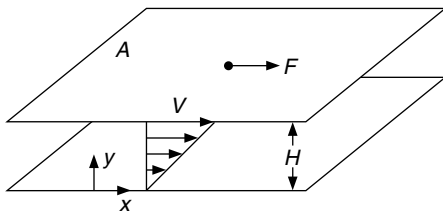


FIG. 6-1 Deformation of a fluid subjected to a shear stress.

Fluids without any solidlike elastic behavior do not undergo any reverse deformation when shear stress is removed, and are called **purely viscous fluids**. The shear stress depends only on the rate of deformation, and not on the extent of deformation (strain). Those which exhibit both viscous and elastic properties are called **viscoelastic fluids**.

Purely viscous fluids are further classified into time-independent and time-dependent fluids. For time-independent fluids, the shear stress depends only on the instantaneous shear rate. The shear stress for time-dependent fluids depends on the past history of the rate of deformation, as a result of structure or orientation buildup or breakdown during deformation.

A **rheogram** is a plot of shear stress versus shear rate for a fluid in simple shear flow, such as that in Fig. 6-1. Rheograms for several types of time-independent fluids are shown in Fig. 6-2. The **Newtonian fluid rheogram** is a straight line passing through the origin. The slope of the line is the viscosity. For a Newtonian fluid, the viscosity is independent of shear rate, and may depend only on temperature and perhaps pressure. By far, the Newtonian fluid is the largest class of fluid of engineering importance. Gases and low molecular weight liquids are generally Newtonian. Newton's law of viscosity is a rearrangement of Eq. (6-1) in which the viscosity is a constant:

$$\tau = \mu \dot{\gamma} = \mu \frac{du}{dy} \quad (6-2)$$

All fluids for which the viscosity varies with shear rate are **non-Newtonian fluids**. For non-Newtonian fluids the viscosity, defined as the ratio of shear stress to shear rate, is often called the **apparent viscosity** to emphasize the distinction from Newtonian behavior. Purely viscous, time-independent fluids, for which the apparent viscosity may be expressed as a function of shear rate, are called **generalized Newtonian fluids**.

Non-Newtonian fluids include those for which a finite stress τ_y is required before continuous deformation occurs; these are called **yield-stress materials**. The **Bingham plastic fluid** is the simplest yield-stress material; its rheogram has a constant slope μ_∞ , called the *infinite shear viscosity*.

$$\tau = \tau_y + \mu_\infty \dot{\gamma} \quad (6-3)$$

Highly concentrated suspensions of fine solid particles frequently exhibit Bingham plastic behavior.

Shear-thinning fluids are those for which the slope of the rheogram decreases with increasing shear rate. These fluids have also been called *pseudoplastic*, but this terminology is outdated and discouraged. Many polymer melts and solutions, as well as some solids suspensions, are shear-thinning. Shear-thinning fluids without yield stresses typically obey a power law model over a range of shear rates.

$$\tau = K \dot{\gamma}^n \quad (6-4)$$

The apparent viscosity is

$$\mu = K \dot{\gamma}^{n-1} \quad (6-5)$$

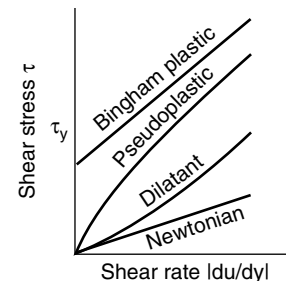


FIG. 6-2 Shear diagrams.

The factor K is the consistency index or power law coefficient, and n is the power law exponent. The exponent n is dimensionless, while K is in units of $\text{kg}/(\text{m} \cdot \text{s}^{2-n})$. For shear-thinning fluids, $n < 1$. The power law model typically provides a good fit to data over a range of one to two orders of magnitude in shear rate; behavior at very low and very high shear rates is often Newtonian. Shear-thinning power law fluids with yield stresses are sometimes called *Herschel-Bulkley fluids*. Numerous other rheological model equations for shear-thinning fluids are in common use.

Dilatant, or shear-thickening, fluids show increasing viscosity with increasing shear rate. Over a limited range of shear rate, they may be described by the power law model with $n > 1$. Dilatancy is rare, observed only in certain concentration ranges in some particle suspensions (Govier and Aziz, pp. 33–34). Extensive discussions of dilatant suspensions, together with a listing of dilatant systems, are given by Green and Grisley (*Trans. Soc. Rheol.*, **12**[1], 13–25 [1968]); Grisley and Green (*AIChE J.*, **17**, 725–728 [1971]); and Bauer and Collins (“Thixotropy and Dilatancy,” in Eirich, *Rheology*, vol. 4, Academic, New York, 1967).

Time-dependent fluids are those for which structural rearrangements occur during deformation at a rate too slow to maintain equilibrium configurations. As a result, shear stress changes with duration of shear. **Thixotropic** fluids, such as mayonnaise, clay suspensions used as drilling muds, and some paints and inks, show decreasing shear stress with time at constant shear rate. A detailed description of thixotropic behavior and a list of thixotropic systems is found in Bauer and Collins (*ibid.*).

Rheopeptic behavior is the opposite of thixotropy. Shear stress increases with time at constant shear rate. Rheopeptic behavior has been observed in bentonite sols, vanadium pentoxide sols, and gypsum suspensions in water (Bauer and Collins, *ibid.*) as well as in some polyester solutions (Steg and Katz, *J. Appl. Polym. Sci.*, **9**, 3, 177 [1965]).

Viscoelastic fluids exhibit elastic recovery from deformation when stress is removed. Polymeric liquids comprise the largest group of fluids in this class. A property of viscoelastic fluids is the *relaxation time*, which is a measure of the time required for elastic effects to decay. Viscoelastic effects may be important with sudden changes in rates of deformation, as in flow startup and stop, rapidly oscillating flows, or as a fluid passes through sudden expansions or contractions where accelerations occur. In many fully developed flows where such effects are absent, viscoelastic fluids behave as if they were purely viscous. In viscoelastic flows, normal stresses perpendicular to the direction of shear are different from those in the parallel direction. These give rise to such behaviors as the *Weissenberg effect*, in which fluid climbs up a shaft rotating in the fluid, and *die swell*, where a stream of fluid issuing from a tube may expand to two or more times the tube diameter.

A parameter indicating whether viscoelastic effects are important is the **Deborah number**, which is the ratio of the characteristic relaxation time of the fluid to the characteristic time scale of the flow. For small Deborah numbers, the relaxation is fast compared to the characteristic time of the flow, and the fluid behavior is purely viscous. For very large Deborah numbers, the behavior closely resembles that of an elastic solid.

Analysis of viscoelastic flows is very difficult. Simple constitutive equations are unable to describe all the material behavior exhibited by viscoelastic fluids even in geometrically simple flows. More complex constitutive equations may be more accurate, but become exceedingly difficult to apply, especially for complex geometries, even with advanced numerical methods. For good discussions of viscoelastic fluid behavior, including various types of constitutive equations, see Bird, Armstrong, and Hassager (*Dynamics of Polymeric Liquids*, vol. 1: *Fluid Mechanics*, vol. 2: *Kinetic Theory*, Wiley, New York, 1977); Middleman (*The Flow of High Polymers*, Interscience (Wiley) New York, 1968); or Astarita and Marrucci (*Principles of Non-Newtonian Fluid Mechanics*, McGraw-Hill, New York, 1974).

Polymer processing is the field which depends most on the flow of non-Newtonian fluids. Several excellent texts are available, including Middleman (*Fundamentals of Polymer Processing*, McGraw-Hill, New York, 1977) and Tadmor and Gogos (*Principles of Polymer Processing*, Wiley, New York, 1979).

There is a wide variety of instruments for measurement of Newtonian viscosity, as well as rheological properties of non-Newtonian fluids. They are described in Van Wazer, Lyons, Kim, and Colwell (*Viscosity and Flow Measurement*, Interscience, New York, 1963); Coleman, Markowitz, and Noll (*Viscometric Flows of Non-Newtonian Fluids*, Springer-Verlag, Berlin, 1966); Dealy and Wissbrun (*Melt Rheology and Its Role in Plastics Processing*, Van Nostrand Reinhold, 1990). Measurement of rheological behavior requires well-characterized flows. Such *rheometric* flows are thoroughly discussed by Astarita and Marrucci (*Principles of Non-Newtonian Fluid Mechanics*, McGraw-Hill, New York, 1974).

KINEMATICS OF FLUID FLOW

Velocity The term *kinematics* refers to the quantitative description of fluid motion or deformation. The rate of deformation depends on the distribution of velocity within the fluid. Fluid velocity \mathbf{v} is a vector quantity, with three cartesian components v_x , v_y , and v_z . The velocity vector is a function of spatial position and time. A **steady** flow is one in which the velocity is independent of time, while in **unsteady** flow \mathbf{v} varies with time.

Compressible and Incompressible Flow An incompressible flow is one in which the density of the fluid is constant or nearly constant. Liquid flows are normally treated as incompressible, except in the context of hydraulic transients (see following). Compressible fluids, such as gases, may undergo incompressible flow if pressure and/or temperature changes are small enough to render density changes insignificant. Frequently, compressible flows are regarded as flows in which the density varies by more than 5 to 10 percent.

Streamlines, Pathlines, and Streaklines These are curves in a flow field which provide insight into the flow pattern. *Streamlines* are tangent at every point to the local instantaneous velocity vector. A *pathline* is the path followed by a material element of fluid; it coincides with a streamline if the flow is steady. In unsteady flow the pathlines generally do not coincide with streamlines. *Streaklines* are curves on which are found all the material particles which passed through a particular point in space at some earlier time. For example, a streakline is revealed by releasing smoke or dye at a point in a flow field. For steady flows, streamlines, pathlines, and streaklines are indistinguishable. In two-dimensional incompressible flows, streamlines are contours of the **stream function**.

One-dimensional Flow Many flows of great practical importance, such as those in pipes and channels, are treated as one-dimensional flows. There is a single direction called the *flow direction*; velocity components perpendicular to this direction are either zero or considered unimportant. Variations of quantities such as velocity, pressure, density, and temperature are considered only in the flow direction. The fundamental conservation equations of fluid mechanics are greatly simplified for one-dimensional flows. A broader category of one-dimensional flow is one where there is only one nonzero velocity component, which depends on only one coordinate direction, and this coordinate direction may or may not be the same as the flow direction.

Rate of Deformation Tensor For general three-dimensional flows, where all three velocity components may be important and may vary in all three coordinate directions, the concept of deformation previously introduced must be generalized. The rate of deformation tensor D_{ij} has nine components. In Cartesian coordinates,

$$D_{ij} = \left(\frac{\partial v_i}{\partial x_j} + \frac{\partial v_j}{\partial x_i} \right) \quad (6-6)$$

where the subscripts i and j refer to the three coordinate directions. Some authors define the deformation rate tensor as one-half of that given by Eq. (6-6).

Vorticity The relative motion between two points in a fluid can be decomposed into three components: rotation, dilatation, and deformation. The rate of deformation tensor has been defined. Dilatation refers to the volumetric expansion or compression of the fluid, and vanishes for incompressible flow. Rotation is described by a tensor $\omega_{ij} = \partial v_i / \partial x_j - \partial v_j / \partial x_i$. The vector of vorticity given by one-half the

6-6 FLUID AND PARTICLE DYNAMICS

curl of the velocity vector is another measure of rotation. In two-dimensional flow in the x - y plane, the vorticity ω is given by

$$\omega = \frac{1}{2} \left(\frac{\partial v_y}{\partial x} - \frac{\partial v_x}{\partial y} \right) \quad (6-7)$$

Here ω is the magnitude of the vorticity vector, which is directed along the z axis. An **irrotational** flow is one with zero vorticity. Irrotational flows have been widely studied because of their useful mathematical properties and applicability to flow regions where viscous effects may be neglected. Such flows without viscous effects are called **inviscid** flows.

Laminar and Turbulent Flow, Reynolds Number These terms refer to two distinct types of flow. In *laminar flow*, there are smooth streamlines and the fluid velocity components vary smoothly with position, and with time if the flow is unsteady. The flow described in reference to Fig. 6-1 is laminar. In *turbulent flow*, there are no smooth streamlines, and the velocity shows chaotic fluctuations in time and space. Velocities in turbulent flow may be reported as the sum of a time-averaged velocity and a velocity fluctuation from the average. For any given flow geometry, a dimensionless **Reynolds number** may be defined for a Newtonian fluid as $Re = LU\rho/\mu$ where L is a characteristic length. Below a critical value of Re the flow is laminar, while above the critical value a transition to turbulent flow occurs. The geometry-dependent critical Reynolds number is determined experimentally.

CONSERVATION EQUATIONS

Macroscopic and Microscopic Balances Three postulates, regarded as laws of physics, are fundamental in fluid mechanics. These are *conservation of mass*, *conservation of momentum*, and *conservation of energy*. In addition, two other postulates, *conservation of moment of momentum* (angular momentum) and the *entropy inequality* (second law of thermodynamics) have occasional use. The conservation principles may be applied either to material systems or to control volumes in space. Most often, control volumes are used. The control volumes may be either of finite or differential size, resulting in either **algebraic** or **differential** conservation equations, respectively. These are often called **macroscopic** and **microscopic** balance equations.

Macroscopic Equations An arbitrary control volume of finite size V_a is bounded by a surface of area A_a with an outwardly directed unit normal vector \mathbf{n} . The control volume is not necessarily fixed in space. Its boundary moves with velocity \mathbf{w} . The fluid velocity is \mathbf{v} . Figure 6-3 shows the arbitrary control volume.

Mass Balance Applied to the control volume, the principle of conservation of mass may be written as (Whitaker, *Introduction to Fluid Mechanics*, Prentice-Hall, Englewood Cliffs, N.J., 1968, Krieger, Huntington, N.Y., 1981)

$$\frac{d}{dt} \int_{V_a} \rho dV + \int_{A_a} \rho(\mathbf{v} - \mathbf{w}) \cdot \mathbf{n} dA = 0 \quad (6-8)$$

This equation is also known as the **continuity** equation.

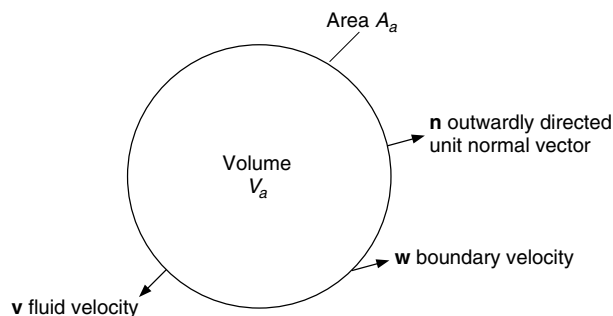


FIG. 6-3 Arbitrary control volume for application of conservation equations.

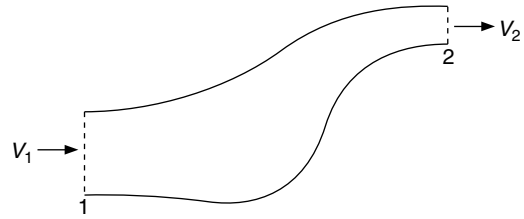


FIG. 6-4 Fixed control volume with one inlet and one outlet.

Simplified forms of Eq. (6-8) apply to special cases frequently found in practice. For a control volume fixed in space with one inlet of area A_1 through which an incompressible fluid enters the control volume at an average velocity V_1 , and one outlet of area A_2 through which fluid leaves at an average velocity V_2 , as shown in Fig. 6-4, the continuity equation becomes

$$V_1 A_1 = V_2 A_2 \quad (6-9)$$

The average velocity across a surface is given by

$$V = (1/A) \int_A v dA$$

where v is the local velocity component perpendicular to the inlet surface. The volumetric flow rate Q is the product of average velocity and the cross-sectional area, $Q = VA$. The average **mass velocity** is $G = \rho V$. For steady flows through fixed control volumes with multiple inlets and/or outlets, conservation of mass requires that the sum of inlet mass flow rates equals the sum of outlet mass flow rates. For incompressible flows through fixed control volumes, the sum of inlet flow rates (mass or volumetric) equals the sum of exit flow rates, whether the flow is steady or unsteady.

Momentum Balance Since momentum is a vector quantity, the momentum balance is a vector equation. Where gravity is the only body force acting on the fluid, the linear momentum principle, applied to the arbitrary control volume of Fig. 6-3, results in the following expression (Whitaker, *ibid.*).

$$\frac{d}{dt} \int_{V_a} \rho \mathbf{v} dV + \int_{A_a} \rho \mathbf{v}(\mathbf{v} - \mathbf{w}) \cdot \mathbf{n} dA = \int_{V_a} \rho \mathbf{g} dV + \int_{A_a} \mathbf{t}_n dA \quad (6-10)$$

Here \mathbf{g} is the gravity vector and \mathbf{t}_n is the force per unit area exerted by the surroundings on the fluid in the control volume. The integrand of the area integral on the left-hand side of Eq. (6-10) is nonzero only on the entrance and exit portions of the control volume boundary. For the special case of steady flow at a mass flow rate \dot{m} through a control volume fixed in space with one inlet and one outlet (Fig. 6-4), with the inlet and outlet velocity vectors perpendicular to planar inlet and outlet surfaces, giving average velocity vectors \mathbf{V}_1 and \mathbf{V}_2 , the momentum equation becomes

$$\dot{m}(\beta_2 \mathbf{V}_2 - \beta_1 \mathbf{V}_1) = -p_1 \mathbf{A}_1 - p_2 \mathbf{A}_2 + \mathbf{F} + M\mathbf{g} \quad (6-11)$$

where M is the total mass of fluid in the control volume. The factor β arises from the averaging of the velocity across the area of the inlet or outlet surface. It is the ratio of the area average of the square of velocity magnitude to the square of the area average velocity magnitude. For a uniform velocity, $\beta = 1$. For turbulent flow, β is nearly unity, while for laminar pipe flow with a parabolic velocity profile, $\beta = 4/3$. The vectors \mathbf{A}_1 and \mathbf{A}_2 have magnitude equal to the areas of the inlet and outlet surfaces, respectively, and are outwardly directed normal to the surfaces. The vector \mathbf{F} is the force exerted on the fluid by the non-flow boundaries of the control volume. It is also assumed that the stress vector \mathbf{t}_n is normal to the inlet and outlet surfaces, and that its magnitude may be approximated by the pressure p . Equation (6-11) may be generalized to multiple inlets and/or outlets. In such cases, the mass flow rates for all the inlets and outlets are not equal. A distinct flow rate \dot{m}_i applies to each inlet or outlet i . To generalize the equation, $-\mathbf{p}\mathbf{A}$ terms for each inlet and outlet, $-\dot{m}\beta\mathbf{V}$ terms for each inlet, and $\dot{m}\beta\mathbf{V}$ terms for each outlet are included.

Balance equations for angular momentum, or moment of momentum, may also be written. They are used less frequently than the linear momentum equations. See Whitaker (*Introduction to Fluid Mechanics*, Prentice-Hall, Englewood Cliffs, N.J., 1968, Krieger, Huntington, N.Y., 1981) or Shames (*Mechanics of Fluids*, 3d ed., McGraw-Hill, New York, 1992).

Total Energy Balance The total energy balance derives from the first law of thermodynamics. Applied to the arbitrary control volume of Fig. 6-3, it leads to an equation for the rate of change of the sum of internal, kinetic, and gravitational potential energy. In this equation, u is the internal energy per unit mass, v is the magnitude of the velocity vector \mathbf{v} , z is elevation, g is the gravitational acceleration, and \mathbf{q} is the heat flux vector:

$$\begin{aligned} \frac{d}{dt} \int_{V_a} \rho \left(u + \frac{v^2}{2} + gz \right) dV + \int_{A_a} \rho \left(u + \frac{v^2}{2} + gz \right) (\mathbf{v} - \mathbf{w}) \cdot \mathbf{n} dA \\ = \int_{A_a} (\mathbf{v} \cdot \mathbf{t}_n) dA - \int_{A_a} (\mathbf{q} \cdot \mathbf{n}) dA \end{aligned} \quad (6-12)$$

The first integral on the right-hand side is the rate of work done on the fluid in the control volume by forces at the boundary. It includes both work done by moving solid boundaries and work done at flow entrances and exits. The work done by moving solid boundaries also includes that by such surfaces as pump impellers; this work is called **shaft work**; its rate is \dot{W}_s .

A useful simplification of the total energy equation applies to a particular set of assumptions. These are a control volume with fixed solid boundaries, except for those producing shaft work, steady state conditions, and mass flow at a rate \dot{m} through a single planar entrance and a single planar exit (Fig. 6-4), to which the velocity vectors are perpendicular. As with Eq. (6-11), it is assumed that the stress vector \mathbf{t}_n is normal to the entrance and exit surfaces and may be approximated by the pressure p . The **equivalent pressure**, $p + \rho gz$, is assumed to be uniform across the entrance and exit. The average velocity at the entrance and exit surfaces is denoted by V . Subscripts 1 and 2 denote the entrance and exit, respectively.

$$h_1 + \alpha_1 \frac{V_1^2}{2} + gz_1 = h_2 + \alpha_2 \frac{V_2^2}{2} + gz_2 - \delta Q - \delta W_s \quad (6-13)$$

Here, h is the enthalpy per unit mass, $h = u + p/\rho$. The shaft work per unit of mass flowing through the control volume is $\delta W_s = \dot{W}_s/\dot{m}$. Similarly, δQ is the heat input per unit of mass. The factor α is the ratio of the cross-sectional area average of the cube of the velocity to the cube of the average velocity. For a uniform velocity profile, $\alpha = 1$. In turbulent flow, α is usually assumed to equal unity; in turbulent pipe flow, it is typically about 1.07. For laminar flow in a circular pipe with a parabolic velocity profile, $\alpha = 2$.

Mechanical Energy Balance, Bernoulli Equation A balance equation for the sum of kinetic and potential energy may be obtained from the momentum balance by forming the scalar product with the velocity vector. The resulting equation, called the *mechanical energy balance*, contains a term accounting for the dissipation of mechanical energy into thermal energy by viscous forces. The mechanical energy equation is also derivable from the total energy equation in a way that reveals the relationship between the dissipation and entropy generation. The macroscopic mechanical energy balance for the arbitrary control volume of Fig. 6-3 may be written, with $p =$ thermodynamic pressure, as

$$\begin{aligned} \frac{d}{dt} \int_{V_a} \rho \left(\frac{v^2}{2} + gz \right) dV + \int_{A_a} \rho \left(\frac{v^2}{2} + gz \right) (\mathbf{v} - \mathbf{w}) \cdot \mathbf{n} dA \\ = \int_{V_a} p \nabla \cdot \mathbf{v} dV + \int_{A_a} (\mathbf{v} \cdot \mathbf{t}_n) dA - \int_{V_a} \Phi dV \end{aligned} \quad (6-14)$$

The last term is the rate of viscous energy dissipation to internal energy, $\dot{E}_v = \int_{V_a} \Phi dV$, also called the rate of viscous losses. These losses are the origin of frictional pressure drop in fluid flow. Whitaker and Bird, Stewart, and Lightfoot provide expressions for the dissipation function Φ for Newtonian fluids in terms of the local velocity gradients. However, when using macroscopic balance equations the local velocity field within the control volume is usually unknown. For such

cases additional information, which may come from empirical correlations, is needed.

For the same special conditions as for Eq. (6-13), the mechanical energy equation is reduced to

$$\alpha_1 \frac{V_1^2}{2} + gz_1 + \delta W_s = \alpha_2 \frac{V_2^2}{2} + gz_2 + \int_{p_1}^{p_2} \frac{dp}{\rho} + l_v \quad (6-15)$$

Here $l_v = \dot{E}_v/\dot{m}$ is the energy dissipation per unit mass. This equation has been called the **engineering Bernoulli equation**. For an incompressible flow, Eq. (6-15) becomes

$$\frac{p_1}{\rho} + \alpha_1 \frac{V_1^2}{2} + gz_1 + \delta W_s = \frac{p_2}{\rho} + \alpha_2 \frac{V_2^2}{2} + gz_2 + l_v \quad (6-16)$$

The Bernoulli equation can be written for incompressible, inviscid flow along a streamline, where no shaft work is done.

$$\frac{p_1}{\rho} + \frac{V_1^2}{2} + gz_1 = \frac{p_2}{\rho} + \frac{V_2^2}{2} + gz_2 \quad (6-17)$$

Unlike the momentum equation (Eq. [6-11]), the Bernoulli equation is not easily generalized to multiple inlets or outlets.

Microscopic Balance Equations Partial differential balance equations express the conservation principles at a point in space. Equations for mass, momentum, total energy, and mechanical energy may be found in Whitaker (ibid.), Bird, Stewart, and Lightfoot (*Transport Phenomena*, Wiley, New York, 1960), and Slattery (*Momentum, Heat and Mass Transfer in Continua*, 2d ed., Krieger, Huntington, N.Y., 1981), for example. These references also present the equations in other useful coordinate systems besides the cartesian system. The coordinate systems are fixed in inertial reference frames. The two most used equations, for mass and momentum, are presented here.

Mass Balance, Continuity Equation The continuity equation, expressing conservation of mass, is written in cartesian coordinates as

$$\frac{\partial \rho}{\partial t} + \frac{\partial \rho v_x}{\partial x} + \frac{\partial \rho v_y}{\partial y} + \frac{\partial \rho v_z}{\partial z} = 0 \quad (6-18)$$

In terms of the **substantial derivative**, D/Dt ,

$$\frac{D\rho}{Dt} \equiv \frac{\partial \rho}{\partial t} + v_x \frac{\partial \rho}{\partial x} + v_y \frac{\partial \rho}{\partial y} + v_z \frac{\partial \rho}{\partial z} = -\rho \left(\frac{\partial v_x}{\partial x} + \frac{\partial v_y}{\partial y} + \frac{\partial v_z}{\partial z} \right) \quad (6-19)$$

The substantial derivative, also called the **material derivative**, is the rate of change in a Lagrangian reference frame, that is, following a material particle. In vector notation the continuity equation may be expressed as

$$\frac{D\rho}{Dt} = -\rho \nabla \cdot \mathbf{v} \quad (6-20)$$

For incompressible flow,

$$\nabla \cdot \mathbf{v} = \frac{\partial v_x}{\partial x} + \frac{\partial v_y}{\partial y} + \frac{\partial v_z}{\partial z} = 0 \quad (6-21)$$

Stress Tensor The stress tensor is needed to completely describe the stress state for microscopic momentum balances in multidimensional flows. The components of the stress tensor σ_{ij} give the force in the j direction on a plane perpendicular to the i direction, using a sign convention defining a positive stress as one where the fluid with the greater i coordinate value exerts a force in the positive i direction on the fluid with the lesser i coordinate. Several references in fluid mechanics and continuum mechanics provide discussions, to various levels of detail, of stress in a fluid (Denn; Bird, Stewart, and Lightfoot; Schlichting; Fung [*A First Course in Continuum Mechanics*, 2d ed., Prentice-Hall, Englewood Cliffs, N.J., 1977]; Truesdell and Toupin [in Flügge, *Handbuch der Physik*, vol. 3/1, Springer-Verlag, Berlin, 1960]; Slattery [*Momentum, Energy and Mass Transfer in Continua*, 2d ed., Krieger, Huntington, N.Y., 1981]).

The stress has an isotropic contribution due to fluid pressure and dilatation, and a **deviatoric** contribution due to viscous deformation effects. The deviatoric contribution for a Newtonian fluid is the three-dimensional generalization of Eq. (6-2):

$$\tau_{ij} = \mu D_{ij} \quad (6-22)$$

6-8 FLUID AND PARTICLE DYNAMICS

The total stress is

$$\sigma_{ij} = (-p + \lambda \nabla \cdot \mathbf{v}) \delta_{ij} + \tau_{ij} \quad (6-23)$$

The identity tensor δ_{ij} is zero for $i \neq j$ and unity for $i = j$. The coefficient λ is a material property related to the **bulk viscosity**, $\kappa = \lambda + 2\mu/3$. There is considerable uncertainty about the value of κ . Traditionally, Stokes' hypothesis, $\kappa = 0$, has been invoked, but the validity of this hypothesis is doubtful (Slattery, *ibid.*). For incompressible flow, the value of bulk viscosity is immaterial as Eq. (6-23) reduces to

$$\sigma_{ij} = -p \delta_{ij} + \tau_{ij} \quad (6-24)$$

Similar generalizations to multidimensional flow are necessary for non-Newtonian constitutive equations.

Cauchy Momentum and Navier-Stokes Equations The differential equations for conservation of momentum are called the **Cauchy momentum equations**. These may be found in general form in most fluid mechanics texts (e.g., Slattery [*ibid.*]; Denn; Whitaker; and Schlichting). For the important special case of an incompressible Newtonian fluid with constant viscosity, substitution of Eqs. (6-22) and (6-24) leads to the **Navier-Stokes equations**, whose three Cartesian components are

$$\begin{aligned} \rho \left(\frac{\partial v_x}{\partial t} + v_x \frac{\partial v_x}{\partial x} + v_y \frac{\partial v_x}{\partial y} + v_z \frac{\partial v_x}{\partial z} \right) \\ = - \frac{\partial p}{\partial x} + \mu \left(\frac{\partial^2 v_x}{\partial x^2} + \frac{\partial^2 v_x}{\partial y^2} + \frac{\partial^2 v_x}{\partial z^2} \right) + \rho g_x \end{aligned} \quad (6-25)$$

$$\begin{aligned} \rho \left(\frac{\partial v_y}{\partial t} + v_x \frac{\partial v_y}{\partial x} + v_y \frac{\partial v_y}{\partial y} + v_z \frac{\partial v_y}{\partial z} \right) \\ = - \frac{\partial p}{\partial y} + \mu \left(\frac{\partial^2 v_y}{\partial x^2} + \frac{\partial^2 v_y}{\partial y^2} + \frac{\partial^2 v_y}{\partial z^2} \right) + \rho g_y \end{aligned} \quad (6-26)$$

$$\begin{aligned} \rho \left(\frac{\partial v_z}{\partial t} + v_x \frac{\partial v_z}{\partial x} + v_y \frac{\partial v_z}{\partial y} + v_z \frac{\partial v_z}{\partial z} \right) \\ = - \frac{\partial p}{\partial z} + \mu \left(\frac{\partial^2 v_z}{\partial x^2} + \frac{\partial^2 v_z}{\partial y^2} + \frac{\partial^2 v_z}{\partial z^2} \right) + \rho g_z \end{aligned} \quad (6-27)$$

In vector notation,

$$\rho \frac{D\mathbf{v}}{Dt} = \frac{\partial \mathbf{v}}{\partial t} + (\mathbf{v} \cdot \nabla) \mathbf{v} = -\nabla p + \mu \nabla^2 \mathbf{v} + \rho \mathbf{g} \quad (6-28)$$

The pressure and gravity terms may be combined by replacing the pressure p by the equivalent pressure $P = p + \rho g z$. The left-hand side terms of the Navier-Stokes equations are the **inertial terms**, while the terms including viscosity μ are the **viscous terms**. Limiting cases under which the Navier-Stokes equations may be simplified include **creeping flows** in which the inertial terms are neglected, **potential flows** (inviscid or irrotational flows) in which the viscous terms are neglected, and **boundary layer** and **lubrication** flows in which certain terms are neglected based on scaling arguments. Creeping flows are described by Happel and Brenner (*Low Reynolds Number Hydrodynamics*, Prentice-Hall, Englewood Cliffs, N.J., 1965); potential flows by Lamb (*Hydrodynamics*, 6th ed., Dover, New York, 1945) and Milne-Thompson (*Theoretical Hydrodynamics*, 5th ed., Macmillan, New York, 1968); boundary layer theory by Schlichting (*Boundary Layer Theory*, 8th ed., McGraw-Hill, New York, 1987); and lubrication theory by Batchelor (*An Introduction to Fluid Dynamics*, Cambridge University, Cambridge, 1967) and Denn (*Process Fluid Mechanics*, Prentice-Hall, Englewood Cliffs, N.J., 1980).

Because the Navier-Stokes equations are first-order in pressure and second-order in velocity, their solution requires one pressure boundary condition and two velocity boundary conditions (for each velocity component) to completely specify the solution. The **no slip** condition, which requires that the fluid velocity equal the velocity of any bounding solid surface, occurs in most problems. Specification of velocity is a type of boundary condition sometimes called a *Dirichlet condition*. Often boundary conditions involve stresses, and thus velocity gradients, rather

than the velocities themselves. Specification of velocity derivatives is a *Neumann boundary condition*. For example, at the boundary between a viscous liquid and a gas, it is often assumed that the liquid shear stresses are zero. In numerical solution of the Navier-Stokes equations, Dirichlet and Neumann, or **essential** and **natural**, boundary conditions may be satisfied by different means.

Fluid statics, discussed in Sec. 10 of the *Handbook* in reference to pressure measurement, is the branch of fluid mechanics in which the fluid velocity is either zero or is uniform and constant relative to an inertial reference frame. With velocity gradients equal to zero, the momentum equation reduces to a simple expression for the pressure field, $\nabla p = \rho \mathbf{g}$. Letting z be directed vertically upward, so that $g_z = -g$ where g is the gravitational acceleration (9.806 m/s²), the pressure field is given by

$$dp/dz = -\rho g \quad (6-29)$$

This equation applies to any incompressible or compressible static fluid. For an incompressible liquid, pressure varies linearly with depth. For compressible gases, p is obtained by integration accounting for the variation of ρ with z .

The **force exerted on a submerged planar surface** of area A is given by $F = p_c A$ where p_c is the pressure at the geometrical **centroid** of the surface. The **center of pressure**, the point of application of the net force, is always lower than the centroid. For details see, for example, Shames, where may also be found discussion of forces on **curved surfaces**, **buoyancy**, and **stability of floating bodies**.

Examples Four examples follow, illustrating the application of the conservation equations to obtain useful information about fluid flows.

Example 1: Force Exerted on a Reducing Bend An incompressible fluid flows through a reducing elbow (Fig. 6-5) situated in a horizontal plane. The inlet velocity V_1 is given and the pressures p_1 and p_2 are measured. Selecting the inlet and outlet surfaces 1 and 2 as shown, the continuity equation Eq. (6-9) can be used to find the exit velocity $V_2 = V_1 A_1 / A_2$. The mass flow rate is obtained by $\dot{m} = \rho V_1 A_1$.

Assume that the velocity profile is nearly uniform so that β is approximately unity. The force exerted on the fluid by the bend has x and y components; these can be found from Eq. (6-11). The x component gives

$$F_x = \dot{m}(V_{2x} - V_{1x}) + p_1 A_{1x} + p_2 A_{2x}$$

while the y component gives

$$F_y = \dot{m}(V_{2y} - V_{1y}) + p_1 A_{1y} + p_2 A_{2y}$$

The velocity components are $V_{1x} = V_1$, $V_{1y} = 0$, $V_{2x} = V_2 \cos \theta$, and $V_{2y} = V_2 \sin \theta$. The area vector components are $A_{1x} = -A_1$, $A_{1y} = 0$, $A_{2x} = A_2 \cos \theta$, and $A_{2y} = A_2 \sin \theta$. Therefore, the force components may be calculated from

$$F_x = \dot{m}(V_2 \cos \theta - V_1) - p_1 A_1 + p_2 A_2 \cos \theta$$

$$F_y = \dot{m} V_2 \sin \theta + p_2 A_2 \sin \theta$$

The force acting on the fluid is \mathbf{F} ; the equal and opposite force exerted by the fluid on the bend is $-\mathbf{F}$.

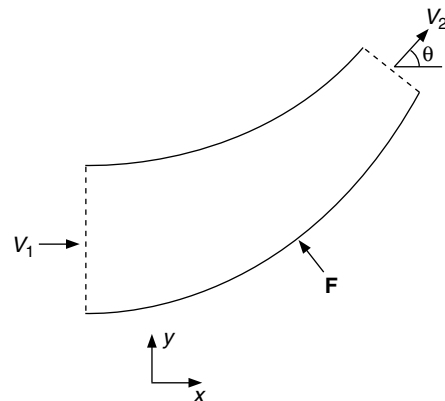


FIG. 6-5 Force at a reducing bend. \mathbf{F} is the force exerted by the bend on the fluid. The force exerted by the fluid on the bend is $-\mathbf{F}$.

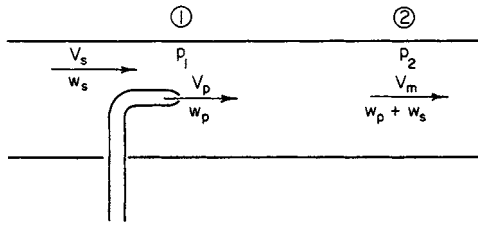


FIG. 6-6 Draft-tube ejector.

Example 2: Simplified Ejector Figure 6-6 shows a very simplified sketch of an ejector, a device that uses a high velocity primary fluid to pump another (secondary) fluid. The continuity and momentum equations may be applied on the control volume with inlet and outlet surfaces 1 and 2 as indicated in the figure. The cross-sectional area is uniform, $A_1 = A_2 = A$. Let the mass flow rates and velocities of the primary and secondary fluids be \dot{m}_p , \dot{m}_s , V_p and V_s . Assume for simplicity that the density is uniform. Conservation of mass gives $\dot{m}_2 = \dot{m}_p + \dot{m}_s$. The exit velocity is $V_2 = \dot{m}_2/(\rho A)$. The principle momentum exchange in the ejector occurs between the two fluids. Relative to this exchange, the force exerted by the walls of the device are found to be small. Therefore, the force term F is neglected from the momentum equation. Written in the flow direction, assuming uniform velocity profiles, and using the extension of Eq. (6-11) for multiple inlets, it gives the pressure rise developed by the device:

$$(p_2 - p_1)A = (\dot{m}_p + \dot{m}_s)V_2 - \dot{m}_p V_p - \dot{m}_s V_s$$

Application of the momentum equation to ejectors of other types is discussed in Lapple (*Fluid and Particle Dynamics*, University of Delaware, Newark, 1951) and in Sec. 10 of the *Handbook*.

Example 3: Venturi Flowmeter An incompressible fluid flows through the venturi flowmeter in Fig. 6-7. An equation is needed to relate the flow rate Q to the pressure drop measured by the manometer. This problem can be solved using the mechanical energy balance. In a well-made venturi, viscous losses are negligible, the pressure drop is entirely the result of acceleration into the throat, and the flow rate predicted neglecting losses is quite accurate. The inlet area is A and the throat area is a .

With control surfaces at 1 and 2 as shown in the figure, Eq. (6-17) in the absence of losses and shaft work gives

$$\frac{p_1}{\rho} + \frac{V_1^2}{2} = \frac{p_2}{\rho} + \frac{V_2^2}{2}$$

The continuity equation gives $V_2 = V_1 A/a$, and $V_1 = Q/A$. The pressure drop measured by the manometer is $p_1 - p_2 = (\rho_m - \rho)g\Delta z$. Substituting these relations into the energy balance and rearranging, the desired expression for the flow rate is found.

$$Q = \frac{1}{A} \sqrt{\frac{2(\rho_m - \rho)g\Delta z}{\rho[(A/a)^2 - 1]}}$$

Example 4: Plane Poiseuille Flow An incompressible Newtonian fluid flows at a steady rate in the x direction between two very large flat plates, as shown in Fig. 6-8. The flow is laminar. The velocity profile is to be found. This example is found in most fluid mechanics textbooks; the solution presented here closely follows Denn.

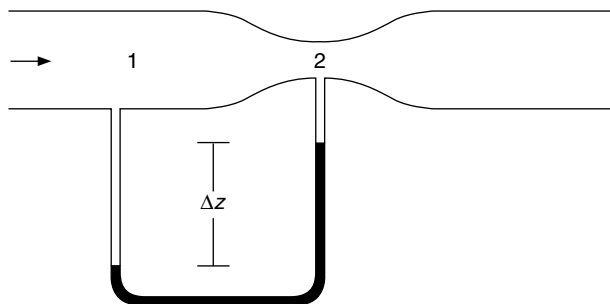


FIG. 6-7 Venturi flowmeter.

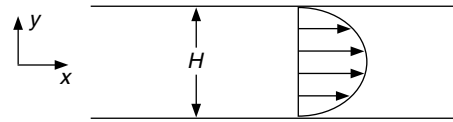


FIG. 6-8 Plane Poiseuille flow.

This problem requires use of the microscopic balance equations because the velocity is to be determined as a function of position. The boundary conditions for this flow result from the no-slip condition. All three velocity components must be zero at the plate surfaces, $y = H/2$ and $y = -H/2$.

Assume that the flow is **fully developed**, that is, all velocity derivatives vanish in the x direction. Since the flow field is infinite in the z direction, all velocity derivatives should be zero in the z direction. Therefore, velocity components are a function of y alone. It is also assumed that there is no flow in the z direction, so $v_z = 0$. The continuity equation Eq. (6-21), with $v_z = 0$ and $\partial v_x/\partial x = 0$, reduces to

$$\frac{dv_y}{dy} = 0$$

Since $v_y = 0$ at $y = \pm H/2$, the continuity equation integrates to $v_y = 0$. This is a direct result of the assumption of fully developed flow.

The Navier-Stokes equations are greatly simplified when it is noted that $v_y = v_z = 0$ and $\partial v_x/\partial x = \partial v_x/\partial z = \partial v_x/\partial t = 0$. The three components are written in terms of the equivalent pressure P :

$$0 = -\frac{\partial P}{\partial x} + \mu \frac{\partial^2 v_x}{\partial y^2}$$

$$0 = -\frac{\partial P}{\partial y}$$

$$0 = -\frac{\partial P}{\partial z}$$

The latter two equations require that P is a function only of x , and therefore $\partial P/\partial x = dP/dx$. Inspection of the first equation shows one term which is a function only of x and one which is only a function of y . This requires that both terms are constant. The pressure gradient $-dP/dx$ is constant. The x -component equation becomes

$$\frac{d^2 v_x}{dy^2} = \frac{1}{\mu} \frac{dP}{dx}$$

Two integrations of the x -component equation give

$$v_x = \frac{1}{2\mu} \frac{dP}{dx} y^2 + C_1 y + C_2$$

where the constants of integration C_1 and C_2 are evaluated from the boundary conditions $v_x = 0$ at $y = \pm H/2$. The result is

$$v_x = \frac{H^2}{8\mu} \left(-\frac{dP}{dx} \right) \left[1 - \left(\frac{2y}{H} \right)^2 \right]$$

This is a **parabolic** velocity distribution. The average velocity $V = (1/H) \int_{-H/2}^{H/2} v_x dy$ is

$$V = \frac{H^2}{12\mu} \left(-\frac{dP}{dx} \right)$$

This flow is one-dimensional, as there is only one nonzero velocity component, v_x , which, along with the pressure, varies in only one coordinate direction.

INCOMPRESSIBLE FLOW IN PIPES AND CHANNELS

Mechanical Energy Balance The mechanical energy balance, Eq. (6-16), for **fully developed** incompressible flow in a straight circular pipe of constant diameter D reduces to

$$\frac{p_1}{\rho} + gz_1 = \frac{p_2}{\rho} + gz_2 + l_v \tag{6-30}$$

In terms of the equivalent pressure, $P \equiv p + \rho gz$,

$$P_1 - P_2 = \rho l_v \tag{6-31}$$

The pressure drop due to frictional losses l_v is proportional to pipe length L for fully developed flow and may be denoted as the (positive) quantity $\Delta P \equiv P_1 - P_2$.

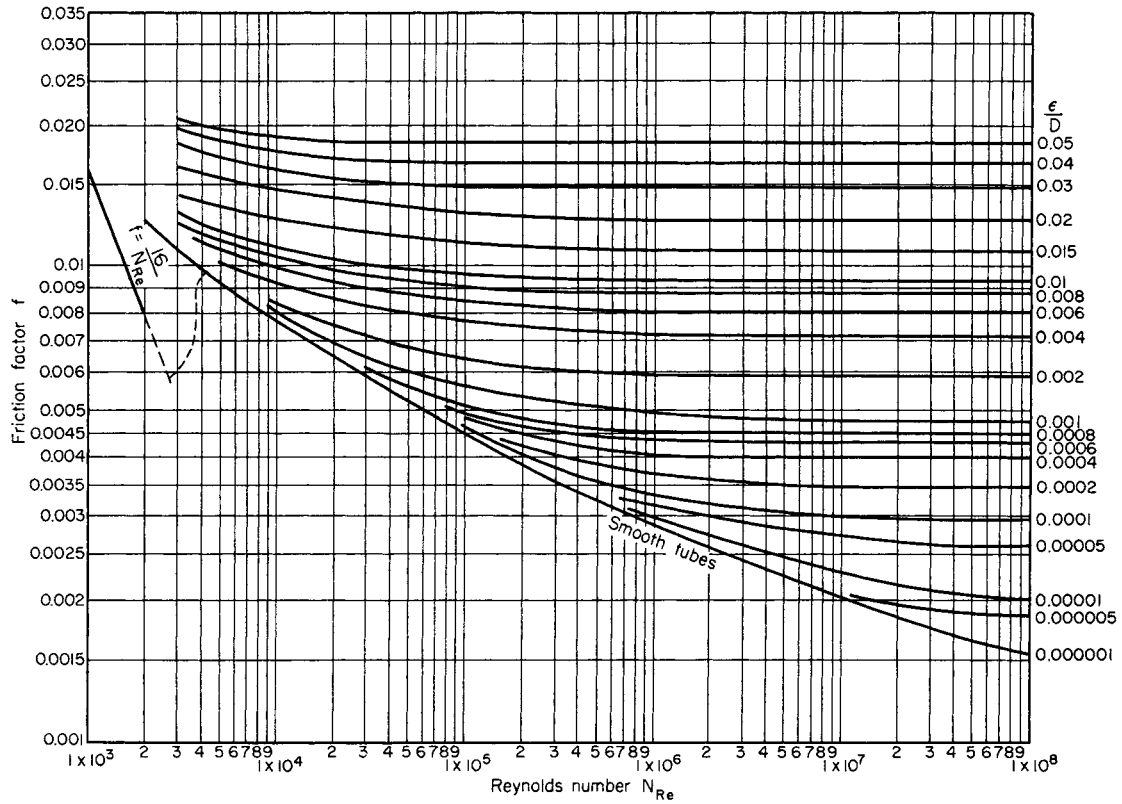


FIG. 6-9 Fanning Friction Factors. Reynolds number $Re = DV\rho/\mu$, where D = pipe diameter, V = velocity, ρ = fluid density, and μ = fluid viscosity. (Based on Moody, *Trans. ASME*, **66**, 671 [1944].)

Friction Factor and Reynolds Number For a Newtonian fluid in a smooth pipe, dimensional analysis relates the frictional pressure drop per unit length $\Delta P/L$ to the pipe diameter D , density ρ , viscosity μ , and average velocity V through two dimensionless groups, the **Fanning friction factor** f and the **Reynolds number** Re .

$$f \equiv \frac{D\Delta P}{2\rho V^2 L} \tag{6-32}$$

$$Re \equiv \frac{DV\rho}{\mu} \tag{6-33}$$

For smooth pipe, the friction factor is a function only of the Reynolds number. In rough pipe, the relative roughness ϵ/D also affects the friction factor. Figure 6-9 plots f as a function of Re and ϵ/D . Values of ϵ for various materials are given in Table 6-1. The Fanning friction factor should not be confused with the Darcy friction factor used by Moody (*Trans. ASME*, **66**, 671 [1944]), which is four times greater. Using the momentum equation, the stress at the wall of the pipe may be expressed in terms of the friction factor:

$$\tau_w = f \frac{\rho V^2}{2} \tag{6-34}$$

Laminar and Turbulent Flow Below a **critical Reynolds number** of about 2,100, the flow is laminar; over the range $2,100 < Re < 5,000$ there is a transition to turbulent flow. Reliable correlations for the friction factor in transitional flow are not available. For laminar flow, the Hagen-Poiseuille equation

$$f = \frac{16}{Re} \quad Re \leq 2,100 \tag{6-35}$$

TABLE 6-1 Values of Surface Roughness for Various Materials*

Material	Surface roughness ϵ , mm
Drawn tubing (brass, lead, glass, and the like)	0.00152
Commercial steel or wrought iron	0.0457
Asphalted cast iron	0.122
Galvanized iron	0.152
Cast iron	0.259
Wood stove	0.183–0.914
Concrete	0.305–3.05
Riveted steel	0.914–9.14

* From Moody, *Trans. Am. Soc. Mech. Eng.*, **66**, 671–684 (1944); *Mech. Eng.*, **69**, 1005–1006 (1947). Additional values of ϵ for various types or conditions of concrete wrought-iron, welded steel, riveted steel, and corrugated-metal pipes are given in Brater and King, *Handbook of Hydraulics*, 6th ed., McGraw-Hill, New York, 1976, pp. 6-12–6-13. To convert millimeters to feet, multiply by 3.281×10^{-3} .

may be derived from the Navier-Stokes equation and is in excellent agreement with experimental data. It may be rewritten in terms of volumetric flow rate, $Q = V\pi D^2/4$, as

$$Q = \frac{\pi\Delta P D^4}{128\mu L} \quad Re \leq 2,100 \tag{6-36}$$

For turbulent flow in smooth tubes, the Blasius equation gives the friction factor accurately for a wide range of Reynolds numbers.

$$f = \frac{0.079}{Re^{0.25}} \quad 4,000 < Re < 10^5 \tag{6-37}$$

The Colebrook formula (Colebrook, *J. Inst. Civ. Eng. [London]*, **11**, 133–156 [1938–39]) gives a good approximation for the f - Re - (ϵ/D) data for rough pipes over the entire turbulent flow range:

$$\frac{1}{\sqrt{f}} = -4 \log \left[\frac{\epsilon}{3.7D} + \frac{1.256}{Re\sqrt{f}} \right] \quad Re > 4,000 \quad (6-38)$$

Equation (6-38) was used to construct the curves in the turbulent flow regime in Fig. 6-9.

An equation by Churchill (*Chem. Eng.*, **84**[24], 91–92 [Nov. 7, 1977]) approximating the Colebrook formula offers the advantage of being explicit in f :

$$\frac{1}{\sqrt{f}} = -4 \log \left[\frac{0.27\epsilon}{D} + \left(\frac{7}{Re} \right)^{0.9} \right] \quad Re > 4,000 \quad (6-39)$$

Churchill also provided a single equation that may be used for Reynolds numbers in laminar, transitional, and turbulent flow, closely fitting $f = 16/Re$ in the laminar regime, and the Colebrook formula, Eq. (6-38), in the turbulent regime. It also gives unique, reasonable values in the transition regime, where the friction factor is uncertain.

$$f = 2 \left[\left(\frac{8}{Re} \right)^{12} + \frac{1}{(A+B)^{32}} \right]^{1/12} \quad (6-40)$$

where

$$A = \left[2.457 \ln \frac{1}{(7/Re)^{0.9} + 0.27\epsilon/D} \right]^{16}$$

and

$$B = \left(\frac{37,530}{Re} \right)^{16}$$

In laminar flow, f is independent of ϵ/D . In turbulent flow, the friction factor for rough pipe follows the smooth tube curve for a range of Reynolds numbers (hydraulically smooth flow). For greater Reynolds numbers, f deviates from the smooth pipe curve, eventually becoming independent of Re . This region, often called *complete turbulence*, is frequently encountered in commercial pipe flows.

Two common pipe flow problems are calculation of pressure drop given the flow rate (or velocity) and calculation of flow rate (or velocity) given the pressure drop. When flow rate is given, the Reynolds number may be calculated directly to determine the flow regime, so that the appropriate relations between f and Re (or pressure drop and flow rate or velocity) can be selected. When flow rate is specified and the flow is turbulent, Eq. (6-39) or (6-40), being explicit in f , may be preferable to Eq. (6-38), which is implicit in f and pressure drop.

When the pressure drop is given and the velocity and flow rate are to be determined, the Reynolds number cannot be computed directly, since the velocity is unknown. Instead of guessing and checking the flow regime, it may be useful to observe that the quantity $Re\sqrt{f} = (D^{3/2}/\mu) \sqrt{\rho \Delta P / (2L)}$, appearing in the Colebrook equation (6-38), does not include velocity and so can be computed directly. The upper limit $Re = 2,100$ for laminar flow and use of Eq. (6-35) corresponds to $Re\sqrt{f} = 183$. For smooth pipe, the lower limit $Re = 4,000$ for the Colebrook equation corresponds to $Re\sqrt{f} = 400$. Thus, at least for smooth pipes, the flow regime can be determined without trial and error from $\Delta P/L$, μ , ρ , and D . When pressure drop is given, Eq. (6-38), being explicit in velocity, is preferable to Eqs. (6-39) and (6-40), which are implicit in velocity.

As Fig. 6-9 suggests, the friction factor is uncertain in the transition range, and a conservative choice should be made for design purposes.

Velocity Profiles In laminar flow, the solution of the Navier-Stokes equation, corresponding to the Hagen-Poiseuille equation, gives the velocity v as a function of radial position r in a circular pipe of radius R in terms of the average velocity $V = Q/A$. The **parabolic** profile, with centerline velocity twice the average velocity, is shown in Fig. 6-10.

$$v = 2V \left(1 - \frac{r^2}{R^2} \right) \quad (6-41)$$

In turbulent flow, the velocity profile is much more blunt, with most of the velocity gradient being in a region near the wall, described by a **universal** velocity profile. It is characterized by a **viscous sublayer**, a **turbulent core**, and a **buffer zone** in between.

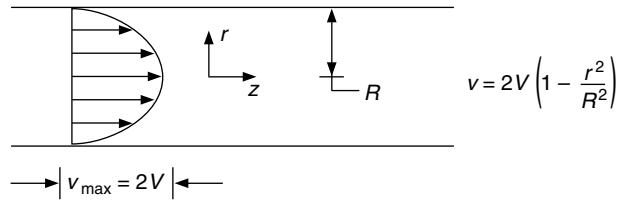


FIG. 6-10 Parabolic velocity profile for laminar flow in a pipe, with average velocity V .

Viscous sublayer

$$u_+ = y_+ \quad \text{for} \quad y_+ < 5 \quad (6-42)$$

Buffer zone

$$u_+ = 5.00 \ln y_+ - 3.05 \quad \text{for} \quad 5 < y_+ < 30 \quad (6-43)$$

Turbulent core

$$u_+ = 2.5 \ln y_+ + 5.5 \quad \text{for} \quad y_+ > 30 \quad (6-44)$$

Here, $u_+ = v/u_\tau$ is the dimensionless, time-averaged axial velocity, $u_\tau = \sqrt{\tau_w/\rho}$ is the **friction velocity** and $\tau_w = f\rho V^2/2$ is the wall stress. The friction velocity is of the order of the root mean square velocity fluctuation perpendicular to the wall in the turbulent core. The dimensionless distance from the wall is $y_+ = y u_\tau \rho / \mu$. The universal velocity profile is valid in the wall region for any cross-sectional channel shape. For incompressible flow in constant diameter circular pipes, $\tau_w = D\Delta P/4L$ where ΔP is the pressure drop in length L . In circular pipes, Eq. (6-44) gives a surprisingly good fit to experimental results over the entire cross section of the pipe, even though it is based on assumptions which are valid only near the pipe wall.

For rough pipes, the velocity profile in the turbulent core is given by

$$u_+ = 2.5 \ln y/\epsilon + 8.5 \quad \text{for} \quad y_+ > 30 \quad (6-45)$$

when the dimensionless roughness $\epsilon_+ = \epsilon u_\tau \rho / \mu$ is greater than 5 to 10; for smaller ϵ_+ , the velocity profile in the turbulent core is unaffected by roughness.

For velocity profiles in the transition region, see Patel and Head (*J. Fluid Mech.*, **38**, part 1, 181–201 [1969]) where profiles over the range $1,500 < Re < 10,000$ are reported.

Entrance and Exit Effects In the entrance region of a pipe, some distance is required for the flow to adjust from upstream conditions to the fully developed flow pattern. This distance depends on the Reynolds number and on the flow conditions upstream. For a uniform velocity profile at the pipe entrance, the computed length in laminar flow required for the centerline velocity to reach 99 percent of its fully developed value is (Dombrowski, Fomeny, Ookawara, and Riza, *Can. J. Chem. Engr.*, **71**, 472–476 [1993])

$$L_{\text{ent}}/D = 0.370 \exp(-0.148Re) + 0.0550Re + 0.260 \quad (6-46)$$

In turbulent flow, the entrance length is about

$$L_{\text{ent}}/D = 40 \quad (6-47)$$

The frictional losses in the entrance region are larger than those for the same length of fully developed flow. (See the subsection, “Frictional Losses in Pipeline Elements,” following.) At the pipe exit, the velocity profile also undergoes rearrangement, but the exit length is much shorter than the entrance length. At low Re , it is about one pipe radius. At $Re > 100$, the exit length is essentially 0.

Residence Time Distribution For laminar Newtonian pipe flow, the cumulative residence time distribution $F(\theta)$ is given by

$$F(\theta) = 0 \quad \text{for} \quad \theta < \frac{\theta_{\text{avg}}}{2}$$

$$F(\theta) = 1 - \frac{1}{4} \left(\frac{\theta_{\text{avg}}}{\theta} \right)^2 \quad \text{for} \quad \theta \geq \frac{\theta_{\text{avg}}}{2} \quad (6-48)$$

where $F(\theta)$ is the fraction of material which resides in the pipe for less than time θ and θ_{avg} is the average residence time, $\theta = V/L$.

The residence time distribution in long transfer lines may be made narrower (more uniform) with the use of **flow inverters** or **static mixing elements**. These devices exchange fluid between the wall and central regions. Variations on the concept may be used to provide effective mixing of the fluid. See Godfrey ("Static Mixers," in Harnby, Edwards, and Nienow, *Mixing in the Process Industries*, 2d ed., Butterworth Heinemann, Oxford, 1992); Etchells and Meyer ("Mixing in Pipelines," in Paul, Atiemo-Obeng, and Kresta, *Handbook of Industrial Mixing*, Wiley Interscience, Hoboken, N.J., 2004).

A theoretically derived equation for laminar flow in helical pipe coils by Ruthven (*Chem. Eng. Sci.*, **26**, 1113–1121 [1971]; **33**, 628–629 [1978]) is given by

$$F(\theta) = 1 - \left(\frac{1}{4}\right) \left[\frac{\theta_{\text{avg}}}{\theta}\right]^{2.51} \quad \text{for} \quad 0.5 < \frac{\theta_{\text{avg}}}{\theta} < 1.63 \quad (6-49)$$

and was substantially confirmed by Trivedi and Vasudeva (*Chem. Eng. Sci.*, **29**, 2291–2295 [1974]) for $0.6 < \text{De} < 6$ and $0.0036 < D/D_c < 0.097$ where $\text{De} = \text{Re}\sqrt{D/D_c}$ is the Dean number and D_c is the diameter of curvature of the coil. Measurements by Saxena and Nigam (*Chem. Eng. Sci.*, **34**, 425–426 [1979]) indicate that such a distribution will hold for $\text{De} > 1$. The residence time distribution for helical coils is narrower than for straight circular pipes, due to the secondary flow which exchanges fluid between the wall and center regions.

In turbulent flow, axial mixing is usually described in terms of turbulent diffusion or dispersion coefficients, from which cumulative residence time distribution functions can be computed. Davies (*Turbulence Phenomena*, Academic, New York, 1972, p. 93) gives $D_L = 1.01\text{vRe}^{0.875}$ for the longitudinal dispersion coefficient. Levenspiel (*Chemical Reaction Engineering*, 2d ed., Wiley, New York, 1972, pp. 253–278) discusses the relations among various residence time distribution functions, and the relation between dispersion coefficient and residence time distribution.

Noncircular Channels Calculation of frictional pressure drop in noncircular channels depends on whether the flow is laminar or turbulent, and on whether the channel is full or open. For **turbulent flow in ducts running full**, the **hydraulic diameter** D_H should be substituted for D in the friction factor and Reynolds number definitions, Eqs. (6-32) and (6-33). The hydraulic diameter is defined as **four times the channel cross-sectional area divided by the wetted perimeter**. For example, the hydraulic diameter for a circular pipe is $D_H = D$, for an annulus of inner diameter d and outer diameter D , $D_H = D - d$, for a rectangular duct of sides a, b , $D_H = ab/[2(a + b)]$. The **hydraulic radius** R_H is defined as **one-fourth** of the hydraulic diameter.

With the hydraulic diameter substituted for D in f and Re , Eqs. (6-37) through (6-40) are good approximations. Note that V appearing in f and Re is the actual average velocity $V = Q/A$; for noncircular pipes; it is **not** $Q/(\pi D_H^2/4)$. The pressure drop should be calculated from the friction factor for noncircular pipes. Equations relating Q to ΔP and D for circular pipes **may not be used** for noncircular pipes with D replaced by D_H because $V \neq Q/(\pi D_H^2/4)$.

Turbulent flow in noncircular channels is generally accompanied by secondary flows perpendicular to the axial flow direction (Schlichting). These flows may cause the pressure drop to be slightly greater than that computed using the hydraulic diameter method. For data on pressure drop in annuli, see Brighton and Jones (*J. Basic Eng.*, **86**, 835–842 [1964]); Okiishi and Serovy (*J. Basic Eng.*, **89**, 823–836 [1967]); and Lawn and Elliot (*J. Mech. Eng. Sci.*, **14**, 195–204 [1972]). For rectangular ducts of large aspect ratio, Dean (*J. Fluids Eng.*, **100**, 215–233 [1978]) found that the numerator of the exponent in the Blasius equation (6-37) should be increased to 0.0868. Jones (*J. Fluids Eng.*, **98**, 173–181 [1976]) presents a method to improve the estimation of friction factors for rectangular ducts using a modification of the hydraulic diameter-based Reynolds number.

The hydraulic diameter method does not work well for **laminar flow** because the shape affects the flow resistance in a way that cannot be expressed as a function only of the ratio of cross-sectional area to wetted perimeter. For some shapes, the Navier-Stokes equations have been integrated to yield relations between flow rate and pressure drop. These relations may be expressed in terms of **equivalent diameters** D_E defined to make the relations reduce to the second form of the Hagen-Poiseuille equation, Eq. (6-36); that is, $D_E \equiv$

$(128Q\mu L/\pi\Delta P)^{1/4}$. **Equivalent diameters are not the same as hydraulic diameters**. Equivalent diameters yield the correct relation between flow rate and pressure drop when substituted into Eq. (6-36), but not Eq. (6-35) because $V \neq Q/(\pi D_E/4)$. Equivalent diameter D_E is not to be used in the friction factor and Reynolds number; $f \neq 16/\text{Re}$ using the equivalent diameters defined in the following. This situation is, by arbitrary definition, opposite to that for the hydraulic diameter D_H used for turbulent flow.

Ellipse, semiaxes a and b (Lamb, *Hydrodynamics*, 6th ed., Dover, New York, 1945, p. 587):

$$D_E = \left(\frac{32a^3b^3}{a^2 + b^2}\right)^{1/4} \quad (6-50)$$

Rectangle, width a , height b (Owen, *Trans. Am. Soc. Civ. Eng.*, **119**, 1157–1175 [1954]):

$$D_E = \left(\frac{128ab^3}{\pi K}\right)^{1/4} \quad (6-51)$$

$a/b =$	1	1.5	2	3	4	5	10	∞
$K =$	28.45	20.43	17.49	15.19	14.24	13.73	12.81	12

Annulus, inner diameter D_1 , outer diameter D_2 (Lamb, op. cit., p. 587):

$$D_E = \left\{ (D_2^2 - D_1^2) \left[D_2^3 + D_1^3 - \frac{D_2^2 - D_1^2}{\ln(D_2/D_1)} \right] \right\}^{1/4} \quad (6-52)$$

For isosceles triangles and regular polygons, see Sparrow (*AIChE J.*, **8**, 599–605 [1962]), Carlson and Irvine (*J. Heat Transfer*, **83**, 441–444 [1961]), Cheng (*Proc. Third Int. Heat Transfer Conf.*, New York, **1**, 64–76 [1966]), and Shih (*Can. J. Chem. Eng.*, **45**, 285–294 [1967]).

The critical Reynolds number for **transition from laminar to turbulent flow** in noncircular channels varies with channel shape. In rectangular ducts, $1,900 < \text{Re}_c < 2,800$ (Hanks and Ruo, *Ind. Eng. Chem. Fundam.*, **5**, 558–561 [1966]). In triangular ducts, $1,600 < \text{Re}_c < 1,800$ (Cope and Hanks, *Ind. Eng. Chem. Fundam.*, **11**, 106–117 [1972]; Bandopadhyay and Hinwood, *J. Fluid Mech.*, **59**, 775–783 [1973]).

Nonisothermal Flow For nonisothermal flow of **liquids**, the friction factor may be increased if the liquid is being cooled or decreased if the liquid is being heated, because of the effect of temperature on viscosity near the wall. In shell and tube heat-exchanger design, the recommended practice is to first estimate f using the bulk mean liquid temperature over the tube length. Then, in laminar flow, the result is divided by $(\mu_w/\mu_c)^{0.23}$ in the case of cooling or $(\mu_w/\mu_c)^{0.38}$ in the case of heating. For turbulent flow, f is divided by $(\mu_w/\mu_c)^{0.11}$ in the case of cooling or $(\mu_w/\mu_c)^{0.17}$ in case of heating. Here, μ_w is the viscosity at the average bulk temperature and μ_c is the viscosity at the average wall temperature (Seider and Tate, *Ind. Eng. Chem.*, **28**, 1429–1435 [1936]). In the case of rough commercial pipes, rather than heat-exchanger tubing, it is common for flow to be in the "complete" turbulence regime where f is independent of Re . In such cases, the friction factor should not be corrected for wall temperature. If the liquid density varies with temperature, the average bulk density should be used to calculate the pressure drop from the friction factor. In addition, a (usually small) correction may be applied for acceleration effects by adding the term $G^2[(1/\rho_2) - (1/\rho_1)]$ from the mechanical energy balance to the pressure drop $\Delta P = P_1 - P_2$, where G is the mass velocity. This acceleration results from small compressibility effects associated with temperature-dependent density. Christiansen and Gordon (*AIChE J.*, **15**, 504–507 [1969]) present equations and charts for frictional loss in laminar nonisothermal flow of Newtonian and non-Newtonian liquids heated or cooled with constant wall temperature.

Frictional dissipation of mechanical energy can result in significant heating of fluids, particularly for very viscous liquids in small channels. Under adiabatic conditions, the bulk liquid temperature rise is given by $\Delta T = \Delta P/C_p \rho$ for incompressible flow through a channel of constant cross-sectional area. For flow of polymers, this amounts to about 4°C per 10 MPa pressure drop, while for hydrocarbon liquids it is about

6°C per 10 MPa. The temperature rise in laminar flow is highly nonuniform, being concentrated near the pipe wall where most of the dissipation occurs. This may result in significant viscosity reduction near the wall, and greatly increased flow or reduced pressure drop, and a flattened velocity profile. Compensation should generally be made for the heat effect when ΔP exceeds 1.4 MPa (203 psi) for adiabatic walls or 3.5 MPa (508 psi) for isothermal walls (Gerard, Steidler, and Appeldoorn, *Ind. Eng. Chem. Fundam.*, **4**, 332–339 [1969]).

Open Channel Flow For flow in **open channels**, the data are largely based on experiments with water in turbulent flow, in channels of sufficient roughness that there is no Reynolds number effect. The hydraulic radius approach may be used to estimate a friction factor with which to compute friction losses. Under conditions of **uniform flow** where liquid depth and cross-sectional area do not vary significantly with position in the flow direction, there is a balance between gravitational forces and wall stress, or equivalently between frictional losses and potential energy change. The mechanical energy balance reduces to $l_v = g(z_1 - z_2)$. In terms of the friction factor and hydraulic diameter or hydraulic radius,

$$l_v = \frac{2fV^2L}{D_H} = \frac{fV^2L}{2R_H} = g(z_1 - z_2) \quad (6-53)$$

The hydraulic radius is the cross-sectional area divided by the wetted perimeter, where the wetted perimeter *does not include the free surface*. Letting $S = \sin \theta =$ channel slope (elevation loss per unit length of channel, $\theta =$ angle between channel and horizontal), Eq. (6-53) reduces to

$$V = \sqrt{\frac{2gSR_H}{f}} \quad (6-54)$$

The most often used friction correlation for open channel flows is due to Manning (*Trans. Inst. Civ. Engrs. Ireland*, **20**, 161 [1891]) and is equivalent to

$$f = \frac{29n^2}{R_H^{1/3}} \quad (6-55)$$

where n is the channel roughness, with dimensions of (length)^{1/6}. Table 6-2 gives roughness values for several channel types.

For gradual changes in channel cross section and liquid depth, and for slopes less than 10°, the momentum equation for a rectangular channel of width b and liquid depth h may be written as a differential equation in the flow direction x .

$$\frac{dh}{dx} (1 - Fr) - Fr \left(\frac{h}{b} \right) \frac{db}{dx} = S - \frac{fV^2(b + 2h)}{2gbh} \quad (6-56)$$

For a given fixed flow rate $Q = Vbh$, and channel width profile $b(x)$, Eq. (6-56) may be integrated to determine the liquid depth profile

TABLE 6-2 Average Values of n for Manning Formula, Eq. (6-55)

Surface	n , m ^{1/6}	n , ft ^{1/6}
Cast-iron pipe, fair condition	0.014	0.011
Riveted steel pipe	0.017	0.014
Vitrified sewer pipe	0.013	0.011
Concrete pipe	0.015	0.012
Wood-stave pipe	0.012	0.010
Planed-plank flume	0.012	0.010
Semicircular metal flumes, smooth	0.013	0.011
Semicircular metal flumes, corrugated	0.028	0.023
Canals and ditches		
Earth, straight and uniform	0.023	0.019
Winding sluggish canals	0.025	0.021
Dredged earth channels	0.028	0.023
Natural-stream channels		
Clean, straight bank, full stage	0.030	0.025
Winding, some pools and shoals	0.040	0.033
Same, but with stony sections	0.055	0.045
Sluggish reaches, very deep pools, rather weedy	0.070	0.057

SOURCE: Brater and King, *Handbook of Hydraulics*, 6th ed., McGraw-Hill, New York, 1976, p. 7-22. For detailed information, see Chow, *Open-Channel Hydraulics*, McGraw-Hill, New York, 1959, pp. 110–123.

$h(x)$. The dimensionless Froude number is $Fr = V^2/gh$. When $Fr = 1$, the flow is **critical**, when $Fr < 1$, the flow is **subcritical**, and when $Fr > 1$, the flow is **supercritical**. Surface disturbances move at a wave velocity $c = \sqrt{gh}$; they cannot propagate upstream in supercritical flows. The **specific energy** E_{sp} is nearly constant.

$$E_{sp} = h + \frac{V^2}{2g} \quad (6-57)$$

This equation is cubic in liquid depth. Below a minimum value of E_{sp} there are no real positive roots; above the minimum value there are two positive real roots. At this minimum value of E_{sp} the flow is critical; that is, $Fr = 1$, $V = \sqrt{gh}$, and $E_{sp} = (3/2)h$. Near critical flow conditions, wave motion and sudden depth changes called **hydraulic jumps** are likely. Chow (*Open Channel Hydraulics*, McGraw-Hill, New York, 1959) discusses the numerous surface profile shapes which may exist in nonuniform open channel flows.

For flow over a sharp-crested weir of width b and height L , from a liquid depth H , the flow rate is given approximately by

$$Q = \frac{2}{3} C_d b \sqrt{2g} (H - L)^{3/2} \quad (6-58)$$

where $C_d \approx 0.6$ is a discharge coefficient. Flow through notched weirs is described under flow meters in Sec. 10 of the *Handbook*.

Non-Newtonian Flow For **isothermal laminar flow** of time-independent non-Newtonian liquids, integration of the Cauchy momentum equations yields the fully developed velocity profile and flow rate–pressure drop relations. For the **Bingham plastic** fluid described by Eq. (6-3), in a pipe of diameter D and a pressure drop per unit length $\Delta P/L$, the flow rate is given by

$$Q = \frac{\pi D^3 \tau_w}{32\mu_\infty} \left[1 - \frac{4\tau_y}{3\tau_w} + \frac{\tau_y^4}{3\tau_w^4} \right] \quad (6-59)$$

where the wall stress is $\tau_w = D\Delta P/(4L)$. The velocity profile consists of a central nondeforming plug of radius $r_p = 2\tau_y/(\Delta P/L)$ and an annular deforming region. The velocity profile in the annular region is given by

$$v_z = \frac{1}{\mu_\infty} \left[\frac{\Delta P}{4L} (R^2 - r^2) - \tau_y (R - r) \right] \quad r_p \leq r \leq R \quad (6-60)$$

where r is the radial coordinate and R is the pipe radius. The velocity of the central, nondeforming plug is obtained by setting $r = r_p$ in Eq. (6-60). When Q is given and Eq. (6-59) is to be solved for τ_w and the pressure drop, multiple positive roots for the pressure drop may be found. The root corresponding to $\tau_w < \tau_y$ is physically unrealizable, as it corresponds to $r_p > R$ and the pressure drop is insufficient to overcome the yield stress.

For a **power law fluid**, Eq. (6-4), with constant properties K and n , the flow rate is given by

$$Q = \pi \left(\frac{\Delta P}{2KL} \right)^{1/n} \left(\frac{n}{1 + 3n} \right) R^{(1 + 3n)/n} \quad (6-61)$$

and the velocity profile by

$$v_z = \left(\frac{\Delta P}{2KL} \right)^{1/n} \left(\frac{n}{1 + n} \right) [R^{(1 + n)/n} - r^{(1 + n)/n}] \quad (6-62)$$

Similar relations for other non-Newtonian fluids may be found in Govier and Aziz and in Bird, Armstrong, and Hassager (*Dynamics of Polymeric Liquids*, vol. 1: *Fluid Mechanics*, Wiley, New York, 1977).

For steady-state laminar flow of any time-independent viscous fluid, at average velocity V in a pipe of diameter D , the Rabinowitsch-Mooney relations give a general relationship for the shear rate at the pipe wall.

$$\dot{\gamma}_w = \frac{8V}{D} \left(\frac{1 + 3n'}{4n'} \right) \quad (6-63)$$

where n' is the slope of a plot of $D\Delta P/(4L)$ versus $8V/D$ on logarithmic coordinates,

$$n' = \frac{d \ln [D\Delta P/(4L)]}{d \ln (8V/D)} \quad (6-64)$$

By plotting capillary viscometry data this way, they can be used directly for pressure drop design calculations, or to construct the rheogram for the fluid. For pressure drop calculation, the flow rate and diameter determine the velocity, from which SV/D is calculated and $D\Delta P/(4L)$ read from the plot. For a Newtonian fluid, $n' = 1$ and the shear rate at the wall is $\dot{\gamma} = SV/D$. For a power law fluid, $n' = n$. To construct a rheogram, n' is obtained from the slope of the experimental plot at a given value of SV/D . The shear rate at the wall is given by Eq. (6-63) and the corresponding shear stress at the wall is $\tau_w = D\Delta P/(4L)$ read from the plot. By varying the value of SV/D , the shear rate versus shear stress plot can be constructed.

The generalized approach of Metzner and Reed (*AIChE J.*, **1**, 434 [1955]) for time-independent non-Newtonian fluids defines a modified Reynolds number as

$$\text{Re}_{\text{MR}} \equiv \frac{D^n V^{2-n} \rho}{K' 8^{n'-1}} \quad (6-65)$$

where K' satisfies

$$\frac{D\Delta P}{4L} = K' \left(\frac{SV}{D} \right)^{n'} \quad (6-66)$$

With this definition, $f = 16/\text{Re}_{\text{MR}}$ is automatically satisfied at the value of SV/D where K' and n' are evaluated. Equation (6-66) may be obtained by integration of Eq. (6-64) only when n' is a constant, as, for example, the cases of Newtonian and power law fluids. For Newtonian fluids, $K' = \mu$ and $n' = 1$; for power law fluids, $K' = K[(1 + 3n)/(4n)]^n$ and $n' = n$. For Bingham plastics, K' and n' are variable, given as a function of τ_w (Metzner, *Ind. Eng. Chem.*, **49**, 1429–1432 [1957]).

$$K = \tau_w^{1-n'} \left[\frac{\mu_\infty}{1 - 4\tau_y/3\tau_w + (\tau_y/\tau_w)^4/3} \right]^{n'} \quad (6-67)$$

$$n' = \frac{1 - 4\tau_y/(3\tau_w) + (\tau_y/\tau_w)^4/3}{1 - (\tau_y/\tau_w)^4} \quad (6-68)$$

For laminar flow of power law fluids in channels of noncircular cross section, see Schechter (*AIChE J.*, **7**, 445–448 [1961]), Wheeler and Wissler (*AIChE J.*, **11**, 207–212 [1965]), Bird, Armstrong, and Hassager (*Dynamics of Polymeric Liquids*, vol. 1: *Fluid Mechanics*, Wiley, New York, 1977), and Skelland (*Non-Newtonian Flow and Heat Transfer*, Wiley, New York, 1967).

Steady-state, fully developed laminar flows of viscoelastic fluids in straight, constant-diameter pipes show no effects of viscoelasticity. The viscous component of the constitutive equation may be used to develop the flow rate–pressure drop relations, which apply downstream of the entrance region after viscoelastic effects have disappeared. A similar situation exists for time-dependent fluids.

The **transition to turbulent flow** begins at Re_{MR} in the range of 2,000 to 2,500 (Metzner and Reed, *AIChE J.*, **1**, 434 [1955]). For Bingham plastic materials, K' and n' must be evaluated for the τ_w condition in question in order to determine Re_{MR} and establish whether the flow is laminar. An alternative method for Bingham plastics is by Hanks (Hanks, *AIChE J.*, **9**, 306 [1963]; **14**, 691 [1968]; Hanks and Pratt, *Soc. Petrol. Engrs. J.*, **7**, 342 [1967]; and Govier and Aziz, pp. 213–215). The transition from laminar to turbulent flow is influenced by **viscoelastic** properties (Metzner and Park, *J. Fluid Mech.*, **20**, 291 [1964]) with the critical value of Re_{MR} increased to beyond 10,000 for some materials.

For **turbulent flow of non-Newtonian fluids**, the design chart of Dodge and Metzner (*AIChE J.*, **5**, 189 [1959]), Fig. 6-11, is most widely used. For Bingham plastic materials in turbulent flow, it is generally assumed that stresses greatly exceed the yield stress, so that the friction factor–Reynolds number relationship for Newtonian fluids applies, with μ_∞ substituted for μ . This is equivalent to setting $n' = 1$ and $\tau_y/\tau_w = 0$ in the Dodge-Metzner method, so that $\text{Re}_{\text{MR}} = DV\rho/\mu_\infty$. Wilson and Thomas (*Can. J. Chem. Eng.*, **63**, 539–546 [1985]) give friction factor equations for turbulent flow of power law fluids and Bingham plastic fluids.

Power law fluids:

$$\frac{1}{\sqrt{f}} = \frac{1}{\sqrt{f_N}} + 8.2 \frac{1-n}{1+n} + 1.77 \ln \left(\frac{1+n}{2} \right) \quad (6-69)$$

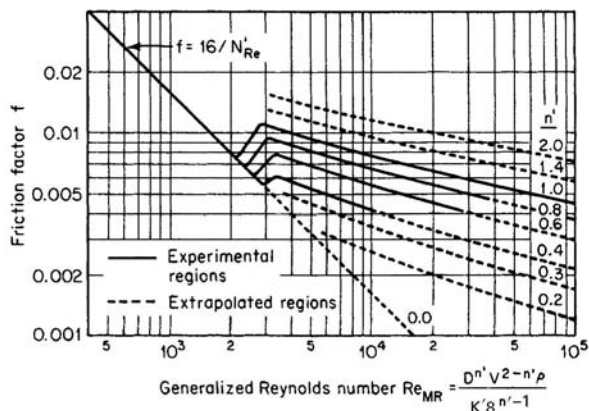


FIG. 6-11 Fanning friction factor for non-Newtonian flow. The abscissa is defined in Eq. (6-65). (From Dodge and Metzner, *Am. Inst. Chem. Eng. J.*, **5**, 189 [1959].)

where f_N is the friction factor for Newtonian fluid evaluated at $\text{Re} = DV\rho/\mu_{\text{eff}}$ where the effective viscosity is

$$\mu_{\text{eff}} = K \left(\frac{3n+1}{4n} \right)^{n-1} \left(\frac{SV}{D} \right)^{n-1} \quad (6-70)$$

Bingham fluids:

$$\frac{1}{\sqrt{f}} = \frac{1}{\sqrt{f_N}} + 1.77 \ln \left(\frac{(1-\xi)^2}{1+\xi} \right) + \xi(10 + 0.884\xi) \quad (6-71)$$

where f_N is evaluated at $\text{Re} = DV\rho/\mu_\infty$ and $\xi = \tau_y/\tau_w$. Iteration is required to use this equation since $\tau_w = f\rho V^2/2$.

Drag reduction in turbulent flow can be achieved by adding soluble high molecular weight polymers in extremely low concentration to Newtonian liquids. The reduction in friction is generally believed to be associated with the viscoelastic nature of the solutions effective in the wall region. For a given polymer, there is a minimum molecular weight necessary to initiate drag reduction at a given flow rate, and a critical concentration above which drag reduction will not occur (Kim, Little, and Ting, *J. Colloid Interface Sci.*, **47**, 530–535 [1974]). Drag reduction is reviewed by Hoyt (*J. Basic Eng.*, **94**, 258–285 [1972]); Little, et al. (*Ind. Eng. Chem. Fundam.*, **14**, 283–296 [1975]) and Virk (*AIChE J.*, **21**, 625–656 [1975]). At maximum possible drag reduction in smooth pipes,

$$\frac{1}{\sqrt{f}} = -19 \log \left(\frac{50.73}{\text{Re}\sqrt{f}} \right) \quad (6-72)$$

or, approximately, $f = \frac{0.58}{\text{Re}^{0.58}}$ (6-73)

for 4,000 < Re < 40,000. The actual drag reduction depends on the polymer system. For further details, see Virk (*ibid.*).

Economic Pipe Diameter, Turbulent Flow The economic optimum pipe diameter may be computed so that the last increment of investment reduces the operating cost enough to produce the required minimum return on investment. For long cross-country pipelines, alloy pipes of appreciable length and complexity, or pipelines with control valves, detailed analyses of investment and operating costs should be made. Peters and Timmerhaus (*Plant Design and Economics for Chemical Engineers*, 4th ed., McGraw-Hill, New York, 1991) provide a detailed method for determining the economic optimum size. For pipelines of the lengths usually encountered in chemical plants and petroleum refineries, simplified selection charts are often adequate. In many cases there is an economic optimum velocity that is nearly independent of diameter, which may be used to estimate the economic diameter from the flow rate. For low-viscosity liquids in schedule 40 steel pipe, economic optimum velocity is typically in the range of 1.8 to 2.4 m/s (5.9 to 7.9 ft/s). For gases with density ranging

from 0.2 to 20 kg/m³ (0.013 to 1.25 lbm/ft³), the economic optimum velocity is about 40 m/s to 9 m/s (131 to 30 ft/s). Charts and rough guidelines for economic optimum size do not apply to multiphase flows.

Economic Pipe Diameter, Laminar Flow Pipelines for the transport of high-viscosity liquids are seldom designed purely on the basis of economics. More often, the size is dictated by operability considerations such as available pressure drop, shear rate, or residence time distribution. Peters and Timmerhaus (ibid., Chap. 10) provide an economic pipe diameter chart for laminar flow. For non-Newtonian fluids, see Skelland (*Non-Newtonian Flow and Heat Transfer*, Chap. 7, Wiley, New York, 1967).

Vacuum Flow When gas flows under high vacuum conditions or through very small openings, the continuum hypothesis is no longer appropriate if the channel dimension is not very large compared to the mean free path of the gas. When the mean free path is comparable to the channel dimension, flow is dominated by collisions of molecules with the wall, rather than by collisions between molecules. An approximate expression based on Brown, et al. (*J. Appl. Phys.*, **17**, 802–813 [1946]) for the mean free path is

$$\lambda = \left(\frac{2\mu}{p}\right) \sqrt{\frac{8RT}{\pi M_w}} \quad (6-74)$$

The Knudsen number Kn is the ratio of the mean free path to the channel dimension. For pipe flow, Kn = λ/D. **Molecular flow** is characterized by Kn > 1.0; continuum viscous (laminar or turbulent) flow is characterized by Kn < 0.01. **Transition** or **slip** flow applies over the range 0.01 < Kn < 1.0.

Vacuum flow is usually described with flow variables different from those used for normal pressures, which often leads to confusion. **Pumping speed** S is the actual volumetric flow rate of gas through a flow cross section. **Throughput** Q is the product of pumping speed and absolute pressure. In the SI system, Q has units of Pa·m³/s.

$$Q = Sp \quad (6-75)$$

The mass flow rate w is related to the throughput using the ideal gas law.

$$w = \frac{M_w}{RT} Q \quad (6-76)$$

Throughput is therefore proportional to mass flow rate. For a given mass flow rate, throughput is independent of pressure. The relation between throughput and pressure drop Δp = p₁ - p₂ across a flow element is written in terms of the **conductance** C. **Resistance** is the reciprocal of conductance. Conductance has dimensions of volume per time.

$$Q = C\Delta p \quad (6-77)$$

The conductance of a series of flow elements is given by

$$\frac{1}{C} = \frac{1}{C_1} + \frac{1}{C_2} + \frac{1}{C_3} + \dots \quad (6-78)$$

while for elements in parallel,

$$C = C_1 + C_2 + C_3 + \dots \quad (6-79)$$

For a vacuum pump of speed S_p withdrawing from a vacuum vessel through a connecting line of conductance C, the pumping speed at the vessel is

$$S = \frac{S_p C}{S_p + C} \quad (6-80)$$

Molecular Flow Under molecular flow conditions, conductance is independent of pressure. It is proportional to √T/M_w, with the proportionality constant a function of geometry. For fully developed pipe flow,

$$C = \frac{\pi D^3}{8L} \sqrt{\frac{RT}{M_w}} \quad (6-81)$$

For an orifice of area A,

$$C = 0.40A \sqrt{\frac{RT}{M_w}} \quad (6-82)$$

TABLE 6-3 Constants for Circular Annuli

D ₂ /D ₁	K	D ₂ /D ₁	K
0	1.00	0.707	1.254
0.259	1.072	0.866	1.430
0.500	1.154	0.966	1.675

Conductance equations for several other geometries are given by Ryans and Roper (*Process Vacuum System Design and Operation*, Chap. 2, McGraw-Hill, New York, 1986). For a circular annulus of outer and inner diameters D₁ and D₂ and length L, the method of Guthrie and Wakerling (*Vacuum Equipment and Techniques*, McGraw-Hill, New York, 1949) may be written

$$C = 0.42K \frac{(D_1 - D_2)^2(D_1 + D_2)}{L} \sqrt{\frac{RT}{M_w}} \quad (6-83)$$

where K is a dimensionless constant with values given in Table 6-3.

For a short pipe of circular cross section, the conductance as calculated for an orifice from Eq. (6-82) is multiplied by a correction factor K which may be approximated as (Kennard, *Kinetic Theory of Gases*, McGraw-Hill, New York, 1938, pp. 306–308)

$$K = \frac{1}{1 + (L/D)} \quad \text{for } 0 \leq L/D \leq 0.75 \quad (6-84)$$

$$K = \frac{1 + 0.8(L/D)}{1 + 1.90(L/D) + 0.6(L/D)^2} \quad \text{for } L/D > 0.75 \quad (6-85)$$

For L/D > 100, the error in neglecting the end correction by using the fully developed pipe flow equation (6-81) is less than 2 percent. For rectangular channels, see Normand (*Ind. Eng. Chem.*, **40**, 783–787 [1948]).

Yu and Sparrow (*J. Basic Eng.*, **70**, 405–410 [1970]) give a theoretically derived chart for slot seals with or without a sheet located in or passing through the seal, giving mass flow rate as a function of the ratio of seal plate thickness to gap opening.

Slip Flow In the transition region between molecular flow and continuum viscous flow, the conductance for fully developed pipe flow is most easily obtained by the method of Brown, et al. (*J. Appl. Phys.*, **17**, 802–813 [1946]), which uses the parameter

$$X = \sqrt{\frac{8}{\pi}} \left(\frac{\lambda}{D}\right) = \left(\frac{2\mu}{p_m D}\right) \sqrt{\frac{RT}{M}} \quad (6-86)$$

where p_m is the arithmetic mean absolute pressure. A correction factor F, read from Fig. 6-12 as a function of X, is applied to the conductance

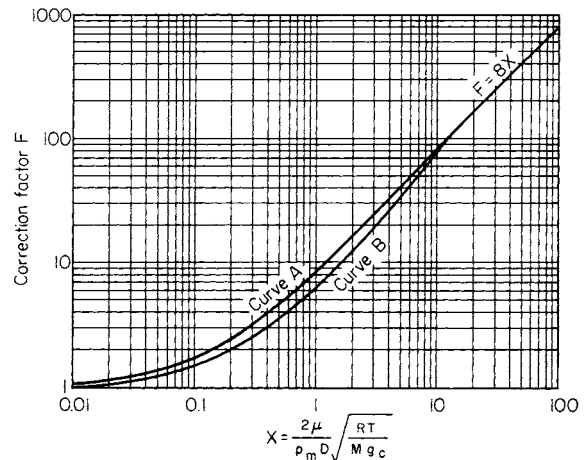


FIG. 6-12 Correction factor for Poiseuille's equation at low pressures. Curve A: experimental curve for glass capillaries and smooth metal tubes. (From Brown, et al., *J. Appl. Phys.*, **17**, 802 [1946].) Curve B: experimental curve for iron pipe (From Riggle, courtesy of E. I. du Pont de Nemours & Co.)

6-16 FLUID AND PARTICLE DYNAMICS

for viscous flow.

$$C = F \frac{\pi D^4 p_m}{128 \mu L} \quad (6-87)$$

For slip flow through **square channels**, see Milligan and Wilkerson (*J. Eng. Ind.*, **95**, 370–372 [1973]). For slip flow through **annuli**, see Maegley and Berman (*Phys. Fluids*, **15**, 780–785 [1972]).

The **pump-down time** θ for evacuating a vessel in the absence of air in-leakage is given approximately by

$$\theta = \left(\frac{V_i}{S_0} \right) \ln \left(\frac{p_1 - p_0}{p_2 - p_0} \right) \quad (6-88)$$

where V_i = volume of vessel plus volume of piping between vessel and pump; S_0 = system speed as given by Eq. (6-80), assumed independent of pressure; p_1 = initial vessel pressure; p_2 = final vessel pressure; and p_0 = lowest pump intake pressure attainable with the pump in question. See Dushman and Lafferty (*Scientific Foundations of Vacuum Technique*, 2d ed., Wiley, New York, 1962).

The amount of inerts which has to be removed by a pumping system after the pump-down stage depends on the in-leakage of air at the various fittings, connections, and so on. Air leakage is often correlated with system volume and pressure, but this approach introduces uncertainty because the number and size of leaks does not necessarily correlate with system volume, and leakage is sensitive to maintenance quality. Ryans and Roper (*Process Vacuum System Design and Operation*, McGraw-Hill, New York, 1986) present a thorough discussion of air leakage.

FRICIONAL LOSSES IN PIPELINE ELEMENTS

The viscous or frictional loss term in the mechanical energy balance for most cases is obtained experimentally. For many common fittings found in piping systems, such as expansions, contractions, elbows, and valves, data are available to estimate the losses. Substitution into the energy balance then allows calculation of pressure drop. A common error is to assume that pressure drop and frictional losses are equivalent. Equation (6-16) shows that in addition to frictional losses, other factors such as shaft work and velocity or elevation change influence pressure drop.

Losses l_v for incompressible flow in sections of straight pipe of constant diameter may be calculated as previously described using the Fanning friction factor:

$$l_v = \frac{\Delta P}{\rho} = \frac{2fV^2L}{D} \quad (6-89)$$

where ΔP = drop in equivalent pressure, $P = p + \rho gz$, with p = pressure, ρ = fluid density, g = acceleration of gravity, and z = elevation. Losses in the fittings of a piping network are frequently termed *minor losses* or *miscellaneous losses*. These descriptions are misleading because in process piping fitting losses are often much greater than the losses in straight piping sections.

Equivalent Length and Velocity Head Methods Two methods are in common use for estimating fitting loss. One, the **equivalent length** method, reports the losses in a piping element as the length of straight pipe which would have the same loss. For turbulent flows, the equivalent length is usually reported as a number of diameters of pipe of the same size as the fitting connection; L_e/D is given as

a fixed quantity, independent of D . This approach tends to be most accurate for a single fitting size and loses accuracy with deviation from this size. For laminar flows, L_e/D correlations normally have a size dependence through a Reynolds number term.

The other method is the **velocity head** method. The term $V^2/2g$ has dimensions of length and is commonly called a *velocity head*. Application of the Bernoulli equation to the problem of frictionless discharge at velocity V through a nozzle at the bottom of a column of liquid of height H shows that $H = V^2/2g$. Thus H is the liquid head corresponding to the velocity V . Use of the velocity head to scale pressure drops has wide application in fluid mechanics. Examination of the Navier-Stokes equations suggests that when the inertial terms dominate the viscous terms, pressure gradients are expected to be proportional to ρV^2 where V is a characteristic velocity of the flow.

In the velocity head method, the losses are reported as a number of velocity heads K . Then, the engineering Bernoulli equation for an incompressible fluid can be written

$$p_1 - p_2 = \alpha_2 \frac{\rho V_2^2}{2} - \alpha_1 \frac{\rho V_1^2}{2} + \rho g(z_2 - z_1) + K \frac{\rho V^2}{2} \quad (6-90)$$

where V is the reference velocity upon which the velocity head loss coefficient K is based. For a section of straight pipe, $K = 4fL/D$.

Contraction and Entrance Losses For a **sudden contraction** at a sharp-edged entrance to a pipe or sudden reduction in cross-sectional area of a channel, as shown in Fig. 6-13a, the loss coefficient based on the downstream velocity V_2 is given for **turbulent flow** in Crane Co. Tech Paper 410 (1980) approximately by

$$K = 0.5 \left(1 - \frac{A_2}{A_1} \right) \quad (6-91)$$

Example 5: Entrance Loss Water, $\rho = 1,000 \text{ kg/m}^3$, flows from a large vessel through a sharp-edged entrance into a pipe at a velocity in the pipe of 2 m/s. The flow is turbulent. Estimate the pressure drop from the vessel into the pipe.

With $A_2/A_1 \rightarrow 0$, the viscous loss coefficient is $K = 0.5$ from Eq. (6-91). The mechanical energy balance, Eq. (6-16) with $V_1 = 0$ and $z_2 - z_1 = 0$ and assuming uniform flow ($\alpha_2 = 1$) becomes

$$p_1 - p_2 = \frac{\rho V_2^2}{2} + 0.5 \frac{\rho V_2^2}{2} = 4,000 + 2,000 = 6,000 \text{ Pa}$$

Note that the total pressure drop consists of 0.5 velocity heads of frictional loss contribution, and 1 velocity head of velocity change contribution. The frictional contribution is a permanent loss of mechanical energy by viscous dissipation. The acceleration contribution is reversible; if the fluid were subsequently decelerated in a frictionless diffuser, a 4,000 Pa pressure rise would occur.

For a **trumpet-shaped** rounded entrance, with a radius of rounding greater than about 15 percent of the pipe diameter (Fig. 6-13b), the turbulent flow loss coefficient K is only about 0.1 (Vennard and Street, *Elementary Fluid Mechanics*, 5th ed., Wiley, New York, 1975, pp. 420–421). Rounding of the inlet prevents formation of the **vena contracta**, thereby reducing the resistance to flow.

For **laminar flow** the losses in sudden contraction may be estimated for area ratios $A_2/A_1 < 0.2$ by an equivalent additional pipe length L_e given by

$$L_e/D = 0.3 + 0.04\text{Re} \quad (6-92)$$

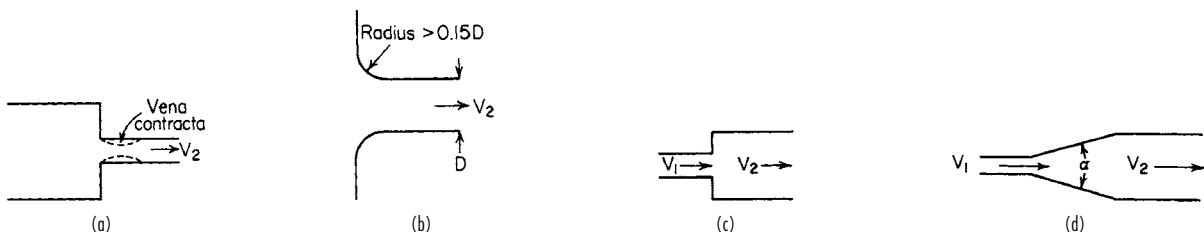


FIG. 6-13 Contractions and enlargements: (a) sudden contraction, (b) rounded contraction, (c) sudden enlargement, and (d) uniformly diverging duct.

where D is the diameter of the smaller pipe and Re is the Reynolds number in the smaller pipe. For laminar flow in the entrance to rectangular ducts, see Shah (*J. Fluids Eng.*, **100**, 177–179 [1978]) and Roscoe (*Philos. Mag.*, **40**, 338–351 [1949]). For creeping flow, $Re < 1$, of power law fluids, the entrance loss is approximately $L_e/D = 0.3n$ (Boger, Gupta, and Tanner, *J. Non-Newtonian Fluid Mech.*, **4**, 239–248 [1978]). For viscoelastic fluid flow in circular channels with sudden contraction, a toroidal vortex forms upstream of the contraction plane. Such flows are reviewed by Boger (*Ann. Review Fluid Mech.*, **19**, 157–182 [1987]).

For creeping flow through **conical converging channels**, inertial acceleration terms are negligible and the viscous pressure drop $\Delta p = \rho l_v$ may be computed by integration of the differential form of the Hagen-Poiseuille equation Eq. (6-36), provided the angle of convergence is small. The result for a power law fluid is

$$\Delta p = 4K \left(\frac{3n+1}{4n} \right)^n \left(\frac{8V_2}{D_2} \right)^n \left\{ \frac{1}{6n \tan(\alpha/2)} \left[1 - \left(\frac{D_2}{D_1} \right)^{3n} \right] \right\} \quad (6-93)$$

where D_1 = inlet diameter
 D_2 = exit diameter
 V_2 = velocity at the exit
 α = total included angle

Equation (6-93) agrees with experimental data (Kemblowski and Kiljanski, *Chem. Eng. J. (Lausanne)*, **9**, 141–151 [1975]) for $\alpha < 11^\circ$. For Newtonian liquids, Eq. (6-93) simplifies to

$$\Delta p = \mu \left(\frac{32V_2}{D_2} \right) \left\{ \frac{1}{6 \tan(\alpha/2)} \left[1 - \left(\frac{D_2}{D_1} \right)^3 \right] \right\} \quad (6-94)$$

For creeping flow through noncircular converging channels, the differential form of the Hagen-Poiseuille equation with equivalent diameter given by Eqs. (6-50) to (6-52) may be used, provided the convergence is gradual.

Expansion and Exit Losses For ducts of any cross section, the frictional loss for a **sudden enlargement** (Fig. 6-13c) with turbulent flow is given by the Borda-Carnot equation:

$$l_v = \frac{V_1^2 - V_2^2}{2} = \frac{V_1^2}{2} \left(1 - \frac{A_1}{A_2} \right)^2 \quad (6-95)$$

where V_1 = velocity in the smaller duct
 V_2 = velocity in the larger duct
 A_1 = cross-sectional area of the smaller duct
 A_2 = cross-sectional area of the larger duct

Equation (6-95) is valid for incompressible flow. For compressible flows, see Benedict, Wyler, Dudek, and Glead (*J. Eng. Power*, **98**, 327–334 [1976]). For an infinite expansion, $A_1/A_2 = 0$, Eq. (6-95) shows that the **exit loss** from a pipe is 1 velocity head. This result is easily deduced from the mechanical energy balance Eq. (6-90), noting that $p_1 = p_2$. This exit loss is due to the dissipation of the discharged jet; there is no pressure drop at the exit.

For creeping Newtonian flow ($Re < 1$), the frictional loss due to a sudden enlargement should be obtained from the same equation for a sudden contraction (Eq. [6-92]). Note, however, that Boger, Gupta, and Tanner (*ibid.*) give an exit friction equivalent length of 0.12 diameter, increasing for power law fluids as the exponent decreases. For laminar flows at higher Reynolds numbers, the pressure drop is twice that given by Eq. (6-95). This results from the velocity profile factor α in the mechanical energy balance being 2.0 for the parabolic laminar velocity profile.

If the transition from a small to a large duct of any cross-sectional shape is accomplished by a **uniformly diverging duct** (see Fig. 6-13d) with a straight axis, the total frictional pressure drop can be computed by integrating the differential form of Eq. (6-89), $dl_v/dx = 2fV^2/D$ over the length of the expansion, provided the total angle α between the diverging walls is less than 7° . For angles between 7° and 45° , the loss coefficient may be estimated as $2.6 \sin(\alpha/2)$ times the loss coefficient for a sudden expansion; see Hooper (*Chem. Eng.*, Nov. 7, 1988). Gibson (*Hydraulics and Its Applications*, 5th ed., Constable, London 1952, p. 93) recommends multiplying the sudden enlargement loss by 0.13 for $5^\circ < \alpha < 7.5^\circ$ and by $0.0110\alpha^{1.22}$ for $7.5^\circ < \alpha <$

35° . For angles greater than 35° to 45° , the losses are normally considered equal to those for a sudden expansion, although in some cases the losses may be greater. Expanding flow through standard pipe reducers should be treated as sudden expansions.

Trumpet-shaped enlargements for turbulent flow designed for constant decrease in velocity head per unit length were found by Gibson (*ibid.*, p. 95) to give 20 to 60 percent less frictional loss than straight taper pipes of the same length.

A special feature of expansion flows occurs when **viscoelastic** liquids are extruded through a die at a low Reynolds number. The extrudate may expand to a diameter several times greater than the die diameter, whereas for a Newtonian fluid the diameter expands only 10 percent. This phenomenon, called **die swell**, is most pronounced with short dies (Graessley, Glasscock, and Crawley, *Trans. Soc. Rheol.*, **14**, 519–544 [1970]). For velocity distribution measurements near the die exit, see Goulden and MacSporran (*J. Non-Newtonian Fluid Mech.*, **1**, 183–198 [1976]) and Whipple and Hill (*AIChE J.*, **24**, 664–671 [1978]). At high flow rates, the extrudate becomes distorted, suffering **melt fracture** at wall shear stresses greater than 10^5 N/m². This phenomenon is reviewed by Denn (*Ann. Review Fluid Mech.*, **22**, 13–34 [1990]). Ramamurthy (*J. Rheol.*, **30**, 337–357 [1986]) has found a dependence of apparent stick-slip behavior in melt fracture to be dependent on the material of construction of the die.

Fittings and Valves For **turbulent flow**, the frictional loss for fittings and valves can be expressed by the equivalent length or velocity head methods. As fitting size is varied, K values are relatively more constant than L_e/D values, but since fittings generally do not achieve geometric similarity between sizes, K values tend to decrease with increasing fitting size. Table 6-4 gives K values for many types of fittings and valves.

Manufacturers of valves, especially control valves, express valve capacity in terms of a flow coefficient C_v , which gives the flow rate through the valve in gal/min of water at 60°F under a pressure drop of 1 lb/in^2 . It is related to K by

$$C_v = \frac{C_1 d^2}{\sqrt{K}} \quad (6-96)$$

where C_1 is a dimensional constant equal to 29.9 and d is the diameter of the valve connections in inches.

For **laminar flow**, data for the frictional loss of valves and fittings are meager (Beck and Miller, *J. Am. Soc. Nav. Eng.*, **56**, 62–83 [1944]; Beck, *ibid.*, **56**, 235–271, 366–388, 389–395 [1944]; De Craene, *Heat. Piping Air Cond.*, **27**[10], 90–95 [1955]; Karr and Schutz, *J. Am. Soc. Nav. Eng.*, **52**, 239–256 [1940]; and Kittredge and Rowley, *Trans. ASME*, **79**, 1759–1766 [1957]). The data of Kittredge and Rowley indicate that K is constant for Reynolds numbers above 500 to 2,000, but increases rapidly as Re decreases below 500. Typical values for K for laminar flow Reynolds numbers are shown in Table 6-5.

Methods to calculate losses for **tee and wye junctions** for dividing and combining flow are given by Miller (*Internal Flow Systems*, 2d ed., Chap. 13, BHRA, Cranfield, 1990), including effects of Reynolds number, angle between legs, area ratio, and radius. Junctions with more than three legs are also discussed. The sources of data for the loss coefficient charts are Blaisdell and Manson (*U.S. Dept. Agric. Res. Serv. Tech. Bull.* 1283 [August 1963]) for combining flow and Gardel (*Bull. Tech. Suisse Romande*, **85**[9], 123–130 [1957]; **85**[10], 143–148 [1957]) together with additional unpublished data for dividing flow.

Miller (*Internal Flow Systems*, 2d ed., Chap. 13, BHRA, Cranfield, 1990) gives the most complete information on losses in **bends and curved pipes**. For turbulent flow in circular cross-section bends of constant area, as shown in Fig. 6-14a, a more accurate estimate of the loss coefficient K than that given in Table 6-4 is

$$K = K^\circ C_{Re} C_o C_f \quad (6-97)$$

where K° , given in Fig. 6-14b, is the loss coefficient for a smooth-walled bend at a Reynolds number of 10^6 . The Reynolds number correction factor C_{Re} is given in Fig. 6-14c. For $0.7 < r/D < 1$ or for $K^\circ < 0.4$, use the C_{Re} value for $r/D = 1$. Otherwise, if $r/D < 1$, obtain C_{Re} from

$$C_{Re} = \frac{K^\circ}{K^\circ + 0.2(1 - C_{Re, r/D=1})} \quad (6-98)$$

TABLE 6-4 Additional Frictional Loss for Turbulent Flow through Fittings and Valves^a

Type of fitting or valve	Additional friction loss, equivalent no. of velocity heads, K
45° ell, standard ^{b,c,d,e,f}	0.35
45° ell, long radius ^c	0.2
90° ell, standard ^{b,c,e,f,g,h}	0.75
Long radius ^{b,c,d,e}	0.45
Square or miter ^h	1.3
180° bend, close return ^{b,c,e}	1.5
Tee, standard, along run, branch blanked off ⁱ	0.4
Used as ell, entering run ^{g,d}	1.0
Used as ell, entering branch ^{e,g,i}	1.0
Branching flow ^{j,k}	1 ^l
Coupling ^{e,e}	0.04
Union ^f	0.04
Gate valve, ^{b,e,m} open	0.17
3/4 open	0.9
1/2 open	4.5
1/4 open	24.0
Diaphragm valve, open	2.3
3/4 open	2.6
1/2 open	4.3
1/4 open	21.0
Globe valve, ^{e,m}	
Bevel seat, open	6.0
1/2 open	9.5
Composition seat, open	6.0
1/2 open	8.5
Plug disk, open	9.0
3/4 open	13.0
1/2 open	36.0
1/4 open	112.0
Angle valve, ^{b,e} open	2.0
Y or blowoff valve, ^{b,m} open	3.0
Plug cock	
θ = 5°	0.05
θ = 10°	0.29
θ = 20°	1.56
θ = 40°	17.3
θ = 60°	206.0
Butterfly valve	
θ = 5°	0.24
θ = 10°	0.52
θ = 20°	1.54
θ = 40°	10.8
θ = 60°	118.0
Check valve, ^{b,e,m} swing	2.0
Disk	10.0
Ball	70.0
Foot valve ^e	15.0
Water meter, ^h disk	7.0
Piston	15.0
Rotary (star-shaped disk)	10.0
Turbine-wheel	6.0

^aLapple, *Chem. Eng.*, **56**(5), 96–104 (1949), general survey reference.
^b"Flow of Fluids through Valves, Fittings, and Pipe," Tech. Pap. 410, Crane Co., 1969.
^cFreeman, *Experiments upon the Flow of Water in Pipes and Pipe Fittings*, American Society of Mechanical Engineers, New York, 1941.
^dGiesecke, *J. Am. Soc. Heat. Vent. Eng.*, **32**, 461 (1926).
^e*Pipe Friction Manual*, 3d ed., Hydraulic Institute, New York, 1961.
^fIto, *J. Basic Eng.*, **82**, 131–143 (1960).
^gGiesecke and Badgett, *Heat. Piping Air Cond.*, **4**(6), 443–447 (1932).
^hSchoder and Dawson, *Hydraulics*, 2d ed., McGraw-Hill, New York, 1934, p. 213.
ⁱHoopes, Isakoff, Clarke, and Drew, *Chem. Eng. Prog.*, **44**, 691–696 (1948).
^jGilman, *Heat. Piping Air Cond.*, **27**(4), 141–147 (1955).
^kMcNown, *Proc. Am. Soc. Civ. Eng.*, **79**, Separate 258, 1–22 (1953); discussion, *ibid.*, **80**, Separate 396, 19–45 (1954). For the effect of branch spacing on junction losses in dividing flow, see Hecker, Nystrom, and Qureshi, *Proc. Am. Soc. Civ. Eng., J. Hydraul. Div.*, **103**(HY3), 265–279 (1977).
^lThis is pressure drop (including friction loss) between run and branch, based on velocity in the mainstream before branching. Actual value depends on the flow split, ranging from 0.5 to 1.3 if mainstream enters run and from 0.7 to 1.5 if mainstream enters branch.
^mLansford, *Loss of Head in Flow of Fluids through Various Types of 1/2-in. Valves*, Univ. Eng. Exp. Sta. Bull. Ser. 340, 1943.

TABLE 6-5 Additional Frictional Loss for Laminar Flow through Fittings and Valves

Type of fitting or valve	Additional frictional loss expressed as K			
	Re = 1,000	500	100	50
90° ell, short radius	0.9	1.0	7.5	16
Gate valve	1.2	1.7	9.9	24
Globe valve, composition disk	11	12	20	30
Plug	12	14	19	27
Angle valve	8	8.5	11	19
Check valve, swing	4	4.5	17	55

SOURCE: From curves by Kirtledge and Rowley, *Trans. Am. Soc. Mech. Eng.*, **79**, 1759–1766 (1957).

The correction C_o (Fig. 6-14d) accounts for the extra losses due to developing flow in the outlet tangent of the pipe, of length L_o . The total loss for the bend plus outlet pipe includes the bend loss K plus the straight pipe frictional loss in the outlet pipe $4fL_o/D$. Note that $C_o = 1$ for L_o/D greater than the termination of the curves on Fig. 6-14d, which indicate the distance at which fully developed flow in the outlet pipe is reached. Finally, the roughness correction is

$$C_f = \frac{f_{\text{rough}}}{f_{\text{smooth}}} \quad (6-99)$$

where f_{rough} is the friction factor for a pipe of diameter D with the roughness of the bend, at the bend inlet Reynolds number. Similarly, f_{smooth} is the friction factor for smooth pipe. For $Re > 10^6$ and $r/D \geq 1$, use the value of C_f for $Re = 10^6$.

Example 6: Losses with Fittings and Valves It is desired to calculate the liquid level in the vessel shown in Fig. 6-15 required to produce a discharge velocity of 2 m/s. The fluid is water at 20°C with $\rho = 1,000 \text{ kg/m}^3$ and $\mu = 0.001 \text{ Pa} \cdot \text{s}$, and the butterfly valve is at $\theta = 10^\circ$. The pipe is 2-in Schedule 40, with an inner diameter of 0.0525 m. The pipe roughness is 0.046 mm. Assuming the flow is turbulent and taking the velocity profile factor $\alpha = 1$, the engineering Bernoulli equation Eq. (6-16), written between surfaces 1 and 2, where the pressures are both atmospheric and the fluid velocities are 0 and $V = 2 \text{ m/s}$, respectively, and there is no shaft work, simplifies to

$$gZ = \frac{V^2}{2} + l_e$$

Contributing to l_e are losses for the entrance to the pipe, the three sections of straight pipe, the butterfly valve, and the 90° bend. Note that no exit loss is used because the discharged jet is outside the control volume. Instead, the $V^2/2$ term accounts for the kinetic energy of the discharging stream. The Reynolds number in the pipe is

$$Re = \frac{DV\rho}{\mu} = \frac{0.0525 \times 2 \times 1000}{0.001} = 1.05 \times 10^5$$

From Fig. 6-9 or Eq. (6-38), at $\epsilon/D = 0.046 \times 10^{-3}/0.0525 = 0.00088$, the friction factor is about 0.0054. The straight pipe losses are then

$$\begin{aligned} l_{e(\text{sp})} &= \left(\frac{4fL}{D}\right) \frac{V^2}{2} \\ &= \left(\frac{4 \times 0.0054 \times (1 + 1 + 1)}{0.0525}\right) \frac{V^2}{2} \\ &= 1.23 \frac{V^2}{2} \end{aligned}$$

The losses from Table 6-4 in terms of velocity heads K are $K = 0.5$ for the sudden contraction and $K = 0.52$ for the butterfly valve. For the 90° standard radius ($r/D = 1$), the table gives $K = 0.75$. The method of Eq. (6-94), using Fig. 6-14, gives

$$\begin{aligned} K &= K^* C_{\text{re}} C_o C_f \\ &= 0.24 \times 1.24 \times 1.0 \times \left(\frac{0.0054}{0.0044}\right) \\ &= 0.37 \end{aligned}$$

This value is more accurate than the value in Table 6-4. The value $f_{\text{smooth}} = 0.0044$ is obtainable either from Eq. (6-37) or Fig. 6-9.

The total losses are then

$$l_e = (1.23 + 0.5 + 0.52 + 0.37) \frac{V^2}{2} = 2.62 \frac{V^2}{2}$$

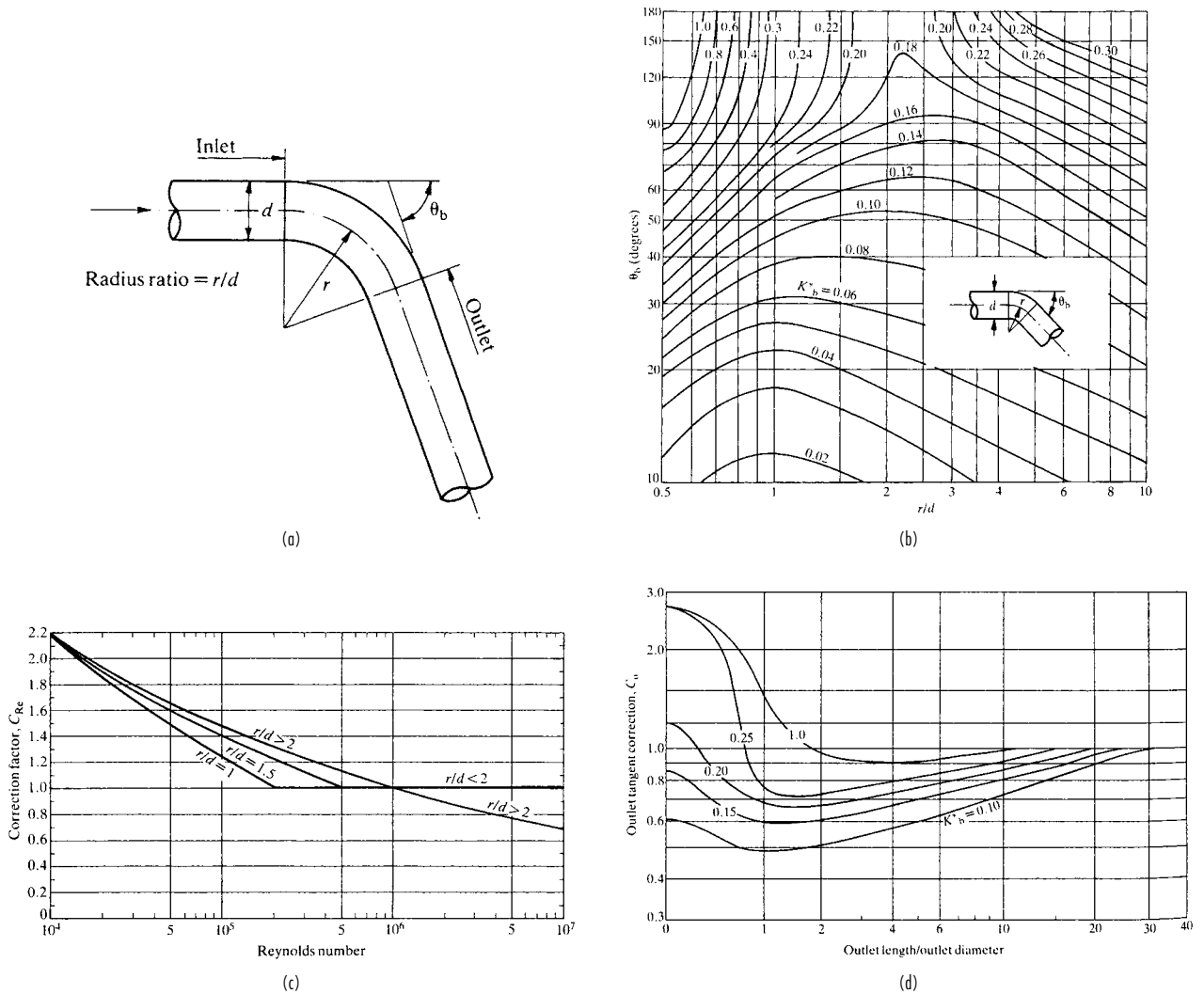


FIG. 6-14 Loss coefficients for flow in bends and curved pipes: (a) flow geometry, (b) loss coefficient for a smooth-walled bend at $Re = 10^6$, (c) Re correction factor, (d) outlet pipe correction factor. (From D. S. Miller; Internal Flow Systems, 2d ed., BHRA, Cranfield, U.K., 1990.)

and the liquid level Z is

$$Z = \frac{1}{g} \left(\frac{V^2}{2} + 2.62 \frac{V^2}{2} \right) = 3.62 \frac{V^2}{2g}$$

$$= \frac{3.62 \times 2^2}{2 \times 9.81} = 0.73 \text{ m}$$

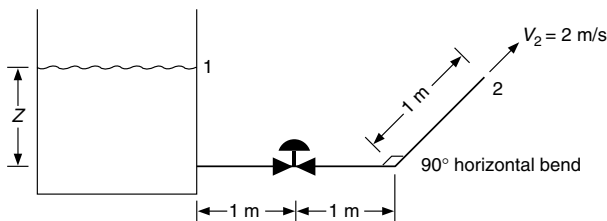


FIG. 6-15 Tank discharge example.

Curved Pipes and Coils For flow through curved pipe or coil, a secondary circulation perpendicular to the main flow called the **Dean effect** occurs. This circulation increases the friction relative to straight pipe flow and stabilizes laminar flow, delaying the transition Reynolds number to about

$$Re_{crit} = 2,100 \left(1 + 12 \sqrt{\frac{D}{D_c}} \right) \quad (6-100)$$

where D_c is the coil diameter. Equation (6-100) is valid for $10 < D_c/D < 250$. The **Dean number** is defined as

$$De = \frac{Re}{(D_c/D)^{1/2}} \quad (6-101)$$

In laminar flow, the friction factor for curved pipe f_c may be expressed in terms of the straight pipe friction factor $f = 16/Re$ as (Hart, *Chem. Eng. Sci.*, **43**, 775-783 [1988])

$$f_c/f = 1 + 0.090 \left(\frac{De^{1.5}}{70 + De} \right) \quad (6-102)$$

6-20 FLUID AND PARTICLE DYNAMICS

For turbulent flow, equations by Ito (*J. Basic Eng.*, **81**, 123 [1959]) and Srinivasan, Nandapurkar, and Holland (*Chem. Eng. [London]* no. 218, CE113-CE119 [May 1968]) may be used, with probable accuracy of ± 15 percent. Their equations are similar to

$$f_c = \frac{0.079}{\text{Re}^{0.25}} + \frac{0.0073}{\sqrt{(D_c/D)}} \quad (6-103)$$

The pressure drop for flow in **spirals** is discussed by Srinivasan, et al. (loc. cit.) and Ali and Seshadri (*Ind. Eng. Chem. Process Des. Dev.*, **10**, 328-332 [1971]). For friction loss in laminar flow through **semi-circular ducts**, see Masliyah and Nandakumar (*AIChE J.*, **25**, 478-487 [1979]); for curved channels of **square cross section**, see Cheng, Lin, and Ou (*J. Fluids Eng.*, **98**, 41-48 [1976]).

For **non-Newtonian (power law) fluids** in coiled tubes, Mashelkar and Devarajan (*Trans. Inst. Chem. Eng. (London)*, **54**, 108-114 [1976]) propose the correlation

$$f_c = (9.07 - 9.44n + 4.37n^2)(D/D_c)^{0.5}(\text{De}')^{-0.768 + 0.122n} \quad (6-104)$$

where De' is a modified Dean number given by

$$\text{De}' = \frac{1}{8} \left(\frac{6n + 2}{n} \right)^n \text{Re}_{\text{MR}} \sqrt{\frac{D}{D_c}} \quad (6-105)$$

where Re_{MR} is the Metzner-Reed Reynolds number, Eq. (6-65). This correlation was tested for the range $\text{De}' = 70$ to 400, $D/D_c = 0.01$ to 0.135, and $n = 0.35$ to 1. See also Oliver and Asghar (*Trans. Inst. Chem. Eng. [London]*, **53**, 181-186 [1975]).

Screens The pressure drop for incompressible flow across a screen of fractional free area α may be computed from

$$\Delta p = K \frac{\rho V^2}{2} \quad (6-106)$$

where ρ = fluid density
 V = superficial velocity based upon the gross area of the screen
 K = velocity head loss

$$K = \left(\frac{1}{C^2} \right) \left(\frac{1 - \alpha^2}{\alpha^2} \right) \quad (6-107)$$

The discharge coefficient for the screen C with aperture D_s is given as a function of screen Reynolds number $\text{Re} = D_s(V/\alpha)\rho/\mu$ in Fig. 6-16 for **plain square-mesh screens**, $\alpha = 0.14$ to 0.79. This curve fits most of the data within ± 20 percent. In the laminar flow region, $\text{Re} < 20$, the discharge coefficient can be computed from

$$C = 0.1\sqrt{\text{Re}} \quad (6-108)$$

Coefficients greater than 1.0 in Fig. 6-16 probably indicate partial pressure recovery downstream of the minimum aperture, due to rounding of the wires.

Grootenhuis (*Proc. Inst. Mech. Eng. [London]*, **A168**, 837-846 [1954]) presents data which indicate that for a series of screens, the total pressure drop equals the number of screens times the pressure drop for one screen, and is not affected by the spacing between screens or their orientation with respect to one another, and presents a correlation for frictional losses across plain square-mesh screens and sintered gauzes. Armour and Cannon (*AIChE J.*, **14**, 415-420 [1968]) give a correlation based on a packed bed model for plain, twill, and "dutch" weaves. For losses through monofilament fabrics see Pedersen (*Filtr. Sep.*, **11**, 586-589 [1975]). For screens **inclined at an angle θ** , use the normal velocity component V'

$$V' = V \cos \theta \quad (6-109)$$

(Carothers and Baines, *J. Fluids Eng.*, **97**, 116-117 [1975]) in place of V in Eq. (6-106). This applies for $\text{Re} > 500$, $C = 1.26$, $\alpha \leq 0.97$, and $0 < \theta < 45^\circ$, for square-mesh screens and diamond-mesh netting. Screens inclined at an angle to the flow direction also experience a tangential stress.

For **non-Newtonian fluids** in slow flow, friction loss across a square-woven or full-twill-woven screen can be estimated by considering the screen as a set of parallel tubes, each of diameter equal to the average minimal opening between adjacent wires, and length twice the diameter, without entrance effects (Carley and Smith, *Polym. Eng. Sci.*, **18**, 408-415 [1978]). For screen stacks, the losses of individual screens should be summed.

JET BEHAVIOR

A **free jet**, upon leaving an outlet, will entrain the surrounding fluid, expand, and decelerate. To a first approximation, total momentum is conserved as jet momentum is transferred to the entrained fluid. For practical purposes, a jet is considered free when its cross-sectional area is less than one-fifth of the total cross-sectional flow area of the region through which the jet is flowing (Elrod, *Heat. Piping Air Cond.*, **26**[3], 149-155 [1954]), and the surrounding fluid is the same as the jet fluid. A **turbulent jet** in this discussion is considered to be a free jet with Reynolds number greater than 2,000. Additional discussion on the relation between Reynolds number and turbulence in jets is given by Elrod (ibid.). Abramowicz (*The Theory of Turbulent Jets*, MIT Press, Cambridge, 1963) and Rajaratnam (*Turbulent Jets*, Elsevier, Amsterdam, 1976) provide thorough discourses on turbulent jets. Hussein, et al. (*J. Fluid Mech.*, **258**, 31-75 [1994]) give extensive

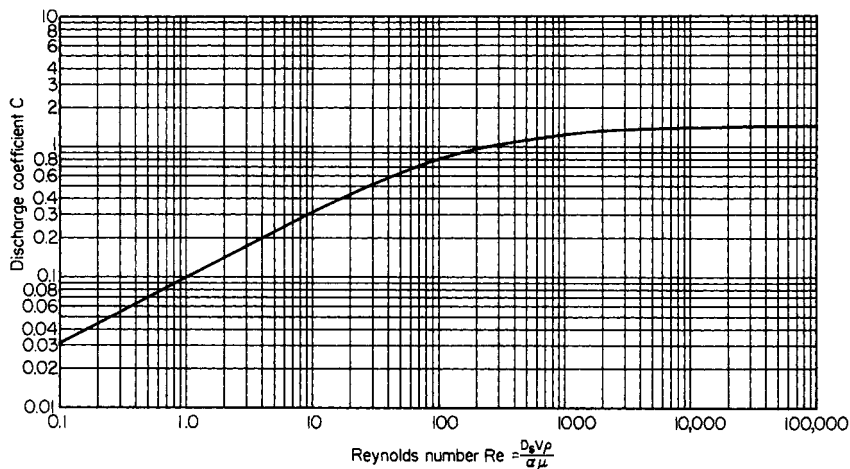


FIG. 6-16 Screen discharge coefficients, plain square-mesh screens. (Courtesy of E. I. du Pont de Nemours & Co.)

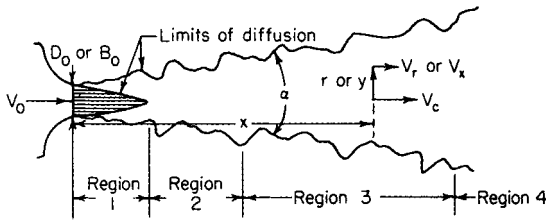


FIG. 6-17 Configuration of a turbulent free jet.

velocity data for a free jet, as well as an extensive discussion of free jet experimentation and comparison of data with momentum conservation equations.

A turbulent free jet is normally considered to consist of four flow regions (Tuve, *Heat. Piping Air Cond.*, **25**[1], 181–191 [1953]; Davies, *Turbulence Phenomena*, Academic, New York, 1972) as shown in Fig. 6-17:

1. Region of flow establishment—a short region whose length is about 6.4 nozzle diameters. The fluid in the conical core of the same length has a velocity about the same as the initial discharge velocity. The termination of this *potential core* occurs when the growing mixing or boundary layer between the jet and the surroundings reaches the centerline of the jet.
2. A transition region that extends to about 8 nozzle diameters.
3. Region of established flow—the principal region of the jet. In this region, the velocity profile transverse to the jet is self-preserving when normalized by the centerline velocity.
4. A terminal region where the residual centerline velocity reduces rapidly within a short distance. For air jets, the residual velocity will reduce to less than 0.3 m/s, (1.0 ft/s) usually considered still air.

Several references quote a length of 100 nozzle diameters for the length of the established flow region. However, this length is dependent on initial velocity and Reynolds number.

Table 6-6 gives characteristics of **rounded-inlet circular jets** and **rounded-inlet infinitely wide slot jets** (aspect ratio > 15). The information in the table is for a homogeneous, incompressible air system under isothermal conditions. The table uses the following nomenclature:

- B_0 = slot height
- D_0 = circular nozzle opening
- q = total jet flow at distance x
- q_0 = initial jet flow rate
- r = radius from circular jet centerline
- y = transverse distance from slot jet centerline
- V_c = centerline velocity
- V_r = circular jet velocity at r
- V_y = velocity at y

Witze (*Am. Inst. Aeronaut. Astronaut. J.*, **12**, 417–418 [1974]) gives equations for the centerline velocity decay of different types of subsonic and supersonic circular free jets. Entrainment of surrounding fluid in the region of flow establishment is lower than in the region of established flow (see Hill, *J. Fluid Mech.*, **51**, 773–779 [1972]). Data of Donald and Singer (*Trans. Inst. Chem. Eng. [London]*, **37**, 255–267 [1959]) indicate that jet angle and the coefficients given in Table 6-6 depend upon the fluids; for a water system, the jet angle for a circular jet is 14° and the entrainment ratio is about 70 percent of that for an air system. Most likely these variations are due to Reynolds number effects which are not taken into account in Table 6-6. Rushton (*AIChE J.*, **26**, 1038–1041 [1980]) examined available published results for circular jets and found that the centerline velocity decay is given by

$$\frac{V_c}{V_0} = 1.41Re^{0.135} \left(\frac{D_0}{x} \right) \quad (6-110)$$

where $Re = D_0V_0\rho/\mu$ is the initial jet Reynolds number. This result corresponds to a jet angle $\tan \alpha/2$ proportional to $Re^{-0.135}$.

TABLE 6-6 Turbulent Free-Jet Characteristics

Where both jet fluid and entrained fluid are air

Rounded-inlet circular jet	
Longitudinal distribution of velocity along jet center line ^a †	
$\frac{V_c}{V_0} = K \frac{D_0}{x}$	for $7 < \frac{x}{D_0} < 100$
$K = 5$	for $V_0 = 2.5$ to 5.0 m/s
$K = 6.2$	for $V_0 = 10$ to 50 m/s
Radial distribution of longitudinal velocity †	
$\log \left(\frac{V_c}{V_r} \right) = 40 \left(\frac{r}{x} \right)^2$	for $7 < \frac{x}{D_0} < 100$
Jet angle ^a †	
$\alpha \approx 20^\circ$	for $\frac{x}{D_0} < 100$
Entrainment of surrounding fluid ‡	
$\frac{q}{q_0} = 0.32 \frac{x}{D_0}$	for $7 < \frac{x}{D_0} < 100$
Rounded-inlet, infinitely wide slot jet	
Longitudinal distribution of velocity along jet centerline †	
$\frac{V_c}{V_0} = 2.28 \left(\frac{B_0}{x} \right)^{0.5}$	for $5 < \frac{x}{B_0} < 2,000$ and $V_0 = 12$ to 55 m/s
Transverse distribution of longitudinal velocity †	
$\log \left(\frac{V_c}{V_x} \right) = 18.4 \left(\frac{y}{x} \right)^2$	for $5 < \frac{x}{B_0} < 2,000$
Jet angle †	
α is slightly larger than that for a circular jet	
Entrainment of surrounding fluid ‡	
$\frac{q}{q_0} = 0.62 \left(\frac{x}{B_0} \right)^{0.5}$	for $5 < \frac{x}{B_0} < 2,000$

^aNottage, Slaby, and Gojsza, *Heat. Piping Air Cond.*, **24**(1), 165–176 (1952).

†Tuve, *Heat. Piping Air Cond.*, **25**(1), 181–191 (1953).

‡Albertson, Dai, Jensen, and Rouse, *Trans. Am. Soc. Civ. Eng.*, **115**, 639–664 (1950), and Discussion, *ibid.*, **115**, 665–697 (1950).

Characteristics of **rectangular jets** of various aspect ratios are given by Elrod (*Heat., Piping, Air Cond.*, **26**[3], 149–155 [1954]). For **slot jets discharging into a moving fluid**, see Weinstein, Osterle, and Forstall (*J. Appl. Mech.*, **23**, 437–443 [1967]). **Coaxial jets** are discussed by Forstall and Shapiro (*J. Appl. Mech.*, **17**, 399–408 [1950]), and **double concentric jets** by Chigier and Beer (*J. Basic Eng.*, **86**, 797–804 [1964]). **Axisymmetric confined jets** are described by Barchilon and Curtet (*J. Basic Eng.*, **777–787** [1964]). **Restrained** turbulent jets of liquid discharging into air are described by Davies (*Turbulence Phenomena*, Academic, New York, 1972). These jets are inherently unstable and break up into drops after some distance. Lienhard and Day (*J. Basic Eng. Trans. AIME*, p. 515 [September 1970]) discuss the breakup of superheated liquid jets which flash upon discharge.

Density gradients affect the spread of a single-phase jet. A jet of lower density than the surroundings spreads more rapidly than a jet of the same density as the surroundings, and, conversely, a denser jet spreads less rapidly. Additional details are given by Keagy and Weller (*Proc. Heat Transfer Fluid Mech. Inst.*, ASME, pp. 89–98, June 22–24 [1949]) and Cleaves and Boelter (*Chem. Eng. Prog.*, **43**, 123–134 [1947]).

Few experimental data exist on **laminar jets** (see Gutfinger and Shinnar, *AIChE J.*, **10**, 631–639 [1964]). Theoretical analysis for velocity distributions and entrainment ratios are available in Schlichting and in Morton (*Phys. Fluids*, **10**, 2120–2127 [1967]).

Theoretical analyses of jet flows for power law **non-Newtonian fluids** are given by Vlachopoulos and Stournaras (*AIChE J.*, **21**, 385–388 [1975]), Mitwally (*J. Fluids Eng.*, **100**, 363 [1978]), and Sridhar and Rankin (*J. Fluids Eng.*, **100**, 500 [1978]).

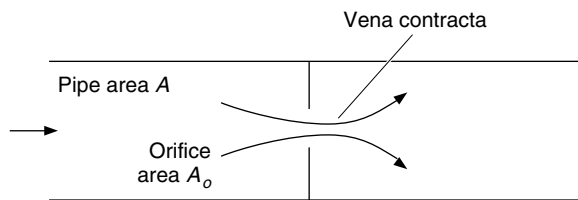


FIG. 6-18 Flow through an orifice.

FLOW THROUGH ORIFICES

Section 10 of this *Handbook* describes the use of orifice meters for flow measurement. In addition, **orifices** are commonly found within pipelines as flow-restricting devices, in perforated pipe distributing and return manifolds, and in perforated plates. Incompressible flow through an orifice in a pipeline, as shown in Fig. 6-18, is commonly described by the following equation for flow rate Q in terms of the pressures P_1 , P_2 , and P_3 ; the orifice area A_o ; the pipe cross-sectional area A ; and the density ρ .

$$\begin{aligned} Q &= v_o A_o = C_o A_o \sqrt{\frac{2(P_1 - P_2)}{\rho[1 - (A_o/A)^2]}} \\ &= C_o A_o \sqrt{\frac{2(P_1 - P_3)}{\rho(1 - A_o/A)[1 - (A_o/A)^2]}} \end{aligned} \quad (6-111)$$

The velocity based on the hole area is v_o . The pressure P_1 is the pressure upstream of the orifice, typically about 1 pipe diameter upstream, the pressure P_2 is the pressure at the **vena contracta**, where the flow passes through a minimum area which is less than the orifice area, and the pressure P_3 is the pressure downstream of the vena contracta after pressure recovery associated with deceleration of the fluid. The velocity of approach factor $1 - (A_o/A)^2$ accounts for the kinetic energy approaching the orifice, and the **orifice coefficient** or **discharge coefficient** C_o accounts for the vena contracta. The location of the vena contracta varies with A_o/A , but is about 0.7 pipe diameter for $A_o/A < 0.25$. The factor $1 - A_o/A$ accounts for pressure recovery. Pressure recovery is complete by about 4 to 8 pipe diameters downstream of the orifice. The permanent pressure drop is $P_1 - P_3$. When the orifice is at the end of pipe, discharging directly into a large chamber, there is negligible pressure recovery, the permanent pressure drop is $P_1 - P_2$, and the last equality in Eq. (6-111) does not apply. Instead, $P_2 = P_3$. Equation (6-111) may also be used for flow across a perforated plate with open area A_o and total area A . The location of the vena contracta and complete recovery would scale not with the vessel or pipe diameter in which the plate is installed, but with the hole diameter and pitch between holes.

The orifice coefficient has a value of about 0.62 at large Reynolds numbers ($Re = D_o V_o \rho / \mu > 20,000$), although values ranging from 0.60 to 0.70 are frequently used. At lower Reynolds numbers, the orifice coefficient varies with both Re and with the area or diameter ratio. See Sec. 10 for more details.

When liquids discharge vertically downward from a pipe of diameter D_p , through orifices into gas, gravity increases the discharge coefficient. Figure 6-19 shows this effect, giving the discharge coefficient in terms of a modified Froude number, $Fr = \Delta p / (\rho g D_p)$.

The orifice coefficient deviates from its value for sharp-edged orifices when the orifice wall thickness exceeds about 75 percent of the orifice diameter. Some pressure recovery occurs within the orifice and the orifice coefficient increases. Pressure drop across **segmental orifices** is roughly 10 percent greater than that for concentric circular orifices of the same open area.

COMPRESSIBLE FLOW

Flows are typically considered **compressible** when the density varies by more than 5 to 10 percent. In practice compressible flows are normally limited to gases, supercritical fluids, and multiphase flows

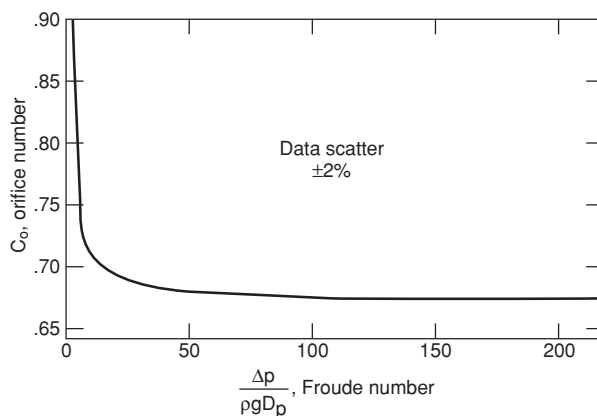


FIG. 6-19 Orifice coefficient vs. Froude number. (Courtesy E. I. duPont de Nemours & Co.)

containing gases. Liquid flows are normally considered incompressible, except for certain calculations involved in **hydraulic transient** analysis (see following) where compressibility effects are important even for nearly incompressible liquids with extremely small density variations. Textbooks on compressible gas flow include Shapiro (*Dynamics and Thermodynamics of Compressible Fluid Flow*, vols. I and II, Ronald Press, New York [1953]) and Zucrow and Hoffman (*Gas Dynamics*, vols. I and II, Wiley, New York [1976]).

In chemical process applications, one-dimensional gas flows through nozzles or orifices and in pipelines are the most important applications of compressible flow. Multidimensional external flows are of interest mainly in aerodynamic applications.

Mach Number and Speed of Sound The **Mach number** $M = V/c$ is the ratio of fluid velocity, V , to the **speed of sound** or **acoustic velocity**, c . The speed of sound is the propagation velocity of infinitesimal pressure disturbances and is derived from a momentum balance. The compression caused by the pressure wave is adiabatic and frictionless, and therefore isentropic.

$$c = \sqrt{\left(\frac{\partial p}{\partial \rho}\right)_s} \quad (6-112)$$

The derivative of pressure p with respect to density ρ is taken at constant entropy s . For an ideal gas,

$$\left(\frac{\partial p}{\partial \rho}\right)_s = \frac{kRT}{M_w}$$

where k = ratio of specific heats, C_p/C_v
 R = universal gas constant (8,314 J/kgmol K)
 T = absolute temperature
 M_w = molecular weight

Hence for an ideal gas,

$$c = \sqrt{\frac{kRT}{M_w}} \quad (6-113)$$

Most often, the Mach number is calculated using the speed of sound evaluated at the local pressure and temperature. When $M = 1$, the flow is **critical** or **sonic** and the velocity equals the local speed of sound. For **subsonic** flow $M < 1$ while **supersonic** flows have $M > 1$. Compressibility effects are important when the Mach number exceeds 0.1 to 0.2. A common error is to assume that compressibility effects are always negligible when the Mach number is small. The proper assessment of whether compressibility is important should be based on relative density changes, not on Mach number.

Isothermal Gas Flow in Pipes and Channels Isothermal compressible flow is often encountered in long transport lines, where there is sufficient heat transfer to maintain constant temperature. Velocities and Mach numbers are usually small, yet compressibility

effects are important when the total pressure drop is a large fraction of the absolute pressure. For an ideal gas with $\rho = pM_w/RT$, integration of the differential form of the momentum or mechanical energy balance equations, assuming a constant friction factor f over a length L of a channel of constant cross section and hydraulic diameter D_H , yields,

$$p_1^2 - p_2^2 = G^2 \frac{RT}{M_w} \left[\frac{4fL}{D_H} + 2 \ln \left(\frac{p_1}{p_2} \right) \right] \quad (6-114)$$

where the mass velocity $G = w/A = \rho V$ is the mass flow rate per unit cross-sectional area of the channel. The logarithmic term on the right-hand side accounts for the pressure change caused by acceleration of gas as its density decreases, while the first term is equivalent to the calculation of frictional losses using the density evaluated at the average pressure $(p_1 + p_2)/2$.

Solution of Eq. (6-114) for G and differentiation with respect to p_2 reveals a maximum mass flux $G_{\max} = p_2 \sqrt{M_w/(RT)}$ and a corresponding exit velocity $V_{2,\max} = \sqrt{RT/M_w}$ and exit Mach number $M_2 = 1/\sqrt{k}$. This apparent **choking** condition, though often cited, is not physically meaningful for isothermal flow because at such high velocities, and high rates of expansion, isothermal conditions are not maintained.

Adiabatic Frictionless Nozzle Flow In process plant pipelines, compressible flows are usually more nearly adiabatic than isothermal. Solutions for adiabatic flows through frictionless nozzles and in channels with constant cross section and constant friction factor are readily available.

Figure 6-20 illustrates adiabatic discharge of a **perfect** gas through a frictionless nozzle from a large chamber where velocity is effectively zero. A perfect gas obeys the ideal gas law $\rho = pM_w/RT$ and also has constant specific heat. The subscript 0 refers to the **stagnation** conditions in the chamber. More generally, stagnation conditions refer to the conditions which would be obtained by isentropically decelerating a gas flow to zero velocity. The minimum area section, or **throat**, of the nozzle is at the nozzle exit. The flow through the nozzle is isentropic because it is frictionless (reversible) and adiabatic. In terms of the exit Mach number M_1 and the upstream stagnation conditions, the flow conditions at the nozzle exit are given by

$$\frac{p_0}{p_1} = \left(1 + \frac{k-1}{2} M_1^2 \right)^{k/(k-1)} \quad (6-115)$$

$$\frac{T_0}{T_1} = 1 + \frac{k-1}{2} M_1^2 \quad (6-116)$$

$$\frac{\rho_0}{\rho_1} = \left(1 + \frac{k-1}{2} M_1^2 \right)^{1/(k-1)} \quad (6-117)$$

The mass velocity $G = w/A$, where w is the mass flow rate and A is the nozzle exit area, at the nozzle exit is given by

$$G = p_0 \sqrt{\frac{kM_w}{RT_0}} \frac{M_1}{\left(1 + \frac{k-1}{2} M_1^2 \right)^{(k+1)/2(k-1)}} \quad (6-118)$$

These equations are consistent with the isentropic relations for a per-

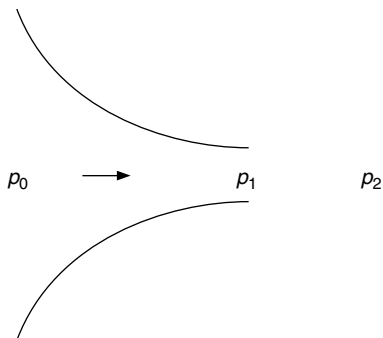


FIG. 6-20 Isentropic flow through a nozzle.

fect gas $p/p_0 = (\rho/\rho_0)^k$, $T/T_0 = (p/p_0)^{(k-1)/k}$. Equation (6-116) is valid for adiabatic flows with or without friction; it does not require isentropic flow. However, Eqs. (6-115) and (6-117) do require isentropic flow.

The exit Mach number M_1 may not exceed unity. At $M_1 = 1$, the flow is said to be **choked**, **sonic**, or **critical**. When the flow is choked, the pressure at the exit is greater than the pressure of the surroundings into which the gas flow discharges. The pressure drops from the exit pressure to the pressure of the surroundings in a series of shocks which are highly nonisentropic. Sonic flow conditions are denoted by * ; sonic exit conditions are found by substituting $M_1 = M_1^* = 1$ into Eqs. (6-115) to (6-118).

$$\frac{p^*}{p_0} = \left(\frac{2}{k+1} \right)^{k/(k-1)} \quad (6-119)$$

$$\frac{T^*}{T_0} = \frac{2}{k+1} \quad (6-120)$$

$$\frac{\rho^*}{\rho_0} = \left(\frac{2}{k+1} \right)^{1/(k-1)} \quad (6-121)$$

$$G^* = p_0 \sqrt{\left(\frac{2}{k+1} \right)^{(k+1)/(k-1)} \left(\frac{kM_w}{RT_0} \right)} \quad (6-122)$$

Note that under choked conditions, the exit velocity is $V = V^* = c^* = \sqrt{kRT^*/M_w}$, not $\sqrt{kRT_0/M_w}$. Sonic velocity must be evaluated at the exit temperature. For air, with $k = 1.4$, the critical pressure ratio p^*/p_0 is 0.5285 and the critical temperature ratio $T^*/T_0 = 0.8333$. Thus, for air discharging from 300 K, the temperature drops by 50 K (90 R). This large temperature decrease results from the conversion of internal energy into kinetic energy and is reversible. As the discharged jet decelerates in the external stagnant gas, it recovers its initial enthalpy.

When it is desired to determine the discharge rate through a nozzle from upstream pressure p_0 to external pressure p_2 , Equations (6-115) through (6-122) are best used as follows. The critical pressure is first determined from Eq. (6-119). If $p_2 > p^*$, then the flow is subsonic (subcritical, unchoked). Then $p_1 = p_2$ and M_1 may be obtained from Eq. (6-115). Substitution of M_1 into Eq. (6-118) then gives the desired mass velocity G . Equations (6-116) and (6-117) may be used to find the exit temperature and density. On the other hand, if $p_2 \leq p^*$, then the flow is choked and $M_1 = 1$. Then $p_1 = p^*$, and the mass velocity is G^* obtained from Eq. (6-122). The exit temperature and density may be obtained from Eqs. (6-120) and (6-121).

When the flow is choked, $G = G^*$ is independent of external downstream pressure. Reducing the downstream pressure will not increase the flow. The mass flow rate under choking conditions is directly proportional to the upstream pressure.

Example 7: Flow through Frictionless Nozzle Air at p_0 and temperature $T_0 = 293$ K discharges through a frictionless nozzle to atmospheric pressure. Compute the discharge mass flux G , the pressure, temperature, Mach number, and velocity at the exit. Consider two cases: (1) $p_0 = 7 \times 10^5$ Pa absolute, and (2) $p_0 = 1.5 \times 10^5$ Pa absolute.

1. $p_0 = 7.0 \times 10^5$ Pa. For air with $k = 1.4$, the critical pressure ratio from Eq. (6-119) is $p^*/p_0 = 0.5285$ and $p^* = 0.5285 \times 7.0 \times 10^5 = 3.70 \times 10^5$ Pa. Since this is greater than the external atmospheric pressure $p_2 = 1.01 \times 10^5$ Pa, the flow is choked and the exit pressure is $p_1 = 3.70 \times 10^5$ Pa. The exit Mach number is 1.0, and the mass flux is equal to G^* given by Eq. (6-118).

$$G^* = 7.0 \times 10^5 \times \sqrt{\left(\frac{2}{1.4+1} \right)^{(1.4+1)/(1.4-1)} \left(\frac{1.4 \times 29}{8314 \times 293} \right)} = 1,650 \text{ kg/m}^2 \cdot \text{s}$$

The exit temperature, since the flow is choked, is

$$T^* = \left(\frac{T^*}{T_0} \right) T_0 = \left(\frac{2}{1.4+1} \right) \times 293 = 244 \text{ K}$$

The exit velocity is $V = Mc = c^* = \sqrt{kRT^*/M_w} = 313$ m/s.

2. $p_0 = 1.5 \times 10^5$ Pa. In this case $p^* = 0.79 \times 10^5$ Pa, which is less than p_2 . Hence, $p_1 = p_2 = 1.01 \times 10^5$ Pa. The flow is unchoked (subsonic). Equation (6-115) is solved for the Mach number.

$$\frac{1.5 \times 10^5}{1.01 \times 10^5} = \left(1 + \frac{1.4-1}{2} M_1^2 \right)^{1.4/(1.4-1)}$$

$$M_1 = 0.773$$

Substitution into Eq. (6-118) gives G .

$$G = 1.5 \times 10^5 \times \sqrt{\frac{1.4 \times 29}{8,314 \times 293}} \times \frac{0.773}{\left(1 + \frac{(1.4-1)}{2} \times 0.773^2\right)^{(1.4+1/2)(1.4-1)}} = 337 \text{ kg/m}^2 \cdot \text{s}$$

The exit temperature is found from Eq. (6-116) to be 261.6 K or -11.5°C . The exit velocity is

$$V = Mc = 0.773 \times \sqrt{\frac{1.4 \times 8314 \times 261.6}{29}} = 250 \text{ m/s}$$

Adiabatic Flow with Friction in a Duct of Constant Cross Section Integration of the differential forms of the continuity, momentum, and total energy equations for a perfect gas, assuming a constant friction factor, leads to a tedious set of simultaneous algebraic equations. These may be found in Shapiro (*Dynamics and Thermodynamics of Compressible Fluid Flow*, vol. I, Ronald Press, New York, 1953) or Zucrow and Hoffmann (*Gas Dynamics*, vol. I, Wiley, New York, 1976). Lapple's (*Trans. AICHE*, **39**, 395–432 [1943]) widely cited graphical presentation of the solution of these equations contained a subtle error, which was corrected by Levenspiel (*AICHE J.*, **23**, 402–403 [1977]). Levenspiel's graphical solutions are presented in Fig. 6-21. These charts refer to the physical situation illustrated in Fig. 6-22, where a perfect gas discharges from stagnation conditions in a large chamber through an isentropic nozzle followed by a duct of length L . The resistance parameter is $N = 4fL/D_H$, where $f = \text{Fanning friction factor}$ and $D_H = \text{hydraulic diameter}$.

The exit Mach number M_2 may not exceed unity. $M_2 = 1$ corresponds to choked flow; sonic conditions may exist only at the pipe exit. The mass velocity G° in the charts is the choked **mass flux for an isentropic nozzle** given by Eq. (6-118). For a pipe of finite length, the mass flux is less than G° under choking conditions. The curves in Fig. 6-21 become vertical at the choking point, where flow becomes independent of downstream pressure.

The equations for nozzle flow, Eqs. (6-114) through (6-118), remain valid for the nozzle section even in the presence of the discharge pipe. Equations (6-116) and (6-120), for the temperature variation, may also be used for the pipe, with M_2, p_2 replacing M_1, p_1 since they are valid for adiabatic flow, with or without friction.

The graphs in Fig. 6-21 are based on accurate calculations, but are difficult to interpolate precisely. While they are quite useful for rough estimates, precise calculations are best done using the equations for one-dimensional adiabatic flow with friction, which are suitable for computer programming. Let subscripts 1 and 2 denote two points along a pipe of diameter D , point 2 being downstream of point 1. From a given point in the pipe, where the Mach number is M , the additional length of pipe required to accelerate the flow to sonic velocity ($M = 1$) is denoted L_{max} and may be computed from

$$\frac{4fL_{\text{max}}}{D} = \frac{1-M^2}{kM^2} + \frac{k+1}{2k} \ln \left(\frac{\frac{k+1}{2} M^2}{1 + \frac{k-1}{2} M^2} \right) \quad (6-123)$$

With $L = \text{length of pipe between points 1 and 2}$, the change in Mach number may be computed from

$$\frac{4fL}{D} = \left(\frac{4fL_{\text{max}}}{D} \right)_1 - \left(\frac{4fL_{\text{max}}}{D} \right)_2 \quad (6-124)$$

Equations (6-116) and (6-113), which are valid for adiabatic flow with friction, may be used to determine the temperature and speed of sound at points 1 and 2. Since the mass flux $G = \rho v = \rho c M$ is constant, and $\rho = PM_w/RT$, the pressure at point 2 (or 1) can be found from G and the pressure at point 1 (or 2).

The additional frictional losses due to pipeline fittings such as elbows may be added to the velocity head loss $N = 4fL/D_H$ using the same velocity head loss values as for incompressible flow. This works well for fittings which do not significantly reduce the channel cross-sectional area, but may cause large errors when the flow area is greatly

reduced, as, for example, by restricting orifices. Compressible flow across restricting orifices is discussed in Sec. 10 of this *Handbook*. Similarly, elbows near the exit of a pipeline may choke the flow even though the Mach number is less than unity due to the nonuniform velocity profile in the elbow. For an abrupt contraction rather than rounded nozzle inlet, an additional 0.5 velocity head should be added to N . This is a reasonable approximation for G , but note that it allocates the additional losses to the pipeline, even though they are actually incurred in the entrance. It is an error to include one velocity head exit loss in N . The kinetic energy at the exit is already accounted for in the integration of the balance equations.

Example 8: Compressible Flow with Friction Losses Calculate the discharge rate of air to the atmosphere from a reservoir at 10^6 Pa gauge and 20°C through 10 m of straight 2-in Schedule 40 steel pipe (inside diameter = 0.0525 m), and 3 standard radius, flanged 90° elbows. Assume 0.5 velocity heads lost for the elbows.

For commercial steel pipe, with a roughness of 0.046 mm, the friction factor for fully rough flow is about 0.0047, from Eq. (6-38) or Fig. 6-9. It remains to be verified that the Reynolds number is sufficiently large to assume fully rough flow. Assuming an abrupt entrance with 0.5 velocity heads lost,

$$N = 4 \times 0.0047 \times \frac{10}{0.0525} + 0.5 + 3 \times 0.5 = 5.6$$

The pressure ratio p_3/p_0 is

$$\frac{1.01 \times 10^5}{(1 \times 10^6 + 1.01 \times 10^5)} = 0.092$$

From Fig. 6-21b at $N = 5.6$, $p_3/p_0 = 0.092$ and $k = 1.4$ for air, the flow is seen to be choked. At the choke point with $N = 5.6$ the critical pressure ratio p_2/p_0 is about 0.25 and G/G° is about 0.48. Equation (6-122) gives

$$G^\circ = 1.101 \times 10^6 \times \sqrt{\left(\frac{2}{1.4+1}\right)^{(1.4+1)(1.4-1)} \left(\frac{1.4 \times 29}{8,314 \times 293.15}\right)} = 2,600 \text{ kg/m}^2 \cdot \text{s}$$

Multiplying by $G/G^\circ = 0.48$ yields $G = 1,250 \text{ kg/m}^2 \cdot \text{s}$. The discharge rate is $w = GA = 1,250 \times \pi \times 0.0525^2/4 = 2.7 \text{ kg/s}$.

Before accepting this solution, the Reynolds number should be checked. At the pipe exit, the temperature is given by Eq. (6-120) since the flow is choked. Thus, $T_2 = T^* = 244.6 \text{ K}$. The viscosity of air at this temperature is about $1.6 \times 10^{-5} \text{ Pa} \cdot \text{s}$. Then

$$\text{Re} = \frac{DV\rho}{\mu} = \frac{DG}{\mu} = \frac{0.0525 \times 1,250}{1.6 \times 10^{-5}} = 4.1 \times 10^6$$

At the beginning of the pipe, the temperature is greater, giving greater viscosity and a Reynolds number of 3.6×10^6 . Over the entire pipe length the Reynolds number is very large and the fully rough flow friction factor choice was indeed valid.

Once the mass flux G has been determined, Fig. 6-21a or 6-21b can be used to determine the pressure at any point along the pipe, simply by reducing $4fL/D_H$ and computing p_2 from the figures, given G , instead of the reverse. Charts for calculation between two points in a pipe with known flow and known pressure at either upstream or downstream locations have been presented by Loeb (*Chem. Eng.*, **76**[5], 179–184 [1969]) and for known downstream conditions by Powley (*Can. J. Chem. Eng.*, **36**, 241–245 [1958]).

Convergent/Divergent Nozzles (De Laval Nozzles) During frictionless adiabatic one-dimensional flow with changing cross-sectional area A the following relations are obeyed:

$$\frac{dA}{A} = \frac{dp}{\rho V^2} (1 - M^2) = \frac{1 - M^2}{M^2} \frac{dp}{\rho} = -(1 - M^2) \frac{dV}{V} \quad (6-125)$$

Equation (6-125) implies that in converging channels, subsonic flows are accelerated and the pressure and density decrease. In diverging channels, subsonic flows are decelerated as the pressure and density increase. In subsonic flow, the converging channels act as nozzles and diverging channels as diffusers. In supersonic flows, the opposite is true. Diverging channels act as nozzles accelerating the flow, while converging channels act as diffusers decelerating the flow.

Figure 6-23 shows a converging/diverging nozzle. When p_2/p_0 is less than the critical pressure ratio (p^*/p_0), the flow will be subsonic in the converging portion of the nozzle, sonic at the throat, and supersonic in the diverging portion. At the throat, where the flow is critical and the velocity is sonic, the area is denoted A^* . The cross-sectional

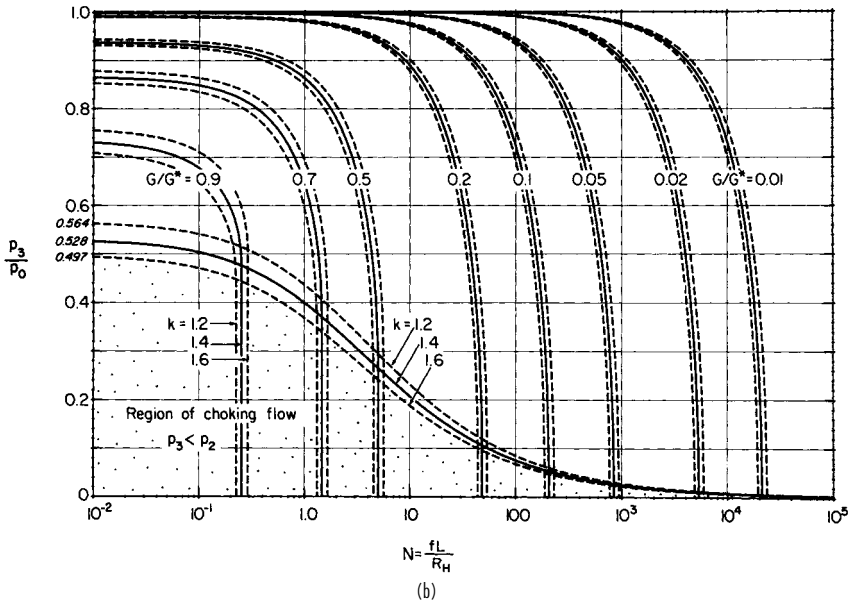
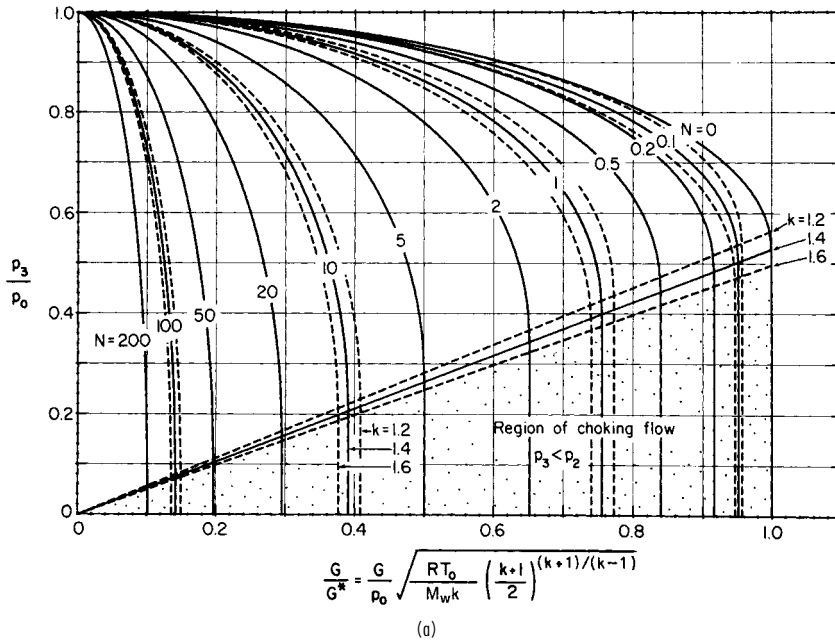


FIG. 6-21 Design charts for adiabatic flow of gases; (a) useful for finding the allowable pipe length for given flow rate; (b) useful for finding the discharge rate in a given piping system. (From Levenspiel, *Am. Inst. Chem. Eng. J.*, **23**, 402 [1977].)

area and pressure vary with Mach number along the converging/diverging flow path according to the following equations for isentropic flow of a perfect gas:

$$\frac{A}{A^*} = \frac{1}{M} \left[\frac{2}{k+1} \left(1 + \frac{k-1}{2} M^2 \right) \right]^{(k+1)/(2(k-1))} \quad (6-126)$$

$$\frac{p_0}{p} = \left(1 + \frac{k-1}{2} M^2 \right)^{k/(k-1)} \quad (6-127)$$

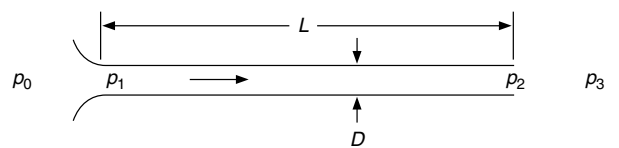


FIG. 6-22 Adiabatic compressible flow in a pipe with a well-rounded entrance.

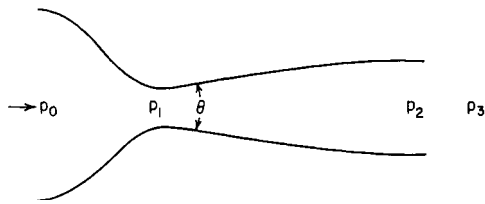


FIG. 6-23 Converging/diverging nozzle.

The temperature obeys the adiabatic flow equation for a perfect gas,

$$\frac{T_0}{T} = 1 + \frac{k-1}{2} M^2 \quad (6-128)$$

Equation (6-128) does not require frictionless (isentropic) flow. The sonic mass flux through the throat is given by Eq. (6-122). With A set equal to the nozzle exit area, the exit Mach number, pressure, and temperature may be calculated. Only if the exit pressure equals the ambient discharge pressure is the ultimate expansion velocity reached in the nozzle. Expansion will be incomplete if the exit pressure exceeds the ambient discharge pressure; shocks will occur outside the nozzle. If the calculated exit pressure is less than the ambient discharge pressure, the nozzle is overexpanded and compression shocks within the expanding portion will result.

The shape of the converging section is a smooth trumpet shape similar to the simple converging nozzle. However, special shapes of the diverging section are required to produce the maximum supersonic exit velocity. Shocks result if the divergence is too rapid and excessive boundary layer friction occurs if the divergence is too shallow. See Liepmann and Roshko (*Elements of Gas Dynamics*, Wiley, New York, 1957, p. 284). If the nozzle is to be used as a thrust device, the diverging section can be conical with a total included angle of 30° (Sutton, *Rocket Propulsion Elements*, 2d ed., Wiley, New York, 1956). To obtain large exit Mach numbers, slot-shaped rather than axisymmetric nozzles are used.

MULTIPHASE FLOW

Multiphase flows, even when restricted to simple pipeline geometry, are in general quite complex, and several features may be identified which make them more complicated than single-phase flow. Flow pattern description is not merely an identification of laminar or turbulent flow. The relative quantities of the phases and the topology of the interfaces must be described. Because of phase density differences, vertical flow patterns are different from horizontal flow patterns, and horizontal flows are not generally axisymmetric. Even when phase equilibrium is achieved by good mixing in two-phase flow, the changing equilibrium state as pressure drops with distance, or as heat is added or lost, may require that interphase mass transfer, and changes in the relative amounts of the phases, be considered.

Wallis (*One-dimensional Two-phase Flow*, McGraw-Hill, New York, 1969) and Govier and Aziz present mass, momentum, mechanical energy, and total energy balance equations for two-phase flows. These equations are based on one-dimensional behavior for each phase. Such equations, for the most part, are used as a framework in which to interpret experimental data. Reliable prediction of multiphase flow behavior generally requires use of data or correlations. **Two-fluid modeling**, in which the full three-dimensional microscopic (partial differential) equations of motion are written for each phase, treating each as a continuum, occupying a volume fraction which is a continuous function of position, is a rapidly developing technique made possible by improved computational methods. For some relatively simple examples not requiring numerical computation, see Pearson (*Chem. Engr. Sci.*, **49**, 727-732 [1994]). Constitutive equations for two-fluid models are not yet sufficiently robust for accurate general-purpose two-phase flow computation, but may be quite good for particular classes of flows.

Liquids and Gases For cocurrent flow of liquids and gases in vertical (upflow), horizontal, and inclined pipes, a very large literature of experimental and theoretical work has been published, with less work on countercurrent and cocurrent vertical downflow. Much of the effort has been devoted to predicting flow patterns, pressure drop, and volume fractions of the phases, with emphasis on fully developed flow. In practice, many two-phase flows in process plants are not fully developed.

The most reliable methods for fully developed gas/liquid flows use **mechanistic models** to predict flow pattern, and use different pressure drop and void fraction estimation procedures for each flow pattern. Such methods are too lengthy to include here, and are well suited to incorporation into computer programs; commercial codes for gas/liquid pipeline flows are available. Some key references for mechanistic methods for flow pattern transitions and flow regime-specific pressure drop and void fraction methods include Taitel and Dukler (*AIChE J.*, **22**, 47-55 [1976]), Barnea, et al. (*Int. J. Multiphase Flow*, **6**, 217-225 [1980]), Barnea (*Int. J. Multiphase Flow*, **12**, 733-744 [1986]), Taitel, Barnea, and Dukler (*AIChE J.*, **26**, 345-354 [1980]), Wallis (*One-dimensional Two-phase Flow*, McGraw-Hill, New York, 1969), and Dukler and Hubbard (*Ind. Eng. Chem. Fundam.*, **14**, 337-347 [1975]). For preliminary or approximate calculations, **flow pattern maps** and flow regime-independent empirical correlations, are simpler and faster to use. Such methods for horizontal and vertical flows are provided in the following.

In **horizontal pipe**, flow patterns for fully developed flow have been reported in numerous studies. Transitions between flow patterns are gradual, and subjective owing to the visual interpretation of individual investigators. In some cases, statistical analysis of pressure fluctuations has been used to distinguish flow patterns. Figure 6-24 (Alves, *Chem. Eng. Progr.*, **50**, 449-456 [1954]) shows seven flow patterns for horizontal gas/liquid flow. **Bubble flow** is prevalent at high ratios of liquid to gas flow rates. The gas is dispersed as bubbles which move at velocity similar to the liquid and tend to concentrate near the top of the pipe at lower liquid velocities. **Plug flow** describes a pattern in which alternate plugs of gas and liquid move along the upper part of the pipe. In **stratified flow**, the liquid flows along the bottom of the pipe and the gas flows over a smooth liquid/gas interface. Similar to stratified flow, **wavy flow** occurs at greater gas velocities and has waves moving in the flow direction. When wave crests are sufficiently high to bridge the pipe, they form frothy slugs which move at much greater than the average liquid velocity. **Slug flow** can cause severe and sometimes dangerous vibrations in equipment because of impact of the high-velocity slugs against bends or other fittings. Slugs may also flood gas/liquid separation equipment.

In **annular flow**, liquid flows as a thin film along the pipe wall and gas flows in the core. Some liquid is entrained as droplets in the gas

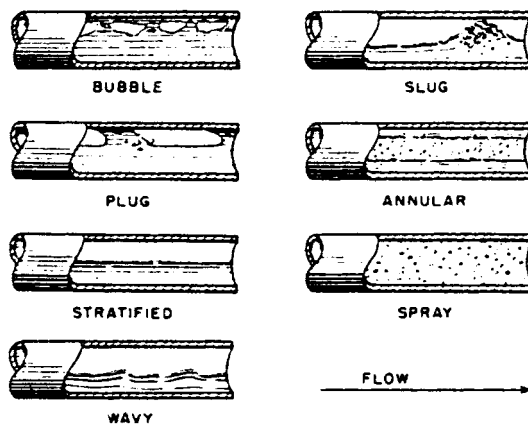


FIG. 6-24 Gas/liquid flow patterns in horizontal pipes. (From Alves, *Chem. Eng. Progr.*, **50**, 449-456 [1954].)

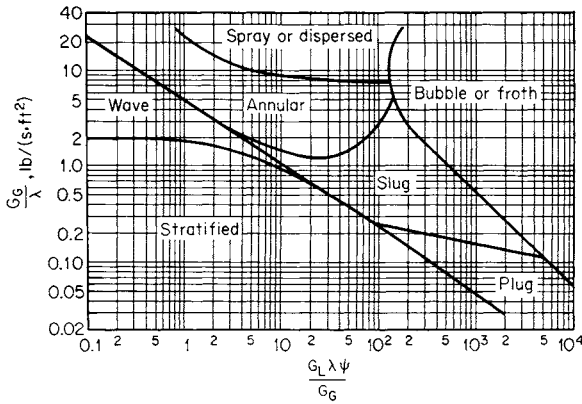


FIG. 6-25 Flow-pattern regions in cocurrent liquid/gas flow through horizontal pipes. To convert $\text{lbm}/(\text{ft}^2 \cdot \text{s})$ to $\text{kg}/(\text{m}^2 \cdot \text{s})$, multiply by 4.8824. (From Baker, *Oil Gas J.*, 53[12], 185–190, 192, 195 [1954].)

core. At very high gas velocities, nearly all the liquid is entrained as small droplets. This pattern is called **spray, dispersed, or mist flow**. Approximate prediction of flow pattern may be quickly done using **flow pattern maps**, an example of which is shown in Fig. 6-25 (Baker, *Oil Gas J.*, 53[12], 185–190, 192–195 [1954]). The Baker chart remains widely used; however, for critical calculations the mechanistic model methods referenced previously are generally preferred for their greater accuracy, especially for large pipe diameters and fluids with physical properties different from air/water at atmospheric pressure. In the chart,

$$\lambda = (\rho'_G \rho'_L)^{1/2} \tag{6-129}$$

$$\psi = \frac{1}{\sigma'} \left[\frac{\mu'_L}{(\rho'_L)^2} \right]^{1/3} \tag{6-130}$$

G_L and G_G are the liquid and gas mass velocities, μ'_L is the ratio of liquid viscosity to water viscosity, ρ'_G is the ratio of gas density to air density, ρ'_L is the ratio of liquid density to water density, and σ' is the ratio of liquid surface tension to water surface tension. The reference properties are at 20°C (68°F) and atmospheric pressure, water density 1,000 kg/m^3 (62.4 lbm/ft^3), air density 1.20 kg/m^3 (0.075 lbm/ft^3), water viscosity 0.001 $\text{Pa} \cdot \text{s}$ (1.0 cP), and surface tension 0.073 N/m (0.0050 lb/ft). The empirical parameters λ and ψ provide a crude accounting for physical properties. The Baker chart is dimensionally inconsistent since the dimensional quantity G_G/λ is plotted against a dimensionless one, $G_L\lambda\psi/G_G$, and so must be used with G_G in $\text{lbm}/(\text{ft}^2 \cdot \text{s})$ units on the ordinate. To convert to $\text{kg}/(\text{m}^2 \cdot \text{s})$, multiply by 4.8824.

Rapid approximate predictions of **pressure drop** for fully developed, incompressible horizontal gas/liquid flow may be made using the method of Lockhart and Martinelli (*Chem. Eng. Prog.*, 45, 39–48 [1949]). First, the pressure drops that would be expected for each of the two phases as if flowing alone in single-phase flow are calculated. The Lockhart-Martinelli parameter X is defined in terms of the ratio of these pressure drops:

$$X = \left[\frac{(\Delta p/L)_L}{(\Delta p/L)_G} \right]^{1/2} \tag{6-131}$$

The two-phase pressure drop may then be estimated from either of the single-phase pressure drops, using

$$\left(\frac{\Delta p}{L} \right)_{TP} = Y_L \left(\frac{\Delta p}{L} \right)_L \tag{6-132}$$

or

$$\left(\frac{\Delta p}{L} \right)_{TP} = Y_G \left(\frac{\Delta p}{L} \right)_G \tag{6-133}$$

where Y_L and Y_G are read from Fig. 6-26 as functions of X . The curve labels refer to the flow regime (laminar or turbulent) found for each of

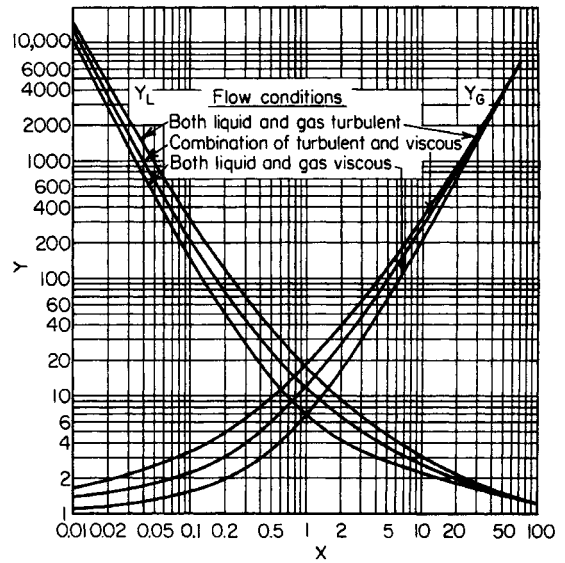


FIG. 6-26 Parameters for pressure drop in liquid/gas flow through horizontal pipes. (Based on Lockhart and Martinelli, *Chem. Eng. Prog.*, 45, 39 [1949].)

the phases flowing alone. The common turbulent-turbulent case is approximated well by

$$Y_L = 1 + \frac{20}{X} + \frac{1}{X^2} \tag{6-134}$$

Lockhart and Martinelli (ibid.) correlated pressure drop data from pipes 25 mm (1 in) in diameter or less within about ± 50 percent. In general, the predictions are high for stratified, wavy, and slug flows and low for annular flow. The correlation can be applied to pipe diameters up to about 0.1 m (4 in) with about the same accuracy.

The **volume fraction**, sometimes called **holdup**, of each phase in two-phase flow is generally not equal to its volumetric flow rate fraction, because of velocity differences, or **slip**, between the phases. For each phase, denoted by subscript i , the relations among superficial velocity V_b , in situ velocity v_b , volume fraction R_b , total volumetric flow rate Q_b , and pipe area A are

$$Q_i = V_i A = v_i R_i A \tag{6-135}$$

$$v_i = \frac{V_i}{R_i} \tag{6-136}$$

The **slip velocity** between gas and liquid is $v_s = v_G - v_L$. For two-phase gas/liquid flow, $R_L + R_G = 1$. A very common mistake in practice is to assume that in situ phase volume fractions are equal to input volume fractions.

For fully developed incompressible horizontal gas/liquid flow, a quick estimate for R_L may be obtained from Fig. 6-27, as a function of the Lockhart-Martinelli parameter X defined by Eq. (6-131). Indications are that liquid volume fractions may be overpredicted for liquids more viscous than water (Alves, *Chem. Eng. Prog.*, 50, 449–456 [1954]), and underpredicted for pipes larger than 25 mm diameter (Baker, *Oil Gas J.*, 53[12], 185–190, 192–195 [1954]).

A method for predicting pressure drop and volume fraction for **non-Newtonian fluids** in annular flow has been proposed by Eisenberg and Weinberger (*AIChE J.*, 25, 240–245 [1979]). Das, Biswas, and Matra (*Can. J. Chem. Eng.*, 70, 431–437 [1993]) studied holdup in both horizontal and vertical gas/liquid flow with non-Newtonian liquids. Farooqi and Richardson (*Trans. Inst. Chem. Engrs.*, 60, 292–305, 323–333 [1982]) developed correlations for holdup and pressure drop for gas/non-Newtonian liquid horizontal flow. They used a modified Lockhart-Martinelli parameter for non-Newtonian

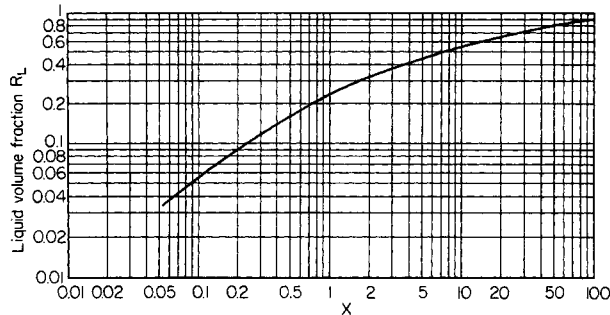


FIG. 6-27 Liquid volume fraction in liquid/gas flow through horizontal pipes. (From Lockhart and Martinelli, *Eng. Prog.*, **45**, 39 [1949].)

liquid holdup. They found that two-phase pressure drop may actually be less than the single-phase liquid pressure drop with shear thinning liquids in laminar flow.

Pressure drop data for a 1-in feed tee with the liquid entering the run and gas entering the branch are given by Alves (*Chem. Eng. Progr.*, **50**, 449–456 [1954]). Pressure drop and division of two-phase **annular flow in a tee** are discussed by Fouda and Rhodes (*Trans. Inst. Chem. Eng. [London]*, **52**, 354–360 [1974]). Flow through tees can result in unexpected flow splitting. Further reading on gas/liquid flow through tees may be found in Mudde, Groen, and van den Akker (*Int. J. Multiphase Flow*, **19**, 563–573 [1993]); Issa and Oliveira (*Computers and Fluids*, **23**, 347–372 [1993]) and Azzopardi and Smith (*Int. J. Multiphase Flow*, **18**, 861–875 [1992]).

Results by Chenoweth and Martin (*Pet. Refiner*, **34**[10], 151–155 [1955]) indicate that single-phase data for **fittings** and **valves** can be used in their correlation for two-phase pressure drop. Smith, Murdock, and Applebaum (*J. Eng. Power*, **99**, 343–347 [1977]) evaluated existing correlations for two-phase flow of steam/water and other gas/liquid mixtures through sharp-edged **orifices** meeting ASTM standards for flow measurement. The correlation of Murdock (*J. Basic Eng.*, **84**, 419–433 [1962]) may be used for these orifices. See also Collins and Gaceta (*J. Basic Eng.*, **93**, 11–21 [1971]), for measurements with steam and water beyond the limits of this correlation.

For pressure drop and holdup in **inclined pipe** with upward or downward flow, see Beggs and Brill (*J. Pet. Technol.*, **25**, 607–617 [1973]); the mechanistic model methods referenced above may also be applied to inclined pipes. Up to 10° from horizontal, upward pipe inclination has little effect on holdup (Gregory, *Can. J. Chem. Eng.*, **53**, 384–388 [1975]).

For fully developed incompressible **cocurrent upflow** of gases and liquids in **vertical pipes**, a variety of flow pattern terminologies and descriptions have appeared in the literature; some of these have been summarized and compared by Govier, Radford, and Dunn (*Can. J. Chem. Eng.*, **35**, 58–70 [1957]). One reasonable classification of patterns is illustrated in Fig. 6-28.

In **bubble flow**, gas is dispersed as bubbles throughout the liquid, but with some tendency to concentrate toward the center of the pipe. In **slug flow**, the gas forms large **Taylor bubbles** of diameter nearly equal to the pipe diameter. A thin film of liquid surrounds the Taylor bubble. Between the Taylor bubbles are liquid slugs containing some bubbles. **Froth** or **churn flow** is characterized by strong intermittency and intense mixing, with neither phase easily described as continuous or dispersed. There remains disagreement in the literature as to whether churn flow is a real fully developed flow pattern or is an indication of large entry length for developing slug flow (Zao and Dukler, *Int. J. Multiphase Flow*, **19**, 377–383 [1993]; Hewitt and Jayanti, *Int. J. Multiphase Flow*, **19**, 527–529 [1993]).

Ripple flow has an upward-moving wavy layer of liquid on the pipe wall; it may be thought of as a transition region to **annular**, **annular mist**, or **film flow**, in which gas flows in the core of the pipe while an annulus of liquid flows up the pipe wall. Some of the liquid is

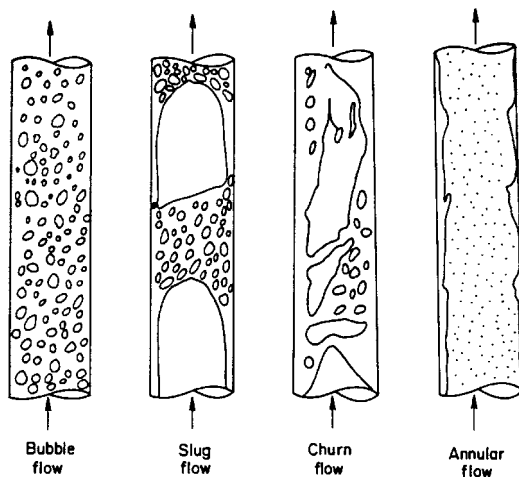


FIG. 6-28 Flow patterns in cocurrent upward vertical gas/liquid flow. (From Taitel, Barnea, and Dukler, *AIChE J.*, **26**, 345–354 [1980]. Reproduced by permission of the American Institute of Chemical Engineers © 1980 AIChE. All rights reserved.)

entrained as droplets in the gas core. **Mist flow** occurs when all the liquid is carried as fine drops in the gas phase; this pattern occurs at high gas velocities, typically 20 to 30 m/s (66 to 98 ft/s).

The correlation by Govier, et al. (*Can. J. Chem. Eng.*, **35**, 58–70 [1957]), Fig. 6-29, may be used for quick estimate of flow pattern.

Slip, or relative velocity between phases, occurs for vertical flow as well as for horizontal. No completely satisfactory, flow regime-independent correlation for volume fraction or holdup exists for vertical flow. Two frequently used flow regime-independent methods are those by Hughmark and Pressburg (*AIChE J.*, **7**, 677 [1961]) and Hughmark (*Chem. Eng. Prog.*, **58**[4], 62 [April 1962]). **Pressure drop in upflow** may be calculated by the procedure described in Hughmark (*Ind. Eng. Chem. Fundam.*, **2**, 315–321 [1963]). The mechanistic, flow regime-based methods are advisable for critical applications.

For **upflow in helically coiled tubes**, the flow pattern, pressure drop, and holdup can be predicted by the correlations of Banerjee, Rhodes, and Scott (*Can. J. Chem. Eng.*, **47**, 445–453 [1969]) and

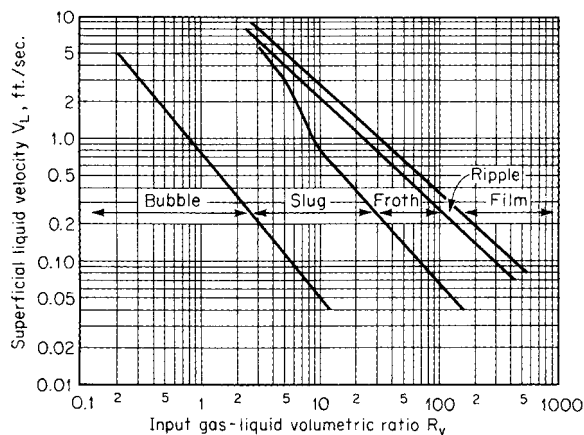


FIG. 6-29 Flow-pattern regions in cocurrent liquid/gas flow in upflow through vertical pipes. To convert ft/s to m/s, multiply by 0.3048. (From Govier, Radford, and Dunn, *Can. J. Chem. Eng.*, **35**, 58–70 [1957].)

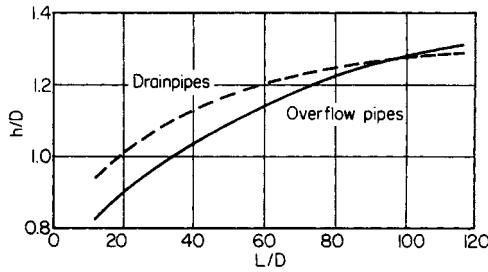


FIG. 6-30 Critical head for drain and overflow pipes. (From Kalinske, Univ. Iowa Stud. Eng., Bull. 26 [1939-1940].)

Akagawa, Sakaguchi, and Ueda (*Bull JSME*, **14**, 564-571 [1971]). Correlations for flow patterns in **downflow** in vertical pipe are given by Oshinowo and Charles (*Can. J. Chem. Eng.*, **52**, 25-35 [1974]) and Barnea, Shoham, and Taitel (*Chem. Eng. Sci.*, **37**, 741-744 [1982]). Use of **drift flux theory** for void fraction modeling in downflow is presented by Clark and Flemmer (*Chem. Eng. Sci.*, **39**, 170-173 [1984]). **Downward inclined** two-phase flow data and modeling are given by Barnea, Shoham, and Taitel (*Chem. Eng. Sci.*, **37**, 735-740 [1982]). Data for **downflow in helically coiled tubes** are presented by Casper (*Chem. Ing. Tech.*, **42**, 349-354 [1970]).

The entrance to a **drain** is flush with a horizontal surface, while the entrance to an **overflow** pipe is above the horizontal surface. When such pipes do not run full, considerable amounts of gas can be drawn down by the liquid. The amount of gas entrained is a function of pipe diameter, pipe length, and liquid flow rate, as well as the drainpipe outlet boundary condition. Extensive data on air entrainment and liquid head above the entrance as a function of water flow rate for pipe diameters from 43.9 to 148.3 mm (1.7 to 5.8 in) and lengths from about 1.22 to 5.18 m (4.0 to 17.0 ft) are reported by Kalinske (*Univ. Iowa Stud. Eng., Bull.* 26, pp. 26-40 [1939-1940]). For heads greater than the critical, the pipes will run full with no entrainment. The critical head h for flow of water in drains and overflow pipes is given in Fig. 6-30. Kalinske's results show little effect of the height of protrusion of overflow pipes when the protrusion height is greater than about one pipe diameter. For conservative design, McDuffie (*AIChE J.*, **23**, 37-40 [1977]) recommends the following relation for minimum liquid height to prevent entrainment.

$$Fr \leq 1.6 \left(\frac{h}{D} \right)^2 \quad (6-137)$$

where the Froude number is defined by

$$Fr \equiv \frac{V_L}{\sqrt{g(\rho_L - \rho_C)D/\rho_L}} \quad (6-138)$$

where g = acceleration due to gravity

V_L = liquid velocity in the drain pipe

ρ_L = liquid density

ρ_C = gas density

D = pipe inside diameter

h = liquid height

For additional information, see Simpson (*Chem. Eng.*, **75**[6], 192-214 [1968]). A critical Froude number of 0.31 to ensure vented flow is widely cited. Recent results (Thorpe, *3d Int. Conf. Multi-phase Flow*, The Hague, Netherlands, 18-20 May 1987, paper K2, and *4th Int. Conf. Multi-phase Flow*, Nice, France, 19-21 June 1989, paper K4) show hysteresis, with different critical Froude numbers for flooding and unflowing of drain pipes, and the influence of end effects. Wallis, Crowley, and Hagi (*Trans. ASME J. Fluids Eng.*, 405-413 [June 1977]) examine the conditions for horizontal discharge pipes to run full.

Flashing flow and **condensing flow** are two examples of multi-phase flow with **phase change**. Flashing flow occurs when pressure drops below the bubble point pressure of a flowing liquid. A frequently

used one-dimensional model for flashing flow through nozzles and pipes is the **homogeneous equilibrium model** which assumes that both phases move at the same in situ velocity, and maintain vapor/liquid equilibrium. It may be shown that a **critical flow** condition, analogous to sonic or critical flow during compressible gas flow, is given by the following expression for the mass flux G in terms of the derivative of pressure p with respect to mixture density ρ_m at constant entropy:

$$G_{\text{crit}} = \rho_m \sqrt{\left(\frac{\partial p}{\partial \rho_m} \right)_s} \quad (6-139)$$

The corresponding acoustic velocity $\sqrt{(\partial p / \partial \rho_m)_s}$ is normally much less than the acoustic velocity for gas flow. The mixture density is given in terms of the individual phase densities and the **quality** (mass flow fraction vapor) x by

$$\frac{1}{\rho_m} = \frac{x}{\rho_C} + \frac{1-x}{\rho_L} \quad (6-140)$$

Choked and unchoked flow situations arise in pipes and nozzles in the same fashion for homogeneous equilibrium flashing flow as for gas flow. For nozzle flow from stagnation pressure p_0 to exit pressure p_1 , the mass flux is given by

$$G^2 = -2\rho_{m1}^2 \int_{p_0}^{p_1} \frac{dp}{\rho_m} \quad (6-141)$$

The integration is carried out over an isentropic flash path: flashes at constant entropy must be carried out to evaluate ρ_m as a function of p . Experience shows that isenthalpic flashes provide good approximations unless the liquid mass fraction is very small. Choking occurs when G obtained by Eq. (6-141) goes through a maximum at a value of p_1 greater than the external discharge pressure. Equation (6-139) will also be satisfied at that point. In such a case the pressure at the nozzle exit equals the choking pressure and flashing shocks occur outside the nozzle exit.

For homogeneous flow in a pipe of diameter D , the differential form of the Bernoulli equation (6-15) rearranges to

$$\frac{dp}{\rho_m} + g dz + \frac{G^2}{\rho_m} d \frac{1}{\rho_m} + 2f \frac{dx'}{D} \frac{G^2}{\rho_m^2} = 0 \quad (6-142)$$

where x' is distance along the pipe. Integration over a length L of pipe assuming constant friction factor f yields

$$G^2 = \frac{-\int_{p_1}^{p_2} \rho_m dp - g \int_{z_1}^{z_2} \rho_m^2 dz}{\ln(\rho_{m1}/\rho_{m2}) + 2fL/D} \quad (6-143)$$

Frictional pipe flow is not isentropic. Strictly speaking, the flashes must be carried out at constant $h + V^2/2 + gz$, where h is the enthalpy per unit mass of the two-phase flashing mixture. The flash calculations are fully coupled with the integration of the Bernoulli equation; the velocity V must be known at every pressure p to evaluate ρ_m . Computational routines, employing the thermodynamic and material balance features of flowsheet simulators, are the most practical way to carry out such flashing flow calculations, particularly when multicomponent systems are involved. Significant simplification arises when the mass fraction liquid is large, for then the effect of the $V^2/2$ term on the flash splits may be neglected. If elevation effects are also negligible, the flash computations are decoupled from the Bernoulli equation integration. For many horizontal flashing flow calculations, this is satisfactory and the flash computations may be carried out first, to find ρ_m as a function of p from p_1 to p_2 , which may then be substituted into Eq. (6-143).

With flashes carried out along the appropriate thermodynamic paths, the formalism of Eqs. (6-139) through (6-143) applies to all homogeneous equilibrium compressible flows, including, for example, flashing flow, ideal gas flow, and nonideal gas flow. Equation (6-118), for example, is a special case of Eq. (6-141) where the quality $x = 1$ and the vapor phase is a perfect gas.

Various **nonequilibrium** and **slip** flow models have been proposed as improvements on the homogeneous equilibrium flow model. See, for example, Henry and Fauske (*Trans. ASME J. Heat Transfer*, 179-187 [May 1971]). Nonequilibrium and slip effects both increase

computed mass flux for fixed pressure drop, compared to homogeneous equilibrium flow. For flow paths greater than about 100 mm, homogeneous equilibrium behavior appears to be the best assumption (Fischer, et al., *Emergency Relief System Design Using DIERS Technology*, AIChE, New York [1992]). For shorter flow paths, the best estimate may sometimes be given by linearly interpolating (as a function of length) between **frozen flow** (constant quality, no flashing) at 0 length and equilibrium flow at 100 mm.

In a series of papers by Leung and coworkers (*AIChE J.*, **32**, 1743–1746 [1986]; **33**, 524–527 [1987]; **34**, 688–691 [1988]; *J. Loss Prevention Proc. Ind.*, **2**[2], 78–86 [April 1989]; **3**[1], 27–32 [January 1990]; *Trans. ASME J. Heat Transfer*, **112**, 524–528, 528–530 [1990]; **113**, 269–272 [1991]) approximate techniques have been developed for homogeneous equilibrium calculations based on pseudo-equation of state methods for flashing mixtures.

Relatively less work has been done on **condensing flows**. Slip effects are more important for condensing than for flashing flows. Soliman, Schuster, and Berenson (*J. Heat Transfer*, **90**, 267–276 [1968]) give a model for condensing vapor in **horizontal pipe**. They assume the condensate flows as an annular ring. The Lockhart-Martinelli correlation is used for the frictional pressure drop. To this pressure drop is added an acceleration term based on homogeneous flow, equivalent to the $C^2 d(1/\rho_m)$ term in Eq. (6-142). Pressure drop is computed by integration of the incremental pressure changes along the length of pipe.

For **condensing vapor in vertical downflow**, in which the liquid flows as a thin annular film, the frictional contribution to the pressure drop may be estimated based on the gas flow alone, using the friction factor plotted in Fig. 6-31, where Re_c is the Reynolds number for the gas flowing alone (Bergelin et al., *Proc. Heat Transfer Fluid Mech. Inst.*, ASME, June 22–24, 1949, pp. 19–28).

$$-\frac{dp}{dz} = \frac{2f_c \rho_c V_c^2}{D} \quad (6-144)$$

To this should be added the $C_c^2 d(1/\rho_c)/dx$ term to account for velocity change effects.

Gases and Solids The flow of gases and solids in **horizontal pipe** is usually classified as either **dilute phase** or **dense phase** flow. Unfortunately, there is no clear delineation between the two types of flow, and the **dense phase** description may take on more than one meaning, creating some confusion (Knowlton et al., *Chem. Eng. Progr.*, **90**[4], 44–54 [April 1994]). For dilute phase flow, achieved at low solids-to-gas weight ratios (loadings), and high gas velocities, the solids may be fully suspended and fairly uniformly dispersed over the pipe cross section (homogeneous flow), particularly for low-density or small particle size solids. At lower gas velocities, the solids may

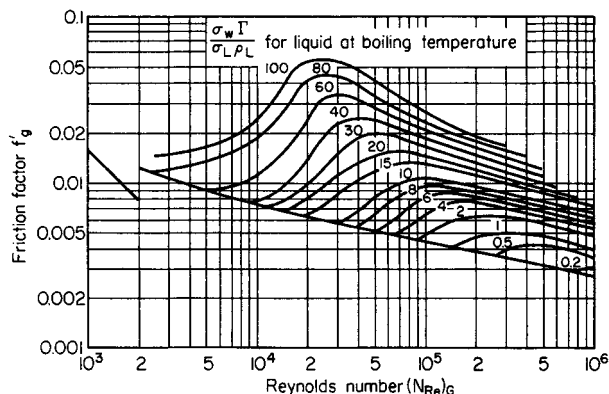


FIG. 6-31 Friction factors for condensing liquid/gas flow downward in vertical pipe. In this correlation $\Gamma/\rho L$ is in ft^2/h . To convert ft^2/h to m^2/s , multiply by 0.00155. (From Bergelin et al., *Proc. Heat Transfer Fluid Mech. Inst.*, ASME, 1949, p. 19.)

bounce along the bottom of the pipe. With higher loadings and lower gas velocities, the particles may settle to the bottom of the pipe, forming dunes, with the particles moving from dune to dune. In dense phase conveying, solids tend to concentrate in the lower portion of the pipe at high gas velocity. As gas velocity decreases, the solids may first form dense moving strands, followed by slugs. Discrete plugs of solids may be created intentionally by timed injection of solids, or the plugs may form spontaneously. Eventually the pipe may become blocked. For more information on flow patterns, see Coulson and Richardson (*Chemical Engineering*, vol. 2, 2d ed., Pergamon, New York, 1968, p. 583); Korn (*Chem. Eng.*, **57**[3], 108–111 [1950]); Patterson (*J. Eng. Power*, **81**, 43–54 [1959]); Wen and Simons (*AIChE J.*, **5**, 263–267 [1959]); and Knowlton et al. (*Chem. Eng. Progr.*, **90**[4], 44–54 [April 1994]).

For the **minimum velocity** required to prevent formation of dunes or settled beds in **horizontal flow**, some data are given by Zenz (*Ind. Eng. Chem. Fundam.*, **3**, 65–75 [1964]), who presented a correlation for the minimum velocity required to keep particles from depositing on the bottom of the pipe. This rather tedious estimation procedure may also be found in Govier and Aziz, who provide additional references and discussion on transition velocities. In practice, the actual conveying velocities used in systems with loadings less than 10 are generally over 15 m/s, (49 ft/s) while for high loadings (>20) they are generally less than 7.5 m/s (24.6 ft/s) and are roughly twice the actual solids velocity (Wen and Simons, *AIChE J.*, **5**, 263–267 [1959]).

Total pressure drop for horizontal gas/solid flow includes acceleration effects at the entrance to the pipe and frictional effects beyond the entrance region. A great number of correlations for pressure gradient are available, none of which is applicable to all flow regimes. Govier and Aziz review many of these and provide recommendations on when to use them.

For **upflow** of gases and solids in **vertical pipes**, the **minimum conveying velocity** for low loadings may be estimated as twice the terminal settling velocity of the largest particles. Equations for terminal settling velocity are found in the “Particle Dynamics” subsection, following. **Choking** occurs as the velocity is dropped below the minimum conveying velocity and the solids are no longer transported, collapsing into solid plugs (Knowlton, et al., *Chem. Eng. Progr.*, **90**[4], 44–54 [April 1994]). See Smith (*Chem. Eng. Sci.*, **33**, 745–749 [1978]) for an equation to predict the onset of choking.

Total pressure drop for vertical upflow of gases and solids includes acceleration and frictional effects also found in horizontal flow, plus potential energy or hydrostatic effects. Govier and Aziz review many of the pressure drop calculation methods and provide recommendations for their use. See also Yang (*AIChE J.*, **24**, 548–552 [1978]).

Drag reduction has been reported for low loadings of small diameter particles (<60 μm diameter), ascribed to damping of turbulence near the wall (Rossettia and Pfeffer, *AIChE J.*, **18**, 31–39 [1972]).

For **dense phase transport in vertical pipes** of small diameter, see Sandy, Daubert, and Jones (*Chem. Eng. Progr.*, **66**, *Symp. Ser.*, 105, 133–142 [1970]).

The **flow of bulk solids through restrictions and bins** is discussed in symposium articles (*J. Eng. Ind.*, **91**[2] [1969]) and by Stepanoff (*Gravity Flow of Bulk Solids and Transportation of Solids in Suspension*, Wiley, New York, 1969). Some problems encountered in discharge from bins include (Knowlton et al., *Chem. Eng. Progr.*, **90**[4], 44–54 [April 1994]) flow stoppage due to **ratholing** or **arching**, **segregation** of fine and coarse particles, **flooding** upon collapse of ratholes, and poor **residence time distribution** when **funnel flow** occurs.

Solid and Liquids Slurry flow may be divided roughly into two categories based on settling behavior (see Etchells in Shamlou, *Processing of Solid-Liquid Suspensions*, Chap. 12, Butterworth-Heinemann, Oxford, 1993). **Nonsettling** slurries are made up of very fine, highly concentrated, or neutrally buoyant particles. These slurries are normally treated as pseudohomogeneous fluids. They may be quite viscous and are frequently non-Newtonian. Slurries of particles that tend to settle out rapidly are called **settling slurries** or **fast-settling slurries**. While in some cases positively buoyant solids are encountered, the present discussion will focus on solids which are more dense than the liquid.

For **horizontal flow of fast-settling slurries**, the following rough description may be made (Govier and Aziz). Ultrafine particles, 10 μm

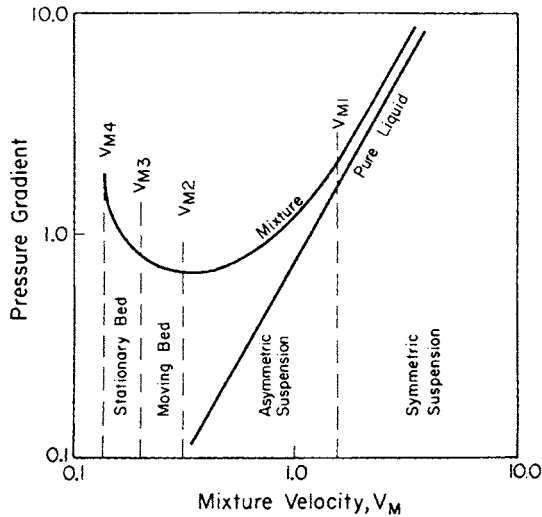


FIG. 6-32 Flow pattern regimes and pressure gradients in horizontal slurry flow. (From Govier and Aziz, *The Flow of Complex Mixtures in Pipes*, Van Nostrand Reinhold, New York, 1972.)

or smaller, are generally fully suspended and the particle distributions are not influenced by gravity. Fine particles 10 to 100 μm (3.3×10^{-5} to 33×10^{-5} ft) are usually fully suspended, but gravity causes concentration gradients. Medium-size particles, 100 to 1000 μm , may be fully suspended at high velocity, but often form a moving deposit on the bottom of the pipe. Coarse particles, 1,000 to 10,000 μm (0.0033 to 0.033 ft), are seldom fully suspended and are usually conveyed as a moving deposit. Ultracoarse particles larger than 10,000 μm (0.033 ft) are not suspended at normal velocities unless they are unusually light.

Figure 6-32, taken from Govier and Aziz, schematically indicates four flow pattern regions superimposed on a plot of pressure gradient vs. mixture velocity $V_M = V_L + V_S = (Q_L + Q_S)/A$ where V_L and V_S are the superficial liquid and solid velocities, Q_L and Q_S are liquid and solid volumetric flow rates, and A is the pipe cross-sectional area. V_{M4} is the transition velocity above which a bed exists in the bottom of the pipe, part of which is stationary and part of which moves by saltation, with the upper particles tumbling and bouncing over one another, often with formation of dunes. With a broad particle-size distribution, the finer particles may be fully suspended. Near V_{M4} , the pressure gradient rapidly increases as V_M decreases. Above V_{M3} , the entire bed moves. Above V_{M2} , the solids are fully suspended; that is, there is no deposit, moving or stationary, on the bottom of the pipe. However, the concentration distribution of solids is asymmetric. This flow pattern is the most frequently used for fast-settling slurry transport. Typical mixture velocities are in the range of 1 to 3 m/s (3.3 to 9.8 ft/s). The minimum in the pressure gradient is found to be near V_{M2} . Above V_{M1} , the particles are symmetrically distributed, and the pressure gradient curve is nearly parallel to that for the liquid by itself.

The most important transition velocity, often regarded as the minimum transport or conveying velocity for settling slurries, is V_{M2} . The Durand equation (Durand, Minnesota Int. Hydraulics Conf., *Proc.*, 89, Int. Assoc. for Hydraulic Research [1953]; Durand and Condolios, *Proc. Colloq. On the Hyd. Transport of Solids in Pipes*, Nat. Coal Board [UK], Paper IV, 39-35 [1952]) gives the minimum transport velocity as

$$V_{M2} = F_L [2gD(s - 1)]^{0.5} \tag{6-145}$$

- where g = acceleration of gravity
- D = pipe diameter
- $s = \rho_s/\rho_L$ = ratio of solid to liquid density
- F_L = a factor influenced by particle size and concentration

Probably F_L is a function of particle Reynolds number and concentration, but Fig. 6-33 gives Durand's empirical correlation for F_L as a function of particle diameter and the input, feed volume fraction

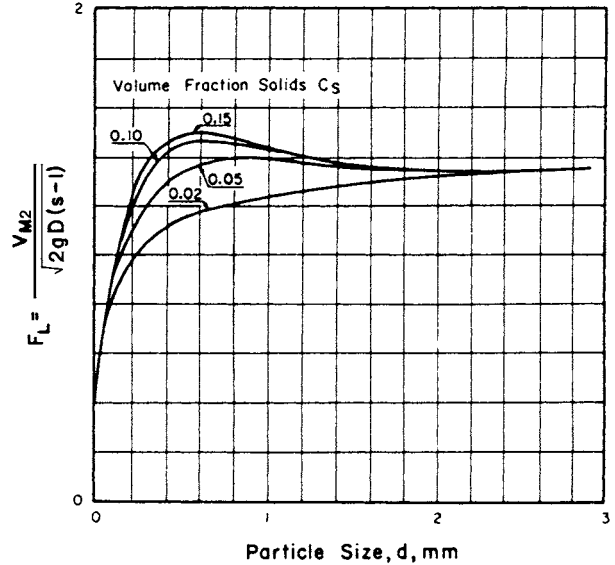


FIG. 6-33 Durand factor for minimum suspension velocity. (From Govier and Aziz, *The Flow of Complex Mixtures in Pipes*, Van Nostrand Reinhold, New York, 1972.)

solids, $C_s = Q_s/(Q_s + Q_L)$. The form of Eq. (6-145) may be derived from turbulence theory, as shown by Davies (*Chem. Eng. Sci.*, **42**, 1667-1670 [1987]).

No single correlation for **pressure drop** in horizontal solid/liquid flow has been found satisfactory for all particle sizes, densities, concentrations, and pipe sizes. However, with reference to Fig. 6-32, the following simplifications may be considered. The minimum pressure gradient occurs near V_{M2} and for conservative purposes it is generally desirable to exceed V_{M2} . When V_{M2} is exceeded, a rough guide for pressure drop is 25 percent greater than that calculated assuming that the slurry behaves as a pseudohomogeneous fluid with the density of the mixture and the viscosity of the liquid. Above the transition velocity to symmetric suspension, V_{M1} , the pressure drop closely approaches the pseudohomogeneous pressure drop. The following correlation by Spells (*Trans. Inst. Chem. Eng. [London]*, **33**, 79-84 [1955]) may be used for V_{M1} .

$$V_{M1}^2 = 0.075 \left(\frac{DV_{M1}\rho_M}{\mu} \right)^{0.775} gD_s(s - 1) \tag{6-146}$$

- where D = pipe diameter
- D_s = particle diameter (such that 85 percent by weight of particles are smaller than D_s)
- ρ_M = the slurry mixture density
- μ = liquid viscosity
- $s = \rho_s/\rho_L$ = ratio of solid to liquid density

Between V_{M2} and V_{M1} the concentration of solids gradually becomes more uniform in the vertical direction. This transition has been modeled by several authors as a concentration gradient where turbulent diffusion balances gravitational settling. See, for example, Karabelas (*AIChE J.*, **23**, 426-434 [1977]).

Published correlations for pressure drop are frequently very complicated and tedious to use, may not offer significant accuracy advantages over the simple guide given here, and many of them are applicable only for velocities above V_{M2} . One which does include the effect of sliding beds is due to Gaessler (Doctoral Dissertation, Technische Hochschule, Karlsruhe, Germany [1967]; reproduced by Govier and Aziz, pp. 668-669). Turian and Yuan (*AIChE J.*, **23**, 232-243 [1977]; see also Turian and Oroskar, *AIChE J.*, **24**, 1144 [1978]) segregated a large body of data into four flow regime groups

and developed empirical correlations for predicting pressure drop in each flow regime.

Pressure drop data for the flow of **paper stock** in pipes are given in the data section of *Standards of the Hydraulic Institute* (Hydraulic Institute, 1965). The flow behavior of fiber suspensions is discussed by Bobkovicz and Gauvin (*Chem. Eng. Sci.*, **22**, 229–241 [1967]), Bugliarello and Daily (*TAPPI*, **44**, 881–893 [1961]), and Daily and Bugliarello (*TAPPI*, **44**, 497–512 [1961]).

In **vertical flow** of fast-settling slurries, the in situ concentration of solids with density greater than the liquid will exceed the feed concentration $C = Q_s/(Q_s + Q_l)$ for upflow and will be smaller than C for downflow. This results from slip between the phases. The **slip velocity**, the difference between the in situ average velocities of the two phases, is roughly equal to the terminal settling velocity of the solids in the liquid. Specification of the slip velocity for a pipe of a given diameter, along with the phase flow rates, allows calculation of in situ volume fractions, average velocities, and holdup ratios by simple material balances. Slip velocity may be affected by particle concentration and by turbulence conditions in the liquid. **Drift-flux theory**, a framework incorporating certain functional forms for empirical expressions for slip velocity, is described by Wallis (*One-Dimensional Two-Phase Flow*, McGraw-Hill, New York, 1969). **Minimum transport velocity** for upflow for design purposes is usually taken as twice the particle settling velocity. **Pressure drop** in vertical pipe flow includes the effects of kinetic and potential energy (elevation) changes and friction. Rose and Duckworth (*The Engineer*, **227**[5,903], 392 [1969]; **227**[5,904], 430 [1969]; **227**[5,905], 478 [1969]; see also Govier and Aziz, pp. 487–493) have developed a calculation procedure including all these effects, which may be applied not only to vertical solid/liquid flow, but also to gas/solid flow and to horizontal flow.

For fast-settling slurries, ensuring conveyance is usually the key design issue while pressure drop is somewhat less important. For **nonsettling slurries** conveyance is not an issue, because the particles do not separate from the liquid. Here, viscous and rheological behavior, which control pressure drop, take on critical importance.

Fine particles, often at high concentration, form nonsettling slurries for which useful design equations can be developed by treating them as homogeneous fluids. These fluids are usually very viscous and often non-Newtonian. Shear-thinning and Bingham plastic behavior are common; dilatancy is sometimes observed. Rheology of such fluids must in general be empirically determined, although theoretical results are available for some very limited circumstances. Further discussion of both fast-settling and nonsettling slurries may be found in Shook (in Shamlou, *Processing of Solid-Liquid Suspensions*, Chap. 11, Butterworth-Heinemann, Oxford, 1993).

FLUID DISTRIBUTION

Uniform fluid distribution is essential for efficient operation of chemical-processing equipment such as contactors, reactors, mixers, burners, heat exchangers, extrusion dies, and textile-spinning chimneys. To obtain optimum distribution, proper consideration must be given to flow behavior in the distributor, flow conditions upstream and downstream of the distributor, and the distribution requirements of the equipment. Even though the principles of fluid distribution have been well developed for more than three decades, they are frequently overlooked by equipment designers, and a significant fraction of process equipment needlessly suffers from maldistribution. In this subsection, guides for the design of various types of fluid distributors, taking into account only the flow behavior within the distributor, are given.

Perforated-Pipe Distributors The simple perforated pipe or sparger (Fig. 6-34) is a common type of distributor. As shown, the flow



FIG. 6-34 Perforated-pipe distributor.

distribution is uniform; this is the case in which pressure recovery due to kinetic energy or momentum changes, frictional pressure drop along the length of the pipe, and pressure drop across the outlet holes have been properly considered. In typical turbulent flow applications, inertial effects associated with velocity changes may dominate frictional losses in determining the pressure distribution along the pipe, unless the length between orifices is large. Application of the momentum or mechanical energy equations in such a case shows that the pressure inside the pipe increases with distance from the entrance of the pipe. If the outlet holes are uniform in size and spacing, the discharge flow will be biased toward the closed end. Disturbances upstream of the distributor, such as pipe bends, may increase or decrease the flow to the holes at the beginning of the distributor. When frictional pressure drop dominates the inertial pressure recovery, the distribution is biased toward the feed end of the distributor.

For turbulent flow, with roughly uniform distribution, assuming a constant friction factor, the combined effect of friction and inertial (momentum) pressure recovery is given by

$$\Delta p = \left(\frac{4fL}{3D} - 2K \right) \frac{\rho V_i^2}{2} \quad (\text{discharge manifolds}) \quad (6-147)$$

where Δp = net pressure drop over the length of the distributor

L = pipe length

D = pipe diameter

f = Fanning friction factor

V_i = distributor inlet velocity

The factor K would be 1 in the case of full momentum recovery, or 0.5 in the case of negligible viscous losses in the portion of flow which remains in the pipe after the flow divides at a takeoff point (Denn, pp. 126–127). Experimental data (Van der Hegge Zijnen, *Appl. Sci. Res.*, **A3**, 144–162 [1951–1953]; and Bailey, *J. Mech. Eng. Sci.*, **17**, 338–347 [1975]), while scattered, show that K is probably close to 0.5 for discharge manifolds. For inertially dominated flows, Δp will be negative. For **return manifolds** the recovery factor K is close to 1.0, and the pressure drop between the first hole and the exit is given by

$$\Delta p = \left(\frac{4fL}{3D} + 2K \right) \frac{\rho V_e^2}{2} \quad (\text{return manifolds}) \quad (6-148)$$

where V_e is the pipe exit velocity.

One means to obtain a desired uniform distribution is to make the average pressure drop across the holes Δp_o large compared to the pressure variation over the length of pipe Δp . Then, the relative variation in pressure drop across the various holes will be small, and so will be the variation in flow. When the area of an individual hole is small compared to the cross-sectional area of the pipe, hole pressure drop may be expressed in terms of the discharge coefficient C_o and the velocity across the hole V_o as

$$\Delta p_o = \frac{1}{C_o^2} \frac{\rho V_o^2}{2} \quad (6-149)$$

Provided C_o is the same for all the holes, the *percent maldistribution*, defined as the percentage variation in flow between the first and last holes, may be estimated reasonably well for small maldistribution by (Senecal, *Ind. Eng. Chem.*, **49**, 993–997 [1957])

$$\text{Percent maldistribution} = 100 \left(1 - \sqrt{\frac{\Delta p_o - |\Delta p|}{\Delta p_o}} \right) \quad (6-150)$$

This equation shows that for 5 percent maldistribution, the pressure drop across the holes should be about 10 times the pressure drop over the length of the pipe. For discharge manifolds with $K = 0.5$ in Eq. (6-147), and with $4fL/3D \ll 1$, the pressure drop across the holes should be 10 times the inlet velocity head, $\rho V_i^2/2$ for 5 percent maldistribution. This leads to a simple design equation.

Discharge manifolds, $4fL/3D \ll 1$, 5% maldistribution:

$$\frac{V_o}{V_i} = \frac{A_p}{A_o} = \sqrt{10C_o} \quad (6-151)$$

Here A_p = pipe cross-sectional area and A_o is the total hole area of the distributor. Use of large hole velocity to pipe velocity ratios promotes perpendicular discharge streams. In practice, there are many cases where the $4fL/3D$ term will be less than unity but not close to zero. In such cases, Eq. (6-151) will be conservative, while Eqs. (6-147), (6-149), and (6-150) will give more accurate design calculations. In cases where $4fL/(3D) > 2$, friction effects are large enough to render Eq. (6-151) nonconservative. When significant variations in f along the length of the distributor occur, calculations should be made by dividing the distributor into small enough sections that constant f may be assumed over each section.

For return manifolds with $K = 1.0$ and $4fL/(3D) \ll 1$, 5 percent maldistribution is achieved when hole pressure drop is 20 times the pipe exit velocity head.

Return manifolds, $4fL/3D \ll 1$, 5% maldistribution:

$$\frac{V_o}{V_e} = \frac{A_p}{A_o} = \sqrt{20C_o} \tag{6-152}$$

When $4fL/3D$ is not negligible, Eq. (6-152) is not conservative and Eqs. (6-148), (6-149), and (6-150) should be used.

One common misconception is that good distribution is always provided by high pressure drop, so that increasing flow rate improves distribution by increasing pressure drop. Conversely, it is mistakenly believed that turndown of flow through a perforated pipe designed using Eqs. (6-151) and (6-152) will cause maldistribution. However, when the distribution is nearly uniform, decreasing the flow rate decreases Δp and Δp_o in the same proportion, and Eqs. (6-151) and (6-152) are still satisfied, preserving good distribution independent of flow rate, as long as friction losses remain small compared to inertial (velocity head change) effects. Conversely, increasing the flow rate through a distributor with severe maldistribution will not generally produce good distribution.

Often, the pressure drop required for design flow rate is unacceptably large for a distributor pipe designed for uniform velocity through uniformly sized and spaced orifices. Several measures may be taken in such situations. These include the following:

1. Taper the diameter of the distributor pipe so that the pipe velocity and velocity head remain constant along the pipe, thus substantially reducing pressure variation in the pipe.
2. Vary the hole size and/or the spacing between holes to compensate for the pressure variation along the pipe. This method may be sensitive to flow rate and a distributor optimized for one flow rate may suffer increased maldistribution as flow rate deviates from design rate.
3. Feed or withdraw from both ends, reducing the pipe flow velocity head and required hole pressure drop by a factor of 4.

The orifice discharge coefficient C_o is usually taken to be about 0.62. However, C_o is dependent on the ratio of hole diameter to pipe diameter, pipe wall thickness to hole diameter ratio, and pipe velocity to hole velocity ratio. As long as all these are small, the coefficient 0.62 is generally adequate.

Example 9: Pipe Distributor A 3-in schedule 40 (inside diameter 7.793 cm) pipe is to be used as a distributor for a flow of 0.010 m³/s of water ($\rho = 1,000 \text{ kg/m}^3$, $\mu = 0.001 \text{ Pa} \cdot \text{s}$). The pipe is 0.7 m long and is to have 10 holes of uniform diameter and spacing along the length of the pipe. The distributor pipe is submerged. Calculate the required hole size to limit maldistribution to 5 percent, and estimate the pressure drop across the distributor.

The inlet velocity computed from $V_i = Q/A = 4Q/(\pi D^2)$ is 2.10 m/s, and the inlet Reynolds number is

$$Re = \frac{DV_i \rho}{\mu} = \frac{0.07793 \times 2.10 \times 1,000}{0.001} = 1.64 \times 10^5$$

For commercial pipe with roughness $\epsilon = 0.046 \text{ mm}$, the friction factor is about 0.0043. Approaching the last hole, the flow rate, velocity, and Reynolds number are about one-tenth their inlet values. At $Re = 16,400$ the friction factor f is about 0.0070. Using an average value of $f = 0.0057$ over the length of the pipe, $4fL/3D$ is 0.068 and may reasonably be neglected so that Eq. (6-151) may be used. With $C_o = 0.62$,

$$\frac{V_o}{V_i} = \frac{A_p}{A_o} = \sqrt{10C_o} = \sqrt{10} \times 0.62 = 1.96$$

With pipe cross-sectional area $A_p = 0.00477 \text{ m}^2$, the total hole area is $0.00477/1.96 = 0.00243 \text{ m}^2$. The area and diameter of each hole are then

$0.00243/10 = 0.000243 \text{ m}^2$ and 1.76 cm. With $V_o/V_i = 1.96$, the hole velocity is $1.96 \times 2.10 = 4.12 \text{ m/s}$ and the pressure drop across the holes is obtained from Eq. (6-149).

$$\Delta p_o = \frac{1}{C_o^2} \frac{\rho V_o^2}{2} = \frac{1}{0.62^2} \times \frac{1,000(4.12)^2}{2} = 22,100 \text{ Pa}$$

Since the hole pressure drop is 10 times the pressure variation in the pipe, the total pressure drop from the inlet of the distributor may be taken as approximately 22,100 Pa.

Further detailed information on pipe distributors may be found in Senecal (*Ind. Eng. Chem.*, **49**, 993–997 [1957]). Much of the information on tapered manifold design has appeared in the pulp and paper literature (Spengos and Kaiser, *TAPPI*, **46**[3], 195–200 [1963]; Madeley, *Paper Technology*, **9**[1], 35–39 [1968]; Mardon, et al., *TAPPI*, **46**[3], 172–187 [1963]; Mardon, et al., *Pulp and Paper Magazine of Canada*, **72**[11], 76–81 [November 1971]; Truffitt, *TAPPI*, **58**[11], 144–145 [1975]).

Slot Distributors These are generally used in sheeting dies for extrusion of films and coatings and in air knives for control of thickness of a material applied to a moving sheet. A simple slotted pipe for turbulent flow conditions may give severe maldistribution because of nonuniform discharge velocity, but also because this type of design does not readily give perpendicular discharge (Koestel and Tuve, *Heat. Piping Air Cond.*, **20**[1], 153–157 [1948]; Senecal, *Ind. Eng. Chem.*, **49**, 993–997 [1957]; Koestel and Young, *Heat. Piping Air Cond.*, **23**[7], 111–115 [1951]). For slots in tapered ducts where the duct cross-sectional area decreases linearly to zero at the far end, the discharge angle will be constant along the length of the duct (Koestel and Young, *ibid.*). One way to ensure an almost perpendicular discharge is to have the ratio of the area of the slot to the cross-sectional area of the pipe equal to or less than 0.1. As in the case of perforated-pipe distributors, pressure variation within the slot manifold and pressure drop across the slot must be carefully considered.

In practice, the following methods may be used to keep the diameter of the pipe to a minimum consistent with good performance (Senecal, *Ind. Eng. Chem.*, **49**, 993–997 [1957]):

1. Feed from both ends.
2. Modify the cross-sectional design (Fig. 6-35); the slot is thus farther away from the influence of feed-stream velocity.
3. Increase pressure drop across the slot; this can be accomplished by lengthening the lips (Fig. 6-35).
4. Use screens (Fig. 6-35) to increase overall pressure drop across the slot.

Design considerations for air knives are discussed by Senecal (*ibid.*). Design procedures for extrusion dies when the flow is laminar, as with highly viscous fluids, are presented by Bernhardt (*Processing of Thermoplastic Materials*, Rheinhold, New York, 1959, pp. 248–281).

Turning Vanes In applications such as ventilation, the discharge profile from slots can be improved by turning vanes. The tapered duct is the most amenable for turning vanes because the discharge angle remains constant. One way of installing the vanes is shown in Fig. 6-36. The vanes should have a depth twice the spacing (*Heating, Ventilating, Air Conditioning Guide*, vol. 38, American Society of Heating, Refrigerating and Air-Conditioning Engineers, 1960, pp. 282–283) and a curvature at the upstream end of the vanes of a circular arc which is tangent to the discharge angle θ of a slot without vanes and perpendicular at the downstream or discharge end of the vanes (Koestel and Young, *Heat. Piping Air Cond.*, **23**[7], 111–115 [1951]). Angle θ can be estimated from

$$\cot \theta = \frac{C_d A_s}{A_d} \tag{6-153}$$

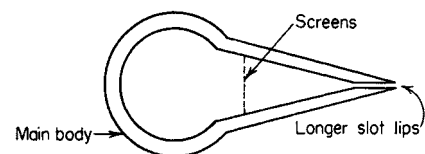


FIG. 6-35 Modified slot distributor.

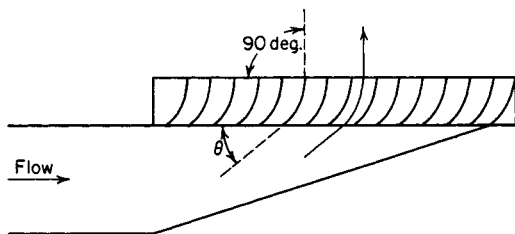


FIG. 6-36 Turning vanes in a slot distributor.

where A_s = slot area
 A_d = duct cross-sectional area at upstream end
 C_d = discharge coefficient of slot

Vanes may be used to improve velocity distribution and reduce frictional loss in bends, when the ratio of bend turning radius to pipe diameter is less than 1.0. For a miter bend with low-velocity flows, simple circular arcs (Fig. 6-37) can be used, and with high-velocity flows, vanes of special airfoil shapes are required. For additional details and references, see Ower and Pankhurst (*The Measurement of Air Flow*, Pergamon, New York, 1977, p. 102); Pankhurst and Holder (*Wind-Tunnel Technique*, Pitman, London, 1952, pp. 92–93); Rouse (*Engineering Hydraulics*, Wiley, New York, 1950, pp. 399–401); and Jorgensen (*Fan Engineering*, 7th ed., Buffalo Forge Co., Buffalo, 1970, pp. 111, 117, 118).

Perforated Plates and Screens A nonuniform velocity profile in turbulent flow through channels or process equipment can be smoothed out to any desired degree by adding sufficient uniform resistance, such as perforated plates or screens across the flow channel, as shown in Fig. 6-38. Stoker (*Ind. Eng. Chem.*, **38**, 622–624 [1946]) provides the following equation for the effect of a uniform resistance on velocity profile:

$$\frac{V_{2,\max}}{V} = \sqrt{\frac{(V_{1,\max}/V)^2 + \alpha_2 - \alpha_1 + \alpha_2 K}{1 + K}} \quad (6-154)$$

Here, V is the area average velocity, K is the number of velocity heads of pressure drop provided by the uniform resistance, $\Delta p = K\rho V^2/2$, and α is the velocity profile factor used in the mechanical energy balance, Eq. (6-13). It is the ratio of the area average of the cube of the velocity, to the cube of the area average velocity V . The shape of the exit velocity profile appears twice in Eq. (6-154), in $V_{2,\max}/V$ and α_2 . Typically, K is on the order of 10, and the desired exit velocity profile

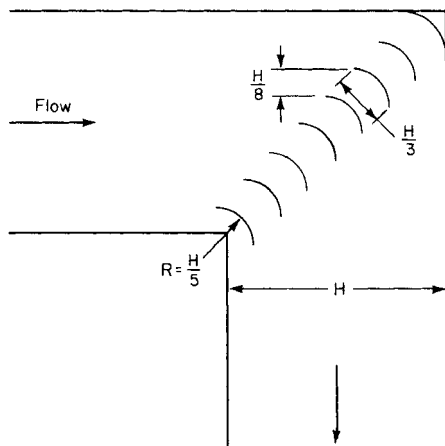


FIG. 6-37 Miter bend with vanes.

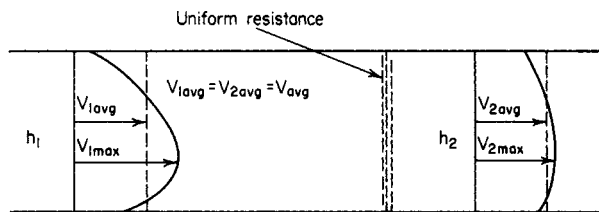


FIG. 6-38 Smoothing out a nonuniform profile in a channel.

is fairly uniform so that $\alpha_2 \sim 1.0$ may be appropriate. Downstream of the resistance, the velocity profile will gradually reestablish the fully developed profile characteristic of the Reynolds number and channel shape. The screen or perforated plate open area required to produce the resistance K may be computed from Eqs. (6-107) or (6-111).

Screens and other flow restrictions may also be used to suppress stream swirl and turbulence (Loehrke and Nagib, *J. Fluids Eng.*, **98**, 342–353 [1976]). Contraction of the channel, as in a venturi, provides further reduction in turbulence level and flow nonuniformity.

Beds of Solids A suitable depth of solids can be used as a fluid distributor. As for other types of distribution devices, a pressure drop of 10 velocity heads is typically used, here based on the superficial velocity through the bed. There are several substantial disadvantages to use of particle beds for flow distribution. Heterogeneity of the bed may actually worsen rather than improve distribution. In general, uniform flow may be found only downstream of the point in the bed where sufficient pressure drop has occurred to produce uniform flow. Therefore, inefficiency results when the bed also serves reaction or mass transfer functions, as in catalysts, adsorbents, or tower packings for gas/liquid contacting, since portions of the bed are bypassed. In the case of trickle flow of liquid downward through column packings, inlet distribution is critical since the bed itself is relatively ineffective in distributing the liquid. Maldistribution of flow through packed beds also arises when the ratio of bed diameter to particle size is less than 10 to 30.

Other Flow Straightening Devices Other devices designed to produce uniform velocity or reduce swirl, sometimes with reduced pressure drop, are available. These include both commercial devices of proprietary design and devices discussed in the literature. For pipeline flows, see the references under flow inverters and static mixing elements previously discussed in the “Incompressible Flow in Pipes and Channels” subsection. For large area changes, as at the entrance to a vessel, it is sometimes necessary to diffuse the momentum of the inlet jet discharging from the feed pipe in order to produce a more uniform velocity profile within the vessel. Methods for this application exist, but remain largely in the domain of proprietary, commercial design.

FLUID MIXING

Mixing of fluids is a discipline of fluid mechanics. Fluid motion is used to accelerate the otherwise slow processes of diffusion and conduction to bring about uniformity of concentration and temperature, blend materials, facilitate chemical reactions, bring about intimate contact of multiple phases, and so on. As the subject is too broad to cover fully, only a brief introduction and some references for further information are given here.

Several texts are available. These include Paul, Atiemo-Obeng, and Kresta (*Handbook of Industrial Mixing*, Wiley-Interscience, Hoboken N.J., 2004); Hamby, Edwards, and Nienow (*Mixing in the Process Industries*, 2d ed., Butterworths, London, 1992); Oldshue (*Fluid Mixing Technology*, McGraw-Hill, New York, 1983); Tatterson (*Fluid Mixing and Gas Dispersion in Agitated Tanks*, McGraw-Hill, New York, 1991); Uhl and Gray (*Mixing*, vols. I–III, Academic, New York, 1966, 1967, 1986); and Nagata (*Mixing: Principles and Applications*, Wiley, New York, 1975). A good overview of stirred tank agitation is given in the series of articles from *Chemical Engineering* (110–114, Dec. 8, 1975; 139–145, Jan. 5, 1976; 93–100, Feb. 2, 1976; 102–110,

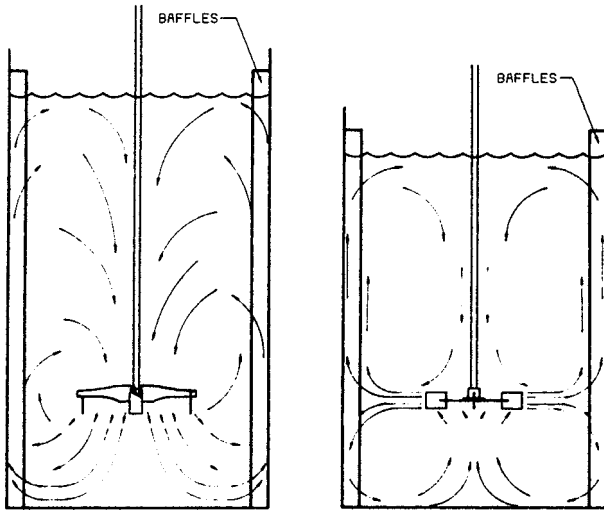


FIG. 6-39 Typical stirred tank configurations, showing time-averaged flow patterns for axial flow and radial flow impellers. (From Oldshue, Fluid Mixing Technology, McGraw-Hill, New York, 1983.)

Apr. 26, 1976; 144-150, May 24, 1976; 141-148, July 19, 1976; 89-94, Aug. 2, 1976; 101-108, Aug. 30, 1976; 109-112, Sept. 27, 1976; 119-126, Oct. 25, 1976; 127-133, Nov. 8, 1976).

Process mixing is commonly carried out in pipeline and vessel geometries. The terms **radial mixing** and **axial mixing** are commonly used. Axial mixing refers to mixing of materials which pass a given point at different times, and thus leads to **backmixing**. For example, backmixing or axial mixing occurs in stirred tanks where fluid elements entering the tank at different times are intermingled.

Mixing of elements initially at different axial positions in a pipeline is axial mixing. Radial mixing occurs between fluid elements passing a given point at the same time, as, for example, between fluids mixing in a pipeline tee.

Turbulent flow, by means of the chaotic eddy motion associated with velocity fluctuation, is conducive to rapid mixing and, therefore, is the preferred flow regime for mixing. **Laminar mixing** is carried out when high viscosity makes turbulent flow impractical.

Stirred Tank Agitation Turbine impeller agitators, of a variety of shapes, are used for stirred tanks, predominantly in turbulent flow. Figure 6-39 shows typical stirred tank configurations and time-averaged flow patterns for axial flow and radial flow impellers. In order to prevent formation of a **vortex**, four vertical baffles are normally installed. These cause top-to-bottom mixing and prevent mixing-ineffective swirling motion.

For a given impeller and tank geometry, the impeller Reynolds number determines the flow pattern in the tank:

$$Re_i = \frac{D^2 N \rho}{\mu} \tag{6-155}$$

where D = impeller diameter, N = rotational speed, and ρ and μ are the liquid density and viscosity. Rotational speed N is typically reported in revolutions per minute, or revolutions per second in SI units. Radians per second are almost never used. Typically, $Re_i > 10^4$ is required for fully turbulent conditions throughout the tank. A wide transition region between laminar and turbulent flow occurs over the range $10 < Re_i < 10^4$.

The power P drawn by the impeller is made dimensionless in a group called the power number:

$$N_p = \frac{P}{\rho N^3 D^5} \tag{6-156}$$

Figure 6-40 shows power number vs. impeller Reynolds number for a typical configuration. The similarity to the friction factor vs. Reynolds number behavior for pipe flow is significant. In laminar flow, the power number is inversely proportional to Reynolds number, reflecting the dominance of viscous forces over inertial forces. In

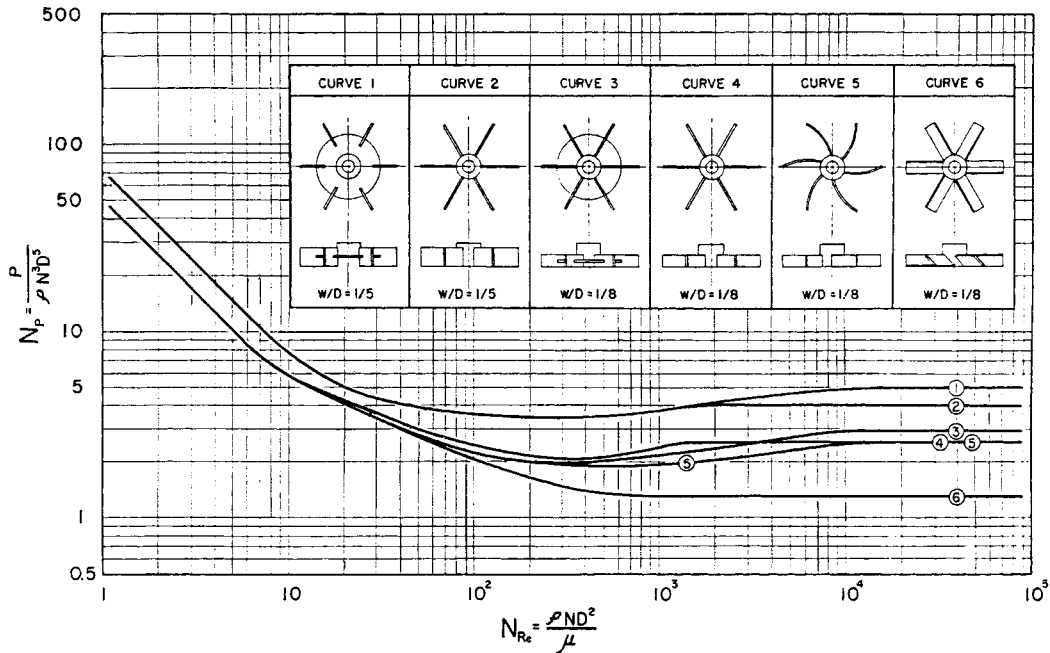


FIG. 6-40 Dimensionless power number in stirred tanks. (Reprinted with permission from Bates, Fondy, and Corpstein, Ind. Eng. Chem. Process Design Develop., 2, 310 [1963].)

turbulent flow, where inertial forces dominate, the power number is nearly constant.

Impellers are sometimes viewed as pumping devices; the total volumetric flow rate Q discharged by an impeller is made dimensionless in a pumping number:

$$N_Q = \frac{Q}{ND^3} \quad (6-157)$$

Blend time t_b , the time required to achieve a specified maximum standard deviation of concentration after injection of a tracer into a stirred tank, is made dimensionless by multiplying by the impeller rotational speed:

$$N_b = t_b N \quad (6-158)$$

Dimensionless pumping number and blend time are independent of Reynolds number under fully turbulent conditions. The magnitude of concentration fluctuations from the final well-mixed value in batch mixing decays exponentially with time.

The design of mixing equipment depends on the desired process result. There is often a tradeoff between operating cost, which depends mainly on power, and capital cost, which depends on agitator size and torque. For some applications bulk flow throughout the vessel is desired, while for others high local turbulence intensity is required. Multiphase systems introduce such design criteria as solids suspension and gas dispersion. In very viscous systems, helical ribbons, extruders, and other specialized equipment types are favored over turbine agitators.

Pipeline Mixing Mixing may be carried out with **mixing tees**, **inline** or **motionless mixing elements**, or in empty pipe. In the latter case, large pipe lengths may be required to obtain adequate mixing. Coaxially injected streams require lengths on the order of 100 pipe diameters. Coaxial mixing in turbulent single-phase flow is characterized by the turbulent diffusivity (eddy diffusivity) D_E which determines the rate of radial mixing. Davies (*Turbulence Phenomena*, Academic, New York, 1972) provides an equation for D_E which may be rewritten as

$$D_E \sim 0.015DV\text{Re}^{-0.125} \quad (6-159)$$

where D = pipe diameter
 V = average velocity
 Re = pipe Reynolds number, $DV\rho/\mu$
 ρ = density
 μ = viscosity

Properly designed tee mixers, with due consideration given to main stream and injected stream momentum, are capable of producing high degrees of uniformity in just a few diameters. Fomey (*Jet Injection for Optimum Pipeline Mixing*, in "Encyclopedia of Fluid Mechanics," vol. 2., Chap. 25, Gulf Publishing, 1986) provides a thorough discussion of tee mixing. Inline or motionless mixers are generally of proprietary commercial design, and may be selected for viscous or turbulent, single or multiphase mixing applications. They substantially reduce required pipe length for mixing.

TUBE BANKS

Pressure drop across tube banks may not be correlated by means of a single, simple friction factor—Reynolds number curve, owing to the variety of tube configurations and spacings encountered, two of which are shown in Fig. 6-41. Several investigators have allowed for configuration and spacing by incorporating spacing factors in their friction factor expressions or by using multiple friction factor plots. Commercial computer codes for heat-exchanger design are available which include features for estimating pressure drop across tube banks.

Turbulent Flow The correlation by Grimson (*Trans. ASME*, **59**, 583–594 [1937]) is recommended for predicting pressure drop for turbulent flow ($\text{Re} \geq 2,000$) across staggered or in-line tube banks for tube spacings $[(a/D_t), (b/D_t)]$ ranging from 1.25 to 3.0. The pressure drop is given by

$$\Delta p = \frac{4fN_r\rho V_{\max}^2}{2} \quad (6-160)$$

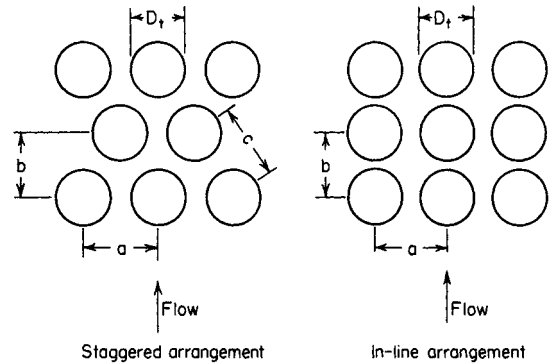


FIG. 6-41 Tube-bank configurations.

where f = friction factor
 N_r = number of rows of tubes in the direction of flow
 ρ = fluid density
 V_{\max} = fluid velocity through the minimum area available for flow

For banks of **staggered tubes**, the friction factor for isothermal flow is obtained from Fig. (6-42). Each "fence" (group of parametric curves) represents a particular Reynolds number defined as

$$\text{Re} = \frac{D_t V_{\max} \rho}{\mu} \quad (6-161)$$

where D_t = tube outside diameter and μ = fluid viscosity. The numbers along each fence represent the transverse and inflow-direction spacings. The upper chart is for the case in which the minimum area for flow is in the transverse openings, while the lower chart is for the case in which the minimum area is in the diagonal openings. In the latter case, V_{\max} is based on the area of the diagonal openings and N_r is the number of rows in the direction of flow minus 1. A critical comparison of this method with all the data available at the time showed an average deviation of the order of ± 15 percent (Boucher and Lapple, *Chem. Eng. Prog.*, **44**, 117–134 [1948]). For tube spacings greater than 3 tube diameters, the correlation by Gunter and Shaw (*Trans. ASME*, **67**, 643–660 [1945]) can be used as an approximation. As an **approximation**, the pressure drop can be taken as 0.72 velocity head (based on V_{\max} per row of tubes for tube spacings commonly encountered in practice (Lapple, et al., *Fluid and Particle Mechanics*, University of Delaware, Newark, 1954).

For banks of **in-line tubes**, f for isothermal flow is obtained from Fig. 6-43. Average deviation from available data is on the order of ± 15 percent. For tube spacings greater than $3D_t$, the charts of Gram, Mackey, and Monroe (*Trans. ASME*, **80**, 25–35 [1958]) can be used. As an **approximation**, the pressure drop can be taken as 0.32 velocity head (based on V_{\max}) per row of tubes (Lapple, et al., *Fluid and Particle Mechanics*, University of Delaware, Newark, 1954).

For turbulent flow through **shallow** tube banks, the average friction factor per row will be somewhat greater than indicated by Figs. 6-42 and 6-43, which are based on 10 or more rows depth. A 30 percent increase per row for 2 rows, 15 percent per row for 3 rows, and 7 percent per row for 4 rows can be taken as the maximum likely to be encountered (Boucher and Lapple, *Chem. Eng. Prog.*, **44**, 117–134 [1948]).

For a **single row of tubes**, the friction factor is given by Curve B in Fig. 6-44 as a function of tube spacing. This curve is based on the data of several experimenters, all adjusted to a Reynolds number of 10,000. The values should be substantially independent of Re for $1,000 < \text{Re} < 100,000$.

For **extended surfaces**, which include fins mounted perpendicularly to the tubes or spiral-wound fins, pin fins, plate fins, and so on, friction data for the specific surface involved should be used. For

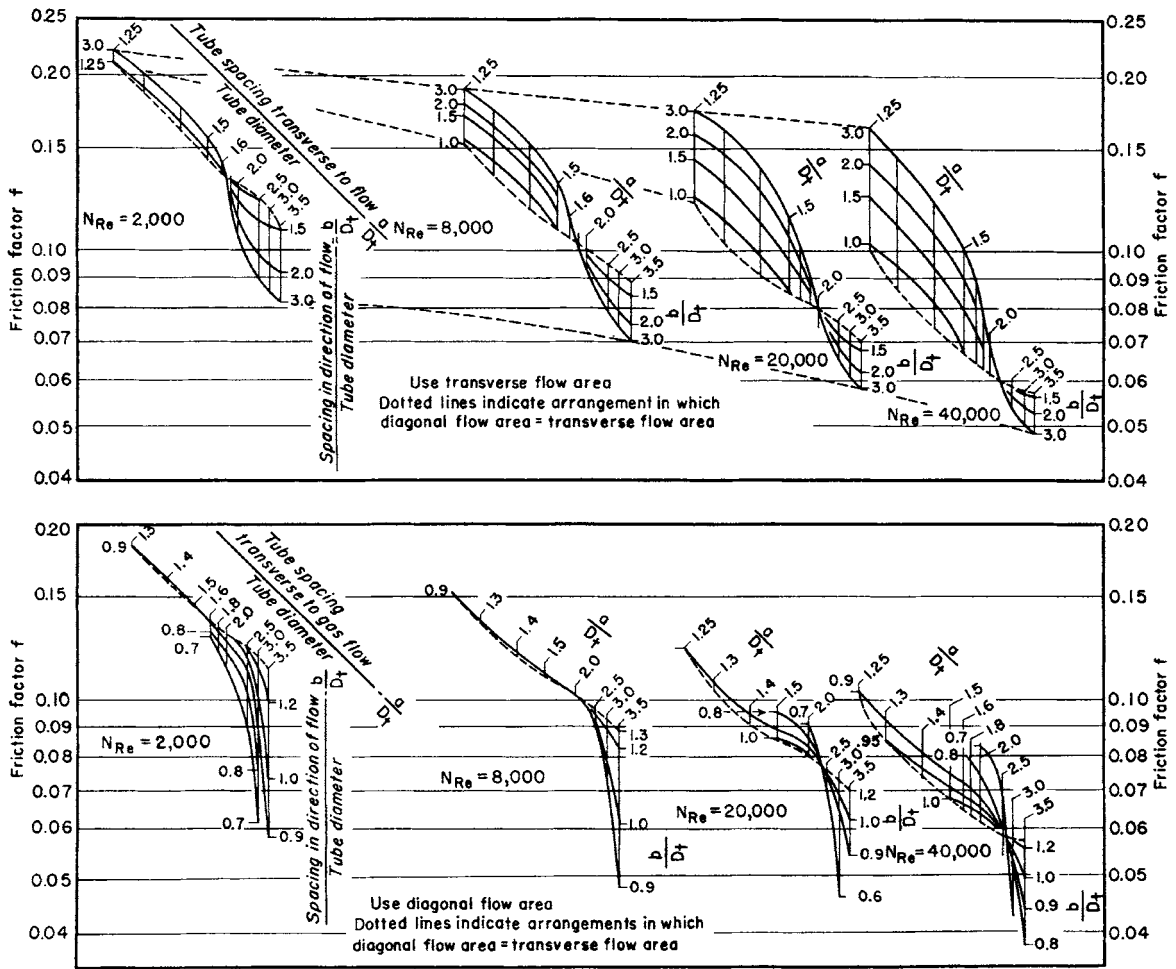


FIG. 6-42 Upper chart: Friction factors for staggered tube banks with minimum fluid flow area in transverse openings. Lower chart: Friction factors for staggered tube banks with minimum fluid flow area in diagonal openings. (From Grimson, *Trans. ASME*, 59, 583 [1937].)

details, see Kays and London (*Compact Heat Exchangers*, 2d ed., McGraw-Hill, New York, 1964). If specific data are unavailable, the correlation by Gunter and Shaw (*Trans. ASME*, 67, 643-660 [1945]) may be used as an approximation.

When a large temperature change occurs in a gas flowing across a tube bundle, gas properties should be evaluated at the mean temperature

$$T_m = T_i + K \Delta T_{lm} \quad (6-162)$$

where T_i = average tube-wall temperature
 K = constant

ΔT_{lm} = log-mean temperature difference between the gas and the tubes

Values of K averaged from the recommendations of Chilton and Genereaux (*Trans. AIChE*, 29, 151-173 [1933]) and Grimson (*Trans. ASME*, 59, 583-594 [1937]) are as follows: for in-line tubes, 0.9 for cooling and -0.9 for heating; for staggered tubes, 0.75 for cooling and -0.8 for heating.

For nonisothermal flow of **liquids** across tube bundles, the friction factor is increased if the liquid is being cooled and decreased if the liquid is being heated. The factors previously given for nonisothermal

flow of liquids in pipes ("Incompressible Flow in Pipes and Channels") should be used.

For two-phase gas/liquid horizontal cross flow through tube banks, the method of Diehl and Unruh (*Pet. Refiner*, 37[10], 124-128 [1958]) is available.

Transition Region This region extends roughly over the range $200 < Re < 2,000$. Figure 6-45 taken from Bergelin, Brown, and Doberstein (*Trans. ASME*, 74, 953-960 [1952]) gives curves for friction factor f_T for five different configurations. Pressure drop for liquid flow is given by

$$\Delta p = \frac{4f_T N_r \rho V_{max}^2}{2} \left(\frac{\mu_s}{\mu_b} \right)^{0.14} \quad (6-163)$$

where N_r = number of major restrictions encountered in flow through the bank (equal to number of rows when minimum flow area occurs in transverse openings, and to number of rows minus 1 when it occurs in the diagonal openings); ρ = fluid density; V_{max} = velocity through minimum flow area; μ_s = fluid viscosity at tube-surface temperature and μ_b = fluid viscosity at average bulk temperature. This method gives the friction factor within about ± 25 percent.

Laminar Region Bergelin, Colburn, and Hull (*Univ. Delaware Eng. Exp. Sta. Bull.*, 2 [1950]) recommend the following equations for

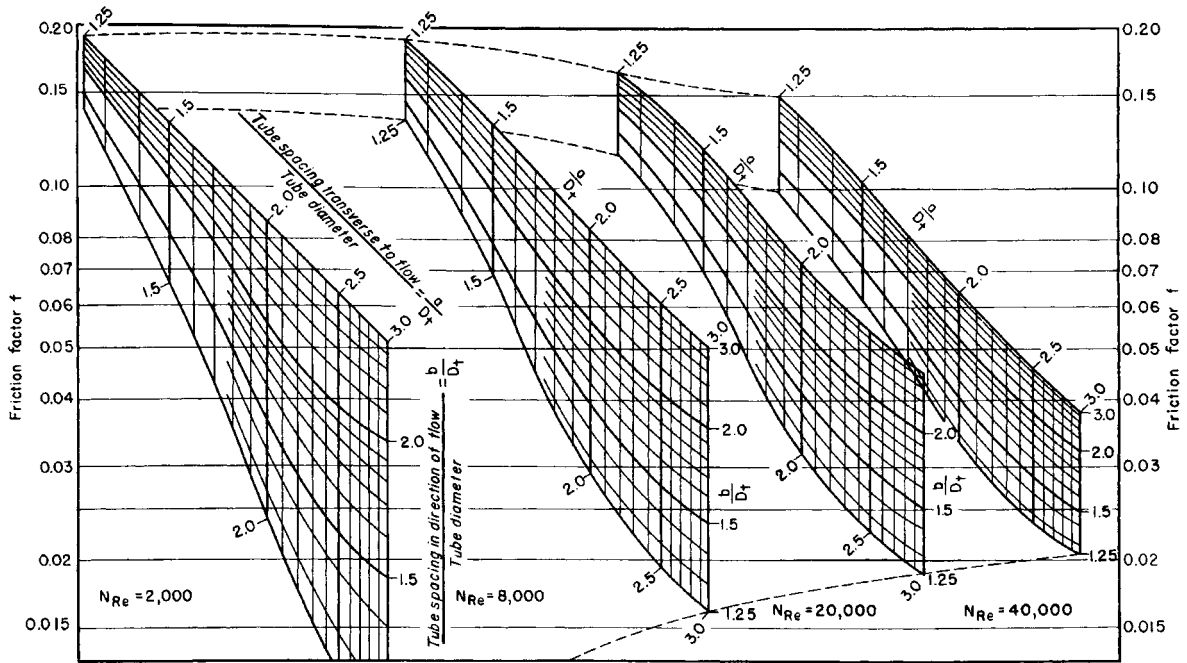


FIG. 6-43 Friction factors for in-line tube banks. (From Grimson, Trans. ASME, 59, 583 [1937].)

pressure drop with laminar flow ($Re_v < 100$) of liquids across banks of plain tubes with pitch ratios P/D_t of 1.25 and 1.50:

$$\Delta p = \frac{280N_r}{Re_v} \left(\frac{D_t}{P}\right)^{1.6} \left(\frac{\mu_s}{\mu_b}\right)^m \left(\frac{\rho V_{max}^2}{2}\right) \quad (6-164)$$

$$m = \frac{0.57}{(Re_v)^{0.25}} \quad (6-165)$$

where $Re_v = D_v V_{max} \rho / \mu_b$; D_v = volumetric hydraulic diameter $[(4 \times \text{free-bundle volume}) / (\text{exposed surface area of tubes})]$; P = pitch (= a for in-line arrangements, = a or c [whichever is smaller] for staggered

arrangements), and other quantities are as defined following Eq. (6-163). Bergelin, et al. (ibid.) show that pressure drop per row is independent of the number of rows in the bank with laminar flow. The pressure drop is predicted within about ± 25 percent.

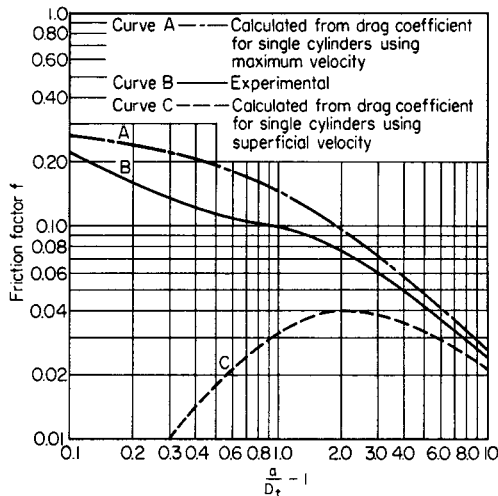


FIG. 6-44 Friction factors vs. transverse spacing for single row of tubes. (From Boucher and Lapple, Chem. Eng. Prog., 44, 117 [1948].)

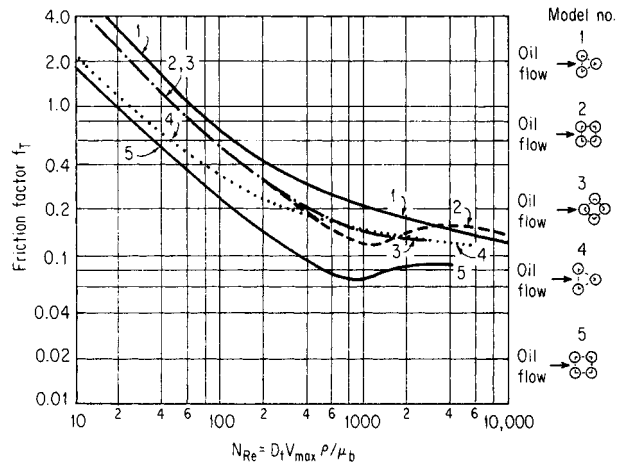


FIG. 6-45 Friction factors for transition region flow across tube banks. (Pitch is the minimum center-to-center tube spacing.) (From Bergelin, Brown, and Doberstein, Trans. ASME, 74, 953 [1952].)

Model	Rows	D_t , in	Pitch/ D_t
1	10	%	1.25
2	10	%	1.25
3	14	%	1.25
4	10	%	1.50
5	10	%	1.50

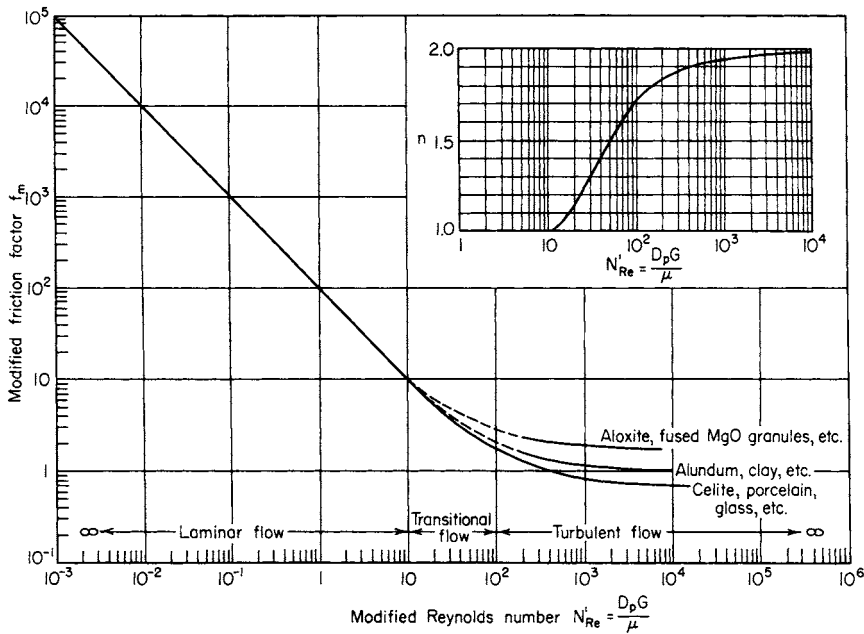


FIG. 6-46 Friction factor for beds of solids. (From Leva, Fluidization, McGraw-Hill, New York, 1959, p. 49.)

The validity of extrapolating Eq. (6-164) to pitch ratios larger than 1.50 is unknown. The correlation of Gunter and Shaw (*Trans. ASME*, **67**, 643-660 [1945]) may be used as an approximation in such cases.

For laminar flow of non-Newtonian fluids across tube banks, see Adams and Bell (*Chem. Eng. Prog.*, **64**, *Symp. Ser.*, **82**, 133-145 [1968]).

Flow-induced **tube vibration** occurs at critical fluid velocities through tube banks, and is to be avoided because of the severe damage that can result. Methods to predict and correct vibration problems may be found in Eisinger (*Trans. ASME J. Pressure Vessel Tech.*, **102**, 138-145 [May 1980]) and Chen (*J. Sound Vibration*, **93**, 439-455 [1984]).

BEDS OF SOLIDS

Fixed Beds of Granular Solids Pressure-drop prediction is complicated by the variety of granular materials and of their packing arrangement. For flow of a **single incompressible fluid** through an incompressible bed of granular solids, the pressure drop may be estimated by the correlation given in Fig. 6-46 (Leva, *Chem. Eng.*, **56**[5], 115-117 [1949]), or *Fluidization*, McGraw-Hill, New York, 1959). The modified friction factor and Reynolds number are defined by

$$f_m \equiv \frac{D_p \rho \phi_s^{3-n} \epsilon^3 |\Delta p|}{2G^2 L (1-\epsilon)^{3-n}} \tag{6-166}$$

$$Re' \equiv \frac{D_p G}{\mu} \tag{6-167}$$

- where $-\Delta p$ = pressure drop
- L = depth of bed
- D_p = average particle diameter, defined as the diameter of a sphere of the same volume as the particle
- ϵ = void fraction
- n = exponent given in Fig. 6-46 as a function of Re'
- ϕ_s = shape factor defined as the area of sphere of diameter D_p divided by the actual surface area of the particle
- G = fluid superficial mass velocity based on the empty chamber cross section
- ρ = fluid density
- μ = fluid viscosity

As for any incompressible single-phase flow, the equivalent pressure $P = p + \rho g z$ where g = acceleration of gravity z = elevation, may be used in place of p to account for gravitational effects in flows with vertical components.

In creeping flow ($Re' < 10$),

$$f_m = \frac{100}{Re'} \tag{6-168}$$

At high Reynolds numbers the friction factor becomes nearly constant, approaching a value of the order of unity for most packed beds.

In terms of S , particle surface area per unit volume of bed,

$$D_p = \frac{6(1-\epsilon)}{\phi_s S} \tag{6-169}$$

Porous Media Packed beds of granular solids are one type of the general class referred to as **porous media**, which include geological formations such as petroleum reservoirs and aquifers, manufactured materials such as sintered metals and porous catalysts, burning coal or char particles, and textile fabrics, to name a few. Pressure drop for incompressible flow across a porous medium has the same qualitative behavior as that given by Leva's correlation in the preceding. At low Reynolds numbers, viscous forces dominate and pressure drop is proportional to fluid viscosity and superficial velocity, and at high Reynolds numbers, pressure drop is proportional to fluid density and to the square of superficial velocity.

Creeping flow ($Re' \ll 1$) through porous media is often described in terms of the **permeability** k and Darcy's law:

$$\frac{-\Delta P}{L} = \frac{\mu}{k} V \tag{6-170}$$

where V = superficial velocity. The SI units for permeability are m^2 . Creeping flow conditions generally prevail in geological porous media. For **multidimensional flows** through **isotropic** porous media, the superficial velocity \mathbf{V} and pressure gradient ∇P vectors replace the corresponding one-dimensional variables in Eq. (6-170).

$$\nabla P = - \frac{\mu}{k} \mathbf{V} \tag{6-171}$$

For isotropic homogeneous porous media (uniform permeability and porosity), the pressure for creeping incompressible single phase-flow may be shown to satisfy the Laplace equation:

$$\nabla^2 p = 0 \quad (6-172)$$

For **anisotropic** or **oriented** porous media, as are frequently found in geological media, permeability varies with direction and a **permeability tensor** \mathbf{K} , with nine components K_{ij} giving the velocity component in the i direction due to a pressure gradient in the j direction, may be introduced. For further information, see Slattery (*Momentum, Energy and Mass Transfer in Continua*, Krieger, Huntington, New York, 1981, pp. 193–218). See also Dullien (*Chem. Eng. J. [Lausanne]*, **10**, 1,034 [1975]) for a review of pressure-drop methods in single-phase flow. Solutions for Darcy's law for several geometries of interest in petroleum reservoirs and aquifers, for both incompressible and compressible flows, are given in Craft and Hawkins (*Applied Petroleum Reservoir Engineering*, Prentice-Hall, Englewood Cliffs, N.J., 1959). See also Todd (*Groundwater Hydrology*, 2nd ed., Wiley, New York, 1980).

For granular solids of **mixed sizes** the average particle diameter may be calculated as

$$\frac{1}{D_p} = \sum_i \frac{x_i}{D_{p,i}} \quad (6-173)$$

where x_i = weight fraction of particles of size $D_{p,i}$.

For **isothermal compressible flow** of a gas with constant compressibility factor Z through a packed bed of granular solids, an equation similar to Eq. (6-114) for pipe flow may be derived:

$$p_1^2 - p_2^2 = \frac{2ZRC^2T}{M_w} \left[\ln \frac{v_2}{v_1} + \frac{2f_m L(1-\epsilon)^{3-n}}{\phi_s^{3-n} \epsilon^3 D_p} \right] \quad (6-174)$$

where p_1 = upstream absolute pressure
 p_2 = downstream absolute pressure
 R = gas constant
 T = absolute temperature
 M_w = molecular weight
 v_1 = upstream specific volume of gas
 v_2 = downstream specific volume of gas

For creeping flow of **power law** non-Newtonian fluids, the method of Christopher and Middleton (*Ind. Eng. Chem. Fundam.*, **4**, 422–426 [1965]) may be used:

$$-\Delta p = \frac{150HLV^n(1-\epsilon)^2}{D_p^2 \phi_s^2 \epsilon^3} \quad (6-175)$$

$$H = \frac{K}{12} \left(9 + \frac{3}{n} \right)^n \left[\frac{D_p^2 \phi_s^2 \epsilon^4}{(1-\epsilon)^2} \right]^{(1-n)/2} \quad (6-176)$$

where $V = G/\rho$ = superficial velocity, K , n = power law material constants, and all other variables are as defined in Eq. (6-166). This correlation is supported by data from Christopher and Middleton (*ibid.*), Gregory and Griskey (*AIChE J.*, **13**, 122–125 [1967]), Yu, Wen, and Bailie (*Can. J. Chem. Eng.*, **46**, 149–154 [1968]), Siskovic, Gregory, and Griskey (*AIChE J.*, **17**, 176–187 [1978]), Kemblowski and Merl (*Chem. Eng. Sci.*, **29**, 213–223 [1974]), and Kemblowski and Dziubinski (*Rheol. Acta*, **17**, 176–187 [1978]). The measurements cover the range $n = 0.50$ to 1.60 , and modified Reynolds number $Re' = 10^{-8}$ to 10 , where

$$Re' = \frac{D_p V^{2-n} \rho}{H} \quad (6-177)$$

For the case $n = 1$ (Newtonian fluid), Eqs. (6-175) and (6-176) give a pressure drop 25 percent less than that given by Eqs. (6-166) through (6-168).

For **viscoelastic fluids** see Marshall and Metzner (*Ind. Eng. Chem. Fundam.*, **6**, 393–400 [1967]), Siskovic, Gregory, and Griskey (*AIChE J.*, **13**, 122–125 [1967]) and Kemblowski and Dziubinski (*Rheol. Acta*, **17**, 176–187 [1978]).

For gas flow through porous media with small pore diameters, the slip flow and molecular flow equations previously given (see the "Vacuum Flow" subsection) may be applied when the pore is of the same or

smaller order as the mean free path, as described by Monet and Vermeulen (*Chem. Eng. Prog.*, **55**, *Symp. Ser.*, **25** [1959]).

Tower Packings For the flow of a **single fluid** through a bed of tower packing, pressure drop may be estimated using the preceding methods. See also Sec. 14 of this *Handbook*. For **countercurrent gas/liquid flow** in commercial tower packings, both structured and unstructured, several sources of data and correlations for pressure drop and flooding are available. See, for example, Strigle (*Random Packings and Packed Towers, Design and Applications*, Gulf Publishing, Houston, 1989; *Chem. Eng. Prog.*, **89**[8], 79–83 [August 1993]), Hughmark (*Ind. Eng. Chem. Fundam.*, **25**, 405–409 [1986]), Chen (*Chem. Eng. Sci.*, **40**, 2139–2140 [1985]), Billet and Mackowiak (*Chem. Eng. Technol.*, **11**, 213–217 [1988]), Krehenwinkel and Knapp (*Chem. Eng. Technol.*, **10**, 231–242 [1987]), Mersmann and Deixler (*Ger. Chem. Eng.*, **9**, 265–276 [1986]), and Robbins (*Chem. Eng. Progr.*, **87**[5], 87–91 [May 1991]). Data and correlations for flooding and pressure drop for structured packings are given by Fair and Bravo (*Chem. Eng. Progr.*, **86**[1], 19–29 [January 1990]).

Fluidized Beds When gas or liquid flows upward through a vertically unconstrained bed of particles, there is a minimum fluid velocity at which the particles will begin to move. Above this minimum velocity, the bed is said to be **fluidized**. Fluidized beds are widely used, in part because of their excellent mixing and heat and mass transfer characteristics. See Sec. 17 of this *Handbook* for detailed information.

BOUNDARY LAYER FLOWS

Boundary layer flows are a special class of flows in which the flow far from the surface of an object is inviscid, and the effects of viscosity are manifest only in a thin region near the surface where steep velocity gradients occur to satisfy the no-slip condition at the solid surface. The thin layer where the velocity decreases from the inviscid, potential flow velocity to zero (relative velocity) at the solid surface is called the **boundary layer**. The thickness of the boundary layer is indefinite because the velocity asymptotically approaches the free-stream velocity at the outer edge. The boundary layer thickness is conventionally taken to be the distance for which the velocity equals 0.99 times the free-stream velocity. The boundary layer may be either laminar or turbulent. Particularly in the former case, the equations of motion may be simplified by scaling arguments. Schlichting (*Boundary Layer Theory*, 8th ed., McGraw-Hill, New York, 1987) is the most comprehensive source for information on boundary layer flows.

Flat Plate, Zero Angle of Incidence For flow over a wide, thin flat plate at zero angle of incidence with a uniform free-stream velocity, as shown in Fig. 6-47, the **critical Reynolds number** at which the boundary layer becomes turbulent is normally taken to be

$$Re_x = \frac{xV\rho}{\mu} = 500,000 \quad (6-178)$$

where V = free-stream velocity
 ρ = fluid density
 μ = fluid viscosity
 x = distance from leading edge of the plate

Uniform free-stream velocity

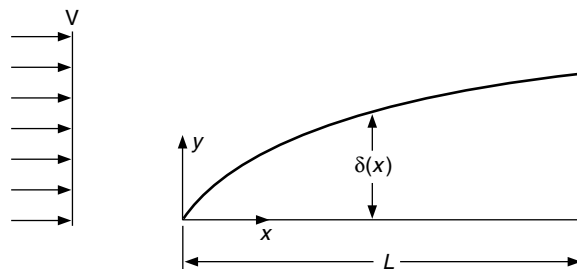


FIG. 6-47 Boundary layer on a flat plate at zero angle of incidence.

However, the transition Reynolds number depends on free-stream turbulence and may range from 3×10^5 to 3×10^6 . The **laminar boundary layer** thickness δ is a function of distance from the leading edge:

$$\delta \approx 5.0x\text{Re}_x^{-0.5} \quad (6-179)$$

The total drag on the plate of length L and width b for a laminar boundary layer, including the drag on both surfaces, is:

$$F_D = 1.328bL\rho V^2\text{Re}_L^{-0.5} \quad (6-180)$$

For **non-Newtonian power law fluids** (Acrivos, Shah, and Peterson, *AIChE J.*, **6**, 312–317 [1960]; Hsu, *AIChE J.*, **15**, 367–370 [1969]),

$$F_D = CbL\rho V^2\text{Re}_L^{-1/(1+n)} \quad (6-181)$$

$n =$	0.2	0.3	0.4	0.5	0.6	0.7	0.8	0.9	1
$C =$	2.075	1.958	1.838	1.727	1.627	1.538	1.460	1.390	1.328

where $\text{Re}'_L = \rho V^{2-n}L^n/K$ and K and n are the power law material constants (see Eq. [6-4]).

For a **turbulent boundary layer**, the thickness may be estimated as

$$\delta \approx 0.37x\text{Re}_x^{-0.2} \quad (6-182)$$

and the total drag force on both sides of the plate of length L is

$$F_D = \left[\frac{0.455}{(\log \text{Re}_L)^{2.58}} - \frac{1,700}{\text{Re}_L} \right] \rho bLV^2 \quad 5 \times 10^5 < \text{Re}_L < 10^9 \quad (6-183)$$

Here the second term accounts for the laminar leading edge of the boundary layer and assumes that the critical Reynolds number is 500,000.

Cylindrical Boundary Layer Laminar boundary layers on cylindrical surfaces, with flow parallel to the cylinder axis, are described by Glauert and Lighthill (*Proc. R. Soc. [London]*, **230A**, 188–203 [1955]), Jaffe and Okamura (*Z. Angew. Math. Phys.*, **19**, 564–574 [1968]), and Stewartson (*Q. Appl. Math.*, **13**, 113–122 [1955]). For a turbulent boundary layer, the total drag may be estimated as

$$F_D = \bar{c}_f \pi r L \rho V^2 \quad (6-184)$$

where r = cylinder radius, L = cylinder length, and the average friction coefficient is given by (White, *J. Basic Eng.*, **94**, 200–206 [1972])

$$\bar{c}_f = 0.0015 + \left[0.30 + 0.015 \left(\frac{L}{r} \right)^{0.4} \right] \text{Re}_L^{-1/3} \quad (6-185)$$

for $\text{Re}_L = 10^6$ to 10^9 and $L/r < 10^6$.

Continuous Flat Surface Boundary layers on continuous surfaces drawn through a stagnant fluid are shown in Fig. 6-48. Figure 6-48a shows the continuous flat surface (Sakiadis, *AIChE J.*, **7**, 26–28,

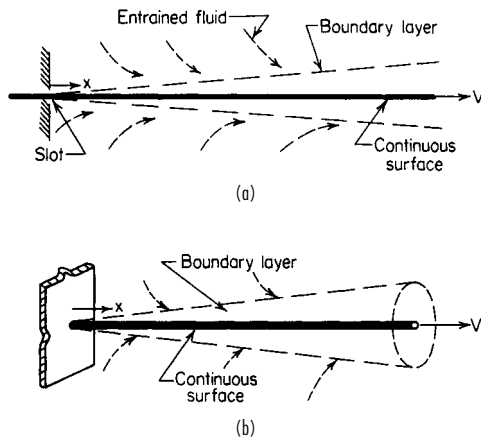


FIG. 6-48 Continuous surface: (a) continuous flat surface, (b) continuous cylindrical surface. (From Sakiadis, *Am. Inst. Chem. Eng. J.*, **7**, 221, 467 [1961].)

221–225, 467–472 [1961]). The critical Reynolds number for transition to turbulent flow may be greater than the 500,000 value for the finite flat-plate case discussed previously (Tsou, Sparrow, and Kurtz, *J. Fluid Mech.*, **26**, 145–161 [1966]). For a laminar boundary layer, the thickness is given by

$$\delta = 6.37x\text{Re}_x^{-0.5} \quad (6-186)$$

and the total drag exerted on the two surfaces is

$$F_D = 1.776bL\rho V^2\text{Re}_L^{-0.5} \quad (6-187)$$

The total flow rate of fluid entrained by the surface is

$$q = 3.232bLV\text{Re}_L^{-0.5} \quad (6-188)$$

The theoretical velocity field was experimentally verified by Tsou, Sparrow, and Goldstein (*Int. J. Heat Mass Transfer*, **10**, 219–235 [1967]) and Szeri, Yates, and Hai (*J. Lubr. Technol.*, **98**, 145–156 [1976]). For **non-Newtonian power law fluids** see Fox, Erickson, and Fan (*AIChE J.*, **15**, 327–333 [1969]).

For a turbulent boundary layer, the thickness is given by

$$\delta = 1.01x\text{Re}_x^{-0.2} \quad (6-189)$$

and the total drag on both sides by

$$F_D = 0.056bL\rho V^2\text{Re}_L^{-0.2} \quad (6-190)$$

and the total entrainment by

$$q = 0.252bLV\text{Re}_L^{-0.2} \quad (6-191)$$

When the laminar boundary layer is a significant part of the total length of the object, the total drag should be corrected by subtracting a calculated turbulent drag for the length of the laminar section and then adding the laminar drag for the laminar section. Tsou, Sparrow, and Goldstein (*Int. J. Heat Mass Transfer*, **10**, 219–235 [1967]) give an improved analysis of the turbulent boundary layer; their data indicate that Eq. (6-190) underestimates the drag by about 15 percent.

Continuous Cylindrical Surface The continuous surface shown in Fig. 6-48b is applicable, for example, for a wire drawn through a stagnant fluid (Sakiadis, *AIChE J.*, **7**, 26–28, 221–225, 467–472 [1961]; Vasudevan and Middleman, *AIChE J.*, **16**, 614 [1970]). The critical-length Reynolds number for transition is $\text{Re}_x = 200,000$. The laminar boundary layer thickness, total drag, and entrainment flow rate may be obtained from Fig. 6-49. The normalized boundary layer thickness and integral friction coefficient are from Vasudevan and Middleman, who used a similarity solution of the boundary layer equations. The drag force over a length x is given by

$$F_D = \bar{C}_f x \frac{\rho V^2}{2} 2\pi r x \quad (6-192)$$

The entrainment flow rate is from Sakiadis, who used an integral momentum approximation rather than the exact similarity solution.

$$q = V\Delta \quad (6-193)$$

Further laminar boundary layer analysis is given by Crane (*Z. Angew. Math. Phys.*, **23**, 201–212 [1972]).

For a turbulent boundary layer, the total drag may be roughly estimated using Eqs. (6-184) and (6-185) for finite cylinders. Measured forces by Kwon and Prevorsek (*J. Eng. Ind.*, **101**, 73–79 [1979]) are greater than predicted this way.

The laminar boundary layer on **deforming continuous surfaces** with velocity varying with axial position is discussed by Vleggaar (*Chem. Eng. Sci.*, **32**, 1517–1525 [1977]) and Crane (*Z. Angew. Math. Phys.*, **26**, 619–622 [1975]).

VORTEX SHEDDING

When fluid flows past objects or through orifices or similar restrictions, vortices may periodically be shed downstream. Objects such as smokestacks, chemical-processing columns, suspended pipelines, and electrical transmission lines can be subjected to damaging vibrations and forces due to the vortices, especially if the shedding frequency is close to a natural vibration frequency of the object. The shedding can

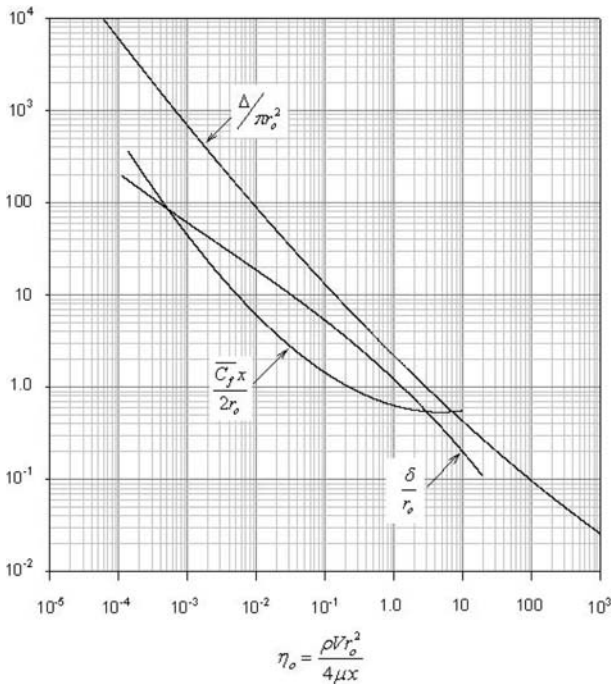


FIG 6-49 Boundary layer parameters for continuous cylindrical surfaces. ($\Delta/\pi r_o^2$ is from Sakiadis, *Am. Inst. Chem. Engr. J.*, **7**, 467 [1961]; $C_f x/2r_o$, and δ/r_o are from Vasudevan and Middleman, *Am. Inst. Chem. Eng. J.*, **16**, 614 [1970].)

also produce sound. See Krzywoblocki (*Appl. Mech. Rev.*, **6**, 393–397 [1953]) and Marris (*J. Basic Eng.*, **86**, 185–196 [1964]).

Development of a vortex street, or *von Kármán vortex street* is shown in Fig. 6-50. Discussions of the vortex street may be found in Panton (pp. 387–393). The Reynolds number is

$$Re = \frac{DV\rho}{\mu} \tag{6-194}$$

where D = diameter of cylinder or effective width of object
 V = free-stream velocity
 ρ = fluid density
 μ = fluid viscosity

For flow past a cylinder, the vortex street forms at Reynolds numbers above about 40. The vortices initially form in the wake, the point of formation moving closer to the cylinder as Re is increased. At a Reynolds number of 60 to 100, the vortices are formed from eddies attached to the cylinder surface. The vortices move at a velocity slightly less than \bar{V} . The frequency of vortex shedding f is given in terms of the Strouhal number, which is approximately constant over a wide range of Reynolds numbers.

$$St \equiv \frac{fD}{V} \tag{6-195}$$

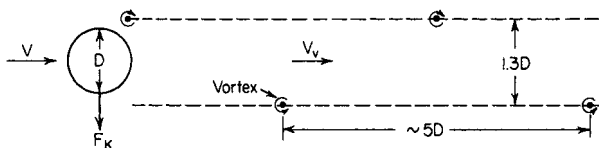


FIG. 6-50 Vortex street behind a cylinder.

For $40 < Re < 200$ the vortices are laminar and the Strouhal number has a nearly constant value of 0.2 for flow past a cylinder. Between $Re = 200$ and 400 the Strouhal number is no longer constant and the wake becomes irregular. Above about $Re = 400$ the vortices become turbulent, the wake is once again stable, and the Strouhal number remains constant at about 0.2 up to a Reynolds number of about 10^5 . Above $Re = 10^5$ the vortex shedding is difficult to see in flow visualization experiments, but velocity measurements still show a strong spectral component at $St = 0.2$ (Panton, p. 392). Experimental data suggest that the vortex street disappears over the range $5 \times 10^5 < Re < 3.5 \times 10^6$, but is reestablished at above 3.5×10^6 (Schlichting).

Vortex shedding exerts alternating lateral forces on a cylinder, perpendicular to the flow direction. Such forces may lead to severe vibration or mechanical failure of cylindrical elements such as heat-exchanger tubes, transmission lines, stacks, and columns when the vortex shedding frequency is close to resonant bending frequency. According to Den Hartog (*Proc. Nat. Acad. Sci.*, **40**, 155–157 [1954]), the vortex shedding and cylinder vibration frequency will shift to the resonant frequency when the calculated shedding frequency is within 20 percent of the resonant frequency. The well-known Tacoma Narrows bridge collapse resulted from resonance between a torsional oscillation and vortex shedding (Panton, p. 392). Spiral strakes are sometimes installed on tall stacks so that vortices at different axial positions are not shed simultaneously. The alternating lateral force F_K , sometimes called the *von Kármán force*, is given by (Den Hartog, *Mechanical Vibrations*, 4th ed., McGraw-Hill, New York, 1956, pp. 305–309):

$$F_K = C_K A \frac{\rho V^2}{2} \tag{6-196}$$

where C_K = von Kármán coefficient
 A = projected area perpendicular to the flow
 ρ = fluid density
 V = free-stream fluid velocity

For a cylinder, $C_K = 1.7$. For a vibrating cylinder, the effective projected area exceeds, but is always less than twice, the actual cylinder projected area (Rouse, *Engineering Hydraulics*, Wiley, New York, 1950).

The following references pertain to discussions of vortex shedding in specific structures: steel stacks (Osler and Smith, *Trans. ASME*, **78**, 1381–1391 [1956]; Smith and McCarthy, *Mech. Eng.*, **87**, 38–41 [1965]); chemical-processing columns (Freese, *J. Eng. Ind.*, **81**, 77–91 [1959]); heat exchangers (Eisinger, *Trans. ASME J. Pressure Vessel Tech.*, **102**, 138–145 [May 1980]; Chen, *J. Sound Vibration*, **93**, 439–455 [1984]; Gainsboro, *Chem. Eng. Prog.*, **64**[3], 85–88 [1968]; “Flow-Induced Vibration in Heat Exchangers,” *Symp. Proc.*, ASME, New York, 1970); suspended pipe lines (Baird, *Trans. ASME*, **77**, 797–804 [1955]); and suspended cable (Steidel, *J. Appl. Mech.*, **23**, 649–650 [1956]).

COATING FLOWS

In coating flows, liquid films are entrained on moving solid surfaces. For general discussions, see Ruschak (*Ann. Rev. Fluid Mech.*, **17**, 65–89 [1985]), Cohen and Gutoff (*Modern Coating and Drying Technology*, VCH Publishers, New York, 1992), and Middleman (*Fundamentals of Polymer Processing*, McGraw-Hill, New York, 1977). It is generally important to control the thickness and uniformity of the coatings.

In **dip coating**, or free withdrawal coating, a solid surface is withdrawn from a liquid pool, as shown in Fig. 6-51. It illustrates many of the features found in other coating flows, as well. Tallmadge and Gutfinger (*Ind. Eng. Chem.*, **59**[11], 19–34 [1967]) provide an early review of the theory of dip coating. The coating flow rate and film thickness are controlled by the withdrawal rate and the flow behavior in the meniscus region. For a withdrawal velocity V and an angle of inclination from the horizontal ϕ , the film thickness h may be

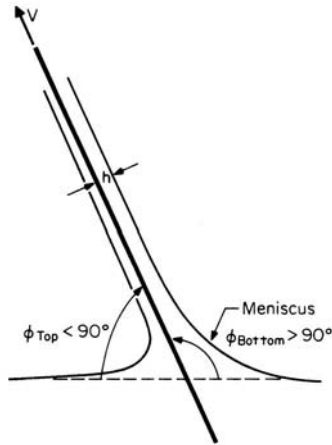


FIG. 6-51 Dip coating.

estimated for low withdrawal velocities by

$$h \left(\frac{\rho g}{\sigma} \right)^{1/2} = \frac{0.944}{(1 - \cos \phi)^{1/2}} Ca^{2/3} \quad (6-197)$$

where g = acceleration of gravity
 $Ca = \mu V / \sigma$ = capillary number
 μ = viscosity
 σ = surface tension

Equation (6-197) is asymptotically valid as $Ca \rightarrow 0$ and agrees with experimental data up to capillary numbers in the range of 0.01 to 0.03. In practice, where high production rates require high withdrawal speeds, capillary numbers are usually too large for Eq. (6-197) to apply. Approximate analytical methods for larger capillary numbers have been obtained by numerous investigators, but none appears wholly satisfactory, and some are based on questionable assumptions (Ruschak, *Ann. Rev. Fluid Mech.*, **17**, 65–89 [1985]). With the availability of high-speed computers and the development of the field of computational fluid dynamics, numerical solutions accounting for two-dimensional flow aspects, along with gravitational, viscous, inertial, and surface tension forces are now the most effective means to analyze coating flow problems.

Other common coating flows include premetered flows, such as **slide** and **curtain coating**, where the film thickness is an independent parameter that may be controlled within limits, and the curvature of the meniscus adjusts accordingly; the closely related **blade coating**; and **roll coating** and **extrusion coating**. See Ruschak (ibid.), Cohen and Gutoff (*Modern Coating and Drying Technology*, VCH Publishers, New York, 1992), and Middleman (*Fundamentals of Polymer Processing*, McGraw-Hill, New York, 1977). For dip coating of wires, see Taughy (*Int. J. Numerical Meth. Fluids*, **4**, 441–475 [1984]).

Many coating flows are subject to instabilities that lead to unacceptable coating defects. Three-dimensional flow instabilities lead to such problems as **ribbing**. Air entrainment is another common defect.

FALLING FILMS

Minimum Wetting Rate The minimum liquid rate required for complete wetting of a vertical surface is about 0.03 to 0.3 kg/m · s for water at room temperature. The minimum rate depends on the geometry and nature of the vertical surface, liquid surface tension, and mass transfer between surrounding gas and the liquid. See Ponter, et al. (*Int. J. Heat Mass Transfer*, **10**, 349–359 [1967]; *Trans. Inst. Chem.*

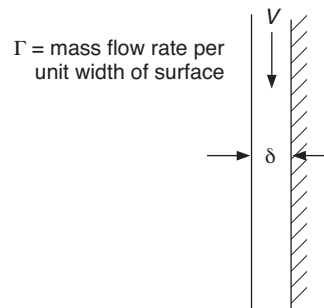


FIG. 6-52 Falling film.

Eng. [London], **45**, 345–352 [1967]), Stainthorp and Allen (*Trans. Inst. Chem. Eng. [London]*, **43**, 85–91 [1967]) and Watanabe, et al. (*J. Chem. Eng. [Japan]*, **8**[1], 75 [1975]).

Laminar Flow For films falling down **vertical flat surfaces**, as shown in Fig. 6-52, or vertical tubes with small film thickness compared to tube radius, laminar flow conditions prevail for Reynolds numbers less than about 2,000, where the Reynolds number is given by

$$Re = \frac{4\Gamma}{\mu} \quad (6-198)$$

where Γ = liquid mass flow rate per unit width of surface and μ = liquid viscosity. For a flat film surface, the following equations may be derived. The film thickness δ is

$$\delta = \left(\frac{3\Gamma\mu}{\rho^2 g} \right)^{1/3} \quad (6-199)$$

The average film velocity is

$$V = \frac{\Gamma}{\rho\delta} = \frac{g\rho\delta^2}{3\mu} \quad (6-200)$$

The downward velocity profile $u(x)$ where $x = 0$ at the solid surface and $x = \delta$ at the liquid/gas interface is given by

$$u = 1.5V \left[\frac{2x}{\delta} - \left(\frac{x}{\delta} \right)^2 \right] \quad (6-201)$$

These equations assume that there is no drag force at the gas/liquid interface, such as would be produced by gas flow. For a flat surface **inclined** at an angle θ with the horizontal, the preceding equations may be modified by replacing g by $g \sin \theta$. For films falling inside vertical tubes with film thickness up to and including the full pipe radius, see Jackson (*AIChE J.*, **1**, 231–240 [1955]).

These equations have generally given good agreement with experimental results for low-viscosity liquids ($< 0.005 \text{ Pa} \cdot \text{s}$) ($< 5 \text{ cP}$) whereas Jackson (ibid.) found film thicknesses for higher-viscosity liquids (0.01 to 0.02 Pa·s (10 to 20 cP) were significantly less than predicted by Eq. (6-197). At Reynolds numbers of 25 or greater, **surface waves** will be present on the liquid film. West and Cole (*Chem. Eng. Sci.*, **22**, 1388–1389 [1967]) found that the surface velocity $u(x = \delta)$ is still within ± 7 percent of that given by Eq. (6-201) even in wavy flow.

For laminar non-Newtonian film flow, see Bird, Armstrong, and Hassager (*Dynamics of Polymeric Liquids*, vol. 1: *Fluid Mechanics*, Wiley, New York, 1977, p. 215, 217), Astarita, Marrucci, and Palumbo (*Ind. Eng. Chem. Fundam.*, **3**, 333–339 [1964]) and Cheng (*Ind. Eng. Chem. Fundam.*, **13**, 394–395 [1974]).

Turbulent Flow In turbulent flow, $Re > 2,000$, for vertical surfaces, the film thickness may be estimated to within ± 25 percent using

$$\delta = 0.304 \left(\frac{\Gamma^{1.75} \mu^{0.25}}{\rho^2 g} \right)^{1/3} \quad (6-202)$$

Replace g by $g \sin \theta$ for a surface inclined at angle θ to the horizontal. The average film velocity is $V = \Gamma/\rho\delta$.

Tallmadge and Gutfinger (*Ind. Eng. Chem.*, **59**[11], 19–34 [1967]) discuss prediction of drainage rates from liquid films on flat and cylindrical surfaces.

Effect of Surface Traction If a drag is exerted on the surface of the film because of motion of the surrounding fluid, the film thickness will be reduced or increased, depending upon whether the drag acts with or against gravity. Thomas and Portalski (*Ind. Eng. Chem.*, **50**, 1081–1088 [1958]), Dukler (*Chem. Eng. Prog.*, **55**[10], 62–67 [1959]), and Kosky (*Int. J. Heat Mass Transfer*, **14**, 1220–1224 [1971]) have presented calculations of film thickness and film velocity. Film thickness data for falling water films with cocurrent and countercurrent air flow in pipes are given by Zhivaikin (*Int. Chem. Eng.*, **2**, 337–341 [1962]), Zabarás, Dukler, and Moalem-Maron (*AIChE J.*, **32**, 829–843 [1986]) and Zabarás and Dukler (*AIChE J.*, **34**, 389–396 [1988]) present studies of film flow in vertical tubes with both cocurrent and countercurrent gas flow, including measurements of film thickness, wall shear stress, wave velocity, wave amplitude, pressure drop, and flooding point for countercurrent flow.

Flooding With countercurrent gas flow, a condition is reached with increasing gas rate for which flow reversal occurs and liquid is carried upward. The mechanism for this flooding condition has been most often attributed to waves either bridging the pipe or reversing direction to flow upward at flooding. However, the results of Zabarás and Dukler (*ibid.*) suggest that flooding may be controlled by flow conditions at the liquid inlet and that wave bridging or upward wave motion does not occur, at least for the 50.8-mm diameter pipe used for their study. Flooding mechanisms are still incompletely understood. Under some circumstances, as when the gas is allowed to develop its normal velocity profile in a “calming length” of pipe beneath the liquid draw-off, the gas superficial velocity at flooding will be increased, and increases with decreasing length of wetted pipe (Hewitt, Lacy, and Nicholls, *Proc. Two-Phase Flow Symp.*, University of Exeter, paper 4H, AERE-4 4614 [1965]). A bevel cut at the bottom of the pipe with an angle 30° from the vertical will increase the flooding velocity in small-diameter tubes at moderate liquid flow rates. If the gas approaches the tube from the side, the taper should be oriented with the point facing the gas entrance. Figures 6-53 and 6-54 give correlations for flooding in tubes with square and slant bottoms (courtesy Holmes, DuPont Co.) The superficial mass velocities of gas and liquid G_G and G_L , and the physical property parameters λ and ψ are the same as those defined for the Baker chart (“Multiphase Flow” subsection, Fig. 6-25). For tubes larger than 50 mm (2 in), flooding velocity appears to be relatively insensitive to diameter and the flooding curves for 1.98-in diameter may be used.

HYDRAULIC TRANSIENTS

Many transient flows of liquids may be analyzed by using the full time-dependent equations of motion for incompressible flow. However,

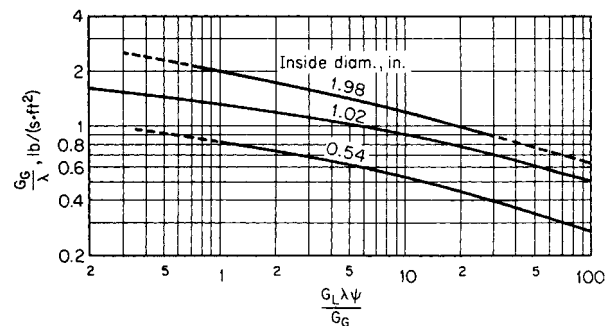


FIG. 6-53 Flooding in vertical tubes with square top and square bottom. To convert $\text{lbm}/(\text{ft}^2 \cdot \text{s})$ to $\text{kg}/(\text{m}^2 \cdot \text{s})$, multiply by 4.8824; to convert in to mm, multiply by 25.4. (Courtesy of E. I. du Pont de Nemours & Co.)

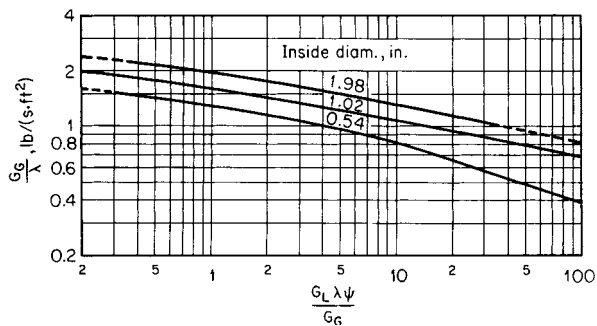


FIG. 6-54 Flooding in vertical tubes with square top and slant bottom. To convert $\text{lbm}/(\text{ft}^2 \cdot \text{s})$ to $\text{kg}/(\text{m}^2 \cdot \text{s})$, multiply by 4.8824; to convert in to mm, multiply by 25.4. (Courtesy of E. I. du Pont de Nemours & Co.)

there are some phenomena that are controlled by the small compressibility of liquids. These phenomena are generally called **hydraulic transients**.

Water Hammer When liquid flowing in a pipe is suddenly decelerated to zero velocity by a fast-closing valve, a pressure wave propagates upstream to the pipe inlet, where it is reflected; a pounding of the line commonly known as **water hammer** is often produced. For an instantaneous flow stoppage of a truly incompressible fluid in an inelastic pipe, the pressure rise would be infinite. Finite compressibility of the fluid and elasticity of the pipe limit the pressure rise to a finite value. The Joukowski formula gives the maximum pressure rise as

$$\Delta p = \rho a \Delta V \tag{6-203}$$

where ρ = liquid density
 ΔV = change in liquid velocity
 a = pressure wave velocity

The wave velocity is given by

$$a = \frac{\sqrt{\beta/\rho}}{\sqrt{1 + (\beta/E)(D/b)}} \tag{6-204}$$

where β = liquid bulk modulus of elasticity
 E = elastic modulus of pipe wall
 D = pipe inside diameter
 b = pipe wall thickness

The numerator gives the wave velocity for perfectly rigid pipe, and the denominator corrects for wall elasticity. This formula is for thin-walled pipes; for thick-walled pipes, the factor D/b is replaced by

$$2 \frac{D_o^2 + D_i^2}{D_o^2 - D_i^2}$$

where D_o = pipe outside diameter
 D_i = pipe inside diameter

Example 10: Response to Instantaneous Valve Closing Compute the wave speed and maximum pressure rise for instantaneous valve closing, with an initial velocity of 2.0 m/s, in a 4-in Schedule 40 steel pipe with elastic modulus 207×10^9 Pa. Repeat for a plastic pipe of the same dimensions, with $E = 1.4 \times 10^9$ Pa. The liquid is water with $\beta = 2.2 \times 10^9$ Pa and $\rho = 1,000 \text{ kg/m}^3$.

For the steel pipe, $D = 102.3 \text{ mm}$, $b = 6.02 \text{ mm}$, and the wave speed is

$$\begin{aligned} a &= \frac{\sqrt{\beta/\rho}}{\sqrt{1 + (\beta/E)(D/b)}} \\ &= \frac{\sqrt{2.2 \times 10^9/1000}}{\sqrt{1 + (2.2 \times 10^9/207 \times 10^9)(102.3/6.02)}} \\ &= 1365 \text{ m/s} \end{aligned}$$

The maximum pressure rise is

$$\begin{aligned} \Delta p &= \rho a \Delta V \\ &= 1,000 \times 1,365 \times 2.0 = 2.73 \times 10^6 \text{ Pa} \end{aligned}$$

For the plastic pipe,

$$\begin{aligned} a &= \frac{\sqrt{2.2 \times 10^9 / 1000}}{\sqrt{1 + (2.2 \times 10^9 / 1.4 \times 10^9)(102.3/6.02)}} \\ &= 282 \text{ m/s} \\ \Delta p &= \rho a \Delta V = 1,000 \times 282 \times 2.0 = 5.64 \times 10^5 \text{ Pa} \end{aligned}$$

The maximum pressure surge is obtained when the valve closes in less time than the period τ required for the pressure wave to travel from the valve to the pipe inlet and back, a total distance of $2L$.

$$\tau = \frac{2L}{a} \tag{6-205}$$

The pressure surge will be reduced when the time of flow stoppage exceeds the pipe period τ , due to cancellation between direct and reflected waves. Wood and Jones (*Proc. Am. Soc. Civ. Eng., J. Hydraul. Div.*, **99**, (HY1), 167–178 [1973]) present charts for reliable estimates of water-hammer pressure for different valve closure modes. Wylie and Streeter (*Hydraulic Transients*, McGraw-Hill, New York, 1978) describe several solution methods for hydraulic transients, including the method of characteristics, which is well suited to computer methods for accurate solutions. A rough approximation for the peak pressure for cases where the valve closure time t_c exceeds the pipe period τ is (Daugherty and Franzini, *Fluid Mechanics with Engineering Applications*, McGraw-Hill, New York, 1985):

$$\Delta p \approx \left(\frac{\tau}{t_c} \right) \rho a \Delta V \tag{6-206}$$

Successive reflections of the pressure wave between the pipe inlet and the closed valve result in alternating pressure increases and decreases, which are gradually attenuated by fluid friction and imperfect elasticity of the pipe. Periods of reduced pressure occur while the reflected pressure wave is traveling from inlet to valve. Degassing of the liquid may occur, as may vaporization if the pressure drops below the vapor pressure of the liquid. Gas and vapor bubbles decrease the wave velocity. Vaporization may lead to what is often called *liquid column separation*; subsequent collapse of the vapor pocket can result in pipe rupture.

In addition to water hammer induced by changes in valve setting, including closure, numerous other hydraulic transient flows are of interest, as, for example (Wylie and Streeter, *Hydraulic Transients*, McGraw-Hill, New York, 1978), those arising from starting or stopping of pumps; changes in power demand from turbines; reciprocating pumps; changing elevation of a reservoir; waves on a reservoir; turbine governor hunting; vibration of impellers or guide vanes in pumps, fans, or turbines; vibration of deformable parts such as valves; draft-tube instabilities due to vortexing; and unstable pump or fan characteristics. Tube failure in heat exchangers may be added to this list.

Pulsating Flow Reciprocating machinery (pumps and compressors) produces flow pulsations, which adversely affect flow meters and process control elements and can cause vibration and equipment failure, in addition to undesirable process results. Vibration and damage can result not only from the fundamental frequency of the pulse producer but also from higher harmonics. Multipiston double-acting units reduce vibrations. Pulsation dampeners are often added. Damping methods are described by M. W. Kellogg Co. (*Design of Piping Systems*, rev. 2d ed., Wiley, New York, 1965). For liquid phase pulsation damping, gas-filled surge chambers, also known as accumulators, are commonly used; see Wylie and Streeter (*Hydraulic Transients*, McGraw-Hill, New York, 1978).

Software packages are commercially available for simulation of hydraulic transients. These may be used to analyze piping systems to reveal unsatisfactory behavior, and they allow the assessment of design changes such as increases in pipe-wall thickness, changes in valve actuation, and addition of check valves, surge tanks, and pulsation dampeners.

Cavitation Loosely regarded as related to water hammer and hydraulic transients because it may cause similar vibration and equipment damage, **cavitation** is the phenomenon of collapse of vapor bubbles in flowing liquid. These bubbles may be formed anywhere the local liquid pressure drops below the vapor pressure, or they may be injected into the liquid, as when steam is sparged into water. Local low-pressure zones may be produced by local velocity increases (in accordance with the Bernoulli equation; see the preceding “Conservation Equations” subsection) as in eddies or vortices, or near boundary contours; by rapid vibration of a boundary; by separation of liquid during water hammer; or by an overall reduction in static pressure, as due to pressure drop in the suction line of a pump.

Collapse of vapor bubbles once they reach zones where the pressure exceeds the vapor pressure can cause objectionable noise and vibration and extensive erosion or pitting of the boundary materials. The critical cavitation number at inception of cavitation, denoted σ_c , is useful in correlating equipment performance data:

$$\sigma_c = \frac{p - p_v}{\rho V^2 / 2} \tag{6-207}$$

where p = static pressure in undisturbed flow
 p_v = vapor pressure
 ρ = liquid density
 V = free-stream velocity of the liquid

The value of the cavitation number for incipient cavitation for a specific piece of equipment is a characteristic of that equipment. Cavitation numbers for various head forms of cylinders, for disks, and for various hydrofoils are given by Holl and Wislicenus (*J. Basic Eng.*, **83**, 385–398 [1961]) and for various surface irregularities by Arndt and Ippen (*J. Basic Eng.*, **90**, 249–261 [1968]), Ball (*Proc. ASCE J. Constr. Div.*, **89**(C02), 91–110 [1963]), and Holl (*J. Basic Eng.*, **82**, 169–183 [1960]). As a guide only, for blunt forms the cavitation number is generally in the range of 1 to 2.5, and for somewhat streamlined forms the cavitation number is in the range of 0.2 to 0.5. Critical cavitation numbers generally depend on a characteristic length dimension of the equipment in a way that has not been explained. This renders scale-up of cavitation data questionable.

For cavitation in flow through orifices, Fig. 6-55 (Thorpe, *Int. J. Multiphase Flow*, **16**, 1023–1045 [1990]) gives the critical cavitation number for inception of cavitation. To use this cavitation number in Eq. (6-207), the pressure p is the orifice backpressure downstream of the vena contracta after full pressure recovery, and V is the average velocity through the orifice. Figure 6-55 includes data from Tullis and Govindarajan (*ASCE J. Hydraul. Div.*, **HY13**, 417–430 [1973]) modified to use the same cavitation number definition; their data also include critical cavitation numbers for 30.50- and 59.70-cm pipes

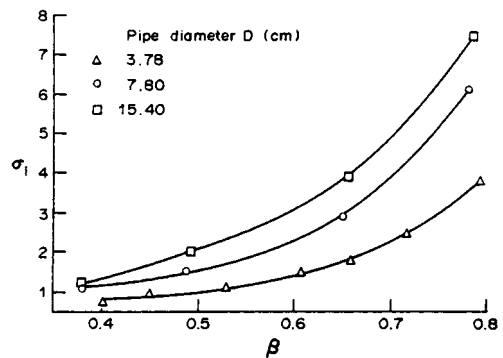


FIG. 6-55 Critical cavitation number vs. diameter ratio β . (Reprinted from Thorpe, “Flow regime transitions due to cavitation in the flow through an orifice,” *Int. J. Multiphase Flow*, **16**, 1023–1045. Copyright © 1990, with kind permission from Elsevier Science, Ltd., The Boulevard, Langford Lane, Kidlington OX5 1GB, United Kingdom.)

(12.00- to 23.50-in). Very roughly, compared with the 15.40-cm pipe, the cavitation number is about 20 percent greater for the 30.50-cm (12.01-in) pipe and about 40 percent greater for the 59.70-cm (23.50-in) diameter pipe. Inception of cavitation appears to be related to release of dissolved gas and not merely vaporization of the liquid. For further discussion of cavitation, see Eisenberg and Tulin (Streeter, *Handbook of Fluid Dynamics*, Sec. 12, McGraw-Hill, New York, 1961).

TURBULENCE

Turbulent flow occurs when the Reynolds number exceeds a critical value above which laminar flow is unstable; the critical Reynolds number depends on the flow geometry. There is generally a transition regime between the critical Reynolds number and the Reynolds number at which the flow may be considered fully turbulent. The transition regime is very wide for some geometries. In turbulent flow, variables such as velocity and pressure fluctuate chaotically; statistical methods are used to quantify turbulence.

Time Averaging In turbulent flows it is useful to define time-averaged and fluctuation values of flow variables such as velocity components. For example, the *x*-component velocity fluctuation v'_x is the difference between the actual instantaneous velocity v_x and the time-averaged velocity \bar{v}_x :

$$v'_x(x, y, z, t) = v_x(x, y, z, t) - \bar{v}_x(x, y, z) \tag{6-208}$$

The actual and fluctuating velocity components are, in general, functions of the three spatial coordinates *x*, *y*, and *z* and of time *t*. The time-averaged velocity \bar{v}_x is independent of time for a **stationary** flow. Nonstationary processes may be considered where averages are defined over time scales long compared to the time scale of the turbulent fluctuations, but short compared to longer time scales over which the time-averaged flow variables change due, for example, to time-varying boundary conditions. The time average over a time interval $2T$ centered at time *t* of a turbulently fluctuating variable $\zeta(t)$ is defined as

$$\bar{\zeta}(t) = \frac{1}{2T} \int_{t-T}^{t+T} \zeta(\tau) d\tau \tag{6-209}$$

where τ = dummy integration variable. For stationary turbulence, $\bar{\zeta}$ does not vary with time.

$$\bar{\zeta} = \lim_{T \rightarrow \infty} \frac{1}{2T} \int_{t-T}^{t+T} \zeta(\tau) d\tau \tag{6-210}$$

The time average of a fluctuation $\bar{\zeta}' = \bar{\zeta} - \bar{\zeta} = 0$. Fluctuation magnitudes are quantified by root mean squares.

$$\bar{v}'_x = \sqrt{\overline{(v'_x)^2}} \tag{6-211}$$

In **isotropic** turbulence, statistical measures of fluctuations are equal in all directions.

$$\bar{v}'_x = \bar{v}'_y = \bar{v}'_z \tag{6-212}$$

In **homogeneous** turbulence, turbulence properties are independent of spatial position. The **kinetic energy of turbulence** *k* is given by

$$k = \frac{1}{2} (\bar{v}'_x{}^2 + \bar{v}'_y{}^2 + \bar{v}'_z{}^2) \tag{6-213}$$

Turbulent velocity fluctuations ultimately dissipate their kinetic energy through viscous effects. Macroscopically, this energy dissipation requires pressure drop, or velocity decrease. The **energy dissipation rate** per unit mass is usually denoted ϵ . For steady flow in a pipe, the average energy dissipation rate per unit mass is given by

$$\epsilon = \frac{2fV^3}{D} \tag{6-214}$$

where ρ = fluid density
f = Fanning friction factor
D = pipe inside diameter

When the continuity equation and the Navier-Stokes equations for incompressible flow are time averaged, equations for the time-averaged

velocities and pressures are obtained which appear identical to the original equations (6-18 through 6-28), except for the appearance of additional terms in the Navier-Stokes equations. Called **Reynolds stress** terms, they result from the nonlinear effects of momentum transport by the velocity fluctuations. In each *i*-component (*i* = *x*, *y*, *z*) Navier-Stokes equation, the following additional terms appear on the right-hand side:

$$\sum_{j=1}^3 \frac{\partial \tau'_{ij}}{\partial x_j}$$

with *j* components also being *x*, *y*, *z*. The Reynolds stresses are given by

$$\tau'_{ij} = -\rho \overline{v'_i v'_j} \tag{6-215}$$

The Reynolds stresses are nonzero because the velocity fluctuations in different coordinate directions are correlated so that $\overline{v'_i v'_j}$ in general is nonzero.

Although direct numerical simulations under limited circumstances have been carried out to determine (unaveraged) fluctuating velocity fields, in general the solution of the equations of motion for turbulent flow is based on the time-averaged equations. This requires semi-empirical models to express the Reynolds stresses in terms of time-averaged velocities. This is the **closure** problem of turbulence. In all but the simplest geometries, numerical methods are required.

Closure Models Many closure models have been proposed. A few of the more important ones are introduced here. Many employ the Boussinesq approximation, simplified here for incompressible flow, which treats the Reynolds stresses as analogous to viscous stresses, introducing a scalar quantity called the turbulent or eddy viscosity μ_t .

$$-\rho \overline{v'_i v'_j} = \mu_t \left(\frac{\partial \bar{v}_i}{\partial x_j} + \frac{\partial \bar{v}_j}{\partial x_i} \right) \tag{6-216}$$

An additional *turbulence pressure* term equal to $-2/3 k \delta_{ij}$, where *k* = turbulent kinetic energy and $\delta_{ij} = 1$ if *i* = *j* and $\delta_{ij} = 0$ if *i* ≠ *j*, is sometimes included in the right-hand side. To solve the equations of motion using the Boussinesq approximation, it is necessary to provide equations for the single scalar unknown μ_t (and *k*, if used) rather than the nine unknown tensor components τ'_{ij} . With this approximation, and using the effective viscosity $\mu_{\text{eff}} = \mu + \mu_t$, the time-averaged momentum equation is similar to the original Navier-Stokes equation, with time-averaged variables and μ_{eff} replacing the instantaneous variables and molecular viscosity. However, solutions to the time-averaged equations for turbulent flow are not identical to those for laminar flow because μ_{eff} is not a constant.

The universal turbulent velocity profile near the pipe wall presented in the preceding subsection "Incompressible Flow in Pipes and Channels" may be developed using the Prandtl mixing length approximation for the eddy viscosity,

$$\mu_t = \rho l_p^2 \left| \frac{d\bar{v}_x}{dy} \right| \tag{6-217}$$

where *l_p* is the Prandtl mixing length. The turbulent core of the universal velocity profile is obtained by assuming that the mixing length is proportional to the distance from the wall. The proportionality constant is one of two constants adjusted to fit experimental data.

The Prandtl mixing length concept is useful for shear flows parallel to walls, but is inadequate for more general three-dimensional flows. A more complicated semiempirical model commonly used in numerical computations, and found in most commercial software for computational fluid dynamics (CFD; see the following subsection), is the *k*- ϵ model described by Launder and Spaulding (*Lectures in Mathematical Models of Turbulence*, Academic, London, 1972). In this model the eddy viscosity is assumed proportional to the ratio k^2/ϵ .

$$\mu_t = \rho C_\mu \frac{k^2}{\epsilon} \tag{6-218}$$

where the value $C_\mu = 0.09$ is normally used. Semiempirical partial differential conservation equations for *k* and ϵ derived from the

Navier-Stokes equations with simplifying closure assumptions are coupled with the equations of continuity and momentum:

$$\frac{\partial}{\partial t} (\rho k) + \frac{\partial}{\partial x_i} (\rho \bar{v}_i k) = \frac{\partial}{\partial x_i} \left(\frac{\mu_t}{\sigma_k} \frac{\partial k}{\partial x_i} \right) + \mu_t \left(\frac{\partial \bar{v}_i}{\partial x_j} + \frac{\partial \bar{v}_j}{\partial x_i} \right) \frac{\partial \bar{v}_i}{\partial x_j} - \rho \epsilon \quad (6-219)$$

$$\frac{\partial}{\partial t} (\rho \epsilon) + \frac{\partial}{\partial x_i} (\rho \bar{v}_i \epsilon) = \frac{\partial}{\partial x_i} \left(\frac{\mu_t}{\sigma_\epsilon} \frac{\partial \epsilon}{\partial x_i} \right) + C_{1\epsilon} \frac{\epsilon \mu_t}{k} \left(\frac{\partial \bar{v}_i}{\partial x_j} + \frac{\partial \bar{v}_j}{\partial x_i} \right) \frac{\partial \bar{v}_i}{\partial x_j} - C_{2\epsilon} \frac{\rho \epsilon^2}{k} \quad (6-220)$$

In these equations summations over repeated indices are implied. The values for the empirical constants $C_{1\epsilon} = 1.44$, $C_{2\epsilon} = 1.92$, $\sigma_k = 1.0$, and $\sigma_\epsilon = 1.3$ are widely accepted (Lauder and Spaulding, *The Numerical Computation of Turbulent Flows*, Imperial Coll. Sci. Tech. London, NTIS N74-12066 [1973]). The $k-\epsilon$ model has proved reasonably accurate for many flows without highly curved streamlines or significant swirl. It usually underestimates flow separation and overestimates turbulence production by normal straining. The $k-\epsilon$ model is suitable for high Reynolds number flows. See Virendra, Patel, Rodi, and Scheuerer (*AIAA J.*, **23**, 1308–1319 [1984]) for a review of low Reynolds number $k-\epsilon$ models.

More advanced models, more complex and computationally intensive, are being developed. For example, the renormalization group theory (Yakhot and Orszag, *J. Scientific Computing*, **1**, 1–51 [1986]; Yakhot, Orszag, Thangam, Gatski, and Speziale, *Phys. Fluids A*, **4**, 1510–1520 [1992]) modification of the $k-\epsilon$ model provides theoretical values of the model constants and provides substantial improvement in predictions of flows with stagnation, separation, normal straining, transient behavior such as vortex shedding, and relaminarization. Stress transport models provide equations for all nine Reynolds stress components, rather than introducing eddy viscosity. Algebraic closure equations for the Reynolds stresses are available, but are no longer in common use. Differential Reynolds stress models (e.g., Launder, Reece, and Rodi, *J. Fluid Mech.*, **68**, 537–566 [1975]) use differential conservation equations for all nine Reynolds stress components.

In **direct numerical simulation** of turbulent flows, the solution of the unaveraged equations of motion is sought. Due to the extreme computational intensity, solutions to date have been limited to relatively low Reynolds numbers in simple geometries. Since computational grids must be sufficiently fine to resolve even the smallest eddies, the computational difficulty rapidly becomes prohibitive as Reynolds number increases. **Large eddy simulations** use models for subgrid turbulence while solving for larger-scale fluctuations.

Eddy Spectrum The energy that produces and sustains turbulence is extracted from velocity gradients in the mean flow, principally through vortex stretching. At Reynolds numbers well above the critical value there is a wide spectrum of eddy sizes, often described as a cascade of energy from the largest down to the smallest eddies. The largest eddies are of the order of the equipment size. The smallest are those for which viscous forces associated with the eddy velocity fluctuations are of the same order as inertial forces, so that turbulent fluctuations are rapidly damped out by viscous effects at smaller length scales. Most of the turbulent kinetic energy is contained in the larger eddies, while most of the dissipation occurs in the smaller eddies. Large eddies, which extract energy from the mean flow velocity gradients, are generally anisotropic. At smaller length scales, the directionality of the mean flow exerts less influence, and **local isotropy** is approached. The range of eddy scales for which local isotropy holds is called the **equilibrium range**.

Davies (*Turbulence Phenomena*, Academic, New York, 1972) presents a good discussion of the spectrum of eddy lengths for well-developed isotropic turbulence. The smallest eddies, usually called *Kolmogorov eddies* (Kolmogorov, *Compt. Rend. Acad. Sci. URSS*, **30**, 301; **32**, 16 [1941]), have a characteristic velocity fluctuation \bar{v}'_k given by

$$\bar{v}'_k = (\nu \epsilon)^{1/4} \quad (6-221)$$

where ν = kinematic viscosity and ϵ = energy dissipation per unit mass. The size of the Kolmogorov eddy scale is

$$l_K = (\nu^3/\epsilon)^{1/4} \quad (6-222)$$

The Reynolds number for the Kolmogorov eddy, $Re_K = l_K \bar{v}'_k/\nu$, is equal to unity by definition. In the equilibrium range, which exists for well-developed turbulence and extends from the medium eddy sizes down to the smallest, the energy dissipation at the smaller length scales is supplied by turbulent energy drawn from the bulk flow and passed down the spectrum of eddy lengths according to the scaling rule

$$\epsilon = \frac{(\bar{v}')^3}{l} \quad (6-223)$$

which is consistent with Eqs. (6-221) and (6-222). For the medium, or energy-containing, eddy size,

$$\epsilon = \frac{(\bar{v}'_e)^3}{l_e} \quad (6-224)$$

For turbulent pipe flow, the friction velocity $u_* = \sqrt{\tau_w/\rho}$ used earlier in describing the universal turbulent velocity profile may be used as an estimate for \bar{v}'_e . Together with the Blasius equation for the friction factor from which ϵ may be obtained (Eq. 6-214), this provides an estimate for the energy-containing eddy size in turbulent pipe flow:

$$l_e = 0.05 D Re^{-1/8} \quad (6-225)$$

where D = pipe diameter and Re = pipe Reynolds number. Similarly, the Kolmogorov eddy size is

$$l_K = 4 D Re^{-0.78} \quad (6-226)$$

Most of the energy dissipation occurs on a length scale about 5 times the Kolmogorov eddy size. The characteristic fluctuating velocity for these energy-dissipating eddies is about 1.7 times the Kolmogorov velocity.

The eddy spectrum is normally described using Fourier transform methods; see, for example, Hinze (*Turbulence*, McGraw-Hill, New York, 1975), and Tennekes and Lumley (*A First Course in Turbulence*, MIT Press, Cambridge, 1972). The spectrum $E(\kappa)$ gives the fraction of turbulent kinetic energy contained in eddies of wavenumber between κ and $\kappa + d\kappa$, so that $k = \int_0^\infty E(\kappa) d\kappa$. The portion of the equilibrium range excluding the smallest eddies, those which are affected by dissipation, is the **inertial subrange**. The Kolmogorov law gives $E(\kappa) \propto \kappa^{-5/3}$ in the inertial subrange.

Several texts are available for further reading on turbulent flow, including Pope (*Turbulent Flows*, Cambridge University Press, Cambridge, U.K., 2000), Tennekes and Lumley (ibid.), Hinze (*Turbulence*, McGraw-Hill, New York, 1975), Landau and Lifshitz (*Fluid Mechanics*, 2d ed., Chap. 3, Pergamon, Oxford, 1987) and Panton (*Incompressible Flow*, Wiley, New York, 1984).

COMPUTATIONAL FLUID DYNAMICS

Computational fluid dynamics (CFD) emerged in the 1980s as a significant tool for fluid dynamics both in research and in practice, enabled by rapid development in computer hardware and software. Commercial CFD software is widely available. Computational fluid dynamics is the numerical solution of the equations of continuity and momentum (Navier-Stokes equations for incompressible Newtonian fluids) along with additional conservation equations for energy and material species in order to solve problems of nonisothermal flow, mixing, and chemical reaction.

Textbooks include Fletcher (*Computational Techniques for Fluid Dynamics*, vol. 1: *Fundamental and General Techniques*, and vol. 2: *Specific Techniques for Different Flow Categories*, Springer-Verlag, Berlin, 1988), Hirsch (*Numerical Computation of Internal and External Flows*, vol. 1: *Fundamentals of Numerical Discretization*, and vol. 2: *Computational Methods for Inviscid and Viscous Flows*, Wiley, New York, 1988), Peyret and Taylor (*Computational Methods for Fluid*

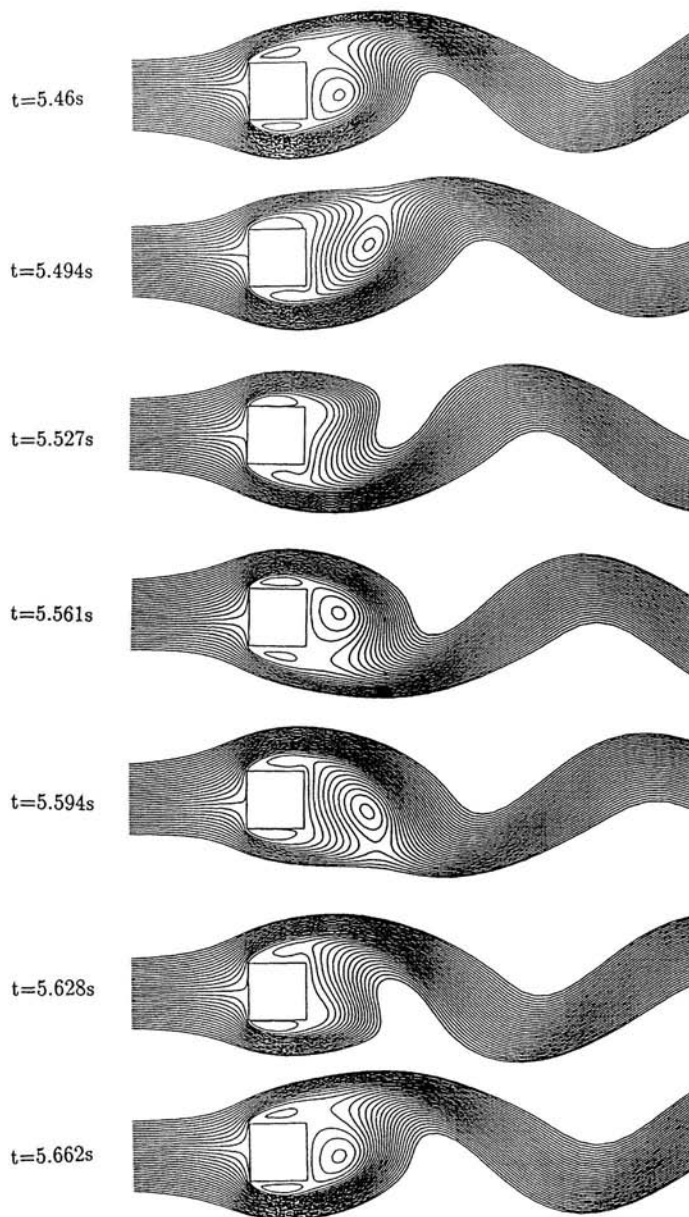


FIG. 6-56 Computational fluid dynamic simulation of flow over a square cylinder, showing one vortex shedding period. (From Choudhury *et al.*, Trans. ASME Fluids Div., TN-076 [1994].)

Flow, Springer-Verlag, Berlin, 1990), Canuto, Hussaini, Quarteroni, and Zang (*Spectral Methods in Fluid Dynamics*, Springer-Verlag, Berlin, 1988), Anderson, Tannehill, and Pletcher (*Computational Fluid Mechanics and Heat Transfer*, Hemisphere, New York, 1984), and Patankar (*Numerical Heat Transfer and Fluid Flow*, Hemisphere, Washington, D.C., 1980).

A wide variety of numerical methods has been employed, but three basic steps are common.

1. **Subdivision or discretization of the flow domain into cells or elements.** There are methods, called *boundary element methods*, in which the surface of the flow domain, rather than the volume, is discretized, but the vast majority of CFD work uses volume discretization. Discretization produces a set of **grid** lines or curves which define a **mesh** and a set of **nodes** at which the flow variables are to be calculated. The equations of motion are solved approximately on a domain defined by the grid. Curvilinear or **body-fitted** coordinate system grids may be used to ensure that the discretized domain accurately represents the true problem domain.

2. **Discretization of the governing equations.** In this step, the exact partial differential equations to be solved are replaced by approximate algebraic equations written in terms of the nodal values of the dependent variables. Among the numerous discretization methods, **finite difference**, **finite volume**, and **finite element** methods are the most common. The *finite difference* method estimates spatial derivatives in terms of the nodal values and spacing between nodes. The governing equations are then written in terms of the nodal unknowns at each interior node. *Finite volume* methods, related to finite difference methods, may be derived by volume integration of the equations of motion, with application of the divergence theorem, reducing by one the order of the differential equations. Equivalently, macroscopic balance equations are written on each cell. *Finite element* methods are weighted residual techniques in which the unknown dependent variables are expressed in terms of **basis functions** interpolating among the nodal values. The basis functions are substituted into the equations of motion, resulting in error residuals which are multiplied by the weighting functions, integrated over the control volume, and set to zero to produce algebraic equations in terms of the nodal unknowns. Selection of the weighting functions defines the various finite element methods. For example, Galerkin's method uses the nodal interpolation basis functions as weighting functions. Each method also has its own method for implementing **boundary conditions**. The end result after discretization of the equations and application of the boundary conditions is a set of algebraic equations for the nodal unknown variables. Discretization in time is also required for the $\partial/\partial t$ time derivative terms in unsteady flow; finite differencing in time is often used. The discretized equations represent an approximation of the exact equations, and their solution gives an approximation for the flow variables. The accuracy of the solution improves as the grid is **refined**; that is, as the number of nodal points is increased.

3. **Solution of the algebraic equations.** For creeping flows with constant viscosity, the algebraic equations are linear and a linear matrix equation is to be solved. Both direct and iterative solvers have been used. For most flows, the nonlinear inertial terms in the momentum equation are important and the algebraic discretized equations are therefore nonlinear. Solution yields the nodal values of the unknowns.

A CFD method called the lattice Boltzmann method is based on modeling the fluid as a set of particles moving with discrete velocities on a discrete grid or lattice, rather than on discretization of the governing continuum partial differential equations. Lattice Boltzmann approximations can be constructed that give the same macroscopic behavior as the Navier-Stokes equations. The method is currently used mainly in academic and research codes, rather than in general-purpose commercial CFD codes. There appear to be significant computational advantages to the lattice Boltzmann method. Lattice Boltzmann simulations incorporating turbulence models, and of multiphase flows and flows with heat transfer, species diffusion, and reaction, have been carried out. For a review of the method, see Chen and Doolen [*Ann. Rev. Fluid Mech.*, **30**, 329 (1998)].

CFD solutions, especially for complex three-dimensional flows, generate very large quantities of solution data. Computer graphics have greatly improved the ability to examine CFD solutions and visualize flow.

CFD methods are used for incompressible and compressible, creeping, laminar and turbulent, Newtonian and non-Newtonian, and isothermal and nonisothermal flows. Chemically reacting flows, particularly in the field of combustion, have been simulated. Solution accuracy must be considered from several perspectives. These include convergence of the algorithms for solving the nonlinear discretized equations and convergence with respect to refinement of the mesh so that the discretized equations better approximate the exact equations and, in some cases, so that the mesh more accurately fits the true geometry. The possibility that steady-state solutions are unstable must always be considered. In addition to numerical sources of error, modeling errors are introduced in turbulent flow, where semiempirical closure models are used to solve time-averaged equations of motion, as discussed previously. Most commercial CFD codes include the $k-\epsilon$ turbulence model, which has been by far the most widely used. More accurate models, such as differential Reynolds stress and renormalization group theory models, are also becoming available. Significant solution error is known to result in some problems from inadequacy of the turbulence model. Closure models for nonlinear chemical reaction source terms may also contribute to inaccuracy.

Large eddy simulation (LES) methods for turbulent flow are available in some commercial CFD codes. LES methods are based on filtering fluctuating variables, so that lower-frequency eddies, with scales larger than the grid spacing, are resolved, while higher-frequency eddies, the subgrid fluctuations, are filtered out. The subgrid-scale Reynolds stress is estimated by a turbulence model. The Smagorinsky model, a one-equation mixing length model, is used in most commercial codes that offer LES options and is also used in many academic and research CFD codes. See Wilcox (*Turbulence Modeling for CFD*, 2d ed., DCW Industries, La Cañada, Calif., 1998).

In its general sense, multiphase flow is not currently solvable by computational fluid dynamics. However, in certain cases reasonable solutions are possible. These include well-separated flows where the phases are confined to relatively well-defined regions separated by one or a few interfaces and flows in which a second phase appears as discrete particles of known size and shape whose motion may be approximately computed with drag coefficient formulations, or rigorously computed with refined meshes applying boundary conditions at the particle surface. **Two-fluid modeling**, in which the phases are treated as overlapping continua, with each phase occupying a volume fraction that is a continuous function of position (and time) is a useful approximation which is becoming available in commercial software. See Elghobashi and Abou-Arab (*J. Physics Fluids*, **26**, 931-938 [1983]) for a $k-\epsilon$ model for two-fluid systems.

Figure 6-56 gives an example CFD calculation for time-dependent flow past a square cylinder at a Reynolds number of 22,000 (Choudhury, et al., *Trans. ASME Fluids Div.*, Lake Tahoe, Nev. [1994]). The computation was done with an implementation of the renormalization group theory $k-\epsilon$ model. The series of contour plots of stream function shows a sequence in time over about 1 vortex-shedding period. The calculated Strouhal number (Eq. [6-195]) is 0.146, in excellent agreement with experiment, as is the time-averaged drag coefficient, $C_D = 2.24$. Similar computations for a circular cylinder at $Re = 14,500$ have given excellent agreement with experimental measurements for St and C_D (*Introduction to the Renormalization Group Method and Turbulence Modeling*, Fluent, Inc., 1993).

DIMENSIONLESS GROUPS

For purposes of data correlation, model studies, and scale-up, it is useful to arrange variables into dimensionless groups. Table 6-7 lists many of the dimensionless groups commonly found in fluid mechanics problems, along with their physical interpretations and areas of application. More extensive tabulations may be found in Catchpole and Fulford (*Ind. Eng. Chem.*, **58**[3], 46-60 [1966]) and Fulford and Catchpole (*Ind. Eng. Chem.*, **60**[3], 71-78 [1968]).

6-50 FLUID AND PARTICLE DYNAMICS

TABLE 6-7 Dimensionless Groups and Their Significance

Name	Symbol	Formula	Physical interpretation	Comments
Archimedes number	Ar	$\frac{gL^3(\rho_p - \rho)\rho}{\mu^3}$	$\frac{\text{inertial forces} \times \text{buoyancy forces}}{(\text{viscous forces})^2}$	Particle settling
Bingham number	Bm	$\frac{\tau_y L}{\mu_\infty V}$	$\frac{\text{yield stress}}{\text{viscous stress}}$	Flow of Bingham plastics = yield number, Y
Bingham Reynolds number	Re _B	$\frac{LV\rho}{\mu_\infty}$	$\frac{\text{inertial force}}{\text{viscous force}}$	Flow of Bingham plastics
Blake number	B	$\frac{V\rho}{\mu(1 - \epsilon)^s}$	$\frac{\text{inertial force}}{\text{viscous force}}$	Beds of solids
Bond number	Bo	$\frac{(\rho_L - \rho_G)L^2g}{\sigma}$	$\frac{\text{gravitational force}}{\text{surface-tension force}}$	Atomization = Eotvos number, Eo
Capillary number	Ca	$\frac{\mu V}{\sigma}$	$\frac{\text{viscous force}}{\text{surface-tension force}}$	Two-phase flows, free surface flows
Cauchy number	C	$\frac{\rho V^2}{\beta}$	$\frac{\text{inertial force}}{\text{compressibility force}}$	Compressible flow, hydraulic transients
Cavitation number	σ	$\frac{p - p_v}{\rho V^2/2}$	$\frac{\text{excess pressure above vapor pressure}}{\text{velocity head}}$	Cavitation
Dean number	D _e	$\frac{Re}{(Dc/D)^{1/2}}$	Reynolds number \times $\frac{\text{inertial force}}{\text{centrifugal force}}$	Flow in curved channels
Deborah number	De	$\lambda\omega$	$\frac{\text{fluid relaxation time}}{\text{flow characteristic time}}$	Viscoelastic flow
Drag coefficient	C _D	$\frac{F_D}{ApV^2/2}$	$\frac{\text{drag force}}{\text{projected area} \times \text{velocity head}}$	Flow around objects, particle settling
Elasticity number	El	$\frac{\lambda\mu}{\rho L^2}$	$\frac{\text{elastic force}}{\text{inertial force}}$	Viscoelastic flow
Euler number	Eu	$\frac{\Delta p}{\rho V^2}$	$\frac{\text{frictional pressure loss}}{2 \times \text{velocity head}}$	Fluid friction in conduits
Fanning friction factor	f	$\frac{D\Delta p}{2\rho V^2 L} = \frac{2\tau_w}{\rho V^2}$	$\frac{\text{wall shear stress}}{\text{velocity head}}$	Fluid friction in conduits Darcy friction factor = 4f
Froude number	Fr	$\frac{V^2}{gL}$	$\frac{\text{inertial force}}{\text{gravity force}}$	Often defined as Fr = V/√gL
Densometric Froude number	Fr'	$\frac{\rho V^2}{(\rho_d - \rho)gL}$	$\frac{\text{inertial force}}{\text{gravity force}}$	or Fr' = $\frac{V}{\sqrt{(\rho_d - \rho)gL/\rho}}$
Hedstrom number	He	$\frac{L^2\tau_y\rho}{\mu_\infty^2}$	Bingham Reynolds number \times Bingham number	Flow of Bingham plastics
Hodgson number	H	$\frac{V'\omega\Delta p}{\bar{q}\bar{p}}$	$\frac{\text{time constant of system}}{\text{period of pulsation}}$	Pulsating gas flow
Mach number	M	$\frac{V}{c}$	$\frac{\text{fluid velocity}}{\text{sonic velocity}}$	Compressible flow
Newton number	Ne	$\frac{\Delta PD}{\rho V^2 L}$	2 \times Fanning friction factor	
Ohnesorge number	Z	$\frac{\mu}{(\rho L\sigma)^{1/2}}$	$\frac{\text{viscous force}}{(\text{inertial force} \times \text{surface tension force})^{1/2}}$	Atomization = $\frac{\text{Weber number}}{\text{Reynolds number}}$
Peclet number	Pe	$\frac{LV}{D}$	$\frac{\text{convective transport}}{\text{diffusive transport}}$	Heat, mass transfer, mixing
Pipeline parameter	Pn	$\frac{aV_o}{2gH}$	$\frac{\text{maximum water-hammer pressure rise}}{2 \times \text{static pressure}}$	Water hammer

TABLE 6-7 Dimensionless Groups and Their Significance (Concluded)

Name	Symbol	Formula	Physical interpretation	Comments	
Power number	Po	$\frac{P}{\rho N^3 L^5}$	$\frac{\text{impeller drag force}}{\text{inertial force}}$	Agitation	
Prandtl velocity ratio	v^+	$\frac{v}{(\tau_w/\rho)^{1/2}}$	velocity normalized by friction velocity	Turbulent flow near a wall, friction velocity = $\sqrt{\tau_w/\rho}$	
Reynolds number	Re	$\frac{LV\rho}{\mu}$	$\frac{\text{inertial force}}{\text{viscous force}}$		
Strouhal number	St	$\frac{f'L}{V}$	vortex shedding frequency \times characteristic flow time scale	Vortex shedding, von Karman vortex streets	
Weber number	We	$\frac{\rho V^2 L}{\sigma}$	$\frac{\text{inertial force}}{\text{surface tension force}}$	Bubble, drop formation	
Nomenclature		SI Units	Nomenclature	SI Units	
a	Wave speed	m/s	P	Power	Watts
A	Projected area	m	\bar{q}	Average volumetric flow rate	m ³ /s
c	Sonic velocity	m/s	s	Particle area/particle volume	1/m
D	Diameter of pipe	m	v	Local fluid velocity	m/s
D_c	Diameter of curvature	m	V	Characteristic or average fluid velocity	m/s
D'	Diffusivity	m ² /s	V'	System volume	m ³
f'	Vortex shedding frequency	1/s	β	Bulk modulus	Pa
F_D	Drag force	N	ϵ	Void fraction	m ³
g	Acceleration of gravity	m/s	λ	Fluid relaxation time	s
H	Static head	m	μ	Fluid viscosity	Pa · s
L	Characteristic length	m	μ_∞	Infinite shear viscosity (Bingham plastics)	Pa · s
N	Rotational speed	1/s	ρ	Fluid density	kg/m ³
p	Pressure	Pa	ρ_G, ρ_L	Gas, liquid densities	kg/m ³
p_v	Vapor pressure	Pa	ρ_d	Dispersed phase density	kg/m ³
\bar{p}	Average static pressure	Pa	σ	Surface tension	N/m
Δp	Frictional pressure drop	Pa	ω	Characteristic frequency or reciprocal time scale of flow	1/s

PARTICLE DYNAMICS

GENERAL REFERENCES: Brodkey, *The Phenomena of Fluid Motions*, Addison-Wesley, Reading, Mass., 1967; Clift, Grace, and Weber, *Bubbles, Drops and Particles*, Academic, New York, 1978; Govier and Aziz, *The Flow of Complex Mixtures in Pipes*, Van Nostrand Reinhold, New York, 1972; Krieger, Huntington, N.Y., 1977; Lapple, et al., *Fluid and Particle Mechanics*, University of Delaware, Newark, 1951; Levich, *Physicochemical Hydrodynamics*, Prentice-Hall, Englewood Cliffs, N.J., 1962; Orr, *Particulate Technology*, Macmillan, New York, 1966; Shook and Roco, *Slurry Flow*, Butterworth-Heinemann, Boston, 1991; Wallis, *One-dimensional Two-phase Flow*, McGraw-Hill, New York, 1969.

DRAG COEFFICIENT

Whenever relative motion exists between a particle and a surrounding fluid, the fluid will exert a drag upon the particle. In steady flow, the drag force on the particle is

$$F_D = \frac{C_D A_P \rho u^2}{2} \quad (6-227)$$

- where F_D = drag force
- C_D = drag coefficient
- A_P = projected particle area in direction of motion
- ρ = density of surrounding fluid
- u = relative velocity between particle and fluid

The drag force is exerted in a direction parallel to the fluid velocity. Equation (6-227) defines the **drag coefficient**. For some solid bodies, such as aerofoils, a lift force component perpendicular to the liquid velocity is also exerted. For free-falling particles, lift

forces are generally not important. However, even spherical particles experience lift forces in shear flows near solid surfaces.

TERMINAL SETTLING VELOCITY

A particle falling under the action of gravity will accelerate until the drag force balances gravitational force, after which it falls at a constant **terminal or free-settling velocity** u_t , given by

$$u_t = \sqrt{\frac{2gm_p(\rho_p - \rho)}{\rho\rho_p A_P C_D}} \quad (6-228)$$

- where g = acceleration of gravity
- m_p = particle mass
- ρ_p = particle density

and the remaining symbols are as previously defined.

Settling particles may undergo fluctuating motions owing to vortex shedding, among other factors. Oscillation is enhanced with increasing separation between the mass and geometric centers of the particle. Variations in mean velocity are usually less than 10 percent. The drag force on a particle fixed in space with fluid moving is somewhat lower than the drag force on a particle freely settling in a stationary fluid at the same relative velocity.

Spherical Particles For spherical particles of diameter d_p , Eq. (6-228) becomes

$$u_t = \sqrt{\frac{4gd_p(\rho_p - \rho)}{3\rho C_D}} \quad (6-229)$$

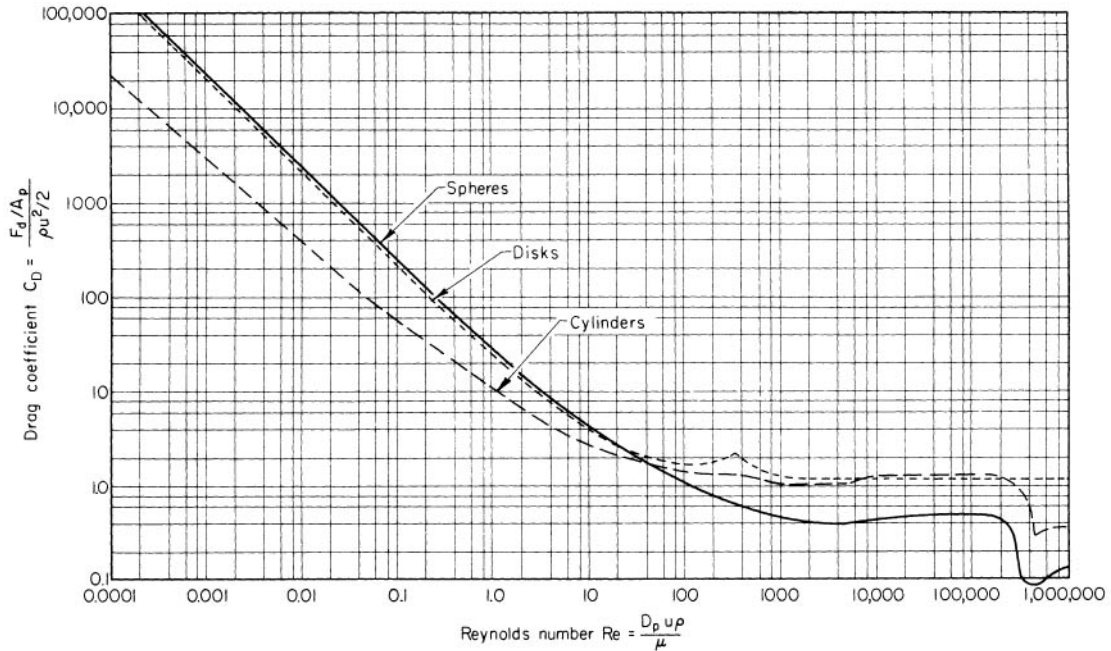


FIG. 6-57 Drag coefficients for spheres, disks, and cylinders; A_p = area of particle projected on a plane normal to direction of motion; C = overall drag coefficient, dimensionless; D_p = diameter of particle; F_d = drag or resistance to motion of body in fluid; Re = Reynolds number, dimensionless; u = relative velocity between particle and main body of fluid; μ = fluid viscosity; and ρ = fluid density. (From Lapple and Shepherd, *Ind. Eng. Chem.*, **32**, 605 [1940].)

The drag coefficient for rigid spherical particles is a function of particle Reynolds number, $Re_p = d_p \rho u / \mu$ where μ = fluid viscosity, as shown in Fig. 6-57. At low Reynolds number, **Stokes' law** gives

$$C_D = \frac{24}{Re_p} \quad Re_p < 0.1 \quad (6-230)$$

which may also be written

$$F_D = 3\pi\mu u d_p \quad Re_p < 0.1 \quad (6-231)$$

and gives for the terminal settling velocity

$$u_t = \frac{gd_p^2(\rho_p - \rho)}{18\mu} \quad Re_p < 0.1 \quad (6-232)$$

In the **intermediate regime** ($0.1 < Re_p < 1,000$), the drag coefficient may be estimated within 6 percent by

$$C_D = \left(\frac{24}{Re_p}\right) \left(1 + 0.14Re_p^{0.70}\right) \quad 0.1 < Re_p < 1,000 \quad (6-233)$$

In the **Newton's law regime**, which covers the range $1,000 < Re_p < 350,000$, $C_D = 0.445$, within 13 percent. In this region, Eq. (6-227) becomes

$$u_t = 1.73 \sqrt{\frac{gd_p(\rho_p - \rho)}{\rho}} \quad 1,000 < Re_p < 350,000 \quad (6-234)$$

Between about $Re_p = 350,000$ and 1×10^6 , the drag coefficient drops dramatically in a **drag crisis** owing to the transition to turbulent flow in the boundary layer around the particle, which delays aft separation, resulting in a smaller wake and less drag. Beyond $Re = 1 \times 10^6$, the drag coefficient may be estimated from (Clift, Grace, and Weber):

$$C_D = 0.19 - \frac{8 \times 10^4}{Re_p} \quad Re_p > 1 \times 10^6 \quad (6-235)$$

Drag coefficients may be affected by turbulence in the free-stream flow; the drag crisis occurs at lower Reynolds numbers when the free

stream is turbulent. Torobin and Guvin (*AIChE J.*, **7**, 615–619 [1961]) found that the drag crisis Reynolds number decreases with increasing free-stream turbulence, reaching a value of 400 when the relative turbulence intensity, defined as $\sqrt{u'}/U_R$ is 0.4. Here $\sqrt{u'}$ is the rms fluctuating velocity and U_R is the relative velocity between the particle and the fluid.

For computing the terminal settling velocity, correlations for drag coefficient as a function of Archimedes number

$$Ar = \frac{gd_p^3(\rho_p - \rho)\rho}{\mu^2} \quad (6-236)$$

may be more convenient than C_D - Re correlations, because the latter are implicit in terminal velocity, and the settling regime is unknown. Karamanev [*Chem. Eng. Comm.* **147**, 75 (1996)] provided a correlation for drag coefficient for settling solid spheres in terms of Ar .

$$C_D = \frac{432}{Ar} (1 + 0.0470Ar^{0.23}) + \frac{0.517}{1 + 154Ar^{-1/3}} \quad (6-237)$$

This equation reduces to Stokes' law $C_D = 24/Re$ in the limit $Ar \rightarrow 0$ and is a fit to data up to about $Ar = 2 \times 10^{10}$, where it gives $C_D = 0.50$, slightly greater than the Newton's law value above. For rising light spheres, which exhibit more energy dissipating lateral motion than do falling dense spheres, Karamanev found that Eq. (6-237) is followed up to $Ar = 13,000$ and that for $Ar > 13,000$, the drag coefficient is $C_D = 0.95$.

For particles settling in **non-Newtonian** fluids, correlations are given by Dallon and Christiansen (Preprint 24C, *Symposium on Selected Papers*, part III, 61st Ann. Mtg. AIChE, Los Angeles, Dec. 1–5, 1968) for spheres settling in shear-thinning liquids, and by Ito and Kajuchi (*J. Chem. Eng. Japan*, **2**[1], 19–24 [1969]) and Pazwash and Robertson (*J. Hydraul. Res.*, **13**, 35–55 [1975]) for spheres settling in Bingham plastics. Beris, Tsamopoulos, Armstrong, and Brown (*J. Fluid Mech.*, **158** [1985]) present a finite element calculation for creeping motion of a sphere through a Bingham plastic.

Nonspherical Rigid Particles The drag on a nonspherical particle depends upon its shape and orientation with respect to the

TABLE 6-8 Free-Fall Orientation of Particles

Reynolds number ^a	Orientation
0.1–5.5	All orientations are stable when there are three or more perpendicular axes of symmetry.
5.5–200	Stable in position of maximum drag.
200–500	Unpredictable. Disks and plates tend to wobble, while fuller bluff bodies tend to rotate.
500–200,000	Rotation about axis of least inertia, frequently coupled with spiral translation.

SOURCE: From Becker, *Can. J. Chem. Eng.*, **37**, 85–91 (1959).

^aBased on diameter of a sphere having the same surface area as the particle.

direction of motion. The orientation in free fall as a function of Reynolds number is given in Table 6-8.

The drag coefficients for **disks** (flat side perpendicular to the direction of motion) and for **cylinders** (infinite length with axis perpendicular to the direction of motion) are given in Fig. 6-57 as a function of Reynolds number. The effect of length-to-diameter ratio for cylinders in the Newton's law region is reported by Knudsen and Katz (*Fluid Mechanics and Heat Transfer*, McGraw-Hill, New York, 1958).

Pettyjohn and Christiansen (*Chem. Eng. Prog.*, **44**, 157–172 [1948]) present correlations for the effect of particle shape on free-settling velocities of **isometric particles**. For $Re < 0.05$, the terminal or free-settling velocity is given by

$$u_t = K_1 \frac{gd_s^2(\rho_p - \rho)}{18\mu} \quad (6-238)$$

$$K_1 = 0.843 \log \left(\frac{\psi}{0.065} \right) \quad (6-239)$$

where ψ = sphericity, the surface area of a sphere having the same volume as the particle, divided by the actual surface area of the particle; d_s = equivalent diameter, equal to the diameter of the equivalent sphere having the same volume as the particle; and other variables are as previously defined.

In the **Newton's law region**, the terminal velocity is given by

$$u_t = \sqrt{\frac{4d_s(\rho_p - \rho)g}{3K_3\rho}} \quad (6-240)$$

$$K_3 = 5.31 - 4.88\psi \quad (6-241)$$

Equations (6-238) to (6-241) are based on experiments on cube-octahedrons, octahedrons, cubes, and tetrahedrons for which the sphericity ψ ranges from 0.906 to 0.670, respectively. See also Clift, Grace, and Weber. A graph of drag coefficient vs. Reynolds number with ψ as a parameter may be found in Brown, et al. (*Unit Operations*, Wiley, New York, 1950) and in Govier and Aziz.

For particles with $\psi < 0.67$, the correlations of Becker (*Can. J. Chem. Eng.*, **37**, 85–91 [1959]) should be used. Reference to this paper is also recommended for **intermediate region** flow. Settling characteristics of nonspherical particles are discussed by Clift, Grace, and Weber, Chaps. 4 and 6.

The terminal velocity of **axisymmetric particles in axial motion** can be computed from Bowen and Masliyah (*Can. J. Chem. Eng.*, **51**, 8–15 [1973]) for low-Reynolds number motion:

$$u_t = \frac{V'}{K_2} \frac{gD_s^2(\rho_p - \rho)}{18\mu} \quad (6-242)$$

$$K_2 = 0.244 + 1.035\Sigma - 0.712\Sigma^2 + 0.441\Sigma^3 \quad (6-243)$$

where D_s = diameter of sphere with perimeter equal to maximum particle projected perimeter

V' = ratio of particle volume to volume of sphere with diameter D_s

Σ = ratio of surface area of particle to surface area of a sphere with diameter D_s

and other variables are as defined previously.

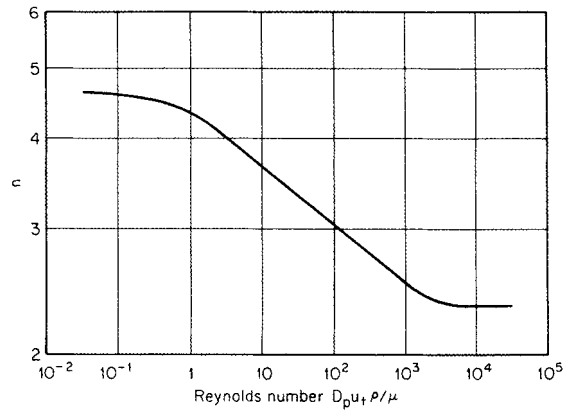


FIG. 6-58 Values of exponent n for use in Eq. (6-242). (From Maude and Whitmore, *Br. J. Appl. Phys.*, **9**, 481 [1958]. Courtesy of the Institute of Physics and the Physical Society.)

Hindered Settling When particle concentration increases, particle settling velocities decrease because of hydrodynamic interaction between particles and the upward motion of displaced liquid. The suspension viscosity increases. Hindered settling is normally encountered in sedimentation and transport of concentrated slurries. Below 0.1 percent volumetric particle concentration, there is less than a 1 percent reduction in settling velocity. Several expressions have been given to estimate the effect of particle volume fraction on settling velocity. Maude and Whitmore (*Br. J. Appl. Phys.*, **9**, 477–482 [1958]) give, for uniformly sized spheres,

$$u_t = u_{t0}(1 - c)^n \quad (6-244)$$

where u_t = terminal settling velocity

u_{t0} = terminal velocity of a single sphere (infinite dilution)

c = volume fraction solid in the suspension

n = function of Reynolds number $Re_p = d_p u_{t0} \rho / \mu$ as given

Fig. 6-58

In the Stokes' law region ($Re_p < 0.3$), $n = 4.65$ and in the Newton's law region ($Re_p > 1,000$), $n = 2.33$. Equation (6-244) may be applied to particles of any size in a polydisperse system, provided the volume fraction corresponding to all the particles is used in computing terminal velocity (Richardson and Shabi, *Trans. Inst. Chem. Eng. [London]*, **38**, 33–42 [1960]). The concentration effect is greater for nonspherical and angular particles than for spherical particles (Steinour, *Ind. Eng. Chem.*, **36**, 840–847 [1944]). Theoretical developments for low-Reynolds number flow assemblages of spheres are given by Happel and Brenner (*Low Reynolds Number Hydrodynamics*, Prentice-Hall, Englewood Cliffs, N.J., 1965) and Famularo and Happel (*AIChE J.*, **11**, 981 [1965]) leading to an equation of the form

$$u_t = \frac{u_{t0}}{1 + \gamma c^{1/3}} \quad (6-245)$$

where γ is about 1.3. As particle concentration increases, resulting in interparticle contact, hindered settling velocities are difficult to predict. Thomas (*AIChE J.*, **9**, 310 [1963]) provides an empirical expression reported to be valid over the range $0.08 < u_t/u_{t0} < 1$:

$$\ln \left(\frac{u_t}{u_{t0}} \right) = -5.9c \quad (6-246)$$

Time-dependent Motion The time-dependent motion of particles is computed by application of Newton's second law, equating the rate of change of particle motion to the net force acting on the particle. Rotation of particles may also be computed from the net torque. For large particles moving through low-density gases, it is usually sufficient to compute the force due to fluid drag from the

relative velocity and the drag coefficient computed for steady flow conditions. For two- and three-dimensional problems, the velocity appearing in the particle Reynolds number and the drag coefficient is the amplitude of the relative velocity. The drag force, not the relative velocity, is to be resolved into vector components to compute the particle acceleration components. Clift, Grace, and Weber (*Bubbles, Drops and Particles*, Academic, London, 1978) discuss the complexities that arise in the computation of transient drag forces on particles when the transient nature of the flow is important. Analytical solutions for the case of a single particle in creeping flow ($Re_p = 0$) are available. For example, the creeping motion of a spherical particle released from rest in a stagnant fluid is described by

$$\rho_p V \frac{dU}{dt} = g(\rho_p - \rho)V - 3\pi\mu d_p U - \frac{\rho}{2} V \frac{dU}{dt} - \left(\frac{3}{2}\right) d_p^3 \sqrt{\pi\mu} \int_0^t \frac{(dU/dt)_{t=s} ds}{\sqrt{t-s}} \quad (6-247)$$

Here, U = particle velocity, positive in the direction of gravity, and V = particle volume. The first term on the right-hand side is the net gravitational force on the particle, accounting for buoyancy. The second is the steady-state Stokes drag (Eq. 6-231). The third is the **added mass** or **virtual mass** term, which may be interpreted as the inertial effect of the fluid which is accelerated along with the particle. The volume of the added mass of fluid is half the particle volume. The last term, the **Basset force**, depends on the entire history of the transient motion, with past motions weighted inversely with the square root of elapsed time. Clift, et al. provide integrated solutions. In **turbulent flows**, particle velocity will closely follow fluid eddy velocities when (Clift et al.)

$$\tau_0 \gg \frac{d_p^2[(2\rho_p/\rho) + 1]}{36\nu} \quad (6-248)$$

where τ_0 = oscillation period or eddy time scale, the right-hand side expression is the **particle relaxation time**, and ν = kinematic viscosity.

Gas Bubbles Fluid particles, unlike rigid solid particles, may undergo deformation and internal circulation. Figure 6-59 shows rise velocity data for air bubbles in stagnant water. In the figure, $Eo = Eotvos\ number, g(\rho_L - \rho_G)d_b/\sigma$, where ρ_L = liquid density, ρ_G = gas density, d_b = bubble diameter, σ = surface tension, and the equivalent diameter d_e is the diameter of a sphere with volume equal to that of

the bubble. Small bubbles (<1-mm [0.04-in] diameter) remain spherical and rise in straight lines. The presence of surface active materials generally renders small bubbles rigid, and they rise roughly according to the drag coefficient and terminal velocity equations for spherical solid particles. Bubbles roughly in the range 2- to 8-mm (0.079- to 0.32-in) diameter assume flattened, ellipsoidal shape, and rise in a zig-zag or spiral pattern. This motion increases dissipation and drag, and the rise velocity may actually decrease with increasing bubble diameter in this region, characterized by rise velocities in the range of 20 to 30 cm/s (0.7 to 1.0 ft/s). Large bubbles, >8-mm (0.32-in) diameter, are greatly deformed, assuming a mushroomlike, spherical cap shape. These bubbles are unstable and may break into smaller bubbles. Carefully purified water, free of surface active materials, allows bubbles to freely circulate even when they are quite small. Under creeping flow conditions $Re_b = d_b\mu_r/\mu_L < 1$, where u_r = bubble rise velocity and μ_L = liquid viscosity, the bubble rise velocity may be computed analytically from the Hadamard-Rybczynski formula (Levich, *Physicochemical Hydrodynamics*, Prentice-Hall, Englewood Cliffs, N.J., 1962, p. 402). When $\mu_G/\mu_L \ll 1$, which is normally the case, the rise velocity is 1.5 times the rigid sphere Stokes law velocity. However, in practice, most liquids, including ordinary distilled water, contain sufficient surface active materials to render small bubbles rigid. Larger bubbles undergo deformation in both purified and ordinary liquids; however, the variation in rise velocity for large bubbles with degree of purity is quite evident in Fig. 6-59. For additional discussion, see Clift, et al., Chap. 7.

Karamanev [op. cit.] provided equations for bubble rise velocity based on the Archimedes number and on use of the bubble projected diameter d_b in the drag coefficient and the bubble equivalent diameter in Ar . The Archimedes number is as defined in Eq. (6-236) except that the density difference is liquid density minus gas density, and d_p is replaced by d_e .

$$u_r = 40.3 \frac{d_e}{d_h} \sqrt{\frac{V^{1/3}}{C_D}} = 40.3 \frac{d_e}{d_h} \sqrt{\frac{(\pi d_e^3/6)^{1/3}}{C_D}} \quad (6-249)$$

$$C_D = \frac{432}{Ar} (1 + 0.0470 Ar^{2/3}) + \frac{0.517}{1 + 154 Ar^{-1/3}} \quad Ar < 13,000 \quad (6-250)$$

$$C_D = 0.95 \quad Ar > 13,000 \quad (6-251)$$

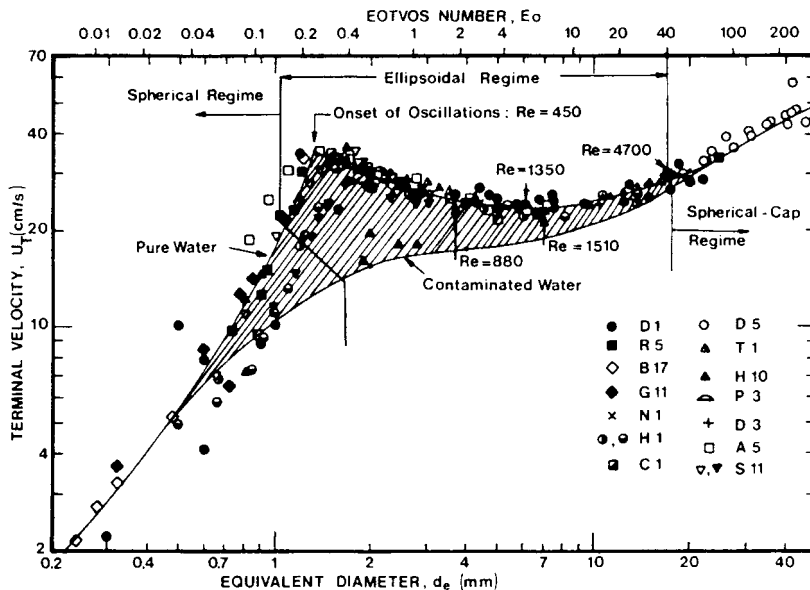


FIG. 6-59 Terminal velocity of air bubbles in water at 20°C. (From Clift, Grace, and Weber, *Bubbles, Drops and Particles*, Academic, New York, 1978).

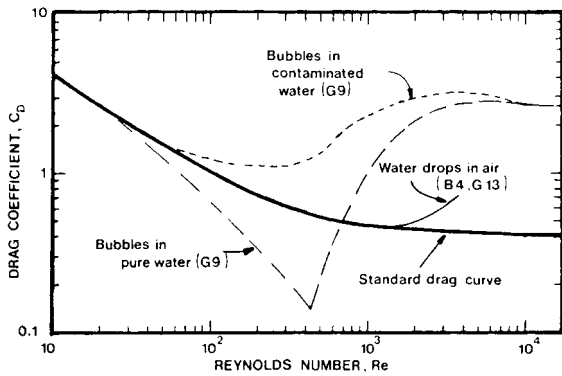


FIG. 6-60 Drag coefficient for water drops in air and air bubbles in water. Standard drag curve is for rigid spheres. (From Clift, Grace, and Weber, Bubbles, Drops and Particles, Academic, New York, 1978.)

$$\frac{d_c}{d_h} = (1 + 0.163Eo^{0.757})^{-1/3} \quad Eo < 40 \quad (6-252)$$

$$\frac{d_c}{d_h} = 0.62 \quad Eo > 40 \quad (6-253)$$

Applied to air bubbles in water, these expressions give reasonable agreement with the contaminated water curve in Fig. 6-59.

Figure 6-60 gives the drag coefficient as a function of bubble or drop Reynolds number for air bubbles in water and water drops in air, compared with the standard drag curve for rigid spheres. Information on bubble motion in **non-Newtonian** liquids may be found in Astarita and Apuzzo (*AIChE J.*, **11**, 815-820 [1965]); Calderbank, Johnson, and Loudon (*Chem. Eng. Sci.*, **25**, 235-256 [1970]); and Acharya, Mashelkar, and Ulbrecht (*Chem. Eng. Sci.*, **32**, 863-872 [1977]).

Liquid Drops in Liquids Very small liquid drops in immiscible liquids behave like rigid spheres, and the terminal velocity can be approximated by use of the drag coefficient for solid spheres up to a Reynolds number of about 10 (Warshay, Bogusz, Johnson, and Kintner, *Can. J. Chem. Eng.*, **37**, 29-36 [1959]). Between Reynolds numbers of 10 and 500, the terminal velocity exceeds that for rigid spheres owing to internal circulation. In normal practice, the effect of drop phase viscosity is neglected. Grace, Wairegi, and Nguyen (*Trans. Inst. Chem. Eng.*, **54**, 167-173 [1976]; Clift, et al., op. cit., pp. 175-177) present a correlation for terminal velocity valid in the range

$$M < 10^{-3} \quad Eo < 40 \quad Re > 0.1 \quad (6-254)$$

- where $M = \text{Morton number} = g\mu^4\Delta\rho/\rho^2\sigma^3$
- $Eo = \text{Eotvos number} = g\Delta\rho d^2/\sigma$
- $Re = \text{Reynolds number} = d\rho u/\mu$
- $\Delta\rho = \text{density difference between the phases}$
- $\rho = \text{density of continuous liquid phase}$
- $d = \text{drop diameter}$
- $\mu = \text{continuous liquid viscosity}$
- $\sigma = \text{surface tension}$
- $u = \text{relative velocity}$

The correlation is represented by

$$J = 0.94H^{0.757} \quad (2 < H \leq 59.3) \quad (6-255)$$

$$J = 3.42H^{0.441} \quad (H > 59.3) \quad (6-256)$$

where
$$H = \frac{4}{3} EoM^{-0.149} \left(\frac{\mu}{\mu_w}\right)^{-0.14} \quad (6-257)$$

$$J = ReM^{0.149} + 0.857 \quad (6-258)$$

Note that the terminal velocity may be evaluated explicitly from

$$u = \frac{\mu}{\rho d} M^{-0.149} (J - 0.857) \quad (6-259)$$

In Eq. (6-257), $\mu = \text{viscosity of continuous liquid}$ and $\mu_w = \text{viscosity of water, taken as } 0.9 \text{ cP } (0.0009 \text{ Pa} \cdot \text{s})$.

For drop velocities in non-Newtonian liquids, see Mhatre and Kintner (*Ind. Eng. Chem.*, **51**, 865-867 [1959]); Marrucci, Apuzzo, and Astarita (*AIChE J.*, **16**, 538-541 [1970]); and Mohan, et al. (*Can. J. Chem. Eng.*, **50**, 37-40 [1972]).

Liquid Drops in Gases Liquid drops falling in stagnant gases appear to remain spherical and follow the rigid sphere drag relationships up to a Reynolds number of about 100. Large drops will deform,

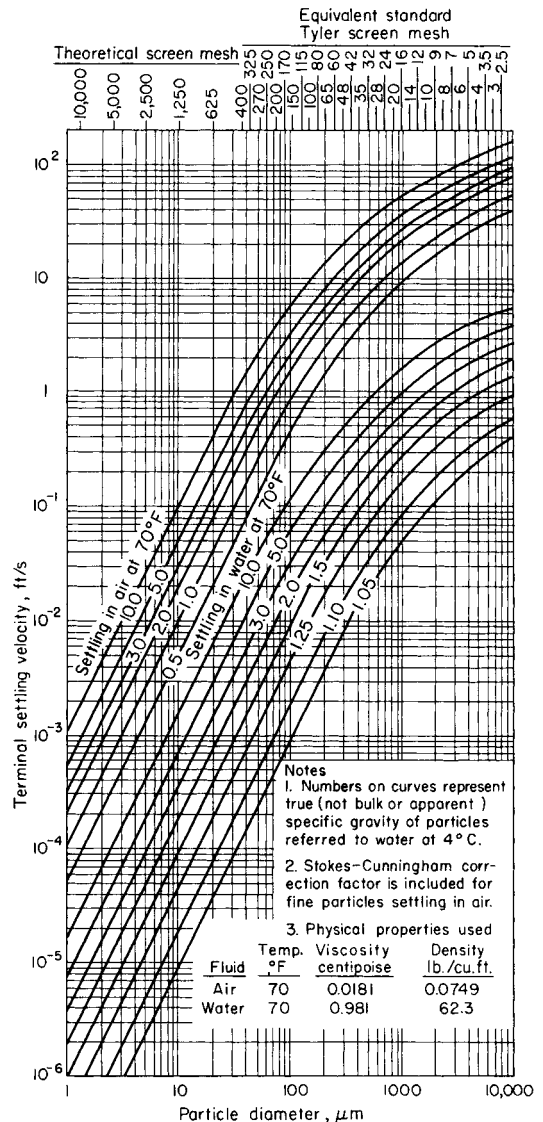


FIG. 6-61 Terminal velocities of spherical particles of different densities settling in air and water at 70°F under the action of gravity. To convert ft/s to m/s, multiply by 0.3048. (From Lapple, et al., Fluid and Particle Mechanics, University of Delaware, Newark, 1951, p. 292.)

6-56 FLUID AND PARTICLE DYNAMICS

with a resulting increase in drag, and in some cases will shatter. The largest water drop which will fall in air at its terminal velocity is about 8 mm (0.32 in) in diameter, with a corresponding velocity of about 9 m/s (30 ft/s). Drops shatter when the Weber number defined as

$$We = \frac{\rho_C u^2 d}{\sigma} \quad (6-260)$$

exceeds a critical value. Here, ρ_C = gas density, u = drop velocity, d = drop diameter, and σ = surface tension. A value of $We_c = 13$ is often cited for the critical Weber number.

Terminal velocities for water drops in air have been correlated by Berry and Prnager (*J. Appl. Meteorol.*, **13**, 108–113 [1974]) as

$$Re = \exp [-3.126 + 1.013 \ln N_D - 0.01912(\ln N_D)^2] \quad (6-261)$$

for $2.4 < N_D < 10^7$ and $0.1 < Re < 3,550$. The dimensionless group N_D (often called the *Best* number [Clift et al.]) is given by

$$N_D = \frac{4\rho\Delta\rho g d^3}{3\mu^2} \quad (6-262)$$

and is proportional to the similar Archimedes and Galileo numbers.

Figure 6-61 gives calculated settling velocities for solid spherical particles settling in air or water using the standard drag coefficient curve for spherical particles. For fine particles settling in air, the **Stokes-Cunningham correction** has been applied to account for particle size comparable to the mean free path of the gas. The correction is less than 1 percent for particles larger than 16 μm settling in air. Smaller particles are also subject to **Brownian motion**. Motion of particles smaller than 0.1 μm is dominated by Brownian forces and gravitational effects are small.

Wall Effects When the diameter of a settling particle is significant compared to the diameter of the container, the settling velocity is

TABLE 6-9 Wall Correction Factor for Rigid Spheres in Stokes' Law Region

β°	k_w	β	k_w
0.0	1.000	0.4	0.279
0.05	0.885	0.5	0.170
0.1	0.792	0.6	0.0945
0.2	0.596	0.7	0.0468
0.3	0.422	0.8	0.0205

SOURCE: From Haberman and Sayre, *David W. Taylor Model Basin Report* 1143, 1958.

* β = particle diameter divided by vessel diameter.

reduced. For rigid spherical particles settling with $Re < 1$, the correction given in Table 6-9 may be used. The factor k_w is multiplied by the settling velocity obtained from Stokes' law to obtain the corrected settling rate. For values of diameter ratio β = particle diameter/vessel diameter less than 0.05, $k_w = 1/(1 + 2.1\beta)$ (Zenz and Othmer, *Fluidization and Fluid-Particle Systems*, Reinhold, New York, 1960, pp. 208–209). In the range $100 < Re < 10,000$, the computed terminal velocity for rigid spheres may be multiplied by k'_w to account for wall effects, where k'_w is given by (Harmathy, *AIChE J.*, **6**, 281 [1960])

$$k'_w = \frac{1 - \beta^2}{\sqrt{1 + \beta^4}} \quad (6-263)$$

For gas bubbles in liquids, there is little wall effect for $\beta < 0.1$. For $\beta > 0.1$, see Uto and Kintner (*AIChE J.*, **2**, 420–424 [1956]), Maneri and Mendelson (*Chem. Eng. Prog.*, **64**, *Symp. Ser.*, **82**, 72–80 [1968]), and Collins (*J. Fluid Mech.*, **28**, part 1, 97–112 [1967]).

SECTION **7**

Reaction Kinetics

PERRY'S CHEMICAL ENGINEERS' HANDBOOK

8TH EDITION



TIBERIU M. LEIB
CARMO J. PEREIRA

Copyright © 2008, 1997, 1984, 1973, 1963, 1950, 1941, 1934 by The McGraw-Hill Companies, Inc. All rights reserved. Manufactured in the United States of America. Except as permitted under the United States Copyright Act of 1976, no part of this publication may be reproduced or distributed in any form or by any means, or stored in a database or retrieval system, without the prior written permission of the publisher.

0-07-154214-0

The material in this eBook also appears in the print version of this title: 0-07-151130-X.

All trademarks are trademarks of their respective owners. Rather than put a trademark symbol after every occurrence of a trademarked name, we use names in an editorial fashion only, and to the benefit of the trademark owner, with no intention of infringement of the trademark. Where such designations appear in this book, they have been printed with initial caps.

McGraw-Hill eBooks are available at special quantity discounts to use as premiums and sales promotions, or for use in corporate training programs. For more information, please contact George Hoare, Special Sales, at george_hoare@mcgraw-hill.com or (212) 904-4069.

TERMS OF USE

This is a copyrighted work and The McGraw-Hill Companies, Inc. (“McGraw-Hill”) and its licensors reserve all rights in and to the work. Use of this work is subject to these terms. Except as permitted under the Copyright Act of 1976 and the right to store and retrieve one copy of the work, you may not decompile, disassemble, reverse engineer, reproduce, modify, create derivative works based upon, transmit, distribute, disseminate, sell, publish or sublicense the work or any part of it without McGraw-Hill’s prior consent. You may use the work for your own noncommercial and personal use; any other use of the work is strictly prohibited. Your right to use the work may be terminated if you fail to comply with these terms.

THE WORK IS PROVIDED “AS IS.” MCGRAW-HILL AND ITS LICENSORS MAKE NO GUARANTEES OR WARRANTIES AS TO THE ACCURACY, ADEQUACY OR COMPLETENESS OF OR RESULTS TO BE OBTAINED FROM USING THE WORK, INCLUDING ANY INFORMATION THAT CAN BE ACCESSED THROUGH THE WORK VIA HYPERLINK OR OTHERWISE, AND EXPRESSLY DISCLAIM ANY WARRANTY, EXPRESS OR IMPLIED, INCLUDING BUT NOT LIMITED TO IMPLIED WARRANTIES OF MERCHANTABILITY OR FITNESS FOR A PARTICULAR PURPOSE. McGraw-Hill and its licensors do not warrant or guarantee that the functions contained in the work will meet your requirements or that its operation will be uninterrupted or error free. Neither McGraw-Hill nor its licensors shall be liable to you or anyone else for any inaccuracy, error or omission, regardless of cause, in the work or for any damages resulting therefrom. McGraw-Hill has no responsibility for the content of any information accessed through the work. Under no circumstances shall McGraw-Hill and/or its licensors be liable for any indirect, incidental, special, punitive, consequential or similar damages that result from the use of or inability to use the work, even if any of them has been advised of the possibility of such damages. This limitation of liability shall apply to any claim or cause whatsoever whether such claim or cause arises in contract, tort or otherwise.

DOI: 10.1036/007151130X

Reaction Kinetics*

Tiberiu M. Leib, Ph.D. *Principal Consultant, DuPont Engineering Research and Technology, E. I. du Pont de Nemours and Company; Fellow, American Institute of Chemical Engineers*

Carmo J. Pereira, Ph.D., MBA *DuPont Fellow, DuPont Engineering Research and Technology, E. I. du Pont de Nemours and Company; Fellow, American Institute of Chemical Engineers*

REFERENCES

BASIC CONCEPTS

Mechanism	7-5
Reaction Rate	7-5
Classification of Reactions	7-5
Effect of Concentration on Rate	7-6
Law of Mass Action	7-6
Effect of Temperature	7-6
Heat of Reaction	7-6
Chemical Equilibrium	7-7
Conversion, Extent of Reaction, Selectivity, and Yield	7-7
Concentration Types	7-8
Stoichiometric Balances	7-8
Single Reactions	7-8
Reaction Networks	7-9
Catalysis	7-9

IDEAL REACTORS

Ideal Batch Reactor	7-11
Batch Reactor (BR)	7-11
Semibatch Reactor (SBR)	7-12
Ideal Continuous Stirred Tank Reactor (CSTR)	7-12
Plug Flow Reactor (PFR)	7-12
Ideal Recycle Reactor	7-12
Examples for Some Simple Reactions	7-13

KINETICS OF COMPLEX HOMOGENEOUS REACTIONS

Chain Reactions	7-14
Phosgene Synthesis	7-14
Ozone Conversion to Oxygen in Presence of Chlorine	7-14
Hydrogen Bromide Synthesis	7-15
Chain Polymerization	7-15
Nonchain Reactions	7-15
Homogeneous Catalysis	7-15

*The contributions of Stanley M. Walas, Ph.D., Professor Emeritus, Department of Chemical and Petroleum Engineering, University of Kansas (Fellow, American Institute of Chemical Engineers), author of this section in the seventh edition, are acknowledged.

The authors of the present section would like to thank Dennie T. Mah, M.S.Ch.E., Senior Consultant, DuPont Engineering Research and Technology, E. I. du Pont de Nemours and Company (Senior Member, American Institute of Chemical Engineers; Member, Industrial Electrolysis and Electrochemical Engineering; Member, The Electrochemical Society), for his contributions to the "Electrochemical Reactions" subsection; and John Villadsen, Ph.D., Senior Professor, Department of Chemical Engineering, Technical University of Denmark, for his contributions to the "Biochemical Reactions" subsection. We acknowledge comments from Peter Harriott, Ph.D., Fred H. Rhodes Professor of Chemical Engineering (retired), School of Chemical and Biomolecular Engineering, Cornell University, on our original outline and on the subject of heat transfer in packed-bed reactors. The authors also are grateful to the following colleagues for reading the manuscript and for thoughtful comments: Thomas R. Keane, DuPont Fellow (retired), DuPont Engineering Research and Technology, E. I. du Pont de Nemours and Company (Senior Member, American Institute of Chemical Engineers); Güray Tosun, Ph.D., Senior Consultant, DuPont Engineering Research and Technology, E. I. du Pont de Nemours and Company (Senior Member, American Institute of Chemical Engineers); and Nitin H. Kollhapure, Ph.D., Senior Consulting Engineer, DuPont Engineering Research and Technology, E. I. du Pont de Nemours and Company (Senior Member, American Institute of Chemical Engineers).

7-2 REACTION KINETICS

Acid-Catalyzed Isomerization of Butene-1	7-15
Enzyme Kinetics	7-15
Autocatalysis	7-16

INTRINSIC KINETICS FOR FLUID-SOLID CATALYTIC REACTIONS

Adsorption Equilibrium	7-16
Dissociation	7-17
Different Sites	7-17
Change in Number of Moles	7-17
Reactant in the Gas Phase	7-17
Chemical Equilibrium in Gas Phase	7-17
No Rate-Controlling Step	7-18
Liquid-Solid Catalytic Reactions	7-18
Biocatalysis	7-18

FLUID-SOLID REACTIONS WITH MASS AND HEAT TRANSFER

Gas-Solid Catalytic Reactions	7-19
External Mass Transfer	7-19
Intraparticle Diffusion	7-20
Intraparticle Diffusion and External Mass-Transfer Resistance	7-22
Heat-Transfer Resistances	7-22
Catalyst Deactivation	7-22
Gas-Solid Noncatalytic Reactions	7-23
Sharp Interface Model	7-23
Volume Reaction Model	7-25

GAS-LIQUID REACTIONS

Reaction-Diffusion Regimes	7-27
----------------------------------	------

GAS-LIQUID-SOLID REACTIONS

Gas-Liquid-Solid Catalytic Reactions	7-28
Polymerization Reactions	7-29
Bulk Polymerization	7-29
Bead Polymerization	7-29
Emulsion Polymerization	7-29
Solution Polymerization	7-29
Polymer Characterization	7-29

Chain Homopolymerization Mechanism and Kinetics	7-30
Step Growth Homopolymerization Mechanism and Kinetics	7-30
Copolymerization	7-30
Biochemical Reactions	7-30
Mechanism	7-31
Monod-Type Empirical Kinetics	7-31
Chemostat with Empirical Kinetics	7-32
Electrochemical Reactions	7-32
Kinetic Control	7-32
Mass-Transfer Control	7-33
Ohmic Control	7-33
Multiple Reactions	7-33

.DETERMINATION OF MECHANISM AND KINETICS

Laboratory Reactors	7-33
Batch Reactors	7-34
Flow Reactors	7-35
Multiphase Reactors	7-35
Solid Catalysts	7-35
Bioreactors	7-35
Calorimetry	7-35
Kinetic Parameters	7-35
Data Analysis Methods	7-36
Differential Data Analysis	7-36
Integral Data Analysis	7-36
The Half-Life Method	7-36
Complex Rate Equations	7-37
Parameter Estimation	7-37
Linear Models in Parameters, Single Reaction	7-37
Nonlinear Models in Parameters, Single Reaction	7-38
Network of Reactions	7-38
Theoretical Methods	7-38
Prediction of Mechanism and Kinetics	7-38
Lumping and Mechanism Reduction	7-38
Multiple Steady States, Oscillations, and Chaotic Behavior	7-39
Software Tools	7-39

Nomenclature and Units

The component A is identified by the subscript a . Thus, the number of moles is n_a ; the fractional conversion is X_a ; the extent of reaction is ζ_a ; the partial pressure is p ; the rate of consumption is r_a ; the molar flow rate is N_a ; the volumetric flow rate is q ; reactor volume is V_r or simply V for batch reactors; the volumetric concentration is $C_a = n_a/V$ or $C_a = N_a/q$; the total pressure is P ; and the temperature is T . Throughout this section, equations are presented without specification of units. Use of any consistent unit set is appropriate.

Following is a listing of typical nomenclature expressed in SI and U.S. Customary System units.

Symbol	Definition	SI units	U.S. Customary System units	Symbol	Definition	SI units	U.S. Customary System units
A, B, C, \dots	Names of substances			p_a	Partial pressure of substance A	Pa	psi
A	Free radical, as CH_3			q	Volumetric flow rate	m^3/s	ft^3/s
a	Activity			Q	Electric charge	Coulomb	
BR	Batch reactor			\bar{R}	Radial position, radius, universal gas constant		
b	Estimate of kinetic parameters, vector			Re	Reynolds number		
C_a	Concentration of substance A	$\text{kg}\cdot\text{mol}/\text{m}^3$	$\text{lb}\cdot\text{mol}/\text{ft}^3$	RgSS	Regression sum of squares		
CSTR	Continuous stirred tank reactor			RSS	Residual sum of squares		
C_0	Initial concentration	$\text{kg}\cdot\text{mol}/\text{m}^3$	$\text{lb}\cdot\text{mol}/\text{ft}^3$	r_a	Rate of reaction of A per unit volume		
c_p	Heat capacity at constant pressure	$\text{kJ}/(\text{kg}\cdot\text{K})$	$\text{Btu}/(\text{lbm}\cdot^\circ\text{F})$	S	Selectivity, stoichiometric matrix, objective function for parameter estimation		
Δc_p	Heat capacity change in a reaction	$\text{kJ}/(\text{kg}\cdot\text{K})$	$\text{Btu}/(\text{lbm}\cdot^\circ\text{F})$	SBR	Semibatch reactor		
D	Diffusivity, dispersion coefficient	m^2/s	ft^2/s	Sc	Schmidt number		
D_e	Effective diffusivity	m^2/s	ft^2/s	Sh	Sherwood number		
D_K	Knudsen diffusivity	m^2/s	ft^2/s	ΔS	Entropy change	$\text{kJ}/(\text{kg}\cdot\text{mol}\cdot\text{K})$	$\text{Btu}/(\text{lb}\cdot\text{mol}\cdot\text{R})$
DP	Degree of polymerization			s	Estimate of variance		
E	Activation energy, enhancement factor for gas-liquid mass transfer with reaction, electrochemical cell potential			t	Time, t statistic		
F	Faraday constant, F statistic			u	Linear velocity	m/s	ft/s
f	Efficiency of initiation in polymerization			V	Volume of reactor, variance-covariance matrix		
f_a	C_a/C_{a0} or n_a/n_{a0} , fraction of A remaining unconverted			v	Molar volume	$\text{m}^3/\text{kg}\cdot\text{mol}$	$\text{ft}^3/\text{lb}\cdot\text{mol}$
Ha	Hatta number			WCLD	Weight chain length distribution		
He	Henry constant for absorption of gas in liquid			WMMD	Weight molecular weight distribution		
ΔG	Free energy change	$\text{kJ}/\text{kg}\cdot\text{mol}$	$\text{Btu}/\text{lb}\cdot\text{mol}$	X	Linear model matrix for parameter estimation, fractional conversion		
ΔH_r	Heat of reaction	$\text{kJ}/\text{kg}\cdot\text{mol}$	$\text{Btu}/\text{lb}\cdot\text{mol}$	X_a	$1 - f_a = 1 - C_a/C_{a0}$ or $1 - n_a/n_{a0}$, fraction of A converted		
I	Initiator for polymerization, modified Bessel functions, electric current			x	Axial position in a reactor, mole fraction in liquid	Variable	
j	Electric current density	A/m^2		Y	Yield; yield coefficient for biochemical reactions		
K_a	Adsorption constant			y	Mole fraction in gas, predicted dependent variable		
K_e	Chemical equilibrium constant			z	x/L , normalized axial position		
k	Specific rate constant of reaction, mass-transfer coefficient			Greek letters			
L	Length of path in reactor	m	ft	α	Fraction of initial catalyst activity, probability of propagation for chain polymerization, confidence level		
LFSS	Lack of fit sum of squares			β	r/R , normalized radial position, fraction of poisoned catalyst, kinetic parameter vector		
M	Average molecular weight in polymers, dead polymer species, monomer			δ	Film thickness or boundary layer thickness, relative change in number of moles by reaction		
m	Number of moles in electrochemical reaction	$\text{kg}\cdot\text{mol}$	$\text{lb}\cdot\text{mol}$	$\delta(t)$	Unit impulse input, Dirac function		
N	Molar flow rate, molar flux			ε	Fraction void space in a packed bed, relative change in number of moles by reaction, residual error, porosity, current efficiency		
NCLD	Number chain length distribution			Φ	Weisz Prater parameter		
NMWD	Number molecular weight distribution			ϕ	Thiele modulus		
n	Number of stages in a CSTR battery, reaction order, number of electrons in electrochemical reaction, number of experiments						
n_a	Number of moles of A present	$\text{kg}\cdot\text{mol}$	$\text{lb}\cdot\text{mol}$				
n_t	Total number of moles	$\text{kg}\cdot\text{mol}$	$\text{lb}\cdot\text{mol}$				
P	Total pressure, live polymer species						
PESS	Pure error sum of squares						
PFR	Plug flow reactor						
p	Number of kinetic parameters						

7-4 REACTION KINETICS

Nomenclature and Units (Concluded)

Symbol	Definition	SI units	U.S. Customary System units	Subscripts	
				Greek letters	
η	Effectiveness factor of porous catalyst, overpotential in electrochemical reactions			d	Deactivation
λ	Parameter for instantaneous gas-liquid reaction, moments in polymer chain length			e	Equilibrium
μ	Viscosity, biomass growth rate, average chain length in polymers			f	Forward reaction, final, formation
ν	μ/ρ , kinematic viscosity, stoichiometric coefficient, fraction of surface covered by adsorbed species			G	Gas
θ	Dimensionless time			i	Component i
ρ	Density	kg/m ³	lbm/ft ³	j	Reaction j
σ	Variance			L	Liquid
τ	Residence time, tortuosity factor			m	Based on mass, mass transfer
ζ	Extent of reaction			max	Maximum biomass growth, maximum extent of reaction
				Subscripts	
act	Activation			n	Chain length in polymers
anode	At anode			o	Oxidized
B	Bed			obs	observed
cathode	At cathode			p	Particle
cell	Electrochemical cell			projected	Electrode projected area
current, j	Current, species j			r	Reverse reaction, reduced
D	Diffusion, dispersion			S	Substrate
				Superscripts	
				s	Solid or catalyst, saturation, surface
				surf	Surface
				v	Based on volume
				x	Biomass
				0	At initial or inlet conditions, as in C_{a0}, n_{a0}, V_0 , at reference temperature
				1/2	Half-life
				Superscripts	
				eq	Equilibrium
				o	At reference temperature
				T	Transposed matrix

REFERENCES

GENERAL REFERENCES: Amundson, *Mathematical Methods in Chemical Engineering—Matrices and Their Application*, Prentice-Hall International, New York, 1966; Aris, *Elementary Chemical Reactor Analysis*, Prentice-Hall, 1969; Astarita, *Mass Transfer with Chemical Reaction*, Elsevier, New York, 1967; Bamford and Tipper (eds.), *Comprehensive Chemical Kinetics*, Elsevier, 1969; Bird, Stewart, and Lightfoot, *Transport Phenomena*, 2d ed., Wiley, New York, 2002; Boudart, *Kinetics of Chemical Processes*, Prentice-Hall, 1968; Boudart and Djega-Mariadassou, *Kinetics of Heterogeneous Catalytic Reactions*, Princeton University Press, Princeton, N.J., 1984; Brotz, *Fundamentals of Chemical Reaction Engineering*, Addison-Wesley, 1965; Butt, *Reaction Kinetics and Reactor Design*, Prentice-Hall, 1980; Butt and Petersen, *Activation, Deactivation and Poisoning of Catalysts*, Academic Press, 1988; Capello and Bielski, *Kinetic Systems: Mathematical Description of Kinetics in Solution*, Wiley, 1972; Carberry, *Chemical and Catalytic Reaction Engineering*, McGraw-Hill, 1976; Carberry and Varma (eds.), *Chemical Reaction and Reactor Engineering*, Dekker, 1987; Chen, *Process Reactor Design*, Allyn & Bacon, 1983; Churchill, *The Interpretation and Use of Rate Data: The Rate Concept*, McGraw-Hill, New York, 1974; Cooper and Jeffreys, *Chemical Kinetics and Reactor Design*, Prentice-Hall, 1971; Cremer and Turner, *Chemical Engineering Practice*, vol. 8: *Chemical Kinetics*, Butterworths, 1965; Davis and Davis, *Fundamentals of Chemical Reaction Engineering*, McGraw-Hill, 2003; Delmon and Froment, *Catalyst Deactivation*, Elsevier, 1980; Denbigh and Turner, *Chemical Reactor Theory*, Cambridge, 1971; Denn, *Process Modeling*, Langman, New York, 1986; Fogler, *Elements of Chemical Reaction Engineering*, 4th ed., Prentice-Hall, 2006; Froment and Bischoff, *Chemical Reactor Analysis and Design*, Wiley, 1990; Froment and Hosten, "Catalytic Kinetics—Modeling," in *Catalysis—Science and Technology*, Springer Verlag, New York, 1981; Harriott, *Chemical Reactor Design*, Dekker, 2003; Hill, *An Introduction to Chemical Engineering Kinetics and Reactor Design*, 2d ed., Wiley, 1990; Holland and Anthony, *Fundamentals of Chemical Reaction Engineering*, Prentice-Hall, 1989; Kafarov, *Cybernetic Methods in Chemistry and Chemical Engineering*, Mir Publishers, 1976; Laidler, *Chemical Kinetics*, Harper & Row, 1987; Lapidus and Amundson (eds.), *Chemical Reactor Theory—A Review*, Prentice-Hall, 1977; Levenspiel, *Chemical Reaction Engineering*, 3d ed., Wiley, 1999; Lewis (ed.), *Techniques of Chemistry*, vol. 4: *Investigation of Rates and Mechanisms of Reactions*, Wiley, 1974; Masel, *Chemical Kinetics and*

Catalysis, Wiley, 2001; Naumann, *Chemical Reactor Design*, Wiley, 1987; Panchenkov and Lebedev, *Chemical Kinetics and Catalysis*, Mir Publishers, 1976; Petersen, *Chemical Reaction Analysis*, Prentice-Hall, 1965; Rase, *Chemical Reactor Design for Process Plants: Principles and Case Studies*, Wiley, 1977; Rose, *Chemical Reactor Design in Practice*, Elsevier, 1981; Satterfield, *Heterogeneous Catalysis in Practice*, McGraw-Hill, 1991; Schmidt, *The Engineering of Chemical Reactions*, Oxford University Press, 1998; Smith, *Chemical Engineering Kinetics*, McGraw-Hill, 1981; Steinfeld, Francisco, and Hasse, *Chemical Kinetics and Dynamics*, Prentice-Hall, 1989; Ulrich, *Guide to Chemical Engineering Reactor Design and Kinetics*, Ulrich, 1993; Van Santen and Neurock, *Molecular Heterogeneous Catalysis: A Conceptual and Computational Approach*, Wiley, 2006; Van Santen and Niemantsverdriet, *Chemical Kinetics and Catalysis, Fundamental and Applied Catalysis*, Plenum Press, New York, 1995; van't Riet and Tramper, *Basic Bioreactor Design*, Dekker, 1991; Walas, *Reaction Kinetics for Chemical Engineers*, McGraw-Hill, 1959; reprint, Butterworths, 1989; Walas, *Chemical Reaction Engineering Handbook of Solved Problems*, Gordon & Breach Publishers, 1995; Westerterp, van Swaaij, and Beenackers, *Chemical Reactor Design and Operation*, Wiley, 1984.

REFERENCES FOR LABORATORY REACTORS: Berty, Laboratory reactors for catalytic studies, in Leach, ed., *Applied Industrial Catalysis*, vol. 1, Academic, 1983, pp. 41–57; Berty, *Experiments in Catalytic Reaction Engineering*, Elsevier, 1999; Danckwerts, *Gas-Liquid Reactions*, McGraw-Hill, 1970; Hoffmann, Industrial Process Kinetics and parameter estimation, in *ACS Advances in Chemistry* **109**:519–534 (1972); Hoffman, Kinetic data analysis and parameter estimation, in de Lasa (ed.), *Chemical Reactor Design and Technology*, Martinus Nijhoff, 1986, pp. 69–105; Horak and Pasek, *Design of Industrial Chemical Reactors from Laboratory Data*, Heiden, Philadelphia, 1978; Rase, *Chemical Reactor Design for Process Plants*, Wiley, 1977, pp. 195–259; Shah, *Gas-Liquid-Solid Reactor Design*, McGraw-Hill, 1979, pp. 149–179; Charpentier, *Mass Transfer Rates in Gas-Liquid Absorbers and Reactors*, in Drew et al., eds., *Advances in Chemical Engineering*, vol. 11, Academic Press, 1981.

The mechanism and corresponding kinetics provide the rate at which the chemical or biochemical species in the reactor system react at the prevailing conditions of temperature, pressure, composition, mixing, flow, heat, and mass transfer. Observable kinetics represent the true intrinsic chemical kinetics only when competing phenomena such as transport of mass and heat are not limiting the rates. The intrinsic chemical mechanism and kinetics are unique to the reaction system. Knowledge of the intrinsic kinetics therefore facilitates reactor selection, choice of optimal operating conditions, and reactor scale-up and design, when combined with understanding of the associated physical and transport phenomena for different reactor scales and types.

This section covers the following key aspects of reaction kinetics:

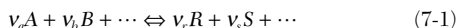
- Chemical mechanism of a reaction system and its relation to kinetics
- Intrinsic rate data using equations that can be correlative, lumped, or based on detailed elementary kinetics
- Catalytic kinetics
- Effect of mass transfer on kinetics in heterogeneous systems
- Intrinsic kinetic rates from experimental data and/or from theoretical calculations
- Kinetic parameter estimation

The use of reaction kinetics for analyzing and designing suitable reactors is discussed in Sec. 19.

BASIC CONCEPTS

MECHANISM

The mechanism describes the reaction steps and the relationship between the reaction rates of the chemical components. A single chemical reaction includes reactants A, B, \dots and products R, S, \dots



where ν_i are the *stoichiometric coefficients* of components A, B, \dots , i.e., the relative number of molecules of A, B, \dots that participate in the reaction. For instance, the HBr synthesis has the global stoichiometry $\text{H}_2 + \text{Br}_2 \rightleftharpoons 2\text{HBr}$.

The *stoichiometry* of the reaction defines the reaction elemental balance (atoms of H and Br, for instance) and therefore relates the number of molecules of reactants and products participating in the reaction. The stoichiometric coefficients are not unique for a given reaction, but their ratios are unique. For instance, for the HBr synthesis above we could have written the stoichiometric equation $\frac{1}{2}\text{H}_2 + \frac{1}{2}\text{Br}_2 \rightleftharpoons \text{HBr}$ as well.

Often several reactions occur simultaneously, resulting in a *network of reactions*. When the network is broken down into *elementary* or *single-event* steps (such as a single electron transfer), the network represents the *true mechanism* of the chemical transformations leading from initial reactants to final products through intermediates. The intermediates can be molecules, ions, free radicals, transition state complexes, and other moieties. A network of *global reactions*, with each reaction representing the combination of a number of elementary steps, does not represent the true mechanism of the chemical transformation but is still useful for global reaction rate calculations, albeit empirically. The stoichiometry can only be written in a unique manner for elementary reactions, since as shown later, the reaction rate for elementary reactions is determined directly by the stoichiometry through the concept of the law of mass action.

REACTION RATE

The *specific rate* of consumption or production of any reaction species i , r_i , is the rate of change of the number of molecules of species i with time per unit volume of reaction medium:

$$r_i = \frac{1}{V} \frac{dn_i}{dt} \quad (7-2)$$

The rate is negative when i represents a *reactant* (dn_i/dt is negative since n_i is decreasing with time) and positive when i represents a *product*

(dn_i/dt positive since n_i is increasing with time). The specific rate of a reaction, e.g., that in Eq. (7-1) is defined as

$$\begin{aligned} r &= -r_i/\nu_i && \text{for reactants} \\ r &= r_i/\nu_i && \text{for products} \end{aligned} \quad (7-3)$$

By this definition, the specific rate of reaction is uniquely defined, and its sign is always positive. Inversely, the rate of reaction of each component or species participating in the reaction is the specific reaction rate multiplied by the species' stoichiometric coefficient with the corrected sign (negative for reactants, positive for products).

CLASSIFICATION OF REACTIONS

Reactions can be classified in several ways. On the basis of *mechanism* they may be

1. *Irreversible*, i.e., the reverse reaction rate is negligible: $A + B \Rightarrow C + D$, e.g., CO oxidation $\text{CO} + \frac{1}{2}\text{O}_2 \Rightarrow \text{CO}_2$
2. *Reversible*: $A + B \rightleftharpoons C + D$, e.g., the water-gas shift $\text{CO} + \text{H}_2\text{O} \rightleftharpoons \text{CO}_2 + \text{H}_2$
3. *Equilibrium*, a special case with zero net rate, i.e., with the forward and reverse reaction rates of a reversible reaction being equal. All reversible reactions, if left to go to completion, end in equilibrium.
4. *Networks of simultaneous reactions*, i.e., consecutive, parallel, complex (combination of consecutive and parallel reactions):



e.g., two-step hydrogenation of acetylene to ethane



A further classification is from the point of view of the number of reactant molecules participating in the reaction, or the *molecularity*:

1. *Unimolecular*: $A \Rightarrow B$, e.g., isomerization of ortho-xylene to para-xylene, O-xylene to P-xylene, or $A \Rightarrow B + C$, e.g., decomposition $\text{CaCO}_3 \Rightarrow \text{CaO} + \text{CO}_2$
2. *Bimolecular*: $A + B \Rightarrow C$ or $2A \Rightarrow B$ or $A + B \Rightarrow C + D$, e.g., $\text{C}_2\text{H}_4 + \text{H}_2 \Rightarrow \text{C}_2\text{H}_6$
3. *Trimolecular*: $A + B + C \Rightarrow D$ or $3A \Rightarrow B$

This last classification has fundamental meaning only when considering elementary reactions, i.e., reactions that constitute a single chemical transformation or a single event, such as a single electron transfer. For elementary reactions, molecularity is rarely higher than 2. Often elementary reactions are not truly unimolecular, since in order for the reaction to occur, energy is required and it is obtained through collision with other molecules such as an inert solvent or gas.

7-6 REACTION KINETICS

Thus the unimolecular reaction $A \Rightarrow B$ could in reality be represented as a bimolecular reaction $A + X \Rightarrow B + X$, i.e., A collides with X to produce B and X , and thus no net consumption of X occurs.

Reactions can be further classified according to the *phases* present. Examples for the more common cases are

1. *Homogeneous gas*, e.g., methane combustion
2. *Homogeneous liquid*, e.g., acid/base reactions to produce soluble salts
3. *Heterogeneous gas-solid*, e.g., HCN synthesis from NH_3 , CH_4 , and air on a solid catalyst
4. *Heterogeneous gas-liquid*, e.g., absorption of CO_2 in amine solutions
5. *Heterogeneous liquid-liquid*, e.g., reaction in immiscible organic and aqueous phases such as synthesis of adipic acid from cyclohexanone and nitric acid
6. *Heterogeneous liquid-solid*, e.g., reaction of limestone with sulfuric acid to make gypsum
7. *Heterogeneous solid-solid*, e.g., self-propagating, high-temperature synthesis of inorganic pure oxides (SHS)
8. *Heterogeneous gas-liquid-solid*, e.g., catalytic Fischer-Tropsch synthesis of hydrocarbons from CO and H_2
9. *Heterogeneous gas-liquid-liquid*, e.g., oxidations or hydrogenations with phase transfer catalysts

Reactions can also be classified with respect to the *mode of operation* in the reaction system as

1. *Isothermal constant volume* (batch)
2. *Isothermal constant pressure* (continuous)
3. *Adiabatic*
4. *Nonisothermal* temperature-controlled (by cooling or heating), batch or continuous

EFFECT OF CONCENTRATION ON RATE

The *concentration* of the reaction components determines the rate of reaction. For instance, for the irreversible reaction



the rate can be represented *empirically* as a power law function of the reactant concentrations such as

$$r = kC_a^a C_b^b \quad C_i = \frac{n_i}{V} \quad (7-5)$$

The exponents a and b represent the *order of the reaction* with respect to components A and B , and the *sum* $a + b$ represents the *overall order of the reaction*. The order can be a positive, zero, or negative number indicating that the rate increases, is independent of, or decreases with an increase in a species concentration, respectively. The exponents can be whole (integral order) or fraction (fractional order). In Eq. (7-5) k is the *specific rate constant* of the reaction, and it is independent of concentrations for elementary reactions only. For global reactions consisting of several elementary steps, k may still be constant over a narrow range of compositions and operating conditions and therefore can be considered constant for limited practical purposes. A further complexity arises for nonideal chemical solutions where activities have to be used instead of concentrations. In this case the rate constant can be a function of composition even for elementary steps (see, for instance, Froment and Bischoff, *Chemical Reactor Analysis and Design*, Wiley, 1990).

When Eq. (7-4) represents a global reaction combining a number of elementary steps, then rate equation (7-5) represents an empirical correlation of the global or overall reaction rate. In this case exponents a and b have no clear physical meaning other than indicating the overall effect of the various concentrations on rate, and they do not have any obvious relationship to the stoichiometric coefficients p and q . This is not so for elementary reactions, as shown in the next subsection. Also, as shown later, power law and rate expressions other than power law (e.g., hyperbolic) can be developed for specific reactions by starting with the mechanism of the elementary steps and making simplifying assumptions that are valid under certain conditions.

LAW OF MASS ACTION

As indicated above, the dependence of rate on concentration can be shown to be of the general form

$$r = kf(C_a, C_b, \dots) \quad (7-6)$$

For elementary reactions, the *law of mass action* states that the rate is proportional to the concentrations of the reactants raised to the power of their respective molecularity. Thus for an elementary irreversible reaction such as (7-4) the rate equation is

$$r = kC_a^p C_b^q \quad (7-7)$$

Hence, the exponents p and q of Eq. (7-7) are the stoichiometric coefficients when the stoichiometric equation truly represents the mechanism of reaction, i.e., when the reactions are elementary. As discussed above, the exponents a and b in Eq. (7-5) identify the order of the reaction, while the stoichiometric coefficients p and q in Eq. (7-7) also identify the molecularity—for elementary reactions these are the same.

EFFECT OF TEMPERATURE

The *Arrhenius equation* relates the specific rate constant to the absolute temperature

$$k = k_0 \exp\left(-\frac{E}{RT}\right) \quad (7-8)$$

where E is called the *activation energy* and k_0 is the *preexponential factor*. As seen from Eq. (7-8), the rate can be a very strongly increasing (exponential) function of temperature, depending on the magnitude of the activation energy E . This equation works well for elementary reactions, and it also works reasonably well for global reactions over a relatively narrow range of temperatures in the absence of mass-transfer limitations. The Arrhenius form represents an energy barrier on the reaction pathway between reactants and products that has to be overcome by the reactant molecules.

The Arrhenius equation can be derived from theoretical considerations using either of two competing theories, the *collision theory* and the *transition state theory*. A more accurate form of Eq. (7-8) includes an additional temperature factor

$$k = k_0 T^m \exp\left(-\frac{E}{RT}\right) \quad 0 < m < 1 \quad (7-9)$$

but the T^m factor is often neglected because of the usually much stronger dependence on temperature of the exponential factor in Eq. (7-9), as m is usually small. When m is larger, as it can be for complex molecules, then the T^m term has to be taken into consideration. For more details, see Masel, *Chemical Kinetics and Catalysis*, Wiley, 2001; Levenspiel, *Chemical Reaction Engineering*, 3d ed., Wiley, 1999).

HEAT OF REACTION

Chemical reactions are accompanied by evolution or absorption of energy. The enthalpy change (difference between the total enthalpy of formation of the products and that of the reactants) is called the *heat of reaction* ΔH_r :

$$\Delta H_r = (v_r H_{fr} + v_s H_{fs} + \dots) - (v_a H_{fa} + v_b H_{fb} + \dots) \quad (7-10)$$

where H_{fi} are the *enthalpies of formation* of components i . The reaction is *exothermic* if heat is produced by the reaction (negative heat of reaction) and *endothermic* if heat is consumed (positive heat of reaction). The magnitude of the effective heat of reaction depends upon temperature and the phases of the reactants and product. To estimate the dependence of the heat of reaction on temperature relative to a

reference temperature T_0 , the following expression can be used, provided there is no phase change:

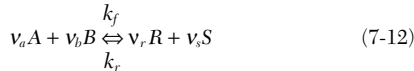
$$\Delta H_r(T) = \Delta H_r(T_0) + \int_{T_0}^T \Delta c_p \, dT \quad (7-11)$$

$$\Delta c_p = (v_a c_{p_a} + v_b c_{p_b} + \dots) - (v_a c_{p_a} + v_b c_{p_b} + \dots)$$

where c_{p_i} are the *heat capacities* of component i . The heat of reaction can be measured by using calorimetry, or it can be calculated by using a variety of thermodynamic methods out of the scope of this chapter (see relevant sections of this handbook, thermodynamic texts, and Bird, Stewart, and Lightfoot, *Transport Phenomena*, 2d ed., John Wiley & Sons, New York, 2002). It is important to accurately capture the energy balance and its relation to the heat of reaction and heat capacities (see also Denn, *Process Modeling*, Langman, New York, 1986, for correct formulations). The coupling of the heat of reaction with the reaction rate through the Arrhenius equation often has a dominating effect on reactor selection and control, and on the laboratory reactor setup required to obtain accurate intrinsic kinetics and mechanism. More on this can be found in Sec. 19.

CHEMICAL EQUILIBRIUM

Often reactions or reaction steps in a network of reactions are at chemical equilibrium; i.e., the rate of the forward reaction equals the rate of the reverse reaction. For instance, for the reversible reaction



with mass action kinetics, the rate may be written as

$$r = r_f - r_r = k_f C_a^v C_b^v - k_r C_r^v C_s^v \quad (7-13)$$

At chemical equilibrium the forward and reverse reaction rates are equal according to the principle of *microscopic reversibility*:

$$r = r_f - r_r = 0 \quad (7-14)$$

The equilibrium constant K_e (based on volumetric concentrations) is defined as the ratio of the forward and reverse rate constants and is related to the composition at equilibrium as follows:

$$K_e = \frac{k_f}{k_r} = \frac{C_R^v C_S^v}{C_A^v C_B^v} \quad (7-15)$$

K_e can be calculated from the free energy change of the reaction. Using the van't Hoff relation, we obtain the dependence of K_e on temperature:

$$\frac{d(\ln K_e)}{dT} = \frac{\Delta H_r}{RT^2} \quad (7-16)$$

Integrating with respect to temperature, we obtain a form similar to the Arrhenius expression of the rate constant for a narrow range of temperature:

$$K_e = K_{e,0} \exp\left(\frac{\Delta H_r}{RT}\right) \quad (7-17)$$

A more general integral form of Eq. (7-16) is

$$\ln K_e(T) = \ln K_e(T_0) + \frac{1}{R} T \int_{T_0}^T \frac{\Delta H_r(T_0) + \int_{T_0}^T \Delta c_p \, dT}{T^2} \, dt \quad (7-18)$$

When a reversible reaction is not at equilibrium, knowledge of K_e can be used to eliminate the rate constant of the reverse reaction by using Eq. (7-15) as follows:

$$r = k_f (C_a^v C_b^v - C_r^v C_s^v / K_e) \quad (7-19)$$

When several reversible reactions occur simultaneously, each reaction r_j is characterized by its equilibrium constant K_{e_j} . When the K_{e_j} are known, the composition at equilibrium can be calculated from a set of equations such as Eq. (7-15) for each reaction.

CONVERSION, EXTENT OF REACTION, SELECTIVITY, AND YIELD

Conversion of a reactant is the number of moles converted per initial or feed moles of a reactant. Thus for component A

$$X_a = 1 - \frac{n_a}{n_{a0}} \quad (7-20)$$

A *limiting reactant* is a reactant whose concentration at the start of the reaction is the least of all reactants relative to the required stoichiometric amount needed for complete conversion. For instance, for the single reaction (7-12), A is the limiting reactant if the initial molar ratio of concentrations of A and B is less than the ratio of their stoichiometric coefficients:

$$\frac{n_{a0}}{n_{b0}} < \frac{v_a}{v_b} \quad (7-21)$$

Once the limiting reactant is depleted, the respective reaction stops even though other (nonlimiting) reactants may still be abundant.

For each reaction or each step in a network of reactions, a unique *extent of reaction* ξ that relates the composition of components that participate in the reaction to each other can be defined. For instance, for the single reaction (7-1):

$$\xi = \frac{n_{a0} - n_a}{v_a} = \frac{n_{b0} - n_b}{v_b} = \dots = -\frac{n_{r0} - n_r}{v_r} = -\frac{n_{s0} - n_s}{v_s} = \dots \quad (7-22)$$

The extent of reaction is related to conversion as follows:

$$\xi = \frac{X_a n_{a0}}{v_a} = \frac{X_b n_{b0}}{v_b} = \dots \quad (7-23)$$

When A is the limiting reactant as in Eq. (7-21), the maximum extent of reaction (with A fully converted) is

$$\xi_{\max} = \frac{n_{a0}}{v_a} \quad (7-24)$$

For multiple reactions with reactants participating in more than one reaction, it is more difficult to determine the limiting reactant and often it is necessary to calculate the concentration as the reactions proceed to determine which reactant is consumed first. When the limiting reactant is depleted, all reactions that use this component as reactant stop, and the corresponding rates become zero.

Selectivity S of a product is the ratio of the rate of production of that product to the rate of production of all products combined. For a single reaction selectivity is trivial—if more than one product occurs, then the selectivity of each product is the ratio of the stoichiometric coefficient of that product to the sum of stoichiometric coefficients of all the products. Thus for reaction (7-1)

$$S_r = \frac{v_r}{v_r + v_s + \dots} \quad (7-25)$$

7-8 REACTION KINETICS

The selectivity of product R for a network of reactions, with all the reactions making the various products included, is

$$S_r = \frac{r_r}{\sum_{\text{all products } i} r_i} \quad (7-26)$$

For instance, for the network of reactions $A + B \xrightarrow{1} C + D$
 $C + E \xrightarrow{2} F + G$, the selectivity to product C is

$$S_c = \frac{r_c}{r_c + r_d + r_f + r_g} = \frac{r_1 - r_2}{(r_1 - r_2) + r_1 + r_2 + r_2} = \frac{r_1 - r_2}{2r_1 + r_2}$$

The *yield* Y of a product R with respect to a reactant A is the ratio of the rate of production of R to that of consumption of A :

$$Y_r = \frac{r_r}{-r_a} \quad (7-27)$$

For a single reaction the yield is trivial and Eq. (7-27) simplifies to the ratio of the respective stoichiometric coefficients:

$$Y_r = \frac{v_r}{v_a} \quad (7-28)$$

The yield quantifies the efficiency of the respective reactant utilization to make the desired products.

CONCENTRATION TYPES

Different concentration types are used for different reaction systems. For gas-phase reactions, *volumetric concentration* or *partial pressures* are equally useful and can be related by the thermodynamic equation of state. For instance, for ideal gases (approximation valid for gases at very low pressure)

$$PV = nRT \quad (7-29)$$

When applied to individual components in a constant-volume system,

$$p_i V = n_i RT \quad (7-30)$$

Using Eq. (7-5), we obtain the relationship between the volumetric concentrations and partial pressures:

$$C_i = \frac{p_i}{RT} \quad (7-31)$$

For an ideal gas the total concentration is

$$C = \frac{P}{RT} \quad (7-32)$$

For higher pressure and nonideal gases, a *compressibility factor* z_i can be used:

$$p_i V = z_i n_i RT \quad \text{and} \quad C_i = \frac{p_i}{z_i RT} \quad (7-33)$$

Other relevant equations of state can also be used for both gases and liquids. This aspect is not in the scope of this section, and the reader is referred to the relevant section of this handbook.

Other concentration units include *mole fractions* for liquid x_i :

$$x_i = \frac{n_i}{\sum n_i} = \frac{C_i}{\sum C_i} = \frac{C_i}{C} \quad (7-34)$$

and for gas y_i :

$$y_i = \frac{n_i}{\sum n_i} = \frac{C_i}{\sum C_i} = \frac{C_i}{C} = \frac{p_i}{\sum p_i} = \frac{p_i}{P} \quad (7-35)$$

The last two terms are only valid for an ideal gas.

STOICHIOMETRIC BALANCES

Single Reactions Equation (7-22) shows that for a single reaction, the number of moles and concentration of all other components can be calculated from the extent of reaction ξ or the conversion based on the limiting reactant, say A , X_a . In terms of number of moles n_i ,

$$\begin{aligned} n_a &= n_{a0} - v_a \xi = n_{a0}(1 - X_a) \\ n_b &= n_{b0} - v_b \xi = n_{b0}(1 - X_b) = n_{b0} - \frac{v_b}{v_a} n_{a0} X_a \\ &\dots \\ n_r &= n_{r0} + v_r \xi = n_{r0} - \frac{v_r}{v_a} n_{a0} X_a \\ n_s &= n_{s0} + v_s \xi = n_{s0} - \frac{v_s}{v_a} n_{a0} X_a \\ &\dots \end{aligned} \quad (7-36)$$

Similarly the number of moles of each component in terms of moles of A , n_{a0} , is

$$\begin{aligned} n_b &= n_{b0} - \frac{v_b}{v_a} (n_{a0} - n_a) \\ &\dots \\ n_r &= n_{r0} + \frac{v_r}{v_a} (n_{a0} - n_a) \\ n_s &= n_{s0} + \frac{v_s}{v_a} (n_{a0} - n_a) \\ &\dots \end{aligned} \quad (7-37)$$

Change in number of moles by the reaction and change in temperature, pressure, and density affect the translation of stoichiometric balances from number of moles to volumetric concentrations. These relationships are different for gases and liquids. For instance, for *constant density* systems (such as many liquid-phase isothermal reactions) or for *constant temperature, constant pressure* gas reaction with no change in number of moles, Eqs. (7-36) and (7-37) can be changed to volumetric concentration C_i by dividing each equation by the constant reaction volume V (e.g., in a batch reactor) and using Eq. (7-5). For example, for the single reaction (7-4) with rate (7-5):

$$\begin{aligned} C_b &= C_{b0} - \frac{q}{p} (C_{a0} - C_a) \\ C_r &= C_{r0} + \frac{r}{p} (C_{a0} - C_a) \\ C_s &= C_{s0} + \frac{s}{p} (C_{a0} - C_a) \end{aligned} \quad (7-38)$$

$$r = k C_a^a \left[C_{b0} - \frac{q}{p} (C_{a0} - C_a) \right]^b = k [C_{a0}(1 - X_a)]^a \left(C_{b0} - \frac{q}{p} C_{a0} X_a \right)^b \quad (7-39)$$

It is best to represent all concentrations in terms of that of the limiting reactant.

Often there is a change in total number of moles due to reaction. Taking the general reaction (7-1), in the gas phase the change in

number of moles relative to moles of component A converted, δ_a , and the total number of moles can be calculated as follows:

$$\delta_a = \frac{v_q + v_s + \dots - v_a - v_b - \dots}{v_a}$$

$$n_a = \sum n_{i0} \quad n = \sum n_i \quad (7-40)$$

$$\frac{n}{n_0} = 1 + y_{a0} \delta_a X_a = 1 + \varepsilon_a X_a$$

$$\varepsilon_a = y_{a0} \delta_a$$

Using the ideal gas law, Eq. (7-29), the volume change depends on conversion as follows:

$$\frac{V}{V_0} = \frac{T}{T_0} \frac{P_0}{P} \frac{n}{n_0} = \frac{T}{T_0} \frac{P_0}{P} (1 + \varepsilon_a X_a) \quad (7-41)$$

Hence, for an isothermal constant-pressure ideal gas reaction system,

$$C_a = \frac{n_a}{V} = \frac{C_{a0}(1 - X_a)}{1 + \varepsilon_a X_a}$$

$$C_b = \frac{n_b}{V} = \frac{C_{b0} - \frac{v_b}{v_a} C_{a0} X_a}{1 + \varepsilon_a X_a}$$

$$\dots$$

$$C_r = \frac{n_r}{V} = \frac{C_{r0} - \frac{v_r}{v_a} C_{a0} X_a}{1 + \varepsilon_a X_a}$$

$$C_s = \frac{n_s}{V} = \frac{C_{s0} - \frac{v_s}{v_a} C_{a0} X_a}{1 + \varepsilon_a X_a}$$

$$\dots$$
(7-42)

Applying this to reaction (7-4) and rate (7-5) gives

$$r = k \left[\frac{C_{a0}(1 - X_a)}{1 + \varepsilon_a X_a} \right]^a \left[\frac{C_{b0} - (q/p) C_{a0} X_a}{1 + \varepsilon_a X_a} \right]^b \quad (7-43)$$

Compare this to Eq. (7-39) where there is no change in number of moles.

Reaction Networks The analysis for single reactions can be extended to a network of reactions by defining an extent of reaction for each reaction, or by choosing a representative reactant concentration for each reaction step. For a complex network, the number of independent extents of reaction required to calculate the concentration of all components is equal to the number of *independent reactions*, which is less than or equal to the total number of reactions in the network. To calculate the number of independent reactions, and to form a set of independent reactions and corresponding independent set of concentrations or extents of reaction, we need to construct the *stoichiometric matrix* and determine its *rank*. The stoichiometric matrix is used to derive a relationship between the concentrations and the independent extents of reaction similar to that of a single reaction.

The stoichiometric matrix is the matrix of the stoichiometric coefficients of the reaction network with negative signs for reactants and positive signs for products. For instance, the hydrodechlorination of Freon 12 (CF_2Cl_2) can proceed with the following consecutive mechanism [Bonarowska et al., "Hydrodechlorination of CCl_2F_2 (CFC-12) over Silica-Supported Palladium-Gold Catalysts," *Appl. Catal. B: Environmental*, **30**:187–193, 2001]:



The stoichiometric matrix S for this network is

$$S = \begin{pmatrix} -1 & 1 & 0 & -1 & 1 \\ 0 & -1 & 1 & -1 & 1 \end{pmatrix}$$

The first row refers to the first reaction and the second row to the second reaction. The columns (species) are in the following order: 1- CF_2Cl_2 , 2- CF_2ClH , 3- CF_2H_2 , 4- H_2 , and 5- HCl . The rank of a matrix is the largest square submatrix obtained by deleting rows and columns, whose determinant is not zero. The rank equals the number of independent reactions. This is also equivalent to stating that there are reactions in the network that are linear combinations of the independent reactions. The rank of S above is 2, since the *determinant* of the first 2×2 submatrix is not zero (there are other 2×2 submatrices that are not zero as well but it is sufficient to have at least one that is not zero):

$$S_1 = \begin{pmatrix} -1 & 1 \\ 0 & -1 \end{pmatrix} \quad \det(S_1) = 1 \neq 0$$

Hence the two reactions are independent. Now if we add another step, which converts Freon 12 directly into the final hydrofluorocarbon CF_2H_2 : $\text{CF}_2\text{Cl}_2 + 2\text{H}_2 \Rightarrow \text{CF}_2\text{H}_2 + 2\text{HCl}$, then the stoichiometric matrix becomes

$$S = \begin{pmatrix} -1 & 1 & 0 & -1 & 1 \\ 0 & -1 & 1 & -1 & 1 \\ -1 & 0 & 1 & -2 & 2 \end{pmatrix}$$

Since the last reaction is a linear combination of the first two (sum), it can be easily proved that the rank remains unchanged at 2. So to conclude, the concentrations of all components in this network can be expressed in terms of two, say H_2 and Freon 12, and the first two reactions form an independent reaction set. In case of more complicated networks it may be difficult to determine the independent reactions by observation alone. In this case the *Gauss-Jordan decomposition* leads to a set of independent reactions (see, e.g., Amundson, *Mathematical Methods in Chemical Engineering—Matrices and Their Application*, Prentice-Hall International, New York, 1966).

For a network of reactions the general procedure is as follows:

1. Generate the reaction network by including all known reaction steps.
2. Generate the corresponding stoichiometric matrix.
3. Calculate the rank of the stoichiometric matrix which equals the number of independent reactions and independent component concentrations required to calculate all the remaining component concentrations.
4. For relatively simple networks, observation allows selection of reactions that are independent—for more complex systems use the Gauss-Jordan elimination to reduce the network to a set of independent (nonzero rows) reactions.

5. Select the independent concentration variables and independent reactions, and use these to calculate all other concentrations and reaction rates.

CATALYSIS

A catalyst is a material that increases the rate of both the forward and reverse reactions of a reaction step, with no net consumption or generation of catalyst by the reaction. A catalyst does not affect the reaction thermodynamics, i.e., the equilibrium composition or the heat of reaction. It does, however, affect the temperature sensitivity of the reaction rate by lowering the activation energy or the energy barrier on the reaction pathway from reactants to products. This allows the reaction to occur faster than the corresponding uncatalyzed reaction at a given temperature. Alternatively, catalytic reactions can proceed at lower temperatures than the corresponding noncatalytic reactions. For a network of reactions, the catalyst is often used to speed up desired reactions and/or to slow down undesired reactions for improved selectivity. On the basis of catalysis, reactions can be further classified into

1. Noncatalytic reactions, e.g., free-radical gas-phase reactions such as combustion of hydrocarbons.

7-10 REACTION KINETICS

2. Homogeneous catalytic reactions with the catalyst being dissolved in the same phase as the reactants and products in a homogeneous reaction medium. Here the catalyst is uniformly distributed throughout the system, e.g., the hydroformylation of olefins in the presence of dissolved Co or Rh carbonyls.

3. Heterogeneous catalytic reactions, with the catalyst, for instance, being a solid in contact with reactants and products in a gas-solid, gas-liquid-solid, or a liquid-solid reaction system. Here the catalyst is not uniformly distributed, and the reaction occurring on the catalyst surface requires, for instance, adsorption of reactants and desorption of products from the solid surface, e.g., the catalytic cracking of gasoil to gasoline and lighter hydrocarbons.

Table 7-1 illustrates the enhancement of the reaction rates by the catalyst—this enhancement can be of many orders of magnitude.

TABLE 7-1 The Rate of Enhancement of Some Reactions in the Presence of a Catalyst

Reaction	Catalyst	Rate enhancement	Temperature, K
Ortho $H_2 \Rightarrow$ para H_2	Pt (solid)	10^{40}	300
$2NH_3 \Rightarrow N_2 + 3H_2$	Mo (solid)	10^{20}	600
$C_2H_4 + H_2 \Rightarrow C_2H_6$	Pt (solid)	10^{42}	300
$H_2 + Br_2 \Rightarrow 2HBr$	Pt (solid)	1×10^8	300
$2NO + 2H_2 \Rightarrow N_2 + 2H_2O$	Ru (solid)	3×10^{16}	500
$CH_3COH \Rightarrow CH_4 + CO$	I_2 (gas)	4×10^6	500
$CH_3CH_3 \Rightarrow C_2H_4 + H_2$	NO_2 (gas)	1×10^9	750
$(CH_3)_3COH \Rightarrow$ $(CH_3)_2CH_2CH_2 + H_2O$	HBr (gas)	3×10^8	750

SOURCE: Masel, *Chemical Kinetics and Catalysis*, Wiley, 2001, Table 12.1.

IDEAL REACTORS

Reactions occur in reactors, and in addition to the intrinsic kinetics, observed reaction rates depend on the reactor type, scale, geometry, mode of operation, and operating conditions. Similarly, understanding of the reactor system used in the kinetic experiments is required to determine the reaction mechanism and intrinsic kinetics. In this section we address the effect of reactor type on observed rates. In Sec. 19 the effect of reactor type on performance (rates, selectivity, yield) is discussed in greater detail.

Material, energy, and momentum balances are essential to fully describe the performance of reactors, and often simplifying assumptions and phenomenological assumptions are needed especially for energy and momentum terms, as indicated in greater detail in Sec. 19

(see also Bird, Stewart, and Lightfoot, *Transport Phenomena*, 2d ed., John Wiley & Sons, New York, 2002). Ideal reactors allow us to simplify the energy, momentum, and material balances, thus focusing the analysis on intrinsic kinetics. A useful classification of ideal reactor types is in terms of their concentration distributions versus reaction time and space. Three types of ideal reactors are considered in this section:

1. Ideal *batch reactors (BRs)* including *semibatch reactors (SBRs)*
2. Ideal *continuously stirred tank reactor (CSTR)*, including single and multiple stages
3. *Plug flow reactor (PFR)* with and without *recycle*

Figure 7-1 shows these types of ideal reactors. Other types of ideal and nonideal reactors are treated in detail in Sec. 19.

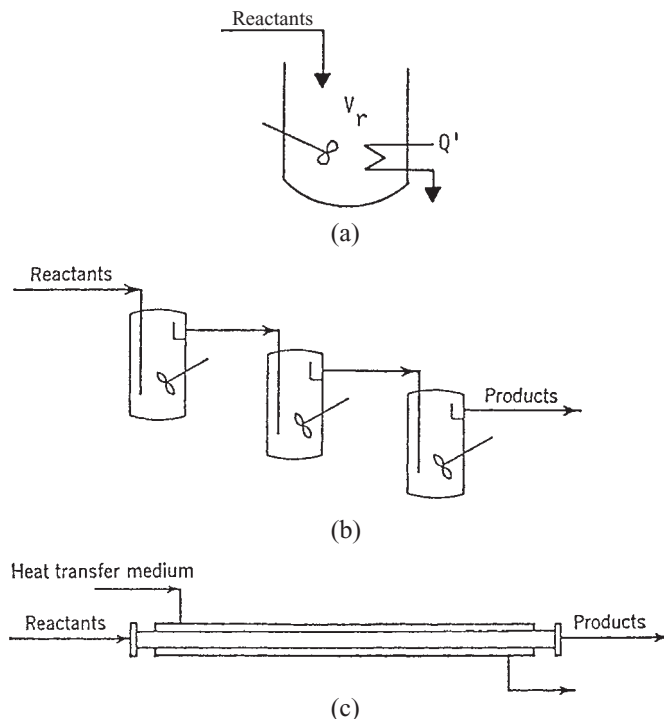


FIG. 7-1 Types of ideal reactors: (a) Batch or semibatch. (b) CSTR or series of CSTRs. (c) Plug flow.

The general form of a balance equation is

$$\text{Input} + \text{sources} - \text{outputs} = \text{accumulation} \quad (7-44)$$

IDEAL BATCH REACTOR

Batch Reactor (BR) Ideal batch reactors (Fig. 7-1a) are tanks provided with agitation for uniform composition and temperature at all times. An ideal batch reactor can be operated under isothermal conditions (constant temperature), temperature-programmed mode (by controlling cooling rate according to a protocol), or adiabatic mode with no heat crossing the reactor boundaries). In adiabatic mode the temperature is increasing, decreasing, or constant as the reaction proceeds for exothermic, endothermic, and thermally neutral reactions, respectively. In the ideal batch reactor, all the reactants are loaded into the reactor and well mixed by agitation before the conditions for reaction initiation (temperature and pressure) are reached; as the reaction proceeds, the concentration varies with time, but at any one time it is uniform throughout due to agitation.

Laboratory batch reactors can be single-phase (e.g., gas or liquid), multiphase (e.g., gas-liquid or gas-liquid-solid), and catalytic or non-catalytic. In this section we limit the discussion to operation at isothermal conditions. This eliminates the need to consider energy, and due to the uniform composition the component material balances are simple ordinary differential equations with time as the independent variable.

An ideal isothermal single-phase batch reactor in which a general reaction network takes place has the following general material balance equation:

$$\frac{dn_i}{dt} = V \sum_j \nu_{ij} r_j \quad n_i = n_{i0} \quad \text{at } t = 0 \quad (7-45)$$

The left-hand side is the accumulation term in moles per second of component i , and the right-hand side is the source term due to chemical reaction also in moles per second, which includes all reactions j that consume or produce component i , and the corresponding stoichiometric coefficients are represented in matrix form as ν_{ij} with a positive sign for products and a negative sign for reactants. This molar

balance is valid for each component since we can multiply each side of the equation by the component molecular weight to obtain the true mass balance equation. In terms of conversion, Eq. (7-45) can be rewritten as

$$\frac{n_{i0} dX_i}{dt} = -V \sum_j \nu_{ij} r_j \quad n_i = n_{i0} \quad \text{at } t = 0 \quad (7-46)$$

and we can integrate this equation to get the *batch reaction time* or *batch residence time* τ_{BR} required to obtain a conversion X_i , starting with initial conversion X_{i0} and ending with final conversion X_{if} :

$$\tau_{BR} = -n_{i0} \int_{X_{i0}}^{X_{if}} \frac{dX_i}{V \sum_j \nu_{ij} r_j} \quad (7-47)$$

To integrate we need to represent all reaction rates r_j in terms of the conversion X_i . For a single reaction this is straightforward [see, e.g., Eq. (7-43)]. However, for a network of reactions, integration of a system of often nonlinear differential equations is required using implicit or semi-implicit integration. For references please see the relevant section of this handbook or any textbook on ordinary differential equations.

A special case of batch reactors is constant-volume or constant-density operation typical of liquid-phase reactions, with volume invariant with time:

$$\frac{dC_i}{dt} = \sum_j \nu_{ij} r_j \quad C_i = C_{i0} \quad \text{at } t = 0 \quad (7-48)$$

A typical concentration profile versus time for a reactant is shown in Fig. 7-2a. Integration of Eq. (7-48) gives the batch residence time

$$\tau_{BR} = \int_{C_{i0}}^{C_{if}} \frac{dC_i}{\sum_j \nu_{ij} r_j} \quad (7-49)$$

For instance, for a single reaction, Eq. (7-43) can be used to describe the reaction rate r_i in terms of one reactant concentration. For reaction networks integration of a system of ordinary differential equations is required.

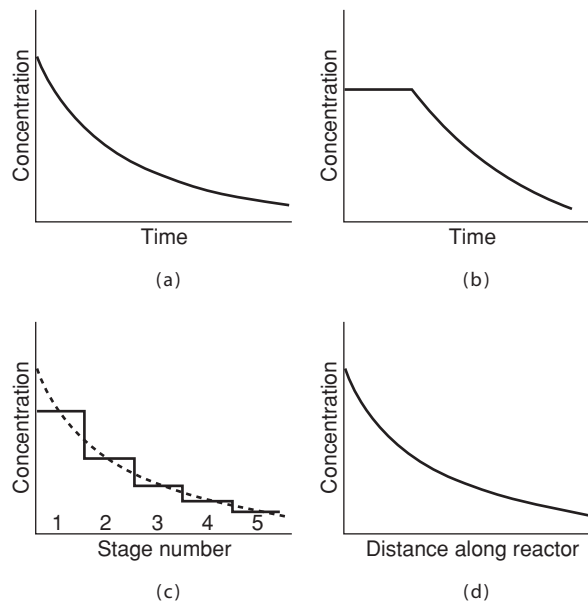


FIG. 7-2 Concentration profiles in batch and continuous flow: (a) Batch time profile. (b) Semibatch time profile. (c) Five-stage CSTRs distance profile. (d) Tubular flow distance profile.

7-12 REACTION KINETICS

Semibatch Reactor (SBR) In semibatch operation, a gas of limited solubility or a liquid reactant may be fed in gradually as it is used up. An ideal isothermal single-phase semibatch reactor in which a general reaction network takes place has the following general material balance equation:

$$\frac{dn_i}{dt} = N_{i0} + V \sum v_{ij} r_j \quad n_i = n_{i0} \quad \text{at } t = 0$$

$$N_{i0} = N_{i0}(t) \quad \text{for } t_{s0i} \leq t \leq t_{s1i} \quad (7-50)$$

The first term on the right-hand side of Eq. (7-50) is the molar feed rate of the components, which can be different for each component, hence the subscript i , and can vary with time. A typical concentration profile versus time for a reactant whose concentration is kept constant initially by controlling the feed rate is shown in Fig. 7-2b. Knowledge of the reaction kinetics allows these ordinary differential equations to be integrated to obtain the reactor composition versus time.

IDEAL CONTINUOUS STIRRED TANK REACTOR (CSTR)

In an ideal continuous stirred tank reactor, composition and temperature are uniform throughout just as in the ideal batch reactor. But this reactor also has a continuous feed of reactants and a continuous withdrawal of products and unconverted reactants, and the effluent composition and temperature are the same as those in the tank (Fig. 7-1b). A CSTR can be operated under transient conditions (due to variation in feed composition, temperature, cooling rate, etc., with time), or it can be operated under steady-state conditions. In this section we limit the discussion to isothermal conditions. This eliminates the need to consider energy balance equations, and due to the uniform composition the component material balances are simple ordinary differential equations with time as the independent variable:

$$\frac{dn_i}{dt} = N_{i0} - N_i + V \sum v_{ij} r_j \quad n_i = n_{i0} \quad \text{at } t = 0 \quad (7-51)$$

At steady state the differential equations simplify to algebraic equations as indicated below:

$$V = - \frac{N_{i0} - N_i}{\sum v_{ij} r_j} \quad (7-52)$$

Equation (7-52) can be expressed in terms of volumetric concentration or in terms of conversions just as we did with the batch reactor. An *apparent residence time* based on feed conditions can be defined for a single-phase CSTR as follows:

$$\tau_{\text{CSTR}} = \frac{V}{q_0} \quad N_{i0} = q_0 C_{i0} \quad N_i = q C_i \quad (7-53)$$

In Eq. (7-53) the feed and effluent molar rates N_{i0} and N_i are expressed in terms of volumetric flow rates q_0 and q (inlet and outlet, respectively) and concentrations. Thus Eq. (7-52) can be rewritten as

$$\tau_{\text{CSTR}} = \frac{C_{i0} - (q/q_0)C_i}{\sum v_{ij} r_j} \quad (7-54)$$

Equation (7-54) allows calculation of the residence time required to achieve a given conversion or effluent composition. In the case of a network of reactions, knowing the reaction rates as a function of volumetric concentrations allows solution of the set of often nonlinear algebraic material balance equations using an implicit solver such as the multi variable Newton-Raphson method to determine the CSTR effluent concentration as a function of the residence time. As for batch reactors, for a single reaction all compositions can be expressed in terms of a component conversion or volumetric concentration, and Eq. (7-54) then becomes a single nonlinear algebraic equation solved by the Newton-Raphson method (for more details on this method see the relevant section in this handbook).

A special case of Eq. (7-54) is a constant-density system (e.g., a liquid-phase reaction), with the true average residence time τ_{CSTR}

$$\tau_{\text{CSTR}} = \frac{C_{i0} - C_i}{\sum v_{ij} r_j} \quad q = q_0 \quad (7-55)$$

When a number of such CSTRs are employed in series, the concentration profile is step-shaped if the abscissa is the total residence time or the stage number as indicated by a typical reactant concentration profile in Fig. 7-2c.

PLUG FLOW REACTOR (PFR)

In a *plug flow reactor* all portions of the feed stream move with the same radially uniform velocity along parallel streamlines and therefore have the same residence time; that is, there is no mixing in the axial direction but complete mixing radially (Fig. 7-1c). As the reaction proceeds, the concentration falls off with distance. A PFR can be operated under either transient conditions or steady-state conditions. In this section we limit the discussion to steady-state conditions. This eliminates the need to consider partial differential equations in time and space. We further limit the discussion to isothermal operation, which together with the defined plug flow also eliminates the need for energy and momentum balance equations. Due to the radially uniform composition, the component material balances are simple ordinary differential equations with axial distance from inlet as the independent variable. An isothermal single-phase steady-state PFR in which a general reaction network takes place has the following general material balance equation:

$$\frac{dN_i}{dV} = \sum v_{ij} r_j \quad N_i = N_{i0} \quad \text{at } V = 0 \quad (7-56)$$

Note the similarity between the ideal batch and the plug flow reactors, Eqs. (7-45) and (7-56), respectively. In terms of conversion, Eq. (7-56) can be written as

$$N_{i0} \frac{dX_i}{dV} = - \sum v_{ij} r_j \quad (7-57)$$

Equation (7-57) can be integrated to calculate the reactor volume required to achieve a given conversion X_i :

$$V = -N_{i0} \int_{X_{i0}}^{X_{if}} \frac{dX_i}{\sum v_{ij} r_j} \quad (7-58)$$

An *apparent residence time* based on feed conditions can be defined for a single-phase PFR as follows:

$$\tau_{\text{PFR}} = \frac{V}{q_0} \quad (7-59)$$

Equation (7-58) becomes

$$\tau_{\text{PFR}} = -C_{i0} \int_{X_{i0}}^{X_{if}} \frac{dX_i}{\sum v_{ij} r_j} \quad (7-60)$$

Equation (7-60) is identical to that of the ideal batch reactor, Eq. (7-47), and the two reactor systems can be modeled in identical fashion.

For a constant-density system with no change in number of moles, with the true residence time τ_{PFR} :

$$\tau_{\text{PFR}} = \int_{C_{i0}}^{C_{if}} \frac{dC_i}{\sum v_{ij} r_j} \quad (7-61)$$

This is identical to the corresponding ideal batch reactor, Eq. (7-49).

Ideal Recycle Reactor All reactor modes can sometimes be advantageously operated with recycling part of the product or intermediate streams. Heated or cooled recycle streams serve to moderate undesirable temperature gradients, and they can be processed for changes in composition such as separating products to remove equilibrium limitations, before being returned. Say the recycle flow rate in

TABLE 7-2 Consecutive and Parallel First-Order Reactions in an Isothermal Constant-Volume Ideal Batch or Plug Flow Reactor.

The independent variable t is either the batch time or the plug flow residence time.

Reaction network	Material balances	Concentration profiles
$A \xrightarrow{1} B \xrightarrow{2} C$	$\frac{dC_a}{dt} = -k_1 C_a$	$C_a = C_{a0} e^{-k_1 t}$
	$\frac{dC_b}{dt} = k_1 C_a - k_2 C_b$	$C_b = C_{b0} e^{-k_2 t} + \frac{k_1 C_{a0}}{k_2 - k_1} (e^{-k_1 t} - e^{-k_2 t})$
	$\frac{dC_c}{dt} = k_2 C_b$	$C_c = C_{a0} + C_{b0} + C_{c0} - C_a - C_b$
$A \xrightarrow{1} B$ $A \xrightarrow{2} C$	$\frac{dC_a}{dt} = -(k_1 + k_2) C_a$	$C_a = C_{a0} e^{-(k_1 + k_2)t}$
	$\frac{dC_b}{dt} = k_1 C_a$	$C_b = C_{b0} + \frac{k_1 C_{a0}}{k_2 + k_1} (1 - e^{-(k_1 + k_2)t})$
	$\frac{dC_c}{dt} = k_2 C_a$	$C_c = C_{a0} + C_{b0} + C_{c0} - C_a - C_b$

a PFR is q_R and the fresh feed rate is q_0 . With a fresh feed concentration of C_0 and a product concentration of C_2 , the composite reactor feed concentration C_1 and the recycle ratio R are

$$C_1 = \frac{C_0 + RC_2}{1 + R} \quad R = \frac{q_R}{q_0} \quad (7-62)$$

The change in concentration across the reactor becomes

$$\Delta C = C_1 - C_2 = \frac{C_2 - C_0}{1 + R} \quad (7-63)$$

Accordingly, the change in concentration (or in temperature) across the reactor can be made as small as desired by increasing the recycle ratio. Eventually, the reactor can become a well-mixed unit with essentially constant concentration and temperature, while substantial differences in composition will concurrently arise between the fresh feed inlet and the product withdrawal outlet, similar to a CSTR. Such an operation is useful for obtaining experimental data for analysis of rate

equations. In the simplest case, where the product is recycled without change in composition, the flow reactor equation at constant density is

$$\tau_{PFR} = (1 + R) \int_{C_{i0}}^{C_{if}} \frac{dC_i}{\sum v_j f_j} \quad (7-64)$$

Hence, recycling increases the residence time or reactor size required to achieve a given conversion, since $1 + R > 1$.

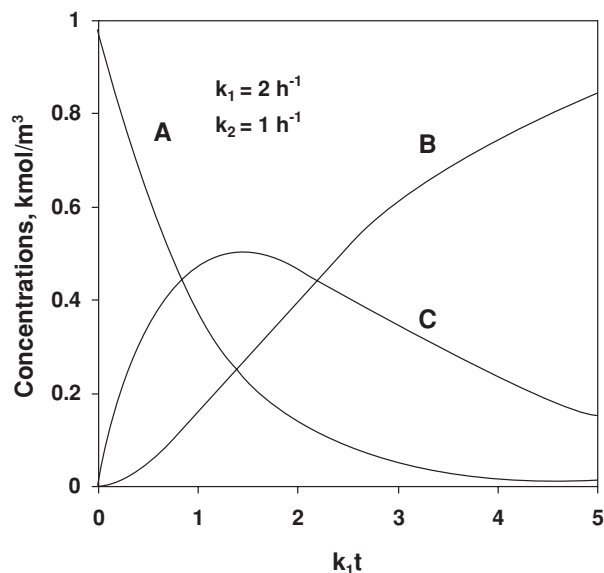
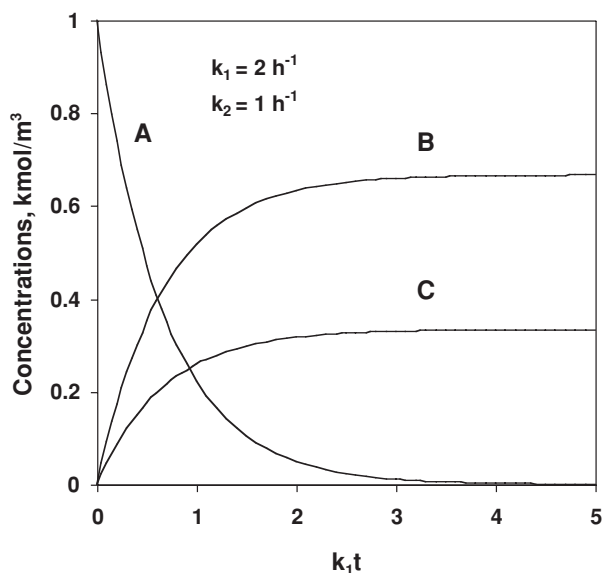
EXAMPLES FOR SOME SIMPLE REACTIONS

Table 7-2 and Figs. 7-3 and 7-4 show the analytical solution of the integrals for two simple first-order reaction systems in an isothermal constant-volume batch reactor or plug flow reactor. Table 7-3 shows the analytical solution for the same reaction systems in an isothermal constant-density CSTR.

Section 19 provides discussion about advantages and disadvantages of CSTRs versus PFR and BR for various reaction systems.

TABLE 7-3 Consecutive and Parallel First-Order Reactions in an Isothermal Constant-Volume Ideal CSTR

Reaction network	Material balances	Concentration profiles
$A \xrightarrow{1} B \xrightarrow{2} C$	$C_{a0} - C_a - \tau k_1 C_a = 0$	$C_a = \frac{C_{a0}}{1 + \tau k_1}$
	$C_{b0} - C_b + \tau(k_1 C_a - k_2 C_b) = 0$	$C_b = \frac{C_{b0}}{1 + \tau k_2} + \frac{\tau k_1 C_{a0}}{(1 + \tau k_1)(1 + \tau k_2)}$
	$C_{c0} - C_c + \tau k_2 C_b = 0$	$C_c = C_{a0} + C_{b0} + C_{c0} - C_a - C_b$
$A \xrightarrow{1} B$ $A \xrightarrow{2} C$	$C_{a0} - C_a - \tau(k_1 + k_2) C_a = 0$	$C_a = \frac{C_{a0}}{1 + \tau(k_1 + k_2)}$
	$C_{b0} - C_b + \tau k_1 C_a = 0$	$C_b = C_{b0} \frac{\tau k_1 C_{a0}}{1 + \tau(k_1 + k_2)}$
	$C_{c0} - C_c + \tau k_2 C_a = 0$	$C_c = C_{a0} + C_{b0} + C_{c0} - C_a - C_b$

FIG. 7-3 Concentration profiles for the reaction $A \rightarrow B \rightarrow C$.FIG. 7-4 Concentration profiles for the reaction $A \rightarrow B$ and $A \rightarrow C$.

KINETICS OF COMPLEX HOMOGENEOUS REACTIONS

Global or complex reactions are not usually well represented by mass action kinetics because the rate results from the combined effect of several simultaneous elementary reactions (each subject to mass action kinetics) that underlie the global reaction. The elementary steps include short-lived and unstable intermediate components such as free radicals, ions, molecules, transition complexes, etc.

The reason many global reactions between stable reactants and products have complex mechanisms is that these unstable intermediates have to be produced in order for the reaction to proceed at reasonable rates. Often simplifying assumptions lead to closed-form kinetic rate expressions even for very complex global reactions, but care must be taken when using these since the simplifying assumptions are valid over limited ranges of compositions, temperature, and pressure. These assumptions can fail completely—in that case the full elementary reaction network has to be considered, and no closed-form kinetics can be derived to represent the complex system as a global reaction.

Typical simplifying assumptions include these:

- *Pseudo-steady-state* approximation for the unstable intermediate; i.e., the concentration of these does not change during reaction
- Equilibrium for certain fast reversible reactions and completion of very fast irreversible steps
- *Rate-determining step(s)*; i.e., the global reaction rate is determined by the rate(s) of the slowest step(s) in the reaction network composing the overall or global reaction

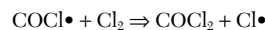
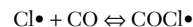
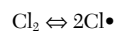
These simplifying assumptions allow elimination of some reaction steps, and representation of free radical and short-lived intermediates concentrations in terms of the concentration of the stable measurable components, resulting in complex non-mass action rate expressions.

Complex reactions can proceed through *chain* or *nonchain* mechanisms. In a *chain reaction*, the active unstable components are produced in an *initiation* step and are repeatedly regenerated through *propagation* steps, and only a small fraction of these are converted to stable components through a *termination* step. Free radicals are examples of such unstable components frequently encountered in chain reactions: free radicals are molecular fragments having one or more unpaired electrons, are usually short-lived (milliseconds), and are highly reactive. They are detectable spectroscopically, and some have been isolated. They occur as initiators and intermediates in such

basic phenomena as oxidation, combustion, photolysis, and polymerization. Several examples of free radical mechanisms possessing non-integral power law or hyperbolic rate equations are cited below. In a *nonchain reaction*, the unstable intermediate, such as an *activated complex* or *transition state complex*, reacts further to produce the products, and it is not regenerated through propagation but is continually made from reactants in stoichiometric quantities.

CHAIN REACTIONS

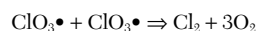
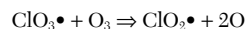
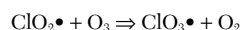
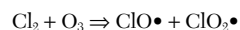
Phosgene Synthesis The global reaction $\text{CO} + \text{Cl}_2 \Rightarrow \text{COCl}_2$ proceeds through the following free radical mechanism:



Assuming the first two reactions are in equilibrium, expressions are found for the concentrations of the free radicals $\text{Cl}\cdot$ and $\text{COCl}\cdot$ in terms of the species CO , Cl_2 , and COCl_2 , and when these are substituted into the mass action rate expression of the third reaction, the rate becomes

$$r_{\text{COCl}_2} = k(\text{CO})(\text{Cl}_2)^{3/2} \quad (7-65)$$

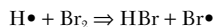
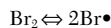
Ozone Conversion to Oxygen in Presence of Chlorine The global reaction $2\text{O}_3 \xrightarrow{\text{Cl}_2} 3\text{O}_2$ in the presence of Cl_2 proceeds through the following sequence:



The chain carriers $\text{ClO}\cdot$, $\text{ClO}_2\cdot$, and $\text{ClO}_3\cdot$ are assumed to attain pseudo-steady state. Then,

$$r_{\text{O}_3} = k(\text{Cl}_2)^{1/2}(\text{O}_3)^{3/2} \quad (7-66)$$

Hydrogen Bromide Synthesis The global reaction $\text{H}_2 + \text{Br}_2 \Rightarrow 2\text{HBr}$ proceeds through the following chain of reactions:

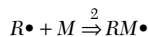


Assuming pseudo-steady state for the concentrations of the free radicals $\text{H}\cdot$ and $\text{Br}\cdot$, the global rate equation becomes

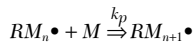
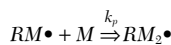
$$r_{\text{HBr}} = \frac{k_1(\text{H}_2)(\text{Br}_2)^{1/2}}{k_2 + \text{HBr}/\text{Br}_2} \quad (7-67)$$

Chain Polymerization For free radical polymerization, the following generic mechanism can be postulated:

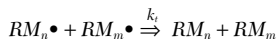
Initiation:



Propagation:



Termination:



The rates of formation of the free radicals $R\cdot$ and $M\cdot$ reach pseudo-steady states, resulting in the following polymerization rate:

$$r_p = k_p(M)(M^*) = k_p \left(\frac{k_i}{k_t} \right)^{1/2} (M)(I)^{1/2} \quad (7-68)$$

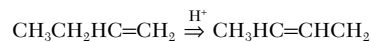
NONCHAIN REACTIONS

Nonchain reactions proceed through an active intermediate to the products. Many homogeneous nonchain reactions are also homogeneously catalyzed reactions, discussed below.

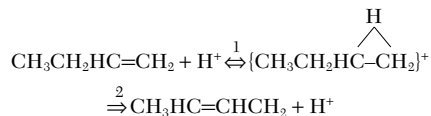
HOMOGENEOUS CATALYSIS

Homogeneous catalysts proceed through an activated or transition state complex between reactant(s) and catalysts, which decomposes into products. Homogeneous catalysts are dissolved in the homogeneous reaction mixture and include among others acids/bases, metal salts, radical initiators, solvents, and enzymes.

Acid-Catalyzed Isomerization of Butene-1 Butene-1 isomerizes to butene-2 in the presence of an acid according to the global reaction



Even though this appears to be a monomolecular reaction, it is not, as it proceeds through the following mechanism:



Assuming reaction 1 is in equilibrium, the reaction rate is

$$r = k_2 K_1 [\text{H}^+] [\text{CH}_3\text{CH}_2\text{HC}=\text{CH}_2] \quad (7-69)$$

Enzyme Kinetics Enzymes are homogeneous catalysts for cellular and enzymatic reactions. The enzyme E and the reactant S are

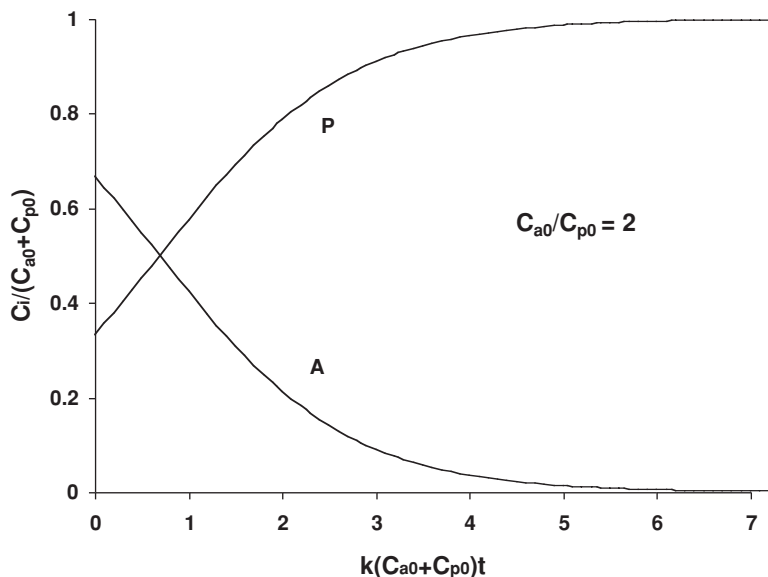
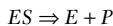
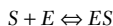


FIG. 7-5 Product concentration profile for the autocatalytic reaction $A + P \Rightarrow 2P$ with rate $r = kC_a C_p$.

7-16 REACTION KINETICS

assumed to form a complex ES that then dissociates into product P and releases the enzyme:



Assuming equilibrium for the first step results in the following rate, developed by Michaelis and Menten [*Biochem. Zeit.*, **49**:333 (1913)] and named Michaelis-Menten kinetics,

$$r_p = -r_s = \frac{k(S)}{K_m + (S)} \quad (7-70)$$

Here K_m is the inverse of the equilibrium constant for the first reaction.

AUTOCATALYSIS

In an autocatalytic reaction, a reactant reacts with a product to make more product. For the reaction to proceed, therefore, product must be present

initially in a batch or in the feed of a continuous reactor. Examples are cell growth in fermentation and combustion of fuels. For instance, the irreversible elementary reaction $A + P \Rightarrow 2P$ has the mass action kinetics

$$r = kC_a C_p \quad (7-71)$$

For an ideal batch reactor (see, e.g., Steinfeld, Francisco, and Hase, *Chemical Kinetics and Dynamics*, Prentice-Hall, 1989):

$$\frac{dC_a}{dt} = -kC_a C_p \quad \frac{dC_p}{dt} = kC_a C_p \quad C_a + C_p = C_{a0} + C_{p0} \quad (7-72)$$

Integration results in the following concentration profile:

$$C_p = \frac{C_{a0} + C_{p0}}{1 + (C_{a0}/C_{p0})e^{-k(C_{a0} + C_{p0})t}} \quad C_a = C_{a0} + C_{p0} - C_p \quad (7-73)$$

Figure 7-5 illustrates the dimensionless concentration profile for the reactant A and product P , $C_i/(C_{a0} + C_{p0})$, for $C_{a0}/C_{p0} = 2$, indicative of a maximum rate at the inflexion point (maximum in slope of the concentration-time curve), typical to autocatalytic reactions.

INTRINSIC KINETICS FOR FLUID-SOLID CATALYTIC REACTIONS

There are a large number of fluid-solid catalytic reactions, mostly gas-solid, including catalytic cracking, oxidation of polluting gases in automotive and power generation catalytic converters, partial oxidation synthesis reactions such as HCN synthesis, chemical vapor deposition, etc. (see, e.g., Sec. 19 for more examples). Examples of solid catalysts include, among others, supported metals, transition metal oxides and sulfides, solid acids and bases, and immobilized homogeneous catalysts and enzymes. Solid catalysts can be a fine powder (suspended in a liquid or fluidized by a flowing gas), cylindrical, spherical, and more-complex-shaped particles (in a packed bed), a thin layer of active components (on the walls of a monolith or a foam) and gauzes. The solid catalyst can be porous with active component distributed throughout the particle volume, or nonporous with active component present on the exposed catalyst external surface alone.

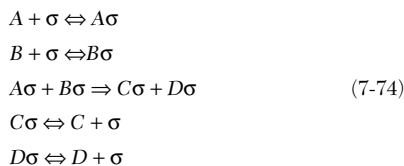
The analysis of Langmuir [*J. Am. Chem. Soc.* **40**:1361 (1918)] and Hinshelwood (*Kinetics of Chemical Change*, Oxford, 1940) form the basis for the simplified treatment of kinetics on heterogeneous catalysts. For a solid catalyzed reaction between gas phase reactants A and B , the postulated mechanism consists of the following steps in series:

1. The reactants from the gas adsorb to bond to active sites on the catalyst surface as molecules or dissociated atoms. The rate of adsorption is proportional to the partial pressure of reactants and to the fraction of uncovered surface sites ϑ_v . More than one type of active site can be present. The adsorption isotherms such as the Langmuir isotherm relate the partial pressure of an adsorbed species to its surface coverage, and the form of this relationship is indicative of the type of adsorption process taking place (see, for more details, Masel, *Chemical Kinetics and Catalysis*, Wiley, 2001).

2. The adsorbed species react on the surface to form adsorbed products. The rate of reaction between adsorbed species is proportional to their adsorbed concentrations on the surface.

3. The adsorbed products desorb into the gas. The rate of desorption of species A is proportional to the fraction of the surface covered by A , ϑ_a .

For instance, for the simple irreversible reaction $A + B \Rightarrow C + D$, the postulated mechanism is



$A\sigma$, $B\sigma$, $C\sigma$, and $D\sigma$ above are adsorbed species on the catalyst surface, and σ is an available active site. We will consider a variety of possible scenarios for this simple solid-catalyzed system. Note that the intrinsic specific reaction rate for such systems is often expressed on a unit mass catalyst basis (r_m) instead of unit reaction volume basis (r_v), and the latter is related to the former through the catalyst loading (mass catalyst/reaction volume) or bed density:

$$r_v = \frac{r_m M_{\text{cat}}}{V} = r_m \rho_B \quad (7-75)$$

ADSORPTION EQUILIBRIUM

Assuming equilibrium for all adsorption steps (e.g., the surface reaction is rate-limiting), the net rates of adsorption of reactants and product are all zero.

$$r_i = k_i p_i \vartheta_v - k_{-i} \vartheta_i \Rightarrow 0 \quad i = a, b, c, d \quad (7-76)$$

A material balance on all sites yields

$$\vartheta_v = 1 - \vartheta_a - \vartheta_b - \vartheta_c - \vartheta_d \quad (7-77)$$

and solving for the surface coverages gives

$$\begin{aligned} \vartheta_a &= \left(\frac{k_a}{k_a - a} \right) p_a \vartheta_v = K_a p_a \vartheta_v & \vartheta_b &= \left(\frac{k_b}{k_b - b} \right) p_b \vartheta_v = K_b p_b \vartheta_v \\ \vartheta_c &= \left(\frac{k_c}{k_c - c} \right) p_c \vartheta_v = K_c p_c \vartheta_v & \vartheta_d &= \left(\frac{k_d}{k_d - d} \right) p_d \vartheta_v = K_d p_d \vartheta_v \end{aligned} \quad (7-78)$$

The fraction of surface not covered is

$$\vartheta_v = \frac{1}{1 + K_a p_a + K_b p_b + K_c p_c + K_d p_d} \quad (7-79)$$

In the denominator, terms may be added for adsorbed inerts (e.g., $K_i p_i$) that may be present, and analogous expressions for the other participants. The rate of reaction or the rate-determining step is that between adsorbed reactant species:

$$r = k_p a p_b \vartheta_c^2 = \frac{k_p a p_b}{(1 + K_a p_a + K_b p_b + K_c p_c + K_d p_d)^2} \quad (7-80)$$

DISSOCIATION

A diatomic molecule A_2 may adsorb dissociatively as atoms



with the result

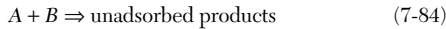
$$\theta_a = \frac{\sqrt{K_a p_a}}{1 + \sqrt{K_a p_a} + K_b p_b + \dots} = \sqrt{K_a p_a} \theta_v \tag{7-82}$$

and the rate-determining step and its rate are



DIFFERENT SITES

When A and B adsorb on chemically different sites σ_1 and σ_2 , the rate of the reaction, with surface reaction controlling,



is

$$r = \frac{k p_a p_b}{(1 + K_a p_a)(1 + K_b p_b)} \tag{7-85}$$

CHANGE IN NUMBER OF MOLES

When the numbers of moles of product is larger than that of the reactants, extra sites are required:

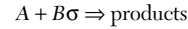


and the rate is

$$r = k \left(\theta_a \theta_v - \frac{\theta_m \theta_n}{K} \right) = \left(p_a - \frac{p_m p_n}{K} \right) \theta_v^2 = \frac{k(p_a - p_m p_n / K)}{(1 + K_a p_a + K_m p_m + K_n p_n)^2} \tag{7-88}$$

REACTANT IN THE GAS PHASE

When A in the gas phase reacts directly with adsorbed B :

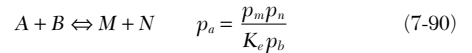


$$r = k p_a \theta_b = k p_a p_b \theta_v = \frac{k p_a p_b}{1 + \sum K_i p_i} \tag{7-89}$$

This mechanism is called the *Ely-Rideal kinetics*.

CHEMICAL EQUILIBRIUM IN GAS PHASE

When A is not in adsorptive equilibrium but it is in chemical equilibrium in the gas phase according to



this expression is substituted for p_a wherever it appears in the rate equation. If the rate-determining step is the surface reaction between adsorbed species, then

$$r = k p_a p_b \theta_v^2 = \frac{k p_m p_n / K_e}{1 + K_a (p_m p_n / K_e p_b) + K_b p_b + K_m p_m + K_n p_n} \tag{7-91}$$

Table 7-4 summarizes some examples of reactions where all substances are in adsorptive equilibrium and the surface reaction controls the rate. In Table 7-5, substance A is not in adsorptive equilibrium, and its adsorption rate is controlling. Details of the derivations of these and some other equations are presented by Yang and Hougen [*Chem. Eng.*

TABLE 7-4 Surface-Reaction Controlling.

Adsorptive equilibrium maintained for all participants.

Reaction	Special condition	Basic rate equation	Driving force	Adsorption term
1. $A \rightarrow M + N$ $A \rightarrow M + N$ $A \rightarrow M + N$	General case Sparsely covered surface Fully covered surface	$r = k \theta_a$ $r = k \theta_a$ $r = k \theta_a$	p_a p_a 1	$1 + K_a p_a + K_m p_m + K_n p_n$ 1 1
2. $A \rightleftharpoons M$		$r = k_1 \theta_a - k_{-1} \theta_m$	$p_a - \frac{p_m}{K}$	$1 + K_a p_a + K_m p_m$
3. $A \rightleftharpoons M + N$	Adsorbed A reacts with vacant site	$r = k_1 \theta_a \theta_v - k_{-1} \theta_m \theta_v$	$p_a - \frac{p_m p_n}{K}$	$(1 + K_a p_a + K_m p_m + K_n p_n)^2$
4. $A_2 \rightleftharpoons M$	Dissociation of A_2 upon adsorption	$r = k_1 \theta_a^2 - k_{-1} \theta_m \theta_v$	$p_a - \frac{p_m}{K}$	$(1 + \sqrt{K_a p_a} + K_m p_m)^2$
5. $A + B \rightarrow M + N$ $A + B \rightarrow M + N$	Adsorbed B reacts with A in gas but not with adsorbed A	$r = k \theta_a \theta_b$ $r = k p_a \theta_b$	$p_a p_b$ $p_a p_b$	$(1 + K_a p_a + K_b p_b + K_m p_m + K_n p_n)^2$ $1 + K_a p_a + K_b p_b + K_m p_m + K_n p_n$
6. $A + B \rightleftharpoons M$		$r = k_1 \theta_a \theta_b - k_{-1} \theta_m \theta_v$	$p_a p_b - \frac{p_m}{K}$	$(1 + K_a p_a + K_b p_b + K_m p_m)^2$
7. $A + B \rightleftharpoons M + N$		$r = k_1 \theta_a \theta_b - k_{-1} \theta_m \theta_n$	$p_a p_b - \frac{p_m p_n}{K}$	$(1 + K_a p_a + K_b p_b + K_m p_m + K_n p_n)^2$
8. $A_2 + B \rightleftharpoons M + N$	Dissociation of A_2 upon adsorption	$r = k_1 \theta_a^2 \theta_b - k_{-1} \theta_m \theta_n \theta_v$	$p_a p_b - \frac{p_m p_n}{K}$	$(1 + \sqrt{K_a p_a} + K_b p_b + K_m p_m + K_n p_n)^3$

NOTE: The rate equation is:

$$r = \frac{k (\text{driving force})}{\text{adsorption term}}$$

When an inert substance I is adsorbed, the term $K_I p_I$ is to be added to the adsorption term.

SOURCE: From Walas, *Reaction Kinetics for Chemical Engineers*, McGraw-Hill, 1959; Butterworths, 1989.

7-18 REACTION KINETICS

TABLE 7-5 Adsorption-Rate Controlling (Rapid Surface Reaction)

Reaction	Special condition	Basic rate equation	Driving force	Adsorption term
1. $A \rightarrow M + N$		$r = kp_a\theta_c$	p_a	$1 + \frac{K_a p_m p_n}{K} + K_m p_m + K_n p_n$
2. $A \rightleftharpoons M$		$r = k \left(p_a \theta_c - \frac{\theta_a}{K_a} \right)$	$p_a - \frac{p_m}{K}$	$1 + \frac{K_a p_m}{K} + K_m p_m$
3. $A \rightleftharpoons M + N$		$r = k \left(p_a \theta_c - \frac{\theta_a}{K_a} \right)$	$p_a - \frac{p_m p_n}{K}$	$1 + \frac{K_a p_m p_n}{K} + K_m p_m + K_n p_n$
4. $A_2 \rightleftharpoons M$	Dissociation of A_2 upon adsorption	$r = k \left(p_a \theta_c^2 - \frac{\theta_a^2}{K_a} \right)$	$p_a - \frac{p_m}{K}$	$\left(1 + \sqrt{\frac{K_a p_m}{K} + K_m p_m} \right)^2$
5. $A + B \rightarrow M + N$	Unadsorbed A reacts with adsorbed B	$r = kp_a\theta_c$	p_a	$1 + \frac{K_a p_m p_n}{K p_b} + K_b p_b + K_m p_m + K_n p_n$
6. $A + B \rightleftharpoons M$		$r = k \left(p_a \theta_c - \frac{\theta_a}{K_a} \right)$	$p_a - \frac{p_m}{K p_b}$	$1 + \frac{K_a p_m}{K p_b} + K_b p_b + K_m p_m$
7. $A + B \rightleftharpoons M + N$		$r = k \left(p_a \theta_c - \frac{\theta_a}{K_a} \right)$	$p_a - \frac{p_m p_n}{K p_b}$	$1 + \frac{K_a p_m p_n}{K p_b} + K_b p_b + K_m p_m + K_n p_n$
8. $A_2 + B \rightleftharpoons M + N$	Dissociation of A_2 upon adsorption	$r = k \left(p_a \theta_c^2 - \frac{\theta_a^2}{K_a} \right)$	$p_a - \frac{p_m p_n}{K p_b}$	$\left(1 + \sqrt{\frac{K_a p_m p_n}{K p_b} + K_b p_b + K_m p_m + K_n p_n} \right)^2$

NOTES: The rate equation is:

$$r = \frac{k (\text{driving force})}{\text{adsorption term}}$$

Adsorption rate of substance A is controlling in each case. When an inert substance I is adsorbed, the term $K_I p_I$ is to be added to the adsorption term.

SOURCE: From Walas, *Reaction Kinetics for Chemical Engineers*, McGraw-Hill, 1959; Butterworths, 1989.

Prog. **46**:146 (1950)], Walas (*Reaction Kinetics for Chemical Engineers*, McGraw-Hill, 1959; Butterworths, 1989, pp. 153–164), and Rase (*Chemical Reactor Design for Process Plants*, vol. 1, Wiley, 1977, pp. 178–191).

NO RATE-CONTROLLING STEP

All the relations developed above assume that only one step is controlling. In a reaction system, changing the operating conditions may shift the control from one step to another. It is therefore also obvious that at certain conditions there is no single step controlling. In that case all the reactions and their respective rates have to be considered, and the adsorbed species cannot be eliminated from the rate expressions to obtain a single closed-form kinetic rate.

LIQUID-SOLID CATALYTIC REACTIONS

An analogous treatment for liquid-solid catalysis can be derived, with partial pressures replaced by liquid volumetric concentrations. Otherwise all the analyses hold.

BIOCATALYSIS

Biochemical reactions such as *aerobic* and *anaerobic fermentations* occur in the presence of living organisms or *cells*, such as bacteria, algae, and yeast. These reactions can be considered as *biocatalyzed* by the organism. Thus in a typical bioreactor a *substrate* (such as glucose) is fed into the *fermenter* or *bioreactor* in the presence of an initial amount of cells. The desired product can be the cells themselves or a secreted chemical called a *metabolite*. In either case the cells multiply in the presence of the substrate, and the rate of production of cells is proportional to the concentration of the cells—hence this process is autocatalytic. In a batch reactor with ample

supply of substrate, this results in *exponential growth* of the culture. A typical cell or biomass growth rate function, called the *Monod kinetics*, is identical in form to the Michaelis-Menten enzyme kinetics in Eq. (7-70):

$$\mu = \frac{\mu_{\max} C_s}{K_s + C_s} \quad (7-92)$$

In Eq. (7-92) μ is the *specific growth rate* of the culture. It is measured in units of reciprocal time (h^{-1}). Growth rate μ is related to the *volumetric growth rate* r_x of the culture: $r_x = C_A \mu$. This means that the true unit of μ is, e.g., (g biomass formed/h)/(g biomass present), where *g biomass* is the *dry-weight* (DW) of the biomass, obtained after evaporation of the water content of the cell (which constitutes about 80 percent of the *wet biomass weight*). Similarly C_s has the unit, e.g., (g DW)/(L medium volume). The variable C_s in Eq. (7-92) is the concentration of the *limiting substrate* in the medium (g/L). There are many substrates (including micronutrients) in the medium, but there is usually just one that determines the specific growth rate. This substrate is often a sugar (most likely glucose) but it could also be a metal ion (Mg^{2+} etc.), or PO_4^{3-} , NH_4^+ , . . . , or perhaps a hormone. The limiting substrate may easily change during a fermentation, and then the rate expression will change.

The two parameters in Eq. (7-92) are the *maximum specific growth rate* μ_{\max} (h^{-1}) and the *saturation constant* K_s (g substrate/L). The value of K_s is obtained as the substrate concentration at which $\mu = 1/2 \mu_{\max}$ (see Fig. 7-6). The form of Eq. (7-92) is entirely empirical, but it incorporates two important features: (1) At high substrate concentration the whole cell machinery is involved in cell synthesis, and the specific growth rate reaches a maximum μ_{\max} ; (2) at low substrate concentration formation of biomass is a first-order rate process (as in any other chemical reaction) and $\mu \rightarrow (\mu_{\max}/K_s)C_s$. Note that for many commonly used microorganisms K_s is much

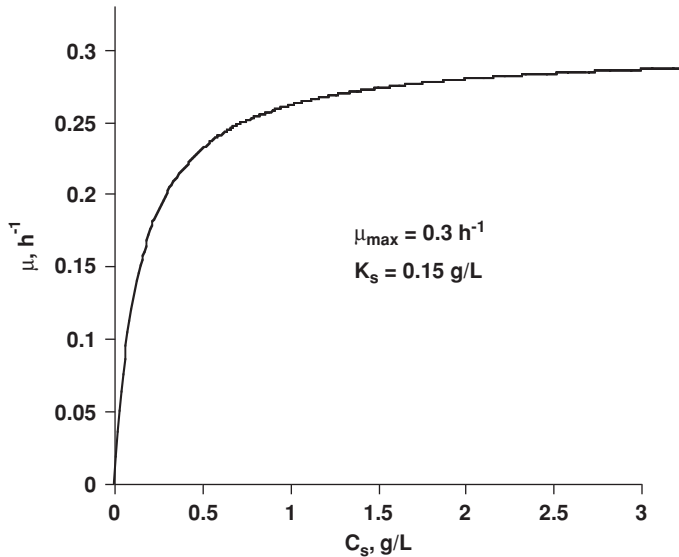


FIG. 7-6 The effect of substrate concentration on specific growth rate.

smaller than the substrate concentration C_s . Thus in batch cultivations K_s is several orders of magnitude smaller than C_s until the very end of the batch, and this is what gives the well-known *exponential growth* [see Eq. (7-93)]. Equation (7-93) applies for batch cultures after an initial *lag phase* when cell machinery is synthesized. Typical values for K_s are 150 mg/L (*Saccharomyces cerevisiae*), 5 to 10 mg/L (lactic bacteria and *E. coli*), and less than 1 mg/L (filamentous fungi).

$$\frac{dC_x}{dt} = \mu C_x \quad C_x = C_{x0} e^{\mu t} \quad (7-93)$$

Equation (7-93) may have to be modified by subtraction of a *death-rate* term $\mu_d C_x$. μ_d may well increase during the batch fermentation in which case the net growth rate of (viable) cells eventually becomes negative, and the concentration of (viable) cells will start to decrease.

FLUID-SOLID REACTIONS WITH MASS AND HEAT TRANSFER

GAS-SOLID CATALYTIC REACTIONS

The Langmuir-Hinshelwood mechanism of adsorption/reaction described above allowed us to relate the gas concentrations and partial pressures in the vicinity of the catalyst surface to the adsorbed species concentration at the active sites, which in turn determined the surface reaction rates. In practice, two additional mass-transfer processes may need to be considered:

1. Diffusion to and from the bulk gas to the external catalyst surface, represented as an external mass-transfer process across a film or boundary layer concentration gradient. For nonporous catalyst this is the only mass-transfer step.

2. Diffusion to and from the catalyst external surface through pores in a porous catalyst particle to active sites inside the catalyst particle where the adsorption and reaction occur, represented as intraparticle diffusion and modeled as a diffusion-reaction process.

External Mass Transfer In a reactor, the solid catalyst is deposited on the surface of narrow tubes (such as monolith or foams), is packed as particles in a tube, or is suspended in slurry or in a fluidized bed as fine particles. For these systems, the bulk concentration of the gas phase approaches that on the catalyst surface if the mass-transfer rate from bulk to surface is substantially larger than the reaction rates on the surface. This, however, is often not the case. The mechanism of mass transfer and reaction on the external catalyst surface includes the following consecutive steps:

1. Mass transfer of gas reactants from the bulk gas to the solid catalyst surface, also called external mass transfer
2. Adsorption, reaction on the surface, and desorption of products, e.g., Langmuir-Hinshelwood kinetics
3. Mass transfer of products from the catalyst surface to the bulk gas

At steady state all these rates are equal.

For example, for a first-order irreversible reaction $A \Rightarrow B$, the rate of mass transfer equals the rate of intrinsic reaction:

$$k_s a_s (C_a - C_{as}) = k C_{as} \quad (7-94)$$

Here a_s is, for instance, the external particle surface area/volume of reactor. Eliminating the surface concentration C_{as} in terms of the observable bulk gas concentration C_a yields the overall specific rate of consumption of A:

$$r_{\text{obs}} = k C_a = \frac{C_a}{1/(k_s a_s) + 1/k} \quad (7-95)$$

$$k_{\text{obs}} = \frac{1}{1/(k_s a_s) + 1/k}$$

Hence the observable overall rate constant k_{obs} is actually a combination of the mass-transfer coefficient and the intrinsic rate

7-20 REACTION KINETICS

coefficient; or in terms of resistances (in units of time) the overall resistance is the sum of the mass transfer and intrinsic kinetic resistance. For this first-order rate case, the overall behavior remains first order in bulk gas concentration. The two limiting cases are mass transfer and reaction control, respectively:

$$\begin{aligned} k_{\text{obs}} = k_s a_s \quad \text{and} \quad r_{\text{obs}} = k_s a_s C_a \quad \text{for } k_s a_s \ll k \quad \text{Mass transfer control} \\ k_{\text{obs}} = k \quad \text{and} \quad r_{\text{obs}} = k C_a \quad \text{for } k_s a_s \gg k \quad \text{Kinetic control} \end{aligned} \quad (7-96)$$

The mass-transfer coefficient depends on the geometry of the solid surface, on the hydrodynamic conditions in the vicinity of the catalyst (which are a function, e.g., of the reactor type, geometry, operating conditions, flow regime), and it also depends on the diffusivity of the gas species. Correlations for the mass-transfer coefficient are a large topic and outside the scope of this section. For more details see Bird, Stewart, and Lightfoot, *Transport Phenomena*, 2d ed., John Wiley & Sons, New York, 2002, and relevant sections in this handbook. For non-first-order kinetics a closed-form relationship such as the series of resistances cannot always be derived, but the steady-state assumption of the consecutive mass and reaction steps still applies.

Intraparticle Diffusion As indicated above, the larger the catalyst surface area per unit reaction volume a_s , the larger the overall reaction rate. For a fixed mass of catalyst, decreasing the particle size increases the total external surface area available for the reaction. Another way to increase the surface area is by providing a porous catalyst with lots of internal surface area. The internal structure of the catalyst determines how accessible these internal sites are to the gas-phase reactant and how easily can the products escape back to the gas. The analysis is based on the pseudo-homogeneous reaction diffusion equation, with the gas reactant diffusing through the pores and reacting at active sites inside the catalyst particle. For a first-order irreversible reaction of species A in an infinite slab geometry, the diffusion-reaction equations describe the decreasing reactant concentration from the external surface to the center of the slab:

$$\begin{aligned} D_{ea} \frac{d^2 C_{ay}}{dy^2} - k C_{ay} = 0 \quad C_{ay}(L) = C_{as} \\ \frac{dC_{ay}}{dy} (0) \end{aligned} \quad (7-97)$$

The concept of effectiveness factor has been developed to calculate the overall reaction rate in terms of the concentration at the external surface C_{as} :

$$r = \eta k C_{as} \quad (7-98)$$

Hence the effectiveness factor is the ratio of the actual rate to that if the reactions were to occur at the external surface concentration, i.e., in absence of intraparticle diffusion resistance:

$$\eta = \frac{(1/L) \int_0^L r(C_{ay}) dy}{r(C_{as})} = \frac{\text{rate with pore diffusion resistance}}{\text{rate at external surface conditions}} \quad (7-99)$$

The effectiveness factor can be written as a function of a dimensionless independent variable called the Thiele modulus, which for a first-order reaction is defined below together with the corresponding effectiveness factor derived by integration of the corresponding diffusion-reaction equation (7-97):

$$\phi_{\text{slab}} = L \sqrt{\frac{k}{D_{ea}}} \quad \eta = \frac{\tanh \phi_{\text{slab}}}{\phi_{\text{slab}}} \quad (7-100)$$

Since the model is pseudo-homogeneous, there is no distinction

between the gas-filled pores and the solid parts of the particle. For most catalysts (except for straight channel monoliths), the diffusion path is not straight and has varying cross section. Hence, the effective diffusivity of A is defined based on the catalyst internal structure and the gas diffusivity of A in the gas mixture as follows:

$$D_{ea} = \frac{\epsilon_s}{\tau} D_a \quad (7-101)$$

The parameters that describe the pore structure are the porosity ϵ_s , accounting for the fact that diffusion only occurs through the gas-filled part of the particle, and the tortuosity τ accounting for the effect of diffusion path length and contraction/expansion of pores along the diffusion path. The diffusion regime depends on the diffusing molecule, pore size, and operating conditions (concentration, temperature, pressure), and this can be visualized in Fig. 7-7. As indicated, the effective diffusion coefficient ranges over many orders of magnitude from very low values in the configurational regime (e.g., in zeolites) to high values in the regular regime.

There is a large body of literature that deals with the proper definition of the diffusivity used in the intraparticle diffusion-reaction model, especially in multicomponent mixtures found in many practical reaction systems. The reader should consult references, e.g., Bird, Stewart, and Lightfoot, *Transport Phenomena*, 2d ed., John Wiley & Sons, New York, 2002; Taylor and Krishna, *Multicomponent Mass Transfer*, Wiley, 1993; and Cussler, *Diffusion Mass Transfer in Fluid Systems*, Cambridge University Press, 1997.

The larger the characteristic length L , the larger the Thiele modulus, the smaller the effectiveness factor, and the steeper the reactant concentration profile in the catalyst particle. A generalized characteristic length definition V_p/S_{px} (particle volume/external particle surface area) brings together the η - ϕ curves for a variety of particle shapes, as illustrated in Table 7-6 and Fig. 7-8 for for slabs, cylinders, and spheres. Here I_0 and I_1 are the corresponding modified Bessel functions of the first kind.

Further generalization of the Thiele modulus and effectiveness factor for a general global reaction and various shapes is

$$\phi = \frac{(V_p/S_{px}) r_a(C_{as})}{\sqrt{\frac{1}{2} \int_{C_{ae}}^{C_{as}} D_{ea}(C_{ay}) r_a(C_{ay}) dC_{ay}}} \quad (7-102)$$

In Eq. (7-102) component A is the limiting reactant. For example, for an n th-order irreversible reaction

$$\phi = \frac{V_p}{S_{px}} \sqrt{\frac{(n+1) k C_{as}^{n-1}}{2 D_{ea}}} \quad (7-103)$$

This generalized Thiele modulus works well with the effectiveness factors for low and high values of the Thiele modulus, but it is not as accurate for intermediate values. However, these differences are not significant, given the uncertainties associated with measuring some of the other key parameters that go into the calculation of the Thiele modulus, e.g., the effective diffusivity and the intrinsic rate constant.

Effect of Intraparticle Diffusion on Observed Order and Activation Energy Taking the n th-order reaction case in the limit of intraparticle diffusion control, i.e., large Thiele modulus, the effectiveness factor is

$$\eta = \frac{1}{\phi} \quad (7-104)$$

the observed rate is

$$r_{\text{obs}} = \eta r = \frac{S_{px}}{V_p} \sqrt{\frac{2 D_{ea} k}{(n+1)}} C_{as}^{(n+1)/2} \quad (7-105)$$

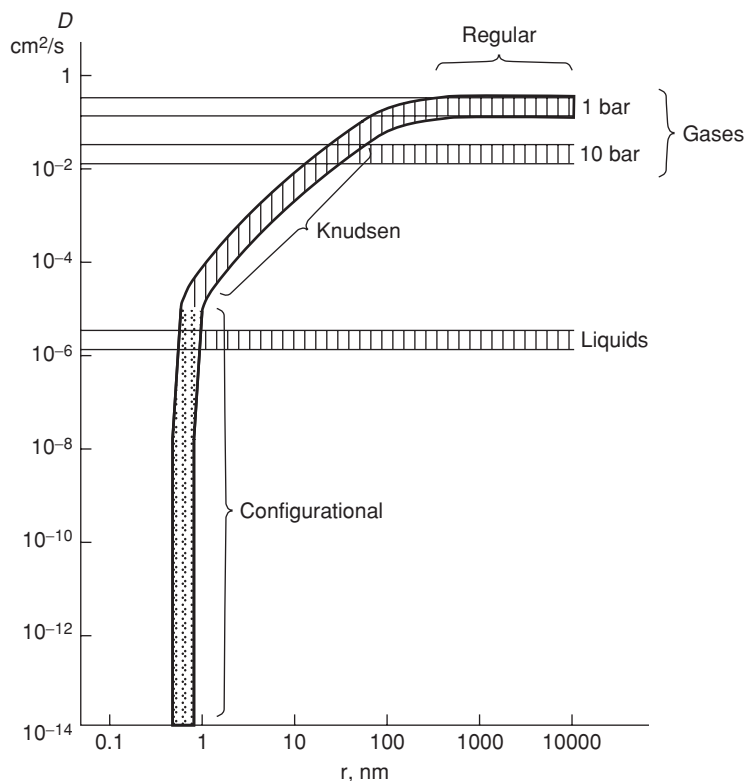


FIG. 7-7 Diffusion regimes in heterogeneous catalysts. [From Weisz, *Trans. Fara. Soc.* **69**: 1696–1705 (1973); Froment and Bischoff, *Chemical Reactor Analysis and Design*, Wiley, 1990, Figure 3.5.1-1.]

and the observed rate constant is

$$k_{\text{obs}} = \eta k = \frac{S_{px}}{V_p} \sqrt{\frac{2}{n+1} D_{\text{eff}} e^{(E_D/RT)} k_0 e^{(E/RT)}} \quad (7-106)$$

Hence, the observed order and activation energy differ from those of the intrinsic n th-order kinetics:

$$n_{\text{obs}} = \frac{n+1}{2} \quad E_{\text{obs}} = \frac{E + E_D}{2} \approx \frac{E}{2} \quad (7-107)$$

Here E_D is the activation energy for diffusion.

TABLE 7-6 Effectiveness Factors for Different Shapes for a First-Order Reaction

Shape	V_p/S_{px}	Effectiveness factor η
Infinite slab	R	$\frac{\tanh \phi}{\phi}$
Infinite cylinder	$R/2$	$\frac{I_1(2\phi)}{\phi I_0(2\phi)}$
Sphere	$R/3$	$\frac{1}{\phi} \left(\frac{3}{\tanh 3\phi} - \frac{1}{\phi} \right)$

The observed and intrinsic reaction order is the same under intraparticle diffusion control only for a first-order reaction. Weisz and Prater [“Interpretation of Measurements in Experimental Catalysis,” *Adv. Catal.* **6**: 144 (1954)] developed general estimates for the observed order and activation energy over the entire range of ϕ :

$$n_{\text{obs}} = n + \frac{n-1}{2} \frac{d \ln \eta}{d \ln \phi} \quad E_{\text{obs}} = E + \frac{E - E_D}{2} \frac{d \ln \eta}{d \ln \phi} \quad (7-108)$$

Weisz and Prater [“Interpretation of Measurements in Experimental Catalysis,” *Adv. Catal.* **6**: 144 (1954)] also developed a general criterion for diffusion limitations, which can guide the lab analysis of rate data:

$$\text{If } \Phi = \left(\frac{3V_p}{S_{px}} \right)^2 \frac{r_{\text{obs}}}{D_{\text{eff}} C_{\text{as}}} \gg 1 \text{ then diffusion-limited} \\ \ll 1 \text{ then no diffusional resistance} \quad (7-109)$$

Effect of Intraparticle Diffusion for Reaction Networks

For multiple reactions, intraparticle diffusion resistance can also affect the observed selectivity and yield. For example, for consecutive reactions intraparticle diffusion resistance reduces the yield of the intermediate (often desired) product if both reactions have the same order. For parallel reactions diffusion resistance reduces the selectivity to the higher-order reaction. For more details see, e.g., Carberry, *Chemical and Catalytic Reaction Engineering*, McGraw-Hill, 1976; and Levenspiel, *Chemical Reaction Engineering*, 3d ed., Wiley, 1999.

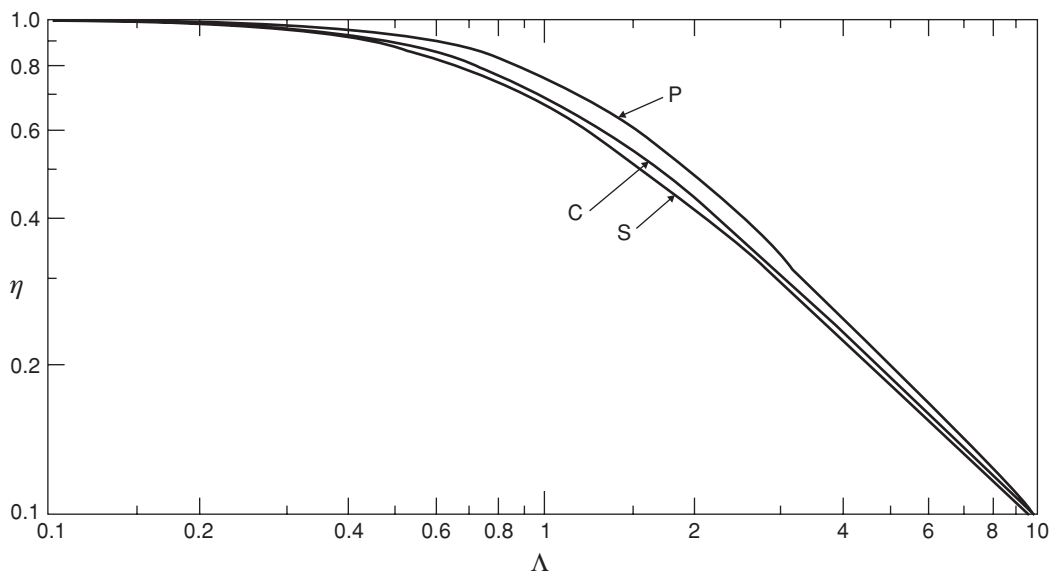


FIG. 7-8 Effectiveness factors for a slab (P), a cylinder (C), and a sphere (S). [Adapted from Fig. 1 in Aris and Bester, "The Effect of Shape on the Effectiveness Factor," Chem. Eng. Sci. **24**: 793 (1969).]

For more complex reactions, the effect of intraparticle diffusion resistance on rate, selectivity, and yield depends on the particulars of the network. Also, the use of the Thiele modulus–effectiveness factor relationships is not as easily applicable, and numerical solution of the diffusion-reaction equations may be required.

Intraparticle Diffusion and External Mass-Transfer Resistance For typical industrial conditions, external mass transfer is important only if there is substantial intraparticle diffusion resistance. This subject has been discussed by Luss, "Diffusion-Reaction Interactions in Catalyst Pellets," in Carberry and Varma (eds.), *Chemical Reaction and Reactor Engineering*, Dekker, 1987. This, however, may not be the case for laboratory conditions, and care must be exerted in including the proper data interpretation. For instance, for a spherical particle with both external and internal mass-transfer limitations and first-order reaction, an overall effectiveness factor η_i can be derived, indicating the series-of-resistances nature of external mass transfer followed by intraparticle diffusion-reaction:

$$\frac{1}{\eta_i} = \frac{1}{\eta} + \frac{\phi^2}{3Sh'} \quad (7-110)$$

$$Sh' = \frac{\epsilon k_p R}{D_{ca}} \quad (7-111)$$

As indicated above, intraparticle diffusion lowers the apparent activation energy. The apparent activation energy is even further lowered under external mass-transfer control. Figure 7-9 illustrates how the rate-controlling step changes with temperature, and as a result the dependence of the apparent first-order rate constant on temperature also changes, from a very strong dependence under kinetic control to virtual independence under external mass-transfer control.

Note that in the limit of external diffusion control, the activation energy $E_{obs} \rightarrow 0$, as can be shown when substituting Eq. (7-110) in Eq. (7-108). For more details on how to represent the combined effect of external and intraparticle diffusion on effectiveness factor for more complex systems, see Luss, "Diffusion-Reaction Interactions in Catalyst Pellets."

Heat-Transfer Resistances A similar analysis regarding external and intraparticle heat-transfer limitations leads to temperature

gradients which add further complexity to the behavior of heterogeneous catalytic systems, including steady-state multiplicity. More details are given in Sec. 19.

Catalyst Deactivation The catalyst life ranges from seconds to minutes to a few days to several years, as the active surface of a catalyst is degraded by chemical, thermal, or mechanical factors. *Chemical deactivation* occurs due to feed or product poisoning or masking. Poisoning may be due to compounds such as P, S, As, Na, and Bi that have free electron pairs and is generally considered irreversible. In some cases a reduced life is simply accepted, as in the case of slow accumulation of trace metals from feed to catalytic cracking; but in other cases the deactivation is too rapid. Sulfur and water are removed from feed to ammonia synthesis, sulfur from feed to platinum reforming, and arsenic from feed to SO₂ oxidation with platinum. Masking may be due to covering of the active sites by contaminants in either the feed or products. Examples of feed masking agents can include Si (from organic silicons) and rust. An example of product masking is coking. Reactivation sometimes is done in place;

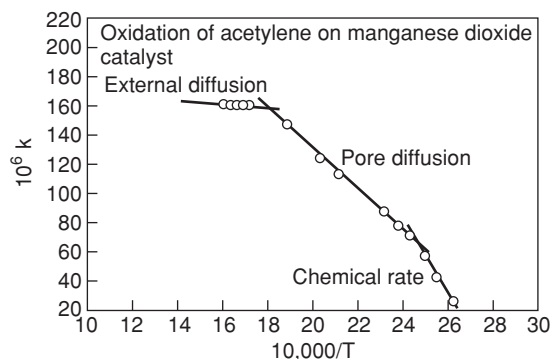


FIG. 7-9 Dependence of the rate-controlling step on temperature.

for instance, coke is burned off cracking catalyst or off nickel and nickel-molybdenum catalysts in a fluidized reactor/regenerator system. *Thermal deactivation* is primarily due to rearrangement of the active sites at high temperature due to *sintering*. Sintering results in agglomeration of active ingredients (lower dispersion). In most cases sintering is irreversible; however Pt/Al₂O₃ catalysts have been regenerated in place by Cl₂ treatment. The catalyst also can be modified by additives, for instance, chromia to nickel to prevent sintering, rhenium to platinum to reduce coking, and so on. *Mechanical deactivation* may be caused by attrition or erosion and subsequent loss of catalyst as fines. The attrition resistance of catalysts is related to the nature of the support and its porosity.

For additional references, see, e.g., Thomas, *Catalytic Processes and Proven Catalysts*, Academic Press, 1970; Butt and Petersen, *Activation, Deactivation and Poisoning of Catalysts*, Academic Press, 1988; and Delmon and Froment, *Catalyst Deactivation*, Elsevier, 1980.

The *activity* α at any time on stream may be simply defined as the ratio of the rate at time t to the rate with fresh catalyst

$$\alpha = \frac{r(t)}{r(t=0)} \quad (7-112)$$

The rate of destruction of active sites and pore structure can be expressed as a kinetic relation that can be generally first- or second-order. For instance, for a second-order dependence,

$$\frac{d\alpha}{dt} = -k_d\alpha^2 \quad (7-113)$$

the corresponding integral is

$$\alpha = \frac{1}{1 + k_d t} \quad (7-114)$$

This type of deactivation mechanism often applies catalyst sintering and coke deactivation. The deactivation rate constant is expected to have an Arrhenius dependence on temperature.

When the feedstock contains constant proportions of reactive impurities, the rate of decline may also depend on the concentration of the main reactant, e.g., for a power law rate

$$\frac{d\alpha}{dt} = -k_d\alpha^p C^q \quad (7-115)$$

Such a differential equation must be solved simultaneously with a rate equation for the main reactant.

The deactivation rate constants are estimated by methods like those for finding constants of any rate equation, given suitable (α , t) data. There are different chemical deactivation mechanisms—two of the most common are described below. For more details see Butt and Petersen, *Activation, Deactivation and Poisoning of Catalysts*, Academic Press, 1988; and Froment and Bischoff, *Chemical Reactor Analysis and Design*, Wiley, 1990. In *uniform deactivation*, the poison is distributed uniformly throughout the pellet and degrades it gradually. In *pore mouth (shell progressive) poisoning*, the poison is so effective that it kills the active site as it enters the pore; hence complete deactivation begins at the mouth and moves gradually inward.

Uniform Deactivation When uniform deactivation occurs, the specific rate declines by a factor $1 - \beta$, where β is the fractional poisoning. β is calculated from the poisoning rate, and it is often assumed to be proportional to the concentration of the poison in the bulk fluid. Then a power law rate equation becomes

$$r = k(1 - \beta)\eta C_s^n \quad (7-116)$$

The effectiveness depends on β through the Thiele modulus

$$\phi = L\sqrt{\frac{k(1 - \beta)C_s^{n-1}}{D_e}} \quad (7-117)$$

To find the effectiveness under poisoned conditions, this form of the Thiele modulus is substituted into the appropriate relation for effectiveness. For example, for a first-order reaction in slab geometry, the effectiveness factor is

$$\eta = \frac{\tanh \phi}{\phi} = \frac{\tanh[L\sqrt{k(1 - \beta)/D_e}]}{L\sqrt{k(1 - \beta)/D_e}} \quad (7-118)$$

Figure 7-10a shows the ratio of the effectiveness factor with uniform poisoning to that without poisoning versus the fraction poisoned for the above case of first-order reaction in a slab.

Pore Mouth (or Shell Progressive) Poisoning This mechanism occurs when the poisoning of a pore surface begins at the mouth of the pore and moves gradually inward. This is a moving boundary problem, and the pseudo-steady-state assumption is made that the boundary moves slowly compared with diffusion of poison and reactants and reaction on the active surface. β is the fraction of the pore that is deactivated. The poison diffuses through the dead zone and deposits at the interface between the dead and active zones. The reactants diffuse across the dead zone without reaction, followed by diffusion-reaction in the active zone.

Figure 7-10b shows simulation results for the ratio of the effectiveness factor with pore mouth poisoning to that without poisoning for a first-order reaction in a slab.

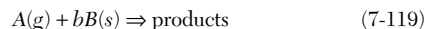
GAS-SOLID NONCATALYTIC REACTIONS

Examples of gas-solid noncatalytic reactions include production of iron from iron ores, roasting of sulfide oxides, combustion of solid fuels, chlorination of Ti ores to make TiCl₄ in the production of TiO₂ pigments, incineration of waste, decomposition of solids to produce gases, e.g., solid propellants and explosives. The kinetic treatment of these reactions has to take into consideration external mass transfer and intraparticle diffusion just as in the case of gas-solid catalytic reactions. However there are major differences, the primary one being consumption of the solid reactant, making the conditions inside the solid particle transient in nature, including change in unreacted particle size, particle density, porosity, etc. For more details see, e.g., Wen ["Noncatalytic Heterogeneous Solid-Fluid Reaction Models," *Ind. Eng. Chem.* **60**(9):34-54 (1968)], Szekeley (in Lapidus and Amundson (eds.), *Chemical Reactor Theory—A Review*, Prentice-Hall, 1977), Doraiswamy and Kulkarni [in Carberry and Varma (eds.), *Chemical Reaction and Reactor Engineering*, Dekker, 1987], and Levenspiel (*Chemical Reaction Engineering*, 3d ed., Wiley, 1999).

The basic steps are identical to those of catalytic gas-solid reactions. However, as indicated above, the process is transient (non-steady-state) due to change in particle size and properties as the reaction progresses.

Several models that describe gas-solid noncatalytic reactions are summarized in Table 7-7. The first two, the sharp interface and volume reaction models, are pseudo-homogeneous, form part of the class of shrinking core models, and can be treated by using the Thiele modulus and effectiveness factor concept. The last three are heterogeneous models.

Sharp Interface Model For a first-order reaction in gas reactant,

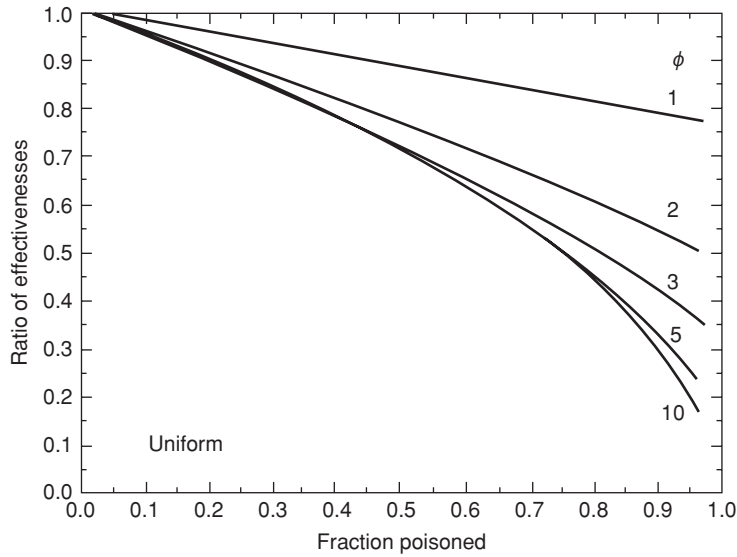


a rate of conversion of the solid B per unit particle volume of

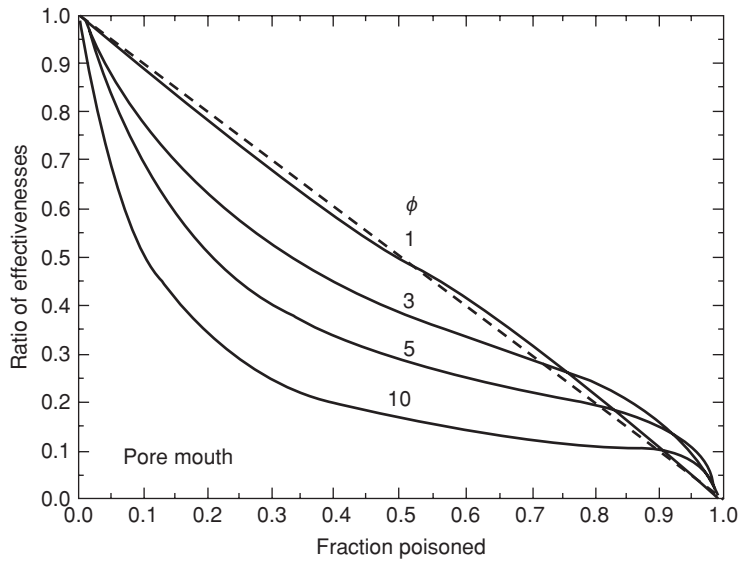
$$r_b = kC_{a0}C_s \quad (7-120)$$

and assuming pseudo-steady state for the gas-phase component, it can be shown that

$$r_{\text{obs}} = \frac{C_{a0}}{\frac{1}{k_p a_p} + \frac{R_p^2}{D_{ca}} \left(\frac{R_p}{R_s} - 1 \right) + \frac{b}{kC_{a0}}} \quad (7-121)$$



(a)



(b)

FIG. 7-10 Poisoning of a first-order reaction. (a) Uniform poisoning. (b) Pore mouth poisoning.

where R_p and R_s are the particle and solid core radii, a_p is the external particle diameter-based interfacial area per particle volume, and k is based on particle volume. Equation (7-121) represents three resistances in series—external mass transfer, diffusion in the reacted (ash) zone, and reaction at the unreacted solid-ash interface.

The conversion of the solid reactant B is obtained from integration of the pseudo-steady-state diffusion model with reaction at the boundary:

$$\frac{1}{r^2} \frac{\partial}{\partial r} \left(D_{ea} r^2 \frac{\partial C_{as}}{\partial r} \right) = 0$$

$$D_{ea} \frac{\partial C_{as}}{\partial r} = \frac{1}{b} k C_{as} C_s \quad \text{at } r = R_s, \quad (7-122)$$

$$D_{ea} \frac{\partial C_{as}}{\partial r} = k_s (C_{a0} - C_{as}) \quad \text{at } r = R_p$$

TABLE 7-7 Noncatalytic Gas-Solid Reaction-Diffusion Models

Model	Main features
Sharp interface model (SIM)	Reacting solid is nonporous. Reacted solid ash is porous. Reaction occurs at the ash-unreacted solid interface.
Volume reaction model	Reacting solid is also porous. Reaction occurs everywhere in the particle.
Grain model	Particle is divided into identical solid spherical grains. Each grain reacts according to the sharp interface model.
Crackling core model	Combination of SIM and grain model.
Nucleation model	Nucleation of metals in metal reduction reactions.

The moving boundary radius R_c is determined from a material balance that relates the unreacted solid volume to the reaction rate. Integration gives the time τ required to achieve a given conversion of the solid B , X_b :

$$\tau = \frac{R_p C_{s0}}{b C_{a0}} \left\{ \frac{1}{3} \left(\frac{1}{k_s} - \frac{R_p}{D_{ea}} \right) X_b + \frac{R_p}{2 D_{ea}} \left[1 - (1 - X_b)^{2/3} \right] + \frac{3b}{C_{s0} R_p k} \left[1 - (1 - X_b)^{1/3} \right] \right\} \quad X_b = 1 - \left(\frac{R_c}{R_p} \right)^3 \quad (7-123)$$

Similar solutions can be obtained for other shapes (Doraiswamy and Kulkarni, in Carberry and Varma (eds.), *Chemical Reaction and Reactor Engineering*, Dekker, 1987). Figure 7-11 shows typical concentration profiles for this case.

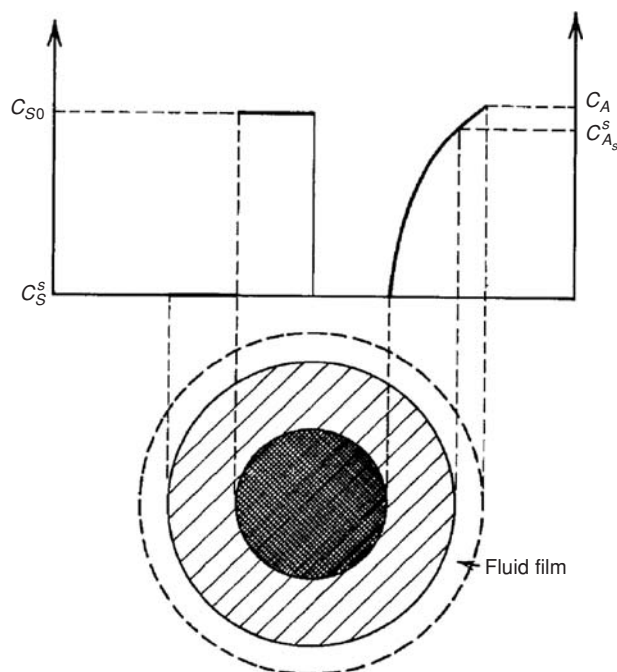


FIG. 7-11 Sharp interface model—concentration profiles. [From Wen, "Noncatalytic Heterogeneous Solid-Fluid Reaction Models," *Ind. Eng. Chem.* **60**(9): 34-54 (1968), Fig. 1.]

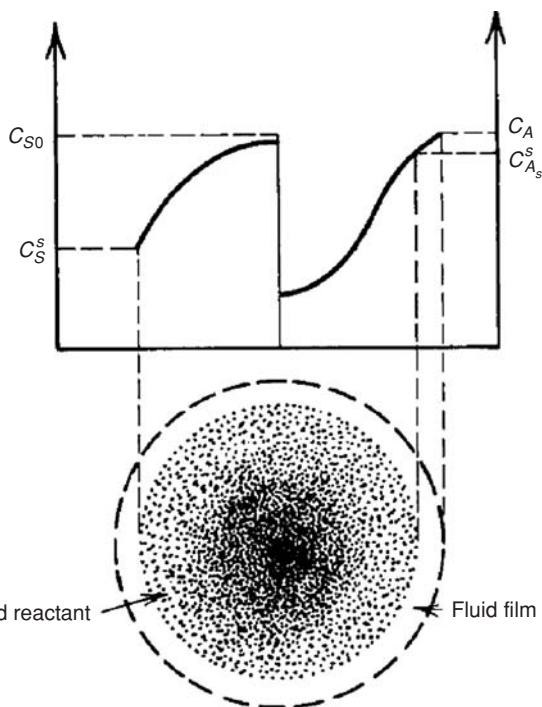


FIG. 7-12 Typical concentration profiles for the volume reaction model. [From Wen, "Noncatalytic Heterogeneous Solid-Fluid Reaction Models," *Ind. Eng. Chem.* **60**(9): 34-54 (1968), Fig. 3.]

Volume Reaction Model A typical concentration profile for the volume reaction model is shown in Fig. 7-12.

A general transient model of diffusion-reaction that uses the effective diffusivity concept described for gas-solid catalytic reactions can be derived here as well, e.g., for a spherical particle:

$$\frac{\partial(\epsilon_s C_{as})}{\partial t} = \frac{1}{r^2} \frac{\partial}{\partial r} \left(D_{ea} r^2 \frac{\partial C_{as}}{\partial r} \right) - r_a \quad \frac{\partial C_s}{\partial t} = -r_s$$

$$C_{as} = C_{as0} \quad C_s = C_{s0} \quad \text{at } t = 0 \quad \frac{\partial C_{as}}{\partial r} = 0 \quad \text{at } r = 0$$

$$D_{ea} \frac{\partial C_{as}}{\partial r} \Big|_{r=R} = k_s (C_a - C_{as}|_{r=R}) \quad (7-124)$$

$$\epsilon_s = \epsilon_{s0} + C_{s0}(v_s - v_p) \left(1 - \frac{C_s}{C_{s0}} \right) \quad \frac{D_{ea}}{D_{ea0}} = \left(\frac{\epsilon_s}{\epsilon_{s0}} \right)^\beta, \quad \beta = 2 - 3 \quad (7-125)$$

Here the porosity and the diffusivity vary with conversion of solid; v_s and v_p are the reactant and product molar volumes. A Thiele modulus ϕ and dimensionless time θ can be defined, e.g., for a rate second-order in A and first-order in S:

$$r = k C_a^2 C_s \quad (7-126)$$

$$\phi = R \sqrt{\frac{k C_{as}(R) C_{s0}}{D_{ea0}}} \quad \theta = b k C_{as0} t \quad (7-127)$$

For the given rate expression, equations (7-124) to (7-127) can be numerically integrated, e.g., in Fig. 7-13 for reaction control and Fig. 7-14 for intraparticle diffusion control, both with negligible external mass-transfer resistance; x is the fractional conversion.

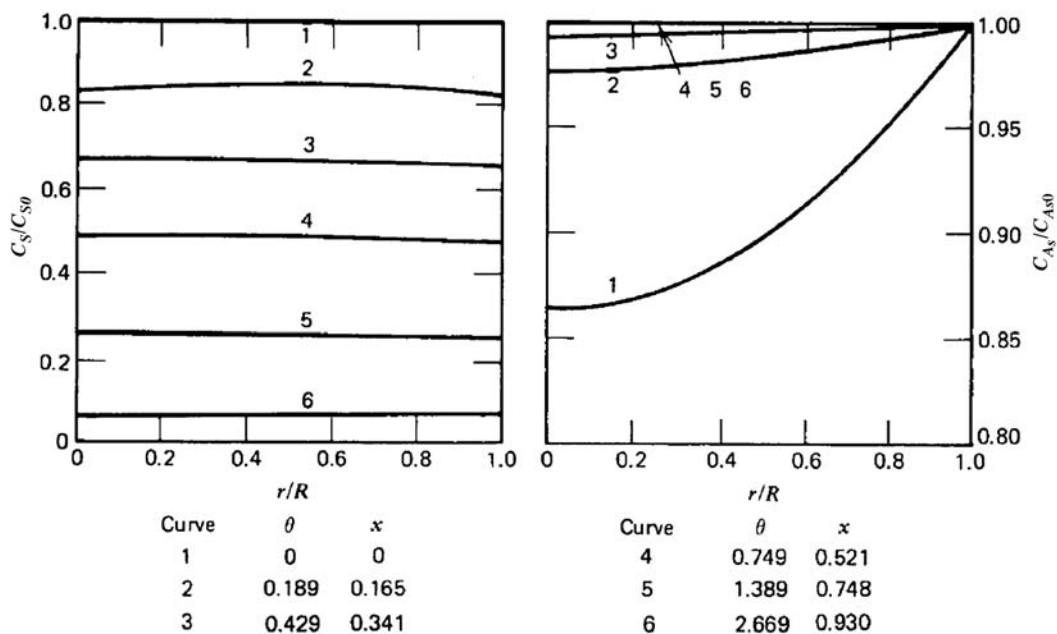


FIG. 7-13 Concentration profiles with reaction control $\phi = 1$, in absence of gas particle mass-transfer resistance. [From Wen, "Noncatalytic Heterogeneous Solid-Fluid Reaction Models," Ind. Eng. Chem. **60**(9): 34-54 (1968), Fig. 11.]

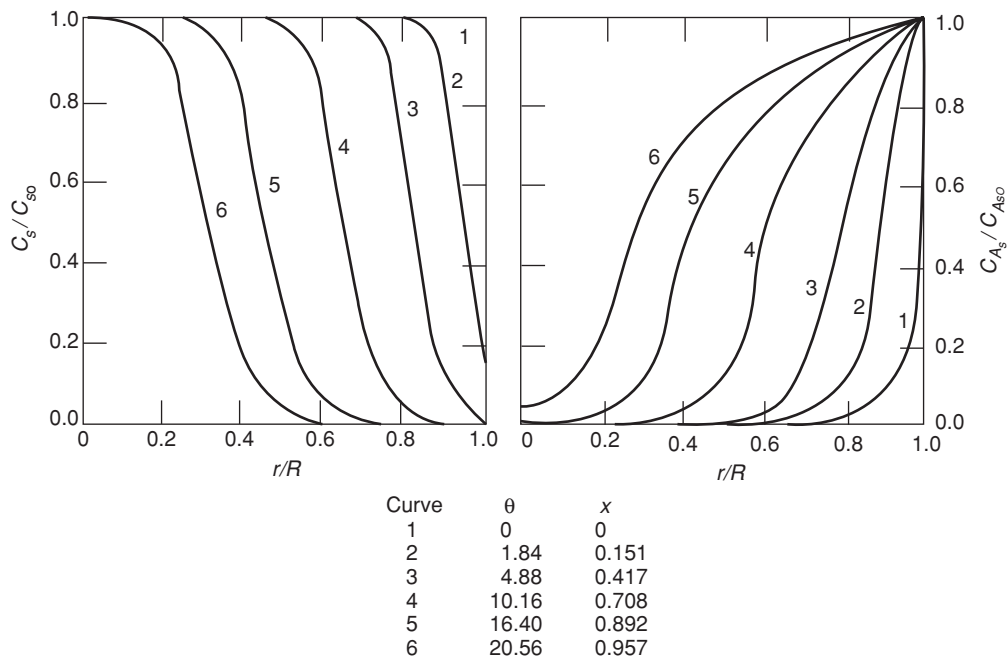


FIG. 7-14 Concentration profiles with intraparticle diffusion control, $\phi = 70$, in absence of gas particle mass-transfer resistance. [From Wen, "Noncatalytic Heterogeneous Solid-Fluid Reaction Models," Ind. Eng. Chem. **60**(9): 34-54 (1968), Fig. 12.]

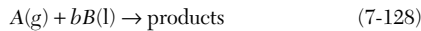
GAS-LIQUID REACTIONS

Many industrial processes employ gas-liquid reactions that can be either noncatalytic or homogeneously catalyzed. These include, for instance, absorption of acid gases (SO₃, NO₂, CO₂), chlorinations (benzene, dodecane, toluene), oxidations (P-Xylene to terephthalic acid, cyclohexane to cyclohexanone and cyclohexanol, acetaldehyde to acetic acid), hydrogenations (olefins, esters to fatty acids), and hydroformylation of olefins to alcohols, to name a few. See also Sec. 19 and Shah (*Gas-Liquid-Solid Reactor Design*, McGraw-Hill, 1979). These reactions include gas reactants dissolving in a liquid and reacting there with a liquid reactant. When determining the kinetics of such reactions from lab data, one needs to understand the mechanism and the controlling steps, just as was the case for heterogeneous gas-solid reactions. The simplest model is the two-film model, and it involves the following consecutive steps for the gaseous reactant:

1. Mass transfer of gas reactant from bulk gas to the gas-liquid interface across the gas film.
2. At the gas-liquid interface, the liquid and gas concentrations of the gaseous reactant are assumed to be at thermodynamic equilibrium.
3. Mass transfer of the dissolved gas reactant to the bulk liquid across the liquid film—if the reaction is fast, the reaction will occur both in the liquid film (in parallel with diffusion) and in the bulk liquid.

For a volatile liquid reactant or a volatile product, these steps are essentially reversed. For a nonvolatile liquid reactant or product, only the reaction and diffusion in the liquid take place. Figure 7-15 describes the absorbing gas concentration profiles in a gas-liquid system.

For a general gas-liquid reaction:



the two-film pseudo-steady-state model is described by the following fluxes across the interface for the gaseous reactant A:

$$\begin{aligned} N_{aG} &= \frac{D_{aG}}{\delta_G} (P_a - P_{ai}) = k_G (P_a - P_{ai}) = N_{aL} = \frac{D_{aL}}{\delta_L} (C_{Lai} - C_{La}) \\ &= k_L (C_{Lai} - C_{La}) \end{aligned} \quad (7-129)$$

Here the subscript *L* denotes liquid, *G* denotes gas, *i* denotes the gas-liquid interface (where the gas and liquid concentrations are in equilibrium). The thickness of the liquid and gas films is not a directly measurable quantity, and instead mass-transfer coefficients are

defined as indicated above. These depend on the diffusivity of the molecule, geometry, flow, and operating conditions; and typical values can be viewed in Sec. 19. In addition to the two-film steady-state model, other more accurate, non-steady-state models have also been developed such as the surface renewal and penetration models (see, e.g., Astarita, *Mass Transfer with Chemical Reaction*, Elsevier, 1967). In many industrial cases of interest, mass-transfer resistance in the gas-film is negligible, especially considering that gas-phase diffusivities are 2 to 3 orders of magnitude larger for the same species than those in the liquid. Hence we drop the subscripts *L* and *G* from the concentrations since the concentrations considered are in the liquid phase only.

REACTION-DIFFUSION REGIMES

Depending on the relative rates of diffusion and reaction, the following diffusion-reaction regimes occur:

- $t_D \ll t_r$ slow reaction regime with reaction control
 - $t_D \gg t_r$ fast reaction regime with diffusion control
 - $t_D \approx t_r$ both reaction and diffusion are important
- (7-130)

$$t_D = \frac{D_a}{k_L^2} \qquad t_r = \frac{C_{ai} - C_{ae}}{r(C_{ai})}$$

Here t_D and t_r are the diffusion and reaction times, respectively, and k_L is the mass-transfer coefficient in the absence of reaction. For the *fast reaction regime*, diffusion and reaction occur in parallel in the liquid film, while for the *slow reaction regime*, there is no reaction in the liquid film and the mass transfer can be considered to occur independently of reaction in a consecutive manner. For the slow reaction regime, the following subregimes can be defined:

- $t_m \ll t_r$ slow reaction kinetic control
 - $t_m \gg t_r$ slow reaction mass-transfer control
 - $t_m \approx t_r$ both reaction and mass transfer are important
- (7-131)

$$t_m = \frac{1}{k_L a}$$

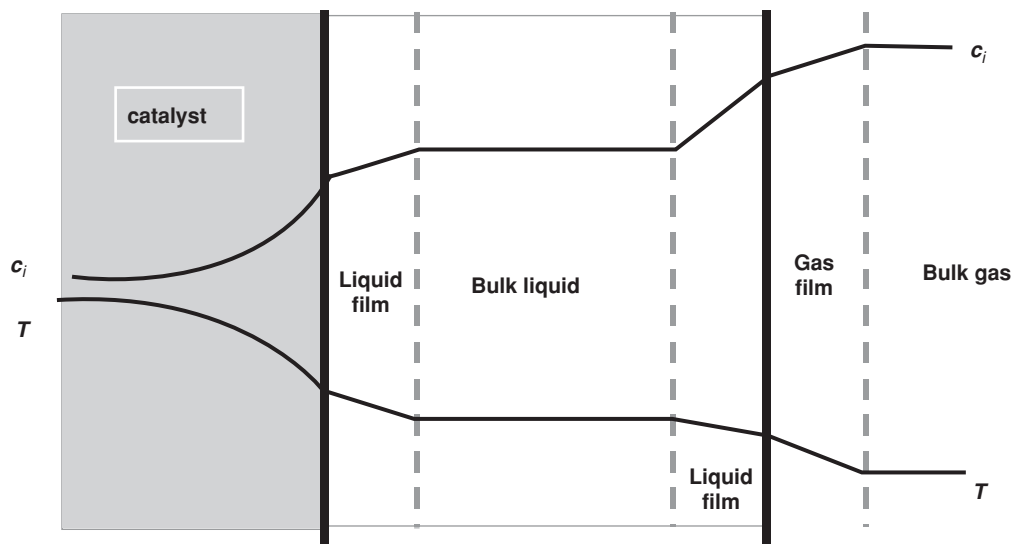


FIG. 7-15 Absorbing gas concentration and temperature profiles (exothermic reaction) in gas-liquid and gas-liquid-solid reactions.

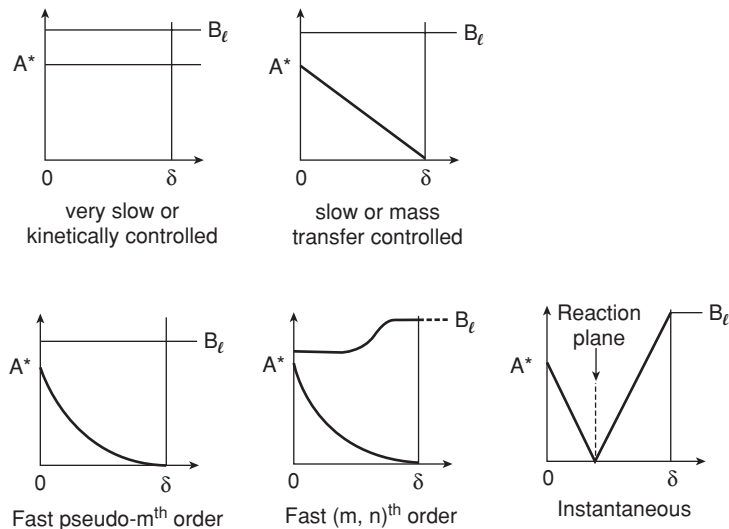


FIG. 7-16 Concentration profiles for the general reaction $A(g) + bB(l) \rightarrow \text{products}$ with the rate $r = kC_a^m C_b^n$. [Adapted from Mills, Ramachandran, and Chaudhari, "Multiphase Reaction Engineering for Fine Chemicals and Pharmaceuticals," *Rev. Chem. Eng.* 8(1-2):1 (1992), Figs. 19 and 20.]

Here t_m is the mass-transfer time. Only under *slow reaction kinetic control regime* can intrinsic kinetics be derived directly from lab data. Otherwise the intrinsic kinetics have to be extracted from the observed rate by using the mass-transfer and diffusion-reaction equations, in a manner similar to those defined for catalytic gas-solid reactions. For instance, in the *slow reaction regime*,

$$r_{a,\text{obs}} = \frac{C_{ai}}{He_a/k_G a + 1/k_1 a + 1/k} \quad (7-132)$$

$$k_{\text{obs}} = \frac{1}{He_a/k_G a + 1/k_1 a + 1/k} \quad (7-133)$$

Here He_a is the Henry constant for the solute a . For the fast reaction regime, instead of the effectiveness factor adjustment for the intrinsic reaction rate, it is customary to define an *enhancement factor* for mass-transfer enhancement by the reaction, defined as the ratio of mass transfer in presence of reaction in the liquid, to mass transfer in absence of reaction:

$$E = k_1/k_{L0} \quad (7-134)$$

Solving the diffusion-reaction equation in the liquid, the enhancement factor can be related to the *Hatta number* Ha , which is similar to the Thiele modulus defined for heterogeneous gas-solid catalysts. Thus, the Hatta number and its relation to the controlling regime are

$$Ha = \frac{t_D}{t_R} = \sqrt{\frac{\text{maximum reaction rate in the film}}{\text{maximum mass transfer rate through film}}}$$

$$Ha \ll 1 \quad \text{slow reaction regime} \quad (7-135)$$

$$Ha \gg 1 \quad \text{fast reaction regime}$$

For instance, for a first-order reaction in the gaseous reactant A (e.g., with large excess of liquid reactant B), the following relates the enhancement factor to the Hatta number:

$$Ha = \delta_L \sqrt{\frac{k}{D_a}} = \frac{\sqrt{kD_a}}{k_{L0}} \quad \text{for } C_b \gg C_{ai} \quad (7-136)$$

$$E = \frac{Ha}{\tanh Ha} \left(1 - \frac{C_a}{C_{ai}} \frac{1}{\cosh Ha} \right) > 1 \quad (7-137)$$

When both A and B have comparable concentrations, then the enhancement factor is an increasing function of an additional parameter:

$$\lambda = \frac{D_b C_b}{b D_a C_{ai}} \quad (7-138)$$

In the limit of an instantaneous reaction, the reaction occurs at a plane where the concentration of both reactants A and B is zero and the flux of A equals the flux of B . The criterion for an instantaneous reaction is

$$Ha^{1/2} \gg \frac{C_b}{b C_{ai}} \quad E_{\infty} = 1 + \lambda \gg 1 \quad (7-139)$$

Figure 7-16 illustrates typical concentration profiles of A and B for the various diffusion-reaction regimes.

GAS-LIQUID-SOLID REACTIONS

GAS-LIQUID-SOLID CATALYTIC REACTIONS

Many solid catalyzed reactions take place with one of the reactants absorbing from the gas phase into the liquid and reacting with a liquid reactant on the surface or inside the pores of a solid catalyst (see Fig. 7-15). Examples include the Fischer-Tropsch synthesis of hydrocarbons from synthesis gas (CO and H_2) in the presence of Fe or Co -

based heterogeneous catalysts, methanol synthesis from synthesis gas ($\text{H}_2 + \text{CO}$) in the presence of heterogeneous CuO/ZnO catalyst, and a large number of noble metal catalyzed hydrogenations among others. For a slow first-order reaction of a gaseous reactant, the concept of resistances in series can be expanded as follows, e.g., for a slurry reactor with fine catalyst powder:

$$r_{a,obs} = \frac{C_{ai}}{\frac{H_e}{k_c a} + \frac{1}{k_{l1} a} + \frac{1}{k_{s1} a} + \frac{1}{k}} \quad k_{obs} = \frac{1}{\frac{H_e}{k_c a} + \frac{1}{k_{l1} a} + \frac{1}{k_{s1} a} + \frac{1}{k}} \quad (7-140)$$

Intraparticle diffusion resistance may become important when the particles are larger than the powders used in slurry reactors, such as for catalytic packed beds operating in trickle flow mode (gas and liquid downflow), in upflow gas-liquid mode, or countercurrent gas-liquid mode. For these the effectiveness factor concept for intraparticle diffusion resistance has to be considered in addition to the other resistances present. See more details in Sec. 19.

POLYMERIZATION REACTIONS

Polymers are high-molecular-weight compounds assembled by the linking of small molecules called monomers. Most polymerization reactions involve two or three phases, as indicated below. There are several excellent references dealing with *polymerization kinetics* and reactors, including Ray in Lapidus and Amundson, (eds.), *Chemical Reactor Theory—A Review*, Prentice-Hall, 1977; Tirrel et al. in Carberry and Varma (eds.), *Chemical Reaction and Reactor Engineering*, Dekker, 1987; and Meyer and Keurentjes (eds.), *Handbook of Polymer Reaction Engineering*, Wiley, 2005.

Polymerization can be classified according to the main phase in which the reaction occurs as liquid (most polymerizations), vapor (e.g., Ziegler Natta polymerization of olefins), and solid phase (e.g., finishing of melt step polymerization). Polymerization reactions occur in liquid phase and can be further subclassified into

1. Bulk mass polymerization:
 - a. Polymer soluble in monomer
 - b. Polymer insoluble in monomer
 - c. Polymer swollen by monomer
2. Solution polymerization
 - a. Polymer soluble in solvent
 - b. Polymer insoluble in solvent
3. Suspension polymerization with initiator dissolved in monomer
4. Emulsion polymerization with initiator dissolved in dispersing medium

Polymerization can be catalytic or noncatalytic, and can be homogeneously or heterogeneously catalyzed. Polymers that form from the liquid phase may remain dissolved in the remaining monomer or solvent, or they may precipitate. Sometimes beads are formed and remain in suspension; sometimes emulsions form. In some processes solid polymers precipitate from a fluidized gas phase. Polymerization processes are also characterized by extremes in temperature, viscosity, and reaction times. For instance, many industrial polymers are mixtures with molecular weights of 10^4 to 10^7 . In polymerization of styrene the viscosity increased by a factor of 10^6 as conversion increased from 0 to 60 percent. The adiabatic reaction temperature for complete polymerization of ethylene is 1800 K (3240°R). Initiators of the chain reactions have concentration as low as 10^{-8} g·mol/L, so they are highly sensitive to small concentrations of poisons and impurities.

Polymerization mechanism and kinetics require special treatment and special mathematical tools due to the very large number of similar reaction steps. Some polymerization types are briefly described next.

Bulk Polymerization The monomer and initiators are reacted with or without mixing, e.g., without mixing to make useful shapes directly. Because of viscosity limitations, stirred bulk polymerization is not carried to completion. For instance, for addition polymerization conversions as low as 30 to 60 percent are achieved, with the remaining monomer stripped out and recycled (e.g., in the case of polystyrene).

Bead Polymerization Bulk reaction proceeds in droplets of 10- to 1000- μ m diameter suspended in water or other medium and insulated from each other by some colloid. A typical suspending agent is polyvinyl alcohol dissolved in water. The polymerization can be done to high conversion. Temperature control is easy because of the moderating thermal effect of the water and its low viscosity. The suspensions sometimes are unstable and agitation may be critical. Examples

are polyvinyl acetate in methanol, copolymers of acrylates and methacrylates, and polyacrylonitrile in aqueous $ZnCl_2$ solution.

Emulsion Polymerization Emulsions have particles of 0.05- to 5.0- μ m diameter. The product is a stable latex, rather than a filterable suspension. Some latexes are usable directly, as in paints, or they may be coagulated by various means to produce very high-molecular-weight polymers. Examples are polyvinyl chloride and butadiene-styrene rubber.

Solution Polymerization These processes may retain the polymer in solution or precipitate it. Examples include polyethylene, the copolymerization of styrene and acrylonitrile in methanol, the aqueous solution of acrylonitrile to precipitate polyacrylonitrile.

Polymer Characterization The physical properties of polymers depend largely on the *molecular weight distribution (MWD)*, which can cover a wide range. Since it is impractical to fractionate the products and reformulate them into desirable ranges of molecular weights, immediate attainment of desired properties must be achieved through the correct choice of reactor type and operating conditions, notably of distributions of residence time and temperature. High viscosities influence those factors. For instance, high viscosities prevalent in bulk and melt polymerizations can be avoided with solution, bead, or emulsion operations. The interaction between the flow pattern in the reactor and the type of reaction affects the MWD. If the period during which the molecule is growing is short compared with the residence time in the reactor, the MWD in a batch reactor is broader than in a CSTR. This situation holds for many free radical and ionic polymerization processes where the reaction intermediates are very short lived. In cases where the growth period is the same as the residence time in the reactor, the MWD is narrower in batch than in CSTR. Polymerizations that have no termination step—for instance, polycondensations—are of this type. This topic is treated by Denbigh [*J. Applied Chem.*, 1:227(1951)].

Four types of MWD can be defined: (1) The *number chain length distribution (NCLD)*, relating the chain length distribution to the number of molecules per unit volume; (2) the *weight chain length distribution (WCLD)* relating the chain length distribution to the weight of molecules per unit volume; (3) the *number molecular weight distribution (NMWD)* relating the chain length distribution to molecular weight; and (4) the *weight molecular weight distribution (WMWD)* relating the weight distribution to molecular weight. Two average molecular weights and corresponding average chain lengths are typically defined: the *number average molecular weight* M_n and the corresponding *number average chain length* μ_n ; and the *weight average molecular weight* M_w and the corresponding *weight average chain length* μ_w . Their ratio is called *polydispersity* and describes the width of the molecular weight distribution.

$$M_n = \frac{w \sum_{j=1}^{\infty} j P_j}{\sum_{j=1}^{\infty} P_j} \quad \mu_n = \frac{\sum_{j=1}^{\infty} j P_j}{\sum_{j=1}^{\infty} P_j} \quad M_w = \frac{w \sum_{j=1}^{\infty} j^2 P_j}{\sum_{j=1}^{\infty} j P_j} \quad \mu_w = \frac{\sum_{j=1}^{\infty} j^2 P_j}{\sum_{j=1}^{\infty} j P_j}$$

$$\text{polydispersity} = \frac{M_w}{M_n} = \frac{\mu_w}{\mu_n} \quad (7-141)$$

The average chain lengths can be related to the *moments* λ_k of the distribution as follows:

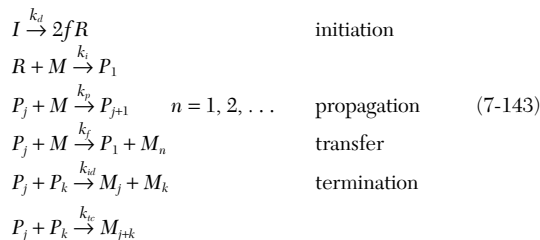
$$\mu_n = \frac{\lambda_1}{\lambda_0} \quad \mu_w = \frac{\lambda_2}{\lambda_1} \quad \text{polydispersity} = \frac{\lambda_0 \lambda_2}{\lambda_1^2} \quad \lambda_k = \sum_{j=1}^{\infty} j^k P_j \quad (7-142)$$

Here P_j is the concentration of the polymer with chain length j —the same symbol is also used for representing the polymer species P_j ; w is the molecular weight of the repeating unit in the chain.

A factor in addition to the residence time distribution and temperature distribution that affects the molecular weight distribution is the type of the chemical reaction (e.g., step or addition polymerization).

Two major polymerization mechanisms are considered: *chain growth* and *step growth*. In addition, polymerization can be *homopolymerization*—a single monomer is used—and *copolymerization* usually with two monomers with complementary functional groups.

Chain Homopolymerization Mechanism and Kinetics Free radical and ionic polymerizations proceed through this type of mechanism, such as styrene polymerization. Here one monomer molecule is added to the chain in each step. The general reaction steps and corresponding rates can be written as follows:



Here P_j is the *growing* or *live polymer*, and M_j is the *dead* or *product polymer*. Assuming reaction steps independent of chain length and assuming pseudo-steady-state approximation for the radicals lead to the following rates for monomer and initiator conversion and live polymer distribution. The growing chains distribution is the most probable distribution [see, e.g., Ray in Lapidus and Amundson (eds.), *Chemical Reactor Theory—A Review*, Prentice-Hall, 1977; Tirrel et al. in Carberry and Varma (eds.), *Chemical Reaction and Reactor Engineering*, Dekker, 1987]:

$$\begin{aligned}
 P_n &= (1 - \alpha)P\alpha^{n-1} \quad \alpha = \frac{k_p M}{(k_p + k_t)M + (k_{tc} + k_{td})P} \\
 P &= \left(\frac{2fk_d I}{k_{tc} + k_{td}} \right)^{1/2} \quad \frac{dI}{dt} = -k_d I \quad (7-144) \\
 r = \frac{dM}{dt} &= -k_p \left(\frac{2fk_d}{k_{tc} + k_{td}} \right)^{1/2} I^{1/2} M \quad DP_n^{\text{inst}} = \frac{k_p M}{(0.5k_{tc} + k_{td})P}
 \end{aligned}$$

Here r is the rate of polymerization, α is the *probability of propagation*, DP_n^{inst} is the *instantaneous degree of polymerization*, i.e., the number of monomer units on the dead polymer, and f is the *initiation efficiency*. Compare r in Eq. (7-144) with the simpler Eq. (7-68). When chain transfer is the primary termination mechanism, such as in anionic polymerization, then the polydispersity is 2.

Mathematically, the infinite set of equations describing the rate of each chain length can be solved by using the z transform method (a discrete method), *continuous variable approximation method*, or the *method of moments* [see, e.g., Ray in Lapidus and Amundson (eds.), *Chemical Reactor Theory—A Review*, Prentice-Hall, 1977].

Typical ranges of the kinetic parameters for low conversion homopolymerization are given in Table 7-8. For more details see Hutchenson in Meyer and Keurentjes (eds.), *Handbook of Polymer Reaction Engineering*, Wiley, 2005.

Step Growth Homopolymerization Mechanism and Kinetics

Here any two growing chains can react with each other. The propagation mechanism is an infinite set of reactions:



TABLE 7-8 Typical Ranges of Kinetic Parameters

Coefficient/concentration	Typical range
k_{ds} , 1/s	10^{-6} – 10^{-4}
f	0.4–0.9
k_p , L/(mol/s)	10^2 – 10^4
k_t , L/(mol/s)	10^6 – 10^8
k_{tr}/k_p	10^{-6} – 10^{-4}
I , mol/L	10^{-4} – 10^{-2}
M , mol/L	1–10

SOURCE: Hutchenson, "Typical Ranges of Kinetic Parameters," in *Handbook of Reaction Engineering*, Wiley, 2005, Table 4.1.

For instance, some nylons are produced through this mechanism. This is usually modeled under the simplifying assumption that the rate constants are independent of chain length. This assumption was proved pretty accurate, and by using the z transform it results in the *Flory distribution*:

$$\begin{aligned}
 P_n &= \frac{P_{10}(P_{10}\tau)^{n-1}}{(P_{10}\tau + 1)^{n+1}} \quad n \geq 1 \quad k_{pnm} = k_p \quad \text{for all } n, m \quad \tau = \int_0^t k_p M dt \\
 \mu_n &= \frac{2 - \alpha}{1 - \alpha} \quad \mu_w = \frac{2}{(1 - \alpha)(2 - \alpha)} \quad \text{polydispersity} = \frac{\mu_w}{\mu_n} = \frac{2}{(2 - \alpha)^2} \\
 \alpha &= \frac{P_{10}\tau}{P_{10}\tau + 1} \quad (7-146)
 \end{aligned}$$

Copolymerization Copolymerization involves more than one monomer, usually two comonomers, as opposed to the single monomer involved in the chain growth and step homopolymerization schemes above. Examples are some nylons, polyesters, and aramids. Here as well there are step growth and chain growth mechanisms, and these are much more complex [see, e.g., Ray in Lapidus and Amundson (eds.), *Chemical Reactor Theory—A Review*, Prentice-Hall, 1977].

BIOCHEMICAL REACTIONS

Mechanism and kinetics in biochemical systems describe the cellular reactions that occur in living cells. Biochemical reactions involve two or three phases. For example, aerobic fermentation involves gas (air), liquid (water and dissolved nutrients), and solid (cells), as described in the "Biocatalysis" subsection above. Bioreactions convert feeds called *substrates* into more *cells* or *biomass* (cell growth), proteins, and *metabolic products*. Any of these can be the desired product in a commercial *fermentation*. For instance, methane is converted to biomass in a commercial process to supply fish meal to the fish farming industry. Ethanol, a metabolic product used in transportation fuels, is obtained by fermentation of corn-based or sugar-cane-based sugars. There is a substantial effort to develop genetically modified biocatalysts that produce a desired metabolite at high yield.

Bioreactions follow the same general laws that govern conventional chemical reactions, but the complexity of the mechanism is higher due to the close coupling of bioreactions and *enzymes* that are turned on (*expressed*) or off (*repressed*) by the cell depending on the conditions in the fermenter and in the cell. Thus the rate expression (7-92) can mainly be used to design bioreaction processes when the culture is in *balanced growth*, i.e., for steady-state cultivations or batch growth for as long as the substrate concentration is much higher than C_s . After a sudden process upset (e.g., a sudden change in substrate concentration or pH), the *control network* of the cell that lies under the *mass flow network* is activated, and dramatic changes in the kinetics of product formation can occur. Table 7-9 summarizes key differences between biochemical and conventional chemical systems [see, e.g., Leib, Pereira, and Villadsen, "Bioreactors, A Chemical Engineering Perspective," *Chem. Eng. Sci.* **56**: 5485–5497 (2001)].

TABLE 7-9 Biological versus Chemical Systems

- There is tighter control on conditions (e.g., pH, temperature, substrate and product concentrations, dissolved O₂ concentration, avoidance of contamination by foreign organisms).
- Pathways can be turned on/off by the microorganism through expression of certain enzymes depending on the substrate type and concentration and operating conditions, leading to a richness of behavior unparalleled in chemical systems.
- The global stoichiometry changes with operating conditions and feed composition; kinetics and stoichiometry obtained from steady-state (chemostat) data cannot be used reliably over a wide range of conditions, unless fundamental models are employed.
- Long-term adaptations (mutations) may occur in response to environment changes that can alter completely the product distribution.
- Only the substrates that maximize biomass growth are utilized even in the presence of multiple substrates.
- Cell energy balance requirements pose additional constraints on the stoichiometry that can make it very difficult to predict flux limitations.

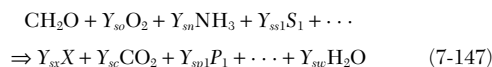
TABLE 7-10 Hierarchy of Kinetic Models in Biological Systems

- Stoichiometric black box models (similar to a single global chemical reaction) represent the biochemistry by a single global reaction with fixed stoichiometric or *yield coefficients* (limited to a narrow range of conditions). Black box models can be used over a wider range of conditions by establishing different sets of yield coefficient for different conditions. These are also needed to establish the quantitative amounts of various nutrients needed for the completion of the bioreaction.
- Unstructured models view the cell as a single component interacting with the fermentation medium, and each bioreaction is considered to be a global reaction, with a corresponding empirical rate expression.
- Structured models include information on individual reactions or groups of reactions occurring in the cell, and cell components such as DNA, RNA, and proteins are included in addition to the primary metabolites and substrates (see, e.g., the active cell model of Nielsen and Villadsen, *Bioreaction Engineering Principles*, 2d ed., Kluwer Academic/Plenum Press, 2003).
- Fundamental models include cell dimensions, transport of substrates and metabolites across the cell membrane, and the elementary cell bioreaction steps and their corresponding enzyme induction mechanism. In recent years further kinetic steps have been added to the above models which are based on the conversion of substrates to metabolites. Thus the kinetics of protein synthesis by *transcription* and *translation* from the *genome* add much further complexity to cell kinetics.

The network of bioreactions is called the *metabolic network*, the series of consecutive steps between key intermediates in the network are called *metabolic pathways*, and the determination of the mechanism and kinetics is called *metabolic flux analysis*. As for chemical systems, there are several levels of mechanistic and kinetic representation and analysis, listed in order of increasing complexity in Table 7-10.

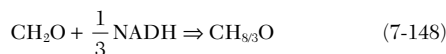
Additional complexity can be included through cell population balances that account for the distribution of cell generation present in the fermenter through use of stochastic models. In this section we limit the discussion to simple black box and unstructured models. For more details on bioreaction systems, see, e.g., Nielsen, Villadsen, and Liden, *Bioreaction Engineering Principles*, 2d ed., Kluwer, Academic/Plenum Press, 2003; Bailey and Ollis, *Biochemical Engineering Fundamentals*, 2d ed., McGraw-Hill, 1986; Blanch and Clark, *Biochemical Engineering*, Marcel Dekker, 1997; and Sec. 19.

Mechanism Stoichiometric balances are done on a C atom basis called *C-moles*, e.g., relative to the substrate (denoted by subscript *s*), and the corresponding stoichiometric coefficients Y_{si} (based on C-mole of the primary substrate) are called *yield coefficients*. For instance,



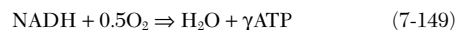
Here the reactants (substrates) are glucose (CH_2O), O_2 , NH_3 , and a sulfur-providing nutrient S_1 , and the products are biomass X, CO_2 , metabolic product P_1 , and H_2O .

The products of bioreactions can be reduced or oxidized, and all feasible pathways have to be *redox neutral*. There are several cofactors that transfer redox power in a pathway or between pathways, each equivalent to the reducing power of a molecule of H_2 , e.g., nicotinamide adenine dinucleotide (NADH), and these have to be included in the stoichiometric balances as H equivalents through redox balancing. For instance, for the reaction of glucose to glycerol (CH_3O), $\frac{1}{3}$ NADH equivalent is consumed:



The stoichiometry in the biochemical literature often does not show H_2O produced by the reaction; however, for complete elemental balance, water has to be included, and this is easily done once an O_2 requirement has been determined based on a redox balance. Likewise for simplicity, the other form of the cofactor [e.g., the oxidized form of the cofactor NADH in Eq. (7-148)] is usually left out. In

addition to C balances, for aerobic systems cell respiration has to be accounted for as well through a stoichiometric equation:



The associated free energy produced or consumed in each reaction is captured in units of adenosine triphosphate (ATP). The ATP stoichiometry is usually obtained from biochemical tables since the energy has to be also balanced for the cell. Thus for Eq. (7-148) the stoichiometric ATP requirement to convert one C-mole of glucose to one C-mole of glycerol is $\frac{1}{3}$. In calculations of the carbon flux distribution in different pathways this ATP requirement has to be added on the left-hand side of the equation. Again the other form of the cofactor ATP is usually left out to simplify the reaction equation.

There are several metabolic pathways that are repeated for many living cells, and these are split into two: *catabolic* or energy-producing and *anabolic* or energy-consuming, the later producing building blocks such as amino acids and the resulting macromolecules such as proteins. Of course the energy produced in catabolic steps has to be balanced by the energy consumed in anabolic steps. Catabolic pathways include the well-studied *glycolysis*, *TCA cycle*, *oxidative phosphorylation*, and *fermentative pathways*. For more details see Stephanopoulos, Aristidou, and Nielsen, *Metabolic Engineering: Principles and Methodologies*, Academic Press, 1998; and Nielsen, Villadsen, and Liden, *Bioreaction Engineering Principles*, 2d ed., Kluwer, Academic/Plenum Press, 2003; Bailey and Ollis, *Biochemical Engineering Fundamentals*, 2d ed., McGraw-Hill, 1986.

Monod-Type Empirical Kinetics Many bioreactions show increased biomass growth rate with increasing substrate concentration at low substrate concentration for the limiting substrate, but no effect of substrate concentration at high concentrations. This behavior can be represented by the Monod equation (7-92). Additional variations on the Monod equation are briefly illustrated below. For two essential substrates the Monod equation can be modified as

$$\mu = \frac{\mu_{\max}C_{s1}C_{s2}}{(K_{s1} + C_{s2})(K_{s2} + C_{s2})} \quad (7-150)$$

This type of rate expression is often used in models for water treatment, and many environmental factors can be included (the effect of, e.g., phosphate, ammonia, volatile fatty acids, etc.). The correlation between parameters in such complicated models is, however, severe, and very often a simple Monod model (7-92) with only one limiting substrate is sufficient.

When *substrate inhibition* occurs,

$$\mu = \frac{\mu_{\max}C_s}{K_s + C_s + K_i/C_s^2} \quad (7-151)$$

O_2 is typically a substrate that in high concentrations leads to substrate inhibition, but a high concentration of the carbon source can also be inhibiting (e.g., in bioremediation of toxic waste a high concentration of the organic substrate can well lead to severe inhibition or death of the microorganism).

When *product inhibition* is present,

$$\mu = \frac{\mu_{\max}C_s}{K_s + C_s} \left(1 - \frac{C_p}{C_{p\max}} \right) \quad (7-152)$$

Here the typical example is the inhibitor effect of ethanol on yeast growth. Considerable efforts are made by the biocompanies to develop yeast strains that are tolerant to high ethanol concentrations since this will give considerable savings in, e.g., production of biofuel by fermentation.

The various component reaction rates for a single reaction can be related to the growth rate by using the stoichiometric (yield) coefficients, e.g., from Eq. (7-147):

$$r_i = Y_{si}\mu C_x = \frac{Y_{si}}{Y_{sx}}\mu C_x \quad (7-153)$$

7-32 REACTION KINETICS

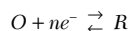
Chemostat with Empirical Kinetics Using the CSTR equation (7-54) for a constant-volume single reaction [Eq. (7-147)], the substrate, biomass, and product material balances are

$$\begin{aligned} \frac{1}{Y_{sx}} \mu C_x + D(C_{s0} - C_s) &= 0 \\ \mu C_x - DC_x &= 0 \rightarrow D = \mu \\ \frac{Y_{sp}}{Y_{sx}} \mu C_x - DC_p &= 0 \end{aligned} \quad (7-154)$$

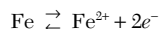
Here C_{s0} is the feed substrate concentration, and D is the *dilution rate*, which at steady-state constant volume is equal to both the feed and effluent volumetric flow rates and to the specific growth rate. The effluent concentrations of substrate, biomass, and products can be calculated by using a suitable expression for the specific growth rate μ such as one of the relevant variants of the Monod kinetics described above.

ELECTROCHEMICAL REACTIONS

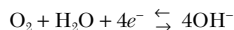
Electrochemical reactions involve coupling between chemical reactions and electric charge transfer and may have two or three phases, for instance, a gas (e.g., H_2 or O_2 evolved at the electrodes or fed as reactants), a liquid (the electrolyte solution), and solids (electrodes). Electrocatalysts may be employed to enhance the reaction for a particular desired product. Hence, electrochemical reactions are heterogeneous reactions that occur at the surface of electrodes and involve the transfer of charge in the form of electrons as part of a chemical reaction. The electrochemical reaction can produce a chemical change by passing an electric current through the system (e.g., electrolysis), or reversely a chemical change can produce electric energy (e.g., using a battery or fuel cell to power an appliance). There are a variety of practical electrochemical reactions, some occurring naturally, such as corrosion, and others used in production of chemicals (e.g., the decomposition of HCl to produce Cl_2 and H_2 , the production of caustic soda and chlorine, the smelting of aluminum), electroplating, and energy generation (e.g., fuel cells and photovoltaics). Electrochemical reactions are reversible and can be generally written as a *reduction-oxidation (redox)* couple:



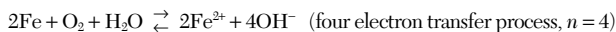
where O is an oxidized and R is a reduced species. For instance, the corrosion process includes oxidation at the *anode*:



and reduction at the *cathode*:



The overall electrochemical reaction is the stoichiometric sum of the anode and cathode reactions:



The anode and cathode reactions are close coupled in that the electric charge is conserved; therefore, the overall production rate is a direct function of the electric charge passed per unit time, the electric current I .

For references on electrochemical reaction kinetics and mechanism, see, e.g., Newman and Thomas-Alvea, *Electrochemical Systems*, 3d ed., Wiley Interscience, 2004; Bard and Faulkner, *Electrochemical Methods: Fundamentals and Applications*, 2d ed., Wiley, 2001; Bethune and Swendeman, "Table of Electrode Potentials and Temperature Coefficients," *Encyclopedia of Electrochemistry*, Van Nostrand Reinhold, New York 1964, pp. 414–424; and Bethune and Swendeman, *Standard Aqueous Electrode Potentials and Temperature Coefficients*, C. A. Hampel Publisher, 1964.

Faraday's law relates the charge transferred by ions in the electrolyte and electrons in the external circuit, to the moles of chemical species reacted (Newman and Thomas-Alvea, *Electrochemical Systems*, 3d ed., Wiley Interscience, 2004):

$$\begin{aligned} Q &= nmF \quad F = 96,485 \text{ C/equiv} \\ I &= \frac{Q}{t} = \frac{\text{charge}}{\text{time}} \quad A \end{aligned} \quad (7-155)$$

where n is the number of equivalents per mole, m is the number of moles, F is the Faraday constant, Q is the charge, and t is time. The total current passed may represent several parallel electrochemical reactions; therefore, we designate a current efficiency for each chemical species. The chemical species production rate (mass/time) is related to the total current passed I , the species *current efficiency* $\epsilon_{\text{current},i}$, and the molecular weight of the chemical species MW_i :

$$\begin{aligned} \dot{m} &= \frac{I \times \epsilon_{\text{current},i} \times MW_i}{nF} = \frac{\text{mass}}{\text{time}} \\ j &= \frac{\text{current}}{\text{area}} = \frac{I}{A_{\text{projected}}} \end{aligned} \quad (7-156)$$

Since electrochemical reactions are heterogeneous at electrode surfaces, the current I is generally normalized by dividing it by the geometric or projected area of the electrode, resulting in the quantity known as the *current density* j , in units of kA/m^2 .

The overall electrochemical cell *equilibrium potential* E°_{cell} , as measured between the cathode and the anode, is related to the Gibbs free energy change for the overall electrochemical reaction:

$$\begin{aligned} \Delta G^\circ &= \Delta H^\circ - T \Delta S^\circ = -nFE^\circ_{\text{cell}} \\ E^\circ_{\text{cell}} &= -\frac{\Delta G^\circ}{nF} = E^\circ_{\text{cathode}} - E^\circ_{\text{anode}} \end{aligned} \quad (7-157)$$

Each electrode reaction, anode and cathode, or half-cell reaction has an associated energy level or electrical potential (volts) associated with it. Values of the standard equilibrium electrode reduction potentials E° at unit activity and $25^\circ C$ may be obtained from the literature (de Bethune and Swendeman Loud, *Encyclopedia of Electrochemistry*, Van Nostrand Reinhold, 1964). The overall electrochemical cell *equilibrium potential* either can be obtained from ΔG values or is equal to the cathode half-cell potential minus the anode half-cell potential, as shown above.

The *Nernst equation* allows one to calculate the *equilibrium potential* E^{eq} when the activity of the reactants or products is not at unity:

$$\begin{aligned} \sum_i \nu_i M_i^{\nu_i} &\rightarrow ne^- \\ E^{\text{eq}} &= E^\circ - \frac{RT}{nF} \ln(\Pi a_i^{\nu_i}) \\ \left(\frac{\partial E}{\partial T} \right)_p &= \frac{\Delta S}{nF} \end{aligned} \quad (7-158)$$

where ν_i is the stoichiometric coefficient of chemical species i (positive for products; negative for reactants), M_i is the symbol for species i , n_i is the charge number of the species, a_i is the activity of the chemical species, E is the *formal potential*, and Π represents the product of all respective activities raised to their stoichiometric powers as required by the reaction. Please note that if the value of the equilibrium potential is desired at another temperature, E° must also be evaluated at the new temperature as indicated.

Kinetic Control In 1905, Julius Tafel experimentally observed that when mass transport was not limiting, the *current density* j of electrochemical reactions exhibited the following behavior:

$$j = a' e^{\eta_{\text{act}}/b'} \quad \text{or} \quad \eta_{\text{act}} = a + b \log j$$

where the quantity η_{act} is known as the *activation overpotential* $E - E^{\text{eq}}$, and is the difference between the actual electrode potential

E and the reversible equilibrium potential of the electrochemical reaction E^{eq} . Thus the driving force for the electrochemical reaction is not the absolute potential; it is the activation overpotential η_{act} .

This relationship between the current density and activation overpotential has been further developed and resulted in the Butler-Volmer equation:

$$r = \frac{j}{nF} = k_f C_o - k_r C_r \quad j = j_0 (e^{-(\alpha_a F/RT)\eta_{act}} - e^{[(1-\alpha_c)F/RT]\eta_{act}})$$

$$\eta_{act} = E - E^{eq} \quad (7-159)$$

Here the reaction rate r is defined per unit electrode area, moles per area per time, j_0 is the *equilibrium exchange current* when $E = E^{eq}$, η_{act} is the *activation overpotential*, and α is the *transfer coefficient*. For large activation overpotentials, the *Tafel empirical equation* applies:

$$\eta_{act} = a + b \log j \quad \text{for } \eta_{act} > 100 \text{ mV, } b = \text{Tafel slope} \quad (7-160)$$

For small activation overpotentials, linearization gives

$$j = j_0 \frac{nF}{RT} \eta_{act} \quad (7-161)$$

Mass-Transfer Control The surface concentration at the electrodes differs significantly from the bulk electrolyte concentration. The Nernst equation applies to the surface concentrations (or activities in case of nonideal solutions):

$$E^{eq} = E^o - \frac{RT}{nF} \ln(\Pi a_{i,surf}^{\nu_i}) \quad (7-162)$$

DETERMINATION OF MECHANISM AND KINETICS

Laboratory data are the predominant source for reaction mechanism and kinetics in industrial practice. However, often laboratory data intended for scoping and demonstration studies rather than for kinetic evaluation have to be used, thus reducing the effectiveness and accuracy of the resulting kinetic model. The following are the steps required to obtain kinetics from laboratory data:

1. Develop initial guesses on mechanism, reaction time scale, and potential kinetic models from the literature, scoping experiments, similar chemistries, and computational chemistry calculations, when possible.

2. Select a suitable laboratory reactor type and scale, and analytical tools for kinetic measurements.

3. Develop a priori factorial experimental design or sequential experimental design.

4. When possible, provide ideal reactor conditions, e.g., good mechanical agitation in batch and CSTR, high velocity flow in PFR.

5. Estimate the limiting diffusion-reaction regimes under the prevailing lab reactor conditions for heterogeneous reactions, and use the appropriate lab reactor model. When possible, operate the reactor under kinetic control.

6. Discriminate between competing mechanisms and kinetic rates by forcing maximum differentiation between competing hypotheses through the experimental design, and by obtaining the best fit of the kinetic data to the proposed kinetic forms.

LABORATORY REACTORS

Selection of the laboratory reactor type and size, and associated feed and product handling, control, and analytical schemes depends on the type of reaction, reaction time scales, and type of analytical methods required. The criteria for selection include equipment cost, ease of operation, ease of data analysis, accuracy, versatility, temperature uniformity, and controllability, suitability for mixed phases, and scale-up

If mass transfer is limiting, then a *limiting current* is obtained for each chemical species i :

$$j_{i,lim} = \frac{nFD_i C_i}{\delta} = nFk_{L,i} C_i \quad (7-163)$$

where D_i is the diffusion coefficient, δ is the boundary layer thickness, and $k_{L,i}$ is the mass-transfer coefficient of species i . The effect of mass transfer is included as follows:

$$j = j_0 \left[\left(1 - \frac{j}{j_{a,lim}} \right) e^{-(\alpha_a F/RT)\eta_{act}} - \left(1 - \frac{j}{j_{c,lim}} \right) e^{[(1-\alpha_c)F/RT]\eta_{act}} \right]$$

$$\frac{C_{i,surf}}{C_i} = \left(1 - \frac{j}{j_{i,lim}} \right) \quad i = o, r \quad (7-164)$$

Ohmic Control The overall electrochemical reactor cell voltage may be dependent on the kinetic and mass-transfer aspects of the electrochemical reactions; however, a third factor is the potential lost within the electrolyte as current is passing through this phase. The potential drops may become dominant and limit the electrochemical reactions requiring an external potential to be applied to drive the reactions or significantly lower the delivered electrical potential in power generation applications such as batteries and fuel cells.

Multiple Reactions With multiple reactions, the total current is the sum of the currents from the individual reactions with anodic currents positive and cathodic currents negative. This is called the *mixed potential principle*. For more details see Bard and Faulkner, *Electrochemical Methods: Fundamentals and Applications*, 2d ed., Wiley, 2001.

feasibility. Many configurations of laboratory reactors have been employed. Rase (*Chemical Reactor Design for Process Plants*, Wiley, 1977) and Shah (*Gas-Liquid-Solid Reactor Design*, McGraw-Hill, 1979) each have about 25 sketches, and Shah's bibliography has 145 items classified into 22 categories of reactor types. Jankowski et al. [*Chemische Technik* 30: 441-446 (1978)] illustrate 25 different kinds of gradientless laboratory reactors for use with solid catalysts.

Laboratory reactors are of two main types:

1. Reactors used to obtain fundamental data on intrinsic chemical rates free of mass-transfer resistances or other complications. Some of the gas-liquid lab reactors, for instance, employ known interfacial areas, thus avoiding the uncertainty regarding the area for gas to liquid mass transfer. When ideal behavior cannot be achieved, intrinsic kinetic estimates need to account for mass- and heat-transfer effects.

2. Reactors used to obtain scale-up data due to their similarity to the reactor intended for the pilot or commercial plant scale. How to scale down from the conceptual commercial or pilot scale to lab scale is a difficult problem in itself, and it is not possible to maintain all key features while scaling down.

The first type is often the preferred one—once the intrinsic kinetics are obtained at “ideal” lab conditions, scale-up is done by using models or correlations that describe large-scale reactor hydrodynamics coupled with the intrinsic kinetics. However, in some cases ideal conditions cannot be achieved, and the laboratory reactor has to be adequately modeled to account for mass and heat transfer and non-ideal mixing effects to enable extraction of intrinsic kinetics. In addition, with homogeneous reactions, attention must be given to prevent wall-catalyzed reactions, which can result in observed kinetics that are fundamentally different from intrinsic homogeneous kinetics. This is a problem for scale-up, due to the high surface/volume ratio in small reactors versus the low surface/volume ratio in large-scale systems, resulting in widely different contributions of wall effects at different scales. Similar issues arise in bioreactors with the potential of

undesirable wall growth of the biocatalyst cells masking the homogeneous growth kinetics. In catalytic reactions certain reactor configurations may enhance undesirable homogeneous reactions, and the importance of these reactions may be different at larger scale, causing potential scale-up pitfalls.

The reaction rate is expressed in terms of chemical compositions of the reacting species, so ultimately the variation of composition with time or space must be found. The composition is determined in terms of a property that is measured by some instrument and calibrated. Among the measures that have been used are titration, pressure, refractive index, density, chromatography, spectrometry, polarimetry, conductimetry, absorbance, and magnetic resonance. Therefore, batch or semibatch data are converted to composition as a function of time (C, t), or to composition and temperature as functions of time (C, T, t), to prepare for kinetic analysis. In a steady CSTR and PFR, the rate and compositions in the effluent are observed as a function of residence time.

When a reaction has many reactive species (which may be the case even for apparently simple processes such as pyrolysis of ethane or synthesis of methanol), a factorial or sequential experimental design should be developed and the data can be subjected to a *response surface analysis* (Box, Hunter, and Hunter, *Statistics for Experimenters*, 2d ed., Wiley Interscience, 2005; Davies, *Design and Analysis of Industrial Experiments*, Oliver & Boyd, 1954). This can result in a black box correlation or statistical model, such as a quadratic (limited to first- and second-order effects) for the variables x_1, x_2 , and x_3 :

$$r = k_1x_1 + k_2x_2 + k_3x_3 + k_{12}x_1x_2 + k_{13}x_1x_3 + k_{23}x_2x_3$$

Analysis of such statistical correlations may reveal the significant variables and interactions and may suggest potential mechanisms and kinetic models, say, of the Langmuir-Hinshelwood type, that could be analyzed in greater detail by a regression process. The variables x_i could be various parameters of heterogeneous processes as well as concentrations. An application of this method to isomerization of *n*-pentane is given by Kittrel and Erjavec [*Ind. Eng. Chem. Proc. Des. Dev.* 7: 321 (1968)].

Table 7-11 summarizes laboratory reactor types that approach the three ideal concepts BR, CSTR and PFR, classified according to reaction types.

TABLE 7-11 Laboratory Reactors

Reaction	Reactor
Homogeneous gas	Isothermal U-tube in temperature-controlled batch
Homogeneous liquid	Mechanically agitated batch or CSTR with jacketed cooling/heating
Catalytic gas-solid	Packed tube in furnace Isothermal U-tube in temperature-controlled bath Rotating basket with jacketed cooling/heating Internal recirculation (Berty) reactor with jacketed cooling/heating
Noncatalytic gas-solid	Packed tube in furnace
Liquid-solid	Packed tube in furnace
Gas-liquid	CSTR with jacketed cooling/heating Fixed interface CSTR Wetted wall Laminar jet
Gas-liquid-solid	Slurry CSTR with jacketed cooling/heating Packed bed with downflow, upflow, or countercurrent
Solid-solid	Packed tube in furnace

For instance, Fig. 7-17 summarizes laboratory reactor types and hydrodynamics for gas-liquid reactions.

Batch Reactors In the simplest kind of investigation, reactants can be loaded into a number of sealed tubes, kept in a thermostatic bath for various periods, shaken mechanically to maintain uniform composition, and analyzed. In terms of cost and versatility, the stirred batch reactor is the unit of choice for homogeneous or heterogeneous slurry reactions including gas-liquid and gas-liquid-solid systems. For multiphase systems the reactants can be semibatch or continuous. The BR is especially suited to reactions with half-lives in excess of 10 min. Samples are taken at time intervals, and the reaction is stopped by cooling, by dilution, or by destroying a residual reactant such as an acid or base; analysis can then be made at a later time. Analytic methods that do not necessitate termination of reaction include noninvasive measurements of (1) the amount of gas produced, (2) the gas pressure in a constant-volume vessel, (3) absorption of light, (4) electrical or thermal conductivity, (5) polarography, (6) viscosity of polymerization, (7) pH and DO probes, and so on. Operation may be isothermal, with the important effect of temperature determined from several isothermal runs, or the composition and temperature may be recorded simultaneously and the


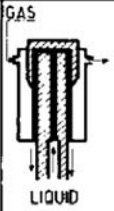
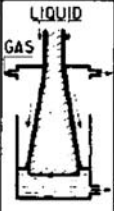
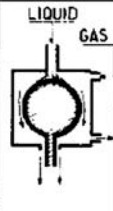
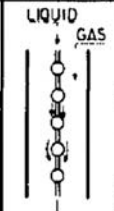

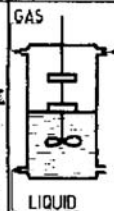
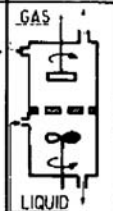
TYPE	LAMINAR JET	CYLINDRICAL WETTED WALL	CONIC WETTED WALL	SPHERICAL WETTED WALL	STRING OF DISKS	ROTATING DRUM	STIRRED VESSEL	STIRRED VESSEL
SCHEME								
k_L cm/sec	0.016 -0.16	$3.6 \cdot 10^{-3}$ -0.016	$5 \cdot 10^{-3}$ -0.011	$5 \cdot 10^{-3}$ -0.016	$3.6 \cdot 10^{-3}$ -0.016	0.016 -0.36	$1.6 \cdot 10^{-3}$ -0.02	$2 \cdot 10^{-3}$ -0.02
CONTACT TIMES	10^{-3} - 10^{-1} sec	10^{-1} -2 sec	0.2-1 sec	0.1-1 sec	10^{-1} -2 sec	$2 \cdot 10^{-4}$ -10 sec	0.06-10 sec	0.08-10 sec
INTERFACIAL AREA	0.3-10 cm ² high precision	10-100 cm ² high precision	80 cm ² high precision	10-40 cm ² high precision	30-360 cm ² moderate precision	diameter 10 cm length 12 cm high precision	80 cm ² good precision	diameter 10 cm length 15 cm 2-30% open

FIG. 7-17 Principal types of laboratory reactors for gas-liquid reactions. [From Fig. 8 in J. C. Charpentier, "Mass Transfer Rates in Gas-Liquid Absorbers and Reactors," in Drew et al. (eds.), *Advances in Chemical Engineering*, vol. 11, Academic Press, 1981.]

data regressed. On the laboratory scale, it is essential to ensure that a BR is stirred to uniform composition, and for critical cases such as high viscosities this should be checked with tracer tests.

Flow Reactors CSTRs and other devices that require flow control are more expensive and difficult to operate. However, CSTRs and PFRs are the preferred laboratory reactors for steady operation. One of the benefits of CSTRs is their isothermicity and the fact that their mathematical representation is algebraic, involving no differential equations, thus making data analysis simpler. For laboratory research purposes, CSTRs are considered feasible for holding times of 1 to 4000 s, reactor volumes of 2 to 1000 cm³ (0.122 to 61 in³), and flow rates of 0.1 to 2.0 cm³/s. Fast reactions and those in the gas phase are generally done in tubular flow reactors, just as they are often done on the commercial scale. Usually it is not possible to measure compositions along a PFR, although temperatures can be measured using a thermowell with fixed or mobile thermocouple bundle. PFRs can be kept at nearly constant temperatures; small-diameter tubes immersed in a fluidized sand bed or molten salt can hold quite constant temperatures of a few hundred degrees. Other PFRs are operated at near adiabatic conditions by providing dual radial temperature control to minimize the radial heat flux, with multiple axial zones. A recycle unit can be operated as a differential reactor with arbitrarily small conversion and temperature change. Test work in a tubular flow unit may be desirable if the intended commercial unit is of that type.

Multiphase Reactors Reactions between gas-liquid, liquid-liquid, and gas-liquid-solid phases are often tested in CSTRs. Other laboratory types are suggested by the commercial units depicted in appropriate sketches in Sec. 19 and in Fig. 7-17 [Charpentier, *Mass Transfer Rates in Gas-Liquid Absorbers and Reactors*, in Drew et al. (eds.), *Advances in Chemical Engineering*, vol. 11, Academic Press, 1981]. Liquids can be reacted with gases of low solubilities in stirred vessels, with the liquid charged first and the gas fed continuously at the rate of reaction or dissolution. Some of these reactors are designed to have known interfacial areas. Most equipment for gas absorption without reaction is adaptable to absorption with reaction. The many types of equipment for liquid-liquid extraction also are adaptable to reactions of immiscible liquid phases.

Solid Catalysts Processes with solid catalysts are affected by diffusion of heat and mass (1) within the pores of the pellet, (2) between the fluid and the particle, and (3) axially and radially within the packed bed. Criteria in terms of various dimensionless groups have been developed to tell when these effects are appreciable, and some of these were discussed above. For more details see Mears [*Ind. Eng. Chem. Proc. Des. Devel.* **10**: 541–547 (1971); *Ind. Eng. Chem. Fund.* **15**: 20–23 (1976)] and Satterfield (*Heterogeneous Catalysis in Practice*, McGraw-Hill, 1991, p. 491). For catalytic investigations, the rotating basket or fixed basket with internal recirculation is the standard device, usually more convenient and less expensive than equipment with external recirculation. In the fixed-basket type, an internal recirculation rate of 10 to 15 or so times the feed rate effectively eliminates external diffusional resistance, and temperature gradients (see, e.g., Berty, *Experiments in Catalytic Reaction Engineering*, Elsevier, 1999). A unit holding 50 cm³ (3.05 in³) of catalyst can operate up to 800 K (1440°R) and 50 bar (725 psi). When deactivation occurs rapidly (in a few seconds during catalytic cracking, for instance), the fresh activity can be maintained with a transport reactor through which both reactants and fresh catalyst flow without slip and with short contact time. Since catalysts often are sensitive to traces of impurities, the time deactivation of the catalyst usually can be evaluated only with commercial feedstock. Physical properties of catalysts also may need to be checked periodically, including pellet size, specific surface, porosity, pore size and size distribution, effective diffusivity, and active metals content and dispersion. The effectiveness of a porous catalyst is found by measuring conversions with successively smaller pellets until no further change occurs. These topics are touched on by Satterfield (*Heterogeneous Catalysis in Industrial Practice*, McGraw-Hill, 1991).

To determine the deactivation kinetics, long-term deactivation studies at constant conditions and at different temperatures are required. In some cases, accelerated aging can be induced to reduce the time required for the experimental work, by either increasing the feed flow

rate (if the deactivation is a result of feed or product poisoning) or increasing the temperature above the standard reaction temperature. These require a good understanding of how the higher-temperature or rate-accelerated deactivation correlates with deactivation at the operating reaction temperature and rate.

Bioreactors There are several types of laboratory bioreactors used with live organisms as biocatalysts:

1. Mechanically agitated batch/semibatch with pH control and nutrients or other species either fed at the start or added continuously based on a recipe or protocol.

2. CSTR to maintain a constant *dilution rate* (the feed rate). These require some means to separate the biocatalyst from the product and recycle to the reactor, such as centrifuge or microfiltration:

a. *Chemostat* controls the flow to maintain a constant fermentation volume.

b. *Turbidostat* controls the biomass or cells concentration.

c. *pH-auxostat* controls pH in the effluent (same as pH in reactor).

d. *Productostat* controls the effluent concentration of one of the metabolic products.

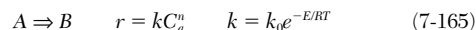
The preferred reactor for kinetics is the chemostat, but semibatch reactors are more often used owing to their simpler operation.

Calorimetry Another category of laboratory systems that can be used for kinetics includes *calorimeters*. These are primarily used to establish temperature effects and thermal runaway conditions, but can also be employed to determine reaction kinetics. Types of calorimeters are summarized in Table 7-12; for more details see Reid, "Differential Microcalorimeters," *J. Physics E: Scientific Instruments*, **9** (1976).

Additional methods of laboratory data acquisition are described in Masel, *Chemical Kinetics and Catalysis*, Wiley, 2001.

KINETIC PARAMETERS

The kinetic parameters are constants that appear in the intrinsic kinetic rate expressions and are required to describe the rate of a reaction or reaction network. For instance, for the simple global *n*th-order reaction with Arrhenius temperature dependence:



The kinetic parameters are k_0 , E , and n , and knowledge of these parameters and the prevailing concentration and temperature fully determines the reaction rate.

For a more complex expression such as the Langmuir-Hinshelwood rate for gas reaction on heterogeneous catalyst surface with equilibrium adsorption of reactants *A* and *B* on two different sites and non-adsorbing products, Eq. (7-85) can be rewritten as

$$r = \frac{k_0 e^{-E/RT} P_a P_b}{(1 + K_{a0} e^{-E_a/RT})(1 + K_{b0} e^{-E_b/RT})} \quad (7-166)$$

and the kinetic parameters are k_0 , E , K_{a0} , E_{a0} , K_{b0} , and E_{b0} .

A number of factors limit the accuracy with which parameters needed for the design of commercial equipment can be determined. The kinetic parameters may be affected by inaccurate accounting for laboratory reactor heat and mass transport, and hydrodynamics; correlations for these are typically determined under nonreacting conditions at ambient temperature and pressure and with nonreactive model fluids and may not be applicable or accurate at reaction conditions. Experimental uncertainty including errors in analysis, measurement,

TABLE 7-12 Calorimetric Methods

Adiabatic	Nonadiabatic
Accelerating rate calorimeter (ARC)	Reaction calorimeter (RC1) + IR
Vent sizing package (VSP) calorimeter	Differential scanning calorimeter (DSC)
PHI-TEC	Thermal gravimetry (TG)
Dewar	Isothermal calorimetry
Automatic pressure tracking adiabatic calorimeter (APTAC)	Differential thermal analysis (DTA)
	Differential microcalorimeters
	Advanced reaction system
	screening tool (ARSSST)

and control is also a contributing factor (see, e.g., Hoffman, "Kinetic Data Analysis and Parameter Estimation," in de Lasa (ed.), *Chemical Reactor Design and Technology*, Martinus Nijhoff, 1986.

DATA ANALYSIS METHODS

In this section we focus on the three main types of ideal reactors: BR, CSTR, and PFR. Laboratory data are usually in the form of concentrations or partial pressures versus batch time (batch reactors), concentrations or partial pressures versus distance from reactor inlet or residence time (PFR), or rates versus residence time (CSTR). Rates can also be calculated from batch and PFR data by differentiating the concentration versus time or distance data, usually by numerical curve fitting first. It follows that a general classification of experimental methods is based on whether the data measure rates directly (differential or direct method) or indirectly (integral of indirect method). Table 7-13 shows the pros and cons of these methods.

Some simple reaction kinetics are amenable to analytical solutions and graphical linearized analysis to calculate the kinetic parameters from rate data. More complex systems require numerical solution of nonlinear systems of differential and algebraic equations coupled with nonlinear parameter estimation or regression methods.

Differential Data Analysis As indicated above, the rates can be obtained either directly from differential CSTR data or by differentiation of integral data. A common way of evaluating the kinetic parameters is by rearrangement of the rate equation, to make it linear in parameters (or some transformation of parameters) where possible. For instance, using the simple n th-order reaction in Eq. (7-165) as an example, taking the natural logarithm of both sides of the equation results in a linear relationship between the variables $\ln r$, $1/T$, and $\ln C_a$:

$$\ln r = \ln k_0 - \frac{E}{RT} + n \ln C_a \quad (7-167)$$

Multilinear regression can be used to find the constants k_0 , E , and n . For constant-temperature (isothermal) data, Eq. (7-167) can be simplified by using the Arrhenius form as

$$\ln r = \ln k + n \ln C_a \quad (7-168)$$

and the kinetic parameters n and k can be determined as the intercept and slope of the best straight-line fit to the data, respectively, as shown in Fig. 7-18.

The preexponential k_0 and activation energy E can be obtained from multiple isothermal data sets at different temperatures by using the linearized form of the Arrhenius equation

$$\ln k = \ln k_0 - \frac{E}{RT} \quad (7-169)$$

as shown in Fig. 7-19.

Integral Data Analysis Integral data such as from batch and PFR relate concentration to time or distance. Integration of the BR equation for an n th-order homogeneous constant-volume reaction yields

TABLE 7-13 Comparison of Direct and Indirect Methods

Direct method	Indirect method
Advantages	Disadvantages
Get rate equation directly	Must infer rate equation
Easy to fit data to a rate law	Hard to analyze rate data
High confidence on final rate equation	Low confidence on final rate equation
Disadvantages	Advantages
Difficult experiment	Easier experiment
Need many runs	Can do a few runs and get important information
Not suitable for very fast or very slow reactions	Suitable for all reactions including very fast or very slow ones

SOURCE: Masel, *Chemical Kinetics and Catalysis*, Wiley, 2001, Table 3.2.

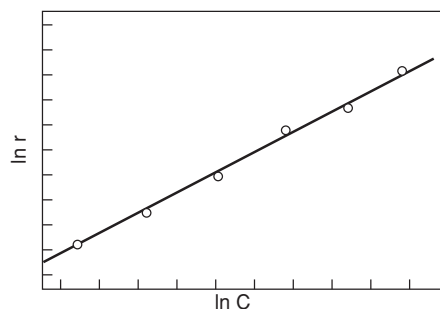


FIG. 7-18 Determination of the rate constant and reaction order.

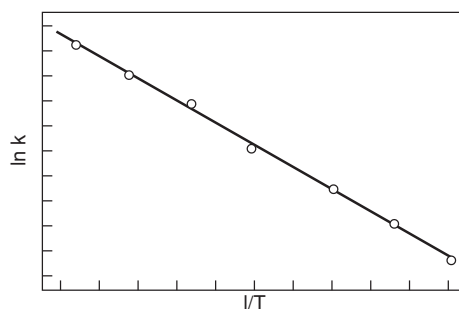


FIG. 7-19 Determination of the activation energy.

$$\ln \frac{C_{a0}}{C_a} = k\tau \quad \text{for } n = 1 \quad (7-170)$$

$$\left(\frac{C_{a0}}{C_a} \right)^{n-1} = 1 + k\tau(n-1)C_{a0}^{n-1} \quad \text{for } n \neq 1$$

For the first-order case, the rate constant k can be obtained directly from the slope of the graph of the left-hand side of Eq. (7-170) versus batch time, as shown in Fig. 7-20.

For orders other than first, plotting the natural log of Eq. (7-170) can at least indicate if the order is larger or smaller than 1, as shown in Fig. 7-21.

The Half-Life Method The half-life is the batch time required to get 50 percent conversion. For an n th-order reaction,

$$\tau_{1/2} = \frac{\ln 2}{k} \quad \text{for } n = 1 \quad (7-171)$$

$$\tau_{1/2} = \frac{2^{n-1} - 1}{(n-1)kC_{a0}^{n-1}} \quad \text{for } n \neq 1$$

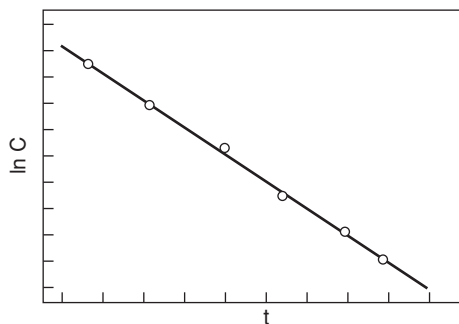


FIG. 7-20 Determination of first-order rate constant from integral data.

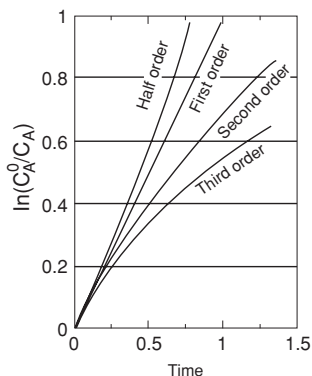


FIG. 7-21 Reaction behavior for n th-order reaction. (Masek, *Chemical Kinetics and Catalysis*, Wiley, 2001, Fig. 3.15.)

Thus for first-order reactions, the *half-life* is constant and independent of the initial reactant concentration and can be used directly to calculate the rate constant k . For non-first-order reactions, Eq. (7-171) can be linearized as follows:

$$\ln \tau_{1/2} = \ln \frac{2^{n-1} - 1}{(n-1)k} - (n-1) \ln C_{a0} \quad \text{for } n \neq 1 \quad (7-172)$$

The reaction order n can be obtained from the slope and the rate constant k from the intercept of the plot of Eq. (7-172), shown in Fig. 7-22.

Complex Rate Equations The examples above are for special cases amenable to simple treatment. Complex rate equations and reaction networks with complex kinetics require individual treatment, which often includes both numerical solvers for the differential and algebraic equations describing the laboratory reactor used to obtain the data and linear or nonlinear parameter estimation.

PARAMETER ESTIMATION

The straightforward method to obtain kinetic parameters from data is the numerical fitting of the concentration data (e.g., from BR or PFR) to integral equations, or the rate data (e.g., from a CSTR or from differentiation of BR or PFR) to rate equations. This is done by parameter estimation methods described here. An excellent reference for experimental design and parameter estimation (illustrated for heterogeneous gas-solid reactions) is the review paper of Froment and Hosten, "Catalytic Kinetics—Modeling," in *Catalysis—Science and Technology*, Springer-Verlag, New York, 1981. Two previous papers devoted to this topic by Hofmann [in *Chemical Reaction Engineering*, ACS *Advances in Chemistry*, **109**: 519–534 (1972); in de Lasa (ed.),

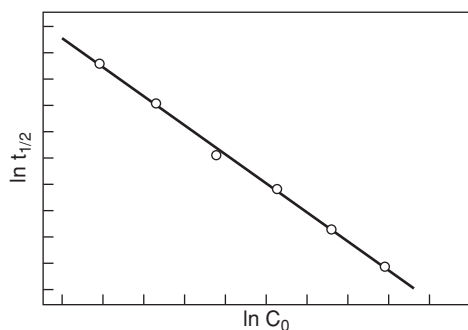


FIG. 7-22 Determination of reaction order and rate constant from half-life data.

Chemical Reactor Design and Technology, Martinus Nijhoff, 1985, pp. 69–105] are also very useful. As indicated above, the acquisition of kinetic data and parameter estimation can be a complex endeavor. It includes statistical design of experiments, laboratory equipment, computer-based data acquisition, complex analytical methods, and statistical evaluation of the data.

Regression is the procedure used to estimate the kinetic parameters by fitting kinetic model predictions to experimental data. When the parameters can be made to appear linear in the kinetic model (through transformations, grouping of parameters, and rearrangement), the regression is linear, and an accurate fit to data can be obtained, provided the form of the kinetic model represents well the reaction kinetics and the data provide enough width in temperature, pressure, and composition for statistically significant estimates. Often such linearization is not possible.

Linear Models in Parameters, Single Reaction We adopt the terminology from Froment and Hosten, "Catalytic Kinetics—Modeling," in *Catalysis—Science and Technology*, Springer-Verlag, New York, 1981. For n observations (experiments) of the concentration vector y for a model linear in the parameter vector β of length $p < n$, the *residual error* ϵ is the difference between the kinetic model-predicted values and the measured data values:

$$\epsilon = y - X\beta = y - \hat{y} \quad (7-173)$$

The linear model is represented as a linear transformation of the parameter vector β through the model matrix X . Estimates b of the true parameters β are obtained by minimizing the *objective function* $S(\beta)$, the *sum of squares of the residual errors*, while varying the values of the parameters:

$$S(\beta) = \epsilon^T \epsilon = \sum_{i=1}^n (y_i - \hat{y}_i)^2 \xrightarrow{\beta} \text{Min} \quad (7-174)$$

This linear optimization problem, subject to constraints on the possible values of the parameters (e.g., requiring positive preexponentials, activation energies, etc.) can be solved to give the estimated parameters:

$$b = (X^T X)^{-1} X^T y \quad (7-175)$$

When the error is *normally distributed* and has zero mean and variance σ^2 , then the *variance-covariance matrix* $V(b)$ is defined as

$$V(b) = (X^T X)^{-1} \sigma^2 \quad (7-176)$$

An estimate for σ^2 , denoted s^2 , is

$$s^2 = \frac{\sum_{i=1}^n (y_i - \hat{y}_i)^2}{n - p} \quad (7-177)$$

When $V(b)$ is known from experimental observations, a *weighted objective function* should be used for optimization of the objective function:

$$S(\beta) = \epsilon^T V^{-1} \epsilon \xrightarrow{\beta} \text{Min} \quad (7-178)$$

and the estimates b are obtained as

$$b = (X^T V^{-1} X)^{-1} X^T V^{-1} y \quad (7-179)$$

The parameter fit is adequate if the *F test* is satisfied, that is, F_c , the calculated F , is larger than the tabulated statistical one at the *confidence level* of $1 - \alpha$:

$$F_c = \frac{\text{LFSS}}{n - p - n_e + 1} \geq F(n - p - n_e + 1, n_e - 1; 1 - \alpha) \quad (7-180)$$

PESS
n_e - 1

7-38 REACTION KINETICS

$$\text{LFSS} = \sum_{i=1}^n (y_i - \hat{y}_i)^2 - \sum_{i=1}^{ne} (y_i - \bar{y}_i)^2 \quad \text{PESS} = \sum_{i=1}^{ne} (y_i - \bar{y}_i)^2$$

Here \bar{y}_i are the averaged values of the data for replicates. Equation (7-180) is valid if there are n replicate experiments and the pure error sum of squares (PESS) is known. Without replicates,

$$F_c = \frac{\frac{\text{RgSS}}{p}}{\frac{\text{RSS}}{n-p}} \geq F(p, n-p; 1-\alpha) \quad \text{RgSS} = \sum_{i=1}^n \hat{y}_i^2$$

$$\text{RSS} = \sum_{i=1}^n (y_i - \hat{y}_i)^2 \quad (7-181)$$

The bounds on the parameter estimates are given by the t statistics:

$$b_i - t\left(n-p; 1 - \frac{\alpha}{2}\right) \leq \beta_i \leq b_i + t\left(n-p; 1 - \frac{\alpha}{2}\right) \quad (7-182)$$

An example of a linear model in parameters is Eq. (7-167), where the parameters are $\ln k_0$, E , and n , and the linear regression can be used directly to estimate these.

Nonlinear Models in Parameters, Single Reaction In practice, the parameters appear often in nonlinear form in the rate expressions, requiring nonlinear regression. Nonlinear regression does not guarantee optimal parameter estimates even if the kinetic model adequately represents the true kinetics and the data width is adequate. Further, the statistical tests of model adequacy apply rigorously only to models linear in parameters, and can only be considered approximate for nonlinear models.

For a general nonlinear model $f(x_i, \beta)$, where x is the vector of the independent model variables and β is the vector of parameters,

$$\varepsilon = y - f(x, \beta) \quad (7-183)$$

An example of a model nonlinear in parameters is Eq. (7-166). Here it is not possible through any number of transformations to obtain a linear form in all the parameters k_0 , E , K_{ab} , E_{aa} , K_{bb} , E_{ab} . Note that for some Langmuir-Hinshelwood rate expressions it is possible to linearize the model in parameters at isothermal conditions and obtain the kinetic constants for each temperature, followed by Arrhenius-type plots to obtain activation energies (see, e.g., Churchill, *The Interpretation and Use of Rate Data: The Rate Concept*, McGraw-Hill, 1974).

Minimization of the sum of squares of residuals does not result in a closed form for nonlinear parameter estimates as for the linear case; rather it requires an iterative numerical solution, and having a reasonable initial estimate for the parameter values and their feasible ranges is critical for success. Also, the minima in the residual sum of squares are local and not global. To obtain global minima that better represent the kinetics over a wide range of conditions, parameter estimation has to be repeated with a wide range of initial parameter guesses to increase the chance of reaching the global minimum. The nonlinear regression procedure typically involves a *steepest descent* optimization search combined with *Newton's linearization* method when a minimum is approached, enhancing the convergence speed [e.g., the *Marquardt-Levenberg* or *Newton-Gauss* method; Marquardt, *J. Soc. Ind. Appl. Math.* **2**: 431 (1963)].

An integral part of the parameter estimation methodology is *mechanism discrimination*, i.e., selection of the best mechanism that would result in the best kinetic model. Nonlinear parameter estimation is an extensive topic and will not be further discussed here. For more details see Froment and Hosten, "Catalytic Kinetics—Modeling," in *Catalysis—Science and Technology*, Springer-Verlag, New York, 1981.

Network of Reactions The statistical parameter estimation for multiple reactions is more complex than for a single reaction. As indicated before, a single reaction can be represented by a single con-

centration [e.g., Eq. 7-39]. With a network of reactions, there are a number of dependent variables equal to the number of stoichiometrically independent reactions, also called *responses*. In this case the objective function has to be modified. For details see Froment and Hosten, "Catalytic Kinetics—Modeling," in *Catalysis—Science and Technology*, Springer-Verlag, New York, 1981.

THEORETICAL METHODS

Prediction of Mechanism and Kinetics Reaction mechanisms for a variety of reaction systems can be predicted to some extent by following a set of heuristic rules derived from experience with a wide range of chemistries. For instance, Masel, *Chemical Kinetics and Catalysis*, Wiley, 2001, chapter 5, enumerates the rules for gas-phase chain and nonchain reactions including limits on activation energies for various elementary steps. Other reaction systems such as ionic reactions, and reactions on metal and acid surfaces, are also discussed by Masel, although these mechanisms are not as well understood. Nevertheless, the rules can lead to computer-generated mechanisms for complex systems such as homogeneous gas-phase combustion and partial oxidation of methane and higher hydrocarbons. Developments in computational chemistry methods allow, in addition to the derivation of most probable elementary mechanisms, prediction of thermodynamic and kinetic reaction parameters for relatively small molecules in homogeneous gas-phase and liquid-phase reactions, and even for some heterogeneous catalytic systems. This is especially useful for complex kinetics where there is no easily discernible rate-determining step, and therefore no simple closed-form global reaction rate can be determined. In particular, estimating a large number of kinetic parameters from laboratory data requires a large number of experiments and use of intermediate reaction components that are not stable or not readily available. The nonlinear parameter estimation with many parameters is difficult, with no assurance that global minima are actually obtained. For such complex systems, computational chemistry estimates are an attractive starting point, requiring experimental validation.

Computational chemistry includes a wide range of methods of varying accuracy and complexity, summarized in Table 7-14. Many of these methods have been implemented as software packages that require high-speed supercomputers or parallel computers to solve realistic reactions. For more details on computational chemistry, see, e.g., Cramer, *Essentials of Computational Chemistry: Theories and Models*, 2d ed., Wiley, 2004.

Lumping and Mechanism Reduction It is often useful to reduce complex reaction networks to a smaller reaction set which still maintains the key features of the detailed reaction network but with a much smaller number of representative species, reactions, and kinetic parameters. Simple examples were already given above for reducing simple networks into global reactions through assumptions such as pseudo-steady state, rate-limiting step, and equilibrium reactions.

In general, *mechanism reduction* can only be used over a limited range of conditions for which the simplified system simulates the original complete reaction network. This reduces the number of kinetic parameters that have to be either estimated from data or calculated by

TABLE 7-14 Computational Chemistry Methods

Abinitio methods (no empirical parameters)	
Electronic structure determination (time-independent Schrodinger equation)	
Hartree-Fock (HF) with corrections	
Quantum Monte Carlo (QMT)	
Density functional theory (DFT)	
Chemical dynamics determination (time-dependent Schrodinger equation)	
Split operator technique	
Multiconfigurational time-dependent Hartree-Fock method	
Semiclassical method	
Semiempirical methods (approximate parts of HF calculations such as two-electron integrals)	
Huckel	
Extended Huckel	
Molecular mechanics (avoids quantum mechanical calculations)	
Empirical methods (group contributions)	
Polanyi linear approximation of activation energy	

using computational chemistry. The simplified system also reduces the computation load for reactor scale-up, design, and optimization.

A type of mechanism reduction called *lumping* is typically performed on a reaction network that consists of a large number of similar reactions occurring between similar species, such as homologous series or molecules having similar functional groups. Such situations occur, for instance, in the oil refining industry, examples including catalytic reforming, catalytic cracking, hydrocracking, and hydrotreating. Lumping is done by grouping similar species, or molecules with similar functional groups, into pseudo components called lumped species. The behavior of the lumped system depends on the initial composition, the distribution of the rate constants in the detailed system, and the form of the rate equation. The two main issues in lumping are

1. Determination of the lump structure that simulates the detailed system over the required range of conditions
2. Determination of the kinetics of the lumped system from general knowledge about the type of kinetics and the overall range of parameters of the detailed system

Lumping has been applied extensively to first-order reaction networks [e.g., Wei and Kuo, "A Lumping Analysis in Monomolecular Reaction Systems," *I&EC Fundamentals* **8**(1): 114–123 (1969); Golikeri and Luss, "Aggregation of Many Coupled Consecutive First Order Reactions," *Chem. Eng. Sci.* **29**: 845–855 (1974)]. For instance, it has been shown that a lumped reaction network of first-order reactions can behave under certain conditions as a global second-order reaction. Where analytical solutions were not available, others, such as Golikeri and Luss, "Aggregation of Many Coupled Consecutive First Order Reactions," *Chem. Eng. Sci.* **29**: 845–855 (1974), developed bounds that bracketed the behavior of the lump for first-order reactions as a function of the initial composition and the rate constant distribution. Lumping has not been applied as successfully to nonlinear or higher-order kinetics. More recent applications of lumping were published, including structure-oriented lumping that lumps similar structural groups, by Quann and Jaffe, "Building Useful Models of Complex Reaction Systems in Petroleum Refining," *Chem. Eng. Sci.* **51**(10): 1615–1635 (1996).

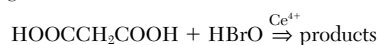
For other types of systems such as highly branched reaction networks for homogeneous gas-phase combustion and combined homogeneous and catalytic partial oxidation, mechanism reduction involves pruning branches and pathways of the reaction network that do not contribute significantly to the overall reaction. This pruning is done by using *sensitivity analysis*. See, e.g., Bui et al., "Hierarchical Reduced Models for Catalytic Combustion: H₂/Air Mixtures near Platinum Surfaces," *Combustion Sci. Technol.* **129**(1–6):243–275 (1997).

Multiple Steady States, Oscillations, and Chaotic Behavior
There are reaction systems whose steady-state behavior depends on

the initial or starting conditions; i.e., for different starting conditions, different steady states can be reached at the same final operating conditions. This behavior is called steady-state multiplicity and is often the result of the interaction of kinetic and transport phenomena having distinct time scales. For some cases, the cause of the multiplicity is entirely reaction-related, as shown below. Associated with steady-state multiplicity is hysteresis, and higher-order instabilities such as self-sustained oscillations and chaotic behavior. The existence of multiple steady states may be relevant to analysis of laboratory data, since faster of slower rates may be observed at the same conditions depending on how the lab reactor is started up.

For example, CO oxidation on heterogeneous Rh catalyst exhibits hysteresis and multiple steady states, and one of the explained causes is the existence of two crystal structures for Rh, each with a different reactivity (Masel, *Chemical Kinetics and Catalysis*, Wiley, 2001, p. 38).

Another well-known example of chemistry-related instability includes the oscillatory behavior of the Bheulousov-Zhabotinsky reaction of malonic acid and bromate in the presence of homogeneous Ce catalyst having the overall reaction



Ce can be in two oxidation states, Ce³⁺ and Ce⁴⁺, and there are competing reaction pathways. Complex kinetic models are required to predict the oscillatory behavior, the most well known being that of Noyes [e.g., Showalter, Noyes, and Bar-Eli, *J. Chem. Phys.* **69**(6): 2514–2524 (1978)].

A large body of work has been done to develop criteria that determine the onset of chemistry and transport chemistry-based instabilities. More details and transport-reaction coupling-related examples are discussed in Sec. 19.

SOFTWARE TOOLS

There are a number of useful software packages that enable efficient analysis of laboratory data for developing the mechanism and kinetics of reactions and for testing the kinetics by using simple reactor models. The reader is referred to search the Internet as some of these software packages change ownership or name. Worth mentioning are the Aspen Engineering Suite (Aspen), the Thermal Safety Software suite (Cheminform St. Petersburg), the Matlab suite (Mathworks), the Chemkin software suite (Reaction Design), the NIST Chemical Kinetics database (NIST), and Gepasi for biochemical kinetics (freeware). The user is advised to experiment and validate any software package with known data and kinetics to ensure robustness and reliability.

SECTION 8

Process Control

PERRY'S CHEMICAL ENGINEERS' HANDBOOK

8TH EDITION



THOMAS F. EDGAR, CECIL L. SMITH
F. GREG SHINSKEY, GEORGE W. GASSMAN
ANDREW W. R. WAITE, THOMAS J. MCAVOY
DALE E. SEBORG

Copyright © 2008, 1997, 1984, 1973, 1963, 1950, 1941, 1934 by The McGraw-Hill Companies, Inc. All rights reserved. Manufactured in the United States of America. Except as permitted under the United States Copyright Act of 1976, no part of this publication may be reproduced or distributed in any form or by any means, or stored in a database or retrieval system, without the prior written permission of the publisher.

0-07-154215-9

The material in this eBook also appears in the print version of this title: 0-07-151131-8.

All trademarks are trademarks of their respective owners. Rather than put a trademark symbol after every occurrence of a trademarked name, we use names in an editorial fashion only, and to the benefit of the trademark owner, with no intention of infringement of the trademark. Where such designations appear in this book, they have been printed with initial caps.

McGraw-Hill eBooks are available at special quantity discounts to use as premiums and sales promotions, or for use in corporate training programs. For more information, please contact George Hoare, Special Sales, at george_hoare@mcgraw-hill.com or (212) 904-4069.

TERMS OF USE

This is a copyrighted work and The McGraw-Hill Companies, Inc. (“McGraw-Hill”) and its licensors reserve all rights in and to the work. Use of this work is subject to these terms. Except as permitted under the Copyright Act of 1976 and the right to store and retrieve one copy of the work, you may not decompile, disassemble, reverse engineer, reproduce, modify, create derivative works based upon, transmit, distribute, disseminate, sell, publish or sublicense the work or any part of it without McGraw-Hill’s prior consent. You may use the work for your own noncommercial and personal use; any other use of the work is strictly prohibited. Your right to use the work may be terminated if you fail to comply with these terms.

THE WORK IS PROVIDED “AS IS.” McGRAW-HILL AND ITS LICENSORS MAKE NO GUARANTEES OR WARRANTIES AS TO THE ACCURACY, ADEQUACY OR COMPLETENESS OF OR RESULTS TO BE OBTAINED FROM USING THE WORK, INCLUDING ANY INFORMATION THAT CAN BE ACCESSED THROUGH THE WORK VIA HYPERLINK OR OTHERWISE, AND EXPRESSLY DISCLAIM ANY WARRANTY, EXPRESS OR IMPLIED, INCLUDING BUT NOT LIMITED TO IMPLIED WARRANTIES OF MERCHANTABILITY OR FITNESS FOR A PARTICULAR PURPOSE. McGraw-Hill and its licensors do not warrant or guarantee that the functions contained in the work will meet your requirements or that its operation will be uninterrupted or error free. Neither McGraw-Hill nor its licensors shall be liable to you or anyone else for any inaccuracy, error or omission, regardless of cause, in the work or for any damages resulting therefrom. McGraw-Hill has no responsibility for the content of any information accessed through the work. Under no circumstances shall McGraw-Hill and/or its licensors be liable for any indirect, incidental, special, punitive, consequential or similar damages that result from the use of or inability to use the work, even if any of them has been advised of the possibility of such damages. This limitation of liability shall apply to any claim or cause whatsoever whether such claim or cause arises in contract, tort or otherwise.

DOI: 10.1036/0071511318

Process Control

Thomas F. Edgar, Ph.D. Professor of Chemical Engineering, University of Texas—Austin
(Section Editor, *Advanced Control Systems, Process Measurements*)

Cecil L. Smith, Ph.D. Principal, Cecil L. Smith Inc. (*Batch Process Control, Telemetry and Transmission, Digital Technology for Process Control, Process Control and Plant Safety*)

F. Greg Shinskey, B.S.Ch.E. Consultant (retired from Foxboro Co.) (*Fundamentals of Process Dynamics and Control, Unit Operations Control*)

George W. Gassman, B.S.M.E. Senior Research Specialist, Final Control Systems, Fisher Controls International, Inc. (*Controllers, Final Control Elements, and Regulators*)

Andrew W. R. Waite, P.Eng. Principal Process Control Consultant, EnTech Control, a Division of Emerson Electric Canada (*Controllers, Final Control Elements, and Regulators*)

Thomas J. McAvoy, Ph.D. Professor of Chemical Engineering, University of Maryland—College Park (*Fundamentals of Process Dynamics and Control*)

Dale E. Seborg, Ph.D. Professor of Chemical Engineering, University of California—Santa Barbara (*Advanced Control Systems*)

FUNDAMENTALS OF PROCESS DYNAMICS AND CONTROL

The General Control System	8-5
Feedback Control	8-5
Feedforward Control	8-5
Computer Control	8-5
Process Dynamics and Mathematical Models	8-5
Open-Loop versus Closed-Loop Dynamics	8-5
Physical Models versus Empirical Models	8-6
Nonlinear versus Linear Models	8-7
Simulation of Dynamic Models	8-7
Laplace Transforms	8-7
Transfer Functions and Block Diagrams	8-8
Continuous versus Discrete Models	8-8
Process Characteristics in Transfer Functions	8-9
Fitting Dynamic Models to Experimental Data	8-12
Feedback Control System Characteristics	8-12
Closing the Loop	8-13
On/Off Control	8-13
Proportional Control	8-14
Proportional-plus-Integral (PI) Control	8-14
Proportional-plus-Integral-plus-Derivative (PID) Control	8-15
Controller Comparison	8-16
Controller Tuning	8-16

Controller Performance Criteria	8-17
Tuning Methods Based on Known Process Models	8-18
Tuning Methods When Process Model Is Unknown	8-19
Set-Point Response	8-19

ADVANCED CONTROL SYSTEMS

Benefits of Advanced Control	8-20
Advanced Control Techniques	8-21
Feedforward Control	8-21
Cascade Control	8-24
Time-Delay Compensation	8-24
Selective and Override Control	8-25
Adaptive Control	8-26
Fuzzy Logic Control	8-26
Expert Systems	8-26
Multivariable Control	8-26
Control Strategies for Multivariable Control	8-27
Decoupling Control Systems	8-27
Pairing of Controlled and Manipulated Variables	8-28
RGA Method for 2×2 Control Problems	8-28
RGA Example	8-29
Model Predictive Control	8-29
Advantages and Disadvantages of MPC	8-29

8-2 PROCESS CONTROL

Economic Incentives for Automation Projects	8-29
Basic Features of MPC	8-30
Implementation of MPC	8-31
Integration of MPC and Online Optimization	8-32
Real-Time Process Optimization	8-32
Essential Features of Optimization Problems	8-33
Development of Process (Mathematical) Models	8-33
Formulation of the Objective Function	8-34
Unconstrained Optimization	8-34
Single-Variable Optimization	8-34
Multivariable Optimization	8-34
Constrained Optimization	8-34
Nonlinear Programming	8-35
Statistical Process Control	8-35
Western Electric Rules	8-37
CUSUM Control Charts	8-38
Process Capability Indices	8-38
Six-Sigma Approach	8-38
Multivariate Statistical Techniques	8-39

UNIT OPERATIONS CONTROL

Piping and Instrumentation Diagrams	8-39
Control of Heat Exchangers	8-40
Steam-Heated Exchangers	8-40
Exchange of Sensible Heat	8-41
Distillation Column Control	8-41
Controlling Quality of a Single Product	8-42
Controlling Quality of Two Products	8-43
Chemical Reactors	8-44
Composition Control	8-44
Temperature Control	8-44
Controlling Evaporators	8-45
Drying Operations	8-46

BATCH PROCESS CONTROL

Batch versus Continuous Processes	8-47
Batches and Recipes	8-47
Routing and Production Monitoring	8-48
Production Scheduling	8-48
Batch Automation Functions	8-49
Interlocks	8-49
Discrete Device States	8-49
Process States	8-49
Regulatory Control	8-49
Sequence Logic	8-49
Industrial Applications	8-50
Batch Reactor Control	8-51
Batch Production Facilities	8-52
Plant	8-52
Equipment Suite	8-52
Process Unit or Batch Unit	8-53
Item of Equipment	8-53
Device	8-53
Structured Batch Logic	8-53
Product Technology	8-53
Process Technology	8-53

PROCESS MEASUREMENTS

General Considerations	8-54
Continuous Measurements	8-54
Accuracy and Repeatability	8-54
Dynamics of Process Measurements	8-55
Selection Criteria	8-55
Calibration	8-55
Temperature Measurements	8-56
Thermocouples	8-56
Resistance Thermometers	8-56
Thermistors	8-56
Filled-System Thermometers	8-57
Bimetal Thermometers	8-57
Pyrometers	8-58
Pressure Measurements	8-58
Liquid-Column Methods	8-58
Elastic Element Methods	8-59
Electrical Methods	8-59
Flow Measurements	8-59
Orifice Meter	8-59

Venturi Meter	8-59
Rotameter	8-60
Turbine Meter	8-60
Vortex-Shedding Flowmeters	8-60
Ultrasonic Flowmeters	8-60
Magnetic Flowmeters	8-60
Coriolis Mass Flowmeters	8-60
Thermal Mass Flowmeters	8-60
Level Measurements	8-60
Float-Actuated Devices	8-60
Head Devices	8-61
Electrical Methods	8-61
Thermal Methods	8-61
Sonic Methods	8-61
Laser Level Transmitters	8-61
Radar Level Transmitters	8-61
Physical Property Measurements	8-61
Density and Specific Gravity	8-61
Viscosity	8-61
Refractive Index	8-61
Dielectric Constant	8-62
Thermal Conductivity	8-62
Chemical Composition Analyzers	8-62
Chromatographic Analyzers	8-62
Infrared Analyzers	8-62
Ultraviolet and Visible-Radiation Analyzers	8-62
Paramagnetism	8-62
Other Analyzers	8-63
Electroanalytical Instruments	8-63
Conductometric Analysis	8-63
Measurement of pH	8-63
Specific-Ion Electrodes	8-63
Moisture Measurement	8-63
Dew Point Method	8-63
Piezoelectric Method	8-63
Capacitance Method	8-63
Oxide Sensors	8-63
Photometric Moisture Analysis	8-64
Other Transducers	8-64
Gear Train	8-64
Differential Transformer	8-64
Hall Effect Sensors	8-64
Sampling Systems for Process Analyzers	8-64
Selecting the Sampling Point	8-64
Sample Withdrawal from Process	8-64
Sample Transport	8-64
Sample Conditioning	8-65

TELEMETERING AND TRANSMISSION

Analog Signal Transmission	8-65
Digital Systems	8-65
Analog Inputs and Outputs	8-65
Pulse Inputs	8-65
Serial Interfaces	8-66
Microprocessor-Based Transmitters	8-66
Transmitter/Actuator Networks	8-66
Filtering and Smoothing	8-66
Alarms	8-67

DIGITAL TECHNOLOGY FOR PROCESS CONTROL

Hierarchy of Information Systems	8-68
Measurement Devices and Final Control Elements	8-68
Safety and Environmental/Equipment Protection	8-68
Regulatory Controls	8-68
Real-Time Optimization	8-68
Production Controls	8-68
Corporate Information Systems	8-69
Digital Hardware in Process Control	8-69
Single-Loop Controllers	8-69
Programmable Logic Controllers	8-69
Personal Computer Controllers	8-69
Distributed Control System	8-69
Distributed Database and the Database Manager	8-70
Data Historian	8-70
Digital Field Communications and Field Bus	8-70
Intermodal Communications	8-70
Process Control Languages	8-71

CONTROLLERS, FINAL CONTROL ELEMENTS, AND REGULATORS

Pneumatic, Electronic, and Digital Controllers	8-71
Pneumatic Controllers	8-71
Electronic (Digital) Controllers	8-72
Control Valves	8-74
Valve Types	8-74
Special Application Valves	8-76
Actuators	8-76
Other Process Valves	8-78
Valves for On/Off Applications	8-78
Pressure Relief Valves	8-78
Check Valves	8-79
Valve Design Considerations	8-79
Materials and Pressure Ratings	8-79
Sizing	8-79
Noise Control	8-81
Cavitation and Flashing	8-82
Seals, Bearings, and Packing Systems	8-82
Flow Characteristics	8-83
Valve Control Devices	8-84

Valve Positioners	8-84
Transducers	8-89
Booster Relays	8-90
Solenoid Valves	8-91
Trip Valves	8-91
Limit Switches and Stem Position Transmitters	8-91
Fire and Explosion Protection	8-91
Environmental Enclosures	8-91
Adjustable-Speed Pumps	8-91
Regulators	8-92
Self-Operated Regulators	8-92
Pilot-Operated Regulators	8-93
Overpressure Protection	8-94

PROCESS CONTROL AND PLANT SAFETY

Role of Automation in Plant Safety	8-94
Integrity of Process Control Systems	8-95
Considerations in Implementation of Safety Interlock Systems	8-95
Interlocks	8-96
Testing	8-96

8-4 PROCESS CONTROL

Nomenclature

Symbol	Definition	Symbol	Definition
A	Area	s	Laplace transform variable
A_a	Actuator area	s	Search direction
A_c	Output amplitude limits	S_i	Step response coefficient
A_v	Amplitude of controlled variable	t	Time
A_1	Cross-sectional area of tank	T	Temperature, target
b	Controller output bias	$T(s)$	Decoupler transfer function
B	Bottoms flow rate	T_b	Base temperature
B_i°	Limit on control	T_f	Exhaust temperature
c_A	Concentration of A	T_R	Reset time
C	Cumulative sum	U	Heat-transfer coefficient
C_d	Discharge coefficient	u, U	Manipulated variable, controller output
C_i	Inlet concentration	V	Volume
C_i°	Limit on control move	V_c	Product value
C_L	Specific heat of liquid	w	Mass flow rate
C_0	Integration constant	w_i	Weighting factor
C_p	Process capability	W	Steam flow rate
C_r	Heat capacity of reactants	x	Mass fraction
C_v	Valve flow coefficient	\bar{x}	Sample mean
D	Distillate flow rate, disturbance	x_i	Optimization variable
D_i°	Limit on output	x_T	Pressure drop ratio factor
e	Error	X	Transform of deviation variable
E	Economy of evaporator	y, Y	Process output, controlled variable, valve travel
f	Function of time	Y_{sp}	Set point
F, f	Feed flow rate	z	Controller tuning law, expansion factor
F_L	Pressure recovery factor	z_i	Feed mole fraction (distillation)
g_c	Unit conversion constant	Z	Compressibility factor
g_i	Algebraic inequality constraint		
G	Transfer function		Greek Symbols
G_c	Controller transfer function	α	Digital filter coefficient
G_d	Disturbance transfer function	a_T	Temperature coefficient of resistance
G_f	Feedforward controller transfer function	β	Resistance thermometer parameter
G_m	Sensor transfer function	γ	Ratio of specific heats
G_p	Process transfer function	δ	Move suppression factor, shift in target value
G_t	Transmitter transfer function	Δq	Load step change
G_v	Valve transfer function	Δt	Time step
h_i	Algebraic equality constraints	ΔT	Temperature change
h_1	Liquid head in tank	Δu	Control move
H	Latent heat of vaporization, control limit or threshold	ε	Spectral emissivity, step size
i	Summation index	ζ	Damping factor (second-order system)
I_i	Impulse response coefficient	θ	Time delay
j	Time index	λ	Relative gain array parameter, wavelength
J	Objective function or performance index	Λ	Relative gain array
k	Time index	ξ	Deviation variable
k_f	Flow coefficient	ρ	Density
k_r	Kinetic rate constant	σ	Stefan-Boltzmann constant, standard deviation
K	Gain, slack parameter	Σ_t	Total response time
K_c	Controller gain	τ	Time constant
K_d	Disturbance transfer function gain	τ_d	Natural period of closed loop, disturbance time constant
K_m	Measurement gain	τ_D	Derivative time (PID controller)
K_p	Process gain	τ_F	Filter time constant
K_u	Ultimate controller gain (stability)	τ_I	Integral time (PID controller)
L	Load variable	τ_P	Process time constant
L_p	Sound pressure level	τ_o	Period of oscillation
M	Manipulated variable	ϕ_{PI}	Phase lag
m_c	Number of constraints		Subscripts
M_c	Mass flow	A	Species A
M_r	Mass of reactants	b	Best
M_w	Molecular weight	c	Controller
n	Number of data points, number of stages or effects	d	Disturbance
N	Number of inputs/outputs, model horizon	eff	Effective
p	Proportional band (%)	f	Feedforward
p_c	Vapor pressure	i	Initial, inlet
p_d	Actuator pressure	L	Load, disturbance
p_i	Pressure	m	Measurement or sensor
p_u	Proportional band (ultimate)	p	Process
q	Radiated energy flux	s	Steady state
q_b	Energy flux to a black body	sp	Set-point value
Q	Flow rate	t	Transmitter
r_c	Number of constraints	u	Ultimate
R	Equal-percentage valve characteristic	v	Valve
R_T	Resistance in temperature sensor		
R_1	Valve resistance		

FUNDAMENTALS OF PROCESS DYNAMICS AND CONTROL

THE GENERAL CONTROL SYSTEM

A process is shown in Fig. 8-1 with a manipulated input U , a load input D , and a controlled output Y , which could be flow, pressure, liquid level, temperature, composition, or any other inventory, environmental, or quality variable that is to be held at a desired value identified as the set point Y_{sp} . The load may be a single variable or an aggregate of variables either acting independently or manipulated for other purposes, affecting the controlled variable much as the manipulated variable does. Changes in load may occur randomly as caused by changes in weather, diurnally with ambient temperature, manually when operators change production rate, stepwise when equipment is switched into or out of service, or cyclically as the result of oscillations in other control loops. Variations in load will drive the controlled variable away from the set point, requiring a corresponding change in the manipulated variable to bring it back. The manipulated variable must also change to move the controlled variable from one set point to another.

An open-loop system positions the manipulated variable either manually or on a programmed basis, without using any process measurements. This operation is acceptable for well-defined processes without disturbances. An automated transfer switch is provided to allow manual adjustment of the manipulated variable in case the process or the control system is not performing satisfactorily.

A closed-loop system uses the measurement of one or more process variables to move the manipulated variable to achieve control. Closed-loop systems may include feedforward, feedback, or both.

Feedback Control In a feedback control loop, the controlled variable is compared to the set point Y_{sp} , with the error E acted upon by the controller to move U in such a way as to minimize the error. This action is specifically negative feedback, in that an increase in error moves U so as to decrease the error. (Positive feedback would cause the error to expand rather than diminish and therefore does not regulate.) The action of the controller is selectable to allow use on process gains of both signs.

The controller has tuning parameters related to proportional, integral, derivative, lag, dead time, and sampling functions. A negative feedback loop will oscillate if the controller gain is too high; but if it is too low, control will be ineffective. The controller parameters must be properly related to the process parameters to ensure closed-loop stability while still providing effective control. This relationship is accomplished, first,

by the proper selection of control modes to satisfy the requirements of the process and, second, by the appropriate tuning of those modes.

Feedforward Control A feedforward system uses measurements of disturbance variables to position the manipulated variable in such a way as to minimize any resulting deviation. The disturbance variables could be either measured loads or the set point, the former being more common. The feedforward gain must be set precisely to reduce the deviation of the controlled variable from the set point.

Feedforward control is usually combined with feedback control to eliminate any offset resulting from inaccurate measurements and calculations and unmeasured load components. The feedback controller can be used as a bias on the feedforward controller or in a multiplicative form.

Computer Control Computers have been used to replace analog PID controllers, either by setting set points of lower-level controllers in supervisory control or by driving valves directly in direct digital control. Single-station digital controllers perform PID control in one or two loops, including computing functions such as mathematical operations, characterization, lags, and dead time, with digital logic and alarms. Distributed control systems provide all these functions, with the digital processor shared among many control loops; separate processors may be used for displays, communications, file servers, and the like. A host computer may be added to perform high-level operations such as scheduling, optimization, and multivariable control. More details on computer control are provided later in this section.

PROCESS DYNAMICS AND MATHEMATICAL MODELS

GENERAL REFERENCES: Seborg, Edgar, and Mellichamp, *Process Dynamics and Control*, Wiley, New York, 2004; Marlin, *Process Control*, McGraw-Hill, New York, 2000; Ogunnaike and Ray, *Process Dynamics Modeling and Control*, Oxford University Press, New York, 1994; Smith and Corripio, *Principles and Practices of Automatic Process Control*, Wiley, New York, 1997.

Open-Loop versus Closed-Loop Dynamics It is common in industry to manipulate coolant in a jacketed reactor in order to control conditions in the reactor itself. A simplified schematic diagram of such a reactor control system is shown in Fig. 8-2. Assume that the reactor temperature is adjusted by a controller that increases the coolant flow in proportion to the difference between the desired reactor temperature and the temperature that is measured. The proportionality constant is K_c . If a small change in the temperature of the inlet stream occurs, then

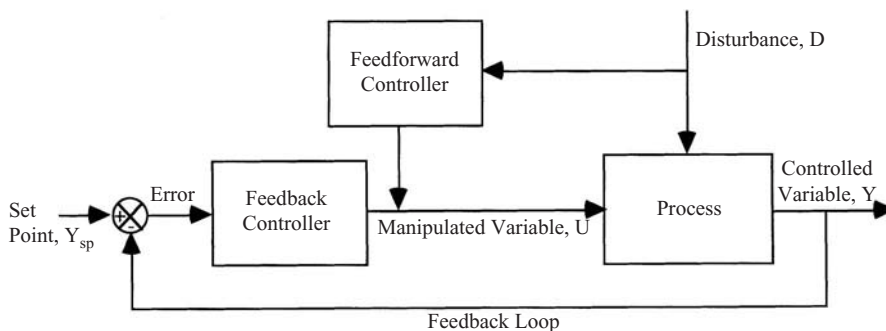


FIG. 8-1 Block diagram for feedforward and feedback control.

8-6 PROCESS CONTROL

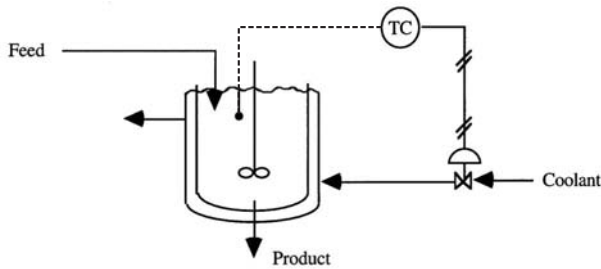


FIG. 8-2 Reactor control system.

depending on the value of K_c , one might observe the reactor temperature responses shown in Fig. 8-3. The top plot shows the case for no control ($K_c = 0$), which is called the open loop, or the normal dynamic response of the process by itself. As K_c increases, several effects can be noted. First, the reactor temperature responds faster and faster. Second, for the initial increases in K , the maximum deviation in the reactor temperature becomes smaller. Both of these effects are desirable so that disturbances from normal operation have as small an effect as possible on the process under study. As the gain is increased further, eventually a point is reached where the reactor temperature oscillates indefinitely, which is undesirable. This point is called the stability limit, where $K_c = K_u$, the ultimate controller gain. Increasing K_c further causes the magnitude of the oscillations to increase, with the result that the control valve will cycle between full open and closed.

The responses shown in Fig. 8-3 are typical of the vast majority of regulatory loops encountered in the process industries. Figure 8-3

shows that there is an optimal choice for K_c , somewhere between 0 (no control) and K_u (stability limit). If one has a dynamic model of a process, then this model can be used to calculate controller settings. In Fig. 8-3, no time scale is given, but rather the figure shows relative responses. A well-designed controller might be able to speed up the response of a process by a factor of roughly 2 to 4. Exactly how fast the control system responds is determined by the dynamics of the process itself.

Physical Models versus Empirical Models In developing a dynamic process model, there are two distinct approaches that can be taken. The first involves models based on first principles, called physical or first principles models, and the second involves empirical models. The conservation laws of mass, energy, and momentum form the basis for developing physical models. The resulting models typically involve sets of differential and algebraic equations that must be solved simultaneously. Empirical models, by contrast, involve postulating the form of a dynamic model, usually as a transfer function, which is discussed below. This transfer function contains a number of parameters that need to be estimated from data. For the development of both physical and empirical models, the most expensive step normally involves verification of their accuracy in predicting plant behavior.

To illustrate the development of a physical model, a simplified treatment of the reactor, shown in Fig. 8-2, is used. It is assumed that the reactor is operating isothermally and that the inlet and exit volumetric flows and densities are the same. There are two components, A and B, in the reactor, and a single first-order reaction of $A \rightarrow B$ takes place. The inlet concentration of A, which we call c_{iA} , varies with time. A dynamic mass balance for the concentration of A, denoted c_A , can be written as follows:

$$V \frac{dc_A}{dt} = Fc_i - Fc_A - k_r V c_A \quad (8-1)$$

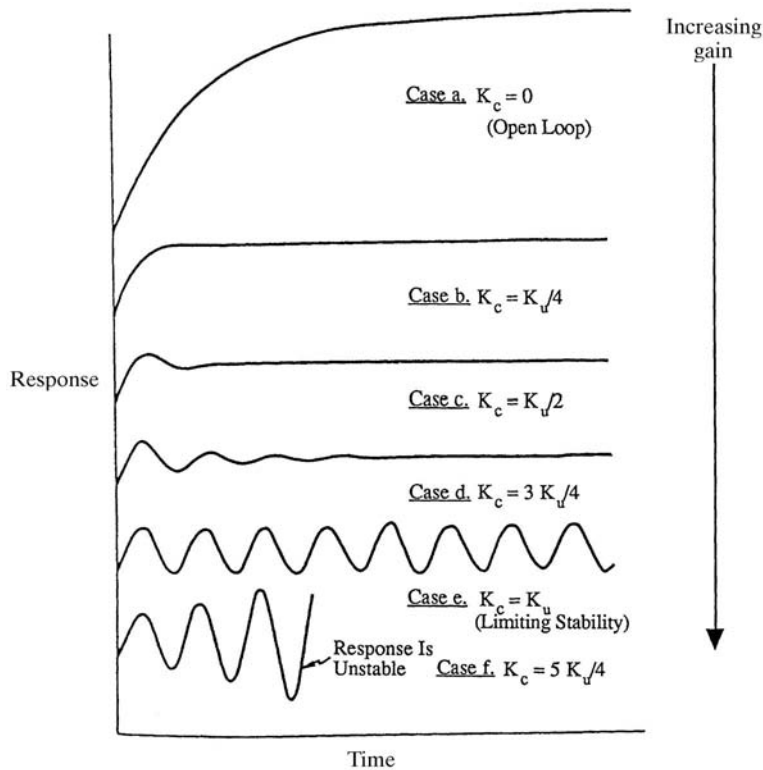


FIG. 8-3 Typical control system responses.

In Eq. (8-1), the flow in of component A is Fc_i , the flow out is Fc_A , and the loss via reaction is $k_r V c_A$, where V = reactor volume and k_r = kinetic rate constant. In this example, c_i is the input, or forcing, variable and c_A is the output variable. If V , F , and k_r are constant, Eq. (8-1) can be rearranged by dividing by $F + k_r V$ so that it contains only two groups of parameters. The result is

$$\tau \frac{dc_A}{dt} = Kc_i - c_A \tag{8-2}$$

where $\tau = V/(F + k_r V)$ and $K = F/(F + k_r V)$. For this example, the resulting model is a first-order differential equation in which τ is called the time constant and K the process gain.

As an alternative to deriving Eq. (8-2) from a dynamic mass balance, one could simply postulate a first-order differential equation to be valid (empirical modeling). Then it would be necessary to estimate values for τ and K so that the postulated model described the reactor's dynamic response. The advantage of the physical model over the empirical model is that the physical model gives insight into how reactor parameters affect the values of τ and K , which in turn affects the dynamic response of the reactor.

Nonlinear versus Linear Models If V , F , and k are constant, then Eq. (8-1) is an example of a linear differential equation model. In a linear equation, the output and input variables and their derivatives appear to only the first power. If the rate of reaction were second-order, then the resulting dynamic mass balance would be

$$V \frac{dc_A}{dt} = Fc_i - Fc_A - k_r V c_A^2 \tag{8-3}$$

Since c_A appears in this equation to the second power, the equation is nonlinear.

The difference between linear systems and nonlinear systems can be seen by considering the steady-state behavior of Eq. (8-1) compared to Eq. (8-3) (the left-hand side is zero; that is, $dc_A/dt = 0$). For a given change in c_i , Δc_i , the change in c_A calculated from Eq. (8-1), Δc_A , is always proportional to Δc_i , and the proportionality constant is K [see Eq. (8-2)]. The change in the output of a system divided by a change in the input to the system is called the *process gain*. Linear systems have constant process gains for all changes in the input. By contrast, Eq. (8-3) gives a Δc_A that varies with Δc_i , which is a function of the concentration levels in the reactor. Thus, depending on the reactor operating conditions, a change in c_i produces different changes in c_A . In this case, the process has a nonlinear gain. Systems with nonlinear gains are more difficult to control than linear systems that have constant gains.

Simulation of Dynamic Models Linear dynamic models are particularly useful for analyzing control system behavior. The insight gained through linear analysis is invaluable. However, accurate dynamic process models can involve large sets of nonlinear equations. Analytical solution of these models is not possible. Thus, in these cases, one must turn to simulation approaches to study process dynamics and the effect of process control. Equation (8-3) will be used to illustrate the simulation of nonlinear processes. If dc_A/dt on the left-hand side of Eq. (8-3) is replaced with its finite difference approximation, one gets

$$c_A(t + \Delta t) = \frac{c_A(t) + \Delta t \cdot [Fc_i(t) - Fc_A(t) - k_r V c_A^2(t)]}{V} \tag{8-4}$$

Starting with an initial value of c_A and given $c_i(t)$, Eq. (8-4) can be solved for $c_A(t + \Delta t)$. Once $c_A(t + \Delta t)$ is known, the solution process can be repeated to calculate $c_A(t + 2\Delta t)$, and so on. This approach is called the Euler integration method; while it is simple, it is not necessarily the best approach to numerically integrating nonlinear differential equations. As discussed in Sec. 3, more sophisticated approaches are available that allow much larger step sizes to be taken but require additional calculations. One widely used approach is the fourth-order Runge Kutta method, which involves the following calculations:

Define

$$f(c_A t) = \frac{Fc_i(t) - Fc_A - k_r V c_A^2}{V} \tag{8-5}$$

then

$$c_A(t + \Delta t) = c_A(t) + \Delta t(m_1 + 2m_2 + 2m_3 + m_4) \tag{8-6}$$

with

$$m_1 = f[c_A(t), t] \tag{8-7}$$

$$m_2 = f\left[c_A(t) + 2\frac{m_1 \Delta t}{2}, t + \frac{\Delta t}{2}\right] \tag{8-8}$$

$$m_3 = f\left[c_A(t) + 2\frac{m_2 \Delta t}{2}, t + \frac{\Delta t}{2}\right] \tag{8-9}$$

$$m_4 = f[c_A(t) + m_3 \Delta t, t + \Delta t] \tag{8-10}$$

In this method, the m_i 's are calculated sequentially in order to take a step in time. Even though this method requires calculation of the four additional m_i values, for equivalent accuracy the fourth-order Runge Kutta method can result in a faster numerical solution, because it permits a larger step Δt to be taken. Increasingly sophisticated simulation packages are being used to calculate the dynamic behavior of processes and to test control system behavior. These packages have good user interfaces, and they can handle stiff systems where some variables respond on a time scale that is much much faster or slower than that of other variables. A simple Euler approach cannot effectively handle stiff systems, which frequently occur in chemical process models. See Sec. 3 of this handbook for more details.

Laplace Transforms When mathematical models are used to describe process dynamics in conjunction with control system analysis, the models generally involve linear differential equations. Laplace transforms are very effective for solving linear differential equations. The key advantage of using Laplace transforms is that they convert differential equations to algebraic equations. The resulting algebraic equations are easier to solve than the original differential equations. When the Laplace transform is applied to a linear differential equation in time, the result is an algebraic equation in a new variable s , called the Laplace variable. To get the solution to the original differential equation, one needs to invert the Laplace transform. Table 8-1 gives a number of useful Laplace transform pairs, and more extensive tables are available (Seborg, Edgar, and Mellichamp, *Process Dynamics and Control*, Wiley, New York, 2004).

To illustrate how Laplace transforms work, consider the problem of solving Eq. (8-2), subject to the initial condition that $c_A = c_i = 0$ at $t = 0$. If c_A were not initially zero, one would define a deviation variable between c_A and its initial value c_{A0} . Then the transfer function would be developed by using this deviation variable. If c_i changes from zero to \bar{c}_i , taking the Laplace transform of both sides of Eq. (8-2) gives

$$\mathcal{L}\left(\tau \frac{dc_A}{dt}\right) = \mathcal{L}(K\bar{c}_i) - \mathcal{L}(c_A) \tag{8-11}$$

TABLE 8-1 Frequently Used Laplace Transforms

Time function $f(t)$	Transform $F(s)$
A	A/s
At	A/s^2
Ae^{-at}	$A/(s + a)$
$A(1 - e^{-t\tau})$	$A/[s(\tau s + 1)]$
$A \sin \omega t$	$A\omega/(s^2 + \omega^2)$
$f(t - \theta)$	$e^{-s\theta}F(s)$
df/dt	$sF(s) - f(0)$
$\int f(t)dt$	$F(s)/s$

8-8 PROCESS CONTROL

Denoting $\mathcal{L}(C_A)$ as $C_A(s)$ and using the relationships in Table 8-1 give

$$\tau s C_A(s) = \frac{K\bar{C}_i}{s} - C_A(s) \quad (8-12)$$

Equation (8-12) can be solved for C_A to give

$$C_A(s) = \frac{K\bar{C}_i/s}{\tau s + 1} \quad (8-13)$$

By using the entries in Table 8-1, Eq. (8-13) can be inverted to give the transient response of c_A as

$$c_A(t) = (K\bar{c}_i)(1 - e^{-t/\tau}) \quad (8-14)$$

Equation (8-14) shows that c_A starts from 0 and builds up exponentially to a final concentration of $K\bar{c}_i$. Note that to get Eq. (8-14), it was only necessary to solve the algebraic Eq. (8-12) and then find the inverse of $C_A(s)$ in Table 8-1. The original differential equation was not solved directly. In general, techniques such as partial fraction expansion must be used to solve higher-order differential equations with Laplace transforms.

Transfer Functions and Block Diagrams A very convenient and compact method of representing the process dynamics of linear systems involves the use of transfer functions and block diagrams. A transfer function can be obtained by starting with a physical model, as discussed previously. If the physical model is nonlinear, first it needs to be linearized around an operating point. The resulting linearized model is then approximately valid in a region around this operating point. To illustrate how transfer functions are developed, Eq. (8-2) will again be used. First, one defines deviation variables, which are the process variables minus their steady-state values at the operating point. For Eq. (8-2), there would be deviation variables for both c_A and c_b , and these are defined as

$$\xi = c_A - \bar{c}_A \quad (8-15)$$

$$\xi_i = c_i - \bar{c}_i \quad (8-16)$$

where the overbar stands for steady state. Substitution of Eqs. (8-15) and (8-16) into Eq. (8-2) gives

$$\tau \frac{d\xi}{dt} = K\xi_i - \xi + (K\bar{c}_i - \bar{c}_A) \quad (8-17)$$

The term in parentheses in Eq. (8-17) is zero at steady state, and thus it can be dropped. Next the Laplace transform is taken, and the resulting algebraic equation is solved.

By denoting $X(s)$ as the Laplace transform of ξ and $X_i(s)$ as the transform of ξ_i , the final transfer function can be written as

$$\frac{X}{X_i} = \frac{K}{\tau s + 1} \quad (8-18)$$

Equation (8-18) is an example of a first-order transfer function. As mentioned above, an alternative to formally deriving Eq. (8-18) involves simply postulating its form and then identifying its two parameters, the process gain K and time constant τ , to fit the process under study. In fitting the parameters, data can be generated by forcing the process. If step forcing is used, then the resulting response is called the process reaction curve. Often transfer functions are placed in block diagrams, as shown in Fig. 8-4. Block diagrams show how changes in an input variable affect an output variable. Block diagrams are a means of concisely representing the dynamics of a process under study. Since linearity is assumed in developing a block diagram, if more than one variable affects an output, the contributions from each can be added.

Continuous versus Discrete Models The preceding discussion has focused on systems where variables change continuously with

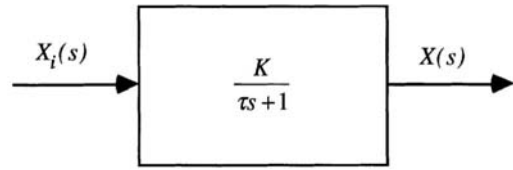


FIG. 8-4 First-order transfer function.

time. Most real processes have variables that are continuous, such as temperature, pressure, and flow. However, some processes involve discrete events, such as the starting or stopping of a pump. In addition, modern plants are controlled by digital computers, which are discrete. In controlling a process, a digital system samples variables at a fixed rate, and the resulting system is a sampled data system. From one sampling instant until the next, variables are assumed to remain fixed at their sampled values. Similarly, in controlling a process, a digital computer sends out signals to control elements, usually valves, at discrete instants of time. These signals remain fixed until the next sampling instant.

Figure 8-5 illustrates the concept of sampling a continuous function. At integer values of the sampling rate Δt , the value of the variable to be sampled is measured and held until the next sampling instant. To deal with sampled data systems, the z transform has been developed. The z transform of the function given in Fig. 8-5 is defined as

$$Z(f) = \sum_{n=0}^{\infty} f(n \Delta t) z^{-n} \quad (8-19)$$

In an analogous manner to Laplace transforms, one can develop transfer functions in the z domain as well as block diagrams. Tables of z transform pairs have been published (Seborg, Edgar, and Mellichamp, *Process Dynamics and Control*, Wiley, New York, 2004) so that the discrete transfer functions can be inverted back to the time domain. The inverse gives the value of the function at the discrete sampling instants. Sampling a continuous variable results in a loss of information. However, in practical applications, sampling is fast enough that the loss is typically insignificant and the difference between continuous and discrete modeling is small in terms of its effect on control. Increasingly, model predictive controllers that make use of discrete dynamic models are being used in the process industries. The purpose of these controllers is to guide a process to optimum operating points. These model predictive control algorithms are typically run at much slower sampling rates than are used for basic control loops such as flow control or pressure control. The discrete dynamic models used are normally developed from data generated

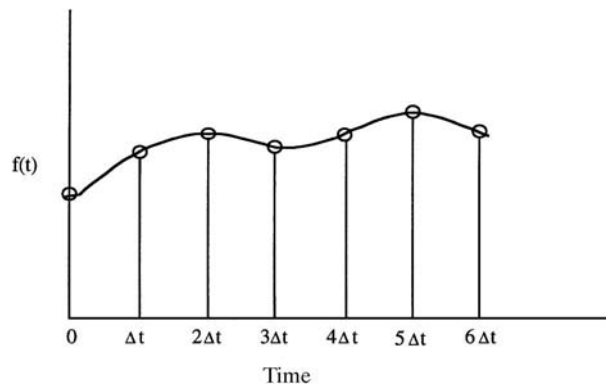


FIG. 8-5 Sampled data example.

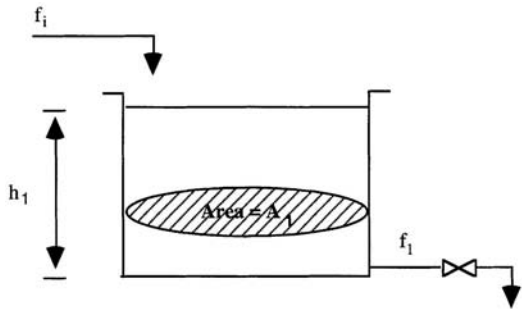


FIG. 8-6 Single tank with exit valve.

from plant testing, as discussed hereafter. For a detailed discussion of modeling sampled data systems, the interested reader is referred to textbooks on digital control (Astrom and Wittenmark, *Computer Controlled Systems*, Prentice-Hall, Englewood Cliffs, N.J., 1997).

Process Characteristics in Transfer Functions In many cases, process characteristics are expressed in the form of transfer functions. In the previous discussion, a reactor example was used to illustrate how a transfer function could be derived. Here, another system involving flow out of a tank, shown in Fig. 8-6, is considered.

Proportional Element First, consider the outflow through the exit valve on the tank. If the flow through the line is turbulent, then Bernoulli's equation can be used to relate the flow rate through the valve to the pressure drop across the valve as

$$f_1 = k_f A_v \sqrt{2g_c(h_1 - h_0)} \tag{8-20}$$

where f_1 = flow rate, k_f = flow coefficient, A_v = cross-sectional area of the restriction, g_c = constant, h_1 = liquid head in tank (pressure at the base of the tank), and h_0 = atmospheric pressure. This relationship between flow and pressure drop across the valve is nonlinear, and it can be linearized around a particular operating point to give

$$f_1 - \bar{f}_1 = \left(\frac{1}{R_1}\right)(h_1 - \bar{h}_1) \tag{8-21}$$

where $R_1 = \bar{f}_1 / (g_c k_f^2 A_v^2)$ is called the resistance of the valve in analogy with an electrical resistance. The transfer function relating changes in flow to changes in head is shown in Fig. 8-7, and it is an example of a pure gain system with no dynamics. In this case, the process gain is $K = 1/R_1$. Such a system has an instantaneous dynamic response, and for a step change in head, there is an immediate step change in flow, as shown in Fig. 8-8. The exact magnitude of the step in flow depends on the operating flow \bar{f}_1 as the definition of R_1 shows.

First-Order Lag (Time Constant Element) Next consider the system to be the tank itself. A dynamic mass balance on the tank gives

$$A_1 \frac{dh_1}{dt} = f_i - f_1 \tag{8-22}$$

where A_1 is the cross-sectional area of the tank and f_i is the inlet flow. By substituting Eq. (8-21) into Eq. (8-22) and following the approach

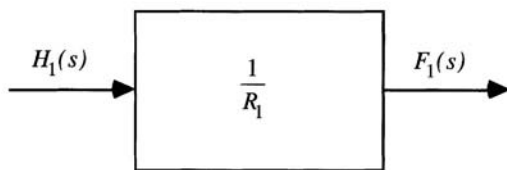


FIG. 8-7 Proportional element transfer function.

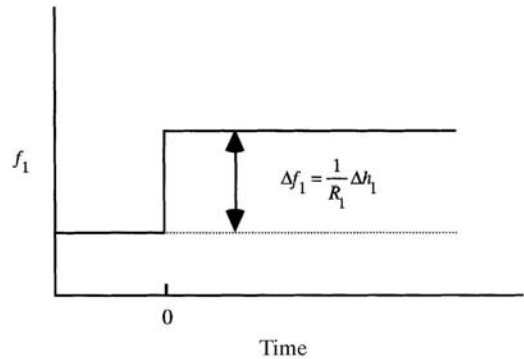


FIG. 8-8 Response of proportional element.

discussed above for deriving transfer functions, one can develop the transfer function relating changes in h_1 to changes in f_1 . The resulting transfer function is another example of a first-order system, shown in Fig. 8-4, and it has a gain $K = R_1$ and a time constant $\tau_1 = R_1 A_1$. For a step change in f_i , h_1 follows a decaying exponential response from its initial value \bar{h}_1 to a final value of $\bar{h}_1 + R_1 \Delta f_i$ (Fig. 8-9). At a time equal to τ_1 , the transient in h_1 is 63 percent finished; and at $3\tau_1$, the response is 95 percent finished. These percentages are the same for all first-order processes. Thus, knowledge of the time constant of a first-order process gives insight into how fast the process responds to sudden input changes.

Capacity Element Now consider the case where the valve in Fig. 8-7 is replaced with a pump. In this case, it is reasonable to assume that the exit flow from the tank is independent of the level in the tank. For such a case, Eq. (8-22) still holds, except that f_1 no longer depends on h_1 . For changes in f_i , the transfer function relating changes in h_1 to changes in f_i is shown in Fig. 8-10. This is an example of a pure capacity process, also called an integrating system. The cross-sectional area of the tank is the chemical process equivalent of an electrical capacitor. If the inlet flow is step forced while the outlet is held constant, then the level builds up linearly, as shown in Fig. 8-11. Eventually the liquid will overflow the tank.

Second-Order Element Because of their linear nature, transfer functions can be combined in a straightforward manner. Consider the two-tank system shown in Fig. 8-12. For tank 1, the transfer function relating changes in f_1 to changes in f_i is

$$\frac{F_1(s)}{F_i(s)} = \frac{1}{A_1 R_1 + 1} \tag{8-23}$$

Since f_1 is the inlet flow to tank 2, the transfer function relating changes in h_2 to changes in f_1 has the same form as that given in Fig. 8-4:

$$\frac{H_2(s)}{F_1(s)} = \frac{R_2}{A_2 R_2 s + 1} \tag{8-24}$$

Equations (8-23) and (8-24) can be multiplied to give the final transfer function relating changes in h_2 to changes in f_i , as shown in Fig. 8-13. This is an example of a second-order transfer function. This transfer function has a gain R_2 and two time constants $A_1 R_1$ and $A_2 R_2$. For two tanks with equal areas, a step change in f_i produces the S-shaped response in level in the second tank shown in Fig. 8-14.

General Second-Order Element Figure 8-3 illustrates the fact that closed-loop systems can exhibit oscillatory behavior. A general second-order transfer function that can exhibit oscillatory behavior is important for the study of automatic control systems. Such a transfer function is given in Fig. 8-15. For a unit step input, the transient responses shown in Fig. 8-16 result. As can be seen, when $\zeta < 1$, the response oscillates; and when $\zeta < 1$, the response is S-shaped. Few open-loop chemical processes exhibit an oscillating response; most exhibit an S-shaped step response.

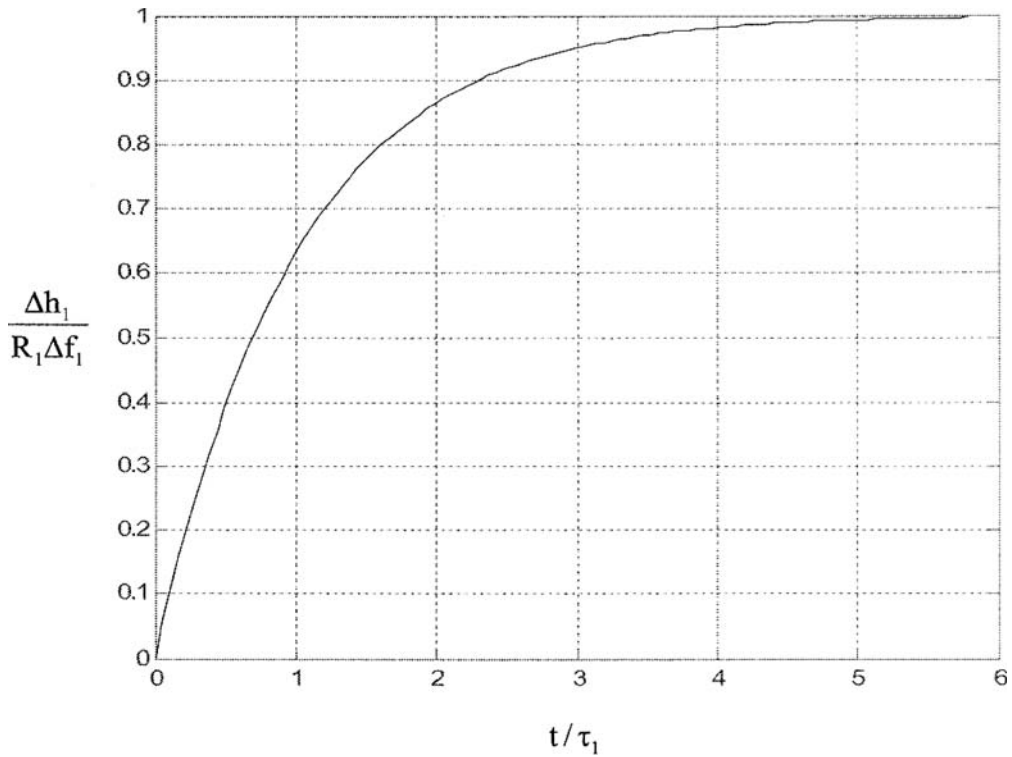


FIG. 8-9 Response of first-order system.

Distance-Velocity Lag (Dead-Time Element) The dead-time or time-delay element, commonly called a distance-velocity lag, is often encountered in process systems. For example, if a temperature-measuring element is located downstream from a heat exchanger, a time delay occurs before the heated fluid leaving the exchanger

arrives at the temperature measurement point. If some element of a system produces a dead time of θ time units, then an input to that unit $f(t)$ will be reproduced at the output as $f(t - \theta)$. The transfer function for a pure dead-time element is shown in Fig. 8-17, and the transient response of the element is shown in Fig. 8-18.

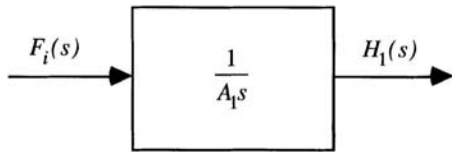


FIG. 8-10 Pure capacity or integrating transfer function.

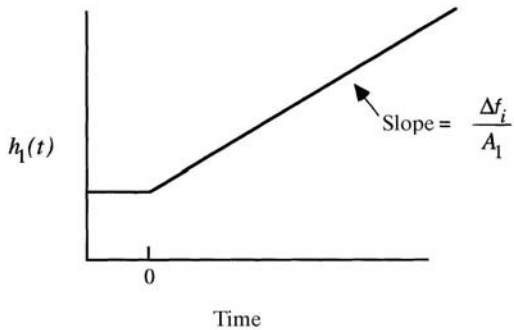


FIG. 8-11 Response of pure capacity system.

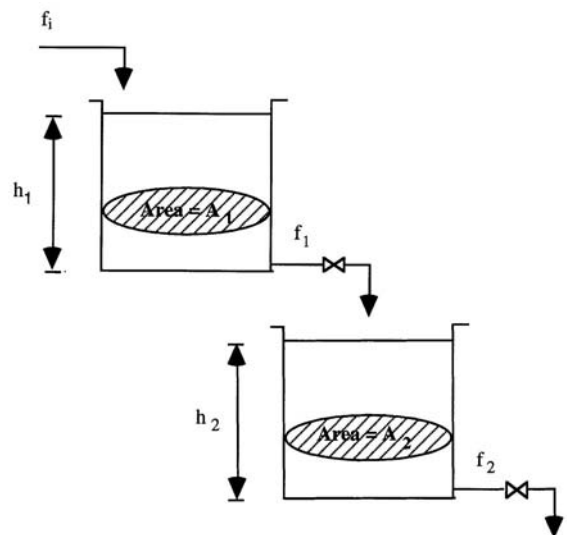


FIG. 8-12 Two tanks in series.

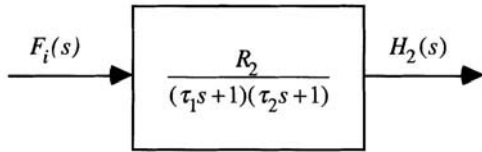


FIG. 8-13 Second-order transfer function.

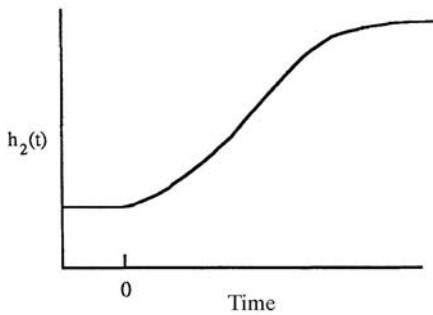


FIG. 8-14 Response of second-order system.

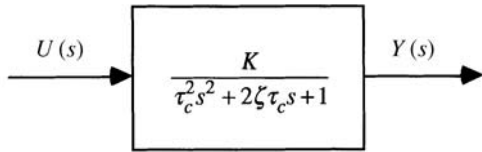


FIG. 8-15 General second-order transfer function.

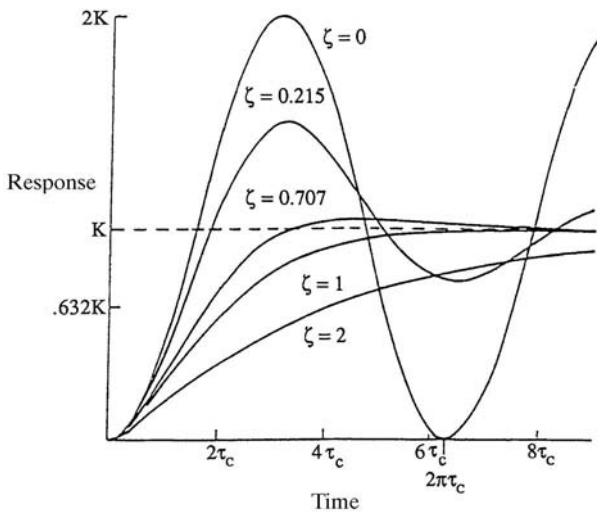


FIG. 8-16 Response of general second-order system.

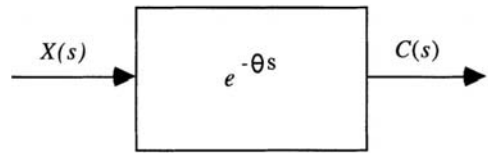


FIG. 8-17 Dead-time transfer function.

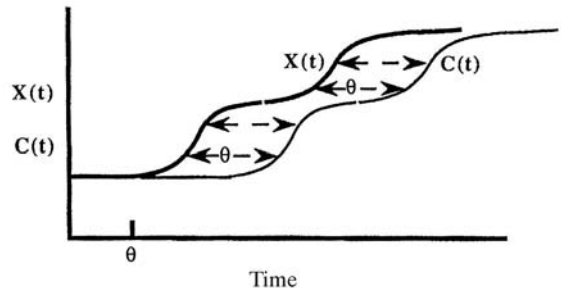


FIG. 8-18 Response of dead-time system.

Higher-Order Lags If a process is described by a series of n first-order lags, the overall system response becomes proportionally slower with each lag added. The special case of a series of n first-order lags with equal time constants has a transfer function given by

$$G(s) = \frac{K}{(\tau s + 1)^n} \quad (8-25)$$

The step response of this transfer function is shown in Fig. 8-19. Note that all curves reach about 60 percent of their final value at $t = n\tau$.

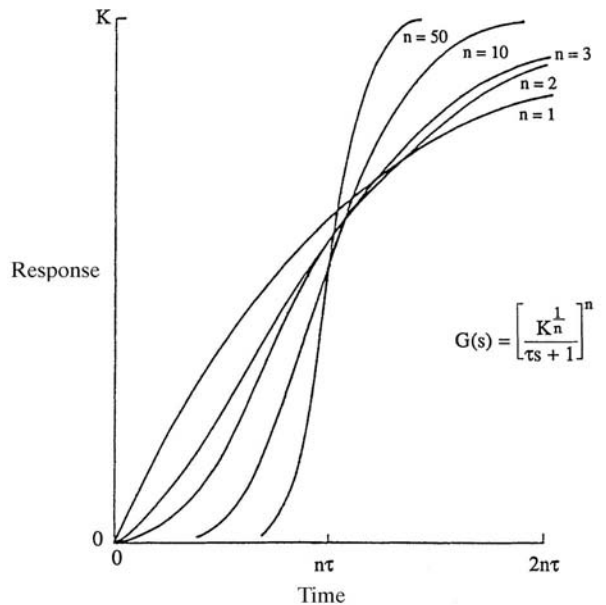


FIG. 8-19 Response of n th-order lags.

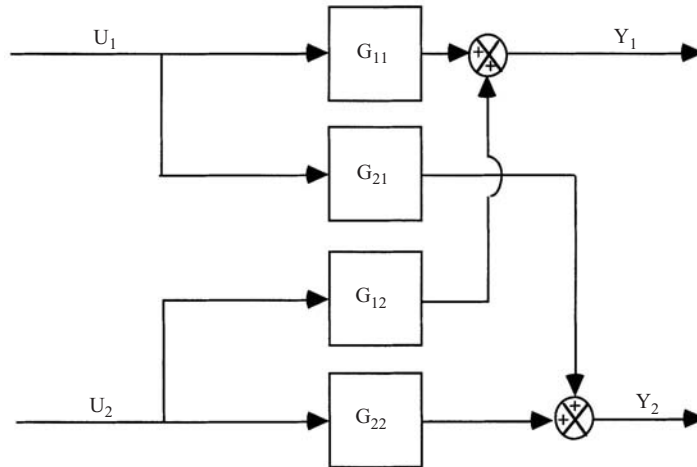


FIG. 8-20 Example of 2×2 transfer function.

Higher-order systems can be approximated by a first- or second-order plus dead-time system for control system design.

Multi-input, Multioutput Systems The dynamic systems considered up to this point have been examples of single-input, single-output (SISO) systems. In chemical processes, one often encounters systems where one input can affect more than one output. For example, assume that one is studying a distillation tower in which both reflux and boil-up are manipulated for control purposes. If the output variables are the top and bottom product compositions, then each input affects both outputs. For this distillation example, the process is referred to as a 2×2 system to indicate the number of inputs and outputs. In general, multi-input, multioutput (MIMO) systems can have n inputs and m outputs with $n \neq m$, and they can be nonlinear. Such a system would be called an $n \times m$ system. An example of a transfer function for a 2×2 linear system is given in Fig. 8-20. Note that since linear systems are involved, the effects of the two inputs on each output are additive. In many process control systems, one input is selected to control one output in a MIMO system. For m outputs there would be m such selections. For this type of control strategy, one needs to consider which inputs and outputs to couple, and this problem is referred to as loop pairing. Another important issue that arises involves interaction between control loops. When one loop makes a change in its manipulated variable, the change affects the other loops in the system. These changes are the direct result of the multivariable nature of the process. In some cases, the interaction can be so severe that overall control system performance is drastically reduced. Finally, some of the modern approaches to process control tackle the MIMO problem directly, and they simultaneously use all manipulated variables to control all output variables rather than pair one input to one output (see later section on multivariable control).

Fitting Dynamic Models to Experimental Data In developing empirical transfer functions, it is necessary to identify model parameters from experimental data. There are a number of approaches to process identification that have been published. The simplest approach involves introducing a step test into the process and recording the response of the process, as illustrated in Fig. 8-21. The x 's in the figure represent the recorded data. For purposes of illustration, the process under study will be assumed to be first-order with dead time and have the transfer function

$$G(s) = \frac{Y(s)}{U(s)} = K \exp(-\theta s) / \tau s + 1 \quad (8-26)$$

The response $y(t)$, produced by Eq. (8-26) can be found by inverting the transfer function, and it is also shown in Fig. 8-21 for a set of

model parameters K , τ , and θ fitted to the data. These parameters are calculated by using optimization to minimize the squared difference between the model predictions and the data, i.e., a least squares approach. Let each measured data point be represented by y_j (measured response), t_j (time of measured response), $j = 1$ to n . Then the least squares problem can be formulated as

$$\min_{\tau, \theta, K} \sum_{j=1}^n [y_j - \hat{y}(t_j)]^2 \quad (8-27)$$

where $\hat{y}(t_j)$ is the predicted value of y at time t_j and n is the number of data points. This optimization problem can be solved to calculate the optimal values of K , τ , and θ . A number of software packages such as Excel Solver are available for minimizing Eq. (8-27).

One operational problem caused by step forcing is the fact that the process under study is moved away from its steady-state operating point. Plant managers may be reluctant to allow large steady-state changes, since normal production will be disturbed by the changes. As a result, alternative methods of forcing actual processes have been developed, and these included pulse testing and pseudo-random binary signal (PRBS) forcing, both of which are illustrated in Fig. 8-22. With pulse forcing, one introduces a step, and then after a period of time the input is returned to its original value. The result is that the process dynamics are excited, but after the forcing the process returns to its original steady state. PRBS forcing involves a series of pulses of fixed height and random duration, as shown in Fig. 8-22. The advantage of PRBS is that forcing can be concentrated on particular frequency ranges that are important for control system design.

Transfer function models are linear, but chemical processes are known to exhibit nonlinear behavior. One could use the same type of optimization objective as given in Eq. (8-27) to determine parameters in nonlinear first-principles models, such as Eq. (8-3) presented earlier. Also, nonlinear empirical models, such as neural network models, have recently been proposed for process applications. The key to the use of these nonlinear empirical models is to have high-quality process data, which allows the important nonlinearities to be identified.

FEEDBACK CONTROL SYSTEM CHARACTERISTICS

GENERAL REFERENCES: Shinskey, *Process Control Systems*, 4th ed., McGraw-Hill, New York, 1996; Seborg, Edgar, and Mellichamp, *Process Dynamics and Control*, Wiley, New York, 1989.

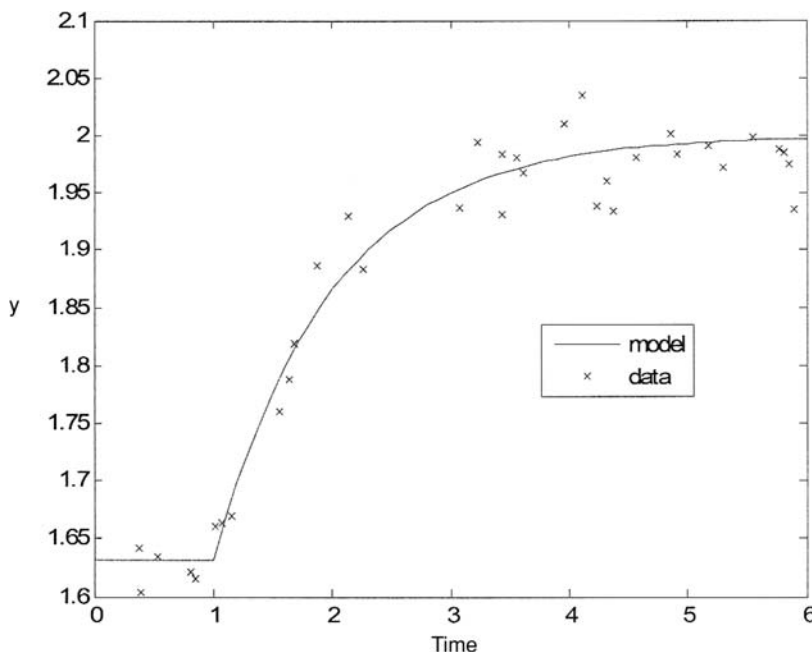


FIG. 8-21 Plot of experimental data and first-order model fit.

There are two objectives in applying feedback control: (1) regulate the controlled variable at the set point following changes in load and (2) respond to set-point changes, the latter called servo operation. In fluid processes, almost all control loops must contend with variations in load, and therefore regulation is of primary importance. While most loops will operate continuously at fixed set points, frequent changes in set points can occur in flow loops and in batch production. The most common mechanism for achieving both objectives is feedback control, because it is the simplest and most universally applicable approach to the problem.

Closing the Loop The simplest representation of the closed feedback loop is shown in Fig. 8-23. The load is shown entering the process at the same point as the manipulated variable because that is the most common point of entry, and because, lacking better information, the elements in the path of the manipulated variable are the best estimates of those in the load path. The load rarely impacts directly on the controlled variable without passing through the dominant lag in the process. Where the load is unmeasured, its current value can be observed as the controller output required to keep the controlled variable Y at set point Y_{sp} .

If the loop is opened—either by placing the controller in manual operation or by setting its gains to zero—the load will have complete influence over the controlled variable, and the set point will have none. Only by closing the loop with controller gain as high as possible will the influence of the load be minimized and that of the set point be maximized. There is a practical limit to the controller gain, however, at the point where the controlled variable develops a uniform oscillation. This is defined as the limit of stability, and it is reached when the product of gains in the loop $\Pi G = G_c G_v G_p$ is equal to 1.0 at the period of the oscillation. If the gain of any element in the loop increases from this condition, oscillations will expand, creating a dangerous situation where safe limits of operation could be exceeded in a few cycles. Consequently, control loops should be left in a condition where the loop gain is less than 1.0 by a safe margin that allows for possible variations in process parameters. Figure 8-24 describes a load response under PID (proportional-integral-derivative) control where the loop is well damped at a loop gain of 0.56; loop gain is then increased to 0.93 and to 1.05, creating a lightly damped and then an expanding cycle, respectively.

In controller tuning, a choice must be made between performance and robustness. Performance is a measure of how well a given con-

troller with certain parameter settings regulates a variable, relative to the best response that can be achieved for that particular process. Robustness is a measure of how small a change in a process parameter is required to bring the loop from its current state to the limit of stability ($\Pi G = 1.0$). The well-damped loop in Fig. 8-24 has a robustness of 79 percent, in that increasing the gain of any element in the loop by a factor of 1/0.56, or 1.79, would bring the loop to the limit of stability. Increasing controller performance by raising its gain can therefore be expected to decrease robustness. Both performance and robustness are functions of the dynamics of the process being controlled, the selection of the controller, and the tuning of the controller parameters.

On/Off Control An on/off controller is used for manipulated variables having only two states. They commonly control temperatures in homes, electric water heaters and refrigerators, and pressure and liquid level in pumped storage systems. On/off control is satisfactory where slow cycling is acceptable, because it always leads to cycling when the load lies between the two states of the manipulated variable. The cycle will be positioned symmetrically about the set point only if the load happens to be equidistant between the two states of the manipulated variable. The period of the symmetric cycle will be approximately 4θ , where θ is the dead time in the loop. If the load is not centered between the states of the manipulated variable, the period will tend to increase and the cycle will follow a sawtooth pattern.

Every on/off controller has some degree of dead band, also known as lockup, or differential gap. Its function is to prevent erratic switching between states, thereby extending the life of contacts and motors. Instead of changing states precisely when the controlled variable crosses the set point, the controller will change states at two different points for increasing and decreasing signals. The difference between these two switching points is the dead band (see Fig. 8-25); it increases the amplitude and period of the cycle, similar to the effects of dead time.

A three-state controller is used to drive either a pair of independent two-state actuators, such as heating and cooling valves, or a bidirectional motorized actuator. The controller is comprised of two on/off controllers, each with dead band, separated by a dead zone. While the controlled variable lies within the dead zone, neither output is energized. This controller can drive a motorized valve to the point where the manipulated variable matches the load, thereby avoiding cycling.

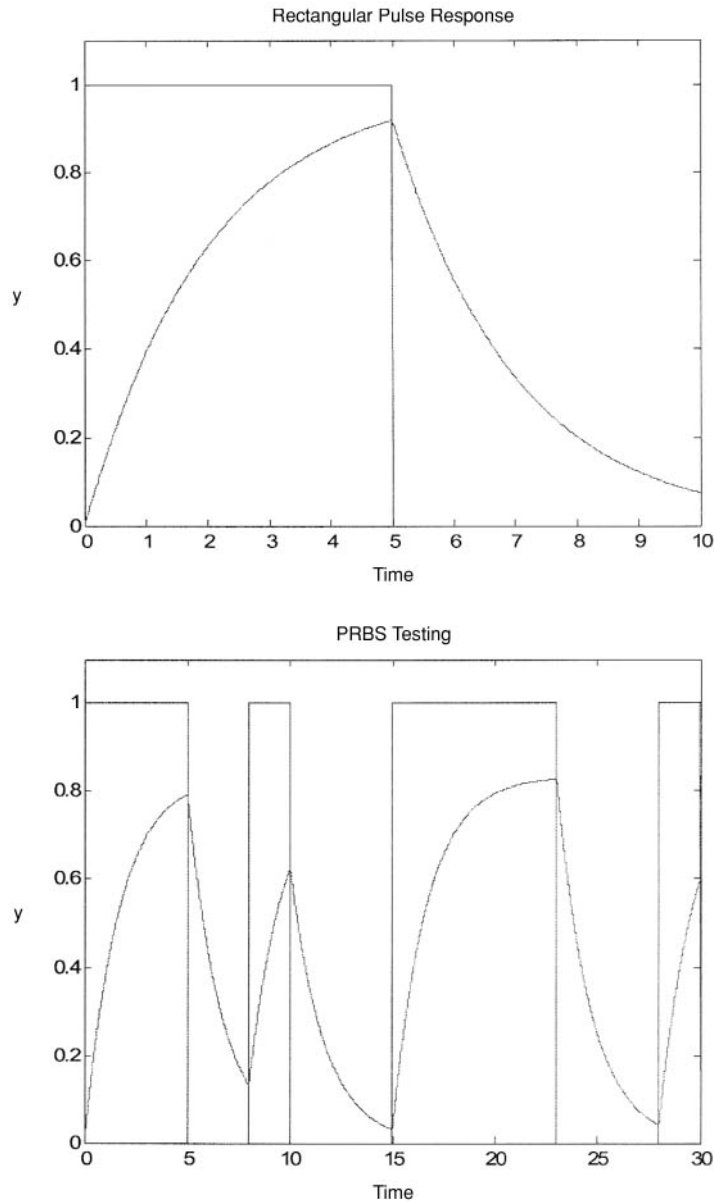


FIG. 8-22 Rectangular pulse response and PRBS testing.

Proportional Control A proportional controller moves its output proportional to the deviation e between the controlled variable y and its set point y_{sp} :

$$u = K_c e + b = \frac{100}{P} e + b \quad (8-28)$$

where $e = \pm(y - y_{sp})$, the sign selected to produce negative feedback. In some controllers, proportional gain K_c is introduced as a pure number; in others, it is set as $100/P$, where P is the proportional band in percent. The output bias b of the controller is also known as manual reset. The proportional controller is not a good regulator, because any change in output required to respond to a change in load results in a corresponding change in the controlled variable. To minimize the resulting offset, the bias

should be set at the best estimate of the load, and the proportional band set as low as possible. Processes requiring a proportional band of more than a few percent may control with unacceptably large values of offset.

Proportional control is most often used to regulate liquid level, where variations in the controlled variable carry no economic penalty and where other control modes can easily destabilize the loop. It is actually recommended for controlling the level in a surge tank when manipulating the flow of feed to a critical downstream process. By setting the proportional band just under 100 percent, the level is allowed to vary over the full range of the tank capacity as inflow fluctuates, thereby minimizing the resulting rate of change of manipulated outflow. This technique is called averaging level control.

Proportional-plus-Integral (PI) Control Integral action eliminates the offset described above by moving the controller output at a

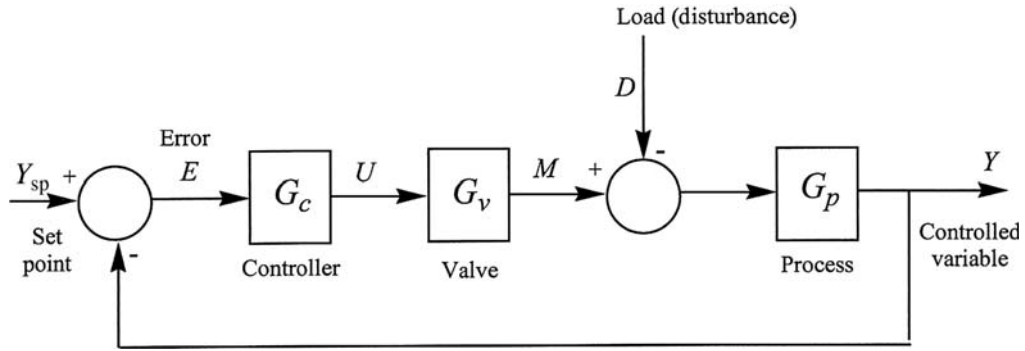


FIG. 8-23 Both load regulation and set-point response require high gains for the feedback controller.

rate proportional to the deviation from set point—the output will then not stop moving until the deviation is zero. Although available alone in an integral controller, it is most often combined with proportional action in a PI controller:

$$u = \frac{100}{P} \left(e + \frac{1}{\tau_i} \int e dt \right) + C_0 \quad (8-29)$$

where τ_i is the integral time constant in minutes; in some controllers it is introduced as integral gain or reset rate $1/\tau_i$ in repeats per minute. The last term in the equation is the constant of integration, the value of the controller output when integration begins. The PI controller is by far the most commonly used controller in the process industries.

Because the integral term lags the proportional term by 90° in phase, the PI controller then always produces a phase lag between 0° and 90° :

$$\phi_{PI} = -\tan^{-1} \frac{\tau_o}{2\pi\tau_i} \quad (8-30)$$

where τ_o is the period of oscillation of the loop. The phase angle should be kept between 15° for lag-dominant processes and 45° for dead-time-dominant processes for optimum results.

Proportional-plus-Integral-plus-Derivative (PID) Control The derivative mode moves the controller output as a function of the rate of change of the controlled variable, which adds phase lead to the controller, increasing its speed of response. It is normally combined with proportional and integral modes. The noninteracting or ideal form of the PID controller appears functionally as

$$u = \frac{100}{P} \left(e + \frac{1}{\tau_i} \int e dt \pm \tau_D \frac{dy}{dt} \right) + C_0 \quad (8-31)$$

where τ_D is the derivative time constant. Note that derivative action is applied to the controlled variable rather than to the deviation, as it should not be applied to the set point; the selection of the sign for the derivative term must be consistent with the action of the controller.

In some PID controllers, the integral and derivative terms are combined serially rather than in parallel, as done in the last equation. This results in interaction between these modes, such that the effective values of the controller parameters differ from their set values as follows:

$$\begin{aligned} \tau_{i,\text{eff}} &= \tau_i + \tau_D \\ \tau_{D,\text{eff}} &= \frac{1}{1/\tau_D + 1/\tau_i} \\ K_c &= \frac{100}{P} \left(1 + \frac{\tau_D}{\tau_i} \right) \end{aligned} \quad (8-32)$$

The performance of the interacting controller is almost as high as that of the noninteracting controller on most processes, but the tuning rules differ because of the above relationships. Both controllers are in common use in digital systems.

There is always a gain limit placed upon the derivative vector—a value of 10 is typical. However, interaction decreases the derivative

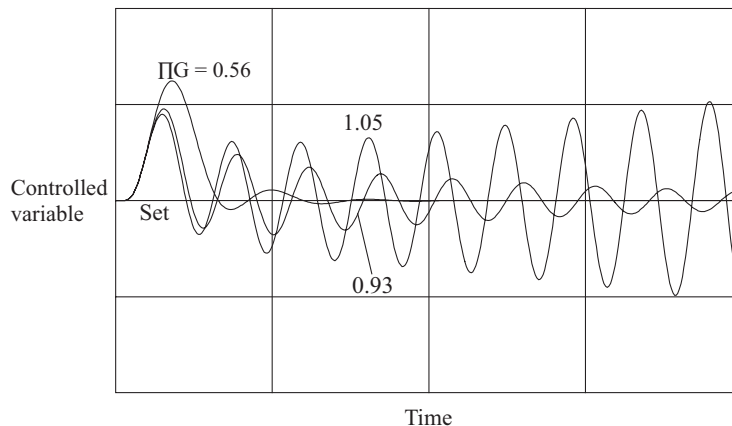


FIG. 8-24 Transition from well-damped load response to instability develops as loop gain increases.

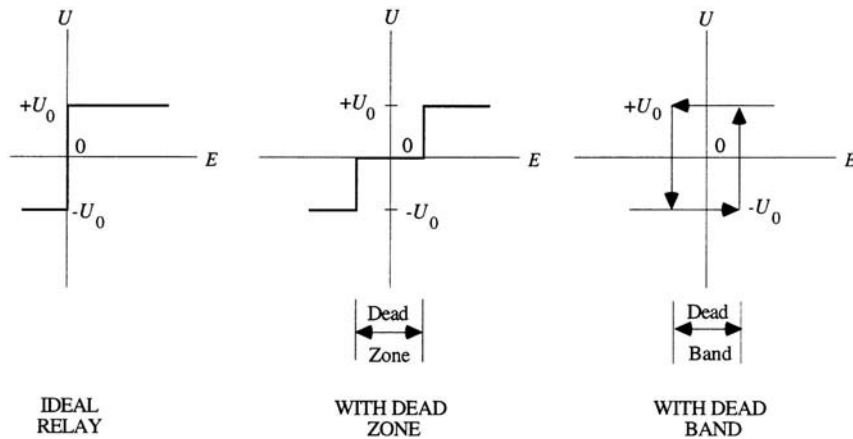


FIG. 8-25 On/off controller characteristics.

gain below this value by the factor $1 + \tau_D/\tau_I$, which is the reason for the decreased performance of the interacting PID controller. Sampling in a digital controller has a similar effect, limiting derivative gain to the ratio of derivative time to the sample interval of the controller. Noise on the controlled variable is amplified by the derivative gain, preventing its use in controlling flow and liquid level. Derivative action is recommended for control of temperature and composition in multiple-capacity processes with little measurement noise.

Controller Comparison Figure 8-26 compares the step load response of a distributed lag without control, and with P, PI, and interacting PID control. A distributed lag is a process whose resistance and capacity are distributed throughout its length—a heat exchanger is characteristic of this class, its heat-transfer surface and heat capacity being uniformly distributed. Other examples include imperfectly stirred tanks and distillation columns—both trayed and packed. The signature of a distributed lag is its open-loop (uncontrolled) step response, featuring a relatively short dead time followed by a dominant lag called $\Sigma\tau$, which is the time required to reach 63.2 percent complete response.

The proportional controller is unable to return the controlled variable to the set point following the step load change, as a deviation is required to sustain its output at a value different from its fixed bias b . The amount of proportional offset produced as a fraction of the uncontrolled offset is $1/(1 + KK_c)$, where K is the steady-state process

gain—in Fig. 8-26, that fraction is 0.13. Increasing K_c can reduce the offset, but with an accompanying loss in damping.

The PI and PID controller were tuned to produce a minimum *integrated absolute error* (IAE). Their response curves are similar in appearance to a gaussian distribution curve, but with a damped cycle in the trailing edge. The peak deviation of the PID response curve is only 0.12 times the uncontrolled offset, occurring at $0.36\Sigma\tau$; the peak deviation of the PI response curve is 0.21 times the uncontrolled offset, occurring at $0.48\Sigma\tau$. These values can be used to predict the load response of any distributed lag whose parameters K and $\Sigma\tau$ are known or can be estimated as described below.

CONTROLLER TUNING

The performance of a controller depends as much on its tuning as on its design. Tuning must be applied by the end user to fit the controller to the controlled process. There are many different approaches to controller tuning, based on the particular performance criteria selected, whether load or set-point changes are more important, whether the process is lag- or dead-time-dominant, and the availability of information about the process dynamics. The earliest definitive work in this field was done at the Taylor Instrument Company by Ziegler and Nichols (*Trans. ASME*, p. 759, 1942), tuning PI and interacting PID

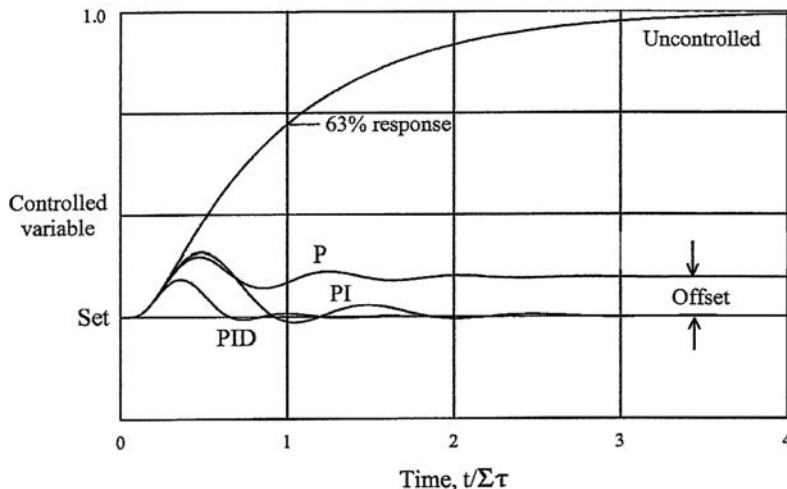


FIG. 8-26 Minimum-IAE tuning gives very satisfactory load response for a distributed lag.

controllers for optimum response to step load changes applied to lag-dominant processes. While these tuning rules are still in use, they do not apply to set-point changes, dead-time-dominant processes, or noninteracting PID controllers (Seborg, Edgar, and Mellichamp, *Process Dynamics and Control*, Wiley, New York, 2004).

Controller Performance Criteria The most useful measures of controller performance in an industrial setting are the maximum deviation in the controlled variable resulting from a disturbance, and its integral. The disturbance could be to the set point or to the load, depending on the variable being controlled and its context in the process. The size of the deviation and its integral are proportional to the size of the disturbance (if the loop is linear at the operating point). While actual disturbances arising in a plant may appear to be random, the controller needs a reproducible test to determine how well it is tuned. The disturbance of choice for test purposes is the step, because it can be applied manually, and by containing all frequencies including zero it exercises all modes of the controller. (The step actually has the same frequency distribution as integrated white noise, a “random walk.”) When tuned optimally for step disturbances, the controller will be optimally tuned for most other disturbances as well.

A step change in set point, however, may be a poor indicator of a loop’s load response. For example, a liquid-level controller does not have to integrate to follow a set-point change, as its steady-state output is independent of the set point. Stepping a flow controller’s set point is

an effective test of its tuning, however, as its steady-state output is proportional to its set point. Other loops should be load-tested: simulate a load change from a steady state at zero deviation by transferring the controller to manual and stepping its output, and then immediately transferring back to automatic before a deviation develops.

Figure 8-27*a* and *b* shows variations in the response of a distributed lag to a step change in load for different combinations of proportional and integral settings of a PI controller. The maximum deviation is the most important criterion for variables that could exceed safe operating levels, such as steam pressure, drum level, and steam temperature in a boiler. The same rule can apply to product quality if violating specifications causes it to be rejected. However, if the product can be accumulated in a downstream storage tank, its average quality is more important, and this is a function of the deviation integrated over the residence time of the tank. Deviation in the other direction, where the product is better than specification, is safe but increases production costs in proportion to the integrated deviation because quality is given away.

For a PI or PID controller, the integrated deviation—better known as integrated error IE—is related to the controller settings

$$IE = \Delta u \frac{P\tau_i}{100} \tag{8-33}$$

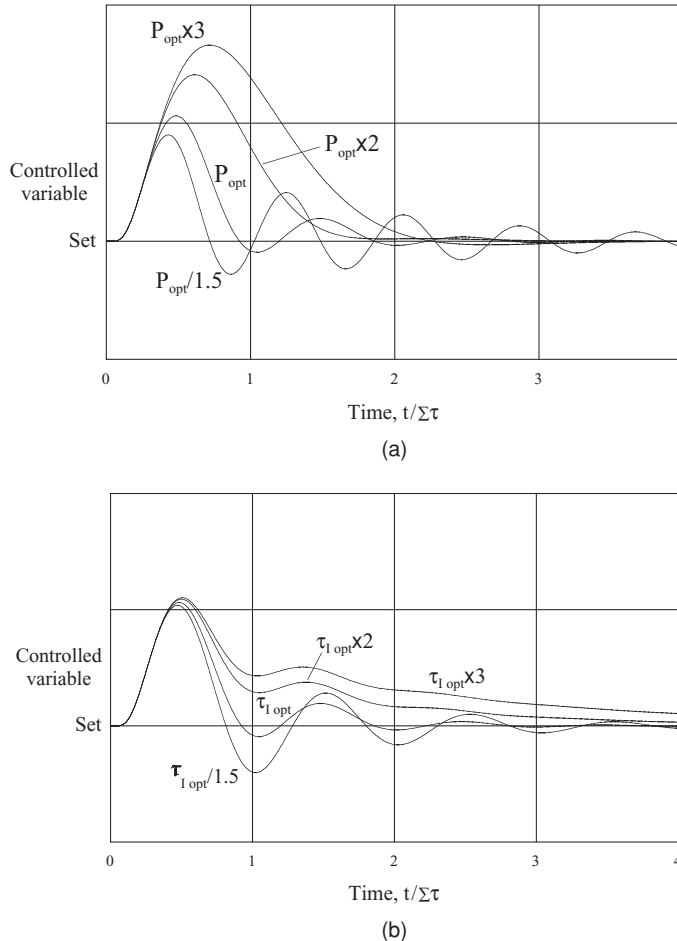


FIG. 8-27 The optimum settings produce minimum-IAE load response. (a) The proportional band primarily affects damping and peak deviation. (b) Integral time determines overshoot.

where Δu is the difference in controller outputs between two steady states, as required by a change in load or set point. The proportional band P and integral time τ_i are the indicated settings of the controller for PI and both interacting and noninteracting PID controllers. Although the derivative term does not appear in the relationship, its use typically allows a 50 percent reduction in integral time and therefore in IE. The integral time in the IE expression should be augmented by the sample interval if the controller is digital, the time constant of any filter used, and the value of any dead-time compensator.

It would appear, from the above, that minimizing IE is simply a matter of minimizing the P and τ_i settings of the controller. However, settings will be reached that produce excessive oscillations, such as shown in the lowest two response curves in Fig. 8-27a and b. It is preferable instead to find a combination of controller settings that minimizes integrated absolute error IAE, which for both load and set-point changes is a well-damped response with minimal overshoot. The curves designated P_{opt} and $\tau_{i,opt}$ in Fig. 8-27 are the same minimum-IAE response to a step change in load for a distributed-lag process under PI control. Because of the very small overshoot, the IAE will be only slightly larger than the IE. Loops that are tuned to minimize IAE tend to give responses that are close to minimum IE and with minimum peak deviation. The other curves in Fig. 8-27a and b describe the effects of individual adjustments to P and τ_i , respectively, around those optimum values and can serve as a guide to fine-tuning a PI controller.

The performance of a controller (and its tuning) must be based on what is achievable for a given process. The concept of best practical IE (IE_b) for a step change in load ΔL to a process consisting of dead time and one or two lags can be estimated (Shinskey, *Process Control Systems*, 4th ed., McGraw-Hill, New York, 1996)

$$IE_b = \Delta L K_L \tau_L (1 - e^{-\theta/\tau_L}) \tag{8-34}$$

where K_L is the gain and τ_L the primary time constant in the load path, and θ the dead time in the manipulated path to the controlled variable. If the load or its gain is unknown, Δu and $\bar{K} (= K_L K_p)$ may be substituted. If the process is non-self-regulating (i.e., an integrator), the relationship is

$$IE_b = \frac{\Delta L \theta^2}{\tau_i} \tag{8-35}$$

where τ_i is the time constant of the process integrator. The peak deviation of the best practical response curve is

$$e_b = \frac{IE_b}{\theta + \tau_2} \tag{8-36}$$

where τ_2 is the time constant of a common secondary lag (e.g., in the measuring device).

TABLE 8-2 Tuning Rules Using Known Process Parameters

Process	Controller	P	τ_i	τ_D
Dead-time-dominant	PI	250K	0.5 θ	
Lag-dominant	PI	106K θ/τ_m	4.0 θ	
	PID _n	77K θ/τ_m	1.8 θ	0.45 θ
	PID _i	106K θ/τ_m	1.5 θ	0.55 θ
Non-self-regulating	PI	106 θ/τ_i	4.0 θ	
	PID _n	78 θ/τ_i	1.9 θ	0.48 θ
	PID _i	108 θ/τ_i	1.6 θ	0.58 θ
Distributed lags	PI	20K	0.50 $\Sigma\tau$	
	PID _n	10K	0.30 $\Sigma\tau$	0.09 $\Sigma\tau$
	PID _i	15K	0.25 $\Sigma\tau$	0.10 $\Sigma\tau$

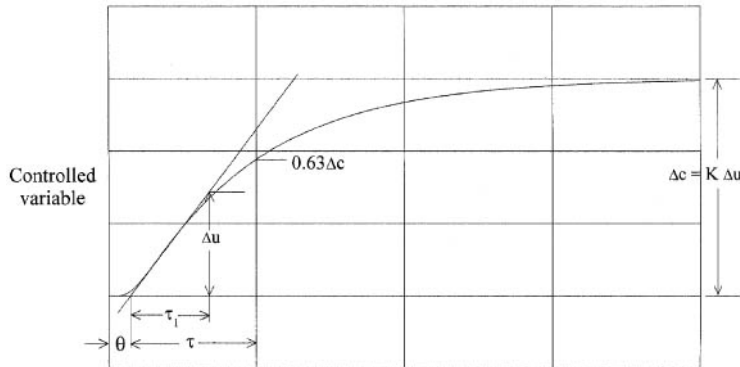
NOTE: n = noninteracting, i = interacting controller modes.

The performance of any controller can be measured against this standard by comparing the IE it achieves in responding to a load change with the best practical IE. Maximum performance levels for PI controllers on lag-dominant processes lie in the 20 to 30 percent range, while for PID controllers they fall between 40 and 60 percent, varying with secondary lags.

Tuning Methods Based on Known Process Models The most accurate tuning rules for controllers have been based on simulation, where the process parameters can be specified and IAE and IE can be integrated during the simulation as an indication of performance. Controller settings are then iterated until a minimum IAE is reached for a given disturbance. Next these optimum settings are related to the parameters of the simulated process in tables, graphs, or equations, as a guide to tuning controllers for processes whose parameters are known (Seborg, Edgar, and Mellichamp, *Process Dynamics and Control*, Wiley, New York, 2004). This is a multidimensional problem, however, in that the relationships change as a function of process type, controller type, and source of disturbance.

Table 8-2 summarizes these rules for minimum-IAE load response for the most common controllers. The process gain and time constant τ_m are obtained from the product of G_v and G_p in Fig. 8-23. Derivative action is not effective for dead-time-dominant processes. Any secondary lag, sampling interval, or filter time constant should be added to dead time θ .

The principal limitation to using these rules is that the true process parameters are often unknown. Steady-state gain K can be calculated from a process model, or determined from the steady-state results of a step test as $\Delta c/\Delta u$, as shown in Fig. 8-28. The test will not be viable, however if the time constant of the process τ_m is longer than a few minutes, since five time constants must elapse to approach a steady state within 1 percent, and unexpected disturbances may intervene. Estimated dead time θ is the time from the step to the intercept of a



Time t

FIG. 8-28 If a steady state can be reached, gain K and time constant τ can be estimated from a step response; if not, use τ_i instead.

TABLE 8-3 Tuning Rules Using Slope and Intercept

Controller	P	τ_i	τ_D
PI	$150\theta/\tau_1$	3.5 θ	
PID _n	$75\theta/\tau_1$	2.1 θ	0.63 θ
PID _i	$113\theta/\tau_1$	1.8 θ	0.70 θ

NOTE: n = noninteracting, i = interacting controller modes.

straight line tangent to the steepest part of the response curve. The estimated time constant τ is the time from that point to 63 percent of the complete response. In the presence of a significant secondary lag, these results will not be completely accurate, however. The time for 63 percent response may be more accurately calculated as the residence time of the process: its volume divided by current volumetric flow rate.

Tuning Methods When Process Model Is Unknown Ziegler and Nichols developed two tuning methods for processes with unknown parameters. The open-loop method uses a step test without waiting for a steady state to be reached and is therefore applicable to very slow processes. Dead time is estimated from the intercept of the steepest tangent to the response curve in Fig. 8-28, whose slope is also used. If the process is non-self-regulating, the controlled variable will continue to follow this slope, changing by an amount equal to Δu in a time equal to its time constant τ_1 . This time estimate τ_1 is used along with θ to tune controllers according to Table 8-3, applicable to lag-dominant processes. If the process is known to be a distributed lag, such as a heat exchanger, distillation column, or stirred tank, then better results will be obtained by converting the estimated values of θ and τ_1 to K and $\Sigma\tau$ and using Table 8-2. The conversion factors are $K = 7.5\theta/\tau_1$ and $\Sigma\tau = 7.0\theta$.

The Ziegler and Nichols closed-loop method requires forcing the loop to cycle uniformly under proportional control, by setting the integral time to maximum and derivative time to zero and reducing the proportional band until a constant-amplitude cycle results. The natural period τ_p of the cycle (the proportional controller contributes no phase shift to alter it) is used to set the optimum integral and derivative time constants. The optimum proportional band is set relative to the undamped proportional band P_u which was found to produce the uniform oscillation. Table 8-4 lists the tuning rules for a lag-dominant process.

A uniform cycle can also be forced by using on-off control to cycle the manipulated variable between two limits. The period of the cycle will be close to τ_p if the cycle is symmetric; the peak-to-peak ampli-

TABLE 8-4 Tuning Rules Using Proportional Cycle

Controller	P	τ_i	τ_D
PI	$1.70P_u$	$0.81\tau_p$	
PID _n	$1.30P_u$	$0.48\tau_p$	$0.11\tau_p$
PID _i	$1.80P_u$	$0.38\tau_p$	$0.14\tau_p$

NOTE: n = noninteracting, i = interacting controller modes.

tude A_c of the controlled variable divided by the difference between the output limits A_u is a measure of process gain at that period and is therefore related to P_u for the proportional cycle:

$$P_u = 100 \frac{\pi}{4} \frac{A_c}{A_u} \tag{8-37}$$

The factor $\pi/4$ compensates for the square wave in the output. Tuning rules are given in Table 8-4.

Set-Point Response All the above tuning methods are intended to minimize IAE for step load changes. When applied to lag-dominant processes, the resulting controller settings produce excessive overshoot of set-point changes. This behavior has led to the practice of tuning to optimize set-point response, which unfortunately degrades the load response of lag-dominant loops. An option has been available with some controllers to remove proportional action from set-point changes, which eliminates set-point overshoot but lengthens settling time. A preferred solution to this dilemma is available in many modern controllers which feature an independent gain adjustment for the set point, through which set-point response can be optimized after the controller has been tuned to optimize load response.

Figure 8-29 shows set-point and load responses of a distributed lag for both set-point and load tuning, including the effects of fractional set-point gain K_s . The set point was stepped at time zero, and the load stepped at time 2.4. With full set-point gain, the PI controller was tuned for minimum-IAE set-point response with $P = 29K$ and $\tau_i = \Sigma\tau$, compared to $P = 20K$ and $\tau_i = 0.50\Sigma\tau$ for minimum-IAE load response. These settings increase its IE for load response by a factor of 2.9, and its peak deviation by 20 percent, over optimum load tuning. However, with optimum load tuning, that same set-point overshoot can be obtained with set-point gain $K_s = 0.54$. The effects of full set-point gain (1.0) and no set-point gain (0) are shown for comparison.

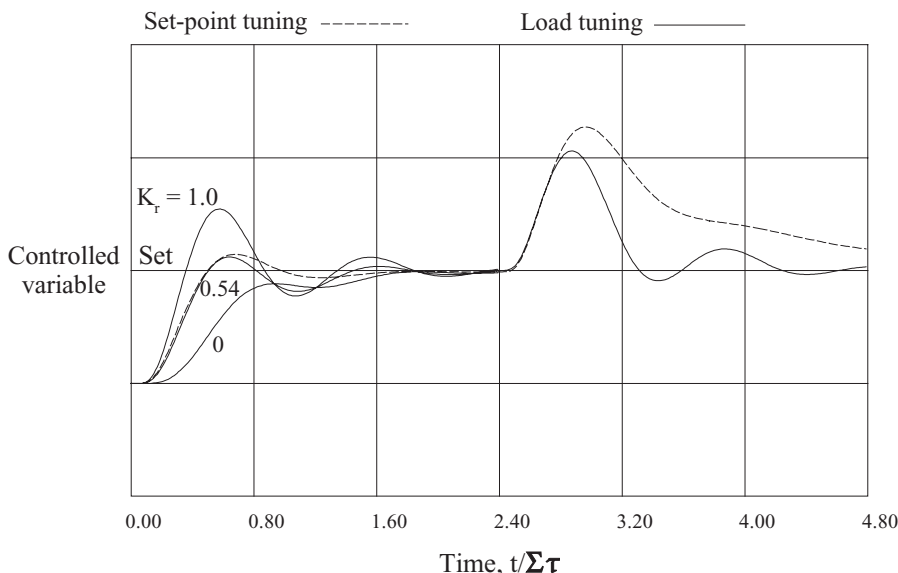


FIG. 8-29 Tuning proportional and integral settings to optimize set-point response degrades load response; using a separate set-point gain adjustment allows both responses to be optimized.

ADVANCED CONTROL SYSTEMS

BENEFITS OF ADVANCED CONTROL

The economics of most processes are determined by the steady-state operating conditions. Excursions from these steady-state conditions usually have a less important effect on the economics of the process, except when the excursions lead to off-specification products. To enhance the economic performance of a process, the steady-state operating conditions must be altered in a manner that leads to more efficient process operation.

The hierarchy shown in Fig. 8-30 indicates that process control activities consist of the following five levels:

- Level 1: Measurement devices and actuators
- Level 2: Safety, environmental/equipment protection
- Level 3: Regulatory control
- Level 4: Real-time optimization
- Level 5: Planning and scheduling

Levels 4 and 5 clearly affect the process economics, as both levels are directed to optimizing the process in some manner. In contrast, levels 1, 2, and 3 would appear to have no effect on process economics. Their direct effect is indeed minimal, although indirectly they can have a major effect. Basically, these levels provide the foundation for all higher levels. A process cannot be optimized until it can be operated consistently at the prescribed targets. Thus, satisfactory regulatory control must be the first goal of any automation effort. In turn, the measurements and actuators provide the process interface for regulatory control.

For most processes, the optimum operating point is determined by a constraint. The constraint might be a product specification (a product stream can contain no more than 2 percent ethane); violation of this constraint causes off-specification product. The constraint might be an equipment limit (vessel pressure rating is 300 psig); violation of this constraint causes the equipment protection mechanism (pressure

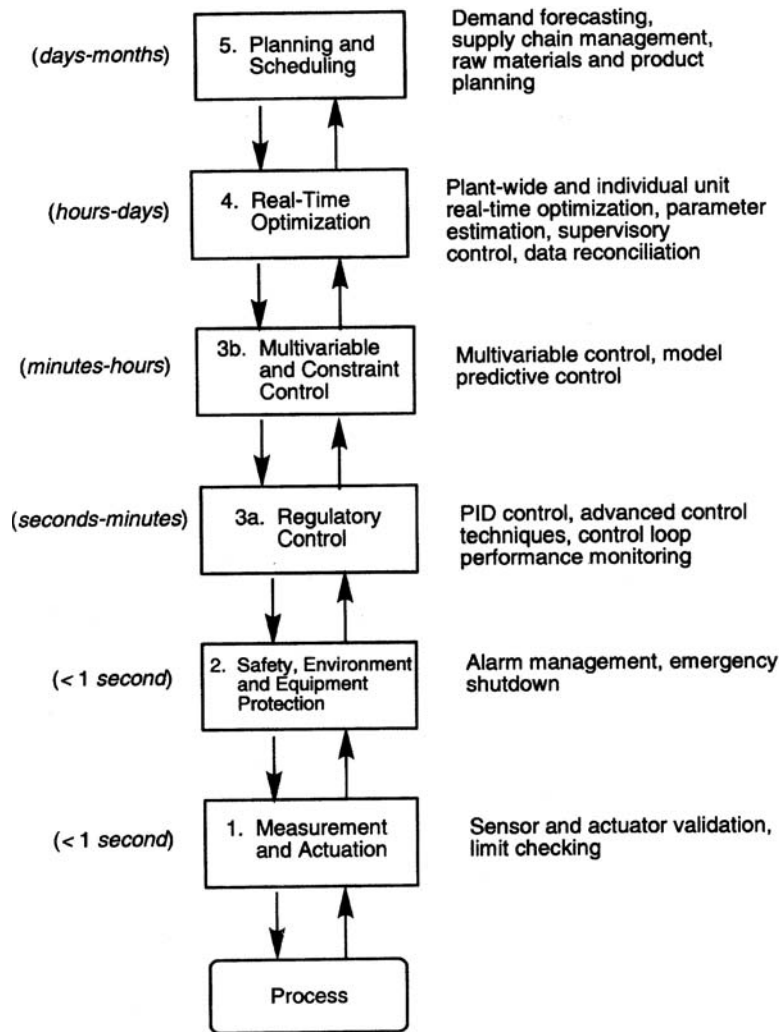


FIG. 8-30 The five levels of process control and optimization in manufacturing. Time scales are shown for each level. (Source: *Seborg et al., Process Dynamics and Control, 2d ed., Wiley, New York, 2004.*)

relief device) to activate. As the penalties are serious, violation of such constraints must be very infrequent.

If the regulatory control system were perfect, the target could be set exactly equal to the constraint (i.e., the target for the pressure controller could be set at the vessel relief pressure). However, no regulatory control system is perfect. Therefore, the value specified for the target must be on the safe side of the constraint, thus allowing the control system some operating margin. How much depends on the following:

1. *The performance of the control system (i.e., how effectively it responds to disturbances).* The faster the control system reacts to a disturbance, the closer the process can be operated to the constraint.

2. *The magnitude of the disturbances to which the control system must respond.* If the magnitude of the major disturbances can be reduced, the process can be operated closer to the constraint.

One measure of the performance of a control system is the variance of the controlled variable from the target. Both improving the control system and reducing the disturbances will lead to a lower variance in the controlled variable.

In a few applications, improving the control system leads to a reduction in off-specification product and thus improved process economics. However, in most situations, the process is operated sufficiently far from the constraint that very little, if any, off-specification product results from control system deficiencies. Management often places considerable emphasis on avoiding off-specification production, so consequently the target is actually set far more conservatively than it should be.

In most applications, simply improving the control system does not directly lead to improved process economics. Instead, the control system improvement must be accompanied by shifting the target closer to the constraint. There is always a cost of operating a process in a conservative manner. The cost may be a lower production rate, a lower process efficiency, a product giveaway, or other. When management places undue emphasis on avoiding off-specification production, the natural reaction is to operate very conservatively, thus incurring other costs.

The immediate objective of an advanced control effort is to reduce the variance in an important controlled variable. However, this effort must be coupled with a commitment to adjust the target for this controlled variable so that the process is operated closer to the constraint. In large-throughput (commodity) processes, very small shifts in operating targets can lead to large economic returns.

ADVANCED CONTROL TECHNIQUES

GENERAL REFERENCES: Seborg, Edgar, and Mellichamp, *Process Dynamics and Control*, Wiley, New York, 2004. Stephanopoulos, *Chemical Process Control: An Introduction to Theory and Practice*, Prentice-Hall, Englewood Cliffs, N.J., 1984. Shinskey, *Process Control Systems*, 4th ed., McGraw-Hill, New York, 1996. Ogunnaike and Ray, *Process Dynamics, Modeling, and Control*, Oxford University Press, New York, 1994.

While the single-loop PID controller is satisfactory in many process applications, it does not perform well for processes with slow dynamics, time delays, frequent disturbances, or multivariable interactions. We discuss several advanced control methods below that can be implemented via computer control, namely, feedforward control, cascade control, time-delay compensation, selective and override control, adaptive control, fuzzy logic control, and statistical process control.

Feedforward Control If the process exhibits slow dynamic response and disturbances are frequent, then the application of feedforward control may be advantageous. Feedforward (FF) control differs from feedback (FB) control in that the primary disturbance or load (D) is measured via a sensor and the manipulated variable (U) is adjusted so that deviations in the controlled variable from the set point are minimized or eliminated (see Fig. 8-31). By taking control action based on measured disturbances rather than controlled variable error, the controller can reject disturbances before they affect the controlled variable Y . To determine the appropriate settings for the manipulated variable, one must develop mathematical models that relate

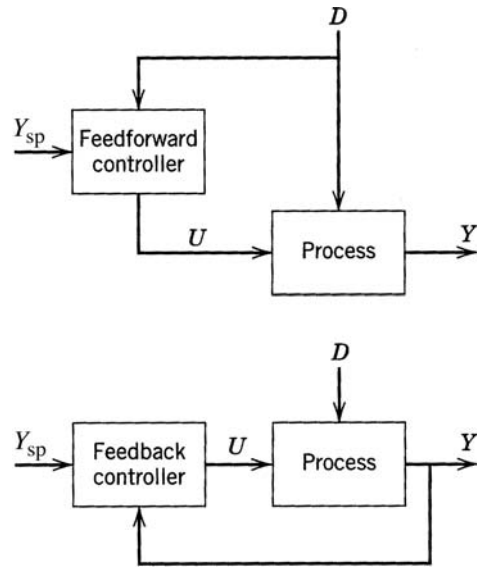


FIG. 8-31 Simplified block diagrams for feedforward and feedback control.

1. The effect of the manipulated variable U on the controlled variable Y
2. The effect of the disturbance D on the controlled variable Y

These models can be based on steady-state or dynamic analysis. The performance of the feedforward controller depends on the accuracy of both models. If the models are exact, then feedforward control offers the potential of perfect control (i.e., holding the controlled variable precisely at the set point at all times because of the ability to predict the appropriate control action). However, since most mathematical models are only approximate and since not all disturbances are measurable, it is standard practice to utilize feedforward control in conjunction with feedback control. Table 8-5 lists the relative advantages and disadvantages of feedforward and feedback control. By combining the two control methods, the strengths of both schemes can be utilized.

FF control therefore attempts to eliminate the effects of measurable disturbances, while FB control would correct for unmeasurable disturbances and modeling errors. This latter case is often referred to as feedback trim. These controllers have become widely accepted in the chemical process industries since the 1960s.

Design Based on Material and Energy Balances Consider a heat exchanger example (see Fig. 8-32) to illustrate the use of FF and FB control. The control objective is to maintain T_2 , the exit liquid temperature, at the desired value (or set point) T_{2sp} despite variations in the inlet liquid flow rate F and inlet liquid temperature T_1 . This is done by manipulating W , the steam flow rate. A feedback control scheme would entail measuring T_2 , comparing T_2 to T_{2sp} , and then adjusting W . A feedforward control scheme requires measuring F and T_1 , and adjusting W (knowing T_{2sp}), in order to control exit temperature T_2 .

Figure 8-33a and b shows the control system diagrams for FB and FF control. A feedforward control algorithm can be designed for the heat exchanger in the following manner. Using a steady-state energy balance and assuming no heat loss from the heat exchanger,

$$WH = FC(T_2 - T_1) \tag{8-38}$$

where H = latent heat of vaporization and C = specific heat of liquid

$$W = \frac{C}{H} F(T_2 - T_1) \tag{8-39}$$

or

$$W = K_1 F(T_2 - T_1) \tag{8-40}$$

TABLE 8-5 Relative Advantages and Disadvantages of Feedforward and Feedback

Advantages	Disadvantages
Feedforward	
<ul style="list-style-type: none"> Acts before the effect of a disturbance has been felt by the system Is good for systems with large time constant or dead time Does not introduce instability in the closed-loop response 	<ul style="list-style-type: none"> Requires direct measurement of all possible disturbances Cannot cope with unmeasured disturbances Is sensitive to process/model error
Feedback	
<ul style="list-style-type: none"> Does not require identification and measurement of any disturbance for corrective action Does not require an explicit process model Is possible to design controller to be robust to process/model errors 	<ul style="list-style-type: none"> Control action not taken until the effect of the disturbance has been felt by the system Is unsatisfactory for processes with large time constants and frequent disturbances May cause instability in the closed-loop response

with

$$K_1 = \frac{C_L}{H} \tag{8-41}$$

Replace T_2 by T_{2sp}

$$W = K_1 F(T_{set} - T_1) \tag{8-42}$$

Equation (8-42) can be used in the FF calculation, assuming one knows the physical properties C and H . Of course, it is probable that the model will contain errors (e.g., unmeasured heat losses, incorrect C or H). Therefore, K_1 can be designated as an adjustable parameter that can be tuned. The use of a physical model for FF control is desirable because it provides a physical basis for the control law and gives an a priori estimate of what the tuning parameters should be. Note that such a model could be nonlinear [e.g., in Eq. (8-42), F and T_{2sp} are multiplied].

Block Diagram Analysis One shortcoming of this feedforward design procedure is that it is based on the steady-state characteristics of the process and, as such, neglects process dynamics (i.e., how fast the controlled variable responds to changes in the load and manipulated variables). Thus, it is often necessary to include “dynamic compensation” in the feedforward controller. The most direct method of designing the FF dynamic compensator is to use a block diagram of a general process, as shown in Fig. 8-34, where G_d represents the disturbance transmitter, G_f is the feedforward controller, G_v relates the disturbance to the controlled variable, G_c is the valve, G_p is the process, G_m is the output transmitter, and G_e is the feedback controller. All blocks correspond to transfer functions (via Laplace transforms).

Using block diagram algebra and Laplace transform variables, the controlled variable $Y(s)$ is given by

$$Y(s) = \frac{G_f G_L(s) + G_d D(s)}{1 + G_m G_c G_v G_p} \tag{8-43}$$

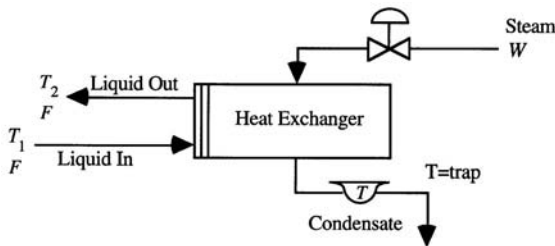
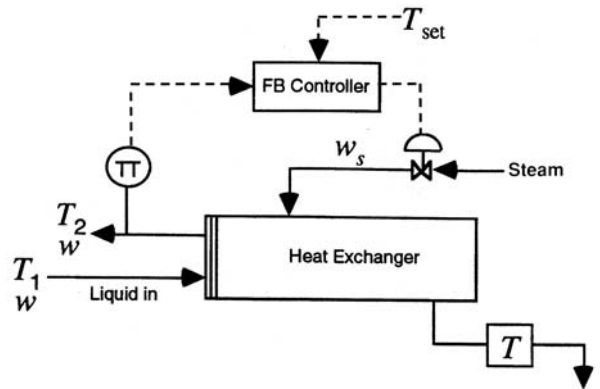


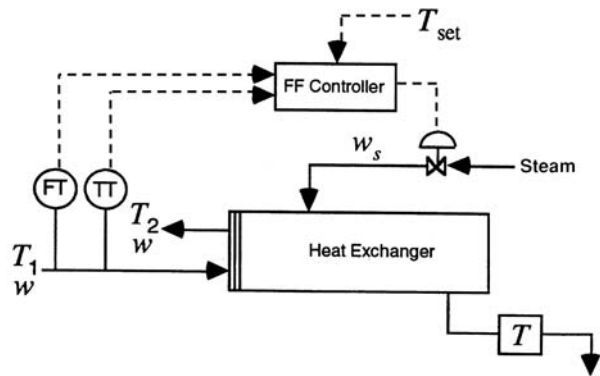
FIG. 8-32 A heat exchanger diagram.

For disturbance rejection [$D(s) \neq 0$] we require that $Y(s) = 0$, or zero error. Solving Eq. (8-43) for G_f gives

$$G_f = \frac{-G_L}{G_v G_c G_p} \tag{8-44}$$



(a)



(b)

FIG. 8-33 (a) Feedback control of a heat exchanger. (b) Feedforward control of a heat exchanger.

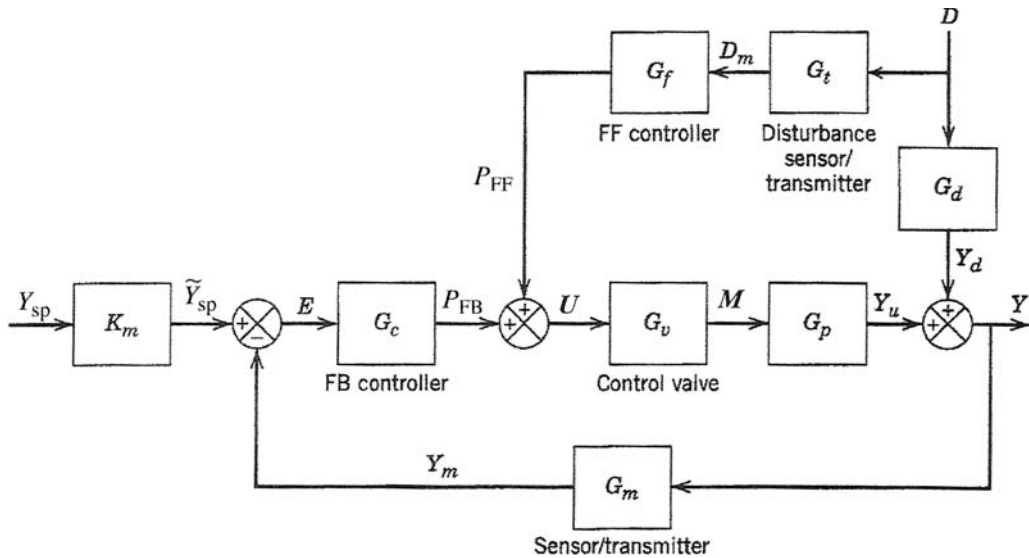


FIG. 8-34 A block diagram of a feedforward-feedback control system. (Source: Seborg et al., Process Dynamics and Control, 2d ed., Wiley, New York, 2004.)

Suppose the dynamics of G_d and G_p are first-order; in addition, assume that $G_c = K_c$ and $G_t = K_t$ (constant gains for simplicity).

$$G_d(s) = \frac{K_d}{\tau_d s + 1} = \frac{Y(s)}{D(s)} \tag{8-45}$$

$$G_p(s) = \frac{K_p}{\tau_p s + 1} = \frac{Y(s)}{U(s)} \tag{8-46}$$

Using Eq. (8-44),

$$G_f(s) = \frac{\tau_p s + 1}{\tau_d s + 1} \cdot \frac{-K_d}{K_p K_c K_t} = \frac{-K(\tau_p s + 1)}{\tau_d s + 1} \tag{8-47}$$

where K is the overall ratio of the gains in Eq. (8-47).

The above FF controller can be implemented by using a digital computer. Figure 8-35*a* and *b* compares typical responses for PID FB control, steady-state FF control ($s = 0$), dynamic FF control, and combined FF/FB control. In practice, the engineer can tune K , τ_p , and τ_d in the field to improve the performance of the FF controller. The feedforward controller can also be simplified to provide steady-state feedforward control. This is done by setting $s = 0$ in $G_f(s)$. This might be appropriate if there is uncertainty in the dynamic models for G_d and G_p .

Other Considerations in Feedforward Control The tuning of feedforward and feedback control systems can be performed independently. In analyzing the effects of the disturbance $D(s)$, as long as there are no model errors. For the feedback loop, therefore, the effects of $D(s)$ can also be ignored, which for the servo case is

$$\frac{Y(s)}{Y_{sp}(s)} = \frac{G_c G_c G_p K_m}{1 + G_c G_c G_p G_m} \tag{8-48}$$

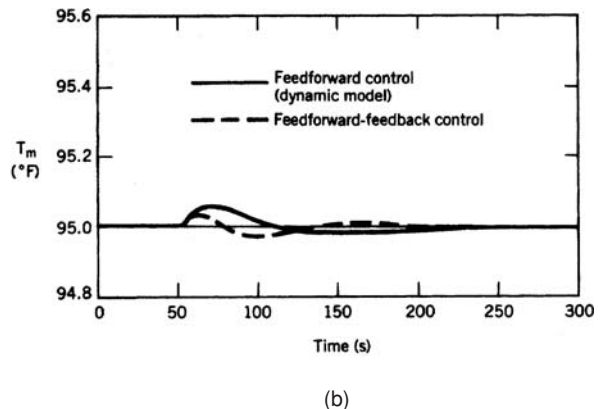
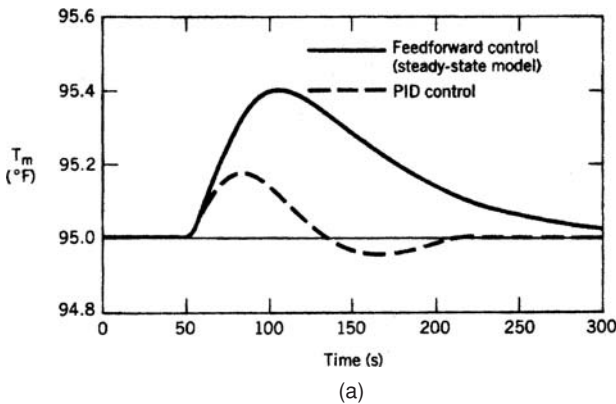


FIG. 8-35 (a) Comparison of FF (steady-state model) and PID FB control for disturbance change. (b) Comparison of FF (dynamic model) and combined FF/FB control.

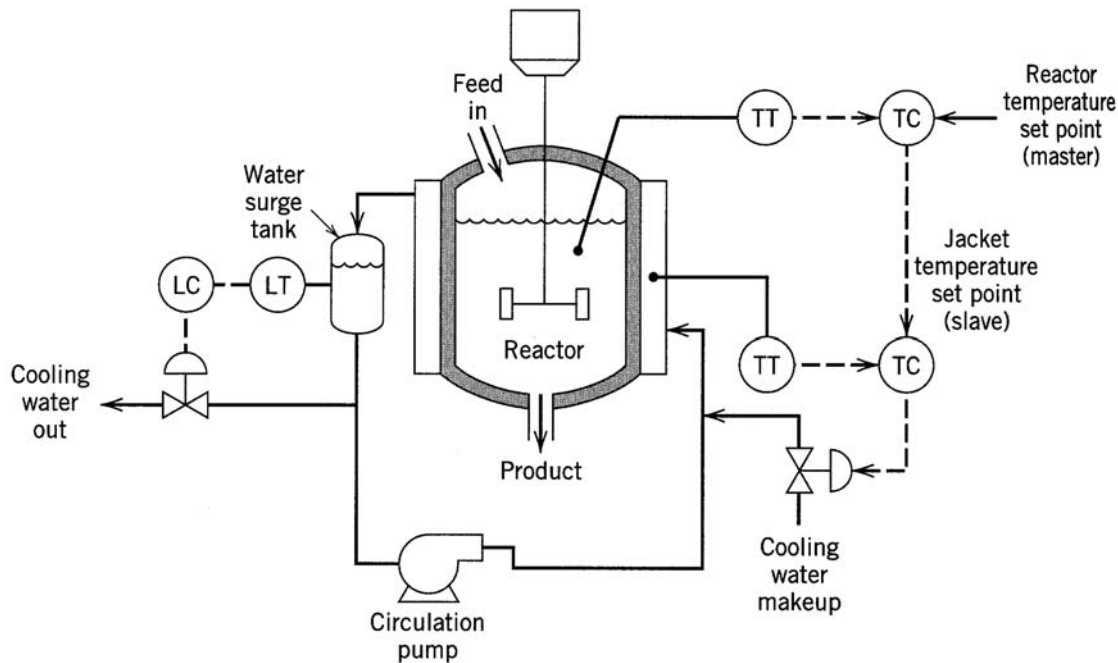


FIG. 8-36 Cascade control of an exothermic chemical reactor. (Source: Seborg et al., *Process Dynamics and Control*, 2d ed., Wiley, New York, 2004.)

Note that the characteristic equation will be unchanged for the FF + FB system; hence system stability will be unaffected by the presence of the FF controller. In general, the tuning of the FF controller can be less conservative than for the case of FB alone, because smaller excursions from the set point will result. This in turn would make the dynamic model $Y(s)$ more accurate.

The tuning of the controller in the feedback loop can be theoretically performed independently of the feedforward loop (i.e., the feedforward loop does not introduce instability in the closed-loop response). For more information on feedforward/feedback control applications and design of such controllers, refer to the general references.

Cascade Control One of the disadvantages of using conventional feedback control for processes with large time lags or delays is that disturbances are not recognized until after the controlled variable deviates from its set point. In these processes, correction by feedback control is generally slow and results in long-term deviation from the set point. One way to improve the dynamic response to load changes is by using a secondary measurement point and a secondary controller; the secondary measurement point is located so that it recognizes the upset condition before the primary controlled variable is affected.

One such approach is called cascade control, which is routinely used in most modern computer control systems. Consider a chemical reactor, where reactor temperature is to be controlled by coolant flow to the jacket of the reactor. The reactor temperature can be influenced by changes in disturbance variables such as feed rate or feed temperature; a feedback controller could be employed to compensate for such disturbances by adjusting a valve on the coolant flow to the reactor jacket. However, suppose an increase occurs in the coolant temperature as a result of changes in the plant coolant system. This will cause a change in the reactor temperature measurement, although such a change will not occur quickly, and the corrective action taken by the controller will be delayed.

Cascade control is one solution to this problem (see Fig. 8-36). Here the jacket temperature is measured, and an error signal is sent from this point to the coolant control valve; this reduces coolant flow,

maintaining the heat-transfer rate to the reactor at a constant level and rejecting the disturbance. The cascade control configuration will also adjust the setting of the coolant control valve when an error occurs in the reactor temperature. The cascade control scheme shown in Fig. 8-36 contains two controllers. The primary controller is the reactor temperature controller. It measures the reactor temperature, compares it to the set point, and computes an output, which is the set point for the coolant flow rate controller. The secondary controller compares this set point to the coolant temperature measurement and adjusts the valve. The principal advantage of cascade control is that the secondary measurement (jacket temperature) is located closer to a potential disturbance in order to improve the closed-loop response.

Figure 8-37 shows the block diagram for a general cascade control system. In tuning of a cascade control system, the secondary controller (in the inner loop) is tuned first with the primary controller in manual. Often only a proportional controller is needed for the secondary loop, because offset in the secondary loop can be treated by using proportional-plus-integral action in the primary loop. When the primary controller is transferred to automatic, it can be tuned by using the techniques described earlier in this section. For more information on theoretical analysis of cascade control systems, see the general references for a discussion of applications of cascade control.

Time-Delay Compensation Time delays are a common occurrence in the process industries because of the presence of recycle loops, fluid-flow distance lags, and dead time in composition measurements resulting from use of chromatographic analysis. The presence of a time delay in a process severely limits the performance of a conventional PID control system, reducing the stability margin of the closed-loop control system. Consequently, the controller gain must be reduced below that which could be used for a process without delay. Thus, the response of the closed-loop system will be sluggish compared to that of the system with no time delay.

To improve the performance of time-delay systems, special control algorithms have been developed to provide time-delay compensation. The Smith predictor technique is the best-known algorithm; a related method is called the analytical predictor. Various investigators have

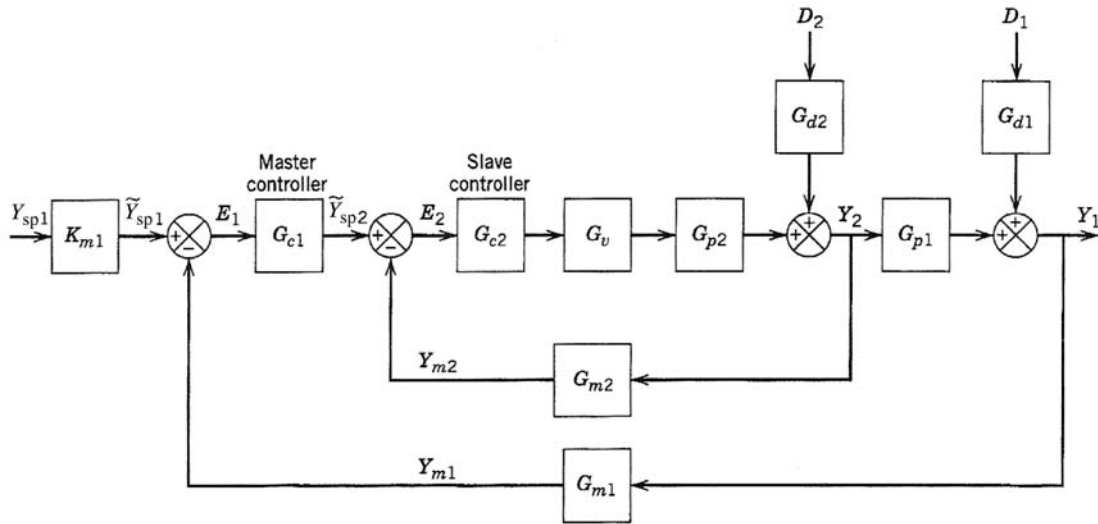


FIG. 8-37 Block diagram of the cascade control system. For a chemical reactor G_{d1} would correspond to a feed temperature or composition disturbance, while G_{d2} would be a change in the cooling water temperature. (Source: Seborg et al., Process Dynamics and Control, 2d ed., Wiley, New York, 2004.)

found that, based on integral squared error, the performance of the Smith predictor can be better than that for a conventional controller, as long as the time delay is known accurately.

The Smith predictor is a model-based control strategy that involves a more complicated block diagram than that for a conventional feedback controller, although a PID controller is still central to the control strategy (see Fig. 8-38). The key concept is based on better coordination of the timing of manipulated variable action. The loop configuration takes into account the fact that the current controlled variable measurement is not a result of the current manipulated variable action, but the value taken θ time units earlier. Time-delay compensation can yield excellent performance; however, if the process model parameters change (especially the time delay), the Smith predictor

performance will deteriorate and is not recommended unless other precautions are taken.

Selective and Override Control When there are more controlled variables than manipulated variables, a common solution to this problem is to use a selector to choose the appropriate process variable from among a number of available measurements. Selectors can be based on multiple measurement points, multiple final control elements, or multiple controllers, as discussed below. Selectors are used to improve the control system performance as well as to protect equipment from unsafe operating conditions.

One type of selector device chooses as its output signal the highest (or lowest) of two or more input signals. This approach is often referred to as auctioneering. On instrumentation diagrams, the symbol

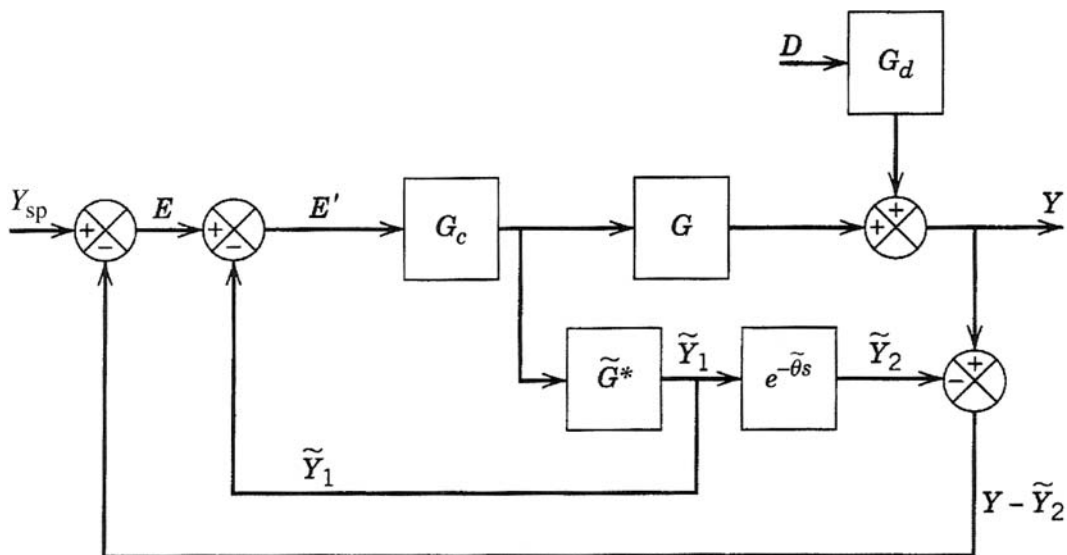


FIG. 8-38 Block diagram of the Smith predictor. (Source: Seborg et al., Process Dynamics and Control, 2d ed., Wiley, New York, 2004.)

> denotes a high selector and < a low selector. For example, a high selector can be used to determine the hot-spot temperature in a fixed-bed chemical reactor. In this case, the output from the high selector is the input to the temperature controller. In an exothermic catalytic reaction, the process may run away due to disturbances or changes in the reactor. Immediate action should be taken to prevent a dangerous rise in temperature. Because a hot spot may potentially develop at one of several possible locations in the reactor, multiple (redundant) measurement points should be employed. This approach minimizes the time required to identify when a temperature has risen too high at some point in the bed.

The use of high or low limits for process variables is another type of selective control, called an override. The feature of antireset windup in feedback controllers is a type of override. Another example is a distillation column with lower and upper limits on the heat input to the column reboiler. The minimum level ensures that liquid will remain on the trays, while the upper limit is determined by the onset of flooding. Overrides are also used in forced-draft combustion control systems to prevent an imbalance between airflow and fuel flow, which could result in unsafe operating conditions.

Other types of selective systems employ multiple final control elements or multiple controllers. In some applications, several manipulated variables are used to control a single process variable (also called split-range control). Typical examples include the adjustment of both inflow and outflow from a chemical reactor to control reactor pressure or the use of both acid and base to control pH in wastewater treatment. In this approach, the selector chooses among several controller outputs which final control element should be adjusted.

Adaptive Control Process control problems inevitably require online tuning of the controller constants to achieve a satisfactory degree of control. If the process operating conditions or the environment changes significantly, the controller may have to be retuned. If these changes occur quite frequently, then adaptive control techniques should be considered. An adaptive control system is one in which the controller parameters are adjusted automatically to compensate for changing process conditions.

The subject of adaptive control is one of current interest. New algorithms continue to be developed, but these need to be field-tested before industrial acceptance can be expected. An adaptive controller is inherently nonlinear and therefore more complicated than the conventional PID controller.

Fuzzy Logic Control The application of fuzzy logic to process control requires the concepts of fuzzy rules and fuzzy inference. A fuzzy rule, also known as a fuzzy IF-THEN statement, has the form

If x then y
 if input1 = high
 and input2 = low
 then output = medium

Three functions are required to perform logical inferencing with fuzzy rules. The fuzzy AND is the product of a rule's input membership values, generating a weight for the rule's output. The fuzzy OR is a normalized sum of the weights assigned to each rule that contributes to a particular decision. The third function used is defuzzification, which generates a crisp final output. In one approach, the crisp output is the weighted average of the peak element values.

With a single feedback control architecture, information that is readily available to the algorithm includes the error signal, difference between the process variable and the set-point variable, change in error from previous cycles to the current cycle, changes to the set-point variable, change of the manipulated variable from cycle to cycle, and change in the process variable from past to present. In addition, multiple combinations of the system response data are available. As long as the irregularity lies in that dimension wherein fuzzy decisions are being based or associated, the result should be enhanced performance. This enhanced performance should be demonstrated in both the transient and steady-state response. If the system tends to have

changing dynamic characteristics or exhibits nonlinearities, fuzzy logic control should offer a better alternative to using constant PID settings. Most fuzzy logic software begins building its information base during the autotune function. In fact, the majority of the information used in the early stages of system start-up comes from the autotune solutions.

In addition to single-loop process controllers, products that have benefited from the implementation of fuzzy logic are camcorders, elevators, antilock braking systems, and televisions with automatic color, brightness, and sound control. Sometimes fuzzy logic controllers are combined with pattern recognition software such as artificial neural networks (Passino and Yurkovich, *Fuzzy Control*, Addison-Wesley, Reading, Mass., 1998; Kosko, *Neural Networks and Fuzzy Systems*, Prentice-Hall, Englewood Cliffs, N.J., 1992).

EXPERT SYSTEMS

An expert system is a computer program that uses an expert's knowledge in a particular domain to solve a narrowly focused, complex problem. An offline system uses information entered manually and produces results in visual form to guide the user in solving the problem at hand. An online system uses information taken directly from process measurements to perform tasks automatically or instruct or alert operating personnel to the status of the plant.

Each expert system has a rule base created by the expert to respond as the expert would to sets of input information. Expert systems used for plant diagnostics and management usually have an open rule base, which can be changed and augmented as more experience accumulates and more tasks are automated. The system begins as an empty shell with an assortment of functions such as equation solving, logic, and simulation, as well as input and display tools to allow an expert to construct a proprietary rule base. The "expert" in this case would be the person or persons having the deepest knowledge about the process, its problems, its symptoms, and remedies. Converting these inputs to meaningful outputs is the principal task in constructing a rule base. First-principles models (deep knowledge) produce the most accurate results, although heuristics are always required to establish limits. Often modeling tools such as artificial neural nets are used to develop relationships among the process variables.

A number of process control vendors offer comprehensive, object-oriented software environments for building and deploying expert systems. Advantages of such software include transforming complex real-time data to useful information through knowledge-based reasoning and analysis, monitoring for potential problems before they adversely impact operations, diagnosing root causes of time-critical problems to speed up resolution, and recommending or taking corrective actions to help ensure successful recovery.

MULTIVARIABLE CONTROL

GENERAL REFERENCES: Shinsky, *Process Control Systems*, 4th ed., McGraw-Hill, New York, 1996. Seborg, Edgar, and Mellichamp, *Process Dynamics and Control*, 2d ed., Wiley, New York, 2004. McAvoy, *Interaction Analysis*, ISA, Research Triangle Park, N.C., 1983.

Process control books and journal articles tend to emphasize problems with a single controlled variable. In contrast, many processes require multivariable control with many process variables to be controlled. In fact, for virtually any important industrial process, at least two variables must be controlled: product quality and throughput. In this section, strategies for multivariable control are considered.

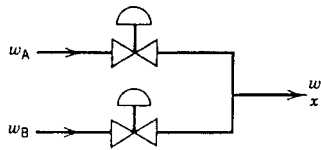
Three examples of simple multivariable control systems are shown in Fig. 8-39. The in-line blending system blends pure components A and B to produce a product stream with flow rate w and mass fraction of A , x . Adjusting either inlet flow rate w_A or w_B affects both of the controlled variables w and x . For the pH neutralization process in Fig. 8-39b, liquid level h and exit stream pH are to be controlled by adjusting the acid and base flow rates w_A and w_B . Each of the manipulated variables affects both of the controlled variables. Thus, both the blending system and the pH neutralization process are said to exhibit

strong process interactions. In contrast, the process interactions for the gas-liquid separator in Fig. 8-39c are not as strong because one manipulated variable, liquid flow rate L , has only a small and indirect effect on one of the controlled variables, pressure P .

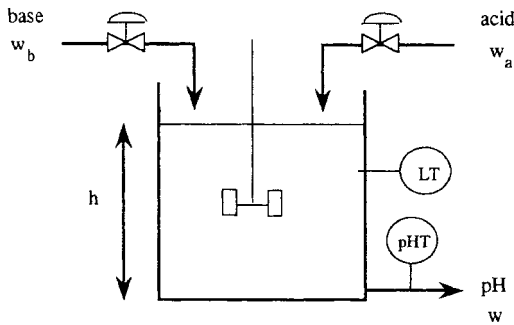
Strong process interactions can cause serious problems if a conventional multiloop feedback control scheme (e.g., either PI or PID controllers) is employed. The process interactions can produce undesirable control loop interactions where the controllers fight each other. Also, it may be difficult to determine the best pairing of controlled and manipulated variables. For example, in the in-line blending process in Fig. 8-39a, should w be controlled with w_A and x with w_B , or vice versa?

Control Strategies for Multivariable Control If a conventional multiloop control strategy performs poorly due to control loop interactions, a number of solutions are available:

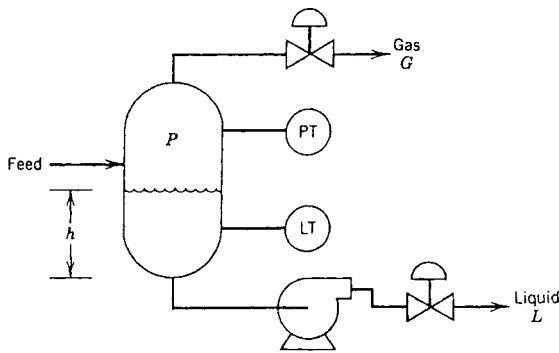
1. Detune one or more of the control loops.
2. Choose different controlled or manipulated variables (or their pairings).



In-line blending system
(a)



pH neutralization process
(b)



Gas liquid separator
(c)

FIG. 8-39 Physical examples of multivariable control problems.

3. Use a decoupling control system.

4. Use a multivariable control scheme (e.g., model predictive control).

Detuning a controller (e.g., using a smaller controller gain or a larger reset time) tends to reduce control loop interactions by sacrificing the performance for the detuned loops. This approach may be acceptable if some of the controlled variables are faster or less important than others.

The selection of controlled and manipulated variables is of crucial importance in designing a control system. In particular, a judicious choice may significantly reduce control loop interactions. For the blending process in Fig. 8-39a, a straightforward control strategy would be to control x by adjusting w_A , and w by adjusting w_B . But physical intuition suggests that it would be better to control x by adjusting the ratio $w_A/(w_A + w_B)$ and to control product flow rate w by the sum $w_A + w_B$. Thus, the new manipulated variables would be $U_1 = w_A/(w_A + w_B)$ and $U_2 = w_A + w_B$. In this control scheme, U_1 affects only x , and U_2 affects only w . Thus, the control loop interactions have been eliminated. Similarly, for the pH neutralization process in Fig. 8-39b, the control loop interactions would be greatly reduced if pH were controlled by $U_1 = w_A/(w_A + w_B)$ and liquid level h were controlled by $U_2 = w_A + w_B$.

Decoupling Control Systems Decoupling control systems provide an alternative approach for reducing control loop interactions. The basic idea is to use additional controllers called decouplers to compensate for undesirable process interactions.

As an illustrative example, consider the simplified block diagram for a representative decoupling control system shown in Fig. 8-40. The two controlled variables Y_1 and Y_2 and two manipulated variables U_1 and U_2 are related by the four process transfer functions G_{p11} , G_{p12} , and so on. For example, G_{p11} denotes the transfer function between U_1 and Y_1 :

$$\frac{Y_1(s)}{U_1(s)} = G_{p11}(s) \tag{8-49}$$

Figure 8-40 includes two conventional feedback controllers: G_{c1} controls Y_1 by manipulating U_1 , and G_{c2} controls Y_2 by manipulating U_2 . The output signals from the feedback controllers serve as input signals to the two decouplers T_{12} and T_{21} . The block diagram is in a simplified form because the disturbance variables and transfer functions for the final control elements and sensors have been omitted.

The function of the decouplers is to compensate for the undesirable process interactions represented by G_{p12} and G_{p21} . Suppose that the process transfer functions are all known. Then the ideal design equations are

$$T_{12}(s) = -\frac{G_{p12}(s)}{G_{p11}(s)} \tag{8-50}$$

$$T_{21}(s) = -\frac{G_{p21}(s)}{G_{p22}(s)} \tag{8-51}$$

These decoupler design equations are very similar to the ones for feedforward control in an earlier section. In fact, decoupling can be interpreted as a type of feedforward control where the input signal is the output of a feedback controller rather than a measured disturbance variable.

In principle, ideal decoupling eliminates control loop interactions and allows the closed-loop system to behave as a set of independent control loops. But in practice, this ideal behavior is not attained for a variety of reasons, including imperfect process models and the presence of saturation constraints on controller outputs and manipulated variables. Furthermore, the ideal decoupler design equations in (8-50) and (8-51) may not be physically realizable and thus would have to be approximated.

In practice, other types of decouplers and decoupling control configurations have been employed. For example, in partial decoupling, only a single decoupler is employed (i.e., either T_{12} or T_{21} in Fig. 8-40

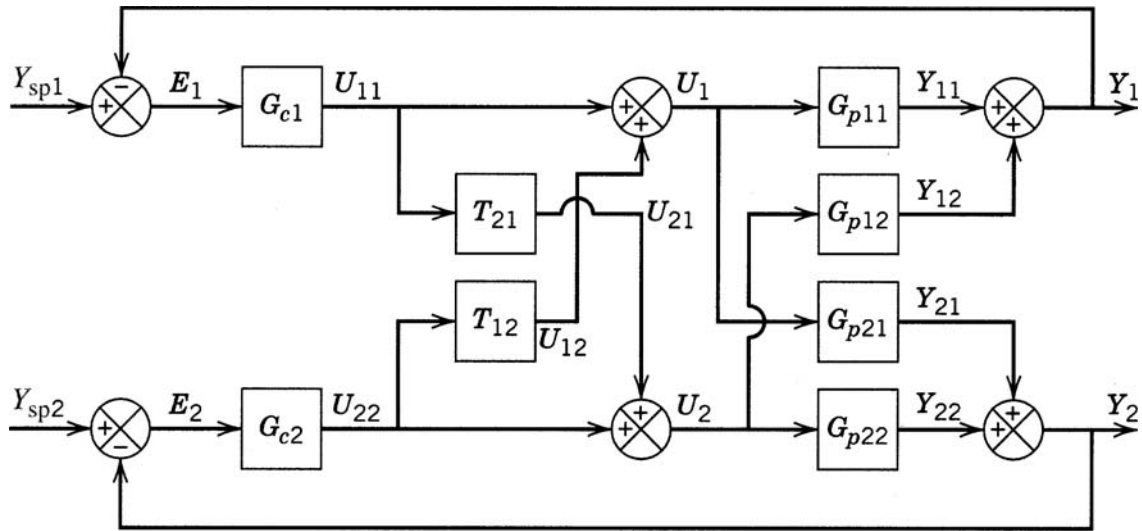


FIG. 8-40 A decoupling control system.

is set equal to zero). This approach tends to be more robust than complete decoupling and is preferred when one of the controlled variables is more important than the other. Static decouplers can be used to reduce the steady-state interactions between control loops. They can be designed by replacing the transfer functions in Eqs. (8-50) and (8-51) with the corresponding steady-state gains

$$T_{12}(s) = -\frac{K_{p12}}{K_{p11}} \quad (8-52)$$

$$T_{21}(s) = -\frac{K_{p21}}{K_{p22}} \quad (8-53)$$

The advantage of static decoupling is that less process information is required, namely, only steady-state gains. Nonlinear decouplers can be used when the process behavior is nonlinear.

Pairing of Controlled and Manipulated Variables A key decision in multiloop control system design is the pairing of manipulated and controlled variables. This is referred to as the controller pairing problem. Suppose there are N controlled variables and N manipulated variables. Then $N!$ distinct control configurations exist. For example, if $N = 5$, then there are 120 different multiloop control schemes. In practice, many would be rejected based on physical insight or previous experience. But a smaller number (say, 5 to 15) may appear to be feasible, and further analysis would be warranted. Thus, it is very useful to have a simple method for choosing the most promising control configuration.

The most popular and widely used technique for determining the best controller pairing is the relative gain array (RGA) method (Bristol, "On a New Measure of Process Interaction," *IEEE Trans. Auto. Control*, **AC-11**: 133, 1966). The RGA method provides two important items of information:

1. A measure of the degree of process interactions between the manipulated and controlled variables
2. A recommended controller pairing

An important advantage of the RGA method is that it requires minimal process information, namely, steady-state gains. Another advantage is that the results are independent of both the physical units used and the scaling of the process variables. The chief disadvantage of the RGA method is that it neglects process dynamics, which can be an important factor in the pairing decision. Thus, the RGA analysis

should be supplemented with an evaluation of process dynamics. Although extensions of the RGA method that incorporate process dynamics have been reported, these extensions have not been widely applied.

RGA Method for 2 × 2 Control Problems To illustrate the use of the RGA method, consider a control problem with two inputs and two outputs. The more general case of $N \times N$ control problems is considered elsewhere (McAvoy, *Interaction Analysis*, ISA, Research Triangle Park, N.C., 1983). As a starting point, it is assumed that a linear, steady-state process model in Eqs. (8-54) and (8-55) is available, where U_1 and U_2 are steady-state values of the manipulated inputs; Y_1 and Y_2 are steady-state values of the controlled outputs; and the K values are steady-state gains. The Y and U variables are deviation variables from nominal steady-state values. This process model could be obtained in a variety of ways, such as by linearizing a theoretical model or by calculating steady-state gains from experimental data or a steady-state simulation.

$$Y_1 = K_{11}U_1 + K_{12}U_2 \quad (8-54)$$

$$Y_2 = K_{21}U_1 + K_{22}U_2 \quad (8-55)$$

By definition, the relative gain λ_{ij} between the i th manipulated variable and the j th controlled variable is defined as

$$\lambda_{ij} = \frac{\text{open-loop gain between } Y_i \text{ and } U_j}{\text{closed-loop gain between } Y_i \text{ and } U_j} \quad (8-56)$$

where the open-loop gain is simply K_{ij} from Eqs. (8-54) and (8-55). The closed-loop gain is defined to be the steady-state gain between U_j and Y_i when the other control loop is closed and no offset occurs in the other controlled variable due to the presence of integral control action. The RGA for the 2×2 process is denoted by

$$\Lambda = \begin{bmatrix} \lambda_{11} & \lambda_{12} \\ \lambda_{21} & \lambda_{22} \end{bmatrix} \quad (8-57)$$

The RGA has the important normalization property that the sum of the elements in each row and each column is exactly 1. Consequently, the RGA in Eq. (8-57) can be written as

$$\Lambda = \begin{bmatrix} \lambda & 1 - \lambda \\ 1 - \lambda & \lambda \end{bmatrix} \quad (8-58)$$

where λ can be calculated from the following formula:

$$\lambda = \frac{1}{1 - K_{12}K_{21}/(K_{11}K_{22})} \quad (8-59)$$

Ideally, the relative gains that correspond to the proposed controller pairing should have a value of 1 because Eq. (8-56) implies that the open- and closed-loop gains are then identical. If a relative gain equals 1, the steady-state operation of this loop will not be affected when the other control loop is changed from manual to automatic, or vice versa. Consequently, the recommendation for the best controller pairing is to pair the controlled and manipulated variables so that the corresponding relative gains are positive and close to 1.

RGA Example To illustrate use of the RGA method, consider the following steady-state version of a transfer function model for a pilot-scale, methanol-water distillation column (Wood and Berry, "Terminal Composition Control of a Binary Distillation Column," *Chem. Eng. Sci.*, **28**: 1707, 1973): $K_{11} = 12.8$, $K_{12} = -18.9$, $K_{21} = 6.6$, and $K_{22} = -19.4$. It follows that $\lambda = 2$ and

$$\Lambda = \begin{pmatrix} 2 & -1 \\ -1 & 2 \end{pmatrix} \quad (8-60)$$

Thus it is concluded that the column is fairly interacting and the recommended controller pairing is to pair Y_1 with U_1 and Y_2 with U_2 .

MODEL PREDICTIVE CONTROL

GENERAL REFERENCES: Qin and Badgwell, *Control Eng. Practice*, **11**: 773, 2003. Rawlings, *IEEE Control Systems Magazine*, **20**(3): 38, 2000). Camacho and Bordons, *Model Predictive Control*, 2d ed., Springer-Verlag, New York, 2004. Maciejowski, *Predictive Control with Constraints*, Prentice-Hall, Upper Saddle River, N.J., 2002. Seborg, Edgar, and Mellichamp, *Process Dynamics and Control*, 2d ed., Wiley, New York, 2004, Chap. 20.

The model-based control strategy that has been most widely applied in the process industries is *model predictive control (MPC)*. It is a general method that is especially well suited for difficult multi-input, multioutput (MIMO) control problems where there are significant interactions between the manipulated inputs and the controlled outputs. Unlike other model-based control strategies, MPC can easily accommodate inequality constraints on input and output variables such as upper and lower limits and rate-of-change limits.

A key feature of MPC is that future process behavior is predicted by using a dynamic model and available measurements. The controller outputs are calculated so as to minimize the difference between the predicted process response and the desired response. At each sampling instant, the control calculations are repeated and the predictions updated based on current measurements. In typical industrial applications, the set point and target values for the MPC calculations are updated by using online optimization based on a steady-state model of the process.

The current widespread interest in MPC techniques was initiated by pioneering research performed by two industrial groups in the 1970s. Shell Oil (Houston, Tex.) reported its Dynamic Matrix Control (DMC) approach in 1979, while a similar technique, marketed as IDCOM, was published by a small French company ADERSA in 1978. Since then, there have been thousands of applications of these and related MPC techniques in oil refineries and petrochemical plants around the world. Thus, MPC has had a substantial impact and is currently the method of choice for difficult multivariable control problems in these industries. However, relatively few applications have been reported in other process industries, even though MPC is a very general approach that is not limited to a particular industry.

Advantages and Disadvantages of MPC Model predictive control offers a number of important advantages in comparison with conventional multiloop PID control:

1. It is a general control strategy for MIMO processes with inequality constraints on input and output variables.
 2. It can easily accommodate difficult or unusual dynamic behavior such as large time delays and inverse responses.
 3. Because the control calculations are based on optimizing control system performance, MPC can be readily integrated with online optimization strategies to optimize plant performance.
 4. The control strategy can be easily updated online to compensate for changes in process conditions, constraints, or performance criteria.
- But current versions of MPC have significant disadvantages in comparison with conventional multiloop control:
1. The MPC strategy is very different from conventional multiloop control strategies and thus initially unfamiliar to plant personnel.
 2. The MPC calculations can be relatively complicated [e.g., solving a linear programming (LP) or quadratic programming (QP) problem at each sampling instant] and thus require a significant amount of computer resources and effort. These optimization strategies are described in the next section.
 3. The development of a dynamic model from plant data is time-consuming, typically requiring days, or even weeks, of around-the-clock plant tests.
 4. Because empirical models are generally used, they are valid only over the range of conditions considered during the plant tests.
 5. Theoretical studies have demonstrated that MPC can perform poorly for some types of process disturbances, especially when output constraints are employed.

Because MPC has been widely used and has had considerable impact, there is a broad consensus that its advantages far outweigh its disadvantages.

Economic Incentives for Automation Projects Industrial applications of advanced process control strategies such as MPC are motivated by the need for improvements regarding safety, product quality, environmental standards, and economic operation of the process. One view of the economics incentives for advanced automation techniques is illustrated in Fig. 8-41. Distributed control systems (DCS) are widely used for data acquisition and conventional single-loop (PID) control. The addition of advanced regulatory control systems such as selective controls, gain scheduling, and time-delay compensation can provide benefits for a modest incremental cost. But

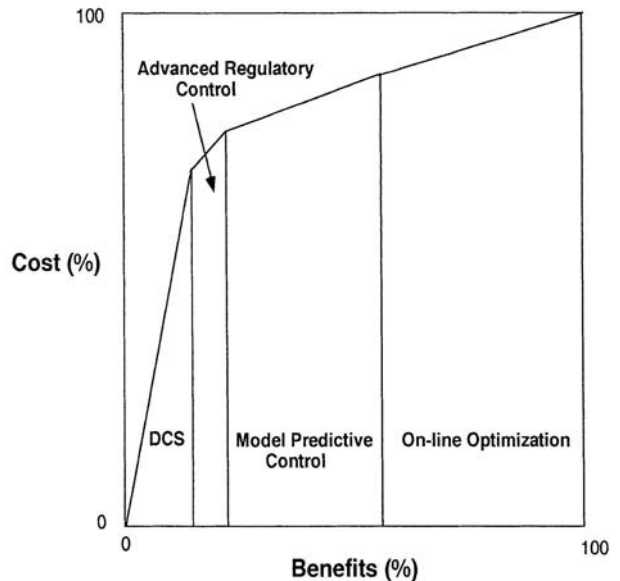


FIG. 8-41 Economic incentives for automation projects in the process industries.

experience has indicated that the major benefits can be obtained for relatively small incremental costs through a combination of MPC and online optimization. The results in Fig. 8-41 are shown qualitatively, rather than quantitatively, because the actual costs and benefits are application-dependent.

A key reason why MPC has become a major commercial and technical success is that there are numerous vendors who are licensed to market MPC products and install them on a turnkey basis. Consequently, even medium-sized companies are able to take advantage of this new technology. Payout times of 3 to 12 months have been widely reported.

Basic Features of MPC Model predictive control strategies have a number of distinguishing features:

1. A dynamic model of the process is used to predict the future outputs over a prediction horizon consisting of the next P sampling periods.
2. A reference trajectory is used to represent the desired output response over the prediction horizon.
3. Inequality constraints on the input and output variables can be included as an option.
4. At each sampling instant, a control policy consisting of the next M control moves is calculated. The control calculations are based on minimizing a quadratic or linear performance index over the prediction horizon while satisfying the constraints.
5. The performance index is expressed in terms of future control moves and the predicted deviations from the reference trajectory.
6. A *receding horizon approach* is employed. At each sampling instant, only the first control move (of the M moves that were calculated) is actually implemented.
7. Then the predictions and control calculations are repeated at the next sampling instant.

These distinguishing features of MPC will now be described in greater detail.

Dynamic Model A key feature of MPC is that a dynamic model of the process is used to predict future values of the controlled outputs. There is considerable flexibility concerning the choice of the dynamic model. For example, a physical model based on first principles (e.g., mass and energy balances) or an empirical model developed from data could be employed. Also, the empirical model could be a linear model (e.g., transfer function, step response model, or state space model) or a nonlinear model (e.g., neural net model). However, most industrial applications of MPC have relied on linear empirical models, which may include simple nonlinear transformations of process variables.

The original formulations of MPC (i.e., DMC and IDCOM) were based on empirical linear models expressed in either step response or impulse response form. For simplicity, we consider only a single-input, single-output (SISO) model. However, the SISO model can be easily generalized to the MIMO models that are used in industrial applications. The step response model relating a single controlled variable y and a single manipulated variable u can be expressed as

$$\hat{y}(k+1) = y_0 + \sum_{i=1}^{N-1} S_i \Delta u(k-i+1) + S_N u(k-N+1) \quad (8-61)$$

where $\hat{y}(k+1)$ is the predicted value of y at the $k+1$ sampling instant, $u(k)$ is the value of the manipulated input at time k , and the model parameters S_i are referred to as the *step response coefficients*. The initial value y_0 is assumed to be known. The change in the manipulated input from one sampling instant to the next is denoted by

$$\Delta u(k) = u(k) - u(k-1) \quad (8-62)$$

The step response model is also referred to as a discrete convolution model.

In principle, the step response coefficients can be determined from the output response to a step change in the input. A typical response to a unit step change in input u is shown in Fig. 8-42. The step response coefficients S_i are simply the values of the output variable at the sampling instants, after the initial value y_0 has been subtracted. Theoretically, they can be determined from a single step response, but, in practice, a num-

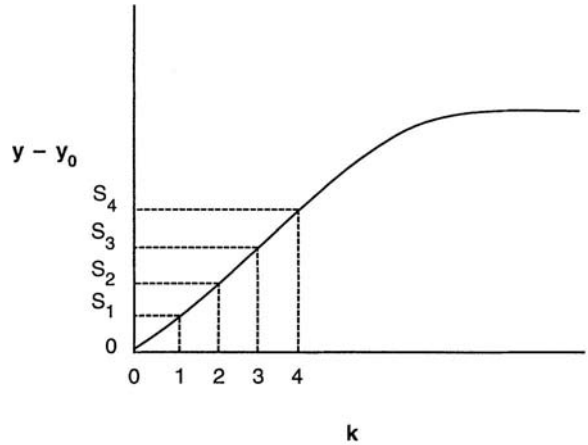


FIG. 8-42 Step response for a unit step change in the input.

ber of “bump tests” are required to compensate for unanticipated disturbances, process nonlinearities, and noisy measurements.

Horizons The step response model in Eq. (8-61) is equivalent to the following impulse response model:

$$\hat{y}(k) = \sum_{i=1}^N h_i u(k-i) + y_0 \quad (8-63)$$

where the impulse response coefficients h_i are related to the step response coefficients by $h_i = S_i - S_{i-1}$. Step and impulse response models typically contain a large number of parameters because the model horizon N is usually quite large ($30 < N < 120$). In fact, these models are often referred to as nonparametric models.

The receding horizon feature of MPC is shown in Fig. 8-43 with the current sampling instant denoted by k . Past and present input signals [$u(i)$ for $i \leq k$] are used to predict the output at the next P sampling instants [$y(k+i)$ for $i = 1, 2, \dots, P$]. The control calculations are performed to generate an M -step control policy [$u(k), u(k+1), \dots, u(k+M-1)$], which optimizes a performance index. The first control action $u(k)$ is implemented. Then at the next sampling instant $k+1$, the prediction and control calculations are repeated in order to determine $u(k+1)$. In Fig. 8-43 the reference trajectory (or target) is considered to be constant. Other possibilities include a gradual or step set-point change that can be generated by online optimization.

Performance Index The performance index for MPC applications is usually a linear or quadratic function of the predicted errors and calculated future control moves. For example, the following quadratic performance index has been widely used:

$$\min_{\Delta u(k)} J = \sum_{i=1}^P Q e^2(k+i) + \sum_{i=1}^M R_i \Delta u^2(k+i-1) \quad (8-64)$$

The value $e(k+i)$ denotes the predicted error at time $k+i$,

$$e(k+i) = y_{sp}(k+i) - \hat{y}(k+i) \quad (8-65)$$

where $y_{sp}(k+i)$ is the set point at time $k+i$ and $\Delta u(k)$ denotes the column vector of current and future control moves over the next M sampling instants:

$$\Delta u(k) = [\Delta u(k), \Delta u(k+1), \dots, \Delta u(k+M-1)]^T \quad (8-66)$$

Equation (8-64) contains two types of design parameters that can also be used for tuning purposes. Weighting factor R_i penalizes large control moves, while weighting factor Q_i allows the predicted errors to be weighed differently at each time step, if desired.

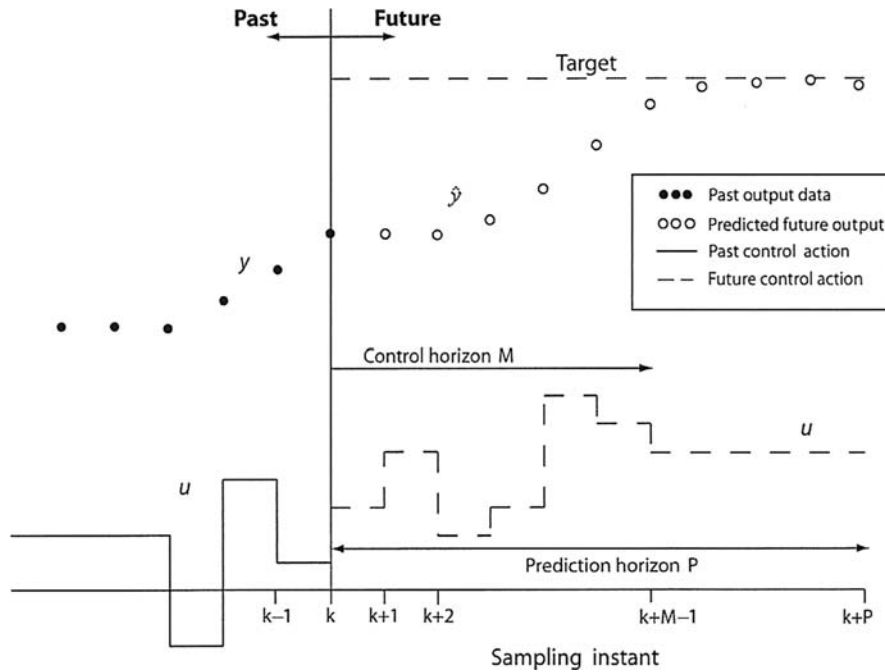


FIG. 8-43 The “moving horizon” approach of model predictive control. (Seborg, Edgar, and Mellichamp, *Process Dynamics and Control, 2d ed.*, Wiley, New York, 2004.)

Inequality Constraints Inequality constraints on the future inputs or their rates of change are widely used in the MPC calculations. For example, if both upper and lower limits are required, the constraints could be expressed as

$$u^-(k) \leq u(k+j) \leq u^+(k) \quad \text{for } j = 0, 1, \dots, M-1 \quad (8-67)$$

$$\Delta u^-(k) \leq \Delta u(k+j) \leq \Delta u^+(k) \quad \text{for } j = 0, 1, \dots, M-1 \quad (8-68)$$

where B_j and C_j are constants. Constraints on the predicted outputs are sometimes included as well:

$$y^-(k) \leq \hat{y}(k+j) \leq y^+(k) \quad \text{for } j = 0, 1, \dots, P \quad (8-69)$$

The minimization of the quadratic performance index in Eq. (8-64), subject to the constraints in Eqs. (8-67) to (8-69) and the step response model in Eq. (8-61), can be formulated as a standard QP (quadratic programming) problem. Consequently, efficient QP solution techniques can be employed. When the inequality constraints in Eqs. (8-67) to (8-69) are omitted, the optimization problem has an analytical solution (Camacho and Bordons, *Model Predictive Control*, 2d ed., Springer-Verlag, New York, 2004; Maciejowski, *Predictive Control with Constraints*, Prentice-Hall, Upper Saddle River, N.J., 2002). If the quadratic terms in Eq. (8-64) are replaced by linear terms, an LP (linear programming) problem results that can also be solved by using standard methods. This MPC formulation for SISO control problems can easily be extended to MIMO problems.

Implementation of MPC For a new MPC application, a cost/benefit analysis is usually performed prior to project approval. Then the steps involved in the implementation of MPC can be summarized as follows (Hokanson and Gerstle, *Dynamic Matrix Control Multivariable Controllers*, in *Practical Distillation Control*, Luyben (ed.), Van Nostrand Reinhold, New York, 1992, p. 248; Qin and Badgwell, *Control Eng. Practice*, **11**: 773, 2003).

Step 1: Initial Controller Design The first step in MPC design is to select the controlled, manipulated, and measured disturbance variables. These choices determine the structure of the MPC system and should be based on process knowledge and control objectives. In typical

applications the number of controlled variables ranges from 5 to 40, and the number of manipulated variables is typically between 5 and 20.

Step 2: Pretest Activity During the pretest activity, the plant instrumentation is checked to ensure that it is working properly and to decide whether additional sensors should be installed. The pretest data can be used to estimate the steady-state gain and approximate settling times for each input/output pair. This information is used to plan the full plant tests of step 3.

As part of the pretest, it is desirable to benchmark the performance of the existing control system for later comparison with MPC performance (step 8).

Step 3: Plant Tests The dynamic model for the MPC calculations is developed from data collected during special plant tests. The excitation for the plant tests usually consists of changing an input variable or a disturbance variable (if possible) from one value to another, using either a series of step changes with different durations or a pseudorandom binary sequence (PRBS). To ensure that sufficient data are obtained for model identification, each input variable is typically moved to a new value, 8 to 15 times during a plant test (Qin and Badgwell, *Control Eng. Practice*, **11**: 773, 2003). Identification during closed-loop operation is becoming more common.

Step 4: Model Development The dynamic model is developed from the plant test data by selecting a model form (e.g., a step response model) and then estimating the model parameters. However, first it is important to eliminate periods of test data where plant upsets or other abnormal situations have occurred. Decisions to omit portions of the test data are based on visual inspection of the data, knowledge of the process, and experience. Parameter estimation is usually based on least squares estimation.

Step 5: Control System Design and Simulation The preliminary control system design from step 1 is critically evaluated and modified, if necessary. Then the MPC design parameters are selected including the sampling periods, weighting factors, and control and prediction horizons. Next, the closed-loop system is simulated, and the MPC design parameters are adjusted, if necessary, to obtain satisfactory control system performance and robustness over the specified range of operating conditions.

Step 6: Operator Interface Design and Operator Training Operator training is important because MPC concepts such as predictive control, multivariable interactions, and constraint handling are very different from conventional regulatory control concepts. Thus, understanding why the MPC system responds the way that it does, especially for unusual operating conditions, can be a challenge for both operators and engineers.

Step 7: Installation and Commissioning After an MPC control system is installed, it is first evaluated in a "prediction mode." Model predictions are compared with measurements, but the process continues to be controlled by the existing control system. After the output predictions are judged to be satisfactory, the calculated MPC control moves are evaluated to determine if they are reasonable. Finally, the MPC software is evaluated during closed-loop operation with the calculated control moves implemented as set points to the DCS control loops. The MPC design parameters are tuned, if necessary. The commissioning period typically requires some troubleshooting and can take as long as, or even longer than, the plant tests of step 3.

Step 8: Measuring Results and Monitoring Performance The evaluation of MPC system performance is not easy, and widely accepted metrics and monitoring strategies are not available. However, useful diagnostic information is provided by basic statistics such as the means and standard deviations for both measured variables and calculated quantities, such as control errors and model residuals. Another useful statistic is the relative amount of time that an input is saturated or a constraint is violated, expressed as a percentage of the total time the MPC system is in service.

Integration of MPC and Online Optimization As indicated in Fig. 8-41, significant potential benefits can be realized by using a combination of MPC and online optimization. At present, most commercial MPC packages integrate the two methodologies in a hierarchical configuration such as the one shown in Fig. 8-44. The MPC calculations

are performed quite often (e.g., every 1 to 10 min) and implemented as set points for PID control loops at the DCS level. The targets and constraints for the MPC calculations are generated by solving a steady-state optimization problem (LP or QP) based on a linear process model. These calculations may be performed as often as the MPC calculations. As an option, the targets and constraints for the LP or QP optimization can be generated from a nonlinear process model using a nonlinear optimization technique. These calculations tend to be performed less frequently (e.g., every 1 to 24 h) due to the complexity of the calculations and the process models.

The combination of MPC and frequent online optimization has been successfully applied in oil refineries and petrochemical plants around the world.

REAL-TIME PROCESS OPTIMIZATION

GENERAL REFERENCES: Biegler, Grossmann, and Westerberg, *Systematic Methods of Chemical Process Design*, Prentice-Hall, Upper Saddle River, N.J., 1997. Darby and White, *On-line Optimization of Complex Process Units*, *Chem. Engr. Prog.*, **84**(10): 51, 1998. Edgar, Himmelblau, and Lasdon, *Optimization of Chemical Processes*, 2d ed., McGraw-Hill, New York, 2001. Forbes, Marlin, and MacGregor, *Model Selection Criteria for Economics-Based Optimizing Control*, *Comp. Chem. Engng.*, **18**: 497, 1994; Marlin and Hrymak, *Real-Time Optimization of Continuous Processes*, *Chem. Proc. Cont V, AIChE Symp. Ser.*, **93**(316): 156, 1997. Narashimhan and Jordache, *Data Reconciliation and Gross Error Detection*, Gulf Publishing, Houston, Tex., 2000. Nash and Sofer, *Linear and Nonlinear Programming*, McGraw-Hill, New York, 1996. Shobrys and White, *Planning, Scheduling, and Control Systems: Why They Cannot Work Together*, *Comp. Chem. Engng.*, **26**: 149, 2002. Timmons, Jackson, and White, *Distinguishing On-line Optimization Benefits from Those of Advanced Controls*, *Hydrocarb. Proc.*, **79**(6): 69, 2000.

The chemical industry has undergone significant changes during the past 20 years due to the increased cost of energy and raw materials, more stringent environmental regulations, and intense worldwide competition. Modifications of both plant design procedures and plant operating conditions have been implemented to reduce costs and meet constraints. One of the most important engineering tools that can be employed in such activities is optimization. As plant computers have become more powerful, the size and complexity of problems that can be solved by optimization techniques have correspondingly expanded. A wide variety of problems in the operation and analysis of chemical plants (as well as many other industrial processes) can be solved by optimization. Real-time optimization means that the process operating conditions (set points) are evaluated on a regular basis and optimized, as shown earlier in level 4 in Fig. 8-28. Sometimes this is called steady-state optimization or supervisory control. This section examines the basic characteristics of optimization problems and their solution techniques and describes some representative benefits and applications in the chemical and petroleum industries.

Typical problems in chemical engineering process design or plant operation have many possible solutions. Optimization is concerned with selecting the best among the entire set of solutions by efficient quantitative methods. Computers and associated software make the computations involved in the selection manageable and cost-effective. Engineers work to improve the initial design of equipment and strive for enhancements in the operation of the equipment once it is installed in order to realize the greatest production, the greatest profit, the maximum cost, the least energy usage, and so on. In plant operations, benefits arise from improved plant performance, such as improved yields of valuable products (or reduced yields of contaminants), reduced energy consumption, higher processing rates, and longer times between shutdowns. Optimization can also lead to reduced maintenance costs, less equipment wear, and better staff utilization. It is helpful to systematically identify the objective, constraints, and degrees of freedom in a process or a plant if such benefits as improved quality of designs, faster and more reliable troubleshooting, and faster decision making are to be achieved.

Optimization can take place at many levels in a company, ranging from a complex combination of plants and distribution facilities down through individual plants, combinations of units, individual pieces of equipment, subsystems in a piece of equipment, or even smaller entities.

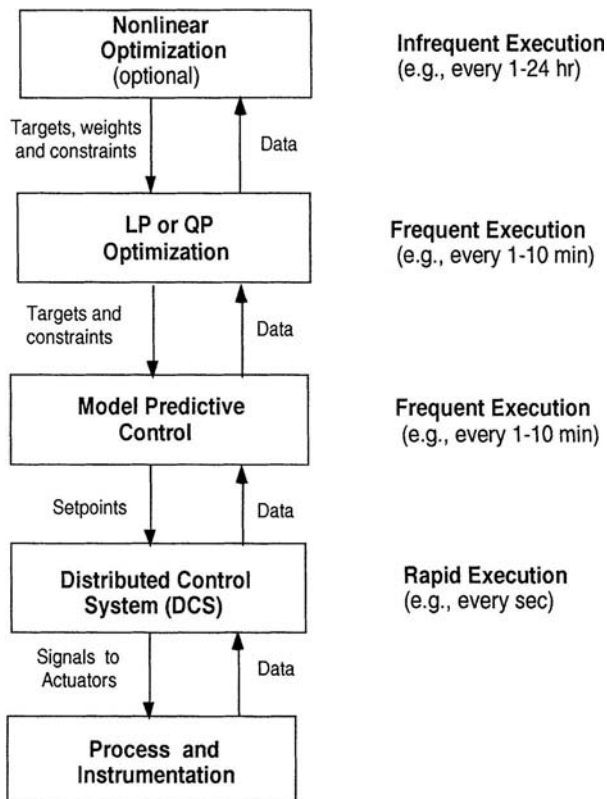


FIG. 8-44 Hierarchical control configuration for MPC and online optimization.

Problems that can be solved by optimization can be found at all these levels.

While process design and equipment specification are usually performed prior to the implementation of the process, optimization of operating conditions is carried out monthly, weekly, daily, hourly, or even every minute. Optimization of plant operations determines the set points for each unit at the temperatures, pressures, and flow rates that are the best in some sense. For example, the selection of the percentage of excess air in a process heater is quite critical and involves a balance on the fuel/air ratio to ensure complete combustion and at the same time make the maximum use of the heating potential of the fuel. Typical day-to-day optimization in a plant minimizes steam consumption or cooling water consumption, optimizes the reflux ratio in a distillation column, or allocates raw materials on an economic basis [Latour, *Hydro. Proc.*, **58**(6): 73, 1979, and **58**(7): 219, 1979].

A real-time optimization (RTO) system determines set-point changes and implements them via the computer control system without intervention from unit operators. The RTO system completes all data transfer, optimization calculations, and set-point implementation before unit conditions change that may invalidate the computed optimum. In addition, the RTO system should perform all tasks without upsetting plant operations. Several steps are necessary for implementation of RTO, including determination of the plant steady state, data gathering and validation, updating of model parameters (if necessary) to match current operations, calculation of the new (optimized) set points, and the implementation of these set points.

To determine if a process unit is at steady state, a program monitors key plant measurements (e.g., compositions, product rates, feed rates, and so on) and determines if the plant is close enough to steady state to start the sequence. Only when all the key measurements are within the allowable tolerances is the plant considered steady and the optimization sequence started. Tolerances for each measurement can be tuned separately. Measured data are then collected by the optimization computer. The optimization system runs a program to screen the measurements for unreasonable data (gross error detection). This validity checking automatically modifies the model updating calculation to reflect any bad data or when equipment is taken out of service. Data validation and reconciliation (online or offline) is an extremely critical part of any optimization system.

The optimization system then may run a parameter-fitting case that updates model parameters to match current plant operation. The integrated process model calculates such items as exchanger heat-transfer coefficients, reactor performance parameters, furnace efficiencies, and heat and material balances for the entire plant. Parameter fitting allows for continual updating of the model to account for plant deviations and degradation of process equipment. After completion of the parameter fitting, the information regarding the current plant constraints, control status data, and economic values for feed products, utilities, and other operating costs is collected. The economic values are updated by the planning and scheduling department on a regular basis. The optimization system then calculates the optimized set points. The steady-state condition of the plant is rechecked after the optimization case is successfully completed. If the plant is still steady, then the values of the optimization targets are transferred to the process control system for implementation. After a line-out period, the process control computer resumes the steady-state detection calculations, restarting the cycle.

Essential Features of Optimization Problems The solution of optimization problems involves the use of various tools of mathematics, which is discussed in detail in Sec. 3. The formulation of an optimization problem requires the use of mathematical expressions. From a practical viewpoint, it is important to mesh properly the problem statement with the anticipated solution technique. Every optimization problem contains three essential categories:

1. An objective function to be optimized (revenue function, cost function, etc.)
2. Equality constraints (equations)
3. Inequality constraints (inequalities)

Categories 2 and 3 comprise the model of the process or equipment; category 1 is sometimes called the economic model.

TABLE 8-6 Six Steps Used to Solve Optimization Problems

- 1 Analyze the process itself so that the process variables and specific characteristics of interest are defined (i.e., make a list of all the variables).
- 2 Determine the criterion for optimization, and specify the objective function in terms of the above variables together with coefficients. This step provides the performance model (sometimes called the economic model, when appropriate).
- 3 Develop via mathematical expressions a valid process or equipment model that relates the input/output variables of the process and associated coefficients. Include both equality and inequality constraints. Use well-known physical principles (mass balances, energy balances), empirical relations, implicit concepts, and external restrictions. Identify the independent and dependent variables (number of degrees of freedom).
- 4 If the problem formulation is too large in scope, (a) break it up into manageable parts and/or (b) simplify the objective function and model.
- 5 Apply a suitable optimization technique to the mathematical statement of the problem.
- 6 Check the answers and examine the sensitivity of the result to changes in the coefficients in the problem and the assumptions.

No single method or algorithm of optimization exists that can be applied efficiently to all problems. The method chosen for any particular case will depend primarily on (1) the character of the objective function, (2) the nature of the constraints, and (3) the number of independent and dependent variables. Table 8-6 summarizes the six general steps for the analysis and solution of optimization problems (Edgar, Himmelblau, and Lasdon, *Optimization of Chemical Processes*, 2d ed., McGraw-Hill, New York, 2001). You do not have to follow the cited order exactly, but you should cover all the steps at some level of detail. Shortcuts in the procedure are allowable, and the easy steps can be performed first. Steps 1, 2, and 3 deal with the mathematical definition of the problem: identification of variables, specification of the objective function, and statement of the constraints. If the process to be optimized is very complex, it may be necessary to reformulate the problem so that it can be solved with reasonable effort. Later in this section, we discuss the development of mathematical models for the process and the objective function (the economic model) in typical RTO applications.

Step 5 in Table 8-6 involves the computation of the optimum point. Quite a few techniques exist to obtain the optimal solution for a problem. We describe several classes of methods below. In general, the solution of most optimization problems involves the use of a digital computer to obtain numerical answers. Over the past 15 years, substantial progress has been made in developing efficient and robust computational methods for optimization. Much is known about which methods are most successful. Virtually all numerical optimization methods involve iteration, and the effectiveness of a given technique can depend on a good first guess for the values of the variables at the optimal solution. After the optimum is computed, a sensitivity analysis for the objective function value should be performed to determine the effects of errors or uncertainty in the objective function, mathematical model, or other constraints.

Development of Process (Mathematical) Models Constraints in optimization problems arise from physical bounds on the variables, empirical relations, physical laws, and so on. The mathematical relations describing the process also comprise constraints. Two general categories of models exist:

1. Those based on physical theory
 2. Those based on strictly empirical descriptions
- Mathematical models based on physical and chemical laws (e.g., mass and energy balances, thermodynamics, chemical reaction kinetics) are frequently employed in optimization applications. These models are conceptually attractive because a general model for any system size can be developed before the system is constructed. On the other hand, an empirical model can be devised that simply correlates input/output data without any physiochemical analysis of the process. For these models, optimization is often used to fit a model to process data, using a procedure called parameter estimation. The well-known least squares curve-fitting procedure is based on optimization theory, assuming that the model parameters are contained linearly in the model. One example is the yield matrix, where the percentage yield of each product in a unit operation is estimated for each feed component

by using process data rather than employing a mechanistic set of chemical reactions.

Formulation of the Objective Function The formulation of objective functions is one of the crucial steps in the application of optimization to a practical problem. You must be able to translate the desired objective to mathematical terms. In the chemical process industries, the objective function often is expressed in units of currency per unit time (e.g., U.S. dollars per week, month, or year) because the normal industrial goal is to minimize costs or maximize profits subject to a variety of constraints.

A typical economic model involves the costs of raw materials, values of products, and costs of production as functions of operating conditions, projected sales figures, and the like. An objective function can be expressed in terms of these quantities; e.g., annual operating profit (\$/yr) might be expressed as

$$J = \sum_N F_s V_s - \sum_r F_r C_r - \text{OC} \quad (8-70)$$

where $J = \text{profit/time}$

$\sum_N F_s V_s = \text{sum of product flow rates times respective product values (income)}$

$\sum_r F_r C_r = \text{sum of feed flows times respective unit costs}$

OC = operating costs/time

Unconstrained Optimization *Unconstrained optimization* refers to the case where no inequality constraints are present and all equality constraints can be eliminated by solving for selected dependent variables followed by substitution for them in the objective function. Very few realistic problems in process optimization are unconstrained. However, the availability of efficient unconstrained optimization techniques is important because these techniques must be applied in real time, and iterative calculations may require excessive computer time. Two classes of unconstrained techniques are single-variable optimization and multivariable optimization.

Single-Variable Optimization Many real-time optimization problems can be reduced to the variation of a single-variable so as to maximize profit or some other overall process objective function. Some examples of single-variable optimization include optimizing the reflux ratio in a distillation column or the air/fuel ratio in a furnace. While most processes actually are multivariable processes with several operating degrees of freedom, often we choose to optimize only the most important variable in order to keep the strategy uncomplicated. One characteristic implicitly required in a single-variable optimization problem is that the objective function J be unimodal in the variable x .

The selection of a method for one-dimensional search is based on the tradeoff between the number of function evaluations and computer time. We can find the optimum by evaluating the objective function at many values of x , using a small grid spacing (Δx) over the allowable range of x values, but this method is generally inefficient. There are three classes of techniques that can be used efficiently for one-dimensional search: indirect, region elimination, and interpolation.

Indirect methods seek to solve the necessary condition $dJ/dx = 0$ by iteration, but these methods are not as popular as the second two classes. Region elimination methods include equal interval search, dichotomous search (or bisection), Fibonacci search, and golden section. These methods do not use information on the shape of the function (other than its being unimodal) and thus tend to be rather conservative. The third class of techniques uses repeated polynomial fitting to predict the optimum. These interpolation methods tend to converge rapidly to the optimum without being very complicated. Two interpolation methods, quadratic and cubic interpolation, are used in many optimization packages.

Multivariable Optimization The numerical optimization of general nonlinear multivariable objective functions requires that efficient and robust techniques be employed. Efficiency is important since iteration is employed. For example, in multivariable "grid" search for a

problem with four independent variables, an equally spaced grid for each variable is prescribed. For 10 values of each of the four variables, 10^4 total function evaluations would be required to find the best answer for the grid intersections, but this result may not be close enough to the true optimum and would require further search. A larger number of variables (say, 20) would require exponentially more computation, so grid search is a very inefficient method for most problems.

In multivariable optimization, the difficulty of dealing with multivariable functions is usually resolved by treating the problem as a series of one-dimensional searches. For a given starting point, a search direction s is specified, and the optimum is found by searching along that direction. The step size ϵ is the distance moved along s . Then a new search direction is determined, followed by another one-dimensional search. The algorithm used to specify the search direction depends on the optimization method selected.

There are two basic types of unconstrained optimization algorithms: (1) those requiring function derivatives and (2) those that do not. Here we give only an overview and refer the reader to Sec. 3 or the references for more details. The nondervative methods are of interest in optimization applications because these methods can be readily adapted to the case in which experiments are carried out directly on the process. In such cases, an actual process measurement (such as yield) can be the objective function, and no mathematical model for the process is required. Methods that do not require derivatives are called direct methods and include sequential simplex (Nelder-Mead) and Powell's method. The sequential simplex method is quite satisfactory for optimization with two or three independent variables, is simple to understand, and is fairly easy to execute. Powell's method is more efficient than the simplex method and is based on the concept of conjugate search directions. This class of methods can be used in special cases but is not recommended for optimization involving more than 6 to 10 variables.

The second class of multivariable optimization techniques in principle requires the use of partial derivatives of the objective function, although finite difference formulas can be substituted for derivatives. Such techniques are called indirect methods and include the following classes:

1. Steepest descent (gradient) method
2. Conjugate gradient (Fletcher-Reeves) method
3. Newton's method
4. Quasi-newton methods

The steepest descent method is quite old and utilizes the intuitive concept of moving in the direction in which the objective function changes the most. However, it is clearly not as efficient as the other three. Conjugate gradient utilizes only first-derivative information, as does steepest descent, but generates improved search directions. Newton's method requires second-derivative information but is very efficient, while quasi-newton retains most of the benefits of Newton's method but utilizes only first-derivative information. All these techniques are also used with constrained optimization.

Constrained Optimization When constraints exist and cannot be eliminated in an optimization problem, more general methods must be employed than those described above, because the unconstrained optimum may correspond to unrealistic values of the operating variables. The general form of a nonlinear programming problem allows for a nonlinear objective function and nonlinear constraints, or

$$\begin{aligned} \text{Minimize} \quad & J(x_1, x_2, \dots, x_n) \\ \text{Subject to} \quad & h_i(x_1, x_2, \dots, x_n) = 0 \quad i = 1, r_c \\ & g_i(x_1, x_2, \dots, x_n) > 0 \quad i = 1, m_c \end{aligned} \quad (8-71)$$

In this case, there are n process variables with r_c equality constraints and m_c inequality constraints. Such problems pose a serious challenge to performing optimization calculations in a reasonable amount of time. Typical constraints in chemical process optimization include operating conditions (temperatures, pressures, and flows have limits), storage capacities, and product purity specifications.

An important class of constrained optimization problems is one in which both the objective function and the constraints are linear. The solution of these problems is highly structured and can be obtained

rapidly. The accepted procedure, linear programming (LP), has become quite popular in the past 20 years, solving a wide range of industrial problems. It is increasingly being used for online optimization. For processing plants, there are several different kinds of linear constraints that may arise, making the LP method of great utility.

1. Production limitation due to equipment throughput restrictions, storage limits, or market constraints
2. Raw material (feedstock) limitation
3. Safety restrictions on allowable operating temperatures and pressures
4. Physical property specifications placed on the composition of the final product. For blends of various products, we usually assume that a composite property can be calculated through the mass-averaging of pure-component physical properties
5. Material and energy balances of the steady-state model

The optimum in linear programming lies at the constraint intersections, which was generalized to any number of variables and constraints by George Dantzig. The simplex algorithm is a matrix-based numerical procedure for which many digital computer codes exist, for both mainframe and microcomputers (Edgar, Himmelblau, and Lasdon, *Optimization of Chemical Processes*, 2d ed., McGraw-Hill, New York, 2001; Nash and Sofer, *Linear and Nonlinear Programming*, McGraw-Hill, New York, 1996). The algorithm can handle virtually any number of inequality constraints and any number of variables in the objective function, and utilizes the observation that only the constraint boundaries need to be examined to find the optimum. In some instances, nonlinear optimization problems even with nonlinear constraints can be linearized so that the LP algorithm can be employed to solve them (called successive linear programming, or SLP). In the process industries, LP and SLP have been applied to a wide range of RTO problems, including refinery scheduling, olefins production, the optimal allocation of boiler fuel, and the optimization of a total plant.

Nonlinear Programming The most general case for optimization occurs when both the objective function and the constraints are nonlinear, a case referred to as nonlinear programming. While the ideas behind the search methods used for unconstrained multivariable problems are applicable, the presence of constraints complicates the solution procedure. All the methods discussed below have been utilized to solve nonlinear programming problems in the field of chemical engineering design and operations. Nonlinear programming is now used extensively in the area of real-time optimization.

One of the older and most accessible NLP algorithms uses iterative linearization and is called the *generalized reduced gradient (GRG) algorithm*. The GRG algorithm employs linear or linearized constraints and uses slack variables to convert all constraints to equality constraints. The GRG algorithm is used in the Excel Solver. CONOPT is a reduced gradient algorithm that works well for large-scale problems and nonlinear constraints. CONOPT and GRG work best for problems in which the number of degrees of freedom is small (the number of constraints is nearly equal to the number of variables).

Successive quadratic programming (SQP) solves a sequence of quadratic programs that approach the solution of the original NLP by linearizing the constraints and using a quadratic approximation to the objective function. Lagrange multipliers are introduced to handle constraints, and the search procedure generally employs some variation of Newton's method, a second-order method that approximates the hessian matrix using first derivatives (Biegler et al., 1997; Edgar et al., 2001). MINOS and NPSOL are software packages that are suitable for problems with large numbers of variables (more variables than equations) and constraints that are linear or nearly linear. *Successive linear programming (SLP)* is used less often for solving RTO problems. It requires linear approximations of both the objective function and the constraints but sometimes exhibits poor convergence to optima that are not located at constraint intersections.

One important class of nonlinear programming techniques is called *quadratic programming (QP)*, where the objective function is quadratic and the constraints are linear. While the solution is iterative, it can be obtained quickly as in linear programming. This is the basis for the newest type of constrained multivariable control algorithms called model predictive control, which is heavily used in the refining industry. See the earlier subsection on model predictive control for more details.

Figure 8-45 gives an overview of which optimization algorithms are appropriate for certain types of RTO problems. Software libraries such as GAMS (General Algebraic Modeling System) or NAG (Numerical Algorithms Group) offer one or more NLP algorithms, but rarely are all algorithms available from a single source. Also there are quite a few good optimization software programs that are free and can be found by a web search. No single NLP algorithm is best for every problem, so several solvers should be tested on a given application. See Edgar, Himmelblau, and Lasdon, *Optimization of Chemical Processes*, McGraw-Hill, New York, 2001.

Linear and nonlinear programming solvers have been interfaced to spreadsheet software for desktop computers. The spreadsheet has become a popular user interface for entering and manipulating numeric data. Spreadsheet software increasingly incorporates analytic tools that are accessible from the spreadsheet interface and permit access to external databases. For example, Microsoft Excel incorporates an optimization-based routine called Solver that operates on the values and formulas of a spreadsheet model. Current versions (4.0 and later) include LP and NLP solvers and mixed integer programming (MIP) capability for both linear and nonlinear problems. The user specifies a set of cell addresses to be independently adjusted (the decision variables), a set of formula cells whose values are to be constrained (the constraints), and a formula cell designated as the optimization objective.

Referring to Fig. 8-30, the highest level of process control, planning and scheduling, also employs optimization extensively, often with variables that are integer. Level 5 sets production goals to meet supply and logistics constraints and addresses time-varying capacity and workforce utilization decisions. Enterprise resource planning (ERP) and supply chain management (SCM) in level 5 refer to the links in a web of relationships involving retailing (sales), distribution, transportation, and manufacturing. Planning and scheduling usually operate over relatively long time scales and tend to be decoupled from the rest of the activities in lower levels. For example, all of the refineries owned by an oil company are usually included in a comprehensive planning and scheduling model. This model can be optimized to obtain target levels and prices for interrefinery transfers, crude oil and product allocations to each refinery, production targets, inventory targets, optimal operating conditions, stream allocations, and blends for each refinery.

Some planning and scheduling problems are mixed-integer optimization problems that involve both continuous and integer problems; whether or not to operate or use a piece of equipment is a binary (on/off) decision that arises in batch processing. Solution techniques for this type of problem include branch and bound methods and global search. This latter approach handles very complex problems with multiple optima by using algorithms such as tabu search, scatter search, simulated annealing, and genetic evolutionary algorithms (see Edgar, Himmelblau, and Lasdon).

STATISTICAL PROCESS CONTROL

In industrial plants, large numbers of process variables must be maintained within specified limits in order for the plant to operate properly. Excursions of key variables beyond these limits can have significant consequences for plant safety, the environment, product quality, and plant profitability. *Statistical process control (SPC)*, also called *statistical quality control (SQC)*, involves the application of statistical techniques to determine whether a process is operating normally or abnormally. Thus, SPC is a process monitoring technique that relies on *quality control charts* to monitor measured variables, especially product quality.

The basic SPC concepts and control chart methodology were introduced by Walter Shewhart in the 1930s. The current widespread interest in SPC techniques began in the 1950s when they were successfully applied first in Japan and then elsewhere. Control chart methodologies are now widely used to monitor product quality and other variables that are measured infrequently or irregularly. The basic SPC methodology is described in introductory statistics textbooks (e.g., Montgomery and Runger, *Applied Statistics and Probability for Engineers*, 3d ed., Wiley, New York, 2002) and some process control textbooks (e.g., Seborg, Edgar, and Mellichamp, *Process Dynamics and Control*, 2d ed., Wiley, New York, 2004).

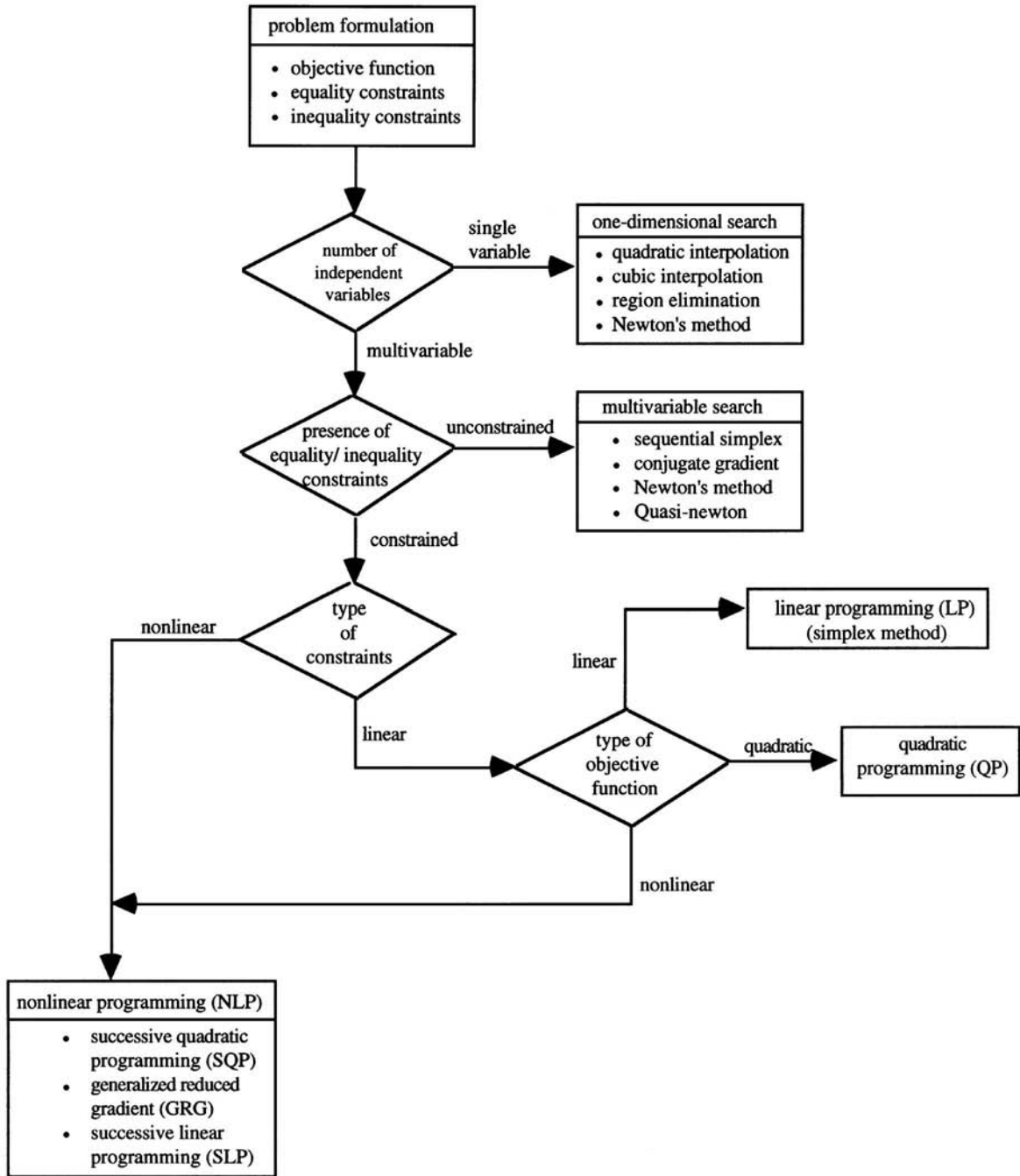


FIG. 8-45 Diagram for selection of optimization techniques with algebraic constraints and objective function.

An example of the most common control chart, the Shewhart chart, is shown in Fig. 8-46. It merely consists of measurements plotted versus sample number with control limits that indicate the range for normal process operation. The plotted data are either an individual measurement x or the sample mean \bar{x} if more than one sample is measured at each sampling instant. The sample mean for k samples is calculated as,

culated as,

$$\bar{x} = \frac{1}{n} \sum_{j=1}^n x_j \tag{8-72}$$

The Shewhart chart in Fig. 8-46 has a *target* (T), an *upper control limit* (UCL), and a *lower control limit* (LCL). The target (or centerline) is the

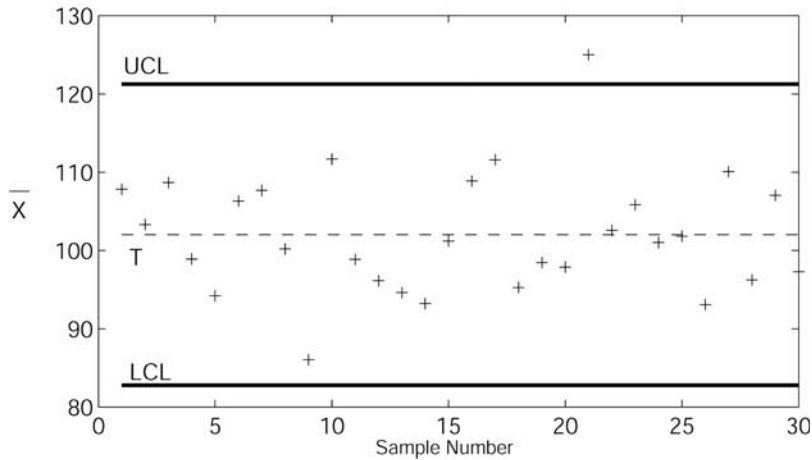


FIG. 8-46 Shewhart chart for sample mean \bar{x} . (Source: Seborg et al., Process Dynamics and Control, 2d ed., Wiley, New York, 2004.)

desired (or expected) value for \bar{x} while the region between UCL and LCL defines the range of normal variability. If all the \bar{x} data are within the control limits, the process operation is considered to be normal or “in a state of control.” Data points outside the control limits are considered to be abnormal, indicating that the process operation is out of control. This situation occurs for the 21st sample. A single measurement slightly beyond a control limit is not necessarily a cause for concern. But frequent or large chart violations should be investigated to determine the root cause.

The major objective in SPC is to use process data and statistical techniques to determine whether the process operation is normal or abnormal. The SPC methodology is based on the fundamental assumption that normal process operation can be characterized by random variations around a mean value. The random variability is caused by the cumulative effects of a number of largely unavoidable phenomena such as electrical measurement noise, turbulence, and random fluctuations in feedstock or catalyst preparation. If this situation exists, the process is said to be *in a state of statistical control* (or *in control*), and the control chart measurements tend to be normally distributed about the mean value. By contrast, frequent control chart violations would indicate abnormal process behavior or an *out-of-control* situation. Then a search would be initiated to attempt to identify the *assignable cause* or the *special cause* of the abnormal behavior

The control limits in Fig. 8-46 (UCL and LCL) are based on the assumption that the measurements follow a normal distribution. Figure 8-47 shows the probability distribution for a normally distributed random variable x with mean μ and standard deviation σ . There is a very high probability (99.7 percent) that any measurement is within 3 standard deviations of the mean. Consequently, the control limits for x are typically chosen to be $T \pm 3\hat{\sigma}$, where $\hat{\sigma}$ is an estimate of σ . This estimate is usually determined from a set of representative data for a period of time when the process operation is believed to be typical. For the common situation in which the plotted variable is the sample mean, its standard deviation is estimated.

Shewhart control charts enable average process performance to be monitored, as reflected by the sample mean. It is also advantageous to monitor process variability. Process variability within a sample of k measurements can be characterized by its range, standard deviation, or sample variance. Consequently, control charts are often used for one of these three statistics.

Western Electric Rules Shewhart control charts can detect abnormal process behavior by comparing individual measurements with control chart limits. But the pattern of measurements can also provide useful information. For example, if 10 consecutive measurements are all increasing, then it is very unlikely that the process is in a

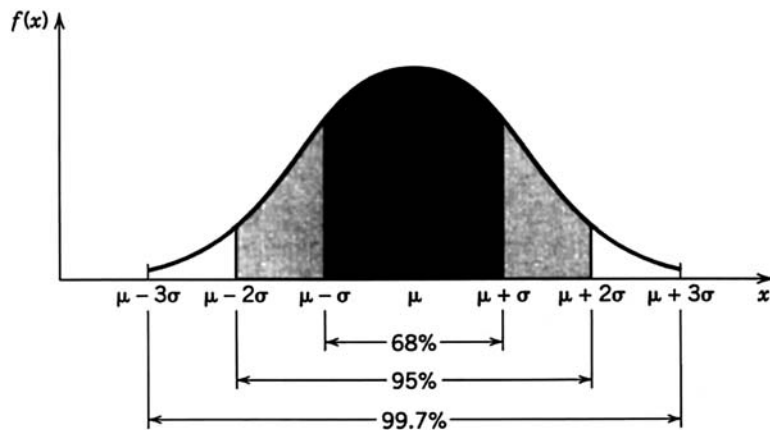


FIG. 8-47 Probabilities associated with the normal distribution. (Source: Montgomery and Runger, Applied Statistics and Probability for Engineers, 3d ed., Wiley, New York, 2002.)

state of control. A wide variety of *pattern tests* (also called *zone rules*) can be developed based on the properties of the normal distribution. For example, the following excerpts from the *Western Electric Rules* (Western Electric Company, *Statistical Quality Control Handbook*, Delmar Printing Company, Charlotte, N.C., 1956; Montgomery and Runger, *Applied Statistics and Probability for Engineers*, 3d ed., Wiley, New York, 2002) indicate that the process is out of control if one or more of the following conditions occur:

1. One data point outside the 3σ control limits
2. Two out of three consecutive data points beyond a 2σ limit
3. Four out of five consecutive data points beyond a 1σ limit and on one side of the centerline
4. Eight consecutive points on one side of the centerline

Note that the first condition is the familiar Shewhart chart limits. Pattern tests can be used to augment Shewhart charts. This combination enables out-of-control behavior to be detected earlier, but the false-alarm rate is higher than that for Shewhart charts alone.

CUSUM Control Charts Although Shewhart charts with 3σ limits can quickly detect large process changes, they are ineffective for small, sustained process changes (e.g., changes smaller than 1.5σ). Alternative control charts have been developed to detect small changes such as the CUSUM control chart. They are often used in conjunction with Shewhart charts. The *cumulative sum (CUSUM)* is defined to be a running summation of the deviations of the plotted variable from its target. If the sample mean is plotted, the cumulative sum at sampling instant k , $C(k)$, is

$$C(k) = \sum_{j=1}^k [\bar{x}(j) - T] \tag{8-73}$$

where T is the target for \bar{x} . During normal process operation, $C(k)$ fluctuates about zero. But if a process change causes a small shift in \bar{x} , $C(k)$ will drift either upward or downward.

The CUSUM control chart was originally developed using a graphical approach based on *V masks*. However, for computer calculations, it is more convenient to use an equivalent algebraic version that consists of two recursive equations

$$C^+(k) = \max[0, \bar{x}(k) - (T + K) + C^+(k - 1)] \tag{8-74}$$

$$C^-(k) = \max[0, (T - K) - \bar{x}(k) + C^-(k - 1)] \tag{8-75}$$

where C^+ and C^- denote the sums for the high and low directions, and K is a constant, the *slack parameter*. The CUSUM calculations are initialized by setting $C^+(0) = C^- = 0 = 0$. A deviation from the target that is larger than K increases either C^+ or C^- . A control limit violation occurs when either C^+ or C^- exceeds a specified control limit (or *threshold*) H . After a limit violation occurs, that sum is reset to zero or to a specified value.

The selection of the threshold H can be based on considerations of *average run length (ARL)*, the average number of samples required to detect a disturbance of specified magnitude. For example, suppose that the objective is to be able to detect if the sample mean \bar{x} has shifted from the target by a small amount δ . The slack parameter K is usually specified as $K = 0.5\delta$. For the ideal situation (e.g., normally distributed, uncorrelated disturbances), ARL values have been tabulated for different values of δ , K , and H . Table 8-7 summarizes ARL

TABLE 8-7 Average Run Lengths for CUSUM Control Charts

Shift from target (in multiples of σ)	ARL for $H = 4\sigma$	ARL for $H = 5\sigma$
0	168.	465.
0.25	74.2	139.
0.50	26.6	38.0
0.75	13.3	17.0
1.00	8.38	10.4
2.00	3.34	4.01
3.00	2.19	2.57

Adapted from Ryan, *Statistical Methods for Quality Improvement*, 2d ed., Wiley, New York, 2000.

values for two values of H and different values of δ . (The values of δ are usually expressed as multiples of the standard deviation σ .) The ARL values indicate the average number of samples before a change of δ is detected. Thus the ARL values for $\delta = 0$ indicate the average time between false alarms, i.e., the average time between successive CUSUM alarms when no shift in \bar{x} has occurred. Ideally, we would like the ARL value to be very large for $\delta = 0$ and small for $\delta \neq 0$. Table 8-7 shows that as the magnitude of the shift δ increases, ARL decreases and thus the CUSUM control chart detects the change faster. Increasing the value of H from 4σ to 5σ increases all the ARL values and thus provides a more conservative approach.

The relative performance of the Shewhart and CUSUM control charts is compared in Fig. 8-48 for a set of simulated data for the tensile strength of a resin. It is assumed that the tensile strength x is normally distributed with a mean of $\mu = 70$ MPa and a standard deviation of $\sigma = 3$ MPa. A single measurement is available at each sampling instant. A constant ($\sigma = 0.5\sigma = 1.5$) was added to $x(k)$ for $k \geq 10$ in order to evaluate each chart's ability to detect a small process shift. The CUSUM chart was designed using $K = 0.5\sigma$ and $H = 5\sigma$.

The Shewhart chart fails to detect the 0.5σ shift in x at $k = 10$. But the CUSUM chart quickly detects this change because a limit violation occurs at $k = 20$. The mean shift can also be detected by applying the Western Electric Rules in the previous section.

Process Capability Indices Also known as *process capability ratios*, these provide a measure of whether an in-control process is meeting its product specifications. Suppose that a quality variable x must have a volume between an *upper specification limit (USL)* and a *lower specification limit (LSL)* in order for product to satisfy customer requirements. The *capability index* C_p is defined as

$$C_p = \frac{USL - LSL}{6\sigma} \tag{8-76}$$

where σ is the standard deviation of x . Suppose that $C_p = 1$ and x is normally distributed. Based on the normal distribution, we would expect that 99.7 percent of the measurements satisfy the specification limits, or equivalently, we would expect that only 2700 out of 1 million measurements would lie outside the specification limits. If $C_p < 1$, the product specifications are satisfied; for $C_p > 1$, they are not. However, capability indices are applicable even when the data are not normally distributed.

A second capability index C_{pk} is based on average process performance \bar{x} as well as process variability σ . It is defined as

$$C_{pk} = \frac{\text{Min}[\bar{x} - LSL, USL - \bar{x}]}{3\sigma} \tag{8-77}$$

Although both C_p and C_{pk} are used, we consider C_{pk} to be superior to C_p for the following reason. If $\bar{x} = T$, the process is said to be "centered" and $C_{pk} = C_p$. But for $\bar{x} \neq T$, C_p does not change, even though the process performance is worse, while C_{pk} does decrease. For this reason, C_{pk} is preferred.

If the standard deviation σ is not known, it is replaced by an estimate $\hat{\sigma}$ in Eqs. (8-76) and (8-77). For situations where there is only a single specification limit, either USL or LSL, the definitions of C_p and C_{pk} can be modified accordingly.

In practical applications, a common objective is to have a capability index of 2.0 while a value greater than 1.5 is considered to be acceptable. If the C_{pk} value is too low, it can be improved by making a change that either reduces process variability or causes \bar{x} to move closer to the target. These improvements can be achieved in a number of ways that include better process control, better process maintenance, reduced variability in raw materials, improved operator training, and process changes.

Six-Sigma Approach Product quality specifications continue to become more stringent as a result of market demands and intense worldwide competition. Meeting quality requirements is especially difficult for products that consist of a very large number of components and for manufacturing processes that consist of hundreds of individual steps. For example, the production of a microelectronic device typically requires 100 to 300 batch processing steps. Suppose

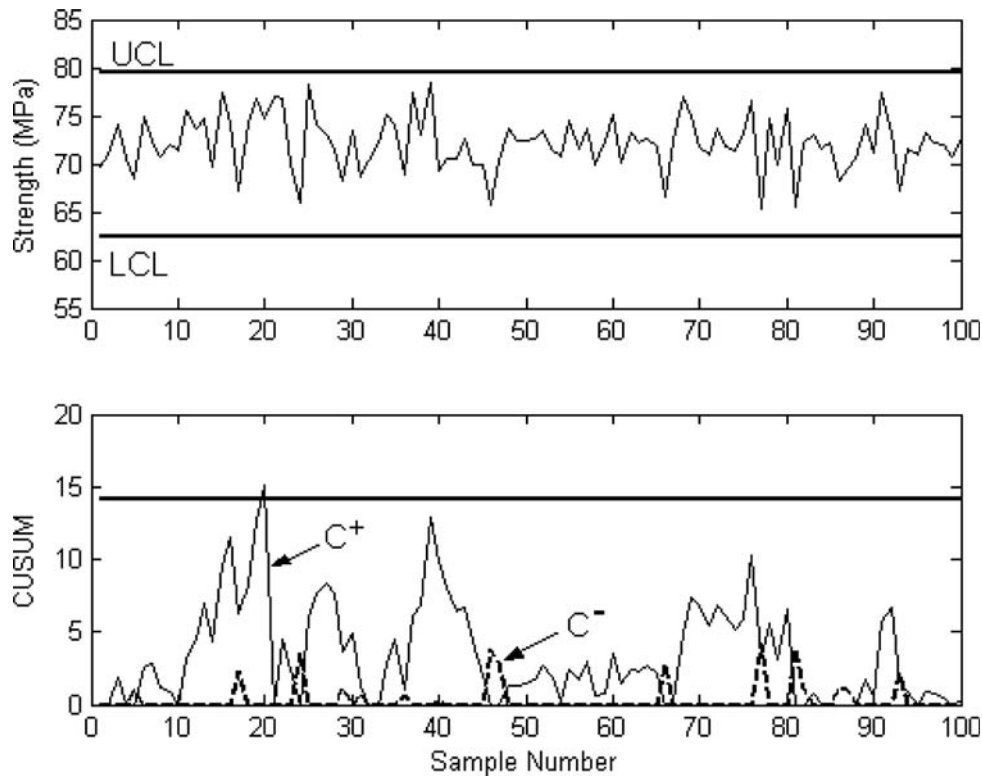


FIG. 8-48 Comparison of Shewhart and CUSUM control charts for the resin example. (Source: Seborg et al., *Process Dynamics and Control*, 2d ed., Wiley, New York, 2004.)

that there are 200 steps and that each one must meet a quality specification for the final product to function properly. If each step is independent of the others and has a 99 percent success rate, the overall yield of satisfactory product is $(0.99)^{200} = 0.134$, or only 13.4 percent. This low yield is clearly unsatisfactory. Similarly, even when a processing step meets 3σ specifications (99.73 percent success rate), it will still result in an average of 2700 “defects” for every 1 million produced. Furthermore, the overall yield for this 200-step process is still only 58.2 percent.

The six-sigma approach was pioneered by the Motorola Corporation in the early 1980s as a strategy for achieving both six-sigma quality and continuous improvement. Since then, other large corporations have adopted companywide programs that apply the six-sigma approach to all their business operations, both manufacturing and nonmanufacturing. Thus, although the six-sigma approach is “data-driven” and based on statistical techniques, it has evolved into a broader management philosophy that has been implemented successfully by many large corpora-

tions. The six-sigma programs have also had a significant financial impact.

Multivariate Statistical Techniques For common SPC monitoring problems, two or more quality variables are important, and they can be highly correlated. For these situations, multivariate (or *multivariate*) SPC techniques can offer significant advantages over the single-variable methods discussed earlier. Multivariate monitoring based on the classical Hotelling’s T^2 statistic (Montgomery, *Introduction to Statistical Quality Control*, 4th ed., Wiley, New York, 2001) can be effective if the data are not highly correlated and the number of variables p is not large (for example, $p < 10$). Fortunately, alternative multivariate monitoring techniques such as *principal-component analysis (PCA)* and *partial least squares (PLS)* methods have been developed that are very effective for monitoring problems with large numbers of variables and highly correlated data [Piovoso and Hoo (eds.), *Special Issue of IEEE Control Systems Magazine*, 22(5), 2002].

UNIT OPERATIONS CONTROL

PIPING AND INSTRUMENTATION DIAGRAMS

GENERAL REFERENCES: Shinsky, *Process Control Systems*, 4th ed., McGraw-Hill, New York, 1996. Luyben, *Practical Distillation Control*, Van Nostrand Reinhold, New York, 1992. Luyben, Tyreus, and Luyben, *Plantwide Process Control*, McGraw-Hill, New York, 1998.

The piping and instrumentation (P&I) diagram provides a graphical representation of the control configuration of the process. P&I diagrams illustrate the measuring devices that provide inputs to the con-

trol strategy, the actuators that will implement the results of the control calculations, and the function blocks that provide the control logic. They may also include piping details such as line sizes and the location of hand valves and condensate traps.

The symbology for drawing P&I diagrams generally follows standards developed by the Instrumentation, Systems, and Automation Society (ISA). The chemicals, refining, and food industries generally follow this standard. The standards are updated from time to time, primarily because the continuing evolution in control system hardware and software provides additional capabilities for implementing

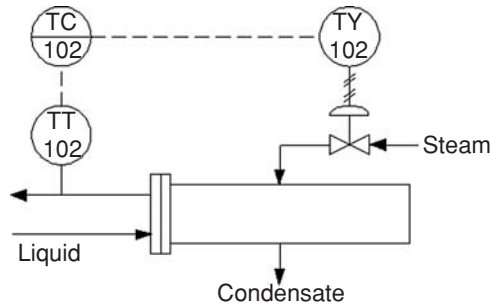


FIG. 8-49 Example of a simplified piping and instrumentation diagram.

control schemes. The ISA symbols are simple and represent a device or function as a circle containing its tag number and identifying the type of variable being controlled, e.g., pressure, and the function performed, e.g., control: PC-105. Examples of extensions of the ISA standard appear on the pages following.

Figure 8-49 presents a simplified P&I diagram for a temperature control loop that applies the ISA symbology. The measurement devices and most elements of the control logic are shown as circles:

1. TT102 is the temperature transmitter.
2. TC102 is the temperature controller.
3. TY102 is the current-to-pneumatic (I/P) transducer.

The symbol for the control valve in Fig. 8-49 is for a pneumatic modulating valve without a valve positioner.

Electronic (4- to 20-mA) signals are represented by dashed lines. In Fig. 8-49, these include the signal from the transmitter to the controller and the signal from the controller to the I/P transducer. Pneumatic signals are represented by solid lines with double crosshatching at regular intervals. The signal from the I/P transducer to the valve actuator is pneumatic.

The ISA symbology provides different symbols for different types of actuators. Furthermore, variations for the controller symbol distinguish control algorithms implemented in distributed control systems from those in panel-mounted single-loop controllers.

CONTROL OF HEAT EXCHANGERS

Steam-Heated Exchangers Steam, the most common heating medium, transfers its latent heat in condensing, causing heat flow to be proportional to steam flow. Thus a measurement of steam flow is essentially a measure of heat transfer. Consider raising a liquid from temperature T_1 to T_2 by condensing steam:

$$Q = WH = MC(T_2 - T_1) \quad (8-78)$$

where W and H are the mass flow of steam and its latent heat, M and C are the mass flow and specific heat of the liquid, and Q is the rate of heat transfer. The response of controlled temperature to steam flow is linear:

$$\frac{dT_2}{dW} = \frac{H}{MC} \quad (8-79)$$

However, the steady-state process gain described by this derivative varies inversely with liquid flow: adding a given increment of heat flow to a smaller flow of liquid produces a greater temperature rise.

Dynamically, the response of liquid temperature to a step in steam flow is that of a distributed lag, shown in Fig. 8-26 (uncontrolled). The time required to reach 63 percent complete response, $\Sigma\tau$, is essentially the residence time of the fluid in the exchanger, which is its volume divided by its flow. The residence time then varies inversely with flow. Table 8-2 gives optimum settings for PI and PID controllers for distributed lags, the proportional band varying directly with steady-state gain, and integral and derivative settings directly with $\Sigma\tau$. Since both these parameters vary inversely with liquid flow, fixed settings for the temperature controller are optimal at only one flow rate.

The variability of the process parameters with flow causes variability in load response, as shown in Fig. 8-50. The PID controller was tuned for optimum (minimum-IAE) load response at 50 percent flow. Each curve represents the response of exit temperature to a 10 percent step in liquid flow, culminating at the stated flow. The 60 percent curve is overdamped and the 40 percent curve is underdamped. The differences in gain are reflected in the amplitude of the deviation, and the differences in dynamics are reflected in the period of oscillation.

If steam flow is linear with controller output, as it is in Fig. 8-50, undamped oscillations will be produced when the flow decreases by

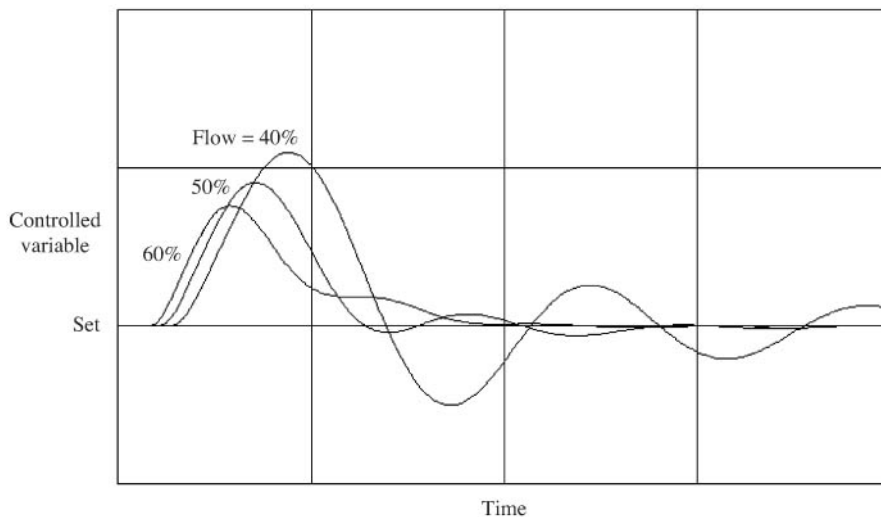


FIG. 8-50 The response of a heat exchanger varies with flow in both gain and dynamics; here the PID temperature controller was tuned for optimum response at 50 percent flow.

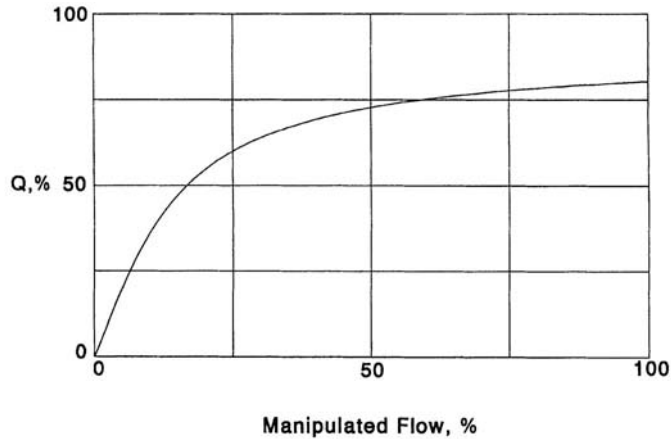


FIG. 8-51 Heat-transfer rate in sensible-heat exchange varies nonlinearly with flow of the manipulated fluid, requiring equal-percentage valve characterization.

one-third from the value at which the controller was optimally tuned—in this example at 33 percent flow. The stable operating range can be extended to one-half the original flow by using an equal-percentage (logarithmic) steam valve, whose gain varies directly with steam flow, thereby compensating for the variable process gain. Further extension requires increasing the integral setting and reducing the derivative setting from their optimum values. The best solution is to adapt all three PID settings to change inversely with measured flow, thereby keeping the controller optimally tuned for all flow rates.

Feedforward control can also be applied, as described previously under “Advanced Control Techniques.” The feedforward system solves Eq. (8-78) for the manipulated set point to the steam flow controller, first by subtracting inlet temperature T_1 from the output of the outlet temperature controller (in place of T_2), and then by multiplying the result by the dynamically compensated liquid flow measurement. If the inlet temperature is not subject to rapid or wide variation, it can be left out of the calculation. Feedforward is capable of a reduction in integrated error as much as a 100-fold, but requires the use of a steam flow loop and lead-lag compensator to approach this effectiveness. Multiplication of the controller output by liquid flow varies the feedback loop gain directly proportional to flow, extending the stable operating range of the feedback loop much as the equal-percentage steam valve did without feedforward. (This system is eminently applicable to control of fired heaters in oil refineries, which commonly provide a circulating flow of hot oil to several distillation columns and are therefore subject to frequent disturbances).

Steam flow is sometimes controlled by manipulating a valve in the condensate line rather than the steam line, because it is smaller and hence less costly. Heat transfer then is changed by raising or lowering the level of condensate flooding the heat-transfer surface, an operation that is slower than manipulating a steam valve. Protection also needs to be provided against an open condensate valve blowing steam into the condensate system.

Exchange of Sensible Heat When there is no change in phase, the rate of heat transfer is no longer linear with the flow of the manipulated stream, but is a function of the mean temperature difference ΔT_m :

$$Q = UA \Delta T_m = M_H C_H (T_{H1} - T_{H2}) = M_C C_C (T_{C2} - T_{C1}) \quad (8-79a)$$

where U and A are the overall heat-transfer coefficient and area and subscripts H and C refer to the hot and cold fluids, respectively. An example would be a countercurrent cooler, where the hot-stream outlet temperature is controlled. Using the logarithmic mean tempera-

ture difference and solving for T_{H2} give

$$T_{H2} = T_{C1} + (T_{H1} - T_{C1}) \frac{1 - M_H C_H / M_C C_C}{\varepsilon - M_H C_H / M_C C_C} \quad (8-79b)$$

where

$$\varepsilon = \exp \left[-UA \left(\frac{1}{M_C C_C} - \frac{1}{M_H C_H} \right) \right] \quad (8-79c)$$

At a given flow of hot fluid, the heat-transfer rate is plotted as a function of coolant flow in Fig. 8-51, as a percentage of its maximum value (corresponding to $T_{C2} = T_{C1}$). The extreme nonlinearity of this relationship requires the use of an equal-percentage coolant valve for gain compensation. The variable dynamics of the distributed lag also apply, limiting the stable operating range in the same way as for the steam-heated exchanger.

Sensible-heat exchangers are also subject to variations in the temperature of the manipulated stream, an increasingly common problem where heat is being recovered at variable temperatures for reuse. Figure 8-52 shows a temperature controller (TC) setting a heat flow controller (QC) in cascade. A measurement of the manipulated flow is multiplied by its temperature difference across the heat exchanger to calculate the current heat-transfer rate, by using the right side of Eq. (8-78). Variations in supply temperature then appear as variations in calculated heat-transfer rate, which the QC can quickly correct by adjusting the manipulated flow. An equal-percentage valve is still required to linearize the secondary loop, but the primary loop of temperature-setting heat flow is linear. Feedforward can be added by multiplying the dynamically compensated flow measurement of the other fluid by the output of the temperature controller.

When a stream is manipulated whose flow is independently determined, such as the flow of a product or of a heat-transfer fluid from a fired heater, a three-way valve is used to divert the required flow to the heat exchanger. This does not alter the linearity of the process or its sensitivity to supply variations, and it even adds the possibility of independent flow variations. The three-way valve should have equal-percentage characteristics, and heat flow control may be even more beneficial.

DISTILLATION COLUMN CONTROL

Distillation columns have four or more closed loops—increasing with the number of product streams and their specifications—all of which interact with one another to some extent. Because of this interaction, there are many possible ways to pair manipulated and controlled variables through controllers and other mathematical functions, with widely differing

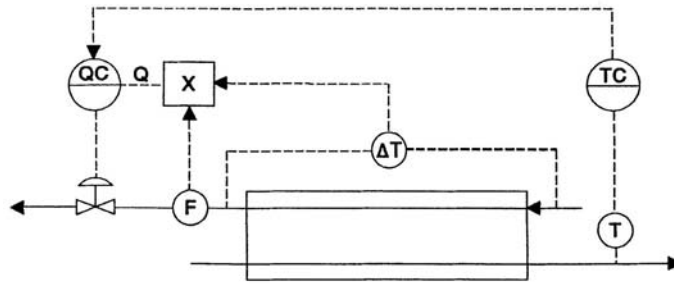


FIG. 8-52 Manipulating heat flow linearizes the loop and protects against variations in supply temperature.

degrees of effectiveness. Columns also differ from one another, so that no single rule of configuring control loops can be applied successfully to all. The following rules apply to the most common separations.

Controlling Quality of a Single Product If one of the products of a column is far more valuable than the other(s), its quality should be controlled to satisfy given specifications, and its recovery should be maximized by minimizing losses of its principal component in other streams. This is achieved by maximizing the reflux ratio consistent with flooding limits on trays, which means maximizing the flow of internal reflux or vapor, whichever is limiting. The same rule should be followed when heating and cooling have little value. A typical example is the separation of high-purity propylene from much lower-valued propane, usually achieved with the waste heat of quench water from the cracking reactors.

The most important factor affecting product quality is the material balance. In separating a feed stream F into distillate D and bottom B products, an overall mole flow balance must be maintained

$$F = D + B \tag{8-80}$$

as well as a balance on each component

$$Fz_i = Dy_i + Bx_i \tag{8-81}$$

where z , y , and x are mole fractions of component i in the respective streams. Combining these equations gives a relationship between the composition of the products and their relative portion of the feed:

$$\frac{D}{F} = 1 - \frac{B}{F} = \frac{z_i - x_i}{y_i - x_i} \tag{8-82}$$

From the above, it can be seen that control of either x_i or y_i requires both product flow rates to change with feed rate and feed composition.

Figure 8-53 shows a propylene-propane fractionator controlled at maximum boil-up by the differential pressure controller (DPC) across the trays. This loop is fast enough to reject upsets in the temperature

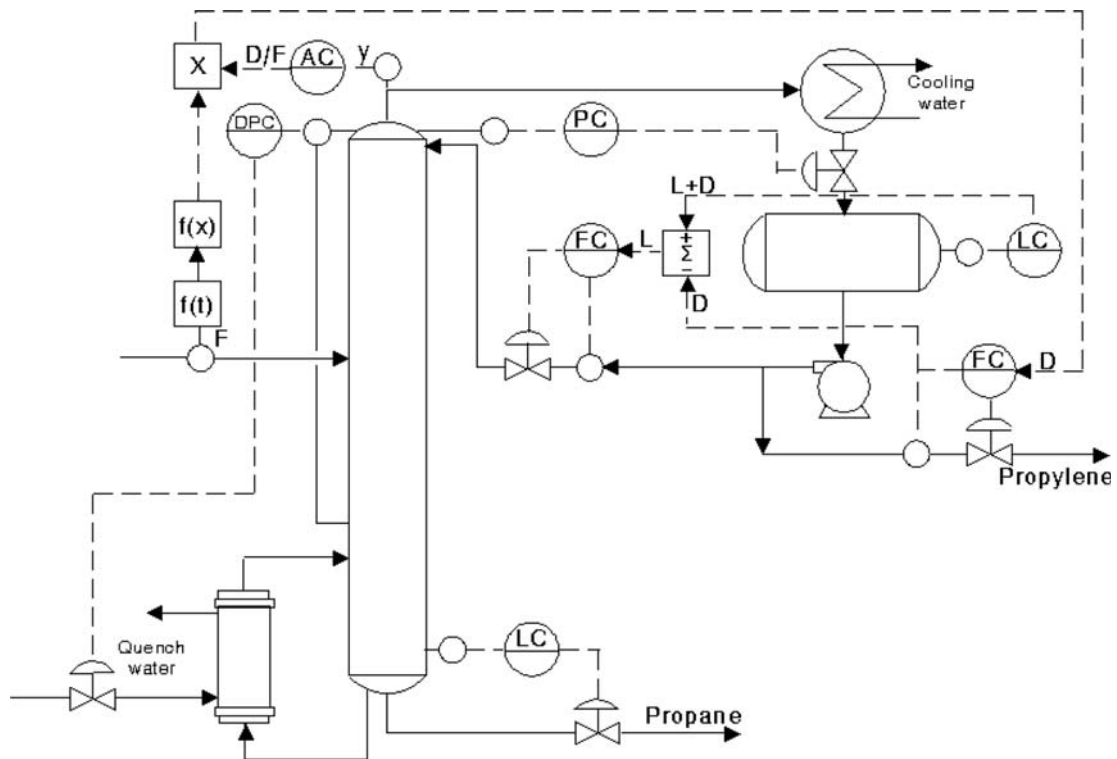


FIG. 8-53 The quality of high-purity propylene should be controlled by manipulating the material balance.

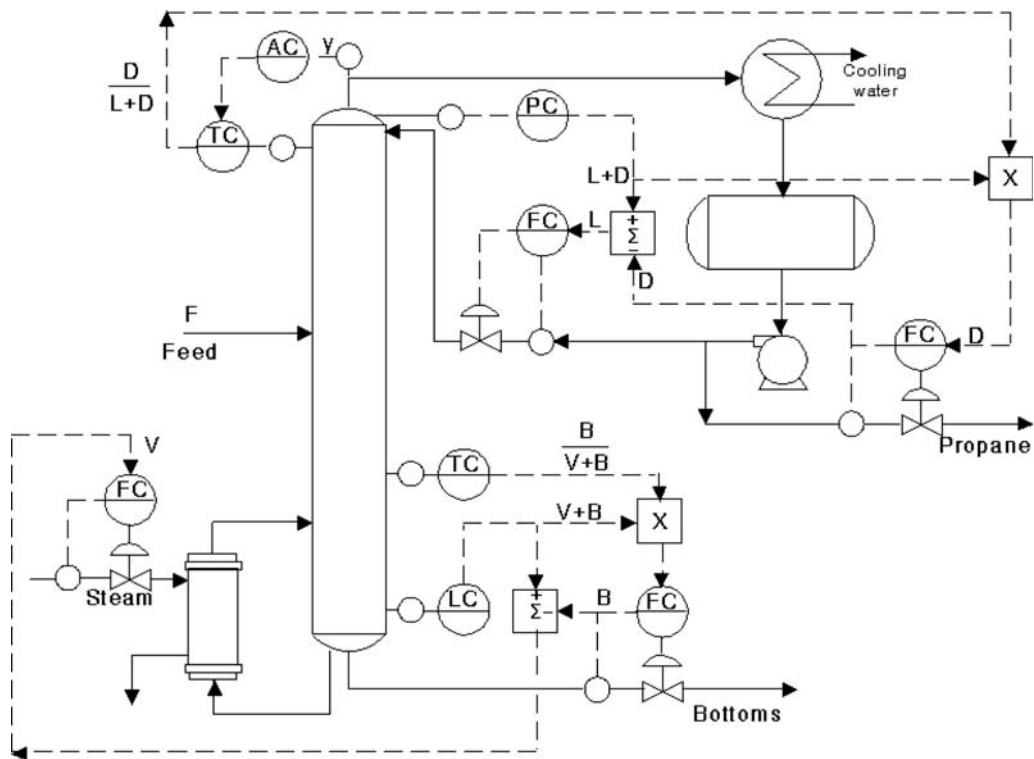


FIG. 8-54 Depropanizers require control of the quality of both products, here using reflux ratio and boil-up ratio manipulation.

of the quench water quite easily. Pressure is controlled by manipulating the heat-transfer surface in the condenser through flooding. If the condenser should become overloaded, pressure will rise above the set point, but this has no significant effect on the other control loops. Temperature measurements on this column are not helpful, as the difference between the component boiling points is too small. Propane content in the propylene distillate is measured by a chromatographic analyzer sampling the overhead vapor for fast response, and it is controlled by the analyzer controller (AC) manipulating the ratio of distillate to feed rates. The feedforward signal from feed rate is dynamically compensated by $f(t)$ and nonlinearly characterized by $f(x)$ to account for variations in propylene recovery as the feed rate changes. Distillate flow can be measured and controlled more accurately than reflux flow by a factor equal to the reflux ratio, which in this column is typically between 10 and 20. Therefore reflux flow is placed under accumulator level control (LC). Yet composition responds to the difference between internal vapor and reflux flow rates. To eliminate the lag inherent in the response of the accumulator level controller, reflux flow is driven by the subtractor in the direction opposite to distillate flow—this is essential to fast response of the composition loop. The gain of converting distillate flow changes to reflux flow changes can even be increased beyond -1 , thereby changing the accumulator level loop from a lag into a dominant lead.

Controlling Quality of Two Products Where the two products have similar values, or where heating and cooling costs are comparable to product losses, the compositions of both products should be controlled. This introduces the possibility of strong interaction between the two composition loops, as they tend to have similar speeds of response. Interaction in most columns can be minimized by controlling distillate composition with reflux ratio and bottom composition with boil-up, or preferably boil-up/bottom flow ratio. These loops are insensitive to variations in feed rate, eliminating the need for feedforward control, and they also reject heat balance upsets quite effectively.

Figure 8-54 shows a depropanizer controlled by reflux and boil-up ratios. The actual mechanism through which these ratios are manipulated is as $D/(L + D)$ and $B/(V + B)$, where L is reflux flow and V is vapor boil-up, which decouples the temperature loops from the liquid-level loops. Column pressure here is controlled by flooding both the condenser and accumulator; however, there is no level controller on the accumulator, so this arrangement will not function with an overloaded condenser. Temperatures are used as indications of composition in this column because of the substantial difference in boiling points between propane and butanes. However, off-key components such as ethane do affect the accuracy of the relationship, so that an analyzer controller is used to set the top temperature controller (TC) in cascade.

If the products from a column are especially pure, even this configuration may produce excessive interaction between the composition loops. Then the composition of the less pure product should be controlled by manipulating its own flow; the composition of the remaining product should be controlled by manipulating the reflux ratio if it is the distillate, or the boil-up ratio if it is the bottom product.

Most sidestream columns have a small flow dedicated to removing an off-key impurity entering the feed, and that stream must be manipulated to control its content in the major product. For example, an ethylene fractionator separates its feed into a high-purity ethylene sidestream, an ethane-rich bottom product, and a small flow of methane overhead. This small flow must be withdrawn to control the methane content in the ethylene product. The key impurities may then be controlled in the same way as in a two-product column.

Most volatile mixtures have a relative volatility that varies inversely with column pressure. Therefore, their separation requires less energy at lower pressure, and savings in the range of 20 to 40 percent have been achieved. Column pressure can be minimized by floating on the condenser, i.e., by operating the condenser with minimal or no restrictions. In some columns, such as the propylene-propane splitter, pressure can be left uncontrolled. Where it cannot, the set point of the

pressure controller can be indexed by an integral-only controller acting to slowly drive the pressure control valve toward a position just short of maximum cooling. In the case of a flooded condenser, the degree of reflux subcooling can be controlled in place of condenser valve position. Where column temperatures are used to indicate product composition, their measurements must be pressure-compensated.

CHEMICAL REACTORS

Composition Control The first requirement for successful control of a chemical reactor is to establish the proper stoichiometry, i.e., to control the flow rates of the reactants in the proportions needed to satisfy the reaction chemistry. In a continuous reactor, this begins by setting ingredient flow rates in ratio to one another. However, because of variations in the purity of the feed streams and inaccuracy in flow metering, some indication of excess reactant such as pH or a composition measurement should be used to trim the ratios. Many reactions are incomplete, leaving one or more reactants unconverted. They are separated from the products of the reaction and recycled to the reactor, usually contaminated with inert components. While reactants can be recycled to complete conversion (extinction), inerts can accumulate to the point of impeding the reaction and must be purged from the system. Inerts include noncondensable gases that must be vented and nonvolatiles from which volatile products must be stripped.

If one of the reactants differs in phase from the others and the product(s), it may be manipulated to close the material balance on that phase. For example, a gas reacting with liquids to produce a liquid product may be added as it is consumed to control reactor pressure; a gaseous purge would be necessary. Similarly, a liquid reacting with a gas to produce a gaseous product could be added as it is consumed to control the liquid level in the reactor; a liquid purge would be required. Where a large excess of one reactant *A* is used to minimize side reactions, the unreacted excess is sent to a storage tank for recycling. Its flow from the recycle storage tank is set in the desired ratio to the flow of reactant *B*, with the flow of fresh *A* manipulated to control the recycle tank level if the feed is a liquid, or tank pressure if it is a gas. Some catalysts travel with the reactants and must be recycled in the same way.

With batch reactors, it may be possible to add all reactants in their proper quantities initially, if the reaction rate can be controlled by temperature control of an exothermic reactor, as the loop includes two dominant lags—concentration of the reactant and heat capacity of the reaction mass—and can easily go unstable. It also presents the unfavorable dynamic of inverse response—increasing feed rate may lower temperature by its sensible heat before the increased reaction rate raises temperature.

Temperature Control Reactor temperature should always be controlled by heat transfer. Endothermic reactions require heat and therefore are eminently self-regulating. Exothermic reactions produce heat, which tends to raise reaction temperature, thereby increasing the reaction rate and producing more heat. This positive feedback is countered by negative feedback in the cooling system, which removes more heat as the reactor temperature rises. Most continuous reactors have enough heat-transfer surface relative to reaction mass that negative feedback dominates and they are self-regulating. But most batch reactors do not, and they are therefore steady-state unstable. Unstable reactors can be controlled if their temperature controller gain can be set high enough, and if their cooling system has enough margin to accommodate the largest expected disturbance in heat load. Stirred-tank reactors are lag-dominant, and their dynamics allow a high controller gain, but plug flow reactors are dead-time-dominant, preventing their temperature controller from providing enough gain to overcome steady-state instability. Therefore unstable plug flow reactors are also uncontrollable, their temperature tending to limit-cycle in a sawtooth wave. A stable reactor can become unstable as its heat-transfer surface fouls, or as the production rate is increased beyond a critical point (Shinsky, "Exothermic Reactors: The Stable, the Unstable, and the Uncontrollable," *Chem. Eng.*, pp. 54–59, March 2002).

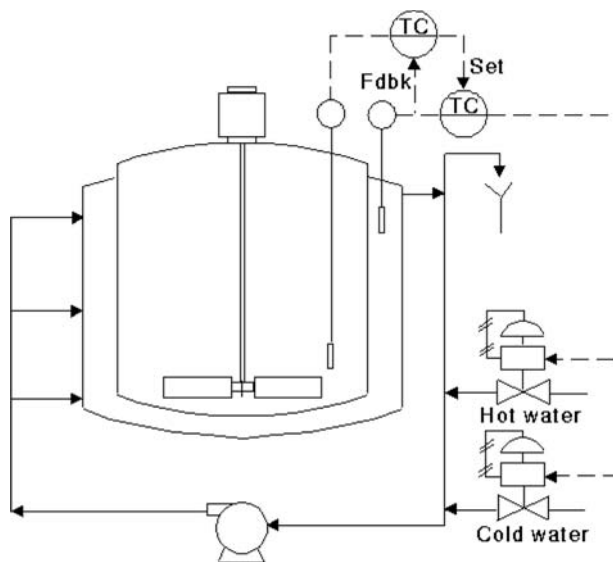


FIG. 8-55 The stirred-tank reactor temperature controller sets the coolant outlet temperature in cascade, with primary integral feedback taken from the secondary temperature measurement.

Figure 8-55 shows the recommended system for controlling the temperature of an exothermic stirred-tank reactor, either continuous or batch. The circulating pump on the coolant loop is absolutely essential to effective temperature control in keeping dead time minimum and constant—without it, dead time varies inversely with cooling load, causing limit-cycling at low loads. Heating is usually required to raise the temperature to reaction conditions, although it is often locked out of a batch reactor once the initiator is introduced. The valves are operated in split range, the heating valve opening from 50 to 100 percent of controller output and the cooling valve opening from 50 to 0 percent. The cascade system linearizes the reactor temperature response, speeds its response, and protects it from disturbances in the cooling system. The flow of heat removed per unit of coolant flow is directly proportional to the temperature rise of the coolant, which varies with both the temperature of the reactor and the rate of heat transfer from it. Using an equal-percentage cooling valve helps compensate for this nonlinearity, but incompletely.

The flow of heat across the heat-transfer surface is linear with both temperatures, leaving the primary loop with a constant gain. Using the coolant exit temperature as the secondary controlled variable as shown in Fig. 8-55 places the jacket dynamics in the secondary loop, thereby reducing the period of the primary loop. This is dynamically advantageous for a stirred-tank reactor because of the slow response of its large heat capacity. However, a plug flow reactor cooled by an external heat exchanger lacks this heat capacity, and requires the faster response of the coolant inlet temperature loop.

Performance and robustness are both improved by using the secondary temperature measurement as the feedback signal to the integral mode of the primary controller. (This feature may be available only with controllers that integrate by positive feedback.) This places the entire secondary loop in the integral path of the primary controller, effectively pacing its integral time to the rate at which the secondary temperature is able to respond. It also permits the primary controller to be left in the automatic mode at all times without integral windup.

The primary time constant of the reactor is

$$\tau_1 = \frac{M_r C_r}{UA} \quad (8-83)$$

where M_r and C_r are the mass and heat capacity of the reactants and U and A are the overall heat-transfer coefficient and area, respectively.

The control system of Fig. 8-55 was tested on a pilot reactor where the heat-transfer area and mass could both be changed by a factor of 2, changing τ_1 by a factor of 4 as confirmed by observations of the rates of temperature rise. Yet neither controller required retuning as τ_1 varied. The primary controller should be PID and the secondary controller at least PI in this system (if the secondary controller has no integral mode, the primary will control with offset). Set-point overshoot in batch reactor control can be avoided by setting the derivative time of the primary controller higher than its integral time, but this is effective only with interacting PID controllers.

CONTROLLING EVAPORATORS

The most important consideration in controlling the quality of concentrate from an evaporator is the forcing of the vapor withdrawal rate to match the flow of excess solvent entering the feed. The mass flow rates of solid material entering and leaving are equal in the steady state

$$M_0 x_0 = M_n x_n \quad (8-84)$$

where M_0 and x_0 are the mass flow and solid fraction of the feed and M_n and x_n are their values in the product after n effects of evaporation. The total solvent evaporated from all the effects must then be

$$\sum W = M_0 - M_n = M_0 \left(1 - \frac{x_0}{x_n} \right) \quad (8-85)$$

For a steam-heated evaporator, each unit of steam W_0 applied produces a known amount of evaporation, based on the number of effects and their fractional economy E :

$$\sum W = nEW_0 \quad (8-86)$$

(A comparable statement can be made with regard to the power applied to a mechanical recompression evaporator.) In summary, the steam flow required to increase the solid content of the feed from x_0

to x_n is

$$W_0 = \frac{M_0(1 - x_0/x_n)}{nE} \quad (8-87)$$

The usual measuring device for feed flow is a magnetic flowmeter, which is a volumetric device whose output F must be multiplied by density ρ to produce mass flow M_0 . For most aqueous solutions fed to evaporators, the product of density and the function of solid content appearing above is linear with density:

$$F\rho \left(1 - \frac{x_0}{x_n} \right) \approx F[1 - m(\rho - 1)] \quad (8-88)$$

where slope m is determined by the desired product concentration and density is in grams per milliliter. The required steam flow in pounds per hour for feed measured in gallons per minute is then

$$W_0 = \frac{500F[1 - m(\rho - 1)]}{nE} \quad (8-89)$$

where the factor of 500 converts gallons per minute of water to pounds per hour. The factor nE is about 1.74 for a double-effect evaporator and 2.74 for a triple-effect. Using a thermocompressor (ejector) driven with 150 lb/in² steam on a single-effect evaporator gives an nE of 2.05; it essentially adds the equivalent of one effect to the evaporator train.

A cocurrent evaporator train with its controls is illustrated in Fig. 8-56. The control system applies equally well to countercurrent or mixed-feed evaporators, the principal difference being the tuning of the dynamic compensator $f(t)$, which must be done in the field to minimize the short-term effects of changes in feed flow on product quality. Solid concentration in the product is usually measured as density; feedback trim is applied by the analyzer controller AC adjusting the slope m of the density function, which is the only term related to x_n . This recalibrates the system whenever x_n must move to a new set point.

The accuracy of the system depends on controlling heat flow; therefore if steam pressure varies, compensation must be applied to correct

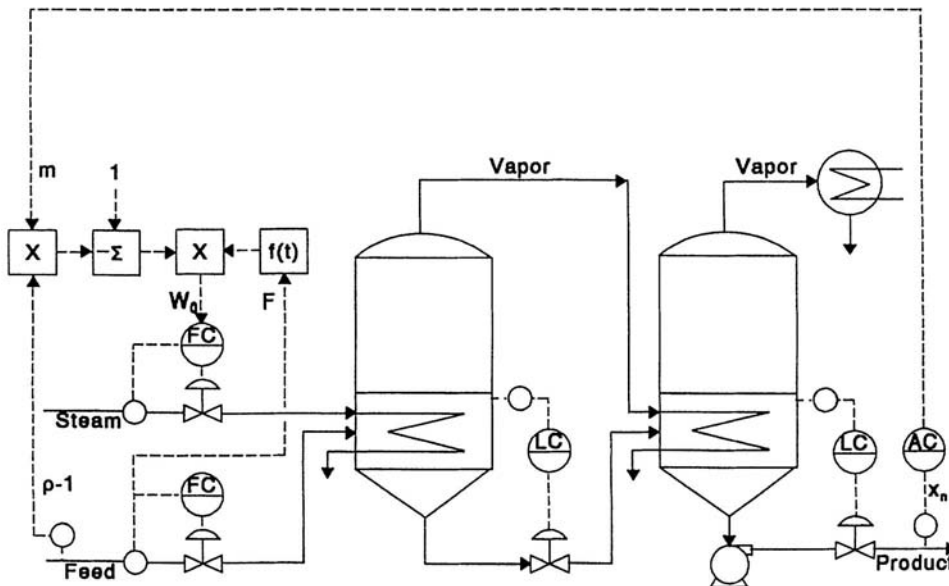


FIG. 8-56 Controlling the evaporators requires matching steam flow and evaporative load, here using feedforward control.

for both steam density and enthalpy as a function of pressure. Some evaporators must use unreliable sources of low-pressure steam. In this case, the measurement of pressure-compensated steam flow can be used to set feed flow by solving the last equation for F , using W_0 as a variable. The steam flow controller would be set for a given production rate, but the dynamically compensated steam flow measurement would be the input signal to calculate the feed flow set point. Both of these configurations are widely used in controlling corn syrup concentrators.

DRYING OPERATIONS

Controlling dryers is much different from controlling evaporators, because online measurements of feed rate and composition and product composition are rarely available. Most dryers transfer moisture from wet feed into hot dry air in a single pass. The process is generally very self-regulating, in that moisture becomes progressively harder to remove from the product as it dries: this is known as falling-rate drying. Controlling the temperature of the air leaving a cocurrent dryer tends to regulate the moisture in the product, as long as the rate and moisture content of the feed and air are reasonably constant. However, at constant outlet air temperature, product moisture tends to rise with all three of these disturbance variables.

In the absence of moisture analyzers, regulation of product quality can be improved by raising the temperature of the exhaust air in proportion to the evaporative load. The evaporative load can be estimated by the loss in temperature of the air passing through the dryer in the steady state. Changes in load are first observed in upsets in exhaust temperature at a given inlet temperature; the controller then responds by returning the exhaust air to its original temperature by changing that of the inlet air.

Figure 8-57 illustrates the simplest application of this principle as the linear relationship

$$T_0 = T_b + K \Delta T \quad (8-90)$$

where T_0 is the set point for exhaust temperature elevated above a base temperature T_b corresponding to zero-load operation and ΔT is the drop in air temperature from inlet to outlet. Coefficient K must be set to regulate product moisture over the expected range of evaporative load. If K is set too low, product moisture will increase with increasing load; if K is set too high, product moisture will decrease with increasing load. While K can be estimated from the model of a dryer, it does depend on the rate-of-drying curve for the product, its mean particle size, and whether the load variations are due primarily to changes in feed rate or feed moisture.

It is important to have the most accurate measurement of exhaust temperature attainable. Note that Fig. 8-57 shows the sensor inserted into the dryer upstream of the rotating seal, because air infiltration there could cause the temperature in the exhaust duct to read low—even lower than the wet-bulb temperature, an impossibility without either substantial heat loss or outside-air infiltration.

The calculation of the exhaust temperature set point forms a positive feedback loop capable of destabilizing the dryer. For example, an increase in evaporative load causes the controller to raise the inlet temperature, which will in turn raise the calculated set point, calling for a further increase in inlet temperature. The gain in the set-point loop K is typically well below the gain of the exhaust temperature measurement responding to the same change in inlet temperature. Negative feedback then dominates in the steady state, but the response of the exhaust temperature measurement is delayed by the dryer. A compensating lag $f(t)$ is shown inserted in the set-point loop to prevent positive feedback from dominating in the short term, which could cause cycling. Lag time can be safely set equal to the integral time of the outlet-air temperature controller.

If product moisture is measured offline, analytical results can be used to adjust K and T_b manually. If an online analyzer is used, the analyzer controller would be most effective in adjusting the bias T_b , as is done in the figure.

While a rotary dryer is shown, commonly used for grains and minerals, this control system has been successfully applied to fluid-bed drying of plastic pellets, air-lift drying of wood fibers, and spray drying of milk solids. The air may be steam-heated as shown or heated by direct combustion of fuel, provided that a representative measurement of inlet air temperature can be made. If it cannot, then evaporative load can be inferred from a measurement of fuel flow, which then would replace ΔT in the set-point calculation.

If the feed flows countercurrent to the air, as is the case when drying granulated sugar, the exhaust temperature does not respond to variations in product moisture. For these dryers, the moisture in the product can better be regulated by controlling its temperature at the point of discharge. Conveyor-type dryers are usually divided into a number of zones, each separately heated with recirculation of air, which raises its wet-bulb temperature. Only the last two zones may require indexing of exhaust air temperature as a function of ΔT .

Batch drying, used on small lots such as pharmaceuticals, begins operation by blowing air at constant inlet temperature through saturated product in constant-rate drying, where ΔT is constant at its maximum value ΔT_c . When product moisture reaches the point where falling-rate drying begins, the exhaust temperature begins to rise. The desired product moisture will be reached at a corresponding exhaust

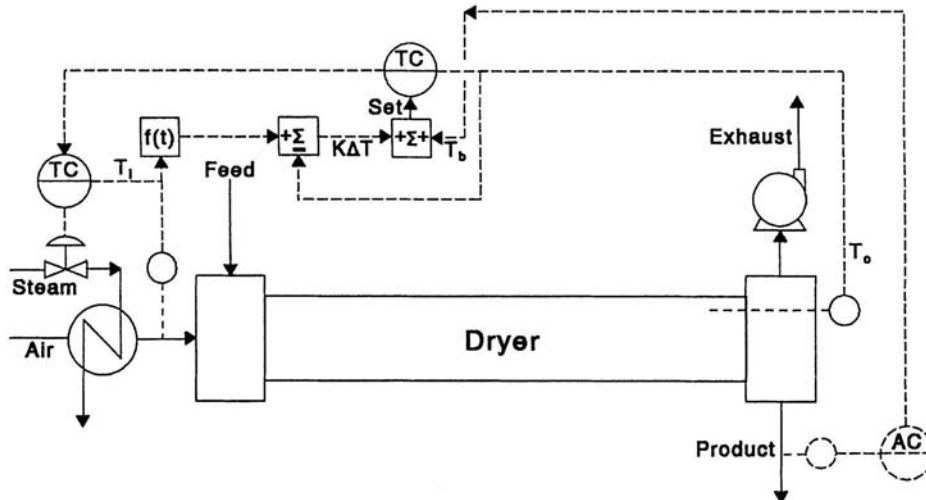


FIG. 8-57 Product moisture from a cocurrent dryer can be regulated through temperature control indexed to heat load.

temperature T_f , which is related to the temperature T_c observed during constant-rate drying, as well as to ΔT_c :

$$T_f = T_c + K \Delta T_c \quad (8-91)$$

The control system requires that the values of T_c and ΔT_c observed during the first minutes of operation be stored as the basis for the above calculation of endpoint. When the exhaust temperature then reaches

the calculated value of T_f , drying is terminated. Coefficient K can be estimated from models, but requires adjustment online to reach product specifications repeatedly. Products having different moisture specifications or particle size will require different settings of K , but the system does compensate for variations in feed moisture, batch size, air moisture, and inlet temperature. Some exhaust air may be recirculated to control the dew point of the inlet air, thereby conserving energy toward the end of the batch and when the ambient air is especially dry.

BATCH PROCESS CONTROL

GENERAL REFERENCES: Fisher, *Batch Control Systems: Design, Application, and Implementation*, ISA, Research Triangle Park, N.C., 1990. Rosenof and Ghosh, *Batch Process Automation*, Van Nostrand Reinhold, New York, 1987.

BATCH VERSUS CONTINUOUS PROCESSES

When one is categorizing process plants, the following two extremes can be identified:

1. *Commodity plants.* These plants are custom-designed to produce large amounts of a single product (or a primary product plus one or more secondary products). An example is a chlorine plant, where the primary product is chlorine and the secondary products are hydrogen and sodium hydroxide. Usually the margins (product value less manufacturing costs) for the products from commodity plants are small, so the plants must be designed and operated for best possible efficiencies. Although a few are batch, most commodity plants are continuous. Factors such as energy costs are life-and-death issues for such plants.

2. *Specialty plants.* These plants are capable of producing small amounts of a variety of products. Such plants are common in fine chemicals, pharmaceuticals, foods, and so on. In specialty plants, the margins are usually high, so factors such as energy costs are important but not life-and-death issues. As the production amounts are relatively small, it is not economically feasible to dedicate processing equipment to the manufacture of only one product. Instead, batch processing is utilized so that several products (perhaps hundreds) can be manufactured with the same process equipment. The key issue in such plants is to manufacture consistently each product in accordance with its specifications.

The above two categories represent the extremes in process configurations. The term *semibatch* designates plants in which some processing is continuous but other processing is batch. Even processes that are considered to be continuous can have a modest amount of batch processing. For example, the reformer unit within a refinery is thought of as a continuous process, but the catalyst regeneration is normally a batch process.

In a continuous process, the conditions within the process are largely the same from one day to the next. Variations in feed composition, plant utilities (e.g., cooling water temperature), catalyst activities, and other variables occur, but normally these changes either are about an average (e.g., feed compositions) or exhibit a gradual change over an extended period (e.g., catalyst activities). Summary data such as hourly averages, daily averages, and the like are meaningful in a continuous process.

In a batch process, the conditions within the process are continually changing. The technology for making a given product is contained in the product recipe that is specific to that product. Such recipes normally state the following:

1. *Raw material amounts.* This is the stuff needed to make the product.

2. *Processing instructions.* This is what must be done with the stuff to make the desired product.

This concept of a recipe is quite consistent with the recipes found in cookbooks. Sometimes the term *recipe* is used to designate only the raw material amounts and other parameters to be used in manufacturing a batch. Although appropriate for some batch processes, this concept is far too restrictive for others. For some products, the differ-

ences from one product to the next are largely physical as opposed to chemical. For such products, the processing instructions are especially important. The term *formula* is more appropriate for the raw material amounts and other parameters, with *recipe* designating the formula and the processing instructions. The above concept of a recipe permits the following three different categories of batch processes to be identified:

1. *Cyclical batch.* Both the formula and the processing instructions are the same from batch to batch. Batch operations within processes that are primarily continuous often fall into this category. The catalyst regenerator within a reformer unit is a cyclical batch process.

2. *Multigrade.* The processing instructions are the same from batch to batch, but the formula can be changed to produce modest variations in the product. In a batch PVC plant, the different grades of PVC are manufactured by changing the formula. In a batch pulp digester, the processing of each batch or cook is the same, but at the start of each cook, the process operator is permitted to change the formula values for chemical-to-wood ratios, cook time, cook temperature, and so on.

3. *Flexible batch.* Both the formula and the processing instructions can change from batch to batch. Emulsion polymerization reactors are a good example of a flexible batch facility. The recipe for each product must detail both the raw materials required and how conditions within the reactor must be sequenced to make the desired product.

Of these, the flexible batch is by far the most difficult to automate and requires a far more sophisticated control system than either the cyclical batch or the multigrade batch facility.

Batches and Recipes Each batch of product is manufactured in accordance with a product recipe, which contains all information (formula and processing instructions) required to make a batch of the product (see Fig. 8-58). For each batch of product, there will be one and only one product recipe. However, a given product recipe is normally used to make several batches of product. To uniquely identify a batch of product, each batch is assigned a unique identifier called the batch ID. Most companies adopt a convention for generating the batch ID, but this convention varies from one company to the next. In most batch facilities, more than one batch of product will be in some stage of production at any given time. The batches in progress may or may not be using the same recipe. The maximum number of batches that can be in progress at any given time is a function of the equipment configuration for the plant.

The existence of multiple batches in progress at a given time presents numerous opportunities for the process operator to make errors, such as charging a material to the wrong batch. Charging a material to the wrong batch is almost always detrimental to the batch to which the material is incorrectly charged. Unless this error is recognized quickly so that the proper charge can be made, the error is also detrimental to the batch to which the charge was supposed to have been made. Such errors usually lead to an off-specification batch, but the consequences could be more serious and could result in a hazardous condition.

Recipe management refers to the assumption of such duties by the control system. Each batch of product is tracked throughout its production, which may involve multiple processing operations on various pieces of processing equipment. Recipe management ensures that all actions specified in the product recipe are performed on each batch of product made in accordance with that recipe. As the batch proceeds from one piece of processing equipment to the next, recipe management

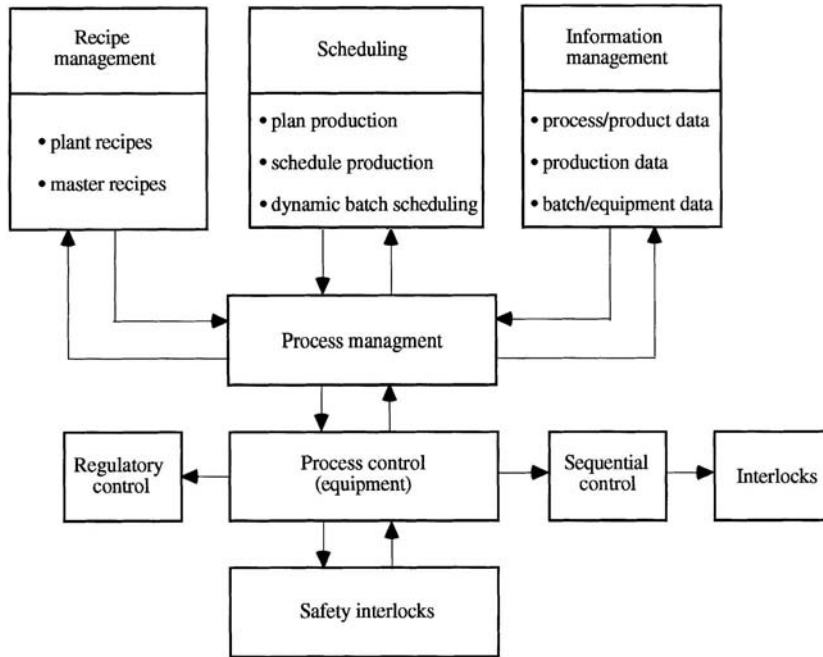


FIG. 8-58 Batch control overview.

is also responsible for ensuring that the proper type of process equipment is used and that this processing equipment is not currently in use by another batch.

By assuming such responsibilities, the control system greatly reduces the incidences where operator error results in off-specification batches. Such a reduction in error is essential to implement just-in-time production practices, where each batch of product is manufactured at the last possible moment. When a batch (or batches) is made today for shipment by overnight truck, there is insufficient time for producing another batch to make up for an off-specification batch.

Routing and Production Monitoring In some facilities, batches are individually scheduled. However, in most facilities, production is scheduled by product runs (also called process orders), where a run is the production of a stated quantity of a given product. From the stated quantity and the standard yield of each batch, the number of batches can be determined. As this is normally more than one batch of product, a production run is normally a sequence of some number of batches of the same product.

In executing a production run, the following issues must be addressed (see Fig. 8-58):

1. *Processing equipment must be dedicated to making the run.* More than one run is normally in progress at a given time. The maximum number of runs simultaneously in progress depends on the equipment configuration of the plant. Routing involves determining which processing equipment will be used for each production run.

2. *Raw material must be utilized.* When a production run is scheduled, the necessary raw materials must be allocated to the production run. As the individual batches proceed, the consumption of raw materials must be monitored for consistency with the allocation of raw materials to the production run.

3. *The production quantity for the run must be achieved by executing the appropriate number of batches.* The number of batches is determined from a standard yield for each batch. However, some batches may achieve yields higher than the standard yield, but other

batches may achieve yields lower than the standard yield. The actual yields from each batch must be monitored, and significant deviations from the expected yields must be communicated to those responsible for scheduling production.

The last two activities are key components of production monitoring, although production monitoring may also involve other activities such as tracking equipment utilization.

Production Scheduling In this regard, it is important to distinguish between scheduling runs (sometimes called long-term scheduling) and assigning equipment to runs (sometimes called routing or short-term scheduling). As used here production scheduling refers to scheduling runs and is usually a corporate-level as opposed to a plant-level function. Short-term scheduling or routing was previously discussed and is implemented at the plant level. The long-term scheduling is basically a material resources planning (MRP) activity involving the following:

1. *Forecasting.* Orders for long-delivery raw materials are issued at the corporate level based on the forecast for the demand for products. The current inventory of such raw materials is also maintained at the corporate level. This constitutes the resources from which products can be manufactured. Functions of this type are now incorporated into supply chain management.

2. *Orders for products.* Orders are normally received at the corporate level and then assigned to individual plants for production and shipment. Although the scheduling of some products is based on required product inventory levels, scheduling based on orders and shipping directly to the customer (usually referred to as just-in-time) avoids the costs associated with maintaining product inventories.

3. *Plant locations and capacities.* While producing a product at the nearest plant usually lowers transportation costs, plant capacity limitations sometimes dictate otherwise. Any company competing in the world economy needs the flexibility to accept orders on a worldwide basis and then assign them to individual plants to be filled. Such a function is logically implemented within the corporate-level information technology framework.

BATCH AUTOMATION FUNCTIONS

Automating a batch facility requires a spectrum of functions.

Interlocks Some of these are provided for safety and are properly called safety interlocks. However, others are provided to avoid mistakes in processing the batch. When safety is not involved, terms such as *permissives* and *process actions* are sometimes used in lieu of interlocks. Some understand the term *interlock* to have a connection to safety (interlock will be subsequently defined as a protective response initiated on the detection of a process hazard).

Discrete Device States Discrete devices such as two-position valves can be driven to either of two possible states. Such devices can be optionally outfitted with limit switches that indicate the state of the device. For two-position valves, the following combinations are possible:

1. No limit switches
2. One limit switch on the closed position
3. One limit switch on the open position
4. Two limit switches

In process control terminology, the discrete device driver is the software routine that generates the output to a discrete device such as a valve and also monitors the state feedback information to ascertain that the discrete device actually attains the desired state. Given the variety of discrete devices used in batch facilities, this logic must include a variety of capabilities. For example, valves do not instantly change states; instead each valve exhibits a travel time for the change from one state to another. To accommodate this characteristic of the field device, the processing logic within the discrete device driver must provide for a user-specified transition time for each field device. When equipped with limit switches, the potential states for a valve are as follows:

1. *Open*. The valve has been commanded to open, and the limit switch inputs are consistent with the open state.
2. *Closed*. The valve has been commanded to close, and the limit switch inputs are consistent with the closed state.
3. *Transition*. This is a temporary state that is only possible after the valve has been commanded to change state. The limit switch inputs are not consistent with the commanded state, but the transition time has not expired.

4. *Invalid*. The transition time has expired, and the limit switch inputs are not consistent with the commanded state for the valve.

The invalid state is an abnormal condition that is generally handled in a manner similar to process alarms. The transition state is not considered to be an abnormal state but may be implemented in either of the following ways:

1. *Drive and wait*. Further actions are delayed until the device attains its commanded state.
2. *Drive and proceed*. Further actions are initiated while the device is in the transition state.

The latter is generally necessary for devices with long travel times, such as flush-fitting reactor discharge valves that are motor-driven. Closing of such valves is normally done via drive and wait; however, drive and proceed is usually appropriate when opening the valve. Although two-state devices are most common, the need occasionally arises for devices with three or more states. For example, an agitator may be on high speed, on slow speed, or off.

Process States Batch processing usually involves imposing the proper sequence of states on the process. For example, a simple blending sequence might be as follows:

1. Transfer specified amount of material from tank A to tank R. The process state is "transfer from A."
2. Transfer specified amount of material from tank B to tank R. The process state is "transfer from B."
3. Agitate for specified time. The process state is "agitate without cooling."
4. Cool (with agitation) to specified target temperature. The process state is "agitate with cooling."

For each process state, the various discrete devices are expected to be in a specified device state. For process state "transfer from A," the device states might be as follows:

1. Tank A discharge valve: open
2. Tank R inlet valve: open

3. Tank A transfer pump: running
4. Tank R agitator: off
5. Tank R cooling valve: closed

For many batch processes, process state representations are a very convenient mechanism for representing the batch logic. A grid or table can be constructed, with the process states as rows and the discrete device states as columns (or vice versa). For each process state, the state of every discrete device is specified to be one of the following:

1. Device state 0, which may be valve closed, agitator off, and so on
2. Device state 1, which may be valve open, agitator on, and so on
3. No change or don't care

This representation is easily understandable by those knowledgeable about the process technology and is a convenient mechanism for conveying the process requirements to the control engineers responsible for implementing the batch logic.

Many batch software packages also recognize process states. A configuration tool is provided to define a process state. With such a mechanism, the batch logic does not need to drive individual devices but can simply command that the desired process state be achieved. The system software then drives the discrete devices to the device states required for the target process state. This normally includes the following:

1. Generating the necessary commands to drive each device to its proper state.
2. Monitoring the transition status of each device to determine when all devices have attained their proper states.
3. Continuing to monitor the state of each device to ensure that the devices remain in their proper states. Should any discrete device not remain in its target state, failure logic must be initiated.

Regulatory Control For most batch processes, the discrete logic requirements overshadow the continuous control requirements. For many batch processes, the continuous control can be provided by simple loops for flow, pressure, level, and temperature. However, very sophisticated advanced control techniques are occasionally applied. As temperature control is especially critical in reactors, the simple feedback approach is replaced by model-based strategies that rival, if not exceed, the sophistication of advanced control loops in continuous plants.

In some installations, alternative approaches for regulatory control may be required. Where a variety of products are manufactured, the reactor may be equipped with alternative heat removal capabilities, including the following:

1. Jacket filled with cooling water. Most such jackets are once-through, but some are recirculating.
2. Heat exchanger in a pump-around loop.
3. Reflux condenser.

The heat removal capability to be used usually depends on the product being manufactured. Therefore, regulatory loops must be configured for each possible option, and sometimes for certain combinations of the possible options. These loops are enabled and disabled depending on the product being manufactured.

The interface between continuous controls and sequence logic (discussed shortly) is also important. For example, a feed might be metered into a reactor at a variable rate, depending on another feed or possibly on reactor temperature. However, the product recipe calls for a specified quantity of this feed. The flow must be totaled (i.e., integrated), and when the flow total attains a specified value, the feed must be terminated. The sequence logic must have access to operational parameters such as controller modes. That is, the sequence logic must be able to switch a controller to manual, automatic, or cascade. Furthermore, the sequence logic must be able to force the controller output to a specified value.

Sequence Logic Sequence logic must not be confused with discrete logic. Discrete logic is especially suitable for interlocks or permissives; e.g., the reactor discharge valve must be closed for the feed valve to be opened. Sequence logic is used to force the process to attain the proper sequence of states. For example, a feed preparation might be to first charge A, then charge B, next mix, and finally cool. Although discrete logic can be used to implement sequence logic, other alternatives are often more attractive.

Sequence logic is often, but not necessarily, coupled with the concept of a process state. Basically, the sequence logic determines when the process should proceed from the current state to the next and sometimes what the next state should be.

Sequence logic must encompass both normal and abnormal process operations. Thus, sequence logic is often viewed as consisting of two distinct but related parts:

1. *Normal logic.* This sequence logic provides for the normal or expected progression from one process state to another.
2. *Failure logic.* This logic provides for responding to abnormal conditions, such as equipment failures.

Of these, the failure logic can easily be the most demanding. The simplest approach is to stop or hold on any abnormal condition and let the process operator sort things out. However, this is not always acceptable. Some failures lead to hazardous conditions that require immediate action; waiting for the operator to decide what to do is not acceptable. The appropriate response to such situations is best determined in conjunction with the process hazards analysis.

No single approach has evolved as the preferred way to implement sequence logic. The approaches utilized include the following:

1. *Discrete logic.* Although sequence logic is different from discrete logic, sequence logic can be implemented using discrete logic capabilities. Simple sequences are commonly implemented as ladder diagrams in programmable logic controllers (PLCs). Sequence logic can also be implemented using the boolean logic functions provided by a distributed control system (DCS), although this approach is now infrequently pursued.

2. *Programming languages.* Traditional procedural languages do not provide the necessary constructs for implementing sequence logic. This necessitates one of the following:

a. *Special languages.* The necessary extensions for sequence logic are provided by extending the syntax of the programming language. This is the most common approach within distributed control systems. The early implementations used BASIC as the starting point for the extensions; the later implementations used C as the starting point. A major problem with this approach is portability, especially from one manufacturer to the next but sometimes from one product version to the next within the same manufacturer's product line.

b. *Subroutine or function libraries.* The facilities for sequence logic are provided via subroutines or functions that can be referenced from programs written in FORTRAN or C. This requires a general-purpose program development environment and excellent facilities to trap the inevitable errors in such programs. Operating systems with such capabilities have long been available on the larger computers, but not for the microprocessors utilized within DCSs. However, such operating systems are becoming more common within DCSs.

3. *State machines.* This technology is commonly applied within the discrete manufacturing industries. However, its migration to process batch applications has been limited.

4. *Graphical implementations.* For sequence logic, the flowchart traditionally used to represent the logic of computer programs must be extended to provide parallel execution paths. Such extensions have been implemented in a graphical representation generally referred to as a sequential function chart, which is a derivative of an earlier technology known as Grafset. As process engineers have demonstrated a strong dislike for ladder logic, most PLC manufacturers now provide sequential function charts either in addition to or as an alternative to ladder logic. Many DCS manufacturers also provide sequential function charts either in addition to or as an alternative to special sequence languages.

INDUSTRIAL APPLICATIONS

An industrial example requiring simple sequence logic is the effluent tank with two sump pumps illustrated in Fig. 8-59. There are two sump pumps, A and B. The tank is equipped with three level switches, one for low level (LL), one for high level (LH), and one for high-high level (LHH). All level switches actuate on rising level. The logic is to be as follows:

1. When level switch LH actuates, start one sump pump. This must alternate between the sump pumps. If pump A is started on this occasion, then pump B must be started on the next occasion.

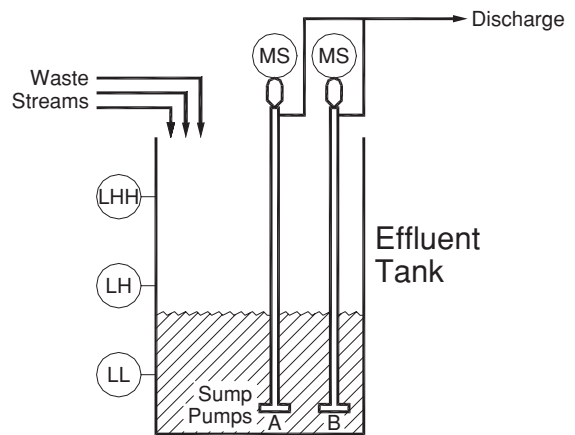


FIG. 8-59 Effluent tank process.

2. When level switch LHH actuates, start the other sump pump.
3. When level switch LL deactuates, stop all sump pumps.

Once a sump pump is started, it is not stopped until level switch LL deactuates. With this logic, one, both, or no sump pump may be running when the level is between LL and LH. Either one or both sump pumps may be running when the level is between LH and LHH.

Figure 8-60a presents the ladder logic implementation of the sequence logic. Ladder diagrams were originally developed for representing hardwired logic, but are now widely used in PLCs. The vertical bar on the left provides the source of power; the vertical bar on the right is ground. If a coil is connected between the power source and ground, the coil will be energized. If a circuit consisting of a set of contacts is inserted between the power source and the coil, the coil will be energized only if power can flow through the circuit. This will depend on the configuration of the circuit and the states of the contacts within the circuit. Ladder diagrams are constructed as rungs, with each rung consisting of a circuit of contacts and an output coil.

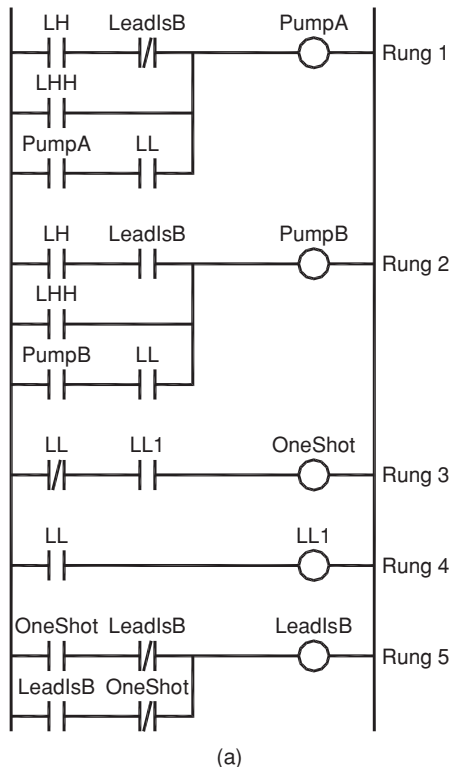
Contacts are represented as vertical bars. A vertical bar represents a normally open contact; power flows through this contact only if the device with which the contact is associated is actuated (energized). Vertical bars separated by a slash represent a normally closed contact; power flows through this contact only if the device with which the contact is associated is not actuated. The level switches actuate on rising level. If the vessel level is below the location of the switch, the normally open contact is open and the normally closed contact is closed. If the level is above the location of the switch, the normally closed contact is closed and the normally open contact is open.

The first rung in Fig. 8-60a is for pump A. It will run if one (or more) of the following conditions is true:

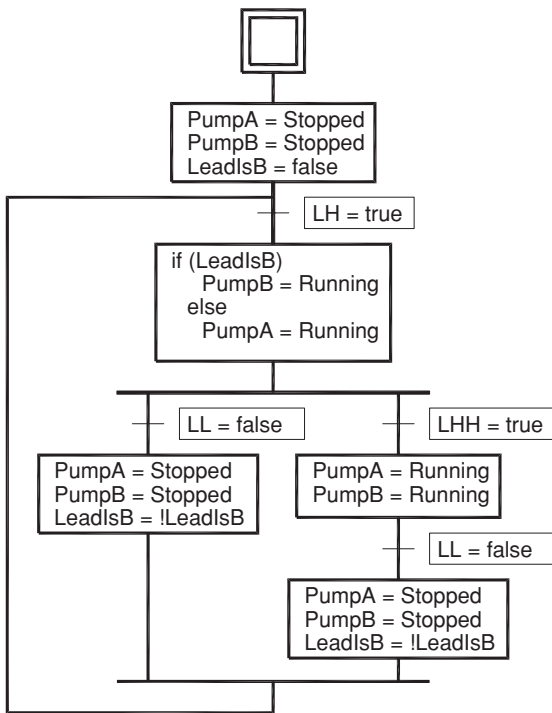
1. Level is above LH and pump A is the lead pump. A coil (designated as LeadIsB) will be subsequently provided to designate the pump to be started next (called the lead pump). If this coil is energized, pump B is the lead pump. Hence, pump A is to be started at LH if this coil is not energized, hence the use of the normally closed contact on coil LeadIsB in the rung of ladder logic for pump A.
2. Level is above LHH.
3. Pump A is running and the level is above LL.

The second rung is an almost identical circuit for pump B. The difference is the use of the normally open contact on the coil LeadIsB.

When implemented as hardwired logic, ladder diagrams are truly parallel logic; i.e., all circuits are active at all instants of time. But when ladder diagrams are implemented in PLCs, the behavior is slightly different. The ladder logic is scanned very rapidly (on the order of 100 times per second), which gives the appearance of parallel logic. But within a scan of ladder logic, the rungs are executed sequentially. This



(a)



(b)

FIG. 8-60 (a) Ladder logic. (b) Sequence logic for effluent tank sump pumps.

permits constructs within ladder logic for PLCs that make no sense in hardwired circuits.

One such construct is for a “one-shot.” Some PLCs provide this as a built-in function, but here it will be presented in terms of separate components. The one-shot is generated by the third rung of ladder logic in Fig. 8-60a. But first examine the fourth rung. The input LL drives the output coil LL1. This coil provides the state of level switch LL on the previous scan of ladder logic. This is used in the third rung to produce the one-shot. Output coil OneShot is energized if

1. LL is not actuated on this scan of ladder logic (note the use of the normally closed contact for LL)
2. LL was actuated on the previous scan of ladder logic (note the use of the normally open contact for LL1)

When LL deactuates, coil OneShot is energized for one scan of ladder logic. OneShot does not energize when LL actuates (a slight modification of the circuit would give a one-shot when LL actuates).

The one-shot is used in the fifth rung of ladder logic to toggle the lead pump. The output coil LeadIsB is energized provided that

1. LeadIsB is energized and OneShot is not energized. Once LeadIsB is energized, it remains energized until the next “firing” of the one-shot.
2. LeadIsB is not energized and OneShot is energized. This causes coil LeadIsB to change states each time the one-shot fires.

Ladder diagrams are ideally suited for representing discrete logic, such as required for interlocks. Sequence logic can be implemented via ladder logic, but usually with some tricks or gimmicks (the one-shot in Fig. 8-60a is such a gimmick). These are well known to those “skilled in the art” of PLC programming. But to others, they can be quite confusing.

Figure 8-60b provides a sequential function chart for the pumps. Sequential function charts consist of steps and transitions. A step consists of actions to be performed, as represented by statements. A transition consists of a logical expression. As long as the logical expression is false, the sequence logic remains at the transition. When the logical expression is true, the sequence logic proceeds to the step following the transition.

The basic constructs of sequential function charts are presented in Fig. 8-61. The basic construct of a sequential function chart is the step-transition-step. But also note the constructs for OR and AND. At the divergent OR, the logic proceeds on only one of the possible paths, specifically, the one whose transition is the first to attain the true condition. At the divergent AND, the logic proceeds on all paths simultaneously, and all must complete to proceed beyond the convergent AND. This enables sequential function charts to provide parallel logic.

In the sequential function chart in Fig. 8-60b for the pumps, the logic is initiated with both pumps stopped and pump A as the lead pump. When LH actuates, the lead pump is started. A divergent OR is used to create two paths:

1. If LL deactuates, both pumps are stopped and the lead pump is swapped.
2. If LHH actuates, both pumps are started (one is already running). Both remain running until LL deactuates, at which time both are stopped. The logic then loops to the transition for LH actuating.

Although not illustrated here, programming languages (either custom sequence languages or traditional languages extended by libraries of real-time functions) are a viable alternative for implementing the logic for the pumps. Graphical constructs such as ladder logic and sequential function charts are appealing to those uncomfortable with traditional programming languages. But in reality, these are programming methodologies.

BATCH REACTOR CONTROL

The reactors in flexible batch chemical plants usually present challenges. Many reactors have multiple mechanisms for heating and/or cooling. The reactor in Fig. 8-62 has three mechanisms:

1. Heat with steam.
2. Cool with cooling tower water.
3. Cool with chilled water.

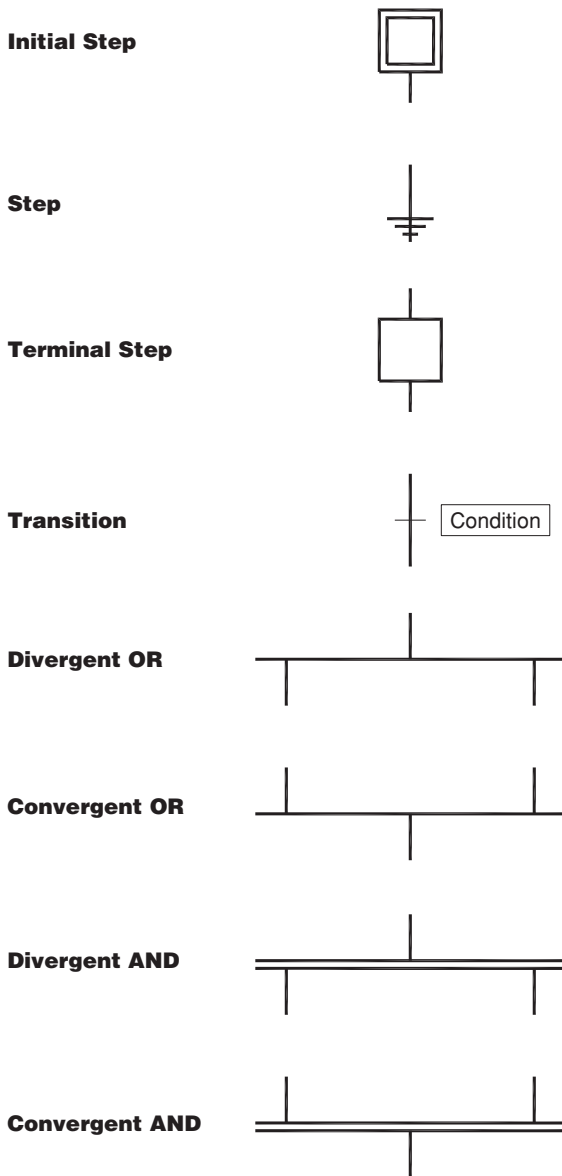


FIG. 8-61 Elements of sequential function charts.

Sometimes glycol is an option; occasionally liquid nitrogen is used to achieve even lower temperatures. Some jacket configurations require sequences for switching between the various modes for heating and cooling (the jacket has to be drained or depressurized before another medium can be admitted).

The reactor in Fig. 8-62 has three mechanisms for pressure control:

1. Vacuum
2. Atmospheric (using the vent and inert valves)
3. Pressure

Some reactors are equipped with multiple vacuum pumps, with different operating modes for moderate vacuum versus high vacuum. Sequence logic is usually required to start vacuum pumps and establish vacuum.

With three options for heating/cooling and three options for pressure, the reactor in Fig. 8-62 has nine combinations of operating modes.

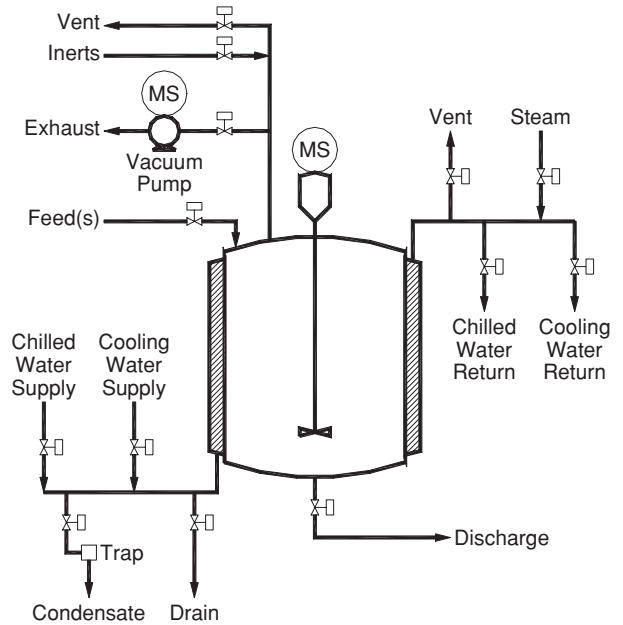


FIG. 8-62 Chemical reactor schematic.

In practice, this is actually a low number. This number increases with features such as

1. Recirculations or pump-arounds containing a heater and/or cooler
2. Reflux condensers that can be operated at total reflux (providing only cooling) or such that some component is removed from the reacting system

These further increase the number of possible combinations. Some combinations may not make sense, may not be used in current production operations, or otherwise can be eliminated. However, the net number of combinations that must be supported tends to be large.

The order in which the systems are activated usually depends on the product being manufactured. Sometimes heating/cooling and pressure control are established simultaneously; sometimes heating/cooling is established first and then pressure control, and sometimes pressure control is established first and then heating/cooling. One has to be very careful when imposing restrictions. Suppose no current products establish pressure control first and then establish heating/cooling. But what about the next product to be introduced? After all, this is a flexible batch facility.

Such challenging applications for recipe management and sequence logic require a detailed analysis of the production equipment and the operations conducted within that production equipment. While applications such as the sump pumps in the effluent tank can be pursued without it, a structured approach is essential in flexible batch facilities.

BATCH PRODUCTION FACILITIES

Especially for flexible batch applications, the batch logic must be properly structured in order to be implemented and maintained in a reasonable manner. An underlying requirement is that the batch process equipment be properly structured. The following structure is appropriate for most batch production facilities.

Plant A plant is the collection of production facilities at a geographic site. The production facilities at a site normally share warehousing, utilities, and the like.

Equipment Suite An equipment suite is the collection of equipment available for producing a group of products. Normally, this

group of products is similar in certain respects. For example, they might all be manufactured from the same major raw materials. Within the equipment suite, material transfer and metering capabilities are available for these raw materials. The equipment suite contains all the necessary types of processing equipment (reactors, separators, and so on) required to convert the raw materials to salable products. A plant may consist of only one suite of equipment, but large plants usually contain multiple equipment suites.

Process Unit or Batch Unit A process unit is a collection of processing equipment that can, at least at certain times, be operated in a manner completely independent of the remainder of the plant. A process unit normally provides a specific function in the production of a batch of product. For example, a process unit might be a reactor complete with all associated equipment (jacket, recirculation pump, reflux condenser, and so on). However, each feed preparation tank is usually a separate process unit. With this separation, preparation of the feed for the next batch can be started as soon as the feed tank is emptied for the current batch.

All but the very simplest equipment suites contain multiple process units. The minimum number of process units is one for each type of processing equipment required to make a batch of product. However, many equipment suites contain multiple process units of each type. In such equipment suites, multiple batches and multiple production runs can be in progress at a given time.

Item of Equipment An item of equipment is a hardware item that performs a specific purpose. Examples are pumps, heat exchangers, agitators, and the like. A process unit could consist of a single item of equipment, but most process units consist of several items of equipment that must be operated in harmony to achieve the function expected of the process unit.

Device A device is the smallest element of interest to batch logic. Examples of devices include measurement devices and actuators.

STRUCTURED BATCH LOGIC

Flexible batch applications must be pursued by using a structured approach to batch logic. In such applications, the same processing equipment is used to make a variety of products. In most facilities, little or no proprietary technology is associated with the equipment itself; the proprietary technology is how this equipment is used to produce each of the products.

The primary objective of the structured approach is to separate cleanly the following two aspects of the batch logic:

Product Technology Basically, this encompasses the product technology, such as how to mix certain molecules to make other molecules. This technology ultimately determines the chemical and physical properties of the final product. The product recipe is the principal source for the product technology.

Process Technology The process equipment permits certain processing operations (e.g., heat to a specified temperature) to be undertaken. Each processing operation will involve certain actions (e.g., opening appropriate valves).

The need to keep these two aspects separated is best illustrated by a situation where the same product is to be made at different plants. While it is possible that the processing equipment at the two plants is identical, this is rarely the case. Suppose one plant uses steam for heating its vessels, but the other uses a hot oil system as the source of heat. When a product recipe requires that material be heated to a specified temperature, each plant can accomplish this objective, but each will go about it in quite different ways. The ideal case for a product recipe is as follows:

1. It contains all the product technology required to make a product.
2. It contains no equipment-dependent information, i.e., no process technology.

In the previous example, such a recipe would simply state that the product must be heated to a specified temperature. Whether heating is undertaken with steam or hot oil is irrelevant to the product technology. By restricting the product recipe to a given product technology, the same product recipe can be used to make products at

different sites. At a given site, the specific approach to be used to heat a vessel is important. The traditional approach is for an engineer at each site to expand the product recipe into a document that explains in detail how the product is to be made at the specific site. This document goes by various names, although standard operating procedure or SOP is a common one. Depending on the level of detail to which it is written, the SOP could specify exactly which valves must be opened to heat the contents of a vessel. Thus, the SOP is site-dependent and contains both product technology and process technology.

In structuring the logic for a flexible batch application, the following organization permits product technology to be cleanly separated from process technology:

- A recipe consists of a formula and one or more processing operations. Ideally, only product technology is contained in a recipe.
- A processing operation consists of one or more phases. Ideally, only product technology is contained in a processing operation.
- A phase consists of one or more actions. Ideally, only process technology is contained in a phase.

In this structure, the recipe and processing operations would be the same at each site that manufactures the product. However, the logic that comprises each phase would be specific to a given site. In the heating example from above, each site would require a phase to heat the contents of the vessel. However, the logic within the phase at one site would accomplish the heating by opening the appropriate steam valves, while the logic at the other site would accomplish the heating by opening the appropriate hot oil valves.

Usually the critical part of structuring batch logic is the definition of the phases. There are two ways to approach this:

1. Examine the recipes for the current products for commonality, and structure the phases to reflect this commonality.

2. Examine the processing equipment to determine what processing capabilities are possible, and write phases to accomplish each possible processing capability.

There is the additional philosophical issue of whether to have a large number of simple phases with few options each, or a small number of complex phases with numerous options. The issues are analogous to structuring a complex computer program into subprograms. Each possible alternative has advantages and disadvantages.

As the phase contains no product technology, the implementation of a phase must be undertaken by those familiar with the process equipment. Furthermore, they should undertake this on the basis that the result will be used to make a variety of products, not just those that are initially contemplated. The development of the phase logic must also encompass all equipment-related safety issues. The phase should accomplish a clearly defined objective, so the implementers should be able to thoroughly consider all relevant issues in accomplishing this objective. The phase logic is defined in detail, implemented in the control system, and then thoroughly tested. Except when the processing equipment is modified, future modifications to the phase should be infrequent. The result should be a very dependable module that can serve as a building block for batch logic.

Even for flexible batch applications, a comprehensive menu of phases should permit most new products to be implemented by using currently existing phases. By reusing existing phases, numerous advantages accrue:

1. The engineering effort to introduce a new recipe at a site is reduced.
2. The product is more likely to be on-spec the first time, thus avoiding the need to dispose of off-spec product.
3. The new product can be supplied to customers sooner, hopefully before competitors can supply the product.

There is also a distinct advantage in maintenance. When a problem with a phase is discovered and the phase logic is corrected, the correction is effectively implemented in all recipes that use the phase. If a change is implemented in the processing equipment, the affected phases must be modified accordingly and then thoroughly tested. These modifications are also effectively implemented in all recipes that use these phases.

PROCESS MEASUREMENTS

GENERAL REFERENCES: Baker, *Flow Measurement Handbook*, Cambridge University Press, New York, 2000. Connell, *Process Instrumentation Applications Manual*, McGraw-Hill, New York, 1966. Dakin, and Culshaw (eds), *Optical Fiber Sensors: Applications, Analysis, and Future Trends*, vol. IV, Artech House, Norwood, Mass., 1997. Dolenc, "Choose the Right Flow Meter," *Chem. Engr. Prog.*, **92**(1): 22, 1996. Johnson, *Process Control Instrumentation Technology*, 6th ed., Prentice-Hall, Upper Saddle River, N.J., 2000. Liptak (ed.), *Instrument Engineers Handbook*, 3d ed., vol. 1: *Process Measurement*, Chilton Books, Philadelphia, 2000. Nichols, *On-Line Process Analyzers*, Wiley, New York, 1988. Seborg, Edgar, and Mellichamp, *Process Dynamics and Control*, Wiley, New York, 2004. Soloman, *Sensors Handbook*, McGraw-Hill, New York, 1999. Spitzer, *Flow Measurement*, 2d ed., ISA, Research Triangle Park, N.C., 2001.

GENERAL CONSIDERATIONS

Process measurements encompass the application of the principles of metrology to the process in question. The objective is to obtain values for the current conditions within the process and to make this information available in a form usable by the control system, process operators, or management information systems. The term *measured variable* or *process variable* designates the process condition that is being determined.

Process measurements fall into two categories:

1. *Continuous measurements.* An example of a continuous measurement is a level measurement device that determines the liquid level in a tank (e.g., in meters).

2. *Discrete measurements.* An example of a discrete measurement is a level switch that indicates the presence or absence of liquid at the location at which the level switch is installed.

In continuous processes, most process control applications rely on continuous measurements. In batch processes, many of the process control applications utilize discrete as well as continuous measurements. In both types of processes, the safety interlocks and process interlocks rely largely on discrete measurements.

Continuous Measurements In most applications, continuous measurements provide more information than discrete measurements. Basically, discrete measurements involve a yes/no decision, whereas continuous measurements may entail considerable signal processing.

The components of a typical continuous measurement device are as follows:

1. *Sensor.* This component produces a signal that is related in a known manner to the process variable of interest. The sensors in use today are primarily of the electrical analog variety, and the signal is in the form of a voltage, a resistance, a capacitance, or some other directly measurable electrical quantity. Prior to the mid-1970s, instruments tended to use sensors whose signal was mechanical and thus compatible with pneumatic technology. Since that time, the fraction of sensors that are digital has grown considerably, often eliminating the need for analog-to-digital conversion.

2. *Signal processing.* The signal from a sensor is usually related in a nonlinear fashion to the process variable of interest. For the output of the measurement device to be linear with respect to the process variable of interest, linearization is required. Furthermore, the signal from the sensor might be affected by variables other than the process variable. In this case, additional variables must be sensed, and the signal from the sensor compensated to account for the other variables. For example, reference junction compensation is required for thermocouples (except when used for differential temperature measurements).

3. *Transmitter.* The measurement device output must be a signal that can be transmitted over some distance. Where electronic analog transmission is used, the low range on the transmitter output is 4 mA, and the upper range is 20 mA. Microprocessor-based transmitters (often referred to as smart transmitters) are usually capable of transmitting the measured variable digitally in engineering units.

Accuracy and Repeatability Definitions of terminology pertaining to process measurements can be obtained from standards available from the Instrumentation, Systems, and Automation Society

(ISA) and from the Scientific Apparatus Makers Association [now Measurement, Control, and Automation Association (MCAA)], both of which are updated periodically. An appreciation of accuracy and repeatability is especially important. Some applications depend on the accuracy of the instrument, but other applications depend on repeatability. Excellent accuracy implies excellent repeatability; however, an instrument can have poor accuracy but excellent repeatability. In some applications, this is acceptable, as discussed below.

Range and Span A continuous measurement device is expected to provide credible values of the measured value between a lower range and an upper range. The difference between the upper range and the lower range is the span of the measurement device. The maximum value for the upper range and the minimum value for the lower range depend on the principles on which the measurement device is based and on the design chosen by the manufacturer of the measurement device. If the measured variable is greater than the upper range or less than the lower range, the measured variable is said to be out of range or the measurement device is said to be overranged.

Accuracy Accuracy refers to the difference between the measured value and the true value of the measured variable. Unfortunately, the true value is never known, so in practice accuracy refers to the difference between the measured value and an accepted standard value for the measured variable.

Accuracy can be expressed in four ways:

1. As an absolute difference in the units of the measured variable
2. As a percent of the current reading
3. As a percent of the span of the measured variable
4. As a percent of the upper range of the span

For process measurements, accuracy as a percent of span is the most common.

Manufacturers of measurement devices always state the accuracy of the instrument. However, these statements always specify specific or reference conditions at which the measurement device will perform with the stated accuracy, with temperature and pressure most often appearing in the reference conditions. When the measurement device is applied at other conditions, the accuracy is affected. Manufacturers usually also provide some statements on how accuracy is affected when the conditions of use deviate from the referenced conditions in the statement of accuracy. Although appropriate calibration procedures can minimize some of these effects, rarely can they be totally eliminated. It is easily possible for such effects to cause a measurement device with a stated accuracy of 0.25 percent of span at reference conditions to ultimately provide measured values with accuracies of 1 percent or less. Microprocessor-based measurement devices usually provide better accuracy than do the traditional electronic measurement devices.

In practice, most attention is given to accuracy when the measured variable is the basis for billing, such as in custody transfer applications. However, whenever a measurement device provides data to any type of optimization strategy, accuracy is very important.

Repeatability Repeatability refers to the difference between the measurements when the process conditions are the same. This can also be viewed from the opposite perspective. If the measured values are the same, repeatability refers to the difference between the process conditions.

For regulatory control, repeatability is of major interest. The basic objective of regulatory control is to maintain uniform process operation. Suppose that on two different occasions, it is desired that the temperature in a vessel be 800°C. The regulatory control system takes appropriate actions to bring the measured variable to 800°C. The difference between the process conditions at these two times is determined by the repeatability of the measurement device.

In the use of temperature measurement for control of the separation in a distillation column, repeatability is crucial but accuracy is not. Composition control for the overhead product would be based on a measurement of the temperature on one of the trays in the rectifying section. A target would be provided for this temperature. However, at

periodic intervals, a sample of the overhead product is analyzed in the laboratory and the information is provided to the process operator. Should this analysis be outside acceptable limits, the operator would adjust the set point for the temperature. This procedure effectively compensates for an inaccurate temperature measurement; however, the success of this approach requires good repeatability from the temperature measurement.

Dynamics of Process Measurements Especially where the measurement device is incorporated into a closed-loop control configuration, dynamics are important. The dynamic characteristics depend on the nature of the measurement device, and on the nature of components associated with the measurement device (e.g., thermowells and sample conditioning equipment). The term *measurement system* designates the measurement device and its associated components.

The following dynamics are commonly exhibited by measurement systems:

- **Time constants.** Where there is a capacity and a throughput, the measurement device will exhibit a time constant. For example, any temperature measurement device has a thermal capacity (mass times heat capacity) and a heat flow term (heat-transfer coefficient and area). Both the temperature measurement device and its associated thermowell will exhibit behavior typical of time constants.
- **Dead time.** Probably the best example of a measurement device that exhibits pure dead time (time delay) is the chromatograph, because the analysis is not available for some time after a sample is injected. Additional dead time results from the transportation lag within the sample system. Even continuous analyzer installations can exhibit dead time from the sample system.
- **Underdamped.** Measurement devices with mechanical components often have a natural harmonic and can exhibit underdamped behavior. The displacer type of level measurement device is capable of such behavior.

While the manufacturers of measurement devices can supply some information on the dynamic characteristics of their devices, interpretation is often difficult. Measurement device dynamics are quoted on varying bases, such as rise time, time to 63 percent response, settling time, etc. Even where the time to 63 percent response is quoted, it might not be safe to assume that the measurement device exhibits first-order behavior.

Where the manufacturer of the measurement device does not supply the associated equipment (thermowells, sample conditioning equipment, etc.), the user must incorporate the characteristics of these components to obtain the dynamics of the measurement system. An additional complication is that most dynamic data are stated for configurations involving reference materials such as water and air. The nature of the process material will affect the dynamic characteristics. For example, a thermowell will exhibit different characteristics when immersed in a viscous organic emulsion than when immersed in water. It is often difficult to extrapolate the available data to process conditions of interest.

Similarly, it is often impossible, or at least very difficult, to experimentally determine the characteristics of a measurement system under the conditions where it is used. It is certainly possible to fill an emulsion polymerization reactor with water and determine the dynamic characteristics of the temperature measurement system. However, it is not possible to determine these characteristics when the reactor is filled with the emulsion under polymerization conditions.

The primary impact of unfavorable measurement dynamics is on the performance of closed-loop control systems. This explains why most control engineers are very concerned with minimizing measurement dynamics, even though the factors considered in dynamics are often subjective.

Selection Criteria The selection of a measurement device entails a number of considerations given below, some of which are almost entirely subjective.

1. **Measurement span.** The measurement span required for the measured variable must lie entirely within the instrument's envelope of performance.
2. **Performance.** Depending on the application, accuracy, repeatability, or perhaps some other measure of performance is appropriate.

Where closed-loop control is contemplated, speed of response must be included.

3. **Reliability.** Data available from the manufacturers can be expressed in various ways and at various reference conditions. Often, previous experience with the measurement device within the purchaser's organization is weighted most heavily.

4. **Materials of construction.** The instrument must withstand the process conditions to which it is exposed. This encompasses considerations such as operating temperatures, operating pressures, corrosion, and abrasion. For some applications, seals or purges may be necessary.

5. **Prior use.** For the first installation of a specific measurement device at a site, training of maintenance personnel and purchases of spare parts might be necessary.

6. **Potential for releasing process materials to the environment.** Fugitive emissions are receiving ever-increasing attention. Exposure considerations, both immediate and long-term, for maintenance personnel are especially important when the process fluid is either corrosive or toxic.

7. **Electrical classification.** Article 500 of the National Electric Code provides for the classification of the hazardous nature of the process area in which the measurement device will be installed. If the measurement device is not inherently compatible with this classification, suitable enclosures must be purchased and included in the installation costs.

8. **Physical access.** Subsequent to installation, maintenance personnel must have physical access to the measurement device for maintenance and calibration. If additional structural facilities are required, they must be included in the installation costs.

9. **Invasive or noninvasive.** The insertion of a probe can result in fouling problems and a need for maintenance. Probe location must be selected carefully for good accuracy and minimal fouling.

10. **Cost.** There are two aspects of the cost:

a. Initial purchase and installation (capital cost).

b. Recurring costs (operational expense). This encompasses instrument maintenance, instrument calibration, consumables (e.g., titrating solutions must be purchased for automatic titrators), and any other costs entailed in keeping the measurement device in service.

Calibration Calibration entails the adjustment of a measurement device so that the value from the measurement device agrees with the value from a standard. The International Standards Organization (ISO) has developed a number of standards specifically directed to calibration of measurement devices. Furthermore, compliance with the ISO 9000 standards requires that the working standard used to calibrate a measurement device be traceable to an internationally recognized standard such as those maintained by the National Institute of Standards and Technology (NIST).

Within most companies, the responsibility for calibrating measurement devices is delegated to a specific department. Often, this department may also be responsible for maintaining the measurement device. The specific calibration procedures depend on the type of measurement device. The frequency of calibration is normally predetermined, but earlier action may be dictated if the values from the measurement device become suspect.

Calibration of some measurement devices involves comparing the measured value with the value from the working standard. Pressure and differential pressure transmitters are calibrated in this manner. Calibration of analyzers normally involves using the measurement device to analyze a specially prepared sample whose composition is known. These and similar approaches can be applied to most measurement devices.

Flow is an important measurement whose calibration presents some challenges. When a flow measurement device is used in applications such as custody transfer, provision is made to pass a known flow through the meter. However, such a provision is costly and is not available for most in-process flowmeters. Without such a provision, a true calibration of the flow element itself is not possible. For orifice meters, calibration of the flowmeter normally involves calibration of the differential pressure transmitter, and the orifice plate is usually only inspected for deformation, abrasion, etc. Similarly, calibration of a magnetic flowmeter normally involves calibration of the voltage

TABLE 8-8 Online Measurement Options for Process Control

Temperature	Flow	Pressure	Level	Composition
Thermocouple	Orifice	Liquid column	Float-activated	Gas-liquid chromatography (GLC)
Resistance temperature detector (RTD)	Venturi	Elastic element	Chain gauge	Mass spectrometry (MS)
Filled-system thermometer	Rotameter	Bourdon tube	Lever	Magnetic resonance analysis (MRA)
Bimetal thermometer	Turbine	Bellow	Magnetically coupled	Infrared (IR) spectroscopy
Pyrometer	Vortex-shedding	Diaphragm	Head devices	Raman spectroscopy
Total radiation	Ultrasonic	Strain gauges	Bubble tube	Ultraviolet (uv) spectroscopy
Photoelectric	Magnetic	Piezoresistive transducers	Electrical (conductivity)	Thermal conductivity
Ratio	Thermal mass	Piezoelectric transducers	Sonic	Refractive index (RI)
Laser	Coriolis	Optical fiber	Laser	Capacitance probe
Surface acoustic wave	Target		Radiation	Surface acoustic wave
Semiconductor			Radar	Electrophoresis
				Electrochemical
				Paramagnetic
				Chemi/bioluminescence
				Tunable diode laser absorption

measurement circuitry, which is analogous to calibration of the differential pressure transmitter for an orifice meter.

In the next section we cover the major types of measurement devices used in the process industries, principally the “big five” measurements: temperature, flow rate, pressure, level, and composition, along with online physical property measurement techniques. Table 8-8 summarizes the different options under each of the principal measurements.

TEMPERATURE MEASUREMENTS

Measurement of the hotness or coldness of a body or fluid is commonplace in the process industries. Temperature-measuring devices utilize systems with properties that vary with temperature in a simple, reproducible manner and thus can be calibrated against known references (sometimes called secondary thermometers). The three dominant measurement devices used in automatic control are thermocouples, resistance thermometers, and pyrometers, and they are applicable over different temperature regimes.

Thermocouples Temperature measurements using thermocouples are based on the discovery by Seebeck in 1821 that an electric current flows in a continuous circuit of two different metallic wires if the two junctions are at different temperatures. The thermocouple may be represented diagrammatically as shown in Fig. 8-63. There A and B are the two metals, and T_1 and T_2 are the temperatures of the junctions. Let T_1 and T_2 be the reference junction (cold junction) and the measuring junction, respectively. If the thermoelectric current i flows in the direction indicated in Fig. 8-63, metal A is customarily referred to as thermoelectrically positive to metal B. Metal pairs used for thermocouples include platinum-rhodium (the most popular and accurate), chromel-alumel, copper-constantan, and iron-constantan. The thermal emf is a measure of the difference in temperature between T_2 and T_1 . In control systems the reference junction is usually located at the emf-measuring device. The reference junction may be held at constant temperature such as in an ice bath or a thermostated oven, or it may be at ambient temperature but electrically compen-

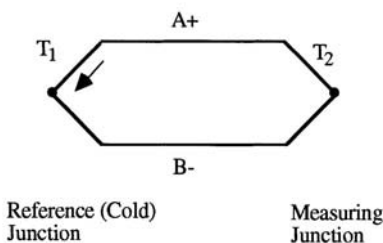


FIG. 8-63 Basic circuit of Seebeck effect.

sated (cold junction compensated circuit) so that it appears to be held at a constant temperature.

Resistance Thermometers The resistance thermometer depends upon the inherent characteristics of materials to change in electrical resistance when they undergo a change in temperature. Industrial resistance thermometers are usually constructed of platinum, copper, or nickel, and more recently semiconducting materials such as thermistors are being used. Basically, a resistance thermometer is an instrument for measuring electrical resistance that is calibrated in units of temperature instead of in units of resistance (typically ohms). Several common forms of bridge circuits are employed in industrial resistance thermometry, the most common being the Wheatstone bridge. A resistance thermometer detector (RTD) consists of a resistance conductor (metal) which generally shows an increase in resistance with temperature. The following equation represents the variation of resistance with temperature ($^{\circ}\text{C}$):

$$R_T = R_0(1 + a_1T + a_2T^2 + \dots + a_nT^n) \tag{8-92}$$

R_0 = resistance at 0°C

The temperature coefficient of resistance, α_T is expressed as

$$\alpha_T = \frac{1}{R_T} \frac{dR_T}{dT} \tag{8-93}$$

For most metals α_T is positive. For many pure metals, the coefficient is essentially constant and stable over large portions of their useful range. Typical resistance versus temperature curves for platinum, copper, and nickel are given in Fig. 8-64, with platinum usually the metal of choice. Platinum has a useful range of -200 to 800°C , while nickel (-80 to 320°C) and copper (-100 to 100°C) are more limited. Detailed resistance versus temperature tables are available from the National Institute of Standards and Technology (NIST) and suppliers of resistance thermometers. Table 8-9 gives recommended temperature measurement ranges for thermocouples and RTDs. Resistance thermometers are receiving increased usage because they are about 10 times more accurate than thermocouples.

Thermistors Thermistors are nonlinear temperature-dependent resistors, and normally only the materials with negative temperature coefficient of resistance (NTC type) are used. The resistance is related to temperature as

$$R_T = R_T \exp\left[\beta\left(\frac{1}{T} - \frac{1}{T_r}\right)\right] \tag{8-94}$$

where α_T is a reference temperature, which is generally 298 K. Thus

$$\alpha_T = \frac{1}{R_T} \frac{dR_T}{dT} \tag{8-95}$$

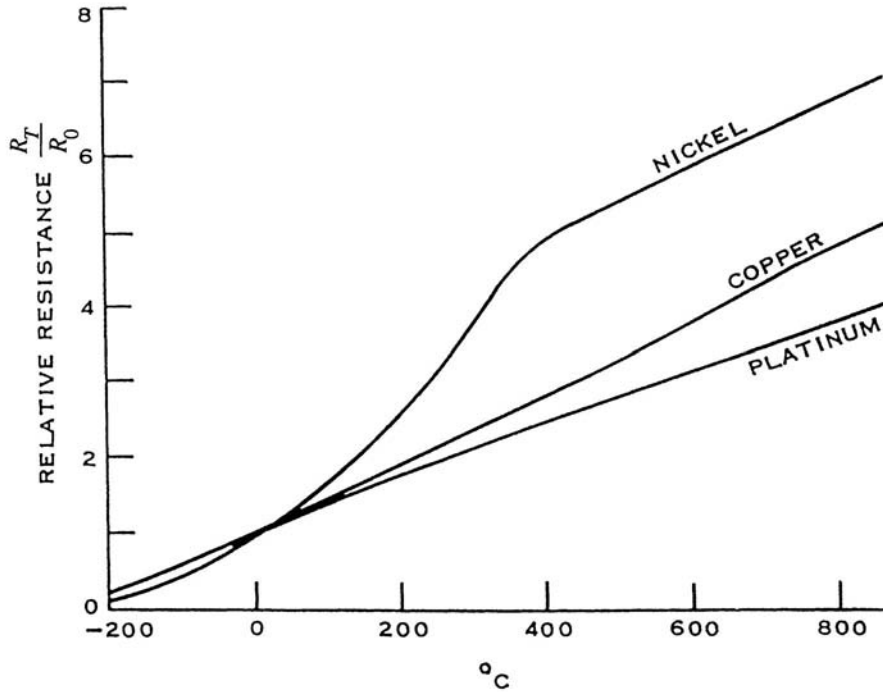


FIG. 8-64 Typical resistance thermometer curves for platinum, copper, and nickel wire, where R_T = resistance at temperature T and R_0 = resistance at 0°C .

The value of β is on the order of 4000, so at room temperature (298 K), $\alpha_T = -0.045$ for thermistor and 0.0035 for 100- Ω platinum RTD. Compared with RTDs, NTC-type thermistors are advantageous in that the detector dimension can be made small, resistance value is higher (less affected by the resistances of the connecting leads), and it has higher temperature sensitivity and low thermal inertia of the sensor. Disadvantages of thermistors to RTDs include nonlinear characteristics and low measuring temperature range.

Filled-System Thermometers The filled-system thermometer is designed to provide an indication of temperature some distance removed from the point of measurement. The measuring element (bulb) contains a gas or liquid that changes in volume, pressure, or vapor pressure with temperature. This change is communicated through a capillary tube to a Bourdon tube or other pressure- or volume-sensitive device. The Bourdon tube responds so as to provide a motion related to the bulb temperature. Those systems that respond to volume changes are completely filled with a liquid. Systems that respond to

pressure changes either are filled with a gas or are partially filled with a volatile liquid. Changes in gas or vapor pressure with changes in bulb temperatures are carried through the capillary to the Bourdon. The latter bulbs are sometimes constructed so that the capillary is filled with a nonvolatile liquid.

Fluid-filled bulbs deliver enough power to drive controller mechanisms and even directly actuate control valves. These devices are characterized by large thermal capacity, which sometimes leads to slow response, particularly when they are enclosed in a thermal well for process measurements. Filled-system thermometers are used extensively in industrial processes for a number of reasons. The simplicity of these devices allows rugged construction, minimizing the possibility of failure with a low level of maintenance, and inexpensive overall design of control equipment. In case of system failure, the entire unit must be replaced or repaired.

As they are normally used in the process industries, the sensitivity and percentage of span accuracy of these thermometers are generally the equal of those of other temperature-measuring instruments. Sensitivity and absolute accuracy are not the equal of those of short-span electrical instruments used in connection with resistance-thermometer bulbs. Also the maximum temperature is somewhat limited.

Bimetal Thermometers Thermostatic bimetal can be defined as a composite material made up of strips of two or more metals fastened together. This composite, because of the different expansion rates of its components, tends to change curvature when subjected to a change in temperature. With one end of a straight strip fixed, the other end deflects in proportion to the temperature change, the square of the length, and inversely as the thickness, throughout the linear portion of the deflection characteristic curve. If a bimetallic strip is wound into a helix or a spiral and one end is fixed, the other end will rotate when heat is applied. For a thermometer with uniform scale divisions, a bimetal must be designed to have linear deflection over the desired temperature range. Bimetal thermometers are used at temperatures ranging from 580 down to -180°C and lower. However, at the low temperatures

TABLE 8-9 Recommended Temperature Measurement Ranges for RTDs and Thermocouples

Resistance Thermometer Detectors (RTDs)	
100V Pt	-200 – $+850^\circ\text{C}$
120V Ni	-80 – $+320^\circ\text{C}$
Thermocouples	
Type B	700 – $+1820^\circ\text{C}$
Type E	-175 – $+1000^\circ\text{C}$
Type J	-185 – $+1200^\circ\text{C}$
Type K	-175 – $+1372^\circ\text{C}$
Type N	0 – $+1300^\circ\text{C}$
Type R	125 – $+1768^\circ\text{C}$
Type S	150 – $+1768^\circ\text{C}$
Type T	-170 – $+400^\circ\text{C}$

8-58 PROCESS CONTROL

the rate of deflection drops off quite rapidly. Bimetal thermometers do not have long-time stability at temperatures above 430°C.

Pyrometers Planck's distribution law gives the radiated energy flux $q_b(\lambda, T)d\lambda$ in the wavelength range λ to $\lambda + d\lambda$ from a black surface:

$$q_b(\lambda, T) = \frac{C_1}{\lambda^5} \frac{1}{e^{C_2/\lambda T} - 1} \quad (8-96)$$

where $C_1 = 3.7418 \times 10^{10} \mu W \cdot \mu m^4 \cdot cm^{-2}$ and $C_2 = 14,388 \mu m \cdot K$.

If the target object is a black body and if the pyrometer has a detector which measures the specific wavelength signal from the object, the temperature of the object can be exactly estimated from Eq. (8-96). While it is possible to construct a physical body that closely approximates black body behavior, most real-world objects are not black bodies. The deviation from a black body can be described by the spectral emissivity

$$\epsilon_T = \frac{q(T)}{q_b(T)} \quad (8-97)$$

where $q(\lambda, T)$ is the radiated energy flux from a real body in the wavelength range λ to $\lambda + d\lambda$ and $0 < \epsilon_{\lambda, T} < 1$. Integrating Eq. (8-96) over all wavelengths gives the Stefan-Boltzmann equation

$$q_b(T) = \int_0^\infty q_b(\lambda, T)d\lambda = \sigma T^4 \quad (8-98)$$

where σ is the Stefan-Boltzmann constant. Similar to Eq. (8-93), the emissivity ϵ_T for the total radiation is

$$\epsilon_T = \frac{q(T)}{q_b(T)} \quad (8-99)$$

where $q(T)$ is the radiated energy flux from a real body with emissivity ϵ_T .

Total Radiation Pyrometers In total radiation pyrometers, the thermal radiation is detected over a large range of wavelengths from the object at high temperature. The detector is normally a thermopile, which is built by connecting several thermocouples in series to increase the temperature measurement range. The pyrometer is calibrated for black bodies, so the indicated temperature T_p should be converted for non-black body temperature.

Photoelectric Pyrometers Photoelectric pyrometers belong to the class of band radiation pyrometers. The thermal inertia of thermal radiation detectors does not permit the measurement of rapidly changing temperatures. For example, the smallest time constant of a thermal detector is about 1 ms while the smallest time constant of a photoelectric detector can be about 1 or 2 s. Photoelectric pyrometers may use photoconductors, photodiodes, photovoltaic cells, or vacuum photocells. Photoconductors are built from glass plates with thin film coatings of 1- μm thickness, using PbS, CdS, PbSe, or PbTe. When the incident radiation has the same wavelength as the materials are able to absorb, the captured incident photons free photoelectrons, which form an electric current. Photodiodes in germanium or silicon are operated with a reverse bias voltage applied. Under the influence of the incident radiation, their conductivity as well as their reverse saturation current is proportional to the intensity of the radiation within the spectral response band from 0.4 to 1.7 μm for Ge and from 0.6 to 1.1 μm for Si. Because of the above characteristics, the operating range of a photoelectric pyrometer can be either spectral or in specific band. Photoelectric pyrometers can be applied for a specific choice of the wavelength.

Disappearing Filament Pyrometers Disappearing filament pyrometers can be classified as spectral pyrometers. The brightness of a lamp filament is changed by adjusting the lamp current until the filament disappears against the background of the target, at which point the temperature is measured. Because the detector is the human eye, it is difficult to calibrate for online measurements.

Ratio Pyrometers The ratio pyrometer is also called the two-color pyrometer. Two different wavelengths are utilized for detecting

the radiated signal. If one uses Wien's law for small values of AT , the detected signals from spectral radiant energy flux emitted at wavelengths λ_1 and λ_2 with emissivities ϵ_{λ_1} and ϵ_{λ_2} are

$$S_{\lambda_1} = KC_1 \epsilon_{\lambda_1} \lambda_1^{-5} \exp\left(\frac{-C_2}{\lambda_1 T}\right) \quad (8-100)$$

$$S_{\lambda_2} = KC_1 \epsilon_{\lambda_2} \lambda_2^{-5} \exp\left(\frac{-C_2}{\lambda_2 T}\right) \quad (8-101)$$

The ratio of the signals S_{λ_1} and S_{λ_2} is

$$\frac{S_{\lambda_1}}{S_{\lambda_2}} = \frac{\epsilon_{\lambda_1}}{\epsilon_{\lambda_2}} \left(\frac{\lambda_2}{\lambda_1}\right)^5 \exp\left[\frac{C_2}{T} \left(\frac{1}{\lambda_2} - \frac{1}{\lambda_1}\right)\right] \quad (8-102)$$

Nonblack or nongray bodies are characterized by the wavelength dependence of their spectral emissivity. Let T_c be defined as the temperature of the body corresponding to the temperature of a black body. If the ratio of its radiant intensities at wavelengths λ_1 and λ_2 equals the ratio of the radiant intensities of the non-black body, whose temperature is to be measured at the same wavelength, then Wien's law gives

$$\frac{\epsilon_{\lambda_1} \exp(-C_2/\lambda_1 T)}{\epsilon_{\lambda_2} \exp(-C_2/\lambda_2 T)} = \frac{\exp(-C_2/\lambda_1 T_c)}{\exp(-C_2/\lambda_2 T_c)} \quad (8-103)$$

where T is the true temperature of the body. Rearranging Eq. (8-103) gives

$$T = \left[\frac{\ln \epsilon_{\lambda_1}/\epsilon_{\lambda_2}}{C_2(1/\lambda_1 - 1/\lambda_2)} + \frac{1}{T_c} \right]^{-1} \quad (8-104)$$

For black or gray bodies, Eq. (8-104) reduces to

$$\frac{S_{\lambda_1}}{S_{\lambda_2}} = \left(\frac{\lambda_2}{\lambda_1}\right)^5 \exp\left[\frac{C_2}{T} \left(\frac{1}{\lambda_2} - \frac{1}{\lambda_1}\right)\right] \quad (8-105)$$

Thus by measuring S_{λ_1} and S_{λ_2} , the temperature T can be estimated.

Accuracy of Pyrometers Most of the temperature estimation methods for pyrometers assume that the object is either a gray body or has known emissivity values. The emissivity of the non-black body depends on the internal state or the surface geometry of the objects. Also the medium through which the thermal radiation passes is not always transparent. These inherent uncertainties of the emissivity values make the accurate estimation of the temperature of the target objects difficult. Proper selection of the pyrometer and accurate emissivity values can provide a high level of accuracy.

PRESSURE MEASUREMENTS

Pressure, defined as force per unit area, is usually expressed in terms of familiar units of weight-force and area or the height of a column of liquid which produces a like pressure at its base. Process pressure-measuring devices may be divided into three groups: (1) those based on the measurement of the height of a liquid column, (2) those based on the measurement of the distortion of an elastic pressure chamber, and (3) electrical sensing devices.

Liquid-Column Methods Liquid-column pressure-measuring devices are those in which the pressure being measured is balanced against the pressure exerted by a column of liquid. If the density of the liquid is known, the height of the liquid column is a measure of the pressure. Most forms of liquid-column pressure-measuring devices are commonly called manometers. When the height of the liquid is

observed visually, the liquid columns are contained in glass or other transparent tubes. The height of the liquid column may be measured in length units or calibrated in pressure units. Depending on the pressure range, water and mercury are the liquids most frequently used. Because the density of the liquid used varies with temperature, the temperature must be taken into account for accurate pressure measurements.

Elastic Element Methods Elastic element pressure-measuring devices are those in which the measured pressure deforms some elastic material (usually metallic) within its elastic limit, the magnitude of the deformation being approximately proportional to the applied pressure. These devices may be loosely classified into three types: Bourdon tube, bellows, and diaphragm.

Bourdon Tube Elements Probably the most frequently used process pressure-indicating device is the C-spring Bourdon tube pressure gauge. Gauges of this general type are available in a wide variety of pressure ranges and materials of construction. Materials are selected on the basis of pressure range, resistance to corrosion by the process materials, and effect of temperature on calibration. Gauges calibrated with pressure, vacuum, compound (combination pressure and vacuum), and suppressed-zero ranges are available.

Bellows Element The bellows element is an axially elastic cylinder with deep folds or convolutions. The bellows may be used unopposed, or it may be restrained by an opposing spring. The pressure to be measured may be applied either to the inside or to the space outside the bellows, with the other side exposed to atmospheric pressure. For measurement of absolute pressure either the inside or the space outside of the bellows can be evacuated and sealed. Differential pressures may be measured by applying the pressures to opposite sides of a single bellows or to two opposing bellows.

Diaphragm Elements Diaphragm elements may be classified into two principal types: those that utilize the elastic characteristics of the diaphragm and those that are opposed by a spring or other separate elastic element. The first type usually consists of one or more capsules, each composed of two diaphragms bonded together by soldering, brazing, or welding. The diaphragms are flat or corrugated circular metallic disks. Metals commonly used in diaphragm elements include brass, phosphor bronze, beryllium copper, and stainless steel. Ranges are available from fractions of an inch of water to over 800 in (200 kPa) gauge. The second type of diaphragm is used for containing the pressure and exerting a force on the opposing elastic element. The diaphragm is a flexible or slack diaphragm of rubber, leather, impregnated fabric, or plastic. Movement of the diaphragm is opposed by a spring which determines the deflection for a given pressure. This type of diaphragm is used for the measurement of extremely low pressure, vacuum, or differential pressure.

Electrical Methods Electrical methods for pressure measurement include strain gauges, piezoresistive transducers, and piezoelectric transducers.

Strain Gauges When a wire or other electrical conductor is stretched elastically, its length is increased and its diameter is decreased. Both of these dimensional changes result in an increase in the electrical resistance of the conductor. Devices utilizing resistance-wire grids for measuring small distortions in elastically stressed materials are commonly called strain gauges. Pressure-measuring elements utilizing strain gauges are available in a wide variety of forms. They usually consist of one of the elastic elements described earlier to which one or more strain gauges have been attached to measure the deformation. There are two basic strain gauge forms: bonded and unbonded. Bonded strain gauges are bonded directly to the surface of the elastic element whose strain is to be measured. The unbonded strain gauge transducer consists of a fixed frame and an armature that moves with respect to the frame in response to the measured pressure. The strain gauge wire filaments are stretched between the armature and frame. The strain gauges are usually connected electrically in a Wheatstone bridge configuration.

Strain gauge pressure transducers are manufactured in many forms for measuring gauge, absolute, and differential pressures and vacuum. Full-scale ranges from 25.4 mm of water to 10,134 MPa are available. Strain gauges bonded directly to a diaphragm pressure-sensitive element usually have an extremely fast response time and are suitable for high-frequency dynamic pressure measurements.

Piezoresistive Transducers A variation of the conventional strain gauge pressure transducer uses bonded single-crystal semiconductor wafers, usually silicon, whose resistance varies with strain or distortion. Transducer construction and electrical configurations are similar to those using conventional strain gauges. A permanent magnetic field is applied perpendicular to the resonating sensor. An alternating current causes the resonator to vibrate, and the resonant frequency is a function of the pressure (tension) of the resonator. The principal advantages of piezoresistive transducers are a much higher bridge voltage output and smaller size. Full-scale output voltages of 50 to 100 mV/V of excitation are typical. Some newer devices provide digital rather than analog output.

Piezoelectric Transducers Certain crystals produce a potential difference between their surfaces when stressed in appropriate directions. Piezoelectric pressure transducers generate a potential difference proportional to a pressure-generated stress. Because of the extremely high electrical impedance of piezoelectric crystals at low frequency, these transducers are usually not suitable for measurement of static process pressures.

FLOW MEASUREMENTS

Flow, defined as volume per unit of time at specified temperature and pressure conditions, is generally measured by positive displacement or rate meters. The term *positive displacement meter* applies to a device in which the flow is divided into isolated measured volumes when the number of fillings of these volumes is counted in some manner. The term *rate meter* applies to all types of flowmeters through which the material passes without being divided into isolated quantities. Movement of the material is usually sensed by a primary measuring element that activates a secondary device. The flow rate is then inferred from the response of the secondary device by means of known physical laws or from empirical relationships.

The principal classes of flow-measuring instruments used in the process industries are variable-head, variable-area, positive-displacement, and turbine instruments; mass flowmeters; vortex-shedding and ultrasonic flowmeters; magnetic flowmeters; and more recently, Coriolis mass flowmeters. Head meters are covered in detail in Sec. 5.

Orifice Meter The most widely used flowmeter involves placing a fixed-area flow restriction (an orifice) in the pipe carrying the fluid. This flow restriction causes a pressure drop which can be related to flow rate. The sharp-edge orifice is popular because of its simplicity, low cost, and the large amount of research data on its behavior. For the orifice meter, the flow rate Q_a for a liquid is given by

$$Q_a = \frac{C_d A_2}{\sqrt{1 - (A_2/A_1)^2}} \cdot \sqrt{\frac{2(p_1 - p_2)}{\rho}} \quad (8-106)$$

where $p_1 - p_2$ is the pressure drop, ρ is the density, A_1 is the pipe cross-sectional area, A_2 is the orifice cross-sectional area, and C_d is the discharge coefficient. The discharge coefficient C_d varies with the Reynolds number at the orifice and can be calibrated with a single fluid, such as water (typically $C_d \approx 0.6$). If the orifice and pressure taps are constructed according to certain standard dimensions, quite accurate (about 0.4 to 0.8 percent error) values of C_d may be obtained. Also note that the standard calibration data assume no significant flow disturbances such as elbows and valves for a certain minimum distance upstream of the orifice. The presence of such disturbances close to the orifice can cause errors of as much as 15 percent. Accuracy in measurements limits the meter to a flow rate range of 3:1. The orifice has a relatively large permanent pressure loss that must be made up by the pumping machinery.

Venturi Meter The venturi tube operates on exactly the same principle as the orifice [see Eq. (8-102)]. Discharge coefficients of venturis are larger than those for orifices and vary from about 0.94 to 0.99. A venturi gives a definite improvement in power losses over an orifice and is often indicated for measuring very large flow rates, where power losses can become economically significant. The initial higher cost of a venturi over an orifice may thus be offset by reduced operating costs.

Rotameter A rotameter consists of a vertical tube with a tapered bore in which a float changes position with the flow rate through the tube. For a given flow rate, the float remains stationary because the vertical forces of differential pressure, gravity, viscosity, and buoyancy are balanced. The float position is the output of the meter and can be made essentially linear with flow rate by making the tube area vary linearly with the vertical distance.

Turbine Meter If a turbine wheel is placed in a pipe containing a flowing fluid, its rotary speed depends on the flow rate of the fluid. A turbine can be designed whose speed varies linearly with flow rate. The speed can be measured accurately by counting the rate at which turbine blades pass a given point, using magnetic pickup to produce voltage pulses. By feeding these pulses to an electronic pulse rate meter one can measure flow rate by summing the pulses during a timed interval. Turbine meters are available with full-scale flow rates ranging from about 0.1 to 30,000 gal/min for liquids and 0.1 to 15,000 ft³/min for air. Nonlinearity can be less than 0.05 percent in the larger sizes. Pressure drop across the meter varies with the square of flow rate and is about 3 to 10 psi at full flow. Turbine meters can follow flow transients quite accurately since their fluid/mechanical time constant is on the order of 2 to 10 ms.

Vortex-Shedding Flowmeters These flowmeters take advantage of vortex shedding, which occurs when a fluid flows past a non-streamlined object (a blunt body). The flow cannot follow the shape of the object and separates from it, forming turbulent vortices or eddies at the object's side surfaces. As the vortices move downstream, they grow in size and are eventually shed or detached from the object. Shedding takes place alternately at either side of the object, and the rate of vortex formation and shedding is directly proportional to the volumetric flow rate. The vortices are counted and used to develop a signal linearly proportional to the flow rate. The digital signals can easily be totaled over an interval of time to yield the flow rate. Accuracy can be maintained regardless of density, viscosity, temperature, or pressure when the Reynolds number is greater than 10,000. There is usually a low flow cutoff point below which the meter output is clamped at zero. This flowmeter is recommended for use with relatively clean, low-viscosity liquids, gases, and vapors, and rangeability of 10:1 to 20:1 is typical. A sufficient length of straight-run pipe is necessary to prevent distortion in the fluid velocity profile.

Ultrasonic Flowmeters An ultrasonic flowmeter is based upon the variable time delays of received sound waves which arise when a flowing liquid's rate of flow is varied. Two fundamental measurement techniques, depending upon liquid cleanliness, are generally used. In the first technique two opposing transducers are inserted in a pipe so that one transducer is downstream from the other. These transducers are then used to measure the difference between the velocity at which the sound travels with the direction of flow and the velocity at which it travels against the direction of flow. The differential velocity is measured either by (1) direct time delays using sound wave burst or (2) frequency shifts derived from beat-together, continuous signals. The frequency measurement technique is usually preferred because of its simplicity and independence of the liquid static velocity. A relatively clean liquid is required to preserve the uniqueness of the measurement path.

In the second technique, the flowing liquid must contain scatters in the form of particles or bubbles which will reflect the sound waves. These scatters should be traveling at the velocity of the liquid. A Doppler method is applied by transmitting sound waves along the flow path and measuring the frequency shift in the returned signal from the scatters in the process fluid. This frequency shift is proportional to liquid velocity.

Magnetic Flowmeters The principle behind these flowmeters is Faraday's law of electromagnetic inductance. The magnitude of the voltage induced in a conductive medium moving at right angles through a magnetic field is directly proportional to the product of the magnetic flux density, the velocity of the medium, and the path length between the probes. A minimum value of fluid conductivity is required to make this approach viable. The presence of multiple phases or undissolved solids can affect the accuracy of the measurement if the velocities of the phases are different from that for straight-run pipe. Magmeters are very accurate over wide flow ranges and are especially

accurate at low flow rates. Typical applications include metering viscous fluids, slurries, or highly corrosive chemicals. Because magmeters should be filled with fluid, the preferred installation is in vertical lines with flow going upward. However, magmeters can be used in tight piping schemes where it is impractical to have long pipe runs, typically requiring lengths equivalent to five or more pipe diameters.

Coriolis Mass Flowmeters Coriolis mass flowmeters utilize a vibrating tube in which Coriolis acceleration of a fluid in a flow loop can be created and measured. They can be used with virtually any liquid and are extremely insensitive to operating conditions, with pressure ranges over 100:1. These meters are more expensive than volumetric meters and range in size from $\frac{1}{16}$ to 6 in. Due to the circuitous path of flow through the meter, Coriolis flowmeters exhibit higher than average pressure changes. The meter should be installed so that it will remain full of fluid, with the best installation in a vertical pipe with flow going upward. There is no Reynolds number limitation with this meter, and it is quite insensitive to velocity profile distortions and swirl, hence there is no requirement for straight piping upstream.

Thermal Mass Flowmeters The trend in the chemical process industries is toward increased usage of mass flowmeters that are independent of changes in pressure, temperature, viscosity, and density. Thermal mass meters are widely used in semiconductor manufacturing and in bioprocessing for control of low flow rates (called mass flow controllers, or MFCs). MFCs measure the heat loss from a heated element, which varies with flow rate, with an accuracy of ± 1 percent. Capacitance probes measure the dielectric constant of the fluid and are useful for flow measurements of slurries and other two-phase flows.

LEVEL MEASUREMENTS

The measurement of level can be defined as the determination of the location of the interface between two fluids, separable by gravity, with respect to a fixed reference plane. The most common level measurement is that of the interface between a liquid and a gas. Other level measurements frequently encountered are the interface between two liquids, between a granular or fluidized solid and a gas, and between a liquid and its vapor.

A commonly used basis for classification of level devices is as follows: float-actuated, displacer, and head devices, and a miscellaneous group which depends mainly on fluid characteristics.

Float-Actuated Devices Float-actuated devices are characterized by a buoyant member which floats at the interface between two fluids. Because a significant force is usually required to move the indicating mechanism, float-actuated devices are generally limited to liquid-gas interfaces. By properly weighting the float, they can be used to measure liquid-liquid interfaces. Float-actuated devices may be classified on the basis of the method used to couple the float motion to the indicating system, as discussed below.

Chain or Tape Float Gauge In these types of gauges, the float is connected to the indicating mechanism by means of a flexible chain or tape. These gauges are commonly used in large atmospheric storage tanks. The gauge-board type is provided with a counterweight to keep the tape or chain taut. The tape is stored in the gauge head on a spring-loaded reel. The float is usually a pancake-shaped hollow metal float, with guide wires from top to bottom of the tank to constrain it.

Lever and Shaft Mechanisms In pressurized vessels, float-actuated lever and shaft mechanisms are frequently used for level measurement. This type of mechanism consists of a hollow metal float and lever attached to a rotary shaft which transmits the float motion to the outside of the vessel through a rotary seal.

Magnetically Coupled Devices A variety of float-actuated level devices which transmit the float motion by means of magnetic coupling have been developed. Typical of this class of devices are magnetically operated level switches and magnetic-bond float gauges. A typical magnetic-bond float gauge consists of a hollow magnet-carrying float which rides along a vertical nonmagnetic guide tube. The follower magnet is connected and drives an indicating dial similar to that on a conventional tape float gauge. The float and guide tube are in contact with the measured fluid and come in a variety of materials for resistance to corrosion and to withstand high pressures or vacuum. Weighted floats for liquid-liquid interfaces are available.

Head Devices A variety of devices utilize hydrostatic head as a measure of level. As in the case of displacer devices, accurate level measurement by hydrostatic head requires an accurate knowledge of the densities of both heavier-phase and lighter-phase fluids. The majority of this class of systems utilize standard pressure and differential pressure measuring devices.

Bubble Tube Systems The commonly used bubble tube system sharply reduces restrictions on the location of the measuring element. To eliminate or reduce variations in pressure drop due to the gas flow rate, a constant differential regulator is commonly employed to maintain a constant gas flow rate. Because the flow of gas through the bubble tube prevents entry of the process liquid into the measuring system, this technique is particularly useful with corrosive or viscous liquids, liquids subject to freezing, and liquids containing entrained solids.

Electrical Methods Two electrical characteristics of fluids, conductivity and dielectric constant, are frequently used to distinguish between two phases for level measurement purposes. An application of electrical conductivity is the fixed-point level detection of a conductive liquid such as high and low water levels. A voltage is applied between two electrodes inserted into the vessel at different levels. When both electrodes are immersed in the liquid, a current flows. Capacitance-type level measurements are based on the fact that the electrical capacitance between two electrodes varies with the dielectric constant of the material between them. A typical continuous level measurement system consists of a rod electrode positioned vertically in a vessel, the other electrode usually being the metallic vessel wall. The electrical capacitance between the electrodes is a measure of the height of the interface along the rod electrode. The rod is usually conductively insulated from process fluids by a coating of plastic. The dielectric constants of most liquids and solids are markedly higher than those of gases and vapors (by a factor of 2 to 5). The dielectric constant of water and other polar liquids is 10 to 20 times that of hydrocarbons and other nonpolar liquids.

Thermal Methods Level-measuring systems may be based on the difference in thermal characteristics between the fluids, such as temperature or thermal conductivity. A fixed-point level sensor based on the difference in thermal conductivity between two fluids consists of an electrically heated thermistor inserted into the vessel. The temperature of the thermistor and consequently its electrical resistance increase as the thermal conductivity of the fluid in which it is immersed decreases. Because the thermal conductivity of liquids is markedly higher than that of vapors, such a device can be used as a point level detector for liquid-vapor interface.

Sonic Methods A fixed-point level detector based on sonic propagation characteristics is available for detection of a liquid-vapor interface. This device uses a piezoelectric transmitter and receiver, separated by a short gap. When the gap is filled with liquid, ultrasonic energy is transmitted across the gap, and the receiver actuates a relay. With a vapor filling the gap, the transmission of ultrasonic energy is insufficient to actuate the receiver.

Laser Level Transmitters These are designed for bulk solids, slurries, and opaque liquids. A laser near the vessel top fires a short pulse of light down to the surface of the process liquid, where it reflects back to a detector at the vessel top. A timing circuit measures the elapsed time and calculates the fluid depth. Lasers are attractive because lasers have no false echoes and can be directed through tight spaces.

Radar Level Transmitters Radar systems operate by beaming microwaves downward, from either a horn or parabolic dish located on top of the vessel. The signal reflects off the fluid surface back to the source after it detects a change in dielectric constant from the vapor to the fluid. The round-trip time is proportional to the distance to the fluid level. Guided-wave radar systems provide a rigid probe or flexible cable to guide the microwave down the height of the tank and back. Guided-wave radar is much more efficient than open-air radar because the guide provides a more focused energy path.

PHYSICAL PROPERTY MEASUREMENTS

Physical property measurements are sometimes equivalent to composition analyzers, because the composition can frequently be inferred from the measurement of a selected physical property.

Density and Specific Gravity For binary or pseudobinary mixtures of liquids or gases or a solution of a solid or gas in a solvent, the density is a function of the composition at a given temperature and pressure. Specific gravity is the ratio of the density of a noncompressible substance to the density of water at the same physical conditions. For nonideal solutions, empirical calibration will give the relationship between density and composition. Several types of measuring devices are described below.

Liquid Column Density may be determined by measuring the gauge pressure at the base of a fixed-height liquid column open to the atmosphere. If the process system is closed, then a differential pressure measurement is made between the bottom of the fixed-height liquid column and the vapor over the column. If vapor space is not always present, the differential pressure measurement is made between the bottom and top of a fixed-height column with the top measurement being made at a point below the liquid surface.

Displacement There are a variety of density measurement devices based on displacement techniques. A hydrometer is a constant-weight, variable-immersion device. The degree of immersion, when the weight of the hydrometer equals the weight of the displaced liquid, is a measure of the density. The hydrometer is adaptable to manual or automatic usage. Another modification includes a magnetic float suspended below a solenoid, the varying magnetic field maintaining the float at a constant distance from the solenoid. Change in position of the float, resulting from a density change, excites an electrical system which increases or decreases the current through the solenoid.

Direct Mass Measurement One type of densitometer measures the natural vibration frequency and relates the amplitude to changes in density. The density sensor is a V-shaped tube held stationary at its node points and allowed to vibrate at its natural frequency. At the curved end of the V is an electrochemical device that periodically strikes the tube. At the other end of the V the fluid is continuously passed through the tube. Between strikes, the tube vibrates at its natural frequency. The frequency changes directly in proportion to changes in density. A pickup device at the curved end of the V measures the frequency and electronically determines the fluid density. This technique is useful because it is not affected by the optical properties of the fluid. However, particulate matter in the process fluid can affect the accuracy.

Radiation-Density Gauges Gamma radiation may be used to measure the density of material inside a pipe or process vessel. The equipment is basically the same as for level measurement, except that here the pipe or vessel must be filled over the effective, irradiated sample volume. The source is mounted on one side of the pipe or vessel and the detector on the other side with appropriate safety radiation shielding surrounding the installation. Cesium 137 is used as the radiation source for path lengths under 610 mm (24 in) and cobalt 60 above 610 mm. The detector is usually an ionization gauge. The absorption of the gamma radiation is a function of density. Since the absorption path includes the pipe or vessel walls, an empirical calibration is used. Appropriate corrections must be made for the source intensity decay with time.

Viscosity Continuous viscometers generally measure either the resistance to flow or the drag or torque produced by movement of an element (moving surface) through the fluid. Each installation is normally applied over a narrow range of viscosities. Empirical calibration over this range allows use on both newtonian and nonnewtonian fluids. One such device uses a piston inside a cylinder. The hydrodynamic pressure of the process fluid raises the piston to a preset height. Then the inlet valve closes, the piston is allowed to free-fall, and the time of travel (typically a few seconds) is a measure of viscosity. Other geometries include the rotation of a spindle inside a sample chamber and a vibrating probe immersed in the fluid. Because viscosity depends on temperature, the viscosity measurement must be thermostated with a heater or cooler.

Refractive Index When light travels from one medium (e.g., air or glass) into another (e.g., a liquid), it undergoes a change of velocity and, if the angle of incidence is not 90°, a change of direction. For a given interface, angle, temperature, and wavelength of light, the amount of deviation or refraction will depend on the composition of

the liquid. If the sample is transparent, the normal method is to measure the refraction of light transmitted through the glass-sample interface. If the sample is opaque, the reflectance near the critical angle at a glass-sample interface is measured. In an online refractometer the process fluid is separated from the optics by a prism material. A beam of light is focused on a point in the fluid which creates a conic section of light at the prism, striking the fluid at different angles (greater than or less than the critical angle). The critical angle depends on the species concentrations; as the critical angle changes, the proportions of reflected and refracted light change. A photodetector produces a voltage signal proportional to the light refracted, when compared to a reference signal. Refractometers can be used with opaque fluids and in streams that contain particulates.

Dielectric Constant The dielectric constant of material represents its ability to reduce the electric force between two charges separated in space. This property is useful in process control for polymers, ceramic materials, and semiconductors. Dielectric constants are measured with respect to vacuum (1.0); typical values range from 2 (benzene) to 33 (methanol) to 80 (water). The value for water is higher than that for most plastics. A measuring cell is made of glass or some other insulating material and is usually doughnut-shaped, with the cylinders coated with metal, which constitute the plates of the capacitor.

Thermal Conductivity All gases and vapor have the ability to conduct heat from a heat source. At a given temperature and physical environment, radiation and convection heat losses will be stabilized, and the temperature of the heat source will mainly depend on the thermal conductivity and thus the composition of the surrounding gases. Thermal conductivity analyzers normally consist of a sample cell and a reference cell, each containing a combined heat source and detector. These cells are normally contained in a metal block with two small cavities in which the detectors are mounted. The sample flows through the sample cell cavity past the detector. The reference cell is an identical cavity with a detector through which a known gas flows. The combined heat source and detectors are normally either wire filaments or thermistors heated by a constant current. Because their resistance is a function of temperature, the sample detector resistance will vary with sample composition while the reference detector resistance will remain constant. The output from the detector bridge will be a function of sample composition.

CHEMICAL COMPOSITION ANALYZERS

Chemical composition is generally the most challenging online measurement. Before the era of online analyzers, messengers were required to deliver samples to the laboratory for analysis and to return the results to the control room. The long time delay involved prevented process adjustment from being made, affecting product quality. The development of online analyzers has automated this approach and reduced the analysis time. However, manual sampling is still frequently employed, especially in the specialty chemical industry where few instruments are commercially available. It is not unusual for a chemical composition analysis system to cost over \$100,000, so it is important to assess the payback of such an investment versus the cost of manual sampling. Potential quality improvements can be an important consideration.

A number of composition analyzers used for process monitoring and control require chemical conversion of one or more sample components preceding quantitative measurement. These reactions include formation of suspended solids for turbidimetric measurement, formation of colored materials for colorimetric detection, selective oxidation or reduction for electrochemical measurement, and formation of electrolytes for measurement by electrical conductance. Some nonvolatile materials may be separated and measured by gas chromatography after conversion to volatile derivatives.

Chromatographic Analyzers These analyzers are widely used for the separation and measurement of volatile compounds and of compounds that can be quantitatively converted to volatile derivatives. The compounds to be measured are separated by placing a portion of the sample in a chromatographic column and carrying the compounds through the column with a gas stream, called gas chroma-

tography, or GC. As a result of the different affinities of the sample components for the column packing, the compounds emerge successively as binary mixtures with the carrier gas. A detector at the column outlet measures a specific physical property that can be related to the concentrations of the compounds in the carrier gas. Both the concentration peak height and the peak height-time integral, i.e., peak area, can be related to the concentration of the compound in the original sample. The two detectors most commonly used for process chromatographs are the thermal conductivity detector and the hydrogen flame ionization detector. Thermal conductivity detectors, discussed earlier, require calibration for the thermal response of each compound. Hydrogen flame ionization detectors are more complicated than thermal conductivity detectors but are capable of 100 to 10,000 times greater sensitivity for hydrocarbons and organic compounds. For ultrasensitive detection of trace impurities, carrier gases must be specially purified.

Typically, all components can be analyzed in a 5- to 10-min time period (although miniaturized GCs are faster). High-performance liquid chromatography (HPLC) can be used to measure dissolved solute levels, including proteins.

Infrared Analyzers Many gaseous and liquid compounds absorb infrared radiation to some degree. The degree of absorption at specific wavelengths depends on molecular structure and concentration. There are two common detector types for nondispersive infrared analyzers. These analyzers normally have two beams of radiation, an analyzing and a reference beam. One type of detector consists of two gas-filled cells separated by a diaphragm. As the amount of infrared energy absorbed by the detector gas in one cell changes, the cell pressure changes. This causes movement in the diaphragm, which in turn causes a change in capacitance between the diaphragm and a reference electrode. This change in electrical capacitance is measured as the output. The second type of detector consists of two thermopiles or two bolometers, one in each of the two radiation beams. The infrared radiation absorbed by the detector is measured by a differential thermocouple output or a resistance thermometer (bolometer) bridge circuit.

There are two common detector types for nondispersive analyzers. These analyzers normally have two beams of radiation, an analyzing and a reference beam. One type of detector consists of two gas-filled cells separated by a diaphragm. As the amount of infrared energy absorbed by the detector gas in one cell changes, the cell pressure changes. This causes movement in the diaphragm, which in turn causes a change in capacitance between the diaphragm and a reference electrode. This change in electrical capacitance is measured as the output. The second type of detector consists of two thermopiles or two bolometers, one in each of the two radiation beams. The infrared radiation absorbed by the detector is measured by a differential thermocouple output or a resistance thermometer (bolometer) bridge circuit. With gas-filled detectors, a chopped light system is normally used in which one side of the detector sees the source through the analyzing beam and the other side sees through the reference beam, alternating at a frequency of a few hertz.

Ultraviolet and Visible-Radiation Analyzers Many gas and liquid compounds absorb radiation in the near-ultraviolet or visible region. For example, organic compounds containing aromatic and carbonyl structural groups are good absorbers in the ultraviolet region. Also many inorganic salts and gases absorb in the ultraviolet or visible region. In contrast, straight chain and saturated hydrocarbons, inert gases, air, and water vapor are essentially transparent. Process analyzers are designed to measure the absorbance in a particular wavelength band. The desired band is normally isolated by means of optical filters. When the absorbance is in the visible region, the term *colorimetry* is used. A phototube is the normal detector. Appropriate optical filters are used to limit the energy reaching the detector to the desired level and the desired wavelength region. Because absorption by the sample is logarithmic if a sufficiently narrow wavelength region is used, an exponential amplifier is sometimes used to compensate and produce a linear output.

Paramagnetism A few gases including O₂, NO, and NO₂ exhibit paramagnetic properties as a result of unpaired electrons. In a nonuniform magnetic field, paramagnetic gases, because of their magnetic susceptibility, tend to move toward the strongest part of the

field, thus displacing diamagnetic gases. Paramagnetic susceptibility of these gases decreases with temperature. These effects permit measurement of the concentration of the strongest paramagnetic gas, oxygen. An oxygen analyzer uses a dumbbell suspended in the magnetic field which is repelled or attracted toward the magnetic field depending on the magnetic susceptibility of the gas.

Other Analyzers Mass spectroscopy (MS) determines the partial pressures of gases in a mixture of directing ionized gases into a detector under a vacuum (10^{-6} torr), and the gas phase composition is then monitored more or less continuously based on the molecular weight of the species (Nichols, 1988). Sometimes GC is combined with MS to obtain a higher level of discrimination of the components present. Fiber-optic sensors are attractive options (although higher-cost) for acquiring measurements in harsh environments such as high temperature or pressure. The transducing technique used by these sensors is optical and does not involve electric signals, so they are immune to electromagnetic interference. Raman spectroscopy uses fiber optics and involves pulsed light scattering by molecules. It has a wide variety of applications in process control. Workman, Koch, and Veltkamp, *Anal. Chem.*, **75**: 2859, 2003.

Significant advances have occurred during the past decade to miniaturize the size of the measurement system in order to make online analysis economically feasible and to reduce the time delays that often are present in analyzers. Recently, chemical sensors have been placed on microchips, even those requiring multiple physical, chemical, and biochemical steps (such as electrophoresis) in the analysis. This device has been called *lab-on-a-chip*. The measurements of chemical composition can be direct or indirect, the latter case referring to applications where some property of the process stream is measured (such as refractive index) and then related to composition of a particular component.

ELECTROANALYTICAL INSTRUMENTS

Conductometric Analysis Solutions of electrolytes in ionizing solvents (e.g., water) conduct current when an electrical potential is applied across electrodes immersed in the solution. Conductance is a function of ion concentration, ionic charge, and ion mobility. Conductance measurements are ideally suited for measurement of the concentration of a single strong electrolyte in dilute solutions. At higher concentrations conductance becomes a complex, nonlinear function of concentration requiring suitable calibration for quantitative measurements.

Measurement of pH The primary detecting element in pH measurement is the glass electrode. A potential is developed at the pH-sensitive glass membrane as a result of differences in hydrogen ion activity in the sample and a standard solution contained within the electrode. This potential measured relative to the potential of the reference electrode gives a voltage which is expressed as pH. Instrumentation for pH measurement is among the most widely used process measurement devices. Rugged electrode systems and highly reliable electronic circuits have been developed for this use.

After installation, the majority of pH measurement problems are sensor-related, mostly on the reference side, including junction plugging, poisoning, and depletion of electrolyte. For the glass (measuring electrode), common difficulties are broken or cracked glass, coating, and etching or abrasion. Symptoms such as drift, sluggish response, unstable readings, and inability to calibrate are indications of measurement problems. Online diagnostics such as impedance measurements, wiring checks, and electrode temperature are now available in most instruments. Other characteristics that can be measured offline include efficiency or slope and asymmetry potential (offset), which indicate whether the unit should be cleaned or changed [Nichols, *Chem. Engr. Prog.*, **90**(12):64, 1994; McMillan, *Chem. Engr. Prog.*, **87**(12):30, 1991].

Specific-Ion Electrodes In addition to the pH glass electrode specific for hydrogen ions, a number of electrodes which are selective for the measurement of other ions have been developed. This selectivity is obtained through the composition of the electrode membrane (glass, polymer, or liquid-liquid) and the composition of the electrode. These electrodes are subject to interference from other ions, and the

response is a function of the total ionic strength of the solution. However, electrodes have been designed to be highly selective for specific ions, and when properly used, these provide valuable process measurements.

MOISTURE MEASUREMENT

Moisture measurements are important in the process industries because moisture can foul products, poison reactions, damage equipment, or cause explosions. Moisture measurements include both absolute moisture methods and relative-humidity methods. The absolute methods provide a primary output that can be directly calibrated in terms of dew point temperature, molar concentration, or weight concentration. Loss of weight on heating is the most familiar of these methods. The relative-humidity methods provide a primary output that can be more directly calibrated in terms of percentage of saturation of moisture.

Dew Point Method For many applications the dew point is the desired moisture measurement. When concentration is desired, the relation between water content and dew point is well known and available. The dew point method requires an inert surface whose temperature can be adjusted and measured, a sample gas stream flowing past the surface, a manipulated variable for adjusting the surface temperature to the dew point, and a means of detecting the onset of condensation.

Although the presence of condensate can be detected electrically, the original and most often used method is the optical detection of change in light reflection from an inert metallic-surface mirror. Some instruments measure the attenuation of reflected light at the onset of condensation. Others measure the increase of light dispersed and scattered by the condensate instead of, or in addition to, the reflected-light measurement. Surface cooling is obtained with an expendable refrigerant liquid, conventional mechanical refrigeration, or thermoelectric cooling. Surface-temperature measurement is usually made with a thermocouple or a thermistor.

Piezoelectric Method A piezoelectric crystal in a suitable oscillator circuit will oscillate at a frequency dependent on its mass. If the crystal has a stable hygroscopic film on its surface, the equivalent mass of the crystal varies with the mass of water sorbed in the film. Thus the frequency of oscillation depends on the water in the film. The analyzer contains two such crystals in matched oscillator circuits. Typically, valves alternately direct the sample to one crystal and a dry gas to the other on a 30-s cycle. The oscillator frequencies of the two circuits are compared electronically, and the output is the difference between the two frequencies. This output is then representative of the moisture content of the sample. The output frequency is usually converted to a variable dc voltage for meter readout and recording. Multiple ranges are provided for measurement from about 1 ppm to near saturation. The dry reference gas is preferably the same as the sample except for the moisture content of the sample. Other reference gases which are adsorbed in a manner similar to the dried sample gas may be used. The dry gas is usually supplied by an automatic dryer. The method requires a vapor sample to the detector. Mist striking the detector destroys the accuracy of measurement until it vaporizes or is washed off the crystals. Water droplets or mist may destroy the hygroscopic film, thus requiring crystal replacement. Vaporization or gas-liquid strippers may sometimes be used for the analysis of moisture in liquids.

Capacitance Method Several analyzers utilize the high dielectric constant of water for its detection in solutions. The alternating electric current through a capacitor containing all or part of the sample between the capacitor plates is measured. Selectivity and sensitivity are enhanced by increasing the concentration of moisture in the cell by filling the capacitor sample cell with a moisture-specific sorbent as part of the dielectric. This both increases the moisture content and reduces the amount of other interfering sample components. Granulated alumina is the most frequently used sorbent. These detectors may be cleaned and recharged easily and with satisfactory reproducibility if the sorbent itself is uniform.

Oxide Sensors Aluminum oxide can be used as a sensor for moisture analysis. A conductivity cell has one electrode node of aluminum,

which is anodized to form a thin film of aluminum oxide, followed by coating with a thin layer of gold (the opposite electrode). Moisture is selectively adsorbed through the gold layer and into the hygroscopic aluminum oxide layer, which in turn determines the electrical conductivity between gold and aluminum oxide. This value can be related to ppm water in the sample. This sensor can operate between near vacuum to several hundred atmospheres, and it is independent of flow rate (including static conditions). Temperature, however, must be carefully monitored. A similar device is based on phosphorous pentoxide. Moisture content influences the electric current between two inert metal electrodes, which are fabricated as a helix on the inner wall of a tubular nonconductive sample cell. For a constant dc voltage applied to the electrodes, a current flows that is proportional to moisture. The moisture is absorbed into the hygroscopic phosphorous pentoxide, where the current electrolyzes the water molecules into hydrogen and oxygen. This sensor will handle moisture up to 1000 ppm and 6-atm pressure. As with the aluminum oxide ion, temperature control is very important.

Photometric Moisture Analysis This analyzer requires a light source, a filter wheel rotated by a synchronous motor, a sample cell, a detector to measure the light transmitted, and associated electronics. Water has two absorption bands in the near-infrared region at 1400 and 1900 nm. This analyzer can measure moisture in liquid or gaseous samples at levels from 5 ppm up to 100 percent, depending on other chemical species in the sample. Response time is less than 1 s, and samples can be run up to 300°C and 400 psig.

OTHER TRANSDUCERS

Other types of transducers used in process measurements include mechanical drivers such as gear trains and electrical drivers such as a differential transformer or a Hall effect (semiconductor-based) sensor.

Gear Train Rotary motion and angular position are easily transduced by various types of gear arrangements. A gear train in conjunction with a mechanical counter is a direct and effective way to obtain a digital readout of shaft rotations. The numbers on the counter can mean anything desired, depending on the gear ratio and the actuating device used to turn the shaft. A pointer attached to a gear train can be used to indicate a number of revolutions or a small fraction of a revolution for any specified pointer rotation.

Differential Transformer These devices produce an ac electrical output from linear movement of an armature. They are very versatile in that they can be designed for a full range of output with any range of armature travel up to several inches. The transformers have one or two primaries and two secondaries connected to oppose each other. With an ac voltage applied to the primary, the output voltage depends on the position of the armature and the coupling. Such devices produce accuracies of 0.5 to 1.0 percent of full scale and are used to transmit forces, pressures, differential pressures, or weights up to 1500 m. They can also be designed to transmit rotary motion.

Hall Effect Sensors Some semiconductor materials exhibit a phenomenon in the presence of a magnetic field which is adaptable to sensing devices. When a current is passed through one pair of wires attached to a semiconductor, such as germanium, another pair of wires properly attached and oriented with respect to the semiconductor will develop a voltage proportional to the magnetic field present and the current in the other pair of wires. Holding the exciting current constant and moving a permanent magnet near the semiconductor produce a voltage output proportional to the movement of the magnet. The magnet may be attached to a process variable measurement device which moves the magnet as the variable changes. Hall effect devices provide high speed of response, excellent temperature stability, and no physical contact.

SAMPLING SYSTEMS FOR PROCESS ANALYZERS

The sampling system consists of all the equipment required to present a process analyzer with a clean representative sample of a process stream and to dispose of that sample. When the analyzer is part of an automatic control loop, the reliability of the sampling system is as important as the reliability of the analyzer or the control equipment.

Sampling systems have several functions. The sample must be withdrawn from the process, transported, conditioned, introduced to the analyzer, and disposed. Probably the most common problem in sample system design is the lack of realistic information concerning the properties of the process material at the sampling point. Another common problem is the lack of information regarding the conditioning required so that the analyzer may utilize the sample without malfunction and treating that the sampling systems become equivalent to miniature online processing plants. These systems possess many of the same fabrication, reliability, and operating problems as small-scale pilot plants except that the sampling system must generally operate reliably for much longer periods of time.

Selecting the Sampling Point The selection of the sampling point is based primarily on supplying the analyzer with a sample whose composition or physical properties are pertinent to the control function to be performed. Other considerations include selecting locations that provide representative homogeneous samples with minimum transport delay, locations which collect a minimum of contaminating material, and locations which are accessible for test and maintenance procedures.

Sample Withdrawal from Process A number of considerations are involved in the design of sample withdrawal devices which will provide representative samples. For example, in a horizontal pipe carrying process fluid, a sample point on the bottom of the pipe will collect a maximum count of rust, scale, or other solid materials being carried along by the process fluid. In a gas stream, such a location will also collect a maximum amount of liquid contaminants. A sample point on the top side of a pipe will, for liquid streams, collect a maximum amount of vapor contaminants being carried along. Bends in the piping which produce swirls or cause centrifugal concentration of the denser phase may cause maximum contamination to be at unexpected locations. Two-phase process materials are difficult to sample for a total-composition representative sample.

A typical method for obtaining a sample of process fluid well away from vessel or pipe walls is an eduction tube inserted through a packing gland. This sampling method withdraws liquid sample and vaporizes it for transporting to the analyzer location. The transport lag time from the end of the probe to the vaporizer is minimized by using tubing having a small internal volume compared with pipe and valve volumes.

This sample probe may be removed for maintenance and reinstalled without shutting down the process. The eduction tube is made of material which will not corrode so that it will slide through the packing gland even after long periods of service. There may be a small amount of process fluid leakage until the tubing is withdrawn sufficiently to close the gate valve. A swaged ferrule on the end of the tube prevents accidental ejection of the eduction tube prior to removal of the packing gland. The section of pipe surrounding the eduction tube and extending into the process vessel provides mechanical protection for the eduction tube.

Sample Transport Transport time—the time elapsed between sample withdrawal from the process and its introduction into the analyzer—should be minimized, particularly if the analyzer is an automatic analyzer-controller. Any sample transport time in the analyzer-controller loop must be treated as equivalent to process dead time in determining conventional feedback controller settings or in evaluating controller performance. Reduction in transport time usually means transporting the sample in the vapor state.

Design considerations for sample lines are as follows:

1. The structural strength or protection must be compatible with the area through which the sample line runs.
2. Line size and length must be small enough to meet transport time requirements without excessive pressure drop or excessive bypass of sample at the analyzer input.
3. Line size and internal surface quality must be adequate to prevent clogging by the contaminants in the sample.
4. The prevention of a change of state of the sample may require installation, refrigeration, or heating of the sample line.
5. Sample line material must be such as to minimize corrosion due to sample or the environment.

Sample Conditioning Sample conditioning usually involves the removal of contaminants or some deleterious component from the sample mixture and/or the adjustment of temperature, pressure, and flow rate of the sample to values acceptable to the analyzer. Some of the more common contaminants which must be removed are rust, scale, corrosion products, deposits due to chemical reactions, and tar. In sampling some process streams, the material to be removed may include the primary process product such as polymer or the main constituent of the stream such as oil. In other

cases the material to be removed is present in trace quantities, e.g., water in an online chromatograph sample which can damage the chromatographic column packing. When contaminants or other materials which will hinder analysis represent a large percentage of the stream composition, their removal may significantly alter the integrity of the sample. In some cases, removal must be done as part of the analysis function so that removed material can be accounted for. In other cases, proper calibration of the analyzer output will suffice.

TELEMETERING AND TRANSMISSION

ANALOG SIGNAL TRANSMISSION

Modern control systems permit the measurement device, the control unit, and the final control element to be physically separated by several hundred meters, if necessary. This requires the transmission of the measured variable from the measurement device to the control unit, and the transmission of the controller output from the control unit to the final control element. In each case, transmission of a single value in only one direction is required. Such requirements can be met by analog signal transmission. A measurement range is defined for the value to be transmitted, and the value is basically transmitted as a percent of the span. For the measured variable, the logical span is the measurement span. For the controller output, the logical span is the range of the final control element (e.g., valve fully closed to valve fully open).

For pneumatic transmission systems, the signal range used for the transmission is 3 to 15 psig. In each pneumatic transmission system, there can be only one transmitter, but there can be any number of receivers. When most measurement devices were pneumatic, pneumatic transmission was the logical choice. However, with the displacement of pneumatic measurement devices by electronic devices, pneumatic transmission is now limited to applications where the unique characteristics of pneumatics make it the logical choice.

In order for electronic transmission systems to be less susceptible to interference from magnetic fields, current is used for the transmission signal instead of voltage. The signal range is 4 to 20 mA. In each circuit or "current loop," there can be only one transmitter. There can be more than one receiver, but not an unlimited number. For each receiver, a 250- Ω range resistor is inserted into the current loop, which provides a 1- to 5-V input to the receiving device. The number of receivers is limited by the power available from the transmitter.

Both pneumatic and electronic transmission use a *live zero*. This enables the receiver to distinguish a transmitted value of 0 percent of span from a transmitter or transmission system failure. Transmission of 0 percent of span provides a signal of 4 mA in electronic transmission. Should the transmitter or the transmission system fail (i.e., an open circuit in a current loop), the signal level would be 0 mA.

For most measurement variable transmissions, the lower range corresponds to 4 mA and the upper range corresponds to 20 mA. On an open circuit, the measured variable would fail to its lower range. In some applications, this is undesirable. For example, in a fired heater that is heating material to a target temperature, failure of the temperature measurement to its lower range value would drive the output of the combustion control logic to the maximum possible firing rate. In such applications, the analog transmission signal is normally inverted, with the upper range corresponding to 4 mA and the lower range corresponding to 20 mA. On an open circuit, the measured variable would fail to its upper range. For the fired heater, failure of the measured variable to its upper range would drive the output of the combustion control logic to the minimum firing rate.

DIGITAL SYSTEMS

With the advent of the microprocessor, digital technology began to be used for data collection, feedback control, and all other information processing requirements in production facilities. Such systems must

acquire data from a variety of measurement devices, and control systems must drive final control elements.

Analog Inputs and Outputs Analog inputs are generally divided into two categories:

1. *High level.* Where the source is a process transmitter, the range resistor in the current loop converts the 4- to 20-mA signal to a 1- to 5-V signal. The conversion equipment can be unipolar (i.e., capable of processing only positive voltages).

2. *Low level.* The most common low-level signals are inputs from thermocouples. These inputs rarely exceed 30 mV and could be zero or even negative. The conversion equipment must be bipolar (i.e., capable of processing positive and negative voltages).

Ultimately, such signals are converted to digital values via an analog-to-digital (A/D) converter. However, the A/D converter is normally preceded by two other components:

1. *Multiplexer.* This permits one A/D converter to service multiple analog inputs. The number of inputs to a multiplexer is usually between 8 and 256.

2. *Amplifier.* As A/D converters require high-level signals, a high-gain amplifier is required to convert low-level signals to high-level signals.

One of the important parameters for the A/D converter is its resolution. The resolution is stated in terms of the number of significant binary digits (bits) in the digital value. As the repeatability of most process transmitters is around 0.1 percent, the minimum acceptable resolution for a bipolar A/D converter is 12 bits, which translates to 11 data bits plus 1 bit for the sign. With this resolution, the analog input values can be represented to 1 part in 2^{11} , or 1 part in 2048. Normally, a 5-V input is converted to a digital value of 2000, which effectively gives a resolution of 1 part in 2000, or 0.05 percent. Very few process control systems utilize resolutions higher than 14 bits, which translates to a resolution of 1 part in 8000, or 0.0125 percent.

For 4- to 20-mA inputs, the resolution is not quite as good as stated above. For a 12-bit bipolar A/D converter, 1 V converts to a digital value of 400. Thus, the range for the digital value is 400 to 2000, making the effective input resolution 1 part in 1600, or 0.0625 percent. Sometimes this is expressed as a resolution of 7.4 bits, where $2^{7.4} = 1600$.

On the output side, dedicated digital-to-analog (D/A) converters are provided for each analog output. Outputs are normally unipolar and require a lower resolution than inputs. A 10-bit resolution is normally sufficient, giving a resolution of 1 part in 1000, or 0.1 percent.

Pulse Inputs Where the sensor within the measurement device is digital, analog-to-digital conversion can be avoided. For rotational devices, the rotational element can be outfitted with a shaft encoder that generates a known number of pulses per revolution. The digital system can process such inputs in any of the following ways:

1. Count the number of pulses over a fixed interval of time.
2. Determine the time for a specified number of pulses.
3. Determine the duration of time between the leading (or trailing) edges of successive pulses.

Of these, the first option is the most commonly used in process applications. Turbine flowmeters are probably the most common example where pulse inputs are used. Another example is a watt-hour meter. Basically any measurement device that involves a rotational element can be interfaced via pulses. Occasionally, a nonrotational measurement device can generate pulse outputs. One example is the

vortex-shedding meter, where a pulse can be generated when each vortex passes over the detector.

Serial Interfaces Some very important measurement devices cannot be reasonably interfaced via either analog or pulse inputs. Two examples are the following:

1. Chromatographs can perform a total composition analysis for a sample. It is possible but inconvenient to provide an analog input for each component. Furthermore, it is often desirable to capture other information, such as the time that the analysis was made (normally the time the sample was injected).

2. Load cells are capable of resolutions of 1 part in 100,000. A/D converters for analog inputs cannot even approach such resolutions.

One approach to interfacing with such devices involves serial interfaces. This has two aspects:

1. *Hardware interface.* The RS-232 interface standard is the basis for most serial interfaces.

2. *Protocol.* This is interpreting the sequence of characters transmitted by the measurement device. There are no standards for protocols, which means that custom software is required.

One advantage of serial interfaces is that two-way communication is possible. For example, a "tare" command can be issued to a load cell.

Microprocessor-Based Transmitters The cost of microprocessor technology has declined to the point where it is economically feasible to incorporate a microprocessor into each transmitter. Such microprocessor-based transmitters are often referred to as *smart* transmitters. As opposed to conventional or *dumb* transmitters, the smart transmitters offer the following capabilities:

1. They check on the internal electronics, such as verifying that the voltage levels of internal power supplies are within specifications.

2. They check on environmental conditions within the instruments, such as verifying that the case temperature is within specifications.

3. They perform compensation of the measured value for conditions within the instrument, such as compensating the output of a pressure transmitter for the temperature within the transmitter. Smart transmitters are much less affected by temperature and pressure variations than are conventional transmitters.

4. They perform compensation of the measured value for other process conditions, such as compensating the output of a capacitance level transmitter for variations in process temperature.

5. They linearize the output of the transmitter. Functions such as square root extraction of the differential pressure for a head-type flowmeter can be done within the instrument instead of within the control system.

6. They configure the transmitter from a remote location, such as changing the span of the transmitter output.

7. They do automatic recalibration of the transmitter. Although this is highly desired by users, the capabilities, if any, in this respect depend on the type of measurement.

Due to these capabilities, smart transmitters offer improved performance over conventional transmitters.

Transmitter/Actuator Networks With the advent of smart transmitters and smart actuators, the limitations of the 4- to 20-mA analog signal transmission retard the full utilization of the capabilities of smart devices. For smart transmitters, the following capabilities are required:

1. *Transmission of more than one value from a transmitter.* Information beyond the measured variable is available from the smart transmitter. For example, a smart pressure transmitter can also report the temperature within its housing. Knowing that this temperature is above normal values permits corrective action to be taken before the device fails. Such information is especially important during the initial commissioning of a plant.

2. *Bidirectional transmission.* Configuration parameters such as span, engineering units, and resolution must be communicated to the smart transmitter.

Similar capabilities are required for smart actuators.

Eventually this technology, generally referred to as field bus, will replace all other forms of transmission (analog, pulse, and serial). Its acceptance by the user community has been slow, mainly due to the absence of a standard. Smart transmitters and smart valves have gained widespread acceptance, but initially the signal transmission continued to be via current loops. During this interim, several manu-

facturers introduced products based on proprietary communications technologies. Most manufacturers released sufficient information for others to develop products using their communications technologies, but those considering doing so found the costs to be an impediment.

A standard is now available, specifically, IEC 61158, "Digital Data Communications for Measurement and Control." In most industries, a standard defines only one way of doing something, but not in the computer industry. IEC 61158 defines five different communications technologies. Several manufacturers had selected a direction, and standards are not immune to commercial considerations. The net result is that one person's "field bus" might not be the same as another's. Most plants select one technology for their field bus, although it is possible to have multiple field bus interfaces on a control system and not have all the same type.

Although there will be winners and losers, most companies find the appealing features of field bus technologies too great to continue with the older technologies. U.S. manufacturers have generally chosen a field bus technology known as Foundation Fieldbus. In Europe, a field bus technology known as Profibus has gained wide acceptance. Probably the major advantages of these technologies lie in installation and commissioning. There are fewer wires and connections in a field bus installation. In most plants, the cost of the wiring is proving to be a minor issue. With fewer wires and connections, errors in field bus installations are fewer and can be located more quickly. The major cost savings prove to be in configuring and commissioning the system. With time, field bus will largely replace analog, pulse, and serial signal transmissions within industrial facilities.

FILTERING AND SMOOTHING

A signal received from a process transmitter generally contains the following components distinguished by their frequency [frequencies are measured in hertz (Hz), with 60-cycle ac being a 60-Hz frequency]:

1. *Low-frequency process disturbances.* The control system is expected to react to these disturbances.

2. *High-frequency process disturbances.* The frequency of these disturbances is beyond the capability of the control system to effectively react.

3. *Measurement noise.*

4. *Stray electrical pickup, primarily 50- or 60-cycle ac.*

The objective of filtering and smoothing is to remove the last three components, leaving only the low-frequency process disturbances. Normally this has to be accomplished by using the proper combination of analog and digital filters. Sampling a continuous signal results in a phenomenon often referred to as aliasing or foldover. To represent a sinusoidal signal, a minimum of four samples are required during each cycle. Consequently, when a signal is sampled at a frequency ω_s , all frequencies higher than $(\pi/2)\omega_s$ cannot be represented at their original frequency. Instead, they are present in the sampled signal with their original amplitude but at a lower-frequency harmonic. Because of the aliasing or foldover issues, a combination of analog and digital filtering is usually required. The sampler (i.e., the A/D converter) must be preceded by an analog filter that rejects those high-frequency components such as stray electrical pickup that would result in foldover when sampled. In commercial products, analog filters are normally incorporated into the input processing hardware by the manufacturer. The software then permits the user to specify digital filtering to remove any undesirable low-frequency components.

On the analog side, the filter is often the conventional resistor-capacitor or RC filter. However, other possibilities exist. For example, one type of A/D converter is called an *integrating A/D* because the converter basically integrates the input signal over a fixed interval of time. By making the interval $\frac{1}{60}$ s, this approach provides excellent rejection of any 60-Hz electrical noise.

On the digital side, the input processing software generally provides for smoothing via the exponentially weighted moving average, which is the digital counterpart to the RC network analog filter. The smoothing equation is as follows:

$$y_i = \alpha x_i + (1 - \alpha)y_{i-1} \quad (8-107)$$

where x_i = current value of input

y_i = current output from filter

y_{i-1} = previous output from filter
 α = filter coefficient

The degree of smoothing is determined by the filter coefficient α , with $\alpha = 1$ being no smoothing and $\alpha = 0$ being infinite smoothing (no effect of new measurements). The filter coefficient α is related to the filter time constant τ_f and the sampling interval Δt by

$$\alpha = 1 - \exp\left(\frac{-\Delta t}{\tau_f}\right) \quad (8-108)$$

or by the approximation

$$\alpha = \frac{\Delta t}{\Delta t + \tau_f} \quad (8-109)$$

Another approach to smoothing is to use the arithmetic moving average, which is represented by

$$y_i = \frac{\sum_{j=1}^n x_{i+1-j}}{n} \quad (8-110)$$

The term *moving* is used because the filter software maintains a storage array with the previous n values of the input. When a new value is received, the oldest value in the storage array is replaced with the new value, and the arithmetic average is recomputed. This permits the filtered value to be updated each time a new input value is received.

In process applications, determining τ_f (or α) for the exponential filter and n for the moving average filter is often done merely by observing the behavior of the filtered value. If the filtered value is "bouncing," the degree of smoothing (that is, τ_f or n) is increased. This can easily lead to an excessive degree of filtering, which will limit the performance of any control system that uses the filtered value. The degree of filtering is best determined from the frequency spectrum of the measured input, but such information is rarely available for process measurements.

ALARMS

The purpose of an alarm is to alert the process operator to a process condition that requires immediate attention. An alarm is said to occur whenever the abnormal condition is detected and the alert is issued. An alarm is said to return to normal when the abnormal condition no longer exists. Analog alarms can be defined on measured variables, calculated variables, controller outputs, and the like. For analog alarms, the following possibilities exist:

1. *High/low alarms.* A high alarm is generated when the value is greater than or equal to the value specified for the high-alarm limit. A low alarm is generated when the value is less than or equal to the value specified for the low-alarm limit.

2. *Deviation alarms.* An alarm limit and a target are specified. A high-deviation alarm is generated when the value is greater than or equal to the target plus the deviation alarm limit. A low-deviation alarm is generated when the value is less than or equal to the target minus the deviation alarm limit.

3. *Trend or rate-of-change alarms.* A limit is specified for the maximum rate of change, usually specified as a change in the measured value per minute. A high-trend alarm is generated when the rate of change of the variable is greater than or equal to the value specified for the trend alarm limit. A low-trend alarm is generated when the rate of change of the variable is less than or equal to the negative of the value specified for the trend alarm limit.

Most systems permit multiple alarms of a given type to be configured for a given value. For example, configuring three high alarms provides a high alarm, a high-high alarm, and a high-high-high alarm.

One operational problem with analog alarms is that noise in the variable can cause multiple alarms whenever its value approaches a limit. This can be avoided by defining a dead band on the alarm. For example, a high alarm would be processed as follows:

1. *Occurrence.* The high alarm is generated when the value is greater than or equal to the value specified for the high-alarm limit.

2. *Return to normal.* The high-alarm return to normal is generated when the value is less than or equal to the high-alarm limit less the dead band.

As the degree of noise varies from one input to the next, the dead band must be individually configurable for each alarm.

Discrete alarms can be defined on discrete inputs, limit switch inputs from on/off actuators, and so on. For discrete alarms, the following possibilities exist:

1. *Status alarms.* An expected or normal state is specified for the discrete value. A status alarm is generated when the discrete value is other than its expected or normal state.

2. *Change-of-state alarm.* A change-of-state alarm is generated on any change of the discrete value.

The expected sequence of events on an alarm is basically as follows:

1. The alarm occurs. This usually activates an audible annunciator.

2. The alarm occurrence is acknowledged by the process operator. When all alarms have been acknowledged, the audible annunciator is silenced.

3. Corrective action is initiated by the process operator.

4. The alarm condition returns to normal.

However, additional requirements are imposed at some plants. Sometimes the process operator must acknowledge the alarm's return to normal. Some plants require that the alarm occurrence be reissued if the alarm remains in the occurred state longer than a specified time. Consequently, some "personalization" of the alarming facilities is done.

When alarms were largely hardware-based (i.e., the panel alarm systems), the purchase and installation of the alarm hardware imposed a certain discipline on the configuration of alarms. With digital systems, the suppliers have made it extremely easy to configure alarms. In fact, it is sometimes easier to configure alarms on a measured value than not to configure the alarms. Furthermore, the engineer assigned the responsibility for defining alarms is often paranoid that an abnormal process condition will go undetected because an alarm has not been configured. When alarms are defined on every measured and calculated variable, the result is an excessive number of alarms, most of which are duplicative and unnecessary.

The accident at the Three Mile Island nuclear plant clearly demonstrated that an alarm system can be counterproductive. An excessive number of alarms can distract the operator's attention from the real problem that needs to be addressed. Alarms that merely tell the operator something that is already known do the same. In fact, a very good definition of a nuisance alarm is one that informs the operator of a situation of which the operator is already aware. The only problem with applying this definition lies determining what the operator already knows.

Unless some discipline is imposed, engineering personnel, especially where contractors are involved, will define far more alarms than plant operations require. This situation may be addressed by simply setting the alarm limits to values such that the alarms never occur. However, changes in alarms and alarm limits are changes from the perspective of the process safety management regulations. It is prudent to impose the necessary discipline to avoid an excessive number of alarms. Potential guidelines are as follows:

1. For each alarm, a specific action is expected from the process operator. Operator actions such as call maintenance are inappropriate with modern systems. If maintenance needs to know, modern systems can inform maintenance directly.

2. Alarms should be restricted to abnormal situations for which the process operator is responsible. A high alarm on the temperature in one of the control system cabinets should not be issued to the process operator. Correcting this situation is the responsibility of maintenance, not the process operator.

3. Process operators are expected to be exercising normal surveillance of the process. Therefore, alarms are not appropriate for situations known to the operator either through previous alarms or through normal process surveillance. The "sleeping operator" problem can be addressed by far more effective means than the alarm system.

4. When the process is operating normally, no alarms should be triggered. Within the electric utility industry, this design objective is

known as *darkboard*. Application of darkboard is especially important in batch plants, where much of the process equipment is operated intermittently.

Ultimately, guidelines such as those above will be taken seriously only if production management pays attention to the process alarms. The consequences of excessive and redundant alarms will be felt primarily by those responsible for production operations. Therefore, production management must make adequate resources available for reviewing and analyzing the proposed alarm configurations.

Another serious distraction to a process operator is the multiple-alarm event, where a single event within the process results in multiple alarms. When the operator must individually acknowledge each alarm, considerable time can be lost in silencing the obnoxious annunciator before the real problem is addressed. Air-handling systems are especially vulnerable to this, where any fluctuation in pressure (e.g., resulting from a blower trip) can cause a number of pressure alarms to occur.

Point alarms (high alarms, low alarms, status alarms, etc.) are especially vulnerable to the multiple-alarm event. This can be addressed in one of two ways:

1. *Ganging alarms*. Instead of individually issuing the point alarms, all alarms associated with a certain aspect of the process

are configured to give a single trouble alarm. The responsibility rests entirely with the operator to determine the nature of the problem.

2. *Intelligent alarms*. Logic is incorporated into the alarm system to determine the nature of the problem and then issue a single alarm to the process operator.

While the intelligent alarm approach is clearly preferable, substantial process analysis is required to support intelligent alarming. Meeting the following two objectives is quite challenging:

1. The alarm logic must consistently detect abnormal conditions within the process.
2. The alarm logic must not issue an alert to an abnormal condition when in fact none exists.

Often the latter case is more challenging than the former. Logically, the intelligent alarm effort must be linked to the process hazards analysis. Developing an effective intelligent alarming system requires substantial commitments of effort, involving process engineers, control systems engineers, and production personnel. Methodologies such as expert systems can facilitate the implementation of an intelligent alarming system, but they must still be based on a sound analysis of the potential process hazards.

DIGITAL TECHNOLOGY FOR PROCESS CONTROL

GENERAL REFERENCES: Auslander and Ridgely, *Design and Implementation of Real-Time Software for the Control of Mechanical Systems*, Prentice-Hall, Upper Saddle River, N.J., 2002. Herb, *Understanding Distributed Processor Systems for Control*, ISA, Research Triangle Park, N.C., 1999. Hughes, *Programmable Controllers*, ISA, Research Triangle Park, N.C., 1997. Johnson, *Process Control Instrumentation Technology*, 6th ed., Prentice-Hall, Upper Saddle River, N.J., 2000. Liptak, *Instrument Engineers Handbook*, Chilton Book Company, Philadelphia, 1995. Webb and Reis, *Programmable Logic Controllers*, 4th ed., Prentice-Hall, Upper Saddle River, N.J., 2002.

Since the 1970s, process controls have evolved from pneumatic analog technology to electronic analog technology to microprocessor-based controls. Electronic and pneumatic controllers have now virtually disappeared from process control systems, which are dominated by programmable electronic systems based on microprocessor technology.

HIERARCHY OF INFORMATION SYSTEMS

Coupling digital controls with networking technology permits information to be passed from level to level within a corporation at high rates of speed. This technology is capable of presenting the measured variable from a flow transmitter installed in a plant in a remote location anywhere in the world to the company headquarters in less than 1 s.

A hierarchical representation of the information flow within a company leads to a better understanding of how information is passed from one layer to the next. Such representations can be developed in varying degrees of detail, and most companies have developed one that describes their specific practices. The following hierarchy consists of five levels, as shown in Fig. 8-30.

Measurement Devices and Final Control Elements This lowest layer couples the control and information systems to the process. The measurement devices provide information on the current conditions within the process. The final control elements permit control decisions to be imposed on the process. Although traditionally analog, smart transmitters and smart valves based on microprocessor technology are now beginning to dominate this layer.

Safety and Environmental/Equipment Protection The level 2 functions play a critical role by ensuring that the process is operating safely and satisfies environmental regulations. Process safety relies on the principle of multiple protection layers that involve groupings of equipment and human actions. One layer includes process control functions, such as alarm management during abnormal situations, and safety instrumented systems for emergency shutdowns. The safety equipment (including sensors and block valves) operates independently of the regular instrumentation used for regulatory control in level 3. Sensor validation techniques can be employed to confirm that the sensors are functioning properly.

Regulatory Controls The objective of this layer is to operate the process at or near the targets supplied by a higher layer in the hierarchy. To achieve consistent process operations, a high degree of automatic control is required from the regulatory layer. The direct result is a reduction in variance in the key process variables. More uniform product quality is an obvious benefit. However, consistent process operation is a prerequisite for optimizing the process operations. To ensure success for the upper-level functions, the first objective of any automation effort must be to achieve a high degree of regulatory control.

Real-Time Optimization Determining the most appropriate targets for the regulatory layer is the responsibility of the RTO layer. Given the current production and quality targets for a unit, RTO determines how the process can be best operated to meet them. Usually this optimization has a limited scope, being confined to a single production unit or possibly even a single unit operation within a production unit. RTO translates changes in factors such as current process efficiencies, current energy costs, cooling medium temperatures, and so on to changes in process operating targets so as to optimize process operations.

Production Controls The nature of the production control logic differs greatly between continuous and batch plants. A good example of production control in a continuous process is refinery optimization. From the assay of the incoming crude oil, the values of the various possible refined products, the contractual commitments to deliver certain products, the performance measures of the various units within a refinery, and the like, it is possible to determine the mix of products that optimizes the economic return from processing this crude. The solution of this problem involves many relationships and constraints and is solved with techniques such as linear programming.

In a batch plant, production control often takes the form of routing or short-term scheduling. For a multiproduct batch plant, determining the long-term schedule is basically a manufacturing resource planning (MRP) problem, where the specific products to be manufactured and the amounts to be manufactured are determined from the outstanding orders, the raw materials available for production, the production capacities of the process equipment, and other factors. The goal of the MRP effort is the long-term schedule, which is a list of the products to be manufactured over a specified period of time (often one week). For each product on the list, a target amount is also specified. To manufacture this amount usually involves several batches. The term *production run* often refers to the sequence of batches required to make the target amount of product, so in effect the long-term schedule is a list of production runs.

Most multiproduct batch plants have more than one piece of equipment of each type. Routing refers to determining the specific pieces of equipment that will be used to manufacture each run on the long-term

production schedule. For example, the plant might have five reactors, eight neutralization tanks, three grinders, and four packing machines. For a given run, a rather large number of routes are possible. Furthermore, rarely is only one run in progress at a given time. The objective of routing is to determine the specific pieces of production equipment to be used for each run on the long-term production schedule. Given the dynamic nature of the production process (equipment failures, insertion/deletion of runs into the long-term schedule, etc.), the solution of the routing problem continues to be quite challenging.

Corporate Information Systems Terms such as *management information systems* (MIS), *enterprise resource planning* (ERP), *supply chain management* (SCM), and *information technology* (IT) are frequently used to designate the upper levels of computer systems within a corporation. From a control perspective, the functions performed at this level are normally long-term and/or strategic. For example, in a processing plant, long-term contracts are required with the providers of the feedstocks. A forecast must be developed for the demand for possible products from the plant. This demand must be translated to needed raw materials, and then contracts executed with the suppliers to deliver these materials on a relatively uniform schedule.

DIGITAL HARDWARE IN PROCESS CONTROL

Digital control technology was first applied to process control in 1959, using a single central computer (and analog backup for reliability). In the mid-1970s, a microcomputer-based process control architecture referred to as a *distributed control system* (DCS) was introduced and rapidly became a commercial success. A DCS consists of some number of microprocessor-based nodes that are interconnected by a digital communications network, often called a data highway. Today the DCS is still dominant, but there are other options for carrying out computer control, such as single-loop controllers, programmable logic controllers, and personal computer controllers. A brief review of each type of controller device is given below; see the following section "Controllers, Final Control Elements, and Regulators" for more details on controller hardware options.

Single-Loop Controllers The single-loop controller (SLC) is the digital equivalent of analog single-loop controllers. It is a self-contained microprocessor-based unit that can be rack-mounted. Many manufacturers produce single processor units that handle cascade control or multiple loops, typically 4, 8, or 16 loops per unit, and incorporate self-tuning or auto-tuning PID control algorithms.

Programmable Logic Controllers Programmable logic controllers (PLCs) are simple digital devices that are widely used to control sequential and batch processes, although they now have additional functions that implement PID control and other mathematical operations. PLCs can be utilized as stand-alone devices or in conjunction with digital computer control systems. Because the logical functions are stored in main memory, one measure of a PLC's capability is its memory scan rate. Most PLCs are equipped with an internal timing capability to delay an action by a prescribed amount of time, to execute an action at a prescribed time, and so on. Newer PLC models often are networked to serve as one component of a DCS, with operator I/O provided by a separate component in the network. A distinction is made between configurable and programmable PLCs. The term *configurable* implies that logical operations (performed on inputs to yield a desired output) are located in PLC memory, perhaps in the form of ladder diagrams by selecting from a PLC menu or by direct interrogation of the PLC. Most control engineers prefer the simplicity of configuring the PLC to the alternative of programming it. However, some batch applications, particularly those involving complex sequencing, are best handled by a programmable approach.

Personal Computer Controllers In comparison with PLCs, PCs have the advantages of lower purchase cost, graphics output, large memory, large selection of software products (including databases and development tools), more programming options (use of C or Java versus ladder logic), richer operating systems, and open networking. PLCs have the following advantages: lower maintenance cost, operating system and hardware optimized for control, fast boot times, ruggedness, low failure rate, longer support for product models, and self-contained units.

A number of vendors have introduced so-called scalable process control systems. Scalable means that the size of the control and instrumentation systems is easily expanded by simply adding more devices. This feature is possible because of the trend toward more openness (i.e., "plug and play" between devices), smaller size, lower cost, greater flexibility, and more off-the-shelf hardware and software in digital control systems. A typical system includes personal computers, an operating system, object-oriented database technology, modular field-mounted controllers, and plug-and-play integration of both system and intelligent field devices. New devices are automatically recognized and configured with the system. Advanced control algorithms can be executed at the PC level.

Distributed Control System Figure 8-65 depicts a representative distributed control system. The DCS consists of many commonly

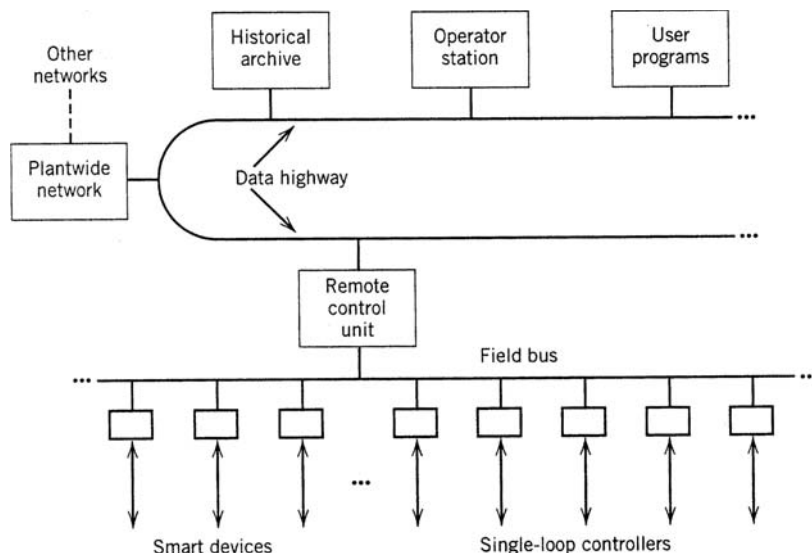


FIG. 8-65 A DCS using a broadband (high-bandwidth) data highway and field bus connected to a single remote control unit that operates smart devices and single-loop controllers.

8-70 PROCESS CONTROL

used components, including multiplexers (MUXs), single-loop and multiple-loop controllers, PLCs, and smart devices. A system includes some of or all the following components:

1. *Control network.* The control network is the communication link between the individual components of a network. Coaxial cable and, more recently, fiber-optic cable have often been used, sometimes with Ethernet protocols. A redundant pair of cables (dual redundant highway) is normally supplied to reduce the possibility of link failure.

2. *Workstations.* Workstations are the most powerful computers in the system, capable of performing functions not normally available in other units. A workstation acts both as an arbitrator unit to route internodal communications and as the database server. An operator interface is supported, and various peripheral devices are coordinated through the workstations. Computationally intensive tasks, such as real-time optimization or model predictive control, are implemented in a workstation. Operators supervise and control processes from these workstations. Operator stations may be connected directly to printers for alarm logging, printing reports, or process graphics.

3. *Remote control units (RCUs).* These components are used to implement basic control functions such as PID control. Some RCUs may be configured to acquire or supply set points to single-loop controllers. Radio telemetry (wireless) may be installed to communicate with MUX units located at great distances.

4. *Application stations.* These separate computers run application software such as databases, spreadsheets, financial software, and simulation software via an OPC interface. OPC is an acronym for object linking and embedding for process control, a software architecture based on standard interfaces. These stations can be used for e-mail and as web servers, for remote diagnosis configuration, and even for operation of devices that have an IP (Internet Protocol) address. Applications stations can communicate with the main database contained in online mass storage systems. Typically hard disk drives are used to store active data, including online and historical databases and nonmemory resident programs. Memory resident programs are also stored to allow loading at system start-up.

5. *Field buses and smart devices.* An increasing number of field-mounted devices are available that support digital communication of the process I/O in addition to, or in place of, the traditional 4- to 20-mA current signal. These devices have greater functionality, resulting in reduced setup time, improved control, combined functionality of separate devices, and control valve diagnostic capabilities. Digital communication also allows the control system to become completely distributed where, e.g., a PID control algorithm could reside in a valve positioner or in a sensor/transmitter.

DISTRIBUTED DATABASE AND THE DATABASE MANAGER

A database is a centralized location for data storage. The use of databases enhances system performance by maintaining complex relations between data elements while reducing data redundancy. A database may be built based on the relational model, the entity relationship model, or some other model. The database manager is a system utility program or programs acting as the gatekeeper to the databases. All functions retrieving or modifying data must submit a request to the manager. Information required to access the database includes the tag name of the database entity, often referred to as a point, the attributes to be accessed, and the values, if modifying. The database manager maintains the integrity of the databases by executing a request only when not processing other conflicting requests. Although a number of functions may read the same data item at the same time, writing by a number of functions or simultaneous read and write of the same data item is not permitted.

To allow flexibility, the database manager must also perform point addition or deletion. However, the ability to create a point type or to add or delete attributes of a point type is not normally required because, unlike other data processing systems, a process control system normally involves a fixed number of point types and related attributes. For example, analog and binary input and output types are required for process I/O points. Related attributes for these point types include tag names, values, and hardware addresses. Different

system manufacturers may define different point types using different data structures. We will discuss other commonly used point types and attributes as they appear.

Data Historian A historical database is built similar to an online database. Unlike their online counterparts, the information stored in a historical database is not normally accessed directly by other subsystems for process control and monitoring. Periodic reports and long-term trends are generated based on the archived data. The reports are often used for planning and system performance evaluations such as statistical process (quality) control. The trends may be used to detect process drifts or to compare process variations at different times.

The historical data are sampled at user-specified intervals. A typical process plant contains a large number of data points, but it is not feasible to store data for all points at all times. The user determines if a data point should be included in the list of archive points. Most systems provide archive-point menu displays. The operators are able to add or delete data points to the archive point lists. The sampling periods are normally some multiples of their base scan frequencies. However, some systems allow historical data sampling of arbitrary intervals. This is necessary when intermediate virtual data points that do not have the scan frequency attribute are involved. The archive point lists are continuously scanned by the historical database software. Online databases are polled for data, and the times of data retrieval are recorded with the data obtained. To conserve storage space, different data compression techniques are employed by various manufacturers.

DIGITAL FIELD COMMUNICATIONS AND FIELD BUS

Microprocessor-based equipment, such as smart instruments and single-loop controllers with digital communications capability, are now used extensively in process plants. A field bus, which is a low-cost protocol, is necessary to perform efficient communication between the DCS and devices that may be obtained from different vendors. Figure 8-65 illustrates a LAN-based DCS with field buses and smart devices connected to a data highway.

Presently, there are several regional and industry-based field bus standards, including the French standard (FIP), the German standard (Profibus), and proprietary standards by DCS vendors, generally in the United States, led by the Fieldbus Foundation, a not-for-profit corporation. As of 2002, international standards organizations had adopted all these field bus standards rather than a single unifying standard. However, there will likely be further developments in field bus standards in the future. A benefit of standardizing the field bus is that it has encouraged third-party traditional equipment manufacturers to enter the smart equipment market, resulting in increased competition and improved equipment quality.

Several manufacturers have made available field bus controllers that reside in the final control element or measurement transmitter. A suitable communications modem is present in the device to interface with a proprietary PC-based, or hybrid analog/digital bus network. At present, field bus controllers are single-loop controllers containing 8- and 16-bit microprocessors that support the basic PID control algorithm as well as other functionalities. Case studies in implementing such digital systems have shown significant reductions in cost of installation (mostly cabling and connections) versus traditional analog field communication.

A general movement has also begun in the direction of using the high-speed Ethernet standard (100 Mbit/s or higher), allowing data transfer by TCP/IP that is used pervasively in computer networking. This would allow any smart device to communicate directly with others in the network or to be queried by the operator regarding its status and settings.

INTERNODAL COMMUNICATIONS

For a group of computers to become a network, intercomputer communication is required. Prior to the 1980s, each system vendor used a proprietary protocol to network its computers. Ad hoc approaches were sometimes used to connect third-party equipment but were not cost-effective with regard to system maintenance, upgrade, and expansion.

The recent introduction of standardized communication protocols has led to a decrease in capital cost. Most current DCS network protocol designs are based on the ISO-OSI seven-layer model with physical, data link, network, transport, session, presentation, and application layers.

An effort in standardizing communication protocols for plant automation was initiated by General Motors in the early 1980s. This work culminated in the Manufacturing Automation Protocol (MAP), which adopted the ISO-OSI standards as its basis. MAP specifies a broadband backbone local-area network (LAN) that incorporates a selection of existing standard protocols suitable for discrete component manufacturing. MAP was intended to address the integration of DCSs used in process control. Subsequently, TCP/IP (Transmission Control Protocol/Internet Protocol) was adopted for communication between nodes that have different operating systems.

Communication programs also act as links to the database manager. When data are requested from a remote node, the database manager transfers the request to the remote node database manager via the communication programs. The remote node communication programs then relay the request to the resident database manager and return the requested data. The remote database access and the existence of communications equipment and software are transparent to the user.

PROCESS CONTROL LANGUAGES

Originally, software for process control utilized high-level programming languages such as FORTRAN and BASIC. Some companies have incorporated libraries of software routines for these languages, but others have developed specialty languages characterized by natural language statements. The most widely adopted user-friendly approach is the fill-in-the-forms or table-driven process control languages (PCLs). Typical PCLs include function block diagrams, ladder logic, and programmable logic. The core of these languages is a num-

ber of basic function blocks or software modules, such as analog in, digital in, analog out, digital out, PID, summer, and splitter. Using a module is analogous to calling a subroutine in conventional FORTRAN or C programs.

In general, each module contains one or more inputs and an output. The programming involves connecting outputs of function blocks to inputs of other blocks via the graphical-user interface. Some modules may require additional parameters to direct module execution. Users are required to fill in templates to indicate the sources of input values, the destinations of output values, and the parameters for forms/tables prepared for the modules. The source and destination blanks may specify process I/O channels and tag names when appropriate. To connect modules, some systems require filling in the tag names of modules originating or receiving data.

Many DCSs allow users to write custom code (similar to BASIC) and attach it to data points, so that the code is executed each time the point is scanned. The use of custom code allows many tasks to be performed that cannot be carried out by standard blocks.

All process control languages contain PID control blocks of different forms. Other categories of function blocks include

1. *Logical operators.* AND, OR, and exclusive OR (XOR) functions.
2. *Calculations.* Algebraic operations such as addition, multiplication, square root extraction, or special function evaluation.
3. *Selectors.* Min and max functions, transferring data in a selected input to the output or the input to a selected output.
4. *Comparators.* Comparison of two analog values and transmission of a binary signal to indicate whether one analog value exceeds the other.
5. *Timers.* Delayed activation of the output for a programmed duration after activation by the input signal.
6. *Process dynamics.* Emulation of a first-order process lag (or lead) and time delay.

CONTROLLERS, FINAL CONTROL ELEMENTS, AND REGULATORS

GENERAL REFERENCES: Driskell, *Control-Valve Selection and Sizing*, ISA, 1983. McMillan, *Process/Industrial Instruments and Controls Handbook*, 5th ed., McGraw-Hill, 1999. Hammit, *Cavitation and Multiphase Flow Phenomena*, McGraw-Hill, 1980. ANSI/ISA-75.25.01, *Test Procedure for Control Valve Response Measurement from Step Inputs*, The Instrumentation Systems and Automation Society, 2000. Norton and Karczub, *Fundamentals of Noise and Vibration Analysis for Engineers*, 2d ed., Cambridge University Press, 2003. Ulanski, *Valve and Actuator Technology*, McGraw-Hill, 1991. Kinsler et al., *Fundamentals of Acoustics*, 4th ed., Wiley. *National Electrical Code Handbook*, 9th ed., National Fire Protection Association, Inc.

External control of the process is achieved by devices that are specially designed, selected, and configured for the intended process control application. The text that follows covers three very common function classifications of process control devices: controllers, final control elements, and regulators.

The process controller is the "master" of the process control system. It accepts a set point and other inputs and generates an output or outputs that it computes from a rule or set of rules that is part of its internal configuration. The controller output serves as an input to another controller or, more often, as an input to a final control element. The final control element typically is a device that affects the flow in the piping system of the process. The final control element serves as an interface between the process controller and the process. Control valves and adjustable speed pumps are the principal types discussed.

Regulators, though not controllers or final control elements, perform the combined function of these two devices (controller and final control element) along with the measurement function commonly associated with the process variable transmitter. The uniqueness, control performance, and widespread usage of the regulator make it deserving of a functional grouping of its own.

PNEUMATIC, ELECTRONIC, AND DIGITAL CONTROLLERS

Pneumatic Controllers The pneumatic controller is an automatic controller that uses variable air pressure as input and output signals. An air supply is also required to "power" the mechanical components of the controller and provide an air source for the controller output signal. Pneumatic controllers were first available in the early 1940s but are now rarely used for large-scale industrial control projects. Pneumatic controllers are still used where cost, ruggedness, or the installation requires an all-pneumatic solution.

Pneumatic process transmitters are used to produce a pressure signal that is proportional to the calibrated range of the measuring element. Of the transmitter range 0 to 100 percent is typically represented by a 0.2- to 1.0-bar (3- to 15-psig) pneumatic signal. This signal is sent through tubing to the pneumatic controller process variable feedback connection. The process variable feedback can also be sensed directly in cases where the sensing element has been incorporated into the controller design. Controllers with integral sensing elements are available that sense pressure, differential pressure, temperature, and level.

The pneumatic controller is designed so that 0 to 100 percent output is also represented by 0.2 to 1.0 bar (3 to 15 psig). The output signal is sent through tubing to the control valve or other final control element. Most pneumatic controllers provide a manual control mode where the output pressure is manually set by operating personnel. The controller design also provides a mechanism to adjust the set point.

Early controller designs required "balancing" of the controller output prior to switching to or from automatic and manual modes. This procedure minimized inadvertent disturbance to the process caused by potentially large differences between the automatic and manual output levels. Later designs featured "bumpless" or "procedureless" automatic-to-manual transfer.

Although the pneumatic controller is often used in single-loop control applications, cascade strategies can be implemented where the controller design supports input of external or remote set-point signals. A balancing procedure is typically required to align the remote set point with the local set point before the controller is switched into cascade mode.

Almost all pneumatic controllers include indicators for process variable, set point, and output. Many controller designs also feature integral chart recorders. There are versions of the pneumatic controller that support combinations of proportional, integral, and derivative actions.

The pneumatic controller can be installed into panel boards that are adjacent to the process being controlled or in a centrally located control room. Field-mountable controllers can be installed directly onto the control valve, a nearby pipestand, or wall in close proximity to the control valve and/or measurement transmitter.

If operated on clean, dry plant air, pneumatic controllers offer good performance and are extremely reliable. In many cases, however, plant air is neither clean nor dry. A poor-quality air supply will cause unreliable performance of pneumatic controllers, pneumatic field measurement devices, and final control elements. The main shortcoming of the pneumatic controller is its lack of flexibility when compared to modern electronic controller designs. Increased range of adjustability, choice of alternative control algorithms, the communication link to the control system, and other features and services provided by the electronic controller make it a superior choice in most of today's applications. Controller performance is also affected by the time delay induced by pneumatic tubing runs. For example, a 100-m run of 6.35-mm ($\frac{1}{4}$ -in) tubing will typically cause 5 s of apparent process dead time, which will limit the control performance of fast processes such as flows and pressures.

Pneumatic controllers continue to be used in areas where it would be hazardous to use electronic equipment, such as locations with flammable or explosive atmospheres or other locations where compressed air is available but where access to electrical services is limited or restricted.

Electronic (Digital) Controllers Almost all the electronic process controllers used today are microprocessor-based, digital devices. In the transition from pneumatic to electronic controllers, a number of analog controller designs were available. Due to the inflexible nature of the analog designs, these controllers have been almost completely replaced by digital designs. The microprocessor-based controllers contain, or have access to, input/output (I/O) interface electronics that allow various types of signals to enter and leave the controller's processor.

The resolution of the analog I/O channels of the controller varies by manufacturer and age of the design. The 12- to 14-bit conversion resolution of the analog input channels is quite common. Conversion resolution of the analog output channels is typically 10- to 12-bit. Newer designs support up to 16 bit input and output resolution. Although 10-bit output resolution had been considered satisfactory for many years, it has recently been identified as a limitation of control performance. This limitation has emerged as the performance of control valve actuators has improved and the use of other high-resolution field devices, such as variable-speed pump drives, has become more prevalent. These improvements have been driven by the need to deliver higher operating efficiencies and improved product specifications through enhanced process control performance.

Sample rates for the majority of digital controllers are adjustable and range from 1 sample every 5 s to 10 samples per second. Some controller designs have fixed sample rates that fall within the same range. Hardwired low-pass filters are usually installed on the analog inputs to the controller to help protect the sampler from aliasing errors.

The real advantage of digital controllers is the substantial flexibility offered by a number of different configuration schemes. The simplest form of configuration is seen in a controller design that features a number of user-selectable control strategies. These strategies are customized by setting "tunable" parameters within the strategy. Another common configuration scheme uses a library of function blocks that can be selected and combined to form the desired control strategy. Each function block has adjustable parameters. Additional configuration schemes include text-based scripting languages, higher-level languages such as Basic or C, and ladder logic.

Some digital controller designs allow the execution rates of control strategy elements to be set independently of each other and indepen-

dently of the I/O subsystem sample rate. Data passed from control element to subsystems that operate at slower sample or execution rates present additional opportunities for timing and aliasing errors.

Distributed Control Systems Some knowledge of the distributed control system (DCS) is useful in understanding electronic controllers. A DCS is a process control system with sufficient performance to support large-scale, real-time process applications. The DCS has (1) an operations workstation with input devices, such as a keyboard, mouse, track ball, or other similar device, and a display device, such as a CRT or LCD panel; (2) a controller subsystem that supports various types of controllers and controller functions; (3) an I/O subsystem for converting analog process input signals to digital data and digital data back to analog output signals; (4) a higher-level computing platform for performing process supervision, historical data trending and archiving functions, information processing, and analysis; and (5) communication networks to tie the DCS subsystems, plant areas, and other plant systems together. The component controllers used in the controller subsystem portion of the DCS can be of various types and include multiloop controllers, programmable logic controllers, personal computer controllers, single-loop controllers, and field bus controllers. The type of electronic controller utilized depends on the size and functional characteristic of the process application being controlled. Personal computers are increasingly being used as DCS operations workstations or interface stations in place of custom-built machines. This is due to the low cost and high performance of the PC. See the earlier section "Digital Technology for Process Control."

Multiloop Controllers The multiloop controller is a DCS network device that uses a single 32-bit microprocessor to provide control functions to many process loops. The controller operates independently of the other devices on the DCS network and can support from 20 to 500 loops. Data acquisition capability for 1000 analog and discrete I/O channels or more can also be provided by this controller. The I/O is typically processed through a subsystem that is connected to the controller through a dedicated bus or network interface. The multiloop controller contains a variety of function blocks (for example, PID, totalizer, lead/lag compensator, ratio control, alarm, sequencer, and boolean) that can be "soft-wired" together to form complex control strategies. The multiloop controller also supports additional configuration schemes including text-based scripting languages, higher-level languages such as Basic or C, and, to a limited extent, ladder logic. The multiloop controller, as part of a DCS, communicates with other controllers and human/machine interface (HMI) devices also on the DCS network.

Programmable Logic Controllers The programmable logic controller (PLC) originated as a solid-state, and far more flexible, replacement for the hardwired relay control panel and was first used in the automotive industry for discrete manufacturing control. Today, PLCs are primarily used to implement boolean logic functions, timers, and counters. Some PLCs offer a limited number of math functions and PID control. PLCs are often used with on/off input and output devices such as limit or proximity switches, solenoid-actuated process control valves, and motor switch gear. PLCs vary greatly in size with the smallest supporting less than 128 I/O channels and the largest supporting more than 1023 I/O channels. Very small PLCs combine processor, I/O, and communications functions into a single, self-contained unit. For larger PLC systems, hardware modules such as the power supply, processor module, I/O modules, communication module, and backplane are specified based on the application. These systems support multiple I/O backplanes that can be chained together to increase the I/O count available to the processor. Discrete I/O modules are available that support high-current motor loads and general-purpose voltage and current loads. Other modules support analog I/O and special-purpose I/O for servomotors, stepping motors, high-speed pulse counting, resolvers, decoders, displays, and keyboards. PLC I/O modules often come with indicators to determine the status of key I/O channels. When used as an alternative to a DCS, the PLC is programmed with a handheld or computer-based loader. The PLC is typically programmed with ladder logic or a high-level computer language such as BASIC, FORTRAN, or C. Programmable logic controllers use 16- or 32-bit microprocessors and offer some form of point-to-point serial communications such as RS-232C, RS-485, or

networked communication such as Ethernet with proprietary or open protocols. PLCs typically execute the boolean or ladder logic configuration at high rates; 10-ms execution intervals are common. This does not necessarily imply that the analog I/O or PID control functions are executed at the same rate. Many PLCs execute the analog program at a much slower rate. Manufacturers' specifications must be consulted.

Personal Computer Controller Because of its high performance at low cost and its unexcelled ease of use, application of the personal computer (PC) as a platform for process controllers is growing. When configured to perform scan, control, alarm, and data acquisition (SCADA) functions and combined with a spreadsheet or database management application, the PC controller can be a low-cost, basic alternative to the DCS or PLC. Using the PC for control requires installation of a board into the expansion slot in the computer, or the PC can be connected to an external I/O module by using a standard communication port on the PC. The communication is typically achieved through a serial interface (RS-232, RS-422, or IEEE-488), universal serial bus (USB), or Ethernet. The controller card/module supports 16- or 32-bit microprocessors. Standardization and high volume in the PC market have produced a large selection of hardware and software tools for PC controllers.

The PC can also be interfaced to a DCS to perform advanced control or optimization functions that are not available within the standard DCS function library.

Single-Loop Controller The single-loop controller (SLC) is a process controller that produces a single output. SLCs can be pneumatic, analog electronic, or microprocessor-based. Pneumatic SLCs are discussed in the pneumatic controller section, and analog electronic SLC is not discussed because it has been virtually replaced by the microprocessor-based design. The microprocessor-based SLC uses an 8- or 16-bit microprocessor with a small number of digital and analog process input channels with control logic for the I/O incorporated within the controller. Analog inputs and outputs are available in the standard ranges (1 to 5 V dc and 4 to 20 mA dc). Direct process inputs for temperature sensors (thermistor RTD and thermocouple types) are available. Binary outputs are also available. The face of the SLC has some form of visible display and pushbuttons that are used to view or adjust control values and configuration. SLCs are available for mounting in panel openings as small as 48 × 48 mm (1.9 × 1.9 in).

The processor-based SLC allows the user to select from a set of predefined control strategies or to create a custom control strategy by using a set of control function blocks. Control function blocks include PID, on/off, lead/lag, adder/subtractor, multiply/divide, filter functions, signal selector, peak detector, and analog track. SLCs feature auto/manual transfer switching, multi-set-point self-diagnostics, gain scheduling, and perhaps also time sequencing. Most processor-based SLCs have self-tuning or auto-tuning PID control algorithms. Sample times for the microprocessor-based SLCs vary from 0.1 to 0.5 s. Low-pass analog electronic filters are usually installed on the process inputs to minimize aliasing errors caused by high-frequency content in the process signal. Input filter time constants are typically in the range of 0.1 to 1 s. Microprocessor-based SLCs may be made part of a DCS by using the communication port (RS-485 is common) on the controller or may be operated in a stand-alone mode independently of the DCS.

Field Bus Controller Field bus technology is a network-based communications system that interconnects measurement and control equipment such as sensors, actuators, and controllers. Advanced field bus systems, intended for process control applications, such as Foundation Fieldbus, enable digital interoperability among these devices and have a built-in capability to distribute the control application across the network. Several manufacturers have made available Foundation Fieldbus devices that support process controller functionality. These controllers, known as field bus controllers, typically reside in the final control element or measurement transmitter, but can be designed into any field bus device. A suitable communications interface connects the Fieldbus segment to the distributed control system. When configuring the control strategy, all or part of the strategy may be loaded into the field bus devices. The remaining part of the control strategy would reside in the DCS itself. The distribution of the control function depends on the processing capacity of the field bus devices, the control strategy, and where it makes sense to perform these functions. Linearization of a control valve could be performed in the digital valve positioner (controller), for

example. Temperature and pressure compensation of a flow measurement could be performed in the flow transmitter processor. The capability of field bus devices varies greatly. Some devices will allow instances of control system function blocks to be loaded and executed, while other devices allow the use of only preconfigured function blocks. Field bus controllers are typically configured as single-loop PID controllers, but cascade or other complex control strategies can be configured depending on the capability of the field bus device. Field bus devices that have native support for process control functions do not necessarily implement the PID algorithm in the same way. It is important to understand these differences so that the controller tuning will deliver the desired closed-loop characteristics. The functionality of field bus devices is projected to increase as the controller market develops.

Controller Reliability and Application Trends Critical process control applications demand a high level of reliability from the electronic controller. Some methods that improve the reliability of electronic controllers include (1) focusing on robust circuit design using quality components; (2) using redundant circuits, modules, or subsystems where necessary; (3) using small backup systems when needed; (4) reducing repair time and using more powerful diagnostics; and (5) distributing functionality to more independent modules to limit the impact of a failed module. Currently, the trend in process control is away from centralized process control and toward an increased number of small distributed control or PLC systems. This trend will put emphasis on the evolution of the field bus controller and continued growth of the PC-based controller. Also, as hardware and software improve, the functionality of the controller will increase, and the supporting hardware will be physically smaller. Hence, the traditional lines between the DCS and the PLC will become less distinct as systems become capable of supporting either function set.

Controller Performance and Process Dynamics The design of a control loop must take the control objectives into account. What do you want this loop to do? And under what operating conditions? There may be control applications that require a single control objective and others that have several control objectives. Control objectives may include such requirements as minimum variance control at steady state, maximum speed of recovery from a major disturbance, maximum speed of set-point response where overshoot and ringing are acceptable, critically damped set-point response with no overshoot, robustness issues, and special start-up or shutdown requirements. The control objectives will define not only the tuning requirements of the controller, but also, to a large extent, the allowable dynamic parameters of the field instruments and process design. Process dynamics alone can prevent control objectives from being realized. Tuning of the controller cannot compensate for an incompatible process or unrealistic control objectives. For most controllers, the difference between the set-point and process feedback signal, the error, is the input to the PID algorithm. The calculated PID output is sent back to the final control element. Every component between the controller output and the process feedback is considered by the controller as the "process" and will directly affect the dynamics and ultimately the performance of the system. This includes not only the dynamics of the physical process, but also the dynamics of the field instruments, signal conditioning equipment, and controller signal processing elements such as filters, scaling, and linearization routines. The choice of final control element can significantly affect the dynamics of the system. If the process dynamics are relatively slow, with time constants of a few minutes or longer, most control valves are fast enough that their contribution to the overall process time response will be negligible. In cases where the process time constants are only a few seconds, the control valve dynamics may become the dominant lag in the overall response. Excessive filtering in the field-sensing devices may also mask the true process dynamics and potentially limit control performance. Often, the design of a control loop and the tuning of the controller are a compromise between a number of different control objectives. When a compromise is unacceptable, gain scheduling or other adaptive tuning routine may be necessary to match the controller response to the most appropriate control objective.

When one is tuning a controller, the form of the PID algorithm must be known. The three common forms of the PID algorithm are parallel

or noninteracting, classical or interacting, and the ISA Standard form. In most cases, a controller with any of these PID forms can be tuned to produce the desired closed-loop response. The actual tuning parameters will be different. The units of the tuning parameters also affect their value. The controller gain parameter is typically represented as a pure gain (K_c), acting on the error, or as proportional band (PB). In cases where the proportional band parameter is used, the equivalent controller gain is equal to 100 divided by the proportional band and represents the percent span that the error must traverse to produce a 100 percent change in the controller output. The proportional band is always applied to the controller error in terms of percent of span and percent of output. Controllers that use a gain tuning parameter commonly scale the error into percent span and use a percent output basis. In some controllers, the error is scaled by using a separate parameter into percent span prior to the PID algorithm. The gain parameter can also be applied to the error in engineering units. Even though most controller outputs are scaled as a percent, in cascade strategies the controller output may need to be scaled to the same span at the slave loop set point. In this case, the controller gain may in fact be required to calculate the controller output in terms of the slave loop engineering units.

The execution rate of a digital controller should be sufficiently fast, compared to the process dynamics, to produce a response that closely approximates that of an analog controller with the same tuning. A general rule of thumb is that the execution interval should be at least 3 times faster than the dominant lag of the process or about 10 times faster than the closed-loop time constant. The controller can be used when the sample rates are slower than this recommendation, but the controller output will consist of a series of coarse steps as compared to a smooth response. This may create stability problems. Some integral and derivative algorithms may not be accurate when the time-based tuning parameters approach the controller execution interval. The analog inputs of the controller are typically protected from aliasing errors through the use of one- or two-pole analog filters. Faster sample rates allow a smaller antialiasing filter and improved input response characteristics. Some controllers or I/O subsystems oversample the analog inputs with respect to the controller execution interval and then process the input data through a digital filter. This technique can produce a more representative measurement with less quantization noise.

Differences in the PID algorithm, controller parameters, units, and other fundamental control functions highlight the importance of understanding the structure of the controller and the requirement of sufficiently detailed documentation. This is especially important for the controller but is also important for the field instruments, final control elements, and device that have the potential to affect the signal characteristics.

CONTROL VALVES

A control valve consists of a valve, an actuator, and usually one or more valve control devices. The valves discussed in this section are applicable to throttling control (i.e., where flow through the valve is regulated to any desired amount between maximum and minimum limits). Other valves such as check, isolation, and relief valves are addressed in the next subsection. As defined, control valves are automatic control devices that modify the fluid flow rate as specified by the controller.

Valve Types Types of valves are categorized according to their design style. These styles can be grouped into type of stem motion—linear or rotary. The valve stem is the rod, shaft, or spindle that connects the actuator with the closure member (i.e., a movable part of the valve that is positioned in the flow path to modify the rate of flow). Movement of either type of stem is known as travel. The major categories are described briefly below.

Globe and Angle The most common linear stem-motion control valve is the globe valve. The name comes from the globular cavities around the port. In general, a port is any fluid passageway, but often the reference is to the passage that is blocked off by the closure member when the valve is closed. In globe valves, the closure member is called a plug. The plug in the valve shown in Fig. 8-66 is guided by a large-diameter port and moves within the port to provide the flow control orifice of the valve. A very popular alternate construction is a cage-guided plug, as illustrated in Fig. 8-67. In many such designs,

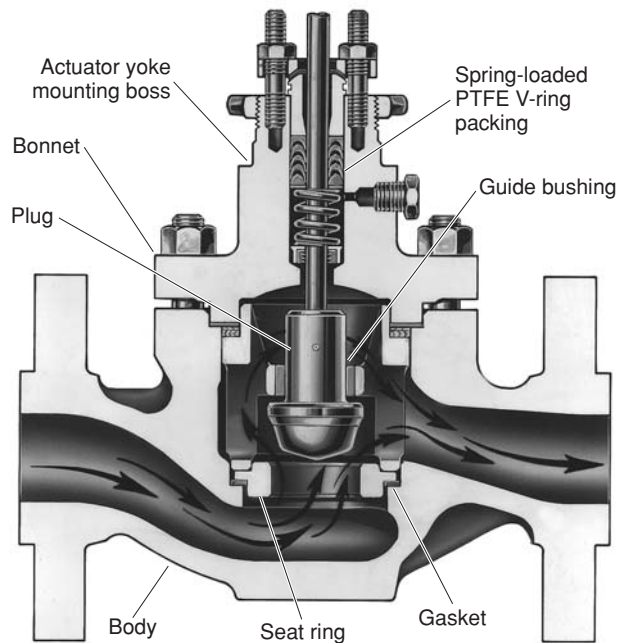


FIG. 8-66 Post-guided contour plug globe valve with metal seat and raised-face flange end connections. (Courtesy Fisher Controls International LLC.)

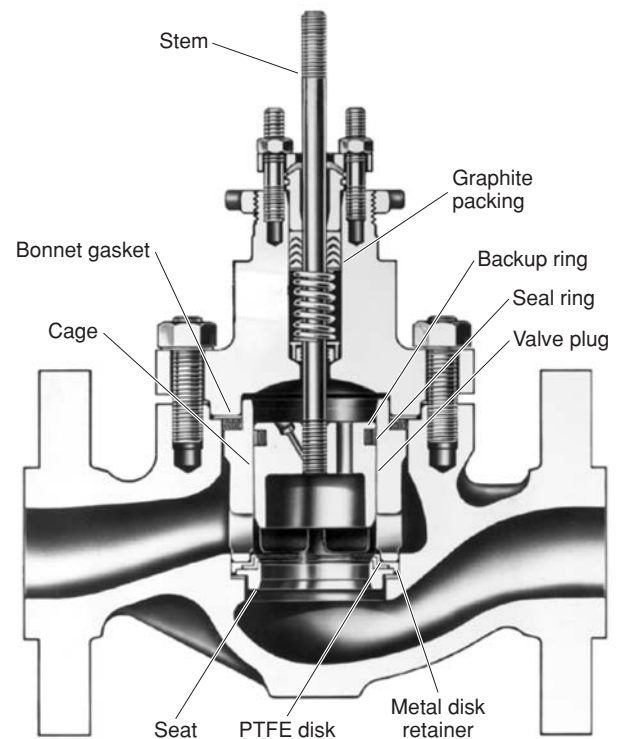


FIG. 8-67 Cage-guided balanced plug globe valve with polymer seat and plug seal. (Courtesy Fisher Controls International LLC.)

openings in the cage provide the flow control orifices. The valve seat is the zone of contact between the moving closure member and the stationary valve body, which shuts off the flow when the valve is closed. Often the seat in the body is on a replaceable part known as a seat ring. This stationary seat can also be designed as an integral part of the cage. Plugs may also be port-guided by wings or a skirt that fits snugly into the seat-ring bore.

One distinct advantage of cage guiding is the use of balanced plugs in single-port designs. The unbalanced plug depicted in Fig. 8-66 is subjected to a static pressure force equal to the port area times the valve pressure differential (plus the stem area times the downstream pressure) when the valve is closed. In the balanced design (Fig. 8-67), note that both the top and bottom of the plug are subjected to the same downstream pressure when the valve is closed. Leakage via the plug-to-cage clearance is prevented by a plug seal. Both plug types are subjected to hydrostatic force due to internal pressure acting on the stem area and to dynamic flow forces when the valve is flowing.

The plug, cage, seat ring, and associated seals are known as the trim. A key feature of globe valves is that they allow maintenance of the trim via a removable bonnet without removing the valve body from the line. Bonnets are typically bolted on but may be threaded in smaller sizes.

Angle valves are an alternate form of the globe valve. They often share the same trim options and have the top-entry bonnet style. Angle valves can eliminate the need for an elbow but are especially useful when direct impingement of the process fluid on the body wall is to be avoided. Sometimes it is not practical to package a long trim within a globe body, so an angle body is used. Some angle bodies are self-draining, which is an important feature for dangerous fluids.

Butterfly The classic design of butterfly valves is shown in Fig. 8-68. Its chief advantage is high capacity in a small package and a very low initial cost. Much of the size and cost advantage is due to the wafer body design, which is clamped between two pipeline flanges. In the simplest design, there is no seal as such, merely a small clearance gap between the disc OD and the body ID. Often a true seal is provided by a resilient material in the body that is engaged via an interference fit with the disc. In a lined butterfly valve, this material covers the entire body ID and extends around the body ends to eliminate the need for pipeline joint gaskets. In a fully lined valve, the disc is also coated to minimize corrosion or erosion.

A high-performance butterfly valve has a disc that is offset from the shaft centerline. This eccentricity causes the seating surface to move away from the seal once the disc is out of the closed position, reducing friction and seal wear. It is also known as an eccentric disc valve; the advantage of the butterfly valve is improved shutoff while maintaining

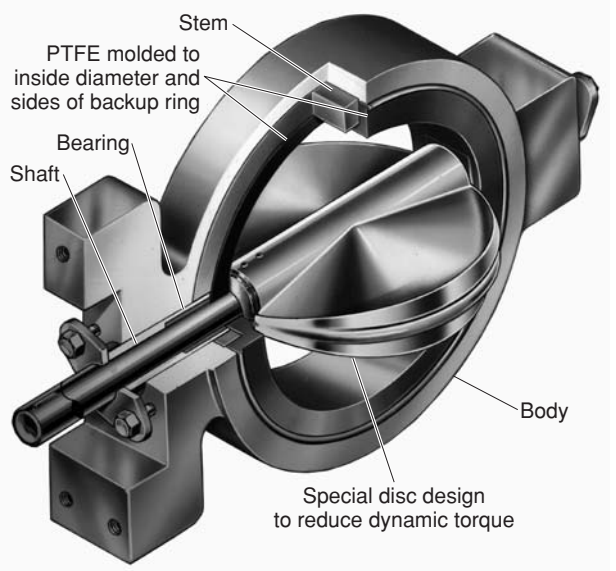


FIG. 8-68 Partial cutaway of wafer-style lined butterfly valve. (Courtesy Fisher Controls International LLC.)

high ultimate capacity at a reasonable cost. This cost advantage relative to other design styles is particularly true in sizes above 6-in nominal pipe size (NPS). Improved shutoff is due to advances in seal technologies, including polymer, flexing metal, combination metal with polymer inserts, and so on, many utilizing pressure assist.

Ball Ball valves get their name from the shape of the closure member. One version uses a full spherical member with a cylindrical bore through it. The ball is rotated one-quarter turn from the full-closed to the full-open position. If the bore is the same diameter as the mating-pipe fitting ID, the valve is referred to as full-bore. If the hole is undersized, the ball valve is considered to be a venturi style. A segmented ball is a portion of a hollow sphere that is large enough to block the port when closed. Segmented balls often have a V-shaped contour along one edge, which provides a desirable flow characteristic (see Fig. 8-69). Both full ball and segmented ball valves are known for

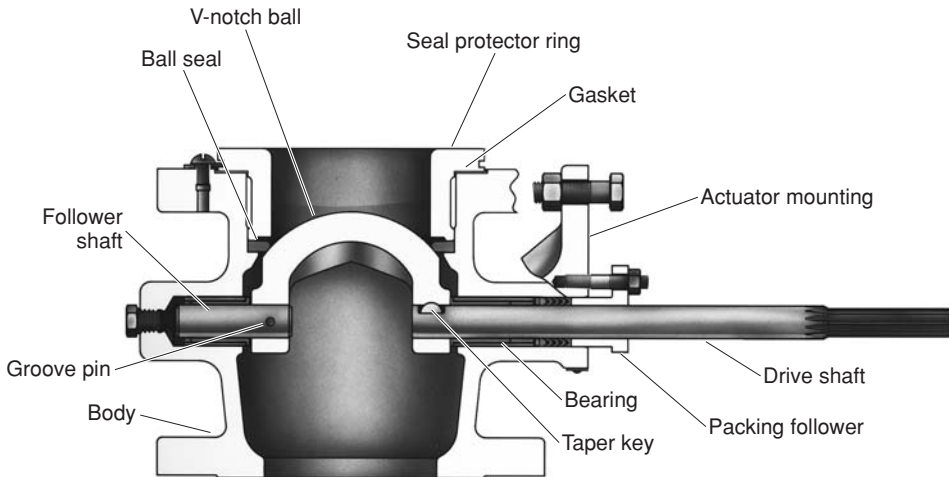


FIG. 8-69 Segmented ball valve. Partial view of actuator mounting shown 90° out of position. (Courtesy Fisher Controls International LLC.)

their low resistance to flow when full open. Shutoff leakage is minimized through the use of flexing or spring-loaded elastomeric or metal seals. Bodies are usually in two or three pieces or have a removable retainer to facilitate installing seals. End connections are usually flanged or threaded in small sizes, although segmented ball valves are offered in wafer style also.

Plug There are two substantially different rotary valve design categories referred to as plug valves. The first consists of a cylindrical or slightly conical plug with a port through it. The plug rotates to vary the flow much as a ball valve does. The body is top-entry but is geometrically simpler than a globe valve and thus can be lined with fluorocarbon polymer to protect against corrosion. These plug valves have excellent shutoff but are generally not for modulating service due to high friction. A variation of the basic design (similar to the eccentric butterfly disc) only makes sealing contact in the closed position and is used for control.

The other rotary plug design is portrayed in Fig. 8-70. The seating surface is substantially offset from the shaft, producing a ball-valve-like motion with the additional cam action of the plug into the seat when closing. In reverse flow, high-velocity fluid motion is directed inward, impinging on itself and only contacting the plug and seat ring.

Multiport This term refers to any valve or manifold of valves with more than one inlet or outlet. For throttling control, the three-way body is used for blending (two inlets, one outlet) or as a diverter (one inlet, two outlets). A three-way valve is most commonly a special globe-like body with special trim that allows flow both over and under the plug. Two rotary valves and a pipe tee can also be used. Special three-, four-, and five-way ball valve designs are used for switching applications.

Special Application Valves

Digital Valves True digital valves consist of discrete solenoid-operated flow ports that are sized according to binary weighing. The valve can be designed with sharp-edged orifices or with streamlined nozzles that can be used for flow metering. Precise control of the throttling control orifice is the strength of the digital valve. Digital valves are mechanically complicated and expensive, and they have considerably reduced maximum flow capacities compared to the globe and rotary valve styles.

Cryogenic Service Valves designed to minimize heat absorption for throttling liquids and gases below 80 K are called cryogenic service

valves. These valves are designed with small valve bodies to minimize heat absorption and long bonnets between the valve and actuator to allow for extra layers of insulation around the valve. For extreme cases, vacuum jacketing can be constructed around the entire valve to minimize heat influx.

High Pressure Valves used for pressures nominally above 760 bar (11,000 psi, pressures above ANSI Class 4500) are often custom-designed for specific applications. Normally, these valves are of the plug type and use specially hardened plug and seat assemblies. Internal surfaces are polished, and internal corners and intersecting bores are smoothed to reduce high localized stresses in the valve body. Steam loops in the valve body are available to raise the body temperature to increase ductility and impact strength of the body material.

High-Viscous Process Used most extensively by the polymer industry, the valve for high-viscous fluids is designed with smooth finished internal passages to prevent stagnation and polymer degradation. These valves are available with integral body passages through which a heat-transfer fluid is pumped to keep the valve and process fluid heated.

Pinch The industrial equivalent of controlling flow by pinching a soda straw is the pinch valve. Valves of this type use fabric-reinforced elastomer sleeves that completely isolate the process fluid from the metal parts in the valve. The valve is actuated by applying air pressure directly to the outside of the sleeve, causing it to contract or pinch. Another method is to pinch the sleeve with a linear actuator with a specially attached foot. Pinch valves are used extensively for corrosive material service and erosive slurry service. This type of valve is used in applications with pressure drops up to 10 bar (145 psi).

Fire-Rated Valves that handle flammable fluids may have additional safety-related requirements for minimal external leakage, minimal internal (downstream) leakage, and operability during and after a fire. Being fire-rated does not mean being totally impervious to fire, but a sample valve must meet particular specifications such as those of American Petroleum Institute (API) 607, Factory Mutual Research Corp. (FM) 7440, or the British Standard 5146 under a simulated fire test. Due to very high flame temperature, metal seating (either primary or as a backup to a burned-out elastomer) is mandatory.

Solids Metering The control valves described earlier are primarily used for the control of fluid (liquid or gas) flow. Sometimes these valves, particularly the ball, butterfly, or sliding gate valves, are used to throttle dry or slurry solids. More often, special throttling mechanisms such as venturi ejectors, conveyers, knife-type gate valves, or rotating vane valves are used. The particular solids-metering valve hardware depends on the volume, density, particle shape, and coarseness of the solids to be handled.

Actuators An actuator is a device that applies the force (torque) necessary to cause a valve's closure member to move. Actuators must overcome pressure and flow forces as well as friction from packing, bearings or guide surfaces, and seals; and must provide the seating force. In rotary valves, maximum friction occurs in the closed position, and the moment necessary to overcome it is referred to as breakout torque. The rotary valve shaft torque generated by steady-state flow and pressure forces is called dynamic torque. It may tend to open or close the valve depending on valve design and travel. Dynamic torque per unit pressure differential is largest in butterfly valves at roughly 70° open. In linear stem-motion valves, the flow forces should not exceed the available actuator force, but this is usually accounted for by default when the seating force is provided.

Actuators often provide a fail-safe function. In the event of an interruption in the power source, the actuator will place the valve in a predetermined safe position, usually either full-open or full-closed. Safety systems are often designed to trigger local fail-safe action at specific valves to cause a needed action to occur, which may not be a complete process or plant shutdown.

Actuators are classified according to their power source. The nature of these sources leads naturally to design features that make their performance characteristics distinct.

Pneumatic Despite the availability of more sophisticated alternatives, the pneumatically driven actuator is still by far the most popular type. Historically the most common has been the spring and diaphragm design (Fig. 8-71). The compressed air input signal fills a

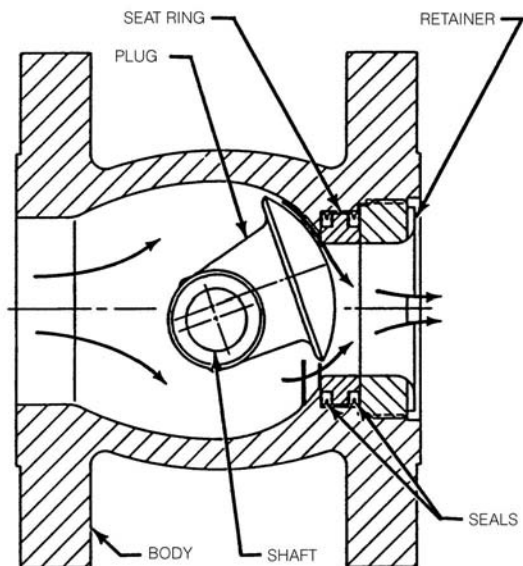


FIG. 8-70 Eccentric plug valve shown in erosion-resistant reverse flow direction. Shaded components can be made of hard metal or ceramic materials. (Courtesy Fisher Controls International LLC.)

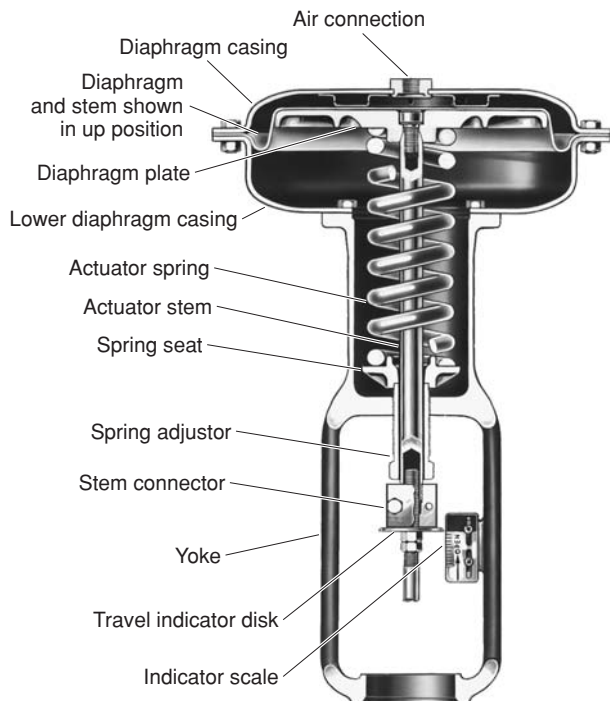


FIG. 8-71 Spring and diaphragm actuator with an “up” fail-safe mode. Spring adjuster allows slight alteration of bench set. (Courtesy Fisher Controls International LLC.)

chamber sealed by an elastomeric diaphragm. The pressure force on the diaphragm plate causes a spring to be compressed and the actuator stem to move. This spring provides the fail-safe function and contributes to the dynamic stiffness of the actuator. If the accompanying valve is “push down to close,” the actuator depicted in Fig. 8-71 will be described as “air to close” or synonymously as fail-open. A slightly different design yields “air to open” or fail-closed action. The spring is typically precompressed to provide a significant available force in the failed position (e.g., to provide seating load). The spring also provides a proportional relationship between the force generated by air pressure and stem position. The pressure range over which a spring and diaphragm actuator strokes in the absence of valve forces is known as the bench set. The chief advantages of spring and diaphragm actuators are their high reliability, low cost, adequate dynamic response, and fail-safe action—all of which are inherent in their simple design.

Alternately, the pressurized chamber can be formed by a circular piston with a seal on its outer edge sliding within a cylindrical bore. Higher operating pressure [6 bar (~ 90 psig) is typical] and longer strokes are possible. Piston actuators can be spring-opposed but many times are in a dual-acting configuration (i.e., compressed air is applied to both sides of the piston with the net force determined from the pressure difference—see Fig. 8-72). Dynamic stiffness is usually higher with piston designs than with spring and diaphragm actuators; see “Positioner/Actuator Stiffness.” Fail-safe action, if necessary, is achieved without a spring through the use of additional solenoid valves, trip valves, or relays. See “Valve Control Devices.”

Motion Conversion Actuator power units with translational output can be adapted to rotary valves that generally need 90° or less rotation. A lever is attached to the rotating shaft, and a link with pivoting means on the end connects to the linear output of the power unit, an arrangement similar to an internal combustion engine crankshaft, connecting rod, and piston. When the actuator piston, or more commonly the diaphragm plate, is designed to tilt, one pivot can be eliminated (see Fig. 8-72). Scotch yoke and rack-and-pinion arrangements are also commonly used, especially with piston power units.

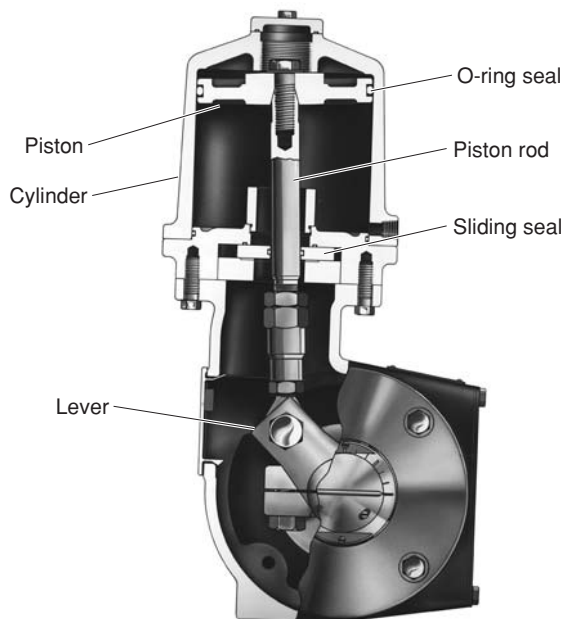


FIG. 8-72 Double-acting piston rotary actuator with lever and tilting piston for motion conversion. (Courtesy Fisher Controls International LLC.)

Friction and the changing mechanical advantage of these motion conversion mechanisms mean the available torque may vary greatly with travel. One notable exception is vane-style rotary actuators whose off-set “piston” pivots, giving direct rotary output.

Hydraulic The design of typical hydraulic actuators is similar to that of double-acting piston pneumatic types. One key advantage is the high pressure [typically 35 to 70 bar (500 to 1000 psi)], which leads to high thrust in a smaller package. The incompressible nature of the hydraulic oil means these actuators have very high dynamic stiffness. The incompressibility and small chamber size connote fast stroking speed and good frequency response. The disadvantages include high initial cost, especially when considering the hydraulic supply. Maintenance is much more difficult than with pneumatics, especially on the hydraulic positioner.

Electrohydraulic actuators have similar performance characteristics and cost/maintenance ramifications. The main difference is that they contain their own electric-powered hydraulic pump. The pump may run continuously or be switched on when a change in position is required. Their main application is remote sites without an air supply when a fail-safe spring return is needed.

Electric The most common electric actuators use a typical motor—three-phase ac induction, capacitor-start split-phase induction, or dc. Normally the motor output passes through a large gear reduction and, if linear motion output is required, a ball screw or thread. These devices can provide large thrust, especially given their size. Lost motion in the gearing system does create backlash, but if not operating across a thrust reversal, this type of actuator has very high stiffness. Usually the gearing system is self-locking, which means that forces on the closure member cannot move it by spinning a nonenergized motor. This behavior is called a lock-in-last-position fail-safe mode. Some gear systems (e.g., low-reduction spur gears) can be backdriven. A solenoid-activated mechanical brake or locking current to motor field coils is added to provide lock-in-last-position fail-safe mode. A battery backup system for a dc motor can guard against power failures. Otherwise, an electric actuator is not acceptable if fail-open/closed action is mandatory. Using electric power requires environmental enclosures and explosion protection, especially in hydrocarbon processing facilities; see the full discussion in “Valve Control Devices.”

Unless sophisticated speed control power electronics is used, position modulation is achieved via bang-zero-bang control. Mechanical inertia causes overshoot, which is (1) minimized by braking and/or (2) hidden by adding dead band to the position control. Without these provisions, high starting currents would cause motors to overheat from constant "hunting" within the position loop. Travel is limited with power interruption switches or with force (torque) electro-mechanical cutouts when the closed position is against a mechanical stop (e.g., a globe valve). Electric actuators are often used for on/off service. Stepper motors can be used instead, and they, as their name implies, move in fixed incremental steps. Through gear reduction, the typical number of increments for 90° rotation ranges from 5000 to 10,000; hence positioning resolution at the actuator is excellent.

An electromagnetic solenoid can be used to directly actuate the plug on very small linear stem-motion valves. A solenoid is usually designed as a two-position device, so this valve control is on/off. Special solenoids with position feedback can provide proportional action for modulating control. Force requirements of medium-sized valves can be met with piloted plug designs, which use process pressure to assist the solenoid force. Piloted plugs are also used to minimize the size of common pneumatic actuators, especially when there is need for high seating load.

Manual A manually positioned valve is by definition not an automatic control valve, but it may be involved with process control. For rotary valves, the manual operator can be as simple as a lever, but a wheel driving a gear reduction is necessary in larger valves. Linear motion is normally created with a wheel turning a screw-type device. A manual override is usually available as an option for the powered actuators listed above. For spring-opposed designs, an adjustable travel stop will work as a one-way manual input. In more complex designs, the handwheel can provide loop control override via an engagement means. Some gear reduction systems of electric actuators allow the manual positioning to be independent of the automatic positioning without declutching.

OTHER PROCESS VALVES

In addition to the throttling control valve, other types of process valves can be used to manipulate a process.

Valves for On/Off Applications Valves are often required for service that is primarily nonthrottling. Valves in this category, depending on the service requirements, may be of the same design as the types used for throttling control or, as in the case of gate valves, different in design. Valves in this category usually have tight shutoff when they are closed and low pressure drops when they are wide open. The on/off valve can be operated manually, such as by handwheel or lever; or automatically, with pneumatic or electric actuators.

Batch Batch process operation is an application requiring on/off valve service. Here the valve is opened and closed to provide reactant, catalyst, or product to and from the batch reactor. Like the throttling control valve, the valve used in this service must be designed to open and close thousands of times. For this reason, valves used in this application are often the same valves used in continuous throttling applications. Ball valves are especially useful in batch operations. The ball valve has a straight-through flow passage that reduces pressure drop in the wide-open state and provides tight shutoff capability when closed. In addition, the segmented ball valve provides for shearing action between the ball and the ball seat that promotes closure in slurry service.

Isolation A means for pressure-isolating control valves, pumps, and other piping hardware for installation and maintenance is another common application for an on/off valve. In this application, the valve is required to have tight shutoff so that leakage is stopped when the piping system is under repair. As the need to cycle the valve in this application is far less than that of a throttling control valve, the wear characteristics of the valve are less important. Also, because many are required in a plant, the isolation valve needs to be reliable, simple in design, and simple in operation.

The gate valve, shown in Fig. 8-73, is the most widely used valve in this application. The gate valve is composed of a gatelike disc that moves perpendicular to the flow stream. The disc is moved up and

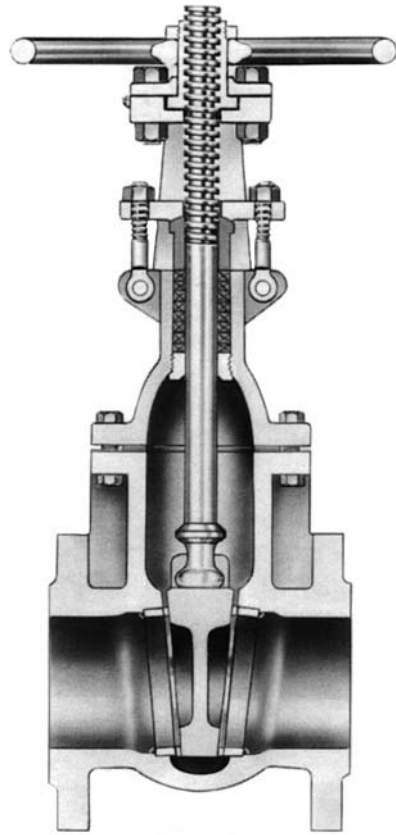


FIG. 8-73 Gate valve. (Courtesy Crane Valves.)

down by a threaded screw that is rotated to effect disc movement. Because the disc is large and at right angles to the process pressure, a large seat loading for tight shutoff is possible. Wear produced by high seat loading during the movement of the disc prohibits the use of the gate valve for throttling applications.

Pressure Relief Valves The pressure relief valve is an automatic pressure-relieving device designed to open when normal conditions are exceeded and to close again when normal conditions are restored. Within this class there are relief valves, pilot-operated pressure relief valves, and safety valves. Relief valves (see Fig. 8-74) have spring-loaded discs that close a main orifice against a pressure source. As pressure rises, the disc begins to rise off the orifice and a small amount of fluid passes through the valve. Continued rise in pressure above the opening pressure causes the disc to open the orifice in a proportional fashion. The main orifice reduces and closes when the pressure returns to the set pressure. Additional sensitivity to overpressure conditions can be improved by adding an auxiliary pressure relief valve (pilot) to the basic pressure relief valve. This combination is known as a pilot-operated pressure relief valve.

The safety valve is a pressure relief valve that is designed to open fully, or pop, with only a small amount of pressure over the rated limit. Where conventional safety valves are sensitive to downstream pressure and may have unsatisfactory operating characteristics in variable backpressure applications, pressure-balanced safety relief valve designs are available to minimize the effect of downstream pressure on performance.

Application and sizing of pressure relief valves, pilot-operated pressure relief valves, and safety valves for use on pressure vessels are found in the ASME Boiler and Pressure Vessel Code, Section VIII, Division 1, "Rules for Construction of Pressure Vessels," Paragraphs UG-125 through UG-137.

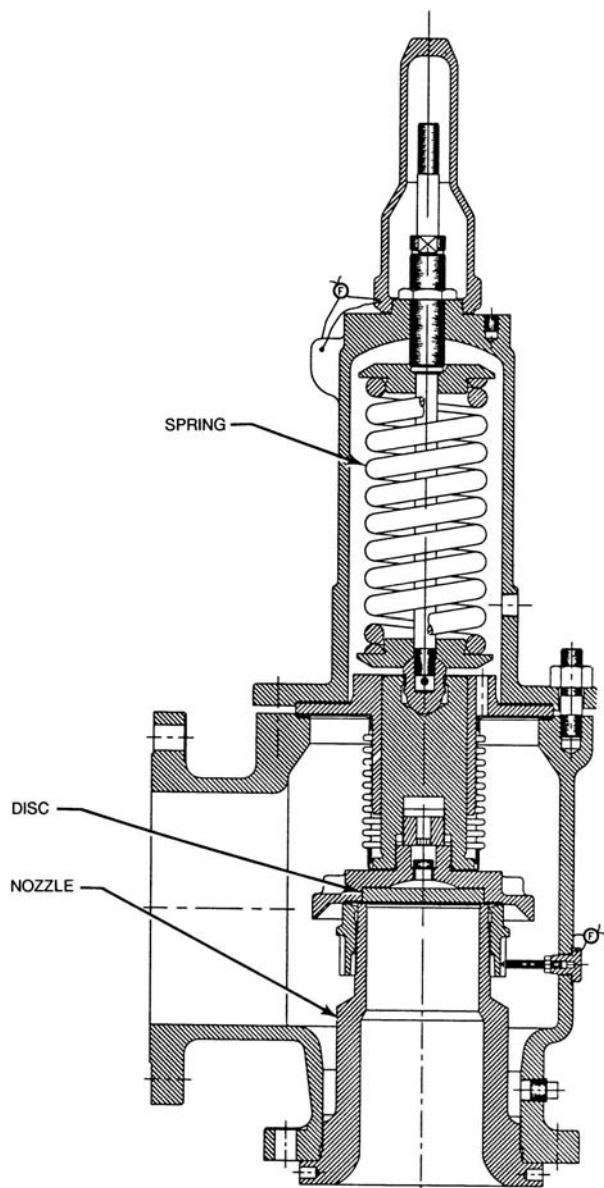


FIG. 8-74 Relief valve. (Courtesy of Teledyne Fluid Systems, Farris Engineering.)

Check Valves The purpose of a check valve is to allow relatively unimpeded flow in the desired direction but to prevent flow in the reverse direction. Two common designs are swing-type and lift-type check valves, the names of which denote the motion of the closure member. In the forward direction, flow forces overcome the weight of the member or a spring to open the flow passage. With reverse pressure conditions, flow forces drive the closure member into the valve seat, thus providing shutoff.

VALVE DESIGN CONSIDERATIONS

Functional requirements and the properties of the controlled fluid determine which valve and actuator types are best for a specific application. If demands are modest and no unique valve features are required, the valve design style selection may be determined solely by

cost. If so, general-purpose globe or angle valves provide exceptional value, especially in sizes less than 3-in NPS and hence are very popular. Beyond type selection, there are many other valve specifications that must be determined properly to ultimately yield improved process control.

Materials and Pressure Ratings Valves must be constructed from materials that are sufficiently immune to corrosive or erosive action by the process fluid. Common body materials are cast iron, steel, stainless steel, high-nickel alloys, and copper alloys such as bronze. Trim materials need better corrosion and erosion resistance due to the higher fluid velocity in the throttling region. High hardness is desirable in erosive and cavitating applications. Heat-treated and precipitation-hardened stainless steels are common. High hardness is also good for guiding, bearing, and seating surfaces; cobalt-chromium alloys are utilized in cast or wrought form and frequently as welded overlays called hard facing. In less stringent situations, chrome plating, heat-treated nickel coatings, and nitriding are used. Tungsten carbide and ceramic trim are warranted in extremely erosive services. See Sec. 25, "Materials of Construction," for specific material properties.

Since the valve body is a pressurized vessel, it is usually designed to comply with a standardized system of pressure ratings. Two common systems are described in the standards ASME B16.34 and EN 12516. Internal pressure limits under these standards are divided into broad classes, with specific limits being a function of material and temperature. Manufacturers also assign their own pressure ratings based on internal design rules. A common insignia is 250 WOG, which means a pressure rating of 250 psig (~17 bar) in water, oil, or gas at ambient temperature. "Storage and Process Vessels" in Sec. 10 provides introductory information on compliance of pressure vessel design to industry codes (e.g., ASME Boiler and Pressure Vessel Code, Section VIII; ASME B31.3 Chemical Plant and Petroleum Refinery Piping).

Valve bodies are also standardized to mate with common piping connections: flanged, butt-welded end, socket-welded end, and screwed end. Dimensional information for some of these joints and class pressure-temperature ratings are included in Sec. 10, "Process Plant Piping." Control valves have their own standardized face-to-face dimensions that are governed by ANSI/ISA Standards S75.08 and S75.22. Butterfly valves are also governed by API 609 and Manufacturers Standardization Society (MSS) SP-67 and SP-68.

Sizing Throttling control valves must be selected to pass the required flow rate, given expected pressure conditions. Sizing is not merely matching the end connection size with surrounding piping; it is a key step in ensuring that the process can be properly controlled. Sizing methods range from simple models based on elementary fluid mechanics to very complex models when unusual thermodynamics or nonideal behaviors occur. Basic sizing practices have been standardized (for example, ANSI-75.01.01) and are implemented as PC-based programs by manufacturers. The following is a discussion of very basic sizing equations and the associated physics.

Regardless of the particular process variable being controlled (e.g., temperature, level, pH), the output of a control valve is the flow rate. The throttling valve performs its function of manipulating the flow rate by virtue of being an adjustable resistance to flow. Flow rate and pressure conditions are normally known when a process is designed, and the valve resistance range must be matched accordingly. In the tradition of orifice and nozzle discharge coefficients, this resistance is embodied in the valve flow coefficient C_v . By applying the principles of conservation of mass and energy, the mass flow rate w kg/h is given for a liquid by

$$w = 27.3C_v\sqrt{\rho(p_1 - p_2)} \quad (8-111)$$

where p_1 and p_2 are upstream and downstream static pressure, bar, respectively. The density of the fluid ρ is expressed in kilograms per cubic meter. This equation is valid for nonvaporizing, turbulent flow conditions for a valve with no attached fittings.

While the above equation gives the relationship between pressure and flow from a macroscopic point of view, it does not explain what is going on inside the valve. Valves create a resistance to flow by restricting the cross-sectional area of the flow passage and by forcing the fluid to change direction as it passes through the body and trim.

The conservation of mass principle dictates that, for steady flow, the product of density, average velocity, and cross-sectional area remain a constant. The average velocity of the fluid stream at the minimum restriction in the valve is therefore much higher than that at the inlet. Note that due to the abrupt nature of the flow contraction that forms the minimum passage, the main fluid stream may separate from the passage walls and form a jet that has an even smaller cross section, the so-called vena contracta. The ratio of minimum stream area to the corresponding passage area is called the contraction coefficient. As the fluid expands from the minimum cross-sectional area to the full passage area in the downstream piping, large amounts of turbulence are generated. Direction changes can also induce significant amounts of turbulence.

Figure 8-75 is an illustration of how the mean pressure changes as fluid moves through a valve. Some of the potential energy that was stored in the fluid by pressurizing it (e.g., the work done by a pump) is first converted to the kinetic energy of the fast-moving fluid at the vena contracta. Some of that kinetic energy turns into the kinetic energy of turbulence. As the turbulent eddies break down into smaller and smaller structures, viscous effects ultimately convert all the turbulent energy to heat. Therefore, a valve converts fluid energy from one form to another.

For many valve constructions, it is reasonable to approximate the fluid transition from the valve inlet to the minimum cross section of the flow stream as an isentropic or lossless process. Using this approximation, the minimum pressure p_{VC} can be estimated from the

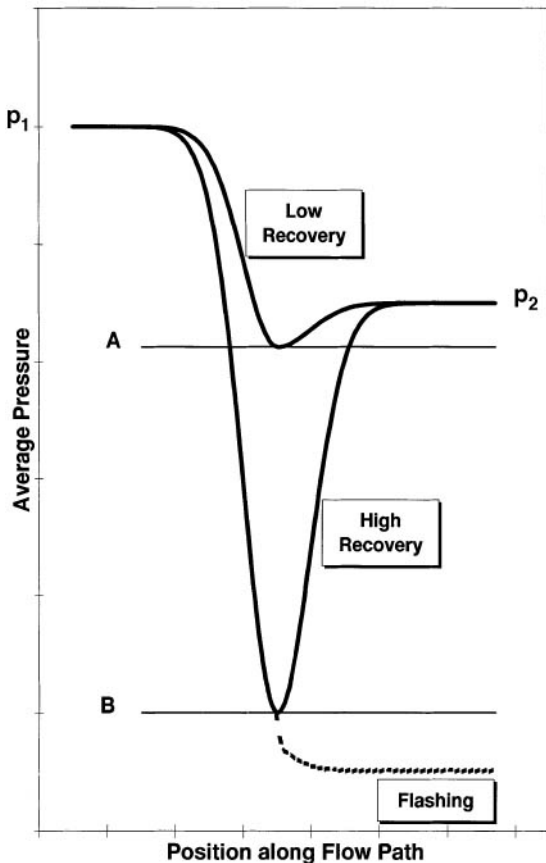


FIG. 8-75 Generic depictions of average pressure at subsequent cross sections throughout a control valve. The F_L values selected for illustration are 0.9 and 0.63 for low and high recovery, respectively. Internal pressure in the high-recovery valve is shown as a dashed line for flashing conditions ($p_2 < p_c$) with $p_c = B$.

Bernoulli relationship. See Sec. 6 ("Fluid and Particle Mechanics") for more background information. Downstream of the vena contracta, the flow is definitely not lossless due to all the turbulence that is generated. As the flow passage area increases and the fluid slows down, some of the kinetic energy of the fluid is converted back to pressure energy as pressure recovers. The energy that is permanently lost via turbulence accounts for the permanent pressure or head loss of the valve. The relative amount of pressure that is recouped determines whether the valve is considered to be high- or low-recovery. The flow passage geometry at and downstream of the vena contracta primarily determines the amount of recovery. The amount of recovery is quantified by the liquid pressure recovery factor F_L .

$$F_L = \sqrt{\frac{p_1 - p_2}{p_1 - p_{VC}}} \quad (8-112)$$

Under some operating conditions, sufficient pressure differential may exist across the valve to cause the vena contracta pressure to drop to the saturation pressure (also known as the *vapor pressure*) of the liquid. If this occurs, a portion of the liquid will vaporize, forming a two-phase, compressible mixture within the valve. If sufficient vapor forms, the flow may *choke*. When a flow is choked, any increase in pressure differential across the valve no longer produces an increase in flow through the valve.

The vena contracta condition at choked flow for pure liquids has been shown to be

$$p_{VC} = F_F p_c \quad (8-113)$$

where

$$F_F = 0.96 - 0.28 \sqrt{\frac{p_c}{p_c}} \quad (8-114)$$

and p_{VC} is the absolute vena contracta pressure under choked conditions, F_F is the liquid critical pressure ratio factor, p_c is the absolute vapor pressure of the liquid at inlet temperature, and p_c is the absolute thermodynamic critical pressure of the fluid.

Equations (8-112) and (8-113) can be used together to determine the pressure differential across the valve at the point where the flow chokes

$$\Delta p_{\text{choked}} = F_L^2 (p_1 - F_F p_c) \quad (8-115)$$

The pressure recovery factor is a constant for any given valve at a given opening. The value of this factor can be established by flow test and is published by the valve manufacturer. If the actual pressure differential across the valve is greater than the choked pressure differential of Eq. (8-115), then Δp_{choked} should be used in Eq. (8-111) to determine the correct valve size. A more complete presentation of sizing relationships is given in ANSI 75.01.01, including provisions for pipe reducers and Reynolds number effects.

Equations (8-111) to (8-115) are restricted to incompressible fluids. For gases and vapors, the fluid density is dependent on pressure. For convenience, compressible fluids are often assumed to follow the ideal gas law model. Deviations from ideal behavior are corrected for, to first order, with nonunity values of compressibility factor Z (see Sec. 2, "Physical and Chemical Data," for definitions and data for common fluids). For compressible fluids

$$w = 94.8 C_v p_1 Y \sqrt{\frac{x M_w}{T_1 Z}} \quad (8-116)$$

where p_1 is in bar absolute, T_1 is inlet temperature in kelvins, M_w is the molecular weight, and x is the dimensionless pressure drop ratio $(p_1 - p_2)/p_1$. The expansion factor Y accounts for changes in the fluid density as the fluid passes through the valve. It is dependent on pressure drop and valve geometry. Experimental data have shown that for

small departures in the ratio of specific heat from that of air (1.4), a simple linear relationship can be used to represent the expansion factor:

$$Y = 1 - \frac{1.4x}{3x_T\gamma} \quad \text{for} \quad x \leq \frac{x_T\gamma}{1.4} \quad (8-117)$$

where γ is the ratio of specific heats and x_T is an experimentally determined factor for a specific valve and is the largest value of x that contributes to flow (i.e., values of x greater than x_T do not contribute to flow).

The terminal value of x , x_T , results from a phenomenon known as choking. Given a nozzle geometry with fixed inlet conditions, the mass flow rate will increase as p_2 is decreased up to a maximum amount at the critical pressure drop. The velocity at the vena contracta has reached sonic, and a standing shock has formed. This shock causes a step change in pressure as flow passes through it, and further reduction in p_2 does not increase mass flow. Thus x_T relates to the critical pressure drop ratio and also accounts for valve geometry effects. The value of x_T varies with flow path geometry and is supplied by the valve manufacturer. In the choked case,

$$x = \frac{x_T\gamma}{1.4} \quad \text{and} \quad Y = 0.67 \quad (8-118)$$

Noise Control Sound is a fluctuation of air pressure that can be detected by the human ear. Sound travels through any fluid (e.g., the air) as a compression/expansion wave. This wave travels radially outward in all directions from the sound source. The pressure wave induces an oscillating motion in the transmitting medium that is superimposed on any other net motion it may have. These waves are reflected, refracted, scattered, and absorbed as they encounter solid objects. Sound is transmitted through solids in a complex array of types of elastic waves. Sound is characterized by its amplitude, frequency, phase, and direction of propagation.

Sound strength is therefore location-dependent and is often quantified as a sound pressure level L_p in decibels based on the root mean square (rms) sound pressure value p_s , where

$$L_p = 10 \log \left(\frac{p_s}{p_{\text{reference}}} \right)^2 \quad (8-119)$$

For airborne sound, the reference pressure is 2×10^{-5} Pa (29×10^{-1} psi), which is nominally the human threshold of hearing at 1000 Hz. The corresponding sound pressure level is 0 dB. A voice in conversation is about 50 dB, and a jackhammer operator is subject to 100 dB. Extreme levels such as a jet engine at takeoff might produce 140 dB at a distance of 3 m, which is a pressure amplitude of 200 Pa (29×10^{-3} psi). These examples demonstrate both the sensitivity and the wide dynamic range of the human ear.

Traveling sound waves carry energy. Sound intensity I is a measure of the power passing through a unit area in a specified direction and is related to p_s . Measuring sound intensity in a process plant gives clues to the location of the source. As one moves away from the source, the fact that the energy is spread over a larger area requires that the sound pressure level decrease. For example, doubling one's distance from a point source reduces L_p by 6 dB. Viscous action from the induced fluid motion absorbs additional acoustic energy. However, in free air, this viscous damping is negligible over short distances (on the order of 1 m).

Noise is a group of sounds with many nonharmonic frequency components of varying amplitudes and random phase. The turbulence generated by a throttling valve creates noise. As a valve converts potential energy to heat, some of the energy becomes acoustic energy as an intermediate step. Valves handling large amounts of compressible fluid through a large pressure change create the most noise because more total power is being transformed. Liquid flows are noisy only under special circumstances, as will be seen in the next subsection. Due to the random nature of turbulence and the broad distribution of length and velocity scales of turbulent eddies, valve-generated sound is

usually random, broad-spectrum noise. The total sound pressure level from two such statistically uncorrelated sources is (in decibels)

$$L_p = 10 \log \frac{(p_{s1})^2 + (p_{s2})^2}{(p_{\text{reference}})^2} \quad (8-120)$$

For example, two sources of equal strength combine to create an L_p that is 3 dB higher.

While noise is annoying to listen to, the real reasons for being concerned about noise relate to its impact on people and equipment. Hearing loss can occur due to long-term exposure to moderately high, or even short exposure to very high, noise levels. The U.S. Occupational Safety and Health Act (OSHA) has specific guidelines for permissible levels and exposure times. The human ear has a frequency-dependent sensitivity to sound. When the effect on humans is the criterion, L_p measurements are weighted to account for the ear's response. This so-called A-weighted scale is defined in ANSI S1.4 and is commonly reported as L_{pA} . Figure 8-76 illustrates the difference between actual and perceived airborne sound pressure levels. At sufficiently high levels, noise and the associated vibration can damage equipment.

There are two approaches to fluid-generated noise control—source or path treatment. Path treatment means absorbing or blocking the transmission of noise after it has been created. The pipe itself is a barrier. The sound pressure level inside a standard schedule pipe is roughly 40 to 60 dB higher than on the outside. Thicker-walled pipe reduces levels somewhat more, and adding acoustical insulation on the outside of the pipe reduces ambient levels up to 10 dB per inch of thickness. Since noise propagates relatively unimpeded inside the

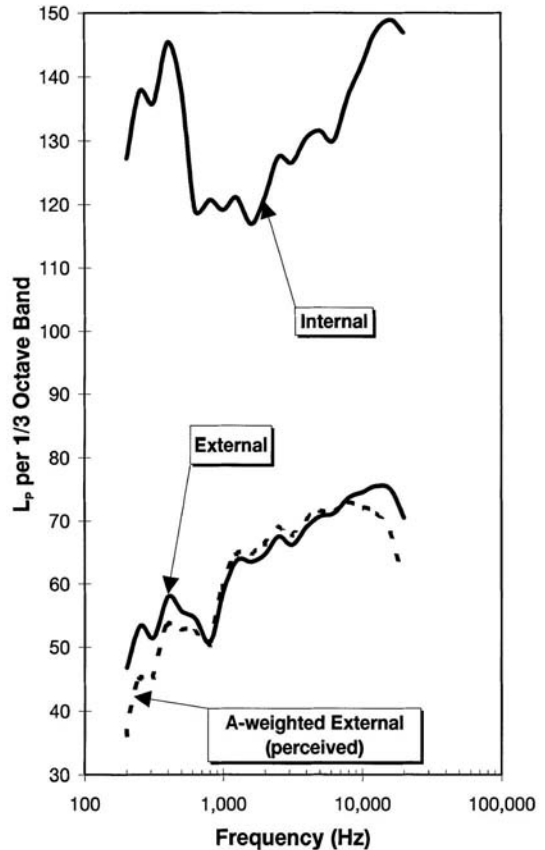


FIG. 8-76 Valve-generated sound pressure level spectrums.

pipe, barrier approaches require the entire downstream piping system to be treated in order to be totally effective. In-line silencers place absorbent material inside the flow stream, thus reducing the level of the internally propagating noise. Noise reductions up to 25 dB can be achieved economically with silencers.

The other approach to valve noise problems is the use of quiet trim. Two basic strategies are used to reduce the initial production of noise—dividing the flow stream into multiple paths and using several flow resistances in series. Sound pressure level L_p is proportional to mass flow and is dependent on vena contracta velocity. If each path is an independent source, it is easy to show from Eq. (8-120) that p_v^2 is inversely proportional to the number of passages; additionally, smaller passage size shifts the predominate spectral content to higher frequencies, where structural resonance may be less of a problem. Series resistances or multiple stages can reduce maximum velocity and/or produce backpressure to keep jets issuing from multiple passages from acting independently. While some of the basic principles are understood, predicting noise for a particle flow passage requires some empirical data as a basis. Valve manufacturers have developed noise prediction methods for the valves they build. ANSI/ISA-75.17 is a public-domain methodology for standard (non-low-noise) valve types, although treatment of some multistage, multipath types is underway. Low-noise hardware consists of special cages in linear stem valves, perforated domes or plates and multichannel inserts in rotary valves, and separate devices that use multiple fixed restrictions.

Cavitation and Flashing From the discussion of pressure recovery it was seen that the pressure at the vena contracta can be much lower than the downstream pressure. If the pressure on a liquid falls below its vapor pressure p_v , the liquid will vaporize. Due to the effect of surface tension, this vapor phase will first appear as bubbles. These bubbles are carried downstream with the flow, where they collapse if the pressure recovers to a value above p_v . This pressure-driven process of vapor bubble formation and collapse is known as cavitation.

Cavitation has three negative side effects in valves—noise and vibration, material removal, and reduced flow. The bubble collapse process is a violent asymmetric implosion that forms a high-speed microjet and induces pressure waves in the fluid. This hydrodynamic noise and the mechanical vibration that it can produce are far stronger than other noise generation sources in liquid flows. If implosions occur adjacent to a solid component, minute pieces of material can be removed, which, over time, will leave a rough, cinderlike surface.

The presence of vapor in the vena contracta region puts an upper limit on the amount of liquid that will pass through a valve. A mixture of vapor and liquid has a lower density than that of the liquid alone. While Eq. (8-111) is not applicable to two-phase flows because pressure changes are redistributed due to varying density and the two phases do not necessarily have the same average velocity, it does suggest that lower density reduces the total mass flow rate. Figure 8-77 illustrates a typical flow rate/pressure drop relationship. As with compressible gas flow at a given p_1 , flow increases as p_2 is decreased until the flow chokes (i.e., no additional fluid will pass). The transition between incompressible and choked flow is gradual because, within the convoluted flow passages of valves, the pressure is actually an uneven distribution at each cross section and consequently vapor formation zones increase gradually. In fact, isolated zones of bubble formation or incipient cavitation often occur at pressure drops well below that at which a reduction in flow is noticeable. The similarity between liquid and gas choking is not serendipitous; it is surmised that the two-phase fluid is traveling at the mixture's sonic velocity in the throat when choked. Complex fluids with components having varying vapor pressures and/or entrained noncondensable gases (e.g., crude oil) will exhibit soft vaporization/implosion transitions.

There are several methods to reduce cavitation or at least its negative side effects. Material damage is slowed by using harder materials and by directing the cavitating stream away from passage walls (e.g., with an angle body flowing down). Sometimes the system can be designed to place the valve in a higher p_2 location or add downstream resistance, which creates backpressure. A low recovery valve has a higher minimum pressure for a given p_2 and so is a means to eliminate the cavitation itself, not just its side effects. In Fig. 8-75, if $p_v < B$, neither valve will cavitate substantially. For $p_v > B$ but $p_v < A$, the high

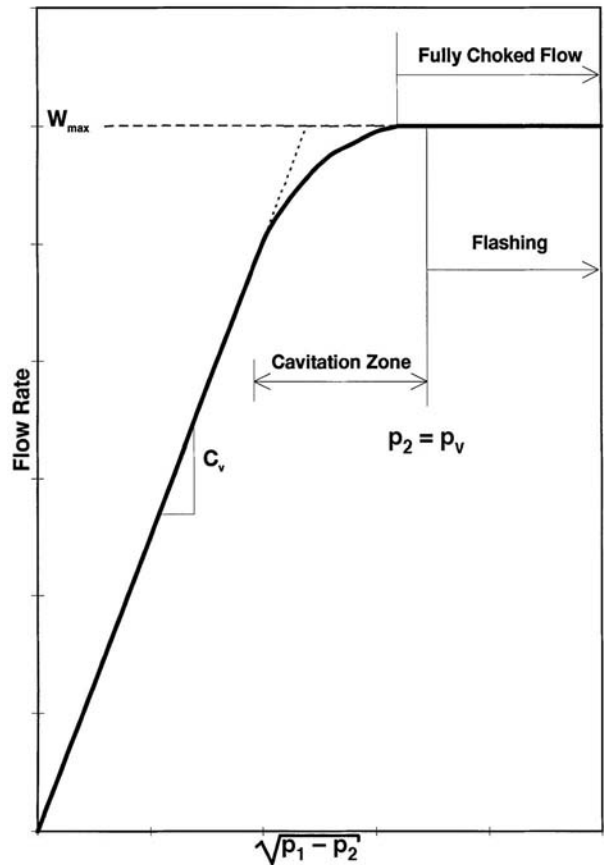


FIG. 8-77 Liquid flow rate versus pressure drop (assuming constant p_1 and p_v).

recovery valve will cavitate substantially, but the low recovery valve will not. Special anticavitation trims are available for globe and angle valves and more recently for some rotary valves. These trims use multiple contraction/expansion stages or other distributed resistances to boost F_1 to values sometimes near unity.

If p_2 is below p_v , the two-phase mixture will continue to vaporize in the body outlet and/or downstream pipe until all liquid phase is gone, a condition known as flashing. The resulting huge increase in specific volume leads to high velocities, and any remaining liquid droplets acquire much of the higher vapor-phase velocity. Impingement of these droplets can produce material damage, but it differs from cavitation damage because it exhibits a smooth surface. Hard materials and directing the two-phase jets away from solid surfaces are means to avoid this damage.

Seals, Bearings, and Packing Systems In addition to their control function, valves often need to provide shutoff. FCI 70-2-1998 and IEC 60534-4 recognize six standard classifications and define their as-shipped qualification tests. Class I is an amount agreed to by user and supplier with no test needed. Classes II, III, and IV are based on an air test with maximum leakage of 0.5 percent, 0.1 percent, and 0.01 percent of rated capacity, respectively. Class V restricts leakage to 5×10^{-6} mL of water per second per millimeter of port diameter per bar differential. Class VI allows 0.15 to 6.75 mL/min of air to escape depending on port size; this class implies the need for interference-fit elastomeric seals. With the exception of class V, all classes are based on standardized pressure conditions that may not represent actual conditions. Therefore, it is difficult to estimate leakage in service. Leakage normally increases over time as seals and seating surfaces become nicked or worn. Leak passages across the seat-contact line, known as

wire drawing, may form and become worse over time—even in hard metal seats under sufficiently high-pressure differentials.

Polymers used for seat and plug seals and internal static seals include PTFE (polytetrafluoroethylene) and other fluorocarbons, polyethylene, nylon, polyether-ether-ketone, and acetal. Fluorocarbons are often carbon- or glass-filled to improve mechanical properties and heat resistance. Temperature and chemical compatibility with the process fluid are the key selection criteria. Polymer-lined bearings and guides are used to decrease friction, which lessens dead band and reduces actuator force requirements. See Sec. 25, “Materials of Construction,” for properties.

Packing forms the pressure-tight seal, where the stem protrudes through the pressure boundary. Packing is typically made from PTFE or, for high temperature, a bonded graphite. If the process fluid is toxic, more sophisticated systems such as dual packing, live-loaded, or a flexible metal bellows may be warranted. Packing friction can significantly degrade control performance. Pipe, bonnet, and internal-trim joint gaskets are typically a flat sheet composite. Gaskets intended to absorb dimensional mismatch are typically made from filled spiral-wound flat stainless-steel wire with PTFE or graphite filler. The use of asbestos in packing and gaskets has been largely eliminated.

Flow Characteristics The relationship between valve flow and valve travel is called the valve flow characteristic. The purpose of flow characterization is to make loop dynamics independent of load, so that a single controller tuning remains optimal for all loads. Valve gain is one factor affecting loop dynamics. In general, gain is the ratio of change in output to change in input. The input of a valve is travel y , and the output is flow w . Since pressure conditions at the valve can depend on flow (hence travel), valve gain is

$$\frac{dw}{dy} = \frac{\partial w}{\partial C_V} \frac{dC_V}{dy} + \frac{\partial w}{\partial p_1} \frac{dp_1}{dy} + \frac{\partial w}{\partial p_2} \frac{dp_2}{dy} \quad (8-121)$$

An inherent valve flow characteristic is defined as the relationship between flow rate and travel, under constant-pressure conditions. Since the rightmost two terms in Eq. (8-121) are zero in this case, the inherent characteristic is necessarily also the relationship between flow coefficient and travel.

Figure 8-78 shows three common inherent characteristics. A linear characteristic has a constant slope, meaning the inherent valve gain is a constant. The most popular characteristic is equal-percentage, which gets its name from the fact that equal changes in travel produce equal-percentage changes in the existing flow coefficient. In other words, the slope of the curve is proportional to C_V , or equivalently that inherent valve gain is proportional to flow. The equal-percentage characteristic can be expressed mathematically by

$$C_V(y) = (\text{rated } C_V) \exp \left[\left(\frac{y}{\text{rated } y} - 1 \right) \ln R \right] \quad (8-122)$$

This expression represents a set of curves parameterized by R . Note that $C_V(y = 0)$ equals $(\text{rated } C_V)/R$ rather than zero; real equal-percentage characteristics deviate from theory at some small travel to meet shutoff requirements. An equal-percentage characteristic provides perfect compensation for a process where the gain is inversely proportional to flow (e.g., liquid pressure). *Quick opening* does not have a standardized mathematical definition. Its shape arises naturally from high-capacity plug designs used in on/off service globe valves. Frequently, pressure conditions at the valve will change with flow rate. This so-called process influence [the rightmost two terms on the right-hand side of Eq. (8-121)] combines with inherent gain to express the installed valve gain. The flow versus travel relationship for a specific set of conditions is called the installed flow characteristic. Typically, valve Δp decreases with load, since pressure losses in the piping system increase with flow. Figure 8-79 illustrates how allocation of total system head to the valve influences the installed flow characteristics. For a linear or quick-opening characteristic, this transition toward a concave down shape would be more extreme. This effect of typical process pressure variation, which causes equal-percentage

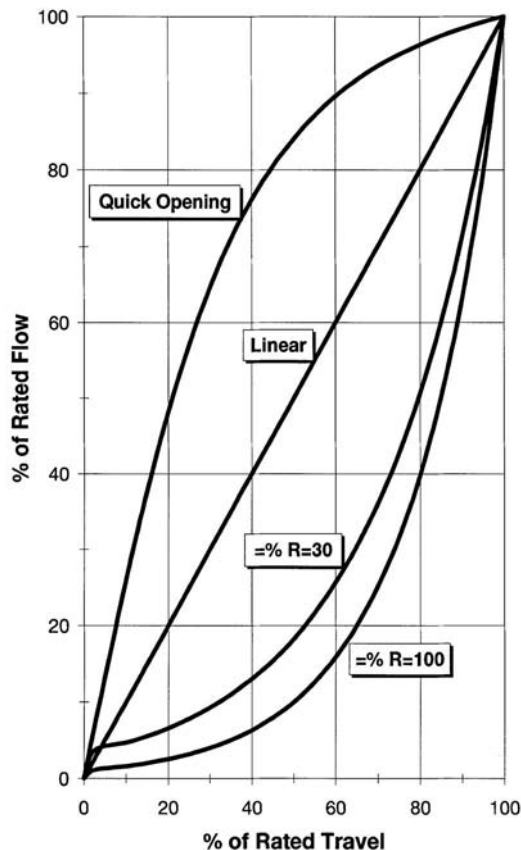


FIG. 8-78 Typical inherent flow characteristics.

characteristics to have fairly constant installed gain, is one reason the equal-percentage characteristic is the most popular.

Due to clearance flow, flow force gradients, seal friction, and the like, flow cannot be throttled to an arbitrarily small value. Installed rangeability is the ratio of maximum to minimum controllable flow. The actuator and positioner, as well as the valve, influence the installed rangeability. Inherent rangeability is defined as the ratio of the largest to the smallest C_V within which the characteristic meets specified criteria (see ISA 75.11). The R value in the equal-percentage definition is a theoretical rangeability only. While high installed rangeability is desirable, it is also important not to oversize a valve; otherwise, turndown (ratio of maximum normal to minimum controllable flow) will be limited.

Sliding stem valves are characterized by altering the contour of the plug when the port and plug determine the minimum (controlling) flow area. Passage area versus travel is also easily manipulated in characterized cage designs. Inherent rangeability varies widely, but typical values are 30 for contoured plugs and 20 to 50 for characterized cages. While these types of valves can be characterized, the degree to which manufacturers conform to the mathematical ideal is revealed by plotting measured C_V versus travel. Note that ideal equal-percentage will plot as a straight line on a semilog graph. Custom characteristics that compensate for a specific process are possible.

Rotary stem-valve designs are normally offered only in their naturally occurring characteristic, since it is difficult to appreciably alter this. If additional characterization is required, the positioner or controller may be characterized. However, these approaches are less direct, since it is possible for device nonlinearity and dynamics to distort the compensation.

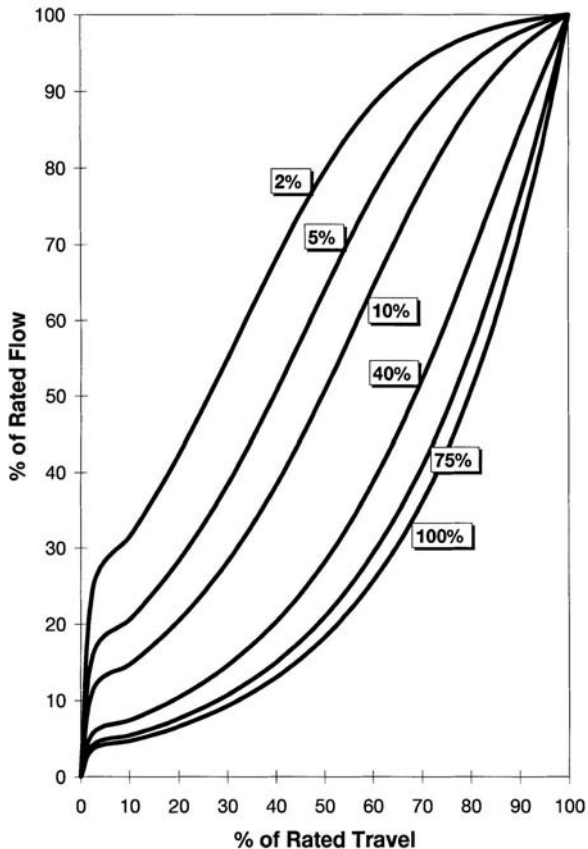


FIG. 8-79 Installed flow characteristic as a function of percent of total system head allocated to the control valve (assuming constant-head pump, no elevation head loss, and an R equal to 30 equal-percentage inherent characteristic).

VALVE CONTROL DEVICES

Devices mounted on the control valve that interface various forms of input signals, monitor and transmit valve position, or modify valve response are valve control devices. In some applications, several auxiliary devices are used together on the same control valve. For example, mounted on the control valve, one may find a current-to-pressure transducer, a valve positioner, a volume booster relay, a solenoid valve, a trip valve, a limit switch, a process controller, and/or a stem position transmitter. Figure 8-80 shows a valve positioner mounted on the yoke leg of a spring and diaphragm actuator.

As most throttling control valves are still operated by pneumatic actuators, the control valve device descriptions that follow relate primarily to devices that are used with pneumatic actuators. The functions of hydraulic and electrical counterparts are very similar. Specific details on a particular valve control device are available from the vendor of the device.

Valve Positioners The valve positioner, when combined with an appropriate actuator, forms a complete closed-loop valve position control system. This system makes the valve stem conform to the input signal coming from the process controller in spite of force loads that the actuator may encounter while moving the control valve. Usually, the valve positioner is contained in its own enclosure and is mounted on the control valve.

The key parts of the positioner/actuator system, shown in Fig. 8-81a, are (1) an input conversion network, (2) a stem position feedback network, (3) a summing junction, (4) an amplifier network, and (5) an actuator.



FIG. 8-80 Valve and actuator with valve positioner attached. (Courtesy Fisher Controls International LLC.)

The input conversion network shown is the interface between the input signal and the summer. This block converts the input current or pressure (from an I/P transducer or a pneumatic process controller) to a voltage, electric current, force, torque, displacement, or other particular variable that can be directly used by the summer. The input conversion usually contains a means to adjust the slope and offset of the block to provide for a means of spanning and zeroing the positioner during calibration. In addition, means for changing the sense (known as "action") of the input/output characteristic are often addressed in this block. Also exponential, logarithmic, or other predetermined characterization can be put in this block to provide a characteristic that is useful in offsetting or reinforcing a nonlinear valve or process characteristic.

The stem position feedback network converts stem travel to a useful form for the summer. This block includes the feedback linkage which varies with actuator type. Depending on positioner design, the stem position feedback network can provide span and zero and characterization functions similar to that described for the input conversion block.

The amplifier network provides signal conversion and suitable static and dynamic compensation for good positioner performance. Control from this block usually reduces to a form of proportional or proportional plus derivative control. The output from this block in the case of a pneumatic positioner is a single connection to the spring and diaphragm actuator or two connections for push/pull operation of a

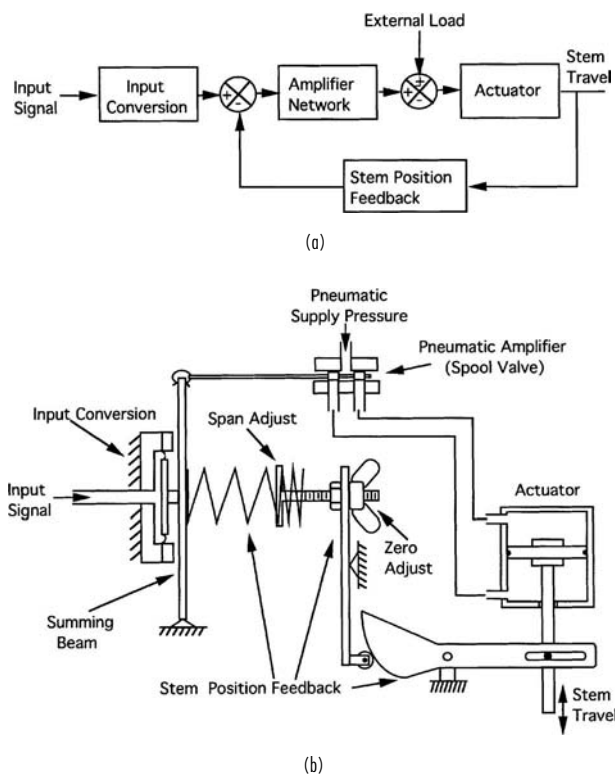


FIG. 8-81 Positioner/actuators. (a) Generic block diagram. (b) Example of a pneumatic positioner/actuator.

springless piston actuator. The action of the amplifier network and the action of the stem position feedback can be reversed together to provide for reversed positioner action.

By design, the gain of the amplifier network shown in Fig. 8-81a is made very large. Large gain in the amplifier network means that only a small proportional deviation will be required to position the actuator through its active range of travel. This means that the signals into the summer track very closely and that the gain of the input conversion block and the stem position feedback block determine the closed-loop relationship between the input signal and the stem travel.

Large amplifier gain also means that only a small amount of additional stem travel deviation will result when large external force loads are applied to the actuator stem. For example, if the positioner's amplifier network has a gain of 50 (and assuming that high packing box friction loads require 25 percent of the actuator's range of thrust to move the actuator), then only 25 percent/50 (or 0.5 percent deviation) between input signal and output travel will result due to valve friction.

Figure 8-81b is an example of a pneumatic positioner/actuator. The input signal is a pneumatic pressure that (1) moves the summing beam, which (2) operates the spool valve amplifier, which (3) provides flow to and from the piston actuator, which (4) causes the actuator to move and continue moving until (5) the feedback force returns the beam to its original position and stops valve travel at a new position. Typical positioner operation is thereby achieved.

Static performance measurements related to positioner/actuator operation include the conformity, measured accuracy, hysteresis, dead band, repeatability, and locked stem pressure gain. Definitions and standardized test procedures for determining these measurements can be found in ISA-S75.13, "Method of Evaluating the Performance of Positioners with Analog Input Signals and Pneumatic Output."

Dynamics of Positioner-Based Control Valve Assemblies

Control valve assemblies are complete, functional units that include the valve body, actuator, positioner, if so equipped, associated linkages, and any auxiliary equipment such as current to pneumatic signal transducers and air supply pressure regulators. Although performance information such as frequency response, sensitivity, and repeatability data may be available for a number of these components individually, it is the performance of the entire assembly that will ultimately determine how well the demand signal from the controller output is transferred through the control valve to the process. The valve body, actuator, and positioner combination is typically responsible for the majority of the control valve assembly's dynamic behavior. On larger actuators, the air supply pressure regulator capacity or other airflow restrictions may limit the control valve assembly's speed of response.

The control valve assembly response can usually be characterized quite well by using a first-order plus dead-time response model. The control valve assembly will also exhibit backlash, stiction, and other non-linear behavior. During normal operation of a control loop, the controller usually makes small output changes from one second to the next. Typically this change is less than 1 percent. With very small controller output changes, e.g., less than 0.1 percent, the control valve assembly may not move at all. As the magnitude of the controller output change increases, eventually the control valve will move. At the threshold of movement, the positional accuracy and repeatability of the control valve are usually quite poor. The speed of response may be quite slow and may occur after a number of seconds of dead time. This poor performance is due to the large backlash and stiction effects relative to the requested movement and the small output change of the positioner. With a further increase in the magnitude of the controller output steps, the behavior of the control valve typically becomes more repeatable and "linear." Dead time usually drops to only a fraction of a second, and the first-order time constant becomes faster. For much larger steps in the controller output, e.g., over 10 percent, the positioner and air supply equipment may be unable to deliver the necessary air volume to maintain the first-order response. In this case, the control valve will exhibit very little dead time, but will be rate-limited and will ramp toward the requested position. It is within the linear region of motion that the potential for the best control performance exists.

When one is specifying a control valve for process control applications, in addition to material, style, and size information, the dynamic response characteristics and maximum allowable dead band (sum of backlash, stiction, and hysteresis effects) *must* be stated. The requirement for the control valve assembly's speed of response is ultimately determined by the dynamic characteristics of the process and the control objectives. Typically, the equivalent first-order time constant specified for the control valve assembly should be at least 5 times faster than the desired controller closed-loop time constant. If this requirement is not met, the tuning of the control loop must be slowed down to accommodate the slow control valve response, otherwise, control robustness and stability may be compromised. The dead band of the control valve assembly is typically the determining factor for control resolution and frequently causes control instability in the form of a "limit" cycle. The controller output will typically oscillate across a range that is 1 to 2 times the magnitude of the control valve dead band. This is very dependent on the nature of the control valve nonlinearities, the process dynamics, and the controller tuning. The magnitude of the process limit cycle is determined by the size of the control valve dead band multiplied by the installed gain of the control valve. For this reason, a high-performance control valve assembly, e.g., with only 0.5 percent dead band, may cause an unacceptably large process limit cycle if the valve is oversized and has a high installed gain. For typical process control applications, the installed gain of the control valve should be in the range of 0.5 to 2 percent of the process variable span per percent of the controller output. The total dead band of the control valve assembly should be less than 1 percent. For applications that require more precise control, the dead band and possibly the installed gain of the control valve must be reduced. Specialized actuators are available that are accurate down to 0.1 percent or less. At this level of performance, however, the design of the valve body, bearings, linkages, and seals starts to become a significant source of dead band.

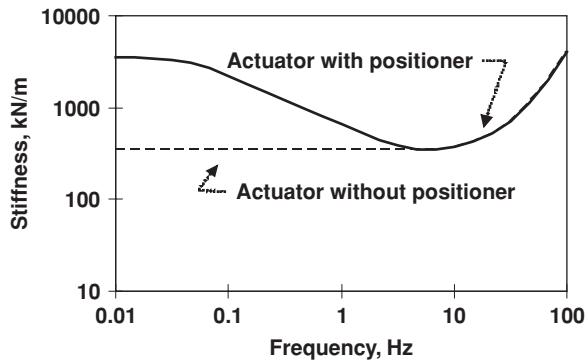


FIG. 8-82 Actuator stiffness as a function of frequency for a 69-in² spring and diaphragm pneumatic actuator. Actuator with positioner exhibits higher stiffness over the lower frequency range compared to that of the pneumatic actuator without a positioner.

Positioner/Actuator Stiffness Minimizing the effect of dynamic loads on valve stem travel is an important characteristic of the positioner/actuator. Stem position must be maintained in spite of changing reaction forces caused by valve throttling. These forces can be random (buffeting force) or can result from a negative-slope force/stem travel characteristic (negative gradient); either could result in valve stem instability and loss of control. To reduce and eliminate the effect of these forces, the effective stiffness of the positioner/actuator must be made sufficiently high to maintain stationary control of the valve stem.

The stiffness characteristic of the positioner/actuator varies with the forcing frequency. Figure 8-82 indicates the stiffness of the positioner/actuator is increased at low frequencies and is directly related to the locked-stem pressure gain provided by the positioner. As frequency increases, a dip in the stiffness curve results from dynamic gain attenuation in the pneumatic amplifiers in the positioner. The value at the bottom of the dip is the sum of the mechanical stiffness of the spring in the actuator and the air spring effect produced by air enclosed in the actuator casing. At yet higher frequencies, actuator inertia dominates and causes a corresponding rise in system stiffness.

The air spring effect results from adiabatic expansion and compression of air in the actuator casing. Numerically, the small perturbation value for air spring stiffness in newtons per meter is given by

$$\text{Air spring rate} = \frac{\gamma p_a A_a^2}{V} \quad (8-123)$$

where γ is the ratio of specific heats (1.4 for air), p_a is the actuator pressure in pascals absolute, A_a is the actuator pressure area in square meters, and V is the internal actuator volume in cubic meters.

Positioner Application Positioners are widely used on pneumatic valve actuators. Often they provide improved process loop control because they reduce valve-related nonlinearity. Dynamically, positioners maintain their ability to improve control valve performance for sinusoidal input frequencies up to about one-half of the positioner bandwidth. At input frequencies greater than this, the attenuation in the positioner amplifier network gets large, and valve nonlinearity begins to affect final control element performance more significantly. Because of this, the most successful use of the positioner occurs when the positioner response bandwidth is greater than twice that of the most dominant time lag in the process loop.

Some typical examples in which the dynamics of the positioner are sufficiently fast to improve process control are the following:

1. In a distributed control system (DCS) process loop with an electronic transmitter. The DCS controller and the electronic transmitter have time constants that are dominant over the positioner response. Positioner operation is therefore beneficial in reducing valve-related nonlinearity.

2. In a process loop with a pneumatic controller and a large process time constant. Here the process time constant is dominant, and the positioner will improve the linearity of the final control element. Some common processes with large time constants that benefit from positioner application are liquid level, temperature, large-volume gas pressure, and mixing.

3. Additional situations in which valve positioners are used:

- a. On springless actuators where the actuator is not usable for throttling control without position feedback.

- b. When split ranging is required to control two or more valves sequentially. In the case of two valves, the smaller control valve is calibrated to open in the lower half of the input signal range, and a larger valve is calibrated to open in the upper half of the input signal range. Calibrating the input command signal range in this way is known as split-range operation and increases the practical range of throttling process flows over that of a single valve.

- c. In open-loop control applications where best static accuracy is needed. On occasion, positioner use can degrade process control. Such is the case when the process controller, process, and process transmitter have time constants that are similar to or smaller than that of the positioner/actuator. This situation is characterized by low process controller proportional gain (gain < 0.5), and hunting or limit cycling of the process variable is observed.

Improvements here can be made by doing one of the following:

1. Install a dominant first-order, low-pass filter in the loop ahead of the positioner and retune the process loop. This should allow increased proportional gain in the process loop and reduce hunting. Possible means for adding the filter include adding it to the firmware of the DCS controller, by adding an external RC network on the output of the process controller or by enabling the filter function in the input of the positioner, if it is available. Also, some transducers, when connected directly to the actuator, form a dominant first-order lag that can be used to stabilize the process loop.

2. Select a positioner with a faster response characteristic.

Processor-Based Positioners When designed around an electronic microcontroller, the valve positioner [now commonly referred to as a *digital valve controller* (DVC)] takes on additional functionality that provides convenience and performance enhancements over the traditional design. The most common form of processor-based positioner, shown in Fig. 8-81, is a digitally communicating stem position controller that operates by using the fundamental blocks shown in Fig. 8-81a. A local display is part of the positioner and provides tag information, command input and travel, servo tuning parameters, and diagnostic information. Often auxiliary sensors are integrated into the device to provide increased levels of functionality and performance. Sensed variables can include actuator pressure, relay input pressure, relay valve position, board temperature, or a discrete input. A 4- to 20-mA valve travel readback circuit is also common. The travel sensor is based on a potentiometer or can be a noncontacting type such as a variable capacitance sensor, Hall effect sensor, or GMR device. Some positioners require a separate connection to an ac or dc supply voltage, but the majority of the designs are "loop-powered," which means that they receive power either through the current input (for positioners that require a 4- to 20-mA analog input signal) or through the digital communications link when the control signal is a digital signal.

Processor-based positioners support automatic travel calibration and automatic response tuning for quick commissioning of the final control element. Features of this type of valve positioner include compensators for improved static and dynamic travel response; diagnostics for evaluating positioner, actuator, and valve health; and the capability to be polled from remote locations through a PC-based application or through a handheld communicator attached to the field wiring. Capability to support custom firmware for special valve applications, such as emergency safety shutdown, is also a characteristic of the processor-based design.

Digital Field Communications To provide increased data transmission capability between valve-mounted devices and the host control system, manufacturers are providing digital network means in their devices. The field networks, commonly known as field buses, compete fiercely in the marketplace and have varying degrees of flexibility and specific application strengths. A prospective field bus

customer is advised to study the available bus technologies and to make a selection based on needs, and not be seduced by the technology itself.

Generally, a field bus protocol must be nonproprietary ("open") so that different vendors of valve devices can design their bus interface to operate properly on the selected field bus network. Users demand that the devices be "interoperable" so that the device will work with other devices on the same segment or can be substituted with a device from an alternate manufacturer. International standardization of some of the protocols is currently underway (for example, IEC 61158) whereas others are sponsored by user groups or foundations that provide democratic upgrades to the standard and provide network compliance testing.

The physical wiring typically used is the plant standard twisted-pair wiring for 4- to 20-mA instrumentation. Because of the networking capability of the bus, more than one device can be supported on a single pair of wires, and thus wiring requirements are reduced. Compared to a host level bus such as Ethernet, field buses exhibit slower communication rates, have longer transmission distance capability (1 to 2 km), use standard two-wire installation, are capable of multidrop busing, can support bus-powered devices, do not have redundant modes of bus operation, and are available for intrinsically safe installations. Devices on the field bus network may be either powered by the bus itself or powered separately.

The simplest digital networks available today support discrete sensors and on/off actuators, including limit switches and motor starters. Networks of this type have fast cycle times and are often used as an alternative to PLC discrete I/O. More sophisticated field networks are designed to support process automation, more complex process transmitters, and throttling valve actuators. These process-level networks are fundamentally continuous and analoglike in operation, and data computation is floating-point. They support communication of materials of construction, calibration and commissioning, device and loop level diagnostics (including information displays outlining corrective action), and unique manufacturer-specific functionality. Some process networks are able to automatically detect, identify, and assign an address to a new device added to the network, thus reducing labor, eliminating addressing errors, and indicating proper network function immediately after the connection is made. Final control elements operated by the process-level network include I/P transducers, motorized valves, digital valve controllers, and transmitters.

A particular field network protocol known as HART[®] (Highway Addressable Remote Transducer) is the most widely used field network protocol. It is estimated that as of 2004 there are more than 14 million HART-enabled devices installed globally and that 70 percent

of all processor-based process measurement and control instruments installed each year use HART communications. HART's popularity is based on its similarity to the traditional 4- to 20-mA field signaling and thus represents a safe, controlled transition to digital field communications without the risk often associated with an abrupt change to a totally digital field bus. With this protocol, the digital communications occur over the same two wires that provide the 4- to 20-mA process control signal without disrupting the process signal. The protocol uses the frequency-shift keying (FSK) technique (see Fig. 8-83) where two individual frequencies, one representing the mark and the other representing the space, are superimposed on the 4- to 20-mA current signal. As the average value of the signals used is zero, there is no dc offset value added to the 4- to 20-mA signal. The HART protocol is principally a master/slave protocol which means that a field device (slave) speaks only when requested by a master device. In this mode of operation, the slave can update the master at a rate of twice per second. An optional communication mode, *burst mode*, allows a HART slave device to continuously broadcast updates without stimulus requests from the master device. Update rates of 3 to 4 updates per second are typical in the burst mode of operation.

HART-enabled devices are provided by the valve device manufacturer at little or no additional cost. The HART network is compatible with existing 4- to 20-mA applications using current plant personnel and practices, provides for a gradual transition from analog to fully digital protocols, and is provided by the valve device manufacturer at little or no additional cost. Contact the HART Communication Foundation for additional information.

Wireless digital communication to and from the final control element is not yet commercially available but is presently being investigated by more than one device manufacturer. The positive attribute of a wireless field network is the reduced cost of a wireless installation compared to a wired installation. Hurdles for wireless transmissions include security from nonnetwork sources, transmission reliability in the plant environment, limited bus speed, and the conservative nature of the process industry relative to change. Initial installations of wireless networks will support secondary variables and diagnostics, then primary control of processes with large time constants, and finally general application to process control. Both point-to-point and mesh architectures are being evaluated for commercialization at the device level. Mesh architectures rely on the other transmitting devices in the area to receive and then pass on any data transmission, thus rerouting communications around sources of interference. Two unlicensed spread spectrum radio bands are the main focus for current wireless development: 900 MHz and 2.4 GHz. The 900-MHz band is unique to North America and has better propagation and penetrating properties than the 2.4-GHz band. The 2.4-GHz band is a worldwide band and has wider channels, allowing much higher data rates. The spread

*HART is a registered trademark of the HART Communication Foundation.

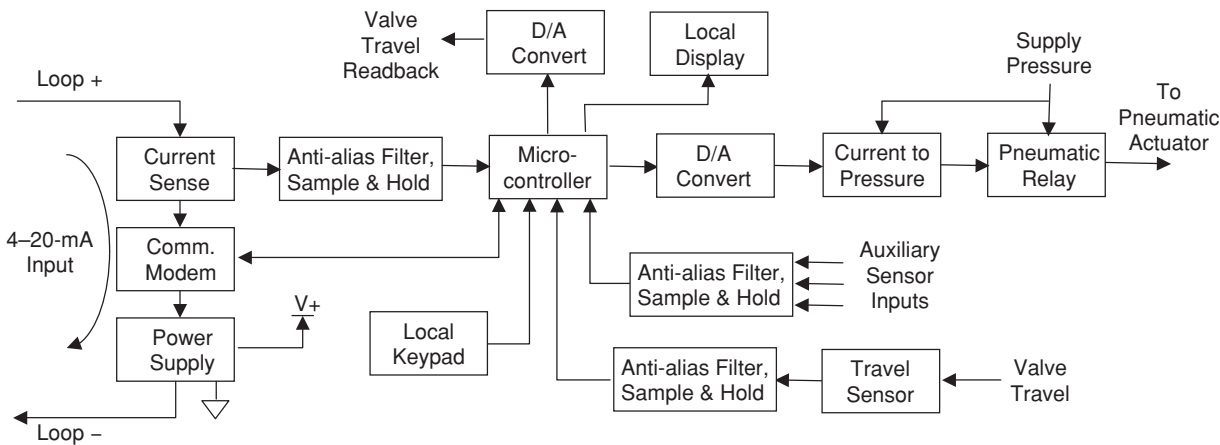


FIG. 8-83 Generic loop powered digital valve controller.

spectrum technique uses multiple frequencies within the radio band to transmit data. Spread spectrum is further divided into the direct sequence technique, where the device changes frequency many times per data bit, and the frequency-hopping technique, where the device transmits a data packet on one frequency and then changes to a different frequency. Because of the rapid growth expected in this decade, the prospective wireless customer is encouraged to review up-to-date literature to determine the state of field wireless commercialization as it applies to her or his specific application.

Diagnostic Capability The rapid proliferation of communicating, processor-based digital valve controllers over the last decade has led to a corresponding rise in diagnostic capability at the control valve. Diagnosing control valve health is critical to plant operation as maintenance costs can be reduced by identifying the valves that are candidates for repair. Less time is spent during plant shutdown repairing valves that do not need repair, which ultimately results in increased online operating time. Valve diagnostics can detect and flag a failed valve more quickly than by any other means, and can be configured to cause the valve to move to its fail-safe position on detection of specified fault conditions. The diagnostic-enabled positioner, when used with its host-based software application, can pinpoint exact components in a given final control element that have failed, and can recommend precise maintenance procedures to follow to remedy the fault condition.

The state variables that provide valve position control are used to diagnose the health of the final control element. In addition, some digital valve controller designs integrate additional sensors into their construction to provide increased diagnostic capability. For example, pressure sensors are provided to detect supply pressure, actuator pressure (upper and lower cylinder pressures in the case of a springless piston actuator), and internal pilot pressure. Also, the position of the pneumatic relay valve is available in some designs to provide quiescent flow data used for leak detection in the actuator.

Valve diagnostics are divided into two types: online and offline. Offline diagnostics are those diagnostics that occur when the control valve is bypassed or otherwise isolated from the process. The offline diagnostic routine manipulates the travel command to the valve and records the corresponding valve travel, actuator pressure, and servodrive value. These parameters are plotted in various combinations to provide hysteresis plus dead-band information, actuator operating pressure as a function of travel, valve friction, servodrive performance, valve seating load, positioner calibration endpoints, and dynamic response traces. Small- and large-amplitude step inputs as well as large slow ramps (exceeding 100 percent of the input range) are common offline test waveforms generated by the diagnostic as command inputs for offline diagnostic tests. Figure 8-84 is an example of one offline diagnostic test performed on a small globe valve actuated by a spring and diaphragm actuator. During this test the command input, travel, actuator pressure, and servodrive level are recorded and plotted as they result from a command input that is slowly ramped by the diagnostic routine (Fig. 8-85a). This diagnostic is extremely useful in detecting problems with the valve/actuator system and can flag potential problems with the final control element before catastrophic failure occurs. For example, Fig. 8-85b indicates the overall tracking capability of the control valve, and Fig. 8-85c indicates the pressure operating range of the actuator and the amount of frictional force resulting from the combined effects of valve packing and valve plug contact. Figure 8-85d displays the level of servodrive required to stroke the valve from one end of travel to the other. The composite operative health of the control valve is determined through comparison of the empirical levels presented in Fig. 8-85 with the manufacturers' recommendations. Recommended maintenance actions result from this comparison.

Online diagnostics are diagnostics that monitor and evaluate conditions at the control valve during normal throttling periods (i.e., during valve-in-service periods). Online diagnostics monitor mean levels and disturbances generated in the normal operation of the valve and typically do not force or generate disturbances on the valve's operation. For example, an online diagnostic can calculate travel deviation relative to the input command and flag a condition where the valve travel has deviated beyond a preset band. Such an event, if it exists for more than a short time, indicates that the valve has lost its ability to track the input

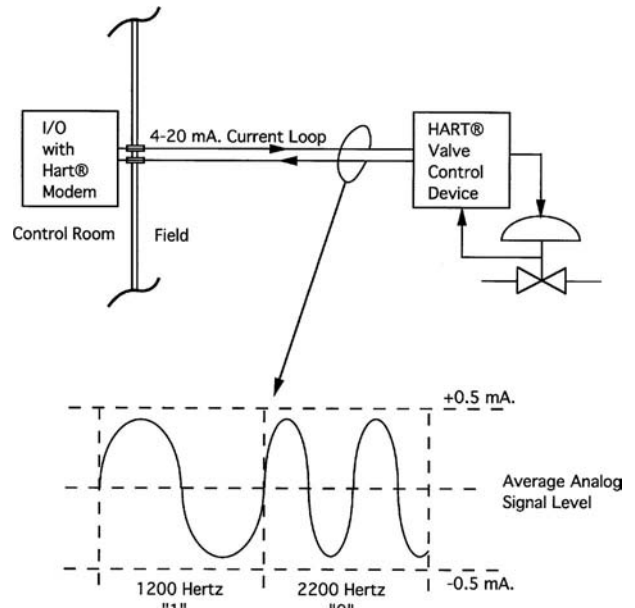


FIG. 8-84 Hybrid point-to-point communications between the control room and the control valve device.

command within specified limits. Additional diagnostics could suggest that the feedback linkage has ceased functioning, or that the valve has stuck, or that some other specific malfunction is the cause of excess travel deviation. The manufacturer of the positioner diagnostic incorporates default limits into the host software application that are used to determine the relative importance of a specific deviation. To quickly indicate the severity of a problem detected by a diagnostic routine, a red, yellow, or green, or "advise, maintenance now, or failed," indication is presented on the user-interface screen for the valve problem diagnosed. Help notes and recommended remedial action are available by pointing and clicking on the diagnostic icon presented on the user's display.

Event-triggered recording is an online diagnostic technique supported in digital valve controllers (DVCs). Functionally a triggering event, such as a valve coming off a travel stop or a travel deviation alert, starts a time-series recording of selected variables. A collection of variables such as the input command, stem travel, actuator pressure, and drive command are stored for several minutes before and after the triggered event. These variables are then plotted as time series for immediate inspection or are stored in memory for later review. Event-triggering diagnostics are particularly useful in diagnosing valves that are closed or full-open for extended periods. In this case the event-triggered diagnostic focuses on diagnostic rich data at the time the valve is actually in operation and minimizes the recording of flat-line data with little diagnostic content. Other online diagnostics detected by DVC manufacturers include excess valve friction, supply pressure failure, relay operation failure, broken actuator spring, current to pressure module failure, actuator diaphragm leaking, and shifted travel calibration.

Safety shutdown valves, which are normally wide open and operate infrequently, are expected to respond to a safety trip command reliably and without fault. To achieve the level of reliability required in this application, the safety valve must be periodically tested to ensure positive operation under safety trip conditions. To test the operation of the shutdown system without disturbing the process, the traditional method is to physically lock the valve stem in the wide-open position and then to electrically operate the pneumatic shutdown solenoid valve. Observing that the pneumatic solenoid valve has properly vented the actuator pressure to zero, the actuator is seen as capable of applying sufficient spring force to close the valve, and a positive safety valve test is indicated. The

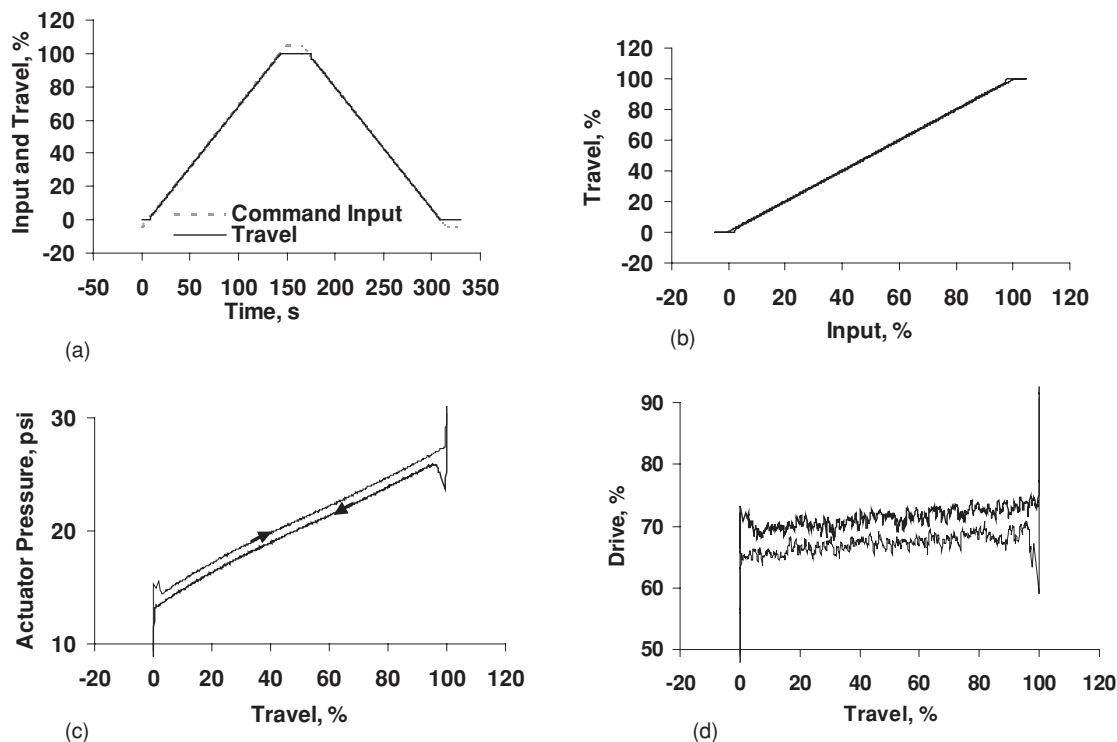


FIG. 8-85 Offline valve diagnostic scan showing results of a diagnostic ramp. (a) The command input and resulting travel. (b) The dynamic scan. (c) The valve signature. (d) The servodrive versus travel plot. The hysteresis shown in the valve signature results from sliding friction due to valve packing and valve plug contact.

pneumatic solenoid valve is then returned to its normal electrical state, the actuator pressure returns to full supply pressure, and the valve stem lock mechanism is removed. This procedure, though necessary to enhance process safety, is time-consuming and takes the valve out of service during the locked stem test. Digital valve controllers are able to validate the operation of a safety shutdown valve by using an online diagnostic referred to as a partial stroke test. The partial stroke test is substituted for the traditional test method described above and does not require the valve to be locked in the wide-open position to perform the test. In a fashion similar to that shown in Fig. 8-85a (the partial stroke diagnostic), the system physically ramps the command input to the positioner from the wide-open position to a new position, pauses at the new position for a few seconds, and then ramps the command input back to the wide-open position (see Fig. 8-86a). During this time, the valve travel measurement is monitored and compared to the input command. If the travel measurement deviates from the input by more than a fixed amount for the configured period of time, the valve is considered to have failed the test and a failed-test message is communicated to the host system. Also during this test, the actuator pressure required to move the valve is detected via a dedicated pressure sensor (see Fig. 8-86b). If the thrust (pressure) required to move the valve during the partial stroke test exceeds the predefined thrust limit for this test, the control valve is determined to have a serious sticking problem, the test is immediately aborted, and the valve is flagged as needing maintenance. The partial stroke test can be automated to perform on a periodic basis, for instance, once a week; or it can be initialized by operator request at any time. The amount of valve travel that occurs during the partial stroke test is typically limited to a minimum valve position of 70 percent open or greater. This limit is imposed to prevent the partial stroking of the safety valve from significantly affecting the process flow through the valve.

Comparison of partial stroke curves from past tests can indicate the gradual degradation of valve components. Use of “overlay” graphics, identification of unhealthy shifts in servodrive, increases in valve friction, and changes in dynamic response provide information leading to a diagnosis of needed maintenance.

In addition to device-level diagnostics, networked final control elements, process controllers, and transmitters can provide “loop” level diagnostics that can detect loops that are operating below expectations. Process variability, time in a limit (saturated) condition, and time in the wrong control mode are metrics used to detect problems in process loop operation.

Transducers The current-to-pressure transducer (I/P transducer) is a conversion interface that accepts a standard 4- to 20-mA input current from the process controller and converts it to a pneumatic output in a standard pneumatic pressure range [normally 0.2 to 1.0 bar (3 to 15 psig) or, less frequently, 0.4 to 2.0 bar (6 to 30 psig)]. The output pressure generated by the transducer is connected directly to the pressure connection on a spring-opposed diaphragm actuator or to the input of a pneumatic valve positioner.

Figure 8-87a is the schematic of a basic I/P transducer. The transducer shown is characterized by (1) an input conversion that generates an angular displacement of the beam proportional to the input current, (2) a pneumatic amplifier stage that converts the resulting angular displacement to pneumatic pressure, and (3) a pressure area that serves as a means to return the beam to very near its original position when the new output pressure is achieved. The result is a device that generates a pressure output that tracks the input current signal. The transducer shown in Fig. 8-88a is used to provide pressure to small load volumes (normally 4.0 in³ or less), such as a positioner or booster input. With only one stage of pneumatic amplification, the flow

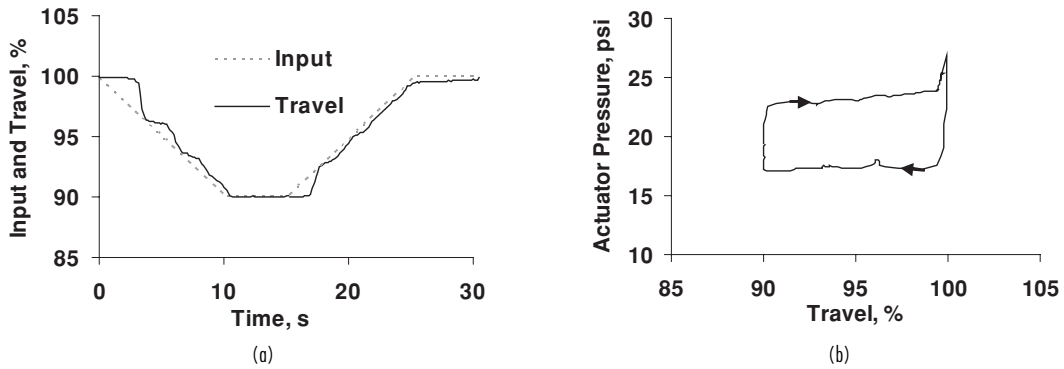


FIG. 8-86 Online partial stroke diagnostic used to validate the operability of a pneumatically operated safety shutdown valve. (a) Input command generated by the diagnostic and resulting travel. (b) Actuator pressure measured over the tested range of travel.

capacity of this transducer is limited and not sufficient to provide responsive load pressure directly to a pneumatic actuator.

The flow capacity of the transducer can be increased by adding a booster relay such as the one shown in Fig. 8-87b. The flow capacity of the booster relay is nominally 50 to 100 times that of the nozzle amplifier shown in Fig. 8-87a and makes the combined transducer/booster suitably responsive to operate pneumatic actuators. This type of transducer is stable for all sizes of load volume and produces measured accuracy (see ANSI/ISA-51.1, "Process Instrumentation Terminology," for the definition of measured accuracy) of 0.5 to 1.0 percent of span.

Better measured accuracy results from the transducer design shown in Fig. 8-87c. In this design, pressure feedback is taken at the output of the booster relay stage and fed back to the main summer. This allows the transducer to correct for errors generated in the pneumatic booster as well as errors in the I/P conversion stage. Also, particularly with the new analog electric and digital versions of this design, PID control is used in the transducer control network to give extremely good static accuracy, fast dynamic response, and reasonable stability into a wide range of load volumes (small instrument bellows to large actuators). Also environmental factors such as temperature change, vibration, and supply pressure fluctuation affect this type of transducer the least. Even a perfectly accurate I/P transducer cannot compensate for stem position errors generated by friction, backlash, and varying force loads coming from the actuator and valve. To do this compensation, a different control valve device—the valve positioner—is required.

Booster Relays The booster relay is a single-stage power amplifier having a fixed gain relationship between the input and output pressures. The device is packaged as a complete stand-alone unit with pipe thread connections for input, output, and supply pressure. The booster amplifier shown in Fig. 8-87b shows the basic construction of the booster relay. Enhanced versions are available that provide specific features such as (1) variable gain to split the output range of a pneumatic controller to operate more than one valve or to provide additional actuator force; (2) low hysteresis for relaying measurement and control signals; (3) high flow capacity for increased actuator stroking speed; and (4) arithmetic, logic, or other compensation functions for control system design.

A particular type of booster relay, called a dead-band booster, is shown in Fig. 8-88. This booster is designed to be used exclusively between the output of a valve positioner and the input to a pneumatic actuator. It is designed to provide extra flow capacity to stroke the actuator faster than with the positioner alone. The dead-band booster is designed intentionally with a large dead band (approximately 5 percent of the input span), elastomer seats for tight shutoff, and an adjustable bypass valve connected between the input and output of the booster. The bypass valve is tuned to provide the best compromise between increased actuator stroking speed and positioner/actuator stability.

With the exception of the dead-band booster, the application of booster relays has diminished somewhat by the increased use of current-to-pressure transducers, electropneumatic positioners, and electronic control systems. Transducers and valve positioners serve much the same functionality as the booster relay in addition to interfacing with the electronic process controller.

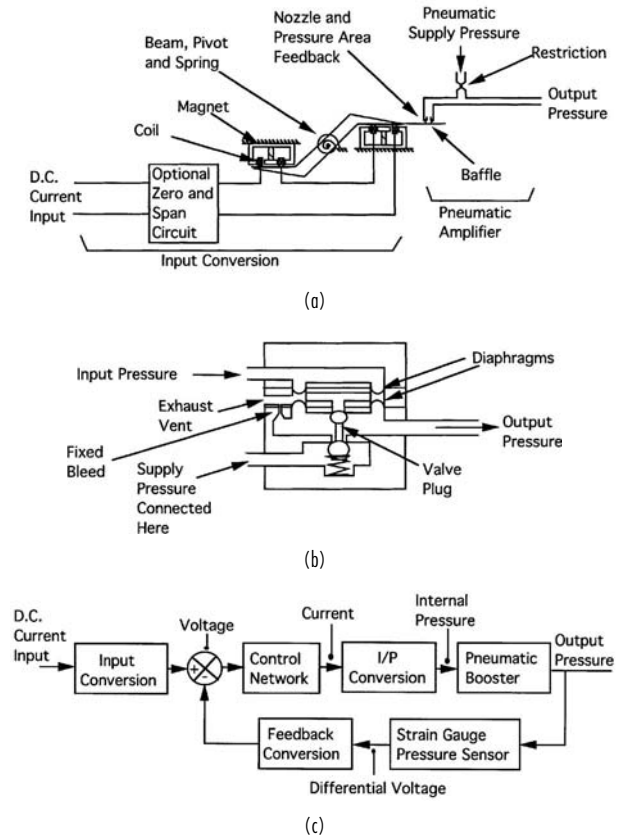


FIG. 8-87 Current-to-pressure transducer component parts. (a) Direct-current-to-pressure conversion. (b) Pneumatic booster amplifier (relay). (c) Block diagram of a modern I/P transducer.

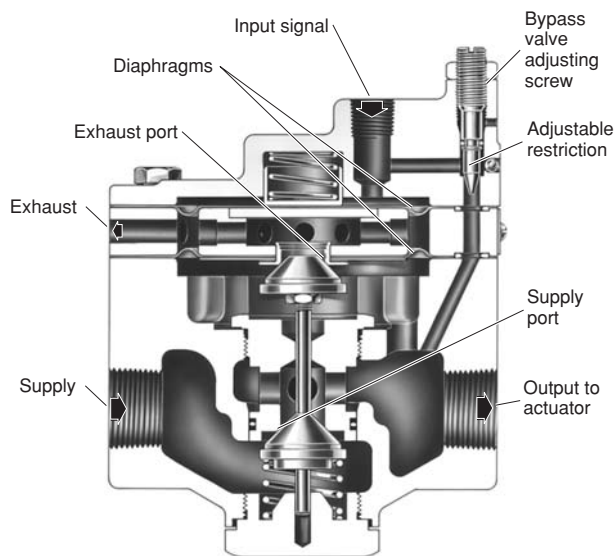


FIG. 8-88 Dead-band booster relay. (Courtesy Fisher Controls International LLC.)

Solenoid Valves The electric solenoid valve has two output states. When sufficient electric current is supplied to the coil, an internal armature moves against a spring to an extreme position. This motion causes an attached pneumatic or hydraulic valve to operate. When current is removed, the spring returns the armature and the attached solenoid valve to the deenergized position. An intermediate pilot stage is sometimes used when additional force is required to operate the main solenoid valve. Generally, solenoid valves are used to pressurize or vent the actuator casing for on/off control valve application and safety shutdown applications.

Trip Valves The trip valve is part of a system used where a specific valve action (i.e., fail up, fail down, or lock in last position) is required when pneumatic supply pressure to the control valve falls below a pre-set level. Trip systems are used primarily on springless piston actuators requiring fail-open or fail-closed action. An air storage or "volume" tank and a check valve are used with the trip valve to provide power to stroke the valve when supply pressure is lost. Trip valves are designed with hysteresis around the trip point to avoid instability when the trip pressure and the reset pressure settings are too close to the same value.

Limit Switches and Stem Position Transmitters Travel limit switches, position switches, and valve position transmitters are devices that detect the component's relative position, when mounted on the valve, actuator, damper, louver, or other throttling element. The switches are used to operate alarms, signal lights, relays, solenoid valves, or discrete inputs into the control system. The valve position transmitter generates a 4- to 20-mA output that is proportional to the position of the valve.

FIRE AND EXPLOSION PROTECTION

Electrical equipment and wiring methods can be sources of ignition in environments with combustible concentrations of gas, liquid, dust, fibers, or flyings. Most of the time it is possible to locate the electronic equipment away from these hazardous areas. However, where electric or electronic valve-mounted instruments must be used in areas where there is a hazard of fire or explosion, the equipment and installation must meet requirements for safety. Articles 500 through 504 of the National Electrical Code cover the definitions and requirements for electrical and electronic equipment used in the class I (flammable gases or vapors), divisions 1 and 2; class II (combustible dust), divisions 1 and 2; and class III (ignitable fibers or flyings), divisions 1 and 2. Division 1 locations are locations with hazardous concentrations of gases, vapors, or combustible dust under normal operating conditions;

hazardous concentration of gases, vapors, or combustible dust that occur frequently due to repair, maintenance, or leakage; or hazardous due to the presence of easily ignitable fibers or materials producing combustible flyings during handling, manufacturing, or use. Division 2 locations are locations that normally do not have ignitable concentrations of gases, vapors, or combustible dust. Division 2 locations might become hazardous through failure of ventilating equipment; adjacent proximity to a class I, division 1 location where ignitable concentrations of gases or vapors might occasionally exist; through dust accumulations on or in the vicinity of the electrical equipment sufficient to interfere with the safe dissipation of heat or by abnormal operation or failure of electrical equipment; or when easily ignitable fibers are stored or handled other than in the process of manufacture. An alternate method used for class I hazardous locations is the European "zone" method described in IEC 60079-10, "Electrical Apparatus for Explosive Gas Atmospheres." The zone designation for class I locations has been adapted by the NEC as an alternate method and is defined in Article 505 of the NEC.

Acceptable protection techniques for electrical and electronic valve accessories used in specific class and division locations include explosion-proof enclosures; intrinsically safe circuits; nonincendive circuits, equipment, and components; dust-ignition-proof enclosures; dusttight enclosures; purged and pressurized enclosures; oil immersion for current-interrupting contacts; and hermetically sealed equipment. Details of these techniques can be found in the *National Electrical Code Handbook*, available from the *National Fire Protection Association*.

Certified testing and approval for control valve devices used in hazardous locations is normally procured by the manufacturer of the device. The manufacturer typically goes to a third-party laboratory for testing and certification. Applicable approval standards are available from CSA, CENELEC, FM, SAA, and UL.

Environmental Enclosures Enclosures for valve accessories are sometimes required to provide protection from specific environmental conditions. The National Electrical Manufacturers Association (NEMA) provides descriptions and test methods for equipment used in specific environmental conditions in NEMA 250. IEC 60529, "Degrees of Protection Provided by Enclosures (IP Code)," describes the European system for classifying the degrees of protection provided by the enclosures of electrical equipment. Rain, windblown dust, hose-directed water, and external ice formation are examples of environmental conditions that are covered by these enclosure standards.

Of growing importance is the electronic control valve device's level of immunity to, and emission of, electromagnetic interference in the chemical valve environment. Electromagnetic compatibility (EMC) for control valve devices is presently mandatory in the European Community and is specified in International Electrotechnical Commission (IEC) 61326, "Electrical Equipment for Measurement Control and Laboratory Use—EMC Requirements." Test methods for EMC testing are found in the series IEC 61000-4, "EMC Compatibility (EMC), Testing and Measurement Techniques." Somewhat more stringent EMC guidelines are found in the German document NAMUR NE21, "Electromagnetic Compatibility of Industrial Process and Laboratory Control Equipment."

ADJUSTABLE-SPEED PUMPS

An alternative to throttling a process with a process control valve and a fixed-speed pump is by adjusting the speed of the process pump and not using a throttling control valve at all. Pump speed can be varied by using variable-speed prime movers such as turbines, motors with magnetic or hydraulic couplings, and electric motors. Each of these methods of modulating pump speed has its own strengths and weaknesses, but all offer energy savings and dynamic performance advantages over throttling with a control valve.

The centrifugal pump directly driven by a variable-speed electric motor is the most commonly used hardware combination for adjustable-speed pumping. The motor is operated by an electronic motor speed controller whose function is to generate the voltage or current waveform required by the motor to make the speed of the motor track the input command signal from the process controller.

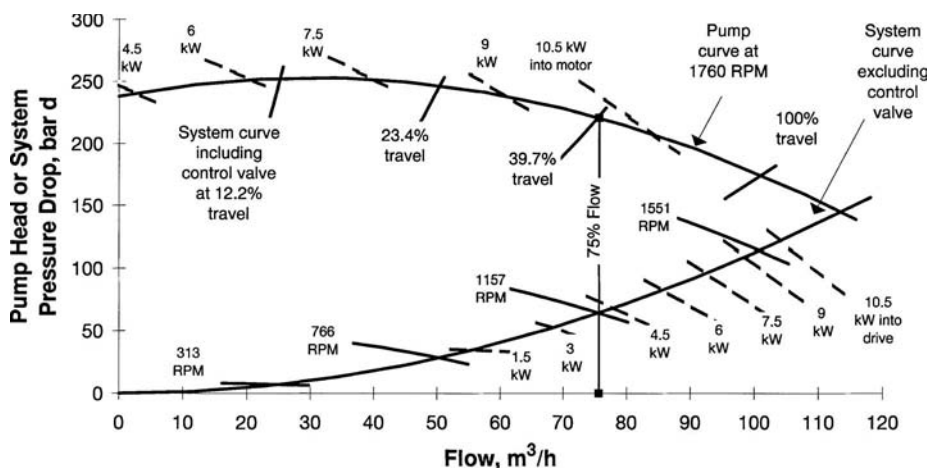


FIG. 8-89 Pressure, flow, and power for throttling a process using a control valve and a constant-speed pump compared to throttling with an adjustable-speed pump.

The most popular form of motor speed control for adjustable-speed pumping is the voltage-controlled pulse-width-modulated (PWM) frequency synthesizer and ac squirrel-cage induction motor combination. The flexibility of application of the PWM motor drive and its 90+ percent electrical efficiency along with the proven ruggedness of the traditional ac induction motor makes this combination popular.

From an energy consumption standpoint, the power required to maintain steady process flow with an adjustable-speed-pump system (three-phase PWM drive and a squirrel-cage induction motor driving a centrifugal pump on water) is less than that required with a conventional control valve and a fixed-speed pump. Figure 8-89 shows this to be the case for a system where 100 percent of the pressure loss is due to flow velocity losses. At 75 percent flow, the figure shows that using the constant-speed pump/control valve results in a 10.1-kW rate, while throttling with the adjustable-speed pump and not using a control valve results in a 4.1-kW rate. This trend of reduced energy consumption is true for the entire range of flows, although amounts vary.

From a dynamic response standpoint, the electronic adjustable-speed pump has a dynamic characteristic that is more suitable in process control applications than those characteristics of control valves. The small amplitude response of an adjustable-speed pump does not contain the dead band or the dead time commonly found in the small amplitude response of the control valve. Nonlinearities associated with friction in the valve and discontinuities in the pneumatic portion of the control valve instrumentation are not present with electronic variable-speed drive technology. As a result, process control with the adjustable-speed pump does not exhibit limit cycles, problems related to low controller gain, and generally degraded process loop performance caused by control valve nonlinearities.

Unlike the control valve, the centrifugal pump has poor or nonexistent shutoff capability. A flow check valve or an automated on/off valve may be required to achieve shutoff requirements. This requirement may be met by automating an existing isolation valve in retrofit applications.

REGULATORS

A regulator is a compact device that maintains the process variable at a specific value in spite of disturbances in load flow. It combines the functions of the measurement sensor, controller, and final control element into one self-contained device. Regulators are available to control pressure, differential pressure, temperature, flow, liquid level, and other basic process variables. They are used to control the differential across a filter press, heat exchanger, or orifice plate. Regulators are used for monitoring pressure variables for redundancy, flow check, and liquid surge relief.

Regulators may be used in gas blanketing systems to maintain a protective environment above any liquid stored in a tank or vessel as the liquid is pumped out. When the temperature of the vessel is suddenly cooled, the regulator maintains the tank pressure and protects the walls of the tank from possible collapse. Regulators are known for their fast dynamic response. The absence of time delay that often comes with more sophisticated control systems makes the regulator useful in applications requiring fast corrective action.

Regulators are designed to operate on the process pressures in the pipeline without any other sources of energy. Upstream and downstream pressures are used to supply and exhaust the regulator. Exhausting is connected back to the downstream piping so that no contamination or leakage to the external environment occurs. This makes regulators useful in remote locations where power is not available or where external venting is not allowed.

The regulator is limited to operating on processes with clean, non-slurry process fluids. The small orifice and valve assemblies contained in the regulator can plug and malfunction if the process fluid that operates the regulator is not sufficiently clean.

Regulators are normally not suited to systems that require constant set-point adjustment. Although regulators are available with capability to respond to remote set-point adjustment, this feature adds complexity to the regulator and may be better addressed by a control-valve-based system. In the simplest of regulators, tuning of the regulator for best control is accomplished by changing a spring, an orifice, or a nozzle.

Self-Operated Regulators Self-operated regulators are the simplest form of regulator. This regulator (see Fig. 8-90a) is composed of a main throttling valve, a diaphragm or piston to sense pressure, and a spring. The self-contained regulator is completely operated by the process fluid, and no outside control lines or pilot stage is used. In general, self-operated regulators are simple in construction, are easy to operate and maintain, and are usually stable devices. Except for some of the pitot-tube types, self-operated regulators have very good dynamic response characteristics. This is so because any change in the controlled variable registers directly and immediately upon the main diaphragm to produce a quick response to the disturbance.

The disadvantage of the self-operated regulator is that it is not generally capable of maintaining a set point as load flow is increased. Because of the proportional nature of the spring and diaphragm-throttling effect, offset from set point occurs in the controlled variable as flow increases. Figure 8-91 shows a typical regulation curve for the self-contained regulator.

Reduced set-point offset with increasing load flow can be achieved by adding a pitot tube to the self-operated regulator. The

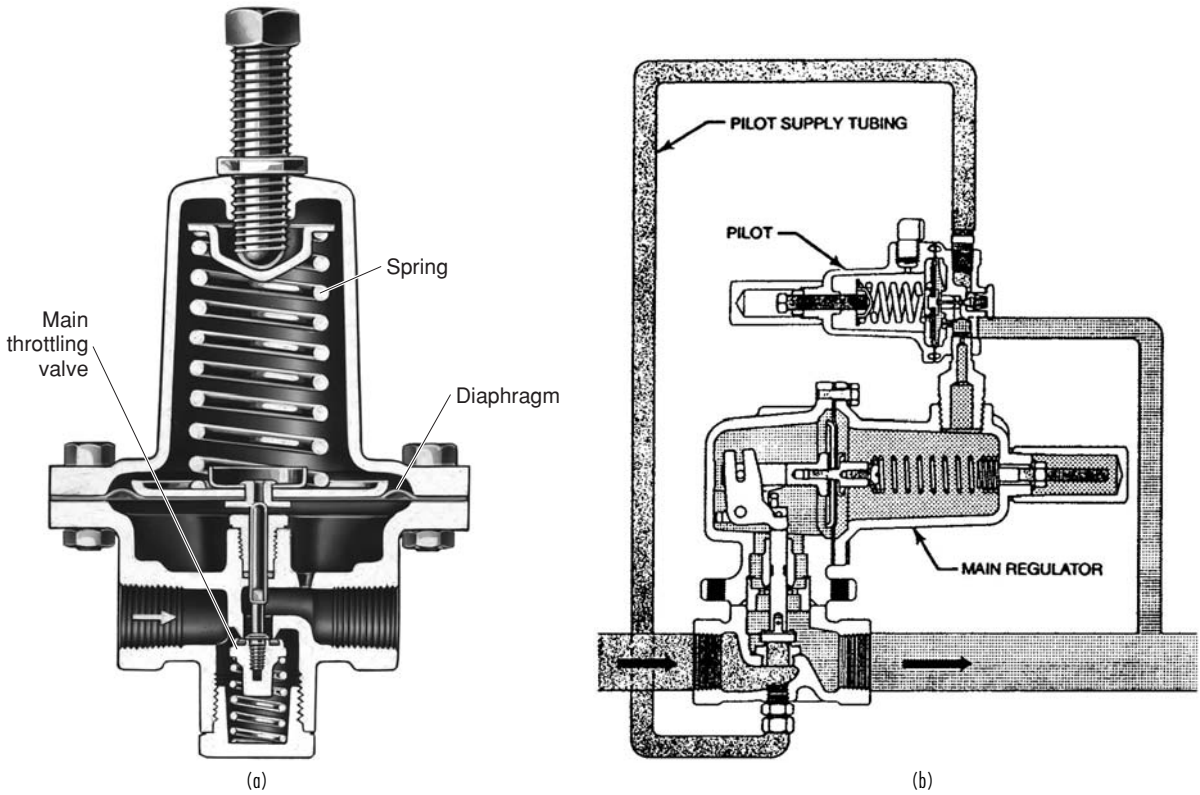


FIG. 8-90 Regulators. (a) Self-operated. (b) Pilot-operated. (Courtesy Fisher Controls International LLC.)

tube is positioned somewhere near the vena contracta of the main regulator valve. As flow through the valve increases, the measured feedback pressure from the pitot tube drops below the control pressure. This causes the main valve to open or boost more than it would if the static value of control pressure were acting on the diaphragm. The resultant effect keeps the control pressure closer to the set point and thus prevents a large drop in process pressure during high-load-flow conditions. Figure 8-91 shows the improvement that the pitot-

tube regulator provides over the regulator without the tube. A side effect of adding a pitot-tube method is that the response of the regulator can be slowed due to the restriction provided by the pitot tube.

Pilot-Operated Regulators Another category of regulators uses a pilot stage to provide the load pressure on the main diaphragm. This pilot is a regulator itself that has the ability to multiply a small change in downstream pressure into a large change in pressure applied to the regulator diaphragm. Due to this high-gain feature, pilot-operated

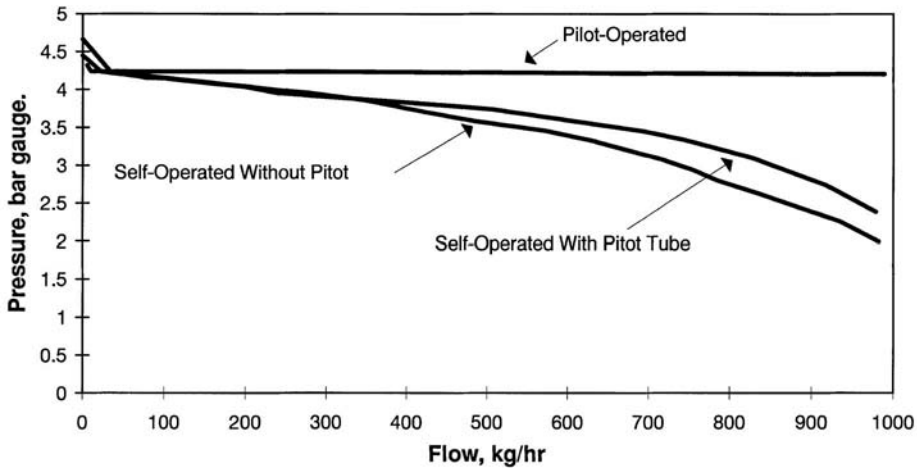


FIG. 8-91 Pressure regulation curves for three regulator types.

regulators can achieve a dramatic improvement in steady-state accuracy over that achieved with a self-operated regulator. Figure 8-91 shows for regulation at high flows the pilot-operated regulator is the best of the three regulators shown.

The main limitation of the pilot-operated regulator is stability. When the gain in the pilot amplifier is raised too much, the loop can become unstable and oscillate or hunt. The two-path pilot regulator (see Fig. 8-90b) is also available. This regulator combines the effects of self-operated and the pilot-operated styles and mathematically produces the equivalent of proportional plus reset control of the process pressure.

Overpressure Protection Figure 8-91 shows a characteristic rise in control pressure that occurs at low or zero flow. This lockup

tail is due to the effects of imperfect plug and seat alignment and the elastomeric effects of the main throttle valve. If, for some reason, the main throttle valve fails to completely shut off, or if the valve shuts off but the control pressure continues to rise for other reasons, the lockup tail could get very large, and the control pressure could rise to extremely high values. Damage to the regulator or the downstream pressure volume could occur.

To avoid this situation, some regulators are designed with a built-in overpressure relief mechanism. Overpressure relief circuits usually are composed of a spring-opposed diaphragm and valve assembly that vents the downstream piping when the control pressure rises above the set-point pressure.

PROCESS CONTROL AND PLANT SAFETY

GENERAL REFERENCE: *Guidelines for Safe Automation of Chemical Processes*, AIChE Center for Chemical Process Safety, New York, 1993.

Accidents in chemical plants make headline news, especially when there is loss of life or the general public is affected in even the slightest way. This increases the public's concern and may lead to government action. The terms *hazard* and *risk* are defined as follows:

- **Hazard.** A potential source of harm to people, property, or the environment.
- **Risk.** Possibility of injury, loss, or an environmental accident created by a hazard.

Safety is the freedom from hazards and thus the absence of any associated risks. Unfortunately, absolute safety cannot be realized.

The design and implementation of safety systems must be undertaken with a view to two issues:

- **Regulatory.** The safety system must be consistent with all applicable codes and standards as well as "generally accepted good engineering practices."
- **Technical.** Just meeting all applicable regulations and "following the crowd" do not relieve a company of its responsibilities. The safety system must work.

The regulatory environment will continue to change. As of this writing, the key regulatory instrument is OSHA 29 CFR 1910.119, "Process Safety Management of Highly Hazardous Chemicals," which pertains to process safety management within plants in which certain chemicals are present.

In addition to government regulation, industry groups and professional societies are producing documents ranging from standards to guidelines. Two applicable standards are IEC 61508, "Functional Safety of Electrical/Electronic/Programmable Electronic Safety-related Systems," and ANSI/ISA S84.01, "Application of Safety Instrumented Systems for the Process Industries." *Guidelines for Safe Automation of Chemical Processes* from the American Institute of Chemical Engineers' Center for Chemical Process Safety (1993) provides comprehensive coverage of the various aspects of safety; and although short on specifics, it is very useful to operating companies developing their own specific safety practices (i.e., it does not tell you what to do, but it helps you decide what is proper for your plant).

The ultimate responsibility for safety rests with the operating company; OSHA 1910.119 is clear on this. Each company is expected to develop (and enforce) its own practices in the design, installation, testing, and maintenance of safety systems. Fortunately, some companies make these documents public. Monsanto's *Safety System Design Practices* was published in its entirety in the proceedings of the International Symposium and Workshop on Safe Chemical Process Automation, Houston, Texas, September 27–29, 1994 (available from the American Institute of Chemical Engineers' Center for Chemical Process Safety).

ROLE OF AUTOMATION IN PLANT SAFETY

As microprocessor-based controls displaced hardwired electronic and pneumatic controls, the impact on plant safety has definitely been positive. When automated procedures replace manual procedures for routine operations, the probability of human errors leading to hazardous situations is lowered. The enhanced capability for presenting information to the process operators in a timely manner and in the most meaningful form increases the operator's awareness of current conditions in the process. Process operators are expected to exercise due diligence in the supervision of the process, and timely recognition of an abnormal situation reduces the likelihood that the situation will progress to the hazardous state. Figure 8-92 depicts the layers of safety protection in a typical chemical plant. Although microprocessor-based process controls enhance plant safety, their primary objective is efficient process operation. Manual operations are automated to reduce variability, to minimize the time required, to increase productivity, and so on. Remaining competitive in the world market demands that the plant be operated in the best manner possible, and microprocessor-based process controls provide numerous functions that make this possible. Safety is never compromised in the effort to increase competitiveness, but enhanced safety is a by-product of the process control function and is not a primary objective. By attempting to maintain process conditions at or near their design values, the process controls also attempt to prevent abnormal conditions from developing within the process.

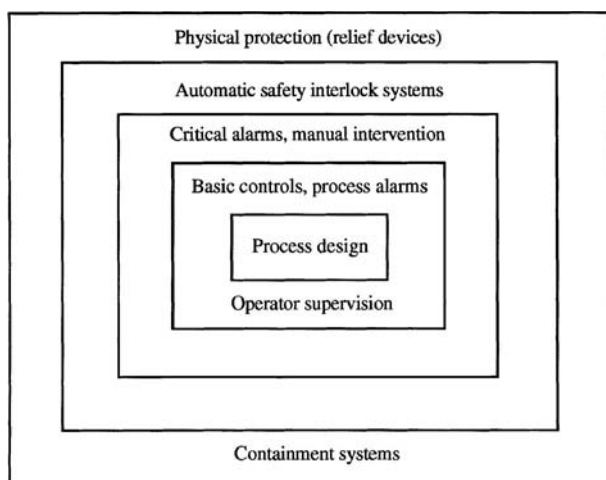


FIG. 8-92 Layers of safety protection in chemical plants.

Although process controls can be viewed as a protective layer, this is really a by-product and not the primary function. Where the objective of a function is specifically to reduce risk, the implementation is normally not within the process controls. Instead, the implementation is within a separate system specifically provided to reduce risk. This system is generally referred to as the safety interlock system.

As safety begins with the process design, an inherently safe process is the objective of modern plant designs. When this cannot be achieved, process hazards of varying severity will exist. Where these hazards put plant workers and/or the general public at risk, some form of protective system is required. Process safety management addresses the various issues, ranging from assessment of the process hazard to ensuring the integrity of the protective equipment installed to cope with the hazard. When the protective system is an automatic action, it is incorporated into the safety interlock system, not within the process controls.

INTEGRITY OF PROCESS CONTROL SYSTEMS

Ensuring the integrity of process controls involves hardware issues, software issues, and human issues. Of these, the hardware issues are usually the easiest to assess and the software issues the most difficult.

The hardware issues are addressed by providing various degrees of redundancy, by providing multiple sources of power and/or an uninterruptible power supply, and the like. The manufacturers of process controls provide a variety of configuration options. Where the process is inherently safe and infrequent shutdowns can be tolerated, nonredundant configurations are acceptable. For more-demanding situations, an appropriate requirement might be that no single component failure be able to render the process control system inoperable. For the very critical situations, triple-redundant controls with voting logic might be appropriate. The difficulty lies in assessing what is required for a given process.

Another difficulty lies in assessing the potential for human errors. If redundancy is accompanied with increased complexity, the resulting increased potential for human errors must be taken into consideration. Redundant systems require maintenance procedures that can correct problems in one part of the system while the remainder of the system is in full operation. When maintenance is conducted in such situations, the consequences of human errors can be rather unpleasant.

The use of programmable systems for process control presents some possibilities for failures that do not exist in hardwired electro-mechanical implementations. Probably of greatest concern are latent defects or "bugs" in the software, either the software provided by the supplier or the software developed by the user. The source of this problem is very simple. There is no methodology available that can be applied to obtain absolute assurance that a given set of software is completely free of defects. Increased confidence in a set of software is achieved via extensive testing, but no amount of testing results in absolute assurance that there are no defects. This is especially true of real-time systems, where the software can easily be exposed to a sequence of events that was not anticipated. Just because the software performs correctly for each event individually does not mean that it will perform correctly when two (or more) events occur at nearly the same time. This is further complicated by the fact that the defect may not be in the programming; it may be in how the software was designed to respond to the events.

The testing of any collection of software is made more difficult as the complexity of the software increases. Software for process control has become progressively complex, mainly because the requirements have become progressively demanding. To remain competitive in the world market, processes must be operated at higher production rates, within narrower operating ranges, closer to equipment limits, and so on. Demanding applications require sophisticated control strategies, which translate to more-complex software. Even with the best efforts of both supplier and user, complex software systems are unlikely to be completely free of defects.

CONSIDERATIONS IN IMPLEMENTATION OF SAFETY INTERLOCK SYSTEMS

Where hazardous conditions can develop within a process, a protective system of some type must be provided. Sometimes this is in the form of process hardware such as pressure relief devices. However, sometimes logic must be provided for the specific purpose of taking the process to a state where the hazardous condition cannot exist. The term *safety interlock system* is normally used to designate such logic.

The purpose of the logic within the safety interlock system is very different from that of the logic within the process controls. Fortunately, the logic within the safety interlock system is normally much simpler than the logic within the process controls. This simplicity means that a hardwired implementation of the safety interlock system is usually an option. Should a programmable implementation be chosen, this simplicity means that latent defects in the software are less likely to be present. Most safety systems only have to do simple things, but they must do them very, very well.

The difference in the nature of process controls and safety interlock systems leads to the conclusion that these two should be physically separated (see Fig. 8-92). That is, safety interlocks should not be piggybacked onto a process control system. Instead, the safety interlocks should be provided by equipment, either hardwired or programmable, that is dedicated to the safety functions. As the process controls become more complex, faults are more likely. Separation means that faults within the process controls have no consequences in the safety interlock system.

Modifications to the process controls are more frequent than modifications to the safety interlock system. Therefore, physically separating the safety interlock system from the process controls provides the following benefits:

1. The possibility of a change to the process controls leading to an unintentional change to the safety interlock system is eliminated.
2. The possibility of a human error in the maintenance of the process controls having consequences for the safety interlock system is eliminated.
3. Management of change is simplified.
4. Administrative procedures for software version control are more manageable.

Separation also applies to the measurement devices and actuators. Although the traditional point of reference for safety interlock systems is a hardwired implementation, a programmed implementation is an alternative. The potential for latent defects in software implementation is a definite concern. Another concern is that solid-state components are not guaranteed to fail to the safe state. The former is addressed by extensive testing; the latter is addressed by manufacturer-supplied and/or user-supplied diagnostics that are routinely executed by the processor within the safety interlock system. Although issues must be addressed in programmable implementations, the hardwired implementations are not perfect either.

Where a programmed implementation is deemed to be acceptable, the choice is usually a programmable logic controller that is dedicated to the safety function. PLCs are programmed with the traditional relay ladder diagrams used for hardwired implementations. The facilities for developing, testing, and troubleshooting PLCs are excellent. However, for PLCs used in safety interlock systems, administrative procedures must be developed and implemented to address the following issues:

1. Version controls for the PLC program must be implemented and rigidly enforced. Revisions to the program must be reviewed in detail and thoroughly tested before implementation in the PLC. The various versions must be clearly identified so that there can be no doubt as to what logic is provided by each version of the program.
2. The version of the program that is currently being executed by the PLC must be known with absolute certainty. It must be impossible for a revised version of the program undergoing testing to be downloaded to the PLC.

Constant vigilance is required to prevent lapses in such administrative procedures.

INTERLOCKS

An interlock is a protective response initiated on the detection of a process hazard. The interlock system consists of the measurement devices, logic solvers, and final control elements that recognize the hazard and initiate an appropriate response. Most interlocks consist of one or more logic conditions that detect out-of-limit process conditions and respond by driving the final control elements to the safe states. For example, one must specify that a valve fails open or fails closed.

The potential that the logic within the interlock could contain a defect or bug is a strong incentive to keep it simple. Within process plants, most interlocks are implemented with discrete logic, which means either hardwired electromechanical devices or programmable logic controllers.

The discrete logic within process plants can be broadly classified as follows:

1. *Safety interlocks.* These are designed to protect the public, the plant personnel, and possibly the plant equipment from process hazards. These are implemented within the safety interlock system.

2. *Process actions.* These are designed to prevent process conditions that would unduly stress equipment (perhaps leading to minor damage), lead to off-specification product, and so on. Basically, the process actions address hazards whose consequences essentially lead to a monetary loss, possibly even a short plant shutdown. Although sometimes referred to as interlocks, process actions address situations that are not deemed to be process hazards.

Implementation of process actions within process control systems is perfectly acceptable. Furthermore, it is also permissible (and probably advisable) for responsible operations personnel to be authorized to bypass or ignore a process action. Safety interlocks must be implemented within the separate safety interlock system. Bypassing or ignoring safety interlocks by operations personnel is simply not permitted. When this is necessary for actions such as verifying that the interlock continues to be functional, such situations must be infrequent and incorporated into the design of the interlock.

Safety interlocks are assigned to categories that reflect the severity of the consequences, should the interlock fail to perform as intended. The specific categories used within a company are completely at the discretion of the company. However, most companies use categories that distinguish among the following:

1. *Hazards that pose a risk to the public.* Complete redundancy is normally required.

2. *Hazards that could lead to injury of company personnel.* Partial redundancy is often required (e.g., redundant measurements but not redundant logic).

3. *Hazards that could result in major equipment damage and consequently lengthy plant downtime.* No redundancy is normally required for these, although redundancy is always an option.

Situations resulting in minor equipment damage that can be quickly repaired do not generally require a safety interlock; however, a process action might be appropriate.

A process hazards analysis is intended to identify the safety interlocks required for a process and to provide the following for each:

1. The hazard that is to be addressed by the safety interlock
2. The classification of the safety interlock
3. The logic for the safety interlock, including inputs from measurement devices and outputs to actuators

The process hazards analysis is conducted by an experienced, multi-disciplinary team that examines the process design, plant equipment, operating procedures, and so on, using techniques such as hazard and operability studies (HAZOP), failure mode and effect analysis (FMEA), and others. The process hazards analysis recommends appropriate measures to reduce the risk, including (but not limited to) the safety interlocks to be implemented in the safety interlock system.

Diversity is recognized as a useful approach to reduce the number of defects. The team that conducts the process hazards analysis does not implement the safety interlocks but provides the specifications for the safety interlocks to another organization for implementation. This organization reviews the specifications for each safety interlock, seeking clarifications as necessary from the process hazards analysis team and bringing any perceived deficiencies to the attention of the process hazards analysis team.

Diversity can be used to further advantage in redundant configurations. Where redundant measurement devices are required, different technology can be used for each. Where redundant logic is required, one can be programmed and one hardwired. Reliability of the interlock systems has two aspects:

1. It must react, should the hazard arise.

2. It must not react when there is no hazard.

Emergency shutdowns often pose risks in themselves, and therefore they should be undertaken only when truly appropriate. The need to avoid extraneous shutdowns is not motivated by a desire simply to avoid disruption in production operations.

Although safety interlocks can inappropriately initiate shutdowns, the process actions are usually the major source of problems. It is possible to configure so many process actions that it is not possible to operate the plant.

TESTING

As part of the detailed design of each safety interlock, written test procedures must be developed for the following purposes:

1. Ensure that the initial implementation complies with the requirements defined by the process hazards analysis team.

2. Ensure that the interlock (hardware, software, and I/O) continues to function as designed. The design must also determine the time interval over which this must be done. Often these tests must be done with the plant in full operation.

The former is the responsibility of the implementation team and is required for the initial implementation and following any modification to the interlock. The latter is the responsibility of plant maintenance, with plant management responsible for seeing that it is done at the specified interval of time.

Execution of each test must be documented, showing when it was done, by whom, and the results. Failures must be analyzed for possible changes in the design or implementation of the interlock. These tests must encompass the complete interlock system, from the measurement devices through the final control elements. Merely simulating inputs and checking the outputs is not sufficient. The tests must duplicate the process conditions and operating environments as closely as possible. The measurement devices and final control elements are exposed to process and ambient conditions and thus are usually the most likely to fail. Valves that remain in the same position for extended periods may stick in that position and not operate when needed. The easiest component to test is the logic; however, this is the least likely to fail.

SECTION 9

Process
Economics

PERRY'S CHEMICAL ENGINEERS' HANDBOOK

8TH EDITION



JAMES R. COUPER
DARRYL W. HERTZ
F. LEE SMITH

Copyright © 2008, 1997, 1984, 1973, 1963, 1950, 1941, 1934 by The McGraw-Hill Companies, Inc. All rights reserved. Manufactured in the United States of America. Except as permitted under the United States Copyright Act of 1976, no part of this publication may be reproduced or distributed in any form or by any means, or stored in a database or retrieval system, without the prior written permission of the publisher.

0-07-154216-7

The material in this eBook also appears in the print version of this title: 0-07-151132-6.

All trademarks are trademarks of their respective owners. Rather than put a trademark symbol after every occurrence of a trademarked name, we use names in an editorial fashion only, and to the benefit of the trademark owner, with no intention of infringement of the trademark. Where such designations appear in this book, they have been printed with initial caps.

McGraw-Hill eBooks are available at special quantity discounts to use as premiums and sales promotions, or for use in corporate training programs. For more information, please contact George Hoare, Special Sales, at george_hoare@mcgraw-hill.com or (212) 904-4069.

TERMS OF USE

This is a copyrighted work and The McGraw-Hill Companies, Inc. (“McGraw-Hill”) and its licensors reserve all rights in and to the work. Use of this work is subject to these terms. Except as permitted under the Copyright Act of 1976 and the right to store and retrieve one copy of the work, you may not decompile, disassemble, reverse engineer, reproduce, modify, create derivative works based upon, transmit, distribute, disseminate, sell, publish or sublicense the work or any part of it without McGraw-Hill’s prior consent. You may use the work for your own noncommercial and personal use; any other use of the work is strictly prohibited. Your right to use the work may be terminated if you fail to comply with these terms.

THE WORK IS PROVIDED “AS IS.” McGRAW-HILL AND ITS LICENSORS MAKE NO GUARANTEES OR WARRANTIES AS TO THE ACCURACY, ADEQUACY OR COMPLETENESS OF OR RESULTS TO BE OBTAINED FROM USING THE WORK, INCLUDING ANY INFORMATION THAT CAN BE ACCESSED THROUGH THE WORK VIA HYPERLINK OR OTHERWISE, AND EXPRESSLY DISCLAIM ANY WARRANTY, EXPRESS OR IMPLIED, INCLUDING BUT NOT LIMITED TO IMPLIED WARRANTIES OF MERCHANTABILITY OR FITNESS FOR A PARTICULAR PURPOSE. McGraw-Hill and its licensors do not warrant or guarantee that the functions contained in the work will meet your requirements or that its operation will be uninterrupted or error free. Neither McGraw-Hill nor its licensors shall be liable to you or anyone else for any inaccuracy, error or omission, regardless of cause, in the work or for any damages resulting therefrom. McGraw-Hill has no responsibility for the content of any information accessed through the work. Under no circumstances shall McGraw-Hill and/or its licensors be liable for any indirect, incidental, special, punitive, consequential or similar damages that result from the use of or inability to use the work, even if any of them has been advised of the possibility of such damages. This limitation of liability shall apply to any claim or cause whatsoever whether such claim or cause arises in contract, tort or otherwise.

DOI: 10.1036/0071511326

Process Economics

James R. Couper, D.Sc. Professor Emeritus, The Ralph E. Martin Department of Chemical Engineering, University of Arkansas—Fayetteville (Section Editor)

Darryl W. Hertz, B.S. Manager, Front-End Loading and Value-Improving Practices Group, KBR (Front-End Loading, Value-Improving Practices)

(Francis) Lee Smith, Ph.D., M.Eng. Principal, Wilcrest Consulting Associates, Houston, Texas (Front-End Loading, Value-Improving Practices)

GENERAL COMMENTS

ACCOUNTING AND FINANCIAL CONSIDERATIONS

Principles of Accounting	9-4
Financial Statements	9-5
Balance Sheet	9-5
Income Statement	9-6
Accumulated Retained Earnings	9-6
Concluding Remarks	9-6
Other Financial Terms	9-6
Financial Ratios	9-7
Relationship Between Balance Sheets and Income Statements	9-7
Financing Assets by Debt and/or Equity	9-7
Cost of Capital	9-9
Working Capital	9-9
Inventory Evaluation and Cost Control	9-9
Budgets and Cost Control	9-10

CAPITAL COST ESTIMATION

Total Capital Investment	9-10
Land	9-10
Fixed Capital Investment	9-10
Example 1: Use of Cost Index	9-13
Example 2: Inflation	9-13
Example 3: Equipment Sizing and Costing	9-13
Estimation of Fixed Capital Investment	9-13
Example 4: Seven-Tenths Rule	9-14
Example 5: Fixed Capital Investment Using the Lang, Hand, and Wroth Methods	9-14
Comments on Significant Cost Items	9-16
Computerized Cost Estimation	9-17
Contingency	9-17
Offsite Capital	9-17
Allocated Capital	9-17
Working Capital	9-17
Start-up Expenses	9-17
Other Capital Items	9-17

MANUFACTURING-OPERATING EXPENSES

Raw Material Expense	9-18
Direct Expenses	9-18
Utilities	9-18
Operating Labor	9-18
Supervision	9-18
Payroll Charges	9-18
Maintenance	9-18
Miscellaneous Direct Expenses	9-18
Environmental Control Expense	9-18
Indirect Expenses	9-20
Depreciation	9-20
Plant Indirect Expenses	9-20
Total Manufacturing Expense	9-20
Packaging and Shipping Expenses	9-20
Total Product Expense	9-20
General Overhead Expense	9-20
Total Operating Expense	9-20
Rapid Manufacturing Expense Estimation	9-20
Scale-up of Manufacturing Expenses	9-21

FACTORS THAT AFFECT PROFITABILITY

Depreciation	9-21
Depletion	9-22
Amortization	9-22
Taxes	9-22
Time Value of Money	9-23
Simple Interest	9-23
Discrete Compound Interest	9-23
Continuous Compound Interest	9-23
Compounding-Discounting	9-23
Effective Interest Rates	9-25
Example 6: Effective Interest Rate	9-27
Example 7: After-Tax Cash Flow	9-27
Cash Flow	9-27
Cumulative Cash Position Table	9-27
Example 8: Cumulative Cash Position Table (Time Zero at Start-up)	9-28

9-2 PROCESS ECONOMICS

Cumulative Cash Position Plot	9-28
Time Zero at Start-up	9-28
PROFITABILITY	
Quantitative Measures of Profitability	9-30
Payout Period Plus Interest	9-30
Net Present Worth	9-30
Discounted Cash Flow	9-30
Example 9: Profitability Calculations	9-32
Qualitative Measures	9-32
Sensitivity Analysis	9-32
Break-Even Analysis	9-32
Strauss Plot	9-32
Tornado Plot	9-32
Relative Sensitivity Plot	9-32
Uncertainty Analysis	9-32
Feasibility Analysis	9-34
OTHER ECONOMIC TOPICS	
Comparison of Alternative Investments	9-35
Net Present Worth (NPW) Method	9-36
Cash Flow Method	9-36

Uniform Annual Cost	9-36
Example 10: Choice among Alternatives	9-36
Replacement Analysis	9-36
Example 11: Replacement Analysis	9-38
Opportunity Cost	9-39
Economic Balance	9-39
Example 12: Optimum Number of Evaporator Effects	9-39
Interactive Systems	9-41
CAPITAL PROJECT EXECUTION AND ANALYSIS	
Front-End Loading	9-41
Introduction	9-41
Characteristics of FEL	9-42
Typical FEL Deliverables	9-47
Value-Improving Practices	9-48
Introduction	9-48
VIP Descriptions	9-50
VIP Planning and Implementation	9-52
VIPs That Apply the Value Methodology	9-53
Sources of Expertise	9-53

GLOSSARY

Nomenclature and Units

Symbol	Definition	Units	Symbol	Definition	Units
A_1	Annual conversion expense at production rate 1	\$	LIFO	Last in, last out (inventory)	lb
A_{TC}	Annual capital outlay	\$	M	Annual raw material expense	\$
B	Constant	Dimensionless	MACRS	Modified Accelerated Cost Recovery System	
C	Cost of equipment	\$	m	Number of interest periods per year	Varies
C_B	Base cost of carbon steel exchanger	\$	m, n, p, q	constants or exponent	Dimensionless
CE	Chemical Engineering cost index	Dimensionless	N	Annual labor requirements	Operators per shift per year
$(C_{FC})_{BL}$	Battery-limits fixed capital investment	\$	n	Number of years, depreciation	Years
$(C_{EQ})_{DEL}$	Delivered equipment cost	\$	P	Principal, present value, present worth	\$
C_{HE}	Purchased equipment cost, heat exchanger	\$	PC	Personal computer	
C_L	Cost of labor	\$	POP	Payout period (no interest)	Years
COE	Cash operating expenses	\$	POP + I	Payout period plus interest	Years
C_p	Equipment cost in base year	\$	Q	Energy transferred	Btu/h
cP	Viscosity	cP	\dot{R}_1, R_2	Annual production rates	lb/yr
D	Depreciation	\$	S	Salvage value or equipment capacity	Various
DCFRROR	Discounted cash flow rate of return	%	SL	Straight-line depreciation	
EBIT	Earnings before interest and taxes	\$	Sp gr	Specific gravity	Dimensionless
e	Naperian logarithm base	2.718	TE	Total expenses	\$
F	Future value, future worth, future amount	\$	T_c	Combined incremental tax rate	%
F	Heat exchanger efficiency factor	Dimensionless	T_f	Incremental federal income tax rate	%
F_B	Heat exchanger design type	Dimensionless	T_s	Incremental state income tax rate	%
FCI	Fixed capital investment	\$	U	Annual utility expenses	\$
FE	Fixed expenses	\$	UAC	Uniform annual cost	\$
FEL	Front-end loading		U_D	Overall heat-transfer coefficient	Btu/(h·ft ² ·F)
FIFO	First in, first out (inventory)	lb	V_e	Asset value at end of year	\$
FOB	Free on board		V_i	Asset value at beginning of year	\$
F_M	Material of construction cost factor	Dimensionless	VE	Variable expenses	\$
F_p	Design pressure cost factor	Dimensionless	VIP	Value-improving practice	
f_1, f_2, f_3	Inflation factors for years 1, 2, and 3	Dimensionless	X	Plant capacity	tons/day
f	Declining-balance factor	Dimensionless	Y	Operating labor	operator-hour/ton per processing step
I	Investment	\$			
IRS	Internal Revenue Service				
i	Nominal interest	%			
i_{eff}	Effective interest	%			
K	Factor for cost index	Dimensionless			

GENERAL REFERENCES: Allen, D. H., *Economic Evaluation of Projects*, 3d ed., Institution of Chemical Engineers, Rugby, England, 1991. Baasel, W. D., *Chemical Engineering Plant Design*, 2d ed., Van Nostrand Reinhold, New York, 1989. Brown, T. R., Hydrocarbon Processing, October 2000, pp. 93–100. Canada, J. R., and J. A. White, *Capital Investment Decision: Analysis for Management and Engineering*, 2d ed., Prentice-Hall, Englewood Cliffs, N.J., 1980. *Chemical Engineering* (ed.), *Modern Cost Engineering*, McGraw-Hill, New York, 1979. Couper, J. R., and W. H. Rader, *Applied Finance and Economic Analysis for Scientists and Engineers*, Van Nostrand Reinhold, New York, 1986. Couper, J. R., and O. T. Beasley, *The Chemical Process Industries: Function and Economics*, Dekker, New York, 2001. Couper, J. R., *Process Engineering Economics*, Dekker, New York, 2003. Garrett, D. E., *Chemical Engineering Economics*, Van Nostrand Reinhold, New York, 1989. Grant, E. L., and W. G. Ireson, *Engineering Economy*, 2d ed., Wiley, New York, 1950. Grant, E. L., W. G. Ireson, and R. S. Leavenworth, *Engineering Economy*, 8th ed., Wiley, New York, 1990. Hackney, J. W., and K. K. Humphreys (eds.), *Control and Management of Capital Projects*, 2d ed., McGraw-Hill, New York, 1992. Hill, D. A., and L. E. Rockley, *Secrets of Successful Financial Management*, Heinemann, London, 1990. Holland, F. A., F. A. Watson, and J. E. Wilkerson, *Introduction to Process Economics*, 2d ed., Wiley, London, 1983. K. K. Humphreys, F. C. Jelen, and J. H. Black (eds.), *Cost and*

Optimization Engineering, 3d ed., McGraw-Hill, New York, 1991. *A Guide to Capital Cost Estimation*, 3d ed., Institution of Chemical Engineers, Rugby, England, 1990. Kharbanda, O. P., and E. A. Stallworthy, *Capital Cost Estimating in the Process Industries*, 2d ed., Butterworth-Heinemann, London, 1988. *How to Read an Annual Report*, Merrill Lynch, New York, 1997. Nickerson, C. B., *Accounting Handbook for Non Accountants*, 2d ed., CBI Publishing, Boston, 1979. Ostwald, P. F., *Engineering Cost Estimating*, 3d ed., Prentice-Hall, Englewood Cliffs, N.J., 1991. Park, W. R., and D. E. Jackson, *Cost Engineering Analysis*, 2d ed., Wiley, New York, 1984. Peters, M. S., and K. D. Timmerhaus, *Plant Design and Economics for Chemical Engineers*, 6th ed., McGraw-Hill, New York, 2003. Popper, H. (ed.), *Modern Cost Estimating Techniques*, McGraw-Hill, New York, 1970. Rose, L. M., *Engineering Investment Decisions: Planning under Uncertainty*, Elsevier, Amsterdam, 1976. Thorne, H. C., and J. B. Weaver (eds.), *Investment Appraisal for Chemical Engineers*, American Institute of Chemical Engineers, New York, 1991. Ulrich, G., and P. T. Vasudevan, *Chemical Engineering Process Design and Economics*, CRC Press, Boca Raton, Fla., 2004. Valle-Riestra, J. F., *Project Evaluation in the Chemical Process Industries*, McGraw-Hill, New York, 1983. Wells, G. L., *Process Engineering with Economic Objectives*, Wiley, New York, 1973. Woods, D. R., *Process Design and Engineering*, Prentice-Hall, Englewood Cliffs, N.J., 1993.

GENERAL COMMENTS

One of the most confusing aspects of process engineering economics is the nomenclature used by various authors and companies. In this part of Sec. 9, generic, descriptive terms have been used. Further, an attempt has been made to bring together most of the methods currently in use for project evaluation and to present them in such a way as to make them amenable to modern computational techniques. Most of the calculations can be performed on handheld calculators equipped with scientific function keys. For calculations requiring greater sophistication than that of handheld calculators, algorithms may be solved by using such programs as MATHCAD, TKSOLVER, etc. Spreadsheets are also used whenever the solution to a problem lends itself to this technique.

The nomenclature in process economics has been developed by accountants, engineers, and others such that there is no one correct set of nomenclature. Often it seems confusing, but one must question

what is meant by a certain term since companies have adopted their own language. A glossary of terms is included at the end of this section to assist the reader in understanding the nomenclature. Further, abbreviations of terms such as DCFRR (discounted cash flow rate of return) are used to reduce the wordiness. The number of letters and numbers used to define a variable has been limited to five. The parentheses are removed whenever the letter group is used to define a variable for a computer. Also, a general symbol is defined for a type variable and is modified by mnemonic subscript, e.g., an annual cash quantity, annual capital outlay A_{TC} , \$/year. Wherever a term like this is introduced, it is defined in the text.

It is impossible to allow for all possible variations of equation requirements, but it is hoped that the nomenclature presented will prove adequate for most purposes and will be capable of logical extension to other more specialized requirements.

ACCOUNTING AND FINANCIAL CONSIDERATIONS

PRINCIPLES OF ACCOUNTING

Accounting has been defined as the art of recording business transactions in a systematic manner. It is the language of business and is used to communicate financial information. Conventions that govern accounting are fairly simple, but their application is complex. In this section, the basic principles are illustrated by a simple example and applied to analyzing a company report. The fair allocation of costs requires considerable technical knowledge of operations, so a close liaison between process engineers and accountants in a company is desirable.

In simplest terms, assets that are the economic resources of a company are balanced against equities that are claims against the firm. In equation form,

$$\text{Assets} = \text{Equities}$$

or
$$\text{Assets} = \text{Liabilities} + \text{Owners' Equity}$$

This dual aspect has led to the *double-entry* bookkeeping system in use today. Any transaction that takes place causes changes in the accounting equation. An increase in assets must be accompanied by one of the following:

- An increase in liabilities
- An increase in stockholders' equity
- An increase in assets

A change in one part of the equation due to an economic transaction must be accompanied by an equal change in another place—therefore, the term *double-entry* bookkeeping. On a page of an account, the left-hand side is designated the *debit* side and the right-hand side is the *credit* side. This convention holds regardless of the type of account. Therefore, for every economic transaction, there is an entry on the debit side balanced by the same entry on the credit side.

All transactions in their original form (receipts and invoices) are recorded chronologically in a *journal*. The date of the transaction together with an account title and a brief description of the transaction is entered. Table 9-1 is an example of a typical journal page for a company. Journal entries are transferred to a *ledger* in a process called *posting*. Separate ledger accounts, such as a revenue account, expense account, liability account, or asset account, may be set up for each major transaction. Table 9-2 shows an example of a typical ledger page. The number of ledger accounts depends on the information that management needs to make decisions. Periodically, perhaps on a monthly basis but certainly on a yearly basis, the ledger sheets are closed and balanced. The ledger sheets are then intermediate documents between journal records and balance sheets, income statements, and retained earnings statements, and they provide information for management and various government reports. For example, a consolidated income statement can be prepared for the ledger, revenue, and expense accounts. In like manner, the asset and liability accounts provide information for balance sheets.

TABLE 9-1 Typical Journal Page

Date	Explanation	LP	Debit	Credit
200X				
Mar 1	Cash	1	\$95,000	
	J. Jones, Capital	2		\$95,000
Mar 4	Property	4	5,000	
	Cash	1		3,000
	Mortgage	3		2,000
Mar 11	Remodeling Bldg.	5	7,800	
	Cash	1		7,800
Mar 13	Equipment	6	62,300	
	Cash	1		10,000
	Note Payable	3		52,300
Apr 4	To J. Jones	2	2,500	
	Cash	1		2,500

SOURCE: J. R. Couper, *Process Engineering Economics*, Dekker, New York, 2003. By permission of Taylor & Francis Books, Inc., Boca Raton, Fla.

FINANCIAL STATEMENTS

A basic knowledge of accounting and financial statements is necessary for a chemical professional to be able to analyze a firm's operation and to communicate with accountants, financial personnel, and managers. Financial reports of a company are important sources of information used by management, owners, creditors, investment bankers, and financial analysts. All publicly held companies are required to submit annual reports to the Securities and Exchange Commission. As with any field a certain basic nomenclature is used to be able to understand the financial operation of a company. It should be emphasized that companies may also have their own internal nomenclature, but some terms are universally accepted. In this section, the common terminology is used.

A financial report contains two important documents—the *balance sheet* and the *income statement*. Two other documents that appear in the financial report are the *accumulated retained earnings* and the *changes in working capital*. All these documents are discussed in the following sections using a fictitious company.

Balance Sheet The balance sheet represents an accounting view of the financial status of a company on a particular date. Table 9-3 is an example of a balance sheet for a company. The date frequently used by corporations is December 31 of any given year, although some companies are now using June 30 or September 30 as the closing date. It is as if the company's operation were frozen in time on that date. The term *consolidated* means that all the balance sheet and income statement data include information from the parent as well as subsidiary operations. The balance sheet consists of two parts: *assets* are the items that the company owns, and *liabilities and stockholders' equity* are what the

company owes to creditors and stockholders. Although the balance sheet has two sides, it is not part of the double-entry accounting system. The balance sheet is not an account but a statement of claims against company assets on the date of the reporting period. The claims are the creditors and the stockholders. Therefore, the total assets must equal the total liabilities plus the stockholders' equity.

Assets are classified as current, fixed, or intangibles. *Current assets* include cash, cash equivalents, marketable securities, accounts receivable, inventories, and prepaid expenses. Cash and cash equivalents are those items that can be easily converted to cash. Marketable securities are securities that a company holds that also may be converted to cash. Accounts receivable are the amounts due a company from customers from material that has been delivered but has not been collected as yet. Customers are given 30, 60, or 90 days in which to pay; however, some customers fail to pay bills on time or may not be able to pay at all. An allowance is made for doubtful accounts. The amount is deducted from the accounts receivables. Inventories include the cost of raw materials, goods in process, and product on hand. Prepaid expenses include insurance premiums paid, charges for leased equipment, and charges for advertising that are paid prior to the receipt of the benefit from these items. The sum of all the above items is the *total current assets*. The term *current* refers to the fact that these assets are easily converted within a year, or more likely in a shorter time, say, 90 days.

Fixed assets are items that have a relatively long life such as land, buildings, and manufacturing equipment. The sum of these items is the *total property, plant, and equipment*. From this total, *accumulated depreciation* is subtracted and the result is *net property and equipment*. Last, an item referred to as *intangibles* includes a variety of items such as patents, licenses, intellectual capital, and goodwill. Intangibles are difficult to evaluate since they have no physical existence; e.g., goodwill is the value of the company's name and reputation. The sum of the *total current assets, net property, and intangibles* is the *total assets*.

Liabilities are the obligations that the company owes to creditors and stockholders. *Current liabilities* are obligations that come due within a year and include *accounts payable* (money owed to creditors for goods and services), *notes payable* (money owed to banks, corporations, or other lenders), *accrued expenses* (salaries and wages to employees, interest on borrowed funds, fees due to professionals, etc.), *income taxes payable, current part of long-term debt, and other current liabilities* due within the year.

Long-term liabilities are the amounts due after 1 year from date of the financial report. They include *deferred income taxes* that a company is permitted to postpone due to accelerated depreciation to encourage investment, (but they must be paid sometime in the future) and *bonds and notes* that do not have to be paid within the year but at some later date. The sum of the *current and long-term liabilities* is the *total liabilities*.

TABLE 9-2 Typical Ledger Page

Cash: Account 01						
200X						
Mar 1 Capital	J-1	\$95,000	Mar 1	Property	J-1	\$3,000
			Mar 11	Remodeling	J-1	7,800
			Mar 13	Equipment	J-1	10,000
			Apr 4	J. Jones	J-1	2,500
Capital: Account 02						
Apr 4 Cash to J. Jones	J-1	\$2,500	Mar 1	Capital	J-1	\$95,000
Accounts Payable: Account 03						
			Mar 4	Mortgage	J-1	\$2,000
			Mar 13	Note Payable	J-1	52,300
Property and Building: Account 04						
Mar 4	J-1	\$5,000				
Mar 11	J-1	7,800				
Equipment: Account 05						
Mar 13	J-1	\$62,300				

SOURCE: J. R. Couper, *Process Engineering Economics*, Dekker, New York, 2003. By permission of Taylor & Francis Books, Inc., Boca Raton, Fla.

9-6 PROCESS ECONOMICS

TABLE 9-3 Consolidated Balance Sheet^a (December 31)

Assets	2005	2004
Current assets		
Cash	\$63,000	\$51,000
Marketable securities	41,000	39,000
Accounts receivable ^b	135,000	126,000
Inventories	149,000	153,000
Prepaid expenses	3,200	2,500
Total current assets	\$391,200	\$371,500
Fixed assets		
Land	35,000	35,000
Buildings	101,000	97,500
Machinery	278,000	221,000
Office equipment	24,000	19,000
Total fixed assets	\$438,000	\$372,500
Less accumulated depreciation	128,000	102,000
Net fixed assets	\$310,000	\$270,500
Intangibles	4,500	4,500
Total assets	\$705,700	\$646,500
Liabilities	2005	2004
Current liabilities		
Accounts payable	\$92,300	\$81,300
Notes payable	67,500	59,500
Accrued expenses payable	23,200	26,300
Federal income taxes payable	18,500	17,500
Total current liabilities	\$201,500	\$184,600
Long-term liabilities		
Debenture bonds, 10.3% due in 2015	110,000	110,000
Debenture bonds, 11.5% due in 2007	125,000	125,000
Deferred income taxes	11,600	10,000
Total liabilities	\$448,100	\$429,600
Stockholder's equity		
Preferred stock, 5% cumulative \$5 par value—200,000 shares	\$10,000	\$10,000
Common stock, \$1 par value 2000 28,000,000 shares 2000X 32,000,000 shares	32,000	28,000
Capital surplus	8,000	6,000
Accumulated retained earnings	207,600	172,900
Total stockholder's equity	\$257,600	\$216,900
Total liabilities and stockholder's equity	\$705,700	\$646,500

^aAll amounts in thousands of dollars.

^bIncludes an allowance for doubtful accounts.

SOURCE: J. R. Couper, *Process Engineering Economics*, Dekker, New York, 2003. By permission of Taylor & Francis Books, Inc., Boca Raton, Fla.

Stockholders' equity is the interest that all stockholders have in a company and is a liability with respect to the company. This category includes *preferred* and *common stock* as well as additional paid-in capital (the amount that stockholders paid above the par value of the stock) and *retained earnings*. These are earnings from accumulated profit that a company earns and are used for reinvestment in the company. The sum of these items is the *stockholders' equity*.

On a balance sheet, the sum of the *total liabilities* and the *stockholders' equity* must equal the *total assets*, hence the term *balance sheet*. Comparing balance sheets for successive years, one can follow changes in various items that will indicate how well the company manages its assets and meets its obligations.

Income Statement An income statement shows the revenue and the corresponding expenses for the year and serves as a guide for how the company may do in the future. Often income statements may show how the company performed for the last two or three years. Table 9-4 is an example of a consolidated income statement.

Net sales are the primary source of revenue from goods and services. This figure includes the amount reported after returned goods, discounts, and allowances for price reductions are taken into account. *Cost of sales* represents all the expenses to convert raw materials to finished products. The major components of these expenses are direct material, direct labor, and overhead. If the cost of sales is subtracted from net sales, the result is the *gross margin*. One of the most important items on the income statement is *depreciation* and *amortization*. Depreciation is an allowance the federal government permits for the

TABLE 9-4 Consolidated Income Statement (December 31)

	2005	2004
Net sales (revenue)	\$932,000	\$850,000
Cost of sales and operating expenses		
Cost of goods sold	692,000	610,000
Depreciation and amortization	40,000	36,000
Sales, general, and administrative expenses	113,500	110,000
Operating profit	\$86,500	\$94,000
Other income (expenses)		
Dividends and interest income	10,000	7,000
Interest expense	(22,000)	(22,000)
Income before provision for income taxes	\$74,500	\$79,000
Provision for federal income taxes	24,500	26,000
Net profit for year	\$50,000	\$53,000

SOURCE: J. R. Couper, *Process Engineering Economics*, Dekker, New York, 2003. By permission of Taylor & Francis Books, Inc., Boca Raton, Fla.

wear and tear as well as the obsolescence of plant and equipment and is treated as an expense. Amortization is the decline in value of intangible assets such as patents, franchises, and goodwill. *Selling, general, and administrative expenses* include the marketing salaries, advertising expenses, travel, executive salaries, as well as office and payroll expenses. When depreciation, amortization, and the sales and administrative expenses are subtracted from the gross margin, the result is the *operating income*. *Dividends and interest income* received by the company are then added. Next *interest expense* earned by the stockholders and *income taxes* are subtracted, yielding the term *income before extraordinary loss*. It is the expenses a company may incur for unusual and infrequent occasions. When all the above items are added or subtracted from the operating income, *net income* (or *loss*) is obtained. This latter term is the "bottom line" often referred to in various reports.

Accumulated Retained Earnings This is an important part of the financial report because it shows how much money has been retained for growth and how much has been paid as dividends to stockholders. When the accumulated retained earnings increase, the company has greater value. The calculation of this value of the retained earnings begins with the previous year's balance. To that figure add the net profit after taxes for the year. Dividends paid to stockholders are then deducted, and the result is the accumulated retained earnings for the year. See Table 9-5.

Concluding Remarks One of the most important sections of an annual report is the "notes." These contain any liabilities that a company may have due to impending litigation that could result in charges or expenses not included in the annual report.

OTHER FINANCIAL TERMS

Profit margin is the ratio of net income to total sales, expressed as a percentage or sometimes quoted as the ratio of profit before interest and taxes to sales, expressed as a percentage. *Operating margin* is obtained by subtracting operating expenses from gross profit expressed as a percentage of sales. *Net worth* is the difference between total assets and total liabilities plus stockholders' equity. *Working capital* is the difference between total current assets and current liabilities.

TABLE 9-5 Accumulated Retained Earnings Statement^a (December 31)

	2005	2004
Balance as of January 1	\$172,900	\$141,850
Net profit for year	50,000	53,000
Total for year	\$222,900	\$194,850
Less dividends paid on:		
Preferred stock	700	700
Common stock	14,600	21,250
Balance December 31	\$207,600	\$172,900

^aAll amounts in thousands of dollars.

SOURCE: J. R. Couper, *Process Engineering Economics*, Dekker, New York, 2003. By permission of Taylor & Francis Books, Inc., Boca Raton, Fla.

FINANCIAL RATIOS

There are many financial ratios of interest to financial analysts. A brief discussion of some of these ratios follows; however, a more complete discussion may be found in Couper (2003).

Liquidity ratios are a measure of a company's ability to pay its short-term debts. *Current ratio* is obtained by dividing the current assets by the current liabilities. Depending on the economic climate, this ratio is 1.5 to 2.0 for the chemical process industries, but some companies operate closer to 1.0. The *quick ratio* is another measure of liquidity and is cash plus marketable securities divided by the current liabilities and is slightly greater than 1.0.

Leverage ratios are an indication of the company's overall debt burden. The *debt/total assets ratio* is determined by dividing the total debt by total assets expressed as a percentage. The industry average is 35 percent. *Debt/equity ratio* is another such ratio. The higher these ratios, the greater the financial risk since if an economic downturn did occur, it might be difficult for a company to meet the creditors' demands. The *times interest earned* is a measure of the extent to which profit could decline before a company is unable to pay interest charges. The ratio is calculated by dividing the *earnings before interest and taxes (EBIT)* by interest charges. The *fixed-charge coverage* is obtained by dividing the income available for meeting fixed charges by the fixed charges.

Activity ratios are a measure of how effectively a firm manages its assets. There are two inventory/turnover ratios in common use today. The *inventory/sales* ratio is found by dividing the inventory by the sales. Another method is to divide the cost of sales by inventory. The *average collection period* measures the number of days that customers' invoices remain unpaid. *Fixed assets* and *total assets turnover* indicate how well the fixed and total assets of the firm are being used.

Profitability ratios are used to determine how well income is being managed. The *gross profit margin* is found by dividing the gross profits by the net sales, expressed as a percentage. The *net operating margin* is equal to the earnings before interest and taxes divided by net sales. Another measure, the *profit margin on sales*, is calculated by dividing the net profit after taxes by net sales. The *return on total assets* ratio is the net profit after taxes divided by the total assets expressed as a percentage. The *return on equity* ratio is the net income after taxes and interest divided by stockholders' equity.

Table 9-6 shows the financial ratios for Tables 9-3 and 9-4. Table 9-7 is a summary of selected financial ratios and industry averages.

RELATIONSHIP BETWEEN BALANCE SHEETS AND INCOME STATEMENTS

There is a relationship between these two documents because information obtained from each is used to calculate the returns on assets and equity. Figure 9-1 is an operating profitability tree for a fictitious

TABLE 9-6 Financial Ratios for Tables 9-3 and 9-4

Liquidity	
Current ratio = \$391,200/\$201,500 = 1.94	
Cash ratio = \$391,200 - 149,000/\$201,500 = 1.20	
Leverage	
Debt/assets ratio = [(\$448,100 - 201,500)/\$705,700] × 100 = 35%	
Times interest earned = \$74,500 - 22,000/\$22,000 = 4.39	
Fixed-charge coverage = \$86,500/\$22,000 = 3.93	
Activity	
Inventory turnover = \$932,000/\$149,000 = 6.25	
Average collection period = \$135,000/(\$932,000/365) = 52.8 days	
Fixed-assets turnover = \$932,000/\$438,000 = 2.13	
Total-assets turnover = \$932,000/\$705,700 = 1.32	
Profitability	
Gross profit margin = [(\$932,000 - 692,000)/\$932,000] × 100 = 25.8%	
Net operating margin = \$74,500/\$932,000 × 100 = 7.99%	
Profit margin on sales = \$50,000/\$932,000 × 100 = 5.36%	
Return on net worth (return on equity)	
= [\$50,000/(\$705,700 - 448,100)] × 100 = 19.4%	
Return on total assets = (\$50,000/\$705,700) × 100 = 7.09%	

company and contains the fixed and variable expenses as reported on internal company reports, such as the manufacturing expense sheet. Figure 9-2 is a financial family tree for the same company depicting the relationship between values in the income statement and the balance sheet.

FINANCING ASSETS BY DEBT AND/OR EQUITY

The various options for obtaining funds to finance new projects are not a simple matter. Significant factors such as the state of the economy, inflation, a company's present indebtedness, and the cost of capital will affect the decision. Should a company incur more long-term debt, or should it seek new venture capital from equity sources? A simple yes or no answer will not suffice because the financial decision is complex. One consideration is the company's position with respect to leverage. If a company has a large proportion of its debt in bonds and preferred stock, the common stock is highly leveraged. Should the earnings decline, say, by 10 percent, the dividends available to common stockholders might be wiped out. The company also might not be able to cover the interest on its bonds without dipping into the accumulated earnings. A high debt/equity ratio illustrates the fundamental weakness of companies with a large amount of debt. When low-interest financing is available, such as for large government projects, the return-on-equity evaluations are used. Such leveraging is tantamount to transferring money from one pocket to another; or, to

TABLE 9-7 Selected Financial Ratios

Item	Equation for calculation	Industry average
Liquidity		
Current ratio	Current assets/current liabilities	1.5-2.0
Cash ratio	Current assets - inventory/current liabilities	1.0-1.5
Leverage		
Debt to total assets	Total debt/total assets	30-40%
Times interest earned	Profit before taxes plus interest charges/interest charges	7.0-8.0
Fixed-charge coverage	Income available for meeting fixed charges/interest charges	6.0
Activity		
Inventory turnover	Sales or revenue/inventory	7.0
Average collection period	Receivables/sales per day	40-60 days
Fixed assets turnover	Sales/fixed assets	2-4
Total assets turnover	Sales/total assets	1-2
Profitability		
Gross profit margin	Net sales - cost of goods sold/sales	25-40%
Net operating margin	Net operating profit before taxes/sales	10-15%
Profit margin on sales	Net profit after taxes/sales	5-8%
Return on net worth (return on equity)	Net profit after taxes/net worth	15%
Return on total assets	Net profit after taxes/total assets	7-10%

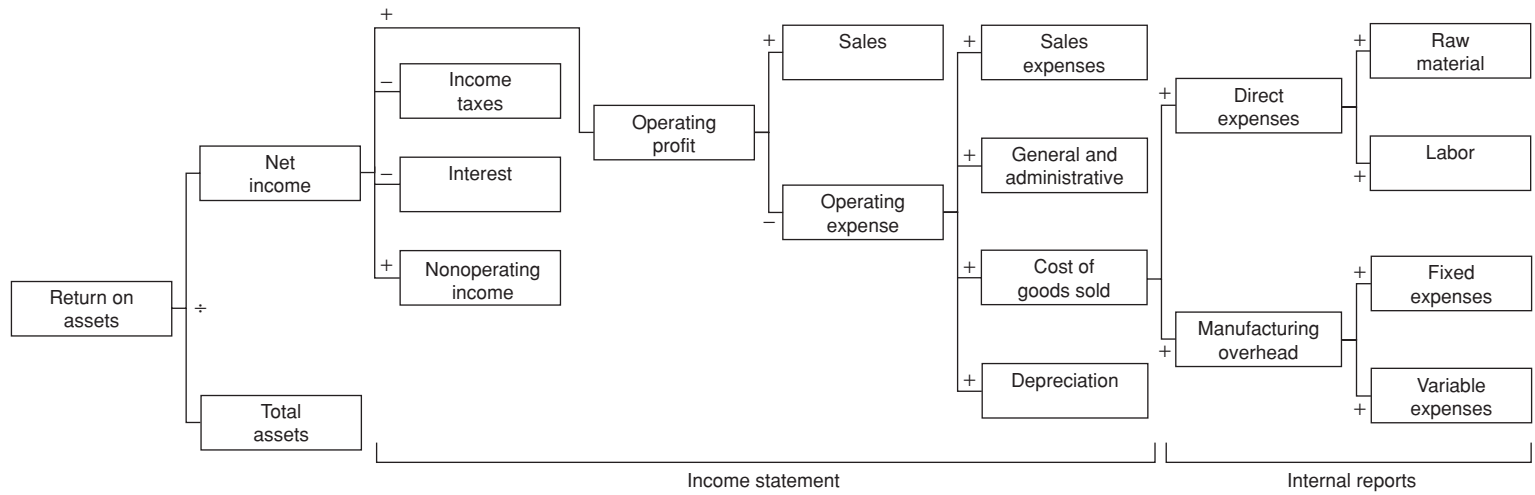


FIG. 9-1 Operating profitability tree. (Source: Adapted from Couper, 2003.)

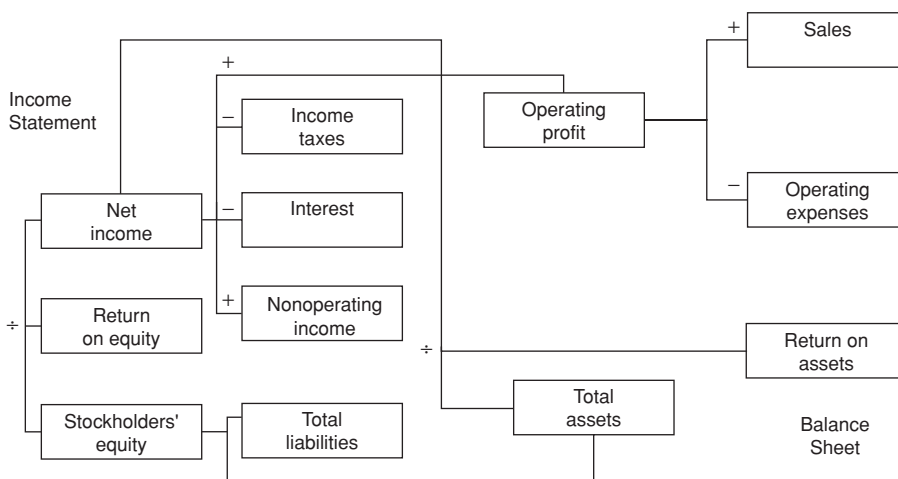


FIG. 9-2 Financial family tree. (Source: Adapted from Couper, 2003.)

put it another way, a company may find itself borrowing from itself. In the chemical process industries, debt/equity ratios of 0.3 to 0.5 are common for industries that are capital-intensive (Couper et al., 2001). Much has been written on the strategies of financing a corporate venture. The correct strategy has to be evaluated from the standpoint of what is best for the company. It must maintain a debt/equity ratio similar to those of successful companies in the same line of business.

COST OF CAPITAL

The cost of capital is what it costs a company to borrow money from all sources, such as loans, bonds, and preferred and common stock. It is an important consideration in determining a company's minimum acceptable rate of return on an investment. A company must make more than the cost of capital to pay its debts and make a profit. From profits, a company pays dividends to the stockholders. If a company ignores the cost of capital to increase dividends to the stockholders, then management is not meeting its obligations to pay off outstanding debts.

A sample calculation of the after-tax weighted cost of capital is found in Table 9-8. Each debt item is divided by the total debt, and

TABLE 9-8 Cost of Capital Illustration

Balance sheet 12/31/XX	Debt, \$M	After-tax yield to maturity, %	After-tax weighted average cost, %
Long-term debt			
Revolving account	5.0	4.5	0.02
4½% debentures	12.0	4.0	0.05
6½% debentures	3.4	4.7	0.02
6¼% debentures	9.4	4.2	0.04
7½% debentures	74.5	4.2	0.30
9¾% loan	125.0	4.4	0.53
Other	23.2	4.4	0.10
Total long-term debt	252.5		1.06
Deferred taxes	67.7	0.0	0
Reserves	16.1	0.0	0
Preferred stock	50.0	8.6	0.42
Shareholders' equity	653.9	15.6	9.80
Total debt	1,040.2		11.28

Each debt item in \$M divided by the total debt times the after-tax yield to maturity equals the after-tax weighted average cost contributing to the cost of capital.

SOURCE: Private communication.

that result is multiplied by the after-tax yield to maturity that equals the after-tax weighted average cost of that debt item contributing to the cost of capital. The information to estimate the cost of capital may be obtained from the annual report, the 10K, or the 10Q reports.

WORKING CAPITAL

The accounting definition of *working capital* is total current assets minus total current liabilities. This information can be found from the balance sheet. Current assets consist chiefly of cash, marketable securities, accounts receivable, and inventories; current liabilities include accounts payable, short-term debts, and the part of the long-term debt currently due. The accounting definition is in terms of the entire company.

For economic evaluation purposes, another definition of working capital is used. It is the funds, in addition to the fixed capital, that a company must contribute to a project. It must be adequate to get the plant in operation and to meet subsequent obligations when they come due. Working capital is not a one-time investment that is known at the project inception, but varies with the sales level and other factors. The relationship of working capital to other project elements may be viewed in the cash flow model (see Fig. 9-9). Estimation of an adequate amount of working capital is found in the section "Capital Investment."

INVENTORY EVALUATION AND COST CONTROL

Under ordinary circumstances, inventories are priced (valued) at some form of cost. The problem in valuating inventory lies in "determining what costs are to be identified with inventories in a given situation" (Nickerson, 1979).

Valuation of materials can be made by using the

- Cost of a specific lot
- Average cost
- Standard cost

Under "cost of a specific lot," those lots to be valued must be identified by referring to related invoices. Many companies use the average cost for valuating inventories. The average used should be weighted by the quantities purchased rather than by an average purchase price. Average cost method tends to spread the effects of short-run price changes and has a tendency to level out profits in those industries that use raw materials whose prices are volatile. For many manufacturing companies, inventory valuation is an important

9-10 PROCESS ECONOMICS

consideration varying in degree of importance. Inventories that are large are subject to significant fluctuations from time to time in size and mix and in prices, costs, and values.

Materials are valued in accordance with their acquisition. Some companies use the first-in, first-out (FIFO) basis. Materials are used in order of their acquisition to minimize losses from deterioration. Another method is last-in, first-out (LIFO) in which materials coming in are the first to leave storage for use. The method used depends on a number of factors. Accounting texts discuss the pros and cons of each method, often giving numerical examples. Some items to consider are income tax considerations and cash flow that motivate management to adopt conservative valuation policies. Tax savings may accrue using one method compared to the other, but they may not be permanent. Whatever method is selected, consistency is important so that comparability of reported figures may be maintained from one time period to another. It is management's responsibility to make the decision regarding the method used. In some countries, government regulations control the method to be used. There are several computer software programs that permit the user to organize, store, search, and manage inventory from a desktop computer.

BUDGETS AND COST CONTROL

A budget is an objective expressed in monetary terms for planning and controlling the resources of a company. Budgeted numbers are

objectives, not achievements. A comparison of actual expenses with budgeted (cost standards) figures is used for control at the company, plant, departmental, or project level. A continuing record of performance should be maintained to provide the data for preparing future budgets (Nickerson, 1979). Often when a company compares actual results with cost standards or budgeted figures, a need for improving operations will surface. For example, if repairs to equipment continuously exceed the budgeted amount, perhaps it is time to consider replacement of that older equipment with a newer, more efficient model. Budgets are usually developed for a 1-year period; however, budgets for various time frames are frequently prepared. For example, in planning future operations, an intermediate time period of, say, 5 years may be appropriate, or for long-range planning the time period selected may be 10 years.

- A cost control system is used
 - To provide early warning of uneconomical or excessive costs in operations
 - To provide relevant feedback to the personnel responsible for developing budgets
 - To develop cost standards
 - To promote a sense of cost consciousness
 - To summarize progress
- Budgetary models based upon mathematical equations are available to determine the effect of changes in variables. There are numerous sources extant in the literature for these models.

CAPITAL COST ESTIMATION

TOTAL CAPITAL INVESTMENT

The *total capital investment* includes funds required to purchase land, design and purchase equipment, structures, and buildings as well as to bring the facility into operation (Couper, 2003). The following is a list of items constituting the total capital investment:

- Land
- Fixed capital investment
- Offsite capital
- Allocated capital
- Working capital
- Start-up expenses
- Other capital items (interest on borrowed funds prior to start-up; catalysts and chemicals; patents, licenses, and royalties; etc.)

Land Land is often acquired by a company some time prior to the building of a manufacturing facility. When a project is committed to be built on this land, the value of the land becomes part of that facility's capital investment.

Fixed Capital Investment When a firm considers the manufacture of a product, a capital cost estimate is prepared. These estimates are required for a variety of reasons such as feasibility studies, the selection of alternative processes or equipment, etc., to provide information for planning capital appropriations or to enable a contractor to bid on a project. Included in the fixed capital investment is the cost of purchasing, delivery, and installation of manufacturing equipment, piping, automatic controls, buildings, structures, insulation, painting, site preparation, environmental control equipment, and engineering and construction costs. The fixed capital investment is significant in developing the economics of a process since this figure is used in estimating operating expenses and calculating depreciation, cash flow, and project profitability. The estimating method used should be the best, most accurate means consistent with the time and money available to prepare the estimate.

Classification of Estimates There are two broad classes of estimates: grass roots and battery limits. Grass-roots estimates include the entire facility, starting with site preparation, buildings and structures, processing equipment, utilities, services, storage facilities, railroad yards, docks, and plant roads. A battery-limits estimate is one in which an imaginary boundary is drawn around the proposed facility to be estimated. It is assumed that all materials, utilities, and services are available in the quality and quantity required to manufacture a product. Only costs within the boundary are estimated.

Quality of Estimates Capital cost estimation is more art than science. An estimator must use considerable judgment in preparing the estimate, and as the estimator gains experience, the accuracy of the estimate improves. There are several types of fixed capital cost estimates:

- *Order-of-magnitude (ratio estimate)*. Rule-of-thumb methods based on cost data from similar-type plants are used. The probable accuracy is -30 percent to +50 percent.
- *Study estimate (factored estimate)*. This type requires knowledge of preliminary material and energy balances as well as major equipment items. It has a probable accuracy of -25 to +30 percent.
- *Preliminary estimate (budget authorization estimate)*. More details about the process and equipment, e.g., design of major plant items, are required. The accuracy is probably -20 to +25 percent.
- *Definitive estimate (project control estimate)*. The data needed for this type of estimate are more detailed than those for a preliminary estimate and include the preparation of specifications and drawings. The probable accuracy is -10 to +15 percent.
- *Detailed estimate (firm estimate)*. Complete specifications, drawings, and site surveys for the plant construction are required, and the estimate has an accuracy of -5 to +10 percent.

Detailed information requirements for each type of estimate may be found in Fig. 9-3.

In periods of high inflation, the results of various estimates and accuracy may overlap. At such times, four categories may be more suitable, namely, study, preliminary, definitive, and detailed categories. At present, some companies employing the *front-end loading (FEL)* process for project definition and execution use three categories:

Project stage	Accuracy
Conceptual	±/40%
Feasibility	±/25%
Definition	±/10%

For more information on the FEL process, see "Capital Project Execution and Analysis" near the end of Sec 9.

Scope The scope is a document that defines a project. It contains words, drawings, and costs. A scope should answer the following questions clearly:

- What product is being manufactured?
- How much is being produced?

ESTIMATING INFORMATION GUIDE
Information Either Required or Available

Estimate types	Detailed (firm)	←	←	←	←	←
	Definitive (project control)	←	←	←	←	←
Estimate types	Preliminary (budget authorization)	←	←	←	←	←
	Study (factored)	←	←	←	←	←
	Order of magnitude (ratio)	←	←	←	←	←
Site	Location General description Site survey Geotechnical report Site plot plan and contours Well-developed site facilities		•	•	•	•
Process flow	Rough sketches Preliminary Engineered		•	•	•	•
Equipment	Rough sizes and construction Engineered specifications Vessel data sheets General arrangement Final arrangement		•	•	•	•
Buildings and structures	Rough sizes and construction Foundation sketches Architectural and construction Preliminary structural design General arrangements and elevations Detailed drawings		•	•	•	•
Utilities and services	Rough quantities Preliminary heat balance Preliminary flow sheets Engineered heat balance Engineered flow sheets Detailed drawings		•	•	•	•
Piping and insulation	Preliminary flow sheets Engineered flow sheets Piping layouts and schedules Insulation rough specifications Insulation applications Insulation details		•	•	•	•
Instrumentation	Preliminary list Engineered list Detail drawings			•	•	•
Electrical	Rough motor list and sizes Engineered list and sizes Substation number and size Preliminary specifications Distribution specifications Preliminary interlocks and controls Engineered single-line diagrams Detailed drawings		•	•	•	•
Work-hours	Engineering and drafting Construction supervision Craft labor		•	•	•	•
Project scope	Product, capacity, location, utilities, and services Building requirements, process, storage, and handling	•	•	•	•	•

FIG. 9-3 Information guide for preparing estimates. (Source: Perry's Chemical Engineers' Handbook, 5th ed., McGraw-Hill, New York, 1973.)

What is the quality of the product?
Where is the product to be produced?
What is the quality of the estimate?
What is the basis for the estimate?
What are the knowns and unknowns with respect to the project?
Before an estimate can be prepared, it is essential to prepare a scope. It may be as simple as a single page, such as for an order-of-

magnitude estimate, or several large manuals, for a detailed estimate. As the project moves forward from inception to a detailed estimate, the scope must be revised and updated to provide the latest information. Changes during the progress of a project are inevitable, but a well-defined scope prepared in advance can help minimize costly changes. If a scope is properly defined, the following results:

9-12 PROCESS ECONOMICS

An understanding between those who prepared the scope (engineering) and those who accept it (management)

A document that indicates clearly what is provided in terms of technology, quality, schedule, and cost

A basis in enough detail to be used in controlling the project and its costs to permit proper evaluation of any proposed changes

A device to permit subsequent evaluation of the performance compared to the intended performance

A document to control the detailed estimate for the final design, construction, and design

Equipment Cost Data The foundation of a fixed capital investment estimate is the equipment cost data. From this information, through the application of factors or percentages based upon the estimator's experience, the fixed capital investment is developed.

These cost data are reported as purchased, delivered, or installed cost. Purchased cost is the price of the equipment FOB at the manufacturer's plant, whereas delivered cost is the purchased price plus the delivery charge to the purchaser's plant FOB. Installed cost means the equipment has been purchased, delivered, uncrated, and placed on a foundation in the purchaser's operating department but does not include piping, electrical, instrumentation, insulation, etc., costs. Perhaps a better name might be *set-in-place cost*.

It is essential to have reliable cost data since the engineer producing the estimate starts with this information and develops the fixed capital cost estimate. The estimator must know the source of the data, the basis for the data, its date, potential errors, and the range over which the data apply. There are many sources of graphical equipment cost data in the literature, but some are old and the latest published data were in the early 1990s. There have been no significant cost data published recently. To obtain current cost data, one should solicit bids from vendors; however, it is essential to impress on the vendor that the information is to be used for preliminary estimates. A disadvantage of using vendor sources is that there is a chance of compromising proprietary information.

Cost-capacity plots of equipment indicate a straight-line relationship on a log-log plot. Figure 9-4 is an example of such a plot. A convenient method of presenting these data is in equation format:

$$C_2 = C_1 \left(\frac{S_2}{S_1} \right)^n \quad (9-1)$$

where C_1 = cost of equipment of capacity S_1
 C_2 = cost of equipment of capacity S_2

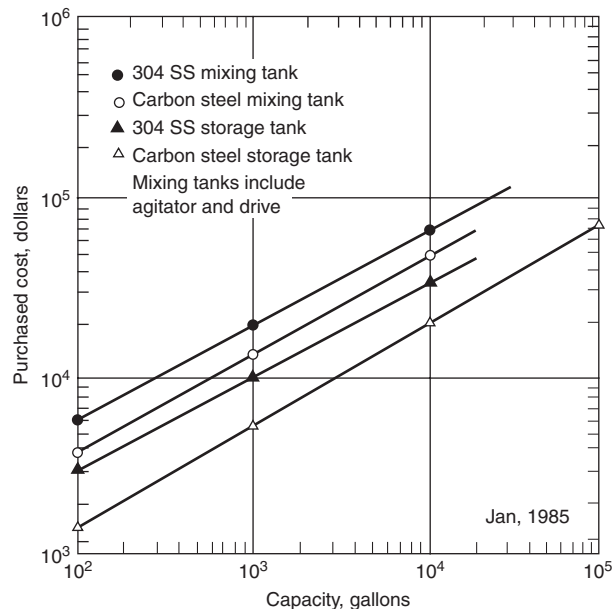


FIG. 9-4 Cost-capacity plot.

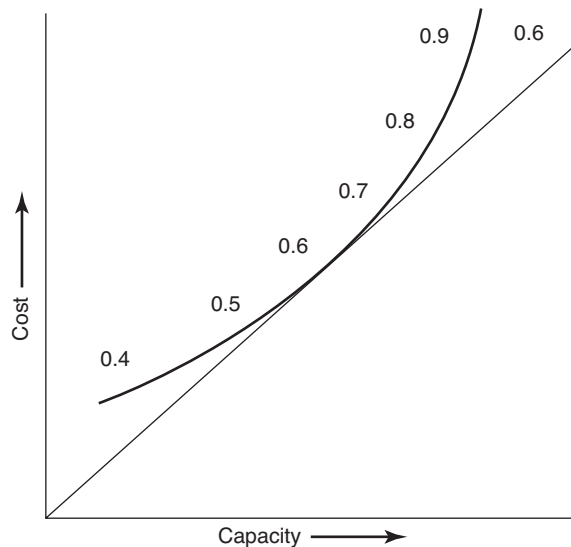


FIG. 9-5 Variation of n on cost-capacity plot.

n = exponent that may vary between 0.4 and 1.2 depending on type of equipment

Equation (9-1) is known as the *six-tenths rule* since the average value for all equipment is about 0.6. D. S. Remer and L. H. Chai (*Chemical Engineering Progress*, August 1990, pp. 77-82) published an extensive list of six-tenths data. Figure 9-5 shows how the exponent may vary from 0.4 to 0.9 for a given equipment item. Data accuracy is the highest in the narrow, middle-range of capacity, but at either end of the plot, the error is great. These errors occur when one correlates cost data with one independent variable when more than one variable is necessary to represent the data, or when pressure, temperature, materials of construction, or design features vary considerably.

A convenient way to display cost-capacity data is by algorithms. They are readily adaptable for computerized cost estimation programs. Algorithm modifiers in equation format may be used to account for temperature, pressure, material of construction, equipment type, etc. Equation (9-2) is an example of obtaining the cost of a shell-and-tube heat exchanger by using such modifiers.

$$C_{HE} = K C_B F_D F_M F_P \quad (9-2)$$

where C_{HE} = purchased equipment cost
 K = factor for cost index based upon a base year
 C_B = base cost of a carbon-steel floating-head exchanger, 150-psig design pressure
 F_D = design-type cost factor if different from that in C_B
 F_M = material-of-construction cost factor
 F_P = design pressure cost factor

Each cost factor is obtained from equations or tables from Couper, 2003, App. C, and have been updated to third-quarter 2002.

Cost Indices Cost data are given as of a specific date and can be converted to more recent costs through the use of cost indices. In general, the indices are based upon constant dollars in a base year and actual dollars in a specific year. In this way, with the proper application of the index, the effect of inflation (or deflation) and price increases by multiplying the historical cost by the ratio of the present cost index divided by the index applicable in the historical year. Labor, material, construction costs, energy prices, and product prices all change at different rates. Most cost indices represent national averages, and local averages may vary considerably. Table 9-9 is a list of selected values of three cost indices of significance in the chemical process industries.

TABLE 9-9 Selected Cost Indices

Year Base	M&S Index ^{(1)a} 1926 = 100	CE index ⁽¹⁾ 1957 – 1959 = 100	Nelson-Farrar index ⁽²⁾ 1946 = 100
1990	915.1	357.6	1225.7
1992	943.1	358.2	1277.3
1994	964.2	368.1	1349.7
1996	1039.1	381.7	1418.9
1998	1061.9	389.5	1477.6
2000	1089.0	394.1	1542.7
2001	1093.9	394.3	1579.7
2002	1104.2	395.6	1642.2
2003	1123.6	402.0	1710.4
2004 (3Q)	1124.7	457.4	1856.1

(1) From 1990 onward, the M&S and CE indices are from *Chemical Engineering* magazine.

(2) The Nelson-Farrar indices from 1990 onward are found in *Oil and Gas Journal*.

^aProcess industry average instead of all industry average.

The chemical engineering (CE) index and the Marshall and Swift index are found in each issue of the magazine *Chemical Engineering*. The *Oil and Gas Journal* reports the *Nelson-Farrar Refinery* indices in the first issue of each quarter. The base years selected for each index are generally periods of low inflation so that the index is stable. The derivation of base values is referred to in the respective publications.

A cost index is used to project a cost from a base year to another selected year. The following equation is used:

$$\text{Cost at } \Theta_2 = \text{cost at } \Theta_1 \left(\frac{\text{index at } \Theta_2}{\text{index at } \Theta_1} \right) \quad (9-3)$$

Example 1: Use of Cost Index A centrifuge cost \$95,000 in 1999. What is the cost of the same centrifuge in third quarter of 2004? Use the CE index.

Solution:

CE index in 1999 = 390.6

CE index in 3d quarter 2004 = 457.4

Cost in 2004 = cost in 1999 (CE index in 3d quarter 2004/ CE index in 1999)

$$= \$95,000 \left(\frac{457.4}{390.6} \right) = \$111,200$$

Inflation When costs are to be projected into the future due to inflation, it is a highly speculative exercise, but it is necessary for estimating investment costs, operating expenses, etc. Inflation is the increase in price of goods without a corresponding increase in productivity. A method for estimating an inflated cost is

$$C_i = (1 + f_1) (1 + f_2) (1 + f_3) C_P \quad (9-4)$$

where C_i = inflated cost

f_1 = inflation rate the first year

f_2 = inflation rate the second year

f_3 = inflation rate the third year

C_P = cost in a base year

The assumed inflation factors f are obtained from federal economic reports, financial sources such as banks and investment houses, and news media. These factors must be reviewed periodically to update estimates.

Example 2: Inflation A dryer today costs \$475,000. The projected inflation rates for the next 3 years are 3, 4.2, and 4.7 percent. Calculate the projected cost in 3 years.

Solution:

$$\begin{aligned} C_i &= (1 + f_1) (1 + f_2) (1 + f_3) C_P \\ &= (1.030) (1.042) (1.047) (\$475,000) = \$533,800 \end{aligned}$$

Equipment Sizing Before equipment costs can be obtained, it is necessary to determine equipment size from material and energy balances. For preliminary estimates, rules of thumb may be used; but for definitive and detailed estimates, detailed equipment calculations must be made.

Example 3: Equipment Sizing and Costing Oil at 490,000 lb/h is to be heated from 100 to 170°F with 145,000 lb/h of kerosene initially at 390°F from another section of a plant. The oil enters at 20 psig and the kerosene at 25 psig. The physical properties are

Oil—0.85 sp gr, 3.5 cP at 135°F, 0.49 sp ht

Kerosene—0.82 sp gr, 0.45 cP, 0.61 sp ht

Estimate the cost of an all-carbon-steel exchanger in late 2004. Assume a counterflow shell-and-tube exchanger.

Solution:

Energy required to heat oil stream $(490,000)(0.49)(170 - 100) = 16,807,000$ Btu/h

$$\begin{aligned} \text{Exit kerosene temperature } T &= 390 - \left(\frac{490,000}{145,000} \right) \left(\frac{0.49}{0.61} \right) (170 - 100) \\ &= 200^\circ \text{F} \end{aligned}$$

$$\text{LMTD} = \frac{220 - 100}{\ln 2.2} = 152^\circ \text{F}$$

Calculate the exchanger efficiency factor, F .

$$P = \frac{170 - 100}{390 - 100} = 0.241$$

$$R = \frac{390 - 200}{170 - 100} = 2.71$$

From Perry $F = 0.88$. Since the factor must be greater than 0.75, the exchanger is satisfactory. Therefore, $\Delta T = (F)(\text{LMTD}) = (0.88)(152) = 134^\circ \text{F}$. Assume $U_D = 50$ Btu/(h·ft²·F).

$$Q = U_D A \Delta T = 16,800,000 = (50)(A)(134)$$

$$A = 2510 \text{ ft}^2$$

Use the cost algorithm cited above.

$$C_B = \exp [8.821 - 0.30863 \ln A + 0.0681(\ln A)^2]$$

$$= \exp [8.821 - 0.30863(7.83) + 0.0681(61.3)] = \$39,300 \text{ base cost}$$

$$F_D = 1.0 \quad F_M = \text{for cs/cs material} = 1.0$$

$$F_P = 1.00 \quad \text{since this exchange is operating below 4 bar}$$

$$\begin{aligned} K &= 1.218 (\text{CE index 4th qtr 2004/CE index 1st qtr 2003}) = 1.218 \left(\frac{463}{406} \right) \\ &= 1.389 \end{aligned}$$

Therefore, $C_{HE} = K C_B F_D F_M F_P = (1.389)(39,300)(1.0)(1.0)(1.0) = \$54,600$.

Estimation of Fixed Capital Investment

Order-of-Magnitude Methods The **ratio method** will give the fixed capital investment per gross annual sales; however, most of these data are from the 1960s, and no recent data have been published. The ratio above is called the *capital ratio*, often used by financial analysts. The reciprocal of the capital ratio is the *turnover ratio* that for various businesses ranges from 4 to 0.3. The chemical industry has an average of about 0.4 to 0.5. The ratio method of obtaining fixed capital investment is rapid but suitable only for order-of-magnitude estimates.

The **exponential method** may be used to obtain a rapid capital cost for a plant based upon existing company data or from published sources such as those of D. S. Remer and L. H. Chai, *Chemical Engineering*,

9-14 PROCESS ECONOMICS

April 1990, pp. 138–175. In the method known as the *seven-tenths rule*, the cost-capacity data for process plants may be correlated by a logarithmic plot similar to the six-tenths plot for equipment. Remer and Chai compiled exponents for a variety of processes and found that the exponents ranged from 0.6 to 0.8. When the data are used to obtain a capital cost for a different-size plant, the estimated capital must be for the same process.

The equation is

$$\text{Cost of plant B} = \text{cost of plant A} \left(\frac{\text{capacity of plant B}}{\text{capacity of plant A}} \right)^{0.7} \quad (9-5)$$

Cost indices may be used to correct costs for time changes.

Example 4: Seven-Tenths Rule A company is considering the manufacture of 150,000 tons annually of ethylene oxide by the direct oxidation of ethylene. According to Remer and Chai (1990), the cost capacity exponent for such a plant is 0.67. A subsidiary of the company built a 100,000-ton annual capacity plant for \$70 million fixed capital investment in 1996. Using the seven-tenths rule, estimate the cost of the proposed new facility in the third quarter 2004.

Solution:

$$\begin{aligned} \text{Cost}_{150} &= \text{Cost}_{100} \left(\frac{\text{Cap}_{150}}{\text{Cap}_{100}} \right)^{0.67} \left(\frac{\text{CE index 3Q 2004}}{\text{CE index 1996}} \right) \\ &= (\$70,000,000) \left(\frac{150,000}{100,000} \right)^{0.67} \left(\frac{457.4}{381.7} \right) = \$110,000,000 \end{aligned}$$

Study Method The single-factor method begins with collecting the delivered cost of various items of equipment and applying one factor to obtain the battery-limits (BL) fixed capital (FC) investment or total capital investment as follows:

$$(C_{\text{FC}})_{\text{BL}} = f \sum (C_{\text{EQ}})_{\text{DEL}} \quad (9-6)$$

where $(C_{\text{FC}})_{\text{BL}}$ = battery-limits fixed capital investment or total capital investment
 $(C_{\text{EQ}})_{\text{DEL}}$ = delivered equipment costs

The single factors include piping, automatic controls, insulation, painting, electrical work, engineering costs, etc. (Couper, 2003). Table 9-10 shows the Lang factors for various types of processing plants. The boundaries between the classifications are not clear-cut, and considerable judgment is required in the selection of the appropriate factors.

Preliminary Estimate Methods A refinement of the Lang factor method is the Hand method. The Hand factors are found in Table 9-11. Equipment is grouped in categories, such as heat exchangers and pumps, and then a factor is applied to each group to obtain the installed cost; finally the groups are summed to give the battery-limits installed cost. Wroth compiled a more detailed list of installation factors; a selection of these can be found in Table 9-12. The Lang and Hand methods start with purchased equipment costs whereas the Wroth method begins with delivered equipment costs, so delivery charges must be included in the Lang and Hand methods. At best the Lang and Hand methods will yield study quality estimates, and the Wroth method might yield a preliminary quality estimate.

Example 5: Fixed Capital Investment Using the Lang, Hand, and Wroth Methods The following is a list of the purchased equipment costs for a proposed processing unit:

Heat exchangers	\$620,000
Distillation towers and internals	975,000
Receivers	320,000

TABLE 9-10 Lang Factors

Type of plant	Lang factors	
	Fixed capital investment	Total capital investment
Solid processing	4.0	4.7
Solid-fluid processing	4.3	5.0
Fluid processing	5.0	6.0

Adapted from M. S. Peters, K. D. Timmerhaus, and R. West, *Plant Design and Economics for Chemical Engineers*, 5th ed., McGraw-Hill, New York, 2004.

TABLE 9-11 Hand Factors

Equipment type	Factor
Fractionating columns	4.0
Pressure vessels	4.0
Heat exchangers	3.5
Fired heaters	2.0
Pumps	4.0
Compressors	2.5
Instruments	4.0
Miscellaneous equipment	2.5

Adapted from W. E. Hand, *Petroleum Refiner*, September 1958, pp. 331–334.

Accumulator drum	125,000
Pumps and motors	220,000
Automatic controls	275,000
Miscellaneous equipment	150,000

Assume delivery charges are 5 percent of the purchased price. Estimate the fixed capital investment 2 years into the future, using the Lang, Hand, and Wroth methods. The inflation rates are 3.5 percent for the first year and 4.0 percent for the second.

Solution:

Equipment	Purchased equipment cost	Delivered equipment cost
Heat exchangers	\$620,000	\$651,000
Distillation towers, internals	975,000	1,024,000
Receivers	320,000	336,000
Accumulator drum	125,000	131,000
Pumps and motors	220,000	231,000
Automatic controls	275,000	289,000
Miscellaneous equipment	150,000	158,000
Total	\$2,685,000	\$2,820,000

Lang method: The Lang factor for a fluid processing unit starting with purchased equipment costs is 5.0. Therefore, fixed capital investment is \$2,820,000 \times 5.0 \times 1.035 \times 1.040 = \$15,177,000.

Hand method: The Hand method begins with purchased equipment costs, and factors are applied from Table 9-11.

TABLE 9-12 Selected Wroth Factors

Equipment	Factor
Blender	2.0
Blowers and fans	2.5
Centrifuge	2.0
Compressors	
Centrifugal (motor-driven)	2.0
Centrifugal (steam-driven, including turbine)	2.0
Reciprocating (steam and gas)	2.3
Reciprocating (motor-driven less motor)	2.3
Ejectors, vacuum	2.5
Furnaces (packaged units)	2.0
Heat exchangers	4.8
Instruments	4.1
Motors, electric	3.5
Pumps	
Centrifugal (motor-driven less motor)	7.0
Centrifugal (steam-driven including turbine)	6.5
Positive-displacement (less motor)	5.0
Reactors (factor as appropriate, equivalent-type equipment)	—
Refrigeration (packaged units)	2.5
Tanks	
Process	4.1
Storage	3.5
Fabricated and field-erected 50,000+ gal	2.0
Towers (columns)	4.0

Abstracted from W. F. Wroth, *Chemical Engineering*, October 17, 1960, p. 204.

Hand method:

Equipment	Purchased equipment cost	Hand factor	Purchased equipment installed cost
Heat exchangers	\$620,000	3.5	\$2,170,000
Distillation towers, internals	975,000	4.0	3,900,000
Receivers	320,000	2.5*	800,000
Accumulator drum	125,000	2.5*	313,000
Pumps and motors	220,000	4.0	880,000
Automatic controls	275,000	4.0	1,100,000
Miscellaneous	150,000	2.5	375,000
TOTAL	\$2,685,000		\$9,538,000

The asterisk on the receivers and accumulators indicates that if these vessels are pressure vessels, a factor of 4.0 should be used instead of 2.5. The total purchased equipment installed is \$9,538,000 for non-pressure vessels and the delivered cost is \$10,015,000. Therefore, the fixed capital investment installed would be $\$10,015,000 \times 1.035 \times 1.040 = \$10,780,000$. Using pressure vessels increases the total purchased equipment cost \$667,000; therefore, the fixed capital investment for this case including inflation would be $\$10,780,000 \times 1.05 \times 1.035 \times 1.04 = \$11,534,000$.

Wroth method:

Equipment	Delivered equipment cost	Wroth factor	Delivered equipment installed cost
Heat exchangers	\$651,000	4.8	\$3,125,000
Distillation towers, internals	1,024,000	4.0	4,096,000
Receivers	336,000	3.5	1,176,000
Accumulator drum	131,000	3.5	459,000
Pumps and motors	231,000	7.0	1,617,000
Automatic controls	289,000	4.1	1,185,000
Miscellaneous	158,000	4.0 (assumed)	632,000
TOTAL	\$2,820,000		\$12,290,000

The total delivered installed equipment cost is the fixed capital investment and, corrected for 2 years of inflation, will be $\$12,290,000 \times 1.035 \times 1.040 = \$13,229,000$.

Therefore, the summary of the fixed capital investment by the various methods is

Lang	\$15,177,000
Hand	11,534,000
Wroth	13,229,000

Experience has shown that the fixed capital investment by the Lang method is generally higher than that of the other methods. Whatever figure is reported to management, it is advisable to state the potential accuracy of these methods.

Brown developed guidelines for the preparation of order-of-magnitude and study capital cost estimates based upon the Lang and Hand methods. Brown modified Lang and Hand methods for materials of construction, instrumentation, and location factors. He found that the modified Hand and Garrett module factor methods gave results within 3.5 percent.

Other multiple-factor methods that have been published in the past are those by C. E. Chilton, *Cost Estimation in the Process Industries*, McGraw-Hill, New York, 1960; M. S. Peters, K. D. Timmerhaus, and R. E. West, *Plant Design and Economics for Chemical Engineers*, 5th ed., McGraw-Hill, New York, 2003; C. A. Miller, *Chemical Engineering*, Sept. 13, 1965, pp. 226–236; and F. A. Holland, F. A. Watson, and V. K. Wilkinson, *Chem. Eng.*, Apr. 1, 1974, pp. 71–76. These methods produced preliminary quality estimates. Most companies have developed their own in-house multiple-factor methods for preliminary cost estimation.

Step-counting methods are based upon a number of processing steps or “functional units.” The concept was first introduced by H. E. Wessel, *Chem. Eng.*, 1952, p. 209. Subsequently, R. D. Hill, *Petrol. Refin.*, **35**(8):106–110, August 1956; F. C. Zevnik and R. L. Buchanan, *Chem. Eng. Progress*, **59**(2):70–77, February 1963; and J. H. Taylor, *Eng. Process Econ.*, **2**:259–267, 1977, further developed the step-counting method.

A step or functional unit is a significant process step including all process equipment and ancillary equipment necessary for operating the unit. A functional unit may be a unit operation, unit process, or separation in which mass and energy are transferred. The sum of all functional units is the total fixed capital investment. Pumping and heat exchangers are considered as part of a functional unit. In-process storage is generally ignored except for raw materials, intermediates, or products. Difficulties are encountered in applying the method due to defining a step. This takes practice and experience. If equipment has been omitted from a step, the resulting estimate is seriously affected. These methods are reported to yield estimates of study quality or at best preliminary quality.

Definitive Estimate Methods Modular methods are an extension of the multiple-factor methods and have been proposed by several authors. One of the most comprehensive methods and one of the earliest was that of K. M. Guthrie, *Chem. Eng.*, **76**:114–142, Mar. 24, 1969. It began with equipment FOB equipment costs, and through the use of factors listed in Table 9-13, the module material cost was obtained. Labor for erection and setting equipment was added to the material cost as well as indirect costs for freight, insurance, engineering, and field expenses to give a total module cost. Such items as contingencies, contractors’ fees, auxiliaries, site development land, and industrial buildings were added if applicable. Since any plant consists of equipment modules, these are summed to give the total fixed capital investment. Unfortunately, the factors and data are old but the concept is useful. Garrett (1989) developed a similar method based upon a variety of equipment modules, starting with purchased equipment costs obtained from plots and applying factors for materials of construction, instrumentation, and plant location. The method provides for all supporting and connecting equipment to make the equipment installation operational. See Table 9-14. T. R. Brown, *Hydrocarbon Processing*, October 2000, pp. 93–100, made modifications to the Garrett method.

Another method, called the *discipline method*, mentioned by L. R. Dysert, *Cost Eng.* **45**(6), June 6, 2003, is similar to the models of

TABLE 9-13 Guthrie Method Factors*

Details	Exchangers			Vessels		Pump and driver	Compressor and driver	Tanks
	Furnaces	Shell and tube	Air-cooled	Vertical	Horizontal			
FOB equipment	1.00	1.00	1.00	1.00	1.00	1.00	1.00	1.00
Piping	0.18	0.46	0.18	0.61	0.42	0.30	0.21	
Concrete	0.10	0.05	0.02	0.10	0.06	0.04	0.12	
Steel		0.03		0.08				
Instruments	0.04	0.10	0.05	0.12	0.06	0.03	0.08	
Electrical	0.02	0.02	0.12	0.05	0.05	0.31	0.16	
Insulation		0.05		0.08	0.05	0.03	0.03	
Paint			0.01	0.01	0.01	0.01	0.01	
Total materials = <i>M</i>	1.34	1.71	1.38	2.05	1.65	1.72	1.61	1.20
Erection and setting (<i>L</i>)	0.30	0.63	0.38	0.95	0.59	0.70	0.58	0.13
χ , excluding site preparation and auxiliaries (<i>M</i> + <i>L</i>)	1.64	2.34	1.76	3.00	2.24	2.42	2.19	1.33
Freight, insurance, taxes, engineering, home office, construction		0.08		0.08	0.08	0.08	0.08	0.08
Overhead or field expense	0.60	0.95	0.70	1.12	0.92	0.97	0.97	
Total module factor	2.24	3.37	2.46	4.20	3.24	3.47	3.24	1.41

*From K. M. Guthrie, *Chem. Eng.*, **76**, 114–142 (Mar. 24, 1969). Based on FOB equipment cost = 100 (carbon steel).

TABLE 9-14 Selected Garrett Module Factors

Equipment type (carbon steel unless otherwise noted)	Module factor
Agitators: dual-bladed turbines/single-blade propellers	2.0
Agitated tanks	2.5
Air conditioning	1.46
Blender, ribbon	2.0
Blowers, centrifugal	2.5
Centrifuges: solid-bowl, screen-bowl, pusher, stainless steel	2.0
Columns: distillation, absorption, etc.	
Horizontal	3.05
Vertical	4.16
Compressors: low-, medium-, high-pressure	2.6 avg.
Coolers, quenchers	2.7
Crystallizers	2.6 avg.
Drives/motors	
Electric, for fans, compressors, pumps	1.5
Electric for other units	2.0
Gasoline	2.0
Turbine: gas and steam	3.5
Dryers	
Fluid bed, spray	2.7
Rotary	2.3
Dust collectors	
Bag filters	2.2
Cyclones, multiclones	3.0
Evaporators, single-effect stainless steel	
Falling film	2.3
Forced circulation	2.9
Fans	2.2
Filters	
Belt, rotary drum and leaf, tilting pan	2.4
Others	2.8
Furnaces	2.1
Heat exchangers	
Air-cooled	2.2
Double-pipe	1.8
Shell-and-tube	3.2
Mills	
Hammer	2.8
Ball, rod	2.3 avg.
Pumps	
Centrifugal	5.0
Reciprocating	3.3
Turbine	1.8
Reactors, jacketed, no agitator	
304 SS	1.8
Glass-lined	2.1
Mild steel	2.3
Vacuum equipment	2.2

SOURCE: Adapted from Garrett (1989).

Guthrie and Garrett. It uses equipment factors to generate separate costs for each of the “disciplines” associated with the installation of equipment, such as installation labor, concrete, structural steel, and piping, to obtain direct field costs for each type of equipment, e.g., heat exchangers, towers, and reactors.

Modular methods, depending on the amount of detail provided, will yield preliminary quality estimates.

Detailed Estimate Method For estimates in the detailed category, a code of account needs to be used to prevent oversight of certain significant items in the capital cost. See Table 9-15. Each item in the code is estimated and provides the capital cost estimate; then this estimate serves for cost control during the construction phase of a project.

Comments on Significant Cost Items

Piping This cost includes the cost of the pipe, installation labor, valves, fittings, supports, and miscellaneous items necessary for complete installation of all pipes in the process. The accuracy of the estimates can be seriously in error by the improper application of estimating techniques to this component. Many pipe estimating methods are extant in the literature.

Two general methods have been used to estimate piping costs when detailed flow sheets are not available. One method is to use a percentage of the FOB equipment costs or a percentage of the fixed capital investment. Typical figures are 80 to 100 percent of the FOB equipment costs or 20 to 30 percent of the fixed capital investment. This method is used

TABLE 9-15 Code of Accounts

Category number	Direct capital cost account titles
010	Equipment items
020	Instrument items
030	Setting and testing equipment
040	Setting and testing instruments
050	Piling
060	Excavation
070	Foundations
080	Supports, platforms, and structures
090	Other building items
100	Fire protection and sprinklers
110	Piping
120	Ductwork
130	Electrical and wiring
140	Site preparation
150	Sewers, drains, and plumbing
160	Underground piping
170	Yards, roads, and fencing
180	Railroads
190	Insulation
200	Painting
210	Walls, masonry, roofs, and roofing
220	Spares
230	Lump-sum contracts
Distributives	
500	Site burden
510	Direct labor burden
530	Construction equipment, tools, and supplies
550	Rental and servicing construction equipment and tools
580	Premium wages and overtime—contractor
670	Temporary facilities
740	Cancellation charges
750	Abandoned design
760	Self-insured losses
790	Unvouchered liabilities
800	In-house engineering
810	Outside engineering
870	Undeveloped design allowances
880	Distributives transferred to expense
890	Contingencies—capital items
Expense	
900	Dismantling
910	Sales and use taxes
920	Repairs expense
930	Relocation and modification expense
940	Start-up relocation and modification expense
990	Contingencies

SOURCE: Private communication.

for preliminary estimates. Another group of methods such as the Dickson “N” method (R. A. Dickson, *Chem. Eng.*, **57**:123–135, Nov. 1947), estimating by weight, estimating by cost per joint, etc., requires a detailed piping takeoff from either PID or piping drawings with piping specifications, material costs, labor expenses, etc. These methods are used for definitive or detailed estimates where accuracy of 10 to 15 percent is required. The takeoff methods must be employed with great care and accuracy by an experienced engineer. A detailed breakdown by plant type for process piping costs is presented in Peters et al. (2003) and in *Perry's Chemical Engineers' Handbook*, 6th ed., 1984.

Electrical This item consists of transformers, wiring, switching gear, as well as instrumentation and control wiring. The installed costs of the electrical items may be estimated as 20 to 40 percent of the delivered equipment costs or 5 to 10 percent of the fixed capital investment for preliminary estimates. As with piping estimation, the process design must be well along toward completion before detailed electrical takeoffs can be made.

Buildings and Structures The cost of the erection of buildings and structures in a chemical process plant as well as the plumbing, heating and ventilation, and miscellaneous building service items may be estimated as 20 to 50 percent of delivered equipment costs or as 10 to 20 percent of the fixed capital investment for a preliminary estimate.

Yards, Railroad Sidings, Roads, etc. This investment includes roads, railroad spurs, docks, and fences. A reasonable figure for preliminary estimates is 15 to 20 percent of the FOB equipment cost or 3 to 7 percent of the fixed capital investment for a preliminary estimate.

Service Facilities For a process plant, utility services such as steam, water, electric power, fuel, compressed air, shop facilities, and a cafeteria require capital expenditures. The cost of these facilities lumped together may be 10 to 20 percent of the fixed capital investment for a preliminary estimate. (*Note:* Buildings, yards, and service facilities must be well defined to obtain a definitive or detailed estimate.)

Environmental Control and Waste Disposal These items are treated as a separate expenditure and are difficult to estimate due to the variety and complexity of the process requirements. Pollution control equipment is generally included as part of the process design. Couper (2003) and Peters et al. (2003) mention that at present there are no general guidelines for estimating these expenditures.

Computerized Cost Estimation With the advent of powerful personal computers (PCs) and software packages, capital cost estimates advanced from large mainframe computers to the PCs. The reasons for using computer cost estimation and economic evaluation packages are time saved on repetitive calculations and reduction in mathematical errors. Numerous computer simulation software packages have been developed over the past two decades. Examples of such software are those produced by ASPEN, ICARUS, CHEMCAD, SUPERPRO, PRO II, HYSYS, etc.; but most do not contain cost estimation software packages. ICARUS developed a PC cost estimation and economic evaluation package called Questimate. This system built a cost estimate from design and equipment cost modules, bulk items, site construction, piping and ductwork, buildings, electrical equipment, instruments, etc., developing worker-hours for engineering and fieldwork costs. This process is similar to quantity takeoff methods to which unit costs are applied. A code of accounts is also provided.

ASPEN acquired ICARUS in 2000 and developed Process Evaluator based on Questimate that is used for conceptual design, known as front-end loading (FEL). More information on FEL and value-improving process (VIP) is found later in Sec. 9. Basic and detailed estimates are coupled with a business decision framework in ASPEN-TECH ICARUS 2000.

EstPro is a process plant cost estimation package for conceptual cost estimation for conceptual design only. It may be obtained from Gulf Publishing, Houston, Tex.

Many companies have developed their own factored estimates using computer spreadsheets based upon their in-house experience and cost database information that they have built from company project history. For detailed estimates, the job is outsourced to design-construction companies that have the staff to perform those estimates.

Whatever package is used, it is recommended that computer-generated costs be spot-checked for reasonable results using a hand-held calculator since errors do occur. Some commercial software companies will develop cost estimation databases in cooperation with a company for site-specific costs.

Contingency This is a provision for unforeseen events that experience has demonstrated are likely to occur. Contingencies are of two types: process and project contingency. In the former, there are uncertainties in

- Equipment and performance
- Integration of old and new process steps
- Scaling up to a large-scale plant size
- Accurate definition of certain process parameters, such as severity of process conditions, number of recycles, process blocks and equipment, multiphase streams, and unusual separations
- No matter how much time and effort are spent preparing estimates, there is a chance of errors occurring due to
 - Engineering errors and omissions
 - Cost and labor rate changes
 - Construction problems
 - Estimating inaccuracies
 - Miscellaneous "unforeseens"
 - Weather-related problems
 - Strikes by fabricators, transportation, and construction personnel

For preliminary estimates, a 15 to 20 percent project contingency should be applied if the process information is firm. As the quality of the estimate moves to definitive and detailed, the contingency value may be lowered to 10 to 15 percent and 5 to 10 percent, respectively. Experience has shown that the smaller the dollar value of the project, the higher the contingency should be.

Offsite Capital These facilities include all structures, equipment, and services that do not enter into the manufacture of a product but are important to the functioning of the plant. Such capital items might be steam-generating and electrical-generating and distribution facilities, well-water cooling tower, and pumping stations for water distribution, etc. Service capital might be auxiliary buildings, such as warehouses, service roads, railroad spurs, material storage, fire protection equipment, and security systems. For estimating purposes, the following percentages of the fixed capital investment might be used:

- Small modification of offsites, 1 to 5 percent
- Restructuring of offsites, 5 to 15 percent
- Major expansion of offsites, 15 to 45 percent
- Grass-roots plants, 45 to 150 percent

Allocated Capital This is capital that is shared due to its proportionate share use in a new facility. Such items include intermediate chemicals, utilities, services and sales, administration, research, and engineering overhead.

Working Capital Working capital is the funds necessary to conduct day-to-day company business. These are funds required to purchase raw materials, supplies, etc. It is continuously liquidated and rejuvenated from the sale of products or services. If an adequate amount of working capital is available, management has the necessary flexibility to cover expenses in case of strikes, delays, fires, etc. Several methods are available for estimating an adequate amount of working capital. They may be broadly classified into percentage and inventory methods. The percentage methods are satisfactory for study and preliminary capital estimates. The percentage methods are of two types: percentage based on capital investment and percentage based upon sales. In the former method, 15 to 25 percent of the total capital investment may be sufficient for preliminary estimates. In the case of certain specialty chemicals where the raw materials are expensive, it is perhaps better to use the percentage of sales method. Such chemicals as flavors, fragrances, perfumes, etc., are in this category. Experience has shown that 15 to 45 percent of sales has been used with 30 to 35 percent being a reasonable average value.

Start-up Expenses Start-up expenses are defined as the total costs directly related to bringing a new manufacturing facility onstream. Start-up time is the time span between the end of construction and the beginning of normal operation. Normal operation is operation at a certain percentage of design capacity or a specified number of days of continuous operation or the ability to make product of a specified purity. Start-up costs are part of the total capital investment and include labor, materials, and overhead for design modifications or changes due to errors on the part of engineering, contractors, costs of tests, final alterations and adjustments. These items cannot be included as contingency because it is known that such work will be necessary before the project is completed. Experience has shown that start-up costs are a percentage of the battery-limits fixed capital investment of the order on average of 3 percent.

Depending on the tax laws in effect, not all start-up costs can be expensed and a portion must be capitalized. Start-up costs can reduce the after-tax earnings during the early years of a project because of a delay in the start-up of production causing a loss of earnings. Construction changes are items of capital cost, and production start-up costs are expensed as an operating expense.

Other Capital Items Paid-up royalties and licenses are considered part of the capital investment since these are replacements for capital to perform process research and development. The initial catalyst and chemical charge, especially for noble metal catalysts and/or in electrolytic processes, is a large amount. These materials are considered to have a life of 1 year. If funds must be borrowed for a new facility, then the interest on borrowed funds during the construction period is capitalized; otherwise, the interest is part of the operating expense.

MANUFACTURING-OPERATING EXPENSES

The estimation of manufacturing expenses has received less attention in the open literature than the estimation of capital requirements. Operating expenses are estimated from proprietary company files. In this section, methods for estimating the elements that constitute operating expenses are presented. Operating expenses consist of the expense of manufacturing a product, packaging and shipping, as well as general overhead expense. These are described later in this section. Figure 9-6 shows an example of a typical manufacturing expense sheet.

RAW MATERIAL EXPENSE

Estimates of the amount of raw material consumed can be obtained from the process material balance. Normally, the raw material expense is the largest expense item in the manufacture of a product. Since yields in a chemical reaction determine the quantity of raw materials consumed, assumed yields may be used to obtain approximate exploratory estimates if possible ranges are given. The prices of the raw materials are published in various trade journals that list material according to form, grade, method of delivery, unit of measure, and cost per unit. The *Chemical Marketing Reporter* is a typical source of these prices. The prices are generally higher than quotations from suppliers, and these latter should be used whenever possible. It may be possible for a company to negotiate the price of a raw material based upon large-quantity use on a long-term basis. With the amount of material used from the material balance and the price of the raw material, the following information can be obtained: annual material consumption, annual material expense, as well as the consumption and expense per unit of product.

Occasionally, by-products may be produced, and if there is a market for these materials, a credit can be given. By-products are treated in the same manner as raw materials and are entered into the manufacturing expense sheet as a credit. If by-products are intermediates for which no market exists, they may be credited to downstream or subsequent operations at a value equivalent to their value as a replacement, or no credit may be obtained.

DIRECT EXPENSES

These are the expenses that are directly associated with the manufacture of a product, e.g., utilities, labor, and maintenance.

Utilities The utility requirements are obtained from the material and energy balances. Utilities include steam, electricity, cooling water, fuel, compressed air, and refrigeration. The current utility prices can be obtained from company plant accounting or from the plant utility supervisor. This person might be able to provide information concerning rate prices for the near future. As requirements increase, the unit cost declines. If large incremental amounts are required, e.g., electricity, it may be necessary to tie the company's utility line to a local utility as a floating source.

With the current energy demands increasing, the unit costs of all utilities are increasing. Any prices quoted need to be reviewed periodically to determine their effect on plant operations. A company utility supervisor is a good source of future price trends. Unfortunately, there are no shortcuts for estimating and projecting utility prices. Utilities are the third largest expense item in the manufacture of a product, behind raw materials and labor.

Operating Labor The most reliable method for estimating labor requirements is to prepare a table of shift, weekend, and vacation coverage. For round-the-clock operation of a continuous process, one operator per shift requires 4.2 operators, if it is assumed that 21 shifts cover the operation and each operator works five, 8-h shifts per week. For batch or semicontinuous operation, it is advisable to prepare a labor table, listing the number of tasks and the number of operators required per task, paying particular attention to primary processing steps such as filtration and distillation that may have several items of equipment per step.

Labor rates may be obtained from the union contract or from a company labor relation supervisor. This person will know the current

labor rates and any potential labor rate increases in the near future. One should not forget shift differential and overtime charges. Once the number of operators per shift has been established, the annual labor expense and unit expense may be estimated. Wessel (*Chem. Eng.*, 59:209-210, July 1952) developed a method for estimating labor requirements for various types of chemical processes in the United States. The equation is applicable for a production rate of 2 to 2000 tons/day (2000 lb/ton).

$$\log Y = -0.783 \log X + 1.252 + B \quad (9-7)$$

where Y = operating labor, operator h/ton per processing step
 X = plant capacity, tons/day
 B = constant depending upon type of process
 + 0.132 (for batch operations that have minimum labor requirements)
 + 0 (for operations with average labor requirements)
 - 0.167 (for a well-instrumented continuous process)

A processing step is one in which a unit operation occurs; e.g., a filtration step might consist of a feed (precoat) tank, pump, filter, and receiver so a processing step may have several items of equipment. By using a flow sheet, the number of processing steps may be counted. The Wessel equation does not take into account changes in labor productivity, but this information can be obtained from each issue of *Chemical Engineering*. Labor productivity varies widely in various sections of this country but even more widely in foreign countries.

Ulrich (1984) developed a table for estimating labor requirements from flow sheets and drawings of the process. Consideration is given to the type and arrangement of equipment, multiplicity of units, and amount of process control equipment. This method is easier to use than the Wessel method and has been updated in a new edition of the original text.

Supervision The approximate expense for supervision of operations depends on process complexity, but 15 to 30 percent of the operating labor expense is reasonable.

Payroll Charges This item includes workers' compensation, social security premiums, unemployment taxes, paid vacations, holidays, and some part of health and dental insurance premiums. The figure has steadily declined from 1980 and now is 30 to 40 percent of operating labor plus supervision expenses.

Maintenance The maintenance expense consists of two components, namely, materials and labor, approximately 60 and 40 percent, respectively. Company records are the best information sources, however, a value of 6 to 10 percent of the fixed capital investment is a reasonable figure. Processes with a large amount of rotating equipment or that operate at extremes of temperature and/or pressure have higher maintenance requirements.

Miscellaneous Direct Expenses These items include operating supplies, clothing and laundry, laboratory expenses, royalties, environmental control expenses, etc.

Item	Basis	Percentage
Operating supplies	Operating labor	5-7
Clothing and laundry	Operating labor	10-15
Laboratory expenses	Operating labor	10-20
Royalties and patents	Sales	1-5

Environmental Control Expense Wastes from manufacturing operations must be disposed of in an environmentally acceptable manner. This direct expense is borne by each manufacturing department. Some companies have their own disposal facilities, or they may contract with a firm that handles the disposal operation. However the wastes are handled, there is an expense. Published data are found in the open literature, some of which have been published by Couper (2003).

TOTAL OPERATING EXPENSES				

PRODUCT:	PLASTICIZER X			
TOTAL SALES (\$/YR):		7200000		
RATED CAPACITY (MM LBS/YR):		12		
LOCATION:				
FIXED CAPITAL INVESTMENT:		800000		
LAND		25000		
WORKING CAPITAL		120000		
OPERATING HOURS (HRS/YR):				
DATE:				
BY:				

RAW MATERIALS:				
MATERIAL	UNIT	ANNUAL QUANTITY	\$/UNIT	\$/YEAR
A AND B	LB	12000000	.23	2760000
				0
				0
				0
GROSS MATERIAL EXPENSE				2760000

BY-PRODUCTS:	UNIT	ANNUAL QUANTITY	\$/UNIT	\$/YEAR
				0
				0
BY-PRODUCT CREDIT				0

NET MATERIAL EXPENSE				2760000

DIRECT EXPENSES:				
	UNIT	ANNUAL QUANTITY	\$/UNIT	\$/YEAR
UTILITIES:				
steam, low pressure				0
steam, medium pressure				0
steam, high pressure	LB	6000000	.003	180000
GROSS STEAM EXPENSE				180000
STEAM CREDIT				0
NET STEAM EXPENSE				180000
electricity	KWH	3000000	.035	105000
cooling water	GALLONS	7200000	.000045	3240
fuel gas				0
other:				0
city water	GALLONS	36000000	.0002	72000
TOTAL UTILITIES COST				540240
LABOR:				
men per shift	4			
annual labor rate per shift	25000			25000
TOTAL LABOR COSTS				100000
SUPERVISION:				
% total of labor expense				0
SUPERVISION EXPENSE=				18000
PAYROLL CHARGES, FRINGE BENEFITS:				
% total of labor expense	40			
PAYROLL EXPENSE				47200
MAINTENANCE				
% of fixed capital investment	8			
MAINTENANCE EXPENSE				64000
SUPPLIES:				
% of operating labor				0
SUPPLIES EXPENSE				1800
LABORATORY:				
laboratory hours per year	900			
cost per hour	30			
TOTAL LABORATORY EXPENSE				27000

FIG. 9-6 Total operating expense sheet.

9-20 PROCESS ECONOMICS

ROYALTIES		
WASTE DISPOSAL:		0
tons per year		
waste charge per ton		0
WASTE DISPOSAL EXPENSE		0
OTHER:		
laundry	6000	6000

TOTAL DIRECT EXPENSE		804240
TOTAL DIRECT + NET MATERIAL COSTS		3564240

INDIRECT EXPENSES:		
DEPRECIATION		
% of fixed capital investment	100	
life of project (yrs)	7	
DEPRECIATION		114000
PLANT INDIRECT EXPENSES		
% of fixed capital investment	5	
PLANT INDIRECT EXPENSES		40000

TOTAL INDIRECT EXPENSES		154000

TOTAL MANUFACTURING EXPENSE:		3718240
PACKAGING, SHIPPING EXPENSE		
rated capacity per	12000000	
dollars per unit	.005	
PACKAGING AND SHIPPING EXPENSE		60000
TOTAL PRODUCTION EXPENSE		3778240
GENERAL OVERHEAD EXPENSES		
percent of annual sales	5	
GENERAL OVERHEAD EXPENSES		360000
TOTAL OPERATING EXPENSE		4138240

FIG. 9-6 (Continued)

INDIRECT EXPENSES

These indirect expenses consist of two major items; depreciation and plant indirect expenses.

Depreciation The Internal Revenue Service allows a deduction for the "exhaustion, wear and tear and normal obsolescence of equipment used in the trade or business." (This topic is treated more fully later in this section.) Briefly, for manufacturing expense estimates, straight-line depreciation is used, and accelerated methods are employed for cash flow analysis and profitability calculations.

Plant Indirect Expenses These expenses cover a wide range of items such as property taxes, personal and property liability insurance premiums, fire protection, plant safety and security, maintenance of plant roads, yards and docks, plant personnel staff, and cafeteria expenses (if one is available). A quick estimate of these expenses based upon company records is on the order of 2 to 4 percent of the fixed capital investment. Hackney presented a method for estimating these expenses based upon a capital investment factor, and a labor factor, but the result is high.

TOTAL MANUFACTURING EXPENSE

The total manufacturing expense for a product is the sum of the raw materials and direct and indirect expenses.

PACKAGING AND SHIPPING EXPENSES

The packaging expense depends on how the product is sold. The package may vary from small containers to fiberpacks to leverpacks, or the product may be shipped via tank truck, tank car, or pipeline. Each product must be considered and the expense of the container included on a case-by-case basis. The shipping expense includes the in-plant movement to warehousing facilities. Product delivery expenses are difficult to estimate because products are shipped in

various amounts to numerous destinations. Often these expenses come under the heading of freight allowed in the sale of a product.

TOTAL PRODUCT EXPENSE

The sum of the total manufacturing expense and the packaging and in-plant shipping expense is the total product expense.

GENERAL OVERHEAD EXPENSE

This expense is often separated from the manufacturing expenses. It includes the expense of maintaining sales offices throughout the country, staff engineering departments, and research and development facilities and administrative offices. All manufacturing departments are expected to share in these expenses so an appropriate charge is made for each product varying between 6 and 15 percent of the product's annual revenue. The wide range in percentage will vary depending on the amount of customer service required due to the nature of the product.

TOTAL OPERATING EXPENSE

The sum of the total product expense and the general overhead expense is the total operating expense. This item ultimately becomes part of the operating expense on the income statement.

RAPID MANUFACTURING EXPENSE ESTIMATION

Holland et al. (1953) developed an expression for estimating annual manufacturing expenses for production rates other than the base case based upon fixed capital investment, labor requirements, and utility expense.

$$A_1 = mC_{fd} + nc_L N_1 + pU_1 \quad (9-8)$$

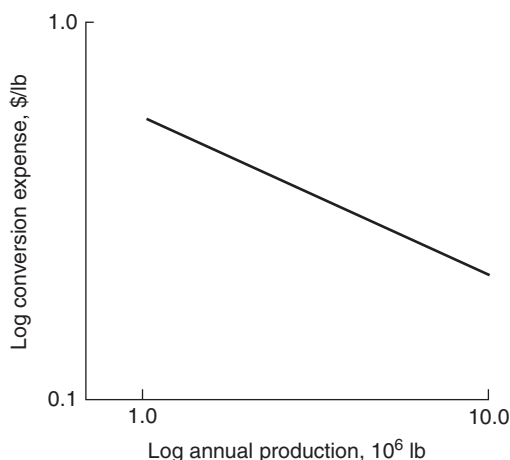


FIG. 9-7 Annual conversion expense as a function of production rate.

where $C_{\text{fc}} =$ fixed capital investment, \$
 $C_L =$ cost of labor, \$ per operator per shift
 $N_1 =$ annual labor requirements, operators/shift/year at rate 1
 $U_1 =$ annual utility expenses at production rate 1
 $A_1 =$ annual conversion expense at rate 1
 $m, n, p =$ constants obtained from company records in consistent units

Equation (9-8) can be modified to include raw materials by adding a term qM_1 , where $q =$ a constant and $M_1 =$ annual raw material expense at rate 1.

SCALE-UP OF MANUFACTURING EXPENSES

If it is desired to estimate the annual manufacturing expense at some rate other than a base case, the following modification may be made:

TABLE 9-16 Typical Labor Requirements for Various Equipment

Equipment	Laborers per unit per shift
Blowers and compressor	0.1–0.2
Centrifuge	0.25–0.50
Crystallizer, mechanical	0.16
Dryers	
Rotary	0.5
Spray	1.0
Tray	0.5
Evaporator	0.25
Filters	
Vacuum	0.125–0.25
Plate and frame	1.0
Rotary and belt	0.1
Heat exchangers	0.1
Process vessels, towers (including auxiliary pumps and exchangers)	0.2–0.5
Reactors	
Batch	1.0
Continuous	0.5

Adapted from G. D. Ulrich, *A Guide to Chemical Engineering Process Design and Economics*, Wiley, New York, 1984.

$$A_2 = mC_{\text{fc}} \left(\frac{R_2}{R_1} \right)^{0.7} + nC_L N_1 \left(\frac{R_2}{R_1} \right)^{0.25} + pU_1 \left(\frac{R_2}{R_1} \right) + qM_1 \left(\frac{R_2}{R_1} \right) \quad (9-9)$$

where $A_2 =$ annual manufacturing expense at production rate 2
 $R_1 =$ production rate 1
 $R_2 =$ production rate 2

Equation (9-9) may also be used to calculate data for a plot of manufacturing expense as a function of annual production rate, as shown in Fig. 9-7. Plots of these data show that the manufacturing expense per unit of production decreases with increasing plant size. The first term in Eq. (9-9) reflects the increase in the capital investment by using the 0.7 power for variations in production rates. Labor varies as the 0.25 power for continuous operations based upon experience. Utilities and raw materials are essentially in direct proportion to the amount of product manufactured, so the exponent of these terms is unity.

FACTORS THAT AFFECT PROFITABILITY

DEPRECIATION

According to the Internal Revenue Service (IRS), *depreciation* is defined as an allowance for the decrease in value of a property over a period of time due to wear and tear, deterioration, and normal obsolescence. The intent is to recover the cost of an asset over a period of time. It begins when a property is placed in a business or trade for the production of income and ends when the asset is retired from service or when the cost of the asset is fully recovered, whichever comes first. Depreciation and taxes are irrevocably tied together. It is essential to be aware of the latest tax law changes because the rules governing depreciation will probably change. Over the past 70 years, there have been many changes in the tax laws of which depreciation is a major component. Couper (2003) discussed the history and development of depreciation accounting. Accelerated depreciation was introduced in the early 1950s to stimulate investment and the economy. It allowed greater depreciation rates in the early years of a project when markets were not well established, manufacturing facilities were coming onstream, and expenses were high due to bringing the facility up to design capacity.

The current methods for determining annual depreciation charges are the *straight-line depreciation* and the *Modified Accelerated Cost Recovery System (MACRS)*. In the straight-line method, the cost of an asset is distributed over its expected useful life such that the annual charge is

$$D = \frac{I + S}{n} \quad \text{\$ per year} \quad (9-10)$$

where $D =$ annual depreciation charge
 $I =$ investment
 $n =$ number of years
 $S =$ salvage value

The MACRS went into effect in January 1987 (Couper, 2003) with six asset recovery periods: 3, 5, 7, 10, 15, and 20 years. It is based upon the declining-balance method. The equation for the declining-balance method is

$$V_e = V_i (1 - f) \quad (9-11)$$

where $V_i =$ value of asset at beginning of year
 $V_e =$ value of asset at end of year
 $f =$ declining-balance factor

For 150 percent declining balance $f = 1.5$, and for 200 percent $f = 2.0$. These factors are applied to the previous year's remaining balance. It is evident that the declining-balance method will not recover the asset that the IRS permits. Therefore, a combination of the declining-balance and straight-line methods forms the basis for the MACRS.

Class lives for selected industries are found in Couper (2003), but most chemical processing equipment falls in the 5-year category and petroleum processing equipment in the 7-year category. For those assets with class lives less than 10 years, a 200 percent declining-balance

9-22 PROCESS ECONOMICS

TABLE 9-17 Depreciation Class Lives and MACRS Recovery Periods

Asset class	Description of asset	Class life, yr	MACRS recovery period, yr
00.12	Information systems	6	5
00.4	Industrial steam and electric generation and/or distribution systems	22	15
13.3	Petroleum refining	16	10
20.3	Manufacture of vegetable oils and vegetable oil products	18	10
20.5	Manufacture of food and beverages	4	3
22.4	Manufacture of textile yarns	8	5
22.5	Manufacture of nonwoven fabrics	10	7
26.1	Manufacture of pulp and paper	13	7
28.0	Manufacture of chemicals and allied products	9.5	5
30.1	Manufacture of rubber products	14	7
30.2	Manufacture of finished plastic products	11	7
32.1	Manufacture of glass products	14	7
32.2	Manufacture of cement	20	15
32.3	Manufacture of other stone and clay products	15	7
33.2	Manufacture of primary nonferrous metals	14	7
32.4	Manufacture of primary steel mill products	15	7
49.223	Substitute natural gas-coal gasification	18	10
49.25	Liquefied natural gas plant	22	15

SOURCE: "How to Depreciate Property," Publication 946, Internal Revenue Service, U.S. Department of Treasury, Washington, 1999.

method with a switch to straight-line in the later years is used. The IRS adopted a half-year convention for both depreciation methods. Under this convention, a property placed in service is considered to be only one-half year irrespective of when during the year the property was placed in service. Table 9-17 is a listing of the class lives, and Table 9-18 contains factors with the half-year convention for both the MACRS and straight-line methods.

Depreciation is entered as an indirect expense on the manufacturing expense sheet based upon the straight-line method. However, when one is determining the after-tax cash flow, straight-line depreciation is removed from the manufacturing expense and the MACRS depreciation is entered. This is illustrated under the section on cash flow.

There are certain terms that apply to depreciation:

- *Depreciation reserve* is the accumulated depreciation at a specific time.
- *Book value* is the original investment minus the accumulated depreciation.
- *Service life* is the time period during which an asset is in service and is economically feasible.
- *Salvage value* is the net amount of money obtained from the sale of a used property over and above any charges involved in the removal and sale of the property.
- *Scrap value* implies that the asset has no further useful life and is sold for the amount of scrap material in it.
- *Economic life* is the most likely period of successful operation before a need arises for subsequent investment in additional equipment as the result of product or process obsolescence or equipment due to wear and tear.

DEPLETION

Depletion is concerned with the diminution of natural resources. Generally depletion does not enter into process economic studies. Rules for determining the amount of depletion are found in the IRS Publication 535.

AMORTIZATION

Amortization is the ratable deduction for the cost of an intangible property over its useful life, perhaps a 15-year life, via straight-line calculations. An example of an intangible property is a franchise, patent, trademark, etc. Two IRS publications, Form 4562 and Publication 535 (1999), established the regulations regarding amortization.

TAXES

Corporations pay an income tax based upon gross earnings, as shown in Table 9-19. Most major corporations pay the federal tax rate of 34 percent on their annual gross earnings. In addition, some states have a stepwise corporate income tax rate. State income tax is deductible as an expense item before the calculation of the federal tax. If T_s is the incremental tax rate and T_f is the incremental federal tax, both expressed as decimals, then the combined incremental rate T_c is

TABLE 9-18 Depreciation Rates for Straight-Line and MACRS Methods

Year	Straight-line half-year convention						MACRS* half-year convention						
	3	5	7	10	15	20	3	5	7	10	15	20	
1	16.67%	10.00%	7.14%	5.0%	3.33%	2.5%	33.33%	20.00%	14.29%	10.00%	5.00%	3.750%	
2	33.33	20.00	14.29	10.0	6.67	5.0	44.45	32.00	24.49	18.00	9.50	7.219	
3	33.33	20.00	14.29	10.0	6.67	5.0	3	14.81	19.20	17.49	14.40	8.55	6.677
4	16.67	20.00	14.28	10.0	6.67	5.0	4	7.41	11.52	12.49	11.52	7.70	6.177
5		20.00	14.29	10.0	6.67	5.0	5		11.52	8.93	9.22	6.93	5.713
6		10.00	14.28	10.0	6.67	5.0	6		5.76	8.92	7.37	6.23	5.285
7			14.29	10.0	6.67	5.0	7			8.93	6.55	5.90	4.888
8			7.14	10.0	6.66	5.0	8			4.46	6.55	5.90	4.522
9				10.0	6.67	5.0	9				6.56	5.91	4.462
10				10.0	6.66	5.0	10				6.55	5.90	4.461
11				5.0	6.67	5.0	11				3.28	5.91	4.462
12					6.66	5.0	12					5.90	4.461
13					6.67	5.0	13					5.91	4.462
14					6.66	5.0	14					5.90	4.461
15					6.67	5.0	15					5.91	4.462
16					3.33	5.0	16					2.95	4.461
17						5.0	17						4.462
18						5.0	18						4.461
19						5.0	19						4.462
20						5.0	20						4.461
21						2.5	21						2.231

*General depreciation system. Declining-balance switching to straight-line. Recovery periods 3, 5, 7, 10, 15, and 20 years.

SOURCE: "How to Depreciate Property," Publication 946, Internal Revenue Service, U.S. Department of Treasury, Washington, 1999.

TABLE 9-19 Corporate Federal Income Tax Rates

Taxable income	Tax rate, %
Annual gross earnings less than \$50,000	15
Annual gross earnings greater than \$50,000 but not over \$75,000	25
Annual gross earnings greater than \$75,000 plus 5% of gross earnings over \$100,000 or \$11,750, whichever is greater	34
Corporations with gross earnings of at least \$335,000 pay a flat rate of 34%	

SOURCE: U.S. Corporate Income Tax Return, Form 1120, Internal Revenue Service, U. S. Department of Treasury, Washington, 1999.

$$T_c = T_s + (1 - T_s)T_f \tag{9-12}$$

If the federal rate is 34 percent and the state rate is 7 percent, then the combined rate is

$$T_c = 0.07 + (1 - 0.07)(0.34) = 0.39$$

Therefore, the combined tax rate is 39 percent.

TIME VALUE OF MONEY

In business, money is either borrowed or loaned. If money is loaned, there is the risk that it may not be repaid. From the lender's standpoint, the funds could have been invested somewhere else and made a profit; therefore, the interest charged for the loan is compensation for the foregone profit. The borrower may look upon this interest as the cost of renting money. The amount of interest charged depends on the scarcity of money, the size of the loan, the length of the loan period, the risk that the lender feels that the loan may not be repaid, and the prevailing economic conditions. Engineers involved in the presentation and/or the evaluation of an investment of funds in a venture, therefore, need to understand the time value of money and how it is applied in the evaluation of projects.

The amount of the loan is called the *principal P*. The longer the time for which the money is loaned, the greater the total amount of interest paid. The *future amount of the money F* is greater than the *principal or present worth P*. The relationship between *F* and *P* depends upon the type of interest used. Table 9-20 is a summary of the nomenclature used in time value of money calculations.

Simple Interest The relationship between *F* and *P* is $F = P(1 + in)$. The interest is charged on the original loan and not on the unpaid balance (Couper and Rader, 1986). The interest is paid at the end of each time interval. Although the simple interest concept still exists, it is seldom used in business.

Discrete Compound Interest In financial transactions, loans or deposits are made using compound interest. The interest is not withdrawn but is added to the principal for that time period. In the next time period, the interest is calculated upon the principal plus the interest from the preceding time period. This process illustrates compound interest. In equation format,

$$\text{Year 1: } P + Pi = P(1 + i) = F_1$$

TABLE 9-20 Interest Nomenclature

Symbol	Definition
<i>F</i>	Future sum Future value Future worth Future amount
<i>P</i>	Principal Present worth Present value Present amount
<i>A</i>	End of period payment in a uniform series

$$\text{Year 2: } P + Pi(1 + i) = P(1 + i)^2 = F_2 \tag{9-13}$$

$$\text{Year } n: P(1 + i)^n = F$$

An interest rate quoted on an annual basis is called *nominal interest*. However, interest may be payable on a semiannual, quarterly, monthly, or daily basis. To determine the amount compounded, the following equation applies:

$$F = P \left(1 + \frac{i}{m} \right)^{mn} \tag{9-14}$$

where *m* = number of interest periods per year
n = number of years
i = nominal interest

Interest calculated for a given time period is known as *discrete compound interest*, with *discrete* referring to a discrete time period. Table 9-21 contains 5 and 6 percent discrete interest factors.

Examples of the use of discrete factors for various applications are found in Table 9-22, assuming that the present time is when the first funds are expended.

Continuous Compound Interest In some companies, namely, petroleum, petrochemical, and chemical companies, money transactions occur hourly or daily, or essentially continuously. The receipts from sales and services are invested immediately upon receipt. The interest on this cash flow is continuously compounded. To use continuous compounding when evaluating projects or investments, one assumes that cash flows continuously.

In continuous compounding, the year is divided into an infinite number of periods. Mathematically, the limit of the interest term is

$$\lim_{n \rightarrow \infty} \left(1 + \frac{r}{m} \right)^{mn} = e^{rn} \tag{9-15}$$

where *n* = number of years
m = number of interest periods per year
r = nominal interest rate
e = base for naperian logarithms

The numerical difference between discrete compound interest and continuous compound interest is small, but when large sums of money are involved, the difference may be significant. Table 9-23 is an abbreviated continuous interest table, assuming that time zero is when start-up occurs. A summary of the equations for discrete compound and continuous compound interest is found in Table 9-24.

Compounding-Discounting When money is moved forward in time from the present to a future time, the process is called *compounding*. The effect of compounding is that the total amount of money increases with time due to interest. *Discounting* is the reverse process, i.e., a sum of money moved backward in time. Figure 9-8 is a

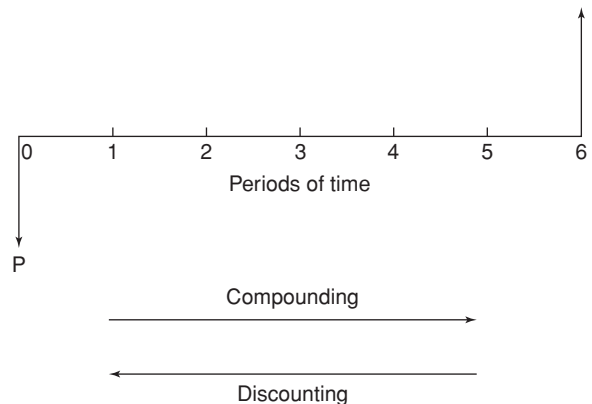


FIG. 9-8 Compounding-discounting diagram.

TABLE 9-21 Discrete Compound Interest Factors*

n	Single payment		Uniform annual series				Single payment		Uniform annual series				n
	Compound-amount factor	Present-worth factor	Sinking-fund factor	Capital-recovery factor	Compound-amount factor	Present-worth factor	Compound-amount factor	Present-worth factor	Sinking-fund factor	Capital-recovery factor	Compound-amount factor	Present-worth factor	
	Given P to find F $(1+i)^n$	Given F to find P $\frac{1}{(1+i)^n}$	Given F to find A $\frac{i}{(1+i)^n - 1}$	Given P to find A $\frac{i(1+i)^n}{(1+i)^n - 1}$	Given A to find F $\frac{(1+i)^n - 1}{i}$	Given A to find P $\frac{1}{i(1+i)^n}$	Given P to find F $(1+i)^n$	Given F to find P $\frac{1}{(1+i)^n}$	Given F to find A $\frac{i}{(1+i)^n - 1}$	Given P to find A $\frac{i(1+i)^n}{(1+i)^n - 1}$	Given A to find F $\frac{(1+i)^n - 1}{i}$	Given A to find P $\frac{1}{i(1+i)^n}$	
5% Compound Interest Factors						6% Compound Interest Factors							
1	1.050	0.9524	1.00000	1.05000	1.000	0.952	1.060	0.9434	1.00000	1.06000	1.000	0.943	1
2	1.103	.9070	.048780	.053780	2.050	1.859	1.124	.8900	0.48544	0.54544	2.060	1.833	2
3	1.158	.8638	.31721	.36721	3.153	2.723	1.191	.8396	.31411	.37411	3.184	2.673	3
4	1.216	.8227	.23201	.28201	4.310	3.546	1.262	.7921	.22859	.28859	4.375	3.465	4
5	1.276	.7835	.18097	.23097	5.526	4.329	1.338	.7473	.17740	.23740	5.637	4.212	5
6	1.340	.7462	.14702	.19702	6.802	5.076	1.419	.7050	.14336	.20336	6.975	4.917	6
7	1.407	.7107	.12282	.17282	8.142	5.786	1.504	.6651	.11914	.17914	8.394	5.582	7
8	1.477	.6768	.10472	.15472	9.549	6.463	1.594	.6274	.10104	.16104	9.897	6.210	8
9	1.551	.6446	.09069	.14069	11.027	7.108	1.689	.5919	.08702	.14702	11.491	6.802	9
10	1.629	.6139	.07940	.12950	12.578	7.722	1.791	.5584	.07587	.13587	13.181	7.360	10
11	1.710	.5847	.07039	.12039	14.207	8.306	1.898	.5268	.06679	.12679	14.972	7.887	11
12	1.796	.5568	.06283	.11283	15.917	8.863	2.012	.4970	.05928	.11928	16.870	8.384	12
13	1.886	.5303	.05646	.10646	17.713	9.394	2.133	.4688	.05296	.11296	18.882	8.853	13
14	1.980	.5051	.05102	.10102	19.599	9.899	2.261	.4423	.04758	.10758	21.015	9.295	14
15	2.079	.4810	.04634	.09634	21.579	10.380	2.397	.4173	.04296	.10296	23.276	9.712	15
16	2.183	.4581	.04227	.09227	23.657	10.838	2.540	.3936	.03895	.09895	25.673	10.106	16
17	2.292	.4363	.03870	.08870	25.840	11.274	2.693	.3714	.03544	.09544	28.213	10.477	17
18	2.407	.4155	.03555	.08555	28.132	11.690	2.854	.3503	.03236	.09236	30.906	10.828	18
19	2.527	.3957	.03275	.08275	30.539	12.085	3.026	.3305	.02962	.08962	33.760	11.158	19
20	2.653	.3769	.03024	.08024	33.066	12.462	3.207	.3118	.02718	.08718	36.786	11.470	20
21	2.786	.3589	.02800	.07800	35.719	12.821	3.400	.2942	.02500	.08500	39.993	11.764	21
22	2.925	.3418	.02597	.07597	38.505	13.163	3.604	.2775	.02305	.08305	43.392	12.042	22
23	3.072	.3256	.02414	.07414	41.430	13.489	3.820	.2618	.02128	.08128	46.996	12.303	23
24	3.225	.3101	.02247	.07247	44.502	13.799	4.049	.2470	.01968	.07968	50.816	12.550	24
25	3.386	.2953	.02095	.07095	47.727	14.094	4.292	.2330	.01823	.07823	54.865	12.783	25
26	3.556	.2812	.01956	.06956	51.113	14.375	4.549	.2198	.01690	.07690	59.156	13.003	26
27	3.733	.2678	.01829	.06829	54.669	14.643	4.822	.2074	.01570	.07570	63.706	13.211	27
28	3.920	.2551	.01712	.06712	58.403	14.898	5.112	.1956	.01459	.07459	68.528	13.406	28
29	4.116	.2429	.01605	.06605	62.323	15.141	5.418	.1846	.01358	.07358	73.640	13.591	29
30	4.322	.2314	.01505	.06505	66.439	15.372	5.743	.1741	.01265	.07265	79.058	13.765	30
31	4.538	.2204	.01413	.06413	70.761	15.593	6.088	.1643	.01179	.07179	84.802	13.929	31
32	4.765	.2099	.01328	.06328	75.299	15.803	6.453	.1550	.01100	.07100	90.890	14.084	32
33	5.003	.1999	.01249	.06249	80.064	16.003	6.841	.1462	.01027	.07027	97.343	14.230	33
34	5.253	.1904	.01176	.06176	85.067	16.193	7.251	.1379	.00960	.06960	104.184	14.368	34
35	5.516	.1813	.01107	.06107	90.320	16.374	7.686	.1301	.00897	.06897	111.435	14.498	35
40	7.040	.1420	.00828	.05828	120.800	17.159	10.286	.0972	.00646	.06646	154.762	15.046	40
45	8.985	.1113	.00626	.05626	159.700	17.774	13.765	.0727	.00470	.06470	212.744	15.456	45
50	11.467	.0872	.00478	.05478	209.348	18.256	18.420	.0543	.00344	.06344	290.336	15.762	50
55	14.636	.0683	.00367	.05367	272.713	18.633	24.650	.0406	.00254	.06254	394.172	15.991	55
60	18.679	.0535	.00283	.05283	353.584	18.929	32.988	.0303	.00188	.06188	533.128	16.161	60
65	23.840	.0419	.00219	.05219	456.798	19.161	44.145	.0227	.00139	.06139	719.083	16.289	65
70	30.426	.0329	.00170	.05170	588.529	19.343	59.076	.0169	.00103	.06103	967.932	16.385	70
75	38.833	.0258	.00132	.05132	756.654	19.485	79.057	.0126	.00077	.06077	1,300.949	16.456	75
80	49.561	.0202	.00103	.05103	971.229	19.596	105.796	.0095	.00057	.06057	1,746.600	16.509	80
85	63.254	.0158	.00080	.05080	1,245.087	19.684	141.579	.0071	.00043	.06043	2,342.982	16.549	85
90	80.730	.0124	.00063	.05063	1,594.607	19.752	189.465	.0053	.00032	.06032	3,141.075	16.579	90
95	103.035	.0097	.00049	.05049	2,040.694	19.806	253.546	.0039	.00024	.06024	4,209.104	16.601	95
100	131.501	.0076	.00038	.05038	2,610.025	19.848	339.302	.0029	.00018	.06018	5,638.368	16.618	100

*Factors presented for two interest rates only. By using the appropriate formulas, values for other interest rates may be calculated.

TABLE 9-22 Examples of the Use of Compound Interest Table

Given: \$2500 is invested now at 5 percent.

Required: Accumulated value in 10 years (i.e., the amount of a given principal).

$$\begin{aligned} \text{Solution:} \quad F &= P(1+i)^n = \$2500 \times 1.05^{10} \\ \text{Compound-amount factor} &= (1+i)^n = 1.05^{10} = 1.629 \\ F &= \$2500 \times 1.629 = \$4062.50 \end{aligned}$$

Given: \$19,500 will be required in 5 years to replace equipment now in use.

Required: With interest available at 3 percent, what sum must be deposited in the bank at present to provide the required capital (i.e., the principal which will amount to a given sum)?

$$\begin{aligned} \text{Solution:} \quad P &= F \frac{1}{(1+i)^n} = \$19,500 \frac{1}{1.03^5} \\ \text{Present-worth factor} &= 1/(1+i)^n = 1/1.03^5 = 0.8626 \\ P &= \$19,500 \times 0.8626 = \$16,821 \end{aligned}$$

Given: \$50,000 will be required in 10 years to purchase equipment.

Required: With interest available at 4 percent, what sum must be deposited each year to provide the required capital (i.e., the annuity which will amount to a given fund)?

$$\begin{aligned} \text{Solution:} \quad A &= F \frac{i}{(1+i)^n - 1} = \$50,000 \frac{0.04}{1.04^{10} - 1} \\ \text{Sinking-fund factor} &= \frac{i}{(1+i)^n - 1} = \frac{0.04}{1.04^{10} - 1} = 0.08329 \\ A &= \$50,000 \times 0.08329 = \$4,164 \end{aligned}$$

Given: \$20,000 is invested at 10 percent interest.

Required: Annual sum that can be withdrawn over a 20-year period (i.e., the annuity provided by a given capital).

$$\begin{aligned} \text{Solution:} \quad A &= P \frac{i(1+i)^n}{(1+i)^n - 1} = \$20,000 \frac{0.10 \times 1.10^{20}}{1.10^{20} - 1} \\ \text{Capital-recovery factor} &= \frac{i(1+i)^n}{(1+i)^n - 1} = \frac{0.10 \times 1.10^{20}}{1.10^{20} - 1} = 0.11746 \\ A &= \$20,000 \times 0.11746 = \$2349.20 \end{aligned}$$

Given: \$500 is invested each year at 8 percent interest.

Required: Accumulated value in 15 years (i.e., amount of an annuity).

$$\begin{aligned} \text{Solution:} \quad F &= A \frac{(1+i)^n - 1}{i} = \$500 \frac{1.08^{15} - 1}{0.08} \\ \text{Compound-amount factor} &= \frac{(1+i)^n - 1}{i} = \frac{1.08^{15} - 1}{0.08} = 27.152 \\ F &= \$500 \times 27.152 = \$13,576 \end{aligned}$$

Given: \$8000 is required annually for 25 years.

Required: Sum that must be deposited now at 6 percent interest.

$$\begin{aligned} \text{Solution:} \quad P &= A \frac{(1+i)^n - 1}{i(1+i)^n} = \$8000 \frac{1.06^{25} - 1}{0.06 \times 1.06^{25}} \\ \text{Present-worth factor} &= \frac{(1+i)^n - 1}{i(1+i)^n} = \frac{1.06^{25} - 1}{0.06 \times 1.06^{25}} = 12.783 \\ P &= \$8000 \times 12.783 = \$102,264 \end{aligned}$$

sketch of this process. The time periods are years, and the interest is normally on an annual basis using end-of-year money flows. The longer the time before money is received, the less it is worth at present.

Effective Interest Rates When an interest rate is quoted, it is *nominal* interest that is stated. These quotes are on an annual basis, however, when compounding occurs that is not the actual or effective interest. According to government regulations, an effective

rate APY must be stated also. The effective interest is calculated by

$$i_{\text{eff}} = \left(1 + \frac{i}{m}\right)^{(m)(1)} - 1 \quad (9-16)$$

The time period for calculating the effective interest rate is 1 year.

TABLE 9-23 Condensed Continuous Interest Table*

Factors for determining zero-time values for cash flows which occur at other than zero time.

Compounding of Cash Flows Which Occur:	1%	5%	10%	15%	20%	25%	30%	35%	40%	50%	60%	70%	80%	90%	100%
A. In an Instant															
$\frac{1}{2}$ year before	1.005	1.025	1.051	1.078	1.105	1.133	1.162	1.191	1.221	1.284	1.350	1.419	1.492	1.568	1.649
1 " "	1.010	1.051	1.105	1.162	1.221	1.284	1.350	1.419	1.492	1.649	1.822	2.014	2.226	2.460	2.718
$1\frac{1}{2}$ " "	1.015	1.078	1.162	1.252	1.350	1.455	1.568	1.690	1.822	2.117	2.460	2.858	3.320	3.857	4.482
2 " "	1.020	1.105	1.221	1.350	1.492	1.649	1.822	2.014	2.226	2.718	3.320	4.055	4.953	6.050	7.389
3 " "	1.030	1.162	1.350	1.568	1.822	2.117	2.460	2.858	3.320	4.482	6.050	8.166	11.023	14.880	20.086
B. Uniformly until Zero Time															
From $\frac{1}{2}$ year before to 0 time	1.002	1.013	1.025	1.038	1.052	1.065	1.079	1.093	1.107	1.136	1.166	1.197	1.230	1.263	1.297
" 1 " " " " "	1.005	1.025	1.052	1.079	1.107	1.136	1.166	1.197	1.230	1.297	1.370	1.448	1.532	1.622	1.718
" $1\frac{1}{2}$ " " " " "	1.008	1.038	1.079	1.121	1.166	1.213	1.263	1.315	1.370	1.489	1.622	1.769	1.933	2.117	2.321
" 2 " " " " "	1.010	1.052	1.107	1.166	1.230	1.297	1.370	1.448	1.532	1.718	1.933	2.182	2.471	2.805	3.194
" 3 " " " " "	1.015	1.079	1.166	1.263	1.370	1.489	1.622	1.769	1.933	2.321	2.805	3.412	4.176	5.141	6.362
Discounting of Cash Flows Which Occur:															
C. In an Instant															
1 year later	.990	.951	.905	.861	.819	.779	.741	.705	.670	.606	.549	.497	.449	.407	.360
2 " "	.980	.905	.819	.741	.670	.606	.549	.497	.449	.368	.301	.247	.202	.165	.135
3 " "	.970	.861	.741	.638	.549	.472	.407	.350	.301	.223	.165	.122	.091	.067	.050
4 " "	.961	.819	.670	.549	.449	.368	.301	.247	.202	.135	.091	.061	.041	.027	.018
5 " "	.951	.779	.606	.472	.368	.286	.223	.174	.135	.082	.050	.030	.018	.011	.007
10 years later	.905	.606	.368	.223	.135	.082	.050	.030	.018	.007	.002	.001	—	—	—
15 " "	.861	.472	.223	.105	.050	.024	.011	.005	.002	.001	—	—	—	—	—
20 " "	.819	.368	.135	.050	.018	.007	.002	.001	—	—	—	—	—	—	—
25 " "	.779	.286	.082	.024	.007	.002	.001	—	—	—	—	—	—	—	—
D. Uniformly over Individual Years															
1st year	.995	.975	.952	.929	.906	.885	.864	.844	.824	.787	.752	.719	.688	.659	.632
2nd "	.985	.928	.861	.799	.742	.689	.640	.595	.552	.477	.413	.357	.309	.268	.232
3rd "	.975	.883	.779	.688	.608	.537	.474	.419	.370	.290	.226	.177	.139	.109	.086
4th "	.966	.840	.705	.592	.497	.418	.351	.295	.248	.176	.124	.088	.062	.044	.032
5th "	.956	.799	.638	.510	.407	.326	.260	.208	.166	.106	.068	.044	.028	.018	.012
6th year	.946	.760	.577	.439	.333	.254	.193	.147	.112	.065	.037	.022	.013	.007	.004
7th "	.937	.723	.522	.378	.273	.197	.143	.103	.075	.039	.020	.011	.006	.003	.002
8th "	.928	.687	.473	.325	.224	.154	.108	.073	.050	.024	.011	.005	.002	.001	.001
9th "	.918	.654	.428	.280	.183	.120	.078	.051	.034	.014	.006	.003	.001	—	—
10th "	.909	.622	.387	.241	.150	.093	.058	.036	.022	.009	.003	.001	—	—	—
E. Uniformly over 5-Year Periods															
1st 5 years	.975	.885	.787	.704	.632	.571	.518	.472	.432	.367	.317	.277	.245	.220	.199
6th through 10th year	.928	.689	.477	.332	.232	.164	.116	.082	.058	.030	.016	.008	.004	.002	.001
11th through 15th year	.883	.537	.290	.157	.086	.047	.026	.014	.008	.002	.001	—	—	—	—
16th through 20th year	.840	.418	.176	.074	.032	.013	.006	.002	.001	—	—	—	—	—	—
21st through 25th year	.799	.326	.106	.035	.012	.004	.001	—	—	—	—	—	—	—	—
F. Declining to Nothing at Constant Rate															
1st 5 years	.983	.922	.852	.791	.736	.687	.643	.603	.568	.506	.456	.413	.377	.347	.320
" 10 " "	.968	.852	.736	.643	.568	.506	.456	.413	.377	.320	.278	.245	.219	.198	.180
" 15 " "	.952	.791	.643	.536	.456	.394	.347	.309	.278	.231	.198	.172	.153	.137	.124
" 20 " "	.936	.736	.568	.456	.377	.320	.278	.245	.219	.180	.153	.133	.117	.105	.095
" 25 " "	.922	.687	.506	.394	.320	.269	.231	.203	.180	.147	.124	.108	.095	.085	.077

*From tables compiled by J. C. Gregory, The Atlantic Refining Co.

TABLE 9-24 Summary of Discrete and Compound Interest Equations

Factor	Find	Given	Discrete compounding		Continuous compounding	
Single payment						
Compound amount	F	P	$F = P(1 + i)^n$	$P(F/P, i, n)$	$F = P(e^{rn})$	$P(F/P, r, n)^\infty$
Present worth	P	F	$P = F \left[\frac{1}{(1 + i)^n} \right]$	$F(P/F, i, n)$	$P = F(e^{-rn})$	$F(P/F, r, n)^\infty$
Uniform series						
Compound amount	F	A	$F = A \left[\frac{(1 + i)^n - 1}{i} \right]$	$A(F/A, i, n)$	$F = A \left(\frac{e^{rn} - 1}{e^r - 1} \right)$	$F(F/A, r, n)^\infty$
Sinking fund	A	F	$A = F \left[\frac{i}{(1 + i)^n - 1} \right]$	$F(A/F, i, n)$	$A = F \left(\frac{e^r - 1}{e^{rn} - 1} \right)$	$F(A/F, r, n)^\infty$
Present worth	P	A	$P = A \left[\frac{(1 + i)^n - 1}{i(1 + i)^n} \right]$	$A(F/A, i, n)$	$P = A \left[\frac{e^{rn} - 1}{e^{rn}(e^r - 1)} \right]$	$A(P/A, r, n)^\infty$
Capital recovery	A	P	$A = P \left[\frac{i(1 + i)^n}{(1 + i)^n - 1} \right]$	$P(A/P, i, n)$	$A = P \left[\frac{e^{rn}(e^r - 1)}{e^{rn} - 1} \right]$	$A(P/A, r, n)^\infty$

Example 6: Effective Interest Rate A person is quoted an 8.33 percent nominal interest rate on a 4-year loan compounded monthly. Determine the effective interest rate.

Solution:

$$i_{\text{eff}} = \left(\frac{1 + i}{m} \right)^{(m)(1)} = \left(\frac{1 + 0.833}{12} \right)^{(12)(1)} - 1 = (1.00694)^{12} - 1 = 1.0865 - 1 = 0.0865$$

The effective interest rate is 8.65 percent.

CASH FLOW

Cash flow is the amount of funds available to a company to meet current operating expenses. Cash flow may be expressed on a before- or after-tax basis. *After-tax cash flow* is defined as the net profit (income) after taxes plus depreciation. It is an integral part of the net present worth (NPW) and discounted cash flow profitability calculations.

The cash flow diagram, also referred to as a cash flow model (Fig. 9-9), shows the relationship between revenue, cash operating expenses, depreciation, and profit. This diagram is similar in many respects to a process flow diagram, but it is in dollars. Revenue is generated from the

sale of a product manufactured in “operations.” Working capital is replenished from sales and may be considered to be in dynamic equilibrium with operations. Leaving the operations box is a stream, “cash operating expenses.” It includes all the cash expenses incurred in the operation but does not include the noncash item depreciation. Since depreciation is an allowance, it is reported on the operating expense sheet, in accordance with the tax laws, as an operating expense item. (See the section “Operating Expense Estimation.”) Depreciation is an internal expense, and this allowance is retained within the company. If the cash operating expenses are subtracted from the revenue, the result is the operating income. If depreciation is subtracted from the operating income, the net profit before taxes results. Federal income taxes are then deducted from the net profit before taxes, giving the net profit after taxes. When depreciation and net profit after taxes are summed, the result is the after-tax cash flow. The terminology in Fig. 9-9 is consistent with that found in most company income statements in company annual reports.

An equation can be developed for cash flow as follows:

$$CF = (R - C - D)(1 - t) + D \tag{9-17}$$

- where R = revenue
- C = cash operating expenses
- D = depreciation
- t = tax rate
- CF = after-tax cash flow

Equation (9-17) can be rearranged algebraically to yield Eq. (9-18)

$$CF = t(D) + (1 - t)(\Delta R) - (1 - t)(\Delta C) \tag{9-18}$$

The term $t \times D$ is only the result of an algebraic manipulation, and no interpretation should be assumed. This term $t \times D$ is the contribution to cash flow from depreciation, and $(1 - t) \times R$ and $(1 - t) \times C$ are the contributions to cash flow from revenues and cash operating expenses, respectively. Example 7 is a sample calculation of the after-tax cash flow and the tabulated results.

Example 7: After-Tax Cash Flow The revenue from the manufacture of a product in the first year of operation is \$9.0 million, and the cash operating expenses are \$4.5 million. Depreciation on the invested capital is \$1.7 million. If the federal income tax rate is 35 percent, calculate the after-tax cash flow.

Solution: The resulting after-tax cash flow is \$3.52 million. See Fig. 9-10.

Cumulative Cash Position Table To organize cash flow calculations, it is suggested that a cumulative cash position table be prepared by using an electronic spreadsheet. For this discussion,

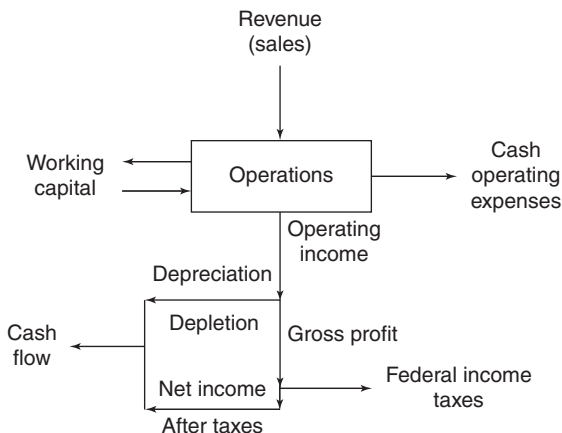


FIG. 9-9 Cash flow model.

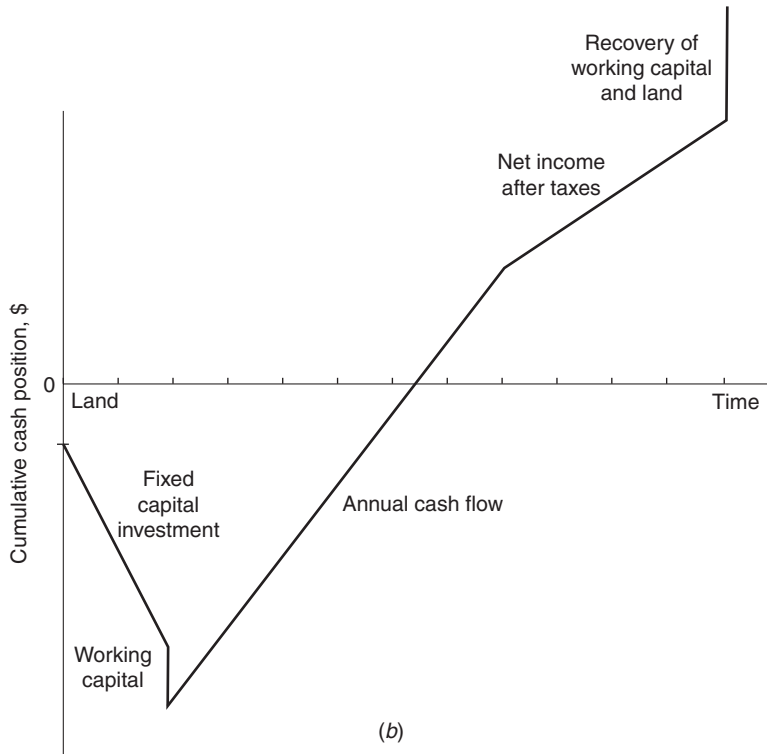
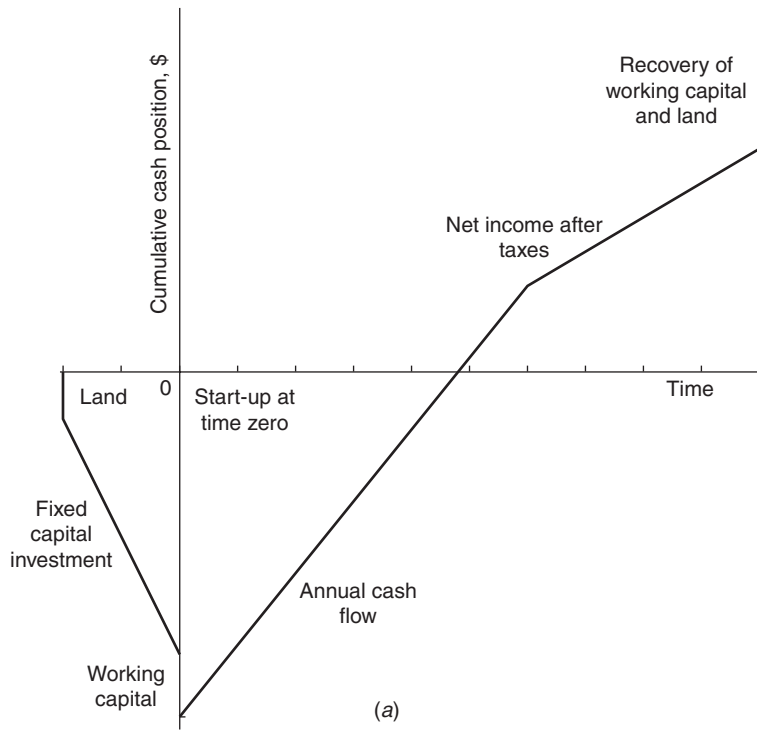


FIG. 9-11 Typical cumulative cash position plot. (a) Time zero is start-up. (b) Time zero occurs when first funds are spent.

PROFITABILITY

In the free enterprise system, companies are in business to make a profit. Management has the responsibility of investing in ventures that are financially attractive by increasing earnings, providing attractive rates of return, and increasing value added. Every viable business has limitations on the capital available for investment; therefore, it will invest in the most economically attractive ventures. The objectives and goals of a company are developed by management. Corporate objectives may include one or several of the following: maximize return on investment, maximize return on stockholders' equity, maximize aggregate earnings, maximize common stock prices, increase market share, increase economic value, increase earnings per share of stock, and increase market value added. These objectives are the ones most frequently listed by executives.

To determine the worthiness of a venture, quantitative and qualitative measures of profitability are considered.

QUANTITATIVE MEASURES OF PROFITABILITY

When a company invests in a venture, the investment must earn more than the cost of capital for it to be worthwhile. A profitability estimate is an attempt to quantify the desirability of taking a risk in a venture.

The *minimum acceptable rate of return (MARR)* for a venture depends on a number of factors such as interest rate, cost of capital, availability of capital, degree of risk, economic project life, and other competing projects. Management will adjust the MARR depending on any of the above factors to screen out the more attractive ventures. When a company invests in a venture, the investment must earn more than the cost of capital and should be able to pay dividends.

Although there have been many quantitative measures suggested through the years, some did not take into account the time value of money. In today's economy, the following measures are the ones most companies use:

- Payout period (POP) plus interest
- Net present worth (NPW)
- Discounted cash flow (DCFROR)

Payout Period Plus Interest Payout period (POP) is the time that will be required to recover the depreciable fixed capital investment from the accrued after-tax cash flow of a project with no interest considerations. In equation format

$$\text{Payout period} = \frac{\text{depreciable fixed capital investment}}{\text{after-tax cash flow}} \quad (9-19)$$

This model does not take into account the time value of money, and no consideration is given to cash flows that occur in a project's later years after the depreciable investment has been recovered. A variation on this method includes interest, called payout period plus interest (POP + I); and the net effect is to increase the payout period. This variation accounts for the time value of money.

Payout period plus interest (POP + I) =

$$\left(\frac{\text{depreciable fixed capital investment}}{\text{after-tax cash flow}} \right)_i \quad (9-20)$$

Neither of these methods makes provision for including land and working capital, and no consideration is given to cash flows that occur in a project's later years after the depreciable fixed investment has been recovered for projects that earn most of their profit in the early years.

Net Present Worth In the net present worth method, an arbitrary time frame is selected as the basis of calculation. This method is the measure many companies use, as it reflects properly the time value of money and its effect on profitability. In equation form

$$\text{Net present worth (NPW)} = \text{present worth of all cash inflows} - \text{present worth of all investment items} \quad (9-21)$$

When the NPW is calculated according to Eq. (9-21), if the result is positive, the venture will earn more than the interest (discount) rate used; conversely, if the NPW is negative, the venture earns less than that rate.

Discounted Cash Flow In the discounted cash flow method, all the yearly after-tax cash flows are discounted or compounded to time zero depending upon the choice of time zero. The following equation is used to solve for the interest rate *i*, which is the discounted cash flow rate of return (DCFROR).

$$\text{DCFROR} = \sum_0^n (\text{after-tax cash flows}) = 0 \quad (9-22)$$

Equation (9-22) may be solved graphically or analytically by an iterative trial-and-error procedure for the value of *i*, which is the discounted cash flow rate of return. It has also been known as the *profitability index*. For a project to be profitable, the interest rate must exceed the cost of capital.

The effect of interest on the cash position of a project is shown in Fig. 9-12. As interest increases, the time to recover the capital expenditures is increased.

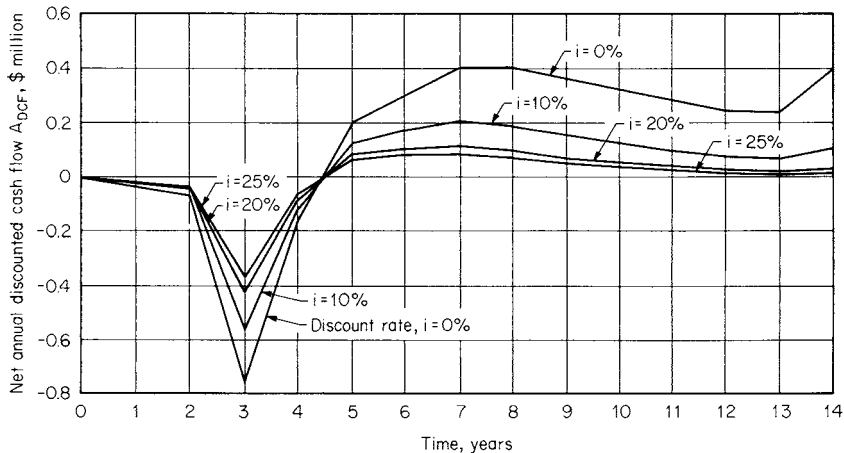


FIG. 9-12 Effect of interest rate on cash flow (time zero occurs when first funds are expanded).

TABLE 9-26 Profitability Analysis for Example 9

Time	Cash flow	20% interest factors	Present worth 20% interest	30% interest factors	Present worth 30% interest	40% interest factors	Present worth 40% interest
-2	-300	1.492	-448	1.822	-547	2.226	-668
-2 to 0	-12,000	1.230	-14,760	1.370	-16,440	1.532	-18,384
0	-2,250	1.000	-2,250	1.000	-2,250	1.000	-2,250
1	6,040	0.906	5,472	0.864	5,219	0.824	4,977
2	7,974	0.742	5,917	0.640	5,103	0.552	4,402
3	8,527	0.608	5,184	0.474	4,042	0.370	3,155
4	8,754	0.497	4,351	0.351	3,073	0.248	2,171
5	9,602	0.407	3,908	0.260	2,497	0.166	1,594
6	9,361	0.333	3,117	0.193	1,807	0.112	1,048
7	6,711	0.273	1,832	0.143	960	0.075	503
8	5,821	0.224	1,304	0.106	617	0.050	291
9	4,862	0.183	890	0.078	379	0.034	165
10	3,471	0.150	561	0.058	217	0.022	82
End 10	2,100	0.135	284	0.050	105	0.018	284
Net present worth			15,362		4,782		-2,360
Discounted cash flow rate of return			33.90%				

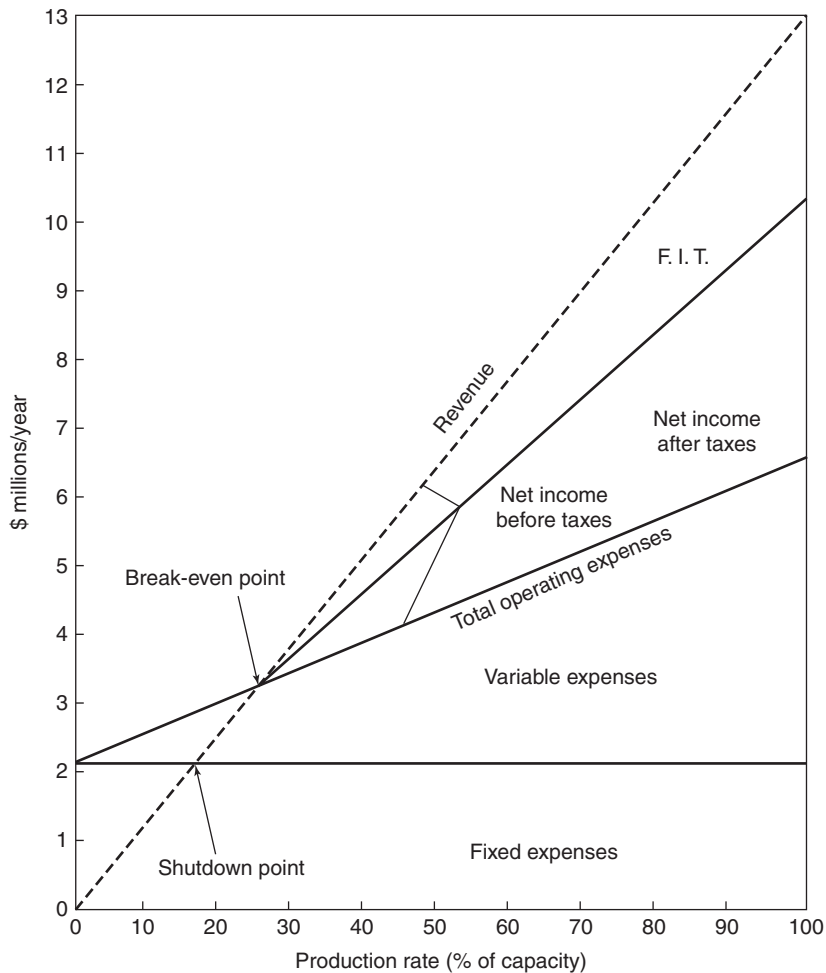


FIG. 9-13 Break-even plot.

9-32 PROCESS ECONOMICS

In the chemical business, operating net profit and cash flow are received on a nearly continuous basis, therefore, there is justification for using the condensed continuous interest tables, such as Table 9-23, in discounted cash flow calculations.

Example 9: Profitability Calculations Example 8 data are used to demonstrate these calculations. Calculate the following:

- Payout period (POP)
- Payout period with interest (POP + I)
- NPW at a 30 percent interest rate
- DCF rate of return

Solution:

a. From Table 9-26, the second column is the cash flow by years with no interest. The payout period occurs where the cumulative cash flow is equal to the fixed capital investment, \$12,000,000 or 1.7 years.

b. In Table 9-26, the payout period at 30 percent interest occurs at 2.4 years.

c. The results of the present worth calculations for 20, 30, and 40 percent interest rates are tabulated. At 30 percent interest, the net present worth is \$4,782,000, and since it is a positive figure, this means the project will earn more than 30 percent interest.

d. Discounted cash flow rate of return is determined by interpolating in Table 9-26. At 30 percent interest the net present worth is positive, and at 40 percent interest it is negative. By definition, the DCFROR occurs when the summation of the net present worth equals zero. This occurs at an interest of 33.9 percent.

QUALITATIVE MEASURES

In addition to quantitative measures, there are certain qualitative measures or intangible factors that may affect the ultimate investment decision. Those most frequently mentioned by management are employee morale, employee safety, environmental constraints, legal constraints, product liability, corporate image, and management goals. Attempts have been made to quantify these intangibles by using an

ordinal or a ranking system, but most have had little or no success. Couper (2003) discussed in greater detail the effect of qualitative measures on the decision-making process.

SENSITIVITY ANALYSIS

Whenever an economic study is prepared, the marketing, capital investment, and operating expense data used are estimates, and therefore a degree of uncertainty exists. Questions arise such as, What if the capital investment is 15 percent greater than the value reported? A sensitivity analysis is used to determine the effect of percentage changes in pertinent variables on the profitability of the project. Such an analysis indicates which variables are most susceptible to change and need further study.

Break-Even Analysis Break-even analysis is a simple form of sensitivity analysis and is a useful concept that can be of value to managers. *Break-even* refers to the point in an operation where income just equals expenses. Figure 9-13 is a pictorial example of the results of a break-even analysis, showing that the break-even point is at 26 percent of production capacity. Management wants to do better than just break even; therefore, such plots can be used as a profit planning tool, for product pricing, production operating level, incremental equipment costs, etc. Another significant point is the *shutdown point* where revenue just equals the fixed expenses. Therefore, if a proposed operation can't make fixed expenses, it should be shut down.

Strauss Plot R. Strauss (*Chem. Eng.*, pp. 112–116, Mar. 25, 1968) developed a sensitivity plot, in Fig. 9-14, in which the ordinate is a measure of profitability and the abscissa is the change in a variable greater than (or less than) the value used in the base case. Where the abscissa crosses the ordinate is the result of the base case of NPW, return, annual worth, etc. The slope of a line on this "spider" plot is the degree of change in profitability resulting from a change in a

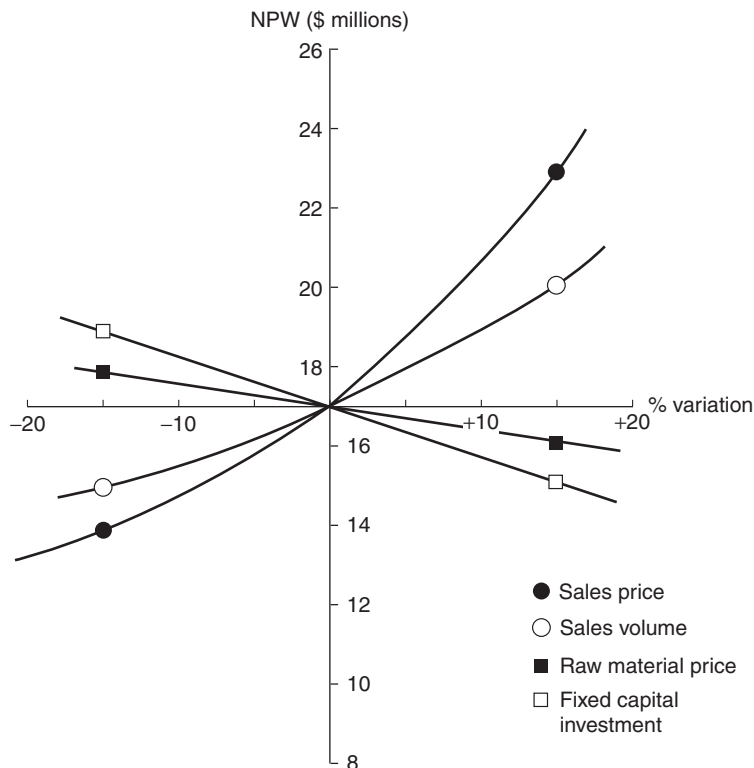


FIG. 9-14 Strauss plot.

variable, selling price, sales volume, investment, etc. The length of the line represents the sensitivity of the variable and its degree of uncertainty. Positive-slope lines are income-related, and negative-slope lines are expense-related. A spreadsheet is useful in developing data for this “what if” plot since numerous scenarios must be prepared to develop the plot.

Tornado Plot Another graphical sensitivity analysis is the “tornado” plot. Its name is derived from the shape of the resulting envelope. As in other methods, a base case is solved first, usually expressing the profitability as the net present worth. In Fig. 9-15, the NPW is a vertical line, and variations in each selected variable above and below the base case are solved and plotted. In this figure, the variables of selling price, sales volume, operating expenses, raw material expenses, share of the market, and investment are plotted. It is apparent that the selling price and sales volume are the critical factors affecting the profitability. A commercial computer program known as @RISK® developed by the Palisade Corporation, Newfield, N.Y., may be used to prepare a tornado plot.

Relative Sensitivity Plot Another type of analysis developed by J. C. Agarwal and I. V. Klumpar (*Chem. Eng.*, pp. 66–72, Sept. 29, 1975) is the relative sensitivity plot. The variables studied are related to those in the base case, and the resulting plot is the relative profitability.

Although sensitivity analyses are easy to prepare and they yield useful information for management, there is a serious disadvantage. Only one variable at a time can be studied. Frequently, there are synergistic effects among variables; e.g., in marketing, the variables such as sales volume, selling price, and market share may have a synergistic effect, and that effect cannot be taken into account. Other inter-related variables such as fixed capital investment, maintenance, and other investment-based items also cannot be represented properly. These disadvantages lead to another management tool—uncertainty analysis.

UNCERTAINTY ANALYSIS

This analysis allows the user to account for variable interaction that is another level of sophistication. Two terms need clarification—

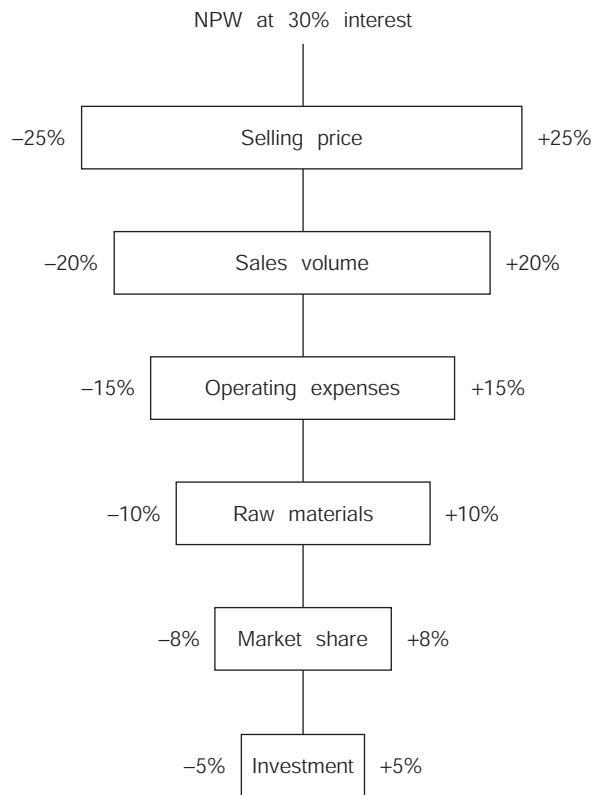


FIG. 9-15 Typical tornado plot. (Source: Adapted from Couper, 2003.)

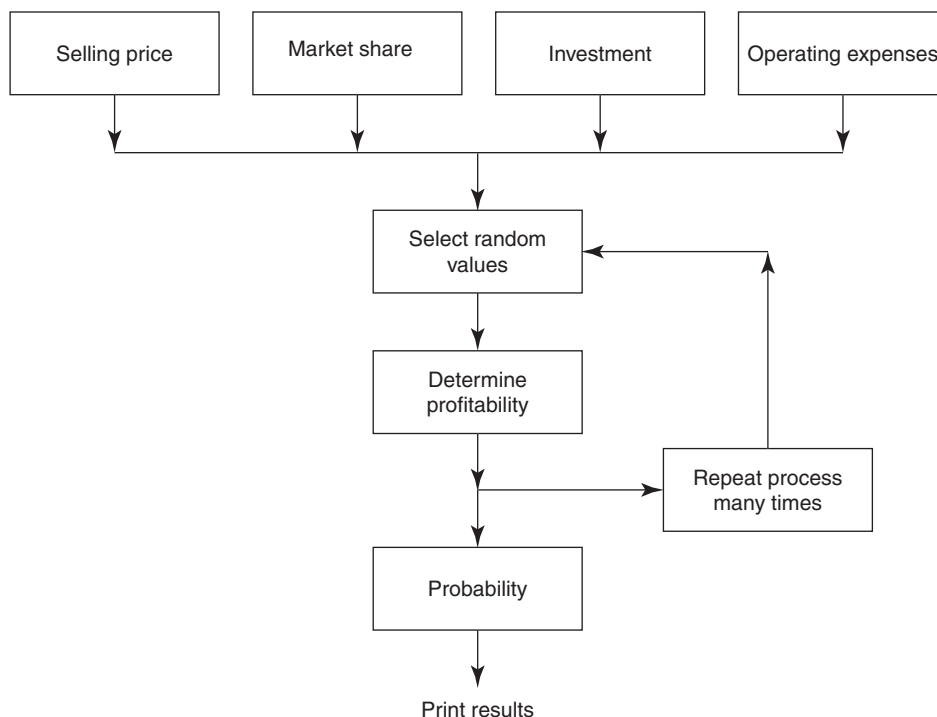


FIG. 9-16 Schematic diagram of Monte Carlo simulation.

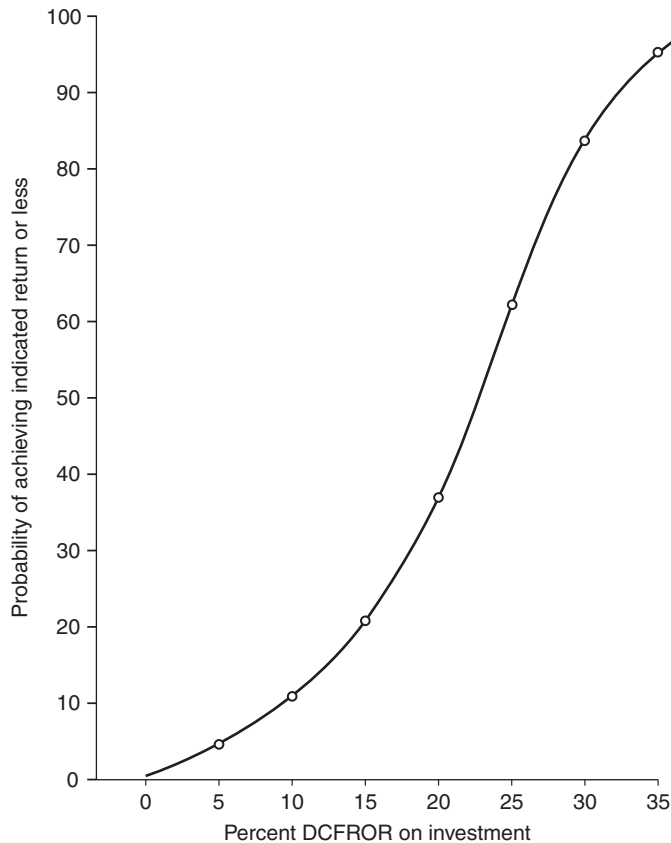


FIG. 9-17 Probability curve for Monte Carlo simulation.

uncertainty and risk. Uncertainty is exactly what the word means—not certain. Risk, however, implies that the probability of achieving a specific outcome is known within certain confidence limits.

Since sensitivity analysis has the shortcoming of being able to inspect only one variable at a time, the next step is to use probability risk analysis, generally referred to as the Monte Carlo technique. R. C. Ross (*Chem. Eng.*, pp. 149–155, Sept. 20, 1971), P. Macalusa (*BYTE*, pp. 179–192, March 1984), and D. B. Hertz (*Harvard Bus. Rev.*, pp. 96–108, Jan-Feb 1968) have written classic articles on the use of the Monte Carlo technique in uncertainty analysis. These articles incorporate subjective probabilities and assumptions of the distribution of errors into the analysis. Each variable is represented by a probability distribution model. Figure 9-16 is a pictorial representation of the steps in the Monte Carlo simulation. The first step is to gather enough data to develop a reasonable probability model. Not all variables follow the normal distribution curve, but perhaps sales volume and sales-related variables do. Studies have shown that capital investment estimates are best represented by a beta distribution. Next the task is to select random values from the various models by using a random number generator and from these data calculate a profitability measure such as NPW or rate of return. The procedure is repeated a number of times to generate a plot of the probability of achieving a given profitability versus profitability. Figure 9-17 is a typical plot. Once the analysis has been performed, the next task is to interpret the results. Management must understand what the results mean and the reliability of the results. Experience can be gained only by performing uncertainty analyses, not just one or two attempts, to develop confidence in

the process. The stakes may be high enough to spend time and learn the method. Software companies such as @RISK or SAS permit the user to develop probability models and perform the Monte Carlo analysis. The results may be plotted as the probability of achieving at least a given return or of achieving less than the desired profitability.

FEASIBILITY ANALYSIS

A feasibility analysis is prepared for the purpose of determining that a proposed investment meets the minimum requirements established

TABLE 9-27 Checklist of Required Information for a Feasibility Analysis

Fixed capital investment
Working capital requirements
Total capital investment
Total manufacturing expense
Packaging and in-plant expense
Total product expense
General overhead expense
Total operating expense
Marketing data
Cash flow analysis
Project profitability
Sensitivity analysis
Uncertainty analysis

TABLE 9-28 Marketing Data Template

Project title:						
Basis: Sales and marketing data are not inflated (20__ dollars)						
		20__		20__		20__
	Amount	%Total	Amount	%Total	Amount	%Total
Total market						
Units						
Average realistic price, \$/unit						
Value, \$						
Estimated product sales (with AR)						
Units						
Average realistic price, \$/unit						
Value, \$						
Current product sales (without AR)						
Units						
Average realistic price, \$/unit						
Value, \$						
Incremental product sales						
Units						
Average realistic price, \$/unit						
Value, \$						
Current product sales displaced by improved product sales						
Units						
Value, \$						
Total improved product sales						
Units						
Value, \$						

NOTE: Table extends to the right to accommodate the number of project years.
AR = appropriation request.

TABLE 9-29 Cash Flow Analysis Template

	Cash flow summary		
	200X	200Y	200Z, etc.*
Investment			
Land			
Fixed capital investment			
Offsite capital			
Allocated capital			
Working capital			
Start-up expenses			
Interest			
Catalysts and chemicals			
Licenses, patents, etc.			
Total capital investment			
Income statement			
Income			
Expenses			
Cash operating expenses			
Depreciation			
Total operating expenses			
Operating income			
Net income before taxes			
Federal income taxes			
Net income after taxes			
Cash flow			
Capital recovery			
Cumulative cash flow			

*Table may be extended to the right to accommodate the number of years of the project.

by management. It should be in sufficient detail to provide management with the facts required to make an investment decision. All the basic information has been discussed in considerable detail in the earlier parts of Sec. 9.

The minimum information required should include, but not be limited to, that in Table 9-27. Forms and spreadsheets are the most succinct method to present the information. The forms should state clearly the fund amounts and the date that each estimate was performed. The forms may be developed so that data for other scenarios may be reported by extending the tables to the right of the page. It is suggested that blank lines be included for any additional information. Finally the engineer preparing the feasibility analysis should make recommendations based upon management's guidelines.

The development of the information required for Table 9-27 was discussed previously in Sec. 9 with the exception of marketing information. An important document for a feasibility analysis is the marketing data so that the latest income projections can be included for management's consideration. As a minimum, the tabulation of sales volume, sales prices, and market share both domestically and globally should be included. Table 9-28 shows a sample of such marketing information.

Other templates may be prepared for total capital investment, working capital, total product expense, general overhead expense, and cash flow. Table 9-29 may be used to organize cash flow data by showing investment, operating expenses, cash flow, and cumulative cash flow.

OTHER ECONOMIC TOPICS

COMPARISON OF ALTERNATIVE INVESTMENTS

Engineers are often confronted with making choices between alternative equipment, designs, procedures, plans or methods. The courses of action require different amounts of capital and different operating expenses. Some basic concepts must be considered before attempting

to use mathematical methods for a solution. It is necessary to clearly define the alternatives and their merits. Flow of money takes the form of expenditures or income. Savings from operations are considered as income or as a reduction in operating expenses. Income taxes and inflation as well as a reasonable return on the investment must be included. Money spent is negative and money earned or saved is positive.

9-36 PROCESS ECONOMICS

Expenditures are of two kinds; instantaneous like land, working capital and capital recovery or uniformly continuous for plant investment, operating expenses, etc. A methodology involving after-tax cash flow is developed to reduce all the above to a manageable format.

In an earlier part of this section, after-tax cash flow was defined as

$$CF = (R - C - D)(1 - t) + D \quad (9-17)$$

where CF = after-tax cash flow

D = depreciation

t = tax rate

S = sales or revenue

C = cash operating expenses (COE)

For the situation in which each case will produce the same revenue or the same benefit, R will equal 0. Rearranging Eq. (9-17) algebraically yields

$$CF = (t)(D) + (1 - t)(S - C) \quad (9-17a)$$

$$\text{or} \quad CF = (t)(D) + (1 - t)(-C) \quad (9-17b)$$

$$CF = (t)(D) - (1 - t)(C) \quad (9-17c)$$

This expression is applied to each alternative. [Note: As mentioned under cash flow, the first term in the above equations, (t)(D), is the result of an algebraic rearrangement, and no other significance should be assumed.]

Several methods are available for determining the choice among alternatives:

Net present worth

Rate of return

Capitalized cost

Cash flow

Uniform annual cost

Humphreys in Jelen and Black, *Cost and Optimization Engineering* (1991), has shown that each of these methods would result in the same decision, but the numerical results will differ.

Net Present Worth Method The NPW method allows the conversion of all money flows to be discounted to the present time. Appropriate interest factors are applied depending on how and when the cash flow enters a venture. They may be instantaneous, as in the purchase of capital equipment, or uniform, as in operating expenses. The alternative with the more positive NPW is the one to be preferred. In some instances, the alternatives may have different lives so the cost analysis must be for the least common multiple number of years. For example, if alternative A has a 2-year life and alternative B has a 3-year life, then 6 years is the least common multiple. The rate of return, capitalized cost, cash flow, and uniform annual cost methods avoid this complication.

Rate of return and capitalized cost methods are discussed at length in Humphreys (1991).

Cash Flow Method Cash flows for each case are determined, and the case that generates the greater cash flow is the preferred one.

Uniform Annual Cost (UAC) Method In the uniform annual cost method, the cost is determined over the entire estimated project life. The least common multiple does not have to be calculated, as in the NPW method. This is the advantage of the UAC method; however, the result obtained by this method is more meaningful than the results obtained by other methods.

The UAC method begins with a calculation for each alternative. If discrete interest is used, the annual cost C is found by multiplying the present worth P by the appropriate discrete interest factor, found in Table 9-21, for the number of years n and the interest rate i. If continuous interest is preferred, the UAC equation is

$$UAC = \frac{NPW}{(\text{years of life})(\text{continuous interest factor})} \quad (9-23)$$

The continuous interest factor may be found from continuous interest equations or from the continuous interest table, Table 9-30. In this table time zero is the present, and all cash flows are discounted back to the present. Note that there are three sections to this table,

depending on the cash flow: uniform, instantaneous, or declining uniformly to zero. One enters the table with the argument $R \times T$, where R is the interest rate expressed as a whole number and T is the time in years to obtain a factor. This factor is then used to calculate the present worth of the cash flow item. All cash flows are summed algebraically, giving the net present worth which is substituted in Eq. (9-23). This procedure is followed for both alternatives, and the alternative that yields the more positive UAC (or the least negative) value is the preferred alternative. In Eq. (9-23) the "factor" is always the uniform factor that annualizes all the various cash flows.

This method of comparing alternatives is demonstrated in Example 10.

Example 10: Choice among Alternatives Two filters are considered for installation in a process to remove solids from a liquid discharge stream to meet environmental requirements. The equipment is to be depreciated over a 7-year period by the straight-line method. The income tax rate is 35 percent, and 15 percent continuous interest is to be used. Assume that the service life is 7 years and there is no capital recovery. Data for the two systems are as follows:

System	B	C
Fixed investment	\$18,000	\$30,000
Annual operating expenses	14,200	4,800

Which alternative is preferred?

Solution:

System B:

Year	Item	Cash flow, \$	Factor	PW, \$
0	Investment	-18,000	1.0	-18,000
0-7	Contribution to cash flow from depreciation	(0.35)(18,000)	0.6191	+3,900
0-7	Contribution to cash flow from operating expense	(1 - 0.35)(7)(14,200)	0.6191	-40,000
			NPW B	-54,100

$$UAC_B = \frac{NPW}{(\text{years of life})(\text{uniform factor})} = \frac{-\$54,100}{(7)(0.6191)} = -\$12,484$$

System C:

Year	Item	Cash flow, \$	Factor	PW, \$
0	Investment	-30,000	1.0	-30,000
0-7	Contribution to cash flow from depreciation	(0.35)(30,000)	0.6191	+6,500
0-10	Contribution to cash flow from operating expense	(1 - 0.35)(10)(4,800)	0.6191	-19,316
			NPW C	-42,816

$$UAC_C = \frac{NPW}{(\text{years of life})(\text{uniform factor})} = \frac{-\$42,816}{(10)(0.6191)} = -\$6,916$$

Alternative C is preferred because it has the more positive UAC.

REPLACEMENT ANALYSIS

During the lifetime of a physical asset, continuation of its use may make it a candidate for replacement. In this type of analysis, a replacement is intended to supplant a similar item performing the same service without plant or equipment expansion. In a chemical plant, *replacement* usually refers to a small part of the processing equipment such as a heat exchanger, filter, or compressor. If the replacement is required due to "physical" deterioration, there is no question of whether to replace the item, but the entire plant may be shut down if it is not replaced. The problem then becomes whether the equipment

TABLE 9-30 Factors for Continuous Discounting

$R \times T$	0	1	2	3	4	5	6	7	8	9
	Uniform									
0	1.0000	.9950	.9901	.9851	.9803	.9754	.9706	.9658	.9610	.9563
10	.9516	.9470	.9423	.9377	.9332	.9286	.9241	.9196	.9152	.9107
20	.9063	.9020	.8976	.8933	.8891	.8848	.8806	.8764	.8722	.8681
30	.8639	.8598	.8558	.8517	.8477	.8437	.8396	.8359	.8319	.8281
40	.8242	.8204	.8166	.8128	.8090	.8053	.8016	.7979	.7942	.7906
50	.7869	.7833	.7798	.7762	.7727	.7692	.7657	.7622	.7588	.7554
60	.7520	.7486	.7453	.7419	.7386	.7353	.7320	.7288	.7256	.7224
70	.7192	.7160	.7128	.7097	.7066	.7035	.7004	.6974	.6944	.6913
80	.6883	.6854	.6824	.6795	.6765	.6736	.6707	.6679	.6650	.6622
90	.6594	.6566	.6538	.6510	.6483	.6455	.6428	.6401	.6374	.6348
100	.6321	.6295	.6269	.6243	.6217	.6191	.6166	.6140	.6115	.6090
110	.6065	.6040	.6015	.5991	.5967	.5942	.5918	.5894	.5871	.5847
120	.5823	.5800	.5777	.5754	.5731	.5708	.5685	.5663	.5640	.5618
130	.5596	.5574	.5552	.5530	.5509	.5487	.5466	.5444	.5423	.5402
140	.5381	.5361	.5340	.5320	.5299	.5279	.5259	.5239	.5219	.5199
150	.5179	.5160	.5140	.5121	.5101	.5082	.5063	.5044	.5025	.5007
160	.4988	.4970	.4951	.4933	.4915	.4897	.4879	.4861	.4843	.4825
170	.4808	.4790	.4773	.4756	.4738	.4721	.4704	.4687	.4671	.4654
180	.4637	.4621	.4604	.4588	.4572	.4555	.4539	.4523	.4507	.4492
190	.4476	.4460	.4445	.4429	.4414	.4399	.4383	.4368	.4353	.4338
200	.4323	.4309	.4294	.4279	.4265	.4250	.4236	.4221	.4207	.4193
210	.4179	.4165	.4151	.4137	.4123	.4109	.4096	.4082	.4069	.4055
220	.4042	.4029	.4015	.4002	.3989	.3976	.3963	.3950	.3937	.3925
230	.3912	.3899	.3887	.3874	.3862	.3849	.3837	.3825	.3813	.3801
240	.3789	.3777	.3765	.3753	.3741	.3729	.3718	.3706	.3695	.3683
250	.3672	.3660	.3649	.3638	.3627	.3615	.3604	.3593	.3582	.3571
260	.3560	.3550	.3539	.3528	.3518	.3507	.3496	.3486	.3476	.3465
270	.3455	.3445	.3434	.3424	.3414	.3404	.3394	.3384	.3374	.3364
280	.3354	.3344	.3335	.3325	.3315	.3306	.3296	.3287	.3277	.3268
290	.3259	.3249	.3240	.3231	.3222	.3212	.3203	.3194	.3185	.3176
300	.3167	.3158	.3150	.3141	.3132	.3123	.3115	.3106	.3098	.3089
310	.3080	.3072	.3064	.3055	.3047	.3039	.3030	.3022	.3014	.3006
320	.2998	.2990	.2982	.2974	.2966	.2958	.2950	.2942	.2934	.2926
330	.2919	.2911	.2903	.2896	.2888	.2880	.2873	.2865	.2858	.2850
340	.2843	.2836	.2828	.2821	.2814	.2807	.2799	.2792	.2785	.2778
350	.2771	.2764	.2757	.2750	.2743	.2736	.2729	.2722	.2715	.2709
360	.2702	.2695	.2688	.2682	.2675	.2669	.2662	.2655	.2649	.2642
370	.2636	.2629	.2623	.2617	.2610	.2604	.2598	.2591	.2585	.2579
380	.2573	.2567	.2560	.2554	.2548	.2542	.2536	.2530	.2524	.2518
390	.2512	.2506	.2500	.2495	.2489	.2483	.2477	.2471	.2466	.2460
400	.2454	.2449	.2443	.2437	.2432	.2426	.2421	.2415	.2410	.2404
	Instantaneous									
0	1.0000	.9900	.9802	.9704	.9608	.9512	.9418	.9324	.9231	.9139
10	.9048	.8958	.8869	.8781	.8694	.8607	.8521	.8437	.8353	.8270
20	.8187	.8106	.8025	.7945	.7866	.7788	.7711	.7634	.7558	.7483
30	.7408	.7334	.7261	.7189	.7118	.7047	.6977	.6907	.6839	.6771
40	.6703	.6637	.6570	.6505	.6440	.6376	.6313	.6250	.6188	.6126
50	.6065	.6005	.5945	.5886	.5827	.5769	.5712	.5655	.5599	.5543
60	.5488	.5434	.5379	.5326	.5273	.5220	.5169	.5117	.5066	.5016
70	.4966	.4916	.4868	.4819	.4771	.4724	.4677	.4630	.4584	.4538
80	.4493	.4449	.4404	.4360	.4317	.4274	.4232	.4190	.4148	.4107
90	.4066	.4025	.3985	.3946	.3906	.3867	.3829	.3791	.3753	.3716
100	.3679	.3642	.3606	.3570	.3535	.3499	.3465	.3430	.3396	.3362
110	.3329	.3296	.3263	.3230	.3198	.3166	.3135	.3104	.3073	.3042
120	.3012	.2982	.2952	.2923	.2894	.2865	.2837	.2808	.2780	.2753
130	.2725	.2698	.2671	.2645	.2618	.2592	.2567	.2541	.2516	.2491
140	.2466	.2441	.2417	.2393	.2369	.2346	.2322	.2299	.2276	.2254
150	.2231	.2209	.2187	.2165	.2144	.2122	.2101	.2080	.2060	.2039
160	.2019	.1999	.1979	.1959	.1940	.1920	.1901	.1882	.1864	.1845
170	.1827	.1809	.1791	.1773	.1755	.1738	.1720	.1703	.1686	.1670
180	.1653	.1637	.1620	.1604	.1588	.1572	.1557	.1541	.1526	.1511
190	.1496	.1481	.1466	.1451	.1437	.1423	.1409	.1395	.1381	.1367
200	.1353	.1340	.1327	.1313	.1300	.1287	.1275	.1262	.1249	.1237
210	.1225	.1212	.1200	.1188	.1177	.1165	.1153	.1142	.1130	.1119
220	.1108	.1097	.1086	.1075	.1065	.1054	.1044	.1033	.1023	.1013
230	.1003	.0993	.0983	.0973	.0963	.0954	.0944	.0935	.0926	.0916
240	.0907	.0898	.0889	.0880	.0872	.0863	.0854	.0846	.0837	.0829
250	.0821	.0813	.0805	.0797	.0789	.0781	.0773	.0765	.0758	.0750
260	.0743	.0735	.0728	.0721	.0714	.0707	.0699	.0693	.0686	.0679
270	.0672	.0665	.0659	.0652	.0646	.0639	.0633	.0627	.0620	.0614
280	.0608	.0602	.0596	.0590	.0584	.0578	.0573	.0567	.0561	.0556
290	.0550	.0545	.0539	.0534	.0529	.0523	.0518	.0513	.0508	.0503
300	.0498	.0493	.0488	.0483	.0478	.0474	.0469	.0464	.0460	.0455
310	.0450	.0446	.0442	.0437	.0433	.0429	.0424	.0420	.0416	.0412

TABLE 9-30 Factors for Continuous Discounting (Concluded)

R × T	0	1	2	3	4	5	6	7	8	9
Instantaneous										
320	.0408	.0404	.0400	.0396	.0392	.0388	.0384	.0380	.0376	.0373
330	.0369	.0365	.0362	.0358	.0354	.0351	.0347	.0344	.0340	.0337
340	.0334	.0330	.0327	.0324	.0321	.0317	.0314	.0311	.0308	.0305
350	.0302	.0299	.0296	.0293	.0290	.0287	.0284	.0282	.0279	.0276
360	.0273	.0271	.0268	.0265	.0263	.0260	.0257	.0255	.0252	.0250
370	.0247	.0245	.0242	.0240	.0238	.0235	.0233	.0231	.0228	.0226
380	.0224	.0221	.0219	.0217	.0215	.0213	.0211	.0209	.0207	.0204
390	.0202	.0200	.0198	.0196	.0194	.0193	.0191	.0189	.0187	.0185
400	.0183	.0181	.0180	.0178	.0176	.0174	.0172	.0171	.0169	.0167
Declining Uniformly to 0										
0	1.0000	.9968	.9934	.9902	.9867	.9836	.9803	.9771	.9739	.9707
10	.9675	.9643	.9612	.9580	.9549	.9518	.9487	.9457	.9426	.9396
20	.9365	.9335	.9305	.9275	.9246	.9216	.9187	.9158	.9129	.9100
30	.9071	.9042	.9013	.8985	.8957	.8929	.8901	.8873	.8845	.8817
40	.8790	.8763	.8735	.8708	.8681	.8655	.8628	.8601	.8575	.8549
50	.8522	.8496	.8470	.8445	.8419	.8393	.8368	.8343	.8317	.8292
60	.8267	.8242	.8218	.8193	.8169	.8144	.8120	.8096	.8072	.8048
70	.8024	.8000	.7977	.7953	.7930	.7906	.7883	.7860	.7837	.7814
80	.7792	.7769	.7746	.7724	.7702	.7679	.7657	.7635	.7613	.7591
90	.7570	.7548	.7526	.7505	.7484	.7462	.7441	.7420	.7399	.7378
100	.7358	.7337	.7316	.7296	.7275	.7255	.7235	.7215	.7195	.7175
110	.7155	.7135	.7115	.7096	.7076	.7057	.7038	.7018	.6999	.6980
120	.6961	.6942	.6923	.6905	.6886	.6867	.6849	.6830	.6812	.6794
130	.6776	.6757	.6739	.6721	.6704	.6686	.6668	.6650	.6633	.6615
140	.6598	.6581	.6563	.6546	.6529	.6512	.6495	.6478	.6461	.6445
150	.6428	.6411	.6395	.6378	.6362	.6345	.6329	.6313	.6297	.6281
160	.6265	.6249	.6233	.6217	.6202	.6186	.6170	.6155	.6139	.6124
170	.6109	.6093	.6078	.6063	.6048	.6033	.6018	.6003	.5988	.5973
180	.5959	.5944	.5929	.5915	.5900	.5886	.5872	.5857	.5843	.5829
190	.5815	.5801	.5787	.5773	.5759	.5745	.5731	.5718	.5704	.5690
200	.5677	.5663	.5650	.5636	.5623	.5610	.5596	.5583	.5570	.5557
210	.5544	.5531	.5518	.5505	.5492	.5480	.5467	.5454	.5442	.5429
220	.5417	.5404	.5392	.5379	.5367	.5355	.5342	.5330	.5318	.5306
230	.5294	.5282	.5270	.5258	.5246	.5234	.5223	.5211	.5199	.5188
240	.5176	.5165	.5153	.5142	.5130	.5119	.5108	.5096	.5085	.5074
250	.5063	.5052	.5041	.5029	.5018	.5008	.4997	.4986	.4975	.4964
260	.4953	.4943	.4932	.4922	.4911	.4900	.4890	.4879	.4869	.4859
270	.4848	.4838	.4828	.4818	.4807	.4797	.4787	.4777	.4767	.4757
280	.4747	.4737	.4727	.4717	.4707	.4698	.4688	.4678	.4669	.4659
290	.4649	.4640	.4630	.4621	.4611	.4602	.4592	.4583	.4574	.4564
300	.4555	.4546	.4537	.4527	.4518	.4509	.4500	.4491	.4482	.4473
310	.4464	.4455	.4446	.4438	.4429	.4420	.4411	.4402	.4394	.4385
320	.4376	.4368	.4359	.4351	.4342	.4334	.4325	.4317	.4308	.4300
330	.4292	.4283	.4275	.4267	.4259	.4251	.4242	.4234	.4226	.4218
340	.4210	.4202	.4194	.4186	.4178	.4170	.4162	.4154	.4147	.4139
350	.4131	.4123	.4115	.4108	.4100	.4092	.4085	.4077	.4070	.4062
360	.4055	.4047	.4040	.4032	.4025	.4017	.4010	.4003	.3995	.3988
370	.3981	.3973	.3966	.3959	.3952	.3945	.3937	.3930	.3923	.3916
380	.3909	.3902	.3895	.3888	.3881	.3874	.3867	.3860	.3854	.3847
390	.3840	.3833	.3826	.3820	.3813	.3806	.3799	.3793	.3786	.3779
400	.3773	.3766	.3760	.3753	.3747	.3740	.3734	.3727	.3721	.3714

SOURCE: Adapted and abridged from Couper, 2003.

should be replaced like for like or whether an alternative should be chosen that may be different in cost and/or efficiency. If the replacement is due to technical obsolescence, the timing of the replacement may be important, especially if a plant expansion may be imminent in the near future. Whatever the situation, the replaced item should not present a bottleneck to the processing. The engineer should understand replacement theory to determine if alternative equipment is adequate for the job but with different costs and timing.

Certain terminology has been developed to identify the equipment under consideration. The item in place is called the *defender*, and the candidate for replacement is called the *challenger*. This terminology and methodology was reported by E. L. Grant and W. G. Ireson in *Engineering Economy*, Wiley, New York, 1950. To apply this method, there are certain rules. The value of the defender asset is a sunk cost and is irrelevant except insofar as it affects cash flow from depreciation for the rest of its life and a tax credit for the book loss if it is

replaced sooner than its depreciation life. A capital cost for the defender is the net capital recovery forgone and the tax credit from the book loss of the defender asset that was not realized. The UAC method will be used and will be computed for each case, using the time period most favorable to each. For the defender it is 1 year and for the challenger it is the full economic life. The UAC for the challenger is handled in the same manner as in the comparison of alternatives. The method is demonstrated in Example 11.

Example 11: Replacement Analysis A 3-year-old reciprocating compressor is being considered for replacement. Its original cost was \$150,000, and it was being depreciated over a 7-year period by the straight-line method. If it is replaced now, the net proceeds from its sale are \$50,000, and it is believed that 1 year from now they will be \$35,000. A new centrifugal compressor can be installed for \$160,000, which would save the company \$2000 per year in operating expenses for the 10-year life. At the end of the 10th year, its net proceeds are estimated to be zero. The 7-year depreciation applies also to the centrifugal

compressor. A 35 percent tax rate may be assumed. The company requires a 15 percent after-tax return on an investment of this type. Should the present compressor be replaced now?

Solution: The UAC method will be used as a basis for comparison. It is assumed that all money flows are continuous, and continuous interest will be used.

Defender case: The basis for this unit will be 1 year. If it is not replaced now, the rules listed above indicate that there is an equivalent of a capital cost for two benefits forgone (given up). They are

1. Net proceeds now at 3 years of \$50,000
2. Tax credit for the loss not realized

Thus net loss forgone = book value at the end of 3 years minus net capital recovery, or

$$NLF_3 = BV_3 - NCR_3$$

where NLF_3 = net loss forgone at end of 3 years
 BV_3 = book value at end of 3 years
 NCR_3 = net capital recovery at end of 3 years

$$NLF_3 = \$150,000 \left(1 - \frac{1}{7}\right) - \$50,000 = \$35,714$$

$$\text{Depreciation for 4th year} = \$150,000 \left(\frac{1}{7}\right) = \$21,429$$

$$NLF_4 = BV_4 - NCR_4 = \$150,000 \left(1 - \frac{4}{7}\right) - \$35,000 = \$29,286$$

Year	Item	Cash flow, \$	Factor	PW, \$
At 0 ^e	Tax credit for net loss forgone	(0.35)(-35,714)	1.0	-12,500
At 0 ^e	Net cash recovery forgone	-50,000	1.0	-50,000
0-1	Contribution to CF from depreciation	(0.35)(-21,429)	0.9286 ^b	6,965
0-1	Contribution to CF from operating expense	(1 - 0.35)(-15,000)	0.9286 ^b	-9,054
End 1	Tax credit for net loss	(0.35)(29,286)	0.8607 ^c	8,822
End 1	Net cash	35,000	0.8607 ^c	30,125
			NPW	-25,642

^aFor the defender case, 0 year is the end of the third year.
^bFrom Table 9-30, uniform section, for the argument $R \times T = 15 \times 1 = 15$.
^cFrom Table 9-30, instantaneous section, for the argument $R \times T = 15 \times 1 = 15$.

$$UAC = \frac{NPW}{(\text{years of life})(\text{uniform factor})} = \frac{-\$25,642}{(1)(0.9286)} = -\$27,614$$

Challenger case:

Year	Item	Cash flow, \$	Factor	PW, \$
0	First cost	-160,000	1.0	-160,000
0-7	Contribution to CF from depreciation	(0.35)(160,000)	0.6191 ^d	56,000
0-10	Contribution	(1 - 0.35)(10)(-13,000)	0.5179 ^e	-43,763
			NPW	-147,763

^dFrom Table 9-30, uniform section, $R \times T = 15 \times 7 = 105$.
^eFrom Table 9-30, uniform section, $R \times T = 15 \times 10 = 150$.

$$UAC = \frac{NPW}{(\text{years of life})(\text{uniform factor})} = \frac{-\$147,763}{(10)(0.5179)} = -\$28,531$$

The UAC for the defender case is less negative (more positive) than that for the challenger case; therefore, the defender should not be replaced now. But there will be a time in the near future when the defender should be replaced, as maintenance and deterioration will increase.

OPPORTUNITY COST

Opportunity cost refers to the cost or value that is forgone or given up because a proposed investment is undertaken, often used as a base case. Perhaps the term should be *lost opportunity*. For example, the profit from production in obsolete facilities is an opportunity cost of

replacing them with more efficient ones. In cost analysis on investments, an incremental approach is often used, and if it is applied properly, the correct cost analysis will result.

ECONOMIC BALANCE

An engineering cost analysis can be used to find either a minimum cost or a maximum profit for a venture. This analysis is called an *economic balance* since it involves the balancing of economic factors to determine optimum design or optimum operating conditions. Such an analysis involves *engineering tradeoffs*. It may be more beneficial to invest more capital to reduce operating expenses or, conversely, incur more operating expenses without the addition of costly capital. An economic balance, then, is a study of all costs, expenses, revenues, and savings that pertain to an operation or perhaps an equipment item size. In this presentation, certain terminology is used; e.g., the term *cost* refers to a one-time purchase of capital equipment. A recurring expense is called an *operating expense*, such as utilities, labor, and maintenance. All costs and operating expenses are related to an arbitrarily designated *controllable* variable such as heat exchanger area, thickness of insulation, or number of units.

There are certain practical considerations that must be recognized in attempting to find the best or optimum condition. Occasionally, a solution may lead to a result for which industrial equipment is not available in the optimum size; therefore, engineering judgment must be exercised. A smaller-diameter pipe might lead to a higher pumping expense but lower pipe costs while a larger-diameter pipe would result in lower pumping expense but higher capital cost. The engineer then encounters an engineering tradeoff that must be resolved.

The essential elements of an economic balance are

- Fixed and variable expenses
 - An allowance for depreciation
 - An acceptable return on the investment
- A total expense equation is

$$TE = FE + VE \tag{9-24}$$

where TE = total expenses
 FE = fixed expenses
 VE = variable expenses

The guidelines for solving a single-variable economic balance consist of the following steps:

1. Determine all expenses that vary as the controllable variable changes and that need to be considered in the balance.
2. Determine whether any operating limitations exist, such as pressure drop in columns where flooding occurs or limiting heads for pipelines for gravity flow.
3. Mathematically express the expenses as a function of the variables related to the equipment; otherwise use variables that define the operation such as temperature, pressure, and concentration. The final expression should include all pertinent expenses, eliminating those that are not significant. Frequently only one variable is used.
4. Ascertain if the optimum size must be one of a number of discrete sizes commercially available or whether it can be any size.
5. Solve the total expense equation either analytically or graphically.

The solution to Eq. (9-24) may be found analytically or graphically. In the analytical method, the fixed and variable expenses are related in equation format to the controllable variable. Example 12 is an engineering balance example of this method. Equation (9-24) can be differentiated with respect to the controllable variable and that result set equal to zero to find the optimum condition. A graphical method involves determining the fixed and variable expenses for a range of equipment sizes. A plot of TE , FE , and VE as a function of the controllable sizes yields a plot identifying the optimum. Figure 9-18 is a graphical solution to the TE equation. Should the optimum result fall between two commercial sizes, then the engineer must exercise judgment in the tradeoff.

Example 12: Optimum Number of Evaporator Effects Determine the number of evaporator effects for the minimum total annual operating

9-40 PROCESS ECONOMICS

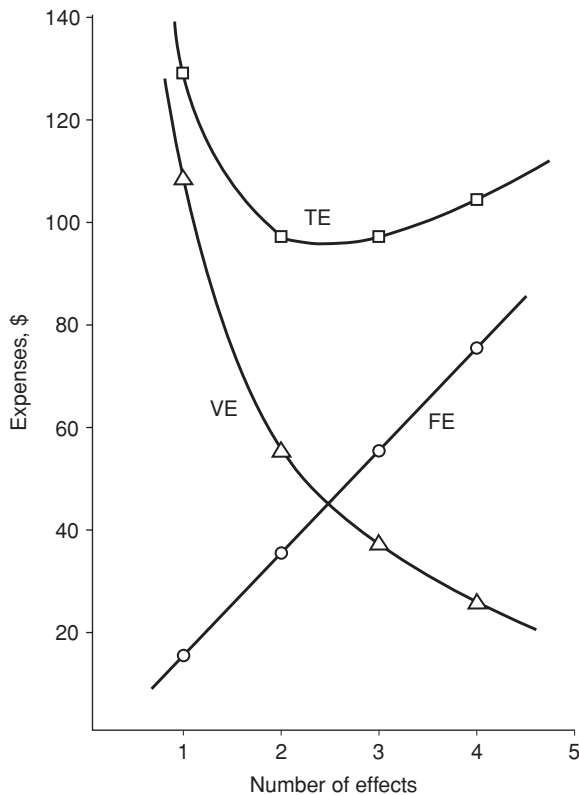


FIG. 9-18 Optimum number of evaporator effects in Example 12.

expense of a small evaporator system to concentrate a colloidal suspension. Steam costs \$3.00 per million Btu (MBtu), and each pound of steam will evaporate 0.8N lb water, with N being the number of effects. The total capital cost of each effect is \$40,000 and has an estimated life of 10 years. The annual maintenance expense is 10 percent of the capital cost. Labor and other expenses not mentioned may be considered to be independent of the number of effects. The system will operate 300 days/yr with 100,000,000 Btu/day evaporator duty. Depreciation on the equipment is by 7-year straight-line method, and the tax rate is 35 percent. Annual net profit after taxes on the investment must be 15 percent for the installed equipment.

Basis: 1 year of operation, duty 10^8 Btu/day. Let N equal the number of effects.

Solution:

Analytical method:

Annual fixed expenses = FE

$$FE = \$40,000N \left(0.143 + 0.100 + \frac{0.15}{1 - 0.35} \right) = \$18,960N$$

dep. maint. profit (return)

Annual variable expenses VE in this example are essentially the steam expenses, and all other variable expenses do not enter into the equation. Therefore

$$VE = 10^8 \text{ Btu/day} \times 300 \text{ day/yr} \times \$3.00/10^6 \text{ Btu} \times 1/(0.8N) = \frac{\$112,500}{N}$$

$$TE = FE + VE = \$18,960N + \frac{\$112,500}{N}$$

Take the derivative of TE with respect to N and set the result equal to zero.

$$\frac{d(TE)}{dN} = 18,960 - \frac{112,500}{N^2} = 0 \quad N = 2.44 \text{ effects}$$

Therefore 3 effects are required.

Graphical method: Assume the number of effects and calculate the fixed, variable, and total expenses for effect.

N	18,960N	112,500/N	TE
1	\$18,960	\$112,500	\$131,460
2	37,920	56,250	94,210
3	56,880	37,500	94,380
4	75,840	28,125	103,965

The minimum TE occurs between 2 and 3 effects, but 3 effects are recommended to evaporate the colloidal solution. Figure 9-18 is a plot of the graphical solution.

In another example involving the reclaiming of a product using an evaporator and a dryer in series, the product is pumped from the discharge of the evaporator to the dryer. See Fig. 9-19. An economic analysis indicated that a 55 percent slurry is optimum, but perhaps such a slurry is too thick to be pumped. Therefore, engineering judgment must be exercised. The slurry was pumped not at 55 percent but at a lesser concentration of 50 percent, although it was not optimum.

When more than one controllable variable affects the economic balance, the solution approach is essentially the same as that for the single-variable case, but determining the optimum is tedious.

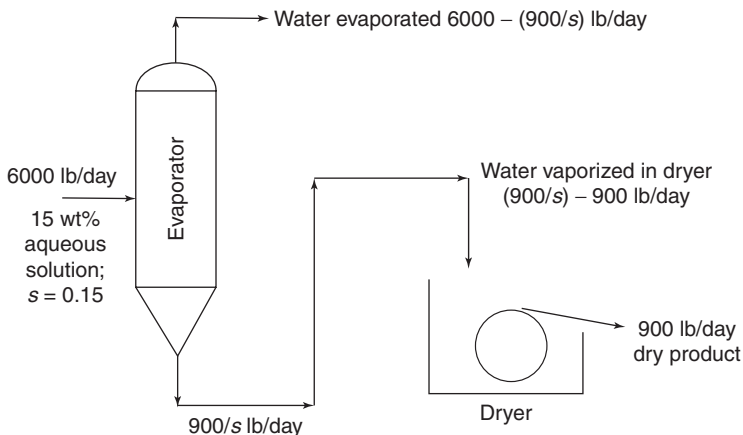


FIG. 9-19 Evaporator-dryer system. (Source: Adapted from Couper, 2003.)

INTERACTIVE SYSTEMS

If the TE does not pass through a minimum or maximum, but continues to decline or to increase with the number of equipment items or equipment size, the next step is to look at the flow sheet for equipment upstream or downstream from the selected item. It may be necessary to group two or more items and treat them as one in the analysis. Such a system is said to be *interactive*, since more than one item affects the optimum results. An example of such an interactive system is the

removal of nitrogen from helium in a natural gas stream. Carbon adsorption is a method for removing nitrogen, but compressors are also required since this is a high-pressure process. If one attempts to find the optimum operating pressure, optimizing on compressor pressure will not result in an optimum condition; and conversely, optimizing on the size of the carbon bed will not yield an optimum. This is an example of an interactive system. Therefore, to find the optimum pressure, both the size of the carbon bed and the compressor pressure must be considered together.

CAPITAL PROJECT EXECUTION AND ANALYSIS

The demands made on business organizations with the arrival of global free trade have made sophisticated management of capital projects, for the purposes of minimizing capital costs and maximizing project profitability, a necessity. Two elements of such sophisticated project management practice are *front-end loading (FEL)* and *value-improving practices (VIPs)*. These two management practices are, and must be, closely integrated activities, as seen in Fig. 9-20. As shown, they are performed during the early stages of a project life cycle, when they can be, and are, effective at influencing a project's profitability. However, they have very different characteristics, as are detailed in the following sections. Properly performed together, FEL and VIPs maximize project profitability by ensuring that all matters that influence project profitability are considered in the most productive manner and at the most optimal time.

FRONT-END LOADING

GENERAL REFERENCES: Porter, James B., E. I. DuPont de Nemours and Company, DuPont's Role in Capital Projects, Proceedings of Government/Industry

Forum: The Owner's Role in Project Management and Pre-project Planning, 2002. Smith, C. C., Improved Project Definition Insures Value-added Performance—Part 1, *Hydrocarbon Processing*, August 2000, pp. 95-99. KBR Front-end Loading Program, data compiled from selected large projects from 1993 through 2003, <http://www.halliburton.com/kbr/index.jsp>. Merrow, E. W., Independent Project Analysis, Inc., 32d Annual Engineering & Construction Contracting Conference, Sept. 28-29, 2000. Merrow, E. W., Independent Project Analysis, Inc., 30th Annual Engineering & Construction Contracting Conference, September 1998. HPI Impact, *Hydrocarbon Processing*, August 2002, p. 23, data obtained from Independent Project Analysis, Inc. PDRI: Project Definition Rating Index— Industrial Projects, p. 5, Construction Industry Institute (CII), University of Texas at Austin, <http://construction-institute.org>, July 1996. Merrow, E. W., Independent Project Analysis, Inc., 32d Annual Engineering & Construction Contracting Conference, Sept. 28-29, 2000.

Introduction Front-end loading (FEL) is the process by which a company develops a detailed definition of the scope of a capital project that meets corporate business objectives. The term *front-end loading* was first coined by the DuPont company in 1987 and has been used throughout the chemical, refining, and oil and gas industries ever since (Porter, James B., E. I. DuPont de Nemours and

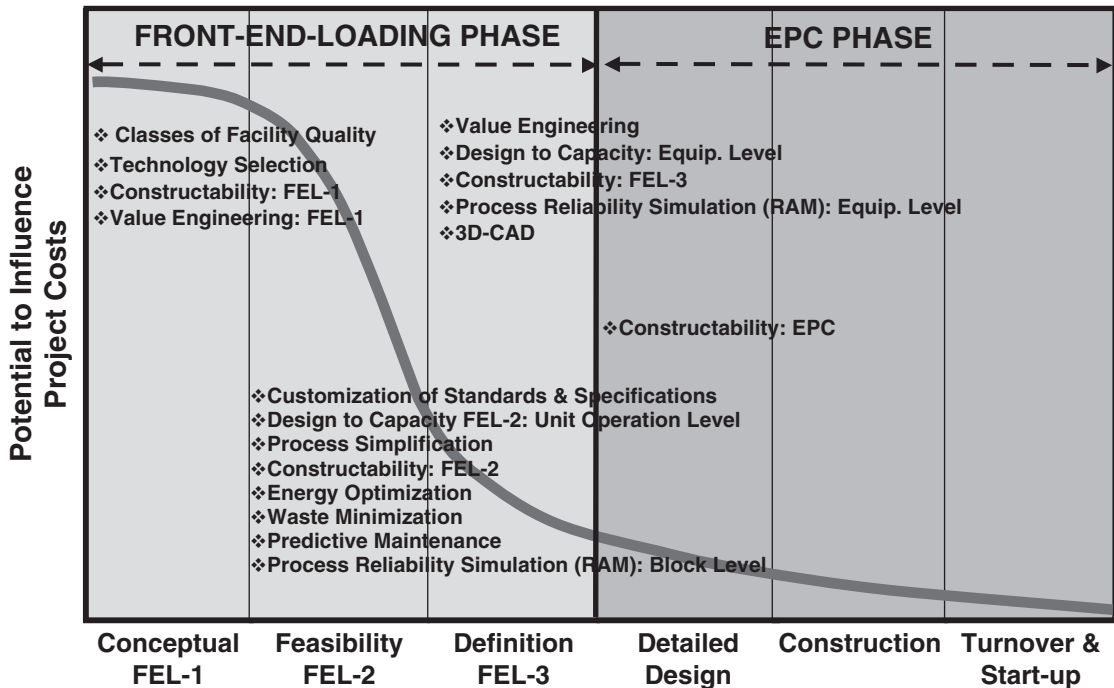


FIG. 9-20 Front-end loading and the implementation of value-improving practices.

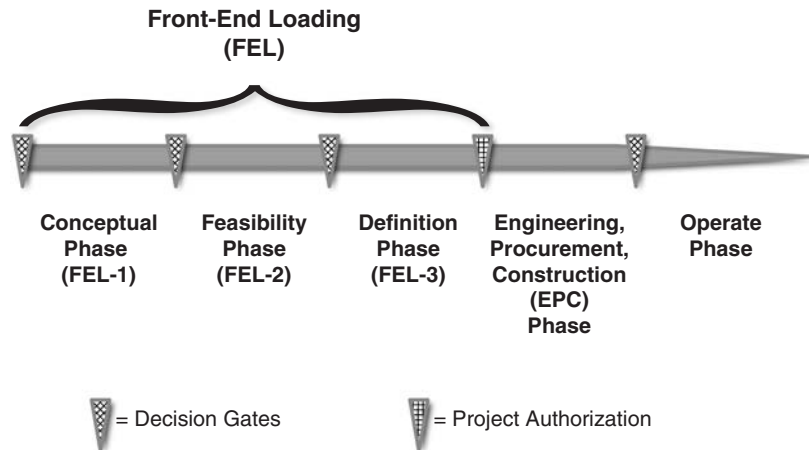


FIG. 9-21 FEL in the capital project life cycle.

Company). The product of the FEL process is a design-basis package of customized information used to support the production of detailed engineering design documents. Completion of the FEL design-basis package typically coincides with project AFE (Authorization for Expenditure) or project authorization. Project authorization is that point in the project life cycle where the owner organization commits the majority of the project's capital investment and contracts.

FEL starts when an idea for a project is first conceived by a research and development group, project engineering group, plant group, or business unit. FEL activity continues until the project is authorized. After initial conception of an idea, organized interaction is required among the various project stakeholders to assemble the project design-basis package for subsequent authorization.

Within the FEL phases, decision points are formally established by the operating company authorizing the initiation of a capital project development effort. These formal decision gates allow for continuity across the enterprise for authorization of additional funding for the next phase of engineering and project definition. Figure 9-21 illustrates the typical decision gates or stage gates for capital projects.

When the level of project definition is sufficient to support a definitive cost estimate for both the entire project and its projected rate of return, major project funding is authorized for expenditure. This is the conclusion of the FEL process and any significant involvement of the process design engineer. Not until the conclusion of the engineering, procurement, and construction (EPC) phase does the process engineer again become involved. At this time, commissioning and start-up become the focus where the validation occurs for all that was done in the FEL phases many months earlier.

Differing terminology used by companies, engineers, and project management teams is often a point of confusion. Most people seem to think they know what all the terms mean. This is never the case. Confirmation of which terminology will be used by all involved in the project is a must. Nearly every operating company and engineering contractor use differing terminology. FEL terminology is often misunderstood and further confused by differing references to which FEL phase the project is actually in. Figure 9-22 provides some idea of the differing terminology for each project phase used by only a few major oil and gas and chemical companies today. These terms change periodically, so diligence in confirming such terminology is a key task for the process engineers to finish, before beginning their work.

The influence of changes on capital projects is considerably affected by when those changes occur. The earlier a change is considered and incorporated into the project scope, the greater its potential influence on the project's profitability and the greater the ease of

incorporating the change. This means that late changes (e.g., in the EPC phase) are far more expensive to implement and are considered very undesirable. Late changes which are potentially advantageous are often not implemented because the cost to implement the change exceeds the benefits of doing so. Conversely, the cost to implement a change at the earlier phases of the project is far lower than making the same change after detailed engineering is underway.

Figure 9-23 shows how quickly this influence curve changes as the typical project progresses (Smith, C. C., *Improved Project Definition Insures Value-added Performance—Part 1*). This is why proactively seeking changes during FEL is far more advantageous to profitability than is allowing those needed changes to be "discovered" during later project phases. This also means that potentially beneficial changes (value improvements) must be sought during FEL, or else they stand a good chance of not being cost-effective to implement during the EPC phase. This is also why seeking operations, maintenance, and construction experience during FEL offers significant profitability advantages over practices which bring such experience onto the project team following FEL.

Characteristics of FEL Front-end loading is a specialized and adaptable work process. This work process translates financial and marketing opportunities to a technical reality in the form of a capital project. It is particularly important that the project be defined in sufficient detail by the engineering deliverables, which are generated by the FEL work process, prior to the point where major funds are authorized. In this manner, overall project risks are identified and sufficiently mitigated to have project funding approved. To achieve this important level of definition, critical decisions must be made and adhered to. In addition, the FEL project team should proactively seek value improvement alternatives and challenge the project premises, scope, and design until such time as implementation of those alternatives loses their profitability and/or technical advantage. By doing so, such value improvements will not develop into costly corrections, which surface later, during the EPC phase.

Goals and Objectives of FEL The FEL work process must enable nearly constant consideration of changes as the work progresses. FEL phases must consider the long-term implications of every aspect of the design. Predictability of equipment and process system life cycle costs must always be balanced with operations and maintenance preferences, as well as the need for the project to maintain its profitability or ROI (return on investment). Additional important goals and objectives of FEL projects are as follows:

- Develop a well-defined and acceptably profitable project.
- Define the primary technical and financial drivers for capital project investment.

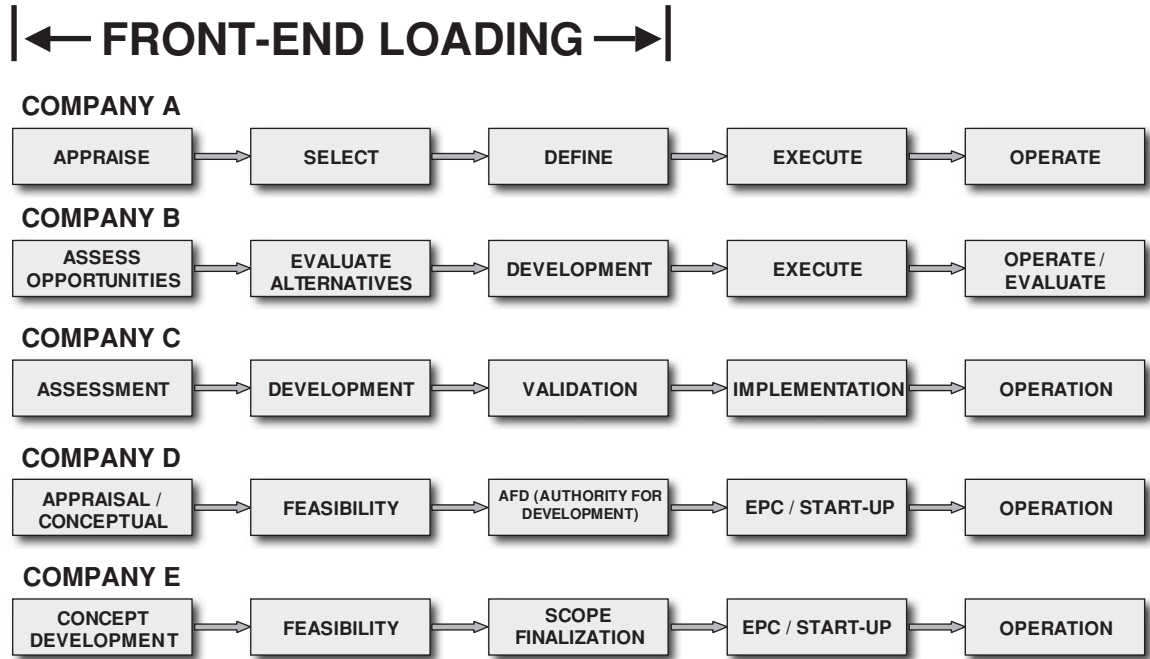


FIG. 9-22 Project life cycle terminology.

- Challenge baseline premises, and purposely seek out and evaluate alternatives and opportunities.
- Minimize changes during the EPC, turnover, and start-up phases.
- Reduce project schedule and capital cost.
- Reduce the business and project execution risk.
- Balance project technical, financial, and operational profitability drivers.

Comparison of FEL Projects with EPC Projects FEL projects are very different from EPC projects. Engineers and project managers having significant experience only with projects in the EPC phase often are unfamiliar with the significant differences between the philosophies and challenges of the FEL phase and the EPC phase of projects. One of the most important (but most subtle) aspects of FEL is the demand during FEL for more highly experienced staff and

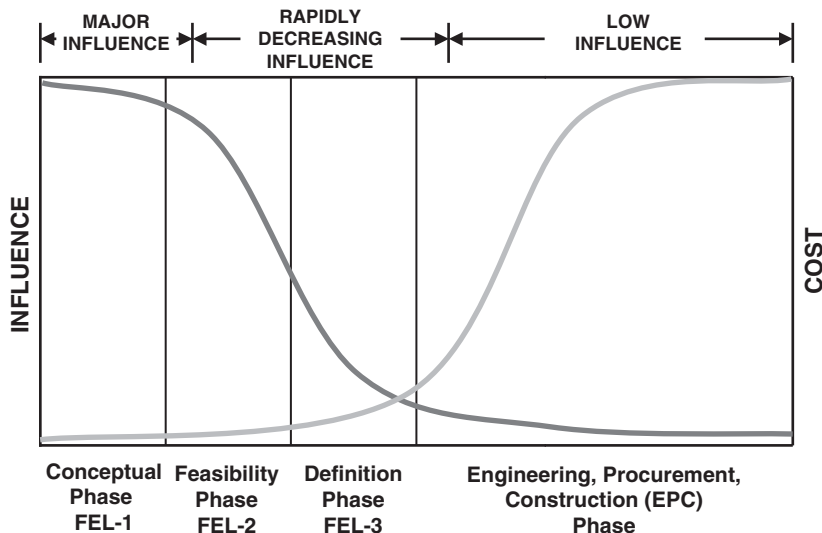


FIG. 9-23 Project life cycle cost-influence curve.

	FEL	EPC
Project State	Undefined	Defined
Changes	Actively Seeks Changes	Actively Resists Changes
Impact of Change	Low	High
Opportunity for Change	High	Low
Contract Type	Typically Reimbursable	Typically Lump Sum
Value Improvement Potential	High	Low
Client Participation	Encouraged	Discouraged
Philosophy	Information-Driven	Deliverable-Driven

FIG. 9-24 FEL projects versus EPC projects.

more sophisticated analysis tools, as compared to EPC projects which have achieved a well-defined project prior to authorization. This is so because of the need in FEL to create, analyze, and implement improvements to what many might consider a “good” design.

In spite of its relatively short duration, FEL proactively seeks to implement the best possible design. The nearly constantly changing environment requires people of many different disciplines and functions to work together to communicate effectively. A well-integrated team always seems to perform best during FEL, if FEL has well-established, informal, and personal interfaces between project groups and organizations. The following describes how the FEL phase is distinguished from the EPC phase:

- FEL proactively seeks data, resources, support, and decision making.
- Projects in the FEL phase place a higher level of importance on close and effective owner-contractor management interfaces.
- FEL demands continuous realignment of client desires and requirements with contractor needs.
- FEL requires greater development of personal relationships that result in respect and trust.
- FEL demands significantly higher frequency of feedback of owner satisfaction.
- FEL emphasizes elimination of low- or zero-value scope.
- FEL improves the capital productivity of projects by using best-available technology.
- FEL focuses on overall project profitability rather than on only cost, schedule, and workhours.
- FEL focuses almost entirely on the owner’s business needs.

Figure 9-24 lists further differences between FEL and EPC projects. Understanding these many differences is very important to the process engineer, in that awareness of them, and the driving forces behind them, will prepare the chemical engineer for the challenging and rewarding environment of FEL projects.

Parameters of FEL Phases Important aspects of each phase of FEL are cost estimate accuracy, cumulative engineering hours spent, and the contingency assigned to the cost estimate. Figure 9-25 lists the typical parameters encountered industrywide (KBR Front-end Loading Program, data compiled from selected large projects from 1993 through 2003). For the capital cost estimate, each operating company may request a slightly different accuracy, which is often project-specific. What is important is the level of engineering required to support such estimating accuracy. This determination is the responsibility of both the owner and the engineering contractor. Agreement on this is critical prior to initiating project work.

The engineering hours spent during each phase of FEL vary widely between small and large projects. This is also true for those projects where new or emerging technology is being applied or where higher

throughput capacities are being applied than previously commercially demonstrated. Projects such as these may require additional engineering to achieve the desired estimate accuracy and project contingency.

FEL Project Performance Characteristics Overall project performance can be enhanced by ensuring that the following characteristics are emphasized during the FEL phases.

- Methodical business and project execution planning is necessary.
- Effective integration of workforce between owner and contractor staff is important.
- Projects with an integrated management team (owner and engineering contractor) have the lowest number of design changes at any project stage.
- Engineering contractor should be brought into project in early FEL phases.
- Clear roles must exist for project team members that relate to the expertise of both owner and contractor staff.
- Effective personal communication is required between owner and contractor organizations and their project team representatives, ensuring extensive site and manufacturing input.
- Schedule and cost goals are set by integrated business and technical project team composed of owner and contractor representatives.

Figure 9-26 illustrates the benefit of good FEL performance on project costs (Merrow, E. W., Independent Project Analysis, Inc., 32d Annual Engineering & Construction Contracting Conference, Sept. 28–29, 2000). Figure 9-27 illustrates the benefit of good FEL performance on critical path schedule (Merrow, E. W., Independent

	FEL-1 (CONCEPTUAL)	FEL-2 (FEASIBILITY)	FEL-3 (DEFINITION)
Cost Estimate Accuracy	±40%	±25%	±10%
Cumulative Engineering Hours Spent	1–5%	5–15%	15–30%
Contingency	15–20%	10–15%	8–12%

FIG. 9-25 Parameters of FEL phases.

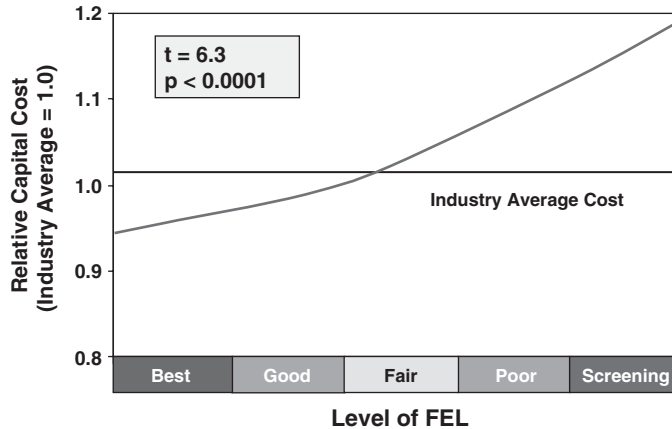


FIG. 9-26 FEL drives better cost performance.

Project Analysis, Inc., 32d Annual Engineering & Construction Contracting Conference, Sept. 28–29, 2000). IPA statistics indicate that significant project financial and schedule benefits can be realized by implementing a thorough FEL effort prior to the EPC phase.

Figure 9-28 presents the benefits of having an integrated project team during FEL on the overall project performance. This performance impacts overall project costs as well as schedule and operability. An integrated project team produces fewer late changes. This means lower capital costs, better and more predictable schedules, and a slightly better operability, as compared statistically to similar projects lacking an integrated management team (Merrow, E. W., Independent Project Analysis, Inc., 30th Annual Engineering & Construction Contracting Conference, September 1998).

In addition, project data indicate that a well-integrated FEL team can produce significantly better project performance in terms of lower capital investment, as compared to projects where FEL teams were not properly integrated. This illustrates the benefits for each engineering team member working closely together with each other team member, to produce the most profitable project results.

Although project teams, once integrated and functioning with clear roles and responsibilities, perform better, this edge can be quickly lost

if key members of that team are changed. The impacts of changes of project managers to a well-integrated FEL team are shown in Fig. 9-29 (HPI Impact, *Hydrocarbon Processing*, p. 23, August 2002, data obtained from Independent Project Analysis, Inc.).

Investment in FEL for Best Project Performance The cost and schedule required to optimally complete the FEL phase of a project are always under pressure and must be justified. This is especially true for “fast-track” projects where the time pressures can be significant. The Construction Industry Institute (CII) has shown that higher levels of preproject planning (i.e., front-end loading) effort can result in significant cost and schedule savings, as seen in Fig. 9-30 (PDRI: Project Definition Rating Index—Industrial Projects, Construction Industry Institute, University of Texas at Austin, July 1996). The process engineer produces the best project performance, when he or she strives, with the entire integrated FEL project team, to define the overall project (not just the process design) as well as possible, prior to AFE.

The level of definition of a project during the FEL phases has a direct influence on the project’s ultimate outcome in terms of the number and impacts of changes in the EPC phase. This level of FEL performance translates to fewer major changes in engineering, construction, and during start-up (Merrow, E. W., Independent Project

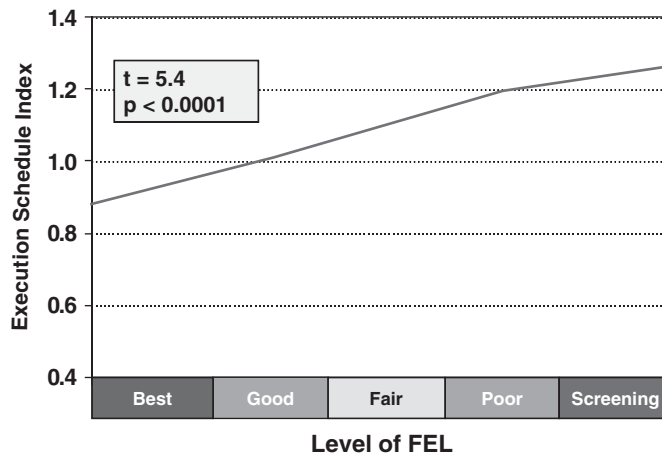


FIG. 9-27 Good FEL speeds execution time.

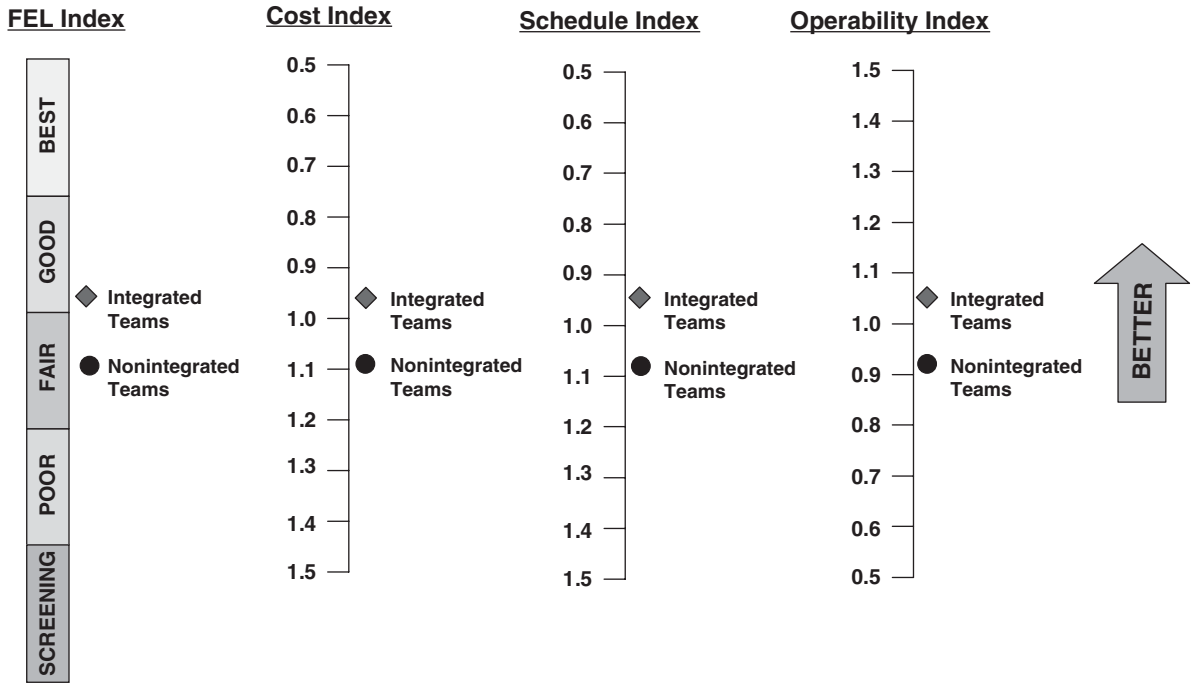


FIG. 9-28 Integrated teams result in better FEL and better overall performance.

Analysis, Inc., 32d Annual Engineering & Construction Contracting Conference, Sept. 28–29, 2000). These conclusions are depicted by Fig. 9-31. A major late change is defined by IPA's data to mean changes made after the start of detailed engineering and involving impacts greater than either 0.5 percent of the total project capital investment or 1 month in critical path project schedule.

These graphs illustrate why better project performance is produced through proactively seeking profit-improving changes as early

as possible. One of the reasons for this observation is that operation, maintenance, and construction expertise is incorporated into the project at the very beginning—during FEL.

This means that the process design engineer should be working closely with these real-world experts as they design processes and their support systems. This also means that to improve overall project performance, achieving the best practical or highest level of definition during FEL is critical. Finally, this high level of definition results in a

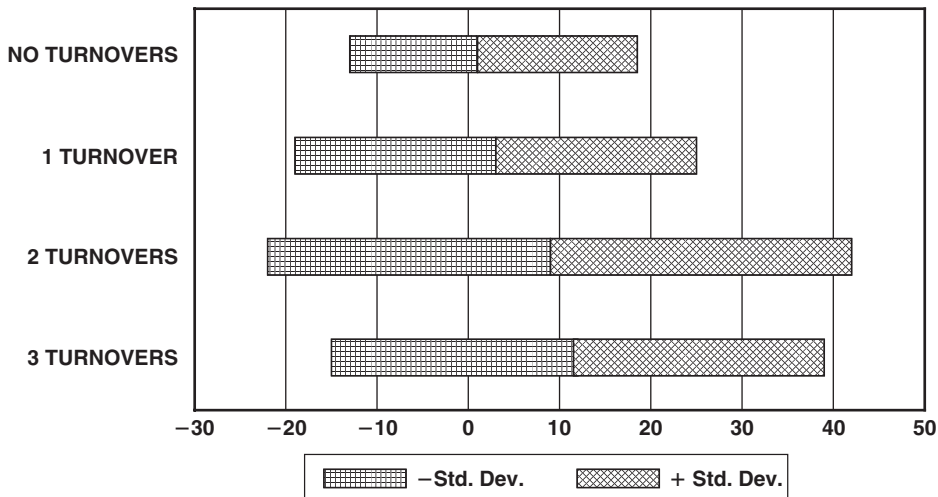


FIG. 9-29 Effects of project manager turnover on cost growth.

LEVEL OF FEL EFFORT	COST	SCHEDULE
High	-4%	-13%
Medium	-2%	+8%
Low	+16%	+26%
Difference	20%	39%

FIG. 9-30 Project performance versus level of FEL effort.

reduced number of changes during the EPC phase. These observations should be the critical goals of all project teams.

The size of capital project also has an influence on FEL outcome based on IPA statistics. IPA's data indicate that small projects benefit more from better project definition prior to the EPC phase than do major projects. The data also indicate that small projects typically have more late changes than do larger projects.

Figure 9-32 illustrates the effect of large projects versus small projects in terms of the impact of late changes (Morrow, E. W., Independent Project Analysis, Inc., 32d Annual Engineering & Construction Contracting Conference, Sept. 28-29, 2000). Figure 9-32 also illustrates that the level of FEL performance directly impacts the number of, and the consequences of, late changes made in projects of any size.

Typical FEL Deliverables Every process engineer assigned to a project should be acutely aware of which deliverables or end products are required by those who must commission their work. This should be very well understood by all parties prior to starting the work. Further, the splits of work (who will do which aspect of the work) must be well understood. Today, it is very common to have multiple operating companies form a joint venture to authorize major projects. It is also common for multiple engineering contractors to form joint ventures to execute the engineering for the FEL phases of the project.

Typical Conceptual Phase (FEL-1) Deliverables These are listed below. Each project will customize these deliverables to suit the particular needs of the project. There is no such thing as a "standard" FEL. Therefore, the process engineer must understand what the details are for each deliverable needed, what the *minimum* level is for the engineering required to meet those requirements, and in which formats that information and data will be needed.

- Strategic business assessment
- Key technology selected and risk identified
- Market assessment for feed, products, and capacity
- Potential sites identified and under evaluation
- Cost estimate (± 40 percent)
- Preliminary project milestone schedule
- Block flow diagrams completed
- Process cases identified
- Critical long-lead equipment identified
- Value-improving practices reports

Typical Feasibility Phase (FEL-2) Deliverables These are listed below. In this phase, emphasis is on determining the best technical and economic flow scheme, as well as the support systems required to provide the necessary annual production rate at the sales quality required. The focus for the process engineer should be on confirming the number and type of process and technology studies needed, as well as the number of alternate cases required to be evaluated and/or simulated.

- Strategic business assessment
- Project schedule level 1
- Cost estimate (± 25 percent)
- Overall project execution strategy
- Contracting and purchasing strategies
- Permitting and regulatory compliance plan
- Soil survey and report
- Project alternatives analysis
- Process flow diagrams for selected option(s)
- Preliminary utility flow diagrams and balances
- Preliminary equipment list and equipment load sheets
- Materials of construction
- Process hazards analysis report
- Value-improving practices reports

Typical Definition Phase (FEL-3) Deliverables These are listed below. In this phase, emphasis is typically on optimizing the best flow scheme and support systems combination. This optimum includes consideration of the plot plan and equipment arrangements for the entire facility. Process optimization cannot be done in isolation. Significant and continuous interaction with operations, maintenance, and construction experts always produces the best results. The emphasis in this phase is on achieving the best practical level of project definition and a good-quality project estimate of ± 10 percent. This level of project definition and cost estimate quality is normally required in order to present to management a candidate project which has the right combination of overall risk and projected economic performance, and thereby secure an AFE.

- Strategic business assessment
- Detailed EPC phase project execution plan
- Detailed EPC phase project master schedule

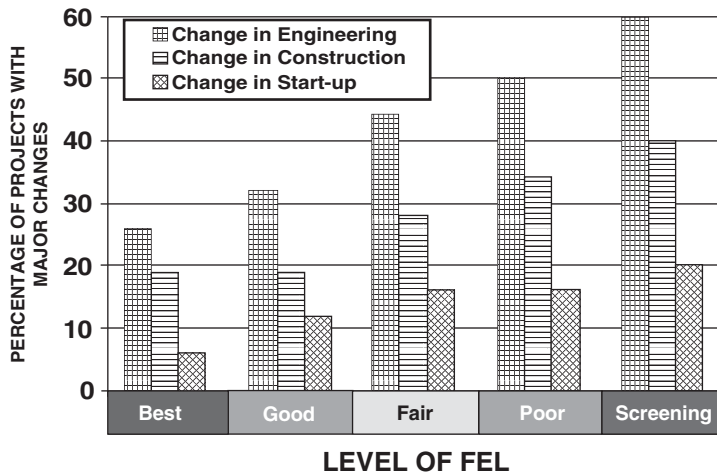


FIG. 9-31 Good FEL drives late changes down.

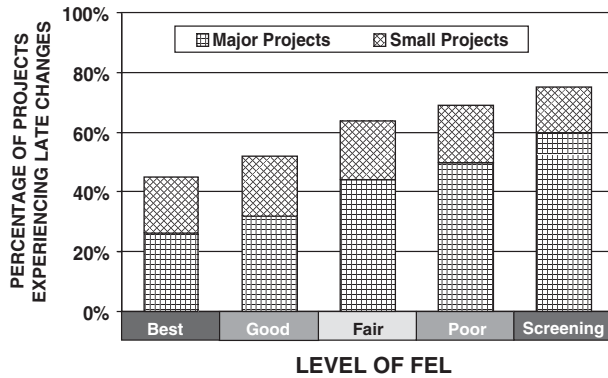


FIG. 9-32 Rate of late major changes is higher for small projects.

- Completed environment permit submittal
- Project plan/project execution plan
 - a. Cash flow plan for EPC phase
 - b. Training, commissioning, and start-up plans
 - c. Contracting plans
 - d. Materials management plan
 - e. Safety process and quality management plan
- Cost estimate (± 10 percent)
- Finalized utility flow diagrams and balances
- P&ID's—issue IPL (issue for plant layout)
- Plot plans and critical equipment layouts
- Equipment list and equipment data sheets
- Single-line electrical diagrams
- Control system summary and control room layout
- Materials of construction
- VIPs reports
- Hazard and operability studies (HAZOP) report

VALUE-IMPROVING PRACTICES

GENERAL REFERENCES: Independent Project Analysis, Inc. (IPA), <http://www.ipaglobal.com>. The Construction Industry Institute (CII), University of Texas at Austin, <http://construction-institute.org>. Lavingia, Jr., N. J., Improve Profitability Through Effective Project Management and TCM, 36th Annual Engineering & Construction Contracting Conference, Sept. 4, 2003. KBR Value Improving Practices Program, 1995 through 2005, <http://www.halliburton.com/kbr/index.jsp>. PDRI: Project Definition Rating Index—Industrial Projects, Construction Industry Institute (CII), University of Texas at Austin, <http://construction-institute.org>, July 1996. Society of American Value Engineers International (SAVE), <http://www.value-eng.org>. KBR experience.

Introduction Value-improving practices (VIPs) are formal structured practices applied to capital projects to improve profitability (or “value”) above that which is attained through the application of proven good engineering and project management practices. VIPs are formal analyses of project characteristics and features performed by small multidisciplinary teams at identified optimum times during the engineering design and development of capital projects.

Application of VIPs to capital projects has been statistically proved to significantly improve project profitability according to Independent Project Analysis, Inc. (IPA) and the Construction Industry Institute (CII). IPA data presented in Fig. 9-33 have been gathered from many capital projects since 1987. These data indicate that about 2.5 percent reduction in the relative capital cost can be expected for high-performing projects due to implementation of good front-end loading, work processes. The best-performing projects are often referred to as “Best Practical” or “Best in Class” projects and represent the upper 20 percent of projects.

However, when FEL improvement is combined with rigorous application of VIPs, the project performance improves to about 10 percent in reduction of relative capital cost (Lavingia, Jr., N. J., Improve Profitability Through Effective Project Management and TCM). Experience of at least one major engineering contractor indicates that about a 20 percent capital cost improvement can be expected through judicious use of their modified VIPs (KBR Value Improving Practices Program, 1995 through 2005). These improved results come about from continual adaptation and improvement of the VIPs themselves to maintain their relevance and ability to improve projects above what the project teams can accomplish by themselves.

The VIPs that have been statistically verified by IPA benchmarking of capital projects are listed below. Each has a different purpose and focus, but all produce project profitability improvements that the project team cannot achieve on its own.

- Classes of facility quality
- Technology selection
- Process simplification
- Constructability
- Customization of standards and specifications
- Energy optimization
- Predictive maintenance
- Waste minimization
- Process reliability simulation
- Value engineering
- Design to capacity
- 3D-CAD

Selection of the most applicable VIPs to be performed during a specific project is the focus of the VIP planning session, which should be held just following project kickoff. Figure 9-34 presents the optimal times during a large project for consideration of VIPs. The duration for FEL has been assumed to be 12 months. Every project will have a

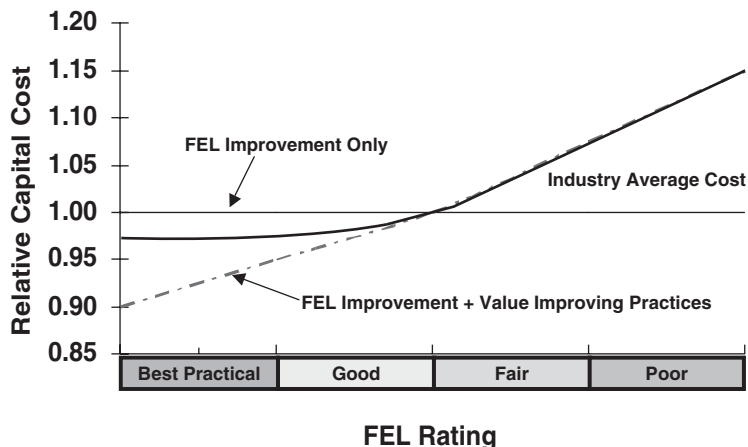


FIG. 9-33 FEL and VIPs drive lower capital investment.

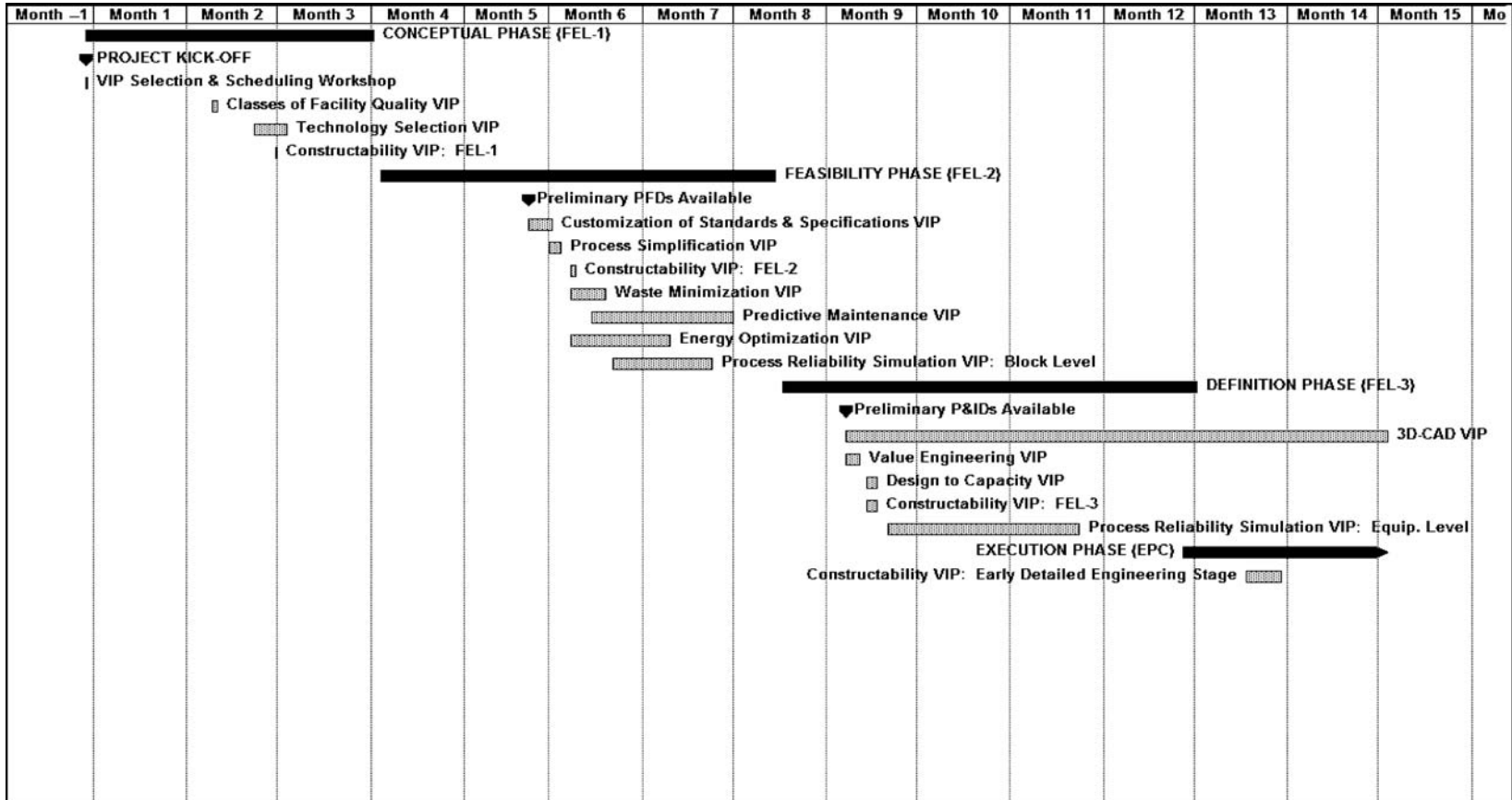


FIG. 9-34 Typical VIP implementation relationship.

unique duration for FEL with each phase dictated by the owner organization. The best times to conduct the VIP workshops should be considered at the project outset. Key anchor points for VIPs are the first appearance of the process flow diagrams (PFDs). The second anchor point for VIPs is the issue of preliminary piping and instrumentation diagrams (P&IDs).

When capital projects are benchmarked by third-party organizations such as IPA or through CII's Project Definition Rating Index (PDRI: Project Definition Rating Index—Industrial Projects, Construction Industry Institute), the implementation of applicable VIPs to the project is a part of their analysis. All the VIPs, when properly implemented, focus on producing better project definition and resultant economic improvements. The level of project definition achieved during FEL phases of the project is the focus of such benchmarking efforts.

VIPs as a group of practices are often described by their characteristics:

- Out-of-the-ordinary practices are used to improve cost, schedule, and/or reliability of capital projects.
- They are used primarily during FEL project phases.
- Formal and documented practices involve repeatable work processes.
- All involve a formal facilitated workshop to confirm the value gained to the project and to formally approve VIP team recommendations.
- All involve stated explicit support from the owner's corporate executive team.
- VIPs must be performed by a trained experienced VIP facilitator—someone who is not a member of the project team
- VIPs are characterized by statistical links between the use of the practice and better project performance which are demonstrated, systematic, repeatable, and proven correlations
- VIPs are also further clarified by what they are not, as below.
- Just "good engineering"
- Simple brainstorming or strategy sessions
- Business as usual
- A special look at some aspect of the project
- Cost reduction or scope reduction exercises
- PFD or P&ID reviews
- Safety reviews
- Audits
- Project readiness reviews

VIP Descriptions

Classes of Facility Quality VIP The class of facility quality VIP determines the appropriate classes of facility quality that would produce the highest value or profitability in terms of

- Capital investment (CAPEX)
- Planned facility life
- Expandability
- Level of automation
- Equipment selection,
- Operating expense (OPEX)
- Environmental controls
- Capacity
- Technology

This VIP individually confirms the best overall design philosophy for the project team, for each of the parameters listed above. Here, the designer first learns how aggressive the owner organization wants the facility design and operation to be in terms of overall risk. For example, if the plant is to have the lowest possible OPEX, then the designer will incorporate greater levels of automation, instrumentation, and robustness of mechanical design in the overall facility.

The results of this VIP are used by the project management team to update its project execution plan for each FEL phase. The class of facility quality VIP provides the best results when conducted prior to executing any other VIP effort in the conceptual phase (FEL-1) of the project.

Technology Selection VIP The technology selection VIP is the application of evaluation criteria aligned with the project's business objectives to identify manufacturing and processing technology that may be superior to that currently used. The goal is to ensure that the technology suite finally selected is the most competitive available. This requires a systematic search, both inside and outside the operating company's organization, to identify emerging technology alternatives. This formal facilitated process is also meant to ensure due diligence for all parties involved and that all emerging and near-commercial alternative

technologies for accomplishing a particular processing function are objectively considered. This VIP is most commonly applied at the unit operation level, although it has also been successfully applied down to the major equipment level (KBR Value Improving Practices Program, 2000 through 2005). This VIP is particularly effective for combating the NIH syndrome ("not-invented-here").

The goals of this VIP are to document which technology evaluation criteria are applicable and then to conduct a formal technology screening and evaluation assessment. The result is a prioritized listing of technology options for each selected application for the project. The preferred time to execute this VIP is the midpoint in the conceptual phase (FEL-1).

Process Simplification VIP The process simplification VIP uses the value methodology and is a formal, rigorous process to search for opportunities to eliminate or combine process and utility system steps or equipment, ultimately resulting in the reduction of investment and operating costs. The focus is the reduction of installed costs and critical path schedule while balancing these value improvements with expected facility operability, flexibility, and overall life cycle costs.

The process simplification VIP does far more than just evaluate and simplify processing steps. This very productive VIP ensures that low- or zero-value functions or equipment included in the project scope are challenged by experienced world-class experts and eliminated, if possible. This VIP tries to systematically differentiate "wants" from "needs" and remove the "wants." It can be especially effective for providing a neutral professional environment for identifying and challenging "sacred cows" and then removing them. Removal of these low- or zero-value functions yields significant profitability improvements to the overall project. Process simplification results in

- Reduced capital costs (CAPEX)
- Improved critical path schedule
- Reduced process inventory
- Increased yields
- Reduced operating and maintenance costs (OPEX)
- Increased productivity
- Incremental capacity gains
- Reduced utility and support systems requirements
- Reduced waste generation

Process simplification is executed in a formal workshop with a trained experienced facilitator. This VIP should always include key participants from each of the project owner's organizations, the engineering contractor organization, key third-party technology licensors, and equipment or systems vendors, where possible. One or more "cold eyes" reviewers or subject matter experts, who have extensive experience, should be included to provide an objective and unbiased perspective.

This VIP also provides a means for integrating overall plantwide systems. The process simplification VIP is typically performed during the feasibility phase (FEL-2) after the preliminary PFDs and heat and material balances become available. However, for very large and complex projects, considerable value has been gained by also performing this VIP at the midpoint or later in the conceptual phase (FEL-1).

Constructability VIP The constructability VIP is the systematic implementation of the latest engineering, procurement and construction concepts and lessons learned, which are consistent with the facility's operations and maintenance requirements. The goal is to enhance construction safety, scope, cost, schedule, and quality.

Since the constructability VIP has seen widespread implementation in industry for capital projects over the last 20 years, in order for this VIP to remain consistent with the definition of a VIP (i.e., above what project teams can do on their own), at least one large engineering and construction company has enhanced this VIP to include a formal facilitated workshop that seeks profitability improvements above those already identified by the project team in the course of its normal work (KBR Value Improving Practices Program, 2001 through 2005). Both work processes described below are mutually additive, flexible, and compatible.

The traditional constructability work process includes the following characteristics:

- Starts at the FEL-1 phase and continues through facility start-up
- Is an ongoing structured program

- Optimizes the combined use of operations, maintenance, engineering, procurement, key vendors, and construction knowledge and experience
- Enhances the achievement of project objectives
- Has construction experts working with the engineering and procurement process that results in construction safety, cost, schedule, and quality savings
- Uses on-project and off-project expertise

The enhanced constructability VIP adds the following to the traditional approach:

- Includes a formal facilitated workshop
- Is held in every engineering phase of the project with a focus on the pertinent aspects of that phase
- Identifies value improvements and their benefits above those already being considered by the traditional constructability work process
- Focuses on the systematic implementation of the latest engineering, procurement, construction concepts, and lessons learned
- Involves a detail review of planning, design, procurement, fabrication, and installation functions to achieve the best overall project safety performance, lowest CAPEX, and the shortest reasonable schedule
- Applies operations and maintenance requirements and expertise
- Includes considerations for operability and maintainability
- Enhances construction safety, scope, cost, schedule, and quality

A formal constructability VIP workshop conducted in the conceptual phase (FEL-1) should focus on the overall project construction strategies regarding site layout, construction and turnaround laydown areas, access to the site for large equipment and modules, modularization, sequencing of heavy lifts, limitations regarding procurement, limitations regarding fabrication and transport, area labor limitations, and coordination with any existing or nearby structures or facilities.

A formal constructability VIP workshop conducted in the feasibility phase (FEL-2) should focus on more specific topics of layout optimization, using a preliminary plot plan and equipment layout for the project. Considerations should include optimum site layout in terms of construction laydown areas; optimum equipment arrangement to reduce piping and steel for structures and piperack; specific sizes and weights for modules; which components will be included in each module; crane locations for heavy lifts; equipment requiring early purchase to allow project schedule to be achieved; further analysis of limitations regarding procurement, fabrication, and area labor availability; and precommissioning, commissioning, and start-up considerations.

A formal constructability VIP workshop conducted in the definition phase (FEL-3) focuses on even greater detail for what was discussed above. In the detailed engineering stage (EPC phase), considerable detail will be reviewed to evaluate how the project can best construct what will be needed. Here, significant application of detailed lessons learned is reviewed and considered.

Constructability VIP workshops should be formal facilitated workshops drawing on personnel from operations, maintenance, and construction in addition to project and owner organization representation.

Customization of Standards and Specifications VIP The customization of standards and specifications VIP is a direct and systematic method to improve project value by selecting the most appropriate codes, standards, and specifications for the project. The goal is to make helpful changes to meet the actual project requirements, ensuring that the codes, standards, and specifications selected do not exceed those required for the project, and maximizing the use of specifications from equipment vendors to obtain the best overall value. This VIP is beyond typical good engineering practices and should not be confused with ongoing systematic improvements in corporate standards and specifications, or with required identification of applicable procurement specifications to be used for the project. This formal VIP takes a combination of project owner and engineering contractor corporate specifications and aggressively seeks profitability improvements consistent with the project's goals and limitations. This VIP maximizes the procurement of off-the-shelf equipment over equipment customized for the project.

Industry experience indicates that project-specific "Fit for Purpose" standards and specifications on the average cost less than the general application of traditional standards. This VIP is best performed early in the feasibility phase (FEL-2), and should include project team members involved from both the project owner and

engineering contractor, as well as appropriate suppliers of major packaged subsystems, modularized equipment, etc.

Energy Optimization VIP The energy optimization VIP is the systematic process for the evaluation of the thermal efficiency of a process (or multiple subunits within a larger process or facility). The goal is to improve the economic utilization of energy. This optimization starts by using the "pinch" technology branch of process energy integration (energy pinch) to identify better process energy exchange options.

Energy pinch (usually just called *pinch*) is a methodology for the conceptual design of process heating, utility, and power systems. Pinch allows the maximization of energy utilization within a process, while minimizing the use of plant utilities. Such minimization is achieved by reusing energy, via process stream-to-process stream heat exchange. A pinch analysis is performed by analyzing the trade-off between the energy which can be recovered and the additional capital costs which must be added to do so. It includes the project's design and thermodynamic constraints (performance targets) available during this preliminary design phase.

The benefits of pinch technology include lower operating costs, occasionally reduced capital cost, improved operability/flexibility, increased throughput, and site-specific process optimization and reduced emissions. Pinch technology can be applied for both grass-roots and retrofit applications. Typical applications include process heat integration as well as sitewide heat and power integration. However, this methodology is profitably applied to the optimization of high-value complex mass flow problems, such as refinery hydrogen network optimization (hydrogen pinch) and wastewater minimization (water pinch).

Once the minimum theoretical energy requirements and applicable process options have been determined, a formal facilitated workshop follows to modify the process or facility to bring the design closer to the thermodynamic optimum within project economic constraints.

The energy optimization VIP is most beneficial for processes where energy and related capital expense are a relatively large fraction of the total operating cost. The benefits result in reduced energy requirements and environmental emissions in balance with project economics. This VIP should be implemented in the feasibility phase (FEL-2) when preliminary PFDs and heat and material balances are available.

Predictive Maintenance VIP The predictive maintenance VIP is the proactive use of sensors and associated controls to monitor the machinery mechanical "health," using both current state and historical trends, to optimize effective planning of all shutdowns and maintenance, thereby detecting equipment abnormalities and diagnosing potential problems before they cause permanent equipment damage. Examples include real-time corrosion monitoring and equipment vibration monitoring. This additional instrumentation is generally economically justified in the case of critical equipment items and key operations. Predictive maintenance reduces maintenance costs, improves the confidence of extending time between turnarounds, improves reliability, and provides a more predictable maintenance schedule for key process equipment. It also minimizes the amount of remaining equipment life that is lost through using only preventive maintenance practices. Preventive maintenance is an older practice which is limited to periodic inspections and repairs to avoid unplanned equipment breakdowns.

For the predictive maintenance VIP to be effective, maintenance personnel from the project owner's organization must be involved in determining key predictive maintenance requirements. Suppliers of critical equipment items (i.e., compressors) are also important participants in this process.

The predictive maintenance VIP is considered by some operating companies and engineering contractors to have become standard practice. For those where it is not already standard practice, this VIP should be initiated in the feasibility phase (FEL-2) and concluded with a formal facilitated workshop and report of recommendations to the project management team.

Waste Minimization VIP The waste minimization VIP involves a formal process stream-by-stream analysis to identify ways to eliminate or reduce the generation of wastes or nonuseful streams within the chemical process itself. For those streams not eliminated or converted to salable by-products, it provides the method for managing the resulting wastes. This VIP incorporates environmental requirements into the facility design and combines life cycle environmental

benefits and positive economic returns through energy reductions, reduced end-of-pipe treatment requirements, and improved raw material yields. The waste reduction hierarchy is to

- Eliminate or minimize the generation of waste through source reduction
- Recycle by use, reuse, or reclamation those potential waste materials that cannot be eliminated or minimized
- Treat all waste that is nevertheless generated to reduce volume, toxicity, or mobility prior to storage or disposal

This VIP is considered by some engineering contractors to have become standard practice. For those where it is not standard practice, the waste minimization VIP should be executed in a formal workshop with an experienced facilitator with project owner and engineering contractor representatives always involved. A “cold eyes” reviewer with extensive experience should also be included to add a nonbiased perspective. The waste minimization VIP should be implemented at the feasibility phase (FEL-2) when preliminary PFDs and heat and material balances are available.

Process Reliability Simulation VIP The process reliability simulation VIP is the use of reliability, availability, and maintainability (RAM) computer simulation modeling of the process and the mechanical reliability of the facility. A principal goal is to optimize the engineering design in terms of life cycle cost, thereby maximizing the project’s potential profitability. The objective is to determine the optimum relationships between maximum production rates and design and operational factors. Process reliability simulation is also applied for safety purposes, since it considers the consequences of specific equipment failures and failure modes.

This VIP is typically led by an engineer experienced in plant operations and the use of the RAM simulation modeling software. The VIP should also directly involve the project owner since that organization would most often supply the historical operating and maintenance information required for the development of the simulation model. This process provides the project team with a more effective means of assessing, early in the design, the cost/benefit impact of changes in design, identification of bottlenecks in the system, simulation of key operating scenarios, determination of equipment-sparing needs, training and maintenance requirements of a facility.

The process reliability simulation VIP should be initiated in the feasibility phase (FEL-2) to produce a block-level RAM model. Based on the results of that model, a more detailed equipment-level RAM model should be developed starting in the definition phase (FEL-3).

Value Engineering VIP The value engineering VIP is a flexible, organized, multidisciplinary team effort directed at analyzing the functions, issues, and essential characteristics of a project, process, technology, or system. The goal is to satisfy those functions, issues, and essential characteristics at the lowest life cycle cost. The value engineering VIP rigorously examines what is needed to meet the business objectives of a project and the elimination of non-value-adding investment. An open-minded attitude by participants is required to effectively remove unneeded scope and in doing so reduce the installed costs of the project. This VIP tries to systematically differentiate “wants” from “needs” and remove the “wants.” Tests for non-income-producing investments include redundancy, overdesign, manufacturing add-ons, upgraded materials of construction, and customized design versus vendor standards.

The value engineering VIP also ensures that low- or zero-value functions or equipment included in the project scope are challenged to be the highest value possible for the project. Removal of these low- or zero-value functions from the project scope, if possible, will most likely yield significant profitability improvements to the overall project. These can encompass the following:

- Misalignment of unit or system capacity or operations capability with respect to the overall facility
- Overly conservative assumptions of the basic design data
- Overly conservative interpretation of how the facilities will be used during peak, seasonal, or upset conditions
- Preinvestment included in the project scope that may not be value added
- Overdesign of equipment or systems to provide uneconomic added flexibility

The value engineering VIP is executed in a formal workshop with a trained experienced technical workshop facilitator. Both the project

owner and the engineering contractor are always involved. Third-party licensors and equipment/system vendors should be included where applicable. One (or more) cold-eyes reviewer with extensive experience should also be included to provide an unbiased perspective.

This VIP leverages the growing accumulation of more detailed project knowledge to test the value of earlier, more generalized scope assumptions. It also tests the presumed added value of different stakeholder requirements, which have influenced the evolution of the project scope. This highly adaptable VIP results in reduced capital costs (CAPEX), improved critical path schedule, reduced process inventory, increased yields, reduced operating and maintenance costs (OPEX), increased productivity, incremental capacity gains, reduced utility and support systems requirements, and reduced waste generation.

The value engineering VIP should be conducted in the definition phase (FEL-3) when the first issue of P&IDs is available.

Design to Capacity VIP The design to capacity VIP systematically evaluates the maximum capacity of major equipment, ancillary piping, valving, instrumentation, and associated engineering calculations and guidelines. The goal is to improve life cycle costs (profitability) by eliminating preinvestment and overdesign. This VIP requires the systematic and formal evaluation of the maximum capacity of each piece of equipment instead of the traditional practice of designing with an extra safety factor or margin to allow for additional catch-up capacity or some future production increase. The goal is also to eliminate overdesign in both calculations and engineering guidelines. This VIP is conducted as a facilitated workshop with both project owner and engineering contractor representation.

This VIP reduces capital investment by confirming minimum required capacities and flexibility necessary only to meet current project business objectives. The workshop drills down to each specific system and subsystem and finally scrutinizes the design of each equipment item. This workshop is often combined with the value engineering VIP, which overlaps significantly. The design to capacity VIP should be conducted in the definition phase (FEL-3) when the first issue of P&IDs is available.

3D-CAD VIP The 3D-CAD VIP is the creation of a detailed three-dimensional (3D) computer model depicting the proposed process and associated equipment along with the optimized plant layout and specific equipment arrangements and orientations. The 3D model can then be used to generate computerized interference checks of bulk material configurations and equipment and extraction of error-free fabrication drawings and material quantities. The goals of this VIP are to reduce engineering and construction rework, improve operability and maintainability, and confirm the incorporation into the design of advantageous human factors (a.k.a. ergonomics) focused on ease of operation and maintenance.

A number of industry-accepted state-of-the-art 3D computer-aided design (CAD) systems have been used for this purpose. The specification-driven 3D-CAD system allows a computer model to be built to allow extraction of drawings from the model for fabrication and erection. The extracted drawings are enhanced in their accuracy by the computer interference detection system which greatly reduces field rework.

The principal benefit of utilizing 3D-CAD is the ability to produce an electronic model that accurately resembles the completed facility. This enables project teams, clients, and constructors to review and agree on the plant design before construction starts. The model can then be used to generate interference checks of bulk material configurations and equipment, as well as the extraction of error-free fabrication drawings and material quantities. The system also utilizes its design review capabilities to confirm proposed designs and obtain approvals from key project stakeholders and owners.

This VIP is considered by most major engineering contractors to have become standard practice. The 3D-CAD VIP model development should be initiated in the feasibility phase (FEL-2) after the plot plan has been finalized and the first issue of P&IDs is available.

VIP Planning and Implementation Each VIP has a unique character, and it should be performed at a certain time and in a certain way to produce the best results for the project. Part of the power of VIPs is that they can be used to improve the overall economics of the project without the need for inordinate additional time or expense. Ironically, the return on investment (ROI) for the cost of implementing each VIP is usually much greater than that ROI for the overall proposed project. For one engineering contractor, *the typical ROI for*

implementing VIPs is at least one order of magnitude higher (KBR Value Improving Practices Program, 2000 through 2005).

It is important to reiterate that the benefits of VIPs cannot be realized by just executing “good engineering.” The application and implementation of VIPs to any project must have the explicit commitment of the owner’s corporation executives. VIP execution must be deliberately and carefully planned in the initial phase of the project. For all projects, this VIP planning meeting should take place immediately following project kickoff. The project management team and the selected VIP facilitator should

- Confirm which VIPs should be applied to the project and when
- Incorporate the planned VIPs into the project scope of work and schedule
- Determine the required workshop resources and best combination of engineering, operations, maintenance, construction, and other expertise for each selected VIP workshop team

VIPs That Apply the Value Methodology Nearly all VIPs are conducted only once in a project at a “sweet spot” where maximum benefit is found. For example, the process simplification VIP is anchored at the first appearance of the preliminary PFDs, while the value engineering VIP and the design to capacity VIP are anchored at the first issue of the P&IDs. Both of these apply the value methodology [Society of American Value Engineers International (SAVE)] that has produced excellent results in industry for more than 55 years. The typical approach and steps for these three unique VIPs are presented below.

Preparation and Planning Before the VIP is begun, the goals, objectives, and scheduled time for the formal workshop must be agreed upon by the integrated project management team. The workshop facilitator must ensure that all the information required for the workshop is available and that the workshop team members have been fully briefed on the VIP’s objectives, methodology, and expectations.

The Formal Workshop The formal workshop is always structured to make maximum use of the multi-disciplinary team’s time and effort. Such workshops typically require no less than 2 days and as many as 5 days depending on the size and complexity of the project. The required workshop length should be determined by the VIP facilitator. A typical process simplification VIP, value engineering VIP, and design to capacity VIP workshop includes the following phases of a typical “job plan” that are supported by the Society of American Value Engineers International.

The information phase In this phase, team members review important background materials and confirm their understanding of the basis for the design of the project, the constraints, and the sensitivity of the relevant capital and operating costs. Here, incorporating important unresolved project issues into the workshop produces more meaningful financial and technical results. Discussion of the issues’ validity and basis are determined during the first day of the workshop. These issues very often become some of the best brainstorming targets for cost and schedule reduction ideas.

A very specific and structured methodology is used which is known as the *Function Analysis System Technique (FAST)*. This function analysis diagramming illustrates the logical or functional relationships and dependencies between different process systems and project activities. These diagrams are then reviewed and critiqued together with the associated costs of selected groups of process functions or project functions. The function analysis can be performed at this stage, but often time can be saved by preparing a draft of these FAST diagrams prior to the workshop with a small group of the workshop team members.

The speculation phase Once the pertinent information and issues have been reviewed and the important functions of each process and project step identified, the team is encouraged to speculate on alternative methods to perform each function and to solve each major project issue. Brainstorming sessions within a creative environment encourage the team to strive for new and innovative ideas.

The conceptual phase The team then reviews the ideas against relevant project criteria such as potential impact on long-term project economics, impact on operations and maintenance costs, effect on the capital cost for the project, validity to the project scope of work, technical risks associated with implementation of the new concept, impact on project schedule, and cost required to implement the improvement. Each study has specific criteria against which proposed alterna-

tives are judged. The ideas are weighted, sorted, grouped, linked, and ranked so that the best of the technically viable ideas are efficiently identified for further detailed study.

The feasibility phase The ideas with the most merit are developed into preliminary two-page written proposals with potential benefits approximated as part of the workshop. Performing this important activity following the formal workshop has been shown to often result in significant loss of potential for implementation. The VIP team expands the ideas ranked highest to obtain additional technical and economic insights and information to support the idea. The proposals are then presented internally, to the assembled VIP workshop team, and discussed to determine whether the ideas retain sufficient technical and economic merit to be recommended by the VIP team to a separate steering committee or project management team.

Experience indicates that having the VIP team perform this stage within the formal workshop produces the best results.

The presentation phase The VIP team formally presents the profitability recommendations consistent with the objectives and constraints of the workshop and their implementation plans to the steering committee or the project management team. The steering committee then approves those recommendations that pass muster and authorizes the project team to begin the implementation effort. Often, this approval is conditional on early validation by subject matter experts within the project owner’s organization, but not present within the workshop. This external feasibility check is meant to provide support to the project team for any additional resources and schedule time needed to fully incorporate the improvements into the project scope of work.

Report and follow-up After completing the intensive VIP workshop, the workshop facilitator completes the written VIP final report for the project record. During this time, the project management team assigns each approved recommendation to a member of the project team, estimates the engineering time and resources required to incorporate the improvement into the project scope of work, and communicates the results of the VIP within the integrated project team. This follow-up action plan creates a very positive and cost-conscious attitude within the project team that leads to further improvements in project value.

Sources of Expertise VIP workshops should be planned and led by a trained experienced facilitator who has significant experience in effectively conducting such VIP workshops. Technical expertise for VIP workshops should be a combination of senior project team members and subject matter experts from the operating company’s organization, the engineering contractor’s organization, licensed technology providers, and any key fabrication or installation subcontractors to be used. Figure 9-35 illustrates the best balance of expertise for VIP workshops (KBR Value Improving Practices Program, 1995 through 2005).

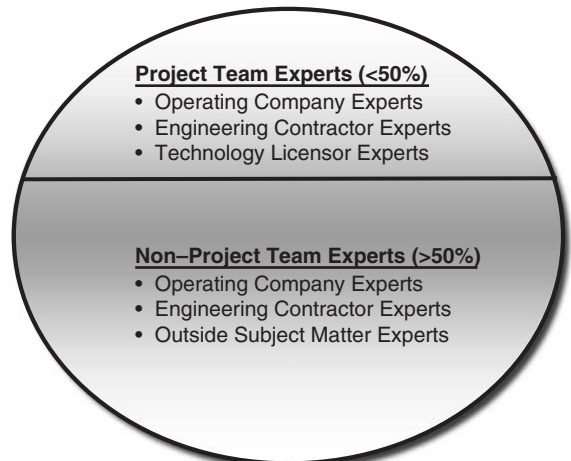


FIG. 9-35 The ideal VIP team makeup.

GLOSSARY

Accounts payable The value of purchased goods and services that are being used but have not been paid.

Accounts receivable Credit extended to customers, usually on a 30-day basis. Cash is set aside to take care of the probability that some customers may not pay their bills.

Administrative basis The accounting method that recognizes revenues and disbursement of funds by receipt of bills or orders and not by cash flow, distinguished from *cash basis*.

Administrative expense An overhead expense due to the general direction of a company beyond the plant level. It includes administrative and office salaries, rent, auditing, accounting, legal, central purchasing and engineering, etc., expenses.

Allocation of expenses A procedure whereby overhead expenses and other indirect charges are assigned back to processing units or to products on what is expected to be an equitable basis. All allocations are somewhat arbitrary.

Amortization Often used interchangeably with *depreciation*, but there is a slight difference depending on whether the life of an asset is known. If the period of time is known to be usually more than a year, this annual expense is *amortization*; however, if the life is estimated, then it is *depreciation*.

Annual net sales Pounds of product sold times the net selling price. *Net* means that any allowances have been subtracted from the gross selling price.

Annual report Management's report to the stockholders and other interested parties at the end of a year of operation showing the status of the company, its activities, funds, income, profits, expenses, and other information.

Appurtenances The auxiliaries to either process or nonprocess equipment: piping, electrical, insulation, instrumentation, etc.

Assets The list of money on hand, marketable securities, monies due, investments, plants, properties, intellectual property, inventory, etc., at cost or market value, whichever is smaller. The assets are what a company (or person) owns.

Balance sheet This is an accounting, historical tabulation of assets, liabilities, and stockholders' equity for a company. The assets must equal the liabilities plus the stockholders' equity.

Battery limit A geographic boundary defining the coverage of a specific project. Usually it takes in the manufacturing area of a proposed plant, including all process equipment but excluding provision for storage, site preparation, utilities, administrative buildings, or auxiliary facilities.

Bonds When one purchases a bond, the company (or person) acquires an interest in debt and becomes a creditor of the company. The purchaser receives the right to receive regular interest payments and the subsequent repayment of the principal.

Book value Current investment value on the company books as the original installed cost less depreciation accruals.

Book value of common stock Net worth of a firm divided by the number of shares of common stock issued at the time of a report.

Break-even chart An economic production chart depicting total revenue and total expenses as functions of operation of a processing facility.

Break-even point The percentage of capacity at which income equals all fixed and variable expenses at that level of operation.

By-product A product made as a consequence of the production of a main product. The by-product may have a market value or a value as a raw material.

Capacity The estimated maximum level of production on a sustained basis.

Capital ratio Ratio of capital investment to sales dollars; the reciprocal of capital turnover.

Capital recovery The process by which original investment in a project is recovered over its life.

Capital turnover The ratio of sales dollars to capital investment; the reciprocal of capital ratio.

Cash Money that is on hand to pay for operating expenses, e.g., wages, salaries, raw materials, supplies, etc., to maintain a liquid financial position.

Cash basis The accounting basis whereby revenue and expense are recorded when cash is received and paid, distinguished from accrual basis.

Cash flow Net income after taxes plus depreciation (and depletion) flowing into the company treasury.

Code of accounts A system in which items of expense or fixed capital such as equipment and material are identified with numerical figures to facilitate accounting and cost control.

Common stock Money paid into a corporation for the purchase of shares of common stock that becomes the permanent capital of the firm. Common stockholders have the right to transfer ownership and may sell the stock to individuals or firms. Common stockholders have the right to vote at annual meetings on company business or may do so by proxy.

Compound interest The interest charges under the condition that interest is charged on previous interest plus principal.

Contingencies An allowance for unforeseeable elements of cost in fixed investment estimates that previous experience has shown to exist.

Continuous compounding A mathematical procedure for evaluating compound interest based upon continuous interest function rather than discrete interest periods.

Conversion expense The expense of converting raw materials to finished product.

Corporation In 1819, defined by Chief Justice Marshall of the Supreme Court as "an artificial being, invisible, intangible and existing only in contemplation of law." It exists by the grace of a state, and the laws of a state govern the procedure for its formation.

Cost of capital The cost of borrowing money from all sources, namely, loans, bonds, and preferred and common stock. It is expressed as an interest rate.

Cost center For accounting purposes, a grouping of equipment and facilities comprising a product manufacturing system.

Cost of sales The sum of the fixed and variable (direct and indirect) expenses for manufacturing a product and delivering it to a customer.

Decision or decision making A program of action undertaken as a result of (1) an established policy or (2) an analysis of variables that can be altered to influence a final result.

Depletion A provision in the tax regulations that allows a business to charge as current expense a noncash expense representing the portion of limited natural resources consumed in the conduct of business.

Depreciation A reasonable allowance by the Internal Revenue Service for the exhaustion, wear and tear, and normal obsolescence of equipment used in a trade or business. The property must have a useful life of more than 1 year. Depreciation is a noncash expense deductible from income for tax purposes.

Design to cost A management technique to achieve system designs that meet cost parameters. Cost as a design parameter is considered on a continuous basis as part of a system's development and production processes.

Direct expense An expense directly associated with the production of a product such as utilities, labor, and maintenance.

Direct labor expense The expense of labor involved in the manufacture of a product or in the production of a service.

Direct material expense The expense associated with materials consumed in the manufacture of a product or the production of a service.

Distribution expense Expense including advertising, preparation of samples, travel, entertainment, freight, warehousing, etc., to distribute a sample or product.

Dollar volume Dollar worth of a product manufactured per unit of time.

Earnings The difference between income and operating expenses.

Economic life The period of commercial use of a product or facility. It may be limited by obsolescence, physical life of equipment, or changing economic conditions.

Economic value added The period dollar profit above the cost of capital. It is a means to measure an organization's value and a way to determine how management's decisions contribute to the value of a company.

Effective interest The true value of interest computed by equations for the compound interest rate for a period of 1 year.

Equity The owner's actual capital held by a company for its operations.

Escalation A provision in actual or estimated cost for an increase in equipment cost, material, labor, expenses, etc., over those specified in an original estimate or contract due to inflation.

External funds Capital obtained by selling stocks or bonds or by borrowing.

FEL (front-end loading) The process by which a company develops a detailed definition of the scope of a capital project that meets corporate business objectives.

FIFO (first in, first out) The valuation of raw material and supplies inventory, meaning first into the company or process is the first used or out.

Financial expense The charges for use of borrowed funds.

Fixed assets The real or material facilities that represent part of the capital in an economic venture.

Fixed capital Item including the equipment and buildings.

Fixed expense An expense that is independent of the rate of output, e.g., depreciation and plant indirect expenses.

Fringe benefits Employee welfare benefits; expenses of employment over and above compensation for actual time worked, such as holidays, vacations, sick leave, insurance.

Full cost accounting Method of pricing goods and services to reflect their true costs, including production, use recycling, and disposal.

Future worth The expected value of capital in the future according to some predetermined method of computation.

Goods manufactured, cost of Total expense (direct and indirect expenses) including overhead charges.

Goods-in-process inventory The holdup of product in a partially finished state.

Goods sold, cost of The total of all expenses before income taxes that is deducted from income (revenue).

Gross-roots plant A complete plant erected on new site including land, site preparation, battery-limits facilities, and auxiliary facilities.

Gross domestic product An indicator of a country's economic activity. It is the sum of all goods and services produced by a nation within its borders.

Gross margin (profit) Total revenue minus cost of goods manufactured.

Gross national product An economic indicator of a country's economic activity. It is the sum of all the goods and services produced by a nation both within and outside its borders.

Income Profit before income taxes or gross income from sales before deduction of expenses.

Income statement The statement of earnings of a firm as approximated by accounting practices, usually covering a 1-year period.

Income tax The tax imposed on corporate profits by the federal and/or state governments.

Indirect expenses Part of the manufacturing expense of a product not directly related to the amount of product manufactured, e.g., depreciation, local taxes, and insurance.

Internal funds Capital available from depreciation and accumulated retained earnings.

Inventory The quantity of raw materials and/or supplies held in a process or in storage.

Last in, first out (LIFO) The valuation of raw materials and supplies, meaning the last material into a process or storage is the first used or out.

Leverage The influence of debt on the earning rate of a company.

Liabilities An accounting term for capital owed by a company.

Life cycle cost Cost of development, acquisition, support, and disposal of a system over its full life.

Manufacturing expense The sum of the raw material, labor, utilities, maintenance, depreciation, local taxes, etc., expenses. It is the sum of the direct and indirect (fixed and variable) manufacturing expenses.

Marginal cost The incremental cost of making one additional unit without additional investment in facilities

Market capitalization The product of the number of shares of common stock outstanding and the share price.

Market value added A certain future economic value added for a company. It is the present value of the future economic value (EVA) generated by a company. It is a measure of how much value a firm has created.

Minimum acceptable rate of return (MARR) The level of return on investment, at or above the cost of capital, chosen as acceptable for discounting or cutoff purposes.

Net sales price Gross sales price minus freight adjustments.

Net worth The sum of the stockholders' investment plus surplus, or total assets minus total liabilities.

Nominal interest The number applied loosely to describe the annual interest rate.

Obsolescence The occurrence of decreasing value of physical assets due to technological changes rather than physical deterioration.

Operating expense The sum of the manufacturing expense for a product and the general, administrative, and selling expenses.

Operating margin The gross margin minus the general, administrative, and selling expenses.

Opportunity cost The estimate of values that are forgone by undertaking one alternative instead of another one.

Payout time (payback period) The time to recover the fixed capital investment from profit plus depreciation. It is usually after taxes but not always.

Preferred stock Stock having claims that it commands over common stock, with the preference related to dividends. The holders of such stock receive dividends before any distribution is made to common stockholders. Preferred stockholders usually do not have voting rights as common stockholders do.

Present worth The value at some datum time (present time) of expenditures, costs, profits, etc., according to a predetermined method of computation. It is the current value of cash flow obtained by discounting.

Production rate The amount of product manufactured in a given time period.

Profitability A term generally applied in a broad sense to the economic feasibility of a proposed venture or an ongoing operation. It is generally considered to be related to return on investment.

Rate of return on investment The efficiency ratio relating profit or cash flow to investment.

Replacement A new facility that takes the place of an older facility with no increase in capacity.

Revenue The net sales received from the sale of a product or a service to a customer.

Sales, administration, research, and engineering expenses (SARE) Overhead expenses incurred as a result of maintaining sales offices and administrative offices and the expense of maintaining research and engineering departments. This item is usually expressed as a percentage of annual net sales.

Sales volume The amount of sales expressed in pounds, gallons, tons, cubic feet, etc., per unit of time.

Salvage value The value that can be realized from equipment or other facilities when taken out of service and sold.

Selling expense Salaries and commissions paid to sales personnel.

Simple interest The interest charges in any time period that is only charged on the principal.

Sinking fund An accounting procedure computed according to a specified procedure to provide capital to replace an asset.

Surplus The excess of earnings over expenses that is not distributed to stockholders.

Tax credit The amount available to a firm as part of its annual return because of deductible expenses for tax purposes. Examples have been research and development expenses, energy tax credit, etc.

Taxes In a manufacturing cost statement, usually property taxes. In an income statement, usually federal and state income taxes.

Time value of money The expected interest rate that capital should or would earn. Money has value with respect to time.

9-56 PROCESS ECONOMICS

Total operating investment The fixed capital investment, backup capital, auxiliary capital, utilities and services capital, and working capital.

Utilities and services capital Electrical substations, plant sewers, water distribution facilities, and occasionally the steam plant.

Value added The difference between the raw material expense and the selling price of that product.

Value-improving practices (VIPs) Formal structured practices applied to capital projects to improve profitability ("or value") above

that which is attained through the application of proven good engineering and project management practices.

Variable expense Any expense that varies directly with production output.

Working capital In the accounting sense, the current assets minus the current liabilities. It consists of the total amount of money invested in raw materials, supplies, goods in process, product inventories, accounts receivable, and cash minus those liabilities due within 1 year.

SECTION 10

Transport and
Storage of
Fluids

PERRY'S CHEMICAL ENGINEERS' HANDBOOK

8TH EDITION



MEHERWAN P. BOYCE, VICTOR H. EDWARDS
TERRY W. COWLEY, TIMOTHY FAN
HUGH D. KAISER, WAYNE B. GEYER
DAVID NADEL, LARRY SKODA
SHAWN TESTONE, KENNETH L. WALTER

Copyright © 2008, 1997, 1984, 1973, 1963, 1950, 1941, 1934 by The McGraw-Hill Companies, Inc. All rights reserved. Manufactured in the United States of America. Except as permitted under the United States Copyright Act of 1976, no part of this publication may be reproduced or distributed in any form or by any means, or stored in a database or retrieval system, without the prior written permission of the publisher.

0-07-154217-5

The material in this eBook also appears in the print version of this title: 0-07-151133-4.

All trademarks are trademarks of their respective owners. Rather than put a trademark symbol after every occurrence of a trademarked name, we use names in an editorial fashion only, and to the benefit of the trademark owner, with no intention of infringement of the trademark. Where such designations appear in this book, they have been printed with initial caps.

McGraw-Hill eBooks are available at special quantity discounts to use as premiums and sales promotions, or for use in corporate training programs. For more information, please contact George Hoare, Special Sales, at george_hoare@mcgraw-hill.com or (212) 904-4069.

TERMS OF USE

This is a copyrighted work and The McGraw-Hill Companies, Inc. (“McGraw-Hill”) and its licensors reserve all rights in and to the work. Use of this work is subject to these terms. Except as permitted under the Copyright Act of 1976 and the right to store and retrieve one copy of the work, you may not decompile, disassemble, reverse engineer, reproduce, modify, create derivative works based upon, transmit, distribute, disseminate, sell, publish or sublicense the work or any part of it without McGraw-Hill’s prior consent. You may use the work for your own noncommercial and personal use; any other use of the work is strictly prohibited. Your right to use the work may be terminated if you fail to comply with these terms.

THE WORK IS PROVIDED “AS IS.” McGRAW-HILL AND ITS LICENSORS MAKE NO GUARANTEES OR WARRANTIES AS TO THE ACCURACY, ADEQUACY OR COMPLETENESS OF OR RESULTS TO BE OBTAINED FROM USING THE WORK, INCLUDING ANY INFORMATION THAT CAN BE ACCESSED THROUGH THE WORK VIA HYPERLINK OR OTHERWISE, AND EXPRESSLY DISCLAIM ANY WARRANTY, EXPRESS OR IMPLIED, INCLUDING BUT NOT LIMITED TO IMPLIED WARRANTIES OF MERCHANTABILITY OR FITNESS FOR A PARTICULAR PURPOSE. McGraw-Hill and its licensors do not warrant or guarantee that the functions contained in the work will meet your requirements or that its operation will be uninterrupted or error free. Neither McGraw-Hill nor its licensors shall be liable to you or anyone else for any inaccuracy, error or omission, regardless of cause, in the work or for any damages resulting therefrom. McGraw-Hill has no responsibility for the content of any information accessed through the work. Under no circumstances shall McGraw-Hill and/or its licensors be liable for any indirect, incidental, special, punitive, consequential or similar damages that result from the use of or inability to use the work, even if any of them has been advised of the possibility of such damages. This limitation of liability shall apply to any claim or cause whatsoever whether such claim or cause arises in contract, tort or otherwise.

DOI: 10.1036/0071511334

Transport and Storage of Fluids

Meherwan P. Boyce, Ph.D., P.E. *Chairman and Principal Consultant, The Boyce Consultancy Group, LLC; Fellow, American Society of Mechanical Engineers; Registered Professional Engineer (Texas) (Section Editor, Measurement of Flow, Pumps and Compressors)*

Victor H. Edwards, Ph.D., P.E. *Process Director, Aker Kvaerner, Inc.; Fellow, American Institute of Chemical Engineers; Member, American Association for the Advancement of Science, American Chemical Society, National Society of Professional Engineers; Life Member, New York Academy of Sciences; Registered Professional Engineer (Texas) (Section Editor, Measurement of Flow)*

Terry W. Cowley, B.S., M.A. *Consultant, DuPont Engineering; Member, American Society of Mechanical Engineers, American Welding Society, National Association of Corrosion Engineers (Polymeric Materials)*

Timothy Fan, P.E., M.Sc. *Chief Project Engineer, Foster Wheeler USA; Member, American Society of Mechanical Engineers, Registered Professional Engineer (Massachusetts and Texas) (Piping)*

Hugh D. Kaiser, P.E., B.S., MBA *Principal Engineer, PB Energy Storage Services, Inc.; Senior Member, American Institute of Chemical Engineers; Registered Professional Engineer (Texas) (Underground Storage of Liquids and Gases, Cost of Storage Facilities, Bulk Transport of Fluids)*

Wayne B. Geyer, P.E. *Executive Vice President, Steel Tank Institute and Steel Plate Fabricators Association; Registered Professional Engineer (Atmospheric Tanks)*

David Nadel, P.E., M.S. *Senior Principal Mechanical Engineer, Aker Kvaerner, Inc.; Registered Professional Engineer (Pressure Vessels)*

Larry Skoda, P.E. *Principal Piping Engineer, Aker Kvaerner, Inc.; Registered Professional Engineer (Texas) (Piping)*

Shawn Testone *Product Manager, De Dietrich Process Systems (Glass Piping and Glass-Lined Piping)*

Kenneth L. Walter, Ph.D. *Process Manager—Technology, Aker Kvaerner, Inc.; Senior Member, American Institute of Chemical Engineers, Sigma Xi, Tau Beta Pi (Storage and Process Vessels)*

MEASUREMENT OF FLOW

Introduction	10-6	Tube Size for Manometers	10-8
Properties and Behavior of Fluids	10-6	Multiplying Gauges	10-8
Total Temperature	10-7	Mechanical Pressure Gauges	10-9
Thermocouples	10-7	Conditions of Use	10-9
Resistive Thermal Detectors (RTDs)	10-7	Calibration of Gauges	10-9
Static Temperature	10-7	Static Pressure	10-10
Dry- and Wet-Bulb Temperatures	10-7	Local Static Pressure	10-10
Pressure Measurements	10-7	Average Static Pressure	10-10
Liquid-Column Manometers	10-8	Specifications for Piezometer Taps	10-10
		Velocity Measurements	10-11

10-2 TRANSPORT AND STORAGE OF FLUIDS

Variables Affecting Measurement	10-11
Velocity Profile Effects	10-11
Other Flow Disturbances	10-11
Pitot Tubes	10-11
Special Tubes	10-13
Traversing for Mean Velocity	10-13
Flowmeters	10-14
Industry Guidelines and Standards	10-14
Classification of Flowmeters	10-14
Differential Pressure Meters	10-14
Velocity Meters	10-14
Mass Meters	10-14
Volumetric Meters	10-14
Variable-Area Meters	10-14
Open-Channel Flow Measurement	10-14
Differential Pressure Flowmeters	10-15
General Principles	10-15
Orifice Meters	10-16
Venturi Meters	10-18
Flow Nozzles	10-19
Critical Flow Nozzle	10-19
Elbow Meters	10-20
Accuracy	10-20
Velocity Meters	10-21
Anemometers	10-21
Turbine Flowmeters	10-21
Mass Flowmeters	10-21
General Principles	10-21
Axial-Flow Transverse-Momentum Mass Flowmeter	10-21
Inferential Mass Flowmeter	10-21
Coriolis Mass Flowmeter	10-22
Variable-Area Meters	10-22
General Principles	10-22
Rotameters	10-22
Two-Phase Systems	10-22
Gas-Solid Mixtures	10-23
Gas-Liquid Mixtures	10-23
Liquid-Solid Mixtures	10-23
Flowmeter Selection	10-23
Weirs	10-23
PUMPS AND COMPRESSORS	
Introduction	10-24
Terminology	10-25
Displacement	10-25
Centrifugal Force	10-25
Electromagnetic Force	10-25
Transfer of Momentum	10-25
Mechanical Impulse	10-25
Measurement of Performance	10-25
Capacity	10-25
Total Dynamic Head	10-25
Total Suction Head	10-25
Static Suction Head	10-26
Total Discharge Head	10-26
Static Discharge Head	10-26
Velocity	10-27
Velocity Head	10-27
Viscosity	10-27
Friction Head	10-27
Work Performed in Pumping	10-27
Pump Selection	10-27
Range of Operation	10-27
Net Positive Suction Head	10-27
Suction Limitations of a Pump	10-27
NPSH Requirements for Other Liquids	10-28
Example 1: NPSH Calculation	10-28
Pump Specifications	10-28
Positive-Displacement Pumps	10-28
Reciprocating Pumps	10-28
Piston Pumps	10-30
Diaphragm Pumps	10-30
Rotary Pumps	10-31
Gear Pumps	10-31
Screw Pumps	10-32
Fluid-Displacement Pumps	10-32
Centrifugal Pumps	10-32
Casings	10-33
Action of a Centrifugal Pump	10-33

Centrifugal Pump Characteristics	10-33
System Curves	10-34
Pump Selection	10-34
Process Pumps	10-34
Sealing the Centrifugal Chemical Pump	10-35
Double-Suction Single-Stage Pumps	10-35
Close-Coupled Pumps	10-35
Canned-Motor Pumps	10-36
Vertical Pumps	10-36
Sump Pumps	10-37
Multistage Centrifugal Pumps	10-37
Propeller and Turbine Pumps	10-37
Axial-Flow (Propeller) Pumps	10-37
Turbine Pumps	10-38
Regenerative Pumps	10-38
Jet Pumps	10-39
Electromagnetic Pumps	10-39
Pump Diagnostics	10-40
Compressors	10-40
Compressor Selection	10-42
Compression of Gases	10-42
Theory of Compression	10-42
Adiabatic Calculations	10-44
Reciprocating Compressors	10-45
Fans and Blowers	10-49
Axial-Flow Fans	10-49
Centrifugal Blowers	10-49
Forward-Curved Blade Blowers	10-50
Backward-Curved Blade Blowers	10-50
Fan Performance	10-52
Continuous-Flow Compressors	10-52
Centrifugal Compressors	10-52
Compressor Configuration	10-53
Impeller Fabrication	10-54
Axial-Flow Compressors	10-54
Positive-Displacement Compressors	10-56
Rotary Compressors	10-56
Ejectors	10-57
Ejector Performance	10-57
Uses of Ejectors	10-58
Vacuum Systems	10-58
Vacuum Equipment	10-58
Sealing of Rotating Shafts	10-59
Noncontact Seals	10-59
Labyrinth Seals	10-59
Ring Seals	10-62
Fixed Seal Rings	10-62
Floating Seal Rings	10-62
Packing Seal	10-62
Mechanical Face Seals	10-63
Mechanical Seal Selection	10-63
Internal and External Seals	10-64
Throttle Bushings	10-64
Materials	10-65
Bearings	10-65
Types of Bearings	10-65
Thrust Bearings	10-66
Thrust-Bearing Power Loss	10-67
Centrifugal Compressor Problems	10-67
Compressor Fouling	10-68
Compressor Failures	10-69
Impeller Problems	10-69
Rotor Thrust Problems	10-69
Journal Bearing Failures	10-70
Thrust Bearing Failures	10-70
Compressor Seal Problems	10-70
Rotor Dynamics	10-70
Vibration Monitoring	10-71
Example 2: Vibration	10-72
PROCESS PLANT PIPING	
Introduction	10-73
Codes and Standards	10-73
Units: Pipe and Tubing Sizes and Ratings	10-73
Pressure-Piping Codes	10-73
National Standards	10-73
Government Regulations: OSHA	10-73
International Regulations	10-74
Code Contents and Scope	10-74
Selection of Pipe System Materials	10-74

General Considerations 10-74
 Specific Material Considerations—Metals 10-75
 Specific Material Considerations—Nonmetals 10-76
Metallic Piping System Components 10-76
 Seamless Pipe and Tubing 10-76
 Welded Pipe and Tubing 10-76
 Tubing 10-77
 Methods of Joining Pipe 10-77
 Flanged Joints 10-81
 Ring Joint Flanges 10-85
 Bolting 10-85
 Miscellaneous Mechanical Joints 10-87
 Pipe Fittings and Bends 10-89
 Valves 10-93
Cast Iron, Ductile Iron, and High-Silicon Iron Piping Systems 10-98
 Cast Iron and Ductile Iron 10-98
 High-Silicon Iron 10-99
Nonferrous Metal Piping Systems 10-99
 Aluminum 10-99
 Copper and Copper Alloys 10-100
 Nickel and Nickel Alloys 10-100
 Titanium 10-101
 Flexible Metal Hose 10-101
Nonmetallic Pipe and Metallic Piping Systems with
 Nonmetallic Linings 10-103
 Cement-Lined Carbon-Steel Pipe 10-103
 Concrete Pipe 10-104
 Glass Pipe and Fittings 10-104
 Glass-Lined Steel Pipe and Fittings 10-105
 Fused Silica or Fused Quartz 10-105
 Plastic-Lined Steel Pipe 10-105
 Rubber-Lined Steel Pipe 10-106
 Plastic Pipe 10-106
 Reinforced-Thermosetting-Resin (RTR) Pipe 10-107
Design of Piping Systems 10-107
 Safeguarding 10-107
 Classification of Fluid Services 10-107
 Category D 10-107
 Category M 10-107
 Design Conditions 10-107
 Effects of Support, Anchor, and Terminal Movements 10-108
 Reduced Ductility 10-108
 Cyclic Effects 10-108
 Air Condensation Effects 10-108
 Design Criteria: Metallic Pipe 10-108
 Limits of Calculated Stresses due to Sustained Loads
 and Displacement Strains 10-111
 Pressure Design of Metallic Components 10-111
 Test Conditions 10-113
 Thermal Expansion and Flexibility: Metallic Piping 10-114
 Reactions: Metallic Piping 10-120
 Pipe Supports 10-122
 Design Criteria: Nonmetallic Pipe 10-123
Fabrication, Assembly, and Erection 10-123
 Welding, Brazing, or Soldering 10-123

Bending and Forming 10-126
 Preheating and Heat Treatment 10-126
 Joining Nonmetallic Pipe 10-126
 Assembly and Erection 10-126
Examination, Inspection, and Testing 10-126
 Examination and Inspection 10-126
 Examination Methods 10-128
 Type and Extent of Required Examination 10-131
 Impact Testing 10-133
 Pressure Testing 10-133
 Cost Comparison of Piping Systems 10-135
 Forces of Piping on Process Machinery and Piping Vibration 10-135
Heat Tracing of Piping Systems 10-135
 Types of Heat-Tracing Systems 10-137
 Choosing the Best Tracing System 10-140

STORAGE AND PROCESS VESSELS

Storage of Liquids 10-140
 Atmospheric Tanks 10-140
 Shop-Fabricated Storage Tanks 10-140
 USTs versus ASTs 10-140
 Aboveground Storage Tanks 10-140
 Pressure Tanks 10-144
 Calculation of Tank Volume 10-144
 Container Materials and Safety 10-145
 Pond Storage 10-146
 Underground Cavern Storage 10-146
Storage of Gases 10-148
 Gas Holders 10-148
 Solution of Gases in Liquids 10-148
 Storage in Pressure Vessels, Bottles, and Pipe Lines 10-148
 Materials 10-149
 Cavern Storage 10-149
 Cost of Storage Facilities 10-149
Bulk Transport of Fluids 10-149
 Pipe Lines 10-149
 Tanks 10-149
 Tank Cars 10-150
 Tank Trucks 10-151
 Marine Transportation 10-151
 Materials of Construction for Bulk Transport 10-151
Pressure Vessels 10-151
 Code Administration 10-151
 ASME Code Section VIII, Division 1 10-152
 ASME Code Section VIII, Division 2 10-155
 Additional ASME Code Considerations 10-155
 Other Regulations and Standards 10-157
 Vessels with Unusual Construction 10-157
 ASME Code Developments 10-158
 Vessel Codes Other than ASME 10-158
 Vessel Design and Construction 10-158
 Care of Pressure Vessels 10-158
 Pressure-Vessel Cost and Weight 10-159

10-4 TRANSPORT AND STORAGE OF FLUIDS

Nomenclature and Units

In this listing, symbols used in the section are defined in a general way and appropriate SI and U.S. customary units are given. Specific definitions, as denoted by subscripts, are stated at the place of application in the section. Some specialized symbols used in the section are defined only at the place of application.

Symbol	Definition	SI units	U.S. customary units	Symbol	Definition	SI units	U.S. customary units
A	Area	m ²	ft ²	K	Fluid bulk modulus of elasticity	N/m ²	lbf/ft ²
A	Factor for determining minimum value of R_1			K_1	Constant in empirical flexibility equation		
A_∞	Free-stream speed of sound			k	Ratio of specific heats	Dimensionless	Dimensionless
a	Area	m ²	ft ²	k	Flexibility factor		
a	Duct or channel width	m	ft	k	Adiabatic exponent c_p/c_v		
a	Coefficient, general			L	Length	m	ft
B	Height	m	ft	L	Developed length of piping between anchors	m	ft
b	Duct or channel height	m	ft	L	Dish radius	m	in
b	Coefficient, general			M	Molecular weight	kg/mol	lb/mol
C	Coefficient, general			M_b, m_i	In-plane bending moment	N-mm	in-lbf
C	Conductance	m ³ /s	ft ³ /s	M_o	Out-plane bending moment	N-mm	in-lbf
C	Sum of mechanical allowances (thread or groove depth) plus corrosion or erosion allowances	mm	in	M_t	Torsional moment	N-mm	in-lbf
C	Cold-spring factor			M_∞	Free stream Mach number		
C	Constant			m	Mass	kg	lb
C_a	Capillary number	Dimensionless	Dimensionless	m	Thickness	m	ft
C_1	Estimated self-spring or relaxation factor			N	Number of data points or items	Dimensionless	Dimensionless
c_p	Constant-pressure specific heat	J/(kg·K)	Btu/(lb·°R)	N	Frictional resistance	Dimensionless	Dimensionless
c_v	Constant-volume specific heat	J/(kg·K)	Btu/(lb·°R)	N	Equivalent full temperature cycles		
D	Diameter	m	ft	N_s	Strouhal number	Dimensionless	Dimensionless
D, D_o	Outside diameter of pipe	mm	in	N_{De}	Dean number	Dimensionless	Dimensionless
d	Diameter	m	ft	N_{Fr}	Froude number	Dimensionless	Dimensionless
E	Modulus of elasticity	N/m ²	lbf/ft ²	N_{Re}	Reynolds number	Dimensionless	Dimensionless
E	Quality factor			N_{We}	Weber number	Dimensionless	Dimensionless
E_a	As-installed Young's modulus	MPa	kip/in ² (ksi)	NPSH	Net positive suction head	m	ft
E_c	Casting quality factor			n	Polytropic exponent		
E_j	Joint quality factor			n	Pulsation frequency	Hz	1/s
E_m	Minimum value of Young's modulus	MPa	kip/in ² (ksi)	n	Constant, general		
F	Force	N	lbf	n	Number of items	Dimensionless	Dimensionless
F	Friction loss	(N·m)/kg	(ft·lbf)/lb	P	Design gauge pressure	kPa	lbf/in ²
F	Correction factor	Dimensionless	Dimensionless	P_{ad}	Adiabatic power	kW	hp
f	Frequency	Hz	1/s	p	Pressure	Pa	lbf/ft ²
f	Friction factor	Dimensionless	Dimensionless	p	Power	kW	hp
f	Stress-range reduction factor			Q	Heat	J	Btu
G	Mass velocity	kg/(s·m ²)	lb/(s·ft ²)	Q	Volume	m ³	ft ³
g	Local acceleration due to gravity	m/s ²	ft/s ²	Q	Volume rate of flow (liquids)	m ³ /h	gal/min
g_c	Dimensional constant	1.0 (kg·m)/(N·s ²)	32.2 (lb·ft)/(lbf·s ²)	Q	Volume rate of flow (gases)	m ³ /h	ft ³ /min (cfm)
H	Depth of liquid	m	ft	q	Volume flow rate	m ³ /s	ft ³ /s
H, h	Head of fluid, height	m	ft	\bar{R}	Gas constant	8314 J/(K·mol)	1545 (ft·lbf)/(mol·°R)
H_{ad}	Adiabatic head	N·m/kg	lbf-ft/lbm	R	Radius	m	ft
h	Flexibility characteristic			R	Electrical resistance	Ω	Ω
h	Height of truncated cone; depth of head	m	in	R	Head reading	m	ft
i	Specific enthalpy	J/kg	Btu/lb	R	Range of reaction forces or moments in flexibility analysis	N or N-mm	lbf or in-lbf
i	Stress-intensification factor			R	Cylinder radius	m	ft
i_i	In-plane stress-intensification factor			R	Universal gas constant	J/(kg·K)	(ft·lbf)/(lbm·°R)
i_o	Out-plane stress-intensification factor			R_a	Estimated instantaneous reaction force or moment at installation temperature	N or N-mm	lbf or in-lbf
I	Electric current	A	A	R_m	Estimated instantaneous maximum reaction force or moment at maximum or minimum metal temperature	N or N-mm	lbf or in-lbf
J	Mechanical equivalent of heat	1.0 (N·m)/J	778 (ft·lbf)/Btu	R_1	Effective radius of miter bend	mm	in
K	Index, constant or flow parameter						

Nomenclature and Units (Concluded)

Symbol	Definition	SI units	U.S. customary units	Symbol	Definition	SI units	U.S. customary units
r	Radius	m	ft	v	Specific volume	m ³ /kg	ft ³ /lb
r	Pressure ratio	Dimensionless	Dimensionless	W	Work	N·m	lb·ft
r_c	Critical pressure ratio			W	Weight	kg	lb
r_k	Knuckle radius	m	in	w	Weight flow rate	kg/s	lb/s
r_2	Mean radius of pipe using nominal wall thickness \bar{T}	mm	in	x	Weight fraction	Dimensionless	Dimensionless
S	Specific surface area	m ² /m ³	ft ² /ft ³	x	Distance or length	m	ft
S	Fluid head loss	Dimensionless	Dimensionless	x	Value of expression $[(p_2/p_1)^{(k-1/k)} - 1]$		
S	Specific energy loss	m/s ²	lb/ft	Y	Expansion factor	Dimensionless	Dimensionless
S	Speed	m ³ /s	ft ³ /s	y	Distance or length	m	ft
S	Basic allowable stress for metals, excluding factor E , or bolt design stress	MPa	kip/in ² (ksi)	y	Resultant of total displacement strains	mm	in
S_A	Allowable stress range for displacement stress	MPa	kip/in ² (ksi)	Z	Section modulus of pipe	mm ³	in ³
S_E	Computed displacement-stress range	MPa	kip/in ² (ksi)	Z	Vertical distance	m	ft
S_L	Sum of longitudinal stresses	MPa	kip/in ² (ksi)	Z_c	Effective section modulus for branch	mm ³	in ³
S_T	Allowable stress at test temperature	MPa	kip/in ² (ksi)	Z	Gas-compressibility factor	Dimensionless	Dimensionless
S_b	Resultant bending stress	MPa	kip/in ² (ksi)	z	Vertical distance	m	ft
S_c	Basic allowable stress at minimum metal temperature expected	MPa	kip/in ² (ksi)	Greek symbols			
S_h	Basic allowable stress at maximum metal temperature expected	MPa	kip/in ² (ksi)	α	Viscous-resistance coefficient	1/m ²	1/ft ²
S_t	Torsional stress	MPa	kip/in ² (ksi)	α	Angle	°	°
s	Specific gravity			σ	Half-included angle	°	°
s	Specific entropy	J/(kg·K)	Btu/(lb·°R)	α, β, θ	Angles	°	°
T	Temperature	K (°C)	°R (°F)	β	Inertial-resistance coefficient	1/m	1/ft
T_s	Effective branch-wall thickness	mm	in	β	Ratio of diameters	Dimensionless	Dimensionless
\bar{T}	Nominal wall thickness of pipe	mm	in	Γ	Liquid loading	kg/(s·m)	lb/(s·ft)
\bar{T}_b	Nominal branch-pipe wall thickness	mm	in	Γ	Pulsation intensity	Dimensionless	Dimensionless
\bar{T}_h	Nominal header-pipe wall thickness	mm	in	δ	Thickness	m	ft
t	Head or shell radius	mm	in	ϵ	Wall roughness	m	ft
t	Pressure design thickness	mm	in	ϵ	Voidage—fractional free volume	Dimensionless	Dimensionless
t	Time	s	s	η	Viscosity, nonnewtonian fluids	Pa·s	lb/(ft·s)
t_m	Minimum required thickness, including mechanical, corrosion, and erosion allowances	mm	in	η_{ad}	Adiabatic efficiency		
t_r	Pad or saddle thickness	mm	in	η_p	Polytropic efficiency		
U	Straight-line distance between anchors	m	ft	θ	Angle	°	°
u	Specific internal energy	J/kg	Btu/lb	λ	Molecular mean free-path length	m	ft
u	Velocity	m/s	ft/s	μ	Viscosity	Pa·s	lb/(ft·s)
V	Velocity	m/s	ft/s	ν	Kinematic viscosity	m ² /s	ft ² /s
V	Volume	m ³	ft ³	ρ	Density	kg/m ³	lb/ft ³
				σ	Surface tension	N/m	lb/ft
				σ_c	Cavitation number	Dimensionless	Dimensionless
				τ	Shear stress	N/m ²	lb/ft ²
				ϕ	Shape factor	Dimensionless	Dimensionless
				ϕ	Angle	°	°
				ϕ	Flow coefficient		
				ψ	Pressure coefficient		
				ψ	Sphericity	Dimensionless	Dimensionless

MEASUREMENT OF FLOW

GENERAL REFERENCES: ASME, *Performance Test Code on Compressors and Exhausters*, PTC 10-1997, American Society of Mechanical Engineers (ASME), New York, 1997. Norman A. Anderson, *Instrumentation for Process Measurement and Control*, 3d ed., CRC Press, Boca Raton, Fla., 1997. Roger C. Baker, *Flow Measurement Handbook: Industrial Designs, Operating Principles, Performance, and Applications*, Cambridge University Press, Cambridge, United Kingdom, 2000. Roger C. Baker, *An Introductory Guide to Flow Measurement*, ASME, New York, 2003. Howard S. Bean, ed., *Fluid Meters—Their Theory and Application—Report of the ASME Research Committee on Fluid Meters*, 6th ed., ASME, New York, 1971. Douglas M. Considine, Editor-in-Chief, *Process/Industrial Instruments and Controls Handbook*, 4th ed., McGraw-Hill, New York, 1993. Bela C. Liptak, Editor-in-Chief, *Process Measurement and Analysis*, 4th ed., CRC Press, Boca Raton, Fla., 2003. Richard W. Miller, *Flow Measurement Engineering Handbook*, 3d ed., McGraw-Hill, New York, 1996. Ower and Pankhurst, *The Measurement of Air Flow*, Pergamon, Oxford, United Kingdom, 1966. Brian Price et al., *Engineering Data Book*, 12th ed., Gas Processors Suppliers Association, Tulsa, Okla., 2004. David W. Spitzer, *Flow Measurement*, 2d ed., Instrument Society of America, Research Triangle Park, N.C., 2001. David W. Spitzer, *Industrial Flow Measurement*, 3d ed., Instrument Society of America, Research Triangle Park, N.C., 2005.

INTRODUCTION

The flow rate of fluids is a critical variable in most chemical engineering applications, ranging from flows in the process industries to environmental flows and to flows within the human body. *Flow* is defined as mass flow or volume flow per unit of time at specified temperature and pressure conditions for a given fluid. This subsection deals with the techniques of measuring pressure, temperature, velocities, and flow rates of flowing fluids. For more detailed discussion of these variables, consult Sec. 8. Section 8 introduces methods of measuring flow rate, temperature, and pressure. This subsection builds on the coverage in Sec. 8 with emphasis on measurement of the flow of fluids.

PROPERTIES AND BEHAVIOR OF FLUIDS

Transportation and the storage of fluids (gases and liquids) involves the understanding of the properties and behavior of fluids. The study of fluid dynamics is the study of fluids and their motion in a force field.

Flows can be classified into two major categories: (a) incompressible and (b) compressible flow. Most liquids fall into the incompressible-flow category, while most gases are compressible in nature. A perfect fluid can be defined as a fluid that is nonviscous and nonconducting. Fluid flow, compressible or incompressible, can be classified by the ratio of the inertial forces to the viscous forces. This ratio is represented by the Reynolds number (N_{Re}). At a low Reynolds number, the flow is considered to be laminar, and at high Reynolds numbers, the

flow is considered to be turbulent. The limiting types of flow are the inertialess flow, sometimes called Stokes flow, and the inviscid flow that occurs at an infinitely large Reynolds number. Reynolds numbers (dimensionless) for flow in a pipe is given as:

$$N_{Re} = \frac{\rho VD}{\mu} \quad (10-1)$$

where ρ is the density of the fluid, V the velocity, D the diameter, and μ the viscosity of the fluid. In fluid motion where the frictional forces interact with the inertia forces, it is important to consider the ratio of the viscosity μ to the density ρ . This ratio is known as the kinematic viscosity (ν). Tables 10-1 and 10-2 give the kinematic viscosity for several fluids. A flow is considered to be *adiabatic* when there is no transfer of heat between the fluid and its surroundings. An isentropic flow is one in which the entropy of each fluid element remains constant.

To fully understand the mechanics of flow, the following definitions explain the behavior of various types of fluids in both their static and flowing states.

A perfect fluid is a nonviscous, nonconducting fluid. An example of this type of fluid would be a fluid that has a very small viscosity and conductivity and is at a high Reynolds number. An ideal gas is one that obeys the equation of state:

$$\frac{P}{\rho} = RT \quad (10-2)$$

where P = pressure, ρ = density, R is the gas constant per unit mass, and T = temperature.

A flowing fluid is acted upon by many forces that result in changes in pressure, temperature, stress, and strain. A fluid is said to be isotropic when the relations between the components of stress and those of the rate of strain are the same in all directions. The fluid is said to be Newtonian when this relationship is linear. These pressures and temperatures must be fully understood so that the entire flow picture can be described.

The *static pressure* in a fluid has the same value in all directions and can be considered as a scalar point function. It is the pressure of a flowing fluid. It is normal to the surface on which it acts and at any given point has the same magnitude irrespective of the orientation of the surface. The static pressure arises because of the random motion in the fluid of the molecules that make up the fluid. In a diffuser or nozzle, there is an increase or decrease in the static pressure due to the change in velocity of the moving fluid.

Total pressure is the pressure that would occur if the fluid were brought to rest in a reversible adiabatic process. Many texts and engineers use the words *total* and *stagnation* to describe the flow characteristics interchangeably. To be accurate, the stagnation pressure

TABLE 10-1 Density, Viscosity, and Kinematic Viscosity of Water and Air in Terms of Temperature

Temperature		Water			Air at a pressure of 760 mm Hg (14.696 lbf/in ²)		
		Density ρ (lbf sec ² /ft ⁴)	Viscosity $\mu \times 10^6$ (lbf sec/ft ²)	Kinematic viscosity $\nu \times 10^6$ (ft ² /sec)	Density ρ (lbf sec ² /ft ⁴)	Viscosity $\mu \times 10^6$ (lbf sec/ft ²)	Kinematic viscosity $\nu \times 10^6$ (ft ² /sec)
(°C)	(°F)						
-20	-4	—	—	—	0.00270	0.326	122
-10	14	—	—	—	0.00261	0.338	130
0	32	1.939	37.5	19.4	0.00251	0.350	140
10	50	1.939	27.2	14.0	0.00242	0.362	150
20	68	1.935	21.1	10.9	0.00234	0.375	160
40	104	1.924	13.68	7.11	0.00217	0.399	183
60	140	1.907	9.89	5.19	0.00205	0.424	207
80	176	1.886	7.45	3.96	0.00192	0.449	234
100	212	1.861	5.92	3.19	0.00183	0.477	264

Conversion factors: 1 kp sec²/m⁴ = 0.01903 lbf sec²/ft⁴ (= slug/ft³)
 1 lbf sec²/ft⁴ = 32.1719 lb/ft³ (lb = lb mass; lbf = lb force)
 1 kp sec²/m⁴ = 9.80665 kg/m³ (kg = kg mass; kp = kg force)
 1 kg/m³ = 16.02 lb/ft³

TABLE 10-2 Kinematic Viscosity

Liquid	Temperature		$\nu \times 10^6$ (ft ² /s)
	°C	°F	
Glycerine	20	68	7319
Mercury	0	32	1.35
Mercury	100	212	0.980
Lubricating oil	20	68	4306
Lubricating oil	40	104	1076
Lubricating oil	60	140	323

is the pressure that would occur if the fluid were brought to rest adiabatically or diabatically.

Total pressure will only change in a fluid if shaft work or work of extraneous forces are introduced. Therefore, total pressure would increase in the impeller of a compressor or pump; it would remain constant in the diffuser. Similarly, total pressure would decrease in the turbine impeller but would remain constant in the nozzles.

Static temperature is the temperature of the flowing fluid. Like static pressure, it arises because of the random motion of the fluid molecules. Static temperature is in most practical installations impossible to measure since it can be measured only by a thermometer or thermocouple at rest relative to the flowing fluid that is moving with the fluid. Static temperature will increase in a diffuser and decrease in a nozzle.

Total temperature is the temperature that would occur when the fluid is brought to rest in a reversible adiabatic manner. Just like its counterpart *total pressure*, *total* and *stagnation temperatures* are used interchangeably by many test engineers.

Dynamic temperature and pressure are the difference between the total and static conditions.

$$P_d = P_T - P_s \quad (10-3)$$

$$T_d = T_T - T_s \quad (10-4)$$

where subscript *d* refers to dynamic, *T* to total, and *s* to static.

Another helpful formula is:

$$P_k = \frac{1}{2} \rho V^2 \quad (10-5)$$

For incompressible fluids, $P_k = P_d$.

TOTAL TEMPERATURE

For most points requiring temperature monitoring, either thermocouples or resistive thermal detectors (RTDs) can be used. Each type of temperature transducer has its own advantages and disadvantages, and both should be considered when temperature is to be measured. Since there is considerable confusion in this area, a short discussion of the two types of transducers is necessary.

Thermocouples The various types of thermocouples provide transducers suitable for measuring temperatures from -330 to 5000°F (-201 to 2760°C). Thermocouples function by producing a voltage proportional to the temperature differences between two junctions of dissimilar metals. By measuring this voltage, the temperature difference can be determined. It is assumed that the temperature is known at one of the junctions; therefore, the temperature at the other junction can be determined. Since the thermocouples produce a voltage, no external power supply is required to the test junction; however, for accurate measurement, a reference junction is required. For a temperature monitoring system, reference junctions must be placed at each thermocouple or similar thermocouple wire installed from the thermocouple to the monitor where there is a reference junction. Properly designed thermocouple systems can be accurate to approximately $\pm 2^\circ\text{F}$ ($\pm 1^\circ\text{C}$).

Resistive Thermal Detectors (RTDs) RTDs determine temperature by measuring the change in resistance of an element due to temperature. Platinum is generally utilized in RTDs because it remains mechanically and electrically stable, resists contaminations, and can be highly refined. The useful range of platinum RTDs is

-454 – 1832°F (-270 – 1000°C). Since the temperature is determined by the resistance in the element, any type of electrical conductor can be utilized to connect the RTD to the indicator; however, an electrical current must be provided to the RTD. A properly designed temperature monitoring system utilizing RTDs can be accurate $\pm 0.02^\circ\text{F}$ ($\pm 0.01^\circ\text{C}$).

STATIC TEMPERATURE

Since this temperature requires the thermometer or thermocouple to be at rest relative to the flowing fluid, it is impractical to measure. It can be, however, calculated from the measurement of total temperature and total and static pressure.

$$T_s = \frac{T_o}{\left(\frac{P_o}{P_s}\right)^{(k-1)/k}} \quad (10-6)$$

DRY- AND WET-BULB TEMPERATURES

The moisture content or humidity of air has an important effect on the properties of the gaseous mixture. Steam in air at any relative humidity less than 100 percent must exist in a superheated condition. The saturation temperature corresponding to the actual partial pressure of the steam in air is called the dew point. This term arose from the fact that when air at less than 100 percent relative humidity is cooled to the temperature at which it becomes saturated, the air has reached the minimum temperature to which it can be cooled without precipitation of the moisture (dew). Dew point can also be defined as that temperature at which the weight of steam associated with a certain weight of dry air is adequate to saturate that weight of air.

The dry-bulb temperature of air is the temperature that is indicated by an ordinary thermometer. When an air temperature is stated without any modifying term, it is always taken to be the dry-bulb temperature. In contrast to dry-bulb, or air, temperature, the term *wet-bulb temperature of the air*, or simply *wet-bulb temperature*, is employed. When a thermometer, with its bulb covered by a wick wetted with water, is moved through air unsaturated with water vapor, the water evaporates in proportion to the capacity of the air to absorb the evaporated moisture, and the temperature indicated by the thermometer drops below the dry-bulb, or air, temperature. The equilibrium temperature finally reached by the thermometer is known as the wet-bulb temperature. The purpose in measuring both the dry-bulb and wet-bulb temperature of the air is to find the exact humidity characteristics of the air from the readings obtained, either by calculation or by use of a psychrometric chart. Instruments for measuring wet-bulb and dry-bulb temperatures are known as psychrometers. A sling psychrometer consists of two thermometers mounted side by side on a holder, with provision for whirling the whole device through the air. The dry-bulb thermometer is bare, and the wet bulb is covered by a wick which is kept wetted with clean water. After being whirled a sufficient amount of time, the wet-bulb thermometer reaches its equilibrium point, and both the wet-bulb and dry-bulb thermometers are then quickly read. Rapid relative movement of the air past the wet-bulb thermometer is necessary to get dependable readings.

For other methods of measuring the moisture content of gases, see Sec. 8.

PRESSURE MEASUREMENTS

Pressure is defined as the force per unit area. Pressure devices measure with respect to the ambient atmospheric pressure: The absolute pressure P_a is the pressure of the fluid (gauge pressure) plus the atmospheric pressure.

Process pressure-measuring devices may be divided into three groups:

1. Those that are based on the height of a liquid column (manometers)
2. Those that are based on the measurement of the distortion of an elastic pressure chamber (mechanical pressure gauges such as Bourdon-tube gauges and diaphragm gauges)

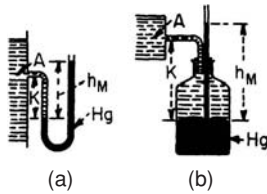


FIG. 10-1 Open manometers.

3. Electric sensing devices (strain gauges, piezoresistive transducers, and piezoelectric transducers)

This subsection contains an expanded discussion of manometric methods. See Sec. 8 for other methods.

Liquid-Column Manometers The **height, or head,** $p_h = \rho h g/g_c$, to which a fluid rises in an open vertical tube attached to an apparatus containing a liquid is a direct measure of the pressure at the point of attachment and is frequently used to show the level of liquids in tanks and vessels. This same principle can be applied with U-tube gauges (Fig. 10-1a) and equivalent devices (such as that shown in Fig. 10-1b) to measure pressure in terms of the head of a fluid other than the one under test. Most of these gauges may be used either as **open** or as **differential manometers**. The manometric fluid that constitutes the measured liquid column of these gauges may be any liquid immiscible with the fluid under pressure. For high pressures and large pressure differences, the gauge liquid is a high-density liquid, generally mercury; for low pressures and small pressure differences, a low-density liquid (e.g., alcohol, water, or carbon tetrachloride) is used.

The **open U tube** (Fig. 10-1a) and the **open gauge** (Fig. 10-1b) each show a reading h_M m (ft) of manometric fluid. If the interface of the manometric fluid and the fluid of which the pressure is wanted is K m (ft) below the point of attachment, A , ρ_A is the density of the latter fluid at A , and ρ_M is that of the manometric fluid, then gauge pressure p_A (lb/ft²) at A is

$$p_A = (h_M \rho_M - K \rho_A)(g/g_c) \quad (10-7)^{\circ}$$

where g = local acceleration due to gravity and g_c = dimensional constant. The head H_A at A as meters (feet) of the fluid at that point is

$$h_A = h_M(\rho_M/\rho_A) - K \quad (10-8)^{\circ}$$

When a gas pressure is measured, unless it is very high, ρ_A is so much smaller than ρ_M that the terms involving K in these formulas are negligible.

The **differential U tube** (Fig. 10-2) shows the pressure difference between taps A and B to be

$$p_A - p_B = [h_M(\rho_M - \rho_A) + K_A \rho_A - K_B \rho_B](g/g_c) \quad (10-9)^{\circ}$$

where h_M is the difference in height of the manometric fluid in the U tube; K_A and K_B are the vertical distances of the upper surface of the

^oThe line leading from the pressure tap to the gauge is assumed to be filled with fluid of the same density as that in the apparatus at the location of the pressure tap; if this is not the case, ρ_A is the density of the fluid actually filling the gauge line, and the value given for h_A must be multiplied by ρ_A/ρ where ρ is the density of the fluid whose head is being measured.

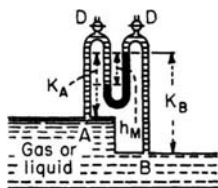


FIG. 10-2 Differential U tube.

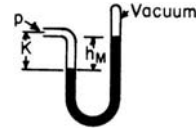


FIG. 10-3 Closed U tube.

manometric fluid above A and B , respectively; ρ_A and ρ_B are the densities of the fluids at A and B , respectively; and ρ_M is the density of the manometric fluid. If either pressure tap is above the higher level of manometric fluid, the corresponding K is taken to be negative. Valve D , which is kept closed when the gauge is in use, is used to vent off gas which may accumulate at these high points.

The **inverted differential U tube**, in which the manometric fluid may be a gas or a light liquid, can be used to measure liquid pressure differentials, especially for the flow of slurries where solids tend to settle out.

Closed U tubes (Fig. 10-3) using mercury as the manometric fluid serve to measure directly the absolute pressure p of a fluid, provided that the space between the closed end and the mercury is substantially a perfect vacuum.

The **mercury barometer** (Fig. 10-4) indicates directly the absolute pressure of the atmosphere in terms of height of the mercury column. Normal (standard) barometric pressure is 101.325 kPa by definition. Equivalents of this pressure in other units are 760 mm mercury (at 0°C), 29.921 inHg (at 0°C), 14.696 lbf/in², and 1 atm. For cases in which barometer readings, when expressed by the height of a mercury column, must be corrected to standard temperature (usually 0°C), appropriate temperature correction factors are given in ASME PTC, op. cit., pp. 23–26; and West, *Handbook of Chemistry and Physics*, 62d ed., Chemical Rubber, Cleveland, 1984, pp. E36–E37.

Tube Size for Manometers To avoid capillary error, tube diameter should be sufficiently large and the manometric fluids of such densities that the effect of capillarity is negligible in comparison with the gauge reading. The effect of capillarity is practically negligible for tubes with inside diameters 12.7 mm (1/2 in) or larger (see ASME PTC, op. cit., p. 15). Small diameters are generally permissible for U tubes because the capillary displacement in one leg tends to cancel that in the other.

The capillary rise in a small vertical open tube of circular cross section dipping into a pool of liquid is given by

$$h = \frac{4\sigma g_c \cos \theta}{gD(\rho_1 - \rho_2)} \quad (10-10)$$

Here σ = surface tension, D = inside diameter, ρ_1 and ρ_2 are the densities of the liquid and gas (or light liquid) respectively, g = local acceleration due to gravity, g_c = dimensional constant, and θ is the contact angle subtended by the heavier fluid. For most organic liquids and water, the contact angle θ is zero against glass, provided the glass is wet with a film of the liquid; for mercury against glass, $\theta = 140^\circ$ (*International Critical Tables*, vol. IV, McGraw-Hill, New York, 1928, pp. 434–435). For further discussion of capillarity, see Schwartz, *Ind. Eng. Chem.*, **61**(1), 10–21 (1969).

Multiplying Gauges To attain the requisite precision in measurement of small pressure differences by liquid-column manometers,

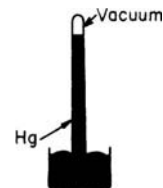


FIG. 10-4 Mercury barometer.

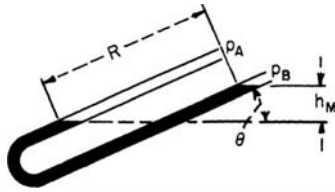


FIG. 10-5 Inclined U tube.

means must often be devised to magnify the readings. Of the schemes that follow, the second and third may give tenfold multiplication; the fourth, as much as thirtyfold. In general, the greater the multiplication, the more elaborate must be the precautions in the use of the gauge if the gain in precision is not to be illusory.

1. *Change of manometric fluid.* In open manometers, choose a fluid of lower density. In differential manometers, choose a fluid such that the difference between its density and that of the fluid being measured is as small as possible.

2. *Inclined U tube (Fig. 10-5).* If the reading R m (ft) is taken as shown and R_0 m (ft) is the zero reading, by making the substitution $h_M = (R - R_0) \sin \theta$, the formulas of preceding paragraphs give $(p_A - p_B)$ when the corresponding upright U tube is replaced by one inclined. For precise work, the gauge should be calibrated because of possible variations in tube diameter and slope.

3. *The draft gauge (Fig. 10-6).* Commonly used for low gas heads, this gauge has for one leg of the U a reservoir of much larger bore than the tubing that forms the inclined leg. Hence variations of level in the inclined tube produce little change in level in the reservoir. Although h_M may be readily computed in terms of reading R and the dimensions of the tube, calibration of the gauge is preferable; often the changes of level in the reservoir are not negligible, and also variations in tube diameter may introduce serious error into the computation. Commercial gauges are often provided with a scale giving h_M directly in height of water column, provided a particular liquid (often not water) fills the tube; failure to appreciate that the scale is incorrect unless the gauge is filled with the specified liquid is a frequent source of error. If the scale reads correctly when the density of the gauge liquid is ρ_0 , then the reading must be multiplied by ρ/ρ_0 if the density of the fluid actually in use is ρ .

4. *Two-fluid U tube (Fig. 10-7).* This is a highly sensitive device for measuring small gas heads. Let A be the cross-sectional area of each of the reservoirs and a that of the tube forming the U; let ρ_1 be the density of the lighter fluid and ρ_2 that of the heavier fluid; and if R is the reading and R_0 its value with zero pressure difference, then the pressure difference is

$$p_A - p_B = (R - R_0) \left(\rho_2 - \rho_1 + \frac{a}{A} \rho_1 \right) \frac{g}{g_c} \quad (10-11)$$

where g = local acceleration due to gravity and g_c = dimensional constant.

When A/a is sufficiently large, the term $(a/A) \rho_1$ in Eq. (10-11) becomes negligible in comparison with the difference $(\rho_2 - \rho_1)$. However, this term should not be omitted without due consideration. In applying Eq. (10-11), the densities of the gauge liquids may not be taken from tables without the possibility of introducing serious error,

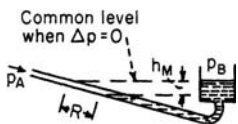


FIG. 10-6 Draft gauge.

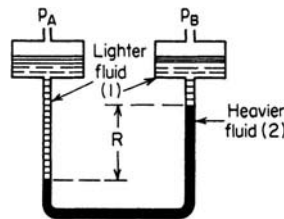


FIG. 10-7 Two-fluid U tube.

for each liquid may dissolve appreciable quantities of the other. Before the gauge is filled, the liquids should be shaken together, and the actual densities of the two layers should be measured for the temperature at which the gauge is to be used. When high magnification is being sought, the U tube may have to be enclosed in a constant-temperature bath so that $(\rho_2 - \rho_1)$ may be accurately known. In general, if highest accuracy is desired, the gauge should be calibrated.

Several **micromanometers**, based on the liquid-column principle and possessing extreme precision and sensitivity, have been developed for measuring minute gas-pressure differences and for calibrating low-range gauges. Some of these micromanometers are available commercially. These micromanometers are free from errors due to capillarity and, aside from checking the micrometer scale, require no calibration.

Mechanical Pressure Gauges The **Bourdon-tube gauge** indicates pressure by the amount of flexion under internal pressure of an oval tube bent in an arc of a circle and closed at one end. These gauges are commercially available for all pressures below atmospheric and for pressures up to 700 MPa (about 100,000 lbf/in²) above atmospheric. Details on Bourdon-type gauges are given by Harland [*Mach. Des.*, 40(22), 69–74 (Sept. 19, 1965)].

A **diaphragm gauge** depends for its indication on the deflection of a diaphragm, usually metallic, when subjected to a difference of pressure between the two faces. These gauges are available for the same general purposes as Bourdon gauges but are not usually employed for high pressures. The aneroid barometer is a type of diaphragm gauge.

Small **pressure transducers with flush-mounted diaphragms** are commercially available for the measurement of either steady or fluctuating pressures up to 100 MPa (about 15,000 lbf/in²). The metallic diaphragms are as small as 4.8 mm (³/₁₆ in) in diameter. The transducer is mounted on the apparatus containing the fluid whose pressure is to be measured so that the diaphragm is flush with the inner surface of the apparatus. Deflection of the diaphragm is measured by unbonded strain gauges and recorded electrically.

With nonnewtonian fluids the pressure measured at the wall with non-flush-mounted pressure gauges may be in error (see subsection "Static Pressure").

Bourdon and diaphragm gauges that show both pressure and vacuum indications on the same dial are called **compound gauges**.

Conditions of Use Bourdon tubes should not be exposed to temperatures over about 65°C (about 150°F) unless the tubes are specifically designed for such operation. When the pressure of a hotter fluid is to be measured, some type of liquid seal should be used to keep the hot fluid from the tube. In using either a Bourdon or a diaphragm gauge to measure gas pressure, if the gauge is below the pressure tap of the apparatus so that liquid can collect in the lead, the gauge reading will be too high by an amount equal to the hydrostatic head of the accumulated liquid.

For measuring pressures of corrosive fluids, slurries, and similar process fluids which may foul Bourdon tubes, a **chemical gauge**, consisting of a Bourdon gauge equipped with an appropriate flexible diaphragm to seal off the process fluid, may be used. The combined volume of the tube and the connection between the diaphragm and the tube is filled with an inert liquid. These gauges are available commercially.

Further details on pressure-measuring devices are found in Sec. 8.

Calibration of Gauges Simple **liquid-column manometers** do not require calibration if they are so constructed as to minimize errors due to capillarity (see subsection "Liquid-Column Manometers"). If the scales used to measure the readings have been checked against a standard, the accuracy of the gauges depends solely upon the precision of determining the position of the liquid surfaces. Hence liquid-column manometers are primary standards used to calibrate other gauges.

For **high pressures** and, with commercial mechanical gauges, even for quite moderate pressures, a deadweight gauge (see ASME PTC, op. cit., pp. 36–41) is commonly used as the primary standard because it is safer and more convenient than use of manometers. When manometers are used as high-pressure standards, an extremely high mercury column may be avoided by connecting a number of the usual U tubes in series. Multiplying gauges are standardized by comparing

10-10 TRANSPORT AND STORAGE OF FLUIDS

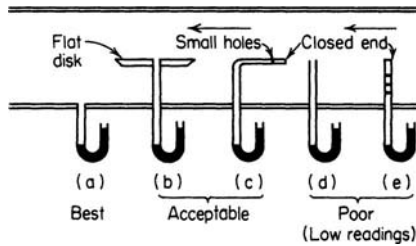


FIG. 10-8 Measurement of static pressure.

them with a micromanometer. Procedure in the calibration of a gauge consists merely of connecting it, in parallel with a standard gauge, to a reservoir wherein constant pressure may be maintained. Readings of the unknown gauge are then made for various reservoir pressures as determined by the standard.

Calibration of **high-vacuum gauges** is described by Sellenger [*Vacuum*, 18(12), 645–650 (1968)].

STATIC PRESSURE

Local Static Pressure In a moving fluid, the local static pressure is equal to the pressure on a surface which moves with the fluid or to the normal pressure (for newtonian fluids) on a stationary surface which parallels the flow. The pressure on such a surface is measured by making a small hole perpendicular to the surface and connecting the opening to a pressure-sensing element (Fig. 10-8a). The hole is known as a piezometer opening or pressure tap.

Measurement of local static pressure is frequently difficult or impractical. If the channel is so small that introduction of any solid object disturbs the flow pattern and increases the velocity, there will be a reduction and redistribution of the static pressure. If the flow is in straight parallel lines, aside from the fluctuations of normal turbulence, the flat disk (Fig. 10-8b) and the bent tube (Fig. 10-8c) give satisfactory results when properly aligned with the stream. Slight misalignments can cause serious errors. Diameter of the disk should be 20 times its thickness and 40 times the static opening; the face must be flat and smooth, with the knife edges made by beveling the underside. The piezometer tube, such as that in Fig. 10-8c, should have openings with size and spacing as specified for a pitot-static tube (Fig. 10-12).

Readings given by open straight tubes (Fig. 10-8d and 10-8e) are too low due to flow separation. Readings of closed tubes oriented perpendicularly to the axis of the stream and provided with side openings (Fig. 10-8e) may be low by as much as two velocity heads.

Average Static Pressure In most cases, the object of a static-pressure measurement is to obtain a suitable average value for substitution in Bernoulli's theorem or in an equivalent flow formula. This can be done simply only when the flow is in straight lines parallel to the confining walls, such as in straight ducts at sufficient distance downstream from bends (2 diameters) or other disturbances. For such streams, the sum of static head and gravitational potential head is the same at all points in a cross section taken perpendicularly to the axis of flow. Thus the exact location of a piezometer opening about the periphery of such a cross section is immaterial provided its elevation is known. However, in stating the static pressure, the custom is to give the value at the elevation corresponding to the centerline of the stream.

With flow in curved passages or with swirling flow, determination of a true average static pressure is, in general, impractical. In metering, straightening vanes are often placed upstream of the pressure tap to eliminate swirl. Figure 10-9 shows various flow equalizers and straighteners.

Specifications for Piezometer Taps The size of a static opening should be small compared with the diameter of the pipe and yet large compared with the scale of surface irregularities. For reliable results, it is essential that (1) the surface in which the hole is made be substantially smooth and parallel to the flow for some distance on either side of the

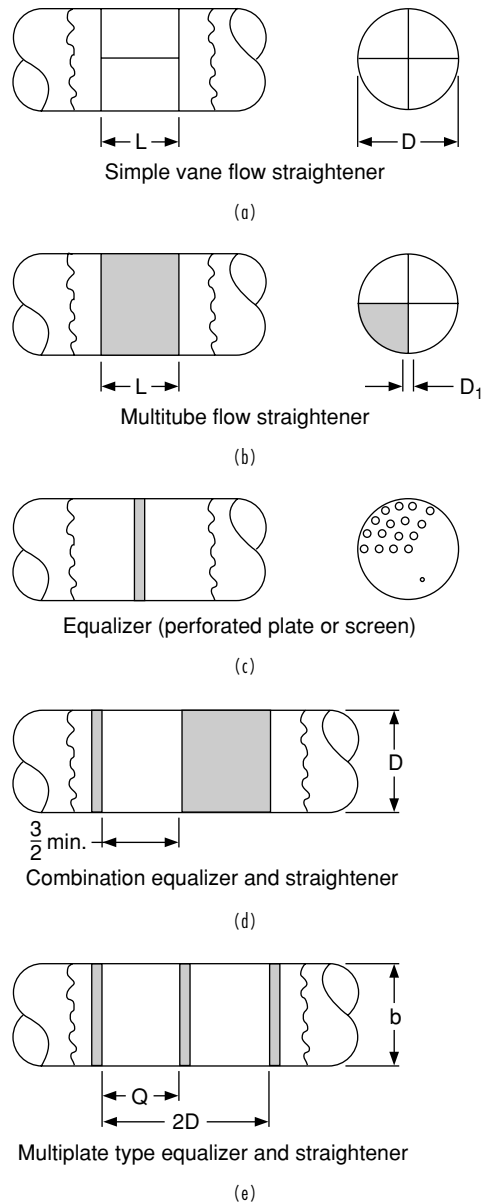


FIG. 10-9 Flow equalizers and straighteners [*Power Test Code 10, Compressors and Exhausters, Amer. Soc. of Mechanical Engineers, 1997*].

opening, and (2) the opening be flush with the surface and possess no "burr" or other irregularity around its edge. Rounding of the edge is often employed to ensure absence of a burr. Pressure readings will be high if the tap is inclined upstream, is rounded excessively on the upstream side, has a burr on the downstream side, or has an excessive countersink or recess. Pressure readings will be low if the tap is inclined downstream, is rounded excessively on the downstream side, has a burr on the upstream side, or protrudes into the flow stream. Errors resulting from these faults can be large.

Recommendations for **pressure-tap dimensions** are summarized in Table 10-3. Data from several references were used in arriving at these composite values. The length of a pressure-tap opening prior to any enlargement in the tap channel should be at least two tap diameters, preferably three or more.

TABLE 10-3 Pressure-Tap Holes

Nominal inside pipe diameter, in	Maximum diameter of pressure tap, mm (in)	Radius of hole-edge rounding, mm (in)
1	3.18 (1/8)	<0.40 (1/64)
2	6.35 (1/4)	0.40 (1/64)
3	9.53 (3/8)	0.40–0.79 (1/64–1/32)
4	12.7 (1/2)	0.79 (1/32)
8	12.7 (1/2)	0.79–1.59 (1/32–1/16)
16	19.1 (3/4)	0.79–1.59 (1/32–1/16)

A **piezometer ring** is a toroidal manifold into which are connected several sidewall static taps located around the perimeter of a common cross section. Its intent is to give an average pressure if differences in pressure other than those due to static head exist around the perimeter. However, there is generally no assurance that a true average is provided thereby. The principal advantage of the ring is that use of several holes in place of a single hole reduces the possibility of completely plugging the static openings.

For information on prediction of static-hole error, see Shaw, *J. Fluid Mech.*, **7**, 550–564 (1960); Livesey, Jackson, and Southern, *Aircr. Eng.*, **34**, 43–47 (February 1962).

For nonnewtonian fluids, pressure readings with taps may also be low because of fluid-elasticity effects. This error can be largely eliminated by using flush-mounted diaphragms.

For information on the pressure-hole error for nonnewtonian fluids, see Han and Kim, *Trans. Soc. Rheol.*, **17**, 151–174 (1973); Novotny and Eckert, *Trans. Soc. Rheol.*, **17**, 227–241 (1973); and Higashitani and Lodge, *Trans. Soc. Rheol.*, **19**, 307–336 (1975).

VELOCITY MEASUREMENTS

Measurement of flow can be based on the measurement of velocity in ducts or pipes by using devices such as pitot tubes and hot wire anemometers. The local velocity is measured at various sections of a conduit and then averaged for the area under consideration.

$$\frac{w}{\rho} = A \times V = Q \tag{10-12}$$

where w = mass flow rate, lb_m/s, kg/s
 ρ = density, lb_m/ft³, kg/m³
 A = area, ft², m²
 V = velocity, ft/s, m/s
 Q = volumetric flow rate, ft³/s, m³/s

Equation (10-12) shows that the fluid density directly affects the relationship between mass flow rate and both velocity and volumetric flow rate. Liquid temperature affects liquid density and hence volumetric flow rate at a constant mass flow rate. Liquid density is relatively insensitive to pressure. Both temperature and pressure affect gas density and thus volumetric flow rate.

Variables Affecting Measurement Flow measurement methods may sense local fluid velocity, volumetric flow rate, total or cumulative volumetric flow (the integral of volumetric flow rate with respect to elapsed time), mass flow rate, and total mass flow.

Velocity Profile Effects Many variables can influence the accuracy of specific flow measurement methods. For example, the velocity profile in a closed conduit affects many types of flow-measuring devices. The velocity of a fluid varies from zero at the wall and at other stationary solid objects in the flow channel to a maximum at a distance from the wall. In the entry region of a conduit, the velocity field may approach plug flow and a constant velocity across the conduit, dropping to zero only at the wall. As a newtonian fluid progresses down a pipe, a velocity profile develops that is parabolic for laminar flow [Eq. (6-41)] and that approaches plug flow for highly turbulent flow. Once a steady flow profile has developed, the flow is said to be fully developed; the length of conduit necessary to achieve fully devel-

oped flow is called the entrance region. For long cylindrical, horizontal pipe ($L < 40D$, where D is the inside diameter of the pipe and L is the upstream length of pipe), the velocity profile becomes fully developed. Velocity profiles in flowing fluids are discussed in greater detail in Sec. 6 (p. 6-11).

For steady-state, isothermal, single-phase, uniform, fully developed newtonian flow in straight pipes, the velocity is greatest at the center of the channel and symmetric about the axis of the pipe. Of those flowmeters that are dependent on the velocity profile, they are usually calibrated for this type of flow. Thus any disturbances in flow conditions can affect flowmeter readings.

Upstream and downstream disturbances in the flow field are caused by valves, elbows, and other types of fittings. Two upstream elbows in two perpendicular planes will impart swirl in the fluid downstream. Swirl, similar to atypical velocity profiles, can lead to erroneous flow measurements. Although the effect is not as great as in upstream flow disturbances, downstream flow disturbances can also lead to erroneous flow measurements.

Other Flow Disturbances Other examples of deviations from fully developed, single-phase newtonian flow include nonnewtonian flow, pulsating flow, cavitation, multiphase flow, boundary layer flows, and nonisothermal flows. See Sec. 6.

Pitot Tubes The combination of pitot tubes in conjunction with sidewall static taps measures local or point velocities by measuring the difference between the total pressure and the static pressure. The pitot tube shown in Fig. 10-10 consists of an impact tube whose opening faces directly into the stream to measure impact pressure, plus one or more sidewall taps to measure local static pressure.

Dynamic pressure may be measured by use of a pitot tube that is a simple impact tube. These tubes measure the pressure at a point where the velocity of the fluid is brought to zero. Pitot tubes must be parallel to the flow. The pitot tube is sensitive to yaw or angle attack. In general angles of attack over 10° should be avoided. In cases where the flow direction is unknown, it is recommended to use a Kiel probe. Figure 10-11 shows a Kiel probe. This probe will read accurately to an angle of about 22° with the flow.

The combined pitot-static tube shown in Fig. 10-12 consists of a jacketed impact tube with one or more rows of holes, 0.51 to 1.02 mm (0.02 to 0.04 in) in diameter, in the jacket to measure the static pressure. Velocity V_0 m/s (ft/s) at the point where the tip is located is given by

$$V_0 = C \sqrt{2g_c \Delta h} = C \sqrt{2g_c (P_T - P_s) / \rho_0} \tag{10-13}$$

where C = coefficient, dimensionless; g_c = dimensional constant; Δh = dynamic pressure ($\Delta h g_c / g_c$), expressed in (N·m)/kg [(ft·lb_f)/lb or ft of fluid flowing]; Δh_s = differential height of static liquid column corresponding to Δh ; g = local acceleration due to gravity; g_c = dimensional constant; p_i = impact pressure; p_0 = local static pressure; and ρ_0 = fluid density measured at pressure p_0 and the local temperature. With gases at velocities above 60 m/s (about 200 ft/s), compressibility becomes important, and the following equation should be used:

$$V_0 = C \sqrt{\frac{2g_c k}{k-1} \left(\frac{p_0}{\rho_0}\right) \left[\left(\frac{p_i}{p_0}\right)^{(k-1)/k} - 1\right]} \tag{10-14}$$

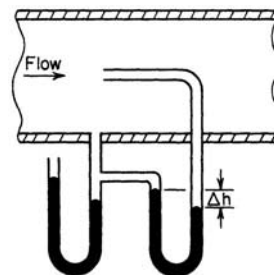


FIG. 10-10 Pitot tube with sidewall static tap.

10-12 TRANSPORT AND STORAGE OF FLUIDS

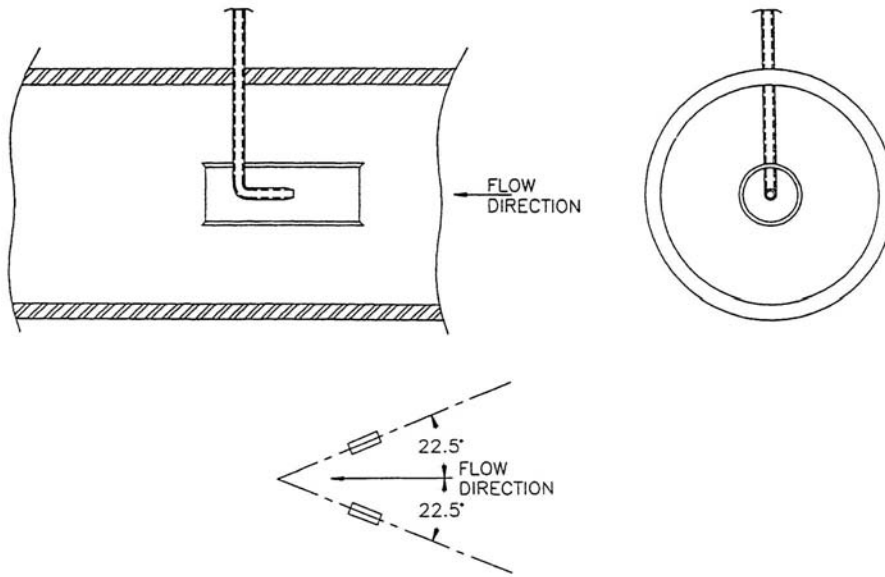


FIG. 10-11 Kiel probe. Accurate measurements can be made at angles up to 22.5° with the flow stream.

where k is the ratio of specific heat at constant pressure to that at constant volume. (See ASME Research Committee on Fluid Meters Report, op. cit., p. 105.) Coefficient C is usually close to 1.00 (± 0.01) for simple pitot tubes (Fig. 10-10) and generally ranges between 0.98 and 1.00 for pitot-static tubes (Fig. 10-12).

There are certain limitations on the range of usefulness of pitot tubes. With gases, the differential is very small at low velocities; e.g., at 4.6 m/s (15.1 ft/s) the differential is only about 1.30 mm (0.051 in) of water (20°C) for air at 1 atm (20°C), which represents a lower limit for 1 percent error even when one uses a micromanometer with a precision of 0.0254 mm (0.001 in) of water. Equation does not apply for Mach numbers greater than 0.7 because of the interference of shock waves. For supersonic flow, local Mach numbers can be calculated from a knowledge of the dynamic and true static pressures. The free stream Mach number (M_∞) is defined as the ratio of the speed of the stream (V_∞) to the speed of sound in the free stream:

$$A_\infty = \sqrt{\left(\frac{\partial P}{\partial \rho}\right)_{s=c}} \quad (10-15)$$

$$M_\infty = \frac{V_\infty}{\sqrt{\left(\frac{\partial P}{\partial \rho}\right)_{s=c}}} \quad (10-16)$$

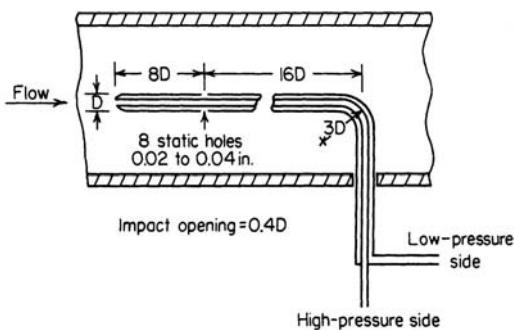


FIG. 10-12 Pitot-static tube.

where S is the entropy. For isentropic flow, this relationship and pressure can be written as:

$$M_\infty = \frac{V_\infty}{\sqrt{kRT_s}} \quad (10-17)$$

The relationships between total and static temperature and pressure are given by the following relationship:

$$\frac{T_T}{T_s} = 1 + \frac{k-1}{2} M^2 \quad (10-18)$$

$$\frac{P_T}{P_s} = \left(1 + \frac{k-1}{2} M^2\right)^{(k-1)/k} \quad (10-19)$$

With **liquids** at low velocities, the effect of the Reynolds number upon the coefficient is important. The coefficients are appreciably less than unity for Reynolds numbers less than 500 for pitot tubes and for Reynolds numbers less than 2300 for pitot-static tubes [see Folsom, *Trans. Am. Soc. Mech. Eng.*, **78**, 1447-1460 (1956)]. Reynolds numbers here are based on the probe outside diameter. Operation at low Reynolds numbers requires prior calibration of the probe.

The pitot-static tube is also sensitive to **yaw** or **angle of attack** than is the simple pitot tube because of the sensitivity of the static taps to orientation. The error involved is strongly dependent upon the exact probe dimensions. In general, angles greater than 10° should be avoided if the velocity error is to be 1 percent or less.

Disturbances upstream of the probe can cause large errors, in part because of the turbulence generated and its effect on the static-pressure measurement. A calming section of at least 50 pipe diameters is desirable. If this is not possible, the use of straightening vanes or a honeycomb is advisable.

The effect of **pulsating flow** on pitot-tube accuracy is treated by Ower et al., op. cit., pp. 310-312. For sinusoidal velocity fluctuations, the ratio of indicated velocity to actual mean velocity is given by the factor $\sqrt{1 + \lambda^2/2}$, where λ is the velocity excursion as a fraction of the mean velocity. Thus, the indicated velocity would be about 6 percent high for velocity fluctuations of ± 50 percent, and pulsations greater than ± 20 percent should be damped to avoid errors greater than 1 percent. The error increases as the frequency of flow oscillations approaches the natural frequency of the pitot tube and the density of

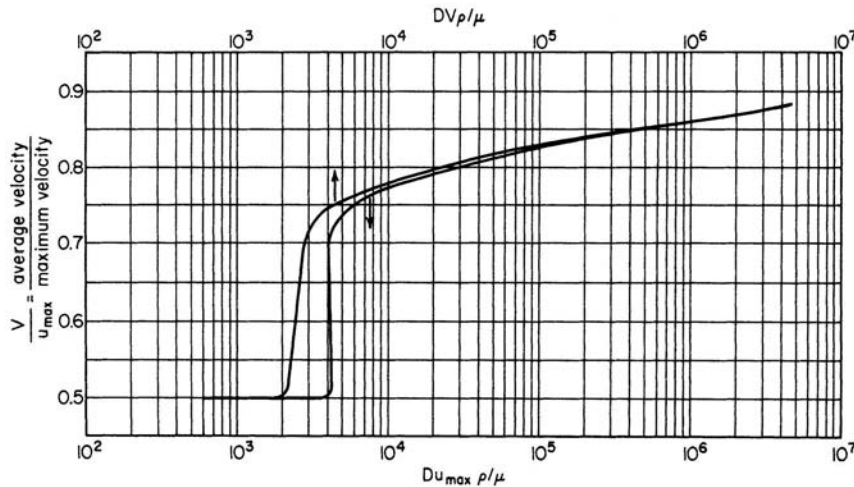


FIG. 10-13 Velocity ratio versus Reynolds number for smooth circular pipes. [Based on data from Rothfus, Archer, Klimas, and Sikchi, *Am. Inst. Chem. Eng. J.*, 3, 208 (1957).]

the measuring fluid approaches the density of the process fluid [see Horlock and Daneshyar, *J. Mech. Eng. Sci.*, **15**, 144–152 (1973)].

Pressures substantially lower than true impact pressures are obtained with pitot tubes in turbulent flow of dilute polymer solutions [see Halliwell and Lewkowicz, *Phys. Fluids*, **18**, 1617–1625 (1975)].

Special Tubes A variety of special forms of the pitot tube have been evolved. Folsom (loc. cit.) gives a description of many of these special types together with a comprehensive bibliography. Included are the impact tube for **boundary-layer** measurements and **shielded total-pressure tubes**. The latter are insensitive to angle of attack up to 40°.

Chue [*Prog. Aerosp. Sci.*, **16**, 147–223 (1975)] reviews the use of the pitot tube and allied pressure probes for impact pressure, static pressure, dynamic pressure, flow direction and local velocity, skin friction, and flow measurements.

A reversed pitot tube, also known as a **pitometer**, has one pressure opening facing upstream and the other facing downstream. Coefficient C for this type is on the order of 0.85. This gives about a 40 percent increase in pressure differential as compared with standard pitot tubes and is an advantage at low velocities. There are commercially available very compact types of pitometers which require relatively small openings for their insertion into a duct.

The **pitot-venturi** flow element is capable of developing a pressure differential 5 to 10 times that of a standard pitot tube. This is accomplished by employing a pair of concentric venturi elements in place of the pitot probe. The low-pressure tap is connected to the throat of the inner venturi, which in turn discharges into the throat of the outer venturi. For a discussion of performance and application of this flow element, see Stoll, *Trans. Am. Soc. Mech. Eng.*, **73**, 963–969 (1951).

Traversing for Mean Velocity Mean velocity in a duct can be obtained by dividing the cross section into a number of equal areas, finding the local velocity at a representative point in each, and averaging the results. In the case of **rectangular passages**, the cross section is usually divided into small squares or rectangles and the velocity is found at the center of each. In circular pipes, the cross section is divided into several equal annular areas as shown in Fig. 10-13. Readings of velocity are made at the intersections of a diameter and the set of circles which bisect the annuli and the central circle.

For an N -point traverse on a circular cross section, make readings on each side of the cross section at

$$100 \times \sqrt{(2n-1)/N} \text{ percent} \quad (n = 1, 2, 3 \text{ to } N/2)$$

of the pipe radius from the center. Traversing several diameters spaced at equal angles about the pipe is required if the velocity distri-

bution is unsymmetrical. With a normal velocity distribution in a circular pipe, a 10-point traverse theoretically gives a mean velocity 0.3 percent high; a 20-point traverse, 0.1 percent high.

For normal velocity distribution in straight circular pipes at locations preceded by runs of at least 50 diameters without pipe fittings or other obstructions, the graph in Fig. 10-13 shows the ratio of mean velocity V to velocity at the center u_{\max} plotted against the Reynolds number, where D = inside pipe diameter, ρ = fluid density, and μ = fluid viscosity, all in consistent units. Mean velocity is readily determined from this graph and a pitot reading at the center of the pipe if the quantity $Du_{\max}\rho/\mu$ is less than 2000 or greater than 5000. The method is unreliable at intermediate values of the Reynolds number.

Methods for determining mean flow rate from probe measurements under nonideal conditions are described by Mandersloot, Hicks, and Langejan [*Chem. Eng. (London)*, no. 232, CE370-CE380 (1969)].

The **hot-wire anemometer** consists essentially of an electrically heated fine wire (generally platinum) exposed to the gas stream whose velocity is being measured. An increase in fluid velocity, other things being equal, increases the rate of heat flow from the wire to the gas, thereby tending to cool the wire and alter its electrical resistance. In a constant-current anemometer, gas velocity is determined by measuring the resulting wire resistance; in the constant-resistance type, gas velocity is determined from the current required to maintain the wire temperature, and thus the resistance, constant. The difference in the two types is primarily in the electric circuits and instruments employed.

The hot-wire anemometer can, with suitable calibration, accurately measure velocities from about 0.15 m/s (0.5 ft/s) to supersonic velocities and detect velocity fluctuations with frequencies up to 200,000 Hz. Fairly rugged, inexpensive units can be built for the measurement of mean velocities in the range of 0.15 to 30 m/s (about 0.5 to 100 ft/s). More elaborate, compensated units are commercially available for use in unsteady flow and turbulence measurements. In calibrating a hot-wire anemometer, it is preferable to use the same gas, temperature, and pressure as will be encountered in the intended application. In this case the quantity $I^2 R_w / \Delta t$ can be plotted against \sqrt{V} , where I = hot-wire current, R_w = hot-wire resistance, Δt = difference between the wire temperature and the gas bulk temperature, and V = mean local velocity. A procedure is given by Wasan and Baid [*Am. Inst. Chem. Eng. J.*, **17**, 729–731 (1971)] for use when it is impractical to calibrate with the same gas composition or conditions of temperature and pressure. Andrews, Bradley, and Hundy [*Int. J. Heat Mass Transfer*, **15**, 1765–1786 (1972)] give a calibration correlation for measurement

of small gas velocities. The hot-wire anemometer is treated in considerable detail in Dean, *op. cit.*, chap. VI; in Ladenburg et al., *op. cit.*, art. F-2; by Grant and Kronauer, *Symposium on Measurement in Unsteady Flow*, American Society of Mechanical Engineers, New York, 1962, pp. 44–53; ASME Research Committee on Fluid Meters Report, *op. cit.*, pp. 105–107; and by Compte-Bellot, *Ann. Rev. Fluid Mech.*, **8**, pp. 209–231 (1976).

The hot-wire anemometer can be modified for liquid measurements, although difficulties are encountered because of bubbles and dirt adhering to the wire. See Stevens, Borden, and Strausser, David Taylor Model Basin Rep. 953, December 1956; Middlebrook and Piret, *Ind. Eng. Chem.*, **42**, 1511–1513 (1950); and Piret et al., *Ind. Eng. Chem.*, **39**, 1098–1103 (1947).

The **hot-film anemometer** has been developed for applications in which use of the hot-wire anemometer presents problems. It consists of a platinum-film sensing element deposited on a glass substrate. Various geometries can be used. The most common involves a wedge with a 30° included angle at the end of a tapered rod. The wedge is commonly 1 mm (0.039 in) long and 0.2 mm (0.0079 in) wide on each face. Compared with the hot wire, it is less susceptible to fouling by bubbles or dirt when used in liquids, has greater mechanical strength when used with gases at high velocities and high temperatures, and can give a higher signal-to-noise ratio. For additional information see Ling and Hubbard, *J. Aeronaut. Sci.*, **23**, 890–891 (1956); and Ling, *J. Basic Eng.*, **82**, 629–634 (1960).

The **heated-thermocouple anemometer** measures gas velocity from the cooling effect of the gas stream flowing across the hot junctions of a thermopile supplied with constant electrical power input. Alternate junctions are maintained at ambient temperature, thus compensating for the effect of ambient temperature. For details see Bunker, *Proc. Instrum. Soc. Am.*, **9**, pap. 54-43-2 (1954).

A glass-coated bead **thermistor anemometer** can be used for the measurement of low fluid velocities, down to 0.001 m/s (0.003 ft/s) in air and 0.0002 m/s (0.0007 ft/s) in water [see Murphy and Sparks, *Ind. Eng. Chem. Fundam.*, **7**, 642–645 (1968)].

The **laser-Doppler anemometer** measures local fluid velocity from the change in frequency of radiation, between a stationary source and a receiver, due to scattering by particles along the wave path. A laser is commonly used as the source of incident illumination. The measurements are essentially independent of local temperature and pressure. This technique can be used in many different flow systems with transparent fluids containing particles whose velocity is actually measured. For a brief review of the laser-Doppler technique see Goldstein, *Appl. Mech. Rev.*, **27**, 753–760 (1974). For additional details see Durst, Melling, and Whitelaw, *Principles and Practice of Laser-Doppler Anemometry*, Academic, New York, 1976.

FLOWMETERS

In the process industries, flow measurement devices are the largest market in the process instrumentation field. Two web sites for process equipment and instrumentation, www.globalspec.com, and www.thomasnet.com, both list more than 800 companies that offer flow measurement products. There are more than one hundred types of flowmeters commercially available. The aforementioned web sites not only facilitate selection and specification of commercial flowmeters, but also provide electronic access to manufacturers' technical literature.

Devices that measure flow can be categorized in two areas as follows:

1. All types of measuring devices in which the material passes without being divided into isolated quantities. Movement of the material is usually sensed by a primary measuring element which activates a secondary device. The flow rate is then inferred from the response of the secondary device by means of known physical laws or from empirical relationships.

2. A positive-displacement meter, which applies to a device in which the flow is divided into isolated measured volumes. The number of fillings of these known volumes are measured with respect to time.

The most common application of flow measurement in process plants is flow in pipes, ducts, and tubing. Table 10-4 lists widely used

flowmeters for these closed conduits as well as the two major classes of open-channel flowmeters. Table 10-4 also lists many other types of flowmeters that are discussed later in this subsection.

This subsection summarizes selection and installation of flowmeters, including the measurement of pressure and velocities of fluids when the flow measurement technique requires it.

INDUSTRY GUIDELINES AND STANDARDS

Because flow measurement is important, many engineering societies and trade organizations have developed flow-related guidelines, standards, and other publications (Table 10-5). The reader should consult the appropriate standards when specifying, installing, and calibrating flow measurement systems.

There are also numerous articles in scholarly journals, trade magazines, and manufacturers' literature related to flow measurement.

Different types of flowmeters differ markedly in their degrees of sensitivity to flow disturbances. In the most extreme cases, obtaining highly accurate flow measurements with certain types of flowmeters may require 60D upstream straight pipe and 20D downstream. Valves can be particularly problematic because their effects on a flowmeter vary with valve position. Numerous types of flow straighteners or conditioners, as shown in Fig. 10-9, can significantly reduce the required run of straight pipe upstream of a given flowmeter.

CLASSIFICATION OF FLOWMETERS

Table 10-4 lists the major classes of flowmeters, along with common examples of each. Brief descriptions are provided in this subsection, followed by more details in subsequent subsections.

Differential Pressure Meters Differential pressure meters or head meters measure the change in pressure across a special flow element. The differential pressure increases with increasing flow rate. The pitot tubes described previously work on this principle. Other examples include orifices [see also Eqs. (6-111) and (8-102), and Fig. 10-14], nozzles (Fig. 10-19), targets, venturis (see also Sec. 8 and Fig. 10-17), and elbow meters. Averaging pitot tubes produce a pressure differential that is based on multiple measuring points across the flow path.

Differential pressure meters are widely used. Temperature, pressure, and density affect gas density and readings of differential pressure meters. For that reason, many commercial flowmeters that are based on measurement of differential pressure often have integral temperature and absolute pressure measurements in addition to differential pressure. They also frequently have automatic temperature and pressure compensation.

Velocity Meters Velocity meters measure fluid velocity. Examples include electromagnetic, propeller, turbine, ultrasonic Doppler, ultrasonic transit time, and vortex meters. Section 8 describes the principles of operation of electromagnetic, turbine, ultrasonic, and vortex flowmeters.

Mass Meters Mass flowmeters measure the rate of mass flow through a conduit. Examples include Coriolis flowmeters and thermal mass flowmeters. Coriolis flowmeters can measure fluid density simultaneously with mass flow rate. This permits calculation of volumetric flow rate as well. Section 8 includes brief descriptions of Coriolis and thermal mass flowmeters.

Volumetric Meters Volumetric meters (also called positive-displacement flowmeters) are devices that mechanically divide a fluid stream into discrete, known volumes and count the number of volumes that pass through the device. See Spitzer (2005, *op. cit.*).

Variable-Area Meters Variable-area meters, which are also called rotameters, offer popular and inexpensive flow measurement devices. These meters employ a float inside a tube that has an internal cross-sectional area that increases with distance upward in the flow path through the tube. As the flow rate increases, the float rises in the tube to provide a larger area for the flowing fluid to pass.

Open-Channel Flow Measurement Open-channel flow measurements are usually based on measurement of liquid level in a flow channel constructed of a specified geometry. The two most common flow channels used are weirs and flumes. See Spitzer (2005, *op. cit.*).

TABLE 10-4 Comparison of Flowmeter Technologies

Flowmeter technology	Accuracy* (+/-)	Turndown	Fluids†	Pipe sizes, ‡ in	Maximum pressure, ‡ psig	Temperature range, ‡ °F	Pipe run	Relative pressure loss
Differential Pressure Meters								
Pitot		8:1	L, G	1 to 96	2.76E-4 to 200	-200 to 750		L
Averaging pitot	1% R	8:1	L, G, S	0.25 to 72	8800	-20 to 2370		L
Orifice							Long	
Square-edged	0.5 to 1.5% R	4:1	L, G, S	0.5 to 40	8800	-4 to 2300		M
Eccentric	2% R	4:1	L, G, S	0.5 to 40	8800	-4 to 2300		M
Segmental	2% R	4:1	L, G, S, SL	0.5 to 40	8800	-4 to 2300		M
Orifice and multi-variable flow transmitter	0.5 to 1% R	10:1	L, G, S	> 0.5	4000	1000		M
Venturi	0.5 to 1.5% R	10:1	L, G, S, SL	1 to 120	8800	-4 to 2300		L
Flow nozzle	0.5 to 2% R	8:1	L, G, S	2 to 80	>1000	<1000		M
V cone	0.5% F	10:1	L, G, S, SL	0.25 to 120	6000	To 400		M
Wedge	0.5 to 5% R	10:1	L, G, S, SL	0.5 to 24	>600	‡		M
Velocity Meters								
Correlation	0.5% R	10:1	L, G, SL	1 to 60	Piping limits	To 600	Long	L
Electromagnetic	0.2 to 2% R	10:1	L	0.15 to 60	5000	-40 to 350	Short	L
Propeller	2% R	15:1	L	2 to 12	230	0 to 300		M
Turbine	0.15 to 1% R	10:1	L, G	0.5 to 30	6000	-450 to 600	Short	M
Ultrasonic Doppler	1 to 30% R	50:1	L, G, SL	0.5 to 200	6000	-40 to 250	Long	L
Ultrasonic transit time	0.5 to 5% R	Down to zero flow	L, G	1 to 540	6000	-40 to 650	Long	L
Vortex	0.5 to 2% R	20:1	L, G, S	0.5 to 16	1500	-330 to 800	Short	M
Mass Meters								
Coriolis	0.1 to 0.3% R	10:1 to 80:1	L, G	0.06 to 12	5700	-400 to 800	None	L, M
Thermal (for gases)	1% F	50:1	G	0.125 to 8	4500	32 to 572	Short	L
Thermal (for liquids)	0.5% F	50:1	L	0.06 to 0.25	4500	40 to 165	Short	L
Volumetric	0.15 to 2% R	10:1	L	0.25 to 16	2000	-40 to 600	None	M to H
Variable area	1 to 5% F	10:1	L, G	0.125 to 6	6000	<1000	None	M
Open-Channel Flowmeters								
Weirs	2 to 5% R	25:1	L	Wide range	NA	NA		L
Flumes	3 to 10% R	40:1	L	Wide range	NA	NA		L

*F = full scale, R = rate. †L = liquid, G = gas, S = steam, SL = slurry.

‡Dependent on the material selection and application. Readers should consult manufacturers for current capabilities.

Adapted from J. Pomroy, *Chemical Engineering*, pp. 94–102, May 1996; J. W. Dolenc, *Chemical Engineering Progress*, pp. 22–32, Jan. 1996; R. C. Baker, *Introductory Guide to Flow Measurement*, American Society of Mechanical Engineers, New York, 2003; R. W. Miller, *Flow Measurement Engineering Handbook*, 3d ed., McGraw-Hill, New York, 1996; D. W. Spitzer, *Industrial Flow Measurement*, 3d ed., The Instrumentation, Systems, and Automation Society, Research Triangle Park, N.C., 2005; and manufacturers' literature at www.globalspec.com.

DIFFERENTIAL PRESSURE FLOWMETERS

General Principles If a constriction is placed in a closed channel carrying a stream of fluid, there will be an increase in velocity, and hence an increase in kinetic energy, at the point of constriction. From an energy balance, as given by Bernoulli's theorem [see Sec. 6, subsection "Energy Balance," Eq. (6-16)], there must be a corresponding reduction in pressure. Rate of discharge from the constriction can be calculated by knowing this pressure reduction, the area available for flow at the constriction, the density of the fluid, and the coefficient of discharge C . The last-named is defined as the ratio of actual flow to the theoretical flow and makes allowance for stream contraction and frictional effects. The metering characteristics of commonly used differential pressure meters are reviewed and grouped by Halmi [*J. Fluids Eng.*, **95**, 127–141 (1973)].

The term **static head** generally denotes the pressure in a fluid due to the head of fluid above the point in question. Its magnitude is given by the application of Newton's law (force = mass \times acceleration). In the case of **liquids** (constant density), the static head p_h Pa (lbf/ft²) is given by

$$p_h = h\rho g/g_c \quad (10-20)$$

where h = head of liquid above the point, m (ft); ρ = liquid density; g = local acceleration due to gravity; and g_c = dimensional constant.

The head developed in a compressor or pump is the energy force per unit mass. In the measuring systems it is often misnamed as (ft) while the units are really ft-lb/lbm or kilojoules.

For a compressor or turbine, it is represented by the following relationship:

$$E = U_1 V_{\theta 1} - U_2 V_{\theta 2} \quad (10-21)$$

TABLE 10-5 Guidelines, Standards, and Other Publications Related to Flow Measurement

Technical society	Number of guidelines and standards*
American Gas Association (AGA)	2
American Petroleum Institute (API)	11
American Society of Heating, Refrigeration, and Air Conditioning Engineers (ASHRAE)	5
American Society of Mechanical Engineers (ASME)	18
ASTM International (ASTM)	17
British Standards Institution (BSI)	100
Deutsches Institut für Normung E. V. (DIN)	48
International Electrotechnical Commission (IEC)	6
Instrumentation, Systems, and Automation Society (ISA)	3
International Organization for Standardization (ISO)	212
SAE International (SAE)	6

*Number of documents identified by searching for *flow measurement* on <http://global.ihl.com>, the web site of a clearinghouse of industry guidelines, codes, and standards.

where U is the blade speed and V_θ is the tangential velocity component of absolute velocity. This equation is known as the Euler equation.

Orifice Meters A **square-edged** or **sharp-edged** orifice, as shown in Fig. 10-14, is a clean-cut square-edged hole with straight walls perpendicular to the flat upstream face of a thin plate placed crosswise of the channel. The stream issuing from such an orifice attains its minimum cross section (vena contracta) at a distance downstream of the orifice which varies with the ratio β of orifice to pipe diameter (see Fig. 10-15).

For a centered circular orifice in a pipe, the pressure differential is customarily measured between one of the following pressure-tap pairs. Except in the case of flange taps, all measurements of distance from the orifice are made from the upstream face of the plate.

1. *Corner taps.* Static holes drilled one in the upstream and one in the downstream flange, with the openings as close as possible to the orifice plate.
2. *Radius taps.* Static holes located one pipe diameter upstream and one-half pipe diameter downstream from the plate.
3. *Pipe taps.* Static holes located $2\frac{1}{2}$ pipe diameters upstream and eight pipe diameters downstream from the plate.

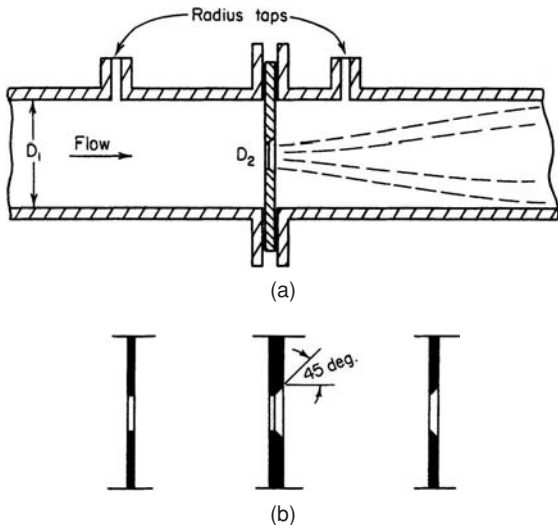


FIG. 10-14 Square-edged or sharp-edged orifices. The plate at the orifice opening must not be thicker than one-thirtieth of the pipe diameter, one-eighth of the orifice diameter, or one-fourth of the distance from the pipe wall to the edge of the opening. (a) Pipe-line orifice. (b) Types of plates.

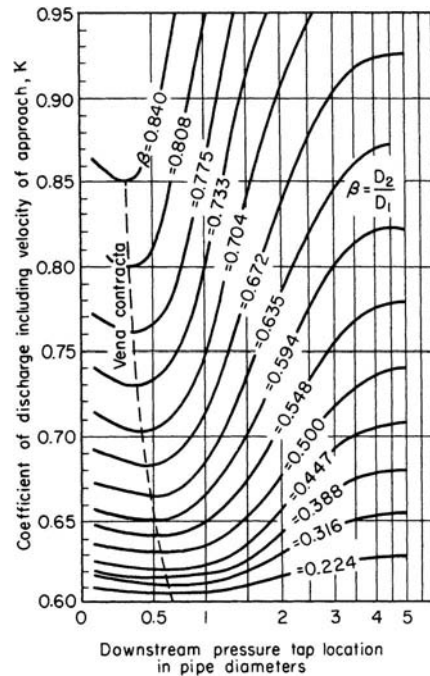


FIG. 10-15 Coefficient of discharge for square-edged circular orifices for $N_{Re} > 30,000$ with the upstream tap located between one and two pipe diameters from the orifice plate. [Spitzglass, *Trans. Am. Soc. Mech. Eng.*, **44**, 919 (1922).]

4. *Flange taps.* Static holes located 25.4 mm (1 in) upstream and 25.4 mm (1 in) downstream from the plate.

5. *Vena-contracta taps.* The upstream static hole is one-half to two pipe diameters from the plate. The downstream tap is located at the position of minimum pressure (see Fig. 10-15).

Radius taps are best from a practical standpoint; the downstream pressure tap is located at about the mean position of the vena contracta, and the upstream tap is sufficiently far upstream to be unaffected by distortion of the flow in the immediate vicinity of the orifice (in practice, the upstream tap can be as much as two pipe diameters from the plate without affecting the results). Vena-contracta taps give the largest differential head for a given rate of flow but are inconvenient if the orifice size is changed from time to time. Corner taps offer the sometimes great advantage that the pressure taps can be built into the plate carrying the orifice. Thus the entire apparatus can be quickly inserted in a pipe line at any convenient flanged joint without having to drill holes in the pipe. Flange taps are similarly convenient, since by merely replacing standard flanges with special orifice flanges, suitable pressure taps are made available. Pipe taps give the lowest differential pressure, the value obtained being close to the permanent pressure loss.

The practical working equation for weight rate of discharge, adopted by the ASME Research Committee on Fluid Meters for use with either gases or liquids, is

$$\begin{aligned}
 w &= q_1 \rho_1 = CYA_2 \sqrt{\frac{2g_c(p_1 - p_2)\rho_1}{1 - \beta^4}} \\
 &= KYA_2 \sqrt{2g_c(p_1 - p_2)\rho_1} \quad (10-22)
 \end{aligned}$$

where A_2 = cross-sectional area of throat; C = coefficient of discharge, dimensionless; g_c = dimensional constant; $K = C/\sqrt{1 - \beta^4}$, dimensionless; p_1, p_2 = pressure at upstream and downstream static pressure taps respectively; q_1 = volumetric rate of discharge measured at upstream pressure and temperature; w = weight rate of discharge; Y = expansion factor, dimensionless; β = ratio of throat diameter to

pipe diameter, dimensionless; and ρ_1 = density at upstream pressure and temperature.

For the case of subsonic flow of a gas ($r_c < r < 1.0$), the expansion factor Y for orifices is approximated by

$$Y = 1 - [(1-r)/k](0.41 + 0.35\beta^4) \quad (10-23)$$

where r = ratio of downstream to upstream static pressure (p_2/p_1), k = ratio of specific heats (c_p/c_v), and β = diameter ratio. (See also Fig. 10-18.) Values of Y for supercritical flow of a gas ($r < r_c$) through orifices are given by Benedict [*J. Basic Eng.*, **93**, 121–137 (1971)]. For the case of **liquids**, expansion factor Y is unity, and Eq. (10-27) should be used, since it allows for any difference in elevation between the upstream and downstream taps.

Coefficient of discharge C for a given orifice type is a function of the Reynolds number N_{Re} (based on orifice diameter and velocity) and diameter ratio β . At Reynolds numbers greater than about 30,000, the coefficients are substantially constant. For square-edged or sharp-edged concentric circular orifices, the value will fall between 0.595 and 0.620 for vena-contracta or radius taps for β up to 0.8 and for flange taps for β up to 0.5. Figure 10-15 gives the coefficient of discharge K , including the velocity-of-approach factor ($1/\sqrt{1-\beta^4}$), as a function of β and the location of the downstream tap. Precise values of K are given in *ASME PTC*, op. cit., pp. 20–39, for flange taps, radius taps, vena-contracta taps, and corner taps. Precise values of C are given in the *ASME Research Committee on Fluid Meters Report*, op. cit., pp. 202–207, for the first three types of taps.

The discharge coefficient of sharp-edged orifices was shown by Benedict, Wyler, and Brandt [*J. Eng. Power*, **97**, 576–582 (1975)] to increase with edge roundness. Typical as-purchased orifice plates may exhibit deviations on the order of 1 to 2 percent from ASME values of the discharge coefficient.

In the transition region (N_{Re} between 50 and 30,000), the coefficients are generally higher than the above values. Although calibration is generally advisable in this region, the curves given in Fig. 10-16 for corner and vena-contracta taps can be used as a guide. In the laminar-flow region ($N_{Re} < 50$), the coefficient C is proportional to $\sqrt{N_{Re}}$. For $1 < N_{Re} < 100$, Johansen [*Proc. R. Soc. (London)*, **A121**, 231–245 (1930)] presents discharge-coefficient data for sharp-edged orifices with corner taps. For $N_{Re} < 1$, Miller and Nemecek [*ASME Paper 58-A-106* (1958)] present correlations giving coefficients for sharp-edged orifices and short-pipe orifices (L/D from 2 to 10). For short-pipe orifices (L/D from 1 to 4), Dickerson and Rice [*J. Basic Eng.*, **91**, 546–548 (1969)] give coefficients for the intermediate range ($27 < N_{Re} < 7000$). See also subsection "Contraction and Entrance Losses."

Permanent pressure loss across a concentric circular orifice with radius or vena-contracta taps can be approximated for turbulent flow by

$$(p_1 - p_4)/(p_1 - p_2) = 1 - \beta^2 \quad (10-24)$$

where p_1 , p_2 = upstream and downstream pressure-tap readings respectively, p_4 = fully recovered pressure (four to eight pipe diameters downstream of the orifice), and β = diameter ratio. See *ASME PTC*, op. cit., Fig. 5.

See Benedict, *J. Fluids Eng.*, **99**, 245–248 (1977), for a general equation for pressure loss for orifices installed in pipes or with plenum inlets. Orifices show higher loss than nozzles or venturis. Permanent pressure loss for laminar flow depends on the Reynolds number in addition to β . See Alvi, Sridharan, and Lakshmana Rao, loc. cit., for details.

For the case of **critical flow** through a square- or sharp-edged concentric circular orifice (where $r \leq r_c$, as discussed earlier in this subsection), use Eqs. (10-31), (10-32), and (10-33) as given for critical-flow nozzles. However, unlike nozzles, the flow through a sharp-edged orifice continues to increase as the downstream pressure drops below that

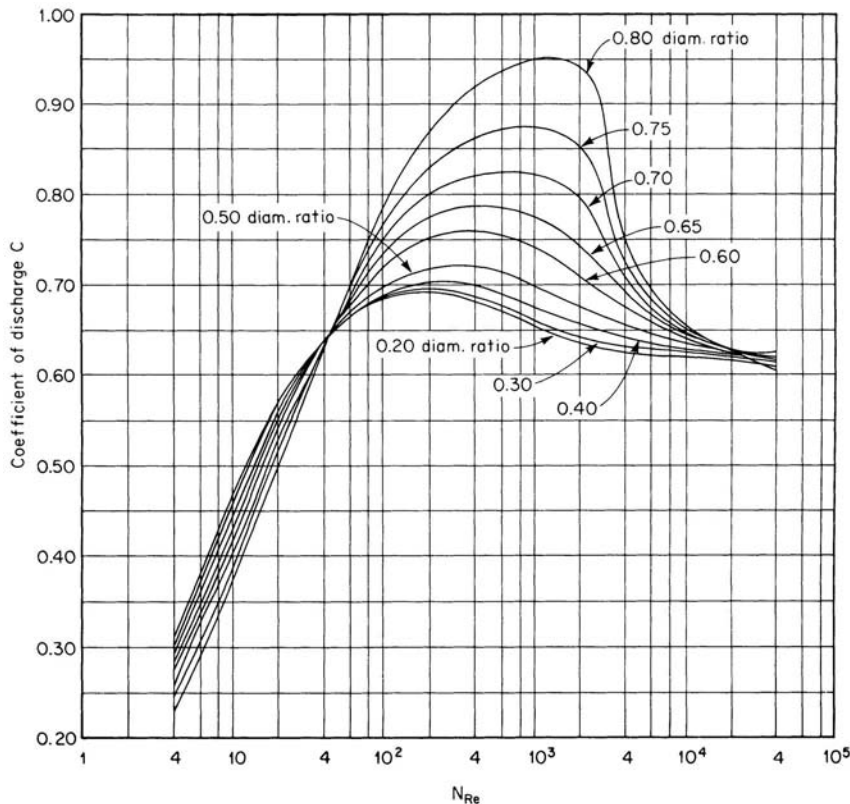


FIG. 10-16 Coefficient of discharge for square-edged circular orifices with corner taps. [*Tuve and Sprenkle, Instruments*, **6**, 201 (1933).]

corresponding to the critical pressure ratio r_c . This is due to an increase in the cross section of the vena contracta as the downstream pressure is reduced, giving a corresponding increase in the coefficient of discharge. At $r = r_c$, C is about 0.75, while at $r \neq 0$, C has increased to about 0.84. See Grace and Lapple, loc. cit.; and Benedict, *J. Basic Eng.*, **93**, 99–120 (1971).

Measurements by Harris and Magnall [*Trans. Inst. Chem. Eng. (London)*, **50**, 61–68 (1972)] with a venturi ($\beta = 0.62$) and orifices with radius taps ($\beta = 0.60 - 0.75$) indicate that the discharge coefficient for **nonnewtonian fluids**, in the range N_{Re} (generalized Reynolds number) 3500 to 100,000, is approximately the same as for newtonian fluids at the same Reynolds number.

Quadrant-edge orifices have holes with rounded edges on the upstream side of the plate. The quadrant-edge radius is equal to the thickness of the plate at the orifice location. The advantages claimed for this type versus the square- or sharp-edged orifice are constant-discharge coefficients extending to lower Reynolds numbers and less possibility of significant changes in coefficient because of erosion or other damage to the inlet shape.

Values of discharge coefficient C and Reynolds numbers limit for constant C are presented in Table 10-6, based on Ramamoorthy and Seetharamiah [*J. Basic Eng.*, **88**, 9–13 (1966)] and Bogema and Monkmeier [*J. Basic Eng.*, **82**, 729–734 (1960)]. At Reynolds numbers above those listed for the upper limits, the coefficients rise abruptly. As Reynolds numbers decrease below those listed for the lower limits, the coefficients pass through a hump and then drop off. According to Bogema, Spring, and Ramamoorthy [*J. Basic Eng.*, **84**, 415–418 (1962)], the hump can be eliminated by placing a fine-mesh screen about three pipe diameters upstream of the orifice. This reduces the lower N_{Re} limit to about 500.

Permanent pressure loss across quadrant-edge orifices for turbulent flow is somewhat lower than given by Eq. (10-24). See Alvi, Sridharan, and Lakshmana Rao, loc. cit., for values of discharge coefficient and permanent pressure loss in laminar flow.

Slotted orifices offer significant advantages over a standard square-edged orifice with an identical open area for homogeneous gases or liquids [G. L. Morrison and K. R. Hall, *Hydrocarbon Processing* **79**, 12, 65–72 (2000)]. The slotted orifice flowmeter only requires compact header configurations with very short upstream pipe lengths and maintains accuracy in the range of 0.25 percent with no flow conditioner. Permanent head loss is less than or equal to that of a standard orifice that has the same β ratio. Discharge coefficients for the slotted orifice are much less sensitive to swirl or to axial velocity profiles. A slotted orifice plate can be a “drop in” replacement for a standard orifice plate.

Segmental and eccentric orifices are frequently used for gas metering when there is a possibility that entrained liquids or solids would otherwise accumulate in front of a concentric circular orifice. This can be avoided if the opening is placed on the lower side of the pipe. For liquid flow with entrained gas, the opening is placed on the upper side. The pressure taps should be located on the opposite side of the pipe from the opening.

Coefficient C for a square-edged eccentric circular orifice (with opening tangent to pipe wall) varies from about 0.61 to 0.63 for β 's from 0.3 to 0.5, respectively, and pipe Reynolds numbers $> 10,000$ for either vena-

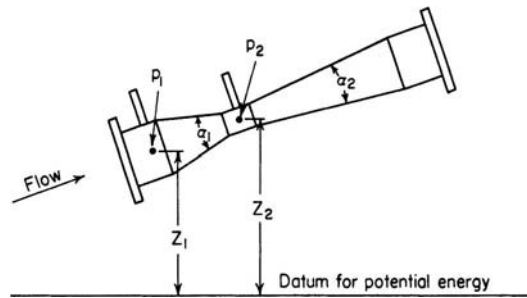


FIG. 10-17 Herschel-type venturi tube.

contracta or flange taps (where $\beta =$ diameter ratio). For square-edged segmental orifices, the coefficient C falls generally between 0.63 and 0.64 for $0.3 \leq \beta \leq 0.5$ and pipe Reynolds numbers $> 10,000$, for vena-contracta or flange taps, where $\beta =$ diameter ratio for an equivalent circular orifice $= \sqrt{\alpha}$ ($\alpha =$ ratio of orifice to pipe cross-sectional areas). Values of expansion factor Y are slightly higher than for concentric circular orifices, and the location of the vena contracta is moved farther downstream as compared with concentric circular orifices. For further details, see ASME Research Committee on Fluid Meters Report, op. cit., pp. 210–213.

For permanent pressure loss with segmental and eccentric orifices with laminar pipe flow see Lakshmana Rao and Sridharan, *Proc. Am. Soc. Civ. Eng., J. Hydraul. Div.*, **98** (HY 11), 2015–2034 (1972).

Annular orifices can also be used to advantage for gas metering when there is a possibility of entrained liquids or solids and for liquid metering with entrained gas present in small concentrations. Coefficient K was found by Bell and Bergelin [*Trans. Am. Soc. Mech. Eng.*, **79**, 593–601 (1957)] to range from about 0.63 to 0.67 for annulus Reynolds numbers in the range of 100 to 20,000 respectively for values of $2L/(D - d)$ less than 1 where $L =$ thickness of orifice at outer edge, $D =$ inside pipe diameter, and $d =$ diameter of orifice disk. The annulus Reynolds number is defined as

$$N_{Re} = (D - d)(G/\mu) \tag{10-25}$$

where $G =$ mass velocity ρV through orifice opening and $\mu =$ fluid viscosity. The above coefficients were determined for β 's ($= d/D$) in the range of 0.95 to 0.996 and with pressure taps located 19 mm ($3/4$ in) upstream of the disk and 230 mm (9 in) downstream in a 5.25-in-diameter pipe.

Venturi Meters The standard Herschel-type venturi meter consists of a short length of straight tubing connected at either end to the pipe line by conical sections (see Fig. 10-17). Recommended proportions (ASME PTC, op. cit., p. 17) are entrance cone angle $\alpha_1 = 21 \pm 2^\circ$, exit cone angle $\alpha_2 = 5$ to 15° , throat length = one throat diameter, and upstream tap located 0.25 to 0.5 pipe diameter upstream of the entrance cone. The straight and conical sections should be joined by smooth curved surfaces for best results. **Rate of discharge** of either gases or liquids through a venturi meter is given by Eq. (10-22).

For the flow of **gases**, expansion factor Y , which allows for the change in gas density as it expands adiabatically from p_1 to p_2 , is given by

$$Y = \sqrt{r^{2/k} \left(\frac{k}{k-1} \right) \left(\frac{1-r^{(k-1)/k}}{1-r} \right) \left(\frac{1-\beta^4}{1-\beta^4 r^{2/k}} \right)} \tag{10-26}$$

for venturi meters and flow nozzles, where $r = p_2/p_1$ and $k =$ specific heat ratio c_p/c_v . Values of Y computed from Eq. (10-26) are given in Fig. 10-18 as a function of r , k , and β .

For the flow of **liquids**, expansion factor Y is unity. The change in potential energy in the case of an inclined or vertical venturi meter must be allowed for. Equation (10-22) is accordingly modified to give

$$w = q_1 \rho = CA_2 \sqrt{\frac{2g_c(p_1 - p_2) + 2g\rho(Z_1 - Z_2)\rho}{1 - \beta^4}} \tag{10-27}$$

TABLE 10-6 Discharge Coefficients for Quadrant-Edge Orifices

β	$C \ddagger$	$K \ddagger$	Limiting N_{Re}^* for constant coefficient†	
			Lower	Upper
0.225	0.770	0.771	5,000	60,000
0.400	0.780	0.790	5,000	150,000
0.500	0.824	0.851	4,000	200,000
0.600	0.856	0.918	3,000	120,000
0.630	0.885	0.964	3,000	105,000

*Based on pipe diameter and velocity.

†For a precision of about ± 0.5 percent.

‡Can be used with corner taps, flange taps, or radius taps.

where g = local acceleration due to gravity and Z_1, Z_2 = vertical heights above an arbitrary datum plane corresponding to the centerline pressure-reading locations for p_1 and p_2 respectively.

Value of the **discharge coefficient** C for a **Herschel-type venturi meter** depends upon the Reynolds number and to a minor extent upon the size of the venturi, increasing with diameter. A plot of C versus pipe Reynolds number is given in *ASME PTC*, op. cit., p. 19. A value of 0.984 can be used for pipe Reynolds numbers larger than 200,000.

Permanent pressure loss for a Herschel-type venturi tube depends upon diameter ratio β and discharge cone angle α_2 . It ranges from 10 to 15 percent of the pressure differential ($p_1 - p_2$) for small angles (5 to 7°) and from 10 to 30 percent for large angles (15°), with the larger losses occurring at low values of β (see *ASME PTC*, op. cit., p. 12). See Benedict, *J. Fluids Eng.*, **99**, 245–248 (1977), for a general equation for pressure loss for venturis installed in pipes or with plenum inlets.

For flow measurement of **steam and water mixtures** with a Herschel-type venturi in 2½-in- and 3-in-diameter pipes, see Collins and Gacesa, *J. Basic Eng.*, **93**, 11–21 (1971).

A variety of **short-tube venturi meters** are available commercially. They require less space for installation and are generally (although not always) characterized by a greater pressure loss than the corresponding Herschel-type venturi meter. Discharge coefficients vary widely for different types, and individual calibration is recommended if the manufacturer's calibration is not available. Results of tests on the Dall flow tube are given by Miner [*Trans. Am. Soc. Mech. Eng.*, **78**, 475–479 (1956)] and Dowdell [*Instrum. Control Syst.*, **33**, 1006–1009 (1960)]; and on the Gentile flow tube (also called Beth flow tube or Foster flow tube) by Hooper [*Trans. Am. Soc. Mech. Eng.*, **72**, 1099–1110 (1950)].

The use of a **multiventuri system** (in which an inner venturi discharges into the throat of an outer venturi) to increase both the differential pressure for a given flow rate and the signal-to-loss ratio is described by Klomp and Sovran [*J. Basic Eng.*, **94**, 39–45 (1972)].

Flow Nozzles A simple form of flow nozzle is shown in Fig. 10-19. It consists essentially of a short cylinder with a flared approach section. The approach cross section is preferably elliptical in shape but may be conical. Recommended contours for long-radius flow nozzles are given in *ASME PTC*, op. cit., p. 13. In general, the length of the straight portion of the throat is about one-half throat diameter, the upstream pressure tap is located about one pipe diameter from the nozzle inlet face, and the downstream pressure tap about one-half pipe diameter from the inlet face. For subsonic flow, the pressures at points 2 and 3 will be practically identical. If a conical inlet is preferred, the inlet and throat geometry specified for a Herschel-type venturi meter can be used, omitting the expansion section.

Rate of discharge through a flow nozzle for subcritical flow can be determined by the equations given for venturi meters, Eq. (10-22) for gases and Eq. (10-27) for liquids. The expansion factor Y for nozzles is the same as that for venturi meters [Eq. (10-26), Fig. 10-18]. The value of the discharge coefficient C depends primarily upon the pipe Reynolds number and to a lesser extent upon the diameter ratio β . Curves of recommended coefficients for long-radius flow nozzles with pressure taps located one pipe diameter upstream and one-half pipe diameter downstream of the inlet face of the nozzle are given in *ASME PTC*, op. cit., p. 15. In general, coefficients range from 0.95 at a pipe Reynolds number of 10,000 to 0.99 at 1,000,000.

The performance characteristics of pipe-wall-tap nozzles (Fig. 10-19) and throat-tap nozzles are reviewed by Wyler and Benedict [*J. Eng. Power*, **97**, 569–575 (1975)].

Permanent pressure loss across a subsonic flow nozzle is approximated by

$$p_1 - p_4 = \frac{1 - \beta^2}{1 + \beta^2} (p_1 - p_2) \quad (10-28)$$

where p_1, p_2, p_4 = static pressures measured at the locations shown in Fig. 10-19; and β = ratio of nozzle throat diameter to pipe diameter, dimensionless. Equation (10-28) is based on a momentum balance assuming constant fluid density (see Lapple et al., *Fluid and Particle Mechanics*, University of Delaware, Newark, 1951, p. 13).

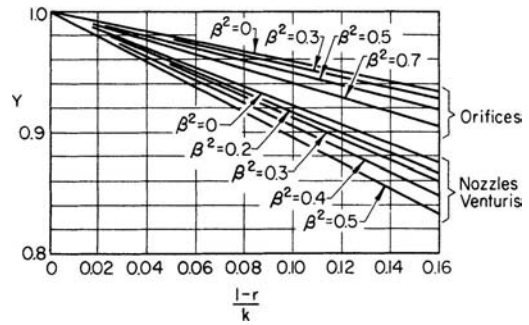


FIG. 10-18 Values of expansion factor Y for orifices, nozzles, and venturis.

See Benedict, loc. cit., for a general equation for pressure loss for nozzles installed in pipes or with plenum inlets. Nozzles show higher loss than venturis. Permanent pressure loss for laminar flow depends on the Reynolds number in addition to β . For details, see Alvi, Sridharan, and Lakshamana Rao, *J. Fluids Eng.*, **100**, 299–307 (1978).

Critical Flow Nozzle For a given set of upstream conditions, the rate of discharge of a gas from a nozzle will increase for a decrease in the absolute pressure ratio p_2/p_1 until the linear velocity in the throat reaches that of sound in the gas at that location. The value of p_2/p_1 for which the acoustic velocity is just attained is called the critical pressure ratio r_c . The actual pressure in the throat will not fall below $p_1 r_c$ even if a much lower pressure exists downstream.

The **critical pressure ratio** r_c can be obtained from the following theoretical equation, which assumes a perfect gas and a frictionless nozzle:

$$r_c^{(1-k)/k} + \left(\frac{k-1}{2}\right) \beta^4 r_c^{2/k} = \frac{k+1}{2} \quad (10-29)$$

This reduces, for $\beta \leq 0.2$, to

$$r_c = \left(\frac{2}{k+1}\right)^{k/(k-1)} \quad (10-30)$$

where k = ratio of specific heats c_p/c_v and β = diameter ratio. A table of values of r_c as a function of k and β is given in the ASME Research Committee on Fluid Meters Report, op. cit., p. 68. For small values of β , $r_c = 0.487$ for $k = 1.667$, 0.528 for $k = 1.40$, 0.546 for $k = 1.30$, and 0.574 for $k = 1.15$.

Under **critical flow conditions**, only the upstream conditions p_1, v_1 , and T_1 need be known to determine flow rate, which, for $\beta \leq 0.2$, is given by

$$w_{\max} = CA_2 \sqrt{g_k k \left(\frac{p_1}{v_1}\right) \left(\frac{2}{k+1}\right)^{(k+1)/(k-1)}} \quad (10-31)$$

For a **perfect gas**, this corresponds to

$$w_{\max} = CA_2 p_1 \sqrt{g_k k \left(\frac{M}{RT_1}\right) \left(\frac{2}{k+1}\right)^{(k+1)/(k-1)}} \quad (10-32)$$

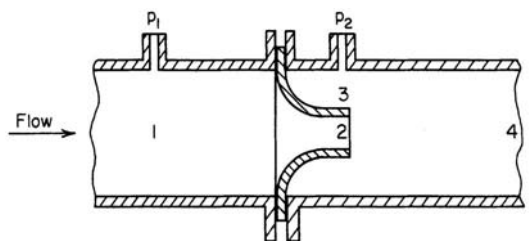


FIG. 10-19 Flow-nozzle assembly.

10-20 TRANSPORT AND STORAGE OF FLUIDS

For air, Eq. (10-31) reduces to

$$w_{\max} = C_1 C A_2 p_1 / \sqrt{T_1} \quad (10-33)$$

where A_2 = cross-sectional area of throat; C = coefficient of discharge, dimensionless; g_c = dimensional constant; k = ratio of specific heats, c_p/c_v ; M = molecular weight; p_1 = pressure on upstream side of nozzle; R = gas constant; T_1 = absolute temperature on upstream side of nozzle; v_1 = specific volume on upstream side of nozzle; C_1 = dimensional constant, 0.0405 SI units (0.533 U.S. customary units); and w_{\max} = maximum-weight flow rate.

Discharge coefficients for critical flow nozzles are, in general, the same as those for subsonic nozzles. See Grace and Lapple, *Trans. Am. Soc. Mech. Eng.*, **73**, 639–647 (1951); and Szanislo, *J. Eng. Power*, **97**, 521–526 (1975). Amberg, Britton, and Seidl [*J. Fluids Eng.*, **96**, 111–123 (1974)] present discharge-coefficient correlations for circular-arc venturi meters at critical flow. For the calculation of the flow of natural gas through nozzles under critical-flow conditions, see Johnson, *J. Basic Eng.*, **92**, 580–589 (1970).

Elbow Meters A pipe elbow can be used as a flowmeter for liquids if the differential centrifugal head generated between the inner and outer radii of the bend is measured by means of pressure taps located midway around the bend. Equation (10-27) can be used, except that the pressure-difference term ($p_1 - p_2$) is now taken to be the differential centrifugal pressure and β is taken as zero if one assumes no change in cross section between the pipe and the bend. The discharge coefficient should preferably be determined by calibration, but as a guide it can be estimated within ± 6 percent for circular pipe for Reynolds numbers greater than 10^5 from $C = 0.98 \sqrt{R_c/2D}$, where R_c = radius of curvature of the centerline and D = inside pipe diameter in consistent units. See Murdock, Foltz, and Gregory, *J. Basic Eng.*, **86**, 498–506 (1964); or the ASME Research Committee on Fluid Meters Report, op. cit., pp. 75–77.

Accuracy Square-edged orifices and venturi tubes have been so extensively studied and standardized that reproducibilities within 1 to 2 percent can be expected between standard meters when new and clean. This is therefore the order of reliability to be had, if one assumes (1) accurate measurement of meter differential, (2) selection of the coefficient of discharge from recommended published literature, (3) accurate knowledge of fluid density, (4) accurate measurement of critical meter dimensions, (5) smooth upstream face of orifice, and (6) proper location of the meter with respect to other flow-disturbing elements in the system. Care must also be taken to avoid even slight corrosion or fouling during use.

Presence of **swirling flow** or an **abnormal velocity distribution** upstream of the metering element can cause serious metering error unless calibration in place is employed or sufficient straight pipe is inserted between the meter and the source of disturbance. Table 10-7 gives the minimum lengths of straight pipe required to avoid appreciable error due to the presence of certain fittings and valves either upstream or downstream of an orifice or nozzle. These values were extracted from plots presented by Sprenkle [*Trans. Am. Soc. Mech. Eng.*, **67**, 345–360 (1945)]. Table 10-7 also shows the reduction in spacing made possible by the use of straightening vanes between the fittings and the meter. Entirely adequate straightening vanes can be provided by fitting a bundle of thin-wall tubes within the pipe. The center-to-center distance between tubes should not exceed one-fourth of the pipe diameter, and the bundle length should be at least 8 times this distance.

The distances specified in Table 10-7 will be conservative if applied to venturi meters. For specific information on requirements for venturi meters, see a discussion by Pardoe appended to Sprenkle (op. cit.). Extensive data on the effect of installation on the coefficients of venturi meters are given elsewhere by Pardoe [*Trans. Am. Soc. Mech. Eng.*, **65**, 337–349 (1943)].

In the presence of **flow pulsations**, the indications of head meters such as orifices, nozzles, and venturis will often be undependable for several reasons. First, the measured pressure differential will tend to be high, since the pressure differential is proportional to the square of flow rate for a head meter, and the square root of the mean differential pressure is always greater than the mean of the square roots of the differential pressures. Second, there is a phase shift as the wave passes through

TABLE 10-7 Locations of Orifices and Nozzles Relative to Pipe Fittings

Type of fitting upstream	$\frac{D_2}{D_1}$	Distances in pipe diameters, D_1		Distance, vanes to orifice	Distance, nearest downstream fitting from orifice
		Distance, upstream fitting to orifice			
		Without straightening vanes	With straightening vanes		
Single 90° ell, tee, or cross used as ell	0.2	6			2
	0.4	6			
	0.6	9	9		
	0.8	20	12	8	4
2 short-radius 90° ells in form of S	0.2	7			2
	0.4	8	8		
	0.6	13	10	6	
	0.8	25	15	11	4
2 long- or short-radius 90° ells in perpendicular planes	0.2	15	9	5	2
	0.4	18	10	6	
	0.6	25	11	7	
	0.8	40	13	9	4
Contraction or enlargement	0.2	8	Vanes have no advantage		2
	0.4	9			
	0.6	10			
	0.8	15			4
Globe valve or stop check	0.2	9	9	5	2
	0.4	10	10	6	
	0.6	13	10	6	
	0.8	21	13	9	4
Gate valve, wide open, or plug cocks	0.2	6	Same as globe valve		2
	0.4	6			
	0.6	8			
	0.8	14			4

the metering restriction which can affect the differential. Third, pulsations can be set up in the manometer leads themselves. Frequency of the pulsation also plays a part. At low frequencies, the meter reading can generally faithfully follow the flow pulsations, but at high frequencies it cannot. This is due to inertia of the fluid in the manometer leads or of the manometric fluid, whereupon the meter would give a reading intermediate between the maximum and minimum flows but having no readily predictable relation to the mean flow. Pressure transducers with flush-mounted diaphragms can be used together with high-speed recording equipment to provide accurate records of the pressure profiles at the upstream and downstream pressure taps, which can then be analyzed and translated into a mean flow rate.

The rather general practice of producing a steady differential reading by placing restrictions in the manometer leads can result in a reading which, under a fixed set of conditions, may be useful in control of an operation but which has no readily predictable relation to the actual average flow. If calibration is employed to compensate for the presence of pulsations, complete reproduction of operating conditions, including source of pulsations and waveform, is necessary to ensure reasonable accuracy.

According to Head [*Trans. Am. Soc. Mech. Eng.*, **78**, 1471–1479 (1956)], a pulsation-intensity limit of $\Gamma = 0.1$ is recommended as a practical pulsation threshold below which the performance of all types of flowmeters will differ negligibly from steady-flow performance (an error of less than 1 percent in flow due to pulsation). Γ is the peak-to-trough flow variation expressed as a fraction of the average flow rate. According to the ASME Research Committee on Fluid Meters Report (op. cit., pp. 34–35), the fractional metering error E for **liquid flow** through a head meter is given by

$$(1 + E)^2 = 1 + \Gamma^2/8 \quad (10-34)$$

When the pulsation amplitude is such as to result in a greater-than-permissible metering error, consideration should be given to installation of a pulsation damper between the source of pulsations and the

flowmeter. References to methods of pulsation-damper design are given in the subsection "Unsteady-State Behavior."

Pulsations are most likely to be encountered in discharge lines from reciprocating pumps or compressors and in lines supplying steam to reciprocating machinery. For **gas flow**, a combination involving a surge chamber and a constriction in the line can be used to damp out the pulsations to an acceptable level. The surge chamber is generally located as close to the pulsation source as possible, with the constriction between the surge chamber and the metering element. This arrangement can be used for either a suction or a discharge line. For such an arrangement, the metering error has been found to be a function of the Hodgson number N_H , which is defined as

$$N_H = Qn \Delta p_s / qp_s \quad (10-35)$$

where Q = volume of surge chamber and pipe between metering element and pulsation source; n = pulsation frequency; Δp_s = permanent pressure drop between metering element and surge chamber; q = average volume flow rate, based on gas density in the surge chamber; and p_s = pressure in surge chamber.

Herning and Schmid [*Z. Ver. Dtsch. Ing.*, **82**, 1107–1114 (1938)] presented charts for a simplex double-acting compressor for the prediction of metering error as a function of the Hodgson number and s , the ratio of piston discharge time to total time per stroke. Table 10-8a gives the minimum Hodgson numbers required to reduce the metering error to 1 percent as given by the charts (for specific heat ratios between 1.28 and 1.37). Schmid [*Z. Ver. Dtsch. Ing.*, **84**, 596–598 (1940)] presented similar charts for a duplex double-acting compressor and a triplex double-acting compressor for a specific heat ratio of 1.37. Table 10-8b gives the minimum Hodgson numbers corresponding to a 1 percent metering error for these cases. The value of $Q \Delta p_s$ can be calculated from the appropriate Hodgson number, and appropriate values of Q and Δp_s selected so as to satisfy this minimum requirement.

VELOCITY METERS

Anemometers An anemometer may be any instrument for measurement of gas velocity, e.g., a pitot tube, but usually the term refers to one of the following types.

The vane **anemometer** is a delicate revolution counter with jeweled bearings, actuated by a small windmill, usually 75 to 100 mm (about 3 to 4 in) in diameter, constructed of flat or slightly curved radially disposed vanes. Gas velocity is determined by using a stopwatch to find the time interval required to pass a given number of meters (feet) of gas as indicated by the counter. The velocity so obtained is inversely proportional to gas density. If the original calibration was carried out in a gas of density ρ_0 and the density of the gas stream being metered is ρ_1 , the true gas velocity can be found as follows: From the calibration curve for the instrument, find $V_{t,0}$ corresponding to the quantity $V_m \sqrt{\rho_1 / \rho_0}$, where V_m = measured velocity. Then the actual velocity $V_{t,1}$ is equal to $V_{t,0} \sqrt{\rho_0 / \rho_1}$. In general, when working with air, the effects of

atmospheric-density changes can be neglected for all velocities above 1.5 m/s (about 5 ft/s). In all cases, care must be taken to hold the anemometer well away from one's body or from any object not normally present in the stream.

Vane anemometers can be used for gas-velocity measurements in the range of 0.3 to 45 m/s (about 1 to 150 ft/s), although a given instrument generally has about a twentyfold velocity range. Bearing friction has to be minimized in instruments designed for accuracy at the low end of the range, while ample rotor and vane rigidity must be provided for measurements at the higher velocities. Vane anemometers are sensitive to shock and cannot be used in corrosive atmospheres. Therefore, accuracy is questionable unless a recent calibration has been made and the history of the instrument subsequent to calibration is known. For additional information, see Ower et al., op. cit., chap. VIII.

Turbine Flowmeters They consist of a straight flow tube containing a turbine which is free to rotate on a shaft supported by one or more bearings and located on the centerline of the tube. Means are provided for magnetic detection of the rotational speed, which is proportional to the volumetric flow rate. Its use is generally restricted to clean, noncorrosive fluids. Additional information on construction, operation, range, and accuracy can be obtained from Baker, pp. 215–252, 2000; Miller, op. cit.; and Spitzer, pp. 303–317, 2005.

The **current meter** is generally used for measuring velocities in open channels such as rivers and irrigation channels. There are two types, the cup meter and the propeller meter. The former is more widely used. It consists of six conical cups mounted on a vertical axis pivoted at the ends and free to rotate between the rigid arms of a U-shaped clevis to which a vaned tailpiece is attached. The wheel rotates because of the difference in drag for the two sides of the cup, and a signal proportional to the revolutions of the wheel is generated. The velocity is determined from the count over a period of time. The current meter is generally useful in the range of 0.15 to 4.5 m/s (about 0.5 to 15 ft/s) with an accuracy of ± 2 percent. For additional information see Creager and Justin, *Hydroelectric Handbook*, 2d ed., Wiley, New York, 1950, pp. 42–46.

Other important classes of velocity meters include electromagnetic flowmeters and ultrasonic flowmeters. Both are described in Sec. 8.

MASS FLOWMETERS

General Principles There are two main types of mass flowmeters: (1) the so-called true mass flowmeter, which responds directly to mass flow rate, and (2) the inferential mass flowmeter, which commonly measures volume flow rate and fluid density separately. A variety of types of true mass flowmeters have been developed, including the following: (a) the Magnus-effect mass flowmeter, (b) the axial-flow, transverse-momentum mass flowmeter, (c) the radial-flow, transverse-momentum mass flowmeter, (d) the gyroscopic transverse-momentum mass flowmeter, and (e) the thermal mass flowmeter. Type b is the basis for several commercial mass flowmeters, one version of which is briefly described here.

Axial-Flow Transverse-Momentum Mass Flowmeter This type is also referred to as an angular-momentum mass flowmeter. One embodiment of its principle involves the use of axial flow through a driven impeller and a turbine in series. The impeller imparts angular momentum to the fluid, which in turn causes a torque to be imparted to the turbine, which is restrained from rotating by a spring. The torque, which can be measured, is proportional to the rotational speed of the impeller and the mass flow rate.

Inferential Mass Flowmeter There are several types in this category, including the following:

1. **Head meters with density compensation.** Head meters such as orifices, venturis, or nozzles can be used with one of a variety of densitometers [e.g., based on (a) buoyant force on a float, (b) hydraulic coupling, (c) voltage output from a piezoelectric crystal, or (d) radiation absorption]. The signal from the head meter, which is proportional to ρV^2 (where ρ = fluid density and V = fluid velocity), is multiplied by ρ given by the densitometer. The square root of the product is proportional to the mass flow rate.

TABLE 10-8a Minimum Hodgson Numbers
Simplex double-acting compressor

s	N_H	s	N_H
0.167	1.31	0.667	0.60
0.333	1.00	0.833	0.43
0.50	0.80	1.00	0.34

TABLE 10-8b Minimum Hodgson Numbers

Duplex double-acting compressor		Triplex double-acting compressor	
s	N_H	s	N_H
0.167	1.00	0.167	0.85
0.333	0.70	0.333	0.30
0.50	0.30	0.50	0.15
0.667	0.10	0.667	0.06
0.833	0.05	0.833	0.00
1.00	0.00	1.00	0.00

2. *Head meters with velocity compensation.* The signal from the head meter, which is proportional to ρV^2 , is divided by the signal from a velocity meter to give a signal proportional to the mass flow rate.

3. *Velocity meters with density compensation.* The signal from the velocity meter (e.g., turbine meter, electromagnetic meter, or sonic velocity meter) is multiplied by the signal from a densitometer to give a signal proportional to the mass flow rate.

Coriolis Mass Flowmeter This type, described in Sec. 8, offers simultaneous direct measurement of both mass flow rate and fluid density. The Coriolis flowmeter is insensitive to upstream and downstream flow disturbances, but its performance is adversely affected by the presence of even a few percent of a gas when measuring a liquid flow.

VARIABLE-AREA METERS

General Principles The underlying principle of an ideal area meter is the same as that of a head meter of the orifice type (see subsection "Orifice Meters"). The stream to be measured is throttled by a constriction, but instead of observing the variation with flow of the differential head across an orifice of fixed size, the constriction of an area meter is so arranged that its size is varied to accommodate the flow while the differential head is held constant.

A simple example of an area meter is a gate valve of the rising-stem type provided with static-pressure taps before and after the gate and a means for measuring the stem position. In most common types of area meters, the variation of the opening is automatically brought about by the motion of a weighted piston or float supported by the fluid. Two different cylinder- and piston-type area meters are described in the ASME Research Committee on Fluid Meters Report, op. cit., pp. 82-83.

Rotameters The rotameter, an example of which is shown in Fig. 10-20, has become one of the most popular flowmeters in the chemical-process industries. It consists essentially of a plummet, or "float," which is free to move up or down in a vertical, slightly tapered tube having its small end down. The fluid enters the lower end of the tube and causes the float to rise until the annular area between the float and the wall of the tube is such that the pressure drop across this constriction is just sufficient to support the float. Typically, the tapered tube is of glass and carries etched upon it a nearly linear scale on which the position of the float may be visually noted as an indication of the flow.

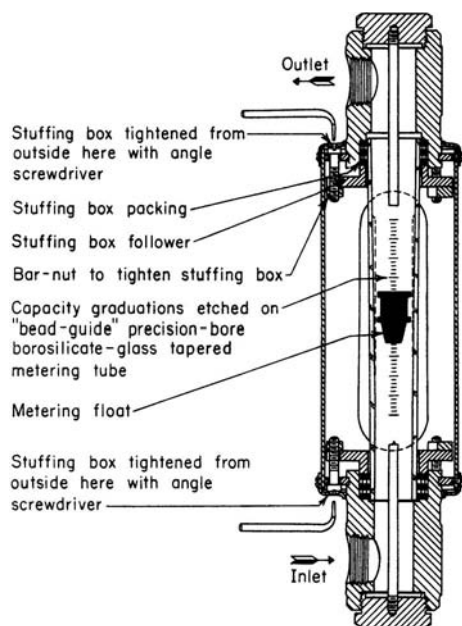


FIG. 10-20 Rotameter.

Interchangeable precision-bore glass tubes and metal metering tubes are available. Rotameters have proved satisfactory both for gases and for liquids at high and at low pressures. A single instrument can readily cover a tenfold range of flow, and by providing floats of different densities a two-hundredfold range is practicable. Rotameters are available with pneumatic, electric, and electronic transmitters for actuating remote recorders, integrators, and automatic flow controllers (see Considine, op. cit., pp. 4-35-4-36, and Sec. 8 of this *Handbook*).

Rotameters require no straight runs of pipe before or after the point of installation. Pressure losses are substantially constant over the whole flow range. In experimental work, for greatest precision, a rotameter should be calibrated with the fluid which is to be metered. However, most modern rotameters are precision-made so that their performance closely corresponds to a master calibration plot for the type in question. Such a plot is supplied with the meter upon purchase.

According to Head [*Trans. Am. Soc. Mech. Eng.*, **76**, 851-862 (1954)], flow rate through a rotameter can be obtained from

$$w = q\rho = KD_f \sqrt{\frac{W_f(\rho_f - \rho)\rho}{\rho_f}} \quad (10-36)$$

and

$$K = \phi \left[\frac{D_t}{D_f}, \frac{\mu}{\sqrt{W_f(\rho_f - \rho)\rho}} \right] \quad (10-37)$$

where w = weight flow rate; q = volume flow rate; ρ = fluid density; K = flow parameter, $m^{1/2}/s$ ($ft^{1/2}/s$); D_f = float diameter at constriction; W_f = float weight; ρ_f = float density; D_t = tube diameter at point of constriction; and μ = fluid viscosity. The appropriate value of K is obtained from a composite correlation of K versus the parameters shown in Eq. (10-37) corresponding to the float shape being used. The relation of D_t to the rotameter reading is also required for the tube taper and size being used.

The ratio of flow rates for two different fluids A and B at the same rotameter reading is given by

$$\frac{w_A}{w_B} = \frac{K_A}{K_B} \sqrt{\frac{(\rho_f - \rho_A)\rho_A}{(\rho_f - \rho_B)\rho_B}} \quad (10-38)$$

A measure of self-compensation, with respect to weight rate of flow, for fluid-density changes can be introduced through the use of a float with a density twice that of the fluid being metered, in which case an increase of 10 percent in ρ will produce a decrease of only 0.5 percent in w for the same reading. The extent of immunity to changes in fluid viscosity depends upon the shape of the float.

According to Baird and Cheema [*Can. J. Chem. Eng.*, **47**, 226-232 (1969)], the presence of square-wave pulsations can cause a rotameter to overread by as much as 100 percent. The higher the pulsation frequency, the less the float oscillation, although the error can still be appreciable even when the frequency is high enough so that the float is virtually stationary. Use of a damping chamber between the pulsation source and the rotameter will reduce the error.

Additional information on rotameter theory is presented by Fischer [*Chem. Eng.*, **59**(6), 180-184 (1952)], Coleman [*Trans. Inst. Chem. Eng.*, **34**, 339-350 (1956)], and McCabe, Smith, and Harriott (*Unit Operations of Chemical Engineering*, 4th ed., McGraw-Hill, New York, 1985, pp. 202-205).

TWO-PHASE SYSTEMS

It is generally preferable to meter each of the individual components of a two-phase mixture separately prior to mixing, since it is difficult to meter such mixtures accurately. Problems arise because of fluctuations in composition with time and variations in composition over the cross section of the channel. Information on metering of such mixtures can be obtained from the following sources.

Gas-Solid Mixtures Carlson, Frazier, and Engdahl [*Trans. Am. Soc. Mech. Eng.*, **70**, 65–79 (1948)] describe the use of a **flow nozzle** and a **square-edged orifice** in series for the measurement of both the gas rate and the solids rate in the flow of a finely divided solid-in-gas mixture. The nozzle differential is sensitive to the flow of both phases, whereas the orifice differential is not influenced by the solids flow.

Farbar [*Trans. Am. Soc. Mech. Eng.*, **75**, 943–951 (1953)] describes how a **venturi meter** can be used to measure solids flow rate in a gas-solids mixture when the gas rate is held constant. Separate calibration curves (solids flow versus differential) are required for each gas rate of interest.

Cheng, Tung, and Soo [*J. Eng. Power*, **92**, 135–149 (1970)] describe the use of an **electrostatic probe** for measurement of solids flow in a gas-solids mixture.

Goldberg and Boothroyd [*Br. Chem. Eng.*, **14**, 1705–1708 (1969)] describe several types of solids-in-gas flowmeters and give an extensive bibliography.

Gas-Liquid Mixtures An empirical equation was developed by Murdock [*J. Basic Eng.*, **84**, 419–433 (1962)] for the measurement of gas-liquid mixtures using **sharp-edged orifice** plates with either radius, flange, or pipe taps.

An equation for use with **venturi meters** was given by Chisholm [*Br. Chem. Eng.*, **12**, 454–457 (1967)]. A procedure for determining steam quality via pressure-drop measurement with upflow through either venturi meters or sharp-edged orifice plates was given by Collins and Gacesa [*J. Basic Eng.*, **93**, 11–21 (1971)].

Liquid-Solid Mixtures Liptak [*Chem. Eng.*, **74**(4), 151–158 (1967)] discusses a variety of techniques that can be used for the measurement of solids-in-liquid suspensions or slurries. These include metering pumps, weigh tanks, magnetic flowmeter, ultrasonic flowmeter, gyroscope flowmeter, etc.

Shirato, Gotoh, Osasa, and Usami [*J. Chem. Eng. Japan*, **1**, 164–167 (January 1968)] present a method for determining the mass flow rate of suspended solids in a liquid stream wherein the liquid velocity is measured by an electromagnetic flowmeter and the flow of solids is calculated from the pressure drops across each of two vertical sections of pipe of different diameter through which the suspension flows in series.

FLOWMETER SELECTION

Web sites for process equipment and instrumentation, such as www.globalspec.com and www.thomasnet.com, are valuable tools when selecting a flowmeter. These search engines can scan the flowmeters manufactured by more than 800 companies for specific products that meet the user's specifications. Table 10-4 was based in part on information from these web sites. Note that the accuracies claimed are achieved only under ideal conditions when the flowmeters are properly installed and calibrated for the application.

The purpose of this subsection is to summarize the preferred applications as well as the advantages and disadvantages of some of the common flowmeter technologies.

Table 10-9 divides flowmeters into four classes. Flowmeters in class I depend on wetted moving parts that can wear, plug, or break. The

potential for catastrophic failure is a disadvantage. However, in clean fluids, class I flowmeters have often proved reliable and stable when properly installed, calibrated, and maintained.

Class II flowmeters have no wetted moving parts to break and are thus not subject to catastrophic failure. However, the flow surfaces such as orifice plates may wear, eventually biasing flow measurements. Other disadvantages of some flowmeters in this class include high pressure drop and susceptibility to plugging. Very dirty and abrasive fluids should be avoided.

Because class III flowmeters have neither moving parts nor obstructions to flow, they are suitable for dirty and abrasive fluids provided that appropriate materials of construction are available.

Class IV flowmeters have sensors mounted external to the pipe, and would thus seem to be ideal, but problems of accuracy and sensitivity have been encountered in early devices. These comparatively new technologies are under development, and these problems may be overcome in the future.

Section 8 outlines the following criteria for selection of measurement devices: measurement span, performance, reliability, materials of construction, prior use, potential for releasing process materials to the environment, electrical classification, physical access, invasive or noninvasive, and life-cycle cost.

Spitzer, op. cit., 2005, cites four intended end uses of the flowmeter: rate indication, control, totalization, and alarm. Thus high accuracy may be important for rate indication, while control may just need good repeatability. Volumetric flow or mass flow indication is another choice.

Baker, op. cit., 2003, identifies the type of fluid (liquid or gas, slurry, multiphase), special fluid constraints (clean or dirty, hygienic, corrosive, abrasive, high flammability, low lubricity, fluids causing scaling). He lists the following flowmeter constraints: accuracy or measurement uncertainty, diameter range, temperature range, pressure range, viscosity range, flow range, pressure loss caused by the flowmeter, sensitivity to installation, sensitivity to pipework supports, sensitivity to pulsation, whether the flowmeter has a clear bore, whether a clamp-on version is available, response time, and ambient conditions. Finally, Baker identifies these environmental considerations: ambient temperature, humidity, exposure to weather, level of electromagnetic radiation, vibration, tamperproof for domestic use, and classification of area requiring explosionproof, intrinsic safety, etc.

Note that the accuracies cited in Table 10-4 can be achieved by those flowmeters only under ideal conditions of application, installation, and calibration. This subsection has only given an introduction to issues to consider in the choice of a flowmeter for a given application. See Baker, op. cit., 2003; Miller, op. cit., 1996; and Spitzer, op. cit., 2005, for further guidance and to obtain application-specific data from flowmeter vendors.

WEIRS

Liquid flow in an open channel may be metered by means of a weir, which consists of a dam over which, or through a notch in which, the liquid flows. The terms “rectangular weir,” “triangular weir,” etc., generally refer to the shape of the notch in a notched weir. All weirs considered here have flat upstream faces that are perpendicular to the bed and walls of the channel.

Sharp-edged weirs have edges like those of square or sharp-edged orifices (see subsection “Orifice Meters”). Notched weirs are ordinarily sharp-edged. Weirs not in the sharp-edged class are, for the most part, those described as **broad-crested weirs**.

The head h_0 on a weir is the liquid-level height above the crest or base of the notch. The head must be measured sufficiently far upstream to avoid the drop in level occasioned by the overflow which begins at a distance about $2h_0$ upstream from the weir. Surface-level measurements should be made a distance of $3h_0$ or more upstream, preferably by using a stilling box equipped with a high-precision level gauge, e.g., a hook gauge or float gauge.

With sharp-edged weirs, the sheet of discharging liquid, called the “nappe,” contracts as it leaves the opening and free discharge occurs. Rounding the upstream edge will reduce the contraction and increase the flow rate for a given head. A clinging nappe may result

TABLE 10-9 Flowmeter Classes

Class I: Flowmeters with wetted moving parts	Class II: Flowmeters with no wetted moving parts
Positive displacement Turbine Variable-area	Differential pressure Vortex Target Thermal
Class III: Obstructionless flowmeters	Class IV: Flowmeters with sensors mounted external to the pipe
Coriolis mass Electromagnetic Ultrasonic	Clamp-on ultrasonic Correlation

Adapted from Spitzer, op. cit., 2005.

10-24 TRANSPORT AND STORAGE OF FLUIDS

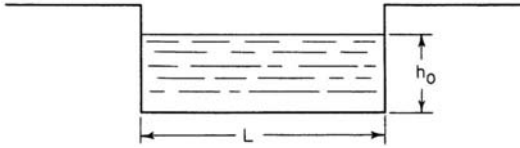


FIG. 10-21 Rectangular weir.

if the head is very small, if the edge is well rounded, or if air cannot flow in beneath the nappe. This, in turn, results in an increase in the discharge rate for a given head as compared with that for a free nappe. For further information on the effect of the nappe, see Gibson, *Hydraulics and Its Applications*, 5th ed., Constable, London, 1952; and Chow, *Open-Channel Hydraulics*, McGraw-Hill, New York, 1959.

Flow through a **rectangular weir** (Fig. 10-21) is given by

$$q = 0.415(L - 0.2h_0)h_0^{1.5} \sqrt{2g} \quad (10-39)$$

where q = volume flow rate, L = crest length, h_0 = weir head, and g = local acceleration due to gravity. This is known as the modified Francis formula for a rectangular sharp-edged weir with two end corrections; it applies when the velocity-of-approach correction is small. The Francis formula agrees with experiments within 3 percent if (1) L is greater than $2h_0$, (2) velocity of approach is 0.6 m/s (2 ft/s) or less, (3) height of crest above bottom of channel is at least $3h_0$, and (4) h_0 is not less than 0.09 m (0.3 ft).

Narrow rectangular notches ($h_0 > L$) have been found to give about 93 percent of the discharge predicted by the Francis formula. Thus

$$q = 0.386Lh_0^{1.5} \sqrt{2g} \quad (10-40)$$

In this case, no end corrections are applied even though the formula applies only for sharp-edged weirs. See Schoder and Dawson, *Hydraulics*, McGraw-Hill, New York, 1934, p. 175, for further details.

The **triangular-notch weir** has the advantage that a single notch can accommodate a wide range of flow rates, although this in turn reduces its accuracy. The discharge for sharp- or square-edged weirs is given by

$$q = (0.31h_0^{2.5} \sqrt{2g}) / \tan \phi \quad (10-41)$$

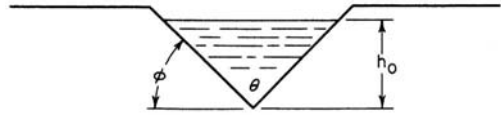


FIG. 10-22 Triangular weir.

See Eq. (10-39) for nomenclature. Angle ϕ is illustrated in Fig. 10-22. Equations (10-39), (10-40), and (10-41) are applicable only to the flow of water. However, for the case of triangular-notch weirs Lenz [*Trans. Am. Soc. Civ. Eng.*, **108**, 759–802 (1943)] has presented correlations predicting the effect of viscosity over the range of 0.001 to 0.15 Pa·s (1 to 150 cP) and surface tension over the range of 0.03 to 0.07 N/m (30 to 70 dyn/cm). His equation predicts about an 8 percent increase in flow for a liquid of 0.1-Pa·s (100-cP) viscosity compared with water at 0.001 Pa·s (1 cP) and about a 1 percent increase for a liquid with one-half of the surface tension of water. For fluids of moderate viscosity, Ranga Raju and Asawa [*Proc. Am. Soc. Civ. Eng., J. Hydraul. Div.*, **103** (HY 10), 1227–1231 (1977)] find that the effect of viscosity and surface tension on the discharge flow rate for rectangular and triangular-notch ($\phi = 45^\circ$) weirs can be neglected when

$$(N_{Re})^{0.2}(N_{We})^{0.6} > 900 \quad (10-42)$$

where N_{Re} (Reynolds number) = $\sqrt{gh_0^3}/v$, g = local acceleration due to gravity, h_0 = weir head, v = kinematic viscosity; N_{We} (Weber number) = $\rho gh_0^2/g_c \sigma$, ρ = density, g_c = dimensional constant, and σ = surface tension.

For the flow of high-viscosity liquids over rectangular weirs, see Slocum, *Can. J. Chem. Eng.*, **42**, 196–200 (1964). His correlation is based on data for liquids with viscosities in the range of 2.5 to 500 Pa·s (25 to 5000 cP), in which range the discharge decreases markedly for a given head as viscosity is increased.

Information on other types of weirs can be obtained from Addison, op. cit.; Gibson, *Hydraulics and Its Applications*, 5th ed., Constable, London, 1952; Henderson, *Open Channel Flow*, Macmillan, New York, 1966; Linford, *Flow Measurement and Meters*, Spon, London, 1949; Lakshmana Rao, "Theory of Weirs," in *Advances in Hydrosience*, vol. 10, Academic, New York, 1975; and Merritt, *Standard Handbook for Civil Engineers*, 2d ed., McGraw-Hill, New York, 1976.

PUMPS AND COMPRESSORS

GENERAL REFERENCES: Meherwan P. Boyce, P.E., *Centrifugal Compressors: A Basic Guide*, Pennwell Books, Tulsa, Okla., 2002; Royce N. Brown, *Compressors: Selection and Sizing*, 3d ed., Gulf Professional Publishing, Houston, Tex., 2005; James Corley, "The Vibration Analysis of Pumps: A Tutorial," Fourth International Pump Symposium, Texas A & M University, Houston, Tex., May 1987; John W. Dufor and William E. Nelson, *Centrifugal Pump Sourcebook*, McGraw-Hill, New York, 1992; *Engineering Data Book*, 12th ed., vol. I, Secs. 12 and 13, Gas Processors Suppliers Association, Tulsa, Okla., 2004; Paul N. Garay, P.E., *Pump Application Desk Book*, Fairmont Press, 1993; *Process Pumps*, IIT Fluid Technology Corporation, 1992; Igor J. Karassik et al., *Pump Handbook*, 3d ed., McGraw-Hill, New York, 2001; Val S. Lobanoff and Robert R. Ross, *Centrifugal Pumps: Design and Application*, 2d ed., Gulf Professional Publishing, Houston, Tex., 1992; A. J. Stephanoff, *Centrifugal and Axial Flow Pumps: Theory, Design, and Application*, 2d ed., Krieger Publishing, Melbourne, Fla., 1992.

INTRODUCTION

The following subsections deal with pumps and compressors. A pump or compressor is a physical contrivance that is used to deliver fluids from one location to another through conduits. The term *pump* is used when the fluid is a liquid, while the term *compressor* is used when the fluid is a gas. The basic requirements to define the applica-

tion are suction and delivery pressures, pressure loss in transmission, and flow rate. Special requirements may exist in food, pharmaceutical, nuclear, and other industries that impose material selection requirements of the pump.

The primary means of transfer of energy to the fluid that causes flow are gravity, displacement, centrifugal force, electromagnetic force, transfer of momentum, mechanical impulse, and a combination of these energy-transfer mechanisms. Displacement and centrifugal force are the most common energy-transfer mechanisms in use.

Pumps and compressors are designed per technical specifications and standards developed over years of operating and maintenance experience. Table 10-10 lists some of these standards for pumps and compressors and for related equipment such as lubrication systems and gearboxes which, if not properly specified, could lead to many operational and maintenance problems with the pumps and compressors. These standards specify design, construction, maintenance, and testing details such as terminology, material selection, shop inspection and tests, drawings, clearances, construction procedures, and so on.

There are four (4) major types of pumps: (1) positive displacement, (2) dynamic (kinetic), (3) lift, and (4) electromagnetic. Piston pumps are positive displacement pumps. The most common centrifugal

TABLE 10-10 Standards Governing Pumps and Compressors

ASME Standards, American Society of Mechanical Engineers, New York
 B73.1-2001, *Specification for Horizontal End Suction Centrifugal Pumps for Chemical Process*
 B73.2-2003, *Specification for Vertical In-Line Centrifugal Pumps for Chemical Process*
 PTC 10, 1997 *Test Code on Compressors and Exhausters*
 PTC 11, 1984 *Fans*
 B19.3-1991, *Safety Standard for Compressors for Process Industries*
 API Standards, American Petroleum Institute, Washington
 API Standard 610, *Centrifugal Pumps for Petroleum, Petrochemical, and Natural Gas Industries*, Adoption of ISO 13709, October 2004
 API Standard 613, *Special Purpose Gear Units for Petroleum, Chemical and Gas Industry Services*, February 2003
 API Standard 614, *Lubrication, Shaft-Sealing, and Control-Oil Systems and Auxiliaries for Petroleum, Chemical and Gas Industry Services*, April 1999
 API Standard 616, *Gas Turbines for the Petroleum, Chemical, and Gas Industry Services*, August 1998
 API Standard 617, *Axial and Centrifugal Compressors and Expanders—Compressors for Petroleum, Chemical, and Gas Industry Services*, June 2003
 API Standard 618, *Reciprocating Compressors for Petroleum, Chemical, and Gas Industry Services*, June 1995
 API Standard 619, *Rotary-Type Positive Displacement Compressors for Petroleum, Petrochemical, and Natural Gas Industries*, December 2004
 API Standard 670, *Machinery Protection Systems*, November 2003
 API Standard 671, *Special Purpose Couplings for Petroleum, Chemical, and Gas Industry Services*, October 1998
 API Standard 672, *Packaged, Integrally Geared, Centrifugal Air Compressors for Petroleum, Chemical, and Gas Industry Services*, March 2004
 API Standard 673, *Centrifugal Fans for Petroleum, Chemical, and Gas Industry Services*, October 2002
 API Standard 674, *Positive Displacement Pumps—Reciprocating*, June 1995
 API Standard 675, *Positive Displacement Pumps—Controlled Volume*, March 2000
 API Standard 677, *General Purpose Gear Units for Petroleum, Chemical, and Gas Industry Services*, April 2006
 API Standard 680, *Packaged Reciprocating Plant and Instrument Air Compressors for General Refinery Services*, October 1987
 API Standard 681, *Liquid Ring Vacuum Pumps and Compressors for Petroleum, Chemical, and Gas Industry Services*, June 2002
 API Standard 682, *Pumps—Shaft Sealing Systems for Centrifugal and Rotary Pumps*, September 2004
 API Standard 685, *Sealless Centrifugal Pumps for Petroleum, Heavy Duty Chemical, and Gas Industry Services*, October 2000
 Hydraulic Institute, Parsippany, N.J. (www.pumps.org)
 ANSI/HI Pump Standards, 2005 (covers centrifugal, vertical, rotary, and reciprocating pumps)
 National Fire Protection Association, Quincy, Mass. (www.nfpa.org)
 Standards for pumps used in fire protection systems

pumps are of dynamic type; ancient bucket-type pumps are lift pumps; and electromagnetic pumps use electromagnetic force and are common in modern reactors. Canned pumps are also becoming popular in the petrochemical industry because of the drive to minimize fugitive emissions. Figure 10-23 shows pump classification:

TERMINOLOGY

Displacement Discharge of a fluid from a vessel by partially or completely displacing its internal volume with a second fluid or by mechanical means is the principle upon which a great many fluid-transport devices operate. Included in this group are reciprocating-piston and diaphragm machines, rotary-vane and gear types, fluid piston compressors, acid eggs, and air lifts.

The large variety of displacement-type fluid-transport devices makes it difficult to list characteristics common to each. However, for most types it is correct to state that (1) they are adaptable to high-pressure operation, (2) the flow rate through the pump is variable (auxiliary damping systems may be employed to reduce the magnitude of pressure pulsation and flow variation), (3) mechanical considerations limit maximum throughputs, and (4) the devices are capable of efficient performance at extremely low-volume throughput rates.

Centrifugal Force Centrifugal force is applied by means of the centrifugal pump or compressor. Though the physical appearance of the many types of centrifugal pumps and compressors varies greatly, the basic function of each is the same, i.e., to produce kinetic energy by the action of centrifugal force and then to convert this energy into pressure by efficiently reducing the velocity of the flowing fluid.

In general, centrifugal fluid-transport devices have these characteristics: (1) discharge is relatively free of pulsation; (2) mechanical design lends itself to high throughputs, capacity limitations are rarely a problem; (3) the devices are capable of efficient performance over a wide range of pressures and capacities even at constant-speed operation; (4) discharge pressure is a function of fluid density; and (5) these are relatively small high-speed devices and less costly.

A device which combines the use of centrifugal force with mechanical impulse to produce an increase in pressure is the axial-flow compressor or pump. In this device the fluid travels roughly parallel to the shaft through a series of alternately rotating and stationary radial blades having airfoil cross sections. The fluid is accelerated in the axial direction by mechanical impulses from the rotating blades; concurrently, a positive-pressure gradient in the radial direction is established in each stage by centrifugal force. The net pressure rise per stage results from both effects.

Electromagnetic Force When the fluid is an electrical conductor, as is the case with molten metals, it is possible to impress an electromagnetic field around the fluid conduit in such a way that a driving force that will cause flow is created. Such pumps have been developed for the handling of heat-transfer liquids, especially for nuclear reactors.

Transfer of Momentum Deceleration of one fluid (motivating fluid) in order to transfer its momentum to a second fluid (pumped fluid) is a principle commonly used in the handling of corrosive materials, in pumping from inaccessible depths, or for evacuation. Jets and eductors are in this category.

Absence of moving parts and simplicity of construction have frequently justified the use of jets and eductors. However, they are relatively inefficient devices. When air or steam is the motivating fluid, operating costs may be several times the cost of alternative types of fluid-transport equipment. In addition, environmental considerations in today's chemical plants often inhibit their use.

Mechanical Impulse The principle of mechanical impulse when applied to fluids is usually combined with one of the other means of imparting motion. As mentioned earlier, this is the case in axial-flow compressors and pumps. The turbine or regenerative-type pump is another device which functions partially by mechanical impulse.

Measurement of Performance The amount of useful work that any fluid-transport device performs is the product of (1) the mass rate of fluid flow through it and (2) the total pressure differential measured immediately before and after the device, usually expressed in the height of column of fluid equivalent under adiabatic conditions. The first of these quantities is normally referred to as **capacity**, and the second is known as **head**.

Capacity This quantity is expressed in the following units. In SI units capacity is expressed in cubic meters per hour (m³/h) for both liquids and gases. In U.S. customary units it is expressed in U.S. gallons per minute (gal/min) for liquids and in cubic feet per minute (ft³/min) for gases. Since all these are volume units, the density or specific gravity must be used for conversion to mass rate of flow. When gases are being handled, capacity must be related to a pressure and a temperature, usually the conditions prevailing at the machine inlet. It is important to note that all heads and other terms in the following equations are expressed in height of column of liquid.

Total Dynamic Head The total dynamic head H of a pump is the total discharge head h_d minus the total suction head h_s .

Total Suction Head This is the reading h_{gs} of a gauge at the suction flange of a pump (corrected to the pump centerline*), plus the barometer reading and the velocity head h_{vs} at the point of gauge attachment:

$$h_s = h_{gs} + \text{atm} + h_{vs} \quad (10-43)$$

If the gauge pressure at the suction flange is less than atmospheric, requiring use of a vacuum gauge, this reading is used for h_{gs} in Eq. (10-43) with a negative sign.

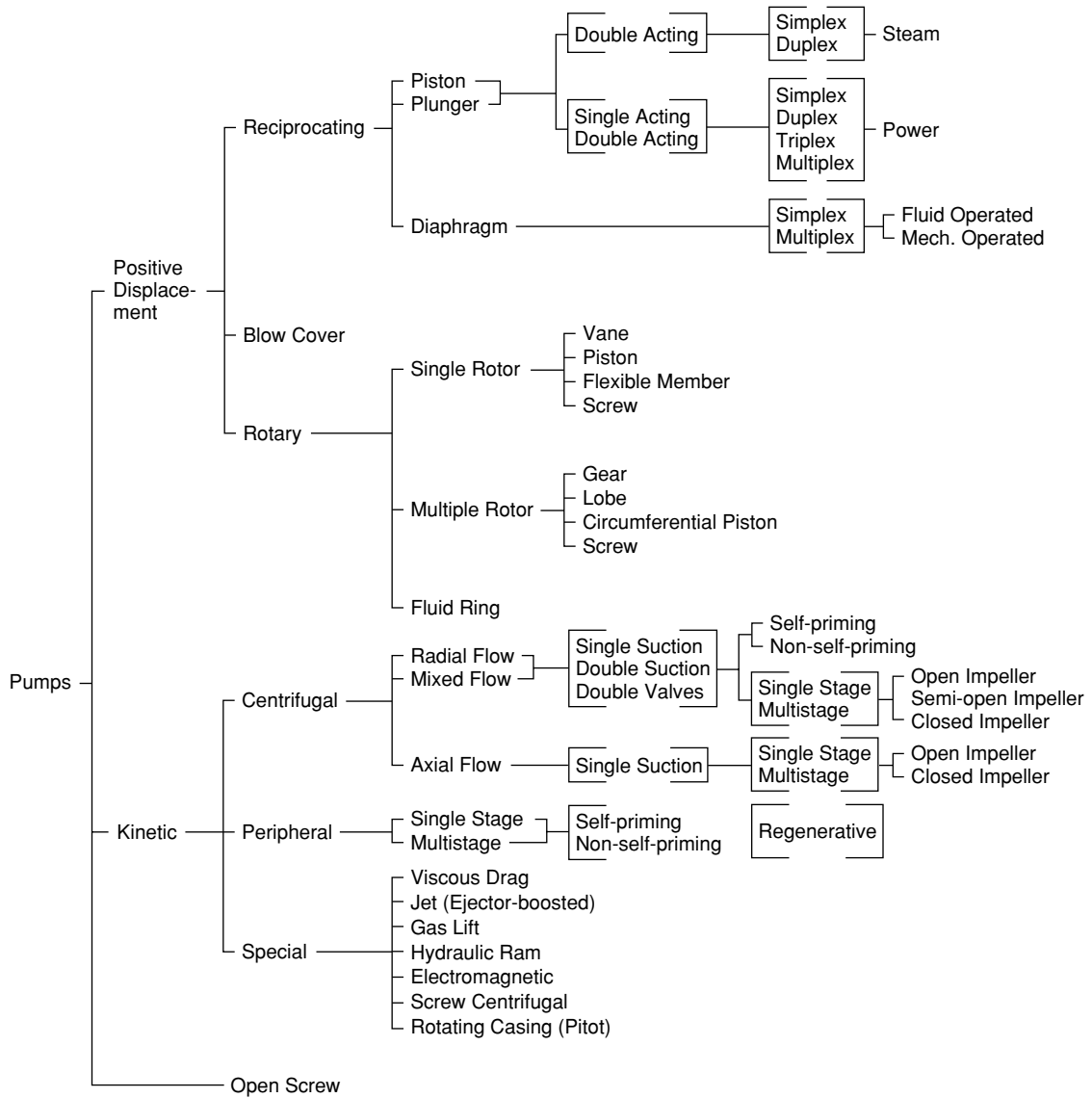


FIG. 10-23 Classification of pumps. (Courtesy of Hydraulic Institute.)

Before installation it is possible to estimate the total suction head as follows:

$$h_s = h_{ss} - h_{fs} \quad (10-44)$$

where h_{ss} = static suction head and h_{fs} = suction friction head.

Static Suction Head The static suction head h_{ss} is the vertical distance measured from the free surface of the liquid source to the pump centerline plus the absolute pressure at the liquid surface.

Total Discharge Head The total discharge head h_d is the reading h_{gd} of a gauge at the discharge flange of a pump (corrected to the pump centerline^o), plus the barometer reading and the velocity head h_{vd} at the point of gauge attachment:

^oOn vertical pumps, the correction should be made to the eye of the suction impeller.

$$h_d = h_{gd} + atm + h_{vd} \quad (10-45)$$

Again, if the discharge gauge pressure is below atmospheric, the vacuum-gauge reading is used for h_{gd} in Eq. (10-45) with a negative sign.

Before installation it is possible to estimate the total discharge head from the static discharge head h_{sd} and the discharge friction head h_{fd} as follows:

$$h_d = h_{sd} + h_{fd} \quad (10-46)$$

Static Discharge Head The static discharge head h_{sd} is the vertical distance measured from the free surface of the liquid in the receiver to the pump centerline, ^o plus the absolute pressure at the liquid surface. **Total static head** h_{ts} is the difference between discharge and suction static heads.

Velocity Since most liquids are practically incompressible, the relation between the quantity flowing past a given point in a given time and the velocity of flow is expressed as follows:

$$Q = Av \tag{10-47}$$

This relationship in SI units is as follows:

$$v \text{ (for circular conduits)} = 3.54 Q/d^2 \tag{10-48}$$

where v = average velocity of flow, m/s; Q = quantity of flow, m³/h; and d = inside diameter of conduit, cm.

This same relationship in U.S. customary units is

$$v \text{ (for circular conduits)} = 0.409 Q/d^2 \tag{10-49}$$

where v = average velocity of flow, ft/s; Q = quantity of flow, gal/min; and d = inside diameter of conduit, in.

Velocity Head This is the vertical distance by which a body must fall to acquire the velocity v .

$$h_v = v^2/2g \tag{10-50}$$

Viscosity (See Sec. 6 for further information.) In flowing liquids the existence of internal friction or the internal resistance to relative motion of the fluid particles must be considered. This resistance is called viscosity. The viscosity of liquids usually decreases with rising temperature. Viscous liquids tend to increase the power required by a pump, to reduce pump efficiency, head, and capacity, and to increase friction in pipe lines.

Friction Head This is the pressure required to overcome the resistance to flow in pipe and fittings. It is dealt with in detail in Sec. 6.

Work Performed in Pumping To cause liquid to flow, work must be expended. A pump may raise the liquid to a higher elevation, force it into a vessel at higher pressure, provide the head to overcome pipe friction, or perform any combination of these. Regardless of the service required of a pump, all energy imparted to the liquid in performing this service must be accounted for; consistent units for all quantities must be employed in arriving at the work or power performed.

When arriving at the performance of a pump, it is customary to calculate its **power output**, which is the product of (1) the total dynamic head and (2) the mass of liquid pumped in a given time. In SI units power is expressed in kilowatts; horsepower is the conventional unit used in the United States.

In SI units,

$$kW = HQ\rho/3.670 \times 10^5 \tag{10-51}$$

where kW is the pump power output, kW; H = total dynamic head, N·m/kg (column of liquid); Q = capacity, m³/h; and ρ = liquid density, kg/m³.

When the total dynamic head H is expressed in pascals, then

$$kW = HQ/3.599 \times 10^6 \tag{10-52}$$

In U.S. customary units,

$$hp = HQs/3.960 \times 10^3 \tag{10-53}$$

where hp is the pump-power output, hp; H = total dynamic head, lbf·ft/lbm (column of liquid); Q = capacity, U.S. gal/min; and s = liquid specific gravity.

When the total dynamic head H is expressed in pounds-force per square inch, then

$$hp = HQ/1.714 \times 10^3 \tag{10-54}$$

The **power input** to a pump is greater than the **power output** because of internal losses resulting from friction, leakage, etc. The efficiency of a pump is therefore defined as

$$\text{Pump efficiency} = (\text{power output})/(\text{power input}) \tag{10-55}$$

PUMP SELECTION

When selecting pumps for any service, it is necessary to know the liquid to be handled, the total dynamic head, the suction and discharge heads, and, in most cases, the temperature, viscosity, vapor pressure, and specific gravity. In the chemical industry, the task of pump selection is frequently further complicated by the presence of

solids in the liquid and liquid corrosion characteristics requiring special materials of construction. Solids may accelerate erosion and corrosion, have a tendency to agglomerate, or require delicate handling to prevent undesirable degradation.

Range of Operation Because of the wide variety of pump types and the number of factors which determine the selection of any one type for a specific installation, the designer must first eliminate all but those types of reasonable possibility. Since range of operation is always an important consideration, Fig. 10-24 should be of assistance. The boundaries shown for each pump type are at best approximate. In most cases, following Fig. 10-24 will select the pump that is best suited for a given application. Low-capacity pumps with high discharge head requirements are best served by positive-displacement pumps. Reciprocating pumps and rotary pumps such as gear and roots rotor-type pumps are examples of positive-displacement pumps. Displacement pumps provide high heads at low capacities which are beyond the capability of centrifugal pumps. Displacement pumps achieve high pressure with low velocities and are thus suited for high-viscosity service and slurry.

The centrifugal pump operates over a very wide range of flows and pressures. For low heads but high flows the axial pump is best suited. Both the centrifugal and axial flow pumps impart energy to the fluid by the rotational speed of the impeller and the velocity it imparts to the fluid.

NET POSITIVE SUCTION HEAD

Net positive suction head available (NPSH)_A is the difference between the total absolute suction pressure at the pump suction nozzle when the pump is running and the vapor pressure at the flowing liquid temperature. All pumps require the system to provide adequate (NPSH)_A. In a positive-displacement pump the (NPSH)_A should be large enough to open the suction valve, to overcome the friction losses within the pump liquid end, and to overcome the liquid acceleration head.

Suction Limitations of a Pump Whenever the pressure in a liquid drops below the vapor pressure corresponding to its temperature, the liquid will vaporize. When this happens within an operating pump, the vapor bubbles will be carried along to a point of higher pressure, where they suddenly collapse. This phenomenon is known as **cavitation**. Cavitation in a pump should be avoided, as it is accompanied by metal removal, vibration, reduced flow, loss in efficiency, and noise. When the absolute suction pressure is low, cavitation may occur in the pump inlet and damage result in the pump suction and on the impeller vanes near the inlet edges. To avoid this phenomenon, it is necessary to maintain a **required net positive suction head**

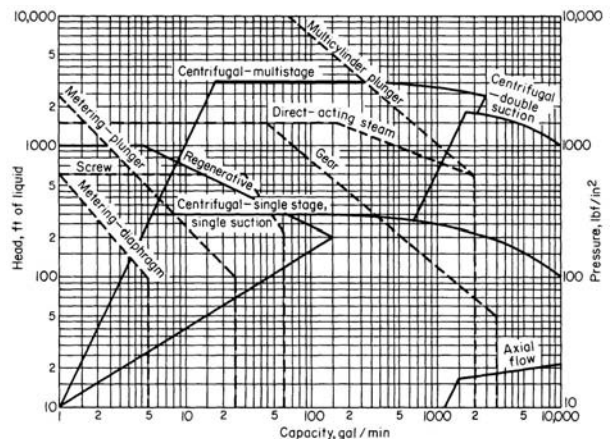


FIG. 10-24 Pump coverage chart based on normal ranges of operation of commercially available types. Solid lines: use left ordinate, head scale. Broken lines: use right ordinate, pressure scale. To convert gallons per minute to cubic meters per hour, multiply by 0.2271; to convert feet to meters, multiply by 0.3048; and to convert pounds-force per square inch to kilopascals, multiply by 6.895.

10-28 TRANSPORT AND STORAGE OF FLUIDS

$(NPSH)_R$, which is the equivalent total head of liquid at the pump centerline less the vapor pressure p . Each pump manufacturer publishes curves relating $(NPSH)_R$ to capacity and speed for each pump.

When a pump installation is being designed, the **available net positive suction head** $(NPSH)_A$ must be equal to or greater than the $(NPSH)_R$ for the desired capacity. The $(NPSH)_A$ can be calculated as follows:

$$(NPSH)_A = h_{ss} - h_{fs} - p \quad (10-56)$$

If $(NPSH)_A$ is to be checked on an existing installation, it can be determined as follows:

$$(NPSH)_A = \text{atm} + h_{gs} - p + h_{es} \quad (10-57)$$

Practically, the NPSH required for operation without cavitation and vibration in the pump is somewhat greater than the theoretical. The actual $(NPSH)_R$ depends on the characteristics of the liquid, the total head, the pump speed, the capacity, and impeller design. Any suction condition which reduces $(NPSH)_A$ below that required to prevent cavitation at the desired capacity will produce an unsatisfactory installation and can lead to mechanical difficulty.

The following two equations usually provide an adequate design margin between $(NPSH)_A$ and $(NPSH)_R$:

$$(NPSH)_A = (NPSH)_R + 5 \text{ ft} \quad (10-58)$$

$$(NPSH)_A = 1.35(NPSH)_R \quad (10-59)$$

Use the larger value of $(NPSH)_A$ calculated with Eqs. (10-58) and (10-59).

NPSH Requirements for Other Liquids NPSH values depend on the fluid being pumped. Since water is considered a standard fluid for pumping, various correction methods have been developed to evaluate NPSH when pumping other fluids. The most recent of these corrective methods has been developed by the Hydraulic Institute and is shown in Fig. 10-25.

The chart shown in Fig. 10-25 is for pure liquids. Extrapolation of data beyond the ranges indicated in the graph may not produce accurate results. Figure 10-25 shows the variation of vapor pressure and NPSH reductions for various hydrocarbons and hot water as a function of temperature. Certain rules apply while using this chart. When using the chart for hot water, if the NPSH reduction is greater than one-half of the NPSH required for cold water, deduct one-half of cold water NPSH to obtain the corrected NPSH. On the other

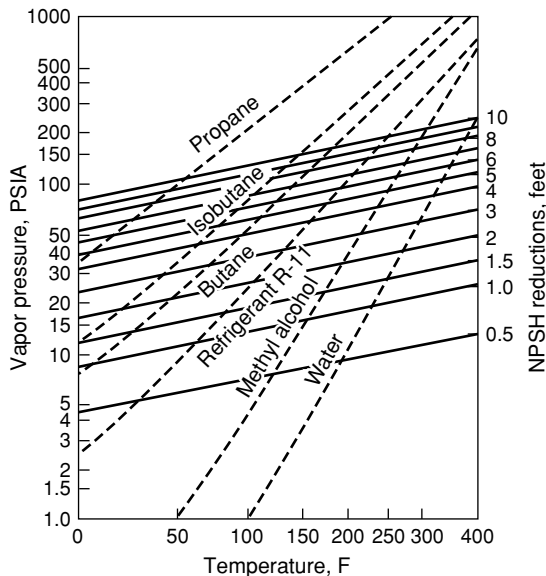


FIG. 10-25 NPSH reductions for pumps handling hydrocarbon liquids and high-temperature water. This chart has been constructed from test data obtained using the liquids shown (*Hydraulic Institute Standards*).

hand, if the value read on the chart is less than one-half of cold water NPSH, deduct this chart value from the cold water NPSH to obtain the corrected NPSH.

Example 1: NPSH Calculation Suppose a selected pump requires a minimum NPSH of 16 ft (4.9 m) when pumping cold water. What will be the NPSH limitation to pump propane at 55°F (12.8°C) with a vapor pressure of 100 psi? Using the chart in Fig. 10-25, NPSH reduction for propane gives 9.5 ft (2.9 m). This is greater than one-half of cold water NPSH of 16 ft (4.9 m). The corrected NPSH is therefore 8 ft (2.2 m) or one-half of cold water NPSH.

PUMP SPECIFICATIONS

Pump specifications depend upon numerous factors but mostly on application. Typically, the following factors should be considered while preparing a specification.

1. Application, scope, and type
2. Service conditions
3. Operating conditions
4. Construction application-specific details and special considerations
 - a. Casing and connections
 - b. Impeller details
 - c. Shaft
 - d. Stuffing box details—lubrications, sealing, etc.
 - e. Bearing frame and bearings
 - f. Baseplate and couplings
 - g. Materials
 - h. Special operating conditions and miscellaneous items

Table 10-11 is based on the API and ASME codes and illustrates a typical specification for centrifugal pumps.

POSITIVE-DISPLACEMENT PUMPS

Positive-displacement pumps and those that approach positive displacement will ideally produce whatever head is impressed upon them by the system restrictions to flow. The maximum head attainable is determined by the power available in the drive (slippage neglected) and the strength of the pump parts. A pressure relief valve on the discharge side should be set to open at a safe pressure for the casing and the internal components of the pump such as piston rods, cylinders, crankshafts, and other components which would be pressurized. In the case of a rotary pump, the total dynamic head developed is uniquely determined for any given flow by the speed at which it rotates.

In general, overall efficiencies of positive-displacement pumps are higher than those of centrifugal equipment because internal losses are minimized. On the other hand, the flexibility of each piece of equipment in handling a wide range of capacities is somewhat limited.

Positive-displacement pumps may be of either the **reciprocating** or the **rotary** type. In all positive-displacement pumps, a cavity or cavities are alternately filled and emptied of the pumped fluid by the action of the pump.

Reciprocating Pumps There are three classes of reciprocating pumps: **piston pumps**, **plunger pumps**, and **diaphragm pumps**. Basically, the action of the liquid-transferring parts of these pumps is the same, a cylindrical piston, plunger, or bucket or a round diaphragm being caused to pass or flex back and forth in a chamber. The device is equipped with valves for the inlet and discharge of the liquid being pumped, and the operation of these valves is related in a definite manner to the motions of the piston. In all modern-design reciprocating pumps, the suction and discharge valves are operated by pressure difference. That is, when the pump is on its suction stroke and the pump cavity is increasing in volume, the pressure is lowered within the pump cavity, permitting the higher suction pressure to open the suction valve and allowing liquid to flow into the pump. At the same time, the higher discharge-line pressure holds the discharge valve closed. Likewise on the discharge stroke, as the pump cavity is decreasing in volume, the higher pressure developed in the pump cavity holds the suction valve closed and opens the discharge valve to expel liquid from the pump into the discharge line.

The *overall efficiency* of these pumps varies from about 50 percent for the small pumps to about 90 percent or more for the larger sizes.

TABLE 10-11 Typical Pump Specification

Specifi- cation	Description	Specifi- cation	Description
1.0	<p>Scope:</p> <p>This specification covers horizontal, end suction, vertically split, single-stage centrifugal pumps with top centerline discharge and “back pullout” feature.</p>		
2.0	<p>Service Conditions:</p> <p>Pump shall be designed to operate satisfactorily with a reasonable service life when operated either intermittently or continuously in typical process applications.</p>		
3.0	<p>Operating Conditions:</p> <p>Capacity _____ U.S. gallons per minute Head (_____ ft total head) (_____ psig). Speed _____ rpm Suction Pressure (_____ ft head) (positive) (lift) (_____ psig) Liquid to be handled _____ Specific gravity _____ Viscosity (_____) Temperature of liquid at inlet _____ °F Solids content _____ % _____ Max. size</p>		
4.0	<p>Pump Construction:</p> <p>4.1 <i>Casing</i>. Casing shall be vertically split with self-venting top centerline discharge, with an integral foot located directly under the casing for added support. All casings shall be of the “back pullout” design with suction and discharge nozzles cast integrally. Casings shall be provided with bosses in suction and discharge nozzles, and in bottom of casing for gauge taps and drain tap. (Threaded taps with plugs shall be provided for these features.)</p> <p>4.2 <i>Casing Connections</i>. Connections shall be A.N.S.I. flat-faced flanges. [Cast iron (125) (250) psig rated] [Duron metal, steel, alloy steel (150) (300) psig rated]</p> <p>4.3 <i>Casing Joint Gasket</i>. A confined-type nonasbestos gasket suitable for corrosive service shall be provided at the casing joint.</p> <p>4.4 <i>Impeller</i>. Fully-open impeller with front edge having contoured vanes curving into the suction for minimum NPSH requirements and maximum efficiency shall be provided. A hex head shall be cast in the eye of the impeller to facilitate removal, and eliminate need for special impeller removing tool. All impellers shall have radial “pump-out” vanes on the back side to reduce stuffing box pressure and aid in eliminating collection of solids at stuffing box throat. Impellers shall be balanced within A.N.S.I. guidelines to ISO tolerances.</p> <p>4.4.1 <i>Impeller Clearance Adjustment</i>. All pumps shall have provisions for adjustment of axial clearance between the leading edge of the impeller and casing. This adjustment shall be made by a precision microdial adjustment at the outboard bearing housing, which moves the impeller forward toward the suction wall of the casing.</p> <p>4.5 <i>Shafts</i>. Shafts shall be suitable for hook-type sleeve. Shaft material shall be (SAE 1045 steel on Duron and 316 stainless steel pumps) or (AISI 316 stainless steel on CD-4MCu pumps and #20 stainless steel pumps). Shaft deflection shall not exceed .005 at the vertical centerline of the impeller.</p> <p>4.6 <i>Shaft Sleeve</i>. Renewable hook-type shaft sleeve that extends through the stuffing box and gland shall be provided. Shaft sleeve shall be (316 stainless steel), (#20 stainless steel) or (XH-800 Ni-chrome-boron coated 316 stainless steel with coated surface hardness of approximately 800 Brinnell).</p> <p>4.7 <i>Stuffing Box</i>. Stuffing box shall be suitable for packing, single (inside or outside) or double-inside mechanical seal without modifications. Stuffing box shall be accurately centered by machined rabbit fits on case and frame adapter.</p> <p>4.7.1 <i>Packed Stuffing Box</i>. The standard packed stuffing box shall consist of five rings of graphited nonasbestos packing; a stainless steel packing base ring in the bottom of the box to prevent extrusion of the packing past the throat; a Teflon seal cage, and a two-piece 316 stainless steel packing gland to ensure even pressure on the packing. Ample space shall be provided for repacking the stuffing box.</p> <p>4.7.1.1 <i>Lubrication-Packed Stuffing Box</i>. A tapped hole shall be provided in the stuffing box directly over the seal cage for lubrication and cooling of the packing. Lubrication liquid shall be supplied (from an external source) (through a by-pass line from the pump discharge nozzle).</p> <p>4.7.2 <i>Stuffing Box with Mechanical Seal</i>. Mechanical seal shall be of the (single inside) (single outside) (double inside) (cartridge) type and (balanced) (unbalanced).</p> <p>Stuffing box is to be (standard) (oversize) (oversize tapered).</p>		
			<p>Suitable space shall be provided in the standard and oversized stuffing box for supplying a (throttle bushing) (dilution control bushing) with single seals. Throttle bushings and dilution control bushings shall be made of (glass-filled Teflon) (a suitable metal material).</p> <p>4.7.2.1 <i>Lubrication—Stuffing Box with Mechanical Seals</i>. Suitable tapped connections shall be provided to effectively lubricate, cool, flush, quench, etc., as required by the application or recommendations of the mechanical seal manufacturer.</p>
4.8	<p>Bearing Frame and Bearings:</p> <p>4.8.1 <i>Bearing Frame</i>. Frames shall be equipped with axial radiating fins extending the length of the frame to aid in heat dissipation. Frame shall be provided with ductile iron outboard bearing housing. Both ends of the frame shall be provided with lip-type oil seals and labyrinth-type deflectors of metallic reinforced synthetic rubber to prevent the entrance of contaminants.</p> <p>4.8.2 <i>Bearings</i>. Pump bearings shall be heavy-duty, antifriction ball-type on both ends. The single row inboard bearing, nearest the impeller, shall be free to float within the frame and shall carry only radial load. The double row outboard bearing (F4-G1 and F4-I1) or duplex angular contact bearing (F4-H1), coupling end, shall be locked in place to carry radial and axial thrust loads. Bearings shall be designed for a minimum life of 20,000 hours in any normal pump operating range.</p>	4.9	<p><i>Bearing Lubrication</i>. Ball bearings shall be oil-mist—lubricated by means of a slinger. The oil slinger shall be mounted on the shaft between the bearings to provide equal lubrication to both bearings. Bulls-eye oil-sight glasses shall be provided on both sides of the frame to provide a positive means of checking the proper oil level from either side of the pump. A tapped and plugged hole shall also be provided in both sides of the frame to mount bottle-type constant-level oilers where desired. A tapped and plugged hole shall be provided on both sides for optional straight-through oil cooling device.</p>
5.0	<p>Baseplate and Coupling:</p> <p>5.1 <i>Baseplate</i>. Baseplates shall be rigid and suitable for mounting pump and motor. Baseplates shall be of channel steel construction.</p> <p>5.2 <i>Coupling</i>. Coupling shall be flexible-spacer type. Coupling shall have at least three-and-one-half-inch spacer length for ease of rotating element removal. Both coupling hubs shall be provided with flats 180° apart to facilitate removal of impeller. Coupling shall not require lubrication.*</p>	6.0	<p>Mechanical Modifications Required for High Temperature:</p> <p>6.1 <i>Modifications Required, Temperature Range 250–350°F</i>. Pumps for operation in this range shall be provided with a water-jacketed stuffing box.</p> <p>6.2 <i>Modifications Required, Temperature Range 351–550°F (Maximum)</i>. Pumps for operation in this range shall be provided with a water-jacketed stuffing box and a water-cooled bearing frame.</p>
		7.0	<p>Materials:</p> <p>Pump materials shall be selected to suit the particular service requirements.</p> <p>7.1 <i>Cast Iron—316 SS Fitted</i>. 15” only; pump shall have cast iron casing and stuffing box cover. 316 SS metal impeller; shaft shall be 1045 steel with 316 SS sleeve.</p> <p>7.2 <i>All Duron Metal</i>. All pump materials shall be Duron metal. Shaft shall be 1045 steel, with 316 SS sleeve. 316 SS metal impeller optional.</p> <p>7.3 <i>All AISI 316 Stainless Steel</i>. All pump materials shall be AISI 316 stainless steel. Shaft should be 1045 steel, with 316 SS sleeve.</p> <p>7.4 <i>All #20 Stainless Steel</i>. All pump materials shall be #20 SS stainless steel. Shaft shall be 316 SS, with #20 SS sleeve.</p> <p>7.5 <i>All CD-4MCu</i>. All pump materials shall be CD-4MCu. Shaft shall be 316 SS, with #20 SS sleeve.</p>
8.0	<p>Miscellaneous:</p> <p>8.1 <i>Nameplates</i>. All nameplates and other data plates shall be stainless steel, suitably secured to the pump.</p> <p>8.2 <i>Hardware</i>. All machine bolts, stud nuts, and capscrews shall be of the hex-head type.</p> <p>8.3 <i>Rotation</i>. Pump shall have clockwise rotation viewed from its driven end.</p> <p>8.4 <i>Parts Numbering</i>. Parts shall be completely identified with a numerical system (no alphabetical letters) to facilitate parts inventory control and stocking. Each part shall be properly identified by a separate number, and those parts that are identical shall have the same number to effect minimum spare parts inventory.</p>		

*Omit if not applicable.

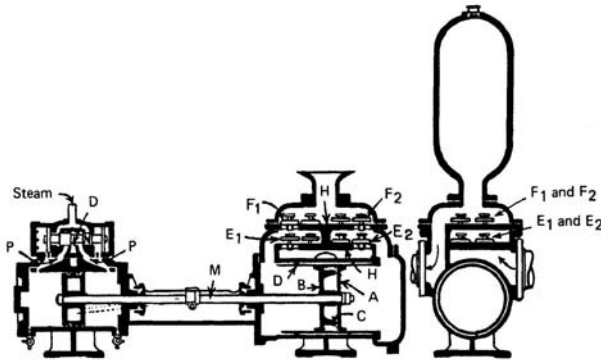


FIG. 10-26 Double-acting steam-driven reciprocating pump.

As shown in Fig. 10-26, reciprocating pumps, except when used for metering service, are frequently provided on the discharge side with gas-charged chambers, the purpose of which is to limit pressure pulsation and to provide a more uniform flow in the discharge line. In many installations, surge chambers are required on the suction side as well. Piping layouts should be studied to determine the most effective size and location. If surge chambers are used, provision should be made to keep the chamber charged with gas. A surge chamber filled with liquid is of no value. A liquid-level gauge is desirable to permit checking the amount of gas in the chamber.

Reciprocating pumps may be of **single-cylinder** or **multicylinder** design. Multicylinder pumps have all cylinders in parallel for increased capacity. Piston-type pumps may be single-acting or double-acting; i.e., pumping may be accomplished from one or both ends of the piston. Plunger pumps are always single-acting. The tabulation in Table 10-12 provides data on the flow variation of reciprocating pumps of various designs.

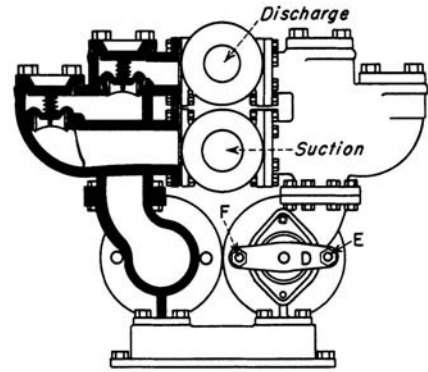
Piston Pumps There are two ordinary types of piston pumps, simplex double-acting pumps and duplex double-acting pumps.

Simplex Double-Acting Pumps These pumps may be direct-acting (i.e., direct-connected to a steam cylinder) or power-driven (through a crank and flywheel from the crosshead of a steam engine). Figure 10-26 is a direct-acting pump, designed for use at pressures up to 0.690 MPa (100 lbf/in²). In this figure, the piston consists of disks A and B, with packing rings C between them. A bronze liner for the water cylinder is shown at D. Suction valves are E₁ and E₂. Discharge valves are F₁ and F₂.

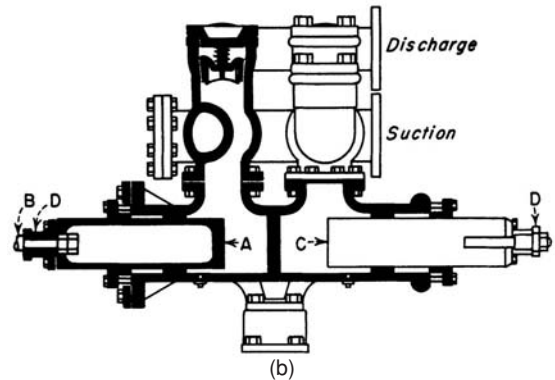
Duplex Double-Acting Pumps These pumps differ primarily from those of the simplex type in having two cylinders whose operation is coordinated. They may be direct-acting, steam-driven, or power-driven with crank and flywheel.

A duplex outside-end-packed **plunger pump** with pot valves, of the type used with hydraulic presses and for similar service, is shown in Fig. 10-27. In this drawing, plunger A is direct-connected to rod B, while plunger C is operated from the rod by means of yoke D and tie rods.

Plunger pumps differ from piston pumps in that they have one or more constant-diameter plungers reciprocating through packing glands and displacing liquid from cylinders in which there is consider-



(a)



(b)

FIG. 10-27 Duplex single-acting plunger pump.

able radial clearance. They are always single-acting, in the sense that only one end of the plunger is used in pumping the liquid.

Plunger pumps are available with one, two, three, four, five, or even more cylinders. Simplex and duplex units are often built in a horizontal design. Those with three or more cylinders are usually of vertical design. The driver may be an electric motor, a steam or gas engine, or a steam turbine. This is the common type of **power pump**. An example, arranged for belt drive, is shown in Fig. 10-28 from which the action may be readily traced.

Occasionally plunger pumps are constructed with opposed cylinders and plungers connected by yokes and tie rods; this arrangement, in effect, constitutes a double-acting unit.

Simplex plunger pumps mounted singly or in gangs with a common drive are quite commonly used as **metering** or **proportioning pumps** (Fig. 10-29). Frequently a variable-speed drive or a stroke-adjusting mechanism is provided to vary the flow as desired. These pumps are designed to measure or control the flow of liquid within a deviation of ± 2 percent with capacities up to 11.35 m³/h (50 gal/min) and pressures as high as 68.9 MPa (10,000 lbf/in²).

Diaphragm Pumps These pumps perform similarly to piston and plunger pumps, but the reciprocating driving member is a flexible diaphragm fabricated of metal, rubber, or plastic. The chief advantage of this arrangement is the elimination of all packing and seals exposed to the liquid being pumped. This, of course, is an important asset for equipment required to handle hazardous or toxic liquids.

A common type of low-capacity diaphragm pump designed for metering service employs a plunger working in oil to actuate a metallic or plastic diaphragm. Built for pressures in excess of 6.895 MPa (1000 lbf/in²) with flow rates up to about 1.135 m³/h (5 gal/min) per cylinder, such pumps possess all the characteristics of plunger-type metering pumps with the added advantage that the pumping head can be mounted in a remote (even a submerged) location entirely separate from the drive.

TABLE 10-12 Flow Variation of Reciprocating Pumps

Number of cylinders	Single- or double-acting	Flow variation per stroke from mean, percent
Single	Single	+220 to -100
Single	Double	+60 to -100
Duplex	Single	+24.1 to -100
Duplex	Double	+6.1 to -21.5
Triplex	Single and double	+1.8 to -16.9
Quintuplex	Single	+1.8 to -5.2

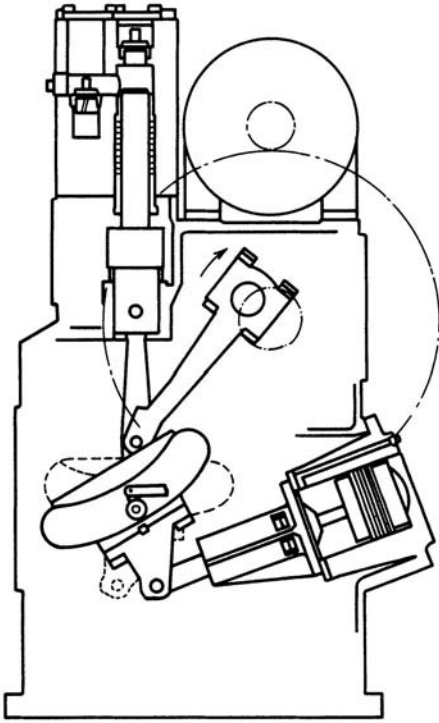


FIG. 10-28 Adrich-Groff variable-stroke power pump. (Courtesy of Ingersoll-Rand.)

Figure 10-30 shows a high-capacity 22.7-m³/h (100-gal/min) pump with actuation provided by a mechanical linkage.

Pneumatically Actuated Diaphragm Pumps (Fig. 10-31) These pumps require no power source other than plant compressed air. They must have a flooded suction, and the pressure is, of course, limited to the available air pressure. Because of their slow speed and large valves, they are well suited to the gentle handling of liquids for which degradation of suspended solids should be avoided.

A major consideration in the application of diaphragm pumps is the realization that diaphragm failure will probably occur eventually. The consequences of such failure should be realistically appraised before selection, and maintenance procedures should be established accordingly.

Rotary Pumps In rotary pumps the liquid is displaced by rotation of one or more members within a stationary housing. Because internal clearances, although minute, are a necessity in all but a few special types, capacity decreases somewhat with increasing pump

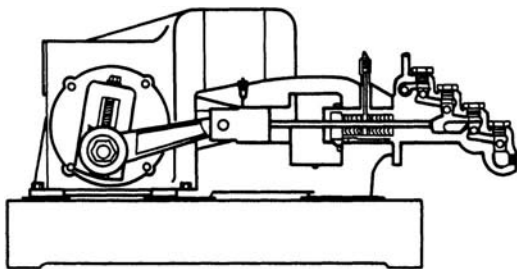


FIG. 10-29 Plunger-type metering pump. (Courtesy of Milton Roy Co.)

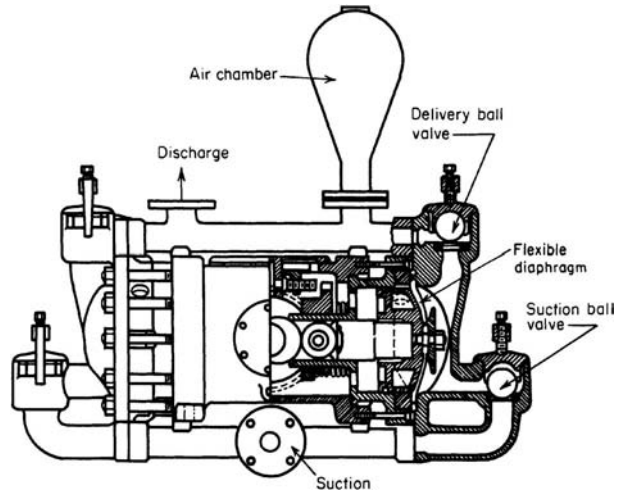


FIG. 10-30 Mechanically actuated diaphragm pump.

differential pressure. Therefore, these pumps are not truly positive-displacement pumps. However, for many other reasons they are considered as such.

The selection of materials of construction for rotary pumps is critical. The materials must be corrosion-resistant, compatible when one part is running against another, and capable of some abrasion resistance.

Gear Pumps When two or more impellers are used in a rotary-pump casing, the impellers will take the form of toothed-gear wheels as in Fig. 10-32, of helical gears, or of lobed cams. In each case, these impellers rotate with extremely small clearance between them and between the surfaces of the impellers and the casing. In Fig. 10-32, the two toothed impellers rotate as indicated by the arrows; the suction connection is at the bottom. The pumped liquid flows into the spaces between the impeller teeth as these cavities pass the suction opening. The liquid is then carried around the casing to the discharge opening, where it is forced out of the impeller teeth mesh. The arrows indicate this flow of liquid.

Rotary pumps are available in two general classes, interior-bearing and exterior-bearing. The **interior-bearing type** is used for handling

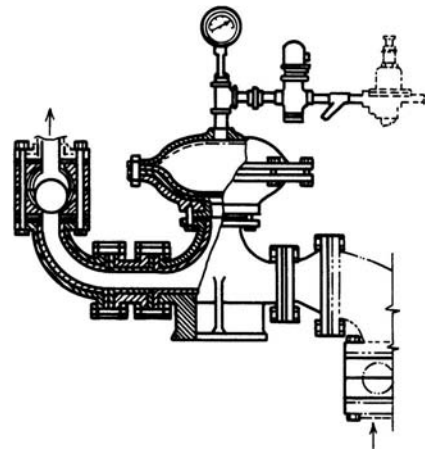


FIG. 10-31 Pneumatically actuated diaphragm pump for slurry service. (Courtesy of Dorr-Oliver Inc.)

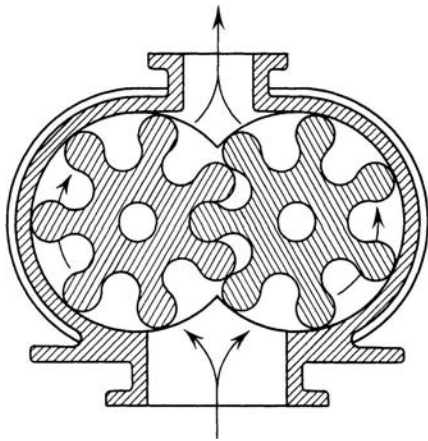


FIG. 10-32 Positive-displacement gear-type rotary pump.

liquids of a lubricating nature, and the **exterior-bearing type** is used with nonlubricating liquids. The interior-bearing pump is lubricated by the liquid being pumped, and the exterior-bearing type is oil-lubricated.

The use of spur gears in gear pumps will produce in the discharge pulsations having a frequency equivalent to the number of teeth on both gears multiplied by the speed of rotation. The amplitude of these disturbances is a function of tooth design. The pulsations can be reduced markedly by the use of rotors with helical teeth. This in turn introduces end thrust, which can be eliminated by the use of double-helical or herringbone teeth.

Screw Pumps A modification of the helical gear pump is the screw pump. Both gear and screw pumps are positive-displacement pumps. Figure 10-33 illustrates a two-rotor version in which the liquid is fed to either the center or the ends, depending upon the direction of rotation, and progresses axially in the cavities formed by the meshing threads or teeth. In three-rotor versions, the center rotor is the driving member while the other two are driven. Figure 10-34 shows still another arrangement, in which a metal rotor of unique design rotates without clearance in an elastomeric stationary sleeve.

Screw pumps, because of multiple dams that reduce slip, are well adapted for producing higher pressure rises, for example, 6.895 MPa (1000 lbf/in²), especially when handling viscous liquids such as heavy oils. The all-metal pumps are generally subject to the same limitations on handling abrasive solids as conventional gear pumps. In addition, the wide bearing spans usually demand that the liquid have considerable lubricity to prevent metal-to-metal contact.

Among the liquids handled by rotary pumps are mineral oils, vegetable oils, animal oils, greases, glucose, viscose, molasses, paints, var-

nish, shellac, lacquers, alcohols, catsup, brine, mayonnaise, sizing, soap, tanning liquors, vinegar, and ink. Some screw-type units are specially designed for the gentle handling of large solids suspended in the liquid.

Fluid-Displacement Pumps In addition to pumps that depend on the mechanical action of pistons, plungers, or impellers to move the liquid, other devices for this purpose employ displacement by a secondary fluid. This group includes air lifts and acid eggs.

The air lift is a device for raising liquid by means of compressed air. In the past it was widely used for pumping wells, but it has been less widely used since the development of efficient centrifugal pumps. It operates by introducing compressed air into the liquid near the bottom of the well. The air-and-liquid mixture, being lighter than liquid alone, rises in the well casing. The advantage of this system of pumping lies in the fact that there are no moving parts in the well. The pumping equipment is an air compressor, which can be located on the surface.

A simplified sketch of an air lift for this purpose is shown in Fig. 10-35. Ingersoll-Rand has developed empirical information on air-lift performance which is available upon request.

An important application of the gas-lift principle involves the extraction of oil from wells. There are several references to both practical and theoretical work involving gas lift performance and related problems. Recommended sources are American Petroleum Institute, *Drilling and Production Practices*, 1952, pp. 257-317, and 1939, p. 266; *Trans. Am. Soc. Mining Metall. Eng.*, **92**, 296-313 (1931), **103**, 170-186 (1933), **118**, 56-70 (1936), **192**, 317-326 (1951), **189**, 73-82 (1950), and **198**, 271-278 (1953); *Trans. Am. Soc. Mining Metall.*, and *Pet. Eng.*, **213** (1958), and **207**, 17-24 (1956); and *Univ. Wisconsin Bull., Eng. Ser.*, **6**, no. 7 (1911, reprinted 1914).

An **acid egg**, or **blowcase**, consists of an egg-shaped container which can be filled with a charge of liquid that is to be pumped. This container is fitted with an inlet pipe for the charge, an outlet pipe for the discharge, and a pipe for the admission of compressed air or gas, as illustrated in Fig. 10-36. Pressure of air or gas on the surface of the liquid forces it out of the discharge pipe. Such pumps can be hand-operated or arranged for semiautomatic or automatic operation.

CENTRIFUGAL PUMPS

The centrifugal pump is the type most widely used in the chemical industry for transferring liquids of all types—raw materials, materials in manufacture, and finished products—as well as for general services of water supply, boiler feed, condenser circulation, condensate return, etc. These pumps are available through a vast range of sizes, in capacities from 0.5 m³/h to 2 × 10⁴ m³/h (2 gal/min to 10³ gal/min), and for discharge heads (pressures) from a few meters to approximately 48 MPa (7000 lbf/in²). The size and type best suited to a particular application can be determined only by an engineering study of the problem.

The primary advantages of a centrifugal pump are simplicity, low first cost, uniform (nonpulsating) flow, small floor space, low maintenance expense, quiet operation, and adaptability for use with a motor or a turbine drive.

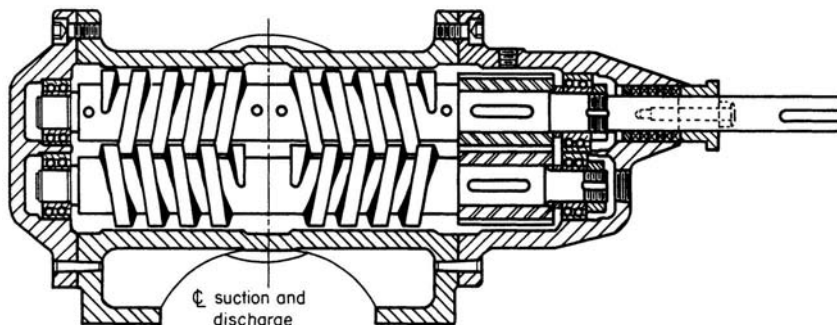


FIG. 10-33 Two-rotor screw pump. (Courtesy of Warren Quimby Pump Co.)

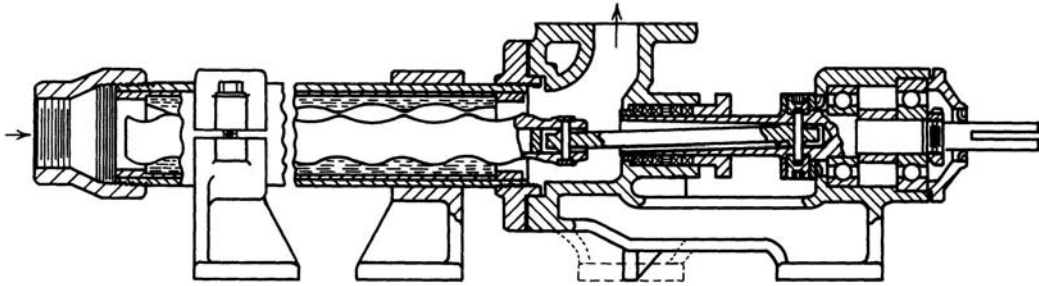


FIG. 10-34 Single-rotor screw pump with an elastomeric lining. (Courtesy of Moyno Pump Division, Robbins & Myers, Inc.)

A centrifugal pump, in its simplest form, consists of an impeller rotating within a casing. The **impeller** consists of a number of blades, either open or shrouded, mounted on a shaft that projects outside the casing. Its axis of rotation may be either horizontal or vertical, to suit the work to be done. **Closed-type**, or **shrouded**, impellers are generally the most efficient. **Open- or semiopen-type** impellers are used for viscous liquids or for liquids containing solid materials and on many small pumps for general service. Impellers may be of the **single-suction** or the **double-suction** type—single if the liquid enters from one side, double if it enters from both sides.

Casings There are three general types of casings, but each consists of a chamber in which the impeller rotates, provided with inlet and exit for the liquid being pumped. The simplest form is the **circular casing**, consisting of an annular chamber around the impeller; no attempt is made to overcome the losses that will arise from eddies and shock when the liquid leaving the impeller at relatively high velocities enters this chamber. Such casings are seldom used.

Volute casings take the form of a spiral increasing uniformly in cross-sectional area as the outlet is approached. The volute efficiently converts the velocity energy imparted to the liquid by the impeller into pressure energy.

A third type of casing is used in **diffuser-type** or turbine pumps. In this type, **guide vanes** or **diffusers** are interposed between the impeller discharge and the casing chamber. Losses are kept to a minimum in a well-designed pump of this type, and improved efficiency is obtained over a wider range of capacities. This construction is often used in multistage high-head pumps.

Action of a Centrifugal Pump Briefly, the action of a centrifugal pump may be shown by Fig. 10-37. Power from an outside source is applied to shaft A, rotating the impeller B within the stationary casing C. The blades of the impeller in revolving produce a reduction in

pressure at the entrance or eye of the impeller. This causes liquid to flow into the impeller from the suction pipe D. This liquid is forced outward along the blades at increasing tangential velocity. The velocity head it has acquired when it leaves the blade tips is changed to pressure head as the liquid passes into the volute chamber and thence out the discharge E.

Centrifugal Pump Characteristics Figure 10-38 shows a typical characteristic curve of a centrifugal pump. It is important to note that at any fixed speed the pump will operate along this curve and at no other points. For instance, on the curve shown, at 45.5 m³/h (200 gal/min) the pump will generate 26.5-m (87-ft) head. If the head is increased to 30.48 m (100 ft), 27.25 m³/h (120 gal/min) will be delivered. It is not possible to reduce the capacity to 27.25 m³/h (120 gal/min) at 26.5-m (87-ft) head unless the discharge is throttled so that 30.48 m (100 ft) is actually generated within the pump. On pumps with variable-speed drivers such as steam turbines, it is possible to change the characteristic curve, as shown by Fig. 10-39.

As shown in Eq. (10-50), the head depends upon the velocity of the fluid, which in turn depends upon the capability of the impeller

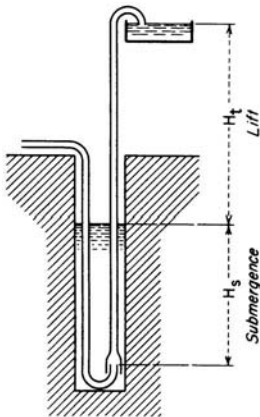


FIG. 10-35 Simplified sketch of an air lift, showing submergence and total head.

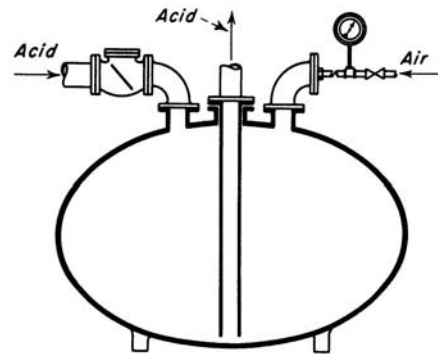


FIG. 10-36 A form of acid egg. External controls required for automatic operation are not shown.

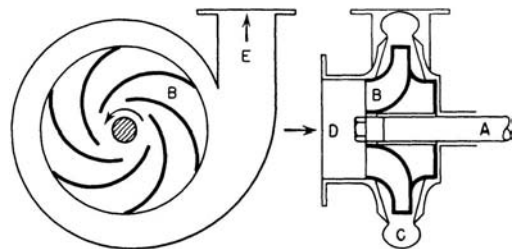


FIG. 10-37 A simple centrifugal pump.

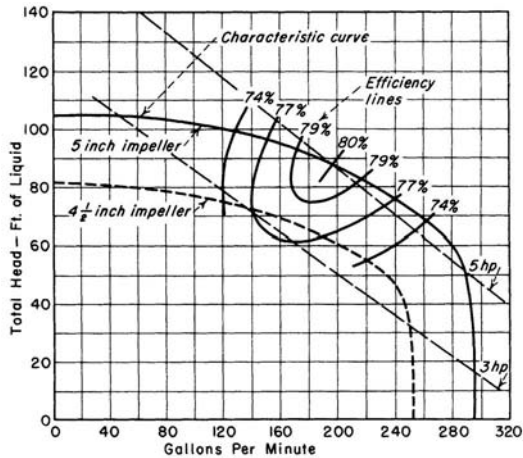


FIG. 10-38 Characteristic curve of a centrifugal pump operating at a constant speed of 3450 r/min. To convert gallons per minute to cubic meters per hour, multiply by 0.2271; to convert feet to meters, multiply by 0.3048; to convert horsepower to kilowatts, multiply by 0.746; and to convert inches to centimeters, multiply by 2.54.

to transfer energy to the fluid. This is a function of the fluid viscosity and the impeller design. It is important to remember that the head produced will be the same for any liquid of the same viscosity. The pressure rise, however, will vary in proportion to the specific gravity.

For quick pump selection, manufacturers often give the most essential performance details for a whole range of pump sizes. Figure 10-40 shows typical performance data for a range of process pumps based on suction and discharge pipes and impeller diameters. The performance data consists of pump flow rate and head. Once a pump meets a required specification, then a more detailed performance data for the particular pump can be easily found based on the curve reference number. Figure 10-41 shows a more detailed pump performance curve that includes, in addition to pump head and flow, the brake horsepower required, NPSH required, number of vanes, and pump efficiency for a range of impeller diameters.

If detailed manufacturer-specified performance curves are not available for a different size of the pump or operating condition, a best

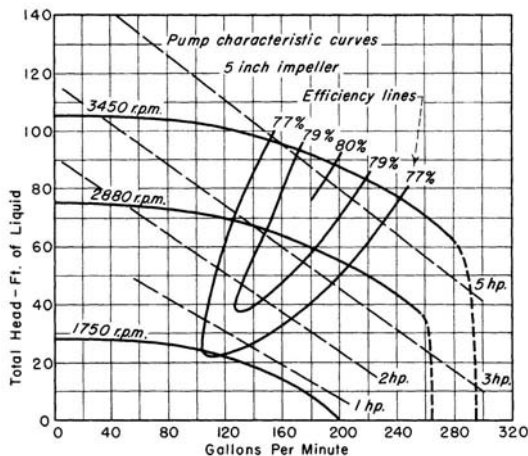


FIG. 10-39 Characteristic curve of a centrifugal pump at various speeds. To convert gallons per minute to cubic meters per hour, multiply by 0.2271; to convert feet to meters, multiply by 0.3048; to convert horsepower to kilowatts, multiply by 0.746; and to convert inches to centimeters, multiply by 2.54.

estimate of the off-design performance of pumps can be obtained through similarity relationship or the affinity laws. These are:

1. Capacity (Q) is proportional to impeller rotational speed (N).
2. Head (h) varies as square of the impeller rotational speed.
3. Brake horsepower (BHP) varies as the cube of the impeller rotational speed.

These equations can be expressed mathematically and appear in Table 10-13.

System Curves In addition to the pump design, the operational performance of a pump depends upon factors such as the downstream load characteristics, pipe friction, and valve performance. Typically, head and flow follow the following relationship:

$$\frac{(Q_2)^2}{(Q_1)^2} = \frac{h_2}{h_1} \quad (10-60)$$

where the subscript 1 refers to the design condition and 2 to the actual conditions. The above equation indicates that head will change as a square of the water flow rate.

Figure 10-42 shows the schematic of a pump, moving a fluid from tank A to tank B, both of which are at the same level. The only force that the pump has to overcome in this case is the pipe friction, variation of which with fluid flow rate is also shown in the figure. On the other for the use shown in Fig. 10-43, the pump in addition to pipe friction should overcome head due to difference in elevation between tanks A and B. In this case, elevation head is constant, whereas the head required to overcome friction depends on the flow rate. Figure 10-44 shows the pump performance requirement of a valve opening and closing.

Pump Selection One of the parameters that is extremely useful in selecting a pump for a particular application is specific speed N_s . Specific speed of a pump can be evaluated based on its design speed, flow, and head:

$$N_s = \frac{NQ^{1/2}}{H^{3/4}} \quad (10-61)$$

where N = rpm, Q is flow rate in gpm, and H is head in ft-lb/lbm.

Specific speed is a parameter that defines the speed at which impellers of geometrically similar design have to be run to discharge one gallon per minute against a one-foot head. In general, pumps with a low specific speed have a low capacity and high specific speed, high capacity. Specific speeds of different types of pumps are shown in Table 10-14 for comparison.

Another parameter that helps in evaluating the pump suction limitations, such as cavitation, is suction-specific speed.

$$S = \frac{NQ^{1/2}}{(\text{NPSH})^{3/4}} \quad (10-62)$$

Typically, for single-suction pumps, suction-specific speed above 11,000 is considered excellent. Below 7000 is poor and 7000–9000 is of an average design. Similarly, for double-suction pumps, suction-specific speed above 14,000 is considered excellent, below 7000 is poor, and 9000–11,000 is average.

Figure 10-45 shows the schematic of specific-speed variation for different types of pumps. The figure clearly indicates that, as the specific speed increases, the ratio of the impeller outer diameter D_1 to inlet or eye diameter D_2 decreases, tending to become unity for pumps of axial-flow type.

Typically, axial flow pumps are of high flow and low head type and have a high specific speed. On the other hand, purely radial pumps are of high head and low flow rate capability and have a low specific speed. Obviously, a pump with a moderate flow and head has an average specific speed.

A typical pump selection chart such as shown in Fig. 10-46 calculates the specific speed for a given flow, head, and speed requirements. Based on the calculated specific speed, the optimal pump design is indicated.

Process Pumps This term is usually applied to single-stage pedestal-mounted units with single-suction overhung impellers and with a single packing box. These pumps are ruggedly designed for

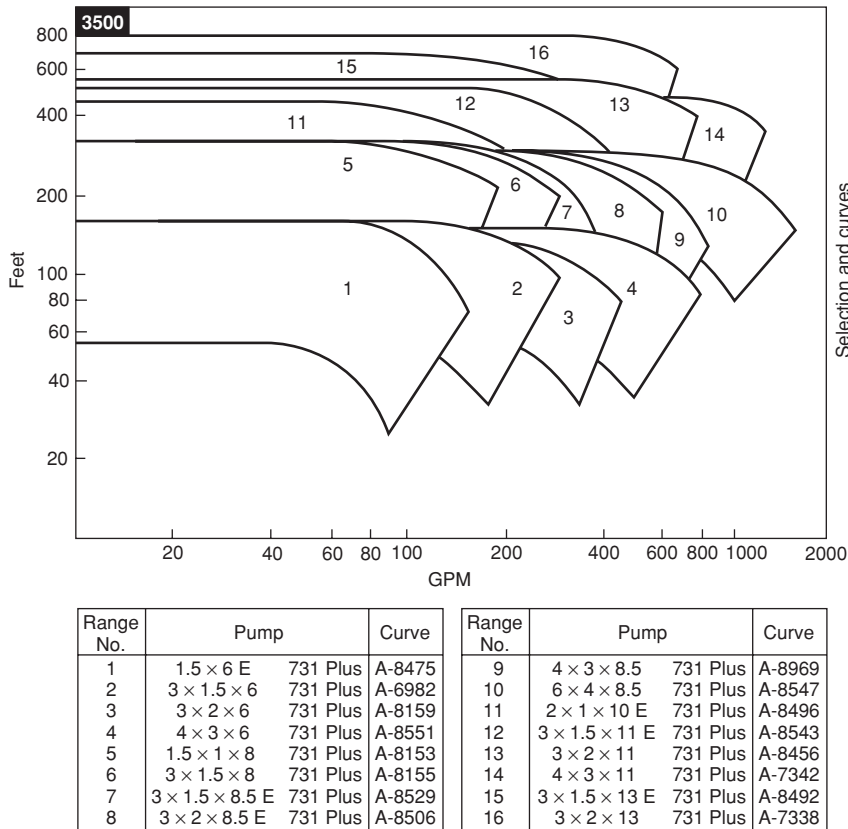


FIG. 10-40 Performance curves for a range of open impeller pumps.

ease in dismantling and accessibility, with mechanical seals or packing arrangements, and are built especially to handle corrosive or otherwise difficult-to-handle liquids.

Specifically but not exclusively for the chemical industry, most pump manufacturers now build to national standards **horizontal and vertical process pumps**. ASME Standards B73.1—2001 and B73.2—2003 apply to the horizontal (Fig. 10-47) and vertical in-line (Fig. 10-48) pumps, respectively.

The horizontal pumps are available for capacities up to 900 m³/h (4000 gal/min); the vertical in-line pumps, for capacities up to 320 m³/h (1400 gal/min). Both horizontal and vertical in-line pumps are available for heads up to 120 m (400 ft). The intent of each ANSI specification is that pumps from all vendors for a given nominal capacity and total dynamic head at a given rotative speed shall be dimensionally interchangeable with respect to mounting, size, and location of suction and discharge nozzles, input shaft, base plate, and foundation bolts.

The vertical in-line pumps, although relatively new additions, are finding considerable use in chemical and petrochemical plants in the United States. An inspection of the two designs will make clear the relative advantages and disadvantages of each.

Chemical pumps are available in a variety of materials. Metal pumps are the most widely used. Although they may be obtained in iron, bronze, and iron with bronze fittings, an increasing number of pumps of ductile-iron, steel, and nickel alloys are being used. Pumps are also available in glass, glass-lined iron, carbon, rubber, rubber-lined metal, ceramics, and a variety of plastics, such units usually being employed for special purposes.

Sealing the Centrifugal Chemical Pump Although detailed treatment of **shaft seals** is presented in the subsection "Sealing of

Rotating Shafts," it is appropriate to mention here the special problems of sealing centrifugal chemical pumps. Current practice demands that packing boxes be designed to accommodate both packing and mechanical seals. With either type of seal, one consideration is of paramount importance in chemical service: the liquid present at the sealing surfaces must be free of solids. Consequently, it is necessary to provide a secondary compatible liquid to flush the seal or packing whenever the process liquid is not absolutely clean.

The use of **packing** requires the continuous escape of liquid past the seal to minimize and to carry away the frictional heat developed. If the effluent is toxic or corrosive, quench glands or catch pans are usually employed. Although packing can be adjusted with the pump operating, leaking mechanical seals require shutting down the pump to correct the leak. Properly applied and maintained **mechanical seals** usually show no visible leakage. In general, owing to the more effective performance of mechanical seals, they have gained almost universal acceptance.

Double-Suction Single-Stage Pumps These pumps are used for general water-supply and circulating service and for chemical service when liquids that are noncorrosive to iron or bronze are being handled. They are available for capacities from about 5.7 m³/h (25 gal/min) up to as high as 1.136 × 10⁴ m³/h (50,000 gal/min) and heads up to 304 m (1000 ft). Such units are available in iron, bronze, and iron with bronze fittings. Other materials increase the cost; when they are required, a standard chemical pump is usually more economical.

Close-Coupled Pumps (Fig. 10-49) Pumps equipped with a built-in electric motor or sometimes steam-turbine-driven (i.e., with pump

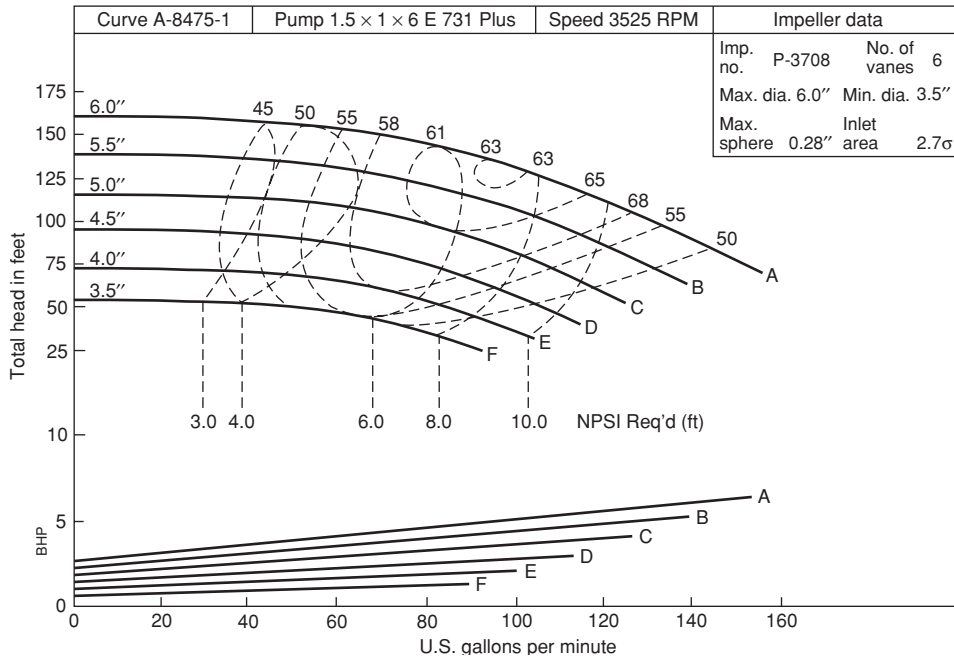


FIG. 10-41 Typical pump performance curve. The curve is shown for water at 85°F. If the specific gravity of the fluid is other than unity, BHP must be corrected.

impeller and driver on the same shaft) are known as close-coupled pumps. Such units are extremely compact and are suitable for a variety of services for which standard iron and bronze materials are satisfactory. They are available in capacities up to about 450 m³/h (2000 gal/min) for heads up to about 73 m (240 ft). Two-stage units in the smaller sizes are available for heads to around 150 m (500 ft).

Canned-Motor Pumps (Fig. 10-50) These pumps command considerable attention in the chemical industry. They are close-coupled units in which the cavity housing the motor rotor and the pump casing are interconnected. As a result, the motor bearings run in the process liquid and all seals are eliminated. Because the process liquid is the bearing lubricant, abrasive solids cannot be tolerated. Standard single-stage canned-motor pumps are available for flows up to 160 m³/h (700 gal/min) and heads up to 76 m (250 ft). Two-stage units are available for heads up to 183 m (600 ft). Canned-motor pumps are being widely used for handling organic solvents, organic heat-transfer liquids, and light oils as well as many clean toxic or hazardous liquids or for installations in which leakage is an economic problem.

Vertical Pumps In the chemical industry, the term **vertical process pump** (Fig. 10-51) generally applies to a pump with a vertical shaft having a length from drive end to impeller of approximately 1 m (3.1 ft) minimum to 20 m (66 ft) or more. Vertical pumps are used as either **wet-pit pumps** (immersed) or **dry-pit pumps** (externally mounted) in conjunction with stationary or mobile tanks containing

difficult-to-handle liquids. They have the following advantages: the liquid level is above the impeller, and the pump is thus self-priming; and the shaft seal is above the liquid level and is not wetted by the pumped liquid, which simplifies the sealing task. When no bottom connections are permitted on the tank (a safety consideration for highly corrosive or toxic liquid), the vertical wet-pit pump may be the only logical choice.

These pumps have the following disadvantages: intermediate or line bearings are generally required when the shaft length exceeds about 3 m (10 ft) in order to avoid shaft resonance problems; these

TABLE 10-13 The Affinity Laws

	Constant impeller diameter	Constant impeller speed
Capacity	$\frac{Q_1}{Q_2} = \frac{N_1}{N_2}$	$\frac{Q_1}{Q_2} = \frac{D_1}{D_2}$
Head	$\frac{H_1}{H_2} = \frac{(N_1)^2}{(N_2)^2}$	$\frac{h_1}{h_2} = \frac{(D_1)^2}{(D_2)^2}$
Brake horsepower	$\frac{BHP_1}{BHP_2} = \frac{(N_1)^3}{(N_2)^3}$	$\frac{BHP_1}{BHP_2} = \frac{(P_1)^3}{(P_2)^3}$

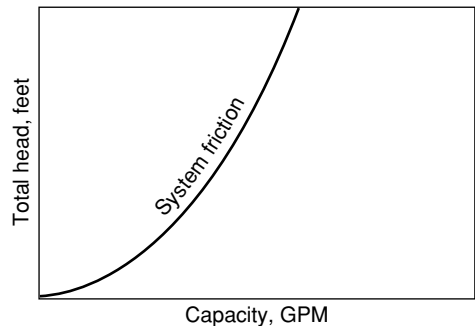
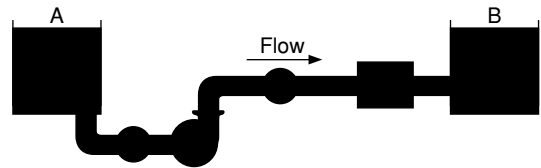


FIG. 10-42 Variation of total head versus flow rate to overcome friction.

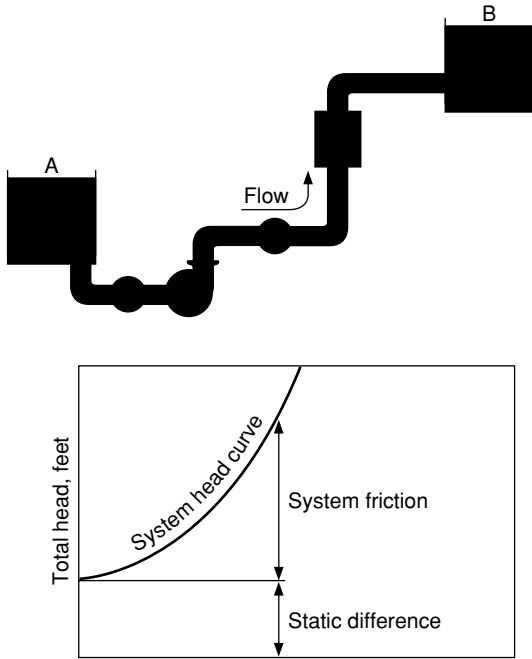


FIG. 10-43 Variation of total head as a function of flow rate to overcome both friction and static head.

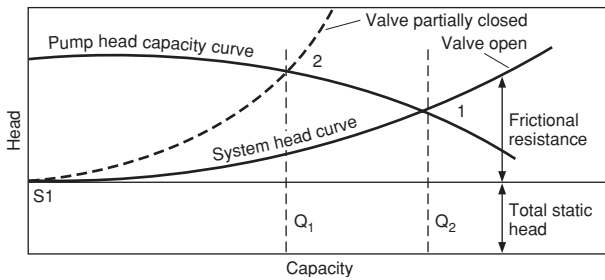


FIG. 10-44 Typical steady-state response of a pump system with a valve fully and partially open.

TABLE 10-14 Specific Speeds of Different Types of Pumps

Pump type	Specific speed range
Below 2,000	Process pumps and feed pumps
2,000–5,000	Turbine pumps
4,000–10,000	Mixed-flow pumps
9,000–15,000	Axial-flow pumps

bearings must be lubricated whenever the shaft is rotating. Since all wetted parts must be corrosion-resistant, low-cost materials may not be suitable for the shaft, column, etc. Maintenance is more costly since the pumps are larger and more difficult to handle.

For abrasive service, vertical cantilever designs requiring no line or foot bearings are available. Generally, these pumps are limited to about a 1-m (3.1-ft) maximum shaft length. Vertical pumps are also used to pump waters to reservoirs. One such application in the Los Angeles water basin has fourteen 4-stage pumps, each pump requiring 80,000 hp to drive them.

Sump Pumps These are small single-stage vertical pumps used to drain shallow pits or sumps. They are of the same general construction as vertical process pumps but are not designed for severe operating conditions.

Multistage Centrifugal Pumps These pumps are used for services requiring heads (pressures) higher than can be generated by a single impeller. All impellers are in series, the liquid passing from one impeller to the next and finally to the pump discharge. The total head then is the summation of the heads of the individual impellers. Deepwell pumps, high-pressure water-supply pumps, boiler-feed pumps, fire pumps, and charge pumps for refinery processes are examples of multistage pumps required for various services.

Multistage pumps may be of the **volute type** (Fig. 10-52), with single- or double-suction impellers (Fig. 10-53), or of the **diffuser type** (Fig. 10-54). They may have horizontally split casings or, for extremely high pressures, 20 to 40 MPa (3000 to 6000 lbf/in²), vertically split barrel-type exterior casings with inner casings containing diffusers, interstage passages, etc.

PROPELLER AND TURBINE PUMPS

Axial-Flow (Propeller) Pumps (Fig. 10-55) These pumps are essentially very-high-capacity low-head units. Normally they are designed for flows in excess of 450 m³/h (2000 gal/min) against heads of 15 m (50 ft) or less. They are used to great advantage in closed-loop circulation systems in which the pump casing becomes merely an

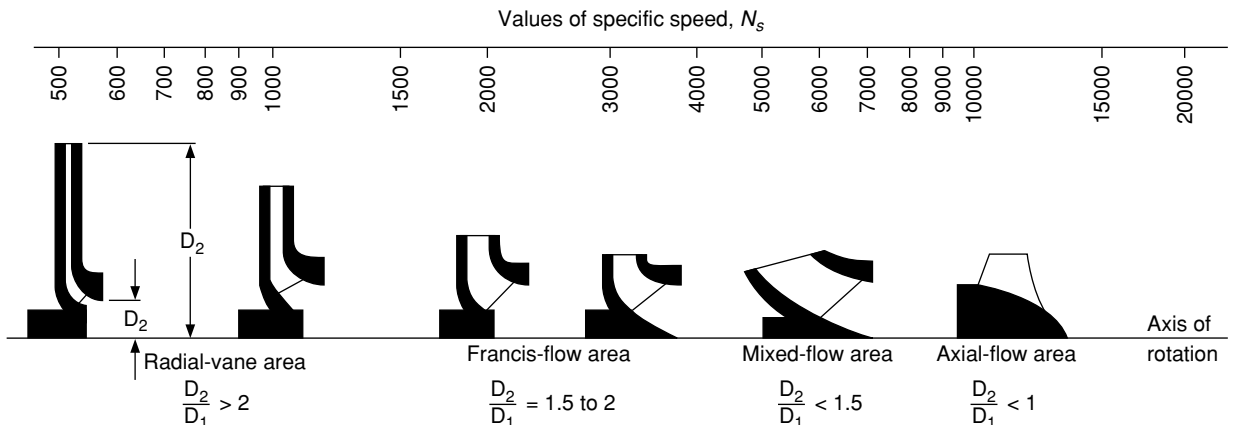


FIG. 10-45 Specific speed variations of different types of pump.

10-38 TRANSPORT AND STORAGE OF FLUIDS

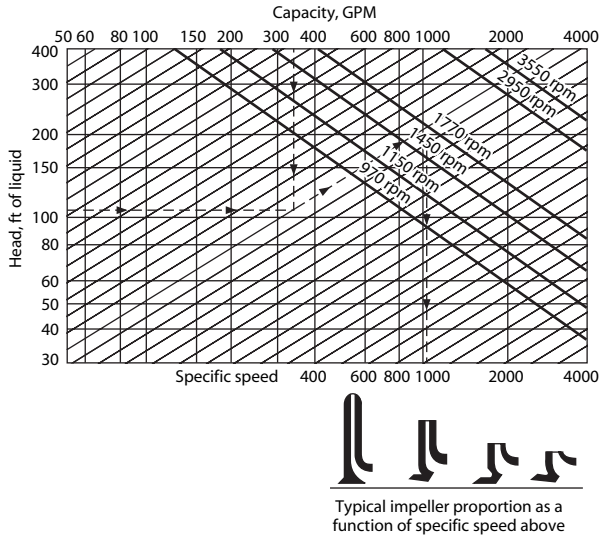


FIG. 10-46 Relationships between specific speed, rotative speed, and impeller proportions (*Worthington Pump Inc., Pump World, vol. 4, no. 2, 1978*).

elbow in the line. A common installation is for calandria circulation. A characteristic curve of an axial-flow pump is given in Fig. 10-56.

Turbine Pumps The term “turbine pump” is applied to units with mixed-flow (part axial and part centrifugal) impellers. Such units are available in capacities from 20 m³/h (100 gal/min) upward for heads up to about 30 m (100 ft) per stage. Turbine pumps are usually vertical.

A common form of turbine pump is the vertical pump, which has the pump element mounted at the bottom of a column that serves as the discharge pipe (see Fig. 10-57). Such units are immersed in the liquid to be pumped and are commonly used for wells, condenser circulating water, large-volume drainage, etc. Another form of the pump has a shell surrounding the pumping element which is connected to the intake pipe. In this form, the pump is used on condensate service in power plants and for process work in oil refineries.

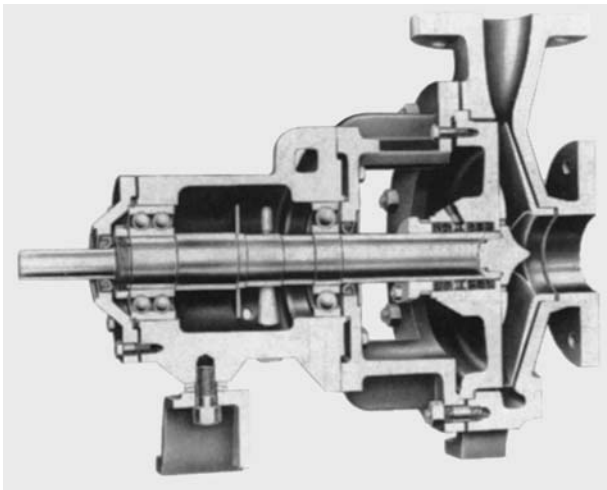


FIG. 10-47 Horizontal process pump conforming to American Society of Mechanical Engineers Standards B73.1—2001.

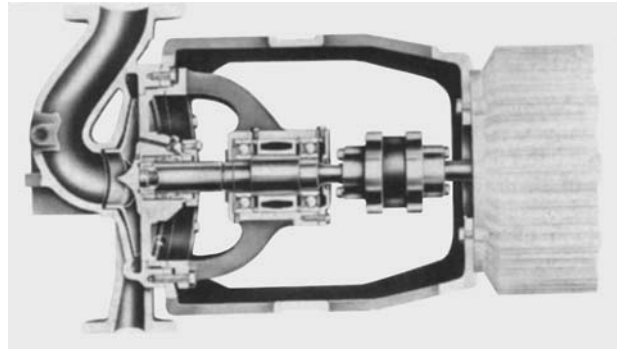


FIG. 10-48 Vertical in-line process pump conforming to ASME standard B73.2—2003. The pump shown is driven by a motor through flexible coupling. Not shown but also conforming to ASME Standard B73.2—2003 are vertical in-line pumps with rigid couplings and with no coupling (impeller-mounted on an extended motor shaft).

Regenerative Pumps Also referred to as turbine pumps because of the shape of the impeller, regenerative pumps employ a combination of mechanical impulse and centrifugal force to produce heads of several hundred meters (feet) at low volumes, usually less than 20 m³/h (100 gal/min). The impeller, which rotates at high speed with small clearances, has many short radial passages milled on each side at the periphery. Similar channels are milled in the mating surfaces of the casing. Upon entering, the liquid is directed into the impeller passages and proceeds in a spiral pattern around the periphery, passing alternately from the impeller to the casing and receiving successive impulses as it does so. Figure 10-58 illustrates a typical performance-characteristic curve.

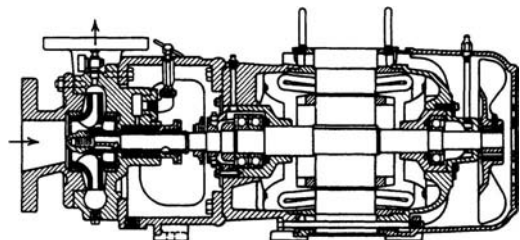


FIG. 10-49 Close-coupled pump.

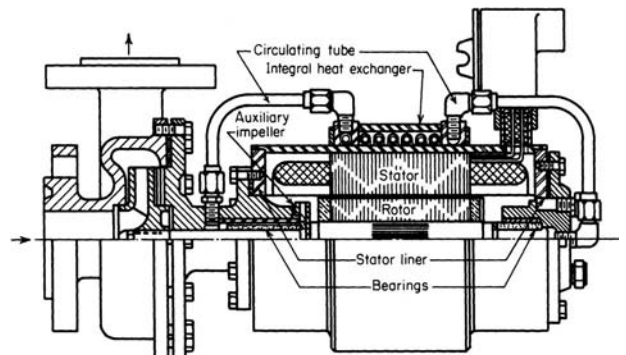


FIG. 10-50 Canned-motor pump. (*Courtesy of Chempump Division, Crane Co.*)

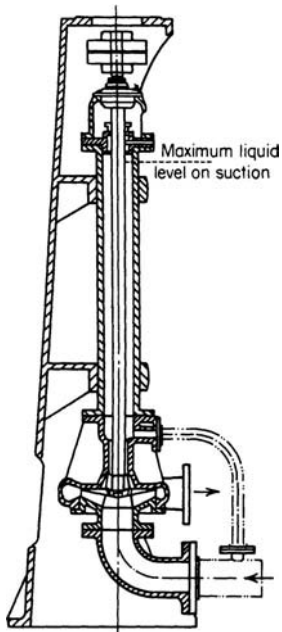


FIG. 10-51 Vertical process pump for dry-pit mounting. (Courtesy of Lawrence Pumps, Inc.)

These pumps are particularly useful when low volumes of low-viscosity liquids must be handled at higher pressures than are normally available with centrifugal pumps. Close clearances limit their use to clean liquids. For very high heads, multistage units are available.

JET PUMPS

Jet pumps are a class of liquid-handling device that makes use of the momentum of one fluid to move another.

Ejectors and injectors are the two types of jet pumps of interest to chemical engineers. The ejector, also called the siphon, exhauster, or eductor, is designed for use in operations in which the head pumped against is low and is less than the head of the fluid used for pumping. The injector is a special type of jet pump, operated by steam and used for boiler feed and similar services, in which the fluid being pumped is discharged into a space under the same pressure as that of the steam being used to operate the injector.

Figure 10-59 shows a simple design for a jet pump of the ejector type. The pumping fluid enters through the nozzle at the left and passes through the venturi nozzle at the center and out of the discharge opening at the right. As it passes into the venturi nozzle, it develops a suction that causes some of the fluid in the suction chamber to be entrained with the stream and delivered through this discharge.

The efficiency of an ejector or jet pump is low, being only a few percent. The head developed by the ejector is also low except in special types. The device has the disadvantage of diluting the fluid pumped by mixing it with the pumping fluid. In steam injectors for boiler feed and similar services in which the heat of the steam is recovered, efficiency is close to 100 percent.

The simple ejector or siphon is widely used, in spite of its low efficiency, for transferring liquids from one tank to another, for lifting acids, alkalis, or solid-containing liquids of an abrasive nature, and for emptying sumps.

ELECTROMAGNETIC PUMPS

The necessity of circulating liquid-metal heat-transfer media in nuclear-reactor systems has led to development of electromagnetic pumps. All electromagnetic pumps utilize the motor principle: a conductor in a magnetic field, carrying a current which flows at right angles to the direction of the field, has a force exerted on it, the force being mutually perpendicular to both the field and the current. In all electromagnetic pumps, the fluid is the conductor. This force, suitably directed in the fluid, manifests itself as a pressure if the fluid is suitably contained. The field and current can be produced in a number of different ways and the force utilized variously.

Both alternating- and direct-current units are available. While dc pumps (Fig. 10-60) are simpler, their high-current requirement is a definite limitation; ac pumps can readily obtain high currents by making use of transformers. Multipole induction ac pumps have been

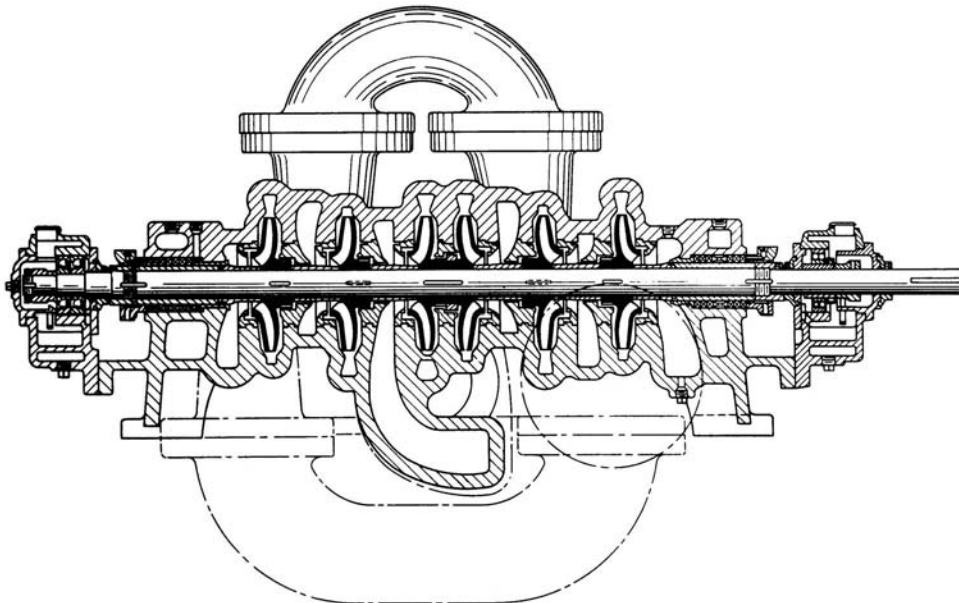


FIG. 10-52 Six-stage volute-type pump.

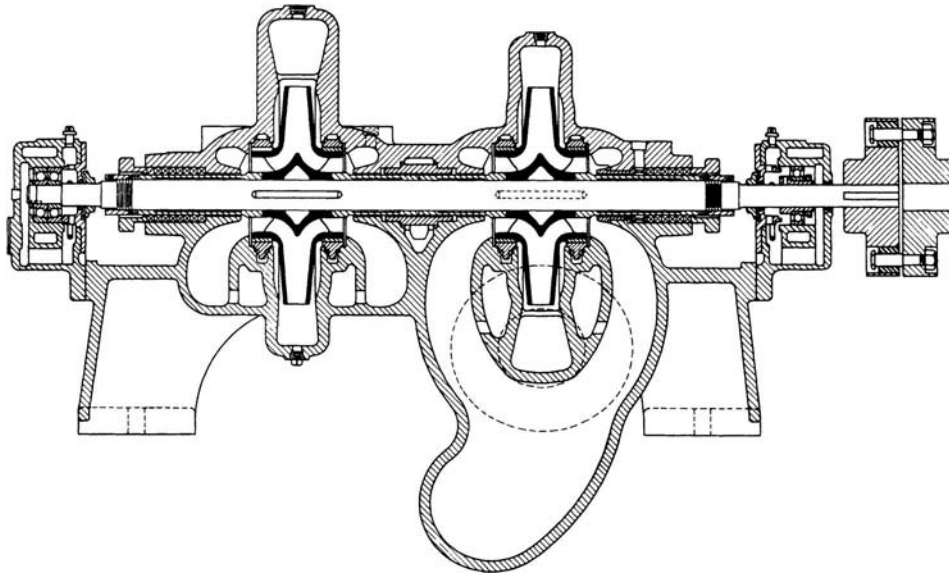


FIG. 10-53 Two-stage pump having double-suction impellers.

built in helical and linear configurations. Helical units are effective for relatively high heads and low flows, while linear induction pumps are best suited to large flows at moderate heads. Electromagnetic pumps are available for flow rates up to $2.271 \times 10^3 \text{ m}^3/\text{h}$ (10,000 gal/min), and pressures up to 2 MPa (300 lbf/in²) are practical. Performance characteristics resemble those of centrifugal pumps.

PUMP DIAGNOSTICS

Pump problems vary over a large range depending on the type of pumps and the usage of the pumps. They can be classified in the following manner by the pump type and the service:

1. *Positive-displacement pumps—reciprocating pumps* problems can be classified into the following categories:
 - a. Compressor valve problems: plate valves, feather valves, concentric disk valves, relief valves
 - b. Piston and rod assembly: piston rings, cylinder chatter, cylinder cooling, piston-rod packing
 - c. Lubrication system
2. *Positive displacement pumps—gear-type and roots-type* problems can be classified into the following categories:
 - a. Rotor dynamic problems: vibration problems, gear problems or roots rotor problems, bearing and seal problems
 - b. Lubrication systems

3. *Continuous flow pumps such as centrifugal pumps* problems can be classified into the following categories:

- a. Cavitation
- b. Capacity flow
- c. Motor overload
- d. Impeller
- e. Bearings and seals
- f. Lubrication systems

Table 10-15 classifies different types of centrifugal pump-related problems, their possible causes, and corrective actions that can be taken to solve some of the more common issues. These problems in the table are classified into three major categories for these type of pumps:

1. Cavitation
2. Capacity flow
3. Motor overload

The use of vibration monitoring to diagnose pump and compressor problems is discussed at the end of the subsection on compressor problems.

COMPRESSORS

A compressor is a device which pressurizes a working fluid. One of the basic purposes of using a compressor is to compress the fluid and to

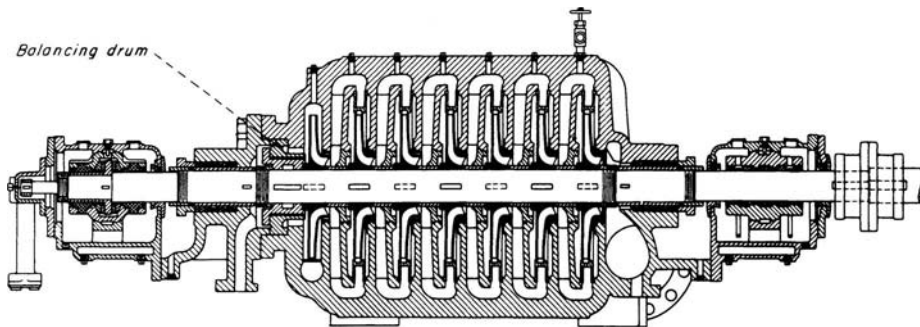


FIG. 10-54 Seven-stage diffuser-type pump.

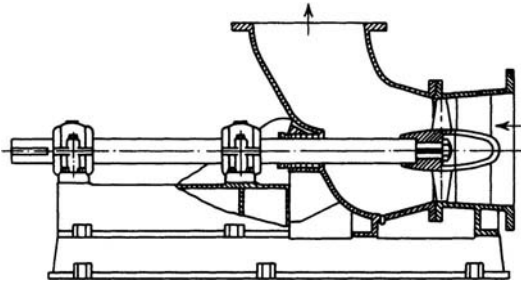


FIG. 10-55 Axial-flow elbow-type propeller pump. (Courtesy of Lawrence Pumps, Inc.)

deliver it at a pressure higher than its original pressure. Compression is required for a variety of purposes, some of which are listed below:

1. To provide air for combustion
2. To transport process fluid through pipelines
3. To provide compressed air for driving pneumatic tools
4. To circulate process fluid within a process

Different types of compressors are shown in Fig. 10-61. Positive-displacement compressors are used for intermittent flow in which successive volumes of fluid are confined in a closed space to increase their pressures. Rotary compressors provide continuous flow. In rotary compressors, rapidly rotating parts (impellers) accelerate fluid to a high speed; this velocity is then converted to additional pressure by gradual deceleration in the diffuser or volute which surrounds the impeller. Positive-displacement compressors can be further classified as either reciprocating or rotary type, as shown in Fig. 10-61. The reciprocating compressor has a piston having a reciprocating motion within a cylinder. The rotary positive-displacement compressors have rotating elements whose positive action results in compression and displacement. The rotary positive-displacement compressors can be further subdivided into sliding vane, liquid piston, straight lobe, and helical lobe compressors. The continuous flow compressors (Fig. 10-61) can be classified as either dynamic compressors or ejectors. Ejectors entrain the in-flowing fluid by using a high-velocity gas or steam jet and then convert the velocity of the mixture to pressure in a diffuser. The dynamic compressors have rotating elements, which accelerate the in-flowing fluid, and convert the velocity head to pressure head, partially in the rotating elements and partially in the stationary diffusers or blade. The dynamic compressors can be further subdivided into centrifugal, axial-flow, and mixed-flow compressors. The main flow of gas in the centrifugal compressor is radial. The flow of gas in an axial com-

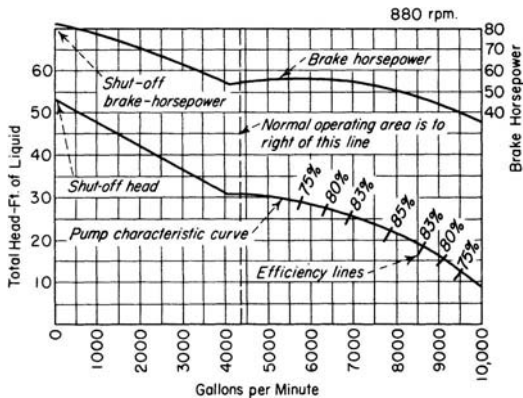


FIG. 10-56 Characteristic curve of an axial-flow pump. To convert gallons per minute to cubic meters per hour, multiply by 0.2271; to convert feet to meters, multiply by 0.3048; and to convert horsepower to kilowatts, multiply by 0.746.

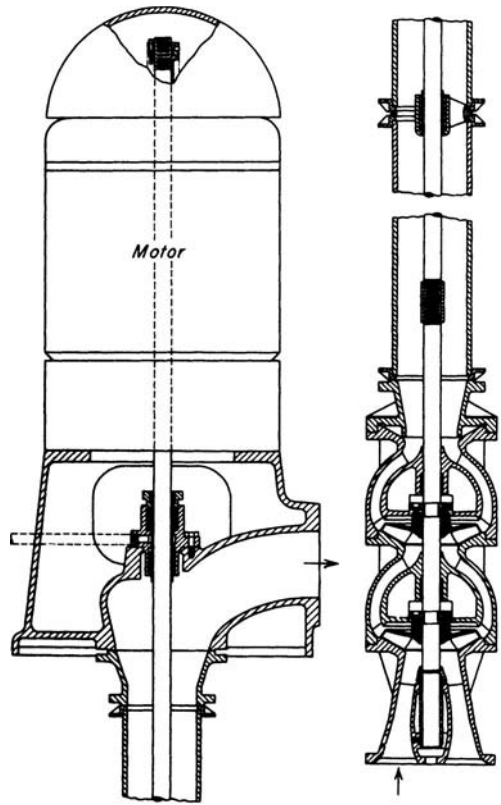


FIG. 10-57 Vertical multistage turbine, or mixed-flow, pump.

pressor is axial, and the mixed-flow compressor combines some characteristics of both centrifugal and axial compressors.

It is not always obvious what type of compressor is needed for an application. Of the many types of compressors used in the process industries, some of the more significant are the centrifugal, axial, rotary, and reciprocating compressors. They fall into three categories, as shown in Fig. 10-62.

For very high flows and low pressure ratios, an axial-flow compressor would be best. Axial-flow compressors usually have a higher efficiency, as seen in Fig. 10-63, but a smaller operating region than does

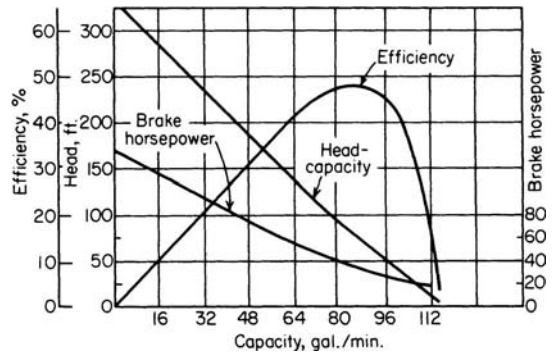


FIG. 10-58 Characteristic curves of a regenerative pump. To convert gallons per minute to cubic meters per hour, multiply by 0.2271; to convert feet to meters, multiply by 0.3048; and to convert horsepower to kilowatts, multiply by 0.746.

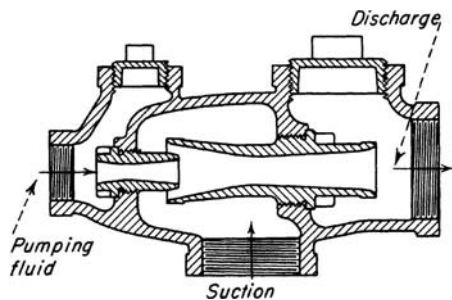


FIG. 10-59 Simple ejector using a liquid-motivating fluid.

a centrifugal machine. Centrifugal compressors operate most efficiently at medium flow rates and high pressure ratios. Rotary and reciprocating compressors (positive-displacement machines) are best used for low flow rates and high pressure ratios. The positive-displacement compressors and, in particular, reciprocating compressors were the most widely used in the process and pipeline industries up to and through the 1960s.

In turbomachinery the centrifugal flow and the axial-flow compressors are the ones used for compressing gases. Positive-displacement compressors such as reciprocating, gear-type, or lobe-type are widely used in the industry for many other applications such as slurry pumping.

The performance characteristics of a single stage of the three main types of compressors are given in Table 10-16. The pressure ratios of the axial and centrifugal compressors have been classified into three groups: industrial, aerospace, and research.

The industrial pressure ratio is low because the operating range needs to be large. The operating range is defined as the range between the surge point and the choke point. The surge point is the point at which the flow is reversed in the compressor. The choke point is the point at which the flow has reached Mach = 1.0, the point where no more flow can get through the unit, a "stone wall." When surge occurs, the flow is reversed, and so are all the forces acting on the compressor, especially the thrust forces. Surge can lead to total destruction of the compressor. Thus surge is a region that must be avoided. Choke conditions cause a large drop in efficiency, but do not lead to destruction of the unit. Note that with the increase in pressure ratio and the number of stages, the operating range is narrowed in axial-flow and centrifugal compressors.

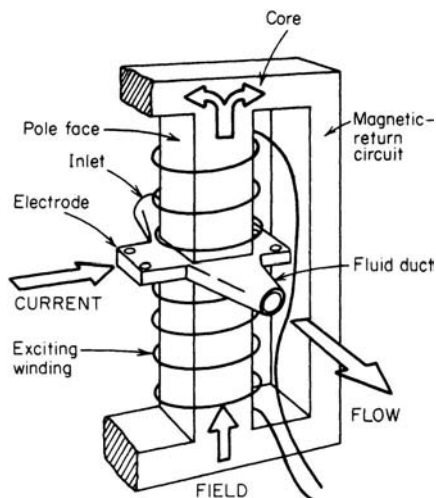


FIG. 10-60 Simplified diagram of a direct-current-operated electromagnetic pump.

Compressor Selection To select the most satisfactory compression equipment, engineers must consider a wide variety of types, each of which offers peculiar advantages for particular applications. Among the major factors to be considered are flow rate, head or pressure, temperature limitations, method of sealing, method of lubrication, power consumption, serviceability, and cost.

To be able to decide which compressor best fits the job, the engineer must analyze the flow characteristics of the units. The following dimensionless numbers describe the flow characteristics.

Reynolds number is the ratio of the inertia forces to the viscous forces

$$N_{Re} = \frac{\rho V D}{\mu} \quad (10-63)$$

where ρ is the density of the gas, V is the velocity of the gas, D is the diameter of the impeller, and μ is the viscosity of the gas.

The specific speed compares the adiabatic head and flow rate in geometrically similar machines at various speeds.

$$N_s = \frac{N \sqrt{Q}}{H_{ad}^{3/4}} \quad (10-64)$$

where N is the speed of rotation of the compressor, Q is the volume flow rate, and H is the adiabatic head.

The specific diameter compares head and flow rates in geometrically similar machines at various diameters

$$D_s = \frac{D H^{1/4}}{\sqrt{Q}} \quad (10-65)$$

The flow coefficient is the capacity of the flow rate of the machine

$$\phi = \frac{Q^1}{N D^3} \quad (10-66)$$

The pressure coefficient is the pressure or the pressure rise of the machine

$$\Psi = \frac{H}{N^2 D^2} \quad (10-67)$$

In selecting the machines of choice, the use of specific speed and diameter best describe the flow. Figure 10-64 shows the characteristics of the three types of compressors. Other considerations in chemical plant service such as problems with gases which may be corrosive or have abrasive solids in suspension must be dealt with. Gases at elevated temperatures may create a potential explosion hazard, while air at the same temperatures may be handled quite normally; minute amounts of lubricating oil or water may contaminate the process gas and so may not be permissible, and for continuous-process use, a high degree of equipment reliability is required, since frequent shutdowns for inspection or maintenance cannot be tolerated.

COMPRESSION OF GASES

Theory of Compression In any continuous compression process the relation of absolute pressure p to volume V is expressed by the formula

$$pV^n = C = \text{constant} \quad (10-68)$$

The plot of pressure versus volume for each value of exponent n is known as the **polytropic** curve. Since the work W performed in proceeding from p_1 to p_2 along any polytropic curve (Fig. 10-65) is

$$W = \int_1^2 p dV \quad (10-69)$$

it follows that the amount of work required is dependent upon the polytropic curve involved and increases with increasing values of n . The path requiring the least amount of input work is $n = 1$, which is equivalent to **isothermal** compression. For **adiabatic** compression (i.e., no heat is being added or taken away during the process), $n = k =$ ratio of specific heat at constant pressure to that at constant volume.

TABLE 10-15 Pump Problems

Possible causes	Corrective action
Cavitating-Type Problems	
Plugged suction screen.	Check for indications of the presence of screen. Remove and clean screen.
Piping gaskets with undersized IDs installed, a very common problem in small pumps.	Install proper-sized gaskets.
Column tray parts or ceramic packing lodged in the impeller eye.	Remove suction piping and debris.
Deteriorated impeller eye due to corrosion.	Replace impeller and overhaul pump.
Flow rate is high enough above design that NPSH for flow rate has increased above NPSH.	Reduce flow rate to that of design.
Lined pipe collapsed at gasket area or ID due to buildup of corrosion products between liner and carbon-steel pipe.	Replace deteriorated piping.
Poor suction piping layout, too many elbows in too many planes, a tee branch almost directly feeding the suction of the other pump, or not enough straight run before the suction flange of the pump.	Redesign piping layout, using fewer elbows and laterals for tees, and have five or more straight pipe diameters before suction flange.
Vertical pumps experience a vortex formation due to loss of submergence required by the pump. Observe the suction surface while the pump is in operation, if possible.	Review causes of vortexing. Consider installation of a vortex breaker such as a bell mouth umbrella or changes to sump design.
Spare pump begins to cavitate when attempt is made to switch it with the running pump. The spare is "backed off" by the running pump because its shutoff head is less than the head produced by the running pump. This is a frequent problem when one pump is turbine-driven and one is motor-driven.	Throttle discharge of running pump until spare can get in system. Slow down running pump if it is a turbine or variable-speed motor.
Suction piping configuration causes adverse fluid rotation when approaching impeller.	Install sufficient straight run of suction piping, or install vanes in piping to break up prerotation.
Velocity of the liquid is too high as it approaches the impeller eye.	Install larger suction piping or reduce flow through pump.
Pump is operating at a low-flow-producing suction recirculation in the impeller eye. This results in a cavitationlike sound.	Install bypass piping back to suction vessel to increase flow through pump. Remember bypass flow may have to be as high as 50 percent of design flow.
Capacity-Type Problems	
Check the discharge block valve opening first. It may be partially closed and thus the problem.	Open block valve completely.
Wear-ring clearances are excessive (closed impeller design).	Overhaul pump. Renew wear rings if clearance is about twice design value for energy and performance reasons.
Impeller-to-case or head clearances are excessive (open impeller design).	Reposition impeller to obtain correct clearance.
Air leaks into the system if the pump suction is below atmospheric pressure.	Take actions as needed to eliminate air leaks.
Increase in piping friction to the discharge vessel due to the following: <ol style="list-style-type: none"> 1. Gate has fallen off the discharge valve stem. 2. Spring is broken in the spring-type check valve. 3. Check valve flapper pin is worn, and flapper will not swing open. 4. Lined pipe collapsing. 5. Control valve stroke improperly set, causing too much pressure drop. 	Take the following actions: <ol style="list-style-type: none"> 1. Repair or replace gate valve. 2. Repair valve by replacing spring. 3. Overhaul check valve; restore proper clearance to pin and flapper bore. 4. Replace damaged pipe. 5. Adjust control valve stroke as necessary.
Suction and/or discharge vessel levels are not correct, a problem mostly seen in lower-speed pumps.	Calibrate level controllers as necessary.
Motor running backward or impeller of double suction design is mounted backward. Discharge pressure developed in both cases is about one-half design value.	Check for proper rotation and mounting of impeller. Reverse motor leads if necessary.
Entrained gas from the process lowering NPSH available.	Reduce entrained gas in liquid by process changes as needed.
Polymer or scale buildup in discharge nozzle areas.	Shut down pump and remove scale or deposits.
Mechanical seal in suction system under vacuum is leaking air into system, causing pump curve to drop.	Change percentage balance of seal faces or increase spring tension.
The pump may have formed a vortex at high flow rates or low liquid level. Does the vessel have a vortex breaker? Does the incoming flow cause the surface to swirl or be agitated?	Reduce flow to design rates. Raise liquid level in suction vessel. Install vortex breaker in suction vessel.
Variable-speed motor running too slowly.	Adjust motor speed as needed.
Bypassing is occurring between volute channels in a double-volute pump casing due to a casting defect or extreme erosion.	Overhaul pump; repair eroded area.
The positions of impellers are not centered with diffuser vanes. Several impellers will cause vibration and lower head output.	Overhaul pump; reposition individual impellers as needed. Reposition whole rotor by changing thrust collar locator spacer.
When the suction system is under vacuum, the spare pump has difficulty getting into system.	Install a positive-pressure steam (from running pump) to fill the suction line from the block valve through the check valve.
Certain pump designs use an internal bypass orifice port to alter head-flow curve. High liquid velocities often erode the orifice, causing the pump to go farther out on the pump curve. The system head curve increase corrects the flow back up the curve.	Overhaul pump, restore orifice to correct size.
Replacement impeller is not correct casting pattern; therefore NPSH required is different.	Overhaul pump, replace impeller with correct pattern.
Volute and cutwater area of casing is severely eroded.	Overhaul pump; replace casing or repair by welding. Stress-relieve after welding as needed.

10-44 TRANSPORT AND STORAGE OF FLUIDS

TABLE 10-15 Pump Problems (Concluded)

Possible causes	Corrective action
Overload Problems	
Polymer buildup between wear surfaces (rings or vanes).	Remove buildup to restore clearances.
Excessive wear ring (closed impeller) or cover-case clearance (open impeller).	Replace wear rings or adjust axial clearance of open impeller. In severe cases, cover or case must be replaced.
Pump circulating excessive liquid back to suction through a breakdown bushing or a diffuser gasket area.	Overhaul pump, replacing parts as needed.
Minimum-flow loop left open at normal rates, or bypass around control valve is open.	Close minimum-flow loop or control valve bypass valve.
Discharge piping leaking under liquid level in sump-type design.	Inspect piping for leakage. Replace as needed.
Electrical switch gear problems cause one phase to have low amperage.	Check out switch gear and repair as necessary.
Specific gravity is higher than design specification.	Change process to adjust specific gravity to design value, or throttle pump to reduce horsepower requirements. This will not correct problem with some vertical turbine pumps that have a flat horsepower-required curve.
Pump motor not sized for end of curve operation.	Replace motor with one of larger size, or reduce flow rate.
Open impeller has slight rub on casing. Most often occurs in operations from 250 to 400°F due to piping strain and differential growth in the pump.	Increase clearance of impeller to casing.
A replacement impeller was not trimmed to the correct diameter.	Remove impeller from pump and turn to correct diameter.

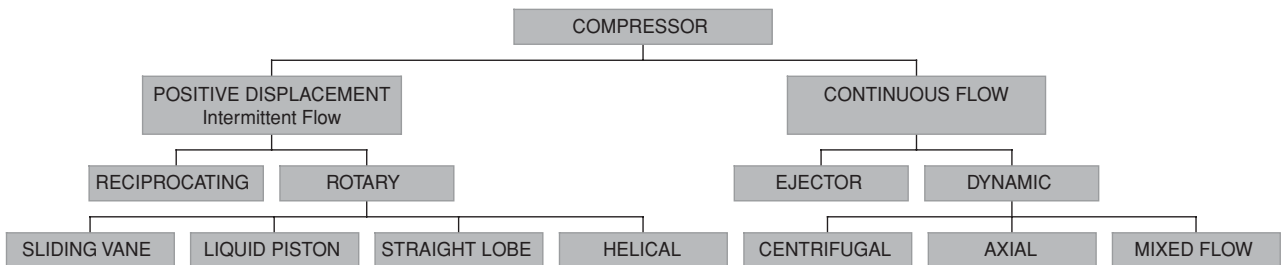


FIG. 10-61 Principal types of compressors.

Since most compressors operate along a polytropic path approaching the adiabatic, compressor calculations are generally based on the adiabatic curve.

Some formulas based upon the adiabatic equation and useful in compressor work are as follows:

Pressure, volume, and temperature relations for perfect gases:

$$p_2/p_1 = (V_1/V_2)^k \quad (10-70)$$

$$T_2/T_1 = (V_1/V_2)^{k-1} \quad (10-71)$$

$$p_2/p_1 = (T_2/T_1)^{k/(k-1)} \quad (10-72)$$

Adiabatic Calculations Adiabatic head is expressed as follows: In SI units,

$$H_{ad} = \frac{k \times ZRT_1}{k-1} \left[\left(\frac{p_2}{p_1} \right)^{(k-1)/k} - 1 \right] \quad (10-73a)$$

where H_{ad} = adiabatic head, N·m/kg; R = gas constant, J/(kg·K) = 8314/molecular weight; T_1 = inlet gas temperature, K; p_1 = absolute inlet pressure, kPa; and p_2 = absolute discharge pressure, kPa.

In U.S. customary units,

$$H_{ad} = \frac{k}{k-1} ZRT_1 \left[\left(\frac{p_2}{p_1} \right)^{(k-1)/k} - 1 \right] \quad (10-73b)$$

where H_{ad} = adiabatic head, ft·lbf/lbm; R = gas constant, (ft·lbf)/(lbm·°R) = 1545/molecular weight; T_1 = inlet gas temperature, °R;

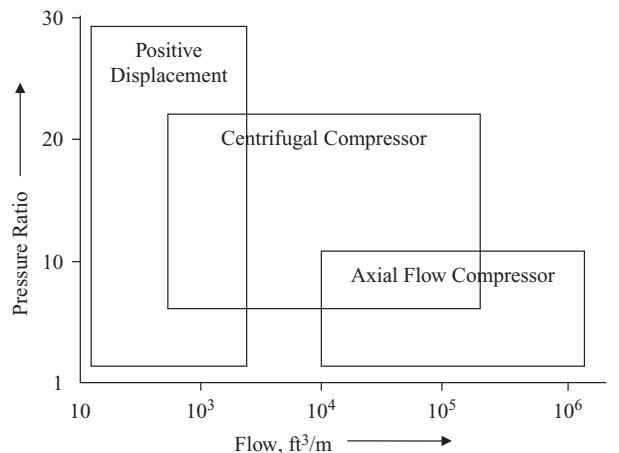


FIG. 10-62 Performance characteristics of different types of compressors.

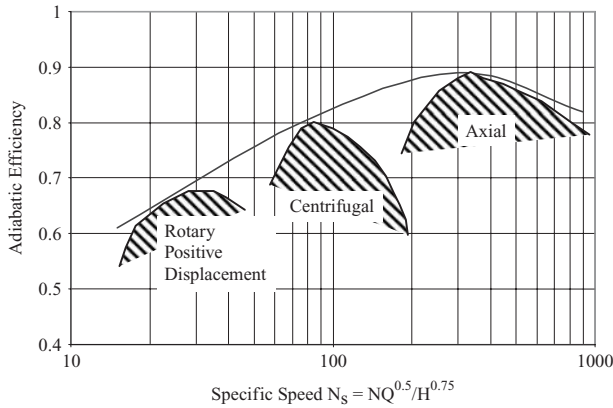


FIG. 10-63 Variation of adiabatic efficiency with specific speed for the three types of compressors.

p_1 = absolute inlet pressure, lbf/in²; and p_2 = absolute discharge pressure, lbf/in².

The **work** expended on the gas during compression is equal to the product of the adiabatic head and the mass flow of gas handled. Therefore, the adiabatic power is as follows:

In SI units,

$$kW_{ad} = \frac{WH_{ad}}{10^3} = \frac{k \times ZWRT_1}{k-1} \left[\left(\frac{p_2}{p_1} \right)^{(k-1)/k} - 1 \right] \quad (10-74a)$$

or
$$kW_{ad} = 2.78 \times 10^{-4} \frac{k}{k-1} Q_1 p_1 \left[\left(\frac{p_2}{p_1} \right)^{(k-1)/k} - 1 \right] \quad (10-75a)$$

where kW_{ad} = power, kW; W = mass flow, kg/s; and Q_1 = volume rate of gas flow, m³/h, at compressor inlet conditions.

In U.S. Customary units,

$$hp_{ad} = \frac{WH_{ad}}{550} = \frac{k}{k-1} \frac{ZWRT_1}{550} \left[\left(\frac{p_2}{p_1} \right)^{(k-1)/k} - 1 \right] \quad (10-74b)$$

or
$$hp_{ad} = \frac{k}{k-1} \frac{Q_1 p_1}{3600} \left[\left(\frac{p_2}{p_1} \right)^{(k-1)/k} - 1 \right] \quad (10-75b)$$

where hp_{ad} = power, hp; W = mass flow, lb/s; and Q_1 = volume rate of gas flow, ft³/min.

Adiabatic discharge temperature is

$$T_2 = T_1(p_2/p_1)^{(k-1)/k} \quad (10-76)$$

The work in a compressor under ideal conditions as previously shown occurs at constant entropy. The actual process is a polytropic process as shown in Fig. 10-65 and given by the equation of state $Pv^n = \text{constant}$.

Adiabatic efficiency is given by the following relationship:

$$\eta_{ad} = \frac{\text{ideal work}}{\text{actual work}} \quad (10-77)$$

In terms of the change in total temperatures the relationship can be written as:

$$\eta_{ad} = \frac{T_2 - T_1}{T_{2a} - T_1} \quad (10-78)$$

where T_{2a} is the total actual discharge temperature of the gas. The adiabatic efficiency can be represented in terms of total pressure change:

$$\eta_{ad} = \frac{\left(\frac{P_2}{P_1} \right)^{(k-1)/k} - 1}{\left(\frac{P_2}{P_1} \right)^{(n-1)/n} - 1} \quad (10-79)$$

Polytropic head can be expressed by the following relationship:

$$H_{poly} = \frac{n}{n-1} ZRT_1 \left[\left(\frac{P_2}{P_1} \right)^{(n-1)/n} - 1 \right] \quad (10-80)$$

Likewise for polytropic efficiency, which is often considered as the small stage efficiency, or the hydraulic efficiency:

$$\eta_{pc} = \frac{(k-1)/k}{(n-1)/n} \quad (10-81)$$

Polytropic efficiency is the limited value of the isentropic efficiency as the pressure ratio approaches 1.0, and the value of the polytropic efficiency is higher than the corresponding adiabatic efficiency.

A characteristic of polytropic efficiency is that the polytropic efficiency of a multistage unit is equal to the stage efficiency if each stage has the same efficiency.

If the compression cycle approaches the isothermal condition, $pV = \text{constant}$, as is the case when several stages with intercoolers are used, a simple approximation of the power is obtained from the following formula:

In SI units,

$$kW = 2.78 \times 10^{-4} Q_1 p_1 \ln p_2/p_1 \quad (10-82a)$$

In U.S. customary units,

$$hp = 4.4 \times 10^{-3} Q_1 p_1 \ln p_2/p_1 \quad (10-82b)$$

Reciprocating Compressors Reciprocating compressors are used mainly when high-pressure head is required at a low flow. Reciprocating compressors are furnished in either single-stage or multistage types. The number of stages is determined by the required compressor ratio p_2/p_1 . The compression ratio per stage is generally limited to 4, although low-capacity units are furnished with compression ratios of 8 and even higher. Generally, the maximum compression ratio is determined by the maximum allowable discharge-gas temperature.

TABLE 10-16 Performance Characteristics of Compressors

Types of compressors	Pressure ratio per stage			Efficiency, %	Operating range surge – choke, %
	Industrial	Aerospace	Research		
Positive displacement	Up to 30	—	—	75–82	—
Centrifugal	1.2–1.9	2.0–7.0	13	75–87 25	Large
Axial	1.05–1.3	1.1–1.45	2.1	80–91	Narrow 3–10

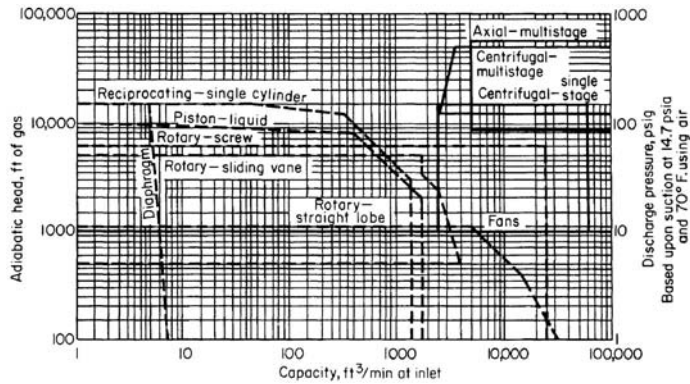


FIG. 10-64 Compressor coverage chart based on the normal range of operation of commercially available types shown. Solid lines: use left ordinate, head. Broken lines: use right ordinate, pressure. To convert cubic feet per minute to cubic meters per hour, multiply by 1.699; to convert feet to meters, multiply by 0.3048; and to convert pounds-force per square inch to kilopascals, multiply by 6.895; $(^{\circ}\text{F} - 32) \div 1.8 = ^{\circ}\text{C}$.

Single-acting air-cooled and water-cooled air compressors are available in sizes up to about 75 kW (100 hp). Such units are available in one, two, three, or four stages for pressure as high as 24 MPa (3500 lbf/in²). These machines are seldom used for gas compression because of the difficulty of preventing gas leakage and contamination of the lubricating oil.

The compressors most commonly used for compressing gases have a crosshead to which the connecting rod and piston rod are connected. This provides a straight-line motion for the piston rod and permits simple packing to be used. Figure 10-66 illustrates a simple single-stage machine of this type having a double-acting piston. Either single-acting (Fig. 10-67) or double-acting pistons (Fig. 10-68) may be used, depending on the size of the machine and the number of stages. In some machines double-acting pistons are used in the first stages and single-acting in the later stages.

On multistage machines, intercoolers are provided between stages. These heat exchangers remove the heat of compression from the gas and reduce its temperature to approximately the temperature existing at the compressor intake. Such cooling reduces the volume of gas going to the high-pressure cylinders, reduces the power required for compression, and keeps the temperature within safe operating limits.

Figure 10-69 illustrates a two-stage compressor end such as might be used on the compressor illustrated in Fig. 10-66.

Compressors with horizontal cylinders such as illustrated in Figs. 10-66 to 10-68 are most commonly used because of their accessibility. However, machines are also built with vertical cylinders and other arrangements such as right-angle (one horizontal and one vertical cylinder) and V-angle.

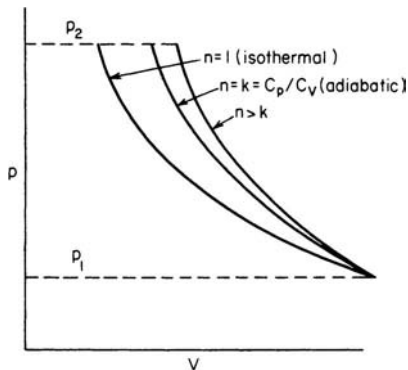


Fig. 10-65 Polytropic compression curves.

Compressors up to around 75 kW (100 hp) usually have a single center-throw crank, as illustrated in Fig. 10-66. In larger sizes compressors are commonly of duplex construction with cranks on each end of the shaft (see Fig. 10-70). Some large synchronous motor-driven units are of four-corner construction; i.e., they are of double-duplex construction with two connecting rods from each of the two crank throws (see Fig. 10-71). Steam-driven compressors have one or more steam cylinders connected directly by piston rod or tie rods to the gas-cylinder piston or crosshead.

Valve Losses Above piston speeds of 2.5 m/s (500 ft/min), suction and discharge valve losses begin to exert significant effects on the actual internal compression ratio of most compressors, depending on the valve port area available. The obvious results are high temperature rise and higher power requirements than might be expected. These effects become more pronounced with higher-molecular-weight gases. Valve problems can be a very major contributor to down time experienced by these machines.

Control Devices In many installations the use of gas is intermittent, and some means of controlling the output of the compressor is therefore necessary. In other cases constant output is required despite variations in discharge pressure, and the control device must operate to maintain a constant compressor speed. Compressor capacity, speed, or pressure may be varied in accordance with requirements. The nature of the control device will depend on the function to be regulated. Regulation of pressure, volume, temperature, or some other factor determines the type of regulation required and the type of the compressor driver.

The most common control requirement is regulation of capacity. Many capacity controls, or unloading devices, as they are usually termed, are actuated by the pressure on the discharge side of the compressor. A falling pressure indicates that gas is being used faster than it is being compressed and that more gas is required. A rising pressure indicates that more gas is being compressed than is being used and that less gas is required.

An obvious method of controlling the capacity of a compressor is to vary the speed. This method is applicable to units driven by variable-speed drivers such as steam pistons, steam turbines, gas engines, diesel engines, etc. In these cases the regulator actuates the steam-admission or fuel-admission valve on the compressor driver and thus controls the speed.

Motor-driven compressors usually operate at constant speed, and other methods of controlling the capacity are necessary. On reciprocating compressors discharging into receivers, up to about 75 kW (100 hp), two types of control are usually available. These are automatic-start-and-stop control and constant-speed control.

Automatic-start-and-stop control, as its name implies, stops or starts the compressor by means of a pressure-actuated switch as the

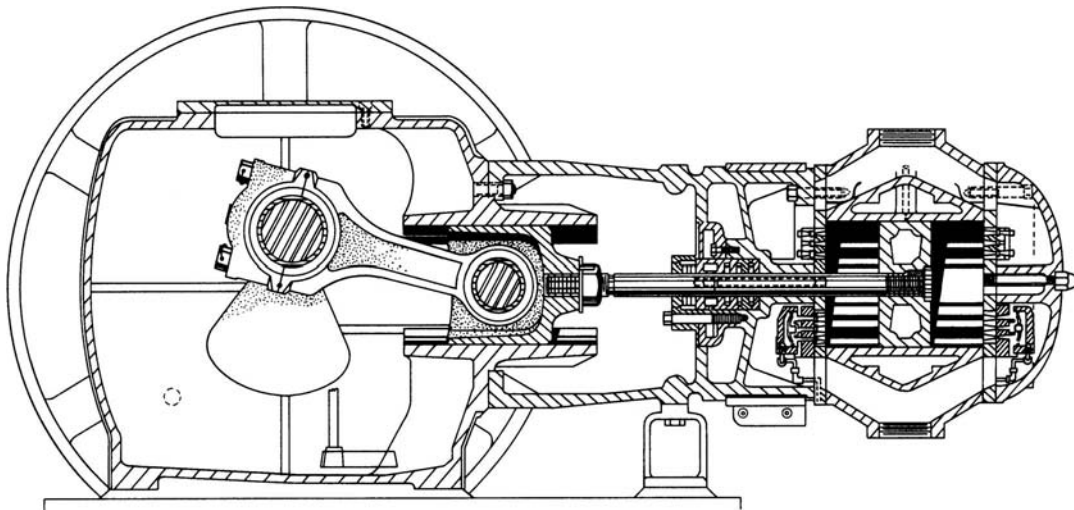


FIG. 10-66 Typical single-stage, double-acting water-cooled compressor.

gas demand varies. It should be used only when the demand for gas will be intermittent.

Constant-speed control should be used when gas demand is fairly constant. With this type of control, the compressor runs continuously but compresses only when gas is needed. Three methods of unloading the compressor with this type of control are in common use: (1) **closed suction unloaders**, (2) **open inlet-valve unloaders**, and (3) **clearance unloaders**. The closed suction unloader consists of a pressure-actuated valve which shuts off the compressor intake. Open inlet-valve unloaders (see Fig. 10-72) operate to hold the compressor inlet valves open and thereby prevent compression. Clearance unloaders (see Fig. 10-73) consist of pockets or small reservoirs which are opened when unloading is desired. The gas is compressed into them on the compression stroke and reexpands into the cylinder on the return stroke, thus preventing the compression of additional gas.

It is sometimes desirable to have a compressor equipped with both constant-speed and automatic-start-and-stop control. When this is done, a switch allows immediate selection of either type.

Motor-driven reciprocating compressors above about 75 kW (100 hp) in size are usually equipped with a step control. This is in reality a variation of constant-speed control in which unloading is accomplished in a series of steps, varying from full load down to no load.

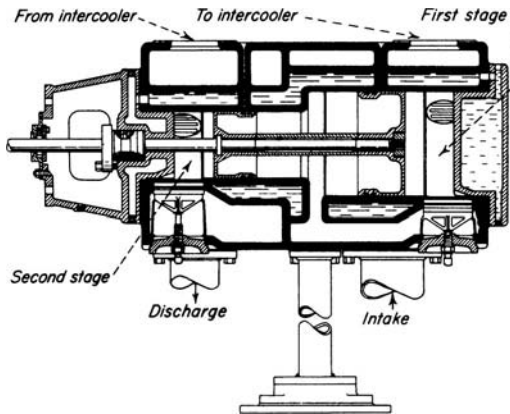


FIG. 10-67 Two-stage single-acting opposed piston in a single step-type cylinder.

Three-step control (full load, one-half load, and no load) is usually accomplished with inlet-valve unloaders. **Five-step control** (full load, three-fourths load, one-half load, one-fourth load, and no load) is accomplished by means of clearance pockets (see Fig. 10-74). On some machines, inlet-valve and clearance-control unloading are used in combination.

Although such control devices are usually automatically operated, manual operation is satisfactory for some services. When manual operation is provided, it often consists of a valve or valves to open and close clearance pockets. In some cases, a movable cylinder head is provided for variable clearance in the cylinder (see Fig. 10-75).

When no capacity control or unloading device is provided, it is necessary to provide bypasses between the inlet and discharge in order that the compressor can be started against no load (see Fig. 10-76).

Nonlubricated Cylinders Most compressors use oil to lubricate the cylinder. In some processes, however, the slightest oil contamination

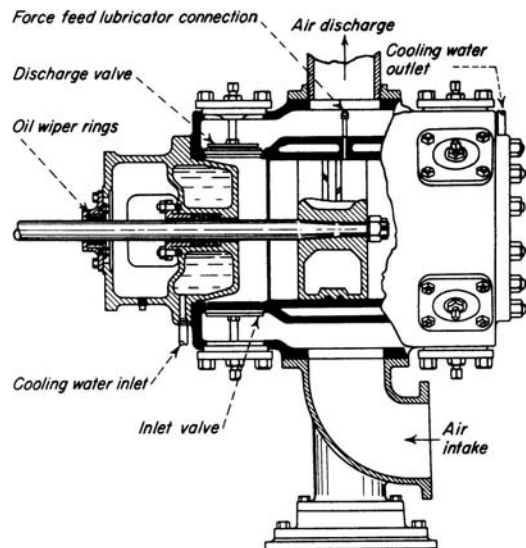


FIG. 10-68 Typical double-acting compressor piston and cylinder.

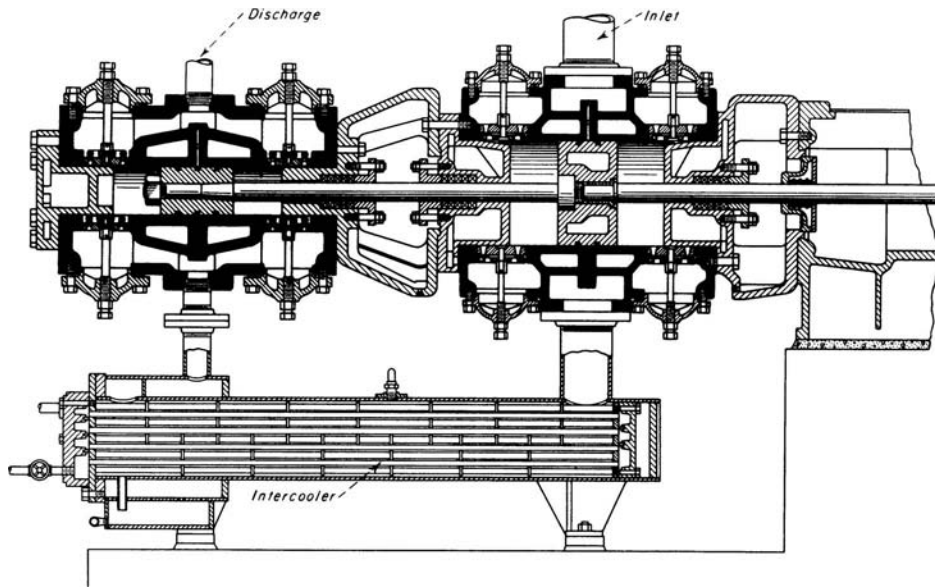


FIG. 10-69 Two-stage double-acting compressor cylinders with intercooler.

is objectionable. For such cases a number of manufacturers furnish a "nonlubricated" cylinder (see Fig. 10-77). The piston on these cylinders is equipped with piston rings of graphitic carbon or Teflon[®] as well as pads or rings of the same material to maintain proper clearance between the piston and the cylinder. Plastic packing of a type that requires no lubricant is used on the stuffing box. Although oil-wiper rings are used on the piston rod where it leaves the compressor frame, minute quantities of oil might conceivably enter the cylinder on the rod. If even such small amounts of oil are objectionable, an extended cylinder connecting piece can be furnished. This simply lengthens the piston rod enough so that no portion of the rod can alternately enter the frame and the cylinder.

In many cases, a small amount of gas leaking through the packing is objectionable. Special connecting pieces are furnished between the cylinder and the frame, which may be either single-compartment or double-compartment. These may be furnished gastight and

vented back to the suction or filled with a sealing gas or fluid and held under a slight pressure.

High-Pressure Compressors There is a definite trend in the chemical industry toward the use of high-pressure compressors with discharge pressures of from 34.5 to 172 MPa (5000 to 25,000 lbf/in²) and with capacities from 8.5×10^3 to 42.5×10^3 m³/h (5000 to 25,000 ft³/min). These require special design, and a complete knowledge of the characteristics of the gas is necessary. In most cases, these types of applications use the barrel-type centrifugal compressor.

The gas usually deviates considerably from the perfect-gas laws, and in many cases temperature or other limitations necessitate a thorough engineering study of the problem. These compressors usually have five, six, seven, or eight stages, and the cylinders must be properly proportioned to meet the various limitations involved and also to balance the load among the various stages. In many cases, scrubbing or other processing is carried on between stages. High-pressure cylinders are steel forgings with single-acting plungers (see Fig. 10-78). The compressors are usually designed so that the pressure load against the plunger is opposed by one or more single-acting pistons of the lower pressure stages. Piston-rod packing is usually of the segmental-ring metallic type. Accurate fitting and correct lubrication are very important. High-pressure compressor valves are designed for the conditions involved. Extremely high-grade engineering and skill are necessary.

Piston-Rod Packing Proper piston-rod packing is important. Many types are available, and the most suitable is determined by the gas handled and the operating conditions for a particular unit.

There are many types and compositions of soft packing, semimetallic packing, and metallic packing. In many cases, metallic packing is to be recommended. A typical low-pressure packing arrangement is shown in Fig. 10-79. A high-pressure packing arrangement is shown in Fig. 10-80.

When wet, volatile, or hazardous gases are handled or when the service is intermittent, an auxiliary packing gland and soft packing are usually employed (see Fig. 10-81).

Metallic Diaphragm Compressors (Fig. 10-82) These are available for small quantities [up to about 17 m³/h (10 ft³/min)] for compression ratios as high as 10:1 per stage. Temperature rise is not a serious problem, as the large wall area relative to the gas volume permits sufficient heat transfer to approach isothermal compression. These compressors possess the advantage of having no seals for the process gas. The diaphragm is actuated hydraulically by a plunger pump.

[®]Du Pont tetrafluoroethylene fluorocarbon resin.

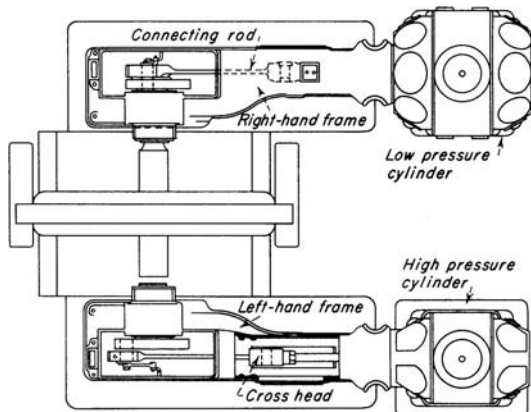


FIG. 10-70 Duplex two-stage compressor (plan view).

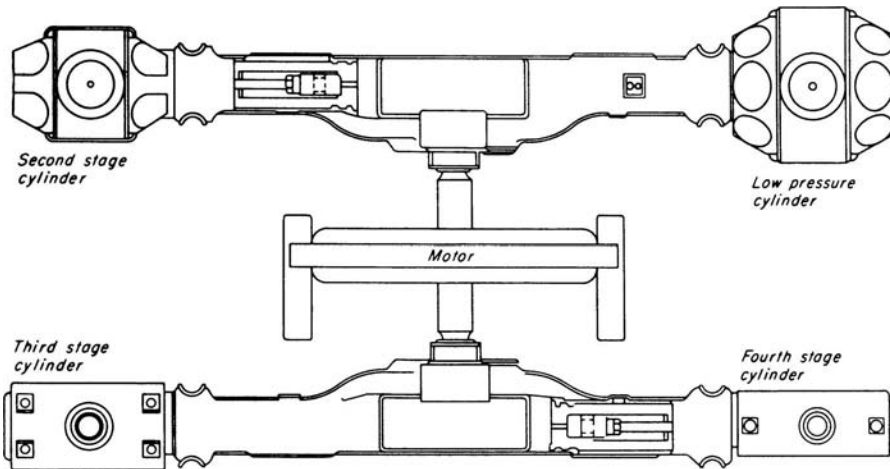


FIG. 10-71 Four-corner four-stage compressor (plan view).

FANS AND BLOWERS

Fans are used for low pressures where generally the delivery pressure is less than 3.447 kPa (0.5 lb/in²), and **blowers** are used for higher pressures. However, they are usually below delivery pressures of 10.32 kPa (1.5 lb/in²). These units can either be centrifugal or the axial-flow type.

Fans and blowers are used for many types of ventilating work such as air-conditioning systems. In large buildings, blowers are often used due to the high delivery pressures needed to overcome the pressure drop in the ventilation system. Most of these blowers are of the centrifugal type. Blowlers are also used to supply draft air to boilers and furnaces. Fans are used to move large volumes of air or gas through ducts, supplying air for drying, conveying material suspended in the gas stream, removing fumes, condensing towers and other high-flow, low-pressure applications.

Axial-Flow Fans These are designed to handle very high flow rates and low pressure. The disc-type fans are similar to those of a household fan. They are usually for general circulation or exhaust work without ducts.

The so-called propeller-type fans with blades that are aerodynamically designed (as seen in Fig. 10-83) can consist of two or more stages. The air in these fans enters in an axial direction and leaves in an axial direction. The fans usually have inlet guide vanes followed by a rotating blade, followed by a stationary (stator) blade.

Centrifugal Blowers These blowers have air or gases entering in the axial direction and being discharged in the radial direction. These blowers have three types of blades: radial or straight blades, forward-curved blades, and backward-curved blades (Figs. 10-84 to 10-86).

Radial blade blowers as seen in Fig. 10-84 are usually used in large-diameter or high-temperature applications. The blades being radial in direction have very low stresses as compared to the backward or forward

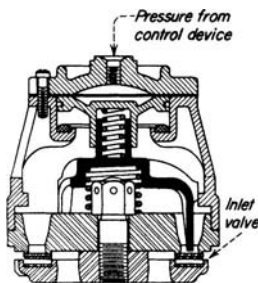


FIG. 10-72 Inlet-valve unloader.

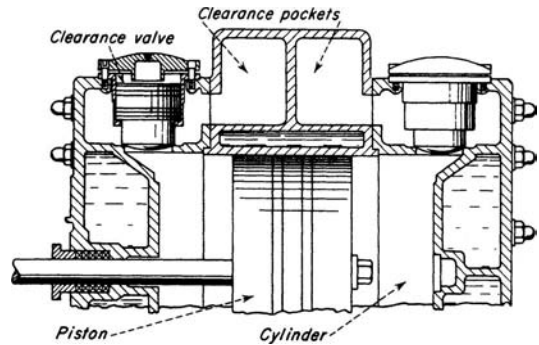


FIG. 10-73 Clearance-control cylinder. (Courtesy of Ingersoll-Rand.)

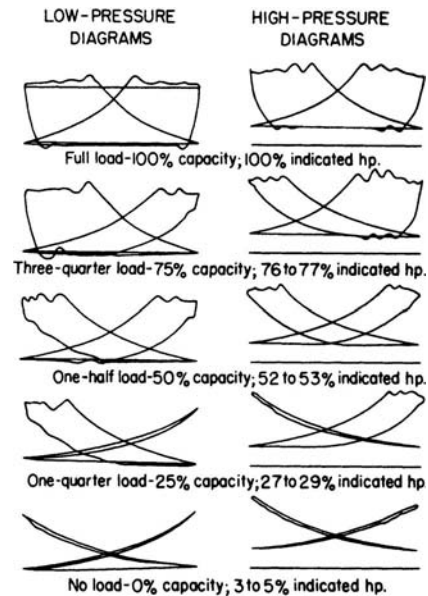


FIG. 10-74 Actual indicator diagram of a two-stage compressor showing the operation of clearance control at five load points.

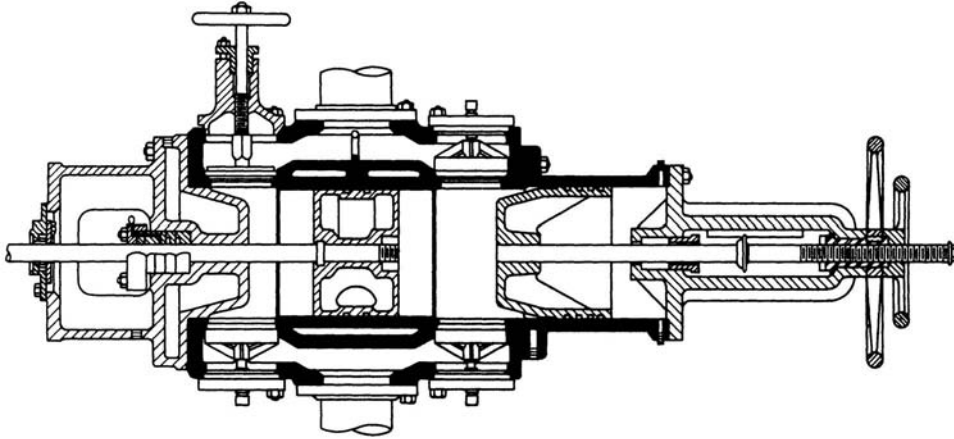


FIG. 10-75 Sectional view of a cylinder equipped with a hand-operated valve lifter on one end and a variable-volume clearance pocket at other end.

curve blades. The rotors have anywhere between 4 to 12 blades and usually operate at low speeds. These fans are used in exhaust work especially for gases at high temperature and with suspensions in the flow stream.

Forward-Curved Blade Blowers These blowers discharge the gas at a very high velocity. The pressure supplied by this blower is lower than that produced in the other two blade characteristics. The number of blades in such a rotor can be large—up to 50 blades—and the speed is high—usually 3600–1800 rpm in 60-cycle countries and 3000–1500 rpm in 50-cycle countries.

Backward-Curved Blade Blowers These blowers are used when a higher discharge pressure is needed. It is used over a wide range of applications. Both the forward and backward curved blades do have much higher stresses than the radial bladed blower.

Starting compressor	Stopping compressor
Start with A and D open	Close ---- C
Close ---- D	Close --- B
Close ----- A	Open ---- A and D
Open ----- B	
Slowly open --- C	

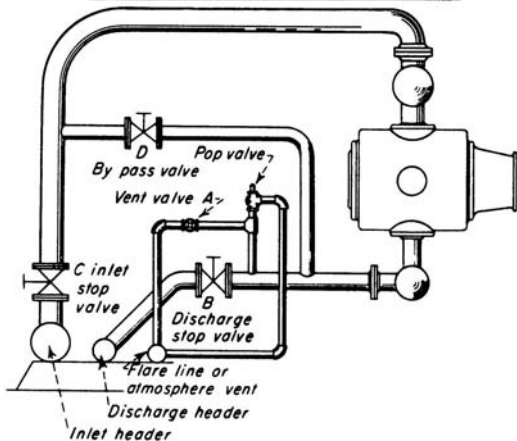


FIG. 10-76 Bypass arrangement for a single-stage compressor. On multistage machines, each stage is bypassed in a similar manner. Such an arrangement is necessary for no-load starting.

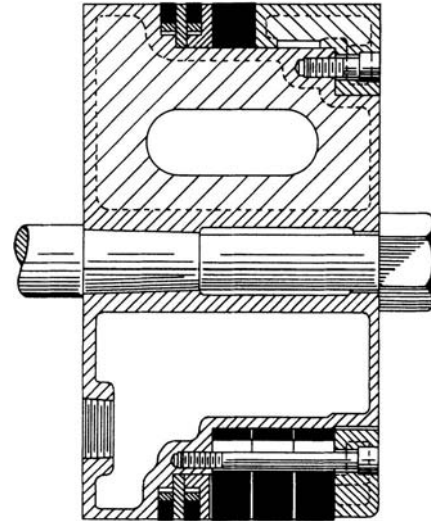


FIG. 10-77 Piston equipped with carbon piston and wearing rings for a non-lubricated cylinder.

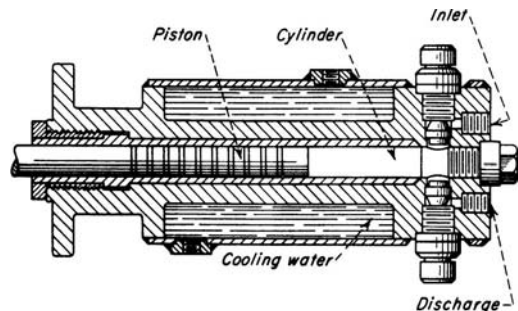


FIG. 10-78 Forged-steel single-acting high-pressure cylinder.

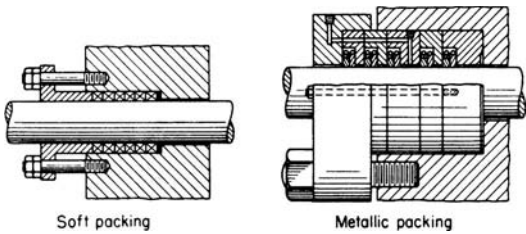


FIG. 10-79 Typical packing arrangements for low-pressure cylinders.

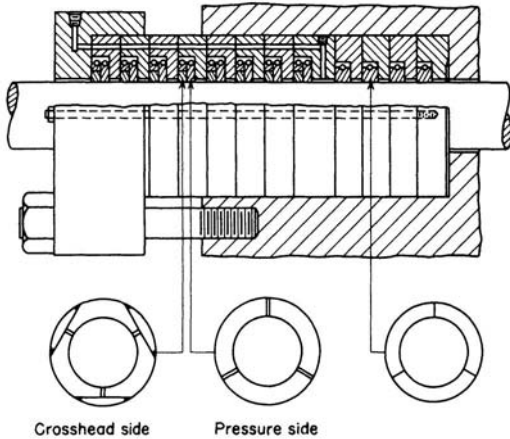


FIG. 10-80 Typical packing arrangement, using metallic packing, for high-pressure cylinders.

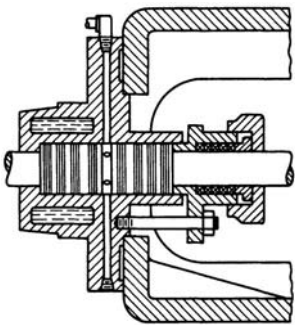


FIG. 10-81 Soft packing in an auxiliary stuffing box for handling gases.

The centrifugal blower produces energy in the air stream by the centrifugal force and imparts a velocity to the gas by the blades. Forward curved blades impart the most velocity to the gas. The scroll-shaped volute diffuses the air and creates an increase in the static pressure by reducing the gas velocity. The change in total pressure occurs in the impeller—this is usually a small change. The static pressure is increased in both the impeller and the diffuser section. Operating efficiencies of the fan range from 40 to 80 percent. The discharge total pressure is the summation of the static pressure and the velocity head. The power needed to drive the fan can be computed as follows.

$$\text{Power (kW)} = 2.72 \times 10^{-5} QP \quad (10-83)$$

where Q is the fan volume (m^3/h) and P is the total discharge pressure

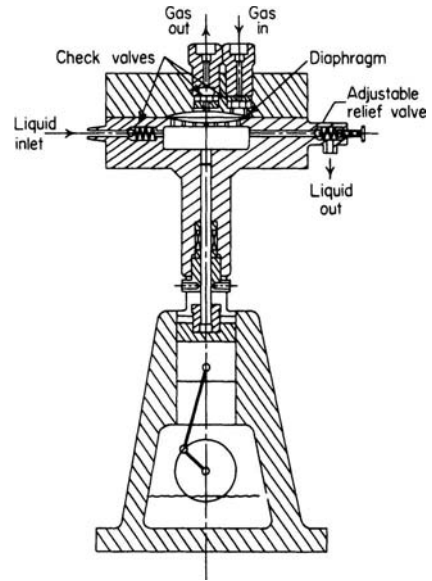


FIG. 10-82 High-pressure, low-capacity compressor having a hydraulically actuated diaphragm. (Pressure Products Industries.)

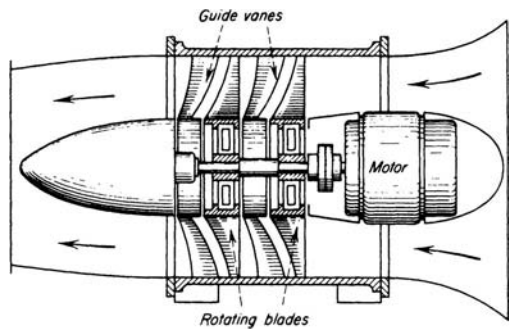


FIG. 10-83 Two-stage axial-flow fan.

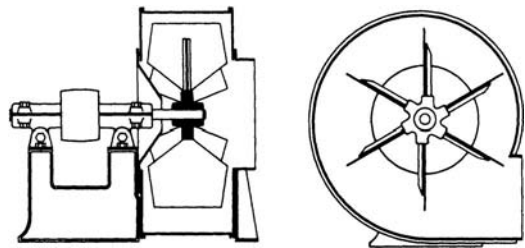


FIG. 10-84 Straight-blade, or steel-plate, fan.

in cm of water column.

In U.S. customary units,

$$\text{hp} = 1.57 \times 10^{-4} Qp \quad (10-84)$$

where hp is the fan power output, hp ; Q is the fan volume, ft^3/min ; and p is the fan-operating pressure, inches water column.

$$\text{Efficiency} = \frac{\text{air power output}}{\text{shaft power input}} \quad (10-85)$$

10-52 TRANSPORT AND STORAGE OF FLUIDS

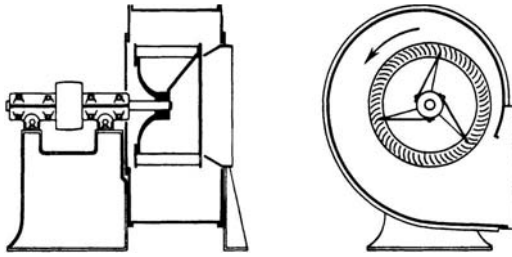


FIG. 10-85 Forward-curved blade, or "scirocco"-type, fan.

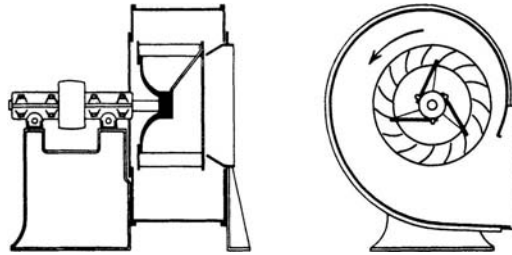


FIG. 10-86 Backward-curved-blade fan.

Fan Performance The performance of a centrifugal fan varies with changes in conditions such as temperature, speed, and density of the gas being handled. It is important to keep this in mind in using the catalog data of various fan manufacturers, since such data are usually based on stated standard conditions. Corrections must be made for variations from these standards. The usual variations are as follows:

When speed varies, (1) capacity varies directly as the speed ratio, (2) pressure varies as the square of the speed ratio, and (3) horsepower varies as the cube of the speed ratio.

When the temperature of air or gas varies, horsepower and pressure vary inversely as the absolute temperature, speed and capacity being constant. See Fig. 10-87.

When the density of air or gas varies, horsepower and pressure vary directly as the density, speed and capacity being constant.

CONTINUOUS-FLOW COMPRESSORS

Continuous-flow compressors are machines where the flow is continuous, unlike positive-displacement machines where the flow is fluctuating. Continuous-flow compressors are also classified as turbomachines. These types of machines are widely used in the chemical and petroleum industry for many services. They are also used extensively in many other industries such as the iron and steel industry, pipeline boosters, and on offshore platforms for reinjection compressors. Continuous-flow machines are usually much smaller in size and produce much less vibration than their counterpart, positive-displacement units.

Centrifugal Compressors The flow in a centrifugal compressor enters the impeller in an axial direction and exits in a radial direction.

In a typical centrifugal compressor, the fluid is forced through the impeller by rapidly rotating impeller blades. The velocity of the fluid is converted to pressure, partially in the impeller and partially in the stationary diffusers. Most of the velocity leaving the impeller is converted into pressure energy in the diffuser as shown in Fig. 10-88. It is normal practice to design the compressor so that half the pressure rise takes place in the impeller and the other half in the diffuser. The diffuser consists of a vaneless space, a vane that is tangential to the impeller, or a combination of both. These vane passages diverge to convert the velocity head into pressure energy.

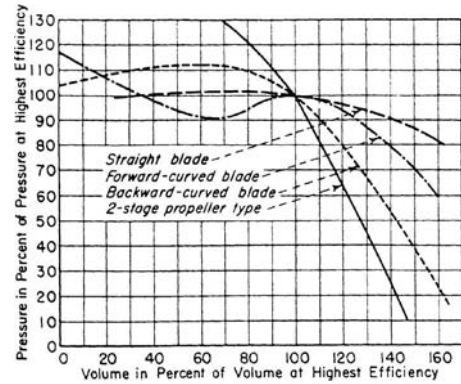


FIG. 10-87 Approximate characteristic curves of various types of fans.

Centrifugal compressors in general are used for higher pressure ratios and lower flow rates compared to lower-stage pressure ratios and higher flow rates in axial compressors. The pressure ratio in a single-stage centrifugal compressor varies depending on the industry and application. In the petrochemical industry the single stage pressure ratio is about 1.2:1. Centrifugal compressors used in the aerospace industry, usually as a compressor of a gas turbine, have pressure ratios between 3:1 to as high as 9:1 per stage.

In the petrochemical industry, the centrifugal compressors consist mainly of casings with multiple stages. In many instances, multiple casings are also used, and to reduce the power required to drive these multiple casings, there are intercoolers between them. Each casing can have up to 9 stages. In some cases, intercoolers are also used between single stages of compressor to reduce the power required for compression. These compressors are usually driven by gas turbines, steam turbines, and electric motors. Speed-increasing gears may be used in conjunction with these drivers to obtain the high speeds at which many of these units operate. Rotative speeds of as high as 50,000 rpm are not uncommon. Most of the petrochemical units run between 9,000 and 15,000 rpm.

The compressor's operating range is between two major regions as seen in Fig. 10-89, which is a performance map of a centrifugal compressor. These two regions are *surge*, which is the lower flow limit of stable operation, and *choke* or *stonewall*, which is the maximum flow through the compressor at a given operating speed. The centrifugal compressor's operating range between surge and choke is reduced as the pressure ratio per stage is increased or the number of stages are added.

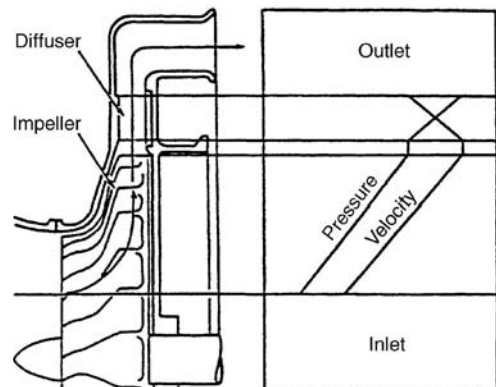


FIG. 10-88 Pressure and velocity through a centrifugal compressor.

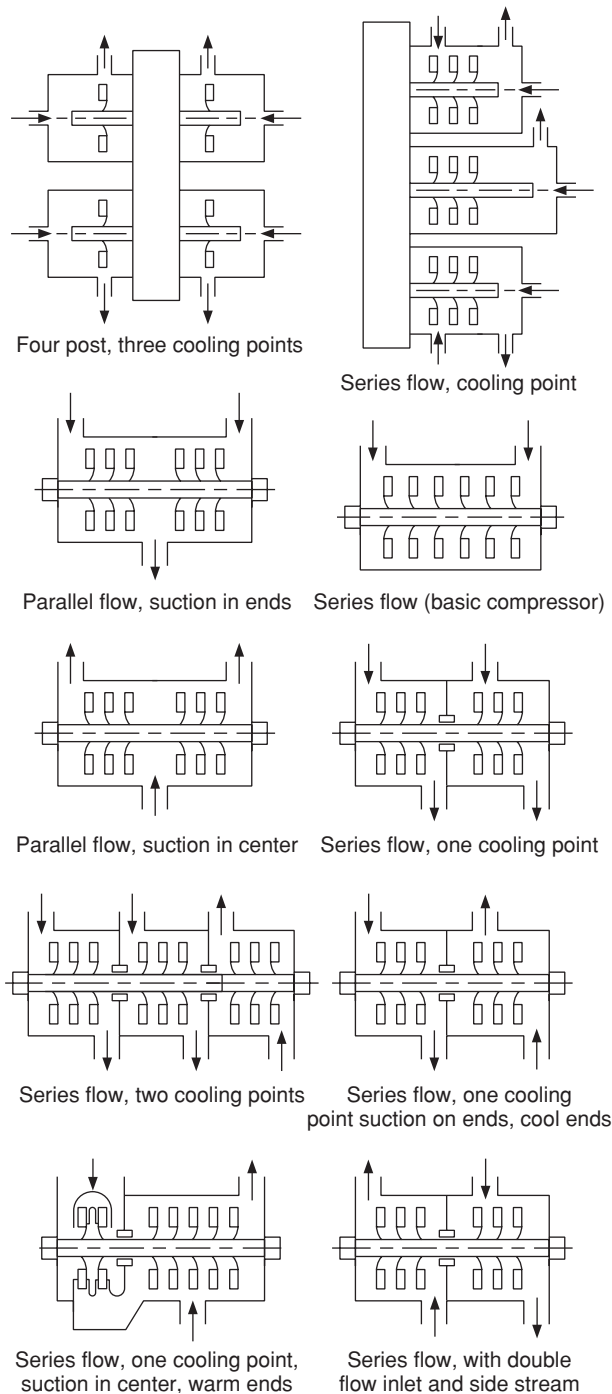


FIG. 10-90 Various configurations of centrifugal compressors.

Impeller Fabrication Centrifugal-compressor impellers are either shrouded or unshrouded. Open, shrouded impellers that are mainly used in single-stage applications are made by investment-casting techniques or by three-dimensional milling. Such impellers are used, in most cases, for the high-pressure-ratio stages. The

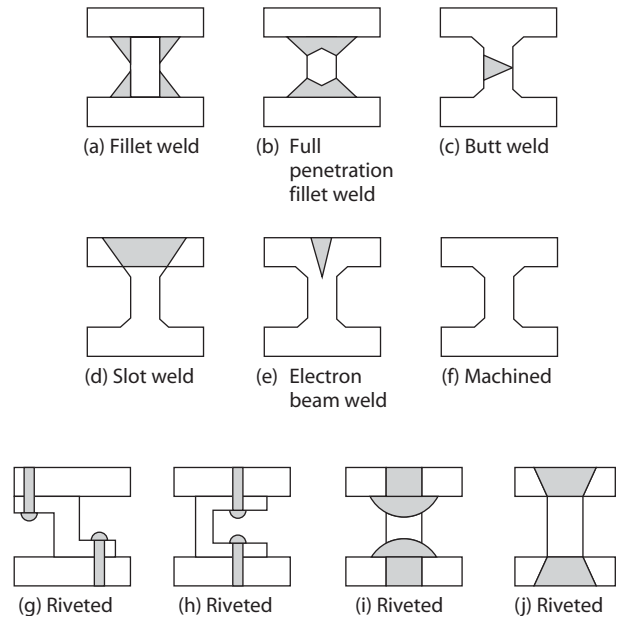


FIG. 10-91 Several fabrication techniques for centrifugal impellers.

shrouded impeller is commonly used in the process compressor because of its low pressure ratio stages. The low tip stresses in this application make it a feasible design. Figure 10-91 shows several fabrication techniques. The most common type of construction is seen in A and B where the blades are fillet-welded to the hub and shroud. In B, the welds are full penetration. The disadvantage in this type of construction is the obstruction of the aerodynamic passage. In C, the blades are partially machined for the covers and then butt-welded down the middle. For backward lean-angled blades, this technique has not been very successful, and there has been difficulty in achieving a smooth contour around the leading edge.

D illustrates a slot-welding technique and is used where blade-passage height is too small (or the backward lean-angle too high) to permit conventional fillet welding. In E, an electron-beam technique is shown. Its major disadvantage is that electron-beam welds should preferably be stressed in tension but, for the configuration of E, they are in shear. The configurations of G through J use rivets. Where the rivet heads protrude into the passage aerodynamic performance is reduced. Riveted impellers were used in the 1960s—they are very rarely used now. Elongation of these rivets occurs at certain critical surge conditions and can lead to major failures.

Materials for fabricating these impellers are usually low-alloy steels, such as AISI 4140 or AISI 4340. AISI 4140 is satisfactory for most applications; AISI 4340 is used for large impellers requiring higher strengths. For corrosive gases, AISI 410 stainless steel (about 12 percent chromium) is used. Monel K-500 is employed in halogen gas atmospheres and oxygen compressors because of its resistance to sparking. Titanium impellers have been applied to chlorine service. Aluminum-alloy impellers have been used in great numbers, especially at lower temperatures (below 300°F). With new developments in aluminum alloys, this range is increasing. Aluminum and titanium are sometimes selected because of their low density. This low density can cause a shift in the critical speed of the rotor, which may be advantageous.

Axial-Flow Compressors Axial-flow compressors are used mainly as compressors for gas turbines. They are also used in the steel industry as blast furnace blowers and in the chemical industry for large nitric acid plants. They are mainly used for applications where the head required is low and the flow large.

Figure 10-92 shows a typical axial-flow compressor. The rotating element consists of a single drum to which are attached several rows

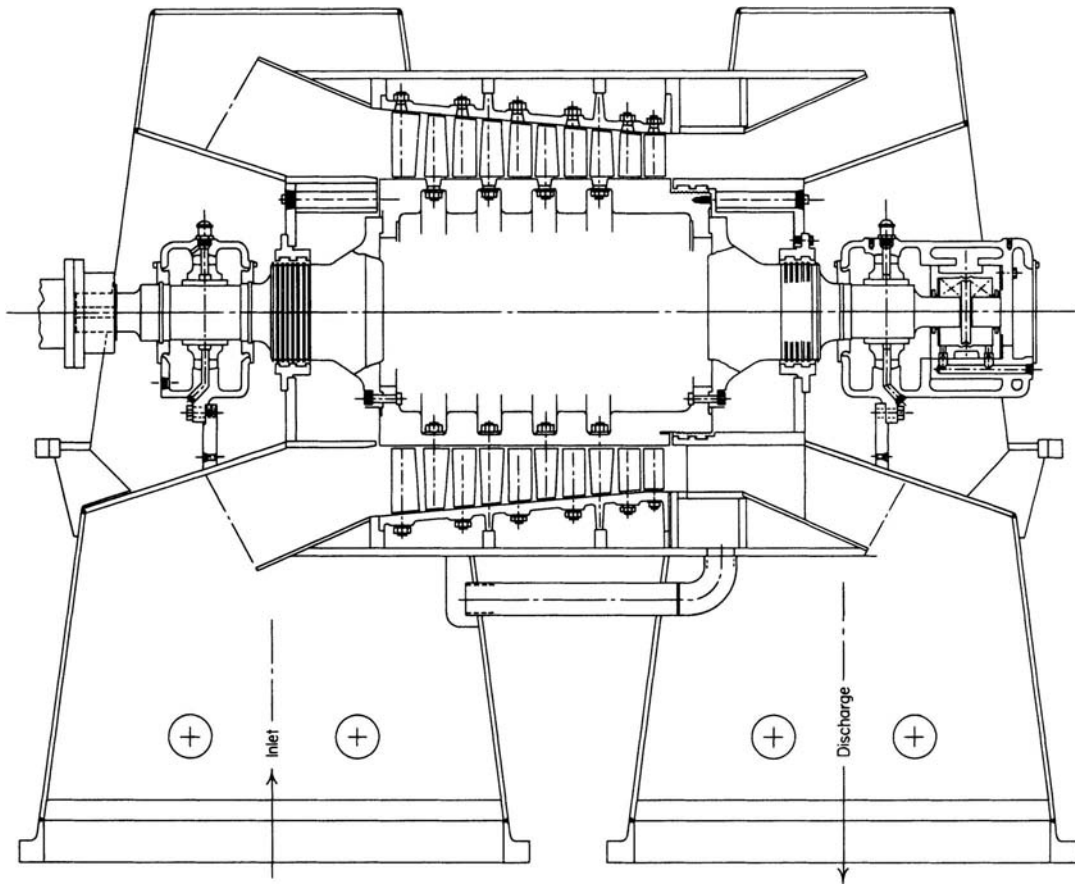


FIG. 10-92 Axial-flow compressor. (Courtesy of Allis-Chalmers Corporation.)

of decreasing-height blades having airfoil cross sections. Between each rotating blade row is a stationary blade row. All blade angles and areas are designed precisely for a given performance and high efficiency. The use of multiple stages permits overall pressure increases up to 30:1. The efficiency in an axial flow compressor is higher than the centrifugal compressor.

Pressure ratio per casing can be comparable with those of centrifugal equipment, although flow rates are considerably higher for a given casing diameter because of the greater area of the flow path. The pressure ratio per stage is less than in a centrifugal compressor. The pressure ratio per stage in industrial compressors is between 1:05 and 1:15, and for aeroturbines, 1.1 and 1.2.

The axial-flow compressors used in gas turbines vary depending on the type of turbines. The industrial-type gas turbine has an axial-flow compressor of a rugged construction. These units have blades that have low aspect ratio ($R = \text{blade height/blade chord}$) with minimum streamline curvature, and the shafts are support on sleeve-type bearings. The industrial gas turbine compressor has also a lower pressure ratio per stage (stage = rotor + stationary blade), giving a low blade loading. This also gives a larger operating range than its counterpart the aero axial gas turbine compressor but considerably less than the centrifugal compressor.

The axial-flow compressors in aero gas turbines are heavily loaded. The aspect ratio of the blades, especially the first few stages, can be as high as 4.0, and the effect of streamline curvature is substantial. The streamline configuration is a function of the annular passage area, the camber and thickness distribution of the blade, and the flow angles at the inlet and outlet of the blades. The

shafts on these units are supported on antifriction bearings (roller or ball bearings).

The operation of the axial-flow compressor is a function of the rotational speed of the blades and the turning of the flow in the rotor. The stationary blades (stator) are used to diffuse the flow and convert the velocity increased in the rotor to a pressure increase. One rotor and one stator make up a stage in a compressor. One additional row of fixed blades (inlet guide vanes) is frequently used at the compressor inlet to ensure that air enters the first stage rotors at the desired angle. In addition to the stators, another diffuser at the exit of the compressor further diffuses the gas and, in the case of gas turbines, controls its velocity entering the combustor. The axial-flow compressor has a much smaller operating range "Surge to Choke" than its counterpart in the centrifugal compressor. Because of the steep characteristics of the head/flow capacity curve, the surge point is usually within 10 percent of the design point.

The axial-flow compressor has three distinct stall phenomena. Rotating stall and individual blade stall are aerodynamic phenomena. Stall flutter is an aeroelastic phenomenon. Rotating stall (propagating stall) consists of large stall zones covering several blade passages and propagates in the direction of the rotor and at some fraction of rotor speed. The number of stall zones and the propagating rates vary considerably. Rotating stall is the most prevalent type of stall phenomenon. Individual blade stall occurs when all the blades around the compressor annulus stall simultaneously without the occurrence of the stall propagation mechanism. The phenomena of stall flutter is caused by self-excitation of the blade and is aeroelastic. It must be distinguished from classic flutter, since classic flutter is a coupled

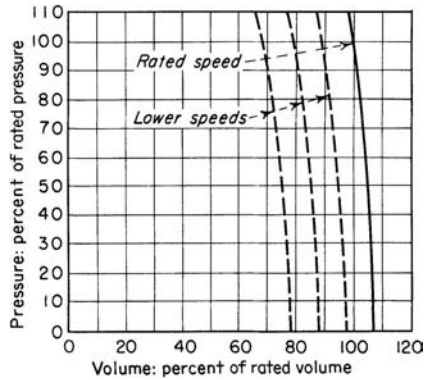


Fig. 10-93 Approximate performance curves for a rotary positive-displacement compressor. The safety valve in discharge line or bypass must be set to operate at a safe value determined by construction.

torsional-flexural vibration that occurs when the freestream velocity over an airfoil section reaches a certain critical velocity. Stall flutter, on the other hand, is a phenomenon that occurs due to the stalling of the flow around a blade. Blade stall causes Karman vortices in the airfoil wake. Whenever the frequency of the vortices coincides with the natural frequency of airfoil, flutter will occur. Stall flutter is a major cause of compressor-blade failure.

Positive-Displacement Compressors Positive-displacement compressors are machines that are essentially constant-volume machines with variable discharge pressures. These machines can be divided into two types:

1. Rotary compressors
2. Reciprocating compressors

Many users consider rotary compressors, such as the "Rootes"-type blower, as turbomachines because their behavior in terms of the rotor dynamics is very close to centrifugal and axial flow machinery. Unlike the reciprocating machines, the rotary machines do not have a very high vibration problem but, like the reciprocating machines, they are positive-displacement machines.

Rotary Compressors Rotary compressors are machines of the positive-displacement type. Such units are essentially constant-volume machines with variable discharge pressure. The volume can be varied only by changing the speed or by bypassing or wasting some of the capacity of the machine. The discharge pressure will vary with the resistance on the discharge side of the system. A characteristic curve typical of the form produced by these rotary units is shown in Fig. 10-93.

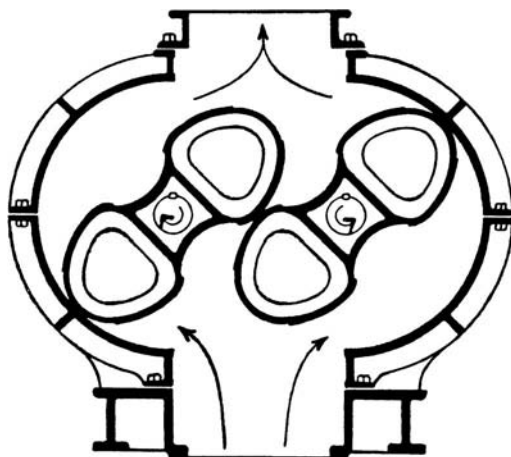


FIG. 10-94 Two-impeller type of rotary positive-displacement blower.

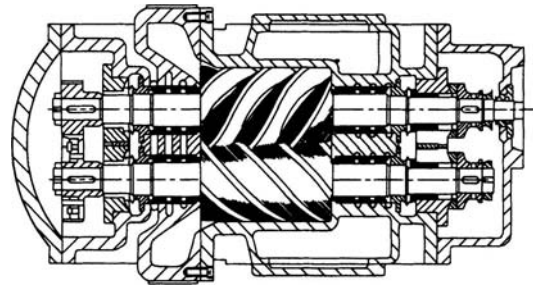


FIG. 10-95 Screw-type rotary compressor.

Rotary compressors are generally classified as of the straight-lobe type, screw type, sliding-vane type, and liquid-piston type.

Straight-Lobe Type This type is illustrated in Fig. 10-94. Such units are available for pressure differentials up to about 83 kPa (12 lbf/in²) and capacities up to 2.549×10^4 m³/h (15,000 ft³/min). Sometimes multiple units are operated in series to produce higher pressures; individual-stage pressure differentials are limited by the shaft deflection, which must necessarily be kept small to maintain rotor and casing clearance.

Screw Type This type of rotary compressor, as shown in Fig. 10-95, is capable of handling capacities up to about 4.248×10^4 m³/h (25,000 ft³/min) at pressure ratios of 4:1 and higher. Relatively small-diameter rotors allow rotative speeds of several thousand rev/min. Unlike the straight-lobe rotary machine, it has male and female rotors whose rotation causes the axial progression of successive sealed cavities. These machines are staged with intercoolers when such an arrangement is advisable. Their high-speed operation usually necessitates the use of suction- and discharge-noise suppressors. The bearings used are sleeve-type bearings. Due to the side pressures experienced, tilting pad bearings are highly recommended.

Sliding-Vane Type This type is illustrated in Fig. 10-96. These units are offered for operating pressures up to 0.86 MPa (125 lbf/in²) and in capacities up to 3.4×10^3 m³/h (2000 ft³/min). Generally, pressure ratios per stage are limited to 4:1. Lubrication of the vanes is required, and the air or gas stream therefore contains lubricating oil.

Liquid-Piston Type This type is illustrated in Fig. 10-97. These compressors are offered as single-stage units for pressure differentials up to about 0.52 MPa (75 lbf/in²) in the smaller sizes and capacities up to 6.8×10^3 m³/h (4000 ft³/min) when used with a lower pressure differential. Staging is employed for higher pressure differentials. These units have found wide application as vacuum pumps on wet-vacuum service. Inlet and discharge ports are located in the impeller hub. As the vaned impeller rotates, centrifugal force drives the sealing liquid

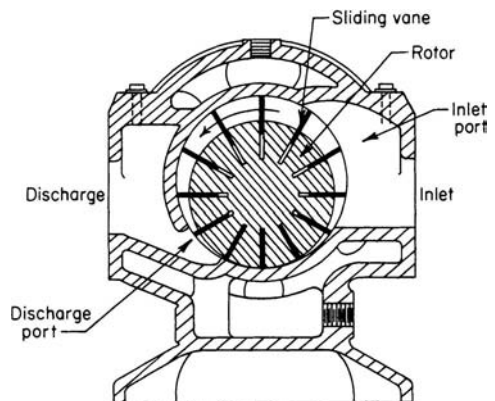


FIG. 10-96 Sliding-vane type of rotary compressor.

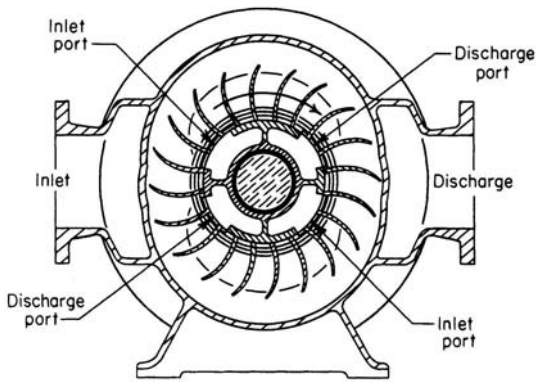


FIG. 10-97 Liquid-piston type of rotary compressor.

against the walls of the elliptical housing, causing the air to be successively drawn into the vane cavities and expelled against discharge pressure. The sealing liquid must be externally cooled unless it is used in a once-through system. A separator is usually employed in the discharge line to minimize carryover of entrained liquid. Compressor capacity can be considerably reduced if the gas is highly soluble in the sealing liquid.

The liquid-piston type of compressor has been of particular advantage when hazardous gases are being handled. Because of the gas-liquid contact and because of the much greater liquid specific heat, the gas-temperature rise is very small.

EJECTORS

An ejector is a simplified type of vacuum pump or compressor which has no pistons, valves, rotors, or other moving parts. Figure 10-98 illustrates a steam-jet ejector. It consists essentially of a nozzle which discharges a high-velocity jet across a suction chamber that is con-

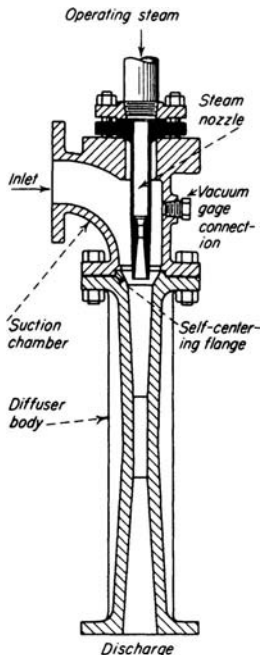


FIG. 10-98 Typical steam-jet ejector.

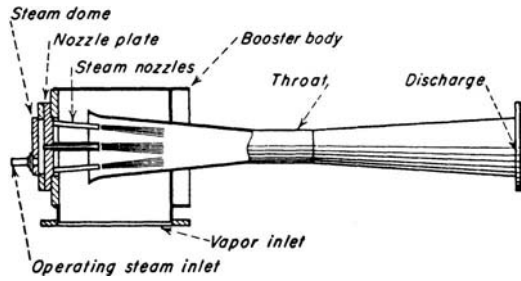


FIG. 10-99 Booster ejector with multiple steam nozzles.

nected to the equipment to be evacuated. The gas is entrained by the steam and carried into a venturi-shaped diffuser which converts the velocity energy into pressure energy. Figure 10-99 shows a large-sized ejector, sometimes called a booster ejector, with multiple nozzles. Nozzles are devices in subsonic flow that have a decreasing area and accelerate the flow. They convert pressure energy to velocity energy. A minimum area is reached when velocity reaches sonic flow. In supersonic flow, the nozzle is an increasing area device. A diffuser in subsonic flow has an increasing area and converts velocity energy into pressure energy. A diffuser in supersonic flow has a decreasing area.

Two or more ejectors may be connected in series or stages. Also, a number of ejectors may be connected in parallel to handle larger quantities of gas or vapor.

Liquid- or air-cooled condensers are usually used between stages. Liquid-cooled condensers may be of either the direct-contact (barometric) or the surface type. By condensing vapor the load on the following stage is reduced, thus minimizing its size and reducing consumption of motive gas. Likewise, a precondenser installed ahead of an ejector reduces its size and consumption if the suction gas contains vapors that are condensable at the temperature condition available. An **aftercondenser** is frequently used to condense vapors from the final stage, although this does not affect ejector performance.

Ejector Performance The performance of any ejector is a function of the area of the motive-gas nozzle and venturi throat, pressure of the motive gas, suction and discharge pressures, and ratios of specific heats, molecular weights, and temperatures. Figure 10-100, based on the assumption of **constant-area mixing**, is useful in evaluating single-stage-ejector performance for compression ratios up to 10 and area ratios up to 100 (see Fig. 10-101 for notation).

For example, assume that it is desired to evacuate air at 2.94 lbf/in² with a steam ejector discharging to 14.7 lbf/in² with available steam pressure of 100 lbf/in². Entering the chart at $p_{03}/p_{0b} = 5.0$, at $p_{0b}/p_{0a} = 2.94/100 = 0.0294$ the optimum area ratio is 12. Proceeding horizontally to the left, w_1/w_a is approximately 0.15 lb of air per 1 lb of steam. This value must be corrected for the temperature and molecular-weight differences of the two fluids by Eq. (10-86).

$$w/w_a = w_1/w_a \sqrt{T_{0a}M_b/T_{0b}M_a} \tag{10-86}$$

In addition, there are empirical correction factors which should be applied. Laboratory tests show that for ejectors with constant-area mixing the actual entrainment and compression ratios will be approximately 90 percent of the calculated values and even less at very small values of p_{0b}/p_{0a} . This compensates for ignoring wall friction in the mixing section and irreversibilities in the nozzle and diffuser. In theory, each point on a given design curve of Fig. 10-100 is associated with an optimum ejector for prevailing operating conditions. Adjacent points on the same curve represent theoretically different ejectors for the new conditions, the difference being that for each ratio of p_{0b}/p_{0a} there is an optimum area for the exit of the motive-gas nozzle. In practice, however, a segment of a given curve for constant A_2/A_1 represents the

*All data are given in U.S. customary units since the charts are in these units. Conversion factors to SI units are given on the charts.

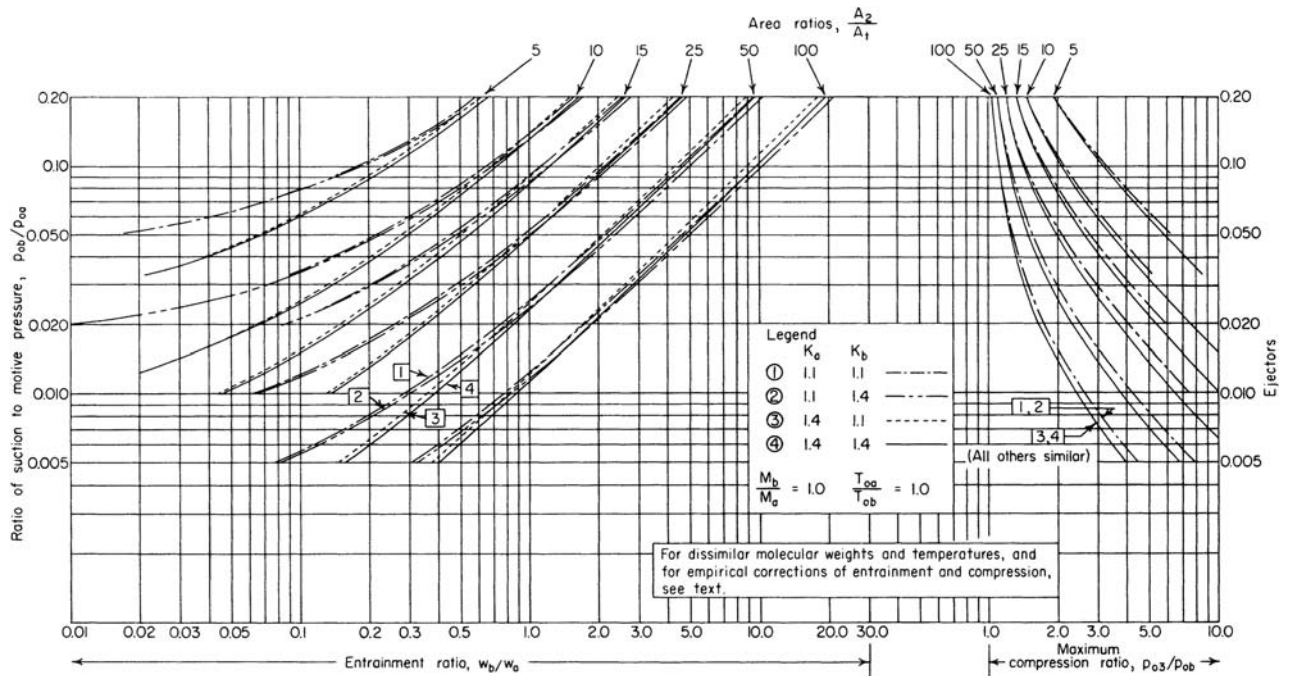


FIG. 10-100 Design curves for optimum single-stage ejectors. [DeFrate and Hoerl, Chem. Eng. Prog., 55, Symp. Ser. 21, 46 (1959).]

performance of a single ejector satisfactorily for estimating purposes, provided that the suction pressure lies within 20 to 130 percent of the design suction pressure and the motive pressure within 80 to 120 percent of design motive pressure. Thus the curves can be used to select an optimum ejector for the design point and to estimate its performance at off-design conditions within the limits noted. Final ejector selection should, of course, be made with the assistance of a manufacturer of such equipment.

Uses of Ejectors For the operating range of steam-jet ejectors in vacuum applications, see the subsection "Vacuum Systems."

The choice of the most suitable type of ejector for a given application depends upon the following factors:

1. *Steam pressure.* Ejector selection should be based upon the minimum pressure in the supply line selected to serve the unit.
2. *Water temperature.* Selection is based on the maximum water temperature.
3. *Suction pressure and temperature.* Overall process requirements should be considered. Selection is usually governed by the minimum suction pressure required (the highest vacuum).
4. *Capacity required.* Again overall process requirements should be considered, but selection is usually governed by the capacity required at the minimum process pressure.

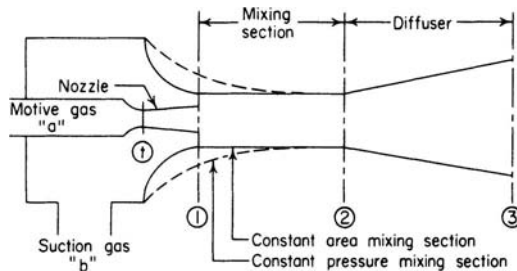


FIG. 10-101 Notation for Fig. 10-100.

Ejectors are easy to operate and require little maintenance. Installation costs are low. Since they have no moving parts, they have long life, sustained efficiency, and low maintenance cost. Ejectors are suitable for handling practically any type of gas or vapor. They are also suitable for handling wet or dry mixtures or gases containing sticky or solid matter such as chaff or dust.

Ejectors are available in many materials of construction to suit process requirements. If the gases or vapors are not corrosive, the diffuser is usually constructed of cast iron and the steam nozzle of stainless steel. For more corrosive gases and vapors, many combinations of materials such as bronze, various stainless-steel alloys, and other corrosion-resistant metals, carbon, and glass can be used.

VACUUM SYSTEMS

Figure 10-102 illustrates the level of vacuum normally required to perform many of the common manufacturing processes. The attainment of various levels is related to available equipment in Fig. 10-103.

Vacuum Equipment The equipment shown in Fig. 10-103 has been discussed elsewhere in this section with the exception of the **diffusion pump**. Figure 10-104 depicts a typical design. A liquid of low absolute vapor pressure is boiled in the reservoir. The vapor is ejected at high velocity in a downward direction through multiple jets and is condensed on the walls, which are cooled by the surrounding coils. Molecules of the gas being pumped enter the vapor stream and are driven downward by collisions with the vapor molecules. The gas molecules are removed through the discharge line by a backing pump such as a rotary oil-sealed unit.

Diffusion pumps operate at very low pressures. The ultimate vacuum attainable depends somewhat upon the vapor pressure of the pump liquid at the temperature of the condensing surfaces. By providing a cold trap between the diffusion pump and the region being evacuated, pressures as low as 10^{-7} mmHg absolute are achieved in this manner. Liquids used for diffusion pumps are mercury and oils of low vapor pressure. Silicone oils have excellent characteristics for this service.

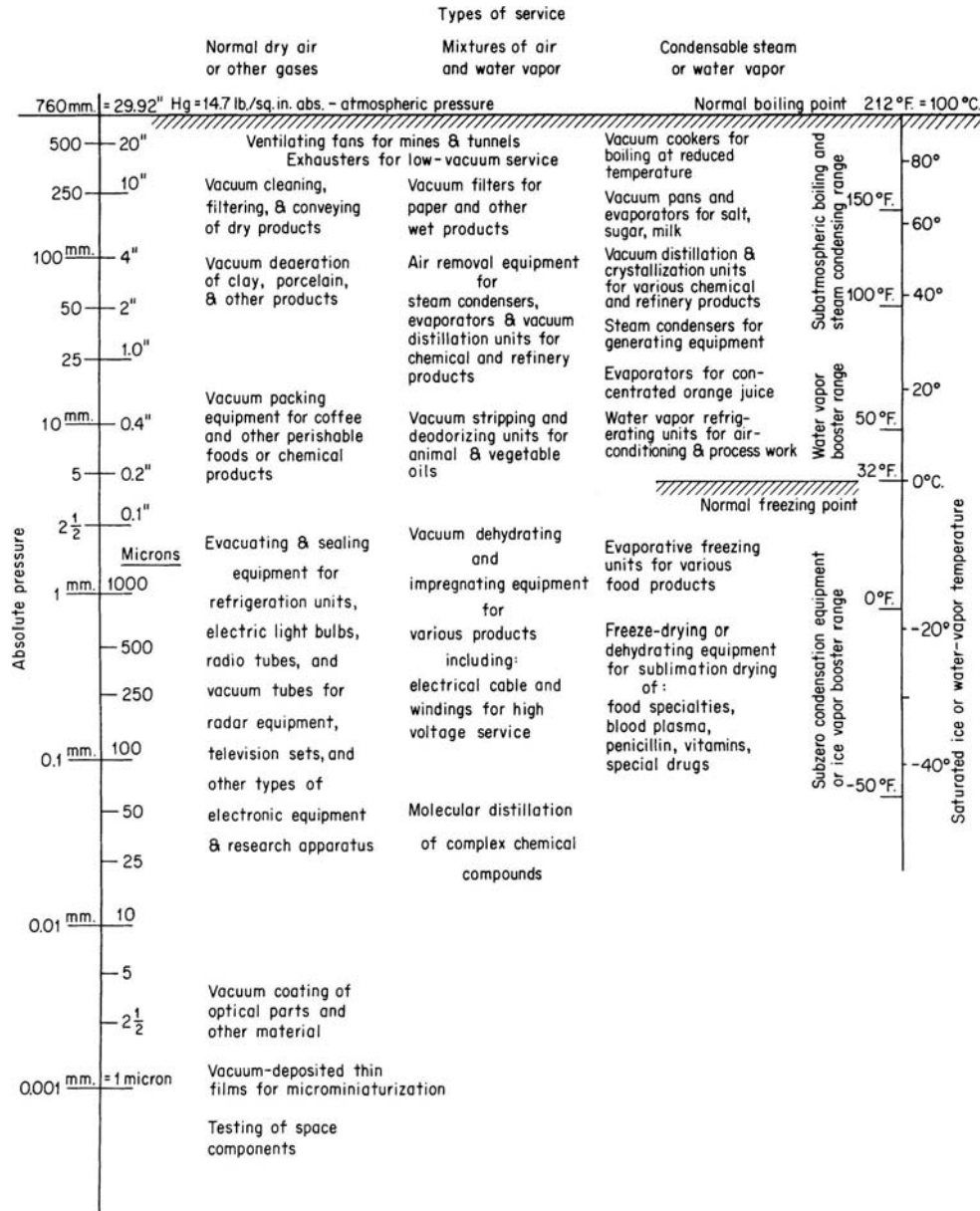


FIG. 10-102 Vacuum levels normally required to perform common manufacturing processes. (Courtesy of Compressed Air magazine.)

SEALING OF ROTATING SHAFTS

Seals are very important and often critical components in large rotating machinery especially on high-pressure and high-speed equipment. The principal sealing systems used between the rotor and stationary elements fall into two main categories: (1) noncontacting seals and (2) face seals. These seals are an integral part of the rotating system, they affect the dynamic operating characteristics of the machine. The stiffness and damping factors will be changed by the seal geometry and pressures. In operation the rotating shafts have both radial and axial movement. Therefore any seal must be flexible and compact to ensure maximum sealing minimum effect on rotor dynamics.

Noncontact Seals Noncontact seals are used extensively in gas service in high speed rotating equipment. These seals have good mechanical reliability and minimum impact on the rotor dynamics of the system. They are not positive sealing. There are two types of non-contact seals: (1) labyrinth seals and (2) ring seals.

Labyrinth Seals The labyrinth is one of the simplest of the many sealing devices. It consists of a series of circumferential strips of metal extending from the shaft or from the bore of the shaft housing to form a cascade of annular orifices. Labyrinth seal leakage is greater than that of clearance bushings, contact seals, or filmriding seals.

The major advantages of labyrinth seals are their simplicity, reliability, tolerance to dirt, system adaptability, very low shaft power

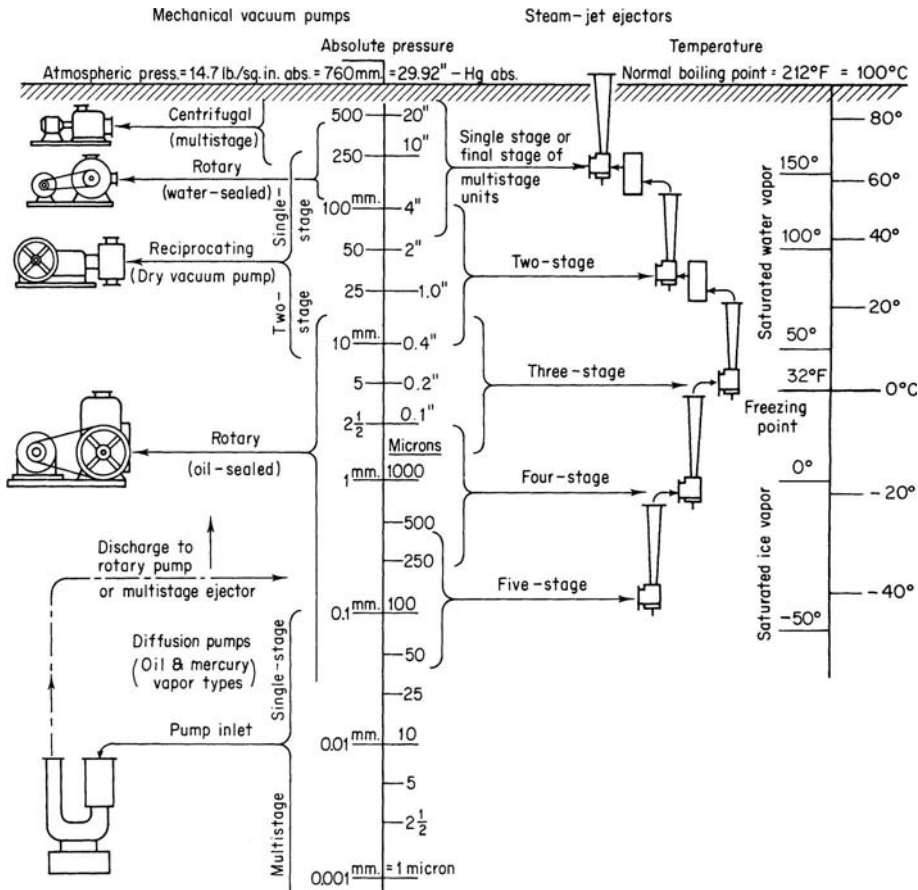


FIG. 10-103 Vacuum levels attainable with various types of equipment. (Courtesy of Compressed Air magazine.)

consumption, material selection flexibility, minimal effect on rotor dynamics, back diffusion reduction, integration of pressure, lack of pressure limitations, and tolerance to gross thermal variations. The major disadvantages are the high leakage, loss of machine efficiency, increased buffering costs, tolerance to ingestion of particulates with

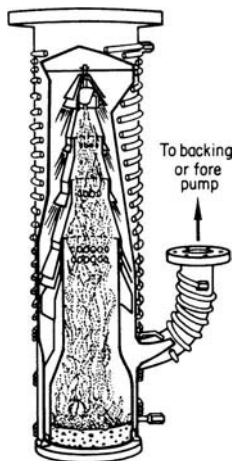
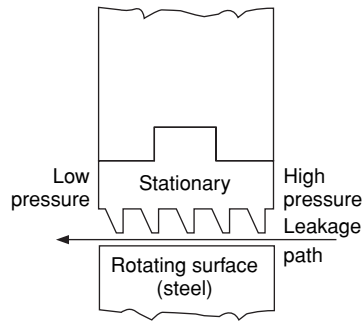


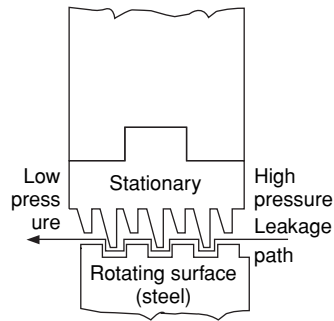
FIG. 10-104 Typical diffusion pump. (Courtesy of Compressed Air magazine.)

resulting damage to other critical items such as bearings, the possibility of the cavity clogging due to low gas velocities or back diffusion, and the inability to provide a simple seal system that meets OSHA or EPA standards. Because of some of the foregoing disadvantages, many machines are being converted to other types of seals.

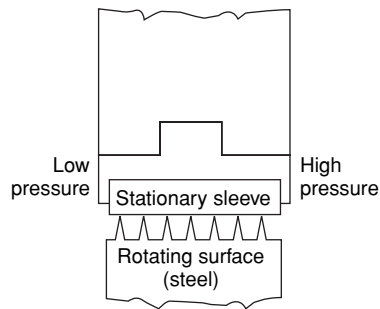
Labyrinth seals are simple to manufacture and can be made from conventional materials. Early designs of labyrinth seals used knife-edge seals and relatively large chambers or pockets between the knives. These relatively long knives are easily subject to damage. The modern, more functional, and more reliable labyrinth seals consist of sturdy, closely spaced lands. Some labyrinth seals are shown in Fig. 10-105. Figure 10-105a is the simplest form of the seal. Figure 10-105b shows a grooved seal; it is more difficult to manufacture but produces a tighter seal. Figure 10-105c and 10-105d is rotating labyrinth-type seals. Figure 10-105e shows a simple labyrinth seal with a buffered gas for which pressure must be maintained above the process gas pressure and the outlet pressure (which can be greater than or less than the atmospheric pressure). The buffered gas produces a fluid barrier to the process gas. The eductor sucks gas from the vent near the atmospheric end. Figure 10-105f shows a buffered, stepped labyrinth. The step labyrinth gives a tighter seal. The matching stationary seal is usually manufactured from soft materials such as bab-bitt or bronze, while the stationary or rotating labyrinth lands are made from steel. This composition enables the seal to be assembled with minimal clearance. The lands can therefore cut into the softer materials to provide the necessary running clearances for adjusting to the dynamic excursions of the rotor. To maintain maximum sealing efficiency, it is essential that the labyrinth lands maintain sharp edges in the direction of the flow.



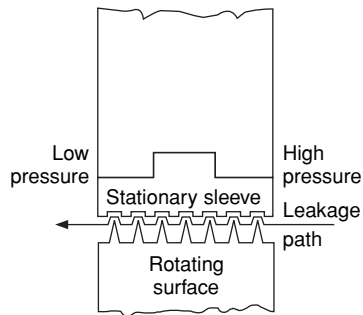
(a) Simplest design. (Labyrinth materials: aluminum, bronze, babbitt or steel)



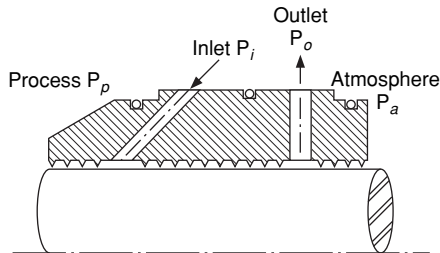
(b) More difficult to manufacture but produces a tighter seal. (Same material as in a.)



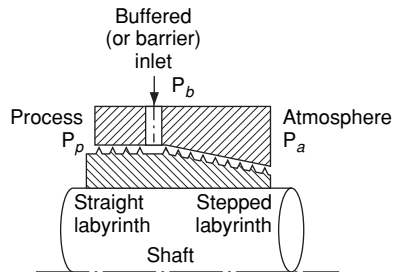
(c) Rotating labyrinth type, before operation. (Sleeve material: babbitt, aluminum, nonmetallic or other soft materials)



(d) Rotating labyrinth, after operation. Radial and axial movement of rotor cuts grooves in sleeve material to simulate staggered type shown in b.



(e) Buffered-vented straight labyrinth



(f) Buffered combination labyrinth

FIG. 10-105 Various configurations of labyrinth seals.

Leakage past these labyrinths is approximately inversely proportional to the square root of the number of labyrinth lands. This translates into the following relationship if leakage is to be cut in half in a four labyrinth seal: The number of labyrinths would have to be increased to 16. The Elgi leakage formula can be modified and written as:

$$m_l = AK \left[\frac{(g/V_o)(P_o - P_n)}{n + \ln(P_n/P_o)} \right]^{1/2} \quad (10-87)$$

where m_l = leakage
 A = leakage area of single throttling

K = labyrinth constant ($K = .9$ for straight labyrinths, $K = .75$ for staggered labyrinths)
 P_o = absolute pressure before the labyrinth
 P_n = absolute pressure after the last labyrinth
 V_o = specific volume before the labyrinth
 n = number of lands

The leakage of a labyrinth seal can be kept to a minimum by providing: (1) minimum clearance between the seal lands and the seal sleeve, (2) sharp edges on the lands to reduce the flow discharge coefficient, and (3) grooves or steps in the flow path for reducing dynamic head carryover from stage to stage.

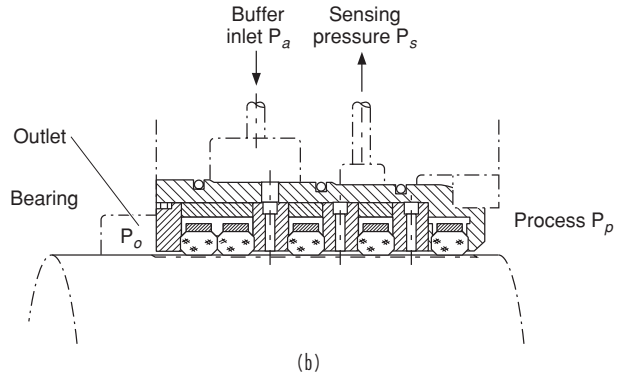
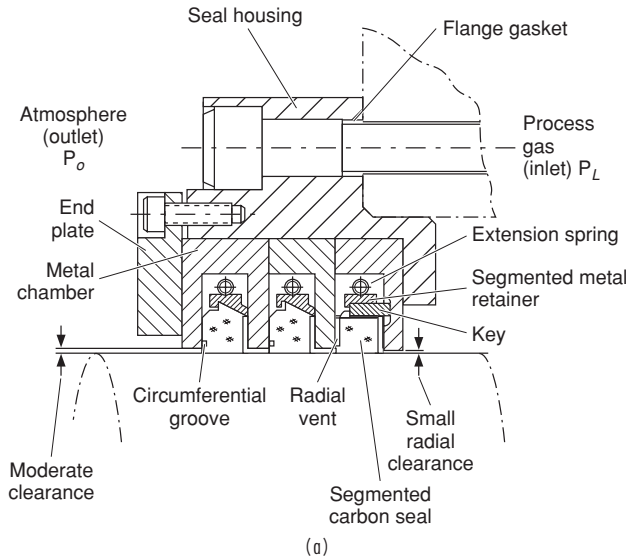


FIG. 10-106 Floating-type restrictive ring seal.

The labyrinth sleeve can be flexibly mounted to permit radial motion for self-aligning effects. In practice, a radial clearance of under 0.008S is difficult to achieve.

Ring Seals The restrictive ring seal is essentially a series of sleeves in which the bores form a small clearance around the shaft. Thus, the leakage is limited by the flow resistance in the restricted area and controlled by the laminar or turbulent friction. There are two types of ring seals: (1) fixed seal rings and (2) floating seal rings. The floating rings permit a much smaller leakage; they can be either the segmented type as shown in Fig. 10-106a or the rigid type as shown in Fig. 10-106b.

Fixed Seal Rings The fixed-seal ring consists of a long sleeve affixed to a housing in which the shaft rotates with small clearances. Long assemblies must be used to keep leakage within a reasonable limit. Long seal assemblies aggravate alignment and rubbing problems, thus requiring shafts to operate below their capacity. The fixed bushing seal operates with appreciable eccentricity and, combined with large clearances, produces large leakages, thus making this kind of seal impractical where leakage is undesirable.

Floating Seal Rings Clearance seals that are free to move in a radial direction are known as floating seals. The floating characteristics permit them to move freely, thus avoiding severe rubs. Due to differential thermal expansion between the shaft and bushing, the bushings should be made of material with a higher coefficient of thermal expansion. This is achieved by shrinking the carbon into a metallic retaining ring with a coefficient of expansion that equals or exceeds that of the shaft material. It is advisable in high shearing applications to lock the bushings against rotation.

Buildup of dirt and other foreign material lodged between the seal ring and seat will create an excessive spin and damage on the floating seal ring unit. It is therefore improper to use soft material such as bab-bitt and silver as seal rings.

Packing Seal A common type of rotating shaft seal consists of packing composed of fibers which are first woven, twisted, or braided into strands and then formed into coils, spirals, or rings. To ensure initial lubrication and to facilitate installation, the basic materials are often impregnated. Common materials are braided and twisted rubber and duck, flax, jute, and metallic braids. The so-called plastic packings can be made up with varying amounts of fiber combined with a binder and lubricant for high-speed applications. Maximum temperatures that base materials of packings withstand and still give good service are as follows:

	°C	°F
Flax	38	100
Cotton	93	200
Duck and rubber	149	300
Rubber	177	350
Metallic (lead-based)	218	425
Metallic (aluminum-based)	552	1025
Metallic (copper-based)	829	1525

Packing may not provide a completely leak-free seal. With shaft surface speeds less than approximately 2.5 m/s (500 ft/min), the packing may be adjusted to seal completely. However, for higher speeds some leakage is required for lubrication, friction reduction, and cooling.

Application of Packing Coils and spirals are cut to form closed or nearly closed rings in the stuffing box. Clearance between ends should be sufficient to allow for fitting and possible expansion due to increased temperature or liquid absorption of the packing while in operation.

The correct form of the ring joint depends on materials and service requirements. Braided and flexible metallic packings usually have butt or square joints (Fig. 10-107a). With other packing material, service experience indicates that rings cut with bevel or skive joints (Fig. 10-107b) are more satisfactory. A slight advantage of the bevel joint over the butt joint is that the bevel permits a certain amount of sliding action, thus absorbing a portion of ring expansion.

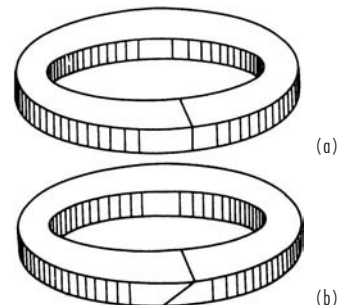


FIG. 10-107 Butt (a) and skive (b) joints for compression packing rings.

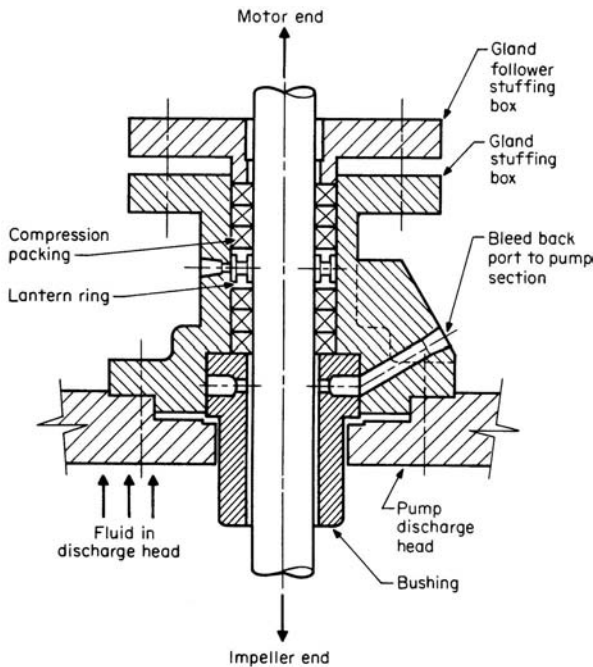


FIG. 10-108 Seal cage or lantern ring. (Courtesy of Crane Packing Co.)

In the manufacture of packings, the proper grade and type of **lubricant** is usually impregnated for each service for which the packing is recommended. However, it may be desirable to replenish the lubricant during the normal life of the packing. Lack of lubrication causes packing to become hard and lose its resiliency, thus increasing friction, shortening packing life, and increasing operating costs.

An effective auxiliary device frequently used with packing and rotary shafts is the **seal cage** (or **lantern ring**), shown in Fig. 10-108. The seal cage provides an annulus around the shaft for the introduction of a lubricant, oil, grease, etc. The seal cage is also used to introduce liquid for cooling, to prevent the entrance of atmospheric air, or to prevent the infiltration of abrasives from the process liquid.

The chief advantage of packing over other types of seals is the ease with which it can be adjusted or replaced. Most equipment is designed so that disassembly of major components is not required to remove or add packing rings. The major disadvantages of a packing-type seal are (1) short life, (2) requirement for frequent adjustment, and (3) need for some leakage to provide lubrication and cooling.

Mechanical Face Seals This type of seal forms a running seal between flat precision-finished surfaces. It is an excellent seal against leakages. The sealing surfaces are planes perpendicular to the rotating shaft, and the forces that hold the contact faces are parallel to the shaft axis. For a seal to function properly, there are four sealing points:

1. Stuffing box face
2. Leakage down the shaft
3. Mating ring in the gland plate
4. Dynamic faces

Mechanical Seal Selection There are many factors that govern the selection of seals. These factors apply to any type of seal:

1. Product
2. Seal environment
3. Seal arrangement
4. Equipment
5. Secondary packing
6. Seal face combinations
7. Seal gland plate
8. Main seal body

Product Physical and chemical properties of the liquid or gas being sealed places constraints on the type of material, design, and arrangement of the seal.

Pressure. Pressure affects the choice of material and whether balanced or unbalanced seal design can be used. Most unbalanced seals are good up to 100 psig stuffing box pressure. Over 100 psig, balanced seals should be used.

Temperature. The temperature of the liquid being pumped is important because it affects the seal face material selection as well as the wear life of the seal face.

Lubricity. In any mechanical seal design, there is rubbing motion between the dynamic seal faces. This rubbing motion is often lubricated by the fluid being pumped. Most seal manufacturers limit the speed of their seals to 90 ft/s (30 m/s). This is primarily due to centrifugal forces acting on the seal, which tends to restrict the seal's axial flexibility.

Abrasion. If there are entrained solids in the liquid, it is desirable to have a flushed single inside type with a face combination of very hard material.

Corrosion. This affects the type of seal body: what spring material, what face material, and what type of elastomer or gasket material. The corrosion rate will affect the decision of whether to use a single or multiple spring design because the spring can usually tolerate a greater amount of corrosion without weakening it appreciably.

Seal Environment The design of the seal environment is based on the product and the four general parameters that regulate it:

1. Pressure control
2. Temperature control
3. Fluid replacement
4. Atmospheric air elimination

Seal Arrangement There are four types of seal arrangements:

1. Double seals are standard with toxic and lethal products, but maintenance problems and seal design contribute to poor reliability. The double face-to-face seal may be a better solution.
2. Do not use a double seal in dirty service—the inside seal will hang up.
3. API standards for balanced and unbalanced seals are good guidelines; too low a pressure for a balanced seal may encourage face lift-off.
4. Arrangement of the seal will determine its success more than the vendor. Over 100 arrangements are available.

Equipment The geometry of the pump or compressor is very important in seal effectiveness. Different pumps with the same shaft diameter and the total differential head can present different sealing problems.

Secondary Packing Much more emphasis should be placed on secondary packing especially if Teflon is used. A wide variation in performance is seen between various seal vendors, depending on seal arrangement there can be differences in mating ring packing.

Seal Face Combinations The dynamics of seal faces is better understood today. Seal-face combinations have come a long way in the past 8–10 years. Stellite is being phased out of the petroleum and petrochemical applications. Better grades of ceramic are available, cost of tungsten has come down, and relapping of tungsten are available near most industrial areas. Silicon carbide is being used in abrasive service.

Seal Gland Plate The seal gland plate is caught in between the pump vendor and the seal vendor. Special glands should be furnished by seal vendors, especially if they require heating, quenching, and drain with a floating-throat bushing. Gland designs are complex and may have to be revisited, especially if seals are changed.

Main Seal Body The term *seal body* makes reference to all rotating parts on a pusher seal, excluding shaft packing and seal ring. In many cases it is the chief reason to avoid a particular design for a particular service.

Basically, most mechanical seals have the following components as seen in Fig. 10-109.

1. Rotating seal ring
2. Stationary seal ring
3. Spring devices to provide pressure
4. Static seals

A loading device such as a spring is needed to ensure that in the event of loss or hydraulic pressure the sealing surfaces are kept closed. The amount of the load on the sealing area is determined by the

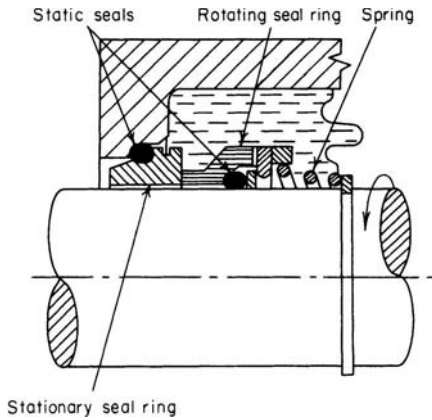


FIG. 10-109 Mechanical-seal components.

degree of “seal balance.” Figure 10-110 shows what seal balance means. A completely balanced seal is when the only force exerted on the sealing surfaces is the spring force; i.e., hydraulic pressure does not act on the sealing surface. The type of spring depends on the space available, loading characteristics, and the seal environment. Based on these considerations, either a single or multiple spring can be used. In small axial space, bellville springs, finger washers, or curved washers can be used.

Shaft-sealing elements can be split up into two groups. The first type may be called pusher-type seals and includes the O-ring, V-ring, U-cup, and wedge configurations. Figure 10-111 shows some typical pusher-type seals. The second type is the bellows-type seals, which differ from the pusher-type seals in that they form a static seal between themselves and the shaft.

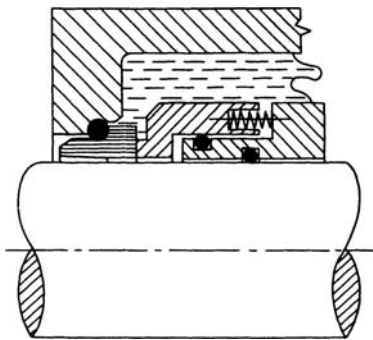


FIG. 10-110 Balanced internal mechanical seal.

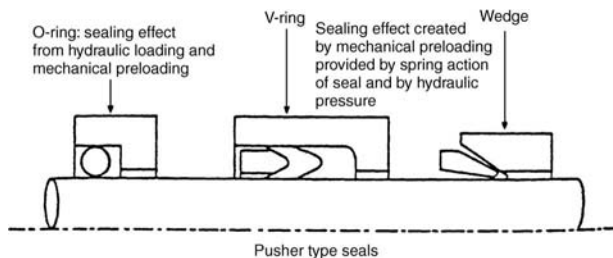


FIG. 10-111 Various types of shaft-sealing elements.

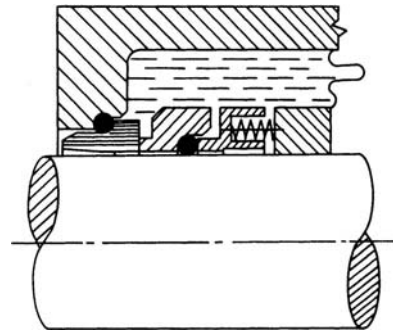


FIG. 10-112 Internal mechanical seal.

Internal and External Seals Mechanical seals are classified broadly as internal or external. **Internal seals** (Fig. 10-112) are installed with all seal components exposed to the fluid sealed. The advantages of this arrangement are (1) the ability to seal against high pressure, since the hydrostatic force is normally in the same direction as the spring force; (2) protection of seal parts from external mechanical damage; and (3) reduction in the shaft length required.

For high-pressure installations, it is possible to balance partially or fully the hydrostatic force on the rotating member of an internal seal by using a stepped shaft or shaft sleeve (Fig. 10-110). This method of relieving face pressure is an effective way of decreasing power consumption and extending seal life.

When abrasive solids are present and it is not permissible to introduce appreciable quantities of a secondary flushing fluid into the process, double internal seals are sometimes used (Fig. 10-113). Both sealing faces are protected by the flushing fluid injected between them even though the inward flow is negligible.

External seals (Fig. 10-114) are installed with all seal components protected from the process fluid. The advantages of this arrangement are that (1) fewer critical materials of construction are required, (2) installation and setting are somewhat simpler because of the exposed position of the parts, and (3) stuffing-box size is not a limiting factor. Hydraulic balancing is accomplished by proper proportioning of the seal face and secondary seal diameters.

Throttle Bushings These bushings (Fig. 10-115) are commonly used with single internal or external seals when solids are present in the fluid and the inflow of a flushing fluid is not objectionable. These close-clearance bushings are intended to serve as flow restrictions through which the maintenance of a small inward flow of flushing fluid prevents the entrance of a process fluid into the stuffing box.

A typical complex seal utilizes both the noncontact and mechanical aspects of sealing. Figure 10-116 shows such a seal with its two major elements. This type of seal will normally have buffering via a labyrinth

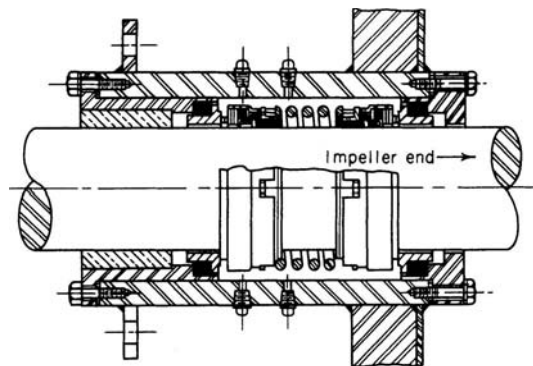


FIG. 10-113 Internal bellows-type double mechanical seal.

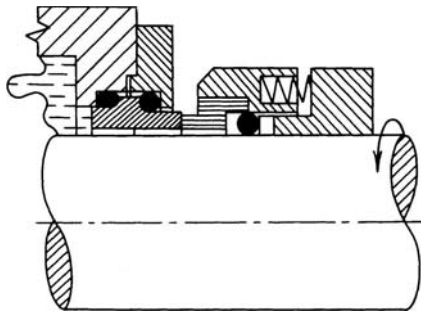


FIG. 10-114 External mechanical seal.

seal and a positive shutdown device. For shutdown, the carbon ring is tightly sandwiched between the rotating seal ring and the stationary sleeve with gas pressure to prevent gas from leaking out when no oil pressure is available.

In operation seal oil pressure is about 30–50 psi over the process gas pressure. The high-pressure oil enters the top and completely fills the seal cavity. A small percentage is forced across the carbon ring seal faces. The rotative speed of the carbon ring can be anywhere between zero and full rotational speed. Oil crossing the seal faces contacts the process gas and therefore is “contaminated oil.” The contaminated oil leaves through the contaminated oil drain to a degassifier for purification. The majority of the oil flows through the uncontaminated seal oil drain.

Materials Springs and other metallic components are available in a wide variety of alloys and are usually selected on the basis of temperature and corrosion conditions. The use of a particular mechanical seal is frequently restricted by the temperature limitations of the organic materials used in the static seals. Most elastomers are limited to about 121°C (250°F). Teflon will withstand temperatures of 260°C (500°F) but softens appreciably above 204°C (400°F). Glass-filled Teflon is dimensionally stable up to 232 to 260°C (450 to 500°F).

One of the most common elements used for seal faces is carbon. Although compatible with most process media, carbon is affected by strong oxidizing agents, including fuming nitric acid, hydrogen chloride, and high-temperature air [above 316°C (600°F)]. Normal mating-face materials for carbon are tungsten or chromium carbide, hard steel, stainless steel, or one of the cast irons.

Other sealing-face combinations that have been satisfactory in corrosive service are carbide against carbide, ceramic against ceramic, ceramic against carbon, and carbon against glass. The ceramics have also been mated with the various hard-facing alloys. When selecting seal materials the possibility of galvanic corrosion must also be considered.

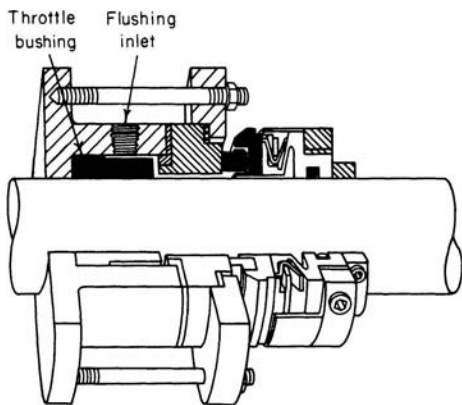
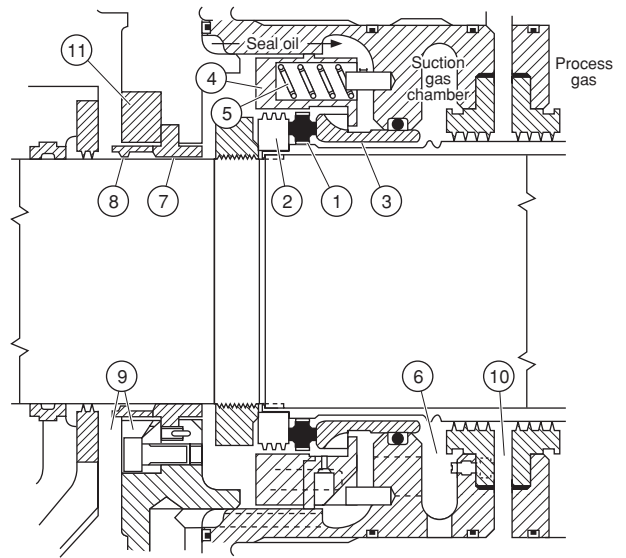


FIG. 10-115 External mechanical seal and throttle bushing.



- | | |
|-----------------------------------|--------------------------------------|
| 1. Rotating carbon ring | 7. Floating babbitt-faced steel ring |
| 2. Rotating seal ring | 8. Seal wiper ring |
| 3. Stationary sleeve | 9. Seal oil drain line |
| 4. Spring retainer | 10. Buffer gas injection port |
| 5. Spring | 11. Bypass orifice |
| 6. Gas and contaminated oil drain | |

FIG. 10-116 Mechanical contact shaft seal.

BEARINGS

Many factors enter into the selection of the proper design for bearings. Some of these factors are:

1. Shaft speed range.
2. Maximum shaft misalignment that can be tolerated.
3. Critical speed analysis and the influence of bearing stiffness on this analysis
4. Loading of the compressor impellers
5. Oil temperatures and viscosity
6. Foundation stiffness
7. Axial movement that can be tolerated
8. Type of lubrication system and its contamination
9. Maximum vibration levels that can be tolerated

Types of Bearings Figure 10-117 shows a number of different types of journal bearings. A description of a few of the pertinent types of journal bearings is given here:

1. *Plain journal.* Bearing is bored with equal amounts of clearance (on the order of one and one-half to two thousandths of an inch per inch of journal diameter) between the journal and bearing.
2. *Circumferential grooved bearing.* Normally the oil groove is half the bearing length. This configuration provides better cooling but reduces load capacity by dividing the bearing into two parts.
3. *Cylindrical bore bearings.* Another common bearing type used in turbines. It has a split construction with two axial oil-feed grooves at the split.
4. *Pressure or pressure dam.* Used in many places where bearing stability is required, this bearing is a plain journal bearing with a pressure pocket cut in the unloaded half. This pocket is approximately 1/32 of an inch deep with a width 50 percent of the bearing length. This groove or channel covers an arc of 135° and terminates abruptly in a sharp-edge dam. The direction of rotation is such that the oil is pumped down the channel toward the sharp edge. Pressure dam bearings are for one direction of rotation. They can be used in conjunction with cylindrical bore bearings as shown in Fig. 10-117.

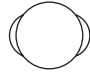
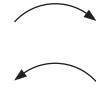


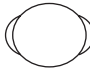
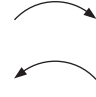

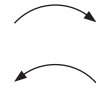



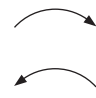
Bearing type	Load capacity	Suitable direction of rotation	Resistance to half-speed whirl	Stiffness and damping
Cylindrical bore 	Good		Worst ↓ Increasing ↓ Best	Moderate
Cylindrical bore with dammed groove 	Good			Moderate
Lemon bore 	Good			Moderate
Three lobe 	Moderate			Good
Offset halves 	Good			Excellent
Tilting pad 	Moderate			Good

FIG. 10-117 Comparison of general bearing types.

5. *Lemon bore or elliptical.* This bearing is bored with shims split line, which are removed before installation. The resulting shape approximates an ellipse with the major axis clearance approximately twice the minor axis clearance. Elliptical bearings are for both directions of rotation.

6. *Three-lobe bearing.* The three-lobe bearing is not commonly used in turbomachines. It has a moderate load-carrying capacity and can be operated in both directions.

7. *Offset halves.* In principle, this bearing acts very similar to a pressure dam bearing. Its load-carrying capacity is good. It is restricted to one direction of rotation.

8. *Tilt-pad bearings.* This bearing is the most common bearing type in today's machines. It consists of several bearing pads posed around the circumference of the shaft. Each pad is able to tilt to assume the most effective working position. This bearing also offers the greatest increase in fatigue life because of the following advantages:

- Thermal conductive backing material to dissipate heat developed in oil film.
- A thin babbitt layer can be centrifugally cast with a uniform thickness of about 0.005 inch. Thick babbitts greatly reduce bearing life. Babbitt thickness in the neighborhood of .01 reduce the bearing life by more than half.
- Oil film thickness is critical in bearing stiffness calculations. In a tilting-pad bearing, one can change this thickness in a number of ways:

(a) change the number of pads; (b) direct the load on or in between the pads; (c) change the axial length of pad.

The previous list contains some of the most common types of journal bearings. They are listed in the order of growing stability. All of the bearings designed for increased stability are obtained at higher manufacturing costs and reduced efficiency. The antiwhirl bearings all impose a parasitic load on the journal, which causes higher-power losses to the bearings and in turn requires higher oil flow to cool the bearing.

Thrust Bearings The most important function of a thrust bearing is to resist the unbalanced force in a machine's working fluid and to maintain the rotor in its position (within prescribed limits). A complete analysis of the thrust load must be conducted. As mentioned earlier, compressors with back-to-back rotors reduce this load greatly on thrust bearings. Figure 10-118 shows a number of thrust-bearing types. Plain, grooved thrust washers are rarely used with any continuous load, and their use tends to be confined to cases where the thrust load is very short duration or possibly occurs at standstill or low speed only. Occasionally, this type of bearing is used for light loads (less than 50 lb/in²), and in these circumstances the operation is probably hydrodynamic due to small distortions present in the nominally flat bearing surface.

When significant continuous loads have to be taken on a thrust washer, it is necessary to machine into the bearing surface a profile to generate a fluid film. This profile can be either a tapered wedge or occasionally a small step.

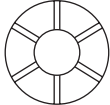

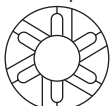







Bearing type	Load capacity	Suitable direction of rotation	Tolerance of changing load/speed	Tolerance of misalignment	Space requirement
Plain washer 	Poor		Good	Moderate	Compact
Taper land Bidirectional 	Moderate		Poor	Poor	Compact
Unidirectional 	Good		Poor	Poor	Compact
Tilting pad Bidirectional 	Good		Good	Good	Greater
Unidirectional 	Good		Good	Good	Greater

FIG. 10-118 Comparison of thrust-bearing types.

The tapered-land thrust bearing, when properly designed, can take and support a load equal to a tilting-pad thrust bearing. With perfect alignment, it can match the load of even a self-equalizing tilting-pad thrust bearing that pivots on the back of the pad along a radial line. For variable-speed operation, tilting-pad thrust bearings as shown in Fig. 10-119 are advantageous when compared to conventional taper-land bearings. The pads are free to pivot to form a proper angle for lubrication over a wide speed range. The self-leveling feature equalizes individual pad loadings and reduces the sensitivity to shaft misalignments that may occur during service. The major drawback of this bearing type is that standard designs require more axial space than a nonequalizing thrust bearing.

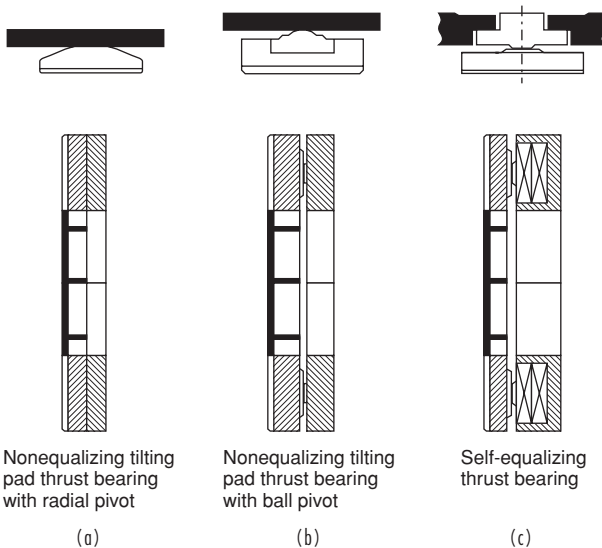


FIG. 10-119 Various types of thrust bearings.

The thrust-carrying capacity can be greatly improved by maintaining pad flatness and removing heat from the loaded zone. By the use of high thermal conductivity backing materials with proper thickness and proper support, the maximum continuous thrust limit can be increased to 1000 psi or more. This new limit can be used to increase either the factor of safety and improve the surge capacity of a given size bearing or reduce the thrust bearing size and consequently the losses generated for a given load.

Since the higher thermal conductivity material (copper or bronze) is a much better bearing material than the conventional steel backing, it is possible to reduce the babbitt thickness to .010–.030 in. Embedded thermocouples and RTDs will signal distress in the bearing if properly positioned. Temperature-monitoring systems have been found to be more accurate than axial-position indicators, which tend to have linearity problems at high temperatures.

In a change from steel-backing to copper-backing, a different set of temperature limiting criteria should be used. Figure 10-120 shows a typical set of curves for the two backing materials. This chart also shows that drain oil temperature is a poor indicator of bearing operating conditions because there is very little change in drain oil temperature from low load to failure load.

Thrust-Bearing Power Loss The power consumed by various thrust bearing types is an important consideration in any system. Power losses must be accurately predicted so that turbine efficiency can be computed and the oil supply system properly designed.

Figure 10-121 shows a typical power consumption in thrust bearings as a function of unit speed. The total power loss is usually about 0.8–10 percent of the total rate power of the unit. New vector lube bearings reduce the horsepower loss by as much as 30 percent. In large vertical pumps, thrust bearings take not only the load caused by the fluid but also the load caused by the weight of the entire assembly (shaft and impellers). In some large pumps these could be about 60 ft (20 m) high and weigh 16 tons. The thrust bearing for such a pump is over 5 ft (1.7 m) in diameter with each thrust pad weighing over 110 lb (50 kg). In such cases, the entire pump assembly is first floated before the unit is started.

CENTRIFUGAL COMPRESSOR PROBLEMS

Compressors in process gas applications suffer from many problems. The following are some of the major categories in which these problems

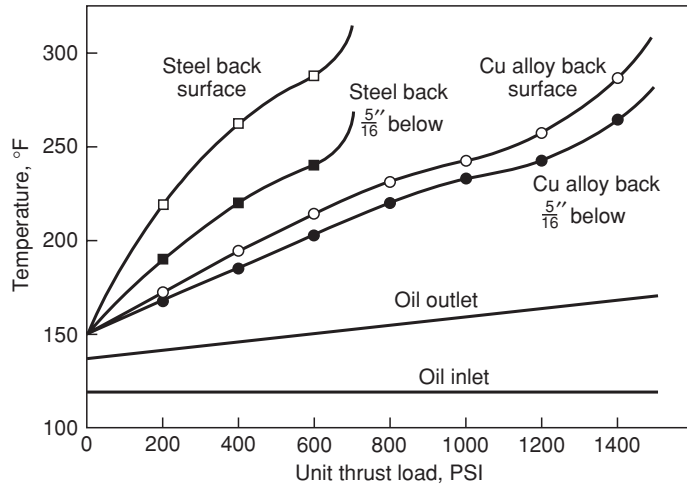


FIG. 10-120 Thrust-bearing temperature characteristics.

fall (see Meherwan P. Boyce, *Centrifugal Compressors: A Basic Guide*, PennWell, 2003):

1. Compressor fouling
2. Compressor failures
3. Impeller problems
4. Rotor thrust problems
5. Seals and bearings problems
6. Bearing maintenance

Compressor Fouling Centrifugal compressors, especially in the process gas applications, suffer greatly from fouling. Fouling is the deposit and nonuniform accumulation of debris in the gas on internal compressor surfaces. Fouling is due to the carryover of liquids and other debris from the suction knockout drums. Debris can roughen compressor surfaces. Polymerization can occur also due to changes in

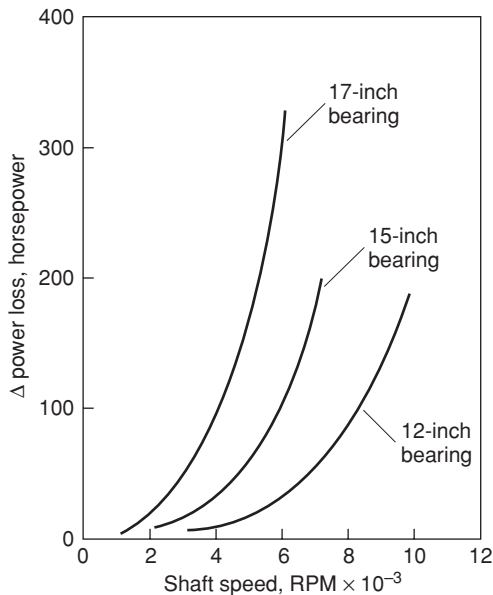


FIG. 10-121 Difference in total-power-loss data test minus catalog frictional losses versus shaft speed for 6 x 6 pad double-element thrust bearings.

process conditions. In wet gas compressors, ethylene plant cracked gas compressors, and polyethylene recycle compressors, the temperature of the gas must be kept below the threshold temperature that would initiate polymerization. The buildup will usually occur on the hub and the shroud with a larger buildup on the shroud at the elbow of the impeller on closed-face impellers. There is also a buildup on the blades, with the buildup usually more on the pressure side than on the suction side. Often the buildup is the heaviest on the pressure side at the blade exit where there is also flow separation.

Techniques to Prevent Fouling in Process Gas Compressors

1. *Condition monitoring of compressor aerodynamic and mechanical parameters.* Vibration monitoring could also alert the operator to fouling problems.

2. *Process control.* Accurate control of process conditions can prevent fouling in applications where polymers can form. Control of temperature is usually the most important. The following are examples of applications that can be affected by excessive process temperature:

- a. Ethylene cracked gas
- b. Linear low-density polyethylene
- c. High-density propylene
- d. Fluid catalytic cracker off-gas (wet gas)
- e. Thermal cracker off-gas (wet gas)
- f. Coker gas

The temperature below which fouling can be prevented varies with each process, compressor, and application. Monitoring of process conditions is necessary to establish a threshold temperature in each case. In some cases, fouling cannot be prevented with an existing compressor. It may be necessary to modify the aerodynamic design and/or add cooling.

3. *On-line solvent injection.* On-line solvent injection is very successful in various processes. The objective of this measure is to *continuously* inject a small amount of solvent to reduce the friction coefficient of the blade and impeller surface and thus prevent fouling of the surface. The injection should be done from the start; otherwise, the foulant could be dislodged and moved downstream, creating a major problem. The downstream areas are much smaller so foulant lodging there could create a blockage.

Air Compressors

1. *Inlet filter.* In air compressors filter selection is an important factor in preventing fouling. Most high-efficiency air filters have a triple-stage filtration system. Also these filters often have rain shades to prevent water from entering the filters. Site conditions play a very important part in the selection of the filters.

Compressor Blade Coating Coatings protect blades against oxidation, corrosion, and cracking problems. Coatings guard the base metal of the compressor from attack. Other benefits include reduced

thermal fatigue from cyclic operation, increased surface smoothness, reduced erosion, and reduced heat flux loading when one is considering thermal barriers. Coatings increase resistance to spalling from light impacts. Coatings also extend compressor life, better endure operational conditions, and serve as a sacrificial layer by allowing the coating to be restriped and recoated on the same base metal.

Compressor Failures In the process industry there are three types of compressors that have very different maintenance problems:

1. Barrel-type compressor
2. Horizontal split casing centrifugal compressor with closed-face impellers
3. Air integral gear-type compressor with open-face impellers

Barrel-Type Compressors Barrel-type compressors are being utilized in the process industry to an increased extent because the barrel design confines gases more effectively than horizontally split cases. This becomes a critical consideration in two areas: high-pressure and low-molecular-weight gas compression. API-617, *Centrifugal Compressors for General Refinery Services*, requires a barrel design based on the molecular percent of hydrogen contained in the process gas and the discharge pressure. API-617 defines high-pressure compressors as units in which the partial pressure of the hydrogen exceeds 200 psig, and specifies that these units be vertically (radially) split. Hydrogen partial pressure is given by the following relationship (in absolute pressures):

$$P_{H_2} = P(\%H_2/100) \quad (10-88)$$

Maximum casing working pressure for axially split compressors (psig) is

$$P_{\text{casing}} = \frac{200}{\%H_2/100} \quad (10-89)$$

The casings should include a minimum of a 1/8-in corrosion allowance. Casing strength and rigidity should limit change of alignment to 0.002 in if it is caused by the worst combination of pressure, torque, or allowable piping stress.

The barrel design is essentially a compressor placed inside a pressure vessel. For higher pressures some manufacturers have merely "beefed up" lower-pressure barrel designs, while others, have perfected unique designs such as the "shear ring" head design. All these designs make extensive use of elastomer O-rings as sealing devices. There are several inherent maintenance problems with barrel-type compressors:

Handling. Barrel-type machines must be removed from their foundations for total maintenance. Because barrel machines weigh up to 30 tons, the handling problems can be formidable.

Inner casing alignment. Since this type of compressor consists of a bundle contained within the pressure walls of the barrel, alignment and positive positioning are often very poor and the bundle is free to move to a certain extent. Bundle length is critical. Interstage leakage may occur if the bundle length is not correct. Assembly errors can be particularly detrimental in the case of a stacked diaphragm design, and care must be exercised to maintain proper impeller-diaphragm positioning. Since the bundle is subjected to discharge pressure on one end and suction pressure on the other, a force builds up that is transmitted from diaphragm to diaphragm, causing high loading on the inlet wall.

Internal leakage. The discharge and suction compartments of the inner bundle on a straight-through flow design are normally separated by a single O-ring. Compressors with side nozzles can have several bundles of O-rings. Excessive bundle-to-barrel clearance may cause leakage past the O-rings. O-rings are frequently pinched and cut across the suction nozzle opening in the barrel, a condition that is hard to prevent and doubly hard to detect if it occurs. Pressure differentials in excess of 400 to 500 psi even using good design practice can cause extrusion and failure of the O-rings. In many cases backup rings to the O-rings have been added to prevent failures. Grooves with O-ring ribbons have been added to the horizontal joints of the bundles of almost all the machines to prevent interstage leakage.

Bearing bracket alignment. In contrast to horizontally split compressors where the bearing brackets are normally an integral part of the lower case half, in barrel machines bearing brackets are bolted to

the barrel heads. Both the bearing brackets *and* the head are removed during the disassembly operation, thus requiring *all* internal alignment to be reestablished each time maintenance work is performed.

Material problems. To limit the physical size of the case or pressure vessel, to limit the rotor bearing span, and to maximize the number of stages within the heavy barrel, the gas path of a barrel is "squeezed" to a greater extent than in a horizontally split machine. This means the diaphragms and inlet guide vanes are intricate shapes with very small openings. Plain gray cast iron is normally used for these shapes because of casting ease and for other economic reasons. The gray iron is not strong enough in many instances to withstand the pressure differentials imposed on it, resulting in failures. Inlet guide vanes have been especially troublesome. On several occasions inlet guide vanes have been fabricated from wrought stainless and carbon steel materials. Replacement diaphragms and inlet guide vanes cast of nodular iron have also been used to alleviate some of these material problems.

Impeller Problems The high-speed rotation of the impeller of a centrifugal compressor imparts the vital aerodynamic velocity to the flow within the gas path. The buffeting effects of the gas flow can cause fatigue failures in the conventional fabricated shrouded impeller due to vibration-induced alternating stresses. These may be of the following types:

1. Resultant vibration in a principal mode
2. Forced-undamped vibration, associated with aerodynamic buffeting or high acoustic energy levels

The vibratory mode most frequently encountered is of the plate type and involves either the shroud or the disc. Fatigue failure generally originates at the impeller outside diameter, adjacent to a vane often due to the vibratory motion of the shroud or disc. The fatigue crack propagates inward along the nodal line, and finally a section of the shroud or disc tears out.

To eliminate failures of the covered impellers when operating at high density levels, the impellers are frequently scalloped between vanes at the outside diameter. The consequent reduction in disc friction also causes a small increase in impeller efficiency. However, there may be a slight reduction in overall efficiency due to higher losses in the diffuser. The advantages of scalloped impellers from a mechanical point of view are large. Several rotors have been salvaged by scalloping the wheels after a partial failure has occurred.

Rotor Thrust Problems Thrust loads in compressors due to aerodynamic forces are affected by impeller geometry, by pressure rise through the compressor, and by internal leakage due to labyrinth clearances. The impeller thrust is calculated by using correction factors to account for internal leakage, and a balance piston size is selected to compensate for the impeller thrust load. The common assumptions made in the calculation are

1. The radial pressure distribution along the outside of the disc cover is essentially balanced.
2. Only the "eye" area is effective in producing thrust.
3. The pressure differential applied to the "eye" area is equal to the difference between the static pressure at the impeller tip, corrected for the pumping action of the disc, and the total pressure at inlet.

These "common assumptions" are grossly erroneous and can be disastrous when applied to high-pressure, barrel-type compressors where a large part of the impeller-generated thrust is compensated by a balance piston. The actual thrust is about 50 percent more than the calculations indicate. The error is less when the thrust is compensated by opposed impellers, because the mistaken assumptions offset each other.

The magnitude of the thrust is considerably affected by leakage at the impeller labyrinth seals. Increased leakage here produces increased thrust independent of balancing piston labyrinth seal clearance or leakage.

The thrust errors are further compounded in the design of the balancing piston, labyrinths, and bleed line. API-617, *Centrifugal Compressors*, specifies that a separate pressure tap connection be provided to indicate the pressure in the balance chamber. It also specifies that the balance line be sized to handle balance piston labyrinth gas leakage at twice the initial clearance without exceeding the load ratings of the thrust bearing, and that thrust bearings for compressors be selected at no more than 50 percent of the bearing manufacturer's

rating. The leaks and the consequential pressure change across the balance piston destabilize the entire rotor system.

Journal Bearing Failures With high-speed machines, simple bearing failures are rare unless they are caused by faulty alignment, distortion, wrong clearance, or dirt. More common are failures caused by vibrations and rotor whirls. Some of these originate in the bearings; others can be amplified or attenuated by the bearings, the bearing cases, and the bearing support structure.

During inspection, all journal bearings should be closely inspected. If the machine has not suffered from excessive vibrations or lubrication problems, the bearings can be reinstalled and utilized.

Four places should be checked for wear during inspection periods:

1. Babbitted shoe surface
2. Pivoting shoe surface and seat in retaining ring
3. Seal ring bore or end plates
4. The shoe thickness at the pivot point or across ball *and* socket (all shoes should be within 0.0005 percent of the same thickness)

Thrust Bearing Failures Tilting pad-type thrust bearings are used in most major pieces of rotating equipment under the general term *Kingsbury type*. A thrust-bearing failure is one of the worst things that can happen to a machine, since it often wrecks the machine. To evaluate the reliability of a thrust bearing arrangement, one must first consider how a failure is initiated and evaluate the merits of the various designs.

Failures caused by bearing overload during normal operation (design error) are rare today, but still far more thrust failures occur than one would expect, considering all the precautions taken by the bearing designer. The causes in the following list are roughly in sequence of importance:

1. *Fluid slugging*. Passing a slug of fluid through a turbine or compressor can increase the thrust to many times its normal level.
2. *Buildup of solids in rotor and/or stator passages ("plugging" of turbine blades)*. This problem should be noticed from performance or pressure distribution in the machine (first-stage pressure) long before the failure occurs.
3. *Off-design operation*. This arises especially from backpressure (vacuum), inlet pressure, extraction pressure, or moisture. Many failures are caused by overload, off-design speed, and flow fluctuations.
4. *Compressor surging*. This problem occurs especially in double-flow machines.
5. *Gear coupling thrust*. This is a frequent cause of failure, especially of upstream thrust bearings. The thrust is caused by friction in the loaded teeth that opposes thermal expansion. Therefore, thrust can get very high, since it has no relation to the normal thrust caused by pressure distribution inside the machine. The coupling thrust may act either way, adding to or subtracting from normal thrust. Much depends on tooth geometry and coupling quality.
6. *Dirt in oil*. This is a common cause of failures, especially when combined with other factors. The oil film at the end of the oil wedge is only a small fraction of a thousandth inch thick. If dirt goes through, it can cause the film to rupture, and the bearing may burn out. Therefore, very fine filtering of the oil is required.
7. *Momentary loss of oil pressure*. This type of failure is usually encountered while switching filters or coolers, or in some instances when the dc pump does not come on-line when the main pumps fail.

The thrust bearings must be closely maintained. This type of bearing consists of pivoted segments or pads (usually six) against which the thrust collar revolves, forming a wedge-shaped oil film. This film plus minute misalignment of the thrust collar and the bearing pads causes movement and wear of the various bearing parts. The erroneous thrust calculations discussed earlier cause the bearing to be loaded more heavily than desired. This accelerates the wear problem. There are seven wear points in the bearing. All these points must be checked for wear:

1. The soft babbitted shoe face
2. The hardened steel shoe insert face
3. The face of the hardened steel upper leveling plate
4. The outer edge of the upper leveling plate
5. The upper edge of lower leveling plate
6. The pivot point of the lower leveling plate
7. The inner face of the base ring

To protect thrust bearings, accurate and reliable instrumentation is now available to monitor thrust bearings well enough to ensure safe continuous operation and to prevent catastrophic failure in the event of an upset to the system.

Temperature sensors, such as RTDs (resistance temperature detectors), thermocouples, and thermistors, can be installed directly in the thrust bearing to measure metal temperature.

Axial proximity probes are another means of monitoring rotor position and the integrity of the thrust bearing. This method detects thrust collar runout and rotor movement. In most cases this ideal positioning of the probes is not possible. Many times the probes are indexed to the rotor or other convenient locations and thus do not truly show the movement of the rotor with respect to the thrust bearing.

A critical installation should have the metal temperature sensors in the thrust pad. Axial proximity probes may be used as a backup system. If metal temperatures are high and the rate of change of those temperatures begins to alter rapidly, thrust-bearing failure should be anticipated.

Compressor Seal Problems The extent of the leakage past the seals where the shaft comes through the casing frequently limits the running time of the compressor, yet the seals and the seal systems are not given adequate treatment in the maintenance manuals or in the operating instructions furnished by the compressor manufacturer.

Shaft seals are divided into the following categories by API Standard 617:

- Labyrinth
- Restrictive carbon rings
- Mechanical (contact) type
- Liquid film or floating bushing type
- Liquid film type with pump bushings

The first two seal categories are usually operated dry, and the last three categories require seal oil consoles either separately or as part of the lube system. Each of these seal designs has its own characteristics and maintenance difficulties.

Oil flows and critical clearances are not spelled out well in either the operating instructions or the maintenance manuals. Because of this, several maintenance technique improvements are needed:

1. *Radial clearances*. Radial clearance between the bushing and the shaft and the length of the bushing must be selected to obtain minimum leakage without exceeding fluid temperature limitations.
2. *Quality control*. The flatness, parallelism, and surface finish of the mating sleeve faces must be carefully controlled to obtain maximum seal effectiveness.
3. *Axial clearances*. Axial clearance between the bushing or sleeve and the housing is critical, there should be 12 to 15 mils of clearance per bushing between the bushing or sleeve and the housing; where the sleeves are mounted back-to-back, there will be 25 to 30 mils of clearance total for the seal.
4. *Seal design*. In higher-pressure seals, more than one outboard (i.e., high differential) sleeve may be used. Generally, it is desirable to use a single sleeve because the inboard sleeve operates with up to 80 percent of the total pressure drop across it. The outer sleeve with the lower differential causes lubrication and cooling problems that can shorten the life of one or both sleeves.
5. *Guidelines*. These should be explicit in indicating oil flow rates and the interaction of various components.
6. *Rules of thumb*. There are a few rules of thumb that help in understanding seal operation and maintenance.
 - a. The oil flow rate will vary: (1) *directly* with the differential pressure and the wetted perimeter of the sleeve; (2) with the *cube* of the radial clearance; (3) with the *square* of the eccentricity of the sleeve and shaft; (4) *inversely* with oil viscosity, temperature, and length of the sleeve.
 - b. Shear work done on the sealing fluid during its passage through the sleeve raises its temperature to a much higher level than may be expected.

ROTOR DYNAMICS

The rotating elements consist of the impeller and the shaft. The shaft should be made of one-piece, heat-treated forged steel, with the shaft ends tapered for coupling fits. Interstage sleeves should be renewable and made of material which is corrosion-resistant in the

specified service. The rotor shaft sensing area observed by the non-contact probes should be concentric with the bearing journals and free of any scratches, marks, or other surface discontinuity. The surface finish should be 16 to 32 μin root mean square, and the area should be demagnetized and treated. Electromechanical runout should not exceed 25 percent of the maximum allowed peak-to-peak vibration amplitude or 0.25 mil, whichever is greater. Although not mentioned in the standard, chrome plating of the shaft in the sensing area is unacceptable. Maximum vibration should not exceed 2.0 mils as given by

$$\text{Vib}_{\text{max}} = \sqrt{\frac{12,000}{\text{rpm}}} + 0.25 \sqrt{\frac{12,000}{\text{rpm}}} \quad (10-90)$$

(Vibration) (runout)

At the trip speed of the driver (105 percent for a gas turbine), the vibration should not exceed this level by more than 0.5 mil.

The impellers can be an open-faced (stationary shroud) or closed-face (rotating shroud) design. As long as the tip velocities are below 1000 ft/s, closed-face impellers can be used. The standards allow the impellers to be welded, riveted, milled, or cast. Riveted impellers are unacceptable, especially if the impeller loading is high. Impellers are to be assembled on the shaft with a shrink fit with or without key. Shrink fits should be carefully done because excessive shrink fits can cause a problem known as hysteresis whirl. In compressors where the impellers require their thrust to be balanced, a balance drum is acceptable and preferred.

The high-speed pumps or compressors must operate in a region away from any critical speed. The amplification factor used to indicate the severity of the critical speed is given by the relationship

$$\text{AF} = \frac{\text{critical speed}}{\text{peak width of "half-power" point}} \quad (10-91)$$

$$\text{AF} = \frac{N_{C1}}{N_2 - N_1} \quad (10-92)$$

where $N_2 - N_1$ is the rpm corresponding to the 0.707 peak critical amplitude.

The amplification factor should be below 8 and preferably above 5. A rotor response plot is shown in Fig. 10-122. The operational speed for units operating below their first critical speed should be at least 20 percent below the critical speed. For units operating above their first critical speed, the operational speed must be at least 15 percent above the critical speed and/or 20 percent below any critical speed. The preferred bearings for the various types of installation are tilting-shoe radial bearings and the self-equalizing tilting pad thrust bearings. Radial and thrust bearings should be equipped with embedded temperature sensors to detect pad surface temperatures.

VIBRATION MONITORING

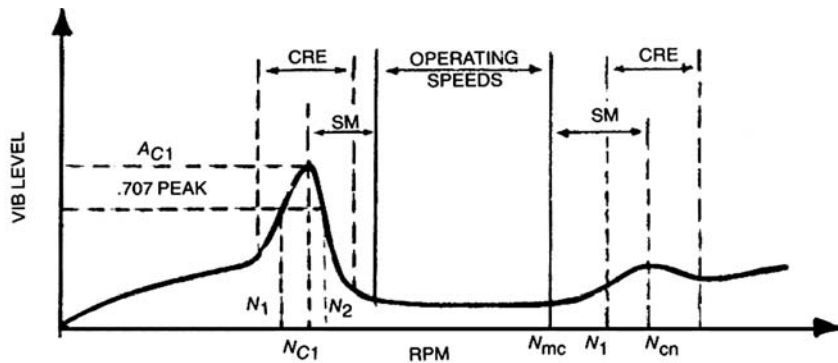
One of the major factors that causes pump failure is vibration, which usually causes seal damage and oil leakage. Vibration in pumps is caused by numerous factors such as cavitation, impeller unbalance, loose bearings, and pipe pulsations.

As the mechanical integrity of the pump system changes, the amplitude of vibration levels change. In some cases, in order to identify the source of vibration, pump speed may have to be varied, as these problems are frequency- or resonance-dependent. Pump impeller imbalance and cavitation are related to this category.

It is advisable in most of these cases to use accelerometers. Displacement probes will not give the high-frequency signals and velocity probes because their mechanical design is very directional and prone to deterioration. Figure 10-123 shows the signal from the various types of probes.

Typically, large-amplitude vibration occurs when the frequency of vibration coincides with that of the natural frequency of the pump system. This results in a catastrophic operating condition that should be avoided. If the natural frequency is close to the upper end of the operating speed range, then the pump system should be stiffened to reduce vibration. On the other hand, if the natural frequency is close to the lower end of the operating range, the unit should be made more flexible. During startup, the pump system may go through its system natural frequency, and vibration can occur. Continuous operation at this operating point should be avoided.

ASME recommends periodic monitoring of all pumps. Pump vibration level should fall within the prescribed limits. The reference vibration level is measured during acceptance testing. This level is specified by the manufacturer.



- N_{C1} = Rotor 1st critical, center frequency, cycles per minute
- N_{cn} = Critical speed, nth
- N_t = Trip speed
- N_{mc} = Maximum continuous speed, 105 percent
- N_1 = Initial (lesser) speed at $.707 \times$ peak amplitude (critical)
- N_2 = Final (greater) speed at $.707 \times$ peak amplitude (critical)
- $N_2 - N_1$ = Peak width at the "half-power" point

- AF = Amplification factor
- $$= \frac{N_{C1}}{N_2 - N_1}$$
- SM = Separation margin
- CRE = Critical response envelope
- N_{C1} = Amplitude @ N_{C1}
- A_{cn} = Amplitude @ N_{cn}

FIG. 10-122 Rotor response plot. This plot is Figure 7 in API Standard 617, *Centrifugal Compressors for General Refinery Services*, 4th ed., 1979. (Courtesy American Petroleum Institute.)

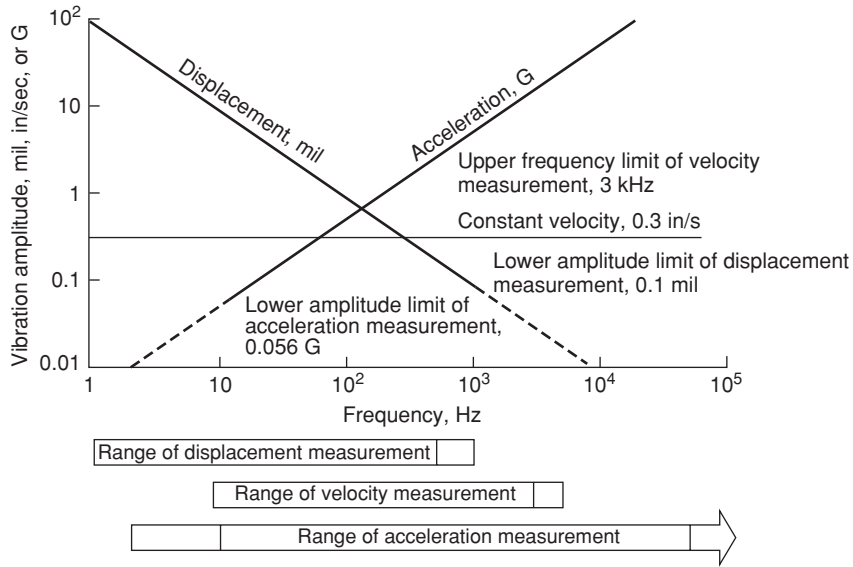


FIG. 10-123 Limitations on machinery vibrations analysis systems and transducers.

TABLE 10-17 Alert Levels

Reference value mils.	Alert mils., μm	Action required mils., μm
$V_r < 0.5$	1.0	1.5
$0.5 < V_r < 2.0$	$2V_r$	$3V_r$
$2.0 < V_r < 5.0$	$2+V_r$	$4+V_r$
$5.0 < V_r$	$1.4V_r$	$1.8V_r$

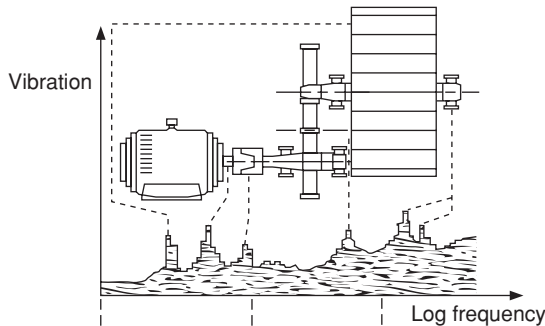
During periodic maintenance, the vibration level should not exceed alert level (see Table 10-17). If the measured level exceeds the alert level then preventive maintenance should be performed, by diagnosing the cause of vibration and reducing the vibration level prior to continued operation.

Typical problems and their vibration frequency ranges are shown in Fig. 10-124.

Collection and analysis of vibration signatures is a complex procedure. By looking at a vibration spectrum, one can identify which components of the pump system are responsible for a particular frequency component. Comparison of vibration signatures at periodic intervals reveals if a particular component is deteriorating. The following example illustrates evaluation of the frequency composition of an electric motor gear pump system.

Example 2: Vibration Consider an electric motor rotating at 1800 rpm driving an 8-vane centrifugal pump rotating at 600 rpm. For this 3:1 speed reduction, assume a gear box having two gears of 100 and 300 teeth. Since 60 Hz is 1 rpm, Motor frequency = $1800/60 = 30$ Hz
 Pump frequency = $600/60 = 10$ Hz
 Gear mesh frequency = $300 \text{ teeth} \times 600 \text{ rpm} = 3000$ Hz
 Vane frequency = $8 \times 600 \text{ rpm} = 80$ Hz
 An ideal vibration spectra for this motor-gear pump assembly would appear as shown in Fig. 10-125.

Figure 10-126 shows an actual pump vibration spectra. In the figure, several amplitude peaks occur at several frequencies.



Frequency range	Low	Medium	High
Fault to be detected	Unbalance Misalignment Bent shaft Oil whirl Eccentricity	Wear Faults in gears	Faults in rolling element bearings

FIG. 10-124 Frequency range of typical machinery faults.

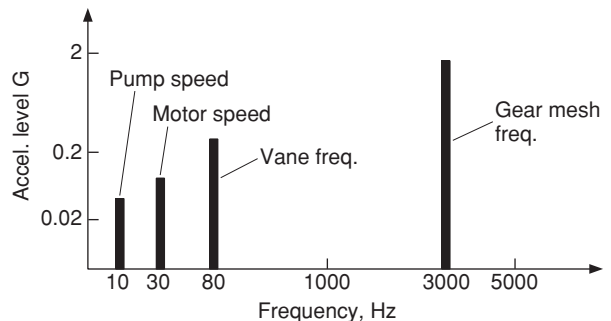


FIG. 10-125 An ideal vibration spectra from an electric motor pump assembly.

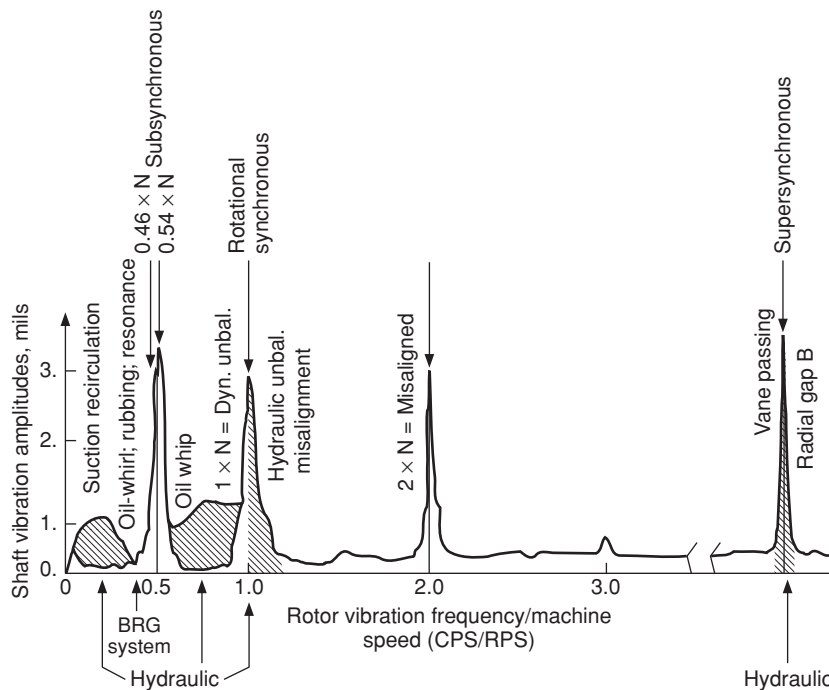


FIG. 10-126 An actual pump vibration spectrum.

PROCESS PLANT PIPING

INTRODUCTION

This section provides general comments that are pertinent to the design of process plant piping. It is intended to provide a convenient summary of commonly used information from various sources. It is not intended to serve as a comprehensive source of requirements or as a substitute for referenced codes, standards, and specifications. It is intended that qualified designers obtain copies of all applicable codes, standards, and specifications and thoroughly review all pertinent requirements of these documents prior to execution of work.

CODES AND STANDARDS

Units: Pipe and Tubing Sizes and Ratings In this subsection pipe and tubing sizes are generally quoted in units of inches. To convert inches to millimeters, multiply by 25.4. Ratings are given in pounds. To convert pounds to kilograms, multiply by 0.454.

Pressure-Piping Codes The code for pressure piping (ASME B31) consists of a number of sections which collectively constitute the code. Table 10-18 shows the status of the B31 code as of July 2005. The sections are published as separate documents for simplicity and convenience. The sections differ extensively.

The Process Piping Code (ASME B31.3) is a subsection of the ASME code for Pressure Piping B31. It was derived from a merging of the code groups for chemical-plant (B31.6) and petroleum-refinery (B31.3) piping into a single committee. Some of the significant requirements of ASME B31.3, Process Piping (2004 edition) are summarized in the following presentation.

Where the word *code* is used in this subsection of the *Handbook* without other identification, it refers to the B31.3 section of ASME B31. The

code has been extensively quoted in this subsection of the *Handbook* with the permission of the publisher. The code is published by and copies are available from the American Society of Mechanical Engineers (ASME), Three Park Avenue, New York, New York 10016-5990.

National Standards The American Society of Mechanical Engineers (ASME) and the American Petroleum Institute (API) have established dimensional standards for the most widely used piping components. Lists of these standards as well as specifications for pipe and fitting materials and testing methods of the American Society for Testing and Materials (ASTM), American Welding Society (AWS) specifications, and standards of the Manufacturers Standardization Society of the Valve and Fittings Industry (MSS) can be found in the ASME B31 code sections. Many of these standards contain pressure-temperature ratings which will be of assistance to engineers in their design function. The use of published standards does not eliminate the need for engineering judgment. For example, although the code calculation formulas recognize the need to provide an allowance for corrosion, the standard rating tables for valves, flanges, fittings, etc., do not incorporate a corresponding allowance. Judgments regarding the suitability of these components are left to the designer.

The introduction to the code sets forth engineering requirements deemed necessary for the safe design and construction of piping systems. While safety is the basic consideration of the code, this factor alone will not necessarily govern final specifications for any pressure piping system.

Designers are cautioned that the code is not a design handbook and does not do away with the need for competent engineering judgment.

Government Regulations: OSHA Sections of the ASME B31 code have been adopted with certain reservations or revisions by some state and local authorities as local codes.

TABLE 10-18 Status of ASME B31 Code for Pressure Piping

ASME B31.3 section number, latest issue, and title	General scope and application
B31.1-2004, <i>Power Piping</i>	Addresses piping typically found in electric power generating stations, industrial and institutional plants, geothermal heating systems, and central and district heating and cooling systems.
B31.2-1968, <i>Fuel Gas Piping</i>	Addresses fuel gas piping systems in and between buildings. The scope includes piping between the outlet of the consumer's meter and the outlet of the first pressure-containing valve upstream of the gas utilization device.
B31.3-2004, <i>Process Piping</i>	Addresses piping typically found in petroleum refineries; chemical, pharmaceutical, textile, paper, semiconductor, and cryogenic plants; and related processing plants and terminals.
B31.4-2002, <i>Pipeline Transportation Systems for Liquid Hydrocarbons and Other Liquids</i>	Addresses piping transporting products which are predominately liquid between plants and terminals. Included are terminals, tank farms, and pumping, regulating, and metering stations.
B31.5-2001, <i>Refrigeration Piping and Heat Transfer Components</i>	Addresses refrigeration piping in packaged units and in commercial and public buildings.
B31.7, <i>Nuclear Power Piping</i>	Withdrawn; see <i>ASME Boiler and Pressure Vessel Code</i> , Sec. 3.
B31.8-2003, <i>Gas Transmission and Distribution Piping Systems</i>	Addresses piping transporting products which are predominately gas between sources and terminals. Included are gas-gathering pipelines and compressor, regulating, and metering stations.
B31.8S-2004, <i>Managing System Integrity of Gas Pipelines</i>	Addresses development and implementation of integrity management systems for gas pipelines.
B31.9-1996, <i>Building Services Piping</i>	Addresses piping outside the scope of ASME B31.1 that is typically found in multiunit residences and in industrial, institutional, commercial, and public buildings.
B31.11-2002, <i>Slurry Transportation Piping Systems</i>	Addresses piping transporting aqueous slurries between plants and terminals and within terminals, pumping, and regulating stations.
B31G-1991, <i>Manual for Determining the Remaining Strength of Corroded Pipelines: A Supplement to ASME B31 Code for Pressure Piping</i>	Addresses methods of determining the remaining strength of corroded pipelines that are within the scope of the <i>ASME B31 Code for Pressure Piping</i> .

Addenda are issued at intervals between publication of complete editions. Information on the latest issues can be obtained from the American Society of Mechanical Engineers, Three Park Avenue, New York, NY 10016-5990; or on the World Wide Web at ASME.org.

The specific requirements for piping systems in certain services have been promulgated as Occupational Safety and Health Administration (OSHA) regulations. These rules and regulations will presumably be revised and supplemented from time to time and may include specific requirements not addressed by the B31 sections.

International Regulations ASME piping codes have been widely used throughout the world for the design of facilities falling within their defined scopes. Although the use of ASME codes is widely acceptable in areas outside the United States, it is essential to identify additional local or national codes or standards that may apply. Such documents may require qualified third-party review and approval of project specifications, facility design, fabrication, material documentation, inspection, and testing. For example, within the European Community, such requirements are imposed by the Pressure Equipment Directive 97/23/EC (also known as the PED). These requirements must be recognized early in the project to avoid costly error.

CODE CONTENTS AND SCOPE

The code prescribes minimum requirements for materials, design, fabrication, assembly, support, erection, examination, inspection, and testing of piping systems subject to pressure or vacuum. The scope of the piping covered by B31.3 is illustrated in Fig. 10-127. It applies to all fluids including fluidized solids and to all services except as noted in the figure.

The code also excludes piping systems designed for internal gauge pressures at or above zero but less than 0.105 MPa (15 lbf/in²) provided the fluid handled is nonflammable, nontoxic, and not damaging to human tissues, and its design temperature is from -29°C (-20°F) through 186°C (366°F). Refer to the code for definitions of nonflammable and nontoxic.

Some of the more significant requirements of ASME B31.3 (2004 edition) have been summarized and incorporated in this section of the *Handbook*. For a more comprehensive treatment of code require-

ments engineers are referred to the B31.3 code and the standards referenced therein.

SELECTION OF PIPE SYSTEM MATERIALS

The selection of material to resist deterioration in service is outside the scope of the B31.3 code (see Sec. 25). Experience has, however, resulted in the following material considerations extracted from the code with the permission of the publisher, the American Society of Mechanical Engineers, New York.

General Considerations* Following are some general considerations which should be evaluated when selecting and applying materials in piping:

1. The possibility of exposure of the piping to fire and the melting point, degradation temperature, loss of strength at elevated temperature, and combustibility of the piping material under such exposure.
2. The susceptibility to brittle failure or failure from thermal shock of the piping material when exposed to fire or to fire-fighting measures, and possible hazards from fragmentation of the material in the event of failure.
3. The ability of thermal insulation to protect piping against failure under fire exposure (e.g., its stability, fire resistance, and ability to remain in place during a fire).
4. The susceptibility of the piping material to crevice corrosion under backing rings, in threaded joints, in socket-welded joints, and in other stagnant, confined areas.
5. The possibility of adverse electrolytic effects if the metal is subject to contact with a dissimilar metal.
6. The compatibility of lubricants or sealants used on threads with the fluid service.

*Extracted from ASME B31.3-2004, Section F323, with permission of the publisher, the American Society of Mechanical Engineers, New York.

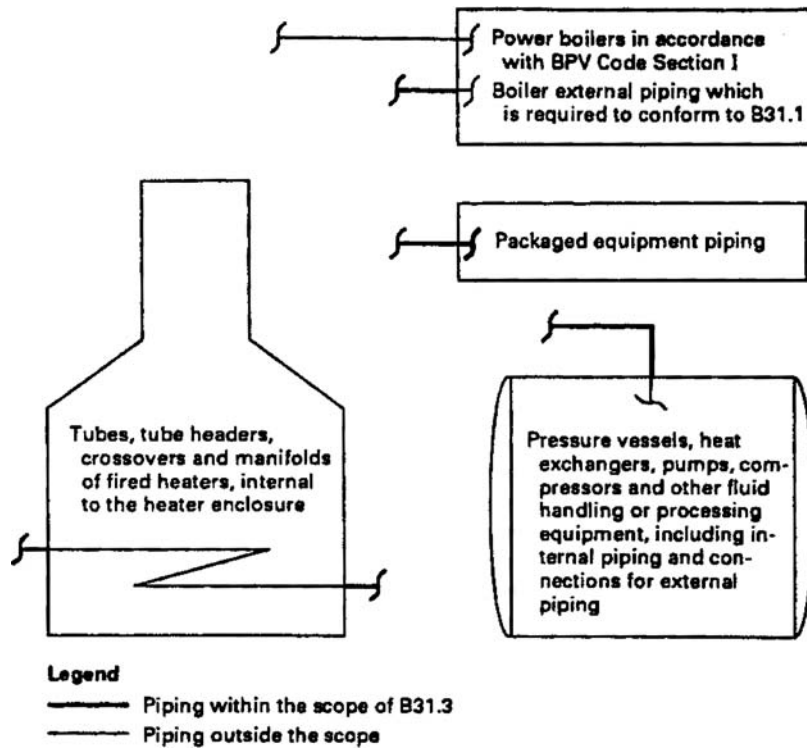


FIG. 10-127 Scope of work covered by process piping code ASME B31.3-2004.

- 7. The compatibility of packing, seals, and O-rings with the fluid service.
- 8. The compatibility of materials, such as cements, solvents, solders, and brazing materials, with the fluid service.
- 9. The chilling effect of sudden loss of pressure on highly volatile fluids as a factor in determining the lowest expected service temperature.
- 10. The possibility of pipe support failure resulting from exposure to low temperatures (which may embrittle the supports) or high temperatures (which may weaken them).
- 11. The compatibility of materials, including sealants, gaskets, lubricants, and insulation, used in strong oxidizer fluid service (e.g., oxygen or fluorine).

Specific Material Considerations—Metals* Following are some specific considerations which should be evaluated when applying certain metals in piping.

- 1. *Irons—cast, malleable, and high silicon (14.5%).* Their lack of ductility and their sensitivity to thermal and mechanical shock.
- 2. *Carbon steel, and low and intermediate alloy steels.*
 - a. The possibility of embrittlement when handling alkaline or strong caustic fluids.
 - b. The possible conversion of carbides to graphite during long time exposure to temperatures above 427°C (800°F) of carbon steels, plain

*Extracted from ASME B31.3-2004, Section F323, with permission of the publisher, the American Society of Mechanical Engineers, New York.

†Titles of referenced documents are:

API RP941, *Steels for Hydrogen Service at Elevated Temperatures and Pressures in Petroleum Refineries and Petrochemical Plants*

NACE MR0175, *Sulfide Stress-Cracking Resistant Metallic Materials for Oil Field Equipment*

NACE RP0472, *Methods and Controls to Prevent In-Service Cracking of Carbon Steel (P-1) Welds in Corrosive Petroleum Refining Environments*

NACE RP0170, *Protection of Austenitic Stainless Steel in Refineries Against Stress Corrosion Cracking by Use of Neutralizing Solutions During Shutdown*

nickel steel, carbon-manganese steel, manganese-vanadium steel, and carbon-silicon steel.

c. The possible conversion of carbides to graphite during long time exposure to temperatures above 468°C (875°F) of carbon-molybdenum steel, manganese-molybdenum-vanadium steel, and chromium-vanadium steel.

d. The advantages of silicon-killed carbon steel (0.1% silicon minimum) for temperatures above 482°C (900°F).

e. The possibility of damage due to hydrogen exposure at elevated temperature (see API RP941); hydrogen damage (blistering) may occur at lower temperatures under exposure to aqueous acid solutions.[†]

f. The possibility of stress corrosion cracking when exposed to cyanides, acids, acid salts, or wet hydrogen sulfide; a maximum hardness limit is usually specified (see NACE MR0175 and RP0472).[†]

g. The possibility of sulfidation in the presence of hydrogen sulfide at elevated temperatures.

3. *High-alloy (stainless) steels.*

a. The possibility of stress corrosion cracking of austenitic stainless steels exposed to media such as chlorides and other halides either internally or externally; the latter can result from improper selection or application of thermal insulation, or from use of marking inks, paints, labels, tapes, adhesives, and other accessory materials containing chlorides or other halides.

b. The susceptibility to intergranular corrosion of austenitic stainless steels sensitized by exposure to temperatures between 427 and 871°C (800 and 1600°F); as an example, stress corrosion cracking of sensitized metal at room temperature by polythionic acid (reaction of oxidizable sulfur compound, water, and air); stabilized or low-carbon grades may provide improved resistance (see NACE RP0170).[†]

c. The susceptibility to intercrystalline attack of austenitic stainless steels on contact with liquid metals (including aluminum, antimony, bismuth, cadmium, gallium, lead, magnesium, tin, and zinc) or their compounds.

d. The brittleness of ferritic stainless steels at room temperature after service at temperature above 371°C (700°F).

4. *Nickel and nickel-base alloys.*

a. The susceptibility to grain boundary attack of nickel and nickel-base alloys not containing chromium when exposed to small quantities of sulfur at temperatures above 316°C (600°F).

b. The susceptibility to grain boundary attack of nickel-base alloys containing chromium at temperatures above 593°C (1100°F) under reducing conditions and above 760°C (1400°F) under oxidizing conditions.

c. The possibility of stress corrosion cracking of nickel-copper Alloy 400 in hydrofluoric acid vapor in the presence of air, if the alloy is highly stressed (including residual stresses from forming or welding).

5. *Aluminum and aluminum alloys.*

a. The compatibility with aluminum of thread compounds used in aluminum threaded joints to prevent seizing and galling.

b. The possibility of corrosion from concrete, mortar, lime, plaster, or other alkaline materials used in buildings or structures.

c. The susceptibility of Alloy nos. 5083, 5086, 5154, and 5456 to exfoliation or intergranular attack; and the upper temperature limit of 66°C (150°F) shown in Appendix A to avoid such deterioration.

6. *Copper and copper alloys.*

a. The possibility of dezincification of brass alloys.

b. The susceptibility to stress corrosion cracking of copper-based alloys exposed to fluids such as ammonia or ammonium compounds.

c. The possibility of unstable acetylide formation when exposed to acetylene.

7. *Titanium and titanium alloys.* The possibility of deterioration of titanium and its alloys above 316°C (600°F).

8. *Zirconium and zirconium alloys.* The possibility of deterioration of zirconium and zirconium alloys above 316°C (600°F).

9. *Tantalum.* Above 299°C (570°F), the possibility of reactivity of tantalum with all gases except the inert gases. Below 299°C, the possibility of embrittlement of tantalum by nascent (monatomic) hydrogen (but not molecular hydrogen). Nascent hydrogen is produced by galvanic action, or as a product of corrosion by certain chemicals.

10. *Metals with enhanced properties.* The possible loss of strength, in a material whose properties have been enhanced by heat treatment, during long-continued exposure to temperatures above the tempering temperature.

11. The desirability of specifying some degree of production impact testing, in addition to the weld procedure qualification tests, when using materials with limited low-temperature service experience below the minimum temperature stated in ASME B31.3 Table A-1.

Specific Material Considerations—Nonmetals Following are some considerations to be evaluated when applying nonmetals in piping. Refer to Tables 10-19, 10-20, and 10-21 for typical temperature limits.

1. *Static charges.* Because of the possibility of producing hazardous electrostatic charges in nonmetallic piping and metallic piping lined with nonmetals, consideration should be given to grounding the metallic components of such systems conveying nonconductive fluids.

2. *Thermoplastics.* If thermoplastic piping is used aboveground for compressed air or other compressed gases, special precautions should be observed. In determining the needed safeguarding for such services, the energetics and the specific failure mechanism need to be evaluated. Encasement of the plastic piping in shatter-resistant material may be considered.

3. *Borosilicate glass.* Take into account its lack of ductility and its sensitivity to thermal and mechanical shock.

METALLIC PIPING SYSTEM COMPONENTS

Metallic pipe systems comprise the majority of applications. Metallic pipe, tubing, and pipe fittings are divided into two main categories: seamless and welded. Both have advantages and disadvantages in terms of economy and function. Specifications governing the production of these products dictate the permissible mechanical and dimensional variations, and code design calculations account for these variations.

Seamless Pipe and Tubing Seamless pipe and tubing may be formed by various methods. A common technique involves piercing solid round forgings, followed by rolling and drawing. Other tech-

TABLE 10-19 Recommended Temperature Limits for Thermoplastic Pipe*

ASTM spec. no.	Material	Recommended temperature limits †,‡			
		Minimum		Maximum	
		°C	°F	°C	°F
...	ABS55535	-40	-40	80	176
...	AP	-18	0	77	170
D 2846	CPVC4120	-18	0	99	210
F 441					
F 442					
...	ECTFE	-40	-40	149	300
...	ETFE	-40	-40	149	300
D 2513	PB2110	-18	0	99	210
D 2662					
D 2666					
D 3000					
D 3309					
D 2104	PE3408	-34	-30	82	180
D 2239					
D 2447					
D 2513					
D 2737					
D 3035					
...	PEEK	-40	-40	250	450
...	PFA	-40	-40	250	450
...	POP2125	-1	30	99	210
...	PP	-1	30	99	210
D 1785	PVC1120	-18	0	66	150
D 2241	PVC1220	-18	0	66	150
D 2513	PVC2110	-18	0	54	130
D 2672	PVC2120	-18	0	66	150
...	PVDC	4	40	71	160
...	PVDF	-18	0	135	275

*Extracted from ASME B31.3-2004, Table B-1, with permission of the publisher, the American Society of Mechanical Engineers, New York.

†These recommended limits are for low-pressure applications with water and other fluids that do not significantly affect the properties of the thermoplastic. The upper temperature limits are reduced at higher pressures, depending on the combination of fluid and expected service life. Lower temperature limits are affected more by the environment, safeguarding, and installation conditions than by strength.

‡These recommended limits apply only to materials listed. Manufacturers should be consulted for temperature limits on specific types and kinds of materials not listed.

niques include forging and boring, extrusion, and static and centrifugal casting. Piercing frequently produces pipe with a less uniform wall thickness and concentricity of bore than is the case with products produced by other methods. Since seamless products have no weld joints, there is no reduction of strength due to weld joint efficiency.

Welded Pipe and Tubing These products are typically made by forming strips or plate into cylinders and seam-welding by various methods. Manufacturing by welding permits the production of larger diameter pipe than is possible with seamless manufacturing methods, as well as larger diameter/wall thickness ratios. While strip and plate thickness may be more closely controlled than is possible for some seamless products, the specifications governing production are not always more stringent for welded products.

Weld quality has the potential of making the weld weaker than the base material. Depending on the welding method and the degree of nondestructive examination required by the product specification or dictated by the designer, the code assigns a joint efficiency ranging from 60 to 100 percent of the strength of the base material. Although

TABLE 10-20 Recommended Temperature Limits for Thermoplastics Used as Linings*

Materials	Minimum		Maximum	
	°C	°F	°C	°F
PFA	-198	-325	260	500
PTFE	-198	-325	260	500
FEP	-198	-325	204	400
ECTFE	-198	-325	171	340
ETFE	-198	-325	149	300
PVDF	-18	0	135	275
PP	-18	0	107	225
PVDC	-18	0	79	175

*Extracted from ASME B31.3-2004, Table A323.4.3, with permission of the publisher, the American Society of Mechanical Engineers, New York.

NOTE: These temperature limits are based on material tests and do not necessarily reflect evidence of successful use as piping component linings in specific fluid services at these temperatures. The designer should consult the manufacturer for specific applications, particularly as temperature limits are approached.

Abbreviations for plastics: ABS, acrylonitrile-butadiene-styrene; CPVC, chlorinated poly vinyl chloride; ECTFE, ethylene-chlorotrifluoroethylene; ETFE, ethylene-tetrafluoroethylene; PB, polybutylene; PE, polyethylene; PEEK, poly ether ether ketone; PFA, perfluoroalkoxy copolymer; POE, poly phenylene oxide; PP, polypropylene; PVC, poly vinyl chloride; PVDC, poly vinylidene chloride; PVDF, poly vinylidene fluoride.

some welding methods have the potential of producing short sections of partially fused joints that may develop into small leaks in corrosive conditions, proper matching of the weld method and the type and extent of examination will result in highly reliable joints that are suitable for use in critical services. Welds must be considered when developing specifications for bending, flaring or expanding welded pipe or tubing.

Tubing Tubing sizes typically reflect the actual outside diameter of the product. Pipe is manufactured to nominal diameters, which are not the same as the actual outside diameters for sizes 12 in and smaller. Facilities within the scope of the ASME B31 codes nearly exclusively use pipe, rather than tubing, for applications external to equipment. Tubing is commonly classified as suitable for either mechanical or pressure applications. Tubing is available in size and wall thickness combinations not normally produced as pipe. Tubing wall thickness (gauge) is specified as either average wall or minimum wall. Minimum wall is more costly than average wall, and because of closer tolerances on thickness and diameter, tubing of either gauge system is generally more costly than pipe. Tubing having outside diameters of 2³/₈, 2⁷/₈, 3¹/₂, and 4¹/₂ in are commonly available; however, these sizes are generally considered to be nonstandard for typical piping applications.

Table 10-22 gives some of the more common standard size and wall-thickness combinations together with capacity and weight.

Methods of Joining Pipe Piping joints must be reliably leak-tight and provide adequate mechanical strength to resist external loads due to thermal expansion, weight, wind, seismic activity, and other factors. Joints for pipe buried in soil may be subjected to unique external loads resulting from thermal expansion and contraction, settlement, and other factors. Joint designs that permit rotation about an axis perpendicular to the longitudinal axis of the pipe may be advantageous in certain situations.

Disassembly frequency and ease should be considered when selecting joining methods. Ideally the method for joining piping system components provides minimum installed cost, maintains its integrity throughout the lifetime of the facility, provides restraint against axial thrust due to internal pressure, provides strength against external loads equal to that of the pipe, permits unrestricted flow with minimum pressure drop, and is free from crevices that may be detrimental to the product or contribute to corrosion or erosion problems.

Joint design and selection generally involves compromising between the ideal and practical. A number of manufacturers produce patented or "proprietary" joints that embody many ideal characteristics. Some are excellent products and are well suited to special applications. Valves and fittings are often available with proprietary joints that have gained wide acceptance; however, consideration should be given to the possible impact on product delivery time and cost.

Welded Joints The most widely used joint in piping systems is the **butt-weld joint** (Fig. 10-128). In all ductile pipe metals which can be welded, pipe, elbows, tees, laterals, reducers, caps, valves, flanges, and V-clamp joints are available in all sizes and wall thicknesses with ends prepared for butt welding. Joint strength equal to the original pipe (except for work-hardened pipes which are annealed by the welding), unimpaired flow pattern, and generally unimpaired corrosion resistance more than compensate for the necessary careful alignment, skilled labor, and equipment required.

Plain-end pipe used for socket-weld joints (Fig. 10-129) is available in all sizes, but fittings and valves with socket-weld ends are limited to sizes 3 in and smaller, for which the extra cost of the socket is outweighed by much easier alignment and less skill needed in welding.

Socket-welded joints are not as resistant to externally applied bending moments as are butt-welded joints, are not easily examined by volumetric nondestructive examination methods such as radiography and ultrasonic, and should not be used where crevice corrosion has been determined to be of concern. However, they are widely used in sizes 2 in and smaller and are quite satisfactory for most applications when used within the limits established by code restrictions and good engineering judgment. Components with socket-welded ends are generally specified as requiring compliance with ASME B16.11, *Forged-Fittings, Socket-Welding and Threaded*.

Branch Connections Branch connections may be made with manufactured tees, fabricated reinforced and nonreinforced branch connections (Fig. 10-130), or manufactured integrally reinforced branch connections. Butt-welded fittings offer the best opportunity

TABLE 10-21 Recommended Temperature Limits for Reinforced Thermosetting Resin Pipe*

Materials		Recommended temperature limits			
		Minimum		Maximum	
Resin	Reinforcing	°C	°F	°C	°F
Epoxy	Glass fiber	-29	-20	149	300
Phenolic	Glass fiber	-29	-20	149	300
Furan	Carbon	-29	-20	93	200
Furan	Glass fiber	-29	-20	93	200
Polyester	Glass fiber	-29	-20	93	200
Vinyl ester	Glass fiber	-29	-20	93	200

*Extracted from ASME B31.3-2004, Table A323.4.2C, with permission of the publisher, the American Society of Mechanical Engineers, New York.

NOTE: These temperature limits apply only to materials listed and do not reflect evidence of successful use in specific fluid services at these temperatures. The designer should consult the manufacturer for specific applications, particularly as the temperature limits are approached.

10-78 TRANSPORT AND STORAGE OF FLUIDS

TABLE 10-22 Properties of Steel Pipe

Nominal pipe size, in	Outside diameter, in	Schedule no.	Wall thickness, in	Inside diameter, in	Cross-sectional area		Circumference, ft, or surface, ft ² /ft of length		Capacity at 1-ft/s velocity		Weight of plain-end pipe, lb/ft
					Metal, in ²	Flow, ft ²	Outside	Inside	U.S. gal/min	lb/h water	
1/8	0.405	10S	0.049	0.307	0.055	0.00051	0.106	0.0804	0.231	115.5	0.19
		40ST, 40S	.068	.269	.072	.00040	.106	.0705	.179	89.5	.24
		80XS, 80S	.095	.215	.093	.00025	.106	.0563	.113	56.5	.31
1/4	0.540	10S	.065	.410	.097	.00092	.141	.107	.412	206.5	.33
		40ST, 40S	.088	.364	.125	.00072	.141	.095	.323	161.5	.42
		80XS, 80S	.119	.302	.157	.00050	.141	.079	.224	112.0	.54
3/8	0.675	10S	.065	.545	.125	.00162	.177	.143	.727	363.5	.42
		40ST, 40S	.091	.493	.167	.00133	.177	.129	.596	298.0	.57
		80XS, 80S	.126	.423	.217	.00098	.177	.111	.440	220.0	.74
1/2	0.840	5S	.065	.710	.158	.00275	.220	.186	1.234	617.0	.54
		10S	.083	.674	.197	.00248	.220	.176	1.112	556.0	.67
		40ST, 40S	.109	.622	.250	.00211	.220	.163	0.945	472.0	.85
		80XS, 80S	.147	.546	.320	.00163	.220	.143	0.730	365.0	1.09
		160	.188	.464	.385	.00117	.220	.122	0.527	263.5	1.31
		XX	.294	.252	.504	.00035	.220	.066	0.155	77.5	1.71
3/4	1.050	5S	.065	.920	.201	.00461	.275	.241	2.072	1036.0	0.69
		10S	.083	.884	.252	.00426	.275	.231	1.903	951.5	0.86
		40ST, 40S	.113	.824	.333	.00371	.275	.216	1.665	832.5	1.13
		80XS, 80S	.154	.742	.433	.00300	.275	.194	1.345	672.5	1.47
		160	.219	.612	.572	.00204	.275	.160	0.917	458.5	1.94
		XX	.308	.434	.718	.00103	.275	.114	0.461	230.5	2.44
1	1.315	5S	.065	1.185	.255	.00768	.344	.310	3.449	1725	0.87
		10S	.109	1.097	.413	.00656	.344	.287	2.946	1473	1.40
		40ST, 40S	.133	1.049	.494	.00600	.344	.275	2.690	1345	1.68
		80XS, 80S	.179	0.957	.639	.00499	.344	.250	2.240	1120	2.17
		160	.250	0.815	.836	.00362	.344	.213	1.625	812.5	2.84
		XX	.358	0.599	1.076	.00196	.344	.157	0.878	439.0	3.66
1 1/4	1.660	5S	.065	1.530	0.326	.01277	.435	.401	5.73	2865	1.11
		10S	.109	1.442	0.531	.01134	.435	.378	5.09	2545	1.81
		40ST, 40S	.140	1.380	0.668	.01040	.435	.361	4.57	2285	2.27
		80XS, 80S	.191	1.278	0.881	.00891	.435	.335	3.99	1995	3.00
		160	.250	1.160	1.107	.00734	.435	.304	3.29	1645	3.76
		XX	.382	0.896	1.534	.00438	.435	.235	1.97	985	5.21
1 1/2	1.900	5S	.065	1.770	0.375	.01709	.497	.463	7.67	3835	1.28
		10S	.109	1.682	0.614	.01543	.497	.440	6.94	3465	2.09
		40ST, 40S	.145	1.610	0.800	.01414	.497	.421	6.34	3170	2.72
		80XS, 80S	.200	1.500	1.069	.01225	.497	.393	5.49	2745	3.63
		160	.281	1.338	1.429	.00976	.497	.350	4.38	2190	4.86
		XX	.400	1.100	1.885	.00660	.497	.288	2.96	1480	6.41
2	2.375	5S	.065	2.245	0.472	.02749	.622	.588	12.34	6170	1.61
		10S	.109	2.157	0.776	.02538	.622	.565	11.39	5695	2.64
		40ST, 40S	.154	2.067	1.075	.02330	.622	.541	10.45	5225	3.65
		80ST, 80S	.218	1.939	1.477	.02050	.622	.508	9.20	4600	5.02
		160	.344	1.687	2.195	.01552	.622	.436	6.97	3485	7.46
		XX	.436	1.503	2.656	.01232	.622	.393	5.53	2765	9.03
2 1/2	2.875	5S	.083	2.709	0.728	.04003	.753	.709	17.97	8985	2.48
		10S	.120	2.635	1.039	.03787	.753	.690	17.00	8500	3.53
		40ST, 40S	.203	2.469	1.704	.03322	.753	.647	14.92	7460	5.79
		80XS, 80S	.276	2.323	2.254	.02942	.753	.608	13.20	6600	7.66
		160	.375	2.125	2.945	.02463	.753	.556	11.07	5535	10.01
		XX	.552	1.771	4.028	.01711	.753	.464	7.68	3840	13.69
3	3.500	5S	.083	3.334	0.891	.06063	.916	.873	27.21	13,605	3.03
		10S	.120	3.260	1.274	.05796	.916	.853	26.02	13,010	4.33
		40ST, 40S	.216	3.068	2.228	.05130	.916	.803	23.00	11,500	7.58
		80XS, 80S	.300	2.900	3.016	.04587	.916	.759	20.55	10,275	10.25
		160	.438	2.624	4.213	.03755	.916	.687	16.86	8430	14.32
		XX	.600	2.300	5.466	.02885	.916	.602	12.95	6475	18.58
3 1/4	4.0	5S	.083	3.834	1.021	.08017	1.047	1.004	35.98	17,990	3.48
		10S	.120	3.760	1.463	.07711	1.047	0.984	34.61	17,305	4.97
		40ST, 40S	.226	3.548	2.680	.06870	1.047	0.929	30.80	15,400	9.11
		80XS, 80S	.318	3.364	3.678	.06170	1.047	0.881	27.70	13,850	12.50
4	4.5	5S	.083	4.334	1.152	.10245	1.178	1.135	46.0	23,000	3.92
		10S	.120	4.260	1.651	.09898	1.178	1.115	44.4	22,200	5.61
		40ST, 40S	.237	4.026	3.17	.08840	1.178	1.054	39.6	19,800	10.79

TABLE 10-22 Properties of Steel Pipe (Continued)

Nominal pipe size, in	Outside diameter, in	Schedule no.	Wall thickness, in	Inside diameter, in	Cross-sectional area		Circumference, ft, or surface, ft ² /ft of length		Capacity at 1-ft/s velocity		Weight of plain-end pipe, lb/ft
					Metal, in ²	Flow, ft ²	Outside	Inside	U.S. gal/min	lb/h water	
5	5.563	80XS, 80S	.337	3.826	4.41	.07986	1.178	1.002	35.8	17,900	14.98
		120	0.438	3.624	5.58	0.07170	1.178	0.949	32.2	16,100	19.00
		160	.531	3.438	6.62	.06647	1.178	0.900	28.9	14,450	22.51
		XX	.674	3.152	8.10	.05419	1.178	0.825	24.3	12,150	27.54
		5S	.109	5.345	1.87	.1558	1.456	1.399	69.9	34,950	6.36
		10S	.134	5.295	2.29	.1529	1.456	1.386	68.6	34,300	7.77
		40ST, 40S	.258	5.047	4.30	.1390	1.456	1.321	62.3	31,150	14.62
		80XS, 80S	.375	4.813	6.11	.1263	1.456	1.260	57.7	28,850	20.78
		120	.500	4.563	7.95	.1136	1.456	1.195	51.0	25,500	27.04
		160	.625	4.313	9.70	.1015	1.456	1.129	45.5	22,750	32.96
		XX	.750	4.063	11.34	.0900	1.456	1.064	40.4	20,200	38.55
		6	6.625	5S	.109	6.407	2.23	.2239	1.734	1.677	100.5
10S	.134			6.357	2.73	.2204	1.734	1.664	98.9	49,450	9.29
40ST, 40S	.280			6.065	5.58	.2006	1.734	1.588	90.0	45,000	18.97
80XS, 80S	.432			5.761	8.40	.1810	1.734	1.508	81.1	40,550	28.57
120	.562			5.501	10.70	.1650	1.734	1.440	73.9	36,950	36.39
160	.719			5.187	13.34	.1467	1.734	1.358	65.9	32,950	45.34
XX	.864			4.897	15.64	.1308	1.734	1.282	58.7	29,350	53.16
5S	.109			8.407	2.915	.3855	2.258	2.201	173.0	86,500	9.93
10S	.148			8.329	3.941	.3784	2.258	2.180	169.8	84,900	13.40
20	.250			8.125	6.578	.3601	2.258	2.127	161.5	80,750	22.36
30	.277			8.071	7.265	.3553	2.258	2.113	159.4	79,700	24.70
40ST, 40S	.322			7.981	8.399	.3474	2.258	2.089	155.7	77,850	28.55
60	.406	7.813	10.48	.3329	2.258	2.045	149.4	74,700	35.64		
80XS, 80S	.500	7.625	12.76	.3171	2.258	1.996	142.3	71,150	43.39		
100	.594	7.437	14.99	.3017	2.258	1.947	135.4	67,700	50.95		
120	.719	7.187	17.86	.2817	2.258	1.882	126.4	63,200	60.71		
140	.812	7.001	19.93	.2673	2.258	1.833	120.0	60,000	67.76		
XX	.875	6.875	21.30	.2578	2.258	1.800	115.7	57,850	72.42		
160	.906	6.813	21.97	.2532	2.258	1.784	113.5	56,750	74.69		
10	10.75	5S	.134	10.482	4.47	.5993	2.814	2.744	269.0	134,500	15.19
		10S	.165	10.420	5.49	.5922	2.814	2.728	265.8	132,900	18.65
		20	.250	10.250	8.25	.5731	2.814	2.685	257.0	128,500	28.04
		30	.307	10.136	10.07	.5603	2.814	2.655	252.0	126,000	34.24
		40ST, 40S	.365	10.020	11.91	.5475	2.814	2.620	246.0	123,000	40.48
		80S, 60XS	.500	9.750	16.10	.5185	2.814	2.550	233.0	116,500	54.74
		80	.594	9.562	18.95	.4987	2.814	2.503	223.4	111,700	64.43
		100	.719	9.312	22.66	.4729	2.814	2.438	212.3	106,150	77.03
		120	.844	9.062	26.27	.4479	2.814	2.372	201.0	100,500	89.29
		140, XX	1.000	8.750	30.63	.4176	2.814	2.291	188.0	94,000	104.13
		160	1.125	8.500	34.02	.3941	2.814	2.225	177.0	88,500	115.64
		12	12.75	5S	0.156	12.438	6.17	.8438	3.338	3.26	378.7
10S	0.180			12.390	7.11	.8373	3.338	3.24	375.8	187,900	24.17
20	0.250			12.250	9.82	.8185	3.338	3.21	367.0	183,500	33.38
30	0.330			12.090	12.88	.7972	3.338	3.17	358.0	179,000	43.77
ST, 40S	0.375			12.000	14.58	.7854	3.338	3.14	352.5	176,250	49.56
40	0.406			11.938	15.74	.7773	3.338	3.13	349.0	174,500	53.52
XS, 80S	0.500			11.750	19.24	.7530	3.338	3.08	338.0	169,000	65.42
60	0.562			11.626	21.52	.7372	3.338	3.04	331.0	165,500	73.15
80	0.688			11.374	26.07	.7056	3.338	2.98	316.7	158,350	88.63
100	0.844			11.062	31.57	.6674	3.338	2.90	299.6	149,800	107.32
120, XX	1.000			10.750	36.91	.6303	3.338	2.81	283.0	141,500	125.49
140	1.125			10.500	41.09	.6013	3.338	2.75	270.0	135,000	139.67
160	1.312	10.126	47.14	.5592	3.338	2.65	251.0	125,500	160.27		
14	14	5S	0.156	13.688	6.78	1.0219	3.665	3.58	459	229,500	23.07
		10S	0.188	13.624	8.16	1.0125	3.665	3.57	454	227,000	27.73
		10	0.250	13.500	10.80	0.9940	3.665	3.53	446	223,000	36.71
		20	0.312	13.376	13.42	0.9750	3.665	3.50	438	219,000	45.61
		30, ST	0.375	13.250	16.05	0.9575	3.665	3.47	430	215,000	54.57
		40	0.438	13.124	18.66	0.9397	3.665	3.44	422	211,000	63.44
		XS	0.500	13.000	21.21	0.9218	3.665	3.40	414	207,000	72.09
		60	0.594	12.812	25.02	0.8957	3.665	3.35	402	201,000	85.05
		80	0.750	12.500	31.22	0.8522	3.665	3.27	382	191,000	106.13
		100	0.938	12.124	38.49	0.8017	3.665	3.17	360	180,000	130.85
		120	1.094	11.812	44.36	0.7610	3.665	3.09	342	171,000	150.79
		140	1.250	11.500	50.07	0.7213	3.665	3.01	324	162,000	170.21
160	1.406	11.188	55.63	0.6827	3.665	2.93	306	153,000	189.11		
16	16	5S	0.165	15.670	8.21	1.3393	4.189	4.10	601	300,500	27.90
		10S	0.188	15.624	9.34	1.3314	4.189	4.09	598	299,000	31.75
		10	0.250	15.500	12.37	1.3104	4.189	4.06	587	293,500	42.05

10-80 TRANSPORT AND STORAGE OF FLUIDS

TABLE 10-22 Properties of Steel Pipe (Concluded)

Nominal pipe size, in	Outside diameter, in	Schedule no.	Wall thickness, in	Inside diameter, in	Cross-sectional area		Circumference, ft, or surface, ft ² /ft of length		Capacity at 1-ft/s velocity		Weight of plain-end pipe, lb/ft		
					Metal, in ²	Flow, ft ²	Outside	Inside	U.S. gal/min	lb/h water			
18	18	20	0.312	15.376	15.38	1.2985	4.189	4.03	578	289,000	52.27		
		30, ST	0.375	15.250	18.41	1.2680	4.189	3.99	568	284,000	62.58		
		40, XS	0.500	15.000	24.35	1.2272	4.189	3.93	550	275,000	82.77		
		60	0.656	14.688	31.62	1.1766	4.189	3.85	528	264,000	107.50		
		80	0.844	14.312	40.19	1.1171	4.189	3.75	501	250,500	136.61		
		100	1.031	13.938	48.48	1.0596	4.189	3.65	474	237,000	164.82		
		120	1.219	13.562	56.61	1.0032	4.189	3.55	450	225,000	192.43		
		140	1.438	13.124	65.79	0.9394	4.189	3.44	422	211,000	223.64		
		160	1.594	12.812	72.14	0.8953	4.189	3.35	402	201,000	245.25		
		5S	0.165	17.670	9.25	1.7029	4.712	4.63	764	382,000	31.43		
		10S	0.188	17.624	10.52	1.6941	4.712	4.61	760	379,400	35.76		
		10	0.250	17.500	13.94	1.6703	4.712	4.58	750	375,000	47.39		
		20	0.312	17.376	17.34	1.6468	4.712	4.55	739	369,500	58.94		
		ST	0.375	17.250	20.76	1.6230	4.712	4.52	728	364,000	70.59		
		30	0.438	17.124	24.16	1.5993	4.712	4.48	718	359,000	82.15		
		XS	0.500	17.000	27.49	1.5763	4.712	4.45	707	353,500	93.45		
40	0.562	16.876	30.79	1.5533	4.712	4.42	697	348,500	104.67				
60	0.750	16.500	40.64	1.4849	4.712	4.32	666	333,000	138.17				
80	0.938	16.124	50.28	1.4180	4.712	4.22	636	318,000	170.92				
100	1.156	15.688	61.17	1.3423	4.712	4.11	602	301,000	207.96				
120	1.375	15.250	71.82	1.2684	4.712	3.99	569	284,500	244.14				
140	1.562	14.876	80.66	1.2070	4.712	3.89	540	270,000	274.22				
160	1.781	14.438	90.75	1.1370	4.712	3.78	510	255,000	308.50				
20	20	5S	0.188	19.624	11.70	2.1004	5.236	5.14	943	471,500	39.78		
		10S	0.218	19.564	13.55	2.0878	5.236	5.12	937	467,500	46.06		
		10	0.250	19.500	15.51	2.0740	5.236	5.11	930	465,000	52.73		
		20, ST	0.375	19.250	23.12	2.0211	5.236	5.04	902	451,000	78.60		
		30, XS	0.500	19.000	30.63	1.9689	5.236	4.97	883	441,500	104.13		
		40	0.594	18.812	36.21	1.9302	5.236	4.92	866	433,000	123.11		
		60	0.812	18.376	48.95	1.8417	5.236	4.81	826	413,000	166.40		
		80	1.031	17.938	61.44	1.7550	5.236	4.70	787	393,500	208.87		
		100	1.281	17.438	75.33	1.6585	5.236	4.57	744	372,000	256.10		
		120	1.500	17.000	87.18	1.5763	5.236	4.45	707	353,500	296.37		
		140	1.750	16.500	100.3	1.4849	5.236	4.32	665	332,500	341.09		
		160	1.969	16.062	111.5	1.4071	5.236	4.21	632	316,000	397.17		
		24	24	5S	0.218	23.564	16.29	3.0285	6.283	6.17	1359	679,500	55.37
				10, 10S	0.250	23.500	18.65	3.012	6.283	6.15	1350	675,000	63.41
				20, ST	0.375	23.250	27.83	2.948	6.283	6.09	1325	662,500	94.62
				XS	0.500	23.000	36.90	2.885	6.283	6.02	1295	642,500	125.49
30	0.562			22.876	41.39	2.854	6.283	5.99	1281	640,500	140.68		
40	0.688			22.624	50.39	2.792	6.283	5.92	1253	626,500	171.29		
60	0.969			22.062	70.11	2.655	6.283	5.78	1192	596,000	238.35		
80	1.219			21.562	87.24	2.536	6.283	5.64	1138	569,000	296.58		
100	1.531			20.938	108.1	2.391	6.283	5.48	1073	536,500	367.39		
120	1.812			20.376	126.3	2.264	6.283	5.33	1016	508,000	429.39		
140	2.062			19.876	142.1	2.155	6.283	5.20	965	482,500	483.12		
160	2.344			19.312	159.5	2.034	6.283	5.06	913	456,500	542.13		
30	30			5S	0.250	29.500	23.37	4.746	7.854	7.72	2130	1,065,000	79.43
				10, 10S	0.312	29.376	29.10	4.707	7.854	7.69	2110	1,055,000	98.93
				ST	0.375	29.250	34.90	4.666	7.854	7.66	2094	1,048,000	118.65
				20, XS	0.500	29.000	46.34	4.587	7.854	7.59	2055	1,027,500	157.53
		30	0.625	28.750	57.68	4.508	7.854	7.53	2020	1,010,000	196.08		

5S, 10S, 40S, and 80S are extracted from Stainless Steel Pipe, ASME B36.19M-1985, with permission of the publisher, the American Society of Mechanical Engineers, New York. ST = standard wall, XS = extra strong wall, XX = double extra strong wall, and Schedules 10 through 160 are extracted from Welded and Seamless Wrought Steel Pipe, ASME B36.10M-1996, with permission of the same publisher. Refer to these standards for a more comprehensive listing of material sizes and wall thicknesses. Decimal thicknesses for respective pipe sizes represent their nominal or average wall dimensions. Mill tolerances as high as ±12½ percent are permitted.

Plain-end pipe is produced by a square cut. Pipe is also shipped from the mills threaded, with a threaded coupling on one end, or with the ends beveled for welding, or grooved or sized for patented couplings.

To convert inches to millimeters, multiply by 25.4; to convert square inches to square millimeters, multiply by 645; to convert feet to meters, multiply by 0.3048; to convert square feet to square meters, multiply by 0.0929; to convert pounds per foot to kilograms per meter, multiply by 1.49; to convert gallons to cubic meters, multiply by 3.7854 × 10⁻³; and to convert pounds to kilograms, multiply by 0.4536.



FIG. 10-128 Butt weld.

for nondestructive examination; however, branch connections are commonly specified for branches smaller than the header, and often best satisfy the design and economic requirements. Design of fabricated branch connections is addressed in the subsection "Pressure Design of Metallic Components: Wall Thickness." Integrally reinforced fittings are generally specified as requiring compliance with Manufacturer's Standardization Society specification MSS SP-97, *Integrally Reinforced Forged Branch Outlet Fittings—Socket Welding, Threaded, and Butt Welding Ends*.

Threaded Joints Pipe with **taper-pipe-thread** ends (Fig. 10-131), per ASME B1.20.1, is available 12 in and smaller, subject to minimum-wall limitations. Fittings and valves with taper-pipe-thread ends are available in most pipe metals.

Principal use of threaded joints is in sizes 2 in and smaller, in metals for which the most economically produced walls are thick enough to withstand pressure and corrosion after reduction in thickness due to threading. For threaded joints over 2 in, assembly difficulty and cost of tools increase rapidly. Careful alignment, required at the start of assembly and during rotation of the components, as well as variation in length produced by diametral tolerances in the threads, severely limits preassembly of the components. Threading is not a precise machining operation, and filler materials known as "pipe dope" are necessary to block the spiral leakage path.

Threads notch the pipe and cause loss of strength and fatigue resistance. Enlargement and contraction of the flow passage at threaded joints creates turbulence; sometimes corrosion and erosion are aggravated at the point where the pipe has already been thinned by threading. The tendency of pipe wrenches to crush pipe and fittings limits the torque available for tightening threaded joints. For low-pressure systems, a slight rotation in the joint may be used to impart flexibility to the system, but this same rotation, unwanted, may cause leaks to develop in higher-pressure systems. In some metals, galling occurs when threaded joints are disassembled.

Straight Pipe Threads These are confined to light-weight couplings in sizes 2 in and smaller (Fig. 10-132). Manufacturers of threaded pipe ship it with such couplings installed on one end of each pipe. The joint obtained is inferior to that obtained with taper threads. The code limits the joint shown in Fig. 10-129 to 1.0 MPa (150 lbf/in²) gauge maximum, 182°C (360°F) maximum, and to nonflammable, nontoxic fluids.

When both components of a threaded joint are of weldable metal, the joint may be **seal-welded** as shown in Fig. 10-133. Seal welds may be used only to prevent leakage of threaded joints. They are not considered as contributing any strength to the joint. This type of joint is limited to new construction and is not suitable as a repair procedure, since pipe dope in the threads would interfere with welding. Careful consideration should be given to the suitability of threaded joints when joining metals having significantly different coefficients of expansion. Thermal expansion and temperature cycling may eventually result in leakage.

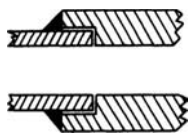
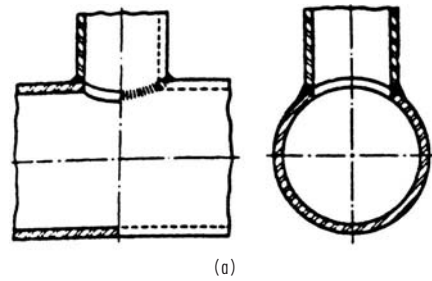
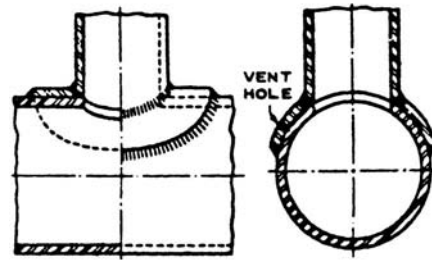


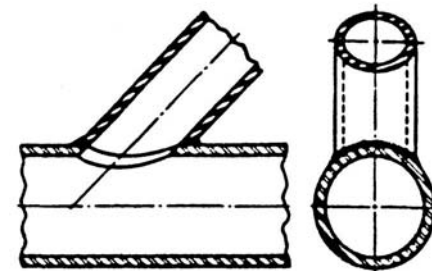
FIG. 10-129 Socket weld.



(a)



(b)



(c)

FIG. 10-130 Branch welds. (a) Without added reinforcement. (b) With added reinforcement. (c) Angular branch.

To assist in assembly and disassembly of both threaded and welded systems, **union joints** (Fig. 10-134) are used. They comprise metal-to-metal or gasketed seats drawn together by a shouldered straight thread nut and are available both in couplings for joining two lengths of pipe and on the ends of some fittings. On threaded piping systems in which disassembly is not contemplated, union joints installed at intervals permit future further tightening of threaded joints. Tightening of heavy unions yields tight joints even if the pipe is slightly misaligned at the start of tightening.

Flanged Joints For sizes larger than 2 in when disassembly is contemplated, the flanged joint (Fig. 10-135) is the most widely used. Figures 10-136 and 10-137 illustrate the wide variety of types and facings available. Though flanged joints consume a large volume of metal, precise machining is required only on the facing. Flanged joints do not impose severe diametral tolerances on the pipe. Alignment tolerances required for flanged joints are reasonably achieved with quality construction practices, and in comparison with taper threaded joints, required wrench sizes are smaller and sealing is more easily and reliably obtained.

Manufacturers offer **flanged-end pipe** in only a few metals. Otherwise, flanges are attached to pipe by various types of joints (Fig. 10-136). The lap joint involves a modification of the pipe which may be formed from the pipe itself or by welding a ring or a lap-joint stub end to it. **Flanged-end fittings** and valves are available in all sizes of most pipe metals.

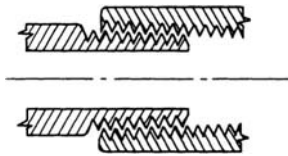


FIG. 10-131 Taper pipe thread.

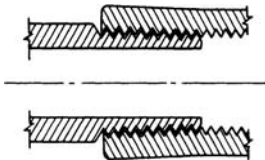


FIG. 10-132 Taper pipe to straight coupling thread.

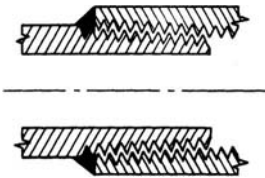


FIG. 10-133 Taper pipe thread seal-welded.

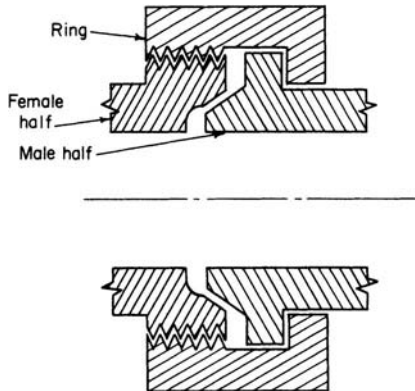


FIG. 10-134 Union.

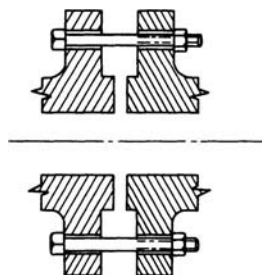


FIG. 10-135 Flanged joint.

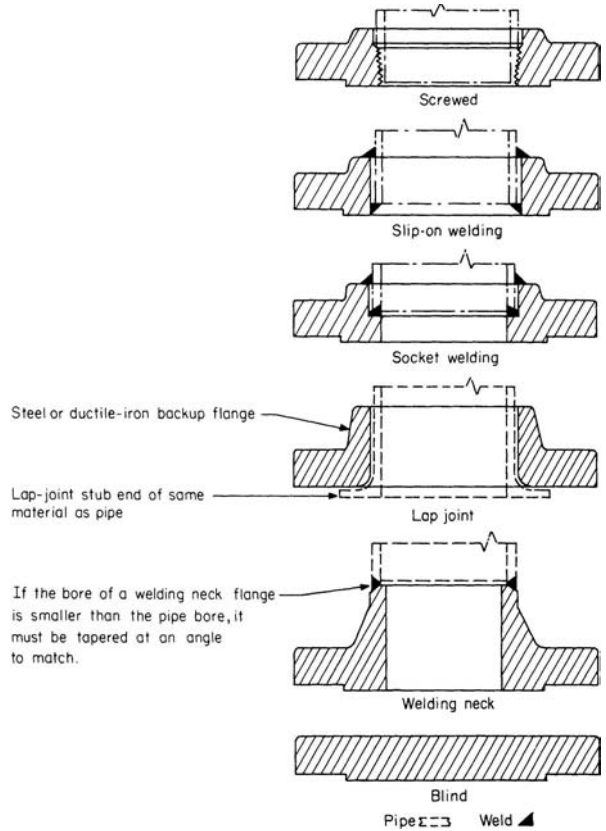


FIG. 10-136 Types of carbon and alloy steel flanges.

Of the flange types shown in Fig. 10-136, welding-neck flanges offer the highest mechanical strength and are the type most suitable for extreme temperatures and cyclic loading. Regardless of the type selected, designers must be aware that the flange's capability to resist external bending moments and maintain its seal does not necessarily match the bending moment capability of the attached pipe.

When selecting the flange type, the designer should review the usage restrictions contained in each section of the ASME B31 code. Each of the other types shown provides significant fabrication and economic advantages and is suitable for many of the routine applications. Lap-joint flanges permit adjustment of the bolt hole orientation and can greatly simplify construction when configurations are complex and bolt hole orientations are difficult to ensure.

Dimensions for alloy and carbon-steel pipe flanges are given in Tables 10-23 through 10-29. The dimensions were extracted from *Pipe Flanges and Flanged Fittings*, ASME B16.5-2003, with permission of the publisher, the American Society of Mechanical Engineers, New York. Dimensions for cast-iron flanges are provided in *Cast Iron Pipe Flanges and Flanged Fittings*, ASME B16.1. Bolt patterns and bolt sizes for Class 125 cast-iron flanges match the ASME B16.5 Class 150 flange dimensions, and bolt patterns for Class 250 cast-iron flanges match the ASME B16.5 Class 300 flange dimensions.

When mating with cast-iron flanged fittings or valves, steel pipe flanges are often preferred to cast-iron flanges because they permit welded rather than screwed assembly to the pipe and because cast-iron pipe flanges, not being reinforced by the pipe, are not so resistant to abuse as flanges cast integrally on cast-iron fittings.

Facing of flanges for alloy and carbon steel pipe and fittings is shown in Fig. 10-137; Class 125 cast-iron pipe and fitting flanges have flat faces, which with full-face gaskets minimize bending stresses; Class 250 cast-iron pipe and fitting flanges have 1.5-mm

TABLE 10-23 Dimensions of ASME B16.5 Class 150 Flanges*

All dimensions in inches

Nominal pipe size	Outside diameter of flange	Thickness of flange, minimum	Diameter of flange, minimum	Diameter of bolt circle	No. of bolts	Length through hub			
						Threaded slip-on socket welding	Lap joint	Welding neck	ANSI B16.1, screwed (125-lb)
1/2	3.50	0.44	2.38	1/2	4	0.62	0.62	1.88	
3/4	3.88	0.50	2.75	1/2	4	0.62	0.62	2.06	
1	4.25	0.56	3.12	1/2	4	0.69	0.69	2.19	0.69
1 1/4	4.62	0.62	3.50	1/2	4	0.81	0.81	2.25	0.81
1 1/2	5.00	0.69	3.88	1/2	4	0.88	0.88	2.44	0.88
2	6.00	0.75	4.75	5/8	4	1.00	1.00	2.50	1.00
2 1/2	7.00	0.88	5.50	5/8	4	1.12	1.12	2.75	1.12
3	7.50	0.94	6.00	5/8	4	1.19	1.19	2.75	1.19
3 1/2	8.50	0.94	7.00	5/8	8	1.25	1.25	2.81	1.25
4	9.00	0.94	7.50	5/8	8	1.31	1.31	3.00	1.31
5	10.00	0.94	8.50	3/4	8	1.44	1.44	3.50	1.44
6	11.00	1.00	9.50	3/4	8	1.56	1.56	3.50	1.56
8	13.50	1.12	11.75	3/4	8	1.75	1.75	4.00	1.75
10	16.00	1.19	14.25	7/8	12	1.94	1.94	4.00	1.94
12	19.00	1.25	17.00	7/8	12	2.19	2.19	4.50	2.19
14	21.00	1.38	18.75	1	12	2.25	3.12	5.00	2.25
16	23.50	1.44	21.25	1	16	2.50	3.44	5.00	2.50
18	25.00	1.56	22.75	1 1/8	16	2.69	3.81	5.00	2.69
20	27.50	1.69	25.00	1 1/8	20	2.88	4.06	5.69	2.88
24	32.00	1.88	29.50	1 1/4	20	3.25	4.38	6.00	3.25

*Dimensions from ASME B16.5-2003, unless otherwise noted. To convert inches to millimeters, multiply by 25.4.

(1/16-in) raised faces (wider than on steel flanges) for the same purpose. Carbon steel and ductile- (nodular-) iron lap-joint flanges are widely used as backup flanges with stub ends in piping systems of austenitic stainless steel and other expensive materials to reduce costs (see Fig. 10-136). The code prohibits the use of ductile-iron flanges at temperatures above 343°C (650°F). When the type of facing affects the length through the hub dimension of flanges, correct dimensions for commonly used facings can be determined from the dimensional data in Fig. 10-137.

Gaskets Gaskets must resist corrosion by the fluids handled. The more expensive male-and-female or tongue-and-groove facings may be required to seat hard gaskets adequately. With these facings the gasket generally cannot blow out. Flanged joints, by placing the gasket material under heavy compression and permitting only edge attack by the fluid handled, can use gasket materials which in other joints might not satisfactorily resist the fluid handled.

Standards to which flanges are manufactured (e.g., ASME B16.1, ASME B16.5, ASME B16.47) typically specify a standard surface finish

TABLE 10-24 Dimensions of ASME B16.5 Class 300 Flanges*

All dimensions in inches

Nominal pipe size	Outside diameter of flange	Thickness of flange, minimum	Diameter of bolt circle	Diameter of bolts	No. of bolts	Length through hub			
						Threaded slip-on socket welding	Lap joint	Welding neck	ANSI B16.1, screwed (Class 250)
1/2	3.75	0.56	2.62	1/2	4	0.88	0.88	2.06	
3/4	4.62	0.62	3.25	5/8	4	1.00	1.00	2.25	
1	4.88	0.69	3.50	5/8	4	1.06	1.06	2.44	0.88
1 1/4	5.25	0.75	3.88	5/8	4	1.06	1.06	2.56	1.00
1 1/2	6.12	0.81	4.50	3/4	4	1.19	1.19	2.69	1.12
2	6.50	0.88	5.00	5/8	8	1.31	1.31	2.75	1.25
2 1/2	7.50	1.00	5.88	3/4	8	1.50	1.50	3.00	1.43
3	8.25	1.12	6.62	3/4	8	1.69	1.69	3.12	1.56
3 1/2	9.00	1.19	7.25	3/4	8	1.75	1.75	3.19	1.62
4	10.00	1.25	7.88	3/4	8	1.88	1.88	3.38	1.75
5	11.00	1.38	9.25	3/4	8	2.00	2.00	3.88	1.88
6	12.50	1.44	10.62	3/4	12	2.06	2.06	3.88	1.94
8	15.00	1.62	13.00	7/8	12	2.44	2.44	4.38	2.19
10	17.50	1.88	15.25	1	16	2.62	3.75	4.62	2.38
12	20.50	2.00	17.75	1 1/8	16	2.88	4.00	5.12	2.56
14	23.00	2.12	20.25	1 1/8	20	3.00	4.38	5.62	2.69
16	25.50	2.25	22.50	1 1/4	20	3.25	4.75	5.75	2.88
18	28.00	2.38	24.75	1 1/4	24	3.50	5.12	6.25	
20	30.50	2.50	27.00	1 1/4	24	3.75	5.50	6.38	
24	36.00	2.75	32.00	1 1/2	24	4.19	6.00	6.62	

*Dimensions from ASME B16.5-2003, unless otherwise noted. To convert inches to millimeters, multiply by 25.4.

10-84 TRANSPORT AND STORAGE OF FLUIDS

TABLE 10-25 Dimensions of ASME B16.5 Class 400 Flanges*

All dimensions in inches

Nominal pipe size	Outside diameter of flange	Thickness of flange, minimum	Diameter of bolt circle	Diameter of bolts	No. of bolts	Length through hub		
						Threaded slip-on socket welding	Lap joint	Welding neck
1/2								
3/4								
1								
1 1/4								
1 1/2								
	Use Class 600 dimensions in these sizes.							
2								
2 1/2								
3								
3 1/2								
4	10.00	1.38	7.88	7/8	8	2.00	2.00	3.50
5	11.00	1.50	9.25	7/8	8	2.12	2.12	4.00
6	12.50	1.62	10.62	7/8	12	2.25	2.25	4.06
8	15.00	1.88	13.00	1	12	2.69	2.69	4.62
10	17.50	2.12	15.25	1 1/4	16	2.88	4.00	4.88
12	20.50	2.25	17.75	1 1/4	16	3.12	4.25	5.38
14	23.00	2.38	20.25	1 1/4	20	3.31	4.62	5.88
16	25.50	2.50	22.50	1 3/4	20	3.69	5.00	6.00
18	28.00	2.62	24.75	1 3/4	24	3.88	5.38	6.50
20	30.50	2.75	27.00	1 1/2	24	4.00	5.75	6.62
24	36.00	3.00	32.00	1 3/4	24	4.50	6.25	6.88

*Dimensions from ASME B16.5-2003. To convert inches to millimeters, multiply by 25.4.

for the gasket seal area. Flange rating and type, flange size, flange facing type, gasket style, commodity, design conditions, and bolting must all be considered to ensure proper seating of the gasket and reliable performance. Unless the user is familiar with gasket design and the particular application being considered, it is highly recommended that the gasket manufacturer be consulted regarding gasket selection. Upon request, gasket manufacturers typically provide assistance in determining the proper material selection and the proper gasket style to ensure an economical choice and a reliable system.

When appropriate for the commodity, elastomer sheet gaskets without fillers are generally the least expensive gasket type. They are

typically limited to Class 150 and temperatures below 120°C (250°F). Composition sheet gaskets are somewhat more expensive than elastomer sheet gaskets. They are generally composed of an elastomer binder with fiber filler. Their use is generally limited to Class 150 and Class 300, and depending on the filler selected the upper temperature limit typically ranges between 205°C (400°F) and 370°C (700°F). Nonelastomer sheet gaskets, such as graphite sheet gaskets, are generally somewhat more expensive than composition sheet gaskets. Their use is typically limited to Class 150 and Class 300, and the upper temperature limit may be 535°C (1000°F) or higher. Spiral-wound gaskets with graphite, PTFE, or other filler are generally appropriate

TABLE 10-26 Dimensions of ASME B16.5 Class 600 Flanges*

All dimensions in inches

Nominal pipe size	Outside diameter of flange	Thickness of flange, minimum	Diameter of bolt circle	Diameter of bolts	No. of bolts	Length through hub		
						Threaded slip-on socket welding	Lap joint	Welding neck
1/2	3.75	0.56	2.62	1/2	4	0.88	0.88	2.06
3/4	4.62	0.62	3.25	3/8	4	1.00	1.00	2.25
1	4.88	0.69	3.50	3/8	4	1.06	1.06	2.44
1 1/4	5.25	0.81	3.88	3/8	4	1.12	1.12	2.62
1 1/2	6.12	0.88	4.50	3/4	4	1.25	1.25	2.75
2	6.50	1.00	5.00	3/8	8	1.44	1.44	2.88
2 1/2	7.50	1.12	5.88	3/4	8	1.62	1.62	3.12
3	8.25	1.25	6.62	3/4	8	1.81	1.81	3.25
3 1/2	9.00	1.38	7.25	7/8	8	1.94	1.94	3.38
4	10.75	1.50	8.50	7/8	8	2.12	2.12	4.00
5	13.00	1.75	10.50	1	8	2.38	2.38	4.50
6	14.00	1.88	11.50	1	12	2.62	2.62	4.62
8	16.50	2.19	13.75	1 1/8	12	3.00	3.00	5.25
10	20.00	2.50	17.00	1 1/4	16	3.38	4.38	6.00
12	22.00	2.62	19.25	1 1/4	20	3.62	4.62	6.12
14	23.75	2.75	20.75	1 3/4	20	3.69	5.00	6.50
16	27.00	3.00	23.75	1 1/2	20	4.19	5.50	7.00
18	29.25	3.25	25.75	1 3/4	20	4.62	6.00	7.25
20	32.00	3.50	28.50	1 3/4	24	5.00	6.50	7.50
24	37.00	4.00	33.00	1 3/4	24	5.50	7.25	8.00

*Dimensions from ASME B16.5-2003. To convert inches to millimeters, multiply by 25.4.

TABLE 10-27 Dimensions of ASME B16.5 Class 900 Flanges*

All dimensions in inches

Nominal pipe size	Outside diameter of flange	Thickness of flange, minimum	Diameter of bolt circle	Diameter of bolts	No. of bolts	Length through hub		
						Threaded slip-on socket welding	Lap joint	Welding neck
1/2								
3/4								
1								
1 1/4								
1 1/2								
2								
2 1/2								
Use Class 1500 dimensions in these sizes.								
3	9.50	1.50	7.50	7/8	8	2.12	2.12	4.00
4	11.50	1.75	9.25	1 1/8	8	2.75	2.75	4.50
5	13.75	2.00	11.00	1 1/4	8	3.12	3.12	5.00
6	15.00	2.19	12.50	1 1/4	12	3.38	3.38	5.50
8	18.50	2.50	15.50	1 3/8	12	4.00	4.50	6.38
10	21.50	2.75	18.50	1 3/8	16	4.25	5.00	7.25
12	24.00	3.12	21.00	1 3/8	20	4.62	5.62	7.88
14	25.25	3.38	22.00	1 1/2	20	5.12	6.12	8.38
16	27.75	3.50	24.25	1 3/4	20	5.25	6.50	8.50
18	31.00	4.00	27.00	1 7/8	20	6.00	7.50	9.00
20	33.75	4.25	29.50	2	20	6.25	8.25	9.75
24	41.00	5.50	35.50	2 1/2	20	8.00	10.50	11.50

*Dimensions from ASME B16.5-2003. To convert inches to millimeters, multiply by 25.4.

for applications more demanding than those handled by sheet gaskets. They are generally more expensive than sheet gaskets and are commonly used in Class 150 through Class 1500 services (and higher) class ratings. Because of their breadth of capabilities and the advantages of standardizing, they are often used when less expensive gaskets would suffice. The solid metal outer ring on spiral-wound gaskets serves to center the gasket and provide blowout resistance. With the proper filler, spiral-wound gaskets and some sheet gaskets provide good sealing under fire conditions.

Ring Joint Flanges Ring joint (RTJ) flanges provide sealing capability for pressure-temperature combinations higher than those for which spiral-wound gaskets are typically used. Depending on the

service, use of RTJ flanges is often considered in Class 900 and higher applications. RTJ flange facings and gaskets are more expensive than the spiral-wound counterparts. The ring material must be softer than the flange seating surface, and corrosion-resistant to the service. They provide good resistance to leakage under fire conditions. RTJ flanges must be separated in the axial direction to permit insertion and removal of the gasket.

Bolting Bolt strength requirements are addressed to some extent by the code and by code-referenced flange standards. Bolts are categorized by the code as high strength, intermediate strength, and low strength. Bolting materials having allowable stresses meeting or exceeding those of ASTM A193 Grade B7 are categorized as high

TABLE 10-28 Dimensions of ASME B16.5 Class 1500 Flanges*

All dimensions in inches

Nominal pipe size	Outside diameter of flange	Thickness of flange, minimum	Diameter of bolt circle	Diameter of bolts	No. of bolts	Length through hub		
						Threaded slip-on socket welding	Lap joint	Welding neck
1/2	4.75	0.88	3.25	3/4	4	1.25	1.25	2.38
3/4	5.12	1.00	3.50	3/4	4	1.38	1.38	2.75
1	5.88	1.12	4.00	7/8	4	1.62	1.62	2.88
1 1/4	6.25	1.12	4.38	7/8	4	1.62	1.62	2.88
1 1/2	7.00	1.25	4.88	1	4	1.75	1.75	3.25
2	8.50	1.50	6.50	7/8	8	2.25	2.25	4.00
2 1/2	9.62	1.62	7.50	1	8	2.50	2.50	4.12
3	10.50	1.88	8.00	1 1/8	8	2.88	2.88	4.62
4	12.25	2.12	9.50	1 1/4	8	3.56	3.56	4.88
5	14.75	2.88	11.50	1 1/2	8	4.12	4.12	6.12
6	15.50	3.25	12.50	1 3/8	12	4.69	4.69	6.75
8	19.00	3.62	15.50	1 3/8	12	5.62	5.62	8.38
10	23.00	4.25	19.00	1 7/8	12	6.25	7.00	10.00
12	26.50	4.88	22.50	2	16	7.12	8.62	11.12
14	29.50	5.25	25.00	2 1/4	16		9.50	11.75
16	32.50	5.75	27.75	2 1/2	16		10.25	12.25
18	36.00	6.38	30.50	2 3/4	16		10.88	12.88
20	38.75	7.00	32.75	3	16		11.50	14.00
24	46.00	8.00	39.00	3 1/2	16		13.00	16.00

*Dimensions from ASME B16.5-2003. To convert inches to millimeters, multiply by 25.4.

TABLE 10-29 Dimensions of ASME B16.5 Class 2500*

All dimensions in inches

Nominal pipe size	Outside diameter of flange	Thickness of flange, minimum	Diameter of bolt circle	Diameter of bolts	No. of bolts	Length through hub		
						Threaded	Lap joint	Welding neck
1/2	5.25	1.19	3.50	3/4	4	1.56	1.56	2.88
3/4	5.50	1.25	3.75	3/4	4	1.69	1.69	3.12
1	6.25	1.38	4.25	7/8	4	1.88	1.88	3.50
1 1/4	7.25	1.50	5.12	1	4	2.06	2.06	3.75
1 1/2	8.00	1.75	5.75	1 1/8	4	2.38	2.38	4.38
2	9.25	2.00	6.75	1	8	2.75	2.75	5.00
2 1/2	10.50	2.25	7.75	1 1/8	8	3.12	3.12	5.62
3	12.00	2.62	9.00	1 1/4	8	3.62	3.62	6.62
4	14.00	3.00	10.75	1 1/2	8	4.25	4.25	7.50
5	16.50	3.62	12.75	1 3/4	8	5.12	5.12	9.00
6	19.00	4.25	14.50	2	8	6.00	6.00	10.75
8	21.75	5.00	17.25	2	12	7.00	7.00	12.50
10	26.50	6.50	21.25	2 1/2	12	9.00	9.00	16.50
12	30.00	7.25	24.38	2 3/4	12	10.00	10.00	18.25

*Dimensions from ASME B16.5-2003. To convert inches to millimeters, multiply by 25.4.

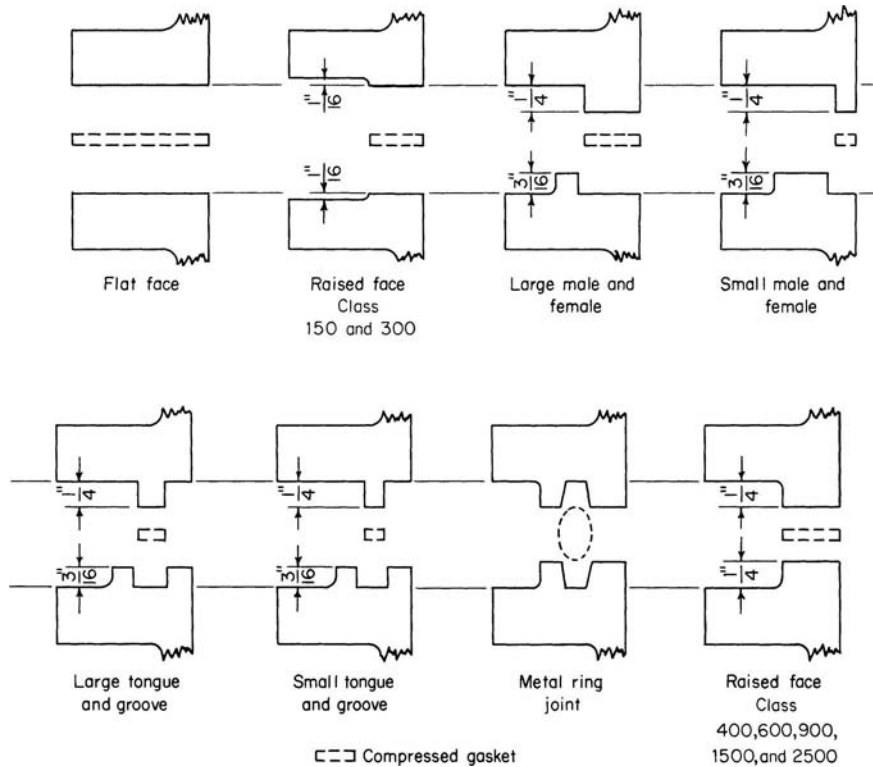


FIG. 10-137 Flange facings, illustrated on welding-neck flanges. (On small male-and-female facings the outside diameter of the male face is less than the outside diameter of the pipe, so this facing does not apply to screwed or slip-on flanges. A similar joint can be made with screwed flanges and threaded pipe by projecting the pipe through one flange and recessing it in the other. However, pipe thicker than Schedule 40 is required to avoid crushing gaskets.) To convert inches to millimeters, multiply by 25.4.

strength. Bolting materials having specified minimum yield strengths of 207 MPa (30 ksi) or less are categorized as low strength. ASTM A307 Grade B is a commonly used specification for low-strength bolting.

The suitability of the strength of any bolting throughout the required temperature range should be verified by the designer. Verification of the suitability of intermediate-strength bolting for the intended joint design is required prior to its use. The code restricts the use of low-strength bolting to nonmetallic gaskets and flanges rated ASME B16.5 Class 300 and lower having bolt temperatures at -29 to 204°C (-20 to 400°F) inclusive. Low-strength bolting is not permitted for use under severe cyclic conditions as defined by the code.

Except when bolting brittle flange materials such as gray cast iron, the code permits the use of high-strength bolting for any style of flanged joint and gasket type combination. Per the code, if either mating flange is specified in accordance with ASME B16.1, ASME B16.24, MSS SP-42, or MSS SP-51, the bolting material shall be no stronger than low-strength unless both mating flanges have a flat face and a full-face gasket is used. Exception to this requirement is permitted if sequence and torque limits for bolt-up are specified, with consideration given to sustained and occasional loads, and displacement strains. When both flanges are flat face and the gasket is full face extending to the outside diameter of the flange, intermediate-strength and high-strength bolts may be used.

Miscellaneous Mechanical Joints

Packed-Gland Joints These joints (Fig. 10-138) require no special end preparation of pipe but do require careful control of the diameter of the pipe. Thus the supplier of the pipe should be notified when packed-gland joints are to be used. Cast- and ductile-iron pipe, fittings, and valves are available with the bell cast on one or more ends. Glands, bolts, and gaskets are shipped with the pipe. Couplings equipped with packed glands at each end, known as Dresser couplings, are available in several metals. The joints can be assembled with small wrenches and unskilled labor, in limited space, and if necessary, under water.

Packed-gland joints are designed to take the same hoop stress as the pipe. They do not resist bending moments or axial forces tending to separate the joints but yield to them to an extent indicated by the manufacturer's allowable-angular-deflection and end movement specifications. Further angular or end movement produces leakage, but end movement can be limited by harnessing or bridling with a combination of rods and welded clips or clamps, or by anchoring to existing or new structures. The crevice between the bell and the spigot may promote corrosion. The joints are widely used in underground lines. They are not affected by limited earth settlement, and friction of the earth is often adequate to prevent end separation. When disassembly by moving pipe axially is not practical, packed-joint couplings which can be slid entirely onto one of the two lengths joined are available.

Poured Joints Figure 10-139 illustrates a poured joint design. With regard to performance and ease of installation, most other joint

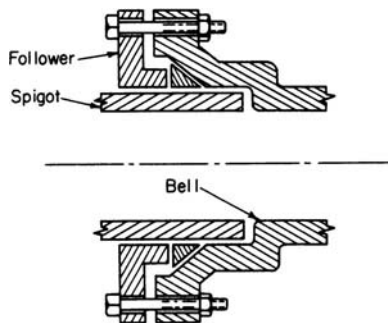


FIG. 10-138 Packed-gland joint.

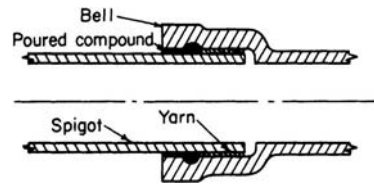


FIG. 10-139 Poured joint.

designs are preferable to poured joints, and their use can generally be avoided.

Push-on Joints These joints (Fig. 10-140) require diametral control of the end of the pipe. They are used for brittle and nonmetallic materials. Pipe, fittings, and valves are furnished with the bells on one or more ends.

Push-on joints do not resist bending moments or axial forces tending to separate the joints but yield to them to an extent limited by the manufacturer's allowable-angular-deflection and end-movement specifications. End movement can be limited by harnessing or bridling with a combination of rods and clamps, or by anchoring to existing or new structures. Some manufacturers offer O-rings with metallic embedments that grip the pipe and prevent axial separation under internal pressure loading. The joints are widely used on underground lines. They are not affected by limited earth settlement, and friction of the earth is often adequate to prevent end separation. A lubricant is used on the O ring during assembly. After this disappears, the O ring bonds somewhat to the spigot and disassembly is very difficult. Disassembly for maintenance is accomplished by cutting the pipe and reassembly by use of a coupling with a packed-gland joint on each end.

Expanded Joints These joints (Fig. 10-141) are confined to the smaller pipe sizes and ductile metals. Various proprietary designs are available in which either the pipe is expanded into the coupling or the

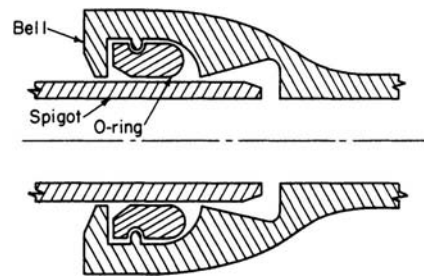


FIG. 10-140 Push-on joint.

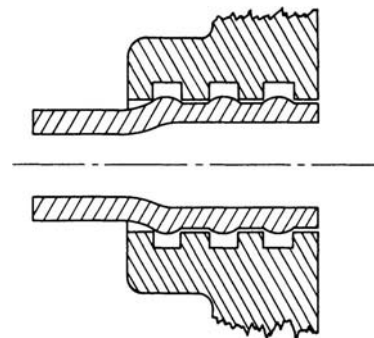


FIG. 10-141 Expanded joint.

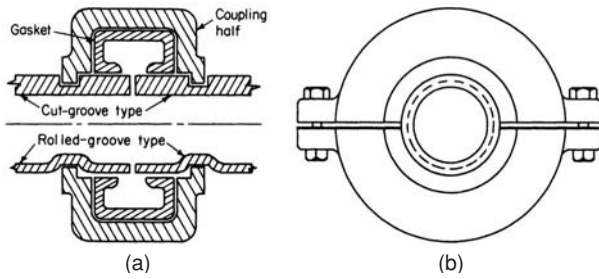


FIG. 10-142 Grooved joint. (a) Section. (b) End view.

coupling is crimped down onto the pipe. In some designs, the seal between the pipe and coupling is metal to metal, while in others elastomer O-rings are employed. Joints of these types typically are quickly and easily made with specialized equipment, and they may be particularly attractive in maintenance applications since no welding is involved. The designer should clearly understand the limitations of the joint design and should verify the success of its long-term service in similar applications.

Grooved Joints These joints (Fig. 10-142) are divided into two classes, cut grooves and rolled grooves. Rolled grooves are preferred because, compared with cut grooves, they are easier to form and reduce the metal wall less. However, they slightly reduce the flow area. They are limited to thin walls of ductile material, while cut grooves, because of their reduction of the pipe wall, are limited to thicker walls. In the larger pipe sizes, some commonly used wall thicknesses are too thick for rolled grooves but too thin for cut grooves. The thinning of the walls impairs resistance to corrosion and erosion but not to internal pressure, because the thinned area is reinforced by the coupling.

Control of outside diameter is important. Permissible minus tolerance is limited, since it impairs the grip of the couplings. Plus tolerance makes it necessary to cut the cut grooves more deeply, increasing the thinning of the wall. Plus tolerance is not a problem with rolled grooves, since they are confined to walls thin enough so that the couplings can compress the pipe. Pipe is available from vendors already grooved and also with heavier-wall grooved ends welded on.

Grooved joints resist axial forces tending to separate the joints. Angular deflection, up to the limit specified by the manufacturer, may be used to absorb thermal expansion and to permit the piping to be laid on uneven ground. Grooved joints provide quick and easy assembly and disassembly when compared with flanges, but may require more support than welded joints.

Gaskets are self-sealing against both internal and external pressure and are available in a wide variety of elastomers. However, successful performance of an elastomer as a flange gasket does not necessarily mean equally satisfactory performance in a grooved joint, since exposure to the fluid in the latter is much greater and hardening has a greater unfavorable effect. It is advisable to select coupling material that is suitably corrosion-resistant with respect to the service; but with proper gasket style it may be permissible to use a coupling material that might otherwise be unacceptable with respect to fluid contamination.

V-Clamp Joints These joints (Fig. 10-143) are attached to the pipe by butt-weld or expanded joints. Theoretically, there is only one relative position of the parts in which the conical surfaces of the clamp are completely in contact with the conical surfaces of the stub ends. In actual practice, there is considerable flexing of the stub ends and the clamp; also complete contact is not required. This permits use of elastomeric gaskets as well as metal gaskets. Fittings are also available with integral conical shouldered ends.

Conical ends vary from machined forgings to roll-formed tubing, and clamps vary from machined forgings to bands to which several roll-formed channels are attached at their centers by spot welding. A hinge may be inserted in the band as a substitute for one of the draw bolts. Latches may also be substituted for draw bolts.

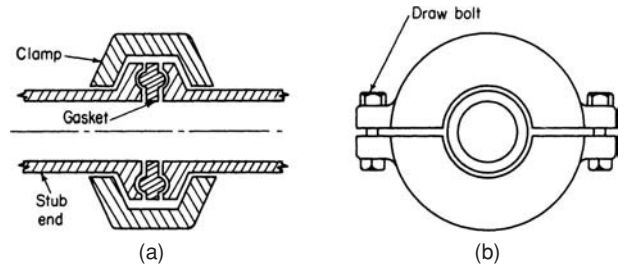


FIG. 10-143 V-clamp joint. (a) Section. (b) End view.

Compared with flanges, V-clamp joints use less metal, require less labor for assembly, and are less likely to leak under wide-range rapid temperature cycling. However, they are more susceptible to failure or damage from overtightening. They are widely used for high-alloy piping subject to periodic cleaning or relocation. Manufactured as forgings, they are used in carbon steel with metal gaskets for very high pressures. They resist both axial strain and bending moments. Each size of each type of joint is customarily rated by the vendor for both internal pressure and bending moment.

Seal Ring Joints These joints (Fig. 10-144) consist of hubs that are attached to pipe ends by welding. Joints of this type are proprietary, and their pressure/temperature ratings and external loading capabilities are established by the manufacturers. Variations of this design are offered by various manufacturers. Many of these designs have been widely used in critical high-pressure/temperature applications. They are particularly cost-effective in high-pressure alloy material applications.

Pressure-Seal Joints These joints (Fig. 10-145) are used for pressures of ASME Class 600 and higher. They use less metal than flanged joints but require much more machining of surfaces. There are several designs, in all of which increasing fluid pressure increases the force holding the sealing surfaces against each other. These joints are widely used as bonnet joints in carbon and alloy steel valves.

Tubing Joints Flared-fitting joints (see Fig. 10-146) are used for ductile tubing when the ratio of wall thickness to the diameter is small enough to permit flaring without cracking the inside surface. The tubing must have a smooth interior surface. The three-piece type avoids torsional strain on the tubing and minimizes vibration fatigue on the flared portion of the tubing. More labor is required for assembly, but the fitting is more resistant to temperature cycling than other tubing fittings and is less likely to be damaged by overtightening. Its efficiency is not impaired by repeated assembly and disassembly. Size is limited because of the large number of machined surfaces. The nut and, in the three-piece type, the sleeve need not be of the same material as the tubing. For these fittings, less control of tubing diameter is required.

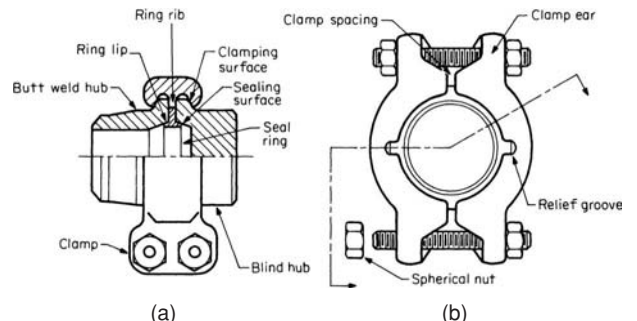


FIG. 10-144 Seal-ring joint. (Courtesy of Gray Tool Co.)

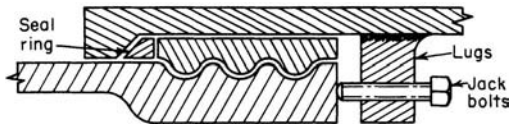
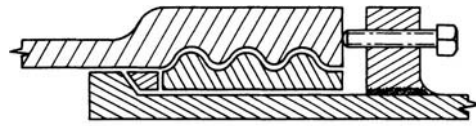


FIG. 10-145 Pressure-seal joint.



Compression-Fitting Joints These joints (Fig. 10-147) are used for ductile tubing with thin walls. The outside of the tubing must be clean and smooth. Assembly consists only of inserting the tubing and tightening the nut. These are the least costly tubing fittings but are not resistant to vibration or temperature cycling.

Bite-Type-Fitting Joints These joints (Fig. 10-148) are used when the tubing has too high a ratio of wall thickness to diameter for flaring, when the tubing lacks sufficient ductility for flaring, and for low assembly-labor cost. The outside of the tubing must be clean and smooth. Assembly consists in merely inserting the tubing and tightening the nut. The sleeve must be considerably harder than the tubing yet still ductile enough to be diametrically compressed and must be as resistant to corrosion by the fluid handled as the tubing. The fittings are resistant to vibration but not to wide-range rapid temperature cycling. Compared with flared fittings, they are less suited for repeated assembly and disassembly, require closer diametral control of the tubing, and are more susceptible to damage from overtightening. They are widely used for oil-filled hydraulic systems at all pressures.

O-ring Seal Joints These joints (Fig. 10-149) are also used for applications requiring heavy-wall tubing. The outside of the tubing must be clean and smooth. The joint may be assembled repeatedly, and as long as the tubing is not damaged, leaks can usually be corrected by replacing the O ring and the antiextrusion washer. This joint is used extensively in oil-filled hydraulic systems.

Soldered Joints These joints (Fig. 10-150) require precise control of the diameter of the pipe or tubing and of the cup or socket in the fitting in order to cause the solder to draw into the clearance between the cup and the tubing by capillary action (Fig. 10-150). Extrusion provides this diametral control, and the joints are most widely used in copper. A 50 percent lead, 50 percent tin solder is used for temperatures up to 93°C (200°F). Careful cleaning of the outside of the tubing and inside of the cup is required.

Heat for soldering is usually obtained from torches. The high conductivity of copper makes it necessary to use large flames for the larger sizes, and for this reason the location in which the joint will be made must be carefully considered. Soldered joints are most widely used in sizes 2 in and smaller for which heat requirements are less burdensome. Soldered joints should not be used in areas where plant fires are likely because exposure to fires results in rapid and complete failure of the joints. Properly made, the joints are completely impervious. The code permits the use of soldered joints only for Category D fluid service and then only if the system is not subject to severe cyclic conditions.

Silver Brazed Joints These are similar to soldered joints except that a temperature of about 600°C (1100°F) is required. A 15 percent silver, 80 percent copper, 5 percent phosphorus solder is used for copper and copper alloys, while 45 percent silver, 15 percent copper, 16 percent zinc, 24 percent cadmium solders are used for copper, copper alloys, carbon steel, and alloy steel. Silver-brazed joints are used for temperatures up to 200°C (400°F). Cast-bronze fittings and valves with preinserted rings of 15 percent silver, 80 percent copper, 5 percent phosphorus brazing alloy are available.

Silver-brazed joints are used when temperature or the combination of temperature and pressure is beyond the range of soldered joints. They are also more reliable in the event of plant fires and are more resistant to vibration. If they are used for fluids that are flammable, toxic, or damaging to human tissue, appropriate safeguarding is required by the code. There are OSHA regulations governing the use of silver brazing alloys containing cadmium and other toxic materials.

Pipe Fittings and Bends Directional changes in piping systems are typically made with bends or welded fittings. Bends are made as either hot bends or cold bends. Cold bending is done at temperatures below the material transformation temperature. Depending on the material and the amount of strain involved, annealing or stress relief may be required after bending. The bend radius that may be achieved for pipe of a given size, material, and thickness depends upon the bending machine capabilities and bending procedures used. When contemplating bending, the bending limitations should be reviewed with the pipe fabricators being considered for the project. Because bends are not generally made to radii as small as those of standard butt-weld or socket-weld fittings, the use of bends must be considered during piping layout. Wall thinning resulting from bending must also be considered when specifying the wall thickness of material that is to be bent. A detailed bending specification that addresses all aspects of bending, including requirements for bending procedure specifications, availability of bending procedure qualification records and bending operator qualification records, the range of bends covered by a single bending procedure qualification, in-process nondestructive examination requirements (including minimum wall thickness verification), dimensional tolerance requirements, etc., should be part of the bending agreement. Some bending operations and subsequent heat treatment can result in tenacious oxide formation on certain materials (such as 9Cr-1Mo-V). Removal of this oxide by conventional means such as abrasive blasting may be very difficult. Methods of avoiding this formation or of removing it should be discussed prior to bending when the application requires a high level of cleanliness, such as is the case with steam supply lines to turbines.

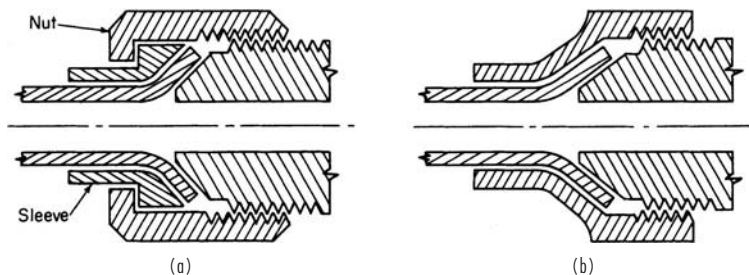


FIG. 10-146 Flared-fitting joint. (a) Three-piece. (b) Two-piece.

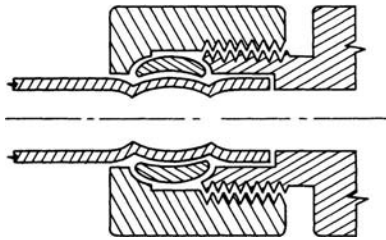


FIG. 10-147 Compression-fitting joint.

Elbow Fittings These fittings may be cast, forged, or hot- or cold-formed from short pieces of pipe or made by welding together pieces of miter-cut pipe. The thinning of pipe during the forming of elbows is compensated for by starting with heavier walls.

Flow in bends and elbow fittings is more turbulent than in straight pipe, thus increasing corrosion and erosion. This can be countered by selecting a component with greater radius of curvature, thicker wall, or smoother interior contour, but this is seldom economical in miter elbows.

Compared with elbow fittings, bends with a centerline radius of three or five nominal pipe diameters save the cost of joints and reduce pressure drop. It is sometimes difficult to nest bends of unequal pipe size when they lie in the same plane.

Flanged fittings are used when pipe is likely to be dismantled for frequent cleaning or extensive revision, or for lined piping systems. They are also used in areas where welding is not permitted. Cast fittings are usually flanged. Table 10-30 gives dimensions for flanged fittings.

Dimensions of carbon and alloy steel **butt-welding fittings** are shown in Table 10-31. Butt-welding fittings are available in the wall thicknesses shown in Table 10-22. Larger sizes and other wall thicknesses are also available. Schedule 5 and Schedule 10 stainless-steel butt-welding fittings are available with extensions for expanding into stainless-steel hubs mechanically locked in carbon steel ASME B16.5 dimension flanges. The use of expanded joints (Fig. 10-141) is restricted by the code.

Depending on the size, forged fittings are available with socket-weld (Fig. 10-129) or screwed ends in sizes 4 in and smaller; however, 2 in is the upper size limit normally used. ASME B16.11 gives minimum dimensions for Class 3000, 6000, and 9000 socket-weld fittings, and for Class 2000, 3000, and 6000 threaded fittings. The use of socket-weld and threaded fittings is restricted by the code.

Steel forged fittings with screwed ends may be installed without pipe dope in the threads and seal-welded (Fig. 10-133) to secure bubble-tight joints.

ASME B16.3-1998 gives pressure ratings and dimensions for Class 150 and Class 300 **malleable-iron threaded fittings**. Primary usage is 2 in and smaller; however, Class 150 fittings are available in 6 in and smaller, and Class 300 fittings are available in 3 in and smaller. Malleable-iron fittings are generally less expensive than forged carbon-

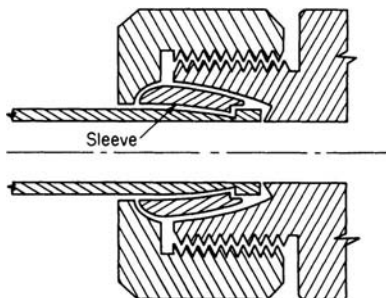


FIG. 10-148 Bite-type-fitting joint.

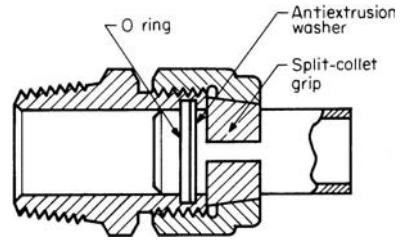


FIG. 10-149 O-ring seal joint. (Courtesy of the Lenz Co.)

steel fittings, but cannot be seal-welded. Threaded ends are typically female; however, male threads or a combination of male and female is available in some fittings. Among other restrictions, the code does not permit the use of malleable iron in severe cyclic conditions, in situations subject to thermal or mechanical shock, or in any fluid service below -29°C (-20°F) or above 343°C (650°F). It also does not permit its use in flammable fluid service at temperatures above 149°C (300°F) or at gauge pressures above 2.76 MPa (400 lbf/in²). ASME B16.3 ratings for Class 150 fittings are 2.07 MPa (300 lbf/in²) at 66°C (150°F) and below and 1.03 MPa (150 lbf/in²) at 186°C (366°F). ASME B16.3 ratings for Class 300 fittings are size-dependent, but at least 6.89 MPa (1000 lbf/in²) at 66°C (150°F) and below and 2.07 MPa (300 lbf/in²) at 288°C (550°F).

ASME B16.4-1998 gives pressure ratings and dimensions for Class 125 and Class 250 **gray-iron (cast-iron) threaded fittings**. Threaded fittings in both classes are available in sizes 12 in and smaller; however, consideration should be given to other types of end connections prior to using threaded fittings in sizes larger than 2 in. Threaded ends are typically female. Cast-iron fittings are less expensive than forged carbon steel fittings, but cannot be seal-welded. The code places significant restrictions on the use of cast iron, and its use is typically limited to low-pressure, noncritical, nonflammable services. Its brittle nature should be considered before using it for compressed gas services. The minimum permissible design temperature is 29°C (-20°F). ASME B16.4 ratings for Class 125 fittings are 1.21 MPa (175 lbf/in²) at 66°C (150°F) and below and 0.86 MPa (125 lbf/in²) at 178°C (353°F). ASME B16.4 ratings for Class 250 fittings are 2.76 MPa (400 lbf/in²) at 66°C (150°F) and below and 1.72 MPa (250 lbf/in²) at 208°C (406°F).

Tees Tees may be cast, forged, or hot- or cold-formed from plate or pipe. Tees are typically stocked with both header (run) ends of the same size. In general, run ends of different sizes are not typically stocked or specified; however, occasionally run ends of different sizes are specified in threaded or socket-welded sizes. Branch connections may be full size or reducing sizes. Branch reductions two sizes smaller than the header are routinely stocked, and it is not typically difficult to purchase reducing tees with branches as small as those listed in ASME B16.9 (i.e., approximately one-half the header size). Economics, stress intensification factors, and nondestructive examination requirements typically dictate the branch connection type.

Reducers Reducers may be cast, forged, or hot- or cold-formed from pipe or plate. End connections may be concentric or eccentric, that is, tangent to the same plane at one point on their circumference. For pipe supported by hangers, concentric reducers permit maintenance

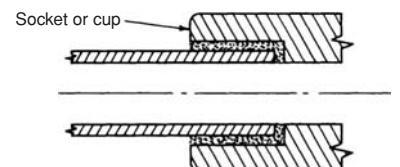
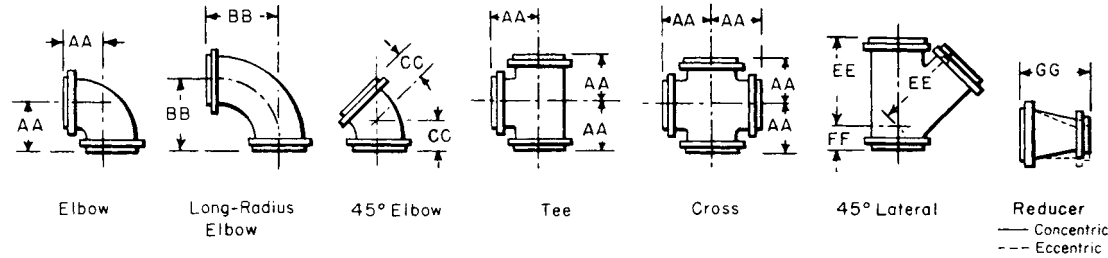


FIG. 10-150 Soldered, brazed, or cemented joint.

TABLE 10-30 Dimensions of Flanged Fittings*

All dimensions in inches



Nominal pipe size	ASME B16.5, Class 150 ASME B16.1, Class 125						ASME B16.5, Class 300 ASME B16.1, Class 250						ASME B16.5, Class 400					ASME B16.5, Class 600				
	AA	BB	CC	EE	FF	GG	AA	BB	CC	EE	FF	GG	AA	CC	EE	FF	GG	AA	CC	EE	FF	GG
½																		3.25	2.00	5.75	1.75	5.00
¾																		3.75	2.50	6.75	2.00	5.00
1	3.50	5.00	1.75	5.75	1.75	4.50	4.00	5.00	2.25	6.50	2.00	4.50	Use Class 600 dimensions in these sizes					4.25	2.50	7.25	2.25	5.00
1¼	3.75	5.50	2.00	6.25	1.75	4.50	4.25	5.50	2.50	7.25	2.25	4.50						4.50	2.75	8.00	2.50	5.00
1½	4.00	6.00	2.25	7.00	2.00	4.50	4.50	6.00	2.75	8.50	2.50	4.50						4.75	3.00	9.00	2.75	5.00
2	4.50	6.50	2.50	8.00	2.50	5.00	5.00	6.50	3.00	9.00	2.50	5.00						5.75	4.25	10.25	3.50	6.00
2½	5.00	7.00	3.00	9.50	2.50	5.50	5.50	7.00	3.50	10.50	2.50	5.50	6.50	4.50	11.50	3.50	6.75					
3	5.50	7.75	3.00	10.00	3.00	6.00	6.00	7.75	3.50	11.00	3.00	6.00	7.00	5.00	12.75	4.00	7.25					
3½	6.00	8.50	3.50	11.50	3.00	6.50	6.50	8.50	4.00	12.50	3.00	6.50	7.50	5.50	14.00	4.50	7.75					
4	6.50	9.00	4.00	12.00	3.00	7.00	7.00	9.00	4.50	13.50	3.00	7.00	8.00	6.00	16.50	4.50	8.75					
5	7.50	10.25	4.50	13.50	3.50	8.00	8.00	10.25	5.00	15.00	3.50	8.00	9.00	6.00	19.50	6.00	10.25					
6	8.00	11.50	5.00	14.50	3.50	9.00	8.50	11.50	5.50	17.50	4.00	9.00	9.75	6.25	21.00	6.50	11.25					
8	9.00	14.00	5.50	17.50	4.50	11.00	10.00	14.00	6.00	20.50	5.00	11.00	11.75	6.75	24.50	7.00	13.25					
10	11.00	16.50	6.50	20.50	5.00	12.00	11.50	16.50	7.00	24.00	5.50	12.00	13.25	7.75	29.50	8.00	15.75					
12	12.00	19.00	7.50	24.50	5.50	14.00	13.00	19.00	8.00	27.50	6.00	14.00	15.00	8.75	31.50	8.50	16.75					
14	14.00	21.50	7.50	27.00	6.00	16.00	15.00	21.50	8.50	31.00	6.50	16.00	16.25	9.25	34.25	9.00	17.75					
16	15.00	24.00	8.00	30.00	6.50	18.00	16.50	24.00	9.50	34.50	7.50	18.00	17.75	10.25	38.50	10.00	19.75					
18	16.50	26.50	8.50	32.00	7.00	19.00	18.00	26.50	10.00	37.50	8.00	19.00	19.25	10.75	42.00	10.50	21.75					
20	18.00	29.00	9.50	35.00	8.00	20.00	19.50	29.00	10.50	40.50	8.50	20.00	20.75	11.25	45.50	11.00	23.75					
24	22.00	34.00	11.00	40.50	9.00	24.00	22.50	34.00	12.00	47.50	10.00	24.00	24.25	12.75	53.00	13.00	27.75					

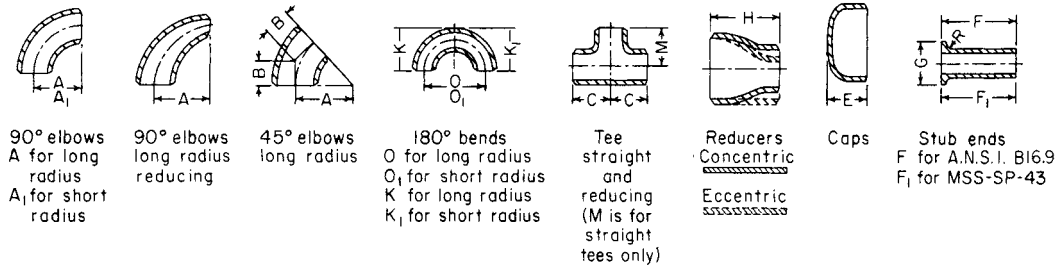
TABLE 10-30 Dimensions of Flanged Fittings* (Concluded)

Nominal pipe size	ASME B16.5, Class 900					ASME B16.5, Class 1500					ASME B16.5, Class 2500				
	AA	CC	EE	FF	GG	AA	CC	EE	FF	GG	AA	CC	EE	FF	GG
	Use Class 1500 dimensions in these sizes														
½						4.25	3.00				5.19				
¾						4.50	3.25				5.37				
1						5.00	3.50	9.00	2.50	5.00	6.06	4.00			
1¼						5.50	4.00	10.00	3.00	5.75	6.87	4.25			
1½						6.00	4.25	11.00	3.50	6.25	7.56	4.75			
2						7.25	4.75	13.25	4.00	7.25	8.87	5.75	15.25	5.25	9.50
2½						8.25	5.25	15.25	4.50	8.25	10.00	6.25	17.25	5.75	10.50
3	7.50	5.50	14.50	4.50	7.75	9.25	5.75	17.25	5.00	9.25	11.37	7.25	19.75	6.75	11.75
4	9.00	6.50	17.50	5.50	9.25	10.75	7.25	19.25	6.00	10.75	13.25	8.50	23.00	7.75	13.50
5	11.00	7.50	21.00	6.50	11.25	13.25	8.75	23.25	7.50	13.75	15.62	10.00	27.25	9.25	15.75
6	12.00	8.00	22.50	6.50	12.25	13.88	9.38	24.88	8.12	14.50	18.00	11.50	31.25	10.50	18.00
8	14.50	9.00	27.50	7.50	14.75	16.38	10.88	29.88	9.12	17.00	20.12	12.75	35.25	11.75	20.50
10	16.50	10.00	31.50	8.50	16.75	19.50	12.00	36.00	10.25	20.25	25.00	16.00	43.25	14.75	25.50
12	19.00	11.00	34.50	9.00	17.75	22.25	13.25	40.75	12.00	23.00	28.00	17.75	49.25	16.25	29.00
14	20.25	11.50	36.50	9.50	19.00	24.75	14.25	44.00	12.50	25.75					
16	22.25	12.50	40.75	10.50	21.00	27.25	16.25	48.25	14.75	28.25					
18	24.00	13.25	45.50	12.00	24.50	30.25	17.75	53.25	16.50	31.50					
20	26.00	14.50	50.25	13.00	26.50	32.75	18.75	57.75	17.75	34.00					
24	30.50	18.00	60.00	15.50	30.50	38.25	20.75	67.25	20.50	39.75					

*Outline drawings show a ¼-in (6.5-mm) raised face machined onto the flange for ASME Class 400 and higher. ASME B16.1 Class 250 and ASME B16.5 Classes 150 and 300 have a ¼-in. (1.5-mm) raised face. ASME B16.1 Class 125 has no raised face. See Tables 10-23 through 10-29 for flange drillings. Dimensions for Class 400 and Class 600 fittings are identical for sizes ½ through 3½ in. Dimensions for Class 900 and Class 1500 fittings are identical for sizes ½ through 2½ in. To convert inches to millimeters, multiply by 25.4. The dimensions were extracted from *Cast Iron Pipe Flanges and Flanged Fittings*, ASME B16.1-1998, and *Pipe Flanges and Flanged Fittings*, ASME B16.5-2003, with permission of the publisher, the American Society of Mechanical Engineers, New York.

TABLE 10-31 Butt-Welding Fittings*

All dimensions in inches



Pipe size	A	K	A1	K1	B	O	O1	M, C	H	E†	G	F	F1	R‡
½	1.50	1.88			0.62	3.00		1.00		1.00	1.38	3.00	2.00	0.12
¾	1.50	2.00			0.75	3.00		1.12	1.50	1.00	1.69	3.00	2.00	0.12
1	1.50	2.19	1.00	1.62	0.88	3.00	2.00	1.50	2.00	1.50	2.00	4.00	2.00	0.12
1¼	1.88	2.75	1.25	2.06	1.00	3.75	2.50	1.88	2.00	1.50	2.50	4.00	2.00	0.19
1½	2.25	3.25	1.50	2.44	1.12	4.50	3.00	2.25	2.50	1.50	2.88	4.00	2.00	0.25
2	3.00	4.19	2.00	3.19	1.38	6.00	4.00	2.50	3.00	1.50	3.62	6.00	2.50	0.31
2½	3.75	5.19	2.50	3.94	1.75	7.50	5.00	3.00	3.50	1.50	4.12	6.00	2.50	0.31
3	4.50	6.25	3.00	4.75	2.00	9.00	6.00	3.38	3.50	2.00	5.00	6.00	2.50	0.38
3½	5.25	7.25	3.50	5.50	2.25	10.50	7.00	3.75	4.00	2.50	5.50	6.00	3.00	0.38
4	6.00	8.25	4.00	6.25	2.50	12.00	8.00	4.12	4.00	2.50	6.19	6.00	3.00	0.44
5	7.50	10.31	5.00	7.75	3.12	15.00	10.00	4.88	5.00	3.00	7.31	8.00	3.00	0.44
6	9.00	12.31	6.00	9.31	3.75	18.00	12.00	5.62	5.50	3.50	8.50	8.00	3.50	0.50
8	12.00	16.31	8.00	12.31	5.00	24.00	16.00	7.00	6.00	4.00	10.62	8.00	4.00	0.50
10	15.00	20.38	10.00	15.38	6.25	30.00	20.00	8.50	7.00	5.00	12.75	10.00	5.00	0.50
12	18.00	24.38	12.00	18.38	7.50	36.00	24.00	10.00	8.00	6.00	15.00	10.00	6.00	0.50
14	21.00	28.00	14.00	21.00	8.75	42.00	28.00	11.00	13.00	6.50	16.25	12.00	6.00	0.50
16	24.00	32.00	16.00	24.00	10.00	48.00	32.00	12.00	14.00	7.00	18.50	12.00	6.00	0.50
18	27.00	36.00	18.00	27.00	11.25	54.00	36.00	13.50	15.00	8.00	21.00	12.00	6.00	0.50
20	30.00	40.00	20.00	30.00	12.50	60.00	40.00	15.00	20.00	9.00	23.00	12.00	6.00	0.50
24	36.00	48.00	24.00	36.00	15.00	72.00	48.00	17.00	20.00	10.50	27.25	12.00	6.00	0.50

*Extracted from *Factory-Made Wrought Butt-Welding Fittings*, ASME B16.9-2003, with permission of the publisher, the American Society of Mechanical Engineers, New York. O and K dimensions of 2.25 and 1.69 in respectively may be furnished for NPS ¾ at the manufacturer's option.

†For wall thicknesses greater than extra heavy, E is greater than shown here for sizes 2 in and larger.

‡For MSS SP-43 type B stub ends, which are designed to be backed up by slip-on flanges, R = ½ in for 4 in and smaller and ⅙ in for 6 through 12 in. To convert inches to millimeters multiply by 25.4.

of the same hanger length; for pipe laid on structural steel, eccentric reducers permit maintaining the same elevation of top of steel. Eccentric reducers with the common tangent plane on the bottom side permit complete drainage of branched horizontal piping systems. With the common tangent plane on the top side, they permit liquid flow in horizontal lines to sweep the line free of gas or vapor.

Reducing Elbow Fittings These permit change of direction and concentric size reduction in the same fitting.

Valves Valve bodies may be cast, forged, machined from bar stock, or fabricated from welded plate. Steel valves are available with screwed or socket-weld ends in the smaller sizes. Bronze and brass screwed-end valves are widely used for low-pressure service in steel systems. Table 10-32 gives contact-surface-of-face to contact-surface-of-face dimensions for flanged ferrous valves and end-to-end dimensions for butt-welding ferrous valves. Drilling of end flanges is shown in Tables 10-23 to 10-29. Bolt holes are located so that the stem is equidistant from the centerline of two bolt holes. Even if removal for maintenance is not anticipated, flanged valves are frequently used instead of butt-welding-end valves because they permit insertion of blanks for isolating sections of a loop piping system.

Ferrous valves are also available in nodular (ductile) iron, which has tensile strength and yield point approximately equal to cast carbon steel at temperatures of 343°C (650°F) and below and only slightly less elongation.

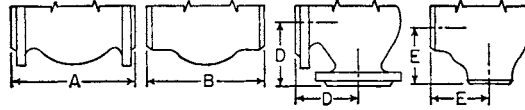
Valves serve not only to regulate the flow of fluids but also to isolate piping or equipment for maintenance without interrupting other connected units. Valve designers attempt to minimize body distortion due to pressure, changes in temperature, and applied loads. The sealing mechanisms of certain valve designs are inherently more tolerant of these factors than are others. The selection of valve type and materials of construction should provide a valve that functions reliably and that is acceptably tight across the sealing surfaces for the lowest lifetime cost. Valve manufacturers are a valuable source of information when evaluating the suitability of specific designs. The principal types are named, described, compared, and illustrated with line diagrams in subsequent subsections. In the line diagrams, the operating stem is shown in solid black, direction of flow by arrows on a thin solid line, and motion of valve parts by arrows on a dotted line. Moving parts are drawn with solid lines in the nearly closed position and with dotted lines in the fully open position. Packing is represented by an X in a square.

Gate Valves These valves are designed in two types (Fig. 10-151). The wedge-shaped-gate, **inclined-seat** type is most commonly used. The wedge gate may be solid or flexible (partly cut into halves by a plane at right angles to the pipe) or split (completely cleft by such a plane). Flexible and split wedges minimize galling of the sealing surfaces by distorting more easily to match angularly misaligned seats. In the double-disk **parallel-seat** type, an inclined-plane device mounted between the disks converts stem force to axial force, pressing the disks against the

10-94 TRANSPORT AND STORAGE OF FLUIDS

TABLE 10-32 Dimensions of Valves*

All dimensions in inches



Nominal valve size	Class 125 cast iron					Class 150 steel, MSS-SP-42 through 12-in size					Class 250 cast iron		
	Flanged end					Flanged end	Welding end	Flanged end and welding end			Flanged end		
	Gate		Globe and lift check A	Angle and lift check D	Swing check A	Gate	Gate	Globe and lift check A and B	Angle and lift check D and E	Swing check A and B	Gate Solid wedge and double disk A	Globe, lift check, and swing check A	Angle and lift check D
	Solid wedge A	Double disk A				Solid wedge and double disk B	Solid wedge and double disk A						
1/4					4	4	4	2	4				
3/8					4	4	4	2	4				
1/2					4 1/4	4 1/4	4 1/4	2 1/4	4 1/4				
3/4					4 3/8	4 3/8	4 3/8	2 1/2	4 3/8				
1					5	5	5	2 3/4	5				
1 1/4					5 1/2	5 1/2	5 1/2	3	5 1/2				
1 1/2					6 1/2	6 1/2	6 1/2	3 1/4	6 1/2				
2	7	7	8	4	8	7	8 1/2	8	4	8	8 1/2	10 1/2	5 1/4
2 1/2	7 1/2	7 1/2	8 1/2	4 1/4	8 1/2	7 1/2	9 1/2	8 1/4	4 1/4	8 1/2	9 1/2	11 1/2	5 3/4
3	8	8	9 1/2	4 3/4	9 1/2	8	11 1/8	9 1/2	4 3/4	9 1/2	11 1/8	12 1/2	6 1/4
3 1/2	8 1/2	8 1/2				†				12	14	7	
4	9	9	11 1/2	5 3/4	11 1/2	9	12	11 1/2	5 3/4	11 1/2	15	15 3/4	7 3/8
5	10	10	13	6 1/2	13	10	15	14	7	13	15 1/2	17 1/2	8 3/4
6	10 1/2	10 1/2	14	7	14	10 1/2	15 1/2	16	8	14	16 1/2	21	10 1/2
8	11 1/2	11 1/2	19 1/2	9 3/4	19 1/2	11 1/2	16 1/2	19 1/2	9 3/4	19 1/2	18	24 1/2	12 1/4
10	13	13	24 1/2	12 1/4	24 1/2	13	18	24 1/2	12 1/4	24 1/2	19 3/4	28	14
12	14	14	27 1/2	13 3/4	27 1/2	14	19 3/4	27 1/2	13 3/4	27 1/2	22 1/2	†	
14	15	†	31	15 1/2	31	15	22 1/2	31	15 1/2	31	24	†	
16	16	†	36	18	†	16	24	36	18	†	26	†	
18	17	†			†	17	26			†	28		
20	18	†			†	18	28			†			
24	20	†			†	20	32			†	31		

Nominal valve size	Class 300 steel				Class 400 steel				Class 600 steel							
	Flanged end and welding end				Flanged end and welding end				Flanged end and welding end							
	Gate		Globe and lift check A and B	Angle and lift check D and E	Swing check A and B	Gate		Globe, lift check, and swing check A and B	Angle and lift check D and E	Gate			Regular globe, regular lift check, swing check A and B	Short pattern† globe, short pattern lift check B	Angle and lift check	
	Solid wedge and double disk A and B	Globe and lift check A and B				Solid wedge A and B	Double disk A and B			Solid wedge A and B	Double disk A and B	Short pattern† B			Regular D and E	Short pattern E
1/2	5 1/2	6	3		6 1/2	7 1/2	6 1/2	3 1/4	6 1/2	7 1/2	6 1/2	7 1/2		3 1/4		
3/4	6	7	3 1/2		7 1/2	8 1/2	7 1/2	3 3/4	7 1/2	8 1/2	7 1/2	8 1/2		3 3/4		
1	6 1/2	8	4	8 1/2	8 1/2	8 1/2	8 1/2	4 1/4	8 1/2	8 1/2	5 1/4	8 1/2	5 1/4	4 1/4		
1 1/4	7 1/2	8 1/2	4 1/4	9	9	9	9	4 1/2	9	9	5 3/4	9	5 3/4	4 1/2		
1 1/2	7 1/2	9	4 1/2	9 1/2	9 1/2	9 1/2	9 1/2	4 3/4	9 1/2	9 1/2	6	9 1/2	6	4 3/4		
2	8 1/2	10 1/2	5 1/4	10 1/2	11 1/2	11 1/2	11 1/2	5 3/4	11 1/2	11 1/2	7	11 1/2	7	5 3/4	4 1/4	
2 1/2	9 1/2	11 1/2	5 3/4	11 1/2	13	13	13	6 1/2	13	13	8 1/2	13	8 1/2	6 1/2	5	
3	11 1/2	12 1/2	6 1/4	12 1/2	14	14	14	7	14	14	10	14	10	7	6	
4	12	14	7	14	16	16	16	8	17	17	12	17	12	8 1/2	7	
5	15	15 3/4	7 3/4	15 3/4	18	18	18	9	20	20	15	20	15	10	8 1/2	
6	15 3/8	17 1/2	8 3/4	17 1/2	19 1/2	19 1/2	19 1/2	9 3/4	22	22	18	22	18	11	10	
8	16 1/2	22	11	21	23 1/2	23 1/2	23 1/2	11 3/4	26	26	23	26	23	13		
10	18	24 1/2	12 1/4	24 1/2	26 1/2	26 1/2	26 1/2	13 1/4	31	31	28	31	28	15 1/2		
12	19 3/4	28	14	28	30	30	30	15	33	33	32	33	32	16 1/2		
14	30			†	32 1/2	30 1/2	†		35	35	35	35	32			
16	33			†	35 1/2	35 1/2	†		39	39	39	†				
18	36			†	38 1/2	38 1/2	†		43	43	43	†				
20	39			†	41 1/2	41 1/2	†		47	47	47	†				
22	43			†	45	45	†		51	51	51	†				
24	45			†	48 1/2	48 1/2	†		55	55	55	†				

TABLE 10-32 Dimensions of Valves (Concluded)

Nominal valve size	Class 900 steel						Class 1500 steel					
	Flanged end and welding end						Flanged end and welding end					
	Gate			Regular globe regular lift check, swing check A and B	Short pattern† globe, short pattern lift check B	Angle and lift check		Gate			Globe, lift check, swing check A and B	Angle and lift check D and E
	Solid wedge A and B	Double disk A and B	Short pattern‡ B			Regular D and E	Short pattern E	Solid wedge A and B	Double disk A and B	Short pattern‡ B		
¾				9		4½					9	4½
1	10		5½	10		5		10		5½	10	5
1¼	11		6½	11		5½		11		6½	11	5½
1½	12		7	12		6		12		7	12	6
2	14½	14½	8½	14½		7¼		14½	14½	8½	14½	7¼
2½	16½	16½	10	16½		8¼		16½	16½	10	16½	8¼
3	15	15	12	15		7½	6	18½	18½	12	18½	9¼
4	18	18	14	18	14	9	7	21½	21½	16	21½	10¾
5	22	22	17	22	17	11	8½	26½	26½	19	26½	13¼
6	24	24	20	24	20	12	10	27¾	27¾	22	27¾	13¾
8	29	29	26	29	26	14½	13	32¾	32¾	28	32¾	16¾
10	33	33	31	33	31	16½	15½	39	39	34	39	19½
12	38	38	36	38	36	19	18	44½	44½	39	44½	22¼
14	40½	40½	39	40½	39	20¼	19½	49½	49½	42	49½	24¾
16	44½	44½	43					54½	54½	47		
18	48	48	†					60½	60½	53		
20	52	52	†					65½	65½	58		
24	61	61	†					76½	76½			

Nominal valve size	Class 2500 steel					
	Flanged end and welding end					
	Gate			Globe, lift check, swing check A and B	Angle and lift check B	
	Solid wedge A and B	Double disk A and B	Short pattern‡ B			
½	10¾			10¾	5¾	
¾	10¾			10¾	5¾	
1	12½		7¾	12½	6¼	
1¼	13¾		9¾	13¾	6¾	
1½	15¾		9¾	15¾	7¾	
2	17¾	17¾	11	17¾	8¾	
2½	20	20	13	20	10	
3	22¾	22¾	14½	22¾	11¾	
4	26½	26½	18	26½	13¼	
5	31¼	31¼	21	31¼	15¾	
6	36	36	24	36	18	
8	40¼	40¼	30	40¼	20¼	
10	50	50	36	50	25	
12	56	56	41	56	28	
14			44			
16			49			
18			55			

NOTE: Outline drawings for flanged valves show ¼-in raised face machined onto flange, as for Class 400 cast-steel valves; Class 150 and 300 cast-steel valves and Class 250 cast-iron valves have ⅙-in raised faces; Class 125 cast-iron have no raised faces.

*Extracted from Face-to-Face and End-to-End Dimensions of Valves, ASME B16.10, with permission of the publisher, the American Society of Mechanical Engineers, New York. To convert inches to millimeters, multiply by 25.4.

†Not shown in ANSI B16.10 but commercially available.

‡These dimensions apply to pressure-seal or flangeless bonnet valves only.

§Solid wedge only.

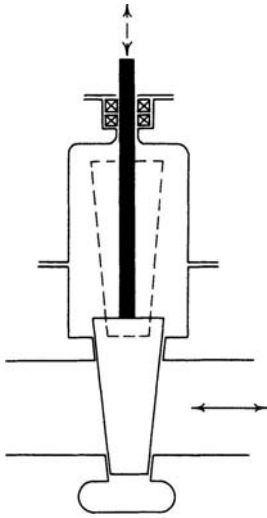


FIG. 10-151 Gate valve.

seats after the disks have been positioned for closing. This gate assembly distorts automatically to match both angular misalignment of the seats and longitudinal shrinkage of the valve body on cooling.

During opening and closing, some parallel-seat designs are more subject to vibration resulting from fluid flow than are wedge gates. Specific applications should be discussed with the manufacturer. In some applications it may be advisable to use a small bypass around the in-line valve to help lower opening and closing forces and to relieve binding between the gate and the seat due to high differential pressure or temperature. Double-disk parallel seat valves should be installed with the stem essentially vertical unless otherwise recommended by the manufacturer. All wedge gate valves are equipped with tongue-and-groove guides to keep the gate sealing surfaces from clattering on the seats and marring them during opening and closing. Depending on the velocity and density of the fluid stream being sheared, these guiding surfaces may be specified as cast, machined, or hard-surfaced and ground.

Gate valves may have nonrising stems, inside-screw rising stems, or outside-screw rising stems, listed in order of decreasing exposure of the stem threads to the fluid handled. Rising-stem valves require more space, but the position of the stem visually indicates the position of the gate. Indication is clearest on the outside-screw rising-stem valves, and on these the stem threads and thrust collars may be lubricated, reducing operating effort. The stem connection to the gate assembly prevents the stem from rotating.

Gate valves are used to minimize pressure drop in the open position and to stop the flow of fluid rather than to regulate it. The problem, when the valve is closed, of pressure buildup in the bonnet from cold liquids expanding or chemical action between fluid and bonnet should be solved by a relief valve or by notching the upstream seat ring.

Globe Valves (Fig. 10-152) These are designed as either inside-screw rising stem or outside-screw rising stem. In most designs the disk is free to rotate on the stem; this prevents galling between the disk and the seat. Various designs are used to maintain alignment between the disk and the seat, and to keep the fluid flow from vibrating or rotating the disk. Disks are typically guided either by the valve stem or against the valve body. Body guiding reduces side thrust loads on the stem. The suitability of each design can be determined by reviewing specific applications with valve manufacturers.

Disk shapes are commonly flat or conical. Conical designs provide either line or area contact between the seat and disk, and are generally more suitable than flat disks for high pressures and temperatures. Needle-type disks provide better flow control and are commonly available in valves 1 in and smaller.

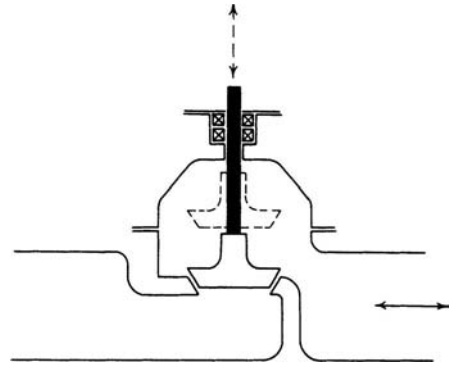


FIG. 10-152 Globe valve.

For certain valve designs, sizes, and applications, globe valves may be installed with the stem in the horizontal position; however, unless approved by the manufacturer, the stem orientation should be vertical. Globe valves are not symmetric with respect to flow. Generally globe valves are installed with pressure under the seat when the valve is in the closed position, and with the flow direction coming from under the seat. Opposite-flow direction provides pressure-assisted seating, lower seating torque requirements, and higher opening torques, and may result in blockage in dirty services. Consult the manufacturer before installing globe valves in the opposite-flow direction.

Pressure drop through globe valves is much greater than that for gate valves. In Y-type globe valves, the stem and seat are at about 45° to the pipe instead of 90° . This reduces pressure drop but presents design challenges with regard to disk alignment.

Globe valves in horizontal lines prevent complete drainage.

Angle Valves These valves are similar to globe valves; the same bonnet, stem, and disk are used for both (Fig. 10-153). They combine an elbow fitting and a globe valve into one component with a substantial saving in pressure drop.

Diaphragm Valves These valves are limited to pressures of approximately 50 lbf/in^2 (Fig. 10-154). The fabric-reinforced diaphragms may be made from natural rubber, from a synthetic rubber, or from natural or synthetic rubbers faced with Teflon[®] fluorocarbon resin. The simple shape of the body makes lining it economical. Elastomers have shorter lives as diaphragms than as linings because of

[®]Du Pont TFE fluorocarbon resin.

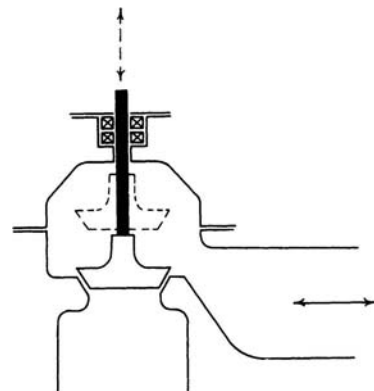


FIG. 10-153 Angle valve.

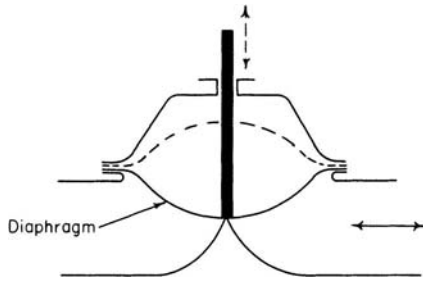


FIG. 10-154 Diaphragm valve.

flexing but still provide satisfactory service. Plastic bodies, which have low moduli of elasticity compared with metals, are practical in diaphragm valves since alignment and distortion are minor problems.

These valves are excellent for fluids containing suspended solids and can be installed in any position. Models in which the dam is very low, reducing pressure drop to a negligible quantity and permitting complete drainage in horizontal lines, are available. However, drainage can be obtained with any model simply by installing it with the stem horizontal. The only maintenance required is replacement of the diaphragm, which can be done very quickly without removing the valve from the line.

Plug Valves These valves (Fig. 10-155) are typically limited to temperatures below 260°C (500°F) since differential expansion between the plug and the body results in seizure. The size and shape of the port divide these valves into different types. In order of increasing cost they are short venturi, reduced rectangular port; long venturi, reduced rectangular port; full rectangular port; and full round port.

In lever-sealed plug valves, tapered plugs are used. The plugs are raised by turning one lever, rotated by another lever, and resealed by the first lever. **Lubricated** plug valves may use straight or tapered plugs. The tapered plugs may be raised slightly, to reduce turning effort, by injection of the lubricant, which also acts as a seal. Plastic is used in nonlubricated plug valves as a body liner, a plug coating, or port seals in the body or on the plug.

In plug valves other than lever-sealed plug valves, the contact area between plug and body is large, and gearing is usually used in sizes 6 in and larger to minimize operating effort. There are several lever-sealed plug valves incorporating mechanisms which convert the rotary motion of a handwheel into sequenced motion of the two levers.

For lubricated plug valves, the lubricant must have limited viscosity change over the range of operating temperature, must have low solubility in the fluid handled, and must be applied regularly. There must be no chemical reaction between the lubricant and the fluid which would harden or soften the lubricant or contaminate the fluid. For these reasons, lubricated plug valves are most often used when there are a large number handling the same or closely related fluids at approximately the same temperature.

Lever-sealed plug valves are used for throttling service. Because of the large contact area between plug and body, if a plug valve is operable, there is little likelihood of leakage when closed, and the handle position is a clearly visible indication of the valve position.

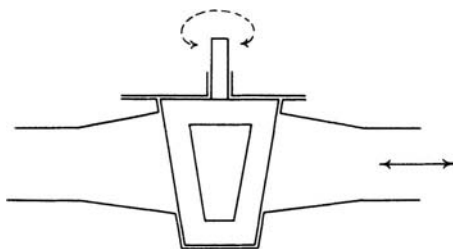


FIG. 10-155 Plug valve.

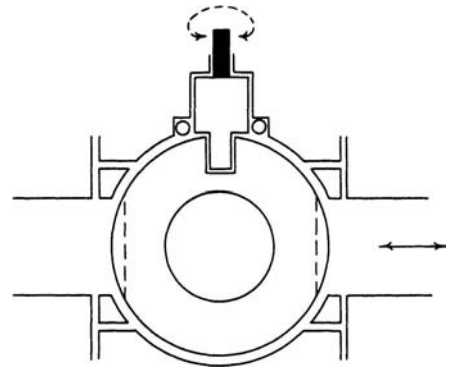


FIG. 10-156 Ball valve; floating ball.

Ball Valves Ball valves (Figs. 10-156 and 10-157) are of two primary designs, floating ball and trunnion-mounted ball. In floating ball designs, the ball is supported by the downstream seat. In trunnion ball designs, the ball is supported by the trunnion and the seat loads are less than those in floating ball valves. Because of operating torque and shutoff pressure ratings, trunnion ball valves are available in larger sizes and higher pressure ratings than floating ball valves.

Both floating and trunnion-mounted designs are available with other design variations that include metal seated valves, soft seated valves, top-entry valves, end-entry valves, and split body valves. Valves in all these design variations are available as either full port or reduced port. *Port* refers to the round-bore fluid flow area through the ball. Full port valves have a bore that is approximately equal to the inside diameter of the mating pipe. Reduced port valves have a bore that is approximately equal to the inside diameter of pipe one size smaller than full bore.

A variety of soft seat materials are available, including PTFE and nylon. Since the shutoff pressure capability of ball valves is limited by the load capabilities of the seat material, the upper temperature limit of soft seated valves is limited by the seat material selection. The shutoff pressure rating of soft seated valves typically declines rapidly with increasing temperature, and the shutoff rating is often less than the body pressure rating. Metal seated valves do not share this characteristic.

For equal port size, ball valves share the low pressure drop characteristics of gate valves. Also as is the case with gate valves, consideration must be given to venting the valve when the expansion of fluid trapped within the body cavity could overpressurize the valve body. Some seat designs are inherently self-venting to either the upstream or the downstream side of the valve. In floating ball valves, venting may result in a unidirectional valve that seats against flow in only one direction.

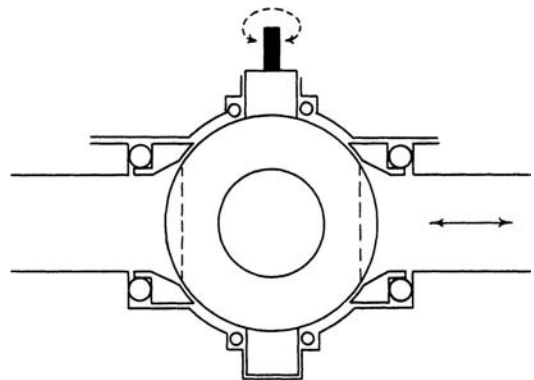


FIG. 10-157 Ball valve; trunnion-mounted ball.

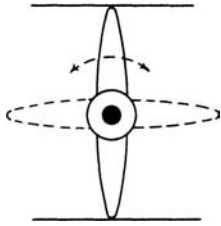


FIG. 10-158 Butterfly valve.

With split body designs, internals must be removed by separating the valve body in the axial direction of the mating pipe. Top-entry design permits removal of the internals through the top of the valve. When valves are butt-welded, top entry may be specified to permit repair without removing the valve from the piping. Top-entry valves are significantly more expensive than split body and end-entry valves, and full port valves are more expensive than reduced port in any body design. Metal seated valves are significantly more expensive than soft seated valves and are typically used only when other types of valves are unsuitable for the application.

Butterfly Valves These valves (Fig. 10-158) occupy less space, are much lighter than other types of block valves, and are available in body styles that include wafer, lugged (drilled-through or tapped), and flanged. They are available in ASME Class 900 and lower pressure ratings. The maximum size available varies with pressure rating. Valves in Class 150 are available in sizes exceeding 60-in diameter. Within limits, they may be used for throttling. Their relatively high pressure drop must be considered during design.

Like ball valves, butterfly valves are fully opened in one-quarter turn and are therefore well suited to automation. *Butterfly Valves: Double Flange, Lug- and Wafer-Type*, API 609, is one of the standards commonly used to specify butterfly valves. API 609 defines two major categories of butterfly valves: Category A and Category B. Category A valves are typically soft seated valves with shell pressure ratings that may be less than the flange rating of the valve. They are typically used for utility services and are commonly referred to as *utility valves*. Category B may be soft seated or metal seated, and must have shell pressure ratings equal to the full pressure rating of the valve flange, and seat ratings that essentially meet the shell rating within the temperature capability of the seat material. Within Category B, valves may be further divided into concentric shaft, double-offset shaft, and triple-offset shaft designs. *Offset* refers to the position of the shaft with respect to seat area. With minor exception, double- and triple-offset valve designs are metal-to-metal seated. They are distinguished from other designs by their exceptional seat tightness (often “zero” leakage) that is maintained throughout the life of the valve. Their tightness exceeds the seat tightness capability and reliability of wedge-type gate valves. Double-offset valves minimize rubbing between the disk and the seat, and triple-offset valves virtually eliminate rubbing. Although double- and triple-offset valves are more expensive than other butterfly valve designs, because of their weight they are often more economical than gate valves for some combinations of pressure class, size, and materials.

Check Valves These valves are used to prevent reversal of flow. They must be located where flow turbulence or instability does not result in chatter (high-frequency opening and closing of the valve) and in systems designed to prevent sudden high-velocity flow reversal which results in slamming upon closure. Many valve manufacturers can provide application advice.

Swing Check Valves These valves (Fig. 10-159) are normally designed for use in horizontal lines or in vertical lines with normally upward flow. Since their seating force is primarily due to pipeline pressure, they may not seal as tightly at low pressures as at higher pressures. When suitable, nonmetallic seats may be used to minimize this problem.

Lift Check Valves These valves (Figs. 10-160 through 10-162) are made in three styles. Vertical lift check valves are for installation in vertical lines with flow normally upward. Globe (or piston) valves with a 90° bonnet (Fig. 10-161) are for installation in horizontal lines, although inclined bonnet versions (approximately 45°) with spring

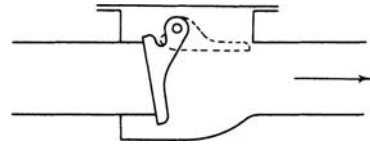


FIG. 10-159 Swing check valve.

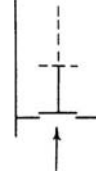


FIG. 10-160 Lift check valve, vertical.

assist may be used in vertical lines with normally upward flow. Globe and angle check valves often incorporate mechanisms to control the opening or closing rate of the piston, or to promote full opening under low-flow conditions. In some designs, spring-assisted closure is available, but this increases pressure drop. Lift check valves should not be used when the fluid contains suspended solids. Ball check valves having designs similar to those in Figs. 10-160 and 10-161 are available in sizes 2 in and smaller. They promote even wear of the seat area and are more suitable for viscous services, or services with limited solids.

Tilting-Disk Check Valves These valves (Fig. 10-163) may be installed in a horizontal line or in lines in which the flow is vertically upward. The pivot point is located so that the distribution of pressure in the fluid handled speeds the closing but arrests slamming. Compared with swing check valves of the same size, pressure drop is less at low velocities but greater at high velocities.

Closure at the instant of flow reversal is most nearly attained with tilting-disk, dual-plate, and specialty axial-flow check valves. However, quick closure is not the solution to all noise, shock, and water hammer problems. External dashpots are available when a controlled rate of closure is desired. Nonmetallic seats are also available.

Dual-Plate Check Valves These valves (Fig. 10-163) occupy less space, are much lighter than other types of check valves, and are available in body styles that include wafer, lugged (drilled-through or tapped), and flanged. They are available in all ASME pressure classes. The maximum size available varies with pressure rating. Valves in Class 150 are available in sizes 60 in or larger. They are available with either metallic or nonmetallic seats. Pressure drop is greater than that in a fully open swing check valve. Plate closure is spring-assisted, and the rate of closure can be controlled with proper spring selection. High-performance valves with fast closure rates are available to address water hammer problems. They typically weigh as little as 15 to 30 percent as much as swing check valves. Because of their weight they are often more economical than other types of check valves.

Valve Trim Various alloys are available for valve parts such as seats, disks, and stems which must retain smooth finish for successful operation. The problem in seat materials is fivefold: (1) resistance to corrosion by the fluid handled and to oxidation at high temperatures, (2) resistance to erosion by suspended solids in the fluid, (3) prevention of galling (seizure at point of contact) by differences in material or hardness or both, (4) maintenance of high strength at high temperature, and (5) avoidance of distortion.

Standard valve trims are defined by standards such as API 600 and API 602. Elastomer or plastic inserts may be specified to achieve bubble-tight shutoff. Valve manufacturers may be consulted for recommended trims.

CAST IRON, DUCTILE IRON, AND HIGH-SILICON IRON PIPING SYSTEMS

Cast Iron and Ductile Iron Cast iron and ductile iron provide more metal for less cost than steel in piping systems and are widely used in low-pressure services in which internal and external corrosion

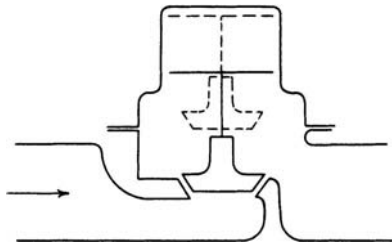


FIG. 10-161 Lift check valve, globe.

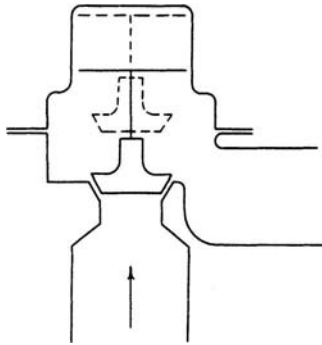


FIG. 10-162 Lift check valve, angle.

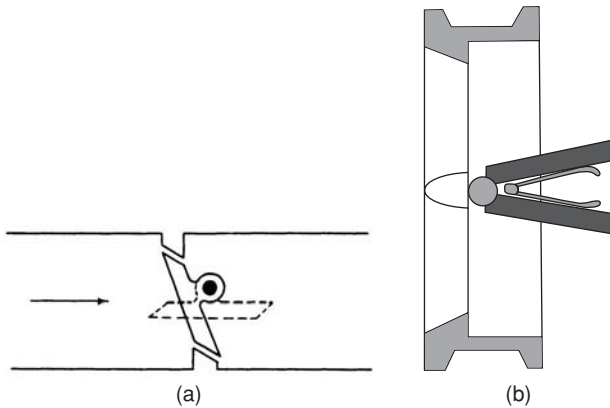


FIG. 10-163 (a) Tilting-disk check valve. (b) Dual-plate check valve.

may cause a considerable loss of metal. They are widely used for underground water distribution. Cement lining is available at a nominal cost for handling water causing tuberculation.

Ductile iron has an elongation of 10 percent or more compared with essentially nil elongation for cast iron and has for all practical purposes supplanted cast iron as a cast piping material. It is usually centrifugally cast. This manufacturing method improves tensile strength and reduces porosity. Ductile-iron pipe is manufactured to AWWA C151/A21.51-2002 and is available in nominal sizes from 3 through 64 in. Wall thicknesses are specified by seven standard thickness classes. Table 10-33 gives the outside diameter and standard thickness for various rated water working pressures for centrifugally cast ductile-iron pipe. The required wall thickness for underground installations increases with internal pressure, depth of laying, and weight of vehicles operating over the pipe. It is reduced by the degree to which the soil surrounding the pipe provides uniform support along the pipe and around the lower 180°.

Tables are provided in AWWA C151/A21.51 for determining wall-thickness-class recommendations for various installation conditions. The poured joint (Fig. 10-139) has been almost entirely superseded by the mechanical joint (Fig. 10-138) and the push-on joint (Fig. 10-140), which are better suited to wet trenches, bad weather, and unskilled labor. Such joints also minimize strain on the pipe from ground settlement. Lengths vary between 5 and 6 m (between 18 and 20 ft), depending on the supplier. Stock fittings are designed for 1.72-MPa (250-lbf/in²) cast iron or 2.41-MPa (350-lbf/in²) ductile iron in sizes through 12 in and for 1.0- and 1.72-MPa (150- and 250-lbf/in²) cast iron or 2.41-MPa (350-lbf/in²) ductile iron in sizes 14 in and larger. Stock fittings include 22½° and 11¼° bends. Ductile-iron pipe is also supplied with flanges that match the dimensions of Class 125 flanges shown in ASME B16.1 (see Table 10-23). These flanges are assembled to the pipe barrel by threaded joints.

High-Silicon Iron Pipe and fittings are cast products of material typically conforming to ASTM A518. Nominal silicon content is 14.5 percent, and nominal carbon content is approximately 0.85 percent. This material is corrosion-resistant to most chemicals, highly abrasion-resistant, and suitable for applications to 260°C (500°F). Applications are primarily gravity drain. Pipe and fittings are available under the trade name Duriron®.

Pipe and fitting sizes typically available are shown in Table 10-34. Pipe and fitting dimensions commonly conform to ASTM A861. Bell and spigot connections are sealed with chemical-resistant rope packing and molten lead. Mechanical joint connections are made with TFE gaskets and stainless steel clamps.

The coefficient of linear expansion of this alloy in the temperature range of 21 to 100°C (70 to 212°F) is $12.2 \times 10^{-6}/^{\circ}\text{C}$ ($6.8 \times 10^{-6}/^{\circ}\text{F}$), which is slightly above that of cast iron (National Bureau of Standards). Since this material has practically no elasticity, the need for expansion joints should be considered. Connections for flanged pipe, fittings, valves, and pumps are made to ASME B16.1, Class 125.

The use of high-silicon iron in flammable-fluid service or in Category M fluid service is prohibited by the code.

NONFERROUS METAL PIPING SYSTEMS

Aluminum Seamless aluminum pipe and tube are produced by extrusion in essentially pure aluminum and in several alloys; 6-, 9-, and 12-m (20-, 30-, and 40-ft) lengths are available. Alloying and mill treatment improve physical properties, but welding reduces them. Essentially pure aluminum has an ultimate tensile strength of 58.6 MPa (8500 lbf/in²) subject to a slight increase by mill treatment which is lost during welding. Alloy 6061, which contains 0.25 percent copper, 0.6 percent silicon, 1 percent magnesium, and 0.25 percent chromium, has an ultimate tensile strength of 124 MPa (18,000 lbf/in²) in the annealed condition, 262 MPa (38,000 lbf/in²), mill-treated as 6061-T6, and 165 MPa (24,000 lbf/in²) at welded joints. Extensive use is made of alloy 1060, which is 99.6 percent pure aluminum, for hydrogen peroxide; of alloy 3003, which contains 1.2 percent manganese, for high-purity chemicals; and of alloys 6063 and 6061 for many other services. Alloy 6063 is the same as 6061 minus the chromium and has slightly lower mechanical properties.

Aluminum is not embrittled by low temperatures and is not subject to external corrosion when exposed to normal atmospheres. At 200°C (400°F) its strength is less than half that at room temperature. It is attacked by alkalis, by traces of copper, nickel, mercury, and other heavy-metal ions, and by prolonged contact with wet insulation. It suffers from galvanic corrosion when coupled to copper, nickel, or lead-base alloys but not when coupled to galvanized iron.

Aluminum pipe schedules conform to those in Table 10-22. Consult suppliers for available sizes and schedules.

Threaded aluminum fittings are seldom recommended for process piping. Wrought fittings with welding ends (see Table 10-31 for dimensions) and with grooved joint ends are available. Wrought 6061-T6 flanges with dimensions per Table 10-23 are also available. Consult suppliers on availability of cast flanges and fittings. Castings manufactured in accordance with ASTM B26 are available in several grades. Refer to Table 10-30 for dimensions. The low strength and

10-100 TRANSPORT AND STORAGE OF FLUIDS

TABLE 10-33 Dimensions of Ductile-Iron Pipe*

Standard thickness for internal pressure†

Pipe size, in	Outside diameter, in	Rated water working pressure, lbf/in ² ‡									
		150		200		250		300		350	
		Thickness, in	Thickness class	Thickness, in	Thickness class	Thickness, in	Thickness class	Thickness, in	Thickness class	Thickness, in	Thickness class
3	3.96	0.25	51	0.25	51	0.25	51	0.25	51	0.25	51
4	4.80	0.26	51	0.26	51	0.26	51	0.26	51	0.26	51
6	6.90	0.25	50	0.25	50	0.25	50	0.25	50	0.25	50
8	9.05	0.27	50	0.27	50	0.27	50	0.27	50	0.27	50
10	11.10	0.29	50	0.29	50	0.29	50	0.29	50	0.29	50
12	13.20	0.31	50	0.31	50	0.31	50	0.31	50	0.31	50
14	15.30	0.33	50	0.33	50	0.33	50	0.33	50	0.33	50
16	17.40	0.34	50	0.34	50	0.34	50	0.34	50	0.34	50
18	19.50	0.35	50	0.35	50	0.35	50	0.35	50	0.35	50
20	21.60	0.36	50	0.36	50	0.36	50	0.36	50	0.39	51
24	25.80	0.38	50	0.38	50	0.38	50	0.41	51	0.44	52
30	32.00	0.39	50	0.39	50	0.43	51	0.47	52	0.51	53
36	38.30	0.43	50	0.43	50	0.48	51	0.53	52	0.58	53
42	44.50	0.47	50	0.47	50	0.53	51	0.59	52	0.65	53
48	50.80	0.51	50	0.51	50	0.58	51	0.65	52	0.72	53
54	57.56	0.57	50	0.57	50	0.65	51	0.73	52	0.81	53

*Extracted from *Ductile Iron Pipe, Centrifugally Cast*, AWWA C151/A21.51-2002, with permission of the publisher, the American Water Works Association, Denver, Colo.

†To convert from inches to millimeters, multiply by 25.4; to convert pounds-force per square inch to megapascals, multiply by 0.006895.

‡These pipe walls are adequate for the rated working pressure plus a surge allowance of 100 lbf/in². For the effect of laying conditions and depth of bury, see ANSI A21.51.

modulus of elasticity of aluminum must be considered when using flanged connections.

Aluminum-body diaphragm and ball valves are used extensively.

Copper and Copper Alloys Seamless pipe and tubing manufactured from copper, bronze, brass, and copper-nickel alloys are produced by extrusion. The availability of pipe or tubing depends on the metallurgy and size. Copper tubing is widely used for plumbing, steam tracing, compressed air, instrument air, and inert gas applications. Copper tubing specifications are generally segregated into three types: water and general service, refrigeration service (characterized by cleanliness requirements), and drain/waste/vent (DWV) service. Tubing is available in the annealed or hard-drawn condition. Hard-drawn products are available only as straight lengths. Annealed products

are often available in coils or as straight lengths. Suppliers should be consulted regarding wall thickness availability and standard lengths; however, many products are available in 3.0-m (10-ft) and 6.1-m (20-ft) straight lengths. Coil lengths are generally 12.2 m (40 ft) to 30 m (100 ft).

ASTM copper tubing specifications for water and general-purpose applications include B75 and B88 (Table 10-35). Tubing, fittings, and solders specified for potable water services must always be approved by the appropriate authority, such as the National Sanitation Foundation (NSF). ASTM copper tubing specifications for refrigeration services include B68 and B280 (Table 10-36). ASTM specifications for DWV services include B306 (1¼ through 8-in OD). Pipe conforming to the diameters shown in Table 10-37 is available as ASTM B42 and B302. ASTM B302 has diameters matching ASTM B42, but is available with thinner walls (Table 10-38). Red brass pipe is available as ASTM B43.

Joints are typically soldered, silver-brazed, or mechanical. When using flare, compression, or other mechanical joint fittings, consideration must be given to the fitting manufacturer's recommendations regarding hardness, minimum and maximum wall thickness, finish requirements, and diameter tolerances. Flanges and flanged fittings are seldom used since soldered and brazed joints can be easily disassembled. Brass and bronze valves are available with female ends for soldering.

70 percent copper, 30 percent nickel and 90 percent copper, 10 percent nickel ASTM B466 are available as seamless pipe (ASTM B466) or welded pipe (ASTM B467) and welding fittings for handling brackish water in Schedule 10 and regular copper pipe thicknesses.

Nickel and Nickel Alloys A wide range of ferrous and nonferrous nickel and nickel-bearing alloys are available. They are usually selected because of their improved resistance to chemical attack or their superior resistance to the effects of high temperature. In general terms their cost and corrosion resistance are somewhat a function of their nickel content. The 300 Series stainless steels are the most generally used. Some other frequently used alloys are listed in Table 10-39 together with their nominal compositions. For metallurgical and corrosion resistance data, see Sec. 25.

TABLE 10-34 High-Silicon Iron Pipe*

Size, inside diam., in	No hub (MJ) ends				Bell-and-spigot ends			
	Out-side diam., in	Wall thick-ness, in	Stand-ard† length, ft	Est. weight per piece, lb	Out-side diam., in	Wall thick-ness, in	Stand-ard† length, ft	Est. weight per piece, lb
1½	2¾ ₁₆	⅝ ₁₆	7	46				
2	2 ¹¹ / ₁₆	⅝ ₁₆	7	56	2 ¹¹ / ₁₆	⅝ ₁₆	7	62
3	3 ⁴⁹ / ₆₄	⅝ ₁₆	7	79	3 ²⁵ / ₃₂	⅝ ₁₆	7	90
4	4 ⁴⁹ / ₆₄	⅝ ₁₆	7	100	4 ²⁵ / ₃₂	⅝ ₁₆	7	114
6					6 ¹ / ₁₆	1 ³ / ₃₂	7	169
8					9	1 ³ / ₃₂	7	234
10					11¾	⅝	7	340
12					13¾	⅝	5	470
15					16¼	7 ₈	5	800

*Extracted from *Standard Specification for High-Silicon Iron Pipe and Fittings*, ASTM A861-2004, with permission of the American Society for Testing and Materials, West Conshocken, Pa.

TABLE 10-35 Dimensions, Weights, and Tolerances in Diameter and Wall Thickness for Nominal or Standard Copper Water Tube Sizes (ASTM B88-2003)*

All tolerances are plus and minus except as otherwise noted.

Nominal standard size, in	Outside diameter, in	Average outside diameter ^a tolerance, in		Wall thickness and tolerances, in						Theoretical weight, lb/ft		
				Type K		Type L		Type M		Type K	Type L	Type M
		Annealed	Drawn	Wall thickness	Tolerance ^b	Wall thickness	Tolerance ^b	Wall thickness	Tolerance ^b			
¼	0.375	0.002	0.001	0.035	0.0035	0.030	0.003	c	c	0.145	0.126	c
⅜	0.500	0.0025	0.001	0.049	0.005	0.035	0.004	0.025	0.002	0.269	0.198	0.145
½	0.625	0.0025	0.001	0.049	0.005	0.040	0.004	0.028	0.003	0.344	0.285	0.204
⅝	0.750	0.0025	0.001	0.049	0.005	0.042	0.004	c	c	0.418	0.362	c
¾	0.875	0.003	0.001	0.065	0.006	0.045	0.004	0.032	0.003	0.641	0.455	0.328
1	1.125	0.0035	0.0015	0.065	0.006	0.050	0.005	0.035	0.004	0.839	0.655	0.465
1¼	1.375	0.004	0.0015	0.065	0.006	0.055	0.006	0.042	0.004	1.04	0.884	0.682
1½	1.625	0.0045	0.002	0.072	0.007	0.060	0.006	0.049	0.005	1.36	1.14	0.940
2	2.125	0.005	0.002	0.083	0.008	0.070	0.007	0.058	0.006	2.06	1.75	1.46
2½	2.625	0.005	0.002	0.095	0.010	0.080	0.008	0.065	0.006	2.93	2.48	2.03
3	3.125	0.005	0.002	0.109	0.011	0.090	0.009	0.072	0.007	4.00	3.33	2.68
3½	3.625	0.005	0.002	0.120	0.012	0.100	0.010	0.083	0.008	5.12	4.29	3.58
4	4.125	0.005	0.002	0.134	0.013	0.110	0.011	0.095	0.010	6.51	5.38	4.66
5	5.125	0.005	0.002	0.160	0.016	0.125	0.012	0.109	0.011	9.67	7.61	6.66
6	6.125	0.005	0.002	0.192	0.019	0.140	0.014	0.122	0.012	13.9	10.2	8.92
8	8.125	0.006	+0.002 -0.004	0.271	0.027	0.200	0.020	0.170	0.017	25.9	19.3	16.5
10	10.125	0.008	+0.002 -0.006	0.338	0.034	0.250	0.025	0.212	0.021	40.3	30.1	25.6
12	12.125	0.008	+0.002 -0.006	0.405	0.040	0.280	0.028	0.254	0.025	57.8	40.4	36.7

* Extracted from ASTM B88-2003 with permission of the publisher, the American Society for Testing and Materials, West Conshohocken, Pa.

^a The average outside diameter of a tube is the average of the maximum and minimum outside diameter, as determined at any one cross section of the tube.

^b Maximum deviation at any one point.

^c Indicates that the material is not generally available or that no tolerance has been established.

Titanium Seamless pipe is available as ASTM B861, and welded pipe is available as ASTM B862. Both standards offer numerous grades of unalloyed and alloyed materials. While the alloys often have higher tensile strengths, corrosion resistance may be sacrificed. Forged or wrought fittings and forged or cast valves are available. For many applications, elastomer-lined valves having carbon-steel or ductile-iron bodies and titanium trim offer an economical alternative to valves with titanium bodies. Titanium pipe is available with wall thicknesses conforming to many of those listed in Table 10-22, including Schedule 10S and Standard Weight. Properly selected and specified, titanium can be a good choice for seawater systems such as offshore fire

water systems. Seamless and welded tubing is manufactured to ASTM B338; however, availability may be limited.

Flexible Metal Hose Flexible hoses provide flexible connections for conveying gases or liquids, wherever rigid pipes are impractical. There are two basic types of flexible hose: corrugated hoses and interlocked hoses. These flexible hoses can absorb vibrations and noise. They can also provide some flexibility for misaligned rigid piping or equipment during construction. Corrugated or interlocked thin brass, bronze, Monel, aluminum, and steel tubes are covered with flexible braided-wire jackets to form flexible metal hose. Both tube and braid are brazed or welded to pipe-thread, union, or flanged ends. Failures are often the

TABLE 10-36a Standard Dimensions and Weights, and Tolerances in Diameter and Wall Thickness for Coil Lengths (ASTM B280-2003*)

Standard size, in	Outside diameter, in (mm)	Wall thickness, in (mm)	Weight, lb/ft (kg/m)	Tolerances	
				Average ^a outside diameter, plus and minus, in (mm)	Wall ^b thickness, plus and minus, in (mm)
¼	0.125 (3.18)	0.030 (0.762)	0.0347 (0.0516)	0.002 (0.051)	0.003 (0.08)
⅜	0.187 (4.75)	0.030 (0.762)	0.0575 (0.0856)	0.002 (0.051)	0.003 (0.08)
½	0.250 (6.35)	0.030 (0.762)	0.0804 (0.120)	0.002 (0.051)	0.0025 (0.08)
⅝	0.312 (7.92)	0.032 (0.813)	0.109 (0.162)	0.002 (0.051)	0.003 (0.08)
¾	0.375 (9.52)	0.032 (0.813)	0.134 (0.199)	0.002 (0.051)	0.003 (0.08)
1	0.500 (12.7)	0.032 (0.813)	0.182 (0.271)	0.002 (0.051)	0.003 (0.08)
1¼	0.625 (15.9)	0.035 (0.889)	0.251 (0.373)	0.002 (0.051)	0.004 (0.11)
1½	0.750 (19.1)	0.042 (0.889)	0.305 (0.454)	0.0025 (0.064)	0.004 (0.11)
2	0.750 (19.1)	0.042 (1.07)	0.362 (0.539)	0.0025 (0.064)	0.004 (0.11)
2½	0.875 (22.3)	0.045 (1.14)	0.455 (0.677)	0.003 (0.076)	0.004 (0.11)
3	1.125 (28.6)	0.050 (1.27)	0.665 (0.975)	0.0035 (0.089)	0.005 (0.13)
3½	1.375 (34.9)	0.055 (1.40)	0.884 (1.32)	0.004 (0.10)	0.006 (0.15)
4	1.625 (41.3)	0.060 (1.52)	1.14 (1.70)	0.0045 (0.11)	0.006 (0.15)

* Extracted from ASTM B280-2003 with permission of the publisher, the American Society for Testing and Materials, West Conshohocken, Pa.

^a The average outside diameter of a tube is the average of the maximum and minimum outside diameters as determined at any one cross section of the tube.

^b The tolerances listed represent the maximum deviation at any point.

TABLE 10-36b Standard Dimensions and Weights, and Tolerances in Diameter and Wall Thickness for Straight Lengths (ASTM B280-2003*)

Note 1—Applicable to drawn temper tube only.

Standard size, in	Outside diameter, in (mm)	Wall thickness, in (mm)	Weight, lb/ft (kg/m)	Tolerances	
				Average ^a outside diameter, plus and minus, in (mm)	Wall ^b thickness, plus and minus, in (mm)
3/8	0.375 (9.52)	0.030 (0.762)	0.126 (0.187)	0.001 (0.025)	0.0035 (0.08)
1/2	0.500 (12.7)	0.035 (0.889)	0.198 (0.295)	0.001 (0.025)	0.004 (0.09)
5/8	0.625 (15.9)	0.040 (1.02)	0.285 (0.424)	0.001 (0.025)	0.004 (0.10)
3/4	0.750 (19.1)	0.042 (1.07)	0.362 (0.539)	0.001 (0.025)	0.004 (0.11)
7/8	0.875 (22.3)	0.045 (1.14)	0.455 (0.677)	0.001 (0.025)	0.004 (0.11)
1 1/8	1.125 (28.6)	0.050 (1.27)	0.655 (0.975)	0.0015 (0.038)	0.004 (0.13)
1 3/8	1.375 (34.9)	0.055 (1.40)	0.884 (1.32)	0.0015 (0.038)	0.006 (0.11)
1 5/8	1.625 (41.3)	0.060 (1.52)	1.14 (1.70)	0.002 (0.051)	0.006 (0.11)
2 1/8	2.125 (54.0)	0.070 (1.78)	1.75 (2.60)	0.002 (0.051)	0.007 (0.15)
2 3/8	2.625 (66.7)	0.080 (2.03)	2.48 (3.69)	0.002 (0.051)	0.008 (0.15)
3 1/8	3.125 (79.4)	0.090 (2.29)	3.33 (4.96)	0.002 (0.051)	0.009 (0.23)
3 3/8	3.625 (92.1)	0.100 (2.54)	4.29 (6.38)	0.002 (0.051)	0.010 (0.25)
4 1/8	4.125 (105)	0.110 (2.79)	5.38 (8.01)	0.002 (0.051)	0.011 (0.28)

*Extracted from ASTM B280-2003, with permission of the publisher, the American Society for Testing and Materials, West Conshohocken, Pa.

^a The average outside diameter of a tube is the average of the maximum and minimum outside diameters as determined at any one cross section of the tube.

^b The tolerances listed represent the maximum deviation at any point.

TABLE 10-37 Copper and Red-Brass Pipe (ASTM B42-2002 and B43-2004)*: Standard Dimensions, Weights, and Tolerances

Standard pipe size, in	Nominal outside diameter, in (mm)	Average outside diameter tolerances, in (mm), all minus†	Nominal wall thickness, in (mm)	Tolerance, in (mm)‡	Theoretical weight, lb/ft (kg/m)	
					Red brass	Copper
Regular pipe						
1/8	0.405 (10.3)	0.004 (0.10)	0.062 (1.57)	0.004 (0.10)	0.253 (0.376)	0.259 (0.385)
1/4	0.540 (13.7)	0.004 (0.10)	0.082 (2.08)	0.005 (0.13)	0.447 (0.665)	0.457 (0.680)
3/8	0.675 (17.1)	0.005 (0.13)	0.090 (2.29)	0.005 (0.13)	0.627 (0.933)	0.641 (0.954)
1/2	0.840 (21.3)	0.005 (0.13)	0.107 (2.72)	0.006 (0.15)	0.934 (1.39)	0.955 (1.42)
3/4	1.050 (26.7)	0.006 (0.15)	0.114 (2.90)	0.006 (0.15)	1.27 (1.89)	1.30 (1.93)
1	1.315 (33.4)	0.006 (0.15)	0.126 (3.20)	0.007 (0.18)	1.78 (2.65)	1.82 (2.71)
1 1/4	1.660 (42.2)	0.006 (0.15)	0.146 (3.71)	0.008 (0.20)	2.63 (3.91)	2.69 (4.00)
1 1/2	1.900 (48.3)	0.006 (0.15)	0.150 (3.81)	0.008 (0.20)	3.13 (4.66)	3.20 (4.76)
2	2.375 (60.3)	0.008 (0.20)	0.156 (3.96)	0.009 (0.23)	4.12 (6.13)	4.22 (6.28)
2 1/2	2.875 (73.0)	0.008 (0.20)	0.187 (4.75)	0.010 (0.25)	5.99 (8.91)	6.12 (9.11)
3	3.500 (88.9)	0.010 (0.25)	0.219 (5.56)	0.012 (0.30)	8.56 (12.7)	8.76 (13.0)
3 1/2	4.000 (102)	0.010 (0.25)	0.250 (6.35)	0.013 (0.33)	11.2 (16.7)	11.4 (17.0)
4	4.500 (114)	0.012 (0.30)	0.250 (6.35)	0.014 (0.36)	12.7 (18.9)	12.9 (19.2)
5	5.562 (141)	0.014 (0.36)	0.250 (6.35)	0.014 (0.36)	15.8 (23.5)	16.2 (24.1)
6	6.625 (168)	0.016 (0.41)	0.250 (6.35)	0.014 (0.36)	19.0 (28.3)	19.4 (28.9)
8	8.625 (219)	0.020 (0.51)	0.312 (7.92)	0.022 (0.56)	30.9 (46.0)	31.6 (47.0)
10	10.750 (273)	0.022 (0.56)	0.365 (9.27)	0.030 (0.76)	45.2 (67.3)	46.2 (68.7)
12	12.750 (324)	0.024 (0.61)	0.375 (9.52)	0.030 (0.76)	55.3 (82.3)	56.5 (84.1)
Extrastrong pipe						
1/8	0.405 (10.3)	0.004 (0.10)	0.100 (2.54)	0.006 (0.15)	0.363 (0.540)	0.371 (0.552)
1/4	0.540 (13.7)	0.004 (0.10)	0.123 (3.12)	0.007 (0.18)	0.611 (0.909)	0.625 (0.930)
3/8	0.675 (17.1)	0.005 (0.13)	0.127 (3.23)	0.007 (0.18)	0.829 (1.23)	0.847 (1.26)
1/2	0.840 (21.3)	0.005 (0.13)	0.149 (3.78)	0.008 (0.20)	1.23 (1.83)	1.25 (1.86)
3/4	1.050 (26.7)	0.006 (0.15)	0.157 (3.99)	0.009 (0.23)	1.67 (2.48)	1.71 (2.54)
1	1.315 (33.4)	0.006 (0.15)	0.182 (4.62)	0.010 (0.25)	2.46 (3.66)	2.51 (3.73)
1 1/4	1.660 (42.2)	0.006 (0.15)	0.194 (4.93)	0.010 (0.25)	3.39 (5.04)	3.46 (5.15)
1 1/2	1.900 (48.3)	0.006 (0.15)	0.203 (5.16)	0.011 (0.28)	4.10 (6.10)	4.19 (6.23)
2	2.375 (60.3)	0.008 (0.20)	0.221 (5.61)	0.012 (0.30)	5.67 (8.44)	5.80 (8.63)
2 1/2	2.875 (73.0)	0.008 (0.20)	0.280 (7.11)	0.015 (0.38)	8.66 (12.9)	8.85 (13.2)
3	3.500 (88.9)	0.010 (0.25)	0.304 (7.72)	0.016 (0.41)	11.6 (17.3)	11.8 (17.6)
3 1/2	4.000 (102)	0.010 (0.25)	0.321 (8.15)	0.017 (0.43)	14.1 (21.0)	14.4 (21.4)
4	4.500 (114)	0.012 (0.30)	0.341 (8.66)	0.018 (0.46)	16.9 (25.1)	17.3 (25.7)
5	5.562 (141)	0.014 (0.36)	0.375 (9.52)	0.019 (0.48)	23.2 (34.5)	23.7 (35.3)
6	6.625 (168)	0.016 (0.41)	0.437 (11.1)	0.027 (0.69)	32.2 (47.9)	32.9 (49.0)
8	8.625 (219)	0.020 (0.51)	0.500 (12.7)	0.035 (0.89)	48.4 (72.0)	49.5 (73.7)
10	10.750 (273)	0.022 (0.56)	0.500 (12.7)	0.040 (1.0)	61.1 (90.9)	62.4 (92.9)

*Copyright American Society for Testing and Materials, West Conshohocken, PA; reprinted/adapted with permission. All tolerances are plus and minus except as otherwise indicated.

†The average outside diameter of a tube is the average of the maximum and minimum outside diameters as determined at any one cross section of the tube.

‡Maximum deviation at any one point.

TABLE 10-38 Hard-Drawn Copper Threadless Pipe (ASTM B302)*

Standard pipe size, in	Nominal dimensions, in (mm)			Cross-sectional area of bore, in ² (cm ²)	Nominal weight, lb/ft (kg/m)	Tolerances, in (mm)	
	Outside diameter	Inside diameter	Wall thickness			Average outside diameter, all minus†	Wall thickness, plus and minus
¼	0.540 (13.7)	0.410 (10.4)	0.065 (1.65)	0.132 (0.852)	0.376 (0.559)	0.004 (0.10)	0.0035 (0.089)
⅜	0.675 (17.1)	0.545 (13.8)	0.065 (1.65)	0.233 (1.50)	0.483 (0.719)	0.004 (0.10)	0.004 (0.10)
½	0.840 (21.3)	0.710 (18.0)	0.065 (1.65)	0.396 (2.55)	0.613 (0.912)	0.005 (0.13)	0.004 (0.10)
¾	1.050 (26.7)	0.920 (23.4)	0.065 (1.65)	0.665 (4.29)	0.780 (1.16)	0.005 (0.13)	0.004 (0.10)
1	1.315 (33.4)	1.185 (30.1)	0.065 (1.65)	1.10 (7.10)	0.989 (1.47)	0.005 (0.13)	0.004 (0.10)
1¼	1.660 (42.2)	1.530 (38.9)	0.065 (1.65)	1.84 (11.9)	1.26 (1.87)	0.006 (0.15)	0.004 (0.10)
1½	1.900 (48.3)	1.770 (45.0)	0.065 (1.65)	2.46 (15.9)	1.45 (2.16)	0.006 (0.15)	0.004 (0.10)
2	2.375 (60.3)	2.245 (57.0)	0.065 (1.65)	3.96 (25.5)	1.83 (272)	0.007 (0.18)	0.006 (0.15)
2½	2.875 (73.0)	2.745 (69.7)	0.065 (1.65)	5.92 (38.2)	2.22 (3.30)	0.007 (0.18)	0.006 (0.15)
3	3.500 (88.9)	3.334 (84.7)	0.083 (2.11)	8.73 (56.3)	3.45 (5.13)	0.008 (0.20)	0.007 (0.18)
3½	4.000 (102)	3.810 (96.8)	0.095 (2.41)	11.4 (73.5)	4.52 (6.73)	0.008 (0.20)	0.007 (0.18)
4	4.500 (114)	4.286 (109)	0.107 (2.72)	14.4 (92.9)	5.72 (8.51)	0.010 (0.25)	0.009 (0.23)
5	5.562 (141)	5.298 (135)	0.132 (3.40)	22.0 (142)	8.73 (13.0)	0.012 (0.30)	0.010 (0.25)
6	6.625 (168)	6.309 (160)	0.158 (4.01)	31.3 (202)	12.4 (18.5)	0.014 (0.36)	0.010 (0.25)
8	8.625 (219)	8.215 (209)	0.205 (5.21)	53.0 (342)	21.0 (31.2)	0.018 (0.46)	0.014 (0.36)
10	10.750 (273)	10.238 (260)	0.256 (6.50)	82.3 (531)	32.7 (48.7)	0.018 (0.46)	0.016 (0.41)
12	12.750 (324)	12.124 (308)	0.313 (7.95)	115 (742)	47.4 (70.5)	0.018 (0.46)	0.020 (0.51)

*Copyright American Society for Testing and Materials, West Conshohocken, PA; reprinted/adapted with permission.
 †The average outside diameter of a tube is the average of the maximum and minimum outside diameters, as determined at any one cross section of the tube.

result of corrosion of the braided-wire jacket or of a poor jacket-to-fitting weld. Maximum recommended temperature for bronze hose is approximately 230°C (450°F). Metal thickness is much less than for straight tube for the same pressure-temperature conditions; so accurate data on corrosion and erosion are required to make proper selection.

NONMETALLIC PIPE AND METALLIC PIPING SYSTEMS WITH NONMETALLIC LININGS

Cement-Lined Carbon-Steel Pipe Cement-lined carbon-steel pipe is made by lining steel pipe with special cement. The cement lin-

ing prevents pickup of iron by the fluid handled, corrosion of the metal by brackish or saline water, and growth of tuberculation. Various grades of cement are available, and the proper grade should be selected to match the application.

Cement-lined pipe in sizes smaller than 1½ in is not generally recommended. Cement-lined carbon steel pipe can be supplied with butt-weld or flanged ends. Butt-welded construction involves the use of special joint grouts at the weld joint and controlled welding procedures. See Table 10-40.

American Water Works Association Standard C205 addresses shop-applied cement mortar lining of pipe sizes 4 in and larger. Fittings are

TABLE 10-39 Common Nickel and Nickel-Bearing Alloys

Common trade name or registered trademark	Code designation	Alloy no.	ASTM specification (pipe)	Nominal composition, %											
				Ni	Cr	Mo	Fe	C ^a	Si ^a	Mn	Cu	Cb	Co	W	
Type 304 stainless steel		S30400	A312	8	18		BAL	0.08	1.00	2.0					
Type 304L stainless steel		S30403	A312	8	18		BAL	0.03	1.00	2.0					
Type 316 stainless steel		S31600	A312	12	16	2	BAL	0.08	1.00	2.0					
Type 316L stainless steel		S31603	A312	12	16	2	BAL	0.03	1.00	2.0					
Carpenter 20cb ^b	Ni-Cr-Fe-Mo-Cu-Cb stabilized	N08020	B464	33	20	2.5	38.5	0.06		2.0	3	1			
Incoloy 800 ^c	Ni-Fe-Cr	N08800	B407	32.5	21		46	0.05	0.5	0.8	0.4				
Incoloy 825 ^c	Ni-Fe-Cr-Mo-Cu	N08825	B423	42	21.5	3	30	0.03	0.2	0.5	2.2				
Hastelloy C-276 ^d	Ni-Mo-Cr low carbon	N10276	B575 ^e	54	15	16	5	0.02	0.08	1				2.5	4
Hastelloy B-2 ^d	Ni-Mo	N10001	B333 ^e	64	1	28	2	0.02	0.1	1					
Inconel 625 ^c	Ni-Cr-Mo-Cb	N06625	B444	61	21.5	9	2.5	0.05	0.2	0.2		4			
Inconel 600 ^c	Ni-Cr-Fe	N06600	B167	76	15.5		8	0.08	0.2	0.5		0.2			
Monel 400 ^c	Ni-Cu	N04400	B165	66			1.2	0.20	0.2	1		31.5			
Nickel 200 ^c	Ni	N02200	B161	99+			0.2	0.08							
Hastelloy C ^d	Ni-Cr-Fe-Mo-Cu	N06007	B622	42	22.2	6.5	19.5	0.05	1	1.5	2	2.2 ^f	2.5 ^g	1 ^c	

^a Maximum.

^b Registered trademark, Carpenter Technology Corp.

^c Registered trademark, Huntington Alloys, Inc.

^d Registered trademark, Cabot Corp.

^e Plate.

^f Cb + Ta.

TABLE 10-40 Cement-Lined Carbon-Steel Pipe*

Stand-ard pipe size, in	Inside diam. after lining, in	Typical thickness of lining, in	Weight, per ft, lb	Stand-ard pipe size, in	Inside diam. after lining, in	Typical thickness of lining, in	Weight per ft, lb
				3	2.70	0.13	8.3
				4	3.60	.16	12.0
				6	5.40	.25	24.0
1½	1.40	.09	3.0	8	7.40	.25	32.0
2	1.80	.10	4.1	10	9.40	.30	43.0
2½	2.20	.10	6.6	12	11.40	.30	55.0

*To convert inches to millimeters, multiply by 25.4; to convert pounds per foot to kilograms per meter, multiply by 1.49.

available as cement mortar lined butt-weld or flanged carbon steel, flanged cast iron, or flanged ductile iron. AWWA C602 addresses in-place (i.e., in situ or field) application of cement mortar lining for pipe sizes 4 in and larger.

Concrete Pipe Concrete piping and nonmetallic piping such as PVC, RTR, and HDPE are commonly used for buried gravity drain and pressurized applications. Common applications for both include construction culverts and forced water mains, sewage, industrial waste, and storm water systems. Some of the factors to be considered when deciding whether to use concrete or nonmetallic piping include local code requirements, pipe size, soil and commodity corrosivity, commodity temperature and pressure, resistance to tuberculin growth, traffic and burial loads, soil conditions and bedding requirements, groundwater level and buoyancy issues, suitability of available joining methods, ability of joints to resist internal pressure thrust without the use of thrust blocks, availability of pressure-rated and non-pressure-rated fittings, shipping weight, load capacity of available construction equipment, requirements for special equipment such as fusion bonding machines, contractor's experience and labor skill level requirements, and final installed cost.

Nonreinforced concrete culvert pipe for gravity drain applications is manufactured to ASTM C14 in strength Classes 1, 2, and 3. It is available with internal diameters 4 through 36 in. Reinforced concrete culvert for gravity drain applications is manufactured to ASTM C76 with internal diameters of 12 through 144 in. Metric sizes are manufactured to ASTM C14M and C76M. Joints are typically bell and spigot (or a similar variation) with rubber gaskets.

Concrete pressure pipe is typically custom-designed to three different specifications. Each design provides a cement mortar lining or concrete interior. It is advisable to consult manufacturers regarding the most appropriate specification for a given application and the availability of fittings. The names of some manufacturers can be obtained through the American Concrete Pressure Pipe Association. American Water Works Association standard AWWA C300 addresses steel cylinder reinforced concrete pressure pipe in inside-diameter sizes 30 through 144 in. AWWA C301 addresses prestressed reinforced pipe with a steel cylinder wrapped with steel wire. Inside-diameter sizes are 16 through 144 in. AWWA C302 addresses circumferentially reinforced pipe without a steel cylinder or prestress. Inside diameter sizes are 12 through 144 in, with continuous pressure ratings to 0.38 MPa (55 lbf/in²) and total pressure (including surge) to 0.45 MPa (65 lbf/in²). AWWA C303 addresses reinforced pipe with a steel cylinder helically wrapped with steel bar. Inside-diameter sizes are 10 through 60 in, with pressure ratings to 2.7-MPa (400 lbf/in²) working pressure. Joints are typically bell and spigot (or a similar variation) with rubber gaskets. In addition to the gasket, grouting is used on the exterior and interior of the joint to seal otherwise exposed steel.

Glass Pipe and Fittings These are made from heat- and chemical-resistant borosilicate glass in accordance with ASTM E-438 Type 1 Class A. This glass is resistant to chemical attack by almost all products, which makes its resistance much more comprehensive than that of other well-known materials. It is highly resistant to water, saline solutions, organic substances, halogens such as chlorine and bromine, and many acids. There are only a few chemicals that can cause noticeable corrosion of the glass surface, such as hydrofluoric acid, concen-

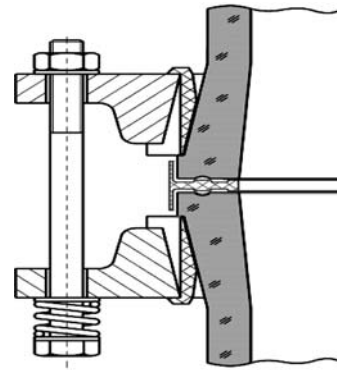


FIG. 10-164 Flanged joint with conical ends. (Adapted with permission of De Dietrich Process Systems, Mountainside, N.J.)

trated phosphoric acid, and strong caustic solutions at elevated temperatures. Some important physical properties are as follows:

- Mean linear expansion coefficient between 20 and 300°C: [(3.3 ± 0.1) × 10⁻⁶]/K
- Mean thermal conductivity between 20 and 200°C: 1.2 W/(m K)
- Mean specific heat capacity between 20 and 100°C: 0.8 kJ/kg(K)
- Mean specific heat capacity between 101 and 200°C: 0.9 kJ/kg(K)
- Density at 20°C: 2.23 kg/dm³

Flanged glass pipe with conical ends (Fig. 10-164) should be used in applications requiring a pressure rating or that are expected to see thermal cycling. Flanged ends are normally required to mate with other glass components (vessels, coil heat exchangers, etc). The flanges are specially designed plastic backing flanges that are cushioned from the glass by either molded plastic or fiber inserts. The liquid seal is provided by means of a gasket that is gripped between the grooved pipe ends.

Glass pipe is made in the sizes shown in Table 10-41. Depending on the nominal diameter, lengths range from 0.075 to 3 m. Design pressure ranges from -0.10 MPa (-14.5 lbf/in²) vacuum to 0.40 MPa (58 lbf/in²) for nominal diameters of 15 through 50 mm, 3 MPa (43 lbf/in²) for nominal diameter of 80 mm, 0.20 MPa (29 lbf/in²) for nominal diameters of 100 and 150 mm, and 0.10 MPa (14.5 lbf/in²) for nominal diameters of 200 and 300 mm. Maximum permissible thermal shock as a general guide is 120 K. Maximum operating temperature is 200°C (248°F). A complete line of fittings is available, and special parts can be made to order. Thermal expansion stresses should be completely relieved by tied PTFE corrugated expansion joints and offsets. Temperature rating may be limited by joint design and materials.

Beaded pipe is used for process waste lines and vent lines. Some applications have also been made in low-pressure and vacuum lines. Beaded end pipe is available in nominal diameters of 1½ through 6 in. For operating conditions manufacturers should be consulted. In this system the ends of the pipe and fittings are formed into a bead, as

TABLE 10-41 Dimensions for Glass Pipe and Flanged Joints (see Fig. 10-165)*

Nominal pipe size, mm	D1	D2	D3	D4	Type
15	16.8	28.6	23	15.5-17.5	A
25	26.5	42.2	34	25-27	A
40	38.5	57.4	48	36.5-39.75	A
50	50.5	70	60.5	48-52	A
80	76	99.2	88	72-78	A
100	104.5	132.6	120.5	97.6-110	A
150	154	185	172	150-156	A
200	203	235	220	197-205	B
300	300	340	321	299-303	B

*Adapted with permission of De Dietrich Process Systems, Mountainside, N.J.

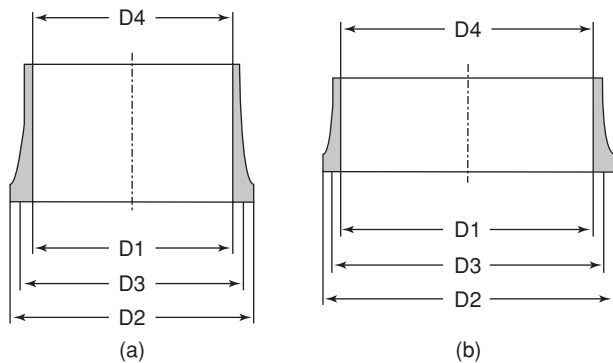


FIG. 10-165 Flanged pipe ends. (Adapted with permission of De Dietrich Process Systems, Mountainside, N.J.)

shown in Fig. 10-166. The coupling consists of a stainless steel outer shell, a rubber collar, and a TFE liner-gasket. When the single coupling nut is tightened, the thick rubber sleeve forces the TFE gasket against the glass to make the seal.

Glass-Lined Steel Pipe and Fittings This pipe is fully resistant to all acids except hydrofluoric and concentrated phosphoric acids at temperatures up to 120°C (248°F). It is also resistant to alkaline solutions at moderate temperatures. Glass-lined steel pipe can be used at temperatures up to 220°C (428°F) under some exposure conditions provided there are no excessive temperature changes. The operating pressure rating of commonly available systems is 1 MPa (145 lb/in²). The glass lining is approximately 1.6 mm (1/16 in) thick. It is made by lining Schedule 40 steel pipe. Fittings are available in glass-lined cast steel. Standard nominal pipe sizes available are 1½ through 8 in. Larger-diameter pipe up to 48 in is available on a custom-order basis. A range of lengths are generally available. See Table 10-42 for dimensional data. Steel split flanges drilled to ANSI B16.5 Class 150 dimensions along with PTFE envelope gaskets are used for the assembly of the system.

Fused Silica or Fused Quartz Containing 99.8 percent silicon dioxide, fused silica or fused quartz can be obtained as opaque or transparent pipe and tubing. The melting point is 1710°C (3100°F). Tensile strength is approximately 48 MPa (7000 lb/in²); specific gravity is about 2.2. The pipe and tubing can be used continuously at temperatures up to 1000°C (1830°F) and intermittently up to 1500°C (2730°F). The material's chief assets are noncontamination of most chemicals in high-temperature service, thermal-shock resistance, and high-temperature electrical insulating characteristics.

Transparent tubing is available in inside diameters from 1 to 125 mm in a range of wall thicknesses. Satin-surface tubing is available in inside diameters from 1/8 to 2 in, and sand-surface pipe and tubing are

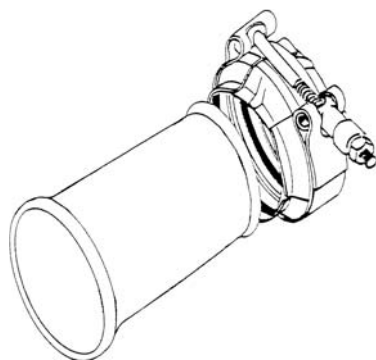


FIG. 10-166 Joint with beaded pipe ends. (Adapted with permission of De Dietrich Process Systems, Mountainside, N.J.)

TABLE 10-42 Glass-Lined Steel Pipe*

Size, in.	Outside diameter, in	Range of standard lengths, in	
		Minimum	Maximum
1½	1.900	6	60
2	2.375	6	84
3	3.500	6	120
4	4.500	6	120
6	6.625	6	120
8	8.625	6	120

*Adapted with permission of De Dietrich Process Systems, Mountainside, N.J. Other manufacturers may offer different standard lengths.

available in ½- to 24-in inside diameters and lengths up to 6 m (20 ft). Sand-surface pipe and tubing are obtainable in wall thicknesses varying from 1/8 to 1 in. Pipe and tubing sections in both opaque and transparent fused silica or fused quartz can be readily machine-ground to special tolerances for pressure joints or other purposes. Also, fused-silica piping and tubing can be reprocessed to meet special-design requirements. Manufacturers should be consulted for specific details.

Plastic-Lined Steel Pipe Use of a variety of polymeric materials as liners for steel pipe rather than as piping systems solves problems which the relatively low tensile strength of the polymer at elevated temperature and high thermal expansion, compared with steel, would produce. The steel outer shell permits much wider spacing of supports, reliable flanged joints, and higher pressure and temperature in the piping. The size range is 1 through 12 in. The systems are flanged with 125-lb cast-iron, 150-lb ductile-iron, and 150- and 300-lb steel flanges. The linings are factory-installed in both pipe and fittings. Lengths are available up to 6 m (20 ft). Lined ball, diaphragm, and check valves and plug cocks are available.

One method of manufacture consists of inserting the liner into an oversize, approximately Schedule 40 steel tube and swaging the assembly to produce iron-pipe-size outside diameter, firmly engaging the liner which projects from both ends of the pipe. Flanges are then screwed onto the pipe, and the projecting liner is hot-flared over the flange faces nearly to the bolt holes. In another method, the liner is pushed into steel pipe having cold-flared laps backed up by flanges at the ends and then hot-flared over the faces of the laps. Pipe lengths made by either method may be shortened in the field and reflared with special procedures and tools. Square and tapered spacers are furnished to adjust for small discrepancies in assembly.

Liner types available are suitable for a wide variety of chemical services, including acids, alkalis, and various solvents. All liners are permeable to some degree, and manufacturers use various methods to vent gas out of the interspace between the liner and casing. All plastics are subject to environmental stress cracking (ESC). ESC can occur even when the liner is chemically resistant to the service. Lined pipe manufacturers should always be consulted regarding liner selections and service applications. Also consult manufacturers regarding vacuum service limits.

Polyvinylidene Chloride Liners Polyvinylidene chloride liners have excellent resistance to hydrochloric acid. Maximum temperature is 80°C (175°F). Polyvinylidene chloride is also known as Saran, a product of the Dow Chemical Co.

Polypropylene Liners Polypropylene liners are used in sulfuric acid service. At 10 to 30 percent concentration the upper temperature limit is 93°C (200°F). Polypropylene is also suitable for higher concentrations at lower temperatures.

Kynar Liners Kynar (Pennwalt Chemicals Corp.) polyvinylidene fluoride liners are used for many chemicals, including bromine and 50 percent hydrochloric acid.

PTFE and PFA Lined Steel Pipe These are available in sizes from 1 through 12 in and in lengths through 6 m (20 ft). Experience has determined that practical upper temperature limits are approximately 204°C (400°F) for PTFE (polytetrafluoroethylene) and PFA (perfluoroalkoxy) and 149°C (300°F) for FEP (fluoroethylene polymer); Class 150 and 300 ductile-iron or steel flanged lined fittings and valves are used. The nonadhesive properties of the liner make it ideal for handling sticky or viscous substances. Thickness of the lining varies from 1.5 to 3.8 mm (60 to 150 mil), depending on pipe size. Only flanged joints are used.

Rubber-Lined Steel Pipe This pipe is made in lengths up to 6 m (20 ft) with seamless, straight seam-welded and some types of spiral-welded pipe using various types of natural and synthetic adhering rubber. The type of rubber is selected to provide the most suitable lining for the specific service. In general, soft rubber is used for abrasion resistance, semihard for general service, and hard for the more severe service conditions. Multiple-ply lining and combinations of hard and soft rubber are available. The thickness of lining ranges from 3.2 to 6.4 mm ($\frac{1}{8}$ to $\frac{1}{4}$ in) depending on the service, the type of rubber, and the method of lining. Cast-steel, ductile-iron, and cast-iron flanged fittings are available rubber-lined. The fittings are usually purchased by the vendor since absence of porosity on the inner surface is essential. Pipe is flanged before rubber lining, and welding elbows and tees may be incorporated at one end of the length of pipe, subject to the conditions that the size of the pipe and the location of the fittings are such that the operator doing the lining can place a hand on any point on the interior surface of the fitting. Welds must be ground smooth on the inside, and a radius is required at the inner edge of the flange face.

The rubber lining is extended out over the face of flanges. With hard-rubber lining, a gasket is required. With soft-rubber lining, a release coating or a polyethylene sheet is required in place of a gasket to avoid bonding of the lining of one flange to the lining on the other and to permit disassembly of the flanged joint. Also, for pressures over 0.86 MPa (125 lbf/in²), the tendency of soft-rubber linings to extrude out between the flanges may be prevented by terminating the lining inside the bolt holes and filling the balance of the space between the flange faces with a spacer of the proper thickness. Hard-rubber-lined gate, diaphragm, and swing check valves are available. In gate valves, the stem, wedge assembly, and seat rings, and in the check valves, the hinge pin, flapper arm, disk, and seat ring must be made of metal resistant to the solution handled.

Plastic Pipe In contrast to other piping materials, plastic pipe is free from internal and external corrosion, is easily cut and joined, and does not cause galvanic corrosion when coupled to other materials. Allowable stresses and upper temperature limits are low. Normal operation is in the creep range. Fluids for which a plastic is not suited penetrate and soften it rather than dissolve surface layers. Coefficients of thermal expansion are high.

Plastic pipe or tubing may be used for a wide variety of services. As with all nonmetallic materials, code restrictions limit the applications in which their use is permitted. In general, their use in flammable or toxic service is limited. Plastic tubing of various types may be used for instrument air-signal connections; however, as is the case with all non-metallic applications, the need for fire resistance must be considered. When used in specialized applications such as potable water or underground fire water, care should be taken to ensure that the specified products are certified by appropriate agencies such as the National Sanitation Foundation and Factory Mutual.

Support spacing must be much closer than for carbon steel. As temperature increases, the allowable stress for many plastic pipes decreases very rapidly, and heat from sunlight or adjacent hot uninsulated equipment has a marked effect. Many plastics deteriorate with exposure to ultraviolet light if not provided with a UV-resistant coating or other surface barrier. Successful economical underground use of plastic pipe does not necessarily indicate similar economies outdoors aboveground.

Methods of joining include threaded joints with IPS dimensions, solvent-welded joints, heat-fused joints, and insert fittings. Schedules 40 and 80 (see Table 10-22) have been used as a source for standardized dimensions at joints. Some plastics are available in several grades with allowable stresses varying by a factor of 2 to 1. For the same plastic, $\frac{1}{2}$ -in Schedule 40 pipe of the strongest grade may have 4 times the allowable internal pressure of the weakest grade of a 2-in Schedule 40 pipe. For this reason, the plastic-pipe industry is shifting to standard dimension ratios (approximately the same ratio of diameter to wall thickness over a wide range of pipe sizes).

ASTM and the Plastics Pipe Institute have established identifications for plastic pipe in which the first group of letters identifies the plastic, the two following numbers identify the grade of that plastic, and the last two numbers represent the design stress in the nearest lower 0.7-MPa (100-lbf/in²) unit at 23°C (73.4°F).

Polyethylene Plastics Pipe Institute (www.plasticpipe.org) is an excellent source of information regarding specification, design, fabrication, and testing of polyethylene piping. Polyethylene (PE) pipe and tubing are available in sizes 48 in and smaller. They have excellent resistance at room temperature to salts, sodium and ammonium hydroxides, and sulfuric, nitric, and hydrochloric acids. High-density polyethylene (HDPE) is often used for underground fire water. Pipe and tubing are produced by extrusion from resins whose density varies with the manufacturing process. Physical properties and therefore wall thickness depend on the particular resin used. In some products, about 3 percent carbon black is added to provide resistance to ultraviolet light. Use of higher-density resin reduces splitting and pinholing in service and increases the strength of the material and the maximum service temperature.

ASTM D2104 covers PE pipe in sizes $\frac{1}{2}$ through 6 in with IPS Schedule 40 outside and inside diameters for insert-fitting joints. ASTM D2239 covers six standard dimension ratios of pipe diameter to wall thickness in sizes $\frac{1}{2}$ through 6 in. ASTM D2447 covers sizes $\frac{1}{2}$ through 12 in with IPS Schedule 40 and 80 outside and inside diameters for use with heat-fusion socket-type and butt-type fittings. ASTM D3035 covers 10 standard dimension ratios of pipe sizes from $\frac{1}{2}$ through 24 in with IPS outside diameters. All these specifications cover various PE materials. Hydrostatic design stresses within the recommended temperature limits are given in Appendix B, Table B-1, of the code. The hydrostatic design stress is the maximum tensile hoop stress due to internal hydrostatic water pressure that can be applied continuously with a high degree of certainty that failure of the pipe will not occur. Both manufacturers and the Plastic Pipe Institute publish literature describing design calculations required to determine the required wall thickness.

Polyethylene water piping is not damaged by freezing. Pipe and tubing 2 in and smaller are shipped in coils several hundred feet in length.

Clamped-insert joints (Fig. 10-167) are used for flexible plastic pipe up through the 2-in size. Friction between the pipe and the spud is developed both by forcing the spud into the pipe and by tightening the clamp. For the larger sizes, which have thicker walls, these methods cannot develop adequate friction. Insert joints also have high pressure drop. Stainless-steel bands are available. Inserts are available in nylon, polypropylene, and a variety of metals.

Joints of all sizes may be made with heat fusion techniques. Fused joints may be made with either electrofusion or conventional heat fusion. Electrofusion joints are made with fittings which have embedded heating wires. Conventional fusion joints are made with special machines which trim the pipe ends, apply heat, and then force them together to form a bond. Consult the manufacturer regarding the sizes for which electrofusion fittings are available.

A significant use for PE and PP pipe is the technique of rehabilitating deteriorated pipe lines by lining them with plastic pipe. Lining an existing pipe with plastic pipe has a large cost advantage over replacing the line, particularly if replacement of the old line would require excavation.

Polyvinyl Chloride Polyvinyl chloride (PVC) pipe and tubing are available with socket fittings for solvent-cemented joints in sizes 24 in and smaller. PVC with gasketed bell and spigot joints is available in sizes 4 through 48 in. Chlorinated polyvinyl chloride (CPVC) pipe and tubing are available with socket fittings for solvent-cemented joints in sizes 4 in and smaller. PVC and CPVC are suitable

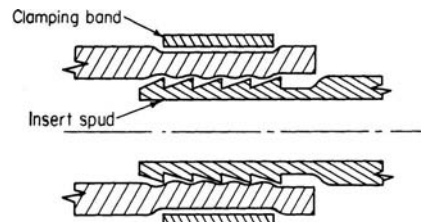


FIG. 10-167 Clamped-insert joint.

for a variety of chemical services and are commonly used for potable water. Consult manufacturers or the Plastics Pipe Institute for chemical resistance data. Hydrostatic design stresses within the temperature limits are given in Appendix B, Table B-1, of the code.

ASTM D1785 covers sizes from 1/4 through 12 in of PVC pipe in IPS Schedules 40, 80, and 120, except that Schedule 120 starts at 1/2 in and is not IPS for sizes from 1/2 through 3 in. ASTM D2241 covers sizes 1/2 through 36 in but with IPS outside diameter and seven standard dimension ratios: 13.5, 17, 21, 26, 32.5, 41, and 64.

ASTM D2513 specifies requirements for thermoplastic materials for buried fuel gas and relining applications. Materials addressed include PE, PVC, and crosslinked polyethylene (PEX). Tubing sizes covered are 1/4 through 1 3/4 in. IPS sizes covered are 1/2 through 12 in. Size availability depends upon the material.

Solvent-cemented joints (Fig. 10-150) are standard, but screwed joints are sometimes used with Schedule 80 pipe. Cemented joints must not be disturbed for 5 min and achieve full strength in 1 day. A wide variety of valve types are available in PVC and CPVC.

Polypropylene Polypropylene (PP) pipe and fittings have excellent resistance to most common organic and mineral acids and their salts, strong and weak alkalis, and many organic chemicals. They are available in sizes 1/2 through 6 in, in Schedules 40 and 80, but are not covered as such by ASTM specifications.

Reinforced-Thermosetting-Resin (RTR) Pipe Glass-reinforced epoxy resin has good resistance to nonoxidizing acids, alkalis, salt water, and corrosive gases. The glass reinforcement is many times stronger at room temperature than plastics, does not lose strength with increasing temperature, and reinforces the resin effectively up to 149°C (300°F). (See Table 10-21 for temperature limits.) The glass reinforcement is located near the outside wall, protected from the contents by a thick wall of resin and protected from the atmosphere by a thin wall of resin. Stock sizes are 2 through 12 in.

Pipe is supplied in 6- and 12-m (20- and 40-ft) lengths. It is more economical for long, straight runs than for systems containing numerous fittings. When the pipe is sawed to nonfactory lengths, it must be sawed very carefully to avoid cracking the interior plastic zone. A two-component cement may be used to bond lengths into socket couplings or flanges or cemented-joint fittings. Curing of the cement is temperature-sensitive; it sets to full strength in 45 min at 93°C (200°F), in 12 h at 38°C (100°F), and in 24 h at 10°C (50°F). Extensive use is made of shop-fabricated flanged preassemblies. Only flanged joints are used to connect to metallic piping systems. Compared with that of other plastics, the ratio of fitting cost to pipe cost is high. Cemented-joint fittings and flanged fittings are available. Internally lined flanged metallic valves are used.

RTR is more flexible than metallic pipe and consequently requires closer support spacing. While the recommended spacing varies among manufacturers and with the type of product, Table 10-43 gives typical hanger-spacing ranges. The pipe fabricator should be consulted for recommended hanger spacing on the specific pipe-wall construction being used.

Epoxy resin has a higher strength at elevated temperatures than polyester resins but is not as resistant to attack by some fluids. Some glass-reinforced epoxy-resin pipe is made with a polyester-resin liner. The coefficient of thermal expansion of glass-reinforced resin pipe is higher than that for carbon steel but much less than that for plastics.

Glass-reinforced polyester is the most widely used reinforced-resin system. A wide choice of polyester resins is available. The bisphenol resins resist strong acids as well as alkaline solutions. The size range is 2 through at least 36 in; the temperature range is shown

TABLE 10-43 Typical Hanger-Spacing Ranges Recommended for Reinforced-Thermosetting-Resin Pipe

Nominal pipe size, in	2	3	4	6	8	10	12
Hanger-spacing range, ft	5-8	6-9	6-10	8-11	9-13	10-14	11-15

NOTE: Consult pipe manufacturer for recommended hanger spacing for the specific RTR pipe being used. Tabulated values are based on a specific gravity of 1.25 for the contents of the pipe. To convert feet to meters, multiply by 0.3048.

in Table 10-21. Diameters are not standardized. Adhesive-cemented socket joints and hand-lay-up reinforced butt joints are used. For the latter, reinforcement consists of layers of glass cloth saturated with adhesive cement.

DESIGN OF PIPING-SYSTEMS

Safeguarding Safeguarding may be defined as the provision of protective measures as required to ensure the safe operation of a proposed piping system. General considerations to be evaluated should include (1) the hazardous properties of the fluid, (2) the quantity of fluid which could be released by a piping failure, (3) the effect of a failure (such as possible loss of cooling water) on overall plant safety, (4) evaluation of effects on a reaction with the environment (i.e., possibility of a nearby source of ignition), (5) the probable extent of exposure of operating or maintenance personnel, and (6) the relative inherent safety of the piping by virtue of materials of construction, methods of joining, and history of service reliability.

Evaluation of safeguarding requirements might include engineered protection against possible failures such as thermal insulation, armor, guards, barricades, and damping for protection against severe vibration, water hammer, or cyclic operating conditions. Simple means to protect people and property such as shields for valve bonnets, flanged joints, and sight glasses should not be overlooked. The necessity for means to shut off or control flow in the event of a piping failure such as block valves or excess-flow valves should be examined.

Classification of Fluid Services The code applies to piping systems as illustrated in Fig. 10-127, but two categories of fluid services are segregated for special consideration as follows:

Category D Category D fluid service is defined as "a fluid service to which all the following apply: (1) the fluid handled is non-flammable and nontoxic; (2) the design gage pressure does not exceed 150 psi (1.0 MPa); and (3) the design temperature is between -20°F (-29°C) and 366°F (186°C)."

Category M Category M fluid service is defined as "a fluid service in which a single exposure to a very small quantity of a toxic fluid, caused by leakage, can produce serious irreversible harm to persons on breathing or bodily contact, even when prompt restorative measures are taken."

The code assigns to the owner the responsibility for identifying those fluid services which are in Categories D and M. The design and fabrication requirements for Class M toxic-service piping are beyond the scope of this *Handbook*. See ASME B31.3—2004, chap. VIII.

Design Conditions Definitions of the temperatures, pressures, and various forces applicable to the design of piping systems are as follows:

Design Pressure The design pressure of a piping system shall not be less than the pressure at the most severe condition of coincident internal or external pressure and temperature resulting in the greatest required component thickness or rating.

Design Temperature The design temperature is the material temperature representing the most severe condition of coincident pressure and temperature. For uninsulated metallic pipe with fluid below 65°C (150°F), the metal temperature is taken as the fluid temperature.

With fluid at or above 65°C (150°F) and without external insulation, the metal temperature is taken as a percentage of the fluid temperature unless a lower temperature is determined by test or calculation. For pipe, threaded and welding-end valves, fittings, and other components with a wall thickness comparable with that of the pipe, the percentage is 95 percent; for flanges and flanged valves and fittings, 90 percent; for lap-joint flanges, 85 percent; and for bolting, 80 percent.

With external insulation, the metal temperature is taken as the fluid temperature unless service data, tests, or calculations justify lower values. For internally insulated pipe, the design metal temperature shall be calculated or obtained from tests.

Ambient Influences If cooling results in a vacuum, the design must provide for external pressure or a vacuum breaker installed; also provision must be made for thermal expansion of contents trapped between or in closed valves. Nonmetallic or nonmetallic-lined pipe may require protection when ambient temperature exceeds design temperature.

Occasional variations of pressure or temperature, or both, above operating levels are characteristic of certain services. If the following criteria are met, such variations need not be considered in determining pressure-temperature design conditions. Otherwise, the most severe conditions of coincident pressure and temperature during the variation shall be used to determine design conditions. (Application of pressures exceeding pressure-temperature ratings of valves may under certain conditions cause loss of seat tightness or difficulty of operation. Such an application is the owner's responsibility.)

All the following criteria must be met:

1. The piping system shall have no pressure-containing components of cast iron or other nonductile metal.
2. Nominal pressure stresses shall not exceed the yield strength at temperature (see S_y data in BPV Code, Sec. II, Part D).
3. Combined longitudinal stresses S_L shall not exceed the limits established in the code (see pressure design of piping components for S_L limitations).
4. The total number of pressure-temperature variations above the design condition shall not exceed 1000 during the life of the piping system.
5. Occasional variations above design conditions shall remain within one of the following limits for pressure design:
 - When the variation lasts no more than 10 h at any one time and no more than 100 h per year, it is permissible to exceed the pressure rating or the allowable stress for pressure design at the temperature of the increased condition by not more than 33 percent.
 - When the variation lasts no more than 50 h at any one time and not more than 500 h per year, it is permissible to exceed the pressure rating or the allowable stress for pressure design at the temperature of the increased condition by not more than 20 percent.

Dynamic Effects Design must provide for impact (hydraulic shock, etc.), wind (exposed piping), earthquake, discharge reactions, and vibrations (of piping arrangement and support).

Weight Effects Weight considerations include (1) live loads (contents, ice, and snow), (2) dead loads (pipe, valves, insulation, etc.), and (3) test loads (test fluid).

Thermal Expansion and Contraction Effects Thermal-expansion and -contraction loads occur when a piping system is prevented from free thermal expansion or contraction as a result of anchors and restraints or undergoes large, rapid temperature changes or unequal temperature distribution because of an injection of cold liquid striking the wall of a pipe carrying hot gas.

Effects of Support, Anchor, and Terminal Movements The effects of movements of piping supports, anchors, and connected equipment shall be taken into account in the design of piping. These movements may result from the flexibility and/or thermal expansion of equipment, supports, or anchors; and from settlement, tidal movements, or wind sway.

Reduced Ductility The harmful effects of reduced ductility shall be taken into account in the design of piping. The effects may, e.g., result from welding, heat treatment, forming, bending, or low operating temperatures, including the chilling effect of sudden loss of pressure on highly volatile fluids. Low ambient temperatures expected during operation shall be considered.

Cyclic Effects Fatigue due to pressure cycling, thermal cycling, and other cyclic loading shall be considered in the design.

Air Condensation Effects At operating temperatures below -191°C (-312°F) in ambient air, condensation and oxygen enrichment occur. These shall be considered in selecting materials, including insulation, and adequate shielding and/or disposal shall be provided.

Design Criteria: Metallic Pipe The code uses three different approaches to design, as follows:

1. It provides for the use of dimensionally standardized components at their published pressure-temperature ratings.
2. It provides design formulas and maximum stresses.
3. It prohibits the use of materials, components, or assembly methods in certain conditions.

Components Having Specific Ratings These are listed in ASME, API, and industry standards. These ratings are acceptable for design pressures and temperatures unless limited in the code. A list of component standards is given in Appendix E of the ASME B31.3 code. Table 10-44 lists pressure-temperature ratings for

TABLE 10-44a Pressure-Temperature Ratings for Group 1.1 Materials (Carbon Steel)*

Nominal designation	Forgings		Castings		Plates		
C-Si	A 105 (1)		A 216 Gr. WCB (1)		A 515 Gr. 70 (1)		
C-Mn-Si	A 350 Gr. LF2 (1)				A 516 Gr. 70 (1), (2)		
C-Mn-Si-V	A 350 Gr. LF6 Cl. 1 (4)				A 537 Cl. 1 (3)		
3½ NI	A 350 Gr. LF 3						
Working pressures by classes, psig							
Class temp., °F	150	300	400	600	900	1500	2500
-20 to 100	285	740	985	1480	2220	3705	6170
200	260	680	905	1360	2035	3395	5655
300	230	655	870	1310	1965	3270	5450
400	200	635	845	1265	1900	3170	5280
500	170	605	805	1205	1810	3015	5025
600	140	570	755	1135	1705	2840	4730
650	125	550	730	1100	1650	2745	4575
700	110	530	710	1060	1590	2655	4425
750	95	505	675	1015	1520	2535	4230
800	80	410	550	825	1235	2055	3430
850	65	320	425	640	955	1595	2655
900	50	230	305	460	690	1150	1915
950	35	135	185	275	410	685	1145
1000	20	85	115	170	255	430	715

NOTES:

- (1) Upon prolonged exposure to temperatures above 800°F, the carbide phase of steel may be converted to graphite. Permissible, but not recommended for prolonged use above 800°F.
- (2) Not to be used over 850°F.
- (3) Not to be used over 700°F.
- (4) Not to be used over 500°F.

TABLE 10-44b Pressure-Temperature Ratings for Group 1.5 Materials (Carbon, 1/2Mo Steel)

Nominal designation	Forgings			Castings			Plates	
C-1/2Mo	A 182 Gr. F1 (1)						A 204 Gr. A (1)	A 204 Gr. B (1)
Working pressures by classes, psig								
Class temp., °F	150	300	400	600	900	1500	2500	
-20 to 100	265	695	930	1395	2090	3480	5805	
200	260	695	930	1395	2090	3480	5805	
300	230	685	915	1375	2060	3435	5725	
400	200	660	885	1325	1985	3310	5520	
500	170	640	855	1285	1925	3210	5350	
600	140	605	805	1210	1815	3025	5040	
650	125	590	785	1175	1765	2940	4905	
700	110	570	755	1135	1705	2840	4730	
750	95	530	710	1065	1595	2660	4430	
800	80	510	675	1015	1525	2540	4230	
850	65	485	650	975	1460	2435	4060	
900	50	450	600	900	1350	2245	3745	
950	35	280	375	560	845	1405	2345	
1000	20	165	220	330	495	825	1370	

NOTE:

(1) Upon prolonged exposure to temperatures above 875°F, the carbide phase of carbon-molybdenum steel may be converted to graphite. Permissible, but not recommended for prolonged use above 875°F.

TABLE 10-44c Pressure-Temperature Ratings for Group 2.1 Materials (Type 304 Stainless Steel)

Nominal designation	Forgings			Castings			Plates	
18Cr-8Ni	A 182 Gr. F304 (1)			A 351 Gr. CF3 (2)			A 240 Gr. 304 (1)	
	A 182 Gr. F304H			A 351 Gr. CF8 (1)			A 240 Gr. 304H	
Working pressures by classes, psig								
Class temp., °F	150	300	400	600	900	1500	2500	
-20 to 100	275	720	960	1440	2160	3600	6000	
200	230	600	800	1200	1800	3000	5000	
300	205	540	715	1075	1615	2690	4480	
400	190	495	660	995	1490	2485	4140	
500	170	465	620	930	1395	2330	3880	
600	140	440	590	885	1325	2210	3680	
650	125	430	575	865	1295	2160	3600	
700	110	420	565	845	1265	2110	3520	
750	95	415	550	825	1240	2065	3440	
800	80	405	540	810	1215	2030	3380	
850	65	395	530	790	1190	1980	3300	
900	50	390	520	780	1165	1945	3240	
950	35	380	510	765	1145	1910	3180	
1000	20	355	470	710	1065	1770	2950	
1050	...	325	435	650	975	1630	2715	
1100	...	255	345	515	770	1285	2145	
1150	...	205	275	410	615	1030	1715	
1200	...	165	220	330	495	825	1370	
1250	...	135	180	265	400	670	1115	
1300	...	115	150	225	340	565	945	
1350	...	95	125	185	280	465	770	
1400	...	75	100	150	225	380	630	
1450	...	60	80	115	175	290	485	
1500	...	40	55	85	125	205	345	

NOTES:

(1) At temperatures over 1000°F, use only when the carbon content is 0.04% or higher.

(2) Not to be used over 800°F.

10-110 TRANSPORT AND STORAGE OF FLUIDS

TABLE 10-44d Pressure-Temperature Ratings for Group 2.2 Materials (Type 316 Stainless Steel)

Nominal designation	Forgings		Castings			Plates	
16Cr-12Ni-2Mo	A 182 Gr. F316 (1) A 182 Gr. F316H		A 351 Gr. CF3M (2) A 351 Gr. CF8M (1)			A 240 Gr. 316 (1) A 240 Gr. 316H	
18Cr-13Ni-3Mo	A 182 Gr. F317 (1)					A 240 Gr. 317 (1)	
19Cr-10Ni-3Mo			A 351 Gr. CG8M (3)				
Working pressures by classes, psig							
Class temp., °F	150	300	400	600	900	1500	2500
-20 to 100	275	720	960	1440	2160	3600	6000
200	235	620	825	1240	1860	3095	5160
300	215	560	745	1120	1680	2795	4660
400	195	515	685	1025	1540	2570	4280
500	170	480	635	955	1435	2390	3980
600	140	450	600	900	1355	2255	3760
650	125	440	590	885	1325	2210	3680
700	110	435	580	870	1305	2170	3620
750	95	425	570	855	1280	2135	3560
800	80	420	565	845	1265	2110	3520
850	65	420	555	835	1255	2090	3480
900	50	415	555	830	1245	2075	3460
950	35	385	515	775	1160	1930	3220
1000	20	365	485	725	1090	1820	3030
1050	...	360	480	720	1080	1800	3000
1100	...	305	405	610	915	1525	2545
1150	...	235	315	475	710	1185	1970
1200	...	185	245	370	555	925	1545
1250	...	145	195	295	440	735	1230
1300	...	115	155	235	350	585	970
1350	...	95	130	190	290	480	800
1400	...	75	100	150	225	380	630
1450	...	60	80	115	175	290	485
1500	...	40	55	85	125	205	345

NOTES:

- (1) At temperatures over 1000°F, use only when the carbon content is 0.04% or higher.
- (2) Not to be used over 850°F.
- (3) Not to be used over 1000°F.

TABLE 10-44e Pressure-Temperature Ratings for Group 2.2 Materials (Type 304L and 316L Stainless Steel)

Nominal designation	Forgings		Castings			Plates	
16Cr-12Ni-2Mo	A 182 Gr. F316L					A 240 Gr. 316L	
18Cr-8Ni	A 182 Gr. F304L (1)					A 240 Gr. 304L (1)	
Working pressures by classes, psig							
Class temp., °F	150	300	400	600	900	1500	2500
-20 to 100	230	600	800	1200	1800	3000	5000
200	195	510	680	1020	1535	2555	4260
300	175	455	610	910	1370	2280	3800
400	160	420	560	840	1260	2100	3500
500	150	395	525	785	1180	1970	3280
600	140	370	495	745	1115	1860	3100
650	125	365	485	730	1095	1825	3040
700	110	360	480	720	1080	1800	3000
750	95	355	470	705	1060	1765	2940
800	80	345	460	690	1035	1730	2880
850	65	340	450	675	1015	1690	2820

NOTE:

- (1) Not to be used over 800°F.

flanges, flanged fittings, and flanged valves, and has been extracted from ASME B16.5 with permission of the publisher, the American Society of Mechanical Engineers, New York. Only a few of the more common materials of construction of piping are reproduced here. See ASME B16.5 for other materials. Flanged joints, flanged valves in the open position, and flanged fittings may be subjected to system hydrostatic tests at a pressure not to exceed the hydrostatic-shell test pressure. Flanged valves in the closed position may be subjected to a system hydrostatic test at a pressure not to exceed 110 percent of the 100°F rating of the valve unless otherwise limited by the manufacturer.

Pressure-temperature ratings for soldered tubing joints are given in ASME B16.22—2001.

Components without Specific Ratings Components such as pipe and butt-welding fittings are generally furnished in nominal thicknesses. Fittings are rated for the same allowable pressures as pipe of the same nominal thickness and, along with pipe, are rated by the rules for pressure design and other provisions of the code.

Limits of Calculated Stresses due to Sustained Loads and Displacement Strains

1. *Internal pressure stresses.* Stresses due to internal pressure shall be considered safe when the wall thickness of the piping component, including any reinforcement, meets the requirements of the pressure design of components defined by the ASME B31.3 code.

2. *External pressure stresses.* Stresses due to external pressure shall be considered safe when the wall thickness of the piping component, and its means of stiffening meet the requirements of the pressure design of components defined by the ASME B31.3 code.

3. *Longitudinal stresses S_L .* The sum of longitudinal stresses S_L in any component in a piping system, due to sustained loads such as pressure and weight, shall not exceed the product $S_h W$, where S_h is the basic allowable stress at maximum metal temperature expected during the displacement cycle under analysis, and W is the weld joint strength reduction factor.

4. *Allowable displacement stress range S_A .* The computed displacement stress range S_E in a piping system shall not exceed the allowable displacement stress range S_A .

$$S_A = f(1.25S_c + 0.25S_h) \tag{10-93}$$

When S_h is greater than S_L , the difference between them may be added to the term $0.25S_h$ in Eq. (10-93). In that case, the allowable stress range is calculated by

$$S_A = f[1.25(S_c + S_h) - S_L] \tag{10-94}$$

- where S_A = allowable displacement stress range
- f = stress range factor (see Fig. 10-168)
- S_c = basic allowable stress at minimum metal temperature expected during displacement cycle under analysis
- S_h = basic allowable stress at maximum metal temperature expected during displacement cycle under analysis
- S_L = longitudinal stresses, including pressure and weight

5. *Weld joint strength reduction factor W .* It is very important to include the weld joint strength reduction factor W in the design consideration. Especially, at elevated temperatures, the long-term strength of weld joints may be lower than the long-term strength of the base material. The weld joint strength reduction factor only applies at weld locations.

Pressure Design of Metallic Components External-pressure stress evaluation of piping is the same as for pressure vessels. But an important difference exists when one is establishing design pressure and wall thickness for internal pressure as a result of the ASME Boiler and Pressure Vessel Code's requirement that the relief-valve setting be not higher than the design pressure. For vessels this means

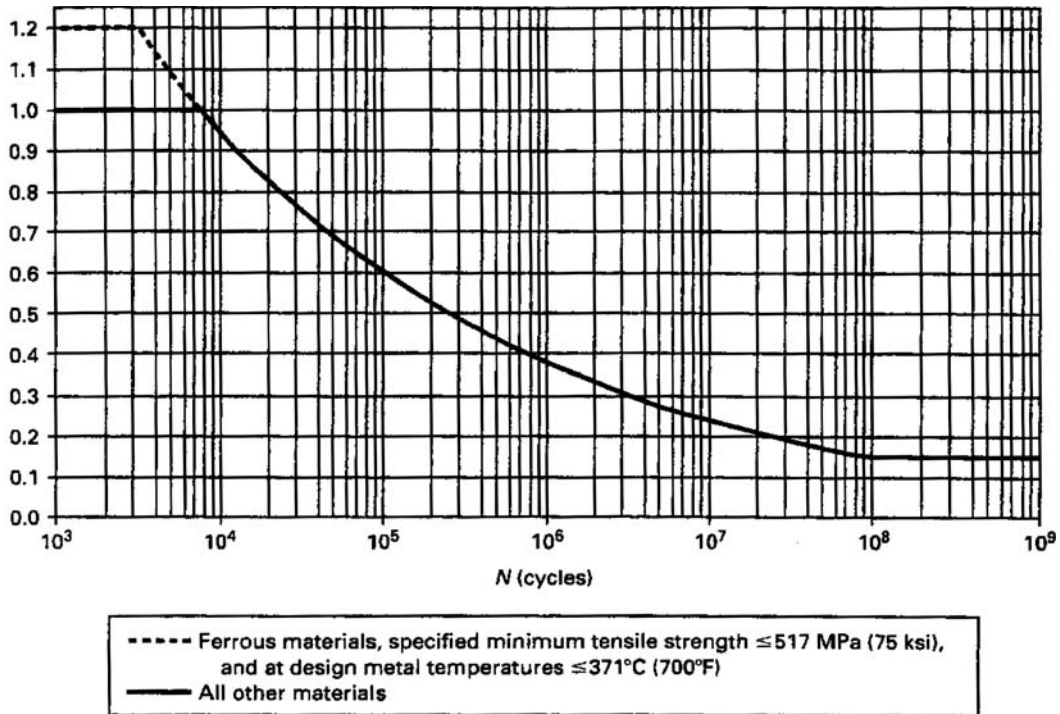


FIG. 10-168 Stress range reduction factor, f . (Reproduced from ASME B31.3-2004 with permission of the publisher, the American Society of Mechanical Engineers, New York.)

10-112 TRANSPORT AND STORAGE OF FLUIDS

that the design is for a pressure 10 percent more or less above the intended maximum operating pressure to avoid popping or leakage from the valve during normal operation. However, on piping the design pressure and temperature are taken as the maximum intended operating pressure and coincident temperature combination which results in the maximum thickness. The temporary increased operating conditions listed under "Design Criteria" cover temporary operation at pressures that cause relief valves to leak or open fully. Allowable stresses for nearly 1000 materials are contained in the code. For convenience, the allowable stresses for commonly used carbon and stainless steels have been extracted from the code and listed in Table 10-44.

For **straight metal pipe under internal pressure** the formula for minimum required wall thickness t_m is applicable for:

1. $t < D/6$. The internal pressure design thickness for straight pipe shall be not less than that calculated in accordance with the equation below. The more conservative Barlow and Lamé equations may also be used. Equation (10-95) includes a factor Y varying with material and temperature to account for the redistribution of circumferential

stress which occurs under steady-state creep at high temperature and permits slightly lesser thickness at this range.

$$t_m = \frac{PD_o}{2(SE + PY)} \div C \quad (10-95)$$

where (in consistent units)

P = design pressure

D_o = outside diameter of pipe

C = sum of allowances for corrosion, erosion, and any thread or groove depth. For threaded components the depth is h of ASME B1.20.1, and for grooved components the depth is the depth removed (0.02 in when no tolerance is specified).

SE = allowable stress (see Table 10-44)

S = basic allowable stress for materials, excluding casting, joint, or structural-grade quality factors

E = quality factor. The quality factor E is one or the product of more than one of the following quality factors: casting quality factor E_c , joint quality factor E_j (see Fig. 10-169).





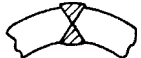
No.	Type of Joint	Type of Seam	Examination	Factor E_j	
1	Furnace but weld, continuous weld		Straight	As required by listed specification	0.60 [Note (1)]
2	Electric resistance weld		Straight or spiral	As required by listed specification	0.85 [Note (1)]
3	Electric fusion weld				
	(a) Single butt weld (with or without filler metal)		Straight or spiral	As required by listed specification or this code	0.80
				Additionally spot radiographed per para. 341.5.1, ASME B31.3	0.90
				Additionally 100% radiographed per para. 344.5.1 and Table 341.3.2, ASME B31.3	1.00
	(b) Double butt weld (with or without filler metal)		Straight or spiral [except as provided in 4(a) below]	As required by listed specification or this code	0.85
				Additionally spot radiographed per para. 341.5.1, ASME B31.3	0.90
				Additionally 100% radiographed per para. 344.5.1 and Table 341.3.2, ASME B31.3	1.00
4	Per specific specification				
	(a) API 5L	Submerged arc weld (SAW) Gas metal arc weld (GMAW) Combined GMAW, SAW	Straight with one or two seams Spiral	As required by specification	0.95
					

FIG. 10-169 Longitudinal weld joint quality factor, E_j . [NOTE (1): It is not permitted to increase the joint quality factor by additional examination for joint 1 or 2.] (Reproduced from ASME B31.3 with permission of the publisher, the American Society of Mechanical Engineers, New York.)

Y = coefficient having value in Table 10-45 valid for $t < D/6$ and for materials shown
 t_m = minimum required thickness, in, including mechanical, corrosion, and erosion allowances

2. $t \geq D/6$ or $P/SE > 0.385$. Calculation of pressure design thickness for straight pipe requires special consideration of factors such as theory of failure, effects of fatigue, and thermal stress.

For flanges of nonstandard dimensions or for sizes beyond the scope of the approved standards, design shall be in accordance with the requirements of the ASME Boiler and Pressure Vessel Code, Sec. VIII, except that requirements for fabrication, assembly, inspection testing, and the pressure and temperature limits for materials of the Piping Code are to prevail. Countermoment flanges of flat face or otherwise providing a reaction outside the bolt circle are permitted if designed or tested in accordance with code requirements under pressure-containing components "not covered by standards and for which design formulas or procedures are not given."

Test Conditions The shell pressure test for flanged fittings shall be at a pressure no less than 1.5 times the 38°C (100°F) pressure rating rounded off to the next higher 1-bar (psi) increment.

In accordance with listed standards, **blind flanges** may be used at their pressure-temperature ratings. The minimum thickness of non-standard blind flanges shall be the same as for a bolted flat cover, in accordance with the rules of the ASME Boiler and Pressure Vessel Code, Sec. VIII.

Operational blanks shall be of the same thickness as blind flanges or may be calculated by the following formula (use consistent units):

$$t = d\sqrt{3P/16SE + C} \quad (10-96)$$

where d = inside diameter of gasket for raised- or flat (plain)-face flanges, or the gasket pitch diameter for retained gasketed flanges

- P = internal design pressure or external design pressure
- S = applicable allowable stress
- E = quality factor
- C = sum of the mechanical allowances

Valves must comply with the applicable standards listed in Appendix E of the code and with the allowable pressure-temperature limits established thereby but not beyond the code-established service or materials limitations. Special valves must meet the same requirements as for countermoment flanges.

The code contains no specific rules for the design of **fittings** other than as branch openings. Ratings established by recognized standards are acceptable, however. ASME Standard B16.5 for steel-flanged fittings incorporates a 1.5 shape factor and thus requires the entire fitting to be 50 percent heavier than a simple cylinder in order to provide reinforcement for openings and/or general shape. ASME B16.9 for butt-welding fittings, on the other hand, requires only that the fittings be able to withstand the calculated bursting strength of the straight pipe with which they are to be used.

The thickness of **pipe bends** shall be determined as for straight pipe, provided the bending operation does not result in a difference between maximum and minimum diameters greater than 8 and 3 percent of the nominal outside diameter of the pipe for internal and external pressure, respectively.

TABLE 10-45 Values of Coefficient Y for $t < D/6$

Materials	Temperature, °C (°F)					
	≤482 (900 and lower)	510 (950)	538 (1000)	566 (1050)	593 (1100)	≥621 (1150 and up)
Ferritic steels	0.4	0.5	0.7	0.7	0.7	0.7
Austenitic steels	0.4	0.4	0.4	0.4	0.5	0.7
Other ductile metals	0.4	0.4	0.4	0.4	0.4	0.4
Cast iron	0.0

The maximum allowable internal pressure for multiple miter bends shall be the lesser value calculated from Eqs. (10-97) and (10-98). These equations are not applicable when θ exceeds 22.5°.

$$P_m = \frac{SEW(T - C)}{r_2} = \left[\frac{T - C}{(T - C) + 0.643 \tan \theta \sqrt{r_2(T - C)}} \right] \quad (10-97)$$

$$P_m = \frac{SEW(T - C)}{r_2} = \left(\frac{R_1 - r_2}{R_1 - 0.5r_2} \right) \quad (10-98)$$

where nomenclature is the same as for straight pipe except as follows (see Fig. 10-170):

- S = stress value for material
- C = sum of mechanical allowances
- r_2 = mean radius of pipe
- R_1 = effective radius of miter bend, defined as the shortest distance from the pipe centerline to the intersection of the planes of adjacent miter joints
- θ = angle of miter cut, °
- α = angle of change in direction at miter joint = 2θ , °
- T = pipe wall thickness
- W = weld joint strength reduction factor
- E = quality factor

For compliance with the code, the value of R_1 shall not be less than that given by Eq. (10-99):

$$R_1 = A/\tan\theta + D/2 \quad (10-99)$$

where A has the following empirical values:

t , in	A
≤ 0.5	1.0
0.5 < t < 0.88	$2(T - C)$
≥ 0.88	$[2(T - C)/3] + 1.17$

Piping branch connections involve the same considerations as pressure-vessel nozzles. However, outlet size in proportion to piping header size is unavoidably much greater for piping. The current Piping Code rules for calculation of branch-connection reinforcement are similar to those of the ASME Boiler and Pressure Vessel Code, Sec. VIII, Division I—2004 for a branch with axis at right angles to the header axis. If the branch connection makes an angle β with the header axis from 45 to 90°, the Piping Code requires that the area to be replaced be increased by dividing it by $\sin \beta$. In such cases the half width of the reinforcing zone measured along the header axis is similarly increased, except that it may not exceed the outside diameter of the header. Some details of commonly used reinforced branch connections are given in Fig. 10-171.

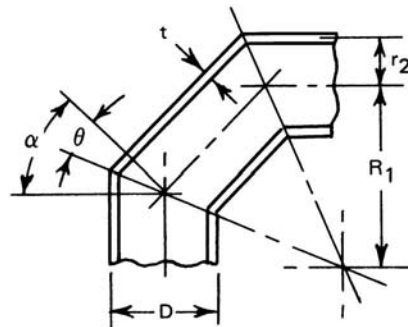


FIG. 10-170 Nomenclature for miter bends. (Extracted from the Process Piping Code, ASME B31.3—2004, with permission of the publisher, the American Society of Mechanical Engineers, New York.)

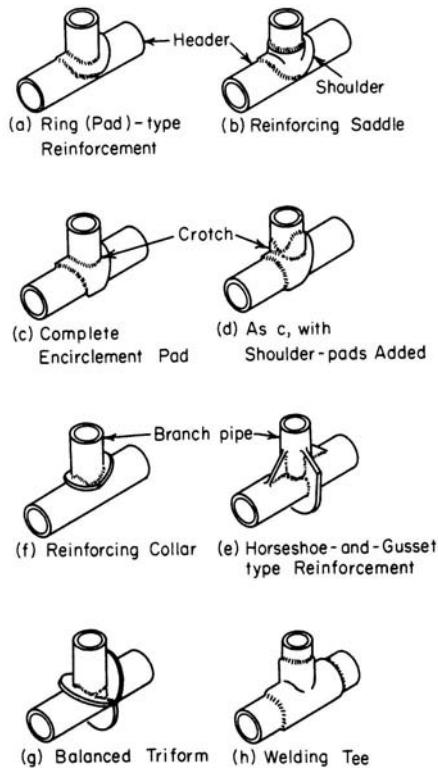


FIG. 10-171 Types of reinforcement for branch connections. (From Kellogg, *Design of Piping Systems*, Wiley, New York, 1965.)

The rules provide that a branch connection has adequate strength for pressure if a fitting (tee, lateral, or cross) is in accordance with an approved standard and is used within the pressure-temperature limitations or if the connection is made by welding a coupling or half coupling (wall thickness not less than the branch anywhere in reinforcement zone or less than extra heavy or 3000 lb) to the run and provided the ratio of branch to run diameters is not greater than one-fourth and that the branch is not greater than 2 in nominal diameter.

Dimensions of extra-heavy couplings are given in the *Steel Products Manual* published by the American Iron and Steel Institute. In ASME B16.11—2001, 2000-lb couplings were superseded by 3000-lb couplings.

ASME B31.3 states that the reinforcement area for resistance to external pressure is to be at least one-half of that required to resist internal pressure.

The code provides no guidance for analysis but requires that external and internal **attachments** be designed to avoid flattening of the pipe, excessive localized bending stresses, or harmful thermal gradients, with further emphasis on minimizing stress concentrations in cyclic service.

The code provides design requirements for **closures** which are flat, ellipsoidal, spherically dished, hemispherical, conical (without transition knuckles), conical convex to pressure, toriconical concave to pressure, and toriconical convex to pressure.

Openings in closures over 50 percent in diameter are designed as flanges in flat closures and as reducers in other closures. Openings of not over one-half of the diameter are to be reinforced as branch connections.

Thermal Expansion and Flexibility: Metallic Piping ASME B31.3 requires that piping systems have sufficient flexibility to prevent thermal expansion or contraction or the movement of piping supports or terminals from causing (1) failure of piping supports from overstress or fatigue; (2) leakage at joints; or (3) detrimental stresses or distortions in piping or in connected equipment (pumps, turbines, or valves, for example), resulting from excessive thrusts or movements in the piping.

To assure that a system meets these requirements, the computed displacement-stress range S_E shall not exceed the allowable stress range S_A [Eqs. (10-93) and (10-94)], the reaction forces R_m [Eq. (10-106)] shall not be detrimental to supports or connected equipment, and movement of the piping shall be within any prescribed limits.

Displacement Strains Strains result from piping being displaced from its unrestrained position:

1. **Thermal displacements.** A piping system will undergo dimensional changes with any change in temperature. If it is constrained from free movement by terminals, guides, and anchors, it will be displaced from its unrestrained position.

2. **Reaction displacements.** If the restraints are not considered rigid and there is a predictable movement of the restraint under load, this may be treated as a compensating displacement.

3. **Externally imposed displacements.** Externally caused movement of restraints will impose displacements on the piping in addition to those related to thermal effects. Such movements may result from causes such as wind sway or temperature changes in connected equipment.

Total Displacement Strains Thermal displacements, reaction displacements, and externally imposed displacements all have equivalent effects on the piping system and must be considered together in determining total displacement strains in a piping system.

Expansion strains may be taken up in three ways: by bending, by torsion, or by axial compression. In the first two cases maximum stress occurs at the extreme fibers of the cross section at the critical location. In the third case the entire cross-sectional area over the entire length is for practical purposes equally stressed.

Bending or torsional flexibility may be provided by bends, loops, or offsets; by corrugated pipe or expansion joints of the bellows type; or by other devices permitting rotational movement. These devices must be anchored or otherwise suitably connected to resist end forces from fluid pressure, frictional resistance to pipe movement, and other causes.

Axial flexibility may be provided by expansion joints of the slipjoint or bellows types, suitably anchored and guided to resist end forces from fluid pressure, frictional resistance to movement, and other causes.

Displacement Stresses Stresses may be considered proportional to the total displacement strain only if the strains are well distributed and not excessive at any point. The methods outlined here and in the code are applicable only to such a system. Poor distribution of strains (unbalanced systems) may result from:

1. Highly stressed small-size pipe runs in series with large and relatively stiff pipe runs

2. Local reduction in size or wall thickness or local use of a material having reduced yield strength (for example, girth welds of substantially lower strength than the base metal)

3. A line configuration in a system of uniform size in which expansion or contraction must be absorbed largely in a short offset from the major portion of the run

If unbalanced layouts cannot be avoided, appropriate analytical methods must be applied to assure adequate flexibility. If the designer determines that a piping system does not have adequate inherent flexibility, additional flexibility may be provided by adding bends, loops, offsets, swivel joints, corrugated pipe, expansion joints of the bellows or slip-joint type, or other devices. Suitable anchoring must be provided.

As contrasted with stress from sustained loads such as internal pressure or weight, displacement stresses may be permitted to cause limited overstrain in various portions of a piping system. When the system is operated initially at its greatest displacement condition, any yielding reduces stress. When the system is returned to its original condition, there occurs a redistribution of stresses which is referred to as self-springing. It is similar to cold springing in its effects.

While stresses resulting from thermal strain tend to diminish with time, the algebraic difference in displacement condition and in either the original (as-installed) condition or any anticipated condition with a greater opposite effect than the extreme displacement condition remains substantially constant during any one cycle of operation. This difference is defined as the displacement-stress range, and it is a determining factor in the design of piping for flexibility. See Eqs. (10-93) and (10-94) for the allowable stress range S_A and Eq. (10-101) for the computed stress range S_E .

Cold Spring Cold spring is the intentional deformation of piping during assembly to produce a desired initial displacement and stress. For pipe operating at a temperature higher than that at which it was installed, cold spring is accomplished by fabricating it slightly shorter than design length. Cold spring is beneficial in that it serves to balance the magnitude of stress under initial and extreme displacement conditions. When cold spring is properly applied, there is less likelihood of overstrain during initial operation; hence, it is recommended especially for piping materials of limited ductility. There is also less deviation from as-installed dimensions during initial operation, so that hangers will not be displaced as far from their original settings.

Inasmuch as the service life of a system is affected more by the range of stress variation than by the magnitude of stress at a given time, no credit for cold spring is permitted in stress-range calculations. However, in calculating the thrusts and moments when actual reactions as well as their range of variations are significant, credit is given for cold spring.

Values of thermal-expansion coefficients to be used in determining total displacement strains for computing the stress range are determined from Table 10-46 as the algebraic difference between the value at design maximum temperature and that at the design minimum temperature for the thermal cycle under analysis.

Values for Reactions Values of thermal displacements to be used in determining total displacement strains for the computation of reactions on supports and connected equipment shall be determined as the algebraic difference between the value at design maximum (or minimum) temperature for the thermal cycle under analysis and the value at the temperature expected during installation.

The as-installed and maximum or minimum moduli of elasticity, E_a and E_m respectively, shall be taken as the values shown in Table 10-47. Poisson's ratio may be taken as 0.3 at all temperatures for all metals.

The allowable stress range for displacement stresses S_A and permissible additive stresses shall be as specified in Eqs. (10-93) and (10-94) for systems primarily stressed in bending and/or torsion. For pipe or piping components containing longitudinal welds the basic allowable stress S may be used to determine S_A .

Nominal thicknesses and outside diameters of pipe and fittings shall be used in flexibility calculations.

In the absence of more directly applicable data, the flexibility factor k and stress-intensification factor i shown in Table 10-48 may be used in flexibility calculations in Eq. (10-102). For piping components or attachments (such as valves, strainers, anchor rings, and bands) not covered in the table, suitable stress-intensification factors may be assumed by comparison of their significant geometry with that of the components shown.

Requirements for Analysis No formal analysis of adequate flexibility is required in systems which (1) are duplicates of successfully operating installations or replacements without significant change of systems with a satisfactory service record; (2) can readily be judged adequate by comparison with previously analyzed systems; or (3) are of uniform size, have no more than two points of fixation, have no intermediate restraints, and fall within the limitations of empirical Eq. (10-100):^o

$$\frac{Dy}{(L - U)^2} \leq K_1 \tag{10-100}$$

- where D = outside diameter of pipe, in (mm)
- y = resultant of total displacement strains, in (mm), to be absorbed by the piping system
- L = developed length of piping between anchors, ft (m)
- U = anchor distance, straight line between anchors, ft (m)
- $K_1 = 0.03$ for U.S. customary units listed
- $= 208.3$ for SI units listed in parentheses

^oWARNING: No general proof can be offered that this equation will yield accurate or consistently conservative results. It is not applicable to systems used under severe cyclic conditions. It should be used with caution in configurations such as unequal leg U bends ($L/U > 2.5$) or near-straight sawtooth runs, or for large thin-wall pipe ($i \geq 5$), or when extraneous displacements (not in the direction connecting anchor points) constitute a large part of the total displacement. There is no assurance that terminal reactions will be acceptably low even if a piping system falls within the limitations of Eq. (10-100).

1. All systems not meeting these criteria shall be analyzed by simplified, approximate, or comprehensive methods of analysis appropriate for the specific case.

2. Approximate or simplified methods may be applied only if they are used in the range of configurations for which their adequacy has been demonstrated.

3. Acceptable comprehensive methods of analysis include analytical and chart methods which provide an evaluation of the forces, moments, and stresses caused by displacement strains.

4. Comprehensive analysis shall take into account stress-intensification factors for any component other than straight pipe. Credit may be taken for the extra flexibility of such a component.

In calculating the flexibility of a piping system between anchor points, the system shall be treated as a whole. The significance of all parts of the line and of all restraints introduced for the purpose of reducing moments and forces on equipment or small branch lines and also the restraint introduced by support friction shall be recognized. Consider all displacements over the temperature range defined by operating and shutdown conditions.

Flexibility Stresses Bending and torsional stresses shall be computed using the as-installed modulus of elasticity E_a and then combined in accordance with Eq. (10-101) to determine the computed displacement stress range S_E , which shall not exceed the allowable stress range S_A [Eqs. (10-93) and (10-94)]:

$$S_E = \sqrt{S_b^2 + 4S_t^2} \tag{10-101}$$

- where S_b = resultant bending stress, lbf/in² (MPa)
- $S_t = M_t/2Z$ = torsional stress, lbf/in² (MPa)
- M_t = torsional moment, in-lbf (N-mm)
- Z = section modulus of pipe, in³ (mm³)

The resultant bending stresses S_b to be used in Eq. (10-101) for elbows and miter bends shall be calculated in accordance with Eq. (10-102), with moments as shown in Fig. (10-172):

$$S_b = \frac{\sqrt{(i_t M_t)^2 + (i_o M_o)^2}}{Z} \tag{10-102}$$

- where S_b = resultant bending stress, lbf/in² (MPa)
- i_t = in-plane stress-intensification factor from Table 10-48
- i_o = out-plane stress-intensification factor from Table 10-48
- M_t = in-plane bending moment, in-lbf (N-mm)
- M_o = out-plane bending moment, in-lbf (N-mm)
- Z = section modulus of pipe, in³ (mm³)

The resultant bending stresses S_b to be used in Eq. (10-101) for branch connections shall be calculated in accordance with Eqs. (10-103) and (10-104), with moments as shown in Fig. 10-173.

For header (legs 1 and 2):

$$S_b = \frac{\sqrt{(i_t M_t)^2 + (i_o M_o)^2}}{Z} \tag{10-103}$$

For branch (leg 3):

$$S_b = \frac{\sqrt{(i_t M_t)^2 + (i_o M_o)^2}}{Z_e} \tag{10-104}$$

- where S_b = resultant bending stress, lbf/in² (MPa)
- Z_e = effective section modulus for branch, in³ (mm³)

$$Z_e = \pi r_s^2 T_s \tag{10-105}$$

- r_s = mean branch cross-sectional radius, in (mm)
- T_s = effective branch wall thickness, in (mm) [lesser of \bar{T}_h and $(i_o)(\bar{T}_b)$]
- \bar{T}_h = thickness of pipe matching run of tee or header exclusive of reinforcing elements, in (mm)

TABLE 10-46 Thermal Coefficients, U.S. Units, for MetalsMean coefficient of linear thermal expansion between 70°F and indicated temperature, $\mu\text{in}/(\text{in}\cdot^{\circ}\text{F})$

Temp., °F	Material															
	Carbon steel carbon-moly- low-chrome (through 3Cr-Mo)	5Cr-Mo through 9Cr-Mo	Austenitic stainless steels 18Cr-8Ni	12Cr, 17Cr, 27Cr	25Cr-20Ni	UNS N04400 Monel 67Ni-30Cu	3½Ni	Copper and copper alloys	Aluminum	Gray cast iron	Bronze	Brass	70Cu-30Ni	UNS N08XXX series Ni-Fe-Cr	UNS N06XXX series Ni-Cr-Fe	Ductile iron
-450	6.30
-425	6.61
-400	6.93
-375	7.24
-350	7.51
-325	5.00	4.70	8.15	4.30	...	5.55	4.76	7.74	9.90	...	8.40	8.20	6.65
-300	5.07	4.77	8.21	4.36	...	5.72	4.90	7.94	10.04	...	8.45	8.24	6.76
-275	5.14	4.84	8.28	4.41	...	5.89	5.01	8.11	10.18	...	8.50	8.29	6.86
-250	5.21	4.91	8.34	4.47	...	6.06	5.15	8.26	10.33	...	8.55	8.33	6.97
-225	5.28	4.98	8.41	4.53	...	6.23	5.30	8.40	10.47	...	8.60	8.37	7.08
-200	5.35	5.05	8.47	4.59	...	6.40	5.45	8.51	10.61	...	8.65	8.41	7.19	4.65
-175	5.42	5.12	8.54	4.64	...	6.57	5.52	8.62	10.76	...	8.70	8.46	7.29	4.76
-150	5.50	5.20	8.60	4.70	...	6.75	5.59	8.72	10.90	...	8.75	8.50	7.40	4.87
-125	5.57	5.26	8.66	4.78	...	6.85	5.67	8.81	11.08	...	8.85	8.61	7.50	4.98
-100	5.65	5.32	8.75	4.85	...	6.95	5.78	8.89	11.25	...	8.95	8.73	7.60	5.10
-75	5.72	5.38	8.83	4.93	...	7.05	5.83	8.97	11.43	...	9.05	8.84	7.70	5.20
-50	5.80	5.45	8.90	5.00	...	7.15	5.88	9.04	11.60	...	9.15	8.95	7.80	5.30
-25	5.85	5.51	8.94	5.05	...	7.22	5.94	9.11	11.73	...	9.23	9.03	7.87	5.40
0	5.90	5.56	8.98	5.10	...	7.28	6.00	9.17	11.86	...	9.32	9.11	7.94	5.50
25	5.96	5.62	9.03	5.14	...	7.35	6.08	9.23	11.99	...	9.40	9.18	8.02	5.58
50	6.01	5.67	9.07	5.19	...	7.41	6.16	9.28	12.12	...	9.49	9.26	8.09	5.66
70	6.07	5.73	9.11	5.24	...	7.48	6.25	9.32	12.25	...	9.57	9.34	8.16	...	7.13	5.74
100	6.13	5.79	9.16	5.29	...	7.55	6.33	9.39	12.39	...	9.66	9.42	8.24	...	7.20	5.82
125	6.19	5.85	9.20	5.34	...	7.62	6.36	9.43	12.53	...	9.75	9.51	8.31	...	7.25	5.87
150	6.25	5.92	9.25	5.40	...	7.70	6.39	9.48	12.67	...	9.85	9.59	8.39	...	7.30	5.92
175	6.31	5.98	9.29	5.45	...	7.77	6.42	9.52	12.81	...	9.93	9.68	8.46	...	7.35	5.97
200	6.38	6.04	9.34	5.50	8.79	7.84	6.45	9.56	12.95	5.75	10.03	9.76	8.54	7.90	7.40	6.02
225	6.43	6.08	9.37	5.54	8.81	7.89	6.50	9.60	13.03	5.80	10.05	9.82	8.58	8.01	7.44	6.08
250	6.49	6.12	9.41	5.58	8.83	7.93	6.55	9.64	13.12	5.84	10.08	9.88	8.63	8.12	7.48	6.14
275	6.54	6.15	9.44	5.62	8.85	7.98	6.60	9.68	13.20	5.89	10.10	9.94	8.67	8.24	7.52	6.20
300	6.60	6.19	9.47	5.66	8.87	8.02	6.65	9.71	13.28	5.93	10.12	10.00	8.71	8.35	7.56	6.25
325	6.65	6.23	9.50	5.70	8.89	8.07	6.69	9.74	13.36	5.97	10.15	10.06	8.76	8.46	7.60	6.31
350	6.71	6.27	9.53	5.74	8.90	8.11	6.73	9.78	13.44	6.02	10.18	10.11	8.81	8.57	7.63	6.37
375	6.76	6.30	9.56	5.77	8.91	8.16	6.77	9.81	13.52	6.06	10.20	10.17	8.85	8.69	7.67	6.43
400	6.82	6.34	9.59	5.81	8.92	8.20	6.80	9.84	13.60	6.10	10.23	10.23	8.90	8.80	7.70	6.48
425	6.87	6.38	9.62	5.85	8.92	8.25	6.83	9.86	13.68	6.15	10.25	10.29	...	8.82	7.72	6.57
450	6.92	6.42	9.65	5.89	8.92	8.30	6.86	9.89	13.75	6.19	10.28	10.35	...	8.85	7.75	6.66
475	6.97	6.46	9.67	5.92	8.92	8.35	6.89	9.92	13.83	6.24	10.30	10.41	...	8.87	7.77	6.75
500	7.02	6.50	9.70	5.96	8.93	8.40	6.93	9.94	13.90	6.28	10.32	10.47	...	8.90	7.80	6.85
525	7.07	6.54	9.73	6.00	8.93	8.45	6.97	9.97	13.98	6.33	10.35	10.53	...	8.92	7.82	6.88
550	7.12	6.58	9.76	6.05	8.93	8.49	7.01	9.99	14.05	6.38	10.38	10.58	...	8.95	7.85	6.92
575	7.17	6.62	9.79	6.09	8.93	8.54	7.04	10.1	14.13	6.42	10.41	10.64	...	8.97	7.88	6.95
600	7.23	6.66	9.82	6.13	8.94	8.58	7.08	10.04	14.20	6.47	10.44	10.69	...	9.00	7.90	6.98
625	7.28	6.70	9.85	6.17	8.94	8.63	7.12	6.52	10.46	10.75	...	9.02	7.92	7.02
650	7.33	6.73	9.87	6.20	8.95	8.68	7.16	6.56	10.48	10.81	...	9.05	7.95	7.04
675	7.38	6.77	9.90	6.23	8.95	8.73	7.19	6.61	10.50	10.86	...	9.07	7.98	7.08
700	7.44	6.80	9.92	6.26	8.96	8.78	7.22	6.65	10.52	10.92	...	9.10	8.00	7.11
725	7.49	6.84	9.95	6.29	8.96	8.83	7.25	6.70	10.55	10.98	...	9.12	8.02	7.14
750	7.54	6.88	9.99	6.33	8.96	8.87	7.29	6.74	10.57	11.04	...	9.15	8.05	7.18
775	7.59	6.92	10.02	6.36	8.96	8.92	7.31	6.79	10.60	11.10	...	9.17	8.08	7.22
800	7.65	6.96	10.05	6.39	8.97	8.96	7.34	6.83	10.62	11.16	...	9.20	8.10	7.25
825	7.70	7.00	10.08	6.42	8.97	9.01	7.37	6.87	10.65	11.22	...	9.22	...	7.27

850	7.75	7.03	10.11	6.46	8.98	9.06	7.40	6.92	10.67	11.28	...	9.25	...	7.31
875	7.79	7.07	10.13	6.49	8.99	9.11	7.43	6.96	10.70	11.34	...	9.27	...	7.34
900	7.84	7.10	10.16	6.52	9.00	9.16	7.45	7.00	10.72	11.40	...	9.30	...	7.37
925	7.87	7.13	10.19	6.55	9.05	9.21	7.47	7.05	10.74	11.46	...	9.32	...	7.41
950	7.91	7.16	10.23	6.58	9.10	9.25	7.49	7.10	10.76	11.52	...	9.35	...	7.44
975	7.94	7.19	10.26	6.60	9.15	9.30	7.52	7.14	10.78	11.57	...	9.37	...	7.47
1000	7.97	7.22	10.29	6.63	9.18	9.34	7.55	7.19	10.80	11.63	...	9.40	...	7.50
1025	8.01	7.25	10.32	6.65	9.20	9.39	10.83	11.69	...	9.42
1050	8.05	7.27	10.34	6.68	9.22	9.43	10.85	11.74	...	9.45
1075	8.08	7.30	10.37	6.70	9.24	9.48	10.88	11.80	...	9.47
1100	8.12	7.32	10.39	6.72	9.25	9.52	10.90	11.85	...	9.50
1125	8.14	7.34	10.41	6.74	9.29	9.57	10.93	11.91	...	9.52
1150	8.16	7.37	10.44	6.75	9.33	9.61	10.95	11.97	...	9.55
1175	8.17	7.39	10.46	6.77	9.36	9.66	10.98	12.03	...	9.57
1200	8.19	7.41	10.48	6.78	9.39	9.70	11.00	12.09	...	9.60
1225	8.21	7.43	10.50	6.80	9.43	9.75	9.64
1250	8.24	7.45	10.51	6.82	9.47	9.79	9.68
1275	8.26	7.47	10.53	6.83	9.50	9.84	9.71
1300	8.28	7.49	10.54	6.85	9.53	9.88	9.75
1325	8.30	7.51	10.56	6.86	9.53	9.92	9.79
1350	8.32	7.52	10.57	6.88	9.54	9.96	9.83
1375	8.34	7.54	10.59	6.89	9.55	10.00	9.86
1400	8.36	7.55	10.60	6.90	9.56	10.04	9.90
1425	10.64	9.94
1450	10.68	9.98
1475	10.72	10.01
1500	10.77	10.05

GENERAL NOTE: For Code references to this table, see para. 319.3.1, ASME B31.3. These data are for use in the absence of more applicable data. It is the designer's responsibility to verify that materials are suitable for the intended service at the temperatures shown.

TABLE 10-48 Flexibility Factor k and Stress Intensification Factor i

Description	Flexibility factor k	Stress intensification factor [Notes (2), (3)]		Flexibility characteristic h	Sketch
		Out-of-plane, i_o	In-plane, i_i		
Welding elbow or pipe bend [Notes (2)], (4)-(7)]	$\frac{1.65}{h}$	$\frac{0.75}{h^{2/3}}$	$\frac{0.9}{h^{2/3}}$	$\frac{\bar{T}R_1}{r_2^2}$	
Closely spaced miter bend $s < r_2 (1 + \tan \theta)$ [Notes (2), (4), (5), (7)]	$\frac{1.52}{h^{5/6}}$	$\frac{0.9}{h^{2/3}}$	$\frac{0.9}{h^{2/3}}$	$\frac{\cot \theta}{2} \left(\frac{s\bar{T}}{r_2^2} \right)$	
Single miter bend or widely spaced miter bend $s \geq r_2 (1 + \tan \theta)$ [Notes (2), (4), (7)]	$\frac{1.52}{h^{5/6}}$	$\frac{0.9}{h^{2/3}}$	$\frac{0.9}{h^{2/3}}$	$\frac{1 + \cot \theta}{2} \left(\frac{\bar{T}}{r_2} \right)$	
Welding tee per ASME B16.9 [Notes (2), (4), (6), (11), (13)]	1	$\frac{0.9}{h^{2/3}}$	$\frac{3}{4} i_o + \frac{1}{4}$	$3.1 \frac{\bar{T}}{r_2}$	
Reinforced fabricated tee with pad or saddle [Notes (2), (4), (8), (12), (13)]	1	$\frac{0.9}{h^{2/3}}$	$\frac{3}{4} i_o + \frac{1}{4}$	$\frac{(\bar{T} + \frac{1}{2} \bar{T}_r)^{2.5}}{\bar{T}^{1.5} r_2}$	
Unreinforced fabricated tee [Notes (2), (4), (12), (13)]	1	$\frac{0.9}{h^{2/3}}$	$\frac{3}{4} i_o + \frac{1}{4}$	$\frac{\bar{T}}{r_2}$	
Extruded welding tee with $r_s \geq 0.05 D_b$ $T_c < 1.5 \bar{T}$ [Notes (2), (4), (13)]	1	$\frac{0.9}{h^{2/3}}$	$\frac{3}{4} i_o + \frac{1}{4}$	$\left(1 + \frac{r_s}{r_2} \right) \frac{\bar{T}}{r_2}$	
Welded-in contour insert [Notes (2), (4), (11), (13)]	1	$\frac{0.9}{h^{2/3}}$	$\frac{3}{4} i_o + \frac{1}{4}$	$3.1 \frac{\bar{T}}{r_2}$	
Branch welded-on fitting (integrally reinforced) [Notes (2), (4), (9), (12)]	1	$\frac{0.9}{h^{2/3}}$	$\frac{0.9}{h^{2/3}}$	$3.3 \frac{\bar{T}}{r_2}$	

TABLE 10-48 Flexibility Factor k and Stress-Intensification Factor i (Concluded)

Description	Flexibility factor k	Stress intensification factor i [Note (1)]
Butt-welded joint, reducer, or weld-neck flange	1	1.0
Double-welded slip-on flange	1	1.2
Fillet welded joint, or socket weld flange or fitting	1	Note (14)
Lap joint flange (with ASME B16.9 lap joint stub)	1	1.6
Threaded pipe joint or threaded flange	1	2.3
Corrugated straight pipe, or corrugated or creased bend [Note (10)]	5	2.5

NOTES:

(1) Stress intensification and flexibility factor data in this table are for use in the absence of more directly applicable data (see para. 319.3.6). Their validity has been demonstrated for $D/T \leq 100$.

(2) The flexibility factor, k , in this table applies to bending in any plane. The flexibility factors, k , and stress intensification factors, i , shall not be less than unity; factors for torsion equal unity. Both factors apply over the effective arc length (shown by heavy centerlines in the sketches) for curved and miter bends, and to the intersection point for tees.

(3) A single intensification factor equal to $0.9/h^{2/3}$ may be used for both i and k , if desired.

(4) The values of k and i can be read directly from Chart A by entering with the characteristic h computed from the formulas given above. Nomenclature is as follows:

- D_b = outside diameter of branch
- R_1 = bend radius of welding elbow or pipe bend
- r_x = see definition in para. 304.3.4(c) and Table 10-48
- r_2 = mean radius of matching pipe
- s = miter spacing at centerline
- \bar{T} = for elbows and miter bends, the nominal wall thickness of the fitting, = for tees, the nominal wall thickness of the matching pipe
- T_c = crotch thickness of branch connections measured at the center of the crotch where shown in the sketches
- \bar{T}_r = pad or saddle thickness
- θ = one-half angle between adjacent miter axes

(5) Where flanges are attached to one or both ends, the values of k and i in this table shall be corrected by the factors C_1 , which can be read directly from Chart B, entering with the computed h .

(6) The designer is cautioned that cast butt-welded fittings may have considerably heavier walls than that of the pipe with which they are used. Large errors may be introduced unless the effect of these greater thicknesses is considered.

(7) In large diameter thin-wall elbows and bends, pressure can significantly affect the magnitudes of k and i . To correct values from the table, divide k by

$$1 + 6 \left(\frac{P}{E} \right) \left(\frac{r_2}{\bar{T}} \right)^{2/3} \left(\frac{R_1}{r_2} \right)^{1/3}$$

divide i by

$$1 + 3.25 \left(\frac{P}{E} \right) \left(\frac{r_2}{\bar{T}} \right)^{2/3} \left(\frac{R_1}{r_2} \right)^{2/3}$$

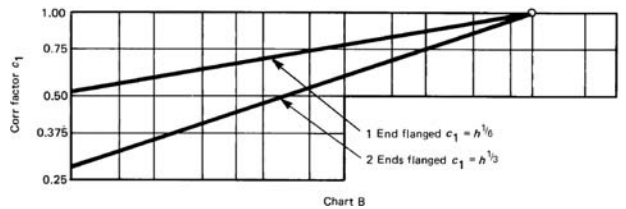
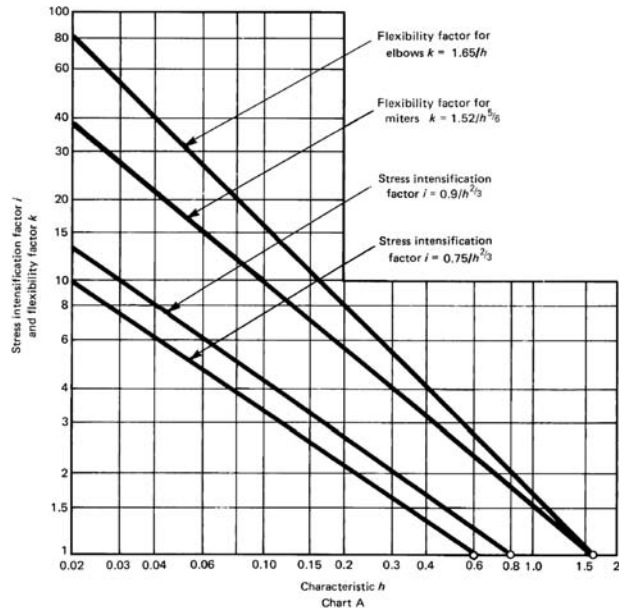
For consistency, use kPa and mm for SI metric, and psi and in, for U.S. customary notation.

- (8) When \bar{T}_r is $> 1\frac{1}{2} \bar{T}$, use $h = 4 \bar{T}/r_2$.
- (9) The designer must be satisfied that this fabrication has a pressure rating equivalent to straight pipe.
- (10) Factors shown apply to bending. Flexibility factor for torsion equals 0.9.
- (11) If $r_x \geq \frac{1}{8} D_b$ and $T_c \geq 1.5 \bar{T}$ a flexibility characteristic of $4.4 \bar{T}/r_2$ may be used.
- (12) The out-of-plane stress intensification factor (SIF) for a reducing branch connection with branch-to-run diameter ratio of $0.5 < d/D < 1.0$ may be nonconservative. A smooth concave weld contour has been shown to reduce the SIF. Selection of the appropriate SIF is the designer's responsibility.
- (13) Stress intensification factors for branch connections are based on tests with at least two diameters of straight run pipe on each side of the branch centerline. More closely loaded branches may require special consideration.
- (14) 2.1 max. or $2.1 \bar{T}/C_x$, but not less than 1.3. C_x is the fillet weld leg length (see Fig. 328.5.2C). For unequal leg lengths, use the smaller leg for C_x .

- \bar{T}_b = thickness of pipe matching branch, in (mm)
- i_o = out-plane stress-intensification factor (Table 10-48)
- i_i = in-plane stress-intensification factor (Table 10-48)

Allowable stress range S_A and permissible additive stresses shall be computed in accordance with Eqs. (10-93) and (10-94).

Required Weld Quality Assurance Any weld at which S_E exceeds $0.8S_A$ for any portion of a piping system and the equivalent number of cycles N exceeds 7000 shall be fully examined in accordance with the requirements for severe cyclic service (presented later in this section).



Reactions: Metallic Piping Reaction forces and moments to be used in the design of restraints and supports and in evaluating the effects of piping displacements on connected equipment shall be based on the reaction range R for the extreme displacement conditions, considering the range previously defined for reactions and using E_a . The designer shall consider instantaneous maximum values of forces and moments in the original and extreme displacement conditions as well as the reaction range in making these evaluations.

Maximum Reactions for Simple Systems For two-anchor systems without intermediate restraints, the maximum instantaneous values

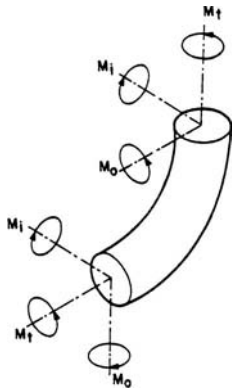


FIG. 10-172 Moments in bends. (Extracted from the Process Piping Code, B31.3—2004, with permission of the publisher, the American Society of Mechanical Engineers, New York.)

of reaction forces and moments may be estimated from Eqs. (10-106) and (10-107).

1. For extreme displacement conditions, R_m . The temperature for this computation is the design maximum or design minimum temperature as previously defined for reactions, whichever produces the larger reaction:

$$R_m = R \left(1 - \frac{2C}{3} \right) \frac{E_m}{E_a} \quad (10-106)$$

where C = cold-spring factor varying from zero for no cold spring to 1.0 for 100 percent cold spring. (The factor $\frac{2}{3}$ is based on experience, which shows that specified cold spring cannot be fully assured even with elaborate precautions.)
 E_a = modulus of elasticity at installation temperature, lbf/in² (MPa)
 E_m = modulus of elasticity at design maximum or design minimum temperature, lbf/in² (MPa)
 R = range of reaction forces or moments (derived from flexibility analysis) corresponding to the full displacement-stress range and based on E_a , lbf or in·lbf (N or N·mm)

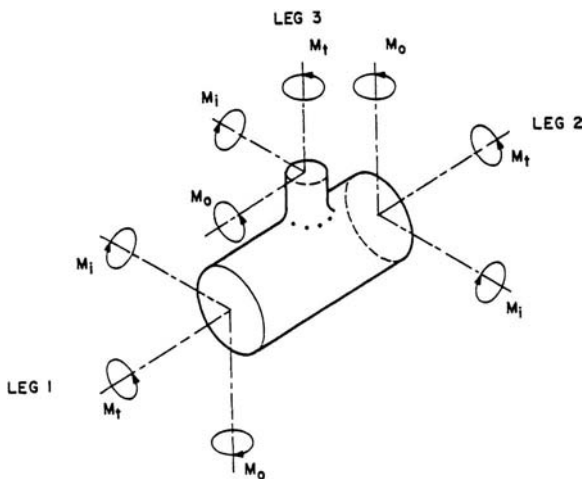


FIG. 10-173 Moments in branch connections. (Extracted from the Process Piping Code, B31.3—2004, with permission of the publisher, the American Society of Mechanical Engineers, New York.)

R_m = estimated instantaneous maximum reaction force or moment at design maximum or design minimum temperature, lbf or in·lbf (N or N·mm)

2. For original condition, R_a . The temperature for this computation is the expected temperature at which the piping is to be assembled.

$$R_a = CR \quad \text{or} \quad C_1R, \text{ whichever is greater} \quad (10-107)$$

where nomenclature is as for Eq. (10-106) and

$C_1 = 1 - (S_i E_d / S_E E_m)$
 = estimated self-spring or relaxation factor (use zero if value of C_1 is negative)

R_a = estimated instantaneous reaction force or moment at installation temperature, lbf or in·lbf (N or N·mm)

S_E = computed displacement-stress range, lbf/in² (MPa). See Eq. (10-101).

S_i = See Eq. (10-93).

Maximum Reactions for Complex Systems For multianchor systems and for two-anchor systems with intermediate restraints, Eqs. (10-106) and (10-107) are not applicable. Each case must be studied to estimate the location, nature, and extent of local overstrain and its effect on stress distribution and reactions.

Acceptable comprehensive methods of analysis are analytical, model-test, and chart methods, which evaluate for the entire piping system under consideration the forces, moments, and stresses caused by bending and torsion from a simultaneous consideration of terminal and intermediate restraints to thermal expansion and include all external movements transmitted under thermal change to the piping by its terminal and intermediate attachments. Correction factors, as provided by the details of these rules, must be applied for the stress intensification of curved pipe and branch connections and may be applied for the increased flexibility of such component parts.

Expansion Joints All the foregoing applies to "stiff piping systems," i.e., systems without expansion joints (see detail 1 of Fig. 10-174). When space limitations, process requirements, or other considerations result in configurations of insufficient flexibility, capacity for deflection within allowable stress range limits may be increased successively by the use of one or more hinged bellows expansion joints, viz., semirigid (detail 2) and nonrigid (detail 3) systems, and expansion effects essentially eliminated by a free-movement joint (detail 4) system. Expansion joints for semirigid and nonrigid systems are restrained against longitudinal and lateral movement by the hinges with the expansion element under bending movement only and are known as "rotation" or "hinged" joints (see Fig. 10-175). Semirigid systems are limited to one plane; nonrigid systems require a minimum of three joints for two-dimensional and five joints for three-dimensional expansion movement.

Joints similar to that shown in Fig. 10-175, except with two pairs of hinge pins equally spaced around a gimbal ring, achieve similar results with a lesser number of joints.

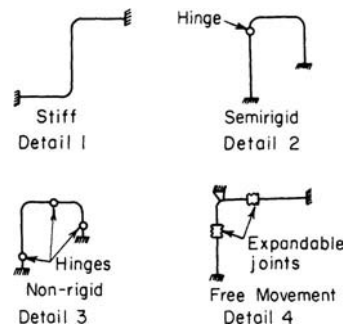


FIG. 10-174 Flexibility classification for piping systems. (From Kellogg, Design of Piping Systems, Wiley, New York, 1965.)

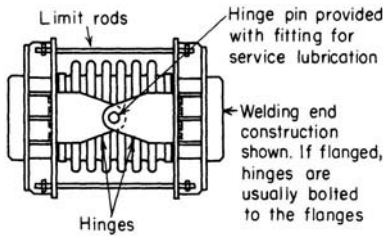


FIG. 10-175 Hinged expansion joint. (From Kellogg, Design of Piping Systems, Wiley, New York, 1965.)

Expansion joints for free-movement systems can be designed for axial or offset movement alone, or for combined axial and offset movements (see Fig. 10-176). For offset movement alone, the end load due to pressure and weight can be transferred across the joint by tie rods or structural members (see Fig. 10-177). For axial or combined movements, anchors must be provided to absorb the unbalanced pressure load and force bellows to deflect.

Commercial bellows elements are usually light-gauge (of the order of 0.05 to 0.10 in thick and are available in stainless and other alloy steels, copper, and other nonferrous materials. Multi-ply bellows, bellows with external reinforcing rings, and toroidal contour bellows are available for higher pressures. Since bellows elements are ordinarily rated for strain ranges which involve repetitive yielding, predictable performance is assured only by adequate fabrication controls and knowledge of the potential fatigue performance of each design. The attendant cold work can affect corrosion resistance and promote susceptibility to corrosion fatigue or stress corrosion; joints in a horizontal position cannot be drained and have frequently undergone pitting or cracking due to the presence of condensate during operation or offstream. For low-pressure essentially nonhazardous service, nonmetallic bellows of fabric-reinforced rubber or special materials are sometimes used. For corrosive service PTFE bellows may be used.

Because of the inherently greater susceptibility of expansion bellows to failure from unexpected corrosion, failure of guides to control joint movements, etc., it is advisable to examine critically their design choice in comparison with a stiff system.

Slip-type expansion joints (Fig. 10-178) substitute packing (ring or plastic) for bellows. Their performance is sensitive to adequate design

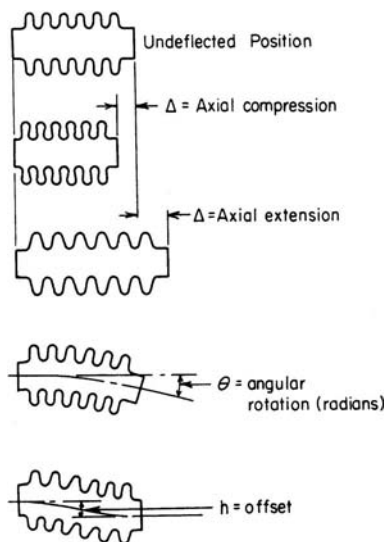


FIG. 10-176 Action of expansion bellows under various movements. (From Kellogg, Design of Piping Systems, Wiley, New York, 1965.)

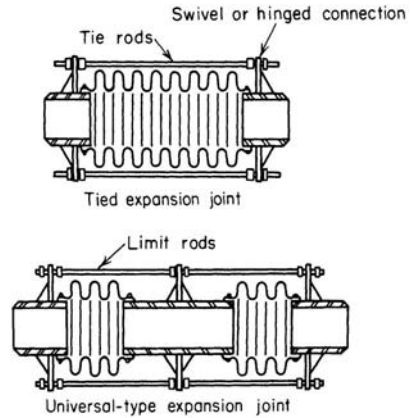


FIG. 10-177 Constrained-bellows expansion joints. (From Kellogg, Design of Piping Systems, Wiley, New York, 1965.)

with respect to guiding to prevent binding and the adequacy of stuffing boxes and attendant packing, sealant, and lubrication. Anchors must be provided for the unbalanced pressure force and for the friction forces to move the joint. The latter can be much higher than the elastic force required to deflect a bellows joint. Rotary packed joints, ball joints, and other special joints can absorb end load.

Corrugated pipe and corrugated and creased bends are also used to decrease stiffness.

Pipe Supports Loads transmitted by piping to attached equipment and supporting elements include weight, temperature- and pressure-induced effects, vibration, wind, earthquake, shock, and thermal expansion and contraction. The design of supports and restraints is based on concurrently acting loads (if it is assumed that wind and earthquake do not act simultaneously).

Resilient and constant-effort-type supports shall be designed for maximum loading conditions including test unless temporary supports are provided.

Though not specified in the code, supports for discharge piping from relief valves must be adequate to withstand the jet reaction produced by their discharge.

The code states further that pipe-supporting elements shall (1) avoid excessive interference with thermal expansion and contraction of pipe which is otherwise adequately flexible; (2) be such that they do not contribute to leakage at joints or excessive sag in piping requiring drainage; (3) be designed to prevent overstress, resonance, or disengagement due to variation of load with temperature; also, so that combined longitudinal stresses in the piping shall not exceed the code allowable limits; (4) be such that a complete release of the piping load will be prevented in the event of spring failure or misalignment, weight transfer, or added load due to test during erection; (5) be of steel or wrought iron; (6) be of alloy steel or protected from temperature when the temperature limit for carbon steel may be exceeded; (7) not be cast

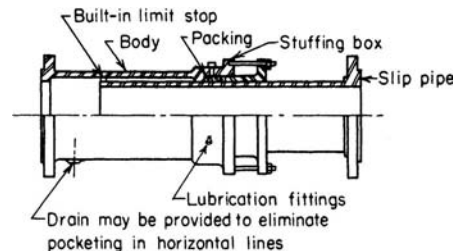


FIG. 10-178 Slip-type expansion joint. (From Kellogg, Design of Piping Systems, Wiley, New York, 1965.)

iron except for roller bases, rollers, anchor bases, etc., under mainly compression loading; (8) not be malleable or nodular iron except for pipe clamps, beam clamps, hanger flanges, clips, bases, and swivel rings; (9) not be wood except for supports mainly in compression when the pipe temperature is at or below ambient; and (10) have threads for screw adjustment which shall conform to ASME B1.1.

A supporting element used as an anchor shall be designed to maintain an essentially fixed position.

To protect terminal equipment or other (weaker) portions of the system, restraints (such as anchors and guides) shall be provided where necessary to control movement or to direct expansion into those portions of the system that are adequate to absorb them. The design, arrangement, and location of restraints shall ensure that expansion-joint movements occur in the directions for which the joint is designed. In addition to the other thermal forces and moments, the effects of friction in other supports of the system shall be considered in the design of such anchors and guides.

Anchors for Expansion Joints Anchors (such as those of the corrugated, omega, disk, or slip type) shall be designed to withstand the algebraic sum of the forces at the maximum pressure and temperature at which the joint is to be used. These forces are:

1. Pressure thrust, which is the product of the effective thrust area times the maximum pressure to which the joint will be subjected during normal operation. (For slip joints the effective thrust area shall be computed by using the outside diameter of the pipe. For corrugated, omega, or disk-type joints, the effective thrust area shall be that area recommended by the joint manufacturer. If this information is unobtainable, the effective area shall be computed by using the maximum inside diameter of the expansion-joint bellows.)

2. The force required to compress or extend the joint in an amount equal to the calculated expansion movement.

3. The force required to overcome the static friction of the pipe in expanding or contracting on its supports, from installed to operating position. The length of pipe considered should be that located between the anchor and the expansion joint.

Support Fixtures Hanger rods may be pipe straps, chains, bars, or threaded rods which permit free movement for thermal expansion or contraction. Sliding supports shall be designed for friction and bearing loads. Brackets shall be designed to withstand movements due to friction in addition to other loads. Spring-type supports shall be designed for weight load at the point of attachment and to prevent misalignment, buckling, or eccentric loading of springs, and provided with stops to prevent spring overtravel. Compensating-type spring hangers are recommended for high-temperature and critical-service piping to make the supporting force uniform with appreciable movement. Counterweight supports shall have stops to limit travel. Hydraulic supports shall be provided with safety devices and stops to support load in the event of loss of pressure. Vibration dampers or sway braces may be used to limit vibration amplitude.

The code requires that the safe load for threaded hanger rods be based on the root area of the threads. This, however, assumes concentric loading. When hanger rods move to a nonvertical position so that the load is transferred from the rod to the supporting structure via the edge of one flat of the nut on the rod, it is necessary to consider the root area to be reduced by one-third. If a clamp is connected to a vertical line to support its weight, it is recommended that shear lugs be welded to the pipe, or that the clamp be located below a fitting or flange, to prevent slippage. Consideration shall be given to the localized stresses induced in the piping by the integral attachment. Typical pipe supports are shown in Fig. 10-179.

Much piping is supported from structures installed for other purposes. It is common practice to use beam formulas for tubular sections to determine stress, maximum deflection, and maximum slope of piping in **spans between supports**. When piping is supported from structures installed for that sole purpose and those structures rest on driven piles, detailed calculations are usually made to determine maximum permissible spans. Limits imposed on maximum slope to make the contents of the line drain to the lower end require calculations made on the weight per foot of the empty line. To avoid interference with other components, maximum deflection should be limited to 25.4 mm (1 in).

Pipe hangers are essentially frictionless but require taller pipe-support structures which cost more than structures on which pipe is laid. Devices that reduce friction between laid pipe subject to thermal movement and its supports are used to accomplish the following:

1. Reduce loads on anchors or on equipment acting as anchors.
2. Reduce the tendency of pipe acting as a column loaded by friction at supports to buckle sideways off supports.
3. Reduce nonvertical loads imposed by piping on its supports so as to minimize cost of support foundations.
4. Reduce longitudinal stress in pipe.

Linear bearing surfaces made of fluorinated hydrocarbons or of graphite and also rollers are used for this purpose.

Design Criteria: Nonmetallic Pipe In using a nonmetallic material, designers must satisfy themselves as to the adequacy of the material and its manufacture, considering such factors as strength at design temperature, impact- and thermal-shock properties, toxicity, methods of making connections, and possible deterioration in service. Rating information, based usually on ASTM standards or specifications, is generally available from the manufacturers of these materials. Particular attention should be given to provisions for the thermal expansion of nonmetallic piping materials, which may be as much as 5 to 10 times that of steel (Table 10-49). Special consideration should be given to the strength of small pipe connections to piping and equipment and to the need for extra flexibility at the junction of metallic and nonmetallic systems.

Table 10-50 gives values for the modulus of elasticity for nonmetals; however, no specific stress-limiting criteria or methods of stress analysis are presented. Stress-strain behavior of most nonmetals differs considerably from that of metals and is less well-defined for mathematic analysis. The piping system should be designed and laid out so that flexural stresses resulting from displacement due to expansion, contraction, and other movement are minimized. This concept requires special attention to supports, terminals, and other restraints.

Displacement Strains The concepts of strain imposed by restraint of thermal expansion or contraction and by external movement described for metallic piping apply in principle to nonmetals. Nevertheless, the assumption that stresses throughout the piping system can be predicted from these strains because of fully elastic behavior of the piping materials is not generally valid for nonmetals.

In thermoplastics and some thermosetting resins, displacement strains are not likely to produce immediate failure of the piping but may result in detrimental distortion. Especially in thermoplastics, progressive deformation may occur upon repeated thermal cycling or on prolonged exposure to elevated temperature.

In brittle nonmetallics (such as porcelain, glass, impregnated graphite, etc.) and some thermosetting resins, the materials show rigid behavior and develop high displacement stresses up to the point of sudden breakage due to overstrain.

Elastic Behavior The assumption that displacement strains will produce proportional stress over a sufficiently wide range to justify an elastic-stress analysis often is not valid for nonmetals. In brittle nonmetallic piping, strains initially will produce relatively large elastic stresses. The total displacement strain must be kept small, however, since overstrain results in failure rather than plastic deformation. In plastic and resin nonmetallic piping strains generally will produce stresses of the overstrained (plastic) type even at relatively low values of total displacement strain.

FABRICATION, ASSEMBLY, AND ERECTION

Welding, Brazing, or Soldering Code requirements dealing with fabrication are more detailed for welding than for other methods of joining, since welding is the predominant method of construction and the method used for the most demanding applications. The code requirements for welding processes and operators are essentially the same as covered in the subsection on pressure vessels (i.e., qualification to Sec. IX of the ASME Boiler and Pressure Vessel Code) except that welding processes are not restricted, the material grouping (P number) must be in accordance with ASME B31.3 Appendix A-1, and welding positions are related to pipe position. The code also permits one fabricator to accept welders or welding operators qualified by another employer

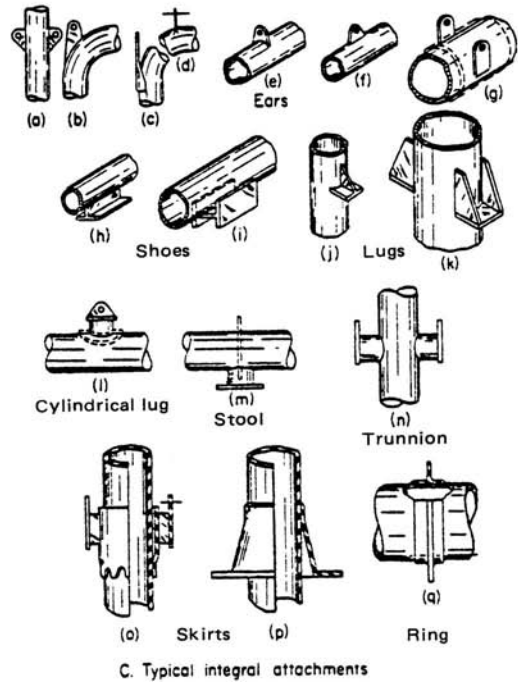
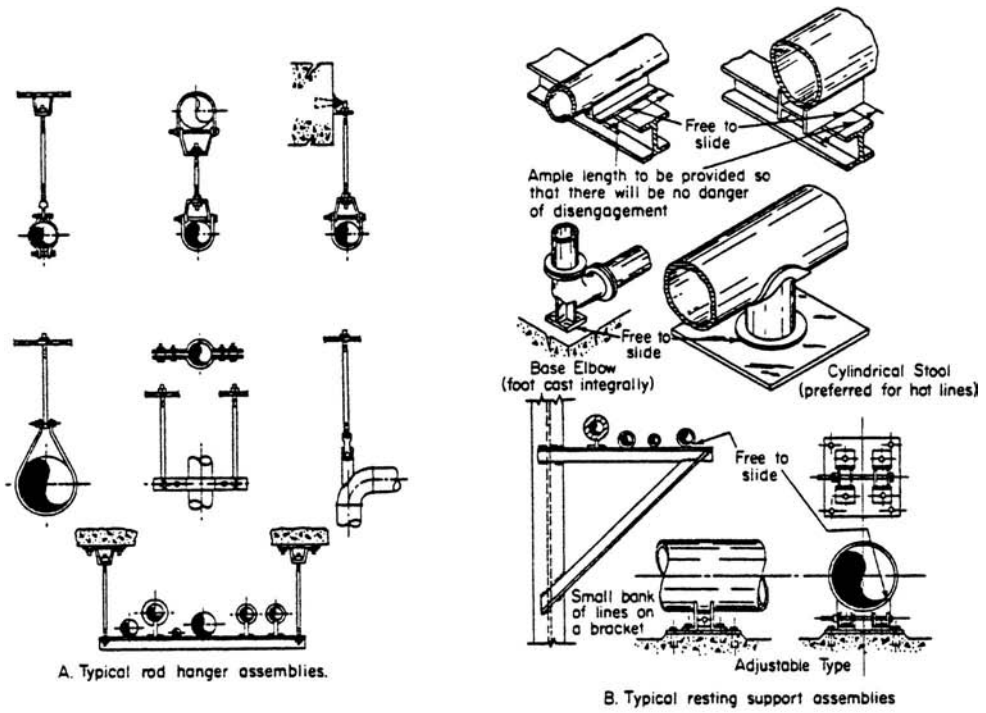


FIG. 10-179 Typical pipe supports and attachments. (From Kellogg, Design of Piping Systems, Wiley, New York, 1965.)

without requalification when welding pipe by the same or equivalent procedure. The code may require that the welding procedure qualification include low-temperature toughness testing (see. Table 10-51).

Filler metal is required to conform with the requirements of Sec. IX. Backing rings (of ferrous material), when used, shall be of weldable quality with sulfur limited to 0.05 percent. Backing rings of nonferrous and nonmetallic materials may be used provided they are proved satisfactory by procedure-qualification tests and provided their use has been approved by the designer.

The code requires internal alignment within the dimensional limits specified in the welding procedure and the engineering design without specific dimensional limitations. Internal trimming is permitted

for correcting internal misalignment provided such trimming does not result in a finished wall thickness before welding of less than required minimum wall thickness t_m . When necessary, weld metal may be deposited on the inside or outside of the component to provide alignment or sufficient material for trimming.

Table 10-53 is a summary of the code acceptance criteria (limits on imperfections) for welds. The defects referred to are illustrated in Fig. 10-180.

Brazing procedures, brazers, and brazing operators must be qualified in accordance with the requirements of Part QB, Sec. IX, ASME Code. At the owner's option, qualification is not required for Category D fluid service not exceeding 93°C (200°F). The clearance between

TABLE 10-49 Thermal Expansion Coefficients, Nonmetals

Material description	Mean coefficients (divide table values by 10 ⁶)			
	in/in, °F	Range, °F	mm/mm, °C	Range, °C
Thermoplastics				
Acetal AP2012	2	...	3.6	...
Acrylonitrile-butadiene-styrene				
ABS 1208	60	...	108	...
ABS 1210	55	45-55	99	7-13
ABS 1316	40	...	72	...
ABS 2112	40	...	72	...
Cellulose acetate butyrate				
CAB MH08	80	...	144	...
CAB S004	95	...	171	...
Chlorinated poly(vinyl chloride)				
CPVC 4120	35	...	63	...
Polybutylene PB 2110	72	...	130	...
Polyether, chlorinated	45	...	81	...
Polyethylene				
PE 1404	100	46-100	180	8-38
PE 2305	90	46-100	162	8-38
PE 2306	80	46-100	144	8-38
PE 3306	70	46-100	126	8-38
PE 3406	60	46-100	108	8-38
Polyphenylene POP 2125	30	...	54	...
Polypropylene				
PP1110	48	33-67	86	1-19
PP1208	43	...	77	...
PP2105	40	...	72	...
Poly(vinyl chloride)				
PVC 1120	30	23-37	54	-5 to +3
PVC 1220	35	34-40	63	1-4
PVC 2110	50	...	90	...
PVC 2112	45	...	81	...
PVC 2116	40	37-45	72	3-7
PVC 2120	30	...	54	...
Poly(vinylidene fluoride)	79	...	142	...
Poly(vinylidene chloride)	100	...	180	...
Polytetrafluoroethylene	55	73-140	99	23-60
Poly(fluorinated ethylenepropylene)	46-58	73-140	83-104	23-60
Poly(perfluoroalkoxy alkane)	67	70-212	121	21-100
Poly(perfluoroalkoxy alkane)	94	212-300	169	100-149
Poly(perfluoroalkoxy alkane)	111	300-408	200	149-209
Reinforced Thermosetting Resins and Reinforced Plastic Mortars				
Glass-epoxy, centrifugally cast	9-13	...	16-23.5	...
Glass-polyester, centrifugally cast	9-15	...	16-27	...
Glass-polyester, filament-wound	9-11	...	16-20	...
Glass-polyester, hand lay-up	12-15	...	21.5-27	...
Glass-epoxy, filament-wound	9-13	...	16-23.5	...
Other Nonmetallic Materials				
Borosilicate glass	1.8	...	3.25	...

GENERAL NOTES:

(a) For Code references to this table, see para. A319.3.1, ASME B31.3—2004. These data are for use in the absence of more applicable data. It is the designer's responsibility to verify that materials are suitable for the intended service at the temperatures shown.

(b) Individual compounds may vary from the values shown. Consult manufacturer for specific values for products.

TABLE 10-50 Modulus of Elasticity, Nonmetals

Material description	E, ksi (73.4°F)	E, MPa (23°C)
Thermoplastics [Note (1)]		
Acetal	410	2,830
ABS, Type 1210	250	1,725
ABS, Type 1316	340	2,345
CAB	120	825
PVC, Type 1120	420	2,895
PVC, Type 1220	410	2,825
PVC, Type 2110	340	2,345
PVC, Type 2116	380	2,620
Chlorinated PVC	420	2,895
Chlorinated polyether	160	1,105
PE, Type 2306	90	620
PE, Type 3306	130	895
PE, Type 3406	150	1,035
Polypropylene	120	825
Poly(vinylidene chloride)	100	690
Poly(vinylidene fluoride)	194	1,340
Poly(tetrafluorethylene)	57	395
Poly(fluorinated ethylenepropylene)	67	460
Poly(perfluoroalkoxy alkane)	100	690
Thermosetting Resins, Axially Reinforced		
Epoxy-glass, centrifugally cast	1,200–1,900	8,275–13,100
Epoxy-glass, filament-wound	1,100–2,000	7,585–13,790
Polyester-glass, centrifugally cast	1,200–1,900	8,275–13,100
Polyester-glass, hand lay-up	800–1,000	5,515–6,895
Other		
Borosilicate glass	9,800	67,570

GENERAL NOTE: For Code references to this table, see para. A319.3.2, ASME B31.3—2004. These data are for use in the absence of more applicable data. It is the designer's responsibility to verify that materials are suitable for the intended service at the temperatures shown.

NOTE:

(1) The modulus of elasticity data shown for thermoplastics are based on short-term tests. The manufacturer should be consulted to obtain values for use under long-term loading.

surfaces to be joined by brazing or soldering shall be no larger than is necessary to allow complete capillary distribution of the filler metal.

The only requirement for solderers is that they follow the procedure in the *Copper Tube Handbook* of the Copper Development Association.

Bending and Forming Pipe may be bent to any radius for which the bend-arc surface will be free of cracks and substantially free of buckles. The use of qualified bends which are creased or corrugated is permitted. Bending may be done by any hot or cold method that produces a product meeting code and service requirements, and that does not have an adverse effect on the essential characteristics of the material. Hot bending and hot forming must be done within a temperature range consistent with material characteristics, end use, and postoperation heat treatment. Postbend heat treatment may be required for bends in some materials; its necessity is dependent upon the type of bending operation and the severity of the bend. Postbend heat treatment requirements are defined in the code.

Piping components may be formed by any suitable hot or cold pressing, rolling, forging, hammering, spinning, drawing, or other method. Thickness after forming shall not be less than required by design. Special rules cover the forming and pressure design verification of flared laps.

The development of fabrication facilities for bending pipe to the radius of commercial butt-welding long-radius elbows and forming flared metallic (Van Stone) laps on pipe are important techniques in reducing welded-piping costs. These techniques save both the cost of the ell or stub end and the welding operation required to attach the fitting to the pipe.

Preheating and Heat Treatment Preheating and postoperation heat treatment are used to avert or relieve the detrimental effects of the high temperature and severe thermal gradients inherent in the

welding of metals. In addition, heat treatment may be needed to relieve residual stresses created during the bending or forming of metals. The code provisions shown in Tables 10-54 and 10-55 represent basic practices which are acceptable for most applications of welding, bending, and forming, but they are not necessarily suitable for all service conditions. The specification of more or less stringent preheating and heat-treating requirements is a function of those responsible for the engineering design.

Refer to the code for rules establishing the thickness to be used in determining PWHT requirements for configurations other than butt welds (e.g., fabricated branch connections and socket welds).

Joining Nonmetallic Pipe All joints should be made in accordance with procedures complying with the manufacturer's recommendations and code requirements. General welding and heat fusion procedures are described in ASTM D-2657. ASTM D2855 describes general solvent-cementing procedures.

Depending on size, thermoplastic piping can be joined with mechanical joints, solvent-cemented joints, hot-gas welding, or heat fusion procedures. Mechanical joints are frequently bell-and-spigot joints which employ an elastomer O-ring gasket. Joints of this type are generally not self-restrained against internal pressure thrust.

Thermosetting resin pipe can be joined with mechanical joints or adhesive-bonded joints. Mechanical joints are generally a variation of gasketed bell-and-spigot joints and may be either nonrestrained or self-restrained. Adhesive-bonded joints are typically bell-and-spigot or butt-and-strap. Butt-and-strap joints join piping components with multiple layers of resin-saturated glass reinforcement.

Assembly and Erection Flanged-joint faces shall be aligned to the design plane to within $\frac{1}{10}$ in/ft (0.5 percent) maximum measured across any diameter, and flange bolt holes shall be aligned to within 3.2-mm ($\frac{1}{8}$ -in) maximum offset. Flanged joints involving flanges with widely differing mechanical properties shall be assembled with extra care, and tightening to a predetermined torque is recommended.

The use of flat washers under bolt heads and nuts is a code requirement when assembling nonmetallic flanges. It is preferred that the bolts extend completely through their nuts; however, a lack of complete thread engagement not exceeding one thread is permitted by the code. The assembly of cast-iron bell-and-spigot piping is covered in AWWA Standard C600.

Screwed joints which are intended to be seal-welded shall be made up without any thread compound.

When installing conductive nonmetallic piping and metallic pipe with nonmetallic linings, consideration should be given to the need to provide electrical continuity throughout the system and to grounding requirements. This is particularly critical in areas with potentially explosive atmospheres.

EXAMINATION, INSPECTION, AND TESTING

This subsection provides a general synopsis of code requirements. It should not be viewed as comprehensive.

Examination and Inspection The code differentiates between examination and inspection. "Examination" applies to quality-control functions performed by personnel of the piping manufacturer, fabricator, or erector. "Inspection" applies to functions performed for the owner by the authorized inspector.

The authorized inspector shall be designated by the owner and shall be the owner, an employee of the owner, an employee of an engineering or scientific organization, or an employee of a recognized insurance or inspection company acting as the owner's agent. The inspector shall not represent or be an employee of the piping erector, the manufacturer, or the fabricator unless the owner is also the erector, the manufacturer, or the fabricator.

The authorized inspector shall have a minimum of 10 years' experience in the design, fabrication, or inspection of industrial pressure piping. Each 20 percent of satisfactory work toward an engineering degree accredited by the Engineers' Council for Professional Development shall be considered equivalent to 1 year's experience, up to 5 years total.

TABLE 10-51 Requirements for Low-Temperature Toughness Tests for Metals*

These toughness requirements are in addition to tests required by the material specification.

	Type of material	Column A Design minimum temperature at or above min. temp. in Table A-1 of ASME B31.3—2004 or Table 10-52		Column B Design minimum temperature below min. temp. in Table A-1 of ASME B31.3—2004 or Table 10-52
Listed Materials	1 Gray cast iron	A-1 No additional requirements		B-1 No additional requirements
	2 Malleable and ductile cast iron: carbon steel per Note (1)	A-2 No additional requirements		B-2 Materials designated in Box 2 shall not be used.
		(a) Base metal	(b) Weld metal and heat affected zone (HAZ) [Note (2)]	
	3 Other carbon steels, low and intermediate alloy steels, high alloy ferritic steels, duplex stainless steels	A-3 (a) No additional requirements	A-3 (b) Weld metal deposits shall be impact tested per para. 323.3. ^c If design min. temp. < -29°C (-20°F), except as provided in Notes (3) and (5), and except as follows: for materials listed for Curves C and D of Table 10-52, where corresponding welding consumables are qualified by impact testing at the design minimum temperature or lower in accordance with the applicable AWS specification, additional testing is not required.	B-3 Except as provided in Notes (3) and (5), heat treat base metal per applicable ASTM specification listed in para. 323.3.2 ^c ; then impact test base metal, weld deposits, and HAZ per para. 323.3 ^c [see Note (2)]. When materials are used at design min. temp. below the assigned curve as permitted by Notes (2) and (3) of Table 10-52, weld deposits and HAZ shall be impact tested [see Note (2)].
	4 Austenitic stainless steels	A-4 (a) If: (1) carbon content by analysis >0.1%; or (2) material is not in solution heat treated condition; then, impact test per para. 323.3 ^c for design min. temp. < -29°C (-20°F) except as provided in Notes (3) and (6)	A-4 (b) Weld metal deposits shall be impact tested per para. 323.3. ^c If design min. temp. < -29°C (-20°F) except as provided in para. 323.2.2 ^b and in Notes (3) and (6)	B-4 Base metal and weld metal deposits shall be impact tested per para. 323.3 ^c . See Notes (2),(3), and (6).
	5 Austenitic ductile iron, ASTM A 571	A-5 (a) No additional requirements	A-5 (b) Welding is not permitted	B-5 Base metal shall be impact tested per para. 323.3. ^c Do not use < -196°C (-320°F). Welding is not permitted.
6 Aluminum, copper, nickel, and their alloys; unalloyed titanium	A-6 (a) No additional requirements	A-6 (b) No additional requirements unless filler metal composition is outside the range for base metal composition; then test per column B-6	B-6 Designer shall be assured by suitable tests [see Note (4)] that base metal, weld deposits, and HAZ are suitable at the design min. temp.	
Unlisted Materials	7 An unlisted material shall conform to a published specification. Where composition, heat treatment, and product form are comparable to those of a listed material, requirements for the corresponding listed material shall be met. Other unlisted materials shall be qualified as required in the applicable section of column B.			

NOTES:

- (1) Carbon steels conforming to the following are subject to the limitations in Box B-2; plates per ASTM A 36, A 283, and A 570; pipe per ASTM A 134 when made from these plates; and pipe per ASTM A 53 Type F and API 5L Gr. A25 butt weld.
- (2) Impact tests that meet the requirements of Table 323.3.1,^c which are performed as part of the weld procedure qualification, will satisfy all requirements of para. 323.2.2.^b and need not be repeated for production welds.
- (3) Impact testing is not required if the design minimum temperature is below -29°C (-20°F) but at or above -104°C (-155°F) and the Stress Ratio defined in Fig. 323.2.2B^b does not exceed 0.3.
- (4) Tests may include tensile elongation, sharp-notch tensile strength (to be compared with unnotched tensile strength), and/or other tests, conducted at or below design minimum temperature. See also para. 323.3.4.^b
- (5) Impact tests are not required when the maximum obtainable Charpy specimen has a width along the notch of less than 2.5 mm (0.098 in). Under these conditions, the design minimum temperature shall not be less than the lower of -48°C (-55°F) or the minimum temperature for the material in Table A-1.
- (6) Impact tests are not required when the maximum obtainable Charpy specimen has a width along the notch of less than 2.5 mm (0.098 in).

^cRefer to the referenced code paragraph for impact testing methods and acceptance.

^bRefer to the referenced code paragraph for comments regarding circumstances under which impact testing can be excluded.

*Table 10-51 and notes have been extracted (with minor modifications) from *Process Piping*, ASME B31.3—2004, with permission of the publisher, the American Society of Mechanical Engineers, New York.

TABLE 10-52 Tabular Values for Minimum Temperatures without Impact Testing for Carbon Steel Materials*

Nominal thickness [Note (6)]		Design minimum temperature							
		Curve A [Note (2)]		Curve B [Note (3)]		Curve C [Note (3)]		Curve D	
mm	in	°C	°F	°C	°F	°C	°F	°C	°F
6.4	0.25	-9.4	15	-28.9	-20	-48.3	-55	-48.3	-55
7.9	0.3125	-9.4	15	-28.9	-20	-48.3	-55	-48.3	-55
9.5	0.375	-9.4	15	-28.9	-20	-48.3	-55	-48.3	-55
10.0	0.394	-9.4	15	-28.9	-20	-48.3	-55	-48.3	-55
11.1	0.4375	-6.7	20	-28.9	-20	-41.7	-43	-48.3	-55
12.7	0.5	-1.1	30	-28.9	-20	-37.8	-36	-48.3	-55
14.3	0.5625	2.8	37	-21.7	-7	-35.0	-31	-45.6	-50
15.9	0.625	6.1	43	-16.7	2	-32.2	-26	-43.9	-47
17.5	0.6875	8.9	48	-12.8	9	-29.4	-21	-41.7	-43
19.1	0.75	11.7	53	-9.4	15	-27.2	-17	-40.0	-40
20.6	0.8125	14.4	58	-6.7	20	-25.0	-13	-38.3	-37
22.2	0.875	16.7	62	-3.9	25	-23.3	-10	-36.7	-34
23.8	0.9375	18.3	65	-1.7	29	-21.7	-7	-35.6	-32
25.4	1.0	20.0	68	0.6	33	-19.4	-3	-34.4	-30
27.0	1.0625	22.2	72	2.2	36	-18.3	-1	-33.3	-28
28.6	1.125	23.9	75	3.9	39	-16.7	2	-32.2	-26
30.2	1.1875	25.0	77	5.6	42	-15.6	4	-30.6	-23
31.8	1.25	26.7	80	6.7	44	-14.4	6	-29.4	-21
33.3	1.3125	27.8	82	7.8	46	-13.3	8	-28.3	-19
34.9	1.375	28.9	84	8.9	48	-12.2	10	-27.8	-18
36.5	1.4375	30.0	86	9.4	49	-11.1	12	-26.7	-16
38.1	1.5	31.1	88	10.6	51	-10.0	14	-25.6	-14
39.7	1.5625	32.2	90	11.7	53	-8.9	16	-25.0	-13
41.3	1.625	33.3	92	12.8	55	-8.3	17	-23.9	-11
42.9	1.6875	33.9	93	13.9	57	-7.2	19	-23.3	-10
44.5	1.75	34.4	94	14.4	58	-6.7	20	-22.2	-8
46.0	1.8125	35.6	96	15.0	59	-5.6	22	-21.7	-7
47.6	1.875	36.1	97	16.1	61	-5.0	23	-21.1	-6
49.2	1.9375	36.7	98	16.7	62	-4.4	24	-20.6	-5
50.8	2.0	37.2	99	17.2	63	-3.3	26	-20.0	-4
51.6	2.0325	37.8	100	17.8	64	-2.8	27	-19.4	-3
54.0	2.125	38.3	101	18.3	65	-2.2	28	-18.9	-2
55.6	2.1875	38.9	102	18.9	66	-1.7	29	-18.3	-1
57.2	2.25	38.9	102	19.4	67	-1.1	30	-17.8	0
58.7	2.3125	39.4	103	20.0	68	-0.6	31	-17.2	1
60.3	2.375	40.0	104	20.6	69	0.0	32	-16.7	2
61.9	2.4375	40.6	105	21.1	70	0.6	33	-16.1	3
63.5	2.5	40.6	105	21.7	71	1.1	34	-15.6	4
65.1	2.5625	41.1	106	21.7	71	1.7	35	-15.0	5
66.7	2.625	41.7	107	22.8	73	2.2	36	-14.4	6
68.3	2.6875	41.7	107	22.8	73	2.8	37	-13.9	7
69.9	2.75	42.2	108	23.3	74	3.3	38	-13.3	8
71.4	2.8125	42.2	108	23.9	75	3.9	39	-13.3	8
73.0	2.875	42.8	109	24.4	76	4.4	40	-12.8	9
74.6	2.9375	42.8	109	25.0	77	4.4	40	-12.2	10
76.2	3.0	43.3	110	25.0	77	5.0	41	-11.7	11

It is the owner's responsibility, exercised through the authorized inspector, to verify that all required examinations and testing have been completed and to inspect the piping to the extent necessary to be satisfied that it conforms to all applicable requirements of the code and the engineering design. This verification may include certifications and records pertaining to materials, components, heat treatment, examination and testing, and qualifications of operators and procedures. The authorized inspector may delegate the performance of inspection to a qualified person.

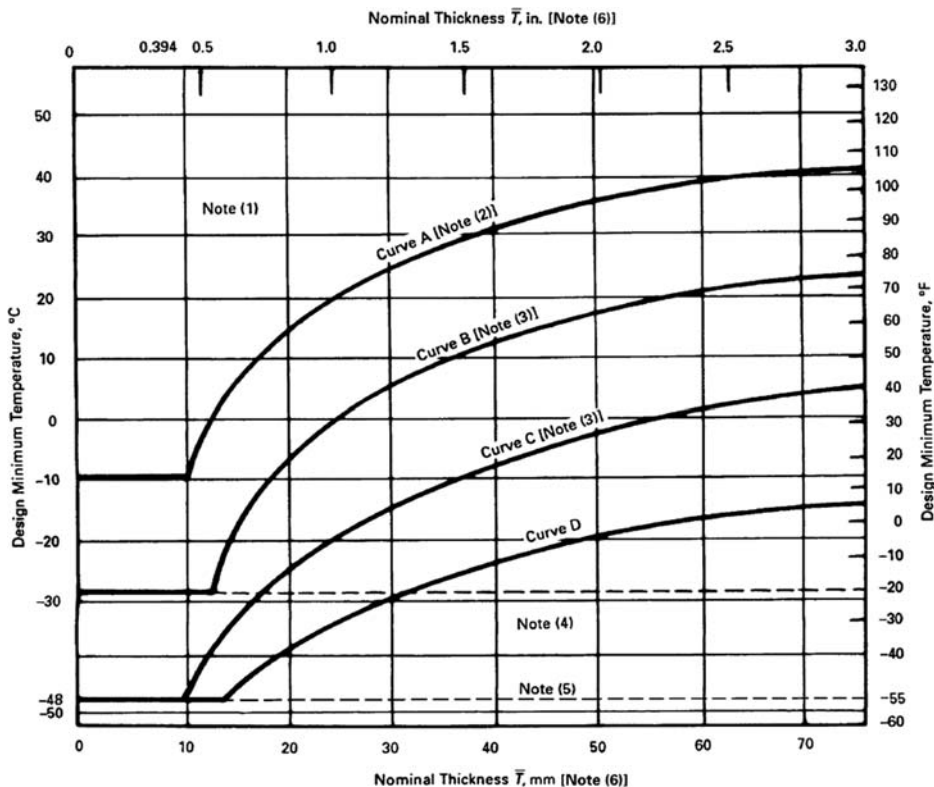
Inspection does not relieve the manufacturer, the fabricator, or the erector of responsibility for providing materials, components, and skill in accordance with requirements of the code and the engineering design, performing all required examinations, and preparing records of examinations and tests for the inspector's use.

Examination Methods The code establishes the types of examinations for evaluating various types of imperfections (see Table 10-56).

Personnel performing examinations other than visual shall be qualified in accordance with applicable portions of SNT TC-1A, *Recommended Practice for Nondestructive Testing Personnel Qualification and Certification*. Procedures shall be qualified as required in Par. T-150, Art. 1, Sec. V of the ASME Code. Limitations on imperfections shall be in accordance with the engineering design but shall at least meet the requirements of the code (see Tables 10-54 and 10-55) for the specific type of examination. Repairs shall be made as applicable.

Visual Examination This consists of observation of the portion of components, joints, and other piping elements that are or can be exposed to view before, during, or after manufacture, fabrication, assembly, erection, inspection, or testing.

TABLE 10-52 Tabular Values for Minimum Temperatures without Impact Testing for Carbon Steel Materials* (Concluded)



NOTES:

- (1) Any carbon steel material may be used to a minimum temperature of -29°C (-20°F) for Category D Fluid Service.
 - (2) X Grades of API SL, and ASTM A 381 materials, may be used in accordance with Curve B if normalized or quenched and tempered.
 - (3) The following materials may be used in accordance with Curve D if normalized:
 - (a) ASTM A 516 Plate, all grades
 - (b) ASTM A 671 Pipe, Grades CE55, CE60, and all grades made with A 516 plate
 - (c) ASTM A 672 Pipe, Grades E55, E60, and all grades made with A 516 plate
 - (4) A welding procedure for the manufacture of pipe or components shall include impact testing of welds and HAZ for any design minimum temperature below -29°C (-20°F), except as provided in Table 10-51, A-3(b).
 - (5) Impact testing in accordance with para. 323.3^a is required for any design minimum temperature below -48°C (-55°F), except as permitted by Note (3) in Table 10-51.
 - (6) For blind flanges and blanks, \bar{T} shall be $1/4$ of the flange thickness.
 - ^aRefer to the referenced code paragraph for impact testing methods and acceptance.
 - ^bRefer to the referenced code paragraph for comments regarding circumstances under which impact testing can be excluded.
- *Table 10-52 and notes have been extracted (with minor modifications) from *Process Piping*, ASME B31.3—2004, with permission of the publisher, the American Society of Mechanical Engineers, New York.

The examination includes verification of code and engineering design requirements for materials and components, dimensions, joint preparation, alignment, welding, bonding, brazing, bolting, threading and other joining methods, supports, assembly, and erection.

Visual examination shall be performed in accordance with Art. 9, Sec. V of the ASME Code.

Magnetic-Particle Examination This examination shall be performed in accordance with Art. 7, Sec. V of the ASME Code.

Liquid-Penetrant Examination This examination shall be performed in accordance with Art. 6, Sec. V of the ASME Code.

Radiographic Examination The following definitions apply to radiography required by the code or by the engineering design:

1. "Random radiography" applies only to girth and miter groove welds. It is radiographic examination of the complete circumference of a specified percentage of the girth butt welds in a designated lot of piping.

2. Unless otherwise specified in engineering design, 100 percent radiography applies only to girth welds, miter groove welds, and fabricated branch connections that utilize butt-type welds to join the header and the branch. The design engineer may, however, elect to designate other types of welds as requiring 100 percent radiography. By definition, 100 percent radiography requires radiographic examination of the complete length of all such welds in a designated lot of piping.

10-130 TRANSPORT AND STORAGE OF FLUIDS

TABLE 10-53 Acceptance Criteria for Welds and Examination Methods for Evaluating Weld Imperfections*

Criteria (A to M) for types of welds and for service conditions [Note (1)]										Examination methods				
Normal and Category M fluid service			Severe cyclic conditions			Category D fluid service				Weld imperfection	Visual	Radiography	Magnetic particle	Liquid penetrant
Type of weld			Type of weld			Type of weld								
Girth, miter groove & branch connection [Note (4)]	Longitudinal groove [Note (2)]	Fillet [Note (3)]	Girth, miter groove & branch connection [Note (4)]	Longitudinal groove [Note (2)]	Fillet [Note (3)]	Girth and miter groove	Longitudinal groove [Note (2)]	Fillet [Note (3)]	Branch connection [Note (4)]					
A	A	A	A	A	A	A	A	A	A	Crack	✓	✓	✓	✓
A	A	A	A	A	A	C	A	N/A	A	Lack of fusion	✓	✓
B	A	N/A	A	A	N/A	C	A	N/A	B	Incomplete penetration	✓	✓
E	E	N/A	D	D	N/A	N/A	N/A	N/A	N/A	Internal porosity	...	✓
G	G	N/A	F	F	N/A	N/A	N/A	N/A	N/A	Internal slag inclusion, tungsten inclusion, or elongated indication	...	✓
H	A	H	A	A	A	I	A	H	H	Undercutting	...	✓
A	A	A	A	A	A	A	A	A	A	Surface porosity or exposed slag inclusion [Note (5)]	✓
N/A	N/A	N/A	J	J	J	N/A	N/A	N/A	N/A	Surface finish	✓
K	K	N/A	K	K	N/A	K	K	N/A	K	Concave root surface (suck up)	✓	✓
L	L	L	L	L	L	M	M	M	M	Weld reinforcement or internal protrusion	✓

Criterion value notes

Criterion		Acceptable value limits [Note (6)]
Symbol	Measure	
A	Extent of imperfection	Zero (no evident imperfection)
B	Depth of incomplete penetration Cumulative length of incomplete penetration	$\leq 1 \text{ mm } (\frac{1}{32} \text{ in})$ and $\leq 0.2\bar{T}_w$ $\leq 38 \text{ mm } (1.5 \text{ in})$ in any 150 mm (6 in) weld length
C	Depth of lack of fusion and incomplete penetration Cumulative length of lack of fusion and incomplete penetration [Note (7)]	$\leq 0.2\bar{T}_w$ $\leq 38 \text{ mm } (1.5 \text{ in})$ in any 150 mm (6 in) weld length
D	Size and distribution of internal porosity	See BPV Code, Section VIII, Division 1, Appendix 4
E	Size and distribution of internal porosity	For $\bar{T}_w \leq 6 \text{ mm } (\frac{1}{4} \text{ in})$, limit is same as D For $\bar{T}_w > 6 \text{ mm } (\frac{1}{4} \text{ in})$, limit is $1.5 \times D$
F	Slag inclusion, tungsten inclusion, or elongated indication Individual length Individual width Cumulative length	$\leq \bar{T}_w/3$ $\leq 2.5 \text{ mm } (\frac{3}{32} \text{ in})$ and $\leq \bar{T}_w/3$ $\leq \bar{T}_w$ in any $12\bar{T}_w$ weld length
G	Slag inclusion, tungsten inclusion, or elongated indication Individual length Individual width Cumulative length	$\leq 2\bar{T}_w$ $\leq 3 \text{ mm } (\frac{1}{8} \text{ in})$ and $\leq \bar{T}_w/2$ $\leq 4\bar{T}_w$ in any 150 mm (6 in) weld length
H	Depth of undercut	$\leq 1 \text{ mm } (\frac{1}{32} \text{ in})$ and $\leq \bar{T}_w/4$
I	Depth of undercut	$\leq 1.5 \text{ mm } (\frac{1}{16} \text{ in})$ and $\leq \bar{T}_w/4$ or $1 \text{ mm } (\frac{1}{32} \text{ in})$
J	Surface roughness	$\leq 500 \text{ min. } Ra$ per ASME B46.1
K	Depth of root surface concavity	Total joint thickness, incl. weld reinf., $\geq \bar{T}_w$
L	Height of reinforcement or internal protrusion [Note (8)] in any plane through the weld shall be within limits of the applicable height value in the tabulation at right, except as provided in Note (9). Weld metal shall merge smoothly into the component surfaces.	For \bar{T}_w mm (in) $\leq 6 (\frac{1}{4})$ $> 6 (\frac{1}{4}), \leq 13 (\frac{1}{2})$ $> 13 (\frac{1}{2}), \leq 25 (1)$ $> 25 (1)$
M	Height of reinforcement or internal protrusion [Note (8)] as described in L. Note (9) does not apply.	Limit is twice the value applicable for L above

Height, mm (in)
$\leq 1.5 (\frac{1}{16})$
$\leq 3 (\frac{1}{8})$
$\leq 4 (\frac{5}{32})$
$\leq 5 (\frac{3}{16})$

TABLE 10-53 Acceptance Criteria for Welds and Examination Methods for Evaluating Weld Imperfections* (Concluded)

GENERAL NOTES:

- Weld imperfections are evaluated by one or more of the types of examination methods. The types and extent of examination shall comply with code requirements and those specified by engineering design.
- "N/A" indicates the code does not establish acceptance criteria or does not require evaluation of this kind of imperfection for this type of weld.
- Check (✓) indicates examination method generally used for evaluating this kind of weld imperfection.
- Ellipsis (...) indicates examination method not generally used for evaluating this kind of weld imperfection.

NOTES:

- Criteria given are for required examination. More stringent criteria may be specified in the engineering design. Other methods of examination may be specified by engineering design to supplement the examination required by the code. The extent of supplementary examination and any acceptance criteria differing from those specified by the code shall be specified by engineering design. Any examination method recognized by the code may be used to resolve doubtful indications. Acceptance criteria shall be those established by the code for the required examination.
- Longitudinal groove weld includes straight and spiral seam. Criteria are not intended to apply to welds made in accordance with component standards recognized by the code (ref. ASME B31.3 Table A1 and Table 326.1); however, alternative leak test requirements dictate that all component welds be examined (see code for specific requirements).
- Fillet weld includes socket and seal welds, and attachment welds for slip-on flanges, branch reinforcement, and supports.
- Branch connection weld includes pressure containing welds in branches and fabricated laps.
- These imperfections are evaluated only for welds ≤ 5 mm ($\frac{3}{16}$ in) in nominal thickness.
- Where two limiting values are separated by *and* the lesser of the values determines acceptance. Where two sets of values are separated by *or* the larger value is acceptable. T_w is the nominal wall thickness of the thinner of two components joined by a butt weld.
- Tightly butted unfused root faces are unacceptable.
- For groove welds, height is the lesser of the measurements made from the surfaces of the adjacent components; both reinforcement and internal protrusion are permitted in a weld. For fillet welds, height is measured from the theoretical throat defined by the code; internal protrusion does not apply.
- For welds in aluminum alloy only, internal protrusion shall not exceed the following values:
 - for thickness ≤ 2 mm ($\frac{3}{64}$ in): 1.5 mm ($\frac{1}{16}$ in)
 - for thickness > 2 mm and ≤ 6 mm ($\frac{1}{4}$ in): 2.5 mm ($\frac{3}{32}$ in)

For external reinforcement and for greater thicknesses, see the tabulation for Symbol L.

*Table 10-53 and notes have been extracted (with minor modifications) from Section 341 of *Process Piping*, ASME B31.3-2004, with permission of the publisher, the American Society of Mechanical Engineers, New York.

3. "Spot radiography" is the practice of making a single-exposure radiograph at a point within a specified extent of welding. Required coverage for a single spot radiograph is as follows:

- For longitudinal welds, at least 150 mm (6 in) of weld length.
- For girth, miter, and branch welds in piping $2\frac{1}{2}$ in NPS and smaller, a single elliptical exposure which encompasses the entire weld circumference, and in piping larger than $2\frac{1}{2}$ in NPS, at least 25 percent of the inside circumference or 150 mm (6 in), whichever is less.

Radiography of components other than castings and of welds shall be in accordance with Art. 2, Sec. V of the ASME Code. Limitations on imperfections in components other than castings and welds shall be as stated in Table 10-53 for the degree of radiography involved.

Ultrasonic Examination Ultrasonic examination of welds shall be in accordance with Art. 5, Sec. V of the ASME Code, except that the modifications stated in Par. 336.4.6 of the code shall be substituted for T542.2.1 and T542.8.1.1. Refer to the code for additional requirements.

Type and Extent of Required Examination The intent of examinations is to provide the examiner and the inspector with reasonable assurance that the requirements of the code and the engineering design have been met. For P-number 3, 4, and 5 materials, examination shall be performed after any heat treatment has been completed.

Examination Normally Required* Piping in normal fluid service shall be examined to the extent specified herein or to any greater extent specified in the engineering design. Acceptance criteria are as stated in the code for Normal Fluid Service unless more stringent requirements are specified.

1. *Visual examination.* At least the following shall be examined in accordance with code requirements:

- Sufficient materials and components, selected at random, to satisfy the examiner that they conform to specifications and are free from defects.
- At least 5 percent of fabrication. For welds, each welder's and welding operator's work shall be represented.
- 100 percent of fabrication for longitudinal welds, except those in components made in accordance with a listed specification. Longi-

tudinal welds required to have a joint efficiency of 0.9 must be spot-radiographed to the extent of 300 mm (12 in) in each 30 m (100 ft) of weld for each welder or welding operator. Acceptance criteria shall comply with code radiography acceptance criteria for Normal Fluid Service.

d. Random examination of the assembly of threaded, bolted, and other joints to satisfy the examiner that they conform to the applicable code requirements for erection and assembly. When pneumatic testing is to be performed, all threaded, bolted, and other mechanical joints shall be examined.

e. Random examination during erection of piping, including checking of alignment, supports, and cold spring.

f. Examination of erected piping for evidence of defects that would require repair or replacement, and for other evident deviations from the intent of the design.

2. Other examination

a. Not less than 5 percent of circumferential butt and miter groove welds shall be examined fully by random radiography or random ultrasonic examination in accordance with code requirements established for these methods. The welds to be examined shall be selected to ensure that the work product of each welder or welding operator doing the production welding is included. They shall also be selected to maximize coverage of intersections with longitudinal joints. When a circumferential weld with intersecting longitudinal weld(s) is examined, at least the adjacent 38 mm ($1\frac{1}{2}$ in) of each intersecting weld shall be examined. In-process examination in accordance with code requirements may be substituted for all or part of the radiographic or ultrasonic examination on a weld-for-weld basis if specified in the engineering design or specifically authorized by the Inspector.

b. Not less than 5 percent of all brazed joints shall be examined by in-process examination in accordance with the code definition of in-process examination, the joints to be examined being selected to ensure that the work of each brazer making the production joints is included.

3. *Certifications and records.* The examiner shall be assured, by examination of certifications, records, and other evidence, that the materials and components are of the specified grades and that they have received required heat treatment, examination, and testing. The examiner shall provide the Inspector with a certification that all the quality control requirements of the code and of the engineering design have been carried out.

*Extracted (with minor editing) from *Process Piping*, ASME B31.3-2004, paragraph 341, with permission of the publisher, the American Society of Mechanical Engineers, New York.

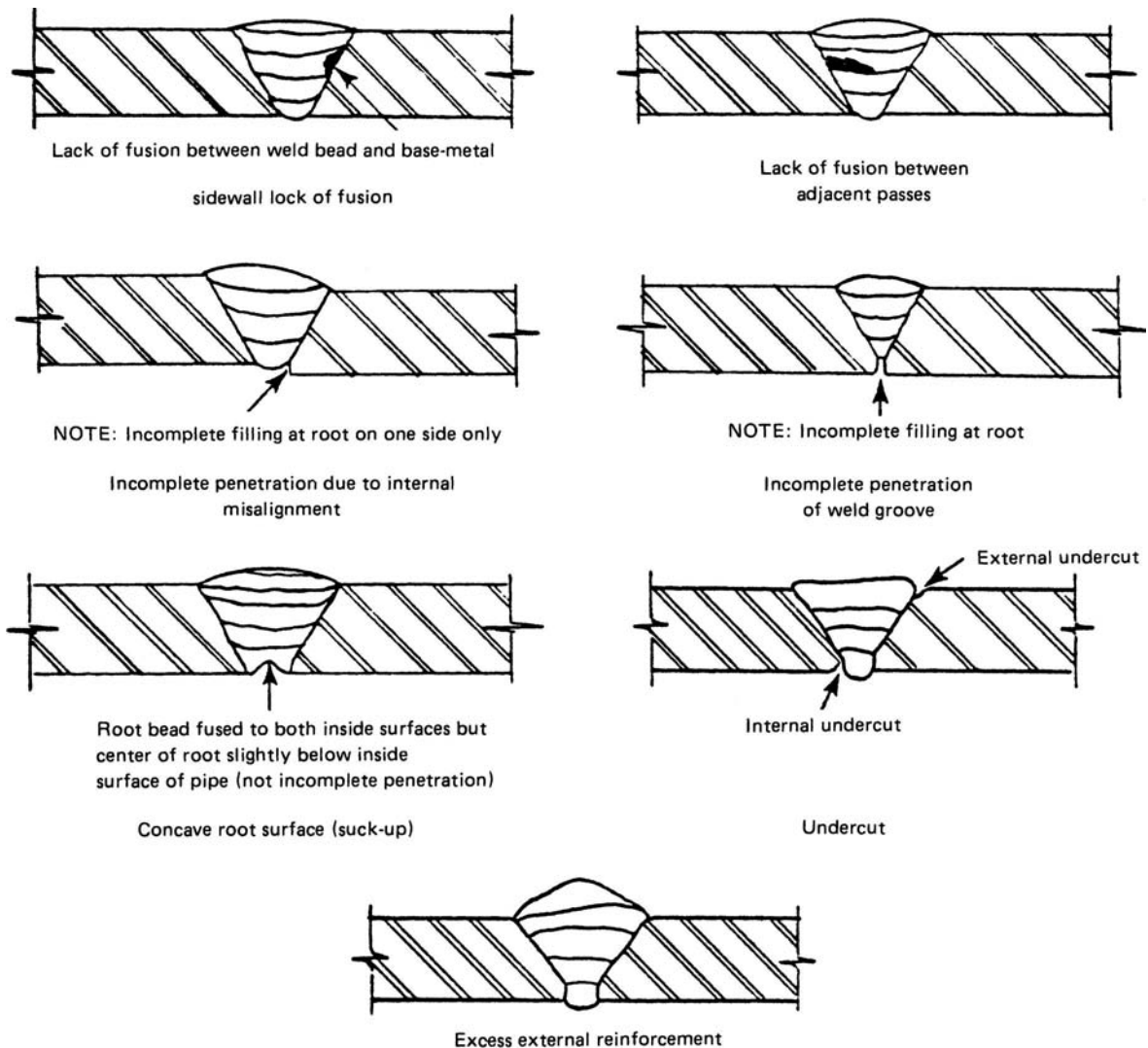


FIG. 10-180 Typical weld imperfections. (Extracted from *Process Piping*, ASME B31.3—2004, with permission of the publisher, the American Society of Mechanical Engineers, New York.)

Examination—Category D Fluid Service^o Piping and piping elements for Category D fluid service as designated in the engineering design shall be visually examined in accordance with code requirements for visual examination to the extent necessary to satisfy the examiner that components, materials, and workmanship conform to the requirements of this code and the engineering design. Acceptance criteria shall be in accordance with code requirements and criteria in Table 10-53, for Category D fluid service, unless otherwise specified.

Examination—Severe Cyclic Conditions^o Piping to be used under severe cyclic conditions shall be examined to the extent specified herein or to any greater extent specified in the engineering design. Acceptance criteria shall be in accordance with code requirements and criteria in Table 10-53, for severe cyclic conditions, unless otherwise specified.

^oExtracted (with minor editing) from *Process Piping*, ASME B31.3—2004, paragraph 341, with permission of the publisher, the American Society of Mechanical Engineers, New York.

1. **Visual examination.** The requirements for Normal Fluid Service apply with the following exceptions.

a. All fabrication shall be examined.

b. All threaded, bolted, and other joints shall be examined.

c. All piping erection shall be examined to verify dimensions and alignment. Supports, guides, and points of cold spring shall be checked to ensure that movement of the piping under all conditions of startup, operation, and shutdown will be accommodated without undue binding or unanticipated constraint.

2. **Other examination.** All circumferential butt and miter groove welds and all fabricated branch connection welds comparable to those recognized by the code (ref. Fig. 10-130) shall be examined by 100% radiography or 100% ultrasonic (if specified in engineering design) in accordance with code requirements. Socket welds and branch connection welds which are not radiographed shall be examined by magnetic particle or liquid penetrant methods in accordance with code requirements.

3. In-process examination in accordance with the code definition, supplemented by appropriate nondestructive examination, may be

TABLE 10-54 Preheat Temperatures*

Base metal P-no. or S-no. [Note (1)]	Weld metal analysis A-no. [Note (2)]	Base metal group	Nominal wall thickness		Specified min. tensile strength, base metal		Min. temperature			
			mm	in.	MPa	ksi	Required °C	Required °F	Recommended °C	Recommended °F
1	1	Carbon steel	<25	<1	≤490	≤71	10	50
			≥25	≥1	All	All	79	175
			All	All	>490	>71	79	175
3	2,11	Alloy steels, Cr ≤ 1/2%	<13	<1/2	≤490	≤71	10	50
			≥13	≥1/2	All	All	79	175
			All	All	>490	>71	79	175
4	3	Alloy steels, 1/2% ≤ Cr ≤ 2%	All	All	All	All	149	300
5A, 5B, 5C	4, 5	Alloy steels, 2 1/4% ≤ Cr ≤ 10%	All	All	All	All	177	350
6	6	High alloy steels martensitic	All	All	All	All	149 ⁴	300 ⁴
7	7	High alloy steels ferritic	All	All	All	All	10	50
8	8, 9	High alloy steels austenitic	All	All	All	All	10	50
9A, 9B	10	Nickel alloy steels	All	All	All	All	93	200
10	...	Cr-Cu steel	All	All	All	All	149-204	300-400
101	...	27Cr steel	All	All	All	All	149 ³	300 ³
11A SG 1	...	8Ni, 9Ni steel	All	All	All	All	10	50
11A SG 2	...	5Ni steel	All	All	All	All	10	50
21-52	All	All	All	All	10	50

*Extracted from *Process Piping*, ASME B31.3—2004, with permission of the publisher, the American Society of Mechanical Engineers, New York.

NOTES:

- (1) P-number or S-number from BPV Code, Section IX, QW/QB-442.
- (2) A-number from Section IX, QW-442.
- (3) Maintain interpass temperature between 177°C and 232°C (350°F and 450°F).
- (4) Maximum interpass temperature 316°C (600°F).

substituted for the examination required in 2 above on a weld-for-weld basis if specified in the engineering design or specifically authorized by the Inspector.

4. *Certification and records.* The requirements established by the code for Normal Fluid Service apply.

Impact Testing In specifying materials, it is critical that the low-temperature limits of materials and impact testing requirements of the applicable code edition be clearly understood. In the recent past, code criteria governing low-temperature limits and requirements for impact testing have undergone extensive revision. The code contains extensive criteria detailing when impact testing is required and describing how it is to be performed. Because of the potentially changing requirements and the complexity of the code requirements, this handbook does not attempt to provide a comprehensive treatment of this subject or a comprehensive presentation of the requirements of the current code edition. Some of the general guidelines are provided here; however, the designer should consult the code to clearly understand additional requirements and special circumstances under which impact testing may be omitted. These exclusions permitted by the code may be significant in selecting materials or establishing material requirements.

In general, materials conforming to ASTM specifications listed by the code may be used at temperatures down to the lowest temperature listed for that material in ASME B31.3 Table A-10. When welding or other operations are performed on these materials, additional low-temperature toughness tests (impact testing) may be required. Refer to Table 10-51 for a general summary of these requirements.

Pressure Testing Prior to initial operation, installed piping shall be pressure-tested to assure tightness except as permitted for Category D fluid service described later. The pressure test shall be main-

tained for a sufficient time to determine the presence of any leaks but not less than 10 min.

If repairs or additions are made following the pressure tests, the affected piping shall be retested except that, in the case of minor repairs or additions, the owner may waive retest requirements when precautionary measures are taken to assure sound construction.

When pressure tests are conducted at metal temperatures near the ductile-to-brittle transition temperature of the material, the possibility of brittle fracture shall be considered.

The test shall be hydrostatic, using water, with the following exceptions. If there is a possibility of damage due to freezing or if the operating fluid or piping material would be adversely affected by water, any other suitable nontoxic liquid may be used. If a flammable liquid is used, its flash point shall not be less than 50°C (120°F), and consideration shall be given to the test environment.

The hydrostatic-test pressure at any point in the system shall be as follows:

- 1. Not less than 1 1/2 times the design pressure.
- 2. For a design temperature above the test temperature, the minimum test pressure shall be as calculated by the following formula:

$$P_T = 1.5PS_T/S \tag{10-108}$$

where P_T = test hydrostatic gauge pressure, MPa (lbf/in²)
 P = internal design pressure, MPa (lbf/in²)
 S_T = allowable stress at test temperature, MPa (lbf/in²)
 S = allowable stress at design temperature, MPa (lbf/in²)
 S_T/S shall not exceed 6.5

If the test pressure as so defined would produce a stress in excess of the yield strength at test temperature, the test pressure may be reduced

10-134 TRANSPORT AND STORAGE OF FLUIDS

TABLE 10-55 Requirements for Heat Treatment*

Base metal P-no. or S-no. [Note (1)]	Weld-metal analysis A-no. [Note (2)]	Base metal group	Nominal wall thickness		Specified min. tensile strength, base metal		Metal temperature range		Holding time			Brinell hardness, max. [Note (4)]
									Nominal wall [Note (3)]		Min. time, h	
			mm	in	MPa	ksi	°C	°F	min/mm	h/in		
1	1	Carbon steel	≤ 19	≤ ¾	All	All	None	None
			> 19	> ¾	All	All	593–649	1100–1200	2.4	1	1	...
3	2, 11	Alloy steels	≤ 19	≤ ¾	≤ 490	≤ 71	None	None
		Cr ½%	> 19	> ¾	All	All	593–718	1100–1325	2.4	1	1	225
			All	All	> 490	> 71	593–718	1100–1325	2.4	1	1	225
4 [Note (5)]	3	Alloy steels, ½% < Cr ≤ 2%	≤ 13	≤ ½	≤ 490	≤ 71	None	None
			> 13	> ½	All	All	704–746	1300–1375	2.4	1	2	225
			All	All	> 490	> 71	704–746	1300–1375	2.4	1	2	225
5A, 5B, 5C [Note (5)]	4, 5	Alloy steels 2¼% ≤ Cr ≤ 10% ≤ 3% Cr and ≤ 0.15% C ≤ 3% Cr and ≤ 0.15% C > 3% Cr or ≤ 0.15% C	≤ 13	≤ ½	All	All	None	None
			> 13	> ½	All	All	704–760	1300–1400	2.4	1	2	241
			All	All	All	All	704–760	1300–1400	2.4	1	2	241
6	6	High-alloy steels: martensitic A 240, Cr. 429	All	All	All	All	732–788	1350–1450	2.4	1	2	241
			All	All	All	All	621–663	1150–1225	2.4	1	2	241
7	7	High-alloy steels: ferritic	All	All	All	All	None	None
8	8, 9	High-alloy steels: austenitic	All	All	All	All	None	None
9A, 9B	10	Nickel alloy steels	≤ 19	≤ ¾	All	All	None	None
			> 19	> ¾	All	All	593–635	1100–1175	1.2	½	1	...
10	...	Cr–Cu steel	All	All	All	All	760–816 [Note (6)]	1400–1500 [Note (6)]	1.2	½	½	...
10H	...	Duplex stainless steel	All	All	All	All	Note (7)	Note (7)	1.2	½	½	...
101	...	27Cr steel	All	All	All	All	663–704 [Note (8)]	1225–1300 [Note (8)]	2.4	1	1	...
11A SG 1	...	8Ni, 9Ni steel	≤ 51	≤ 2	All	All	None	None
			> 51	> 2	All	All	552–585 [Note (9)]	1025–1085 [Note (9)]	2.4	1	1	...
11A SG 2	...	5Ni steel	> 51	> 2	All	All	552–585 [Note (9)]	1025–1085 [Note (9)]	2.4	1	1	...
62	...	Zr R60705	All	All	All	All	538–593 [Note (10)]	1000–1100 [Note (10)]	Note (10)	Note (10)	1	...

* Extracted from *Process Piping*, ASME B31.3—2004, with permission of the publisher, the American Society of Mechanical Engineers, New York.

NOTES:

- (1) P-number or S-number from BPV Code, Section IX, QW/QB-422.
 - (2) A-number from Section IX, QW-442.
 - (3) For holding time in SI metric units, use min/mm (minutes per mm thickness). For U.S. units, use h/in thickness.
 - (4) See para. 331.1.7.^a
 - (5) See Appendix F, para. F331.1.^a
 - (6) Cool as rapidly as possible after the hold period.
 - (7) Postweld heat treatment is neither required nor prohibited, but any heat treatment applied shall be as required in the material specification.
 - (8) Cooling rate to 649°C (1200°F) shall be less than 56°C (100°F)/h; thereafter, the cooling rate shall be fast enough to prevent embrittlement.
 - (9) Cooling rate shall be > 167°C (300°F)/h to 316°C (600°F).
 - (10) Heat treat within 14 days after welding. Hold time shall be increased by ½ h for each 25 mm (1 in) over 25 mm thickness. Cool to 427°C (800°F) at a rate ≤ 278°C (500°F)/h, per 25 mm (1 in) nominal thickness, 278°C (500°F)/h max. Cool in still air from 427°C (800°F).
- ^a Refer to the referenced code paragraph for details.

to the maximum pressure that will not exceed the yield strength at test temperature. If the test liquid in the system is subject to thermal expansion, precautions shall be taken to avoid excessive pressure.

A preliminary air test at not more than 0.17-MPa (25-lbf/in²) gauge pressure may be made prior to hydrostatic test in order to locate major leaks.

If hydrostatic testing is not considered practicable by the owner, a pneumatic test in accordance with the following procedure may be substituted, using air or another nonflammable gas.

If the piping is tested pneumatically, the test pressure shall be 110 percent of the design pressure. When pneumatically testing nonmetallic

materials, assure that the materials are suitable for compressed gas. Pneumatic testing involves a hazard due to the possible release of energy stored in compressed gas. Therefore, particular care must be taken to minimize the chance of brittle failure of metals and thermoplastics. The test temperature is important in this regard and must be considered when material is chosen in the original design. Any pneumatic test shall include a preliminary check at not more than 0.17-MPa (25-lbf/in²) gauge pressure. The pressure shall be increased gradually in steps providing sufficient time to allow the piping to equalize strains during test and to check for leaks. Once test pressure has been achieved, the pressure shall be reduced to design pressure prior to examining for leakage.

TABLE 10-56 Types of Examination for Evaluating Imperfections*

Type of imperfection	Type of examination			
	Visual	Liquid-penetrant or magnetic-particle	Ultrasonic or radiographic	
			Random	100%
Crack	X	X	X	X
Incomplete penetration	X		X	X
Lack of fusion	X		X	X
Weld undercutting	X			
Weld reinforcement	X			
Internal porosity			X	X
External porosity	X			
Internal slag inclusions			X	X
External slag inclusions	X			
Concave root surface	X		X	X

*Extracted from the Chemical Plant and Petroleum Refinery Piping Code, ANSI B31.3—1980, with permission of the publisher, the American Society of Mechanical Engineers, New York. For code acceptance criteria (limits on imperfections) for welds see Table 10-53.

At the owner's option, a piping system used only for Category D fluid service as defined in the subsection "Classification of Fluid Service" may be tested at the normal operating conditions of the system during or prior to initial operation by examining for leaks at every joint not previously tested. A preliminary check shall be made at not more than 0.17-MPa (25-lbf/in²) gauge pressure when the contained fluid is a gas or a vapor. The pressure shall be increased gradually in steps providing sufficient time to allow the piping to equalize strains during testing and to check for leaks.

Tests alternative to those required by these provisions may be applied under certain conditions described in the code.

Piping required to have a sensitive leak test shall be tested by the gas-and bubble-formation testing method specified in Art. 10, Sec. V of the ASME Boiler and Pressure Vessel Code or by another method demonstrated to have equal or greater sensitivity. The sensitivity of the test shall be at least (100 Pa·mL)/s [(10³ atm·mL)/s] under test conditions.

Records shall be kept of each piping installation during the testing.

COST COMPARISON OF PIPING SYSTEMS

Piping may represent as much as 25 percent of the cost of a chemical-process plant. The installed cost of piping systems varies widely with the materials of construction and the complexity of the system. A study of piping costs shows that the most economical choice of material for a simple straight piping run may not be the most economical for a complex installation made up of many short runs involving numerous fittings and valves. The economics also depends heavily on the pipe size and fabrication techniques employed. Fabrication methods such as bending to standard long-radius-elbow dimensions and machine-flaring lap joints have a large effect on the cost of fabricating pipe from ductile materials suited to these techniques. Cost reductions of as high as 35 percent are quoted by some custom fabricators utilizing advanced techniques; however, the basis for pricing comparisons should be carefully reviewed.

Figure 10-181 is based on data extracted from a comparison of the installed cost of piping systems of various materials published by the Dow Chemical Co. The chart shows the relative cost ratios for systems of various materials based on two installations, one consisting of 152 m (500 ft) of 2-in pipe in a complex piping arrangement and the other of 305 m (1000 ft) of 2-in pipe in a straight-run piping arrangement. Figure 10-181 is based on field-fabrication construction techniques using welding stubs, the method commonly used by contractors. A considerably different ranking would result from using other construction methods such as machine-formed lap joints and bends in place of welding elbows. Piping-cost experience shows that it is difficult to generalize and reflect accurate piping-cost comparisons. Although the prices for many of the metallurgies shown in Fig. 10-181 are very volatile even over short periods, Fig. 10-181 may still be used as a reasonable initial estimate of the relative cost of metallic materials. The cost of nonmetallic materials and lined metallic materials versus

solid alloy materials should be carefully reviewed prior to material selection. For an accurate comparison the cost for each type of material must be estimated individually on the basis of the actual fabrication and installation methods that will be used, pipe sizes and the conditions anticipated for the proposed installation.

FORCES OF PIPING ON PROCESS MACHINERY AND PIPING VIBRATION

The reliability of process rotating machinery is affected by the quality of the process piping installation. Excessive external forces and moments upset casing alignment and can reduce clearance between motor and casing. Further, the bearings, seals, and coupling can be adversely affected, resulting in repeated failures that may be correctly diagnosed as misalignment, and may have excessive piping forces as the root causes. Most turbine and compressor manufacturers have prescribed specification or will follow NEMA standards for allowable nozzle loading. For most of the pumps, API or ANSI pump standards will be followed when evaluating the pump nozzle loads. Pipe support restraints need to be placed at the proper locations to protect the machinery nozzles during operation.

Prior to any machinery alignment procedure, it is imperative to check for machine pipe strain. This is accomplished by the placement of dial indicators on the shaft and then loosening the hold-down bolts. Movements of greater than 1 mil are considered indication of a pipe strain condition.

This is an important practical problem area, as piping vibration can cause considerable downtime or even pipe failure.

Pipe vibration is caused by:

1. Internal flow (pulsation)
2. Plant machinery (such as compressors, pumps)

Pulsation can be problematic and difficult to predict. Pulsations are also dependent on acoustic resonance characteristics. For reciprocating equipment, such as reciprocating compressors and pumps, in some cases, an analog (digital) study needs to be performed to identify the deficiency in the piping and pipe support systems as well as to evaluate the performance of the machine during operation. The study will also provide recommendations on how to improve the machine and piping system's performance.

When a pulsation frequency coincides with a mechanical or acoustic resonance, severe vibration can result. A common cause for pulsation is the presence of flow control valves or pressure regulators. These often operate with high pressure drops (i.e., high flow velocities), which can result in the generation of severe pulsation. Flashing and cavitation can also contribute.

Modern-day piping design codes can model the vibration situation, and problems can thus be resolved in the design phases.

HEAT TRACING OF PIPING SYSTEMS

Heat tracing is used to maintain pipes and the material that pipes contain at temperatures above the ambient temperature. Two common uses of heat tracing are preventing water pipes from freezing and maintaining fuel oil pipes at high enough temperatures such that the viscosity of the fuel oil will allow easy pumping. Heat tracing is also used to prevent the condensation of a liquid from a gas and to prevent the solidification of a liquid commodity.

A heat-tracing system is often more expensive on an installed cost basis than the piping system it is protecting, and it will also have significant operating costs. A study on heat-tracing costs by a major chemical company showed installed costs of \$31/ft to \$142/ft and yearly operating costs of \$1.40/ft to \$16.66/ft. In addition to being a major cost, the heat-tracing system is an important component of the reliability of a piping system. A failure in the heat-tracing system will often render the piping system inoperable. For example, with a water freeze protection system, the piping system may be destroyed by the expansion of water as it freezes if the heat-tracing system fails.

The vast majority of heat-traced pipes are insulated to minimize heat loss to the environment. A heat input of 2 to 10 watts per foot is generally required to prevent an insulated pipe from freezing. With high wind speeds, an uninsulated pipe could require well over 100

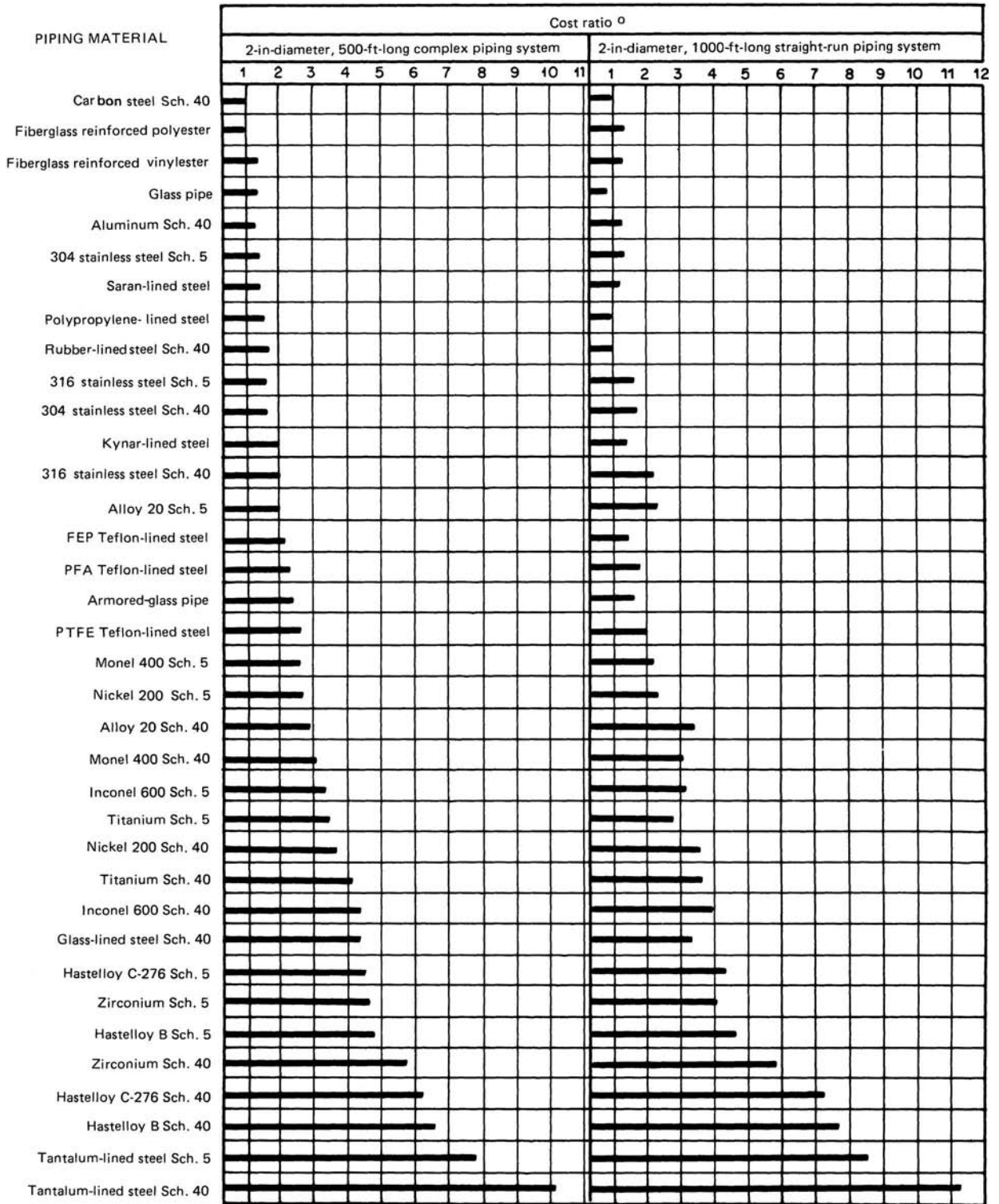


FIG. 10-181 Cost rankings and cost ratios for various piping materials. This figure is based on field-fabrication construction techniques using welding stubs, as this is the method most often employed by contractors. A considerably different ranking would result from using other construction methods, such as machined-formed lap joints, for the alloy pipe. °Cost ratio = (cost of listed item)/(cost of Schedule 40 carbon steel piping system, field-fabricated by using welding stubs). (Extracted with permission from *Installed Cost of Corrosion Resistant Piping*, copyright 1977, Dow Chemical Co.)

watts per foot to prevent freezing. Such a high heat input would be very expensive.

Heat tracing for insulated pipes is generally only required for the period when the material in the pipe is not flowing. The heat loss of an insulated pipe is very small compared to the heat capacity of a flowing fluid. Unless the pipe is extremely long (several thousands of feet), the temperature drop of a flowing fluid will not be significant.

The three major methods of avoiding heat tracing are:

1. Changing the ambient temperature around the pipe to a temperature that will avoid low-temperature problems. Burying water pipes below the frost line or running them through a heated building are the two most common examples of this method.

2. Emptying a pipe after it is used. Arranging the piping such that it drains itself when not in use, can be an effective method of avoiding the need for heat tracing. Some infrequently used lines can be pigged or blown out with compressed air. This technique is not recommended for commonly used lines due to the high labor requirement.

3. Arranging a process such that some lines have continuous flow can eliminate the need for tracing these lines. This technique is generally not recommended because a failure that causes a flow stoppage can lead to blocked or broken pipes.

Some combination of these techniques may be used to minimize the quantity of traced pipes. However, the majority of pipes containing fluids that must be kept above the minimum ambient temperature are generally going to require heat tracing.

Types of Heat-Tracing Systems Industrial heat-tracing systems are generally fluid systems or electrical systems. In fluid systems, a pipe or tube called the *tracer* is attached to the pipe being traced, and a warm fluid is put through it. The tracer is placed under the insulation. Steam is by far the most common fluid used in the tracer, although ethylene glycol and more exotic heat-transfer fluids are used. In electrical systems, an electrical heating cable is placed against the pipe under the insulation.

Fluid Tracing Systems Steam tracing is the most common type of industrial pipe tracing. In 1960, over 95 percent of industrial tracing systems were steam traced. By 1995, improvements in electric heating technology increased the electric share to 30 to 40 percent. Fluid systems other than steam are rather uncommon and account for less than 5 percent of tracing systems.

Half-inch copper tubing is commonly used for steam tracing. Three-eighths-inch tubing is also used, but the effective circuit length is then decreased from 150 ft to about 60 ft. In some corrosive environments, stainless steel tubing is used.

In addition to the tracer, a steam tracing system (Fig. 10-182) consists of steam supply lines to transport steam from the existing steam lines to the traced pipe, a steam trap to remove the condensate and hold back the steam, and in most cases a condensate return system to return the condensate to the existing condensate return system. In the past, a significant percentage of condensate from steam tracing was simply dumped to drains, but increased energy costs and environmental rules have caused almost all condensate from new steam tracing systems to be returned. This has significantly increased the initial cost of steam tracing systems.

Applications requiring accurate temperature control are generally limited to electric tracing. For example, chocolate lines cannot be exposed to steam temperatures or the product will degrade and if caustic soda is heated above 65°C (150°F) it becomes extremely corrosive to carbon steel pipes.

For some applications, either steam or electricity is simply not available and this makes the decision. It is rarely economic to install a steam boiler just for tracing. Steam tracing is generally considered only when a boiler already exists or is going to be installed for some other primary purpose. Additional electric capacity can be provided in most situations for reasonable costs. It is considerably more expensive to supply steam from a long distance than it is to provide electricity. Unless steam is available close to the pipes being traced, the automatic choice is usually electric tracing.

For most applications, particularly in processing plants, either steam tracing or electric tracing could be used, and the correct choice is dependent on the installed costs and the operating costs of the competing systems.

Economics of Steam Tracing versus Electric Tracing The question of the economics of various tracing systems has been examined thoroughly. All of these papers have concluded that electric tracing is generally less expensive to install and significantly less expensive to operate. Electric tracing has significant cost advantages in terms of installation because less labor is required than steam tracing. However, it is clear that there are some special cases where steam tracing is more economical.

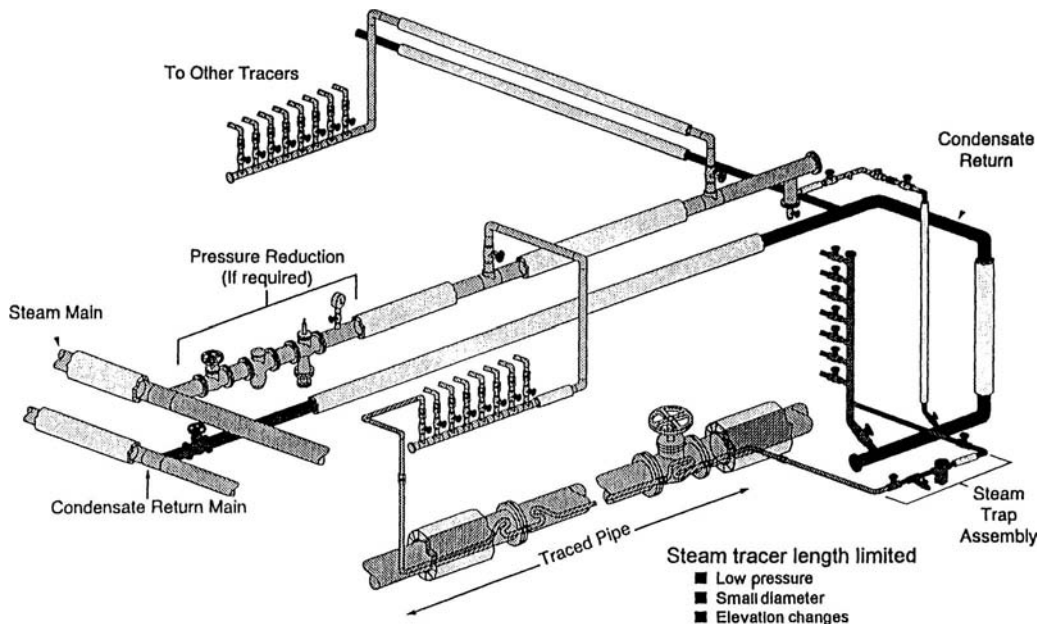


FIG. 10-182 Steam tracing system.

TABLE 10-57 Steam versus Electric Tracing*

Temperature maintained	TIC		Ratio S/E	TOC		Ratio S/E
	Steam	Electric		Steam	Electric	
50°F	22,265	7,733	2.88	1,671	334	5.00
150°F	22,265	13,113	1.70	4,356	1,892	2.30
250°F	22,807	17,624	1.29	5,348	2,114	2.53
400°F	26,924	14,056	1.92	6,724	3,942	1.71

*Specifications: 400 feet of four-inch pipe, \$25/hr labor, \$0.07/kWh, \$4.00/1,000# steam, 100-foot supply lines. TIC = total installed cost; TOC = total operating costs.

The two key variables in the decision to use steam tracing or electric tracing are the temperature at which the pipe must be maintained and the distance to the supply of steam and a source of electric power.

Table 10-57 shows the installed costs and operating costs for 400 ft of 4-in pipe, maintained at four different temperatures, with supply lengths of 100 ft for both electricity and steam and \$25/h labor.

The major advantages of a steam tracing system are:

1. *High heat output.* Due to its high temperature, a steam tracing system provides a large amount of heat to the pipe. There is a very high heat transfer rate between the metallic tracer and a metallic pipe. Even with damage to the insulation system, there is very little chance of a low temperature failure with a steam-tracing system.

2. *High reliability.* Many things can go wrong with a steam-tracing system but very few of the potential problems lead to a heat-tracing failure. Steam traps fail, but they usually fail in the open position, allowing for a continuous flow of steam to the tracer. Other problems such as steam leaks that can cause wet insulation are generally prevented from becoming heat-tracing failures by the extremely high heat output of a steam tracer. Also, a tracing tube is capable of withstanding a large amount of mechanical abuse without failure.

3. *Safety.* While steam burns are fairly common, there are generally fewer safety concerns than with electric tracing.

4. *Common usage.* Steam tracing has been around for many years and many operators are familiar with the system. Because of this familiarity, failures due to operator error are not very common.

The weaknesses of a steam-tracing system are:

1. *High installed costs.* The incremental piping required for the steam supply system and the condensate return system must be installed, insulated, and, in the case of the supply system, additional

steam traps are often required. The tracer itself is not expensive, but the labor required for installation is relatively high. Studies have shown that steam tracing systems typically cost from 50 to 150 percent more than a comparable electric-tracing system.

2. *Energy inefficiency.* A steam-tracing system's total energy use is often more than 20 times the actual energy requirement to keep the pipe at the desired temperature. The steam tracer itself puts out significantly more energy than required. The steam traps use energy even when they are properly operating and waste large amounts of energy when they fail in the open position, which is the common failure mode. Steam leaks waste large amounts of energy, and both the steam supply system and the condensate return system use significant amounts of energy.

3. *Poor temperature control.* A steam-tracing system offers very little temperature control capability. The steam is at a constant temperature (50 psig steam is 300°F) usually well above that desired for the pipe. The pipe will reach an equilibrium temperature somewhere between the steam temperature and the ambient temperature. However, the section of pipe against the steam tracer will effectively be at the steam temperature. This is a serious problem for temperature-sensitive fluids such as food products. It also represents a problem with fluids such as bases and acids, which are not damaged by high temperatures but often become extremely corrosive to piping systems at high temperatures.

4. *High maintenance costs.* Leaks must be repaired and steam traps must be checked and replaced if they have failed. Numerous studies have shown that, due to the energy lost through leaks and failed steam traps, an extensive maintenance program is an excellent investment. Steam maintenance costs are so high that for low-temperature maintenance applications, total steam operating costs are sometimes greater than electric operating costs, even if no value is placed on the steam.

Electric Tracing An electric-tracing system (see Fig. 10-183) consists of an electric heater placed against the pipe under the thermal insulation, the supply of electricity to the tracer, and any control or monitoring system that may be used (optional). The supply of electricity to the tracer usually consists of an electrical panel and electrical conduit or cable trays. Depending on the size of the tracing system and the capacity of the existing electrical system, an additional transformer may be required.

Advantages of Electric Tracing

1. *Lower installed and operating costs.* Most studies have shown that electric tracing is less expensive to install and less expensive to

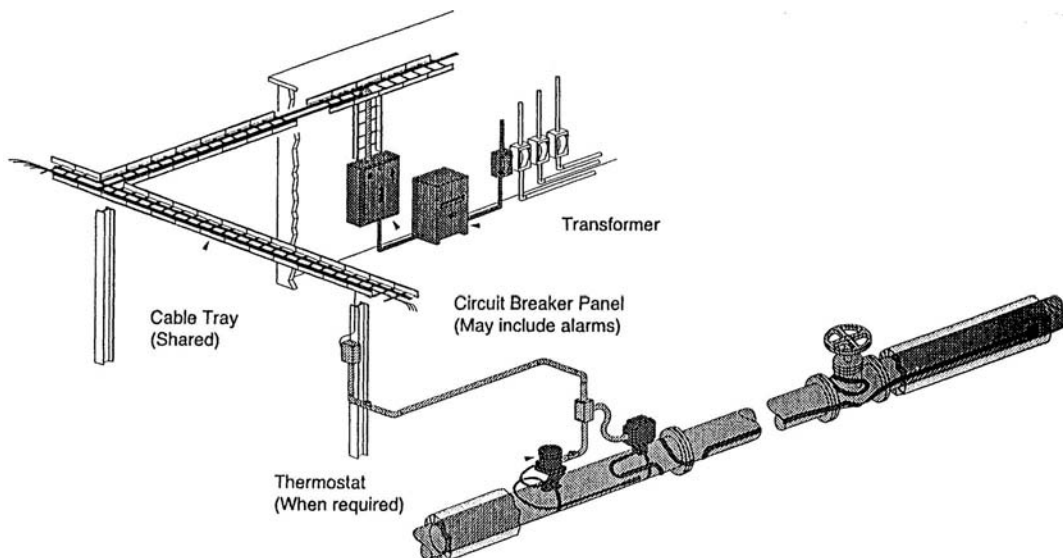


FIG. 10-183 Electrical heat tracing system.

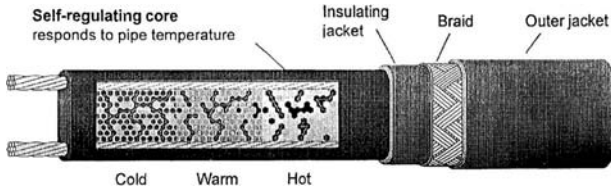


FIG. 10-184 Self-regulating heating cable.

operate. This is true for most applications. However, for some applications, the installed costs of steam tracing are equal to or less than electric tracing.

2. *Reliability.* In the past, electric heat tracing had a well-deserved reputation for poor reliability. However, since the introduction of self-regulating heaters in 1971, the reliability of electric heat tracing has improved dramatically. Self-regulating heaters cannot destroy themselves with their own heat output. This eliminates the most common failure mode of polymer-insulated constant wattage heaters. Also, the technology used to manufacture mineral-insulated cables, high-temperature electric heat tracing, has improved significantly, and this has improved their reliability.

3. *Temperature control.* Even without a thermostat or any control system, an electric tracing system usually provides better temperature control than a steam tracing system. With thermostatic or electronic control, very accurate temperature control can be achieved.

4. *Safety.* The use of self-regulating heaters and ground leakage circuit breakers has answered the safety concerns of most engineers considering electric tracing. Self-regulating heaters eliminate the problems from high-temperature failures, and ground leakage circuit breakers minimize the danger of an electrical fault to ground, causing injury or death.

5. *Monitoring capability.* One question often asked about any heat-tracing system is, "How do I know it is working?" Electric tracing now has available almost any level of monitoring desired. The temperature at any point can be monitored with both high and low alarm capability. This capability has allowed many users to switch to electric tracing with a high degree of confidence.

6. *Energy efficiency.* Electric heat tracing can accurately provide the energy required for each application without the large additional energy use of a steam system. Unlike steam tracing systems, other parts of the system do not use significant amounts of energy.

Disadvantages of Electric Tracing

1. *Poor reputation.* In the past, electric tracing has been less than reliable. Due to past failures, some operating personnel are unwilling to take a chance on any electric tracing.

2. *Design requirements.* A slightly higher level of design expertise is required for electric tracing than for steam tracing.

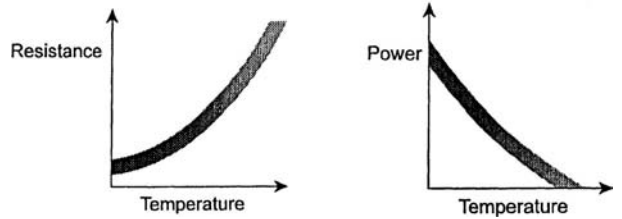


FIG. 10-185 Self-regulation.

3. *Lower power output.* Since electric tracing does not provide a large multiple of the required energy, it is less forgiving to problems such as damaged insulation or below design ambient temperatures. Most designers include a 10 to 20 percent safety factor in the heat loss calculation to cover these potential problems. Also, a somewhat higher than required design temperature is often specified to provide an additional safety margin. For example, many water systems are designed to maintain 50°F to prevent freezing.

Types of Electric Tracing *Self-regulating electric tracing* (see Fig. 10-184) is by far the most popular type of electric tracing. The heating element in a self-regulating heater is a conductive polymer between the bus wires. This conductive polymer increases its resistance as its temperature increases. The increase in resistance with temperature causes the heater to lower its heat output at any point where its temperature increases (Fig. 10-185). This self-regulating effect eliminates the most common failure mode of constant wattage electric heaters, which is destruction of the heater by its own heat output.

Because self-regulating heaters are parallel heaters, they may be cut to length at any point without changing their power output per unit of length. This makes them much easier to deal with in the field. They may be terminated, teed, or spliced in the field with hazardous-area-approved components.

MI Cables Mineral insulated cables (Fig. 10-186) are the electric heat tracers of choice for high-temperature applications. High-temperature applications are generally considered to maintain temperatures above 250°F or exposure temperatures above 420°F where self-regulating heaters cannot be used. MI cable consists of one or two heating wires, magnesium oxide insulation (from whence it gets its name), and an outer metal sheath. Today the metal sheath is generally inconel. This eliminates both the corrosion problems with copper sheaths and the stress cracking problems with stainless steel.

MI cables can maintain temperatures up to 1200°F and withstand exposure to up to 1500°F. The major disadvantage of MI cable is that it must be factory-fabricated to length. It is very difficult to terminate

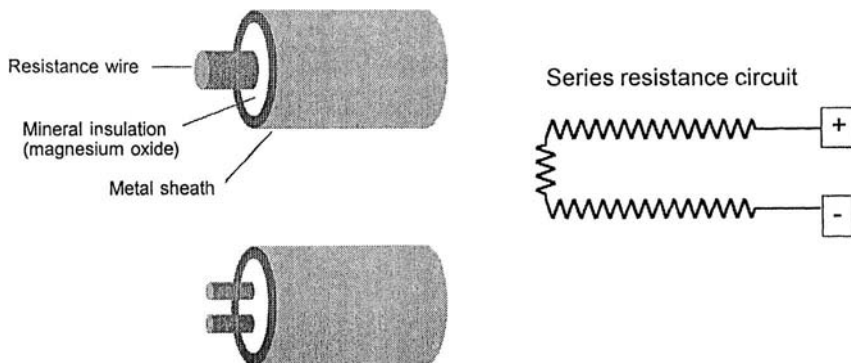


FIG. 10-186 Mineral insulated cable (MI cable).

or splice the heater in the field. This means pipe measurements are necessary before the heaters are ordered. Also, any damage to an MI cable generally requires a complete new heater. It's not as easy to splice in a good section as with self-regulating heaters.

Polymer-Insulated Constant Wattage Electric Heaters These are slightly cheaper than self-regulating heaters, but they are generally being replaced with self-regulating heaters due to inferior reliability. These heaters tend to destroy themselves with their own heat output when they are overlapped at valves or flanges. Since overlapping self-regulating heaters is the standard installation technique, it is difficult to prevent this technique from being used on the similar-looking constant-wattage heaters.

SECT (Skin-Effect Current Tracing) This is a special type of electric tracing employing a tracing pipe, usually welded to the pipe being traced, that is used for extremely long lines. With SECT tracing circuits, up to 10 miles can be powered from one power point. All SECT systems are specially designed by heat-tracing vendors.

Impedance Tracing This uses the pipe being traced to carry the current and generate the heat. Less than 1 percent of electric heat-tracing systems use this method. Low voltages and special electrical isolation techniques are used. Impedance heating is useful when extremely high heat densities are required, like when a pipe containing aluminum metal must be melted from room temperature on a regular basis. Most impedance systems are specially designed by heat tracing vendors.

Choosing the Best Tracing System Some applications require either steam tracing or electric tracing regardless of the relative economics. For example, a large line that is regularly allowed to cool and needs to be quickly heated would require steam tracing because of its much higher heat output capability. In most heat-up applications, steam tracing is used with heat-transfer cement, and the heat output is increased by a factor of up to 10. This is much more heat than would be

practical to provide with electric tracing. For example, a half-inch copper tube containing 50 psig steam with heat transfer cement would provide over 1100 Btu/hr/ft to a pipe at 50°F. This is over 300 watts per foot or more than 15 times the output of a high-powered electric tracer.

Table 10-57 shows that electric tracing has a large advantage in terms of cost at low temperatures and smaller but still significant advantages at higher temperatures. Steam tracing does relatively better at higher temperatures because steam tracing supplies significantly more power than is necessary to maintain a pipe at low temperatures. Table 10-57 indicates that there is very little difference between the steam tracing system at 50°F and the system at 250°F. However, the electric system more than doubles in cost between these two temperatures because more heaters, higher powered heaters, and higher temperature heaters are required.

The effect of supply lengths on a 150°F system can be seen from Table 10-58. Steam supply pipe is much more expensive to run than electrical conduit. With each system having relatively short supply lines (40 ft each) the electric system has only a small cost advantage (10 percent, or a ratio of 1.1). This ratio is 2.1 at 50°F and 0.8 at 250°F. However, as the supply lengths increase, electric tracing has a large cost advantage.

TABLE 10-58 Effect of Supply Lengths

Ratio of steam TIC to electric TIC maintained at 150°F

Steam supply length	Electric supply length		
	40 feet	100 feet	300 feet
40 feet	1.1	1.0	0.7
100 feet	1.9	1.7	1.1
300 feet	4.9	4.2	2.9

STORAGE AND PROCESS VESSELS

STORAGE OF LIQUIDS

Atmospheric Tanks The term *atmospheric tank* as used here applies to any tank that is designed to operate at pressures from atmospheric through 3.45 kPag (0.5 psig). It may be either open to the atmosphere or enclosed. Atmospheric tanks may be either shop-fabricated or field-erected. The most common application is storage of fuel for transportation and power generation. See the subsections "Pressure Tanks" and "Pressure Vessels" later in this section.

Shop-Fabricated Storage Tanks A shop-fabricated storage tank is a storage tank constructed at a tank manufacturer's plant and transported to a facility for installation. In general, tanks 190 m³ (50,000 gal) and under can be shop-fabricated and shipped in one piece to an installation site. Shop-fabricated storage tanks may be either underground storage tanks (USTs) or aboveground storage tanks (ASTs).

USTs versus ASTs For decades, USTs were the standard means of storing petroleum and chemicals in quantities of 190 m³ (50,000 gal) or less. However, during the 1990s, many industrial and commercial facilities shifted to ASTs for hazardous product storage. Reasons include the ability to visually monitor the storage tank as well as to avoid perceived risks and the myriad regulations surrounding underground storage tanks. Nonetheless, AST installations are also subject to certain regulations and codes, particularly fire codes.

The choice of utilizing USTs or ASTs is driven by numerous factors. Local authorities having jurisdiction may allow only underground storage. Total required storage capacity factored against available real estate may also preclude the use of ASTs. In addition, ASTs are subject to minimum distance separations from one another and from buildings, property lines, and public ways. ASTs are visually monitorable, yet that same attribute may be aesthetically undesirable. Other considerations are adequate protection against spills, vandal-

ism, and vehicular damage. Additionally, central design elements regarding product transfer and system functionality must be taken into account.

USTs are subject to myriad EPA regulations as well as fire codes. Further, a commonly cited drawback is the potential for unseen leaks and subsequent environmental damage and cleanup. However, advances in technology have addressed these concerns. Corrosion protection and leak detection are now standard in all UST systems. Sophisticated tank and pipe secondary containment systems have been developed to meet the EPA's secondary containment mandate for underground storage of nonpetroleum chemicals. Computerized in-tank monitoring devices for tracking inventory, evolutionary tank integrity testing equipment, statistical inventory reconciliation analysis, leak-free dry-disconnect pipe and hose joints for loading/unloading, and in-tank fill shutoff valves are just a few of the many pieces of equipment which have surfaced as marketplace solutions.

Properly designed and installed in accordance with industry standards, regulations, and codes, both UST and AST systems are reliable and safe. Because of space limitations and the prevalence of ASTs at plant sites, only ASTs will be discussed further.

Aboveground Storage Tanks Aboveground storage tanks are classified as either field-erected or shop-fabricated. The latter is typically 190-m³ (50,000-gal) capacity or less and is able to be shipped over the highway, while larger tanks are more economically erected in the field. Whereas field-erected tanks likely constitute the majority of total AST storage *capacity*, shop-fabricated ASTs constitute the clear majority of the total *number* of ASTs in existence today. Most of these shop-fabricated ASTs store flammable or combustible liquids at atmospheric pressure and have 45-m³ (12,000-gal) capacity or smaller.

Shop-fabricated ASTs can be designed and fabricated as pressure vessels, but are more typically vented to atmosphere. They are oriented

for either horizontal or vertical installation and are made in either cylindrical or rectangular form. Tanks are often secondarily contained and may also include insulation for fire safety or temperature control. Compartmented ASTs are also available. Over 90 percent of the atmospheric tank applications store some sort of hydrocarbon. Within that, a majority are used to store fuels for motor vehicle dispensing.

Fire Codes Many chemicals are classified as either flammable or combustible or subject to fire codes. All hydrocarbon tanks are classified as flammable or combustible. Notably, with the tremendous increase in the use of ASTs at private fleet fueling facilities in the 1990s, fire codes were rapidly modified to address the understandable safety concerns. In the United States, two principal organizations publish fire codes pertinent to underground storage tanks, with each state adopting all or part of the respective codes.

The **National Fire Protection Association (NFPA)** has developed several principal codes pertaining to the storage of flammable and combustible liquids:

NFPA 30, Flammable and Combustible Liquids Code (2003)

NFPA 30A, Code for Motor Fuel Dispensing Facilities and Repair Garages (2003)

NFPA 31, Standard for the Installation of Oil Burning Equipment

The **International Code Council (ICC)** was formed by the consolidation of three formerly separate fire code organizations: International Conference of Building Officials (ICBO), which had published the Uniform Fire Code under its fire service arm, the International Fire Code Institute (IFCI); Building Officials and Code Administrators (BOCA), which had published the National Fire Prevention Code; and Southern Building Congress Code International (SBCCI), which had published the Standard Fire Prevention Code. When the three groups merged in 2000, in part to develop a common fire code, the individual codes became obsolete; however, they are noted above since references to them may periodically surface. The consolidated code is **IFC-2006, International Fire Code**.

The **Canadian Commission on Building and Fire Codes (CCBFC)** developed a recommended model code to permit adoption by various regional authorities. The National Research Council of Canada publishes the model code document **National Fire Code of Canada (1995)**.

Standards Third-party standards for AST fabrication have evolved significantly over the past two decades, as have various recommended practice guidelines for the installation and operations of AST systems. Standards developed by Underwriters Laboratories (UL) have been perhaps the most predominant guidelines—in fact, ASTs are often categorized according to the UL standard that they meet, such as “a UL 142 tank.”

Underwriters Laboratories Inc. standards for steel ASTs storing flammable and combustible liquids include the following:

UL 142, Steel Aboveground Tanks for Flammable and Combustible Liquids, 9th ed., covers steel atmospheric tanks intended for aboveground storage of noncorrosive, stable, flammable, and combustible liquids that have a specific gravity not exceeding that of water. UL 142 applies to single-wall and double-wall horizontal carbon-steel and stainless steel tanks up to 190 m³ (50,000 gal), with a maximum diameter of 3.66 m (12 ft) and a maximum length-to-diameter ratio of 8 : 1. A formula from *Roark's Formulas for Stress and Strain* has been incorporated within UL 58 to calculate minimum steel wall thicknesses. UL 142 also applies to vertical tanks up to 10.7 m (35 ft) in height. UL 142 has been the primary AST standard since its development in 1922.

Tanks covered by these requirements can be fabricated in cylindrical or rectangular configurations. The standard covers secondary contained tanks, either of dual-wall construction or a tank in a steel dike or bund. It also provides listings for special AST constructions, such as those used under generators for backup power. These tanks are fabricated, inspected, and tested for leakage before shipment from the factory as completely assembled vessels.

UL 142 provides details for steel type, wall thickness, compartments and bulkheads, manways, and other fittings and appurtenances. Issues relating to leakage, venting, and the ability of the tank to with-

stand the development of internal pressures encountered during operation and production leak testing are also addressed.

These requirements do not apply to large field-erected storage tanks covered by the Standard for Welded Steel Tanks for Oil Storage, ANSI/API 650, or the Specification for Field-Welded Tanks for Storage of Production Liquids, API 12D; or to the Specification for Shop-Welded Tanks for Storage of Production Liquids, API 12F.

UL 2085, Protected Aboveground Tanks for Flammable and Combustible Liquids, covers shop-fabricated, aboveground atmospheric protected tanks intended for storage of stable, flammable or combustible liquids that have a specific gravity not greater than 1.0 and that are compatible with the material and construction of the tank.

The UL 2085 tank construction is intended to limit the heat transferred to the primary tank when the AST is exposed to a 2-h hydrocarbon pool fire of 1093°C (2000°F). The tank must be insulated to withstand the test without leakage and with an average maximum temperature rise on the primary tank not exceeding 127°C (260°F). Temperatures on the inside surface of the primary tank cannot exceed 204°C (400°F).

UL 2085 also provides criteria for resistance against vehicle impact, ballistic impact, and fire hose impact. These tanks are also provided with integral secondary containment intended to prevent any leakage from the primary tank from entering the environment.

UL 2080, Fire Resistant Tanks for Flammable and Combustible Liquids, is similar to UL 2085 tanks, except with an average maximum temperature rise on the primary tank limited to 427°C (800°F) during a 2-h pool fire. Temperatures on the inside surface of the primary tank cannot exceed 538°C (1000°F).

UL 2244, Standard for Aboveground Flammable Liquid Tank Systems, covers factory-fabricated, preengineered aboveground atmospheric tank systems intended for dispensing flammable or combustible liquids, such as gasoline or diesel fuel, into motor vehicles, generators, or aircraft.

UL 80, Steel Tanks for Oil-Burner Fuel, covers the design and construction of welded steel tanks of the atmospheric type with a maximum capacity of 0.23 to 2.5 m³ (60 to 660 gal) intended for unenclosed installation inside of buildings or for outside aboveground applications as permitted by the Standard for Installation of Oil-Burning Equipment, NFPA 31, primarily for the storage and supply of fuel oil for oil burners.

UL 2245, Below-Grade Vaults for Flammable Liquid Storage Tanks, covers below-grade vaults intended for the storage of flammable or combustible liquids in an aboveground atmospheric tank. Below-grade vaults, constructed of a minimum of 150 mm (6 in) of reinforced concrete or other equivalent noncombustible material, are designed to contain one aboveground tank, which can be a compartment tank. Adjacent vaults may share a common wall. The lid of the vault may be at grade or below. Vaults provide a safe means to install hazardous tanks so that the system is accessible to the operator without unduly exposing the public.

Southwest Research Institute (SwRI) standards for steel ASTs storing flammable and combustible liquids include the following:

SwRI 93-01, Testing Requirements for Protected Aboveground Flammable Liquid/Fuel Storage Tanks, includes tests to evaluate the performance of ASTs under fire, hose stream, ballistics, heavy vehicular impact, and different environments. This standard requires pool-fire resistance similar to that of UL 2085.

SwRI 97-04, Standard for Fire Resistant Tanks, includes tests to evaluate the performance of ASTs under fire and hose stream. This standard is similar to UL 2080 in that the construction is exposed to a 2-h hydrocarbon pool fire of 1093°C (2000°F). However, SwRI 97-04 is concerned only with the integrity of the tank after the 2-h test and not concerned with the temperature inside the tank due to the heat transfer. As a result, UL 142 tanks have been tested to the SwRI standard and passed. Secondary containment with insulation is not necessarily an integral component of the system.

Underwriters Laboratories of Canada (ULC) publishes a number of standards for aboveground tanks and accessories. All the following pertain to the aboveground storage of flammable liquids and combustible liquids such as gasoline, fuel oil, or similar products with a relative density not greater than 1.0:

ULC S601, Shop Fabricated Steel Aboveground Horizontal Tanks for Flammable and Combustible Liquids, covers single- and double-wall cylindrical horizontal steel nonpressure tanks. These requirements do not cover tanks of capacities greater than 200 m³.

ULC S630, Shop Fabricated Steel Aboveground Vertical Tanks for Flammable and Combustible Liquids, covers single- and double-wall cylindrical vertical steel nonpressure tanks.

ULC S643, Shop Fabricated Steel Utility Tanks for Flammable and Combustible Liquids, covers single- and double-wall cylindrical horizontal steel nonpressure tanks.

ULC S653-94, Aboveground Steel Contained Tank Assemblies for Flammable and Combustible Liquids, covers steel contained tank assemblies.

ULC S655, Aboveground Protected Tank Assemblies for Flammable and Combustible Liquids, covers shop-fabricated primary tanks that provided with secondary containment and protective encasement and are intended for stationary installation and use in accordance with

1. National Fire Code of Canada, Part 4
2. CAN/CSA-B139, Installation Code for Oil Burning Equipment
3. The Environmental Code of Practice for Aboveground Storage Tank Systems Containing Petroleum Products
4. The requirements of the authority having jurisdiction

ULC/ORD C142.20, Secondary Containment for Aboveground Flammable and Combustible Liquid Storage Tanks, covers secondary containments for aboveground primary tanks.

ULC S602, Aboveground Steel Tanks for the Storage of Combustible Liquids Intended to Be Used as Heating and/or Generator Fuels, covers the design and construction of tanks of the nonpressure type, intended for installation inside or outside buildings. This standard covers single-wall tanks and tanks with secondary containment, having a maximum capacity of 2.5 m³.

The **Petroleum Equipment Institute (PEI)** has developed a recommended practice for AST system installation: **PEI-RP200, RP 200, Recommended Practices for Installation of Aboveground Storage Systems for Motor Vehicle Fueling**.

The **American Petroleum Institute (API)** has developed a series of standards and specifications involving ASTs:

API 12F, Shop Welded Tanks for Storage of Production Liquids RP 12R1, Setting, Maintenance, Inspection, Operation, and Repair of Tanks in Production Service

RP 575, Inspection of Atmospheric and Low Pressure Storage Tanks

RP 579, Fitness-For-Service

API 650, Welded Steel Tanks for Oil Storage

API 652, Lining of Aboveground Storage Tank Bottoms

API 653, Tank Inspection, Repair, Alteration, and Reconstruction

API 2350, Overfill Protection for Storage Tanks in Petroleum Facilities (overfill is the primary cause of AST releases)

The **American Society of Mechanical Engineers (ASME)** has developed a standard for welded aluminum-alloy storage tanks: **B96.1, Welded Aluminum-Alloy Storage Tanks** (1999), covers the design, materials, fabrication, erection, inspection, and testing requirements for welded aluminum alloy (field-erected or shop-fabricated) aboveground, vertical, cylindrical, flat bottom, open or closed-top tanks storing liquids under pressures approximating atmospheric pressure at ambient temperatures.

The **American Water Works Association (AWWA)** has many standards dealing with water handling and storage. A list of its publications is given in the *AWWA Handbook* (annually). **AWWA D100, Standard for Steel Tanks—Standpipes, Reservoirs, and Elevated Tanks for Water Storage**, contains rules for design and fabrication. Although AWWA tanks are intended for water, they could be used for the storage of other liquids.

The **Steel Tank Institute (STI)** publishes construction standards and recommended installation practices pertaining to ASTs fabricated to STI technologies. STI's recommended installation practices are notable for their applicability to similar respective technologies:

SP001-06, Standard for Inspection of In-Service Shop Fabricated Aboveground Tanks for Storage of Combustible and Flammable Liquids

R912-00, Installation Instructions for Shop Fabricated Aboveground Storage Tanks for Flammable, Combustible Liquids

F921, Standard for Aboveground Tanks with Integral Secondary Containment

Standard for Fire Resistant Tanks (Flameshield)

Standard for Fireguard Thermally Insulated Aboveground Storage Tanks

F911, Standard for Diked Aboveground Storage Tanks

The **National Association of Corrosion Engineers (NACE International)** has developed the following to protect the soil side of bottoms of on-grade carbon-steel storage tanks: **NACE RP0193-01, Standard Recommended Practice—External Cathodic Protection of On-Grade Metallic Storage Tank Bottoms**.

Environmental Regulations A key **United States Environmental Protection Agency (US EPA)** requirement for certain aboveground storage facilities is the development and submittal of Spill Prevention Control and Countermeasure (SPCC) Plans within 40 CFR 112, the Oil Pollution Prevention regulation, which in turn is part of the Clean Water Act (CWA). SPCC Plans and Facility Response Plans pertain to facilities which may discharge oil into groundwater or storm runoff, which in turn may flow into navigable waters. Enacted in 1973, these requirements were principally used by owners of large, field-fabricated aboveground tanks predominant at that time, although the regulation applied to all bulk containers larger than 2.5 m³ (660 gal) and included the requirement for a Professional Engineer to certify the spill plan.

In July 2002, the US EPA issued a final rule amending 40 CFR 112 which included differentiation of shop-fabricated from field-fabricated ASTs. The rule also includes new subparts outlining the requirements for various classes of oil, revises the applicability of the regulation, amends the requirements for completing SPCC Plans, and makes other modifications.

The revised rule also states that all bulk storage container installations must provide a secondary means of containment for the entire capacity of the largest single container, with sufficient freeboard to contain precipitation, and that such containment is sufficiently impervious to contain discharged oil. US EPA encourages the use of industry standards to comply with the rules. Many owners of shop-fabricated tanks have opted for double-wall tanks built to STI or UL standards as a means to comply with this requirement.

State and Local Jurisdictions Due to the manner in which aboveground storage tank legislation was promulgated in 1972 for protection of surface waters from oil pollution, state environmental agencies did not receive similar jurisdiction as they did within the underground storage tank rules. Nonetheless, many state environmental agencies, state fire marshals, or Weights and Measures departments—including Minnesota, Florida, Wisconsin, Virginia, Oklahoma, Missouri, Maryland, Delaware, and Michigan—are presently regulating aboveground storage tanks through other means. Other regulations exist for hazardous chemicals and should be consulted for specific requirements.

Aboveground Storage Tank Types and Options Most hydrocarbon storage applications use carbon steel as the most economical and available material that provides suitable strength and compatibility for the specific storage application. For vertical tanks installed on grade, corrosion protection can be given to exterior tank bottoms in contact with soil. The interior of the tank can incorporate special coatings and linings (e.g., polymer, glass, or other metals). Some chemical storage applications will dictate that the storage tank be made from a stainless steel or nickel alloy. Fiberglass-reinforced plastic (FRP), polyethylene, or polypropylene may be used for nonflammable storage in smaller sizes. Suppliers can be contacted to verify the appropriate material to be used.

As stated earlier, shop-fabricated ASTs are often categorized according to the standards to which the tanks are fabricated, e.g., a UL 142 or UL 2085 tank. That said, however, there are defined categories such as diked tanks, protected tanks, fire-resistant tanks, and insulated tanks. It's critical, then, for the tank buyer or specifier to know precisely what is required or desired given the application, code requirements, and/or owner/operator preferences—and to discuss this with the tank contractor and/or manufacturer.

Cylindrical or rectangular tanks storing flammable and combustible liquids (UL 142 ASTs) will normally comply with UL 142. The Seventh Edition published in 1993 was particularly notable, as it incorporated secondary containment designs (diking or steel secondary containment tanks) and rectangular tank designs.

Rectangular tanks became a desirable option for small tanks, typically less than 7.6 m³ (2000 gal), as operators liked the accessibility of the flat top to perform operations and maintenance without the need for special ladders or catwalks.

Posttensioned concrete is frequently used for tanks to about 57,000 m³ (15 × 10⁶ gal), usually containing water. Their design is treated in detail by Creasy (*Prestressed Concrete Cylindrical Tanks*, Wiley, New York, 1961). For the most economical design of large open tanks at ground levels, he recommends limiting vertical height to 6 m (20 ft). Seepage can be a problem if unlined concrete is used with some liquids (e.g., gasoline).

Elevated tanks can supply a large flow when required, but pump capacities need be only for average flow. Thus, they may save on pump and piping investment. They also provide flow after pump failure, an important consideration for fire systems.

Open tanks may be used to store materials that will not be harmed by water, weather, or atmospheric pollution. Otherwise, a roof, either fixed or floating, is required. **Fixed roofs** are usually either domed or coned. Large tanks have coned roofs with intermediate supports. Since negligible pressure is involved, snow and wind are the principal design loads. Local building codes often give required values.

Fixed-roof atmospheric tanks require **vents** to prevent pressure changes which would otherwise result from temperature changes and withdrawal or addition of liquid. API Standard 2000, Venting Atmospheric and Low Pressure Storage Tanks, gives practical rules for conservative vent design. The principles of this standard can be applied to fluids other than petroleum products. Excessive losses of volatile liquids, particularly those with flash points below 38°C (100°F), may result from the use of open vents on fixed-roof tanks. Sometimes vents are manifolded and led to a vent tank, or the vapor may be extracted by a recovery system.

An effective way of preventing vent loss is to use one of the many types of **variable-volume tanks**. These are built under API Standard 650. They may have floating roofs of the double-deck or the single-deck type. There are lifter-roof types in which the roof either has a skirt moving up and down in an annular liquid seal or is connected to the tank shell by a flexible membrane. A fabric expansion chamber housed in a compartment on top of the tank roof also permits variation in volume.

Floating roofs must have a seal between the roof and the tank shell. If not protected by a fixed roof, they must have drains for the removal of water, and the tank shell must have a "wind girder" to avoid distortion. An industry has developed to retrofit existing tanks with floating roofs. Much detail on the various types of tank roofs is given in manufacturers' literature. Figure 10-187 shows types. These roofs cause less condensation buildup and are highly recommended.

Fire-Rated or Insulated ASTs: Protected and Fire-Resistant These ASTs have received much attention within the fire regulatory community, particularly for motor fuel storage and dispensing appli-

cations and generator base tanks. National model codes have been revised to allow this type of storage aboveground.

An insulated tank can be a protected tank, built to third-party standards UL 2085 and/or SwRI 93-01, or a fire-resistant tank built to UL 2080 or SwRI 97-04. Protected tanks were developed in line with NFPA requirements and terminology, while fire-resistant ASTs were developed in line with Uniform Fire Code (now International Fire Code) requirements and terminology. Both protected tanks and fire-resistant tanks must pass a 1093°C (2000°F), 2-h fire test.

The insulation properties of many fire-rated ASTs marketed today are typically provided by concrete; i.e., the primary steel tank is surrounded by concrete. Due to the weight of concrete, this design is normally limited to small tanks. Another popular AST technology meeting all applicable code requirements for insulated tanks and fabricated to UL 2085 is a tank that utilizes a lightweight monolithic thermal insulation in between two walls of steel to minimize heat transfer from the outer tank to the inner tank and to make tank handling more palatable.

A **secondary containment AST** to prevent contamination of our environment has become a necessity for all hazardous liquid storage, regardless of its chemical nature, in order to minimize liability and protect neighboring property. A number of different regulations exist, but the regulations with the greatest impact are fire codes and the US EPA SPCC rules for oil storage.

In 1991, the Spill Prevention Control and Countermeasure (SPCC) rule proposed a revision to require secondary containment that was impermeable for at least 72 h after a release occurred. The 2003 promulgated EPA SPCC rule no longer mandates a 72-h containment requirement, instead opting to require means to contain releases until they can be detected and removed. Nonetheless, the need for impermeable containment continues to position steel as a material of choice for shop-fabricated tanks. However, release prevention barriers made from plastic or concrete can also meet US EPA requirements when frequently inspected for releases.

Diked ASTs Fire codes dictate flammable and combustible liquid tanks have spill control in the form of dike, remote impounding, or small secondary containment tanks. The dike must contain the content of the largest tank to prevent hazardous liquids from endangering the public and property. Traditional bulk storage systems will include multiple tanks within a concrete or earthen dike wall.

From a shop-fabricated tank manufacturer's perspective, a diked AST generally refers to a steel tank within a factory-fabricated steel box, or dike. An example of a diked AST is the STI F911 standard, providing an open-topped steel rectangular dike and floor as support and secondary containment of a UL 142 steel tank. The dike will contain 110 percent of the tank capacity; as rainwater may already have collected in the dike, the additional 10 percent acts as freeboard should a catastrophic failure dump a full tank's contents into a dike. Many fabricators offer steel dikes with rain shields to prevent precipitation from collecting.

A **double-wall AST** of steel fulfills the same function as a diked AST with rain shield. Double-wall designs consist of a steel wrap over a horizontal or vertical steel storage tank. The steel wrap provides an intimate, secondary containment over the primary tank. One such design is the Steel Tank Institute's F921 standard, based upon

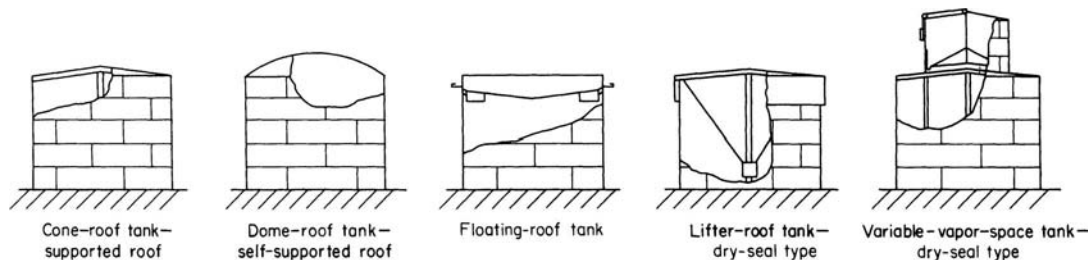


FIG. 10-187 Some types of atmospheric storage tanks.

UL 142-listed construction for the primary tank, outer containment, associated tank supports or skids.

Venting of ASTs is critical, since they are exposed to greater ambient temperature fluctuations than are USTs. Properly designed and sized venting, both normal (atmospheric) and emergency, is required. Normal vents permit the flow of air or inert gas into and out of the tank. The vent line must be large enough to accommodate the maximum filling or withdrawal rates without exceeding the allowable stress for the tank.

Fire codes' recommended installation procedures also detail specifics on pressure/vacuum venting devices and vent line flame arresters. For example, codes mandate different ventilation requirements for Class I-A liquids versus Class I-B or I-C liquids. Tank vent piping is generally not manifolded unless required for special purposes such as air pollution control or vapor recovery. As always, local codes must be consulted.

Emergency venting prevents an explosion during a fire or other emergency. All third-party laboratory standards except UL 80 include emergency relief provisions, since these tanks are designed for atmospheric pressure conditions.

Separation distances are also important. Aboveground storage tanks must be separated from buildings, property lines, fuel dispensers and delivery trucks in accordance with the level of safety the tank design provides, depending upon whether they are constructed of traditional steel or are vault/fire-resistant.

For most chemical storage tanks, codes such as NFPA 30 and the International Fire Code give specific separation distances. For motor vehicle fueling applications, the codes are more stringent on separation requirements due to a greater exposure of the public to the hazards. Hence codes such as NFPA 30A establish variable separation distances depending upon whether the facility is private or public.

Separation distance requirements may dictate whether a tank buyer purchases a traditional steel UL 142 tank, a fire-resistant tank, or a tank in a vault. For example, NFPA 30, NFPA 30A, and the IFC codes allow UL 2085 tanks to be installed closer to buildings and property lines, thereby reducing the real estate necessary to meet fire codes.

Under NFPA 30A, dispensers may be installed directly over vaults or upon fire-resistant tanks at fleet-type installations, whereas a 7.6- to 15.2-m (25- to 50-ft) separation distance is required at retail-type service station installations. The IFC only allows gasoline and diesel to be dispensed from ASTs, designed with a 2-h fire rating. Non-2-h fire-rated UL 142 tanks dispensing diesel can be installed upon approval of the local authority.

Maintenance and Operations Water in any storage system can cause myriad problems from product quality to system degradation due to corrosion from trace contaminants and microbial action. Subsequently, any operations and maintenance program must include a proactive program of monitoring for water—and removing it if found. Other operations and maintenance procedures would include periodic integrity testing and corrosion control for vertical tank bottoms. Additional guidance is available from organizations such as the American Petroleum Institute (API), Petroleum Equipment Institute (PEI), ASTM International, National Oilheat Research Alliance (NORA), and Steel Tank Institute (STI). Also see the Steel Tank Institute document *Keeping Water Out of Your Storage System* (<http://www.steel-tank.com/library/pubs/waterinfuel tanks.pdf>).

Integrity testing and visual inspection requirements are discussed in the SPCC requirements, Subpart B, Para. 112.8 c (6). Chemical tanks storing toluene and benzene, e.g., are subject to the rule in addition to traditional fuels. But the need for a good inspection program is recommended regardless of applicable regulations. Both visual inspection and another testing technique are required. Comparison records must be kept, and frequent inspections must be made of the outside of the tank and system components for signs of deterioration, discharges, or accumulation of oil inside diked areas.

For inspection of large field-erected tanks, API 653, *Tank Inspection, Repair, Alteration, and Reconstruction*, is referenced by the US EPA. A certified inspector must inspect tanks. US EPA references the Steel Tank Institute Standard SP001-06, *Standard for Inspection of In-Service Shop Fabricated Aboveground Tanks for Storage of Combustible and Flammable Liquids*, as an industry standard that may assist an owner or operator with the integrity testing and inspection of shop-fabricated tanks. The STI SP001-06 standard includes inspec-

tion techniques for all types of shop-fabricated tanks—horizontal cylindrical, vertical, and rectangular. SP001-06 also addresses tanks that rest directly on the ground or on release prevention barriers, tanks that are elevated on supports, and tanks that are either single- or double-wall using a risk-based approach.

Pressure Tanks Vertical cylindrical tanks constructed with domed or coned roofs, which operate at pressures above several hundred pascals (a few pounds per square foot) but which are still relatively close to atmospheric pressure, can be built according to API Standard 650. The pressure force acting against the roof is transmitted to the shell, which may have sufficient weight to resist it. If not, the uplift will act on the tank bottom. The strength of the bottom, however, is limited, and if it is not sufficient, an anchor ring or a heavy foundation must be used. In the larger sizes uplift forces limit this style of tank to very low pressures.

As the size or the pressure goes up, curvature on all surfaces becomes necessary. Tanks in this category, up to and including a pressure of 103.4 kPa (15 lbf/in²), can be built according to API Standard 620. Shapes used are spheres, ellipsoids, toroidal structures, and circular cylinders with torispherical, ellipsoidal, or hemispherical heads. The ASME Pressure Vessel Code (Sec. VIII of the ASME Boiler and Pressure Vessel Code), although not required below 103.4 kPa (15 lbf/in²), is also useful for designing such tanks.

Tanks that could be subjected to vacuum should be provided with vacuum-breaking valves or be designed for vacuum (external pressure). The ASME Pressure Vessel Code contains design procedures.

Calculation of Tank Volume A tank may be a single geometrical element, such as a cylinder, a sphere, or an ellipsoid. It may also have a compound form, such as a cylinder with hemispherical ends or a combination of a toroid and a sphere. To determine the volume, each geometrical element usually must be calculated separately. Calculations for a full tank are usually simple, but calculations for partially filled tanks may be complicated.

To calculate the volume of a **partially filled horizontal cylinder** refer to Fig. 10-188. Calculate the angle α in degrees. Any units of length can be used, but they must be the same for H , R , and L . The liquid volume

$$V = LR^2 \left(\frac{\alpha}{57.30} - \sin \alpha \cos \alpha \right) \quad (10-109)$$

This formula may be used for any depth of liquid between zero and the full tank, provided the algebraic signs are observed. If H is greater than R , $\sin \alpha \cos \alpha$ will be negative and thus will add numerically to $\alpha/57.30$. Table 10-59 gives liquid volume, for a partially filled horizontal cylinder, as a fraction of the total volume, for the dimensionless ratio H/D or $H/2R$.

The **volumes of heads** must be calculated separately and added to the volume of the cylindrical portion of the tank. The four types of heads most frequently used are the standard dished head,^o torispherical or ASME head, ellipsoidal head, and hemispherical head. Dimensions and volumes for all four of these types are given in *Lukens Spun*

^oThe standard dished head does not comply with the ASME Pressure Vessel Code.

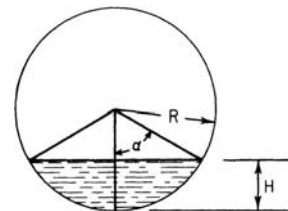


FIG. 10-188 Calculation of partially filled horizontal tanks. H = depth of liquid; R = radius; D = diameter; L = length; α = half of the included angle; and $\cos \alpha = 1 - H/R = 1 - 2H/D$.

TABLE 10-59 Volume of Partially Filled Horizontal Cylinders

H/D	Fraction of volume	H/D	Fraction of volume	H/D	Fraction of volume	H/D	Fraction of volume
0.01	0.00169	0.26	0.20660	0.51	0.51273	0.76	0.81545
.02	.00477	.27	.21784	.52	.52546	.77	.82625
.03	.00874	.28	.22921	.53	.53818	.78	.83688
.04	.01342	.29	.24070	.54	.55088	.79	.84734
.05	.01869	.30	.25231	.55	.56356	.80	.85762
.06	.02450	.31	.26348	.56	.57621	.81	.86771
.07	.03077	.32	.27587	.57	.58884	.82	.87760
.08	.03748	.33	.28779	.58	.60142	.83	.88727
.09	.04458	.34	.29981	.59	.61397	.84	.89673
.10	.05204	.35	.31192	.60	.62647	.85	.90594
.11	.05985	.36	.32410	.61	.63892	.86	.91491
.12	.06797	.37	.33636	.62	.65131	.87	.92361
.13	.07639	.38	.34869	.63	.66364	.88	.93203
.14	.08509	.39	.36108	.64	.67590	.89	.94015
.15	.09406	.40	.37353	.65	.68808	.90	.94796
.16	.10327	.41	.38603	.66	.70019	.91	.95542
.17	.11273	.42	.39858	.67	.71221	.92	.96252
.18	.12240	.43	.41116	.68	.72413	.93	.96923
.19	.13229	.44	.42379	.69	.73652	.94	.97550
.20	.14238	.45	.43644	.70	.74769	.95	.98131
.21	.15266	.46	.44912	.71	.75930	.96	.98658
.22	.16312	.47	.46182	.72	.77079	.97	.99126
.23	.17375	.48	.47454	.73	.78216	.98	.99523
.24	.18455	.49	.48727	.74	.79340	.99	.99831
.25	.19550	.50	.50000	.75	.80450	1.00	1.00000

Heads, Lukens Inc., Coatesville, Pennsylvania. Approximate volumes can also be calculated by the formulas in Table 10-60. Consistent units must be used in these formulas.

A partially filled horizontal tank requires the determination of the partial volume of the heads. The Lukens catalog gives approximate volumes for partially filled (axis horizontal) standard ASME and ellipsoidal heads. A formula for **partially filled heads** (excluding conical), by Doolittle [*Ind. Eng. Chem.*, **21**, 322-323 (1928)], is

$$V = 0.215H^2(3R - H) \tag{10-110}$$

where in consistent units V = volume, R = radius, and H = depth of liquid. Doolittle made some simplifying assumptions which affect the

volume given by the equation, but the equation is satisfactory for determining the volume as a fraction of the entire head. This fraction, calculated by Doolittle's formula, is given in Table 10-61 as a function of H/D_i (H is the depth of liquid, and D_i is the inside diameter). Table 10-61 can be used for standard dished, torispherical, ellipsoidal, and hemispherical heads with an error of less than 2 percent of the volume of the entire head. The error is zero when $H/D_i = 0, 0.5,$ and 1.0 . Table 10-61 cannot be used for conical heads.

When a tank volume cannot be calculated or when greater precision is required, **calibration** may be necessary. This is done by draining (or filling) the tank and measuring the volume of liquid. The measurement may be made by weighing, by a calibrated fluid meter, or by repeatedly filling small measuring tanks which have been calibrated by weight.

Container Materials and Safety Storage tanks are made of almost any structural material. Steel and reinforced concrete are most widely used. Plastics and glass-reinforced plastics are used for tanks up to about 230 m³ (60,000 gal). Resistance to corrosion, light weight, and lower cost are their advantages. Plastic and glass coatings are also applied to steel tanks. Aluminum and other nonferrous metals are used when their special properties are required. When expensive metals such as tantalum are required, they may be applied as tank linings or as clad metals.

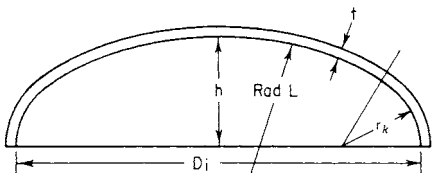
Some grades of steel listed by API and AWWA Standards are of lower quality than is customarily used for pressure vessels. The stresses allowed by these standards are also higher than those allowed by the ASME Pressure Vessel Code. Small tanks containing nontoxic substances are not particularly hazardous and can tolerate a reduced factor of safety. Tanks containing highly toxic substances and very large tanks containing any substance can be hazardous. The designer must consider the magnitude of the hazard. The possibility of brittle behavior of ferrous metal should be taken into account in specifying materials (see subsection "Safety in Design").

Volume 1 of National Fire Codes (National Fire Protection Association, Quincy, Massachusetts) contains recommendations (Code 30) for venting, drainage, and dike construction of tanks for **flammable liquids**.

Container Insulation Tanks containing materials above atmospheric temperature may require insulation to reduce loss of heat. Almost any of the commonly used insulating materials can be employed. Calcium silicate, glass fiber, mineral wool, cellular glass, and plastic foams are among those used. Tanks exposed to weather must have jackets or protective coatings, usually asphalt, to keep water out of the insulation.

Tanks with contents at lower than atmospheric temperature may require insulation to minimize heat absorption. The insulation must have

TABLE 10-60 Volumes of Heads*



Type of head	Knuckle radius, r_k	h	L	Volume	% Error	Remarks
Standard dished	Approx. $3t$		Approx. D_i	Approx. $0.050D_i^3 + 1.65tD_i^2$	± 10	h varies with t
Torispherical or A.S.M.E.	$0.06L$		D_i	$0.0809D_i^3$	± 0.1 ± 8	r_k must be the larger of $0.06L$ and $3t$
Torispherical or A.S.M.E.	$3t$		D_i	Approx. $0.513hD_i^2$		
Ellipsoidal		$D_i/4$		$\pi D_i^2 h/6$	0	Standard proportions
Ellipsoidal		$D_i/2$		$\pi D_i^3/24$	0	
Hemispherical			$D_i/2$	$\pi D_i^3/12$	0	
Conical				$\pi h(D_i^2 + D_i d + d^2)/12$	0	Truncated cone h = height d = diameter at small end

*Use consistent units.

TABLE 10-61 Volume of Partially Filled Heads on Horizontal Tanks*

H/D _i	Fraction of volume	H/D _i	Fraction of volume	H/D _i	Fraction of volume	H/D _i	Fraction of volume
0.02	0.0012	0.28	0.1913	0.52	0.530	0.78	0.8761
.04	.0047	.30	.216	.54	.560	.80	.8960
.06	.0104	.32	.242	.56	.590	.82	.9145
.08	.0182	.34	.268	.58	.619	.84	.9314
.10	.0280	.36	.295	.60	.648	.86	.9467
.12	.0397	.38	.323	.62	.677	.88	.9603
.14	.0533	.40	.352	.64	.705	.90	.9720
.16	.0686	.42	.381	.66	.732	.92	.9818
.18	.0855	.44	.410	.68	.758	.94	.9896
.20	.1040	.46	.440	.70	.784	.96	.9953
.22	.1239	.48	.470	.72	.8087	.98	.9988
.24	.1451	.50	.500	.74	.8324	1.00	1.0000
.26	.1676			.76	.8549		

*Based on Eq. (10-110).

a vapor barrier at the outside to prevent condensation of atmospheric moisture from reducing its effectiveness. An insulation not damaged by moisture is preferable. The insulation techniques presently used for refrigerated systems can be applied (see subsection "Low-Temperature and Cryogenic Storage").

Tank Supports Large vertical atmospheric steel tanks may be built on a base of about 150 cm (6 in) of sand, gravel, or crushed stone if the subsoil has adequate bearing strength. It can be level or slightly coned, depending on the shape of the tank bottom. The porous base provides drainage in case of leaks. A few feet beyond the tank perimeter the surface should drop about 1 m (3 ft) to assure proper drainage of the subsoil. API Standard 650, Appendix B, and API Standard 620, Appendix C, give recommendations for tank foundations.

The bearing pressure of the tank and contents must not exceed the **bearing strength** of the soil. Local building codes usually specify allowable soil loading. Some approximate bearing values are:

	kPa	Tons/ft ²
Soft clay (can be crumbled between fingers)	100	1
Dry fine sand	200	2
Dry fine sand with clay	300	3
Coarse sand	300	3
Dry hard clay (requires a pick to dig it)	350	3.5
Gravel	400	4
Rock	1000-4000	10-40

For high, heavy tanks, a foundation ring may be needed. Prestressed concrete tanks are sufficiently heavy to require foundation rings. Foundations must extend below the frost line. Some tanks that are not flat-bottomed may also be supported by soil if it is suitably graded and drained. When soil does not have adequate bearing strength, it may be excavated and backfilled with a suitable soil, or piles capped with a concrete mat may be required.

Spheres, spheroids, and toroids use steel or concrete saddles or are supported by columns. Some may rest directly on soil. Horizontal cylindrical tanks should have two rather than multiple saddles to avoid indeterminate load distribution. Small horizontal tanks are sometimes supported by legs. Most tanks must be designed to resist the reactions of the saddles or legs, and they may require reinforcing. Neglect of this can cause collapse. Tanks without stiffeners usually need to make contact with the saddles on at least 2.1 rad (120°) of their circumference. An elevated steel tank may have either a circle of steel columns or a large central steel standpipe. Concrete tanks usually have concrete columns. Tanks are often supported by buildings.

Pond and Underground Storage Low-cost liquid materials, if they will not be damaged by rain or atmospheric pollution, may be stored in **ponds**. A pond may be excavated or formed by damming a ravine. To prevent loss by seepage, the soil which will be submerged may require

treatment to make it sufficiently impervious. This can also be accomplished by lining the pond with concrete, plastic film, or some other barrier. Prevention of seepage is especially necessary if the pond contains material that could contaminate present or future water supplies.

Underground Cavern Storage Large volumes of liquids are often stored below ground in artificial caverns as an economical alternative to aboveground tanks and other modes of storage. The liquid to be stored must tolerate water, brine, and other contaminants that are usually present to some degree in the cavern. The liquids that are most commonly stored are natural gas liquids (NGLs), LPGs, crude oil, and refined petroleum products. If the liquid is suitable for cavern storage, this method may be less expensive, safer, and more secure than other storage modes.

There are two types of caverns used for storing liquids. *Hard rock (mined)* caverns are constructed by mining rock formations such as shale, granite, limestone, and many other types of rock. *Solution-mined* caverns are constructed by dissolution processes, i.e., solution mining or leaching a mineral deposit, most often salt (sodium chloride). The salt deposit may take the form of a massive salt dome or thinner layers of bedded salt that are stratified between layers of rock. Hard rock and solution-mined caverns have been constructed in the United States and many other parts of the world.

Mined Caverns Caverns mined in hard rock are generally situated 100 to 150 m (325 to 500 ft) below ground level. These caverns are constructed by excavating rock with conventional drill-and-blast mining methods. The excavated cavern consists of a grouping of interconnecting tunnels or storage "galleries." Mined caverns have been constructed for volumes ranging from as little as 3200 to 800,000 m³ [20,000 API barrels° (bbl) to 5 million bbl]. Figure 10-189 illustrates a typical mined cavern for liquid storage.

Hard rock caverns are designed so that the internal storage pressure is at all times less than the hydrostatic head of the water contained in the surrounding rock matrix. Thus, the depth of a cavern determines its maximum allowable operating pressure. Groundwater that continuously seeps into hard rock caverns in permeable formations is periodically pumped out of the cavern. The maximum operating pressure of the cavern is established after a thorough geological and hydrogeological evaluation is made of the rock formation and the completed cavern is pressure-tested.

Salt Caverns Salt caverns are constructed in both *domal salt*, more commonly referred to as "salt domes," and *bedded salt*, which consists of a body of salt sandwiched between layers of rock. The greatest total volume of underground liquid storage in the United States is stored in salt dome caverns. A salt dome is a large body, mostly consisting of sodium chloride, which over geologic time moved upward thousands of feet from extensive halite deposits deep below the earth's crust. There are numerous salt domes in the United States and other parts of the world [see Harben, P. W., and R. L. Bates, "Industrial Minerals Geology and World Deposits," *Metal Bulletin Plc*, UK, pp. 229-234 (1990)]. An individual salt dome may exceed 1 mi in diameter and contain many storage caverns. The depth to the top of a salt dome may range from a few hundred to several thousand feet, although depths to about 1070 m (3500 ft) are commercially viable for cavern development. The extent of many salt domes allows for caverns of many different sizes and depths to be developed. The extensive nature of salt domes has allowed the development of caverns as large as 5.7 × 10⁶ m³ (36 million bbl) (US DOE Bryan Mound Strategic Petroleum Reserve) and larger; however, cavern volumes of 159,000 to 1.59 × 10⁶ m³ (1 to 10 million bbl) are more common for liquid storage.

The benefits of salt are its high compressive strength of 13.8 to 27.6 MPa (2000 to 4000 psi), its impermeability to hydrocarbon liquids and gases, and its non-chemically reactive (inert) nature. Due to the impervious nature of salt, the maximum allowed storage pressure gradient in this type of cavern is greater than that of a mined cavern. A typical storage pressure gradient for liquids is about 18 kPa/m of depth (0.80 psi/ft) to the bottom of the well casing. Actual maximum and minimum allowable operating pressure gradients are determined from geologic evaluations and rock mechanics studies. Typical depths to the top of a salt cavern may range from 500 to 4000 ft (about 150 to 1200 m).

°One API barrel = 42 US gal = 5.615 ft³ = 0.159 m³.

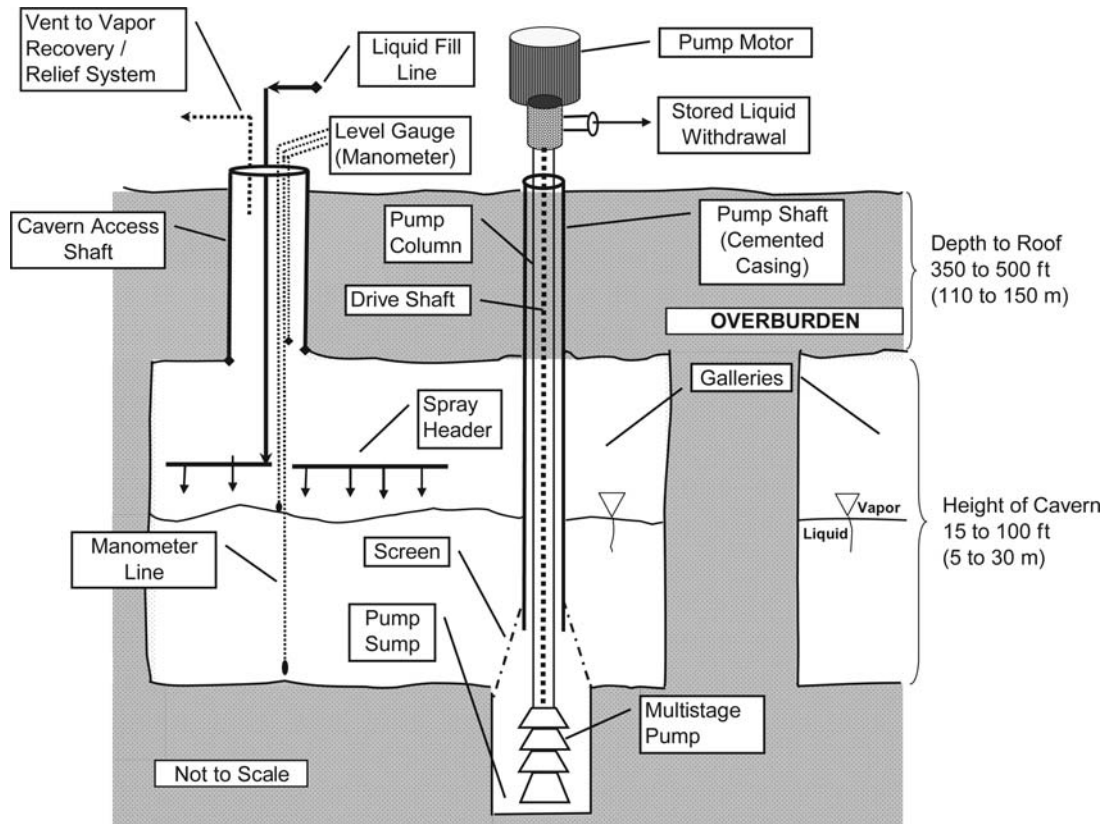


FIG. 10-189 Mined cavern.

Therefore, the maximum storage pressure (2760 to 32,060 kPag, or 400 to 3200 psig) usually exceeds the vapor pressure of all commonly stored hydrocarbon liquids. Higher-vapor-pressure products such as ethylene or ethane cannot be stored in relatively shallow caverns.

Salt caverns are developed by solution mining, a process (leaching) in which water is injected to dissolve the salt. Approximately 7 to 10 units of fresh water are required to leach 1 unit of cavern volume. Figure 10-190 illustrates the leaching process for two caverns. Modern salt dome caverns are shaped as relatively tall, slender cylinders. The leaching process produces nearly saturated brine from the cavern. Brine may be disposed into nearby disposal wells or offshore disposal fields, or it may be supplied to nearby plants as a feedstock for manufacturing of caustic (NaOH) and chlorine (Cl₂). The final portion of the produced brine is retained and stored in artificial surface ponds or tanks to be used to displace the stored liquid from the cavern.

Salt caverns are usually developed using a single well, although some employ two or more wells. The well consists of a series of concentric casings that protect the water table and layers of rock and sediments (overburden) that lie above the salt dome. The innermost well casing is referred to as the last cemented or well "production" casing and is cemented in place, sealing the cavern and protecting the surrounding geology. Once the last cemented casing is in place, a borehole is drilled from the bottom of the well, through the salt to the design cavern depth. For single-well leaching, two concentric tubing strings are then suspended in the well. A liquid, such as diesel, or a gas is then injected through the outer annular space and into the top of the cavern to act as a "blanket" to prevent undesired leaching of the top of the cavern. Water is then injected into one of the suspended tubing strings, and brine is withdrawn from the other. During the leaching process, the flow path for the injected water is alternated between the innermost

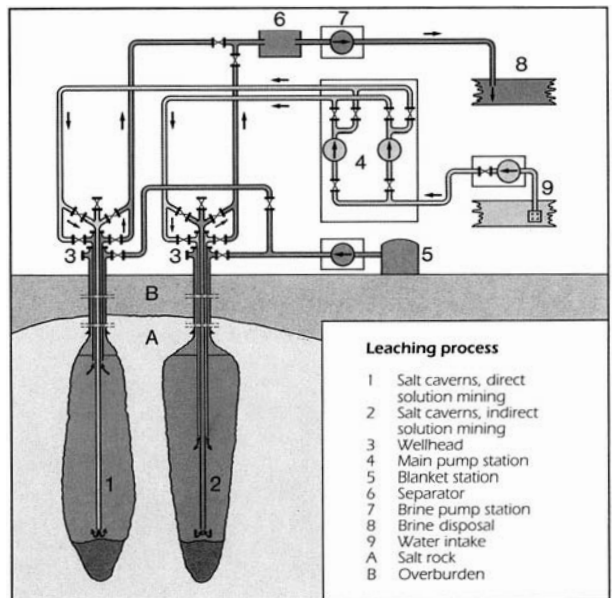


FIG. 10-190 Cavern leaching process.

tubing and the inner annulus, and these strings are periodically raised upward to control the cavern shape. A typical salt dome cavern may require 18 to 30 months of leaching time, whereas smaller, bedded salt caverns may be developed in a shorter time frame.

Brine-Compensated Storage As the stored product is pumped into the cavern, brine is displaced into an aboveground brine storage reservoir. To withdraw the product from the cavern, brine is pumped back into the cavern, displacing the stored liquid. This method of product transfer is termed *brine-compensated*, and caverns that operate in this fashion remain liquid-filled at all times. Figure 10-191 illustrates brine-compensated storage operations.

Uncompensated Storage Hard rock caverns and a few bedded salt caverns do not use brine for product displacement. This type of storage operation is referred to as pumpout or *uncompensated* storage operations. When the cavern is partially empty of liquid, the void space is filled with the vapor that is in equilibrium with the stored liquid. When liquid is introduced into the cavern, it compresses and condenses this saturated vapor phase. In some cases, vapor may be vented to the surface where it may be refrigerated and recycled to the cavern.

Submersible pumps or vertical line shaft pumps are used for withdrawing the stored liquid. Vertical line shaft pumps are suited for depths of no more than several hundred feet. Figure 10-189 illustrates an example of uncompensated storage operations.

Water is also stored underground when suitable formations are available. When an excess of surface water is available part of the time, the excess is treated, if required, and pumped into the ground to be retrieved when needed. Sometimes pumping is unnecessary, and it will seep into the ground.

Underground chambers are also constructed in frozen earth (see subsection "Low-Temperature and Cryogenic Storage"). Underground tunnel or tank storage is often the most practical way of storing hazardous or radioactive materials, such as proposed at Yucca Mountain, Nevada. A cover of 30 m (100 ft) of rock or dense earth can exert a pressure of about 690 kPa (100 lbf/in²).

STORAGE OF GASES

Gas Holders Gas is sometimes stored in expandable gas holders of either the liquid-seal or dry-seal type. The liquid-seal holder is a familiar sight. It has a cylindrical container, closed at the top, and

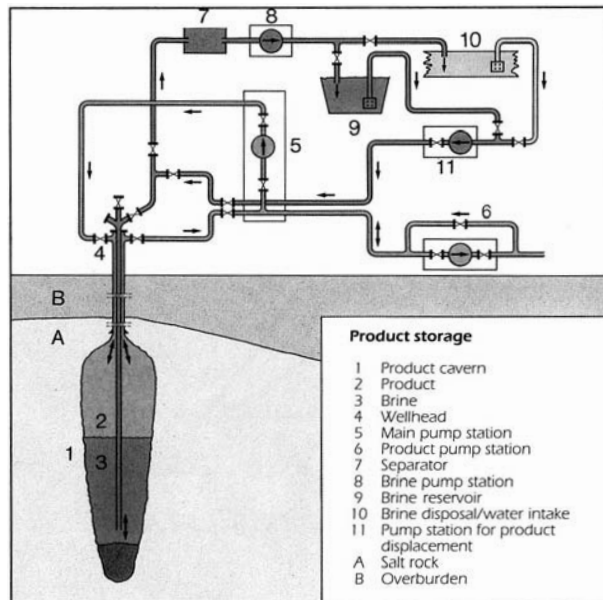


FIG. 10-191 Brine-compensated storage.

varies its volume by moving it up and down in an annular water-filled seal tank. The seal tank may be staged in several lifts (as many as five). Seal tanks have been built in sizes up to 280,000 m³ (10 × 10⁶ ft³). The dry-seal holder has a rigid top attached to the sidewalls by a flexible fabric diaphragm which permits it to move up and down. It does not involve the weight and foundation costs of the liquid-seal holder. Additional information on gas holders can be found in *Gas Engineers Handbook*, Industrial Press, New York, 1966.

Solution of Gases in Liquids Certain gases will dissolve readily in liquids. In some cases in which the quantities are not large, this may be a practical storage procedure. Examples of gases that can be handled in this way are ammonia in water, acetylene in acetone, and hydrogen chloride in water. Whether or not this method is used depends mainly on whether the end use requires the anhydrous or the liquid state. Pressure may be either atmospheric or elevated. The solution of acetylene in acetone is also a safety feature because of the instability of acetylene.

Storage in Pressure Vessels, Bottles, and Pipe Lines The distinction between pressure vessels, bottles, and pipes is arbitrary. They can all be used for storing gases under pressure. A storage pressure vessel is usually a permanent installation. Storing a gas under pressure not only reduces its volume but also in many cases liquefies it at ambient temperature. Some gases in this category are carbon dioxide, several petroleum gases, chlorine, ammonia, sulfur dioxide, and some types of Freon. Pressure tanks are frequently installed underground.

Liquefied petroleum gas (LPG) is the subject of API Standard 2510, The Design and Construction of Liquefied Petroleum Gas Installations at Marine and Pipeline Terminals, Natural Gas Processing Plants, Refineries, and Tank Farms. This standard in turn refers to:

1. National Fire Protection Association (NFPA) Standard 58, Standard for the Storage and Handling of Liquefied Petroleum Gases
2. NFPA Standard 59, Standard for the Storage and Handling of Liquefied Petroleum Gases at Utility Gas Plants
3. NFPA Standard 59A, Standard for the Production, Storage, and Handling of Liquefied Natural Gas (LNG)

The API Standard gives considerable information on the construction and safety features of such installations. It also recommends minimum distances from property lines. The user may wish to obtain added safety by increasing these distances.

The term **bottle** is usually applied to a pressure vessel that is small enough to be conveniently portable. Bottles range from about 57 L (2 ft³) down to CO₂ capsules of about 16.4 mL (1 in³). Bottles are convenient for small quantities of many gases, including air, hydrogen, nitrogen, oxygen, argon, acetylene, Freon, and petroleum gas. Some are one-time-use disposable containers.

Pipe Lines A pipe line is not ordinarily a storage device. Pipes, however, have been buried in a series of connected parallel lines and used for storage. This avoids the necessity of providing foundations, and the earth protects the pipe from extremes of temperature. The economics of such an installation would be doubtful if it were designed to the same stresses as a pressure vessel. Storage is also obtained by increasing the pressure in operating pipe lines and thus using the pipe volume as a tank.

Low-Temperature and Cryogenic Storage This type is used for gases that liquefy under pressure at atmospheric temperature. In cryogenic storage the gas is at, or near to, atmospheric pressure and remains liquid because of low temperature. A system may also operate with a combination of pressure and reduced temperature. The term "cryogenic" usually refers to temperatures below -101°C (-150°F). Some gases, however, liquefy between -101°C and ambient temperatures. The principle is the same, but cryogenic temperatures create different problems with insulation and construction materials.

The liquefied gas must be maintained at or below its boiling point. Refrigeration can be used, but the usual practice is to cool by evaporation. The quantity of liquid evaporated is minimized by insulation. The vapor may be vented to the atmosphere (wasteful), it may be compressed and reliquefied, or it may be used.

At very low temperatures with liquid air and similar substances, the tank may have double walls with the interspace evacuated. The well-known Dewar flask is an example. Large tanks and even pipe

lines are now built this way. An alternative is to use double walls without vacuum but with an insulating material in the interspace. Perlite and plastic foams are two insulating materials employed in this way. Sometimes both insulation and vacuum are used.

Materials Materials for liquefied-gas containers must be suitable for the temperatures, and they must not be brittle. Some carbon steels can be used down to -59°C (-75°F), and low-alloy steels to -101°C (-150°F) and sometimes -129°C (-200°F). Below these temperatures austenitic stainless steel (AISI 300 series) and aluminum are the principal materials. (See discussion of brittle fracture on p.10-160.)

Low temperatures involve problems of **differential thermal expansion**. With the outer wall at ambient temperature and the inner wall at the liquid boiling point, relative movement must be accommodated. Some systems for accomplishing this are patented. The Gaz Transport of France reduces dimensional change by using a thin inner liner of Invar. Another patented French system accommodates this change by means of the flexibility of thin metal which is creased. The creases run in two directions, and the form of the crossings of the creases is a feature of the system.

Low-temperature tanks may be installed underground to take advantage of the insulating value of the earth. Frozen-earth storage is also used. The frozen earth forms the tank. Some installations using this technique have been unsuccessful because of excessive heat absorption.

Cavern Storage Gases are also stored below ground in salt caverns. The most common type of gas stored in caverns is natural gas, although hydrogen and air have also been stored. Hydrogen storage requires special consideration in selecting metallurgy for the wellhead and the tubular goods. Air is stored for the purpose of providing compressed air energy for peak shaving power plants. Two such plants are in operation, one in the United States (Alabama), the other in Germany. A discussion of the Alabama plant is presented in *History of First U.S. Compressed Air Energy Storage (CAES) Plant (110-MW-26 h)*, vol. 1, *Early CAES Development*, Electric Power Research Institute (EPRI), Palo Alto, Calif. (1992).

Since salt caverns contain brine and other contaminants, the type of gas to be stored should not be sensitive to the presence of contaminants. If the gas is determined suitable for cavern storage, then cavern storage may not offer only economic benefits and enhanced safety and security; salt caverns also offer relatively high rates of deliverability compared to reservoir and aquifer storage fields. Solution-mined gas storage caverns in salt formations operate as *uncompensated* storage—no fluid is injected into the well to displace the compressed gas.

Surface gas handling facilities for storage caverns typically include receipt and delivery measurement stations, gas compressors, and gas processing equipment. When compressors are required for cavern injection and/or withdrawal, banks of positive-displacement-type compressors are used, since this compressor type is well suited for handling the highly variable compression ratios and flow rates associated with cavern injection and withdrawal operations. Cavern withdrawal operations typically involve single or multiple pressure reduction stations and full or partial gas dehydration. Large pressure throttling requirements often require heating the gas upon withdrawal, and injection of methanol to help control hydrate formation is also often necessary.

An in-depth discussion on natural gas storage in underground caverns may be found in *Gas Engineering and Operating Practices, Supply*, Book S-1, Part 1, *Underground Storage of Natural Gas*, and Part 2, Chapter 2, "Leached Caverns," American Gas Association, Arlington, Va. (1990).

Additional References API Recommended Practice 1114, *Design of Solution-Mined Underground Storage Facilities*, 1st ed., Washington, June, 1994. API 1115, *Operation of Solution-Mined Underground Storage Facilities*, 1st ed., Washington, September 1994. LeFond, Stanley J., *Handbook of World Salt Resources, Monographs in Geoscience*, Department of Geology, Columbia University, New York, 1969. *SME Mining Engineering Handbook*, 2d ed., vol. 2, 1992.

COST OF STORAGE FACILITIES

Contractors' bids offer the most reliable information on cost. Order-of-magnitude costs, however, may be required for preliminary studies. One way of estimating them is to obtain cost information from similar

facilities and scale it to the proposed installation. Costs of steel storage tanks and vessels have been found to vary approximately as the 0.6 to 0.7 power of their weight [see Happel, *Chemical Process Economics*, Wiley, 1958, p. 267; also Williams, *Chem. Eng.*, **54**(12), 124 (1947)]. All estimates based on the costs of existing equipment must be corrected for changes in the price index from the date when the equipment was built. Considerable uncertainty is involved in adjusting data more than a few years old.

Based on a survey in 1994 for storage tanks, the prices for field-erected tanks are for multiple-tank installations erected by the contractor on foundations provided by the owner. Some cost information on tanks is given in various references cited in Sec. 9. Cost data vary considerably from one reference to another.

Prestressed (posttensioned) concrete tanks cost about 20 percent more than steel tanks of the same capacity. Once installed, however, concrete tanks require very little maintenance. A true comparison with steel would, therefore, require evaluating the maintenance cost of both types.

BULK TRANSPORT OF FLUIDS

Transportation is often an important part of product cost. Bulk transportation may provide significant savings. When there is a choice between two or more forms of transportation, the competition may result in rate reduction. Transportation is subject to considerable regulation, which will be discussed in some detail under specific headings.

Pipe Lines For quantities of fluid which an economic investigation indicates are sufficiently large and continuous to justify the investment, pipe lines are one of the lowest-cost means of transportation. They have been built up to 1.22 m (48 in) or more in diameter and about 3200 km (2000 mi) in length for oil, gas, and other products. Water is usually not transported more than 160 to 320 km (100 to 200 miles), but the conduits may be much greater than 1.22 m (48 in) in diameter. Open canals are also used for water transportation.

Petroleum pipe lines before 1969 were built to ASA (now ANSI) Standard B31.4 for liquids and Standard B31.8 for gas. These standards were seldom mandatory because few states adopted them. The U.S. Department of Transportation (DOT), which now has responsibility for pipe-line regulation, issued Title 49, Part 192—Transportation of Natural Gas and Other Gas by Pipeline: Minimum Safety Standards, and Part 195—Transportation of Liquids by Pipeline. These contain considerable material from B31.4 and B31.8. They allow generally higher stresses than the ASME Pressure Vessel Code would allow for steels of comparable strength. The enforcement of their regulations is presently left to the states and is therefore somewhat uncertain.

Pipe-line pumping stations usually range from 16 to 160 km (10 to 100 miles) apart, with maximum pressures up to 6900 kPa (1000 lb/in^2) and velocities up to 3 m/s (10 ft/s) for liquid. Gas pipe lines have higher velocities and may have greater spacing of stations.

Tanks Tank cars (single and multiple tank), tank trucks, portable tanks, drums, barrels, carboys, and cans are used to transport fluids (see Figs. 10-192 to 10-194). Interstate transportation is regulated by the DOT. There are other regulating agencies—state, local, and private. Railroads make rules determining what they will accept, some states require compliance with DOT specifications on intrastate movements, and tunnel authorities as well as fire chiefs apply restrictions. Water shipments involve regulations of the U.S. Coast Guard. The American Bureau of Shipping sets rules for design and construction which are recognized by insurance underwriters.

The most pertinent **DOT regulations** (*Code of Federal Regulations*, Title 49, Parts 171–179 and 397) were published by R. M. Graziano (then agent and attorney for carriers and freight forwarders) in his tariff titled *Hazardous Materials Regulations of the Department of Transportation* (1978). New tariffs identified by number are issued at intervals, and interim revisions are sent out. Agents change at intervals.

Graziano's tariff lists many regulated (dangerous) commodities (Part 172, DOT regulations) for transportation. This includes those that are poisonous, flammable, oxidizing, corrosive, explosive, radioactive, and compressed gases. Part 178 covers specifications for

10-150 TRANSPORT AND STORAGE OF FLUIDS

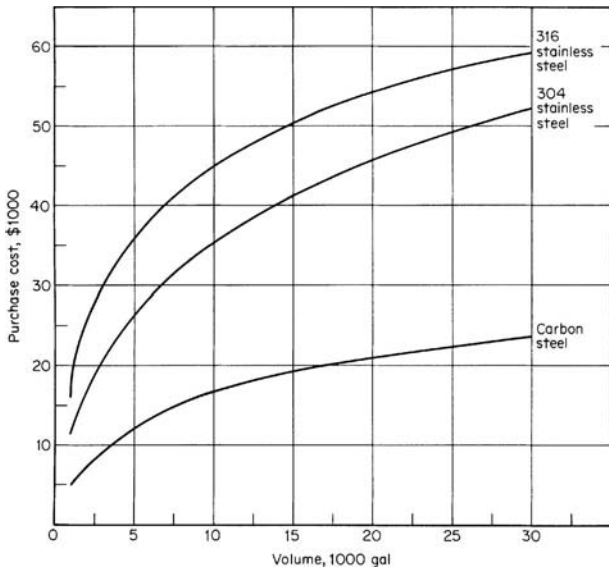


FIG. 10-192 Cost of shop-fabricated tanks in mid-1980 with 1/4-in walls. Multiplying factors on carbon steel costs for other materials are: carbon steel, 1.0; rubber-lined carbon steel, 1.5; aluminum, 1.6; glass-lined carbon steel, 4.5; and fiber-reinforced plastic, 0.75 to 1.5. Multiplying factors on type 316 stainless-steel costs for other materials are: 316 stainless steel, 1.0; Monel, 2.0; Inconel, 2.0; nickel, 2.0; titanium, 3.2; and Hastelloy C, 3.8. Multiplying factors for wall thicknesses different from 1/4 in are:

Thickness, in	Carbon steel	304 stainless steel	316 stainless steel
1/2	1.4	1.8	1.8
3/4	2.1	2.5	2.6
1	2.7	3.3	3.5

To convert gallons to cubic meters, multiply by 3.785×10^{-3} .

all types of containers from carboys to large portable tanks and tank trucks. Part 179 deals with tank-car construction.

An Association of American Railroads (AAR) publication, *Specifications for Tank Cars*, covers many requirements beyond the DOT regulations.

Some additional details are given later. Because of frequent changes, it is always necessary to check the latest rules. The **shipper**, not the carrier, has the ultimate responsibility for shipping in the correct container.

Tank Cars These range in size from about 7.6 to 182 m³ (2000 to 48,000 gal), and a car may be single or multiunit. The DOT now limits them to 130 m³ (34,500 gal) and 120,000 kg (263,000 lb) gross mass. Large cars usually result in lower investment per cubic meter

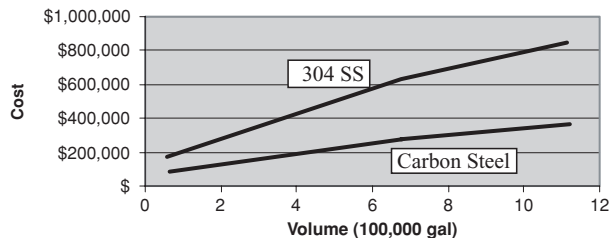


FIG. 10-193 Cost (± 30 percent) of field-erected, domed, flat-bottom API 650 tanks, October 2005, includes concrete foundation and typical nozzles, ladders, and platforms. 1 gal = 0.003785 m³.

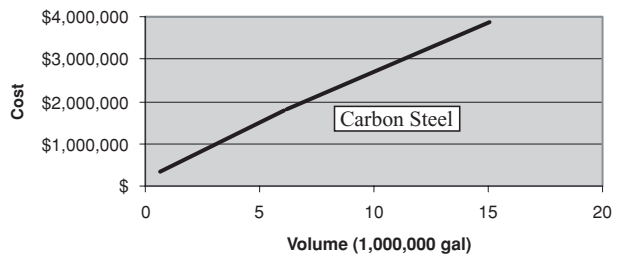


FIG. 10-194 Cost (± 30 percent) of field-erected, floating roof tanks, October 2005, includes concrete foundation and typical nozzles, ladders, and platforms. 1 gal = 0.003785 m³.

and take lower shipping rates. Cars may be insulated to reduce heating or cooling of the contents. Certain liquefied gases may be carried in insulated cars; temperatures are maintained by evaporation (see subsection "Low-Temperature and Cryogenic Storage"). Cars may be heated by steam coils or by electricity. Some products are loaded hot, solidify in transport, and are melted for removal. Some low-temperature cargoes must be unloaded within a given time (usually 30 days) to prevent pressure buildup.

Tank cars are classified as pressure or general-purpose. Pressure cars have relief-valve settings of 517 kPa (75 lbf/in²) and above. Those designated as general-purpose cars are, nevertheless, pressure vessels and may have relief valves or rupture disks. The DOT specification code number indicates the type of car. For instance, 105A500W indicates a pressure car with a test pressure of 3447 kPa (500 lbf/in²) and a relief-valve setting of 2585 kPa (375 lbf/in²). In most cases, loading and unloading valves, safety valves, and vent valves must be in a dome or an enclosure.

Companies shipping dangerous materials sometimes build tank cars with metal thicker than required by the specifications in order to reduce the possibility of leakage during a wreck or fire. The punching of couplers or rail ends into heads of tanks is a hazard.

Older tank cars have a center sill or beam running the entire length of the car. Most modern cars have no continuous sill, only short stub sills at each end. Cars with full sills have tanks anchored longitudinally at the center of the sill. The anchor is designed to be weaker than either the tank shell or the doubler plate between anchor and shell. Cars with stub sills have similar safeguards. Anchors and other parts are designed to meet AAR requirements.

The impact forces on car couplers put high stresses in sills, anchors, and doublers. This may start fatigue cracks in the shell, particularly at the corners of welded doubler plates. With brittle steel in cold weather, such cracks sometimes cause complete rupture of the tank. Large end radii on the doublers and tougher steels will reduce this hazard. Inspection of older cars can reveal cracks before failure.

A difference between tank cars and most pressure vessels is that tank cars are designed in terms of the theoretical ultimate or bursting strength of the car. The test pressure is usually 40 percent of the bursting pressure (sometimes less). The safety valves are set at 75 percent of the test pressure. Thus, the maximum operating pressure is usually 30 percent of the bursting pressure. This gives a nominal factor of safety of 3.3, compared with 3.5 for Division 1 of the ASME Pressure Vessel Code.

The DOT rules require that pressure cars have relief valves designed to limit pressure to 82.5 percent (with certain exceptions) of test pressure (110 percent of maximum operating pressure) when exposed to fire. Appendix A of AAR Specifications deals with the flow capacity of relief devices. The formulas apply to cars in the upright position with the device discharging vapor. They may not protect the car adequately when it is overturned and the device is discharging liquid.

Appendix B of AAR Specifications deals with the certification of facilities. Fabrication, repairing, testing, and specialty work on tank cars must be done in certified facilities. The AAR certifies shops to build cars of certain materials, to do test work on cars, or to make certain repairs and alterations.

Tank Trucks These trucks may have single, compartmented, or multiple tanks. Many of their requirements are similar to those for tank cars, except that thinner shells are permitted in most cases. Trucks for nonhazardous materials are subject to few regulations other than the normal highway laws governing all motor vehicles. But trucks carrying hazardous materials must comply with DOT regulations, Parts 173, 177, 178, and 397. Maximum weight, axle loading, and length are governed by state highway regulations. Many states have limits in the vicinity of 31,750 kg (70,000 lb) total mass, 14,500 kg (32,000 lb) for tandem axles, and 18.3 m (60 ft) or less overall length. Some allow tandem trailers.

Truck cargo tanks (for dangerous materials) are built under Part 173 and Subpart J of Part 178, DOT regulations. This includes Specifications MC-306, MC-307, MC-312, and MC-331. MC-331 is required for compressed gas. Subpart J requires tanks for pressures above 345 kPa (50 lbf/in²) in one case and 103 kPa (15 lbf/in²) in another to be built according to the ASME Pressure Vessel Code. A particular issue of the code is specified.

Because of the demands of highway service, the DOT specifications have a number of requirements in addition to the ASME Code. These include design for impact forces and rollover protection for fittings.

Portable tanks, drums, or bottles are shipped by rail, ship, air, or truck. Portable tanks containing hazardous materials must conform to DOT regulations, Parts 173 and 178, Subpart H.

Some tanks are designed to be shipped by trailer and transferred to railcars or ships (see following discussion).

Marine Transportation Seagoing tankers are for high tonnage. The traditional tanker uses the ship structure as a tank. It is subdivided into a number of tanks by means of transverse bulkheads and a center-line bulkhead. More than one product can be carried. An elaborate piping system connects the tanks to a pumping plant which can discharge or transfer the cargo. Harbor and docking facilities appear to be the only limit to tanker size. The largest crude oil tanker size to date is about 560,000 deadweight tons. In the United States, tankers are built to specifications of the American Bureau of Shipping and the U.S. Coast Guard.

Low-temperature liquefied gases are shipped in special ships with insulation between the hull and an inner tank. The largest LNG carrier's capacity is about 145,000 m³. Poisonous materials are shipped in separate tanks built into the ship. This prevents tank leakage from contaminating harbors. Separate tanks are also used to transport pressurized gases.

Barges are used on inland waterways. Popular sizes are up to 16 m (52½ ft) wide by 76 m (250 ft) long, with 2.6 m (8½ ft) to 4.3 m (14 ft) draft. Cargo requirements and waterway limitations determine design. Use of barges of uniform size facilitates rafting them together.

Portable tanks may be stowed in the holds of conventional cargo ships or special container ships, or they may be fastened on deck.

Container ships have guides in the hold and on deck which hold boxlike containers or tanks. The tank is latched to a trailer chassis and hauled to shipside. A movable gantry, sometimes permanently installed on the ship, hoists the tank from the trailer and lowers it into the guides on the ship. This system achieves large savings in labor, but its application is sometimes limited by lack of agreement between ship operators and unions.

Portable tanks for regulated commodities in marine transportation must be designed and built under Coast Guard regulations (see discussion under "Pressure Vessels").

Materials of Construction for Bulk Transport Because of the more severe service, construction materials for transportation usually are more restricted than for storage. Most large pipe lines are constructed of steel conforming to API Specification 5L or 5LX. Most tanks (cars, etc.) are built of pressure-vessel steels or AAR specification steels, with a few of aluminum or stainless steel. Carbon steel tanks may be lined with rubber, plastic, nickel, glass, or other materials. In many cases this is practical and cheaper than using a stainless-steel tank. Other materials for tank construction may be proposed and used if approved by the appropriate authorities (AAR and DOT).

PRESSURE VESSELS

This discussion of pressure vessels is intended as an overview of the codes most frequently used for the design and construction of pressure

vessels. Chemical engineers who design or specify pressure vessels should determine the federal and local laws relevant to the problem and then refer to the most recent issue of the pertinent code or standard before proceeding. Laws, codes, and standards are frequently changed.

A pressure vessel is a closed container of limited length (in contrast to the indefinite length of piping). Its smallest dimension is considerably larger than the connecting piping, and it is subject to pressures above 7 or 14 kPa (1 or 2 lbf/in²). It is distinguished from a boiler, which in most cases is used to generate steam for use external to itself.

Code Administration The American Society of Mechanical Engineers has written the ASME Boiler and Pressure Vessel Code, which contains rules for the design, fabrication, and inspection of boilers and pressure vessels. The ASME Code is an American National Standard. Most states in the United States and all Canadian provinces have passed legislation which makes the ASME Code or certain parts of it their legal requirement. Only a few jurisdictions have adopted the code for all vessels. The others apply it to certain types of vessels or to boilers. States employ inspectors (usually under a chief boiler inspector) to enforce code provisions. The authorities also depend a great deal on insurance company inspectors to see that boilers and pressure vessels are maintained in a safe condition.

The ASME Code is written by a large committee and many subcommittees, composed of engineers appointed by the ASME. The Code Committee meets regularly to review the code and consider requests for its revision, interpretation, or extension. **Interpretation and extension** are accomplished through "code cases." The decisions are published in *Mechanical Engineering*. Code cases are also mailed to those who subscribe to the service. A typical code case might be the approval of the use of a metal which is not presently on the list of approved code materials. Inquiries relative to code cases should be addressed to the secretary of the ASME Boiler and Pressure Vessel Committee, American Society of Mechanical Engineers, New York.

A new edition of the code is issued every 3 years. Between editions, alterations are handled by issuing semiannual addenda, which may be purchased by subscription. The ASME considers any issue of the code to be adequate and safe, but some government authorities specify certain issues of the code as their legal requirement.

Inspection Authority The National Board of Boiler and Pressure Vessel Inspectors is composed of the chief inspectors of states and municipalities in the United States and Canadian provinces which have made any part of the Boiler and Pressure Vessel Code a legal requirement. This board promotes uniform enforcement of boiler and pressure-vessel rules. One of the board's important activities is providing examinations for, and commissioning of, inspectors. Inspectors so qualified and employed by an insurance company, state, municipality, or Canadian province may inspect a pressure vessel and permit it to be stamped ASME—NB (National Board). An inspector employed by a vessel user may authorize the use of only the ASME stamp. The ASME Code Committee authorizes fabricators to use the various ASME stamps. The stamps, however, may be applied to a vessel only with the approval of the inspector.

The ASME Boiler and Pressure Vessel Code consists of eleven sections as follows:

- I. Power Boilers
- II. Materials
 - a. Ferrous
 - b. Nonferrous
 - c. Welding rods, electrodes, and filler metals
 - d. Properties
- III. Rules for Construction of Nuclear Power Plant Components
- IV. Heating Boilers
- V. Nondestructive Examination
- VI. Rules for Care and Operation of Heating Boilers
- VII. Guidelines for the Care of Power Boilers
- VIII. Pressure Vessels
 - IX. Welding and Brazing Qualifications
 - X. Fiber-Reinforced Plastic Pressure Vessels
 - XI. Rules for Inservice Inspection of Nuclear Power Plant Components

Pressure vessels (as distinguished from boilers) are involved with Secs. II, III, V, VIII, IX, X, and XI. Section VIII, Division 1, is the

Pressure Vessel Code as it existed in the past (and will continue). Division 1, was brought out as a means of permitting higher design stresses while ensuring at least as great a degree of safety as in Division 1. These two divisions plus Secs. III and X will be discussed briefly here. They refer to Secs. II and IX.

ASME Code Section VIII, Division 1 Most pressure vessels used in the process industry in the United States are designed and constructed in accordance with Sec. VIII, Division 1 (see Fig. 10-195). This division is divided into three subsections followed by appendixes.

Introduction The Introduction contains the scope of the division and defines the responsibilities of the user, the manufacturer, and the inspector. The scope defines pressure vessels as containers for the containment of pressure. It specifically excludes vessels having an internal pressure not exceeding 103 kPa (15 lbf/in²) and further states that the rules are applicable for pressures not exceeding 20,670 kPa (3000 lbf/in²). For higher pressures it is usually necessary to deviate from the rules in this division.

The scope covers many other less basic exclusions, and inasmuch as the scope is occasionally revised, except for the most obvious cases, it is prudent to review the current issue before specifying or designing pressure vessels to this division. Any vessel which meets all the requirements of this division may be stamped with the code *U* symbol even though exempted from such stamping.

Subsection A This subsection contains the general requirements applicable to all materials and methods of construction. Design temperature and pressure are defined here, and the loadings to be considered in design are specified. For stress failure and yielding, this section of the code uses the maximum-stress theory of failure as its criterion.

This subsection refers to the tables elsewhere in the division in which the maximum allowable tensile-stress values are tabulated. The basis for the establishment of these allowable stresses is defined in detail in Appendix P; however, as the safety factors used were very important in establishing the various rules of this division, it is noted that the safety factors for internal-pressure loads are 3.5 on ultimate strength and 1.6 or 1.5 on yield strength, depending on the material. For external-pressure loads on cylindrical shells, the safety factors are 3 for both elastic buckling and plastic collapse. For other shapes subject to external pressure and for longitudinal shell compression, the safety factors are 3.5 for both elastic buckling and plastic collapse. Longitudinal compressive stress in cylindrical elements is limited in this subsection by the lower of either stress failure or buckling failure.

Internal-pressure design rules and formulas are given for cylindrical and spherical shells and for ellipsoidal, torispherical (often called ASME heads), hemispherical, and conical heads. The formulas given assume membrane-stress failure, although the rules for heads include consideration for buckling failure in the transition area from cylinder to head (knuckle area).

Longitudinal joints in cylinders are more highly stressed than circumferential joints, and the code takes this fact into account. When forming heads, there is usually some thinning from the original plate thickness in the knuckle area, and it is prudent to specify the minimum allowable thickness at this point.

Unstayed flat heads and covers can be designed by very specific rules and formulas given in this subsection. The stresses caused by pressure on these members are bending stresses, and the formulas include an allowance for additional edge moments induced when the head, cover, or blind flange is attached by bolts. Rules are provided for quick-opening closures because of the risk of incomplete attachment or opening while the vessel is pressurized. Rules for braced and stayed surfaces are also provided.

External-pressure failure of shells can result from overstress at one extreme or from elastic instability at the other or at some intermediate loading. The code provides the solution for most shells by using a number of charts. One chart is used for cylinders where the shell diameter-to-thickness ratio and the length-to-diameter ratio are the variables. The rest of the charts depict curves relating the geometry of cylinders and spheres to allowable stress by curves which are determined from the modulus of elasticity, tangent modulus, and yield strength at temperatures for various materials or classes of materials. The text of this subsection explains how the allowable stress is deter-

mined from the charts for cylinders, spheres, and hemispherical, ellipsoidal, torispherical, and conical heads.

Frequently cost savings for cylindrical shells can result from reducing the effective length-to-diameter ratio and thereby reducing shell thickness. This can be accomplished by adding circumferential stiffeners to the shell. Rules are included for designing and locating the stiffeners.

Openings are always required in pressure-vessel shells and heads. Stress intensification is created by the existence of a hole in an otherwise symmetrical section. The code compensates for this by an area-replacement method. It takes a cross section through the opening, and it measures the area of the metal of the required shell that is removed and replaces it in the cross section by additional material (shell wall, nozzle wall, reinforcing plate, or weld) within certain distances of the opening centerline. These rules and formulas for calculation are included in Subsec. A.

When a cylindrical shell is drilled for the insertion of multiple tubes, the shell is significantly weakened and the code provides rules for tube-hole patterns and the reduction in strength that must be accommodated.

Fabrication tolerances are covered in this subsection. The tolerances permitted for shells for external pressure are much closer than those for internal pressure because the stability of the structure is dependent on the symmetry. Other paragraphs cover repair of defects during fabrication, material identification, heat treatment, and impact testing.

Inspection and testing requirements are covered in detail. Most vessels are required to be hydrostatic-tested (generally with water) at 1.3 times the maximum allowable working pressure. Some enameled (glass-lined) vessels are permitted to be hydrostatic-tested at lower pressures. Pneumatic tests are permitted and are carried to at least 1¼ times the maximum allowable working pressure, and there is provision for proof testing when the strength of the vessel or any of its parts cannot be computed with satisfactory assurance of accuracy. Pneumatic or proof tests are rarely conducted.

Pressure-relief-device requirements are defined in Subsec. A. Set point and maximum pressure during relief are defined according to the service, the cause of overpressure, and the number of relief devices. Safety, safety relief, relief valves, rupture disk, breaking pin, and rules on tolerances for the relieving point are given.

Testing, certification, and installation rules for relieving devices are extensive. Every chemical engineer responsible for the design or operation of process units should become very familiar with these rules. The pressure-relief-device paragraphs are the only parts of Sec. VIII, Division 1, that are concerned with the installation and ongoing operation of the facility; all other rules apply only to the design and manufacture of the vessel.

Subsection B This subsection contains rules pertaining to the methods of fabrication of pressure vessels. Part UW is applicable to welded vessels. Service restrictions are defined. Lethal service is for "lethal substances," which are defined as poisonous gases or liquids of such a nature that a very small amount of the gas or the vapor of the liquid mixed or unmixed with air is dangerous to life when inhaled. It is stated that it is the user's responsibility to advise the designer or manufacturer if the service is lethal. All vessels in lethal service shall have all butt-welded joints fully radiographed, and when practical, joints shall be butt-welded. All vessels fabricated of carbon or low-alloy steel shall be postweld-heat-treated.

Low-temperature service is defined as being below -29°C (-20°F), and impact testing of many materials is required. The code is restrictive in the type of welding permitted.

Unfired steam boilers with design pressures exceeding 345 kPa (50 lbf/in²) have restrictive rules on welded-joint design, and all butt joints require full radiography.

Pressure vessels subject to direct firing have special requirements relative to welded-joint design and postweld heat treatment.

This subsection includes rules governing welded-joint designs and the degree of radiography, with efficiencies for welded joints specified as functions of the quality of joint. These efficiencies are used in the formulas in Subsec. A for determining vessel thicknesses.

Details are provided for head-to-shell welds, tube sheet-to-shell welds, and nozzle-to-shell welds. Acceptable forms of welded stay-bolts and plug and slot welds for staying plates are given here.

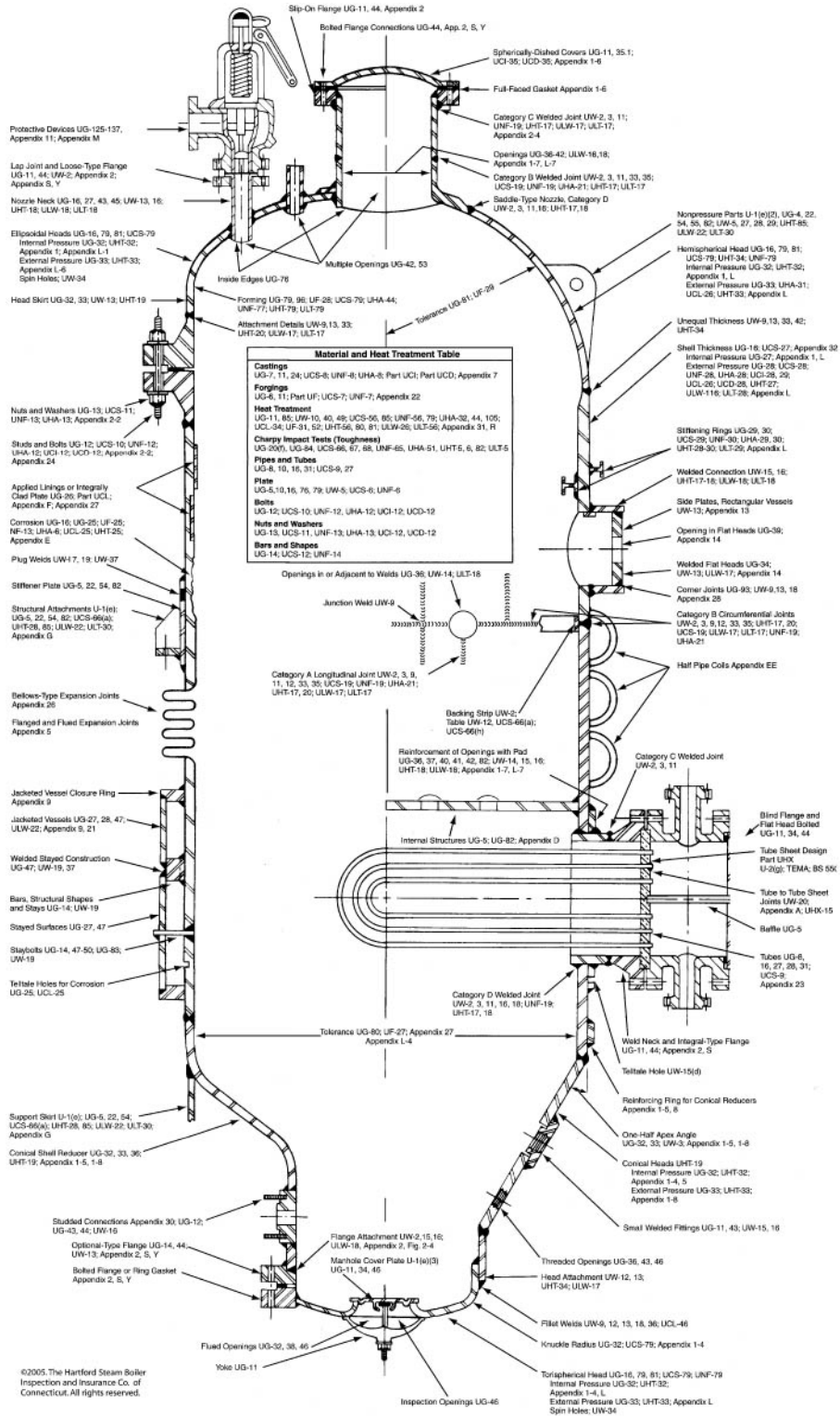


FIG. 10-195 Quick reference guide to ASME Boiler and Pressure Vessel Code Section VIII, Division 1 (2004 edition). (Reprinted with permission of publisher, HSB Global Standards, Hartford, Conn.)

©2005, The Hartford Steam Boiler Inspection and Insurance Co. of Connecticut. All rights reserved.

ORGANIZATION				GENERAL NOTES			
Introduction	Scope and Applicability			Code Jurisdiction for Piping.....U-1	Nameplates, Stamping and Reports.....UG-115-120;		
Subsection A	Part UG-General requirements for all construction and all materials			Design Pressure.....UG-21; UG-98; UCD-3	UHT-115; ULW-115; ULT-115; App. W & 18		
Subsection B	Requirements for methods of fabrication			Design Temperature.....UG-20; UCL-24; UCD-3	Nondestructive Examination		
Part UB	Welding			Dimpled or Embossed Assemblies...Appendix 17	a. Liquid Penetrant.....Appendix 8		
Part UF	Forging			Inspector's Responsibility.....U-2; UG-90	b. Magnetic Particle.....Appendix 6		
Part UB	Brazing			Loadings.....UG-22; Appendix G, H	c. Radiography.....UW-51, 52		
Subsection C	Requirements for classes of material			Low Temperature Service.....UW-2; UCS-66-68;	d. Ultrasonic.....Appendix 12		
Part UCS	Carbon and low alloy steels			UHA-51; Part ULT	Porosity Charts.....Appendix 4		
Part UNF	Nonferrous materials			Manufacturer's Responsibility.....U-2; UG-90	Pressure Tests.....UG-99, 100, 101; UW-50;		
Part UHA	High alloy steels			Material, General.....UG-4, 10, 11, 15	UCI-99; UCD-99; ULT-99		
Part UCI	Cast iron			a. Bolts and Studs.....UG-12	Quality Control System.....U-2; Appendix 10		
Part UCL	Clad plate and corrosion resistant liners			b. Castings.....UG-7	Quick Actuating Closures...U-1; UG-35; App. FF		
Part UCD	Cast ductile iron			c. Forgings.....UG-6	Service Restrictions.....UW-2; UB-3;		
Part UHT	Ferritic steels with tensile properties enhanced by heat treatment			d. Nuts and Washers.....UG-13	UCL-3; UCD-2		
Part ULW	Layered Construction			e. Pipes and Tubes.....UG-8	Stress, Maximum Allowable.....UG-23; App. P;		
Part ULT	Low Temperature Materials			f. Plates.....UG-5	UCS-23; UNF-23; UHA-23; UCD-23;		
Part UHX	Rules for Shell and Tube Heat Exchangers			g. Rod and Bar.....UG-14	UHT-23; ULT-23; UCL-23; UCI-23;		
Mandatory Appendices 1-33				h. Standard Parts.....UG-11, 44	User's Responsibility.....UG-125; U-2		
Nonmandatory Appendices A-Y, DD, EE, FF, GG				i. Welding.....UG-9	Welding Preheat Recommendations.....Appendix R		
				Material Identification, Marking and Certification.....UG-77, 93, 94	UW-26 thru 29;		
				Material Tolerances.....UG-16	ULT-82; UHT-82; UHA-52; UNF-95		

PARA.	REQUIREMENTS/REMARKS	PT	MT	UT	RT	PARA.	REQUIREMENTS/REMARKS	PT	MT	UT
UG-24	General requirements for castings.....X	X	X	X	X	UCL-35	Vessels or parts of vessels constructed of clad plate and those having applied corrosion resistant linings			
UG-93	General requirements for the inspection of all materials.....X	X	X			UCL-36	Chromium stainless steel cladding or lining.....			
UW-11	Radiographic and ultrasonic examination required for pressure vessels and vessel parts (also see UW-51, UW-52)			X	X	UCD-78	Repair of defects in cast ductile iron pressure vessels and vessel parts			
UW-42	Surface weld metal buildup.....X	X	X			UHT-57	Pressure vessels or vessel parts constructed of ferritic steels having tensile properties enhanced by heat treatment	X	X	
UW-50	Welds on pneumatically tested vessels.....X	X	X			UHT-83	Metal removal accomplished by methods involving melting on pressure vessels and vessel parts constructed of ferritic steels having tensile properties enhanced by heat treatment	X	X	
UF-31	Vessels fabricated from SA-372 forging material to be liquid quenched and tempered	X	X			UHT-85	Removal of temporary welds on pressure vessels and vessel parts constructed of ferritic steels having tensile properties enhanced by heat treatment	X	X	
UF-32	Finished welds after postweld heat treatment.....X	X	X			ULW-51	Inner shells and inner heads of layered pressure vessels			
UF-37	Repair welds in forgings.....X	X	X			ULW-52	Welded joints in the layers of layered pressure vessels	X	X	
UF-55	Vessels constructed of SA-372 Class VIII material.....			X		ULW-53	Step welded girth joints in the layers of layered pressure vessels	X	X	
UCS-57	Examination in addition to UW-11 for butt welded joints on carbon and low alloy steel pressure vessels and vessel parts				X	ULW-54	Butt welded joints in layered pressure vessels.....			
UNF-57	Examination in addition to UW-11 for pressure vessels and vessel parts constructed of nonferrous materials				X	ULW-55	Flat head and tube sheet welded joints in layered pressure vessels	X	X	
UNF-58	All groove and fillet welds in vessels constructed of certain nonferrous materials				X	ULW-56	Nozzle and communicating chamber welded joints in layered pressure vessels	X	X	
UHA-33	Exceptions for radiographic examinations of high alloy steel vessels				X	ULW-57	Random spot examinations and repairs of welds in layered pressure vessels	X	X	
UHA-34	Austenitic chromium-nickel alloy steel butt and fillet welds				X	ULT-57	Welds in pressure vessels and vessel parts constructed of materials having increased design stress values due to low temperature applications	X	X	
UCI-78	Repair of defects in cast iron pressure vessels and vessel parts	X	X		X					

Qualifications of Personnel Performing Section VIII, Division 1 Nondestructive Examinations			
Examination	Reference	Examination	Reference
PT	Appendix 8	UT	Appendix 12
MT	Appendix 6	RT	UW-51

FIG. 10-195 (Continued)

Rules for the welded fabrication of pressure vessels cover welding processes, manufacturer's record keeping on welding procedures, welder qualification, cleaning, fit-up alignment tolerances, and repair of weld defects. Procedures for postweld heat treatment are detailed. Checking the procedures and welders and radiographic and ultrasonic examination of welded joints are covered.

Requirements for vessels fabricated by forging in Part UF include unique design requirements with particular concern for stress risers, fabrication, heat treatment, repair of defects, and inspection. Vessels fabricated by brazing are covered in Part UB. Brazed vessels cannot be used in lethal service, for unfired steam boilers, or for direct firing. Permitted brazing processes as well as testing of brazed joints for strength are covered. Fabrication and inspection rules are also included.

Subsection C This subsection contains requirements pertaining to classes of materials. Carbon and low-alloy steels are governed by Part UCS, nonferrous materials by Part UNF, high-alloy steels by Part UHA, and steels with tensile properties enhanced by heat treatment by Part UHT. Each of these parts includes tables of maximum allowable stress values for all code materials for a range of metal temperatures. These stress values include appropriate safety factors. Rules governing the application, fabrication, and heat treatment of the vessels are included in each part.

Part UHT also contains more stringent details for nozzle welding that are required for some of these high-strength materials. Part UCI has rules for cast-iron construction, Part UCL has rules for welded vessels of clad plate as lined vessels, and Part UCD has rules for ductile-iron pressure vessels.

A relatively recent addition to the code is Part ULW, which contains requirements for vessels fabricated by layered construction. This type of construction is most frequently used for high pressures, usually in excess of 13,800 kPa (2000 lbf/in²).

There are several methods of layering in common use: (1) thick layers shrunk together; (2) thin layers, each wrapped over the other and the longitudinal seam welded by using the prior layer as backup; and (3) thin layers spirally wrapped. The code rules are written for either thick or thin layers. Rules and details are provided for all the usual welded joints and nozzle reinforcement. Supports for layered vessels require special consideration, in that only the outer layer could contribute to the support. For lethal service only the inner shell and inner heads need comply with the requirements in Subsec. B. Inasmuch as radiography would not be practical for inspection of many of the welds, extensive use is made of magnetic-particle and ultrasonic inspection. When radiography is required, the code warns the inspector

that indications sufficient for rejection in single-wall vessels may be acceptable. Vent holes are specified through each layer down to the inner shell to prevent buildup of pressure between layers in the event of leakage at the inner shell.

Mandatory Appendixes These include a section on supplementary design formulas for shells not covered in Subsec. A. Formulas are given for thick shells, heads, and dished covers. Another appendix gives very specific rules, formulas, and charts for the design of bolted-flange connections. The nature of these rules is such that they are readily programmable for a digital computer, and most flanges now are designed by using computers. One appendix includes only the charts used for calculating shells for external pressure discussed previously. Jacketed vessels are covered in a separate appendix in which very specific rules are given, particularly for the attachment of the jacket to the inner shell. Other appendixes cover inspection and quality control.

Nonmandatory Appendixes These cover a number of subjects, primarily suggested good practices and other aids in understanding the code and in designing with the code. Several current nonmandatory appendixes will probably become mandatory.

Figure 10-195 illustrates a pressure vessel with the applicable code paragraphs noted for the various elements. Additional important paragraphs are referenced at the bottom of the figure.

ASME Code Section VIII, Division 2 Paragraph AG-100e of Division 2 states: "In relation to the rules of Division 1 of Section VIII, these rules of Division 2 are more restrictive in the choice of materials which may be used but permit higher design stress intensity values to be employed in the range of temperatures over which the design stress intensity value is controlled by the ultimate strength or the yield strength; more precise design procedures are required and some common design details are prohibited; permissible fabrication procedures are specifically delineated and more complete testing and inspection are required." Most Division 2 vessels fabricated to date have been large or intended for high pressure and, therefore, expensive when the material and labor savings resulting from smaller safety factors have been greater than the additional engineering, administrative, and inspection costs.

The organization of Division 2 differs from that of Division 1.

Part AG This part gives the scope of the division, establishes its jurisdiction, and sets forth the responsibilities of the user and the manufacturer. Of particular importance is the fact that no upper limitation in pressure is specified and that a user's design specification is required. The user or the user's agent shall provide requirements for intended operating conditions in such detail as to constitute an adequate basis for selecting materials and designing, fabricating, and inspecting the vessel. The user's design specification shall include the method of supporting the vessel and any requirement for a fatigue analysis. If a fatigue analysis is required, the user must provide information in sufficient detail so that an analysis for cyclic operation can be made.

Part AM This part lists permitted individual construction materials, applicable specifications, special requirements, design stress-intensity values, and other property information. Of particular importance are the ultrasonic-test and toughness requirements. Among the properties for which data are included are thermal conductivity and diffusivity, coefficient of thermal expansion, modulus of elasticity, and yield strength. The design stress-intensity values include a safety factor of 3 on ultimate strength at temperature or 1.5 on yield strength at temperature.

Part AD This part contains requirements for the design of vessels. The rules of Division 2 are based on the maximum-shear theory of failure for stress failure and yielding. Higher stresses are permitted when wind or earthquake loads are considered. Any rules for determining the need for fatigue analysis are given here.

Rules for the design of shells of revolution under internal pressure differ from the Division 1 rules, particularly the rules for formed heads when plastic deformation in the knuckle area is the failure criterion. Shells of revolution for external pressure are determined on the same criterion, including safety factors, as in Division 1. Reinforcement for openings uses the same area-replacement method as Division 1; however, in many cases the reinforcement metal must be closer to the opening centerline.

The rest of the rules in Part AD for flat heads, bolted and studded connections, quick-actuating closures, and layered vessels essentially

duplicate Division 1. The rules for support skirts are more definitive in Division 2.

Part AF This part contains requirements governing the fabrication of vessels and vessel parts.

Part AR This part contains rules for pressure-relieving devices.

Part AI This part contains requirements controlling inspection of vessel.

Part AT This part contains testing requirements and procedures.

Part AS This part contains requirements for stamping and certifying the vessel and vessel parts.

Appendixes Appendix 1 defines the basis used for defining stress-intensity values. Appendix 2 contains external-pressure charts, and Appendix 3 has the rules for bolted-flange connections; these two are exact duplicates of the equivalent appendixes in Division 1.

Appendix 4 gives definitions and rules for stress analysis for shells, flat and formed heads, and tube sheets, layered vessels, and nozzles including discontinuity stresses. Of particular importance are Table 4-120.1, "Classification of Stresses for Some Typical Cases," and Fig. 4-130.1, "Stress Categories and Limits of Stress Intensity." These are very useful in that they clarify a number of paragraphs and simplify stress analysis.

Appendix 5 contains rules and data for stress analysis for cyclic operation. Except in short-cycle batch processes, pressure vessels are usually subject to few cycles in their projected lifetime, and the endurance-limit data used in the machinery industries are not applicable. Curves are given for a broad spectrum of materials, covering a range from 10 to 1 million cycles with allowable stress values as high as 650,000 lbf/in². This low-cycle fatigue has been developed from strain-fatigue work in which stress values are obtained by multiplying the strains by the modulus of elasticity. Stresses of this magnitude cannot occur, but strains do. The curves given have a factor of safety of 2 on stress or 20 on cycles.

Appendix 6 contains requirements of experimental stress analysis, Appendix 8 has acceptance standards for radiographic examination, Appendix 9 covers nondestructive examination, Appendix 10 gives rules for capacity conversions for safety valves, and Appendix 18 details quality-control-system requirements.

The remaining appendixes are nonmandatory but useful to engineers working with the code.

General Considerations Most pressure vessels for the chemical-process industry will continue to be designed and built to the rules of Sec. VIII, Division 1. While the rules of Sec. VIII, Division 2, will frequently provide thinner elements, the cost of the engineering analysis, stress analysis and higher-quality construction, material control, and inspection required by these rules frequently exceeds the savings from the use of thinner walls.

Additional ASME Code Considerations

ASME Code Sec. III: Nuclear Power Plant Components This section of the code includes vessels, storage tanks, and concrete containment vessels as well as other nonvessel items.

ASME Code Sec. X: Fiberglass-Reinforced-Plastic Pressure Vessels This section is limited to four types of vessels: bag-molded and centrifugally cast, each limited to 1000 kPa (150 lbf/in²); filament-wound with cut filaments limited to 10,000 kPa (1500 lbf/in²); and filament-wound with uncut filaments limited to 21,000 kPa (3000 lbf/in²). Operating temperatures are limited to the range from +66°C (150°F) to -54°C (-65°F). Low modulus of elasticity and other property differences between metal and plastic required that many of the procedures in Sec. X be different from those in the sections governing metal vessels. The requirement that at least one vessel of a particular design and fabrication shall be tested to destruction has prevented this section from being widely used. The results from the combined fatigue and burst test must give the design pressure a safety factor of 6 to the burst pressure.

Safety in Design Designing a pressure vessel in accordance with the code will, under most circumstances, provide adequate safety. In the code's own words, however, the rules "cover minimum construction requirements for the design, fabrication, inspection, and certification of pressure vessels." The significant word is "minimum." The **ultimate responsibility** for safety rests with the user and the designer. They must decide whether anything beyond code requirements is necessary. The code cannot foresee and provide for all the

unusual conditions to which a pressure vessel might be exposed. If it tried to do so, the majority of pressure vessels would be unnecessarily restricted. Some of the conditions that a vessel might encounter are unusually low temperatures, unusual thermal stresses, stress ratcheting caused by thermal cycling, vibration of tall vessels excited by von Karman vortices caused by wind, very high pressures, runaway chemical reactions, repeated local overheating, explosions, exposure to fire, exposure to materials that rapidly attack the metal, containment of extremely toxic materials, and very large sizes of vessels. Large vessels, although they may contain nonhazardous materials, could, by their very size, create a serious hazard if they burst. The failure of the Boston molasses tank in 1919 killed 12 people. For pressure vessels which are outside code jurisdiction, there are sometimes special hazards in very-high-strength materials and plastics. There may be many others which the designers should recognize if they encounter them.

Metal fatigue, when it is present, is a serious hazard. Section VIII, Division 1, mentions rapidly fluctuating pressures. Division 2 and Sec. III do require a fatigue analysis. In extreme cases vessel contents may affect the fatigue strength (endurance limit) of the material. This is corrosion fatigue. Although most ASME Code materials are not particularly sensitive to corrosion fatigue, even they may suffer an endurance limit loss of 50 percent in some environments. High-strength heat-treated steels, on the other hand, are very sensitive to corrosion fatigue. It is not unusual to find some of these which lose 75 percent of their endurance in corrosive environments. In fact, in corrosion fatigue many steels do not have an endurance limit. The curve of stress versus cycles to failure (*S/N* curve) continues to slope downward regardless of the number of cycles.

Brittle fracture is probably the most insidious type of pressure-vessel failure. Without brittle fracture, a pressure vessel could be pressurized approximately to its ultimate strength before failure. With brittle behavior some vessels have failed well below their design pressures (which are about 25 percent of the theoretical bursting pressures). In order to reduce the possibility of brittle behavior, Division 2 and Sec. III require impact tests.

The subject of brittle fracture has been understood only since about 1950, and knowledge of some of its aspects is still inadequate. A notched or cracked plate of pressure-vessel steel, stressed at 66°C (150°F), would elongate and absorb considerable energy before breaking. It would have a ductile or plastic fracture. As the temperature is lowered, a point is reached at which the plate would fail in a brittle manner with a flat fracture surface and almost no elongation. The transition from ductile to brittle fracture actually takes place over a temperature range, but a point in this range is selected as the **transition temperature**. One of the ways of determining this temperature is the Charpy impact test (see ASTM Specification E-23). After the transition temperature has been determined by laboratory impact tests, it must be correlated with service experience on full-size plates. The literature on brittle fracture contains information on the relation of impact tests to service experience on some carbon steels.

A more precise but more elaborate method of dealing with the ductile-brittle transition is the **fracture-analysis diagram**. This uses a transition known as the **nil-ductility temperature** (NDT), which is determined by the drop-weight test (ASTM Standard E208) or the drop-weight tear test (ASTM Standard E436). The application of this diagram is explained in two papers by Pellini and Puzak [*Trans. Am. Soc. Mech. Eng.*, 429 (October 1964); *Welding Res. Coun. Bull.* 88, 1963].

Section VIII, Division 1, is rather lax with respect to brittle fracture. It allows the use of many steels down to -29°C (-20°F) without a check on toughness. Occasional brittle failures show that some vessels are operating below the nil-ductility temperature, i.e., the lower limit of ductility. Division 2 has resolved this problem by requiring impact tests in certain cases. Tougher grades of steel, such as the SA516 steels (in preference to SA515 steel), are available for a small price premium. Stress relief, steel made to fine-grain practice, and normalizing all reduce the hazard of brittle fracture.

Nondestructive testing of both the plate and the finished vessel is important to safety. In the analysis of fracture hazards, it is important to know the size of the flaws that may be present in the completed vessel. The four most widely used methods of examination are radiographic, magnetic-particle, liquid-penetrant, and ultrasonic.

Radiographic examination is either by x-rays or by gamma radiation. The former has greater penetrating power, but the latter is more portable. Few x-ray machines can penetrate beyond 300-mm (12-in) thickness.

Ultrasonic techniques use vibrations with a frequency between 0.5 and 20 MHz transmitted to the metal by a transducer. The instrument sends out a series of pulses. These show on a cathode-ray screen as they are sent out and again when they return after being reflected from the opposite side of the member. If there is a crack or an inclusion along the way, it will reflect part of the beam. The initial pulse and its reflection from the back of the member are separated on the screen by a distance which represents the thickness. The reflection from a flaw will fall between these signals and indicate its magnitude and position. Ultrasonic examination can be used for almost any thickness of material from a fraction of an inch to several feet. Its use is dependent upon the shape of the body because irregular surfaces may give confusing reflections. Ultrasonic transducers can transmit pulses normal to the surface or at an angle. Transducers transmitting pulses that are oblique to the surface can solve a number of special inspection problems.

Magnetic-particle examination is used only on magnetic materials. Magnetic flux is passed through the part in a path parallel to the surface. Fine magnetic particles, when dusted over the surface, will concentrate near the edges of a crack. The sensitivity of magnetic-particle examination is proportional to the sine of the angle between the direction of the magnetic flux and the direction of the crack. To be sure of picking up all cracks, it is necessary to probe the area in two directions.

Liquid-penetrant examination involves wetting the surface with a fluid which penetrates open cracks. After the excess liquid has been wiped off, the surface is coated with a material which will reveal any liquid that has penetrated the cracks. In some systems a colored dye will seep out of cracks and stain whitewash. Another system uses a penetrant that becomes fluorescent under ultraviolet light.

Each of these four popular methods has its advantages. Frequently, best results are obtained by using more than one method. Magnetic particles or liquid penetrants are effective on surface cracks. Radiography and ultrasonics are necessary for subsurface flaws. *No known method of nondestructive testing can guarantee the absence of flaws.* There are other less widely used methods of examination. Among these are eddy-current, electrical-resistance, acoustics, and thermal testing. *Nondestructive Testing Handbook* [Robert C. McMaster (ed.), Ronald, New York, 1959] gives information on many testing techniques.

The **eddy-current technique** involves an alternating-current coil along and close to the surface being examined. The electrical impedance of the coil is affected by flaws in the structure or changes in composition. Commercially, the principal use of eddy-current testing is for the examination of tubing. It could, however, be used for testing other things.

The **electrical-resistance method** involves passing an electric current through the structure and exploring the surface with voltage probes. Flaws, cracks, or inclusions will cause a disturbance in the voltage gradient on the surface. Railroads have used this method for many years to locate transverse cracks in rails.

The **hydrostatic test** is, in one sense, a method of examination of a vessel. It can reveal gross flaws, inadequate design, and flange leaks. Many believe that a hydrostatic test guarantees the safety of a vessel. This is not necessarily so. A vessel that has passed a hydrostatic test is probably safer than one that has not been tested. It can, however, still fail in service, even on the next application of pressure. Care in material selection, examination, and fabrication do more to guarantee vessel integrity than the hydrostatic test.

The ASME Codes recommend that hydrostatic tests be run at a temperature that is usually above the nil-ductility temperature of the material. This is, in effect, a pressure-temperature treatment of the vessel. When tested in the relatively ductile condition above the nil-ductility temperature, the material will yield at the tips of cracks and flaws and at points of high residual weld stress. This procedure will actually reduce the residual stresses and cause a redistribution at crack tips. The vessel will then be in a safer condition for subsequent operation. This procedure is sometimes referred to as **notch nullification**.

It is possible to design a hydrostatic test in such a way that it probably will be a proof test of the vessel. This usually requires, among other things, that the test be run at a temperature as low as and

preferably lower than the minimum operating temperature of the vessel. Proof tests of this type are run on vessels built of ultrahigh-strength steel to operate at cryogenic temperatures.

Other Regulations and Standards Pressure vessels may come under many types of regulation, depending on where they are and what they contain. Although many states have adopted the ASME Boiler and Pressure Vessel Code, either in total or in part, any state or municipality may enact its own requirements. The federal government regulates some pressure vessels through the Department of Transportation, which includes the Coast Guard. If pressure vessels are shipped into foreign countries, they may face additional regulations.

Pressure vessels carried aboard United States-registered ships must conform to rules of the **U.S. Coast Guard**. Subchapter F of Title 46, *Code of Federal Regulations*, covers marine engineering. Of this, Parts 50 through 61 and 98 include pressure vessels. Many of the rules are similar to those in the ASME Code, but there are differences.

The **American Bureau of Shipping** (ABS) has rules that insurance underwriters require for the design and construction of pressure vessels which are a permanent part of a ship. Pressure cargo tanks may be permanently attached and come under these rules. Such tanks supported at several points are independent of the ship's structure and are distinguished from "integral cargo tanks" such as those in a tanker. ABS has pressure vessel rules in two of its publications. Most of them are in *Rules for Building and Classing Steel Vessels*.

Standards of Tubular Exchanger Manufacturers Association (TEMA) give recommendations for the construction of tubular heat exchangers. Although TEMA is not a regulatory body and there is no legal requirement for the use of its standards, they are widely accepted as a good basis for design. By specifying TEMA standards, one can obtain adequate equipment without having to write detailed specifications for each piece. TEMA gives formulas for the thickness of tube sheets. Such formulas are not in ASME Codes. (See further discussion of TEMA in Sec. 11.)

Vessels with Unusual Construction High pressures create design problems. The ASME Code Sec. VIII, Division 1, applies to vessels rated for pressures up to 20,670 kPa (3000 lbf/in²). Division 2 is unlimited. At high pressures, special designs not necessarily in accordance with the code are sometimes used. At such pressures, a vessel designed for ordinary low-carbon-steel plate, particularly in large diameters, would become too thick for practical fabrication by ordinary methods. The alternatives are to make the vessel of high-strength plate, use a solid forging, or use multilayer construction.

High-strength steels with tensile strengths over 1380 MPa (200,000 lbf/in²) are limited largely to applications for which weight is very important. Welding procedures are carefully controlled, and preheat is used. These materials are brittle at almost any temperature, and vessels must be designed to prevent brittle fracture. Flat spots and variations in curvature are avoided. Openings and changes in shape require appropriate design. The maximum permissible size of flaws is determined by fracture mechanics, and the method of examination must assure as much as possible that larger flaws are not present. All methods of nondestructive testing may be used. Such vessels require the most sophisticated techniques in design, fabrication, and operation.

Solid forgings are frequently used in construction for pressure vessels above 20,670 kPa (3000 lbf/in²) and even lower. Almost any shell thickness can be obtained, but most of them range between 50 and 300 mm (2 and 12 in). The ASME Code lists forging materials with tensile strengths from 414 to 930 MPa (from 60,000 to 135,000 lbf/in²). Brittle fracture is a possibility, and the hazard increases with thickness. Furthermore, some forging alloys have nil-ductility temperatures as high as 121°C (250°F). A forged vessel should have an NDT at least 17°C (30°F) below the design temperature. In operation, it should be slowly and uniformly heated at least to NDT before it is subjected to pressure. During construction, nondestructive testing should be used to detect dangerous cracks or flaws. Section VIII of the ASME Code, particularly Division 2, gives design and testing techniques.

As the size of a forged vessel increases, the sizes of ingot and handling equipment become larger. The cost may increase faster than the weight. The problems of getting sound material and avoiding brittle fracture also become more difficult. Some of these problems are avoided by use of **multilayer construction**. In this type of vessel, the

heads and flanges are made of forgings, and the cylindrical portion is built up by a series of layers of thin material. The thickness of these layers may be between 3 and 50 mm (1/8 and 2 in), depending on the type of construction. There is an inner lining which may be different from the outer layers.

Although there are multilayer vessels as small as 380-mm (15-in) inside diameter and 2400 mm (8 ft) long, their principal advantage applies to the larger sizes. When properly made, a multilayer vessel is probably safer than a vessel with a solid wall. The layers of thin material are tougher and less susceptible to brittle fracture, have less probability of defects, and have the statistical advantage of a number of small elements instead of a single large one. The heads, flanges, and welds, of course, have the same hazards as other thick members. Proper attention is necessary to avoid cracks in these members.

There are several assembly techniques. One frequently used is to form successive layers in half cylinders and butt-weld them over the previous layers. In doing this, the welds are staggered so that they do not fall together. This type of construction usually uses plates from 6 to 12 mm (1/4 to 1/2 in) thick. Another method is to weld each layer separately to form a cylinder and then shrink it over the previous layers. Layers up to about 50-mm (2-in) thickness are assembled in this way. A third method of fabrication is to wind the layers as a continuous sheet. This technique is used in Japan. The Wickel construction, fabricated in Germany, uses helical winding of interlocking metal strip. Each method has its advantages and disadvantages, and choice will depend upon circumstances.

Because of the possibility of voids between layers, it is preferable not to use multilayer vessels in applications where they will be subjected to fatigue. Inward thermal gradients (inside temperature lower than outside temperature) are also undesirable.

Articles on these vessels have been written by Fratcher [*Pet. Refiner*, 34(11), 137 (1954)] and by Strelzoff, Pan, and Miller [*Chem. Eng.*, 75(21), 143-150 (1968)].

Vessels for high-temperature service may be beyond the temperature limits of the stress tables in the ASME Codes. Section VIII, Division 1, makes provision for construction of pressure vessels up to 650°C (1200°F) for carbon and low-alloy steel and up to 815°C (1500°F) for stainless steels (300 series). If a vessel is required for temperatures above these values and above 103 kPa (15 lbf/in²), it would be necessary, in a code state, to get permission from the state authorities to build it as a special project. Above 815°C (1500°F), even the 300 series stainless steels are weak, and creep rates increase rapidly. If the metal which resists the pressure operates at these temperatures, the vessel pressure and size will be limited. The vessel must also be expendable because its life will be short. Long exposure to high temperature may cause the metal to deteriorate and become brittle. Sometimes, however, economics favor this type of operation.

One way to circumvent the problem of low metal strength is to use a metal inner liner surrounded by insulating material, which in turn is confined by a pressure vessel. The liner, in some cases, may have perforations which will allow pressure to pass through the insulation and act on the outer shell, which is kept cool to obtain normal strength. The liner has no pressure differential acting on it and, therefore, does not need much strength. Ceramic linings are also useful for high-temperature work.

Lined vessels are used for many applications. Any type of lining can be used in an ASME Code vessel, provided it is compatible with the metal of the vessel and the contents. Glass, rubber, plastics, rare metals, and ceramics are a few types. The lining may be installed separately, or if a metal is used, it may be in the form of clad plate. The cladding on plate can sometimes be considered as a stress-carrying part of the vessel.

A **ceramic lining** when used with high temperature acts as an insulator so that the steel outer shell is at a moderate temperature while the temperature at the inside of the lining may be very high. Ceramic linings may be of unstressed brick, or prestressed brick, or cast in place. Cast ceramic linings or unstressed brick may develop cracks and are used when the contents of the vessel will not damage the outer shell. They are usually designed so that the high temperature at the inside will expand them sufficiently to make them tight in the outer (and cooler) shell. This, however, is not usually sufficient to prevent some penetration by the product.

Prestressed-brick linings can be used to protect the outer shell. In this case, the bricks are installed with a special thermosetting-resin mortar. After lining, the vessel is subjected to internal pressure and heat. This expands the steel vessel shell, and the mortar expands to take up the space. The pressure and temperature must be at least as high as the maximum that will be encountered in service. After the mortar has set, reduction of pressure and temperature will allow the vessel to contract, putting the brick in compression. The upper temperature limit for this construction is about 190°C (375°F). The installation of such linings is highly specialized work done by a few companies. Great care is usually exercised in operation to protect the vessel from exposure to unsymmetrical temperature gradients. Side nozzles and other unsymmetrical designs are avoided insofar as possible.

Concrete pressure vessels may be used in applications that require large sizes. Such vessels, if made of steel, would be too large and heavy to ship. Through the use of posttensioned (prestressed) concrete, the vessel is fabricated on the site. In this construction, the reinforcing steel is placed in tubes or plastic covers, which are cast into the concrete. Tension is applied to the steel after the concrete has acquired most of its strength.

Concrete nuclear reactor vessels, of the order of magnitude of 15-m (50-ft) inside diameter and length, have inner linings of steel which confine the pressure. After fabrication of the liner, the tubes for the cables or wires are put in place and the concrete is poured. High-strength reinforcing steel is used. Because there are thousands of reinforcing tendons in the concrete vessel, there is a statistical factor of safety. The failure of 1 or even 10 tendons would have little effect on the overall structure.

Plastic pressure vessels have the *advantages of chemical resistance* and light weight. Above 103 kPa (15 lbf/in²), with certain exceptions, they must be designed according to the ASME Code Section X (see "Storage of Gases") and are confined to the three types of approved code construction. Below 103 kPa (15 lbf/in²), any construction may be used. Even in this pressure range, however, the code should be used for guidance. Solid plastics, because of low strength and creep, can be used only for the lowest pressures and sizes. A stress of a few hundred pounds-force per square inch is the maximum for most plastics. To obtain higher strength, the filled plastics or filament-wound vessels, specified by the code, must be used. Solid-plastic parts, however, are often employed inside a steel shell, particularly for heat exchangers.

Graphite and ceramic vessels are used fully armored; that is, they are enclosed within metal pressure vessels. These materials are also used for boxlike vessels with backing plates on the sides. The plates are drawn together by tie bolts, thus putting the material in compression so that it can withstand low pressure.

ASME Code Developments At the time of this publication, ASME Section VIII is currently being rewritten and reorganized into three classes. Class 1 will be for low-pressure vessels employing spot radiography. Class 2 will be for vessels requiring full radiography. Class 3 will be for vessels experiencing fatigue. This rewriting effort is also using material stress levels similar to those of competing vessel codes from Europe and Asia.

Vessel Codes Other than ASME Different design and construction rules are used in other countries. Chemical engineers concerned with pressure vessels outside the United States must become familiar with local pressure-vessel laws and regulations. *Boilers and Pressure Vessels*, an international survey of design and approval requirements published by the British Standards Institution, Maylands Avenue, Hemel Hempstead, Hertfordshire, England, in 1975, gives pertinent information for 76 political jurisdictions.

The British Code (British Standards) and the German Code (*A. D. Merkblätter*) in addition to the ASME Code are most commonly permitted, although Netherlands, Sweden, and France also have codes. The major difference between the codes lies in factors of safety and in whether or not ultimate strength is considered. ASME Code, Sec. VIII, Division 1, vessels are generally heavier than vessels built to the other codes; however, the differences in allowable stress for a given material are less in the higher temperature (creep) range.

Engineers and metallurgists have developed alloys to comply economically with individual codes. In Germany, where design stress is determined from yield strength and creep-rupture strength and no

allowance is made for ultimate strength, steels which have a very high yield-strength-to-ultimate-strength ratio are used.

Other differences between codes include different bases for the design of reinforcement for openings and the design of flanges and heads. Some codes include rules for the design of heat-exchanger tube sheets, while others (ASME Code) do not. The Dutch Code (*Grondslagen*) includes very specific rules for calculation of wind loads, while the ASME Code leaves this entirely to the designer.

There are also significant differences in construction and inspection rules. Unless engineers make a detailed study of the individual codes and keep current, they will be well advised to make use of responsible experts for any of the codes.

Vessel Design and Construction The ASME Code lists a number of loads that must be considered in designing a pressure vessel. Among them are impact, weight of the vessel under operating and test conditions, superimposed loads from other equipment and piping, wind and earthquake loads, temperature-gradient stresses, and localized loadings from internal and external supports. In general, the code gives no values for these loads or methods for determining them, and no formulas are given for determining the stresses from these loads. Engineers must be knowledgeable in mechanics and strength of materials to solve these problems.

Some of the problems are treated by Brownell and Young, *Process Equipment Design*, Wiley, New York, 1959. ASME papers treat others, and a number of books published by the ASME are collections of papers on pressure-vessel design: *Pressure Vessels and Piping Design: Collected Papers, 1927-1959*; *Pressure Vessels and Piping Design and Analysis*, four volumes; and *International Conference: Pressure Vessel Technology*, published annually.

Throughout the year the Welding Research Council publishes bulletins which are final reports from projects sponsored by the council, important papers presented before engineering societies, and other reports of current interest which are not published in *Welding Research*. A large number of the published bulletins are pertinent for vessel designers.

Care of Pressure Vessels Protection against **excessive pressure** is largely taken care of by code requirements for relief devices. Exposure to fire is also covered by the code. The code, however, does not provide for the possibility of local overheating and weakening of a vessel in a fire. Insulation reduces the required relieving capacity and also reduces the possibility of local overheating.

A pressure-reducing valve in a line leading to a pressure vessel is not adequate protection against overpressure. Its failure will subject the vessel to full line pressure.

Vessels that have an operating cycle which involves the solidification and remelting of solids can develop excessive pressures. A solid plug of material may seal off one end of the vessel. If heat is applied at that end to cause melting, the expansion of the liquid can build up a high pressure and possibly result in yielding or rupture. Solidification in connecting piping can create similar problems.

Some vessels may be exposed to a runaway chemical reaction or even an explosion. This requires relief valves, rupture disks, or, in extreme cases, a frangible roof design or barricade (the vessel is expendable). A vessel with a large rupture disk needs anchors designed for the jet thrust when the disk blows.

Vacuum must be considered. It is nearly always possible that the contents of a vessel might contract or condense sufficiently to subject it to an internal vacuum. If the vessel cannot withstand the vacuum, it must have vacuum-breaking valves.

Improper operation of a process may result in the vessel's **exceeding design temperature**. Proper control is the only solution to this problem. Maintenance procedures can also cause excessive temperatures. Sometimes the contents of a vessel may be burned out with torches. If the flame impinges on the vessel shell, overheating and damage may occur.

Excessively low temperature may involve the hazard of brittle fracture. A vessel that is out of use in cold weather could be at a sub-zero temperature and well below its nil-ductility temperature. In startup, the vessel should be warmed slowly and uniformly until it is above the NDT. A safe value is 38°C (100°F) for plate if the NDT is unknown. The vessel should not be pressurized until this temperature is exceeded. Even after the NDT has been passed, excessively rapid heating or cooling can cause high thermal stresses.

Corrosion is probably the greatest threat to vessel life. Partially filled vessels frequently have severe pitting at the liquid-vapor interface. Vessels usually do not have a corrosion allowance on the outside. Lack of protection against the weather or against the drip of corrosive chemicals can reduce vessel life. Insulation may contain damaging substances. Chlorides in insulating materials can cause cracking of stainless steels. Water used for hydrotesting should be free of chlorides.

Pressure vessels should be **inspected periodically**. No rule can be given for the frequency of these inspections. Frequency depends on operating conditions. If the early inspections of a vessel indicate a low corrosion rate, intervals between inspections may be lengthened. Some vessels are inspected at 5-year intervals; others, as frequently as once a year. Measurement of corrosion is an important inspection item. One of the most convenient ways of measuring thickness (and corrosion) is to use an ultrasonic gauge. The location of the corrosion and whether it is uniform or localized in deep pits should be observed and reported. Cracks, any type of distortion, and leaks should be observed. Cracks are particularly dangerous because they can lead to sudden failure. Insulation is usually left in place during inspection of insulated vessels. If, however, severe external corrosion is suspected, the insulation should be removed. All forms of nondestructive testing are useful for examinations.

There are many ways in which a pressure vessel can suffer **mechanical damage**. The shells can be dented or even punctured, they can be dropped or have hoisting cables improperly attached, bolts can be broken, flanges are bent by excessive bolt tightening, gasket contact faces can be scratched and dented, rotating paddles can drag against the shell and cause wear, and a flange can be bolted up with a gasket half in the groove and half out. Most of these forms of damage can be prevented by care and common sense. If damage is repaired by straightening, as with a dented shell, it may be necessary to stress-relieve the repaired area. Some steels are susceptible to embrittlement by aging after severe straining. A safer procedure is to cut out the damaged area and replace it.

The National Board Inspection Code, published by the National Board of Boiler and Pressure Vessel Inspectors, Columbus, Ohio, is helpful. Any repair, however, is acceptable if it is made in accordance with the rules of the Pressure Vessel Code.

Care in **reassembling** the vessel is particularly important. Gaskets should be properly located, particularly if they are in grooves. Bolts should be tightened in proper sequence. In some critical cases and with large bolts, it is necessary to control bolt tightening by torque wrenches, micrometers, patented bolt-tightening devices, or heating bolts. After assembly, vessels are sometimes given a hydrostatic test.

Pressure-Vessel Cost and Weight Figure 10-196 can be used for estimating carbon-steel vessel cost when a weight estimate is not available and Fig. 10-197 with a weight estimate. Weight and cost include skirts and other supports. The cost is based on several 2005 pressure-vessels. Costs are for vessels not of unusual design. Complicated vessels could cost considerably more. Guthrie [*Chem. Eng.*, 76(6), 114-142 (1969)] also gives pressure-vessel cost data.

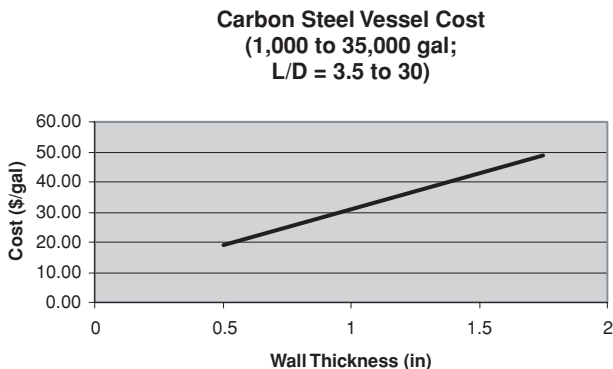


FIG. 10-196 Carbon-steel pressure-vessel cost as a function of wall thickness. 1 gal = 0.003875 cm³; 1 in = 0.0254 m. (Courtesy of E. S. Fox, Ltd.)

Carbon Steel Vessel Cost
(1,000 to 35,000 gal;
L/D = 3.5 to 30)

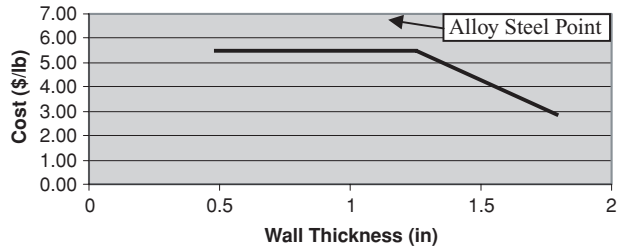


FIG. 10-197 Carbon-steel pressure-vessel cost as a function of wall thickness. 1 gal = 0.003875 cm³; 1 in = 0.0254 m; 1 lb = 0.4536 kg. (Courtesy of E. S. Fox, Ltd.)

When vessels have complicated construction (large, heavy bolted connections, support skirts, etc.), it is preferable to estimate their weight and apply a unit cost in dollars per pound.

Pressure-vessel weights are obtained by calculating the cylindrical shell and heads separately and then adding the weights of nozzles and attachments. Steel weighs 7817 kg/m³ (488 lb/ft³). Metal in heads can be approximated by calculating the area of the blank (disk) used for forming the head. The required diameter of blank can be calculated by multiplying the head outside diameter by the approximate factors given in Table 10-62. These factors make no allowance for the straight flange which is a cylindrical extension that is formed on the head. The blank diameter obtained from these factors must be increased by twice the length of straight flange, which is usually 1½ to 2 in but can be up to several inches in length. Manufacturers' catalogs give weights of heads.

Forming a head thin in certain areas. To obtain the required minimum thickness of a head, it is necessary to use a plate that is initially thicker. Table 10-63 gives allowances for additional thickness.

Nozzles and flanges may add considerably to the weight of a vessel. Their weights can be obtained from manufacturers' catalogs (Taylor Forge Division of Gulf & Western Industries, Inc., Tube Turns Inc., Ladish Co., Lenape Forge, and others). Other parts such as skirts, legs, support brackets, and other details must be calculated.

TABLE 10-62 Factors for Estimating Diameters of Blanks for Formed Heads

	Ratio d/t	Blank diameter factor
ASME head	Over 50	1.09
	30-50	1.11
	20-30	1.15
Ellipsoidal head	Over 20	1.24
	10-20	1.30
Hemispherical head	Over 30	1.60
	18-30	1.65
	10-18	1.70

d = head diameter
 t = nominal minimum head thickness

TABLE 10-63 Extra Thickness Allowances for Formed Heads*

Minimum head thickness, in	Extra thickness, in		
	ASME and ellipsoidal		Hemispherical
	Head o.d. up to 150 in incl.	Head o.d. over 150 in	
Up to 0.99	1/16	1/8	3/16
1 to 1.99	1/8	1/8	3/8
2 to 2.99	1/4	1/4	5/8

*Lukens, Inc.

SECTION 11

Heat-Transfer
Equipment

PERRY'S CHEMICAL ENGINEERS' HANDBOOK

8TH EDITION



RICHARD L. SHILLING, PATRICK M. BERNHAGEN
VICTOR M. GOLDSCHMIDT, PREDRAG S. HRNJAK
DAVID JOHNSON, KLAUS D. TIMMERHAUS

Copyright © 2008, 1997, 1984, 1973, 1963, 1950, 1941, 1934 by The McGraw-Hill Companies, Inc. All rights reserved. Manufactured in the United States of America. Except as permitted under the United States Copyright Act of 1976, no part of this publication may be reproduced or distributed in any form or by any means, or stored in a database or retrieval system, without the prior written permission of the publisher.

0-07-154218-3

The material in this eBook also appears in the print version of this title: 0-07-151134-2.

All trademarks are trademarks of their respective owners. Rather than put a trademark symbol after every occurrence of a trademarked name, we use names in an editorial fashion only, and to the benefit of the trademark owner, with no intention of infringement of the trademark. Where such designations appear in this book, they have been printed with initial caps.

McGraw-Hill eBooks are available at special quantity discounts to use as premiums and sales promotions, or for use in corporate training programs. For more information, please contact George Hoare, Special Sales, at george_hoare@mcgraw-hill.com or (212) 904-4069.

TERMS OF USE

This is a copyrighted work and The McGraw-Hill Companies, Inc. (“McGraw-Hill”) and its licensors reserve all rights in and to the work. Use of this work is subject to these terms. Except as permitted under the Copyright Act of 1976 and the right to store and retrieve one copy of the work, you may not decompile, disassemble, reverse engineer, reproduce, modify, create derivative works based upon, transmit, distribute, disseminate, sell, publish or sublicense the work or any part of it without McGraw-Hill’s prior consent. You may use the work for your own noncommercial and personal use; any other use of the work is strictly prohibited. Your right to use the work may be terminated if you fail to comply with these terms.

THE WORK IS PROVIDED “AS IS.” McGRAW-HILL AND ITS LICENSORS MAKE NO GUARANTEES OR WARRANTIES AS TO THE ACCURACY, ADEQUACY OR COMPLETENESS OF OR RESULTS TO BE OBTAINED FROM USING THE WORK, INCLUDING ANY INFORMATION THAT CAN BE ACCESSED THROUGH THE WORK VIA HYPERLINK OR OTHERWISE, AND EXPRESSLY DISCLAIM ANY WARRANTY, EXPRESS OR IMPLIED, INCLUDING BUT NOT LIMITED TO IMPLIED WARRANTIES OF MERCHANTABILITY OR FITNESS FOR A PARTICULAR PURPOSE. McGraw-Hill and its licensors do not warrant or guarantee that the functions contained in the work will meet your requirements or that its operation will be uninterrupted or error free. Neither McGraw-Hill nor its licensors shall be liable to you or anyone else for any inaccuracy, error or omission, regardless of cause, in the work or for any damages resulting therefrom. McGraw-Hill has no responsibility for the content of any information accessed through the work. Under no circumstances shall McGraw-Hill and/or its licensors be liable for any indirect, incidental, special, punitive, consequential or similar damages that result from the use of or inability to use the work, even if any of them has been advised of the possibility of such damages. This limitation of liability shall apply to any claim or cause whatsoever whether such claim or cause arises in contract, tort or otherwise.

DOI: 10.1036/0071511342

Heat-Transfer Equipment*

Richard L. Shilling, P.E., B.S.M., B.E.M.E. *Vice President of Engineering, Koch Heat Transfer Company LP; American Society of Mechanical Engineers (Section Editor, Shell-and-Tube Heat Exchangers, Hairpin/Double-Pipe Heat Exchangers, Air-Cooled Heat Exchangers, Heating and Cooling of Tanks, Fouling and Scaling, Heat Exchangers for Solids, Thermal Insulation, Thermal Design of Evaporators, Evaporators)*

Patrick M. Bernhagen, P.E., B.S.M.E. *Sales Manager—Fired Heater, Foster Wheeler North America Corp.; American Society of Mechanical Engineers (Compact and Nontubular Heat Exchangers)*

Victor M. Goldschmidt, Ph.D., P.E. *Professor Emeritus, Mechanical Engineering, Purdue University (Air Conditioning)*

Predrag S. Hrnjak, Ph.D., V.Res. *Assistant Professor, University of Illinois at Urbana-Champaign; Principal Investigator—U of I Air Conditioning and Refrigeration Center; Assistant Professor, University of Belgrade; International Institute of Chemical Engineers; American Society of Heat, Refrigerating, and Air Conditioning Engineers (Refrigeration)*

David Johnson, P.E., M.S.C.E. *Heat Exchanger Specialist, A&A Technology, B.P. p.l.c.; American Institute of Chemical Engineers; American Society of Mechanical Engineers; API Subcommittee on Heat Transfer Equipment; API 660/ISO 16812, API 661/ISO 13706, API 662/ISO 15547 (Thermal Design of Heat Exchangers, Condensers, Reboilers)*

Klaus D. Timmerhaus, Ph.D., P.E. *Professor and President's Teaching Scholar, University of Colorado; Fellow, American Institute of Chemical Engineers, American Society for Engineering Education, American Association for the Advancement of Science; Member, American Astronautical Society, National Academy of Engineering, Austrian Academy of Science, International Institute of Refrigeration, American Society of Heat, Refrigerating, and Air Conditioning Engineers, American Society of Environmental Engineers, Engineering Society for Advancing Mobility on Land, Sea, Air, and Space, Sigma Xi, The Research Society (Cryogenic Processes)*

THERMAL DESIGN OF HEAT-TRANSFER EQUIPMENT

Introduction to Thermal Design	11-4	Thermal Design for Single-Phase Heat Transfer	11-5
Approach to Heat-Exchanger Design	11-4	Double-Pipe Heat Exchangers	11-5
Overall Heat-Transfer Coefficient	11-4	Baffled Shell-and-Tube Exchangers	11-7
Mean Temperature Difference	11-4	Thermal Design of Condensers	11-11
Countercurrent or Cocurrent Flow	11-4	Single-Component Condenser	11-11
Reversed, Mixed, or Cross-Flow	11-5	Multicomponent Condensers	11-12
		Thermal Design of Reboilers	11-13

*The prior and substantial contributions of Frank L. Rubin (Section Editor, Sixth Edition) and Dr. Kenneth J. Bell (Thermal Design of Heat Exchangers, Condensers, Reboilers), Dr. Thomas M. Flynn (Cryogenic Processes), and F. C. Standiford (Thermal Design of Evaporators, Evaporators), who were authors for the Seventh Edition, are gratefully acknowledged.

11-2 HEAT-TRANSFER EQUIPMENT

Kettle Reboilers	11-13	Tube-Bundle Bypassing	11-44
Vertical Thermosiphon Reboilers	11-13	Helical Baffles	11-45
Forced-Recirculation Reboilers	11-13	Longitudinal Flow Baffles	11-45
Thermal Design of Evaporators	11-13	Corrosion in Heat Exchangers	11-45
Forced-Circulation Evaporators	11-14	Materials of Construction	11-45
Long-Tube Vertical Evaporators	11-14	Bimetallic Tubes	11-45
Short-Tube Vertical Evaporators	11-15	Clad Tube Sheets	11-46
Miscellaneous Evaporator Types	11-16	Nonmetallic Construction	11-46
Heat Transfer from Various Metal Surfaces	11-16	Fabrication	11-46
Effect of Fluid Properties on Heat Transfer	11-17	Shell-and-Tube Exchanger Costs	11-46
Effect of Noncondensables on Heat Transfer	11-18		
Batch Operations: Heating and Cooling of Vessels	11-18		
Nomenclature	11-18	HAIRPIN/DOUBLE-PIPE HEAT EXCHANGERS	
Applications	11-18	Principles of Construction	11-48
Effect of External Heat Loss or Gain	11-19	Finned Double Pipes	11-48
Internal Coil or Jacket Plus External Heat Exchange	11-19	Multitube Hairpins	11-48
Equivalent-Area Concept	11-19	Design Applications	11-49
Nonagitated Batches	11-20		
Storage Tanks	11-20	AIR-COOLED HEAT EXCHANGERS	
Thermal Design of Tank Coils	11-20	Air Cooled Heat Exchangers	11-49
Nomenclature	11-20	Forced and Induced Draft	11-49
Maintenance of Temperature	11-20	Tube Bundle	11-50
Heating	11-20	Tubing	11-51
Heating and Cooling of Tanks	11-21	Finned-Tube Construction	11-51
Tank Coils	11-21	Fans	11-51
Teflon Immersion Coils	11-22	Fan Drivers	11-51
Bayonet Heaters	11-22	Fan Ring and Plenum Chambers	11-52
External Coils and Tracers	11-22	Air-Flow Control	11-52
Jacketed Vessels	11-22	Air Recirculation	11-52
Extended or Finned Surfaces	11-22	Trim Coolers	11-52
Finned-Surface Application	11-22	Humidification Chambers	11-52
High Fins	11-23	Evaporative Cooling	11-53
Low Fins	11-23	Steam Condensers	11-53
Fouling and Scaling	11-23	Air-Cooled Overhead Condensers	11-53
Control of Fouling	11-23	Air-Cooled Heat-Exchanger Costs	11-53
Fouling Transients and Operating Periods	11-24	Design Considerations	11-53
Removal of Fouling Deposits	11-24		
Fouling Resistances	11-24	COMPACT AND NONTUBULAR HEAT EXCHANGERS	
Typical Heat-Transfer Coefficients	11-24	Compact Heat Exchangers	11-54
Thermal Design for Solids Processing	11-24	Plate-and-Frame Exchangers	11-54
Conductive Heat Transfer	11-24	Gasketed-Plate Exchangers	11-54
Contactive (Direct) Heat Transfer	11-29	Description	11-54
Convective Heat Transfer	11-30	Applications	11-54
Radiative Heat Transfer	11-30	Design	11-55
Scraped-Surface Exchangers	11-31	Welded- and Brazed-Plate Exchangers	11-57
		Combination Welded-Plate Exchangers	11-57
		Spiral-Plate Exchangers	11-57
		Description	11-57
		Applications	11-57
		Design	11-57
		Brazed-Plate-Fin Heat Exchangers	11-58
		Design and Application	11-58
		Plate-Fin Tubular Exchangers (PFE)	11-58
		Description	11-58
		Applications	11-58
		Design	11-58
		Printed-Circuit Heat Exchangers	11-58
		Spiral-Tube Exchangers (STE)	11-59
		Description	11-59
		Applications	11-59
		Design	11-59
		Graphite Heat Exchangers	11-59
		Description	11-59
		Applications and Design	11-59
		Cascade Coolers	11-59
		Bayonet-Tube Exchangers	11-59
		Atmospheric Sections	11-60
		Nonmetallic Heat Exchangers	11-60
		PVDF Heat Exchangers	11-60
		Ceramic Heat Exchangers	11-60
		Teflon Heat Exchangers	11-60
		HEAT EXCHANGERS FOR SOLIDS	
		Equipment for Solidification	11-60
		Table Type	11-61
		Agitated-Pan Type	11-61
		Vibratory Type	11-61
		Belt Types	11-61
		Rotating-Drum Type	11-62
		Rotating-Shelf Type	11-62
TEMA-STYLE SHELL-AND-TUBE HEAT EXCHANGERS			
Types and Definitions	11-33		
TEMA Numbering and Type Designations	11-33		
Functional Definitions	11-35		
General Design Considerations	11-35		
Selection of Flow Path	11-35		
Construction Codes	11-35		
Tube Bundle Vibration	11-36		
Testing	11-36		
Principal Types of Construction	11-36		
Fixed-Tube-Sheet Heat Exchangers	11-36		
U-Tube Heat Exchanger	11-37		
Packed-Lantern-Ring Exchanger	11-39		
Outside-Packed Floating-Head Exchanger	11-39		
Internal Floating-Head Exchanger	11-40		
Pull-Through Floating-Head Exchanger	11-40		
Falling-Film Exchangers	11-40		
Tube-Side Construction	11-41		
Tube-Side Header	11-41		
Special High-Pressure Closures	11-41		
Tube-Side Passes	11-41		
Tubes	11-41		
Rolled Tube Joints	11-41		
Welded Tube Joints	11-41		
Double-Tube-Sheet Joints	11-43		
Shell-Side Construction	11-43		
Shell Sizes	11-43		
Shell-Side Arrangements	11-43		
Baffles and Tube Bundles	11-43		
Segmental Baffles	11-43		
Rod Baffles	11-43		
Tie Rods and Spacers	11-44		
Impingement Baffle	11-44		
Vapor Distribution	11-44		

Equipment for Fusion of Solids	11-63
Horizontal-Tank Type	11-63
Vertical Agitated-Kettle Type	11-63
Mill Type	11-63
Heat-Transfer Equipment for Sheeted Solids	11-63
Cylinder Heat-Transfer Units	11-63
Heat-Transfer Equipment for Divided Solids	11-64
Fluidized-Bed Type	11-65
Moving-Bed Type	11-65
Agitated-Pan Type	11-65
Kneading Devices	11-65
Shelf Devices	11-66
Rotating-Shell Devices	11-66
Conveyor-Belt Devices	11-67
Spiral-Conveyor Devices	11-67
Double-Cone Blending Devices	11-68
Vibratory-Conveyor Devices	11-68
Elevator Devices	11-69
Pneumatic-Conveying Devices	11-69
Vacuum-Shelf Types	11-70

THERMAL INSULATION

Insulation Materials	11-70
Materials	11-70
Thermal Conductivity (<i>K</i> Factor)	11-70
Finishes	11-70
System Selection	11-71
Cryogenic High Vacuum	11-71
Low Temperature	11-71
Moderate and High Temperature	11-72
Economic Thickness of Insulation	11-72
Recommended Thickness of Insulation	11-73
Example 1	11-76
Example 2	11-76
Example 3	11-76
Installation Practice	11-76
Pipe	11-76
Method of Securing	11-76
Double Layer	11-76
Finish	11-76
Tanks, Vessels, and Equipment	11-76
Method of Securing	11-76
Finish	11-76

AIR CONDITIONING

Introduction	11-76
Comfort Air Conditioning	11-76
Industrial Air Conditioning	11-76
Ventilation	11-76
Air-Conditioning Equipment	11-77
Central Systems	11-77
Unitary Refrigerant-Based Air-Conditioning Systems	11-77
Load Calculation	11-77

REFRIGERATION

Introduction	11-78
Basic Principles	11-78
Basic Refrigeration Methods	11-79
Mechanical Refrigeration (Vapor-Compression Systems)	11-79
Vapor-Compression Cycles	11-79
Multistage Systems	11-79
Cascade System	11-82
Equipment	11-82
Compressors	11-82
Positive-Displacement Compressors	11-83
Centrifugal Compressors	11-85
Condensers	11-85
Evaporators	11-87
System Analysis	11-87
System, Equipment, and Refrigerant Selection	11-90
Other Refrigerant Systems Applied in the Industry	11-90
Absorption Refrigeration Systems	11-90
Steam-Jet (Ejector) Systems	11-94

Multistage Systems	11-96
Capacity Control	11-96
Refrigerants	11-96
Secondary Refrigerants (Antifreezes or Brines)	11-97
Organic Compounds (Inhibited Glycols)	11-98
Safety in Refrigeration Systems	11-98

CRYOGENIC PROCESSES

Introduction	11-99
Properties of Cryogenic Fluids	11-99
Properties of Solids	11-99
Structural Properties at Low Temperatures	11-99
Thermal Properties at Low Temperatures	11-100
Electrical Properties at Low Temperatures	11-100
Superconductivity	11-100
Refrigeration and Liquefaction	11-100
Principles	11-100
Expansion Types of Refrigerators	11-100
Miniature Refrigerators	11-103
Thermodynamic Analyses of Cycles	11-103
Process Equipment	11-103
Heat Exchangers	11-103
Expanders	11-104
Separation and Purification Systems	11-104
Air-Separation Systems	11-104
Helium and Natural-Gas Systems Separation	11-106
Gas Purification	11-106
Storage and Transfer Systems	11-107
Insulation Principles	11-107
Types of Insulation	11-107
Storage and Transfer Systems	11-108
Cryogenic Instrumentation	11-108
Pressure	11-109
Liquid Level	11-109
Flow	11-109
Temperature	11-109
Safety	11-109
Physiological Hazards	11-109
Materials and Construction Hazards	11-109
Flammability and Explosion Hazards	11-110
High-Pressure Gas Hazards	11-110
Summary	11-110

EVAPORATORS

Primary Design Problems	11-110
Heat Transfer	11-110
Vapor-Liquid Separation	11-110
Selection Problems	11-110
Product Quality	11-110
Evaporator Types and Applications	11-111
Forced-Circulation Evaporators	11-111
Swirl Flow Evaporators	11-111
Short-Tube Vertical Evaporators	11-112
Long-Tube Vertical Evaporators	11-112
Horizontal-Tube Evaporators	11-113
Miscellaneous Forms of Heating Surface	11-114
Evaporators without Heating Surfaces	11-114
Utilization of Temperature Difference	11-114
Vapor-Liquid Separation	11-114
Evaporator Arrangement	11-116
Single-Effect Evaporators	11-116
Thermocompression	11-116
Multiple-Effect Evaporation	11-116
Seawater Evaporators	11-117
Evaporator Calculations	11-118
Single-Effect Evaporators	11-118
Thermocompression Evaporators	11-118
Flash Evaporators	11-118
Multiple-Effect Evaporators	11-119
Optimization	11-119
Evaporator Accessories	11-119
Condensers	11-119
Vent Systems	11-120
Salt Removal	11-120
Evaporator Operation	11-121

THERMAL DESIGN OF HEAT-TRANSFER EQUIPMENT

INTRODUCTION TO THERMAL DESIGN

Designers commonly use computer software to design heat exchangers. The best sources of such software are Heat Transfer Research, Inc. (HTRI), and Heat Transfer and Fluid Flow Services (HTFS), a division of ASPENTECH. These are companies that develop proprietary correlations based on their research and provide software that utilizes these correlations. However, it is important that engineers understand the fundamental principles that lie beneath the framework of the software. Therefore, design methods for several important classes of process heat-transfer equipment are presented in the following portions of Sec. 11. Mechanical descriptions and specifications of equipment are given in this section and should be read in conjunction with the use of this material. It is impossible to present here a comprehensive treatment of heat-exchanger selection, design, and application. The best general references in this field are Hewitt, Shires, and Bott, *Process Heat Transfer*, CRC Press, Boca Raton, FL, 1994; and Schlünder (ed.), *Heat Exchanger Design Handbook*, Begell House, New York, 2002.

Approach to Heat-Exchanger Design The proper use of basic heat-transfer knowledge in the design of practical heat-transfer equipment is an art. Designers must be constantly aware of the differences between the idealized conditions for and under which the basic knowledge was obtained and the real conditions of the mechanical expression of their design and its environment. The result must satisfy process and operational requirements (such as availability, flexibility, and maintainability) and do so economically. An important part of any design process is to consider and offset the consequences of error in the basic knowledge, in its subsequent incorporation into a design method, in the translation of design into equipment, or in the operation of the equipment and the process. Heat-exchanger design is not a highly accurate art under the best of conditions.

The design of a process heat exchanger usually proceeds through the following steps:

1. Process conditions (stream compositions, flow rates, temperatures, pressures) must be specified.
2. Required physical properties over the temperature and pressure ranges of interest must be obtained.
3. The type of heat exchanger to be employed is chosen.
4. A preliminary estimate of the size of the exchanger is made, using a heat-transfer coefficient appropriate to the fluids, the process, and the equipment.
5. A first design is chosen, complete in all details necessary to carry out the design calculations.
6. The design chosen in step 5 is evaluated, or *rated*, as to its ability to meet the process specifications with respect to both heat transfer and pressure drop.
7. On the basis of the result of step 6, a new configuration is chosen if necessary and step 6 is repeated. If the first design was inadequate to meet the required heat load, it is usually necessary to increase the size of the exchanger while still remaining within specified or feasible limits of pressure drop, tube length, shell diameter, etc. This will sometimes mean going to multiple-exchanger configurations. If the first design more than meets heat-load requirements or does not use all the allowable pressure drop, a less expensive exchanger can usually be designed to fulfill process requirements.
8. The final design should meet process requirements (within reasonable expectations of error) at lowest cost. The lowest cost should include operation and maintenance costs and credit for ability to meet long-term process changes, as well as installed (capital) cost. Exchangers should not be selected entirely on a lowest-first-cost basis, which frequently results in future penalties.

* This assumption is vital but is usually omitted or less satisfactorily stated as "each stream is well mixed at each point." In a heat exchanger with substantial bypassing of the heat-transfer surface, e.g., a typical baffled shell-and-tube exchanger, this condition is not satisfied. However, the error is in some degree offset if the same MTD formulation used in reducing experimental heat-transfer data to obtain the basic correlation is used in applying the correlation to design a heat exchanger. The compensation is not in general exact, and insight and judgment are required in the use of the MTD formulations. Particularly, in the design of an exchanger with a very close temperature approach, bypassing may result in an exchanger that is inefficient and even thermodynamically incapable of meeting specified outlet temperatures.

Overall Heat-Transfer Coefficient The basic design equation for a heat exchanger is

$$dA = dQ/U \Delta T \quad (11-1)$$

where dA is the element of surface area required to transfer an amount of heat dQ at a point in the exchanger where the overall heat-transfer coefficient is U and where the overall bulk temperature difference between the two streams is ΔT . The overall heat-transfer coefficient is related to the individual film heat-transfer coefficients and fouling and wall resistances by Eq. (11-2). Basing U_o on the outside surface area A_o results in

$$U_o = \frac{1}{1/h_o + R_{do} + xA_o/k_w A_{wm} + (1/h_i + R_{di})A_o/A_i} \quad (11-2)$$

Equation (11-1) can be formally integrated to give the outside area required to transfer the total heat load Q_T :

$$A_o = \int_0^{Q_T} \frac{dQ}{U_o \Delta T} \quad (11-3)$$

To integrate Eq. (11-3), U_o and ΔT must be known as functions of Q . For some problems, U_o varies strongly and nonlinearly throughout the exchanger. In these cases, it is necessary to evaluate U_o and ΔT at several intermediate values and numerically or graphically integrate. For many practical cases, it is possible to calculate a constant mean overall coefficient U_{om} from Eq. (11-2) and define a corresponding mean value of ΔT_m , such that

$$A_o = Q_T/U_{om} \Delta T_m \quad (11-4)$$

Care must be taken that U_o does not vary too strongly, that the proper equations and conditions are chosen for calculating the individual coefficients, and that the mean temperature difference is the correct one for the specified exchanger configuration.

Mean Temperature Difference The temperature difference between the two fluids in the heat exchanger will, in general, vary from point to point. The mean temperature difference (ΔT_m or MTD) can be calculated from the terminal temperatures of the two streams if the following assumptions are valid:

1. All elements of a given fluid stream have the same thermal history in passing through the exchanger.*
2. The exchanger operates at steady state.
3. The specific heat is constant for each stream (or if either stream undergoes an isothermal phase transition).
4. The overall heat-transfer coefficient is constant.
5. Heat losses are negligible.

Countercurrent or Cocurrent Flow If the flow of the streams is either *completely* countercurrent or completely cocurrent or if one or both streams are isothermal (condensing or vaporizing a pure component with negligible pressure change), the correct MTD is the logarithmic-mean temperature difference (LMTD), defined as

$$\text{LMTD} = \Delta T_m = \frac{(t'_1 - t''_2) - (t'_2 - t''_1)}{\ln \left(\frac{t'_1 - t''_2}{t'_2 - t''_1} \right)} \quad (11-5a)$$

for *countercurrent flow* (Fig. 11-1a) and

$$\text{LMTD} = \Delta T_m = \frac{(t'_1 - t''_1) - (t'_2 - t''_2)}{\ln \left(\frac{t'_1 - t''_1}{t'_2 - t''_2} \right)} \quad (11-5b)$$

for *cocurrent flow* (Fig. 11-1b)

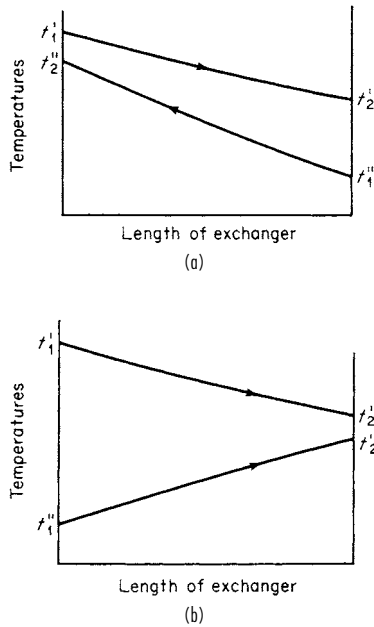


FIG. 11-1 Temperature profiles in heat exchangers. (a) Countercurrent. (b) Cocurrent.

If U is not constant but a linear function of ΔT , the correct value of $U_{om}\Delta T_m$ to use in Eq. (11-4) is [Colburn, *Ind. Eng. Chem.*, **25**, 873 (1933)]

$$U_{om}\Delta T_m = \frac{U_o''(t_1' - t_2'') - U_o'(t_2' - t_1'')}{\ln \left(\frac{U_o''(t_1' - t_2'')}{U_o'(t_2' - t_1'')} \right)} \quad (11-6a)$$

for *countercurrent flow*, where U_o'' is the overall coefficient evaluated when the stream temperatures are t_1' and t_2'' and U_o' is evaluated at t_2' and t_1'' . The corresponding equation for *cocurrent flow* is

$$U_{om}\Delta T_m = \frac{U_o''(t_1' - t_1'') - U_o'(t_2' - t_2'')}{\ln \left(\frac{U_o''(t_1' - t_1'')}{U_o'(t_2' - t_2'')} \right)} \quad (11-6b)$$

where U_o' is evaluated at t_2' and t_2'' and U_o'' is evaluated at t_1' and t_1'' . To use these equations, it is necessary to calculate two values of U_o .

The use of Eq. (11-6) will frequently give satisfactory results even if U_o is not strictly linear with temperature difference.

Reversed, Mixed, or Cross-Flow If the flow pattern in the exchanger is not completely countercurrent or cocurrent, it is necessary to apply a **correction factor** F_T by which the LMTD is multiplied to obtain the appropriate MTD. These corrections have been mathematically derived for flow patterns of interest, still by making assumptions 1 to 5 [see Bowman, Mueller, and Nagle, *Trans. Am. Soc. Mech. Eng.*, **62**, 283 (1940) or Hewitt, et al. op. cit.]. For a common flow pattern, the 1-2 exchanger (Fig. 11-2), the correction factor F_T is given in Fig. 11-4a, which is also valid for finding F_T for a 1-2 exchanger in which the shell-side flow direction is reversed from that shown in Fig. 11-2. Figure 11-4a is also applicable with negligible error to exchangers with one shell pass and any number of tube passes. Values of F_T less than 0.8 (0.75 at the very lowest) are generally unacceptable because the exchanger configuration chosen is inefficient; the chart is difficult to read accurately; and even a small violation of the first assumption

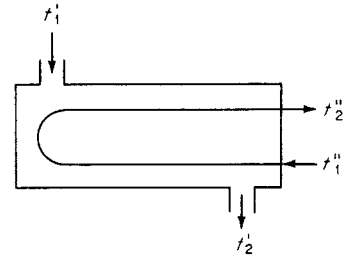


FIG. 11-2 Diagram of a 1-2 exchanger (one well-baffled shell pass and two tube passes with an equal number of tubes in each pass).

underlying the MTD will invalidate the mathematical derivation and lead to a thermodynamically inoperable exchanger.

Correction-factor charts are also available for exchangers with more than one shell pass provided by a longitudinal shell-side baffle. However, these exchangers are seldom used in practice because of mechanical complications in their construction. Also thermal and physical leakages across the longitudinal baffle further reduce the mean temperature difference and are not properly incorporated into the correction-factor charts. Such charts are useful, however, when it is necessary to construct a multiple-shell exchanger train such as that shown in Fig. 11-3 and are included here for two, three, four, and six separate identical shells and two or more tube passes per shell in Fig. 11-4b, c, d, and e. If only one tube pass per shell is required, the piping can and should be arranged to provide pure countercurrent flow, in which case the LMTD is used with no correction.

Cross-flow exchangers of various kinds are also important and require correction to be applied to the LMTD calculated by assuming countercurrent flow. Several cases are given in Fig. 11-4f, g, h, i, and j.

Many other MTD correction-factor charts have been prepared for various configurations. The F_T charts are often employed to make approximate corrections for configurations even in cases for which they are not completely valid.

THERMAL DESIGN FOR SINGLE-PHASE HEAT TRANSFER

Double-Pipe Heat Exchangers The design of double-pipe heat exchangers is straightforward. It is generally conservative to

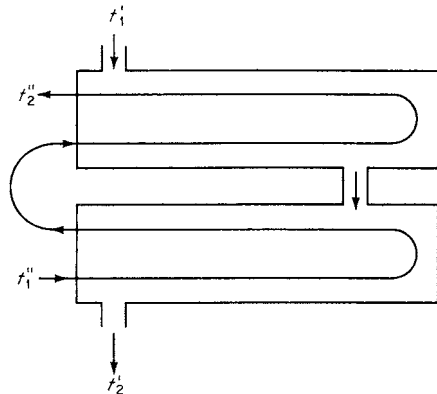


FIG. 11-3 Diagram of a 2-4 exchanger (two separate identical well-baffled shells and four or more tube passes).

*This task can be avoided if a hydrocarbon stream is the limiting resistance by the use of the caloric temperature charts developed by Colburn [*Ind. Eng. Chem.*, **25**, 873 (1933)].

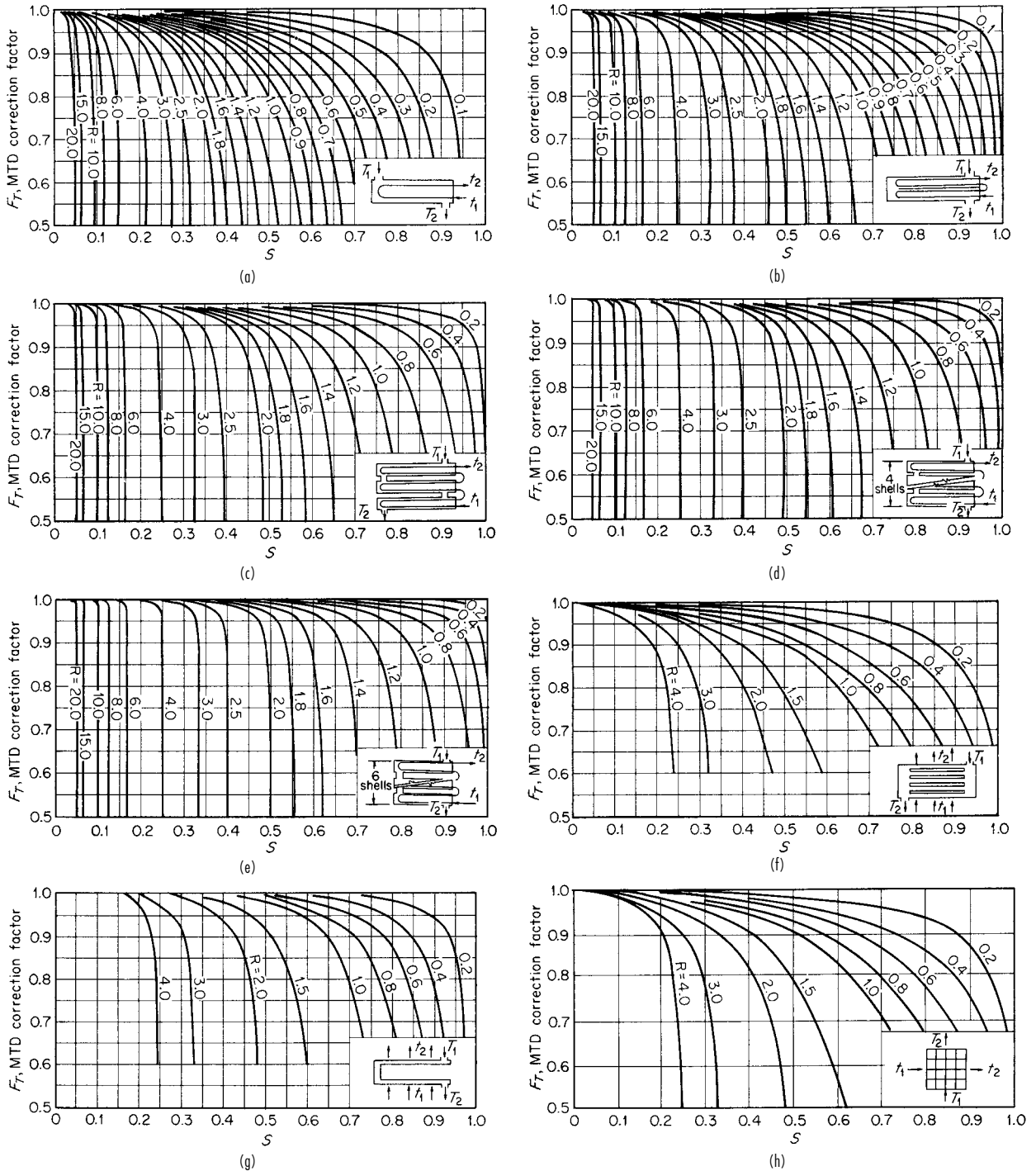


FIG. 11-4 LMTD correction factors for heat exchangers. In all charts, $R = (T_1 - T_2)/(t_2 - t_1)$ and $S = (t_2 - t_1)/(T_1 - t_1)$. (a) One shell pass, two or more tube passes. (b) Two shell passes, four or more tube passes. (c) Three shell passes, six or more tube passes. (d) Four shell passes, eight or more tube passes. (e) Six shell passes, twelve or more tube passes. (f) Cross-flow, one shell pass, one or more parallel rows of tubes. (g) Cross-flow, two passes, two rows of tubes; for more than two passes, use $F_T = 1.0$. (h) Cross-flow, one shell pass, one tube pass, both fluids unmixed. (i) Cross-flow (drip type), two horizontal passes with U-bend connections (trombone type). (j) Cross-flow (drip type), helical coils with two turns.

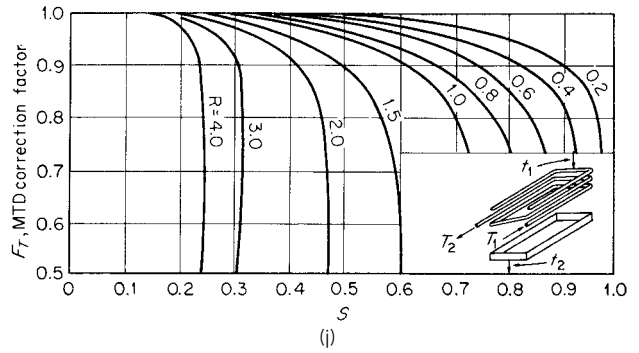
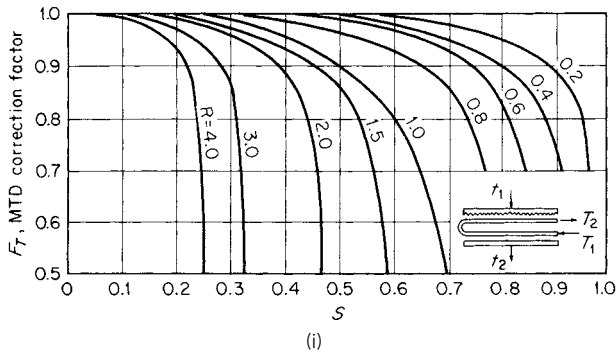


FIG. 11-4 (Continued)

neglect natural-convection and entrance effects in turbulent flow. In laminar flow, natural convection effects can increase the theoretical Graetz prediction by a factor of 3 or 4 for fully developed flows. Pressure drop is calculated by using the correlations given in Sec. 6.

If the inner tube is longitudinally finned on the outside surface, the equivalent diameter is used as the characteristic length in both the Reynolds-number and the heat-transfer correlations. The fin efficiency must also be known to calculate an effective outside area to use in Eq. (11-2).

Fittings contribute strongly to the pressure drop on the annulus side. General methods for predicting this are not reliable, and manufacturer's data should be used when available.

Double-pipe exchangers are often piped in complex series-parallel arrangements on both sides. The MTD to be used has been derived for some of these arrangements and is reported in Kern (*Process Heat Transfer*, McGraw-Hill, New York, 1950). More complex cases may require trial-and-error balancing of the heat loads and rate equations for subsections or even for individual exchangers in the bank.

Baffled Shell-and-Tube Exchangers The method given here is based on the research summarized in Final Report, Cooperative Research Program on Shell and Tube Heat Exchangers, Univ. Del. Eng. Exp. Sta. Bull. 5 (June 1963). The method assumes that the shell-side heat transfer and pressure-drop characteristics are equal to those of the ideal tube bank corresponding to the cross-flow sections of the exchanger, modified for the distortion of flow pattern introduced by the baffles and the presence of leakage and bypass flow through the various clearances required by mechanical construction.

It is assumed that process conditions and physical properties are known and the following are known or specified: tube outside diameter D_o , tube geometrical arrangement (unit cell), shell inside diameter D_s , shell outer tube limit D_{ol} , baffle cut l_c , baffle spacing l_s , and number of sealing strips N_s . The effective tube length between tube sheets L may be either specified or calculated after the heat-transfer coefficient has been determined. If additional specific information (e.g., tube-baffle clearance) is available, the exact values (instead of estimates) of certain parameters may be used in the calculation with some improvement in accuracy. To complete the rating, it is necessary to know also the tube material and wall thickness or inside diameter.

This rating method, though apparently generally the best in the open literature, is not extremely accurate. An exhaustive study by Palen and Taborek [*Chem. Eng. Prog. Symp. Ser. 92*, 65, 53 (1969)] showed that this method predicted shell-side coefficients from about 50 percent low to 100 percent high, while the pressure-drop range was from about 50 percent low to 200 percent high. The mean error for heat transfer was about 15 percent low (safe) for all Reynolds numbers, while the mean error for pressure drop was from about 5 percent low (unsafe) at Reynolds numbers above 1000 to about 100 percent high at Reynolds numbers below 10.

Calculation of Shell-Side Geometrical Parameters

1. Total number of tubes in exchanger N_t . If not known by direct count, estimate using Eq. (11-74) or (11-75).

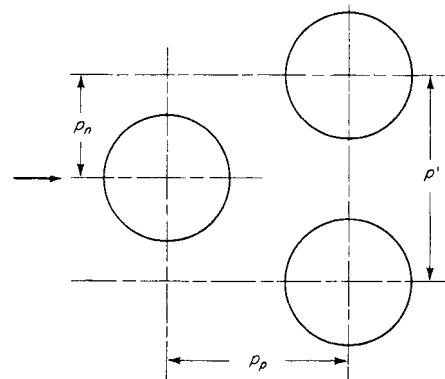
2. Tube pitch parallel to flow p_p and normal to flow p_n . These quantities are needed only for estimating other parameters. If a detailed drawing of the exchanger is available, it is better to obtain these other parameters by direct count or calculation. The pitches are described by Fig. 11-5 and read therefrom for common tube layouts.

3. Number of tube rows crossed in one cross-flow section N_c . Count from exchanger drawing or estimate from

$$N_c = \frac{D_s [1 - 2(l_c/D_s)]}{p_p} \tag{11-7}$$

4. Fraction of total tubes in cross-flow F_c

$$F_c = \frac{1}{\pi} \left[\pi + 2 \frac{D_s - 2l_c}{D_{ol}} \sin \left(\cos^{-1} \frac{D_s - 2l_c}{D_{ol}} \right) - 2 \cos^{-1} \frac{D_s - 2l_c}{D_{ol}} \right] \tag{11-8}$$



Tube O.D. D_o , in.	Tube pitch p' , in.	Layout	p_p , in.	p_n , in.
0.625	0.812		0.704	0.406
0.750	0.938		0.814	0.469
0.750	1		1.000	1.000
0.750	1		0.707	0.707
0.750	1		0.866	0.500
1.000	1.250		1.250	1.250
1.000	1.250		0.884	0.884
1.000	1.250		1.082	0.625

FIG. 11-5 Values of tube pitch for common tube layouts. To convert inches to meters, multiply by 0.0254. Note that D_o , p' , p_p , and p_n have units of inches.

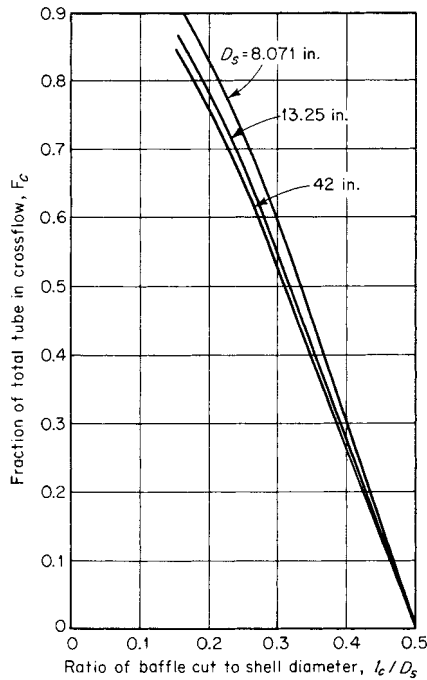


FIG. 11-6 Estimation of fraction of tubes in cross-flow F_c [Eq. (11-8)]. To convert inches to meters, multiply by 0.0254. Note that l_c and D_s have units of inches.

F_c is plotted in Fig. 11-6. This figure is strictly applicable only to splitting, floating-head construction but may be used for other situations with minor error.

5. Number of effective cross-flow rows in each window N_{cw}

$$N_{cw} = \frac{0.8l_c}{p_p} \quad (11-9)$$

6. Cross-flow area at or near centerline for one cross-flow section S_m

a. For rotated and in-line square layouts:

$$S_m = l_s \left[D_s - D_{out} + \frac{D_{out} - D_o}{p_n} (p' - D_o) \right] \text{m}^2 \text{ (ft}^2\text{)} \quad (11-10a)$$

b. For triangular layouts:

$$S_m = l_s \left[D_s - D_{out} + \frac{D_{out} - D_o}{p'} (p' - D_o) \right] \text{m}^2 \text{ (ft}^2\text{)} \quad (11-10b)$$

7. Fraction of cross-flow area available for bypass flow F_{bp}

$$F_{bp} = \frac{(D_s - D_{out})l_s}{S_m} \quad (11-11)$$

8. Tube-to-baffle leakage area for one baffle S_{tb} . Estimate from

$$S_{tb} = bD_o N_T (1 + F_c) \text{m}^2 \text{ (ft}^2\text{)} \quad (11-12)$$

where $b = (6.223)(10^{-4})$ (SI) or $(1.701)(10^{-4})$ (U.S. customary). These values are based on Tubular Exchanger Manufacturers Association (TEMA) Class R construction which specifies $1/32$ -in diametral clearance between tube and baffle. Values should be modified if extra tight or loose construction is specified or if clogging by dirt is anticipated.

9. Shell-to-baffle leakage area for one baffle S_{sb} . If diametral shell-baffle clearance δ_{sb} is known, S_{sb} can be calculated from

$$S_{sb} = \frac{D_s \delta_{sb}}{2} \left[\pi - \cos^{-1} \left(1 - \frac{2l_c}{D_s} \right) \right] \text{m}^2 \text{ (ft}^2\text{)} \quad (11-13)$$

where the value of the term $\cos^{-1} \left(1 - 2l_c/D_s \right)$ is in radians and is between 0 and $\pi/2$. S_{sb} is plotted in Fig. 11-7, based on TEMA Class R standards. Since pipe shells are generally limited to diameters

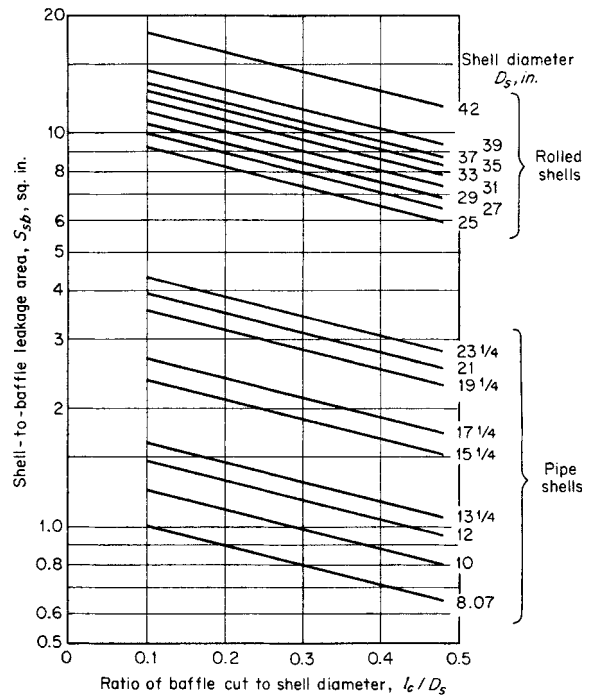


FIG. 11-7 Estimation of shell-to-baffle leakage area [Eq. (11-13)]. To convert inches to meters, multiply by 0.0254; to convert square inches to square meters, multiply by $(6.45)(10^{-4})$. Note that l_c and D_s have units of inches.

below 24 in, the larger sizes are shown by using the rolled-shell specification. Allowance should be made for especially tight or loose construction.

10. Area for flow through window S_w . This area is obtained as the difference between the gross window area S_{wg} and the window area occupied by tubes S_{wt} :

$$S_w = S_{wg} - S_{wt} \quad (11-14)$$

$$S_{wg} = \frac{D_s^2}{4} \left[\cos^{-1} \left(1 - 2 \frac{l_c}{D_s} \right) - \left(1 - 2 \frac{l_c}{D_s} \right) \sqrt{1 - \left(1 - 2 \frac{l_c}{D_s} \right)^2} \right] \text{m}^2 \text{ (ft}^2\text{)} \quad (11-15)$$

S_{wg} is plotted in Fig. 11-8. S_{wt} can be calculated from

$$S_{wt} = (N_T/8)(1 - F_c)\pi D_o^2 \text{m}^2 \text{ (ft}^2\text{)} \quad (11-16)$$

11. Equivalent diameter of window D_w [required only if laminar flow, defined as $(N_{Re})_s \leq 100$, exists]

$$D_w = \frac{4S_w}{(\pi/2)N_T(1 - F_c)D_o + D_s\theta_b} \text{m (ft)} \quad (11-17)$$

where θ_b is the baffle-cut angle given by

$$\theta_b = 2 \cos^{-1} \left(1 - \frac{2l_c}{D_s} \right) \text{rad} \quad (11-18)$$

12. Number of baffles N_b

$$N_b = \frac{L - 2le}{l_s} + 1 \quad (11-19)$$

where le is the entrance/exit baffle spacing, often different from the central baffle spacing. The effective tube length L must be known to calculate N_b , which is needed to calculate shell-side pressure drop. In designing an exchanger, the shell-side coefficient may be calculated and the required exchanger length for heat transfer obtained before N_b is calculated.

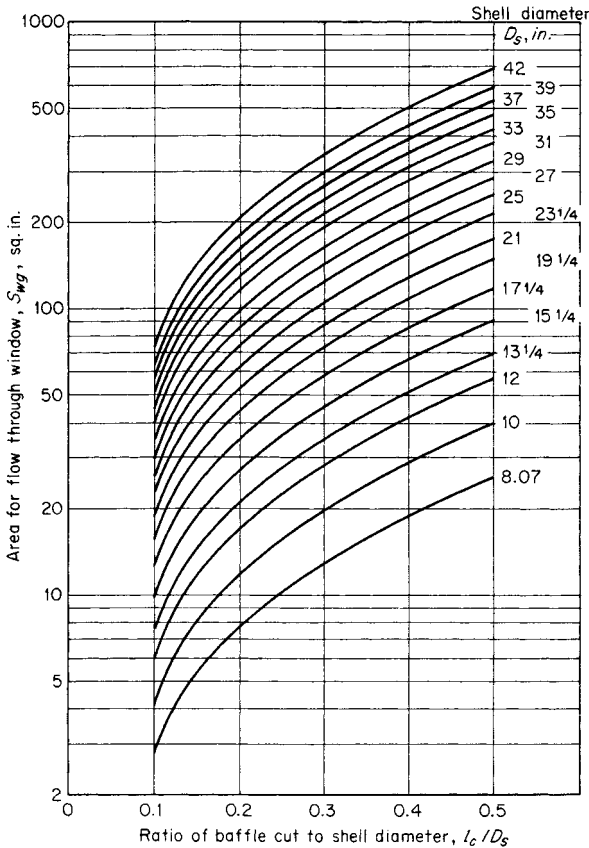


FIG. 11-8 Estimation of window cross-flow area [Eq. (11-15)]. To convert inches to meters, multiply by 0.0254. Note that l_c and D_s have units of inches.

Shell-Side Heat-Transfer Coefficient Calculation

1. Calculate the shell-side Reynolds number $(N_{Re})_s$.

$$(N_{Re})_s = D_s W / \mu_b S_m \tag{11-20}$$

where W = mass flow rate and μ_b = viscosity at bulk temperature. The arithmetic mean bulk shell-side fluid temperature is usually adequate to evaluate all bulk properties of the shell-side fluid. For large temperature ranges or for viscosity that is very sensitive to temperature change, special care must be taken, such as using Eq. (11-6).

2. Find j_k from the ideal-tube bank curve for a given tube layout at the calculated value of $(N_{Re})_s$, using Fig. 11-9, which is adapted from

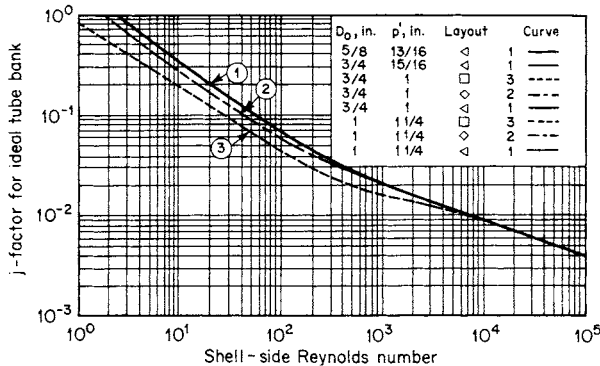


FIG. 11-9 Correlation of j factor for ideal tube bank. To convert inches to meters, multiply by 0.0254. Note that p' and D_s have units of inches.

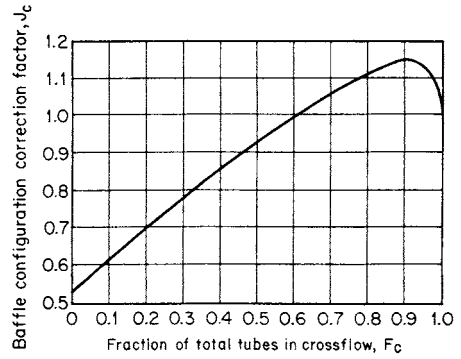


FIG. 11-10 Correction factor for baffle-configuration effects.

ideal-tube-bank data obtained at Delaware by Bergelin et al. [Trans. Am. Soc. Mech. Eng., 74, 953 (1952)] and the Grimison correlation [Trans. Am. Soc. Mech. Eng., 59, 583 (1937)].

3. Calculate the shell-side heat-transfer coefficient for an ideal tube bank h_k .

$$h_k = j_k c \frac{W}{S_m} \left(\frac{k}{c\mu} \right)^{2/3} \left(\frac{\mu_b}{\mu_w} \right)^{0.14} \tag{11-21}$$

where c is the specific heat, k is the thermal conductivity, and μ_w is the viscosity evaluated at the mean surface temperature.

4. Find the correction factor for baffle-configuration effects J_c from Fig. 11-10.

5. Find the correction factor for baffle-leakage effects J_l from Fig. 11-11.

6. Find the correction factor for bundle-bypassing effects J_b from Fig. 11-12

7. Find the correction factor for adverse temperature-gradient buildup at low Reynolds number J_r :

- a. If $(N_{Re})_s < 100$, find J_r^* from Fig. 11-13, knowing N_b and $(N_c + N_{ce})$.
- b. If $(N_{Re})_s \leq 20$, $J_r = J_r^*$.
- c. If $20 < (N_{Re})_s < 100$, find J_r from Fig. 11-14, knowing J_r^* and $(N_{Re})_s$.

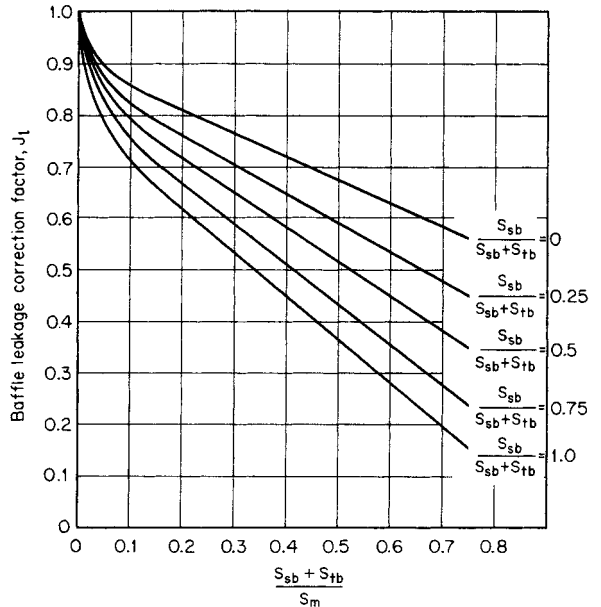


FIG. 11-11 Correction factor for baffle-leakage effects.

11-10 HEAT-TRANSFER EQUIPMENT

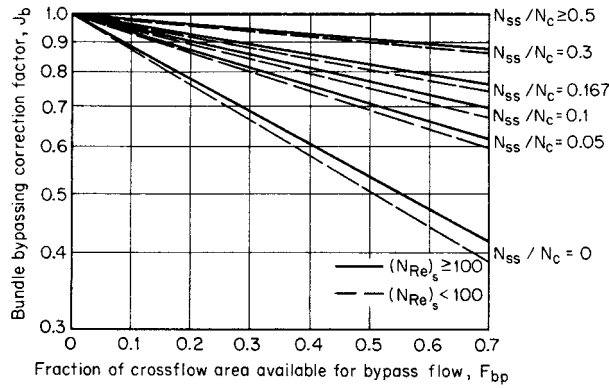


FIG. 11-12 Correction factor for bypass flow.

8. Calculate the shell-side heat-transfer coefficient for the exchanger h_s from

$$h_s = h_k J_c J_j J_b J_r \quad (11-22)$$

Shell-Side Pressure-Drop Calculation

1. Find f_k from the ideal-tube-bank friction-factor curve for the given tube layout at the calculated value of $(N_{Re})_s$ using Fig. 11-15a for triangular and rotated square arrays and Fig. 11-15b for in-line square arrays. These curves are adapted from Bergelin et al. and Grimison (loc. cit.).

2. Calculate the pressure drop for an ideal cross-flow section.

$$\Delta P_{bk} = b \frac{f_k W^2 N_c}{\rho S_m^2} \left(\frac{\mu_w}{\mu_b} \right)^{0.14} \quad (11-23)$$

where $b = (2.0)(10^{-3})$ (SI) or $(9.9)(10^{-5})$ (U.S. customary).

3. Calculate the pressure drop for an ideal window section. If $(N_{Re})_s \geq 100$,

$$\Delta P_{wk} = b \frac{W^2 (2 + 0.6 N_{cw})}{S_m S_w \rho} \quad (11-24a)$$

where $b = (5)(10^{-4})$ (SI) or $(2.49)(10^{-5})$ (U.S. customary).

If $(N_{Re})_s < 100$,

$$\Delta P_{wk} = b_1 \frac{\mu_b W}{S_m S_w \rho} \left(\frac{N_{cw}}{p' - D_o} + \frac{l_s}{D_w^2} \right) + b_2 \frac{W^2}{S_m S_w \rho} \quad (11-24b)$$

where $b_1 = (1.681)(10^{-5})$ (SI) or $(1.08)(10^{-4})$ (U.S. customary), and $b_2 = (9.99)(10^{-4})$ (SI) or $(4.97)(10^{-5})$ (U.S. customary).

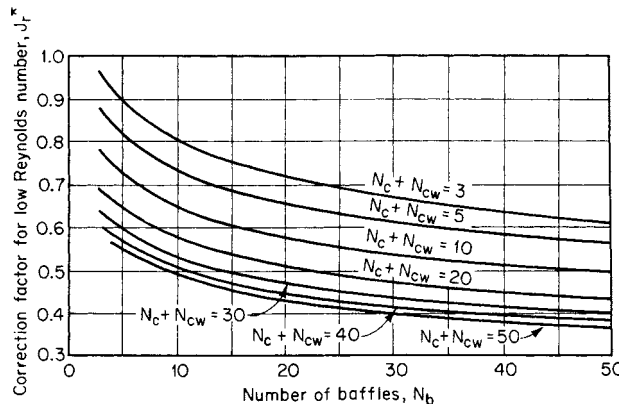


FIG. 11-13 Basic correction factor for adverse temperature gradient at low Reynolds numbers.

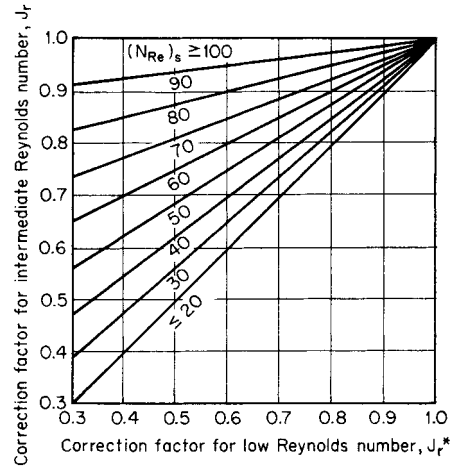
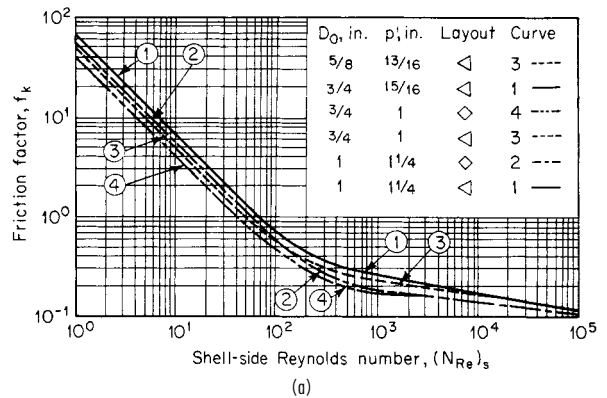


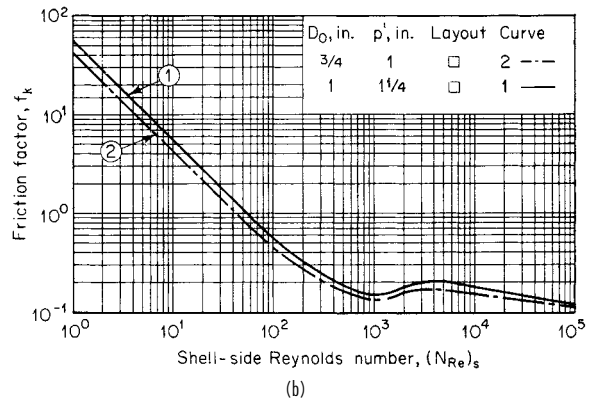
FIG. 11-14 Correction factor for adverse temperature gradient at intermediate Reynolds numbers.

4. Find the correction factor for the effect of baffle leakage on pressure drop R_l from Fig. 11-16. Curves shown are not to be extrapolated beyond the points shown.

5. Find the correction factor for bundle bypass R_b from Fig. 11-17.



(a)



(b)

FIG. 11-15 Correction of friction factors for ideal tube banks. (a) Triangular and rotated square arrays. (b) In-line square arrays.

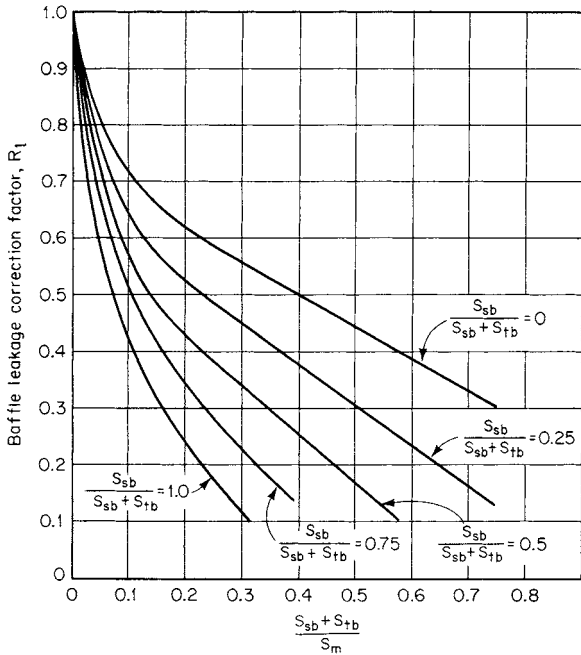


FIG. 11-16 Correction factor for baffle-leakage effect on pressure drop.

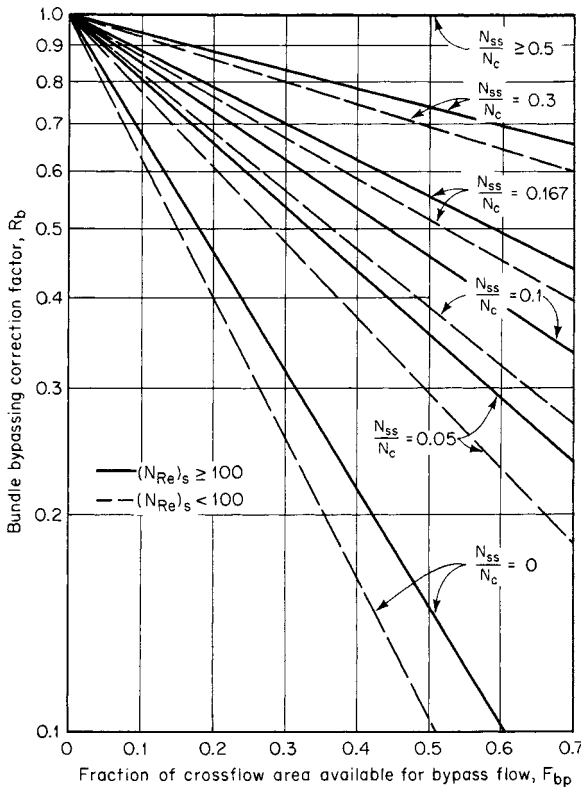


FIG. 11-17 Correction factor on pressure drop for bypass flow.

6. Calculate the *pressure drop across the shell side* (excluding nozzles). Units for pressure drop are lbf/ft².

$$\Delta P_s = [(N_b - 1)(\Delta P_{bk})R_b + N_b \Delta P_{ak}]R_t + 2 \Delta P_{bh}R_b \left(1 + \frac{N_{ac}}{N_c}\right) \quad (11-25)$$

The values of h_s and ΔP_s calculated by this procedure are for clean exchangers and are intended to be as accurate as possible, not conservative. A fouled exchanger will generally give lower heat-transfer rates, as reflected by the dirt resistances incorporated into Eq. (11-2), and higher pressure drops. Some estimate of **fouling effects** on pressure drop may be made by using the methods just given by assuming that the fouling deposit blocks the leakage and possibly the bypass areas. The fouling may also decrease the clearance between tubes and significantly increase the pressure drop in cross-flow.

THERMAL DESIGN OF CONDENSERS

Single-Component Condensers

Mean Temperature Difference In condensing a single component at its saturation temperature, the entire resistance to heat transfer on the condensing side is generally assumed to be in the layer of condensate. A mean condensing coefficient is calculated from the appropriate correlation and combined with the other resistances in Eq. (11-2). The overall coefficient is then used with the LMTD (no F_T correction is necessary for isothermal condensation) to give the required area, even though the condensing coefficient and hence U are not constant throughout the condenser.

If the vapor is **superheated** at the inlet, the vapor may first be desuperheated by sensible heat transfer from the vapor. This occurs if the surface temperature is above the saturation temperature, and a single-phase heat-transfer correlation is used. If the surface is below the saturation temperature, condensation will occur directly from the superheated vapor, and the effective coefficient is determined from the appropriate condensation correlation, using the saturation temperature in the LMTD. To determine whether or not condensation will occur directly from the superheated vapor, calculate the surface temperature by assuming single-phase heat transfer.

$$T_{\text{surface}} = T_{\text{vapor}} - \frac{U}{h} (T_{\text{vapor}} - T_{\text{coolant}}) \quad (11-26)$$

where h is the sensible heat-transfer coefficient for the vapor, U is calculated by using h , and both are on the same area basis. If $T_{\text{surface}} > T_{\text{saturation}}$, no condensation occurs at that point and the heat flux is actually higher than if $T_{\text{surface}} \leq T_{\text{saturation}}$ and condensation did occur. It is generally conservative to design a pure-component desuperheater-condenser as if the entire heat load were transferred by condensation, using the saturation temperature in the LMTD.

The design of an integral **condensate subcooling section** is more difficult, especially if close temperature approach is required. The condensate layer on the surface is on the average subcooled by one-third to one-half of the temperature drop across the film, and this is often sufficient if the condensate is not reheated by raining through the vapor. If the condensing-subcooling process is carried out inside tubes or in the shell of a vertical condenser, the single-phase subcooling section can be treated separately, giving an area that is added onto that needed for condensation. If the subcooling is achieved on the shell side of a horizontal condenser by flooding some of the bottom tubes with a weir or level controller, the rate and heat-balance equations must be solved for each section to obtain the area required.

Pressure drop on the condensing side reduces the final condensing temperature and the MTD and should always be checked. In designs requiring close approach between inlet coolant and exit condensate (subcooled or not), underestimation of pressure drop on the condensing side can lead to an exchanger that cannot meet specified terminal temperatures. Since pressure-drop calculations in two-phase flows such as condensation are relatively inaccurate, designers must consider carefully the consequences of a larger-than-calculated pressure drop.

Horizontal In-Shell Condensers The mean **condensing coefficient** for the outside of a bank of horizontal tubes is calculated from Eq. (5-93) for a single tube, corrected for the number of tubes

in a vertical row. For undisturbed laminar flow over all the tubes, Eq. (5-97) is, for realistic condenser sizes, overly conservative because of rippling, splashing, and turbulent flow (*Process Heat Transfer*, McGraw-Hill, New York, 1950). Kern proposed an exponent of $-1/6$ on the basis of experience, while Freon-11 data of Short and Brown (*General Discussion on Heat Transfer*, Institute of Mechanical Engineers, London, 1951) indicate independence of the number of tube rows. It seems reasonable to use no correction for inviscid liquids and Kern's correction for viscous condensates. For a cylindrical tube bundle, where N varies, it is customary to take N equal to two-thirds of the maximum or centerline value.

Baffles in a horizontal in-shell condenser are oriented with the cuts vertical to facilitate drainage and eliminate the possibility of flooding in the upward cross-flow sections. **Pressure drop** on the vapor side can be estimated by the data and method of Diehl and Unruh [*Pet. Refiner*, **36**(10), 147 (1957); **37**(10), 124 (1958)].

High vapor velocities across the tubes enhance the condensing coefficient. There is no correlation in the open literature to permit designers to take advantage of this. Since the vapor flow rate varies along the length, an incremental calculation procedure would be required in any case. In general, the pressure drops required to gain significant benefit are above those allowed in most process applications.

Vertical In-Shell Condensers Condensers are often designed so that condensation occurs on the outside of vertical tubes. Equation (5-88) is valid as long as the condensate film is laminar. When it becomes turbulent, Fig. 5-10 or Colburn's equation [*Trans. Am. Inst. Chem. Eng.*, **30**, 187 (1933-1934)] may be used.

Some judgment is required in the use of these correlations because of construction features of the condenser. The tubes must be supported by baffles, usually with maximum cut (45 percent of the shell diameter) and maximum spacing to minimize pressure drop. The flow of the condensate is interrupted by the baffles, which may draw off or redistribute the liquid and which will also cause some splashing of free-falling drops onto the tubes.

For **subcooling**, a liquid inventory may be maintained in the bottom end of the shell by means of a weir or a liquid-level-controller. The subcooling heat-transfer coefficient is given by the correlations for natural convection on a vertical surface [Eqs. (5-33a), (5-33b)], with the pool assumed to be well mixed (isothermal) at the subcooled condensate exit temperature. Pressure drop may be estimated by the shell-side procedure.

Horizontal In-Tube Condensers Condensation of a vapor inside horizontal tubes occurs in kettle and horizontal thermosiphon reboilers and in air-cooled condensers. In-tube condensation also offers certain advantages for condensation of multicomponent mixtures, discussed in the subsection "Multicomponent Condensers." The various in-tube correlations are closely connected to the **two-phase flow pattern** in the tube [*Chem. Eng. Prog. Symp. Ser.*, **66**(102), 150 (1970)]. At low flow rates, when gravity dominates the flow pattern, Eq. (5-101) may be used. At high flow rates, the flow and heat transfer are governed by vapor shear on the condensate film, and Eq. (5-100a) is valid. A simple and generally conservative procedure is to calculate the coefficient for a given case by both correlations and use the *larger* one.

Pressure drop during condensation inside horizontal tubes can be computed by using the correlations for two-phase flow given in Sec. 6 and neglecting the pressure recovery due to deceleration of the flow.

Vertical In-Tube Condensation Vertical-tube condensers are generally designed so that vapor and liquid flow cocurrently downward; if pressure drop is not a limiting consideration, this configuration can result in higher heat-transfer coefficients than shell-side condensation and has particular advantages for multicomponent condensation. If gravity controls, the mean heat-transfer coefficient for condensation is given by Figs. 5-9 and 5-10. If vapor shear controls, Eq. (5-99a) is applicable. It is generally conservative to calculate the coefficients by both methods and choose the *higher* value. The pressure drop can be calculated by using the Lockhart-Martinelli method [*Chem. Eng. Prog.*, **45**, 39 (1945)] for friction loss, neglecting momentum and hydrostatic effects.

Vertical in-tube condensers are often designed for **reflux or knock-back application** in reactors or distillation columns. In this

case, vapor flow is upward, countercurrent to the liquid flow on the tube wall; the vapor shear acts to thicken and retard the drainage of the condensate film, reducing the coefficient. Neither the fluid dynamics nor the heat transfer is well understood in this case, but Soliman, Schuster, and Berenson [*J. Heat Transfer*, **90**, 267-276 (1968)] discuss the problem and suggest a computational method. The Diehl-Koppány correlation [*Chem. Eng. Prog. Symp. Ser.* **92**, **65** (1969)] may be used to estimate the maximum allowable vapor velocity at the tube inlet. If the vapor velocity is great enough, the liquid film will be carried upward; this design has been employed in a few cases in which only part of the stream is to be condensed. This velocity cannot be accurately computed, and a very conservative (high) outlet velocity must be used if unstable flow and flooding are to be avoided; 3 times the vapor velocity given by the Diehl-Koppány correlation for incipient flooding has been suggested as the design value for completely stable operation.

Multicomponent Condensers

Thermodynamic and Mass-Transfer Considerations *Multicomponent vapor mixture* includes several different cases: all the components may be liquids at the lowest temperature reached in the condensing side, or there may be components which dissolve substantially in the condensate even though their boiling points are below the exit temperature, or one or more components may be both noncondensable and nearly insoluble.

Multicomponent condensation always involves sensible-heat changes in the vapor and liquid along with the latent-heat load. Compositions of both phases in general change through the condenser, and **concentration gradients** exist in both phases. Temperature and concentration profiles and transport rates at a point in the condenser usually cannot be calculated, but the binary cases have been treated: condensation of one component in the presence of a completely insoluble gas [Colburn and Hougen, *Ind. Eng. Chem.*, **26**, 1178-1182 (1934); and Colburn and Edison, *Ind. Eng. Chem.*, **33**, 457-458 (1941)] and condensation of a binary vapor [Colburn and Drew, *Trans. Am. Inst. Chem. Eng.*, **33**, 196-215 (1937)]. It is necessary to know or calculate diffusion coefficients for the system, and a reasonable approximate method to avoid this difficulty and the reiterative calculations is desirable. To integrate the point conditions over the total condensation requires the temperature, composition enthalpy, and flow-rate profiles as functions of the heat removed. These are calculated from component thermodynamic data if the vapor and liquid are assumed to be in equilibrium at the local vapor temperature. This assumption is not exactly true, since the condensate and the liquid-vapor interface (where equilibrium does exist) are intermediate in temperature between the coolant and the vapor.

In calculating the condensing curve, it is generally assumed that the vapor and liquid flow collinearly and in intimate contact so that composition equilibrium is maintained between the total streams at all points. If, however, the condensate drops out of the vapor (as can happen in horizontal shell-side condensation) and flows to the exit without further interaction, the remaining vapor becomes excessively enriched in light components with a decrease in condensing temperature and in the temperature difference between vapor and coolant. The result may be not only a small reduction in the amount of heat transferred in the condenser but also an inability to condense totally the light ends even at reduced throughput or with the addition of more surface. To prevent the liquid from segregating, in-tube condensation is preferred in critical cases.

Thermal Design If the controlling resistance for heat and mass transfer in the vapor is sensible-heat removal from the cooling vapor, the following design equation is obtained:

$$A = \int_0^{Q_T} \frac{1 + U'Z_H/h_{sc}}{U'(T_c - T_v)} dQ \quad (11-27)$$

U' is the overall heat-transfer coefficient between the vapor-liquid interface and the coolant, including condensate film, dirt and wall resistances, and coolant. The condensate film coefficient is calculated from the appropriate equation or correlation for pure vapor condensation for the geometry and flow regime involved, using mean liquid properties. Z_H is the ratio of the sensible heat removed from the

vapor-gas stream to the total heat transferred; this quantity is obtained from thermodynamic calculations and may vary substantially from one end of the condenser to the other, especially when removing vapor from a noncondensable gas. The sensible-heat-transfer coefficient for the vapor-gas stream h_{vg} is calculated by using the appropriate correlation or design method for the geometry involved, neglecting the presence of the liquid. As the vapor condenses, this coefficient decreases and must be calculated at several points in the process. T_v and T_c are temperatures of the vapor and of the coolant respectively. This procedure is similar in principle to that of Ward [*Petro/Chem. Eng.*, **32**(11), 42-48 (1960)]. It may be nonconservative for condensing steam and other high-latent-heat substances, in which case it may be necessary to increase the calculated area by 25 to 50 percent.

Pressure drop on the condensing side may be estimated by judicious application of the methods suggested for pure-component condensation, taking into account the generally nonlinear decrease of vapor-gas flow rate with heat removal.

THERMAL DESIGN OF REBOILERS

For a **single-component reboiler design**, attention is focused upon the mechanism of heat and momentum transfer at the hot surface. In *multicomponent systems*, the light components are preferentially vaporized at the surface, and the process becomes limited by their rate of diffusion. The net effect is to decrease the effective temperature difference between the hot surface and the bulk of the boiling liquid. If one attempts to vaporize too high a fraction of the feed liquid to the reboiler, the temperature difference between surface and liquid is reduced to the point that nucleation and vapor generation on the surface are suppressed and heat transfer to the liquid proceeds at the lower rate associated with single-phase natural convection. The only safe procedure in design for wide-boiling-range mixtures is to vaporize such a limited fraction of the feed that the boiling point of the remaining liquid mixture is still at least 5.5°C (10°F) below the surface temperature. Positive flow of the unvaporized liquid through and out of the reboiler should be provided.

Kettle Reboilers It has been generally assumed that kettle reboilers operate in the pool boiling mode, but with a lower peak heat flux because of vapor binding and blanketing of the upper tubes in the bundle. There is some evidence that vapor generation in the bundle causes a high circulation rate through the bundle. The result is that, at the lower heat fluxes, the kettle reboiler actually gives higher heat-transfer coefficients than a single tube. Present understanding of the recirculation phenomenon is insufficient to take advantage of this in design. Available nucleate pool boiling correlations are only very approximate, failing to account for differences in the nucleation characteristics of different surfaces. The Mostinski correlation [Eq. (5-102)] and the McNelly correlation [Eq. (5-103)] are generally the best for single components or narrow-boiling-range mixtures at low fluxes, though they may give errors of 40 to 50 percent. Experimental heat-transfer coefficients for pool boiling of a given liquid on a given surface should be used if available. The bundle **peak heat flux** is a function of tube-bundle geometry, especially of tube-packing density; in the absence of better information, the Palen-Small modification [Eq. (5-108)] of the Zuber maximum-heat-flux correlation is recommended.

A general method for analyzing kettle reboiler performance is by Fair and Klip, *Chem. Eng. Prog.* **79**(3), 86 (1983). It is effectively limited to computer application.

Kettle reboilers are generally assumed to require negligible pressure drop. It is important to provide good longitudinal liquid flow paths within the shell so that the liquid is uniformly distributed along the entire length of the tubes and excessive local vaporization and vapor binding are avoided.

This method may also be used for the thermal design of **horizontal thermosiphon reboilers**. The recirculation rate and pressure profile of the thermosiphon loop can be calculated by the methods of Fair [*Pet. Refiner*; **39**(2), 105-123 (1960)].

Vertical Thermosiphon Reboilers Vertical thermosiphon reboilers operate by natural circulation of the liquid from the still through the downcomer to the reboiler and of the two-phase mixture

from the reboiler through the return piping. The flow is induced by the hydrostatic pressure imbalance between the liquid in the downcomer and the two-phase mixture in the reboiler tubes. Thermosiphons do not require any pump for recirculation and are generally regarded as less likely to foul in service because of the relatively high two-phase velocities obtained in the tubes. Heavy components are not likely to accumulate in the thermosiphon, but they are more difficult to design satisfactorily than kettle reboilers, especially in vacuum operation. Several shortcut methods have been suggested for thermosiphon design, but they must generally be used with caution. The method due to Fair (loc. cit.), based upon two-phase flow correlations, is the most complete in the open literature but requires a computer for practical use. Fair also suggests a shortcut method that is satisfactory for preliminary design and can be reasonably done by hand.

Forced-Recirculation Reboilers In forced-recirculation reboilers, a pump is used to ensure circulation of the liquid past the heattransfer surface. Force-recirculation reboilers may be designed so that boiling occurs inside vertical tubes, inside horizontal tubes, or on the shell side. For forced boiling inside vertical tubes, Fair's method (loc. cit.) may be employed, making only the minor modification that the recirculation rate is fixed and does not need to be balanced against the pressure available in the downcomer. Excess pressure required to circulate the two-phase fluid through the tubes and back into the column is supplied by the pump, which must develop a positive pressure increase in the liquid.

Fair's method may also be modified to design forced-recirculation reboilers with horizontal tubes. In this case the hydrostatic-head-pressure effect through the tubes is zero but must be considered in the two-phase return lines to the column.

The same procedure may be applied in principle to design of forced-recirculation reboilers with shell-side vapor generation. Little is known about two-phase flow on the shell side, but a reasonable estimate of the friction pressure drop can be made from the data of Diehl and Unruh [*Pet. Refiner*; **36**(10), 147 (1957); **37**(10), 124 (1958)]. No void-fraction data are available to permit accurate estimation of the hydrostatic or acceleration terms. These may be roughly estimated by assuming homogeneous flow.

THERMAL DESIGN OF EVAPORATORS

Heat duties of evaporator heating surfaces are usually determined by conventional heat and material balance calculations. Heating surface areas are normally, but not always taken as those in contact with the material being evaporated. It is the heat transfer ΔT that presents the most difficulty in deriving or applying heat-transfer coefficients. The total ΔT between heat source and heat sink is never all available for heat transfer. Since energy usually is carried to and from an evaporator body or effect by condensible vapors, loss in pressure represents a loss in ΔT . Such losses include pressure drop through entrainment separators, friction in vapor piping, and acceleration losses into and out of the piping. The latter loss has often been overlooked, even though it can be many times greater than the friction loss. Similarly, friction and acceleration losses past the heating surface, such as in a falling film evaporator, cause a loss of ΔT that may or may not have been included in the heat transfer ΔT when reporting experimental results. Boiling-point rise, the difference between the boiling point of the solution and the condensing point of the solvent at the same pressure, is another loss. Experimental data are almost always corrected for boiling-point rise, but plant data are suspect when based on temperature measurements because vapor at the point of measurement may still contain some superheat, which represents but a very small fraction of the heat given up when the vapor condenses but may represent a substantial fraction of the actual net ΔT available for heat transfer. A ΔT loss that must be considered in forced-circulation evaporators is that due to temperature rise through the heater, a consequence of the heat being absorbed there as sensible heat. A further loss may occur when the heater effluent flashes as it enters the vapor-liquid separator. Some of the liquid may not reach the surface and flash to equilibrium with the vapor pressure in the separator, instead of recirculating to the heater, raising the average temperature at which heat is absorbed and further reducing the net ΔT . Whether or not these ΔT losses are allowed for in the heat-transfer coefficients reported

depends on the method of measurement. Simply basing the liquid temperature on the measured vapor head pressure may ignore both—or only the latter if temperature rise through the heater is estimated separately from known heat input and circulation rate. In general, when calculating overall heat-transfer coefficients from individual-film coefficients, all of these losses must be allowed for, while when using reported overall coefficients care must be exercised to determine which losses may already have been included in the heat transfer ΔT .

Forced-Circulation Evaporators In evaporators of this type in which hydrostatic head prevents boiling at the heating surface, **heat-transfer coefficients** can be predicted from the usual correlations for condensing steam (Fig. 5-10) and forced-convection sensible heating [Eq. (5-50)]. The liquid film coefficient is improved if boiling is not completely suppressed. When only the film next to the wall is above the boiling point, Boarts, Badger, and Meisenberg [*Ind. Eng. Chem.*, **29**, 912 (1937)] found that results could be correlated by Eq. (5-50) by using a constant of 0.0278 instead of 0.023. In such cases, the course of the liquid temperature can still be calculated from known circulation rate and heat input.

When the bulk of the liquid is boiling in part of the tube length, the film coefficient is even higher. However, the liquid temperature starts dropping as soon as full boiling develops, and it is difficult to estimate the course of the temperature curve. It is certainly safe to estimate heat transfer on the basis that no bulk boiling occurs. Fragen and Badger [*Ind. Eng. Chem.*, **28**, 534 (1936)] obtained an **empirical correlation** of overall heat-transfer coefficients in this type of evaporator, based on the ΔT at the heater inlet:

In U.S. customary units

$$U = 2020D^{0.57}(V_s)^{3.6/L}/\mu^{0.25} \Delta T^{0.1} \quad (11-28)$$

where D = mean tube diameter, V_s = inlet velocity, L = tube length, and μ = liquid viscosity. This equation is based primarily on experiments with copper tubes of 0.022 m (8/8 in) outside diameter, 0.00165 m (16 gauge), 2.44 m (8 ft) long, but it includes some work with 0.0127-m (1/2-in) tubes 2.44 m (8 ft) long and 0.0254-m (1-in) tubes 3.66 m (12 ft) long.

Long-Tube Vertical Evaporators In the rising-film version of this type of evaporator, there is usually a nonboiling zone in the bottom section and a boiling zone in the top section. The length of the nonboiling zone depends on heat-transfer characteristics in the two zones and on pressure drop during two-phase flow in the boiling zone. The work of Martinelli and coworkers [Lockhart and Martinelli, *Chem. Eng. Prog.*, **45**, 39–48 (January 1949); and Martinelli and Nelson, *Trans. Am. Soc. Mech. Eng.*, **70**, 695–702 (August 1948)] permits a prediction of pressure drop, and a number of correlations are available for estimating film coefficients of heat transfer in the two zones. In estimating pressure drop, integrated curves similar to those presented by Martinelli and Nelson are the easiest to use. The curves for pure water are shown in Figs. 11-18 and 11-19, based on the assumption that the flow of both vapor and liquid would be turbulent if each were flowing alone in the tube. Similar curves can be prepared if one or both flows are laminar or if the properties of the liquid differ appreciably from the properties of pure water. The **acceleration pressure drop** ΔP_a is calculated from the equation

$$\Delta P_a = br_2G^2/32.2 \quad (11-29)$$

where $b = (2.6)(10^7)$ (SI) and 1.0 (U.S. customary) and using r_2 from Fig. 11-18. The frictional pressure drop is derived from Fig. 11-19, which shows the ratio of two-phase pressure drop to that of the entering liquid flowing alone.

Pressure drop due to hydrostatic head can be calculated from liquid holdup R_1 . For nonfoaming dilute aqueous solutions, R_1 can be estimated from $R_1 = 1/[1 + 2.5(V/L)(\rho_1/\rho_v)^{1/2}]$. Liquid holdup, which represents the ratio of liquid-only velocity to actual liquid velocity, also appears to be the principal determinant of the convective coefficient in the boiling zone (Dengler, Sc.D. thesis, MIT, 1952). In other words, the convective coefficient is that calculated from Eq. (5-50) by using the liquid-only velocity divided by R_1 in the Reynolds number. Nucleate boiling augments convective heat transfer, primarily when ΔT 's are high and the convective coefficient is low [Chen, *Ind. Eng. Chem. Process Des. Dev.*, **5**, 322 (1966)].

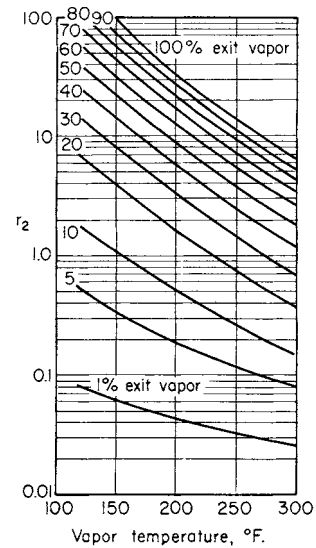


FIG. 11-18 Acceleration losses in boiling flow. $^{\circ}\text{C} = (^{\circ}\text{F} - 32)/1.8$.

Film coefficients for the **boiling of liquids other than water** have been investigated. Coulson and McNelly [*Trans. Inst. Chem. Eng.*, **34**, 247 (1956)] derived the following relation, which also correlated the data of Badger and coworkers [*Chem. Metall. Eng.*, **46**, 640 (1939); *Chem. Eng.*, **61**(2), 183 (1954); and *Trans. Am. Inst. Chem. Eng.*, **33**, 392 (1937); **35**, 17 (1939); **36**, 759 (1940)] on water:

$$N_{Nu} = (1.3 + bD)(N_{Pr})^{0.9}(N_{Re})^{0.23}(N_{Re/g})^{0.34} \left(\frac{\rho_l}{\rho_g}\right)^{0.25} \left(\frac{\mu_g}{\mu_l}\right) \quad (11-30)$$

where $b = 128$ (SI) or 39 (U.S. customary), N_{Nu} = Nusselt number based on liquid thermal conductivity, D = tube diameter, and the remaining terms are dimensionless groupings of liquid Prandtl number, liquid Reynolds number, vapor Reynolds number, and ratios of densities and viscosities. The Reynolds numbers are calculated on the basis of each fluid flowing by itself in the tube.

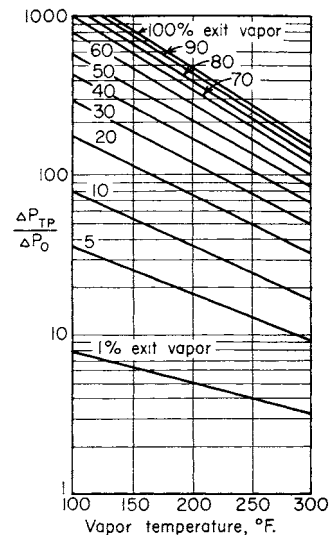


FIG. 11-19 Friction pressure drop in boiling flow. $^{\circ}\text{C} = (^{\circ}\text{F} - 32)/1.8$.

Additional corrections must be applied when the fraction of vapor is so high that the remaining liquid does not wet the tube wall or when the velocity of the mixture at the tube exits approaches sonic velocity. McAdams, Woods, and Bryan (*Trans. Am. Soc. Mech. Eng.*, 1940), Dengler and Addoms (loc. cit.), and Stroebe, Baker, and Badger [*Ind. Eng. Chem.*, **31**, 200 (1939)] encountered dry-wall conditions and reduced coefficients when the weight fraction of vapor exceeded about 80 percent. Schweppe and Foust [*Chem. Eng. Prog.*, **49**, *Symp. Ser.* 5, 77 (1953)] and Harvey and Foust (ibid., p. 91) found that "sonic choking" occurred at surprisingly low flow rates.

The simplified method of calculation outlined includes no allowance for the **effect of surface tension**. Stroebe, Baker, and Badger (loc. cit.) found that by adding a small amount of surface-active agent the boiling-film coefficient varied inversely as the square of the surface tension. Coulson and Mehta [*Trans. Inst. Chem. Eng.*, **31**, 208 (1953)] found the exponent to be -1.4. The higher coefficients at low surface tension are offset to some extent by a higher pressure drop, probably because the more intimate mixture existing at low surface tension causes the liquid fraction to be accelerated to a velocity closer to that of the vapor. The pressure drop due to acceleration ΔP_a derived from Fig. 11-18 allows for some slippage. In the limiting case, such as might be approached at low surface tension, the acceleration pressure drop in which "fog" flow is assumed (no slippage) can be determined from the equation

$$\Delta P'_a = \frac{y(V_g - V_l)G^2}{g_c} \quad (11-31)$$

where y = fraction vapor by weight
 V_g, V_l = specific volume gas, liquid
 G = mass velocity

While the foregoing methods are valuable for detailed evaporator design or for evaluating the effect of changes in conditions on performance, they are cumbersome to use when making preliminary designs or cost estimates. Figure 11-20 gives the general range of **overall long-tube vertical- (LTV) evaporator heat-transfer coefficients** usually encountered in commercial practice. The higher coefficients are encountered when evaporating dilute solutions and the lower range when evaporating viscous liquids. The dashed curve represents the approximate lower limit, for liquids with viscosities of about 0.1 Pa-s (100 cP). The LTV evaporator does not work well at low temperature differences, as indicated by the results shown in Fig. 11-21 for seawater in 0.051-m (2-in), 0.0028-m (12-gauge) brass tubes 7.32 m (24 ft) long (W. L. Badger Associates, Inc., U.S. Department of the Interior, Office of Saline Water Rep. 26, December 1959, OTS

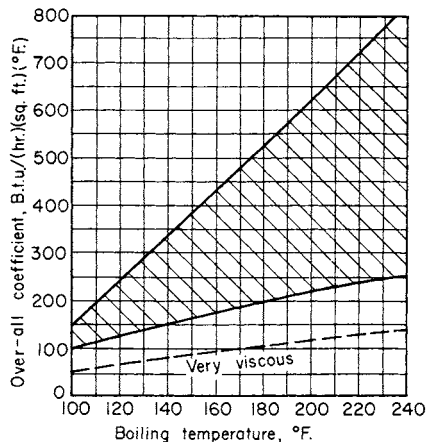


FIG. 11-20 General range of long-tube vertical- (LTV) evaporator coefficients. °C = (°F - 32)/1.8; to convert British thermal units per hour-square foot-degrees Fahrenheit to joules per square meter-second-kelvins, multiply by 5.6783.

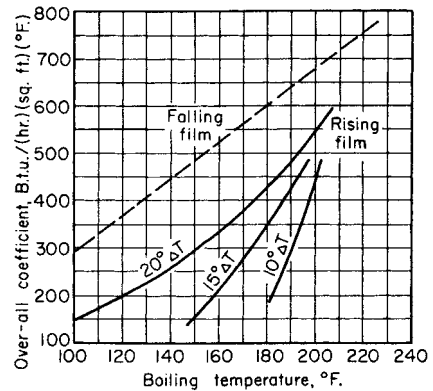


FIG. 11-21 Heat-transfer coefficients in LTV seawater evaporators. °C = (°F - 32)/1.8; to convert British thermal units per hour-square foot-degrees Fahrenheit to joules per square meter-second-kelvins, multiply by 5.6783.

Publ. PB 161290). The feed was at its boiling point at the vapor-head pressure, and feed rates varied from 0.025 to 0.050 kg/(s-tube) [200 to 400 lb/(h-tube)] at the higher temperature to 0.038 to 0.125 kg/(s-tube) [300 to 1000 lb/(h-tube)] at the lowest temperature.

Falling film evaporators find their widest use at low temperature differences—also at low temperatures. Under most operating conditions encountered, heat transfer is almost all by pure convection, with a negligible contribution from nucleate boiling. Film coefficients on the condensing side may be estimated from Dukler's correlation, [*Chem. Eng. Prog.*, **55**, 62 1950]. The same Dukler correlation presents curves covering falling film heat transfer to non-boiling liquids that are equally applicable to the falling film evaporator [Sinek and Young, *Chem. Eng. Prog.*, **58**, No. 12, 74 (1962)]. Kunz and Yerazunis [*J. Heat Transfer* **8**, 413 (1969)] have since extended the range of physical properties covered, as shown in Fig. 11-22. The boiling point in the tubes of such an evaporator is higher than in the vapor head because of both frictional-pressure drop and the head needed to accelerate the vapor to the tube-exit velocity. These factors, which can easily be predicted, make the overall apparent coefficients somewhat lower than those for nonboiling conditions. Figure 11-21 shows overall apparent heat-transfer coefficients determined in a falling-film seawater evaporator using the same tubes and flow rates as for the rising-film tests (W. L. Badger Associates, Inc., loc. cit.).

Short-Tube Vertical Evaporators Coefficients can be estimated by the same detailed method described for recirculating LTV evaporators. Performance is primarily a function of temperature level, temperature difference, and viscosity. While liquid level can also have an important influence, this is usually encountered only at levels lower than considered safe in commercial operation. **Overall heat-transfer coefficients** are shown in Fig. 11-23 for a basket-type evaporator (one with an annular downtake) when boiling water with 0.051-m (2-in) outside-diameter 0.0028-m-wall (12-gauge), 1.22-m-(4-ft)-long steel tubes [Badger and Shepard, *Chem. Metall. Eng.*, **23**, 281 (1920)]. Liquid level was maintained at the top tube sheet. Foust, Baker, and Badger [*Ind. Eng. Chem.*, **31**, 206 (1939)] measured recirculating velocities and heat-transfer coefficients in the same evaporator except with 0.064-m (2.5-in) 0.0034-m-wall (10-gauge), 1.22-m-(4-ft)-long tubes and temperature differences from 7 to 26°C (12 to 46°F). In the normal range of liquid levels, their results can be expressed as

$$U_c = \frac{b(\Delta T_c)^{0.22} N_{Pr}^{0.4}}{(V_g - V_l)^{0.37}} \quad (11-32)$$

where b = 153 (SI) or 375 (U.S. customary) and the subscript c refers to true liquid temperature, which under these conditions was about 0.56°C (1°F) above the vapor-head temperature. This work was done with water.

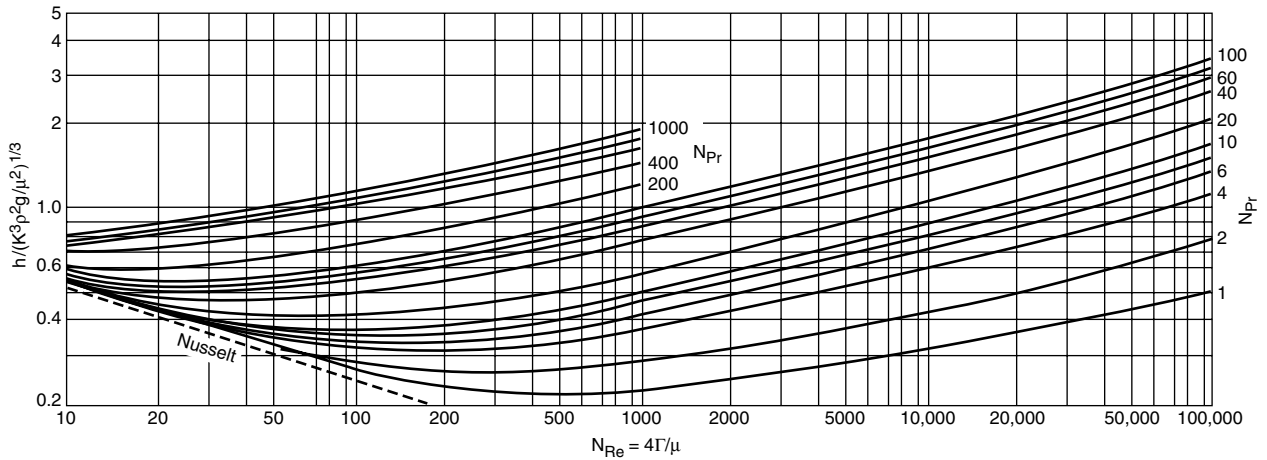


FIG. 11-22 Kunz and Yerazunis Correlation for falling-film heat transfer.

No detailed tests have been reported for the performance of propeller calandrias. Not enough is known regarding the performance of the propellers themselves under the cavitating conditions usually encountered to permit predicting circulation rates. In many cases, it appears that the propeller does no good in accelerating heat transfer over the transfer for natural circulation (Fig. 11-23).

Miscellaneous Evaporator Types **Horizontal-tube evaporators** operating with partially or fully submerged heating surfaces behave in much the same way as short-tube verticals, and heat-transfer coefficients are of the same order of magnitude. Some test results for water were published by Badger [*Trans. Am. Inst. Chem. Eng.*, **13**, 139 (1921)]. When operating unsubmerged, their heat transfer performance is roughly comparable to the falling-film vertical tube evaporator. Condensing coefficients inside the tubes can be derived from Nusselt's theory which, based on a constant-heat flux rather than a constant film ΔT , gives:

$$\frac{h}{(k^3 \rho^2 g / \mu^2)^{1/3}} = 1.59(4\Gamma/\mu)^{-1/3} \quad (11-33a)$$

For the boiling side, a correlation based on seawater tests gave:

$$\frac{h}{(k^3 \rho^2 g / \mu^2)^{1/3}} = 0.0147(4\Gamma/\mu)^{1/3}(D)^{-1/3} \quad (11-33b)$$

where Γ is based on feed-rate per unit length of the top tube in each vertical row of tubes and D is in meters.

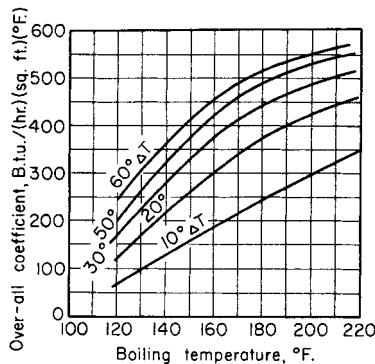


FIG. 11-23 Heat-transfer coefficients for water in short-tube evaporators. $^{\circ}\text{C} = (^{\circ}\text{F} - 32)/1.8$; to convert British thermal units per hour-square foot-degrees Fahrenheit to joules per square meter-second-kelvins, multiply by 5.6783.

Heat-transfer coefficients in clean coiled-tube evaporators for seawater are shown in Fig. 11-24 [Hillier, *Proc. Inst. Mech. Eng. (London)*, **1B**(7), 295 (1953)]. The tubes were of copper.

Heat-transfer coefficients in **agitated-film evaporators** depend primarily on liquid viscosity. This type is usually justifiable only for very viscous materials. Figure 11-25 shows general ranges of overall coefficients [Hauschild, *Chem. Ing. Tech.*, **25**, 573 (1953); Lindsey, *Chem. Eng.*, **60**(4), 227 (1953); and Leniger and Veldstra, *Chem. Ing. Tech.*, **31**, 493 (1959)]. When used with nonviscous fluids, a wiped-film evaporator having fluted external surfaces can exhibit very high coefficients (Lustenader et al., *Trans. Am. Soc. Mech. Eng.*, Paper 59-SA-30, 1959), although at a probably unwarranted first cost.

Heat Transfer from Various Metal Surfaces In an early work, Pridgeon and Badger [*Ind. Eng. Chem.*, **16**, 474 (1924)] published test results on copper and iron tubes in a horizontal-tube evaporator that indicated an extreme **effect of surface cleanliness** on heat-transfer coefficients. However, the high degree of cleanliness needed for high coefficients was difficult to achieve, and the tube layout and liquid level were changed during the course of the tests so as to make direct comparison of results difficult. Other workers have found little or no effect of conditions of surface or tube material on boiling-film

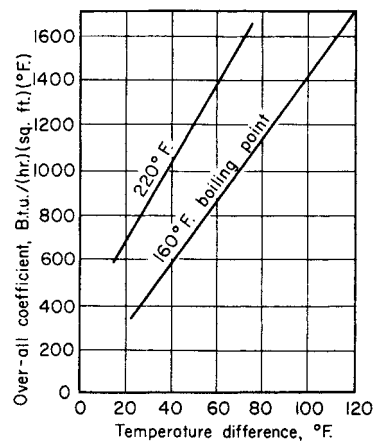


FIG. 11-24 Heat-transfer coefficients for seawater in coil-tube evaporators. $^{\circ}\text{C} = (^{\circ}\text{F} - 32)/1.8$; to convert British thermal units per hour-square foot-degrees Fahrenheit to joules per square meter-second-kelvins, multiply by 5.6783.

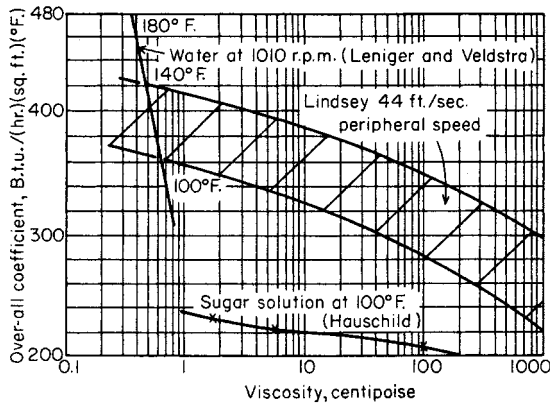


FIG. 11-25 Overall heat-transfer coefficients in agitated-film evaporators. °C = (°F - 32)/1.8; to convert British thermal units per hour-square foot-degrees Fahrenheit to joules per square meter-second-kelvins, multiply by 5.6783; to convert centipoises to pascal-seconds, multiply by 10⁻³.

coefficients in the range of commercial operating conditions [Averin, *Izv. Akad. Nauk SSSR Otd. Tekh. Nauk*, no. 3, p. 116, 1954; and Coulson and McNelly, *Trans. Inst. Chem. Eng.*, **34**, 247 (1956)].

Work in connection with desalination of seawater has shown that **specialty modified surfaces** can have a profound effect on heat-transfer coefficients in evaporators. Figure 11-26 (Alexander and Hoffman, Oak Ridge National Laboratory TM-2203) compares overall coefficients for some of these surfaces when boiling fresh water in 0.051-m (2-in) tubes 2.44-m (8-ft) long at atmospheric pressure in both upflow and downflow. The area basis used was the nominal outside area. Tube 20 was a smooth 0.0016-m- (0.062-in-) wall aluminum brass tube that had accumulated about 6 years of fouling in seawater

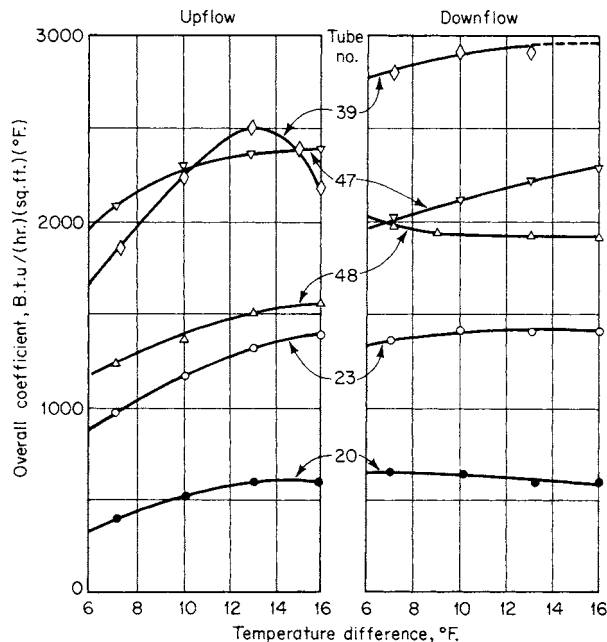


FIG. 11-26 Heat-transfer coefficients for enhanced surfaces. °C = (°F - 32)/1.8; to convert British thermal units per hour-square foot-degrees Fahrenheit to joules per square meter-second-kelvins, multiply by 5.6783. (By permission from Oak Ridge National Laboratory TM-2203.)

service and exhibited a fouling resistance of about (2.6)/(10⁻⁵) (m²·s·K)/J [0.00015 (ft²·h·°F)/Btu]. Tube 23 was a clean aluminum tube with 20 spiral corrugations of 0.0032-m (1/8-in) radius on a 0.254-m (10-in) pitch indented into the tube. Tube 48 was a clean copper tube that had 50 longitudinal flutes pressed into the wall (General Electric double-flute profile, Diedrich, U.S. Patent 3,244,601, Apr. 5, 1966). Tubes 47 and 39 had a specially patterned porous sintered-metal deposit on the boiling side to promote nucleate boiling (Minton, U.S. Patent 3,384,154, May 21, 1968). Both of these tubes also had steam-side coatings to promote dropwise condensation—parlyene for tube 47 and gold plating for tube 39.

Of these special surfaces, only the **double-fluted tube** has seen extended services. Most of the gain in heat-transfer coefficient is due to the condensing side; the flutes tend to collect the condensate and leave the lands bare [Carnavos, *Proc. First Int. Symp. Water Desalination*, **2**, 205 (1965)]. The condensing-film coefficient (based on the actual outside area, which is 28 percent greater than the nominal area) may be approximated from the equation

$$h = b \left(\frac{k^3 \rho^2 g}{\mu^2} \right)^{1/3} \left(\frac{\mu \lambda}{L} \right)^{1/3} \left(\frac{q}{A} \right)^{-0.833} \quad (11-34a)$$

where $b = 2100$ (SI) or 1180 (U.S. customary). The boiling-side coefficient (based on actual inside area) for salt water in downflow may be approximated from the equation

$$h = 0.035(k^3 \rho^2 g / \mu^2)^{1/3} (4\Gamma / \mu)^{1/3} \quad (11-34b)$$

The boiling-film coefficient is about 30 percent lower for pure water than it is for salt water or seawater. There is as yet no accepted explanation for the superior performance in salt water. This phenomenon is also seen in evaporation from smooth tubes.

Effect of Fluid Properties on Heat Transfer Most of the heat-transfer data reported in the preceding paragraphs were obtained with water or with dilute solutions having properties close to those of water. Heat transfer with other materials will depend on the type of evaporator used. For forced-circulation evaporators, methods have been presented to calculate the effect of changes in fluid properties. For natural-circulation evaporators, **viscosity** is the most important variable as far as aqueous solutions are concerned. Badger (*Heat Transfer and Evaporation*, Chemical Catalog, New York, 1926, pp. 133-134) found that, as a rough rule, overall heat-transfer coefficients varied in inverse proportion to viscosity if the boiling film was the main resistance to heat transfer. When handling molasses solutions in a forced-circulation evaporator in which boiling was allowed to occur in the tubes, Coates and Badger [*Trans. Am. Inst. Chem. Eng.*, **32**, 49 (1936)] found that from 0.005 to 0.03 Pa·s (5 to 30 cP) the overall heat-transfer coefficient could be represented by $U = b/\mu_j^{1.24}$, where $b = 2.55$ (SI) or 7043 (U.S. customary). Fragen and Badger [*Ind. Eng. Chem.*, **28**, 534 (1936)] correlated overall coefficients on sugar and sulfite liquor in the same evaporator for viscosities to 0.242 Pa·s (242 cP) and found a relationship that included the viscosity raised only to the 0.25 power.

Little work has been published on the effect of viscosity on heat transfer in the long-tube vertical evaporator. Cessna, Leintz, and Badger [*Trans. Am. Inst. Chem. Eng.*, **36**, 759 (1940)] found that the overall coefficient in the nonboiling zone varied inversely as the 0.7 power of viscosity (with sugar solutions). Coulson and Mehta [*Trans. Inst. Chem. Eng.*, **31**, 208 (1953)] found the exponent to be -0.44, and Stroebe, Baker, and Badger (loc. cit.) arrived at an exponent of -0.3 for the effect of viscosity on the film coefficient in the boiling zone.

Kerr (Louisiana Agr. Exp. Sta. Bull. 149) obtained plant data shown in Fig. 11-27 on various types of full-sized evaporators for cane sugar. These are invariably forward-fecity evaporators concentrating to about 50° Brix, corresponding to a viscosity on the order of 0.005 Pa·s (5 cP) in the last effect. In Fig. 11-27 curve A is for short-tube verticals with central downtake, B is for standard horizontal tube evaporators, C is for Lillie evaporators (which were horizontal-tube machines with no liquor level but having recirculating liquor showered over the tubes), and D is for long-tube vertical evaporators. These curves show apparent coefficients, but sugar solutions have boiling-point rises low enough not to affect the results noticeably. Kerr also obtained the data

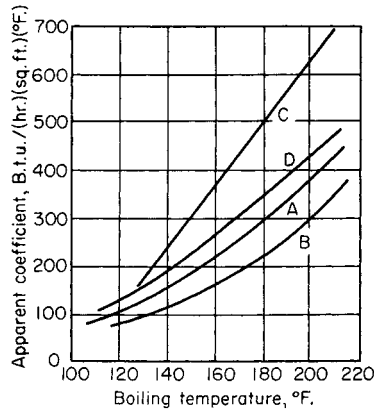


FIG. 11-27 Kerr's tests with full-sized sugar evaporators. °C = (°F - 32)/1.8; to convert British thermal units per hour-square foot-degrees Fahrenheit to joules per square meter-second-kelvins, multiply by 5.6783.

shown in Fig. 11-28 on a laboratory short-tube vertical evaporator with 0.44- by 0.61-m (1¾- by 24-in) tubes. This work was done with sugar juices boiling at 57°C (135°F) and an 11°C (20°F) temperature difference.

Effect of Noncondensables on Heat Transfer Most of the heat transfer in evaporators does not occur from pure steam but from vapor evolved in a preceding effect. This vapor usually contains inert gases—from air leakage if the preceding effect was under vacuum, from air entrained or dissolved in the feed, or from gases liberated by decomposition reactions. To prevent these inerts from seriously impeding heat transfer, the gases must be channeled past the heating surface and vented from the system while the gas concentration is still quite low. The influence of inert gases on heat transfer is due partially to the effect on ΔT of lowering the partial pressure and hence condensing temperature of the steam. The primary effect, however, results from the formation at the heating surface of an insulating blanket of gas through which the steam must diffuse before it can condense. The latter effect can be treated as an added resistance or fouling factor equal to 6.5 × 10⁻⁵ times the local mole percent inert gas (in J⁻¹·s·m²·K) [Standiford, *Chem. Eng. Prog.*, **75**, 59-62 (July 1979)]. The effect on ΔT is readily calculated from Dalton's law. Inert-gas concentrations may vary by a factor of 100 or more between vapor inlet and vent outlet, so these relationships should be integrated through the tube bundle.

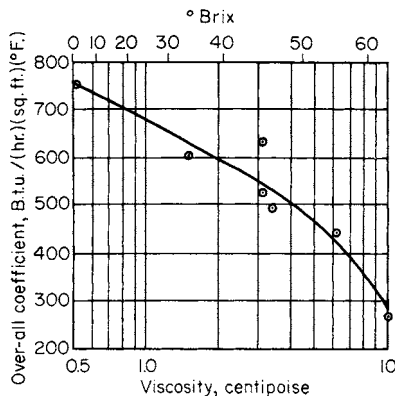


FIG. 11-28 Effect of viscosity on heat transfer in short-tube vertical evaporator. To convert centipoises to pascal-seconds, multiply by 10⁻³; to convert British thermal units per hour-square foot-degrees Fahrenheit to joules per square meter-second-kelvins, multiply by 5.6783.

**BATCH OPERATIONS:
HEATING AND COOLING OF VESSELS**

Nomenclature (Use consistent units.) A = heat-transfer surface; C, c = specific heats of hot and cold fluids respectively; L₀ = flow rate of liquid added to tank; M = mass of fluid in tank; T, t = temperature of hot and cold fluids respectively; T₁, t₁ = temperatures at beginning of heating or cooling period or at inlet; T₂, t₂ = temperature at end of period or at outlet; T₀, t₀ = temperature of liquid added to tank; U = coefficient of heat transfer; and W, w = flow rate through external exchanger of hot and cold fluids respectively.

Applications One typical application in heat transfer with batch operations is the heating of a reactor mix, maintaining temperature during a reaction period, and then cooling the products after the reaction is complete. This subsection is concerned with the heating and cooling of such systems in either unknown or specified periods.

The technique for deriving expressions relating time for heating or cooling agitated batches to coil or jacket area, heat-transfer coefficients, and the heat capacity of the vessel contents was developed by Bowman, Mueller, and Nagle [*Trans. Am. Soc. Mech. Eng.*, **62**, 283-294 (1940)] and extended by Fisher [*Ind. Eng. Chem.*, **36**, 939-942 (1944)] and Chaddock and Sanders [*Trans. Am. Inst. Chem. Eng.*, **40**, 203-210 (1944)] to external heat exchangers. Kern (*Process Heat Transfer*, McGraw-Hill, New York, 1950, Chap. 18) collected and published the results of these investigators.

The assumptions made were that (1) U is constant for the process and over the entire surface, (2) liquid flow rates are constant, (3) specific heats are constant for the process, (4) the heating or cooling medium has a constant inlet temperature, (5) agitation produces a uniform batch fluid temperature, (6) no partial phase changes occur, and (7) heat losses are negligible. The developed equations are as follows. If any of the assumptions do not apply to a system being designed, new equations should be developed or appropriate corrections made. Heat exchangers are counterflow except for the 1-2 exchangers, which are one-shell-pass, two-tube-pass, parallel-flow counterflow.

Coil-in-Tank or Jacketed Vessel: Isothermal Heating Medium

$$\ln (T_1 - t_1)/(T_1 - t_2) = UA\theta/Mc \quad (11-35)$$

Cooling-in-Tank or Jacketed Vessel: Isothermal Cooling Medium

$$\ln (T_1 - t_1)/(T_2 - t_1) = UA\theta/MC \quad (11-35a)$$

Coil-in-Tank or Jacketed Vessel: Nonisothermal Heating Medium

$$\ln \frac{T_1 - t_1}{T_1 - t_2} = \frac{WC}{Mc} \left(\frac{K_1 - 1}{K_1} \right) \theta \quad (11-35b)$$

where $K_1 = e^{UA/WC}$

Coil-in-Tank: Nonisothermal Cooling Medium

$$\ln \frac{T_1 - t_1}{T_2 - t_1} = \frac{wc}{MC} \left(\frac{K_2 - 1}{K_2} \right) \theta \quad (11-35c)$$

where $K_2 = e^{UA/wc}$

External Heat Exchanger: Isothermal Heating Medium

$$\ln \frac{T_1 - t_1}{T_1 - t_2} = \frac{wc}{Mc} \left(\frac{K_2 - 1}{K_2} \right) \theta \quad (11-35d)$$

External Exchanger: Isothermal Cooling Medium

$$\ln \frac{T_1 - t_1}{T_2 - t_1} = \frac{WC}{MC} \left(\frac{K_1 - 1}{K_1} \right) \theta \quad (11-35e)$$

External Exchanger: Nonisothermal Heating Medium

$$\ln \frac{T_1 - t_1}{T_1 - t_2} = \left(\frac{K_3 - 1}{M} \right) \left(\frac{wWC}{K_3wc - WC} \right) \theta \quad (11-35f)$$

where $K_3 = e^{UA(1/WC - 1/wc)}$

External Exchanger: Nonisothermal Cooling Medium

$$\ln \frac{T_1 - t_1}{T_2 - t_1} = \left(\frac{K_4 - 1}{M} \right) \left(\frac{Wwc}{K_4wc - WC} \right) \theta \quad (11-35g)$$

where $K_4 = e^{UA(1/WC - 1/wc)}$

External Exchanger with Liquid Continuously Added to Tank: Isothermal Heating Medium

$$\ln \frac{t_1 - t_0 - \frac{w}{L_0} \left(\frac{K_2 - 1}{K_2} \right) (T_1 - t_1)}{t_2 - t_0 - \frac{w}{L_0} \left(\frac{K_2 - 1}{K_2} \right) (T_1 - t_2)} = \left[\frac{w}{L_0} \left(\frac{K_2 - 1}{K_2} \right) + 1 \right] \ln \frac{M + L_0 \theta}{M} \quad (11-35h)$$

If the addition of liquid to the tank causes an average endothermic or exothermic heat of solution, $\pm q_s$ /kg (Btu/lb) of makeup, it may be included by adding $\pm q_s/c_0$ to both the numerator and the denominator of the left side. The subscript 0 refers to the makeup.

External Exchanger with Liquid Continuously Added to Tank: Isothermal Cooling Medium

$$\ln \frac{T_0 - T_1 - \frac{W}{L_0} \left(\frac{K_1 - 1}{K_1} \right) (T_1 - t_1)}{T_0 - T_2 - \frac{W}{L_0} \left(\frac{K_1 - 1}{K_1} \right) (T_2 - t_1)} = \left[1 - \frac{W}{L_0} \left(\frac{K_1 - 1}{K_1} \right) \right] \ln \frac{M + L_0 \theta}{M} \quad (11-35i)$$

The heat-of-solution effects can be included by adding $\pm q_s/C_0$ to both the numerator and the denominator of the left side.

External Exchanger with Liquid Continuously Added to Tank: Nonisothermal Heating Medium

$$\ln \frac{t_0 - t_1 + \frac{wWC(K_5 - 1)(T_1 - t_1)}{L_0(K_5WC - wc)}}{t_0 - t_2 + \frac{wWC(K_5 - 1)(T_1 - t_2)}{L_0(K_5WC - wc)}} = \left[\frac{wWC(K_5 - 1)}{L_0(K_5WC - wc)} + 1 \right] \ln \frac{M + L_0 \theta}{M} \quad (11-35j)$$

where $K_5 = e^{(UA/wc)(1 - wc/WC)}$

The heat-of-solution effects can be included by adding $\pm q_s/c_0$ to both the numerator and the denominator of the left side.

External Exchanger with Liquid Continuously Added to Tank: Nonisothermal Cooling Medium

$$\ln \frac{T_0 - T_1 - \frac{Wwc(K_6 - 1)(T_1 - t_1)}{L_0(K_6wc - WC)}}{T_0 - T_2 - \frac{Wwc(K_6 - 1)(T_2 - t_1)}{L_0(K_6wc - WC)}} = \left[\frac{Wwc(K_6 - 1)}{L_0(K_6wc - WC)} + 1 \right] \ln \frac{M + L_0 \theta}{M} \quad (11-35k)$$

where $K_6 = e^{(UA/WC)(1 - WC/wc)}$

The heat-of-solution effects can be included by adding $\pm q_s/c_0$ to both the numerator and the denominator of the left side.

Heating and Cooling Agitated Batches: 1-2 Parallel Flow-Counterflow

$$\frac{UA}{wc} = \frac{1}{\sqrt{R^2 + 1}} \ln \frac{2 - S(R + 1 - \sqrt{R^2 + 1})}{2 - S(R + 1 + \sqrt{R^2 + 1})} \quad (11-35l)$$

$$R = \frac{T_1 - T_2}{t' - t} = \frac{wc}{WC} \quad \text{and} \quad S = \frac{t' - t}{T_1 - t}$$

$$\frac{2 - S(R + 1 - \sqrt{R^2 + 1})}{2 - S(R + 1 + \sqrt{R^2 + 1})} = e^{(UA/wc)\sqrt{R^2 + 1}} = K_7 \quad (11-35m)$$

$$S = \frac{2(K_7 - 1)}{K_7(R + 1 + R^2 + 1) - (R + 1 - R^2 + 1)}$$

External 1-2 Exchanger: Heating

$$\ln (T_1 - t_1)/(T_1 - t_2) = (Sw/M)\theta \quad (11-35n)$$

External 1-2 Exchanger: Cooling

$$\ln (T_1 - t_1)/(T_2 - t_1) = S(wc/MC)\theta \quad (11-35o)$$

The cases of multipass exchangers with liquid continuously added to the tank are covered by Kern, as cited earlier. An alternative method for all multipass-exchanger gases, including those presented as well as cases with two or more shells in series, is as follows:

1. Determine UA for using the applicable equations for counter-flow heat exchangers.
2. Use the initial batch temperature T_1 or t_1 .
3. Calculate the outlet temperature from the exchanger of each fluid. (This will require trial-and-error methods.)
4. Note the F_T correction factor for the corrected mean temperature difference. (See Fig. 11-4.)
5. Repeat steps 2, 3, and 4 by using the final batch temperature T_2 and t_2 .
6. Use the average of the two values for F , then increase the required multipass UA as follows:

$$UA(\text{multipass}) = UA(\text{counterflow})/F_T$$

In general, values of F_T below 0.8 are uneconomical and should be avoided. F_T can be raised by increasing the flow rate of either or both of the flow streams. Increasing flow rates to give values well above 0.8 is a matter of economic justification.

If F_T varies widely from one end of the range to the other, F_T should be determined for one or more intermediate points. The average should then be determined for each step which has been established and the average of these taken for use in step 6.

Effect of External Heat Loss or Gain If heat loss or gain through the vessel walls cannot be neglected, equations which include this heat transfer can be developed by using energy balances similar to those used for the derivations of equations given previously. Basically, these equations must be modified by adding a heat-loss or heat-gain term.

A simpler procedure, which is probably acceptable for most practical cases, is to ratio UA or θ either up or down in accordance with the required modification in total heat load over time θ .

Another procedure, which is more accurate for the external-heat-exchanger cases, is to use an equivalent value for MC (for a vessel being heated) derived from the following energy balance:

$$Q = (Mc)_c(t_2 - t_1) = Mc(t_2 - t_1) + U'A'(MTD')\theta \quad (11-35p)$$

where Q is the total heat transferred over time θ , $U'A'$ is the heat-transfer coefficient for heat loss times the area for heat loss, and MTD' is the mean temperature difference for the heat loss.

A similar energy balance would apply to a vessel being cooled.

Internal Coil or Jacket Plus External Heat Exchanger This case can be most simply handled by treating it as two separate problems. M is divided into two separate masses M_1 and $(M - M_1)$, and the appropriate equations given earlier are applied to each part of the system. Time θ , of course, must be the same for both parts.

Equivalent-Area Concept The preceding equations for batch operations, particularly Eq. 11-35 can be applied for the calculation of heat loss from tanks which are allowed to cool over an extended period of time. However, different surfaces of a tank, such as the top (which would not be in contact with the tank contents) and the bottom, may have coefficients of heat transfer which are different from those of the vertical tank walls. The simplest way to resolve this difficulty is to use an equivalent area A_e in the appropriate equations where

$$A_e = A_b U_b / U_s + A_t U_t / U_s + A_s \quad (11-35q)$$

TABLE 11-1 Typical Values for Use with Eqs. (11-36) to (11-44)*

Application	Fluid	U_s	A_s
Tanks on legs, outdoors, not insulated	Oil	3.7	$0.22 A_b + A_s + A_s$
	Water at 150°F.	5.1	$0.16 A_b + A_s + A_s$
Tanks on legs, outdoors, insulated 1 in.	Oil	0.45	$0.7 A_s + A_s + A_s$
	Water	0.43	$0.67 A_s + A_s + A_s$
Tanks on legs, indoors, not insulated	Oil	1.5	$0.53 A_s + A_s + A_s$
	Water	1.8	$0.35 A_s + A_s + A_s$
Tanks on legs, indoors, insulated 1 in.	Oil	0.36	$0.8 A_s + A_s + A_s$
	Water	0.37	$0.73 A_s + A_s + A_s$
Flat-bottom tanks, † outdoors, not insulated	Oil	3.7	$0.22 A_s + A_s + 0.43 D_i$
	Water	5.1	$0.16 A_s + A_s + 0.31 D_i$
Flat-bottom tanks, † outdoors, insulated 1 in.	Oil	0.36	$0.7 A_s + A_s + 3.9 D_i$
	Water	0.37	$0.16 A_s + A_s + 3.7 D_i$
Flat-bottom tanks, indoors, not insulated	Oil	1.5	$0.53 A_s + A_s + 1.1 D_i$
	Water	1.8	$0.35 A_s + A_s + 0.9 D_i$
Flat-bottom tanks, indoors, insulated 1 in.	Oil	0.36	$0.8 A_s + A_s + 4.4 D_i$
	Water	0.37	$0.73 A_s + A_s + 4.5 D_i$

*Based on typical coefficients.

†The ratio $(t - t_o)/(t - t')$ assumed at 0.85 for outdoor tanks. °C = (°F - 32)/1.8; to convert British thermal units per hour-square foot-degrees Fahrenheit to joules per square meter-second-kelvins, multiply by 5.6783.

and the subscripts b , s , and t refer to the bottom, sides, and top respectively. U is usually taken as U_s . Table 11-1 lists typical values for U_s and expressions for A_s for various tank configurations.

Nonagitated Batches Cases in which vessel contents are vertically stratified, rather than uniform in temperature, have been treated by Kern (op. cit.). These are of little practical importance except for tall, slender vessels heated or cooled with external exchangers. The result is that a smaller exchanger is required than for an equivalent agitated batch system that is uniform.

Storage Tanks The equations for batch operations with agitation may be applied to storage tanks even though the tanks are not agitated. This approach gives conservative results. The important cases (nonsteady state) are:

1. *Tanks cool; contents remain liquid.* This case is relatively simple and can easily be handled by the equations given earlier.
2. *Tanks cool, contents partially freeze, and solids drop to bottom or rise to top.* This case requires a two-step calculation. The first step is handled as in case 1. The second step is calculated by assuming an isothermal system at the freezing point. It is possible, given time and a sufficiently low ambient temperature, for tank contents to freeze solid.
3. *Tanks cool and partially freeze; solids form a layer of self-insulation.* This complex case, which has been known to occur with heavy hydrocarbons and mixtures of hydrocarbons, has been discussed by Stuhlberg [*Pet. Refiner*, **38**, 143 (Apr. 1, 1959)]. The contents in the center of such tanks have been known to remain warm and liquid even after several years of cooling.

It is very important that a melt-out riser be installed whenever tank contents are expected to freeze on prolonged shutdown. The purpose is to provide a molten chimney through the crust for relief of thermal expansion or cavitation if fluids are to be pumped out or recirculated through an external exchanger. An external heat tracer, properly located, will serve the same purpose but may require more remelt time before pumping can be started.

THERMAL DESIGN OF TANK COILS

The thermal design of tank coils involves the determination of the area of heat-transfer surface required to maintain the contents of the tank at a constant temperature or to raise or lower the temperature of the contents by a specified magnitude over a fixed time.

Nomenclature A = area; A_b = area of tank bottom; A_s = area of coil; A_s = equivalent area; A_s = area of sides; A_t = area of top; A_1 = equivalent area receiving heat from external coils; A_2 = equivalent area not covered with external coils; D_i = diameter of tank; F = design (safety) factor; h = film coefficient; h_a = coefficient of ambient air; h_c = coefficient of coil; h_h = coefficient of heating medium; h_i = coefficient of liquid phase of tank contents or tube-side coefficient referred to

outside of coil; h_s = coefficient of insulation; k = thermal conductivity; k_g = thermal conductivity of ground below tank; M = mass of tank contents when full; t = temperature; t_a = temperature of ambient air; t_d = temperature of dead-air space; t_f = temperature of contents at end of heating; t_g = temperature of ground below tank; t_h = temperature of heating medium; t_o = temperature of contents at beginning of heating; U = overall coefficient; U_b = coefficient at tank bottom; U_c = coefficient of coil; U_d = coefficient of dead air to the tank contents; U_i = coefficient through insulation; U_s = coefficient at sides; U_t = coefficient at top; and U_2 = coefficient at area A_2 .

Typical coil coefficients are listed in Table 11-2. More exact values can be calculated by using the methods for natural convection or forced convection given elsewhere in this section.

Maintenance of Temperature Tanks are often maintained at temperature with internal coils if the following equations are assumed to be applicable:

$$q = U_s A_s (T - t') \tag{11-36}$$

and

$$A_c = q/U_c (MTD) \tag{11-36a}$$

These make no allowance for unexpected shutdowns. One method of allowing for shutdown is to add a safety factor to Eq. 11-36a.

In the case of a tank maintained at temperature with internal coils, the coils are usually designed to cover only a portion of the tank. The temperature t_d of the dead-air space between the coils and the tank is obtained from

$$U_d A_1 (t_d - t) = U_2 A_2 (t - t') \tag{11-37}$$

The heat load is

$$q = U_d A_1 (t_d - t) + A_1 U_i (t_d - t') \tag{11-38}$$

The coil area is

$$A_c = \frac{qF}{U_c (t_h - t_d)_m} \tag{11-39}$$

where F is a safety factor.

Heating

Heating with Internal Coil from Initial Temperature for Specified Time

$$Q = Wc(t_f - t_o) \tag{11-40}$$

$$A_c = \left[\frac{Q}{\theta_h} + U_s A_s \left(\frac{t_f + t_o}{2} - t' \right) \right] \left[\frac{1}{U_c [t_h - (t_f + t_o)/2]} \right] (F) \tag{11-41}$$

where θ_h is the length of heating period. This equation may also be used when the tank contents have cooled from t_f to t_o and must be

TABLE 11-2 Overall Heat-Transfer Coefficients for Coils Immersed in Liquids
U Expressed as Btu/(h · ft² · °F)

Substance inside coil	Substance outside coil	Coil material	Agitation	<i>U</i>
Steam	Water	Lead	Agitated	70
Steam	Sugar and molasses solutions	Copper	None	50–240
Steam	Boiling aqueous solution			600
Cold water	Dilute organic dye intermediate	Lead	Turboagitator at 95 r.p.m.	300
Cold water	Warm water	Wrought iron	Air bubbled into water surrounding coil	150–300
Cold water	Hot water	Lead	0.40 r.p.m. paddle stirrer	90–360
Brine	Amino acids		30 r.p.m.	100
Cold water	25% oleum at 60°C.	Wrought iron	Agitated	20
Water	Aqueous solution	Lead	500 r.p.m. sleeve propeller	250
Water	8% NaOH		22 r.p.m.	155
Steam	Fatty acid	Copper (pancake)	None	96–100
Milk	Water		Agitation	300
Cold water	Hot water	Copper	None	105–180
60°F. water	50% aqueous sugar solution	Lead	Mild	50–60
Steam and hydrogen at 1500 lb./sq. in.	60°F. water	Steel		100–165
Steam 110–146 lb./sq. in. gage	Vegetable oil	Steel	None	23–29
Steam	Vegetable oil	Steel	Various	39–72
Cold water	Vegetable oil	Steel	Various	29–72

NOTES: Chilton, Drew, and Jebens [*Ind. Eng. Chem.*, **36**, 510 (1944)] give film coefficients for heating and cooling agitated fluids using a coil in a jacketed vessel. Because of the many factors affecting heat transfer, such as viscosity, temperature difference, and coil size, the values in this table should be used primarily for preliminary design estimates and checking calculated coefficients.
 °C = (°F – 32)/1.8; to convert British thermal units per hour-square foot-degrees Fahrenheit to joules per square meter-second-kelvins, multiply by 5.6783.

reheated to *t_f*. If the contents cool during a time *θ_c*, the temperature at the end of this cooling period is obtained from

$$\ln \left(\frac{t_f - t'}{t_o - t'} \right) = \frac{U_s A_c \theta_c}{Wc} \tag{11-42}$$

Heating with External Coil from Initial Temperature for Specified Time The temperature of the dead-air space is obtained from

$$U_d A_1 [t_d - 0.5(t_f - t_o)] = U_2 A_2 [0.5(t_f - t_o) - t'] + Q/\theta_h \tag{11-43}$$

The heat load is

$$q = U_1 A_1 (t_d - t') + U_2 A_2 [0.5(t_f - t_o) - t'] + Q/\theta_h \tag{11-44}$$

The coil area is obtained from Eq. 11-39. The safety factor used in the calculations is a matter of judgment based on confidence in the design. A value of 1.10 is normally not considered excessive. Typical design parameters are shown in Tables 11-1 and 11-2.

HEATING AND COOLING OF TANKS

Tank Coils **Pipe tank coils** are made in a wide variety of configurations, depending upon the application and shape of the vessel. **Helical** and **spiral** coils are most commonly shop-fabricated, while the **hairpin** pattern is generally field-fabricated. The helical coils are used principally in process tanks and pressure vessels when large areas

for rapid heating or cooling are required. In general, heating coils are placed low in the tank, and cooling coils are placed high or distributed uniformly through the vertical height.

Stocks which tend to solidify on cooling require uniform coverage of the bottom or agitation. A maximum spacing of 0.6 m (2 ft) between turns of 50.8-mm (2-in) and larger pipe and a close approach to the tank wall are recommended. For smaller pipe or for low-temperature heating media, closer spacing should be used. In the case of the common hairpin coils in vertical cylindrical tanks, this means adding an encircling ring within 152 mm (6 in) of the tank wall (see Fig. 11-29a for this and other typical coil layouts). The coils should be set directly on the bottom or raised not more than 50.8 to 152 mm (2 to 6 in), depending upon the difficulty of remelting the solids, in order to permit free movement of product within the vessel. The coil inlet should be above the liquid level (or an internal melt-out riser installed) to provide a molten path for liquid expansion or venting of vapors.

Coils may be sloped to facilitate drainage. When it is impossible to do so and remain close enough to the bottom to get proper remelting, the coils should be blown out after usage in cold weather to avoid damage by freezing.

Most coils are firmly clamped (but not welded) to supports. **Supports** should allow expansion but be rigid enough to prevent uncontrolled motion (see Fig. 11-29b). Nuts and bolts should be securely fastened. Reinforcement of the inlet and outlet connections through the tank wall is recommended, since bending stresses due to thermal expansion are usually high at such points.

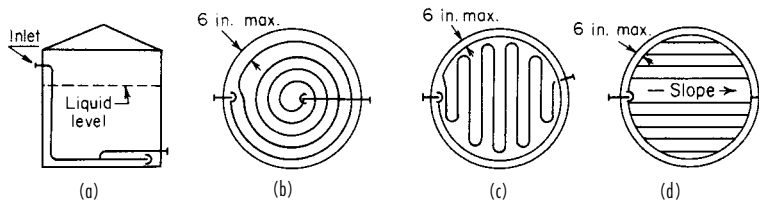


FIG. 11-29a Typical coil designs for good bottom coverage. (a) Elevated inlet on spiral coil. (b) Spiral with recirculating ring. (c) Hairpin with encircling ring. (d) Ring header type.

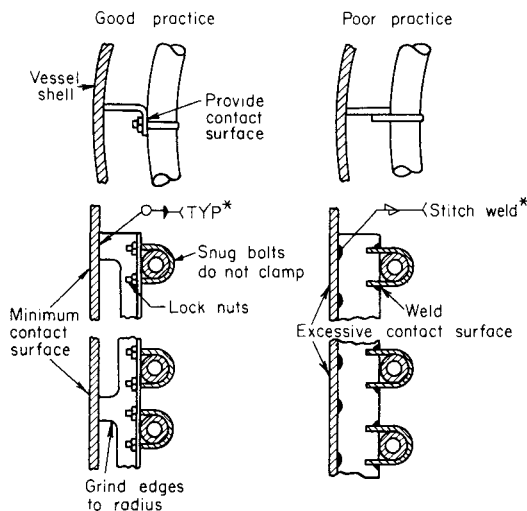


FIG. 11-29b Right and wrong ways to support coils. [*Chem. Eng.*, 172 (May 16, 1960).]

In general, 50.8- and 63.4-mm (2- and 2½-in) coils are the most economical for shop fabrication and 38.1- and 50.8-mm (1½- and 2-in) for field fabrication. The tube-side heat-transfer coefficient, high-pressure, or layout problems may lead to the use of smaller-size pipe.

The wall thickness selected varies with the service and material. Carbon steel coils are often made from schedule 80 or heavier pipe to allow for corrosion. When stainless-steel or other high-alloy coils are not subject to corrosion or excessive pressure, they may be of schedule 5 or 10 pipe to keep costs at a minimum, although high-quality welding is required for these thin walls to assure trouble-free service.

Methods for calculating heat loss from tanks and the sizing of tank coils have been published by Stuhlbarg [*Pet. Refiner*, **38**, 143 (April 1959)].

Fin-tube coils are used for fluids which have poor heat-transfer characteristics to provide more surface for the same configuration at reduced cost or when temperature-driven fouling is to be minimized. Fin tubing is not generally used when bottom coverage is important.

Fin-tube tank heaters are compact prefabricated bundles which can be brought into tanks through manholes. These are normally installed vertically with longitudinal fins to produce good convection currents. To keep the heaters low in the tank, they can be installed horizontally with helical fins or with perforated longitudinal fins to prevent entrapment. Fin tubing is often used for heat-sensitive material because of the lower surface temperature for the same heating medium, resulting in a lesser tendency to foul.

Plate or panel coils made from two metal sheets with one or both embossed to form passages for a heating or cooling medium can be used in lieu of pipe coils. Panel coils are relatively light in weight, easy to install, and easily removed for cleaning. They are available in a range of standard sizes and in both flat and curved patterns. Process tanks have been built by using panel coils for the sides or bottom. A serpentine construction is generally utilized when liquid flows through the unit. Header-type construction is used with steam or other condensing media.

Standard **glass coils** with 0.18 to 11.1 m² (2 to 120 ft²) of heat-transfer surface are available. Also available are plate-type units made of **impervious graphite**.

Teflon Immersion Coils Immersion coils made of Teflon fluorocarbon resin are available with 2.5-mm (0.10-in) ID tubes to increase overall heat-transfer efficiency. The flexible bundles are available with 100, 160, 280, 500, and 650 tubes with standard lengths

varying in 0.6-m (2-ft) increments between 1.2 and 4.8 m (4 and 16 ft). These coils are most commonly used in metal-finishing baths and are adaptable to service in reaction vessels, crystallizers, and tanks where corrosive fluids are used.

Bayonet Heaters A bayonet-tube element consists of an outer and an inner tube. These elements are inserted into tanks and process vessels for heating and cooling purposes. Often the outer tube is of expensive alloy or nonmetallic (e.g., glass, impervious graphite), while the inner tube is of carbon steel. In glass construction, elements with 50.8- or 76.2-mm (2- or 3-in) glass pipe [with lengths to 2.7 m (9 ft)] are in contact with the external fluid, with an inner tube of metal.

External Coils and Tracers Tanks, vessels, and pipe lines can be equipped for heating or cooling purposes with external coils. These are generally 9.8 to 19 mm (¾ to ¾ in) so as to provide good distribution over the surface and are often of soft copper or aluminum, which can be bent by hand to the contour of the tank or line. When necessary to avoid "hot spots," the tracer is so mounted that it does not touch the tank.

External coils spaced away from the tank wall exhibit a coefficient of around 5.7 W/(m²·°C) [1 Btu/(h·ft² of coil surface·°F)]. Direct contact with the tank wall produces higher coefficients, but these are difficult to predict since they are strongly dependent upon the degree of contact. The use of **heat-transfer cements** does improve performance. These puttylike materials of high thermal conductivity are troweled or caulked into the space between the coil and the tank or pipe surface.

Costs of the cements (in 1960) varied from 37 to 63 cents per pound, with requirements running from about 0.27 lb/ft of ¾-in outside-diameter tubing to 1.48 lb/ft of 1-in pipe. Panel coils require ½ to 1 lb/ft². A rule of thumb for preliminary estimating is that the per-foot installed cost of tracer with cement is about double that of the tracer alone.

Jacketed Vessels Jacketing is often used for vessels needing frequent cleaning and for glass-lined vessels which are difficult to equip with internal coils. The jacket eliminates the need for the coil yet gives a better overall coefficient than external coils. However, only a limited heat-transfer area is available. The conventional jacket is of simple construction and is frequently used. It is most effective with a condensing vapor. A liquid heat-transfer fluid does not maintain uniform flow characteristics in such a jacket. Nozzles, which set up a swirling motion in the jacket, are effective in improving heat transfer. Wall thicknesses are often high unless reinforcement rings are installed.

Spiral baffles, which are sometimes installed for liquid services to improve heat transfer and prevent channeling, can be designed to serve as reinforcements. A spiral-wound channel welded to the vessel wall is an alternative to the spiral baffle which is more predictable in performance, since cross-baffle leakage is eliminated, and is reportedly lower in cost [Feichtinger, *Chem. Eng.*, **67**, 197 (Sept. 5, 1960)].

The half-pipe jacket is used when high jacket pressures are required. The flow pattern of a liquid heat-transfer fluid can be controlled and designed for effective heat transfer. The dimple jacket offers structural advantages and is the most economical for high jacket pressures. The low volumetric capacity produces a fast response to temperature changes.

EXTENDED OR FINNED SURFACES

Finned-Surface Application Extended or finned surfaces are often used when one film coefficient is substantially lower than the other, the goal being to make $h_o A_{oc} \approx h_i A_i$. A few typical fin configurations are shown in Fig. 11-30a. Longitudinal fins are used in double-pipe exchangers. Transverse fins are used in cross-flow and shell-and-tube configurations. High transverse fins are used mainly with low-pressure gases; low fins are used for boiling and condensation of nonaqueous streams as well as for sensible-heat transfer. Finned surfaces have been proven to be a successful means of controlling temperature driven fouling such as coking and scaling. Fin spacing should be great enough to avoid entrapment of particulate matter in the fluid stream (5 mm minimum spacing).

The area added by the fin is not as efficient for heat transfer as bare tube surface owing to resistance to conduction through the fin. The

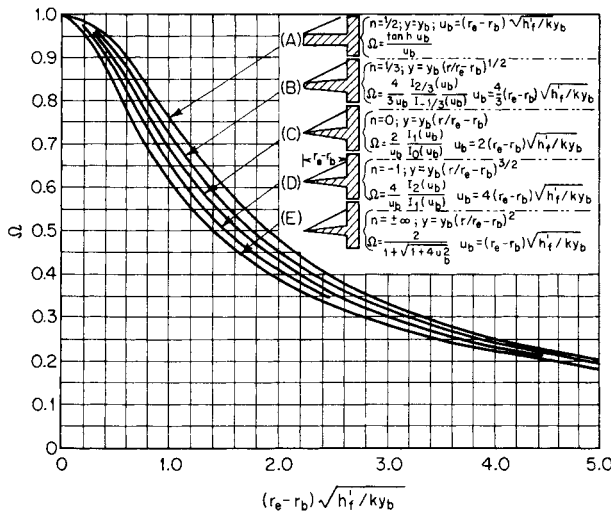


FIG. 11-30a Efficiencies for several longitudinal fin configurations.

effective heat-transfer area is

$$A_{oe} = A_{uf} + A_f \Omega \tag{11-45}$$

The fin efficiency is found from mathematically derived relations, in which the film heat-transfer coefficient is assumed to be constant over the entire fin and temperature gradients across the thickness of the fin have been neglected (see Kraus, *Extended Surfaces*, Spartan Books, Baltimore, 1963). The efficiency curves for some common fin configurations are given in Figs. 11-30a and 11-30b.

High Fins To calculate heat-transfer coefficients for cross-flow to a transversely finned surface, it is best to use a correlation based on experimental data for that surface. Such data are not often available, and a more general correlation must be used, making allowance for the possible error. Probably the best general correlation for bundles of finned tubes is given by Schmidt [*Kaltetechnik*, 15, 98–102, 370–378 (1963)]:

$$hD_r/k = K(D_r \rho V'_{max} / \mu)^{0.625} R_f^{-0.375} N_{Pr}^{1/3} \tag{11-46}$$

where $K = 0.45$ for staggered tube arrays and 0.30 for in-line tube

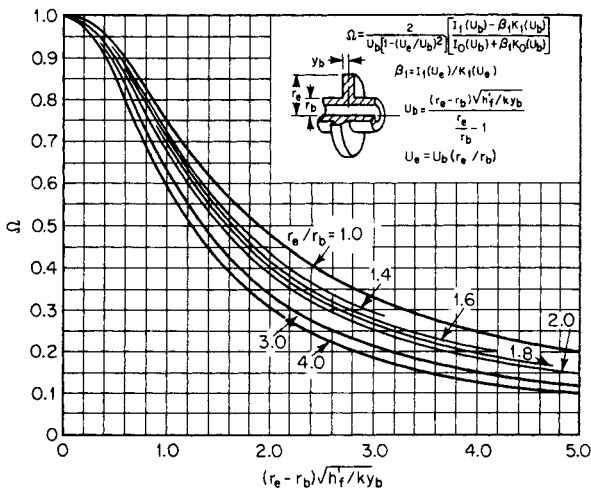


FIG. 11-30b Efficiencies for annular fins of constant thickness.

arrays: D_r is the root or base diameter of the tube; V'_{max} is the maximum velocity through the tube bank, i.e., the velocity through the minimum flow area between adjacent tubes; and R_f is the ratio of the total outside surface area of the tube (including fins) to the surface of a tube having the same root diameter but without fins.

Pressure drop is particularly sensitive to geometrical parameters, and available correlations should be extrapolated to geometries different from those on which the correlation is based only with great caution and conservatism. The best correlation is that of Robinson and Briggs [*Chem. Eng. Prog.*, 62, *Symp. Ser.* 64, 177–184 (1966)].

Low Fins Low-finned tubing is generally used in shell-and-tube configurations. For sensible-heat transfer, only minor modifications are needed to permit the shell-side method given earlier to be used for both heat transfer and pressure [see Briggs, Katz, and Young, *Chem. Eng. Prog.*, 59(11), 49–59 (1963)]. For condensing on low-finned tubes in horizontal bundles, the Nusselt correlation is generally satisfactory for low-surface-tension [$\sigma < (3)(10^{-6})\text{N/m}$ (30 dyn/cm)] condensates; fins of finned surfaces should not be closely spaced for high-surface-tension condensates (notably water), which do not drain easily.

The modified Palen-Small method can be employed for reboiler design using finned tubes, but the maximum flux is calculated from A_{ov} , the total outside heat-transfer area including fins. The resulting value of q_{max} refers to A_{ov} .

FOULING AND SCALING

Fouling refers to any change in the solid boundary separating two heat transfer fluids, whether by dirt accumulation or other means, which results in a decrease in the rate of heat transfer occurring across that boundary. Fouling may be classified by mechanism into six basic categories:

1. *Corrosion fouling.* The heat transfer surface reacts chemically with elements of the fluid stream producing a less conductive, corrosion layer on all or part of the surface.
2. *Biofouling.* Organisms present in the fluid stream are attracted to the warm heat-transfer surface where they attach, grow, and reproduce. The two subgroups are microfouling such as slime and algae and macrofouling such as snails and barnacles.
3. *Particulate fouling.* Particles held in suspension in the flow stream will deposit out on the heat-transfer surface in areas of sufficiently lower velocity.
4. *Chemical reaction fouling* (ex.—Coking). Chemical reaction of the fluid takes place on the heat-transfer surface producing an adhering solid product of reaction.
5. *Precipitation fouling* (ex.—Scaling). A fluid containing some dissolved material becomes supersaturated with respect to this material at the temperatures seen at the heat-transfer surface. This results in a crystallization of the material which “plates out” on the warmer surface.
6. *Freezing fouling.* Overcooling of a fluid below the fluid’s freezing point at the heat-transfer surface causes solidification and coating of the heat-transfer surface.

Control of Fouling Once the combination of mechanisms contributing to a particular fouling problem are recognized, methods to substantially reduce the fouling rate may be implemented. For the case of **corrosion fouling**, the common solution is to choose a less corrosive material of construction balancing material cost with equipment life. In cases of **biofouling**, the use of copper alloys and/or chemical treatment of the fluid stream to control organism growth and reproduction are the most common solutions.

In the case of **particulate fouling**, one of the more common types, insuring a sufficient flow velocity and minimizing areas of lower velocities and stagnant flows to help keep particles in suspension is the most common means of dealing with the problem. For water, the recommended tubeside minimum velocity is about 0.9 to 1.0 m/s. This may not always be possible for moderate to high-viscosity fluids where the resulting pressure drop can be prohibitive.

Special care should be taken in the application of any velocity requirement to the shellside of segmental-baffled bundles due to the many different flow streams and velocities present during operation, the unavoidable existence of high-fouling areas of flow stagnation, and

the danger of flow-induced tube vibration. In general, shellside-particulate fouling will be greatest for segmentally baffled bundles in the regions of low velocity and the TEMA-fouling factors (which are based upon the use of this bundle type) should be used. However, since the 1940's, there have been a host of successful, low-fouling exchangers developed, some tubular and some not, which have in common the elimination of the cross-flow plate baffle and provide practically no regions of flow stagnation at the heat-transfer surface. Some examples are the plate and frame exchanger, the spiral plate exchanger, and the twisted tube exchanger, all of which have dispensed with baffles altogether and use the heat-transfer surface itself for bundle support. The general rule for these designs is to provide between 25 and 30 percent excess surface to compensate for potential fouling, although this can vary in special applications.

For the remaining classifications—**polymerization, precipitation, and freezing**—fouling is the direct result of temperature extremes at the heat-transfer surface and is reduced by reducing the temperature difference between the heat-transfer surface and the bulk-fluid stream. Conventional wisdom says to increase velocity, thus increasing the local heat-transfer coefficient to bring the heat-transfer surface temperature closer to the bulk-fluid temperature. However, due to a practical limit on the amount of heat-transfer coefficient increase available by increasing velocity, this approach, although better than nothing, is often not satisfactory by itself.

A more effective means of reducing the temperature difference is by using, in concert with adequate velocities, some form of extended surface. As discussed by Shilling (*Proceedings of the 10th International Heat Transfer Conference*, Brighton, U.K., 4, p. 423), this will tend to reduce the temperature extremes between fluid and heat transfer surface and not only reduce the rate of fouling but make the heat exchanger generally less sensitive to the effects of any fouling that does occur. In cases where unfinned tubing in a triangular tube layout would not be acceptable because fouling buildup and eventual mechanical cleaning are inevitable, extended surface should be used only when the exchanger construction allows access for cleaning.

Fouling Transients and Operating Periods Three common behaviors are noted in the development of a fouling film over a period of time. One is the so-called *asymptotic fouling* in which the speed of fouling resistance increase decreases over time as it approaches some asymptotic value beyond which no further fouling can occur. This is commonly found in temperature-driven fouling. A second is *linear fouling* in which the increase in fouling resistance follows a straight line over the time of operation. This could be experienced in a case of severe particulate fouling where the accumulation of dirt during the time of operation did not appreciably increase velocities to mitigate the problem. The third, *falling rate fouling*, is neither linear nor asymptotic but instead lies somewhere between these two extremes. The rate of fouling decreases with time but does not appear to approach an asymptotic maximum during the time of operation. This is the most common type of fouling in the process industry and is usually the result of a combination of different fouling mechanisms occurring together.

The optimum operating period between cleanings depends upon the rate and type of fouling, the heat exchanger used (i.e. baffle type, use of extended surface, and velocity and pressure drop design constraints), and the ease with which the heat exchanger may be removed from service for cleaning. As noted above, care must be taken in the use of fouling factors for exchanger design, especially if the exchanger configuration has been selected specifically to minimize fouling accumulation. An oversurfaced heat exchanger which will not foul enough to operate properly can be almost as much a problem as an undersized exchanger. This is especially true in steam-heated exchangers where the ratio of design MTD to minimum achievable MTD is less than U_{clean} divided by U_{fouled} .

Removal of Fouling Deposits Chemical removal of fouling can be achieved in some cases by weak acid, special solvents, and so on. Other deposits adhere weakly and can be washed off by periodic operation at very high velocities or by flushing with a high-velocity steam or water jet or using a sand-water slurry. These methods may be applied to both the shell side and tube side without pulling the bundle. Many fouling deposits, however, must be removed by positive

mechanical action such as rodding, turbing, or scraping the surface. These techniques may be applied inside of tubes without pulling the bundle but can be applied on the shellside only after bundle removal. Even then there is limited access because of the tube pitch and rotated square or large triangular layouts are recommended. In many cases, it has been found that designs developed to minimize fouling often develop a fouling layer which is more easily removed.

Fouling Resistances There are no published methods for predicting fouling resistances a priori. The accumulated experience of exchanger designers and users was assembled more than 40 years ago based primarily upon segmental-baffled exchanger bundles and may be found in the *Standards of Tubular Exchanger Manufacturers Association* (TEMA). In the absence of other information, the fouling resistances contained therein may be used.

TYPICAL HEAT-TRANSFER COEFFICIENTS

Typical overall heat-transfer coefficients are given in Tables 11-3 through 11-8. Values from these tables may be used for preliminary estimating purposes. They should not be used in place of the design methods described elsewhere in this section, although they may serve as a useful check on the results obtained by those design methods.

THERMAL DESIGN FOR SOLIDS PROCESSING

Solids in divided form, such as powders, pellets, and lumps, are heated and/or cooled in chemical processing for a variety of objectives such as solidification or fusing (Sec. 11), drying and water removal (Sec. 20), solvent recovery (Secs. 13 and 20), sublimation (Sec. 17), chemical reactions (Sec. 20), and oxidation. For process and mechanical-design considerations, see the referenced sections.

Thermal design concerns itself with sizing the equipment to effect the heat transfer necessary to carry on the process. The design equation is the familiar one basic to all modes of heat transfer, namely,

$$A = Q/U \Delta t \quad (11-47)$$

where A = effective heat-transfer surface, Q = quantity of heat required to be transferred, Δt = temperature difference of the process, and U = overall heat-transfer coefficient. It is helpful to define the modes of heat transfer and the corresponding overall coefficient as U_{co} = overall heat-transfer coefficient for (indirect through-a-wall) conduction, U_{co} = overall heat-transfer coefficient for the little-used convection mechanism, U_{ct} = heat-transfer coefficient for the *contactive* mechanism in which the gaseous-phase heat carrier passes directly through the solids bed, and U_{ra} = heat-transfer coefficient for radiation.

There are two general methods for determining numerical values for U_{co} , U_{cv} , U_{ct} , and U_{ra} . One is by analysis of actual operating data. Values so obtained are used on geometrically similar systems of a size not too different from the equipment from which the data were obtained. The second method is predictive and is based on the material properties and certain operating parameters. Relative values of the coefficients for the various modes of heat transfer at temperatures up to 980°C (1800°F) are as follows (Holt, Paper 11, Fourth National Heat Transfer Conference, Buffalo, 1960):

Convective	1
Radiant	2
Conductive	20
Contactive	200

Because heat-transfer equipment for solids is generally an adaptation of a primarily material-handling device, the area of heat transfer is often small in relation to the overall size of the equipment. Also peculiar to solids heat transfer is that the Δt varies for the different heat-transfer mechanisms. With a knowledge of these mechanisms, the Δt term generally is readily estimated from temperature limitations imposed by the burden characteristics and/or the construction.

Conductive Heat Transfer Heat-transfer equipment in which heat is transferred by conduction is so constructed that the solids load (burden) is separated from the heating medium by a wall.

For a high proportion of applications, Δt is the log-mean temperature difference. Values of U_{co} are reported in Secs. 11, 15, 17, and 19.

TABLE 11-3 Typical Overall Heat-Transfer Coefficients in Tubular Heat Exchangers

$$U = \text{Btu}/(^{\circ}\text{F} \cdot \text{ft}^2 \cdot \text{h})$$

Shell side	Tube side	Design U	Includes total dirt	Shell side	Tube side	Design U	Includes total dirt
Liquid-liquid media							
Aroclor 1248	Jet fuels	100-150	0.0015	Dowtherm vapor	Dowtherm liquid	80-120	.0015
Cutback asphalt	Water	10-20	.01	Gas-plant tar	Steam	40-50	.0055
Demineralized water	Water	300-500	.001	High-boiling hydrocarbons V	Water	20-50	.003
Ethanol amine (MEA or DEA) 10-25% solutions	Water or DEA, or MEA solutions	140-200	.003	Low-boiling hydrocarbons A	Water	80-200	.003
Fuel oil	Water	15-25	.007	Hydrocarbon vapors (partial condenser)	Oil	25-40	.004
Fuel oil	Oil	10-15	.008	Organic solvents A	Water	100-200	.003
Gasoline	Water	60-100	.003	Organic solvents high NC, A	Water or brine	20-60	.003
Heavy oils	Heavy oils	10-40	.004	Organic solvents low NC, V	Water or brine	50-120	.003
Heavy oils	Water	15-50	.005	Kerosene	Water	30-65	.004
Hydrogen-rich reformer stream	Hydrogen-rich reformer stream	90-120	.002	Kerosene	Oil	20-30	.005
Kerosene or gas oil	Water	25-50	.005	Naphtha	Water	50-75	.005
Kerosene or gas oil	Oil	20-35	.005	Naphtha	Oil	20-30	.005
Kerosene or jet fuels	Trichlorethylene	40-50	.0015	Stabilizer reflux vapors	Water	80-120	.003
Jacket water	Water	230-300	.002	Steam	Feed water	400-1000	.0005
Lube oil (low viscosity)	Water	25-50	.002	Steam	No. 6 fuel oil	15-25	.0055
Lube oil (high viscosity)	Water	40-80	.003	Steam	No. 2 fuel oil	60-90	.0025
Lube oil	Oil	11-20	.006	Sulfur dioxide	Water	150-200	.003
Naphtha	Water	50-70	.005	Tall-oil derivatives, vegetable oils (vapor)	Water	20-50	.004
Naphtha	Oil	25-35	.005	Water	Aromatic vapor-stream azeotrope	40-80	.005
Organic solvents	Water	50-150	.003	Gas-liquid media			
Organic solvents	Brine	35-90	.003	Air, N ₂ , etc. (compressed)	Water or brine	40-80	.005
Organic solvents	Organic solvents	20-60	.002	Air, N ₂ , etc., A	Water or brine	10-50	.005
Tall oil derivatives, vegetable oil, etc.	Water	20-50	.004	Water or brine	Air, N ₂ (compressed)	20-40	.005
Water	Caustic soda solutions (10-30%)	100-250	.003	Water or brine	Air, N ₂ , etc., A	5-20	.005
Water	Water	200-250	.003	Water	Hydrogen containing natural-gas mixtures	80-125	.003
Wax distillate	Water	15-25	.005	Vaporizers			
Wax distillate	Oil	13-23	.005	Anhydrous ammonia	Steam condensing	150-300	.0015
Condensing vapor-liquid media				Chlorine	Steam condensing	150-300	.0015
Alcohol vapor	Water	100-200	.002	Chlorine	Light heat-transfer oil	40-60	.0015
Asphalt (450°F.)	Dowtherm vapor	40-60	.006	Propane, butane, etc.	Steam condensing	200-300	.0015
Dowtherm vapor	Tall oil and derivatives	60-80	.004	Water	Steam condensing	250-400	.0015

NC = noncondensable gas present.

V = vacuum.

A = atmospheric pressure.

Dirt (or fouling factor) units are (h · ft² · °F)/Btu.

To convert British thermal units per hour-square foot-degrees Fahrenheit to joules per square meter-second-kelvins, multiply by 5.6783; to convert hours per square foot-degree Fahrenheit-British thermal units to square meters per second-kelvin-joules, multiply by 0.1761.

TABLE 11-4 Typical Overall Heat-Transfer Coefficients in Refinery Service

$$\text{Btu}/(^{\circ}\text{F} \cdot \text{ft}^2 \cdot \text{h})$$

Fluid	API gravity	Fouling factor (one stream)	Reboiler, steam-heated	Condenser, water-cooled*	Exchangers, liquid to liquid (tube-side fluid designation appears below)			Reboiler (heating liquid designated below)			Condenser (cooling liquid designated below)			
					C	G	H	C	G†	K	D	F	G	J
A Propane		0.001	160	95	85	85	80	110	95	35				
B Butane		.001	155	90	80	75	75	105	90	35	80	55	40	30
C 400°F. end-point gasoline	50	.001	120	80	70	65	60	65	50	30				
D Virgin light naphtha	70	.001	140	85	70	55	55	75	60	35	75			
E Virgin heavy naphtha	45	.001	95	75	65	55	50	55	45	30	70	50	35	30
F Kerosene	40	.001	85	60	60	55	50		45	25		50	35	30
G Light gas oil	30	.002	70	50	60	50	50		40	25	70	45	30	30
H Heavy gas oil	22	.003	60	45	55	50	45	50	40	20	70	40	30	20
J Reduced crude	17	.005			55	45	40							
K Heavy fuel oil (tar)	10	.005			50	40	35							

Fouling factor, water side 0.0002; heating or cooling streams are shown at top of columns as C, D, F, G, etc.; to convert British thermal units per hour-square foot-degrees Fahrenheit to joules per square meter-second-kelvins, multiply by 5.6783; to convert hours per square foot-degree Fahrenheit-British thermal units to square meters per second-kelvin-joules, multiply by 0.1761.

*Cooler, water-cooled, rates are about 5 percent lower.

†With heavy gas oil (H) as heating medium, rates are about 5 percent lower.

11-26 HEAT-TRANSFER EQUIPMENT

TABLE 11-5 Overall Coefficients for Air-Cooled Exchangers on Bare-Tube Basis

Btu/(°F · ft ² · h)			
Condensing	Coefficient	Liquid cooling	Coefficient
Ammonia	110	Engine-jacket water	125
Freon-12	70	Fuel oil	25
Gasoline	80	Light gas oil	65
Light hydrocarbons	90	Light hydrocarbons	85
Light naphtha	75	Light naphtha	70
Heavy naphtha	65	Reformer liquid streams	70
Reformer reactor effluent	70	Residuum	15
Low-pressure steam	135	Tar	7
Overhead vapors	65		
Gas cooling	Operating pressure, lb./sq. in. gage	Pressure drop, lb./sq. in.	Coefficient
Air or flue gas	50	0.1 to 0.5	10
	100	2	20
	100	5	30
Hydrocarbon gas	35	1	35
	125	3	55
	1000	5	80
Ammonia reactor stream			85

Bare-tube external surface is 0.262 ft²/ft.
 Fin-tube surface/bare-tube surface ratio is 16.9.
 To convert British thermal units per hour-square foot-degrees Fahrenheit to joules per square meter-second-kelvins, multiply by 5.6783; to convert pounds-force per square inch to kilopascals, multiply by 6.895.

A predictive equation for U_{co} is

$$U_{co} = \left(\frac{h}{h - 2ca/d_m} \right) \left(\frac{2ca}{d_m} \right) \quad (11-48)$$

where h = wall film coefficient, c = volumetric heat capacity, d_m = depth of the burden, and α = thermal diffusivity. Relevant thermal

properties of various materials are given in Table 11-9. For details of terminology, equation development, numerical values of terms in typical equipment and use, see Holt [*Chem. Eng.*, **69**, 107 (Jan. 8, 1962)].

Equation (11-48) is applicable to burdens in the solid, liquid, or gaseous phase, either static or in laminar motion; it is applicable to solidification equipment and to divided-solids equipment such as metal belts, moving trays, stationary vertical tubes, and stationary-shell fluidizers.

Fixed (or packed) bed operation occurs when the fluid velocity is low or the particle size is large so that fluidization does not occur. For such operation, Jakob [*Heat Transfer*, vol. 2, Wiley, New York, 1957] gives

$$hD_p/k = b_1 b D_i^{0.17} (D_p G/\mu)^{0.83} (c\mu/k) \quad (11-49a)$$

where $b_1 = 1.22$ (SI) or 1.0 (U.S. customary), $h = U_{co}$ = overall coefficient between the inner container surface and the fluid stream,

$$b = .2366 + .0092 \left(\frac{D_p}{D_i} \right) - 4.0672 \left(\frac{D_p}{D_i} \right)^2 + 18.229 \left(\frac{D_p}{D_i} \right)^3 - 11.837 \left(\frac{D_p}{D_i} \right)^4 \quad (11-49b)$$

D_p = particle diameter, D_i = vessel diameter, (note that D_p/D_i has units of foot per foot in the equation), G = superficial mass velocity, k = fluid thermal conductivity, μ = fluid viscosity, and c = fluid specific heat. Other correlations are those of Leva [*Ind. Eng. Chem.*, **42**, 2498 (1950)]:

$$h = 0.813 \frac{k}{D_i} e^{-6D_p/D_i} \left(\frac{D_p G}{\mu} \right)^{0.90} \quad \text{for } \frac{D_p}{D_i} < 0.35 \quad (11-50a)$$

$$h = 0.125 \frac{k}{D_i} \left(\frac{D_p G}{\mu} \right)^{0.75} \quad \text{for } 0.35 < \frac{D_p}{D_i} < 0.60 \quad (11-50b)$$

and Calderbank and Pogerski [*Trans. Inst. Chem. Eng. (London)*, **35**, 195 (1957)]:

$$hD_p/k = 3.6(D_p G/\mu \epsilon_v)^{0.365} \quad (11-51)$$

where ϵ_v = fraction voids in the bed.

TABLE 11-6 Panel Coils Immersed in Liquid: Overall Average Heat-Transfer Coefficients*
 U expressed in Btu/(h · ft² · °F)

Hot side	Cold side	Clean-surface coefficients		Design coefficients, considering usual fouling in this service		
		Natural convection	Forced convection	Natural convection	Forced convection	
Heating applications:	Steam	250-500	300-550	100-200	150-275	
	Steam	50-70	110-140	40-45	60-110	
	Steam	40-60	100-130	35-40	50-100	
	Steam	20-40	70-90	15-30	60-80	
	Steam	15-35	50-70	15-25	40-60	
	Steam	35-45	45-55	20-35	35-45	
	Steam	35-45	45-55	25-35	40-50	
	Steam	2-4	5-10	1-3	4-8	
	Steam	20-40	70-90	15-30	60-80	
	High temperature hot water	Watery solutions	115-140	200-250	70-100	110-160
	High temperature heat-transfer oil	Tar or asphalt	12-30	45-65	10-20	30-50
	Dowtherm or Aroclor	Tar or asphalt	15-30	50-60	12-20	30-50
	Cooling applications:	Water	110-135	195-245	65-95	105-155
		Water	10-15	25-45	7-10	15-25
Water		8-12	20-30	5-8	10-20	
Water		7-10	18-26	4-7	8-15	
Water		2-4	5-10	1-3	4-8	
Freon or ammonia		Watery solution	35-45	60-90	20-35	40-60
Calcium or sodium brine		Watery solution	100-120	175-200	50-75	80-125

*Tranter Manufacturing, Inc.

NOTE: To convert British thermal units per hour-square foot-degrees Fahrenheit to joules per square meter-second-kelvins, multiply by 5.6783.

TABLE 11-7 Jacketed Vessels: Overall Coefficients

Jacket fluid	Fluid in vessel	Wall material	Overall U^*	
			Btu/(h · ft ² · °F)	J/(m ² · s · K)
Steam	Water	Stainless steel	150–300	850–1700
Steam	Aqueous solution	Stainless steel	80–200	450–1140
Steam	Organics	Stainless steel	50–150	285–850
Steam	Light oil	Stainless steel	60–160	340–910
Steam	Heavy oil	Stainless steel	10–50	57–285
Brine	Water	Stainless steel	40–180	230–1625
Brine	Aqueous solution	Stainless steel	35–150	200–850
Brine	Organics	Stainless steel	30–120	170–680
Brine	Light oil	Stainless steel	35–130	200–740
Brine	Heavy oil	Stainless steel	10–30	57–170
Heat-transfer oil	Water	Stainless steel	50–200	285–1140
Heat-transfer oil	Aqueous solution	Stainless steel	40–170	230–965
Heat-transfer oil	Organics	Stainless steel	30–120	170–680
Heat-transfer oil	Light oil	Stainless steel	35–130	200–740
Heat-transfer oil	Heavy oil	Stainless steel	10–40	57–230
Steam	Water	Glass-lined CS	70–100	400–570
Steam	Aqueous solution	Glass-lined CS	50–85	285–480
Steam	Organics	Glass-lined CS	30–70	170–400
Steam	Light oil	Glass-lined CS	40–75	230–425
Steam	Heavy oil	Glass-lined CS	10–40	57–230
Brine	Water	Glass-lined CS	30–80	170–450
Brine	Aqueous solution	Glass-lined CS	25–70	140–400
Brine	Organics	Glass-lined CS	20–60	115–340
Brine	Light oil	Glass-lined CS	25–65	140–370
Brine	Heavy oil	Glass-lined CS	10–30	57–170
Heat-transfer oil	Water	Glass-lined CS	30–80	170–450
Heat-transfer oil	Aqueous solution	Glass-lined CS	25–70	140–400
Heat-transfer oil	Organics	Glass-lined CS	25–65	140–370
Heat-transfer oil	Light oil	Glass-lined CS	20–70	115–400
Heat-transfer oil	Heavy oil	Glass-lined CS	10–35	57–200

*Values listed are for moderate nonproximity agitation. CS = carbon steel.

A technique for calculating radial temperature gradients in a packed bed is given by Smith (*Chemical Engineering Kinetics*, McGraw-Hill, New York, 1956).

Fluidization occurs when the fluid flow rate is great enough so that the pressure drop across the bed equals the weight of the bed. As stated previously, the solids film thickness adjacent to the wall d_m is difficult to measure and/or predict. Wen and Fau [*Chem. Eng.*, 64(7),

254 (1957)] give for *external walls*:

$$h = bk(c, \rho_s)^{0.4} (G\eta/\mu N_f)^{0.36} \quad (11-51a)$$

where $b = 0.29$ (SI) or 11.6 (U.S. customary), c_s = heat capacity of solid, ρ_s = particle density, η = fluidization efficiency (Fig. 11-31) and N_f = bed expansion ratio (Fig. 11-32). For *internal walls*, Wen

TABLE 11-8 External Coils; Typical Overall Coefficients*

U expressed in Btu/(h · ft² · °F)

Type of coil	Coil spacing, in.†	Fluid in coil	Fluid in vessel	Temp. range, °F.	U ‡ without cement	U with heat-transfer cement
¾ in. o.d. copper tubing attached with bands at 24-in. spacing	2	5 to 50 lb./sq. in. gage steam	Water under light agitation	158–210	1–5	42–46
	3½			158–210	1–5	50–53
	6¼			158–210	1–5	60–64
	12½ or greater			158–210	1–5	69–72
¾ in. o.d. copper tubing attached with bands at 24-in. spacing	2	50 lb./sq. in. gage steam	No. 6 fuel oil under light agitation	158–258	1–5	20–30
	3½			158–258	1–5	25–38
	6¼			158–240	1–5	30–40
	12½ or greater			158–238	1–5	35–46
Panel coils		50 lb./sq. in. gage steam	Boiling water	212	29	48–54
			Water	158–212	8–30	19–48
			No. 6 fuel oil	228–278	6–15	24–56
			Water	130–150	7	15
			No. 6 fuel oil	130–150	4	9–19

*Data courtesy of Thermon Manufacturing Co.

†External surface of tubing or side of panel coil facing tank.

‡For tubing, the coefficients are more dependent upon tightness of the coil against the tank than upon either fluid. The low end of the range is recommended.

NOTE: To convert British thermal units per hour-square foot-degrees Fahrenheit to joules per square meter-second-kelvins, multiply by 5.6783; to convert inches to meters, multiply by 0.0254; and to convert pounds-force per square inch to kilopascals, multiply by 6.895.

TABLE 11-9 Thermal Properties of Various Materials as Affecting Conductive Heat Transfer

Material	Thermal conductivity, B.t.u./(hr.)(sq. ft.)(°F./ft.)	Volume specific heat, B.t.u./cu. ft.)(°F.)	Thermal diffusivity, sq. ft./hr.
Air	0.0183	0.016	1.143
Water	0.3766	62.5	0.0755
Double steel plate, sand divider	0.207	19.1	0.0108
Sand	0.207	19.1	0.0108
Powdered iron	0.0533	12.1	0.0044
Magnetite iron ore	0.212	63	0.0033
Aerocat catalysts	0.163	20	0.0062
Table salt	0.168	12.6	0.0133
Bone char	0.0877	16.9	0.0051
Pitch coke	0.333	16.2	0.0198
Phenolformaldehyde resin granules	0.0416	10.5	0.0042
Phenolformaldehyde resin powder	0.070	10	0.0070
Powdered coal	0.070	15	0.0047

To convert British thermal units per hour-square foot-degrees Fahrenheit to joules per meter-second-kelvins, multiply by 1.7307; to convert British thermal units per cubic foot-degrees Fahrenheit to joules per cubic meter-kelvins, multiply by (6.707)(10³); and to convert square feet per hour to square meters per second, multiply by (2.581)(10⁻⁵).

and Fau give

$$h_i = bhG^{-0.37} \tag{11-51b}$$

where $b = 0.78$ (SI) or 9 (U.S. customary), h_i is the coefficient for internal walls, and h is calculated from Eq. (11-51a). G_{mf} , the minimum fluidizing velocity, is defined by

$$G_{mf} = \frac{b\rho_g^{1.1}(\rho_s - \rho_g)^{0.9}D_p^2}{\mu} \tag{11-51c}$$

where $b = (1.23)(10^{-2})$ (SI) or $(5.23)(10^5)$ (U.S. customary).

Wender and Cooper [*Am. Inst. Chem. Eng. J.*, **4**, 15 (1958)] developed an empirical correlation for *internal walls*:

$$\frac{hD_p/k}{1 - \epsilon_v} \left(\frac{k}{c_p} \right)^{0.43} = bC_R \left(\frac{D_p G}{\mu} \right)^{0.23} \left(\frac{c_s}{c_g} \right)^{0.80} \left(\frac{\rho_s}{\rho_g} \right)^{0.66} \tag{11-52a}$$

where $b = (3.51)(10^{-4})$ (SI) or 0.033 (U.S. customary) and C_R = correction for displacement of the immersed tube from the axis of the

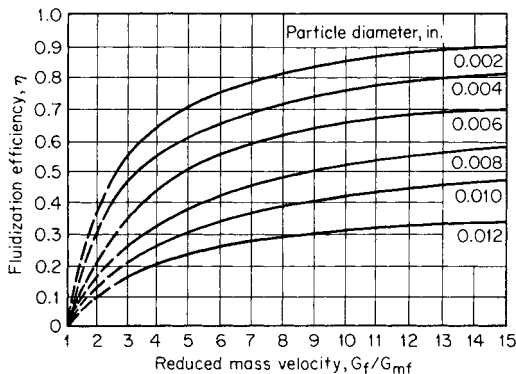


FIG. 11-31 Fluidization efficiency.

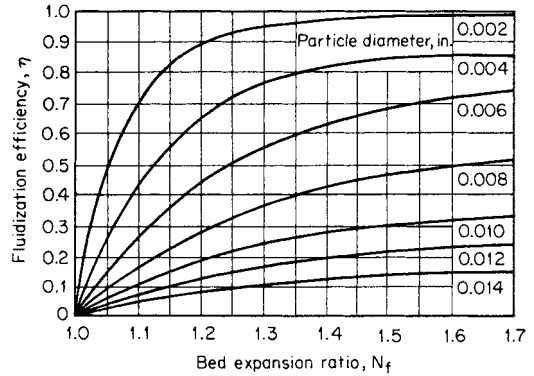


FIG. 11-32 Bed expansion ratio.

vessel (see the reference). For external walls:

$$\frac{hD_p}{k_g(1 - \epsilon_v)(c_s\rho_s/c_g\rho_g)} = f(1 + 7.5e^{-x}) \tag{11-52b}$$

where $x = 0.44L_Hc_s/D_p c_g$ and f is given by Fig. 11-33. An important feature of this equation is inclusion of the ratio of bed depth to vessel diameter L_H/D_p .

For **dilute fluidized beds** on the shell side of an unbaffled tubular bundle Genetti and Knudsen [*Inst. Chem. Eng. (London) Symp. Ser.* 3,172 (1968)] obtained the relation:

$$\frac{hD_p}{k} = \frac{5\phi(1 - \epsilon_v)}{\left[1 + \frac{580}{N_{Re}} \left(\frac{k_s}{D_p^{1.5} c_s \rho_g^{0.5}} \right) \left(\frac{\rho_s}{\rho_g} \right)^{1.1} \left(\frac{G_{mf}}{G} \right)^{7/3} \right]^2} \tag{11-53a}$$

where ϕ = particle surface area per area of sphere of same diameter. When particle transport occurred through the bundle, the heat-transfer coefficients could be predicted by

$$j_H = 0.14(N_{Re}/\phi)^{-0.68} \tag{11-53b}$$

In Eqs. (11-53a) and (11-53b), N_{Re} is based on particle diameter and superficial fluid velocity.

Zenz and Othmer (see "Introduction: General References") give an excellent summary of fluidized bed-to-wall heat-transfer investigations.

Solidification involves heavy heat loads transferred essentially at a steady temperature difference. It also involves the varying values of liquid- and solid-phase thickness and thermal diffusivity. When these are substantial and/or in the case of a liquid flowing over a changing solid layer interface, Siegel and Savino (ASME Paper 67-WA/HT-34, November 1967) offer equations and charts for prediction of the layer-growth time. For solidification (or melting) of a slab or a semi-infinite bar, initially at its transition temperature, the position of the interface is given by the one-dimensional Newmann's solution given in Carslaw and Jaeger (*Conduction of Heat in Solids*, Clarendon Press, Oxford, 1959).

Later work by Hashem and Sliepcevich [*Chem. Eng. Prog.*, **63**, *Symp. Ser.* 79, 35, 42 (1967)] offers more accurate second-order finite-difference equations.

The heat-transfer rate is found to be substantially higher under conditions of **agitation**. The heat transfer is usually said to occur by combined conductive and convective modes. A discussion and explanation are given by Holt [*Chem. Eng.*, **69**(1), 110 (1962)]. Prediction of U_{co} by Eq. (11-48) can be accomplished by replacing α by α_e , the effective thermal diffusivity of the bed. To date so little work has been performed in evaluating the effect of mixing parameters that few predictions can be made. However, for agitated liquid-phase devices Eq. (18-19) is applicable. Holt (loc. cit.) shows that this equation can be converted for solids heat transfer to yield

$$U_{co} = a'c_s D_i^{-0.3} N^{0.7} (\cos \omega)^{0.2} \tag{11-54}$$

where D_i = agitator or vessel diameter; N = turning speed, r/min; ω = effective angle of repose of the burden; and a' is a proportionality con-

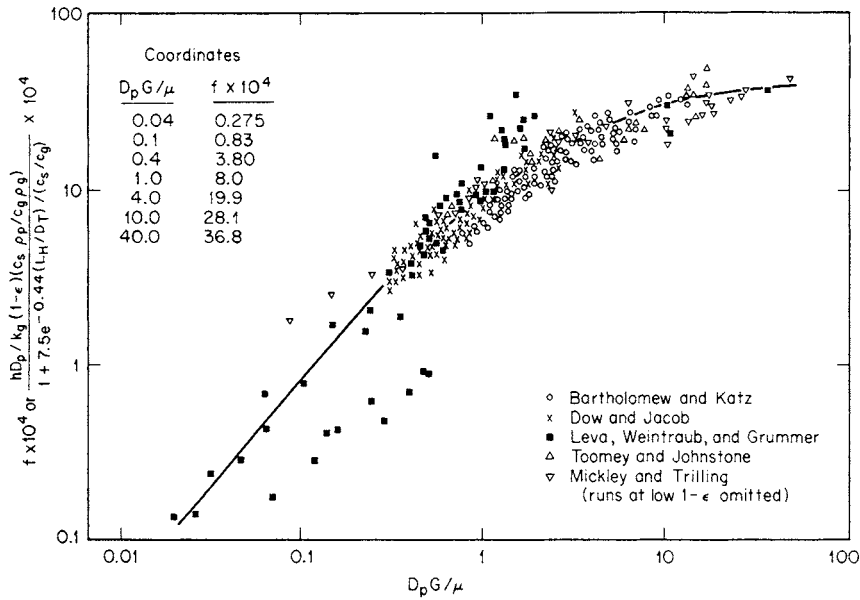


FIG. 11-33 *f* factor for Eq. (11-52*b*).

stant. This is applicable for such devices as agitated pans, agitated kettles, spiral conveyors, and rotating shells.

The solids passage time through **rotary devices** is given by Saemann [Chem. Eng. Prog., 47, 508, (1951)]:

$$\theta = 0.318L \sin \omega / S_r N D_i \quad (11-55a)$$

and by Marshall and Friedman [Chem. Eng. Prog., 45, 482-493, 573-588 (1949)]:

$$\theta = (0.23L / S_r N^{0.9} D_i) \pm (0.6BLG / F_a) \quad (11-55b)$$

where the second term of Eq. (11-55*b*) is positive for counterflow of air, negative for concurrent flow, and zero for indirect rotary shells. From these equations a predictive equation is developed for rotary-shell devices, which is analogous to Eq. (11-54):

$$U_{co} = \frac{b' c_s D_i N^{0.9} Y}{(\Delta t) L \sin \omega} \quad (11-56)$$

where θ = solids-bed passage time through the shell, min; S_r = shell slope; L = shell length; Y = percent fill; and b' is a proportionality constant.

Vibratory devices which constantly agitate the solids bed maintain a relatively constant value for U_{co} such that

$$U_{co} = a' c_s \alpha_e \quad (11-57)$$

with U_{co} having a nominal value of 114 J/(m²·s·K) [20 Btu/(h·ft²·°F)].

Contactive (Direct) Heat Transfer Contactive heat-transfer equipment is so constructed that the particulate burden in solid phase is directly exposed to and permeated by the heating or cooling medium (Sec. 20). The carrier may either heat or cool the solids. A large amount of the industrial heat processing of solids is effected by this mechanism. Physically, these can be classified into packed beds and various degrees of agitated beds from dilute to dense fluidized beds.

The temperature difference for heat transfer is the log-mean temperature difference when the particles are large and/or the beds packed, or the difference between the inlet fluid temperature t_3 and average exhausting fluid temperature t_4 , expressed $\Delta t_{4,3}$, for small particles. The use of the log mean for packed beds has been confirmed by Thodos and Wilkins (Second American Institute of Chemical Engineers-IIQPR Meeting, Paper 30D, Tampa, May 1968). When fluid and solid flow directions are axially concurrent and particle size is

small, as in a vertical-shell fluid bed, the temperature of the exiting solids t_2 (which is also that of exiting gas t_4) is used as $\Delta_3 t_2$, as shown by Levenspiel, Olson, and Walton [Ind. Eng. Chem., 44, 1478 (1952)], Marshall [Chem. Eng. Prog., 50, Monogr. Ser. 2, 77 (1954)], Leva (Fluidization, McGraw-Hill, New York, 1959), and Holt (Fourth Int. Heat Transfer Conf. Paper 11, American Institute of Chemical Engineers-American Society of Mechanical Engineers, Buffalo, 1960). This temperature difference is also applicable for well-fluidized beds of small particles in cross-flow as in various vibratory carriers.

The **packed-bed-to-fluid heat-transfer coefficient** has been investigated by Baumeister and Bennett [Am. Inst. Chem. Eng. J., 4, 69 (1958)], who proposed the equation

$$j_H = (h/cG)(c\mu/k)^{2/3} = a N_{Re}^m \quad (11-58)$$

where N_{Re} is based on particle diameter and superficial fluid velocity. Values of a and m are as follows:

D_i/D_p (dimensionless)	a	m
10.7	1.58	-0.40
16.0	0.95	-0.30
25.7	0.92	-0.28
>30	0.90	-0.28

Glaser and Thodos [Am. Inst. Chem. Eng. J., 4, 63 (1958)] give a correlation involving individual particle shape and bed porosity. Kunii and Suzuki [Int. J. Heat Mass Transfer, 10, 845 (1967)] discuss heat and mass transfer in packed beds of fine particles.

Particle-to-fluid heat-transfer coefficients in gas fluidized beds are predicted by the relation (Zenz and Othmer, op. cit.)

$$\frac{hD_p}{k} = 0.017(D_p G_{mf}/\mu)^{1.21} \quad (11-59a)$$

where G_{mf} is the superficial mass velocity at incipient fluidization.

A more general equation is given by Frantz [Chem. Eng., 69(20), 89 (1962)]:

$$hD_p/k = 0.015(D_p G/\mu)^{1.6}(c\mu/k)^{0.67} \quad (11-59b)$$

where h is based on true gas temperature.

Bed-to-wall coefficients in dilute-phase transport generally can be predicted by an equation of the form of Eq. (5-50). For example,

Bonilla et al. (American Institute of Chemical Engineers Heat Transfer Symp., Atlantic City, N.J., December 1951) found for 1- to 2- μm chalk particles in water up to 8 percent by volume that the coefficient on Eq. (5-50) is 0.029 where k , ρ , and c were arithmetic weighted averages and the viscosity was taken equal to the coefficient of rigidity. Farber and Morley [*Ind. Eng. Chem.*, **49**, 1143 (1957)] found the coefficient on Eq. (5-50) to be 0.025 for the upward flow of air transporting silica-alumina catalyst particles at rates less than 2 kg solids/kg air (2 lb solids/lb air). Physical properties used were those of the transporting gas. See Zenz and Othmer (op. cit.) for additional details covering wider porosity ranges.

The thermal performance of **cylindrical rotating shell** units is based upon a volumetric heat-transfer coefficient

$$U_{ct} = \frac{Q}{V_r(\Delta T)} \quad (11-60a)$$

where V_r = volume. This term indirectly includes an area factor so that thermal performance is governed by a cross-sectional area rather than by a heated area. Use of the heated area is possible, however:

$$U_{ct} = \frac{Q}{(\Delta_3 t_2)A} \quad \text{or} \quad \frac{Q}{(\Delta_3 t_4)A} \quad (11-60b)$$

For **heat transfer directly to solids**, predictive equations give directly the volume V or the heat-transfer area A , as determined by heat balance and airflow rate. For devices with gas flow normal to a fluidized-solids bed,

$$A = \frac{Q}{\Delta t_p (c p_g) (F_g)} \quad (11-61)$$

where $\Delta t_p = \Delta_3 t_4$ as explained above, $c p$ = volumetric specific heat, and F_g = gas flow rate. For air, $c p$ at normal temperature and pressure is about 1100 J/(m³·K) [0.0167 Btu/(ft³·°F)]; so

$$A = \frac{bQ}{(\Delta_3 t_4)F_g} \quad (11-62)$$

where $b = 0.0009$ (SI) or 60 (U.S. customary). Another such equation, for stationary vertical-shell and some horizontal rotary-shell and pneumatic-transport devices in which the gas flow is parallel with and directionally concurrent with the fluidized bed, is the same as Eq. (11-62) with $\Delta_3 t_4$ replaced by $\Delta_3 t_2$. If the operation involves drying or chemical reaction, the heat load Q is much greater than for sensible-heat transfer only. Also, the gas flow rate to provide moisture carry-off and stoichiometric requirements must be considered and simultaneously provided. A good treatise on the latter is given by Pinkey and Plint (*Miner. Process.*, June 1968, p. 17).

Evaporative cooling is a special patented technique that often can be advantageously employed in cooling solids by contactive heat transfer. The drying operation is terminated *before* the desired final moisture content is reached, and solids temperature is at a moderate value. The cooling operation involves contacting the burden (preferably fluidized) with air at normal temperature and pressure. The air adiabatically absorbs and carries off a large part of the moisture and, in doing so, picks up heat from the warm (or hot) solids particles to supply the latent heat demand of evaporation. For entering solids at temperatures of 180°C (350°F) and less with normal heat-capacity values of 0.85 to 1.0 kJ/(kg·K) [0.2 to 0.25 Btu/(lb·°F)], the effect can be calculated by:

1. Using 285 m³ (1000 ft³) of airflow at normal temperature and pressure at 40 percent relative humidity to carry off 0.45 kg (1 lb) of water [latent heat 2326 kJ/kg (1000 Btu/lb)] and to lower temperature by 22 to 28°C (40 to 50°F).

2. Using the lowered solids temperature as t_3 and calculating the remainder of the heat to be removed in the regular manner by Eq. (11-62). The required air quantity for (2) must be equal to or greater than that for (1).

When the solids heat capacity is higher (as is the case for most organic materials), the temperature reduction is inversely proportional to the heat capacity.

A nominal result of this technique is that the required airflow rate and equipment size is about two-thirds of that when evaporative cooling is not used. See Sec. 20 for equipment available.

Convective Heat Transfer Equipment using the true convective mechanism when the heated particles are mixed with (and remain with) the cold particles is used so infrequently that performance and sizing equations are not available. Such a device is the pebble heater as described by Norton (*Chem. Metall. Eng.*, July 1946). For operation data, see Sec. 9.

Convective heat transfer is often used as an adjunct to other modes, particularly to the conductive mode. It is often more convenient to consider the agitative effect a performance-improvement influence on the thermal diffusivity factor α , modifying it to α_e , the effective value.

A *pseudo-convective heat-transfer* operation is one in which the heating gas (generally air) is passed over a bed of solids. Its use is almost exclusively limited to drying operations (see Sec. 12, tray and shelf dryers). The operation, sometimes termed direct, is more akin to the conductive mechanism. For this operation, Tsao and Wheelock [*Chem. Eng.*, **74**(13), 201 (1967)] predict the heat-transfer coefficient when radiative and conductive effects are absent by

$$h = bG^{0.5} \quad (11-63)$$

where $b = 14.31$ (SI) or 0.0128 (U.S. customary), h = convective heat transfer, and G = gas flow rate.

The **drying rate** is given by

$$K_{cv} = \frac{h(T_d - T_w)}{\lambda} \quad (11-64)$$

where K_{cv} = drying rate, for constant-rate period, kg/(m²·s) [lb/(h·ft²)]; T_d and T_w = respective dry-bulb and wet-bulb temperatures of the air; and λ = latent heat of evaporation at temperature T_w . Note here that the temperature-difference determination of the operation is a simple linear one and of a steady-state nature. Also note that the operation is a function of the airflow rate. Further, the solids are granular with a fairly uniform size, have reasonable capillary voids, are of a firm texture, and have the particle surface wetted.

The coefficient h is also used to predict (in the constant-rate period) the total overall air-to-solids heat-transfer coefficient U_{cv} by

$$1/U_{cv} = 1/h + x/k \quad (11-65)$$

where k = solids thermal conductivity and x is evaluated from

$$x = \frac{z(X_c - X_o)}{X_c - X_e} \quad (11-65a)$$

where z = bed (or slab) thickness and is the total thickness when drying and/or heat transfer is from one side only but is one-half of the thickness when drying and/or heat transfer is simultaneously from both sides; X_o , X_c , and X_e are respectively the initial (or feed-stock), critical, and equilibrium (with the drying air) moisture contents of the solids, all in kg H₂O/kg dry solids (lb H₂O/lb dry solids). This coefficient is used to predict the *instantaneous* drying rate

$$-\frac{W}{A} \frac{dX}{d\theta} = \frac{U_{cv}(T_d - T_w)}{\lambda} \quad (11-66)$$

By rearrangement, this can be made into a design equation as follows:

$$A = -\frac{W\lambda(dX/d\theta)}{U_{cv}(T_d - T_w)} \quad (11-67)$$

where W = weight of dry solids in the equipment, λ = latent heat of evaporation, and θ = drying time. The reader should refer to the full reference article by Tsao and Wheelock (loc. cit.) for other solids conditions qualifying the use of these equations.

Radiative Heat Transfer Heat-transfer equipment using the radiative mechanism for divided solids is constructed as a "table" which is stationary, as with trays, or moving, as with a belt, and/or agitated, as with a vibrated pan, to distribute and expose the burden in a plane parallel to (but not in contact with) the plane of the radiant-heat sources. Presence of air is not necessary (see Sec. 12 for vacuum-shelf dryers and Sec. 22 for resublimation). In fact, if air in the intervening space has a high humidity or CO₂ content, it acts as an energy absorber, thereby depressing the performance.

For the radiative mechanism, the temperature difference is evaluated as

$$\Delta t = T_e^4 - T_r^4 \quad (11-68)$$

where T_e = absolute temperature of the radiant-heat source, K (°R); and T_r = absolute temperature of the bed of divided solids, K (°R).

Numerical values for U_{ra} for use in the general design equation may be calculated from experimental data by

$$U_{ra} = \frac{Q}{A(T_e^4 - T_r^4)} \quad (11-69)$$

The literature to date offers practically no such values. However, enough proprietary work has been performed to present a reliable evaluation for the comparison of mechanisms (see "Introduction: Modes of Heat Transfer").

For the radiative mechanism of heat transfer to solids, the rate equation for parallel-surface operations is

$$q_m = b(T_e^4 - T_r^4)i_f \quad (11-70)$$

where $b = (5.67)(10^{-8})(\text{SI})$ or $(0.172)(10^{-8})(\text{U.S. customary})$, q_m = radiative heat flux, and i_f = an interchange factor which is evaluated from

$$1/i_f = 1/e_s + 1/e_r - 1 \quad (11-70a)$$

where e_s = coefficient of emissivity of the source and e_r = "emissivity" (or "absorptivity") of the receiver, which is the divided-solids bed. For the emissivity values, particularly of the heat source e_s , an important consideration is the wavelength at which the radiant source emits as well as the flux density of the emission. Data for these values are available from Polentz [*Chem. Eng.*, **65**(7), 137; (8), 151 (1958)] and Adlam [*Radiant Heating*, Industrial Press, New York, p. 40]. Both give radiated flux density versus wavelength at varying temperatures. Often, the seemingly cooler but longer wavelength source is the better selection.

Emitting sources are (1) pipes, tubes, and platters carrying steam, 2100 kPa (300 lbf/in²); (2) electrical-conducting glass plates, 150 to 315°C (300 to 600°F) range; (3) light-bulb type (tungsten-filament resistance heater); (4) modules of refractory brick for gas burning at high temperatures and high fluxes; and (5) modules of quartz tubes, also operable at high temperatures and fluxes. For some emissivity values see Table 11-10.

For *predictive work*, where U_{ra} is desired for sizing, this can be obtained by dividing the flux rate q_m by Δt :

$$U_{ra} = q_m / (T_e^4 - T_r^4) = i_f b \quad (11-71)$$

where $b = (5.67)(10^{-8})$ (SI) or $(0.172)(10^{-8})$ (U.S. customary). Hence:

$$A = \frac{Q}{U_{ra}(T_e^4 - T_r^4)} \quad (11-72)$$

where A = bed area of solids in the equipment.

Important considerations in the application of the foregoing equations are:

1. Since the temperature of the emitter is generally known (pre-selected or readily determined in an actual operation), the absorptivity value e_r is the unknown. This absorptivity is partly a measure of the ability of radiant heat to penetrate the body of a solid particle (or a moisture film) instantly, as compared with diffusional heat transfer by conduction. Such instant penetration greatly reduces processing time and case-hardening effects. Moisture release and other mass transfer, however, still progress by diffusional means.

2. In one of the major applications of radiative devices (drying), the surface-held moisture is a good heat absorber in the 2- to 7- μm wavelength range. Therefore, the absorptivity, color, and nature of the solids are of little importance.

3. For drying, it is important to provide a small amount of venting air to carry away the water vapor. This is needed for two reasons. First, water vapor is a good absorber of 2- to 7- μm energy. Second, water-vapor accumulation depresses further vapor release by the solids. If the air over the solids is kept fairly dry by venting, very little heat is carried off, because dry air does not absorb radiant heat.

4. For some of the devices, when the overall conversion efficiency has been determined, the application is primarily a matter of computing the required heat load. It should be kept in mind, however, that

there are two conversion efficiencies that must be differentiated. One measure of efficiency is that with which the source converts input energy to output radiated energy. The other is the overall efficiency that measures the proportion of input energy that is actually absorbed by the solids. This latter is, of course, the one that really matters.

Other applications of radiant-heat processing of solids are the toasting, puffing, and baking of foods and the low-temperature roasting and preheating of plastic powder or pellets. Since the determination of heat loads for these operations is not well established, bench and pilot tests are generally necessary. Such processes require a fast input of heat and higher heat fluxes than can generally be provided by indirect equipment. Because of this, infrared-equipment size and space requirements are often much lower.

Although direct contactive heat transfer can provide high temperatures and heat concentrations and at the same time be small in size, its use may not always be preferable because of undesired side effects such as drying, contamination, case hardening, shrinkage, off color, and dusting.

When radiating and receiving surfaces are not in parallel, as in rotary-kiln devices, and the solids burden bed may be only intermittently exposed and/or agitated, the calculation and procedures become very complex, with photometric methods of optics requiring consideration. The following equation for heat transfer, which allows for convective effects, is commonly used by designers of **high-temperature furnaces**:

$$q_m = Q/A = b\sigma [(T_g/100)^4 - (T_s/100)^4] \quad (11-73)$$

where $b = 5.67$ (SI) or 0.172 (U.S. customary); Q = total furnace heat transfer; σ = an emissivity factor with recommended values of 0.74 for gas, 0.75 for oil, and 0.81 for coal; A = effective area for absorbing heat (here the solids burden exposed area); T_g = exiting-combustion-gas absolute temperature; and T_s = absorbing surface temperature.

In rotary devices, reradiation from the exposed shell surface to the solids bed is a major design consideration. A treatise on furnaces, including radiative heat-transfer effects, is given by Ellwood and Danatos [*Chem. Eng.*, **73**(8), 174 (1966)]. For discussion of radiation heat-transfer computational methods, heat fluxes obtainable, and emissivity values, see Schornshort and Viskanta (ASME Paper 68-H 7-32), Sherman (ASME Paper 56-A-111), and the following subsection.

SCRAPED-SURFACE EXCHANGERS

Scraped-surface exchangers have a rotating element with spring-loaded scraper blades to scrape the inside surface (Fig. 11-34). Generally a

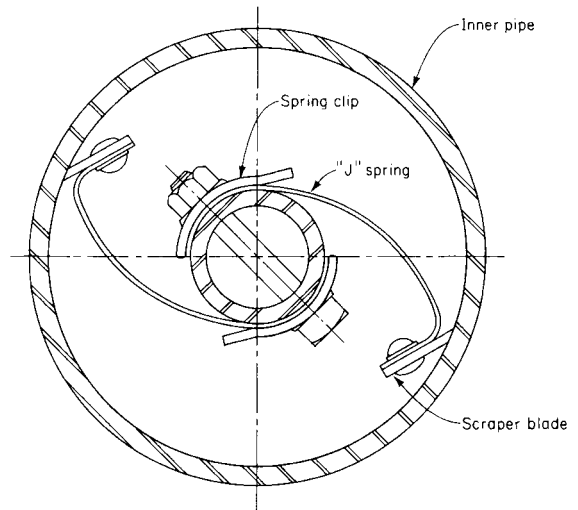


FIG. 11-34 Scraper blade of scraped-surface exchanger. (Henry Vogt Machine Co., Inc.)

11-32 HEAT-TRANSFER EQUIPMENT

TABLE 11-10 Normal Total Emissivity of Various Surfaces

A. Metals and Their Oxides					
Surface	<i>t</i> , °F.°	Emissivity°	Surface	<i>t</i> , °F.°	Emissivity°
Aluminum			Sheet steel, strong rough oxide layer	75	0.80
Highly polished plate, 98.3% pure	440–1070	0.039–0.057	Dense shiny oxide layer	75	0.82
Polished plate	73	0.040	Cast plate:		
Rough plate	78	0.055	Smooth	73	0.80
Oxidized at 1110°F	390–1110	0.11–0.19	Rough	73	0.82
Aluminum-surfaced roofing	100	0.216	Cast iron, rough, strongly oxidized	100–480	0.95
Calorized surfaces, heated at 1110°F.			Wrought iron, dull oxidized	70–680	0.94
Copper	390–1110	0.18–0.19	Steel plate, rough	100–700	0.94–0.97
Steel	390–1110	0.52–0.57	High temperature alloy steels (see Nickel Alloys)		
Brass			Molten metal		
Highly polished:			Cast iron	2370–2550	0.29
73.2% Cu, 26.7% Zn	476–674	0.028–0.031	Mild steel	2910–3270	0.28
62.4% Cu, 36.8% Zn, 0.4% Pb, 0.3% Al	494–710	0.033–0.037	Lead		
82.9% Cu, 17.0% Zn	530	0.030	Pure (99.96%), unoxidized	260–440	0.057–0.075
Hard rolled, polished:			Gray oxidized	75	0.281
But direction of polishing visible	70	0.038	Oxidized at 390°F	390	0.63
But somewhat attacked	73	0.043	Mercury	32–212	0.09–0.12
But traces of stearin from polish left on	75	0.053	Molybdenum filament	1340–4700	0.096–0.292
Polished	100–600	0.096	Monel metal, oxidized at 1110°F	390–1110	0.41–0.46
Rolled plate, natural surface	72	0.06	Nickel		
Rubbed with coarse emery	72	0.20	Electroplated on polished iron, then polished	74	0.045
Dull plate	120–660	0.22	Technically pure (98.9% Ni, + Mn), polished	440–710	0.07–0.087
Oxidized by heating at 1110°F	390–1110	0.61–0.59	Electroplated on pickled iron, not polished	68	0.11
Chromium; see Nickel Alloys for Ni-Cr steels	100–1000	0.08–0.26	Wire	368–1844	0.096–0.186
Copper			Plate, oxidized by heating at 1110°F	390–1110	0.37–0.48
Carefully polished electrolytic copper	176	0.018	Nickel oxide	1200–2290	0.59–0.86
Commercial, emiered, polished, but pits remaining	66	0.030	Nickel alloys		
Commercial, scraped shiny but not mirror-like	72	0.072	Chromnickel	125–1894	0.64–0.76
Polished	242	0.023	Nickelin (18–32 Ni; 55–68 Cu; 20 Zn), gray oxidized	70	0.262
Plate, heated long time, covered with thick oxide layer	77	0.78	KA-2S alloy steel (8% Ni; 18% Cr), light silvery, rough, brown, after heating	420–914	0.44–0.36
Plate heated at 1110°F	390–1110	0.57	After 42 hr. heating at 980°F	420–980	0.62–0.73
Cuprous oxide	1470–2010	0.66–0.54	NCT-3 alloy (20% Ni; 25% Cr), brown, splotted, oxidized from service	420–980	0.90–0.97
Molten copper	1970–2330	0.16–0.13	NCT-6 alloy (60% Ni; 12% Cr), smooth, black, firm adhesive oxide coat from service	520–1045	0.89–0.82
Gold			Platinum		
Pure, highly polished	440–1160	0.018–0.035	Pure, polished plate	440–1160	0.054–0.104
Iron and steel			Strip	1700–2960	0.12–0.17
Metallic surfaces (or very thin oxide layer):			Filament	80–2240	0.036–0.192
Electrolytic iron, highly polished	350–440	0.052–0.064	Wire	440–2510	0.073–0.182
Polished iron	800–1880	0.144–0.377	Silver		
Iron freshly emiered	68	0.242	Polished, pure	440–1160	0.0198–0.0324
Cast iron, polished	392	0.21	Polished	100–700	0.0221–0.0312
Wrought iron, highly polished	100–480	0.28	Steel, see Iron		
Cast iron, newly turned	72	0.435	Tantalum filament	2420–5430	0.194–0.31
Polished steel casting	1420–1900	0.52–0.56	Tin—bright tinned iron sheet	76	0.043 and 0.064
Ground sheet steel	1720–2010	0.55–0.61	Tungsten		
Smooth sheet iron	1650–1900	0.55–0.60	Filament, aged	80–6000	0.032–0.35
Cast iron, turned on lathe	1620–1810	0.60–0.70	Filament	6000	0.39
Oxidized surfaces:			Zinc		
Iron plate, pickled, then rusted red	68	0.612	Commercial, 99.1% pure, polished	440–620	0.045–0.053
Completely rusted	67	0.685	Oxidized by heating at 750°F.	750	0.11
Rolled sheet steel	70	0.657	Galvanized sheet iron, fairly bright	82	0.228
Oxidized iron	212	0.736	Galvanized sheet iron, gray oxidized	75	0.276
Cast iron, oxidized at 1100°F	390–1110	0.64–0.78			
Steel, oxidized at 1100°F	390–1110	0.79			
Smooth oxidized electrolytic iron	260–980	0.78–0.82			
Iron oxide	930–2190	0.85–0.89			
Rough ingot iron	1700–2040	0.87–0.95			
B. Refractories, Building Materials, Paints, and Miscellaneous					
Asbestos			Carbon		
Board	74	0.96	T-carbon (Gebr. Siemens) 0.9% ash (this started with emissivity at 260°F. of 0.72, but on heating changed to values given)	260–1160	0.81–0.79
Paper	100–700	0.93–0.945	Carbon filament	1900–2560	0.526
Brick			Candle soot	206–520	0.952
Red, rough, but no gross irregularities	70	0.93	Lampblack-waterglass coating	209–362	0.959–0.947
Silica, unglazed, rough	1832	0.80			
Silica, glazed, rough	2012	0.85			
Grog brick, glazed	2012	0.75			
See Refractory Materials below.					

TABLE 11-10 Normal Total Emissivity of Various Surfaces (Concluded)

A. Metals and Their Oxides					
Surface	<i>t</i> , °F.°	Emissivity°	Surface	<i>t</i> , °F.°	Emissivity°
Same	260–440	0.957–0.952	Oil paints, sixteen different, all colors	212	0.92–0.96
Thin layer on iron plate	69	0.927	Aluminum paints and lacquers		
Thick coat	68	0.967	10% Al, 22% lacquer body, on rough or smooth surface	212	0.52
Lampblack, 0.003 in. or thicker	100–700	0.945	26% Al, 27% lacquer body, on rough or smooth surface	212	0.3
Enamel, white fused, on iron	66	0.897	Other Al paints, varying age and Al content	212	0.27–0.67
Glass, smooth	72	0.937	Al lacquer, varnish binder, on rough plate	70	0.39
Gypsum, 0.02 in. thick on smooth or blackened plate	70	0.903	Al paint, after heating to 620°F	300–600	0.35
Marble, light gray, polished	72	0.931	Paper, thin		
Oak, planed	70	0.895	Pasted on tinned iron plate	66	0.924
Oil layers on polished nickel (lube oil)	68		On rough iron plate	66	0.929
Polished surface, alone		0.045	On black lacquered plate	66	0.944
+0.001-in. oil		0.27	Plaster, rough lime	50–190	0.91
+0.002-in. oil		0.46	Porcelain, glazed	72	0.924
+0.005-in. oil		0.72	Quartz, rough, fused	70	0.932
Infinitely thick oil layer		0.82	Refractory materials, 40 different poor radiators	1110–1830	$\left[\begin{matrix} 0.65 \\ 0.70 \\ 0.80 \\ 0.85 \end{matrix} \right] - \left[\begin{matrix} 0.75 \\ 0.85 \end{matrix} \right]$
Oil layers on aluminum foil (linseed oil)			good radiators		
Al foil	212	0.087†	Roofing paper	69	0.91
+1 coat oil	212	0.561	Rubber		
+2 coats oil	212	0.574	Hard, glossy plate	74	0.945
Paints, lacquers, varnishes			Soft, gray, rough (reclaimed)	76	0.859
Snowwhite enamel varnish or rough iron plate	73	0.906	Serpentine, polished	74	0.900
Black shiny lacquer, sprayed on iron	76	0.875	Water	32–212	0.95–0.963
Black shiny shellac on tinned iron sheet	70	0.821			
Black matte shellac	170–295	0.91			
Black lacquer	100–200	0.80–0.95			
Flat black lacquer	100–200	0.96–0.98			
White lacquer	100–200	0.80–0.95			

°When two temperatures and two emissivities are given, they correspond, first to first and second to second, and linear interpolation is permissible. °C = (°F – 32)/1.8.
 †Although this value is probably high, it is given for comparison with the data by the same investigator to show the effect of oil layers. See Aluminum, Part A of this table.

double-pipe construction is used; the scraping mechanism is in the inner pipe, where the process fluid flows; and the cooling or heating medium is in the outer pipe. The most common size has 6-in inside and 8-in outside pipes. Also available are 3- by 4-in, 8- by 10-in, and 12- by 14-in sizes (in × 25.4 = mm). These double-pipe units are commonly connected in series and arranged in double stands.

For **chilling** and **crystallizing** with an evaporating refrigerant, a 27-in shell with seven 6-in pipes is available (Henry Vogt Machine Co.). In direct contact with the scraped surface is the process fluid which may

deposit crystals upon chilling or be extremely fouling or of very high viscosity. Motors, chain drives, appropriate guards, and so on are required for the rotating element. For chilling service with a refrigerant in the outer shell, an accumulator drum is mounted on top of the unit.

Scraped-surface exchangers are particularly suitable for heat transfer with crystallization, heat transfer with severe fouling of surfaces, heat transfer with solvent extraction, and heat transfer of high-viscosity fluids. They are extensively used in paraffin-wax plants and in petrochemical plants for crystallization.

TEMA-STYLE SHELL-AND-TUBE HEAT EXCHANGERS

TYPES AND DEFINITIONS

TEMA-style shell-and-tube-type exchangers constitute the bulk of the unfired heat-transfer equipment in chemical-process plants, although increasing emphasis has been developing in other designs. These exchangers are illustrated in Fig. 11-35, and their features are summarized in Table 11-11.

TEMA Numbering and Type Designation Recommended practice for the designation of TEMA-style shell-and-tube heat exchangers by numbers and letters has been established by the Tubular Exchanger Manufacturers Association (TEMA). This information from the sixth edition of the TEMA Standards is reproduced in the following paragraphs.

It is recommended that heat-exchanger size and type be designated by numbers and letters.

1. *Size.* Sizes of shells (and tube bundles) shall be designated by numbers describing shell (and tube-bundle) diameters and tube lengths as follows:

2. *Diameter.* The nominal diameter shall be the inside diameter of the shell in inches, rounded off to the nearest integer. For kettle reboilers the nominal

diameter shall be the port diameter followed by the shell diameter, each rounded off to the nearest integer.

3. *Length.* The nominal length shall be the tube length in inches. Tube length for straight tubes shall be taken as the actual overall length. For U tubes the length shall be taken as the straight length from end of tube to bend tangent.

4. *Type.* Type designation shall be by letters describing stationary head, shell (omitted for bundles only), and rear head, in that order, as indicated in Fig. 11-1.

Typical Examples (A) Split-ring floating-heat exchanger with removable channel and cover, single-pass shell, 591-mm (23¼-in) inside diameter with tubes 4.9 m (16 ft) long. SIZE 23–192 TYPE AES.

(B) U-tube exchanger with bonnet-type stationary head, split-flow shell, 483-mm (19-in) inside diameter with tubes 21-m (7-ft) straight length. SIZE 19–84 TYPE CBU.

(C) Pull-through floating-heat-kettle-type reboiler having stationary head integral with tube sheet, 584-mm (23-in) port diameter and 940-mm (37-in) inside shell diameter with tubes 4.9-m (16-ft) long. SIZE 23/37–192 TYPE CKT.

(D) Fixed-tube sheet exchanger with removable channel and cover, bonnet-type rear head, two-pass shell, 841-mm (33½-in) diameter with tubes 2.4 m (8-ft) long. SIZE 33–96 TYPE AFM.

(E) Fixed-tube sheet exchanger having stationary and rear heads integral with tube sheets, single-pass shell, 432-mm (17-in) inside diameter with tubes 4.9-m (16-ft) long. SIZE 17–192 TYPE CEN.

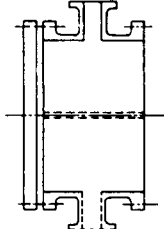
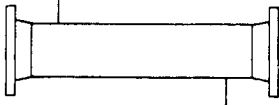
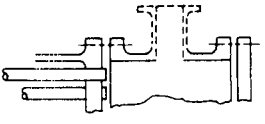
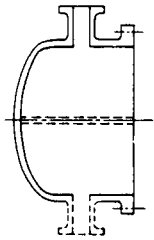
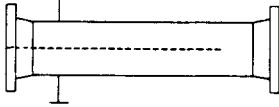
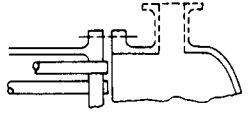
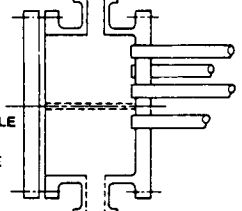
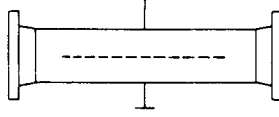
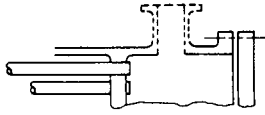
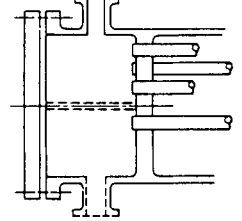
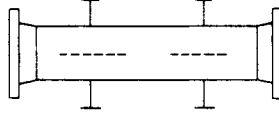
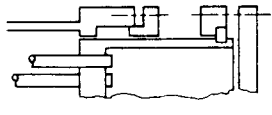
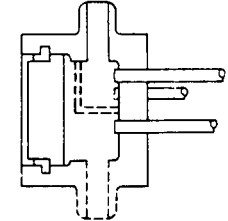
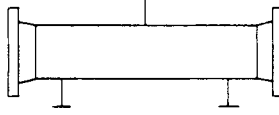
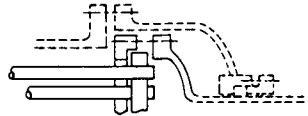
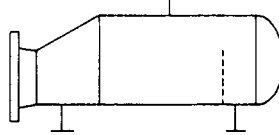
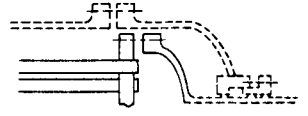
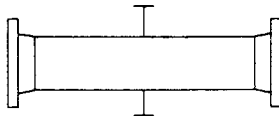
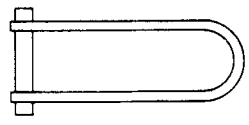
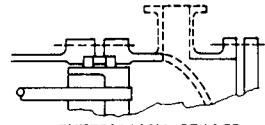
FRONT END STATIONARY HEAD TYPES		SHELL TYPES		REAR END HEAD TYPES	
A	 CHANNEL AND REMOVABLE COVER	E	 ONE PASS SHELL	L	 FIXED TUBESHEET LIKE "A" STATIONARY HEAD
B	 BONNET (INTEGRAL COVER)	F	 TWO PASS SHELL WITH LONGITUDINAL BAFFLE	M	 FIXED TUBESHEET LIKE "B" STATIONARY HEAD
C	 REMOVABLE TUBE BUNDLE ONLY CHANNEL INTEGRAL WITH TUBE-SHEET AND REMOVABLE COVER	G	 SPLIT FLOW	N	 FIXED TUBESHEET LIKE "N" STATIONARY HEAD
N	 CHANNEL INTEGRAL WITH TUBE-SHEET AND REMOVABLE COVER	H	 DOUBLE SPLIT FLOW	P	 OUTSIDE PACKED FLOATING HEAD
D	 SPECIAL HIGH PRESSURE CLOSURE	J	 DIVIDED FLOW	S	 FLOATING HEAD WITH BACKING DEVICE
		K	 KETTLE TYPE REBOILER	T	 PULL THROUGH FLOATING HEAD
		X	 CROSS FLOW	U	 U-TUBE BUNDLE
				W	 EXTERNALLY SEALED FLOATING TUBESHEET

FIG. 11-35 TEMA-type designations for shell-and-tube heat exchangers. (Standards of Tubular Exchanger Manufacturers Association, 6th ed., 1978.)

TABLE 11-11 Features of TEMA Shell-and-Tube-Type Exchangers*

Type of design	Fixed tube sheet	U-tube	Packed lantern-ring floating head	Internal floating head (split backing ring)	Outside-packed floating head	Pull-through floating head
T.E.M.A. rear-head type	L or M or N	U	W	S	P	T
Relative cost increases from A (least expensive) through E (most expensive)	B	A	C	E	D	E
Provision for differential expansion	Expansion joint in shell	Individual tubes free to expand	Floating head	Floating head	Floating head	Floating head
Removable bundle	No	Yes	Yes	Yes	Yes	Yes
Replacement bundle possible	No	Yes	Yes	Yes	Yes	Yes
Individual tubes replaceable	Yes	Only those in outside row†	Yes	Yes	Yes	Yes
Tube cleaning by chemicals inside and outside	Yes	Yes	Yes	Yes	Yes	Yes
Interior tube cleaning mechanically	Yes	Special tools required	Yes	Yes	Yes	Yes
Exterior tube cleaning mechanically:						
Triangular pitch	No	No‡	No‡	No‡	No‡	No‡
Square pitch	No	Yes	Yes	Yes	Yes	Yes
Hydraulic-jet cleaning:						
Tube interior	Yes	Special tools required	Yes	Yes	Yes	Yes
Tube exterior	No	Yes	Yes	Yes	Yes	Yes
Double tube sheet feasible	Yes	Yes	No	No	Yes	No
Number of tube passes	No practical limitations	Any even number possible	Limited to one or two passes	No practical limitations§	No practical limitations	No practical limitations§
Internal gaskets eliminated	Yes	Yes	Yes	No	Yes	No

NOTE: Relative costs A and B are not significantly different and interchange for long lengths of tubing.

*Modified from page a-8 of the Patterson-Kelley Co. Manual No. 700A, Heat Exchangers.

†U-tube bundles have been built with tube supports which permit the U-bends to be spread apart and tubes inside of the bundle replaced.

‡Normal triangular pitch does not permit mechanical cleaning. With a wide triangular pitch, which is equal to 2 (tube diameter plus cleaning lane)/√3, mechanical cleaning is possible on removable bundles. This wide spacing is infrequently used.

§For odd number of tube side passes, floating head requires packed joint or expansion joint.

Functional Definitions Heat-transfer equipment can be designated by type (e.g., fixed tube sheet, outside packed head, etc.) or by function (chiller, condenser, cooler, etc.). Almost any type of unit can be used to perform any or all of the listed functions. Many of these terms have been defined by Donahue [*Pet. Process.*, 103 (March 1956)].

Equipment	Function
Chiller	Cools a fluid to a temperature below that obtainable if water only were used as a coolant. It uses a refrigerant such as ammonia or Freon.
Condenser	Condenses a vapor or mixture of vapors, either alone or in the presence of a noncondensable gas.
Partial condenser	Condenses vapors at a point high enough to provide a temperature difference sufficient to preheat a cold stream of process fluid. This saves heat and eliminates the need for providing a separate preheater (using flame or steam).
Final condenser	Condenses the vapors to a final storage temperature of approximately 37.8°C (100°F). It uses water cooling, which means that the transferred heat is lost to the process.
Cooler	Cools liquids or gases by means of water.
Exchanger	Performs a double function: (1) heats a cold fluid by (2) using a hot fluid which it cools. None of the transferred heat is lost.
Heater	Imparts sensible heat to a liquid or a gas by means of condensing steam or Dowtherm.
Reboiler	Connected to the bottom of a fractionating tower, it provides the reboil heat necessary for distillation. The heating medium may be either steam or a hot-process fluid.
Thermosiphon reboiler	Natural circulation of the boiling medium is obtained by maintaining sufficient liquid head to provide for circulation.
Forced-circulation reboiler	A pump is used to force liquid through the reboiler.
Steam generator	Generates steam for use elsewhere in the plant by using the available high-level heat in tar or a heavy oil.

Superheater	Heats a vapor above the saturation temperature.
Vaporizer	A heater which vaporizes part of the liquid.
Waste-heat boiler	Produces steam; similar to steam generator, except that the heating medium is a hot gas or liquid produced in a chemical reaction.

GENERAL DESIGN CONSIDERATIONS

Selection of Flow Path In selecting the flow path for two fluids through an exchanger, several general approaches are used. The tube-side fluid is more corrosive or dirtier or at a higher pressure. The shell-side fluid is a liquid of high viscosity or a gas.

When alloy construction for one of the two fluids is required, a carbon steel shell combined with alloy tube-side parts is less expensive than alloy in contact with the shell-side fluid combined with carbon steel headers.

Cleaning of the inside of tubes is more readily done than cleaning of exterior surfaces.

For gauge pressures in excess of 2068 kPa (300 lbf/in²) for one of the fluids, the less expensive construction has the high-pressure fluid in the tubes.

For a given pressure drop, higher heat-transfer coefficients are obtained on the shell side than on the tube side.

Heat-exchanger shutdowns are most often caused by fouling, corrosion, and erosion.

Construction Codes "Rules for Construction of Pressure Vessels, Division 1," which is part of Section VIII of the ASME Boiler and Pressure Vessel Code (American Society of Mechanical Engineers), serves as a construction code by providing minimum standards. New editions of the code are usually issued every 3 years. Interim revisions are made semiannually in the form of addenda. Compliance with ASME Code requirements is mandatory in much of the United States and Canada. Originally these rules were not prepared for heat exchangers. However, the welded joint between tube sheet and shell of the fixed-tube-sheet heat exchanger is now included. A nonmandatory appendix on tube-to-tube-sheet joints is also included. Additional rules for heat exchangers are being developed.

Standards of Tubular Exchanger Manufacturers Association, 6th ed., 1978 (commonly referred to as the TEMA Standards), serve to supplement and define the ASME Code for all shell-and-tube-type heat-exchanger applications (other than double-pipe construction). TEMA Class R design is "for the generally severe requirements of petroleum and related processing applications. Equipment fabricated in accordance with these standards is designed for safety and durability under the rigorous service and maintenance conditions in such applications." TEMA Class C design is "for the generally moderate requirements of commercial and general process applications," while TEMA Class B is "for chemical process service."

The mechanical-design requirements are identical for all three classes of construction. The differences between the TEMA classes are minor and were listed by Rubin [*Hydrocarbon Process.*, 59, 92 (June 1980)].

Among the topics of the TEMA Standards are nomenclature, fabrication tolerances, inspection, guarantees, tubes, shells, baffles and support plates, floating heads, gaskets, tube sheets, channels, nozzles, end flanges and bolting, material specifications, and fouling resistances.

Shell and Tube Heat Exchangers for General Refinery Services, API Standard 660, 4th ed., 1982, is published by the American Petroleum Institute to supplement both the TEMA Standards and the ASME Code. Many companies in the chemical and petroleum processing fields have their own standards to supplement these various requirements. *The Interrelationships between Codes, Standards, and Customer Specifications for Process Heat Transfer Equipment* is a symposium volume which was edited by F. L. Rubin and published by ASME in December 1979. (See discussion of pressure-vessel codes in Sec. 6.)

Design pressures and temperatures for exchangers usually are specified with a margin of safety beyond the conditions expected in service. Design pressure is generally about 172 kPa (25 lb/in²) greater than the maximum expected during operation or at pump shutoff. Design temperature is commonly 14°C (25°F) greater than the maximum temperature in service.

Tube Bundle Vibration Damage from tube vibration has become an increasing problem as plate baffled heat exchangers are designed for higher flow rates and pressure drops. The most effective method of dealing with this problem is the avoidance of cross flow by use of tube support baffles which promote only longitudinal flow. However, even then, strict attention must be given the bundle area under the shell inlet nozzle where flow is introduced through the side of the shell. TEMA has devoted an entire section in its standards to this topic. In general, the mechanisms of tube vibration are as follows:

Vortex Shedding The vortex-shedding frequency of the fluid in cross-flow over the tubes may coincide with a natural frequency of the tubes and excite large resonant vibration amplitudes.

Fluid-Elastic Coupling Fluid flowing over tubes causes them to vibrate with a whirling motion. The mechanism of fluid-elastic coupling occurs when a "critical" velocity is exceeded and the vibration then becomes self-excited and grows in amplitude. This mechanism frequently occurs in process heat exchangers which suffer vibration damage.

Pressure Fluctuation Turbulent pressure fluctuations which develop in the wake of a cylinder or are carried to the cylinder from upstream may provide a potential mechanism for tube vibration. The tubes respond to the portion of the energy spectrum that is close to their natural frequency.

Acoustic Coupling When the shell-side fluid is a low-density gas, acoustic resonance or coupling develops when the standing waves in the shell are in phase with vortex shedding from the tubes. The standing waves are perpendicular to the axis of the tubes and to the direction of cross-flow. Damage to the tubes is rare. However, the noise can be extremely painful.

Testing Upon completion of shop fabrication and also during maintenance operations it is desirable hydrostatically to test the shell side of tubular exchangers so that visual examination of tube ends can be made. Leaking tubes can be readily located and serviced. When leaks are determined without access to the tube ends, it is necessary to reroll or reweld all the tube-to-tube-sheet joints with possible damage to the satisfactory joints.

Testing for leaks in heat exchangers was discussed by Rubin [*Chem. Eng.*, 68, 160-166 (July 24, 1961)].

Performance testing of heat exchangers is described in the American Institute of Chemical Engineers' *Standard Testing Procedure for Heat Exchangers*, Sec. 1. "Sensible Heat Transfer in Shell-and-Tube-Type Equipment."

PRINCIPAL TYPES OF CONSTRUCTION

Figure 11-36 shows details of the construction of the TEMA types of shell-and-tube heat exchangers. These and other types are discussed in the following paragraphs.

Fixed-Tube-Sheet Heat Exchangers Fixed-tube-sheet exchangers (Fig. 11-36*b*) are used more often than any other type, and the frequency of use has been increasing in recent years. The tube sheets are welded to the shell. Usually these extend beyond the shell and serve as flanges to which the tube-side headers are bolted. This construction requires that the shell and tube-sheet materials be weldable to each other.

When such welding is not possible, a "blind"-gasket type of construction is utilized. The blind gasket is not accessible for maintenance or replacement once the unit has been constructed. This construction is used for steam surface condensers, which operate under vacuum.

The tube-side header (or channel) may be welded to the tube sheet, as shown in Fig. 11-35 for type C and N heads. This type of construction is less costly than types B and M or A and L and still offers the advantage that tubes may be examined and replaced without disturbing the tube-side piping connections.

There is no limitation on the number of tube-side passes. Shell-side passes can be one or more, although shells with more than two shell-side passes are rarely used.

Tubes can completely fill the heat-exchanger shell. Clearance between the outermost tubes and the shell is only the minimum necessary for fabrication. Between the inside of the shell and the baffles some clearance must be provided so that baffles can slide into the shell. Fabrication tolerances then require some additional clearance between the outside of the baffles and the outermost tubes. The edge distance between the outer tube limit (OTL) and the baffle diameter must be sufficient to prevent vibration of the tubes from breaking through the baffle holes. The outermost tube must be contained within the OTL. Clearances between the inside shell diameter and OTL are 13 mm (½ in) for 635-mm-(25-in)- inside-diameter shells and up, 11 mm (⅞ in) for 254- through 610-mm (10- through 24-in) pipe shells, and slightly less for smaller-diameter pipe shells.

Tubes can be replaced. Tube-side headers, channel covers, gaskets, etc., are accessible for maintenance and replacement. Neither the shell-side baffle structure nor the blind gasket is accessible. During tube removal, a tube may break within the shell. When this occurs, it is most difficult to remove or to replace the tube. The usual procedure is to plug the appropriate holes in the tube sheets.

Differential expansion between the shell and the tubes can develop because of differences in length caused by thermal expansion. Various types of expansion joints are used to eliminate excessive stresses caused by expansion. The need for an expansion joint is a function of both the amount of differential expansion and the cycling conditions to be expected during operation. A number of types of expansion joints are available (Fig. 11-37).

a. *Flat plates.* Two concentric flat plates with a bar at the outer edges. The flat plates can flex to make some allowance for differential expansion. This design is generally used for vacuum service and gauge pressures below 103 kPa (15 lb/in²). All are subject to severe stress during differential expansion.

b. *Flanged-only heads.* The flat plates are flanged (or curved). The diameter of these heads is generally 203 mm (8 in) or more greater than the shell diameter. The welded joint at the shell is subject to the stress referred to before, but the joint connecting the heads is subjected to less stress during expansion because of the curved shape.

c. *Flared shell or pipe segments.* The shell may be flared to connect with a pipe section, or a pipe may be halved and quartered to produce a ring.

d. *Formed heads.* A pair of dished-only or elliptical or flanged and dished heads can be used. These are welded together or connected by a ring. This type of joint is similar to the flanged-only-head type but apparently is subject to less stress.

e. *Flanged and flued heads.* A pair of flanged-only heads is provided with concentric reverse flue holes. These heads are relatively expensive because of

the cost of the fluing operation. The curved shape of the heads reduces the amount of stress at the welds to the shell and also connecting the heads.

f. Toroidal. The toroidal joint has a mathematically predictable smooth stress pattern of low magnitude, with maximum stresses at sidewalls of the corrugation and minimum stresses at top and bottom.

The foregoing designs were discussed as ring expansion joints by Kopp and Sayre, "Expansion Joints for Heat Exchangers" (ASME Misc. Pap., vol. 6, no. 211). All are statically indeterminate but are subjected to analysis by introducing various simplifying assumptions. Some joints in current industrial use are of lighter wall construction than is indicated by the method of this paper.

g. Bellows. Thin-wall bellows joints are produced by various manufacturers. These are designed for differential expansion and are tested for axial and transverse movement as well as for cyclical life. Bellows may be of stainless steel, nickel alloys, or copper. (Aluminum, Monel, phosphor bronze, and titanium bellows have been manufactured.) Welding nipples of the same composition as the heat-exchanger shell are generally furnished. The bellows may be hydraulically formed from a single piece of metal or may consist of welded pieces. External insulation covers of carbon steel are often provided to protect the light-gauge bellows from damage. The cover also prevents insulation from interfering with movement of the bellows (see *h*).

h. Toroidal bellows. For high-pressure service the bellows type of joint has been modified so that movement is taken up by thin-wall small-diameter bellows of a toroidal shape. Thickness of parts under high pressure is reduced considerably (see *f*).

Improper handling during manufacture, transit, installation, or maintenance of the heat exchanger equipped with the thin-wall-bellows type

or toroidal type of expansion joint can damage the joint. In larger units these light-wall joints are particularly susceptible to damage, and some designers prefer the use of the heavier walls of formed heads.

Chemical-plant exchangers requiring expansion joints most commonly have used the flanged-and-flued-head type. There is a trend toward more common use of the light-wall-bellows type.

U-Tube Heat Exchanger (Fig. 11-36*d*) The tube bundle consists of a stationary tube sheet, U tubes (or hairpin tubes), baffles or support plates, and appropriate tie rods and spacers. The tube bundle can be removed from the heat-exchanger shell. A tube-side header (stationary head) and a shell with integral shell cover, which is welded to the shell, are provided. Each tube is free to expand or contract without any limitation being placed upon it by the other tubes.

The U-tube bundle has the advantage of providing minimum clearance between the outer tube limit and the inside of the shell for any of the removable-tube-bundle constructions. Clearances are of the same magnitude as for fixed-tube-sheet heat exchangers.

The number of tube holes in a given shell is less than that for a fixed-tube-sheet exchanger because of limitations on bending tubes of a very short radius.

The U-tube design offers the advantage of reducing the number of joints. In high-pressure construction this feature becomes of considerable importance in reducing both initial and maintenance costs. The use of U-tube construction has increased significantly with the development

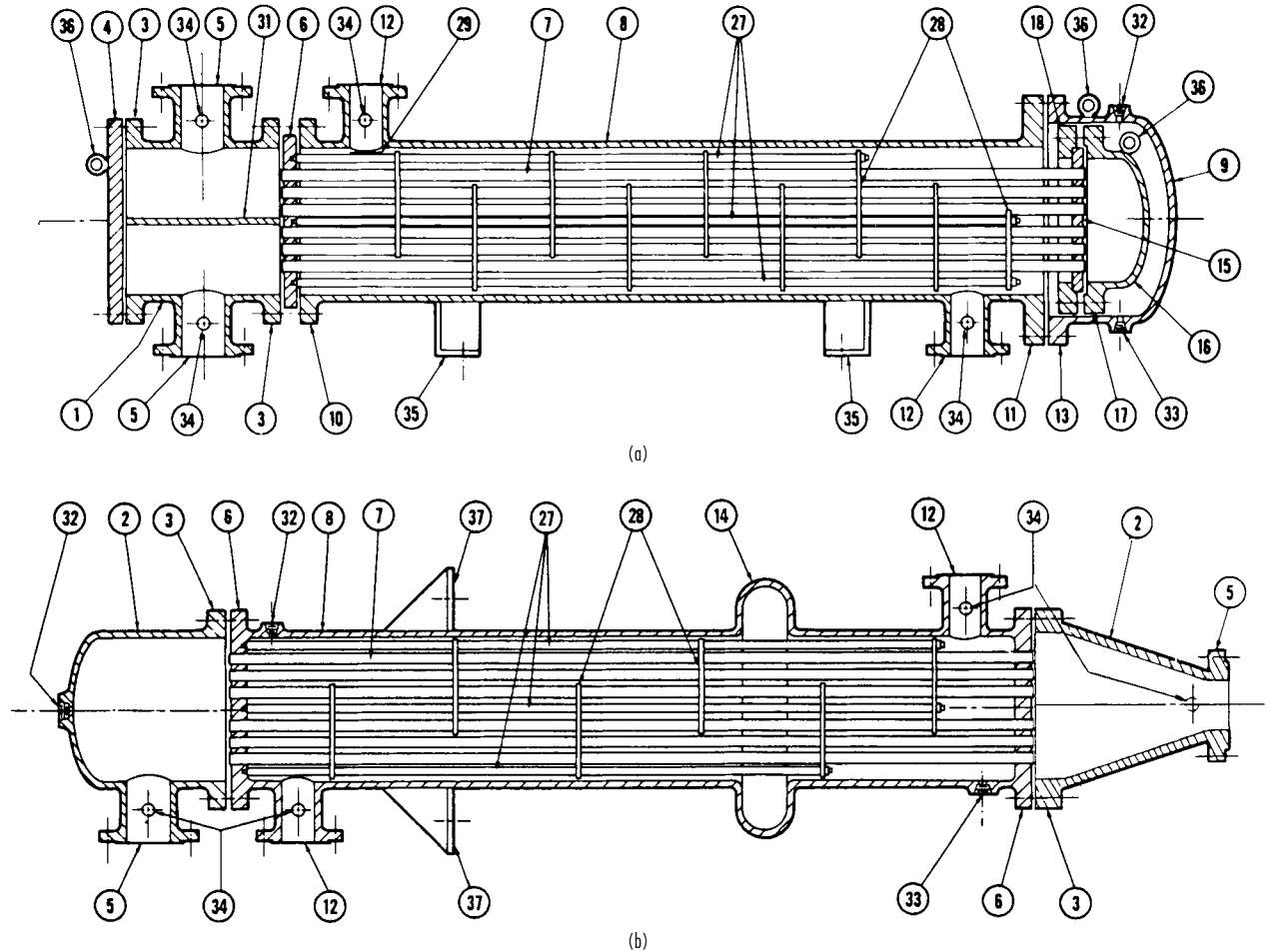


FIG. 11-36 Heat-exchanger-component nomenclature. (a) Internal-floating-head exchanger (with floating-head backing device). Type AES. (b) Fixed-tube-sheet exchanger. Type BEM. (Standards of the Tubular Exchanger Manufacturers Association, 6th ed., 1978.)

11-38 HEAT-TRANSFER EQUIPMENT

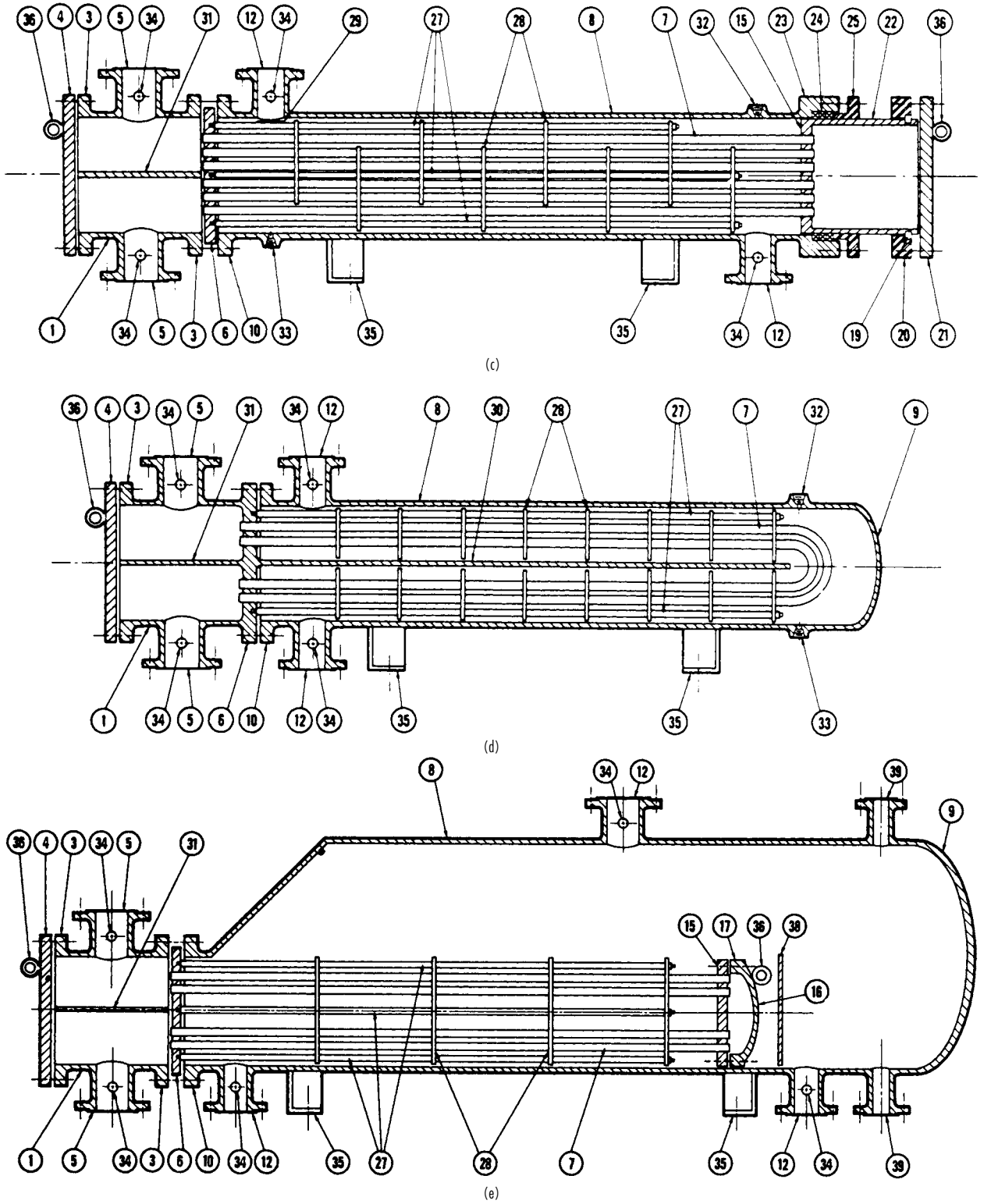
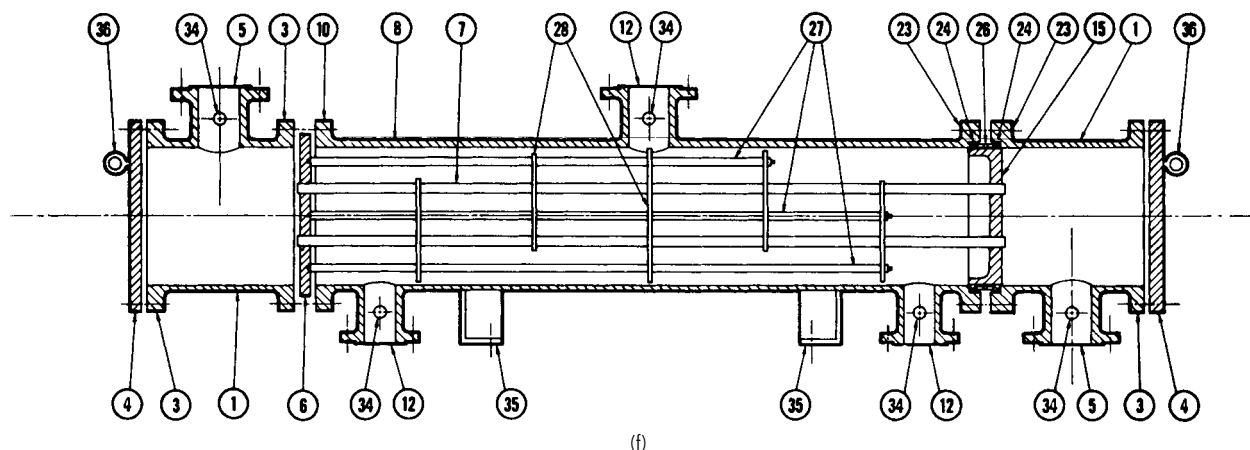


FIG. 11-36 (Continued) Heat-exchanger-component nomenclature. (c) Outside-packed floating-head exchanger. Type AEP. (d) U-tube heat exchanger. Type CFU. (e) Kettle-type floating-head reboiler. Type AKT. (Standards of the Tubular Exchanger Manufacturers Association, 6th ed., 1978.)



- | | |
|---------------------------------------------|------------------------------------------|
| 1. Stationary Head—Channel | 20. Slip-on Backing Flange |
| 2. Stationary Head—Bonnet | 21. Floating Head Cover—External |
| 3. Stationary Head Flange—Channel or Bonnet | 22. Floating Tubesheet Skirt |
| 4. Channel Cover | 23. Packing Box Flange |
| 5. Stationary Head Nozzle | 24. Packing |
| 6. Stationary Tubesheet | 25. Packing Gland |
| 7. Tubes | 26. Lantern Ring |
| 8. Shell | 27. Tie Rods and Spacers |
| 9. Shell Cover | 28. Transverse Baffles or Support Plates |
| 10. Shell Flange—Stationary Head End | 29. Impingement Plate |
| 11. Shell Flange—Rear Head End | 30. Longitudinal Baffle |
| 12. Shell Nozzle | 31. Pass Partition |
| 13. Shell Cover Flange | 32. Vent Connection |
| 14. Expansion Joint | 33. Drain Connection |
| 15. Floating Tubesheet | 34. Instrument Connection |
| 16. Floating Head Cover | 35. Support Saddle |
| 17. Floating Head Flange | 36. Lifting Lug |
| 18. Floating Head Backing Device | 37. Support Bracket |
| 19. Split Shear Ring | 38. Weir |
| | 39. Liquid Level Connection |

FIG. 11-36 (Continued) Heat-exchanger-component nomenclature. (f) Exchanger with packed floating tube sheet and lantern ring. Type AJW. (Standards of the Tubular Exchanger Manufacturers Association, 6th ed., 1978.)

of hydraulic tube cleaners, which can remove fouling residues from both the straight and the U-bend portions of the tubes.

Mechanical cleaning of the inside of the tubes was described by John [*Chem. Eng.*, **66**, 187-192 (Dec. 14, 1959)]. Rods and conventional mechanical tube cleaners cannot pass from one end of the U tube to the other. Power-driven tube cleaners, which can clean both the straight legs of the tubes and the bends, are available.

Hydraulic jetting with water forced through spray nozzles at high pressure for cleaning tube interiors and exteriors of removal bundles is reported by Canaday ("Hydraulic Jetting Tools for Cleaning Heat Exchangers," ASME Pap. 58-A-217, unpublished).

The tank suction heater, as illustrated in Fig. 11-38, contains a U-tube bundle. This design is often used with outdoor storage tanks for heavy fuel oils, tar, molasses, and similar fluids whose viscosity must be lowered to permit easy pumping. Usually the tube-side heating medium is steam. One end of the heater shell is open, and the liquid being heated passes across the outside of the tubes. Pumping costs can be reduced without heating the entire contents of the tank. Bare tube and integral low-fin tubes are provided with baffles. Longitudinal

fin-tube heaters are not baffled. Fins are most often used to minimize the fouling potential in these fluids.

Kettle-type reboilers, evaporators, etc., are often U-tube exchangers with enlarged shell sections for vapor-liquid separation. The U-tube bundle replaces the floating-heat bundle of Fig. 11-36e.

The U-tube exchanger with copper tubes, cast-iron header, and other parts of carbon steel is used for water and steam services in office buildings, schools, hospitals, hotels, etc. Nonferrous tube sheets and admiralty or 90-10 copper-nickel tubes are the most frequently used substitute materials. These standard exchangers are available from a number of manufacturers at costs far below those of custom-built process-industry equipment.

Packed-Lantern-Ring Exchanger (Fig. 11-36f) This construction is the least costly of the straight-tube removable bundle types. The shell- and tube-side fluids are each contained by separate rings of packing separated by a lantern ring and are installed at the floating tube sheet. The lantern ring is provided with weep holes. Any leakage passing the packing goes through the weep holes and then drops to the ground. Leakage at the packing will not result in mixing within the exchanger of the two fluids.

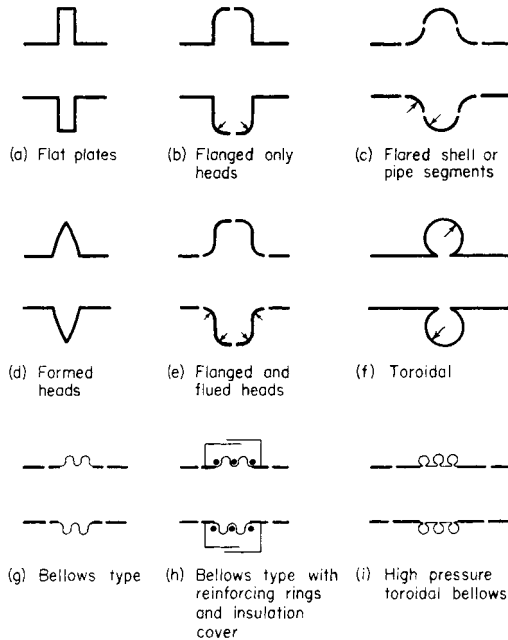


FIG. 11-37 Expansion joints.

The width of the floating tube sheet must be great enough to allow for the packings, the lantern ring, and differential expansion. Sometimes a small skirt is attached to a thin tube sheet to provide the required bearing surface for packings and lantern ring.

The clearance between the outer tube limit and the inside of the shell is slightly larger than that for fixed-tube-sheet and U-tube exchangers. The use of a floating-tube-sheet skirt increases this clearance. Without the skirt the clearance must make allowance for tube-hole distortion during tube rolling near the outside edge of the tube sheet or for tube-end welding at the floating tube sheet.

The packed-lantern-ring construction is generally limited to design temperatures below 191°C (375°F) and to the mild services of water, steam, air, lubricating oil, etc. Design gauge pressure does not exceed 2068 kPa (300 lbf/in²) for pipe shell exchangers and is limited to 1034 kPa (150 lbf/in²) for 610- to 1067-mm- (24- to 42-in-) diameter shells.

Outside-Packed Floating-Head Exchanger (Fig. 11-36c) The shell-side fluid is contained by rings of packing, which are compressed within a stuffing box by a packing follower ring. This construction was frequently used in the chemical industry, but in recent years usage has decreased. The removable-bundle construction accommodates differential expansion between shell and tubes and is used for shell-side

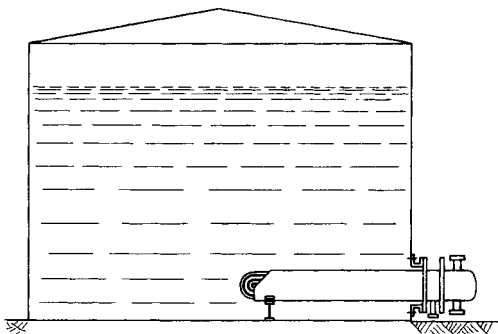


FIG. 11-38 Tank suction heater.

service up to 4137 kPa gauge pressure (600 lbf/in²) at 316°C (600°F). There are no limitations upon the number of tube-side passes or upon the tube-side design pressure and temperature. The outside-packed floating-head exchanger was the most commonly used type of removable-bundle construction in chemical-plant service.

The floating-tube-sheet skirt, where in contact with the rings of packing, has fine machine finish. A split shear ring is inserted into a groove in the floating-tube-sheet skirt. A slip-on backing flange, which in service is held in place by the shear ring, bolts to the external floating-head cover.

The floating-head cover is usually a circular disk. With an odd number of tube-side passes, an axial nozzle can be installed in such a floating-head cover. If a side nozzle is required, the circular disk is replaced by either a dished head or a channel barrel (similar to Fig. 11-36f) bolted between floating-head cover and floating-tube-sheet skirt.

The outer tube limit approaches the inside of the skirt but is farther removed from the inside of the shell than for any of the previously discussed constructions. Clearances between shell diameter and bundle OTL are 22 mm (7/8 in) for small-diameter pipe shells, 44 mm (1 3/4 in) for large-diameter pipe shells, and 58 mm (2 1/8 in) for moderate-diameter plate shells.

Internal Floating-Head Exchanger (Fig. 11-36a) The internal floating-head design is used extensively in petroleum-refinery service, but in recent years there has been a decline in usage.

The tube bundle is removable, and the floating tube sheet moves (or floats) to accommodate differential expansion between shell and tubes. The outer tube limit approaches the inside diameter of the gasket at the floating tube sheet. Clearances (between shell and OTL) are 29 mm (1 1/8 in) for pipe shells and 37 mm (1 7/16 in) for moderate-diameter plate shells.

A split backing ring and bolting usually hold the floating-head cover at the floating tube sheet. These are located beyond the end of the shell and within the larger-diameter shell cover. Shell cover, split backing ring, and floating-head cover must be removed before the tube bundle can pass through the exchanger shell.

With an even number of tube-side passes the floating-head cover serves as return cover for the tube-side fluid. With an odd number of passes a nozzle pipe must extend from the floating-head cover through the shell cover. Provision for both differential expansion and tube-bundle removal must be made.

Pull-Through Floating-Head Exchanger (Fig. 11-36e) Construction is similar to that of the internal-floating-head split-backing-ring exchanger except that the floating-head cover bolts directly to the floating tube sheet. The tube bundle can be withdrawn from the shell without removing either shell cover or floating-head cover. This feature reduces maintenance time during inspection and repair.

The large clearance between the tubes and the shell must provide for both the gasket and the bolting at the floating-head cover. This clearance is about 2 to 2 1/2 times that required by the split-ring design. Sealing strips or dummy tubes are often installed to reduce bypassing of the tube bundle.

Falling-Film Exchangers Falling-film shell-and-tube heat exchangers have been developed for a wide variety of services and are described by Sack [*Chem. Eng. Prog.*, **63**, 55 (July 1967)]. The fluid enters at the top of the vertical tubes. Distributors or slotted tubes put the liquid in film flow in the inside surface of the tubes, and the film adheres to the tube surface while falling to the bottom of the tubes. The film can be cooled, heated, evaporated, or frozen by means of the proper heat-transfer medium outside the tubes. Tube distributors have been developed for a wide range of applications. Fixed tube sheets, with or without expansion joints, and outside-packed-head designs are used.

Principal advantages are high rate of heat transfer, no internal pressure drop, short time of contact (very important for heat-sensitive materials), easy accessibility to tubes for cleaning, and, in some cases, prevention of leakage from one side to another.

These falling-film exchangers are used in various services as described in the following paragraphs.

Liquid Coolers and Condensers Dirty water can be used as the cooling medium. The top of the cooler is open to the atmosphere for

access to tubes. These can be cleaned without shutting down the cooler by removing the distributors one at a time and scrubbing the tubes.

Evaporators These are used extensively for the concentration of ammonium nitrate, urea, and other chemicals sensitive to heat when minimum contact time is desirable. Air is sometimes introduced in the tubes to lower the partial pressure of liquids whose boiling points are high. These evaporators are built for pressure or vacuum and with top or bottom vapor removal.

Absorbers These have a two-phase flow system. The absorbing medium is put in film flow during its fall downward on the tubes as it is cooled by a cooling medium outside the tubes. The film absorbs the gas which is introduced into the tubes. This operation can be concurrent or countercurrent.

Freezers By cooling the falling film to its freezing point, these exchangers convert a variety of chemicals to the solid phase. The most common application is the production of sized ice and paradichlorobenzene. Selective freezing is used for isolating isomers. By melting the solid material and refreezing in several stages, a higher degree of purity of product can be obtained.

TUBE-SIDE CONSTRUCTION

Tube-Side Header The tube-side header (or stationary head) contains one or more flow nozzles.

The **bonnet** (Fig. 11-35B) bolts to the shell. It is necessary to remove the bonnet in order to examine the tube ends. The fixed-tube-sheet exchanger of Fig. 11-36*b* has bonnets at both ends of the shell.

The **channel** (Fig. 11-35A) has a removable channel cover. The tube ends can be examined by removing this cover without disturbing the piping connections to the channel nozzles. The channel can bolt to the shell as shown in Fig. 11-36*a* and *c*. The Type C and Type N channels of Fig. 11-35 are welded to the tube sheet. This design is comparable in cost with the bonnet but has the advantages of permitting access to the tubes without disturbing the piping connections and of eliminating a gasketed joint.

Special High-Pressure Closures (Fig. 11-35D) The channel barrel and the tube sheet are generally forged. The removable channel cover is seated in place by hydrostatic pressure, while a shear ring subjected to shearing stress absorbs the end force. For pressures above 6205 kPa (900 lbf/in²) these designs are generally more economical than bolted constructions, which require larger flanges and bolting as pressure increases in order to contain the end force with bolts in tension. Relatively light-gauge internal pass partitions are provided to direct the flow of tube-side fluids but are designed only for the differential pressure across the tube bundle.

Tube-Side Passes Most exchangers have an even number of tube-side passes. The fixed-tube-sheet exchanger (which has no shell cover) usually has a return cover without any flow nozzles as shown in Fig. 11-35M; Types L and N are also used. All removable-bundle designs (except for the U tube) have a floating-head cover directing the flow of tube-side fluid at the floating tube sheet.

Tubes Standard heat-exchanger tubing is $\frac{1}{4}$, $\frac{3}{8}$, $\frac{1}{2}$, $\frac{5}{8}$, $\frac{3}{4}$, 1, 1 $\frac{1}{4}$, and 1 $\frac{1}{2}$ in in outside diameter (in \times 25.4 = mm). Wall thickness is measured in Birmingham wire gauge (BWG) units. A comprehensive list of tubing characteristics and sizes is given in Table 11-12. The most commonly used tubes in chemical plants and petroleum refineries are 19- and 25-mm ($\frac{3}{4}$ - and 1-in) outside diameter. Standard tube lengths are 8, 10, 12, 16, and 20 ft, with 20 ft now the most common (ft \times 0.3048 = m).

Manufacturing tolerances for steel, stainless-steel, and nickel-alloy tubes are such that the tubing is produced to either average or minimum wall thickness. Seamless carbon steel tube of minimum wall thickness may vary from 0 to 20 percent above the nominal wall thickness. Average-wall seamless tubing has an allowable variation of plus or minus 10 percent. Welded carbon steel tube is produced to closer tolerances (0 to plus 18 percent on minimum wall; plus or minus 9 percent on average wall). Tubing of aluminum, copper, and their alloys can be drawn easily and usually is made to minimum wall specifications.

Common practice is to specify **exchanger surface** in terms of total external square feet of tubing. The effective outside heat-transfer surface is based on the length of tubes measured between the inner faces

of tube sheets. In most heat exchangers there is little difference between the total and the effective surface. Significant differences are usually found in high-pressure and double-tube-sheet designs.

Integrally finned tube, which is available in a variety of alloys and sizes, is being used in shell-and-tube heat exchangers. The fins are radially extruded from thick-walled tube to a height of 1.6 mm ($\frac{1}{16}$ in) spaced at 1.33 mm (19 fins per inch) or to a height of 3.2 mm ($\frac{1}{8}$ in) spaced at 2.3 mm (11 fins per inch). External surface is approximately 2 $\frac{1}{2}$ times the outside surface of a bare tube with the same outside diameter. Also available are 0.93-mm- (0.037-in-) high fins spaced 0.91 mm (28 fins per inch) with an external surface about 3.5 times the surface of the bare tube. Bare ends of nominal tube diameter are provided, while the fin height is slightly less than this diameter. The tube can be inserted into a conventional tube bundle and rolled or welded to the tube sheet by the same means, used for bare tubes. An integrally finned tube rolled into a tube sheet with double serrations and flared at the inlet is shown in Fig. 11-39. Internally finned tubes have been manufactured but have limited application.

Longitudinal fins are commonly used in double-pipe exchangers upon the outside of the inner tube. U-tube and conventional removable tube bundles are also made from such tubing. The ratio of external to internal surface generally is about 10 or 15:1.

Transverse fins upon tubes are used in low-pressure gas services. The primary application is in air-cooled heat exchangers (as discussed under that heading), but shell-and-tube exchangers with these tubes are in service.

Rolled Tube Joints Expanded tube-to-tube-sheet joints are standard. Properly rolled joints have uniform tightness to minimize tube fractures, stress corrosion, tube-sheet ligament pushover and enlargement, and dishing of the tube sheet. Tubes are expanded into the tube sheet for a length of two tube diameters, or 50 mm (2 in), or tube-sheet thickness minus 3 mm ($\frac{1}{8}$ in). Generally tubes are rolled for the last of these alternatives. The expanded portion should never extend beyond the shell-side face of the tube sheet, since removing such a tube is extremely difficult. Methods and tools for tube removal and tube rolling were discussed by John [*Chem. Eng.*, **66**, 77-80 (Dec. 28, 1959)], and rolling techniques by Bach [*Pet. Refiner*, **39**, 8, 104 (1960)].

Tube ends may be projecting, flush, flared, or beaded (listed in order of usage). The flare or bell-mouth tube end is usually restricted to water service in condensers and serves to reduce erosion near the tube inlet.

For moderate general process requirements at gauge pressures less than 2058 kPa (300 lbf/in²) and less than 177°C (350°F), tube-sheet holes without grooves are standard. For all other services with expanded tubes at least two grooves in each tube hole are common. The number of grooves is sometimes changed to one or three in proportion to tube-sheet thickness.

Expanding the tube into the **grooved tube holes** provides a stronger joint but results in greater difficulties during tube removal.

Welded Tube Joints When suitable materials of construction are used, the tube ends may be welded to the tube sheets. Welded joints may be seal-welded "for additional tightness beyond that of tube

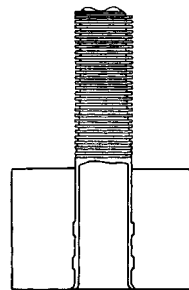


FIG. 11-39 Integrally finned tube rolled into tube sheet with double serrations and flared inlet. (Woverine Division, UOP, Inc.)

TABLE 11-12 Characteristics of Tubing (From Standards of the Tubular Exchanger Manufacturers Association, 8th Ed., 1999; 25 North Broadway, Tarrytown, N.Y.)

Tube O.D., in.	B.W.G. gage	Thickness, in.	Internal area, in. ²	Sq. ft. external surface per foot length	Sq. ft. internal surface per foot length	Weight per ft. length, steel, lb*	Tube I.D., in.	Moment of inertia, in. ⁴	Section modulus, in. ³	Radius of gyration, in.	Constant C†	O.D. I.D.	Transverse metal area, in. ²
1/4	22	0.028	0.0296	0.0654	0.0508	0.066	0.194	0.00012	0.00098	0.0791	46	1.289	0.0195
	24	0.022	0.0333	0.0654	0.0539	0.054	0.206	0.00010	0.00083	0.0810	52	1.214	0.0158
	26	0.018	0.0360	0.0654	0.0560	0.045	0.214	0.00009	0.00071	0.0823	56	1.168	0.0131
	27	0.016	0.0373	0.0654	0.0571	0.040	0.218	0.00008	0.00065	0.0829	58	1.147	0.0118
3/8	18	0.049	0.0603	0.0982	0.0725	0.171	0.277	0.00068	0.0036	0.1166	94	1.354	0.0502
	20	0.035	0.0731	0.0982	0.0798	0.127	0.305	0.00055	0.0029	0.1208	114	1.230	0.0374
	22	0.028	0.0799	0.0982	0.0835	0.104	0.319	0.00046	0.0025	0.1231	125	1.176	0.0305
	24	0.022	0.0860	0.0982	0.0867	0.083	0.331	0.00038	0.0020	0.1250	134	1.133	0.0244
1/2	16	0.065	0.1075	0.1309	0.0969	0.302	0.370	0.0021	0.0086	0.1555	168	1.351	0.0888
	18	0.049	0.1269	0.1309	0.1052	0.236	0.402	0.0018	0.0071	0.1604	198	1.244	0.0694
	20	0.035	0.1452	0.1309	0.1126	0.174	0.430	0.0014	0.0056	0.1649	227	1.163	0.0511
	22	0.028	0.1548	0.1309	0.1162	0.141	0.444	0.0012	0.0046	0.1672	241	1.126	0.0415
5/8	12	0.109	0.1301	0.1636	0.1066	0.601	0.407	0.0061	0.0197	0.1865	203	1.536	0.177
	13	0.095	0.1486	0.1636	0.1139	0.538	0.435	0.0057	0.0183	0.1904	232	1.437	0.158
	14	0.083	0.1655	0.1636	0.1202	0.481	0.459	0.0053	0.0170	0.1939	258	1.362	0.141
	15	0.072	0.1817	0.1636	0.1259	0.426	0.481	0.0049	0.0156	0.1972	283	1.299	0.125
	16	0.065	0.1924	0.1636	0.1296	0.389	0.495	0.0045	0.0145	0.1993	300	1.263	0.114
	17	0.058	0.2035	0.1636	0.1333	0.352	0.509	0.0042	0.0134	0.2015	317	1.228	0.103
	18	0.049	0.2181	0.1636	0.1380	0.302	0.527	0.0037	0.0119	0.2044	340	1.186	0.089
	19	0.042	0.2299	0.1636	0.1416	0.262	0.541	0.0033	0.0105	0.2067	359	1.155	0.077
	20	0.035	0.2419	0.1636	0.1453	0.221	0.555	0.0028	0.0091	0.2090	377	1.126	0.065
	3/4	10	0.134	0.1825	0.1963	0.1262	0.833	0.482	0.0129	0.0344	0.2229	285	1.556
11		0.120	0.2043	0.1963	0.1335	0.808	0.510	0.0122	0.0326	0.2267	319	1.471	0.238
12		0.109	0.2223	0.1963	0.1393	0.747	0.532	0.0116	0.0309	0.2299	347	1.410	0.219
13		0.095	0.2463	0.1963	0.1466	0.665	0.560	0.0107	0.0285	0.2340	384	1.339	0.195
14		0.083	0.2679	0.1963	0.1529	0.592	0.584	0.0098	0.0262	0.2376	418	1.284	0.174
15		0.072	0.2884	0.1963	0.1587	0.522	0.606	0.0089	0.0238	0.2411	450	1.238	0.153
16		0.065	0.3019	0.1963	0.1623	0.476	0.620	0.0083	0.0221	0.2433	471	1.210	0.140
17		0.058	0.3157	0.1963	0.1660	0.429	0.634	0.0076	0.0203	0.2455	492	1.183	0.126
18		0.049	0.3339	0.1963	0.1707	0.367	0.652	0.0067	0.0178	0.2484	521	1.150	0.108
20		0.035	0.3632	0.1963	0.1780	0.268	0.680	0.0050	0.0134	0.2531	567	1.103	0.079
7/8	10	0.134	0.2894	0.2291	0.1589	1.062	0.607	0.0221	0.0505	0.2662	451	1.442	0.312
	11	0.120	0.3167	0.2291	0.1662	0.969	0.635	0.0208	0.0475	0.2703	494	1.378	0.285
	12	0.109	0.3390	0.2291	0.1720	0.893	0.657	0.0196	0.0449	0.2736	529	1.332	0.262
	13	0.095	0.3685	0.2291	0.1793	0.792	0.685	0.0180	0.0411	0.2778	575	1.277	0.233
	14	0.083	0.3948	0.2291	0.1856	0.703	0.709	0.0164	0.0374	0.2815	616	1.234	0.207
	15	0.072	0.4197	0.2291	0.1914	0.618	0.731	0.0148	0.0337	0.2850	655	1.197	0.182
	16	0.065	0.4359	0.2291	0.1950	0.563	0.745	0.0137	0.0312	0.2873	680	1.174	0.165
	17	0.058	0.4525	0.2291	0.1987	0.507	0.759	0.0125	0.0285	0.2896	706	1.153	0.149
	18	0.049	0.4742	0.2291	0.2034	0.433	0.777	0.0109	0.0249	0.2925	740	1.126	0.127
	20	0.035	0.5090	0.2291	0.2107	0.314	0.805	0.0082	0.0187	0.2972	794	1.087	0.092
1	8	0.165	0.3526	0.2618	0.1754	1.473	0.670	0.0392	0.0784	0.3009	550	1.493	0.433
	10	0.134	0.4208	0.2618	0.1916	1.241	0.732	0.0350	0.0700	0.3098	656	1.366	0.365
	11	0.120	0.4536	0.2618	0.1990	1.129	0.760	0.0327	0.0654	0.3140	708	1.316	0.332
	12	0.109	0.4803	0.2618	0.2047	1.038	0.782	0.0307	0.0615	0.3174	749	1.279	0.305
	13	0.095	0.5153	0.2618	0.2121	0.919	0.810	0.0280	0.0559	0.3217	804	1.235	0.270
	14	0.083	0.5463	0.2618	0.2183	0.814	0.834	0.0253	0.0507	0.3255	852	1.199	0.239
	15	0.072	0.5755	0.2618	0.2241	0.714	0.856	0.0227	0.0455	0.3291	898	1.168	0.210
	16	0.065	0.5945	0.2618	0.2278	0.650	0.870	0.0210	0.0419	0.3314	927	1.149	0.191
	18	0.049	0.6390	0.2618	0.2361	0.498	0.902	0.0166	0.0332	0.3367	997	1.109	0.146
	20	0.035	0.6793	0.2618	0.2435	0.361	0.930	0.0124	0.0247	0.3414	1060	1.075	0.106
1-1/4	7	0.180	0.6221	0.3272	0.2330	2.059	0.890	0.0890	0.1425	0.3836	970	1.404	0.605
	8	0.165	0.6648	0.3272	0.2409	1.914	0.920	0.0847	0.1355	0.3880	1037	1.359	0.562
	10	0.134	0.7574	0.3272	0.2571	1.599	0.982	0.0742	0.1187	0.3974	1182	1.273	0.470
	11	0.120	0.8012	0.3272	0.2644	1.450	1.010	0.0688	0.1100	0.4018	1250	1.238	0.426
	12	0.109	0.8365	0.3272	0.2702	1.330	1.032	0.0642	0.1027	0.4052	1305	1.211	0.391
	13	0.095	0.8825	0.3272	0.2775	1.173	1.060	0.0579	0.0926	0.4097	1377	1.179	0.345
	14	0.083	0.9229	0.3272	0.2838	1.036	1.084	0.0521	0.0833	0.4136	1440	1.153	0.304
	16	0.065	0.9852	0.3272	0.2932	0.824	1.120	0.0426	0.0682	0.4196	1537	1.116	0.242
	18	0.049	1.0423	0.3272	0.3016	0.629	1.152	0.0334	0.0534	0.4250	1626	1.085	0.185
	20	0.035	1.0936	0.3272	0.3089	0.455	1.180	0.0247	0.0395	0.4297	1706	1.059	0.134
1-1/2	10	0.134	1.1921	0.3927	0.3225	1.957	1.232	0.1354	0.1806	0.4853	1860	1.218	0.575
	12	0.109	1.2908	0.3927	0.3356	1.621	1.282	0.1159	0.1545	0.4933	2014	1.170	0.476
	14	0.083	1.3977	0.3927	0.3492	1.257	1.334	0.0931	0.1241	0.5018	2180	1.124	0.369
	16	0.065	1.4741	0.3927	0.3587	0.997	1.370	0.0756	0.1008	0.5079	2300	1.095	0.293
2	11	0.120	2.4328	0.5236	0.4608	2.412	1.760	0.3144	0.3144	0.6660	3795	1.136	0.709
	12	0.109	2.4941	0.5236	0.4665	2.204	1.782	0.2904	0.2904	0.6697	3891	1.122	0.648
	13	0.095	2.5730	0.5236	0.4739	1.935	1.810	0.2586	0.2588	0.6744	4014	1.105	0.569
	14	0.083	2.6417	0.5236	0.4801	1.701	1.834	0.2300	0.2300	0.6784	4121	1.091	0.500

*Weights are based on low-carbon steel with a density of 0.2836 lb/cu. in. For other metals multiply by the following factors: aluminum, 0.35; titanium, 0.58; A.I.S.I. 400 Series S/steels, 0.99; A.I.S.I. 300 Series S/steels, 1.02; aluminum bronze, 1.04; aluminum brass, 1.06; nickel-chrome-iron, 1.07; Admiralty, 1.09; nickel, 1.13; nickel-copper, 1.12; copper and cupro-nickels, 1.14.

$$\dagger \text{Liquid velocity} = \frac{\text{lb per tube hour}}{C \times \text{sp gr of liquid}} \quad \text{ft/s (sp gr of water at 60°F = 1.0)}$$

rolling" or may be strength-welded. Strength-welded joints have been found satisfactory in very severe services. Welded joints may or may not be rolled before or after welding.

The variables in tube-end welding were discussed in two unpublished papers (Emhardt, "Heat Exchanger Tube-to-Tubesheet Joints," ASME Pap. 69-WA/HT-47; and Reynolds, "Tube Welding for Conventional and Nuclear Power Plant Heat Exchangers," ASME Pap. 69-WA/HT-24), which were presented at the November 1969 meeting of the American Society of Mechanical Engineers.

Tube-end rolling before welding may leave lubricant from the tube expander in the tube hole. Fouling during normal operation followed by maintenance operations will leave various impurities in and near the tube ends. Satisfactory welds are rarely possible under such conditions, since tube-end welding requires extreme cleanliness in the area to be welded.

Tube expansion after welding has been found useful for low and moderate pressures. In high-pressure service tube rolling has not been able to prevent leakage after weld failure.

Double-Tube-Sheet Joints This design prevents the passage of either fluid into the other because of leakage at the tube-to-tubesheet joints, which are generally the weakest points in heat exchangers. Any leakage at these joints admits the fluid to the gap between the tube sheets. Mechanical design, fabrication, and maintenance of double-tube-sheet designs require special consideration.

SHELL-SIDE CONSTRUCTION

Shell Sizes Heat-exchanger shells are generally made from standard-wall steel pipe in sizes up to 305-mm (12-in) diameter; from 9.5-mm (3/8-in) wall pipe in sizes from 356 to 610 mm (14 to 24 in); and from steel plate rolled at discrete intervals in larger sizes. Clearances between the outer tube limit and the shell are discussed elsewhere in connection with the different types of construction.

The following formulae may be used to estimate tube counts for various bundle sizes and tube passes. The estimated values include the removal of tubes to provide an entrance area for shell nozzle sizes of one-fifth the shell diameter. Due to the large effect from other parameters such as design pressure/corrosion allowance, baffle cuts, seal strips, and so on, these are to be used as estimates only. Exact tube counts are part of the design package of most reputable exchanger design software and are normally used for the final design.

Triangular tube layouts with pitch equal to 1.25 times the tube outside diameter:

$$C = 0.75 (D/d) - 36; \text{ where } D = \text{Bundle O.D. } d = \text{Tube O.D.}$$

$$\text{Range of accuracy: } -24 \leq C \leq 24.$$

$$1 \text{ Tube Pass: } N_t = 1298. + 74.86C + 1.283C^2 - .0078C^3 - .0006C^4 \quad (11-74a)$$

$$2 \text{ Tube Pass: } N_t = 1266. + 73.58C + 1.234C^2 - .0071C^3 - .0005C^4 \quad (11-74b)$$

$$4 \text{ Tube Pass: } N_t = 1196. + 70.79C + 1.180C^2 - .0059C^3 - .0004C^4 \quad (11-74c)$$

$$6 \text{ Tube Pass: } N_t = 1166. + 70.72C + 1.269C^2 - .0074C^3 - .0006C^4 \quad (11-74d)$$

Square tube layouts with pitch equal to 1.25 times the tube outside diameter:

$$C = (D/d) - 36.; \text{ where } D = \text{Bundle O.D. } d = \text{Tube O.D.}$$

$$\text{Range of accuracy: } -24 \leq C \leq 24.$$

$$1 \text{ Tube Pass: } N_t = 593.6 + 33.52C + .3782C^2 - .0012C^3 + .0001C^4 \quad (11-75a)$$

$$2 \text{ Tube Pass: } N_t = 578.8 + 33.36C + .3847C^2 - .0013C^3 + .0001C^4 \quad (11-75b)$$

$$4 \text{ Tube Pass: } N_t = 562.0 + 33.04C + .3661C^2 - .0016C^3 + .0002C^4 \quad (11-75c)$$

$$6 \text{ Tube Pass: } N_t = 550.4 + 32.49C + .3873C^2 - .0013C^3 + .0001C^4 \quad (11-75d)$$

Shell-Side Arrangements The **one-pass shell** (Fig. 11-35E) is the most commonly used arrangement. Condensers from single component vapors often have the nozzles moved to the center of the shell for vacuum and steam services.

A solid longitudinal baffle is provided to form a two-pass shell (Fig. 11-35F). It may be insulated to improve thermal efficiency. (See further discussion on baffles). A two-pass shell can improve thermal effectiveness at a cost lower than for two shells in series.

For **split flow** (Fig. 11-35G), the longitudinal baffle may be solid or perforated. The latter feature is used with condensing vapors.

A **double-split-flow** design is shown in Fig. 11-35H. The longitudinal baffles may be solid or perforated.

The **divided flow** design (Fig. 11-35J), mechanically is like the one-pass shell except for the addition of a nozzle. Divided flow is used to meet low-pressure-drop requirements.

The **kettle reboiler** is shown in Fig. 11-35K. When nucleate boiling is to be done on the shell-side, this common design provides adequate dome space for separation of vapor and liquid above the tube bundle and surge capacity beyond the weir near the shell cover.

BAFFLES AND TUBE BUNDLES

The **tube bundle** is the most important part of a tubular heat exchanger. The tubes generally constitute the most expensive component of the exchanger and are the one most likely to corrode. Tube sheets, baffles, or support plates, tie rods, and usually spacers complete the bundle.

Minimum **baffle spacing** is generally one-fifth of the shell diameter and not less than 50.8 mm (2 in). Maximum baffle spacing is limited by the requirement to provide adequate support for the tubes. The maximum unsupported tube span in inches equals $74 d^{0.75}$ (where d is the outside tube diameter in inches). The unsupported tube span is reduced by about 12 percent for aluminum, copper, and their alloys.

Baffles are provided for heat-transfer purposes. When shell-side baffles are not required for heat-transfer purposes, as may be the case in condensers or reboilers, tube supports are installed.

Segmental Baffles Segmental or cross-flow baffles are standard. Single, double, and triple segmental baffles are used. Baffle cuts are illustrated in Fig. 11-40. The double segmental baffle reduces cross-flow velocity for a given baffle spacing. The triple segmental baffle reduces both cross-flow and long-flow velocities and has been identified as the "window-cut" baffle.

Baffle cuts are expressed as the ratio of segment opening height to shell inside diameter. Cross-flow baffles with horizontal cut are shown in Fig. 11-36a, c, and f. This arrangement is not satisfactory for horizontal condensers, since the condensate can be trapped between baffles, or for dirty fluids in which the dirt might settle out. Vertical-cut baffles are used for side-to-side flow in horizontal exchangers with condensing fluids or dirty fluids. Baffles are notched to assure complete drainage when the units are taken out of service. (These notches permit some bypassing of the tube bundle during normal operation.)

Tubes are most commonly arranged on an equilateral triangular pitch. Tubes are arranged on a square pitch primarily for mechanical cleaning purposes in removable-bundle exchangers.

Maximum baffle cut is limited to about 45 percent for single segmental baffles so that every pair of baffles will support each tube. Tube bundles are generally provided with baffles cut so that at least one row of tubes passes through all the baffles or support plates. These tubes hold the entire bundle together. In pipe-shell exchangers with a horizontal baffle cut and a horizontal pass rib for directing tube-side flow in the channel, the maximum baffle cut, which permits a minimum of one row of tubes to pass through all baffles, is approximately 33 percent in small shells and 40 percent in larger pipe shells.

Maximum shell-side heat-transfer rates in forced convection are apparently obtained by cross-flow of the fluid at right angles to the tubes. In order to maximize this type of flow some heat exchangers are built with segmental-cut baffles and with "no tubes in the window" (or the baffle cutout). Maximum baffle spacing may thus equal maximum unsupported-tube span, while conventional baffle spacing is limited to one-half of this span.

The maximum baffle spacing for no tubes in the window of single segmental baffles is unlimited when intermediate supports are provided. These are cut on both sides of the baffle and therefore do not affect the flow of the shell-side fluid. Each support engages all the tubes; the supports are spaced to provide adequate support for the tubes.

Rod Baffles Rod or bar baffles have either rods or bars extending through the lanes between rows of tubes. A baffle set can consist of a baffle with rods in all the vertical lanes and another baffle with rods in all the horizontal lanes between the tubes. The shell-side flow is uniform and parallel to the tubes. Stagnant areas do not exist.

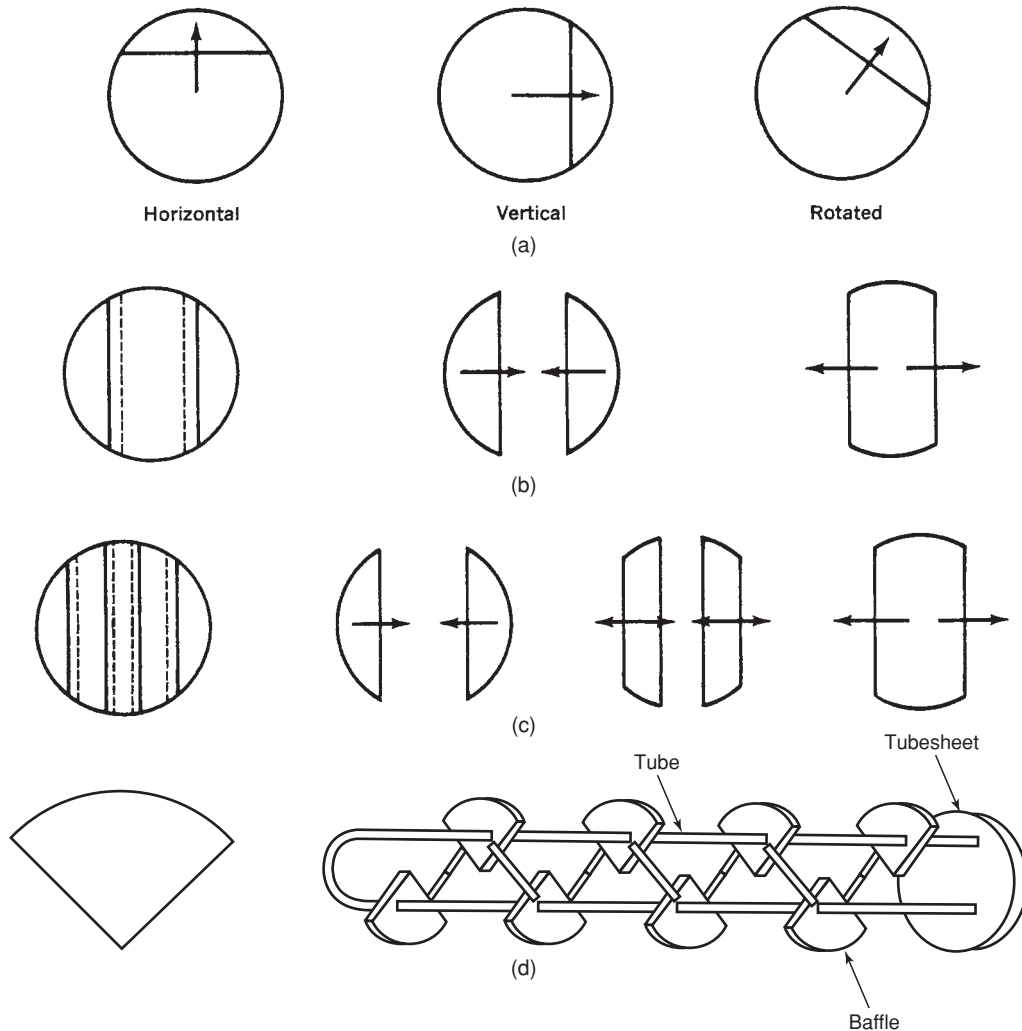


FIG. 11-40 Plate baffles. (a) Baffle cuts for single segmental baffles. (b) Baffle cuts for double segmental baffles. (c) Baffle cuts for triple segmental baffles. (d) Helical baffle construction.

One device uses four baffles in a baffle set. Only half of either the vertical or the horizontal tube lanes in a baffle have rods. The new design apparently provides a maximum shell-side heat-transfer coefficient for a given pressure drop.

Tie Rods and Spacers Tie rods are used to hold the baffles in place with spacers, which are pieces of tubing or pipe placed on the rods to locate the baffles. Occasionally baffles are welded to the tie rods, and spacers are eliminated. Properly located tie rods and spacers serve both to hold the bundle together and to reduce bypassing of the tubes.

In very large fixed-tube-sheet units, in which concentricity of shells decreases, baffles are occasionally welded to the shell to eliminate bypassing between the baffle and the shell.

Metal baffles are standard. Occasionally plastic baffles are used either to reduce corrosion or in vibratory service, in which metal baffles may cut the tubes.

Impingement Baffle The tube bundle is customarily protected against impingement by the incoming fluid at the shell inlet nozzle when the shell-side fluid is at a high velocity, is condensing, or is a two-phase fluid. Minimum entrance area about the nozzle is generally equal to the inlet nozzle area. Exit nozzles also require adequate area

between the tubes and the nozzles. A full bundle without any provision for shell inlet nozzle area can increase the velocity of the inlet fluid by as much as 300 percent with a consequent loss in pressure.

Impingement baffles are generally made of rectangular plate, although circular plates are more desirable. Rods and other devices are sometimes used to protect the tubes from impingement. In order to maintain a maximum tube count the impingement plate is often placed in a conical nozzle opening or in a dome cap above the shell.

Impingement baffles or flow-distribution devices are recommended for axial tube-side nozzles when entrance velocity is high.

Vapor Distribution Relatively large shell inlet nozzles, which may be used in condensers under low pressure or vacuum, require provision for uniform vapor distribution.

Tube-Bundle Bypassing Shell-side heat-transfer rates are maximized when bypassing of the tube bundle is at a minimum. The most significant bypass stream is generally between the outer tube limit and the inside of the shell. The clearance between tubes and shell is at a minimum for fixed-tube-sheet construction and is greatest for straight-tube removable bundles.

Arrangements to reduce tube-bundle bypassing include:
Dummy tubes. These tubes do not pass through the tube sheets and can be located close to the inside of the shell.

Tie rods with spacers. These hold the baffles in place but can be located to prevent bypassing.

Sealing strips. These longitudinal strips either extend from baffle to baffle or may be inserted in slots cut into the baffles.

Dummy tubes or tie rods with spacers may be located within the pass partition lanes (and between the baffle cuts) in order to ensure maximum bundle penetration by the shell-side fluid.

When tubes are omitted from the tube layout to provide entrance area about an impingement plate, the need for sealing strips or other devices to cause proper bundle penetration by the shell-side fluid is increased.

Helical Baffles An increasingly popular variant to the segmental baffle is the helical baffle. These are quadrant-shaped plate baffles installed at an angle to the axial bundle centerline to produce a pseudo-spiraling flow down the length of the tube bundle (Fig. 11-40d). This baffle has the advantage of producing shell-side heat-transfer coefficients similar to those of the segmental baffle with much less shell-side pressure loss for the same size of shell. In the case of equal pressure drops, the helical baffle exchanger will be smaller than the segmental baffle exchanger; or, for identical shell sizes, the helical baffle exchanger will permit a much higher throughput of flow for the same process inlet/outlet temperatures.

A great amount of proprietary research has been conducted by a few companies into the workings of helical baffled heat exchangers. The only known open literature method for estimating helical baffle performance has been "Comparison of Correction Factors for Shell-and-Tube Heat Exchangers with Segmental or Helical Baffles" by Stehlik, Nemcansky, Kral, and Swanson [*Heat Transfer Engineering*, 15(1), 55-65].

Unique design variables for helical baffles include the baffle angle, adjacent baffle contact diameter (which sets the baffle spacing and is usually about half of the shell I.D.), and the number of baffle starts (i.e., number of intermediate baffle starts). Of course, consideration is also given to the tube layout, tube pitch, use of seal strips, and all the other configuration characteristics common to any plate baffled bundle.

A helical baffle bundle built in this way produces two distinct flow regions. The area outside of the adjacent baffle contact diameter tends to produce a stable helical cross flow. However, inside the diameter where adjacent baffles touch is a second region where vortical flow is induced but in which the intensity of the rotational component tends to decrease as one approaches the center of the bundle. For a fixed flow rate and helix angle, this tendency may be minimized by the proper selection of the baffle contact diameter. With the correct selection, stream temperatures may be made to be close to uniform across the bundle cross section through the shell. However, below a critical velocity (for the baffle configuration and fluid state), the tendency for nonuniformity of temperatures increases as velocity decreases until ever-increasing portions of the central core surface area pinch out with respect to temperature and become ineffective for further heat transfer.

The design approach involves varying the baffle spacing for the primary purpose of balancing the flows in the two regions and maximizing the effectiveness of the total surface area. In many cases, a shallower helix angle is chosen in conjunction with the baffle spacing in order to minimize the central core component while still achieving a reduced overall bundle pressure drop.

Longitudinal Flow Baffles In fixed-tube-sheet construction with multipass shells, the baffle is usually welded to the shell and positive assurance against bypassing results. Removable tube bundles have a sealing device between the shell and the longitudinal baffle. Flexible light-gauge sealing strips and various packing devices have been used. Removable U-tube bundles with four tube-side passes and two shell-side passes can be installed in shells with the longitudinal baffle welded in place.

In split-flow shells the longitudinal baffle may be installed without a positive seal at the edges if design conditions are not seriously affected by a limited amount of bypassing.

Fouling in petroleum-refinery service has necessitated rough treatment of tube bundles during cleaning operations. Many refineries

avoid the use of longitudinal baffles, since the sealing devices are subject to damage during cleaning and maintenance operations.

CORROSION IN HEAT EXCHANGERS

Some of the special considerations in regard to heat-exchanger corrosion are discussed in this subsection. A more extended presentation in Sec. 23 covers corrosion and its various forms as well as materials of construction.

Materials of Construction The most common material of construction for heat exchangers is carbon steel. Stainless-steel construction throughout is sometimes used in chemical-plant service and on rare occasions in petroleum refining. Many exchangers are constructed from dissimilar metals. Such combinations are functioning satisfactorily in certain services. Extreme care in their selection is required since electrolytic attack can develop.

Carbon steel and alloy combinations appear in Table 11-13 "Alloys" in chemical- and petrochemical-plant service in approximate order of use are stainless-steel series 300, nickel, Monel, copper alloy, aluminum, Inconel, stainless-steel series 400, and other alloys. In petroleum-refinery service the frequency order shifts, with copper alloy (for water-cooled units) in first place and low-alloy steel in second place. In some segments of the petroleum industry copper alloy, stainless series 400, low-alloy steel, and aluminum are becoming the most commonly used alloys.

Copper-alloy tubing, particularly inhibited admiralty, is generally used with cooling water. Copper-alloy tube sheets and baffles are generally of naval brass.

Aluminum alloy (and in particular alclad aluminum) tubing is sometimes used in water service. The alclad alloy has a sacrificial aluminum-alloy layer metallurgically bonded to a core alloy.

Tube-side headers for water service are made in a wide variety of materials: carbon steel, copper alloy, cast iron, and lead-lined or plastic-lined or specially painted carbon steel.

Bimetallic Tubes When corrosive requirements or temperature conditions do not permit the use of a single alloy for the tubes, bimetallic (or duplex) tubes may be used. These can be made from almost any possible combination of metals. Tube sizes and gauges can be varied. For thin gauges the wall thickness is generally divided equally between the two components. In heavier gauges the more expensive component may comprise from a fifth to a third of the total thickness.

The component materials comply with applicable ASTM specifications, but after manufacture the outer component may increase in hardness beyond specification limits, and special care is required during the tube-rolling operation. When the harder material is on the outside, precautions must be exercised to expand the tube properly. When the inner material is considerably softer, rolling may not be practical unless ferrules of the soft material are used.

In order to eliminate galvanic action the outer tube material may be stripped from the tube ends and replaced with ferrules of the inner tube material. When the end of a tube with a ferrule is expanded or welded to a tube sheet, the tube-side fluid can contact only the inner tube material, while the outer material is exposed to the shell-side fluid.

Bimetallic tubes are available from a small number of tube mills and are manufactured only on special order and in large quantities.

TABLE 11-13 Dissimilar Materials in Heat-Exchanger Construction

Part	Relative use	1	2	3	4	5	6
	Relative cost	A	B	C	D	C	E
Tubes		●	●	●	●	●	●
Tube sheets			●	●	●	●	●
Tube-side headers				●	●		
Baffles					●	●	●
Shell							●

Carbon steel replaced by an alloy when ● appears.
 Relative use: from 1 (most popular) through 6 (least popular) combinations.
 Relative cost: from A (least expensive) to E (most expensive).

Clad Tube Sheets Usually tube sheets and other exchanger parts are of a solid metal. Clad or bimetallic tube sheets are used to reduce costs or because no single metal is satisfactory for the corrosive conditions. The alloy material (e.g., stainless steel, Monel) is generally bonded or clad to a carbon steel backing material. In fixed-tube-sheet construction a copper-alloy-clad tube sheet can be welded to a steel shell, while most copper-alloy tube sheets cannot be welded to steel in a manner acceptable to ASME Code authorities.

Clad tube sheets in service with carbon steel backer material include stainless-steel types 304, 304L, 316, 316L, and 317, Monel, Inconel, nickel, naval rolled brass, copper, admiralty, silicon bronze, and titanium. Naval rolled brass and Monel clad on stainless steel are also in service.

Ferrous-alloy-clad tube sheets are generally prepared by a weld overlay process in which the alloy material is deposited by welding upon the face of the tube sheet. Precautions are required to produce a weld deposit free of defects, since these may permit the process fluid to attack the base metal below the alloy. Copper-alloy-clad tube sheets are prepared by brazing the alloy to the carbon steel backing material.

Clad materials can be prepared by bonding techniques, which involve rolling, heat treatment, explosive bonding, etc. When properly manufactured, the two metals do not separate because of thermal-expansion differences encountered in service. Applied tube-sheet facings prepared by tack welding at the outer edges of alloy and base metal or by bolting together the two metals are in limited use.

Nonmetallic Construction Shell-and-tube exchangers with glass tubes 14 mm (0.551 in) in diameter and 1 mm (0.039 in) thick with tube lengths from 2.015 m (79.3 in) to 4.015 m (158 in) are available. Steel shell exchangers have a maximum design pressure of 517 kPa (75 lbf/in²). Glass shell exchangers have a maximum design gauge pressure of 103 kPa (15 lbf/in²). Shell diameters are 229 mm (9 in), 305 mm (12 in), and 457 mm (18 in). Heat-transfer surface ranges from 3.16 to 51 m² (34 to 550 ft²). Each tube is free to expand, since a Teflon sealer sheet is used at the tube-to-tube-sheet joint.

Impervious graphite heat-exchanger equipment is made in a variety of forms, including outside-packed-head shell-and-tube exchangers. They are fabricated with impervious graphite tubes and tube-side head-

ers and metallic shells. Single units containing up to 1300 m² (14,000 ft²) of heat-transfer surface are available.

Teflon heat exchangers of special construction are described later in this section.

Fabrication Expanding the tube into the tube sheet reduces the tube wall thickness and work-hardens the metal. The induced stresses can lead to **stress corrosion**. Differential expansion between tubes and shell in fixed-tube-sheet exchangers can develop stresses, which lead to stress corrosion.

When austenitic stainless-steel tubes are used for corrosion resistance, a close fit between the tube and the tube hole is recommended in order to minimize work hardening and the resulting loss of corrosion resistance.

In order to facilitate removal and replacement of tubes it is customary to roller-expand the tubes to within 3 mm (1/8 in) of the shell-side face of the tube sheet. A 3-mm- (1/8-in-) long gap is thus created between the tube and the tube hole at this tube-sheet face. In some services this gap has been found to be a focal point for corrosion.

It is standard practice to provide a chamfer at the inside edges of tube holes in tube sheets to prevent cutting of the tubes and to remove burrs produced by drilling or reaming the tube sheet. In the lower tube sheet of vertical units this chamfer serves as a pocket to collect material, dirt, etc., and to serve as a corrosion center.

Adequate venting of exchangers is required both for proper operation and to reduce corrosion. Improper venting of the water side of exchangers can cause alternate wetting and drying and accompanying chloride concentration, which is particularly destructive to the series 300 stainless steels.

Certain corrosive conditions require that special consideration be given to complete drainage when the unit is taken out of service. Particular consideration is required for the upper surfaces of tube sheets in vertical heat exchangers, for sagging tubes, and for shell-side baffles in horizontal units.

SHELL-AND-TUBE EXCHANGER COSTS

Basic costs of shell-and-tube heat exchangers made in the United States of carbon steel construction in 1958 are shown in Fig. 11-41.

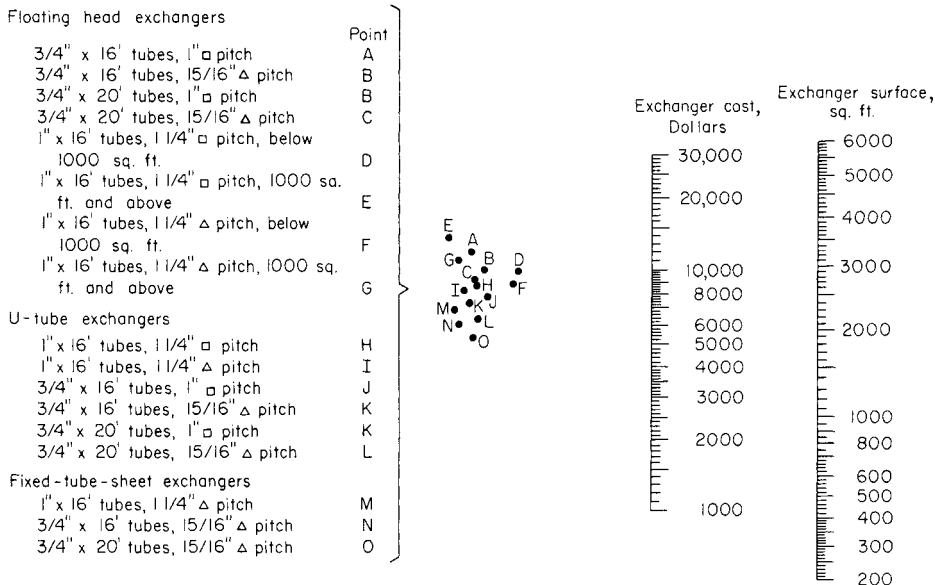


FIG. 11-41 Costs of basic exchangers—all steel, TEMA Class R, 150 lbf/in², 1958. To convert pounds-force per square inch to kilopascals, multiply by 6.895; to convert square feet to square meters, multiply by 0.0929; to convert inches to millimeters, multiply by 25.4; and to convert feet to meters, multiply by 0.3048.

TABLE 11-14 Extras for Pressure and Alloy Construction and Surface and Weights*

Percent of steel base price, 1500-lbf/in² working pressure

Pressure†	Shell diameters, in												
	12	14	16	18	20	22	24	27	30	33	36	39	42
300 lbf/in ²	7	7	8	8	9	9	10	11	11	12	13	14	15
450 lbf/in ²	18	19	20	21	22	23	24	27	29	31	32	33	35
600 lbf/in ²	28	29	31	33	35	37	39	40	41	32	44	45	50
Alloy													
All-steel heat exchanger	100	100	100	100	100	100	100	100	100	100	100	100	100
Tube sheets and baffles													
Naval rolled brass	14	17	19	21	22	22	22	22	22	23	24	24	25
Monel	24	31	35	37	39	39	40	40	41	41	41	41	42
1¼ Cr, ½ Mo	6	7	7	7	8	8	8	8	9	10	10	10	11
4-6 Cr, ½ Mo	19	22	24	25	26	26	26	25	25	25	26	26	26
11-13 Cr (stainless 410)	21	24	26	27	27	27	27	27	27	27	27	27	28
Stainless 304	22	27	29	30	31	31	31	31	30	30	30	31	31
Shell and shell cover													
Monel	45	48	51	52	53	52	52	51	49	47	45	44	44
1¼ Cr, ½ Mo	20	22	24	25	25	25	24	22	20	19	18	17	17
4-6 Cr, ½ Mo	28	31	33	35	35	35	34	32	30	28	27	26	26
11-13 Cr (stainless 410)	29	33	35	36	36	36	35	34	32	30	29	27	27
Stainless 304	32	34	36	37	38	37	37	35	33	31	30	29	28
Channel and floating-head cover													
Monel	40	42	42	43	42	41	40	37	34	32	31	40	30
1¼ Cr, ½ Mo	23	24	24	25	24	24	23	22	21	21	21	20	20
4-6 Cr, ½ Mo	36	37	38	38	37	36	34	31	29	27	26	25	24
11-13 Cr (stainless 410)	37	38	39	39	38	37	35	32	30	28	27	26	25
Stainless 304	37	39	39	39	38	37	36	33	31	29	28	26	26
Surface													
Surface, ft ² , internal floating head, ¾-in OD by 1-in square pitch, 16 ft 0-in, tube‡	251	302	438	565	726	890	1040	1470	1820	2270	2740	3220	3700
1-in OD by 1¼-in square pitch, 16-ft 0-in tube§	218	252	352	470	620	755	876	1260	1560	1860	2360	2770	3200
Weight, lb, internal floating head, 1-in OD, 14 BWG tube	2750	3150	4200	5300	6600	7800	9400	11,500	14,300	17,600	20,500	24,000	29,000

*Modified from E. N. Sieder and G. H. Elliot, *Pet. Refiner*, **39**(5), 223 (1960).

†Total extra is 0.7 × pressure extra on shell side plus 0.3 × pressure extra on tube side.

‡Fixed-tube-sheet construction with ¾-in OD tube on 1½-in triangular pitch provides 36 percent more surface.

§Fixed-tube-sheet construction with 1-in OD tube on 1¼-in triangular pitch provides 18 percent more surface.

¶For an all-steel heat exchanger with mixed design pressures the total extra for pressure is 0.7 × pressure extra on shell side plus 0.3 × pressure extra tube side.

For an exchanger with alloy parts and a design pressure of 150 lbf/in², the alloy extras are added. For shell and shell cover the combined alloy-pressure extra is the alloy extra times the shell-side pressure extra/100. For channel and floating-head cover the combined alloy-pressure extra is the alloy extra times the tube-side pressure extra/100. For tube sheets and baffles the combined alloy-pressure extra is the alloy extra times the higher-pressure extra times 0.9/100. (The 0.9 factor is included since baffle thickness does not increase because of pressure.)

NOTE: To convert pounds-force per square inch to kilopascals, multiply by 6.895; to convert square feet to square meters, multiply by 0.0929; and to convert inches to millimeters, multiply by 25.4.

Cost data for shell-and-tube exchangers from 15 sources were correlated and found to be consistent when scaled by the Marshall and Swift index [Woods et al., *Can. J. Chem. Eng.*, **54**, 469-489 (December 1976)].

Costs of shell-and-tube heat exchangers can be estimated from Fig. 11-41 and Tables 11-14 and 11-15. These 1960 costs should be updated by use of the Marshall and Swift Index, which appears in each issue of *Chemical Engineering*. Note that during periods of high and low demand for heat exchangers the prices in the marketplace may vary significantly from those determined by this method.

Small heat exchangers and exchangers bought in small quantities are likely to be more costly than indicated.

Standard heat exchangers (which are in some instances off-the-shelf items) are available in sizes ranging from 1.9 to 37 m² (20 to 400 ft²) at costs lower than for custom-built units. Steel costs are approximately one-half, admiralty tube-side costs are two-thirds, and stainless costs are three-fourths of those for equivalent custom-built exchangers.

Kettle-type-reboiler costs are 15 to 25 percent greater than for equivalent internal-floating-head or U-tube exchangers. The higher extra is applicable with relatively large kettle-to-port-diameter ratios

and with increased internals (e.g., vapor-liquid separators, foam breakers, sight glasses).

To estimate exchanger costs for varying construction details and alloys, first determine the base cost of a similar heat exchanger of basic construction (carbon steel, Class R, 150 lbf/in²) from Fig. 11-41. From Table 11-14, select appropriate extras for higher pressure rating and for alloy construction of tube sheets and baffles, shell and shell cover, and channel and floating-head cover. Compute these extras in accordance with the notes below the table. For tubes other than welded carbon steel, compute the extra by multiplying the exchanger surface by the appropriate cost per square foot from Table 11-15.

When points for 20-ft-long tubes do not appear in Fig. 11-41, use 0.95 times the cost of the equivalent 16-ft-long exchanger. Length variation of steel heat exchangers affects costs by approximately \$1 per square foot. Shell diameters for a given surface are approximately equal for U-tube and floating-head construction.

Low-fin tubes (1/16-in-high fins) provide 2.5 times the surface per lineal foot. Surface required should be divided by 2.5; then use Fig. 11-41 to determine basic cost of the heat exchanger. Actual surface times extra costs (from Table 11-15) should then be added to determine cost of fin-tube exchanger.

TABLE 11-15 Base Quantity Extra Cost for Tube Gauge and Alloy
Dollars per square foot

	¾-in OD tubes			1-in OD tubes		
	16 BWG	14 BWG	12 BWG	16 BWG	14 BWG	12 BWG
Carbon steel	0	0.02	0.06	0	0.01	0.07
Admiralty	0.78	1.20	1.81	0.94	1.39	2.03
(T-11) 1¼ Cr, ½ Mo	1.01	1.04	1.11	0.79	0.82	0.95
(T-5) 4-6 Cr	1.61	1.65	1.74	1.28	1.32	1.48
Stainless 410 welded	2.62	3.16	4.12	2.40	2.89	3.96
Stainless 410 seamless	3.10	3.58	4.63	2.84	3.31	4.47
Stainless 304 welded	2.50	3.05	3.99	2.32	2.83	3.88
Stainless 304 seamless	3.86	4.43	5.69	3.53	4.08	5.46
Stainless 316 welded	3.40	4.17	5.41	3.25	3.99	5.36
Stainless 316 seamless	7.02	7.95	10.01	6.37	7.27	9.53
90-10 cupronickel	1.33	1.89	2.67	1.50	2.09	2.90
Monel	4.25	5.22	6.68	4.01	4.97	6.47
Low fin						
Carbon steel	0.22	0.23		0.18	0.19	
Admiralty	0.58	0.75		0.70	0.87	
90-10 cupronickel	0.72	0.96		0.86	1.06	

NOTE: To convert inches to millimeters, multiply by 25.4.

HAIRPIN/DOUBLE-PIPE HEAT EXCHANGERS

PRINCIPLES OF CONSTRUCTION

Hairpin heat exchangers (often also referred to as “double pipes”) are characterized by a construction form which imparts a U-shaped appearance to the heat exchanger. In its classical sense, the term *double pipe* refers to a heat exchanger consisting of a pipe within a pipe, usually of a straight-leg construction with no bends. However, due to the need for removable bundle construction and the ability to handle differential thermal expansion while avoiding the use of expansion joints (often the weak point of the exchanger), the current U-shaped configuration has become the standard in the industry (Fig. 11-42). A further departure from the classical definition comes when more than one pipe or tube is used to make a tube bundle, complete with tubesheets and tube supports similar to the TEMA style exchanger.

Hairpin heat exchangers consist of two shell assemblies housing a common set of tubes and interconnected by a return-bend cover referred to as the *bonnet*. The shell is supported by means of bracket assemblies designed to cradle both shells simultaneously. These brackets are configured to permit the modular assembly of many hairpin sections into an exchanger bank for inexpensive future-expansion capability and for providing the very long thermal lengths demanded by special process applications.

The bracket construction permits support of the exchanger without fixing the supports to the shell. This provides for thermal movement of the shells within the brackets and prevents the transfer of thermal stresses into the process piping. In special cases the brackets may be welded to the shell. However, this is usually avoided due to the resulting loss of flexibility in field installation and equipment reuse at other sites and an increase in piping stresses.

The hairpin heat exchanger, unlike the removable bundle TEMA styles, is designed for bundle insertion and removal from the return end rather than the tubesheet end. This is accomplished by means of removable split rings which slide into grooves machined around the outside of each tubesheet and lock the tubesheets to the external closure flanges. This provides a distinct advantage in maintenance since bundle removal

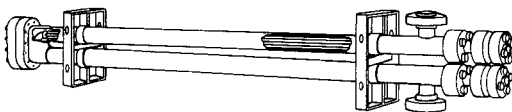


FIG. 11-42 Double-pipe-exchanger section with longitudinal fins. (Brown Fin-tube Co.)

takes place at the exchanger end furthest from the plant process piping without disturbing any gasketed joints of this piping.

FINNED DOUBLE PIPES

The design of the classical single-tube double-pipe heat exchanger is an exercise in pure longitudinal flow with the shellside and tubeside coefficients differing primarily due to variations in flow areas. Adding longitudinal fins gives the more common double-pipe configuration (Table 11-16). Increasing the number of tubes yields the *multitube* hairpin.

MULTITUBE HAIRPINS

For years, the slightly higher mechanical-design complexity of the hairpin heat exchanger relegated it to only the smallest process requirements with shell sizes not exceeding 100 mm. In the early 1970s the maximum available sizes were increased to between 300 and 400 mm depending upon the manufacturer. At the present time, due to recent advances in design technology, hairpin exchangers are routinely produced in shell sizes between 50 (2 in) and 800 mm (30 in) for a wide range of pressures and temperatures and have been made in larger sizes as well. Table 11-17 gives common hairpin tube counts and areas for 19 mm (¾ in) O.D. tubes arranged on a 24 mm (1¼ in) triangular tube layout.

The hairpin width and the centerline distance of the two legs (shells) of the hairpin heat exchanger are limited by the outside diameter of the closure flanges at the tubesheets. This diameter, in turn, is a function of the design pressures. As a general rule, for low-to-moderate design pressures (less than 15 bar), the center-to-center distance is approximately

TABLE 11-16 Double-Pipe Hairpin Section Data

Shell pipe O.D.		Inner pipe O.D.		Fin height		Fin count	Surface-area-per-unit length	
mm	in	mm	in	mm	in	(max)	sq m/m	sq ft/ft
60.33	2.375	25.4	1.000	12.7	0.50	24	0.692	2.27
88.9	3.500	48.26	1.900	12.7	0.50	36	1.07	3.51
114.3	4.500	48.26	1.900	25.4	1.00	36	1.98	6.51
114.3	4.500	60.33	2.375	19.05	0.75	40	1.72	5.63
114.3	4.500	73.03	2.875	12.70	0.50	48	1.45	4.76
141.3	5.563	88.9	3.500	17.46	0.6875	56	2.24	7.34
168.3	6.625	114.3	4.500	17.46	0.6875	72	2.88	9.44

TABLE 11-17 Multitube Hairpin Section Data

Size	Shell O.D.		Shell thickness		Tube count	Surface area for 6.1 m (20 ft.) nominal length	
	mm	in	mm	in		19 mm	sq m
03-MT	88.9	3.500	5.49	0.216	5	3.75	40.4
04-MT	114.3	4.500	6.02	0.237	9	6.73	72.4
05-MT	141.3	5.563	6.55	0.258	14	10.5	113.2
06-MT	168.3	6.625	7.11	0.280	22	16.7	179.6
08-MT	219.1	8.625	8.18	0.322	42	32.0	344.3
10-MT	273.1	10.75	9.27	0.365	68	52.5	564.7
12-MT	323.9	12.75	9.53	0.375	109	84.7	912.1
14-MT	355.6	14.00	9.53	0.375	136	107.	1159.
16-MT	406.4	16.00	9.53	0.375	187	148.	1594.
18-MT	457.2	18.00	9.53	0.375	241	191.	2054.
20-MT	508.0	20.00	9.53	0.375	304	244.	2622.
22-MT	558.8	22.00	9.53	0.375	380	307.	3307.
24-MT	609.6	24.00	9.53	0.375	463	378.	4065.
26-MT	660.4	26.00	9.53	0.375	559	453.	4879.
28-MT	711.2	28.00	9.53	0.375	649	529.	5698.
30-MT	762.0	30.00	11.11	0.4375	752	630.	6776.

1.5 to 1.8 times the shell outside diameter, with this ratio decreasing slightly for the larger sizes.

One interesting consequence of this fact is the inability to construct a hairpin tube bundle having the smallest radius bends common to a conventional U-tube, TEMA shell, and tube bundle. In fact, in the larger hairpin sizes the tubes might be better described as curved rather than bent. The smallest U-bend diameters are greater than the outside diameter of shells less than 300 mm in size. The U-bend diameters are greater than 300 mm in larger shells. As a general rule, mechanical tube cleaning around the radius of a U-bend may be accomplished with a flexible shaft-cleaning tool for bend diameters greater than ten times the tube's inside diameter. This permits the tool to pass around the curve of the tube bend without binding.

In all of these configurations, maintaining longitudinal flow on both the shellside and tubeside allows the decision for placement of a fluid

stream on either one side or the other to be based upon design efficiency (mass flow rates, fluid properties, pressure drops, and velocities) and not because there is any greater tendency to foul on one side than the other. Experience has shown that, in cases where fouling is influenced by flow velocity, overall fouling in tube bundles is less in properly designed longitudinal flow bundles where areas of low velocity can be avoided without flow-induced tube vibration.

This same freedom of stream choice is not as readily applied when a segmental baffle is used. In those designs, the baffle's creation of low velocities and stagnant flow areas on the outside of the bundle can result in increased shellside fouling at various locations of the bundle. The basis for choosing the stream side in those cases will be similar to the common shell and tube heat exchanger. At times a specific selection of stream side must be made regardless of tube-support mechanism in expectation of an unresolvable fouling problem. However, this is often the exception rather than the rule.

DESIGN APPLICATIONS

One benefit of the hairpin exchanger is its ability to handle high tube-side pressures at a lower cost than other removable-bundle exchangers. This is due in part to the lack of pass partitions at the tubesheets which complicate the gasketing design process. Present mechanical design technology has allowed the building of dependable, removable-bundle, hairpin multitubes at tubeside pressures of 825 bar (12,000 psi).

The best known use of the hairpin is its operation in true counter-current flow which yields the most efficient design for processes that have a close temperature approach or temperature cross. However, maintaining countercurrent flow in a tubular heat exchanger usually implies one tube pass for each shell pass. As recently as 30 years ago, the lack of inexpensive, multiple-tube pass capability often diluted the advantages gained from countercurrent flow.

The early attempts to solve this problem led to investigations into the area of heat transfer augmentation. This familiarity with augmentation techniques inevitably led to improvements in the efficiency and capacity of the small heat exchangers. The result has been the application of the hairpin heat exchanger to the solution of unique process problems, such as dependable, once-through, convective boilers offering high-exit qualities, especially in cases of process-temperature crosses.

AIR-COOLED HEAT EXCHANGERS

AIR-COOLED HEAT EXCHANGERS

Atmospheric air has been used for many years to cool and condense fluids in areas of water scarcity. During the 1960s the use of air-cooled heat exchangers grew rapidly in the United States and elsewhere. In Europe, where seasonal variations in ambient temperatures are relatively small, air-cooled exchangers are used for the greater part of process cooling. In some new plants all cooling is done with air. Increased use of air-cooled heat exchangers has resulted from lack of available water, significant increases in water costs, and concern for water pollution.

Air-cooled heat exchangers include a tube bundle, which generally has spiral-wound fins upon the tubes, and a fan, which moves air across the tubes and is provided with a driver. Electric motors are the most commonly used drivers; typical drive arrangements require a V belt or a direct right-angle gear. A plenum and structural supports are basic components. Louvers are often used:

A bay generally has two tube bundles installed in parallel. These may be in the same or different services. Each bay is usually served by two (or more) fans and is furnished with a structure, a plenum, and other attendant equipment.

The location of air-cooled heat exchangers must consider the large space requirements and the possible recirculation of heated air because of the effect of prevailing winds upon buildings, fired heaters, towers, various items of equipment, and other air-cooled exchangers.

Inlet air temperature at the exchanger can be significantly higher than the ambient air temperature at a nearby weather station. See *Air-Cooled Heat Exchangers for General Refinery Services*, API Standard 661, 2d ed., January 1978, for information on refinery-process air-cooled heat exchangers.

Forced and Induced Draft The forced-draft unit, which is illustrated in Fig. 11-43 pushes air across the finned tube surface. The fans are located below the tube bundles. The induced-draft design has the fan above the bundle, and the air is pulled across the finned tube surface. In theory, a primary advantage of the forced-draft unit is that less power is required. This is true when the air-temperature rise exceeds 30°C (54°F).

Air-cooled heat exchangers are generally arranged in banks with several exchangers installed side by side. The height of the bundle aboveground must be one-half of the tube length to produce an inlet velocity equal to the face velocity. This requirement applies both to ground-mounted exchangers and to those pipe-rack-installed exchangers which have a fire deck above the pipe rack.

The forced-draft design offers better accessibility to the fan for on-stream maintenance and fan-blade adjustment. The design also provides a fan and V-belt assembly, which are not exposed to the hot-air stream that exits from the unit. Structural costs are less, and mechanical life is longer.

Induced-draft design provides more even distribution of air across the bundle, since air velocity approaching the bundle is relatively low.

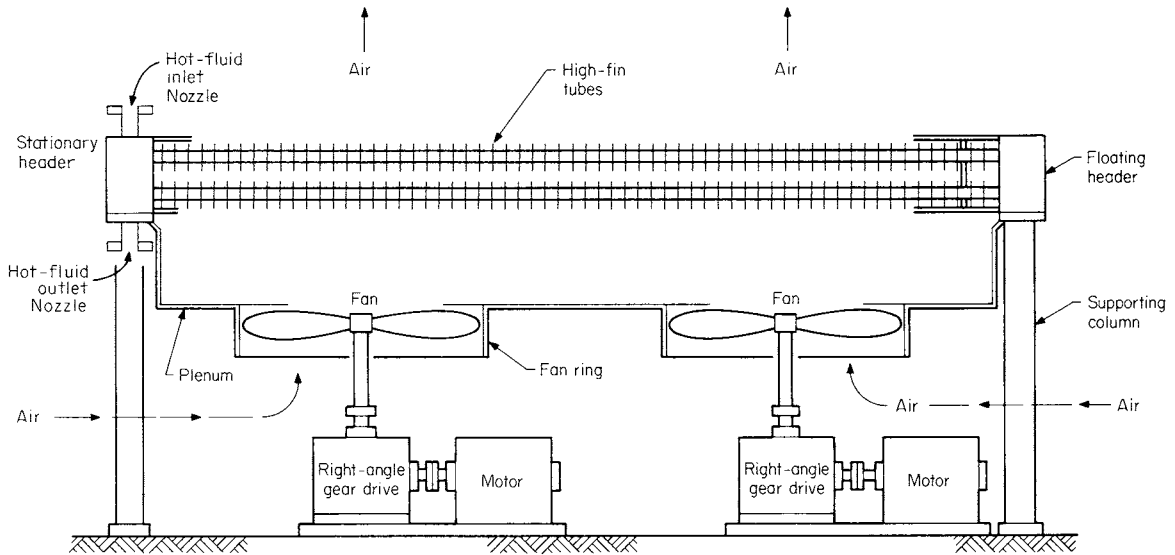


FIG. 11-43 Forced-draft air-cooled heat exchanger. [Chem. Eng., 114 (Mar. 27, 1978).]

This design is better suited for exchangers designed for a close approach of product outlet temperature to ambient-air temperature.

Induced-draft units are less likely to recirculate the hot exhaust air, since the exit air velocity is several times that of the forced-draft unit. Induced-draft design more readily permits the installation of the air-cooled equipment above other mechanical equipment such as pipe racks or shell-and-tube exchangers.

In a service in which sudden temperature change would cause upset and loss of product, the induced-draft unit gives more protection in that only a fraction of the surface (as compared with the forced-draft unit) is exposed to rainfall, sleet, or snow.

Tube Bundle The principal parts of the tube bundle are the finned tubes and the header. Most commonly used is the plug header, which is a welded box that is illustrated in Fig. 11-44. The finned tubes are described in a subsequent paragraph. The components of a tube bundle are identified in the figure.

The second most commonly used header is a cover-plate header. The cover plate is bolted to the top, bottom, and end plates of the

header. Removing the cover plate provides direct access to the tubes without the necessity of removing individual threaded plugs.

Other types of headers include the bonnet-type header, which is constructed similarly to the bonnet construction of shell-and-tube heat exchangers; manifold-type headers, which are made from pipe and have tubes welded into the manifold; and billet-type headers, made from a solid piece of material with machined channels for distributing the fluid. Serpentine-type tube bundles are sometimes used for very viscous fluids. A single continuous flow path through pipe is provided.

Tube bundles are designed to be rigid and self-contained and are mounted so that they expand independently of the supporting structure.

The face area of the tube bundle is its length times width. The net free area for air flow through the bundle is about 50 percent of the face area of the bundle.

The standard air face velocity (FV) is the velocity of standard air passing through the tube bundle and generally ranges from 1.5 to 3.6 m/s (300 to 700 ft/min).

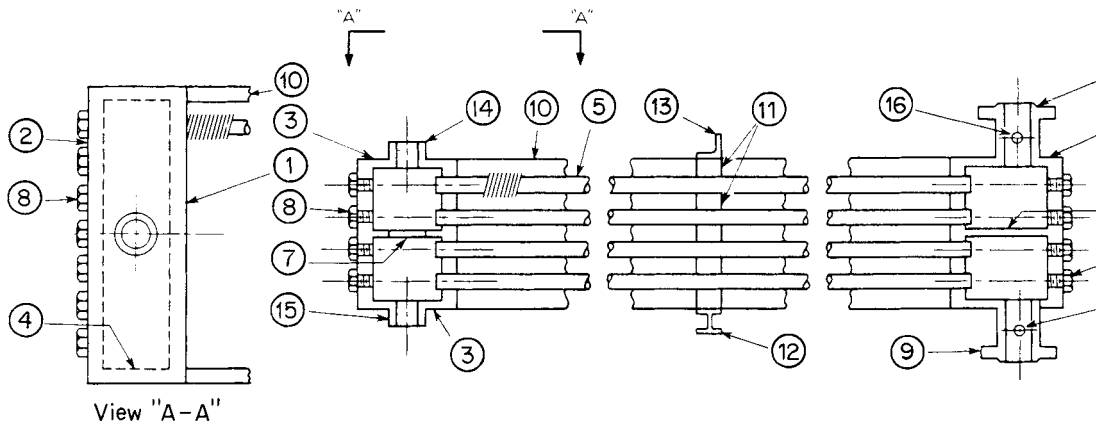


FIG. 11-44 Typical construction of a tube bundle with plug headers: (1) tube sheet; (2) plug sheet; (3) top and bottom plates; (4) end plate; (5) tube; (6) pass partition; (7) stiffener; (8) plug; (9) nozzle; (10) side frame; (11) tube spacer; (12) tube-support cross member; (13) tube keeper; (14) vent; (15) drain; (16) instrument connection. (API Standard 661.)

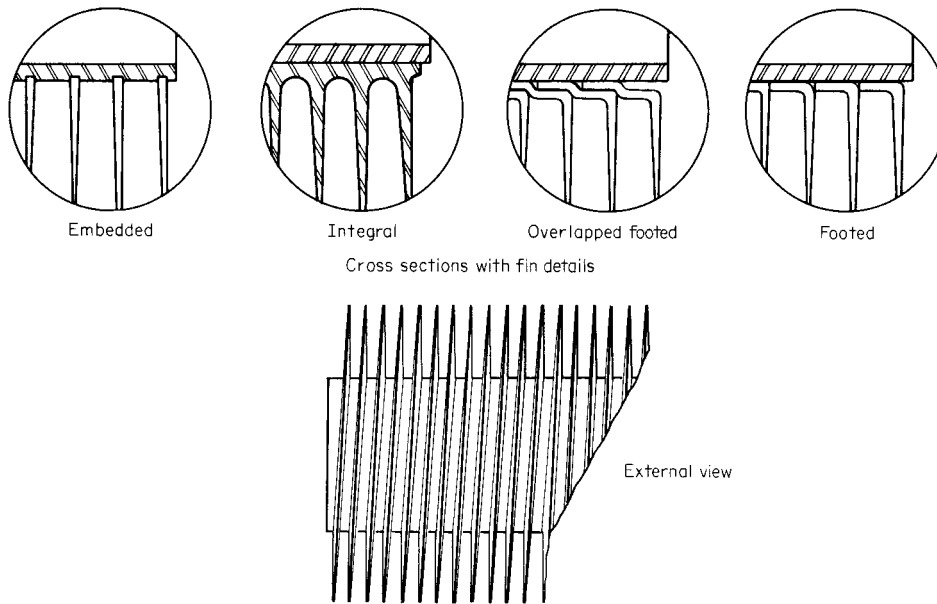


FIG. 11-45 Finned-tube construction.

tubing The 25.4-mm (1-in) outside-diameter tube is most commonly used. Fin heights vary from 12.7 to 15.9 mm (0.5 to 0.625 in), fin spacing from 3.6 to 2.3 mm (7 to 11 per linear inch), and tube triangular pitch from 50.8 to 63.5 mm (2.0 to 2.5 in). Ratio of extended surface to bare-tube outside surface varies from about 7 to 20. The 38-mm (1½-in) tube has been used for flue-gas and viscous-oil service. Tube size, fin heights, and fin spacing can be further varied.

Tube lengths vary and may be as great as 18.3 m (60 ft). When tube length exceeds 12.2 m (40 ft), three fans are generally installed in each bay. Frequently used tube lengths vary from 6.1 to 12.2 m (20 to 40 ft).

Finned-Tube Construction The following are descriptions of commonly used finned-tube constructions (Fig. 11-45).

1. *Embedded.* Rectangular-cross-section aluminum fin which is wrapped under tension and mechanically embedded in a groove 0.25 ± 0.05 mm (0.010 ± 0.002 in) deep, spirally cut into the outside surface of a tube.

2. *Integral (or extruded).* An aluminum outer tube from which fins have been formed by extrusion, mechanically bonded to an inner tube or liner.

3. *Overlapped footed.* L-shaped aluminum fin wrapped under tension over the outside surface of a tube, with the tube fully covered by the overlapped feet under and between the fins.

4. *Footed.* L-shaped aluminum fin wrapped under tension over the outside surface of a tube with the tube fully covered by the feet between the fins.

5. *Bonded.* Tubes on which fins are bonded to the outside surface by hot-dip galvanizing, brazing, or welding.

Typical metal design temperatures for these finned-tube constructions are 399°C (750°F) embedded, 288°C (550°F) integral, 232°C (450°F) overlapped footed, and 177°C (350°F) footed.

Tube ends are left bare to permit insertion of the tubes into appropriate holes in the headers or tube sheets. Tube ends are usually roller-expanded into these tube holes.

Fans Axial-flow fans are large-volume, low-pressure devices. Fan diameters are selected to give velocity pressures of approximately 2.5 mm (0.1 in) of water. Total fan efficiency (fan, driver, and transmission device) is about 75 percent, and fan drives usually have a minimum of 95 percent mechanical efficiency.

Usually fans are provided with four or six blades. Larger fans may have more blades. Fan diameter is generally slightly less than the width of the bay.

At the fan-tip speeds required for economical performance, a large amount of noise is produced. The predominant source of noise is vortex shedding at the trailing edge of the fan blade. Noise control of air-cooled exchangers is required by the Occupational Safety and Health Act (OSHA). API Standard 661 (*Air-Cooled Heat Exchangers for General Refinery Services*, 2d ed., January 1978) has the purchaser specifying sound-pressure-level (SPL) values per fan at a location designated by the purchaser and also specifying sound-power-level (PWL) values per fan. These are designated at the following octave-band-center frequencies: 63, 125, 250, 1000, 2000, 4000, 8000, and also the dBA value (the dBA is a weighted single-value sound-pressure level).

Reducing the fan-tip speed results in a straight-line reduction in air flow while the noise level decreases. The API Standard limits fan-tip speed to 61 m/s (12,000 ft/min) for typical constructions. Fan-design changes which reduce noise include increasing the number of fan blades, increasing the width of the fan blades, and reducing the clearance between fan tip and fan ring.

Both the quantity of air and the developed static pressure of fans in air-cooled heat exchangers are lower than indicated by fan manufacturers' test data, which are applicable to testing-facility tolerances and not to heat-exchanger constructions.

The axial-flow fan is inherently a device for moving a consistent volume of air when blade setting and speed of rotation are constant. Variation in the amount of air flow can be obtained by adjusting the blade angle of the fan and the speed of rotation. The blade angle can be either (1) permanently fixed, (2) hand-adjustable, or (3) automatically adjusted. Air delivery and power are a direct function of blade pitch angle.

Fan mounting should provide a minimum of one-half to three-fourths diameter between fan and ground on a forced-draft heat exchanger and one-half diameter between tubes and fan on an induced-draft cooler.

Fan blades can be made of aluminum, molded plastic, laminated plastic, carbon steel, stainless steel, and Monel.

Fan Drivers Electric motors or steam turbines are most commonly used. These connect with gears or V belts. (Gas engines connected through gears and hydraulic motors either direct-connected or connected through gears are in use. Fans may be driven by a prime mover such as a compressor with a V-belt takeoff from the flywheel to a jack shaft and then through a gear or V belt to the fan. Direct motor drive is generally limited to small-diameter fans.)

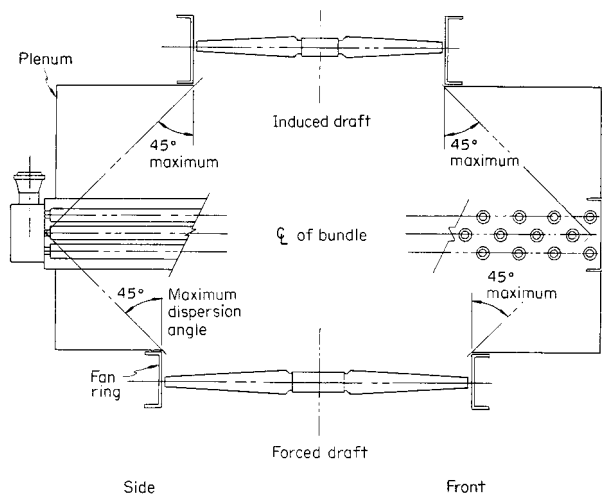


FIG. 11-46 Fan dispersion angle. (API Standard 661.)

V-belt drive assemblies are generally used with fans 3 m (10 ft) and less in diameter and motors of 22.4 kW (30 hp) and less.

Right-angle gear drive is preferred for fans over 3 m (10 ft) in diameter, for electric motors over 22.4 kW (30 hp), and with steam-turbine drives.

Fan Ring and Plenum Chambers The air must be distributed from the circular fan to the rectangular face of the tube bundle. The air velocity at the fan is between 3.8 and 10.2 m/s (750 and 2000 ft/in). The plenum-chamber depth (from fan to tube bundle) is dependent upon the fan dispersion angle (Fig. 11-46), which should have a maximum value of 45°.

The fan ring is made to commercial tolerances for the relatively large diameter fan. These tolerances are greater than those upon closely machined fan rings used for small-diameter laboratory-performance testing. Fan performance is directly affected by this increased clearance between the blade tip and the ring, and adequate provision in design must be made for the reduction in air flow. API Standard 661 requires that fan-tip clearance be a maximum of 0.5 percent of the fan diameter for diameters between 1.9 and 3.8 m (6.25 and 12.5 ft). Maximum clearance is 9.5 mm (3/8 in) for smaller fans and 19 mm (3/4 in) for larger fans.

The depth of the fan ring is critical. Worsham (ASME Pap. 59-PET-27, Petroleum Mechanical Engineering Conference, Houston, 1959) reports an increase in flow varying from 5 to 15 percent with the same power consumption when the depth of a fan ring was doubled. The percentage increase was proportional to the volume of air and static pressure against which the fan was operating.

When making a selection, the stall-out condition, which develops when the fan cannot produce any more air regardless of power input, should be considered.

Air-Flow Control Process operating requirements and weather conditions are considered in determining the method of controlling air flow. The most common methods include simple on-off control, on-off step control (in the case of multiple-driver units), two-speed-motor control, variable-speed drivers, controllable fan pitch, manually or automatically adjustable louvers, and air recirculation.

Winterization is the provision of design features, procedures, or systems for air-cooled heat exchangers to avoid process-fluid operating problems resulting from low-temperature inlet air. These include fluid freezing, pour point, wax formation, hydrate formation, laminar flow, and condensation at the dew point (which may initiate corrosion). Freezing points for some commonly encountered fluids in refinery service include: benzene, 5.6°C (42°F); *p*-xylene 15.5°C (55.9°F); cyclohexane, 6.6°C (43.8°F); phenol, 40.9°C (105.6°F); monoethanolamine, 10.3°C (50.5°F); and diethanolamine, 25.1°C (77.2°F). Water solutions

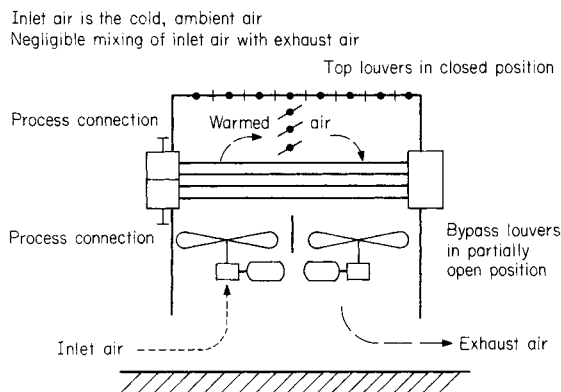


FIG. 11-47 Contained internal recirculation (with internal louvers). [*Hydrocarbon Process*, 59, 148-149 (October 1980).]

of these organic compounds are likely to freeze in air-cooled exchangers during winter service. Paraffinic and olefinic gases (C_1 through C_4) saturated with water vapor form hydrates when cooled. These hydrates are solid crystals which can collect and plug exchanger tubes.

Air-flow control in some services can prevent these problems. Cocurrent flow of air and process fluid during winter may be adequate to prevent problems. (Normal design has countercurrent flow of air and process fluid.) In some services when the hottest process fluid is in the bottom tubes, which are exposed to the lowest-temperature air, winterization problems may be eliminated.

Following are references which deal with problems in low-temperature environments: Brown and Benkley, "Heat Exchangers in Cold Service—A Contractor's View," *Chem. Eng. Prog.*, 70, 59-62 (July 1974); Franklin and Munn, "Problems with Heat Exchangers in Low Temperature Environments," *Chem. Eng. Prog.*, 70, 63-67 (July 1974); Newell, "Air-Cooled Heat Exchangers in Low Temperature Environments: A Critique," *Chem. Eng. Prog.*, 70, 86-91 (October 1974); Rubin, "Winterizing Air Cooled Heat Exchangers," *Hydrocarbon Process.*, 59, 147-149 (October 1980); Shipes, "Air-Cooled Heat Exchangers in Cold Climates," *Chem. Eng. Prog.*, 70, 53-58 (July 1974).

Air Recirculation Recirculation of air which has been heated as it crosses the tube bundle provides the best means of preventing operating problems due to low-temperature inlet air. Internal recirculation is the movement of air within a bay so that the heated air which has crossed the bundle is directed by a fan with reverse flow across another part of the bundle. Wind skirts and louvers are generally provided to minimize the entry of low-temperature air from the surroundings. Contained internal recirculation uses louvers within the bay to control the flow of warm air in the bay as illustrated in Fig. 11-47. Note that low-temperature inlet air has access to the tube bundle.

External recirculation is the movement of the heated air within the bay to an external duct, where this air mixes with inlet air, and the mixture serves as the cooling fluid within the bay. Inlet air does not have direct access to the tube bundle; an adequate mixing chamber is essential. Recirculation over the end of the exchanger is illustrated in Fig. 11-48. Over-the-side recirculation also is used. External recirculation systems maintain the desired low temperature of the air crossing the tube bundle.

Trim Coolers Conventional air-cooled heat exchangers can cool the process fluid to within 8.3°C (15°F) of the design dry-bulb temperature. When a lower process outlet temperature is required, a trim cooler is installed in series with the air-cooled heat exchanger. The water-cooled trim cooler can be designed for a 5.6 to 11.1°C (10 to 20°F) approach to the wet-bulb temperature (which in the United States is about 8.3°C (15°F) less than the dry-bulb temperature). In arid areas the difference between dry- and wet-bulb temperatures is much greater.

Humidification Chambers The air-cooled heat exchanger is provided with humidification chambers in which the air is cooled to a

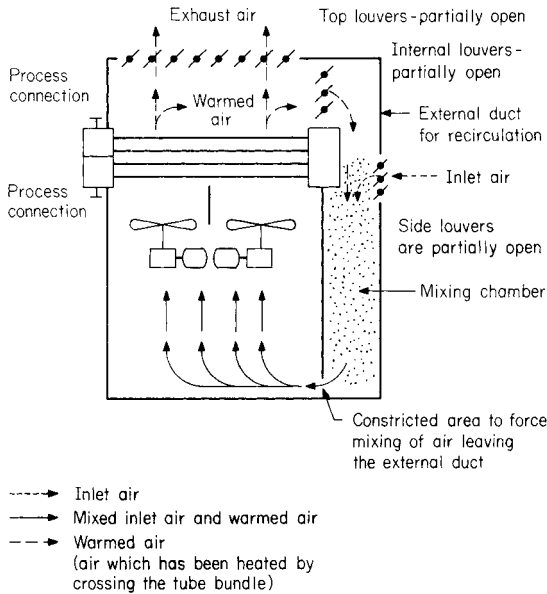


FIG. 11-48 External recirculation with adequate mixing chamber. [*Hydrocarbon Process*, 59, 148-149 (October 1980).]

close approach to the wet-bulb temperature before entering the finned-tube bundle of the heat exchanger.

Evaporative Cooling The process fluid can be cooled by using evaporative cooling with the sink temperature approaching the wet-bulb temperature.

Steam Condensers Air-cooled steam condensers have been fabricated with a single tube-side pass and several rows of tubes. The bottom row has a higher temperature difference than the top row, since the air has been heated as it crosses the rows of tubes. The bottom row condenses all the entering steam before the steam has traversed the length of the tube. The top row, with a lower temperature driving force, does not condense all the entering steam. At the exit header, uncondensed steam flows from the top row into the bottom row. Since noncondensable gases are always present in steam, these accumulate within the bottom row because steam is entering from both ends of the tube. Performance suffers.

Various solutions have been used. These include orifices to regulate the flow into each tube, a "blow-through steam" technique with a vent condenser, complete separation of each row of tubes, and inclined tubes.

Air-Cooled Overhead Condensers Air-cooled overhead condensers (AOC) have been designed and installed above distillation columns as integral parts of distillation systems. The condensers generally have inclined tubes, with air flow over the finned surfaces induced by a fan. Prevailing wind affects both structural design and performance.

AOC provide the additional advantages of reducing ground-space requirements and piping and pumping requirements and of providing smoother column operation.

The downflow condenser is used mainly for nonisothermal condensation. Vapors enter through a header at the top and flow downward. The reflux condenser is used for isothermal and small-temperature-change conditions. Vapors enter at the bottom of the tubes.

AOC usage first developed in Europe but became more prevalent in the United States during the 1960s. A state-of-the-art article was published by Dehne [*Chem. Eng. Prog.*, 64, 51 (July 1969)].

Air-Cooled Heat-Exchanger Costs The cost data that appear in Table 11-18 are unchanged from those published in the 1963 edition of this *Handbook*. In 1969 Guthrie [*Chem. Eng.*, 75, 114 (Mar. 24, 1969)] presented cost data for field-erected air-cooled

TABLE 11-18 Air-Cooled Heat-Exchanger Costs (1970)

Surface (bare tube), sq. ft.	500	1000	2000	3000	5000
Cost for 12-row-deep bundle, dollars/square foot	9.0	7.6	6.8	5.7	5.3
Factor for bundle depth:					
6 rows	1.07	1.07	1.07	1.12	1.12
4 rows	1.2	1.2	1.2	1.3	1.3
3 rows	1.25	1.25	1.25	1.5	1.5

Base: Bare-tube external surface 1 in. o.d. by 12 B.W.G. by 24 ft. 0 in. steel tube with 8 aluminum fins per inch 5/8-in. high. Steel headers. 150 lb./sq. in. design pressure. V-belt drive and explosion-proof motor. Bare-tube surface 0.262 sq. ft./ft. Fin-tube surface/bare-tube surface ratio is 16.9.

Factors: 20 ft. tube length 1.05
 30 ft. tube length 0.95
 18 B.W.G. admiralty tube 1.04
 16 B.W.G. admiralty tube 1.12

NOTE: To convert feet to meters, multiply by 0.3048; to convert square feet to square meters, multiply by 0.0929; and to convert inches to millimeters, multiply by 25.4.

exchangers. These costs are only 25 percent greater than those of Table 11-18 and include the costs of steel stairways, indirect subcontractor charges, and field-erection charges. Since minimal field costs would be this high (i.e., 25 percent of purchase price), the basic costs appear to be unchanged. (Guthrie indicated a cost band of plus or minus 25 percent.) Preliminary design and cost estimating of air-cooled heat exchangers have been discussed by J. E. Lerner [*Simplified Air Cooler Estimating*, *Hydrocarbon Process*, 52, 93-100 (February 1972)].

Design Considerations

1. *Design dry-bulb temperature.* The typically selected value is the temperature which is equalled or exceeded 2½ percent of the time during the warmest consecutive 4 months. Since air temperatures at industrial sites are frequently higher than those used for these weather-data reports, it is good practice to add 1 to 3°C (2 to 6°F) to the tabulated value.

2. *Air recirculation.* Prevailing winds and the locations and elevations of buildings, equipment, fired heaters, etc., require consideration. All air-cooled heat exchangers in a bank are of one type, i.e., all forced-draft or all induced-draft. Banks of air-cooled exchangers must be placed far enough apart to minimize air recirculation.

3. *Wintertime operations.* In addition to the previously discussed problems of winterization, provision must be made for heavy rain, strong winds, freezing of moisture upon the fins, etc.

4. *Noise.* Two identical fans have a noise level 3 dBa higher than one fan, while eight identical fans have a noise level 9 dBa higher than a single fan. Noise level at the plant site is affected by the exchanger position, the reflective surfaces near the fan, the hardness of these surfaces, and noise from adjacent equipment. The extensive use of air-cooled heat exchangers contributes significantly to plant noise level.

5. *Ground area and space requirements.* Comparisons of the overall space requirements for plants using air cooling versus water cooling are not consistent. Some air-cooled units are installed above other equipment—pipe racks, shell-and-tube exchangers, etc. Some plants avoid such installations because of safety considerations, as discussed later.

6. *Safety.* Leaks in air-cooled units are directly to the atmosphere and can cause fire hazards or toxic-fume hazards. However, the large air flow through an air-cooled exchanger greatly reduces any concentration of toxic fluids. Segal [*Pet. Refiner*, 38, 106 (April 1959)] reports that air-fin coolers "are not located over pumps, compressors, electrical switchgear, control houses and, in general, the amount of equipment such as drums and shell-and-tube exchangers located beneath them are minimized."

Pipe-rack-mounted air-cooled heat exchangers with flammable fluids generally have concrete fire decks which isolate the exchangers from the piping.

7. *Atmospheric corrosion.* Air-cooled heat exchangers should not be located where corrosive vapors and fumes from vent stacks will pass through them.

8. *Air-side fouling.* Air-side fouling is generally negligible.
9. *Process-side cleaning.* Either chemical or mechanical cleaning on the inside of the tubes can readily be accomplished.
10. *Process-side design pressure.* The high-pressure process fluid is always in the tubes. Tube-side headers are relatively small as compared with water-cooled units when the high pressure is generally on the shell side. High-pressure design of rectangular headers is complicated. The plug-type header is normally used for design gauge pressures to 13,790 kPa (2000 lbf/in²) and has been used to 62,000 kPa (9000 lbf/in²). The use of threaded plugs at these pressures creates problems. Removable cover plate headers are generally limited to gauge pressures of 2068 kPa (300 lbf/in²). The expensive billet-type header is used for high-pressure service.
11. *Bond resistance.* Vibration and thermal cycling affect the bond resistance of the various types of tubes in different manners and thus affect the amount of heat transfer through the fin tube.
12. *Approach temperature.* The approach temperature, which is the difference between the process-fluid outlet temperature and the design dry-bulb air temperature, has a practical minimum of 8 to 14°C (15 to 25°F). When a lower process-fluid outlet temperature is required, an air-humidification chamber can be provided to reduce the inlet air temperature toward the wet-bulb temperature. A 5.6°C (10°F) approach is feasible. Since typical summer wet-bulb design temperatures in the United States are 8.3°C (15°F) lower than dry-bulb temperatures, the outlet process-fluid temperature can be 3°C (5°F) below the dry-bulb temperature.

13. *Mean-temperature-difference (MTD) correction factor.* When the outlet temperatures of both fluids are identical, the MTD correction factor for a 1:2 shell-and-tube exchanger (one pass shell side, two or more passes tube side) is approximately 0.8. For a single-pass air-cooled heat exchanger the factor is 0.91. A two-pass exchanger has a factor of 0.96, while a three-pass exchanger has a factor of 0.99 when passes are arranged for counterflow.

14. *Maintenance cost.* Maintenance for air-cooled equipment as compared with shell-and-tube coolers (complete with cooling-tower costs) indicates that air-cooling maintenance costs are approximately 0.3 to 0.5 those for water-cooled equipment.

15. *Operating costs.* Power requirements for air-cooled heat exchangers can be lower than at the summer design condition provided that an adequate means of air-flow control is used. The annual power requirement for an exchanger is a function of the means of air-flow control, the exchanger service, the air-temperature rise, and the approach temperature.

When the mean annual temperature is 16.7°C (30°F) lower than the design dry-bulb temperature and when both fans in a bay have automatically controllable pitch of fan blades, annual power required has been found to be 22, 36, and 54 percent respectively of that needed at the design condition for three process services [Frank L. Rubin, "Power Requirements Are Lower for Air-Cooled Heat Exchangers with AV Fans," *Oil Gas J.*, 165-167 (Oct. 11, 1982)]. Alternatively, when fans have two-speed motors, these deliver one-half of the design flow of air at half speed and use only one-eighth of the power of the full-speed condition.

COMPACT AND NONTUBULAR HEAT EXCHANGERS

COMPACT HEAT EXCHANGERS

With equipment costs rising and limited available plot space, compact heat exchangers are gaining a larger portion of the heat exchange market. Numerous types use special enhancement techniques to achieve the required heat transfer in smaller plot areas and, in many cases, less initial investment. As with all items that afford a benefit there is a series of restrictions that limit the effectiveness or application of these special heat exchanger products. In most products discussed some of these considerations are presented, but a thorough review with reputable suppliers of these products is the only positive way to select a compact heat exchanger. The following guidelines will assist in qualifying one of these.

PLATE-AND-FRAME EXCHANGERS

There are two major types gasketed and welded-plate heat exchangers. Each shall be discussed individually.

GASKETED-PLATE EXCHANGERS (G. PHE)

Description This type is the fastest growing of the compact exchangers and the most recognized (see Fig. 11-49). A series of corrugated alloy material channel plates, bounded by elastomeric gaskets are hung off and guided by longitudinal carrying bars, then compressed by large-diameter tightening bolts between two pressure retaining frame plates (cover plates). The frame and channel plates have portholes which allow the process fluids to enter alternating flow passages (the space between two adjacent-channel plates). Gaskets around the periphery of the channel plate prevent leakage to the atmosphere and also prevent process fluids from coming in contact with the frame plates. No interfluid leakage is possible in the port area due to a dual-gasket seal.

The frame plates are typically epoxy-painted carbon-steel material and can be designed per most pressure vessel codes. Design limitations are in the Table 11-19. The channel plates are always an alloy material with 304SS as a minimum (see Table 11-19 for other materials).

Channel plates are typically 0.4 to 0.8 mm thick and have corrugation depths of 2 to 10 mm. Special Wide Gap (WG PHE) plates are available, in limited sizes, for slurry applications with depths of approximately 16 mm. The channel plates are compressed to achieve metal-to-metal contact for pressure-retaining integrity. These narrow gaps and high number of contact points which change fluid flow direction, combine to create a very high turbulence between the plates. This means high individual-heat-transfer coefficients (up to 14,200 W/m² °C), but also very high pressure drops per length as well. To compensate, the channel plate lengths are usually short, most under 2 and few over 3 meters in length. In general, the same pressure drops as conventional exchangers are used without loss of the enhanced heat transfer.

Expansion of the initial unit is easily performed in the field without special considerations. The original frame length typically has an additional capacity of 15-20 percent more channel plates (i.e., surface area). In fact, if a known future capacity is available during fabrication stages, a longer carrying bar could be installed, and later, increasing the surface area would be easily handled. When the expansion is needed, simply untighten the carrying bolts, pull back the frame plate, add the additional channel plates, and tighten the frame plate.

Applications Most PHE applications are liquid-liquid services but there are numerous steam heater and evaporator uses from their heritage in the food industry. Industrial users typically have chevron style channel plates while some food applications are washboard style.

Fine particulate slurries in concentrations up to 70 percent by weight are possible with standard channel spacings. Wide-gap units are used with larger particle sizes. Typical particle size should not exceed 75 percent of the *single* plate (not total channel) gap.

Close temperature approaches and tight temperature control possible with PHE's and the ability to sanitize the entire heat transfer surface easily were a major benefit in the food industry.

Multiple services in a single frame are possible.

Gasket selection is one of the most critical and limiting factors in PHE usage. Table 11-20 gives some guidelines for fluid compatibility. Even trace fluid components need to be considered. The higher the operating temperature and pressure, the shorter the anticipated gasket life. *Always* consult the supplier on gasket selection and obtain an estimated or guaranteed lifetime.

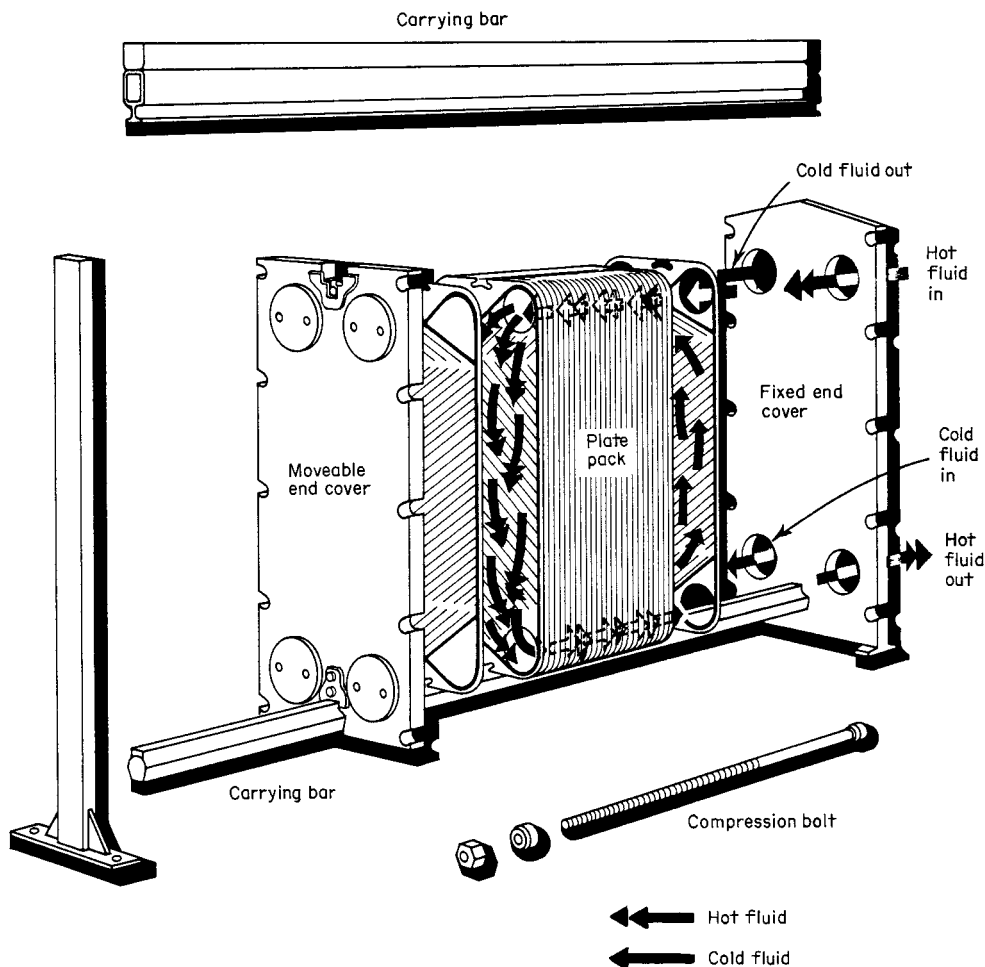


FIG. 11-49 Plate-and-frame heat exchanger. Hot fluid flows down between alternate plates, and cold fluid flows up between alternate plates. (Thermal Division, Alfa-Laval, Inc.)

The major applications are, but not limited to, as follows:

- Temperature cross applications (lean/rich solvent)
- Close approaches (fresh water/seawater)
- Viscous fluids (emulsions)
- Sterilized surface required (food, pharmaceutical)
- Polished surface required (latex, pharmaceutical)
- Future expansion required
- Space restrictions
- Barrier coolant services (closed-loop coolers)
- Slurry applications (TiO₂, Kaolin, precipitated calcium carbonate, and beet sugar raw juice)

Design Plate exchangers are becoming so commonplace that there is now an API 662 document available for the specification of these products. In addition, commercial computer programs are available from HTRI among others. Standard channel-plate designs, unique to each manufacturer, are developed with limited modifications of each plates' corrugation depths and included angles. Manufacturers combine their different style plates to custom-fit each service. Due to the possible combinations, it is impossible to present a way to exactly size PHEs. However, it is possible to estimate areas for new units and to predict performance of existing

units with different conditions (chevron-type channel plates are presented).

The fixed length and limited corrugation included angles on channel plates makes the NTU method of sizing practical. (Waterlike fluids are assumed for the following examples).

$$NTU = \frac{\Delta t \text{ of either side}}{LMTD} \tag{11-76}$$

Most plates have NTU values of 0.5 to 4.0, with 2.0 to 3.0 as the most common, (multipass shell and tube exchangers are typically less than 0.75). The more closely the fluid profile matches that of the channel plate, the smaller the required surface area. Attempting to increase the service NTU beyond the plate's NTU capability causes oversurfacing (inefficiency).

True sizing from scratch is impractical since a pressure balance on a channel-to-channel basis, from channel closest to inlet to furthest, must be achieved and when mixed plate angles are used; this is quite a challenge. Computer sizing is not just a benefit, it is a necessity for supplier's selection. Averaging methods are recommended to perform any sizing calculations.

From the APV heat-transfer handbook—*Design & Application of Paraflow-Plate Heat Exchangers* and J. Marriott's article, "Where and How To Use Plate Heat Exchangers," *Chemical Engineering*, April 5,

TABLE 11-19 Compact Exchanger Applications Guide

Design conditions	G. PHE	W. PHE	WG. PHE	BHE	DBL	MLT	STE	CP	SHE	THE
Design temperature °C	165	150	150	185	+500	+500	+500	450	+400	+500
Minimum metal temp °C	-30	-30	-30	-160	-160	-160	-160	-160	-160	-160
Design pressure MPa	2.5	2.5	0.7	3.1	+20	+20	+20	3.1	2.0	+20
Inspect for leakage	Yes	Partial	Yes	No	Yes	Yes	Yes	Partial	Yes	Yes
Mechanical cleaning	Yes	Yes/no	Yes	No	Yes	Yes	Yes/no	Yes	Yes	Yes
Chemical cleaning	Yes	Yes	Yes	Yes	Yes	Yes	Yes	Yes	Yes	Yes
Expansion capability	Yes	Yes	Yes	No	No	No	No	No	No	No
Repair	Yes	Yes/no	Yes	No	Yes	Yes	Partial	Partial	Partial	Yes
Temperature cross	Yes	Yes	Yes	Yes	Yes	Yes	Yes	Yes	Yes	No°
Surface area/unit m ²	1850	900	250	50	10	150	60	275	450	High
Holdup volume	Low	Low	Low	Low	Med	Med	Low	Low	Med	High

Materials	G. PHE	W. PHE	WG. PHE	BHE	DBL	MLT	STE	CP	SHE	THE
Mild steel	No	No	No	No	Yes	Yes	Yes	Yes	Yes	Yes
Stainless	Yes	Yes	Yes	Yes	Yes	Yes	Yes	Yes	Yes	Yes
Titanium	Yes	Yes	Yes	No	Yes	Yes	Yes	Yes	Yes	Yes
Hastalloy	Yes	Yes	No	No	Yes	Yes	Yes	Yes	Yes	Yes
Nickel	Yes	Yes	No	No	Yes	Yes	Yes	Yes	Yes	Yes
Alloy 20	Yes	Yes	No	No	Yes	Yes	Yes	Yes	Yes	Yes
Incoloy 825	Yes	Yes	No	No	Yes	Yes	Yes	Yes	Yes	Yes
Monel	Yes	Yes	No	No	Yes	Yes	Yes	Yes	Yes	Yes
Impervious graphite	Yes	No	No	No	No	No	No	No	No	Yes

Service	G. PHE	W. PHE	WG. PHE	BHE	DBL	MLT	STE	CP	SHE	THE
Clean fluids	A	A	A	A	A	A	A	A	A	A
Gasket incompatibility	D	A/D	D	A	A	A	A	A	A	A
Medium viscosity	A/B	A/B	A/B	B	A	A	A/B	A/B	A	A
High viscosity	A/B	A/B	A/B	D	A	A	A/B	A/B	A	A
Slurries & pulp (fine)	B/D	D	A/B	C	A	A/B	C	B	A	A/D
Slurries & pulp (coarse)	D	D	B	D	A	B/C	D	B	A	A/D
Refrigerants	D	A	D	A	A	A	B/C	A	A	A
Thermal fluids	D	A/B	D	A/B	A	A	C	A	A	A
Vent condensers	D	D	D	D	A/D	A	A	B/C	A	A
Process condenser	D	C	D	D	A/D	A	A	B/C	B	A
Vacuum reboil/cond	D	D	B	D	A/D	B	A	B/C	B	A/C
Evaporator	D	C	C	A	B	B	A	B/C	C	A
Tight temp control	A	A	A	A	A	A	A	B	A	C
High scaling	B	B	A	D	A	A/B	B/C	B	B	A/D

° Multipass
 Adapted from Alfa-Laval and Vicarb literature
 A—Very good C—Fair
 B—Good D—Poor

TABLE 11-20 Elastomer Selection Guide

	Uses	Avoid
Nitrile (NBR)	Oil resistant Fat resistant Food stuffs Mineral oil Water	Oxidants Acids Aromatics Alkalies Alcohols
Resin cured butyl (IIR)	Acids Lyes Strong alkalies Strong phosphoric acid Dilute mineral acids Ketones Amines Water	Fats and fatty acids Petroleum oils Chlorinated hydrocarbons Liquids with dissolved chlorine Mineral oil Oxygen rich demin. water Strong oxidants
Ethylene-propylene (EPDM)	Oxidizing agents Dilute acids Amines Water (Mostly any IIR fluid)	Oils Hot & conc. acids Very strong oxidants Fats & fatty acids Chlorinated hydrocarbons
Viton (FKM, FPM)	Water Petroleum oils Many inorganic acids (Most all NBR fluids)	Amines Ketones Esters Organic acids Liquid ammonia

1971, there are the following equations for plate heat transfer.

$$Nu = \frac{hDe}{k} = 0.28 * (Re)^{0.65} * (Pr)^{0.4} \quad (11-77)$$

where De = 2 × depth of single-plate corrugation

$$G = \frac{W}{Np * w * De} \quad (11-78)$$

Width of the plate (*w*) is measured from inside to inside of the channel gasket. If not available, use the tear-sheet drawing width and subtract two times the bolt diameter and subtract another 50 mm. For depth of corrugation ask supplier, or take the compressed plate pack dimension, divide by the number of plates and subtract the plate thickness from the result. The number of passages (*Np*) is the number of plates minus 1 then divided by 2.

Typical overall coefficients to start a rough sizing are as below. Use these in conjunction with the NTU calculated for the process. The closer the NTU matches the plate (say between 2.0 and 3.0), the higher the range of listed coefficients can be used. The narrower (smaller) the depth of corrugation, the higher the coefficient (and pressure drop), but also the lower the ability to carry through any particulate.

Water-water	5700–7400 W/(m ² °C)
Steam-water	5700–7400 W/(m ² °C)
Glycol/Glycol	2300–4000 W/(m ² °C)
Amine/Amine	3400–5000 W/(m ² °C)
Crude/Emulsion	400–1700 W/(m ² °C)

Pressure drops typically can match conventional tubular exchangers. Again from the APV handbook an average correlation is as follows:

$$\Delta P = \frac{2fG^2L}{g\rho De} \quad (11-79)$$

where $f = 2.5 (GDe/\mu)^{-0.3}$
 $g =$ gravitational constant

Fouling factors are typically $\frac{1}{10}$ of TEMA values or a percent oversurfacing of 10–20 percent is used (J. Kerner, "Sizing Plate Exchangers," *Chemical Engineering*, November 1993).

LMTD is calculated like a 1 pass-1 pass shell and tube with no F correction factor required in most cases.

Overall coefficients are determined like shell and tube exchangers; that is, sum all the resistances, then invert. The resistances include the hot-side coefficient, the cold-side coefficient, the fouling factor (usually only a total value not individual values per fluid side) and the wall resistance.

WELDED- AND BRAZED-PLATE EXCHANGERS (W. PHE & BHE)

The title of this group of plate exchangers has been used for a great variety of designs for various applications from normal gasketed-plate exchanger services to air-preheater services on fired heaters or boilers. The intent here is to discuss more traditional heat-exchanger designs, not the heat-recovery designs on fired equipment flue-gas streams. Many similarities exist between these products but the manufacturing techniques are quite different due to the normal operating conditions these units experience.

To overcome the gasket limitations, PHE manufacturers have developed welded-plate exchangers. There are numerous approaches to this solution: weld plate pairs together with the other fluid-side conventionally gasketed, weld up both sides but use a horizontal stacking of plates method of assembly, entirely braze the plates together with copper or nickel brazing, diffusion bond then pressure form plates and bond etched, passage plates.

Most methods of welded-plate manufacturing do not allow for inspection of the heat-transfer surface, mechanical cleaning of that surface, and have limited ability to repair or plug off damage channels. Consider these limitations when the fluid is heavily fouling, has solids, or in general the repair or plugging ability for severe services.

One of the previous types has an additional consideration of the brazing material to consider for fluid compatibility. The brazing compound entirely coats both fluid's heat-transfer surfaces.

The second type, a Compabloc (CP) from Alpha-Laval Thermal, has the advantage of removable cover plates, similar to air-cooled exchanger headers, to observe both fluids surface area. The fluids flow at 90° angles to each other on a horizontal plane. LMTD correction factors approach 1.0 for Compabloc just like the other welded and gasketed PHEs. Hydroblasting of Compabloc surfaces is also possible. The Compabloc has higher operating conditions than PHE's or W-PHE.

The performances and estimating methods of welded PHEs match those of gasketed PHEs in most cases, but normally the Compabloc, with larger depth of corrugations, can be lower in overall coefficient. Some extensions of the design operating conditions are possible with welded PHEs, most notably is that cryogenic applications are possible. Pressure vessel code acceptance is available on most units.

COMBINATION WELDED-PLATE EXCHANGERS

Plate exchangers are well known for their high efficiency but suffer from limitations on operating pressure. Several companies have rectified this limitation by placing the welded plate exchanger inside a pressure vessel to withstand the pressure. One popular application is the feed effluent exchange in a catalytic reforming plant for oil refineries. Large volumes of gases with some liquids require cross-exchange to feed a reactor system. Close temperature approaches and lower pressure drops are required. These combined units provide an economic alternative to shell-and-tube exchangers.

SPIRAL-PLATE EXCHANGERS (SHE)

Description The *spiral-plate heat exchanger* (SHE) may be one exchanger selected primarily on its virtues and not on its initial cost. SHEs offer high reliability and on-line performance in many severely fouling services such as slurries.

The SHE is formed by rolling two strips of plate, with welded-on spacer studs, upon each other into clock-spring shape. This forms two passages. Passages are sealed off on one end of the SHE by welding a bar to the plates; hot and cold fluid passages are sealed off on opposite ends of the SHE. A single rectangular flow passage is now formed for each fluid, producing very high shear rates compared to tubular designs. Removable covers are provided on each end to access and clean the entire heat transfer surface. Pure countercurrent flow is achieved and LMTD correction factor is essentially = 1.0.

Since there are no dead spaces in a SHE, the helical flow pattern combines to entrain any solids and create high turbulence creating a self-cleaning flow passage.

There are no thermal-expansion problems in spirals. Since the center of the unit is not fixed, it can torque to relieve stress.

The SHE can be expensive when only one fluid requires a high-alloy material. Since the heat-transfer plate contacts both fluids, it is required to be fabricated out of the higher alloy. SHEs can be fabricated out of any material that can be cold-worked and welded.

The channel spacings can be different on each side to match the flow rates and pressure drops of the process design. The spacer studs are also adjusted in their pitch to match the fluid characteristics.

As the coiled plate spirals outward, the plate thickness increases from a minimum of 2 mm to a maximum (as required by pressure) up to 10 mm. This means relatively thick material separates the two fluids compared to tubing of conventional exchangers. Pressure vessel code conformance is a common request.

Applications The most common applications that fit SHE are slurries. The rectangular channel provides high shear and turbulence to sweep the surface clear of blockage and causes no distribution problems associated with other exchanger types. A localized restriction causes an increase in local velocity which aids in keeping the unit free flowing. Only fibers that are long and stringy cause SHE to have a blockage it cannot clear itself.

As an additional antifoulant measure, SHEs have been coated with a phenolic lining. This provides some degree of corrosion protection as well, but this is not guaranteed due to pinholes in the lining process.

There are three types of SHE to fit different applications:

Type I is the spiral-spiral flow pattern. It is used for all heating and cooling services and can accommodate temperature crosses such as lean/rich services in one unit. The removable covers on each end allow access to one side at a time to perform maintenance on that fluid side. Never remove a cover with one side under pressure as the unit will telescope out like a collapsible cup.

Type II units are the condenser and reboiler designs. One side is spiral flow and the other side is in cross flow. These SHEs provide very stable designs for vacuum condensing and reboiling services. A SHE can be fitted with special mounting connections for reflux-type vent-condenser applications. The vertically mounted SHE directly attaches on the column or tank.

Type III units are a combination of the Type I and Type II where part is in spiral flow and part is in cross flow. This SHE can condense and subcool in a single unit.

The unique channel arrangement has been used to provide on-line cleaning, by switching fluid sides to clean the fouling (caused by the fluid that previously flowed there) off the surface. Phosphoric acid coolers use pond water for cooling and both sides foul; water, as you expect, and phosphoric acid deposit crystals. By reversing the flow sides, the water dissolves the acid crystals and the acid clears up the organic fouling. SHEs are also used as oleum coolers, sludge coolers/heaters, slop oil heaters, and in other services where multiple-flow-passage designs have not performed well.

Design A thorough article by P. E. Minton of Union Carbide called "Designing Spiral-Plate Heat Exchangers," appeared in *Chemical Engineering*, May 4, 1970. It covers the design in detail. Also an

article in *Chemical Engineering Progress* titled "Applications of Spiral Plate Heat Exchangers" by A. Hargis, A. Beckman, and J. Loicano appeared in July 1967, provides formulae for heat-transfer and pressure-drop calculations.

Spacings are from 6.35 to 31.75 mm (in 6.35 mm increments) with 9.5 mm the most common. Stud densities are 60 × 60 to 110 × 110 mm, the former the most common. The width (measured to the spiral flow passage), is from 150 to 2500 mm (in 150 mm increments). By varying the spacing and the width, separately for each fluid, velocities can be maintained at optimum rates to reduce fouling tendencies or utilize the allowable pressure drop most effectively. Diameters can reach 1500 mm. The total surface areas exceed 465 sqm. Materials that work harder are not suitable for spirals since hot-forming is not possible and heat treatment after forming is impractical.

$$Nu = \frac{HDe}{k} = 0.0315 (Re)^{0.8} (Pr)^{0.25} (\mu/\mu_w)^{0.17} \quad (11-80)$$

where $De = 2 \times \text{spacing}$
Flow area = width × spacing

$$\Delta P = \frac{LV^2 p}{1.705E03} * 1.45 \quad (1.45 \text{ for } 60 \times 60 \text{ mm studs}) \quad (11-81)$$

LMTD and overall coefficient are calculated like in PHE section above.

BRAZED-PLATE-FIN HEAT EXCHANGER

Brazed-aluminum-plate-fin heat exchangers (or core exchangers or cold boxes) as they are sometimes called, were first manufactured for the aircraft industry during World War II. In 1950, the first tonnage air-separation plant with these compact, lightweight, reversing heat exchangers began producing oxygen for a steel mill. Aluminum-plate-fin exchangers are used in the process and gas-separation industries, particularly for services below -45°C.

Core exchangers are made up of a stack of rectangular sheets of aluminum separated by a wavy, usually perforated, aluminum fin. Two ends are sealed off to form a passage (see Fig. 11-50). The layers have the wavy fins and sealed ends alternating at 90° to each. Aluminum half-pipe-type headers are attached to the open ends to route the fluids into the alternating passages. Fluids usually flow at this same 90° angle to each other. Variations in the fin height, number of passages, and the length and width of the prime sheet allow for the core exchanger to match the needs of the intended service.

Design conditions range in pressures from full vacuum to 96.5 bar g and in temperatures from -269°C to 200°C. This is accomplished meeting the quality standards of most pressure vessel codes.

Design and Application Brazed plate heat exchangers have two design standards that are available. One is ALPEMA, the Brazed Aluminum Plate-Fin Heat Exchanger Manufacturers' Association, and the other is the API 662 document for plate heat exchangers.

Applications are varied for this highly efficient, compact exchanger. Mainly it is seen in the cryogenic fluid services of air-separation plants, refrigeration trains like in ethylene plants, and in natural-gas processing plants. Fluids can be all vapor, liquid, condensing, or vaporizing. Multifluid exchangers and multiservice cores, that is one exchanger with up to 10 different fluids, are common for this type of product.

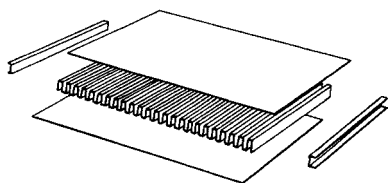


FIG. 11-50 Exploded view of a typical plate-fin arrangement. (Trane Co.)

Cold boxes are a group of cores assembled into a single structure or module, prepiped for minimum field connections. (Data obtained from ALTEC INTERNATIONAL, now Chart Industries. For detailed information refer to *GPSA Engineering Handbook* Section 9.)

PLATE-FIN TUBULAR EXCHANGERS (PFE)

Description These shell and tube exchangers are designed to use a group of tightly spaced plate fins to increase the shellside heat transfer performance as fins do on double-pipe exchangers. In this design, a series of very thin plates (fins), usually of copper or aluminum material, are punched to the same pattern as the tube layout, spaced very close together, and mechanically bonded to the tube. Fin spacing is 315–785 FPM (Fins Per Meter) with 550 FPM most common. The fin thicknesses are 0.24 mm for aluminum and 0.19 mm for copper. Surface-area ratios over bare prime-tube units can be 20:1 to 30:1. The cost of the additional plate-fin material, without a reduction in shell diameter in many cases, and increased fabrication has to be offset by the total reduction of plot space and prime tube-surface area. The more costly the prime tube or plot space cost, the better the pay-out for this design. A rectangular tube layout is normally used, *no tubes in the window* (NTIW). The window area (where no tubes are) of the plate-fins are cut out. This causes a larger shell diameter for a given tube count compared to conventional tubular units. A dome area on top and bottom of the inside of the shell has been created for the fluid to flow along the tube length. In order to exit the unit the fluid must flow across the plate-finned tube bundle with extremely low pressure loss. The units from the outside and from the tubeside appear like any conventional shell and tube exchanger.

Applications Two principal applications are rotating equipment oil coolers and compressor inter- and after-coolers. Although seemingly different applications, both rely on the shellside finning to enhance the heat transfer of low heat-transfer characteristic fluids, viscous oils, and gases. By nature of the fluids and their applications, both are near servicing. The tightly spaced fins would be a maintenance problem otherwise.

Design The economics usually work out in the favor of gas coolers when the centrifugal machine's flow rate reaches about 5000 scfm. The pressure loss can be kept to 7.0 kPa in most cases. When the ratio of A_{h1} to A_{h2} is 20:1, is another point to consider these plate-fin designs. Vibration is practically impossible with this design, and uses in reciprocating compressors are possible due to this.

Marine and hydraulic-oil coolers use these characteristics to enhance the coefficient of otherwise poorly performing fluids. The higher metallurgies in marine applications like 90/10 Cu-Ni afford the higher cost of plate-fin design to be offset by the less amount of alloy material being used. On small hydraulic coolers, these fins usually allow one to two size smaller coolers for the package and save skid space and initial cost.

Always check on metallurgy compatibility and cleanliness of the shellside fluid! (Data provided by Bos-Hatten and ITT-Standard.)

PRINTED-CIRCUIT HEAT EXCHANGERS

These are a variation of the welded or brazed plate heat exchangers but using a chemical etching process to form the flow channels and diffusion bonding technique to secure the plates together. These units have the high heat-transfer characteristics and extended operating conditions that welded or brazed units have, but the diffusion process makes the bond the same strength as that of the prime plate material. The chemical etching, similar to that used in printed circuitry, allows greater flexibility in flow channel patterns than any other heat exchanger. This type of heat exchanger is perhaps the most compact design of all due to the infinite variations in passage size, layout, and direction.

Headers are welded on the core block to direct the fluids into the appropriate passages. The all-metal design allows very high operating conditions for both temperature and pressure. The diffusion bonding provides a near-homogeneous material for fluids that are corrosive or require high purity.

These exchangers can handle gases, liquids, and two-phase applications. It has the greatest potential in cryogenic, refrigeration, gas

processing, and corrosive chemical applications. Other applications are possible with the exception of fluids containing solids: the narrow passages, like most plate exchangers, are conducive to plugging.

SPIRAL-TUBE EXCHANGERS (STE)

Description These exchangers are typically a series of stacked helical-coiled tubes connected to manifolds, then inserted into a casing or shell. They have many advantages like spiral-plate designs, such as avoiding differential expansion problems, acceleration effects of the helical flow increasing the heat transfer coefficient, and compactness of plot area. They are typically selected because of their economical design.

The most common form has both sides in helical flow patterns, pure countercurrent flow is followed and the LMTD correction factor approaches 1.0. Temperature crosses are possible in single units. Like the spiral-plate unit, different configurations are possible for special applications.

Tube material includes any that can be formed into a coil, but usually copper, copper alloys, and stainless steel are most common. The casing or shell material can be cast iron, cast steel, cast bronze, fabricated steel, stainless, and other high-alloy materials. Units are available with pressure vessel code conformance.

The data provided herein has been supplied by Graham Mfg. for their units called Heliflow.

Applications The common Heliflow applications are tank-vent condensers, sample coolers, pump-seal coolers, and steam-jet vacuum condensers. Instant water heaters, glycol/water services, and cryogenic vaporizers use the spiral tube's ability to reduce thermally induced stresses caused in these applications.

Many other applications are well suited for spiral tube units but many believe only small surface areas are possible with these units. Graham Mfg. states units are available to 60 m². Their ability to polish the surfaces, double-wall the coil, use finned coil, and insert static mixers, among others configurations in design, make them quite flexible. Tubeside design pressures can be up to 69000 kPa. A cross-flow design on the external surface of the coil is particularly useful in steam-jet ejector condensing service. These Heliflow units, can be made very cost-effective, especially in small units. The main differences, compared to spiral plate, is that the tubeside cannot be cleaned except chemically and that multiple flow passages make tubeside slurry applications (or fouling) impractical.

Design The fluid flow is similar to the spiral-plate exchangers, but through parallel tube passages. Graham Mfg. has a liquid-liquid sizing pamphlet available from their local distributor. An article by M.A. Noble, J.S. Kamlani, and J.J. McKetta "Heat Transfer in Spiral Coils", was published in *Petroleum Engineer*, April 1952 p. 723, discussing sizing techniques.

The tubeside fluid must be clean or at least chemically cleanable. With a large number of tubes in the coil, cleaning of inside surfaces is not totally reliable. Fluids that attack stressed materials such as chlorides should be reviewed as to proper coil-material selection. Fluids that contain solids can be a problem due to erosion of relatively thin coil materials unlike the thick plates in spiral-plate units and multiple, parallel, fluid passages compared to a single passage in spiral-plate units.

GRAPHITE HEAT EXCHANGERS

Impervious graphite exchangers now come in a variety of geometries to suit the particular requirements of the service. They include cubic block form, drilled cylinder block, shell and tube, and plate and frame.

Description Graphite is one of three crystalline forms of carbon. The other two are diamond and charcoal. Graphite has a hexagonal crystal structure, diamond is cubic, and charcoal is amorphous. Graphite is inert to most chemicals and resists corrosion attack. It is however porous and to be used, it must be impregnated with a resin sealer. Two main resins used are phenolic and PTFE with furan (one currently being phased out of production). Selection of resins include chemical compatibility, operating temperatures, and type of unit to be used. For proper selection, consult with a graphite supplier.

Shell-and-tube units in graphite were started by Karbate in 1939. The European market started using block design in the 1940s. Both technologies utilize the high thermal conductivity of the graphite material to compensate for the poor mechanical strength. The thicker materials needed to sustain pressure do not adversely impede the heat transfer. Maximum design pressures range from 0.35 to 1.0 kPa depending on type and size of exchanger. Design temperature is dependent on the fluids and resin selection, the maximum is 230 °C.

In all situations, the graphite heat transfer surface is contained within a metal structure or a shell (graphite lined on process side) to maintain the design pressure. For shell and tube units, the design is a packed floating tubesheet at both ends within a shell and channel. For stacked block design, the standardize blocks are glued together with special adhesives and compressed within a framework that includes manifold connections for each fluid. The cylindrical block unit is a combination of the above two with blocks glued together and surrounded by a pressure retaining shell. Pressure vessel code conformance of the units is possible due to the metallic components of these designs. Since welding of graphite is not possible, the selection and application of the adhesives used are critical to the proper operating of these units. Tube to tubesheet joints are glued since rolling of tubes into tubesheet is not possible. The packed channels and gasketed manifold connections are two areas of additional concern when selecting sealants for these units.

Applications and Design The major applications for these units are in the acid-related industries. Sulfuric, phosphoric, and hydrochloric acids require either very costly metals or impervious graphite. Usually graphite is the more cost-effective material to be used. Applications are increasing in the herbicide and pharmaceutical industries as new products with chlorine and fluorine compounds expand. Services are coolers, condensers, and evaporators, basically all services requiring this material. Types of units are shell-and-tube, block-type (circular and rectangular), and plate-and-frame-type exchangers. The design of the shell-and-tube units are the same as any but the design characteristics of tubes, spacing, and thickness are unique to the graphite design. The block and plate and frame also can be evaluated using techniques previously addressed but again, the unique characteristics of the graphite materials require input from a reputable supplier. Most designs will need the supplier to provide the most cost-effective design for the immediate and future operation of the exchangers. Also, consider the entire system design as some condensers and/or evaporators can be integral with their associated column.

CASCADE COOLERS

Cascade coolers are a series of standard pipes, usually manifolded in parallel, and connected in series by vertically or horizontally oriented U-bends. Process fluid flows inside the pipe entering at the bottom and water trickles from the top downward over the external pipe surface. The water is collected from a trough under the pipe sections, cooled, and recirculated over the pipe sections. The pipe material can be any of the metallic and also glass, impervious graphite, and ceramics. The tubeside coefficient and pressure drop is as in any circular duct. The water coefficient (with Re number less than 2100) is calculated from the following equation by W.H. McAdams, T.B. Drew, and G.S. Bays Jr., from the ASME trans. **62**, 627-631 (1940).

$$h = 218 * (G'/D_o)^{1/3} \text{ (W/m}^2 \text{ }^\circ\text{C)} \text{ (11-82)}$$

$$G' = m/(2L)$$

$$m = \text{water rate (kg/hr)}$$

$$L = \text{length of each pipe section (meter)}$$

$$D_o = \text{outside diameter of pipe (meter)}$$

LMTD corrections are per Fig. 11-4 *i* or *j* depending on U-bend orientation.

BAYONET-TUBE EXCHANGERS

This type of exchanger gets its name from its design which is similar to a bayonet sword and its associated scabbard or sheath. The bayonet tube is a smaller-diameter tube inserted into a larger-diameter tube

that has been capped at one end. The fluid flow is typically entering the inner tube, exiting, hitting the cap of the larger tube, and returning the opposite direction in the annular area. The design eliminates any thermal expansion problems. It also creates a unique nonfreeze-type tube-side for steam heating of cryogenic fluids, the inner tube steam keeps the annulus condensate from freezing against the cold shellside fluid. This design can be expensive on a surface-area basis due to the need of a double channel design and only the outer tube surface is used to transfer heat. LMTD calculations for nonisothermal fluid are quite extensive and those applications are far too few to attempt to define it. The heat transfer is like the annular calculation of a double-pipe unit. The shellside is a conventional-baffled shell-and-tube design.

ATMOSPHERIC SECTIONS

These consist of a rectangular bundle of tubes in similar fashion to air cooler bundles, placed just under the cooled water distribution section of a cooling tower. It, in essence, combines the exchanger and cooling tower into a single piece of equipment. This design is only practical for single-service cooler/condenser applications, and expansion capabilities are not provided. The process fluid flows inside the tubes and the cooling tower provides cool water that flows over the outside of the tube bundle. Water quality is critical for these applications to prevent fouling or corrosive attack on the outside of the tube surfaces and to prevent blockage of the spray nozzles. The initial and operating costs are lower than separate cooling tower and exchanger. Principal applications now are in the HVAC, Refrigeration and Industrial systems. Sometimes these are called "Wet Surface Air Coolers."

$$h = 1729 [(m^2/hr)/\text{face area } m^2]^{1/3} \quad (11-83)$$

NONMETALLIC HEAT EXCHANGERS

Another growing field is that of nonmetallic heat exchanger designs which typically are of the shell and tube or coiled-tubing type. The graphite units were previously discussed but numerous other materials are available. The materials include Teflon, PVDF, glass, ceramic, and others as the need arises.

When using these types of products, consider the following topics and discuss the application openly with experienced suppliers.

1. The tube-to-tubesheet joint, how is it made? Many use "O" rings to add another material to the selection process. Preference should be given to a fusing technique of similar material.
2. What size tube or flow passage is available? Small tubes plug unless filtration is installed. Size of filtering is needed from the supplier.
3. These materials are very sensitive to temperature and pressure. Thermal or pressure shocks must be avoided.
4. Thermal conductivity of these materials is very low and affects the overall coefficient. When several materials are compatible, explore all of them, as final cost is not always the same as raw material costs.

HEAT EXCHANGERS FOR SOLIDS

This section describes equipment for heat transfer to or from solids by the indirect mode. Such equipment is so constructed that the solids load (burden) is separated from the heat-carrier medium by a wall; the two phases are never in direct contact. Heat transfer is by conduction based on diffusion laws. Equipment in which the phases are in direct contact is covered in other sections of this *Handbook*, principally in Sec. 20.

Some of the devices covered here handle the solids burden in a static or laminar-flowing bed. Other devices can be considered as continuously agitated kettles in their heat-transfer aspect. For the latter, unit-area performance rates are higher.

Computational and graphical methods for predicting performance are given for both major heat-transfer aspects in Sec. 10. In solids heat processing with indirect equipment, the engineer should remember that the heat-transfer capability of the wall is many times that of the

PVDF HEAT EXCHANGERS

These shell-and-tube-type exchangers are similar to the Teflon designs but have some mechanical advantages over Teflon units. First the tubes are available in 9.5 mm sizes which reduces the chances of plugging that are found in Teflon units with unfiltered fluids. Second, the material has higher strength even at lower temperatures almost double. Larger units are possible with PVDF materials.

Tube to tubesheet joints, a weakness of most nonmetallic units, are fused by special techniques that do not severely affect the chemical suitability of the unit. Some nonmetallics use Teflon or "O" rings that add an extra consideration to material selection.

The shell is usually a steel design and, like the graphite units before, can obtain pressure-vessel certification.

CERAMIC HEAT EXCHANGERS

These include glass, silicon carbide, and similar variations. Even larger tubes are available in these materials, up to 19-mm diameter. They have high thermal conductivities and are usually very smooth surfaces to resist fouling. Very high material/fluid compatibility is seen for these products, not many fluids are excluded. Brittleness is a consideration of these materials and a complete discussion of the service with an experienced supplier is warranted. The major selection criteria to explore is the use of "O" rings and other associated joints at tubesheet. The shell is steel in most cases.

TEFLON HEAT EXCHANGERS

Teflon tube shell-and-tube heat exchangers (Ametek) made with tubes of chemically inert Teflon fluorocarbon resin are available. The tubes are 0.25-in OD by 0.20-in ID, 0.175-in OD by 0.160-in ID, or 0.125-in OD by 0.100-in ID (in \times 25.4 equal mm). The larger tubes are primarily used when pressure-drop limitations or particles reduce the effectiveness of smaller tubes. These heat exchangers generally operate at higher pressure drops than conventional units and are best suited for relatively clean fluids. Being chemically inert, the tubing has many applications in which other materials corrode. Fouling is negligible because of the antistick properties of Teflon.

The heat exchangers are of single-pass, countercurrent-flow design with removable tube bundles. Tube bundles are made of straight flexible tubes of Teflon joined together in integral honeycomb tube sheets. Baffles and O-ring gaskets are made of Teflon. Standard shell diameters are 102, 204, and 254 mm (4, 8, and 10 in). Tube counts range from 105 to 2000. Surface varies from 1.9 to 87 m² (20 to 940 ft²). Tube lengths vary from 0.9 to 4.9 m (3 to 16 ft). At 37.8°C (100°F) maximum operating gauge pressures are 690 kPa (100 lbf/in²) internal and 379 kPa (55 lbf/in²) external. At 149°C (300°F) the maximum pressures are 207 kPa (30 lbf/in²) internal and 124 kPa (18 lbf/in²) external.

solids burden. Hence the solids properties and bed geometry govern the rate of heat transfer. This is more fully explained earlier in this section. Only limited resultant (not predictive) and "experience" data are given here.

EQUIPMENT FOR SOLIDIFICATION

A frequent operation in the chemical field is the removal of heat from a material in a molten state to effect its conversion to the solid state. When the operation is carried on batchwise, it is termed casting, but when done continuously, it is termed flaking. Because of rapid heat transfer and temperature variations, jacketed types are limited to an initial melt temperature of 232°C (450°F). Higher temperatures [to 316°C (600°F)] require extreme care in jacket design and cooling-liquid flow pattern. Best performance and greatest capacity are

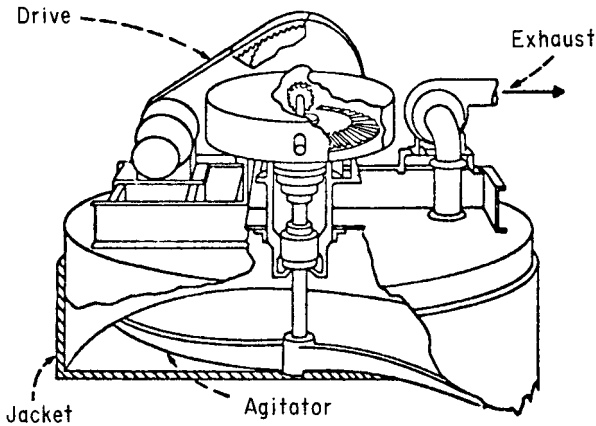


FIG. 11-51 Heat-transfer equipment for solidification (with agitation); agitated-pan type.

obtained by (1) holding precooling to the minimum and (2) optimizing the cake thickness. The latter cannot always be done from the heat-transfer standpoint, as size specifications for the end product may dictate thickness.

Table Type This is a simple flat metal sheet with slightly up-turned edges and jacketed on the underside for coolant flow. For many years this was the mainstay of food processors. Table types are still widely used when production is in small batches, when considerable batch-to-batch variation occurs, for pilot investigation, and when the cost of continuous devices is unjustifiable. Slab thicknesses are usually in the range of 13 to 25 mm ($\frac{1}{2}$ to 1 in). These units are homemade, with no standards available. Initial cost is low, but operating labor is high.

Agitated-Pan Type A natural evolution from the table type is a circular flat surface with jacketing on the underside for coolant flow and the added feature of a stirring means to sweep over the heat-transfer surface. This device is the agitated-pan type (Fig. 11-51). It is a batch-operation device. Because of its age and versatility it still serves a variety of heat-transfer operations for the chemical-process industries. While the most prevalent designation is agitated-pan dryer (in this mode, the burden is heated rather than cooled), considerable use is made of it for solidification applications. In this field, it is particularly suitable for processing burdens that change phase (1)

slowly, by "thickening," (2) over a wide temperature range, (3) to an amorphous solid form, or (4) to a soft semigummy form (versus the usual hard crystalline structure).

The stirring produces the end product in the desired divided-solids form. Hence, it is frequently termed a "granulator" or a "crystallizer." A variety of factory-made sizes in various materials of construction are available. Initial cost is modest, while operating cost is rather high (as is true of all batch devices), but the ability to process "gummy" burdens and/or simultaneously effect two unit operations often yields an economical application.

Vibratory Type This construction (Fig. 11-52) takes advantage of the burden's special needs and the characteristic of vibratory actuation. A flammable burden requires the use of an inert atmosphere over it and a suitable nonhazardous fluid in the jacket. The vibratory action permits construction of rigid self-cleaning chambers with simple flexible connections. When solidification has been completed and vibrators started, the intense vibratory motion of the whole deck structure (as a rigid unit) breaks free the friable cake [up to 76 mm (3 in) thick], shatters it into lumps, and conveys it up over the dam to discharge. Heat-transfer performance is good, with overall coefficient U of about $68 \text{ W}/(\text{m}^2 \cdot ^\circ\text{C})$ [$12 \text{ Btu}/(\text{h} \cdot \text{ft}^2 \cdot ^\circ\text{F})$] and values of heat flux q in the order of $11,670 \text{ W}/\text{m}^2$ [$3700 \text{ Btu}/(\text{h} \cdot \text{ft}^2)$]. Application of timing-cycle controls and a surge hopper for the discharge solids facilitates automatic operation of the caster and continuous operation of subsequent equipment.

Belt Types The patented metal-belt type (Fig. 11-53a), termed the "water-bed" conveyor, features a thin wall, a well-agitated fluid side for a thin water film (there are no rigid welded jackets to fail), a stainless-steel or Swedish-iron conveyor belt "floated" on the water with the aid of guides, no removal knife, and cleanliness. It is mostly used for cake thicknesses of 3.2 to 15.9 mm ($\frac{1}{8}$ to $\frac{3}{8}$ in) at speeds up to 15 m/min (50 ft/min), with 45.7-m (150-ft) pulley centers common. For 25- to 32-mm (1- to $1\frac{1}{4}$ -in) cake, another belt on top to give two-sided cooling is frequently used. Applications are in food operations for cooling to harden candies, cheeses, gelatins, margarines, gums, etc.; and in chemical operations for solidification of sulfur, greases, resins, soaps, waxes, chloride salts, and some insecticides. Heat transfer is good, with sulfur solidification showing values of $q = 5800 \text{ W}/\text{m}^2$ [$1850 \text{ Btu}/(\text{h} \cdot \text{ft}^2)$] and $U = 96 \text{ W}/(\text{m}^2 \cdot ^\circ\text{C})$ [$17 \text{ Btu}/(\text{h} \cdot \text{ft}^2 \cdot ^\circ\text{F})$] for a 7.9-mm ($\frac{5}{16}$ -in) cake.

The submerged metal belt (Fig. 11-53b) is a special version of the metal belt to meet the peculiar handling properties of pitch in its solidification process. Although adhesive to a dry metal wall, pitch will not stick to the submerged wetted belt or rubber edge strips. Submergence helps to offset the very poor thermal conductivity through two-sided heat transfer.

A fairly recent application of the water-cooled metal belt to solidification duty is shown in Fig. 11-54. The operation is termed pastillizing

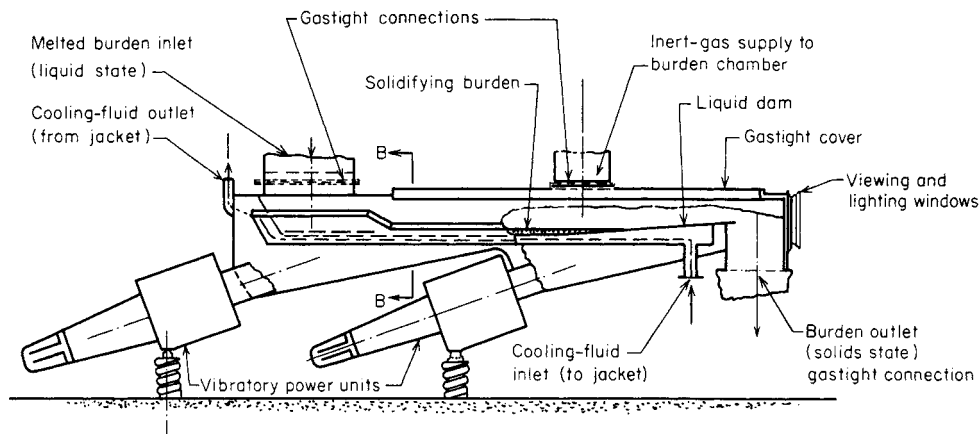


FIG. 11-52 Heat-transfer equipment for batch solidification; vibrating-conveyor type. (Courtesy of Jeffrey Mfg. Co.)

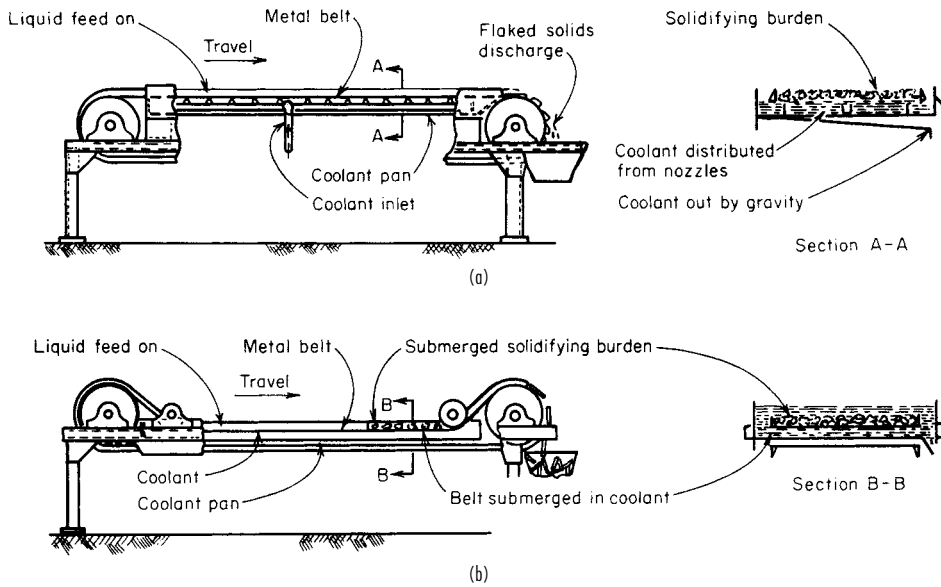


FIG. 11-53 Heat-transfer equipment for continuous solidification. (a) Cooled metal belt. (Courtesy of Sandvik, Inc.) (b) Submerged metal belt. (Courtesy of Sandvik, Inc.)

from the form of the solidified end product, termed "pastilles." The novel feature is a one-step operation from the molten liquid to a fairly uniformly sized and shaped product without intermediate operations on the solid phase.

Another development features a nonmetallic belt [*Plast. Des. Process.*, **13** (July 1968)]. When rapid heat transfer is the objective, a glass-fiber, Teflon-coated construction in a thickness as little as 0.08 mm (0.003 in) is selected for use. No performance data are available, but presumably the thin belt permits rapid heat transfer while taking advantage of the nonsticking property of Teflon. Another development [*Food Process. Mark.*, **69** (March 1969)] is extending the capability of belt solidification by providing use of subzero temperatures.

Rotating-Drum Type This type (Fig. 11-55a and b) is not an adaptation of a material-handling device (though volumetric material throughput is a first consideration) but is designed specifically for heat-transfer service. It is well engineered, established, and widely used. The twin-drum type (Fig. 11-55b) is best suited to thin [0.4- to 6-mm ($\frac{1}{64}$ to $\frac{1}{4}$ -in)] cake production. For temperatures to 149°C (300°F) the coolant water is piped in and siphoned out. Spray application of coolant water to the inside is employed for high-temperature work, permitting feed temperatures to at least 538°C (1000°F), or double those for jacketed equipment. Vaporizing refrigerants are readily applicable for very low temperature work.

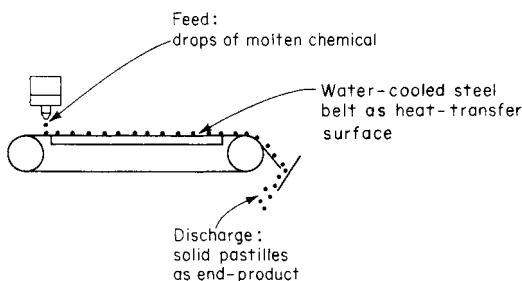


FIG. 11-54 Heat-transfer equipment for solidification; belt type for the operation of pastillization. (Courtesy of Sandvik, Inc.)

The burden must have a definite solidification temperature to assure proper pickup from the feed pan. This limitation can be overcome by side feeding through an auxiliary rotating spreader roll. Application limits are further extended by special feed devices for burdens having oxidation-sensitive and/or supercooling characteristics. The standard double-drum model turns downward, with adjustable roll spacing to control sheet thickness. The newer twin-drum model (Fig. 11-55b) turns upward and, though subject to variable cake thickness, handles viscous and indefinite solidification-temperature-point burden materials well.

Drums have been successfully applied to a wide range of chemical products, both inorganic and organic, pharmaceutical compounds, waxes, soaps, insecticides, food products to a limited extent (including lard cooling), and even flake-ice production. A novel application is that of using a water-cooled roll to pick up from a molten-lead bath and turn out a 1.2-m- (4-ft-) wide continuous sheet, weighing 4.9 kg/m² (1 lb/ft²), which is ideal for a sound barrier. This technique is more economical than other sheeting methods [*Mech. Eng.*, **631** (March 1968)].

Heat-transfer performance of drums, in terms of reported heat flux is: for an 80°C (176°F) melting-point wax, 7880 W/m² [2500 Btu/(h·ft²)]; for a 130°C (266°F) melting-point organic chemical, 20,000 W/m² [6500 Btu/(h·ft²)]; and for high- [318°C (604°F)] melting-point caustic soda (water-sprayed in drum), 95,000 to 125,000 W/m² [30,000 to 40,000 Btu/(h·ft²)], with overall coefficients of 340 to 450 W/(m²·°C) [60 to 80 Btu/(h·ft²·°F)]. An innovation that is claimed often to increase these performance values by as much as 300 percent is the addition of hoods to apply impinging streams of heated air to the solidifying and drying solids surface as the drums carry it upward [*Chem. Eng.*, **74**, 152 (June 19, 1967)]. Similar rotating-drum indirect heat-transfer equipment is also extensively used for drying duty on liquids and thick slurries of solids (see Sec. 20).

Rotating-Shelf Type The patented **Roto-shelf** type (Fig. 11-55c) features (1) a large heat-transfer surface provided over a small floor space and in a small building volume, (2) easy floor cleaning, (3) non-hazardous machinery, (4) stainless-steel surfaces, (5) good control range, and (6) substantial capacity by providing as needed 1 to 10 shelves operated in parallel. It is best suited for thick-cake production and burden materials having an indefinite solidification temperature. Solidification of liquid sulfur into 13- to 19-mm- ($\frac{1}{2}$ - to $\frac{3}{4}$ -in-) thick

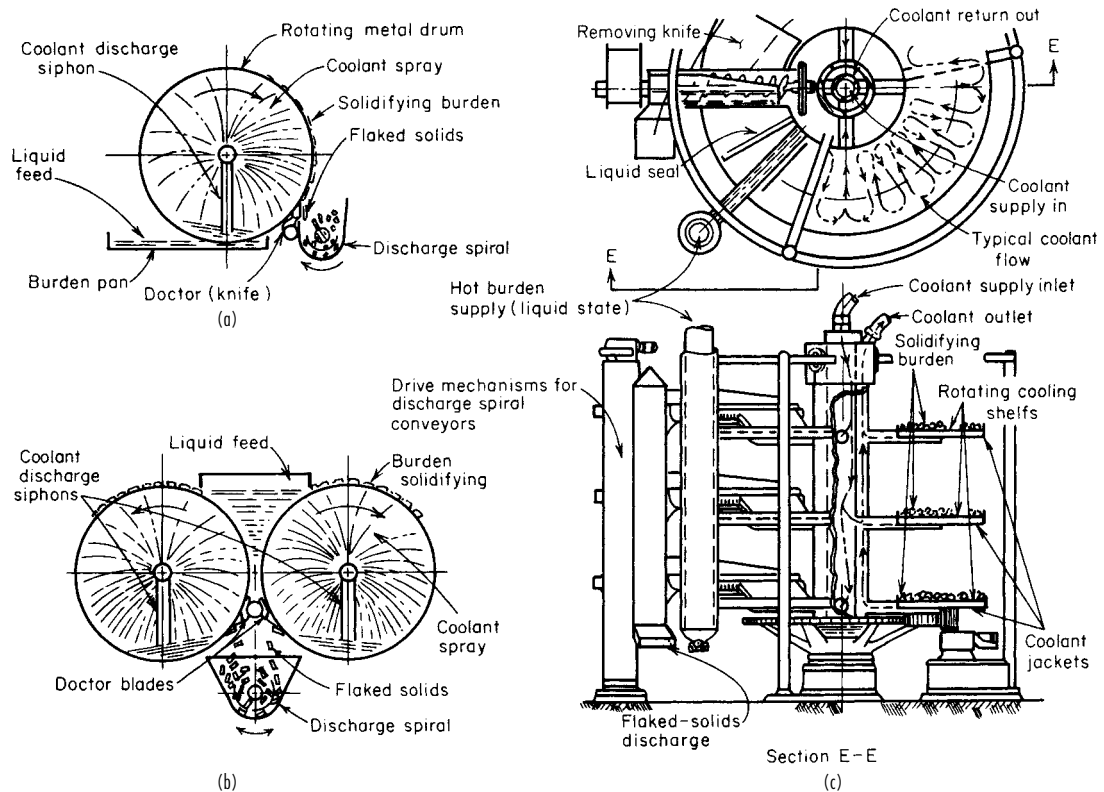


FIG. 11-55 Heat-transfer equipment for continuous solidification. (a) Single drum. (b) Twin drum. (c) Roto-shelf. (Courtesy of Buflovak Division, Blaw-Knox Food & Chemical Equipment, Inc.)

lumps is a successful application. Heat transfer, by liquid-coolant circulation through jackets, limits feed temperatures to 204°C (400°F). Heat-transfer rate, controlled by the thick cake rather than by equipment construction, should be equivalent to the belt type. Thermal performance is aided by applying water sprayed directly to the burden top to obtain two-sided cooling.

EQUIPMENT FOR FUSION OF SOLIDS

The thermal duty here is the opposite of solidification operations. The indirect heat-transfer equipment suitable for one operation is not suitable for the other because of the material-handling rather than the thermal aspects. Whether the temperature of transformation is a definite or a ranging one is of little importance in the selection of equipment for fusion. The burden is much agitated, but the beds are deep. Only fair overall coefficient values may be expected, although heat-flux values are good.

Horizontal-Tank Type This type (Fig. 11-56a) is used to transfer heat for melting or cooking dry powdered solids, rendering lard from meat-scrap solids, and drying divided solids. Heat-transfer coefficients are 17 to 85 W/(m²·°C) [3 to 15 Btu/(h·ft²·°F)] for drying and 28 to 140 W/(m²·°C) [5 to 25 Btu/(h·ft²·°F)] for vacuum and/or solvent recovery.

Vertical Agitated-Kettle Type Shown in Fig. 11-56b this type is used to cook, melt to the liquid state, and provide or remove reaction heat for solids that vary greatly in "body" during the process so that material handling is a real problem. The virtues are simplicity and 100 percent cleanability. These often outweigh the poor heat-transfer aspect. These devices are available from the small jacketed type illustrated to huge cast-iron direct-underfired bowls for calcining gypsum.

Temperature limits vary with construction; the simpler jackets allow temperatures to 371°C (700°F) (as with Dowtherm), which is not true of all jacketed equipment.

Mill Type Figure 11-56c shows one model of roll construction used. Note the ruggedness, as it is a *power device* as well as one for *indirect* heat transfer, employed to knead and heat a mixture of dry powdered-solid ingredients with the objective of reacting and reforming via fusion to a consolidated product. In this compounding operation, frictional heat generated by the kneading may require heat-flow reversal (by cooling). Heat-flow control and temperature-level considerations often predominate over heat-transfer performance. Power and mixing considerations, rather than heat transfer, govern. The two-roll mill shown is employed in compounding raw plastic, rubber, and rubberlike elastomer stocks. Multiple-roll mills less knives (termed calenders) are used for continuous sheet or film production in widths up to 2.3 m (7.7 ft). Similar equipment is employed in the chemical compounding of inks, dyes, paint pigments, and the like.

HEAT-TRANSFER EQUIPMENT FOR SHEETED SOLIDS

Cylinder Heat-Transfer Units Sometimes called "can" dryers or drying rolls, these devices are differentiated from drum dryers in that they are used for solids in flexible continuous-sheet form, whereas drum dryers are used for liquid or paste forms. The construction of the individual cylinders, or drums, is similar in most respects to that of drum dryers. Special designs are used to obtain uniform distribution of steam within large drums when uniform heating across the drum surface is critical.

A cylinder dryer may consist of one large cylindrical drum, such as the so-called Yankee dryer, but more often it comprises a number of

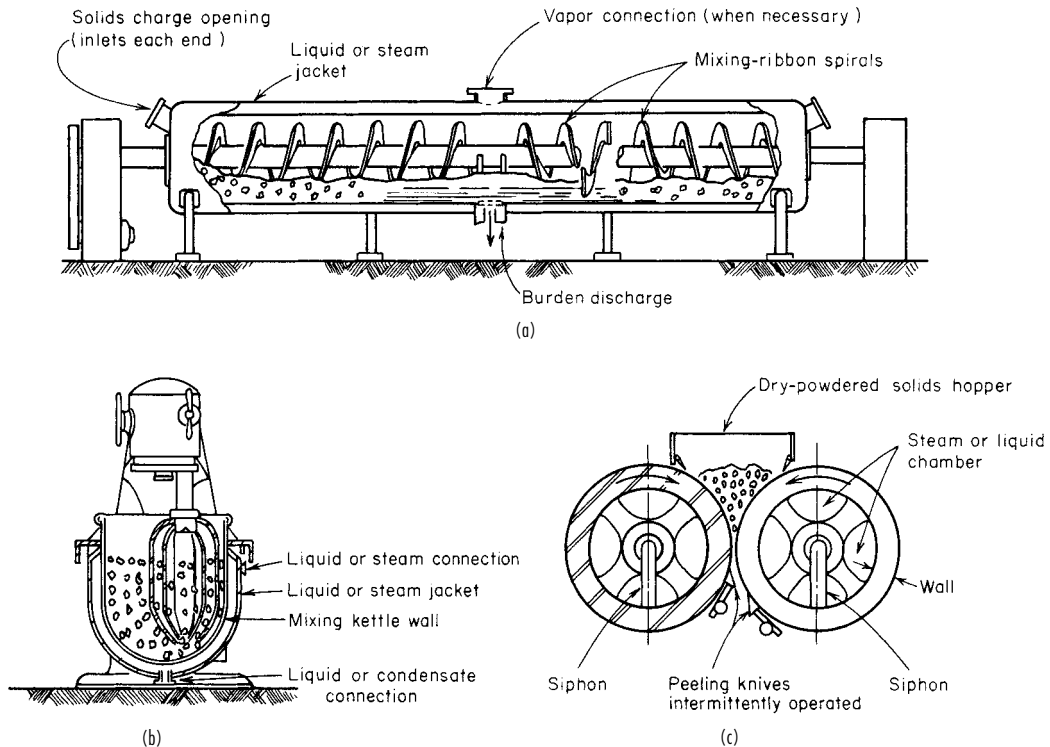


FIG. 11-56 Heat-transfer equipment for fusion of solids. (a) Horizontal-tank type. (Courtesy of Struthers Wells Corp.) (b) Agitated kettle. (Courtesy of Read-Standard Division, Capital Products Co.) (c) Double-drum mill. (Courtesy of Farrel-Birmingham Co.)

drums arranged so that a continuous sheet of material may pass over them in series. Typical of this arrangement are Fourdrinier-paper-machine dryers, cellophane dryers, slashers for textile piece goods and fibers, etc. The multiple cylinders are arranged in various ways. Generally they are staggered in two horizontal rows. In any one row, the cylinders are placed close together. The sheet material contacts the undersurface of the lower rolls and passes over the upper rolls, contacting 60 to 70 percent of the cylinder surface. The cylinders may also be arranged in a single horizontal row, in more than two horizontal rows, or in one or more vertical rows. When it is desired to contact only one side of the sheet with the cylinder surface, unheated guide rolls are used to conduct the sheeting from one cylinder to the next. For sheet materials that shrink on processing, it is frequently necessary to drive the cylinders at progressively slower speeds through the dryer. This requires elaborate individual electric drives on each cylinder.

Cylinder dryers usually operate at atmospheric pressure. However, the Minton paper dryer is designed for operation under vacuum. The drying cylinders are usually heated by steam, but occasionally single cylinders may be gas-heated, as in the case of the Pease blueprinting machine. Upon contacting the cylinder surface, wet sheet material is first heated to an equilibrium temperature somewhere between the wet-bulb temperature of the surrounding air and the boiling point of the liquid under the prevailing total pressure. The heat-transfer resistance of the vapor layer between the sheet and the cylinder surface may be significant.

These cylinder units are applicable to almost any form of sheet material that is not injuriously affected by contact with steam-heated metal surfaces. They are used chiefly when the sheet possesses certain properties such as a tendency to shrink or lacks the mechanical strength necessary for most types of continuous-sheeting air dryers. Applications are to dry films of various sorts, paper pulp in sheet form, paper sheets, paperboard, textile piece goods and fibers, etc. In some cases, imparting a special finish to the surface of the sheet may be an objective.

The **heat-transfer performance capacity** of cylinder dryers is not easy to estimate without a knowledge of the sheet temperature, which, in turn, is difficult to predict. According to published data, steam temperature is the largest single factor affecting capacity. Overall evaporation rates based on the total surface area of the dryers cover a range of 3.4 to 23 kg water/(h·m²) [0.7 to 4.8 lb water/(h·ft²)].

The value of the **coefficient of heat transfer** from steam to sheet is determined by the conditions prevailing on the inside and on the surface of the dryers. Low coefficients may be caused by (1) poor removal of air or other noncondensables from the steam in the cylinders, (2) poor removal of condensate, (3) accumulation of oil or rust on the interior of the drums, and (4) accumulation of a fiber lint on the outer surface of the drums. In a test reported by Lewis et al. [*Pulp Pap. Mag. Can.*, 22 (February 1927)] on a sulfite-paper dryer, in which the actual sheet temperatures were measured, a value of 187 W/(m²·°C) [33 Btu/(h·ft²·°F)] was obtained for the coefficient of heat flow between the steam and the paper sheet.

Operating-cost data for these units are meager. Power costs may be estimated by assuming 1 hp per cylinder for diameters of 1.2 to 1.8 m (4 to 6 ft). Data on labor and maintenance costs are also lacking.

The size of commercial cylinder dryers covers a wide range. The individual rolls may vary in diameter from 0.6 to 1.8 m (2 to 6 ft) and up to 8.5 m (28 ft) in width. In some cases, the width of rolls decreases throughout the dryer in order to conform to the shrinkage of the sheet. A single-cylinder dryer, such as the Yankee dryer, generally has a diameter between 2.7 and 4.6 m (9 and 15 ft).

HEAT-TRANSFER EQUIPMENT FOR DIVIDED SOLIDS

Most equipment for this service is some adaptation of a *material-handling* device whether or not the transport ability is desired. The old vertical tube and the vertical shell (fluidizer) are exceptions. Material-handling problems, plant transport needs, power, and maintenance are

prime considerations in equipment selection and frequently overshadow heat-transfer and capital-cost considerations. Material handling is generally the most important aspect. Material-handling characteristics of the divided solids may vary during heat processing. The body changes are usually important in drying, occasionally significant for heating, and only on occasion important for cooling. The ability to minimize effects of changes is a major consideration in equipment selection. Dehydration operations are better performed on contactive apparatus (see Sec. 12) that provides air to carry off released water vapor before a semiliquid form develops.

Some types of equipment are convertible from heat removal to heat supply by simply changing the temperature level of the fluid or air. Other types require an auxiliary change. Others require constructional changes. Temperature limits for the equipment generally vary with the thermal operation. The kind of thermal operation has a major effect on heat-transfer values. For drying, overall coefficients are substantially higher in the presence of substantial moisture for the constant-rate period than in finishing. However, a stiff "body" occurrence due to moisture can prevent a normal "mixing" with an adverse effect on the coefficient.

Fluidized-Bed Type Known as the cylindrical fluidizer, this operates with a bed of fluidized solids (Fig. 11-57). It is an indirect heat-transfer version of the contactive type in Sec. 17. An application disadvantage is the need for batch operation unless some short circuiting can be tolerated. Solids-cooling applications are few, as they can be more effectively accomplished by the fluidizing gas via the contactive mechanism that is referred to in Sec. 11. Heating applications are many and varied. These are subject to one shortcoming, which is the dissipation of the heat input by carry-off in the fluidizing gas. Heat-transfer performance for the indirect mode to solids has been outstanding, with overall coefficients in the range of 570 to 850 W/(m²·°C) [100 to 150 Btu/(h·ft²·°F)]. This device with its thin film does for solids what the falling-film and other thin-film techniques do for fluids, as shown by Holt (Pap. 11, 4th National Heat-Transfer Conference, August 1960). In a design innovation with high heat-transfer capability, heat is supplied indirectly to the fluidized solids through the walls of in-bed, horizontally placed, finned tubes [Petrie, Freeby, and Buckham, *Chem. Eng. Prog.*, **64**(7), 45 (1968)].

Moving-Bed Type This concept uses a single-pass tube bundle in a vertical shell with the divided solids flowing by gravity in the tubes. It is little used for solids. A major difficulty in divided-solids applications is the problem of charging and discharging with uniformity. A second is poor heat-transfer rates. Because of these limitations, this tube-bundle type is not the workhorse for solids that it is for liquid and gas-phase heat exchange.

However, there are applications in which the nature of a specific chemical reactor system requires indirect heating or cooling of a

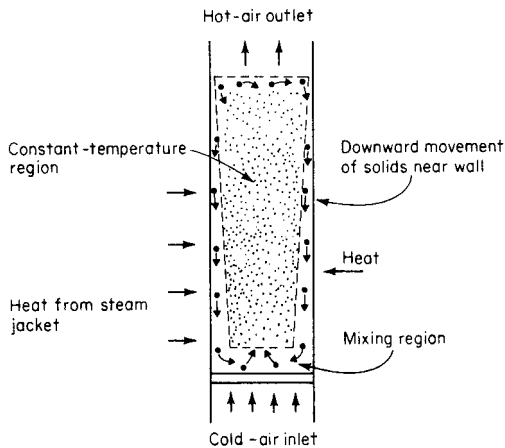


FIG. 11-57 Heat-transfer equipment for divided solids; stationary vertical-shell type. The indirect fluidizer.

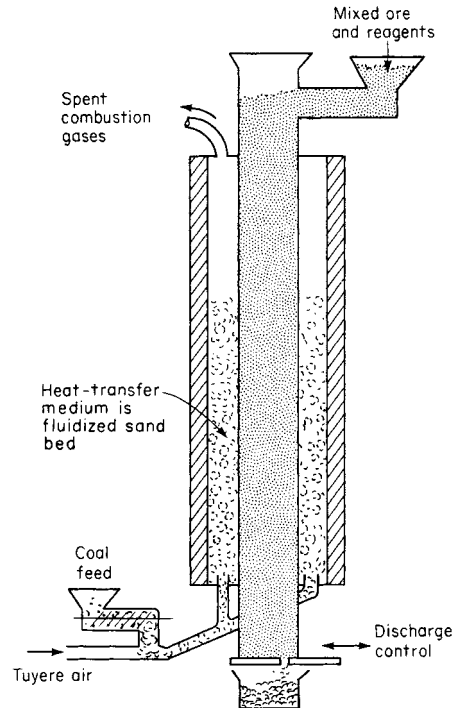


FIG. 11-58 Stationary vertical-tube type of indirect heat-transfer equipment with divided solids inside tubes, laminar solids flow and steady-state heat conditions.

moving bed of divided solids. One of these is the segregation process which through a gaseous reaction frees chemically combined copper in an ore to a free copper form which permits easy, efficient subsequent recovery [Pinkey and Plint, *Miner. Process.*, 17-30 (June 1968)]. The apparatus construction and principle of operation are shown in Fig. 11-58. The functioning is abetted by a novel heat-exchange provision of a fluidized sand bed in the jacket. This provides a much higher unit heat-input rate (coefficient value) than would the usual low-density hot-combustion-gas flow.

Agitated-Pan Type This device (Fig. 11-52) is not an adaptation of a material-handling device but was developed many years ago primarily for heat-transfer purposes. As such, it has found wide application. In spite of its batch operation with high attendant labor costs, it is still used for processing divided solids when no phase change is occurring. Simplicity and easy cleanout make the unit a wise selection for handling small, experimental, and even some production runs when quite a variety of burden materials are heat-processed. Both heating and cooling are feasible with it, but greatest use has been for drying [see Sec. 12 and Uhl and Root, *Chem. Eng. Prog.*, **63**(7), 8 (1967)]. This device, because it can be readily covered (as shown in the illustration) and a vacuum drawn or special atmosphere provided, features versatility to widen its use. For drying granular solids, the heat-transfer rate ranges from 28 to 227 W/(m²·°C) [5 to 40 Btu/(h·ft²·°F)]. For atmospheric applications, thermal efficiency ranges from 65 to 75 percent. For vacuum applications, it is about 70 to 80 percent. These devices are available from several sources, fabricated of various metals used in chemical processes.

Kneading Devices These are closely related to the agitated pan but differ as being primarily mixing devices with heat transfer a secondary consideration. Heat transfer is provided by jacketed construction of the main body and is effected by a coolant, hot water, or steam. These devices are applicable for the compounding of divided solids by mechanical rather than chemical action. Application is largely in the pharmaceutical and food-processing industries. For a

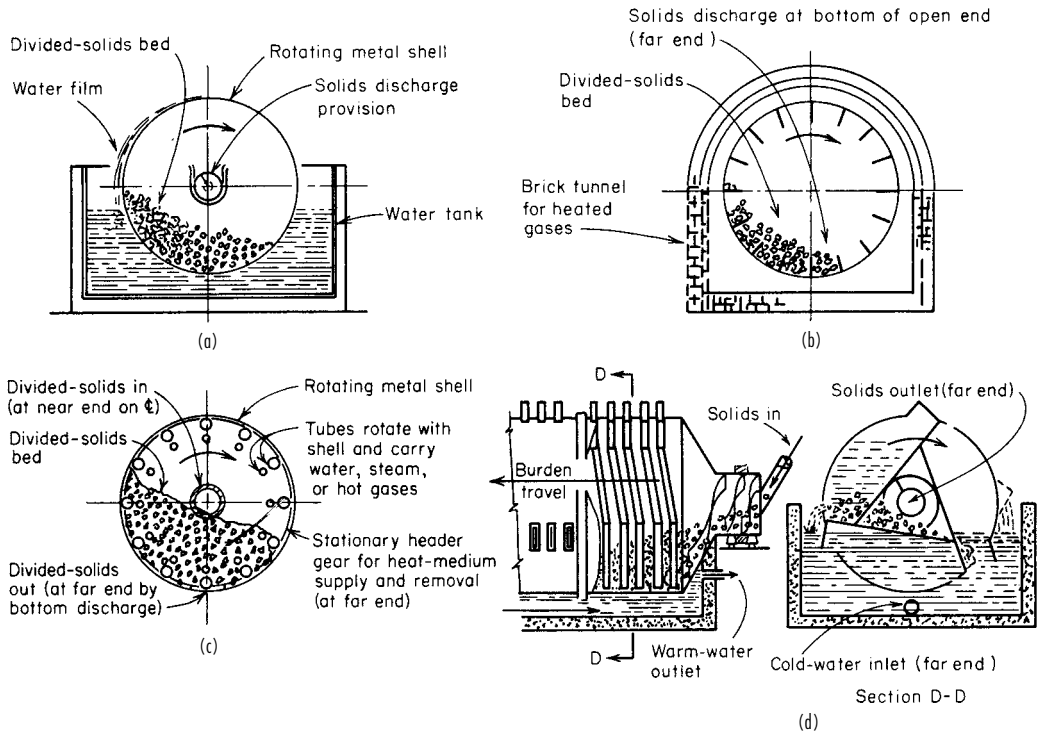


FIG. 11-59 Rotating shells as indirect heat-transfer equipment. (a) Plain. (Courtesy of BSP Corp.) (b) Flighted. (Courtesy of BSP Corp.) (c) Tubed. (d) Deep-finned type. (Courtesy of Link-Belt Co.)

more complete description, illustrations, performance, and power requirements, refer to Sec. 19.

Shelf Devices Equipment having heated and/or cooled shelves is available but is little used for divided-solids heat processing. Most extensive use of stationary shelves is freezing of packaged solids for food industries and for freeze drying by sublimation (see Sec. 22).

Rotating-Shell Devices These (see Fig. 11-59) are installed horizontally, whereas stationary-shell installations are vertical. Material-handling aspects are of greater importance than thermal performance. Thermal results are customarily given in terms of overall coefficient on the basis of the total area provided, which varies greatly with the design. The effective use, chiefly percent fill factor, varies widely, affecting the reliability of stated coefficient values. For performance calculations see Sec. 10 on heat-processing theory for solids. These devices are variously used for cooling, heating, and drying and are the workhorses for heat-processing divided solids in the large-capacity range. Different modifications are used for each of the three operations.

The **plain** type (Fig. 11-59a) features simplicity and yet versatility through various end-construction modifications enabling wide and varied applications. Thermal performance is strongly affected by the "body" characteristics of the burden because of its dependency for material handling on frictional contact. Hence, performance ranges from well-agitated beds with good thin-film heat-transfer rates to poorly agitated beds with poor thick-film heat-transfer rates. Temperature limits in application are (1) low-range cooling with shell dipped in water, 400°C (750°F) and less; (2) intermediate cooling with forced circulation of tank water, to 760°C (1400°F); (3) primary cooling, above 760°C (1400°F), water copiously sprayed and loading kept light; (4) low-range heating, below steam temperature, hot-water dip; and (5) high-range heating by tempered combustion gases or ribbon radiant-gas burners.

The **flighted** type (Fig. 11-59b) is a first-step modification of the plain type. The simple flight addition improves heat-transfer performance. This type is most effective on semifluid burdens which slide readily. Flighted models are restricted from applications in which soft-cake sticking occurs, breakage must be minimized, and abrasion is severe. A special flighting is one having the cross section compartmented into four lesser areas with ducts between. Hot gases are drawn through the ducts en route to the stack to provide about 75 percent more heating surface, improving efficiency and capacity with a modest cost increase. Another similar unit has the flights made in a triangular-duct cross section with hot gases drawn through.

The **tubed-shell** type (Fig. 11-59c) is basically the same device more commonly known as a "steam-tube rotary dryer" (see Sec. 20). The rotation, combined with slight inclination from the horizontal, moves the shell-side solids through it continuously. This type features good mixing with the objective of increased heat-transfer performance. Tube-side fluid may be water, steam, or combustion gas. Bottom discharge slots in the shell are used so that heat-transfer-medium supply and removal can be made through the ends; these restrict wide-range loading and make the tubed type inapplicable for floody materials. These units are seldom applicable for sticky, soft-caking, scaling, or heat-sensitive burdens. They are not recommended for abrasive materials. This type has high thermal efficiency because heat loss is minimized. **Heat-transfer coefficient** values are: water, 34 W/(m²·°C) [6 Btu/(h·ft²·°F)]; steam, same, with heat flux reliably constant at 3800 W/m² [1200 Btu/(h·ft²)]; and gas, 17 W/(m²·°C) [3 Btu/(h·ft²·°F)], with a high temperature difference. Although from the preceding discussion the device may seem rather limited, it is nevertheless widely used for drying, with condensing steam predominating as the heat-carrying fluid. But with water or refrigerants flowing in the tubes, it is also effective for cooling operations. The units are custom-built by several manufacturers in a wide range of sizes and materials.

A few fabricators that specialize in this type of equipment have accumulated a vast store of data for determining application sizing.

The patented **deep-finned** type in Fig. 11-59d is named the "Rotofin cooler." It features loading with a small layer thickness, excellent mixing to give a good effective diffusivity value, and a thin fluid-side film. Unlike other rotating-shell types, it is installed horizontally, and the burden is moved positively by the fins acting as an Archimedes spiral. Rotational speed and spiral pitch determine travel time. For cooling, this type is applicable to both secondary and intermediate cooling duties. Applications include solids in small lumps [9 mm ($\frac{3}{4}$ in)] and granular size [6 mm and less ($\frac{1}{4}$ to 0 in)] with no larger pieces to plug the fins, solids that have a free-flowing body characteristic with no sticking or caking tendencies, and drying of solids that have a low moisture and powder content unless special modifications are made for substantial vapor and dust handling. Thermal performance is very good, with overall coefficients to 110 W/(m²·°C) [20 Btu/(h·ft²·°F)], with one-half of these coefficients nominal for cooling based on the total area provided (nearly double those reported for other indirect rotaries).

Conveyor-Belt Devices The metal-belt type (Fig. 11-55) is the only device in this classification of material-handling equipment that has had serious effort expended on it to adapt it to indirect heat-transfer service with divided solids. It features a lightweight construction of a large area with a thin metal wall. Indirect-cooling applications have been made with poor thermal performance, as could be expected with a static layer. Auxiliary plowlike mixing devices, which are considered an absolute necessity to secure any worthwhile results for this service, restrict applications.

Spiral-Conveyor Devices Figure 11-60 illustrates the major adaptations of this widely used class of material-handling equipment to indirect heat-transfer purposes. These conveyors can be considered for heat-transfer purposes as continuously agitated kettles. The adaptation of Fig. 11-60d offers a batch-operated version for evaporation duty. For this service, all are package-priced and package-shipped items requiring few, if any, auxiliaries.

The **jacketed solid-flight** type (Fig. 11-60a) is the standard low-cost (parts-basis-priced) material-handling device, with a simple jacket added and employed for secondary-range heat transfer of an

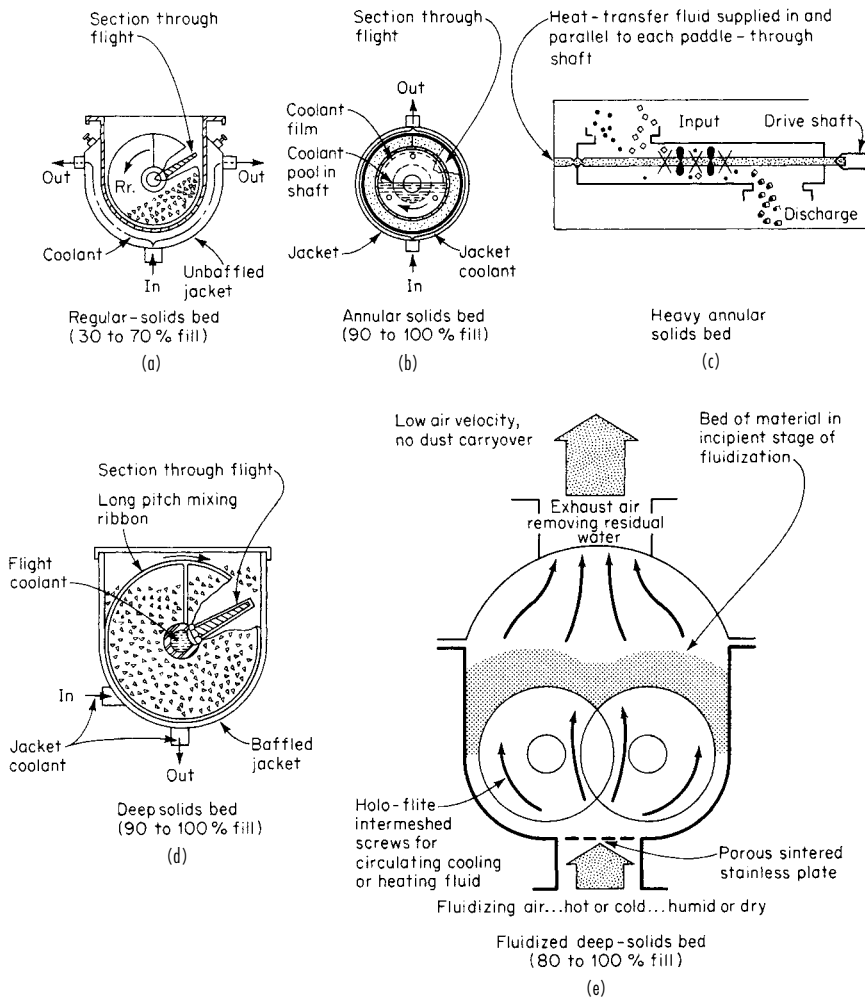


FIG. 11-60 Spiral-conveyor adaptations as heat-transfer equipment. (a) Standard jacketed solid flight. (Courtesy of Jeffrey Mfg. Co.) (b) Small spiral, large shaft. (Courtesy of Fuller Co.) (c) "Porcupine" medium shaft. (Courtesy of Bethlehem Corp.) (d) Large spiral, hollow flight. (Courtesy of Rietz Mfg. Co.) (e) Fluidized-bed large spiral, helical flight. (Courtesy of Western Precipitation Division, Joy Mfg. Co.)

incidental nature. Heat-transfer coefficients are as low as 11 to 34 W/(m²·°C) [2 to 6 Btu/(h·ft²·°F)] on sensible heat transfer and 11 to 68 W/(m²·°C) [2 to 12 Btu/(h·ft²·°F)] on drying because of substantial static solids-side film.

The **small-spiral-large-shaft** type (Fig. 11-60*b*) is inserted in a solids-product line as pipe banks are in a fluid line, solely as a heat-transfer device. It features a thin burden ring carried at a high rotative speed and subjected to two-sided conduction to yield an estimated heat-transfer coefficient of 285 W/(m²·°C) [50 Btu/(h·ft²·°F)], thereby ranking thermally next to the shell-fluidizer type. This device for powdered solids is comparable with the Votator of the fluid field.

Figure 11-60*c* shows a fairly new spiral device with a medium-heavy annular solids bed and having the combination of a jacketed, stationary outer shell with moving paddles that carry the heat-transfer fluid. A unique feature of this device to increase volumetric throughput, by providing an overall greater temperature drop, is that the heat medium is supplied to and withdrawn from the rotor paddles by a parallel piping arrangement in the rotor shaft. This is a unique flow arrangement compared with the usual series flow. In addition, the rotor carries burden-agitating spikes which give it the trade name of Porcupine Heat-Processor (*Chem. Equip. News*, April 1966; and Uhl and Root, AIChE Prepr. 21, 11th National Heat-Transfer Conference, August 1967).

The **large-spiral hollow-flight** type (Fig. 11-60*d*) is an adaptation, with external bearings, full fill, and salient construction points as shown, that is highly versatile in application. Heat-transfer coefficients are 34 to 57 W/(m²·°C) [6 to 10 Btu/(h·ft²·°F)] for poor, 45 to 85 W/(m²·°C) [8 to 15 Btu/(h·ft²·°F)] for fair, and 57 to 114 W/(m²·°C) [10 to 20 Btu/(h·ft²·°F)] for wet conductors. A popular version of this employs two such spirals in one material-handling chamber for a pug-mill agitation of the deep solids bed. The spirals are seldom heated. The shaft and shell are heated.

Another deep-bed spiral-activated solids-transport device is shown by Fig. 11-60*e*. The flights carry a heat-transfer medium as well as the jacket. A unique feature of this device which is purported to increase heat-transfer capability in a given equipment space and cost is the dense-phase fluidization of the deep bed that promotes agitation and moisture removal on drying operations.

Double-Cone Blending Devices The original purpose of these devices was mixing (see Sec. 19). Adaptations have been made; so many models now are primarily for indirect heat-transfer processing. A jacket on the shell carries the heat-transfer medium. The mixing action, which breaks up agglomerates (but also causes some degradation), provides very effective burden exposure to the heat-transfer surface. On drying operations, the vapor release (which in a static bed is a slow diffusional process) takes place relatively quickly. To provide vapor removal from the burden chamber, a hollow shaft is used. Many of these devices carry the hollow-shaft feature a step further by adding a rotating seal and drawing a vacuum. This increases thermal performance notably and makes the device a natural for solvent-recovery operations.

These devices are replacing the older tank and spiral-conveyor devices. Better provisions for speed and ease of fill and discharge (without powered rotation) minimize downtime to make this batch-operated device attractive. Heat-transfer coefficients ranging from 28 to 200 W/(m²·°C) [5 to 35 Btu/(h·ft²·°F)] are obtained. However, if caking on the heat-transfer walls is serious, then values may drop to 5.5 or 11 W/(m²·°C) [1 or 2 Btu/(h·ft²·°F)], constituting a misapplication. The double cone is available in a fairly wide range of sizes and construction materials. The users are the fine-chemical, pharmaceutical, and biological-preparation industries.

A novel variation is a cylindrical model equipped with a tube bundle to resemble a shell-and-tube heat exchanger with a bloated shell [*Chem. Process.*, 20 (Nov. 15, 1968)]. Conical ends provide for redistribution of burden between passes. The improved heat-transfer performance is shown by Fig. 11-61.

Vibratory-Conveyor Devices Figure 11-62 shows the various adaptations of vibratory material-handling equipment for indirect heat-transfer service on divided solids. The basic vibratory-equipment data are given in Sec. 21. These indirect heat-transfer adaptations feature simplicity, nonhazardous construction, nondegradation, nondusting, no wear, ready conveying-rate variation [1.5 to 4.5 m/min (5 to 15 ft/min)], and good heat-transfer coefficient—115 W/(m²·°C)

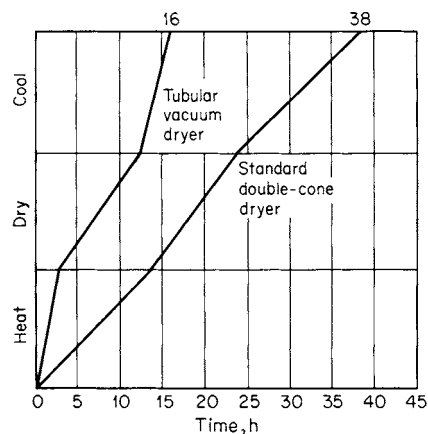


FIG. 11-61 Performance of tubed, blender heat-transfer device.

[20 Btu/(h·ft²·°F)] for sand. They usually require feed-rate and distribution auxiliaries. They are suited for heating and cooling of divided solids in powdered, granular, or moist forms but no sticky, liquefying, or floody ones. Terminal-temperature differences less than 11°C (20°F) on cooling and 17°C (30°F) on heating or drying operations are seldom practical. These devices are for medium and light capacities.

The **heavy-duty jacketed** type (Fig. 11-62*a*) is a special custom-built adaptation of a heavy-duty vibratory conveyor shown in Fig. 11-60. Its application is continuously to cool the crushed material [from about 177°C (350°F)] produced by the vibratory-type “caster” of Fig. 11-53. It does not have the liquid dam and is made in longer lengths that employ L, switchback, and S arrangements on one floor. The capacity rate is 27,200 to 31,700 kg/h (30 to 35 tons/h) with heat-transfer coefficients in the order of 142 to 170 W/(m²·°C) [25 to 30 Btu/(h·ft²·°F)]. For heating or drying applications, it employs steam to 414 kPa (60 lbf/in²).

The **jacketed or coolant-spraying** type (Fig. 11-62*b*) is designed to assure a very thin, highly agitated liquid-side film and the same initial coolant temperature over the entire length. It is frequently employed for transporting substantial quantities of hot solids, with cooling as an incidental consideration. For heating or drying applications, hot water or steam at a gauge pressure of 7 kPa (1 lbf/in²) may be employed. This type is widely used because of its versatility, simplicity, cleanability, and good thermal performance.

The **light-duty jacketed** type (Fig. 11-62*c*) is designed for use of air as a heat carrier. The flow through the jacket is highly turbulent and is usually counterflow. On long installations, the air flow is parallel to every two sections for more heat-carrying capacity and a fairly uniform surface temperature. The outstanding feature is that a wide range of temperature control is obtained by merely changing the heat-carrier temperature level from as low as atmospheric moisture condensation will allow to 204°C (400°F). On heating operations, a very good thermal efficiency can be obtained by insulating the machine and recycling the air. While heat-transfer rating is good, the heat-removal capacity is limited. Cooler units are often used in series with like units operated as dryers or when clean water is unavailable. Drying applications are for heat-sensitive [49 to 132°C (120° to 270°F)] products; when temperatures higher than steam at a gauge pressure of 7 kPa (1 lbf/in²) can provide are wanted but heavy-duty equipment is too costly; when the jacket-corrosion hazard of steam is unwanted; when headroom space is at a premium; and for highly abrasive burden materials such as fritted or crushed glasses and porcelains.

The **tiered arrangement** (Fig. 11-62*d*) employs the units of Fig. 11-62 with either air or steam at a gauge pressure of 7 kPa (1 lbf/in²) as a heat medium. These are custom-designed and built to provide a large amount of heat-transfer surface in a small space with the minimum of transport and to provide a complete processing system. These

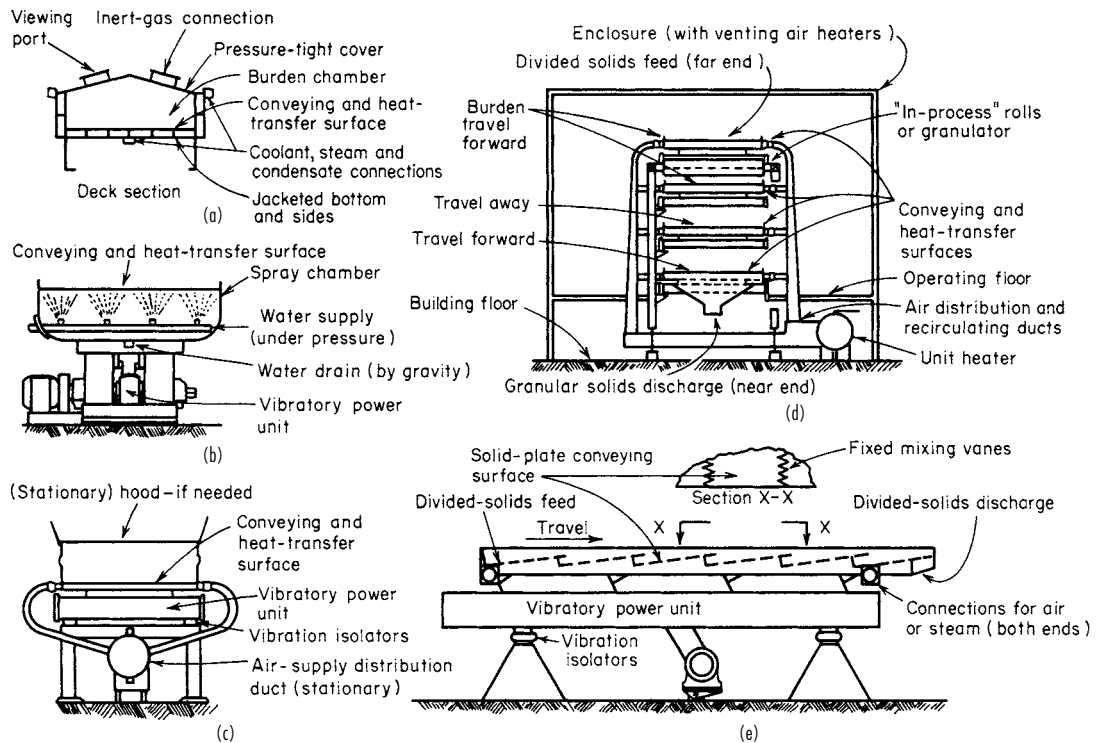


FIG. 11-62 Vibratory-conveyor adaptations as indirect heat-transfer equipment. (a) Heavy-duty jacketed for liquid coolant or high-pressure steam. (b) Jacketed for coolant spraying. (c) Light-duty jacketed construction. (d) Jacketed for air or steam in tiered arrangement. (e) Jacketed for air or steam with Mix-R-Step surface. (Courtesy of Jeffrey Mfg. Co.)

receive a damp material, resize while in process by granulators or rolls, finish dry, cool, and deliver to packaging or tableting. The applications are primarily in the fine-chemical, food, and pharmaceutical manufacturing fields.

The **Mix-R-Step** type in Fig. 11-62e is an adaptation of a vibratory conveyor. It features better heat-transfer rates, practically doubling the coefficient values of the standard flat surface and trebling heat-flux values, as the layer depth can be increased from the normal 13 to 25 and 32 mm ($\frac{1}{2}$ to 1 and $1\frac{1}{4}$ in). It may be provided on decks jacketed for air, steam, or water spray. It is also often applicable when an infrared heat source is mounted overhead to supplement the indirect or as the sole heat source.

Elevator Devices The **vibratory elevating-spiral** type (Fig. 11-63) adapts divided-solids-elevating material-handling equipment to heat-transfer service. It features a large heat-transfer area over a small floor space and employs a reciprocating shaker motion to effect transport. Applications, layer depth, and capacities are restricted, as burdens must be of such "body" character as to convey uphill by the microhopping-transport principle. The type lacks self-emptying ability. Complete washdown and cleaning is a feature not inherent in any other elevating device. A typical application is the cooling of a low-density plastic powder at the rate of 544 kg/h (1200 lb/h).

Another elevator adaptation is that for a **spiral-type elevating** device developed for ground cement and thus limited to fine powdery burdens. The spiral operates inside a cylindrical shell, which is externally cooled by a falling film of water. The spiral not only elevates the material in a thin layer against the wall but keeps it agitated to achieve high heat-transfer rates. Specific operating data are not available [Chem. Eng. Prog., 68(7), 113 (1968)]. The falling-water film, besides being ideal thermally, by virtue of no jacket pressure very greatly reduces the hazard that the cooling water may contact the water-sensitive burden in process. Surfaces wet by water are accessible for

cleaning. A fair range of sizes is available, with material-handling capacities to 60 tons/h.

Pneumatic-Conveying Devices See Sec. 21 for descriptions, ratings, and design factors on these devices. Use is primarily for transport purposes, and heat transfer is a very secondary consideration. Applications have largely been for plastics in powder and pellet forms.

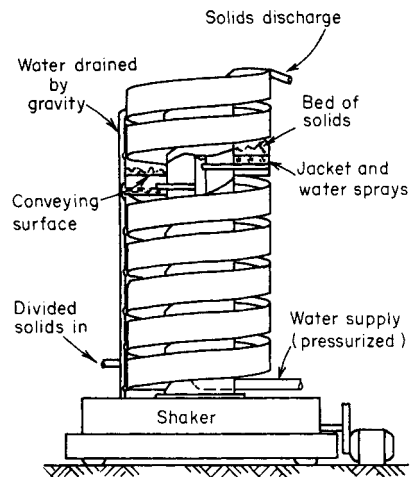


FIG. 11-63 Elevator type as heat-transfer equipment. (Courtesy of Carrier Conveyor Corp.)

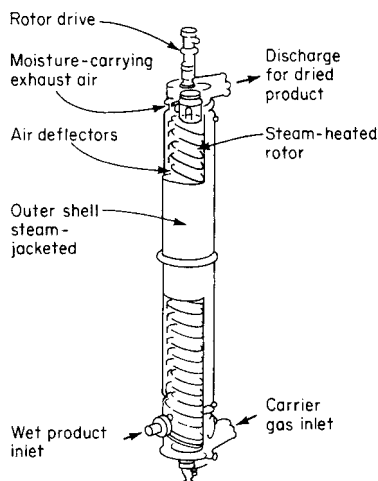


FIG. 11-64 A pneumatic-transport adaptation for heat-transfer duty. (Courtesy of Werner & Pfleiderer Corp.)

By modifications, needed cooling operations have been simultaneously effected with transport to stock storage [*Plast. Des. Process.*, **28** (December 1968)].

Heat-transfer aspects and performance were studied and reported on by Depew and Farbar (ASME Pap. 62-HT-14, September 1962). Heat-transfer coefficient characteristics are similar to those shown in Sec. 11 for the indirectly heated fluid bed. Another frequent application on plastics is a small, rather incidental but necessary amount of drying required for plastic pellets and powders on receipt when

shipped in bulk to the users. Pneumatic conveyors modified for heat transfer can handle this readily.

A pneumatic-transport device designed primarily for heat-sensitive products is shown in Fig. 11-64. This was introduced into the United States after 5 years' use in Europe [*Chem. Eng.*, **76**, 54 (June 16, 1969)].

Both the shell and the rotor carry steam as a heating medium to effect indirect transfer as the burden briefly contacts those surfaces rather than from the transport air, as is normally the case. The rotor turns slowly (1 to 10 r/min) to control, by deflectors, product distribution and prevent caking on walls. The carrier gas can be inert, as nitrogen, and also recycled through appropriate auxiliaries for solvent recovery. Application is limited to burdens that (1) are fine and uniformly graded for the pneumatic transport, (2) dry very fast, and (3) have very little, if any, sticking or decomposition characteristics. Feeds can carry 5 to 100 percent moisture (dry basis) and discharge at 0.1 to 2 percent. Wall temperatures range from 100 to 170°C (212 to 340°F) for steam and lower for a hot-water-heat source. Pressure drops are in order of 500 to 1500 mmH₂O (20 to 60 inH₂O). Steam consumption approaches that of a contractive-mechanism dryer down to a low value of 2.9 kg steam/kg water (2.9 lb steam/lb water). Available burden capacities are 91 to 5900 kg/h (200 to 13,000 lb/h).

Vacuum-Shelf Types These are very old devices, being a version of the table type. Early-day use was for drying (see Sec. 12). Heat transfer is slow even when supplemented by vacuum, which is 90 percent or more of present-day use. The newer vacuum blender and cone devices are taking over many applications. The slow heat-transfer rate is quite satisfactory in a major application, freeze drying, which is a sublimation operation (see Sec. 22 for description) in which the water must be retained in the solid state during its removal. Then slow diffusional processes govern. Another extensive application is freezing packaged foods for preservation purposes.

Available sizes range from shelf areas of 0.4 to 67 m² (4 to 726 ft²). These are available in several manufacturers' standards, either as system components or with auxiliary gear as packaged systems.

THERMAL INSULATION

Materials or combinations of materials which have air- or gas-filled pockets or void spaces that retard the transfer of heat with reasonable effectiveness are thermal insulators. Such materials may be particulate and/or fibrous, with or without binders, or may be assembled, such as multiple heat-reflecting surfaces that incorporate air- or gas-filled void spaces.

The ability of a material to retard the flow of heat is expressed by its thermal **conductivity** (for unit thickness) or **conductance** (for a specific thickness). Low values for thermal conductivity or conductance (or high thermal resistivity or resistance value) are characteristics of thermal insulation.

Heat is transferred by radiation, conduction, and convection. Radiation is the primary mode and can occur even in a vacuum. The amount of heat transferred for a given area is relative to the temperature differential and emissivity from the radiating to the absorbing surface. Conduction is due to molecular motion and occurs within gases, liquids, and solids. The tighter the molecular structure, the higher the rate of transfer. As an example, steel conducts heat at a rate approximately 600 times that of typical thermal-insulation materials. Convection is due to mass motion and occurs only in fluids. The prime purpose of a thermal-insulation system is to minimize the amount of heat transferred.

INSULATION MATERIALS

Materials Thermal insulations are produced from many materials or combinations of materials in various forms, sizes, shapes, and thickness. The most commonly available materials fall within the following categories:

Fibrous or cellular—mineral. Alumina, asbestos, glass, perlite, rock, silica, slag, or vermiculite.

Fibrous or cellular—organic. Cane, cotton, wood, and wood bark (cork).

Cellular organic plastics. Elastomer, polystyrene, polyisocyanate, polyisocyanurate, and polyvinyl acetate.

Cements. Insulating and/or finishing.

Heat-reflecting metals (reflective). Aluminum, nickel, stainless steel.

Available forms. Blanket (felt and batt), block, cements, loose fill, foil and sheet, formed or foamed in place, flexible, rigid, and semi-rigid.

The actual thicknesses of piping insulation differ from the nominal values. Dimensional data of ASTM Standard C585 appear in Table 11-21.

Thermal Conductivity (K Factor) Depending on the type of insulation, the thermal conductivity (K factor) can vary with age, manufacturer, moisture content, and temperature. Typical published values are shown in Fig. 11-65. Mean temperature is equal to the arithmetic average of the temperatures on both sides of the insulating material.

Actual system heat loss (or gain) will normally exceed calculated values because of projections, axial and longitudinal seams, expansion-contraction openings, moisture, workers' skill, and physical abuse.

Finishes Thermal insulations require an external covering (finish) to provide protection against entry of water or process fluids, mechanical damage, and ultraviolet degradation of foamed materials. In some cases the finish can reduce the flame-spread rating and/or provide fire protection.

The finish may be a coating (paint, asphaltic, resinous, or polymeric), a membrane (coated felt or paper, metal foil, or laminate of plastic, paper, foil or coatings), or sheet material (fabric, metal, or plastic).

TABLE 11-21 Thicknesses of Piping Insulation

in mm	Insulation, nominal thickness															
	Outer diameter		1 25		1½ 38		2 51		2½ 64		3 76		3½ 89		4 102	
Nominal iron-pipe size, in	Approximate wall thickness															
	in		mm		in		mm		in		mm		in		mm	
½	0.84	21	1.01	26	1.57	40	2.07	53	2.88	73	3.38	86	3.88	99	4.38	111
¾	1.05	27	0.90	23	1.46	37	1.96	50	2.78	71	3.28	83	3.78	96	4.28	109
1	1.32	33	1.08	27	1.58	40	2.12	54	2.64	67	3.14	80	3.64	92	4.14	105
1¼	1.66	42	0.91	23	1.66	42	1.94	49	2.47	63	2.97	75	3.47	88	3.97	101
1½	1.90	48	1.04	26	1.54	39	2.35	60	2.85	72	3.35	85	3.85	98	4.42	112
2	2.38	60	1.04	26	1.58	40	2.10	53	2.60	66	3.10	79	3.60	91	4.17	106
2½	2.88	73	1.04	26	1.86	47	2.36	60	2.86	73	3.36	85	3.92	100	4.42	112
3	3.50	89	1.02	26	1.54	39	2.04	52	2.54	65	3.04	77	3.61	92	4.11	104
3½	4.00	102	1.30	33	1.80	46	2.30	58	2.80	71	3.36	85	3.86	98	4.36	111
4	4.50	114	1.04	26	1.54	39	2.04	52	2.54	65	3.11	79	3.61	92	4.11	104
4½	5.00	127	1.30	33	1.80	46	2.30	58	2.86	73	3.36	85	3.86	98	4.48	114
5	5.56	141	0.99	25	1.49	38	1.99	51	2.56	65	3.06	78	3.56	90	4.18	106
6	6.62	168	0.96	24	1.46	37	2.02	51	2.52	64	3.02	77	3.65	93	4.15	105
7	7.62	194			1.52	39	2.02	51	2.52	64	3.15	80	3.65	93	4.15	105
8	8.62	219			1.52	39	2.02	51	2.65	67	3.15	80	3.65	93	4.15	105
9	9.62	244			1.52	39	2.15	55	2.65	67	3.15	80	3.65	93	4.15	105
10	10.75	273			1.58	40	2.08	53	2.58	66	3.08	78	3.58	91	4.08	104
11	11.75	298			1.58	40	2.08	53	2.58	66	3.08	78	3.58	91	4.08	104
12	12.75	324			1.58	40	2.08	53	2.58	66	3.08	78	3.58	91	4.08	104
14	14.00	356			1.46	37	1.96	50	2.46	62	2.96	75	3.46	88	3.96	101
Over 14, up to and including 36					1.46	37	1.96	50	2.46	62	2.96	75	3.46	88	3.96	101

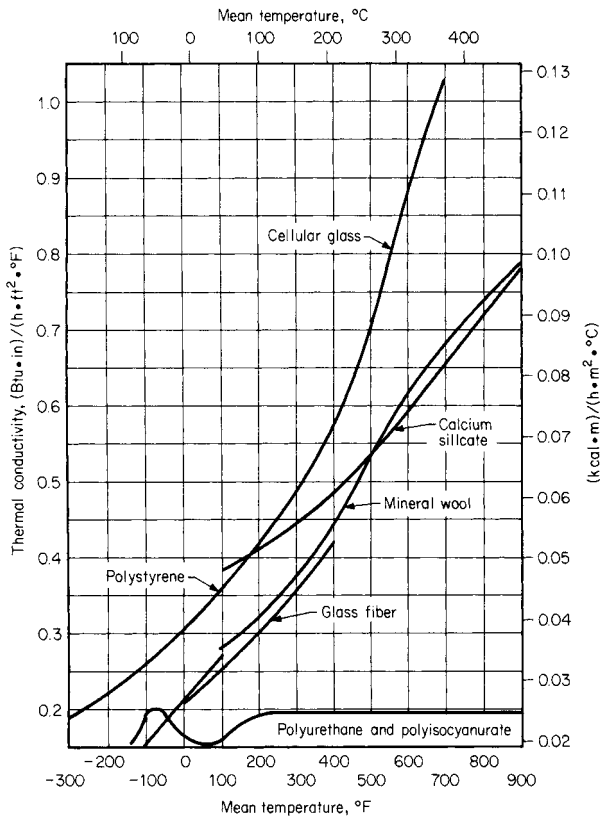


FIG. 11-65 Thermal conductivity of insulating materials.

Finishes for systems operating below 2°C (35°F) must be sealed and retard vapor transmission. Those from 2°C (35°F) through 27°C (80°F) should retard vapor transmission (to prevent surface condensation), and those above 27°C (80°F) should prevent water entry and allow moisture to escape.

Metal finishes are more durable, require less maintenance, reduce heat loss, and, if uncoated, increase the surface temperature on hot systems.

SYSTEM SELECTION

A combination of insulation and finish produces the thermal-insulation system. Selection of these components depends on the purpose for which the system is to be used. No single system performs satisfactorily from the cryogenic through the elevated-temperature range. Systems operating below freezing have a low vapor pressure, and atmospheric moisture is pushed into the insulation system, while the reverse is true for hot systems. Some general guidelines for system selection follow.

Cryogenic [-273 to -101°C (-459 to -150°F)] High Vacuum
 This technique is based on the Dewar flask, which is a double-walled vessel with reflective surfaces on the evacuated side to reduce radiation losses. Figure 11-66 shows a typical laboratory-size Dewar. Figure 11-67 shows a semiportable type. Radiation losses can be further reduced by filling the cavity with powders such as perlite or silica prior to pulling the vacuum.

Multilayer Multilayer systems consist of series of radiation-reflective shields of low emittance separated by fillers or spacers of very low conductance and exposed to a high vacuum.

Foamed or Cellular Cellular plastics such as polyurethane and polystyrene do not hold up or perform well in the cryogenic temperature range because of permeation of the cell structure by water vapor, which in turn increases the heat-transfer rate. Cellular glass holds up better and is less permeable.

Low Temperature [-101 to -1°C (-150 to +30°F)] Cellular glass, glass fiber, polyurethane foam, and polystyrene foam are frequently used for this service range. A vapor-retarder finish with a

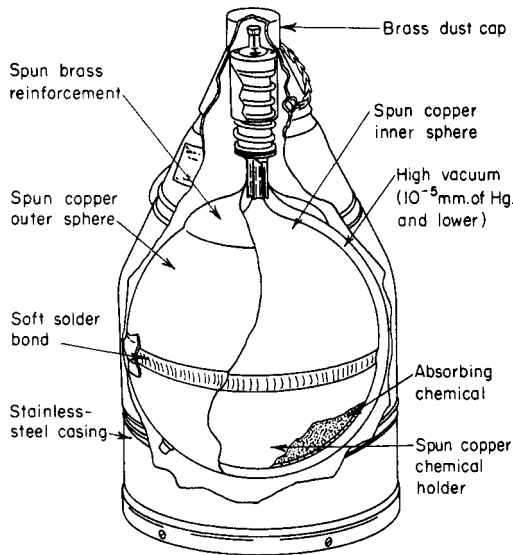


FIG. 11-66 Dewar flask.

perm rating less than 0.02 is required. In addition, it is good practice to coat all contact surfaces of the insulation with a vapor-retardant mastic to prevent moisture migration when the finish is damaged or is not properly maintained. Closed-cell insulation should not be relied on as the vapor retarder. Hairline cracks can develop, cells can break

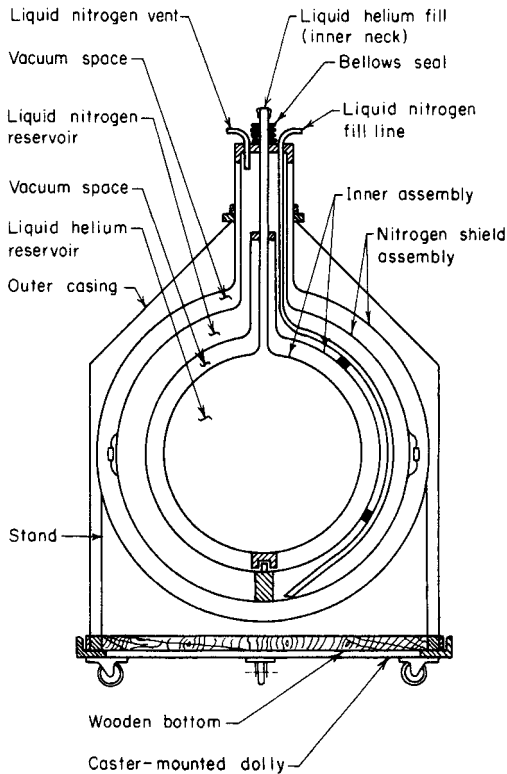


FIG. 11-67 Hydrogen bottle.

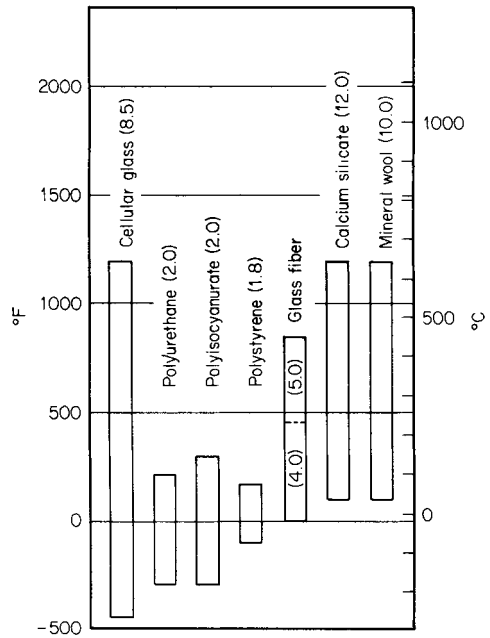


FIG. 11-68 Insulating materials and applicable temperature ranges.

down, glass-fiber binders are absorbent, and moisture can enter at joints between all materials.

Moderate and High Temperature [over 2°C (36°F)] Cellular or fibrous materials are normally used. See Fig. 11-68 for nominal temperature range. Nonwicking insulation is desirable for systems operating below 100°C (212°F).

Other Considerations Autoignition can occur if combustible fluids are absorbed by wicking-type insulations. **Chloride stress corrosion** of austenitic stainless steel can occur when chlorides are concentrated on metal surfaces at or above approximately 60°C (140°F). The chlorides can come from sources other than the insulation. Some calcium silicates are formulated to exceed the requirements of the MIL-I-24244A specification. **Fire resistance** of insulations varies widely. Calcium silicate, cellular glass, glass fiber, and mineral wool are fire-resistant but do not perform equally under actual fire conditions. A steel jacket provides protection, but aluminum does not.

Traced pipe performs better with a nonwicking insulation which has low thermal conductivity. Underground systems are very difficult to keep dry permanently. Methods of insulation include factory-preinsulated pouring types and conventionally applied types. Corrosion can occur under wet insulation. A protective coating, applied directly to the metal surface, may be required.

ECONOMIC THICKNESS OF INSULATION

Optimal economic insulation thickness may be determined by various methods. Two of these are the minimum-total-cost method and the incremental-cost method (or marginal-cost method). The minimum-total-cost method involves the actual calculations of lost energy and insulation costs for each insulation thickness. The thickness producing the lowest total cost is the optimal economic solution. The optimum thickness is determined to be the point where the last dollar invested in insulation results in exactly \$1 in energy-cost savings ("ETI—Economic Thickness for Industrial Insulation," Conservation Pap. 46, Federal Energy Administration, August 1976). The incremental-cost method provides a simplified and direct solution for the least-cost thickness.

The total-cost method does not in general provide a satisfactory means for making most insulation investment decisions, since an

economic return on investment is required by investors and the method does not properly consider this factor. Return on investment is considered by Rubin ("Piping Insulation—Economics and Profits," in *Practical Considerations in Piping Analysis*, ASME Symposium, vol. 69, 1982, pp. 27–46). The incremental method used in this reference requires that each incremental 1/2 in of insulation provide the predetermined return on investment. The minimum thickness of installed insulation is used as a base for calculations. The incremental installed capital cost for each additional 1/2 in of insulation is determined. The energy saved for each increment is then determined. The value of this energy varies directly with the temperature level [e.g., steam at 538°C

(1000°F) has a greater value than condensate at 100°C (212°F)]. The final increment selected for use is required either to provide a satisfactory return on investment or to have a suitable payback period.

Recommended Thickness of Insulation Indoor insulation thickness appears in Table 11-22, and outdoor thickness appears in Table 11-23. These selections were based upon calcium silicate insulation with a suitable aluminum jacket. However, the variation in thickness for fiberglass, cellular glass, and rock wool is minimal. Fiberglass is available for maximum temperatures of 260, 343, and 454°C (500, 650, and 850°F). Rock wool, cellular glass, and calcium silicate are used up to 649°C (1200°F).

TABLE 11-22 Indoor Insulation Thickness, 80°F Still Ambient Air*

Pipe size, in	Insulation thickness, in	Minimum pipe temperature, °F									
		Energy cost, \$/million Btu									
		1	2	3	4	5	6	7	8		
3/4	1 1/2	950	600	550	400	350	300	250	250		
	2				1100	1000	900	800	750		
	2 1/2				1750	1050	950	850	800		
	3									1200	
1	1 1/2	1200	800	600	500	450	400	350	300		
	2			1200	1000	900	800	700	700		
	2 1/2					1200	1050	1000	900		
	3						1100	1150	950		
1 1/2	1 1/2	1100	750	550	450	400	400	350	300		
	2			1000	850	700	650	600	500		
	2 1/2				1050	900	800	750	650		
	3						1150	1100	1000		
2	1 1/2	1050	700	500	450	400	350	300	300		
	2			1050	850	750	700	600	600		
	2 1/2			1100	950	1000	750	700	650		
	3				1200	1050	950	850	800		
3	1 1/2	950	650	500	400	350	300	300	250		
	2			1100	900	700	600	550	450		
	2 1/2				1050	850	750	650	500	500	
	3					1050	950	800	750	700	
4	1 1/2	950	600	500	400	350	300	300	250		
	2			1100	850	700	600	550	450		
	2 1/2				1200	1000	850	750	700	650	
	3					1050	900	800	750	700	
	3 1/2								800	750	700
	4								1150	1150	1050
6	1 1/2	600	350	300	250	250	200	200	200		
	2			1100	850	700	600	550	500	500	
	2 1/2				900	800	650	600	550	550	
	3				1150	1000	850	750	700	600	
	3 1/2							1100	1000	900	
	4									1200	
8	2		1000	800	650	550	500	450	400		
	2 1/2			1050	850	700	600	550	500	450	
	3					1050	900	800	750	700	
	3 1/2							1200	1100	1000	900
	4								1150	1150	
10	2		1100	850	700	650	550	500	450		
	2 1/2			1200	900	750	700	600	550	500	
	3				1050	900	750	700	600	550	
	3 1/2							1200	1050	950	
	4									1200	
12	2	1150	750	600	500	400	400	350	300		
	2 1/2			1000	800	650	550	500	450	400	
	3				1200	1000	900	800	700	650	
	3 1/2							1200	1100	1000	900
	4								1150	1050	950
	4 1/2								1200	1100	1000
14	2	1050	650	550	450	400	350	300	300		
	2 1/2			1000	800	650	550	500	450	400	
	3				1100	950	800	700	650	600	
	3 1/2							1150	1000	950	850
	4							1200	1050	1000	900
	4 1/2								1200	1100	1000

TABLE 11-22 Indoor Insulation Thickness, 80°F Still Ambient Air* (Concluded)

Pipe size, in	Insulation thickness, in	Minimum pipe temperature, °F							
		Energy cost, \$/million Btu							
		1	2	3	4	5	6	7	8
16	2	950	650	500	400	350	300	300	300
	2½		1000	800	700	600	550	500	450
	3		1200	950	800	700	600	550	500
	3½					1150	1050	950	850
	4					1200	1100	1000	900
	4½						1150	1050	950
18	2	1000	650	500	400	350	350	300	300
	2½		950	750	600	550	500	450	400
	3		1150	900	750	650	550	500	500
	3½					1200	1100	1000	900
	4						1150	1050	950
	4½						1200	1100	1000
20	2	1050	700	550	450	400	350	350	300
	2½		1000	800	600	550	500	450	400
	3		1150	900	750	650	550	500	500
	3½						1100	1000	950
	4						1150	1050	1000
	4½							1200	1100
24	2	950	600	500	400	350	300	300	250
	2½		1150	900	750	650	550	500	450
	3			1050	900	750	700	600	550
	3½					1100	1000	900	800
	4					1150	1050	950	850
	4½						1150	1050	950

*Aluminum-jacketed calcium silicate insulation with an emissivity factor of 0.05. To convert inches to millimeters, multiply by 25.4, to convert dollars per 1 million British thermal units to dollars per 1 million kilojoules, multiply by 0.948, °C = 5/9 (°F - 32).

TABLE 11-23 Outdoor Insulation Thickness, 7.5-mi/h Wind, 60°F Air*

Pipe size, in	Thickness, in	Minimum pipe temperature, °F							
		Energy cost, \$/million Btu							
		1	2	3	4	5	6	7	8
¾	1	450	300	250	250	200	200	150	150
	1½	800	500	400	300	250	250	200	200
	2			1150	950	850	750	700	650
	2½			1100	1000	900	800	750	700
1	1	400	300	250	200	200	150	150	150
	1½	1000	650	500	400	350	300	300	250
	2			1100	900	800	700	600	600
	2½				1200	1050	950	850	800
	3					1100	1000	900	850
1½	1	350	250	200	200	150	150	150	150
	1½	900	600	450	350	300	300	250	250
	2		100	850	700	600	550	500	450
	2½			1150	950	800	750	700	600
	3					1200	1050	1000	900
2	1	350	250	200	150	150	150	150	150
	1½	900	550	450	400	300	300	250	250
	2		1150	900	750	650	600	550	500
	2½			1000	850	750	650	600	550
	3				1050	950	850	750	700
3	1	300	200	150	150	150	150	150	150
	1½	750	500	400	300	250	250	250	200
	2		950	750	600	500	450	400	350
	2½		1150	950	750	650	600	500	500
	3			1150	1000	850	750	650	600
4	1	250	200	150	150	150	150	150	150
	1½	750	500	350	300	250	250	200	200
	2		950	750	600	500	450	400	350
	2½			1050	900	700	650	600	550
	3			1100	950	750	700	650	600
	3½						1200	1100	1000

TABLE 11-23 Outdoor Insulation Thickness, 7.5-mi/h Wind, 60°F Air* (Concluded)

Pipe size, in	Thickness, in	Minimum pipe temperature, °F							
		Energy cost, \$/million Btu							
		1	2	3	4	5	6	7	8
6	1	250	150	150	150	150	150	150	150
	1½	450	300	200	200	150	150	150	150
	2		900	700	600	500	450	400	350
	2½		1050	800	650	600	500	450	400
	3			1050	900	750	700	600	550
	3½					1150	1050	950	850
	4							1200	1150
8	1	250	200	150	150	150	150	150	150
	2		850	650	550	450	400	350	350
	2½		900	700	600	500	450	400	400
	3			1100	950	800	750	700	600
	3½					1150	1000	950	850
	4							1050	1000
10	2	200	150	150	150	150	150	150	150
	2½		1000	800	650	550	500	450	400
	3		1200	950	800	700	600	550	500
	3½					1100	1000	900	800
	4							1150	1050
	4½							1200	1100
12	1½	250	150	150	150	150	150	150	150
	2	950	600	500	400	350	300	250	250
	2½		900	700	550	500	400	400	350
	3			1100	900	800	700	650	550
	3½					1100	1000	900	850
	4					1150	1050	950	900
	4½					1200	1100	1000	950
14	1½	250	150	150	150	150	150	150	150
	2	850	550	400	350	300	250	250	250
	2½		850	650	550	500	400	400	400
	3			1000	850	700	650	550	500
	3½				1200	1000	950	850	800
	4					1050	1000	900	850
	4½						1100	1000	950
16	1½	250	150	150	150	150	150	150	150
	2	800	500	350	300	300	250	250	200
	2½		900	700	550	500	450	400	350
	3		1000	850	700	600	500	450	400
	3½				1200	1000	950	850	800
	4					1100	1000	900	850
	4½					1150	1000	950	900
18	1½	250	150	150	150	150	150	150	150
	2	850	550	400	350	300	250	250	200
	2½		800	650	500	450	400	350	350
	3		1000	800	650	550	500	450	400
	3½					1100	1000	900	850
20	1½	150	150	150	150	150	150	150	150
	2	900	550	450	350	300	300	250	250
	2½		850	650	550	450	400	350	350
	3		1000	800	650	550	500	450	400
	3½					1150	1050	950	900
	4					1200	1100	1000	950
24	1½	150	150	150	150	150	150	150	150
	2	800	500	400	300	250	250	200	200
	2½		950	750	650	550	500	450	400
	3		1150	950	750	650	600	550	500
	3½				1150	1000	900	800	750
	4				1200	1050	950	850	800
	4½						1050	950	850

*Aluminum-jacketed calcium silicate insulation with an emissivity factor of 0.05. To convert inches to millimeters, multiply by 25.4; to convert miles per hour to kilometers per hour, multiply by 1.609; and to convert dollars per 1 million British thermal units to dollars per 1 million kilojoules, multiply by 0.948; °C = 5/9 (°F - 32).

The tables were based upon the cost of energy at the end of the first year, a 10 percent inflation rate on energy costs, a 15 percent interest cost, and a present-worth pretax profit of 40 percent per annum on the last increment of insulation thickness. Dual-layer insulation was used for 3½-in and greater thicknesses. The tables and a full explanation of their derivation appear in a paper by F. L. Rubin (op. cit.). Alternatively, the selected thicknesses have a payback period on the last nominal ½-in increment of 1.44 years as presented in a later paper by Rubin ["Can You Justify More Piping Insulation?" *Hydrocarbon Process.*, 152–155 (July 1982)].

Example 1 For 24-in pipe at 371°C (700°F) with an energy cost of \$4/million Btu, select 2-in thickness for indoor and 2½-in for outdoor locations. [A 2½-in thickness would be chosen at 399°C (750°F) indoors and 3½-in outdoors.]

Example 2 For 16-in pipe at 343°C (650°F) with energy valued at \$5/million Btu, select 2½-in insulation indoors [use 3-in thickness at 371°C (700°F)]. Outdoors choose 3-in insulation [use 3½-in dual-layer insulation at 538°C (1000°F)].

Example 3 For 12-in pipe at 593°C (1100°F) with an energy cost of \$6/million Btu, select 3½-in thickness for an indoor installation and 4½-in thickness for an outdoor installation.

INSTALLATION PRACTICE

Pipe Depending on diameter, pipe is insulated with cylindrical half, third, or quarter sections or with flat segmental insulation. Fittings and valves are insulated with preformed insulation covers or with individual pieces cut from sectional straight pipe insulation.

Method of Securing Insulation with factory-applied jacketing may be secured with adhesive on the overlap, staples, tape, or wire, depending on the type of jacket and the outside diameter. Insulation which has a separate jacket is wired or banded in place before the jacket (finish) is applied.

Double Layer Pipe expansion is a significant factor at temperatures above 600°F (316°C). Above this temperature, insulation should be applied in a double layer with all joints staggered to prevent excessive heat loss and high surface temperature at joints opened by pipe

expansion. This procedure also minimizes thermal stresses in the insulation.

Finish Covering for cylindrical surfaces ranges from asphalt-saturated or saturated and coated organic and asbestos paper, through laminates of such papers and plastic films or aluminum foil, to medium-gauge aluminum, galvanized steel, or stainless steel. Fittings and irregular surfaces may be covered with fabric-reinforced mastics or preformed metal or plastic covers. Finish selection depends on function and location. Vapor-barrier finishes may be in sheet form or a mastic, which may or may not require reinforcing, depending on the method of application, and additional protection may be required to prevent mechanical abuse and/or provide fire resistance. Criteria for selecting other finishes should include protection of insulation against water entry, mechanical abuse, or chemical attack. Appearance, life-cycle cost, and fire resistance may also be determining factors. Finish may be secured with tape, adhesive, bands, or screws. Fasteners which will penetrate vapor-retarder finishes should not be used.

Tanks, Vessels, and Equipment Flat, curved, and irregular surfaces such as tanks, vessels, boilers, and breechings are normally insulated with flat blocks, beveled lags, curved segments, blankets, or spray-applied insulation. Since no general procedure can apply to all materials and conditions, it is important that manufacturers' specifications and instructions be followed for specific insulation applications.

Method of Securing On small-diameter cylindrical vessels, the insulation may be secured by banding around the circumference. On larger cylindrical vessels, banding may be supplemented with angle-iron ledges to support the insulation and prevent slipping. On large flat and cylindrical surfaces, banding or wiring may be supplemented with various types of welded studs or pins. Breather springs may be required with bands to accommodate expansion and contraction.

Finish The materials are the same as for pipe and should satisfy the same criteria. Breather springs may be required with bands.

ADDITIONAL REFERENCES: *ASHRAE Handbook and Product Directory: Fundamentals*, American Society of Heating, Refrigerating and Air Conditioning Engineers, Atlanta, 1981. Turner and Malloy, *Handbook of Thermal Insulation Design Economics for Pipes and Equipment*, Krieger, New York, 1980. Turner and Malloy, *Thermal Insulation Handbook*, McGraw-Hill, New York, 1981.

AIR CONDITIONING

INTRODUCTION

Air Conditioning is the process of treating air so as to control simultaneously its temperature, humidity, cleanliness, and distribution to meet the requirements of the conditioned space. The portions relating only to temperature and humidity control will be discussed here. For detailed discussions of air cleanliness and distribution, refer, for example, to the current edition of the *HVAC Applications* volume of the *A.S.H.R.A.E. Handbooks* (ASHRAE, 1791 Tullie Circle, N.E., Atlanta, Ga.). Applications of air conditioning include the promotion of human comfort and the maintenance of proper conditions for the manufacture, processing, and preserving of material and equipment. Also, in industrial environments where, for economical or other reasons, conditions cannot be made entirely comfortable, air conditioning may be used for maintaining the efficiency and health of workers at safe tolerance limits.

COMFORT AIR CONDITIONING

Comfort is influenced by temperature, humidity, air velocity, radiant heat, clothing, and work intensity. Psychological factors may also influence comfort, but their discussion is beyond the scope of this handbook. The reader is referred to Chap. 42 of the *HVAC Applications* volume of the *A.S.H.R.A.E. Handbooks* for a full discussion of the control of noise, which must also be considered in air-conditioning design. Figure 5 in Chap. 8 of the *HVAC Fundamentals* volume of the *A.S.H.R.A.E. Handbooks* relates the variables of ambient temperature, dew point temperature (or humidity ratio) to comfort under clothing and activity conditions typical for office space occupancy. It also shows boundary values for ET^* , the effective temperature index. This index combines temperature and moisture conditions into a

single index representing the temperature of an environment at 50 percent relative humidity resulting in the same heat transfer from the skin as for the actual case. Hence, the ET^* for 50 percent relative humidity is equal in value to the ambient dry-bulb temperature.

INDUSTRIAL AIR CONDITIONING

Industrial buildings have to be designed according to their intended use. For instance, the manufacture of hygroscopic materials (paper, textiles, foods, etc.) will require relatively tight controls of relative humidity. On the other hand, the storage of furs will demand relatively low temperatures, while the ambient in a facility manufacturing refractories might be acceptable at notably higher temperatures. Chapter 12 of the *HVAC Applications* volume of the *A.S.H.R.A.E. Handbooks* provides extensive tables of suggested temperatures and humidities for industrial air conditioning.

VENTILATION

In the design of comfort air-conditioning systems, odors arising from occupants, cooking, or other sources must be controlled. This is accomplished by introducing fresh air or purified recirculated air in sufficient quantities to reduce odor concentrations to an acceptable level by dilution. Recommended fresh-air requirements for different types of buildings are called for in A.S.H.R.A.E. standard 62-1989 "Ventilation for Acceptable Indoor Air Quality." These values range in the order of 15 to 30 cfm per person, according to application.

In industrial air-conditioning systems, harmful environmental gases, vapors, dusts, and fumes are often encountered. These contaminants can be controlled by exhaust systems at the source, by dilution

ventilation, or by a combination of the two methods. When exhaust systems are used, it is necessary to introduce sufficient fresh air into the air-conditioned area to make up for that exhausted. Generally, low exhaust systems are used where the contaminant sources are concentrated and/or where the contaminant may be highly toxic. Where the contaminant comes from widely dispersed points, however, dilution ventilation is usually employed. Combinations of the two systems sometimes provide the least expensive installation. dilution ventilation is not appropriate for cases where large volumes of contaminant are released and cases where the employees must work near the contaminant source. The selection of dilution ventilation for cases with potential fire or smoke should be accompanied by careful study. Details for design of dilution ventilation systems are given in Chap. 25 of the *HVAC Applications* volume of the *A.S.H.R.A.E. Handbooks*. Chapter 27 of the same volume discusses industrial exhaust systems. Exhaust stacks should be high enough to adequately disperse the contaminated air and to prevent recirculation into fresh air intakes (Chap. 14 of the 1993 *HVAC Fundamentals* volume of the *A.S.H.R.A.E. Handbooks*). Depending on the contaminant and air pollution legislation, it may be necessary to reduce the contaminant emission rate by such methods as filtering, scrubbing, catalytic oxidation, or incineration.

AIR-CONDITIONING EQUIPMENT

Basically, an air-conditioning system consists of a fan unit which forces a mixture of fresh outdoor air and room air through a series of devices which act upon the air to clean it, to increase or decrease its temperature, and to increase or decrease its water-vapor content or humidity. In general, air conditioning equipment can be classified into two broad types: central (sometimes called field erected) and unitary (or packaged).

CENTRAL SYSTEMS

Figure 11-69 describes a typical central system. Either water or direct-expansion refrigerant coils or air washers may be used for cooling. Steam or hot-water coils are available for heating. Humidification may be provided by target-type water nozzles, pan humidifiers, air washers,

or sprayed coils. Air cleaning is usually provided by cleanable or throw-away filters. Central-station air-conditioning units in capacities up to about 50,000 cu ft/min are available in prefabricated units.

The principle types of refrigeration equipment used in large central systems are: Reciprocating (up to 300 hp); helical rotary (up to 750 tons); absorption (up to 2000 tons); and centrifugal (up to 10,000 tons). The drives for the reciprocating, rotary, and centrifugal compressors may be electric motors, gas or steam turbines, or gas or diesel engines. The heat rejected from the condensers usually calls for cooling towers or air-cooled condensers; in some cases evaporative cooling might be practical.

UNITARY REFRIGERANT-BASED AIR-CONDITIONING SYSTEMS

These systems include window-mounted air conditioners and heat pumps, outdoor unitary equipment, indoor unitary equipment, unitary self-contained systems, and commercial self-contained systems. These are described in detail in the *HVAC Systems and Equipment* volume of the *A.S.H.R.A.E. Handbooks*. A detailed analysis of the proposed installation is usually necessary to select the air conditioning equipment which is best in overall performance. Each type of air conditioner has its own particular advantages and disadvantages. Important factors to be considered in the selection of air conditioning equipment are degree of temperature and humidity control required, investment, owning, and operating costs, and space requirements. Another important factor is the building itself, that is, whether it is new or existing construction. For example, for existing buildings where it may be inadvisable to install air-supply ducts, the self-contained or unit-type air conditioner may offer the greatest advantages in reduced installation costs. For large industrial processes where close temperature and humidity control are required, a central station system is usually employed.

LOAD CALCULATION

First step in the solution of an air-conditioning problem is to determine the proper design temperature conditions. Since both outdoor and indoor temperatures greatly influence the size of the equipment, the designer must exercise good judgment in selecting the proper conditions for his/her particular case. Table 11-24 lists winter and summer outdoor temperature conditions in common use for comfort applications for various United States cities. For critical-process air conditioning, it may be desirable to use a different set of outdoor temperature conditions. However, it is seldom good practice to design for the extreme maximum or minimum outside conditions. (See the 1993 *HVAC Fundamentals* volume of the *A.S.H.R.A.E. Handbooks*).

After the proper inside and summer outside temperature conditions for comfort and temperature conditions for process air conditioning have been selected, the next step is to calculate the space cooling load, which is made up of sensible heat and latent heat loads. The sensible heat load consists of (1) transmission through walls, roofs, floors, ceilings, and window glass, (2) solar and sky radiation, (3) heat gains from infiltration of outside air, (4) heat gains from people, lights, appliances, and power equipment (including the supply-air fan motor), and (5) heat to be removed from materials or products brought in at higher than room temperature. The latent heat load includes loads due to moisture (1) given off from people, appliances, and products and (2) from infiltration of outside air. The space total heat load is the sum of the sensible heat load and latent heat load of the space. The total refrigeration load consists of the total space load plus the sensible and latent heat loads from the outside air introduced at the conditioning unit.

The procedure for load calculation in nonresidential buildings should account for thermal mass (storage) effects as well as occupancy and other uses affecting the load. The load can in turn be strongly dependent on the nature of the building utilization; as an example, lightning might be a major component in the thermal load for a high-rise office building causing a need for cooling even in winter days. There are various approaches to load calculation, some requiring elaborate computer models. Chapter 26 of the 1993 *HVAC Fundamentals* volume of the *A.S.H.R.A.E. Handbooks* presents a step-by-step outline of the current methods in practice for load calculation.

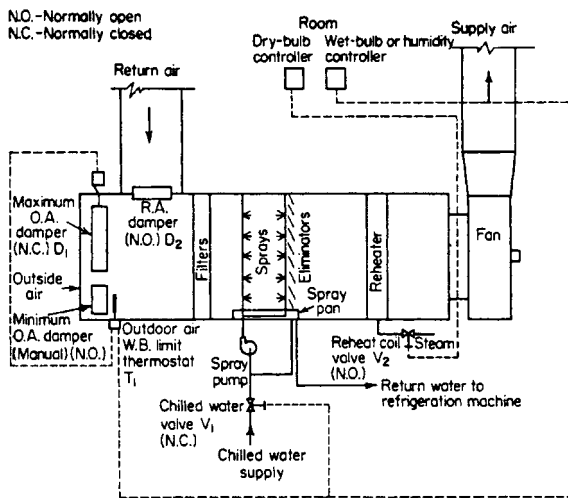


FIG. 11-69 Typical central-station air-conditioning unit and control system. On a rising room wet-bulb temperature, the wet-bulb branch-line air pressure increases through the reverse-acting outdoor-air wet-bulb temperature-limit thermostat T_1 to open gradually the maximum outdoor-air damper D_1 and simultaneously close return-air damper D_2 , then gradually open chilled-water valve V_1 . On a rising room dry-bulb temperature, the dry-bulb branch-line air pressure gradually increases to close reheat steam valve V_2 . When outdoor wet-bulb temperature exceeds the set point of the outdoor-air wet-bulb-limit thermostat T_1 , which is set at the return-air wet-bulb temperature, this thermostat decreases branch-line pressure to close gradually maximum outdoor damper D_1 and simultaneously open return-air damper D_2 . The reverse sequences are followed during the heating season.

TABLE 11-24 Outdoor Design Temperatures*

City-state	Winter	Summer		City-state	Winter	Summer	
	Dry bulb, °F.	Dry bulb, °F.	Wet bulb, °F.		Dry bulb, °F.	Dry bulb, °F.	Wet bulb, °F.
Akron, Ohio	-5	95	75	Milwaukee, Wis.	-15	95	75
Albany, N.Y.	-10	93	75	Minneapolis, Minn.	-20	95	75
Albuquerque, N.M.	0	95	70	Nashville, Tenn.	0	95	78
Atlanta, Ga.	10	95	76	New Haven, Conn.	0	95	75
Baltimore, Md.	0	95	78	New Orleans, La.	20	95	80
Billings, Mont.	-25	90	66	New York, N.Y.	0	95	75
Birmingham, Ala.	10	95	78	Newark, N.J.	0	95	75
Bloomfield, N.J.	0	95	75	Norfolk, Va.	15	95	78
Boise, Idaho	-10	95	65	Oakland, Calif.	30	85	65
Boston, Mass.	0	92	75	Oklahoma City, Okla.	0	101	77
Bridgeport, Conn.	0	95	75	Omaha, Nebr.	-10	95	78
Buffalo, N.Y.	-5	93	73	Peoria, Ill.	-10	96	76
Charleston, S.C.	15	95	78	Philadelphia, Pa.	0	95	78
Chattanooga, Tenn.	10	95	76	Phoenix, Ariz.	0	105	76
Chicago, Ill.	-10	95	75	Pittsburgh, Pa.	-5	95	75
Cincinnati, Ohio	0	95	78	Portland, Me.	-5	90	73
Cleveland, Ohio	0	95	75	Portland, Ore.	10	90	68
Columbus, Ohio	-10	95	76	Providence, R.I.	0	93	75
Dallas, Tex.	0	100	78	Reno, Nev.	-5	95	65
Dayton, Ohio	0	95	78	Richmond, Va.	15	95	78
Denver, Colo.	-10	95	64	Roanoke, Va.	0	95	76
Des Moines, Iowa	-15	95	78	Rochester, N.Y.	-5	95	75
Detroit, Mich.	-10	95	75	St. Louis, Mo.	0	95	78
Duluth, Minn.	-25	93	73	St. Paul, Minn.	-20	95	75
East Orange, N.J.	0	95	75	Salt Lake City, Utah	-10	95	65
El Paso, Tex.	10	100	69	San Antonio, Tex.	20	100	78
Erie, Pa.	-5	93	75	San Francisco, Calif.	35	85	65
Fitchburg, Mass.	-10	93	75	Schenectady, N.Y.	-10	93	75
Flint, Mich.	-10	95	75	Seranton, Pa.	-5	95	75
Fort Wayne, Ind.	-10	95	75	Seattle, Wash.	15	85	65
Fort Worth, Tex.	10	100	78	Shreveport, La.	20	100	78
Grand Rapids, Mich.	-10	95	75	Sioux City, Iowa	-20	95	78
Hartford, Conn.	0	93	75	Spokane, Wash.	-15	93	65
Houston, Tex.	20	95	80	Springfield, Mass.	-10	93	75
Indianapolis, Ind.	-10	95	76	Syracuse, N.Y.	-10	93	75
Jacksonville, Fla.	25	95	78	Tampa, Fla.	30	95	78
Jersey City, N.J.	0	95	75	Toledo, Ohio	-10	95	75
Kansas City, Mo.	-10	100	76	Tucson, Ariz.	25	105	72
Lincoln, Nebr.	-10	95	78	Tulsa, Okla.	0	101	77
Little Rock, Ark.	5	95	78	Washington, D.C.	0	95	78
Long Beach, Calif.	35	90	70	Wichita, Kans.	-10	100	75
Los Angeles, Calif.	35	90	70	Wilmington, Del.	0	95	78
Louisville, Ky.	0	95	78	Worcester, Mass.	0	93	75
Memphis, Tenn.	0	95	78	Youngstown, Ohio	-5	95	75
Miami, Fla.	35	91	79				

*Carrier, Cherne, Grant, and Roberts, *Modern Air Conditioning, Heating, and Ventilating*, 3d ed., p. 531, Pitman, New York, 1959.

REFRIGERATION

INTRODUCTION

Refrigeration is a process where heat is transferred from a lower- to a higher-temperature level by doing work on a system. In some systems heat transfer is used to provide the energy to drive the refrigeration cycle. All refrigeration systems are heat pumps ("pumps energy from a lower to a higher potential"). The term heat pump is mostly used to describe refrigeration system applications where heat rejected to the condenser is of primary interest.

There are many means to obtain refrigerating effect, but here three will be discussed: mechanical vapor refrigeration cycles, absorption and steam jet cycles due to their significance for industry.

Basic Principles Since refrigeration is the practical application of the thermodynamics, comprehending the basic principles of thermodynamics is crucial for full understanding of refrigeration. Section 4 includes a through approach to the theory of thermodynamics. Since our goal is to understand refrigeration processes, cycles are of the crucial interest.

The Carnot refrigeration cycle is reversible and consists of adiabatic (isentropic due to reversible character) compression (1-2), isothermal rejection of heat (2-3), adiabatic expansion (3-4) and isothermal addition of heat (4-1). The temperature-entropy diagram is shown in Fig. 11-70. The Carnot cycle is an unattainable ideal which serves as a standard of comparison and it provides a convenient guide to the temperatures that should be maintained to achieve maximum effectiveness.

The measure of the system performance is *coefficient of performance* (COP). For refrigeration applications COP is the ratio of heat removed from the low-temperature level (Q_{low}) to the energy input (W):

$$COP_R = \frac{Q_{low}}{W} \quad (11-84)$$

For the heat pump (HP) operation, heat rejected at the high temperature (Q_{high}) is the objective, thus:

$$COP_{HP} = \frac{Q_{high}}{W} = \frac{Q + W}{W} = COP_R + 1 \quad (11-85)$$

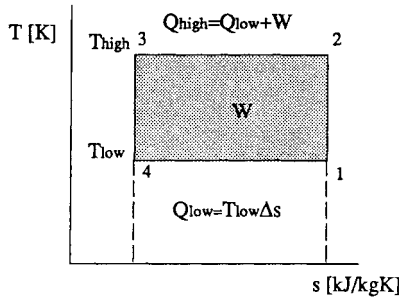


FIG. 11-70 Temperature-entropy diagram of the Carnot cycle.

For a Carnot cycle (where $\Delta Q = T\Delta s$), the COP for the refrigeration application becomes (note that T is absolute temperature [K]):

$$COP_R = \frac{T_{low}}{T_{high} - T_{low}} \quad (11-86)$$

and for heat pump application:

$$COP_{HP} = \frac{T_{high}}{T_{high} - T_{low}} \quad (11-87)$$

The COP in real refrigeration cycles is always less than for the ideal (Carnot) cycle and there is constant effort to achieve this ideal value.

Basic Refrigeration Methods Three basic methods of refrigeration (mentioned above) use similar processes for obtaining refrigeration effect: evaporation in the evaporator, condensation in the condenser where heat is rejected to the environment, and expansion in a flow restrictor. The main difference is in the way compression is being done (Fig. 11-71): using mechanical work (in compressor), thermal energy (for absorption and desorption), or pressure difference (in ejector).

In the next figure (Fig. 11-72) basic refrigeration systems are displayed more detailed. More elaborated approach is presented in the text.

MECHANICAL REFRIGERATION (VAPOR-COMPRESSION SYSTEMS)

Vapor-Compression Cycles The most widely used refrigeration principle is vapor compression. Isothermal processes are realized through isobaric evaporation and condensation in the tubes. Standard vapor compression refrigeration cycle (counterclockwise Rankine cycle) is marked in Fig. 11-72a) by 1, 2, 3, 4.

Work that could be obtained in turbine is small, and iturbine is substituted for an expansion valve. For the reasons of proper compressor

function, wet compression is substituted for an compression of dry vapor.

Although the T - s diagram is very useful for thermodynamic analysis, the pressure enthalpy diagram is used much more in refrigeration practice due to the fact that both evaporation and condensation are isobaric processes so that heat exchanged is equal to enthalpy difference $\Delta Q = \Delta h$. For the ideal, isentropic compression, the work could be also presented as enthalpy difference $\Delta W = \Delta h$. The vapor compression cycle (Rankine) is presented in Fig. 11-73 in p - h coordinates.

Figure 11-74 presents actual versus standard vapor-compression cycle. In reality, flow through the condenser and evaporator must be accompanied by pressure drop. There is always some subcooling in the condenser and superheating of the vapor entering the compressor-suction line, both due to continuing process in the heat exchangers and the influence of the environment. Subcooling and superheating are usually desirable to ensure only liquid enters the expansion device. Superheating is recommended as a precaution against droplets of liquid being carried over into the compressor.

There are many ways to increase cycle efficiency (COP). Some of them are better suited to one, but not for the other refrigerant. Sometimes, for the same refrigerant, the impact on COP could be different for various temperatures. One typical example is the use of a liquid-to-suction heat exchanger (Fig. 11-75).

The suction vapor coming from the evaporator could be used to subcool the liquid from the condenser. Graphic interpretation in T - s diagram for such a process is shown in Fig. 11-76. The result of the use of suction line heat exchanger is to increase the refrigeration effect ΔQ and to increase the work by ΔW . The change in COP is then:

$$\Delta COP = COP' - COP = \frac{Q + \Delta Q}{(P + \Delta P) - Q/P} \quad (11-88)$$

When dry, or superheated, vapor is used to subcool the liquid, the COP in R12 systems will increase, and decrease the COP in NH_3 systems. For R22 systems it could have both effects, depending on the operating regime. Generally, this measure is advantageous (COP is improved) for fluids with high, specific heat of liquid (less-inclined saturated-liquid line on the p - h diagram), small heat of evaporation h_{fg} , when vapor-specific heat is low (isobars in superheated regions are steep), and when the difference between evaporation and condensation temperature is high. Measures to increase COP should be studied for every refrigerant. Sometimes the purpose of the suction-line heat exchanger is not only to improve the COP, but to ensure that only the vapor reaches the compressor, particularly in the case of a malfunctioning expansion valve.

The system shown in Fig. 11-75 is direct expansion where dry or slightly superheated vapor leaves the evaporator. Such systems are predominantly used in small applications because of their simplicity and light weight. For the systems where efficiency is crucial (large industrial systems), recirculating systems (Fig. 11-77) are more appropriate.

Ammonia refrigeration plants are almost exclusively built as recirculating systems. The main advantage of recirculating versus direct expansion systems is better utilization of evaporator surface area. The diagram showing influence of quality on the local heat-transfer coefficients is shown in figure 11-90. It is clear that heat-transfer characteristics will be better if the outlet quality is lower than 1. Circulation could be achieved either by pumping (mechanical or gas) or using gravity (thermosiphon effect: density of pure liquid at the evaporator entrance is higher than density of the vapor-liquid mixture leaving the evaporator). The circulation ratio (ratio of actual mass flow rate to the evaporated mass flow rate) is higher than 1 and up to 5. Higher values are not recommended due to a small increase in heat-transfer rate for a significant increase in pumping costs.

Multistage Systems When the evaporation and condensing pressure (or temperature) difference is large, it is prudent to separate compression in two stages. The use of multistage systems opens up the opportunity to use flash-gas removal and intercooling as measures to improve performance of the system. One typical two-stage system with two evaporating temperatures and both flash-gas removal and intercooling is shown in figure 11-78. The purpose of the flash-tank intercooler is to: (1) separate vapor created in the expansion process,

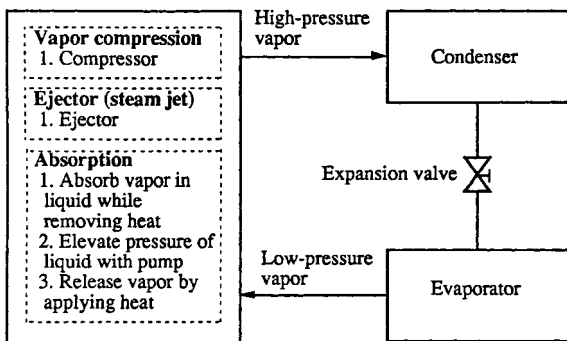


FIG. 11-71 Methods of transforming low-pressure vapor into high-pressure vapor in refrigeration systems (Stoecker, Refrigeration and Air Conditioning).

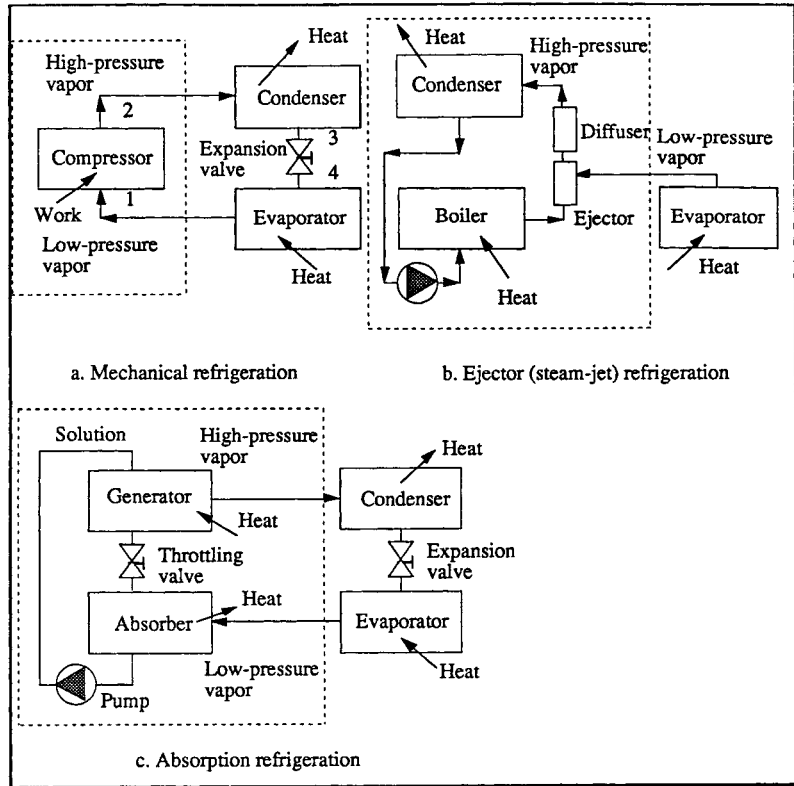


FIG. 11-72 Basic refrigeration systems.

(2) cool superheated vapor from compressor discharge, and (3) to eventually separate existing droplets at the exit of the medium-temperature evaporator. The first measure will decrease the size of the low-stage compressor because it will not wastefully compress the portion of the flow which cannot perform the refrigeration and second will decrease the size of the high-stage compressor due to lowering

the specific volume of the vapor from the low-stage compressor discharge, positively affecting operating temperatures of the high-stage compressor due to cooling effect.

If the refrigerating requirement at a low-evaporating temperature is Q_l and at the medium level is Q_m , then mass flow rates (m_l and m_m

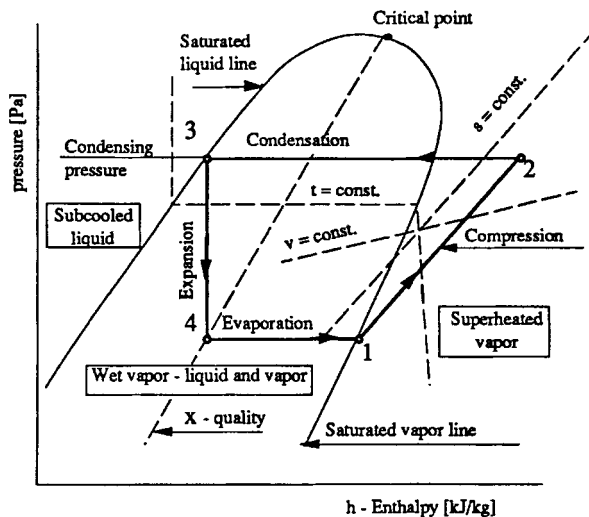


FIG. 11-73 p-h diagram for vapor-compression cycle.

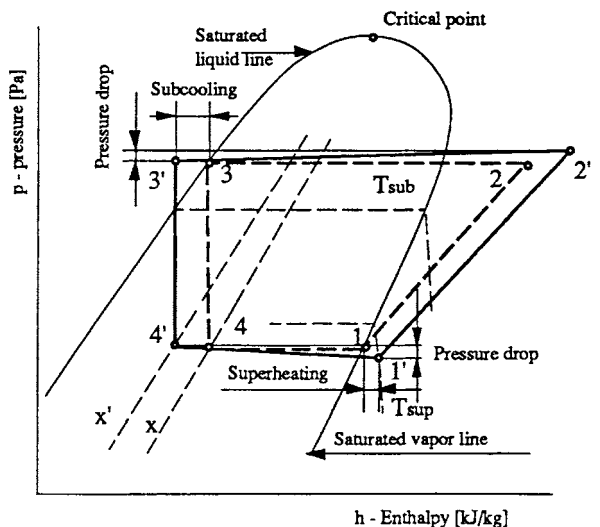


FIG. 11-74 Actual vapor-compression cycle compared with standard cycle.

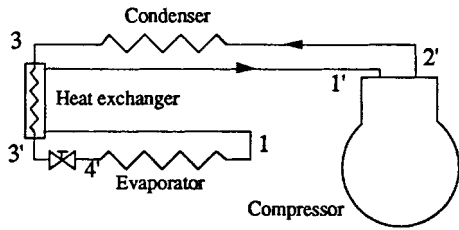


FIG. 11-75 Refrigeration system with a heat exchanger to subcool the liquid from the condenser.

respectively) needed are:

$$m_1 = \frac{Q_l}{h_1 - h_8} = \frac{Q_l}{h_1 - h_7} \quad (11-89)$$

$$m_m = \frac{Q_m}{h_3 - h_6} \quad (11-90)$$

The mass flow rate at the flash-tank inlet m_i consists of three components ($m_i = m_1 + m_{sup} + m_{flash}$):

- m_l = liquid at p_m feeding low temperature evaporator,
- m_{sup} = liquid at p_m to evaporate in flash tank to cool superheated discharge,
- m_{flash} = flashed refrigerant, used to cool remaining liquid.

Vapor component is:

$$m_{flash} = x_m * m_i \quad (11-91)$$

and liquid component is:

$$(1 - x_m) * m_i = m_1 + m_{sup} \quad (11-92)$$

Liquid part of flow to cool superheated compressor discharge is determined by:

$$m_{sup} = \frac{Q_l}{h_1 - h_8} * \frac{h_2 - h_3}{h_3 - h_7} = m_1 * \frac{h_2 - h_3}{h_{fgm}} \quad (11-93)$$

Since the quality x_m is:

$$x_m = \frac{h_6 - h_7}{h_3 - h_7} \quad (11-94)$$

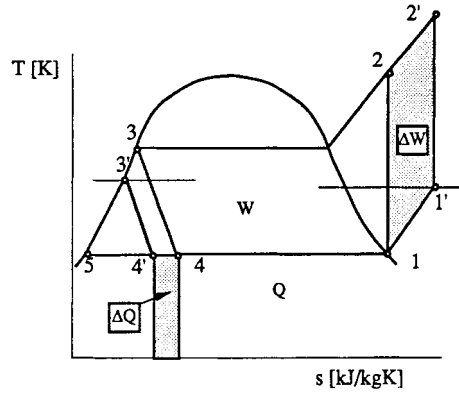


FIG. 11-76 Refrigeration system with a heat exchanger to subcool the liquid from the condenser.

mass flow rate through condenser and high-stage compressor m_h is finally:

$$m_h = m_m + m_i \quad (11-95)$$

The optimum intermediate pressure for the two-stage refrigeration cycles is determined as the geometric mean between evaporation

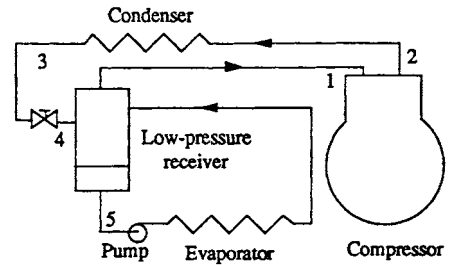


FIG. 11-77 Recirculation system.

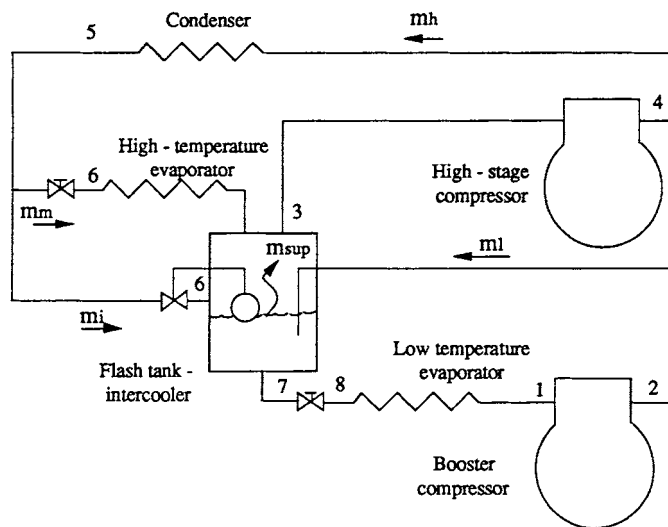


FIG. 11-78 Typical two-stage system with two evaporating temperatures, flash-gas removal, and intercooling.

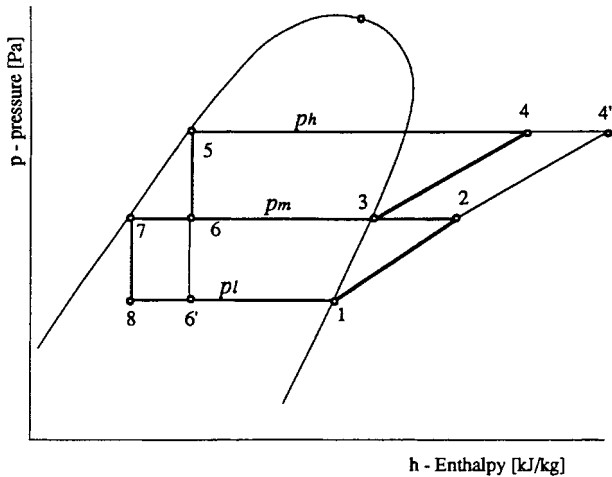


FIG. 11-79 Pressure enthalpy diagram for typical two-stage system with two evaporating temperatures, flash-gas removal, and intercooling.

pressure (p_l) and condensing pressure (p_h , Fig. 11-79):

$$p_m = (\text{sqrt}) \left(\frac{p_h}{p_l} \right)$$

based on equal pressure ratios for low- and high-stage compressors. Optimum interstage pressure is slightly higher than the geometric mean of the suction and the discharge pressures, but, due to very flat optimum of power versus interstage pressure relation geometric mean, it is widely accepted for determining the intermediate pressure. Required pressure of intermediate-level evaporator may dictate interstage pressure other than determined as optimal.

Two-stage systems should be seriously considered when the evaporating temperature is below -20°C . Such designs will save on power and reduce compressor discharge temperatures, but will increase initial cost.

Cascade System This is a reasonable choice in cases when the evaporating temperature is very low (below -60°C). When condensing pressures are to be in the rational limits, the same refrigerant has a high, specific volume at very low temperatures, requiring a large compressor. The evaporating pressure may be below atmospheric, which could cause moisture and air infiltration into the system if there is a leak. In other words, when the temperature difference between the medium that must be cooled and the environment is too high to be served with one refrigerant, it is wise to use different refrigerants in the high and low stages. Figure 11-80 shows a cascade system

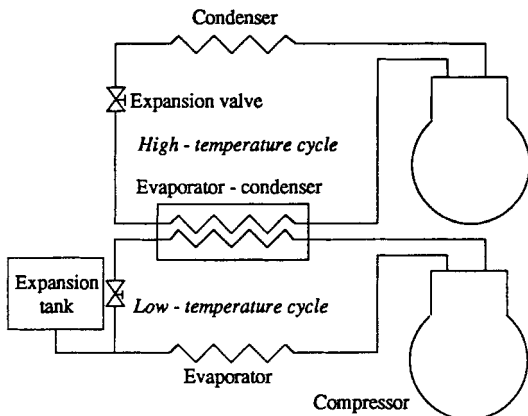


FIG. 11-80 Cascade system.

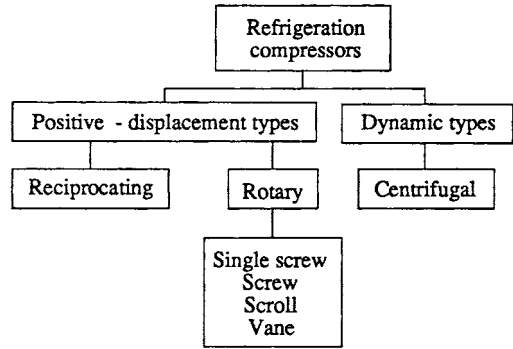


FIG. 11-81 Types of refrigeration compressors.

schematic diagram. There are basically two independent systems linked via a heat exchanger: the evaporator of the high-stage and the condenser of the low-stage system.

EQUIPMENT

Compressors These could be classified by one criteria (the way the increase in pressure is obtained) as positive-displacement and dynamic types as shown in Fig. 11-81 (see Sec. 10 for drawings and mechanical description of the various types of compressors). *Positive-displacement compressors* (PDC) are the machines that increase the pressure of the vapor by reducing the volume of the chamber. Typical PDC are reciprocating (in a variety of types) or rotary as screw (with one and two rotors), vane, scroll, and so on. Centrifugal or turbocompressors are machines where the pressure is raised converting some of kinetic energy obtained by a rotating mechanical element which continuously adds angular momentum to a steadily flowing fluid, similar to a fan or pump.

Generally, reciprocating compressors dominate in the range up to 300 kW refrigeration capacity. Centrifugal compressors are more accepted for the range over 500 kW, while screw compressors are in between with a tendency to go toward smaller capacities. The vane and the scroll compressors are finding their places primarily in very low capacity range (domestic refrigerators and the air conditioners), although vane compressors could be found in industrial compressors. Frequently, screw compressors operate as boosters, for the base load, while reciprocating compressors accommodate the variation of capacity, in the high stage. The major reason is for such design is the advantageous operation of screw compressors near full load and in design conditions, while reciprocating compressors seem to have better efficiencies at part-load operation than screw.

Using other criteria, compressors are classified as *open*, *semihhermetic* (*accessible*), or *hermetic*. Open type is characterized by shaft extension out of compressor where it is coupled to the driving motor. When the electric motor is in the same housing with the compressor mechanism, it could be either hermetic or accessible (semihhermetic). Hermetic compressors have welded enclosures, not designed to be repaired, and are generally manufactured for smaller capacities (seldom over 30 kW), while semihhermetic or an accessible type is located in the housing which is tightened by screws. Semihhermetic compressors have all the advantages of hermetic (no sealing of moving parts, e.g., no refrigerant leakage at the seal shaft, no external motor mounting, no coupling alignment) and could be serviced, but it is more expensive.

Compared to other applications, refrigeration capacities in the chemical industry are usually high. That leads to wide usage of either centrifugal, screw, or high-capacity rotary compressors. Most centrifugal and screw compressors use economizers to minimize power and suction volume requirements. Generally, there is far greater use of open-drive type compressors in the chemical plants than in air-conditioning, commercial, or food refrigeration. Very frequently, compressor lube oil systems are provided with auxiliary oil pumps, filters, coolers, and other equipment to permit maintenance and repair without shut down.

Positive-Displacement Compressors *Reciprocating compressors* are built in different sizes (up to about one megawatt refrigeration capacity per unit). Modern compressors are high-speed, mostly direct-coupled, single-acting, from one to mostly eight, and occasionally up to sixteen cylinders.

Two characteristics of compressors for refrigeration are the most important: refrigerating capacity and power. Typical characteristics are as presented in the Fig. 11-82.

Refrigerating capacity Q_c is the product of mass flow rate of refrigerant m and refrigerating effect R which is (for isobaric evaporation) $R = h_{\text{evaporator outlet}} - h_{\text{evaporator inlet}}$. Power P required for the compression, necessary for the motor selection, is the product of mass flow rate m and work of compression W . The latter is, for the isentropic compression, $W = h_{\text{discharge}} - h_{\text{suction}}$. Both of these characteristics could be calculated for the ideal (without losses) and for the actual compressor. Ideally, the mass flow rate is equal to the product of the compressor displacement V_i per unit time and the gas density ρ : $m = V_i \cdot \rho$. The compressor displacement rate is volume swept through by the pistons (product of the cylinder number n , and volume of cylinder $V = \text{stroke} \cdot d^2 \pi / 4$) per second. In reality, the actual compressor delivers less refrigerant.

Ratio of the actual flow rate (entering compressor) to the displacement rate is the volumetric efficiency η_{va} . The volumetric efficiency is less than unity due to: reexpansion of the compressed vapor in clearance volume, pressure drop (through suction and discharge valves, strainers, manifolds, etc.), internal gas leakage (through the clearance between piston rings and cylinder walls, etc.), valve inefficiencies, and due to expansion of the vapor in the suction cycle caused by the heat exchanged (hot cylinder walls, oil, motor, etc.).

Similar to volumetric efficiency, isentropic (adiabatic) efficiency η_a is the ratio of the work required for isentropic compression of the gas to work input to the compressor shaft. The adiabatic efficiency is less than one mainly due to pressure drop through the valve ports and other restricted passages and the heating of the gas during compression.

Figure 11-83 presents the compression on a pressure-volume diagram for an ideal compressor with clearance volume (thin lines) and

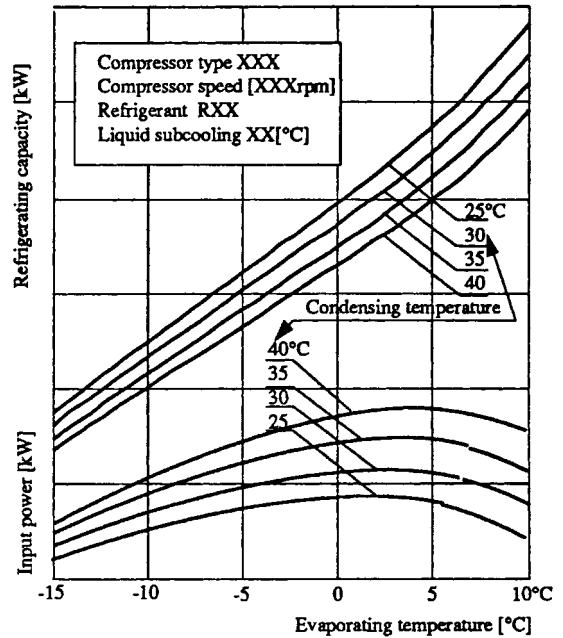


FIG. 11-82 Typical capacity and power-input curves for reciprocating compressor.

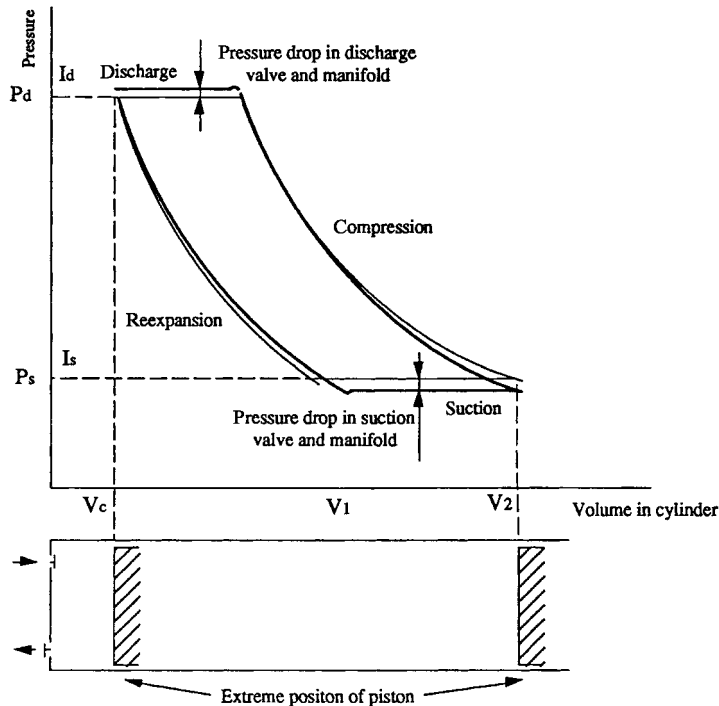


FIG. 11-83 Pressure-volume diagram of an ideal (thin line) and actual (thick line) reciprocating compressor.

actual (thick lines). Compression in an ideal compressor without clearance is extended using dashed lines to the points I_d (end of discharge), line $I_d - I_s$ (suction), and I_s (beginning of suction). The area surrounded by the lines of compression, discharge, reexpansion and intake presents the work needed for compression. Actual compressor only appears to demand less work for compression due to smaller area in the p - V diagram. Mass flow rate for an ideal compressor is higher, which cannot be seen in the diagram. In reality, an actual compressor will have diabatic compression and reexpansion and higher-discharge and lower-suction pressures due to pressure drops in valves and lines. The slight increase in the pressure at the beginning of the discharge and suction is due to forces needed to initially open valves.

When the suction pressure is lowered, the influence of the clearance will increase, causing in the extreme cases the entire volume to be used for reexpansion, which drives the volumetric efficiency to zero.

There are various options for capacity control of reciprocating refrigeration compressors:

1. Opening the suction valves by some external force (oil from the lubricating system, discharge gas, electromagnets . . .).
2. Gas bypassing—returning discharge gas to suction (within the compressor or outside the compressor).
3. Controlling suction pressure by throttling in the suction line.
4. Controlling discharge pressure.
5. Adding reexpansion volume.
6. Changing the stroke.
7. Changing the compressor speed.

The first method is used most frequently. The next preference is for the last method, mostly used in small compressors due to problems with speed control of electrical motors. Other means of capacity control are very seldom utilized due to thermodynamic inefficiencies and design difficulties. Energy losses in a compressor, when capacity regulation is provided by lifting the suction valves, are due to friction of gas flowing in and out the unloaded cylinder. This is shown in Fig. 11-84 where the comparison is made for ideal partial load operation, reciprocating, and screw compressors.

Rotary compressors are also PDC types, but where refrigerant flow rotates during compression. Unlike the reciprocating type, rotary compressors have a built-in volume ratio which is defined as volume in cavity when the suction port is closed ($V_s = m * v_s$) over the volume in the cavity when the discharge port is uncovered ($V_d = m * v_d$). Built-in volume ratio determines for a given refrigerant and conditions the pressure ratio which is:

$$\frac{p_d}{p_s} = \left(\frac{v_s}{v_d} \right)^n \quad (11-96)$$

where n represents the polytropic exponent of compression.

In other words, in a reciprocating compressor the discharge valve opens when the pressure in the cylinder is slightly higher than the pressure in the high-pressure side of the system, while in rotary compressors the discharge pressure will be established only by inlet conditions and built-in volume ratio regardless of the system discharge pressure. Very seldom are the discharge and system (condensing)

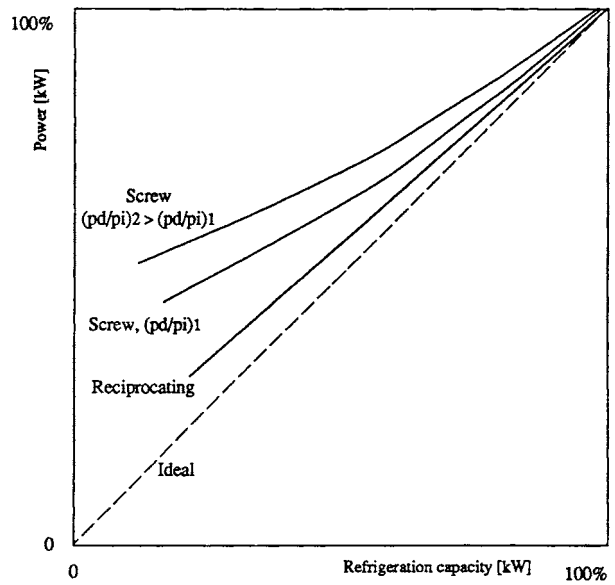


FIG. 11-84 Typical power-refrigeration capacity data for different types of compressors during partial, unloaded operation.

pressure equal, causing the situation shown in Fig. 11-85. When condensing pressure (p) is lower than discharge (p_2), shown as case (a), “over compression” will cause energy losses presented by the horn on the diagram. If the condensing pressure is higher, in the moment when the discharge port uncovers there will be flow of refrigerant backwards into the compressor, causing losses shown in Fig. 11-85b and the last stage will be only discharge without compression. The case when the compressor discharge pressure is equal to the condensing pressure is shown in the Fig. 11-85c.

Double helical rotary (twin) screw compressors consist of two mating helically grooved rotors (male and female) with asymmetric profile, in a housing formed by two overlapped cylinders, with inlet and outlet ports. Developed relatively recently (in 1930s) the first twin screw compressors were used for air, and later (1950s) became popular for refrigeration. Screw compressors have some advantages over reciprocating compressors (fewer moving parts and more compact) but also some drawbacks (lower efficiency at off-design conditions, as discussed above, higher manufacturing cost due to complicated screw geometry, large separators and coolers for oil which is important as a sealant). Figure 11-86 shows the oil circuit of a screw compressor. Oil cooling could be provided by water, glycol, or refrigerant either in the heat-exchanger-utilizing-thermosiphon effect or the using-direct-expansion concept.

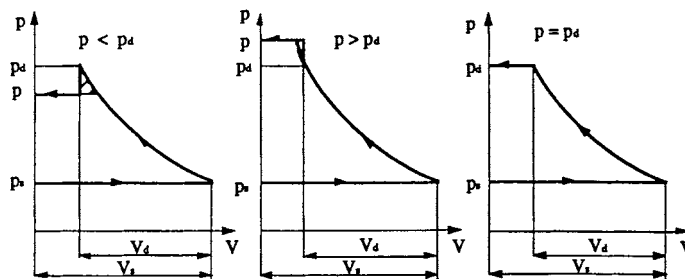


FIG. 11-85 Matching compressor built-in pressure ratio with actual pressure difference.

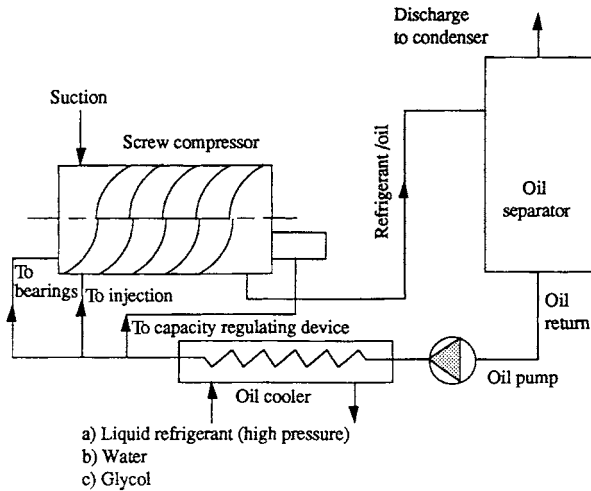


FIG. 11-86 Oil cooling in a screw compressor.

In order to overcome some inherent disadvantages, screw compressors have been initially used predominantly as booster (low-stage) compressors, and following development in capacity control and decreasing prices, they are widely used for high-stage applications. There are several methods for capacity regulation of screw compressors. One is variable speed drive, but a more economical first-cost concept is a slide valve that is used in some form by practically all screw compressors.

The slide is located in the compressor casting below the rotors, allowing internal gas recirculation without compression. Slide valve is operated by a piston located in a hydraulic cylinder and actuated by high-pressure oil from both sides. When the compressor is started, the slide valve is fully open and the compressor is unloaded. To increase capacity, a solenoid valve on the hydraulic line opens, moving the piston in the direction of increasing capacity. In order to increase part-load efficiency, the slide valve is designed to consist of two parts, one traditional slide valve for capacity regulation and other for built-in volume adjustment.

Single screw compressors are a newer design (early 1960s) compared to twin screw compressors, and are manufactured in the range of capacity from 100 kW to 4 MW. The compressor screw is cylindrical with helical grooves mated with two star wheels (gaterotors) rotating in opposite direction from one another. Each tooth acts as the piston in the rotating "cylinder" formed by screw flute and cylindrical main-rotor casting.

As compression occurs concurrently in both halves of the compressor, radial forces are oppositely directed, resulting in negligible net-radial loads on the rotor bearings (unlike twin screw compressors), but there are some loads on the star wheel shafts.

Scroll compressors are currently used in relatively small-sized installations, predominantly for residential air-conditioning (up to 50 kW). They are recognized for low-noise operation. Two scrolls (free-standing, involute spirals bounded on one side by a flat plate) facing each other form a closed volume while one moves in a controlled orbit around a fixed point on the other, fixed scroll.

The suction gas which enters from the periphery is trapped by the scrolls. The closed volumes move radially inward until the discharge port is reached, when vapor is pressed out. The orbiting scroll is driven by a short-throw crank mechanism. Similar to screw compressors, internal leakage should be kept low, and is occurring in gaps between cylindrical surfaces and between the tips of the involute and the opposing scroll base plate.

Similar to the screw compressor, the scroll compressor is a constant-volume-ratio machine. Losses occur when operating conditions of the compressor do not match the built-in volume ratio (see Fig. 11-85).

Vane compressors are used in small, hermetic units, but sometimes as booster compressors in industrial applications. Two basic types are

fixed (roller) or single-vane type and the *rotating* or multiple-vane type. In the single-vane type the rotor (called roller) is eccentrically placed in the cylinder so these two are always in contact. The contact line make the first separation between the suction and discharge chambers while the vane (spring-loaded divider) makes the second. In the multiple-vane compressors the rotor and the cylinder are not in the contact. The rotor has two or more sliding vanes which are held against the cylinder by centrifugal force. In the vane rotary compressors, no suction valves are needed. Since the gas enters the compressor continuously, gas pulsations are at minimum. Vane compressors have a high volumetric efficiency because of the small clearance volume and consequent low reexpansion losses. Rotary vane compressors have a low weight-to-displacement ratio, which makes them suitable for transport applications.

Centrifugal Compressors These are sometimes called turbo-compressors and mostly serve refrigeration systems in the capacity range 200 to 10,000 kW. The main component is a spinning impeller wheel, backwards curved, which imparts energy to the gas being compressed. Some of the kinetic energy converts into pressure in a volute. Refrigerating centrifugal compressors are predominantly multistage, compared to other turbocompressors, that produce high-pressure ratios.

The torque T (Nm) the impeller ideally imparts to the gas is:

$$T = m (u_{\text{tang,out}} r_{\text{out}} - u_{\text{tang,in}} r_{\text{in}}) \quad (11-97)$$

where: m (kg/s) = mass flow rate
 r_{out} (m) = radius of exit of impeller
 r_{in} (m) = radius of exit of impeller
 $u_{\text{tang,out}}$ (m/s) = tangential velocity of refrigerant leaving impeller
 $u_{\text{tang,in}}$ (m/s) = tangential velocity of refrigerant entering impeller

When refrigerant enters essentially radially, $u_{\text{tang,in}} = 0$ and torque becomes:

$$T = m * u_{\text{tang,out}} * r_{\text{out}} \quad (11-98)$$

The power P (W), is the product of torque and rotative speed ω [1/s] so is

$$P = T * \omega = m * u_{\text{tang,out}} * r_{\text{out}} * \omega \quad (11-99)$$

which for $u_{\text{tang,out}} = r_{\text{out}} * \omega$ becomes

$$P = m * u_{\text{tang,out}}^2 \quad (11-100)$$

or for isentropic compression

$$P = m * \Delta h \quad (11-101)$$

The performance of a centrifugal compressor (discharge to suction-pressure ratio vs. the flow rate) for different speeds is shown in Fig. 11-87. Lines of constant efficiencies show the maximum efficiency. Unstable operation sequence, called surging, occurs when compressors fails to operate in the range left of the surge envelope. It is characterized by noise and wide fluctuations of load on the compressor and the motor. The period of the cycle is usually 2 to 5 s, depending upon the size of the installation.

The capacity could be controlled by: (1) adjusting the prerotation vanes at the impeller inlet, (2) varying the speed, (3) varying the condenser pressure, and (4) bypassing discharge gas. The first two methods are predominantly used.

Condensers These are heat exchangers that convert refrigerant vapor to a liquid. Heat is transferred in three main phases: (1) desuperheating, (2) condensing, and (3) subcooling. In reality condensation occurs even in the superheated region and subcooling occurs in the condensation region. Three main types of refrigeration condensers are: air cooled, water cooled, and evaporative.

Air-cooled condensers are used mostly in air-conditioning and for smaller-refrigeration capacities. The main advantage is availability of cooling medium (air) but heat-transfer rates for the air side are far below values when water is used as a cooling medium. Condensation always occurs inside tubes, while the air side uses extended surface (fins).

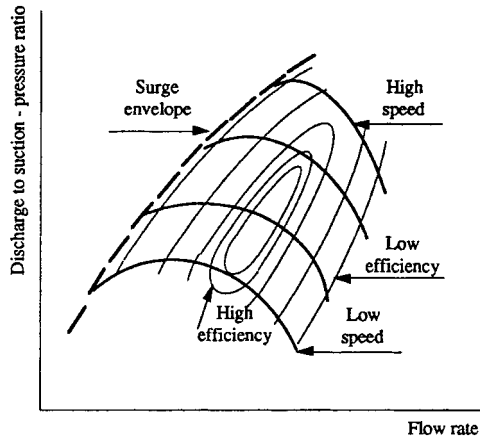


FIG. 11-87 Performance of the centrifugal compressor.

The most common types of water-cooled refrigerant condensers are: (1) shell-and-tube, (2) shell-and-coil, (3) tube-in-tube, and (4) brazed-plate. *Shell-and-tube* condensers are built up to 30 MW capacity. Cooling water flows through the tubes in a single or multipass circuit. Fixed-tube sheet and straight-tube construction are common. Horizontal layout is typical, but sometimes vertical is used. Heat-transfer coefficients for the vertical types are lower due to poor condensate drainage, but less water of lower purity can be utilized. Condensation always occurs on the tubes, and often the lower portion of the shell is used as a receiver. In *shell-and-coil* condensers water circulates through one or more continuous or assembled coils contained within the shell while refrigerant condenses outside. The tubes cannot be mechanically cleaned nor replaced. *Tube-in-tube* condensers could be found in versions where condensation occurs either in the inner tube or in the annulus. Condensing coefficients are more difficult to predict, especially in the cases where tubes are formed in spiral. Mechanical cleaning is more complicated, sometimes impossible, and tubes are not replaceable. *Brazed-plate* condensers are constructed of plates brazed together to make up an assembly of separate channels. The plates are typically stainless steel, wave-style corrugated, enabling high heat-transfer rates. Performance calculation is difficult, with very few correlations available. The main advantage is the highest performance/volume (mass) ratio and the lowest refrigerant charge. The last mentioned advantage seems to be the most important feature for many applications where minimization of charge inventory is crucial.

Evaporative condensers (Fig. 11-88) are widely used due to lower condensing temperatures than in the air-cooled condensers and also lower than the water-cooled condenser combined with the cooling tower. Water demands are far lower than for water-cooled condensers. The chemical industry uses shell-and-tube condensers widely, although the use of air-cooled condensing equipment and evaporative condensers is on the increase.

Generally, cooling water is of a lower quality than normal, having also higher mud and silt content. Sometimes even replaceable copper tubes in shell-and-tube heat exchangers are required. It is advisable to use cupronickel instead of copper tubes (when water is high in chlorides) and to use conservative water side velocities (less than 2 m/s for copper tubes).

Evaporative condensers are used quite extensively. In most cases commercial evaporative condensers are not totally suitable for chemical plants due to the hostile atmosphere which usually abounds in vapor and dusts which can cause either chemical (corrosion) or mechanical problems (plugging of spray nozzles).

Air-cooled condensers are similar to evaporative in that the service dictates either the use of more expensive alloys in the tube construction or conventional materials of greater wall thickness.

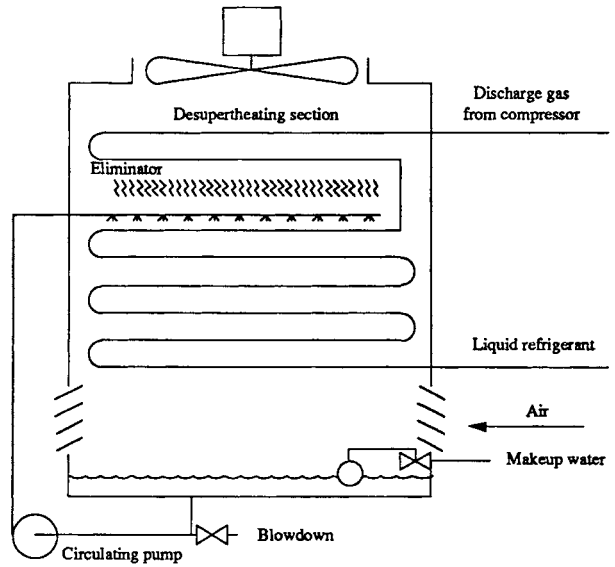


FIG. 11-88 Evaporative condenser with desuperheating coil.

Heat rejected in the condenser Q_{Cd} consists of heat absorbed in the evaporator Q_{Evap} and energy W supplied by the compressor:

$$Q_{Cd} = Q_{Evap} + W \quad (11-102)$$

For the actual systems, compressor work will be higher than for ideal for the isentropic efficiency and other losses. In the case of hermetic or accessible compressors where an electrical motor is cooled by the refrigerant, condenser capacity should be:

$$Q_{Cd} = Q_{Evap} + P_{EM} \quad (11-103)$$

It is common that compressor manufacturers provide data for the ratio of the heat rejected at the condenser to the refrigeration capacity as shown in Fig. 11-89. The solid line represents data for the open compressors while the dotted line represents the hermetic and accessible compressors. The difference between solid and dotted line is due

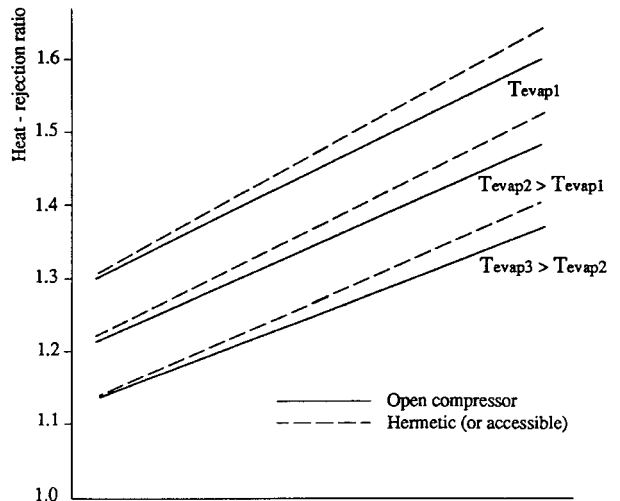


FIG. 11-89 Typical values of the heat-rejection ratio of the heat rejected at the condenser to the refrigerating capacity.

to all losses (mechanical and electrical in the electrical motor). Condenser design is based on the value:

$$Q_{Cd} = Q_{Evap} * \text{heat-rejection ratio} \quad (11-104)$$

Thermal and mechanical design of heat exchangers (condensers and evaporators) is presented earlier in this section.

Evaporators These are heat exchangers where refrigerant is evaporated while cooling the product, fluid, or body. Refrigerant could be in direct contact with the body that is being cooled, or some other medium could be used as secondary fluid. Mostly air, water, or antifreeze are fluids that are cooled. Design is strongly influenced by the application. Evaporators for air cooling will have in-tube evaporation of the refrigerant, while liquid chillers could have refrigerant evaporation inside or outside the tube. The heat-transfer coefficient for evaporation inside the tube (vs. length or quality) is shown in the Fig. 11-90. Fundamentals of the heat transfer in evaporators, as well as design aspects, are presented in Sec. 11. We will point out only some specific aspects of refrigeration applications.

Refrigeration evaporators could be classified according to the method of feed as either direct (dry) expansion or flooded (liquid overfeed). In dry-expansion the evaporator's outlet is dry or slightly superheated vapor. This limits the liquid feed to the amount that can be completely vaporized by the time it reaches the end of evaporator. In the liquid overfeed evaporator, the amount of liquid refrigerant circulating exceeds the amount evaporated by the circulation number. Decision on the type of the system to be used is one of the first in the design process. Direct-expansion evaporator is generally applied in smaller systems where compact design and the low first costs are crucial. Control of the refrigerant mass flow is then obtained by either a thermoexpansion valve or a capillary tube. Figure 11-90 suggests that the evaporator surface is the most effective in the regions with quality which is neither low nor high. In dry-expansion evaporators, inlet qualities are 10–20 percent, but when controlled by the thermoexpansion valve, vapor at the outlet is not only dry, but even superheated.

In recirculating systems saturated liquid ($x = 0$) is entering the evaporator. Either the pump or gravity will deliver more refrigerant liquid than will evaporate, so outlet quality could be lower than one. The ratio of refrigerant flow rate supplied to the evaporator overflow rate of refrigerant vaporized is the circulation ratio, n . When n increases, the coefficient of heat transfer will increase due to the wetted outlet of the evaporator and the increased velocity at the inlet (Fig. 11-91). In the range of $n = 2$ to 4, the overall U value for air cooler increases roughly by 20 to 30 percent compared to the direct-expansion case. Circulation rates higher than four are not efficient.

The price for an increase in heat-transfer characteristics is a more complex system with more auxiliary equipment: low-pressure receivers, refrigerant pumps, valves, and controls. Liquid refrigerant is predominantly pumped by mechanical pumps, however, sometimes gas at condensing pressure is used for pumping, in the variety of concepts.

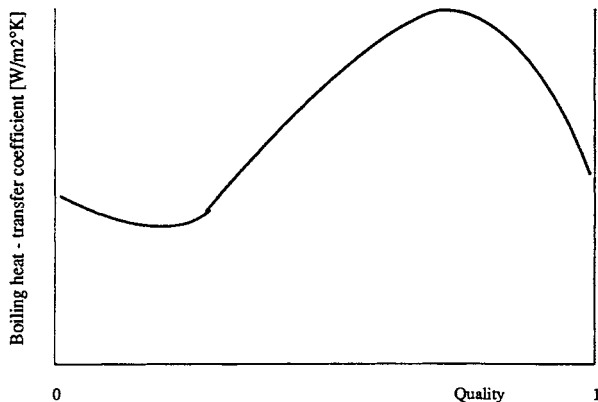


FIG. 11-90 Heat-transfer coefficient for boiling inside the tube.

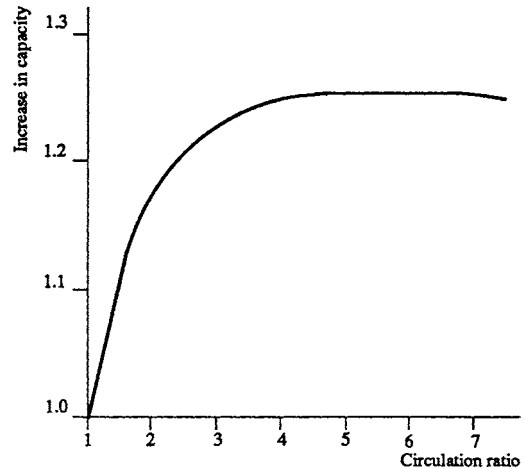


FIG. 11-91 Effect of circulation ratio on the overall heat-transfer coefficient of an air-cooling coil.

The important characteristics of the refrigeration evaporators is the presence of the oil. The system is contaminated with oil in the compressor, in spite of reasonably efficient oil separators. Some systems will recirculate oil, when miscible with refrigerant, returning it to the compressor crankcase. This is found mostly in the systems using halocarbon refrigerants. Although oils that are miscible with ammonia exist, immiscibles are predominantly used. This inhibits the ammonia systems from recirculating the oil. In systems with oil recirculation when halocarbons are used special consideration should be given to proper sizing and layout of the pipes. Proper pipeline configuration, slopes, and velocities (to ensure oil circulation under all operating loads) are essential for good system operation. When refrigerant is lighter than the oil in systems with no oil recirculation, oil will be at the bottom of every volume with a top outlet. Then oil must be drained periodically to avoid decreasing the performance of the equipment.

It is essential for proper design to have the data for refrigerant-oil miscibility under all operating conditions. Some refrigerant-oil combinations will always be miscible, some always immiscible, but some will have both characteristics, depending on temperatures and pressures applied. Defrosting is the important issue for evaporators which are cooling air below freezing. Defrosting is done periodically, actuated predominantly by time relays, but other frost indicators are used (temperature, visual, or pressure-drop sensors). Defrost technique is determined mostly by fluids available and tolerable complexity of the system. Defrosting is done by the following mechanisms when the system is off:

- Hot (or cool) refrigerant gas (the predominant method in industrial applications)
- Water (defrosting from the outside, unlike hot gas defrost)
- Air (only when room temperature is above freezing)
- Electricity (for small systems where hot-gas defrost will be to complex and water is not available)
- Combinations of above.

System Analysis Design calculations are made on the basis of the close to the highest refrigeration load, however the system operates at the design conditions very seldom. The purpose of regulating devices is to adjust the system performance to cooling demands by decreasing the effect or performance of some component. Refrigeration systems have inherent self-regulating control which the engineer could rely on to a certain extent. When the refrigeration load starts to decrease, less refrigerant will evaporate. This causes a drop in evaporation temperature (as long as compressor capacity is unchanged) due to the imbalance in vapor being taken by the compressor and produced by evaporation in evaporator. With a drop in evaporation pressure, the compressor capacity will decrease due to: (1) lower vapor density

(lower mass flow for the same volumetric flow rate) and (2) decrease in volumetric efficiency. On the other hand, when the evaporation temperature drops, for the unchanged temperature of the medium being cooled, the evaporator capacity will increase due to increase in the mean-temperature difference between refrigerant and cooled medium, causing a positive effect (increase) on the cooling load. With a decrease in the evaporation temperature the heat-rejection factor will increase causing an increase of heat rejected to the condenser, but refrigerant mass flow rate will decrease due to compressor characteristics. These will have an opposite effect on condenser load. Even a simplified analysis demonstrates the necessity for better understanding of system performance under different operating conditions. Two methods could be used for more accurate analysis. The traditional method of refrigeration-system analysis is through determination of balance points, while in recent years, system analysis is performed by system simulation or mathematical modeling, using mathematical (equation solving) rather than graphical (intersection of two curves) procedures. Systems with a small number of components such as the vapor-compression refrigeration system could be analyzed both ways. Graphical presentation, better suited for understanding trends is not appropriate for more complex systems, more detailed component description, and frequent change of parameters. There is a variety of different mathematical models tailored to fit specific systems, refrigerants, resources available, demands, and complexity. Although limited in its applications, graphical representation is valuable as the starting tool and for clear understanding of the system performance.

Refrigeration capacity q_e and power P curves for the reciprocating compressor are shown in Fig. 11-92. They are functions of temperatures of evaporation and condensation:

$$q_e = q_e(t_{\text{evap}}, t_{\text{cd}}) \quad (11-105a)$$

and
$$P = P(t_{\text{evap}}, t_{\text{cd}}) \quad (11-105b)$$

where q_e (kW) = refrigerating capacity
 P (kW) = power required by the compressor
 t_{evap} (°C) = evaporating temperature
 t_{cd} (°C) = condensing temperature.

A more detailed description of compressor performance is shown in the section on the refrigeration compressors.

Condenser performance, shown in figure 11-93, could be simplified as:

$$q_{\text{cd}} = F(t_{\text{cd}} - t_{\text{amb}}) \quad (11-105c)$$

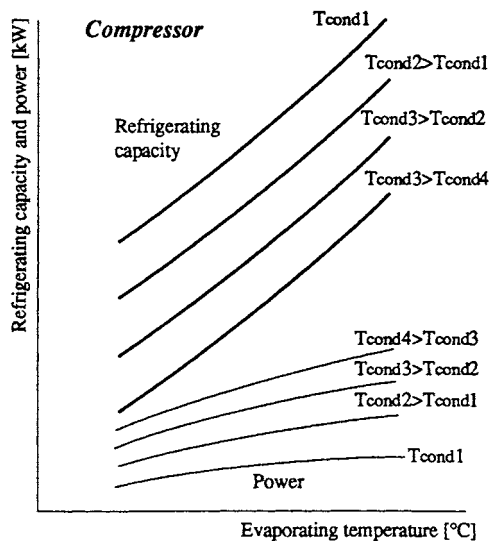


FIG. 11-92 Refrigerating capacity and power requirement for the reciprocating compressor.

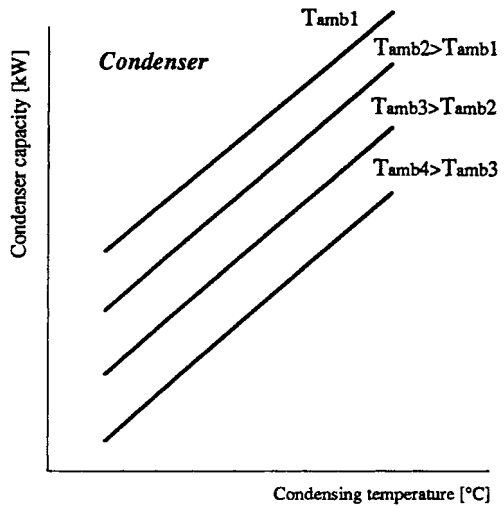


FIG. 11-93 Condenser performance.

where q_{cd} (kW) = capacity of condenser;
 F (kW/°C) = capacity of condenser per unit inlet temperature difference ($F = U * A$);
 t_{amb} (°C) = ambient temperature (or temperature of condenser cooling medium).

In this analysis F will be constant but it could be described more accurately as a function of parameters influencing heat transfer in the condenser (temperature, pressure, flow rate, fluid thermodynamical, and thermophysical characteristics . . .).

Condenser performance should be expressed as “evaporating effect” to enable matching with compressor and evaporator performance. Condenser “evaporating effect” is the refrigeration capacity of an evaporator served by a particular condenser. It is the function of the cycle, evaporating temperature, and the compressor. The “evaporating effect” could be calculated from the heat-rejection ratio q_{cd}/q_e :

$$q_e = \frac{q_{\text{cd}}}{\text{heat-rejection ratio}} \quad (11-105d)$$

The heat-rejection rate is presented in Fig. 11-94 (or Fig. 11-89).

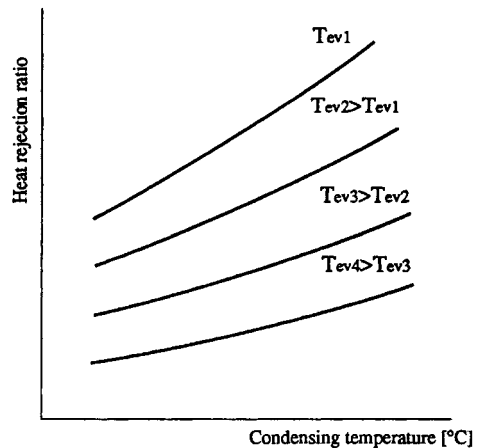


FIG. 11-94 Heat-rejection ratio.

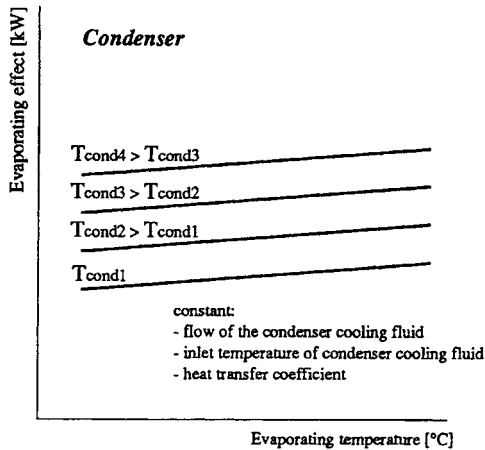


FIG. 11-95 Condenser evaporating effect.

Finally, the evaporating effect of the condenser is shown in Fig. 11-95.

The performance of the condensing-unit (compressor and condenser) subsystem could be developed as shown in Fig. 11-96 by superimposing two graphs, one for compressor performance and the other for condenser evaporating effect.

Evaporator performance could be simplified as:

$$q_e = F_{evap}(t_{amb} - t_{evap}) \quad (11-106)$$

where q_e (kW) = evaporator capacity
 F_e (kW/°C) = evaporator capacity per unit inlet temperature difference
 t_{amb} (°C) = ambient temperature (or temperature of cooled body or fluid).

The diagram of the evaporator performance is shown in the Fig. 11-97. The character of the curvature of the lines (variable heat-transfer rate) indicates that the evaporator is cooling air. Influences of the flow rate of cooled fluid are also shown in this diagram; i.e., higher flow rate will increase heat transfer. The same effect could be shown in the condenser-performance curve. It is omitted only for the reasons of simplicity.

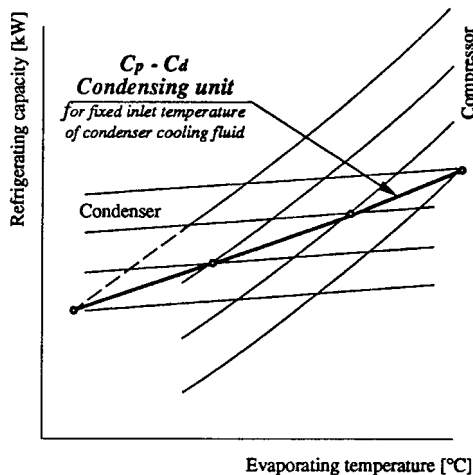


FIG. 11-96 Balance points of compressor and condenser determines performance of condensing unit for fixed temperature of condenser cooling fluid (flow rate and heat-transfer coefficient are constant).

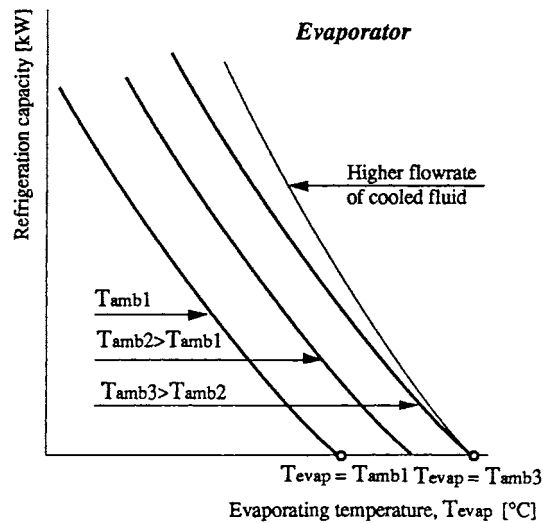


FIG. 11-97 Refrigerating capacity of evaporator.

The performance of the complete system could be predicted by superimposing the diagrams for the condensing unit and the evaporator, as shown in Fig. 11-98. Point 1 reveals a balance for constant flows and inlet temperatures of chilled fluid and fluid for condenser cooling. When this point is transferred in the diagram for the condensing unit in the Figs. 11-95 or 11-96, the condensing temperature could be determined. When the temperature of entering fluid in the evaporator t_{amb1} is lowered to t_{amb2} the new operating conditions will be determined by the state at point 2. Evaporation temperature drops from t_{evap1} to t_{evap2} . If the evaporation temperature should be unchanged, the same reduction of inlet temperature could be achieved by reducing the capacity of the condensing unit from C_p to C_p^* . The new operating point 3 shows reduction in capacity for Δ due to the reduction in the compressor or the condenser capacity.

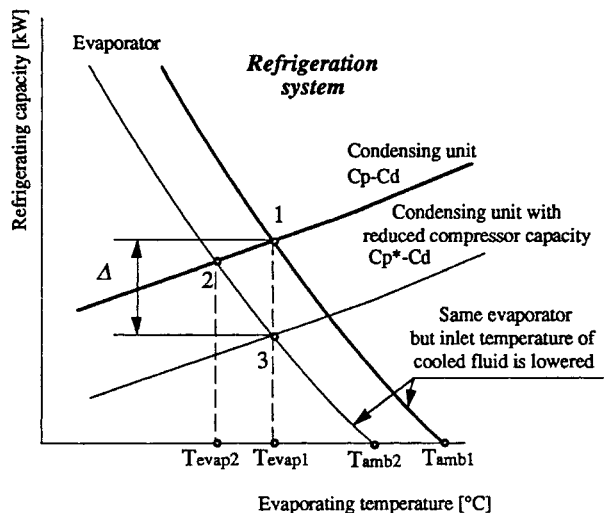


FIG. 11-98 Performance of complete refrigeration system (1), when there is reduction in heat load (2), and when for the same ambient (or inlet in evaporator) evaporation temperature is maintained constant by reducing capacity of compressor/condenser part (3).

Mathematical modeling is essentially the same process, but the description of the component performance is generally much more complex and detailed. This approach enables a user to vary more parameters easier, look into various possibilities for intervention, and predict the response of the system on different influences. Equation-solving does not necessarily have to be done by successive substitution or iteration as this procedure could suggest.

System, Equipment, and Refrigerant Selection There is no universal rule which can be used to decide which system, equipment type, or refrigerant is the most appropriate for a given application. A number of variables influence the final-design decision:

- Refrigeration load
- Type of installation
- Temperature level of medium to be cooled
- Condensing media characteristics: type (water, air, . . .), temperature level, available quantities
- Energy source for driving the refrigeration unit (electricity, natural gas, steam, waste heat)
- Location and space available (urban areas, sensitive equipment around, limited space . . .)
- Funds available (i.e. initial vs. run-cost ratio)
- Safety requirements (explosive environment, aggressive fluids, . . .)
- Other demands (compatibility with existing systems, type of load, compactness, level of automatization, operating life, possibility to use process fluid as refrigerant)

Generally, vapor *compression systems* are considered first. They can be used for almost every task. Whenever it is possible, prefabricated elements or complete units are recommended. Reciprocating compressors are widely used for lower rates, more uneven heat loads (when frequent and wider range of capacity reduction is required). They ask for more space and have higher maintenance costs than centrifugal compressors, but are often the most economical in first costs. Centrifugal compressors are considered for huge capacities, when the evaporating temperature is not too low. Screw compressors are considered first when space in the machine room is limited, when system is operating long hours, and when periods between service should be longer.

Direct-expansions are more appropriate for smaller systems which should be compact, and where there are just one or few evaporators. Overfeed (recirculation) systems should be considered for all applications where first cost for additional equipment (surge drums, low-pressure receivers, refrigerant pumps, and accessories) is lower than the savings for the evaporator surface.

Choice of refrigerant is complex and not straightforward. For industrial applications, advantages of ammonia (thermodynamical and economical) overcome drawbacks which are mostly related to possible low-toxic and panics created by accidental leaks when used in urban areas. Halocarbons have many advantages (not toxic, not explosive, odorless . . .), but environmental issues and slightly inferior thermodynamical and thermophysical properties compared to ammonia or hydrocarbons as well as rising prices are giving the chance to other options. When this text was written the ozone-depletion issue was not resolved, R22 was still used but facing phase-out, and R134a was considered to be the best alternative for CFCs and HCFCs, having similar characteristics to the already banned R12. Very often, fluid to be cooled is used as a refrigerant in the chemical industry. Use of secondary refrigerants in combination with the ammonia central-refrigeration unit is becoming a viable alternative in many applications.

Absorption systems will be considered when there is low-cost low-pressure steam or waste heat available and evaporation temperature and refrigeration load are relatively high. Typical application range is for water chilling at 7–10°C, and capacities from 300 kW to 5 MW in a single unit. The main drawback is the difficulty in maintaining a tight system with the highly corrosive lithium bromide, and an operating pressure in the evaporator and the absorber below atmospheric.

Ejector (steam-jet) refrigeration systems are used for similar applications, when chilled water-outlet temperature is relatively high, when relatively cool condensing water and cheap steam at 7 bar are available, and for similar high duties (0.3–5 MW). Even though these systems usually have low first and maintenance costs, there are not many steam-jet systems running.

OTHER REFRIGERATION SYSTEMS APPLIED IN THE INDUSTRY

Absorption Refrigeration Systems Two main absorption systems are used in industrial application: lithium bromide-water and ammonia-water. Lithium bromide-water systems are limited to evaporation temperatures above freezing because water is used as the refrigerant, while the refrigerant in an ammonia-water system is ammonia and consequently it can be applied for the lower-temperature requirements.

Single-effect indirect-fired lithium bromide cycle is shown in Fig. 11-99. The machine consists of five major components:

Evaporator is the heat exchanger where refrigerant (water) evaporates (being sprayed over the tubes) due to low pressure in the vessel. Evaporation chills water flow inside the tubes that bring heat from the external system to be cooled.

Absorber is a component where strong absorber solution is used to absorb the water vapor flashed in the evaporator. A solution pump sprays the lithium bromide over the absorber tube section. Cool water is passing through the tubes taking refrigeration load, heat of dilution, heat to cool condensed water, and sensible heat for solution cooling.

Heat exchanger is used to improve efficiency of the cycle, reducing consumption of steam and condenser water.

Generator is a component where heat brought to a system in a tube section is used to restore the solution concentration by boiling off the water vapor absorbed in the absorber.

Condenser is an element where water vapor, boiled in the generator, is condensed, preparing pure water (refrigerant) for discharge to an evaporator.

Heat supplied to the generator is boiling weak (dilute) absorbent solution on the outside of the tubes. Evaporated water is condensed on the outside of the condenser tubes. Water utilized to cool the condenser is usually cooled in the cooling tower. Both condenser and generator are located in the same vessel, being at the absolute pressure of about 6 kPa. The water condensate passes through a liquid trap and enters the evaporator. Refrigerant (water) boils on the evaporator tubes and cools the water flow that brings the refrigeration load. Refrigerant that is not evaporated flows to the recirculation pump to be sprayed over the evaporator tubes. Solution with high water concentration that enters the generator increases in concentration as water evaporates. The resulting strong, absorbent solution (solution with low water concentration) leaves the generator on its way to the heat exchanger. There the stream of high water concentration that flows to the generator cools the stream of solution with low water concentration that flows to the second vessel. The solution with low water concentration is distributed over the absorber tubes. Absorber and evaporator are located in the same vessel, so the refrigerant evaporated on the evaporator tubes is readily absorbed into the absorbent solution. The pressure in the second vessel during the operation is 7 kPa (absolute). Heat of absorption and dilution are removed by cooling water (usually from the cooling tower). The resulting solution with high water concentration is pumped through the heat exchanger to the generator, completing the cycle. Heat exchanger increases the efficiency of the system by preheating, that is, reducing the amount of heat that must be added to the high water solution before it begins to evaporate in the generator.

The absorption machine operation is analyzed by the use of a lithium bromide-water equilibrium diagram, as shown in Fig. 11-100. Vapor pressure is plotted against the mass concentration of lithium bromide in the solution. The corresponding saturation temperature for a given vapor pressure is shown on the left-hand side of the diagram. The line in the lower right corner of the diagram is the crystallization line. It indicates the point at which the solution will begin to change from liquid to solid, and this is the limit of the cycle. If the solution becomes overconcentrated, the absorption cycle will be interrupted owing to solidification, and capacity will not be restored until the unit is desolidified. This normally requires the addition of heat to the outside of the solution heat exchanger and the solution pump.

The diagram in Fig. 11-101 presents enthalpy data for LiBr-water solutions. It is needed for the thermal calculation of the cycle. Enthalpies for water and water vapor can be determined from the table of properties of water. The data in Fig. 11-101 are applicable to

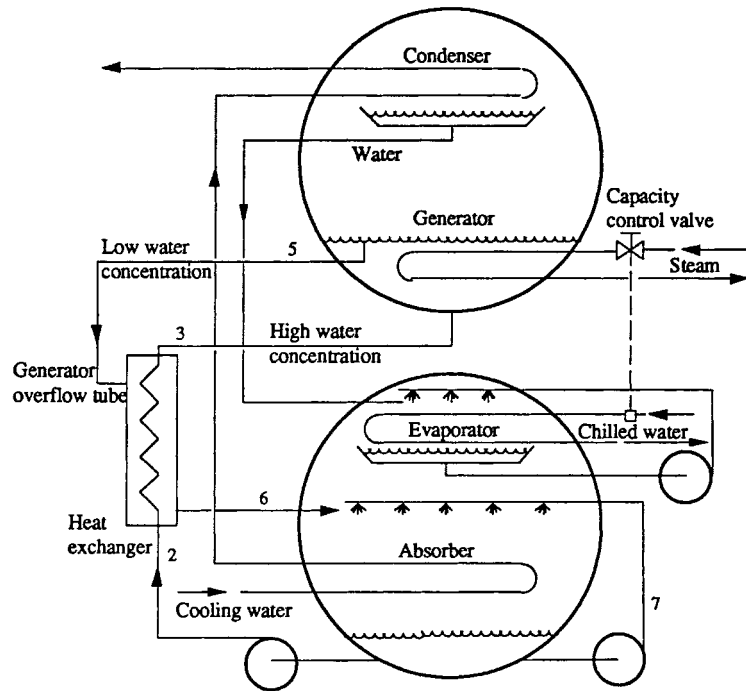


FIG. 11-99 Two-shell lithium bromide-water cycle chiller.

saturated or subcooled solutions and are based on a zero enthalpy of liquid water at 0°C and a zero enthalpy of solid LiBr at 25°C. Since the zero enthalpy for the water in the solution is the same as that in conventional tables of properties of water, the water property tables can be used in conjunction with diagram in Fig. 11-100.

Coefficient of performance of the absorption cycle is defined on the same principle as for the mechanical refrigeration:

$$COP_{abs} = \frac{\text{useful effect}}{\text{heat input}} = \frac{\text{refrigeration rate}}{\text{heat input at generator}}$$

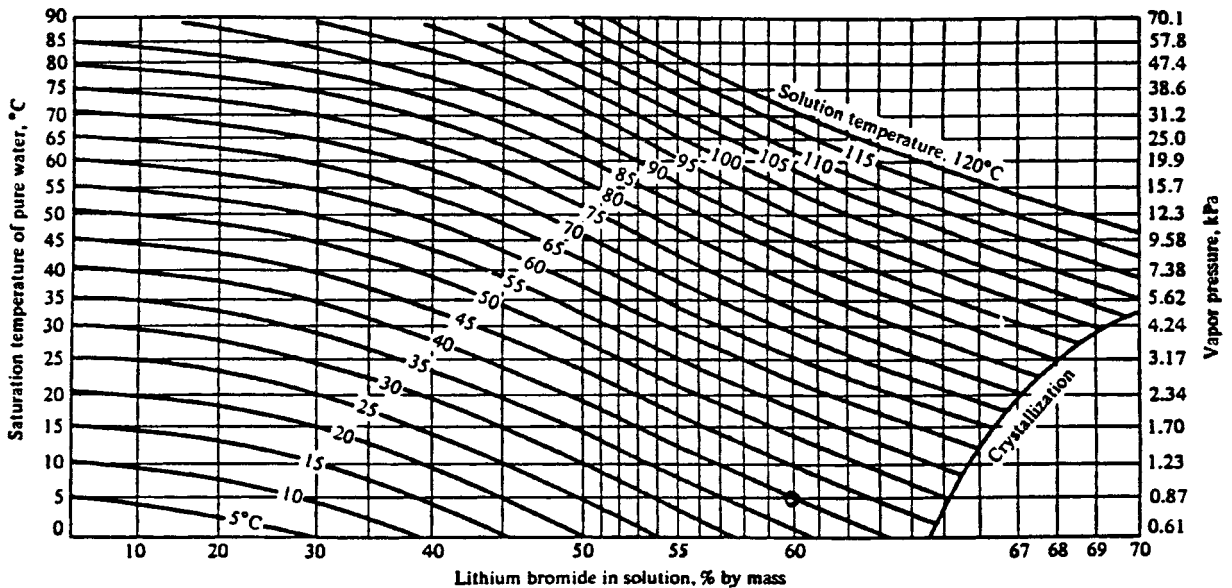


FIG. 11-100 Temperature-pressure-concentration diagram of saturated LiBr-water solutions (W. F. Stoecker and J. W. Jones: Refrigeration and Air-Conditioning)

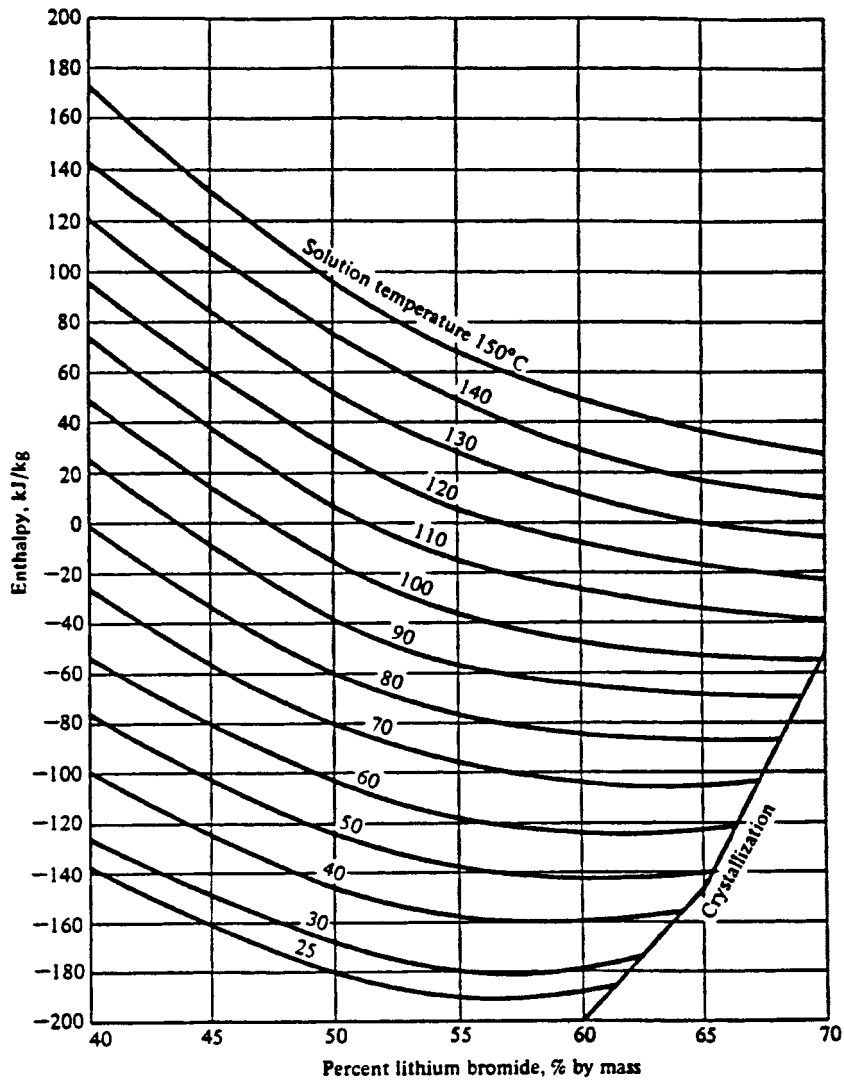


FIG. 11-101 Enthalpy of LiBr-water solutions (W. F. Stoecker and J. W. Jones: Refrigeration and Air-Conditioning).

but it should be noted that here denominator for the COP_{abs} is heat while for the mechanical refrigeration cycle it is work. Since these two forms of energy are not equal, COP_{abs} is not as low (0.6–0.8) as it appears compared to COP for mechanical system (2.5–3.5).

The double-effect absorption unit is shown in Fig. 11-102. All major components and operation of the double-effect absorption machine is similar to that for the single-effect machine. The primary generator, located in the vessel 1, is using an external heat source to evaporate water from dilute-absorbent (high water concentration) solution. Water vapor readily flows to the generator II where it is condensed on the tubes. The absorbent (LiBr) intermediate solution from generator I will pass through the heat exchanger on the way to the generator II where it is heated by the condensing water vapor. The throttling valve reduces pressure from vessel 1 (about 103 kPa absolute) to that of vessel 2. Following the reduction of pressure some water in the solution flashes to vapor, which is liquefied at the condenser. In the high temperature heat exchanger intermediate solution heats the weak (high water concentration) solution stream coming

from the low temperature heat exchanger. In the low temperature heat exchanger strong solution is being cooled before entering the absorber. The absorber is on the same pressure as the evaporator. The double-effect absorption units achieve higher COPs than the single stage.

The ammonia-water absorption system was extensively used until the fifties when the LiBr-water combination became popular. Figure 11-103 shows a simplified ammonia-water absorption cycle. The refrigerant is ammonia, and the absorbent is dilute aqueous solution of ammonia. Ammonia-water systems differ from water-lithium bromide equipment to accommodate major differences: Water (here absorbent) is also volatile, so the regeneration of weak water solution to strong water solution is a fractional distillation. Different refrigerant (ammonia) causes different, much higher pressures: about 1100–2100 kPa absolute in condenser.

Ammonia vapor from the evaporator and the weak water solution from the generator are producing strong water solution in the absorber. Strong water solution is then separated in the rectifier producing (1)

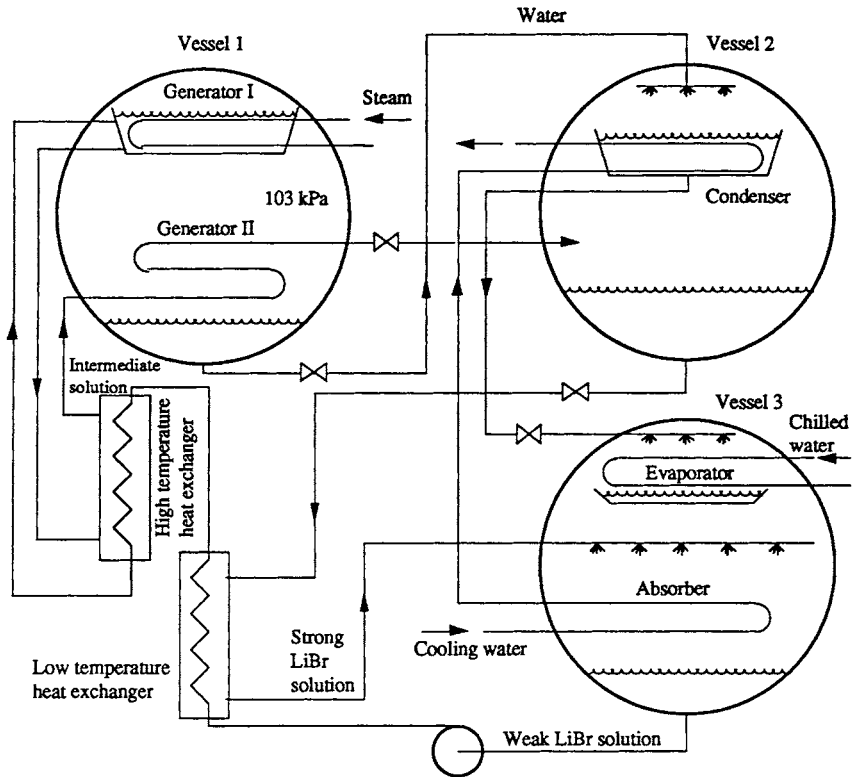


FIG. 11-102 Double-effect absorption unit.

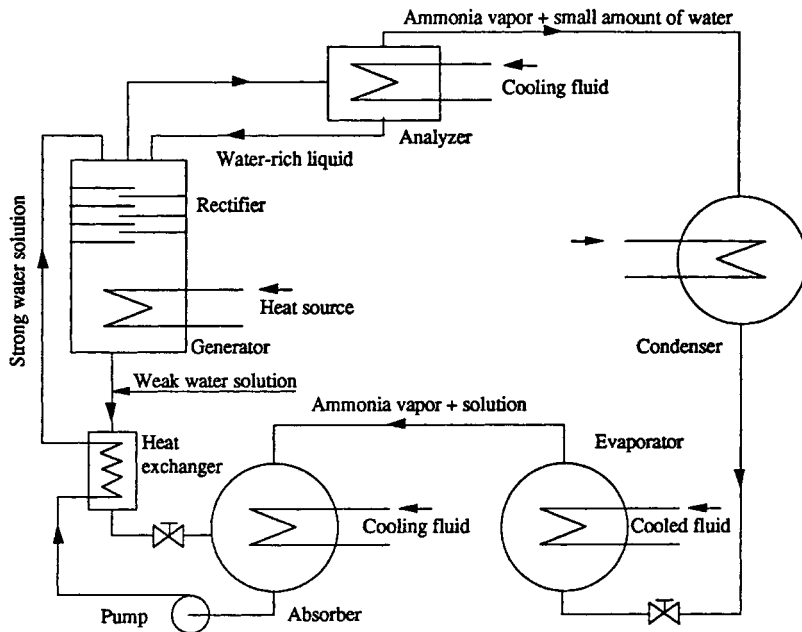


FIG. 11-103 Simplified ammonia-water absorption cycle.

ammonia with some water vapor content and (2) very strong water solution at the bottom, in the generator. Heat in the generator vaporizes ammonia and the weak solution returns to absorber. On its way to the absorber the weak solution stream passes through the heat exchanger, heating strong solution from the absorber on the way to the rectifier. The other stream, mostly ammonia vapor but with some water-vapor content flows to the condenser. To remove water as much as possible, the vapor from the rectifier passes through the analyzer where it is additionally cooled. The remaining water escaped from the analyzer pass as liquid through the condenser and the evaporator to the absorber.

Ammonia-water units can be arranged for single-stage or cascaded two-stage operation. The advantage of two-staging is it creates the possibility of utilizing only part of the heat on the higher and the rest on the lower temperature level but the price is increase in first cost and heat required.

Ammonia-water and lithium bromide-water systems operate under comparable COP. The ammonia-water system is capable achieving evaporating temperatures below 0°C because the refrigerant is ammonia. Water as the refrigerant limits evaporating temperatures to no lower than freezing, better to 3°C. Advantage of the lithium bromide-water system is that it requires less equipment and operates at lower pressures. But this is also a drawback, because pressures are below atmospheric, causing air infiltration in the system which must be purged periodically. Due to corrosion problems, special inhibitors must be used in the lithium-bromide-water system. The infiltration of air in the ammonia-water system is also possible, but when evaporating temperature is below -33°C. This can result in formation of corrosive ammonium carbonate.

Further readings: ASHRAE Handbook 1994 Refrigeration Systems and Applications; Bogart, M., 1981: *Ammonia Absorption Refrigeration in Industrial Processes*, Gulf Publishing Co. Houston; Stoecker, W. F., and Jones, J. W., 1982: *Refrigeration and Air-Conditioning*, McGraw-Hill Book Company, New York.

Steam-Jet (Ejector) Systems These systems substitute an ejector for a mechanical compressor in a vapor compression system. Since refrigerant is water, maintaining temperatures lower than the environment requires that the pressure of water in the evaporator must be below atmospheric. A typical arrangement for the steam-jet refrigeration cycle is shown in Fig. 11-104.

Main Components The main components of steam-jet refrigeration systems are:

1. **Primary steam ejector:** A kinetic device that utilizes the momentum of a high-velocity jet to entertain and accelerate a slower-moving medium into which it is directed. High-pressure steam is delivered to the nozzle of the ejector. The steam expands while flowing through the nozzle where the velocity increases rapidly. The velocity of steam leaving the nozzle is around 1200 m/s. Because of this high velocity, flash vapor from the tank is continually aspirated into the moving steam. The mixture of steam and flash vapor then enters the diffuser section where the velocity is gradually reduced because of increasing cross-sectional area. The energy of the high-velocity steam compresses the vapor during its passage through the diffuser, raising its temperature above the temperature of the condenser cooling water.

2. **Condenser:** The component of the system where the vapor condenses and where the heat is rejected. The rate of heat rejected is:

$$Q_{\text{cond}} = (W_s + W_w) hfg \quad (11-107)$$

where: Q_{cond} = heat rejection (kW)

W_s = primary booster steam rate (kg/s)

W_w = flash vapor rate (kg/s)

hfg = latent heat (kJ/kg)

The condenser design, surface area, and condenser cooling water quantity should be based on the highest cooling water temperature likely to be encountered. If the inlet cooling water temperature becomes hotter than the design, the primary booster (ejector) may cease functioning because of the increase in condenser pressure.

Two types of condensers could be used: the surface condenser (shown in Fig. 11-104) and the barometric or jet condenser (Fig. 11-105). The surface condenser is of shell-and-tube design with water flowing through the tubes and steam condensed on the outside surface. In the jet condenser, condensing water and the steam being condensed are mixed directly, and no tubes are provided. The jet condenser can be barometric or a low-level type. The barometric condenser requires a height of ~10 m above the level of the water in the hot well. A tailpipe of this length is needed so that condenser water and condensate can drain by gravity. In the low-level jet type, the tailpipe is eliminated, and it becomes necessary to remove the condenser water and condensate

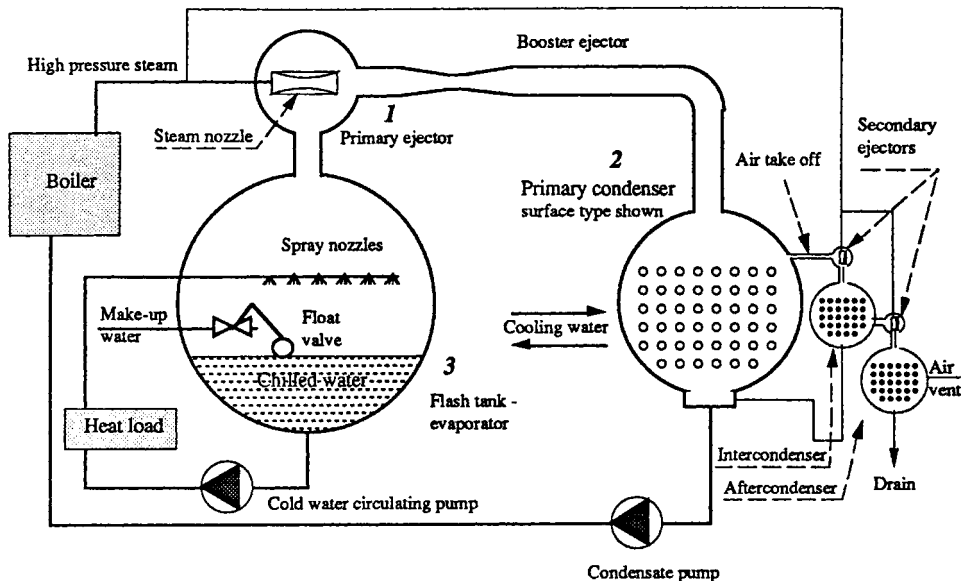


FIG. 11-104 Ejector (steam-jet) refrigeration cycle (with surface-type condenser).

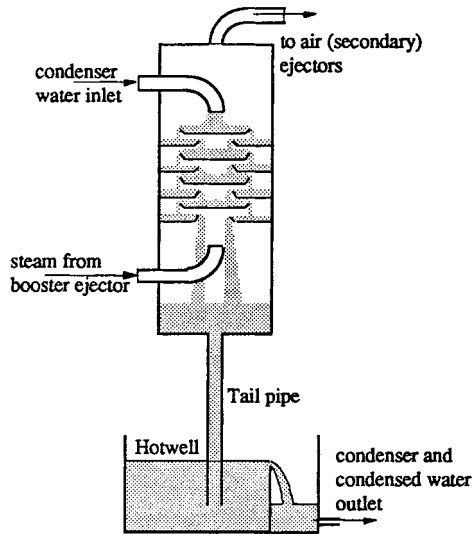


FIG. 11-105 Barometric condenser for steam-jet system.

by pumping from the condenser to the hot well. The main advantages of the jet condenser are low maintenance with the absence of tubes and the fact that condenser water of varying degrees of cleanliness may be used.

3. *Flash tank.* This is the evaporator of the ejector system and is usually a large-volume vessel where large water-surface area is needed for efficient evaporative cooling action. Warm water returning from the process is sprayed into the flash chamber through nozzles (sometimes cascades are used for maximizing the contact surface, being less susceptible to carryover problems) and the cooled effluent is pumped from the bottom of the flash tank.

When the steam supply to one ejector of a group is closed, some means must be provided to prevent the pressure in the condenser and flash tank from equalizing through that ejector. A compartmental flash tank is frequently used for such purposes. With this arrangement, partitions are provided so that each booster is operating on its own flash tank. When the steam is shut off to any booster, the valve to the inlet spray water to that compartment also is closed.

A float valve is provided to control the supply of makeup water to replace the water vapor that has flashed off. The flash tank should be insulated.

Applications The steam-jet refrigeration is suited for:

1. Processes where direct vaporization is used for concentration or drying of heat-sensitive foods and chemicals, where, besides elimination of the heat exchanger, preservation of the product quality is an important advantage.

2. Enabling the use of hard or even sea water for heat rejection e.g. for absorption of gases (CO_2 , SO_2 , ClO_2 . . .) in chilled water (desorption is provided simultaneously with chilling) when a direct contact barometric condenser is used.

Despite being simple, rugged, reliable, requiring low maintenance, low cost, and vibration free, steam-jet systems are not widely accepted in water chilling for air-conditioning due to characteristics of the cycle.

Factors Affecting Capacity Ejector (steam-jet) units become attractive when cooling relatively high-temperature chilled water with a source of about 7 bar gauge waste steam and relatively cool condensing water. The factors involved with steam-jet capacity include the following:

1. *Steam pressure.* The main boosters can operate on steam pressures from as low as 0.15 bar up to 7 bar gauge. The quantity of steam required increases rapidly as the steam pressure drops (Fig. 11-106). The best steam rates are obtained with about 7 bar. Above this pressure the change in quantity of steam required is practically

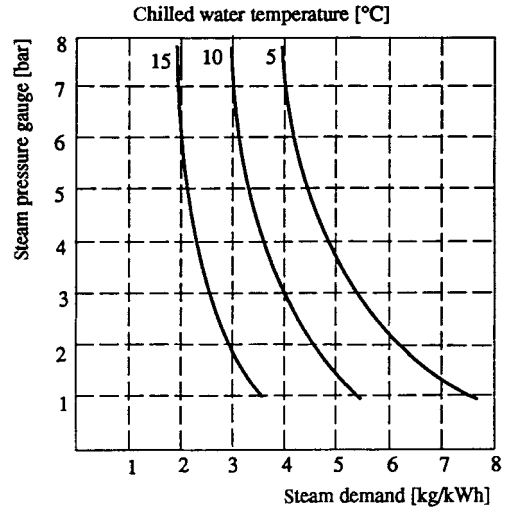


FIG. 11-106 Effect of steam pressure on steam demand at 38°C condenser temperature (ASHRAE 1983 Equipment Handbook).

negligible. Ejectors must be designed for the highest available steam pressure, to take advantage of the lower steam consumption for various steam-inlet pressures.

The secondary ejector systems used for removing air require steam pressures of 2.5 bar or greater. When the available steam pressure is lower than this, an electrically driven vacuum pump is used for either the final secondary ejector or for the entire secondary group. The secondary ejectors normally require 0.2–0.3 kg/h of steam per kW of refrigeration capacity.

2. *Condenser water temperature.* In comparison with other vapor-compression systems, steam-jet machines require relatively large water quantities for condensation. The higher the inlet-water temperature, the higher are the water requirements (Fig. 11-107). The condensing water temperature has an important effect on steam rate per refrigeration effect, rapidly decreasing with colder condenser cooling water. Figure 11-108 presents data on steam rate versus condenser water inlet for given chilled-water outlet temperatures and steam pressure.

3. *Chilled-water temperature.* As the chilled-water outlet temperature decreases, the ratio of steam/refrigeration effect decreases, thus increasing condensing temperatures and/or increasing the condensing-water requirements.

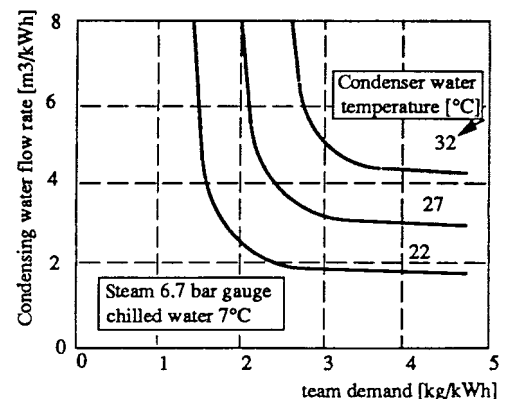


FIG. 11-107 Steam demand versus condenser-water flow rate.

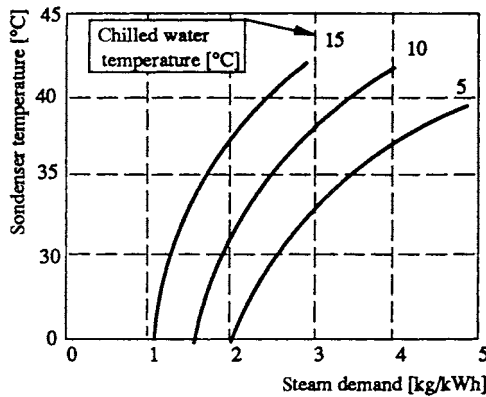


FIG. 11-108 Steam demand versus chilled-water temperature for typical steam-jet system (ASHRAE 1983 Equipment Handbook).

Unlike other refrigeration systems, the chilled-water flow rate is of no particular importance in steam-jet system design, because there is, due to direct heat exchange, no influence of evaporator tube velocities and related temperature differences on heat-transfer rates. Widely varying return chilled-water temperatures have little effect on steam-jet equipment.

Multistage Systems The majority of steam-jet systems being currently installed are multistage. Up to five stage systems are in commercial operation.

Capacity Control The simplest way to regulate the capacity of most steam vacuum refrigeration systems is to furnish several primary boosters in parallel and operate only those required to handle the heat load. It is not uncommon to have as many as four main boosters on larger units for capacity variation. A simple automatic on-off type of control may be used for this purpose. By sensing the chilled-water temperature leaving the flash tank, a controller can turn steam on and off to each ejector as required.

Additionally, two other control systems which will regulate steam flow or condenser-water flow to the machine are available. As the condenser-water temperature decreases during various periods of the year, the absolute condenser pressure will decrease. This will permit the ejectors to operate on less steam because of the reduced discharge pressure. Either the steam flow or the condenser water quantities can be reduced in order to lower operating costs at other than design periods. The arrangement selected depends on cost considerations between the two flow quantities. Some systems have been arranged for a combination of the two, automatically reducing steam flow down to a point, followed by a reduction in condenser-water flow. For maximum operating efficiency, automatic control systems are usually justifiable in keeping operating cost to a minimum without excessive operator attention. In general, steam savings of about 10 percent of rated booster flow are realized for each 2.5°C reduction in condensing-water temperature below the design point.

In some cases, with relatively cold inlet condenser water it has been possible to adjust automatically the steam inlet pressure in response to

chilled-water outlet temperatures. In general, however, this type of control is not possible because of the differences in temperature between the flash tank and the condenser. Under usual conditions of warm condenser-water temperatures, the main ejectors must compress water vapor over a relatively high ratio, requiring an ejector with entirely different operating characteristics. In most cases, when the ejector steam pressure is throttled, the capacity of the jet remains almost constant until the steam pressure is reduced to a point at which there is a sharp capacity decrease. At this point, the ejectors are unstable, and the capacity is severely curtailed. With a sufficient increase in steam pressure, the ejectors will once again become stable and operate at their design capacity. In effect, steam jets have a vapor-handling capacity fixed by the pressure at the suction inlet. In order for the ejector to operate along its characteristic pumping curve, it requires a certain minimum steam flow rate which is fixed for any particular pressure in the condenser. (For further information on the design of ejectors, see Sec. 6)

Further reading and reference: ASHRAE 1983 *Equipment Handbook*; Spencer, E., 1961, *New Development in Steam Vacuum Refrigeration*, ASHRAE Transactions Vol. 67, p. 339.

Refrigerants A refrigerant is any body or substance which acts as a cooling agent by absorbing heat from another body or substance which has to be cooled. Primary refrigerants are those that are used in the refrigeration systems, where they alternately vaporize and condense as they absorb or give off heat respectively. Secondary refrigerants are heat transfer fluids or heat carriers. Refrigerant pairs in absorption systems are ammonia-water and lithium bromide-water, while steam (water) is used as a refrigerant in ejector systems. Refrigerants used in the mechanical refrigeration systems are far more numerous.

A list of the most significant refrigerants is presented in the *ASHRAE Handbook Fundamentals*. More data are shown in the Chap. 3 of this handbook—"Physical and Chemical Data." Due to rapid changes in refrigerant, issue readers are advised to consult the most recent data and publications at the time of application.

The first refrigerants were natural: air, ammonia, CO₂, SO₂, and so on. Fast expansion of refrigeration in the second and third quarters of the 20th century is marked by the new refrigerants, chlorofluorocarbons (CFC) and hydrochlorofluorocarbons (HCFC). They are halocarbons which contain one or more of three halogens chlorine, fluorine, and bromine (Fig. 11-109). These refrigerants introduced many advantageous qualities compared to most of the existing refrigerants: odorless, nonflammable, nonexplosive, compatible with the most engineering materials, reasonably high COP, and nontoxic.

In the last decade, the refrigerant issue is extensively discussed due to the accepted hypothesis that the chlorine and bromine atoms from halocarbons released to the environment were using up ozone in the stratosphere, depleting it specially above the polar regions. Montreal Protocol and later agreements ban use of certain CFCs and halon compounds. It seems that all CFCs and most of the HCFCs will be out of production by the time this text will be published.

Chemical companies are trying to develop safe and efficient refrigerant for the refrigeration industry and application, but uncertainty in CFC and HCFC substitutes is still high. When this text was written HFCs were a promising solution. That is true especially for the R134a which seems to be the best alternative for R12. Substitutes for R22 and R502 are still under debate. Numerous ecologists and chemists are for

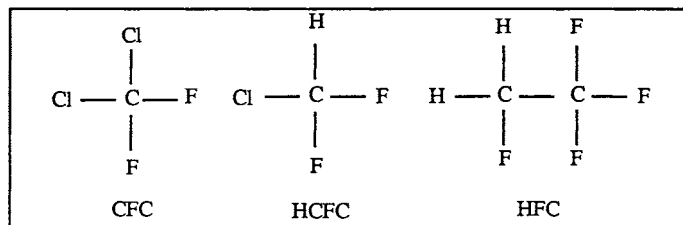


FIG. 11-109 Halocarbon refrigerants.

an extended ban on HFCs as well, mostly due to significant use of CFCs in production of HFCs. Extensive research is ongoing to find new refrigerants. Many projects are aimed to design and study refrigerant mixtures, both azeotropic (mixture which behaves physically as a single, pure compound) and zeotropic having desirable qualities for the processes with temperature glides in the evaporator and the condenser.

Ammonia (R717) is the single natural refrigerant being used extensively (beside halocarbons). It is significant in industrial applications for its excellent thermodynamic and thermophysical characteristics. Many engineers are considering ammonia as a CFC substitute for various applications. Significant work is being done on reducing the refrigerant inventory and consequently problems related to leaks of this fluid with strong odor. There is growing interest in hydrocarbons in some countries, particularly in Europe. Indirect cooling (secondary refrigeration) is under reconsideration for many applications.

Due to the vibrant refrigerant issue it will be a challenge for every engineer to find the best solution for the particular application, but basic principles are the same. Good refrigerant should be:

- Safe: nontoxic, nonflammable, and nonexplosive
- Environmentally friendly
- Compatible with materials normally used in refrigeration: oils, metals, elastomers, etc.
- Desirable thermodynamic and thermophysical characteristics:
 - High latent heat
 - Low specific volume of vapor
 - Low compression ratio
 - Low viscosity
 - Reasonably low pressures for operating temperatures
 - Low specific heat of liquid
 - High specific heat of vapor
 - High conductivity and other heat transfer related characteristics
 - Reasonably low compressor discharge temperatures
 - Easily detected if leaking
 - High dielectric constant
 - Good stability

Secondary Refrigerants (Antifreezes or Brines) These are mostly liquids used for transporting heat energy from the remote heat

source (process heat exchanger) to the evaporator of the refrigeration system. Antifreezes or brines do not change state in the process, but there are examples where some secondary refrigerants are either changing state themselves, or just particles which are carried in them.

Indirect refrigeration systems are more prevalent in the chemical industry than in the food industry, commercial refrigeration, or comfort air-conditioning. This is even more evident in the cases where a large amount of heat is to be removed or where a low temperature level is involved. Advantage of an indirect system is centralization of refrigeration equipment, which is specially important for relocation of refrigeration equipment in a nonhazardous area, both for people and equipment.

Salt Brines The typical curve of freezing point is shown in Fig. 11-110. Brine of concentration x (water concentration is $1-x$) will not solidify at 0°C (freezing temperature for water, point A). When the temperature drops to B, the first crystal of ice is formed. As the temperature decreases to C, ice crystals continue to form and their mixture with the brine solution forms the slush. At the point C there will be part ice in the mixture $l_2/(l_1 + l_2)$, and liquid (brine) $l_1/(l_1 + l_2)$. At point D there is mixture of m_1 parts eutectic brine solution D_1 [concentration $m_1/(m_1 + m_2)$], and m_2 parts of ice [concentration $m_2/(m_1 + m_2)$]. Cooling the mixture below D solidifies the entire solution at the eutectic temperature. Eutectic temperature is the lowest temperature that can be reached with no solidification.

It is obvious that further strengthening of brine has no effect, and can cause a different reaction—salt sometimes freezes out in the installations where concentration is too high.

Sodium chloride, an ordinary salt (NaCl), is the least expensive per volume of any brine available. It can be used in contact with food and in open systems because of its low toxicity. Heat transfer coefficients are relatively high. However, its drawbacks are it has a relatively high freezing point and is highly corrosive (requires inhibitors thus must be checked on a regular schedule).

Calcium chloride (CaCl₂) is similar to NaCl. It is the second lowest-cost brine, with a somewhat lower freezing point (used for temperatures as low as -37°C). Highly corrosive and not appropriate for direct contact with food. Heat transfer coefficients are rapidly reduced at

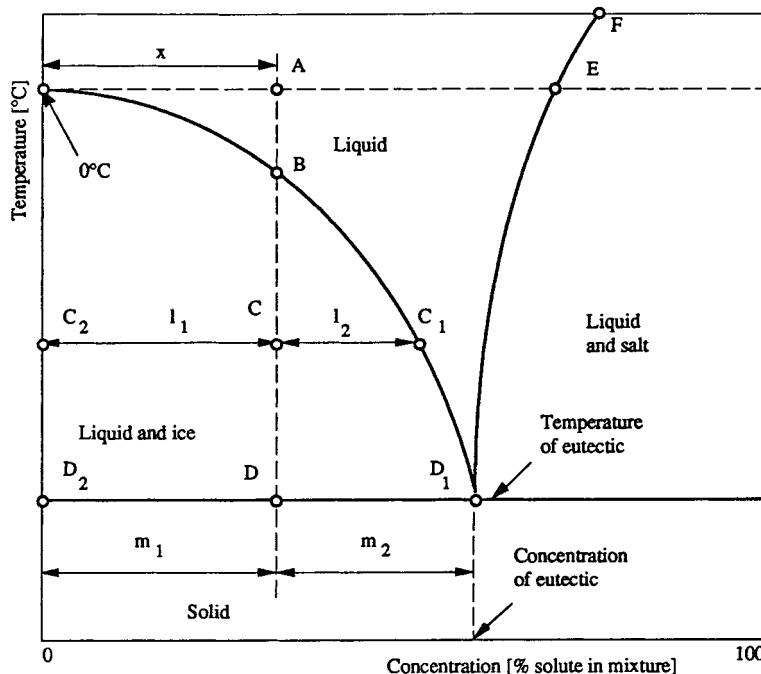


FIG. 11-110 Phase diagram of the brine.

temperatures below -20°C . The presence of magnesium salts in either sodium or calcium chloride is undesirable because they tend to form sludge. Air and carbon dioxide are contaminants and excessive aeration of the brine should be prevented by use of close systems. Oxygen, required for corrosion, normally comes from the atmosphere and dissolves in the brine solution. Dilute brines dissolve oxygen more readily and are generally more corrosive than concentrated brines. It is believed that even a closed brine system will not prevent the infiltration of oxygen.

To adjust alkaline condition to pH 7.0–8.5 use caustic soda (to correct up to 7.0) or sodium dichromate (to reduce excessive alkalinity below pH 8.5). Such slightly alkaline brines are generally less corrosive than neutral or acid ones, although with high alkalinity the activity may increase.

If the untreated brine has the proper pH value, the acidifying effect of the dichromate may be neutralized by adding commercial flake caustic soda (76 percent pure) in quantity that corresponds to 27 percent of sodium dichromate used. Caustic soda must be thoroughly dissolved in warm water before it is added to the brine.

Recommended inhibitor (sodium dichromate) concentrations are 2 kg/m^3 of CaCl_2 and 3.2 kg/m^3 of NaCl brine. Sodium dichromate when dissolved in water or brine makes the solution acid. Steel, iron, copper, or red brass can be used with brine circulating systems. Calcium chloride systems are generally equipped with all-iron-and-steel pumps and valves to prevent electrolysis in event of acidity. Copper and red brass tubing are used for calcium chloride evaporators. Sodium chloride systems are using all-iron or all-bronze pumps.

Organic Compounds (Inhibited Glycols) *Ethylene glycol* is colorless and practically odorless and completely miscible with water. Advantages are low volatility and relatively low corrosivity when properly inhibited. Main drawbacks are relatively low heat-transfer coefficients at lower temperatures due to high viscosities (even higher than for propylene glycol). It is somewhat toxic, but less harmful than methanol water solutions. It is not appropriate for food industry and should not stand in open containers. Preferably waters that are classified as soft and are low in chloride and sulfate ions should be used for preparation of ethylene glycol solution.

Pure ethylene glycol freezes at -12.7°C . Exact composition and temperature for eutectic point are unknown, since solutions in this region turn to viscous, glassy mass that makes it difficult to determine the true freezing point. For the concentrations lower than eutectic, ice forms on freezing, while on the concentrated, solid glycol separates from the solution.

Ethylene glycol normally has pH of 8.8 to 9.2 and should not be used below 7.5. Addition of more inhibitor can not restore the solution to original condition. Once inhibitor has been depleted, it is recommended that the old glycol be removed from the system and the new charge be installed.

Propylene glycol is very similar to ethylene glycol, but it is not toxic and is used in direct contact with food. It is more expensive and, having higher viscosity, shows lower heat transfer coefficients.

Methanol water is an alcohol-base compound. It is less expensive than other organic compounds and, due to lower viscosity, has better heat transfer and pressure drop characteristics. It is used up to -35°C . Disadvantages are (1) considered more toxic than ethylene glycol and thus more suitable for outdoor applications (2) flammable and could be assumed to be a potential fire hazard.

For ethylene glycol systems copper tubing is often used (up to 3 in), while pumps, cooler tubes, or coils are made of iron, steel, brass, copper, or aluminum. Galvanized tubes should not be used in ethylene glycol systems because of reaction of the inhibitor with the zinc.

Methanol water solutions are compatible with most materials but in sufficient concentration will badly corrode aluminum.

Ethanol water is a solution of denatured grain alcohol. Its main advantage is that it is nontoxic and thus is widely used in the food and chemical industry. By using corrosion inhibitors it could be made non-corrosive for brine service. It is more expensive than methanol water and has somewhat lower heat transfer coefficients. As an alcohol derivate it is flammable.

Secondary refrigerants shown below, listed under their generic names, are sold under different trade names. Some other secondary refrigerants appropriate for various refrigeration application will be

listed under their trade names. More data could be obtained from the manufacturer.

Syltherm XLT (Dow Corning Corporation). A silicone polymer (Dimethyl Polysiloxane); recommended temperature range -70°C to 250°C ; odorless; low in acute oral toxicity; noncorrosive toward metals and alloys commonly found in heat transfer systems.

Syltherm 800 (Dow Corning Corporation). A silicone polymer (Dimethyl Polysiloxane); recommended temperature range -40°C to 400°C ; similar to Syltherm XLT, more appropriate for somewhat higher temperatures; flash point is 160°C .

D-limonene (Florida Chemicals). A compound of optically active terpene ($\text{C}_{10}\text{H}_{16}$) derived as an extract from orange and lemon oils; limited data shows very low viscosity at low temperatures—only one centipoise at -50°C ; natural substance having questionable stability.

Therminol D-12 (Monsanto). A synthetic hydrocarbon; clear liquid; recommended range -40°C to 250°C ; not appropriate for contact with food; precautions against ignitions and fires should be taken with this product; could be found under trade names Santotherm or Gilotherm.

Therminol LT (Monsanto). Akybenzene, synthetic aromatic ($\text{C}_{10}\text{H}_{14}$); recommended range -70°C to -180°C ; not appropriate for contact with food; precautions against ignitions and fire should be taken dealing with this product.

Dowtherm J (Dow Corning Corporation). A mixture of isomers of an alkylated aromatic; recommended temperature range -70°C to 300°C ; noncorrosive toward steel, common metals and alloys; combustible material; flash point 58°C ; low toxic; prolonged and repeated exposure to vapors should be limited 10 ppm for daily exposures of eight hours.

Dowtherm Q (Dow Corning Corporation). A mixture of dyphenylene-hane and alkylated aromatics; recommended temperature range -30°C to 330°C ; combustible material; flash point 120°C ; considered low toxic, similar to Dowtherm J.

Safety in Refrigeration Systems This is of paramount importance and should be considered at every stage of installation.

The design engineer should have safety as the primary concern by choosing suitable system and refrigerant; selecting components, choosing materials and thicknesses of vessels, pipes, and relief valves of pressure vessels, proper venting of machine rooms, and arranging the equipment for convenient access for service and maintenance (piping arrangements, valve location, machine room layout, etc.). He or she should conform to the stipulation of the safety codes, which is also important for the purpose of professional liability.

During construction and installation, the installer's good decisions and judgments are crucial for safety, because design documentation never specifies all details. This is especially important when there is reconstruction or repair while the facility has been charged.

During operation the plant is in the hands of the operating personnel. They should be properly trained and familiar with the installation. Very often, accidents are caused by an improper practice, such as making an attempt to repair when proper preparation is not made. Operators should be trained in first-aid procedures and how to respond to emergencies.

Most frequently needed standards and codes are listed below, and the reader can find comments in: W. F. Stoecker: *Industrial Refrigeration*, Vol. 2, Ch. 12, Business News Publishing Co., Troy, MI, 1995; *ASHRAE Handbook Refrigeration System and Applications*, 1994, Ch. 51. Some important standards and codes on safety that a refrigeration engineer should consult are: ANSI/ASHRAE Standard 15-92—Safety Code for Mechanical Refrigeration, ASHRAE, Atlanta GA, 1992; ANSI/ASHRAE Standard 34-92—Number Designation of Refrigerants, ASHRAE, Atlanta GA, 1992; ANSI/ASME Boiler and Pressure Vessel Code, ASME, New York, 1989; ANSI/ASME Code for Pressure Piping, B31, B31.5-1987, ASME, New York, 1987; ANSI/IIAR 2—1984, Equipment, Design and Installation of Ammonia Mechanical Refrigeration Systems, IIAR, Chicago, 1984; IIAR Minimum Safety Criteria for a Safe Ammonia Refrigeration Systems, Bulletin 109; IIAR, IIAR Start-up, Inspection, and Maintenance of Ammonia Mechanical Refrigeration Systems, Bulletin 110, Chicago, 1988; IIAR Recommended Procedures in Event of Ammonia Spills, Bulletin No. 106, IIAR, Chicago, 1977; A Guide to Good Practices for the Operation of an Ammonia Refrigeration System, IIAR Bulletin R1, 1983.

CRYOGENIC PROCESSES

INTRODUCTION

Cryogenics, the production of low temperatures, is a major business in the United States with an annual market in 2003 of almost 14 billion dollars. It is a very diverse supporting technology, a means to an end and not an end in itself. For example, the combined production of oxygen and nitrogen, obtained by the cryogenic separation of air, accounts for 15 percent of the total annual U.S. production of 2.9×10^{11} kg (639 billion lb) of organics and inorganics (2003 *C & EN Annual Report*). Liquid hydrogen production, in the last four decades, has risen from laboratory quantities to a level of over 2.2 kg/s, first spurred by nuclear weapons development and later by the United States space program. Similarly, the space age increased the need for liquid helium by more than a factor of ten, requiring the construction of large plants to separate helium from natural gas by cryogenic means. The demands for energy have likewise accelerated the construction of large base-load liquefied natural gas (LNG) plants around the world and have been responsible for the associated domestic LNG industry of today with its use of peak shaving plants.

Freezing as a means of preserving food dates back to 1840. However, today the food industry uses large quantities of liquid nitrogen for this purpose and uses the refrigerant in frozen-food transport systems. In biological applications liquid-nitrogen cooled containers are routinely used to preserve whole blood, tissue, bone marrow, and animal semen for extended periods of time. Cryogenic surgery has become accepted in curing such involuntary disorders as Parkinson's disease. Medical analysis of patients has increased in sophistication with the use of *magnetic resonance imaging* (MRI) which utilizes cryogenically cooled superconducting magnets. Finally, one must recognize the role that cryogenics plays in the chemical-processing industry with the recovery of valuable feedstocks from natural gas streams, upgrading the heat content of fuel gas, purification of various process and waste streams, production of ethylene, as well as other chemical processes.

PROPERTIES OF CRYOGENIC FLUIDS

There are presently several database programs of thermodynamic properties data developed specifically for fluids commonly associated with low temperature processing including helium, hydrogen, neon, nitrogen, oxygen, argon, and methane. For example, the NIST Standard Reference Database 12, Version 3.0 includes a total of 34 thermophysical properties for seventeen fluids in the database. Cryodata Inc. provides a similar computer version for 28 pure fluids as well as for mixtures incorporating many of these fluids. To fully appreciate the major effort in developing these thermophysical properties, consult the presentation by Jacobsen and coworkers (*Thermodynamics Properties of Cryogenic Fluids*, Plenum Press, New York, 1997). A few peculiarities associated with the fluids of helium, hydrogen, oxygen, and air need to be noted below.

Liquid helium-4 can exist in two different liquid phases: liquid helium I, the normal liquid, and liquid helium II, the superfluid, since under certain conditions the latter fluid acts as if it had no viscosity. The phase transition between the two liquid phases is identified as the lambda line and where this transition intersects the vapor-pressure curve is designated as the lambda point. Thus, there is no triple point for this fluid as for other fluids. In fact, solid helium can only exist under a pressure of 2.5 MPa or more.

A unique property of hydrogen is that it can exist in two different molecular forms: orthohydrogen and parahydrogen. (This is also true for deuterium, an isotope of hydrogen with an atomic mass of 2.) The thermodynamic equilibrium composition of the ortho- and para-varieties is temperature dependent. The equilibrium mixture of 75 percent orthohydrogen and 25 percent parahydrogen at ambient temperatures is recognized as normal hydrogen.

In contrast to other cryogenic fluids, liquid oxygen is slightly magnetic. It is also chemically reactive, particularly with hydrocarbon materials. Oxygen thus presents a safety problem and requires extra precautions in handling.

Since air is a mixture of predominantly nitrogen, oxygen, and a host of lesser impurities, there has been less interest in developing precise thermodynamic properties. A widely used correlation of thermodynamic properties is that published by NIST (NIST Database 72, NIST AIRPROPS, Version 1.0).

PROPERTIES OF SOLIDS

A knowledge of the properties and behavior of materials used in any cryogenic system is essential for proper design considerations. Often the choice of materials for the construction of cryogenic equipment will be dictated by other considerations besides mechanical properties as, for example, thermal conductivity (heat transfer along a structural member), thermal expansivity (expansion and contraction during cycling between ambient and low temperatures), and density (mass of the system). Since properties at low temperatures are often significantly different from those at ambient temperature, there is no substitute for test data on a truly representative sample specimen when designing for the limit of effectiveness of a cryogenic material or structure. For example, some metals including elements, intermetallic compounds and alloys exhibit the phenomenon of superconductivity at very low temperatures. The properties that are affected when a material becomes superconducting include specific heat, thermal conductivity, electrical resistance, magnetic permeability, and thermoelectric effect. As a result, the use of superconducting metals in the construction of equipment for temperatures lower than 10 K needs to be evaluated carefully. (High temperature superconductors because of their brittle ceramic structure are generally not considered as construction materials.)

Structural Properties at Low Temperatures It is most convenient to classify metals by their lattice symmetry for low temperature mechanical properties considerations. The *face-centered-cubic* (fcc) metals and their alloys are most often used in the construction of cryogenic equipment. Al, Cu Ni, their alloys, and the austenitic stainless steels of the 18-8 type are fcc and do not exhibit an impact ductile-to-brittle transition at low temperatures. As a general rule, the mechanical properties of these metals with the exception of 2024-T4 aluminum, improve as the temperature is reduced. Since annealing of these metals and alloys can affect both the ultimate and yield strengths, care must be exercised under these conditions.

The *body-centered-cubic* (bcc) metals and alloys are normally classified as undesirable for low temperature construction. This class includes Fe, the martensitic steels (low carbon and the 400-series stainless steels), Mo, and Nb. If not brittle at room temperature, these materials exhibit a ductile-to-brittle transition at low temperatures. Cold working of some steels, in particular, can induce the austenite-to-martensite transition.

The *hexagonal-close-packed* (hcp) metals generally exhibit mechanical properties intermediate between those of the fcc and bcc metals. For example Zn encounters a ductile-to-brittle transition whereas Zr and pure Ti do not. The latter and their alloys with a hcp structure remain reasonably ductile at low temperatures and have been used for many applications where weight reduction and reduced heat leakage through the material have been important. However, small impurities of O, N, H, and C can have a detrimental effect on the low temperature ductility properties of Ti and its alloys.

Plastics increase in strength as the temperature is decreased, but this is also accompanied by a rapid decrease in elongation in a tensile test and a decrease in impact resistance. Teflon and glass-reinforced plastics retain appreciable impact resistance as the temperature is lowered. The glass-reinforced plastics also have high strength-to-weight and strength-to-thermal conductivity ratios. All elastomers, on the other hand, become brittle at low temperatures. Nevertheless, many of these materials including rubber, Mylar, and nylon can be used for static seal gaskets provided they are highly compressed at room temperature prior to cooling.

The strength of glass under constant loading also increases with decrease in temperature. Since failure occurs at a lower stress when

the glass surface contains surface defects, the strength can be improved by tempering the surface.

Thermal Properties at Low Temperatures The thermodynamic properties of most gases at low temperature approximate quite closely those of an ideal gas, and thus the ideal equation of state is adequate for most cryogenic engineering designs. However, the heat capacity of an ideal gas depends on its molecular composition. In most cryogenic gases, electronic and vibrational degrees of freedom are not excited, while rotational contributions to the specific heat at constant-volume conditions have reached their full classical value. Under these conditions the heat capacity depends only on whether the gas is composed of isolated atoms, linear molecules, or nonlinear molecules. The values for C_v , the heat capacity at constant volume are $3/2R$, $5/2R$ and $3R$, respectively, where R is the universal gas constant. For C_p , the heat capacity at constant pressure, the corresponding values are $5/2R$, $7/2R$, and $4R$, respectively. The C_v data for a number of real gases presented by Barron and White (*Heat Capacity and Thermal Expansion at Low Temperatures*, Kluwer Academic/Plenum Publisher, New York, 1999, p. 132) show that these values provide a good approximation over wide ranges in temperatures, although there are large deviations for hydrogen below about 200 K and for methane at higher temperatures due to vibrational excitation. For solids, the Debye model developed with the aid of statistical mechanics and quantum theory gives a satisfactory representation of the specific heat with temperature. Procedures for calculating values of Θ_D , the Debye characteristic temperature, using either elastic constants, the compressibility, the melting point, or the temperature dependence of the expansion coefficient are outlined by Barron (*Cryogenic Systems, 2d ed.*, Oxford University Press, 1985, pp. 24–29).

Adequate prediction of the thermal conductivity for pure metals can be made by means of the Wiedeman-Franz law which states that the ratio of the thermal conductivity to the product of the electrical conductivity and the absolute temperature is a constant. This ratio for high-conductivity metals extrapolates essentially to the Sommerfeld value of $2.449 \times 10^{-8} \text{ W } \Omega/\text{K}^2$ at 0 K, but falls considerably below it at higher temperatures. High-purity aluminum and copper exhibit peaks in thermal conductivity between 20 to 50 K, but these peaks are rapidly suppressed with increased impurity levels and cold work of the metal. Some metals including Monel, Inconel, stainless steel, and structural and aluminum alloys show a steady decrease in thermal conductivity with a decrease in temperature.

All cryogenic liquids except hydrogen and helium have thermal conductivities that increase as the temperature is decreased. For these two exceptions, the thermal conductivity decreases with a decrease in temperature. The kinetic theory of gases correctly predicts the decrease in thermal conductivity of all gases when the temperature is lowered.

The expansion coefficient of a solid can be estimated with the aid of an approximate thermodynamic equation of state for solids which equates the thermal expansion coefficient β with the quantity $\gamma C_v \rho/B$ where γ is the Grüneisen dimensionless ratio, C_v is the specific heat of the solid, ρ is the density of the material, and B is the bulk modulus. For fcc metals the average value of the Grüneisen constant is near 2.3. However, there is a tendency for this constant to increase with atomic number.

Electrical Properties at Low Temperatures The electrical resistivity of most pure metallic elements at ambient and moderately low temperatures is approximately proportional to the absolute temperature. At very low temperatures, however, the resistivity (with the exception of superconductors) approaches a residual value almost independent of temperature. Alloys, on the other hand, have resistivities much higher than those of their constituent elements and resistance-temperature coefficients that are quite low. The electrical resistivity of alloys as a consequence is largely independent of temperature and may often be of the same magnitude as the room temperature value.

Superconductivity The physical state in which all resistance to the flow of direct-current electricity disappears is defined as superconductivity. The Bardeen-Cooper-Schrieffer (BCS) theory has been reasonably successful in accounting for most of the basic features observed of the superconducting state for *low-temperature superconductors* (LTS) operating below 23 K. The advent of the ceramic *high-temperature superconductors* (HTS) by Bednorz and Miller (*Z. Phys.*

TABLE 11-25 Composition and Critical Temperature T_c for HTS Materials

Formula*	Accepted notation	Forms reported		Critical T_c , K
Y-Ba-Cu-O†	YBCO	123	124	80–92
Bi-Sr-Ca-Cu-O	BSCCO	2212	2223	80–110
Tl-Ba-Ca-Cu-O	TBCCO	Several		to 125
Hg-Ba-Ca-Cu-O	HBCCO	1201	1223	95–155‡

*Subscripts for compounds are not listed since there are generally several forms that can be produced (see column 3).

†Other rare earths may be substituted for Y (yttrium) providing new compounds with somewhat different properties.

‡Highest T_c obtained while subjecting sample to external pressure.

B64, 189, 1989) has called for modifications to existing theories which are still actively being debated. The massive interest in the new superconductors that can be cooled with liquid nitrogen is presently underway with many new applications.

Three important characteristics of the superconducting state are the critical temperature, the critical magnetic field, and the critical current. These parameters many times can be varied by using different materials or giving them special metallurgical treatments.

The alloy *niobium titanium* (NbTi) and the intermetallic compound of *niobium and tin* (Nb₃Sn) are the most technologically advanced LTS materials presently available. Even though NbTi has a lower critical field and critical current density, it is often selected because its metallurgical properties favor convenient wire fabrication. In contrast, Nb₃Sn is a very brittle material and requires wire fabrication under very well-defined temperature conditions. However, the recent discovery by Akimitsu and coworkers (*Nature* **10**, 63, 2001) of the superconducting property of MgBr₂ has spurred new activity in the development of still another LTS conductor for magnetic coils.

There are essentially four families of high-temperature superconductors under investigation for practical magnet applications. Table 11-25 shows that all HTS are copper oxide ceramics even though the oxygen content may vary. However, this variation generally has little effect on the physical properties of importance to superconductivity.

The most widely used development in HTS wire production is the powder-in-tube procedure with BSCCO ceramic materials. In this procedure very fine HTS powder, placed inside of a hollow silver tube, is fused as the tube length is mechanically increased to form a wire. Very high magnetic fields with this wire have been reported at 4 K; however, performance degrades substantially above 20 to 30 K.

HTS materials, because of their ceramic nature, are quite brittle. This has introduced problems relative to the winding of superconducting magnets. One solution is to first wind the magnet with the powder-in-tube wire before the ceramic powder has been bonded and then heat treat the desired configuration to form the final product. Another solution is to form the superconductor into such fine filaments that they remain sufficiently flexible even after the powder has been heat treated.

REFRIGERATION AND LIQUEFACTION

A process for producing refrigeration or liquefaction at cryogenic temperatures usually involves ambient compression of a process fluid with heat rejection to a coolant. During the compression process, the enthalpy and entropy of the fluid are decreased. At the cryogenic temperature where heat is absorbed, the enthalpy and entropy are increased. The reduction in temperature of the process fluid is usually accomplished by heat exchange with a colder fluid and then followed by an expansion. This expansion may take place using either a throttling device (isenthalpic expansion) with only a reduction in temperature or a work-producing device (isentropic expansion) in which both temperature and enthalpy are decreased. Because of liquid withdrawal, a liquefaction system experiences an unbalanced flow in the heat exchanger while a refrigeration system with no liquid withdrawal system usually operates with a balanced flow in the heat exchanger, except where a portion of the flow is diverted through the work-producing expander.

Principles The performance of a real refrigerator is measured by the coefficient of performance, COP, defined as

$$\text{COP} = \frac{Q}{W} = \frac{\text{heat removed at low temperature}}{\text{net work input}} \quad (11-108)$$

Another means of comparing the performance of a practical refrigerator is by the use of the figure of merit, FOM, defined as

$$\text{FOM} = \frac{\text{COP}}{\text{COP}_i} \quad (11-109)$$

where COP is the coefficient of performance of the actual refrigerator system and COP_i is the coefficient of performance for the thermodynamically ideal system. For a liquefier, the FOM is generally specified as

$$\text{FOM} = \frac{W_i/\dot{m}_l}{W/\dot{m}_l} \quad (11-110)$$

where W_i is the work of compression for the ideal cycle, W is the work of compression for the actual cycle, and \dot{m}_l is the mass rate liquefied in the ideal or actual cycle.

The methods of refrigeration and/or liquefaction generally used include (1) vaporization of a liquid, (2) application of the Joule-Thomson effect in a gas, and (3) expansion of a gas in a work-producing engine. Normal commercial refrigeration generally is accomplished in a vapor-compression process. Temperatures to about 200 K can be obtained by cascading vapor-compression processes in which refrigeration is accomplished by liquid evaporation. Below this temperature, isenthalpic or isentropic expansions are generally used either singly or in combination. With few exceptions, refrigerators using these methods also absorb heat by vaporization of the liquid.

If refrigeration is to be accomplished at a temperature range where no suitable liquid exists to absorb heat by evaporation, then a cold gas must be available to absorb the heat. This is generally accomplished by using a work-producing expansion engine.

Expansion Types of Refrigerators A thermodynamic process utilizing isenthalpic expansion to obtain cryogenic temperatures, and commonly referred to as the simple Linde or J-T cycle, is shown schematically with its corresponding temperature-entropy diagram in Fig. 11-111. The gaseous refrigerant is compressed at ambient temperature while essentially rejecting heat isothermally to a coolant. The compressed refrigerant is cooled countercurrently in a heat exchanger by the cold gas stream leaving the liquid reservoir before it enters the throttling valve. Upon expansion, Joule-Thomson cooling further reduces the temperature until, at steady state, a portion of the refrigerant is liquefied. For a refrigerator, the unliquefied fraction and the vapor formed by liquid evaporation from the absorbed heat Q are warmed in the heat exchanger before returning to the intake of the compressor. Assuming no heat inleaks, as well as negligible kinetic and potential energy changes in the fluid, the refrigeration duty Q is equivalent to $\dot{m}(h_1 - h_2)$, where the subscripts refer to the locations

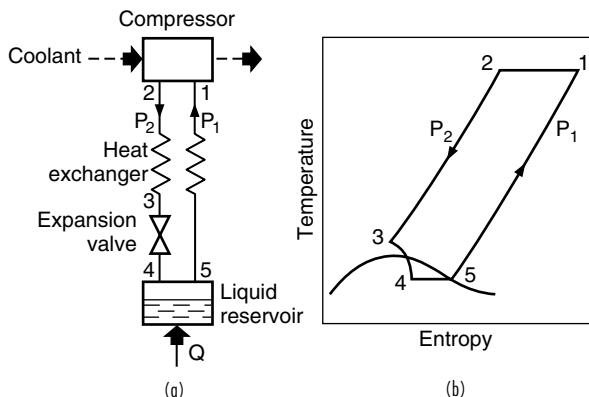


FIG. 11-111 Refrigerator using simple J-T cycle.

shown on Fig. 11-111. Applying Eq. 11-108, the coefficient of performance for the ideal J-T refrigerator is given by

$$\text{COP} = \frac{h_1 - h_2}{T_1[s_1 - s_2 - (h_1 - h_2)]} \quad (11-111)$$

For a simple J-T liquefier, the liquefied portion is continuously withdrawn from the reservoir and only the unliquefied portion of the fluid is warmed in the countercurrent heat exchanger and returned to the compressor. The fraction y that is liquefied is obtained by applying the first law to the heat exchanger, J-T valve, and liquid reservoir. This results in

$$y = \frac{h_1 - h_2}{h_1 - h_f} \quad (11-112)$$

where h_f is the specific enthalpy of the liquid being withdrawn. Maximum liquefaction occurs when the difference between h₁ and h₂ is maximized. To account for heat leak, q_L, the relation needs to be modified to

$$y = \frac{h_1 - h_2 - q_L}{h_1 - h_f} \quad (11-113)$$

with a resultant decrease in the fraction liquefied.

Refrigerants used in this process have a critical temperature well below ambient; consequently liquefaction by direct compression is not possible. In addition, the inversion temperature of the refrigerant must be above ambient temperature to provide initial cooling by the J-T process. Auxiliary refrigeration is required if the simple J-T cycle is to be used to liquefy neon, hydrogen, or helium whose inversion temperatures are below ambient. Liquid nitrogen is the optimum refrigerant for hydrogen and neon liquefaction systems, while liquid hydrogen is the normal refrigerant for helium liquefaction systems.

To reduce the work of compression in this cycle a two-stage or dual-pressure process may be used whereby the pressure is reduced by two successive isenthalpic expansions. Since the isothermal work of compression is approximately proportional to the logarithm of the pressure ratio, and the Joule-Thomson cooling is roughly proportional to the pressure difference, there is a greater reduction in compressor work than in refrigerating performance for this dual-pressure process.

In a work-producing expansion, the temperature of the process fluid is always reduced; hence, cooling does not depend on being below the inversion temperature prior to expansion. Additionally, the work-producing expansion results in a larger amount of cooling than in an isenthalpic expansion over the same pressure difference.

In large systems utilizing expanders, the work produced during expansion is conserved. In small refrigerators, the energy from the expansion is usually expended in a gas or hydraulic pump, or other suitable device. A schematic of a simple cold-gas refrigerator using this expansion principle and the corresponding temperature-entropy diagram is shown in Fig. 11-112. Gas compressed isothermally at ambient temperature is cooled in a heat exchanger by gas being warmed on its return to the compressor intake. Further cooling takes

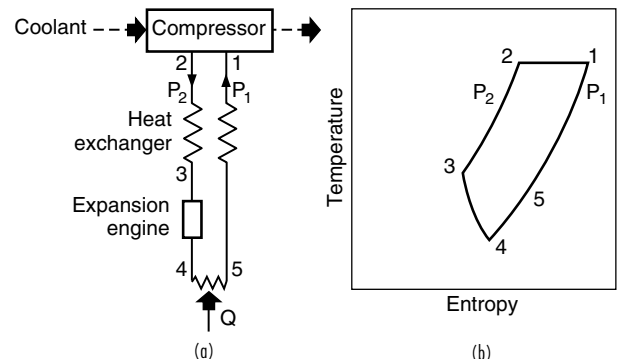


FIG. 11-112 Cold-gas refrigerator.

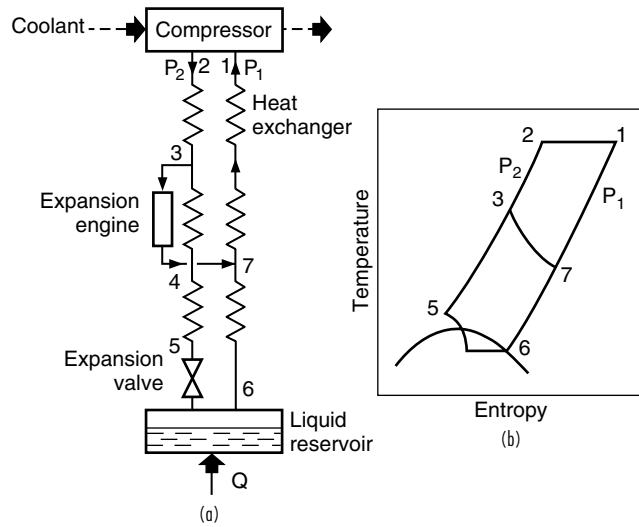


FIG. 11-113 Claude cycle refrigerator utilizing both expansion processes.

place during the engine expansion. In practice this expansion is never truly isentropic, and is reflected by path 3-4 on the temperature-entropy diagram. This specific refrigerant produces a cold gas which absorbs heat from 4-5 and provides a method of refrigeration that can be used to obtain temperatures between those of the boiling points of the lower-boiling cryogenes.

It is not uncommon to utilize both the isentropic and isenthalpic expansions in a cycle. This is done to avoid the technical difficulties associated with the formation of liquid in the expander. The Claude or expansion engine cycle is an example of a combination of these methods and is shown in Fig. 11-113 along with the corresponding temperature-entropy diagram.

The mixed refrigerant cycle was developed to meet the need for liquefying large quantities of natural gas to minimize transportation costs of this fuel. This cycle resembles the classic cascade cycle in principle and may best be understood by referring to that cycle. In the latter, the natural gas stream after purification is cooled successively by vaporization of propane, ethylene, and methane. Each refrigerant may be vaporized at two or three pressure levels to increase the natural gas cooling efficiency, but at a cost of considerable increased process complexity.

Cooling curves for natural gas liquefaction by the cascade process are shown in Fig. 11-114. It is evident that the cascade cycle efficiency can be improved by increasing the number of refrigerants employed.

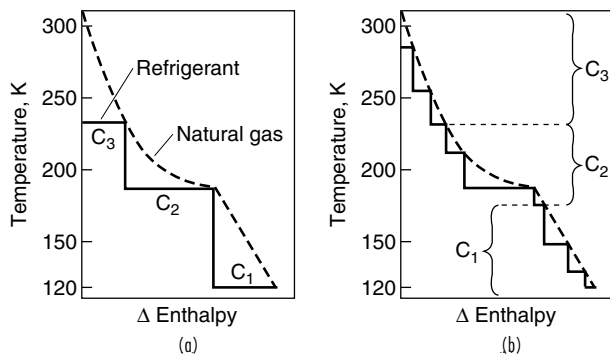


FIG. 11-114 Three- and nine-level cascade cycle cooling curve for natural gas.

For the same refrigeration capacity, the actual work required for the nine-level cascade cycle depicted is approximately 80 percent of that required by the three-level cascade cycle. This increase in efficiency is achieved by minimizing the temperature difference between the refrigerant and the natural gas stream throughout each increment of the cooling curve.

The mixed refrigerant cycle is a variation of the cascade cycle and involves the circulation of a single multicomponent refrigerant stream. The simplification of the compression and heat exchange services in such a cycle can offer potential for reduced capital expenditure over the conventional cascade cycle.

Figure 11-115 shows the basic concepts for a mixed refrigerant cycle (Gaumer, *Advances in Cryogenic Engineering* Vol. 31, Plenum, New York, 1986, p. 1095). Variations of the cycle are proprietary with those cryogenic engineering firms that have developed the technology. However, all of the mixed refrigerant processes use a carefully prepared refrigerant mix which is repeatedly condensed, vaporized, separated, and expanded. Thus, these processes require

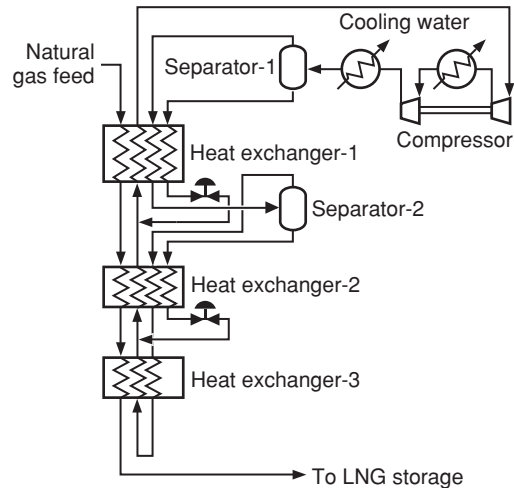


FIG. 11-115 Mixed-refrigerant cycle.

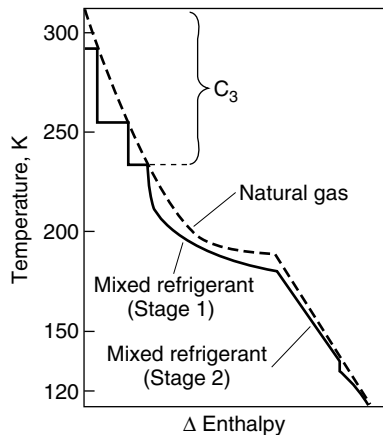


FIG. 11-116 Propane precooled mixed-refrigerant cycle cooling curve for natural gas.

more complete knowledge of the thermodynamic properties of gaseous mixtures than those required in the expander or classical cascade cycles. This is particularly evident when cooling curves similar to the one shown in Fig. 11-116 are desired. An inspection of the mixed refrigerant cycle also shows that these processes must routinely handle two-phase flows in the heat exchangers.

Miniature Refrigerators Expanded space and science projects have provided a need for miniature cryogenic coolers designated as cryocoolers. Such coolers provide useful cooling from a fraction of a watt to several watts at temperature levels from 1 to 90 K. These coolers are used to increase the sensitivity and signal-to-noise ratio of detectors by providing the required cryogenic operating temperatures as well as cooling the optical components to decrease the detector background radiation. The types of coolers developed to meet various specific requirements include solid cryogen coolers, radiative coolers, mechanical coolers, ^3He adsorption coolers, adiabatic demagnetization refrigerators, and liquid helium storage systems. Mechanical coolers are generally classified as regenerative or recuperative. Regenerative coolers use reciprocating components that move the working fluid back and forth through a regenerator. The recuperative coolers, on the other hand, use countercurrent heat exchangers to accomplish the heat transfer operation. The Stirling, Gifford-McMahon, and pulse tube cycles are typically regenerative coolers while the Joule-Thomson and Brayton cycles are associated with recuperative coolers.

The miniature split single-stage Stirling cooler developed by Philips Laboratories produces 5 W of cooling at 65 K with the aid of linear motors and magnetically moving parts. A smaller split Stirling cycle cooler that uses a stacked diaphragm spring rather than magnetic means to levitate the piston and displacer has been developed at Oxford University (Bradshaw, et al., *Advances in Cryogenic Engineering*, Vol. 31, Plenum, New York, 1986, p. 801). The promise of higher reliability has spurred interest in the *pulse-tube refrigerator* (PTR). In the latest version of this device, an orifice and reservoir have been added to the warm end of the pulse tube (OPTR) to permit control of the phase shift required for optimum resonance in the system.

The Joule-Thomson cycle has also benefited from creative thinking. For example, Little (6th International Cryocooler Conference, Naval Postgraduate School, Monterey, CA, 1989, p. 3) has introduced a new method of fabricating J-T refrigerators using a photolithographic manufacturing process in which gas channels for the heat exchangers, expansion capillary, and liquid reservoir are etched on planar, glass substrates that are fused together to form the sealed refrigerator. These microminiature refrigerators have been made in a wide range of sizes and capacities.

Mixtures of highly polar gases are receiving considerable attention for J-T cycles since the magnitude of the Joule-Thomson coefficient

increases with nonideality of the gas. For example, for pure nitrogen with a high pressure of 5 MPa, a low pressure of 0.1 MPa, and an ambient temperature of 300 K, the ideal efficiency at 77 K is only 8.6 percent of Carnot. For a mixture of 40% nitrogen, 17% methane, 15% ethane, and 28% propane, the ideal efficiency for the same operating conditions is 52 percent of Carnot. The higher efficiency possible permits the use of compressors for domestic and commercial refrigeration, thereby reducing the overall costs of the cryogenic unit.

Thermodynamic Analyses of Cycles The thermodynamic quality measure of either a piece of equipment or an entire process is its reversibility. The second law, or more precisely the entropy increase, is an effective guide to this degree of irreversibility. However, to obtain a clearer picture of what these entropy increases mean, it has become convenient to relate such an analysis to the additional work that is required to overcome these irreversibilities. The fundamental equation for such an analysis is

$$W = W_{\text{rev}} + T_o \sum \dot{m} \Delta s \quad (11-114)$$

where the total work, W , is the sum of the reversible work, W_{rev} , plus a summation of the losses in availability for various unit operations in the analysis. Application of this method has been demonstrated numerically by Timmerhaus and Flynn (*Cryogenic Process Engineering*, Plenum Press, 1989, p. 175).

Numerous analyses and comparisons of refrigeration and liquefaction cycles are available in the literature. Great care must be exercised in accepting these comparisons since it is quite difficult to put all processes on a strictly comparable basis. Many assumptions need to be made in the course of the calculations, and these can have considerable effect on the conclusions. Major factors upon which assumptions generally have to be made include heat leak, temperature differences in the exchangers, efficiencies of compressors and expanders, number of stages of compression, fraction of expander work recovered, state of expander exhaust, purity and condition of inlet gases, pressure drop due to fluid flow, and so on. In view of this fact, differences in power requirements of 10 to 20 percent can readily be due to differences in assumed variables and can negate the advantage of one cycle over another. Barron (*Cryogenic Systems, 2d ed.*, Oxford University Press, New York, 1985, p. 94) has made an analysis of some of the more common liquefaction systems described earlier that emphasize this point rather well.

PROCESS EQUIPMENT

The equipment normally associated with cryogenic systems includes heat exchangers, compressors, expanders, throttling valves, and storage containers. Since the reciprocal or centrifugal compressors used generally operate at ambient temperatures, their operating principles are not covered here but in Sec. 10. Storage containers, are discussed later in Sec. 11.

Heat Exchangers Since most cryogens, with the exception of helium II behave as classical fluids, well-established principles of mechanics and thermodynamics at ambient temperature also apply for cryogens. Thus, similar conventional heat transfer correlations have been formulated for simple low-temperature heat exchangers. These correlations are described in terms of well-known dimensionless quantities such as the Nusselt, Reynolds, Prandtl, and Grashof numbers.

Because of the need to operate more efficiently at low temperatures, the simple heat exchangers have generally been replaced with more sophisticated types. Guidance for the development of such units for low-temperature service include the following factors:

1. Small temperature differences between inlet and exit streams to enhance efficiency.
2. Large surface area-to-volume ratio to minimize heat leak.
3. High heat transfer to reduce surface area.
4. Low mass to minimize start-up time.
5. Multichannel capability to minimize the number of units.
6. High-pressure capability to provide design flexibility.
7. Minimum pressure drop to reduce compression costs.
8. High reliability with minimal maintenance to reduce shutdowns.

Problems sometimes occur in trying to minimize the temperature difference at the cold end of the heat exchanger, particularly if the specific heat of the warm fluid decreases with decreasing temperature as is the case with gaseous hydrogen.

The selection of an exchanger for low-temperature operation is usually determined by the process-design requirements, mechanical-design limitations, and economic considerations. Laboratory needs are generally met by concentric tube and extended surface exchangers, while industrial needs are most often met by the coiled-tube, plate-fin, reversing, and regenerator types of exchangers.

The coiled-tube heat exchanger offers unique advantages, especially when dealing with low-temperature design conditions where (1) simultaneous heat transfer between more than two streams is desired, (2) a large number of heat transfer units is required, and (3) high operating pressures are involved. Heat transfer for single-phase flow of either gas or liquid on the tubeside is generally well represented by either the Colburn correlation or modified forms of the Dittus-Boelter relationship.

The shape of the cooling and warming curves in coiled-tube heat exchangers is affected by the pressure drop in both the tube and shell-sides of the heat exchanger. This is particularly important for two-phase flows of multicomponent systems. For example, an increase in pressure drop on the shellside causes boiling to occur at a higher temperature, while an increase in pressure drop on the tubeside will cause condensation to occur at a lower temperature. The net result is both a decrease in the effective temperature difference between the two streams and a requirement for additional heat transfer area to compensate for these losses.

Plate-fin heat exchangers are about nine times as compact as conventional shell-and-tube heat exchangers with the same amount of surface area, weigh less than conventional heat exchangers, and withstand design pressures up to 6 MPa for temperatures between 4 and 340 K. Flow instability frequently becomes a limiting design parameter for plate-fin heat exchangers handling either boiling or condensing two-phase flows. This results in lower optimum economic mass flow velocities for plate-fin heat exchangers when compared with coiled-tube heat exchangers. The use of fins or extended surfaces in plate-fin or similar exchangers greatly increases the heat transfer area. Calculations using finned surfaces are outlined earlier in Sec. 11.

There are two basic approaches to heat-exchanger design for low temperatures: (1) the effectiveness-NTU approach and (2) the *log-mean-temperature-difference* (LMTD) approach. The LMTD approach is used most frequently when all the required mass flows are known and the area of the exchanger is to be determined. The effectiveness-NTU approach is used more often when the inlet temperatures and the flow rates are specified for an exchanger with fixed area and the outlet temperatures are to be determined. Both methods are described earlier in Sec. 11.

System performance in cryogenic liquefiers and refrigerators is directly related to the effectiveness of the heat exchangers used in the system. For example, the liquid yield for a simple J-T cycle as given by Eq. 11-112 needs to be modified to

$$y = \frac{(h_1 - h_2) - (1 - \epsilon)(h_1 - h_g)}{(h_1 - h_f) - (1 - \epsilon)(h_1 - h_g)} \quad (11-115)$$

if the heat exchanger is less than 100 percent effective. Likewise, the heat exchanger ineffectiveness increases the work required for the system by an amount of

$$\Delta \dot{W} = \dot{m}(h_1 - h_g)(1 - \epsilon) \quad (11-116)$$

Uninterrupted operation of heat exchangers at low temperatures requires removal of essentially all impurities present in the streams that are to be cooled. Equipment is readily available for the satisfactory removal of these impurities by both chemical and physical methods, but at increased operating expense. Another effective method for also accomplishing this impurity removal utilizes reversing heat exchangers. Proper functioning of the reversing heat exchanger is dependent upon the relationship between the pressures and temperatures of the two streams. Since the pressures are generally fixed by other factors, the purification function of the heat exchanger is normally controlled by selecting the right temperature difference

throughout the heat exchanger. To assure that reevaporation takes place, these differences must be such that the vapor pressure of the impurity is greater than the partial pressure of the impurity in the purging stream.

Another type of reversing heat exchanger is the regenerator as detailed by Ackerman (*Cryogenic Regenerative Heat Exchangers*, Plenum Press, New York, 1997). As with all reversing heat exchangers, regenerators provide the simultaneous cooling and purification of gases in low-temperature processes. As noted earlier, reversing heat exchangers usually operate continuously. Regenerators do not operate continuously; instead, they operate by periodically storing heat in a packing during the first half of the cycle and then giving up this stored heat to the fluid during the second half of the cycle. Typically, a regenerator consists of two identical columns, which are packed with a porous solid material with a high heat capacity such as metal ribbon, through which the gases flow.

The low cost of the packing material, its large surface-area-per-unit volume, and the low-pressure drops encountered provide compelling arguments for utilizing regenerators. However, the intercontamination of fluid streams, caused by the periodic flow reversals, and the problems associated with designing regenerators to handle three or more fluids, has restricted their use to simple fluids, and favored adoption of plate-fin reversing heat exchangers.

Expanders The primary function of cryogenic expansion equipment is the reduction of the temperature of the gas being expanded to provide needed refrigeration. The expansion of a fluid to produce refrigeration may be carried out in two distinct ways: (1) in an expander where mechanical work is produced, and (2) in a Joule-Thomson valve where no work is produced.

Mechanical Expanders Reciprocating expanders are very similar in concept and design to reciprocating compressors. Generally these units are used with inlet pressures of 4 to 20 MPa. These machines operate at speeds up to 500 rpm. The thermal efficiencies (actual enthalpy difference/maximum possible enthalpy difference) range from about 75 percent for small units to 85 percent for large machines.

Turboexpanders have replaced reciprocating expanders in high-power installations as well as in small helium liquefiers. Sizes range from 0.75 to 7500 kW with flow rates up to 28 million m³/day. Today's large-tonnage air-separation plants are a reality due to the development of highly reliable and efficient turboexpanders. These expanders are being selected over other cryogenic equipment because of their ability to handle condensed ethane and heavier hydrocarbons. This type of expander usually weighs and costs less and requires less space and operating personnel.

Turboexpanders can be classified as either axial or radial. Axial flow expanders have either impulse or reaction type blades and are suitable for multistage expanders because they permit a much easier flow path from one stage to the next. However, radial turboexpanders have lower stresses at a given tip speed, which permits them to run at higher speeds. This results in higher efficiencies with correspondingly lower energy requirements. As a consequence, most turboexpanders built today are of the radial type.

Joule-Thomson Valves The principal function of a J-T valve is to obtain isenthalpic cooling of the gas flowing through the valve. These valves generally are needle-type valves modified for cryogenic operation. They are an important component in most refrigeration systems, particularly in the last stage of the liquefaction process. Joule-Thomson valves also offer an attractive alternative to turboexpanders for small-scale gas-recovery applications.

SEPARATION AND PURIFICATION SYSTEMS

The energy required to reversibly separate gas mixtures is the same as that necessary to isothermally compress each component in the mixture from the partial pressure of the gas in the mixture to the final pressure of the mixture. This reversible isothermal work is given by the familiar relation

$$\frac{-W_i}{\dot{m}} = T(s_1 - s_2) - (h_1 - h_2) \quad (11-117)$$

where s_1 and h_1 refer to conditions before the separation and s_2 and h_2 refer to conditions after the separation. For a binary system, and assuming a perfect gas for both components, Eq. (11-117) simplifies to

$$\frac{-W_i}{\dot{m}} = RT \left(n_A \ln \frac{P_T}{p_A} + n_B \ln \frac{P_T}{p_B} \right) \quad (11-118)$$

where n_A and n_B are the moles of A and B in the mixture, p_A and p_B are the partial pressures of these two components in the mixture, and P_T is the total pressure of the mixture. The figure of merit for a separation system is defined similar to that for a liquefaction system; see Eq. (11-110).

If the mixture to be separated is essentially a binary, both the McCabe-Thiele and the Ponchon-Savarit methods outlined in Sec. 13, with the appropriate cryogenic properties, can be used to obtain the ideal number of stages required. It should be noted, however, that it is not satisfactory in the separation of air to treat it as a binary mixture of oxygen and nitrogen if high purity (99 percent or better) oxygen is desired. The separation of oxygen from argon is a more difficult separation than oxygen from nitrogen and would require correspondingly many more plates. In fact, if the argon is not extracted from air, only 95 percent oxygen would be produced. The other rare gas constituents of air (helium, neon, krypton, and xenon) are present in such small quantities and have boiling points so far removed from those of oxygen and nitrogen that they introduce no important complications.

Air-Separation Systems Of the various separation schemes available today, the simplest is known as the Linde single-column system shown in Fig. 11-117 and first introduced in 1902. In it, purified compressed air passes through a precooling heat exchanger (if oxygen gas is the desired product, a three-channel exchanger for air, waste nitrogen, and oxygen gas is used; if liquid oxygen is to be recovered from the bottom of the column, a two-channel exchanger for air and waste nitrogen is employed), then through a coil in the boiler of the rectifying column where it is further cooled (acting at the same time as the boiler heat source); following this, it expands essentially to atmospheric pressure through a J-T valve and reenters the top of the column with the liquid providing the required reflux. Rectification occurs as liquid and vapor on each plate establish equilibrium. If oxygen gas is to be the product, purified air need only be compressed to a pressure of 3 to 6 MPa; if the product is to be liquid oxygen, a compressor outlet pressure of 20 MPa is necessary. Note that the Linde single-column separation system is simply a J-T liquefaction system

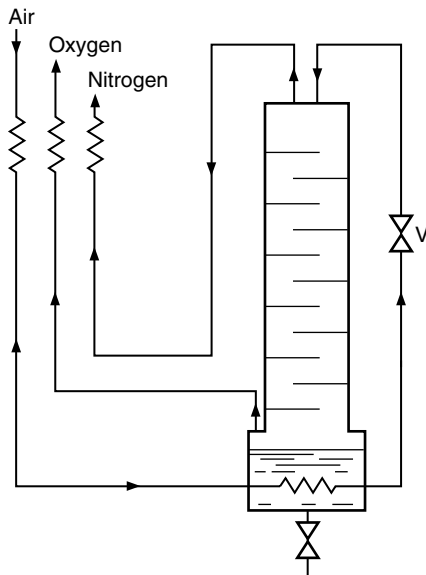


FIG. 11-117 Linde single-column air separator.

with a substitution of a rectification column for the liquid reservoir. However, any of the other liquefaction systems discussed earlier could have been used to furnish the liquid for the column.

In a simple single-column process, although the oxygen purity is high, the nitrogen effluent stream is impure. The equilibrium vapor concentration of the overhead nitrogen effluent for an initial liquid mixture of 21 percent oxygen/79 percent nitrogen at 100 kPa is about 6 to 7 percent oxygen. Thus, the nitrogen waste gas stream with such an impurity may only be usable as a purge gas for certain conditions.

The impurity problem noted in the previous paragraph was solved by the introduction of the Linde double-column system shown in Fig. 11-118. Two rectification columns are placed one on top of the other (hence the name double-column system).

In this system the liquid air is introduced at an intermediate point B into the lower column, and a condenser-evaporator at the top of the lower column makes the arrangement a complete reflux distillation column which delivers almost pure nitrogen at E. In order for the column simultaneously to deliver pure oxygen, the oxygen-rich liquid (about 45 percent O₂) from the bottom boiler is introduced at an intermediate level C in the upper column. The reflux and rectification in the upper column produce pure oxygen at the bottom and pure nitrogen at the top provided all major impurities are first removed from the column. More than enough liquid nitrogen is produced in the lower column for the needed reflux in both columns. Since the condenser must condense nitrogen vapor by evaporating liquid oxygen, it is necessary to operate the lower column at a higher pressure, about 500 kPa, while the upper column is operated at approximately 110 kPa. This requires a reduction in the pressure of the fluids from the lower column as they are admitted to the upper column.

In the cycle shown, gaseous oxygen and nitrogen are withdrawn at room temperature. Liquid oxygen could be withdrawn from point A and liquid nitrogen from point E, but in this case more refrigeration would be needed.

Even the best modern low-temperature air separation plant has an efficiency only a small fraction of the theoretical optimum, that is, about 15 to 20 percent. The principal sources of inefficiency are threefold: (1) the nonideality of the refrigerating process, (2) the imperfection of the heat exchangers, and (3) losses of refrigeration through heat leak.

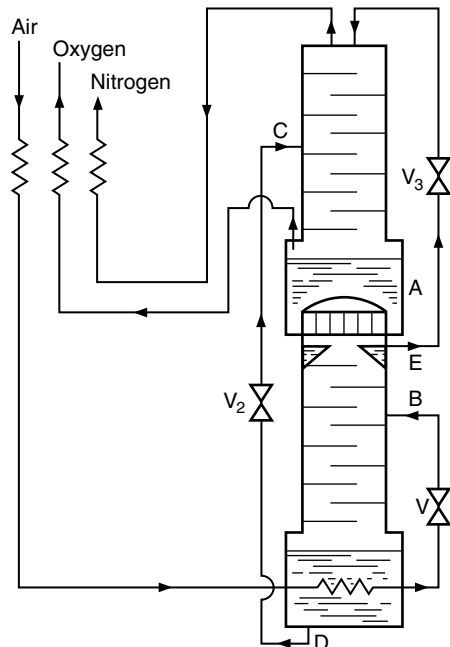


FIG. 11-118 Linde double-column air separator.

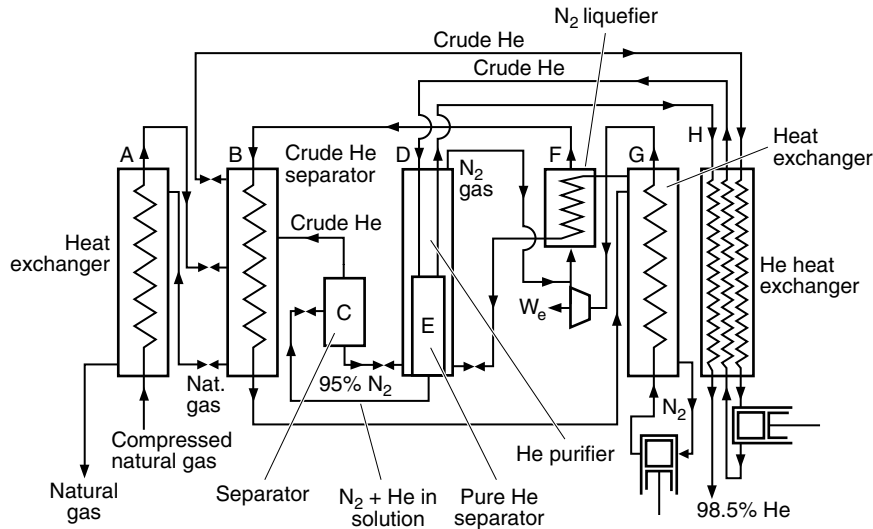


FIG. 11-119 Typical helium-separation plant as operated by the U.S. Bureau of Mines.

Helium and Natural-Gas Systems Separation Helium is produced primarily by separation of helium-rich natural gas. The helium content of the natural gas from plants operated by the U.S. Bureau of Mines normally has varied from 1 to 2 percent while the nitrogen content of the natural gas has varied from 12 to 80 percent. The remainder of the natural gas is methane, ethane, and heavier hydrocarbons.

A Bureau of Mines system for the separation of helium from natural gas is shown in Fig. 11-119. Since the major constituents of natural gas have boiling points very much different from that of helium, a distillation column is not necessary and the separation can be accomplished with condenser-evaporators.

The need to obtain greater recoveries of the C_2 , C_3 , and C_4 's in natural gas has resulted in the expanded use of low-temperature processing of these streams. The majority of the natural gas processing at low temperatures to recover light hydrocarbons is now accomplished using the turboexpander cycle. Feed gas is normally available from 1 to 10 MPa. The gas is first dehydrated to a dew point of 200 K and lower. After dehydration the feed is cooled with cold residue gas. Liquid produced at this point is separated before entering the expander and sent to the condensate stabilizer. The gas from the separator is expanded in a turboexpander where the exit stream can contain as much as 20 wt % liquid. This two-phase mixture is sent to the top section of the stabilizer which separates the two phases. The liquid is used as reflux in this unit while the cold gas exchanges heat with the fresh feed and is recompressed by the expander-driven compressor. Many variations to this cycle are possible and have been used in actual plants.

Gas Purification The nature and concentration of impurities to be removed depends on the type of process involved. For example, in the production of large quantities of oxygen, various impurities must be removed to avoid plugging of the cold process lines or to avoid buildup of hazardous contaminants. The impurities in air that would contribute most to plugging would be water and carbon dioxide. Helium, hydrogen, and neon, on the other hand, will accumulate on the condensing side of the condenser-reboiler located between the two separation columns and will reduce the rate of heat transfer unless removed by intermittent purging. The buildup of acetylene, however, can prove to be dangerous even though the feed concentration in the air is no greater than 0.04 ppm.

Refrigeration purification is a relatively simple method for removing water, carbon dioxide, and certain other contaminants from a process stream by condensation or freezing. (Either regenerators or reversing heat exchangers may be used for this purpose since a flow

reversal is periodically necessary to reevaporate and remove the solid deposits.) The effectiveness of this method depends upon the vapor pressure of the impurities relative to that of the major components of the process stream at the refrigeration temperature. Thus, assuming ideal gas behavior, the maximum impurity content in a gas stream after refrigeration would be inversely proportional to its vapor pressure. However, due to the departure from ideality at higher pressures, the impurity content will be considerably higher than predicted for the ideal situation. For example, the actual water vapor content in air will be over four times that predicted by ideal gas behavior at a temperature of 228 K and a pressure of 20 MPa.

Purification by a solid adsorbent is one of the most common low-temperature methods for removing impurities. Materials such as silica gel, carbon, and synthetic zeolites (molecular sieves) are widely used as adsorbents because of their extremely large effective surface areas. Most of the gels and carbon have pores of varying sizes in a given sample, but the synthetic zeolites are manufactured with closely controlled pore-size openings ranging from about 0.4 to 1.3 nm. This makes them even more selective than other adsorbents since it permits separation of gases on the basis of molecular size.

Information needed in the design of low-temperature adsorbents includes the equilibrium between the solid and gas and the rate of adsorption. Equilibrium data for the common systems generally are available from the suppliers of such material. The rate of adsorption is usually very rapid and the adsorption is essentially complete in a relatively narrow zone of the adsorber. If the concentration of the adsorbed gas is more than a trace, then heat of adsorption may also be a factor of importance in the design. (The heat of adsorption is usually of the same order or larger than the normal heat associated with the phase change.) Under such situations it is generally advisable to design the purification in two steps, that is, first removing a significant portion of the impurity either by condensation or chemical reaction and then completing the purification with a low-temperature adsorption system. A scheme combining the condensation and adsorption is shown in Fig. 11-120.

In normal plant operation at least two adsorption purifiers are employed—one in service while the other is desorbed of its impurities. Often there is an advantage in using an additional purifier by placing this unit in series with the adsorption unit to provide a backup if impurities are not trapped by the first unit. Cooling of the purifier must utilize some of the purified gas to avoid adsorption during this period.

Experience in air separation plant operations and other cryogenic processing plants has shown that local freeze-out of impurities such as

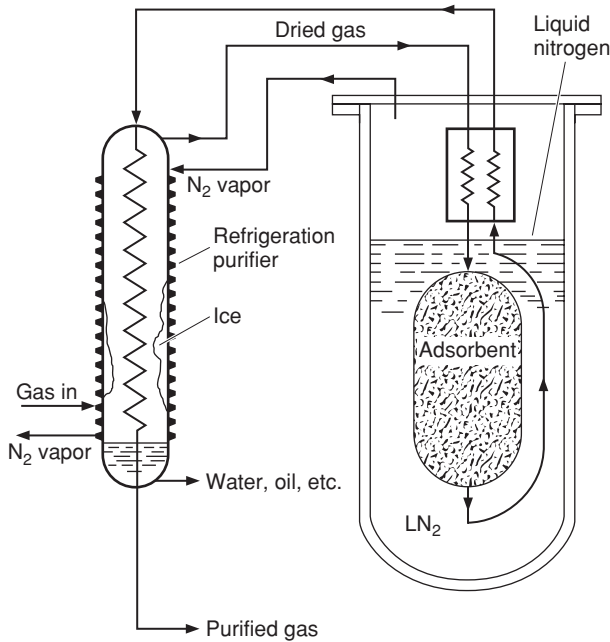


FIG. 11-120 Purifier using refrigeration and adsorption schemes in series.

carbon dioxide can occur at concentrations well below the solubility limit. For this reason, the carbon dioxide content of the feed gas subject to the minimum operating temperature is usually kept below 50 ppm. The amine process and the molecular sieve adsorption process are the most widely used methods for carbon dioxide removal. The amine process involves adsorption of the impurity by a lean aqueous organic amine solution. With sufficient amine recirculation rate, the carbon dioxide in the treated gas can be reduced to less than 25 ppm. Oxygen is removed by a catalytic reaction with hydrogen to form water.

STORAGE AND TRANSFER SYSTEMS

Storage vessels range in type from low-performance containers, insulated by rigid foam or fibrous insulation where the liquid in the container evaporates in a few hours, up to high-performance containers, insulated with multilayer insulations where less than 0.1 percent of the fluid contents is evaporated per day. In the more effective units, the storage container consists of an inner vessel which encloses the cryogenic fluid to be stored and an outer vessel or vacuum jacket. The latter maintains the vacuum necessary to make the insulation effective and at the same time serves as a vapor barrier to the migration of water and other condensibles to the cold surface of the inner vessel. Improvements have been made in the insulation used in these containers, but the vacuum-insulated double-walled Dewar is still the basic idea for high-performance cryogenic-fluid container design.

Insulation Principles The effectiveness of a liquefier or refrigerator is highly dependent upon the heat leak entering such a system. Since heat removal becomes more costly with a lowering in temperature as demonstrated by the Carnot limitation, most cryogenic systems employ some form of insulation to minimize the effect. The insulation strategy is to minimize radiative heat transfer, minimize convective heat transfer, and use only a minimum of solid conductance media. Factors considered in the selection of the most suitable insulation include its ruggedness, convenience, volume, weight, ease of fabrication and handling, and thermal effectiveness and cost. It is common practice to use an experimentally obtained apparent thermal conductivity to characterize the thermal effectiveness of various insulations. Typical k_a values for insulations used in cryogenic service are listed in Table 11-26.

TABLE 11-26 Representative Apparent Thermal Conductivity Values

Type of insulation	$k_a, mW/m \cdot K (77-300K)$
Pure vacuum, 1.3×10^{-4} Pa	5
Foam insulation	26-35
Nonevacuated powders (perlite, silica aerogel)	19-44
Evacuated powders and fibers (1.3×10^{-1} Pa)	1-2
Opacified powdered insulations (1.3×10^{-1} Pa)	3.5×10^{-1}
Multilayer insulations (1.3×10^{-4} Pa)	$1.7-4 \times 10^{-3}$

Types of Insulation Cryogenic insulations have generally been divided into five general categories: high vacuum, multilayer insulation, powder, foam, and special insulations. Each is discussed in turn in the following sections.

Vacuum Insulation Heat transport across an evacuated space (1.3×10^{-4} Pa or lower), is by radiation and by conduction through the residual gas. The heat transfer by radiation generally is predominant and can be approximated by

$$\frac{\dot{Q}_r}{A_1} = \sigma (T_2^4 - T_1^4) \left[\frac{1}{e_1} + \frac{A_1}{A_2} \left(\frac{1}{e_2} - 1 \right) \right]^{-1} \quad (11-119)$$

where \dot{Q}_r/A_1 is the heat transfer by radiation-per-unit area, σ is the Stefan-Boltzmann constant, and e is the emissivity of the surfaces. Subscript 2 refers to the hot surface and subscript 1 refers to the cold surface. The bracketed term on the right-hand side of this relation is designated as the overall emissivity factor, F_e .

The insertion of low-emissivity floating shields within the evacuated space can effectively reduce the heat transport by radiation. The effect of the shields is to greatly reduce the emissivity factor. For example, for N shields or $(N + 2)$ surfaces, an emissivity of the outer and inner surface of e_o , and an emissivity of the shields of e_s , the emissivity factor reduces to

$$\left[2 \left(\frac{1}{e_o} + \frac{1}{e_s} - 1 \right) + \frac{(N-1)(2-e_s)}{e_s} \right]^{-1} \quad (11-120)$$

In essence, one properly located low-emissivity shield can reduce the radiant heat transfer to around one-half of the rate without the shield, two shields can reduce this to around one-fourth of the rate without the shield, and so on.

Multilayer Insulation Multilayer insulation consists of alternating layers of highly reflecting material, such as aluminum foil or aluminized Mylar, and a low-conductivity spacer material or insulator, such as fiberglass mat or paper, glass fabric, or nylon net, all under high vacuum. When properly applied at the optimum density, this type of insulation can have an apparent thermal conductivity as low as 10 to 50 $\mu W/m \cdot K$ between 20 and 300 K.

For a highly evacuated (on the order of 1.3×10^{-4} Pa) multilayer insulation, heat is transferred primarily by radiation and solid conduction through the spacer material. The apparent thermal conductivity of the insulation material under these conditions may be determined from

$$k_a = \frac{1}{N/\Delta x} \left\{ h_s + \frac{\sigma e T_2^3}{2-e} \left[1 + \left(\frac{T_1}{T_2} \right)^2 \right] \left(1 + \frac{T_1}{T_2} \right) \right\} \quad (11-121)$$

where $N/\Delta x$ is the number of complete layers (reflecting shield plus spacer) of the insulation-per-unit thickness, h_s is the solid conductance of the spacer material, σ is the Stefan-Boltzmann constant, e is the effective emissivity of the reflecting shield, and T_2 and T_1 are the temperatures of the warm and cold sides of the insulation, respectively. It is evident that the apparent thermal conductivity can be reduced by increasing the layer density up to a certain point. It is not obvious from the above relation that a compressive load affects the apparent thermal conductivity and thus the performance of a multilayer insulation. However, under a compressive load the solid conductance increases much more rapidly than $N/\Delta x$ resulting in an overall increase in k_a . Plots of heat flux versus compressive load on a logarithmic scale result in straight lines with slopes between 0.5 and 0.67.

The effective thermal conductivity values generally obtained in practice are at least a factor of two greater than the one-dimensional thermal conductivity values measured in the laboratory with carefully

controlled techniques. This degradation in insulation thermal performance is caused by the combined presence of edge exposure to isothermal boundaries, gaps, joints, or penetrations in the insulation blanket required for structural supports, fill and vent lines, and high lateral thermal conductivity of these insulation systems.

Powder Insulation A method of realizing some of the benefits of multiple floating shields without incurring the difficulties of awkward structural complexities is to use evacuated powder insulation. The penalty incurred in the use of this type of insulation, however, is a tenfold reduction in the overall thermal effectiveness of the insulation system over that obtained for multilayer insulation. In applications where this is not a serious factor, such as LNG storage facilities, and investment cost is of major concern, even unevacuated powder-insulation systems have found useful applications. The variation in apparent mean thermal conductivity of several powders as a function of interstitial gas pressure is shown in the familiar S-shaped curves of Fig. 11-121.

The apparent thermal conductivity of powder insulation at cryogenic temperatures is generally obtained from

$$k_a = \frac{k_g}{1 - V_r(1 - k_g/k_s)} \quad (11-122)$$

where k_g is the thermal conductivity of the gas within the insulation, k_s is the thermal conductivity of the powder, and V_r is the ratio of solid volume to the total volume. The amount of heat transport due to radiation through the powders can be reduced by the addition of metallic powders. A mixture containing approximately 40 to 50 wt % of a metallic powder gives the optimum performance.

Foam Insulation Since foams are not homogeneous materials, their apparent thermal conductivity is dependent upon the bulk density of the insulation, the gas used to foam the insulation, and the mean temperature of the insulation. Heat conduction through a foam is determined by convection and radiation within the cells and by conduction in the solid structure. Evacuation of a foam is effective in reducing its thermal conductivity, indicating a partially open cellular structure, but the resulting values are still considerably higher than either multilayer or evacuated powder insulations.

Data on the thermal conductivity for a variety of foams used at cryogenic temperatures have been presented by Kropschot (*Cryogenic Technology*, R. W. Vance, ed., Wiley, New York, 1963, p. 239). Of all the foams, polyurethane and polystyrene have received the widest use at

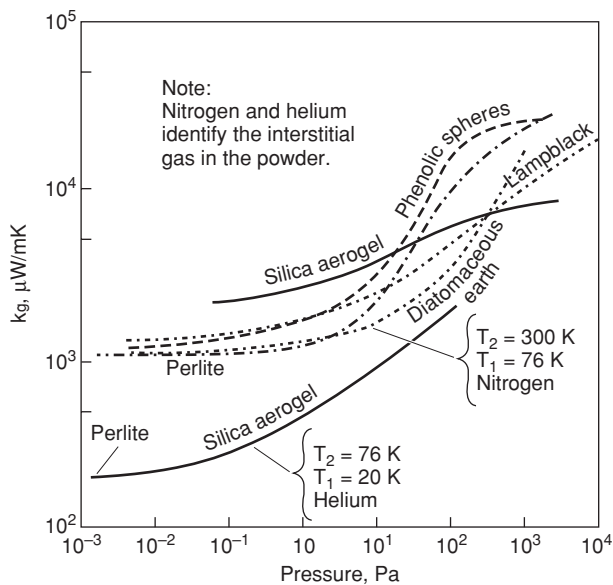


FIG. 11-121 Apparent mean thermal conductivities of several powder insulations as a function of interstitial gas pressure.

low temperatures. The major disadvantage of foams is that they tend to crack upon repeated thermal cycling and lose their insulation value.

Storage and Transfer Systems In general, heat leak into a storage or transfer system for a cryogen is by (1) radiation and conduction through the insulation, and (2) conduction through any inner shell or transfer-line supports, piping leads, and access ports. Conduction losses are reduced by introducing long heat-leak paths, by making the cross sections for heat flow small, and by using materials with low thermal conductivity. Radiation losses, a major factor in the heat leak through insulations, are reduced with the use of radiation shields, such as multilayer insulation, boil-off vapor-cooled shields, and opacifiers in powder insulation.

Several considerations must be met when designing the inner vessel. The material of construction selected must be compatible with the stored cryogen. Nine percent nickel steels are acceptable for the higher-boiling cryogens ($T > 75 \text{ K}$) while many aluminum alloys and austenitic steels are usually structurally acceptable throughout the entire temperature range. Because of its high thermal conductivity, aluminum is not a recommended material for piping and supports that must cross the insulation space. A change to a material of lower thermal conductivity for this purpose introduces a transition joint of a dissimilar material. Since such transition joints are generally mechanical in nature, leaks into the vacuum space develop upon repeated temperature cycling. In addition, the larger thermal coefficient of expansion of aluminum can pose still further support and cooldown problems.

Economic and cooldown considerations dictate that the shell of the storage container be as thin as possible. As a consequence, the inner container is designed to withstand only the internal pressure and bending forces while stiffening rings are used to support the weight of the fluid. The minimum thickness of the inner shell for a cylindrical vessel under such a design arrangement is given by Sec. VIII of the *ASME Boiler and Pressure Vessel Code*.

Since the outer shell of the storage container is subjected to atmospheric pressure on one side and evacuated conditions going down to $1.3 \times 10^{-4} \text{ Pa}$ on the other, consideration must be given to provide ample thickness of the material to withstand collapsing or buckling. Failure by elastic instability is covered by the ASME Code, in which design charts are available for the design of cylinders and spheres subjected to external pressure. Stiffening rings are also used on the outer shell to support the weight of the inner container and its contents as well as maintaining the sphericity of the shell.

The outer shell is normally constructed of carbon steel for economic reasons, unless aluminum is required to reduce the weight. Stainless-steel standoffs must be provided on the carbon steel outer shell for all piping penetrations to avoid direct contact with these penetrations when they are cold.

There are a variety of methods for supporting the inner shell within the outer shell and the cold transfer line within the outer line. Materials that have a high strength to thermal conductivity ratio are selected for these supports. Design of these supports for the inner shell must allow for shipping loads which may be several orders higher than in-service loads. Compression supports such as legs or pads may be used, but tension supports are more common. These may take the form of cables, welded straps, threaded bars, or a combination of these to provide restraint of the inner shell in several directions.

Most storage containers for cryogens are designed for a 10 percent ullage volume. The latter permits reasonable vaporization of the contents due to heat leak without incurring too rapid a buildup of the pressure in the container. This, in turn, permits closure of the container for short periods of time to either avoid partial loss of the contents or to transport flammable or hazardous cryogens safely from one location to another.

CRYOGENIC INSTRUMENTATION

Even though the combined production of cryogenic nitrogen and oxygen exceeds the production of any other chemical in the United States, the cryogenic industry does not appear to warrant a separate product line of instruments for diagnostic and control purposes. Low-temperature thermometry is the one exception. The general approach

generally is that instruments developed for the usual CPI needs must be modified or accepted as is for cryogenic use.

Quite often problems arise when instruments for normal service are subjected to low temperature use. Since some metals become brittle at low temperatures, the instrument literally falls apart. Elastomeric gaskets and seals contract faster with decreasing temperatures than the surrounding metal parts, and the seal often is lost. Even hermetically sealed instruments can develop pin holes or small cracks to permit cryogenic liquids to enter these cases with time. Warming the instrument causes the trapped liquid to vaporize, sometimes generating excessive gas pressure and failure of the case.

Therefore, the first task in adapting normal instruments to cryogenic service is simply to give them a severe thermal shock by immersing them in liquid nitrogen repeatedly, and checking for mechanical integrity. This is the general issue; specific issues according to each type of measurement are discussed below.

Pressure This parameter is usually measured by the flush-mounted pressure transducer which consists of a force-summing device (bellow, diaphragm, bourdon tube, etc.) that translates the pressure into a displacement. The latter is then measured by an analog device (strain gage, piezoelectric crystal, variable distance between capacitor plates, and the like). Since these elements are likely to be made of different materials (bronze diaphragm, stainless-steel case, semiconductor strain gage), each will react to the temperature change in a different way. This is especially serious during cooldown, when the transient nature of material and construction prohibits all of the pressure-gage elements from being at the same temperature at the same time. Under steady-state conditions it is often possible to provide some temperature compensation through the well-known instrument technique of common-mode-rejection. Such compensation is generally not successful during transient temperature fluctuations. Only two courses of action are open: (1) hand-check each type of pressure transducer for thermal noise by thermally shocking it with immersion in liquid nitrogen; and (2) simplify the pressure-transducer construction to eliminate differences between materials. Some success has been observed in the latter area by manufacturers who make very small pressure sensing elements from a single semiconductor chip. The miniature size of these devices helps to reduce or eliminate temperature gradients across the device. The single-element nature of the pressure-gage assembly reduces differences in materials of construction.

Liquid Level The measurements for dense fluids such as liquid oxygen and liquid nitrogen are made in the conventional CPI approach using floats. Sight glasses cannot be used since radiation and thermal conduction would cause the cryogenic fluid within the sight glass to boil. The very light cryogenics, liquid helium and liquid hydrogen, cannot sustain a float. Liquid hydrogen has the density of Styrofoam,TM about 70 g/l, making floating devices impractical. Some electrical analog is used for hydrogen and helium, most frequently a linear concentric-tube electrical capacitor. The dielectric constant of cryogenics is related to their density by the Clausius-Mosotti relation. As the liquid level rises, the greater dielectric constant of the liquid between the tubes causes the overall capacitance to vary in a linear fashion. For best accuracy, these capacitance liquid-level measuring devices should be calibrated in place.

Flow The measurement of cryogenic fluids is most troublesome. Flow rate is not a natural physical parameter, like temperature, but is a derived quantity. A measurement of mass (or volume) must be made over a time interval to derive the flow rate. Because of this, any flow meter is only as good as its calibration. At this time, there is no national capability for calibrating cryogenic flowmeters. From data developed early in the nation's space program, considerable confidence has been developed in turbine-type flowmeters and in pressure-drop-type flowmeters. If all the usual ASTM guidelines are followed for meter installation, and if adequate temperature corrections are applied to changes in dimensions, then such meters can have an accuracy of ± 1 percent of their water calibrations. For very small flow applications, the Coriolis meters are promising. Vortex shedding flow meters appear useful for very large flow rates. Nonetheless, an actual calibration on the cryogen of interest is the only proof of accuracy.

Temperature The level of the temperature measurement (4 K, 20 K, 77 K, or higher) is the first issue to be considered. The second issue is the range needed (e.g., a few degrees around 90 K or 1 to 400 K). If the temperature level is that of air separation or liquefying of natural gas (LNG), then the favorite choice is the platinum resistance thermometer (PRT). Platinum, as with all pure metals, has an electrical resistance that goes to zero as the absolute temperature decreases to zero. Accordingly, the lower useful limit of platinum is about 20 K, or liquid hydrogen temperatures. Below 20 K, semiconductor thermometers (germanium-, carbon-, or silicon-based) are preferred. Semiconductors have just the opposite resistance-temperature dependence of metals—their resistance increases as the temperature is lowered, as fewer valence electrons can be promoted into the conduction band at lower temperatures. Thus, semiconductors are usually chosen for temperatures from about 1 to 20 K.

If the temperature range of interest is large, say 1 to 400 K, then diode thermometers are recommended. Diodes have other advantages compared to resistance thermometers. By contrast, diode thermometers are very much smaller and faster. By selection of diodes all from the same melt, they may be made interchangeable. That is, one diode has the same calibration curve as another, which is not always the case with either semiconductor or metallic-resistance thermometers. It is well known, however, that diode thermometers may rectify an ac field, and thus may impose a dc noise on the diode output. Adequate shielding is required.

Special applications, such as in high-magnetic fields, require special thermometers. The carbon-glass and strontium-titanate resistance thermometers have the least magnetoresistance effects.

Thermocouples are unsurpassed for making temperature-difference measurements. The thermoelectric power of thermocouple materials makes them adequate for use at liquid-air temperatures and above. At 20 K and below, the thermoelectric power drops to a few $\mu\text{V/K}$, and their use in this range is as much art as science.

A descriptive flowchart has been prepared by Sparks (*Materials at Low Temperatures*, ASM, Metal Park, OH, 1983) to show the temperature range of cryogenic thermometers in general use today. Pavese and Molinar (*Modern Gas-Based Temperature and Pressure Measurements*, Plenum, New York, 1992) provide details on gas- and vapor-pressure thermometry at these temperatures.

SAFETY

Past experience has shown that cryogenic fluids can be used safely in industrial environments as well as in typical laboratories provided all facilities are properly designed and maintained, and personnel handling these fluids are adequately trained and supervised. There are many hazards associated with cryogenic fluids. However, the principal ones are those associated with the response of the human body and the surroundings to the fluids and their vapors, and those associated with reactions between the fluids and their surroundings. Edeskuty and Stewart (*Safety in Handling Cryogenic Fluids*, Plenum Press, New York, 1996) provide a detailed examination of these various hazards.

Physiological Hazards Severe cold "burns" may be inflicted if the human body comes in contact with cryogenic fluids or with surfaces cooled by cryogenic fluids. Damage to the skin or tissue is similar to an ordinary burn. Because the body is composed mainly of water, the low temperature effectively freezes the tissue—damaging or destroying it. The severity of the burn depends upon the contact area and the contact time with prolonged contact resulting in deeper burns. Cold burns are accompanied by stinging sensations and pain similar to those of ordinary burns. The ordinary reaction is to withdraw that portion of the body that is in contact with the cold surface. Severe burns are seldom sustained if withdrawal is possible. Cold gases may not be damaging if the turbulence in the gas is low, particularly since the body can normally adjust for a heat loss of $95 \text{ J/m}^2\text{s}$ for an area of limited exposure. If the heat loss becomes much greater than this, the skin temperature drops and freezing of the affected area may ensue. Freezing of facial tissue will occur in about 100 s if the heat loss is $2,300 \text{ J/m}^2\text{s}$.

Materials and Construction Hazards Construction materials for noncryogenic service usually are chosen on the basis of tensile strength, fatigue life, weight, cost, ease of fabrication, corrosion

resistance, and so on. When working with low temperatures the designer must consider the ductility of the material since low temperatures, as noted earlier, have the effect of making some construction materials brittle or less ductile. Some materials become brittle at low temperatures but still can absorb considerable impact, while others become brittle and lose their impact strength.

Flammability and Explosion Hazards In order to have a fire or an explosion requires the combination of an oxidant, a fuel, and an ignition source. Generally the oxidizer will be oxygen. The latter may be available from a variety of sources including leakage or spillage, condensation of air on cryogenically cooled surfaces below 90 K, and buildup, as a solid impurity in liquid hydrogen. The fuel may be almost any noncompatible material or flammable gas; compatible materials can also act as fuels in the presence of extreme heat (strong ignition sources). The ignition source may be a mechanical or electrostatic spark, flame, impact, heat by kinetic effects, friction, chemical reaction, and so on. Certain combinations of oxygen, fuel, and ignition sources will always result in fire or explosion. The order of magnitude of flammability and detonability limits for fuel-oxidant gaseous mixtures of two widely used cryogenics is shown in Table 11-27.

High-Pressure Gas Hazards Potential hazards also exist in highly compressed gases because of their stored energy. In cryogenic systems such high pressures are obtained by gas compression during liquefaction or refrigeration, by pumping of liquids to high pressure followed by evaporation, and by confinement of cryogenic liquids with

TABLE 11-27 Flammability and Detonability Limits of Hydrogen and Methane Gas

Mixture	Flammability Limits (mol %)	Detonability Limits (mol %)
H ₂ -air	4-75	20-65
H ₂ -O ₂	4-95	15-90
CH ₄ -air	5-15	6-14
CH ₄ -O ₂	5-61	10-50

subsequent evaporation. If this confined gas is suddenly released through a rupture or break in a line, a significant thrust may be experienced. For example, the force generated by the rupture of a 2.5-cm diameter valve located on a 13.9-MPa pressurized gas cylinder would be over 6670 N.

SUMMARY

It is obvious that the best designed facility is no better than the attention that is paid to safety. The latter is not considered once and forgotten. Rather, it is an ongoing activity that requires constant attention to every conceivable hazard that might be encountered. Because of its importance, safety, particularly at low temperatures, has received a large focus in the literature with its own safety manual prepared by NIST as well as by the British Cryogenics Council.

EVAPORATORS

GENERAL REFERENCES: Badger and Banchero, *Introduction to Chemical Engineering*, McGraw-Hill, New York, 1955. Standiford, *Chem. Eng.*, **70**, 158-176 (Dec. 9, 1963). *Testing Procedure for Evaporators*, American Institute of Chemical Engineers, 1979. *Upgrading Evaporators to Reduce Energy Consumption*, ERDA Technical Information Center, Oak Ridge, Tenn., 1977.

PRIMARY DESIGN PROBLEMS

Heat Transfer This is the most important single factor in evaporator design, since the heating surface represents the largest part of evaporator cost. Other things being equal, the type of evaporator selected is the one having the highest heat-transfer cost coefficient under desired operating conditions in terms of J/s·K (British thermal units per hour per degree Fahrenheit) per dollar of installed cost. When power is required to induce circulation past the heating surface, the coefficient must be even higher to offset the cost of power for circulation.

Vapor-Liquid Separation This design problem may be important for a number of reasons. The most important is usually prevention of entrainment because of value of product lost, pollution, contamination of the condensed vapor, or fouling or corrosion of the surfaces on which the vapor is condensed. Vapor-liquid separation in the vapor head may also be important when spray forms deposits on the walls, when vortices increase head requirements of circulating pumps, and when short circuiting allows vapor or unflashed liquid to be carried back to the circulating pump and heating element.

Evaporator performance is rated on the basis of **steam economy**—kilograms of solvent evaporated per kilogram of steam used. Heat is required (1) to raise the feed from its initial temperature to the boiling temperature, (2) to provide the minimum thermodynamic energy to separate liquid solvent from the feed, and (3) to vaporize the solvent. The first of these can be changed appreciably by reducing the boiling temperature or by heat interchange between the feed and the residual product and/or condensate. The greatest increase in steam economy is achieved by reusing the vaporized solvent. This is done in a **multiple-effect evaporator** by using the vapor from one effect as the heating medium for another effect in which boiling takes place at

a lower temperature and pressure. Another method of increasing the utilization of energy is to employ a **thermoccompression** evaporator, in which the vapor is compressed so that it will condense at a temperature high enough to permit its use as the heating medium in the same evaporator.

Selection Problems Aside from heat-transfer considerations, the selection of type of evaporator best suited for a particular service is governed by the characteristics of the feed and product. Points that must be considered are crystallization, salting and scaling, product quality, corrosion, and foaming. In the case of a **crystallizing evaporator**, the desirability of producing crystals of a definite uniform size usually limits the choice to evaporators having a positive means of circulation. **Salting**, which is the growth on body and heating-surface walls of a material having a solubility that increases with increase in temperature, is frequently encountered in crystallizing evaporators. It can be reduced or eliminated by keeping the evaporating liquid in close or frequent contact with a large surface area of crystallized solid. **Scaling** is the deposition and growth on body walls, and especially on heating surfaces, of a material undergoing an irreversible chemical reaction in the evaporator or having a solubility that decreases with an increase in temperature. Scaling can be reduced or eliminated in the same general manner as salting. Both salting and scaling liquids are usually best handled in evaporators that do not depend on boiling to induce circulation. **Fouling** is the formation of deposits other than salt or scale and may be due to corrosion, solid matter entering with the feed, or deposits formed by the condensing vapor.

Product Quality Considerations of product quality may require low holdup time and low-temperature operation to avoid thermal degradation. The low holdup time eliminates some types of evaporators, and some types are also eliminated because of poor heat-transfer characteristics at low temperature. Product quality may also dictate special materials of construction to avoid metallic contamination or a catalytic effect on decomposition of the product. **Corrosion** may also influence evaporator selection, since the advantages of evaporators having high heat-transfer coefficients are more apparent when expensive materials of construction are indicated. Corrosion and erosion are frequently more severe in evaporators than in other types of

equipment because of the high liquid and vapor velocities used, the frequent presence of solids in suspension, and the necessary concentration differences.

EVAPORATOR TYPES AND APPLICATIONS

Evaporators may be classified as follows:

1. Heating medium separated from evaporating liquid by tubular heating surfaces.
2. Heating medium confined by coils, jackets, double walls, flat plates, etc.
3. Heating medium brought into direct contact with evaporating liquid.
4. Heating by solar radiation.

By far the largest number of industrial evaporators employ tubular heating surfaces. Circulation of liquid past the heating surface may be induced by boiling or by mechanical means. In the latter case, boiling may or may not occur at the heating surface.

Forced-Circulation Evaporators (Fig. 11-122 a, b, c) Although it may not be the most economical for many uses, the forced-circulation (FC) evaporator is suitable for the widest variety of evaporator applications. The use of a pump to ensure circulation past the heating surface makes possible separating the functions of heat transfer, vapor-liquid separation, and crystallization. The pump withdraws liquor from the flash chamber and forces it through the heating element back to the flash chamber. Circulation is maintained regardless of the evaporation rate; so this type of evaporator is well suited to **crystallizing operation**, in which solids must be maintained in suspension at all times. The liquid velocity past the heating surface is limited only by the pumping power needed or available and by accelerated corrosion and erosion at the higher velocities. **Tube velocities** normally range from a minimum of about 1.2 m/s (4 ft/s) in salt evaporators with copper or brass tubes and liquid containing 5 percent or more solids up to about 3 m/s (10 ft/s) in caustic evaporators having nickel tubes and liquid containing only a small amount of solids. Even higher velocities can be used when corrosion is not accelerated by erosion.

Highest heat-transfer coefficients are obtained in FC evaporators when the liquid is allowed to boil in the tubes, as in the type shown in Fig. 11-122a. The heating element projects into the vapor head, and the liquid level is maintained near and usually slightly below the top tube sheet. This type of FC evaporator is not well suited to salting solutions because boiling in the tubes increases the chances of salt deposit on the walls and the sudden flashing at the tube exits promotes excessive nucleation and production of fine crystals. Consequently, this type of evaporator is seldom used except when there are headroom limitations or when the liquid forms neither salt nor scale.

Swirl Flow Evaporators One of the most significant problems in the thermal design of once-through, tube-side evaporators is the poor predictability of the loss of ΔT upon reaching the critical heat flux condition. This situation may occur through flashing due to a high wall temperature or due to process needs to evaporate most of, if not all, the liquid entering the evaporator. It is the result of sensible heating of the vapor phase which accumulates at the heat-transfer surface, dries out the tube wall, and blocks the transfer of heat to the remaining liquid.

In some cases, even with correctly predicted heat-transfer coefficients, the unexpected ΔT loss can reduce the actual performance of the evaporator by as much as 200 percent below the predicted performance. The best approach is to maintain a high level of mixing of the phases through the heat exchanger near the heat-transfer surface.

The use of swirl flow, whereby a rotational vortex is imparted to the boiling fluid to centrifuge the liquid droplets out to the tube wall, has proved to be the most reliable means to correct for and eliminate this loss of ΔT . The use of this technique almost always corrects the design to operate as well as or better than predicted. Also, the use of swirl flow eliminates the need to determine between horizontal or vertical orientation for most two-phase velocities. Both orientations work about the same in swirl flow.

Many commercially viable methods of inducing swirl flow inside of tubes are available in the form of either swirl flow tube inserts (twisted tapes, helical cores, spiral wire inserts) or special tube configurations

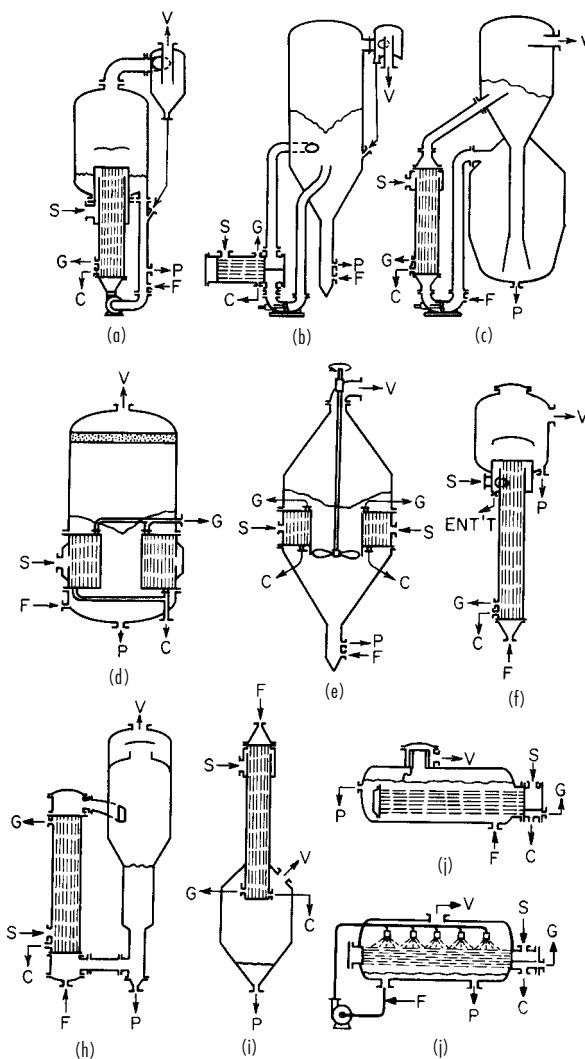


FIG. 11-122 Evaporator types. (a) Forced circulation. (b) Submerged-tube forced circulation. (c) Oslo-type crystallizer. (d) Short-tube vertical. (e) Propeller calandria. (f) Long-tube vertical. (g) Recirculating long-tube vertical. (h) Falling film. (i, j) Horizontal-tube evaporators. C = condensate; F = feed; G = vent; P = product; S = steam; V = vapor; ENT = separated entrainment outlet.

(Twisted Tube[®], internal spiral fins). All are designed to impart a natural swirl component to the flow inside the tubes. Each has been proved to solve the problem of tube-side vaporization at high vapor qualities up to and including complete tube-side vaporization.

By far the largest number of forced-circulation evaporators are of the submerged-tube type, as shown in Fig. 11-122b. The heating element is placed far enough below the liquid level or return line to the flash chamber to prevent boiling in the tubes. Preferably, the hydrostatic head should be sufficient to prevent boiling even in a tube that is plugged (and hence at steam temperature), since this prevents salting of the entire tube. Evaporators of this type sometimes have horizontal heating elements (usually two-pass), but the vertical single-pass heating element is used whenever sufficient headroom is available. The vertical element usually has a lower friction loss and is easier to clean or retube than a horizontal heater. The submerged-tube forced-circulation evaporator is relatively immune to salting in the tubes, since no supersaturation is generated by evaporation in the tubes. The

tendency toward scale formation is also reduced, since supersaturation in the heating element is generated only by a controlled amount of heating and not by both heating and evaporation.

The type of **vapor** head used with the FC evaporator is chosen to suit the product characteristics and may range from a simple centrifugal separator to the crystallizing chambers shown in Fig. 11-122*b* and *c*. Figure 11-122*b* shows a type frequently used for common salt. It is designed to circulate a slurry of crystals throughout the system. Figure 11-122*c* shows a submerged-tube FC evaporator in which heating, flashing, and crystallization are completely separated. The crystallizing solids are maintained as a fluidized bed in the chamber below the vapor head and little or no solids circulate through the heater and flash chamber. This type is well adapted to growing coarse crystals, but the crystals usually approach a spherical shape, and careful design is required to avoid production of fines in the flash chamber.

In a submerged-tube FC evaporator, all heat is imparted as sensible heat, resulting in a temperature rise of the circulating liquor that reduces the overall temperature difference available for heat transfer. Temperature rise, tube proportions, tube velocity, and head requirements on the circulating pump all influence the selection of circulation rate. Head requirements are frequently difficult to estimate since they consist not only of the usual friction, entrance and contraction, and elevation losses when the return to the flash chamber is above the liquid level but also of increased friction losses due to flashing in the return line and vortex losses in the flash chamber. Circulation is sometimes limited by vapor in the pump suction line. This may be drawn in as a result of inadequate vapor-liquid separation or may come from vortices near the pump suction connection to the body or may be formed in the line itself by short circuiting from heater outlet to pump inlet of liquor that has not flashed completely to equilibrium at the pressure in the vapor head.

Advantages of forced-circulation evaporators:

1. High heat-transfer coefficients
2. Positive circulation
3. Relative freedom from salting, scaling, and fouling

Disadvantages of forced-circulation evaporators:

1. High cost
2. Power required for circulating pump
3. Relatively high holdup or residence time

Best applications of forced-circulation evaporators:

1. Crystalline product
2. Corrosive solutions
3. Viscous solutions

Frequent difficulties with forced-circulation evaporators:

1. Plugging of tube inlets by salt deposits detached from walls of equipment
 2. Poor circulation due to higher than expected head losses
 3. Salting due to boiling in tubes
 4. Corrosion-erosion
-

Short-Tube Vertical Evaporators (Fig. 11-122*d*) This is one of the earliest types still in widespread commercial use. Its principal use at present is in the evaporation of cane-sugar juice. Circulation past the heating surface is induced by boiling in the tubes, which are usually 50.8 to 76.2 mm (2 to 3 in) in diameter by 1.2 to 1.8 m (4 to 6 ft) long. The body is a vertical cylinder, usually of cast iron, and the tubes are expanded into horizontal tube sheets that span the body diameter. The circulation rate through the tubes is many times the feed rate; so there must be a return passage from above the top tube sheet to below the bottom tube sheet. Most commonly used is a central well or **downtake** as shown in Fig. 11-122*d*. So that friction losses through the downtake do not appreciably impede circulation up through the tubes, the area of the downtake should be of the same order of magnitude as the combined cross-sectional area of the tubes. This results in a downtake almost half of the diameter of the tube sheet.

Circulation and heat transfer in this type of evaporator are strongly affected by the liquid "level." Highest heat-transfer coefficients are achieved when the level, as indicated by an external gauge glass, is only about halfway up the tubes. Slight reductions in level below the opti-

mum result in incomplete wetting of the tube walls with a consequent increased tendency to foul and a rapid reduction in capacity. When this type of evaporator is used with a liquid that can deposit salt or scale, it is customary to operate with the liquid level appreciably higher than the optimum and usually appreciably above the top tube sheet.

Circulation in the standard short-tube vertical evaporator is dependent entirely on boiling, and when boiling stops, any solids present settle out of suspension. Consequently, this type is seldom used as a crystallizing evaporator. By installing a propeller in the downtake, this objection can be overcome. Such an evaporator, usually called a **propeller calandria**, is illustrated in Fig. 11-122*e*. The propeller is usually placed as low as possible to reduce cavitation and is shrouded by an extension of the downtake well. The use of the propeller can sometimes double the capacity of a short-tube vertical evaporator. The evaporator shown in Fig. 11-122*e* includes an elutriation leg for salt manufacture similar to that used on the FC evaporator of Fig. 11-122*b*. The shape of the bottom will, of course, depend on the particular application and on whether the propeller is driven from above or below. To avoid salting when the evaporator is used for crystallizing solutions, the liquid level must be kept appreciably above the top tube sheet.

Advantages of short-tube vertical evaporators:

1. High heat-transfer coefficients at high temperature differences
2. Low headroom
3. Easy mechanical descaling
4. Relatively inexpensive

Disadvantages of short-tube vertical evaporators:

1. Poor heat transfer at low temperature differences and low temperature
2. High floor space and weight
3. Relatively high holdup
4. Poor heat transfer with viscous liquids

Best applications of short-tube vertical evaporators:

1. Clear liquids
 2. Crystalline product if propeller is used
 3. Relatively noncorrosive liquids, since body is large and expensive if built of materials other than mild steel or cast iron
 4. Mild scaling solutions requiring mechanical cleaning, since tubes are short and large in diameter
-

Long-Tube Vertical Evaporators (Fig. 11-122*f, g, h*) More total evaporation is accomplished in this type than in all others combined because it is normally the **cheapest per unit of capacity**. The long-tube vertical (LTV) evaporator consists of a simple one-pass vertical shell-and-tube heat exchanger discharging into a relatively small vapor head. Normally, no liquid level is maintained in the vapor head, and the residence time of liquor is only a few seconds. The tubes are usually about 50.8 mm (2 in) in diameter but may be smaller than 25.4 mm (1 in). Tube length may vary from less than 6 to 10.7 m (20 to 35 ft) in the rising film version and to as great as 20 m (65 ft) in the falling film version. The evaporator is usually operated single-pass, concentrating from the feed to discharge density in just the time that it takes the liquid and evolved vapor to pass through a tube. An extreme case is the caustic high concentrator, producing a substantially anhydrous product at 370°C (700°F) from an inlet feed of 50 percent NaOH at 149°C (300°F) in one pass up 22-mm- (8/8-in-) outside-diameter nickel tubes 6 m (20 ft) long. The largest use of LTV evaporators is for concentrating black liquor in the pulp and paper industry. Because of the long tubes and relatively high heat-transfer coefficients, it is possible to achieve higher single-unit capacities in this type of evaporator than in any other.

The LTV evaporator shown in Fig. 11-122*f* is typical of those commonly used, especially for black liquor. Feed enters at the bottom of the tube and starts to boil partway up the tube, and the mixture of liquid and vapor leaving at the top at high velocity impinges against a deflector placed above the tube sheet. This deflector is effective both as a primary separator and as a foam breaker.

In many cases, as when the ratio of feed to evaporation or the ratio of feed to heating surface is low, it is desirable to provide for **recirculation of product** through the evaporator. This can be done in the type shown in Fig. 11-122*f* by adding a pipe connection between

the product line and the feed line. Higher recirculation rates can be achieved in the type shown in Fig. 11-122g, which is used widely for condensed milk. By extending the enlarged portion of the vapor head still lower to provide storage space for liquor, this type can be used as a batch evaporator.

Liquid temperatures in the tubes of an LTV evaporator are far from uniform and are difficult to predict. At the lower end, the liquid is usually not boiling, and the liquor picks up heat as sensible heat. Since entering liquid velocities are usually very low, true heat-transfer coefficients are low in this nonboiling zone. At some point up the tube, the liquid starts to boil, and from that point on the liquid temperature decreases because of the reduction in static, friction, and acceleration heads until the vapor-liquid mixture reaches the top of the tubes at substantially vapor-head temperature. Thus the true temperature difference in the boiling zone is always less than the total temperature difference as measured from steam and vapor-head temperatures.

Although the true heat-transfer coefficients in the boiling zone are quite high, they are partially offset by the reduced temperature difference. The point in the tubes at which boiling starts and at which the maximum temperature is reached is sensitive to operating conditions, such as feed properties, feed temperature, feed rate, and heat flux. Figure 11-123 shows typical variations in liquid temperature in tubes of an LTV evaporator operating at a constant terminal temperature difference. Curve 1 shows the normal case in which the feed is not boiling at the tube inlet. Curve 2 gives an indication of the temperature difference lost when the feed enters at the boiling point. Curve 3 is for exactly the same conditions as curve 2 except that the feed contained 0.01 percent Teepol to reduce surface tension [Coulson and Mehta, *Trans. Inst. Chem. Eng.*, **31**, 208 (1953)]. The surface-active agent yields a more intimate mixture of vapor and liquid, with the result that liquid is accelerated to a velocity more nearly approaching the vapor velocity, thereby increasing the pressure drop in the tube. Although the surface-active agent caused an increase of more than 100 percent in the true heat-transfer coefficient, this was more than offset by the reduced temperature difference so that the net result was a reduction in evaporator capacity. This sensitivity of the LTV evaporator to changes in operating conditions is less pronounced at high than at low temperature differences and temperature levels.

The **falling-film** version of the LTV evaporator (Fig. 11-122h) eliminates these problems of hydrostatic head. Liquid is fed to the tops of the tubes and flows down the walls as a film. Vapor-liquid separation usually takes place at the bottom, although some evaporators of this type are arranged for vapor to rise through the tube counter-currently to the liquid. The pressure drop through the tubes is usually very small, and the boiling-liquid temperature is substantially the same as the vapor-head temperature. The falling-film evaporator is widely used for concentrating **heat-sensitive materials**, such as fruit juices, because the holdup time is very small, the liquid is not overheated during passage through the evaporator, and heat-transfer coefficients are high even at low boiling temperatures.

The principal problem with the falling-film LTV evaporator is that of **feed distribution** to the tubes. It is essential that all tube surfaces be wetted continually. This usually requires recirculation of the liquid unless the ratio of feed to evaporation is quite high. An alternative to the simple recirculation system of Fig. 11-122h is sometimes used when the feed undergoes an appreciable concentration change and the product is viscous and/or has a high boiling point rise. The feed chamber and vapor head are divided into a number of liquor com-

partments, and separate pumps are used to pass the liquor through the various banks of tubes in series, all in parallel as to steam and vapor pressures. The actual distribution of feed to the individual tubes of a falling-film evaporator may be accomplished by orifices at the inlet to each tube, by a perforated plate above the tube sheet, or by one or more spray nozzles.

Both rising- and falling-film LTV evaporators are generally unsuited to salting or severely scaling liquids. However, both are widely used for black liquor, which presents a mild scaling problem, and also are used to carry solutions beyond saturation with respect to a crystallizing salt. In the latter case, deposits can usually be removed quickly by increasing the feed rate or reducing the steam rate in order to make the product unsaturated for a short time. The falling-film evaporator is not generally suited to liquids containing solids because of difficulty in plugging the feed distributors. However, it has been applied to the evaporation of saline waters saturated with CaSO_4 and containing 5 to 10 percent CaSO_4 seeds in suspension for scale prevention (Anderson, ASME Pap. 76-WA/Pwr-5, 1976).

Because of their simplicity of construction, compactness, and generally high heat-transfer coefficients, LTV evaporators are well suited to service with corrosive liquids. An example is the reconcentration of rayon spin-bath liquor, which is highly acid. These evaporators employ impervious graphite tubes, lead, rubber-covered or impervious graphite tube sheets, and rubber-lined vapor heads. Polished stainless-steel LTV evaporators are widely used for food products. The latter evaporators are usually similar to that shown in Fig. 11-122g, in which the heating element is at one side of the vapor head to permit easy access to the tubes for cleaning.

Advantages of long-tube vertical evaporators:

1. Low cost
2. Large heating surface in one body
3. Low holdup
4. Small floor space
5. Good heat-transfer coefficients at reasonable temperature differences (rising film)
6. Good heat-transfer coefficients at all temperature differences (falling film)

Disadvantages of long-tube vertical evaporators:

1. High headroom
2. Generally unsuitable for salting and severely scaling liquids
3. Poor heat-transfer coefficients of rising-film version at low temperature differences
4. Recirculation usually required for falling-film version

Best applications of long-tube vertical evaporators:

1. Clear liquids
2. Foaming liquids
3. Corrosive solutions
4. Large evaporation loads
5. High temperature differences—rising film, low temperature differences—falling film
6. Low-temperature operation—falling film
7. Vapor compression operation—falling film

Frequent difficulties with long-tube vertical evaporators:

1. Sensitivity of rising-film units to changes in operating conditions
2. Poor feed distribution to falling-film units

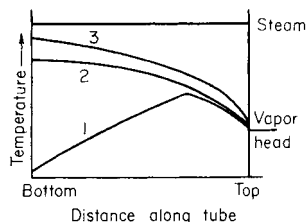


FIG. 11-123 Temperature variations in a long-tube vertical evaporator.

Horizontal-Tube Evaporators (Fig. 11-122i) In these types the steam is inside and the liquor outside the tubes. The submerged-tube version of Fig. 11-122i is seldom used except for the preparation of boiler feedwater. Low entrainment loss is the primary aim; the horizontal cylindrical shell yields a large disengagement area per unit of vessel volume. Special versions use deformed tubes between restrained tube sheets that crack off much of a scale deposit when sprayed with cold water. By showering liquor over the tubes in the version of Fig. 11-122f hydrostatic head losses are eliminated and heat-transfer performance is improved to that of the falling-film tubular type of Fig. 11-122h. Originally called the Lillie, this evaporator is now also called the spray-film or simply the horizontal-tube evaporator. Liquid distribution over the tubes is accomplished by sprays or perforated plates above the topmost tubes. Maintaining this distribution

through the bundle to avoid overconcentrating the liquor is a problem unique to this type of evaporator. It is now used primarily for seawater evaporation.

Advantages of horizontal-tube evaporators:

1. Very low headroom
2. Large vapor-liquid disengaging area—submerged-tube type
3. Relatively low cost in small-capacity straight-tube type
4. Good heat-transfer coefficients
5. Easy semiautomatic descaling—bent-tube type

Disadvantages of horizontal-tube evaporators:

1. Unsuitable for salting liquids
2. Unsuitable for scaling liquids—straight-tube type
3. High cost—bent-tube type
4. Maintaining liquid distribution—film type

Best applications of horizontal-tube evaporators:

1. Limited headroom
 2. Small capacity
 3. Nonscaling nonsalting liquids—straight-tube type
 4. Severely scaling liquids—bent-tube type
-

Miscellaneous Forms of Heating Surface Special evaporator designs are sometimes indicated when heat loads are small, special product characteristics are desired, or the product is especially difficult to handle. **Jacketed kettles**, frequently with agitators, are used when the product is very viscous, batches are small, intimate mixing is required, and/or ease of cleaning is an important factor. Evaporators with steam in coiled **tubes** may be used for small capacities with scaling liquids in designs that permit “cold shocking,” or complete withdrawal of the coil from the shell for manual scale removal. Other designs for scaling liquids employ flat-plate heat exchangers, since in general a scale deposit can be removed more easily from a flat plate than from a curved surface. One such design, the **channel-switching evaporator**, alternates the duty of either side of the heating surface periodically from boiling liquid to condensing vapor so that scale formed when the surface is in contact with boiling liquid is dissolved when the surface is next in contact with condensing vapor.

Agitated thin-film evaporators employ a heating surface consisting of one large-diameter tube that may be either straight or tapered, horizontal or vertical. Liquid is spread on the tube wall by a rotating assembly of blades that either maintain a close clearance from the wall or actually ride on the film of liquid on the wall. The expensive construction limits application to the most difficult materials. High agitation [on the order of 12 m/s (40 ft/s) rotor-tip speed] and power intensities of 2 to 20 kW m² (0.25 to 2.5 hp/ft²) permit handling extremely viscous materials. Residence times of only a few seconds permit concentration of heat-sensitive materials at temperatures and temperature differences higher than in other types [Mutzenberg, Parker, and Fischer. *Chem. Eng.*, **72**, 175–190 (Sept. 13, 1965)]. High feed-to-product ratios can be handled without recirculation.

Economic and process considerations usually dictate that agitated thin-film evaporators be operated in single-effect mode. Very high temperature differences can then be used; many are heated with Dowtherm or other high-temperature media. This permits achieving reasonable capacities in spite of the relatively low heat-transfer coefficients and the small surface that can be provided in a single tube [to about 20 m² (200 ft²)]. The structural need for wall thicknesses of 6 to 13 mm (¼ to ½ in) is a major reason for the relatively low heat-transfer coefficients when evaporating water-like materials.

Evaporators without Heating Surfaces The **submerged-combustion** evaporator makes use of combustion gases bubbling through the liquid as the means of heat transfer. It consists simply of a tank to hold the liquid, a burner and gas distributor that can be lowered into the liquid, and a combustion-control system. Since there are no heating surfaces on which scale can deposit, this evaporator is well suited to use with severely scaling liquids. The ease of constructing the tank and burner of special alloys or nonmetallic materials makes practical the handling of highly corrosive solutions. However, since the vapor is mixed with large quantities of noncondensable gases, it is impossible to reuse the heat in this vapor, and installations are usually

limited to areas of low fuel cost. One difficulty frequently encountered in the use of submerged-combustion evaporators is a high entrainment loss. Also, these evaporators cannot be used when control of crystal size is important.

Disk or cascade evaporators are used in the pulp and paper industry to recover heat and entrained chemicals from boiler stack gases and to effect a final concentration of the black liquor before it is burned in the boiler. These evaporators consist of a horizontal shaft on which are mounted disks perpendicular to the shaft or bars parallel to the shaft. The assembly is partially immersed in the thick black liquor so that films of liquor are carried into the hot-gas stream as the shaft rotates.

Some forms of **flash evaporators** require no heating surface. An example is a recrystallizing process for separating salts having normal solubility curves from salts having inverse solubility curves, as in separating sodium chloride from calcium sulfate [Richards, *Chem. Eng.*, **59**(3), 140 (1952)]. A suspension of raw solid feed in a recirculating brine stream is heated by direct steam injection. The increased temperature and dilution by the steam dissolve the salt having the normal solubility curve. The other salt remains undissolved and is separated from the hot solution before it is flashed to a lower temperature. The cooling and loss of water on flashing cause recrystallization of the salt having the normal solubility curve, which is separated from the brine before the brine is mixed with more solid feed for recycling to the heater. This system can be operated as a multiple effect by flashing down to the lower temperature in stages and using flash vapor from all but the last stage to heat the recycle brine by direct injection. In this process no net evaporation occurs from the total system, and the process cannot be used to concentrate solutions unless heating surfaces are added.

UTILIZATION OF TEMPERATURE DIFFERENCE

Temperature difference is the driving force for evaporator operation and usually is limited, as by compression ratio in vapor-compression evaporators and by available steam-pressure and heat-sink temperature in single- and multiple-effect evaporators. A fundamental objective of evaporator design is to make as much of this total temperature difference available for heat transfer as is economically justifiable. Some losses in temperature difference, such as those due to *boiling point rise* (BPR), are unavoidable. However, even these can be minimized, as by passing the liquor through effects or through different sections of a single effect in series so that only a portion of the heating surface is in contact with the strongest liquor.

Figure 11-124 shows approximate BPR losses for a number of process liquids. A correlation for concentrated solutions of many inorganic salts at the atmospheric pressure boiling point [Meranda and Furter, *J. Ch. and E. Data* **22**, 315-7 (1977)] is

$$\text{BPR} = 104.9N_2^{1.14} \quad (11-123)$$

where N_2 is the mole fraction of salts in solution. Correction to other pressures, when heats of solution are small, can be based on a constant ratio of vapor pressure of the solution to that of water at the same temperature.

The principal reducible loss in ΔT is that due to friction and to entrance and exit losses in vapor piping and entrainment separators. Pressure-drop losses here correspond to a reduction in condensing temperature of the vapor and hence a loss in available ΔT . These losses become most critical at the low-temperature end of the evaporator, both because of the increasing specific volume of the vapor and because of the reduced slope of the vapor-pressure curve. Sizing of vapor lines is part of the economic optimization of the evaporator, extra costs of larger vapor lines being balanced against savings in ΔT , which correspond to savings in heating-surface requirements. It should be noted that entrance and exit losses in vapor lines usually exceed by severalfold the straight-pipe friction losses, so they cannot be ignored.

VAPOR-LIQUID SEPARATION

Product losses in evaporator vapor may result from foaming, splashing, or entrainment. Primary separation of liquid from vapor is accomplished in the vapor head by making the horizontal plan area large

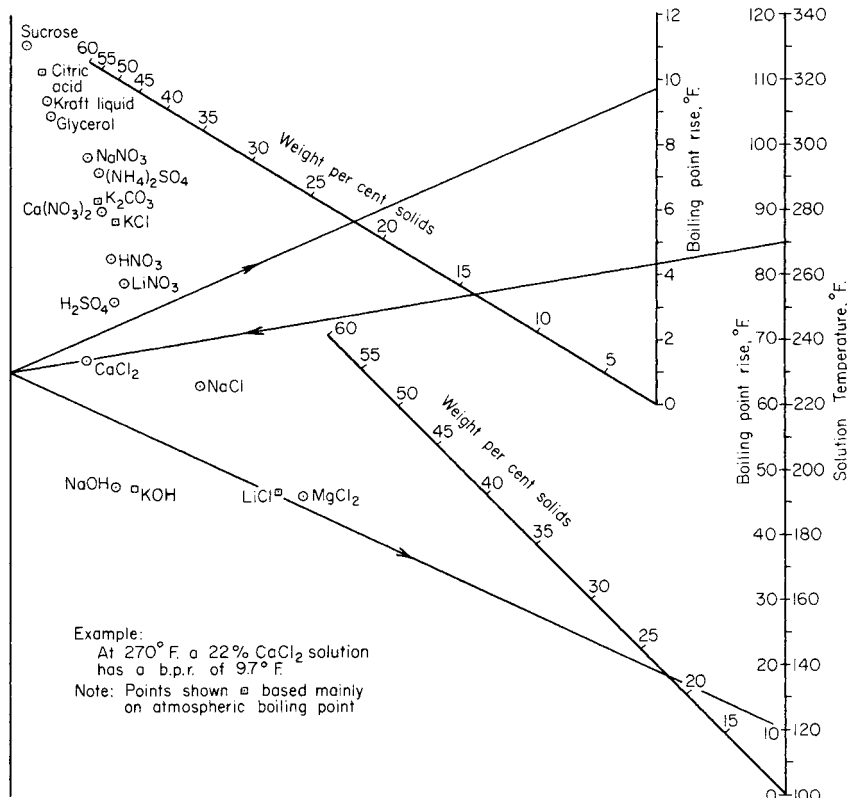


FIG. 11-124 Boiling-point rise of aqueous solutions. °C = 5/9 (°F - 32).

enough so that most of the entrained droplets can settle out against the rising flow of vapor. Allowable velocities are governed by the Souders-Brown equation: $V = k\sqrt{(\rho_1 - \rho_2)/\rho_2}$, in which k depends on the size distribution of droplets and the decontamination factor F desired. For most evaporators and for F between 100 and 10,000, $k \cong 0.245/(F - 50)^{0.4}$ (Standiford, *Chemical Engineers' Handbook*, 4th ed., McGraw-Hill, New York, 1963, p. 11-35). Higher values of k (to about 0.15) can be tolerated in the falling-film evaporator, where most of the entrainment separation occurs in the tubes, the vapor is scrubbed by liquor leaving the tubes, and the vapor must reverse direction to reach the outlet.

Foaming losses usually result from the presence in the evaporating liquid of colloids or of surface-tension depressants and finely divided solids. Antifoam agents are often effective. Other means of combating foam include the use of steam jets impinging on the foam surface, the removal of product at the surface layer, where the foaming agents seem to concentrate, and operation at a very low liquid level so that hot surfaces can break the foam. Impingement at high velocity against a baffle tends to break the foam mechanically, and this is the reason that the long-tube vertical, forced-circulation, and agitated-film evaporators are particularly effective with foaming liquids. Operating at lower temperatures and/or higher-dissolved solids concentrations may also reduce foaming tendencies.

Splashing losses are usually insignificant if a reasonable height has been provided between the liquid level and the top of the vapor head. The height required depends on the violence of boiling. Heights of 2.4 to 3.6 m (8 to 12 ft) or more are provided in short-tube vertical evaporators, in which the liquid and vapor leaving the tubes are projected upward. Less height is required in forced-circulation evaporators, in which the liquid is given a centrifugal motion or is projected downward as by a baffle. The same is true of long-tube vertical evaporators, in which the rising vapor-liquid mixture is projected against a baffle.

Entrainment losses by flashing are frequently encountered in an evaporator. If the feed is above the boiling point and is introduced above or only a short distance below the liquid level, entrainment losses may be excessive. This can occur in a short-tube-type evaporator if the feed is introduced at only one point below the lower tube sheet (Kerr, Louisiana Agric. Expt. Stn. Bull. 149, 1915). The same difficulty may be encountered in forced-circulation evaporators having too high a temperature rise through the heating element and thus too wide a flashing range as the circulating liquid enters the body. Poor vacuum control, especially during startup, can cause the generation of far more vapor than the evaporator was designed to handle, with a consequent increase in entrainment.

Entrainment separators are frequently used to reduce product losses. There are a number of specialized designs available, practically all of which rely on a change in direction of the vapor flow when the vapor is traveling at high velocity. Typical separators are shown in Fig. 11-122, although not necessarily with the type of evaporator with which they may be used. The most common separator is the cyclone, which may have either a top or a bottom outlet as shown in Fig. 11-122a and b or may even be wrapped around the heating element of the next effect as shown in Fig. 11-122f. The separation efficiency of a cyclone increases with an increase in inlet velocity, although at the cost of some pressure drop, which means a loss in available temperature difference. Pressure drop in a cyclone is from 10 to 16 velocity heads [Lawrence, *Chem. Eng. Prog.*, 48, 241 (1952)], based on the velocity in the inlet pipe. Such cyclones can be sized in the same manner as a cyclone dust collector (using velocities of about 30 m/s (100 ft/s) at atmospheric pressure) although sizes may be increased somewhat in order to reduce losses in available temperature difference.

Knitted wire mesh serves as an effective entrainment separator when it cannot easily be fouled by solids in the liquor. The mesh is available in woven metal wire of most alloys and is installed as a blanket

across the top of the evaporator (Fig. 11-122*d*) or in a monitor of reduced diameter atop the vapor head. These separators have low-pressure drops, usually on the order of 13 mm ($\frac{1}{2}$ in) of water, and collection efficiency is above 99.8 percent in the range of vapor velocities from 2.5 to 6 m/s (8 to 20 ft/s) [Carpenter and Othmer, *Am. Inst. Chem. Eng. J.*, **1**, 549 (1955)]. Chevron (hook-and-vane) type separators are also used because of their higher-allowable velocities or because of their reduced tendency to foul with solids suspended in the entrained liquid.

EVAPORATOR ARRANGEMENT

Single-Effect Evaporators Single-effect evaporators are used when the required capacity is small, steam is cheap, the material is so corrosive that very expensive materials of construction are required, or the vapor is so contaminated that it cannot be reused. Single-effect evaporators may be operated in batch, semibatch, or continuous-batch modes or continuously. Strictly speaking, **batch evaporators** are ones in which filling, evaporating, and emptying are consecutive steps. This method of operation is rarely used since it requires that the body be large enough to hold the entire charge of feed and the heating element be placed low enough so as not to be uncovered when the volume is reduced to that of the product. The more usual method of operation is **semibatch**, in which feed is continually added to maintain a constant level until the entire charge reaches final density. **Continuous-batch** evaporators usually have a continuous feed and, over at least part of the cycle, a continuous discharge. One method of operation is to circulate from a storage tank to the evaporator and back until the entire tank is up to desired concentration and then finish in batches. **Continuous evaporators** have essentially continuous feed and discharge, and concentrations of both feed and product remain substantially constant.

Thermocompression The simplest means of reducing the energy requirements of evaporation is to compress the vapor from a single-effect evaporator so that the vapor can be used as the heating medium in the same evaporator. The compression may be accomplished by mechanical means or by a steam jet. In order to keep the compressor cost and power requirements within reason, the evaporator must work with a fairly narrow temperature difference, usually from about 5.5 to 11°C (10° to 20°F). This means that a large evaporator heating surface is needed, which usually makes the vapor-compression evaporator more expensive in first cost than a multiple-effect evaporator. However, total installation costs may be reduced when purchased power is the energy source, since the need for boiler and heat sink is eliminated. Substantial savings in operating cost are realized when electrical or mechanical power is available at a low cost relative to low-pressure steam, when only high-pressure steam is available to operate the evaporator, or when the cost of providing cooling water or other heat sink for a multiple-effect evaporator is high.

Mechanical thermocompression may employ reciprocating, rotary positive-displacement, centrifugal, or axial-flow compressors. Positive-displacement compressors are impractical for all but the smallest capacities, such as portable seawater evaporators. Axial-flow compressors can be built for capacities of more than 472 m³/s (1×10^6 ft³/min). Centrifugal compressors are usually cheapest for the intermediate-capacity ranges that are normally encountered. In all cases, great care must be taken to keep entrainment at a minimum, since the vapor becomes superheated on compression and any liquid present will evaporate, leaving the dissolved solids behind. In some cases a vapor-scrubbing tower may be installed to protect the compressor. A mechanical recompression evaporator usually requires more heat than is available from the compressed vapor. Some of this extra heat can be obtained by preheating the feed with the condensate and, if possible, with the product. Rather extensive heat-exchange systems with close approach temperatures are usually justified, especially if the evaporator is operated at high temperature to reduce the volume of vapor to be compressed. When the product is a solid, an elutriation leg such as that shown in Fig. 11-122*b* is advantageous, since it cools the product almost to feed temperature. The remaining heat needed to maintain the evaporator in operation must be obtained from outside sources.

While theoretical compressor power requirements are reduced slightly by going to lower evaporating temperatures, the volume of

vapor to be compressed and hence compressor size and cost increase so rapidly that low-temperature operation is more expensive than high-temperature operation. The requirement of low temperature for fruit-juice concentration has led to the development of an evaporator employing a **secondary fluid**, usually Freon or ammonia. In this evaporator, the vapor is condensed in an exchanger cooled by boiling Freon. The Freon, at a much higher vapor density than the water vapor, is then compressed to serve as the heating medium for the evaporator. This system requires that the latent heat be transferred through two surfaces instead of one, but the savings in compressor size and cost are enough to justify the extra cost of heating surface or the cost of compressing through a wider temperature range.

Steam-jet thermocompression is advantageous when steam is available at a pressure appreciably higher than can be used in the evaporator. The steam jet then serves as a reducing valve while doing some useful work. The efficiency of a steam jet is quite low and falls off rapidly when the jet is not used at the vapor-flow rate and terminal pressure conditions for which it was designed. Consequently multiple jets are used when wide variations in evaporation rate are expected. Because of the low first cost and the ability to handle large volumes of vapor, steam-jet thermocompressors are used to increase the economy of evaporators that must operate at low temperatures and hence cannot be operated in multiple effect. The steam-jet thermocompression evaporator has a heat input larger than that needed to balance the system, and some heat must be rejected. This is usually done by venting some of the vapor at the suction of the compressor.

Multiple-Effect Evaporation Multiple-effect evaporation is the principal means in use for economizing on energy consumption. Most such evaporators operate on a continuous basis, although for a few difficult materials a continuous-batch cycle may be employed. In a multiple-effect evaporator, steam from an outside source is condensed in the heating element of the first effect. If the feed to the effect is at a temperature near the boiling point in the first effect, 1 kg of steam will evaporate almost 1 kg of water. The first effect operates at (but is not controlled at) a boiling temperature high enough so that the evaporated water can serve as the heating medium of the second effect. Here almost another kilogram of water is evaporated, and this may go to a condenser if the evaporator is a double-effect or may be used as the heating medium of the third effect. This method may be repeated for any number of effects. Large evaporators having six and seven effects are common in the pulp and paper industry, and evaporators having as many as 17 effects have been built. As a first approximation, the **steam economy** of a multiple-effect evaporator will increase in proportion to the number of effects and usually will be somewhat less numerically than the number of effects.

The increased steam economy of a multiple-effect evaporator is gained at the expense of evaporator first cost. The total heat-transfer surface will increase substantially in proportion to the number of effects in the evaporator. This is only an approximation since going from one to two effects means that about half of the heat transfer is at a higher temperature level, where heat-transfer coefficients are generally higher. On the other hand, operating at lower temperature differences reduces the heat-transfer coefficient for many types of evaporator. If the material has an appreciable boiling-point elevation, this will also lower the available temperature difference. The only accurate means of predicting the changes in steam economy and surface requirements with changes in the number of effects is by detailed heat and material balances together with an analysis of the effect of changes in operating conditions on heat-transfer performance.

The approximate **temperature distribution** in a multiple-effect evaporator is under the control of the designer, but once built, the evaporator establishes its own equilibrium. Basically, the effects are a number of series resistances to heat transfer, each resistance being approximately proportional to $1/U_n A_n$. The total available temperature drop is divided between the effects in proportion to their resistances. If one effect starts to scale, its temperature drop will increase at the expense of the temperature drops across the other effects. This provides a convenient means of detecting a drop in heat-transfer coefficient in an effect of an operating evaporator. If the steam pressure and final vacuum do not change, the temperature in the effect that is scaling will decrease and the temperature in the preceding effect will increase.

The feed to a multiple-effect evaporator is usually transferred from one effect to another in series so that the ultimate product concentration is reached only in one effect of the evaporator. In **backward-feed** operation, the raw feed enters the last (coldest) effect, the discharge from this effect becomes the feed to the next-to-the-last effect, and so on until product is discharged from the first effect. This method of operation is advantageous when the feed is cold, since much less liquid must be heated to the higher temperature existing in the early effects. It is also used when the product is so viscous that high temperatures are needed to keep the viscosity low enough to give reasonable heat-transfer coefficients. When product viscosity is high but a hot product is not needed, the liquid from the first effect is sometimes flashed to a lower temperature in one or more stages and the flash vapor added to the vapor from one or more later effects of the evaporator.

In **forward-feed** operation, raw feed is introduced in the first effect and passed from effect to effect parallel to the steam flow. Product is withdrawn from the last effect. This method of operation is advantageous when the feed is hot or when the concentrated product would be damaged or would deposit scale at high temperature. Forward feed simplifies operation when liquor can be transferred by pressure difference alone, thus eliminating all intermediate liquor pumps. When the feed is cold, forward feed gives a low steam economy since an appreciable part of the prime steam is needed to heat the feed to the boiling point and thus accomplishes no evaporation. If forward feed is necessary and feed is cold, steam economy can be improved markedly by preheating the feed in stages with vapor bled from intermediate effects of the evaporator. This usually represents little increase in total heating surface or cost since the feed must be heated in any event and shell-and-tube heat exchangers are generally less expensive per unit of surface area than evaporator heating surface.

Mixed-feed operation is used only for special applications, as when liquor at an intermediate concentration and a certain temperature is desired for additional processing.

Parallel feed involves the introduction of raw feed and the withdrawal of product at each effect of the evaporator. It is used primarily when the feed is substantially saturated and the product is a solid. An example is the evaporation of brine to make common salt. Evaporators of the types shown in Fig. 11-122*b* or *e* are used, and the product is withdrawn as a slurry. In this case, parallel feed is desirable because the feed washes impurities from the salt leaving the body.

Heat-recovery systems are frequently incorporated in an evaporator to increase the steam economy. Ideally, product and evaporator condensate should leave the system at a temperature as low as possible. Also, heat should be recovered from these streams by exchange with feed or evaporating liquid at the highest possible temperature. This would normally require separate liquid-liquid heat exchangers, which add greatly to the complexity of the evaporator and are justifiable only in large plants. Normally, the loss in thermodynamic availability due to flashing is tolerated since the flash vapor can then be used directly in the evaporator effects. The most commonly used is a **condensate flash** system in which the condensate from each effect but the first (which normally must be returned to the boiler) is flashed in successive stages to the pressure in the heating element of each succeeding effect of the evaporator. Product flash tanks may also be used in a backward- or mixed-feed evaporator. In a forward-feed evaporator, the principal means of heat recovery may be by use of **feed preheaters** heated by vapor bled from each effect of the evaporator. In this case, condensate may be either flashed as before or used in a separate set of exchangers to accomplish some of the feed preheating. A feed preheated by last-effect vapor may also materially reduce condenser water requirements.

Seawater Evaporators The production of potable water from saline waters represents a large and growing field of application for evaporators. Extensive work done in this field to 1972 was summarized in the annual *Saline Water Conversion Reports* of the Office of Saline Water, U.S. Department of the Interior. **Steam economies** on the order of 10 kg evaporation/kg steam are usually justified because (1) unit production capacities are high, (2) fixed charges are low on capital used for public works (i.e., they use long amortization periods and have low interest rates, with no other return on investment considered), (3) heat-transfer performance is comparable with that of

pure water, and (4) properly treated seawater causes little deterioration due to scaling or fouling.

Figure 11-125*a* shows a **multiple-effect** (falling-film) flow sheet as used for seawater. Twelve effects are needed for a steam economy of 10. Seawater is used to condense last-effect vapor, and a portion is then treated to prevent scaling and corrosion. Treatment usually consists of acidification to break down bicarbonates, followed by deaeration, which also removes the carbon dioxide generated. The treated seawater is then heated to successively higher temperatures by a portion of the vapor from each effect and finally is fed to the evaporating surface of the first effect. The vapor generated therein and the partially concentrated liquid are passed to the second effect, and so on until the last effect. The feed rate is adjusted relative to the steam rate so that the residual liquid from the last effect can carry away all the salts in solution, in a volume about one-third of that of the feed. Condensate formed in each effect but the first is flashed down to the following effects in sequence and constitutes the product of the evaporator.

As the feed-to-steam ratio is increased in the flow sheet of Fig. 11-125*a*, a point is reached where all the vapor is needed to preheat the feed and none is available for the evaporator tubes. This limiting case is the **multistage flash evaporator**, shown in its simplest form in Fig. 11-125*b*. Seawater is treated as before and then pumped through a number of feed heaters in series. It is given a final boost in temperature with prime steam in a **brine heater** before it is flashed down in series to provide the vapor needed by the feed heaters. The amount of steam required depends on the approach-temperature difference in the feed heaters and the flash range per stage. Condensate from the feed heaters is flashed down in the same manner as the brine.

Since the flow being heated is identical to the total flow being flashed, the temperature rise in each heater is equal to the flash range in each flasher. This temperature difference represents a loss from the temperature difference available for heat transfer. There are thus two ways of increasing the steam economy of such plants: increasing the heating surface and increasing the number of stages. Whereas the number of effects in a multiple-effect plant will be about 20 percent greater than the steam economy, the number of stages in a flash plant will be 3 to 4 times the steam economy. However, a large number of stages can be provided in a single vessel by means of internal bulkheads. The heat-exchanger tubing is placed in the same vessel, and the tubes usually are continuous through a number of stages. This requires ferrules or special close tube-hole clearances where the tubes pass through the internal bulkheads. In a plant for a steam economy of 10, the ratio of flow rate to heating surface is usually such that the seawater must pass through about 152 m of 19-mm (500 ft of ¾-in) tubing before it reaches the brine heater. This places a limitation on the physical arrangement of the vessels.

Inasmuch as it requires a flash range of about 61°C (110°F) to produce 1 kg of flash vapor for every 10 kg of seawater, the multistage flash evaporator requires handling a large volume of seawater relative to the product. In the flow sheet of Fig. 11-125*b* all this seawater must be deaerated and treated for scale prevention. In addition, the last-stage vacuum varies with the ambient seawater temperature, and ejector equipment must be sized for the worst condition. These difficulties can be eliminated by using the **recirculating multistage flash** flow sheet of Fig. 11-125*c*. The last few stages, called the **reject stages**, are cooled by a flow of seawater that can be varied to maintain a reasonable last-stage vacuum. A small portion of the last-stage brine is blown down to carry away the dissolved salts, and the balance is recirculated to the **heat-recovery stages**. This arrangement requires a much smaller makeup of fresh seawater and hence a lower treatment cost.

The multistage flash evaporator is similar to a multiple-effect forced-circulation evaporator, but with all the forced-circulation heaters in series. This has the advantage of requiring only one large-volume forced-circulation pump, but the sensible heating and short-circuiting losses in available temperature differences remain. A disadvantage of the flash evaporator is that the liquid throughout the system is at almost the discharge concentration. This has limited its industrial use to solutions in which no great concentration differences are required between feed and product and to where the liquid can be heated through wide temperature ranges without scaling. A partial remedy is

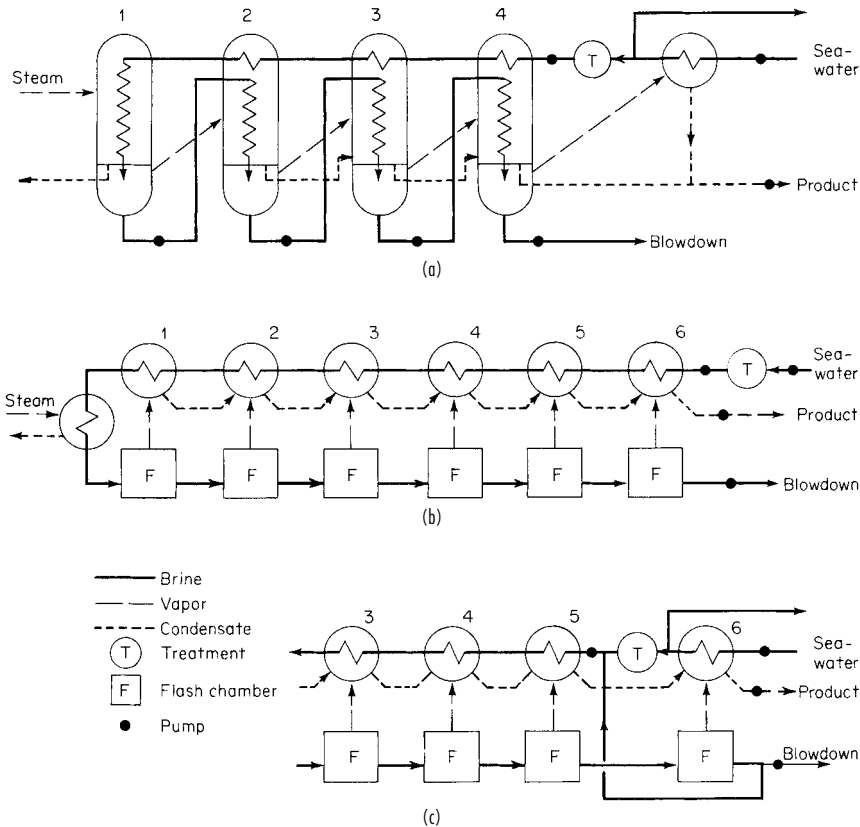


FIG. 11-125 Flow sheets for seawater evaporators. (a) Multiple effect (falling film). (b) Multistage flash (once-through). (c) Multistage flash (recirculating).

to arrange several multistage flash evaporators in series, the heat-rejection section of one being the brine heater of the next. This permits independent control of concentration but eliminates the principal advantage of the flash evaporator, which is the small number of pumps and vessels required. An unusual feature of the flash evaporator is that fouling of the heating surfaces reduces primarily the steam economy rather than the capacity of the evaporator. Capacity is not affected until the heat-rejection stages can no longer handle the increased flashing resulting from the increased heat input.

EVAPORATOR CALCULATIONS

Single-Effect Evaporators The heat requirements of a single-effect continuous evaporator can be calculated by the usual methods of stoichiometry. If enthalpy data or specific heat and heat-of-solution data are not available, the heat requirement can be estimated as the sum of the heat needed to raise the feed from feed to product temperature and the heat required to evaporate the water. The latent heat of water is taken at the vapor-head pressure instead of at the product temperature in order to compensate partially for any heat of solution. If sufficient vapor-pressure data are available for the solution, methods are available to calculate the true latent heat from the slope of the Dühring line [Othmer, *Ind. Eng. Chem.*, **32**, 841 (1940)].

The heat requirements in batch evaporation are the same as those in continuous evaporation except that the temperature (and sometimes pressure) of the vapor changes during the course of the cycle. Since the enthalpy of water vapor changes but little relative to temperature, the difference between continuous and batch heat requirements is almost always negligible. More important usually is the effect of variation of

fluid properties, such as viscosity and boiling-point rise, on heat transfer. These can only be estimated by a step-by-step calculation.

In selecting the **boiling temperature**, consideration must be given to the effect of temperature on heat-transfer characteristics of the type of evaporator to be used. Some evaporators show a marked drop in coefficient at low temperature—more than enough to offset any gain in available temperature difference. The condenser cooling-water temperature and cost must also be considered.

Thermocompression Evaporators Thermocompression-evaporator calculations [Pridgeon, *Chem. Metall. Eng.*, **28**, 1109 (1923); Peter, *Chimia (Switzerland)*, **3**, 114 (1949); Petzold, *Chem. Ing. Tech.*, **22**, 147 (1950); and Weimer, Dolf, and Austin, *Chem. Eng. Prog.*, **76**(11), 78 (1980)] are much the same as single-effect calculations with the added complication that the heat supplied to the evaporator from compressed vapor and other sources must exactly balance the heat requirements. Some knowledge of compressor efficiency is also required. Large axial-flow machines on the order of 236-m³/s (500,000-ft³/min) capacity may have efficiencies of 80 to 85 percent. Efficiency drops to about 75 percent for a 14-m³/s (30,000-ft³/min) centrifugal compressor. Steam-jet compressors have thermodynamic efficiencies on the order of only 25 to 30 percent.

Flash Evaporators The calculation of a heat and material balance on a flash evaporator is relatively easy once it is understood that the temperature rise in each heater and temperature drop in each flasher must all be substantially equal. The steam economy E , kg evaporation/kg of 1055-kJ steam (lb/lb of 1000-Btu steam) may be approximated from

$$E = \left(1 - \frac{\Delta T}{1250}\right) \frac{\Delta T}{Y + R + \Delta T/N} \quad (11-124)$$

where ΔT is the total temperature drop between feed to the first flasher and discharge from the last flasher. °C; N is the number of flash stages; Y is the approach between vapor temperature from the first flasher and liquid leaving the heater in which this vapor is condensed. °C (the approach is usually substantially constant for all stages); and R . °C (is the sum of the boiling-point rise and the short-circuiting loss in the first flash stage. The expression for the mean effective temperature difference Δt available for heat transfer then becomes

$$\Delta t = \frac{\Delta T}{N \ln \frac{1 - \Delta T/1250 - RE/\Delta T}{1 - \Delta T/1250 - RE/\Delta T - E/N}} \quad (11-125)$$

Multiple-Effect Evaporators A number of approximate methods have been published for estimating performance and heating-surface requirements of a multiple-effect evaporator [Coates and Pressburg, *Chem. Eng.*, **67**(6), 157 (1960); Coates, *Chem. Eng. Prog.*, **45**, 25 (1949); and Ray and Carnahan, *Trans. Am. Inst. Chem. Eng.*, **41**, 253 (1945)]. However, because of the wide variety of methods of feeding and the added complication of feed heaters and condensate flash systems, the only certain way of determining performance is by detailed heat and material balances. Algebraic solutions may be used, but if more than a few effects are involved, trial-and-error methods are usually quicker. These frequently involve trial-and-error within trial-and-error solutions. Usually, if condensate flash systems or feed heaters are involved, it is best to start at the first effect. The basic steps in the calculation are then as follows:

1. Estimate temperature distribution in the evaporator, taking into account boiling-point elevations. If all heating surfaces are to be equal, the temperature drop across each effect will be approximately inversely proportional to the heat-transfer coefficient in that effect.

2. Determine total evaporation required, and estimate steam consumption for the number of effects chosen.

3. From assumed feed temperature (forward feed) or feed flow (backward feed) to the first effect and assumed steam flow, calculate evaporation in the first effect. Repeat for each succeeding effect, checking intermediate assumptions as the calculation proceeds. Heat input from condensate flash can be incorporated easily since the condensate flow from the preceding effects will have already been determined.

4. The result of the calculation will be a feed to or a product discharge from the last effect that may not agree with actual requirements. The calculation must then be repeated with a new assumption of steam flow to the first effect.

5. These calculations should yield liquor concentrations in each effect that make possible a revised estimate of boiling-point rises. They also give the quantity of heat that must be transferred in each effect. From the heat loads, assumed temperature differences, and heat-transfer coefficients, heating-surface requirements can be determined. If the distribution of heating surface is not as desired, the entire calculation may need to be repeated with revised estimates of the temperature in each effect.

6. If sufficient data are available, heat-transfer coefficients under the proposed operating conditions can be calculated in greater detail and surface requirements readjusted.

Such calculations require considerable judgment to avoid repetitive trials but are usually well worth the effort. Sample calculations are given in the American Institute of Chemical Engineers *Testing Procedure for Evaporators* and by Badger and Banchemo, *Introduction to Chemical Engineering*, McGraw-Hill, New York, 1955. These balances may be done by computer but programming time frequently exceeds the time needed to do them manually, especially when variations in flow sheet are to be investigated. The MASSBAL program of SACDA, London, Ont., provides a considerable degree of flexibility in this regard. Another program, not specific to evaporators, is ASPEN PLUS by Aspen Tech., Cambridge, MA. Many such programs include simplifying assumptions and approximations that are not explicitly stated and can lead to erroneous results.

Optimization The primary purpose of evaporator design is to enable production of the necessary amount of satisfactory product at the lowest total cost. This requires economic-balance calculations that

may include a great number of variables. Among the possible variables are the following:

1. Initial steam pressure versus cost or availability.
2. Final vacuum versus water temperature, water cost, heat-transfer performance, and product quality.
3. Number of effects versus steam, water, and pump power cost.
4. Distribution of heating surface between effects versus evaporator cost.
5. Type of evaporator versus cost and continuity of operation.
6. Materials of construction versus product quality, tube life, evaporator life, and evaporator cost.
7. Corrosion, erosion, and power consumption versus tube velocity.
8. Downtime for retubing and repairs.
9. Operating-labor and maintenance requirements.
10. Method of feeding and use of heat-recovery systems.
11. Size of recovery heat exchangers.
12. Possible withdrawal of steam from an intermediate effect for use elsewhere.
13. Entrainment separation requirements.

The type of evaporator to be used and the materials of construction are generally selected on the basis of past experience with the material to be concentrated. The method of feeding can usually be decided on the basis of known feed temperature and the properties of feed and product. However, few of the listed variables are completely independent. For instance, if a large number of effects is to be used, with a consequent low temperature drop per effect, it is impractical to use a natural-circulation evaporator. If expensive materials of construction are desirable, it may be found that the forced-circulation evaporator is the cheapest and that only a few effects are justifiable.

The variable having the greatest influence on total cost is the number of effects in the evaporator. An economic balance can establish the optimum number where the number is not limited by such factors as viscosity, corrosiveness, freezing point, boiling-point rise, or thermal sensitivity. Under present United States conditions, savings in steam and water costs justify the extra capital, maintenance, and power costs of about seven effects in large commercial installations when the properties of the fluid are favorable, as in black-liquor evaporation. Under governmental financing conditions, as for plants to supply fresh water from seawater, evaporators containing from 12 to 30 or more effects can be justified.

As a general rule, the optimum number of effects increases with an increase in steam cost or plant size. Larger plants favor more effects, partly because they make it easier to install heat-recovery systems that increase the steam economy attainable with a given number of effects. Such recovery systems usually do not increase the total surface needed but do require that the heating surface be distributed between a greater number of pieces of equipment.

The most common evaporator design is based on the use of the same heating surface in each effect. This is by no means essential since few evaporators are "standard" or involve the use of the same patterns. In fact, there is no reason why all effects in an evaporator must be of the same type. For instance, the cheapest salt evaporator might use propeller calandrias for the early effects and forced-circulation effects at the low-temperature end, where their higher cost per unit area is more than offset by higher heat-transfer coefficients.

Bonilla [*Trans. Am. Inst. Chem. Eng.*, **41**, 529 (1945)] developed a simplified method for distributing the heating surface in a multiple-effect evaporator to achieve minimum cost. If the cost of the evaporator per unit area of heating surface is constant throughout, then minimum cost and area will be achieved if the ratio of area to temperature difference $A/\Delta T$ is the same for all effects. If the cost per unit area z varies, as when different tube materials or evaporator types are used, then $zA/\Delta T$ should be the same for all effects.

EVAPORATOR ACCESSORIES

Condensers The vapor from the last effect of an evaporator is usually removed by a condenser. **Surface condensers** are employed when mixing of condensate with condenser cooling water is not desired. They are for the most part shell-and-tube condensers with

vapor on the shell side and a multipass flow of cooling water on the tube side. Heat loads, temperature differences, sizes, and costs are usually of the same order of magnitude as for another effect of the evaporator. Surface condensers use more cooling water and are so much more expensive that they are never used when a direct-contact condenser is suitable.

The most common type of direct-contact condenser is the countercurrent **barometric condenser**, in which vapor is condensed by rising against a rain of cooling water. The condenser is set high enough so that water can discharge by gravity from the vacuum in the condenser. Such condensers are inexpensive and are economical on water consumption. They can usually be relied on to maintain a vacuum corresponding to a saturated-vapor temperature within 2.8°C (5°F) of the water temperature leaving the condenser [How, *Chem. Eng.*, **63**(2), 174 (1956)]. The ratio of water consumption to vapor condensed can be determined from the following equation:

$$\frac{\text{Water flow}}{\text{Vapor flow}} = \frac{H_c - h_2}{h_2 - h_1} \quad (11-126)$$

where H_c = vapor enthalpy and h_1 and h_2 = water enthalpies entering and leaving the condenser. Another type of direct-contact condenser is the **jet or wet condenser**, which makes use of high-velocity jets of water both to condense the vapor and to force noncondensable gases out the tailpipe. This type of condenser is frequently placed below barometric height and requires a pump to remove the mixture of water and gases. Jet condensers usually require more water than the more common barometric-type condensers and cannot be throttled easily to conserve water when operating at low evaporation rates.

Vent Systems Noncondensable gases may be present in the evaporator vapor as a result of leakage, air dissolved in the feed, or decomposition reactions in the feed. When the vapor is condensed in the succeeding effect, the noncondensables increase in concentration and impede heat transfer. This occurs partially because of the reduced partial pressure of vapor in the mixture but mainly because the vapor flow toward the heating surface creates a film of poorly conducting gas at the interface. (See page 11-14 for means of estimating the effect of noncondensable gases on the steam-film coefficient.) The most important means of reducing the influence of noncondensables on heat transfer is by properly channeling them past the heating surface. A positive vapor-flow path from inlet to vent outlet should be provided, and the path should preferably be tapered to avoid pockets of low velocity where noncondensables can be trapped. Excessive clearances and low-resistance channels that could bypass vapor directly from the inlet to the vent should be avoided [Standiford, *Chem. Eng. Prog.*, **75**, 59–62 (July 1979)].

In any event, noncondensable gases should be vented well before their concentration reaches 10 percent. Since gas concentrations are difficult to measure, the usual practice is to overvent. This means that an appreciable amount of vapor can be lost.

To help conserve steam economy, venting is usually done from the steam chest of one effect to the steam chest of the next. In this way, excess vapor in one vent does useful evaporation at a steam economy only about one less than the overall steam economy. Only when there are large amounts of noncondensable gases present, as in beet-sugar evaporation, is it desirable to pass the vents directly to the condenser to avoid serious losses in heat-transfer rates. In such cases, it can be worthwhile to recover heat from the vents in separate heat exchangers, which preheat the entering feed.

The noncondensable gases eventually reach the condenser (unless vented from an effect above atmospheric pressure to the atmosphere or to auxiliary vent condensers). These gases will be supplemented by air dissolved in the condenser water and by carbon dioxide given off on decomposition of bicarbonates in the water if a barometric condenser is used. These gases may be removed by the use of a water-jet-type condenser but are usually removed by a separate vacuum pump.

The vacuum pump is usually of the steam-jet type if high-pressure steam is available. If high-pressure steam is not available, more expensive mechanical pumps may be used. These may be either a water-ring (Hytor) type or a reciprocating pump.

The primary source of noncondensable gases usually is air dissolved in the condenser water. Figure 11-126 shows the dissolved-gas content

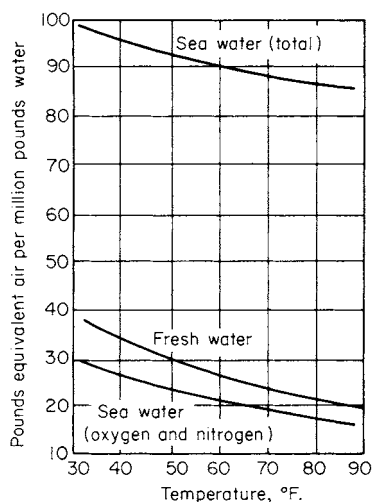


FIG. 11-126 Gas content of water saturated at atmospheric pressure. °C = 5/9 (°F – 32).

of fresh water and seawater, calculated as equivalent air. The lower curve for seawater includes only dissolved oxygen and nitrogen. The upper curve includes carbon dioxide that can be evolved by complete breakdown of bicarbonate in seawater. Breakdown of bicarbonates is usually not appreciable in a condenser but may go almost to completion in a seawater evaporator. The large increase in gas volume as a result of possible bicarbonate breakdown is illustrative of the uncertainties involved in sizing vacuum systems.

By far the largest load on the vacuum pump is water vapor carried with the noncondensable gases. Standard power-plant practice assumes that the mixture leaving a surface condenser will have been cooled 4.2°C (7.5°F) below the saturation temperature of the vapor. This usually corresponds to about 2.5 kg of water vapor/kg of air. One advantage of the countercurrent barometric condenser is that it can cool the gases almost to the temperature of the incoming water and thus reduce the amount of water vapor carried with the air.

In some cases, as with pulp-mill liquors, the evaporator vapors contain constituents more volatile than water, such as methanol and sulfur compounds. Special precautions may be necessary to minimize the effects of these compounds on heat transfer, corrosion, and condensate quality. They can include removing most of the condensate countercurrent to the vapor entering an evaporator-heating element, channeling vapor and condensate flow to concentrate most of the “foul” constituents into the last fraction of vapor condensed (and keeping this condensate separate from the rest of the condensate), and flashing the warm evaporator feed to a lower pressure to remove much of the foul constituents in only a small amount of flash vapor. In all such cases, special care is needed to properly channel vapor flow past the heating surfaces so there is a positive flow from steam inlet to vent outlet with no pockets, where foul constituents or noncondensibles can accumulate.

Salt Removal When an evaporator is used to make a crystalline product, a number of means are available for concentrating and removing the salt from the system. The simplest is to provide settling space in the evaporator itself. This is done in the types shown in Fig. 11-122*b*, *c*, and *e* by providing a relatively quiescent zone in which the salt can settle. Sufficiently high slurry densities can usually be achieved in this manner to reach the limit of pumpability. The evaporators are usually placed above barometric height so that the slurry can be discharged intermittently on a short time cycle. This permits the use of high velocities in large lines that have little tendency to plug.

If the amount of salts crystallized is on the order of a ton an hour or less, a salt trap may be used. This is simply a receiver that is connected to the bottom of the evaporator and is closed off from the evaporator periodically for emptying. Such traps are useful when insufficient headroom is available for gravity removal of the solids. However, traps require a

great deal of labor, give frequent trouble with the shutoff valves, and also can upset evaporator operation completely if a trap is reconnected to the evaporator without first displacing all air with feed liquor.

EVAPORATOR OPERATION

The two principal elements of evaporator control are *evaporation rate* and *product concentration*. Evaporation rate in single- and multiple-effect evaporators is usually achieved by steam-flow control. Conventional-control instrumentation is used (see Sec. 22), with the added precaution that pressure drop across meter and control valve, which reduces temperature difference available for heat transfer, not be excessive when maximum capacity is desired. Capacity control of thermocompression evaporators depends on the type of compressor; positive-displacement compressors can utilize speed control or variations in operating pressure level. Centrifugal machines normally utilize adjustable inlet-guide vanes. Steam jets may have an adjustable spindle in the high-pressure orifice or be arranged as multiple jets that can individually be cut out of the system.

Product concentration can be controlled by any property of the solution that can be measured with the requisite accuracy and reliability. The preferred method is to impose control on rate of product withdrawal. Feed rates to the evaporator effects are then controlled by their

levels. When level control is impossible, as with the rising-film LTV, product concentration is used to control the feed rate—frequently by rationing of feed to steam with the ration reset by product concentration, sometimes also by feed concentration. Other controls that may be needed include vacuum control of the last effect (usually by air bleed to the condenser) and temperature-level control of thermocompression evaporators (usually by adding makeup heat or by venting excess vapor, or both as feed or weather conditions vary). For more control detail, see *Measurement and Control in Water Desalination*, N. Lior, ed., pp. 241–305, Elsevier Science Publ. Co., NY, 1986.

Control of an evaporator requires more than proper instrumentation. Operator logs should reflect changes in basic characteristics, as by use of **pseudo heat-transfer** coefficients, which can detect obstructions to heat flow, hence to capacity. These are merely the ratio of any convenient measure of heat flow to the temperature drop across each effect. **Dilution** by wash and seal water should be monitored since it absorbs evaporative capacity. Detailed tests, routine measurements, and operating problems are covered more fully in *Testing Procedure for Evaporators* (loc. cit.) and by Standiford [*Chem. Eng. Prog.*, **58**(11), 80 (1962)].

By far the best application of computers to evaporators is for working up operators' data into the basic performance parameters such as heat-transfer coefficients, steam economy, and dilution.

SECTION 12

Psychrometry,
Evaporative
Cooling, and
Solids Drying

PERRY'S CHEMICAL ENGINEERS' HANDBOOK

8TH EDITION



LARRY R. GENSKOW, WAYNE E. BEIMESCH
JOHN P. HECHT, IAN KEMP, TIM LANGRISH
CHRISTIAN SCHWARTZBACH, F. LEE SMITH

Copyright © 2008, 1997, 1984, 1973, 1963, 1950, 1941, 1934 by The McGraw-Hill Companies, Inc. All rights reserved. Manufactured in the United States of America. Except as permitted under the United States Copyright Act of 1976, no part of this publication may be reproduced or distributed in any form or by any means, or stored in a database or retrieval system, without the prior written permission of the publisher.

0-07-154219-1

The material in this eBook also appears in the print version of this title: 0-07-151135-0.

All trademarks are trademarks of their respective owners. Rather than put a trademark symbol after every occurrence of a trademarked name, we use names in an editorial fashion only, and to the benefit of the trademark owner, with no intention of infringement of the trademark. Where such designations appear in this book, they have been printed with initial caps.

McGraw-Hill eBooks are available at special quantity discounts to use as premiums and sales promotions, or for use in corporate training programs. For more information, please contact George Hoare, Special Sales, at george_hoare@mcgraw-hill.com or (212) 904-4069.

TERMS OF USE

This is a copyrighted work and The McGraw-Hill Companies, Inc. (“McGraw-Hill”) and its licensors reserve all rights in and to the work. Use of this work is subject to these terms. Except as permitted under the Copyright Act of 1976 and the right to store and retrieve one copy of the work, you may not decompile, disassemble, reverse engineer, reproduce, modify, create derivative works based upon, transmit, distribute, disseminate, sell, publish or sublicense the work or any part of it without McGraw-Hill’s prior consent. You may use the work for your own noncommercial and personal use; any other use of the work is strictly prohibited. Your right to use the work may be terminated if you fail to comply with these terms.

THE WORK IS PROVIDED “AS IS.” McGRAW-HILL AND ITS LICENSORS MAKE NO GUARANTEES OR WARRANTIES AS TO THE ACCURACY, ADEQUACY OR COMPLETENESS OF OR RESULTS TO BE OBTAINED FROM USING THE WORK, INCLUDING ANY INFORMATION THAT CAN BE ACCESSED THROUGH THE WORK VIA HYPERLINK OR OTHERWISE, AND EXPRESSLY DISCLAIM ANY WARRANTY, EXPRESS OR IMPLIED, INCLUDING BUT NOT LIMITED TO IMPLIED WARRANTIES OF MERCHANTABILITY OR FITNESS FOR A PARTICULAR PURPOSE. McGraw-Hill and its licensors do not warrant or guarantee that the functions contained in the work will meet your requirements or that its operation will be uninterrupted or error free. Neither McGraw-Hill nor its licensors shall be liable to you or anyone else for any inaccuracy, error or omission, regardless of cause, in the work or for any damages resulting therefrom. McGraw-Hill has no responsibility for the content of any information accessed through the work. Under no circumstances shall McGraw-Hill and/or its licensors be liable for any indirect, incidental, special, punitive, consequential or similar damages that result from the use of or inability to use the work, even if any of them has been advised of the possibility of such damages. This limitation of liability shall apply to any claim or cause whatsoever whether such claim or cause arises in contract, tort or otherwise.

DOI: 10.1036/0071511350

Psychrometry, Evaporative Cooling, and Solids Drying*

Larry R. Genskow *Technical Director, Corporate Engineering Technologies, The Procter & Gamble Company; Advisory Associate Editor, Drying Technology—An International Journal; Member, International Advisory Committee, International Drying Symposia (Section Editor)*

Wayne E. Beimesch, Ph.D. *Technical Associate Director, Corporate Engineering, The Procter & Gamble Company; Member, The Controlled Release Society; Member, Institute for Liquid Atomization and Spray Systems*

John P. Hecht, Ph.D. *Senior Engineer, The Procter & Gamble Company*

Ian C. Kemp, M.A. (Cantab), C.Eng. *Senior Technical Manager, GlaxoSmithKline; Fellow, Institution of Chemical Engineers; Associate Member, Institution of Mechanical Engineers*

Tim Langrish, D.Phil. *School of Chemical and Biomolecular Engineering, The University of Sydney (Australia)*

Christian Schwartzbach, M.Sc. *Manager, Technology Development (retired), Niro A/S*

(Francis) Lee Smith, Ph.D., M.Eng. *Principal, Wilcrest Consulting Associates, Houston, Texas; Member, American Institute of Chemical Engineers, Society of American Value Engineers, Water Environment Federation, Air and Waste Management Association (Biofiltration)*

PSYCHROMETRY		
Terminology	12-4	
Calculation Formulas	12-5	
Relationship between Wet-Bulb and Adiabatic Saturation Temperatures	12-5	
Psychrometric Charts	12-6	
Examples Illustrating Use of Psychrometric Charts	12-8	
Example 1: Determination of Moist Air Properties	12-8	
Example 2: Air Heating	12-8	
Example 3: Evaporative Cooling	12-9	
Example 4: Cooling and Dehumidification	12-10	
Example 5: Cooling Tower	12-10	
Example 6: Recirculating Dryer	12-12	
Psychrometric Calculations	12-13	
Psychrometric Software and Tables	12-13	
		Psychrometric Calculations—Worked Examples 12-14
		Example 7: Determination of Moist Air Properties 12-14
		Example 8: Calculation of Humidity and Wet-Bulb Condition 12-15
		Example 9: Calculation of Psychrometric Properties of Acetone/Nitrogen Mixture 12-16
		Measurement of Humidity 12-16
		Dew Point Method 12-16
		Wet-Bulb Method 12-16
		EVAPORATIVE COOLING
		Introduction 12-17
		Principles 12-17

*The contributions of Paul Y. McCormick, George A. Schurr, and Eno Bagnoli of E. I. du Pont de Nemours & Co., and Charles G. Moyers and Glenn W. Baldwin of Union Carbide Corporation to material that was used from the fifth to seventh editions are acknowledged.

The assistance of Kwok-Lun Ho, Ph.D., Principal Engineering Consultant, in the preparation of the present section is acknowledged.

12-2 PSYCHROMETRY, EVAPORATIVE COOLING, AND SOLIDS DRYING

Cooling Towers	12-17	Product Quality Considerations	12-38
Cooling Tower Theory	12-17	Overview	12-38
Example 10: Calculation of Mass-Transfer Coefficient Group	12-18	Transformations Affecting Product Quality	12-38
Example 11: Application of Nomograph for Cooling Tower Characteristics	12-19	Additional Reading	12-40
Mechanical Draft Towers	12-19	Solids-Drying Equipment—General Aspects	12-40
Example 12: Application of Sizing and Horsepower Charts	12-20	Classification of Dryers	12-40
Example 13: Application of Sizing Chart	12-20	Description of Dryer Classification Criteria	12-40
Cooling Tower Operation	12-20	Subclassifications	12-47
Example 14: Calculation of Makeup Water	12-21	Selection of Drying Equipment	12-48
Fan Horsepower	12-21	Dryer Selection Considerations	12-48
Pumping Horsepower	12-21	Drying Tests	12-50
Fogging and Plume Abatement	12-22	Dryer Modeling, Design, and Scale-up	12-50
Thermal Performance	12-22	General Principles	12-50
New Technologies	12-22	Levels of Dryer Modeling	12-50
Applications of Evaporative Cooling Towers	12-22	Types of Dryer Calculations	12-50
Natural Draft Towers, Cooling Ponds, Spray Ponds	12-22	Heat and Mass Balance	12-50
Wet Surface Air Coolers (WSACs)	12-22	Scoping Design Calculations	12-51
Principles	12-22	Example 19: Drying of Particles	12-51
Wet Surface Air Cooler Basics	12-22	Scaling Models	12-52
Common WSAC Applications and Configurations	12-24	Example 20: Sealing of Data	12-52
WSAC for Closed-Circuit Cooling Systems	12-24	Detailed or Rigorous Models	12-52
Water Conservation Applications—"Wet-Dry" Cooling	12-25	Example 21: Sizing of a Cascading Rotary Dryer	12-53
		Computational Fluid Dynamics (CFD)	12-54
		Design and Scale-up of Individual Dryer Types	12-54
		Additional Reading	12-56
		Dryer Descriptions	12-56
		Batch Tray Dryers	12-56
		Continuous Tray and Gravity Dryers	12-59
		Continuous Band and Tunnel Dryers	12-63
		Batch Agitated and Rotating Dryers	12-65
		Example 22: Calculations for Batch Dryer	12-70
		Continuous Agitated Dryers	12-71
		Continuous Rotary Dryers	12-71
		Example 23: Sizing of a Cascading Rotary Dryer	12-76
		Fluidized and Spouted Bed Dryers	12-82
		Dryers with Liquid Feeds	12-87
		Example 24: Heat-Transfer Calculations	12-88
		Dryers for Films and Sheets	12-89
		Spray Dryers	12-90
		Industrial Designs and Systems	12-94
		Pneumatic Conveying Dryers	12-97
		Other Dryer Types	12-104
		Field Effects Drying—Drying with Infrared, Radio-Frequency, and Microwave Methods	12-105
		Operation and Troubleshooting	12-106
		Troubleshooting	12-106
		Dryer Operation	12-107
		Dryer Safety	12-107
		Environmental Considerations	12-108
		Control and Instrumentation	12-108
		Drying Software	12-109
SOLIDS-DRYING FUNDAMENTALS			
Introduction	12-26		
Terminology	12-26		
Mass and Energy Balances	12-26		
Example 15: Overall Mass and Energy Balance on a Sheet Dryer	12-27		
Thermodynamics	12-28		
Mechanisms of Moisture Transport within Solids	12-29		
Drying Kinetics	12-29		
Drying Curves and Periods of Drying	12-29		
Introduction to Internal and External Mass-Transfer Control—Drying of a Slab	12-30		
Mathematical Modeling of Drying	12-30		
Numerical Modeling of Drying Kinetics	12-30		
Example 16: Air Drying of a Thin Layer of Paste	12-31		
Simplified Kinetic Models	12-33		
Example 17: Drying a Pure Water Drop	12-33		
Concept of a Characteristic Drying Rate Curve	12-34		
Experimental Methods	12-35		
Measurement of Drying Curves	12-35		
Performing a Mass and Energy Balance on a Large Industrial Dryer	12-36		
Drying of Nonaqueous Solvents	12-36		
Practical Considerations	12-36		
Physical Properties	12-37		
Example 18: Preparation of a Psychrometric Chart	12-37		

Nomenclature and Units

Symbol	Definition	SI units	U.S. Customary System units	Symbol	Definition	SI units	U.S. Customary System units
A	Area	m^2	ft^2	f	Relative drying rate	—	—
a_w	Water activity	—	—	G	Gas mass flow rate	kg/s	lb/h
a_w^{vapor}	Activity of water in the vapor phase	—	—	g	Acceleration due to gravity, $9.81 m/s^2$	m/s^2	ft/s^2
a_w^{solid}	Activity of water in the solid	—	—	H	Enthalpy of a pure substance	J/kg	Btu/lb
c	Concentration	kg/m^3	lb/ft^3	ΔH_{vap}	Heat of vaporization	J/kg	Btu/lb
C_p	Specific heat capacity at constant pressure	$J/(kg \cdot K)$	$Btu/(lb \cdot ^\circ F)$	h	Heat-transfer coefficient	$W/(m^2 \cdot K)$	$Btu/(ft^2 \cdot h \cdot ^\circ F)$
C_w	Concentration of water in the solid	kg/m^3	lbm/ft^3	I	Humid enthalpy (dry substance and associated moisture or vapor)	J/kg	Btu/lb
$\mathcal{D}(w)$	Diffusion coefficient of water in a solid or liquid as a function of moisture content	m^2/s	ft^2/s	J	Mass flux (of evaporating liquid)	$kg/(m^2 \cdot s)$	$lb/(ft^2 \cdot h)$
\mathcal{D}	Diffusion coefficient	m^2/s	ft^2/s	k	Mass-transfer coefficient	m/s	$lb/(ft^2 \cdot h \cdot atm)$
d	Diameter (particle)	m	in	k_{air}	Thermal conductivity of air	$W/(m \cdot K)$	$Btu/(ft \cdot h \cdot ^\circ F)$
E	Power	W	Btu/h	k_c	Mass-transfer coefficient for a concentration driving force	m/s	ft^2/s
F	Solids or liquid mass flow rate	kg/s	lb/h	k_p	Mass transfer coefficient for a partial pressure driving force	$kg/(m^2 \cdot s)$	$lbm/(ft^2 \cdot s)$
F	Mass flux of water at surface	$kg/(m^2 \cdot s)$	$lbm/(ft^2 \cdot s)$				

Nomenclature and Units (Concluded)

Symbol	Definition	SI units	U.S. Customary System units	Symbol	Definition	SI units	U.S. Customary System units
<i>L</i>	Length; length of drying layer	m	ft	<i>X</i>	Solids moisture content (dry basis)	—	—
<i>M</i>	Molecular weight	kg/mol	lb/mol	<i>Y</i>	Mass ratio	—	—
<i>m</i>	Mass	kg	lb	<i>z</i>	Distance coordinate	m	ft
<i>m_{solids}</i>	Mass of dry solids	kg	lbm	Dimensionless groups			
<i>N</i>	Specific drying rate ($-dX/dt$)	1/s	1/s	<i>Ar</i>	Archimedes number, $(gd^3\rho_c/\mu^2)(\rho_F - \rho_C)$	—	—
<i>N</i>	Rotational speed (drum, impeller, etc.)	1/s	rpm	<i>Bi</i>	Biot number, $h \cdot L/\kappa$	—	—
<i>P</i>	Total pressure	kg/(m·s ²)	lbf/in ²	<i>Cr</i>	Crashof number, $L^3 \cdot \rho^2 \cdot \beta g \Delta T / \mu^2$	—	—
<i>P_w^{bulk}</i>	Partial pressure of water vapor in the air far from the drying material	kg/m·s ²	lbf/in ²	<i>Nu</i>	Nusselt number, hd_p/κ	—	—
<i>P_w^{surface}</i>	Partial pressure of water vapor in the air at the solid interface	kg/m·s ²	lbf/in ²	<i>Pr</i>	Prandtl number, $\mu C_p/\kappa$	—	—
<i>p</i>	Partial pressure/vapor pressure of component	kg/(m·s ²)	lbf/in ²	<i>Re</i>	Reynolds number, $\rho d_p U/\mu$	—	—
<i>p_{pure}^{sat}</i>	Pure component vapor pressure	kg/(m·s ²)	lbf/in ²	<i>Sc</i>	Schmidt number, $\mu/\rho D$	—	—
<i>p_w^{air}</i>	Partial pressure of water vapor in air	kg/(m·s ²)	lbf/in ²	<i>Sh</i>	Sherwood number, $k_y d_p/D$	—	—
<i>Q</i>	Heat-transfer rate	W	Btu/h	<i>Le</i>	Lewis = Sc/Pr	—	—
<i>q</i>	Heat flux	W/m ²	Btu/(ft ² ·h)	Greek letters			
<i>R</i>	Universal gas constant, 8314 J/(kmol·K)	J/(mol·K)	Btu/(mol·°F)	α	Slope	—	—
<i>R</i>	Droplet radius	m	ft	β	Psychrometric ratio	—	—
<i>r</i>	Radius; radial coordinate	m	ft	ϵ	Voidage (void fraction)	—	—
RH	Relative humidity	—	—	ζ	Dimensionless distance	—	—
<i>S</i>	Percentage saturation	—	—	η	Efficiency	—	—
<i>s</i>	Solid-fixed coordinate	Depends on geometry		θ	Dimensionless time	—	—
<i>T</i>	Absolute temperature	K	°R	κ	Thermal conductivity	W/(m·K)	Btu/(ft·h·°F)
<i>T, t</i>	Temperature	°C	°F	λ	Latent heat of evaporation	J/kg	Btu/lb
<i>t</i>	Time	s	h	μ	Absolute viscosity	kg/(m·s)	lb/(ft·s)
<i>U</i>	Velocity	m/s	ft/s	μ_{air}	Viscosity of air	kg/(m·s)	lbm/(ft·s)
<i>u</i>	Mass of water/mass of dry solid	—	—	ρ	Density	kg/m ³	lb/ft ³
<i>V</i>	Volume	m ³	ft ³	ρ_{air}	Air density	kg/m ³	lbm/ft ³
<i>V</i>	Air velocity	m/s	ft/s	ρ_s	Mass concentration of solids	kg/m ³	lbm/ft ³
<i>v</i>	Specific volume	m ³ /kg	ft ³ /lb	ρ_s^o	Density of dry solid	kg/m ³	lbm/ft ³
<i>v_{droplet}</i>	Droplet volume	m ³	ft ³	ρ_w^o	Density of pure water	kg/m ³	lbm/ft ³
<i>w</i>	Wet-basis moisture content	—	—	τ	Residence time of solids	s	h
<i>w_{avg dry-basis}</i>	Average wet-basis moisture content	—	—	Φ	Characteristic (dimensionless) moisture content	—	—
				ψ	Relative humidity	%	%

PSYCHROMETRY

GENERAL REFERENCES ASHRAE 2002 *Handbook: Fundamentals*, SI Edition, American Society of Heating, Refrigeration and Air-Conditioning Engineers, Atlanta, Ga., 2002, Chap. 6, "Psychrometrics," Chap. 19.2, "Sorbents and Desiccants." *Aspen Process Manual* (Internet knowledge base), Aspen Technology, 2000 onward. *Humidity and Dewpoint*, British Standard BS 1339 (rev.). Humidity and dewpoint, Pt. 1 (2002); Terms, definitions and formulae, Pt. 2 (2005); Psychrometric calculations and tables (including spreadsheet), Pt. 3 (2004); Guide to humidity measurement, British Standards Institution, Gunnersbury, United Kingdom. Cook and DuMont, *Process Drying Practice*, McGraw-Hill, New York, 1991, Chap. 6. Keey, *Drying of Loose and Particulate Materials*, Hemisphere, New York, 1992. Poling, Prausnitz, and O'Connell, *The Properties of Gases and Liquids*, 5th ed., McGraw-Hill, New York, 2000. Earlier editions: 1st/2d editions, Reid and Sherwood (1958/1966); 3d ed., Reid, Prausnitz, and Sherwood (1977); 4th ed., Reid, Prausnitz, and Poling (1986). Soiminen, "A Prospectively Transformed Psychrometric Chart and Its Application to Drying Calculations," *Drying Technol.* 4(2): 295-305 (1986). Sonntag, "Important New Values of the Physical Constants of 1986, Vapor Pressure Formulations Based on the ITS-90, and Psychrometer Formulae," *Zeitschrift für Meteorologie*, 40(5):340-344 (1990). Treybal, *Mass-Transfer Operations*, 3d ed., McGraw-Hill, New York, 1980. Wexler, *Humidity and Moisture*, vol. 1, Reinhold, New York, 1965.

Psychrometry is concerned with the determination of the properties of gas-vapor mixtures. These are important in calculations for

humidification and dehumidification, particularly in cooling towers, air-conditioning systems, and dryers. The first two cases involve the air-water vapor system at near-ambient conditions, but dryers normally operate at elevated temperatures and may also use elevated or subatmospheric pressures and other gas-solvent systems.

Principles involved in determining the properties of other systems are the same as with air-water vapor, with one major exception. Whereas the psychrometric ratio (ratio of heat-transfer coefficient to product of mass-transfer coefficient and humid heat, terms defined in the following subsection) for the air-water system can be taken as 1, the ratio for other systems in general does not equal 1. This has the effect of making the adiabatic saturation temperature different from the wet-bulb temperature. Thus, for systems other than air-water vapor, accurate calculation of psychrometric and drying problems is complicated by the necessity for point-to-point calculation of the temperature of the evaporating surface. For example, for the air-water system, the temperature of the evaporating surface will be constant during the constant-rate drying period even though the temperature and humidity of the gas stream change. For other systems, the temperature of the evaporating surface would change.

12-4 PSYCHROMETRY, EVAPORATIVE COOLING, AND SOLIDS DRYING

TABLE 12-1 Interconversion Formulas for Air-Water System, to 3 Significant Figures

$T =$ temperature in kelvins (K); $P =$ total pressure in pascals (Pa or N/m ²)				
Convert from:	Y (or ppm _w) ^a	y	p	Y_v
Convert to:				
Absolute humidity (mixing ratio) Y (kg·kg ⁻¹)	1	$Y = \frac{0.622Y}{1 - Y}$	$Y = \frac{0.622p}{P - p}$	$Y = \frac{0.622}{0.002167P/(Y_v T) - 1}$
Mole fraction y (mol·mol ⁻¹)	$y = \frac{Y}{0.622 + Y}$	1	$y = \frac{p}{P}$	$y = \frac{461.5Y_v T}{P}$
Vapor pressure p (Pa)	$p = \frac{PY}{0.622 + Y}$	$p = yP$	1	$p = 461.5Y_v T$
Volumetric humidity Y_v (kg·m ⁻³)	$Y_v = \frac{0.002167PY}{(0.622 + Y)T}$	$Y_v = \frac{0.002167yP}{T}$	$Y_v = \frac{0.002167p}{T}$	1

TERMINOLOGY

Terminology and nomenclature pertinent to psychrometry are given below. There is often considerable confusion between dry and wet basis, and between mass, molar, and volumetric quantities, in both definitions and calculations. Dry- and wet-basis humidity are similar at ambient conditions but can differ significantly at elevated humidities, e.g., in dryer exhaust streams. Complete interconversion formulas between four key humidity parameters are given in Table 12-1 for the air-water system and in Table 12-2 for a general gas-vapor system.

Definitions related to humidity, vapor pressure, saturation, and volume are as follows; the most useful are absolute humidity, vapor pressure, and relative humidity.

Absolute humidity Y Mass of water (or solvent) vapor carried by unit mass of dry air (or other carrier gas). It is also known as the **mixing ratio**, **mass ratio**, or **dry-basis humidity**. Preferred units are lb/lb or kg/kg, but g/kg and gr/lb are often used, as are ppm_w and ppb_w (parts per million/billion by weight); ppm_w = 10⁶ Y , ppb_w = 10⁹ Y .

Specific humidity Y_w Mass of vapor per unit mass of gas-vapor mixture. Also known as mass fraction or wet-basis humidity, and much more rarely used than dry-basis absolute humidity. $Y_w = Y/(1 + Y)$; $Y = Y_w/(1 - Y_w)$.

Mole ratio z Number of moles of vapor per mole of gas (dry basis), mol/mol; $z = (M_g/M_v)Y$, where M_v = molecular weight of vapor and M_g = molecular weight of gas. It may also be expressed as ppm, and ppb_v (parts per million/billion by volume); ppm_v = 10⁶ z , ppb_v = 10⁹ z .

Mole fraction y Number of moles of vapor per mole of gas-vapor mixture (wet basis); $y = z/(1 + z)$; $z = y/(1 - y)$. If a mixture contains m_v kg and n_v mol of vapor (e.g., water) and m_g kg and n_g mol of non-condensable gas (e.g., air), with $m_v = n_v M_v$ and $m_g = n_g M_g$, then the four quantities above are defined by

$$Y = \frac{m_v}{m_g} \quad Y_w = \frac{m_v}{m_g + m_v} \quad z = \frac{n_v}{n_g} \quad y = \frac{n_v}{n_g + n_v}$$

Volumetric humidity Y_v Mass of vapor per unit volume of gas-vapor mixture. It is sometimes, confusingly, called the absolute humidity, but it is really a vapor concentration; preferred units are kg/m³ or lb/ft³, but g/m³ and gr/ft³ are also used. It is inconvenient for calculations because it depends on temperature and pressure and on the units system; absolute humidity Y is always preferable for heat and mass balances. It is proportional to the specific humidity (wet basis); $Y_v = Y_w \rho_g$, where ρ_g is the **humid gas density** (mass of gas-vapor mixture per unit volume, wet basis). Also

$$Y_v = \frac{M_v P n_v}{RT(n_g + n_v)}$$

Vapor pressure p Partial pressure of vapor in gas-vapor mixture, and is proportional to the mole fraction of vapor; $p = yP$, where $P =$ total pressure, in the same units as p (Pa, N/m², bar, atm, or psi). Hence

$$p = \frac{n_v}{n_g + n_v} P$$

Saturation vapor pressure p_s Pressure exerted by pure vapor at a given temperature. When the vapor partial pressure p in the gas-vapor mixture at a given temperature equals the saturation vapor pressure p_s at the same temperature, the air is **saturated** and the absolute humidity is designated the **saturation humidity Y_s** .

Relative humidity RH or Ψ The partial pressure of vapor divided by the saturation vapor pressure at the given temperature, usually expressed as a percentage. Thus $RH = 100p/p_s$.

Percentage absolute humidity (percentage saturation) S Ratio of absolute humidity to saturation humidity, given by $S = 100Y/Y_s = 100p(P - p_s)/[p_s(P - p)]$. It is much less commonly used than relative humidity.

Dew point T_{dew} or saturation temperature Temperature at which a given mixture of water vapor and air becomes saturated on cooling; i.e., the temperature at which water exerts a vapor pressure equal to the partial pressure of water vapor in the given mixture.

TABLE 12-2 Interconversion Formulas for a General Gas-Vapor System

$M_g, M_v =$ molal mass of gas and vapor, respectively; $R = 8314$ J/(kmol·K); $T =$ temperature in kelvins (K); $P =$ total pressure in pascals (Pa or N/m ²)				
Convert from:	Y (or ppm _w)	y	p	Y_v
Convert to:				
Absolute humidity (mixing ratio) Y (kg·kg ⁻¹)	1	$Y = \frac{M_v y}{M_g(1 - Y)}$	$Y = \frac{pM_v}{(P - p)M_g}$	$Y = \frac{M_v}{M_g(PM_v/Y_v RT - 1)}$
Mole fraction y (mol·mol ⁻¹)	$y = \frac{Y}{M_v/M_g + Y}$	1	$y = \frac{p}{P}$	$y = \frac{Y_v RT}{PM_v}$
Vapor pressure p (Pa)	$p = \frac{PY}{M_v/M_g + Y}$	$p = yP$	1	$p = \frac{Y_v RT}{M_v}$
Volumetric humidity Y_v (kg·m ⁻³)	$Y_v = \frac{M_v}{RT} \frac{PY}{M_v/M_g + Y}$	$Y_v = \frac{M_v y P}{RT}$	$Y_v = \frac{M_v p}{RT}$	1

Humid volume v Volume in cubic meters (cubic feet) of 1 kg (1 lb) of dry air and the water vapor it contains.

Saturated volume v_s Humid volume when the air is saturated.

Terms related to heat balances are as follows:

Humid heat C_s Heat capacity of unit mass of dry air and the moisture it contains. $C_s = C_{pg} + C_{pv}Y$, where C_{pg} and C_{pv} are the heat capacities of dry air and water vapor, respectively, and both are assumed constant. For approximate engineering calculations at near-ambient temperatures, in SI units, $C_s = 1 + 1.9Y$ kJ/(kg·K) and in U.S. units, $C_s = 0.24 + 0.45Y$ (Btu/(lb·°F)).

Humid enthalpy H Heat content at a given temperature T of unit mass of dry air and the moisture it contains, relative to a datum temperature T_0 , usually 0°C. As water is liquid at 0°C, the humid enthalpy also contains a term for the latent heat of water. If heat capacity is invariant with temperature, $H = (C_{pg} + C_{pv}Y)(T - T_0) + \lambda_0 Y$, where λ_0 is the latent heat of water at 0°C, 2501 kJ/kg (1075 Btu/lb). In practice, for accurate calculations, it is often easier to obtain the vapor enthalpy H_v from steam tables, when $H = H_g + H_v = C_{pg}T + H_v$.

Adiabatic saturation temperature T_{as} Final temperature reached by a small quantity of vapor-gas mixture into which water is evaporating. It is sometimes called the thermodynamic wet-bulb temperature.

Wet-bulb temperature T_{wb} Dynamic equilibrium temperature attained by a liquid surface from which water is evaporating into a flowing airstream when the rate of heat transfer to the surface by convection equals the rate of mass transfer away from the surface. It is very close to the adiabatic saturation temperature for the air-water system, but not for most other vapor-gas systems; see later.

CALCULATION FORMULAS

Table 12-1 gives formulas for conversion between absolute humidity, mole fraction, vapor pressure, and volumetric humidity for the air-water system, and Table 12-2 does likewise for a general gas-vapor system. Where relationships are not included in the definitions, they are given below.

In U.S. units, the formulas are the same except for the volumetric humidity Y_v . Because of the danger of confusion with pressure units, it is recommended that in both Tables 12-1 and 12-2, Y_v be calculated in SI units and then converted.

Volumetric humidity is also related to absolute humidity and humid gas density by

$$Y_v = Y_w \rho_g = \frac{Y}{1 + Y} \rho_g \tag{12-1}$$

Two further useful formulas are as follows:

Parameter	General vapor-gas system	Air-water system, SI units, to 3 significant figures	Eq. no.
Density of humid gas (moist air) ρ_g (kg/m ³)	$\rho_g = \frac{M_g}{RT} \left(P - p + \frac{M_v}{M_g} p \right)$	$\rho_g = \frac{P - 0.378p}{287.1T}$	(12-2)
Humid volume v per unit mass of dry air (m ³ /kg)	$v = \frac{RT}{M_g(P - p)} = \frac{RT}{P} \times \left(\frac{1}{M_g} + \frac{Y}{M_v} \right)$	$v = \frac{461.5T}{P} (0.622 + Y)$	(12-3)

From Eq. (12-2), the density of dry air at 0°C (273.15 K) and 1 atm (101,325 Pa) is 1.292 kg/m³ (0.08065 lb/ft³). Note that the density of moist air is always lower than that of dry air.

Equation (12-3) gives the humid volume of dry air at 0°C (273.15 K) and 1 atm as 0.774 m³/kg (12.4 ft³/lb). For moist air, humid volume is not the reciprocal of humid gas density; $v = (1 + Y)/\rho_g$.

The **saturation vapor pressure** of water is given by Sonntag (1990) in pascals (N/m²) at absolute temperature T (K).

Over water:

$$\ln p_s = -6096.9385T^{-1} + 21.2409642 - 2.711193 \times 10^{-2}T + 1.673952 \times 10^{-5}T^2 + 2.433502 \ln T \tag{12-4a}$$

Over ice:

$$\ln p_s = -6024.5282T^{-1} + 29.32707 + 1.0613868 \times 10^{-2}T - 1.3198825 \times 10^{-5}T^2 - 0.49382577 \ln T \tag{12-4b}$$

Simpler equations for saturation vapor pressure are the Antoine equation and Magnus formula. These are slightly less accurate, but easier to calculate and also easily reversible to give T in terms of p . For the Antoine equation, given below, coefficients for numerous other solvent-gas systems are given in Poling, Prausnitz, and O’Connell, *The Properties of Gases and Liquids*, 5th ed., McGraw-Hill, 2000.

$$\ln p_s = C_0 - \frac{C_1}{T - C_2} \quad T = \frac{C_1}{C_0 - \ln p_s} + C_2 \tag{12-5}$$

Values for Antoine coefficients for the air-water system are given in Table 12-3. The standard values give vapor pressure within 0.1 percent of steam tables over the range 50 to 100°C, but an error of nearly 3 percent at 0°C. The alternative coefficients give a close fit at 0 and 100°C and an error of less than 1.2 percent over the intervening range.

The Sonntag equation strictly only applies to water vapor with no other gases present (i.e., in a partial vacuum). The vapor pressure of a gas mixture, e.g., water vapor in air, is given by multiplying the pure liquid vapor pressure by an enhancement factor f , for which various equations are available (see British Standard BS 1339 Part 1, 2002). However, the correction is typically less than 0.5 percent, except at elevated pressures, and it is therefore usually neglected for engineering calculations.

RELATIONSHIP BETWEEN WET-BULB AND ADIABATIC SATURATION TEMPERATURES

If a stream of air is intimately mixed with a quantity of water in an adiabatic system, the temperature of the air will drop and its humidity will increase. If the equilibration time or the number of transfer units approaches infinity, the air-water mixture will reach saturation. The **adiabatic saturation temperature T_{as}** is given by a heat balance between the initial unsaturated vapor-gas mixture and the final saturated mixture at thermal equilibrium:

$$C_s(T - T_{as}) = \lambda_{as}(Y_{as} - Y) \tag{12-6}$$

This equation has to be reversed and solved iteratively to obtain Y_{as} (absolute humidity at adiabatic saturation) and hence T_{as} (the calculation is divergent in the opposite direction). Approximate direct formulas are available from various sources, e.g., British Standard BS 1339 (2002) and Liley (*Int. J. Mech. Engg. Educ.* 21(2), 1993). The latent heat of evaporation evaluated at the adiabatic saturation temperature is λ_{as} ,

TABLE 12-3 Alternative Sets of Values for Antoine Coefficients for the Air-Water System

		C_0	C_1	C_2	C_0	C_1	C_2
Standard values	p in Pa	23.1963	3816.44	46.13 K	p in mmHg	18.3036	3816.44
Alternative values	p in Pa	23.19	3830	44.83 K	p in mmHg	18.3	3830

which may be obtained from steam tables; humid heat C_s is evaluated at initial humidity Y . On a psychrometric chart, the adiabatic saturation process almost exactly follows a **constant-enthalpy line**, as the sensible heat given up by the gas-vapor mixture exactly balances the latent heat of the liquid that evaporates back into the mixture. The only difference is due to the sensible heat added to the water to take it from the datum temperature to T_{as} . The adiabatic saturation line differs from the constant-enthalpy line as follows, where C_{PL} is the specific heat capacity of the liquid:

$$H_{as} - H = C_{PL}T_{as}(Y_{as} - Y) \quad (12-7)$$

Equation (12-7) is useful for calculating the adiabatic saturation line for a given T_{as} and gives an alternative iterative method for finding T_{as} , given T and Y ; compared with Eq. (12-6), it is slightly more accurate and converges faster, but the calculation is more cumbersome.

The **wet-bulb temperature** is the temperature attained by a fully wetted surface, such as the wick of a wet-bulb thermometer or a droplet or wet particle undergoing drying, in contact with a flowing unsaturated gas stream. It is regulated by the rates of vapor-phase heat and mass transfer to and from the wet bulb. Assuming mass transfer is controlled by diffusion effects and heat transfer is purely convective:

$$h(T - T_{wb}) = k_y \lambda_{wb} (Y_{wb} - Y) \quad (12-8)$$

where k_y is the corrected mass-transfer coefficient [$\text{kg}/(\text{m}^2 \cdot \text{s})$], h is the heat-transfer coefficient [$\text{kW}/(\text{m}^2 \cdot \text{K})$], Y_{wb} is the saturation mixing ratio at T_{wb} , and λ_{wb} is the latent heat (kJ/kg) evaluated at T_{wb} . Again, this equation must be solved iteratively to obtain T_{wb} and Y_{wb} .

In practice, for any practical psychrometer or wetted droplet or particle, there is significant extra heat transfer from radiation. For an Assmann psychrometer at near-ambient conditions, this is approximately 10 percent. This means that any measured real value of T_{wb} is slightly higher than the “pure convective” value in the definition. It is often more convenient to obtain wet-bulb conditions from adiabatic saturation conditions (which are much easier to calculate) by the following formula:

$$\frac{T - T_{wb}}{Y_{wb} - Y} = \frac{T - T_{as}}{Y_{as} - Y} \beta \quad (12-9)$$

where the psychrometric ratio $\beta = \overline{C}_s k_y / h$ and \overline{C}_s is the mean value of the humid heat over the range from T_{as} to T .

The advantage of using β is that it is approximately constant over normal ranges of temperature and pressure for any given pair of vapor and gas values. This avoids having to estimate values of heat- and mass-transfer coefficients α and k_y from uncertain correlations. For the air-water system, considering convective heat transfer alone, $\beta \sim 1.1$. In practice, there is an additional contribution from radiation, and β is very close to 1. As a result, the wet-bulb and adiabatic saturation temperatures differ by less than 1°C for the air-water system at near-ambient conditions (0 to 100°C, $Y < 0.1 \text{ kg}/\text{kg}$) and can be taken as equal for normal calculation purposes. Indeed, typically the T_{wb} measured by a practical psychrometer or at a wetted solid surface is closer to T_{as} than to the “pure convective” value of T_{wb} .

However, for nearly all other vapor-gas systems, particularly for organic solvents, $\beta < 1$, and hence $T_{wb} > T_{as}$. This is illustrated in Fig. 12-5. For these systems the psychrometric ratio may be obtained by determining h/k_y from heat- and mass-transfer analogies such as the Chilton-Colburn analogy. The basic form of the equation is

$$\beta = \left(\frac{\text{Sc}}{\text{Pr}} \right)^n = \text{Le}^{-n} \quad (12-10)$$

Sc is the Schmidt number for mass-transfer properties, Pr is the Prandtl number for heat-transfer properties, and Le is the Lewis number $\kappa / (C_p \rho_g \mathcal{D})$, where κ is the gas thermal conductivity and \mathcal{D} is the diffusion coefficient for the vapor through the gas. Experimental and theoretical values of the exponent n range from 0.56 [Bedingfield and Drew, *Ind. Eng. Chem.*, **42**:1164 (1950)] to $\frac{2}{3} = 0.667$ [Chilton and Colburn, *Ind. Eng. Chem.*, **26**:1183 (1934)]. A detailed discussion is given by Keey (1992). Values of β for any system can be estimated from the specific heats, diffusion coefficients, and other data given in Sec. 2. See the example below.

For calculation of wet-bulb (and adiabatic saturation) conditions, the most commonly used formula in industry is the **psychrometer equation**. This is a simple, linear formula that gives vapor pressure directly if the wet-bulb temperature is known, and is therefore ideal for calculating humidity from a wet-bulb measurement using a psychrometer, although the calculation of wet-bulb temperature from humidity still requires an iteration.

$$p = p_{wb} - AP(T - T_{wb}) \quad (12-11)$$

where A is the psychrometer coefficient. For the air-water system, the following formulas based on equations given by Sonntag [*Zeitschrift für Meteorologie*, **40**(5): 340–344 (1990)] may be used to give A for T_{wb} up to 30°C; they are based on extensive experimental data for Assmann psychrometers.

Over water (wet-bulb temperature):

$$A = 6.5 \times 10^{-4} (1 + 0.000944T_{wb}) \quad (12-12a)$$

Over ice (ice-bulb temperature):

$$A_i = 5.72 \times 10^{-4} \quad (12-12b)$$

For other vapor-gas systems, A is given by

$$A = \frac{M_g C_s}{M_v \beta \lambda_{wb}} \quad (12-13)$$

Here β is the psychrometric coefficient for the system. As a cross-check, for the air-water system at 20°C wet-bulb temperature, 50°C dry-bulb temperature, and absolute humidity 0.002 kg/kg, $C_s = (1.006 + 1.9 \times 0.002) = 1.01 \text{ kJ}/(\text{kg} \cdot \text{K})$ and $\lambda_{wb} = 2454 \text{ kJ}/\text{kg}$. Since $M_g = 28.97 \text{ kg}/\text{kmol}$ and $M_v = 18.02 \text{ kg}/\text{kmol}$, Eq. (12-12) gives A as $6.617 \times 10^{-4} / \beta$, compared with Sonntag’s value of 6.653×10^{-4} at this temperature, giving a value for the psychrometric coefficient β of 0.995; that is, $\beta \approx 1$, as expected for the air-water system.

PSYCHROMETRIC CHARTS

Psychrometric charts are plots of humidity, temperature, enthalpy, and other useful parameters of a gas-vapor mixture. They are helpful for rapid estimates of conditions and for visualization of process operations such as humidification and drying. They apply to a given system at a given pressure, the most common of course being air-water at atmospheric pressure. There are four types, of which the Grosvenor and Mollier types are most widely used:

The **Grosvenor chart** plots temperature (abscissa) against humidity (ordinate). Standard charts produced by ASHRAE and other groups, or by computer programs, are usually of this type. The saturation line is a curve from bottom left to top right, and curves for constant relative humidity are approximately parallel to this. Lines from top left to bottom right may be of either constant wet-bulb temperature or constant enthalpy, depending on the chart. The two are not quite identical, so if only one is shown, correction factors are required for the other parameter. Examples are shown in Figs. 12-1 (SI units), 12-2a (U.S. Customary System units, medium temperature), and 12-2b (U.S. Customary System units, high temperature).

The **Bowen chart** is a plot of enthalpy (abscissa) against humidity (ordinate). It is convenient to be able to read enthalpy directly, especially for near-adiabatic convective drying where the operating line approximately follows a line of constant enthalpy. However, it is very difficult to read accurately because the key information is compressed in a narrow band near the saturation line. See Cook and DuMont, *Process Drying Practice*, McGraw-Hill, New York, 1991, chap. 6.

The **Mollier chart** plots humidity (abscissa) against enthalpy (lines sloping diagonally from top left to bottom right). Lines of constant temperature are shallow curves at a small slope to the horizontal. The chart is nonorthogonal (no horizontal lines) and hence a little difficult to plot and interpret initially. However, the area of greatest interest is expanded, and they are therefore easy to read accurately. They tend to cover a wider

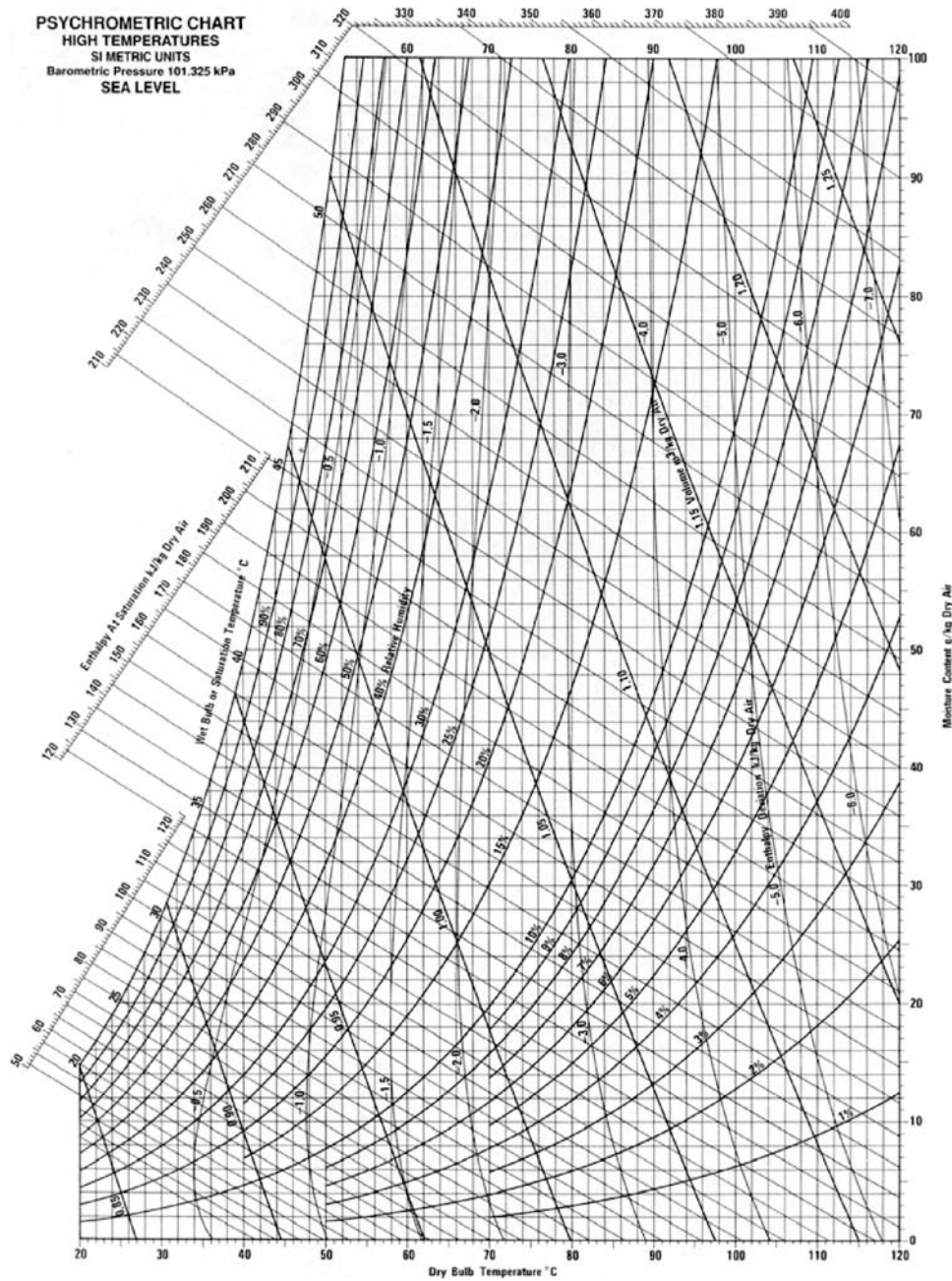


FIG. 12-1 Grosvenor psychrometric chart for the air-water system at standard atmospheric pressure, 101,325 Pa, SI units. (Courtesy Carrier Corporation.)

temperature range than Grosvenor charts, so are useful for dryer calculations. The slope of the enthalpy lines is normally $-1/\lambda$, where λ is the latent heat of evaporation. Adiabatic saturation lines are not quite parallel to constant-enthalpy lines and are slightly curved; the deviation increases as humidity increases. Figure 12-3 shows an example.

The **Salen-Soininen** perspectively transformed **chart** is a triangular plot. It is tricky to plot and read, but covers a much wider range of humidity than do the other types of chart (up to 2 kg/kg) and is thus very effective for high-humidity mixtures and calculations near the

boiling point, e.g., in pulp and paper drying. See Soinen, *Drying Technol.* 4(2): 295-305 (1986).

Figure 12-4 shows a psychrometric chart for combustion products in air. The thermodynamic properties of moist air are given in Table 12-1. Figure 12-4 shows a number of useful additional relationships, e.g., specific volume and latent heat variation with temperature. Accurate figures should always be obtained from physical properties tables or by calculation using the formulas given earlier, and these charts should only be used as a quick check for verification.

12-8 PSYCHROMETRY, EVAPORATIVE COOLING, AND SOLIDS DRYING

In the past, psychrometric charts have been used to perform quite precise calculations. To do this, additive corrections are often required for enthalpy of added water or ice, and for variations in barometric pressure from the standard level (101,325 Pa, 14.696 lb/in², 760 mmHg, 29.921 inHg). It is preferable to use formulas, which give an accurate figure at any set of conditions. Psychrometric charts and tables can be used as a rough cross-check that the result has been calculated correctly. Table 12-4 gives values of saturation humidity, specific volume, enthalpy, and entropy of saturated moist air at selected conditions. Below the freezing point, these become virtually identical to the values for dry air, as saturation humidity is very low. For pressure corrections, an altitude increase of approximately 900 ft gives a pressure decrease of 1 inHg (0.034 bar). For a recorded wet-bulb temperature of 50°F (10°C), this gives an increase in humidity of 1.9 gr/lb (0.00027 kg/kg) and the enthalpy increases by 0.29 Btu/lb (0.68 kJ/kg). This correction increases roughly proportionately for further changes in pressure, but climbs sharply as wet-bulb temperature is increased; when T_{wb} reaches 100°F (38°C), $\Delta Y = 11.2$ gr/lb (0.0016 kg/kg) and $\Delta H = 1.77$ Btu/lb (4.12 kJ/kg). Equivalent, more detailed tables in SI units can be found in the ASHRAE Handbook.

Examples Illustrating Use of Psychrometric Charts In these examples the following nomenclature is used:

- t = dry-bulb temperatures, °F
- t_w = wet-bulb temperature, °F
- t_d = dewpoint temperature, °F
- H = moisture content, lb water/lb dry air
- ΔH = moisture added to or rejected from the airstream, lb water/lb dry air
- h' = enthalpy at saturation, Btu/lb dry air
- D = enthalpy deviation, Btu/lb dry air
- $h = h' + D$ = true enthalpy, Btu/lb dry air
- h_w = enthalpy of water added to or rejected from system, Btu/lb dry air

- q_a = heat added to system, Btu/lb dry air
- q_r = heat removed from system, Btu/lb dry air

Subscripts 1, 2, 3, etc., indicate entering and subsequent states.

Example 1: Determination of Moist Air Properties Find the properties of moist air when the dry-bulb temperature is 80°F and the wet-bulb temperature is 67°F.

Solution: Read directly from Fig. 12-2a (Fig. 12-6a shows the solution diagrammatically).

- Moisture content $H = 78$ gr/lb dry air
= 0.011 lb water/lb dry air
- Enthalpy at saturation $h' = 31.6$ Btu/lb dry air
- Enthalpy deviation $D = -0.1$ Btu/lb dry air
- True enthalpy $h = 31.5$ Btu/lb dry air
- Specific volume $v = 13.8$ ft³/lb dry air
- Relative humidity = 51 percent
- Dew point $t_d = 60.3^\circ\text{F}$

Example 2: Air Heating Air is heated by a steam coil from 30°F dry-bulb temperature and 80 percent relative humidity to 75°F dry-bulb temperature. Find the relative humidity, wet-bulb temperature, and dew point of the heated air. Determine the quantity of heat added per pound of dry air.

Solution: Reading directly from the psychrometric chart (Fig. 12-2a),

- Relative humidity = 15 percent
- Wet-bulb temperature = 51.5°F
- Dew point = 25.2°F

The enthalpy of the inlet air is obtained from Fig. 12-2a as $h_1 = h'_1 + D_1 = 10.1 + 0.06 = 10.16$ Btu/lb dry air; at the exit, $h_2 = h'_2 + D_2 = 21.1 - 0.1 = 21$ Btu/lb dry air. The heat added equals the enthalpy difference, or

$$q_a = \Delta h = h_2 - h_1 = 21 - 10.16 = 10.84 \text{ Btu/lb dry air}$$

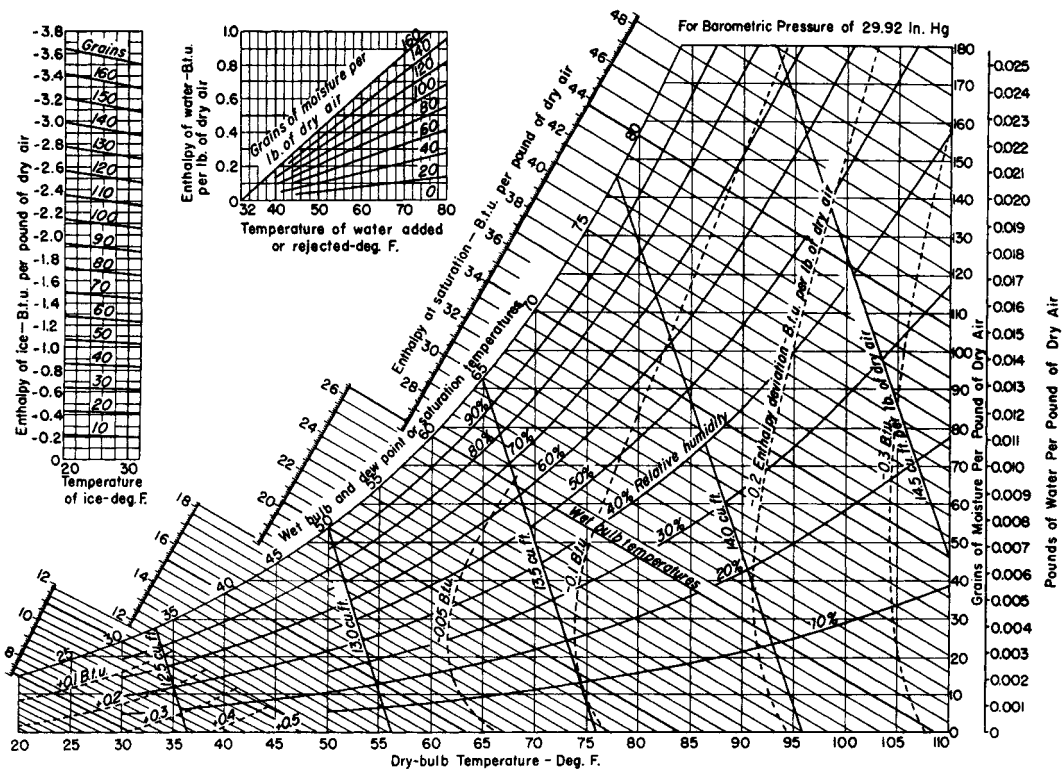


FIG. 12-2a Grosvenor psychrometric chart (medium temperature) for the air-water system at standard atmospheric pressure, 29.92 inHg, U.S. Customary units. (Courtesy Carrier Corporation.)

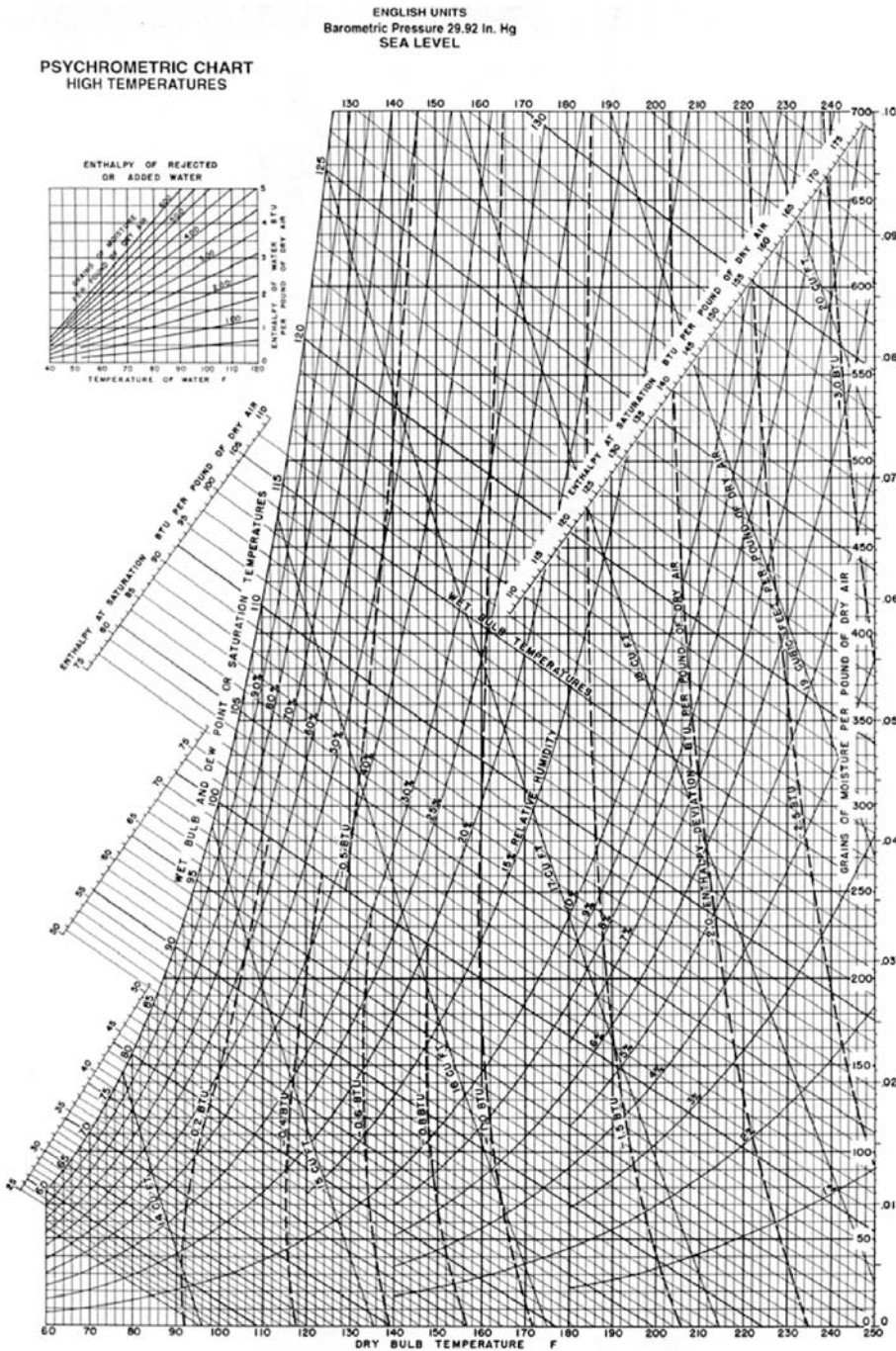


FIG. 12-2b Grosvenor psychrometric chart (high-temperature) for the air-water system at standard atmospheric pressure, 29.92 in.Hg, U.S. Customary units. (Source: Carrier Corporation.)

If the enthalpy deviation is ignored, the heat added q_a is $\Delta h = 21.1 - 10.1 = 11$ Btu/lb dry air, or the result is 1.5 percent high. Figure 12-6b shows the heating path on the psychrometric chart.

Example 3: Evaporative Cooling Air at 95°F dry-bulb temperature and 70°F wet-bulb temperature contacts a water spray, where its relative humidity is increased to 90 percent. The spray water is recirculated; makeup water

enters at 70°F. Determine exit dry-bulb temperature, wet-bulb temperature, change in enthalpy of the air, and quantity of moisture added per pound of dry air.

Solution: Figure 12-6c shows the path on a psychrometric chart. The leaving dry-bulb temperature is obtained directly from Fig. 12-2a as 72.2°F. Since the spray water enters at the wet-bulb temperature of 70°F and there is no heat added to or removed from it, this is by definition an adiabatic process and there

12-10 PSYCHROMETRY, EVAPORATIVE COOLING, AND SOLIDS DRYING

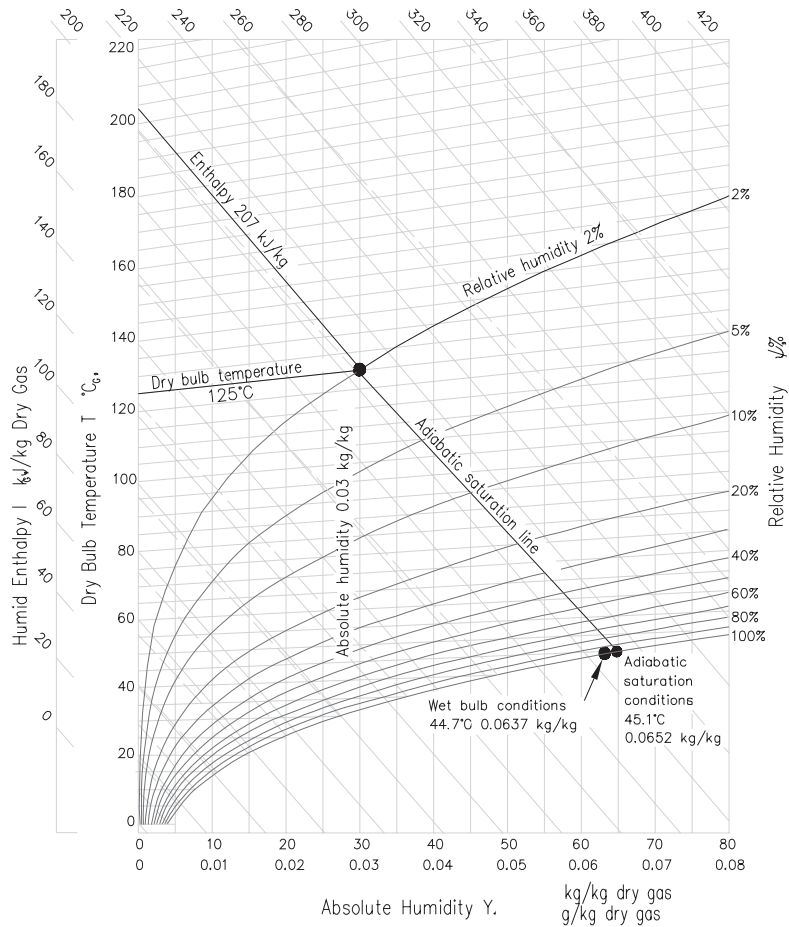


FIG. 12-3 Mollier psychrometric chart for the air-water system at standard atmospheric pressure, 101,325 Pa SI units, plots humidity (abscissa) against enthalpy (lines sloping diagonally from top left to bottom right). (Source: Aspen Technology.)

will be no change in wet-bulb temperature. The only change in enthalpy is that from the heat content of the makeup water. This can be demonstrated as follows:

Inlet moisture $H_1 = 70$ gr/lb dry air

Exit moisture $H_2 = 107$ gr/lb dry air

$\Delta H = 37$ gr/lb dry air

Inlet enthalpy $h_1 = h'_1 + D_1 = 34.1 - 0.22$

$= 33.88$ Btu/lb dry air

Exit enthalpy $h_2 = h'_2 + D_2 = 34.1 - 0.02$

$= 34.08$ Btu/lb dry air

Enthalpy of added water $h_w = 0.2$ Btu/lb dry air (from small diagram, 37 gr at 70°F)

Then

$$q_a = h_2 - h_1 + h_w = 34.08 - 33.88 + 0.2 = 0$$

Example 4: Cooling and Dehumidification Find the cooling load per pound of dry air resulting from infiltration of room air at 80°F dry-bulb temperature and 67°F wet-bulb temperature into a cooler maintained at 30°F dry-bulb and 28°F wet-bulb temperature, where moisture freezes on the coil, which is maintained at 20°F.

Solution: The path followed on a psychrometric chart is shown in Fig. 12-6d.

$$\begin{aligned} \text{Inlet enthalpy } h_1 &= h'_1 + D_1 = 31.62 - 0.1 \\ &= 31.52 \text{ Btu/lb dry air} \end{aligned}$$

$$\begin{aligned} \text{Exit enthalpy } h_2 &= h'_2 + D_2 = 10.1 + 0.06 \\ &= 10.16 \text{ Btu/lb dry air} \end{aligned}$$

Inlet moisture $H_1 = 78$ gr/lb dry air

Exit moisture $H_2 = 19$ gr/lb dry air

Moisture rejected $\Delta H = 59$ gr/lb dry air

Enthalpy of rejected moisture = -1.26 Btu/lb dry air (from small diagram of Fig. 12-2a)

$$\begin{aligned} \text{Cooling load } q_r &= 31.52 - 10.16 + 1.26 \\ &= 22.62 \text{ Btu/lb dry air} \end{aligned}$$

Note that if the enthalpy deviations were ignored, the calculated cooling load would be about 5 percent low.

Example 5: Cooling Tower Determine water consumption and amount of heat dissipated per 1000 ft³/min of entering air at 90°F dry-bulb temperature and 70°F wet-bulb temperature when the air leaves saturated at 110°F and the makeup water is at 75°F.

Solution: The path followed is shown in Fig. 12-6e.

Exit moisture $H_2 = 416$ gr/lb dry air

Inlet moisture $H_1 = 78$ gr/lb dry air

Moisture added $\Delta H = 338$ gr/lb dry air

Enthalpy of added moisture $h_w = 2.1$ Btu/lb dry air (from small diagram of Fig. 12-2b)

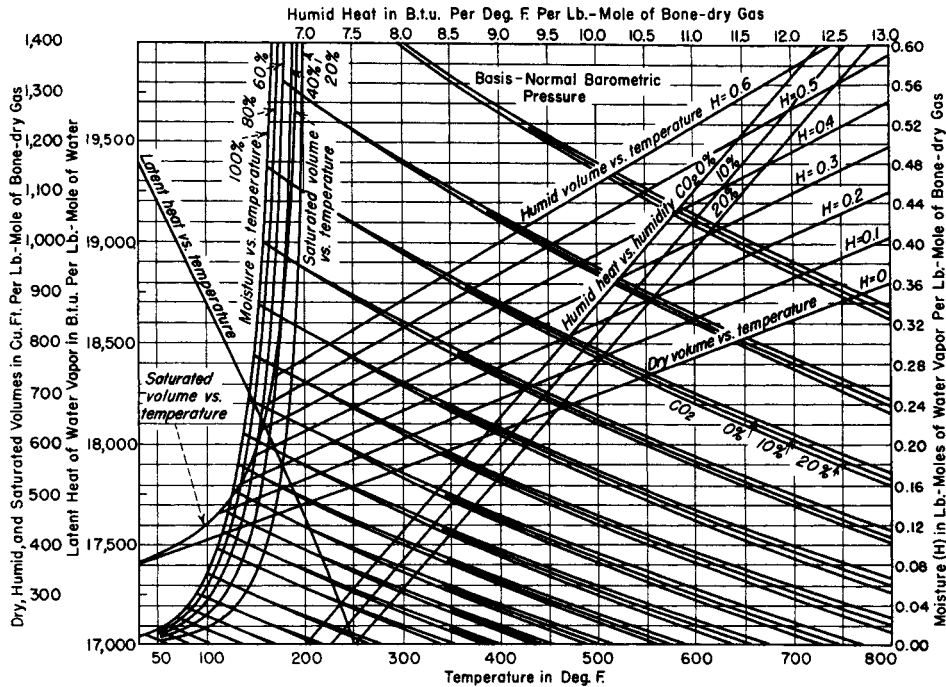


FIG. 12-4 Grosvenor psychrometric chart for air and flue gases at high temperatures, molar units [Hatta, Chem. Metall. Eng., 37:64 (1930)].

TABLE 12-4 Thermodynamic Properties of Saturated Air (U.S. Customary Units, at Standard Atmospheric Pressure, 29.921 inHg)

Temp. T, °F	Saturation humidity H _s	Volume, ft ³ /lb dry air			Enthalpy, Btu/lb dry air			Entropy, Btu/(°F·lb dry air)			Condensed water			Temp. T, °F
		v _a	v _{as}	v _s	h _a	h _{as}	h _s	s _a	s _{as}	s _s	Enthalpy, Btu/lb h _w	Entropy, Btu/(lb·°F) s _w	Vapor pressure, inHg p _s	
-150	6.932 × 10 ⁻⁹	7.775	.000	7.775	36.088	.000	36.088	0.09508	.00000	0.09508	218.77	0.4800	3.301 × 10 ⁻⁶	-150
-100	9.772 × 10 ⁻⁷	9.046	.000	9.046	24.037	.001	24.036	0.05897	.00000	0.05897	201.23	0.4277	4.666 × 10 ⁻⁵	-100
-50	4.163 × 10 ⁻⁵	10.313	.001	10.314	12.012	.043	11.969	0.02766	.00012	0.02754	181.29	0.3758	1.991 × 10 ⁻³	-50
0	7.872 × 10 ⁻⁴	11.578	.015	11.593	0.000	.835	0.835	0.00000	.00192	0.00192	158.93	0.3244	0.037645 × 10 ⁻²	0
10	1.315 × 10 ⁻³	11.831	.025	11.856	2.402	1.401	3.803	.00518	.00314	.00832	154.17	0.3141	0.062858	10
20	2.152 × 10 ⁻³	12.084	.042	12.126	4.804	2.302	7.106	.01023	.00504	.01527	149.31	0.3039	0.10272	20
30	3.454 × 10 ⁻³	12.338	.068	12.406	7.206	3.709	10.915	.01519	.00796	.02315	144.36	0.2936	0.16452	30
32	3.788 × 10 ⁻³	12.388	.075	12.463	7.686	4.072	11.758	.01617	.00870	.02487	143.36	0.2916	0.18035	32
32 ^a	3.788 × 10 ⁻³	12.388	.075	12.463	7.686	4.072	11.758	.01617	.00870	.02487	0.04	0.0000	0.18037	32 ^a
40	5.213 × 10 ⁻³	12.590	.105	12.695	9.608	5.622	15.230	.02005	.01183	.03188	8.09	.0162	.24767	40
50	7.658 × 10 ⁻³	12.843	.158	13.001	12.010	8.291	20.301	.02481	.01711	.04192	18.11	.0361	.36240	50
60	1.108 × 10 ⁻²	13.096	.233	13.329	14.413	12.05	26.46	.02948	.02441	.05389	28.12	.0555	.52159	60
70	1.582 × 10 ⁻²	13.348	.339	13.687	16.816	17.27	34.09	.03405	.03437	.06842	38.11	.0746	.73915	70
80	2.233 × 10 ⁻²	13.601	0.486	14.087	19.221	24.47	43.69	0.03854	0.04784	0.08638	48.10	0.0933	1.0323	80
90	3.118 × 10 ⁻²	13.853	.692	14.545	21.625	34.31	55.93	.04295	.06596	.10890	58.08	.1116	1.4219	90
100	4.319 × 10 ⁻²	14.106	.975	15.081	24.029	47.70	71.73	.04729	.09016	.13745	68.06	.1296	1.9333	100
110	5.944 × 10 ⁻²	14.359	1.365	15.724	26.434	65.91	92.34	.05155	.1226	.1742	78.03	.1472	2.5966	110
120	8.149 × 10 ⁻²	14.611	1.905	16.516	28.841	90.70	119.54	.05573	.1659	.2216	88.01	.1646	3.4474	120
130	0.1116	14.864	2.652	17.516	31.248	124.7	155.9	.05985	.2245	.2844	98.00	.1817	4.5272	130
140	0.1534	15.117	3.702	18.819	33.655	172.0	205.7	.06390	.3047	.3686	107.99	.1985	5.8838	140
150	0.2125	15.369	5.211	20.580	36.063	239.2	275.3	.06787	.4169	.4848	117.99	.2150	7.5722	150
160	0.2990	15.622	7.446	23.068	38.472	337.8	376.3	.07179	.5793	.6511	128.00	.2313	9.6556	160
170	0.4327	15.874	10.938	26.812	40.882	490.6	531.5	.07565	.8273	.9030	138.01	.2473	12.203	170
180	0.6578	16.127	16.870	32.997	43.292	748.5	791.8	.07946	1.240	1.319	148.03	.2631	15.294	180
190	1.099	16.379	28.580	44.959	45.704	1255	1301	.08320	2.039	2.122	158.07	.2786	19.017	190
200	2.295	16.632	60.510	77.142	48.119	2629	2677	.08689	4.179	4.266	168.11	.2940	23.468	200

NOTE: Compiled by John A. Goff and S. Gratch. See also Keenan and Kaye. *Thermodynamic Properties of Air*, Wiley, New York, 1945. Enthalpy of dry air taken as zero at 0°F. Enthalpy of liquid water taken as zero at 32°F.

To convert British thermal units per pound to joules per kilogram, multiply by 2326; to convert British thermal units per pound dry air-degree Fahrenheit to joules per kilogram-kelvin, multiply by 4186.8; and to convert cubic feet per pound to cubic meters per kilogram, multiply by 0.0624.

^a Extrapolated to represent metastable equilibrium with undercooled liquid.

12-12 PSYCHROMETRY, EVAPORATIVE COOLING, AND SOLIDS DRYING

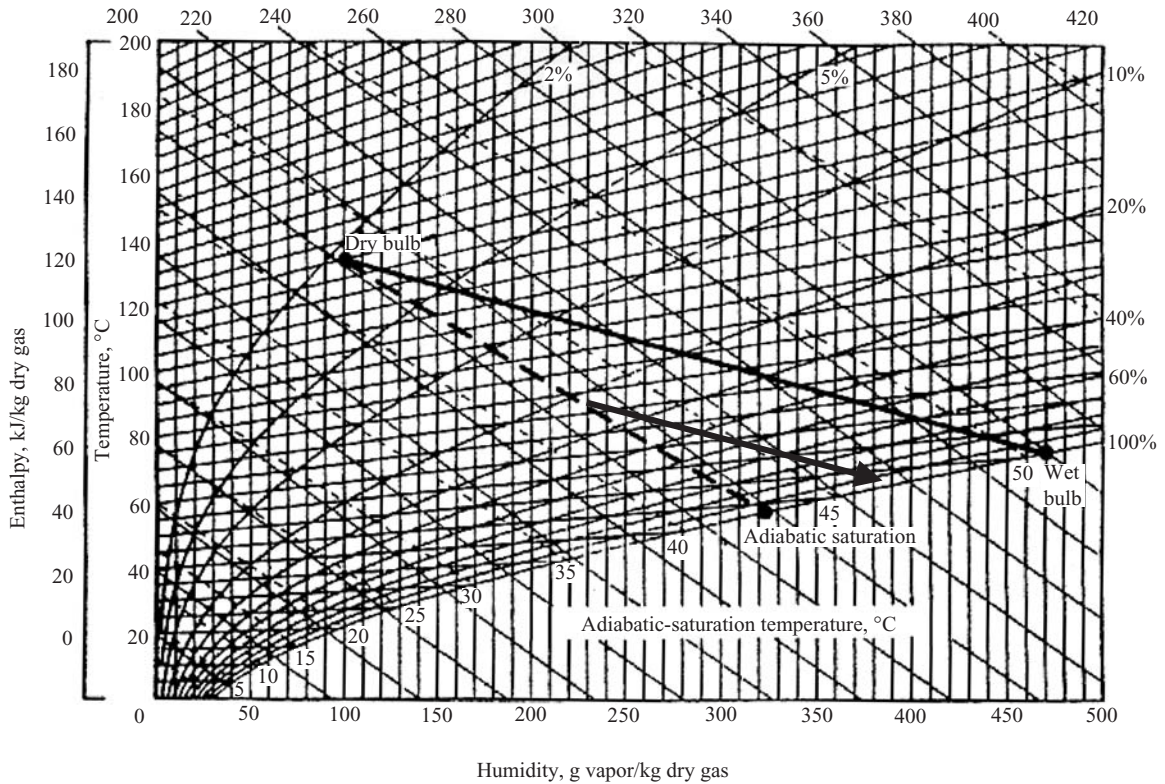


FIG. 12-5 Mollier chart showing changes in T_{wb} during an adiabatic saturation process for an organic system (nitrogen-toluene).

If greater precision is desired, h_w can be calculated as

$$h_w = (338/7000)(1)(75 - 32) = 2.08 \text{ Btu/lb dry air}$$

$$\text{Enthalpy of inlet air } h_1 = h'_1 + D_1 = 34.1 - 0.18 = 33.92 \text{ Btu/lb dry air}$$

$$\text{Enthalpy of exit air } h_2 = h'_2 + D_2 = 92.34 + 0 = 92.34 \text{ Btu/lb dry air}$$

$$\begin{aligned} \text{Heat dissipated} &= h_2 - h_1 - h_w \\ &= 92.34 - 33.92 - 2.08 \\ &= 56.34 \text{ Btu/lb dry air} \end{aligned}$$

$$\text{Specific volume of inlet air} = 14.1 \text{ ft}^3/\text{lb dry air}$$

$$\text{Total heat dissipated} = \frac{(1000)(56.34)}{14.1} = 3990 \text{ Btu/min}$$

Example 6: Recirculating Dryer A dryer is removing 100 lb water/h from the material being dried. The air entering the dryer has a dry-bulb temperature of 180°F and a wet-bulb temperature of 110°F. The air leaves the dryer at 140°F. A portion of the air is recirculated after mixing with room air having a dry-bulb temperature of 75°F and a relative humidity of 60 percent. Determine the quantity of air required, recirculation rate, and load on the preheater if it is assumed that the system is adiabatic. Neglect heatup of the feed and of the conveying equipment.

Solution: The path followed is shown in Fig. 12-6f.

$$\text{Humidity of room air } H_1 = 0.0113 \text{ lb/lb dry air}$$

$$\text{Humidity of air entering dryer } H_3 = 0.0418 \text{ lb/lb dry air}$$

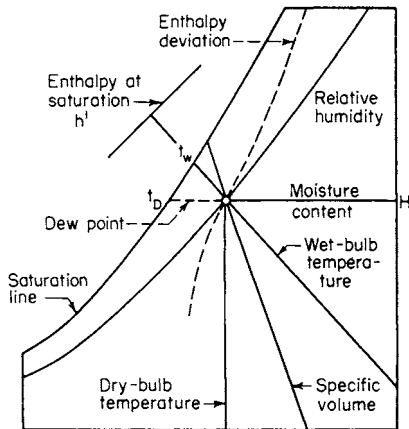


FIG. 12-6a Diagram of psychrometric chart showing the properties of moist air.

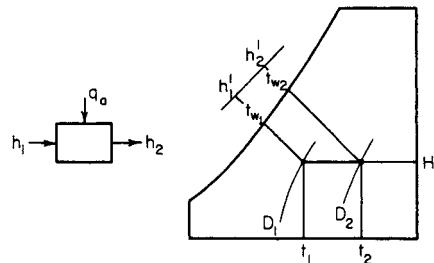


FIG. 12-6b Heating process

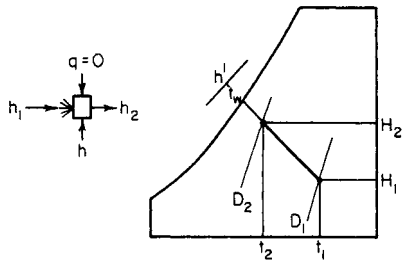


FIG. 12-6c Spray or evaporative cooling.

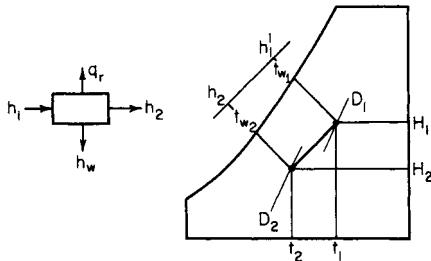


FIG. 12-6d Cooling and dehumidifying process.

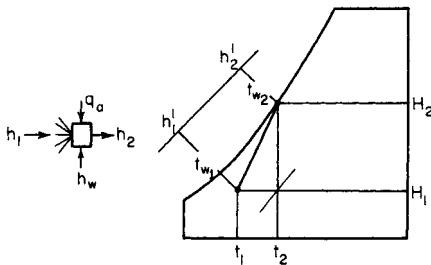


FIG. 12-6e Cooling tower.

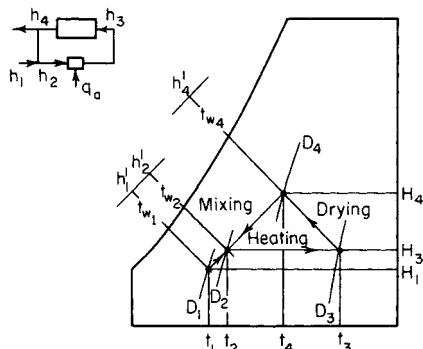


FIG. 12-6f Drying process with recirculation.

Humidity of air leaving dryer $H_4 = 0.0518$ lb/lb dry air
 Enthalpy of room air $h_1 = 30.2 - 0.3$
 $= 29.9$ Btu/lb dry air
 Enthalpy of entering air $h_3 = 92.5 - 1.3$
 $= 91.2$ Btu/lb dry air
 Enthalpy of leaving air $h_4 = 92.5 - 0.55$
 $= 91.95$ Btu/lb dry air

Quantity of air required is $100/(0.0518 - 0.0418) = 10,000$ lb dry air/h. At the dryer inlet the specific volume is 17.1 ft³/lb dry air. Air volume is $(10,000)(17.1)/60 = 2850$ ft³/min. Fraction exhausted is

$$\frac{X}{W_a} = \frac{0.0518 - 0.0418}{0.0518 - 0.0113} = 0.247$$

where X = quantity of fresh air and W_a = total airflow. Thus 75.3 percent of the air is recirculated. Load on the preheater is obtained from an enthalpy balance

$$q_a = 10,000(91.2) - 2470(29.9) - 7530(91.95) = 146,000 \text{ Btu/h}$$

PSYCHROMETRIC CALCULATIONS

Table 12-5 gives the steps required to perform the most common humidity calculations, using the formulas given earlier.

Methods (i) to (iii) are used to find the humidity and dew point from temperature readings in a wet- and dry-bulb psychrometer. Method (iv) is used to find the humidity and dew point from a relative humidity measurement at a given temperature.

Methods (v) and (vi) give the adiabatic saturation and wet-bulb temperatures from absolute humidity (or relative humidity) at a given temperature.

Method (vii) gives the absolute and relative humidity from a dew point measurement.

Method (viii) allows the calculation of all the main parameters if the absolute humidity is known, e.g., from a mass balance on a process plant.

Method (ix) converts the volumetric form of absolute humidity to the mass form (mixing ratio).

Method (x) allows the dew point to be corrected for pressure. The basis is that the mole fraction $y = p/P$ is the same for a given mixture composition at all values of total pressure P . In particular, the dew point measured in a compressed air duct can be converted to the dew point at atmospheric pressure, from which the humidity can be calculated. It is necessary to check that the temperature change associated with compression or expansion does not bring the dry-bulb temperature to a point where condensation can occur. Also, at these elevated pressures, it is strongly advisable to apply the enhancement factor (see BS 1339).

Psychrometric Software and Tables As an alternative to using charts or individual calculations, lookup tables have been published for many years for common psychrometric conversions, e.g., to find relative humidity given the dry-bulb and wet-bulb temperatures. These were often very extensive. To give precise coverage of T_{wb} in 1°C or 0.1°C steps, a complete table would be needed for each individual dry-bulb temperature.

Software is available that will perform calculations of humidity parameters for any point value, and for plotting psychrometric charts. Moreover, British Standard BS 1339 Part 2 (2006) provides functions as macros which can be embedded into any Excel-compatible spreadsheet. Users can therefore generate their own tables for any desired combination of parameters as well as perform point calculations. Hence, the need for published lookup tables has been eliminated. However, this software, like the previous lookup tables, is only valid for the air-water system. For other vapor-gas systems, the equations given in previous sections must be used.

Software may be effectively used to draw psychrometric charts or perform calculations. A wide variety of other psychrometric software may be found on the Internet, but quality varies considerably; the

12-14 PSYCHROMETRY, EVAPORATIVE COOLING, AND SOLIDS DRYING

TABLE 12-5 Calculation Methods for Various Humidity Parameters

	Known	Required	Method
i.	T, T_{wb}	Y	Find saturation vapor pressure p_{wb} at wet-bulb temperature T_{wb} from Eq. (12-4). Find actual vapor pressure p at dry-bulb temperature T from psychrometer equation (12-11). Find mixing ratio Y by conversion from p (Table 12-1).
ii.	T, T_{wb}	T_{dp}, d_e	Find p if necessary by method (i) above. Find dew point T_{dp} from Eq. (12-4) by calculating the T corresponding to p [iteration required; Antoine equation (12-5) gives a first estimate]. Calculate volumetric humidity Y_v , using Eq. (12-1).
iii.	T, T_{wb}	%RH (ψ)	Use method (i) to find p . Find saturation vapor pressure p_s at T from Eq. (12-4). Now relative humidity %RH = $100p/p_s$.
iv.	$T, \%RH$	Y, d_e	Find saturation vapor pressure p_s at T from Eq. (12-4). Actual vapor pressure $p = p_s(\%RH/100)$. Convert to Y (Table 12-1). Find Y_v from Eq. (12-1).
v.	$T, \%RH$ (or T, Y)	T_{as}	Use method (iv) to find p and Y . Make an initial estimate of T_{as} , say, using a psychrometric chart. Calculate Y_{as} from Eq. (12-6). Find p from Table 12-1 and T_{as} from Antoine equation (12-5). Repeat until iteration converges (e.g., using spreadsheet). Alternative method: Evaluate enthalpy H_{est} at these conditions and H at initial conditions. Find H_{as} from Eq. (12-7) and compare with H_{est} . Make new estimate of Y_{as} which would give H_{est} equal to H_{as} . Find p from Table 12-1 and T_{as} from Antoine equation (12-5). Reevaluate H_{as} from Eq. (12-7) and iterate to refine value of Y_{as} .
vi.	$T, \%RH$ (or T, Y)	T_{wb}	Use method (iv) to find p and Y . Make an initial estimate of T_{wb} , e.g., using a psychrometric chart, or (for air-water system) by estimating adiabatic saturation temperature T_{as} . Find p_{wb} from psychrometer equation (12-11). Calculate new value of T_{wb} corresponding to p_{wb} by reversing Eq. (12-4) or using the Antoine equation (12-5). Repeat last two steps to solve iteratively for T_{wb} (computer program is preferable method).
vii.	T, T_{dp}	$Y, \%RH$	Find saturation vapor pressure at dew point T_{dp} from Eq. (12-4); this is the actual vapor pressure p . Find Y from Table 12-1. Find saturation vapor pressure p_s at dry-bulb temperature T from Eq. (12-4). Now %RH = $100p/p_s$.
viii.	T, Y	$T_{dp}, d_e, \%RH, T_{wb}$	Find p by conversion from Y (Table 12-1). Then use method (ii), (iii), or (v) as appropriate.
ix.	T, Y_v	Y	Find specific humidity Y_w from Eqs. (12-2) and (12-1). Convert to absolute humidity Y using $Y = Y_w/(1 - Y_w)$.
x.	T_{dp} at P_1 (elevated)	T_{dp} at P_2 (ambient)	Find vapor pressure p_1 at T_{dp} and P_1 from Eq. (12-4). Convert to vapor pressure p_2 at new pressure P_2 by the formula $p_2 = p_1 P_2/P_1$. Find new dew point T_{dp} from Eq. (12-4) by calculating the T corresponding to p_2 [iteration required as in (ii)].

source and basis of the calculation methods should be carefully checked before using the results. In particular, most methods only apply for the air-water system at moderate temperatures (below 100°C). For high-temperature dryer calculations, only software stated as suitable for this range should be used.

Reliable sources include the following:

1. The American Society of Agricultural Engineers (ASAE): <http://www.asae.org>. Psychrometric data in chart and equation form in both SI and English units. Charts for temperature ranges of -35 to 600°F in USCS units and -10 to 120°C in SI units. Equations and calculation procedures. Air-water system and Grosvenor (temperature-humidity) charts only.

2. The American Society of Heating, Refrigerating and Air-Conditioning Engineers (ASHRAE): <http://www.ashrae.org>. Psychrometric Analysis CD with energy calculations and creation of custom charts at virtually any altitude or pressure. Detailed scientific basis given in ASHRAE Handbook. Air-water system and Grosvenor charts only.

3. Carrier Corporation, a United Technologies Company: <http://www.training.carrier.com>. PSYCH+, computerized psychrometric chart and instructional guide, including design of air conditioning processes and/or cycles. Printed psychrometric charts also supplied. Air-water system and Grosvenor charts only.

4. Linric Company: <http://www.linric.com>. PsycPro generates custom psychrometric charts in English (USCS) or metric (SI) units, based on ASHRAE formulas. Air-water system and Grosvenor charts only.

5. Aspen Technology: <http://www.aspentech.com>. PSYCHIC, one of the Process Tools, generates customized psychrometric charts. Mollier and Bowen enthalpy-humidity charts are produced in addition to Grosvenor. Any gas-vapor system can be handled as well as air-water; data supplied for common organic solvents. Can draw operating lines and spot points, as shown in Fig. 12-7.

6. British Standards Institution: <http://www.bsonline.bsi-global.com>. British Standard BS 1339 Part 2 is a spreadsheet-based software program providing functions based on latest internationally agreed

upon standards. It calculates all key psychrometric parameters and can produce a wide range of psychrometric tables. Users can embed the functions in their own spreadsheets to do psychrometric calculations. Air-water system only (although BS 1339 Part 1 text gives full calculation methods for other gas-vapor systems). SI (metric) units. It does not plot psychrometric charts.

7. Akton Associates provides digital versions of psychrometry charts.

Psychrometric Calculations—Worked Examples

Example 7: Determination of Moist Air Properties An air-water mixture is found from the heat and mass balance to be at 60°C (333 K) and 0.025 kg/kg (25 g/kg) absolute humidity. Calculate the other main parameters for the mixture. Take atmospheric pressure as 101,325 Pa.

Method: Consult item (vi) in Table 12-5 for the calculation methodology.

From the initial terminology section, specific humidity $Y_w = 0.02439$ kg/kg, mole ratio $z = 0.0402$ kmol/kmol, mole fraction $y = 0.03864$ kmol/kmol.

From Table 12-1, vapor pressure $p = 3915$ Pa (0.03915 bar) and volumetric humidity $Y_v = 0.02547$ kg/m³. Dew point is given by the temperature corresponding to p at saturation. From the reversed Antoine equation (12-5), $T_{dp} = 3830/(23.19 - \ln 3915) + 44.83 = 301.58$ K = 28.43°C.

Relative humidity is the ratio of actual vapor pressure to saturation vapor pressure at dry-bulb temperature. From the Antoine equation (12-5), $p_s = \exp[23.19 - 3830/(333.15 - 44.83)] = 20,053$ Pa (new coefficients), or $p_s = \exp[23.1963 - 3816.44/(333.15 - 46.13)] = 19,921$ Pa (old coefficients).

From Sonntag equation (12-4), $p_s = 19,948$ Pa; difference from Antoine is less than 0.5 percent. Relative humidity = $100 \times 3915/19,948 = 19.6$ percent. From a psychrometric chart, e.g., Fig. 12-1, a humidity of 0.025 kg/kg at $T = 60^\circ\text{C}$ lies very close to the adiabatic saturation line for 35°C. Hence a good first estimate for T_{as} and T_{wb} will be 35°C. Refining the estimate of T_{wb} by using the psychrometer equation and iterating gives

$$p_{wb} = 3915 + 6.46 \times 10^{-4} (1.033)(101,325) (60 - 35) = 5605$$

From the Antoine equation,

$$T_{wb} = 3830/(23.19 - \ln 5605) + 44.83 = 307.9$$
 K = 34.75°C

Second iteration:

$$p_{wb} = 3915 + 6.46 \times 10^{-4} (1.033)(101,325)(60 - 34.75) = 5622$$

$$T_{wb} = 307.96$$
 K = 34.81°C.

To a sensible level of precision, $T_{wb} = 34.8^\circ\text{C}$.

Mollier Chart for Nitrogen/Acetone at 10 kPa

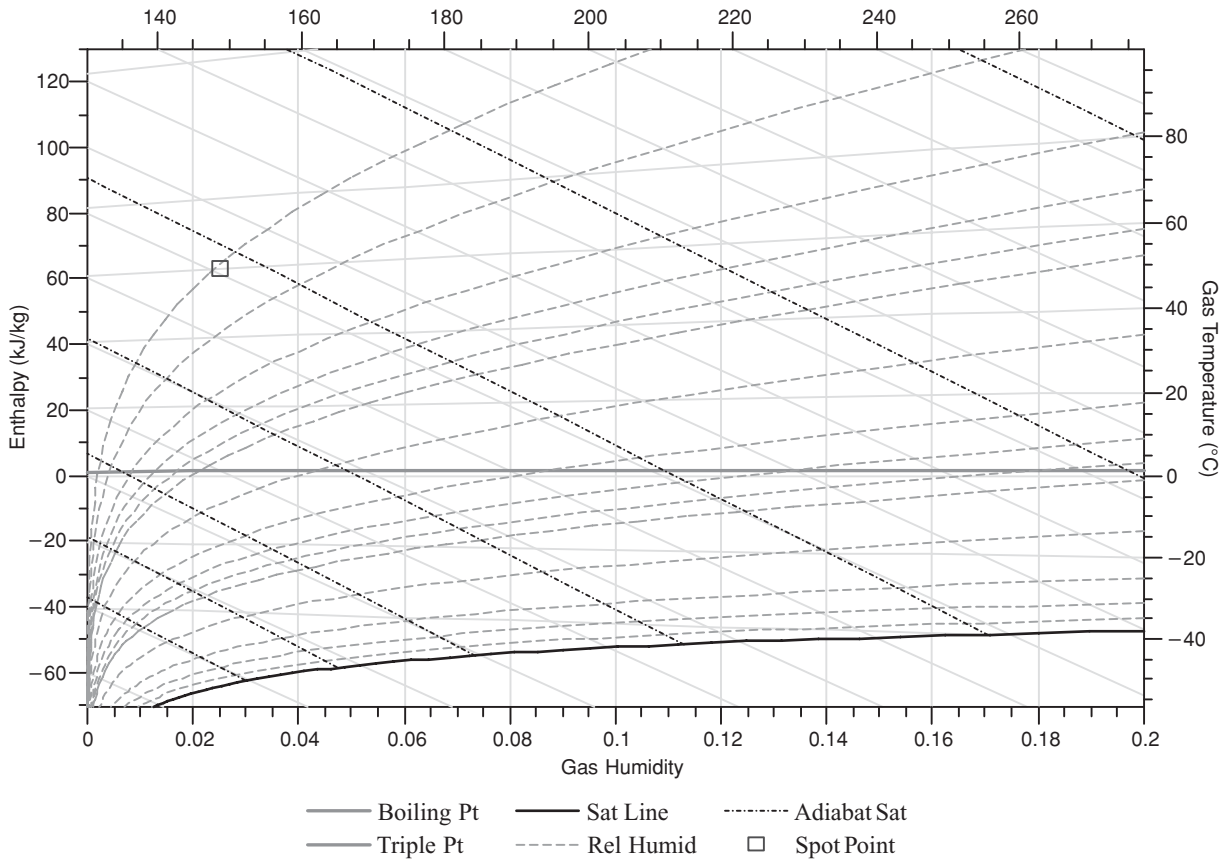


FIG. 12-7 Mollier psychrometric chart (from PSYCHIC software program) showing determination of adiabatic saturation temperature plots humidity (abscissa) against enthalpy (lines sloping diagonally from top left to bottom right). (Courtesy AspenTech.)

From Table 12-1 $Y_{wb} = 5622 \times 0.622 / (101,325 - 5622) = 0.0365(4)$ kg/kg.
 Enthalpy of original hot air is approximately given by $H = (C_{p_g} + C_{p_v} Y)(T - T_0) + \lambda_0 Y = (1 + 1.9 \times 0.025) \times 60 + 2501 \times 0.025 = 62.85 + 62.5 = 125.35$ kJ/kg. A more accurate calculation can be obtained from steam tables; $C_{p_g} = 1.005$ kJ/(kg·K) over this range, H_g at $60^\circ\text{C} = 2608.8$ kJ/kg, $H = 60.3 + 65.22 = 125.52$ kJ/kg.
 Calculation (v), method 1: if $T_{as} = 34.8$, from Eq. (12-6), with $C_s = 1 + 1.9 \times 0.025 = 1.048$ kJ/(kg·K), $\lambda_{as} = 2419$ kJ/kg (steam tables), $Y_{as} = 0.025 + 1.048/2419 (60 - 34.8) = 0.0359(2)$ kg/kg. From Table 12-1, $p = 5530$ Pa. From the Antoine equation (12-5), $T_{as} = 3830 / (23.19 - \ln 5530) + 44.83 = 307.65$ K = 34.52°C . Repeat until iteration converges (e.g., using spreadsheet). Final value $T_{as} = 34.57^\circ\text{C}$, $Y_{as} = 0.0360$ kg/kg.
 Enthalpy check: From Eq. (12-7), $H_{as} - H = 4.1868 \times 34.57 \times (0.036 - 0.025) = 1.59$ kJ/kg. So $H_{as} = 127.11$ kJ/kg. Compare H_{as} calculated from enthalpies; H_g at $34.57^\circ\text{C} = 2564$ kJ/kg, $H_{as} = 34.90 + 92.29 = 127.19$ kJ/kg. The iteration has converged successfully.
 Note that T_{as} is 0.2°C lower than T_{wb} , and Y_{as} is 0.0005 kg/kg lower than Y_{wb} , both negligible differences.

Example 8: Calculation of Humidity and Wet-Bulb Condition A dryer exhaust which can be taken as an air-water mixture at 70°C (343.15 K) is measured to have a relative humidity of 25 percent. Calculate the humidity parameters and wet-bulb conditions for the mixture. Pressure is 1 bar (100,000 Pa).
 Method: Consult item (v) in Table 12-5 for the calculation methodology.

From the Antoine equation (12-5), using standard coefficients (which give a better fit in this temperature range), $p_s = \exp[23.1963 - 3816.44 / (343.15 - 46.13)] = 31,170$ Pa. Actual vapor pressure $p = 25$ percent of 31,170 = 7792 Pa (0.078 bar).
 From Table 12-1, absolute humidity $Y = 0.05256$ kg/kg and volumetric humidity $Y_v = 0.0492$ kg/m³. From the terminology section, mole fraction $y = 0.0779$ kmol/kmol, mole ratio $z = 0.0845$ kmol/kmol, specific humidity $Y_w = 0.04994$ kg/kg.

Dew point $T_{dp} = 3816.44 / (23.1963 - \ln 7792) + 46.13 = 314.22$ K = 41.07°C .

From the psychrometric chart, a humidity of 0.0526 kg/kg at $T = 70^\circ\text{C}$ falls just below the adiabatic saturation line for 45°C . Estimate T_{as} and T_{wb} as 45°C . Refining the estimate of T_{wb} by using the psychrometer equation and iterating gives

$$p_{wb} = 7792 + 6.46 \times 10^{-4} (1.0425)(10^5)(70 - 45) = 9476$$

From the Antoine equation,

$$T_{wb} = 3816.44 / (23.1963 - \ln 9476) + 46.13 = 317.96$$
 K = 44.81°C

Second iteration (taking $T_{wb} = 44.8$):

$$p_{wb} = 9489 \quad T_{wb} = 317.99$$
 K = 44.84°C

The iteration has converged.

Example 9: Calculation of Psychrometric Properties of Acetone/Nitrogen Mixture A mixture of nitrogen N_2 and acetone CH_3COCH_3 is found from the heat and mass balance to be at 60°C (333 K) and 0.025 kg/kg (25 g/kg) absolute humidity (same conditions as in Example 7). Calculate the other main parameters for the mixture. The system is under vacuum at 100 mbar (0.1 bar, 10,000 Pa).

Additional data for acetone and nitrogen are obtained from *The Properties of Gases and Liquids* (Prausnitz et al.). Molecular weight (molal mass) M_g for nitrogen = 28.01 kg/kmol; M_g for acetone = 58.08 kg/kmol. Antoine coefficients for acetone are 16.6513, 2940.46, and 35.93, with p_s in **mmHg** and T in **K**. Specific heat capacity of nitrogen is approximately 1.014 kJ/(kg·K). Latent heat of acetone is 501.1 kJ/kg at the boiling point. The psychrometric ratio for the nitrogen-acetone system is not given, but the diffusion coefficient \mathcal{D} can be roughly evaluated as 1.34×10^{-5} , compared to 2.20×10^{-5} for water in air. As the psychrometric ratio is linked to $\mathcal{D}^{2/3}$, it can be estimated as 0.72, which is in line with tabulated values for similar organic solvents (e.g., propanol).

Method: Consult item (vi) in Table 12-5 for the calculation methodology.

From the terminology, specific humidity $Y_w = 0.02439\text{ kg/kg}$, the same as in Example 7. Mole ratio $z = 0.0121\text{ kmol/kmol}$, mole fraction $y = 0.01191\text{ kmol/kmol}$ —lower than in Example 7 because molecular weights are different.

From the Antoine equation (12-5),

$$\ln p_s = C_0 - \frac{C_1}{T - C_2} = 16.6513 - \frac{2940.46}{T - 35.93}$$

Since $T = 60^\circ\text{C}$, $\ln p_s = 6.758$, $p_s = 861.0\text{ mmHg}$. Hence $p_s = 1.148\text{ bar} = 1.148 \times 10^5\text{ Pa}$. The saturation vapor pressure is higher than atmospheric pressure; this means that acetone at 60°C must be above its normal boiling point. Check; T_{bp} for acetone = 56.5°C .

Vapor pressure $p = yP = 0.01191 \times 10,000 = 119.1\text{ Pa}$ (0.001191 bar)—much lower than before because of the reduced total pressure. This is 0.89 mmHg . Volumetric humidity $Y_v = 0.0025\text{ kg/m}^3$ —again substantially lower than at 1 atm.

Dew point is the temperature where p_s equals p' . From the reversed Antoine equation (12-5),

$$T = \frac{C_1}{C_0 - \ln p_s} + C_2$$

so

$$T_{\text{dp}} = \frac{2940}{16.6513 - \ln 0.89} + 35.93 = 211.27\text{ K} = -61.88^\circ\text{C}$$

This very low dew point is due to the low boiling point of acetone and the low concentration.

Relative humidity is the ratio of actual vapor pressure to saturation vapor pressure at dry-bulb temperature. So $p = 119.1\text{ Pa}$, $p_s = 1.148 \times 10^5\text{ Pa}$, $\text{RH} = 0.104\text{ percent}$ —again very low.

A special psychrometric chart would need to be constructed for the acetone-nitrogen system to get first estimates (this can be done using PSYCHIC, as shown in Fig. 12-7). A humidity of 0.025 kg/kg at $T = 60^\circ\text{C}$ lies just below the adiabatic saturation line for -40°C . The wet-bulb temperature will not be the same as T_{as} for this system; as the psychrometric ratio β is less than 1, T_{wb} should be significantly above T_{as} . However, let us assume no good first estimate is available and simply take T_{wb} to be 0°C initially.

When using the psychrometer equation, we will need to use Eq. (12-13) to obtain the value of the psychrometer coefficient. Using the tabulated values above, we obtain $A = 0.00135$, about double the value for air-water. We must remember that the estimate will be very rough because of the uncertainty in the value of β . Refining the estimate of T_{wb} by using the psychrometer equation and iterating gives

$$p_{\text{wb}} = 119.1 + 1.35 \times 10^{-3} (10^4) (60 - 0) = 932.3\text{ Pa} = 7.0\text{ mmHg}$$

From the Antoine equation,

$$T_{\text{wb}} = 2940 / (16.6513 - \ln 7) + 35.93 = 235.84\text{ K} = -37.3^\circ\text{C}$$

Second iteration:

$$p_{\text{wb}} = 119.1 + 1.35 \times 10^{-3} (10^4) (60 + 37.3) = 1433\text{ Pa} = 10.7\text{ mmHg}$$

$$T_{\text{wb}} = 241.85\text{ K} = -31.3^\circ\text{C}$$

Third iteration:

$$p_{\text{wb}} = 119.1 + 1.35 \times 10^{-3} (10^4) (60 + 31.3) = 1352\text{ Pa} = 10.1\text{ mmHg}$$

$$T_{\text{wb}} = 241.0\text{ K} = -32.1^\circ\text{C}$$

The iteration has converged successfully, despite the poor initial guess. The wet-bulb temperature is -32°C ; given the levels of error in the calculation, it will be meaningless to express this to any greater level of precision.

In a similar way, adiabatic saturation temperature can be calculated from Eq. (12-6) by taking the first guess as -40°C and assuming the humid heat to be $1.05\text{ kJ}/(\text{kg} \cdot \text{K})$ including the vapor:

$$Y_{\text{as}} = Y + \frac{C_{s2}}{\lambda_{\text{as}}} (T - T_{\text{as}}) \\ = 0.025 + \left(\frac{1.05}{501.1} \right) (60 + 40) = 0.235\text{ kg/kg}$$

From Table 12-2,

$$p_{\text{as}} = 1018\text{ Pa} = 7.63\text{ mmHg}$$

From Antoine,

$$T_{\text{as}} = 237.05\text{ K} = -36.1^\circ\text{C}$$

Second iteration:

$$Y_{\text{as}} = 0.025 + (1.05/501.1)(60 + 36.1) = 0.226\text{ kg/kg} \quad p_{\text{as}} = 984\text{ Pa} = 7.38\text{ mmHg}$$

From Antoine,

$$T_{\text{as}} = 236.6\text{ K} = -36.6^\circ\text{C}$$

This has converged. A more accurate figure could be obtained with more refined estimates for C_s and λ_{wb} .

MEASUREMENT OF HUMIDITY

Dew Point Method The dew point of wet air is measured directly by observing the temperature at which moisture begins to form on an artificially cooled, polished surface.

Optical dew point hygrometers employing this method are the most commonly used fundamental technique for determining humidity. Uncertainties in temperature measurement of the polished surface, gradients across the surface, and the appearance or disappearance of fog have been much reduced in modern instruments. Automatic mirror cooling, e.g., thermoelectric, is more accurate and reliable than older methods using evaporation of a low-boiling solvent such as ether, or external coolants (e.g., vaporization of solid carbon dioxide or liquid air, or water cooling). Contamination effects have also been reduced or compensated for, but regular recalibration is still required, at least once a year.

Wet-Bulb Method In the past, probably the most commonly used method for determining the humidity of a gas stream was the measurement of wet- and dry-bulb temperatures. The wet-bulb temperature is measured by contacting the air with a thermometer whose bulb is covered by a wick saturated with water. If the process is adiabatic, the thermometer bulb attains the wet-bulb temperature. When the wet- and dry-bulb temperatures are known, the humidity is readily obtained from charts such as Figs. 12-1 through 12-4. To obtain reliable information, care must be exercised to ensure that the wet-bulb thermometer remains wet and that radiation to the bulb is minimized. The latter is accomplished by making the relative velocity between wick and gas stream high [a velocity of 4.6 m/s (15 ft/s) is usually adequate for commonly used thermometers] or by the use of radiation shielding. In the **Assmann psychrometer** the air is drawn past the bulbs by a motor-driven fan. Making sure that the wick remains wet is a mechanical problem, and the method used depends to a large extent on the particular arrangement. Again, as with the dew point method, errors associated with the measurement of temperature can cause difficulty.

For measurement of atmospheric humidities the **sling or whirling psychrometer** is widely used to give a quick and cheap, but inaccurate, estimate. A wet- and dry-bulb thermometer is mounted in a sling which is whirled manually to give the desired gas velocity across the bulb.

In addition to the mercury-in-glass thermometer, other temperature-sensing elements may be used for psychrometers. These include resistance thermometers, thermocouples, bimetal thermometers, and thermistors.

Electric hygrometers have been the fastest-growing form of humidity measurement in recent years. They measure the electrical resistance, capacitance, or impedance of a film of moisture-absorbing materials exposed to the gas. A wide variety of sensing

elements have been used. Often, it is relative humidity which is measured.

Mechanical hygrometers utilizing materials such as human hair, wood fiber, and plastics have been used to measure humidity. These methods rely on a change in dimension with humidity. They are not suitable for process use.

Other hygrometric techniques in process and laboratory use include electrolytic and piezoelectric hygrometers, infrared and mass

spectroscopy, and vapor pressure measurement, e.g., by a Pirani gauge.

The **gravimetric method** is accepted as the most accurate humidity-measuring technique. In this method a known quantity of gas is passed over a moisture-absorbing chemical such as phosphorus pentoxide, and the increase in weight is determined. It is mainly used for calibrating standards and measurements of gases with SO_x present.

EVAPORATIVE COOLING

GENERAL REFERENCES: 2005 ASHRAE *Handbook of Fundamentals*, "Climatic Design Information," Chap. 28, ASHRAE, Atlanta, Ga.; ASHRAE *Handbook and Product Directory: Equipment*, ASHRAE, Atlanta, 2001.

INTRODUCTION

Evaporative cooling, using recirculated cooling water systems, is the method most widely used throughout the process industries for employing water to remove process waste heat, rejecting that waste heat into the environment. Maintenance considerations (water-side fouling control), through control of makeup water quality and control of cooling water chemistry, form one reason for this preference. Environmental considerations, by minimizing consumption of potable water, minimizing the generation and release of contaminated cooling water, and controlling the release into the environment of chemicals from leaking heat exchangers (HX), form the second major reason.

Local ambient climatic conditions, particularly the maximum summer wet-bulb temperature, determine the design of the evaporative equipment. Typically, the wet-bulb temperature used for design is the 0.4 percent value, as listed in the ASHRAE *Handbook of Fundamentals*, equivalent to 35-h exceedance per year on average.

The first subsection below presents the classic cooling tower (CT), the evaporative cooling technology most widely used today. The second subsection presents the wet surface air cooler (WSAC), a more recently perfected technology, combining within one piece of equipment the functions of cooling tower, circulated cooling water system, and HX tube bundle. The most common application for WSACs is in the direct cooling of process streams. However, the closed-circuit cooling tower, employing WSACs for cooling the circulated cooling water (replacing the CT), is an important alternative WSAC application, presented at the end of this section.

To minimize the total annualized costs for evaporative cooling is a complex engineering task in itself, separate from classic process design (Sec. 24, "Minimizing the Annualized Costs for Process Energy"). The evaluation and the selection of the best option for process cooling impact many aspects of how the overall project will be optimally designed (utilities supply, reaction and separations design, pinch analyses, 3D process layout, plot plan, etc.). Therefore, evaluation and selection of the evaporative cooling technology system should be performed at the start of the project design cycle, during conceptual engineering (Sec. 9, "Process Economics," "Value Improving Practices"), when the potential to influence project costs is at a maximum value (Sec. 9, *VIP Figure 9-33*). The relative savings achievable for selection of the optimum heat rejection technology option can frequently exceed 25 percent, for the installed cost for the technology alone.

PRINCIPLES

The processes of cooling water are among the oldest known. Usually water is cooled by exposing its surface to air. Some of the processes are slow, such as the cooling of water on the surface of a pond; others are comparatively fast, such as the spraying of water into air. These processes all involve the exposure of water surface to air in varying degrees.

The heat-transfer process involves (1) latent heat transfer owing to vaporization of a small portion of the water and (2) sensible heat transfer owing to the difference in temperatures of water and air. Approximately 80 percent of this heat transfer is due to latent heat and 20 percent to sensible heat.

Theoretical possible heat removal per pound of air circulated in a cooling tower depends on the temperature and moisture content of air. An indication of the moisture content of the air is its wet-bulb temperature. Ideally, then, the wet-bulb temperature is the lowest theoretical temperature to which the water can be cooled. Practically, the cold water temperature approaches but does not equal the air wet-bulb temperature in a cooling tower; this is so because it is impossible to contact all the water with fresh air as the water drops through the wetted fill surface to the basin. The magnitude of approach to the wet-bulb temperature is dependent on the tower design. Important factors are air-to-water contact time, amount of fill surface, and breakup of water into droplets. In actual practice, cooling towers are seldom designed for approaches closer than 2.8°C (5°F).

COOLING TOWERS*

GENERAL REFERENCES: *Counterflow Cooling Tower Performance*, Pritchard Corporation, Kansas City, Mo., 1957; Hensley, "Cooling Tower Energy," *Heat Piping Air Cond.* (October 1981); Kelley and Swenson, *Chem. Eng. Prog.* **52**: 263 (1956); McAdams, *Heat Transmission*, 3d ed., McGraw-Hill, New York, 1954, pp. 356-365; Merkel, *Z. Ver. Dtsch. Ing. Forsch.*, no. 275 (1925); *The Parallel Path Wet-Dry Cooling Tower*, Marley Co., Mission Woods, Kan., 1972; *Performance Curves*, Cooling Tower Institute, Houston, Tex., 1967; *Plume Abatement and Water Conservation with Wet-Dry Cooling Tower*, Marley Co., Mission Woods, Kan., 1973; Tech. Bull. R-54-P-5, R-58-P-5, Marley Co., Mission Woods, Kan., 1957; Wood and Betts, *Engineer*, **189**(4912), **377**(4913), **349** (1950); Zivi and Brand, *Refriger. Eng.*, **64**(8): 31-34, 90 (1956); Hensley, *Cooling Tower Fundamentals*, 2d ed., Marley Cooling Technologies, 1998; Mortensen and Gagliardo, *Impact of Recycled Water Use in Cooling Towers*, TP-04-12, Cooling Technology Institute, 2004; www.cti.org; www.ashrae.org; www.marleyct.com.

Cooling Tower Theory The most generally accepted theory of the cooling tower heat-transfer process is that developed by Merkel (op. cit.). This analysis is based upon **enthalpy potential difference** as the driving force.

Each particle of water is assumed to be surrounded by a film of air, and the enthalpy difference between the film and surrounding air provides the driving force for the cooling process. In the integrated form the Merkel equation is

$$\frac{KaV}{L} = \int_{t_2}^{t_1} \frac{C_L dT}{h' - h} \quad (12-14a)$$

where K = mass-transfer coefficient, lb water/(h·ft²); a = contact area, ft²/ft³ tower volume; V = active cooling volume, ft³/ft² of plan area; L = water rate, lb/(h·ft²); C_L = heat capacity of water, Btu/(lb·°F); h' = enthalpy of saturated air at water temperature, Btu/lb; h = enthalpy of

*The contributions of Ken Mortensen, and coworkers, of Marley Cooling Technologies, Overland Park, Kansas, toward the review and update of this subsection are acknowledged.

12-18 PSYCHROMETRY, EVAPORATIVE COOLING, AND SOLIDS DRYING

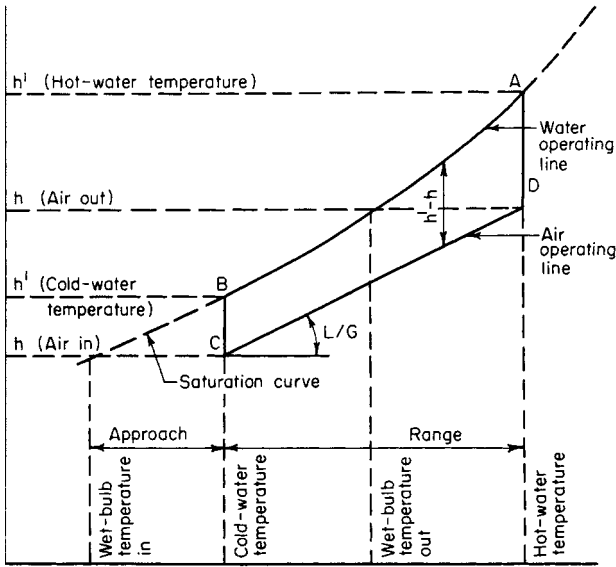


FIG. 12-8a Cooling-tower process heat balance. (Marley Co.)

airstream, Btu/lb; and T_1 and T_2 = entering and leaving water temperatures, °F. The right-hand side of Eq. (12-14a) is entirely in terms of air and water properties and is independent of tower dimensions.

Figure 12-8a illustrates water and air relationships and the driving potential which exist in a counterflow tower, where air flows parallel but opposite in direction to water flow. An understanding of this diagram is important in visualizing the cooling tower process.

The water operating line is shown by line AB and is fixed by the inlet and outlet tower water temperatures. The air operating line begins at C, vertically below B and at a point having an enthalpy corresponding to that of the entering wet-bulb temperature. Line BC represents the initial driving force $h' - h$. In cooling water at 1°F, the enthalpy per pound of air is increased 1 Btu multiplied by the ratio of pounds of water to pound of air. The liquid-gas ratio L/G is the slope of the operating line. The air leaving the tower is represented by point D. The cooling range is the projected length of line CD on the temperature scale. The cooling tower approach is shown on the diagram as the difference between the cold water temperature leaving the tower and the ambient wet-bulb temperature.

The coordinates refer directly to the temperature and enthalpy of any point on the water operating line but refer directly only to the enthalpy of a point on the air operating line. The corresponding wet-bulb temperature of any point on CD is found by projecting the point horizontally to the saturation curve, then vertically to the temperature coordinate. The integral [Eq. (12-14a)] is represented by the area ABCD in the diagram. This value is known as the **tower characteristic**, varying with the L/G ratio.

For example, an increase in entering wet-bulb temperature moves the origin C upward, and the line CD shifts to the right to maintain a constant KaV/L . If the cooling range increases, line CD lengthens. At a constant wet-bulb temperature, equilibrium is established by moving the line to the right to maintain a constant KaV/L . On the other hand, a change in L/G ratio changes the slope of CD, and the tower comes to equilibrium with a new KaV/L .

To predict tower performance, it is necessary to know the required tower characteristics for fixed ambient and water conditions. The tower characteristic KaV/L can be determined by integration. The Chebyshev method is normally used for numerically evaluating the integral, whereby

$$\frac{KaV}{L} = \int_{T_2}^{T_1} \frac{dT}{h_w - h_a} \cong \frac{T_1 - T_2}{4} \left(\frac{1}{\Delta h_1} + \frac{1}{\Delta h_2} + \frac{1}{\Delta h_3} + \frac{1}{\Delta h_4} \right)$$

where h_w = enthalpy of air-water vapor mixture at bulk water temperature, Btu/lb dry air

h_a = enthalpy of air-water vapor mixture at wet-bulb temperature, Btu/lb dry air

Δh_1 = value of $h_w - h_a$ at $T_2 + 0.1(T_1 - T_2)$

Δh_2 = value of $h_w - h_a$ at $T_2 + 0.4(T_1 - T_2)$

Δh_3 = value of $h_w - h_a$ at $T_1 - 0.4(T_1 - T_2)$

Δh_4 = value of $h_w - h_a$ at $T_1 - 0.1(T_1 - T_2)$

Example 10: Calculation of Mass-Transfer Coefficient Group

Determine the theoretically required KaV/L value for a cooling duty from 105°F inlet water, 85°F outlet water, 78°F ambient wet-bulb temperature, and an L/G ratio of 0.97.

From the air-water vapor-mixture tables, the enthalpy h_1 of the ambient air at 78°F wet-bulb temperature is 41.58 Btu/lb.

$$h_2 \text{ (leaving air)} = 41.58 + 0.97(105 - 85) = 60.98 \text{ Btu/lb}$$

$T, ^\circ\text{F}$	h_{water}	h_{air}	$h_w - h_a$	$1/\Delta h$
$T_2 = 85$	49.43	$h_1 = 41.58$		
$T_2 + 0.1(20) = 87$	51.93	$h_1 + 0.1L/G(20) = 43.52$	$\Delta h_1 = 8.41$	0.119
$T_2 + 0.4(20) = 93$	60.25	$h_1 + 0.4L/G(20) = 49.34$	$\Delta h_2 = 10.91$	0.092
$T_1 - 0.4(20) = 97$	66.55	$h_2 - 0.4L/G(20) = 53.22$	$\Delta h_3 = 13.33$	0.075
$T_1 - 0.1(20) = 103$	77.34	$h_2 - 0.1L/G(20) = 59.04$	$\Delta h_4 = 18.30$	0.055
$T_1 = 105$	81.34	$h_2 = 60.98$		0.341

$$\frac{KaV}{L} = \frac{105 - 85}{4} (0.341) = 1.71$$

A quicker but less accurate method is by the use of a nomograph (Fig. 12-8b) prepared by Wood and Betts (op. cit.).

Mechanical draft cooling towers normally are designed for L/G ratios ranging from 0.75 to 1.50; accordingly, the values of KaV/L vary from 0.50 to 2.50. With these ranges in mind, an example of the use of the nomograph will readily explain the effect of changing variables.

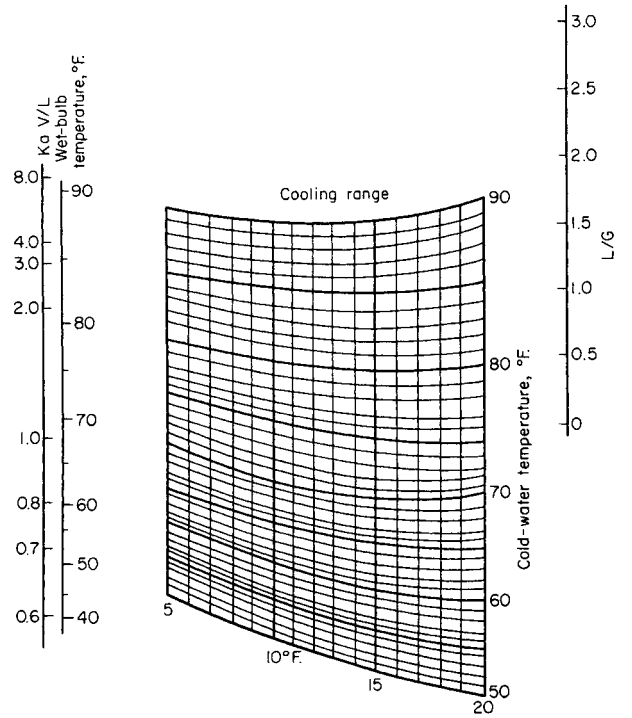


FIG. 12-8b Nomograph of cooling tower characteristics. [Wood and Betts, Engineer, 189(4912), 337 (1950).]

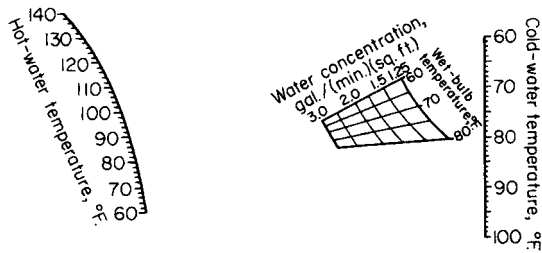


FIG. 12-8c Sizing chart for a counterflow induced-draft cooling tower. For induced-draft towers with (1) an upspray distributing system with 24 ft of fill or (2) a flume-type distributing system and 32 ft of fill. The chart will give approximations for towers of any height. (Ecodyne Corp.)

Example 11: Application of Nomograph for Cooling Tower Characteristics If a given tower is operating with 20°F range, a cold water temperature of 80°F, and a wet-bulb temperature of 70°F, a straight line may be drawn on the nomograph. If the L/G ratio is calculated to be 1.0, then KaV/L may be established by a line drawn through L/G 1.0 and parallel to the original line. The tower characteristic KaV/L is thus established at 1.42. If the wet-bulb temperature were to drop to 50°F, then KaV/L and L/G ratios may be assumed to remain constant. A new line parallel to the original will then show that for the same range the cold-water temperature will be 70°F.

The nomograph provides an approximate solution; degree of accuracy will vary with changes in cooling as well as from tower to tower. Once the theoretical cooling tower characteristic has been determined by numerical integration or from the nomograph for a given cooling duty, it is necessary to design the cooling tower fill and air distribution to meet the theoretical tower characteristic. The Pritchard Corporation (op. cit.) has developed performance data on various tower fill designs. These data are too extensive to include here, and those interested should consult this reference. See also Baker and Mart (Marley Co., Tech. Bull. R-52-P-10, Mission Woods, Kan.) and Zivi and Brand (loc. cit.).

Mechanical Draft Towers Two types of mechanical draft towers are in use today: the forced-draft and the induced-draft. In the **forced-draft tower** the fan is mounted at the base, and air is forced in at the bottom and discharged at low velocity through the top. This arrangement has the advantage of locating the fan and drive outside the tower, where it is convenient for inspection, maintenance, and repairs. Since the equipment is out of the hot, humid top area of the tower, the fan is not subjected to corrosive conditions. However, because of the low exit-air velocity, the forced-draft tower is subjected to excessive recirculation of the humid exhaust vapors back into the air intakes. Since the wet-bulb temperature of the exhaust air is considerably above the wet-bulb temperature of the ambient air, there is a decrease in performance evidenced by an increase in cold (leaving) water temperature.

The **induced-draft tower** is the most common type used in the United States. It is further classified into counterflow and cross-flow design, depending on the relative flow directions of water and air. Thermodynamically, the **counterflow arrangement** is more efficient, since the coldest water contacts the coldest air, thus obtaining maximum enthalpy potential. The greater the cooling ranges and the more difficult the approaches, the more distinct are the advantages of the counterflow type. For example, with an L/G ratio of 1, an ambient wet-bulb temperature of 25.5°C (78°F), and an inlet water temperature of 35°C (95°F), the counterflow tower requires a KaV/L characteristic of 1.75 for a 2.8°C (5°F) approach, while a cross-flow tower requires a characteristic of 2.25 for the same approach. However, if the approach is increased to 3.9°C (7°F), both types of tower have approximately the same required KaV/L (within 1 percent).

The **cross-flow tower** manufacturer may effectively reduce the tower characteristic at very low approaches by increasing the air quantity to give a lower L/G ratio. The increase in airflow is not necessarily achieved by increasing the air velocity but primarily by lengthening the tower to increase the airflow cross-sectional area. It appears then that the cross-flow fill can be made progressively longer in the direction perpendicular to the airflow and shorter in the direction of the airflow until it almost loses its inherent potential-difference disadvantage. However, as this is done, fan power consumption increases.

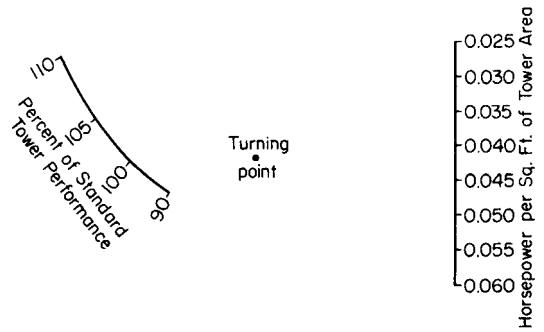


FIG. 12-8d Horsepower chart for a counterflow induced-draft cooling tower. [Fluor Corp. (now Ecodyne Corp.)]

Ultimately, the economic choice between counterflow and cross-flow is determined by the effectiveness of the fill, design conditions, water quality, and the costs of tower manufacture.

Performance of a given type of cooling tower is governed by the ratio of the weights of air to water and the time of contact between water and air. In commercial practice, the variation in the ratio of air to water is first obtained by keeping the air velocity constant at about 350 ft/(min·ft² of active tower area) and varying the water concentration, gal/(min·ft² of tower area). As a secondary operation, air velocity is varied to make the tower accommodate the cooling requirement.

Time of contact between water and air is governed largely by the time required for the water to discharge from the nozzles and fall through the tower to the basin. The time of contact is therefore obtained in a given type of unit by varying the height of the tower. Should the time of contact be insufficient, no amount of increase in the ratio of air to water will produce the desired cooling. It is therefore necessary to maintain a certain minimum height of cooling tower. When a wide approach of 8 to 11°C (15 to 20°F) to the wet-bulb temperature and a 13.9 to 19.4°C (25 to 35°F) cooling range are required, a relatively low cooling tower will suffice. A tower in which the water travels 4.6 to 6.1 m (15 to 20 ft) from the distributing system to the basin is sufficient. When a moderate approach and a cooling range of 13.9 to 19.4°C (25 to 35°F) are required, a tower in which the water travels 7.6 to 9.1 m (25 to 30 ft) is adequate. Where a close approach of 4.4°C (8°F) with a 13.9 to 19.4°C (25 to 35°F) cooling range is required, a tower in which the water travels from 10.7 to 12.2 m (35 to 40 ft) is required. It is usually not economical to design a cooling tower with an approach of less than 2.8°C (5°F).

Figure 12-8c shows the relationship of the hot water, cold water, and wet-bulb temperatures to the water concentration.⁶ From this, the **minimum area** required for a given performance of a well-designed counterflow induced-draft cooling tower can be obtained. Figure 12-8d gives the horsepower per square foot of tower area required for a given performance. These curves do not apply to parallel or cross-flow cooling, since these processes are not so efficient as the counterflow process. Also, they do not apply when the approach to the cold water temperature is less than 2.8°C (5°F). These charts should be considered approximate and for preliminary estimates only. Since many factors not shown in the graphs must be included in the computation, the manufacturer should be consulted for final design recommendations.

The cooling performance of any tower containing a given depth of filling varies with the **water concentration**. It has been found that maximum contact and performance are obtained with a tower having a water concentration of 2 to 5 gal/(min·ft² of ground area). Thus the

⁶See also London, Mason, and Boelter, loc. cit.; Lichtenstein, loc. cit.; Simpson and Sherwood, *J. Am. Soc. Refrig. Eng.*, 52:535, 574 (1946); Simons, *Chem. Metall. Eng.*, 49(5):138; (6): 83 (1942); 46: 208 (1939); and Hutchinson and Spivey, *Trans. Inst. Chem. Eng.*, 20:14 (1942).

problem of calculating the size of a cooling tower becomes one of determining the proper concentration of water required to obtain the desired results. Once the necessary water concentration has been established, the tower area can be calculated by dividing the gallons per minute circulated by the water concentration in gallons per minute square foot. The required tower size then is a function of the following:

1. Cooling range (hot water temperature minus cold water temperature)
2. Approach to wet-bulb temperature (cold water temperature minus wet-bulb temperature)
3. Quantity of water to be cooled
4. Wet-bulb temperature
5. Air velocity through the cell
6. Tower height

Example 12: Application of Sizing and Horsepower Charts
To illustrate the use of the charts, assume the following conditions:

- Hot water temperature $T_1, ^\circ\text{F} = 102$
- Cold water temperature $T_2, ^\circ\text{F} = 78$
- Wet-bulb temperature $t_w, ^\circ\text{F} = 70$
- Water rate, gal/min = 2000

A straight line in Fig. 12-8c, connecting the points representing the design water and wet-bulb temperature, shows that a water concentration of 2 gal/(ft²·min) is required. The area of the tower is calculated as 1000 ft² (quantity of water circulated divided by water concentration).

Fan horsepower is obtained from Fig. 12-8d. Connecting the point representing 100 percent of standard tower performance with the turning point and extending this straight line to the horsepower scale show that it will require 0.041 hp/ft² of actual effective tower area. For a tower area of 1000 ft², 41.0 fan hp is required to perform the necessary cooling.

Suppose that the actual commercial tower size has an area of only 910 ft². Within reasonable limits, the shortage of actual area can be compensated for by an increase in air velocity through the tower. However, this requires boosting fan horsepower to achieve 110 percent of standard tower performance. From Fig. 12-8d, the fan horsepower is found to be 0.057 hp/ft² of actual tower area, or 0.057 × 910 = 51.9 hp.

On the other hand, if the actual commercial tower area is 1110 ft², the cooling equivalent to 1000 ft² of standard tower area can be accomplished with less air and less fan horsepower. From Fig. 12-8d, the fan horsepower for a tower operating at 90 percent of standard performance is 0.031 hp/ft² of actual tower area, or 34.5 hp.

This example illustrates the sensitivity of fan horsepower to small changes in tower area. The importance of designing a tower that is slightly oversize in ground area and of providing plenty of fan capacity becomes immediately apparent.

Example 13: Application of Sizing Chart Assume the same cooling range and approach as used in Example 12 except that the wet-bulb temperature is lower. Design conditions would then be as follows:

- Water rate, gal/min = 2000
- Temperature range $T_1 - T_2, ^\circ\text{F} = 24$
- Temperature approach $T_2 - t_w, ^\circ\text{F} = 8$
- Hot water temperature $T_1, ^\circ\text{F} = 92$
- Cold water temperature $T_2, ^\circ\text{F} = 68$
- Wet-bulb temperature $t_w, ^\circ\text{F} = 60$

From Fig. 12-8c, the water concentration required to perform the cooling is 1.75 gal/(ft²·min), giving a tower area of 1145 ft² versus 1000 ft² for a 70°F wet-bulb temperature. This shows that the lower the wet-bulb temperature for the same cooling range and approach, the larger the area of the tower required and therefore the more difficult the cooling job.

Figure 12-8e illustrates the type of performance curve furnished by the cooling tower manufacturer. This shows the variation in performance with changes in wet-bulb and hot water temperatures while the water quantity is maintained constant.

Cooling Tower Operation

Water Makeup Makeup requirements for a cooling tower consist of the summation of evaporation loss, drift loss, and blowdown. Therefore,

$$W_m = W_e + W_d + W_b \tag{12-14b}$$

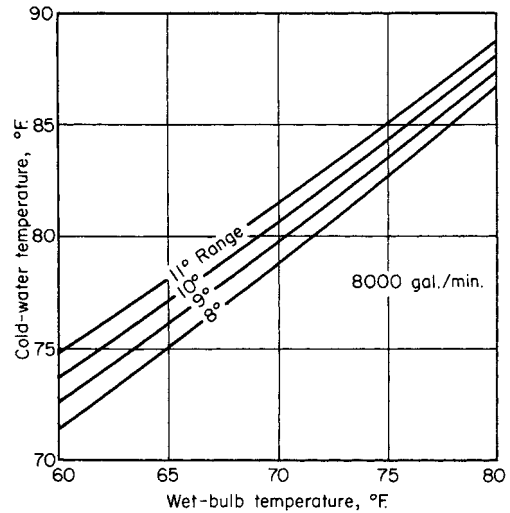


FIG. 12-8e Typical cooling-tower performance curve.

where W_m = makeup water, W_d = drift loss, and W_b = blowdown (consistent units: m³/h or gal/min).

Evaporation loss can be estimated by

$$W_e = 0.00085W_c(T_1 - T_2) \tag{12-14c}$$

where W_c = circulating water flow, m³/h or gal/min at tower inlet, and $T_1 - T_2$ = inlet water temperature minus outlet water temperature, °F. The 0.00085 evaporation constant is a good rule-of-thumb value. The actual evaporation rate will vary by season and climate.

Drift loss can be estimated by

$$W_d = 0.0002W_e$$

Drift is entrained water in the tower discharge vapors. Drift loss is a function of the drift eliminator design and is typically less than 0.02 percent of the water supplied to the tower with the new developments in eliminator design.

Blowdown discards a portion of the concentrated circulating water due to the evaporation process in order to lower the system solids concentration. The amount of blowdown can be calculated according to the number of cycles of concentration required to limit scale formation. "Cycles of concentration" is the ratio of dissolved solids in the recirculating water to dissolved solids in the makeup water. Since chlorides remain soluble on concentration, cycles of concentration are best expressed as the ratio of the chloride contents of the circulating and makeup waters. Thus, the blowdown quantities required are determined from

$$\text{Cycles of concentration} = \frac{W_e + W_b + W_d}{W_b + W_d} \tag{12-14d}$$

or
$$W_b = \frac{W_e - (\text{cycles} - 1)W_d}{\text{cycles} - 1} \tag{12-14e}$$

Cycles of concentration involved with cooling tower operation normally range from three to five cycles. For water qualities where operating water concentrations must be below 3 to control scaling, blowdown quantities will be large. The addition of acid or scale-inhibiting chemicals can limit scale formation at higher cycle levels with such a water, and will allow substantially reduced water usage for blowdown.

The blowdown equation (12-14e) translates to calculated percentages of the cooling system circulating water flow exiting to drain, as listed in Table 12-6. The blowdown percentage is based on the cycles targeted and the cooling range. The range is the difference between the system hot water and cold water temperatures.

TABLE 12.6 Blowdown (%)

Range, °F	2X	3X	4X	5X	6X
10	0.83	0.41	0.26	0.19	0.15
15	1.26	0.62	0.41	0.30	0.24
20	1.68	0.83	0.55	0.41	0.32
25	2.11	1.04	0.69	0.51	0.41
30	2.53	1.26	0.83	0.62	0.49

It is the open nature of evaporative cooling systems, bringing in external air and water continuously, that determines the unique water problems these systems exhibit. Cooling towers (1) concentrate solids by the mechanisms described above and (2) wash air. The result is a buildup of dissolved solids, suspended contaminants, organics, bacteria, and their food sources in the circulating cooling water. These unique evaporative water system problems must be specifically addressed to maintain cooling equipment in good working order.

Example 14: Calculation of Makeup Water Determine the amount of makeup required for a cooling tower with the following conditions:

Inlet water flow, m ³ /h (gal/min)	2270 (10,000)
Inlet water temperature, °C (°F)	37.77 (100)
Outlet water temperature, °C (°F)	29.44 (85)
Drift loss, percent	0.02
Concentration cycles	5

Evaporation loss:

$$W_e, \text{ m}^3/\text{h} = 0.00085 \times 2270 \times (37.77 - 29.44) \times (1.8^\circ\text{F}/^\circ\text{C}) = 28.9$$

$$W_e, \text{ gal/min} = 127.5$$

Drift loss

$$W_d, \text{ m}^3/\text{h} = 2270 \times 0.0002 = 0.45$$

$$W_d, \text{ gal/min} = 2$$

Blowdown

$$W_b, \text{ m}^3/\text{h} = 6.8$$

$$W_b, \text{ gal/min} = 29.9$$

Makeup

$$W_m, \text{ m}^3/\text{h} = 28.9 + 0.45 + 6.8 = 36.2$$

$$W_m, \text{ gal/min} = 159.4$$

Fan Horsepower In evaluating cooling tower ownership and operating costs, fan horsepower requirements can be a significant factor. Large air quantities are circulated through cooling towers at exit velocities of about 10.2 m/s (2000 ft/min) maximum for induced-draft towers. Fan airflow quantities depend upon tower design factors, including such items as type of fill, tower configuration, and thermal performance conditions.

The effective output of the fan is the static air horsepower (SAHP), which is obtained by the following equation:

$$\text{SAHP} = - \frac{Q(h_s)(d)}{33,000(12)}$$

where Q = air volume, ft³/min; h_s = static head, in of water; and d = density of water at ambient temperature, lb/ft³.

Cooling tower fan horsepower can be reduced substantially as the ambient wet-bulb temperature decreases if two-speed fan motors are used. Theoretically, operating at half speed will reduce airflow by 50 percent while decreasing horsepower to one-eighth of that of full-speed operation. However, actual half-speed operation will require about 17 percent of the horsepower at full speed as a result of the inherent motor losses at lighter loads.

Figure 12-8f shows a typical plot of outlet water temperatures when a cooling tower is operated (1) in the fan-off position, (2) with the fan

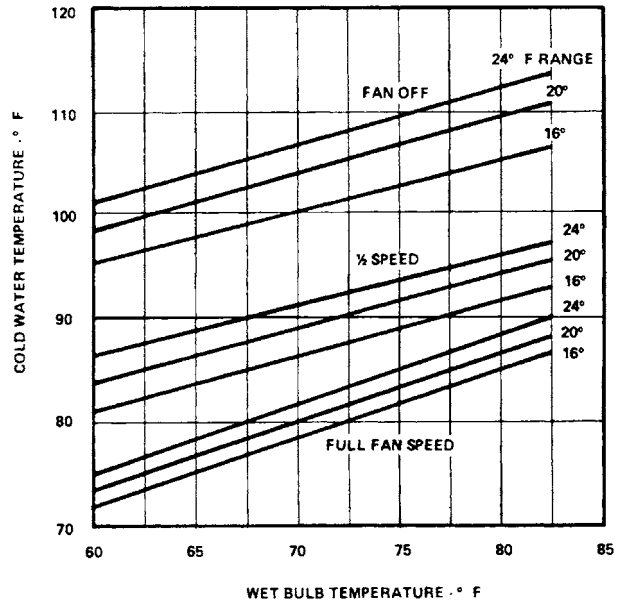


FIG. 12-8f Typical plot of cooling-tower performance at varying fan speeds.

at half speed, and (3) with the fan at full speed. Note that at decreasing wet-bulb temperatures the water leaving the tower during half-speed operation could meet design water temperature requirements of, say, 85°F. For example, for a 60°F wet-bulb, 20°F range, a leaving-water temperature slightly below 85°F is obtained with design water flow over the tower. If the fan had a 100-hp motor, 83 hp would be saved when operating it at half speed. In calculating savings, one should not overlook the advantage of having colder tower water available for the overall water circulating system.

Recent developments in cooling tower fan energy management also include automatic variable-pitch propeller-type fans and inverter-type devices to permit variable fan speeds. These schemes involve tracking the load at a constant outlet water temperature.

The variable-pitch arrangement at constant motor speed changes the pitch of the blades through a pneumatic signal from the leaving water temperature. As the thermal load and/or the ambient wet-bulb temperature decreases, the blade pitch reduces airflow and less fan energy is required.

Inverters make it possible to control a variable-speed fan by changing the frequency modulation. Standard alternating-current fan motors may be speed-regulated between 0 and 60 Hz. In using inverters for this application, it is important to avoid frequencies that would result in fan critical speeds.

Even though tower fan energy savings can result from these arrangements, they may not constitute the best system approach. Power plant steam condensers and refrigeration units, e.g., can take advantage of colder tower water to reduce power consumption. Invariably, these system savings are much larger than cooling tower fan savings with constant leaving water temperatures. A refrigeration unit condenser can utilize inlet water temperatures down to 12.8°C (55°F) to reduce compressor energy consumption by 25 to 30 percent.

Pumping Horsepower Another important factor in analyzing cooling tower selections, especially in medium to large sizes, is the portion of pump horsepower directly attributed to the cooling tower. A counterflow type of tower with spray nozzles will have a pumping head equal to static lift plus nozzle pressure loss. A cross-flow type of tower with gravity flow enables a pumping head to equal static lift. A reduction in tower height therefore reduces static lift, thus reducing pump horsepower:

$$\text{Pump bhp} = \frac{W_c h_t}{3960(\text{pump efficiency})} \quad (12-14f)$$

where W_c = water recirculation rate, gal/min, and h_t = total head, ft.

Fogging and Plume Abatement A phenomenon that occurs in cooling tower operation is fogging, which produces a highly visible plume and possible icing hazards. Fogging results from mixing warm, highly saturated tower discharge air with cooler ambient air that lacks the capacity to absorb all the moisture as vapor. While in the past visible plumes have not been considered undesirable, properly locating towers to minimize possible sources of complaints has now received the necessary attention. In some instances, guyed high fan stacks have been used to reduce ground fog. Although tall stacks minimize the ground effects of plumes, they can do nothing about water vapor saturation or visibility. The persistence of plumes is much greater in periods of low ambient temperatures.

More recently, environmental aspects have caused public awareness and concern over any visible plume, although many laypersons misconstrue cooling tower discharge as harmful. This has resulted in a new development for plume abatement known as a wet-dry cooling tower configuration. Reducing the relative humidity or moisture content of the tower discharge stream will reduce the frequency of plume formation. Figure 12-8g shows a "parallel path" arrangement that has been demonstrated to be technically sound but at substantially increased tower investment. Ambient air travels in parallel streams through the top dry-surface section and the evaporative section. Both sections benefit thermally by receiving cooler ambient air with the wet and dry airstreams mixing after leaving their respective sections. Water flow is arranged in series, first flowing to the dry coil section and then to the evaporation fill section. A "series path" airflow arrangement, in which dry coil sections can be located before or after the air traverses the evaporative section, also can be used. However, series-path airflow has the disadvantage of water impingement, which could result in coil scaling and restricted airflow.

Wet-dry cooling towers incorporating these designs are being used for large-tower industrial applications. At present they are not available for commercial applications.

Thermal Performance The thermal performance of the evaporative cooling tower is critical to the overall efficiency of cooling systems. Modern electronic measurement instrumentation allows accurate verification of cooling tower capability. Testing and tracking of the cooling tower capability are a substantial consideration in measuring cooling system performance. Cooling tower testing is a complex

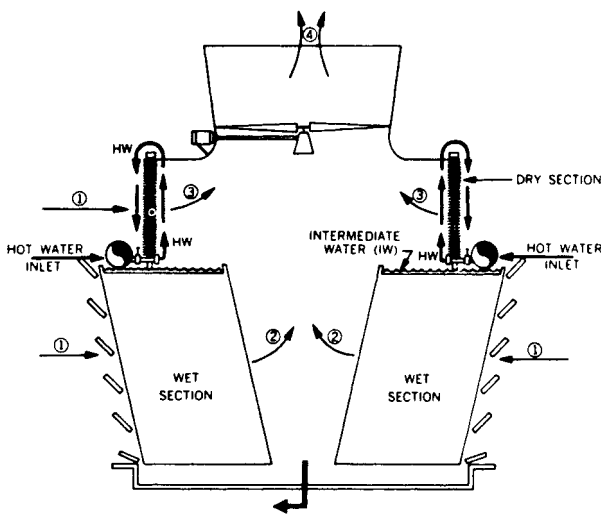


FIG. 12-8g Parallel-path cooling-tower arrangement for plume abatement. (Marley Co.)

activity that requires significant expertise in the art. Consult a competent testing company if such verification is desired.

New Technologies The cooling tower business is constantly changing in an attempt to improve efficiencies of evaporative cooling products. A significant thermal performance improvement over the splash-type fills, covered extensively in the writings above, can be achieved by using film-type fill. Film fills are formed plastic sheets separated by spacing knobs that allow water and air to flow easily between paired plastic surfaces. Fully wetted water flow over these panels creates an extensive "film" of evaporative surface on the plastic. Film fill is more sensitive to water quality than are splash-type fills.

These film fills are not sized via the graphical methods illustrated above for splash fills. They are selected by using manufacturers' proprietary sizing programs, which are based on extensive testing data. Such programs can be obtained by contacting manufacturers and/or industry trade organizations.

Applications for Evaporative Cooling Towers Cooling towers are commonly used in many commercial and industrial processes including

- Power generation (fossil fuel, nuclear)
- Industrial process (refinery, chemical production, plastic molding)
- Comfort cooling (HVAC)

Natural Draft Towers, Cooling Ponds, Spray Ponds Natural draft towers are primarily suited to very large cooling water quantities, and the reinforced concrete structures used are as large as 80 m in diameter and 105 m high.

When large ground areas are available, large cooling ponds offer a satisfactory method of removing heat from water. A pond may be constructed at a relatively small investment by pushing up earth in an earth dike 2 to 3 m high.

Spray ponds provide an arrangement for lowering the temperature of water by evaporative cooling and in so doing greatly reduce the cooling area required in comparison with a cooling pond.

Natural draft towers, cooling ponds, and spray ponds are infrequently used in new construction today in the chemical processing industry. Additional information may be found in previous Perry's editions.

WET SURFACE AIR COOLER (WSAC)

GENERAL REFERENCES: Kals, "Wet Surface Aircoolers," *Chem. Engg.* July 1971; Kals, "Wet Surface Aircoolers: Characteristics and Usefulness," AIChE-ASME Heat Transfer Conference, Denver, Colo., August 6-9, 1972; Elliott and Kals, "Air Cooled Condensers," *Power*, January 1990; Kals, "Air Cooled Heat Exchangers: Conventional and Unconventional," *Hydrocarbon Processing*, August 1994; Hutton, "Properly Apply Closed Circuit Evaporative Cooling," *Chem. Engg. Progress*, October 1996; Hutton, "Improved Plant Performance through Evaporative Steam Condensing," ASME 1998 International Joint Power Conference, Baltimore, Md., August 23-26, 1998; <http://www.niagarablower.com/wsac.htm>; <http://www.baltimoreaircoil.com>.

Principles Rejection of waste process heat through a cooling tower (CT) requires transferring the heat in two devices in series, using two different methods of heat transfer. This requires two temperature driving forces in series: first, sensible heat transfer, from the process stream across the heat exchanger (HX) into the cooling water, and, second, sensible and latent heat transfer, from the cooling water to atmosphere across the CT. Rejecting process heat with a wet surface air cooler transfers the waste heat in a single device by using a single-unit operation. The single required temperature driving force is lower, because the WSAC does not require the use of cooling water sensible heat to transfer heat from the process stream to the atmosphere. A WSAC tube cross section (Fig. 12-8h) shows the characteristic external tube surface having a continuous flowing film of evaporating water, which cascades through the WSAC tube bundle. Consequently, process streams can be economically cooled to temperatures much closer to the ambient wet-bulb temperature (WBT), as low as to within 2.2°C (4°F), depending on the process requirements and economics for the specific application.

Wet Surface Air Cooler Basics The theory and principles for the design of WSACs are a combination of those known for evaporative cooling tower design and HX design. However, the design practices for engineering WSAC equipment remain a largely proprietary, technical

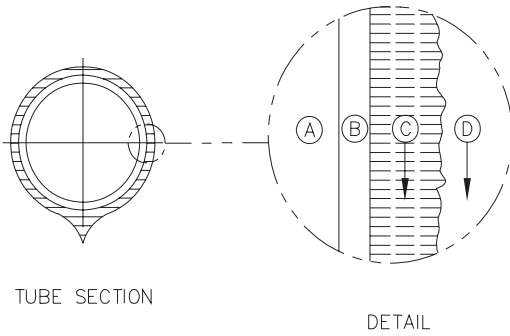


FIG. 12-8h WSAC tube cross-section. Using a small T, heat flows from (A) the process stream, through (B) the tube, through (C) the flowing film of evaporating water, into (D) flowing ambient air.

art, and the details are not presented here. Any evaluation of the specifics and economics for any particular application requires direct consultation with a reputable vendor.

Because ambient air is contacted with evaporating water within a WSAC, from a distance a WSAC has a similar appearance to a CT (Fig. 12-8i). Economically optimal plot plan locations for WSACs can vary: integrated into, or with, the process structure, remote to it, in a pipe rack, etc.

In the WSAC the evaporative cooling occurs on the wetted surface of the tube bundle. The wetting of the tube bundle is performed by recirculating water the short vertical distance from the WSAC collection basin, through the spray nozzles, and onto the top of the bundle (Fig. 12-8j). The tube bundle is completely deluged with this cascading flow of water. Using water application rates between 12 and 24 (m³/h)/m² (5 and 10 gpm/ft²), the tubes have a continuous, flowing external water film, minimizing the potential for water-side biological fouling, sediment deposition, etc. Process inlet temperatures are limited to a maximum of about 85°C (185°F), to prevent external water-side mineral scaling. However, higher process inlet temperatures can be accepted, by incorporating bundles of dry, air-cooled finned tubing within the WSAC unit, to reduce the temperature of the process stream to an acceptable level before it enters the wetted evaporative tube bundles.

The WSAC combines within one piece of equipment the functions of cooling tower, circulated cooling water system, and water-cooled HX. In the basic WSAC configuration (Fig. 12-8k), ambient air is drawn in and



FIG. 12-8j Nozzles spraying onto wetted tube bundle in a WSAC unit.

down through the tube bundle. This airflow is cocurrent with the evaporating water flow, recirculated from the WSAC collection basin sump to be sprayed over the tube bundles. This downward cocurrent flow pattern minimizes the generation of water mist (drift). At the bottom of the WSAC, the air changes direction through 180°, disengaging entrained fine water droplets. Drift eliminators can be added to meet very low drift requirements. Because heat is extracted from the tube surfaces by water latent heat (and not sensible heat), only about 75 percent as much circulating water is required in comparison to an equivalent CT-cooling water-HX application.

The differential head of the circulation water pump is relatively small, since dynamic losses are modest (short vertical pipe and a low ΔP spray nozzle) and the hydraulic head is small, only about 6 m (20 ft) from the basin to the elevation of the spray header. Combined, the pumping energy demand is about 35 percent that for an equivalent CT application. The capital cost for this complete water system is also relatively small. The pumps and motors are smaller, the piping has a smaller diameter and is much shorter, and the required piping structural support is almost negligible, compared to an equivalent CT application. WSAC fan horsepower is typically about 25 percent less than that for an equivalent CT.

A WSAC is **inherently less sensitive to water-side fouling**. This is due to the fact that the deluge rate prevents the adhesion of waterborne material which can cause fouling within a HX. A WSAC

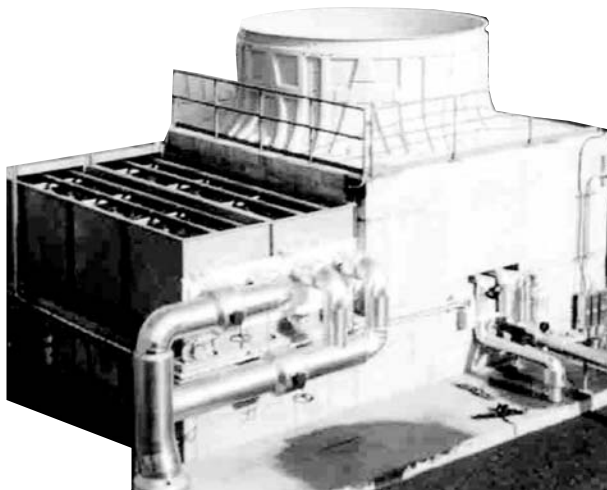


FIG. 12-8i Overhead view of a single-cell WSAC.

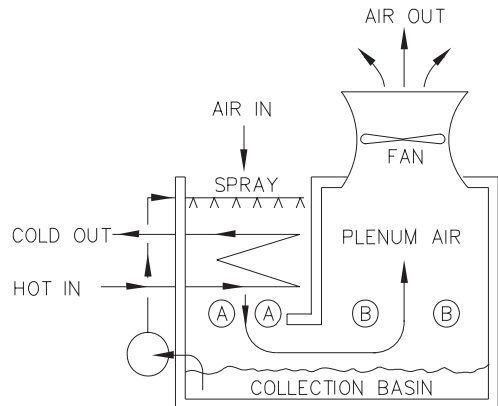


FIG. 12-8k Basic WSAC configuration.

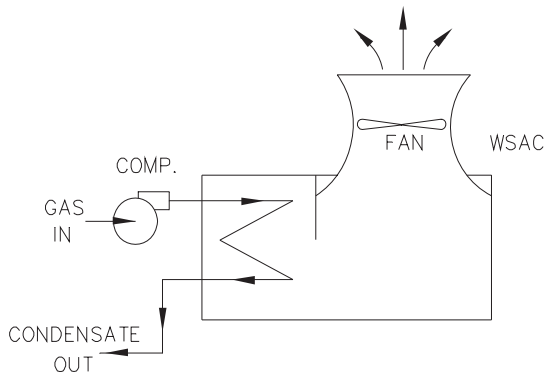


FIG. 12-8l WSAC configuration for condensing a compressed gas. A lower condensing pressure reduces compressor operating horsepower.

can accept relatively contaminated makeup water, such as CT blowdown, treated sewage plant effluent, etc. WSACs can endure **more cycles of concentration without fouling than can a CT application**. This higher practical operating concentration reduces the relative volume for the evaporative cooling blowdown, and therefore also reduces the relative volume of required makeup water. For facilities designed for **zero liquid discharge**, the higher practical WSAC blowdown concentration reduces the size and the operating costs for the downstream water treatment system. Since a hot process stream provides the unit with a heat source, a **WSAC has intrinsic freeze protection** while operating.

Common WSAC Applications and Configurations Employment of a WSAC can reduce process system operating costs that are not specific to the WSAC unit itself. A common WSAC application is **condensation of compressed gas** (Fig. 12-8l). A compressed gas can be condensed in a WSAC at a lower pressure, by condensing at a temperature closer to the ambient WBT, typically 5.5°C (10°F) above the WBT. This reduced condensation pressure reduces costs, by reducing gas compressor motor operating horsepower. Consequently, WSACs are widely applied for **condensing refrigerant gases**, for HVAC, process chillers, ice makers, gas-turbine inlet air cooling, chillers, etc. WSACs are also used directly to **condense lower-molecular-weight hydrocarbon streams**, such as ethane, ethylene, propylene, and LPG. A related WSAC application is the **cooling of compressed gases** (CO_2 , N_2 , methane, LNG, etc.), which directly reduces gas compressor operating costs (inlet and interstage cooling) and indirectly reduces downstream condensing costs (aftercooling the compressed gas to reduce the downstream refrigeration load).

For combined cycle electric power generation, employment of a **WSAC increases steam turbine efficiency**. Steam turbine exhaust can be condensed at a lower pressure (higher vacuum) by condensing at a temperature closer to the ambient WBT, typically 15°C (27°F) above the WBT. This reduced condensation pressure results in a lower turbine discharge pressure, **increasing electricity generation** by increasing output shaft power (Fig. 12-8m). Due to standard WSAC configurations, a second cost advantage is gained at the turbine itself. The **steam turbine can be placed at grade**, rather than being mounted on an elevated platform, by venting horizontally into the WSAC, rather than venting downward to condensers located below the platform elevation, as is common for conventional water-cooled vacuum steam condensers.

A WSAC can **eliminate chilled water use**, for process cooling applications with required temperatures close to and just above the ambient WBT, typically about 3.0 to 5.5°C (5 to 10°F) above the WBT. This WSAC application can eliminate both chiller capital and operating costs. In such an application, either the necessary process temperature is below the practical CT water supply temperature, or they are so close to it that the use of CT water is uneconomical (a low-HX LMDT).

WSACs can be designed to **simultaneously cool several process streams in parallel separate tube bundles within a single cell** of a

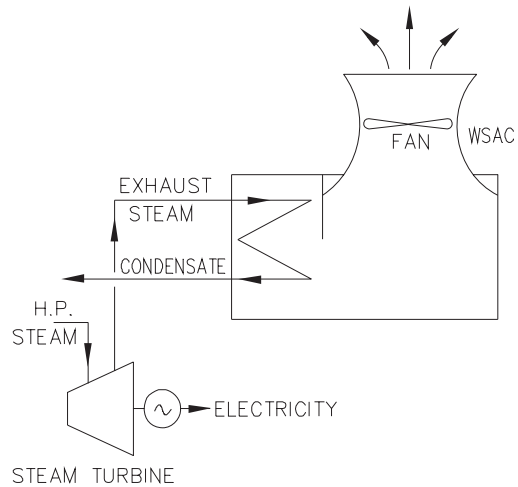


FIG. 12-8m WSAC configuration with electricity generation. A lower steam condensing pressure increases the turbine horsepower extracted.

WSAC (Fig. 12-8n). Often one of the streams is closed-circuit cooling water to be used for remote cooling applications. These might be applications not compatible with a WSAC (rotating seals, bearings, cooling jackets, internal reactor cooling coils, etc.) or merely numerous, small process streams in small HXs.

WSAC for Closed-Circuit Cooling Systems A closed-circuit cooling system as defined by the Cooling Technology Institute (CTI) employs a closed loop of circulated fluid (typically water) remotely as a cooling medium. By definition, this medium is cooled by **water evaporation involving no direct fluid contact** between the air and the enclosed circulated cooling medium. Applied in this manner, a WSAC can be used as the evaporative device to cool the circulated cooling medium, used remotely to cool process streams. This configuration completely isolates the cooling water (and the hot process streams) from the environment (Fig. 12-8o).

The closed circuit permits complete control of the cooling water chemistry, which permits **minimizing** the cost for **water-side materials of construction** and eliminating water-side fouling of, and fouling heat-transfer resistance in, the HXs (or jackets, reactor coils, etc.). **Elimination of water-side fouling** is particularly helpful for high-temperature cooling applications, especially where heat recovery may otherwise be impractical (quench oils, low-density polyethylene reactor cooling, etc.).

Closed-circuit cooling **minimizes circulation pumping horsepower**, which must overcome only dynamic pumping losses. This results through recovery of the returning circulated cooling water hydraulic head. A closed-circuit system can be designed for **operation at elevated pressures**, to guarantee that any process HX leak will be into the

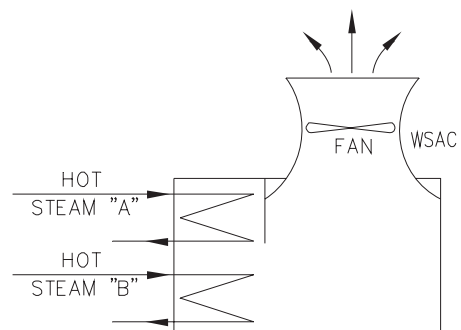


FIG. 12-8n WSAC configuration with parallel streams.

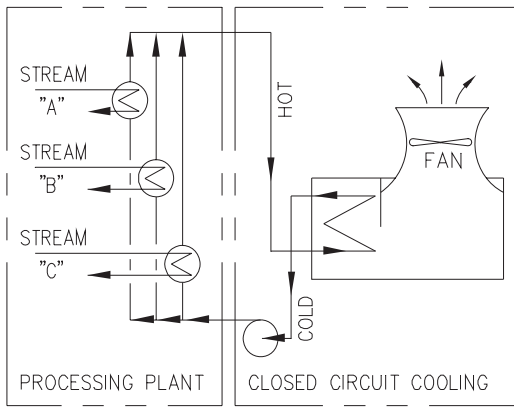


FIG. 12-8o WSAC configuration with no direct fluid contact.

process. Such high-pressure operation is economical, since the system overpressure is not lost during return flow to the circulation pump.

Closed-circuit cooling **splits the water chemistry needs** into two isolated systems: the **evaporating section**, exposed to the environment, and the **circulated cooling section**, isolated from the environment. Typically, this split reduces total water chemistry costs and water-related operations and maintenance problems. On the other hand, the split permits the effective **use of a low-quality or contaminated makeup water** for evaporative cooling, or a water source having severe seasonal quality problems, such as high sediment loadings.

If **highly saline water is used** for the evaporative cooling, a **reduced flow of makeup saline water** would need to be supplied to the WSAC. This reduction results from using latent cooling rather than sensible cooling to reject the waste heat. This consequence reduces the substantial capital investment required for the saline water supply and return systems (canal structures) and pump stations, and the saline supply pumping horsepower. (When saline water is used as the evaporative medium, special attention is paid to materials of construction and spray water chemical treatment due to the aggravated corrosion and scaling tendencies of this water.)

Water Conservation Applications—"Wet-Dry" Cooling A modified and hybridized form of a WSAC can be used to provide what is called "wet-dry" cooling for water conservation applications (Fig. 12-8p). A hybridized combination of air-cooled dry finned tubes, standard wetted bare tubes, and wet deck surface area permits the WSAC to **operate without water in cold weather**, reducing water consumption by about 75 percent of the total for an equivalent CT application.

Under design conditions of maximum summer WBT, the unit operates with spray water deluging the wetted tube bundle. The exiting water then flows down into and through the wet deck surface, where the water is cooled adiabatically to about the WBT, and then to the sump.

As the WBT drops, the process load is shifted from the wetted tubes to the dry finned tubes. By bypassing the process stream around the wetted tubes, cooling water evaporation (consumption) is proportionally reduced.

When the WBT drops to the "switch point," the process bypassing has reached 100 percent. This switch point WBT is at or above 5°C (41°F). As the ambient temperature drops further, adiabatic evaporative cooling continues to be used, to lower the dry-bulb temperature

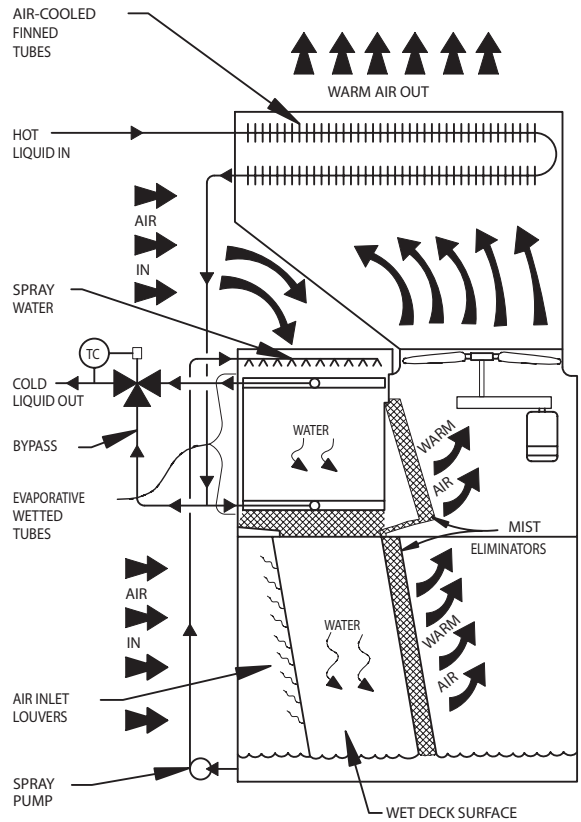


FIG. 12-8p As seasonal ambient temperatures drop, the "wet-dry" configuration for a WSAC progressively shifts the cooling load from evaporative to convective cooling.

to below the switch point temperature. This guarantees that the entire cooling load can be cooled in the dry finned tube bundle.

The use of water is discontinued after ambient dry-bulb temperatures fall below the switch point temperature, since the entire process load can be cooled using only cold fresh ambient air. By using this three-step load-shifting practice, total wet-dry cooling water consumption is about 25 percent of that consumption total experienced with an equivalent CT application.

Wet-dry cooling permits **significant reduction of water consumption**, which is useful where makeup water supplies are limited or where water treatment costs for blowdown are high. Because a WSAC (unlike a CT) has a heat source (the hot process stream), wet-dry cooling avoids various cold-weather-related CT problems. **Fogging and persistent plume formation can be minimized or eliminated** during colder weather. **Freezing and icing problems can be eliminated** by designing a wet-dry system for water-free operation during freezing weather, typically below 5°C (41°F). **In the arctic**, or regions of extreme cold, **elimination of freezing fog conditions** is realized by not evaporating any water during freezing weather.

SOLIDS-DRYING FUNDAMENTALS

GENERAL REFERENCES: Cook and DuMont, *Process Drying Practice*, McGraw-Hill, New York, 1991. *Drying Technology—An International Journal*, Taylor and Francis, New York. Hall, *Dictionary of Drying*, Marcel Dekker, New York, 1979. Keey, *Introduction to Industrial Drying Operations*, Pergamon, New York, 1978. Keey, *Drying of Loose and Particulate Materials*, Hemisphere, New York, 1992. Masters, *Spray Drying Handbook*,

Wiley, New York, 1990. Mujumdar, *Handbook of Industrial Drying*, Marcel Dekker, New York, 1987. Nonhebel and Moss, *Drying of Solids in the Chemical Industry*, CRC Press, Cleveland, Ohio, 1971. Strumillo and Kudra, *Drying: Principles, Application and Design*, Gordon and Breach, New York, 1986. van't Land, *Industrial Drying Equipment*, Marcel Dekker, New York, 1991.

INTRODUCTION

Drying is the process by which volatile materials, usually water, are evaporated from a material to yield a solid product. Drying is a heat- and mass-transfer process. Heat is necessary to evaporate water. The latent heat of vaporization of water is about 2500 J/g, which means that the drying process requires a significant amount of energy. Simultaneously, the evaporating material must leave the drying material by diffusion and/or convection.

Heat transfer and mass transfer are not the only concerns when one is designing or operating a dryer. The product quality (color, particle density, hardness, texture, flavor, etc.) is also very strongly dependent on the drying conditions and the physical and chemical transformations occurring in the dryer.

Understanding and designing a drying process involves measurement and/or calculation of the following:

1. Mass and energy balances
2. Thermodynamics
3. Mass- and heat-transfer rates
4. Product quality considerations

The section below explains how these factors are measured and calculated and how the information is used in engineering practice.

TERMINOLOGY

Generally accepted terminology and definitions are given alphabetically in the following paragraphs.

Absolute humidity is the mass ratio of water vapor (or other solvent mass) to dry air.

Activity is the ratio of the fugacity of a component in a system relative to the standard-state fugacity. In a drying system, it is the ratio of the vapor pressure of a solvent (e.g., water) in a mixture to the pure solvent vapor pressure at the same temperature. Boiling occurs when the vapor pressure of a component in a liquid exceeds the ambient total pressure.

Bound moisture in a solid is that liquid which exerts a vapor pressure less than that of the pure liquid at the given temperature. Liquid may become bound by retention in small capillaries, by solution in cell or fiber walls, by homogeneous solution throughout the solid, by chemical or physical adsorption on solid surfaces, and by hydration of solids.

Capillary flow is the flow of liquid through the interstices and over the surface of a solid, caused by liquid-solid molecular attraction.

Constant-rate period (unhindered) is that drying period during which the rate of water removal per unit of drying surface is constant, assuming the driving force is also constant.

Convection is heat or mass transport by bulk flow.

Critical moisture content is the average moisture content when the constant-rate period ends, assuming the driving force is also constant.

Diffusion is the molecular process by which molecules, moving randomly due to thermal energy, migrate from regions of high chemical potential (usually concentration) to regions of lower chemical potential.

Dry basis expresses the moisture content of wet solid as kilograms of water per kilogram of bone-dry solid.

Equilibrium moisture content is the limiting moisture to which a given material can be dried under specific conditions of air temperature and humidity.

Evaporation is the transformation of material from a liquid state to a vapor state.

Falling-rate period (hindered drying) is a drying period during which the instantaneous drying rate continually decreases.

Fiber saturation point is the moisture content of cellular materials (e.g., wood) at which the cell walls are completely saturated while the cavities are liquid-free. It may be defined as the equilibrium moisture content as the humidity of the surrounding atmosphere approaches saturation.

Free moisture content is that liquid which is removable at a given temperature and humidity. It may include bound and unbound moisture.

Funicular state is that condition in drying a porous body when capillary suction results in air being sucked into the pores.

Hygroscopic material is material that may contain bound moisture.

Initial moisture distribution refers to the moisture distribution throughout a solid at the start of drying.

Internal diffusion may be defined as the movement of liquid or vapor through a solid as the result of a concentration difference.

Latent heat of vaporization is the specific enthalpy change associated with evaporation.

Moisture content of a solid is usually expressed as moisture quantity per unit weight of the dry or wet solid.

Moisture gradient refers to the distribution of water in a solid at a given moment in the drying process.

Nonhygroscopic material is material that can contain no bound moisture.

Pendular state is that state of a liquid in a porous solid when a continuous film of liquid no longer exists around and between discrete particles so that flow by capillary cannot occur. This state succeeds the funicular state.

Permeability is the resistance of a material to bulk or convective, pressure-driven flow of a fluid through it.

Relative humidity is the partial pressure of water vapor divided by the vapor pressure of pure water at a given temperature. In other words, the relative humidity describes how close the air is to saturation.

Sensible heat is the energy required to increase the temperature of a material without changing the phase.

Unaccomplished moisture change is the ratio of the free moisture present at any time to that *initially* present.

Unbound moisture in a hygroscopic material is that moisture in excess of the equilibrium moisture content corresponding to saturation humidity. All water in a nonhygroscopic material is unbound water.

Vapor pressure is the partial pressure of a substance in the gas phase that is in equilibrium with a liquid or solid phase of the pure component.

Wet basis expresses the moisture in a material as a percentage of the weight of the wet solid. Use of a dry-weight basis is recommended since the percentage change of moisture is constant for all moisture levels. When the wet-weight basis is used to express moisture content, a 2 or 3 percent change at high moisture contents (above 70 percent) actually represents a 15 to 20 percent change in evaporative load. See Fig. 12-9 for the relationship between the dry- and wet-weight bases.

MASS AND ENERGY BALANCES

The most basic type of calculation for a dryer is a mass and energy balance. This calculation only quantifies the conservation of mass and energy in the system; by itself it does not answer important questions of rate and quality.

Some examples here illustrate the calculations. Experimental determination of the values used in these calculations is discussed in a later section.

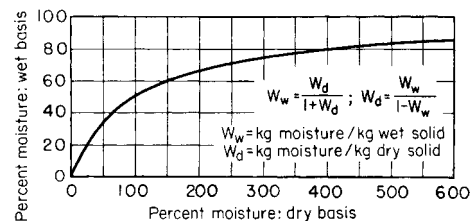


FIG. 12-9 Relationship between wet-weight and dry-weight bases.

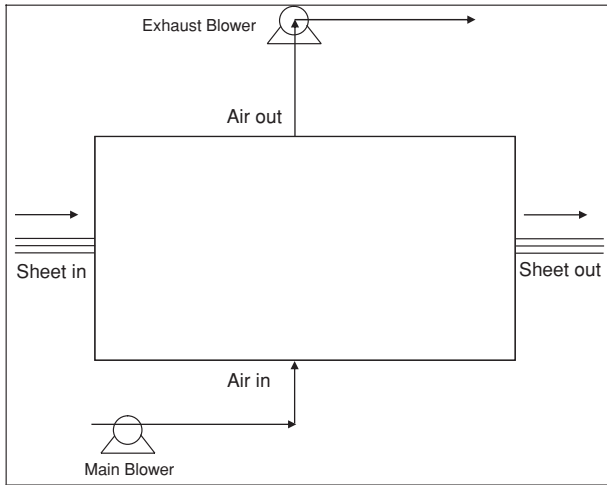


FIG. 12-10 Overall mass and energy balance diagram.

Example 15 illustrates a generic mass and energy balance. Other examples are given in the sections on fluidized bed dryers and rotary dryers.

Example 15: Overall Mass and Energy Balance on a Sheet Dryer Figure 12-10 shows a simple sheet drying system. Hot air enters the dryer and contacts a wet sheet. The sheet leaves a dryer with a lower moisture content, and the air leaves the dryer with a higher humidity.

Given: Incoming wet sheet mass flow rate is 100 kg/h. It enters with 20 percent water on a wet basis and leaves at 1 percent water on a wet basis. The airflow rate is 1000 kg/h, with an absolute humidity of 0.01 g water/g dry air. The incoming air temperature is 170°C. The sheet enters at 20°C and leaves at 90°C.

Relevant physical constants: $C_{p, \text{air}} = 1 \text{ kJ}/(\text{kg} \cdot ^\circ\text{C})$, $C_{p, \text{sheet}} = 2.5 \text{ kJ}/(\text{kg} \cdot ^\circ\text{C})$, $C_{p, \text{liquid water}} = 4.184 \text{ kJ}/(\text{kg} \cdot ^\circ\text{C})$, $C_{p, \text{water vapor}} = 2 \text{ kJ}/(\text{kg} \cdot ^\circ\text{C})$ (for superheated steam at low partial pressures). Latent heat of vaporization of water at 20°C = $\lambda_w = 2454 \text{ J/g}$

Find the following:

1. The absolute humidity of the exiting airstream
2. The exit air temperature

Solution: Answering the questions above involves an overall mass and energy balance. Only the mass and enthalpy of the streams need to be considered to answer the two questions above. Only the streams entering the overall process need to be considered. In this example, wet-basis moisture content (and therefore total mass flow rate including moisture) will be used. Since the same mass of air flows in and out of the dryer, there are no equations to solve for the dry air.

The mass balance is given by the following equations:

$$F_{\text{dry sheet in}} = F_{\text{dry sheet out}} \quad (12-15)$$

$$F_{\text{liquid water in}} = F_{\text{liquid water out}} + F_{\text{evaporated}} \quad (12-16)$$

$$G_{\text{dry air in}} = G_{\text{dry air out}} \quad (12-17)$$

$$G_{\text{water vapor in}} + F_{\text{evaporated}} = G_{\text{water vapor out}} \quad (12-18)$$

The wet-basis moisture contents of the incoming and outgoing sheet are given by

$$w_{\text{in}} = \frac{F_{\text{liquid water in}}}{F_{\text{liquid water in}} + F_{\text{dry sheet in}}} \quad (12-19)$$

$$w_{\text{out}} = \frac{F_{\text{liquid water out}}}{F_{\text{liquid water out}} + F_{\text{dry sheet out}}} \quad (12-20)$$

The relationship between the total airflow, the dry airflow, and the absolute humidity is given by

$$G_{\text{dry air}} = G_{\text{air}} \frac{1}{1 + Y} = 1000 \text{ kg/h} \frac{1}{1 + 0.01} = 990 \text{ kg/h}$$

The absolute humidity of each airstream is given by

$$Y_{\text{in}} = \frac{G_{\text{water vapor in}}}{G_{\text{dry air in}}} \quad (12-21)$$

$$Y_{\text{out}} = \frac{G_{\text{water vapor out}}}{G_{\text{dry air out}}} \quad (12-22)$$

The mass flow rates of the dry sheet and the liquid water in can be calculated from the overall sheet flow rate and the incoming moisture content:

$$G_{\text{liquid water in}} = G_{\text{sheet}} w_{\text{in}} = (100 \text{ kg/h})(0.2) = 20 \text{ kg/h} \quad (12-23)$$

$$F_{\text{dry sheet}} = F_{\text{sheet}}(1 - w_{\text{in}}) = (100 \text{ kg/h})(0.8) = 80 \text{ kg/h} \quad (12-24)$$

The mass flow rates of the dry air and incoming water vapor can be calculated from the overall airflow rate and the incoming absolute humidity:

$$G_{\text{water vapor in}} = G_{\text{dry air}} Y_{\text{in}} = (990 \text{ kg/h})(0.01) = 9.9 \text{ kg/h} \quad (12-25)$$

To calculate the exiting absolute humidity, Eq. (12-22) is used. But the evaporation rate $G_{\text{evaporated}}$ is needed. This is calculated from Eqs. (12-16) and (12-20).

$$F_{\text{liquid water out}} = \frac{w_{\text{out}}}{1 - w_{\text{out}}} F_{\text{dry sheet out}} = \frac{0.01}{0.99} \cdot 80 \text{ kg/h} = 0.8 \text{ kg/h} \quad (12-20, \text{ rearranged})$$

$$G_{\text{evaporated}} = F_{\text{liquid water in}} - F_{\text{liquid water out}} = 20 - 0.8 \text{ kg/h} = 19.2 \text{ kg/h} \quad (12-26)$$

Equation (12-18) is now used to calculate the mass flow of water vapor out of the dryer:

$$G_{\text{water vapor out}} = 9.9 \text{ kg/h} + 19.2 \text{ kg/h} = 29.1 \text{ kg/h} \quad (12-27)$$

Now the absolute humidity of the exiting air is readily calculated from Eq. (12-22):

$$Y_{\text{out}} = \frac{G_{\text{water vapor out}}}{G_{\text{dry air}}} = \frac{29.1}{990} = 0.0294 \quad (12-28)$$

Next an energy balance must be used to estimate the outgoing air temperature. The following general equation is used:

$$H_{\text{dry air in}} + H_{\text{water vapor in}} + H_{\text{dry sheet in}} + H_{\text{liquid water in}} = H_{\text{dry air out}} + H_{\text{water vapor out}} + H_{\text{dry sheet out}} + H_{\text{liquid water out}} + \text{heat loss to surroundings} \quad (12-29)$$

Heat losses to the environment are often difficult to quantify, but they can be neglected for a first approximation. This assumption is more valid for large systems than small systems. It is neglected in this example.

Evaluation of the energy balance terms can be done in a couple of ways. Values of the enthalpies above can be calculated by using a consistent reference, or the equation can be rearranged in terms of enthalpy differences. The latter approach will be used here, as shown by Eq. (12-30).

$$\Delta H_{\text{dry air}} + \Delta H_{\text{water vapor}} + \Delta H_{\text{evaporation}} + \Delta H_{\text{liquid water}} + \Delta H_{\text{dry sheet}} = 0 \quad (12-30)$$

The enthalpy change due to evaporation $\Delta H_{\text{evaporation}}$ is given by $F_{\text{evaporated}} \lambda_w$. To evaluate λ_w rigorously, a decision has to be made on the calculational path of the evaporating water since this water is both heating and evaporating. Typically, a two-step path is used—*isothermal evaporation and heating of either phase*. The incoming liquid water can all be heated to the outlet temperature of the sheet, and then the heat of vaporization at the outlet temperature can be used; or the evaporation can be calculated as occurring at the inlet temperature, and the water vapor is heated from the inlet temperature to the outlet temperature. Alternatively a three-step path based on latent heat at the datum (0°C) may be used. All these methods of calculation are equivalent, since the enthalpy is a state function; but in this case, the second method is preferred since the outlet temperature is unknown. In the calculation, the water will be evaporated at 20°C, heated to the air inlet temperature 170°C, and then cooled to the outlet temperature. Alternatively, this enthalpy change can be calculated directly by using tabular enthalpy values available on the psychrometric chart or Mollier diagram.

The terms in these equations can be evaluated by using

$$\begin{aligned} \Delta H_{\text{dry air}} &= G_{\text{dry air}} C_{p, \text{air}} (T_{\text{air in}} - T_{\text{air out}}) \\ &= (990.1 \text{ kg/h}) [1 \text{ kJ}/(\text{kg} \cdot ^\circ\text{C})] [(170 - T_{\text{air out}}) \text{ kJ/h}] \end{aligned} \quad (12-31)$$

$$\begin{aligned} \Delta H_{\text{water vapor}} &= G_{\text{water vapor out}} C_{p, \text{water vapor}} (T_{\text{air in}} - T_{\text{air out}}) \\ &= (29.1 \text{ kg/h}) [2 \text{ kJ}/(\text{kg} \cdot ^\circ\text{C})] [(170 - T_{\text{air out}}) \text{ kJ/h}] \end{aligned} \quad (12-32)$$

12-28 PSYCHROMETRY, EVAPORATIVE COOLING, AND SOLIDS DRYING

From steam tables, ΔH_{vap} at $20^\circ\text{C} = 2454 \text{ kJ/kg}$, $h_l = 84 \text{ kJ/kg}$, and h_g at 170°C (superheated, low pressure) = 2820 kJ/kg .

$$\begin{aligned} -\Delta H_{\text{evaporation}} &= -C_{\text{evaporated}} \cdot \Delta H_{\text{vap}} \\ &= (-19.2 \text{ kg/h}) \\ [2736 \text{ kJ/kg (from steam table)}] \\ &= -52,530 \text{ kJ/h} \end{aligned} \quad (12-33)$$

$$\begin{aligned} \Delta H_{\text{liquid water}} &= F_{\text{liquid water out}} C_{p, \text{liquid water}} (T_{\text{sheet, in}} - T_{\text{sheet, out}}) \\ &= (0.8 \text{ kg/h}) [4.18 \text{ kJ/(kg} \cdot ^\circ\text{C)}] [(20^\circ\text{C} - 90^\circ\text{C})] = -234 \text{ kJ/h} \end{aligned} \quad (12-34)$$

$$\begin{aligned} \Delta H_{\text{dry sheet}} &= F_{\text{dry sheet}} C_{p, \text{sheet}} (T_{\text{sheet, in}} - T_{\text{sheet, out}}) \\ &= (80 \text{ kg/h}) [2.5 \text{ kJ/(kg} \cdot ^\circ\text{C)}] [(20^\circ\text{C} - 90^\circ\text{C})] = -14,000 \text{ kJ/h} \end{aligned}$$

Putting this together gives

$$(990.1)(1)(170 - T_{\text{air, out}}) + (29.1)(2)(170 - T_{\text{air, out}}) - 52,530 - 293 - 14,000 = 0$$

$$T_{\text{air, out}} = 106^\circ\text{C}$$

THERMODYNAMICS

The thermodynamic driving force for evaporation is the difference in chemical potential or water activity between the drying material and the gas phase. Although drying of water is discussed in this section, the same concepts apply analogously for solvent drying.

For a pure water drop, the driving force for drying is the difference between the vapor pressure of water and the partial pressure of water in the gas phase. The rate of drying is proportional to this driving force; please see the discussion on drying kinetics later in this chapter.

$$\text{Rate} \propto (p_{\text{pure}}^{\text{sat}} - p_{w, \text{air}})$$

The activity of water in the gas phase is defined as the ratio of the partial pressure of water to the vapor pressure of pure water, which is also related to the definition of relative humidity.

$$a_w^{\text{vapor}} = \frac{p_w}{p_{\text{pure}}^{\text{sat}}} = \frac{\% \text{RH}}{100}$$

The activity of water in a mixture or solid is defined as the ratio of the vapor pressure of water in the mixture to that of a reference, usually the vapor pressure of pure water. In solids drying or drying of solutions, the vapor pressure (or water activity) is lower than that for pure water. Therefore, the water activity value equals 1 for pure water and < 1 when binding is occurring. This is caused by thermodynamic interactions between the water and the drying material. In many standard drying references, this is called *bound water*.

$$a_w^{\text{solid}} = \frac{p_{\text{mixture}}^{\text{sat}}}{p_{\text{pure}}^{\text{sat}}}$$

When a solid sample is placed into a humid environment, water will transfer from the solid to the air or vice versa until equilibrium is established. At thermodynamic equilibrium, the water activity is equal in both phases:

$$a_w^{\text{vapor}} = a_w^{\text{solid}} = a_w$$

Sorption isotherms quantify how tightly water is bound to a solid. The goal of obtaining a sorption isotherm for a given solid is to measure the equilibrium relationship between the percentage of water in the sample and the vapor pressure of the mixture. The sorption isotherm describes how dry a product can get if contacted with humid air for an infinite amount of time. An example of a sorption isotherm is shown in Fig. 12-11. In the sample isotherm, a feed material dried with 50 percent relative humidity air ($a_w = 0.5$) will approach a moisture content of 10 percent on a dry basis. Likewise, a material kept in a sealed container will create a headspace humidity according to the isotherm; a 7 percent moisture sample in the example below will create a 20 percent relative humidity ($a_w = 0.2$) headspace in a sample jar or package.

Strictly speaking, the equilibrium moisture content of the sample in a given environment should be independent of the initial condition of

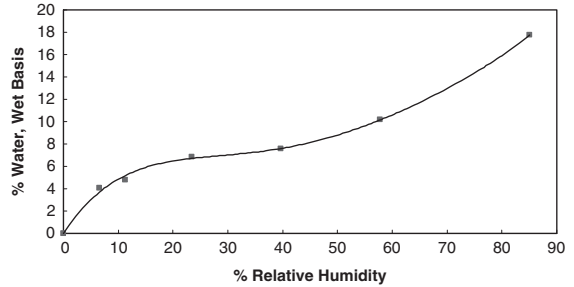


FIG. 12-11 Example of a sorption isotherm (coffee at 22°C).

the sample. However, there are cases where the sorption isotherm of an initially wet sample (sometimes called a desorption isotherm) is different from that of an identical, but initially dry sample. This is called hysteresis and can be caused by irreversible changes in the sample during wetting or drying, micropore geometry in the sample, and other factors. Paper products are notorious for isotherm hysteresis. Most materials show little or no hysteresis.

Sorption isotherms cannot generally be predicted from theory. They need to be measured experimentally. The simplest method of measuring a sorption isotherm is to generate a series of controlled-humidity environments by using saturated salt solutions, allow a solid sample to equilibrate in each environment, and then analyze the solid for moisture content.

The basic apparatus is shown in Fig. 12-12, and a table of salts is shown in Table 12-7. It is important to keep each chamber sealed and to be sure that crystals are visible in the salt solution to ensure that the liquid is saturated. Additionally, the solid should be ground into a powder to facilitate mass transfer. Equilibration can take 2 to 3 weeks. Successive moisture measurements should be used to ensure that the sample has equilibrated, i.e., achieved a steady value. Care must be taken when measuring the moisture content of a sample; this is described later in the chapter.

Another common method of measuring a sorption isotherm is to use a dynamic vapor sorption device. This machine measures the weight change of a sample when exposed to humidity-controlled air. A series of humidity points are programmed into the unit, and it automatically delivers the proper humidity to the sample and monitors the weight. When the weight is stable, an equilibrium point is noted and the air humidity is changed to reflect the next setting in the series. When one is using this device, it is critical to measure and record the starting moisture of the sample, since the results are often reported as a percent of change rather than a percent of moisture.

There are several advantages to the dynamic vapor sorption device. First, any humidity value can be dialed in, whereas salt solutions are not available for every humidity value and some are quite toxic. Second, since the weight is monitored as a function of time, it is clear when equilibrium is reached. The dynamic devices also give the sorption/desorption rates, although these can easily be misused (see the drying kinetics section later). The salt solution method, on



FIG. 12-12 Sorption isotherm apparatus. A saturated salt solution is in the bottom of the sealed chamber; samples sit on a tray in the headspace.

TABLE 12-7 Maintenance of Constant Humidity

Solid phase	Max. temp., °C	% Humidity
H ₃ PO ₄ · <i>a</i> H ₂ O	24.5	9
ZnCl ₂ · <i>a</i> H ₂ O	20	10
KC ₂ H ₃ O ₂	168	13
LiCl·H ₂ O	20	15
KC ₂ H ₃ O ₂	20	20
KF	100	22.9
NaBr	100	22.9
CaCl ₂ ·6H ₂ O	24.5	31
CaCl ₂ ·6H ₂ O	20	32.3
CaCl ₂ ·6H ₂ O	18.5	35
CrO ₃	20	35
CaCl ₂ ·6H ₂ O	10	38
CaCl ₂ ·6H ₂ O	5	39.8
K ₂ CO ₃ ·2H ₂ O	24.5	43
K ₂ CO ₃ ·2H ₂ O	18.5	44
Ca(NO ₃) ₂ ·4H ₂ O	24.5	51
NaHSO ₄ ·H ₂ O	20	52
Mg(NO ₃) ₂ ·6H ₂ O	24.5	52
NaClO ₃	100	54
Ca(NO ₃) ₂ ·4H ₂ O	18.5	56
Mg(NO ₃) ₂ ·6H ₂ O	18.5	56
NaBr·2H ₂ O	20	58
Mg(C ₂ H ₃ O ₂) ₄ ·4H ₂ O	20	65
NaNO ₂	20	66
(NH ₄) ₂ SO ₄	108.2	75
(NH ₄) ₂ SO ₄	20	81
NaC ₂ H ₃ O ₂ ·3H ₂ O	20	76
Na ₂ S ₂ O ₃ ·5H ₂ O	20	78
NH ₄ Cl	20	79.5
NH ₄ Cl	25	79.3
NH ₄ Cl	30	77.5
KBr	20	84
Tl ₂ SO ₄	104.7	84.8
KHSO ₄	20	86
Na ₂ CO ₃ ·10H ₂ O	24.5	87
K ₂ CrO ₄	20	88
NaBrO ₃	20	92
Na ₂ CO ₃ ·10H ₂ O	18.5	92
Na ₂ SO ₄ ·10H ₂ O	20	93
Na ₂ HPO ₄ ·12H ₂ O	20	95
NaF	100	96.6
Pb(NO ₃) ₂	20	98
TlNO ₃	100.3	98.7
TlCl	100.1	99.7

For a more complete list of salts, and for references to the literature, see *International Critical Tables*, vol. 1, p. 68.

the other hand, is significantly less expensive to buy and maintain. Numerous samples can be placed in humidity chambers and run in parallel while a dynamic sorption device can process only one sample at a time.

An excellent reference on all aspects of sorption isotherms is by Bell and Labuza, *Moisture Sorption*, 2d ed., American Association of Cereal Chemists, 2000.

MECHANISMS OF MOISTURE TRANSPORT WITHIN SOLIDS

Drying requires moisture to travel to the surface of a material. There are several mechanisms by which this can occur:

1. *Diffusion of moisture through solids.* Diffusion is a molecular process, brought about by random wanderings of individual molecules. If all the water molecules in a material are free to migrate, they tend to diffuse from a region of high moisture concentration to one of lower moisture concentration, thereby reducing the moisture gradient and equalizing the concentration of moisture.

2. *Convection of moisture within a liquid or slurry.* If a flowable solution is drying into a solid, then liquid motion within the material brings wetter material to the surface.

3. *Evaporation of moisture within a solid and gas transport out of the solid by diffusion and/or convection.* Evaporation can occur within a solid if it is boiling or porous. Subsequently vapor must move out of the sample.

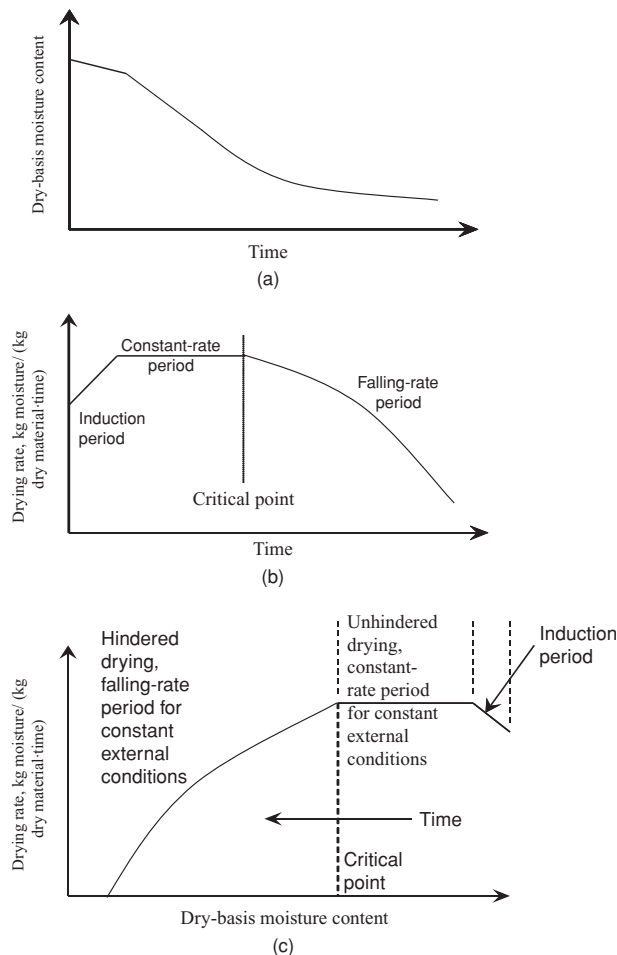
4. *Capillary flow of moisture in porous media.* The reduction of liquid pressure within small pores due to surface tension forces causes liquid to flow in porous media by capillary action.

DRYING KINETICS

This section discusses the rate of drying. The kinetics of drying dictates the size of industrial drying equipment, which directly affects the capital and operating costs of a process involving drying. The rate of drying can also influence the quality of a dried product since other simultaneous phenomena can be occurring, such as heat transfer and shrinkage due to moisture loss.

Drying Curves and Periods of Drying The most basic and essential kinetic information on drying is a *drying curve*. A drying curve describes the drying kinetics and how they change during drying. The drying curve is affected by the material properties, size or thickness of the drying material, and drying conditions. In this section, the general characteristics of drying curves and their uses are described. Experimental techniques to obtain drying curves are discussed in the “Experimental Methods” section and uses of drying curves for scale-up are discussed in “Dryer Modeling Design and Scale-up.”

Several representations of a typical drying curve are shown in Fig. 12-13. The top plot, Fig. 12-13a, is the moisture content (dry basis) as a function of time. The middle plot, Fig. 12-13b, is the drying rate as a function of time, the derivative of the top plot. The bottom plot,


FIG. 12-13 Several common representations of a typical drying curve.

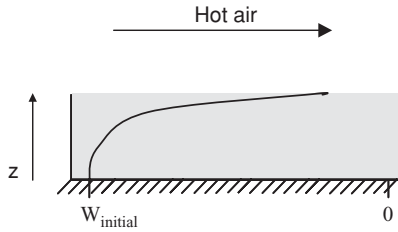


FIG. 12-14 Drying of a slab.

Fig. 12-13c, is the drying rate as affected by the average moisture content of the drying material. Since the material loses moisture as time passes, the progression of time in this bottom plot is from right to left.

Some salient features of the drying curve show the different periods of drying. These are common periods, but not all occur in every drying process. The first period of drying is called the induction period. This period occurs when material is being heated early in drying. The second period of drying is called the constant-rate period. During this period, the surface remains wet enough to maintain the vapor pressure of water on the surface. Once the surface dries sufficiently, the drying rate decreases and the falling-rate period occurs. This period can also be referred to as *hindered drying*.

Figure 12-13 shows the transition between constant- and falling-rate periods of drying occurring at the critical point. The *critical point* refers to the average moisture content of a material at this transition.

The sections below show examples of drying curves and the phenomena that give rise to common shapes.

Introduction to Internal and External Mass-Transfer Control—Drying of a Slab The concepts in drying kinetics are best illustrated with a simple example—air drying of a slab. Consider a thick slab of homogeneous wet material, as shown in Fig. 12-14. In this particular example, the slab is dried on an insulating surface under constant conditions. The heat for drying is carried to the surface with hot air, and air carries water vapor from the surface. At the same time, a moisture gradient forms within the slab, with a dry surface and a wet interior. The curved line is the representation of the gradient. At the bottom the slab ($z = 0$), the material is wet and the moisture content is drier at the surface.

The following processes must occur to dry the slab:

1. Heat transfer from the air to the surface of the slab
2. Mass transfer of water vapor from the surface of the slab to the bulk air
3. Mass transfer of moisture from the interior of the slab to the surface of the slab

Depending on the drying conditions, thickness, and physical properties of the slab, any of the above steps can be rate-limiting. Figure 12-15 shows two examples of rate-limiting cases.

The top example shows the situation of *external rate control*. In this situation, the heat transfer to the surface and/or the mass transfer from the surface in the vapor phase is slower than mass transfer to the surface from the bulk of the drying material. In this limiting case, the moisture gradient in the material is minimal, and the rate of drying will be constant as long as the average moisture content remains high enough to maintain a high water activity (see the section on thermodynamics for a discussion of the relationship between moisture content and water vapor pressure). External rate control leads to the observation of a constant-rate period drying curve.

The bottom example shows the opposite situation: *internal rate control*. In the case of heating from the top, internal control refers to a slow rate of mass transfer from the bulk of the material to the surface of the material. Diffusion, convection, and capillary action (in the case of porous media) are possible mechanisms for mass transfer of moisture to the surface of the slab. In the internal rate control situation, moisture is removed from the surface by the air faster than moisture is transported to the surface. This regime is caused by relatively thick layers or high values of the mass- and heat-transfer coefficients in the air. Internal rate control leads to the observation of a falling-rate period drying curve.

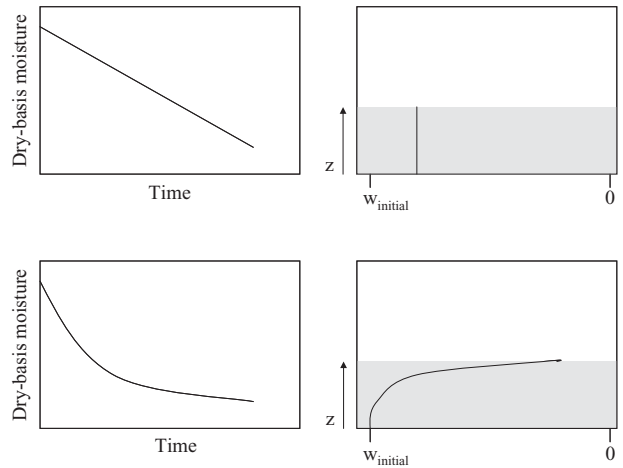


FIG. 12-15 Drying curves and corresponding moisture gradients for situations involving external heat and mass-transfer control and internal mass-transfer control.

Generally speaking, drying curves show both behaviors. When drying begins, the surface is often wet enough to maintain a constant-rate period and is therefore externally controlled. But as the material dries, the mass-transfer rate of moisture to the surface often slows, causing the rate to decrease since the lower moisture content on the surface causes a lower water vapor pressure. However, some materials begin dry enough that there is no observable constant-rate period.

MATHEMATICAL MODELING OF DRYING

Mathematical models can be powerful tools to help engineers understand drying processes. Models can be either purchased or homemade. Several companies offer software packages to select dryers, perform scale-up calculations, and simulate dryers.

Homemade models are often mass and energy balance spreadsheets, simplified kinetic models, or the simultaneous solution of the convection diffusion and heat equations together with nonlinear isotherms. All levels of models have their place.

This section begins with the most rigorous and numerical models. These models are potentially the most accurate, but require physical property data and simultaneous solution of differential and algebraic equations. Generally speaking, simpler models are more accessible to engineers and easier to implement. They can be very useful as long as the inherent limitations are understood.

Numerical Modeling of Drying Kinetics This section summarizes a numerical approach toward modeling drying from a fundamental standpoint. In other words, predictions are made from the appropriate sets of differential and algebraic equations, together with physical properties of the drying medium and drying material. Statistical methods of data analysis, e.g., design of experiments, are not covered.

The approach in this section is lagrangian; i.e., the model is for a drying object (particle, drop, sheet, etc.) as it moves through the drying process in time. More complicated models can use an eulerian frame of reference by simulating the dryer with material moving into and out of the dryer.

The approach taken in this example also assumes that the mechanism of mass transport is by diffusion. This is not always the case and can be significantly incorrect, especially in the case of drying of porous materials.

Any fundamental mathematical model of drying contains mass and energy balances, constitutive equations for mass- and heat-transfer rates, and physical properties. Table 12-8 shows the differential mass balance equations that can be used for common geometries. Note there are two sets of differential mass balances—one including shrinkage and one not including shrinkage. When moisture leaves a drying material, the material can either shrink, or develop porosity, or both.

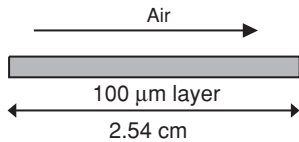
TABLE 12-8 Mass-Balance Equations for Drying Modeling When Diffusion Is Mass-Transfer Mechanism of Moisture Transport

Case	Mass balance without shrinkage	Mass balance with shrinkage
Slab geometry	$\frac{\partial C_w}{\partial t} = \frac{\partial}{\partial z} \left[\mathcal{D}(w) \frac{\partial C_w}{\partial z} \right]$ <p>At top surface, $-\mathcal{D}(w) \frac{\partial C_w}{\partial z}_{\text{top surface}} = k_p \frac{P_w^{\text{bulk}} - P_w^{\text{surface}}}{P - P_w^{\text{surface}}}$</p> <p>At bottom surface, $\frac{\partial C_w}{\partial z}_{\text{bottom surface}} = 0$</p>	$\frac{\partial u}{\partial t} = \frac{\partial}{\partial s} \left[\mathcal{D}(w) \frac{\partial u}{\partial s} \right] \quad \frac{\partial s}{\partial z} = \rho_s$ <p>At top surface, $-\mathcal{D}(w) \frac{\partial u}{\partial s}_{\text{top surface}} = k_p \frac{P_w^{\text{bulk}} - P_w^{\text{surface}}}{P - P_w^{\text{surface}}}$</p> <p>At bottom surface, $\frac{\partial u}{\partial s}_{\text{bottom surface}} = 0$</p>
Cylindrical geometry	$\frac{\partial C_w}{\partial t} = \frac{1}{r} \frac{\partial}{\partial r} \left[r \mathcal{D}(w) \frac{\partial C_w}{\partial r} \right]$ <p>At surface, $-\mathcal{D}(w) \frac{\partial C_w}{\partial r}_{\text{surface}} = k_p \frac{P_w^{\text{bulk}} - P_w^{\text{surface}}}{P - P_w^{\text{surface}}}$</p> <p>At center, $\frac{\partial C_w}{\partial r}_{\text{center}} = 0$</p>	$\frac{\partial u}{\partial t} = \frac{\partial}{\partial s} \left[\rho_s^2 \mathcal{D}(w) \frac{\partial u}{\partial s} \right] \quad \frac{\partial s}{\partial z} = r \rho_s$ <p>At surface, $-\mathcal{D}(w) r \frac{\partial u}{\partial s}_{\text{surface}} = k_p \frac{P_w^{\text{bulk}} - P_w^{\text{surface}}}{P - P_w^{\text{surface}}}$</p> <p>At center, $\frac{\partial u}{\partial s}_{\text{surface}} = 0$</p>
Spherical geometry	$\frac{\partial C_w}{\partial t} = \frac{1}{r^2} \frac{\partial}{\partial r} \left[r^2 \mathcal{D}(w) \frac{\partial C_w}{\partial r} \right]$ <p>At surface, $-\mathcal{D}(w) \frac{\partial C_w}{\partial r}_{\text{surface}} = k_p \frac{P_w^{\text{bulk}} - P_w^{\text{surface}}}{P - P_w^{\text{surface}}}$</p> <p>At center, $\frac{\partial C_w}{\partial r}_{\text{center}} = 0$</p>	$\frac{\partial u}{\partial t} = \frac{\partial}{\partial s} \left[\rho_s^4 \mathcal{D}(w) \frac{\partial u}{\partial s} \right] \quad \frac{\partial s}{\partial z} = r^2 \rho_s$ <p>At surface, $-\mathcal{D}(w) r^2 \frac{\partial u}{\partial s}_{\text{surface}} = k_p \frac{P_w^{\text{bulk}} - P_w^{\text{surface}}}{P - P_w^{\text{surface}}}$</p> <p>At center, $\frac{\partial u}{\partial s}_{\text{bottom surface}} = 0$</p>

The variable u is the dry-basis moisture content. The equations that include shrinkage are taken from Van der Lijn, doctoral thesis, Wageningen (1976).

The equations in Table 12-8 are insufficient on their own. Some algebraic relationships are needed to formulate a complete problem, as illustrated in Example 16. Equations for the mass- and heat-transfer coefficients are also needed for the boundary conditions presented in Table 12-8. These require the physical properties of the air, the object geometry, and Reynolds number. Example 16 shows the solution for a problem using numerical modeling. This example shows some of the important qualitative characteristics of drying.

Example 16: Air Drying of a Thin Layer of Paste Simulate the drying kinetics of 100 μm of paste initially containing 50 percent moisture (wet-basis) with dry air at 60°C, 0 percent relative humidity air at velocities of 1, 10, or 1000 m/s (limiting case) and at 60°C, 0 percent relative humidity air at 1 m/s. The diffusion coefficient of water in the material is constant at $1 \times 10^{-10} \text{ m}^2/\text{s}$. The length of the layer in the airflow direction is 2.54 cm.



Physical property data: Sorption isotherm data fit well to the following equation:

$$w = 3.10 \left(\frac{\%RH}{100} \right)^5 - 6.21 \left(\frac{\%RH}{100} \right)^4 + 4.74 \left(\frac{\%RH}{100} \right)^3 - 1.70 \left(\frac{\%RH}{100} \right)^2 + 0.378 \left(\frac{\%RH}{100} \right)$$

- Solid density = 1150 kg/m³
- Heat of vaporization = 2450 J/g
- Solid heat capacity: 2.5 J/(g·K)
- Water heat capacity: 4.184 J/(g·K)

Solution: The full numerical model needs to include shrinkage since the material is 50 percent water initially and the thickness will decrease from 100 to 46.5 μm during drying. Assuming the layer is viscous enough to resist convection in the liquid, diffusion is the dominant liquid-phase transport mechanism.

Table 12-8 gives the mass balance equation:

$$\frac{\partial u}{\partial t} = \frac{\partial}{\partial s} \left[\mathcal{D}(w) \frac{\partial u}{\partial s} \right] \quad \frac{\partial s}{\partial z} = \rho_s$$

At top surface,

$$-\mathcal{D}(w) \frac{\partial u}{\partial s}_{\text{top surface}} = k_p \frac{P_w^{\text{bulk}} - P_w^{\text{surface}}}{P - P_w^{\text{surface}}}$$

At bottom surface,

$$\frac{\partial u}{\partial s}_{\text{bottom surface}} = 0$$

The temperature is assumed to be uniform through the thickness of the layer.

$$(1 + w_{\text{avg,dry-basis}}) \cdot m_{\text{solids}} C_p \cdot \frac{dT_{\text{layer}}}{dt} = [h(T_{\text{air}} - T_{\text{layer}}) - F \cdot \Delta H_{\text{vap}}] A$$

Mass- and heat-transfer coefficients are given by

$$\text{Nu} = \frac{hL}{k_{\text{air}}} = 0.664 \cdot \text{Re}^{0.5} \cdot \text{Pr}^{0.333}$$

$$\text{Sh} = \frac{k_c L}{\mathcal{D}_{\text{air/water}}} = 0.664 \cdot \text{Re}^{0.5} \cdot \text{Sc}^{0.333}$$

$$k_p = k_c \cdot \rho_{\text{air}}$$

The Reynolds number uses the length of the layer L in the airflow direction:

$$\text{Re} = \frac{VL\rho_{\text{air}}}{\mu_{\text{air}}}$$

where V = air velocity.

12-32 PSYCHROMETRY, EVAPORATIVE COOLING, AND SOLIDS DRYING

The Prandtl and Schmidt numbers, Pr and Sc, for air are given by

$$\text{Pr} = \frac{C_{p,\text{air}} \mu_{\text{air}}}{k_{\text{air}}} = 0.70 \quad \text{Sc} = \frac{\mu_{\text{air}}}{\rho_{\text{air}} D_{\text{air/water}}} = 0.73$$

The following algebraic equations are also needed:

$$\frac{1}{\rho} = \frac{w}{\rho_w} + \frac{1-w}{\rho_s} \quad \text{density of wet material (assumes volume additivity)}$$

$$C_w = w \cdot \rho \quad \text{concentration of water}$$

$$\rho_s = (1-w)\rho \quad \text{concentration of solids}$$

$$\frac{\%RH}{100} = \frac{P_{w,\text{surface}}}{P_{w,\text{sat}}} \quad \text{definition of relative humidity}$$

$$\text{Antoine equation for vapor pressure of water} \quad P_{w,\text{sat}} = 0.01 \exp \left(16.262 - \frac{3800}{226.3 + T_{\text{liquid/solid}}} \right)$$

Result: The results of the simulation are shown in Fig. 12-16. The top plot shows the average moisture content of the layer as a function of time, the middle plot shows the drying rate as a function of time, and the bottom plot shows the moisture gradient in each layer after 10 s of drying.

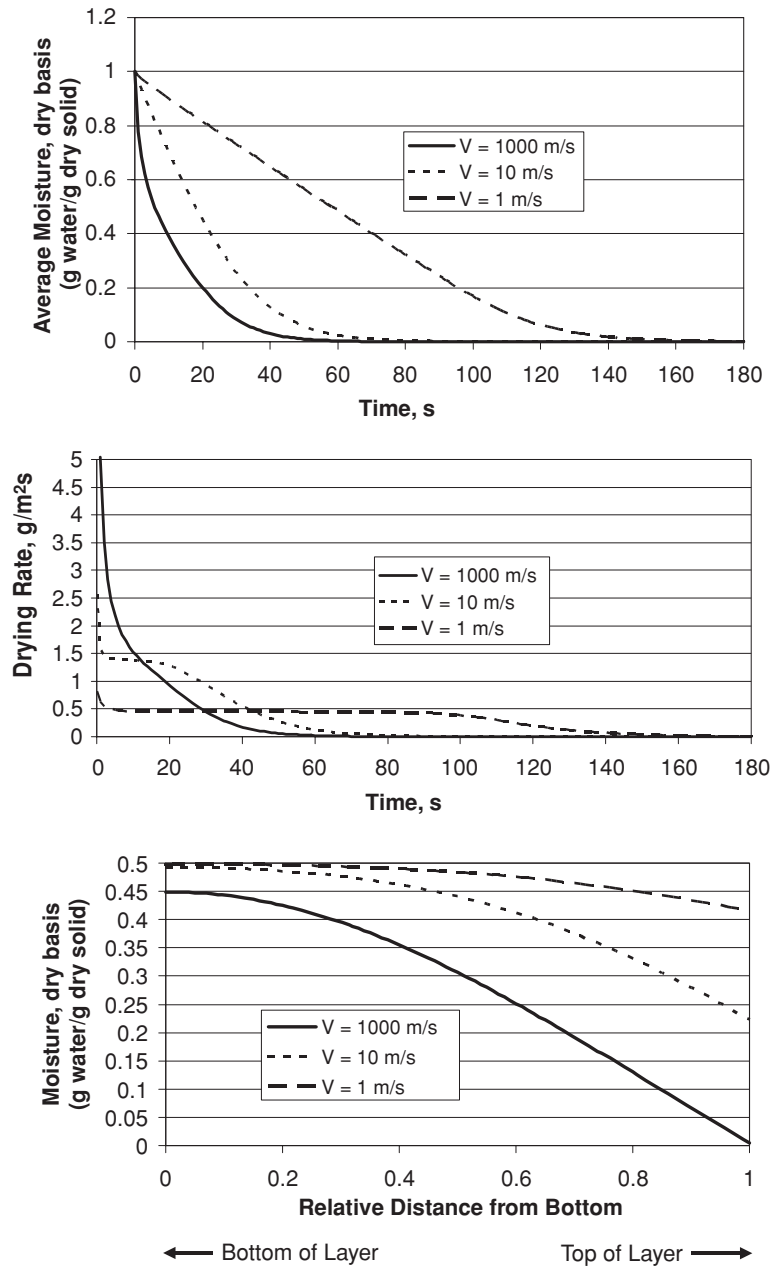


FIG. 12-16 Simulation results for thin layer drying example.

At a velocity of 1 m/s, drying occurs at a constant rate for nearly the entire process; at 10 m/s, drying begins at a high constant rate and then enters a falling-rate period; and at 1000 m/s (limiting case), there is no constant-rate period. These results illustrate the relationships between the external air conditions, drying rate, and moisture gradient. At high air velocity, the drying rate is faster, but becomes limited by internal diffusion and a steep moisture gradient forms. As the air velocity increases, the drying rate becomes less sensitive to air velocity.

The equation set in this example was solved by using a differential-algebraic equation solver called gPROMS from Process Systems Enterprises (www.pse.com). It can also be solved with other software and programming languages such as FORTRAN. Example 16 is too complicated to be done on a spreadsheet.

Simplified Kinetic Models This section presents several examples of simplified kinetic models. A model of the constant-rate period is shown in Example 17. During the constant-rate period, the drying rate is controlled by gas-phase mass and heat transfer. This is easier than modeling the falling-rate period, since the properties of air and water (or other gas-phase molecules) are well understood. Modeling the falling-rate period requires knowledge of and/or assumptions about the physical properties of the drying material.

Example 17: Drying a Pure Water Drop (Marshall, *Atomization & Spray Drying*, 1986.) Calculate the time to dry a drop of water, given the air temperature and relative humidity as a function of drop size.

Solution: Assume that the drop is drying at the wet-bulb temperature. Begin with an energy balance [Eq. (12-35)]

$$\text{Mass flux} = \frac{h(T_{\text{air}} - T_{\text{drop}})}{\Delta H_{\text{vap}}} \quad (12-35)$$

Next, a mass balance is performed on the drop. The change in mass equals the flux times the surface area.

$$\rho \frac{dV_{\text{droplet}}}{dt} = -A \cdot \text{mass flux} \quad (12-36)$$

Evaluating the area and volume for a sphere gives

$$\rho \cdot 4\pi R^2 \frac{dR}{dt} = -4\pi R^2 \cdot \text{mass flux} \quad (12-37)$$

Combining Eqs. (12-35) and (12-37) and simplifying gives

$$\rho \frac{dR}{dt} = \frac{-h(T_{\text{air}} - T_{\text{drop}})}{\Delta H_{\text{vap}}} \quad (12-38)$$

A standard correlation for heat transfer to a sphere is given by (Ranz and Marshall, 1952)

$$\text{Nu} = \frac{h(2R)}{k_{\text{air}}} = 2 + 0.6 \cdot \text{Re}^{0.5} \text{Pr}^{0.33} \quad (12-39)$$

For small drop sizes or for stagnant conditions, the Nusselt number has a limiting value of 2.

$$\text{Nu} = \frac{h(2R)}{k_{\text{air}}} = 2 \quad (12-40)$$

$$h = \frac{k_{\text{air}}}{R} \quad (12-41)$$

Inserting into Eq. (12-38) gives

$$R \frac{dR}{dt} = \frac{k_{\text{air}}(T_{\text{air}} - T_{\text{drop}})}{\rho \Delta H_{\text{vap}}} \quad (12-42)$$

Integration yields

$$\frac{R^2}{2} - \frac{R_0^2}{2} = \frac{k_{\text{air}}(T_{\text{air}} - T_{\text{drop}})t}{\rho \Delta H_{\text{vap}}} \quad (12-43)$$

where R_0 = initial drop radius, m.

Now the total lifetime of a drop can be calculated from Eq. (12-43) by setting $R = 0$:

$$t = \frac{\rho \Delta H_{\text{vap}} R_0^2}{2k_{\text{air}}(T_{\text{air}} - T_{\text{drop}})} \quad (12-44)$$

The effects of drop size and air temperature are readily apparent from Eq. (12-44). The temperature of the drop is the wet-bulb temperature and can be obtained from a psychrometric chart, as described in the previous section. Sample results are plotted in Fig. 12-17.

The above solution for drying of a pure water drop cannot be used to predict the drying rates of drops containing solids. Drops containing solids will not shrink uniformly and will develop internal concentration gradients (falling-rate period) in most cases.

Modeling of the falling-rate period is usually done by treating the drying problem as a diffusion problem, where the rate-limiting step is the diffusion of moisture from deep within the solid to the surface.

One of the attractions of treating drying as a diffusion problem is its relative simplicity compared with more complex models for moisture movement. This renders the approach tractable for hand calculations, and these calculations are often appropriate given the wide variability in diffusion coefficients and permeabilities both within and between

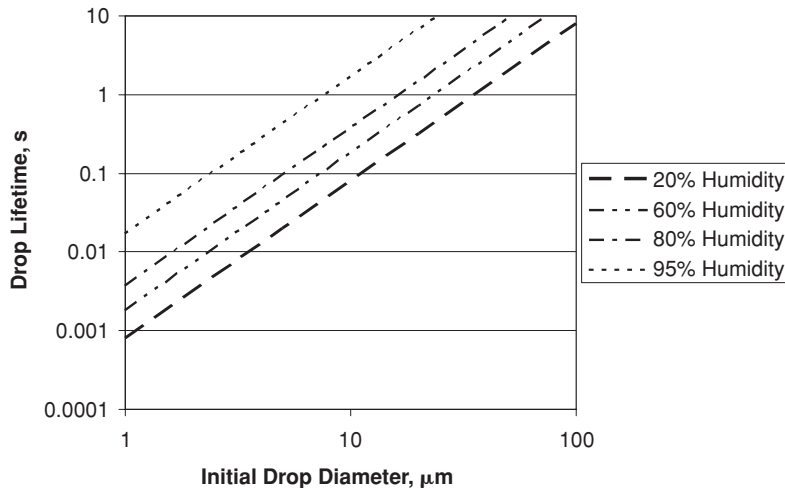


FIG. 12-17 Drying time of pure water drops as function of relative humidity at 25°C.

12-34 PSYCHROMETRY, EVAPORATIVE COOLING, AND SOLIDS DRYING

materials. The simplicity of this approach is also useful when one is optimizing processing conditions, where the number of calculations, even with modern workstations, is considerable. Moreover, this diffusion approach works well for predicting both average moisture contents and moisture-content profiles for some materials.

The three main driving forces which have been used within diffusion models (moisture content, partial pressure of water vapor, and chemical potential) will now be discussed. Attempts to predict diffusion coefficients theoretically will also be reviewed, together with experimental data for fitted diffusion coefficients and their dependence on temperature and moisture content.

Waananen et al. (1993), in their review of drying models, note that most models in their final form express the driving force for moisture movement in terms of a moisture concentration gradient. However, the true potential for transfer may be different, namely, differences in chemical potential, as explored in greater detail by Keey et al. (2000). In theory, the diffusion coefficient will be independent of moisture concentration only if the moisture is unbound, but concentration-independent diffusion coefficients have been successfully used in some cases over a wide range of moisture contents.

Since the true driving force is the chemical potential difference, transfer will occur between two moist bodies in the direction of falling chemical potential rather than decreasing moisture content. Moisture may flow from the drier body to the wetter one.

At low moisture contents, Perré and Turner (1996) suggest that there seems to be little difference between the predictions of drying models with driving forces based on gradients in chemical potential, moisture content, and partial pressure of water vapor, indicating that the simplest approach (a moisture content driving force) might be most practical. The majority of work involving the use of diffusion models has used moisture content driving forces. Hence, there is some empirical support for the use of moisture content driving forces.

In this model, described by Fick's second law, we have

$$\frac{\partial X}{\partial t} = \mathcal{D} \frac{\partial^2 X}{\partial z^2} \quad (12-45)$$

where X is the free moisture content above the equilibrium moisture content, t is time, z is the distance coordinate perpendicular to the airstream, and \mathcal{D} is the diffusion coefficient. Sherwood (1929) was the first to use this approach, and he made the following additional assumptions:

- The diffusion coefficient \mathcal{D} is constant.
- The initial moisture content in the material is uniform.
- Surface material comes into equilibrium with the surrounding air instantaneously, so that the resistance of the boundary layer outside the material is negligible.

Translated to mathematical terms, the last two of these assumptions are

$$t = 0 \quad X = X_i \quad (12-46)$$

$$z = \delta \quad X = X_e \quad (\text{at the surface}) \quad (12-47)$$

where δ is the half thickness of the board. This approach allowed Eq. (12-45) to be integrated to yield a predicted moisture content profile. This moisture content profile may be integrated to give average moisture contents, with the characteristic moisture content $\bar{\Phi}$ being defined as before, $\bar{\Phi} = (\bar{X} - X_e)/(X_i - X_e)$, where \bar{X} is the volume-averaged moisture content and X_i and X_e are the initial and equilibrium moisture contents, respectively. The equation for the characteristic moisture content is

$$\bar{\Phi} = \frac{8}{\pi^2} \sum_{n=0}^{\infty} \frac{1}{(2n+1)^2} \exp \left[- \left(\frac{2n+1}{2} \right)^2 \pi^2 \tau \right] \quad (12-48)$$

With this model, a characteristic parameter which governs the extent of drying is the mass-transfer Fourier number τ , defined as follows:

$$\tau = \frac{\mathcal{D}t}{\delta^2} \quad (12-49)$$

If drying is controlled by diffusion, then for the same drying conditions, doubling the thickness of the material should increase the drying time to the same final moisture content fourfold.

If the diffusion coefficient is constant, the moisture content profile through a material for the steady-state movement of moisture through it would be linear. However, drying is not a steady-state process. When the moisture content change occurs over almost the entire half thickness of the material, in other words when the size of the fully wet region is very small, the moisture content profiles can be shown to be parabolic during drying if the diffusion coefficient is constant.

The surface of the material does not necessarily come instantly to equilibrium. The surface of the material is only at equilibrium with the drying air during the falling-rate period. Although dry patches have been seen and photographed on the surface of moist granular beds as they dry out (Oliver and Clarke, 1973), fine porous material can have a significant fraction of its exposed surface dry before the evaporation from the whole surface is affected (Suzuki et al., 1972; Schlinder, 1988) due to the buffering effect of the external boundary layer.

Concept of a Characteristic Drying Rate Curve In 1958, van Meel observed that the drying rate curves, during the falling-rate period, for a specific material often show the same shape (Figs. 12-18 and 12-19), so that a single characteristic drying curve can be drawn for the material being dried. Strictly speaking, the concept should only

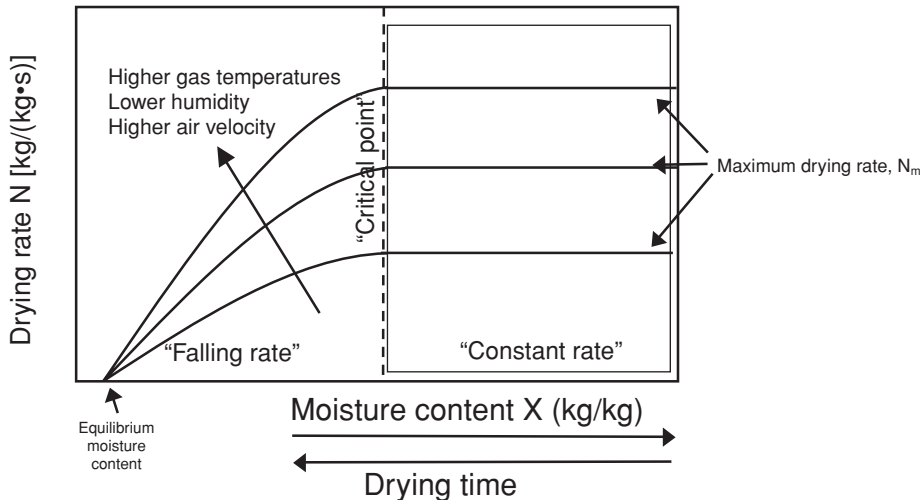


FIG. 12-18 Drying curves for a given material at different constant external conditions.

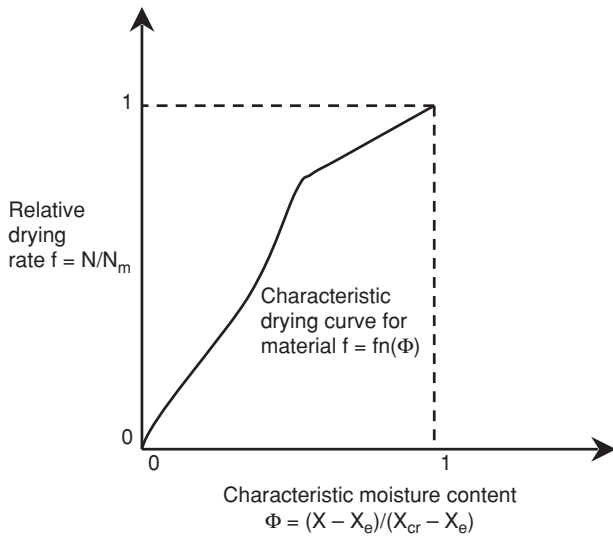


FIG. 12-19 Characteristic drying curve.

apply to materials of the same specific size (surface area to material ratio) and thickness, but Keyy (1992) shows evidence that it applies over a somewhat wider range with reasonable accuracy. In the absence of experimental data, a linear falling-rate curve is often a reasonable first guess for the form of the characteristic function (good approximation for milk powder, fair for ion-exchange resin, silica gel). At each volume-averaged, free moisture content, it is assumed that there is a corresponding specific drying rate relative to the unhindered drying rate in the first drying period that is independent of the external drying conditions. *Volume-averaged* means averaging over the volume (distance cubed for a sphere) rather than just the distance. The relative drying rate is defined as

$$f = \frac{N}{N_m} \tag{12-50}$$

where N is the drying rate, N_m is the rate in the constant-rate period, and the characteristic moisture content becomes

$$\Phi = \frac{\bar{X} - X_e}{X_{cr} - X_e} \tag{12-51}$$

where \bar{X} is the volume-averaged moisture content, X_{cr} is the moisture content at the critical point, and X_e is that at equilibrium. Thus, the drying curve is normalized to pass through the point (1,1) at the critical point of transition in drying behavior and the point (0,0) at equilibrium.

This representation leads to a simple lumped-parameter expression for the drying rate in the falling-rate period, namely,

$$N = fN_m = f[k\phi_m(Y_w - Y_C)] \tag{12-52}$$

Here k is the external mass-transfer coefficient, ϕ_m is the humidity-potential coefficient (corrects for the humidity not being a strictly true representation of the driving force; close to unity most of the time), Y_w is the humidity above a fully wetted surface, and Y_C is the bulk-gas humidity. Equation (12-52) has been used extensively as the basis for understanding the behavior of industrial drying plants owing to its simplicity and the separation of the parameters that influence the drying process: the material itself f , the design of the dryer k , and the process conditions $\phi_m(Y_w - Y_C)f$.

For example, suppose (with nonhygroscopic solids, $X_e = 0$ kg/kg) that we have a linear falling-rate curve, with a maximum drying rate N_m of 0.5 kg moisture/(kg dry solids · s) from an initial moisture content of 1 kg moisture/kg dry solids. If the drying conditions around the sample are constant, what is the time required to dry the material to a moisture content of 0.2 kg moisture/kg dry solids?

$$N = \frac{X}{1 \text{ kg kg}^{-1}} 0.5 \text{ kg kg}^{-1} \text{ s}^{-1}$$

Given that the drying rate dX/dt is equal to N , we have

$$t = \int_{0.2}^1 \frac{dX}{N} = \int_{0.2}^1 \frac{dX}{X(0.5)} = 2 \int_{0.2}^1 \frac{dX}{X} = 2 \ln \frac{1}{0.2} = 3.21 \text{ s} \tag{12-53}$$

The characteristic drying curve, however, is clearly a gross approximation. A common drying curve will be found only if the volume-averaged moisture content reflects the moistness of the surface in some fixed way.

For example, in the drying of impermeable timbers, for which the surface moisture content reaches equilibrium quickly, there is unlikely to be any significant connection between the volume-averaged and the surface moisture contents, so the concept is unlikely to apply. While the concept might not be expected to apply to the same material with different thickness, e.g., Pang finds that it applies for different thicknesses in the drying of softwood timber (Keyy, 1992), its applicability appears to be wider than the theory might suggest. A paper by Kemp and Oakley (2002) explains that many of the errors in the assumptions in this method often cancel out, meaning that the concept has wide applicability.

Keyy and Suzuki (1974) have explored the conditions for which a characteristic curve might apply, using a simplified analysis based on an evaporative front receding through a porous mass. Their analysis shows that a unique curve pertains only when the material is thinly spread and the permeability to moisture is large. Internal diffusion often controls drying as the material becomes very dry, but the result of Keyy and Suzuki suggests that the uniqueness of the curve, in theory, depends on drying not being significantly controlled by internal diffusion. One might expect, then, to find characteristic drying curves for small, microporous particles dried individually, and there is a sufficient body of data to suggest that a characteristic drying curve may be found to describe the drying of discrete particles below 20 mm in diameter over a range of conditions that normally exist within a commercial dryer. Nevertheless, Kemp and Oakley (1992) find that many of the deviations from the assumptions, in practice, cancel out, so that the limitation suggested by Keyy and Suzuki (diffusion not controlling) is not as severe as might be expected.

An example of the application of a linear characteristic drying curve is given in the section on rotary dryers.

EXPERIMENTAL METHODS

Lab-, pilot-, and plant-scale experiments all play important roles in drying research. Lab-scale experiments are often necessary to study product characteristics and physical properties; pilot-scale experiments are often used in proof-of-concept process tests and to generate larger quantities of sample material; and plant-scale experiments are often needed to diagnose processing problems and to start or change a full-scale process.

Measurement of Drying Curves Measuring and using experimental drying curves can be difficult. Typically, this is a three-step process. The first step is to collect samples at different times of drying, the second step is to analyze each sample for moisture, and the third step is to interpret the data to make process decisions.

Solid sample collection techniques depend on the type of dryer. Since a drying curve is the moisture content as a function of time, it must be possible to obtain material before the drying process is complete. There are several important considerations when sampling material for a drying curve:

1. The sampling process needs to be fast relative to the drying process. Drying occurring during or after sampling can produce misleading results. Samples must be sealed prior to analysis. Plastic bags do not provide a sufficient seal.

2. In heterogeneous samples, the sample must be large enough to accurately represent the composition of the mixture.

Table 12-9 outlines some sampling techniques for various dryer types.

Moisture measurement techniques are critical to the successful collection and interpretation of drying data. The key message of this section is that the moisture value almost certainly depends on the measurement technique and that it is essential to have a *consistent*

TABLE 12-9 Sample Techniques for Various Dryer Types

Dryer type	Sampling method
Fluid bed dryer Sheet dryer	Sampling cup (see Fig. 12-20) Collect at end of dryer. Increase speed to change the drying time.
Tray dryer Indirect dryer	Record initial moisture and mass of tray with time. Decrease residence time with higher flow rate and sample at exit.
Spray dryer	Residence time of product is difficult to determine and change. Special probes have been developed to sample partially dried powder in different places within the dryer (ref. Langrish).

technique when measuring moisture. Table 12-10 compares and contrasts some different techniques for moisture measurement.

The most common method is gravimetric ("loss-on-drying"). A sample is weighed in a sample pan or tray and placed into an oven or heater at some high temperature for a given length of time. The sample is weighed again after drying. The difference in weight is then assumed to be due to the complete evaporation of water from the sample. The sample size, temperature, and drying time are all important factors. A very large or thick sample may not dry completely in the given time; a very small sample may not accurately represent the composition of a heterogeneous sample. A low temperature can fail to completely dry the sample, and a temperature that is too high can burn the sample, causing an artificially high loss of mass.

Usually, solid samples are collected as described, but in some experiments, it is more convenient to measure the change in humidity of the air due to drying. This technique requires a good mass balance of the system and is more common in lab-scale equipment than pilot- or plant-scale equipment.

Performing a Mass and Energy Balance on a Large Industrial Dryer Measuring a mass and energy balance on a large dryer is often necessary to understand how well the system is operating and how much additional capacity may be available. This exercise can also be used to detect and debug gross problems, such as leaks and product buildup.

There are several steps to this process.

1. Draw a sketch of the overall process including all the flows of mass into and out of the system. Look for places where air can leak into or out of the system. There is no substitute for physically walking around the equipment to get this information.

2. Decide on the envelope for the mass and energy balance. Some dryer systems have hot-air recycle loops and/or combustion or steam heating systems. It is not always necessary to include these to understand the dryer operation.

3. Decide on places to measure airflows and temperatures and to take feed and product samples. Drying systems and other process equipment are frequently not equipped for such measurements; the system may need minor modification, such as the installation of ports into pipes for pitot tubes or humidity probes. These ports must not leak when a probe is in place.

4. Take the appropriate measurements and calculate the mass and energy balances.

The measurements are inlet and outlet temperatures, humidities, and flow rates of the air inlets and outlets as well as the moisture and temperature of the feed and dry solids. The following are methods for each of the measurements:

Airflow Rate This is often the most difficult to measure. Fan curves are often available for blowers but are not always reliable. A small pitot tube can be used (see Sec. 22, "Waste Management," in this Handbook) to measure local velocity. The best location to use a pitot tube is in a straight section of pipe. Measurements at multiple positions in the cross section of the pipe or duct are advisable, particularly in laminar flow or near elbows and other flow disruptions.

Air Temperature A simple thermocouple can be used in most cases, but in some cases special care must be taken to ensure that wet or sticky material does not build up on the thermocouple. A wet thermocouple will yield a low temperature from evaporative cooling.

Air Humidity Humidity probes need to be calibrated before use, and the absolute humidity (or both the relative humidity and temperature) needs to be recorded. If the probe temperature is below the dew point of the air in the process, then condensation on the probe will occur until the probe heats.

Feed and Exit Solids Rate These are generally known, particularly for a unit in production. Liquids can be measured by using a bucket and stopwatch. Solids can be measured in a variety of ways.

Feed and Exit Solids Moisture Content These need to be measured using an appropriate technique, as described above. Use the same method for both the feed and exit solids. Don't rely on formula sheets for feed moisture information.

Figure 12-20 shows some common tools used in these measurements.

DRYING OF NONAQUEOUS SOLVENTS

Practical Considerations Removal of nonaqueous solvents from a material presents several practical challenges. First, solvents are often flammable and require drying either in an inert environment, such as superheated steam or nitrogen, or in a gas phase comprised solely of solvent vapor. The latter will occur in indirect or

TABLE 12-10 Moisture Determination Techniques

Method	Principle	Advantages	Disadvantages
Gravimetric (loss on drying)	Water evaporates when sample is held at a high temperature. Difference in mass is recorded.	Simple technique. No extensive calibration methods are needed. Lab equipment is commonly available.	Method is slow. Measurement time is several minutes to overnight (depending on material and accuracy). Generally not suitable for process control. Does not differentiate between water and other volatile substances.
IR/NIR	Absorption of infrared radiation by water is measured.	Fast method. Suitable for very thin layers or small particles.	Only surface moisture is detected. Extensive calibration is needed.
RF/microwave	Absorption of RF or microwave energy is measured.	Fast method. Suitable for large particles.	Extensive calibration is needed.
Equilibrium relative humidity (ERH)	The equilibrium relative humidity headspace above sample in a closed chamber is measured. Sorption isotherm is used to determine moisture.	Relatively quick method. Useful particularly if a final moisture specification is in terms of water activity (to retard microorganism growth).	May give misleading results since the surface of the material will equilibrate with the air. Large particles with moisture gradients can give falsely low readings. Measurement of relative humidity can be imprecise.
Karl Fischer titration	Chemical titration that is water-specific. Material can be either added directly to a solvent or heated in an oven, with the headspace purged and bubbled through solvent.	Specific to water only and very precise. Units can be purchased with an autosampler. Measurement takes only a few minutes.	Equipment is expensive and requires solvents. Minimal calibration required. Sample size is small, which may pose a problem for heterogeneous mixtures.

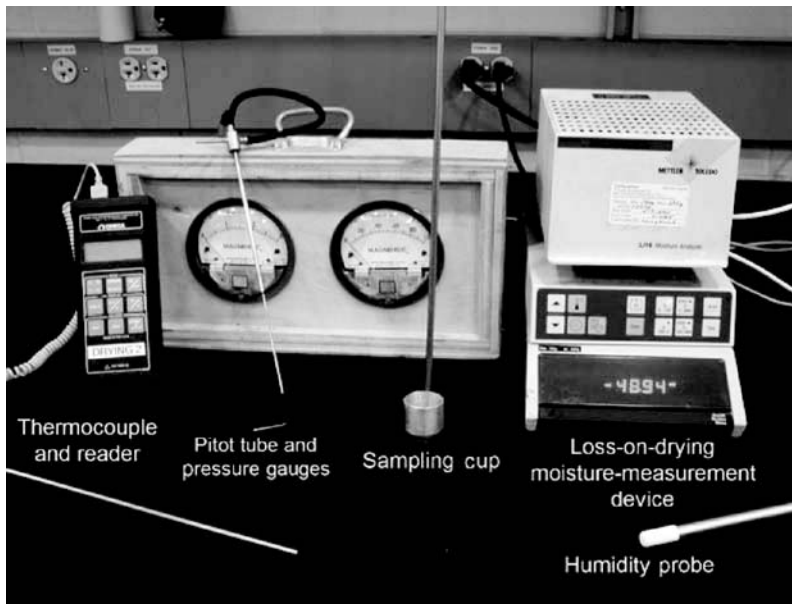


FIG. 12-20 Variety of tools used to measure mass and energy balances on dryers.

vacuum drying equipment. Second, the solvent vapor must be collected in an environmentally acceptable manner.

An additional practical consideration is the remaining solvent content that is acceptable in the final product. Failure to remove all the solvent can lead to problems such as toxicity of the final solid or can cause the headspace of packages, such as drums, to accumulate solvent vapor.

Physical Properties The physical properties that are important in solvent drying are the same as those for an aqueous system. The vapor pressure of a solvent is the most important property since it provides the thermodynamic driving force for drying. Acetone (BP 57°C), for example, can be removed from a solid at atmospheric pressure readily by boiling, but glycerol (BP 200°C) will dry only very slowly. Like water, a solvent may become bound to the solid and have a lower vapor pressure. This effect should be considered when one is designing a solvent-drying process.

Example 18: Preparation of a Psychrometric Chart Make a psychrometric chart for dipropylene glycol. It has a molecular weight of 134.2 g/mol and a normal boiling temperature of 228°C, and the latent heat of vaporization is 65.1 kJ/mol.

The Clausius-Clapeyron equation can be used to estimate the vapor pressure of dipropylene glycol as a function of temperature, with the boiling temperature as a reference.

$$\ln \frac{P_{T_1}^{\text{sat}}}{P_{T_2}^{\text{sat}}} = \frac{-\Delta H_{\text{vap}}}{R} \left(\frac{1}{T_1} - \frac{1}{T_2} \right)$$

where $P_{T_1}^{\text{sat}}$, $P_{T_2}^{\text{sat}}$ = vapor pressures of the solvent at absolute temperatures T_1 and T_2

$$\Delta H_{\text{vap}} = \text{latent heat of vaporization, J/mol}$$

$$R = \text{gas constant, } 8.314 \text{ J/(mol}\cdot\text{K)}$$

Since the boiling temperature is 228°C, 501.15 K and 1 bar were used as T_2 and P_2 . The latent heat value is 65.1 kJ/mol.

Once the vapor pressure of dipropylene glycol is known at a given temperature, the mass of dipropylene glycol/mass of dry air can be calculated. Since dipropylene glycol is the only liquid, the partial pressure of dipropylene glycol equals the vapor pressure.

$$P_{\text{dipropylene glycol}} = P_{\text{dipropylene glycol}}^{\text{sat}}$$

The mole fraction of dipropylene glycol is the partial pressure divided by the total system pressure, taken to equal 1 bar.

$$y_{\text{dipropylene glycol}} = \frac{P_{\text{dipropylene glycol}}}{P}$$

The saturation mole ratio of dipropylene glycol to air is given by the following.

$$\text{Mole ratio} = \frac{y_{\text{dipropylene glycol}}}{1 - y_{\text{dipropylene glycol}}}$$

The saturation mass ratio of dipropylene glycol to air is calculated by multiplying by the molecular weights. The mass ratio as a function of temperature gives the saturation curve, as shown in Fig. 12-21.

$$\begin{aligned} \text{Saturation mass ratio} &= \frac{\text{g dipropylene glycol}}{\text{g dry air}} \\ &= \frac{\text{molecular weight of dipropylene glycol}}{\text{molecular weight of dry air}} \cdot \frac{y_{\text{dipropylene glycol}}}{1 - y_{\text{dipropylene glycol}}} \end{aligned}$$

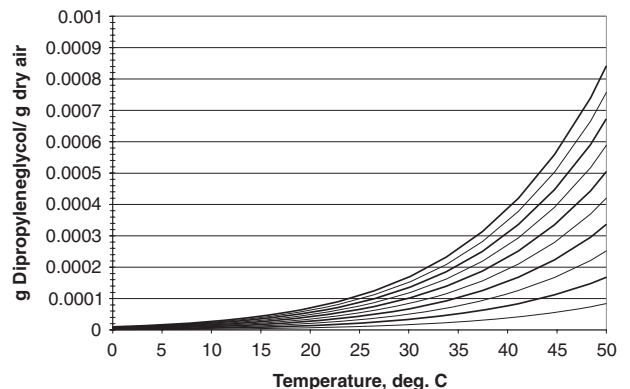


FIG. 12-21 An example of a solvent psychrometric chart.

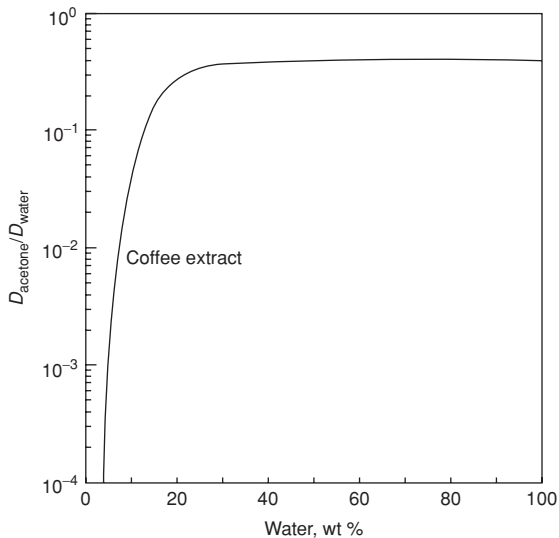


FIG. 12-22 The ratio of the diffusion coefficients of acetone to water in instant coffee as a function of moisture content (taken from Thijssen et al., *De Ingenieur*, JRC, 80, Nr. 47 (1968)]. Acetone has a much higher vapor pressure than water, but is selectively retained in coffee during drying.

Each relative humidity curve is proportional to the saturation value.

$$\text{Mass ratio} = \left(\frac{\%RH}{100} \right) \cdot \text{saturation mass ratio}$$

Diffusion of nonaqueous solvents through a material can be slow. The diffusion coefficient is directly related to the size of the diffusing molecule, so molecules larger than water typically have diffusion coefficients that have a much lower value. This phenomenon is known as *selective diffusion*. Large diffusing molecules can become kinetically trapped in the solid matrix. Solvents with a lower molecular weight will often evaporate from a material faster than a solvent with a higher molecular weight, even if the vapor pressure of the larger molecule is higher. Some encapsulation methods rely on selective diffusion; an example is instant coffee production using spray drying, where volatile flavor and aroma components are retained in particles more than water, even though they are more volatile than water, as shown in Fig. 12-22.

PRODUCT QUALITY CONSIDERATIONS

Overview The drying operation usually has a very strong influence on final product quality and product performance measures. And the final product quality strongly influences the value of the product. Generally, a specific particle or unit size, a specific density, a specific color, and a specific target moisture are desired. Naturally every product is somewhat different, but these are usually the first things we need to get right.

Target Moisture This seems obvious, but it's very important to determine the right moisture target before we address other drying basics. Does biological activity determine the target, flowability of the powder, shelf life, etc.? Sometimes a very small (1 to 2 percent) change in the target moisture will have a very big impact on the size of the dryer required. This is especially true for difficult-to-dry products with flat falling-rate drying characteristics. Therefore, spend the time necessary to get clear on what really determines the moisture target. And as noted earlier in this subsection, care should be taken to define a moisture measurement method since results are often sensitive to the method.

Particle Size Generally a customer or consumer wants a very specific particle size—and the narrower the distribution, the better. No one wants lumps or dust. The problem is that some attrition and

sometimes agglomeration occur during the drying operation. We may start out with the right particle size, but we must be sure the dryer we've selected will not adversely affect particle size to the extent that it becomes a problem. And some dryers will treat particles more gently than others. Particle size is also important from a segregation standpoint. See Sec. 18, "Solid-Solid Operations and Equipment." And of course fine particles can also increase the risk of fire or explosion.

Density Customers and consumers are generally also very interested in getting the product density they have specified or expect. If the product is a consumer product and going into a box, then the density needs to be correct to fill the box to the appropriate level. If density is important, then product shrinkage during drying can be an important harmful transformation to consider. This is particularly important for biological products for which shrinkage can be very high. This is why freeze drying can be the preferred dryer for many of these materials.

Solubility Many dried products are rewet either during use by the consumer or by a customer during subsequent processing. Shrinkage can again be a very harmful transformation. Many times shrinkage is a virtually irreversible transformation which creates an unacceptable product morphology. Case hardening is a phenomenon that occurs when the outside of the particle or product initially shrinks to form a very hard and dense skin that does not easily rewet. A common cause is capillary collapse, discussed along with shrinkage below.

Flowability If we're considering particles, powders, and other products that are intended to flow, then this is a very important consideration. These materials need to easily flow from bins, hoppers, and out of boxes for consumer products. Powder flowability is a measurable characteristic using rotational shear cells (Peschl) or translational shear cells (Jenike) in which the powder is consolidated under various normal loads, and then the shear force is measured, enabling a complete yield locus curve to be constructed. This can be done at various powder moistures to create a curve of flowability versus moisture content. Some minimal value is necessary to ensure free flow. Additional information on these devices and this measure can be found in Sec. 21, "Solid-Solid Operations and Processing."

Color Product color is usually a very important product quality attribute, and a change in color can be caused by several different transformations.

Transformations Affecting Product Quality Drying, as with any other unit operation, has both productive and harmful transformations that occur. The primary productive transformation is water removal of course, but there are many harmful transformations that can occur and adversely affect product quality. The most common of these harmful transformations includes product shrinkage; attrition or agglomeration; loss of flavor, aroma, and nutritional value; browning reactions; discoloration; stickiness; and flowability problems. These were discussed briefly above, but are worth a more in-depth review.

Shrinkage Shrinkage is a particularly important transformation with several possible mechanisms to consider. It's usually especially problematic with food and other biological materials, but is a very broadly occurring phenomenon. Shrinkage generally affects solubility, wettability, texture and morphology, and absorbency. It can be observed when drying lumber when it induces stress cracking and during the drying of coffee beans prior to roasting. Tissue, towel, and other paper products undergo some shrinkage during drying. And many chemical products shrink as water evaporates, creating voids and capillaries prone to collapse as additional water evaporates. As we consider capillary collapse, there are several mechanisms worth mentioning.

Surface tension—the capillary suction created by a receding liquid meniscus can be extremely high.

Plasticization—an evaporating solvent which is also a plasticizer of polymer solute product will lead to greater levels of collapse and shrinkage.

Electric charge effects—the van der Waals and electrostatic forces can also be a strong driver of collapse and shrinkage.

Surface Tension These effects are very common and worth a few more comments. Capillary suction created by a receding liquid meniscus can create very high pressures for collapse. The quantitative

expression for the pressure differential across a liquid-fluid interface was first derived by Laplace in 1806. The meniscus, which reflects the differential, is affected by the surface tension of the fluid. Higher surface tensions create greater forces for collapse. These strong capillary suction pressures can easily collapse a pore. We can reduce these suction pressures by using low-surface-tension fluids or by adding surfactants, in the case of water, which will also significantly reduce surface tension (from 72 to 30 dyn/cm).

The collapse can also be reduced with some dryer types. Freeze drying and heat pump drying can substantially reduce collapse, but of course, the capital cost of these dryers sometimes makes them prohibitive. At the other extreme, dryers which rapidly flash off the moisture can reduce collapse. This mechanism can also be affected by particle size such that the drying is primarily boundary-layer-controlled. When the particle size becomes sufficiently small, moisture can diffuse to the surface at a rate sufficient to keep the surface wetted. This has been observed in a gel-forming food material when the particle size reached 150 to 200 μm (Genskow, "Considerations in Drying Consumer Products," *Proceedings International Drying Symposium*, Versailles, France, 1988).

Biochemical Degradation Biochemical degradation is another harmful transformation that occurs with most biological products. There are four key reactions to consider: lipid oxidation, Maillard browning, protein denaturation, and various enzyme reactions. These reactions are both heat- and moisture-dependent such that control of temperature and moisture profiles can be very important during drying.

Lipid oxidation. Lipid oxidation is normally observed as a product discoloration and can be exacerbated with excess levels of bleach. It is catalyzed by metal ions, enzymes, and pigments. Acidic compounds can be used to complex the metal ions. Synthetic antioxidants, such as butylated hydroxytoluene (BHT) and butylated hydroxyanisole (BHA) can be added to the product, but are limited and coming under increased scrutiny due to toxicology concerns. It may be preferable to use natural antioxidants such as lecithin or vitamin E or to dry under vacuum or in an inert (nitrogen, steam) atmosphere.

Protein denaturation. Protein denaturation is normally observed as an increase in viscosity and a decrease in wettability. It is temperature-sensitive, generally occurring between 40 and 80°C. A common drying process scheme is to dry thermally and under wet-bulb drying conditions without overheating and then vacuum, heat-pump, or freeze-dry to the target moisture.

Enzyme reactions. Enzymatic browning is caused by the enzyme polyphenol oxidase which causes phenols to oxidize to ortho-quinones. The enzyme is active between pH 5 to 7. A viable process scheme again is to dry under vacuum or in an inert (nitrogen, steam) atmosphere.

Maillard browning reaction. This nonenzymatic reaction is observed as a product discoloration, which in some products creates an attractive coloration. The reaction is temperature-sensitive, and normally the rate passes through a maximum and then falls as the product becomes drier. The reaction can be minimized by minimizing the drying temperature, reducing the pH to acidic, or adding an inhibitor such as sulfur dioxide or metabisulfate. A viable process scheme again is to dry thermally and under wet-bulb drying conditions without overheating and then vacuum, heat-pump, or freeze-dry to the target moisture.

Some of the above reactions can be minimized by reducing the particle size and using a monodisperse particle size distribution. The small particle size will better enable wet-bulb drying, and the monodisperse size will reduce overheating of the smallest particles.

Stickiness, Lumping, and Caking These are not characteristics we generally want in our products. They generally connote poor product quality, but can be a desirable transformation if we are trying to enlarge particle size through agglomeration. Stickiness, lumping, and caking are phenomena which are dependent on product moisture and product temperature. The most general description of this phenomenon can be described by measuring the cohesion (particle to particle) of powders as described below. A related measure is adhesion—particle-to-wall interactions. Finally, sticky point is a special case for materials which undergo glass transitions.

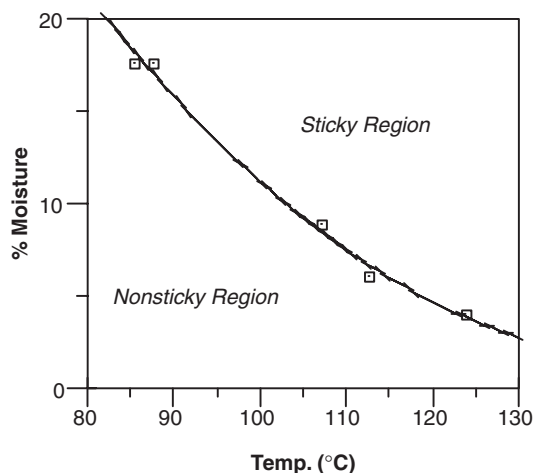


FIG. 12-23 Detergent stickiness curve.

The sticky point can be determined by using a method developed by Lazar and later by Downton [Downton, Flores-Luna, and King, "Mechanism of Stickiness in Hygroscopic, Amorphous Powders," *I&EC Fundamentals* 21: 447 (1982)]. In the simplest method, a sample of the product, at a specific moisture, is placed in a closed tube which is suspended in a water bath. A small stirrer is used to monitor the torque needed to "stir" the product. The water bath temperature is slowly increased until the torque increases. This torque increase indicates a sticky point temperature for that specific moisture. The test is repeated with other product moistures until the entire stickiness curve is determined. A typical curve is shown in Fig. 12-23.

As noted, a sticky point mechanism is a glass transition—the transition when a material changes from the glassy state to the rubbery liquid state. Glass transitions are well documented in food science (Levine and Slade). Roos and Karel [Roos and Karel, "Plasticizing Effect of Water on Thermal Behavior and Crystallization of Amorphous Food Models," *J. Food Sci.* 56(1): 38–43 (1991)] have demonstrated that for these types of products, the glass transition temperature follows the sticky point curve within about 2°C. This makes it straightforward to measure the stickiness curve by using a differential scanning calorimeter (DSC). Somewhat surprisingly, even materials which are not undergoing glass transitions exhibit this behavior, as demonstrated with the detergent stickiness curve above.

Lumping and caking can be measured by using the rotational shear cells (Peschl) or translational shear cells (Jenike) noted above for measuring flowability. The powder is consolidated under various normal loads, and then the shear force is measured, enabling a complete yield locus curve to be constructed. This can be done at various powder moistures to create a curve of "cake strength" versus moisture content. Slurries and dry solids are free-flowing, and there is a cohesion/adhesion peak at an intermediate moisture content, typically when voids between particles are largely full of liquid. A variety of other test methods for handling properties and flowability are available.

Product quality was addressed quite comprehensively by Evangelos Tsotsas at the 2d Nordic Drying Conference [Tsotsas, "Product Quality in Drying—Luck, Trial, Experience, or Science?" 2d Nordic Drying Conference, Copenhagen, Denmark, 2003]. Tsotsos notes that 31 percent of the papers at the 12th International Drying Symposium refer to product quality. The top 5 were color (12 percent), absence of chemical degradation (10 percent), absence of mechanical damage (9 percent), bulk density (8 percent), and mechanical properties (7 percent). These are all properties that are reasonably straightforward to measure. They are physical properties, and we are familiar with them for the most part. However, down the list at a rank

of 20 with only 2 percent of the papers dealing with it, we have sensory properties.

This is the dilemma—sensory properties should rank very high, but they don't because we lack the tools to measure them effectively. For the most part, these quality measures are subjective rather than objective, and frequently they require direct testing with consumers to determine efficacy of a particular product attribute. So the issue is really a lack of physical measurement tools that directly assess the performance measures important to the consumer of the product. The lack of objective performance measures and unknown mechanistic equations also makes mathematical modeling very difficult for addressing quality problems.

The good news is that there has been a shift from the macro to the meso and now to the microscale in drying science. We have some very powerful analytical tools to help us understand the transformations that are occurring at the meso and microscale.

ADDITIONAL READING

- Keey, *Drying of Loose and Particulate Materials*. Hemisphere, New York, 1992.
- Keey, Langrish, and Walker, *Kiln Drying of Lumber*, Springer-Verlag, Heidelberg, 2000.
- Keey and Suzuki, "On the Characteristic Drying Curve," *Int. J. Heat Mass Transfer* **17**:1455–1464 (1974).
- Kemp and Oakley, "Modeling of Particulate Drying in Theory and Practice," *Drying Technol.* **20**(9):1699–1750 (2002).
- Kock et al., "Design, Numerical Simulation and Experimental Testing of a Modified Probe for Measuring Temperatures and Humidities in Two-Phase Flow," *Chem. Eng. J.* **76**(1):49–60 (2000).
- Liou and Bruin, "An Approximate Method for the Nonlinear Diffusion Problem with a Power Relation between the Diffusion Coefficient and Concentration. 1. Computation of Desorption Times," *Int. J. Heat Mass Transfer* **25**:1209–1220 (1982a).
- Liou and Bruin, "An Approximate Method for the Nonlinear Diffusion Problem with a Power Relation between the Diffusion Coefficient and Concentration. 2. Computation of the Concentration Profile," *Int. J. Heat Mass Transfer* **25**:1221–1229 (1982b).
- Marshall, "Atomization and Spray Drying," *AICHE Symposium Series*, No. 2, p. 89 (1986).
- Oliver and Clarke, "Some Experiments in Packed-Bed Drying," *Proc. Inst. Mech. Engrs.* **187**:515–521 (1973).
- Perré and Turner, "The Use of Macroscopic Equations to Simulate Heat and Mass Transfer in Porous Media," in Turner and Mujumdar (eds.), *Mathematical Modeling and Numerical Techniques in Drying Technology*, Marcel Dekker, New York, 1996, pp. 83–156.
- Ranz and Marshall, "Evaporation from Drops," *Chem. Eng. Prog.* **48**(3):141–146 and **48**(4):173–180 (1952).
- Schoeber and Thijssen, "A Short-cut Method for the Calculation of Drying Rates for Slabs with Concentration-Dependent Diffusion Coefficient," *AICHE Symposium Series*, **73**(163):12–24 (1975).
- Schlünder, "On the Mechanism of the Constant Drying Rate Period and Its Relevance to Diffusion Controlled Catalytic Gas Phase Reactions," *Chem. Eng. Sci.* **43**:2685–2688 (1988).
- Sherwood, "The Drying of Solids," *Ind. and Eng. Chem.* **21**(1):12–16 (1929).
- Suzuki et al., "Mass Transfer from a Discontinuous Source," *Proc. PACHEC '72*, Kyoto, Japan, **3**:267–276 (1972).
- Thijssen et al., *De Ingenieur, JRG*, **80**(47) (1968).
- Thijssen and Coumans, "Short-cut Calculation of Non-isothermal Drying Rates of Shrinking and Non-shrinking Particles Containing an Expanding Gas Phase," *Proc. 4th Int. Drying Symp., IDS '84*, Kyoto, Japan, **1**:22–30 (1984).
- Van der Lijn, doctoral thesis, Wageningen, 1976.
- van Meel, "Adiabatic Convection Batch Drying with Recirculation of Air," *Chem. Eng. Sci.* **9**:36–44 (1958).
- Viollez and Suarez, "Drying of Shrinking Bodies," *AICHE J.* **31**:1566–1568 (1985).
- Waananan, Litchfield, and Okos, "Classification of Drying Models for Porous Solids," *Drying Technol.* **11**(1):1–40 (1993).

SOLIDS-DRYING EQUIPMENT—GENERAL ASPECTS

GENERAL REFERENCES: *Aspen Process Manual (Internet knowledge base)*, Aspen Technology, 2000 onward. Cook and DuMont, *Process Drying Practice*, McGraw-Hill, New York, 1991. *Drying Technology—An International Journal*, Taylor and Francis, New York, 1982 onward. Hall, *Dictionary of Drying*, Marcel Dekker, New York, 1979. Keey, *Introduction to Industrial Drying Operations*, Pergamon, New York, 1978. Mujumdar (ed.), *Handbook of Industrial Drying*, Marcel Dekker, New York, 1995. van't Land, *Industrial Drying Equipment*, Marcel Dekker, New York, 1991.

CLASSIFICATION OF DRYERS

Drying equipment may be classified in several ways. Effective classification is vital in selection of the most appropriate dryer for the task and in understanding the key principles on which it operates. The main categories are as follows:

1. Form of feed and product—particulate (solid or liquid feed), sheet, slab
2. Mode of operation—batch or continuous
3. Mode of heat transfer—convective (direct), conductive (indirect), radiative, or dielectric
4. Condition of solids—static bed, moving bed, fluidized or dispersed
5. Gas-solids contacting—parallel flow, perpendicular flow, or through-circulation
6. Gas flow pattern—cross-flow, cocurrent, or countercurrent

Other important features of the drying system are the type of carrier gas (air, inert gas, or superheated steam/solvent), use of gas or solids recycle, type of heating (indirect or direct-fired), and operating pressure (atmospheric or vacuum). However, these are primarily related to the choice of the overall system and operating conditions, not to the individual dryer used, and are discussed briefly at the end of this section. The relative importance of the different categories depends on the purpose of the classification. For distinguishing differences in dryer design, construction, and operation, categories 2 and 3 are particularly useful. A classification chart of drying equipment on this basis is shown in Table 12-11, and the grouping in "Solids-Drying Equipment—Specific Types" follows this pattern. Simplified diagrams for batch and continuous dryers are shown in Figs. 12-24 and 12-25, respectively. However, in the selection of a group of dryers for preliminary consideration in a given drying problem, the most important factor is often category 1, the form, handling characteristics, and physical properties of the wet material. (See Table 12-12.)

In Table 12-11, dryers in round brackets are semicontinuous forms of batch dryers, not commonly used. Dryers in square brackets are semibatch forms of continuous dryers, also fairly rare.

The feed type is a very basic description; *particulate* can also include powders, granules, pastes, pellets, performs, etc.; *liquid/slurry* also includes solutions and sludges. Table 12-12 gives a more comprehensive classification based on particle size and handling properties.

Description of Dryer Classification Criteria

1. Form of Feed and Product Dryers are specifically designed for particular feed and product forms; dryers handling films, sheets, slabs, and bulky artifacts form a clear subset. Most dryers are for particulate products, but the feed may range from a solution or slurry (free-flowing liquid) through a sticky paste to wet filter cakes, powders, or granules (again relatively free-flowing). The ability to successfully mechanically handle the feed and product is a key factor in dryer selection (see Table 12-12).

The drying kinetics (rate of drying, and hence required drying time) also depend strongly on solids properties, particularly particle size and porosity. The surface area/mass ratio and the internal pore structure control the extent to which an operation is diffusion-limited, i.e., diffusion into and out of the pores of a given solids particle, not through the voids among separate particles.

2. Mode of Operation Batch dryers are typically used for low throughputs (averaging under 50 kg/h), long drying times, or where the overall process is predominantly batch. Continuous dryers dominate for high throughputs (over 1 ton/h), high evaporation rates, and where the rest of the process is continuous. Often, there are batch and continuous dryers working on similar principles, but one batch dryer has two or more continuous equivalents, using different methods to move the solids through the dryer. For example, batch tray dryers (nonagitated solids) are equivalent to turbo-tray and plate dryers (vertical gravity transport) and to band dryers (horizontal mechanical transport). Also, dryers which are inherently continuous can be operated in semibatch mode (e.g., small-scale spray dryers) and vice versa.

3. Mode of Heat Transfer

Direct (convective) dryers The general operating characteristics of direct dryers are these:

TABLE 12-11 Classification of Drying Equipment

Dryer group	Feed type	Dryer type	Heating mode	Synonyms and variants
Batch tray Nonagitated	Particulate	Cross-circulated tray Perforated tray Contact/vacuum tray	Cross-circulation Through-circulation Conduction	Atmospheric tray Through-circulation, drying room Vacuum oven, vacuum shelf
Batch agitated Mechanical agitation	Particulate	Vertical pan Conical Spherical Horizontal pan	Conduction Conduction Conduction Conduction	Vertical agitated Sidescrew, Nauta Turbosphere Batch paddle, ploughshare
Continuous tray Nonagitated	Particulate	Turbo-tray Plate Cascade Moving bed	Cross-circulation Conduction Through-circulation Through-circulation	Rotating tray/shelf, Wyssmont Turbo-dryer Krauss-Maffei Wenger Tower, silo, gravity
Continuous band/tunnel Nonagitated	Particulate	Tunnel Perforated band Contact/vacuum band	Cross-circulation Through-circulation Conduction	Moving truck/trolleys Atmospheric band/belt, vibrated bed Vacuum belt, vibrated tray
Continuous agitated Mechanical agitation	Particulate	Paddle, low-speed Paddle, high-speed High-speed convective paddle	Conduction Conduction Through-circulation	Horizontal agitated, Disc, Porcupine, Nara Solidaire Rapid, Forberg
Continuous rotary Rotational agitation	Particulate	Indirect rotary Rotary louvre Cascading rotary	Conduction Through-circulation Dispersion	Steam-tube, Louisville Rotolouvre Direct rotary, rotary drum
Continuous dispersion Airborne transport	Particulate	Fluidized bed Vibrofluidized bed Pneumatic conveying Spin-flash	Dispersion Dispersion Dispersion Dispersion	Well-mixed/plug-flow fluid bed Vibrated fluid bed Flash, ring, swept mill Swirl fluidizer
Continuous special	Particulate	Spouted bed (Freeze)	Dispersion Conduction	Circulating fluid bed Continuous freeze
Continuous liquid feed	Liquid/slurry	Radiofrequency/microwave Spray Spray/fluidized bed Fluid bed granulator Thin-film Drum (Filter-dryer)	Radiation Dispersion Dispersion Dispersion Conduction Conduction Conduction	Dielectric Atomizing Spray/belt Recirculating inert balls Evaporator-dryer, wiped-film, LUWA Film-drum Nutsche, Rosenmund
Continuous sheet/film	Film/sheet	Centrifuge-dryer Cylinder Yankee Rotary through Stenter Flotation Continuous oven Infrared	Through-circulation Conduction Conduction Through-circulation Through-circulation Through-circulation Conduction Radiation	Henkel Paper machine, roller Impingement Tenter, range (textiles) Coanda, floating web Festoon, Spooner oven Curing

- a. Direct contacting of hot gases with the solids is employed for solids heating and vapor removal.
- b. Drying temperatures may range up to 1000 K, the limiting temperature for most common structural metals. At higher temperatures, radiation becomes an important heat-transfer mechanism.
- c. At gas temperatures below the boiling point, the vapor content of gas influences the rate of drying and the final moisture content of the solid. With gas temperatures above the boiling point throughout,

- the vapor content of the gas has only a slight retarding effect on the drying rate and final moisture content. Thus, superheated vapors of the liquid being removed (e.g., steam) can be used for drying.
- d. For low-temperature drying, dehumidification of the drying air may be required when atmospheric humidities are excessively high.
- e. The lower the final moisture content, the more fuel per pound of water evaporated, that a direct dryer consumes.

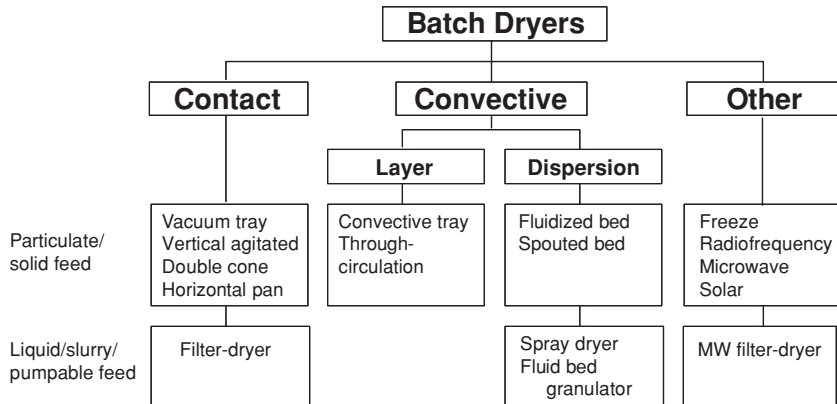


FIG. 12-24 Classification of batch dryers.

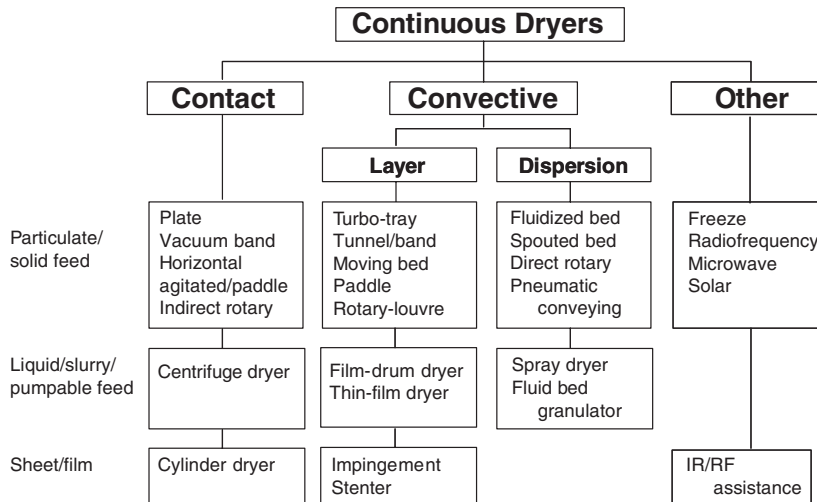


FIG. 12-25 Classification of continuous dryers.

f. Efficiency increases with an increase in the inlet gas temperature for a constant exhaust temperature.

g. Because large amounts of gas are required to supply all the heat for drying, dust recovery equipment may be very large and expensive, especially when drying very small particles.

Indirect (contact or conductive) dryers These differ from direct dryers with respect to heat transfer and vapor removal:

a. Heat is transferred to the wet material by conduction through a solid retaining wall, usually metallic.

b. Surface temperatures may range from below freezing in the case of freeze dryers to above 800 K in the case of indirect dryers heated by combustion products.

c. Indirect dryers are suited to drying under reduced pressures and inert atmospheres, to permit the recovery of solvents and to prevent the occurrence of explosive mixtures or the oxidation of easily decomposed materials.

d. Indirect dryers using condensing fluids as the heating medium are generally economical from the standpoint of heat consumption, since they furnish heat only in accordance with the demand made by the material being dried.

e. Dust recovery and dusty or hazardous materials can be handled more satisfactorily in indirect dryers than in direct dryers.

Miscellaneous dryers

a. **Infrared dryers** depend on the transfer of radiant energy to evaporate moisture. The radiant energy is supplied electrically by infrared lamps, by electric resistance elements, or by incandescent refractories heated by gas. The last method has the added advantage of convection heating. Infrared heating is not widely used in the chemical industries for the removal of moisture. Its principal use is in baking or drying paint films (curing) and in heating thin layers of materials. It is sometimes used to give supplementary heating on the initial rolls of paper machines (cylinder dryers).

b. **Dielectric dryers (radio-frequency or microwave)** have not as yet found a wide field of application, but are increasingly used. Their fundamental characteristic of generating heat within the solid indicates potentialities for drying massive geometric objects such as wood, sponge-rubber shapes, and ceramics, and for evening out moisture gradients in layers of solids. Power costs are generally much higher than the fuel costs of conventional methods; a small amount of dielectric heating (2 to 5 percent) may be combined with thermal heating to maximize the benefit at minimum operating cost. The high capital costs of these dryers must be balanced against product and process improvements.

4. Condition of Solids In solids-gas contacting equipment, the solids bed can exist in any of the following four conditions.

Static This is a dense bed of solids in which each particle rests upon another at essentially the settled bulk density of the solids phase. Specifically, *there is no relative motion among solids particles* (Fig. 12-26).

Moving This is a slightly expanded bed of solids in which the particles are separated only enough to flow one over another. Usually the flow is downward under the force of gravity (Fig. 12-27a), but upward motion by mechanical lifting or agitation may also occur within the process vessel (Fig. 12-27b). In some cases, lifting of the solids is accomplished in separate equipment, and solids flow in the presence of the gas phase is downward only. The latter is a moving bed as usually defined in the petroleum industry. In this definition, *solids motion is achieved by either mechanical agitation or gravity force*.

Fluidized This is an expanded condition in which the solids particles are supported by drag forces caused by the gas phase passing through the interstices among the particles at some critical velocity. The superficial gas velocity upward is less than the terminal settling velocity of the solids particles; the gas velocity is not sufficient to entrain and convey continuously all the solids. Specifically, the solids phase and the gas phase are intermixed and *together behave as a boiling fluid* (Fig. 12-28). The gas forms the continuous phase, but the bulk density is not much lower than a continuous packed bed of solids.

Dispersed or dilute. This is a fully expanded condition in which the solids particles are so widely separated that they exert essentially no influence upon one another. Specifically, the solids phase is so fully dispersed in the gas that the *density of the suspension is essentially that of the gas phase alone* (Fig. 12-29). Commonly, this situation exists when the gas velocity at all points in the system exceeds the terminal settling velocity of the solids and the particles can be lifted and continuously conveyed by the gas; however, this is not always true. Cascading rotary dryers, countercurrent-flow spray dryers, and gravity settling chambers such as prilling towers are three exceptions in which gas velocity is insufficient to entrain the solids completely.

Cascading (direct) rotary dryers with lifters illustrate all four types of flow in a single dryer. Particles sitting in the lifters (flights) are a static bed. When they are in the rolling bed at the bottom of the dryer, or rolling off the top of the lifters, they form a moving bed. They form a falling curtain which is initially dense (fluidized) but then spreads out and becomes dispersed.

Dryers where the solid forms the continuous phase (static and moving beds) are called **layer dryers**, while those where the gas forms the continuous phase (fluidized and dispersed solids) are classified as **dispersion dryers**. Gas-particle heat and mass transfer is much faster in dispersion dryers, and these are therefore often favored where high drying rates, short drying times, or high solids throughput is required.

TABLE 12-12 Classification of Commercial Dryers Based on Feed Materials Handled

	Liquids	Slurries	Pastes and sludges	Free-flowing powders	Granular, crystalline, or fibrous solids	Large solids, special forms and shapes	Continuous sheets	Discontinuous sheets
Type of dryer	True and colloidal solutions; emulsions. Examples: inorganic salt solutions, extracts, milk, blood, waste liquors, rubber latex	Pumpable suspensions. Examples: pigment slurries, soap and detergents, calcium carbonate, bentonite, clay slip, lead concentrates	Examples: filter-press cakes, sedimentation sludges, centrifuged solids, starch	100-mesh (150 µm) or less. Relatively free-flowing in wet state. Dusty when dry. Examples: centrifuged precipitates	Larger than 100-mesh (150 µm). Examples: rayon staple, salt crystals, sand, ores, potato strips, synthetic rubber	Examples: pottery, brick, rayon cakes, shotgun shells, hats, painted objects, rayon skeins, lumber	Examples: paper, impregnated fabrics, cloth, cellophane, plastic sheets	Examples: veneer, wallboard, photograph prints, leather, foam rubber sheets
Vacuum freeze. Indirect type, batch or continuous operation	Expensive. Usually used only for high-value products such as pharmaceuticals; products, which are heat-sensitive and readily oxidized.	See comments under Liquids.	See comments under Liquids.	See comments under Liquids.	Expensive. Usually used on pharmaceuticals and related products which cannot be dried successfully by other means. Applicable to fine chemicals	See comments under Granular solids.	Applicable in special cases such as emulsion-coated films	See comments under Granular solids.
Vacuum tray/shelf. Indirect type, batch operation	Not applicable	Relatively expensive. Applicable for small-batch production	Relatively expensive. Suitable for batch operation, small capacities. Useful for heat-sensitive or readily oxidizable materials. Solvents can be recovered.	See comments under Pastes and Sludges.	Suitable for batch operation, small capacities. Useful for heat-sensitive or readily oxidizable materials. Solvents can be recovered.	See comments under Granular solids.	Not applicable	See comments under Granular solids.
Pan. Indirect type, batch operation including vertical agitated pan, spherical, conical, filter-dryer, double-cone tumbler	Atmospheric or vacuum. Suitable for small batches. Easily cleaned. Solvents can be recovered. Material agitated while dried.	See comments under Liquids.	See comments under Liquids.	See comments under Liquids.	Suitable for small batches. Easily cleaned. Material is agitated during drying, causing some degradation and/or balling up.	Not applicable	Not applicable	Not applicable
Vacuum horizontal agitated and rotary. indirect type, batch operation. Includes indirect rotary, horizontal pan	Not applicable, except when pumping slowly on dry "heel"	May have application in special cases when pumping onto dry "heel"	Material usually cakes to dryer walls and agitator. Special precautions needed, e.g., cleaning hooks, twin screws. Solvents can be recovered.	Suitable for nonsticking materials. Useful for large batches of heat-sensitive materials and for solvent recovery.	Useful for large batches of heat-sensitive materials or where solvent is to be recovered. Product will suffer some grinding action, or may ball up. Dust collectors may be required.	Not applicable	Not applicable	Not applicable
Screw conveyor and indirect rotary. Indirect type, continuous operation. Includes paddle, horizontal agitated and steam-tube dryers, rotary kilns.	Applicable with dry-product recirculation	Applicable with dry-product recirculation	Generally requires recirculation of dry product. Little dusting occurs.	Chief advantage is low dust loss. Well suited to most materials and capacities, particularly those requiring drying at steam temperature	Low dust loss. Material must not stick or be temperature-sensitive	Not applicable	Not applicable	Not applicable

TABLE 12-12 Classification of Commercial Dryers Based on Feed Materials Handled (Concluded)

Type of dryer	Liquids	Slurries	Pastes and sludges	Free-flowing powders	Granular, crystalline, or fibrous solids	Large solids, special forms and shapes	Continuous sheets	Discontinuous sheets
Vibrating tray, vacuum band. Indirect type, continuous operation	Not applicable	Not usually applicable. Belt with raised edges possible, but rare	Not usually applicable due to feed and discharge problems	Suitable for free-flowing materials	Suitable for free-flowing materials that can be conveyed on a vibrating tray or belt	Not applicable	Not applicable	Not applicable
Drum. Indirect type, continuous operation	Single, double, or twin. Atmospheric or vacuum operation. Product flaky and usually dusty. Maintenance costs may be high.	See comments under Liquids. Twin-drum dryers are widely used.	Can be used only when paste or sludge can be made to flow. See comments under Liquids.	Not applicable	Not applicable	Not applicable	Not applicable	Not applicable
Cylinder. Indirect type, continuous operation	Not applicable	Not applicable	Not applicable	Not applicable	Not applicable	Not applicable	Suitable for thin or mechanically weak sheets which can be dried in contact with a heated surface. Special surface effects obtainable	Suitable for materials which need not be dried flat and which will not be injured by contact with hot drum
Tray and compartment. Direct type, batch operation. Includes cross-circulated tray	Not applicable	For very small batch production. Laboratory drying	Suited to batch operation. At large capacities, investment and operating costs are high. Long drying times	Dusting may be a problem. See comments under Pastes and Sludges.	Suited to batch operation. At large capacities, investment and operating costs are high. Long drying times	See comments under Granular solids.	Not applicable	See comments under Granular solids.
Batch through-circulation. Direct type, batch operation includes perforated tray, drying room	Not applicable	Not applicable	Suitable only if material can be preformed. Suited to batch operation. Shorter drying time than tray dryers	Not applicable	Usually not suited for materials smaller than 30-mesh (0.5 mm). Suited to small capacities and batch operation	Primarily useful for small objects	Not applicable	Not applicable
Tunnel/continuous tray. Direct type, continuous operation. Includes tunnel, turbo-tray	Not applicable	Not applicable	Suitable for small- and large-scale production	See comments under Pastes and Sludges. Vertical turbo-tray applicable	Essentially large-scale, semi-continuous tray drying	Suited to a wide variety of shapes and forms, especially tunnel type. Operation can be made continuous. Widely used	Not applicable	Suited for leather, wallboard, veneer
Continuous through-circulation (nonagitated). Direct type, continuous operation. Includes perforated band, moving bed, centrifuge-dryer.	Not applicable	Only crystal filter dryer or centrifuge dryer may be suitable.	Suitable for materials that can be preformed. Will handle large capacities	Not applicable	Usually not suited for materials smaller than 30-mesh (0.5 mm). Material does not tumble or mix.	Suited to smaller objects that can be loaded on each other. Can be used to convey materials through heated zones	Not applicable	Special designs are required. Suited to veneers
Continuous through-circulation (agitated/rotary). Direct type, continuous operation. Includes high-speed convective paddle, rotary-louvre.	Not applicable	Applicable with special high-speed fountain-type dryers, e.g., Hazemag Rapid, Forberg	Suitable for materials that can be preformed. Will handle large capacities. Rotary-louvre requires dry-product recirculation.	Not generally applicable, except rotary-louvre in certain cases	Usually not suited for materials smaller than 30-mesh (0.5 mm). Material is tumbled and mixed, may suffer attrition in paddle dryers.	Not applicable	Not applicable	Not applicable

Direct rotary. Direct-type, continuous operation	Applicable with dry-product recirculation	Applicable with dry-product recirculation	Suitable only if product does not stick to walls and does not dust. Recirculation of product may prevent sticking.	Suitable for most materials and especially for high capacities, provided dusting is not too severe	Suitable for most materials especially for high capacities. Dusting or crystal abrasion will limit its use.	Not applicable	Not applicable	Not applicable
Fluid beds. Direct type, batch or continuous	Applicable only as fluid bed granulator with inert bed or dry-solids recirculator	See comments under Liquids.	See comments under Liquids.	Suitable, if not too dusty. Internal coils can supplement heating, especially for fine powders. Suitable for high capacities.	Suitable for crystals, granules, and very short fibers. Suitable for high capacities	Not applicable	Use hot inert particles for contacting; rare	Use hot inert particles for contacting; rare
Spouted beds. Direct type, batch or continuous	Applicable only with inert bed or dry-solids recirculator. Usable to grow large particles by layering	See comments under Liquids.	See comments under Liquids.	Not applicable	Suitable for large particles and granules over 20-mesh (800 µm) which are spoutable	Not applicable unless objects are spoutable (conveyable in gas stream)	Use hot inert particles for contacting; rare	Use hot inert particles for contacting; rare
Pneumatic conveying. Direct-type, continuous operation includes flash, spin-flash, and ring dryers.	See comments under Slurries.	Can be used only if product is recirculated (backmixed) to make feed suitable for handling	Usually requires recirculation of dry product to make suitable feed. Well suited to high capacities. Disintegration usually required	Suitable for materials that are easily suspended in a gas stream and lose moisture readily. Well suited to high capacities	Suitable for materials conveyable in a gas stream. Well suited to high capacities. Only surface moisture usually removed. Product may suffer physical degradation.	Not applicable	Not applicable	Not applicable
Spray. Direct type, continuous operation. Rotary atomizer, pressure nozzle, or two-fluid nozzle. Includes combined spray-fluid bed and spray-belt dryers	Suited for large capacities. Product is usually powdery, spherical, and free-flowing. High temperatures can sometimes be used with heat-sensitive materials. Products generally have low bulk density.	See comments under Liquids. Pressure-nozzle atomizers subject to erosion	Requires special pumping equipment to feed the atomizer. See comments under Liquids.	Not applicable unless feed is pumpable	Not applicable	Not applicable	Not applicable	Not applicable
Continuous sheeting. Direct-type, continuous operation includes stenter, Yankee, impingement.	Not applicable	Not applicable	Not applicable	Not applicable	Not applicable	Not applicable	Generally high capacity. Different types are available for different requirements. Suitable for drying without contacting hot surfaces	Not applicable
Infrared. Batch or continuous operation. Electric heating or gas-fired	Only for thin films. Can be used in combination with other dryers such as drum.	See comments under Liquids.	See comments under Liquids (only for thin layers).	Only for thin layers	Primarily suited to drying surface moisture. Not suited for thick layers	Specially suited for drying and baking paint and enamels	Useful when space is limited. Usually used in conjunction with other methods, e.g., in drying paper coatings	Useful for laboratory work or in conjunction with other methods
Dielectric. Batch or continuous operation includes microwave, radio-frequency (RF)	Expensive, may be used in small batch filter-dryers, often as supplement to thermal heating. Sometimes useful in combination with other dryers.	See comments under Liquids.	See comments under Liquids.	Expensive, may be used on small batch dryers, often as supplement to thermal heating	Expensive, can assist thermal drying especially to dry center of large granules/pellets	Rapid drying of large objects suited to this method	Applications for final stages of paper and textile dryers	Successful on foam rubber. Not fully developed on other materials



FIG. 12-26 Solids bed in static condition (tray dryer).

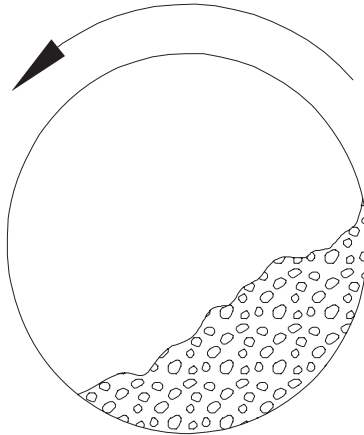


FIG. 12-27a Horizontal moving bed.

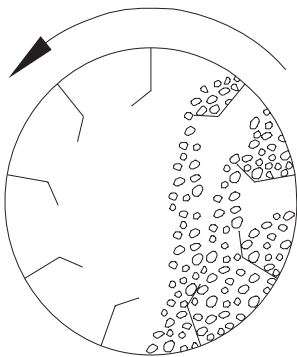


FIG. 12-27b Moving solids bed in a rotary dryer with lifters.

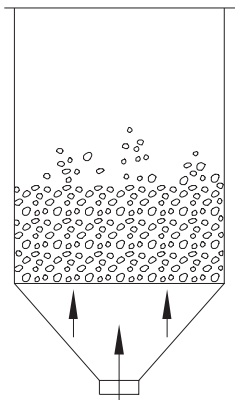


FIG. 12-28 Fluidized solids bed.

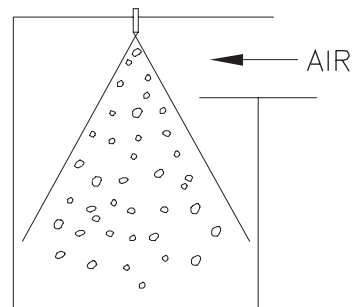


FIG. 12-29 Solids in a dilute condition near the top of a spray dryer.

Layer dryers are very suitable for slow-drying materials requiring a long residence time.

Because in a gas-solids-contacting operation heat transfer and mass transfer take place at the solids' surfaces, maximum process efficiency can be expected with a maximum exposure of solids surface to the gas phase, together with thorough mixing of gas and solids. Both are important. Within any arrangement of particulate solids, gas is present in the voids among the particles and contacts all surfaces except at the points of particle contact. When the solids are fluidized or dispersed, the gas moves past them rapidly, and external heat- and mass-transfer rates are high. When the solids bed is in a static or slightly moving condition, however, gas within the voids is cut off from the main body of the gas phase and can easily become saturated, so that local drying rates fall to low or zero values. Some transfer of energy and mass may occur by diffusion, but it is usually insignificant. The problem can be much reduced by using through-circulation of gas instead of cross-circulation, or by agitating and mixing the solids.

Solids Agitation and Mixing There are four alternatives:

1. No agitation, e.g., tray and band dryers. This is desirable for friable materials. However, drying rates can be extremely low, particularly for cross-circulation and vacuum drying.
2. Mechanical agitation, e.g., vertical pan and paddle dryers. This improves mixing and drying rates, but may give attrition depending on agitator speed; and solids may stick to the agitator, as shown in Fig. 12-30.
3. Vessel rotation, e.g., double-cone and rotary dryers. Mixing and heat transfer are better than for static dryers but may be less than for mechanical agitation. Formation of balls and lumps may be a problem.
4. Airborne mixing, e.g., fluidized beds and flash and spray dryers. Generally there is excellent mixing and mass transfer, but feed must be dispersible and entrainment and gas cleaning are higher. Mechanical vibration may also be used to assist solids movement in some dryers.

Solids transport In continuous dryers, the solids must be moved through the dryer. The main methods of doing this are

1. Gravity flow (usually vertical), e.g., turbo-tray, plate and moving-bed dryers, and rotary dryers (due to the slope)

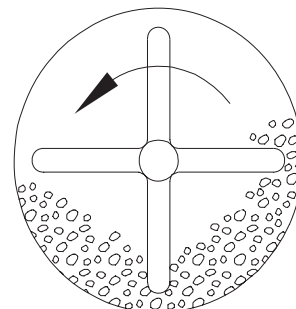


FIG. 12-30 Paddle dryer.

2. Mechanical conveying (usually horizontal), e.g., band, tunnel, and paddle dryers

3. Airborne transport, e.g., fluidized beds and flash and spray dryers

Solids flow pattern For most continuous dryers, the solids are basically in plug-flow; backmixing is low for nonagitated dryers but can be extensive for mechanical, rotary, or airborne agitation. Exceptions are well-mixed fluidized beds, fluid-bed granulators, and spouted beds (well-mixed) and spray and spray/fluidized-bed units (complex flow patterns).

5. Gas-Solids Contacting Where there is a significant gas flow, it may contact a bed of solids in the following ways:

a. Parallel flow or cross-circulation. The direction of gas flow is parallel to the surface of the solids phase. Contacting is primarily at the interface between phases, with possibly some penetration of gas into the voids among the solids near the surface. The solids bed is usually in a static condition (Fig. 12-31).

b. Perpendicular flow or impingement. The direction of gas flow is normal to the phase interface. The gas impinges on the solids bed. Again the solids bed is usually in a static condition (Fig. 12-32). This most commonly occurs when the solids are a continuous sheet, film, or slab.

c. Through circulation. The gas penetrates and flows through interstices among the solids, circulating more or less freely around the individual particles (Fig. 12-33). This may occur when solids are in static, moving, fluidized, or dilute conditions.

6. Gas Flow Pattern in Dryer Where there is a significant gas flow, it may be in cross-flow, cocurrent, or countercurrent flow compared with the direction of solids movement.

a. Cocurrent gas flow. The gas phase and solids particles both flow in the same direction (Fig. 12-34).

b. Countercurrent gas flow. The direction of gas flow is exactly opposite to the direction of solids movement.

c. Cross-flow of gas. The direction of gas flow is at a right angle to that of solids movement, across the solids bed (Fig. 12-35). The difference between these is shown most clearly in the gas and solids temperature profiles along the dryer. For cross-flow dryers, all solids particles are exposed to the same gas temperature, and the solids temperature approaches the gas temperature near the end of

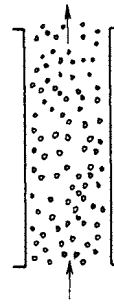


FIG. 12-34 Cocurrent gas-solids flow in a vertical-lift dilute-phase pneumatic conveyor dryer.

drying (Fig. 12-36). In cocurrent dryers, the gas temperature falls throughout the dryer, and the final solids temperature is much lower than that for the cross-flow dryer (Fig. 12-37). Hence cocurrent dryers are very suitable for drying heat-sensitive materials, although it is possible to get a solids temperature peak inside the dryer. Conversely, countercurrent dryers give the most even temperature gradient throughout the dryer, but the exiting solids come into contact with the hottest, driest gas (Fig. 12-38). These can be used to heat-treat the solids or to give low final moisture content (minimizing the local equilibrium moisture content) but are obviously unsuitable for thermally sensitive solids.

Subclassifications

Heater This may be an indirect heat exchanger or a direct-fired burner, or heating may be electrical (including RF/microwave absorption).

Gas Circuit This may be open-cycle (once-through) or closed-cycle (gas recycle, often using inert gas). A closed-cycle system with a direct-fired burner can be operated as a self-inerting system with reduced oxygen concentration.

Solids Feeders These convey the solids into the dryer and may also perform as a metering or sealing dryer. Dry solids may be back-mixed into the wet feed if the latter is sticky and difficult to handle. See Sec. 21.

Gas-Solids Separations After the solids and gas have been brought together and mixed in a gas-solids contactor, it becomes necessary to separate the two phases, particularly for dispersion dryers where the solids loading in the exhaust gas can be very high. If the solids are sufficiently coarse and the gas velocity sufficiently low, it is possible to effect a complete gravitational separation in the primary contactor. Applications of this type are rare, however, and supplementary dust collection equipment is commonly required. The recovery step may even dictate the type of primary contacting device selected. For example, in treating an extremely friable solid material, a deep fluidized-solids contactor might overload the collection system with fines, whereas the more gentle contacting of a traveling-screen contactor

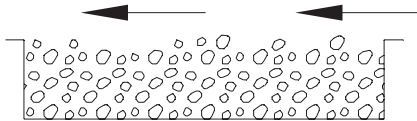


FIG. 12-31 Parallel gas flow over a static bed of solids.

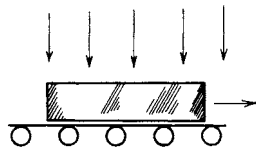


FIG. 12-32 Circulating gas impinging on a large solid object in perpendicular flow, in a roller-conveyor dryer.

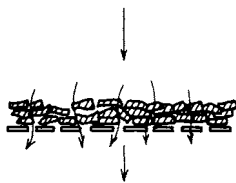


FIG. 12-33 Gas passing through a bed of preformed solids, in through-circulation on a perforated-band dryer.

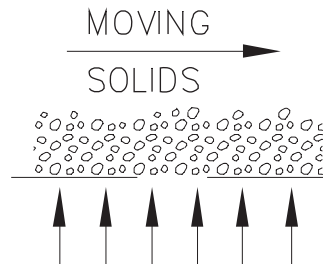


FIG. 12-35 Cross-flow of gas and solids in a fluid bed or band dryer.

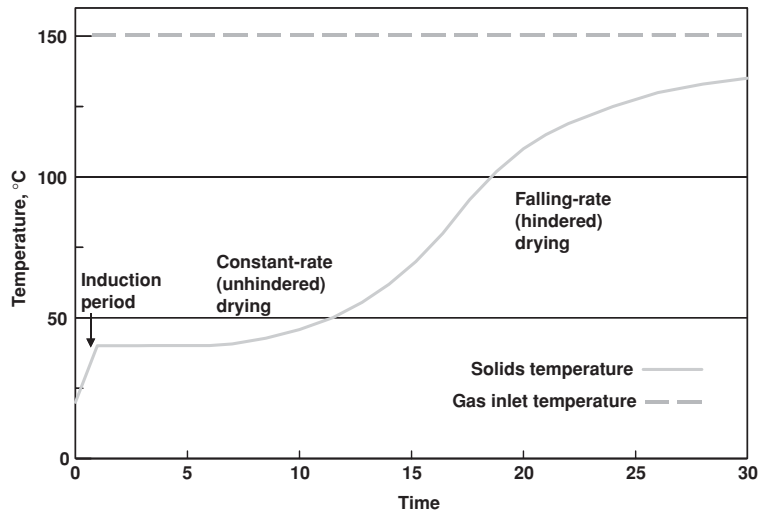


FIG. 12-36 Temperature profiles along a continuous plug-flow dryer for cross-flow of gas and solids. (Aspen Technology Inc.)

would be expected to produce a minimum of fines by attrition. Therefore, although gas solids separation is usually considered as separate and distinct from the primary contacting operation, it is usually desirable to evaluate the separation problem at the same time as contacting methods are evaluated. Methods are noted later in “Environmental Considerations.” The subject is covered in depth in Sec. 17, “Gas-Solids Operations.”

SELECTION OF DRYING EQUIPMENT

Dryer Selection Considerations Dryer selection is a challenging task and rarely clear-cut. For 500- μm particles, there may be several different dryer types which are likely to handle the task well, at similar cost. For 5- μm particles, there may be no dryers that are fully suitable, and the task is to find the “least bad”!

Dryer classification often helps to reveal the broad choices for which equipment is suitable. For instance:

- Batch dryers are almost invariably used for mean throughputs below 50 kg/h and continuous dryers above 1 ton/h; in the intervening range, either may be suitable.
- Liquid or slurry feeds, large artifacts, or continuous sheets and films require completely different equipment to particulate feeds.
- Particles and powders below 1 mm are effectively dried in dispersion or contact dryers, but most through-circulation units are unsuitable. Conversely, for particles of several millimeters or above, through-circulation dryers, rotary dryers, and spouted beds are very suitable.
- Through-circulation and dispersion convective dryers (including fluidized-bed, rotary, and pneumatic types), and agitated or rotary contact dryers, generally give better drying rates than nonagitated cross-circulated or contact tray dryers.
- Nonagitated dryers (including through-circulation) may be preferable for fragile particles where it is desired to avoid attrition.
- For organic solvents, or solids which are highly flammable, are toxic, or decompose easily, contact dryers are often preferable to

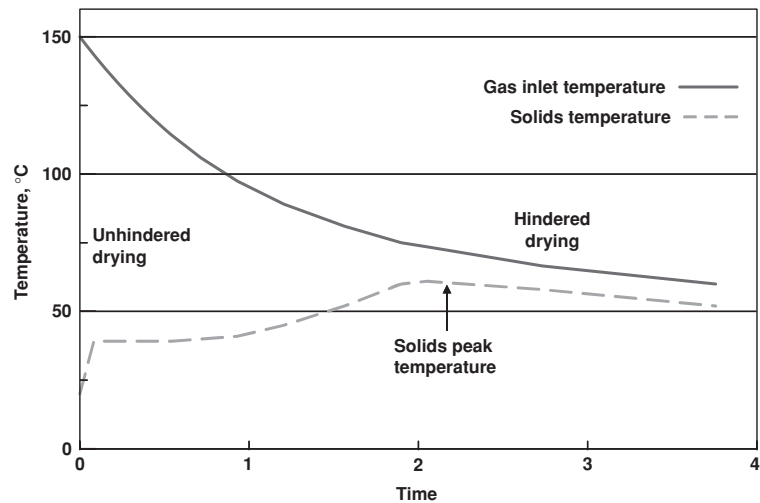


FIG. 12-37 Temperature profiles along a continuous plug-flow dryer for cocurrent flow of gas and solids. (Aspen Technology Inc.)

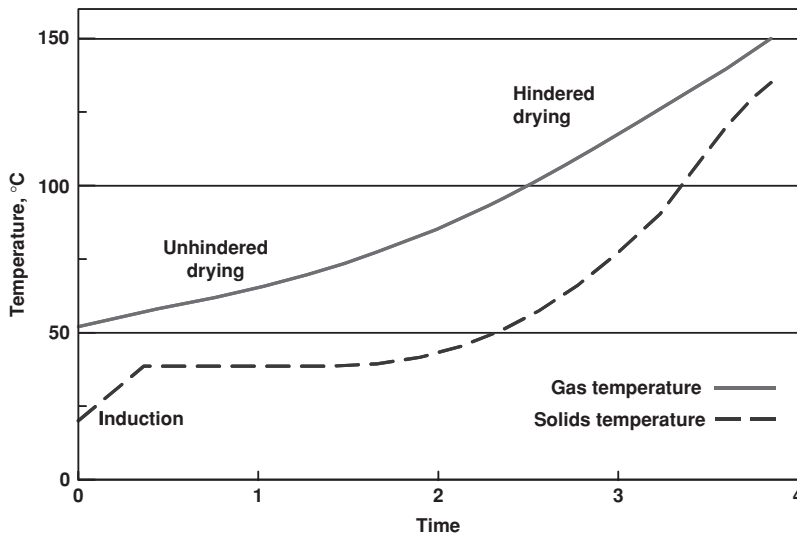


FIG. 12-38 Temperature profiles along a continuous plug-flow dryer for countercurrent flow of gas and solids. (Aspen Technology Inc.)

convective, as containment is better and environmental emissions are easier to control. If a convective dryer is used, a closed-cycle system using an inert carrier gas (e.g., nitrogen) is often required.

- Cocurrent, vacuum, and freeze dryers can be particularly suitable for heat-sensitive materials.

A detailed methodology for dryer selection, including the use of a rule-based expert system, has been described by Kemp [*Drying Technol.* **13**(5-7): 1563-1578 (1995) and **17**(7 and 8): 1667-1680 (1999)].

A simpler step-by-step procedure is given here.

1. *Initial selection of dryers.* Select those dryers which appear best suited to handling the wet material and the dry product, which fit into the continuity of the process as a whole, and which will produce a product of the desired physical properties. This preliminary selection can be made with the aid of Table 12-12, which classifies the various types of dryers on the basis of the materials handled.

2. *Initial comparison of dryers.* The dryers so selected should be evaluated approximately from available cost and performance data. From this evaluation, those dryers which appear to be uneconomical or unsuitable from the standpoint of performance should be eliminated from further consideration.

3. *Drying tests.* Drying tests should be conducted in those dryers still under consideration. These tests will determine the optimum operating conditions and the product characteristics and will form the basis for firm quotations from equipment vendors.

4. *Final selection of dryer.* From the results of the drying tests and quotations, the final selection of the most suitable dryer can be made.

The important factors to consider in the preliminary selection of a dryer are the following:

1. Properties of the material being handled
 - a. Physical characteristics when wet (stickiness, cohesiveness, adhesiveness, flowability)
 - b. Physical characteristics when dry
 - c. Corrosiveness
 - d. Toxicity
 - e. Flammability
 - f. Particle size
 - g. Abrasiveness
2. Drying characteristics of the material
 - a. Type of moisture (bound, unbound, or both)
 - b. Initial moisture content (maximum and range)
 - c. Final moisture content (maximum and range)
 - d. Permissible drying temperature

- e. Probable drying time for different dryers
 - f. Level of nonwater volatiles
3. Flow of material to and from the dryer
 - a. Quantity to be handled per hour (or batch size and frequency)
 - b. Continuous or batch operation
 - c. Process prior to drying
 - d. Process subsequent to drying
 4. Product quality
 - a. Shrinkage
 - b. Contamination
 - c. Uniformity of final moisture content
 - d. Decomposition of product
 - e. Overdrying
 - f. State of subdivision
 - g. Product temperature
 - h. Bulk density
 5. Recovery problems
 - a. Dust recovery
 - b. Solvent recovery
 6. Facilities available at site of proposed installation
 - a. Space
 - b. Temperature, humidity, and cleanliness of air
 - c. Available fuels
 - d. Available electric power
 - e. Permissible noise, vibration, dust, or heat losses
 - f. Source of wet feed
 - g. Exhaust-gas outlets

The physical nature of the material to be handled is the primary item for consideration. A slurry will demand a different type of dryer from that required by a coarse crystalline solid, which, in turn, will be different from that required by a sheet material (Table 12-12).

Following preliminary selection of suitable types of dryers, a rough evaluation of the size and cost should be made to eliminate those which are obviously uneconomical. Information for this evaluation can be obtained from material presented under discussion of the various dryer types. When data are inadequate, preliminary cost and performance data can usually be obtained from the equipment manufacturer. In comparing dryer performance, the factors in the preceding list which affect dryer performance should be properly weighed. The possibility of eliminating or simplifying processing steps which precede or follow drying, such as filtration, grinding, or conveying, should be carefully considered.

Drying Tests These tests should establish the optimum operating conditions, the ability of the dryer to handle the material physically, product quality and characteristics, and dryer size. The principal manufacturers of drying equipment are usually prepared to perform the required tests on dryers simulating their equipment. Occasionally, simple laboratory experiments can serve to reduce further the number of dryers under consideration.

Once a given type and size of dryer have been installed, the product characteristics and drying capacity can be changed only within relatively narrow limits. Thus it is more economical and far more satisfactory to experiment in small-scale units than on the dryer that is finally installed.

On the basis of the results of the drying tests that establish size and operating characteristics, formal quotations and guarantees should be obtained from dryer manufacturers. Initial costs, installation costs, operating costs, product quality, dryer operability, and dryer flexibility can then be given proper weight in final evaluation and selection.

Effective scale-up from tests to industrial equipment is obviously very important, and it was covered in a special issue of *Drying Technol.* 12 (1 and 2): 1–452 (1994).

DRYER MODELING, DESIGN, AND SCALE-UP

General Principles Models and calculations on dryers can be categorized in terms of (1) the level of complexity used and (2) the purpose or type of calculation (design, performance rating, or scale-up). A fully structured approach to dryer modeling can be developed from these principles, as described below and in greater detail by Kemp and Oakley (2002).

Levels of Dryer Modeling Modeling can be carried out at four different levels, depending on the amount of data available and the level of detail and precision required in the answer.

Level 1. *Heat and mass balances.* These balances give information on the material and energy flows to and from the dryer, but say nothing about the required equipment size or the performance which a given dryer is capable of.

Level 2. *Scoping* Approximate or scoping calculations give rough sizes and throughputs (mass flow rates) for dryers, using simple data and making some simplifying assumptions. Either heat-transfer control or first-order drying kinetics is assumed.

Level 3. *Scaling* Scaling calculations give overall dimensions and performance figures for dryers by scaling up drying curves from small-scale or pilot-plant experiments.

Level 4. *Detailed* Rigorous or detailed methods aim to track the temperature and drying history of the solids and find local conditions inside the dryer. Naturally, these methods use more complex modeling techniques with many more parameters and require many more input data.

Types of Dryer Calculations The user may wish to either design a new dryer or improve the performance of an existing one. Three types of calculations are possible:

- Design of a new dryer to perform a given duty, using information from the process flowsheet and physical properties databanks
- Performance calculations for an existing dryer at a new set of operating conditions
- Scale-up from laboratory-scale or pilot-plant experiments to a full-scale dryer

Solids drying is very difficult to model reliably, particularly in the falling-rate period which usually has the main effect on determining the overall drying time. Falling-rate drying kinetics depend strongly on the internal moisture transport within a solid. This is highly dependent on the internal structure, which in turn varies with the upstream process, the solids formation step, and often between individual batches. Hence, many key drying parameters within solids (e.g., diffusion coefficients) cannot be predicted from theory alone, or obtained from physical property databanks; practical measurements are required. Because of this, experimental work is almost always necessary to design a dryer accurately, and scale-up calculations are more reliable than design based only on thermodynamic data. The experiments are used to verify the theoretical model and find the difficult-to-measure parameters; the full-scale dryer can then be modeled more realistically.

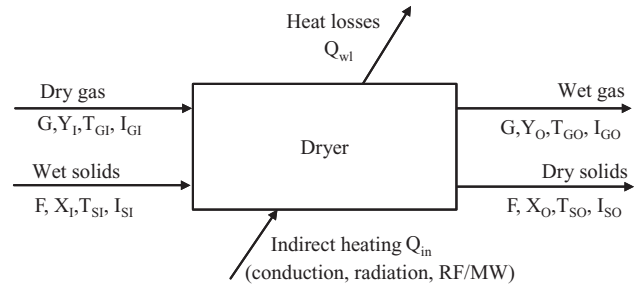


FIG. 12-39 Heat and material flows around a continuous dryer.

Heat and Mass Balance The heat and mass balance on a generic continuous dryer is shown schematically in Fig. 12-39. In this case, mass flows and moisture contents are given on a dry basis.

The **mass balance** is usually performed on the principal solvent and gives the evaporation rate \dot{E} (kg/s). In a contact or vacuum dryer, this is approximately equal to the exhaust vapor flow, apart from any noncondensibles. In a convective dryer, this gives the increased outlet humidity of the exhaust. For a continuous dryer at steady-state operating conditions,

$$\dot{E} = F(X_1 - X_0) = G(Y_0 - Y_1) \quad (12-54)$$

This assumes that the dry gas flow G and dry solids flow F do not change between dryer inlet and outlet. Mass balances can also be performed on the overall gas and solids flows to allow for features such as air leaks and solids entrainment in the exhaust gas stream.

In a design mode calculation (including scale-up), the required solids flow rate, inlet moisture content X_1 and outlet moisture X_0 are normally specified, and the evaporation rate and outlet gas flow are calculated. In performance mode, the calculation is normally reversed; the evaporation rate under new operating conditions is found, and the new solids throughput or outlet moisture content is back-calculated.

For a batch dryer with a dry mass m of solids, a mass balance only gives a snapshot at one point during the drying cycle and an instantaneous drying rate, given by

$$\dot{E} = m \left(-\frac{dX}{dt} \right) = G(Y_0 - Y_1) \quad (12-55)$$

The **heat balance** on a continuous dryer takes the generic form

$$GI_{G1} + FI_{S1} + Q_m = GI_{G0} + FI_{S0} + Q_{wl} \quad (12-56)$$

Here I is the enthalpy (kJ/kg dry material) of the solids or gas plus their associated moisture. Enthalpy of the gas includes the latent heat term for the vapor. Expanding the enthalpy terms gives

$$G(C_{s1}T_{G1} + \lambda Y_1) + F(C_{PS} + X_1 C_{PL})T_{S1} + Q_m = G(C_{s0}T_{G0} + \lambda Y_0) + F(C_{PS} + X_0 C_{PL})T_{S0} + Q_{wl} \quad (12-57)$$

Here C_s is the humid heat $C_{PC} + YC_{PV}$. In convective dryers, the left-hand side is dominated by the sensible heat of the hot inlet gas $GC_{s1}T_{G1}$; in contact dryers, the heat input from the jacket Q_m is dominant. In both cases, the largest single term on the right-hand side is the latent heat of the vapor $G\lambda Y_0$. Other terms are normally below 10 percent. *This shows why the operating line of a convective dryer on a psychrometric chart is roughly parallel to a constant-enthalpy line.*

The corresponding equation for a batch dryer is

$$GI_{G1} + Q_m = GI_{G0} + m \frac{dI_s}{dt} + Q_{wl} \quad (12-58)$$

Further information on heat and mass balances, including practical challenges on industrial dryers and a worked example, is given in the "Drying Fundamentals" section.

Scoping Design Calculations In scoping calculations, some approximate dryer dimensions and drying times are obtained based mainly on a heat and mass balance, without measuring a drying curve or other experimental drying data. They allow the cross-sectional area of convective dryers and the volume of batch dryers to be estimated quite accurately, but are less effective for other calculations and can give overoptimistic results.

Continuous Convective Dryers In design mode, the required solids throughput F and the inlet and outlet moisture content X_I and X_O are known, as is the ambient humidity Y_I . If the inlet gas temperature T_{CI} is chosen, the outlet gas conditions (temperature T_{CO} and humidity Y_O) can be found, either by calculation or (more simply and quickly) by using the constant-enthalpy lines on a psychrometric chart. However, it may be necessary to allow for heat losses and sensible heating of solids, which typically reduce the useful enthalpy of the inlet gas by 10 to 20 percent. Also, if tightly bound moisture is being removed, the heat of wetting to break the bonds should be allowed for. The gas mass flow rate G can now be calculated, as it is the only unknown in the mass balance on the solvent [Eq. (12-56)]. A typical gas velocity U_G along the dryer is now chosen, for example, 20 m/s for a flash dryer, 0.5 m/s for a fluidized bed, and 3 m/s for a cocurrent rotary dryer. For through-circulation and dispersion dryers, the cross-sectional area A is given by

$$A = \frac{G}{\rho_{CI}U_G} = \frac{F(X_I - X_O)}{\rho_{CI}U_G(Y_O - Y_I)} \quad (12-59)$$

The dryer diameter, or linear dimensions of a rectangular bed, can then be calculated. The result is usually accurate within 10 percent, and can be further improved by better estimates of velocity and heat losses. In performance mode, the equation is reversed to find the gas flow rate from $G = \rho_{CI}U_GA$.

The method gives no information about solids residence time or dryer length. A minimum drying time t_{\min} can be calculated by evaluating the maximum (unhindered) drying rate N_{cr} , assuming gas-phase heat-transfer control and estimating a gas-to-solids heat-transfer coefficient. The simple equation (12-60) then applies:

$$t_{\min} = \frac{X_I - X_O}{N_{cr}} \quad (12-60)$$

Alternatively, it may be assumed that first-order falling-rate kinetics apply throughout the drying process, and scale the estimated drying time by using Eq. (12-63). However, these crude methods can give serious underestimates of the required drying time, and it is much better to measure the drying time experimentally and apply scaling (level 3) methods.

Continuous Contact Dryers The key parameter is the area of the heat-transfer surface A_S . In design mode, this can be found from the equation:

$$A_S = \frac{Q}{h_{WS} \Delta T_{WS}} = \frac{E\lambda_{ev}}{h_{WS} \Delta T_{WS}} = \frac{F(X_I - X_O)\lambda_{ev}}{h_{WS} \Delta T_{WS}} \quad (12-61)$$

Here Q is the rate of heat transfer from the heated wall to the solids, and ΔT_{WS} is the temperature driving force. The latent heat of evaporation λ_{ev} should allow for bound moisture and heating of solids and vapor to the final temperature. A typical wall-to-solids heat-transfer coefficient h_{WS} for the given dryer type should be used. The calculation is less accurate than the one for convective dryers. Again, the heat-transfer rate is assumed to be the overall limiting factor.

If the drying process is strongly limited by falling-rate drying kinetics, the calculated size of dryer corresponding to the given heating surface A_S may not give sufficient solids residence time to reach the desired final moisture content. Again, experimental measurement of a drying curve is strongly recommended.

Batch Dryers If the batch size is stipulated, the requirement is simply that the dryer be able to physically contain the volume of the solids, and the dryer volume and dimensions can thus be calculated directly. Solids residence time must then be calculated. Equation (12-61) can be reversed and modified to give

$$t_{CR} = \frac{m_s(X_I - X_O)\lambda_{ev}}{h_{WS}\Delta T_{WS}A_S} \quad (12-62)$$

Heat-transfer control and constant-rate drying are assumed. Again, the calculation will be inaccurate and overoptimistic for falling-rate drying, and it is preferable to measure a drying curve and use a scaling calculation, as outlined in the next section. It is possible to compare the surface area/volume ratios of various types of dryers and deduce how their drying times will compare with each other (see "Drying Equipment—Batch Agitated and Rotary Dryers").

Falling-Rate Kinetics To correct from a calculated constant-rate (unhindered) drying time t_{CR} to first-order falling-rate kinetics, the following equation is used, where X_1 is the initial, X_2 the final, and X_E the equilibrium moisture content (all must be dry-basis):

$$\frac{t_{FR}}{t_{CR}} = \frac{X_1 - X_E}{X_1 - X_2} \ln \left(\frac{X_1 - X_E}{X_2 - X_E} \right) \quad (12-63)$$

Note that $t_{FR} \geq t_{CR}$. Likewise, to convert to a two-stage drying process with constant-rate drying down to X_{cr} and first-order falling-rate drying beyond, the equation is

$$\frac{t_{2S}}{t_{CR}} = \frac{X_1 - X_{cr}}{X_1 - X_2} + \frac{X_{cr} - X_E}{X_1 - X_2} \ln \left(\frac{X_{cr} - X_E}{X_2 - X_E} \right) \quad (12-64)$$

Scale-up Effects As dryers get larger, if the drying rate is either controlled by heat transfer (unhindered or constant-rate drying) or proportional to it (first-order drying kinetics following the characteristic drying curve), then the drying rate N (kg/kg/s) and drying time t will be proportional to the ratio between the area over which heat enters and the mass or volume of solids.

For most types of dryer, it is found that the specific drying rate (SDR), which is a mass flux (evaporation rate per unit area), is constant for a given set of operating conditions. The concept is described by Moyers [Drying Technol. 12(1 and 2):393 (1994)]. For convective layer dryers, both through-circulation and cross-circulation, mass increases proportionately to bed area if layer depth remains constant; hence the drying time should remain the same. This is also true of fluidized beds and of contact dryers where the solids rest as a layer on a heated plate (tray, vacuum band, plate, film-drum, and thin-film dryers). However, for mechanically agitated and rotating contact dryers (vertical pan, conical, double-cone tumbler, and paddle), the heat-transfer surface area increases as the square of dryer diameter and volume as the cube, and hence drying time increases with the cube root of batch size:

$$\frac{t_2}{t_1} = \left(\frac{m_2}{m_1} \right)^{1/3} \quad (12-65)$$

Providing additional internal heating surfaces, such as heated agitators or steam tubes in paddle or rotary dryers, gives a higher area/volume ratio and faster drying, so these will be the preferred contact dryer types for large batches or high throughput. This applies if the drying rate is proportional to the rate of heat supply. For a continuous dryer, heating the agitator allows a smaller dryer for a given solids throughput; for a batch dryer with fixed batch size, a heated agitator shortens the required drying time. However, if a minimum residence time is required to allow removal of tightly bound moisture, there will be little or no gain from providing very large amounts of heat-transfer area.

Again, these methods take no account of the actual drying kinetics of the particle, which are included in the next section.

Example 19: Drying of Particles A convective dryer is to be used to dry 720 kg/h (0.2 kg/s) of particulate material from 0.2 to 0.02 kg/kg moisture content (all flows and moistures on dry basis), using air at 180°C and 0.005 kg/kg humidity. Estimate the required air flow rate and dryer size for a fluidized-bed dryer (0.5 m/s inlet velocity) and a pneumatic conveying dryer (20 m/s inlet velocity). Assume outlet RH is approximately 20 percent. What is the effect of 10 percent heat losses?

Solution: Using a psychrometric chart with $T_{CI} = 180^\circ\text{C}$, the outlet gas temperature is approximately 70°C, $Y_O = 0.048$ kg/kg with no losses, or 0.040 kg/kg with 10 percent losses.

From the mass balance, Eq. (12-54): $0.2(0.2 - 0.02) = W_G(Y_O - 0.005)$. Hence $W_G = 0.837$ kg/s (no losses) or 1.03 kg/s (10 percent losses).

The cross-sectional area of the dryer is obtained from Eq. (12-59), by taking ρ_C at 180°C as 0.78 kg/m³. For the fluidized-bed dryer, assuming 10 percent losses: $A_B = 1.03/(0.5 \times 0.78) = 2.64$ m². For a circular bed, $D = 1.83$ m. For the pneumatic conveying dryer, assuming 10 percent losses, $A_{cs} = 1.03/(20 \times 0.78) = 0.066$ m². For a circular duct, $D = 0.29$ m; for a square duct, $D = 0.257$ m.

A similar example for batch dryers may be found in the section "Batch Agitated and Rotating Dryers," including constant-rate and falling-rate kinetics and scale-up from an experimental test result.

SCALING MODELS

These models use experimental data from drying kinetics tests in a laboratory, pilot-plant or full-scale dryer, and are thus more accurate and reliable than methods based only on estimated drying kinetics. They treat the dryer as a complete unit, with drying rates and air velocities averaged over the dryer volume, except that, if desired, the dryer can be subdivided into a small number of sections. These methods are used for layer dryers (tray, oven, horizontal-flow band, and vertical-flow plate types) and for a simple estimate of fluidized-bed dryer performance. For batch dryers, they can be used for scale-up by refining the scoping design calculation.

The basic principle is to take an experimental drying curve and perform two transformations: (1) from test operating conditions to full-scale operating conditions and (2) for test dimensions to full-scale dryer dimensions. If the operating conditions of the test (e.g., temperature, gas velocity, agitation rate) are the same as those for the full-scale plant, the first correction is not required.

Scaling models are the main design method traditionally used by dryer manufacturers. Pilot-plant test results are scaled to a new set of conditions on a dryer with greater airflow or surface area by empirical rules, generally based on the external driving forces (temperature, vapor pressure, or humidity driving forces). By implication, therefore, a characteristic drying curve concept is again being used, scaling the external heat and mass transfer and assuming that the internal mass transfer changes in proportion. A good example is the set of rules described under "Fluidized-Bed Dryers," which include the effects of temperature, gas velocity, and bed depth on drying time in the initial test and the full-scale dryer.

The integral model is a development of a simple scale-up model which allows for mixing and residence time effects, first suggested for fluidized beds by Vanecek et al. (1964, 1966). The mean outlet moisture content is given by summing the product of the particle moisture content and the probability that it emerges at time t :

$$\bar{X} = \int_0^{\infty} E(t)X(t) dt \tag{12-66}$$

Here $X(t)$ is the drying curve, corrected as before to the new scale and new operating conditions, and $E(t)$ is the residence time function, which must be known. This approach has been used successfully for well-mixed fluidized beds. For pure plug flow, $E(t)$ is a spike (Green's function) and $\bar{X} = X(t)$.

Scale-up of Batch Dryers We can use the same equations as before but base drying time on an experimental value rather than one obtained from an unhindered drying calculation.

Example 20: Scaling of Data An experimental batch drying curve has been measured at 100°C, and drying time was 2 h. Estimate the drying time at (a) 100°C and (b) 150°C for (i) a fluidized-bed dryer and (ii) a conical vacuum dryer at 100-mbar absolute pressure, for a batch size 10 times greater than that of the test. Assume for the fluidized bed that temperature driving forces are proportional to $T - T_{wb}$ and batch drying time is proportional to bed depth, and for the conical dryer that the solids temperature is equal to the saturation temperature at 100-mbar pressure (46°C for water vapor).

Solution:

(i) For the fluid bed, $T = 100^\circ\text{C}$ and 150°C , $T_{wb} = 30^\circ\text{C}$ and 38°C , respectively. The increase in heat transfer and drying rate for case (b) is a factor of $112/70 = 1.6$.

The bed could be scaled up by increasing the bed area by a factor of 10 and keeping depth z constant, in which case drying time will remain at 2 h for case (a) and become $2/1.6 = 1.25$ h for case (b).

Alternatively, all dimensions could be scaled up proportionately; as $V = \rho D^2 z$, D and z will increase by $\sqrt[3]{10} = 2.16$. Drying time then becomes 4.32 h for (a) and 2.70 h for (b).

(ii) For the conical dryer, in case (b), temperature driving force increases by a factor of $104/54 = 1.93$. From Eq. (12-65), linear dimensions and drying time all scale up by a factor of $\sqrt{10}$. Drying time becomes 4.32 h for (a) and $2\sqrt{10}/1.93 = 2.24$ h for (b).

DETAILED OR RIGOROUS MODELS

These models aim to predict local conditions within the dryer and the transient condition of the particles and gas in terms of temperature, moisture content, velocity, etc. Naturally, they require much more input data. There are many published models of this type in the academic literature. They give the possibility of more detailed results, but the potential cumulative errors are also greater.

- Incremental models track the local conditions of the gas and particles through the dryer, mainly in one dimension. They are especially suitable for cocurrent and countercurrent dryers, e.g., flash (pneumatic conveying) and rotary dryers. The air conditions are usually treated as uniform across the cross-section and dependent only on axial position. This method can also be used to determine local conditions (e.g., temperature) where a simpler model has been used to find the overall drying rate. A two- or three-dimensional grid can also be used, e.g., modeling vertical and horizontal variations in a band dryer or plug-flow fluidized bed.
- Complex three-dimensional models, e.g., CFD (computational fluid dynamics), aim to solve the gas conditions and particle motion throughout the dryer. They are the only effective models for spray dryers because of the complex swirling flow pattern; they can also be used to find localized conditions in other dryers.

Incremental Model The one-dimensional incremental model is a key analysis tool for several types of dryers. A set of simultaneous equations is solved at a given location (Fig. 12-40), and the simulation moves along the dryer axis in a series of steps or increments—hence the name. The procedure may be attempted by hand if a few large steps (say, 5 to 10) are used; but for an accurate simulation, a computer program is needed and thousands of increments may be used.

Increments may be stated in terms of time (dt), length (dz), or moisture content (dX). A set of six simultaneous equations is then solved, and ancillary calculations are also required, e.g., to give local values of gas and solids properties. The generic set of equations (for a time increment Δt) is as follows:

Heat transfer to particle: $Q_P = h_{PG}A_P(T_G - T_S)$ (12-67)

Mass transfer from particle:
 $\frac{-dX}{dt} = \text{function}(X, Y, T_P, T_G, h_{PG}, A_P)$ (12-68)

Mass balance on moisture: $G\Delta Y = -F\Delta X = F \frac{-dX}{dt} \Delta t$ (12-69)

Heat balance on particle: $\Delta T_S = \frac{Q_P \Delta t - \lambda_{es} m_P \Delta X}{m_P(C_{PS} + C_{PL}X)}$ (12-70)

Heat balance for increment:
 $-\Delta T_G = \frac{F(C_{PS} + C_{PL}X) \Delta T_S + G(\lambda_{og} + C_{PY}T_G) \Delta Y + \Delta Q_{wl}}{G(C_{PG} + C_{PY})}$ (12-71)

Particle transport: $\Delta z = U_S \Delta t$ (12-72)

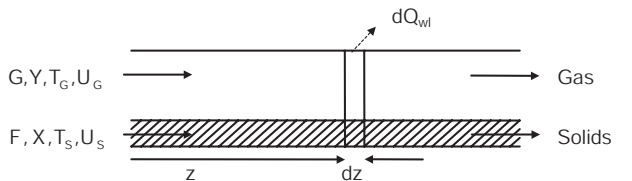


FIG. 12-40 Principle of the incremental model.

The mass and heat balance equations are the same for any type of dryer, but the particle transport equation is completely different, and the heat- and mass-transfer correlations are also somewhat different as they depend on the environment of the particle in the gas (i.e., single isolated particles, agglomerates, clusters, layers, fluidized beds, or packed beds). The mass-transfer rate from the particle is regulated by the drying kinetics and is thus obviously material-dependent (at least in falling-rate drying).

The model is effective and appropriate for dryers where both solids and gas are approximately in axial plug flow, such as pneumatic conveying and cascading rotary dryers. However, it runs into difficulties where there is recirculation or radial flow.

The incremental model is also useful for measuring variations in local conditions such as temperature, solids moisture content, and humidity along the axis of a dryer (e.g., plug-flow fluidized bed), through a vertical layer (e.g., tray or band dryers), or during a batch drying cycle (using time increments, not length). It can be applied in these situations even though the integral model has been used to determine the overall kinetics and drying time.

Example 21: Sizing of a Cascading Rotary Dryer The average gas velocity passing through a cocurrent, adiabatic, cascading rotary dryer is 4 m/s. The particles moving through the dryer have an average diameter of 5 mm, a solids density of 600 kg/m³, and a shape factor of 0.75. The particles enter with a moisture content of 0.50 kg/kg (dry basis) and leave with a moisture content of 0.15 kg/kg (dry basis). The drying rate may be assumed to decrease linearly with average moisture content, with no unhindered ("constant-rate") drying period. In addition, let us assume that the solids are nonhygroscopic (so that the equilibrium moisture content is zero; hygroscopic means that the equilibrium moisture content is nonzero).

The inlet humidity is 0.10 kg/kg (dry basis) due to the use of a direct-fired burner, and the ratio of the flow rates of dry solids to dry gas is unity ($F/G = 1$). The gas temperature at the inlet to the dryer is 800°C, and the gas may be assumed to behave as a pure water vapor/air mixture.

What is the gas-phase residence time that is required?

Data:

$U = 4 \text{ m/s}$	$X_i = 0.50 \text{ kg/kg}$	$F/G = 1$
$d_{PSM} = 0.005 \text{ m}$	$X_o = 0.15 \text{ kg/kg}$	$T_{GI} = 800^\circ\text{C}$
$\rho_p = 600 \text{ kg/m}^3$	$X_{cr} = 0.50 \text{ kg/kg}$	$Y_i = 0.10 \text{ kg/kg}$
$\alpha_p = 0.75$	$X_e = 0.0 \text{ kg/kg}$	

Application of concept of characteristic drying curve: A linear-falling rate curve implies the following equation for the drying kinetics:

$$f = \Phi \quad \text{assumption of linear drying kinetics} \quad (12-73)$$

where f is the drying rate relative to the initial drying rate.

$$f = \frac{N}{N_{\text{initial}}}$$

Since the material begins drying in the falling-rate period, the critical moisture content can be taken as the initial moisture content. The equilibrium moisture content is zero since the material is not hygroscopic.

$$\Phi = \frac{\bar{X} - X_{eq}}{X_{cr} - X_{eq}} = \frac{\bar{X}}{0.5}$$

Application of mass balances (theory): A mass balance around the inlet and any section of the dryer is shown in Fig. 12-41.

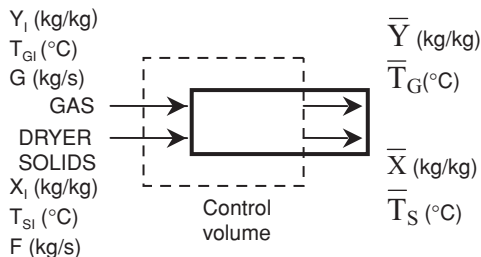


FIG. 12-41 Mass balance around a typical section of a cocurrent dryer.

The essential idea is to calculate the average gas humidity \bar{Y} at each average moisture content \bar{X} .

A differential mass balance on the air at any position in the bed is given below.

$$F \cdot dX = -G \cdot dy$$

$$-\frac{dY}{dX} = \frac{F}{G} = \frac{Y - Y_i}{X_i - \bar{X}} \quad (12-74)$$

where Y = gas humidity, kg moisture/kg dry gas
 X = solids moisture content, kg moisture/kg dry solids
 W_G = flow rate of dry gas, kg dry gas/s
 W_S = flow rate of dry solids, kg dry solids/s

Application of mass balances: Plugging in the numbers gives the relationship between absolute humidity and moisture in the solids at any position.

$$\frac{\bar{Y} - 0.1}{0.5 - \bar{X}} = 1 = \frac{F}{G}$$

$$\bar{Y} = 0.6 - \bar{X}$$

$$Y_o = 0.6 - 0.15 = 0.45 \text{ kg/kg}$$

From Mollier chart: $T_{wb} = 79^\circ\text{C}$ $Y_s^o = 0.48 \text{ kg/kg}$

For the whole dryer, $\bar{Y} = 0.275 \text{ kg/kg}$

The mass balance information is important, but not the entire answer to the question. Now the residence time can be calculated from the kinetics.

Application of concept of characteristic drying curve to estimating drying rates in practice (theory): The overall (required) change in moisture content is divided into a number of intervals of size ΔX . The sizes of the intervals need not be the same and should be finer where the fastest moisture content change occurs. For the sake of simplicity, this example will use intervals of uniform size. Then the application of the concept of a characteristic drying curve gives the following outcomes.

$$-\frac{d\bar{X}}{dt} = \text{drying rate in interval}$$

$$= \frac{f \cdot k \cdot \phi \cdot \frac{A_p}{\rho_p} \cdot \frac{A_p}{V_p} (Y_s^o - \bar{Y})}{V_p} \quad (12-75)$$

where f = relative drying rate in interval (dimensionless)

\bar{Y} = average humidity in interval, kg/kg

ϕ = humidity potential coefficient, close to unity

ρ_p = density of dry solids, kg/m³

Y_s^o = humidity at saturation, from the adiabatic saturation contour on Mollier chart

$$\frac{A_p}{V_p} = \frac{\text{particle surface area}}{\text{particle volume}} = \frac{6}{\phi_p \cdot d_{PSM}} \quad (12-76)$$

d_{PSM} = Sauter-mean particle diameter for mixture (volume-surface diameter), m

ϕ_p = particle shape factor, unity for spheres (dimensionless)

k = mass-transfer coefficient, kg/(m²·s), obtained from the heat-transfer coefficient (often easier to obtain) using the Chilton-Colburn analogy

$$k \cdot \phi = \frac{\delta}{C_{py}} h \quad (12-77)$$

δ = psychrometric ratio, close to unity for air/water vapor system

C_{py} = humid heat capacity = $C_{pG} + Y C_{pV}$

C_{pG} = specific heat capacity of dry gas (air), J/(kg·K)

C_{pV} = specific heat capacity of water vapor, J/(kg·K)

h = heat-transfer coefficient, W/(m²·K)

Define

Re_p = particle Reynolds number

$$= \frac{U \cdot d_{PSM}}{\nu} \quad (12-78)$$

U = relative velocity between gas and particles; in cascading rotary dryers, this is almost constant throughout the dryer and close to the superficial gas velocity U_{Gsuper}

ν = kinematic viscosity of gas at average T_G in dryer, m²/s

12-54 PSYCHROMETRY, EVAPORATIVE COOLING, AND SOLIDS DRYING

For cascading rotary dryers:

$$\begin{aligned} Nu_p &= \text{particle Nusselt number} \\ &= \min(0.03 Re_p^{1.3}, 2 + 0.6 Re_p^{0.5} Pr^{0.3}) \end{aligned} \quad (12-79)$$

$$h = \frac{\lambda_G}{d_{PSM}} Nu_p \quad (12-80)$$

λ_G = thermal conductivity of gas, W/(m·K)

Application of concept of characteristic drying curve to estimating drying rates in practice

GAS PROPERTIES

$$\begin{aligned} v &= 15 \times 10^{-6} \text{ m}^2/\text{s} \\ Pr &= 0.7 \\ \lambda_G &= 0.02 \text{ W}/(\text{m}\cdot\text{K}) \\ C_{PG} &= 1050 \text{ J}/(\text{kg}\cdot\text{K}) \\ C_{PV} &= 2000 \text{ J}/(\text{kg}\cdot\text{K}) \\ C_{PR} &= 1050 + 0.275 \cdot 2000 = 1600 \text{ J}/(\text{kg}\cdot\text{K}) \end{aligned}$$

We might do a more accurate calculation by calculating the gas properties at the conditions for each interval.

HEAT AND MASS-TRANSFER COEFFICIENTS

$$\begin{aligned} Re_p &= \frac{U \cdot d_{PSM}}{v} = \frac{4 \cdot 0.005}{15 \times 10^{-6}} = 1333 \\ Nu &= \min[0.03(1333)^{1.3}, 2 + 0.6(1333)^{0.5} 0.7^{0.3}] \\ &= 21.5 \\ h &= \frac{0.02}{0.005} 21.5 = 86 \text{ W}/(\text{m}^2 \cdot \text{K}) \\ k &= \frac{86}{1600} = 0.054 \text{ kg}/(\text{m}^2 \cdot \text{s}) \end{aligned} \quad (12-81)$$

$$\begin{aligned} \frac{A_p}{V_p} &= \frac{6}{0.75 \cdot 0.005} = 1600 \text{ m}^{-1} \\ \frac{d\bar{X}}{dt} &= f \frac{0.054 \cdot 1600}{600} (0.48 - \bar{Y}) \\ &= 0.14f(0.48 - \bar{Y}) \end{aligned}$$

The particle temperature is obtained by analogy with the falling-rate expression for the drying rate (Keey, 1978). This procedure assumes that the particles reach a quasi-steady state temperature when they are resting on flights after cascading through the gas. The heat-transfer Fourier number typically approaches unity for the dwell time on the flights, meaning that the temperature distribution in the particles at the end of the dwell time is almost uniform. The heat-transfer Fourier number Fo is defined as $\alpha t/d_p^2$, where d_p is the particle diameter, t is time, and α is the thermal diffusivity. The thermal diffusivity α is the ratio of the thermal conductivity to the product of the density and the specific heat capacity.

The energy accumulation term in the energy balance for a particle is assumed to be zero. As above, this assumption can be justified because of the significant resting time that particles remain on a flight during the time that it is lifted around the drum. This quasi-steady state temperature in the energy balance, neglecting the energy accumulation term, is

$$h(T_G - T_s) = fN_w$$

where N_w is the maximum (unhindered) drying rate. For completely unhindered drying, $f = 1$ and T_s is the wet-bulb temperature T_w , so that

$$f = \frac{T_G - T_s}{T_G - T_w}$$

Under these conditions, the solids temperature may be obtained from the equation

$$T_s = T_G - f(T_G - T_w) \quad (12-82)$$

This procedure has been used to calculate the average solids temperature in the eighth column of Table 12-13. This approach to the energy balance has been indicated experimentally for rendered meat solids through the accurate prediction of the maximum particle temperatures.

This procedure gives the particle residence time in the gas (38 s), and a typical variation of process conditions through a cocurrent cascading rotary dryer is shown in Fig. 12-42. We want the total residence time, which is the sum of the time in the gas τ_c and the time soaking on the flights τ_s . Figure 12-43 shows the enthalpy humidity chart used to generate the results in Table 12-13. There is an incomplete final row in Table 12-13 because the first two columns refer to the inlets and the outlets of the control volumes, while the remaining columns refer to the average conditions inside the control volumes, which are assumed to be the average of the inlet and outlet conditions. Hence column 3 (\bar{X}) is the average of the inlet and outlet moisture contents for each of the cells in column 2 (X_i). Column 4 (\bar{Y}) follows from column 3, using Eq. (12-74). Column 5 (\bar{T}_G) follows from column 4, using the enthalpy humidity chart in Fig. 12-43. Column 6 (T_{wb}) is read off the same enthalpy humidity chart. Column 7 (f) follows from the linear falling-rate curve, using the average moisture contents in column 3. Column 8 (T_s) comes from columns 5 (\bar{T}_G), 7 (f), and the energy balance in Eq. (12-82), while column 9 ($d\bar{X}/dt$) comes from columns 4 (\bar{Y}), 7 (f), and Eq. (12-81). The final column comes from the difference between inlet and outlet moisture contents in column 2, divided by the average drying rate in column 9.

Computational Fluid Dynamics (CFD) CFD provides a very detailed and accurate model of the gas phase, including three-dimensional effects and swirl. Where localized flow patterns have a major effect on the overall performance of a dryer and the particle history, CFD can give immense improvements in modeling and in understanding of physical phenomena. Conversely, where the system is well mixed or drying is dominated by falling-rate kinetics and local conditions are unimportant, CFD modeling will give little or no advantage over conventional methods, but will incur a vastly greater cost in computing time.

CFD has been extensively applied in recent years to spray dryers (Langrish and Fletcher, 2001), but it has also been useful for other local three-dimensional swirling flows, e.g., around the feed point of pneumatic conveying dryers (Kemp et al., 1991), and for other cases where airflows affect drying significantly, e.g., local overdrying and warping in timber stacks (Langrish, 1999).

Design and Scale-up of Individual Dryer Types

Oven and Tray Dryers Scale up from tests with an oven or single tray at identical conditions (temperature, airflow or pressure, layer thickness, and agitation, if any). The total area of trays required is then proportional to the mass of material to be dried, compared to the small-scale test.

TABLE 12-13 The Variation in Process Conditions for the Example of a Cocurrent Cascading Rotary Dryer

Interval	$ X_i, \text{ kg/kg} $	$ \bar{X}, \text{ kg/kg} $	$ \bar{Y}, \text{ kg/kg} $	$ \bar{T}_G, ^\circ\text{C} $	$ T_{wb}, ^\circ\text{C} $	$ f = \Phi $	$ \bar{T}_s, ^\circ\text{C} $	$ d\bar{X}/dt, \text{ kg}/(\text{kg}\cdot\text{s}) $	$ \Delta t_{ps}, \text{ s} $
1	0.500	0.478	0.122	720	79.0	0.956	107	0.04656	0.94
2	0.456	0.434	0.166	630	78.5	0.869	151	0.03683	1.19
3	0.412	0.391	0.209	530	78.5	0.781	177	0.02820	1.55
4	0.369	0.347	0.253	430	78.0	0.694	186	0.02067	2.12
5	0.325	0.303	0.297	340	78.0	0.606	181	0.01424	3.07
6	0.281	0.259	0.341	250	78.0	0.519	161	0.00892	4.91
7	0.238	0.216	0.384	200	78.0	0.431	147	0.00470	9.32
8	0.194	0.172	0.428	130	78.0	0.344	112	0.00158	27.73
out	0.150	Total required gas-phase residence time (s) = 50.82 s (summation of last column)							

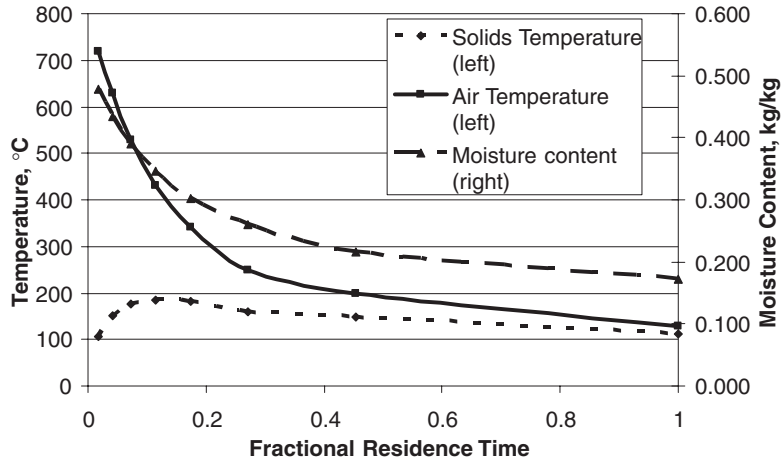


FIG. 12-42 Typical variation of process conditions through a cocurrent cascading rotary dryer.

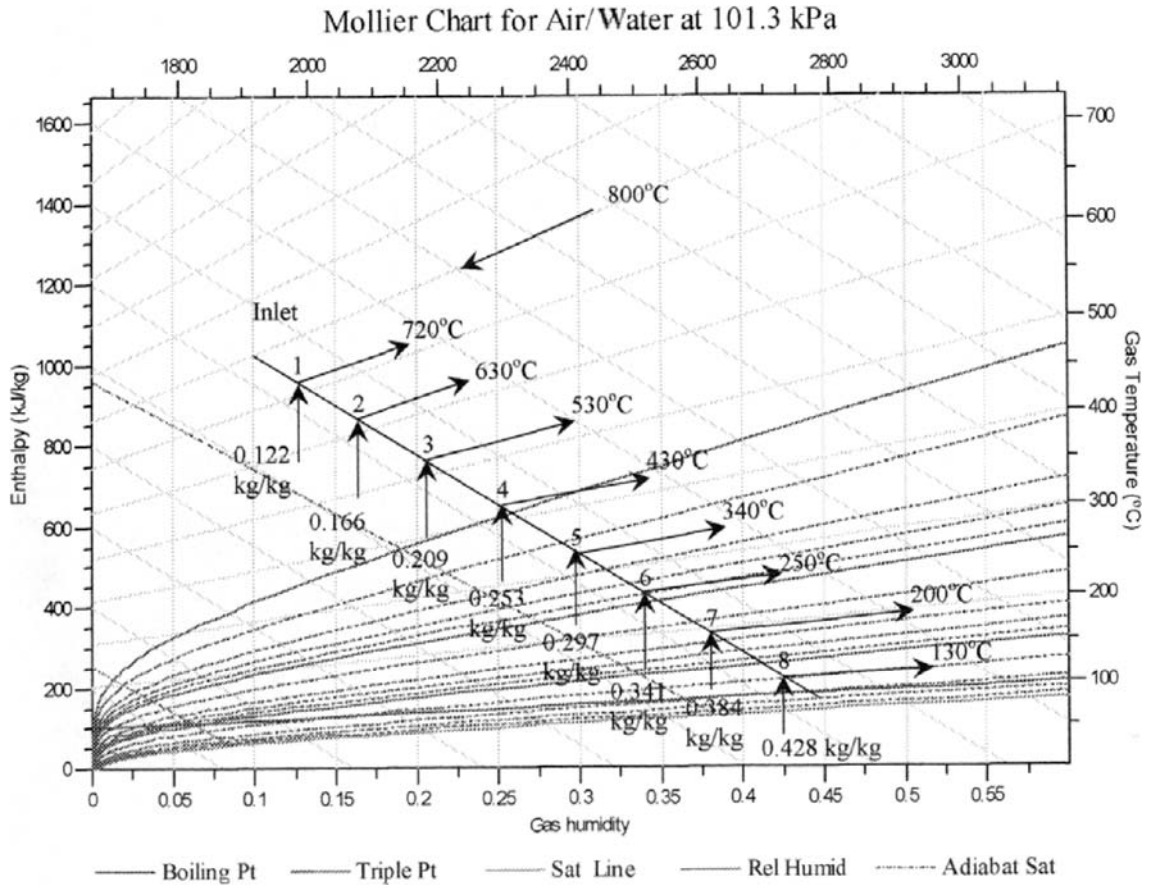


FIG. 12-43 Enthalpy humidity chart used to generate the results in Table 12-13 plots humidity (abscissa) against enthalpy (lines sloping diagonally from top left to bottom right).

Agitated and Rotating Batch Dryers Scale up from pilot-plant tests in a small-scale dryer at the same temperature and pressure and similar agitation conditions. As noted under scoping design, scale-up depends on the surface area/volume ratio, and hence normally to the one-third power of mass. Results from one dryer type may be extrapolated to a different type if assumptions are made on the heat transfer coefficients in both dryers; obviously this is less reliable than measurements on the same dryer type.

Fluidized-Bed Dryers In design mode, the required gas flow rate can be obtained from a heat and mass balance. Bed cross-sectional area is found from the scoping design calculation; the required gas velocity should be found from fluidization tests, but for initial design purposes, a typical value is 0.5 m/s.

For scale-up based on an experimentally recorded batch drying curve, including performance mode calculations and altering operating conditions, Kemp and Oakley (2002) showed that the drying time for a given range of moisture content ΔX scales according to the relationship

$$\frac{\Delta\tau_2}{\Delta\tau_1} = Z = \frac{(m_B/A)_2 G_1 (T_{Cl} - T_{ub})_1 (1 - e^{-fNTU_z})_1}{(m_B/A)_1 G_2 (T_{Cl} - T_{ub})_2 (1 - e^{-fNTU_z})_2} \quad (12-83)$$

where 1 denotes experimental or original conditions and 2 denotes full-scale or new conditions; Z is the normalization factor; G is gas mass flux; m_B/A is bed mass per unit area, proportional to bed depth z ; NTU is number of transfer units through the bed; and f is falling-rate kinetics factor. This method can be used to scale a batch drying curve section by section. Almost always, one of two simplified limiting cases applies, known as type A and type B normalization. In type A, $f(NTU)$ is high, the exponential term is negligible, and the drying time is proportional to $G(T_{Cl} - T_{ub})/(m_B/A)$. This applies to all fast-drying materials and the vast majority of other materials, even well into the falling-rate period. In type B, $f(NTU)$ is low, and expanding the exponential term shows that drying time is simply proportional to $T_{Cl} - T_{ub}$. This applies to a few very slow-drying materials, at very low moisture contents or where drying kinetics is completely controlled by internal moisture movement (e.g., wheat and grain, which have thick cell walls).

For a typical pilot-plant experiment, the fluidization velocity and temperature driving forces are similar to those of the full-size bed, but the bed diameter and depth are much less. Hence, for type A normalization, the m_B/A term dominates. Z is much greater than 1, and the drying time in the full-scale bed is typically 5 to 10 times that in the pilot-plant.

The drying time, bed area, solids throughput, and bed depth expressed as m_B/A are linked by

$$W_s = \frac{A_B}{\tau_s} \left(\frac{m_B}{A_B} \right) \quad (12-84)$$

The consequence is that increasing gas velocity is beneficial for type A normalization (giving reduced drying time and either a higher throughput or a smaller bed area) but gives no real benefit for type B; likewise, increasing bed depth is beneficial for type B (giving either a higher throughput or a smaller bed area with the same drying time) but not type A. However, using unnecessarily high gas velocity or an unnecessarily deep bed increases pressure drop and operating costs.

Cascading Rotary Dryers In design mode, the required gas flow rate can be obtained from a heat and mass balance. Bed cross-sectional area is found from the scoping design calculation (a typical gas velocity is 3 m/s for cocurrent and 2 m/s for countercurrent units). Length is normally between 5 and 10 times drum diameter (an L/D value of 8 can be used for initial estimation) or can be calculated by using an incremental model (see worked example).

Entrainment Dryers In design mode, the required gas flow rate can be obtained from a heat and mass balance. For pneumatic conveying dryers, duct cross-sectional area and diameter are found from the scoping design calculation (if required gas velocity is unknown, a typical value is 20 m/s). Duct length can be estimated by an incremental model, but some parameters are hard to obtain and conditions change rapidly near the feed point, so the model is most effective for scaling up from pilot-plant data; see Kemp and Oakley (2002). Spray

dryer chamber design is complex, and sizing should normally be done by manufacturers.

ADDITIONAL READING

- Kemp, Bahu, and Oakley, "Modeling Vertical Pneumatic Conveying Dryers," *Drying '91* (7th Int. Drying Symp., Prague, Czechoslovakia, Aug. 1990), Mujumdar et al. (eds.), Elsevier, 1991, pp. 217–227.
- Kemp and Oakley, "Modeling of Particulate Drying in Theory and Practice," *Drying Technol.* **20**(9): 1699–1750 (2002).
- Langrish, "The Significance of the Gaps between Boards in Determining the Moisture Content Profiles in the Drying of Hardwood Timber," *Drying Technol.* **17**(Pt. 7–8): 1481–1494 (1999).
- Langrish and Fletcher, "Spray Drying of Food Ingredients and Applications of CFD in Spray Drying," *Chemical Engineering and Processing* **40**(4): 345–354 (2001).
- Vanecek, Picka, and Najmr, "Some Basic Information on the Drying of Granulated NPK Fertilisers," *Int. Chem. Eng.* **4** (1): 93–99 (1964).
- Vanecek, Picka, and Najmr, *Fluidized Bed Drying*, Leonard Hill, London, 1966.

DRYER DESCRIPTIONS

GENERAL REFERENCES: *Aspen Process Manual* (Internet knowledge base), Aspen Technology, 2000 onward. Baker (ed.), *Industrial Drying of Foods*, Blaikie, London, 1997; Cook and DuMont, *Process Drying Practice*, McGraw-Hill, 1991. *Drying Technology—An International Journal*, Marcel Dekker, New York, 1982 onward. Keey, *Drying of Loose and Particulate Materials*, Hemisphere, New York, 1992. Masters, *Spray Drying Handbook*, Wiley, New York, 1990. Mujumdar (ed.), *Handbook of Industrial Drying*, Marcel Dekker, New York, 1995. Nonhebel and Moss, *Drying of Solids in the Chemical Industry*, CRC Press, Cleveland Ohio, 1971. van't Land, *Industrial Drying Equipment*, Marcel Dekker, New York, 1991.

Batch Tray Dryers

Description A tray or compartment dryer is an enclosed, insulated housing in which solids are placed upon tiers of trays in the case of particulate solids or stacked in piles or upon shelves in the case of large objects. Heat transfer may be *direct* from gas to solids by circulation of large volumes of hot gas or *indirect* by use of heated shelves, radiator coils, or refractory walls inside the housing. In indirect-heat units, excepting vacuum-shelf equipment, circulation of a small quantity of gas is usually necessary to sweep moisture vapor from the compartment and prevent gas saturation and condensation. Compartment units are employed for the heating and drying of lumber, ceramics, sheet materials (supported on poles), painted and metal objects, and all forms of particulate solids.

Classification Batch; nonagitated; layer; convective (cross-circulation or through-circulation) or contact/conduction.

Field of Application Because of the high labor requirements usually associated with loading or unloading the compartments, batch compartment equipment is rarely economical except in the following situations:

1. A long heating cycle is necessary because the size of the solid objects or permissible heating temperature requires a long holdup for internal diffusion of heat or moisture. This case may apply when the cycle will exceed 12 to 24 h.

2. The production of several different products requires strict batch identity and thorough cleaning of equipment between batches. This is a situation existing in many small multiproduct plants, e.g., for pharmaceuticals or specialty chemicals.

3. The quantity of material to be processed does not justify investment in more expensive, continuous equipment. This case would apply in many pharmaceutical drying operations.

Further, because of the nature of solids-gas contacting, which is usually by parallel flow and rarely by through-circulation, heat transfer and mass transfer are comparatively inefficient. For this reason, use of tray and compartment equipment is restricted primarily to ordinary drying and heat-treating operations. Despite these harsh limitations, when the listed situations do exist, economical alternatives are difficult to develop.

Auxiliary Equipment If noxious gases, fumes, or dust is given off during the operation, dust or fume recovery equipment will be

necessary in the exhaust gas system. Wet scrubbers are employed for the recovery of valuable solvents from dryers. To minimize heat losses, thorough insulation of the compartment with brick, asbestos, or other insulating compounds is necessary. Modern fabricated dryer compartment panels usually have 7.5 to 15 cm of blanket insulation placed between the internal and external sheet-metal walls. Doors and other access openings should be gasketed and tight. In the case of tray and truck equipment, it is usually desirable to have available extra trays and trucks so that they can be preloaded for rapid emptying and loading of the compartment between cycles. Air filters and gas dryers are occasionally employed on the inlet air system for direct-heat units.

Vacuum-shelf dryers require auxiliary stream jets or other vacuum-producing devices, intercondensers for vapor removal, and occasionally wet scrubbers or (heated) bag-type dust collectors.

Uniform depth of loading in dryers and furnaces handling particulate solids is essential to consistent operation, minimum heating cycles, or control of final moisture. After a tray has been loaded, the bed should be leveled to a uniform depth. Special preform devices, noodle extruders, pelletizers, etc., are employed occasionally for preparing pastes and filter cakes so that screen bottom trays can be used and the advantages of through-circulation approached.

Control of tray and compartment equipment is usually maintained by control of the circulating air temperature (and humidity) and rarely by the solids temperature. On vacuum units, control of the absolute pressure and heating-medium temperature is utilized. In direct dryers, cycle controllers are frequently employed to vary the air temperature or velocity across the solids during the cycle; e.g., high air temperatures may be employed during a constant-rate drying period while the solids surface remains close to the air wet-bulb temperature. During the falling-rate periods, this temperature may be reduced to prevent case hardening or other degrading effects caused by overheating the solids surfaces. In addition, higher air velocities may be employed during early drying stages to improve heat transfer; however, after surface drying has been completed, this velocity may need to be reduced to prevent dusting. Two-speed circulating fans are employed commonly for this purpose.

Direct-Heat Tray Dryers Satisfactory operation of tray-type dryers depends on maintaining a constant temperature and a uniform air velocity over all the material being dried.

Circulation of air at velocities of 1 to 10 m/s is desirable to improve the surface heat-transfer coefficient and to eliminate stagnant air pockets. Proper airflow in tray dryers depends on sufficient fan capacity, on the design of ductwork to modify sudden changes in direction, and on properly placed baffles. *Nonuniform airflow is one of the most serious problems in the operation of tray dryers.*

Tray dryers may be of the tray-truck or the stationary-tray type. In the former, the trays are loaded on trucks which are pushed into the dryer; in the latter, the trays are loaded directly into stationary racks within the dryer. Trucks may be fitted with flanged wheels to run on tracks or with flat swivel wheels. They may also be suspended from and moved on monorails. Trucks usually contain two tiers of trays, with 18 to 48 trays per tier, depending upon the tray dimensions.

Trays may be square or rectangular, with 0.5 to 1 m² per tray, and may be fabricated from any material compatible with corrosion and temperature conditions. When the trays are stacked in the truck, there should be a clearance of not less than 4 cm between the material in one tray and the bottom of the tray immediately above. When material characteristics and handling permit, the trays should have screen bottoms for additional drying area. Metal trays are preferable to non-metallic trays, since they conduct heat more readily. Tray loadings range usually from 1 to 10 cm deep.

Steam is the usual heating medium, and a standard heater arrangement consists of a main heater before the circulating fan. When steam is not available or the drying load is small, electric heat can be used. For temperatures above 450 K, products of combustion can be used, or indirect-fired air heaters.

Air is circulated by propeller or centrifugal fans; the fan is usually mounted within or directly above the dryer. Above 450 K, external or water-cooled bearings become necessary. Total pressure drop through

the trays, heaters, and ductwork is usually in the range of 2.5 to 5 cm of water. Air recirculation is generally in the order of 80 to 95 percent except during the initial drying stage of rapid evaporation. Fresh air is drawn in by the circulating fan, frequently through dust filters. In most installations, air is exhausted by a separate small exhaust fan with a damper to control air recirculation rates.

Prediction of heat- and mass-transfer coefficients in direct heat tray dryers In convection phenomena, heat-transfer coefficients depend on the geometry of the system, the gas velocity past the evaporating surface, and the physical properties of the drying gas. In estimating drying rates, the use of heat-transfer coefficients is preferred because they are usually more reliable than mass-transfer coefficients. In calculating mass-transfer coefficients from drying experiments, the partial pressure at the surface is usually inferred from the measured or calculated temperature of the evaporating surface. Small errors in temperature have negligible effect on the heat-transfer coefficient but introduce relatively large errors in the partial pressure and hence in the mass-transfer coefficient.

For many cases in drying, the heat-transfer coefficient is proportional to U_g^n , where U_g is an appropriate local gas velocity. For flow parallel to plane plates, the exponent n has been reported to range from 0.35 to 0.8. The differences in exponent have been attributed to differences in flow pattern in the space above the evaporating surface, particularly whether it is laminar or turbulent, and whether the length is sufficient to allow fully developed flow. In the absence of applicable specific data, the heat-transfer coefficient for the parallel-flow case can be taken, for estimating purposes, as

$$h = \frac{8.5J^{0.8}}{D_c^{0.2}} \quad (12-85)$$

where h is the heat-transfer coefficient, W/(m²·K) [or J/s·m²·K]; J is the gas mass flux, kg/(m²·S); and D_c is a characteristic dimension of the system. The experimental data have been weighted in favor of an exponent of 0.8 in conformity with the usual Colburn j factor, and average values of the properties of air at 370 K have been incorporated. Typical values are in the range 10 to 50 W/(m²·K).

Experimental data for drying from flat surfaces have been correlated by using the equivalent diameter of the flow channel or the length of the evaporating surface as the characteristic length dimension in the Reynolds number. However, the validity of one versus the other has not been established. The proper equivalent diameter probably depends at least on the geometry of the system, the roughness of the surface, and the flow conditions upstream of the evaporating surface. For most tray drying calculations, the equivalent diameter (4 times the cross-sectional area divided by the perimeter of the flow channel) should be used.

For airflow impinging normally to the surface from slots, nozzles, or perforated plates, the heat-transfer coefficient can be obtained from the data of Friedman and Mueller (*Proceedings of the General Discussion on Heat Transfer*, Institution of Mechanical Engineers, London, and American Society of Mechanical Engineers, New York, 1951, pp. 138–142). These investigators give

$$h = \alpha J^{0.78} \quad (12-86)$$

where the gas mass flux J is based on the total heat-transfer area and is dependent on the plate open area, hole or slot size, and spacing between the plate, nozzle, or slot and the heat-transfer surface.

Most efficient performance is obtained with plates having open areas equal to 2 to 3 percent of the total heat-transfer area. The plate should be located at a distance equal to four to six hole (or equivalent) diameters from the heat-transfer surface.

Data from tests employing multiple slots, with a correction calculated for slot width, were reported by Korger and Kizek [*Int. J. Heat Mass Transfer*, London, 9:337 (1966)].

Another well-known correlation has been used to predict heat- and mass-transfer coefficients for air impinging on a surface from arrays of holes (jets). This correlation uses relevant geometric properties such as the diameter of the holes, the distance between the holes, and the distance between the holes and the sheet [Martin, "Heat and Mass Transfer Between Impinging Gas Jets and Solid

12-58 PSYCHROMETRY, EVAPORATIVE COOLING, AND SOLIDS DRYING

Surfaces," *Advances in Heat Transfer*, vol. 13, Academic Press, 1977, pp. 1-66].

$$\frac{Sh}{Sc^{0.42}} = \frac{Nu}{Pr^{0.42}} = \left[1 + \left(\frac{H/D}{0.6/\sqrt{f}} \right)^6 \right]^{-0.05} \times \sqrt{f} \frac{1 - 2.2\sqrt{f}}{1 + 0.2(H/D - 6)\sqrt{f}} \times Re^{2/3}$$

where D = diameter of nozzle, m

$$f = \frac{\pi}{2\sqrt{3}} \left(\frac{D}{L_D} \right)^2$$

H = distance from nozzle to sheet, m
 L_D = average distance between nozzles, m
 Nu = Nusselt number
 Pr = Prandtl number

$$Re = \frac{wD}{\nu}, \text{ Reynolds number}$$

Sc = Schmidt number
 Sh = Sherwood number
 w = velocity of air at nozzle exit, m/s
 ν = kinematic viscosity of air, m²/s

The heat- and mass-transfer coefficients were then calculated from the definitions of the Nusselt and Sherwood numbers.

$$Nu = \frac{hD}{k_{th}} \quad \text{where } k_{th} = \text{thermal conductivity of air, W/(m}\cdot\text{K)}$$

D = diameter of holes in air bars, m

$$Sh = \frac{k_m D}{diff} \quad \text{where } diff = \text{diffusion coefficient of water vapor in air, m}^2/\text{s}$$

Air impingement is commonly employed for drying sheets, film, thin slabs, and coatings. The temperature driving force must also be found. When radiation and conduction are negligible, the temperature of the evaporating surface approaches the wet-bulb temperature and is readily obtained from the humidity and dry-bulb temperatures. Frequently, however, radiation and conduction cause the temperature of the evaporating surface to exceed the wet-bulb temperature. When this occurs, the true surface temperature must be estimated. The easiest way is to use a psychrometric chart and to change the slope of the adiabatic saturation line; a typical figure for the additional radiation is about 10 percent. In many cases this is canceled out by heat losses and

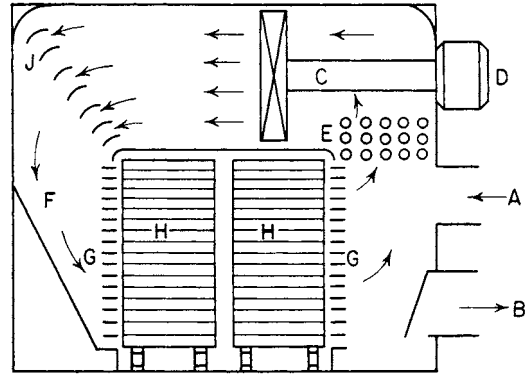


FIG. 12-44 Double-truck tray dryer. (A) Air inlet duct. (B) Air exhaust duct with damper. (C) Adjustable-pitch fan 1 to 15 hp. (D) Fan motor. (E) Fin heaters. (F) Plenum chamber. (G) Adjustable air blast nozzles. (H) Trucks and trays. (J) Turning vanes.

the heat required to warm the solid, leaving the dryer approximately adiabatic.

As with many drying calculations, the most reliable design method is to perform experimental tests and to scale up. By measuring performance on a single tray with similar layer depth, air velocity, and temperature, the SDR (specific drying rate) concept can be applied to give the total area and number of trays required for the full-scale dryer.

Performance data for direct heat tray dryers A standard two-truck dryer is illustrated in Fig. 12-44. Adjustable baffles or a perforated distribution plate is normally employed to develop 0.3 to 1.3 cm of water pressure drop at the wall through which air enters the truck enclosure. This will enhance the uniformity of air distribution, from top to bottom, among the trays. In three (or more) truck ovens, air reheat coils may be placed between trucks if the evaporative load is high. Means for reversing airflow direction may also be provided in multiple-truck units.

Performance data on some typical tray and compartment dryers are tabulated in Table 12-14. These indicate that an overall rate of evaporation of 0.0025 to 0.025 kg water/(s·m²) of tray area may be expected from tray and tray-truck dryers. The thermal efficiency of this type of dryer will vary from 20 to 50 percent, depending on the drying temperature used and the humidity of the exhaust air. In drying to very low moisture contents under temperature restrictions, the thermal efficiency may be on the order of 10 percent. The major operating cost for a tray dryer is the labor involved in loading and unloading the trays. About 2 labor-hours is required to load and unload a standard

TABLE 12-14 Manufacturer's Performance Data for Tray and Tray-Truck Dryers*

Material	Color	Chrome yellow	Toluidine red	Half-finished Titone	Color
Type of dryer	2-truck	16-tray dryer	16-tray	3-truck	2-truck
Capacity, kg product/h	11.2	16.1	1.9	56.7	4.8
Number of trays	80	16	16	180	120
Tray spacing, cm	10	10	10	7.5	9
Tray size, cm	60 × 75 × 4	65 × 100 × 2.2	65 × 100 × 2	60 × 70 × 3.8	60 × 70 × 2.5
Depth of loading, cm	2.5 to 5	3	3.5	3	
Initial moisture, % bone-dry basis	207	46	220	223	116
Final moisture, % bone-dry basis	4.5	0.25	0.1	25	0.5
Air temperature, °C	85-74	100	50	95	99
Loading, kg product/m ²	10.0	33.7	7.8	14.9	9.28
Drying time, h	33	21	41	20	96
Air velocity, m/s	1.0	2.3	2.3	3.0	2.5
Drying, kg water evaporated/(h·m ²)	0.59	65	0.41	1.17	0.11
Steam consumption, kg/kg water evaporated	2.5	3.0	—	2.75	
Total installed power, kW	1.5	0.75	0.75	2.25	1.5

*Courtesy of Wolverine Proctor & Schwartz, Inc.

two-truck tray dryer. In addition, about one-third to one-fifth of a worker's time is required to supervise the dryer during the drying period. Power for tray and compartment dryers will be approximately 1.1 kW per truck in the dryer. Maintenance will run from 3 to 5 percent of the installed cost per year.

Batch Through-Circulation Dryers These may be either of shallow bed or deep bed type. In the first type of batch through-circulation dryer, heated air passes through a stationary permeable bed of the wet material placed on removable screen-bottom trays suitably supported in the dryer. This type is similar to a standard tray dryer except that hot air passes through the wet solid instead of across it. The pressure drop through the bed of material does not usually exceed about 2 cm of water. In the second type, deep perforated-bottom trays are placed on top of plenum chambers in a closed-circuit hot air circulating system. In some food-drying plants, the material is placed in finishing bins with perforated bottoms; heated air passes up through the material and is removed from the top of the bin, reheated, and recirculated. The latter types involve a pressure drop through the bed of material of 1 to 8 cm of water at relatively low air rates. Table 12-15 gives performance data on three applications of batch through-circulation dryers. Batch through-circulation dryers are restricted in application to granular materials (particle size typically 1 mm or greater) that permit free flow-through circulation of air. Drying times are usually much shorter than in parallel-flow tray dryers. Design methods are included in the subsection "Continuous Through-Circulation Dryers."

Contact Tray and Vacuum-Shelf Dryers Vacuum-shelf dryers are indirectly heated batch dryers consisting of a vacuum-tight chamber usually constructed of cast iron or steel plate, heated, supporting shelves within the chamber, a vacuum source, and usually a condenser. One or two doors are provided, depending on the size of the chamber. The doors are sealed with resilient gaskets of rubber or similar material. It is also possible, but much less common, to operate at atmospheric pressure without vacuum.

Hollow shelves of flat steel plate are fastened permanently inside the vacuum chamber and are connected in parallel to inlet and outlet headers. The heating medium, entering through one header and passing through the hollow shelves to the exit header, is generally steam, ranging in pressure from 700 kPa gauge to subatmospheric pressure for low-temperature operations. Low temperatures can be provided by circulating hot water, and high temperatures can be obtained by circulating hot oil or Dowtherm. Some small dryers employ electrically heated shelves. The material to be dried is placed in pans or trays on the heated shelves. The trays are generally of metal to ensure good heat transfer between the shelf and the tray.

Vacuum-shelf dryers may vary in size from 1 to 24 shelves, the largest chambers having overall dimensions of 6 m wide, 3 m long, and 2.5 m high.

Vacuum is applied to the chamber, and vapor is removed through a large pipe which is connected to the chamber in such a manner that if the vacuum is broken suddenly, the in-rushing air will not greatly disturb the bed of material being dried. This line leads to a condenser where moisture or solvent that has been vaporized is condensed. The noncondensable exhaust gas goes to the vacuum source, which may be a wet or dry vacuum pump or a steam-jet ejector.

Vacuum-shelf dryers are used extensively for drying pharmaceuticals, temperature-sensitive or easily oxidizable materials, and materials so valuable that labor cost is insignificant. They are particularly useful for handling small batches of materials wet with toxic or valuable solvents. Recovery of the solvent is easily accomplished without danger of passing through an explosive range. Dusty materials may be dried with negligible dust loss. Hygroscopic materials may be completely dried at temperatures below that required in atmospheric dryers. The equipment is employed also for freeze-drying processes, for metallizing-furnace operations, and for the manufacture of semiconductor parts in controlled atmospheres. All these latter processes demand much lower operating pressures than do ordinary drying operations.

Design methods for vacuum-shelf dryers Heat is transferred to the wet material by conduction through the shelf and bottom of the tray and by radiation from the shelf above. The critical moisture content will not be necessarily the same as for atmospheric tray drying, as the heat-transfer mechanisms are different.

During the constant-rate period, moisture is rapidly removed. Often 50 percent of the moisture will evaporate in the first hour of a 6- to 8-h cycle. The drying time has been found to be proportional to between the first and second power of the depth of loading. Shelf vacuum dryers operate in the range of 1 to 25 mmHg pressure. For size-estimating purposes, a heat-transfer coefficient of 20 J/(m²·s·K) may be used. The area employed in this case should be the shelf area in direct contact with the trays. Trays should be maintained as flatly as possible to obtain maximum area of contact with the heated shelves. For the same reason, the shelves should be kept free from scale and rust. Air vents should be installed on steam-heated shelves to vent noncondensable gases. The heating medium should not be applied to the shelves until after the air has been evacuated from the chamber, to reduce the possibility of the material's overheating or boiling at the start of drying. Case hardening can sometimes be avoided by retarding the rate of drying in the early part of the cycle.

Performance data for vacuum-shelf dryers The purchase price of a vacuum-shelf dryer depends upon the cabinet size and number of shelves per cabinet. For estimating purposes, typical prices (1985) and auxiliary equipment requirements are given in Table 12-16. Installed cost of the equipment will be roughly 100 percent of the carbon-steel purchase cost.

The thermal efficiency of a vacuum-shelf dryer is usually on the order of 60 to 80 percent. Table 12-17 gives operating data for one organic color and two inorganic compounds. Labor may constitute 50 percent of the operating cost; maintenance, 20 percent. Annual maintenance costs amount to 5 to 10 percent of the total installed cost. Actual labor costs will depend on drying time, facilities for loading and unloading trays, etc. The power required for these dryers is only that for the vacuum system; for vacuums of 680 to 735 mmHg, the power requirements are on the order of 0.06 to 0.12 kW/m² tray surface.

Continuous Tray and Gravity Dryers Continuous tray dryers are equivalent to batch tray dryers, but with the solids moving between trays by a combination of mechanical movement and gravity. Gravity (moving-bed) dryers are normally through-circulation convective dryers with no internal trays where the solids gradually descend by gravity. In all these types, the net movement of solids is vertically downward.

Classification Continuous; nonagitated (except for turnover when falling between trays); layer; convective (cross-circulation or through-circulation) or contact/conduction; vertical solids movement by gravity and mechanical agitation.

Turbo-Tray Dryers The turbo-tray dryer (also known as rotating tray, rotating shelf, or Wyssmont TURBO-DRYER[®]) is a continuous

TABLE 12-15 Performance Data for Batch Through-Circulation Dryers*

Kind of material	Granular polymer	Vegetable	Vegetable seeds
Capacity, kg product/h	122	42.5	27.7
Number of trays	16	24	24
Tray spacing, cm	43	43	43
Tray size, cm	91.4 × 104	91.4 × 104	85 × 98
Depth of loading, cm	7.0	6	4
Physical form of product	Crumbs	0.6-cm diced cubes	Washed seeds
Initial moisture content, % dry basis	11.1	669.0	100.0
Final moisture content, % dry basis	0.1	5.0	9.9
Air temperature, °C	88	77 dry-bulb	36
Air velocity, superficial, m/s	1.0	0.6 to 1.0	1.0
Tray loading, kg product/m ²	16.1	5.2	6.7
Drying time, h	2.0	8.5	5.5
Overall drying rate, kg water evaporated/(h·m ²)	0.89	11.86	1.14
Steam consumption, kg/kg water evaporated	4.0	2.42	6.8
Installed power, kW	7.5	19	19

*Courtesy of Wolverine Proctor & Schwartz, Inc.

TABLE 12-16 Standard Vacuum-Shelf Dryers*

Shelf area, m ²	Floor space, m ²	Weight average, kg	Pump capacity, m ³ /s	Pump motor, kW	Condenser area, m ²	Price/m ² (1995)	
						Carbon steel	304 stainless steel
0.4-1.1	4.5	540	0.024	1.12	1	\$110	\$170
1.1-2.2	4.5	680	0.024	1.12	1	75	110
2.2-5.0	4.6	1130	0.038	1.49	4	45	65
5.0-6.7	5.0	1630	0.038	1.49	4	36	65
6.7-14.9	6.4	3900	0.071	2.24	9	27	45
16.7-21.1	6.9	5220	0.071	2.24	9	22	36

*Stokes Vacuum, Inc.

dryer consisting of a stack of rotating annular shelves in the center of which turbo-type fans revolve to circulate the air over the shelves. Wet material enters through the roof, falling onto the top shelf as it rotates beneath the feed opening. After completing 1 r, the material is wiped by a stationary wiper through radial slots onto the shelf below, where it is spread into a uniform pile by a stationary leveler. The action is repeated on each shelf, with transfers occurring once in each revolution. From the last shelf, material is discharged through the bottom of the dryer (Fig. 12-45). The steel-frame housing consists of removable insulated panels for access to the interior. All bearings and lubricated parts are exterior to the unit with the drives located under the housing. Parts in contact with the product may be of steel or special alloy. The trays can be of any sheet material.

The rate at which each fan circulates air can be varied by changing the pitch of the fan blades. In final drying stages, in which diffusion controls or the product is light and powdery, the circulation rate is considerably lower than in the initial stage, in which high evaporation rates prevail. In the majority of applications, air flows through the dryer upward in counterflow to the material. In special cases, required drying conditions dictate that airflow be cocurrent or both counter-current and cocurrent with the exhaust leaving at some level between solids inlet and discharge. A separate cold-air-supply fan is provided if the product is to be cooled before being discharged.

By virtue of its vertical construction, the turbo-type tray dryer has a stack effect, the resulting draft being frequently sufficient to operate the dryer with natural draft. Pressure at all points within the dryer is maintained close to atmospheric. Most of the roof area is used as a breeching, lowering the exhaust velocity to settle dust back into the dryer.

Heaters can be located in the space between the trays and the dryer housing, where they are not in direct contact with the product, and thermal efficiencies up to 3500 kJ/kg (1500 Btu/lb) of water evaporated can be obtained by reheating the air within the dryer. For materials which have a tendency to foul internal heating surfaces, an external heating system is employed.

The turbo-tray dryer can handle materials from thick slurries [1 million N·s/m² (100,000 cP) and over] to fine powders. Filterpress cakes are granulated before feeding. Thixotropic materials are fed directly from a rotary filter by scoring the cake as it leaves the drum. Pastes can be extruded onto the top shelf and subjected to a hot blast of air to make them firm and free-flowing after 1 r.

TABLE 12-17 Performance Data of Vacuum-Shelf Dryers

Material	Sulfur black	Calcium carbonate	Calcium phosphate
Loading, kg dry material/m ²	25	17	33
Steam pressure, kPa gauge	410	410	205
Vacuum, mmHg	685-710	685-710	685-710
Initial moisture content, % (wet basis)	50	50.3	30.6
Final moisture content, % (wet basis)	1	1.15	4.3
Drying time, h	8	7	6
Evaporation rate, kg/(s·m ²)	8.9 × 10 ⁻⁴	7.9 × 10 ⁻⁴	6.6 × 10 ⁻⁴

The turbo-tray dryer is manufactured in sizes from package units 2 m in height and 1.5 m in diameter to large outdoor installations 20 m in height and 11 m in diameter. Tray areas range from 1 m² up to about 2000 m². The number of shelves in a tray rotor varies according to space available and the minimum rate of transfer required, from as few as 12 shelves to as many as 58 in the largest units. Standard construction permits operating temperatures up to 615 K, and high-temperature heaters permit operation at temperatures up to 925 K.

A recent innovation has enabled TURBO-DRYER[®] to operate with very low inert gas makeup. Wyssmont has designed a tank housing that is welded up around the internal structure rather than the column-and-gasket panel design that has been the Wyssmont standard for many years. In field-erected units, the customer does the welding in the field; in packaged units, the tank-type welding is done in the shop. The tank-type housing finds particular application for operation under positive pressure. On the standard design, doors with explosion latches and gang latch operators are used. In the tank-type design,

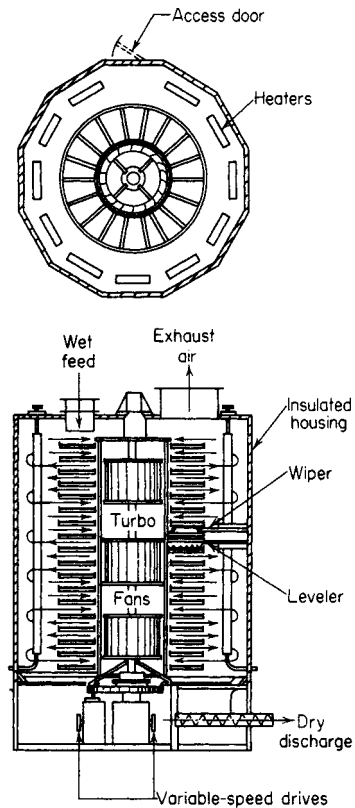


FIG. 12-45 TURBO-DRYER[®]. (Wyssmont Company, Inc.)

tight-sealing manway-type openings permit access to the interior. Tank-type housing designs have been requested when drying solvent wet materials and for applications where the material being dried is highly toxic and certainty is required that no toxic dust get out.

Design methods for turbo-tray dryers The heat- and mass-transfer mechanisms are similar to those in batch tray dryers, except that constant turning over and mixing of the solids significantly improve drying rates. Design must usually be based on previous installations or pilot tests by the manufacturer; apparent heat-transfer coefficients are typically 30 to 60 J/(m²·s·K) for dry solids and 60 to 120 J/(m²·s·K) for wet solids. Turbo-tray dryers have been employed successfully for the drying and cooling of calcium hypochlorite, urea crystals, calcium chloride flakes, and sodium chloride crystals. The Wyssmont "closed-circuit" system, as shown in Fig. 12-46, consists of the turbo-tray dryer with or without internal heaters, recirculation fan, condenser with receiver and mist eliminators, and reheater. Feed and discharge are through a sealed wet feeder and lock, respectively. This method is used for continuous drying without leakage of fumes, vapors, or dust to the atmosphere. A unified approach for scaling up dryers such as turbo-tray, plate, conveyor, or any other dryer type that forms a defined layer of solids next to a heating source is the SDR (specific drying rate) method described by Moyers [*Drying Technol.* 12(1 & 2): 393-417 (1994)].

Performance and cost data for turbo-tray dryers Performance data for four applications of closed-circuit drying are included in Table 12-18. Operating, labor, and maintenance costs compare favorably with those of direct heat rotating equipment.

Plate Dryers The plate dryer is an indirectly heated, fully continuous dryer available for three modes of operation: atmospheric, gastight, or full vacuum. The dryer is of vertical design, with horizontal, heated plates mounted inside the housing. The plates are heated by hot water, steam, or thermal oil, with operating temperatures up to 320°C possible. The product enters at the top and is conveyed through the dryer by a product transport system consisting of a central-rotating shaft with arms and plows. (See dryer schematic, Fig. 12-47.) The thin product layer [approximately ½-in (12-mm) depth] on the surface of the plates, coupled with frequent product turnover by the conveying system, results in short retention times (approximately 5 to 40 min), true plug flow of the material, and uniform drying. The vapors are removed from the dryer by a small amount of heated purge gas or by vacuum. The material of construction of the plates and housing is normally stainless steel, with special metallurgies also available. The drive unit is located at the bottom of the dryer and supports the central-rotating shaft. Typical speed of the dryer is 1 to 7 rpm. Full-opening doors are located on two adjacent sides of the dryer for easy access to dryer internals.

The plate dryer may vary in size from 5 to 35 vertically stacked plates with a heat-exchange area between 3.8 and 175 m². The largest unit available has overall dimensions of 3 m (w) by 4 m (l) by 10 m (h). Depending

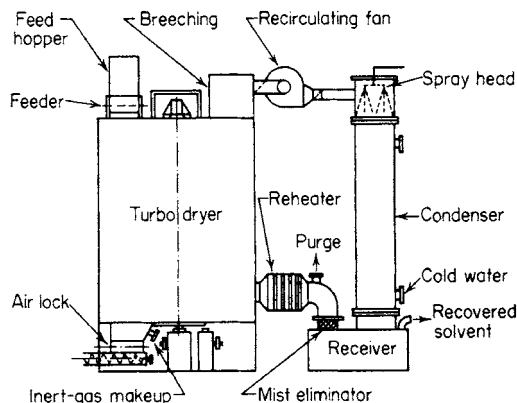


FIG. 12-46 TURBO-DRYER® in closed circuit for continuous drying with solvent recovery. (Wyssmont Company, Inc.)

upon the loose-bulk density of the material and the overall retention time, the plate dryer can process up to 5000 kg/h of wet product.

The plate dryer is limited in its scope of applications only in the consistency of the feed material (the products must be friable, free-flowing, and not undergo phase changes) and drying temperatures up to 320°C. Applications include specialty chemicals, pharmaceuticals, foods, polymers, pigments, etc. Initial moisture or volatile level can be as high as 65 percent, and the unit is often used as a final dryer to take materials to a bone-dry state, if necessary. The plate dryer can also be used for heat treatment, removal of waters of hydration (bound moisture), solvent removal, and as a product cooler.

The atmospheric plate dryer is a dust-tight system. The dryer housing is an octagonal, panel construction, with operating pressure in the range of ±0.5 kPa gauge. An exhaust air fan draws the purge air through the housing for removal of the vapors from the drying process. The purge air velocity through the dryer is in the range of 0.1 to 0.15 m/s, resulting in minimal dusting and small dust filters for the exhaust air. The air temperature is normally equal to the plate temperature. The vapor-laden exhaust air is passed through a dust filter or a scrubber (if necessary) and is discharged to the atmosphere. Normally, water is the volatile to be removed in this type of system.

The gastight plate dryer, together with the components of the gas recirculation system, forms a closed system. The dryer housing is semi-cylindrical and is rated for a nominal pressure of 5 kPa gauge. The flow rate of the recirculating purge gas must be sufficient to absorb the vapors generated from the drying process. The gas temperature must be adjusted according to the specific product characteristics and the

TABLE 12-18 Turbo-Dryer® Performance Data in Wyssmont Closed-Circuit Operations*

Material dried	Antioxidant	Water-soluble polymer	Antibiotic filter cake	Petroleum coke
Dried product, kg/h	500	85	2400	227
Volatiles composition	Methanol and water	Xylene and water	Alcohol and water	Methanol
Feed volatiles, % wet basis	10	20	30	30
Product volatiles, % wet basis	0.5	4.8	3.5	0.2
Evaporation rate, kg/h	53	16	910	302
Type of heating system	External	External	External	External
Heating medium	Steam	Steam	Steam	Steam
Drying medium	Inert gas	Inert gas	Inert gas	Inert gas
Heat consumption, J/kg	0.56 × 10 ⁶	2.2 × 10 ⁶	1.42 × 10 ⁶	1.74 × 10 ⁶
Power, dryer, kW	1.8	0.75	12.4	6.4
Power, recirculation fan, kW	5.6	5.6	37.5	15
Materials of construction	Stainless-steel interior	Stainless-steel interior	Stainless-steel interior	Carbon steel
Dryer height, m	4.4	3.2	7.6	6.5
Dryer diameter, m	2.9	1.8	6.0	4.5
Recovery system	Shell-and-tube condenser	Shell-and-tube condenser	Direct-contact condenser	Shell-and-tube condenser
Condenser cooling medium	Brine	Chilled water	Tower water	Chilled water
Location	Outdoor	Indoor	Indoor	Indoor
Approximate cost of dryer (2004)	\$300,000	\$175,000	\$600,000	\$300,000
Dryer assembly	Packaged unit	Packaged unit	Field-erected unit	Field-erected unit

*Courtesy of Wyssmont Company, Inc.

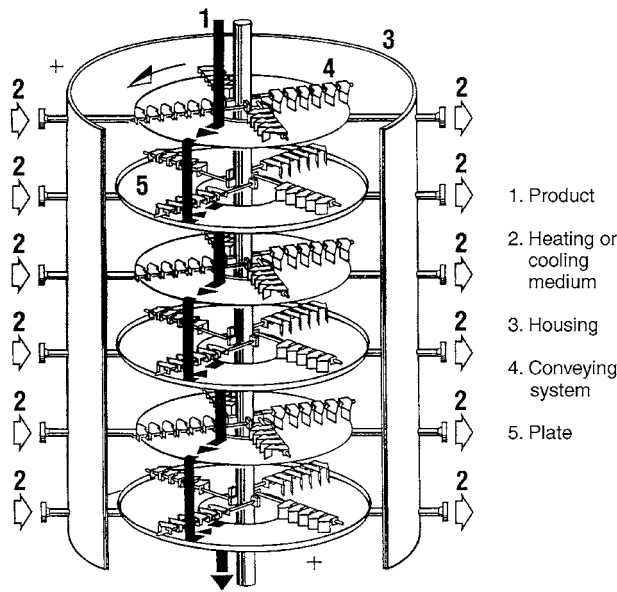


FIG. 12-47 Indirect heat continuous plate dryer for atmospheric, gastight, or full-vacuum operation. (Krauss Maffei.)

type of volatile. After condensation of the volatiles, the purge gas (typically nitrogen) is recirculated back to the dryer via a blower and heat exchanger. Solvents such as methanol, toluene, and acetone are normally evaporated and recovered in the gastight system.

The vacuum plate dryer is provided as part of a closed system. The vacuum dryer has a cylindrical housing and is rated for full-vacuum operation (typical pressure range of 3 to 27 kPa absolute). The exhaust vapor is evacuated by a vacuum pump and is passed through a condenser for solvent recovery. There is no purge gas system required for operation under vacuum. Of special note in the vacuum-drying system are the vacuum feed and discharge locks, which allow for continuous operation of the plate dryer under full vacuum.

Comparison data—plate dryers Comparative studies have been done on products under both atmospheric and vacuum drying conditions. See Fig. 12-48. These curves demonstrate (1) the improvement in drying achieved with elevated temperature and (2) the impact to

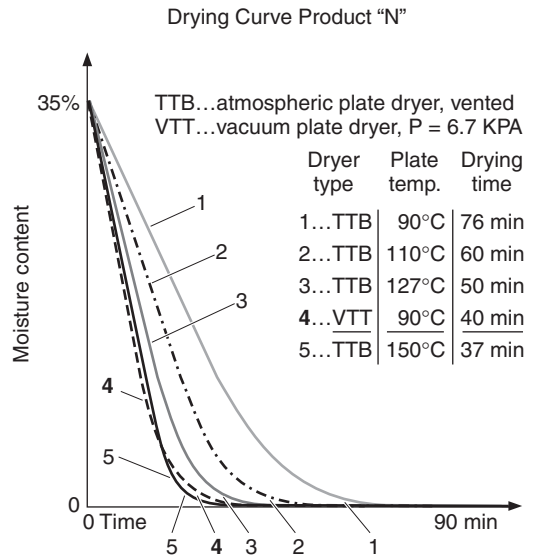


FIG. 12-48 Plate dryer drying curves demonstrating impact of elevated temperature and/or operation under vacuum. (Krauss Maffei.)

the drying process obtained with vacuum operation. Note that curve 4 at 90°C, pressure at 6.7 kPa absolute, is comparable to the atmospheric curve at 150°C. Also, the comparative atmospheric curve at 90°C requires 90 percent more drying time than the vacuum condition. The dramatic improvement with the use of vacuum is important to note for heat-sensitive materials.

The above drying curves have been generated via testing on a plate dryer simulator. The test unit duplicates the physical setup of the production dryer; therefore linear scale-up from the test data can be made to the full-scale dryer. Because of the thin product layer on each plate, drying in the unit closely follows the normal type of drying curve in which the constant-rate period (steady evolution of moisture or volatiles) is followed by the falling-rate period of the drying process. This results in higher heat-transfer coefficients and specific drying capacities on the upper plates of the dryer as compared to the lower plates. The average specific drying capacity for the plate dryer is in the range of 2 to 20 kg/(m²·h) (based on final dry product). Performance data for typical applications are shown on Table 12-19.

TABLE 12-19 Plate Dryer Performance Data for Three Applications*

Product	Plastic additive	Pigment	Foodstuff
Volatiles	Methanol	Water	Water
Production rate, dry	362 kg/hr	133 kg/hr	2030 kg/hr
Inlet volatiles content	30%	25%	4%
Final volatiles content	0.1%	0.5%	0.7%
Evaporative rate	155 kg/hr	44 kg/hr	70 kg/hr
Heating medium	Hot water	Steam	Hot water
Drying temperature	70°C	150°C	90°C
Dryer pressure	11 kPa abs	Atmospheric	Atmospheric
Air velocity	NA	0.1 m/sec	0.2 m/sec
Drying time, min	24	23	48
Heat consumption, kcal/kg dry product	350	480	100
Power, dryer drive	3 kW	1.5 kW	7.5 kW
Material of construction	SS 316L/316Ti	SS 316L/316Ti	SS 316L/316Ti
Dryer height	5 m	2.6 m	8.2 m
Dryer footprint	2.6 m diameter	2.2 m by 3.0 m	3.5 m by 4.5 m
Location	Outdoors	Indoors	Indoors
Dryer assembly	Fully assembled	Fully assembled	Fully assembled
Power, exhaust fan	NA	2.5 kW	15 kW
Power, vacuum pump	20 kW	NA	NA

*Krauss Maffei

Gravity or Moving-Bed Dryers A body of solids in which the particles, consisting of granules, pellets, beads, or briquettes, flow downward by gravity at substantially their normal settled bulk density through a vessel in contact with gases is defined frequently as a **moving-bed** or **tower dryer**. Moving-bed equipment is frequently used for grain drying and plastic pellet drying, and it also finds application in blast furnaces, shaft furnaces, and petroleum refining. Gravity beds are also employed for the cooling and drying of extruded pellets and briquettes from size enlargement processes.

A gravity dryer consists of a stationary vertical, usually cylindrical housing with openings for the introduction of solids (at the top) and removal of solids (at the bottom), as shown schematically in Fig. 12-49. Gas flow is through the solids bed and may be cocurrent or countercurrent and, in some instances, cross-flow. By definition, the rate of gas flow upward must be less than that required for fluidization.

Fields of application One of the major advantages of the gravity-bed technique is that it lends itself well to true intimate countercurrent contacting of solids and gases. This provides for efficient heat transfer and mass transfer. Gravity-bed contacting also permits the use of the solid as a heat-transfer medium, as in pebble heaters.

Gravity vessels are applicable to coarse granular free-flowing solids which are comparatively dust-free. The solids must possess physical properties in size and surface characteristics so that they will not stick together, bridge, or segregate during passage through the vessel. The presence of significant quantities of fines or dust will close the passages among the larger particles through which the gas must penetrate, increasing pressure drop. Fines may also segregate near the sides of the bed or in other areas where gas velocities are low, ultimately completely sealing off these portions of the vessel. The high efficiency of gas-solids contacting in gravity beds is due to the uniform distribution of gas throughout the solids bed; hence choice of feed and its preparation are important factors to successful operation. Preforming techniques such as pelleting and briquetting are employed frequently for the preparation of suitable feed materials.

Gravity vessels are suitable for low-, medium-, and high-temperature operation; in the last case, the housing will be lined completely with refractory brick. Dust recovery equipment is minimized in this type of operation since the bed actually performs as a dust collector itself, and dust in the bed will not, in a successful application, exist in large quantities.

Other advantages of gravity beds include flexibility in gas and solids flow rates and capacities, variable retention times from minutes to several hours, space economy, ease of start-up and shutdown, the

potentially large number of contacting stages, and ease of control by using the inlet and exit gas temperatures.

Maintenance of a uniform rate of solids movement downward over the entire cross-section of the bed is one of the most critical operating problems encountered. For this reason gravity beds are designed to be as high and narrow as practical. In a vessel of large cross section, discharge through a conical bottom and center outlet will usually result in some degree of "ratholing" through the center of the bed. Flow through the center will be rapid while essentially stagnant pockets are left around the sides. To overcome this problem, multiple outlets may be provided in the center and around the periphery; table unloaders, rotating plows, wide moving grates, and multiple-screw unloaders are employed; insertion of inverted cone baffles in the lower section of the bed, spaced so that flushing at the center is retarded, is also a successful method for improving uniformity of solids movement. Fortunately, the problems are less critical in gravity dryers, which are usually for slow drying of large particles, than in applications such as catalytic reactors, where disengagement of gas from solids at the top of the tower can also present serious difficulties.

Continuous Band and Tunnel Dryers This group of dryers is variously known as band, belt, conveyor, or tunnel dryers.

Classification Continuous; nonagitated; layer; convective (cross-circulation or through-circulation) or contact/conduction; horizontal movement by mechanical means.

Continuous tunnels are batch truck or tray compartments, operated in series. The solids to be processed are placed in trays or on trucks which move progressively through the tunnel in contact with hot gases. Operation is **semicontinuous**; when the tunnel is filled, one truck is removed from the discharge end as each new truck is fed into the inlet end. In some cases, the trucks move on tracks or mono-rails, and they are usually conveyed mechanically, employing chain drives connecting to the bottom of each truck.

Belt-conveyor and screen-conveyor (band) dryers are truly continuous in operation, carrying a layer of solids on an endless conveyor.

Continuous tunnel and conveyor dryers are more suitable than (multiple) batch compartments for large-quantity production, usually giving investment and installation savings. In the case of truck and tray tunnels, labor savings for loading and unloading are not significant compared with those for batch equipment. Belt and screen conveyors which are truly continuous represent major labor savings over batch operations but require additional investment for automatic feeding and unloading devices.

Airflow can be totally **cocurrent**, **countercurrent**, or a combination of both. In addition, **cross-flow** designs are employed frequently, with the heating air flowing back and forth across the trucks or belt in series. Reheat coils may be installed after each cross-flow pass to maintain constant-temperature operation; large propeller-type circulating fans are installed at each stage, and air may be introduced or exhausted at any desirable points. Tunnel equipment possesses maximum flexibility for any combination of airflow and temperature staging. When handling granular, particulate solids which do not offer high resistance to airflow, perforated or screen-type belt conveyors are employed with **through-circulation** of gas to improve heat- and mass-transfer rates, almost invariably in cross-flow. Contact drying is also possible, usually under vacuum, with the bands resting on heating plates (vacuum band dryer).

Tunnel Dryers In tunnel equipment, the solids are usually heated by direct contact with hot gases. In high-temperature operations, radiation from walls and refractory lining may be significant also. The air in a direct heat unit may be heated directly or indirectly by combustion or, at temperature below 475 K, by finned steam coils.

Applications of tunnel equipment are essentially the same as those for batch tray and compartment units previously described, namely, practically all forms of particulate solids and large solid objects. Continuous tunnel or conveyor ovens are employed also for drying refractory shapes and for drying and baking enameled pieces. In many of these latter, the parts are suspended from overhead chain conveyors.

Auxiliary equipment and the special design considerations discussed for batch trays and compartments apply also to tunnel equipment. For size-estimating purposes, tray and truck tunnels and

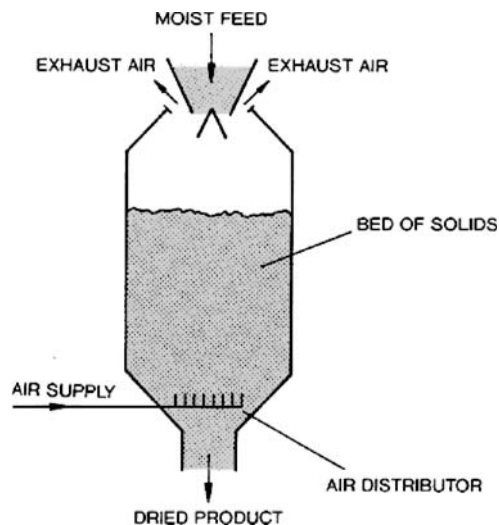


FIG. 12-49 Moving-bed gravity dryer.

furnaces can be treated in the same manner as discussed for batch equipment.

Ceramic tunnel kilns handling large irregular-shaped objects must be equipped for precise control of temperature and humidity conditions to prevent cracking and condensation on the product. The internal mechanism causing cracking when drying clay and ceramics have been studied extensively. Information on ceramic tunnel kiln operation and design is reported fully in publications such as *The American Ceramic Society Bulletin*, *Ceramic Industry*, and *Transactions of the British Ceramic Society*.

Another use of tunnel dryers is for drying leather. Moisture content is initially around 50 percent but must not be reduced below about 15 percent, or else the leather will crack and be useless. To avoid this, a high-humidity atmosphere is maintained by gas recycle, giving a high equilibrium moisture content.

Continuous Through-Circulation Band Dryers Continuous through-circulation dryers operate on the principle of blowing hot air through a permeable bed of wet material passing continuously through the dryer. Drying rates are high because of the large area of contact and short distance of travel for the internal moisture.

The most widely used type is the **horizontal conveyor dryer** (also called perforated band or conveying-screen dryer), in which wet material is conveyed as a layer, 2 to 15 cm deep (sometimes up to 1 m), on a horizontal mesh screen, belt, or perforated apron, while heated air is blown either upward or downward through the bed of material. This dryer consists usually of a number of individual sections, complete with fan and heating coils, arranged in series to form a housing or tunnel through which the conveying screen travels. As shown in the sectional view in Fig. 12-50, the air circulates through the wet material and is reheated before reentering the bed. It is not uncommon to circulate the hot gas upward in the wet end and downward in the dry end, as shown in Fig. 12-51. A portion of the air is exhausted continuously by one or more exhaust fans, not shown in the sketch, which handle air from several sections. Since each section can be operated independently, extremely flexible operation is possible, with high temperatures usually at the wet end, followed by lower temperatures; in some cases a unit with cooled or specially humidified air is employed for final conditioning. The **maximum pressure drop** that can be taken through the bed of solids without developing leaks or air bypassing is roughly 50 mm of water.

Through-circulation drying requires that the wet material be in a state of granular or pelleted subdivision so that hot air may be readily blown through it. Many materials meet this requirement without special preparation. Others require special and often elaborate pretreatment to render them suitable for through-circulation drying. The process of converting a wet solid to a form suitable for through-circulation of air is called **preforming**, and often the success or failure of this contacting method depends on the preforming step. Fibrous, flaky, and coarse granular materials are usually amenable to drying without preforming. They can be loaded directly onto the conveying screen by suitable spreading feeders of the oscillating-belt or vibrating type or by spiked drums or belts feeding from bins.

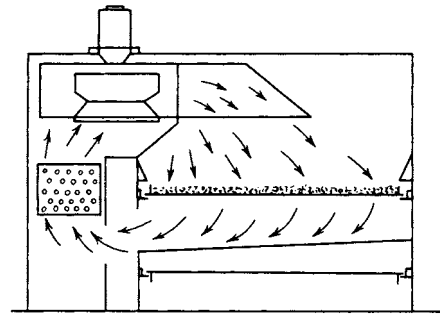


FIG. 12-50 Section view of a continuous through-circulation conveyor dryer. (Proctor & Schwartz, Inc.)

When materials must be preformed, several methods are available, depending on the physical state of the wet solid.

1. Relatively dry materials such as centrifuge cakes can sometimes be granulated to give a suitably porous bed on the conveying screen.

2. Pasty materials can often be preformed by extrusion to form spaghetti-like pieces, about 6 mm in diameter and several centimeters long.

3. Wet pastes that cannot be granulated or extruded may be predried and preformed on a steam-heated finned drum. Preforming on a finned drum may be desirable also in that some predrying is accomplished.

4. Thixotropic filter cakes from rotary vacuum filters that cannot be preformed by any of the above methods can often be scored by knives on the filter, the scored cake discharging in pieces suitable for through-circulation drying.

5. Material that shrinks markedly during drying is often reloaded during the drying cycle to 2 to 6 times the original loading depth. This is usually done after a degree of shrinkage which, by opening the bed, has destroyed the effectiveness of contact between the air and solids.

6. In a few cases, powders have been pelleted or formed in briquettes to eliminate dustiness and permit drying by through-circulation. Table 12-20 gives a list of materials classified by preforming methods suitable for through-circulation drying.

Steam-heated air is the usual heat-transfer medium employed in these dryers, although combustion gases may be used also. Temperatures above 600 K are not usually feasible because of the problems of lubricating the conveyor, chain, and roller drives. Recirculation of air is in the range of 60 to 90 percent of the flow through the bed. Conveyors may be made of wire-mesh screen or perforated-steel plate. The minimum practical screen opening size is about 30-mesh (0.5 mm). Multiple bands in series may be used.

Vacuum band dryers utilize heating by conduction and are a continuous equivalent of vacuum tray (shelf) dryers, with the moving

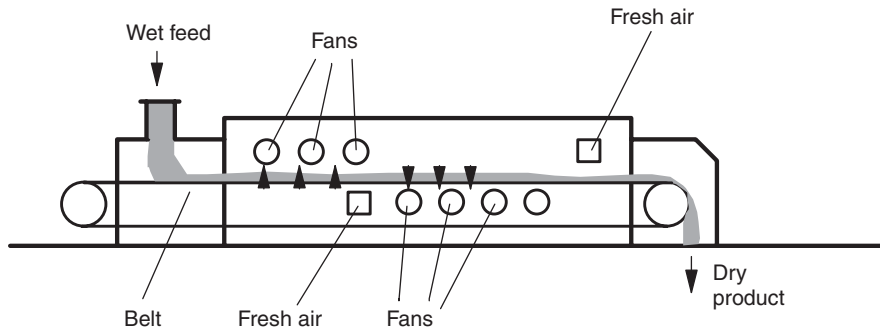


FIG. 12-51 Longitudinal view of a continuous through-circulation conveyor dryer with intermediate airflow reversal.

TABLE 12-20 Methods of Preforming Some Materials for Through-Circulation Drying

No preforming required	Scored on filter	Granulation	Extrusion	Finned drum	Flaking on chilled drum	Briquetting and squeezing
Cellulose acetate Silica gel Scoured wool Sawdust Rayon waste Fluorspar Tapioca Breakfast food Asbestos fiber Cotton linters Rayon staple	Starch Aluminum hydrate	Kaolin Cryolite Lead arsenate Cornstarch Cellulose acetate Dye intermediates	Calcium carbonate White lead Lithopone Titanium dioxide Magnesium carbonate Aluminum stearate Zinc stearate	Lithopone Zinc yellow Calcium carbonate Magnesium carbonate	Soap flakes	Soda ash Cornstarch Synthetic rubber

bands resting on heating plates. Drying is usually relatively slow, and it is common to find several bands stacked above one another, with material falling to the next band and flowing in opposite directions on each pass, to reduce dryer length and give some product turnover.

Design Methods for Continuous Band Dryers In actual practice, design of a continuous through-circulation dryer is best based upon data taken in pilot-plant tests. Loading and distribution of solids on the screen are rarely as nearly uniform in commercial installations as in test dryers; 50 to 100 percent may be added to the test drying time for commercial design.

A mathematical method of a through-circulation dryer has been developed by Thygeson [*Am. Inst. Chem. Eng. J.* **16**(5):749 (1970)]. Rigorous modeling is possible with a two-dimensional incremental model, with steps both horizontally along the belt and vertically through the layer; nonuniformity of the layer across the belt could also be allowed for if desired. Heat-transfer coefficients are typically in the range of 100 to 200 W/(m²·K) and the relationship $h_c = 12(\rho_g U_g d_p)^{0.5}$ may be used for a first estimate, where ρ_g is gas density (kg/m³); U_g , local gas velocity (m/s); and d_p , particle diameter (m). For 5-mm particles and air at 1 m/s, 80°C and 1 kg/m³ [mass flux 1 kg/(m²·s)] this gives $h_c = 170$ W/(m²·K).

Performance and Cost Data for Continuous Band and Tunnel Dryers Experimental performance data are given in Table 12-21 for numerous common materials. Performance data from several commercial through-circulation conveyor dryers are given in Table 12-22. Labor requirements vary depending on the time required for feed adjustments, inspection, etc. These dryers may consume as little as 1.1 kg of steam/kg of water evaporated, but 1.4 to 2 is a more common range. Thermal efficiency is a function of final moisture required and percent air recirculation.

Conveying-screen dryers are fabricated with conveyor widths from 0.3- to 4.4-m sections 1.6 to 2.5 m long. Each section consists of a sheet-metal enclosure, insulated sidewalls and roof, heating coils, a circulating fan, inlet air distributor baffles, a fines catch pan under the conveyor, and a conveyor screen (Fig. 12-51). Table 12-23 gives approximate purchase costs for equipment with type 304 stainless-steel hinged conveyor screens and includes steam-coil heaters, fans, motors, and a variable-speed conveyor drive. Cabinet and auxiliary equipment fabrication is of aluminumized steel or stainless-steel materials. Prices do not include temperature controllers, motor starters, preform equipment, or auxiliary feed and discharge conveyors. These may add \$75,000 to \$160,000 to the dryer purchase cost (2005 costs).

Batch Agitated and Rotating Dryers

Description An *agitated dryer* is defined as one on which the housing enclosing the process is stationary while solids movement is accomplished by an internal mechanical agitator. A rotary dryer is one in which the outer housing rotates. Many forms are in use, including batch and continuous versions. The batch forms are almost invariably heated by conduction with operation under vacuum. Vacuum is used in conjunction with drying or other chemical operations when low solids temperatures must be maintained because heat will cause damage to the product or change its nature; when air combines with the

product as it is heated, causing oxidation or an explosive condition; when solvent recovery is required; and when materials must be dried to extremely low moisture levels.

Vertical agitated pan, spherical and conical dryers are mechanically agitated; tumbler or double-cone dryers have a rotating shell. All these types are typically used for the drying of solvent or water-wet, free-flowing powders in small batch sizes of 1000 L or less, as frequently found in the pharmaceutical, specialty chemical, and fine chemicals industries. Corrosion resistance and cleanliness are often important, and common materials of construction include SS 304 and 316, and Hastelloy. The batch nature of operation is of value in the pharmaceutical industry to maintain batch identification. In addition to pharmaceutical materials, the conical mixer dryer is used to dry polymers, additives, inorganic salts, and many other specialty chemicals. As the size increases, the ratio of jacket heat-transfer surface area to volume falls, extending drying times. For larger batches, horizontal agitated pan dryers are more common, but there is substantial overlap of operating ranges. Drying times may be reduced for all types by heating the internal agitator, but this increases complexity and cost.

Classification Batch; mechanical or rotary agitation; layer; contact/conduction.

Mechanical versus rotary agitation Agitated dryers are applicable to processing solids which are relatively free-flowing and granular when discharged as product. Materials which are not free-flowing in their feed condition can be treated by recycle methods as described in the subsection "Continuous Rotary Dryers." In general, agitated dryers have applications similar to those of rotating vessels. Their chief advantages compared with the latter are twofold. (1) Large-diameter rotary seals are not required at the solids and gas feed and exit points because the housing is stationary, and for this reason gas leakage problems are minimized. Rotary seals are required only at the points of entrance of the mechanical agitator shaft. (2) Use of a mechanical agitator for solids mixing introduces shear forces which are helpful for breaking up lumps and agglomerates. Balling and pelleting of sticky solids, an occasional occurrence in rotating vessels, can be prevented by special agitator design. The problems concerning dusting of fine particles in direct-heat units are identical to those discussed under "Continuous Rotary Dryers."

Vacuum processing All these types of dryer usually operate under vacuum, especially when drying heat-sensitive materials or when removing flammable organic solvents rather than water. The heating medium is hot water, steam, or thermal oil, with most applications in the temperature range of 50 to 150°C and pressures in the range of 3 to 30 kPa absolute. The vapors generated during the drying process are evacuated by a vacuum pump and passed through a condenser for recovery of the solvent. A dust filter is normally mounted over the vapor discharge line as it leaves the dryer, thus allowing any entrapped dust to be pulsed back into the process area. Standard cloth-type dust filters are available, along with sintered metal filters.

In vacuum processing and drying, a major objective is to create a large temperature-driving force between the jacket and the product. To accomplish this purpose at fairly low jacket temperatures, it is necessary to reduce the internal process pressure so that the liquid being removed will boil at a lower vapor pressure. It is not always economical, however,

TABLE 12-21 Experimental Through-Circulation Drying Data for Miscellaneous Materials

Material	Physical form	Moisture contents, kg/kg dry solid			Inlet-air temperature, K	Depth of bed, cm	Loading, kg product/m ²	Air velocity, m/s × 10 ¹	Experimental drying time, s × 10 ⁻²
		Initial	Critical	Final					
Alumina hydrate	Briquettes	0.105	0.06	0.00	453	6.4	60.0	6.0	18.0
Alumina hydrate	Scored filter cake	9.60	4.50	1.15	333	3.8	1.6	11.0	90.0
Alumina hydrate	Scored filter cake	5.56	2.25	0.42	333	7.0	4.6	11.0	108.0
Aluminum stearate	0.7-cm extrusions	4.20	2.60	0.003	350	7.6	6.5	13.0	36.0
Asbestos fiber	Flakes from squeeze rolls	0.47	0.11	0.008	410	7.6	13.6	9.0	5.6
Asbestos fiber	Flakes from squeeze rolls	0.46	0.10	0.0	410	5.1	6.3	9.0	3.6
Asbestos fiber	Flakes from squeeze rolls	0.46	0.075	0.0	410	3.8	4.5	11.0	2.7
Calcium carbonate	Preformed on finned drum	0.85	0.30	0.003	410	3.8	16.0	11.5	12.0
Calcium carbonate	Preformed on finned drum	0.84	0.35	0.0	410	8.9	25.7	11.7	18.0
Calcium carbonate	Extruded	1.69	0.98	0.255	410	1.3	4.9	14.3	9.0
Calcium carbonate	Extruded	1.41	0.45	0.05	410	1.9	5.8	10.2	12.0
Calcium stearate	Extruded	2.74	0.90	0.0026	350	7.6	8.8	5.6	57.0
Calcium stearate	Extruded	2.76	0.90	0.007	350	5.1	5.9	6.0	42.0
Calcium stearate	Extruded	2.52	1.00	0.0	350	3.8	4.4	10.2	24.0
Cellulose acetate	Granulated	1.14	0.40	0.09	400	1.3	1.4	12.7	1.8
Cellulose acetate	Granulated	1.09	0.35	0.0027	400	1.9	2.7	8.6	7.2
Cellulose acetate	Granulated	1.09	0.30	0.0041	400	2.5	4.1	5.6	10.8
Cellulose acetate	Granulated	1.10	0.45	0.004	400	3.8	6.1	5.1	18.0
Clay	Granulated	0.277	0.175	0.0	375	7.0	46.2	10.2	19.2
Clay	1.5-cm extrusions	0.28	0.18	0.0	375	12.7	100.0	10.7	43.8
Cryolite	Granulated	0.456	0.25	0.0026	380	5.1	34.2	9.1	24.0
Fluorspar	Pellets	0.13	0.066	0.0	425	5.1	51.4	11.6	7.8
Lead arsenate	Granulated	1.23	0.45	0.043	405	5.1	18.1	11.6	18.0
Lead arsenate	Granulated	1.25	0.55	0.054	405	6.4	22.0	10.2	24.0
Lead arsenate	Extruded	1.34	0.64	0.024	405	5.1	18.1	9.4	36.0
Lead arsenate	Extruded	1.31	0.60	0.0006	405	8.4	26.9	9.2	42.0
Kaolin	Formed on finned drum	0.28	0.17	0.0009	375	7.6	44.0	9.2	21.0
Kaolin	Formed on finned drum	0.297	0.20	0.005	375	11.4	56.3	12.2	15.0
Kaolin	Extruded	0.443	0.20	0.008	375	7.0	45.0	10.16	18.0
Kaolin	Extruded	0.36	0.14	0.0033	400	9.6	40.6	15.2	12.0
Kaolin	Extruded	0.36	0.21	0.0037	400	19.0	80.7	10.6	30.0
Lithopone (finished)	Extruded	0.35	0.065	0.0004	408	8.2	63.6	10.2	18.0
Lithopone (crude)	Extruded	0.67	0.26	0.0007	400	7.6	41.1	9.1	51.0
Lithopone	Extruded	0.72	0.28	0.0013	400	5.7	28.9	11.7	18.0
Magnesium carbonate	Extruded	2.57	0.87	0.001	415	7.6	11.0	11.4	17.4
Magnesium carbonate	Formed on finned drum	2.23	1.44	0.0019	418	7.6	13.2	8.6	24.0
Mercuric oxide	Extruded	0.163	0.07	0.004	365	3.8	66.5	11.2	24.0
Silica gel	Granular	4.51	1.85	0.15	400	3.8-0.6	3.2	8.6	15.0
Silica gel	Granular	4.49	1.50	0.215	340	3.8-0.6	3.4	9.1	63.0
Silica gel	Granular	4.50	1.60	0.218	325	3.8-0.6	3.5	9.1	66.0
Soda salt	Extruded	0.36	0.24	0.008	410	3.8	22.8	5.1	51.0
Starch (potato)	Scored filter cake	0.866	0.55	0.069	400	7.0	26.3	10.2	27.0
Starch (potato)	Scored filter cake	0.857	0.42	0.082	400	5.1	17.7	9.4	15.0
Starch (corn)	Scored filter cake	0.776	0.48	0.084	345	7.0	26.4	7.4	54.0
Starch (corn)	Scored filter cake	0.78	0.56	0.098	380	7.0	27.4	7.6	24.0
Starch (corn)	Scored filter cake	0.76	0.30	0.10	345	1.9	7.7	6.7	15.0
Titanium dioxide	Extruded	1.2	0.60	0.10	425	3.0	6.8	13.7	6.3
Titanium dioxide	Extruded	1.07	0.65	0.29	425	8.2	16.0	8.6	6.0
White lead	Formed on finned drum	0.238	0.07	0.001	355	6.4	76.8	11.2	30.0
White lead	Extruded	0.49	0.17	0.0	365	3.8	33.8	10.2	27.0
Zinc stearate	Extruded	4.63	1.50	0.005	360	4.4	4.2	8.6	36.0

to reduce the internal pressure to extremely low levels because of the large vapor volumes thereby created. It is necessary to compromise on operating pressure, considering leakage, condensation problems, and the size of the vapor lines and pumping system. Very few vacuum dryers operate below 5 mmHg pressure on a commercial scale. Air in-leakage through gasket surfaces will be in the range of 0.2 kg/(h-linear m of gasketed surface) under these conditions. To keep vapor partial pressure and solids temperature low without pulling excessively high vacuum, a nitrogen bleed may be introduced, particularly in the later stages of drying. The vapor and solids surface temperatures then fall below the vapor boiling point, toward the wet-bulb temperature.

Vertical Agitated Dryers This classification includes vertical pan dryers, filter dryers, and spherical and conical dryers.

Vertical pan dryer The basic vertical pan dryer consists of a short, squat vertical cylinder (Fig. 12-52 and Table 12-24) with an outer heating jacket and an internal rotating agitator, again with the axis

vertical, which mixes the solid and sweeps the base of the pan. Heat is supplied by circulation of hot water, steam, or thermal fluid through the jacket; it may also be used for cooling at the end of the batch cycle, using cooling water or refrigerant. The agitator is usually a plain set of solid blades, but may be a ribbon-type screw or internally heated blades. Product is discharged from a door at the lower side of the wall. Sticky materials may adhere to the agitator or be difficult to discharge.

Filter dryer The basic Nutsche filter dryer is like a vertical pan dryer, but with the bottom heated plate replaced by a filter plate. Hence, a slurry can be fed in and filtered, and the wet cake dried in situ. These units are especially popular in the pharmaceutical industry, as containment is good and a difficult wet solids transfer operation is eliminated by carrying out both filtration and drying in the same vessel. Drying times tend to be longer than for vertical pan dryers as the bottom plate is no longer heated. Some types (e.g., Mitchell Thermovac,

TABLE 12-22 Performance Data for Continuous Through-Circulation Dryers*

	Kind of material						
	Inorganic pigment	Cornstarch	Fiber staple		Charcoal briquettes	Gelatin	Inorganic chemical
Capacity, kg dry product/h	712	4536	1724 Stage A, 57.04 Stage B, 35.12		5443	295	862
Approximate dryer area, m ²	22.11	66.42			52.02	104.05	30.19
Depth of loading, cm	3	4			16	5	4
Air temperature, °C	120	115 to 140	130 to 100	100	135 to 120	32 to 52	121 to 82
Loading, kg product/m ²	18.8	27.3	3.5	3.3	182.0	9.1	33
Type of conveyor, mm	1.59 by 6.35 slots	1.19 by 4.76 slots	2.57-diameter holes, perforated plate		8.5 × 8.5 mesh screen	4.23 × 4.23 mesh screen	1.59 × 6.35 slot
Preforming method or feed	Rolling extruder	Filtered and scored	Fiber feed		Pressed	Extrusion	Rolling extruder
Type and size of preformed particle, mm	6.35-diameter extrusions	Scored filter cake	Cut fiber		64 × 51 × 25	2-diameter extrusions	6.35-diameter extrusions
Initial moisture content, % bone-dry basis	120	85.2	110		37.3	300	111.2
Final moisture content, % bone-dry basis	0.5	13.6	9		5.3	11.1	1.0
Drying time, min	35	24	11		105	192	70
Drying rate, kg water evaporated/(h·m ²)	38.39	42.97	17.09		22.95	9.91	31.25
Air velocity (superficial), m/s	1.27	1.12	0.66		1.12	1.27	1.27
Heat source per kg water evaporated, steam kg/kg gas (m ³ /kg)	Gas	Steam	Steam		Waste heat	Steam	Gas
Installed power, kW	0.11	2.0	1.73			2.83	0.13
	29.8	119.3	194.0		82.06	179.0	41.03

*Courtesy of Wolverine Proctor & Schwartz, Inc.

Krauss-Maffei TNT) invert the unit between the filtration and drying stages to avoid this problem.

Spherical dryer Sometimes called the *turbosphere*, this is another agitated dryer with a vertical axis mixing shaft, but rotation is typically faster than in the vertical pan unit, giving improved mixing and heat transfer. The dryer chamber is spherical, with solids discharge through a door or valve near the bottom.

Conical mixer dryer This is a vertically oriented conical vessel with an internally mounted rotating screw. Figure 12-53 shows a schematic of a typical conical mixer dryer. The screw rotates about its own axis (speeds up to 100 rpm) and around the interior of the vessel (speeds up to 0.4 rpm). Because it rotates around the full circumference of the vessel, the screw provides a self-cleaning effect for the heated vessel walls, as well as effective agitation; it may also be internally heated. Either top-drive (via an internal rotating arm) or bottom-drive (via a universal joint) may be used; the former is more common. The screw is cantilevered in the vessel and requires no additional support (even in vessel sizes up to 20-m³ operating volume). Cleaning of the dryer is facilitated with CIP systems that can be used for cleaning, and/or the vessel can be completely flooded with water or solvents. The dryer makes maximum use of the product-heated areas—the filling volume of the vessel (up to the knuckle of the dished head) is the usable product loading. In some recent applications, microwaves have been used to provide additional energy input and shorten drying times.

In the bottom-drive system, the vessel cover is free of drive components, allowing space for additional process nozzles, manholes, explosion venting, etc., as well as a temperature lance for direct, continuous product temperature measurement in the vessel. The top cover of the vessel is easily heated by either a half-pipe coil or heat tracing, which ensures that no vapor condensation will occur in the process area.

TABLE 12-23 Conveyor-Screen-Dryer Costs*

Length	2.4-m-wide conveyor	3.0-m-wide conveyor
7.5 m	\$8600/m ²	\$7110/m ²
15 m	\$6700/m ²	\$5600/m ²
22.5 m	\$6200/m ²	\$5150/m ²
30 m	\$5900/m ²	\$4950/m ²

*National Drying Machinery Company, 1996.

Because there are no drive components in the process area, the risk of batch failures due to contamination from gear lubricants is eliminated. However, the bottom joint requires especially careful design, maintenance, and sealing. The disassembly of the unit is simplified, as all work on removing the screw can be done without vessel entry. For disassembly, the screw is simply secured from the top, and the drive components are removed from the bottom of the dryer.

Horizontal Pan Dryer This consists of a stationary cylindrical shell, mounted horizontally, in which a set of agitator blades mounted on a revolving central shaft stirs the solids being treated. They tend to be used for larger batches than vertical agitated or batch rotating dryers. Heat is supplied by circulation of hot water, steam, or Dowtherm through the jacket surrounding the shell and, in larger units, through the hollow central shaft. The agitator can be of many different forms, including simple paddles, ploughshare-type blades, a single discontinuous spiral, or a double continuous spiral. The outer blades are set as closely as possible to the wall without touching, usually leaving a gap of 0.3 to 0.6 cm. Modern units occasionally employ spring-loaded shell scrapers mounted on the blades. The dryer is charged through a port at the top and emptied through one or more discharge nozzles at the bottom. Vacuum is applied and maintained by any of the conventional methods, i.e., steam jets, vacuum pumps, etc.

A similar type, the batch indirect rotary dryer, consists of a rotating horizontal cylindrical shell, suitably jacketed. Vacuum is applied to this unit through hollow trunnions with suitable packing glands. Rotary glands must be used also for admitting and removing the heating medium from the jacket. The inside of the shell may have lifting bars, welded longitudinally, to assist agitation of the solids. Continuous rotation is needed while emptying the solids, and a circular dust hood is frequently necessary to enclose the discharge-nozzle turning circle and prevent serious dust losses to the atmosphere during unloading. A typical vacuum rotary dryer is illustrated in Fig. 12-54. Sealing tends to be more difficult where the entire shell rotates compared to the horizontal pan, where only the central agitator shaft rotates, since the seal diameter is smaller in the latter case. Conversely, a problem with a stationary shell is that it can be difficult to empty the final “heel” of material out of the bottom of the cylinder. If batch integrity is important, this is an advantage for the rotary variant over the horizontal pan.

Heated Agitators For all agitated dryers, in addition to the jacket heated area, heating the agitator with the same medium as the

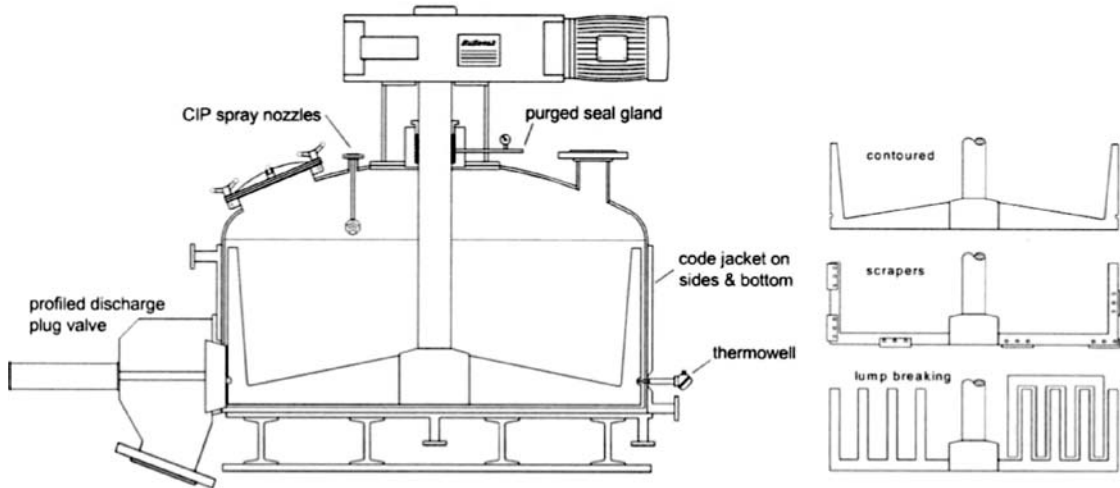


FIG. 12-52 Vertical pan dryer. (Buflovak Inc.)

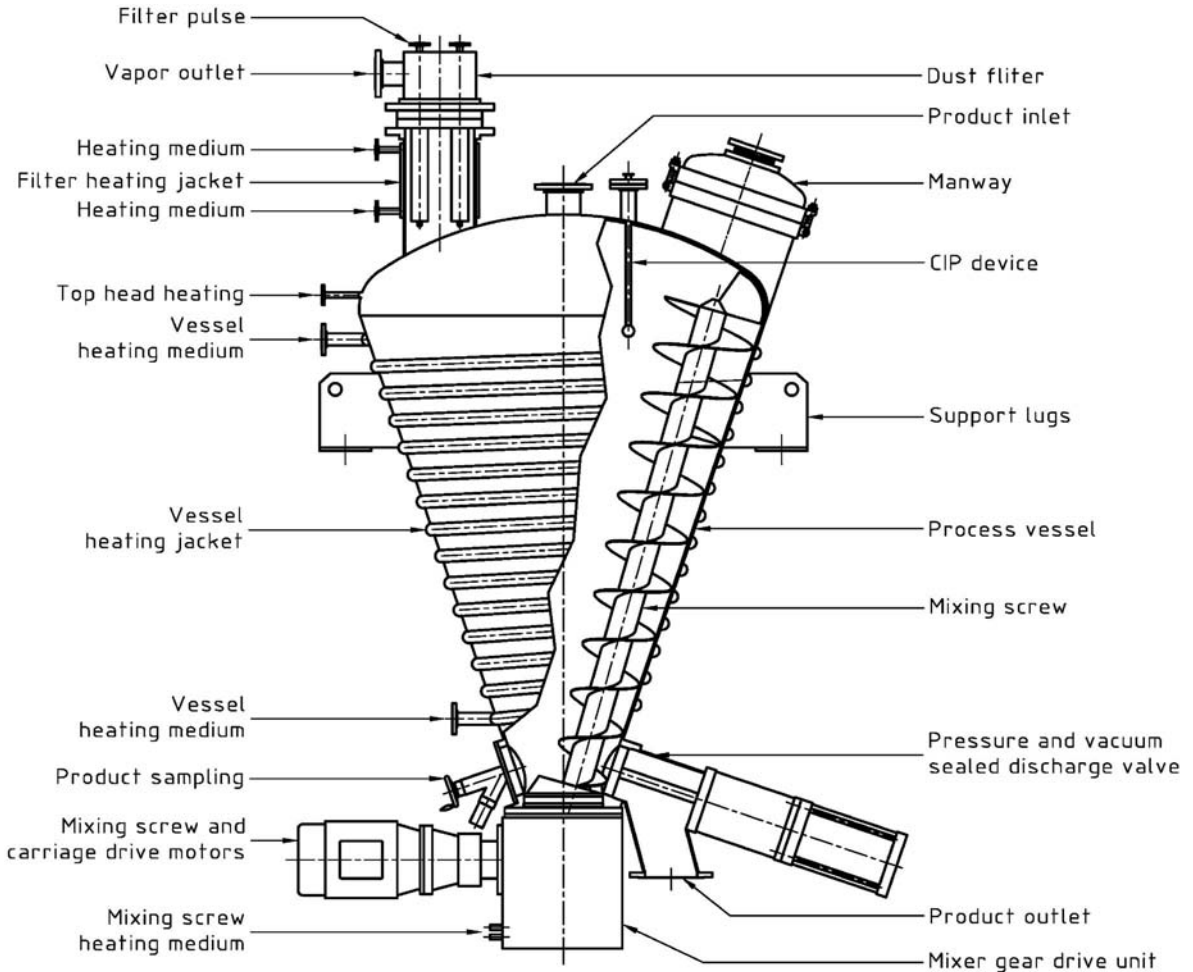


FIG. 12-53 Bottom-drive conical mixer dryer. (Krauss Maffei.)

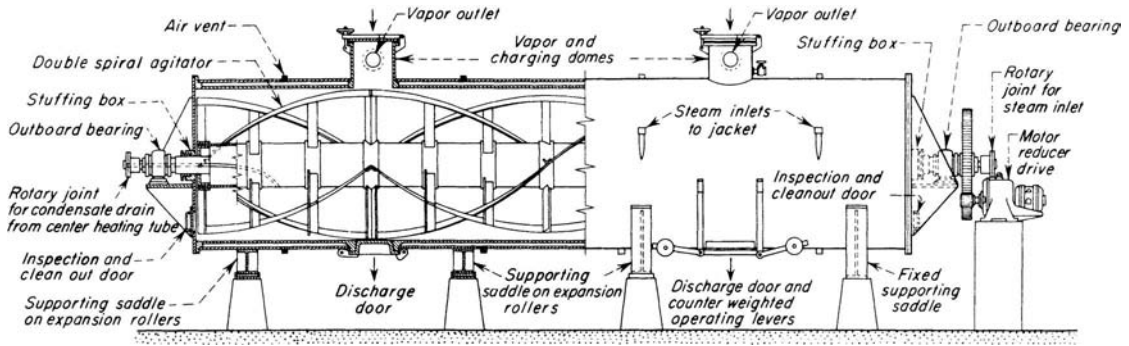


FIG. 12-54 A typical horizontal pan vacuum dryer. (Blaw-Knox Food & Chemical Equipment, Inc.)

jacket (hot water, steam, or thermal oil) will increase the heat-exchange area. This is usually accomplished via rotary joints. Obviously, heating the screw or agitator will mean shorter batch drying times, which yields higher productivity and better product quality due to shorter exposure to the drying temperature, but capital and maintenance costs will be increased. In pan and conical dryers the area is increased only modestly, by 15 to 30 percent; but in horizontal pan and paddle dryers, the opportunity is much greater and indeed the majority of the heat may be supplied through the agitator.

Also, the mechanical power input of the agitator can be a significant additional heat source, and microwave assistance has also been used in filter dryers and conical dryers to shorten drying times (and is feasible in other types).

Tumbler or Double-Cone Dryers These are rotating batch vacuum dryers, as shown in Fig. 12-55. Some types are an offset cylinder, but a double-cone shape is more common. They are very common in the pharmaceutical and fine chemicals industries. The gentle rotation can give less attrition than in some mechanically agitated dryers; on the other hand, formation of lumps and balls is more likely. The sloping walls of the cones permit more rapid emptying of solids when the dryer is in a stationary position, compared to a horizontal cylinder, which requires continuous rotation during emptying to convey product to the discharge nozzles. Several new designs of the double-cone type employ internal tubes or plate coils to provide additional heating surface.

On all rotating dryers, the vapor outlet tube is stationary; it enters the shell through a rotating gland and is fitted with an elbow and an upward extension so that the vapor inlet, usually protected by a felt dust filter, will be at all times near the top of the shell.

Design, Scale-up, and Performance Like all batch dryers, agitated and rotating dryers are primarily sized to physically contain the required batch volume. Note that the nominal capacity of most dryers is significantly lower than their total internal volume, because of the headspace needed for mechanical drives, inlet ports, suction lines,

dust filters, etc. Care must be taken to determine whether a stated "percentage fill" is based on nominal capacity or geometric volume. Vacuum dryers are usually filled to 50 to 65 percent of their total shell volume.

The standard scoping calculation methods for batch conduction drying apply. The rate of heat transfer from the heating medium through the dryer wall to the solids can be expressed by the usual formula

$$Q = hA \Delta T_m \tag{12-87}$$

where Q = heat flux, J/s [Btu/h]; h = overall heat-transfer coefficient, $J/(m^2 \cdot s \cdot K)$ [Btu/(h·ft² jacket area·°F)]; A = total jacket area, m² (ft²); and ΔT_m = log-mean-temperature driving force from heating medium to the solids, K (°F).

The overall heat-transfer rate is almost entirely dependent upon the film coefficient between the inner jacket wall and the solids, which depends on the dryer type and agitation rate, and to a large extent on the solids characteristics. Overall coefficients may range from 30 to 200 $J/(m^2 \cdot s \cdot K)$, based upon total area if the dryer walls are kept reasonably clean. Coefficients as low as 5 or 10 may be encountered if caking on the walls occurs.

For estimating purposes without tests, a reasonable coefficient for ordinary drying, and without taking the product to absolute dryness, may be assumed at $h = 50 J/(m^2 \cdot s \cdot K)$ for mechanically agitated dryers (although higher figures have been quoted for conical and spherical dryers) and 35 $J/(m^2 \cdot s \cdot K)$ for rotating units. The true heat-transfer coefficient is usually higher, but this conservative assumption makes some allowance for the slowing down of drying during the falling-rate period. However, if at all possible, it is always preferable to do pilot-plant tests to establish the drying time of the actual material. Drying trials are conducted in small pilot dryers (50- to 100-L batch units) to determine material handling and drying retention times. Variables such as drying temperature, vacuum level, and screw speed are analyzed during the

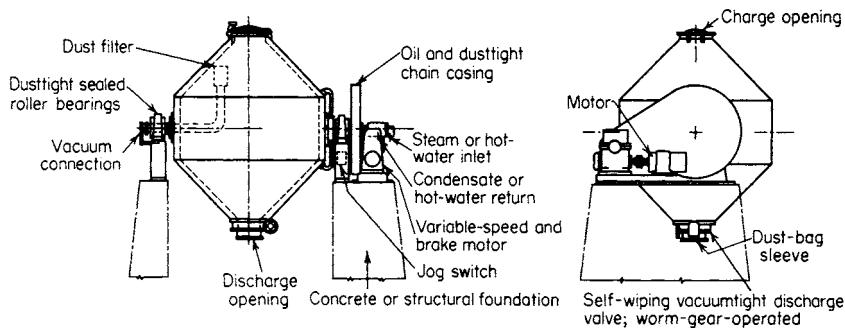


FIG. 12-55 Rotating (double-cone) vacuum dryer. (Stokes Vacuum, Inc.)

12-70 PSYCHROMETRY, EVAPORATIVE COOLING, AND SOLIDS DRYING

TABLE 12-24 Dimensions of Vertical Pan Dryers (Buflovak Inc.)

I.D., ft	Product depth, ft	Working volume, ft ³	USG	Jacketed height, ft	Jacketed area, ft ²			Discharge door, in	
					Cylinder wall	Bottom	Total		
3	0.75	5.3	40	1.0	9	7	16	5	8
4	1	12.6	94	2.0	25	13	38	6	8
5	1	19.6	147	2.0	31	20	51	8	9
6	1	28.3	212	2.0	38	28	66	8	9
8	1	50.3	377	2.0	50	50	101	8	9
10	1.5	117.8	884	3.0	94	79	173	12	12

test trials. Scale-up to larger units is done based upon the area/volume ratio of the pilot unit versus the production dryer. In most applications, the overall drying time in the production models is in the range of 2 to 24 h.

Agitator or rotation speeds range from 3 to 8 rpm. Faster speeds yield a slight improvement in heat transfer but consume more power and in some cases, particularly in rotating units, can cause more “balling up” and other stickiness-related problems.

In all these dryers, the surface area tends to be proportional to the square of the diameter D^2 , and the volume to diameter cubed D^3 . Hence the area/volume ratio falls as diameter increases, and drying times increase. It can be shown that the ratio of drying times in the production and pilot-plant dryers is proportional to the cube root of the ratio of batch volumes. However, if the agitator of the production unit is heated, the drying time increase can be reduced or reversed. Table 12-25 gives basic geometric relationships for agitated and rotating batch dryers, which can be used for approximate size estimation or (with great caution) for extrapolating drying times obtained from one dryer type to another. Note that these do not allow for nominal capacity or partial solids fill. For the paddle (horizontal pan) dryer with heated agitator, R is the ratio of the heat transferred through the agitator to that through the walls, which is proportional to the factor hA for each case.

Example 22: Calculations for Batch Dryer For a 10-m³ batch of material containing 5000 kg dry solids and 30 percent moisture (dry basis), estimate the size of vacuum dryers required to contain the batch at 50 percent volumetric fill. Jacket temperature is 200°C, applied pressure is 100 mbar (0.1 bar), and the solvent is water (take latent heat as 2400 kJ/kg). Assuming the heat-transfer coefficient based on the total surface area to be 50 W/(m²·K) for all

types, calculate the time to dry to 5 percent for (a) unhindered (constant-rate) drying throughout, (b) first-order falling-rate (hindered) drying throughout, (c) if experiment shows the actual drying time for a conical dryer to be 12.5 h and other cases are scaled accordingly. Take $R = 5$ with the heated agitator. Assume material is nonhygroscopic (equilibrium moisture content $X_E = 0$).

Solution: The dryer volume V must be 20 m³, and the diameter is calculated from column 4 of Table 12-25, assuming the default L/D ratios. Table 12-26 gives the results. Water at 100 mbar boils at 46°C so take ΔT as 200 – 46 = 154°C. Then Q is found from Eq. (12-87). The methods used are given in the section “Equipment—General, Scoping Design.” For constant-rate drying throughout, drying time $t_{CR} =$ evaporation rate/heat input rate and was given by Eq. (12-62):

$$t_{CR} = \frac{m_s(X_O - X_f)\lambda_{ev}}{h_{WS}\Delta T_{WS}A_s} = \frac{5000(0.3 - 0.05)2400}{0.05(154A_s)} \quad (12-62)$$

This gives t_{CR} as 389,610/ A_s s or 108.23/ A_s h. Values for A_s and calculated times for the various dryer types are given in Table 12-26.

For falling-rate drying throughout, time t_{FR} is given by Eq. (12-63); the multiplying factor for drying time is 1.2 ln 6 = 2.15 for all dryer types.

$$\frac{t_{FR}}{t_{CR}} = \frac{X_1 - X_E}{X_1 - X_2} \ln \left(\frac{X_1 - X_E}{X_2 - X_E} \right) = \frac{0.3}{0.25} \ln \frac{0.3}{0.05} \quad (12-63)$$

If the material showed a critical moisture content, the calculation could be split into two sections for constant-rate and falling-rate drying. Likewise, the experimental drying time t_{opt} for the conical dryer is 12.5 h which is a factor of 3.94 greater than the constant-rate drying time. A very rough estimate of drying times for the other dryer types has then been made by applying the same scaling factor (3.94) to their constant-rate drying times. Two major sources of error are possible: (1) The drying kinetics could differ between dryers; and (2) if the

TABLE 12-25 Calculation of Key Dimensions for Various Batch Contact Dryers (Fig. 12-55a Shows the Geometries)

Dryer type	Volume as $f(D)$	Typical L/D	Diameter as $f(V)$	Surface area as $f(D)$	Ratio A/V
Tumbler/double-cone	$V = \frac{\pi D^3}{12} \left(\frac{L}{D} \right)$	1.5	$D = \left[\frac{12V}{\pi(L/D)} \right]^{1/3}$	$A = \frac{\pi D^2}{2} \left[\left(\frac{L}{D} \right)^2 + 1 \right]^{1/2}$	$\frac{A}{V} = \frac{6}{D} \left[1 + \left(\frac{D}{L} \right)^2 \right]^{1/2}$
Vertical pan	$V = \frac{\pi D^3}{4} \left(\frac{L}{D} \right)$	0.5	$D = \left[\frac{4V}{\pi(L/D)} \right]^{1/3}$	$A = \pi D^2 \left(\frac{L}{D} + \frac{1}{4} \right)$	$\frac{A}{V} = \frac{4}{D} \left(1 + \frac{D}{4L} \right)$
Spherical	$V = \frac{\pi D^3}{6} \left(\frac{L}{D} \right)$	1	$D = \left[\frac{6V}{\pi(L/D)} \right]^{1/3}$	$A = \pi D^2 \left(\frac{L}{D} \right)$	$\frac{A}{V} = \frac{6}{D}$
Filter dryer	$V = \frac{\pi D^3}{4} \left(\frac{L}{D} \right)$	0.5	$D = \left[\frac{4V}{\pi(L/D)} \right]^{1/3}$	$A = \pi D^2 \left(\frac{L}{D} \right)$	$\frac{A}{V} = \frac{4}{D}$
Conical agitated	$V = \frac{\pi D^3}{12} \left(\frac{L}{D} \right)$	1.5	$D = \left[\frac{12V}{\pi(L/D)} \right]^{1/3}$	$A = \frac{\pi D^2}{2} \left[\left(\frac{L}{D} \right)^2 + \frac{1}{4} \right]^{1/2}$	$\frac{A}{V} = \frac{6}{D} \left[1 + \frac{1}{4} \left(\frac{D}{L} \right)^2 \right]^{1/2}$
Paddle (horizontal agitated)	$V = \frac{\pi D^3}{4} \left(\frac{L}{D} \right)$	5	$D = \left[\frac{4V}{\pi(L/D)} \right]^{1/3}$	$A = \pi D^2 \left(\frac{L}{D} \right)$	$\frac{A}{V} = \frac{4}{D}$
Paddle, heated agitator	$V = \frac{\pi D^3}{4} \left(\frac{L}{D} \right)$	5	$D = \left[\frac{4V}{\pi(L/D)} \right]^{1/3}$	$A = \pi D^2 \left(\frac{L}{D} \right) (1 + R)$	$\frac{A}{V} = \frac{4}{D} (1 + R)$

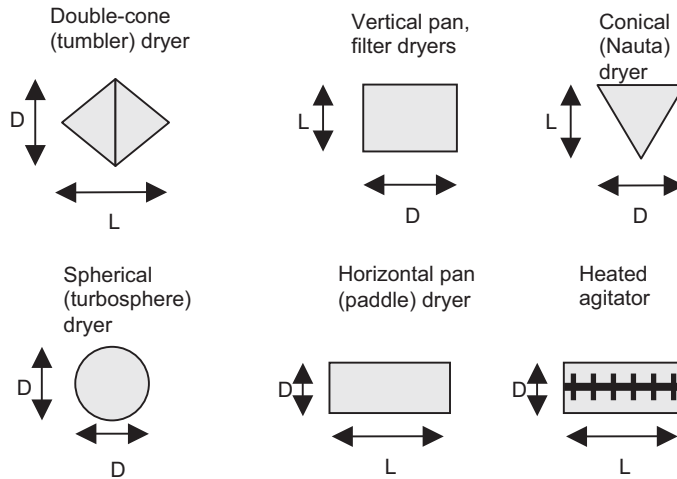


FIG. 12-55a Basic geometries for batch dryer calculations.

estimated heat-transfer coefficient for either the base case or the new dryer type is in error, the scaling factor will be wrong. All drying times have been shown in hours, as this is more convenient than seconds.

The paddle with heated agitator has the shortest drying time, and the filter dryer the longest (because the bottom plate is unheated). Other types are fairly comparable. The spherical dryer would usually have a higher heat-transfer coefficient and shorter drying time than shown.

Performance and Cost Data for Batch Vacuum Rotary Dryers

Typical performance data for horizontal pan vacuum dryers are given in Table 12-27. Size and cost data for rotary agitator units are given in Table 12-28. Data for double-cone rotating units are in Table 12-29.

Continuous Agitated Dryers

Description These dryers, often known as paddle or horizontal agitated dryers, consist of one or more horizontally mounted shells with internal mechanical agitators, which may take many different forms. They are a continuous equivalent of the horizontal pan dryer and are similar in construction, but usually of larger dimensions. They have many similarities to continuous indirect rotary dryers and are sometimes classed as rotary dryers, but this is a misnomer because the outer shell does not rotate, although in some types there is an inner shell which does. Frequently, the internal agitator is heated, and a wide variety of designs exist. Often, two intermeshing agitators are used. There are important variants with high-speed agitator rotation and supplementary convective heating by hot air.

Classification Continuous; mechanical agitation and transport; layer; contact/conduction or convective (through-circulation).

The basic differences are in type of agitator, the two key factors being heat-transfer area and solids handling/stickiness characteristics. Unfortunately, the types giving the highest specific surface area (multiple tubes and coils) are often also the ones most liable to fouling and blockage and most difficult to clean. Figure 12-56 illustrates a number of different agitator types.

The most common problem with paddle dryers (and with their closely related cousins, steam-tube and indirect rotary dryers) is the

buildup of sticky deposits on the surface of the agitator or outer jacket. This leads, first, to reduced heat-transfer coefficients and slower drying and, second, to blockages and stalling of the rotor. Also, thermal decomposition and loss of product quality can result. The problem is usually most acute at the feed end of the dryer, where the material is wettest and stickiest. A wide variety of different agitator designs have been devised to try to reduce stickiness problems and enhance cleanability while providing a high heat-transfer area. Many designs incorporate a high torque drive combined with rugged shaft construction to prevent rotor stall during processing, and stationary mixing elements are installed in the process housing which continually clean the heat-exchange surfaces of the rotor to minimize any crust buildup and ensure an optimum heat-transfer coefficient at all times. Another alternative is to use two parallel intermeshing shafts, as in the Nara paddle dryer (Fig. 12-57). Suitably designed continuous paddle and batch horizontal pan dryers can handle a wide range of product consistencies (dilute slurries, pastes, friable powders) and can be used for processes such as reactions, mixing, drying, cooling, melting, sublimation, distilling, and vaporizing. Bearing supports are usually provided at both ends of the unit for shaft support.

Design Methods for Paddle Dryers Product trials are conducted in small pilot dryers (8- to 60-L batch or continuous units) to determine material handling and process retention times. Variables such as drying temperature, pressure level, and shaft speed are analyzed during the test trials. For initial design purposes, the heat-transfer coefficient for paddle dryers is typically in the range of 10 W/(m²·K) (light, free-flowing powders) up to 150 W/(m²·K) (dilute slurries). However, it is preferable to scale up from the test results, finding the heat-transfer coefficient by backcalculation and scaling up on the basis of total area of heat-transfer surfaces, including heated agitators. Typical length/diameter ratios are between 5 and 8, similar to rotary dryers and greater than some batch horizontal pan dryers.

Continuous Rotary Dryers A rotary dryer consists of a cylinder that rotates on suitable bearings and that is usually slightly inclined to the horizontal. The cylinder length may range from 4 to more than 10 times

TABLE 12-26 Comparative Dimensions and Drying Times for Various Batch Contact Dryers

Dryer type	<i>h</i> , kW/(m ² ·K)	<i>L/D</i>	<i>D</i> , m	<i>L</i> , m	<i>A</i> , m ²	<i>t</i> _{CR} , h	<i>t</i> _{FR} , h	<i>t</i> _{expt} , h
Tumbler/double-cone	0.05	1.5	3.71	5.56	38.91	2.78	5.98	11.0
Vertical pan	0.05	0.5	3.71	1.85	32.37	3.34	7.19	13.2
Spherical	0.05	1	3.37	3.37	35.63	3.04	6.54	12.0
Filter dryer	0.05	0.5	3.71	1.85	21.58	5.01	10.77	19.8
Conical agitated	0.05	1.5	3.71	5.56	34.12	3.17	6.82	12.5
Paddle (horizontal agitated)	0.05	5	1.72	8.60	46.50	2.33	5.01	9.2
Paddle, heated agitator	0.05	5	1.72	8.60	278.99	0.39	0.83	1.52

12-72 PSYCHROMETRY, EVAPORATIVE COOLING, AND SOLIDS DRYING

TABLE 12-27 Performance Data of Vacuum Rotary Dryers*

Material	Diameter × length, m	Initial moisture, % dry basis	Steam pressure, Pa × 10 ³	Agitator speed, r/min	Batch dry weight, kg	Final moisture, % dry basis	Pa × 10 ³	Time, h	Evaporation, kg/(h·m ²)
Cellulose acetate	1.5 × 9.1	87.5	97	5.25	610	6	90–91	7	1.5
Starch	1.5 × 9.1	45–48	103	4	3630	12	88–91	4.75	7.3
Sulfur black	1.5 × 9.1	50	207	4	3180	1	91	6	4.4
Fuller's earth/mineral spirit	0.9 × 3.0	50	345	6	450	2	95	8	5.4

*Stokes Vacuum, Inc.

the diameter, which may vary from less than 0.3 to more than 3 m. Solids fed into one end of the drum are carried through it by gravity, with rolling, bouncing and sliding, and drag caused by the airflow either retarding or enhancing the movement, depending on whether the dryer is cocurrent or countercurrent. It is possible to classify rotary dryers into direct-fired, where heat is transferred to the solids by direct exchange between the gas and the solids, and indirect, where the heating medium is separated from physical contact with the solids by a metal wall or tube. Many rotary dryers contain flights or lifters, which are attached to the inside of the drum and which cascade the solids through the gas as the drum rotates.

For handling large quantities of granular solids, a cascading rotary dryer is often the equipment of choice. If the material is not naturally free-flowing, recycling of a portion of the final dry product may be used to precondition the feed, either in an external mixer or directly inside the drum. Hanging link chains and/or scrapper chains are also used for sticky feed materials.

Their operating characteristics when performing heat- and mass-transfer operations make them suitable for the accomplishment of drying, chemical reactions, solvent recovery, thermal decompositions, mixing, sintering, and agglomeration of solids. The specific types included are the following:

Direct cascading rotary dryer (cooler). This is usually a bare metal cylinder but with internal flights (shelves) which lift the material and drop it through the airflow. It is suitable for low- and medium-temperature operations, the operating temperature being limited primarily by the strength characteristics of the metal employed in fabrication.

Direct rotary dryer (cooler). As above but without internal flights.
Direct rotary kiln. This is a metal cylinder lined on the interior with insulating block and/or refractory brick. It is suitable for high-temperature operations.

Indirect steam-tube dryer. This is a bare metal cylinder provided with one or more rows of metal tubes installed longitudinally in the shell. It is suitable for operation up to available steam temperatures or in processes requiring water cooling of the tubes.

Indirect rotary calciner. This is a bare metal cylinder surrounded on the outside by a fired or electrically heated furnace. It is suitable for operation at medium temperatures up to the maximum that can be tolerated by the metal wall of the cylinder, usually 650 to 700 K for carbon steel and 800 to 1025 K for stainless steel.

Direct Roto-Louvre dryer. This is one of the more important special types, differing from the direct rotary unit in that true through-circulation of gas through the solids bed is provided. Like the direct rotary, it is suitable for low- and medium-temperature operation.

Direct heat rotary dryer. The direct heat units are generally the simplest and most economical in operation and construction, when the solids and gas can be permitted to be in contact. In design mode, the required gas flow rate can be obtained from a heat and mass balance. Bed cross-sectional area is found from a scoping design calculation (a typical gas velocity is 3 m/s for cocurrent and 2 m/s for countercurrent units). Length is normally between 5 and 10 times drum diameter (an L/D value of 8 can be used for initial estimation) or can be calculated by using an incremental model (see Examples 21 and 23).

A typical schematic diagram of a rotary dryer is shown in Fig. 12-58, while Fig. 12-59 shows typical lifting flight designs.

Classification Continuous; agitation and transport by rotation/gravity; layer (dispersion for cascading rotary dryers); convective (through-circulation) or contact/conduction.

Residence Time, Standard Configuration The residence time in a rotary dryer τ represents the average time that particles are present in the equipment, so it must match the required drying time.

Traditional approaches For rotary kilns, without lifting flights, Sullivan et al. (U.S. Bureau of Mines Tech. Paper 384) gave an early formula:

$$\tau = \frac{106.2L\sqrt{\gamma}}{N_m D \tan \alpha} \quad (12-88)$$

Here, the natural angle of repose of the material is γ , which increases as the material becomes more cohesive and less free-flowing, and the residence time τ is in seconds, but the rotation rate N_m is in revolutions per minute (rpm), not per second. The Friedman and Marshall equation [Chem. Eng. Progr. 45(8): 482 (1949)] is derived from this, with an additional term to account for air drag on the solids:

$$\tau = \frac{13.8L}{N_m^{0.9} D \alpha} \pm \frac{590.6LG}{d_p^{0.5} G} \quad (12-89)$$

Here d_p is the particle size, in micrometers, while F and G are the mass flow rates of solids and gas, respectively. This formula has been frequently reported and includes a correction factor to the initial constant term to reflect actual experimental results. Friedman and Marshall took the angle of repose for the solids to be 40° and introduced a 0.9 power for the rotational speed, which had questionable justification within the accuracy of the data. The second term represents the airflow drag term and is negative for cocurrent flow and positive for countercurrent flow.

TABLE 12-28 Standard Rotary Vacuum Dryers*

Diameter, m	Length, m	Heating surface, m ²	Working capacity, m ³ †	Agitator speed, r/min	Drive, kW	Weight, kg	Purchase price (1995)	
							Carbon steel	Stainless steel (304)
0.46	0.49	0.836	0.028	7½	1.12	540	\$ 43,000	\$ 53,000
0.61	1.8	3.72	0.283	7½	1.12	1,680	105,000	130,000
0.91	3.0	10.2	0.991	6	3.73	3,860	145,000	180,000
0.91	4.6	15.3	1.42	6	3.73	5,530	180,000	205,000
1.2	6.1	29.2	3.57	6	7.46	11,340	270,000	380,000
1.5	7.6	48.1	6.94	6	18.7	15,880	305,000	440,000
1.5	9.1	57.7	8.33	6	22.4	19,050	330,000	465,000

*Stokes Vacuum, Inc. Prices include shell, 50-lb/in²-gauge jacket, agitator, drive, and motor; auxiliary dust collectors, condensers.

†Loading with product level on or around the agitator shaft.

TABLE 12-29 Standard (Double-Cone) Rotating Vacuum Dryers*

Working capacity, m ³	Total volume, m ³	Heating surface, m ²	Drive, kW	Floor space, m ²	Weight, kg	Purchase cost (1995)	
						Carbon steel	Stainless steel
0.085	0.130	1.11	.373	2.60	730	\$ 32,400	\$ 38,000
0.283	0.436	2.79	.560	2.97	910	37,800	43,000
0.708	1.09	5.30	1.49	5.57	1810	50,400	57,000
1.42	2.18	8.45	3.73	7.15	2040	97,200	106,000
2.83	4.36	13.9	7.46	13.9	3860	198,000	216,000
4.25	6.51	17.5	11.2	14.9	5440	225,000	243,000
7.08	10.5	*38.7	11.2	15.8	9070	324,000	351,000
9.20	13.9	*46.7	11.2	20.4	9980	358,000	387,000
11.3	16.0	*56.0	11.2	26.0	10,890	378,000	441,000

*Stokes Vacuum, Inc. Price includes dryer, 15-lb/in² jacket, drive with motor, internal filter, and trunnion supports for concrete or steel foundations. Horsepower is established on 65 percent volume loading of material with a bulk density of 50 lb/ft³. Models of 250 ft³, 325 ft³, and 400 ft³ have extended surface area.

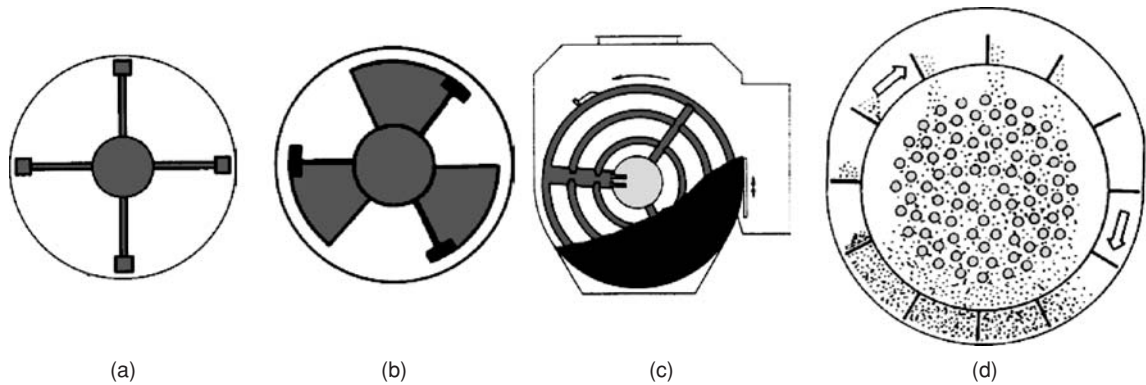


FIG. 12-56 Typical agitator designs for paddle (horizontal agitated) dryers. (a) Simple unheated agitator. (b) Heated cut-flight agitator. (c) Multicoil unit. (d) Tube bundle.

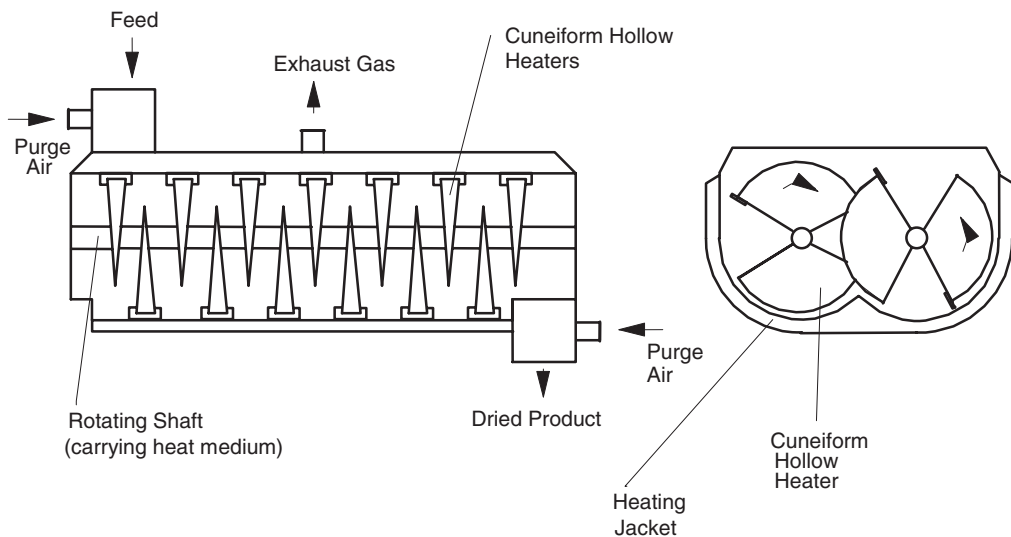


FIG. 12-57 Nara twin-shaft paddle dryer.

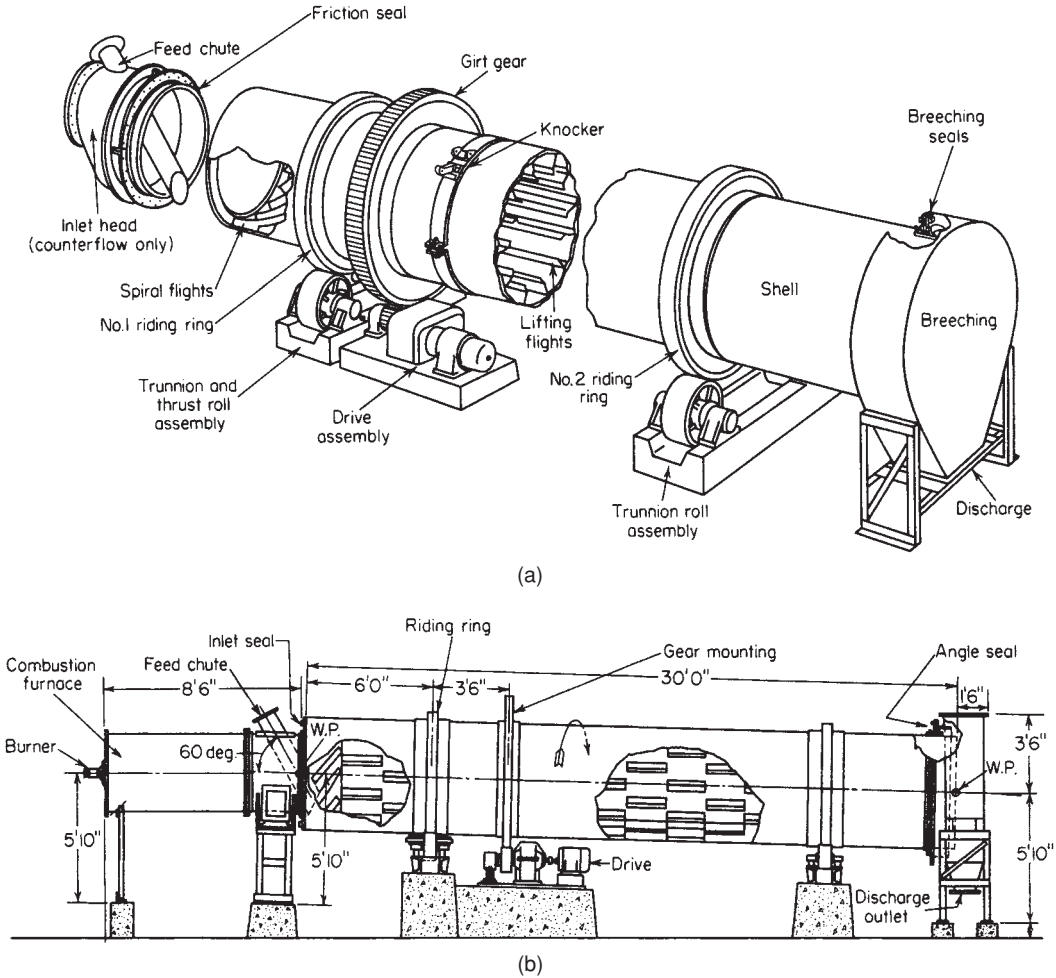


FIG. 12-58 Component arrangement (a) and elevation (b) of countercurrent direct-heat rotary dryer. (Air Preheater Company, Raymond® & Bartlett Snow™ Products.)

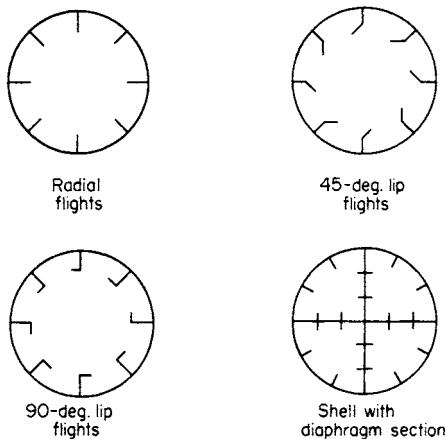


FIG. 12-59 Typical lifting flight designs.

Saeman and Mitchell [*Chem. Eng. Progr.* **50**(9):467 (1954)] proposed the following expression:

$$\tau = \frac{L}{f_H N D (\tan \alpha \pm k_m U_G)} \quad (12-90)$$

Here f_H is a *cascade factor*, with values typically between 2 and π , increasing as solids holdup increases, and k_m is an empirical constant (dimensional) for a given material. The superficial gas velocity through the empty drum is U_G . It was assumed that the airborne particle velocity was proportional to the air velocity. Two empirical constants f_H and k_m are also required to use the equation, and these are not generally available.

Schofield and Glikin [*Trans. IChemE* **40**:183 (1962)] analyzed particle motion from flights and airborne drag, obtaining

$$\tau = \frac{L}{\bar{y} \bar{\theta} N [\sin \alpha - (K U_G^2 / g)]} \quad (12-91)$$

Here \bar{y} is the mean distance of fall of the particles, $\bar{\theta}$ is the mean angle moved by particles in flights, and K is a dimensional drag constant. At

small angles α , $\sin \alpha \approx \tan \alpha$, and they noted that $\bar{y} \bar{\theta} \approx 2D$, so their final Eq. (12-91) is similar to that of Saeman and Mitchell (1954).

The above equations mainly differ in whether the drag term is additive or subtractive (as with Friedman and Marshall) or in the denominator (as with Saeman and Mitchell, and Schofield and Glikin). Some workers, including Sullivan et al. (1927), have neglected the effect of air drag completely. However, the general experience with rotary dryers is that the effect of air velocity and hence of air drag is very substantial, suggesting that neglecting air drag in any equation or analysis is unlikely to be sufficient unless the air velocity is very low. The formulas link L and τ , which is reasonably convenient for dryer performance assessment, but inconvenient for dryer design, where neither L nor τ is initially known.

Modern analysis Matchett and Baker [J. Sep. Proc. Technol. 8:11 (1987)] provided a complete analysis of particle motion in rotary dryers. They considered both the airborne phase (particles falling through air) and the dense phase (particles in the flights or the rolling bed at the bottom). Typically, particles spend 90 to 95 percent of the time in the dense phase, but the majority of the drying takes place in the airborne phase. In the direction parallel to the dryer axis, most particle movement occurs through four mechanisms: by gravity and air drag in the airborne phase, and by bouncing, and sliding and rolling, in the dense phase. The combined particle velocity in the airborne phase is U_{p1} , which is the sum of the gravitational and air drag components for cocurrent dryers and the difference between them for countercurrent dryers. The dense-phase velocity, arising from bouncing, sliding, and rolling, is denoted U_{p2} .

Papadakis et al. [Dry. Tech. 12(1&2):259 (1994)] rearranged the Matchett and Baker model from its original "parallel" form into a more computationally convenient "series" form. The sum of the calculated residence times in the airborne and dense phases, τ_c and τ_s , respectively, is the total solids residence time. The dryer length is simply the sum of the distances travelled in the two phases.

$$\tau = \tau_c + \tau_s \tag{12-92}$$

$$L = \tau_c U_{p1} + \tau_s U_{p2} \tag{12-93}$$

For airborne phase motion, the velocity U_{p1}^o due to the gravitational component is given approximately by

$$U_{p1}^o = \sqrt{\frac{gD_e}{2 \cos \alpha}} K_{fall} \tan \alpha \tag{12-94}$$

where D_e is the effective diameter, which is the distance actually fallen by the particles. When one is designing a dryer, this parameter will not be known until the flight width is decided. And K_{fall} is a parameter that allows for particles falling from a number of positions, with different times of flight and lifting times, and is generally between 0.7 and 1. The velocity U_{p1}^o due to the gravitational component is most conveniently expressed as

$$U_{p1}^o = \sqrt{\frac{gD}{2}} \tan \alpha K_{fall} \sqrt{\frac{D_e}{D \cos \alpha}} = \sqrt{\frac{gD}{2}} \tan \alpha K_{\kappa} \tag{12-95}$$

The drag force gives a velocity component U_{p1}^d that must be obtained from experimental correlations, and combining these components gives U_{p1} .

Bouncing, rolling, and sliding are not so easily analyzed theoretically. Matchett and Baker suggested that the dense-phase velocity could be characterized in terms of a dimensionless dense-phase velocity number a , through the equation

$$a = \frac{U_{p2}}{N \cdot D \cdot \tan \alpha} \tag{12-96}$$

Other workers suggested that, in underloaded and design-loaded dryers, bouncing was a significant transport mechanism, whereas for overloaded dryers, rolling (kilning) was important. Bouncing mechanisms can depend on the airborne phase velocity U_{p1} , since this affects the angle at which the particles hit the bottom of the kiln and the dis-

tance they move forward. Rolling mechanisms would be expected to depend on the depth of the bottom bed, and hence on the difference between the actual holdup H and the design-loaded holdup H^o .

As an example of the typical numbers involved, Matchett and Baker [J. Sep. Proc. Technol., 9:5 (1988)] used their correlations to assess the data of Saeman and Mitchell for an industrial rotary dryer with $D = 1.83$ m and $L = 10.67$ m, with a slope of 4° , 0.067 m/m. For a typical run with $U_c = 0.98$ m/s and $N = 0.08$ r/s, they calculated that $U_{p1}^o = 0.140$ m/s, $U_{p1}^d = -0.023$ m/s, $U_{p1} = 0.117$ m/s, and $U_{p2} = -0.02$ m/s. The dryer modeled was countercurrent and therefore had a greater slope and lower gas velocity than those of a cocurrent unit; for the latter, U_{p1}^o would be lower and U_{p1}^d positive and larger. The ratio τ_s/τ_c is approximately 12 in this case, so that the distance traveled in dense-phase motion would be about twice that in the airborne phase.

Kemp and Oakley [Dry. Tech., 20(9):1699 (2002)] showed that the ratio τ_c/τ_s can be found by comparing the average time of flight from the top of the dryer to the bottom t_f to the average time required for the particles to be lifted by the flights t_d . They derived the following equation:

$$\frac{\tau_s}{\tau_c} = \frac{t_d}{t_f} = \frac{K_{\beta}}{N} \sqrt{\frac{g}{D}} \tag{12-97}$$

Here all the unknowns have been rolled into a single dimensionless parameter K_{β} , given by

$$K_{\beta} = \frac{\theta}{\pi \sqrt{2} \sin \theta} \sqrt{\frac{D}{D_e}} \tag{12-98}$$

Here D_e is the effective diameter (internal diameter between lips of flights), and the solids are carried in the flights for an angle 2θ , on average, before falling. Kemp and Oakley concluded that K_{β} can be taken to be 0.4 to a first (and good) approximation. For overloaded dryers with a large rolling bed, K_{β} will increase. The form of Eq. (12-97) is very convenient for design purposes since it does not require D_e , which is unknown until a decision has been made on the type and geometry of the flights.

The model of Matchett and Baker has been shown by Kemp (Proc. IDS 2004, B, 790) to be similar in form to that proposed by Saeman and Mitchell:

$$\tau = \frac{1.1L}{ND \left[\tan \alpha \cdot (K_{\kappa}/K_{\beta} \sqrt{2} + a) + (1/K_{\beta}) \sqrt{\frac{1}{gD}} \cdot U_{p1}^d \right]} \tag{12-99}$$

In Eq. (12-99), $K_{\kappa}/(K_{\beta} \sqrt{2})$ will typically be on the order of unity, and reported values of a are in the range of 1 to 4. The airborne gravity component is usually smaller than the dense-phase motion but is not negligible. The sum of these two terms is essentially equivalent to the factor f_{fl} in Saeman and Mitchell's equation.

Heat- and Mass-Transfer Estimates Many rotary dryer studies have correlated heat- and mass-transfer data in terms of an overall volumetric heat-transfer coefficient $U_{c,a}$ [W/(m³·K)], defined by

$$Q = U_{c,a} \cdot V_{dryer} \cdot \Delta T_m \tag{12-100}$$

Here Q is the overall rate of heat transfer between the gas and the solids (W), V_{dryer} is the dryer volume (m³), and ΔT_m is an average temperature driving force (K). When one is calculating the average temperature driving force, it is important to distinguish between the case of heat-transfer with dry particles, where the change in the particle temperature is proportional to the change in the gas temperature, and the case of drying particles, where the particle temperature does not change so significantly. Where the particles are dry, the average temperature difference is the logarithmic mean of the temperature differences between the gas and the solids at the inlet and outlet of the dryer, although Miller et al. (1942) took the logarithmic temperature difference as the average temperature difference even when the particles were drying. The volumetric heat-transfer coefficient itself consists of a heat-transfer coefficient U_c based on the effective area of contact between the gas and the solids, and the ratio a of this area to

TABLE 12-30 Values of the Index n in Correlations for the Volumetric Heat-Transfer Coefficient (after Baker, 1983)

Author(s)	Exponent n
Saeman and Mitchell (1954)	0
Friedman and Marshall (1949)	0.16
Aiken and Polsak (1982)	0.37
Miller et al. (1942)	0.46–0.60
McCormick (1962)	0.67
Myklestad (1963)	0.80

the dryer volume. Thus, this procedure eliminates the need to specify where most of the heat-transfer occurs (e.g., to material in the air, on the flights, or in the rolling bed). Empirical correlations are of the form

$$U_v a = \frac{K' U_{G\text{super}}^n}{D} \quad (12-101)$$

where K' depends on the solids properties, the flight geometry, the rotational speed, and the dryer holdup. Table 12-30 gives the values of n chosen by various authors.

McCormick (1962) reworked the data of Miller et al. (1942), Friedman and Marshall (1949), and Saeman and Mitchell (1954) with a view to obtaining a single correlation of the form of Eq. (12-101) for the volumetric heat-transfer coefficient. He demonstrated that all the data could be correlated with values of the exponent n from 0.46 to 0.67. Although the evidence was far from conclusive, he believed that a value of 0.67 for the exponent n was most reliable. Individual values of the constant K' were obtained from the results of each of the workers cited above. He found that it was a function of the solids properties, the flight geometry, the rotational speed, and the dryer holdup, but that there was insufficient evidence available to relate K' to these parameters.

A comparison between the correlations of various workers was made by Baker (1983), and this is given in Table 12-31. A 2-m-diameter dryer containing 16 flights was chosen as the basis for the comparisons. With the exception of the results of Myklestad (1963), the values of $U_v a$ were calculated by using the values of K' and a value of n of 0.67, as obtained by McCormick (1963). A 17-fold variation in the predicted values of $U_v a$ can be observed at both 1 and 3 m/s. The reason for this is not readily apparent. With the exception of the commercial data correlation of Miller et al. (1942), the results were all obtained in pilot-scale rigs having diameters ranging from 0.2 to 0.3 m. Differences in equipment size are therefore not likely to be the cause of the variation. Hence the variation must be attributed to a combination of experimental errors and differences in the experimental conditions which are unaccounted for in the correlations.

An alternative procedure is the use of a conventional film heat-transfer coefficient h_f [W/(m²·K)]

$$Q = h_f \cdot A_s \cdot \Delta T \quad (12-102)$$

Here Q is the local heat-transfer rate (W), A_s is the total surface area of all the particles (m²), and ΔT is the temperature difference between the gas and the solids (K). The method has the advantages that h_f can

TABLE 12-31 Summary of the Predictions Using the Correlations for the Volumetric Heat-Transfer Coefficients of Various Authors (after Baker, 1983)

Author(s)	$U_v a$, W/(m ³ ·K)	
	$U_{G\text{super}} = 1$ m/s	$U_{G\text{super}} = 3$ m/s
Miller et al. (1942)		
Commercial data	248	516
Pilot-scale data	82	184
Friedman and Marshall (1949)	67	138
Saeman and Mitchell (1954)	495–1155	1032–2410
Myklestad (1963)	423	1019

be determined by relatively simple tests (or calculated from appropriate correlations in the literature), variations in operating conditions can be allowed for, and analogies between heat and mass transfer allow the film coefficients for these processes to be related. However, the area for heat transfer must be estimated under the complex conditions of gas-solids interaction present in particle cascades. Schofield and Glikin (1962) estimated this area to be the surface area of particles per unit mass $6/(\rho_p d_p)$, multiplied by the fraction of solids in the drum that are cascading through the gas at any moment, which was estimated as the fraction of time spent by particles cascading through the gas:

$$A_s = \frac{6}{\rho_p d_p} \frac{t_f}{t_f + t_d} \quad (12-103)$$

Schofield and Glikin estimated the heat-transfer coefficient by using the correlation given by McAdams (1954), which correlates data for gas-to-particle heat transfer in air to about 20 percent over a range of Reynolds numbers (Re_p , defined in the previous section) between 17 and 70,000:

$$Nu_p = 0.33 \cdot Re_p^{1/2} \quad (12-104)$$

Here the particle Nusselt number is Nu_p , where $Nu_p = h_f d_p / k_C$, and k_C is the thermal conductivity of the gas [W/(m·K)]. They stated that the heat-transfer rates predicted by this procedure were much larger than those measured on an industrial cooler, which is probably due to the particles on the inside of the cascades not experiencing the full gas velocity. Kamke and Wilson (1986) used a similar approach to model the drying of wood chips, but used the Ranz-Marshall (1952) equation to predict the heat-transfer coefficient:

$$Nu_p = 2 + 0.6 \cdot Re_p^{1/2} \cdot Pr_C \quad (12-105)$$

where Pr_C is the Prandtl number of the gas.

Drying Time Estimates Sometimes, virtually all the drying takes place in the airborne phase. Under such circumstances, the airborne-phase residence time τ_C and the drying time are virtually the same, and the required drying time can be estimated from equivalent times in drying kinetics experiments, e.g., using a thin-layer test (Langrish, D.Phil. thesis, 1988).

An example of how to incorporate the concept of the characteristic drying curve into a design calculation is given in Example 23.

Example 23: Sizing of a Cascading Rotary Dryer The average gas velocity passing through a cocurrent, adiabatic, cascading rotary dryer is 4 m/s. The particles moving through the dryer have an average diameter of 5 mm, a solids density of 600 kg/m³, and a shape factor of 0.75. The particles enter with a moisture content of 0.50 kg/kg (dry basis) and leave with a moisture content of 0.15 kg/kg (dry basis). The drying kinetics may be assumed to be linear, with no unhindered (constant-rate) drying period. In addition, let us assume that the solids are nonhygroscopic (so that the equilibrium moisture content is zero; hygroscopic means that the equilibrium moisture content is nonzero).

The inlet humidity is 0.10 kg/kg (dry basis) due to the use of a direct-fired burner, and the ratio of the flow rates of dry solids to dry gas is unity. The gas temperature at the inlet to the dryer is 800°C, and the gas may be assumed to behave as a pure water vapor/air mixture.

The gas-phase residence time that is required was calculated in the fundamentals section to be 38.0 s.

How does this gas-phase residence time relate to the total residence time that is required and to the dryer dimensions?

Application of residence time calculations (practice): Suppose that this dryer has a slope α of 4° and a diameter D of 1.5 m, operating at a rotational speed N of 0.04 r/s. We already know that the gas velocity through the drum $U_{G\text{super}}$ is 4 m/s, and that the particles have a mean diameter d_p of 5 mm and a particle density ρ_p of 600 kg/m³. As a first estimate, suppose that the gas density ρ_C is 1 kg/m³ and the gas viscosity μ_C is 1.8×10^{-5} kg/(m·s).

Now $K_R/(K_R \sqrt{2}) \approx 1$, $K_R \approx 0.4$, $K_{fall} \approx 1$, and a is within the range of 1 to 4, say, 2.5, and U_{p1}^* is estimated by the following calculation, for Reynolds numbers up to 220.

$$U_{p1}^* = 7.45 \times 10^{-4} Re^{2.2} \frac{\mu U_{G\text{super}} t_f^*}{\rho_p d_p^2} \quad (12-106)$$

Above this Reynolds number, the following equation was recommended by Matchett and Baker (1987):

$$U_{p1}^d = 125 \frac{\mu U_{Gsuper} t_a^*}{\rho_r d_p^2} \tag{12-107}$$

Here Re is the Reynolds number ($U_{Gsuper} d_p \rho / \mu$) and t_f is the average time of flight of a particle in the airborne phase.

$$t_f = \left(\frac{2D}{g \cos \alpha} \right)^{1/2} K_{fall} \tag{12-108}$$

Substituting in the numbers gives

$$t_f = \left(\frac{2 \cdot 1.5 \text{ m}}{9.81 \text{ m/s}^2 \cdot \cos 4^\circ} \right)^{1/2} 1.0 = 0.554 \text{ s}$$

$$Re = \frac{4 \text{ m/s} \cdot 0.005 \text{ m} \cdot 1 \text{ kg/m}^3}{1.8 \times 10^{-5} (\text{kg/m} \cdot \text{s})} = 1100$$

$$U_{p1}^d = 125 \frac{1.8 \times 10^5 \text{ kg/(m} \cdot \text{s)} \cdot 4 \text{ m/s} \cdot 0.554 \text{ s}}{(600 \text{ kg/m}^3)(0.005 \text{ m})^2}$$

$$= 0.332 \text{ m/s}$$

$$\frac{\tau}{L} = \frac{1.1}{0.04 \text{ s}^{-1} \cdot 1.5 \text{ m}}$$

$$\times \left[\frac{\tan 4^\circ \cdot (1 + 2.5) + \frac{1}{0.4} \sqrt{\frac{1}{9.81 \text{ m/s}^2 \cdot 1.5 \text{ m}}}}{\dots} \right]$$

$$= 30 \text{ s/m}$$

$$\frac{\tau_s}{\tau_c} = \frac{t_d}{t_f} = \frac{K_{\beta}}{N} \sqrt{\frac{g}{D}} = \frac{0.4}{0.04 \text{ s}^{-1}} \sqrt{\frac{9.81 \text{ m/s}^2}{1.5 \text{ m}}} = 25.6$$

Now, the required gas-phase residence time τ_c is 38.0 s. The ratio of solids to gas-phase residence times now gives us the required solids-phase residence time τ_s of $25.6 \times 38.0 \text{ s} = 972 \text{ s}$, and a total residence time of $972 + 38 = 1010 \text{ s}$. If the total residence time per unit length is 30 s/m, then the required dryer length is $1010 \text{ s}/(30 \text{ s/m}) = 34.2 \text{ m}$. The dryer length/diameter ratio is therefore $34.2 \text{ m}/1.5 \text{ m} = 22.8$, which is significantly larger than the recommended ratio of between 5:1 and 10:1. The remedy would then be to use a larger dryer diameter and repeat these calculations. The larger dryer diameter would decrease the gas velocity, slowing the particle velocity along the drum, increasing the residence time per unit length, and hence decreasing the required drum length, to give a more normal length/diameter ratio.

Performance and Cost Data for Direct Heat Rotary Dryers
 Table 12-32 gives estimating-price data for direct rotary dryers employing steam-heated air. Higher-temperature operations requiring combustion chambers and fuel burners will cost more. The total installed cost of rotary dryers including instrumentation, auxiliaries, allocated building space, etc., will run from 150 to 300 percent of the purchase cost. Simple erection costs average 10 to 20 percent of the purchase cost.

Operating costs will include 5 to 10 percent of one worker's time, plus power and fuel required. Yearly maintenance costs will range from 5 to 10 percent of total installed costs. Total power for fans, dryer drive, and feed and product conveyors will be in the range of $0.5D^2$ to $1.0D^2$. Thermal efficiency of a high-temperature direct heat rotary dryer will range from 55 to 75 percent and, with steam-heated air, from 30 to 55 percent.

A representative list of materials dried in direct heat rotary dryers is given in Table 12-33.

Indirect Heat Rotary Steam-Tube Dryers Probably the most common type of indirect heat rotary dryer is the steam-tube dryer (Fig. 12-60). Steam-heated tubes running the full length of the cylinder are fastened symmetrically in one, two, or three concentric rows inside the cylinder and rotate with it. Tubes may be simple pipe with condensate draining by gravity into the discharge manifold or bayonet type. Bayonet-type tubes are also employed when units are used as water-tube coolers. When handling sticky materials, one row of tubes is preferred. These are occasionally shielded at the feed end of the dryer to prevent buildup of solids behind them. Lifting flights are usually inserted behind the tubes to promote solids agitation.

Wet feed enters the dryer through a chute or screw feeder. The product discharges through peripheral openings in the shell in ordinary dryers. These openings also serve to admit purge air to sweep moisture or other evolved gases from the shell. In practically all cases, gas flow is countercurrent to solids flow. To retain a deep bed of material within the dryer, normally 10 to 20 percent fillage, the discharge openings are supplied with removable chutes extending radially into the dryer. These, on removal, permit complete emptying of the dryer.

Steam is admitted to the tubes through a revolving steam joint into the steam side of the manifold. Condensate is removed continuously, by gravity through the steam joint to a condensate receiver and by means of lifters in the condensate side of the manifold. By employing simple tubes, noncondensables are continuously vented at the other ends of the tubes through Sarco-type vent valves mounted on an auxiliary manifold ring, also revolving with the cylinder.

Vapors (from drying) are removed at the feed end of the dryer to the atmosphere through a natural-draft stack and settling chamber or wet scrubber. When employed in simple drying operations with 3.5×10^5 to

TABLE 12-32 Warm-Air Direct-Heat Cocurrent Rotary Dryers: Typical Performance Data*

Dryer size, m × m	1.219 × 7.62	1.372 × 7.621	1.524 × 9.144	1.839 × 10.668	2.134 × 12.192	2.438 × 13.716	3.048 × 16.767
Evaporation, kg/h	136.1	181.4	226.8	317.5	408.2	544.3	861.8
Work, 10 ⁶ J/h	3.61	4.60	5.70	8.23	1.12	1.46	2.28
Steam, kg/h at kg/m ² gauge	317.5	408.2	521.6	725.7	997.9	131.5	2041
Discharge, kg/h	408	522	685	953	1270	1633	2586
Exhaust velocity, m/min	70	70	70	70	70	70	70
Exhaust volume, m ³ /min	63.7	80.7	100.5	144.4	196.8	257.7	399.3
Exhaust fan, kW	3.7	3.7	5.6	7.5	11.2	18.6	22.4
Dryer drive, kW	2.2	5.6	5.6	7.5	14.9	18.6	37.3
Shipping weight, kg	7700	10,900	14,500	19,100	35,800	39,900	59,900
Price, FOB Chicago	\$158,000	\$168,466	\$173,066	\$204,400	\$241,066	\$298,933	\$393,333

*Courtesy of Swenson Process Equipment Inc.

NOTE:

Material: heat-sensitive solid

Maximum solids temperature: 65°C

Feed conditions: 25 percent moisture, 27°C

Product conditions: 0.5 percent moisture, 65°C

Inlet-air temperature: 165°C

Exit-air temperature: 71°C

Assumed pressure drop in system: 200 mm

System includes finned air heaters, transition piece, dryer, drive, product collector, duct, and fan.

Prices are for carbon steel construction and include entire dryer system (November, 1994).

For 304 stainless-steel fabrication, multiply the prices given by 1.5.

TABLE 12-33 Representative Materials Dried in Direct-Heat Rotary Dryers*

Material dried	Moisture content, % (wet basis)		Heat efficiency, %
	Initial	Final	
High-temperature:			
Sand	10	0.5	61
Stone	6	0.5	65
Fluorspar	6	0.5	59
Sodium chloride (vacuum salt)	3	0.04	70-80
Sodium sulfate	6	0.1	60
Ilmenite ore	6	0.2	60-65
Medium-temperature:			
Copperas	7	1 (moles)	55
Ammonium sulfate	3	0.10	50-60
Cellulose acetate	60	0.5	51
Sodium chloride (grainer salt)	25	0.06	35
Cast-iron borings	6	0.5	50-60
Styrene	5	0.1	45
Low-temperature:			
Oxalic acid	5	0.2	29
Vinyl resins	30	1	50-55
Ammonium nitrate prills	4	0.25	30-35
Urea prills	2	0.2	20-30
Urea crystals	3	0.1	50-55

*Taken from *Chem. Eng.*, June 19, 1967, p. 190, Table III.

10×10^5 Pa steam, draft is controlled by a damper to admit only sufficient outside air to sweep moisture from the cylinder, discharging the air at 340 to 365 K and 80 to 90 percent saturation. In this way, shell gas velocities and dusting are minimized. When used for solvent recovery or other processes requiring a sealed system, sweep gas is recirculated through a scrubber-gas cooler and blower.

Steam manifolds for pressures up to 10^6 Pa are of cast iron. For higher pressures, the manifold is fabricated from plate steel, stay-bolted, and welded. The tubes are fastened rigidly to the manifold faceplate and are supported in a close-fitting annular plate at the other end to permit expansion. Packing on the steam neck is normally graphite asbestos. Ordinary rotating seals are similar in design with

allowance for the admission of small quantities of outside air when the dryer is operated under a slight negative internal pressure.

Steam-tube dryers are used for the continuous drying, heating, or cooling of granular or powdery solids which cannot be exposed to ordinary atmospheric or combustion gases. They are especially suitable for fine dusty particles because of the low gas velocities required for purging of the cylinder. Tube sticking is avoided or reduced by employing recycle, shell knockers, etc., as previously described; tube scaling by sticky solids is one of the major hazards to efficient operation. The dryers are suitable for drying, solvent recovery, and chemical reactions. Steam-tube units have found effective employment in soda ash production, replacing more expensive indirect-heat rotary calciners.

Special types of steam-tube dryers employ packed and purged seals on all rotating joints, with a central solids-discharge manifold through the steam neck to reduce the seal diameter. This manifold contains the product discharge conveyor and a passage for the admission of sweep gas. Solids are removed from the shell by special volute lifters and dropped into the discharge conveyor. Units have been fabricated for operation at 76 mm of water, internal shell pressure, with no detectable air leakage.

Design methods for indirect heat rotary steam-tube dryers Heat-transfer coefficients in steam-tube dryers range from 30 to 85 $W/(m^2 \cdot K)$. Coefficients will increase with increasing steam temperature because of increased heat transfer by radiation. In units carrying saturated steam at 420 to 450 K, the heat flux UT will range from 6300 W/m^2 for difficult-to-dry and organic solids to 1890 to 3790 W/m^2 for finely divided inorganic materials. The effect of steam pressure on heat-transfer rates up to 8.6×10^5 Pa is illustrated in Fig. 12-61.

Performance and cost data for indirect heat rotary steam-tube dryers Table 12-34 contains data for a number of standard sizes of steam-tube dryers. Prices tabulated are for ordinary carbon steel construction. Installed costs will run from 150 to 300 percent of purchase cost.

The thermal efficiency of steam-tube units will range from 70 to 90 percent, if a well-insulated cylinder is assumed. This does not allow for boiler efficiency, however, and is therefore not directly comparable with direct heat units such as the direct heat rotary dryer or indirect heat calciner.

Operating costs for these dryers include 5 to 10 percent of one person's time. Maintenance will average 5 to 10 percent of total installed cost per year.

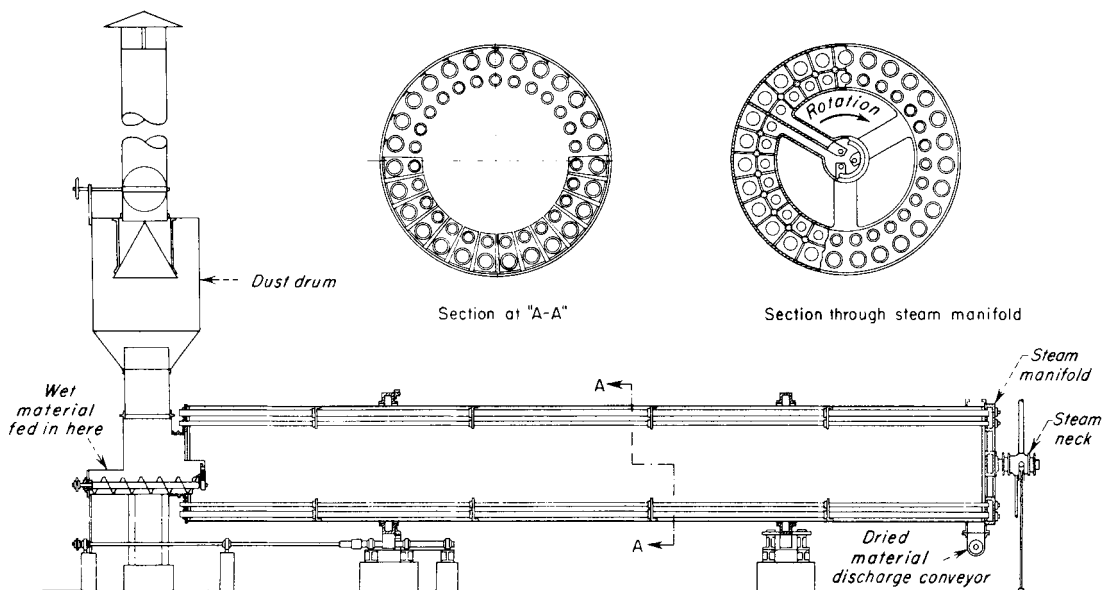


FIG. 12-60 Steam-tube rotary dryer.

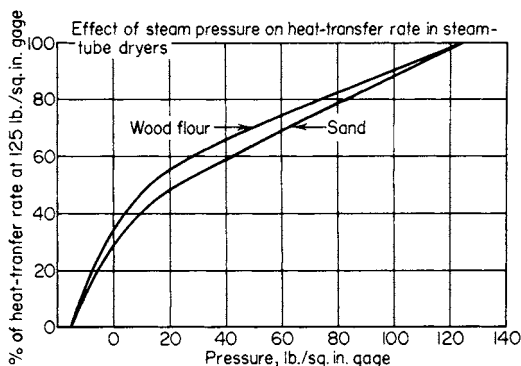


FIG. 12-61 Effect of steam pressure on the heat-transfer rate in steam-tube dryers.

Table 12-35 outlines typical performance data from three drying applications in steam-tube dryers.

Indirect Rotary Calciners and Kilns These large-scale rotary processors are used for very high temperature operations. Operation is similar to that of rotary dryers. For additional information, refer to Perry's 7th Edition, pages 12-56 to 12-58.

Indirect Heat Calciners Indirect heat rotary calciners, either batch or continuous, are employed for heat treating and drying at higher temperatures than can be obtained in steam-heated rotating equipment. They generally require a minimum flow of gas to purge the cylinder, to reduce dusting, and are suitable for gas-sealed operation with oxidizing, inert, or reducing atmospheres. Indirect calciners are widely utilized, and some examples of specific applications are as follows:

1. Activating charcoal
2. Reducing mineral high oxides to low oxides
3. Drying and devolatilizing contaminated soils and sludges
4. Calcination of alumina oxide-based catalysts
5. Drying and removal of sulfur from cobalt, copper, and nickel
6. Reduction of metal oxides in a hydrogen atmosphere
7. Oxidizing and "burning off" of organic impurities
8. Calcination of ferrites

This unit consists essentially of a cylindrical retort, rotating within a stationary insulation-lined furnace. The latter is arranged so that fuel combustion occurs within the annular ring between the retort and the furnace. The retort cylinder extends beyond both ends of the furnace. These end extensions carry the riding rings and drive gear. Material may be fed continuously at one end and discharged continuously at the other. Feeding and solids discharging are usually accomplished with screw feeders or other positive feeders to prevent leakage of gases into or out of the calciner.

In some cases in which it is desirable to cool the product before removal to the outside atmosphere, the discharge end of the cylinder is provided with an additional extension, the exterior of which is water-spray-cooled. In cocurrent flow calciners, hot gases from the interior of the heated portion of the cylinder are withdrawn through a special extraction tube. This tube extends centrally through the cooled section to prevent flow of gas near the cooled-shell surfaces and possible condensation. Frequently a separate cooler is used, isolated from the calciner by an air lock.

To prevent sliding of solids over the smooth interior of the shell, agitating flights running longitudinally along the inside wall are frequently provided. These normally do not shower the solids as in a direct heat vessel but merely prevent sliding so that the bed will turn over and constantly expose new surface for heat and mass transfer. To prevent scaling of the shell interior by sticky solids, cylinder scraper and knocker arrangements are occasionally employed. For example, a scraper chain is fairly common practice in soda ash calciners, while knockers are frequently utilized on metallic-oxide calciners.

Because indirect heat calciners frequently require close-fitting gas seals, it is customary to support all parts on a self-contained frame, for sizes up to approximately 2 m in diameter. The furnace can employ electric heating elements or oil and/or gas burners as the heat source for the process. The hardware would be zoned down the length of the furnace to match the heat requirements of the process. Process control is normally by shell temperature, measured by thermocouples or radiation pyrometers. When a special gas atmosphere must be maintained inside the cylinder, positive rotary gas seals, with one or more pressurized and purged annular chambers, are employed. The diaphragm-type seal is suitable for pressures up to 5 cm of water, with no detectable leakage.

In general, the temperature range of operation for indirect heat calciners can vary over a wide range, from 475 K at the low end to approximately 1475 K at the high end. All types of carbon steel, stainless, and

TABLE 12-34 Standard Steam-Tube Dryers*

Size, diameter × length, m	Tubes		m ² of free area	Dryer speed, r/min	Motor size, hp	Shipping weight, kg	Estimated price
	No. OD (mm)	No. OD (mm)					
0.965 × 4.572	14 (114)		21.4	6	2.2	5,500	\$152,400
0.965 × 6.096	14 (114)		29.3	6	2.2	5,900	165,100
0.965 × 7.620	14 (114)		36.7	6	3.7	6,500	175,260
0.965 × 9.144	14 (114)		44.6	6	3.7	6,900	184,150
0.965 × 10.668	14 (114)		52.0	6	3.7	7,500	196,850
1.372 × 6.096	18 (114)	18 (63.5)	58.1	4.4	3.7	10,200	203,200
1.372 × 7.620	18 (114)	18 (63.5)	73.4	4.4	3.7	11,100	215,900
1.372 × 9.144	18 (114)	18 (63.5)	88.7	5	5.6	12,100	228,600
1.372 × 10.668	18 (114)	18 (63.5)	104	5	5.6	13,100	243,840
1.372 × 12.192	18 (114)	18 (63.5)	119	5	5.6	14,200	260,350
1.372 × 13.716	18 (114)	18 (63.5)	135	5.5	7.5	15,000	273,050
1.829 × 7.62	27 (114)	27 (76.2)	118	4	5.6	19,300	241,300
1.829 × 9.144	27 (114)	27 (76.2)	143	4	5.6	20,600	254,000
1.829 × 10.668	27 (114)	27 (76.2)	167	4	7.5	22,100	266,700
1.829 × 12.192	27 (114)	27 (76.2)	192	4	7.5	23,800	278,400
1.829 × 13.716	27 (114)	27 (76.2)	217	4	11.2	25,700	292,100
1.829 × 15.240	27 (114)	27 (76.2)	242	4	11.2	27,500	304,800
1.829 × 16.764	27 (114)	27 (76.2)	266	4	14.9	29,300	317,500
1.829 × 18.288	27 (114)	27 (76.2)	291	4	14.9	30,700	330,200
2.438 × 12.192	90 (114)		394	3	11.2	49,900	546,100
2.438 × 15.240	90 (114)		492	3	14.9	56,300	647,700
2.438 × 18.288	90 (114)		590	3	14.9	63,500	736,600
2.438 × 21.336	90 (114)		689	3	22.4	69,900	838,200
2.438 × 24.387	90 (114)		786	3	29.8	75,300	927,100

*Courtesy of Swenson Process Equipment Inc. (prices from November, 1994). Carbon steel fabrication; multiply by 1.75 for 304 stainless steel.

TABLE 12-35 Steam-Tube Dryer Performance Data

	Class 1	Class 2	Class 3
Class of materials handled	High-moisture organic, distillers' grains, brewers' grains, citrus pulp	Pigment filter cakes, blanc fixe, barium carbonate, precipitated chalk	Finely divided inorganic solids, water-ground mica, water-ground silica, flotation concentrates
Description of class	Wet feed is granular and damp but not sticky or muddy and dries to granular meal	Wet feed is pasty, muddy, or sloppy; product is mostly hard pellets	Wet feed is crumbly and friable; product is powder with very few lumps
Normal moisture content of wet feed, % dry basis	233	100	54
Normal moisture content of product, % dry basis	11	0.15	0.5
Normal temperature of wet feed, K	310-320	280-290	280-290
Normal temperature of product, K	350-355	380-410	365-375
Evaporation per product, kg	2	1	0.53
Heat load per lb product, kJ	2250	1190	625
Steam pressure normally used, kPa gauge	860	860	860
Heating surface required per kg product, m ²	0.34	0.4	0.072
Steam consumption per kg product, kg	3.33	1.72	0.85

alloy construction are used, depending upon temperature, process, and corrosion requirements. Fabricated-alloy cylinders can be used over the greater part of the temperature range; however, the greater creep-stress abilities of cast alloys makes their use desirable for the highest calciner cylinder temperature applications.

Design methods for calciners In indirect heat calciners, heat transfer is primarily by radiation from the cylinder wall to the solids bed. The thermal efficiency ranges from 30 to 65 percent. By utilization of the furnace exhaust gases for preheated combustion air, steam production, or heat for other process steps, the thermal efficiency can be increased considerably. The limiting factors in heat transmission lie in the conductivity and radiation constants of the shell metal and solids bed. If the characteristics of these are known, equipment may be accurately sized by employing the Stefan-Boltzmann radiation equation. Apparent heat-transfer coefficients will range from 17 W/(m²·K) in low-temperature operations to 85 W/(m²·K) in high-temperature processes.

Cost data for calciners Power, operating, and maintenance costs are similar to those previously outlined for direct and indirect heat rotary dryers. Estimating purchase costs for preassembled and frame-mounted rotary calciners with carbon steel and type 316 stainless-steel cylinders are given in Table 12-36 together with size, weight, and motor requirements. Sale price includes the cylinder, ordinary angle seals, furnace, drive, feed conveyor, burners, and controls. Installed cost may be estimated, not including building or foundation costs, at up to 50 percent of the purchase cost. A layout of a typical continuous calciner with an extended cooler section is illustrated in Fig. 12-62.

Small batch retorts, heated electrically or by combustion, are widely used as carburizing furnaces and are applicable also to chemical processes involving the heat treating of particulate solids. These are mounted on a structural-steel base, complete with cylinder, furnace, drive motor, burner, etc. Units are commercially available in diameters

from 0.24 to 1.25 m and lengths of 1 to 2 m. Continuous retorts with helical internal spirals are employed for metal heat-treating purposes. Precise retention control is maintained in these operations. Standard diameters are 0.33, 0.5, and 0.67 m with effective lengths up to 3 m. These vessels are employed in many small-scale chemical process operations which require accurate control of retention. Their operating characteristics and applications are identical to those of the larger indirect heat calciners.

Direct Heat Roto-Louvre Dryer One of the more important special types of rotating equipment is the Roto-Louvre dryer. As illustrated in Fig. 12-63, hot air (or cooling air) is blown through louvres in a double-wall rotating cylinder and up through the bed of solids. The latter moves continuously through the cylinder as it rotates. Constant turnover of the bed ensures uniform gas contacting for heat and mass transfer. The annular gas passage behind the louvres is partitioned so that contacting air enters the cylinder only beneath the solids bed. The number of louvres covered at any one time is roughly 30 percent. Because air circulates through the bed, fillages of 13 to 15 percent or greater are employed.

Roto-Louvre dryers range in size from 0.8 to 3.6 m in diameter and from 2.5 to 11 m long. The largest unit is reported capable of evaporating 5500 kg/h of water. Hot gases from 400 to 865 K may be employed. Because gas flow is through the bed of solids, high pressure drop, from 7 to 50 cm of water, may be encountered within the shell. For this reason, both a pressure inlet fan and an exhaust fan are provided in most applications to maintain the static pressure within the equipment as closely as possible to atmospheric. This prevents excessive in-leakage or blowing of hot gas and dust to the outside. For pressure control, one fan is usually operated under fixed conditions, with an automatic damper control on the other, regulated by a pressure detector-controller.

In heating or drying applications, when cooling of the product is desired before discharge to the atmosphere, cool air is blown through

TABLE 12-36 Indirect-Heat Rotary Calciners: Sizes and Purchase Costs*

Diameter, ft	Overall cylinder length	Heated cylinder length	Cylinder drive motor hp	Approximate Shipping weight, lb	Approximate sale price in carbon steel construction†	Approximate sale price in No. 316 stainless construction
4	40 ft	30 ft	7.5	50,000	\$275,000	\$325,000
5	45 ft	35 ft	10	60,000	375,000	425,000
6	50 ft	40 ft	20	75,000	475,000	550,000
7	60 ft	50 ft	30	90,000	550,000	675,000

* ABB Raymond (Bartlett-Snow™).

† Prices for November, 1994.

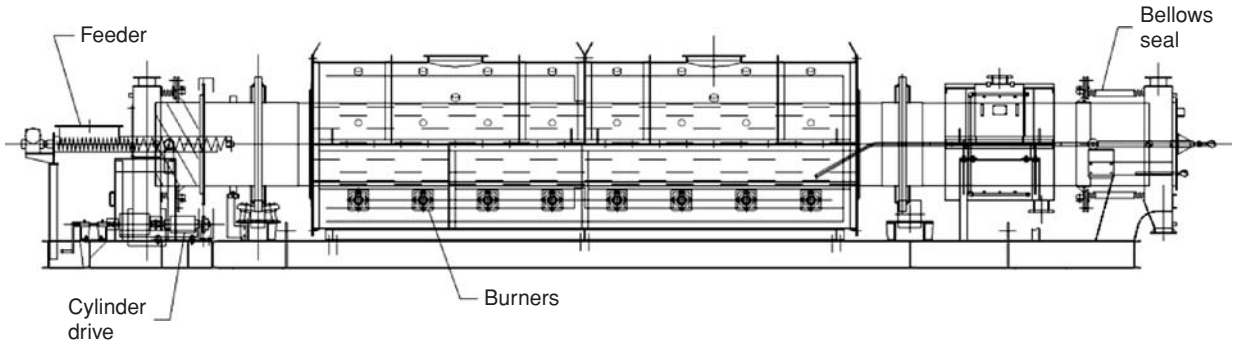


FIG. 12-62 Gas-fired rotary calciner with integral cooler. (Air Preheater Company, Raymond & Bartlett Snow™ Products.)

a second annular space, outside the inlet hot-air annulus, and released through the louvers at the solids discharge end of the shell.

Roto-Louvre dryers are suitable for processing coarse granular solids which do not offer high resistance to airflow, do not require intimate gas contacting, and do not contain significant quantities of dust.

Heat transfer and mass transfer from the gas to the surface of the solids are extremely efficient; hence the equipment size required for a given duty is frequently less than that required when an ordinary direct heat rotary vessel with lifting flights is used. Purchase price savings are partially balanced, however, by the more complex construction of the Roto-Louvre unit. A Roto-Louvre dryer will have a capacity roughly 1.5 times that of a single-shell rotary dryer of the same size under equivalent operating conditions. Because of the cross-flow method of heat exchange, the average t is not a simple function of inlet and outlet t 's. There are currently no published data which permit the sizing of equipment without pilot tests as recommended by the manufacturer. Three applications of Roto-Louvre dryers are outlined in Table 12-37. Installation, operating, power, and maintenance costs will be similar to those experienced with ordinary direct heat rotary dryers. Thermal efficiency will range from 30 to 70 percent.

Additional Reading

Aiken and Polsak, "A Model for Rotary Dryer Computation," in Mujumdar (ed.), *Drying '82*, Hemisphere, New York, 1982, pp. 32-35.
 Baker, "Cascading Rotary Dryers," Chap. 1 in Mujumdar (ed.), *Advances in Drying*, vol. 2, pp. 1-51, Hemisphere, New York, 1983.

Friedman and Mahall, "Studies in Rotary Drying, Part 1. Holdup and Dusting, Part 2. Heat and Mass Transfer," *Chem. Eng. Progr.*, **45**:482-493, 573-588 (1949).
 Hirose and Shinohara, "Volumetric Heat Transfer Coefficient and Pressure Drop in Rotary Dryers and Coolers," 1st Int. Symp. on Drying, **8** (1978).
 Kamke and Wilson, "Computer Simulation of a Rotary Dryer. Part 1. Retention Time, Part 2. Heat and Mass Transfer," *AIChE J.* **32**:263-275 (1986).
 Kemp, "Comparison of Particle Motion Correlations for Cascading Rotary Dryers," *Drying 2004—Proceedings of the 14th International Drying Symposium (IDS 2004)*, São Paulo, Brazil, Aug. 22-25, 2004, vol. B., pp. 790-797.
 Kemp and Oakley, "Modeling of Particulate Drying in Theory and Practice," *Drying Technol.* **20**(9):1699-1750 (2002).
 Langrish, "The Mathematical Modeling of Cascading Rotary Dryers," DPhil Thesis, University of Oxford, 1988.
 Matchett and Baker, "Particle Residence Times in Cascading Rotary Dryers. Part 1—Derivation of the Two-Stream Model," *J. Separ. Proc. Technol.* **8**: 11-17 (1987).
 Matchett and Baker, "Particle Residence Times in Cascading Rotary Dryers. Part 2—Application of the Two-Stream Model to Experimental and Industrial Data," *J. Separ. Proc. Technol.* **9**:5 (1988).
 McCormick, "Gas Velocity Effects on Heat Transfer in Direct Heat Rotary Dryers," *Chem. Eng. Progr.* **58**:57-61 (1962).
 Miller, Smith, and Schuette, "Factors Influencing the Operation of Rotary Dryers. Part 2. The Rotary Dryer as a Heat Exchanger," *Trans. AIChE* **38**: 841-864 (1942).
 Mykkestad, "Heat and Mass Transfer in Rotary Dryers," *Chem. Eng. Progr. Symp. Series* **59**:129-137 (1963).
 Papadakis et al., "Scale-up of Rotary Dryers," *Drying Technol.* **12**(1&2): 259-278 (1994).
 Ranz and Marshall, "Evaporation from Drops, Part 1," *Chem. Eng. Progr.* **48**: 123-142, 251-257 (1952).

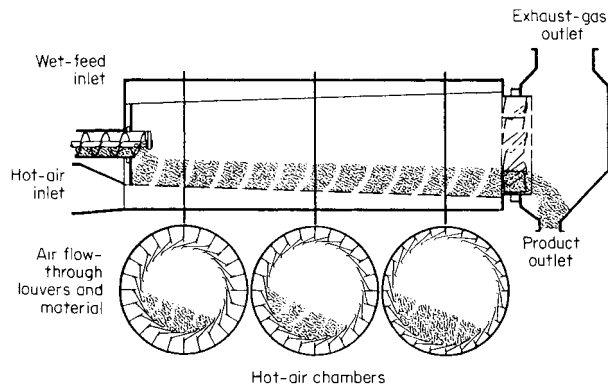


FIG. 12-63 FMC Link-Belt Roto-Louvre Dryer.

TABLE 12-37 Manufacturer's Performance Data for FMC Link-Belt Roto-Louvre Dryers*

Material dried	Ammonium sulfate	Foundry sand	Metallurgical coke
Dryer diameter	2 ft 7 in	6 ft 4 in	10 ft 3 in
Dryer length	10 ft	24 ft	30 ft
Moisture in feed, % wet basis	2.0	6.0	18.0
Moisture in product, % wet basis	0.1	0.5	0.5
Production rate, lb/h	2500	32,000	38,000
Evaporation rate, lb/h	50	2130	8110
Type of fuel	Steam	Gas	Oil
Fuel consumption	255 lb/h	4630 ft ³ /h	115 gal/h
Calorific value of fuel	837 Btu/lb	1000 Btu/ft ³	150,000 Btu/gal
Efficiency, Btu, supplied per lb evaporation	4370	2170	2135
Total power required, hp	4	41	78

*Material Handling Systems Division, FMC Corp. To convert British thermal units to kilojoules, multiply by 1.06; to convert horsepower to kilowatts, multiply by 0.746.

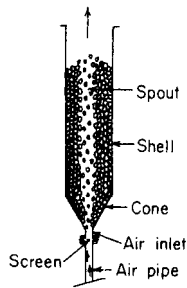


FIG. 12-64 Schematic diagram of spouted bed. [Mathur and Gishler, *Am. Inst. Chem. Eng. J.*, 1, 2, 15 (1955).]

Saeman and Mitchell, "Analysis of Rotary Dryer Performance," *Chem. Eng. Progr.* 50(9):467-475 (1954).

Schofield and Glikin, "Rotary Dryers and Coolers for Granular Fertilizers," *Trans. IChemE* 40:183-190 (1962).

Sullivan, Maier, and Ralston, "Passage of Solid Particles through Rotary Cylindrical Kilns," U.S. Bureau of Mines Tech. Paper, 384, 44 (1927).

Fluidized and Spouted Bed Dryers

Spouted Beds The spouted bed technique was developed primarily for solids which are too coarse to be handled in fluidized beds.

Although their applications overlap, the methods of gas-solids mixing are completely different. A schematic view of a spouted bed is given in Fig. 12-64. Mixing and gas-solids contacting are achieved first in a fluid "spout," flowing upward through the center of a loosely packed bed of solids. Particles are entrained by the fluid and conveyed to the top of the bed. They then flow downward in the surrounding annulus as in an ordinary gravity bed, countercurrently to gas flow. The mechanisms of gas flow and solids flow in spouted beds were first described by Mathur and Gishler [*Am. Inst. Chem. Eng. J.* 1(2):157-164 (1955)]. Drying studies have been carried out by Cowan [*Eng. J.* 41:5, 60-64 (1958)], and a theoretical equation for predicting the minimum fluid velocity necessary to initiate spouting was developed by Madonna and Lama [*Am. Inst. Chem. Eng. J.* 4(4):497 (1958)]. Investigations to determine maximum spoutable depths and to develop theoretical relationships based on vessel geometry and operating variables have been carried out by Lefroy [*Trans. Inst. Chem. Eng.* 47(5):T120-128 (1969)] and Reddy [*Can. J. Chem. Eng.* 46(5):329-334 (1968)].

Gas flow in a spouted bed is partially through the spout and partially through the annulus. About 30 percent of the gas entering the system immediately diffuses into the downward-flowing annulus. Near the top of the bed, the quantity in the annulus approaches 66 percent of the total gas flow; the gas flow through the annulus at any point in the bed equals that which would flow through a loosely packed solids bed under the same conditions of pressure drop. Solids flow in the annulus is both downward and slightly inward. As the fluid spout rises in the bed, it entrains more and more particles, losing velocity and gas into the annulus. The volume of solids displaced by the spout is roughly 6 percent of the total bed.

On the basis of experimental studies, Mathur and Gishler derived an empirical correlation to describe the minimum fluid flow necessary for spouting, in 3- to 12-in.-diameter columns:

$$u = \frac{D_p}{D_c} \left(\frac{D_o}{D_c} \right)^{0.33} \left[\frac{2gL(\rho_s - \rho_f)}{\rho_f} \right]^{0.5} \quad (12-109)$$

where u = superficial fluid velocity through the bed, ft/s; D_p = particle diameter, ft; D_c = column (or bed) diameter, ft; D_o = fluid inlet orifice diameter, ft; L = bed height, ft; ρ_s = absolute solids density, lb/ft³; ρ_f = fluid density, lb/ft³; and $g = 32.2$ ft/s², gravity acceleration.

To convert feet per second to meters per second, multiply by 0.305; to convert pounds per cubic foot to kilograms per cubic meter, multiply by 16. In SI units, $g = 9.8$ m/s². The inlet orifice diameter, air rate, bed diameter, and bed depth were all found to be critical and interdependent:

1. In a given-diameter bed, deeper beds can be spouted as the gas inlet orifice size is decreased. Using air, a 12-in.-diameter bed containing 0.125- by 0.250-in wheat can be spouted at a depth of over 100 in with a 0.8-in orifice, but at only 20 in with a 2.4-in orifice.

2. Increasing bed diameter increases spoutable depth. By employing a bed/orifice diameter ratio of 12 for air spouting, a 9-in.-diameter bed was spouted at a depth of 65 in while a 12-in.-diameter bed was spouted at 95 in.

3. As indicated by Eq. (12-109), the superficial fluid velocity required for spouting increases with bed depth and orifice diameter and decreases as the bed diameter is increased.

Employing wood chips, Cowan's drying studies indicated that the volumetric heat-transfer coefficient obtainable in a spouted bed is at least twice that in a direct heat rotary dryer. By using 20- to 30-mesh Ottawa sand, fluidized and spouted beds were compared. The volumetric coefficients in the fluid bed were 4 times those obtained in a spouted bed. Mathur dried wheat continuously in a 12-in.-diameter spouted bed, followed by a 9-in.-diameter spouted bed cooler. A drying rate of roughly 100 lb/h of water was obtained by using 450 K inlet air. Six hundred pounds per hour of wheat was reduced from 16 to 26 percent to 4 percent moisture. Evaporation occurred also in the cooler by using sensible heat present in the wheat. The maximum drying bed temperature was 118°F, and the overall thermal efficiency of the system was roughly 65 percent. Some aspects of the spouted bed technique are covered by patent (U.S. Patent 2,786,280).

Cowan reported that significant size reduction of solids occurred when cellulose acetate was dried in a spouted bed, indicating its possible limitations for handling other friable particles.

Direct Heat Vibrating Conveyor Dryers Information on vibrating conveyors and their mechanical construction is given in Sec. 19, "Solid-Solid Operations and Equipment." The vibrating conveyor dryer is a modified form of fluidized-bed equipment, in which fluidization is maintained by a combination of pneumatic and mechanical forces. The heating gas is introduced into a plenum beneath the conveying deck through ducts and flexible hose connections and passes up through a screen, perforated, or slotted conveying deck, through the fluidized bed of solids, and into an exhaust hood (Fig. 12-65). If ambient air is employed for cooling, the sides of the plenum may be open and a simple exhaust system used; however, because the gas distribution plate may be designed for several inches of water pressure drop to ensure a uniform velocity distribution through the bed of solids, a combination pressure-blower exhaust-fan system is desirable to balance the pressure above the

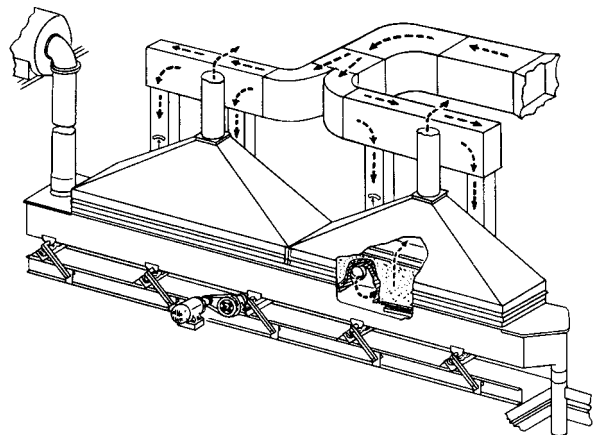


FIG. 12-65 Vibrating conveyor dryer. (Carrier Vibrating Equipment, Inc.)

TABLE 12-38 Table for Estimating Maximum Superficial Air Velocities through Vibrating-Conveyor Screens*

Mesh size	Velocity, m/s	
	2.0 specific gravity	1.0 specific gravity
200	0.22	0.13
100	0.69	0.38
50	1.4	0.89
30	2.6	1.8
20	3.2	2.5
10	6.9	4.6
5	11.4	7.9

*Carrier Vibrating Equipment, Inc.

deck with the outside atmosphere and prevent gas in-leakage or blowing at the solids feed and exit points.

Units are fabricated in widths from 0.3 to 1.5 m. Lengths are variable from 3 to 50 m; however, most commercial units will not exceed a length of 10 to 16 m per section. Power required for the vibrating drive will be approximately 0.4 kW/m² of deck.

In general, this equipment offers an economical heat-transfer area for first cost as well as operating cost. Capacity is limited primarily by the air velocity which can be used without excessive dust entrainment. Table 12-38 shows limiting air velocities suitable for various solids particles. Usually, the equipment is satisfactory for particles larger than 100 mesh in size. [The use of indirect heat conveyors eliminates the problem of dust entrainment, but capacity is limited by the heat-transfer coefficients obtainable on the deck (see Sec. 11)].

When a stationary vessel is employed for fluidization, all solids being treated must be fluidized; nonfluidizable fractions fall to the bottom of the bed and may eventually block the gas distributor. The addition of mechanical vibration to a fluidized system offers the following advantages:

1. Equipment can handle nonfluidizable solids fractions. Although these fractions may drop through the bed to the screen, directional-throw vibration will cause them to be conveyed to the discharge end of the conveyor. Prescreening or sizing of the feed is less critical than in a stationary fluidized bed.

2. Because of mechanical vibration, incipient channeling is reduced.

3. Fluidization may be accomplished with lower pressures and gas velocities. This has been evidenced on vibratory units by the fact that fluidization stops when the vibrating drive is stopped. Vibrating conveyor dryers are suitable for free-flowing solids containing mainly surface moisture. Retention is limited by conveying speeds which range from 0.02 to 0.12 m/s. Bed depth rarely exceeds 7 cm, although units are fabricated to carry 30- to 46-cm-deep beds; these also employ plate and pipe coils suspended in the bed to provide additional heat-transfer area. Vibrating dryers are not suitable for fibrous materials which mat or for sticky solids which may ball or adhere to the deck.

For estimating purposes for direct heat drying applications, it can be assumed that the average exit gas temperature leaving the solids bed will approach the final solids discharge temperature on an ordinary unit carrying a 5- to 15-cm-deep bed. Calculation of the heat load and selection of an inlet air temperature and superficial velocity (Table 12-38) will then permit approximate sizing, provided an approximation of the minimum required retention time can be made.

Vibrating conveyors employing direct contacting of solids with hot, humid air have also been used for the agglomeration of fine powders, chiefly for the preparation of agglomerated water-dispersible food products. Control of inlet air temperature and dew point permits the uniform addition of small quantities of liquids to solids by condensation on the cool incoming-particle surfaces. The wetting section of the conveyor is followed immediately by a warm-air-drying section and particle screening.

Fluidized-Bed Dryers The basic principles of fluid-bed technology are thoroughly described in Sec. 17, "Gas-Solid Operations and Equipment." Originally conceived as a heterogeneous chemical reactor, the use of this technology in connection with drying processes has increased considerably during the last several decades. The technol-

ogy offers the following advantages when compared with other drying methods:

- It has no moving parts.
- It provides rapid heat and mass exchange between gas and particles.
- It provides high heat-transfer rates between the gas/particle bed and immersed objects such as heating panels.
- It provides intensive mixing of solids, leading to homogeneous conditions and reliable control of the drying process.

The fluid-bed technology can be applied to continuous as well as batch processes.

As described in Sec. 17, the process parameter of the highest importance is the gas velocity in the fluidized bed, referred to as the fluidizing velocity or the superficial gas velocity. This velocity is of nominal character since the flow field will be disturbed and distorted by the presence of the solid phase and the turbulent fluctuations created by the gas/solid interaction.

The fluid bed consists of a layer of particles suspended partly by a bed plate with perforations or a grid and partly by the fluidizing gas flowing through the bed plate. If the gas velocity is low, the gas will merely percolate through a bed of particles that appear to be fixed. At a higher velocity the particles will start to move under influence of the aerodynamic forces, and at the point where the pressure drop reaches the equivalent of the weight per unit of area, all the particles will tend to be moving in suspension, also called the incipiently fluidized state. The particle layer behaves as a liquid, and the bed volume expands considerably. At even higher velocities the motion will be stronger, and the excess gas flow will tend to appear as bubbles. In this state the particle layer will undergo vigorous mixing, while still appearing as a dense layer of fluidlike material or a boiling liquid. If the gas velocity is further increased, the solid phase will change into a slugging mode where gas bubbles throw lumps of solid material away from the bed surface. Even further increase will result in the solid phase being entrained by the gas flow and will appear as a lean phase undergoing transport or movement by the gas phase. Most fluid-bed drying processes are adjusted to operate safely below slugging conditions. Figure 12-66 shows a view into an operating drying fluid bed.



FIG. 12-66 Fluid bed for drying in operation. (Niro A/S.)

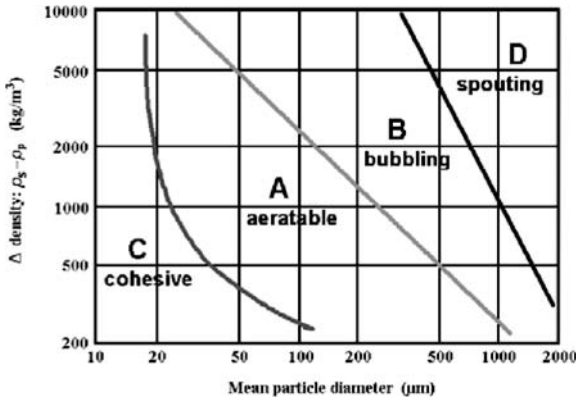


FIG. 12-67 Geldart diagram.

Proper design and operation of a fluid bed installation for drying requires consideration of several important topics. Among these are

- Ability of the material to be fluidized
- Drying characteristics of the material
- The fluidization velocity
- The design of the fluid-bed plate
- The operating conditions
- The mode of operation

Ability of the material to be fluidized has been investigated by Geldart, resulting in the well-known Geldart diagram, a version of which is shown in Fig. 12-67. The general knowledge to be derived from the Geldart diagram is that particulate material can be handled successfully in a fluid bed only if it is not too fine or too coarse. It must also have flowability. Fluid beds are best suited for particles that are regular in shape, not too sticky, and with a mean particle size between 20 μm and 10 mm. Particles of needle- or leaflike shape should be considered as nonfluidizable.

Drying characteristics of the material can be difficult to determine, but a test in a small batch fluid bed can reveal the drying curve of the material, as shown in Fig. 12-68. The drying curve clearly shows that the surface moisture is rapidly evaporated while the material is maintained at a low temperature close to the wet-bulb temperature of the drying gas. At a certain time the surface water has disappeared, and the so-called transition point has been reached. From here on the drying rate is controlled by internal diffusion inside the material, and the drying curve becomes characteristic for the individual material. While the moisture content of the material decreases, the bed temperature increases while approaching the inlet temperature of the drying air. The total drying time to reach the final moisture and the

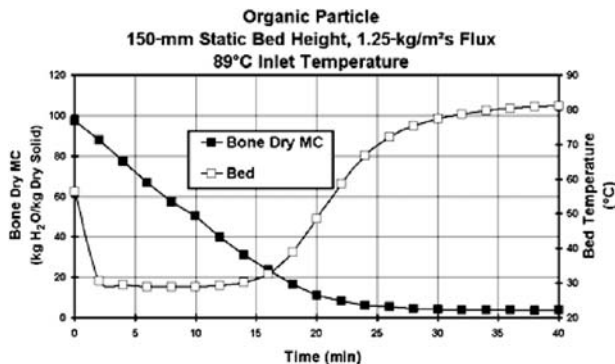


FIG. 12-68 Drying curve of organic material.

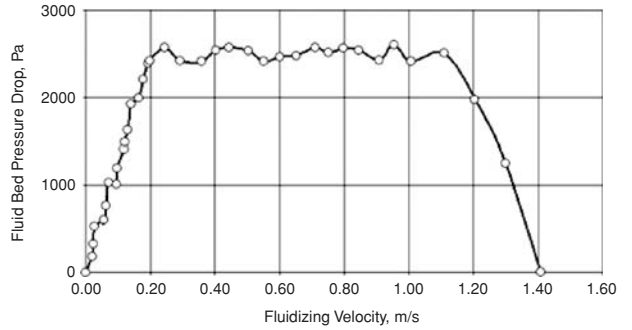


FIG. 12-69 Fluid-bed pressure drop versus fluidizing velocity. (Niro A/S.)

heat sensitivity of the material are important parameters for design of an industrial plant.

The fluidization velocity is of major importance, as indicated in the introduction. Each material will have individual requirements for the gas velocity and pressure drop to provide good fluidization. An investigation of the relationship between fluidization velocity and bed pressure drop for a given material may result in a diagram such as shown in Fig. 12-69. The results are illustrative and intended to give a clear picture of the relationship. The minimum fluidization velocity may be calculated from the Wen and Yu correlation given in Sec. 17.

At a fluidizing velocity below the value required for minimum or incipient fluidization, the pressure drop over the bed will increase proportionally with the velocity. Above a certain critical velocity, the pressure drop corresponds to the weight of the fluidized mass of material and remains roughly at this value even at higher velocities. The critical velocity for a given material may be estimated by methods mentioned in Sec. 17. At a much higher value of the fluidizing velocity, the material in the bed ceases to appear as a moving layer, and it is gradually carried away. Accordingly the pressure drop falls to zero. The fluidizing velocity value that will serve a drying task best cannot be derived exactly from the diagram. However, as a general recommendation, a value between the critical value and the value where the pressure drop falls off will be right. A first choice could be a factor of 2 to 5 times the minimum fluidization velocity. Further clarification must be derived from test work with the actual material.

The design of the fluid-bed plate is important for several reasons. First, the plate is responsible for the distribution of the drying or fluidization gas. This requires an even pattern of orifices in the plate and a sufficient pressure drop over the plate. As a general rule, the following guideline may be recommended:

$$\Delta P_{\text{plate}} = \frac{1}{2} \Delta P_{\text{powder}}$$

with the following limits: ΔP_{plate} minimum 500 Pa, ΔP_{plate} maximum 2500 Pa.

The estimation of the pressure drop in design situations may be difficult except for the case of the traditional perforated sheet with cylindrical holes perpendicular to the plane of the plate, as shown in Fig. 12-70. For this type of plate the formula of McAllister et al. may be useful. A calculation using this formula will show that a plate giving a required pressure drop of 1500 Pa and a typical fluidizing velocity of 0.35 m/s will need an open area of roughly 1 percent. Provided by a plate of 1-mm thickness and 1-mm-diameter holes, this requires approximately 12,500 holes per square meter.



FIG. 12-70 Traditional perforated plate for fluid-bed application.

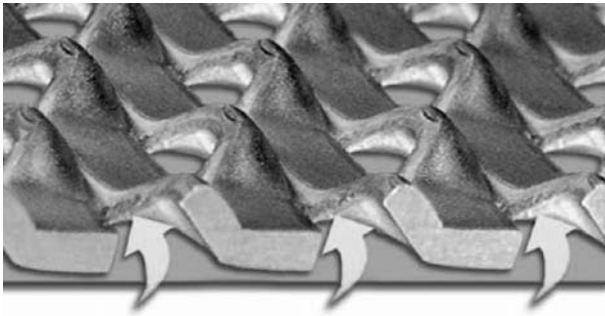


FIG. 12-71 Conidur® plate for fluid-bed application. (Hein, Lehmann Trenn- und Fördertechnik GmbH.)

However, this type of plate is being replaced in most fluid-bed applications due to its inherent disadvantages, which are caused by the difficulties of punching holes of smaller diameter than the thickness of the plate itself. The result is that the plates are weak and are prone to sifting back of the finer particles. The perpendicular flow pattern also means that the plate does not provide a transport capacity for lumps of powder along the plane of the plate.

This transport capacity is provided by plate of so-called gill types of which there are two distinct categories. One category is the type where plates are punched in a very fine regular pattern, not only to provide holes or orifices but also to deform the plate so that each orifice acquires a shape suited for acceleration of the gas flow in magnitude and direction. An example of this type is shown in Fig. 12-71, representing the Conidur® trademark.

The particular feature of Conidur® sheets is the specific hole shape which creates a directional airflow to help in discharging the product and to influence the retention time in the fluid bed. The special method of manufacturing Conidur® sheets enables finishing of fine perforations in sheets with an initial thickness many times over the hole width. Perforations of only 100 µm in an initial sheet thickness of 0.7 mm are possible. With holes this small 1 m² of plate may comprise several hundred thousand individual orifices.

The capacity of contributing to the transport of powder in the plane of the plate due to the horizontal component of the gas velocity is also the present for the second category of plates of the gill-type. Figure 12-72 shows an example.

In this type of plate, the holes or orifices are large and the number of gills per square meter is just a few thousand. The gas flow through each of the gills has a strong component parallel to the plate, providing powder transport capacity as well as a cleaning effect. The gills are punched individually or in groups and can be oriented individually to provide a possibility of articulating the horizontal transport effect.

In certain applications in the food and pharmaceutical industries, the nonsifting property of a fluid-bed plate is particularly appreciated. This property of a gill-type plate can be enhanced as illustrated in Fig. 12-73, where the hole after punching is additionally deformed so that the gill overlaps the orifice.

The fifth and final type of fluid-bed plate to be mentioned here is the so-called bubble plate type. Illustrated in Fig. 12-74, it is in principle a gill-type plate. The orifice is cut out of the plate, and the bub-



FIG. 12-72 GILL PLATE™ for fluid-bed application. (Niro A/S.)



FIG. 12-73 NON-SIFTING GILL PLATE™. (Patented by Niro A/S.)



FIG. 12-74 BUBBLE PLATE™. (Patented by Niro A/S.)

ble is subsequently pressed so that the orifice is oriented in a predominantly horizontal direction. A fluid-bed plate will typically have only 1600 holes per square meter. By this technology a combination of three key features is established. The plate is nonsifting, it has transport capacity that can be articulated through individual orientation of bubbles, and it is totally free of cracks that may compromise sanitary aspects of the installation.

The operating conditions of a fluid bed are to a high degree dictated by the properties of the material to be dried, as already indicated. One parameter can be chosen regardless of the fluidization process, namely, the fluidization air temperature. For most products, however, the temperature is of primary importance, since the fluidized state results in very high heat-transfer rates so that heat sensitivity may restrict temperature and thereby prolong process time.

To achieve the most favorable combination of conditions to carry out a fluid-bed drying process, it is necessary to consider the different modes of fluid-bed drying available.

Industrial fluid-bed drying The first major distinction between fluid-bed types is the choice of mode: batch or continuous.

Batch fluid beds may appear in several forms. The process chamber has a perforated plate or screen in the bottom and a drying gas outlet at the top, usually fitted with an internal filter. The drying gas enters the fluid bed through a plenum chamber below the perforated plate and leaves through the filter arrangement. The batch of material is enclosed in the process chamber for the duration of the process.

Figure 12-75 shows a sketch of a typical batch fluid-bed dryer as used in the food and pharmaceutical industries. The process chamber is conic in order to create a freeboard velocity in the upper part of the chamber that is lower than the fluidizing velocity just above the plate.

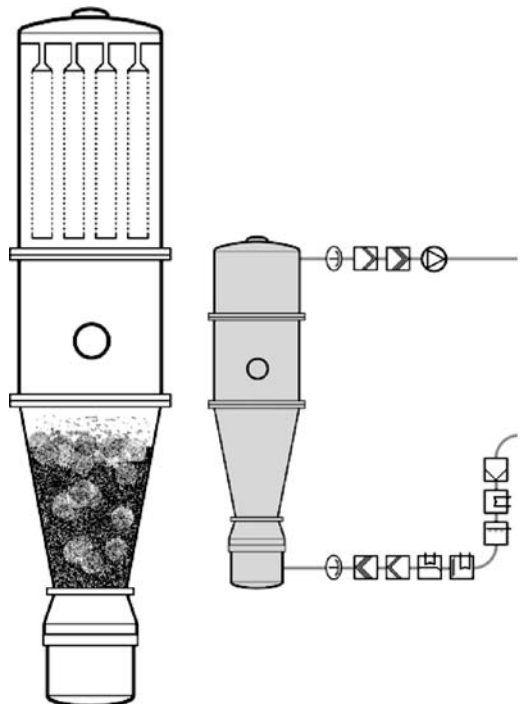


FIG. 12-75 Batch-type fluid-bed. (Aeromatic-Fielder.)

The enclosed product batch is prevented from escaping the process chamber and will therefore allow a freer choice of fluidizing velocity than is the case in a continuous fluid bed, as described later.

The right-hand side of Fig. 12-75 illustrates in symbol form the drying gas supply system comprising fan, filters of various grade, pre-heater, moisturizer, dehumidifier, final heater, and fast-closure valves. This arrangement is necessary for products with extreme quality requirements such as found in pharmaceutical production.

The drying can be carried out very like the process indicated in Fig. 12-68. The versatile drying gas supply system will allow the drying gas temperature and humidity to be controlled throughout the drying process to optimize process time and to minimize overheating of the product.

Continuous fluid beds may be even more varied than batch fluid beds. The main distinction between continuous fluid beds will be according to the solids flow pattern in the dryer. The continuous fluid bed will have an inlet point for moist granular material to be dried and an outlet for the dried material. If the moist material is immediately fluidizable, it can be introduced directly onto the plate and led through the bed in a plug-flow pattern that will enhance control of product residence time and temperature control. If the moist granular material is sticky or cohesive due to surface moisture and therefore needs a certain degree of drying before fluidization, it can be handled by a backmix fluid bed, to be described later.

Continuous plug-flow beds are designed to lead the solids flow along a distinct path through the bed. Baffles will be arranged to prevent or limit solids mixing in the horizontal direction. Thereby the residence time distribution of the solids becomes narrow. The bed may be of cylindrical or rectangular shape.

The temperature and moisture contents of the solids will vary along the path of solids through the bed and thereby enable the solids to come close to equilibrium with the drying gas. A typical plug-flow fluid bed is shown in Fig. 12-76.

Continuous plug-flow beds of stationary as well as vibrating type may benefit strongly from use of the gill-type fluid-bed plates with the capacity for controlling the movement of powder along the plate and around bends and corners created by baffles. Proper use of these means may make it possible to optimize the combination of fluidization velocity, bed layer height, and powder residence time.

Continuous backmix beds are used in particular when the moist granular material needs a certain degree of drying before it can fluidize. By distributing the material over the surface of an operating fluid bed arranged for total solids mixing, also called backmix flow, it will be absorbed by the dryer material in the bed, and lumping as well as sticking to the chamber surfaces will be avoided. The distribution of the feed can be arranged in different ways, among which a rotary thrower

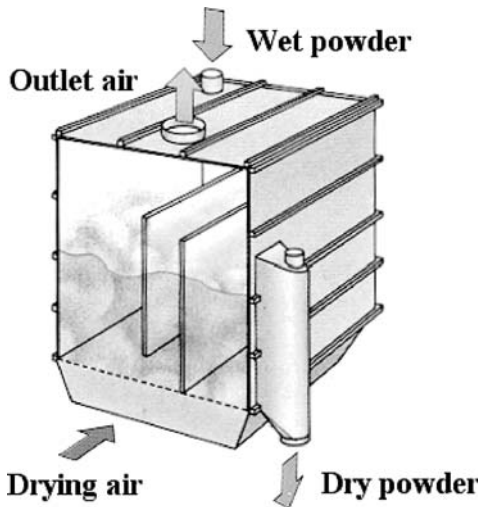


FIG. 12-76 Continuous plug-flow fluid bed. (Niro A/S.)

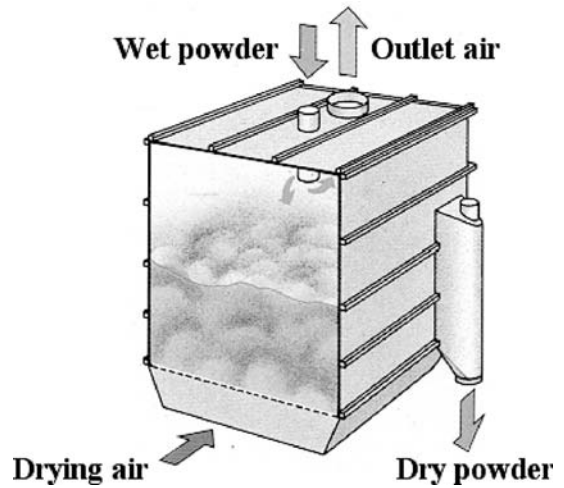


Figure 12-77 Continuous back-mix fluid bed. (Niro A/S.)

is an obvious choice. A typical backmix fluid bed is shown in Fig. 12-77. Backmix fluid beds can be of box-shaped design or cylindrical.

The whole mass of material in the backmix fluid bed will be totally mixed, and all powder particles in the bed will experience the same air temperature regardless of their position on the drying curve illustrated in Fig. 12-68. The residence time distribution becomes very wide, and part of the material may get a very long residence time while another part may get a very short time.

Continuous contact fluid beds are common in the chemical industry as the solution to the problem arising from materials requiring low fluidizing air temperature due to heat sensitivity and high energy input to complete the drying operation. An illustration of a Niro CONTACT FLUIDIZER™ is shown in Fig. 12-78.

The main feature of the contact fluid bed is the presence of heating panels, which are plate or tube structures submerged in the fluidized-bed layer and heated internally by an energy source such as steam, water, or oil. The fluidized state of the bed provides very high heat-transfer rates between the fluidizing gas, the fluidized material, and any objects submerged in the bed. The result is that a very significant portion of the required energy input can be provided by the heating panels without

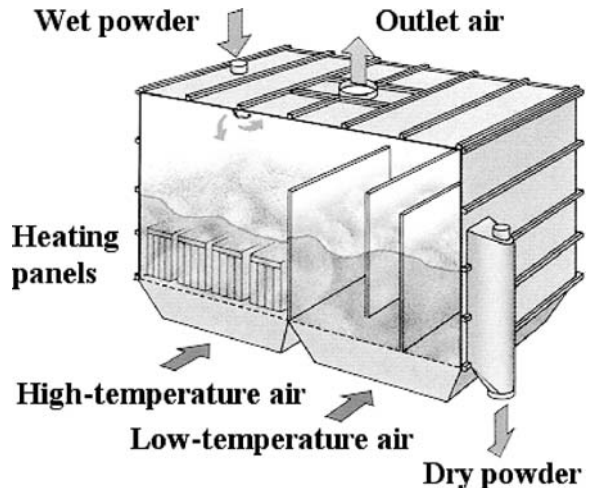


FIG. 12-78 Continuous CONTACT FLUIDIZER™. (Niro A/S.)

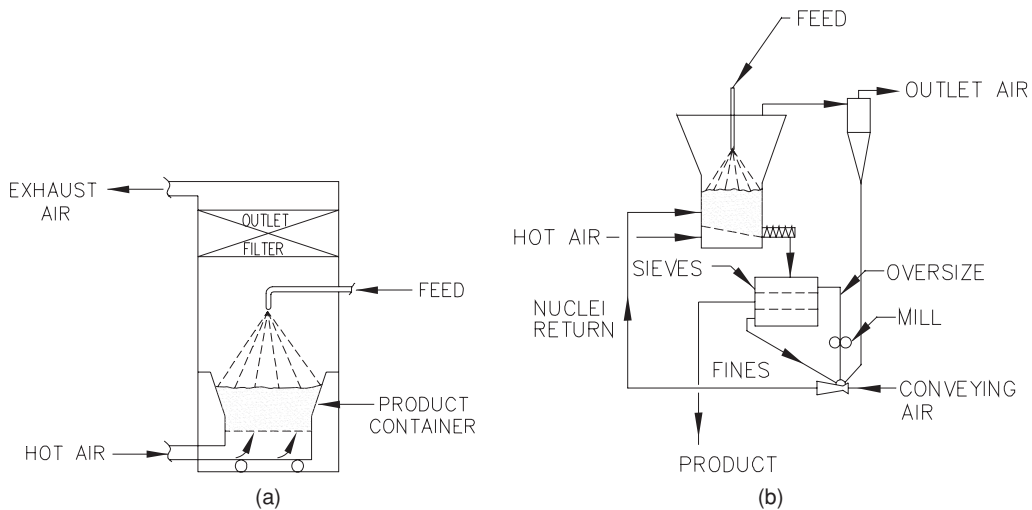


FIG. 12-79 Fluid-bed granulators. (a) Batch; (b) continuous.

risk of overheating the material. The fluidized state of the bed ensures that the material in the bed will flow with little restriction around the heating panels.

The CONTACT FLUIDIZER™ shown in Fig. 12-78 has a number of other features which in combination lead to compact design, high thermal efficiency, and low gas throughput: The first section of the bed is a backmix bed complete with rotary powder distributor and high-temperature fluidizing air supply. It takes care of the drying of the surface moisture, which is controlled mainly by heat supply. The heating panels are distributed over the whole bed volume of this section. The second section of the bed is a plug-flow bed with a fluidizing gas supply adjusted in both temperature and velocity to fit the requirements for the time-controlled diffusion drying of the powder present in this section.

The CONTACT FLUIDIZER™ is primarily used in the polymer industry for drying of polymer powders in high tonnages. Sizewise the individual units become very large, and units with a total fluid-bed area in excess of 60 m² are in operation.

Design methods for fluid beds When fluid-bed technology can be applied to drying of granular products, significant advantages compared to other drying processes can be observed. Design variables such as fluidizing velocity, critical moisture content for fluidization, and residence time required for drying to the specified residual moisture must, however, be established by experimental or pilot test before design steps can be taken. Reliable and highly integrated fluid-bed systems of either batch or continuous type can be designed, but only by using a combination of such pilot test and industrial experience. Scale-up rules are given by Kemp and Oakley (2002).

Additional Reading

- Davidson and Harrison, *Fluidized Particles*, Cambridge University Press, 1963.
 Geldart, *Powder Technol.* **6**:201–205 (1972).
 Geldart, *Powder Technol.* **7**:286–292 (1973).
 Grace, “Fluidized-Bed Hydrodynamics,” Chap. 8.1 in *Handbook of Multiphase Systems*, McGraw-Hill, New York, 1982.
 Gupta and Mujumdar, “Recent Developments in Fluidized Bed Drying,” Chap. 5 in Mujumdar (ed.), *Advances in Drying*, vol. 2, Hemisphere, Washington, D.C., 1983, p. 155.
 Kemp and Oakley, “Modeling of Particulate Drying in Theory and Practice,” *Drying Technol.* **20**(9): 1699–1750 (2002).
 McAllister et al., “Perforated-Plate Performance,” *Chem. Eng. Sci.* **9**:25–35 (1958).
 Poersch, *Aufbereitungs-Technik*, **4**: 205–218 (1983).
 Richardson, “Incipient Fluidization and Particulate Systems,” Chap. 2 in Davidson and Harrison (eds.), *Fluidization*, Academic Press, London, 1972.
 Romankows, “Drying,” Chap. 12 in Davidson and Harrison (eds.), *Fluidization*, Academic Press, London, 1972.
 Vanacek, Drbohlár, and Markvard, *Fluidized Bed Drying*, Leonard Hill, London, 1965.

Dryers with Liquid Feeds If the feed is a liquid, paste, slurry, or solution, special equipment is required. The available choices are as follows:

Spray Dryers A pumpable feed is atomized into droplets by a rotary or nozzle atomizer, as described under “Entrainment Dryers.” An integral fluid bed or belt may be added below the dryer to give longer residence time and some agglomeration. Semibatch and continuous operation is possible.

Fluidized-Bed Granulator A slurry or solution is sprayed onto a fluidized bed of particles, as shown in Fig. 12-79. The difference from the spray fluid bed is that the spray is still liquid when it contacts the particles, so that layered growth or surface agglomeration occurs, producing stronger large particles or agglomerates. Both batch and continuous forms exist (the latter involving continuous solids recycle with classification). In an older variant, the bed may be of inert balls, and the solid forming on the outside is periodically knocked off. Dryer construction and operation are largely as described under “Fluid-Bed Dryers.”

Drum (Film-Drum) Dryers A film of liquid or paste is spread onto the outer surface of a rotating, internally heated drum. Drying occurs by conduction, and at the end of the revolution the dry product, which can be in the form of powder, flakes, or chips and typically is 100 to 300 μm thick, is removed by a doctor’s knife. Drum dryers cannot handle feedstocks which do not adhere to metal, products which dry to a glazed film, or thermoplastics. The drum is heated normally by condensing steam or in vacuum drum dryers by hot water. Figure 12-80 shows three of the many possible forms. The dip feed system is the simplest and most common arrangement but is not suitable for viscous or pasty materials. The nip feed system is usually employed on double-drum dryers, especially for viscous materials, but it cannot handle lumpy or abrasive solids. The latter are usually applied by roller, and this is also effective for sticky and pasty materials. Spray and splash devices are used for feeding heat-sensitive, low-viscosity materials. Vacuum drum dryers are simply conventional units encased in a vacuum chamber with a suitable air lock for product discharge. Air impingement is also used as a secondary heat source on drum and can dryers, as shown in Fig. 12-81.

Contact Drying (Special thanks to R. B. Keey for the following example of contact drying.) In contact drying, the moist material covers a hot surface which supplies the heat required for the drying process.

Let us consider a moist material lying on a hot flat plate of infinite extent. Figure 12-82 illustrates the temperature profile for the fall in temperature from T_H in the heating fluid to T_C in the surrounding air. It is assumed that the temperatures remain steady, unhindered drying takes place, and there is no air-gap between the material being dried and the heating surface.

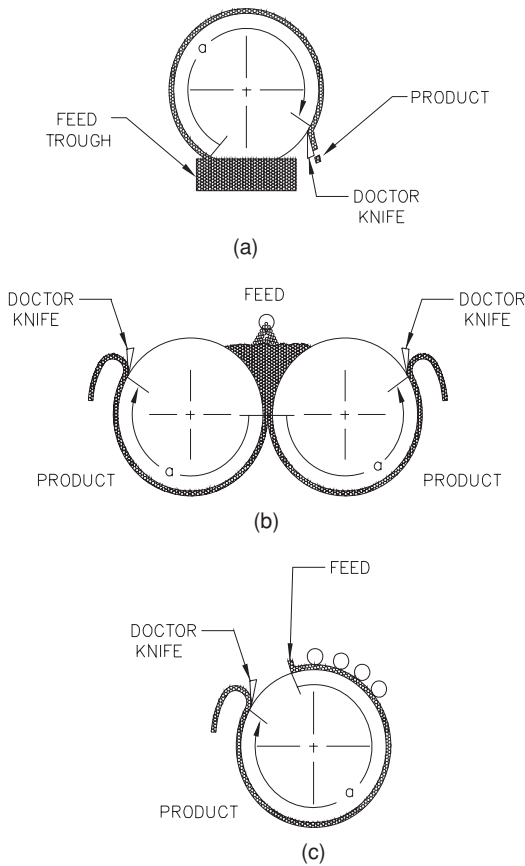


FIG. 12-80 Main types of drum dryers. (a) Dip; (b) nip; (c) roller.

The heat conducted through the wall and material is dissipated by evaporation of moisture and convection from the moist surface to the surrounding air. A heat balance yields

$$U(T_H - T_S) = N_W \Delta H_{VS} + h_C(T_S - T_C) \quad (12-110)$$

where U is the overall heat-transfer coefficient. This coefficient is found from the reciprocal law of summing resistances in series:

$$\frac{1}{U} = \frac{1}{h_H} + \frac{b_B}{\lambda_B} + \frac{b_s}{\lambda_s} \quad (12-111)$$

in which h_H is the heat-transfer coefficient for convection inside the heating fluid. If condensing steam is used, this coefficient is very large normally and the corresponding resistance $1/h_H$ is negligible. Rearrangement of Eq. (12-110) yields an expression for the maximum drying rate

$$N_W = \frac{U(T_H - T_S) - h_C(T_S - T_C)}{\Delta H_{VS}} \quad (12-112)$$

Equation (12-112), as it stands, would give an overestimate of the maximum drying rate for the case of contact drying over heated rolls, when there are significant heat losses from the ends of the drum and only part of the drum's surface can be used for drying. In the roller drying arrangements shown in Fig. 12-80, only a fraction a of the drum's periphery is available from the point of pickup to the point where the solids are peeled off.

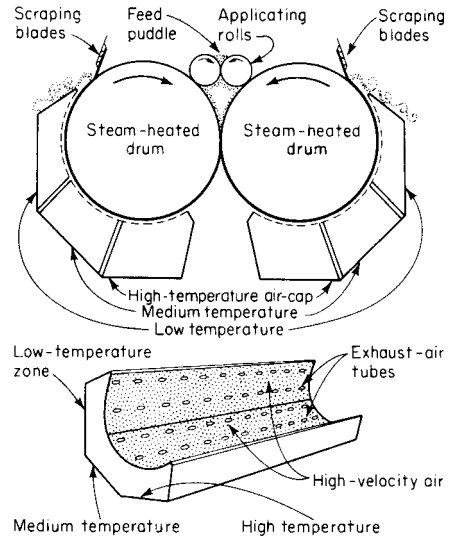


FIG. 12-81 Example of the use of air impingement in drying as a secondary heat source on a double-drum dryer (Chem. Eng., 197, June 19, 1967.)

Let q_E be the heat loss per unit area from the ends. The ratio of the end areas to cylindrical surface, from a drum of diameter D and length L , is $2(\frac{1}{4}\pi D^2)/\pi DL$ or $D/2L$. Equation (12-112) for the maximum drying rate under roller drying conditions thus becomes

$$N_W = \frac{aU(T_H - T_S) - h_C(T_S - T_C) - Dq_E/2L}{\Delta H_{VS}} \quad (12-113)$$

The total evaporation from the drum is $N_w a(\pi DL)$. Equation (12-113) could be refined further, as it neglects the effect caused by the small portion of the drum's surface being covered by the slurry in the feed trough, as well as thermal conduction through the axial shaft to the bearing mounts. The use of Eq. (12-113) to estimate the maximum drying rate is illustrated in Example 24.

Example 24: Heat-Transfer Calculations A single rotating drum of 1.250-m diameter and 3 m wide is internally heated by saturated steam at 0.27 MPa. As the drum rotates, a film of slurry 0.1 mm thick is picked up and dried. The dry product is removed by a knife, as shown in Fig. 12-80a. About three-quarters of the drum's surface is available for evaporating moisture. Estimate the maximum drying rate when the outside air temperature T_C is 15°C and the surface temperature 50°C, and compare the effectiveness of the unit with a dryer without end effects and in which all the surface could be used for drying.

Data:

- Heat-transfer coefficient h_C 50 W/(m²·K)
- Thickness of cylinder wall b_B 10 mm
- Thermal conductivity of wall λ_B 40 W/(m·K)
- Thermal conductivity of slurry film λ_s 0.10 W/(m·K)
- Film transfer coefficient for condensing steam h_H 2.5 kW/(m²·K)

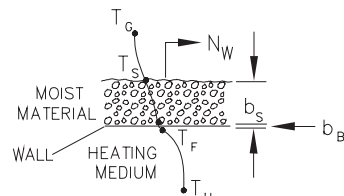


FIG. 12-82 Temperature profile in conductive drying.

Overall heat-transfer coefficient U : The thermal resistances are as follows:

Steamside $1/2.5 = 0.40 \text{ m}^2\text{K/kW}$
 Wall $0.01/0.04 = 0.25 \text{ m}^2\text{K/kW}$
 Filmside $0.0001/0.1 \times 10^{-3} = 1.0 \text{ m}^2\text{K/kW}$
 \therefore Overall resistance $= 0.40 + 0.25 + 1.0 = 1.65 \text{ m}^2\text{K/kW}$
 $U = 1/1.65 = 0.606 \text{ kW}/(\text{m}^2 \cdot \text{K})$

Wall temperature T_B : At 0.27 MPa, the steam temperature is 130°C. If it is assumed that the temperature drops between the steam and the film surface are directionally proportional to the respective thermal resistances, it follows that

$$\frac{T_H - T_B}{T_H - T_s} = \frac{0.40 + 0.25}{1.65} = 0.3939$$

$$\therefore T_B = T_H - 0.3939(T_H - T_s)$$

$$= 130 - 0.3939(130 - 50)$$

$$= 98.5^\circ\text{C}$$

Heat losses from ends q_E : For an emissivity ~ 1 and an air temperature of 15°C with a drum temperature of 98.5°C, one finds [see Eq. (12-119)],

$$q_E = 1184 \text{ W/m}^2$$

Maximum drying rate N_W : From Eq. (12-113),

$$N_W = \frac{aU(T_H - T_s) - h_c(T_s - T_G) - Dq_E/2L}{\Delta H_{VS}}$$

$$= \frac{0.75 \times 0.606(130 - 50) - 0.05(50 - 15) - (1.25 \times 1.184)/6}{2382} \quad (12-114)$$

$$= 0.0144 \text{ kg}/(\text{m}^2 \cdot \text{s})$$

The ideal maximum rate is given by Eq. (12-112) for an endless surface:

$$N_N = \frac{U(T_H - T_s) - h_c(T_s - T_G)}{\Delta H_{VS}}$$

$$= \frac{0.606(130 - 50) - 0.05(50 - 15)}{2382} \quad (12-115)$$

$$= 0.0196 \text{ kg}/(\text{m}^2 \cdot \text{s})$$

Therefore the effectiveness of the dryer is $0.0144/0.0196 = 0.735$.

The predicted thermal efficiency η is

$$\eta = 1 - \frac{h_c(T_s - T_G + Dq_E/2L)}{aU(T_H - T_s)}$$

$$= 1 - \frac{0.05(50 - 15) + (1.25 \times 1.184)/6}{0.75 \times 0.606(130 - 50)} \quad (12-116)$$

$$= 0.945$$

These estimates may be compared with the range of values found in practice, as shown in Table 12-39 (Nonhebel and Moss, *Drying of Solids in the Chemical Industry*, Butterworths, London, 1971, p. 168).

The typical performance is somewhat less than the estimated maximum evaporative capacity, although values as high as 25 g/(m²·s) have been reported. As the solids dry out, so the thermal resistance of the film increases and the evaporation falls off accordingly. Heat losses through the bearing of the drum shaft have been neglected, but the effect of radiation is accounted for in the value of h_c taken. In the case of drying organic pastes, the heat losses have been determined to be 2.5 kW/m² over the whole surface, compared with 1.75 kW/m² estimated here for the cylindrical surface. The inside surface of the drum has been assumed to be clean, and scale would reduce the heat transfer markedly.

For constant hygrothermal conditions, the base temperature T_b is directly proportional to the thickness of the material over the hot surface. When the wet-

TABLE 12-39 Operating Information

	This estimate	Typical range
Specific evaporation, g/(m ² ·s)	14.4	7-11
Thermal efficiency	0.945	0.4-0.7

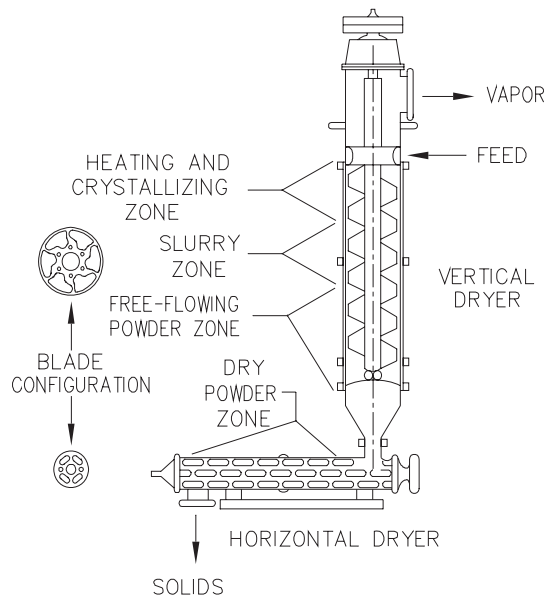


FIG. 12-83 Continuous thin-film dryer.

bulb temperature is high and the layer of material is thick enough, the temperature T_b will reach the boiling point of the moisture. Under these conditions, a mixed vapor-air layer interposes between the material and the heating surface. This is known as the Leidenfrost effect, and the phenomenon causes a greatly increased thermal resistance to heat transfer to hinder drying.

Thin-Film Dryers Evaporation and drying take place in a single unit, normally a vertical chamber with a vertical rotating agitator which almost touches the internal surface. The feed is distributed in a thin layer over the heated inner wall and may go through liquid, slurry, paste, and wet solid forms before emerging at the bottom as a dry solid. These dryers are based on wiped-film or scraped-surface (Luwa-type) evaporators and can handle viscous materials and deal with the "cohesion peak" experienced by many materials at intermediate moisture contents. They also offer good containment. Disadvantages are complexity, limited throughput, and the need for careful maintenance. Continuous or semibatch operation is possible. A typical unit is illustrated in Fig. 12-83.

Filter Dryers Basically this is a Nutsche filter (Sec. 18, "Liquid-Solid Operations and Equipment") followed by a batch dryer, usually of vertical pan type (see "Batch Agitated and Rotating Dryers" section). They are popular in the pharmaceutical and specialty chemicals industries as two unit operations are performed in the same piece of equipment without intermediate solids transfer, and containment is good.

Centrifuge Dryers Usually they are batch or continuous filtering centrifuges (Sec. 18, "Liquid-Solid Operations and Equipment") with hot air being blown over the solids in the discharge section. Manufacturers include Heinkel and Bird-Humboldt.

Pastelike feeds can be handled by some dryers for particulate materials, if either they do not require free-flowing feeds or some dry product can be backmixed with the wet feed to improve its handling.

Dryers for Films and Sheets The construction of dryers where both the feed and the product are in the form of a sheet, web, or film is markedly different from that for dryers used in handling particulate materials. The main users are the paper and textile industries. Almost invariably the material is formed into a very long sheet (often hundreds or thousands of meters long) which is dried in a continuous process. The sheet is wound onto a bobbin at the exit from the dryer; again, this may be 1 or 2 m in diameter. Alternatively, the sheet may be chopped into shorter sections.

Cylinder Dryers and Paper Machines The most common type of dryer in papermaking is the cylinder dryer (Fig. 12-84), which is a

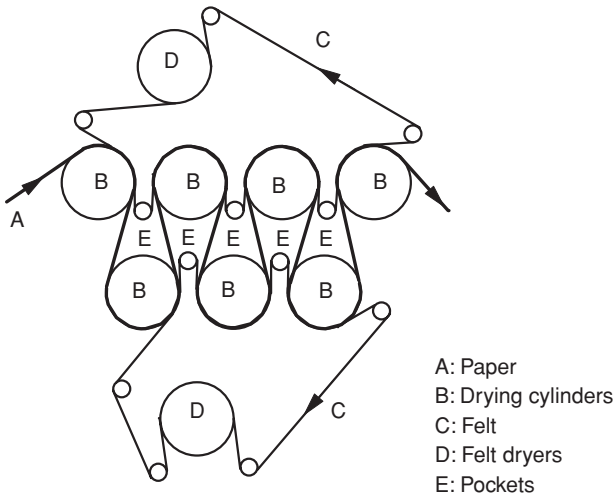


FIG. 12-84 Cylinder dryer (paper machine).

contact dryer. The paper web is taken on a convoluted path during which it wraps around the surface of cylinders which are internally heated by steam or hot water. In papermaking, the sheet must be kept taut, and a large number of cylinders are used, with only short distances between them and additional small unheated rollers to maintain the tension. Normally, a continuous sheet of felt is also used to hold the paper onto the cylinders, and this also becomes damp and is dried on a separate cylinder.

Most of the heating is conductive, through contact with the drums. However, infrared assistance is frequently used in the early stages of modern paper machines. This gets the paper sheet up to the wet-bulb temperature more rapidly, evaporates more surface moisture, and allows the number of cylinders to be reduced for a given throughput. Hot air jets (jet foil dryer) may also be used to supplement heating at the start of the machine. Infrared and dielectric heating may also be used in the later stages to assist the drying of the interior of the sheet.

Although paper is the most common application, multicylinder dryers can also be used for polymer films and other sheet-type feeds.

Convective dryers may be used as well in papermaking. In the Yankee dryer (Fig. 12-85), high-velocity hot airstreams impinging on the

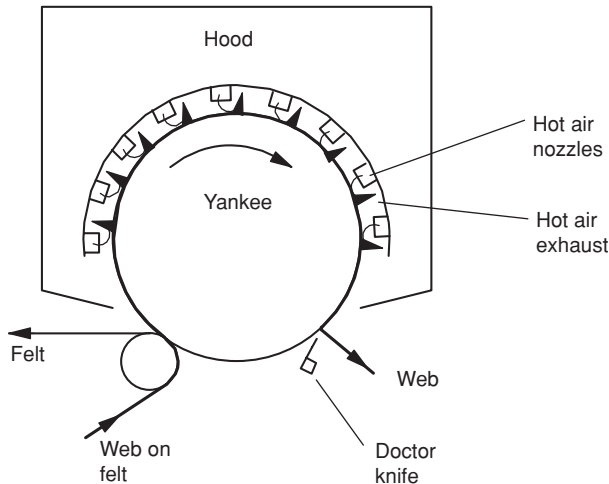


Fig. 12-85 Yankee dryer.

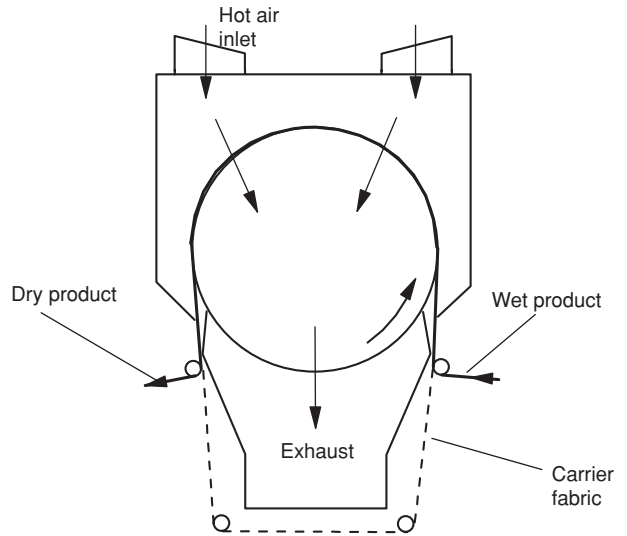


FIG. 12-86 Rotary through-dryer.

web surface give heating by cross-convection. The “Yankees” are bars holding the web in place. Normally the cylinder is also internally heated, giving additional conduction heating of the lower bed surface. In the rotary through-dryer (Fig. 12-86), the drum surface is perforated and hot air passes from the outside to the center of the drum, so that it is a through-circulation convective dryer.

Another approach to drying of sheets has been to suspend or “float” the web in a stream of hot gas, using the Coanda effect, as illustrated in Fig. 12-87. Air is blown from both sides, and the web passes through as an almost flat sheet (with a slight “ripple”). The drying time is reduced because the heat transfer from the impinging hot air jets is faster than that from stagnant hot air in a conventional oven. It is essential to control the tension of the web very accurately. The technique is particularly useful for drying coated paper, as the expansive surface coating can stick to cylinder drums.

Stenters (Tenters) and Textile Dryers These are the basic type of dryer used for sheets or webs in the textile industry. The sheet is held by its edges by clips (clip stenter) or pins (pin stenter), which not only suspend the sheet but also keep it taut and regulate its width—a vital consideration in textile drying. Drying is by convection; hot air is introduced from one or both sides, passes over the surface of the sheet, and permeates through it. Infrared panels may also be used to supply additional heat. A schematic diagram of the unit is shown in Fig. 12-88. A typical unit is 1.4 m wide and handles 2 to 4 t/h of material.

Heavy-duty textiles with thick webs may need a long residence time, and the web can be led up and down in “festoons” to reduce dryer length. Substantial improvements in drying rates have been obtained with radio-frequency heating assistance.

Air impingement dryers as in Fig. 12-87 may also be used for textiles.

Spray Dryers Spray drying is a drying process for transformation of a pumpable liquid feed in the form of a solution, dispersion, slurry, or paste into a particulate dried product in one single operation. The process comprises atomization of the feed followed by intense contact with hot air.

Due to the very large surface area created by the atomization of the feed, rapid evaporation occurs from the surface of each particle or droplet in the spray. The magnitude of the surface area can be illustrated by a simple calculation. Atomization of 1 L of water into a uniform spray of 100- μm droplets results in approximately 1.9×10^9 individual particles with a combined surface area of 60 m^2 . A realistic spray with variation of the droplet size may have a substantially higher number of droplets and a somewhat higher surface area. The dry

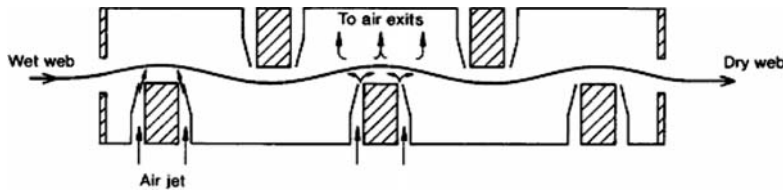


FIG. 12-87 Air flotation (impingement) dryer.

particulate product is formed while the spray droplets are still suspended in the hot drying air. The spray drying process is concluded by product recovery and separation from the drying air.

Spray drying belongs to the family of suspended particle processing (SPP) systems. Other members of this family are fluid-bed drying, flash drying, spray granulation, spray reaction, spray cooling, and spray absorption.

Drying Principles In the spray drying process or operation, the liquid to be removed by drying is predominantly water. Certain special products are produced with use of organic solvents, which are removed in a spray drying process. The drying principles involved for aqueous as well as nonaqueous systems are the same.

The liquid or moisture in a spray droplet is present in two basic forms: bound and unbound moisture. The nature of the solid and the liquid matter determines the drying characteristics of the product.

The category of bound moisture comprises water retained in small capillaries in the solid, water absorbed on solid surfaces, water bound as solutions in cells or fiber walls, and water bound as crystal water in chemical combination with the solid. Bound water exerts an equilibrium vapor pressure lower than that of pure water at the same temperature.

The category of unbound moisture can be described as the moisture in excess of the bound moisture. A hygroscopic material may contain bound as well as unbound moisture. A nonhygroscopic material contains unbound moisture only. The equilibrium vapor pressure of unbound water is equal to that of pure water at the same temperature.

The free moisture in a particle is the moisture in excess of the equilibrium moisture and may consist of unbound and some bound moisture. Only free moisture can be removed by evaporation during spray drying.

The mechanism of moisture flow in a droplet during spray drying is mainly diffusion supplemented by capillary flow. The drying characteristics of the droplet depend on the balance of bound and unbound as each category has distinct features.

The presence of unbound moisture in the droplet means that the drying proceeds at a constant high rate as long as the moisture diffusion within the droplet is able to maintain saturated surface conditions. When the diffusional and capillary flows can no longer maintain these conditions, a critical point is reached and the drying rate will decline until equilibrium moisture content is reached. The evaporation of bound moisture is strongly dependent on the nature of the solid matter in the spray droplet.

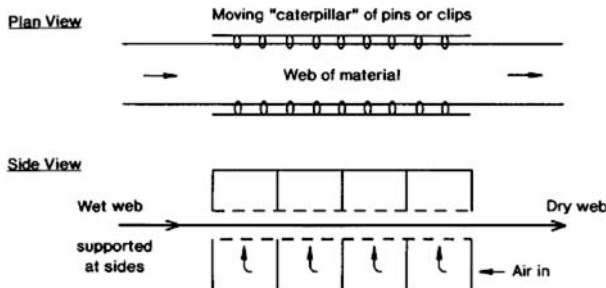


FIG. 12-88 Stenter or tenter for textile drying.

A spray drying plant comprises four process stages, as shown in Table 12-40.

Atomization Stage Spray drying is often used in industrial processes characterized by high production rates. Although the three different methods of atomization indicated in Table 12-40 are the same as those for many other atomization or spray forming processes, the relative weight of the methods is special for spray drying with rotary atomizers and hydraulic pressure nozzles having a very broad application, while two-fluid nozzles are only used to a smaller extent in specialized applications.

Rotary Atomizer Figure 12-89 shows a rotary atomizer in operation. The liquid feed is supplied to the atomizer by gravity or hydraulic pressure. A liquid distributor system leads the feed to the inner part of a rotating wheel. Since the wheel is mounted on a spindle supported by bearings in the atomizer structure, the liquid distributor is usually formed as an annular gap or a ring of holes or orifices concentric with the spindle and wheel. The liquid is forced to follow the wheel either by friction or by contact with internal vanes in the wheel. Due to the high centrifugal forces acting on the liquid, it moves rapidly toward the rim of the wheel, where it is ejected as a film or a series of jets or ligaments. By interaction with the surrounding air the liquid breaks up to form a spray of droplets of varying size. The spray pattern is virtually horizontal with a spray angle said to be 180°. The mean droplet size of the spray depends strongly on the atomizer wheel speed and to a much lesser degree on the feed rate and the feed physical properties such as viscosity. More details about spray characteristics such as droplet size distribution will be given below.

As indicated above, the atomizer wheel speed is the important parameter influencing the spray droplet size and thus the particle size of the final product. The atomizer machine will normally have the capability to operate the wheel at the required speed. More important for the atomization process is the selection of a wheel capable of handling a specific liquid feed with characteristic properties such as abrasiveness, high viscosity, nonnewtonian behavior, or tendency to coagulate.

The most common design of atomizer wheel has radial vanes, as shown in Fig.12-90. This wheel type is widely used in the chemical industry and is virtually blockage-free and simple to operate, even at very high speed. For high-capacity applications, the number and height of the vanes may be increased to maintain limited liquid film thickness conditions on each vane.

Wheels with radial vanes have one important drawback, i.e., their capacity for pumping large amounts of air through the wheel. This so-called air pumping effect causes unwanted product aeration, resulting in powders of low bulk density for some sensitive spray dried products.

TABLE 12-40 Stages of Spray Drying

Process stages of spray drying	Methods
1. Atomization	Rotary atomization Pressure nozzle atomization Two-fluid nozzle atomization
2. Spray/hot air contact	Cocurrent flow Countercurrent flow Mixed flow
3. Evaporation	Drying Particle shape formation
4. Product recovery	Drying chamber Dry collector Wet collectors



FIG. 12-89 Rotary atomizer operation. (Niro.)

Unwanted air pumping effect and product aeration can be reduced through careful wheel design involving change of the shape of the vanes that may appear as forward-curved. This wheel type is used widely in the dairy industry to produce powders of high bulk density. The powder bulk density may increase as much as 15 percent when a curved vane wheel is replacing a radial vane wheel of standard design.

Another way of reducing the air pumping effect is to reduce the space between the vanes so that the liquid feed takes up a larger fraction of the available cross-sectional area. This feature is used with consequence in the so-called bushing wheels such as shown in Fig.12-91. This wheel combines two important design aspects. The air pumping effect is reduced by reducing the flow area to a number of circular orifices, each 5 to 10 mm in diameter. By placing these orifices or nozzles in replaceable bushings or inserts made of very hard materials such as technical ceramics, i.e., alumina or silicon carbide, a substantially abrasion-resistant atomizer wheel design is achieved. This feature is very important in a number of spray drying applications with abrasive feeds, which would wear down a standard vaned wheel in a matter of hours. With an abrasion-resistant wheel, almost unlimited lifetime can be expected for the atomizer wheel structure and several thousand hours for replaceable bushings.

The rotary atomizer machines are high-speed machines traditionally built with a step-up gear to increase the speed from the 3000 or 3600 rpm of the standard two-pole electric motors to 10,000 to 20,000 rpm normally required to achieve sufficiently fine atomization. Newer designs feature high-speed electric motors with frequency control of the atomizer speed. Table 12-41 gives the main operational param-

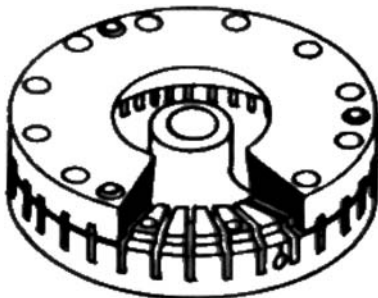


FIG. 12-90 Rotary atomizer wheel with radial vanes. (Niro.)

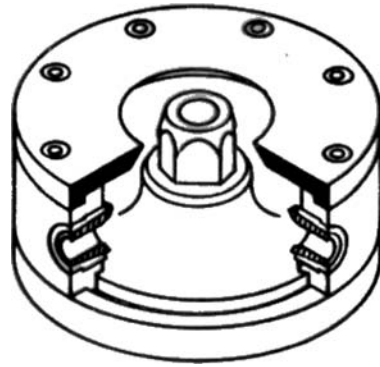


FIG. 12-91 Abrasion-resistant bushing atomizer wheel. (Niro.)

eters for three typical atomizers covering the wide range of capacity and size.

The F800 atomizer is the largest rotary atomizer offered to industry today. It has the capability of handling up to 200 t/h in one single atomizer. The capacity limit of an atomizer is normally its maximum power rating. As indicated above, the atomizer wheel speed is the important parameter influencing the spray droplet size. The wheel speed also determines the power consumption of the atomizer. It can be shown that the atomizer power consumption exclusive mechanical losses amount to

$$P_s = \frac{U^2}{3600}$$

where P_s = specific power consumption, kWh/t and U = peripheral velocity, m/s.

Since the atomizer wheel peripheral speed is proportional to the rotational speed, the maximum feed rate that can be handled by a rotary atomizer declines with the square of the rotational speed. The maximum feed rates indicated in Table 12-41 are therefore not available in the higher end of the speed ranges.

The rotary atomizer has one distinct advantage over other means of atomization. The degree or fineness of atomization achieved at a given speed is only slightly affected by changes in the feed rate. In other words, the rotary atomizer has a large turndown capability.

The larger atomizer machines cited in Table 12-41 represent a range of very large rotary atomizers available to industry. They are equipped with epicyclic-type gearboxes complete with a lubrication system. An extensive monitoring system is integrated in each machine.

Many atomization duties involve much lower capacities than foreseen for this range of atomizers. A full range of smaller rotary atomizers are available with nominal capacities down to less than 100 kg/h. Various designs may be seen with either belt drive or worm gears. Designs without gears are available with high-speed electric motor drive. Table 12-41 gives data for a smaller atomizer machine (FS1.5). It belongs to a family of high-speed machines without gears and lubrication systems capable of operating under the strictest requirements

TABLE 12-41 Operational Parameters for Atomizers (Niro)

Rotary atomizer designs				
Atomizer type		FS1.5	F160	F800
Nominal power rating	kW	1.5	160	1000
Maximum feed rate	t/h	0.3	50	200
Atomizer wheel diameter	mm	90	240	350
Typical gear ratio	#	1:1	4.4:1	2.9:1
Minimum speed	rpm	10,000	6,000	8,800
Maximum speed	rpm	30,000	18,200	11,500
Typical peripheral velocity	m/s	141	165	161
Typical specific power	kWh/t	5.5	7.6	7.2

for noncontamination of the product and in explosion-prone environments.

Hydraulic pressure nozzle In hydraulic pressure nozzle atomizers, the liquid feed is fed to the nozzle under pressure. In the nozzle orifice the pressure energy is converted to kinetic energy. The internal parts of the nozzle are normally designed to apply a certain amount of swirl to the feed flow so that it issues from the orifice as a high-speed film in the form of a cone with a desired vertex angle. This film disintegrates readily into droplets due to instability. The vertex or spray angle is normally on the order of 50° to 80°, a much narrower spray pattern than is seen with rotary atomizers. This means that spray drying chamber designs for pressure nozzle atomization differ substantially from designs used with rotary atomizers. The droplet size distribution produced by a pressure nozzle atomizer varies inversely with the pressure and to some degree with feed rate and viscosity. The capacity of a pressure nozzle varies with the square root of the pressure. To obtain a certain droplet size, the pressure nozzle must operate very close to the design pressure and feed rate. This implies that the pressure nozzle has very little turndown capability.

Hydraulic pressure nozzles cannot combine the capability for fine atomization with high feed capacity in one single unit. Many spray dryer applications, where pressure nozzles are applied, therefore require multinozzle systems with the consequence that start-up, operational control, and shutdown procedures become more complicated.

Two-fluid nozzle atomization In two-fluid nozzle atomizers, the liquid feed is fed to the nozzle under marginal or no pressure conditions. An additional flow of gas, normally air, is fed to the nozzle under pressure. Near the nozzle orifice, internally or externally, the two fluids (feed and pressurized gas) are mixed and the pressure energy is converted to kinetic energy. The flow of feed disintegrates into droplets during the interaction with the high-speed gas flow which may have sonic velocity.

The spray angle obtained with two-fluid nozzles is normally on the order of 10° to 20°, a very narrow spray pattern that is related to the spread of a free jet of gas. Spray drying chamber designs for two-fluid nozzle atomization are very specialized according to the application.

The droplet size produced by a two-fluid nozzle atomizer varies inversely with the ratio of gas to liquid and with the pressure of the atomization gas. The capacity of a two-fluid nozzle is not linked to its atomization performance. Therefore two-fluid nozzles can be attributed with some turndown capability.

Two-fluid nozzles share with pressure nozzles the lack of high feed capacity combined with fine atomization in one single unit. Many spray dryer applications with two-fluid nozzle atomization have a very high number of individual nozzles. The main advantage of two-fluid nozzles is the capability to achieve very fine atomization.

Choice of atomizer system The choice of atomizer system for a specific spray drying operation depends upon the particle size distribution required in the final dried product. It also depends upon the physical and chemical properties of the feed liquid.

In cases where the different types of atomizer means produce similar particle size distributions, the rotary atomizer may be preferred due to its greater flexibility and ease of operation. When one is comparing the atomizer types, the rotary atomizer has distinct advantages. (1) It can handle high feed rates in one single unit, (2) it can handle abrasive feeds with minimal wear, and (3) it has negligible blockage tendencies due to the large flow ports in the atomizer wheel. (4) It is a low-pressure system that can be served by a simple feed supply system, and (5) droplet size control is simple through wheel speed adjustment.

Although it lacks the flexibility of the rotary atomizer, the pressure nozzle is nevertheless widely used in spray drying applications. For many products the requirement for nondusty appearance calls for large mean particle size and lack of a fines fraction that cannot be met with a rotary atomizer. In the other end of the particle size range, some products require finer particles than are practically achievable with a rotary atomizer. This is the range where two-fluid nozzles are applied. The following guidelines may be used as an indication of the particle sizes obtainable in spray dryers:

- For spray dryers with rotary atomizer, the mean size of the dried product varies from 40 to 110 μm, although larger product mean sizes can be produced in large-diameter chambers.

- For spray dryers with pressure nozzle atomization, the mean particle size of the dried product varies in the range from 50 to 250 μm.
- For spray dryers with two-fluid nozzle atomization, the mean particle size of the dried product varies in the range from 15 to 50 μm.

The different means of atomization can also be compared in terms of energy power consumption. As indicated in Table 12-41, typical specific power figures for rotary atomizers are in the range of 5 to 11 kWh/t. Similar figures can be calculated for pressure and two-fluid nozzle systems, i.e., the pumping energy of the feed and the compression energy of the atomization gas. Any such calculation will show that similar median particle sizes are obtained for a given atomization energy independent of the means of atomization. None of the three types stand out as being energy-efficient. The hydraulic pressure nozzle is best suited for relatively coarse atomization, because pressures higher than 300 bar are impractical. Rotary atomizers are limited, because the wheel peripheral speeds required for very fine atomization put the wheel material under extreme tensile stress.

Droplet size distributions obtained with any means mentioned here are relatively well represented by a Rosin-Rammler distribution with an exponent of approximately 2. This means that approximately 80 percent of the droplet population mass is in the range of 0.39 to 1.82 times the median droplet size.

Theoretical prediction of mean particle sizes is difficult and of little practical importance, since the selection of spray drying operational parameters is based on experience and pilot-scale test work. The scientific literature, however, contains numerous estimation formulas to help predict the droplet sizes in sprays. Table 12-42 provides nomenclature for these estimation formulas.

For rotary atomizers median droplet sizes can be estimated from the following empirical equation of obscure origin:

$$d_{50} = K_r \times \dot{m}_L^{0.15} \times D^{-0.8} \times N^{-0.05} \times \omega^{-0.75} \times \mu_L^{0.07}$$

For hydraulic pressure nozzles the following formula proposed by Lefebvre may be used:

$$d_{50} = K_p \times \dot{m}_L^{0.25} \times \Delta P_L^{-0.5} \times (\sigma_L \times \mu_L)^{0.25} \times \rho_A^{-0.25}$$

Similarly, a range of equations or formulas are available for prediction of droplet size for sprays from two-fluid nozzles. The most widely cited in the literature is the Nukiyama-Tanasawa equation, which, however, is complicated and of doubtful validity at high flow rates. A much simpler equation has been proposed by Geng Wang et al.:

$$d_{50} = K_t \times \rho_A^{-0.325} \times \left(\frac{\dot{m}_L}{\dot{m}_L \times U_L + \dot{m}_A \times U_A} \right)^{0.55}$$

If any difference between the atomization means mentioned here were to be pointed out, it would be the tendency for two-fluid nozzles to have the wider particle size distribution and narrower pressure nozzles with rotary atomizers in between.

TABLE 12-42 Nomenclature for Atomization Equations

d_{50} = mass median droplet size	m
K_r = empirical factor	0.008
K_p = empirical factor	4.0
K_t = empirical factor	0.1
\dot{m}_L = liquid feed rate	kg/s
D = wheel diameter	m
N = number of vanes	#
ω = atomizer wheel speed	rad/s
μ_L = liquid viscosity	Pa · s
ΔP_L = atomization pressure	Pa
ρ_A = air density	kg/m ³
σ_L = liquid surface tension	N/m
\dot{m}_A = atomization gas rate	kg/s
U_L = liquid velocity	m/s
U_A = atomization gas velocity	m/s

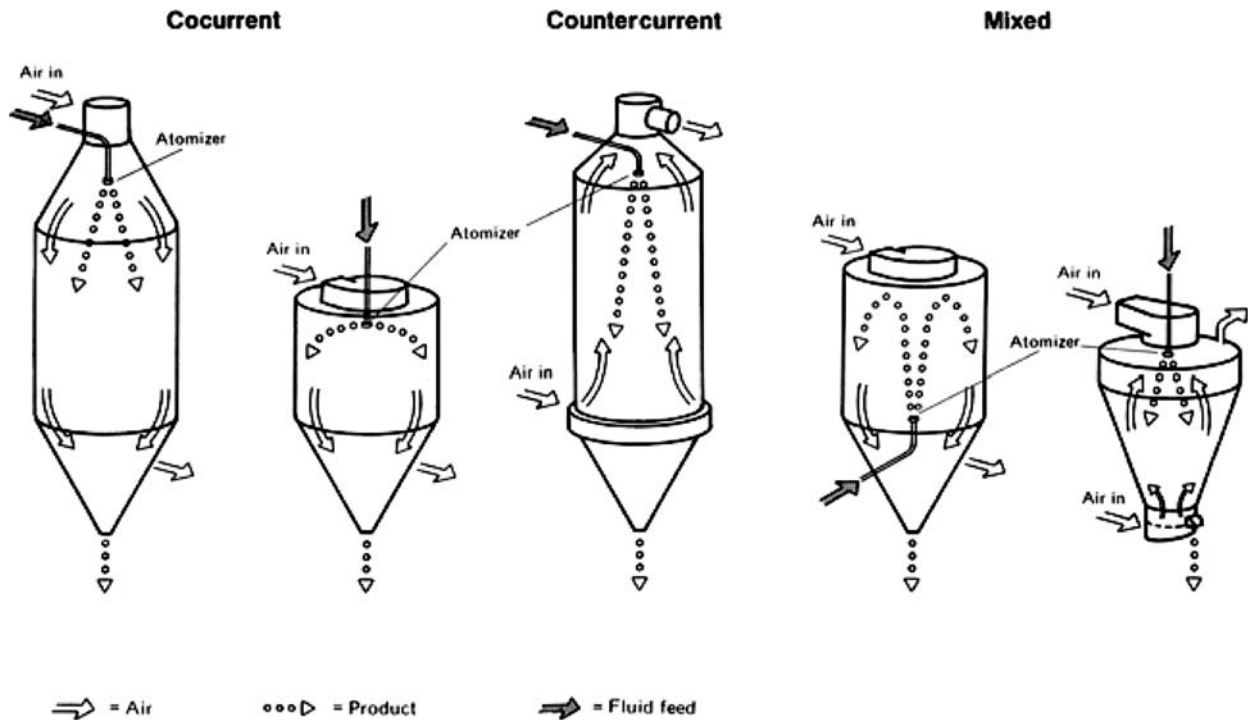


FIG. 12-92 Different forms of spray/hot air contact. (Niro.)

Spray/Hot Air Contact Atomization is first and most important process stage in spray drying. The final result of the process does, however, to a very large degree depend on the second stage, the spray/hot air contact. The way the spray of droplets is contacted by the hot air or gas carrying the thermal energy required to evaporate the moisture in the droplets is important for the quality of the product. In general terms three possible forms can be defined. These are as depicted in Fig. 12-92:

- Cocurrent flow
- Countercurrent flow
- Mixed flow

Different drying chamber forms and different methods of hot air introduction accompany the different flow pattern forms and are selected according to

- Required particle size in product specification
- Required particle form
- Temperature or heat sensitivity of the dried particle

In general terms, selection of chamber design and flow pattern form follows these guidelines:

- Use cocurrent spray drying for heat-sensitive products of fine as well as coarse particle size, where the final product temperature must be kept lower than the dryer outlet temperature.
- Use countercurrent spray drying for products which are not heat-sensitive, but may require some degree of heat treatment to obtain a special characteristic, i.e., porosity or bulk density. In this case the final powder temperature may be higher than the dryer outlet temperature.
- Use mixed-flow spray drying when a coarse product is required and the product can withstand short time exposure to heat without adverse effects on dried product quality.

Evaporation Stage Evaporation takes place from a moisture film which establishes on the droplet surface. The droplet surface temperature is kept low and close to the adiabatic saturation temper-

ature of the drying air. As the temperature of the drying air drops off and the solids content of the droplet/particle increases, the evaporation rate is reduced. The drying chamber design must provide a sufficient residence time in suspended condition for the particle to enable completion of the moisture removal.

During the evaporation stage the atomized spray droplet size distribution may undergo changes as the droplets shrink, expand, collapse, fracture, or agglomerate.

Dry Product Recovery Product recovery is the last stage of the spray drying process. Two distinct systems are used:

- In two-point discharge, primary discharge of a coarse powder fraction is achieved by gravity from the base of the drying chamber. The fine fraction is recovered by secondary equipment downstream of the chamber air exit.
- In single-point discharge, total recovery of dry product is accomplished in the dryer separation equipment.

Collection of powder from an airstream is a large subject of its own. In spray drying, dry collection of powder in a nondestructive way is achieved by use of cyclones, filters with textile bags or metallic cartridges, and electrostatic precipitators.

With the current emphasis on environmental protection, many spray dryers are equipped with additional means to collect even the finest fraction. This collection is often destructive to the powder. Equipment in use are wet scrubbers, bag or other kinds of filters, and in a few cases incinerators.

Industrial Designs and Systems Thousands of different products are processed in spray dryers representing a wide range of feed and product properties as well as drying conditions. The flexibility of the spray drying concept, which is the main reason for this wide application, is described by the following systems.

Plant Layouts Figure 12-93a shows a standard cocurrent cone-based chamber with roof gas disperser. The chamber can have either single- or two-point discharge and can be equipped with rotary or

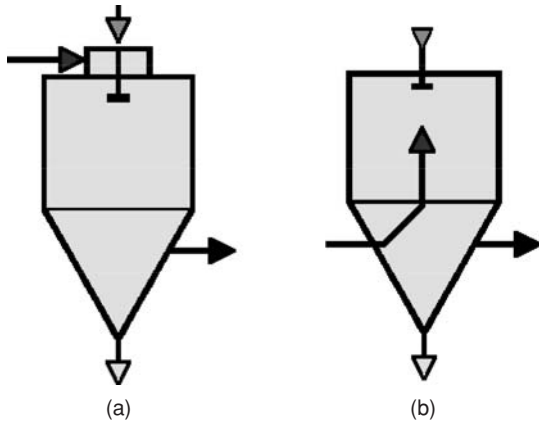


FIG. 12-93 (a) Standard cocurrent and (b) high-temperature chambers.

nozzle atomization. Fine or moderately coarse powders can be produced. This type of dryer finds application in dairy, food, chemical, pharmaceutical, agrochemical, and polymer industries.

Figure 12-93b shows a high-temperature chamber with the hot gas distributor arranged internally on the centerline of the chamber. The atomizer is rotary. Inlet temperature in the range of 600 to 1000°C can be utilized in the drying of non-heat-sensitive products in the chemical and mining industries. Kaolin and mineral flotation concentrates are typical examples.

Figure 12-94a shows a cocurrent cone-based tall form chamber with roof gas disperser. This chamber design is used primarily with pressure nozzle atomization to produce powders of large particle sizes with a minimum of agglomeration. The chamber can be equipped with an oversize cone section to maximize powder discharge from the chamber bottom. This type of dryer is used for dyestuffs, baby foods, detergents, and instant coffee powder.

Figure 12-94b shows a countercurrent flow chamber with pressure nozzle atomization. This design is in limited use because it cannot produce heat-sensitive products. Detergent powder is the main application.

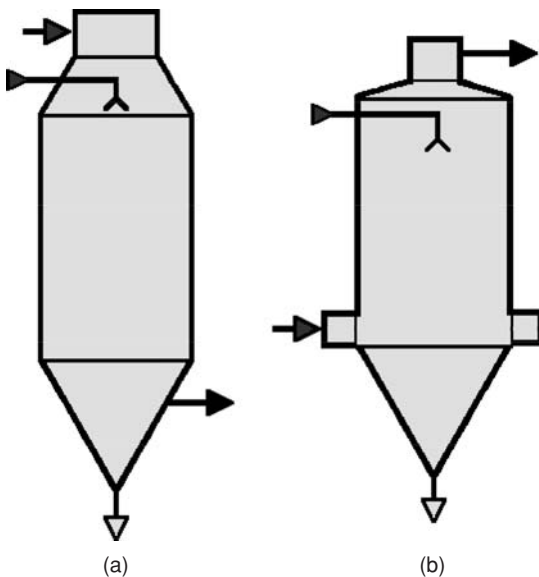


FIG. 12-94 Tall form: (a) cocurrent and (b) countercurrent chambers.

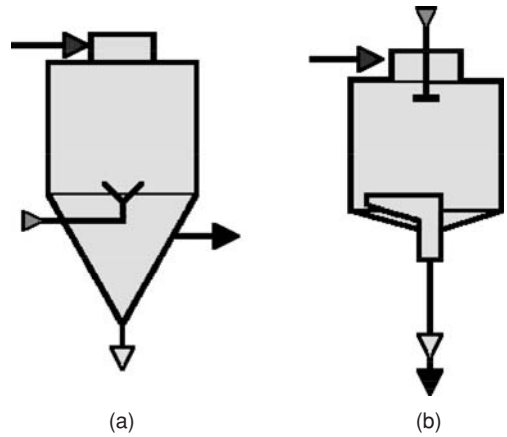


FIG. 12-95 (a) Mixed-flow and (b) flat chambers.

Figure 12-95a shows a mixed-flow chamber with pressure nozzle atomization arranged in so-called fountain mode. This design is ideal for producing a coarse product in a limited-size low-cost drying chamber. This type of dryer is used extensively for ceramic products. Figure 12-95b shows a flat-based cocurrent chamber as used with limited building height. Powder removal requires a sweeping suction device. One of few advantages is ease of access for manual cleaning. These are widely used in production of flavoring materials.

Figure 12-96a shows an integrated fluid-bed chamber which represents the latest development in spray dryer design. The final stage of the drying process is accomplished in a fluid bed located in the lower cone of the chamber. This type of operation allows lower outlet temperatures to be used, leading to fewer temperature effects on the powder and higher energy efficiency. Figure 12-96b shows an integrated belt chamber where product is sprayed onto a moving belt, which also acts as the air exhaust filter. It is highly suitable for slowly crystallizing and high-fat products. Previous operational difficulties derived from hygienic problems on the belt have been overcome, and the integrated belt dryer is now moving the limits of products that can be dried by spray drying.

Atomization/Gas Disperser Arrangement Some of the above-mentioned layouts allow a choice of atomization means while others are restricted to a particular choice. The arrangement of the gas distributor means will be closely related to the choice of atomizer. A

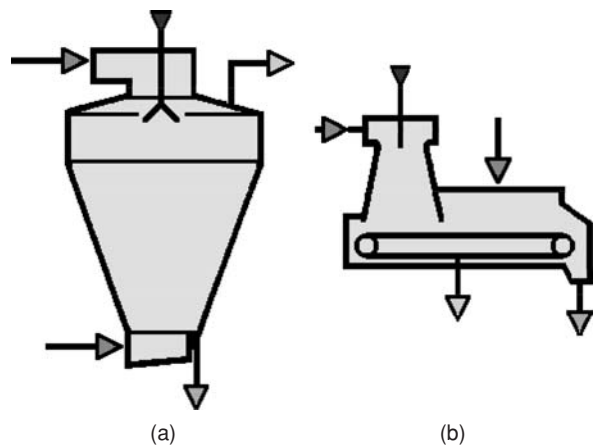


FIG. 12-96 (a) Integrated fluid-bed and (b) belt designs.

rotary atomizer will generally be arranged in a roof gas disperser as suited for the chambers in Figs. 12-93 and 12-95. The hot gas or air enters through a scroll-shaped housing which distributes the air evenly into an annular gap entry with adjustable guide vanes. The geometry and adjustment of the entry gap may determine the success of the drying process. Figure 12-95b shows an alternative arrangement of a rotary atomizer with a central gas disperser such as suited for the high-temperature spray dryer layout.

Hot Air Supply System All the above-mentioned chamber layouts can be used in open-cycle, partial recycle, or closed-cycle layouts. The selection is based on the needs of operation, feed, and powder specification and on environmental considerations.

An open-cycle layout is by far the most common in industrial spray drying. The open layout involves intake of drying air from the atmosphere and discharge of exhaust air to the atmosphere. Drying air can be supplemented by a waste heat source to reduce overall fuel consumption. The heater may be direct, i.e., natural gas burner, or indirect by steam-heated heat exchanger.

A closed-cycle layout is used for drying inflammable or toxic solvent feedstocks. The closed-cycle layout ensures complete solvent recovery and prevents explosion and fire risks. The reason for the use of a solvent system is often to avoid oxidation/degradation of the dried product. Consequently closed-cycle plants are gastight installations operating with an inert drying medium, usually nitrogen. These plants operate at a slight gauge pressure to prevent inward leakage of air.

Partial recycle is used in a plant type applied for products of moderate sensitivity toward oxygen. The atmospheric drying air is heated in a direct fuel-burning heater. Part of the exhaust air, depleted of its oxygen content by the combustion, is condensed in a condenser and recycled to the heater. This type of plant is also designated self-inertizing.

Industrial Applications As mentioned above, thousands of products are spray dried. The most common products may be classified as follows:

- Agrochemicals
- Catalysts
- Ceramics
- Chemicals
- Dyestuffs
- Foodstuffs
- Pharmaceuticals

Table 12-43 shows some of the operational parameters associated with specific and typical products. For each of these product groups and any other product, successful drying depends on the proper selection of a plant concept and proper selection of operational parameters, in particular inlet and outlet temperatures and the atomization method. These parameters are traditionally established through pilot-scale test work, and leading suppliers on the spray drying market often have extensive test stations to support their sales efforts.

Table 12-43 shows the variety of process parameters used in practical applications of spray drying. The air temperatures are traditionally established through experiments and test work. The inlet temperatures reflect the heat sensitivity of the different products, and the outlet temperatures the willingness of the products to release moisture. The percent water in feed parameter is an indication of feed viscosity

and other properties that influence the pumpability and behavior under atomization of the individual feeds.

As a consequence, the amount of drying air or gas required for drying one unit of feed or product varies considerably. Table 12-43 shows for the individual products the ratio of drying gas to evaporation as well as the ratio of drying gas to product on a mass basis. The calculation behind the table neglects the variation of thermodynamic properties with temperature and the variation of residual moisture in each product.

A quick scoping estimate of the size of an industrial spray dryer can be made on this basis. The required evaporation rate or product rate can be multiplied by the relevant ratio from the table to give the mass flow rate of the drying gas. The next step would be to calculate the size of a spray drying chamber to allow the drying gas at outlet conditions approximately 25 s of residence time. A cylindrical chamber with diameter *D* and height *H* equal to *D* and a 60° conical bottom has a nominal volume of

$$V_{\text{chamber}} = \frac{\pi}{4} D^3 \times \left(H + \frac{\sqrt{3}}{2} D \right) = 1.47 \times D^3$$

Accordingly a zinc sulfate spray dryer with a drying capacity of 2 t/h would require a drying gas flow rate of approximately 8.45 kg/s. With an outlet gas density of 0.89 kg/m³ and the above-mentioned gas residence time, this results in a required chamber volume of

$$V_{\text{chamber}} = 8.44 \text{ kg/s} / 0.89 \text{ kg/m}^3 \times 25 \text{ s} = 237 \text{ m}^3$$

The chamber size now becomes

$$D = \sqrt[3]{\frac{237}{1.47}} = 5.5 \text{ m}$$

A similar calculation for the other products based on a powder capacity of 2 t/h would reveal a variation of gas flow rates from 8.4 to 114 kg/s and chamber diameters from 5.5 to 12.7 m.

The selection of the plant concept involves the drying modes illustrated in Figs. 12-93 through 12-96. For different products a range of plant concepts are available to secure successful drying at the lowest cost. Three different concepts are illustrated in Figs. 12-97, 12-98, and 12-99.

Figure 12-97 shows a traditional spray dryer layout with a cone-based chamber and roof gas disperser. The chamber has two-point discharge and rotary atomization. The powder leaving the chamber bottom as well as the fines collected by the cyclone is conveyed pneumatically to a conveying cyclone from where the product discharges. A bag filter serves as the common air pollution control system.

Figure 12-98 shows closed-cycle spray dryer layout used to dry certain products with a nonaqueous solvent in an inert gas flow. The background for this may be product sensitivity to water and oxygen or severe explosion risk. Typical products can be tungsten carbide or pharmaceuticals.

Figure 12-99 shows an integrated fluid-bed chamber layout of the type used to produce agglomerated product. The drying process is accomplished in several stages, the first being a spray dryer with atomization. The second stage is an integrated static fluid bed located in the lower cone of the chamber. The final stages are completed in external

TABLE 12-43 Some Products That Have Been Successfully Spray Dried

Product	Air temperature, K		Water in feed, %	Air/evap. ratio, kg/kg	Air/prod. ratio, kg/kg	Product	Air temperature, K		Water in feed, %	Air/evap. ratio, kg/kg	Air/prod. ratio, kg/kg
	In	Out					In	Out			
Animal blood	440	345	65	27.6	51.3	Detergent A	505	395	50	25.4	25.4
Yeast	500	335	86	15.7	96.2	Detergent B	510	390	63	22.8	38.8
Zinc sulfate	600	380	55	12.4	15.2	Detergent C	505	395	40	25.8	17.2
Lignin	475	365	63	24.3	41.4	Manganese sulfate	590	415	50	16.3	16.3
Aluminum hydroxide	590	325	93	9.7	128.4	Aluminum sulfate	415	350	70	40.5	94.4
Silica gel	590	350	95	10.9	206.5	Urea resin A	535	355	60	14.8	22.1
Magnesium carbonate	590	320	92	9.5	108.7	Urea resin B	505	360	70	18.3	42.7
Tanning extract	440	340	46	26.4	22.5	Sodium sulfide	500	340	50	16.5	16.5
Coffee extract	420	355	70	40.6	94.8	Pigment	515	335	73	14.4	39.0

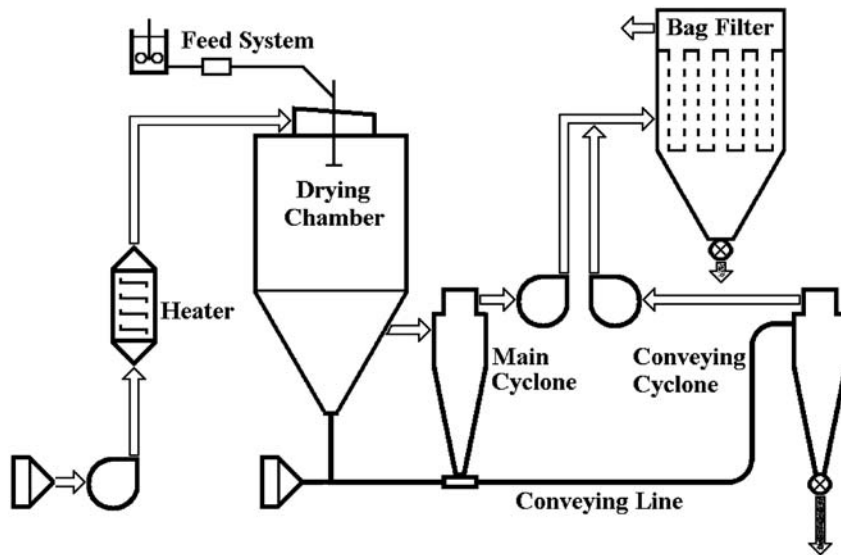


FIG. 12-97 Spray dryer with rotary atomizer and pneumatic powder conveying. (Niro.)

fluid beds of the vibrating type. This type of operation allows lower outlet temperatures to be used, leading to fewer temperature effects on the powder and higher energy efficiency. The chamber has a mixed-flow concept with air entering and exiting at the top of the chamber. This chamber is ideal for heat-sensitive, sticky products. It can be used with pressure nozzle as well as rotary atomization. An important feature is the return of fine particles to the chamber to enhance the agglomeration effect. Many products have been made feasible for spray drying by the development of this concept, which was initially aimed at the food and dairy industry. Recent applications have, however, included dyestuffs, agrochemicals, polymers, and detergents.

Additional Reading

Bayvel and Orzechowski, *Liquid Atomization*, Taylor & Francis, New York, 1993.
 Geng Wang et al., "An Experimental Investigation of Air-Assist Non-Swirl Atomizer Sprays," *Atomisation and Spray Technol.* 3:13-36 (1987).

Lefebvre, *Atomization and Sprays*, Hemisphere, New York, 1989.
 Marshall, "Atomization and Spray Drying," *Chem. Eng. Prog. Mng. Series* 50(2) (1954).
 Masters, *Spray Drying in Practice*, SprayDryConsult International ApS, Denmark, 2002.
 Walzel, "Zerstäuben von Flüssigkeiten," *Chem.-Ing.-Tech.* 62 (1990) Nr. 12, S. 983-994.

Pneumatic Conveying Dryers A gas-solids contacting operation in which the solids phase exists in a dilute condition is termed a *dispersion system*. It is often called a pneumatic system because, in most cases, the quantity and velocity of the gas are sufficient to lift and convey the solids against the forces of gravity and friction. (These systems are sometimes incorrectly called flash dryers when in fact the moisture is not actually "flashed" off. True flash dryers are sometimes used for soap drying to describe moisture removal when pressure is

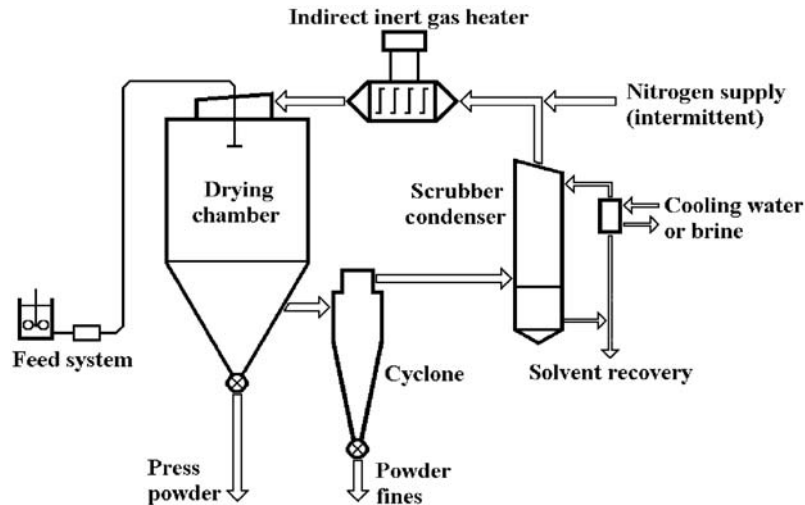


FIG. 12-98 Spray dryer with rotary atomizer and closed-cycle layout. (Niro.)

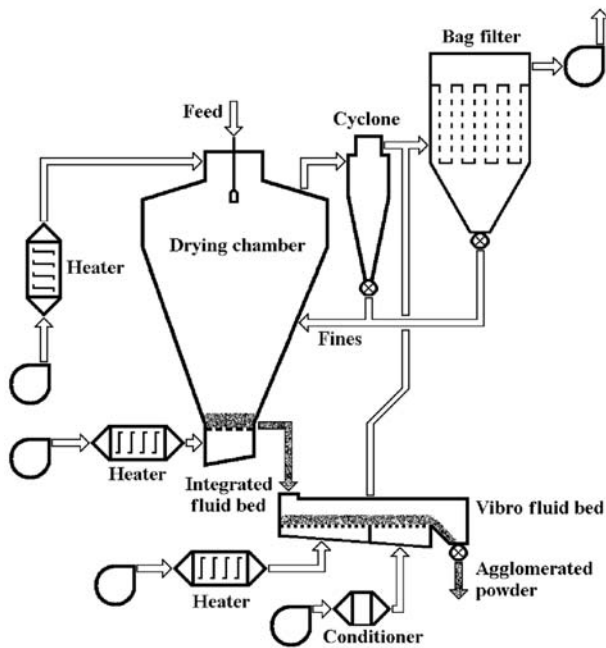


FIG. 12-99 Spray dryer with nozzle atomizer and integrated fluid bed. (Niro.)

quickly reduced.) Pneumatic systems may be distinguished by two characteristics:

1. Retention of a given solids particle in the system is on the average very short, usually no more than a few seconds. This means that any process conducted in a pneumatic system cannot be diffusion-controlled. The reaction must be mainly a surface phenomenon, or the solids particles must be so small that heat transfer and mass transfer from the interiors are essentially instantaneous.

2. On an energy-content basis, the system is balanced at all times; i.e., there is sufficient energy in the gas (or solids) present in the system at any time to complete the work on all the solids (or gas) present at the same time. This is significant in that there is no lag in response to control changes or in starting up and shutting down the system; no partially processed residual solids or gas need be retained between runs.

It is for these reasons that pneumatic equipment is especially suitable for processing heat-sensitive, easily oxidized, explosive, or flammable materials which cannot be exposed to process conditions for extended periods.

Gas flow and solids flow are usually cocurrent, one exception being a countercurrent flow spray dryer. The method of gas-solids contacting is best described as through-circulation; however, in the dilute condition, solids particles are so widely dispersed in the gas that they exhibit apparently no effect upon one another, and they offer essentially no resistance to the passage of gas among them.

Pneumatic Conveyor Dryers Pneumatic conveyor dryers, often also referred to as flash dryers, comprise a long tube or duct carrying a gas at high velocity, a fan to propel the gas, a suitable feeder for addition and dispersion of particulate solids in the gas stream, and a cyclone collector or other separation equipment for final recovery of solids from the gas.

The solids feeder may be of any type: Screw feeders, venturi sections, high-speed grinders, and dispersion mills are employed. For pneumatic conveyors, selection of the correct feeder to obtain thorough initial dispersion of solids in the gas is of major importance. For example, by employing an air-swept hammer mill in a drying operation, 65 to 95 percent of the total heat may be transferred within the mill itself if all the drying gas is passed through it. Fans may be of the

induced-draft or the forced-draft type. The former is usually preferred because the system can then be operated under a slight negative pressure. Dust and hot gas will not be blown out through leaks in the equipment. Cyclone separators are preferred for low investment. If maximum recovery of dust or noxious fumes is required, the cyclone may be followed by a wet scrubber or bag collector.

In ordinary heating and cooling operations, during which there is no moisture pickup, continuous recirculation of the conveying gas is frequently employed. Also, solvent recovery operations employing continuously recirculated inert gas with intercondensers and gas reheaters are carried out in pneumatic conveyors.

Pneumatic conveyors are suitable for materials which are granular and free-flowing when dispersed in the gas stream, so they do not stick on the conveyor walls or agglomerate. Sticky materials such as filter cakes may be dispersed and partially dried by an air-swept disintegrator in many cases. Otherwise, dry product may be recycled and mixed with fresh feed, and then the two dispersed together in a disintegrator. Coarse material containing internal moisture may be subjected to fine grinding in a hammer mill. The main requirement in all applications is that the operation be instantaneously completed; internal diffusion of moisture must not be limiting in drying operations, and particle sizes must be small enough that the thermal conductivity of the solids does not control during heating and cooling operations. Pneumatic conveyors are rarely suitable for abrasive solids. Pneumatic conveying can result in significant particle size reduction, particularly when crystalline or other friable materials are being handled. This may or may not be desirable but must be recognized if the system is selected. The action is similar to that of a fluid-energy grinder.

Pneumatic conveyors may be single-stage or multistage. The former is employed for evaporation of small quantities of surface moisture. Multistage installations are used for difficult drying processes, e.g., drying heat-sensitive products containing large quantities of moisture and drying materials initially containing internal as well as surface moisture.

Typical single- and two-stage drying systems are illustrated in Figs. 12-100, 12-101, and 12-102. Figure 12-100 illustrates the flow diagram of a single-stage dryer with a paddle mixer, a screw conveyor followed by a rotary disperser for introduction of the feed into the airstream at the throat of a venturi section. The drying takes place in the drying column after which the dry product is collected in a cyclone. A diverter introduces the option of recycling part of the product into the mixer in order to handle somewhat sticky products. The environmental requirements are met with a wet scrubber in the exhaust stream.

Figure 12-101 illustrates a two-stage dryer where the initial feed material is dried in a flash dryer by using the spent drying air from the second stage. This semidried product is then introduced into the second-stage flash dryer for contact with the hottest air. This concept is in use in the pulp and paper industry. Its use is limited to materials that are dry enough on the surface after the first-stage to avoid plugging of the first-stage cyclone. The main advantage of the two-stage concept is the heat economy which is improved considerably over that of the single-stage concept.

Figure 12-102 is an elevation view of an actual single-stage dryer, employing an integral coarse-fraction classifier, used to separate undried particles for recycle.

Several typical products dried in pneumatic conveyors are described in Table 12-44.

Design methods for pneumatic conveyor dryers Depending upon the temperature sensitivity of the product, inlet air temperatures between 125 and 750°C are employed. With a heat-sensitive solid, a high initial moisture content should permit use of a high inlet air temperature. Evaporation of surface moisture takes place at essentially the wet-bulb air temperature. Until this has been completed, by which time the air will have cooled significantly, the surface-moisture film prevents the solids temperature from exceeding the wet-bulb temperature of the air. Pneumatic conveyors are used for solids having initial moisture contents ranging from 3 to 90 percent, wet basis. The air quantity required and solids-to-gas loading are fixed by the moisture load, the inlet air temperature, and, frequently, the exit air humidity. If the last is too great to permit complete drying, i.e., if the

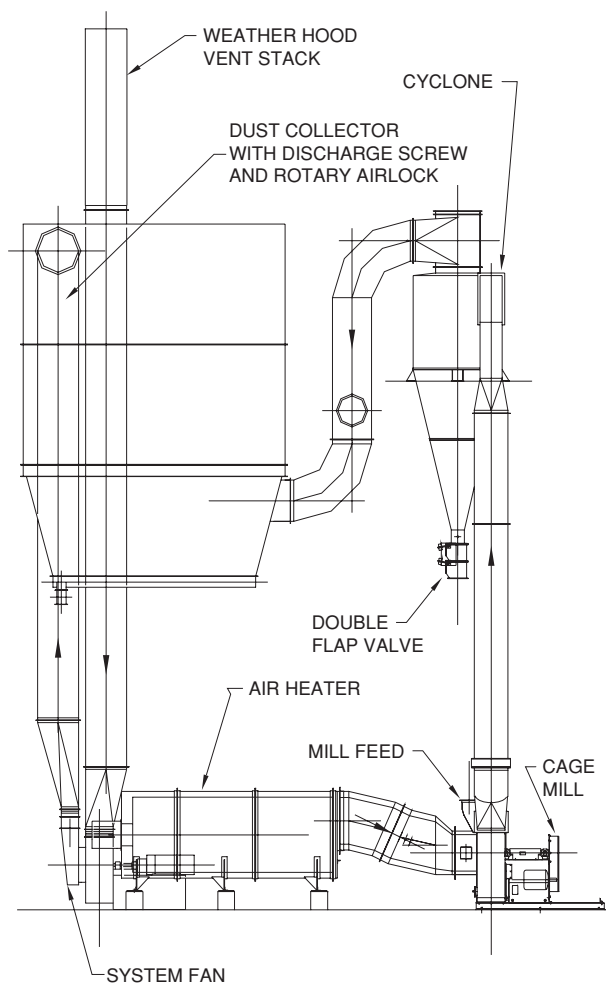


FIG. 12-100 Flow diagram of single-stage flash dryer. (Air Preheater Company, Raymond® & Bartlett Snow™ Products.)

exit air humidity is above that in equilibrium with the product at required dryness, then the solids/gas ratio must be reduced together with the inlet air temperature.

The gas velocity in the conveying duct must be sufficient to convey the largest particle. This may be calculated accurately by methods given in Sec. 17, "Gas-Solids Operations and Equipment." For estimating purposes, a velocity of 25 m/s, calculated at the exit air temperature, is frequently employed. If mainly surface moisture is present, the temperature driving force for drying will approach the log mean of the inlet and exit gas wet-bulb depressions. (The exit solids temperature will approach the exit gas dry-bulb temperature.)

Observation of operating conveyors indicates that the solids are rarely uniformly dispersed in the gas phase. With infrequent exceptions, the particles move in a streaklike pattern, following a streamline along the duct wall where the flow velocity is at a minimum. Complete or even partial diffusion in the gas phase is rarely experienced even with low-specific-gravity particles. Air velocities may approach 20 to 30 m/s. It is doubtful, however, that even finer and lighter materials reach more than 80 percent of this speed, while heavier and larger fractions may travel at much slower rates [Fischer, *Mech. Eng.*, 81(11): 67-69 (1959)]. Very little information and few operating data

on pneumatic conveyor dryers which would permit a true theoretical basis for design have been published.

Therefore, firm design always requires pilot tests. It is believed, however, that the significant velocity effect in a pneumatic conveyor is the difference in velocities between gas and solids, which is strongly linked to heat- and mass-transfer coefficients and is the reason why a major part of the total drying actually occurs in the feed input section.

For estimating purposes, the conveyor cross-section is fixed by the assumed air velocity and quantity. The standard scoping design method is used, obtaining the required gas flow rate from a heat and mass balance, and the duct cross-sectional area and diameter from the gas velocity (if unknown, a typical value is 20 m/s). An incremental mode may be used to predict drying conditions along the duct. However, several parameters are hard to obtain, and conditions change rapidly near the feed point. Hence, for reliable estimates of drying time and duct length, pilot-plant tests should always be used. A conveyor length larger than 50 diameters is rarely required. The length of the full-scale dryer should always be somewhat larger than required in pilot-plant tests, because wall effects are higher in small-diameter ducts. This gives greater relative velocity (and thus higher heat transfer) and lower particle velocity in the pilot-plant dryer, both effects giving a shorter length than the full-scale dryer for a given amount of drying. If desired, the length difference on scale-up can be predicted by using the incremental model and using the pilot-plant data to back-calculate the uncertain parameters; see Kemp, *Drying Technol.* 12(1&2):279 (1994) and Kemp and Oakley (2002).

An alternative method of estimating dryer size very roughly is to estimate a volumetric heat-transfer coefficient [typical values are around 2000 J/(m³·s·K)] and thus calculate dryer volume.

Pressure drop in the system may be computed by methods described in Sec. 6, "Fluid and Particle Dynamics." To prevent excessive leakage into or out of the system, which may have a total pressure drop of 2000 to 4000 Pa, rotary air locks or screw feeders are employed at the solids inlet and discharge.

The conveyor and collector parts are thoroughly insulated to reduce heat losses in drying and other heating operations. Operating control is maintained usually by control of the exit gas temperature, with the inlet gas temperature varied to compensate for changing feed conditions. A constant solids feed rate must be maintained.

Ring Dryers The ring dryer is a development of flash, or pneumatic conveyor, drying technology, designed to increase the versatility of application of this technology and overcome many of its limitations.

One of the great advantages of flash drying is the very short retention time, typically no more than a few seconds. However, in a conventional flash dryer, residence time is fixed, and this limits its application to materials in which the drying mechanism is not diffusion-controlled and where a range of moisture within the final product is acceptable. The ring dryer offers two advantages over the flash dryer. First, residence time is controlled by the use of an adjustable internal classifier that allows fine particles, which dry quickly, to leave while larger particles, which dry slowly, have an extended residence time within the system. Second, the combination of the classifier with an internal mill can allow simultaneous grinding and drying with control of product particle size and moisture. Available with a range of different feed systems to handle a variety of applications, the ring dryer provides wide versatility.

The essential difference between a conventional flash dryer and the ring dryer is the manifold centrifugal classifier. The manifold provides classification of the product about to leave the dryer by using differential centrifugal force. The manifold, as shown in Fig. 12-103, uses the centrifugal effect of an airstream passing around the curve to concentrate the product into a moving layer, with the dense material on the outside and the light material on the inside.

This enables the adjustable splitter blades within the manifold classifier to segregate the denser, wetter material and return it for a further circuit of drying. Fine, dried material is allowed to leave the dryer with the exhaust air and to pass to the product collection system. This selective extension of residence time ensures a more evenly dried material than is possible from a conventional flash

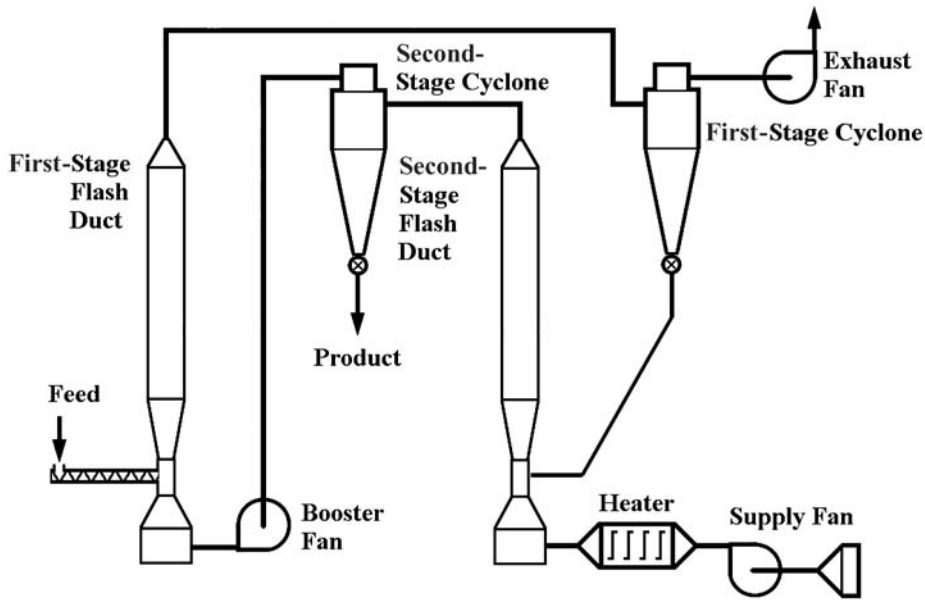


FIG. 12-101 Flow diagram of countercurrent two-stage flash dryer. (Niro.)

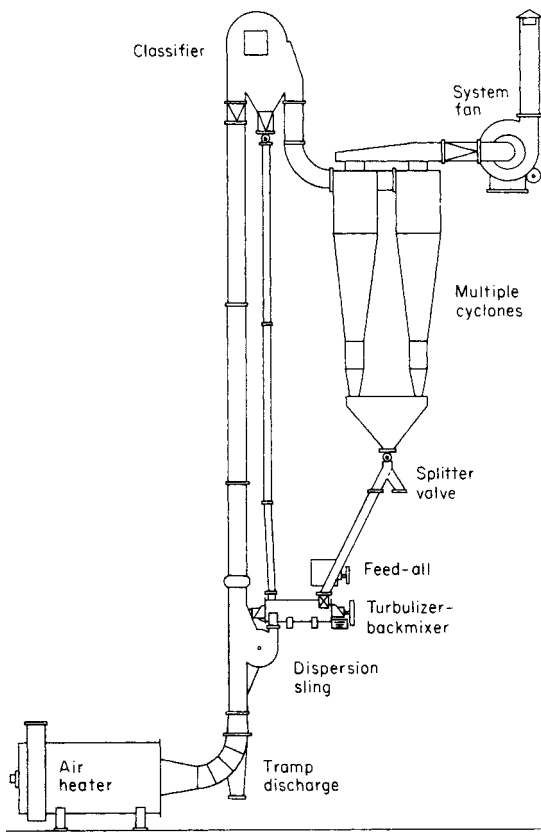


FIG. 12-102 Flow diagram of Strong Scott flash dryer with integral coarse-fraction classifier. (Bepex Corp.)

dryer. Many materials that have traditionally been regarded as difficult to dry can be processed to the required moisture content in a ring dryer. The recycle requirements of products in different applications can vary substantially depending upon the scale of operation, ease of drying, and finished-product specification. The location of reintroduction of undried material back into the drying medium has a significant impact upon the dryer performance and final-product characteristics.

Three configurations of the ring dryer have been developed to offer flexibility in design and optimal performance:

1. *Single-stage manifold-vertical configuration* The feed ring dryer (see Fig. 12-104) is similar to a flash dryer but incorporates a single-stage classifier, which diverts 40 to 60 percent of the product back to the feed point. The feed ring dryer is ideally suited for materials which neither are heat-sensitive nor require a high degree of classification. An advantage of this configuration is that it can be manufactured to very large sizes to achieve high evaporative capacities.

2. *Full manifold-horizontal configuration* The full ring dryer (see Fig. 12-105) incorporates a multistage classifier which allows much higher recycle rates than the single-stage manifold. This configuration usually incorporates a disintegrator which provides adjustable amounts of product grinding depending upon the speed and manifold setting. For sensitive or fine materials, the disintegrator can be omitted. Alternative feed locations are available to suit the material sensitivity and the final-product requirements. The full ring configuration gives a very high degree of control of both residence time and particle size, and is used for a wide variety of applications from small production rates of pharmaceutical and fine chemicals to large production rates of food products, bulk chemicals, and minerals. This is the most versatile configuration of the ring dryer.

3. *P-type manifold-vertical configuration* The P-type ring dryer (see Fig. 12-106) incorporates a single-stage classifier and was developed specifically for use with heat-sensitive materials. The undried material is reintroduced into a cool part of the dryer in which it recirculates until it is dry enough to leave the circuit.

An important element in optimizing the performance of a flash or ring dryer is the degree of dispersion at the feed point. Maximizing the product surface area in this region of highest evaporative

TABLE 12-44 Typical Products Dried in Pneumatic Conveyor Dryers (Barr-Rosin)

Material	Initial moisture, wet basis, %	Final moisture, wet basis, %	Plant configuration
Expandable polystyrene beads	3	0.1	Single-stage flash
Coal fines	23	1.0	Single-stage flash
Polycarbonate resin	25	10	Single-stage flash
Potato starch	42	20	Single-stage flash
Aspirin	22	0.1	Single-stage flash
Melamine	20	0.05	Single-stage flash
Com gluten meal	60	10	Feed-type ring dryer
Maize fiber	60	18	Feed-type ring dryer
Distillers dried grains (DDGs)	65	10	Feed type ring dryer
Vital wheat gluten	70	7	Full-ring dryer
Casein	50	10	Full-ring dryer
Tricalcium phosphate	30	0.5	Full-ring dryer
Zeolite	45	20	Full-ring dryer
Orange peels	82	10	Full-ring dryer
Modified com starch	40	10	P-type ring dryer
Methylcellulose	45	25	P-type ring dryer

driving force is a key objective in the design of this type of dryer. Ring dryers are fed using similar equipment to conventional flash dryers. Ring dryers with vertical configuration are normally fed by a flooded screw and a disperser which propels the wet feed into a high-velocity venturi, in which the bulk of the evaporation takes place. The full ring dryer normally employs an air-swept disperser or mill within the drying circuit to provide screenless grinding when required. Together with the manifold classifier this ensures a product with a uniform particle size. For liquid, slurry, or pasty feed materials, backmixing of the feed with a portion of the dry product will be carried out to produce a conditioned friable material. This further increases the versatility of the ring dryer, allowing it to handle sludge and slurry feeds with ease.

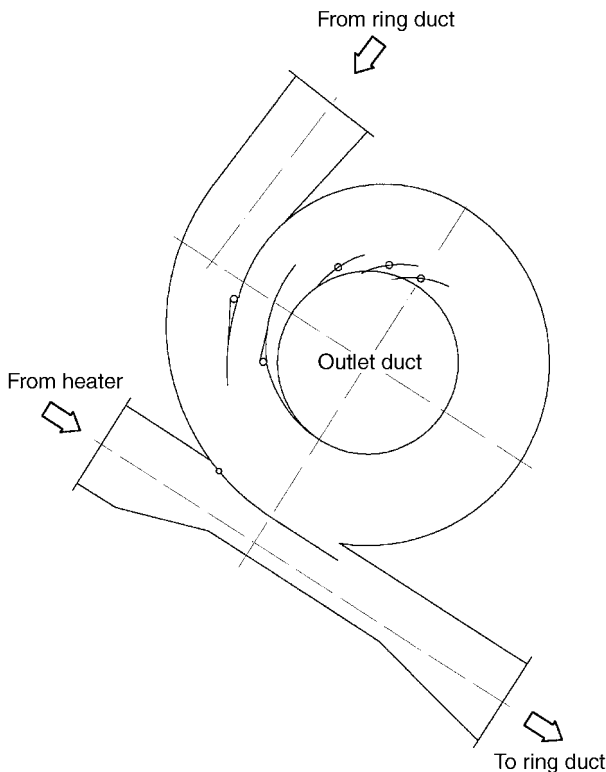


FIG. 12-103 Full manifold classifier for ring dryer. (Barr-Rosin.)

Dried product is collected in either cyclones or bag filters depending upon the product-particle properties. When primary collection is carried out in cyclones, secondary collection in a bag filter or scrubber is usually necessary to comply with environmental regulations. A rotary valve is used to provide an air lock at the discharge point. Screws are utilized to combine product from multiple cyclones or large bag filters. If required, a portion of the dried product is separated from the main stream and returned to the feed system for use as backmix.

Design methods for ring dryers Depending on the temperature sensitivity of the material to be processed, air inlet temperatures as high as 750°C can be utilized. Even with heat-sensitive solids, high feed moisture content may permit the use of high air inlet temperature since evaporation of surface moisture takes place at the wet-bulb air temperature. Until the surface moisture has been removed, it will prevent the solids temperature from exceeding the air wet-bulb temperature, by which time the air will generally have cooled significantly. Ring dryers have been used to process materials with feed moisture contents between 2 and 95 percent, weight fraction. The product moisture content has been controlled to values from 20 percent down to less than 1 percent.

The air velocity required and air/solids ratio are determined by the evaporative load, the air inlet temperature, and the exhaust air humidity. Too high an exhaust air humidity would prevent complete drying, so then a lower air inlet temperature and air/solids ratio would be required. The air velocity within the dryer must be sufficient to convey the largest particle, or agglomerate. The air/solids ratio must be high enough to convey both the product and backmix, together with internal recycle from the manifold. For estimating purposes a velocity of 25 m/s, calculated at dryer exhaust conditions, is appropriate both for pneumatic conveyor and ring dryers.

Agitated Flash Dryers Agitated flash dryers produce fine powders from feeds with high solids contents, in the form of filter cakes, pastes, or thick, viscous liquids. Many continuous dryers are unable to dry highly viscous feeds. Spray dryers require a pumpable feed. Conventional flash dryers often require backmixing of dry product to the feed in order to fluidize. Other drying methods for viscous pastes and filter cakes are well known, such as contact, drum, band, and tray dryers. They all require long processing time, large floor space, high maintenance, and aftertreatment such as milling.

The agitated flash dryer offers a number of process advantages, such as ability to dry pastes, sludges, and filter cakes to a homogeneous, fine powder in a single-unit operation; continuous operation; compact layout; effective heat- and mass-transfer short drying times; negligible heat loss and high thermal efficiency; and easy access and cleanliness.

The agitated flash dryer (Fig. 12-107) consists of four major components: feed system, drying chamber, heater, and exhaust air system. Wet feed enters the feed tank, which has a slow-rotating impeller to break up large particles. The level in the feed tank is maintained by a

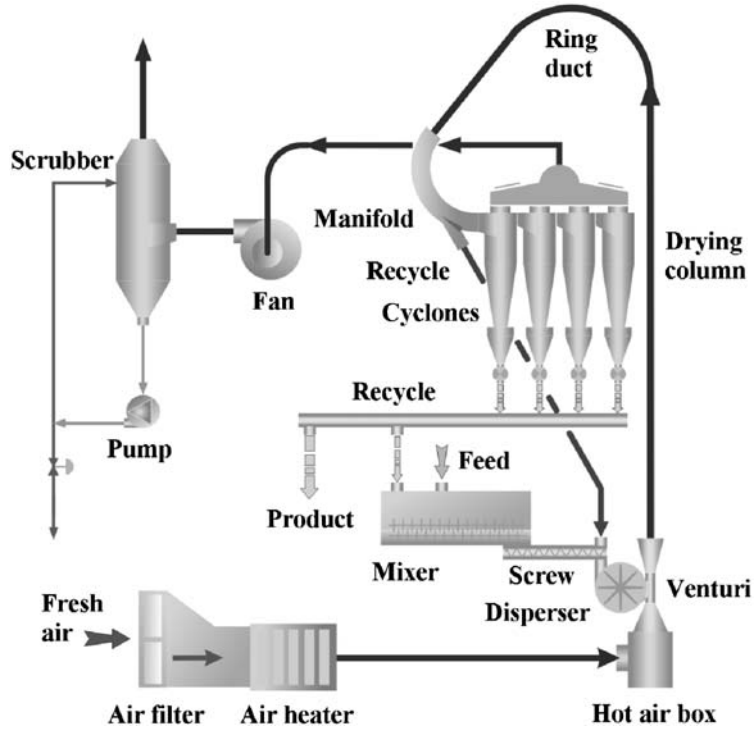


FIG. 12-104 Flow diagram of feed-type ring dryer. (Barr-Rosin.)

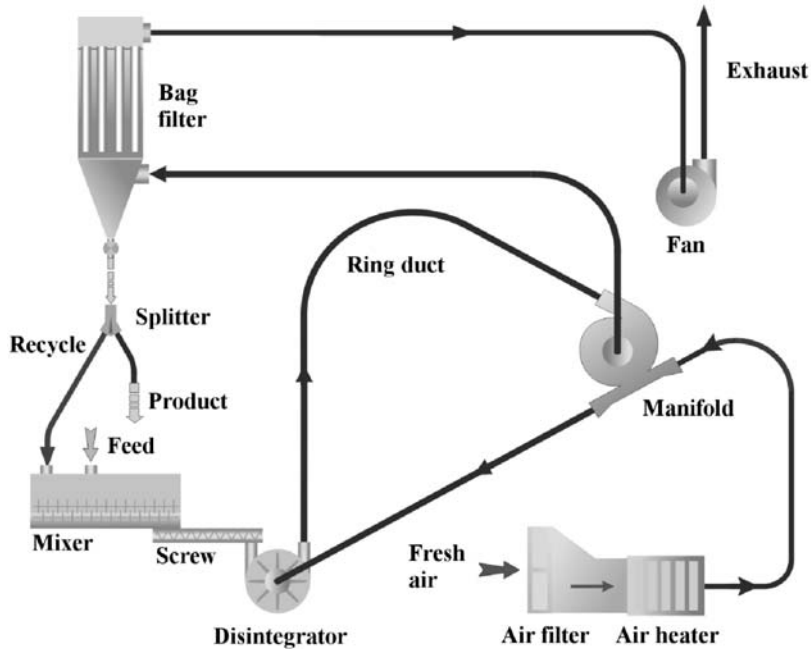


FIG. 12-105 Flow diagram of full manifold-type ring dryer. (Barr-Rosin.)

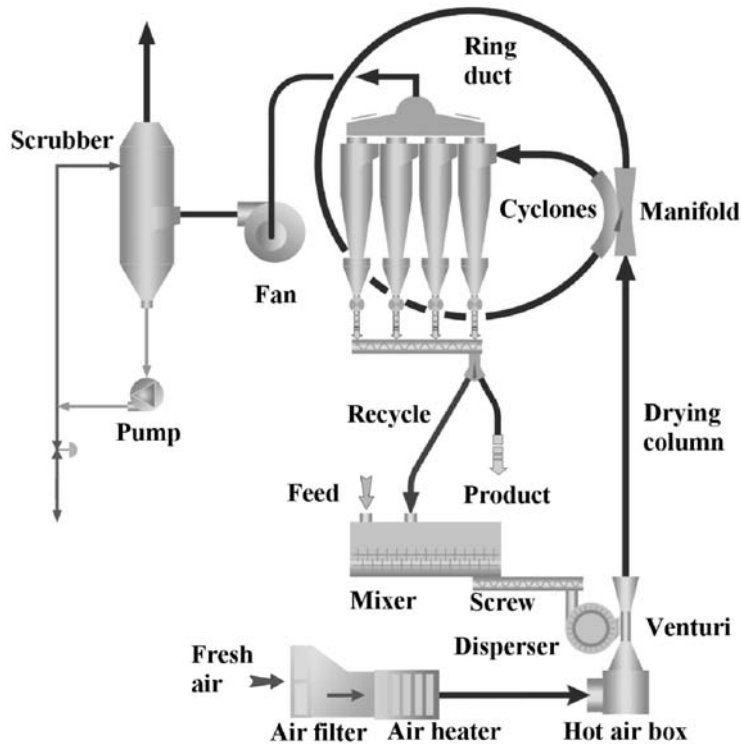


FIG. 12-106 Flow diagram of P-type ring dryer. (Barr-Rosin.)

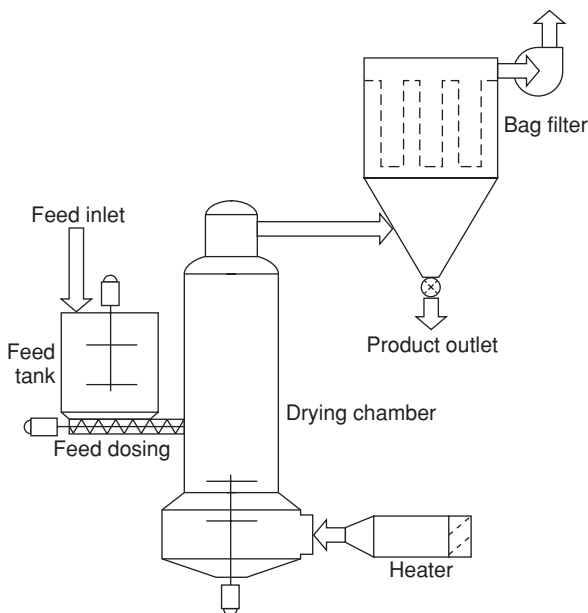


FIG. 12-107 Agitated flash dryer with open cycle. (Niro, Inc.)

level controller. The feed is metered at a constant rate into the drying chamber via a screw conveyor mounted under the feed tank. If the feed is shear thinning and can be pumped, the screw feeder can be replaced by a positive displacement pump.

The drying chamber is the heart of the system consisting of three important components: air disperser, rotating disintegrator, and drying section. Hot, drying air enters the air disperser tangentially and is introduced into the drying chamber as a swirling airflow. The swirling airflow is established by a guide-vane arrangement. The rotating disintegrator is mounted at the base of the drying chamber. The feed, exposed to the hot, swirling airflow and the agitation of the rotating disintegrator, is broken up and dried. The fine dry particles exit with the exhaust air and are collected in the bag filter. The speed of the rotating disintegrator controls the particle size. The outlet air temperature controls the product moisture content.

The drying air is heated either directly or indirectly, depending upon the feed material, powder properties, and available fuel source. The heat sensitivity of the product determines the drying air temperature. The highest possible value is used to optimize thermal efficiency. A bag filter is usually recommended for collecting the fine particles produced. The exhaust fan maintains a slight vacuum in the dryer, to prevent powder leakage into the surroundings. The appropriate process system is selected according to the feed and powder characteristics, available heating source, energy utilization, and operational health and safety requirements.

Open systems use atmospheric air for drying. In cases where products pose a potential for dust explosion, plants are provided with pressure relief or suppression systems. For recycle systems, the drying system medium is recycled, and the evaporated solvent recovered as condensate. There are two alternative designs. In the self-inertizing mode, oxygen content is held below 5 percent by combustion control at the heater. This is recommended for products with serious dust

explosion hazards. In the inert mode, nitrogen is the drying gas. This is used when an organic solvent is evaporated or product oxidation during drying must be prevented.

Design methods The size of the agitated flash dryer is based on the evaporation rate required. The operating temperatures are product-specific. Once established, they determine the airflow requirements. The drying chamber is designed based on air velocity (approximately 3 to 4 m/s) and residence time (product-specific).

Other Dryer Types

Freeze Dryer Industrial freeze drying is carried out in two steps:

1. Freezing of the food or beverage product
2. Freeze drying, i.e., sublimation drying of the ice content and desorption drying of the bound or crystal water content

Freeze drying differs from conventional drying in that when ice is sublimated, only water vapor is transported within the product, causing no displacement of soluble substances such as sugars, salts, and acids. In all conventional drying systems in which water is dried, the water containing the soluble substances is transported to the product surface by capillary action. The water will evaporate from the surface, leaving the soluble substances displaced on the product surface. The major advantages of freeze drying are therefore

- Preservation of original flavor, aroma, color, shape, and texture
- Very little shrinkage, resulting in excellent and instant rehydration characteristics
- Negligible product loss
- Minimal risk of cross-contamination

The freeze drying process is today used widely for a number of products including vegetables, fruits, meat, fish, and beverage products, such as

- Instant coffee for which excellent flavor and aroma retention are of special importance
- Strawberries for which excellent color preservation is of special importance
- Chives for which shape preservation is of special importance

Freezing The freezing methods applied for solid products are all conventional freezing methods such as blast freezing, individual quick freezing (IQF), or similar.

The products maintain their natural cell structure, and the aim is to freeze the free water to pure ice crystals, leaving the soluble substances as high concentrates or even crystallized. To ensure good stability of the product during storage, a product temperature of -20 to -30°C should be achieved to ensure that more than 95 percent of the free water is frozen.

Liquid products have no cell structure, thus the structure of the freeze dried products is formed by the freezing process. The intercrystalline matrix of the concentrated product giving the structure of the freeze dried product is formed around the ice crystals. The size of the ice crystals is a function of the freezing time. Quick freezing results in small ice crystals, slow freezing in large ice crystals. The structure of the matrix determines the freeze drying performance as well as the appearance, mechanical strength, and solubility rate. Small ice crystals lead to light color (high surface reflection of light), diffusion restrictions for vapor transport inside the product, and a good mechanical strength of the freeze dried product. Large ice crystals lead to the opposite results.

Thus the freezing method must be carefully adapted to the quality criteria of the finished product. The preferred methods are

- Drum freezing, by which a thin slab of 1.5 to 3 mm is frozen within 1.5 to 3 min
- Belt freezing, by which a slab of 6 to 10 mm passing through different freezing zones is frozen during 10 to 20 min
- Foaming, used to influence the structure and mainly to control the density of the freeze dried product

Freeze drying Freeze drying of foods takes place in a freeze dryer at vacuum levels of 0.4 to 1.3 mbar absolute, corresponding to sublimation temperatures from -30 to -17°C depending on the product requirements. The main components of the freeze dryer are

- The vacuum chamber, heating plates, and vapor traps, all built into the freeze dryer

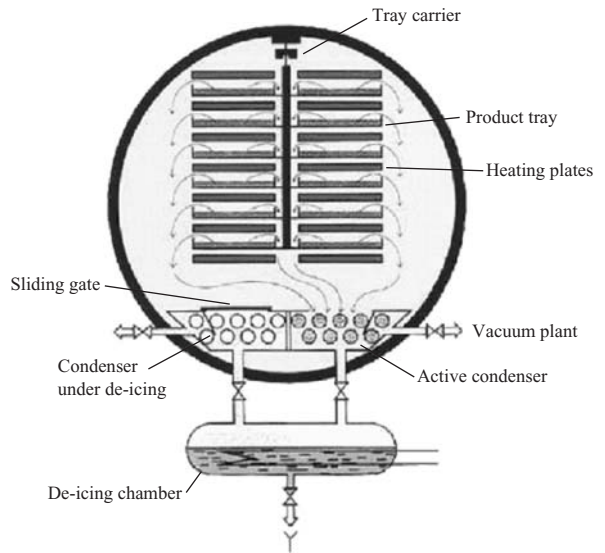


FIG. 12-108 Cross-section of RAY™ batch freeze dryer. (Niro A/S.)

- The external systems, such as the transport system for the product trays, the deicing system, and the support systems for supply of heat, vacuum, and refrigeration

Batch freeze drying The frozen product is carried in trays, and the trays are carried in tray trollies suspended in an overhead rail system for easy transport and quick loading and unloading. The freeze dryer as illustrated in Fig. 12-108 is charged with 3 to 6 trolley loads depending on the size of the freeze dryer. The trollies place the trays between the heating plates for radiation heat transfer. Radiation is preferred to ensure an even heat transfer over the large heating surface, typically $2 \times (70 \text{ to } 140 \text{ m}^2)$. The distribution of the heating medium (water or thermal oil) to the heating plates and the flow rate inside the plates are very important factors. To avoid uneven drying, the surface temperature difference of the heating plates should not exceed 2 to 3°C at maximum load.

When the loading is completed, the freeze dryer is closed and vacuum applied.

The operation vacuum should be reached quickly (within 10 min) to avoid the risk of product melting. For the same reason, the heating plates are cooled to approximately 25°C . When the operation vacuum is achieved, the heating plate temperature is raised quickly to the maximum drying temperature restricted by the capacity of the vapor traps, to perform the sublimation drying as quickly as possible for capacity reasons. During this period, the product is kept cool by the sublimation, and approximately 75 to 80 percent of the free water is sublimated.

The capability of the freeze drying plant to perform during this period is vital for efficient operation. To maintain the required sublimation temperature, the surface temperature of the ice layer on the vapor trap condenser must compensate for the pressure loss of the vapor flow from the sublimation front to the condenser.

The evaporation temperature of the refrigerant must further compensate for the temperature difference through the ice layer to the evaporating refrigerant.

With the flow rate at 1 mbar of approximately $1 \text{ m}^3/(\text{s} \cdot \text{m}^2)$ of tray area), the thermodynamic design of the vapor trap is the main issue for a well-designed freeze dryer.

A built-in vapor trap allowing a large opening for the vapor flow to the condenser and a continuous deicing (CDI) system, reducing the ice layer on the condenser to a maximum of 6 to 8 mm, are important features of a modern freeze drying plant. Approximately 75 percent of the energy costs relate to the refrigeration plant, and if the requirement

TABLE 12-45 Freeze Dryer, Performance Data, Niro RAY™ and CONRAD™ Types

	Tray area, m ²	Typical sublimation capacity		Electricity consumption, kWh/kg, sublimated	Steam consumption, kg/kg sublimated
		Flat tray, kg/h	Ribbed tray, kg/h		
RAY Batch Plant—1 mbar					
RAY 75	68	68	100	1.1	2.2
RAY 100	91	91	136	1.1	2.2
RAY 125*	114	114	170	1.1	2.2
CONRAD Continuous Plant—1 mbar					
CONRAD 300	240	240	360	1.0	2.0
CONRAD 400	320	320	480	1.0	2.0
CONRAD 500*	400	400	600	1.0	2.0

*Other sizes available.

of the evaporation temperature is 10°C lower than optimum, the energy consumption of the refrigeration plant will increase by approximately 50 percent.

At the end of the sublimation drying, the product surface temperature reaches the maximum allowable product temperature, requiring that the temperature of the heating plates be lowered gradually, and the drying will change to desorption drying. The temperature will finally be kept constant at the level of the maximum allowable product temperature until the residual moisture has been reduced to 2 to 3 percent, which is a typical level for a freeze dried product.

Continuous freeze drying From the description of batch freeze drying, it can be seen that the utility requirements vary considerably. During sublimation drying the requirements are 2 to 2.5 times the average requirement. To overcome this peak load and to meet the market request for high unit capacities, continuous freeze dryer designs have been developed. The special features are twofold:

- The tray transport system is a closed-loop system in which the trays pass one by one under the tray filler, where frozen product is automatically filled into the trays at a preset weight. The full tray is charged to the vacuum lock which is then evacuated to the drier vacuum level. Then the tray is pushed into the dryer and grabbed by an elevator which is filled stepwise with a stack of trays. Next a full stack of trays is pushed into the drying area whereby each of the stacks inside the drying area will move one step forward. Thus the last stack containing the finished, freeze dried product will be pushed out of the drying area to an outlet elevator which will be emptied stepwise by discharge of the trays through the outlet vacuum lock. From the outlet vacuum lock the trays are pushed to the emptying station for emptying and then returned to the tray filler.
- As the tray stacks are pushed forward through the freeze dryer, they pass through various temperature zones. The temperature zones form the heating profile, high temperatures during the sublimation drying, medium temperatures during the transition period toward desorption drying, and low temperatures during the final desorption drying. The temperature profile is selected so that overheating of the dry surface is avoided.

Design methods The size of the freeze drying plant is based on the average sublimation capacity required as well as on the product type and form. The external systems for batch plants must be designed for a peak load of 2 to 2.5 times the average capacity in the case of a single plant. Further, a batch plant is not available for drying all the time. A modern batch freeze dryer with the CDI system loses approximately 30 min per batch. Typically, 2 to 3 batches will be freeze dried per day. The evaporation temperature of the refrigeration plant depends on the required vacuum. At 1 mbar it will be -35 to -40°C depending on the vapor trap performance. Sample data are shown in Table 12-45.

Field Effects Drying—Drying with Infrared, Radio-Frequency, and Microwave Methods

Dielectric Methods (Radio-Frequency and Microwave) Schiffmann (1995) defines dielectric (radio-frequency) frequencies as covering the range of 1 to 100 MHz, while microwave frequencies range from 300 MHz to 300 GHz. The devices used for generating microwaves are called magnetrons and klystrons.

Water molecules are dipolar (i.e., they have an asymmetric charge center), and they are normally randomly oriented. The rapidly changing polarity of a microwave or radio-frequency field attempts to pull these dipoles into alignment with the field. As the field changes polarity, the dipoles return to a random orientation before being pulled the other way. This buildup and decay of the field, and the resulting stress on the molecules, causes a conversion of electric field energy to stored potential energy, then to random kinetic or thermal energy. Hence dipolar molecules such as water absorb energy in these frequency ranges. The power developed per unit volume P_e by this mechanism is

$$P_e = kE^2 f \epsilon' \tan \delta = kE^2 f \epsilon'' \tag{12-117}$$

where k is a dielectric constant, depending on the units of measurement, E is the electric field strength (V/m³), f is the frequency, ϵ' is the relative dielectric constant or relative permeability, $\tan \delta$ is the loss tangent or dissipation factor, and ϵ'' is the loss factor.

The field strength and the frequency are dependent on the equipment, while the dielectric constant, dissipation factor, and loss factor are material-dependent. The electric field strength is also dependent on the location of the material within the microwave/radio-frequency cavity (Turner and Ferguson, 1995), which is one reason why domestic microwave ovens have rotating turntables (so that the food is exposed to a range of microwave intensities). This mechanism is the major one for the generation of heat within materials by these electromagnetic fields.

There is also a heating effect due to ionic conduction, since the ions (sodium, chloride, and hydroxyl) in the water inside materials are accelerated and decelerated by the changing electric field. The collisions which occur as a result of the rapid accelerations and decelerations lead to an increase in the random kinetic (thermal) energy of the material. This type of heating is not significantly dependent on either temperature or frequency, and the power developed per unit volume P_e from this mechanism is

$$P_e = E^2 q n \mu \tag{12-118}$$

where q is the amount of electric charge on each of the ions, n is the charge density (ions/m³), and μ is the level of mobility of the ions.

Schiffmann (1995) indicates that the dielectric constant of water is over an order of magnitude higher than that of most underlying materials, and the overall dielectric constant of most materials is usually nearly proportional to moisture content up to a critical moisture content, often around 20 to 30 percent. Hence microwave and radio-frequency methods preferentially heat and dry wetter areas in most materials, a process which tends to give more uniform final moisture contents. The dielectric constant of air is very low compared with that of water, so lower density usually means lower heating rates. For water and other small molecules, the effect of increasing temperature is to decrease the heating rate slightly, hence leading to a self-limiting effect.

Other effects (frequency, conductivity, specific heat capacity, etc.) are discussed by Schiffmann (1995), but are less relevant because the range of available frequencies (which do not interfere with radio transmissions) is small (2.45 GHz, 910 MHz). Lower frequencies lead

to greater penetration depths into material than higher frequencies, with 2.45-GHz frequencies sometimes having penetration depths as low as 1 in. For in-depth heating (“volumetric heating”), radio frequencies, with lower frequencies and longer wavelengths, are often used.

Infrared Methods Infrared radiation is commonly used in the dehydration of coated films and to even out the moisture content profiles in the drying of paper and boards. The mode of heating is essentially on the material surface, and IR sources are relatively inexpensive compared with dielectric sources.

The heat flux obtainable from an IR source is given by

$$q = F\alpha\epsilon (T_{\text{source}}^4 - T_{\text{drying material}}^4) \quad (12-119)$$

where q = heat flux, W/m^2 ; α = Stefan-Boltzmann constant = $5.67 \times 10^{-8} W/(m^2 \cdot K^4)$; ϵ = emissivity; F = view factor; and T = absolute temperature of the source or drying material.

The emissivity is a property of the material. The limiting value is 1 (blackbody); shiny surfaces have a low value of emissivity. The view factor is a fractional value that depends on the geometric orientation of the source with respect to the heating object.

It is very important to recognize the T^4 dependence on the heat flux. IR sources need to be very hot to give appreciable heat fluxes. Therefore, IR sources should not be used with flammable materials. Improperly designed IR systems can also overheat materials and equipment.

OPERATION AND TROUBLESHOOTING

Troubleshooting Dryer troubleshooting is not extensively covered in the literature, but a systematic approach has been proposed by Kemp and Gardiner (2001). The main steps of the algorithm are as follows:

- *Problem definition*—definition of the dryer problem to be solved.
- *Data gathering*—collection of relevant information, e.g., plant operating data
- *Data analysis*—e.g., heat and mass balance—and *identification of the cause of the problem*
- *Conclusions and actions*—selection and implementation of a solution in terms of changes to process conditions, equipment, or operating procedures
- *Performance auditing*—monitoring to ensure that the problem was permanently solved

There is often a danger in practice that the pressure to get the plant back into production as soon as possible may lead to some of these stages being omitted. Even if a short-term fix has been found, it is highly desirable to make sure what the problem really was, to see whether there are better ways of solving it in the long term, and to check that the problem really has been solved (sometimes it reappears later, e.g., when a temporarily cleaned heat exchanger becomes fouled again, or climatic conditions return to previous values).

The algorithm might also be considered as a “plant doctor.” The doctor collects data, or symptoms, and makes a diagnosis of the cause or causes of the problem. Then alternative solutions, or treatments, are considered and a suitable choice is made. The results of the treatment are reviewed (i.e., the process is monitored) to ensure that the “patient” has returned to full health. See Fig. 12-109.

The algorithm is an excellent example of the “divergent-convergent” (brainstorming) method of problem solving. It is important to list all possible causes and solutions, no matter how ridiculous they may initially seem; there may actually be some truth in them, or they may lead to a new and better idea.

Problem Categorization In the problem definition stage, it is extremely useful to categorize the problem, as the different broad groups require different types of solution. Five main categories of dryer problems can be identified:

1. Drying performance (outlet moisture content too high, throughput too low)
2. Materials handling (dried material too sticky to get out of dryer, causing blockage)
3. Product quality (too many fines in product or bulk density too low)

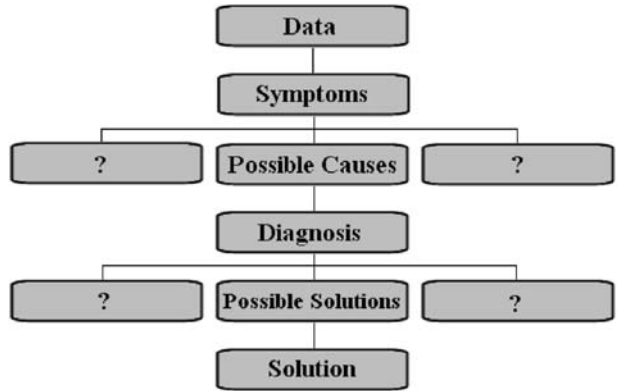


FIG. 12-109 Schematic diagram of algorithm for dryer troubleshooting.

4. Mechanical breakdown (catastrophic sudden failure)
5. Safety, health, and environmental (SHE) issues

Experience suggests that the majority of problems are of the first three types, and these are about equally split over a range of industries and dryer types. Ideally, unforeseen SHE problems will be rare, as these will have been identified in the safety case before the dryer is installed or during commissioning. Likewise, major breakdowns should be largely avoided by a planned maintenance program.

Drying Performance Problems Performance problems can be further categorized as

1. Heat and mass balance deficiencies (not enough heat input to do the evaporation)
2. Drying kinetics (drying too slowly, or solids residence time in dryer too short)
3. Equilibrium moisture limitations (reaching a limiting value, or regaining moisture in storage)

For the heat and mass balance, the main factors are

- Solids throughput
- Inlet and outlet moisture content
- Temperatures and heat supply rate
- Leaks and heat losses

As well as problem-solving, these techniques can be used for performance improvement and debottlenecking.

Drying kinetics, which are affected by temperature, particle size, and structure, are limited by external heat and mass transfer to and from the particle surface in the early stages, but internal moisture transport is the main parameter at lower moisture.

Equilibrium moisture content increases with higher relative humidity, or with lower temperature. Problems that depend on the season of the year, or vary between day and night (both suggesting a dependence on ambient temperature and humidity), are often related to equilibrium moisture content.

Materials Handling Problems The vast majority of handling problems in a dryer concern sticky feedstocks. Blockages can be worse than performance problems as they can close down a plant completely, without warning. Most stickiness, adhesion, caking, and agglomeration problems are due to *mobile liquid bridges* (surface moisture holding particles together). These are extensively described in particle technology textbooks. Unfortunately, these forces tend to be at a maximum when the solid forms the continuous phases and surface moisture is present, which is the situation for most filter and centrifuge cakes at discharge. By comparison, slurries (where the liquid forms the continuous phase) and dry solids (where all surface moisture has been eliminated) are relatively free-flowing and give fewer problems.

Other sources of problems include electrostatics (most marked with fine and dry powders) and *immobile liquid bridges*, the so-called sticky-point phenomenon. This latter is sharply temperature-dependent, with only a weak dependence on moisture content, in contrast to mobile

liquid bridges. It occurs for only a small proportion of materials, but is particularly noticeable in amorphous powders and foods and is often linked to the glass transition temperature.

Product Quality Problems (These do not include moisture level of the main solvent.) Many dryer problems either concern product quality or cannot be solved without considering the effect of any changes on product quality. Thus it is a primary consideration in most troubleshooting, although product quality measurements are specific to the particular product, and it is difficult to generalize. However, typical properties may include color, taste (not easily quantifiable), bulk density, viscosity of a paste or dispersion, dispersibility, or rate of solution. Others are more concerned with particle size, size distribution (e.g., coarse or fine fraction), or powder handling properties such as rate of flow through a standard orifice. These property measurements are nearly always made off-line, either by the operator or by the laboratory, and many are very difficult to characterize in a rigorous quantitative manner. (See also "Fundamentals" Section.)

Storage problems, very common in industry, result if the product from a dryer is free-flowing when packaged, but has caked and formed solid lumps when received by the customer. Sometimes, the entire internal contents of a bag or drum have welded together into a huge lump, making it impossible to discharge.

Depending on the situation, there are at least three different possible causes:

1. *Equilibrium moisture content*—hygroscopic material is absorbing moisture from the air on cooling.

2. *Incomplete drying*—product is continuing to lose moisture in storage.

3. *Psychrometry*—humid air is cooling and reaching its dew point.

The three types of problem have some similarities and common features, but the solution to each one is different. Therefore, it is essential to understand which mechanism is actually occurring.

Option 1: The material is hygroscopic and is absorbing moisture back from the air in storage, where the cool air has a higher relative humidity than the hot dryer exhaust. **Solution:** Pack and seal the solids immediately on discharge in tough impermeable bags (usually double- or triple-lined to reduce the possibility of tear and pinholes), and minimize the ullage (airspace above the solids in the bags) so that the amount of moisture that can be absorbed is too low to cause any significant problem. Dehumidifying the air to the storage area is also possible, but often very expensive.

Option 2: The particles are emerging with some residual moisture, and continue to dry after being stored or bagged. As the air and solids cool down, the moisture in the air comes out as dew and condenses on the surface of the solids, causing caking by mobile liquid bridges. **Solution:** If the material is meeting its moisture content specification, cool the product more effectively before storage, to stop the drying process. If the outlet material is wetter than specification, alter dryer operating conditions or install a postdryer.

Option 3: Warm, wet air is getting into the storage area or the bags, either because the atmosphere is warm with a high relative humidity (especially in the tropics) or because dryer exhaust air has been allowed to enter. As in option 2, when the temperature falls, the air goes below its dew point and condensation occurs on the walls of the storage area or inside the bags, or on the surface of the solids, leading to caking. **Solution:** Avoid high-humidity air in the storage area. Ensure the dryer exhaust is discharged a long way away. If the ambient air humidity is high, consider cooling the air supply to storage to bring it below its dew point and reduce its absolute humidity.

See Kemp and Gardiner, "An Outline Method for Troubleshooting and Problem-Solving in Dryers," *Drying Technol.* 19(8):1875–1890 (2001).

Dryer Operation

Start-up Considerations It is important to start up the heating system before introducing product into the dryer. This will minimize condensation and subsequent product buildup on dryer walls. It is also important to minimize off-quality production by not overdrying or underdrying during the start-up period. Proper control system design can aid in this regard. The dryer turndown ratio is also an

important consideration during start-up. Normally the dryer is started up at the lowest end of the turndown ratio, and it is necessary to match heat input with capacity load.

Shutdown Considerations The sequence for dryer shutdown is also very important and depends on the type of dryer. The sequence must be thoroughly thought through to prevent significant off-quality product or a safety hazard. The outlet temperature during shutdown is a key operating variable to follow.

Energy Considerations The first consideration is to minimize moisture content of the dryer feed, e.g., with dewatering equipment, and to establish as high an outlet product moisture target as possible. Other energy considerations vary widely by dryer type. In general, heating with gas, fuel oil, and steam is significantly more economical than heating with electricity. Hence RF, microwave, and infrared drying is energy-intensive. Direct heating is more efficient than indirect in most situations. Sometimes air recycle (direct or indirect) can be effective to reduce energy consumption. And generally operating at high inlet temperatures is more economical.

Recycle In almost all situations, the process system must be able to accommodate product recycle. The question is, How to handle it most effectively, considering product quality, equipment size, and energy?

Improvement Considerations The first consideration is to evaluate mass and energy balances to identify problem areas. This will identify air leaks and excessive equipment heat losses and will enable determination of overall energy efficiency.

A simplified heat balance will show what might need to be done to debottleneck a convective (hot gas) dryer, i.e., increase its production rate F .

$$F(X_I - X_O)\lambda_{ev} \approx GC_{PG}(T_{CI} - T_{CO}) - Q_{del}$$

Before proceeding along this line, however, it is necessary to establish that the dryer is genuinely heat and mass balance limited. If the system is controlled by kinetics or equilibria, changing the parameters may have undesirable side effects, e.g., increasing the product moisture content.

The major alternatives are then as follows (assuming gas specific heat capacity C_{PG} and latent heat of evaporation λ_{ev} are fixed):

1. Increase gas flow rate G —usually increases pressure drop, so new fans and gas cleaning equipment may be required.

2. Increase inlet gas temperature T_{CI} —usually limited by risk of thermal damage to product.

3. Decrease outlet gas temperature T_{CO} —but note that this increases NTUs, outlet humidity, and relative humidity, and reduces both temperature and humidity driving forces. Hence it may require a longer drying time and a larger dryer, and may also increase equilibrium and outlet moistures X_E and X_O .

4. Reduce inlet moisture content X_I , say, by dewatering by gas blowing, centrifuging, vacuum or pressure filtration, or a predryer.

5. Reduce heat losses Q_{del} by insulation, removing leaks, etc.

Dryer Safety This section discusses some of the key considerations in dryer safety. General safety considerations are discussed in Sec. 23, "Safety and Handling of Hazardous Materials," and should be referred to for additional guidance.

Fires, explosions, and, to a lesser extent, runaway decompositions are the primary hazards associated with drying operations. The outbreak of fire is a result of ignition which may or may not be followed by an explosion. A hazardous situation is possible if

1. The product is combustible
2. The product is wetted by a flammable solvent
3. The dryer is direct-fired

An explosion can be caused by dust or flammable vapors, both of which are fires that rapidly propagate, causing a pressure rise in a confined space.

Dust Explosions Dispersion dryers can be more hazardous than layer-type dryers if we are drying a solid combustible material which is then dispersed in air, particularly if the product is a fine particle size. If this finely dispersed product is then exposed to an ignition source, an explosion can result. The following conditions (van't Land, *Industrial Drying Equipment*, Marcel Dekker, New York, 1991) will be conducive to fire and explosion hazard:

1. Small particle sizes, generally less than 75 μm , which are capable of propagating a flame
2. Dust concentrations within explosive limits, generally 10 to 60 g/m^3
3. Ignition source energy of 10 to 1000 mJ or as low as 5 mJ for highly explosive dust sources
4. Atmosphere supporting combustion

Since most product and hence dust compositions vary widely, it is generally necessary to do quantitative testing in approved test equipment.

Flammable Vapor Explosions This can be a problem for products wetted by flammable solvents if the solvent concentration exceeds 0.2% v/v in the vapor phase. The ignition energy of vapor-air mixtures is lower (< 1 mJ) than that of dust-air suspensions. Many of these values are available in the literature, but testing may sometimes be required.

Ignition Sources There are many possible sources of an ignition, and they need to be identified and addressed by both designers and operators. A few of the most common ignition sources are

1. Spontaneous combustion
2. Electrostatic discharge
3. Electric or frictional sparks
4. Incandescent solid particles from heating system

Safety hazards must be addressed with proper dryer design specifications. The following are a few key considerations in dryer design.

Inert system design The dryer atmosphere is commonly inerted with nitrogen, but superheated steam or self-inertized systems are also possible. Self-inertized systems are not feasible for flammable solvent systems. These systems must be operated with a small overpressure to ensure no oxygen ingress. And continuous on-line oxygen concentration monitoring is required to ensure that oxygen levels remain well below the explosion hazard limit.

Relief venting Relief vents that are properly sized relieve and direct dryer explosions to protect the dryer and personnel if an explosion does occur. Normally they are simple pop-out panels with a minimum length of ducting to direct the explosion away from personnel or other equipment.

Suppression systems Suppression systems typically use an inert gas such as carbon dioxide to minimize the explosive peak pressure rise and fire damage. Dryer operating pressure must be properly monitored to detect the initial pressure rise followed by shutdown of the dryer operating systems and activation of the suppression system.

Clean design Care should be taken in the design of both the dryer and dryer ancillary (cyclones, filters, etc.) equipment to eliminate ledges, crevices, and other obstructions which can lead to dust and product buildup. Smooth drying equipment walls will minimize deposits. This can go a long way in prevention. No system is perfect, of course, and a routine cleaning schedule is also recommended.

Start-up and shutdown Start-up and shutdown situations must be carefully considered when designing a dryer system. These situations can create higher than normal dust and solvent concentrations. This coupled with elevated temperatures can create a hazard well beyond normal continuous operation.

Environmental Considerations Environmental considerations are continuing to be an increasingly important aspect of dryer design and operation as environmental regulations are tightened. The primary environmental problems associated with drying are particulate and volatile organic compound (VOC) emissions. Noise can be an issue with certain dryer types.

Environmental Regulations These vary by country, and it is necessary to know the specific regulations in the country in which the dryer will be installed. It is also useful to have some knowledge of the direction of regulations so that the environmental control system is not obsolete by the time it becomes operational.

Particulate emission problems can span a wide range of hazards. Generally there are limits on both toxic and nontoxic particles in terms of annual and peak emissions limits. Particles can present toxic, bacterial, viral, and other hazards to human, animal, and plant life.

Likewise, VOC emissions can span a wide range of hazards and issues from toxic gases to smelly gases.

Environmental Control Systems We should consider environmental hazards before the drying operation is even considered. The focus should be on minimizing the hazards created in the upstream

processing operations. After potential emissions are minimized, these hazards must be dealt with during dryer system design and then subsequently with proper operational and maintenance procedures.

Particle Emission Control Equipment The four most common methods of particulate emissions control are as follows:

1. **Cyclone separators** The advantage of cyclones is they have relatively low capital and operating costs. The primary disadvantage is that they become increasingly ineffective as the particle size decreases. As a general rule of thumb, we can say that they are 100 percent efficient with particles larger than 20 μm and 0 percent efficient with particles smaller than 1 μm . Cyclones can also be effective precleaning devices to reduce the load on downstream bag filters.

2. **Scrubbers** The more general classification is wet dedusters, the most common of which is the wet scrubber. The advantage of wet scrubbers is that they can remove fine particles that the cyclone does not collect. The disadvantages are they are more costly than cyclones and they can turn air contamination into water contamination, which may then require additional cleanup before the cleaning water is put to the sewer.

3. **Bag filters** The advantages of filters are that they can remove very fine particles and bag technologies continue to improve and enable ever-smaller particles to be removed without excessive pressure drops or buildup. The primary disadvantages are higher cost relative to cyclones and greater maintenance costs, especially if frequent bag replacement is necessary.

4. **Electrostatic precipitators** The capital cost of these systems is relatively high, and maintenance is critical to effective operation.

VOC Control Equipment The four most prevalent equipment controls are

1. **Scrubbers** Similar considerations as above apply.

2. **Absorbers** These systems use a high-surface-area absorbent, such as activated carbon, to remove the VOC absorbate.

3. **Condensers** These systems are generally only feasible for recovering solvents from nonaqueous wetted products.

4. **Thermal and catalytic incinerators** These can be quite effective and are generally a low capital and operating cost solution, except in countries with high energy costs.

Noise Noise analysis and abatement is a very specialized area. Generally, the issue with dryers is associated with the fans, particularly for systems requiring fans that develop very high pressures. Noise is a very big issue that needs to be addressed with pulse combustion dryers and can be an issue with very large dryers such as rotary dryers and kilns.

Additional considerations regarding environmental control and waste management can be found in Secs. 22, "Waste Management," and 23, "Process Safety."

Control and Instrumentation The purpose of the control and instrumentation system is to provide a system that enables the process to produce the product at the desired moisture target and that meets other quality control targets discussed earlier (density, particle size, color, solubility, etc.). This segment discusses key considerations for dryer control and instrumentation. Additional more detailed information can be found in Sec. 8, "Process Control."

Proper control of product quality starts with the dryer selection and design. Sometimes two-stage or multistage systems are required to meet product quality targets. Multistage systems enable us to better control temperature and moisture profiles during drying. Assuming the proper dryer design has been selected, we must then design the control and instrumentation system to ensure we meet all product quality targets.

Manual versus Automatic Control Dryers can be controlled either manually or automatically. Generally lab-, pilot-, and small-scale production units are controlled manually. These operations are usually batch systems, and manual operation provides lower cost and greater flexibility. The preferred mode for large-scale, continuous dryers is automatic.

Key Control Variables Product moisture and product temperature are key control variables. Ideally both moisture and temperature measurement are done on-line, but frequently moisture measurement is done off-line and temperature (or exhaust air temperature) becomes the primary control variable. And generally, inlet temperature

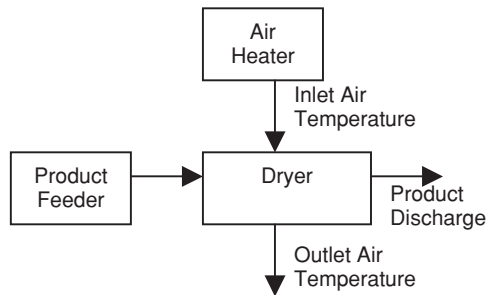


FIG. 12-110 Typical dryer system.

will control the rate of production and outlet temperature will control the product moisture and other product quality targets.

Common Control Schemes Two relatively simple, but common control schemes in many dryer systems (Fig. 12-110) are as follows:

1. Outlet air temperature is controlled by feed rate regulation with inlet temperature controlled by gas heater regulation.
2. Outlet air temperature is controlled by heater regulation with feed rate held constant.

Alternatively, product temperatures can replace air temperatures with the advantage of better control and the disadvantage of greater maintenance of the product temperature sensors.

Other Instrumentation and Control

Pressure Pressure and equipment pressure drops are important to proper dryer operation. Most dryers are operated under vacuum. This prevents dusting to the environment, but excess leakage in decreases dryer efficiency. Pressure drops are especially important for stable fluid-bed operation.

Air (gas) flow rate Obviously gas flows are another important parameter for proper dryer operation. Pitot tubes are useful when a system has no permanent gas flow sensors. Averaging pitot tubes work well in permanent installations. The devices work best in straight sections of ductwork which are sometimes difficult to find and make accurate measurement a challenge.

Product feed rate It's important to know that product feed rates and feed rate changes are sometimes used to control finished product moistures. Weigh belts are common for powdered products, and there is a wide variety of equipment available for liquid feeds. Momentum devices are inexpensive but less accurate.

Humidity The simplest method is sometimes the best. Wet- and dry-bulb temperature measurement to get air humidity is simple and works well for the occasional gas humidity measurement. The problem

with permanent humidity measurement equipment is the difficulty of getting sensors robust enough to cope with a hot, humid, and sometimes dusty environment.

Interlocks Interlocks are another important feature of a well-designed control and instrumentation system. Interlocks are intended to prevent damage to the dryer system or to personnel, especially during the critical periods of start-up and shutdown. The following are a few key interlocks to consider in a typical dryer system.

Drying chamber damage This type of damage can occur when the chamber is subjected to significant vacuum when the exhaust fans are started up before the supply fans.

Personnel injury This interlock is to prevent injury due to entering the dryer during operation, but more typically to prevent dryer start-up with personnel in the main chamber or inlet or exhaust air ductwork on large dryers. This typically involves microswitches on access doors coupled with proper door lock devices and tags.

Assurance of proper startup and shutdown These interlocks ensure, e.g., that the hot air system is started up before the product feed system and that the feed system is shut down before the hot air system.

Heater system There are a host of important heater system interlocks to prevent major damage to the entire drying system. Additional details can be found in Sec. 23, "Process Safety."

Drying Software Several software programs for psychrometric charts and calculations are available and are described in the "Psychrometry" section.

Dryers are included as modules in standard process simulators such as Aspen Plus and HYSYS (Aspen Technology), Pro/II (Simsci/Invensys) and Unisim (Honeywell), and the prototype Solidsim solids process simulator. These are confined (as of 2006) to heat and mass balances or, at most, simple scoping design.

Many higher-level dryer models have been produced by researchers and universities, but they are not commercially available. Windows-based drying programs are available in the Process Tools (Aspen Technology), including a psychrometric chart, dryer selection expert system, dryer scoping design, and fluid-bed dryer simulation. Some CFD programs (e.g., Fluent, CFX) include a module for spray dryers.

In addition to textbooks, a detailed online knowledge base, the Process Manual, is available from Aspen Technology (see www.processmanual.com). This covers equipment, scientific background, design, and operation for drying and 10 other technical areas in solids and separation processes. Company and university licenses are available.

Detailed reviews of drying software packages given by Menshutina and Kudra, *Drying Technol.* **19**(8):1825–1850 (2001); and by Kemp, Chap. 7 in *Modern Drying Technology*, vol. 1, Wiley-VCH (2007), and *Drying Technol.* **25** (2007).

SECTION **13**

Distillation

PERRY'S CHEMICAL ENGINEERS' HANDBOOK

8TH EDITION



M. F. DOHERTY, Z. T. FIDKOWSKI
M. F. MALONE, R. TAYLOR

Copyright © 2008, 1997, 1984, 1973, 1963, 1950, 1941, 1934 by The McGraw-Hill Companies, Inc. All rights reserved. Manufactured in the United States of America. Except as permitted under the United States Copyright Act of 1976, no part of this publication may be reproduced or distributed in any form or by any means, or stored in a database or retrieval system, without the prior written permission of the publisher.

0-07-154220-5

The material in this eBook also appears in the print version of this title: 0-07-151136-9.

All trademarks are trademarks of their respective owners. Rather than put a trademark symbol after every occurrence of a trademarked name, we use names in an editorial fashion only, and to the benefit of the trademark owner, with no intention of infringement of the trademark. Where such designations appear in this book, they have been printed with initial caps.

McGraw-Hill eBooks are available at special quantity discounts to use as premiums and sales promotions, or for use in corporate training programs. For more information, please contact George Hoare, Special Sales, at george_hoare@mcgraw-hill.com or (212) 904-4069.

TERMS OF USE

This is a copyrighted work and The McGraw-Hill Companies, Inc. (“McGraw-Hill”) and its licensors reserve all rights in and to the work. Use of this work is subject to these terms. Except as permitted under the Copyright Act of 1976 and the right to store and retrieve one copy of the work, you may not decompile, disassemble, reverse engineer, reproduce, modify, create derivative works based upon, transmit, distribute, disseminate, sell, publish or sublicense the work or any part of it without McGraw-Hill’s prior consent. You may use the work for your own noncommercial and personal use; any other use of the work is strictly prohibited. Your right to use the work may be terminated if you fail to comply with these terms.

THE WORK IS PROVIDED “AS IS.” McGRAW-HILL AND ITS LICENSORS MAKE NO GUARANTEES OR WARRANTIES AS TO THE ACCURACY, ADEQUACY OR COMPLETENESS OF OR RESULTS TO BE OBTAINED FROM USING THE WORK, INCLUDING ANY INFORMATION THAT CAN BE ACCESSED THROUGH THE WORK VIA HYPERLINK OR OTHERWISE, AND EXPRESSLY DISCLAIM ANY WARRANTY, EXPRESS OR IMPLIED, INCLUDING BUT NOT LIMITED TO IMPLIED WARRANTIES OF MERCHANTABILITY OR FITNESS FOR A PARTICULAR PURPOSE. McGraw-Hill and its licensors do not warrant or guarantee that the functions contained in the work will meet your requirements or that its operation will be uninterrupted or error free. Neither McGraw-Hill nor its licensors shall be liable to you or anyone else for any inaccuracy, error or omission, regardless of cause, in the work or for any damages resulting therefrom. McGraw-Hill has no responsibility for the content of any information accessed through the work. Under no circumstances shall McGraw-Hill and/or its licensors be liable for any indirect, incidental, special, punitive, consequential or similar damages that result from the use of or inability to use the work, even if any of them has been advised of the possibility of such damages. This limitation of liability shall apply to any claim or cause whatsoever whether such claim or cause arises in contract, tort or otherwise.

DOI: 10.1036/0071511369

Distillation*

M. F. Doherty, Ph.D. Professor of Chemical Engineering, University of California—Santa Barbara (Section Editor)

Z. T. Fidkowski, Ph.D. Process Engineer, Air Products and Chemicals Inc. (Distillation Systems)

M. F. Malone, Ph.D. Professor of Chemical Engineering and Dean of Engineering, University of Massachusetts—Amherst (Batch Distillation)

R. Taylor, Ph.D. Professor of Chemical Engineering, Clarkson University (Simulation of Distillation Processes)

INTRODUCTION TO DISTILLATION OPERATIONS

General Principles	13-4
Equilibrium and Nonequilibrium-Stage Concepts	13-5
Related Separation Operations	13-5

THERMODYNAMIC DATA AND MODELS

Phase Equilibrium Data	13-6
Graphical K Value Correlations	13-8
Analytical K Value Correlations	13-9

SINGLE-STAGE EQUILIBRIUM FLASH CALCULATIONS

Bubble Point and Dew Point	13-15
Isothermal Flash	13-15
Adiabatic Flash	13-16
Other Flash Specifications	13-16
Three-Phase Flash	13-16
Complex Mixtures	13-16

GRAPHICAL METHODS FOR BINARY DISTILLATION

Phase Equilibrium Diagrams	13-17
McCabe-Thiele Method	13-18
Operating Lines	13-18
Thermal Condition of the Feed	13-19
Equilibrium-Stage Construction	13-19
Total Column Construction	13-21
Feed-Stage Location	13-22
Minimum Stages	13-22
Minimum Reflux	13-24
Intermediate Reboilers and Condensers	13-24
Optimum Reflux Ratio	13-24
Difficult Separations	13-24

Equation-Based Design Methods	13-25
Stage Efficiency	13-25
Miscellaneous Operations	13-25

APPROXIMATE MULTICOMPONENT DISTILLATION METHODS

Fenske-Underwood-Gilliland (FUG) Shortcut Method	13-25
Example 1: Calculation of FUG Method	13-26
Kremser Equation	13-28
Example 2: Calculation of Kremser Method	13-28

SIMULATION OF DISTILLATION PROCESSES

Equilibrium-Stage Modeling	13-30
The MESH Equations (The $2c + 3$ Formulation)	13-30
Degrees-of-Freedom Analysis and Problem Formulation	13-31
The $2c + 1$ Formulation	13-32
The $c + 3$ Formulation	13-32
Condenser and Reboiler	13-32
Solution of the MESH Equations	13-32
Tearing Methods	13-33
Inside-Out Methods	13-33
Simultaneous Convergence Methods	13-33
Continuation Methods (for Really Difficult Problems)	13-33
Other Methods	13-34
Examples	13-34
Example 3: Simple Distillation Column	13-34
Example 4: Light Hydrocarbon Distillation	13-36
Example 5: Absorber	13-38
Example 6: Reboiled Stripper	13-38
Example 7: An Industrial <i>i</i> -Butane/ <i>n</i> -Butane Fractionator	13-41
Efficiencies	13-43
Example 8: The Industrial <i>i</i> -Butane/ <i>n</i> -Butane Fractionator (Again)	13-44
Example 9: HETP of a Packed Absorber	13-45

* Certain portions of this section draw heavily on the work of J. D. Seader, Jeffrey J. Sirola, and Scott D. Barnicki, authors of this section in the 7th edition.

13-2 DISTILLATION

Using a Simulator to Solve Distillation Problems	13-45
Example 10: Multiple Steady States in Distillation.....	13-46
Nonequilibrium Modeling	13-46
Degrees of Freedom.....	13-49
Physical Properties	13-49
Flow Models	13-49
Mass-Transfer Coefficients.....	13-50
Example 11: Mass-Transfer Coefficient in a Tray Column.....	13-50
Example 12: Mass-Transfer Coefficients in a Packed Column.....	13-51
Solving the NEQ Model Equations.....	13-51
Equipment Design	13-51
Example 13: A Nonequilibrium Model of a C_4 Splitter	13-51
Maxwell-Stefan Approach	13-52
Example 14: The Need for Rigorous Maxwell-Stefan-Based NEQ Models	13-52
Software for Distillation Column Simulations	13-55

DEGREES OF FREEDOM AND DESIGN VARIABLES

Definitions	13-55
Analysis of Elements	13-56
Analysis of Units	13-56
Other Units and Complex Processes	13-58

DISTILLATION SYSTEMS

Possible Configurations of Distillation Columns	13-59
Thermally Coupled Systems and Dividing Wall Columns	13-60
Thermodynamic Efficiency	13-65
Heat Integration	13-65
Imbalanced Feeds	13-67

ENHANCED DISTILLATION

Azeotropy	13-68
Residue Curve Maps and Distillation Region Diagrams	13-69
Applications of RCM and DRD.....	13-71
Azeotropic Distillation	13-81
Exploiting Homogeneous Azeotropes	13-81

Exploiting Pressure Sensitivity.....	13-82
Exploiting Boundary Curvature	13-83
Exploiting Azeotropy and Liquid-Phase Immiscibility.....	13-85
Design and Operation of Azeotropic Distillation Columns	13-87
Extractive Distillation	13-87
Solvent Effects in Extractive Distillation.....	13-88
Extractive Distillation Design and Optimization	13-89
Solvent Screening and Selection	13-91
Extractive Distillation by Salt Effects	13-93
Reactive Distillation	13-93
Simulation, Modeling, and Design Feasibility	13-94
Mechanical Design and Implementation Issues	13-95
Process Applications	13-97
Synthesis of Multicomponent Separation Systems	13-98

PETROLEUM AND COMPLEX-MIXTURE DISTILLATION

Characterization of Petroleum and Petroleum Fractions.....	13-99
Applications of Petroleum Distillation	13-102
Design Procedures	13-103
Example 15: Simulation Calculation of an Atmospheric Tower.....	13-107

BATCH DISTILLATION

Simple Batch Distillation	13-109
Batch Distillation with Rectification	13-109
Operating Methods	13-110
Approximate Calculation Procedures for Binary Mixtures.....	13-111
Batch Rectification at Constant Reflux	13-112
Batch Rectification at Constant Distillate Composition.....	13-113
Other Operating Methods and Optimization	13-113
Effects of Column Holdup.....	13-113
Shortcut Methods for Multicomponent Batch Rectification	13-114
Calculation Methods and Simulation	13-114
Constant-Level Distillation	13-114
Alternative Equipment Configurations	13-115
Batch Distillation of Azeotropic Mixtures	13-116

Nomenclature and Units

Symbol	Definition	SI units	U.S. Customary System units	Symbol	Definition	SI units	U.S. Customary System units
<i>A</i>	Absorption factor			<i>h</i>	Height	m	ft
<i>A</i>	Area	m ²	ft ²	<i>h</i>	Heat-transfer coefficient	kW/m ²	Btu/(ft ² ·h)
<i>C</i>	Number of chemical species			<i>k</i>	Mass-transfer coefficient	m/s	ft/h
<i>D</i>	Distillate flow rate	kg·mol/s	lb·mol/h	<i>l</i>	Component flow rate in liquid	kg·mol/s	lb·mol/h
<i>D</i>	Diffusion coefficient	m ² /s	ft ² /h	<i>p</i>	Pressure	kPa	psia
<i>E</i>	Efficiency			<i>q</i>	Measure of thermal condition of feed		
<i>E</i>	Energy flux	kW/m ²	Btu/(ft ² ·h)	<i>q</i>	Heat flux	kW/m ²	Btu/(ft ² ·h)
<i>E</i>	Energy transfer rate	kW	Btu/h	<i>q_c</i>	Condenser duty	kW	Btu/h
<i>F</i>	Feed flow rate	kg·mol/s	lb·mol/h	<i>q_r</i>	Reboiler duty	kW	Btu/h
<i>H</i>	Column height	m	ft	<i>r</i>	Sidestream ratio		
<i>H</i>	Enthalpy	J/(kg·mol)	Btu/(lb·mol)	<i>s</i>	Liquid-sidestream ratio		
<i>H</i>	Liquid holdup	kg·mol	lb·mol	<i>t</i>	Time	s	h
<i>H</i>	Height of a transfer unit	m	ft	<i>u</i>	Velocity	m/s	ft/h
<i>K</i>	Vapor-liquid equilibrium ratio (<i>K</i> value)			<i>v</i>	Component flow rate in vapor	kg·mol/s	lb·mol/h
<i>K_D</i>	Chemical equilibrium constant for dimerization			<i>w</i>	Weight fraction		
<i>K_L</i>	Liquid-liquid distribution ratio			<i>x</i>	Mole fraction in liquid		
<i>L</i>	Liquid flow rate	kg·mol/s	lb·mol/h	<i>y</i>	Mole fraction in vapor		
<i>N</i>	Number of equilibrium stages			<i>z</i>	Mole fraction in feed		
<i>N_c</i>	Number of relationships			Creek Symbols			
<i>N_i</i>	Number of design variables			<i>α</i>	Relative volatility		
<i>N_{min}</i>	Minimum number of equilibrium stages			<i>γ</i>	Activity coefficient		
<i>N_p</i>	Number of phases			<i>ε</i>	TBK efficiency		
<i>N_r</i>	Number of repetition variables			<i>ξ</i>	Dimensionless time		
<i>N_o</i>	Number of variables			<i>ρ</i>	Density	kg/m ³	lb/ft ³
<i>N_l</i>	Rate of mass transfer	kg·mol/s	lb·mol/h	<i>μ</i>	Viscosity	N/m ²	
<i>N</i>	Molar flux	kg·mol/(m ² ·s)	lb·mol/(ft ² ·h)	<i>σ</i>	Surface tension	N/m	
<i>N</i>	Number of transfer units			<i>θ</i>	Time for batch distillation	s	h
<i>P</i>	Pressure	Pa	psia	<i>Θ</i>	Parameter in Underwood equations		
<i>P^{sat}</i>	Vapor pressure	Pa	psia	<i>Φ</i>	Fugacity coefficient of pure component		
<i>Q</i>	Heat-transfer rate	kW	Btu/h	<i>Φ̂</i>	Fugacity coefficient in mixture		
<i>Q_c</i>	Condenser duty	kW	Btu/h	<i>Φ_A</i>	Fraction of a component in feed vapor that is not absorbed		
<i>Q_r</i>	Reboiler duty	kW	Btu/h	<i>Φ_S</i>	Fraction of a component in entering liquid that is not stripped		
<i>R</i>	External-reflux ratio			<i>Ψ</i>	Factor in Gilliland correlation		
<i>R_{min}</i>	Minimum-reflux ratio			Subscripts and Superscripts			
<i>S</i>	Sidestream flow rate	kg·mol/s	lb·mol/h	EQ	Equilibrium		
<i>S</i>	Stripping factor			<i>f</i>	Froth		
<i>S</i>	Vapor-sidestream ratio			<i>hk</i>	Heavy key		
<i>Sc</i>	Schmidt number			<i>i</i>	Component index		
<i>T</i>	Temperature	K	°R	<i>j</i>	Stage index		
<i>U</i>	Liquid-sidestream rate	kg·mol/s	lb·mol/h	<i>L</i>	Liquid		
<i>V</i>	Vapor flow rate	kg·mol/s	lb·mol/h	<i>lk</i>	Light key		
<i>W</i>	Vapor-sidestream rate	kg·mol/s	lb·mol/h	<i>MV</i>	Murphree vapor		
<i>X</i>	Relative mole fraction in liquid phase			<i>o</i>	Overall		
<i>Y</i>	Relative mole fraction in vapor phase			<i>s</i>	Superficial		
<i>a</i>	Activity			<i>t</i>	Mixture or total		
<i>a</i>	Area	m ²	ft ²	<i>V</i>	Vapor		
<i>b</i>	Component flow rate in bottoms	kg·mol/s	lb·mol/h	<i>°</i>	Equilibrium composition		
<i>c</i>	Number of chemical species			Acronyms			
<i>c</i>	Molar density	kg·mol/m ³	lb·mol/ft ³	HETP	Height equivalent to a theoretical plate		
<i>d</i>	Component flow rate in distillate	kg·mol/s	lb·mol/h	n.b.p.	Normal boiling point (1-atm pressure)		
<i>d</i>	Mass-transfer driving force			NTU	Number of transfer units		
<i>e</i>	Rate of heat transfer	kW	Btu/h				
<i>f</i>	Component flow rate in feed	kg·mol/s	lb·mol/h				
<i>f</i>	Fugacity	Pa	psia				

GENERAL REFERENCES: Billet, *Distillation Engineering*, Chemical Publishing, New York, 1979. Doherty and Malone, *Conceptual Design of Distillation Systems*, McGraw-Hill, New York, 2001. Fair and Bolles, "Modern Design of Distillation Columns," *Chem. Eng.*, **75**(9), 156 (Apr. 22, 1968). Fredenslund, Gmehling, and Rasmussen, *Vapor-Liquid Equilibria Using UNIFAC, A Group Contribution Method*, Elsevier, Amsterdam, 1977. Friday and Smith, "An Analysis of the Equilibrium Stage Separation Problem—Formulation and Convergence," *AIChE J.*, **10**, 698 (1964). Hengstebeck, *Distillation—Principles and Design Procedures*, Reinhold, New York, 1961. Henley and Seader, *Equilibrium-Stage Separation Operations in Chemical Engineering*, Wiley, New York, 1981. Hoffman, *Azeotropic and Extractive Distillation*, Wiley, New York, 1964. Holland, *Fundamentals and Modeling of Separation Processes*, Prentice-Hall, Englewood Cliffs, N.J., 1975. Holland, *Fundamentals of Multicomponent Distillation*, McGraw-Hill,

New York, 1981. King, *Separation Processes*, 2d ed., McGraw-Hill, New York, 1980. Kister, *Distillation Design*, McGraw-Hill, New York, 1992. Kister, *Distillation Operation*, McGraw-Hill, New York, 1990. Robinson and Gilliland, *Elements of Fractional Distillation*, 4th ed., McGraw-Hill, New York, 1950. Rousseau, ed., *Handbook of Separation Process Technology*, Wiley-Interscience, New York, 1987. Seader, "The B. C. (Before Computers) and A.D. of Equilibrium-Stage Operations," *Chem. Eng. Educ.*, **14**(2) (Spring 1985). Seader, *Chem. Eng. Progress*, **85**(10), 41 (1989). Smith, *Design of Equilibrium Stage Processes*, McGraw-Hill, New York, 1963. Seader and Henley, *Separation Process Principles*, Wiley, New York, 1998. Taylor and Krishna, *Multicomponent Mass Transfer*, Wiley, New York, 1993. Treybal, *Mass Transfer Operations*, 3d ed., McGraw-Hill, New York, 1980. *Ullmann's Encyclopedia of Industrial Chemistry*, vol. **B3**, VCH, Weinheim, 1988. Van Winkle, *Distillation*, McGraw-Hill, New York, 1967.

INTRODUCTION TO DISTILLATION OPERATIONS

GENERAL PRINCIPLES

Separation operations achieve their objective by the creation of two or more coexisting zones which differ in temperature, pressure, composition, and/or phase state. Each molecular species in the mixture to be separated responds in a unique way to differing environments offered by these zones. Consequently, as the system moves toward equilibrium, each species establishes a different concentration in each zone, and this results in a separation between the species.

The separation operation called *distillation* utilizes vapor and liquid phases at essentially the same temperature and pressure for the coexisting zones. Various kinds of devices such as *random* or *structured packings* and *plates* or *trays* are used to bring the two phases into intimate contact. Trays are stacked one above the other and enclosed in a cylindrical shell to form a *column*. Packings are also generally contained in a cylindrical shell between hold-down and support plates. The column may be operated continuously or in batch mode depending on a number of factors such as scale and flexibility of operations and solids content of feed. A typical tray-type continuous distillation column plus major external accessories is shown schematically in Fig. 13-1.

The *feed* material, which is to be separated into fractions, is introduced at one or more points along the column shell. Because of the difference in density between vapor and liquid phases, liquid runs down the column, cascading from tray to tray, while vapor flows up the column, contacting liquid at each tray.

Liquid reaching the bottom of the column is partially vaporized in a heated *reboiler* to provide *boil-up*, which is sent back up the column. The remainder of the bottom liquid is withdrawn as *bottoms*, or bottom product. Vapor reaching the top of the column is cooled and condensed to liquid in the *overhead condenser*. Part of this liquid is returned to the column as *reflux* to provide liquid overflow. The remainder of the overhead stream is withdrawn as *distillate*, or overhead product. In some cases only part of the vapor is condensed so that a vapor distillate can be withdrawn.

This overall flow pattern in a distillation column provides counter-current contacting of vapor and liquid streams on all the trays through the column. Vapor and liquid phases on a given tray approach thermal, pressure, and composition equilibria to an extent dependent upon the efficiency of the contacting tray.

The *lighter* (lower-boiling temperature) components tend to concentrate in the vapor phase, while the *heavier* (higher-boiling temperature) components concentrate in the liquid phase. The result is a vapor phase that becomes richer in light components as it passes up the column and a liquid phase that becomes richer in heavy components as it cascades downward. The overall separation achieved between the distillate and the bottoms depends primarily on the *relative volatilities* of the components, the number of contacting trays in each column section, and the ratio of the liquid-phase flow rate to the vapor-phase flow rate in each section.

If the feed is introduced at one point along the column shell, the column is divided into an upper section, which is often called the *rectifying* section, and a lower section, which is often referred to as the *stripping* section. In *multiple-feed* columns and in columns from

which a liquid or vapor *sidestream* is withdrawn, there are more than two column sections between the two end-product streams. The notion of a column section is a useful concept for finding alternative *systems* (or *sequences*) of columns for separating multicomponent mixtures, as described below in the subsection Distillation Systems.

All separation operations require energy input in the form of heat or work. In the conventional distillation operation, as typified in Fig. 13-1, energy required to separate the species is added in the form of heat to the reboiler at the bottom of the column, where the temperature is highest. Also heat is removed from a condenser at the top of the column, where the temperature is lowest. This frequently results in a

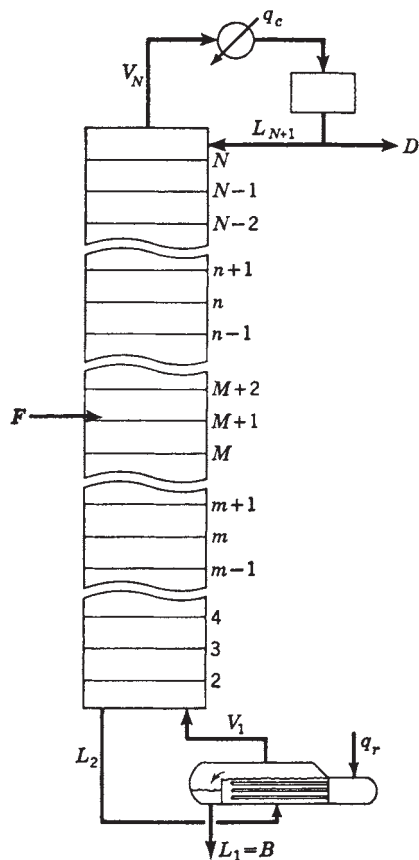


FIG. 13-1 Schematic diagram and nomenclature for a simple continuous distillation column with one feed, a total overhead condenser, and a partial reboiler.

large energy-input requirement and low overall thermodynamic efficiency, especially if the heat removed in the condenser is wasted. Complex distillation operations that offer higher thermodynamic efficiency and lower energy-input requirements have been developed and are also discussed below in the subsection Distillation Systems.

Batch distillation is preferred for small feed flows or seasonal production which is carried out intermittently in "batch campaigns." In this mode the feed is charged to a still which provides vapor to a column where the separation occurs. Vapor leaving the top of the column is condensed to provide liquid reflux back to the column as well as a distillate stream containing the product. Under normal operation, this is the only stream leaving the device. In addition to the batch rectifier just described, other batch configurations are possible as discussed in the subsection Batch Distillation. Many of the concepts and methods discussed for continuous distillation are useful for developing models and design methods for batch distillation.

EQUILIBRIUM AND NONEQUILIBRIUM-STAGE CONCEPTS

The transfer processes taking place in an actual distillation column are a complicated interplay between the thermodynamic phase equilibrium properties of the mixture, rates of intra- and interphase mass and energy transport, and multiphase flows. Simplifications are necessary to develop tractable models. The landmark concept of the *equilibrium-stage model* was developed by Sorel in 1893, in which the liquid in each stage is considered to be well mixed and such that the vapor and liquid streams leaving the stage are in thermodynamic equilibrium with each other. This is needed so that thermodynamic phase equilibrium relations can be used to determine the temperature and composition of the equilibrium streams at a given pressure. A hypothetical column composed of equilibrium stages (instead of actual contact trays) is

designed to accomplish the separation specified for the actual column. The number of hypothetical equilibrium stages required is then converted to a number of actual trays by means of *tray efficiencies*, which describe the extent to which the performance of an actual contact tray duplicates the performance of an equilibrium stage. Alternatively and preferably, tray inefficiencies can be accounted for by using rate-based models that are described below.

Use of the equilibrium-stage concept separates the design of a distillation column into three major steps: (1) Thermodynamic data and methods needed to predict equilibrium-phase compositions are assembled. (2) The number of equilibrium stages and the energy input required to accomplish a specified separation, or the separation that will be accomplished in a given number of equilibrium stages for a given energy input, are calculated. (3) The number of equilibrium stages is converted to an equivalent number of actual contact trays or height of packing, and the column diameter is determined. Much of the third step is eliminated if a rate-based model is used. This section deals primarily with equilibrium and rate-based models of distillation. Section 4 covers the first step, but a summary of methods and some useful data are included in this section. Section 14 covers equipment design.

RELATED SEPARATION OPERATIONS

The simple and complex distillation operations just described all have two things in common: (1) Both rectifying and stripping sections are provided so that a separation can be achieved between two components that are adjacent in volatility; and (2) the separation is effected only by the addition and removal of energy and not by the addition of any mass separating agent (MSA) such as in liquid-liquid extraction.

Sometimes, alternative single- or multiple-stage vapor-liquid separation operations, of the types shown in Fig. 13-2, may be more suitable than distillation for the specified task.

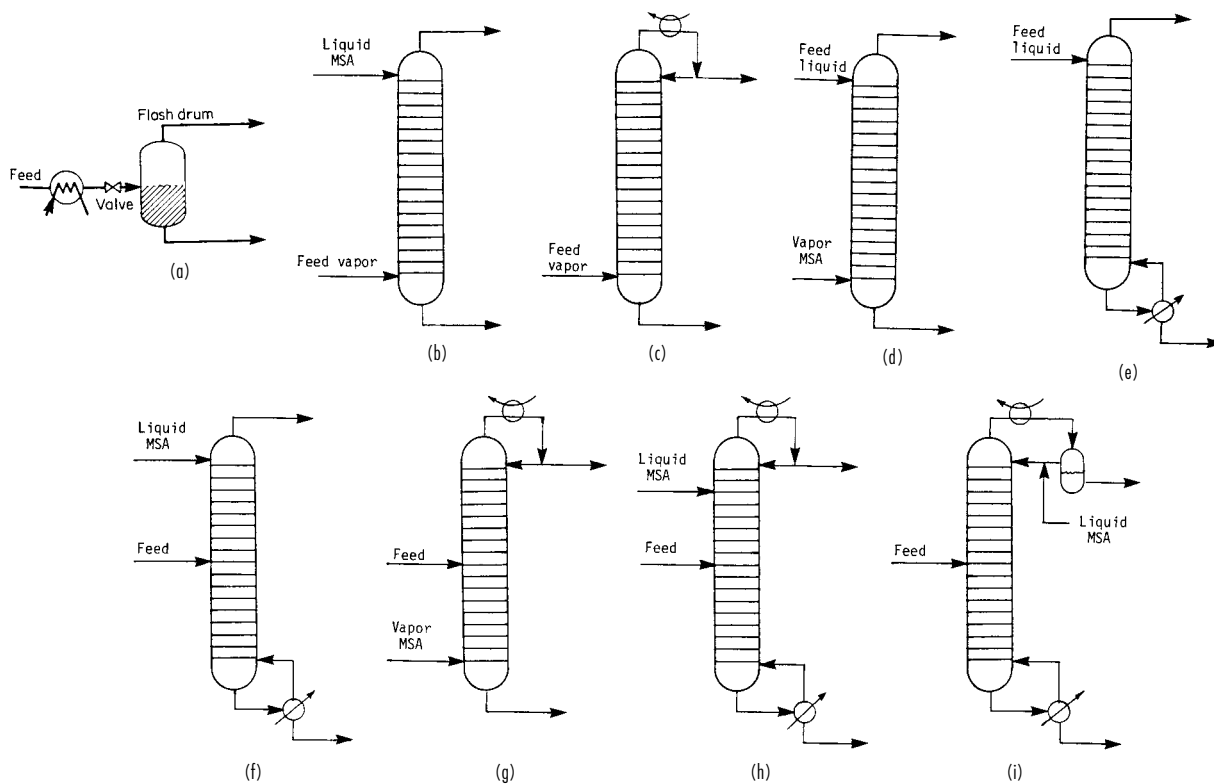


FIG. 13-2 Separation operations related to distillation. (a) Flash vaporization or partial condensation. (b) Absorption. (c) Rectifier. (d) Stripping. (e) Reboiled stripping. (f) Reboiled absorption. (g) Refluxed stripping. (h) Extractive distillation. (i) Azeotropic distillation.

A single-stage flash, as shown in Fig. 13-2a, may be appropriate if (1) the relative volatility between the two components to be separated is very large; (2) the recovery of only one component in one of the two product streams is to be achieved, without regard to the separation of the other components; or (3) only a partial separation is to be made. A common example is the separation of light gases such as hydrogen and methane from aromatics. The desired temperature and pressure of a flash may be established by the use of heat exchangers, a valve, a compressor, and/or a pump upstream of the vessel, used to separate the product vapor and liquid phases. Depending on the original condition of the feed, it may be partially condensed or partially vaporized in a so-called flash operation.

If the recovery of only one component is required rather than a sharp separation between two components of adjacent volatility, their absorption or stripping in a single section of stages may be sufficient. If the feed is vapor at separation conditions, absorption is used either with a liquid MSA absorbent of relatively low volatility, as in Fig. 13-2b, or with reflux produced by an overhead partial condenser, as in Fig. 13-2c. The choice usually depends on the ease of partially condensing the overhead vapor or of recovering and recycling the absorbent. If the feed is liquid at separation conditions, stripping is used, either with an externally supplied vapor stripping agent of relatively high volatility, as shown in Fig. 13-2d, or with boil-up produced by a partial reboiler, as in Fig. 13-2e. The choice depends on the ease of partially reboiling the bottoms or of recovering and recycling the stripping agent.

If a relatively sharp separation is required between two components of adjacent volatility, but either an undesirably low temperature is required to produce reflux at the column operating pressure or an undesirably high temperature is required to produce boil-up, then refluxed stripping, as shown in Fig. 13-2g, or reboiled absorption, as shown in Fig. 13-2f, may be used. In either case, the choice of MSA follows the same consideration given for simple absorption and stripping.

When the volatility difference between the two components to be separated is so small that a very large number of stages would be required, then extractive distillation, as shown in Fig. 13-2h, should be considered. Here, an MSA is selected that increases the volatility difference sufficiently to reduce the stage requirement to a reasonable number. Usually, the MSA is a polar compound of low volatility that leaves in the bottoms, from which it is recovered and recycled. It is introduced in an appreciable amount near the top stage of the column so as to affect the volatility difference over most of the stages. Some reflux to the top stage is used to minimize the MSA content in the distillate. An alternative to extractive distillation is azeotropic distillation, which is shown in Fig. 13-2i in just one of its many modes. In a common mode, an MSA that forms a heterogeneous minimum-boiling azeotrope with one or more components of the feed is used. The azeotrope is taken overhead, and the MSA-rich phase is decanted and returned to the top of the column as reflux.

Numerous other multistaged configurations are possible. One important variation of a stripper, shown in Fig. 13-2d, is a refluxed stripper, in which an overhead condenser is added. Such a configuration is sometimes used to steam-strip sour water containing NH_3 , H_2O , phenol, and HCN.

All the separation operations shown in Fig. 13-2, as well as the simple and complex distillation operations described earlier, are referred to here as distillation-type separations because they have much in common with respect to calculations of (1) thermodynamic properties, (2) vapor-liquid equilibrium stages, and (3) column sizing. In fact, as will be evident from the remaining treatment of this section, the trend is toward single generalized digital computer program packages that compute many or all distillation-type separation operations.

This section also includes a treatment of distillation-type separations from a rate-based point of view that uses principles of mass- and heat-transfer rates. Section 14 also presents details of that subject as applied to absorption and stripping.

THERMODYNAMIC DATA AND MODELS

Reliable thermodynamic data are essential for the accurate design or analysis of distillation columns. Failure of equipment to perform at specified levels is often attributable, at least in part, to the lack of such data.

This subsection summarizes and presents examples of phase equilibrium data currently available to the designer. The thermodynamic concepts used are presented in the subsection Thermodynamics of Sec. 4.

PHASE EQUILIBRIUM DATA

For a binary mixture, pressure and temperature fix the equilibrium vapor and liquid compositions. Thus, experimental data are frequently presented in the form of tables of vapor mole fraction y and liquid mole fraction x for one constituent over a range of temperature T for a fixed pressure P or over a range of pressure for a fixed temperature. A small selection of such data, at a pressure of 101.3 kPa (1 atm, 1.013 bar), for four nonideal binary systems is given in Table 13-1. More extensive presentations and bibliographies of such data may be found in Hala, Wichterle, Polak, and Boublik (*Vapor-Liquid Equilibrium Data at Normal Pressures*, Pergamon, Oxford, 1968); Hirata, Ohe, and Nagahama (*Computer Aided Data Book of Vapor-Liquid Equilibria*, Elsevier, Amsterdam, 1975); Wichterle, Linek, and Hala (*Vapor-Liquid Equilibrium Data Bibliography*, Elsevier, Amsterdam, 1973, Supplement I, 1976, Supplement II, 1979); Ohe (*Vapor-Liquid Equilibrium Data*, Elsevier, Amsterdam, 1989); Ohe (*Vapor-Liquid Equilibrium Data at High Pressure*, Elsevier, Amsterdam, 1990); Walas (*Phase Equilibria in Chemical Engineering*, Butterworth, Boston, 1985); and, particularly, Gmehling and Onken [*Vapor-Liquid Equilibrium Data Collection*, DECHEMA Chemistry Data ser., vol. 1 (parts 1–10), Frankfurt, 1977]. Extensive databases of phase equilibrium measurements are readily available in most process simulators together with models for correlating, interpolating, and extrapolating

(care is needed here) the data. Many of these simulators also provide graphical display of the data for easy visualization and interpretation.

For application to distillation (a nearly isobaric process) binary-mixture data are frequently plotted, for a fixed pressure, as y versus x , with a line of 45° slope included for reference, and as T versus y and x , as shown in Figs. 13-3 to 13-8. In some binary systems, one of the components is more volatile than the other over the entire composition range. This is the case in Figs. 13-3 and 13-4 for the benzene-toluene system at pressures of both 101.3 and 202.6 kPa (1 and 2 atm), where benzene is more volatile than toluene.

For other binary systems, one of the components is more volatile over only a part of the composition range. Two systems of this type, ethyl acetate-ethanol and chloroform-acetone, are shown in Figs. 13-5 to 13-7. Figure 13-5 shows that chloroform is less volatile than acetone below a concentration of 66 mol % chloroform and that ethyl acetate is more volatile than ethanol below a concentration of 53 mol % ethyl acetate. Above these concentrations, volatility is reversed. Such mixtures are known as azeotropic mixtures, and the composition in which the reversal occurs, which is the composition in which vapor and liquid compositions are equal, is the azeotropic composition, or azeotrope. The azeotropic liquid may be homogeneous or heterogeneous (two immiscible liquid phases). Two of the binary mixtures of Table 13-1 form homogeneous azeotropes. Non-azeotrope-forming mixtures such as benzene and toluene in Figs. 13-3 and 13-4 can be separated by simple distillation into two essentially pure products. By contrast, simple distillation of azeotropic mixtures will at best yield the azeotrope and one essentially pure species. The distillate and bottoms products obtained depend upon the feed composition and whether a minimum-boiling azeotrope is formed as with the ethyl acetate-ethanol mixture in Fig. 13-6 or a maximum-boiling azeotrope is formed as with the chloroform-acetone mixture in Fig. 13-7. For example, if a mixture of 30 mol % chloroform and 70 mol % acetone is fed to a simple distillation column, such as that

TABLE 13-1 Constant-Pressure Liquid-Vapor Equilibrium Data for Selected Binary Systems

Component		Temperature, °C	Mole fraction A in		Total pressure, kPa	Reference				
A	B		Liquid	Vapor						
Acetone	Chloroform	62.50	0.0817	0.0500	101.3	1				
		62.82	0.1390	0.1000						
		63.83	0.2338	0.2000						
		64.30	0.3162	0.3000						
		64.37	0.3535	0.3500						
		64.35	0.3888	0.4000						
		64.02	0.4582	0.5000						
		63.33	0.5299	0.6000						
		62.23	0.6106	0.7000						
		60.72	0.7078	0.8000						
		58.71	0.8302	0.9000						
		57.48	0.9075	0.9500						
		Acetone	Water	74.80			0.0500	0.6381	101.3	2
				68.53			0.1000	0.7301		
65.26	0.1500			0.7716						
63.59	0.2000			0.7916						
61.87	0.3000			0.8124						
60.75	0.4000			0.8269						
59.95	0.5000			0.8387						
59.12	0.6000			0.8532						
58.29	0.7000			0.8712						
57.49	0.8000			0.8950						
56.68	0.9000			0.9335						
56.30	0.9500			0.9627						
Ethyl acetate	Ethanol			78.3	0.0	0.0	101.3	3		
		76.6	0.050	0.102						
		75.5	0.100	0.187						
		73.9	0.200	0.305						
		72.8	0.300	0.389						
		72.1	0.400	0.457						
		71.8	0.500	0.516						
		71.8	0.540	0.540						
		71.9	0.600	0.576						
		72.2	0.700	0.644						
		73.0	0.800	0.726						
		74.7	0.900	0.837						
		76.0	0.950	0.914						
		77.1	1.000	1.000						
Ethylene glycol	Water	69.5	0.0	0.0	30.4	4				
		76.1	0.23	0.002						
		78.9	0.31	0.003						
		83.1	0.40	0.010						
		89.6	0.54	0.020						
		103.1	0.73	0.06						
		118.4	0.85	0.13						
		128.0	0.90	0.22						
		134.7	0.93	0.30						
		145.0	0.97	0.47						
		160.7	1.00	1.00						

NOTE: To convert degrees Celsius to degrees Fahrenheit, °C = (°F - 32)/1.8. To convert kilopascals to pounds-force per square inch, multiply by 0.145.

¹Kojima, Kato, Sunaga, and Hashimoto, *Kagaku Kogaku*, **32**, 337 (1968).

²Kojima, Tochigi, Seki, and Watase, *Kagaku Kogaku*, **32**, 149 (1968).

³Chu, Getty, Brennecke, and Paul, *Distillation Equilibrium Data*, New York, 1950.

⁴Trimble and Potts, *Ind. Eng. Chem.*, **27**, 66 (1935).

shown in Fig. 13-1, operating at 101.3 kPa (1 atm), the distillate could approach pure acetone and the bottoms could approach the maximum-boiling azeotrope.

An example of heterogeneous-azeotrope formation is shown in Fig. 13-8 for the water-normal butanol system at 101.3 kPa. At liquid compositions between 0 and 3 mol % butanol and between 40 and 100 mol % butanol, the liquid phase is homogeneous. Phase splitting into two separate liquid phases (one with 3 mol % butanol and the other with 40 mol % butanol) occurs for any overall liquid composition between 3 and 40 mol % butanol. A minimum-boiling heterogeneous azeotrope occurs at 92°C (198°F) when the vapor composition and the overall composition of the two liquid phases are 25 mol % butanol.

For mixtures containing more than two species, an additional degree of freedom is available for each additional component. Thus, for a four-component system, the equilibrium vapor and liquid compositions are fixed only if the pressure, temperature, and mole fractions of two com-

ponents are set. Representation of multicomponent vapor-liquid equilibrium data in tabular or graphical form of the type shown earlier for binary systems is either difficult or impossible. Instead, such data, as well as binary-system data, are commonly represented in terms of K values (vapor-liquid equilibrium ratios), which are defined by

$$K_i = \frac{y_i}{x_i} \quad (13-1)$$

and are correlated empirically or theoretically in terms of temperature, pressure, and phase compositions in the form of tables, graphs, and equations. The K values are widely used in multicomponent distillation calculations, and the ratio of the K values of two species, called the relative volatility,

$$\alpha_{ij} = \frac{K_i}{K_j} \quad (13-2)$$

13-8 DISTILLATION

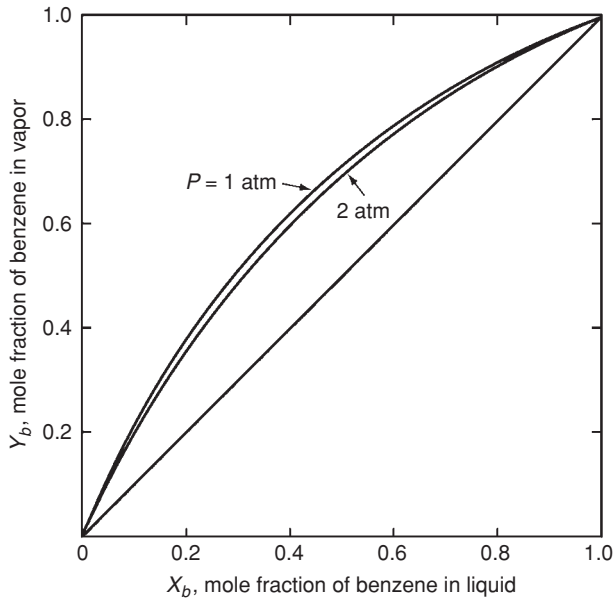


FIG. 13-3 Isobaric y - x curves for benzene-toluene. (Brian, Staged Cascades in Chemical Processing, Prentice-Hall, Englewood Cliffs, N.J., 1972.)

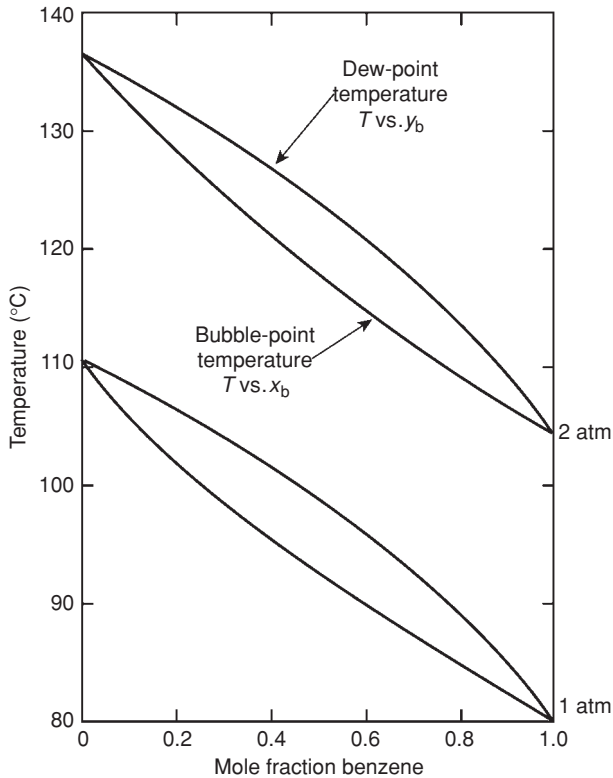


FIG. 13-4 Isobaric vapor-liquid equilibrium curves for benzene-toluene. (Brian, Staged Cascades in Chemical Processing, Prentice-Hall, Englewood Cliffs, N.J., 1972.)

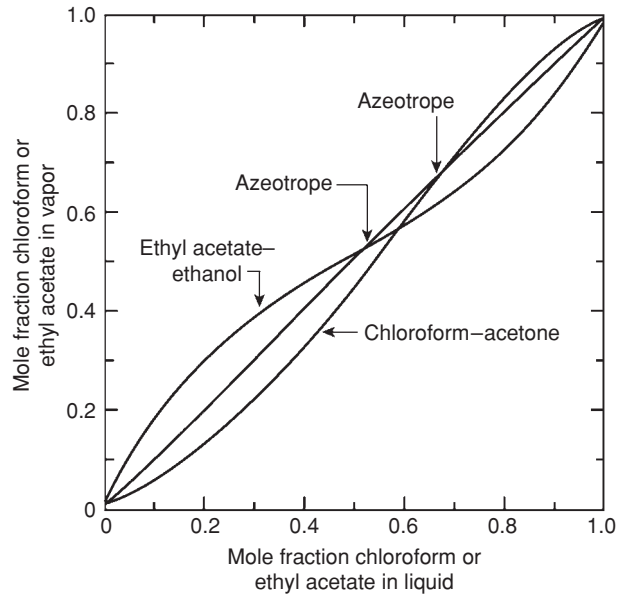


FIG. 13-5 Vapor-liquid equilibria for the ethyl acetate-ethanol and chloroform-acetone systems at 101.3 kPa (1 atm).

is a convenient index of the relative ease or difficulty of separating components i and j by distillation. Rarely is distillation used on a large scale if the relative volatility is less than 1.05, with i more volatile than j .

GRAPHICAL K VALUE CORRELATIONS

As discussed in Sec. 4, the K value of a species is a complex function of temperature, pressure, and equilibrium vapor- and liquid-phase compositions. However, for mixtures of compounds of similar molecular structure and size, the K value depends mainly on temperature and pressure. For example, several major graphical K value correlations are available for light-hydrocarbon systems. The easiest to use are the DePriester charts [*Chem. Eng. Prog. Symp. Ser. 7*, **49**, 1 (1953)],

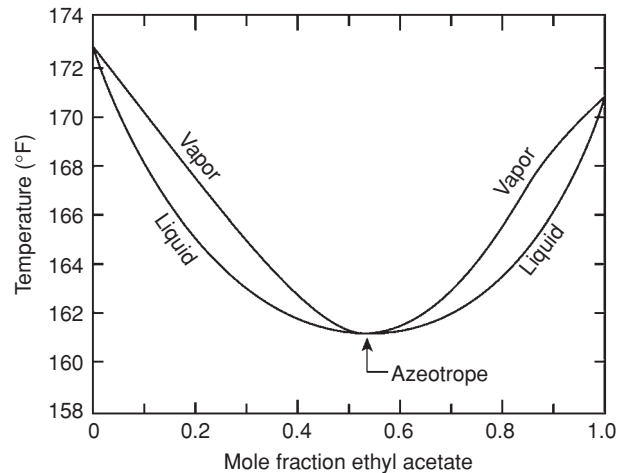


FIG. 13-6 Liquid boiling points and vapor condensation temperatures for minimum-boiling azeotropic mixtures of ethyl acetate and ethanol at 101.3-kPa (1-atm) total pressure.

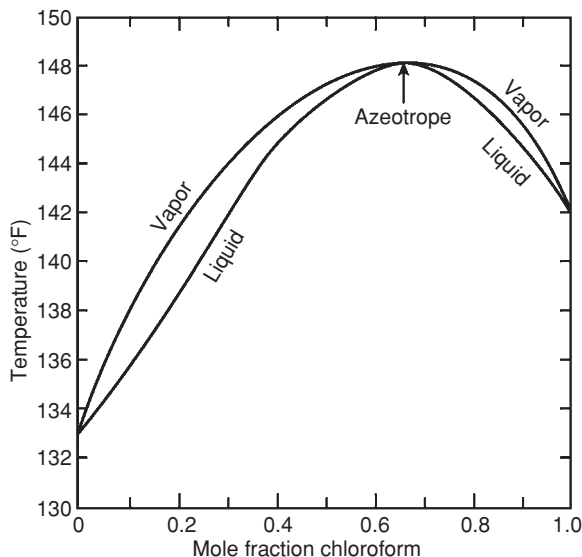


FIG. 13-7 Liquid boiling points and vapor condensation temperatures for maximum-boiling azeotrope mixtures of chloroform and acetone at 101.3-kPa (1-atm) total pressure.

which cover 12 hydrocarbons (methane, ethylene, ethane, propylene, propane, isobutane, isobutylene, *n*-butane, isopentane, *n*-pentane, *n*-hexane, and *n*-heptane). These charts are a simplification of the Kellogg charts (*Liquid-Vapor Equilibria in Mixtures of Light Hydrocarbons*, MWK Equilibrium Constants, *Polyco Data*, 1950) and include additional experimental data. The Kellogg charts, and hence the DePriester charts, are based primarily on the Benedict-Webb-Rubin equation of state [*Chem. Eng. Prog.*, **47**, 419 (1951); **47**, 449 (1951)], which can represent both the liquid and the vapor phases and can predict *K* values quite accurately when the equation constants are available for the components in question.

A trial-and-error procedure is required with any *K* value correlation that takes into account the effect of composition. One cannot calculate *K* values until phase compositions are known, and those cannot be known until the *K* values are available to calculate them. For *K* as a

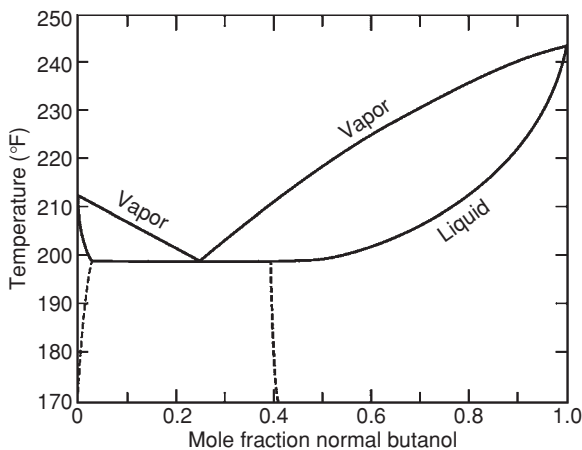


FIG. 13-8 Vapor-liquid equilibrium data for an *n*-butanol-water system at 101.3 kPa (1 atm); phase splitting and heterogeneous-azeotrope formation.

function of *T* and *P* only, the DePriester charts provide good starting values for the iteration. These nomographs are shown in Fig. 13-9a and b. SI versions of these charts have been developed by Dadyburjor [*Chem. Eng. Prog.*, **74**(4), 85 (1978)].

The Kellogg and DePriester charts and their subsequent extensions and generalizations use the molar average boiling points of the liquid and vapor phases to represent the composition effect. An alternative measure of composition is the convergence pressure of the system, which is defined as that pressure at which the *K* values for all the components in an isothermal mixture converge to unity. It is analogous to the critical point for a pure component in the sense that the two phases become indistinguishable. The behavior of a complex mixture of hydrocarbons for a convergence pressure of 34.5 MPa (5000 psia) is illustrated in Fig. 13-10.

Two major graphical correlations based on convergence pressure as the third parameter (besides temperature and pressure) are the charts published by the Gas Processors Association (GPA, *Engineering Data Book*, 9th ed., Tulsa, 1981) and the charts of the American Petroleum Institute (API, *Technical Data Book—Petroleum Refining*, New York, 1966) based on the procedures from Hadden and Grayson [*Hydrocarbon Process., Pet. Refiner*, **40**(9), 207 (1961)]. The former uses the method proposed by Hadden [*Chem. Eng. Prog. Symp. Ser. 7*, **49**, 53 (1953)] for the prediction of convergence pressure as a function of composition. The basis for Hadden's method is illustrated in Fig. 13-11, where it is shown that the critical loci for various mixtures of methane-propane-pentane fall within the area circumscribed by the three binary loci. (This behavior is not always typical of more nonideal systems.) The critical loci for the ternary mixtures vary linearly, at constant temperature, with weight percent propane on a methane-free basis. The essential point is that critical loci for mixtures are independent of the concentration of the lightest component in a mixture. This permits representation of a multicomponent mixture as a pseudobinary. The light component in this pseudobinary is the lightest species present (to a reasonable extent) in the multicomponent mixture. The heavy component is a pseudosubstance whose critical temperature is an average of all other components in the multicomponent mixture. This pseudocritical point can then be located on a *P-T* diagram containing the critical points for all compounds covered by the charts, and a critical locus can be drawn for the pseudobinary by interpolation between various real binary curves. Convergence pressure for the mixture at the desired temperature is read from the assumed loci at the desired system temperature. This method is illustrated in the left half of Fig. 13-12 for the methane-propane-pentane ternary. Associated *K* values for pentane at 104°C (220°F) are shown to the right as a function of mixture composition (or convergence pressure).

The GPA convergence pressure charts are primarily for alkane and alkene systems but do include charts for nitrogen, carbon dioxide, and hydrogen sulfide. The charts may not be valid when appreciable amounts of naphthenes or aromatics are present; the API charts use special procedures for such cases. Useful extensions of the convergence pressure concept to more varied mixtures include the nomographs of Winn [*Chem. Eng. Prog. Symp. Ser. 2*, **48**, 121 (1952)], Hadden and Grayson (op. cit.), and Cajander, Hipkin, and Lenoir [*J. Chem. Eng. Data*, **5**, 251 (1960)].

ANALYTICAL *K* VALUE CORRELATIONS

The widespread availability and use of digital computers for distillation calculations have given impetus to the development of analytical expressions for *K* values. McWilliams [*Chem. Eng.*, **80**(25), 138 (1973)] presents a regression equation and accompanying regression coefficients that represent the DePriester charts of Fig. 13-9. Regression equations and coefficients for various versions of the GPA convergence pressure charts are available from the GPA.

Preferred analytical correlations are less empirical and most often are theoretically based on one of two exact thermodynamic formulations, as derived in Sec. 4. When a single pressure-volume-temperature (*P-V-T*) equation of state is applicable to both vapor and liquid phases, the formulation used is

$$K_i = \frac{\hat{\Phi}_i^L}{\hat{\Phi}_i^V} \quad (13-3)$$

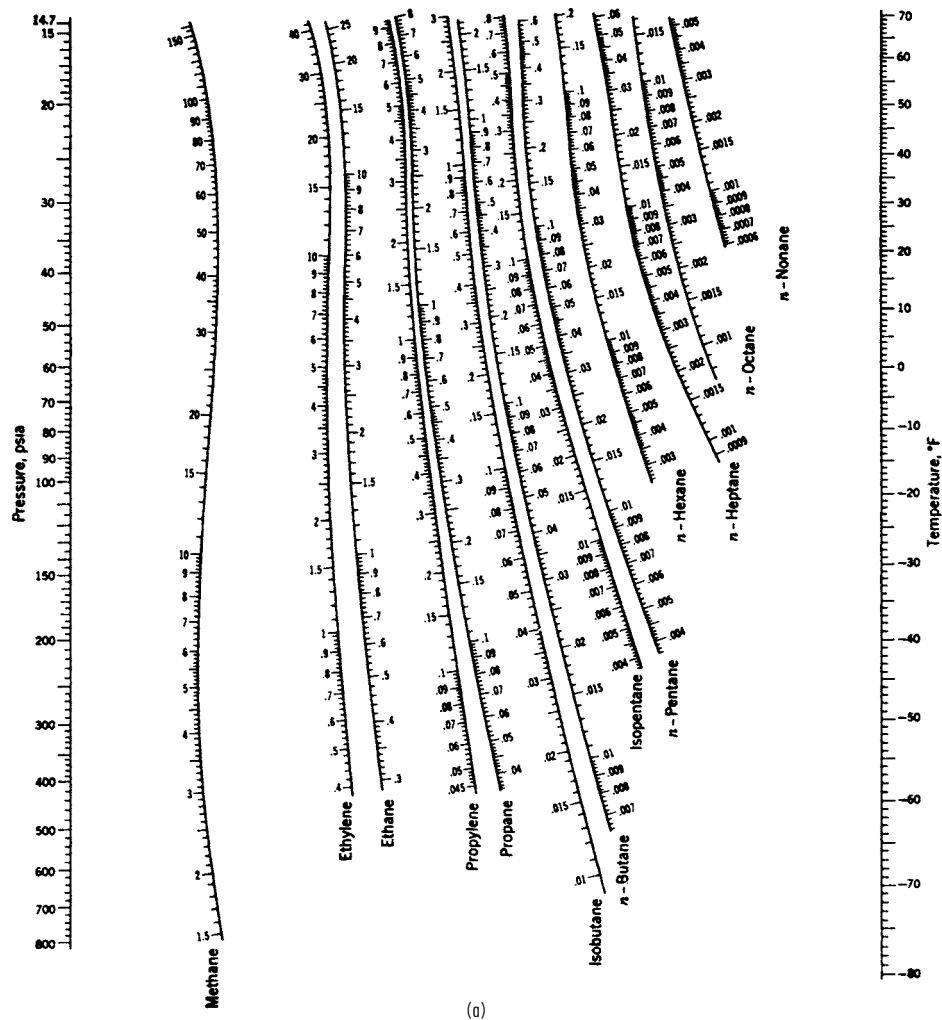


FIG. 13-9 The K values ($K = y/x$) in light-hydrocarbon systems. (a) Low-temperature range. (b) High-temperature range. [DePriester, Chem. Eng. Prog. Symp., Ser. 7, **49**, 1 (1953).]

where the mixture fugacity coefficients $\hat{\Phi}_i^L$ for the liquid and $\hat{\Phi}_i^V$ for the vapor are derived by classical thermodynamics from the P - V - T expression. Consistent equations for enthalpy can be similarly derived.

Until recently, equations of state that have been successfully applied to Eq. (13-3) have been restricted to mixtures of nonpolar compounds, namely, hydrocarbons and light gases. These equations include those of Benedict-Webb-Rubin (BWR), Soave (SRK) [*Chem. Eng. Sci.*, **27**, 1197 (1972)], who extended the remarkable Redlich-Kwong equation, and Peng-Robinson (PR) [*Ind. Eng. Chem. Fundam.*, **15**, 59 (1976)]. The SRK and PR equations belong to a family of so-called cubic equations of state. The Starling extension of the BWR equation (*Fluid Thermodynamic Properties for Light Petroleum Systems*, Gulf, Houston, 1973) predicts K values and enthalpies of the normal paraffins up through n -octane, as well as isobutane, isopentane, ethylene, propylene, nitrogen, carbon dioxide, and hydrogen sulfide, including the cryogenic region. Computer programs for K values derived from the SRK, PR, and other equations of state are widely available in all computer-aided process design and simulation programs. The ability of the SRK correlation to predict K values even when the pressure approaches the convergence pressure is shown for a multicomponent system in Fig. 13-13. Similar results are achieved with the PR correlation. The Wong-Sandler

mixing rules for cubic equations of state now permit such equations to be extended to mixtures of organic chemicals, as shown in a reformulated version by Orbey and Sandler [*AIChE J.*, **41**, 683 (1995)].

An alternative K value formulation that has received wide application to mixtures containing polar and/or nonpolar compounds is

$$K_i = \frac{\gamma_i^L \Phi_i^L}{\hat{\Phi}_i^V} \quad (13-4)$$

where different equations of state may be used to predict the pure-component liquid fugacity coefficient Φ_i^L and the vapor-mixture fugacity coefficient, and any one of a number of mixture free-energy models may be used to obtain the liquid activity coefficient γ_i^L . At low to moderate pressures, accurate prediction of the latter is crucial to the application of Eq. (13-4).

When either Eq. (13-3) or Eq. (13-4) can be applied, the former is generally preferred because it involves only a single equation of state applicable to both phases and thus would seem to offer greater consistency. In addition, the quantity Φ_i^L in Eq. (13-4) is hypothetical for any components that are supercritical. In that case, a modification of Eq. (13-4) that uses Henry's law is sometimes applied.

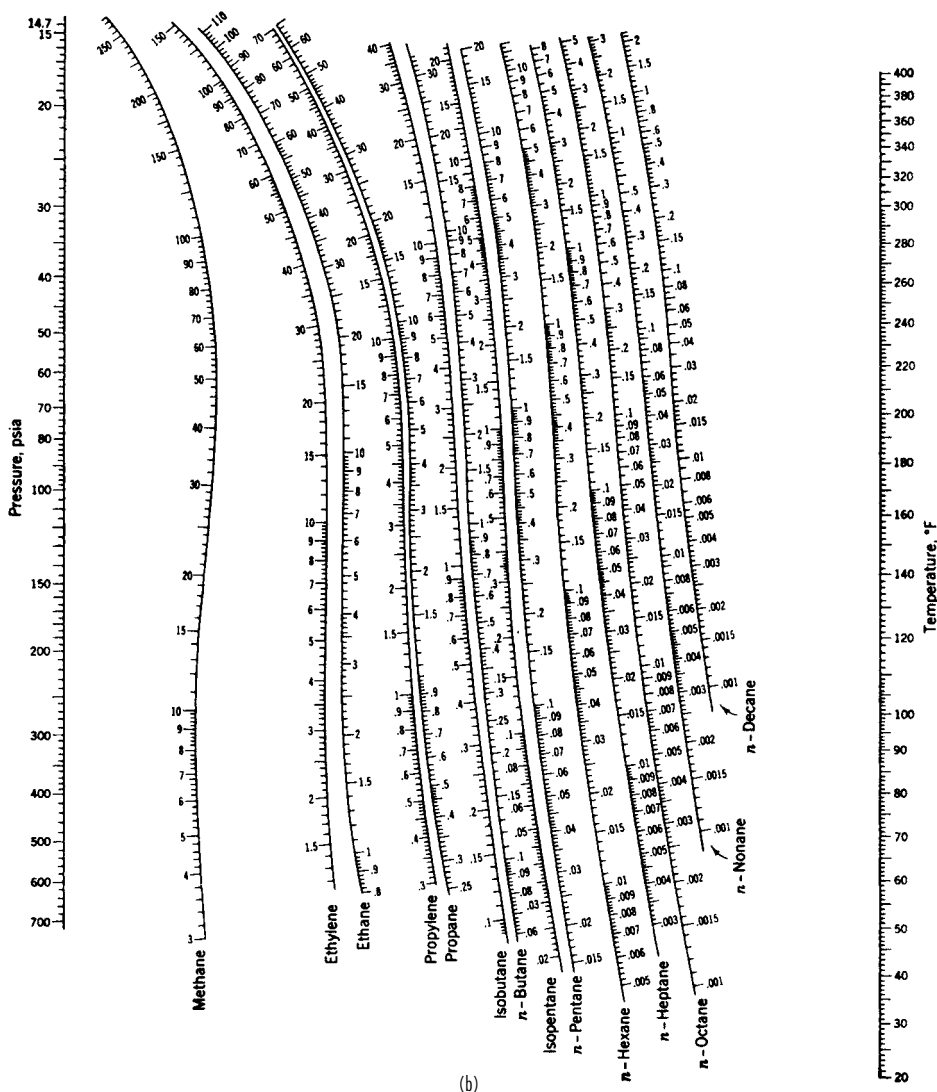


FIG. 13-9 (Continued)

For mixtures of hydrocarbons and light gases, Chao and Seader (CS) [AICHE J., 7, 598 (1961)] applied Eq. (13-4) by using an empirical expression for Φ_i^L based on the generalized corresponding-states P - V - T correlation of Pitzer et al., the Redlich-Kwong equation of state for Φ_i^V , and the regular solution theory of Scatchard and Hildebrand for γ_i^L . The predictive ability of the last-named theory is exhibited in Fig. 13-14 for the heptane-toluene system at 101.3 kPa (1 atm). Five pure-component constants for each species (T_v , P_v , ω , δ , and v^L) are required to use the CS method which, when applied within the restrictions discussed by Lenoir and Koppány [Hydrocarbon Process., 46(11), 249 (1967)], gives good results. Revised coefficients of Grayson and Streed (GS) (Paper 20-P07, Sixth World Pet. Conf. Frankfurt, June, 1963) for the Φ_i^L expression permit application of the CS correlation to higher temperatures and pressures and give improved predictions for hydrogen. Jin, Greenkorn, and Chao [AICHE J., 41, 1602 (1995)] present a revised correlation for the standard-state liquid fugacity of hydrogen, applicable from 200 to 730 K.

For mixtures containing polar substances, more complex predictive equations for γ_i^L that involve binary-interaction parameters for each

pair of components in the mixture are required for use in Eq. (13-4), as discussed in Sec. 4. Six popular expressions are the Margules, van Laar, Wilson, NRTL, UNIFAC, and UNIQUAC equations. The preferred expressions for representing activity coefficients are the NRTL and UNIQUAC equations. Extensive listings of binary-interaction parameters for use in all but the UNIFAC equation are given by Gmehling and Onken (op. cit.). They obtained the parameters for binary systems at 101.3 kPa (1 atm) from best fits of the experimental T - y - x equilibrium data by setting Φ_i^L and Φ_i^V to their ideal-gas, ideal-solution limits of 1.0 and P^{sat}/P , respectively, with the vapor pressure P^{sat} given by a three-constant Antoine equation, whose values they tabulate. Table 13-2 lists their parameters for selected binary systems based on the binary system activity coefficient equation forms given in Table 13-3.

Consistent Antoine vapor pressure constants and liquid molar volumes are listed in Table 13-4. The Wilson equation is particularly useful for systems that are highly nonideal but do not undergo phase splitting, as exemplified by the ethanol-hexane system, whose activity coefficients are shown in Fig. 13-15. For systems such as this, in which activity coefficients in dilute regions may exceed values of

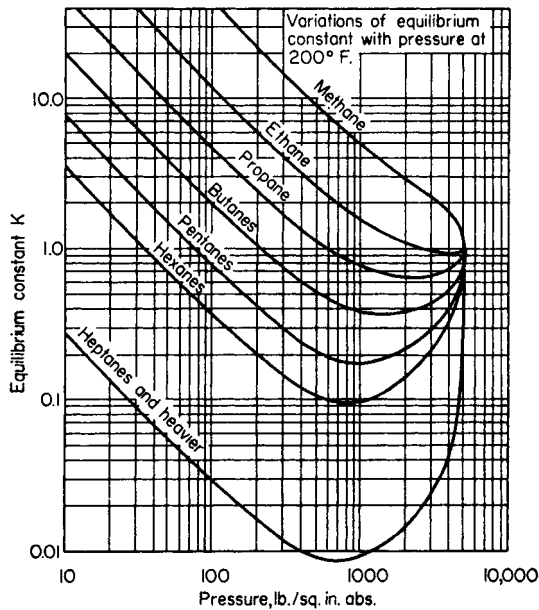


FIG. 13-10 Typical variation of K values with total pressure at constant temperature for a complex mixture. Light hydrocarbons in admixture with crude oil. [Katz and Hachmuth, *Ind. Eng. Chem.*, **29**, 1072 (1937).]

approximately 7.5, the van Laar equation erroneously predicts phase splitting.

Tables 13-2 and 13-4 include data on formic acid and acetic acid, two substances that tend to dimerize in the vapor phase according to the chemical equilibrium expression

$$K_D = \frac{P_D}{P_M^2} = 10^{A+B/T} \quad (13-5)$$

where K_D is the chemical equilibrium constant for dimerization, P_D and P_M are partial pressures of dimer and monomer, respectively, in torr,

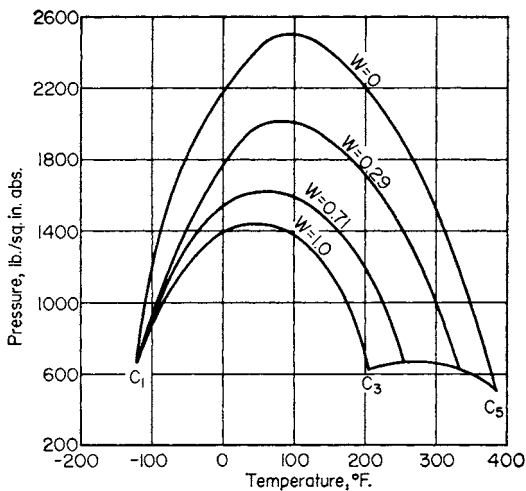


FIG. 13-11 Critical loci for a methane-propane-pentane system according to Hadden [Chem. Eng. Prog. Symp. Sec. 7, **49**, 53 (1953)]. Parameter W is weight fraction propane on a methane-free basis.

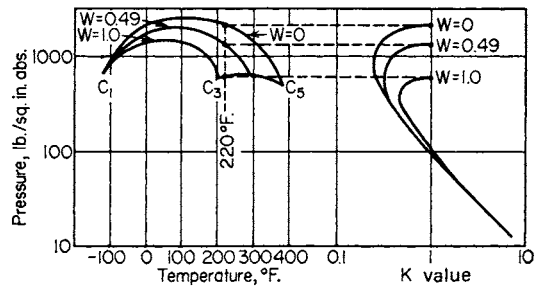


FIG. 13-12 Effect of mixture composition on K value for n -pentane at 104°C (220°F). The K values are shown for various values of W , weight fraction propane on a methane-free basis for the methane-propane-pentane system. [Hadden, *Chem. Eng. Prog. Symp. Sec. 7*, **49**, 58 (1953).]

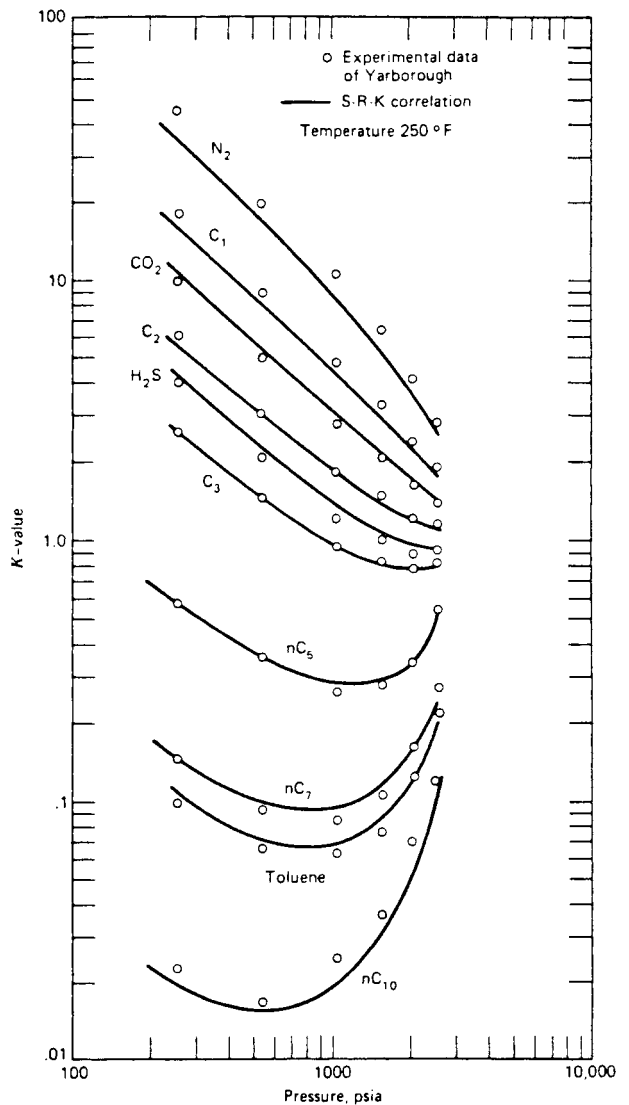


FIG. 13-13 Comparison of experimental K value data and SRK correlation. [Hendley and Seader, *Equilibrium-Stage Separation Operations in Chemical Engineering*, Wiley, New York, 1981; data of Yarborough, *J. Chem. Eng. Data*, **17**, 129 (1972).]

TABLE 13-2 Binary-Interaction Parameters*

System	Margules		van Laar		Wilson (cal/mol)	
	\bar{A}_{12}	\bar{A}_{21}	A_{12}	A_{21}	$(\lambda_{12} - \lambda_{11})$	$(\lambda_{21} - \lambda_{22})$
Acetone (1), chloroform (2)	-0.8404	-0.5610	-0.8643	-0.5899	116.1171	-506.8519
Acetone (1), methanol (2)	0.6184	0.5788	0.6184	0.5797	-114.4047	545.2942
Acetone (1), water (2)	2.0400	1.5461	2.1041	1.5555	344.3346	1482.2133
Carbon tetrachloride (1), benzene (2)	0.0948	0.0922	0.0951	0.0911	7.0459	59.6233
Chloroform (1), methanol (2)	0.8320	1.7365	0.9356	1.8860	-361.7944	1694.0241
Ethanol (1), benzene (2)	1.8362	1.4717	1.8570	1.4785	1264.4318	266.6118
Ethanol (1), water (2)	1.6022	0.7947	1.6798	0.9227	325.0757	953.2792
Ethyl acetate (1) ethanol (2)	0.8557	0.7476	0.8552	0.7526	58.8869	570.0439
n-Hexane (1), ethanol (2)	1.9398	2.7054	1.9195	2.8463	320.3611	2189.2896
Methanol (1), benzene (2)	2.1411	1.7905	2.1623	1.7925	1666.4410	227.2126
Methanol (1), ethyl acetate (2)	1.0016	1.0517	1.0017	1.0524	982.2689	-172.9317
Methanol (1), water (2)	0.7923	0.5434	0.8041	0.5619	82.9876	520.6458
Methyl acetate (1), methanol (2)	0.9605	1.0120	0.9614	1.0126	-93.8900	847.4348
1-Propanol (1), water (2)	2.7070	0.7172	2.9095	1.1572	906.5256	1396.6398
2-Propanol (1), water (2)	2.3319	0.8976	2.4702	1.0938	659.5473	1230.2080
Tetrahydrofuran (1), water (2)	2.8258	1.9450	3.0216	1.9436	1475.2583	1844.7926
Water (1), acetic acid (2)	0.4178	0.9533	0.4973	1.0623	705.5876	111.6579
Water (1), 1-butanol (2)	0.8608	3.2051	1.0996	4.1760	1549.6600	2050.2569
Water (1), formic acid (2)	-0.2966	-0.2715	-0.2935	-0.2757	-310.1060	1180.8040

* Abstracted from Gmehling and Onken, *Vapor-Liquid Equilibrium Data Collection*, DECHEMA Chemistry Data ser., vol. 1 (parts 1-10). Frankfurt, 1977.

and T is in kelvins. Values of A and B for the first four normal aliphatic acids are

	A	B
Formic acid	-10.743	3083
Acetic acid	-10.421	3166
n-Propionic acid	-10.843	3316
n-Butyric acid	-10.100	3040

As shown by Marek and Standart [*Collect. Czech. Chem. Commun.*, **19**, 1074 (1954)], it is preferable to correlate and use liquid-phase activity coefficients for the dimerizing component by considering separately the partial pressures of the monomer and dimer. For example, for a binary system of components 1 and 2, when only compound 1 dimerizes in the vapor phase, the following equations apply if an ideal gas is assumed:

$$P_1 = P_D + P_M \quad (13-6)$$

$$y_1 = \frac{P_M + 2P_D}{P} \quad (13-7)$$

These equations when combined with Eq. (13-5) lead to the following equations for liquid-phase activity coefficients in terms of measurable quantities:

$$\gamma_1 = \frac{P y_1}{P_1^{\text{sat}} x_1} \left\{ \frac{1 + (1 + 4K_D P_1^{\text{sat}})^{0.5}}{1 + [1 + 4K_D P y_1 (2 - y_1)]^{0.5}} \right\} \quad (13-8)$$

$$\gamma_2 = \frac{P y_2}{P_2^{\text{sat}} x_2} \left(\frac{2(1 - y_1) + [1 + 4K_D P y_1 (2 - y_1)]^{0.5}}{(2 - y_1) \{1 + [1 + 4K_D P y_1 (2 - y_1)]^{0.5}\}} \right) \quad (13-9)$$

Detailed procedures, including computer programs for evaluating binary-interaction parameters from experimental data and then using these parameters to predict K values and phase equilibria, are given in terms of the UNIQUAC equation by Prausnitz et al. (*Computer Calculations for Multicomponent Vapor-Liquid and Liquid-Liquid Equilibria*, Prentice-Hall, Englewood Cliffs, N.J., 1980) and in terms of the UNIFAC group contribution method by Fredenslund, Gmehling, and Rasmussen (*Vapor-Liquid Equilibria Using UNIFAC*, Elsevier, Amsterdam, 1980). Both use the method of Hayden and O'Connell [*Ind. Eng. Chem. Process Des. Dev.*, **14**, 209 (1975)] to compute $\hat{\Phi}_i^V$ in Eq. (13-4). When the system temperature is greater than the critical

TABLE 13-3 Activity-Coefficient Equations in Binary Form for Use with Parameters and Constants in Tables 13-2 and 13-4

Type of equation	Adjustable parameters	Equations in binary form
Margules	\bar{A}_{12}	$\ln \gamma_1 = [\bar{A}_{12} + 2(\bar{A}_{21} - \bar{A}_{12})x_1]x_2^2$
	\bar{A}_{21}	$\ln \gamma_2 = [\bar{A}_{21} + 2(\bar{A}_{12} - \bar{A}_{21})x_2]x_1^2$
van Laar	A_{12}	$\ln \gamma_1 = A_{12} \left(\frac{A_{21}x_2}{A_{12}x_1 + A_{21}x_2} \right)^2$
	A_{21}	$\ln \gamma_2 = A_{21} \left(\frac{A_{12}x_1}{A_{12}x_1 + A_{21}x_2} \right)^2$
Wilson	$\lambda_{12} - \lambda_{11}$	$\ln \gamma_1 = -\ln(x_1 + \Lambda_{12}x_2) + x_2 \left(\frac{\Lambda_{12}}{x_1 + \Lambda_{12}x_2} - \frac{\Lambda_{21}}{\Lambda_{21}x_1 + x_2} \right)$
	$\lambda_{21} - \lambda_{22}$	$\ln \gamma_2 = -\ln(x_2 + \Lambda_{21}x_1) - x_1 \left(\frac{\Lambda_{12}}{x_1 + \Lambda_{12}x_2} - \frac{\Lambda_{21}}{\Lambda_{21}x_1 + x_2} \right)$

$$\text{where } \Lambda_{12} = \frac{v_2^L}{v_1^L} \exp\left(-\frac{\lambda_{12} - \lambda_{11}}{RT}\right), \Lambda_{21} = \frac{v_1^L}{v_2^L} \exp\left(-\frac{\lambda_{21} - \lambda_{22}}{RT}\right)$$

v_i^L = molar volume of pure-liquid component i

λ_{ij} = interaction energy between components i and j , $\lambda_{ij} = \lambda_{ji}$

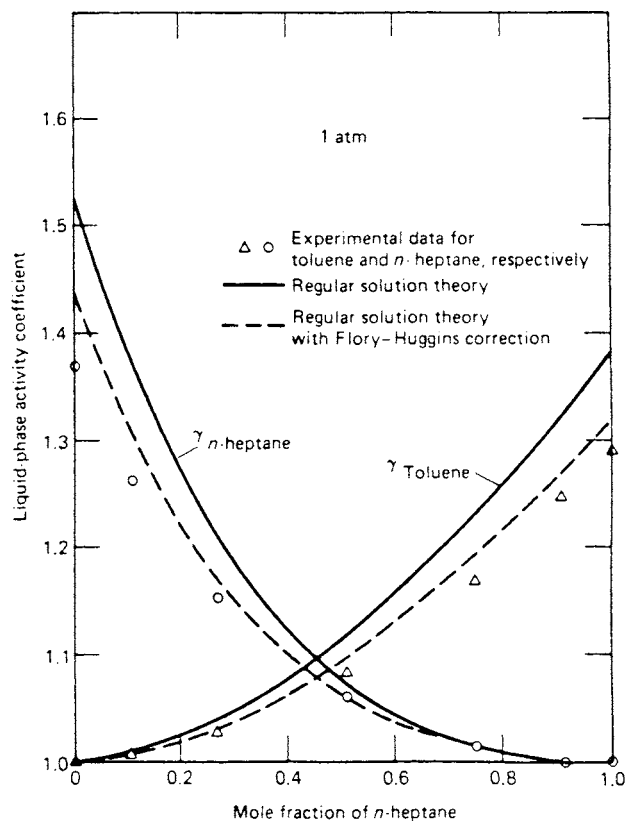


FIG. 13-14 Liquid-phase activity coefficients for an *n*-heptane-toluene system at 101.3 kPa (1 atm). [Henley and Seader, *Equilibrium-Stage Separation Operations in Chemical Engineering*, Wiley, New York, 1981; data of Yerazunis et al., *AIChE J.*, **10**, 660 (1964).]

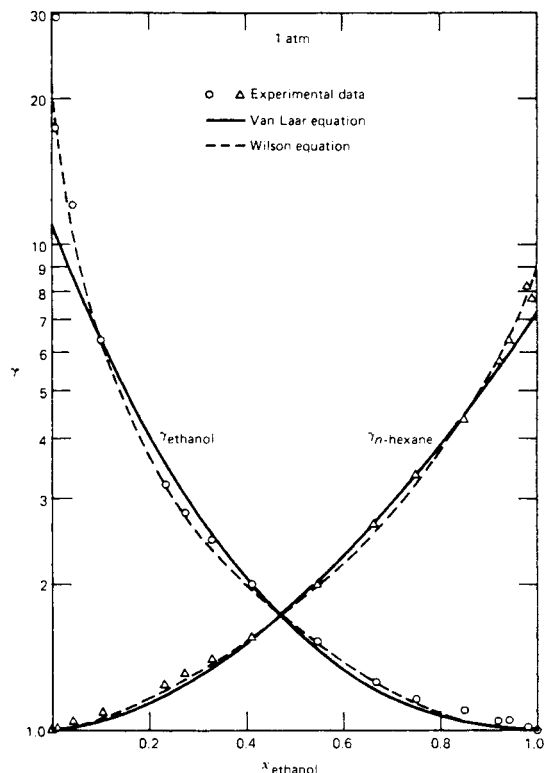


FIG. 13-15 Liquid-phase activity coefficients for an ethanol-*n*-hexane system. [Henley and Seader, *Equilibrium-Stage Separation Operations in Chemical Engineering*, Wiley, New York, 1981; data of Sinor and Weber, *J. Chem. Eng. Data*, **5**, 243-247 (1960).]

TABLE 13-4 Antoine Vapor-Pressure Constants and Liquid Molar Volume*

Species	Antoine constants†			Applicable temperature region, °C	v^L , liquid molar volume, cm ³ /g-mol
	A	B	C		
Acetic acid	8.02100	1936.010	258.451	18-118	57.54
Acetone	7.11714	1210.595	229.664	(-13)-55	74.05
Benzene	6.87987	1196.760	219.161	8-80	89.41
1-Butanol	7.36366	1305.198	173.427	89-126	91.97
Carbon tetrachloride	6.84083	1177.910	220.576	(-20)-77	97.09
Chloroform	6.95465	1170.966	226.232	(-10)-60	80.67
Ethanol	7.58670	1281.590	193.768	78-203	58.68
Ethanol	8.11220	1592.864	226.184	20-93	58.68
Ethyl acetate	7.10179	1244.951	217.881	16-76	98.49
Formic acid	6.94459	1295.260	218.000	36-108	37.91
<i>n</i> -Hexane	6.91058	1189.640	226.280	(-30)-170	131.61
Methanol	8.08097	1582.271	239.726	15-84	40.73
Methyl acetate	7.06524	1157.630	219.726	2-56	79.84
1-Propanol	8.37895	1788.020	227.438	(-15)-98	75.14
2-Propanol	8.87829	2010.320	252.636	(-26)-83	76.92
Tetrahydrofuran	6.99515	1202.290	226.254	23-100	81.55
Water	8.07131	1730.630	233.426	1-100	18.07

* Abstracted from Gmehling and Onken, *Vapor-Liquid Equilibrium Data Collection*, DECHEMA Chemistry Data ser., vol. 1 (parts 1-10), Frankfurt, 1977.

† Antoine equation is $\log P^{\text{sat}} = A - B/(T + C)$ with P^{sat} in torr and T in °C.

NOTE: To convert degrees Celsius to degrees Fahrenheit, °F = 1.8°C + 32. To convert cubic centimeters per gram-mole to cubic feet per pound-mole, multiply by 0.016.

temperature of one or more components in the mixture, Prausnitz et al. use a Henry's law constant $H_{i,M}$ in place of the product $\gamma_i^L \Phi_i^L$ in Eq. (13-4). Otherwise Φ_i^L is evaluated from vapor pressure data with a Poynting saturated-vapor fugacity correction. When the total pressure is less than about 202.6 kPa (2 atm) and all components in the mixture have a critical temperature that is greater than the system temperature, then $\Phi_i^L = P_i^{\text{sat}}/P$ and $\Phi_i^V = 1.0$. Equation (13-4) then reduces to

$$K_i = \frac{\gamma_i^L P_i^{\text{sat}}}{P} \quad (13-10)$$

SINGLE-STAGE EQUILIBRIUM FLASH CALCULATIONS

The simplest continuous distillation process is the adiabatic single-stage equilibrium flash process pictured in Fig. 13-16. Feed temperature and the pressure drop across the valve are adjusted to vaporize the feed to the desired extent, while the drum provides disengaging space to allow the vapor to separate from the liquid. The expansion across the valve is at constant enthalpy, and this fact can be used to calculate T_2 (or T_1 to give a desired T_2).

A degrees-of-freedom analysis indicates that the variables subject to the designer's control are $C + 3$ in number. The most common way to use these is to specify the feed rate, composition, and pressure ($C + 1$ variables) plus the drum temperature T_2 and pressure P_2 . This operation will give one point on the *equilibrium flash curve* shown in Fig. 13-17. This curve shows the relation at constant pressure between the fraction V/F of the feed flashed and the drum temperature. The temperature at $V/F = 0.0$ when the first bubble of vapor is about to form (saturated liquid) is the *bubble point* temperature of the feed mixture, and the value at $V/F = 1.0$ when the first droplet of liquid is about to form (saturated vapor) is the *dew point* temperature.

BUBBLE POINT AND DEW POINT

For a given drum pressure and feed composition, the bubble and dew point temperatures bracket the temperature range of the equilibrium flash. At the bubble point temperature, the total vapor pressure exerted by the mixture becomes equal to the confining drum pressure, and it follows that $\sum y_i = 1.0$ in the bubble formed. Since $y_i = K_i x_i$ and since the x_i 's still equal the feed compositions (denoted by z_i), calculation of the bubble point temperature involves a trial-and-error search for the temperature which, at the specified pressure, makes $\sum K_i z_i = 1.0$. If instead the temperature is specified, one can find the bubble point pressure that satisfies this relationship.

At the dew point temperature y_i still equals z_i and the relationship $\sum x_i = \sum z_i / K_i = 1.0$ must be satisfied. As in the case of the bubble point, a trial-and-error search for the dew point temperature at a specified pressure is involved. Or, if the temperature is specified, the dew point pressure can be calculated.

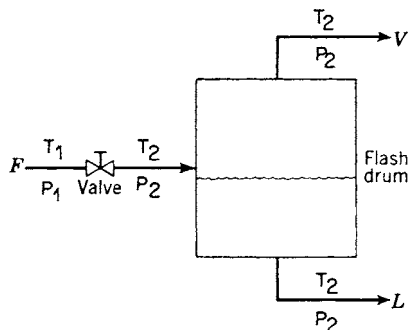


FIG. 13-16 Equilibrium flash separator.

which is referred to as a modified Raoult's law K value. If, furthermore, the liquid phase is ideal, then $\gamma_i^L = 1.0$ and

$$K_i = \frac{P_i^{\text{sat}}}{P} \quad (13-11)$$

which is referred to as a Raoult's law K value that is dependent solely on the vapor pressure P_i^{sat} of the component in the mixture. The UNIFAC method is being periodically updated with new group contributions; e.g., see Hansen et al. [*Ind. Eng. Chem. Res.*, **30**, 2352 (1991)].

ISOTHERMAL FLASH

The calculation for a point on the flash curve that is intermediate between the bubble point and the dew point is referred to as an isothermal flash calculation because T_2 is specified. Except for an ideal binary mixture, procedures for calculating an isothermal flash are iterative. A popular and recommended method is the following, due to Rachford and Rice [*J. Pet. Technol.*, **4**(10), sec. 1, p. 19, and sec. 2, p. 3 (October 1952)]. The component mole balance ($Fz_i = Vy_i + Lx_i$), phase distribution relation ($K_i = y_i/x_i$), and total mole balance ($F = V + L$) can be combined to give

$$x_i = \frac{z_i}{1 + (V/F)(K_i - 1)} \quad (13-12)$$

$$y_i = \frac{K_i z_i}{1 + (V/F)(K_i - 1)} \quad (13-13)$$

Since $\sum x_i - \sum y_i = 0$,

$$f\left(\frac{V}{F}\right) = \sum_i \frac{z_i(1 - K_i)}{1 + (V/F)(K_i - 1)} = 0 \quad (13-14)$$

Equation (13-14) is solved iteratively for V/F , followed by the calculation of values of x_i and y_i from Eqs. (13-12) and (13-13) and L from the total mole balance. Any one of a number of numerical root-finding procedures such as the Newton-Raphson, secant, false-position, or bisection method can be used to solve Eq. (13-14). Values of K_i are constants if they are independent of liquid and vapor compositions. Then the resulting calculations are straightforward. Otherwise, the K_i values must be periodically updated for composition effects, perhaps

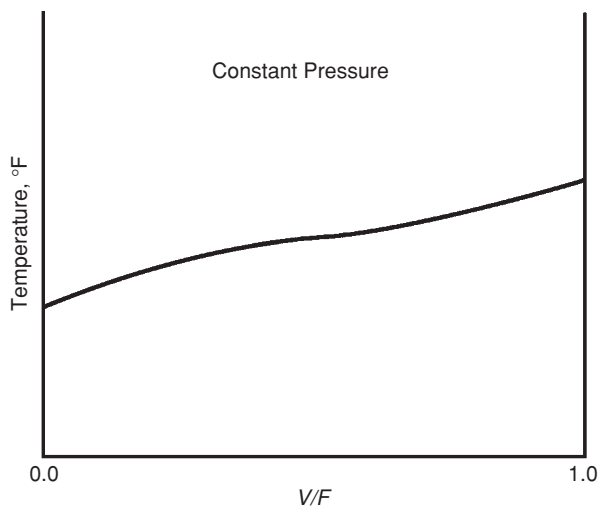


FIG. 13-17 Equilibrium flash curve.

13-16 DISTILLATION

after each iteration, using prorated values of x_i and y_i from Eqs. (13-12) and (13-13). Generally the iterations are continued until the change in the absolute value of V/F is sufficiently small and until the absolute value of the residual $f(V/F)$ is close to zero. When converged, $\sum x_i$ and $\sum y_i$ will each be very close to a value of 1, and, if desired, T_1 can be computed from an energy balance around the valve if no heat exchanger is used. Alternatively, if T_1 is fixed, as mentioned earlier, a heat exchanger must be added before, after, or in place of the valve with the required heat duty being calculated from an energy balance. The limits of applicability of Eqs. (13-12) to (13-14) are the bubble point, at which $\dot{V} = 0$ and $x_i = z_i$, and the dew point, at which $L = 0$ and $y_i = z_i$. At these limits Eq. (13-14) reduces to the bubble point equation

$$\sum_i K_i x_i = 1 \quad (13-15)$$

and the dew point equation, respectively,

$$\sum_i \frac{y_i}{K_i} = 1 \quad (13-16)$$

For a *binary feed*, specification of the flash drum temperature and pressure fixes the equilibrium-phase compositions, which are related to the K values by

$$x_1 = \frac{1 - K_2}{K_1 - K_2} \quad \text{and} \quad y_1 = \frac{K_1 K_2 - K_1}{K_2 - K_1}$$

The mole balance can be rearranged to

$$\frac{V}{F} = \frac{z_1(K_1 - K_2)/(1 - K_2) - 1}{K_1 - 1}$$

If K_1 and K_2 are functions of temperature and pressure only (ideal solutions), the flash curve can be calculated directly without iteration.

ADIABATIC FLASH

In Fig. 13-16, if P_2 and the feed-stream conditions (that is, F, z_i, T_1, P_1) are known, then the calculation of T_2, V, L, y_i , and x_i is referred to as an adiabatic flash. In addition to Eqs. (13-12) to (13-14) and the total mole balance, the following energy balance around both the valve and the flash drum combined must be included:

$$H^F F = H^V V + H^L L \quad (13-17)$$

By taking a basis of $F = 1.0$ mol and eliminating L with the total mole balance, Eq. (13-17) becomes

$$f_2[V, T_2] = H^F - V(H^V - H^L) - H^L = 0 \quad (13-18)$$

With T_2 now unknown, Eq. (13-14) becomes

$$f_1[V, T_2] = \sum_i \frac{z_i(1 - K_i)}{1 + V(K_i - 1)} = 0 \quad (13-19)$$

A number of iterative procedures have been developed for solving Eqs. (13-18) and (13-19) simultaneously for V and T_2 . Frequently, and especially if the feed contains components of a narrow range of volatility, convergence is rapid for a tearing method in which a value of T_2 is assumed, Eq. (13-19) is solved iteratively by the isothermal flash procedure, and, using that value of V , Eq. (13-18) is solved iteratively for a new approximation of T_2 , which is then used to initiate the next cycle

until T_2 and V converge. However, if the feed contains components of a wide range of volatility, it may be best to invert the sequence and assume a value for V , solve Eq. (13-19) for T_2 , solve Eq. (13-18) for V , and then repeat the cycle. If the K values and/or enthalpies are sensitive to the unknown phase compositions, it may be necessary to solve Eqs. (13-18) and (13-19) simultaneously by a Newton or other suitable iterative technique. Alternatively, the two-tier method of Boston and Britt [*Comput. Chem. Eng.*, **2**, 109 (1978)], which is also suitable for difficult isothermal flash calculations, may be applied.

OTHER FLASH SPECIFICATIONS

Flash drum specifications in addition to (P_2, T_2) and (P_2 , adiabatic) are possible but must be applied with care, as discussed by Michelsen [*Comp. Chem. Engng.*, **17**, 431 (1993)]. Most computer-aided process design and simulation programs permit a wide variety of flash specifications.

THREE-PHASE FLASH

Single-stage equilibrium flash calculations become considerably more complex when an additional liquid phase can form, as in mixtures of water with hydrocarbons, water with ethers, and water with higher alcohols (containing four or more carbon atoms). Procedures for computing such situations are referred to as three-phase flash methods, which are given for the general case by Henley and Rosen (*Material and Energy Balance Computations*, Wiley, New York, 1968, chap. 8). When the two liquid phases are almost mutually insoluble, they can be considered separately and relatively simple procedures apply, as discussed by Smith (*Design of Equilibrium Stage Processes*, McGraw-Hill, New York, 1963). Condensation of such mixtures may result in one liquid phase being formed before the other. Computer-aided process design and simulation programs all contain a Gibbs free-energy routine that can compute a three-phase flash by minimization of the Gibbs free energy. Many important and subtle aspects of three-phase flash calculations are discussed by Michelsen [*Fluid Phase Equil.*, **9**, 1, 21 (1982)], McDonald and Floudas [*AIChE J.*, **41**, 1798 (1995)], and Wasylkiewicz et al. [*Ind. Eng. Chem. Research*, **35**, 1395 (1996)].

COMPLEX MIXTURES

Feed analyses in terms of component compositions are usually not available for complex hydrocarbon mixtures with a final normal boiling point above about 38°C (100°F) (*n*-pentane). One method of handling such a feed is to break it down into pseudocomponents (narrow-boiling fractions) and then estimate the mole fraction and K value for each such component. Edmister [*Ind. Eng. Chem.*, **47**, 1685 (1955)] and Maxwell (*Data Book on Hydrocarbons*, Van Nostrand, Princeton, N.J., 1958) give charts that are useful for this estimation. Once K values are available, the calculation proceeds as described above for multicomponent mixtures. Another approach to complex mixtures is to obtain an American Society for Testing and Materials (ASTM) or true-boiling point (TBP) curve for the mixture and then use empirical correlations to construct the atmospheric-pressure equilibrium flash vaporization (EFV) curve, which can then be corrected to the desired operating pressure. A discussion of this method and the necessary charts is presented in a later subsection Petroleum and Complex-Mixture Distillation.

GRAPHICAL METHODS FOR BINARY DISTILLATION

Multistage distillation under continuous, steady-state operating conditions is widely used in practice to separate a variety of mixtures. Table 13-5, taken from the study of Mix, Dweck, Weinberg, and Armstrong [*AIChE Symp. Ser.* **76**, 192, 10 (1980)] lists key components along with typical stage requirements to perform the separation for 27 industrial distillation processes. The design of multistage columns can be accomplished by graphical techniques when the feed mixture contains only two components. The x - y diagram method developed by McCabe and Thiele [*Ind. Eng. Chem.*, **17**, 605 (1925)]

uses only phase equilibrium and mole balance relationships. The method assumes an adiabatic column (no heat losses through the column walls) and constant latent heat for the binary mixture at all compositions (which requires, among other things, equal latent heat for both components). The method is exact only for those systems in which energy effects on vapor and liquid rates leaving the stages are negligible. However, the approach is simple and gives a useful first estimate of the column design which can be refined by using the enthalpy composition diagram method of Ponchon [*Tech. Mod.*, **13**,

TABLE 13-5 Key Components and Typical Number of (Real) Stages Required to Perform the Separation for Distillation Processes of Industrial Importance

Key components	Typical number of trays
Hydrocarbon systems	
Ethylene-ethane	73
Propylene-propane	138
Propyne-1-3-butadiene	40
1-3 Butadiene-vinyl acetylene	130
Benzene-toluene	34, 53
Benzene-ethyl benzene	20
Benzene-diethyl benzene	50
Toluene-ethyl benzene	28
Toluene-xylenes	45
Ethyl benzene-styrene	34
<i>o</i> -Xylene- <i>m</i> -xylene	130
Organic systems	
Methanol-formaldehyde	23
Dichloroethane-trichloroethane	30
Acetic acid-acetic anhydride	50
Acetic anhydride-ethylene diacetate	32
Vinyl acetate-ethyl acetate	90
Ethylene glycol-diethylene glycol	16
Cumene-phenol	38
Phenol-acetophenone	39, 54
Aqueous systems	
HCN-water	15
Acetic acid-water	40
Methanol-water	60
Ethanol-water	60
Isopropanol-water	12
Vinyl acetate-water	35
Ethylene oxide-water	50
Ethylene glycol-water	16

20, 55 (1921)] and Savarit [*Arts Metiers*, **65**, 142, 178, 241, 266, 307 (1922)]. This approach uses the energy balance in addition to mole balance and phase equilibrium relationships and is rigorous when enough calorimetric data are available to construct the diagram without assumptions.

With the widespread availability of computers, the preferred approach to design is equation-based since it provides answers rapidly and repeatedly without the tedium of redrawing graphs. Such an approach is especially useful for sensitivity analysis, which gives insight into how a design changes under variations or uncertainty in design parameters such as thermodynamic properties; feed flow rate, composition, temperature, and pressure; and desired product compositions. Nevertheless, diagrams are useful for quick approximations, for interpreting the results of equation-based methods, and for demonstrating the effect of various design variables. The x - y diagram is the most convenient for these purposes, and its use is developed in detail here. The use of the enthalpy composition diagram is given by Smith (*Design of Equilibrium Stage Processes*, McGraw-Hill, New York, 1963) and Henley and Seader (*Equilibrium-Stage Separation Operations in Chemical Engineering*, Wiley, New York, 1981). An approximate equation-based approach based on the enthalpy composition diagram was proposed by Peters [*Ind. Eng. Chem.*, **14**, 476 (1922)] with additional aspects developed later by others. Doherty and Malone (*Conceptual Design of Distillation Systems*, McGraw-Hill, 2001, app. A) describe this method for binary mixtures and extend it to multicomponent systems. The approach is exact when the enthalpy composition surfaces are linear.

PHASE EQUILIBRIUM DIAGRAMS

Three types of binary phase equilibrium curves are shown in Fig. 13-18. The y - x diagram is almost always plotted for the component that is the more volatile (denoted by the subscript 1) in the region where distillation is to take place. Curve A shows the common case in which component 1 remains more volatile over the entire composition range. Curve B is typical of many systems (e.g., ethanol-water) in which the

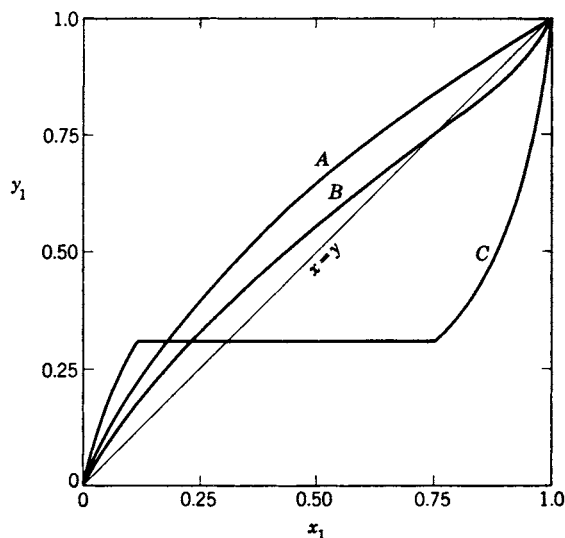


FIG. 13-18 Typical binary equilibrium curves. Curve A, system with normal volatility. Curve B, system with homogeneous azeotrope (one liquid phase). Curve C, system with heterogeneous azeotrope (two liquid phases in equilibrium with one vapor phase).

component that is more volatile at low values of x_1 becomes less volatile than the other component at high values of x_1 . The vapor and liquid compositions are identical for the homogeneous azeotrope where curve B crosses the 45° diagonal (that is, $x_1 = y_1$). A heterogeneous azeotrope is formed by curve C, in which there are two equilibrium liquid phases and one equilibrium vapor phase.

An azeotrope limits the separation that can be obtained between components by simple distillation. For the system described by curve B, the maximum overhead-product concentration that could be obtained from a feed with $z_1 = 0.25$ is the azeotropic composition. Similarly, a feed with $x_1 = 0.9$ could produce a bottom-product composition no lower than the azeotrope.

The phase rule permits only two variables to be specified arbitrarily in a binary two-phase mixture at equilibrium. Consequently, the curves in Fig. 13-18 can be plotted at either constant temperature or constant pressure but not both. The latter is more common, and data in Table 13-1 correspond to that case. The y - x diagram can be plotted in mole, weight, or volume fractions. The units used later for the phase flow rates must, of course, agree with those used for the equilibrium data. Mole fractions, which are almost always used, are applied here.

It is sometimes permissible to assume constant *relative volatility* to approximate the equilibrium curve quickly. Then by applying Eq. (13-2) to components 1 and 2,

$$\alpha = \frac{K_1}{K_2} = \frac{y_1 x_2}{x_1 y_2}$$

which can be rewritten as (using $x_2 = 1 - x_1$ and $y_2 = 1 - y_1$)

$$y_1 = \frac{x_1 \alpha}{1 + (\alpha - 1)x_1} \quad (13-20)$$

With a constant value for α this equation provides a simple, approximate expression for representing the equilibrium $y = x$ diagram. Doherty and Malone (*Conceptual Design of Distillation Systems*, McGraw-Hill, 2001, sec. 2.3) discuss this approximation in greater detail and give a selection of binary mixtures for which the approximation is reasonable. At a constant pressure of 1 atm these include benzene + toluene, $\alpha = 2.34$; benzene + *p*-xylene, $\alpha = 4.82$; and hexane + *p*-xylene, $\alpha = 7.00$.

McCABE-THIELE METHOD

Operating Lines The McCabe-Thiele method is based upon representation of the material balance equations as operating lines on the y - x diagram. The lines are made straight by the assumption of *constant molar overflow*, which eliminates the need for an energy balance. The liquid-phase flow rate is assumed to be constant from tray to tray in each section of the column between addition (feed) and withdrawal (product) points. If the liquid rate is constant, the vapor rate must also be constant.

The constant-molar-overflow assumption rests on several underlying thermodynamic assumptions. The most important one is equal molar heats of vaporization for the two components. The other assumptions are adiabatic operation (no heat leaks) and no heat of mixing or sensible heat effects. These assumptions are most closely approximated for close-boiling isomers. The result of these assumptions on the calculation method can be illustrated with Fig. 13-19, which shows two material balance envelopes cutting through the top section (above the top feed stream or sidestream) of the column. If the liquid flow rate L_{n+1} is assumed to be identical to L_{n-1} , then $V_n = V_{n-2}$ and the component material balance for both envelopes 1 and 2 can be represented by

$$y_n = \left(\frac{L}{V}\right)x_{n+1} + \frac{Dx_D}{V} \quad (13-21)$$

where y and x have a stage subscript n or $n + 1$, but L and V need be identified only with the section of the column to which they apply. Equation (13-21) has the analytical form of a straight line where L/V is the slope and Dx_D/V is the y intercept at $x = 0$.

The effect of a sidestream withdrawal point is illustrated by Fig. 13-20. The material balance equation for the column section below the sidestream is

$$y_n = \frac{L'}{V'}x_{n+1} + \frac{Dx_D + Sx_s}{V'} \quad (13-22)$$

where the primes designate the L and V below the sidestream. Since the sidestream must be a saturated phase, $V = V'$ if a liquid sidestream is withdrawn and $L = L'$ if it is a vapor.

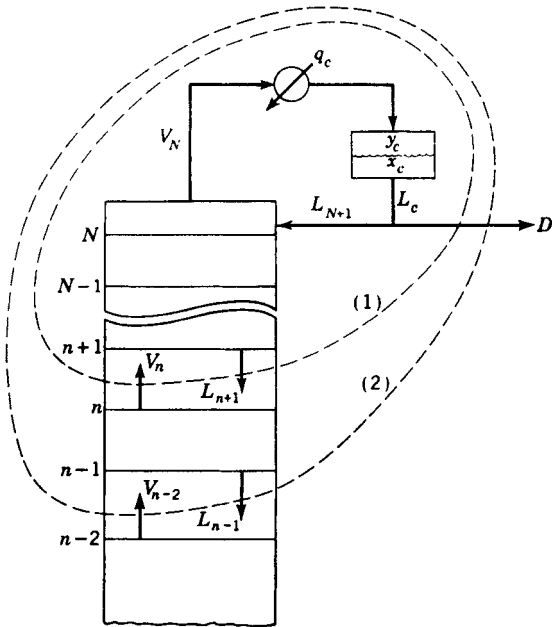


FIG. 13-19 Two material balance envelopes in the top section of a distillation column.

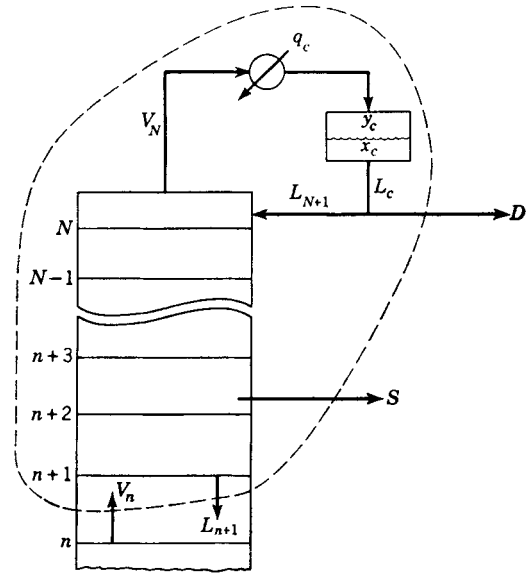


FIG. 13-20 Material balance envelope which contains two external streams D and S , where S represents a sidestream product withdrawn above the feed plate.

If the sidestream in Fig. 13-20 is a feed (not necessarily a saturated liquid or vapor), the balance for the section below the feed becomes

$$y_n = \frac{L'}{V'}x_{n+1} + \frac{Dx_D - Fz_F}{V'} \quad (13-23)$$

Similar equations can be written for the bottom section of the column. For the envelope shown in Fig. 13-21,

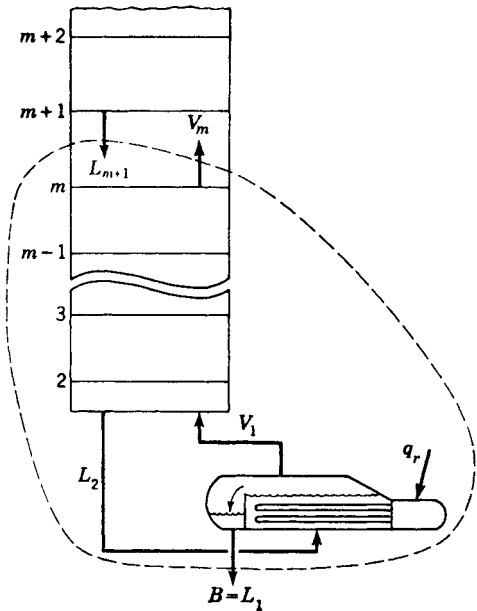


FIG. 13-21 Material balance envelope around the bottom end of the column. The partial reboiler is equilibrium stage 1.

$$y_m = \frac{L'}{V'} x_{m+1} - \frac{Bx_B}{V'} \quad (13-24)$$

where the subscript m is used to identify the stage number in the bottom section.

Equations such as (13-21) through (13-24), when plotted on the y - x diagram, furnish a set of *operating lines*. A point on an operating line represents two *passing streams*, and the operating line itself is the locus of all possible pairs of passing streams within the column section to which the line applies.

An operating line can be located on the y - x diagram if (1) two points on the line are known or (2) one point and the slope are known. The known points on an operating line are usually its intersection with the y - x diagonal and/or its intersection with another operating line.

The slope L/V of the operating line is termed the *internal reflux ratio*. This ratio in the operating line equation for the top section of the column [see Eq. (13-21)] is related to the *external reflux ratio* $R = L_{N+1}/D$ by

$$\frac{L}{V} = \frac{L_{N+1}}{V_N} = \frac{RD}{(1+R)D} = \frac{R}{1+R} \quad (13-25)$$

when the reflux stream L_{N+1} is a saturated liquid.

Thermal Condition of the Feed The slope of the operating line changes whenever a feed stream or a sidestream is passed. To calculate this change, it is convenient to introduce a quantity q which is defined by the following equations for a feed stream F :

$$L' = L + qF \quad (13-26)$$

$$V = V' + (1 - q)F \quad (13-27)$$

The primes denote the streams below the stage to which the feed is introduced. The value of q is a measure of the thermal condition of the feed and represents the moles of saturated liquid formed in the feed stage per mole of feed. The value of q for a particular feed can be estimated from

$$q = \frac{\text{energy to convert 1 mol of feed to saturated vapor}}{\text{molar heat of vaporization}}$$

It takes on the following values for various thermal conditions of the feed:

Subcooled liquid feed:	$q > 1$
Saturated liquid feed:	$q = 1$
Partially flashed feed:	$0 < q < 1$
Saturated vapor feed:	$q = 0$
Superheated vapor feed:	$q < 0$

Equations analogous to (13-26) and (13-27) can be written for a sidestream, but the value of q will be either 1 or 0 depending upon whether the sidestream is taken from the liquid or the vapor stream.

The quantity q can be used to derive the " q line equation" for a feed stream or a sidestream. The q line is the locus of all points of intersection of the two operating lines, which meet at the feed stream or sidestream stage. This intersection must occur along that section of the q line between the equilibrium curve and the $y = x$ diagonal. At the point of intersection, the same y , x point must satisfy both the operating line equation above the feed stream (or sidestream) stage and the one below the feed stream (or sidestream) stage. Subtracting one equation from the other gives for a feed stage

$$(V - V')y = (L - L')x + Fz_F$$

which, when combined with Eqs. (13-26) and (13-27), gives the q line equation

$$y = \frac{q}{q-1}x - \frac{z_F}{q-1} \quad (13-28)$$

A q line construction for a partially flashed feed is given in Fig. 13-22. It is easily shown that the q line must intersect the diagonal at z_F .

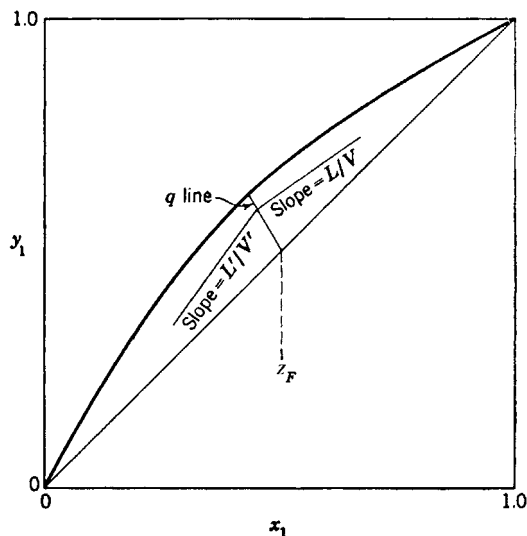


FIG. 13-22 Typical intersection of the two operating lines at the q line for a feed stage. The q line shown is for a partially flashed feed.

The slope of the q line is $q/(q-1)$. All five q line cases are shown in Fig. 13-23. Note that when $q = 1$, the q line has infinite slope and is vertical.

The derivation of Eq. (13-28) assumes a single-feed column and no sidestream. However, the same result is obtained for other column configurations. Typical q line constructions for sidestream stages are shown in Fig. 13-24. Note that the q line for a sidestream must always intersect the diagonal at the composition (y_s or x_s) of the sidestream. Figure 13-24 also shows the intersections of the operating lines with the diagonal construction line. The top operating line must always intersect the diagonal at the overhead-product composition x_D . This can be shown by substituting $y = x$ in Eq. (13-21) and using $V - L = D$ to reduce the resulting equation to $x = x_D$. Similarly (except for columns in which open steam is introduced at the bottom), the bottom operating line must always intersect the diagonal at the bottom-product composition x_B .

Equilibrium-Stage Construction Use of the equilibrium curve and the operating lines to "step off" equilibrium stages is illustrated in Fig. 13-25. The plotted portions of the equilibrium curve (curved) and the operating line (straight) cover the composition range existing in the column section shown in the lower right-hand corner of the figure. If y_n and x_n represent the compositions (in terms of the more volatile

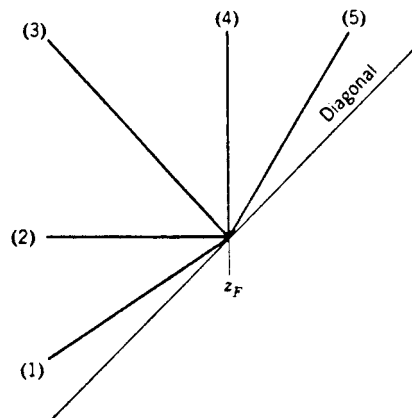


FIG. 13-23 All five cases of q lines: (1) superheated vapor feed, (2) saturated vapor feed, (3) partially vaporized feed, (4) saturated liquid feed, and (5) subcooled liquid feed. Slope of q line is $q/(q-1)$.

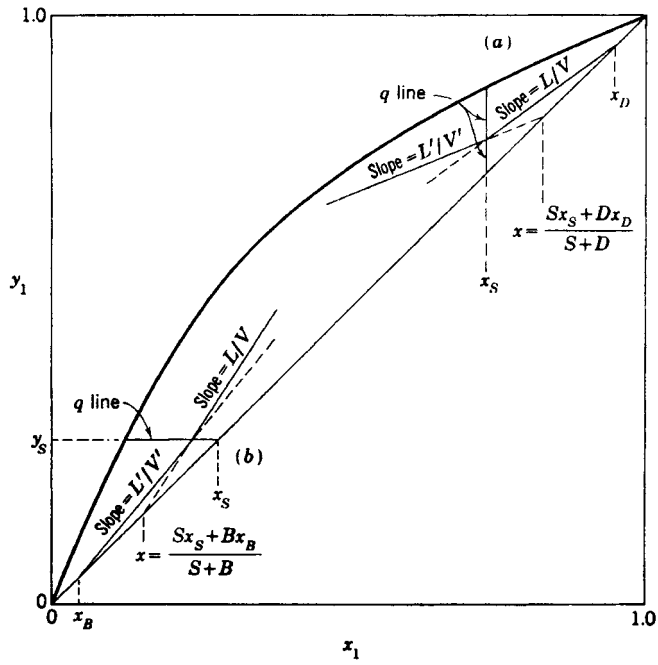


FIG. 13-24 Typical construction for a sidestream showing the intersection of the two operating lines with the q line and with the x - y diagonal. (a) Liquid sidestream near the top of the column. (b) Vapor sidestream near the bottom of the column.

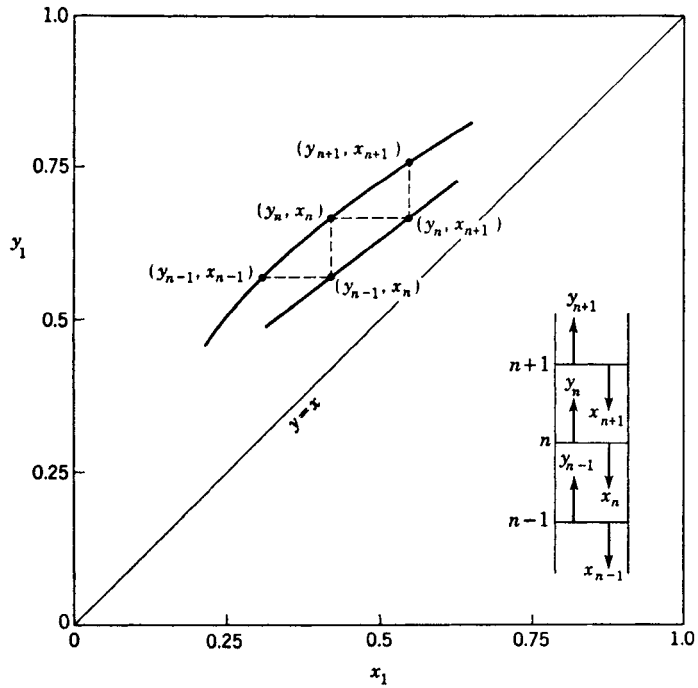


FIG. 13-25 Illustration of how equilibrium stages can be located on the x - y diagram through the alternating use of the equilibrium curve and the operating line.

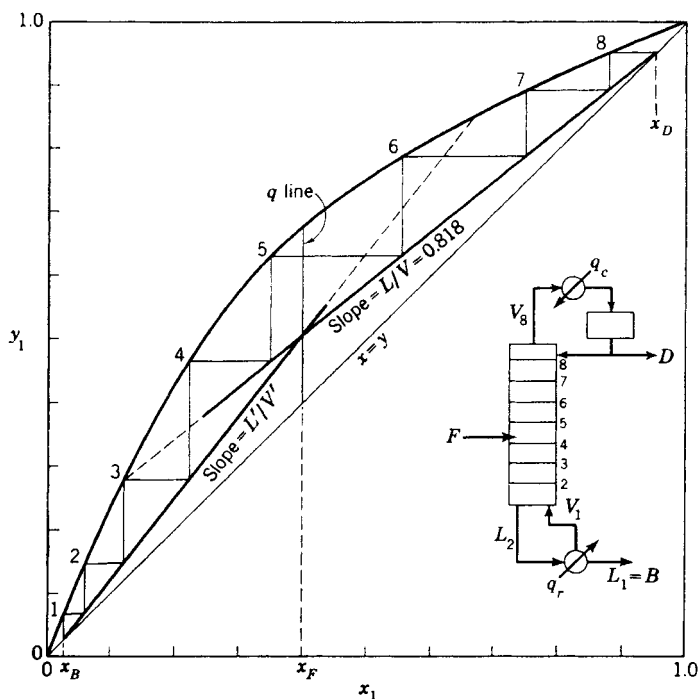


FIG. 13-26 Construction for a column with a bubble point feed, a total condenser, and a partial reboiler.

component) of the equilibrium vapor and liquid leaving stage n , then point (y_n, x_n) on the equilibrium curve must represent the equilibrium stage n . The operating line is the locus for compositions of all possible pairs of passing streams within the section, and therefore a horizontal line (dashed) at y_n must pass through the point (y_n, x_{n+1}) on the operating line since y_n and x_{n+1} represent passing streams. Likewise, a vertical line (dashed) at x_n must intersect the operating line at point (y_{n-1}, x_n) . The equilibrium stages above and below stage n can be located by a vertical line through (y_n, x_{n+1}) to find (y_{n+1}, x_{n+1}) and a horizontal line through (y_{n-1}, x_n) to find (y_{n-1}, x_{n-1}) . This procedure can be repeated by alternating the use of equilibrium and operating lines upward or downward through the column to find the total number of equilibrium stages.

Total Column Construction The graphical construction for an entire column is shown in Fig. 13-26. The process, pictured in the lower right-hand corner of the diagram, is an existing column with a number of actual trays equivalent to eight equilibrium stages. A partial reboiler (equivalent to an equilibrium stage) and a total condenser are used. This column configuration has $C + 2N + 9$ design variables (degrees of freedom) which must be specified to define one unique operation [see subsection Degrees of Freedom and Design Variables, especially Fig. 13-62 and Eq. (13-111)]. These may be used as follows as the basis for a graphical solution:

Specifications	Degrees of freedom
Stage pressures (including reboiler)	N
Condenser pressure	1
Stage heat leaks (except reboiler)	$N - 1$
Pressure and heat leak in reflux divider	2
Feed stream	$C + 2$
Feed-stage location	1
Total number of stages N	1
One overhead purity	1
Reflux temperature	1
Eternal reflux ratio	1
	$C + 2N + 9$

Pressures can be specified at any level below the safe working pressure of the column. The condenser pressure will be set at 275.8 kPa (40 psia), and all pressure drops within the column will be neglected. The equilibrium curve in Fig. 13-26 represents data at that pressure. All heat leaks will be assumed to be zero. The feed composition is 40 mol % of the more volatile component 1, and the feed rate is 0.126 kg-mol/s (1000 lb-mol/h) of saturated liquid ($q = 1$). The feed-stage location is fixed at stage 4 and the total number of stages at eight.

The overhead purity is specified as $x_D = 0.95$. The reflux temperature is the bubble point temperature (saturated reflux), and the external reflux ratio is set at $R = 4.5$.

Answers are desired to the following two questions. First, what bottom-product composition x_B will the column produce under these specifications? Second, what is the value of the top vapor rate V_N in this operation, and will it exceed the maximum vapor rate capacity for this column, which is assumed to be 0.252 kg-mol/s (2000 lb-mol/h) at the top-tray conditions?

The solution is started by using Eq. (13-25) to convert the external reflux ratio of 4.5 to an internal reflux ratio of $L/V = 0.818$. The distillate composition $x_D = 0.95$ is then located on the diagonal, and the upper operating line is drawn as shown in Fig. 13-26.

If the x_B value were known, the bottom operating line could be immediately drawn from the x_B value on the diagonal up to its required intersection point with the upper operating line on the feed q line. In this problem, since the number of stages is fixed, the value of x_B which gives a lower operating line that will require exactly eight stages must be found by trial and error. An x_B value is assumed, and the resulting lower operating line is drawn. The stages can be stepped off by starting from either x_B or x_D ; x_B was used in this case.

Note that the lower operating line is used until the fourth stage is passed, at which time the construction switches to the upper operating line. This is necessary because the vapor and liquid streams passing each other between the fourth and fifth stages must fall on the upper line.

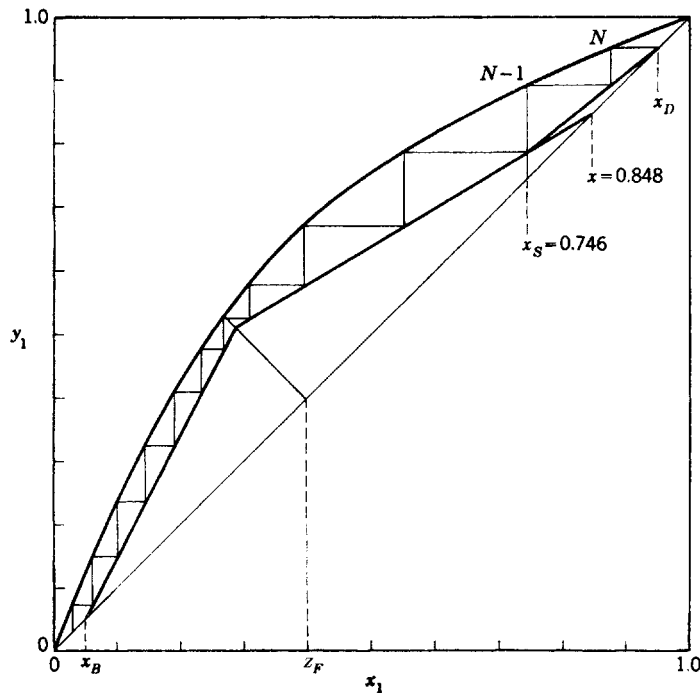


FIG. 13-27 Graphical solution for a column with a partially flashed feed, a liquid sidestream, and a total condenser.

The x_B that requires exactly eight equilibrium stages is $x_B = 0.026$. An overall component balance gives $D = 0.051$ kg-mol/s (405 lb-mol/h). Then

$$\begin{aligned} V_N = V_B = L_{N+1} + D = D(R + 1) &= 0.051(4.5 + 1.0) \\ &= 0.280 \text{ kg-mol/s (2230 lb-mol/h)} \end{aligned}$$

which exceeds the column capacity of 0.252 kg-mol/s (2007 lb-mol/h). This means that the column cannot provide an overhead-product yield of 40.5 percent at 95 percent purity. Either the purity specification must be reduced, or we must be satisfied with a lower yield. If the distillate specification ($x_D = 0.95$) is retained, the reflux rate must be reduced. This will cause the upper operating line to pivot upward around its fixed point of $x_D = 0.95$ on the diagonal. The new intersection of the upper line with the q line will lie closer to the equilibrium curve. The x_B value must then move upward along the diagonal because the eight stages will not "reach" as far as before. The higher x_B composition will reduce the recovery of component 1 in the 95 percent overhead product.

Another entire column with a partially vaporized feed, a liquid sidestream rate equal to D withdrawn from the second stage from the top, and a total condenser is shown in Fig. 13-27. The specified compositions are $z_F = 0.40$, $x_B = 0.05$, and $x_D = 0.95$. The specified L/V ratio in the top section is 0.818. These specifications permit the top operating line to be located and the two top stages stepped off to determine the liquid sidestream composition $x_s = 0.746$. The operating line below the sidestream must intersect the diagonal at the "blend" of the sidestream and the overhead stream. Since S was specified to be equal to D in rate, the intersection point is

$$x = \frac{(1.0)(0.746) + (1.0)(0.95)}{1.0 + 1.0} = 0.848$$

This point plus the point of intersection of the two operating lines on the sidestream q line (vertical at $x_s = 0.746$) permits the location of the

middle operating line. (The slope of the middle operating line could also have been used.) The lower operating line must run from the specified x_B value on the diagonal to the required point of intersection on the feed q line. The stages are stepped off from the top down in this case. The sixth stage from the top is the feed stage, and a total of about 11.4 stages are required to reach the specified $x_B = 0.05$.

Fractional equilibrium stages have meaning. The 11.4 will be divided by a tray efficiency, and the rounding up to an integral number of actual trays should be done after that division. For example, if the average tray efficiency for the process modeled in Fig. 13-27 is 80 percent, then the number of actual trays required is $11.4/0.8 = 14.3$, which is rounded up to 15.

Feed-Stage Location The optimum feed-stage location is that location which, with a given set of other operating specifications, will result in the widest separation between x_D and x_B for a given number of stages. Or, if the number of stages is not specified, the optimum feed location is the one that requires the lowest number of stages to accomplish a specified separation between x_D and x_B . Either of these criteria will always be satisfied if the operating line farthest from the equilibrium curve is used in each step, as in Fig. 13-26.

It can be seen from Fig. 13-26 that the optimum feed location would have been the fifth tray for that operation. If a new column were being designed, that should be the designer's choice. However, when an existing column is being modeled, the feed stage on the diagram should correspond as closely as possible to the actual feed tray in the column. It can be seen that a badly mislocated feed (a feed that requires one to remain with an operating line until it closely approaches the equilibrium curve) can be very wasteful insofar as the effectiveness of the stages is concerned.

Minimum Stages A column operating at total reflux is represented in Fig. 13-28a. Enough material has been charged to the column to fill the reboiler, the trays, and the overhead condensate drum to their working levels. The column is then operated with no feed and with all the condensed overhead stream returned as reflux ($L_{N+1} = V_N$ and $D = 0$). Also all the liquid reaching the reboiler is

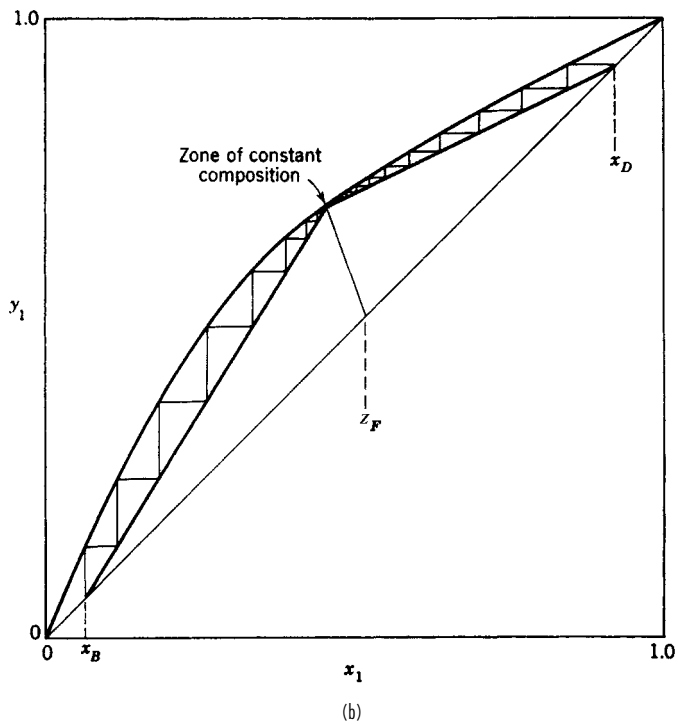
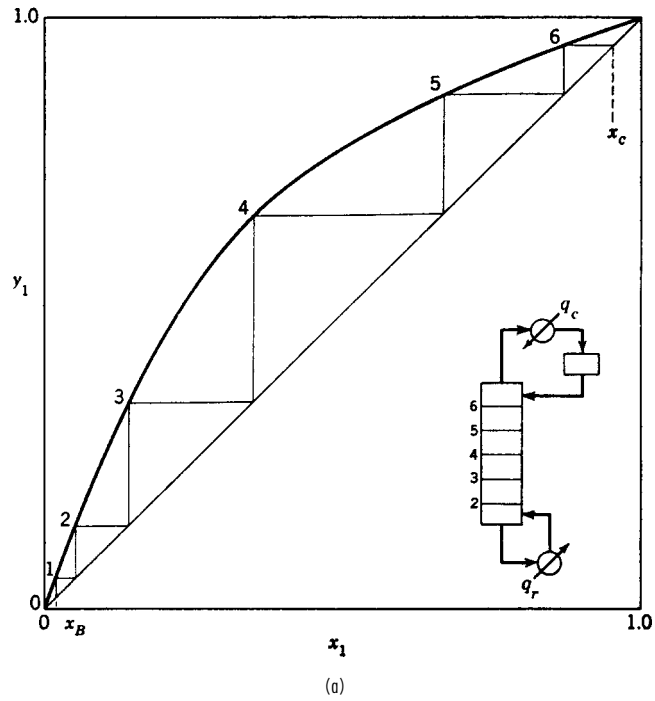


FIG. 13-28 McCabe-Thiele diagrams for limiting cases. (a) Minimum stages for a column operating at total reflux with no feeds or products. (b) Minimum reflux for a binary system of normal volatility.

vaporized and returned to the column as vapor. Since F , D , and B are all zero, $L_{n+1} = V_n$ at all points in the column. With a slope of unity ($L/V = 1.0$), the operating line must coincide with the diagonal throughout the column. Total reflux operation gives the minimum number of stages required to effect a specified separation between x_B and x_D .

Minimum Reflux The minimum reflux ratio is defined as that ratio which if decreased by an infinitesimal amount would require an infinite number of stages to accomplish a specified separation between two components. The concept has meaning only if a separation between two components is specified and the number of stages is not specified. Figure 13-28b illustrates the minimum reflux condition. As the reflux ratio is reduced, the two operating lines swing upward, pivoting around the specified x_B and x_D values, until one or both touch the equilibrium curve. For equilibrium curves shaped like the one shown, the contact occurs at the feed q line, resulting in a *feed pinch point*. Often an equilibrium curve will dip down closer to the diagonal at higher compositions. In such cases, the upper operating line may make contact before its intersection point on the q line reaches the equilibrium curve, resulting in a *tangent pinch point*. Wherever the contact appears, the intersection of the operating line with the equilibrium curve produces a pinch point which contains a very large number of stages, and a zone of constant composition is formed (see Doherty and Malone, 2001, chap. 3 and sec. 4.6 for additional information).

Intermediate Reboilers and Condensers When a large temperature difference exists between the ends of the column due to a wide boiling point difference between the components, intermediate reboilers and/or condensers may be used to add heat at a lower temperature, or remove heat at a higher temperature, respectively. [A distillation column of this type is shown in *Perry's Chemical Engineers' Handbook*, 7th ed. (1986), Fig. 13-2a.] A column operating with an intermediate reboiler and an intermediate condenser in addition to a regular reboiler and a condenser is illustrated with the solid lines in Fig. 13-29. The dashed lines correspond to simple distillation with only a bottoms reboiler and an overhead condenser. Total boiling and condensing heat loads are the same for both columns. As shown by Kayihan [*AIChE Symp. Ser.* 76, 192, 1 (1980)], the addition of intermediate reboilers and intermediate condensers increases thermodynamic efficiency but requires additional stages, as is clear from the positions of the operating lines in Fig. 13-29.

Optimum Reflux Ratio The general effect of the operating reflux ratio on fixed costs, operating costs, and the sum of these is shown in Fig. 13-30. In ordinary situations, the minimum on the total cost curve will generally occur at an operating reflux ratio in the inter-

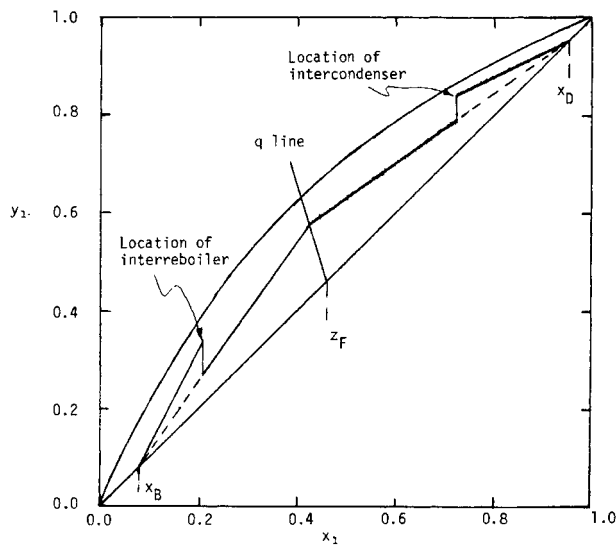


FIG. 13-29 McCabe-Thiele diagram for columns with and without an intermediate reboiler and an intermediate condenser.

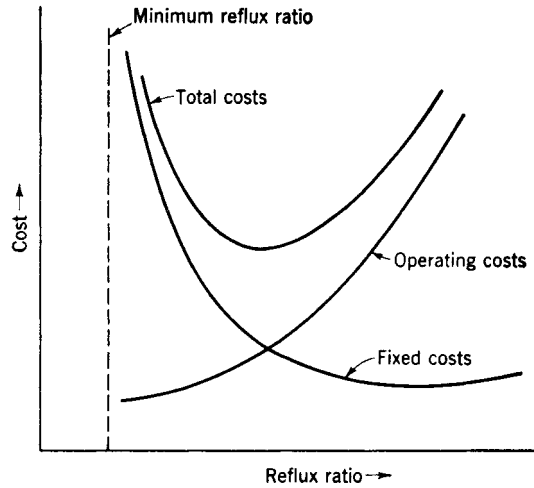


FIG. 13-30 Location of the optimum reflux for a given feed and specified separation.

val 1.1 to 2 times the minimum value. Generally, the total cost curve rises slowly from its minimum value as the operating reflux ratio increases, and very steeply as the operating reflux ratio decreases. In the absence of a detailed cost analysis for the specific separation of interest, it is recommended to select operating reflux ratios closer to 1.5 to 2.0 times the minimum value (see Doherty and Malone, 2001, chap. 6 for additional discussion).

Difficult Separations Some binary separations may pose special problems because of extreme purity requirements for one or both

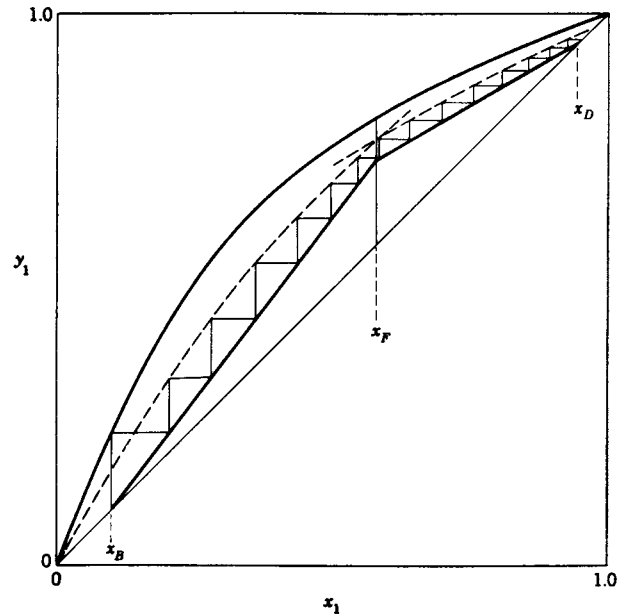


FIG. 13-31 Application of a 50 percent Murphree vapor-phase efficiency to each stage (excluding the reboiler) in the column. Each step in the diagram corresponds to an actual stage.

products or because of a relative volatility close to 1. The y - x diagram is convenient for stepping off stages at extreme purities if it is plotted on log-log paper. However, such cases are best treated by equation-based design methods.

Equation-Based Design Methods Exact design equations have been developed for mixtures with constant relative volatility. Minimum stages can be computed with the Fenske equation, minimum reflux from the Underwood equation, and the total number of stages in each section of the column from either the Smoker equation (*Trans. Am. Inst. Chem. Eng.*, **34**, 165 (1938); the derivation of the equation is shown, and its use is illustrated by Smith, op. cit.), or Underwood's method. A detailed treatment of these approaches is given in Doherty and Malone (op. cit., chap. 3). Equation-based methods have also been developed for nonconstant relative volatility mixtures (including nonideal and azeotropic mixtures) by Julka and Doherty [*Chem. Eng. Sci.*, **45**, 1801 (1990); *Chem. Eng. Sci.*, **48**, 1367 (1993)], and Fidkowski et al. [*AIChE J.*, **37**, 1761 (1991)]. Also see Doherty and Malone (op. cit., chap. 4).

Stage Efficiency The use of the *Murphree plate efficiency* is particularly convenient on y - x diagrams. The Murphree efficiency is defined for the vapor phase as

$$E^{MV} = \frac{y_n - y_{n-1}}{y_n^* - y_{n-1}} \quad (13-29)$$

where y_n^* is the composition of the vapor that would be in equilibrium with the liquid leaving stage n and is the value read from the equilibrium curve. The y_{n-1} and y_n are the actual (nonequilibrium) values for vapor streams leaving the $n-1$ and n stages, respectively. Note that

APPROXIMATE MULTICOMPONENT DISTILLATION METHODS

Some approximate calculation methods for the solution of multicomponent, multistage separation problems continue to serve useful purposes even though computers are available to provide more rigorous solutions. The available phase equilibrium and enthalpy data may not be accurate enough to justify the longer rigorous methods. Or in extensive design and optimization studies, a large number of cases can be worked quickly and cheaply by an approximate method to define roughly the optimum specifications, which can then be investigated more exactly with a rigorous method.

Two approximate multicomponent shortcut methods for simple distillation are the Smith-Brinkley (SB) method, which is based on an analytical solution of the finite-difference equations that can be written for staged separation processes when stages and interstage flow rates are known or assumed, and the Fenske-Underwood-Gilliland (FUG) method, which combines Fenske's total reflux equation and Underwood's minimum reflux equation with a graphical correlation by Gilliland that relates actual column performance to total and minimum reflux conditions for a specified separation between two key components. Thus, the SB and FUG methods are rating and design methods, respectively. Both methods work best when mixtures are nearly ideal.

The SB method is not presented here, but is presented in detail in the 6th edition of *Perry's Chemical Engineers' Handbook*. Extensions of the SB method to nonideal mixtures and complex configurations are developed by Eckert and Hlavacek [*Chem. Eng. Sci.*, **33**, 77 (1978)] and Eckert [*Chem. Eng. Sci.*, **37**, 425 (1982)], respectively, but are not discussed here. However, the approximate and very useful method of Kremser [*Nat. Pet. News*, **22**(21), 43 (May 21, 1930)] for application to absorbers and strippers is discussed at the end of this subsection.

FENSKE-UNDERWOOD-GILLILAND (FUG) SHORTCUT METHOD

In this approach, Fenske's equation [*Ind. Eng. Chem.*, **24**, 482 (1932)] is used to calculate N_{\min} , which is the number of plates required to make a specified separation at total reflux, i.e., the minimum value of N . Underwood's equations [*J. Inst. Pet.*, **31**, 111 (1945); **32**, 598 (1946);

for the y_{n-1} and y_n values we assume that the vapor streams are completely mixed and uniform in composition. An analogous efficiency can be defined for the liquid phase.

The application of a 50 percent Murphree vapor-phase efficiency on a y - x diagram is illustrated in Fig. 13-31. A pseudoequilibrium curve is drawn halfway (on a vertical line) between the operating lines and the true equilibrium curve. The true equilibrium curve is used for the first stage (the partial reboiler is assumed to be an equilibrium stage), but for all other stages the vapor leaving each stage is assumed to approach the equilibrium value y_n^* only 50 percent of the way. Consequently, the steps in Fig. 13-31 represent actual trays.

In general, application of a constant efficiency to each stage as in Fig. 13-31 will not give the same answer as obtained when the number of equilibrium stages (obtained by using the true equilibrium curve) is divided by the same efficiency factor.

The prediction and use of stage efficiencies are described in detail in Sec. 14. Alternative approaches based on mass-transfer rates are preferred, as described in the subsection below, Nonequilibrium Modeling.

Miscellaneous Operations The y - x diagrams for several other column configurations have not been presented here. The omitted items are *partial condensers*, *rectifying columns* (feed introduced to the bottom stage), *stripping columns* (feed introduced to the top stage), total reflux in the top section but not in the bottom section, multiple feeds, and introduction of *open steam* to the bottom stage to eliminate the reboiler. These configurations are discussed in Smith (op. cit.) and Henley and Seader (op. cit.), who also describe the more rigorous Ponchon-Savarit method, which is not covered here.

32, 614 (1946); and *Chem. Eng. Prog.*, **44**, 603 (1948)] are used to estimate the minimum reflux ratio R_{\min} . The empirical correlation of Gilliland [*Ind. Eng. Chem.*, **32**, 1220 (1940)] shown in Fig. 13-32 then uses these values to give N for any specified R , or R for any specified N . Limitations of the Gilliland correlation are discussed by Henley and Seader (*Equilibrium-Stage Separation Operations in Chemical Engineering*, Wiley, New York, 1981). The following equation, developed by Molokanov et al. [*Int. Chem. Eng.*, **12**(2), 209 (1972)], satisfies the endpoints and fits the Gilliland curve reasonably well:

$$\frac{N - N_{\min}}{N + 1} = 1 - \exp\left(\frac{1 + 54.4\Psi}{11 + 117.2\Psi} \times \frac{\Psi - 1}{\Psi^{0.5}}\right) \quad (13-30)$$

where $\Psi = (R - R_{\min})/(R + 1)$.

The Fenske total reflux equation can be written as

$$\left(\frac{x_i}{x_r}\right)_D = (\alpha_i)^{N_{\min}} \left(\frac{x_i}{x_r}\right)_B \quad (13-31)$$

or as
$$N_{\min} = \frac{\log[(Dx_D/Bx_B)/(Bx_B/Dx_D)]}{\log \alpha_i} \quad (13-32)$$

where i is any component and r is an arbitrarily selected reference component in the definition of relative volatilities

$$\alpha_i = \frac{K_i}{K_r} = \frac{y_i x_r}{y_r x_i} \quad (13-33)$$

The particular value of α_i used in Eqs. (13-31) and (13-32) is the effective value calculated from Eq. (13-34) defined in terms of values for each stage in the column by

$$\alpha_i^N = \alpha_{iN} \alpha_{iN-1} \cdots \alpha_{i2} \alpha_{i1} \quad (13-34)$$

Equations (13-31) and (13-32) are exact relationships between the splits obtained for components i and r in a column at total reflux.

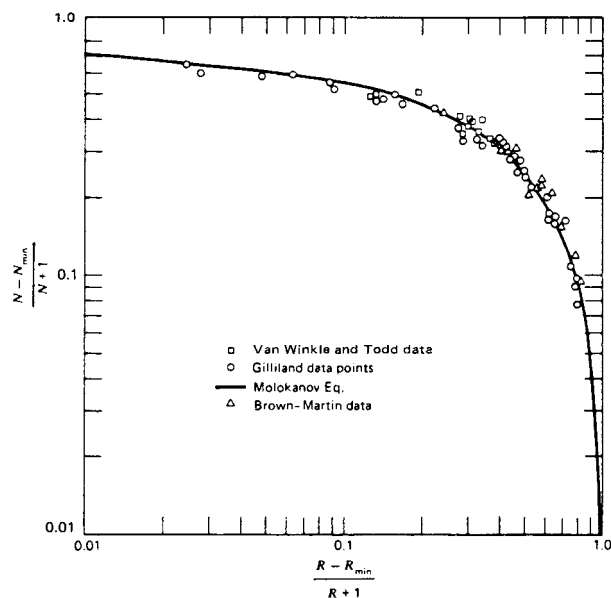


FIG. 13-32 Comparison of rigorous calculations with Gilliland correlation. [Henley and Seader, *Equilibrium-Stage Separation Operations in Chemical Engineering*, Wiley, New York, 1981; data of Van Winkle and Todd, *Chem. Eng.*, **78**(21), 136 (Sept. 20, 1971); data of Gilliland, *Elements of Fractional Distillation, 4th ed.*, McGraw-Hill, New York, 1950; data of Brown and Martin, *Trans. Am. Inst. Chem. Eng.*, **35**, 679 (1939).]

However, the value of α_i must always be estimated, and this is where the approximation enters. It is usually estimated from

$$\alpha = (\alpha_{\text{top}} \alpha_{\text{bottom}})^{1/2} \quad (13-35)$$

or
$$\alpha = (\alpha_{\text{top}} \alpha_{\text{middle}} \alpha_{\text{bottom}})^{1/3} \quad (13-36)$$

As a side note, the separation that will be accomplished in a column with a known number of equilibrium stages can often be reasonably well estimated by specifying the split of one component (designated as the reference component r), setting N_{min} equal to 40 to 60 percent of the number of equilibrium stages (not actual trays), and then using Eq. (13-32) to estimate the splits of all the other components. This is an iterative calculation because the component splits must first be arbitrarily assumed to give end compositions that can be used to give initial end-temperature estimates. The α_{top} and α_{bottom} values corresponding to these end temperatures are used in Eq. (13-5) to give α_i values for each component. The iteration is continued until the α_i values do not change from trial to trial.

The Underwood minimum reflux equations of main interest are those that apply when some of the components do not appear in either the distillate or the bottom products at minimum reflux. These equations are

$$\sum_i \frac{\alpha_i (x_{iD})_{\text{min}}}{\alpha_i - \Theta} = R_{\text{min}} + 1 \quad (13-37)$$

and
$$\sum_i \frac{\alpha_i z_{iF}}{\alpha_i - \Theta} = 1 - q \quad (13-38)$$

The relative volatilities α_i are defined by Eq. (13-33), R_{min} is the minimum reflux ratio, and q describes the thermal condition of the feed (1 for a saturated liquid feed and 0 for a saturated vapor feed). The z_{iF} values are available from the given feed composition. The Θ is the common root for the top section equations and the bottom section

equations developed by Underwood for a column at minimum reflux with separate zones of constant composition in each section. The common root value must fall between α_{hk} and α_{lk} , where hk and lk stand for *heavy key* and *light key*, respectively. The *key components* are the ones the designer wants to separate. In the butane-pentane splitter problem in Example 1, the light key is n -C₄ and the heavy key is i -C₅.

The α_i values in Eqs. (13-37) and (13-38) are effective values obtained from Eq. (13-35) or Eq. (13-36). Once these values are available, Θ can be calculated in a straightforward iteration from Eq. (13-38). Since the α - Θ difference can be small, Θ should be determined to four decimal places to avoid numerical difficulties.

The $(x_{iD})_{\text{min}}$ values in Eq. (13-37) are minimum reflux values, i.e., the overhead composition that would be produced by the column operating at the minimum reflux with an infinite number of stages. When the light key and the heavy key are adjacent in relative volatility and the specified split between them is sharp or the relative volatilities of the other components are not close to those of the two keys, only the two keys will distribute at minimum reflux and the $(x_{iD})_{\text{min}}$ values are easily determined. This is often the case and is the only one considered here. Other cases in which some of or all the nonkey components distribute between distillate and bottom products are discussed in detail by Henley and Seader (op. cit.).

The FUG method is convenient for new column design with the following specifications:

1. A value for R/R_{min}
2. Desired split on the reference component (usually chosen as the heavy key)
3. Desired split on one other component (usually the light key)

However, the total number of equilibrium stages N , N/N_{min} , or the external reflux ratio can be substituted for one of these three specifications. Note that the feed location is automatically specified as the optimum one; this is assumed in the Underwood equations. The assumption of saturated liquid reflux is also inherent in the Fenske and Underwood equations (i.e., the reflux is *not* subcooled). An important limitation on the Underwood equations is the assumption of constant molar overflow. As discussed by Henley and Seader (op. cit.), this assumption can lead to a prediction of the minimum reflux that is considerably lower than the actual value. No such assumption is inherent in the Fenske equation. An exact calculation technique for minimum reflux is given by Tavana and Hansen [*Ind. Eng. Chem. Process Des. Dev.*, **18**, 154 (1979)]. Approximate explicit expressions for minimum reflux for various types of splits in three- and four-component mixtures were developed by Glinos and Malone [*Ind. Eng. Chem. Process Des. Dev.*, **23**, 764 (1984)] as well as lumping rules for applying their expressions to mixtures containing more than four components. These expressions are fairly accurate (usually within 5 percent of the exact value for R_{min}) and are extremely convenient for using in the FUG method since they remove the tedious calculation of R_{min} via the Underwood equations. A computer program for the FUG method is given by Chang [*Hydrocarbon Process.*, **60**(8), 79 (1980)]. The method is best applied to mixtures that form ideal or nearly ideal solutions, and should not be used for strongly nonideal or azeotropic mixtures.

Example 1: Application of FUG Method A large butane-pentane splitter is to be shut down for repairs. Some of its feed will be diverted temporarily to an available smaller column, which has only 11 trays plus a partial reboiler. The feed enters on the middle tray. Past experience with similar feeds indicates that the 11 trays plus the reboiler are roughly equivalent to 10 equilibrium stages and that the column has a maximum top vapor capacity of 1.75 times the feed rate on a mole basis. The column will operate at a condenser pressure of 827.4 kPa (120 psia). The feed will be at its bubble point ($q = 1.0$) at the feed tray conditions and has the following composition on the basis of 0.0126 kg-mol/s (100 lb-mol/h):

Component	Fx_{iF}
C ₃	5
<i>i</i> -C ₄	15
<i>n</i> -C ₄	25
<i>i</i> -C ₅	20
<i>n</i> -C ₅	35
	100

The original column normally has less than 7 mol % *i*-C₅ in the overhead and less than 3 mol % *n*-C₄ in the bottom product when operating at a distillate rate of $D/F = 0.489$. Can these product purities be produced on the smaller column at $D/F = 0.489$?

Pressure drops in the column will be neglected, and the K values will be read at 827 kPa (120 psia) in both column sections from the DePriester nomograph in Fig. 13-9b. When constant molar overflow is assumed in each section, the rates in pound moles per hour in the upper and lower sections are as follows:

Top section	Bottom section
$D = (0.489)(100) = 48.9$	$B = 100 - 48.9 = 51.1$
$V = (1.75)(100) = 175$	$V' = V = 175$
$L = 175 - 48.9 = 126.1$	$L' = L + F = 226.1$
$\frac{V}{L} = 1.388$	$\frac{V'}{L'} = 0.7739$

$$\frac{L}{L'} = \frac{126.1}{226.1} = 0.5577$$

$$R = \frac{126.1}{48.9} = 2.579$$

NOTE: To convert pound-moles per hour to kilogram-moles per second, multiply by 1.26×10^{-3} .

Application of the FUG method is demonstrated on the splitter. Specifications necessary to model the existing column include these:

1. $N = 10$, total number of equilibrium stages
2. Optimum feed location (which may or may not reflect the actual location)
3. Maximum V/F at the top tray of 1.75
4. Split on one component given in the following paragraphs

The solution starts with an assumed arbitrary split of all the components to give estimates of top and bottom compositions that can be used to get initial end temperatures. The α_i 's evaluated at these temperatures are averaged with the α at the feed-stage temperature (assumed to be the bubble point of the feed) by using Eq. (13-36). The initial assumption for the split on *i*-C₅ is $Dx_D/Bx_B = 3.15/16.85$. As mentioned earlier, N_{min} usually ranges from 0.4N to 0.6N, and the initial N_{min} value assumed here will be $(0.6)(10) = 6.0$. Equation (13-32) can be rewritten as

$$\left(\frac{Dx_D}{F x_F - Dx_D} \right)_i = \alpha_i^{6.0} \left(\frac{3.15}{16.85} \right) = \alpha_i^{6.0} (0.1869)$$

or
$$Dx_{iD} = \frac{0.1869 \alpha_i^{6.0}}{1 + 0.1869 \alpha_i^{6.0}} F x_{iF}$$

The evaluation of this equation for each component is as follows:

Component	α_i	$\alpha_i^{6.0}$	$0.1869 \alpha_i^{6.0}$	$F x_{iF}$	$D x_{iD}$	$B x_{iB}$
C ₃	5.00			5	5.0	0.0
<i>i</i> -C ₄	2.63	330	61.7	15	14.8	0.2
<i>n</i> -C ₄	2.01	66	12.3	25	25.1	1.9
<i>i</i> -C ₅	1.00	1.00	0.187	20	3.15	16.85
<i>n</i> -C ₅	0.843	0.36	0.0672	35	2.20	32.80
				100	48.25	51.75

The end temperatures corresponding to these product compositions are 344 K (159°F) and 386 K (236°F). These temperatures plus the feed bubble point temperature of 358 K (185°F) provide a new set of α_i 's which vary only slightly from those used earlier. Consequently, the $D = 48.25$ value is not expected to vary greatly and will be used to estimate a new *i*-C₅ split. The desired distillate

composition for *i*-C₅ is 7 percent; so it will be assumed that $Dx_D = (0.07)(48.25) = 3.4$ for *i*-C₅ and that the split on that component will be 3.4/16.6. The results obtained with the new α_i 's and the new *i*-C₅ split are as follows:

Component	$\alpha_i^{6.0}$	$0.2048 \alpha_i^{6.0}$	$F x_{iF}$	$D x_{iD}$	$B x_{iB}$	x_{iD}	x_{iB}
C ₃			5	5.0	0.0	0.102	0.000
<i>i</i> -C ₄	322	65.9	15	14.8	0.2	0.301	0.004
<i>n</i> -C ₄	68	13.9	25	23.3	1.7	0.473	0.033
<i>i</i> -C ₅	1.00	0.205	20	3.4	16.6	0.069	0.327
<i>n</i> -C ₅	0.415	0.085	35	2.7	32.3	0.055	0.636
			100	49.2	50.8	1.000	1.000

The calculated *i*-C₅ composition in the overhead stream is 6.9 percent, which is close enough to the target value of 7.0 for now.

Table 13-6 shows subsequent calculations using the Underwood minimum reflux equations. The α and x_D values in Table 13-6 are those from the Fenske total reflux calculation. As noted earlier, the x_D values should be those at minimum reflux. This inconsistency may reduce the accuracy of the Underwood method; but to be useful, a shortcut method must be fast, and it has not been shown that a more rigorous estimation of x_D values results in an overall improvement in accuracy. The calculated R_{min} is 0.9426. The actual reflux assumed is obtained from the specified maximum top vapor rate of 0.022 kg-mol/s [175 lb-(mol/h)] and the calculated D of 49.2 (from the Fenske equation).

$$L_{N+1} = V_N - D$$

$$R = \frac{V_N}{D} - 1 = \frac{175}{49.2} - 1 = 2.557$$

The values of $R_{min} = 0.9426$, $R = 2.557$, and $N = 10$ are now used with the Gilliland correlation in Fig. 13-32 or Eq. (13-30) to check the initially assumed value of 6.0 for N_{min} . Equation (13-30) gives $N_{min} = 6.95$, which differs from the assumed value.

Repetition of the calculations with $N_{min} = 7$ gives $R = 2.519$, $R_{min} = 0.9782$, and a calculated check value of $N_{min} = 6.85$, which is close enough. The final product compositions and the α values used are as follows:

Component	α_i	$D x_{iD}$	$B x_{iB}$	x_{iD}	x_{iB}
C ₃	4.98	5.00	0	0.1004	0.0
<i>i</i> -C ₄	2.61	14.91	0.09	0.2996	0.0017
<i>n</i> -C ₄	2.02	24.16	0.84	0.4852	0.0168
<i>i</i> -C ₅	1.00	3.48	16.52	0.0700	0.3283
<i>n</i> -C ₅	0.851	2.23	32.87	0.0448	0.6532
		49.78	50.32	1.0000	1.0000

These results indicate that the 7 percent composition of *i*-C₅ in D and the 3 percent composition of *i*-C₄ in B obtained in the original column can also be obtained with the smaller column. These results disagree somewhat with the answers obtained from a rigorous computer solution, as shown in the following comparison. However, given the approximations that went into the FUG method, the agreement is good.

Component	x_D		x_B	
	Rigorous	FUG	Rigorous	FUG
C ₃	0.102	0.100	0.0	0.0
<i>i</i> -C ₄	0.299	0.300	0.006	0.002
<i>n</i> -C ₄	0.473	0.485	0.037	0.017
<i>i</i> -C ₅	0.073	0.070	0.322	0.328
<i>n</i> -C ₅	0.053	0.045	0.635	0.653
	1.000	1.000	1.000	1.000

TABLE 13-6 Application of Underwood Equations

Component	x_F	α	αx_F	$\theta = 1.36$		$\theta = 1.365$		x_D	αx_D	$\alpha - \theta$	$\frac{\alpha x_D}{\alpha - \theta}$
				$\alpha - \theta$	$\frac{\alpha x_F}{\alpha - \theta}$	$\alpha - \theta$	$\frac{\alpha x_F}{\alpha - \theta}$				
					$\alpha - \theta$		$\frac{\alpha x_F}{\alpha - \theta}$				
C ₃	0.05	4.99	0.2495	3.63	0.0687	3.625	0.0688	0.102	0.5090	3.6253	0.1404
<i>i</i> -C ₄	0.15	2.62	0.3930	1.26	0.3119	1.255	0.3131	0.301	0.7886	1.2553	0.6282
<i>n</i> -C ₄	0.25	2.02	0.5050	0.66	0.7651	0.655	0.7710	0.473	0.9555	0.6553	1.4581
<i>i</i> -C ₅	0.20	1.00	0.2000	-0.36	-0.5556	-0.365	-0.5479	0.069	0.0690	-0.3647	-0.1892
<i>n</i> -C ₅	0.35	0.864	0.3024	-0.496	-0.6097	-0.501	-0.6036	0.055	0.0475	-0.5007	-0.0949
	1.00				-0.0196		+0.0014	1.000			1.9426 = $R_m + 1$

Interpolation gives $\theta = 1.3647$.

KREMSER EQUATION

Starting with the classical method of Kremser (op. cit.), approximate methods of increasing complexity have been developed to calculate the behavior of groups of equilibrium stages for a countercurrent cascade, such as is used in simple absorbers and strippers of the type shown in Fig. 13-2b and d. However, none of these methods can adequately account for stage temperatures that are considerably higher or lower than the two entering stream temperatures for absorption and stripping, respectively, when appreciable composition changes occur. Therefore, only the simplest form of the Kremser method is presented here. Fortunately, rigorous computer methods described later can be applied when accurate results are required. The Kremser method is most useful for making preliminary estimates of absorbent and stripping agent flow rates or equilibrium-stage requirements. The method can also be used to extrapolate quickly results of a rigorous solution to a different number of equilibrium stages.

Consider the general adiabatic countercurrent cascade of Fig. 13-33 where v and ℓ are molar component flow rates. Regardless of whether the cascade is an absorber or a stripper, components in the entering vapor will tend to be absorbed and components in the entering liquid will tend to be stripped. If more moles are stripped than absorbed, the cascade is a stripper; otherwise, the cascade is an absorber. The Kremser method is general and applies to either case. Application of component material balance and phase equilibrium equations successively to stages 1 through $N - 1$, 1 through $N - 2$, etc., as shown by Henley and Seader (op. cit.), leads to the following equations originally derived by Kremser. For each component i ,

$$(v_i)_N = (v_i)_0(\Phi_i)_A = (\ell_i)_{N+1}[1 - (\Phi_i)_S] \quad (13-39)$$

where
$$(\Phi_i)_A = \frac{(A_i)_e - 1}{(A_i)_e^{N+1} - 1} \quad (13-40)$$

is the fraction of component i in the entering vapor that is not absorbed,
$$(\Phi_i)_S = \frac{(S_i)_e - 1}{(S_i)_e^{N+1} - 1} \quad (13-41)$$

is the fraction of component i in the entering liquid that is not stripped,
$$(A_i)_e = \left(\frac{L}{K_i V} \right)_e \quad (13-42)$$

is the effective or average absorption factor for component i , and
$$(S_i)_e = \frac{1}{(A_i)_e} \quad (13-43)$$

is the effective or average stripping factor for component i . When the entering streams are at the same temperature and pressure and negligible absorption and stripping occur, effective component absorption and stripping factors are determined simply by entering stream conditions. Thus, if K values are composition-independent, then

$$(A_i)_e = \frac{1}{(S_i)_e} = \frac{L_{N+1}}{K_i(T_{N+1}, P_{N+1})V_0} \quad (13-44)$$

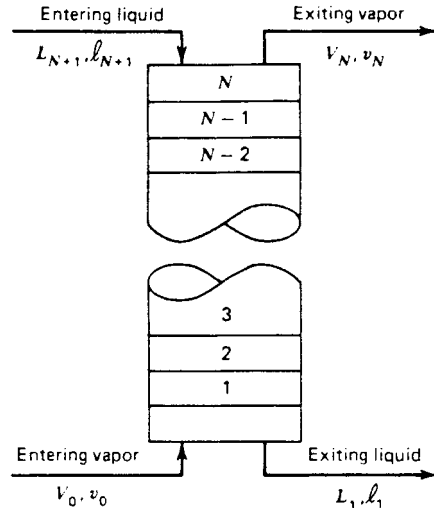


FIG. 13-33 General adiabatic countercurrent cascade for simple absorption or stripping.

When entering stream temperatures differ and/or moderate to appreciable absorption and/or stripping occurs, values of A_i and S_i should be based on effective average values of L , V , and K_i in the cascade. However, even then Eq. (13-44) with T_{N+1} replaced by $(T_{N+1} + T_0)/2$ may be able to give a first-order approximation of $(A_i)_e$. In the case of an absorber, $L_{N+1} < L_e$ and $V_0 > V_e$ will be compensated to some extent by $K_i((T_{N+1} + T_0)/2, P) < K_i(T_e, P)$. A similar compensation, but in opposite directions, will occur in the case of a stripper. Equations (13-40) and (13-41) are plotted in Fig. 13-34. Components having large values of A_e or S_e absorb or strip, respectively, to a large extent. Corresponding values of Φ_A and Φ_S approach a value of 1 and are almost independent of the number of equilibrium stages.

An estimate of the minimum absorbent flow rate for a specified amount of absorption from the entering gas of some key component K for a cascade with an infinite number of equilibrium stages is obtained from Eq. (13-40) as

$$(L_{N+1})_{\min} = K_K V_0 [1 - (\Phi_K)_A] \quad (13-45)$$

The corresponding estimate of minimum stripping agent flow rate for a stripper is obtained as

$$(V_0)_{\min} = \frac{L_{N+1} [1 - (\Phi_K)_S]}{K_K} \quad (13-46)$$

Example 2: Calculation of Kremser Method For the simple absorber specified in Fig. 13-35, a rigorous calculation procedure as described below gives the results in Table 13-7. Values of Φ were computed from component

TABLE 13-7 Results of Calculations for Simple Absorber of Fig. 13-35

Component	N = 6 (rigorous method)				N = 12 (Kremser method)					
	(lb-mol)/h		$(\Phi_i)_A$	$(\Phi_i)_S$	$(A_i)_e$	$(S_i)_e$	(lb-mol)/h		$(\Phi_i)_A$	$(\Phi_i)_S$
	$(v_i)_6$	$(\ell_i)_1$					$(v_i)_{12}$	$(\ell_i)_1$		
C_1	147.64	12.36	0.9228		0.0772		147.64	12.36	0.9228	
C_2	276.03	94.97	0.7460		0.2541		275.98	94.02	0.7459	
C_3	105.42	134.58	0.4393		0.5692		103.46	136.54	0.4311	
nC_4	1.15	23.85	0.0460		1.3693		0.16	24.84	0.0063	
nC_5	0.0015	4.9985	0.0003		3.6		0	5.0	0.0	
Absorber oil	0.05	164.95		0.9997		0.0003	0.05	164.95		0.9997
Totals	530.29	435.71					527.29	437.71		

NOTE: To convert pound-moles per hour to kilogram-moles per hour, multiply by 0.454.

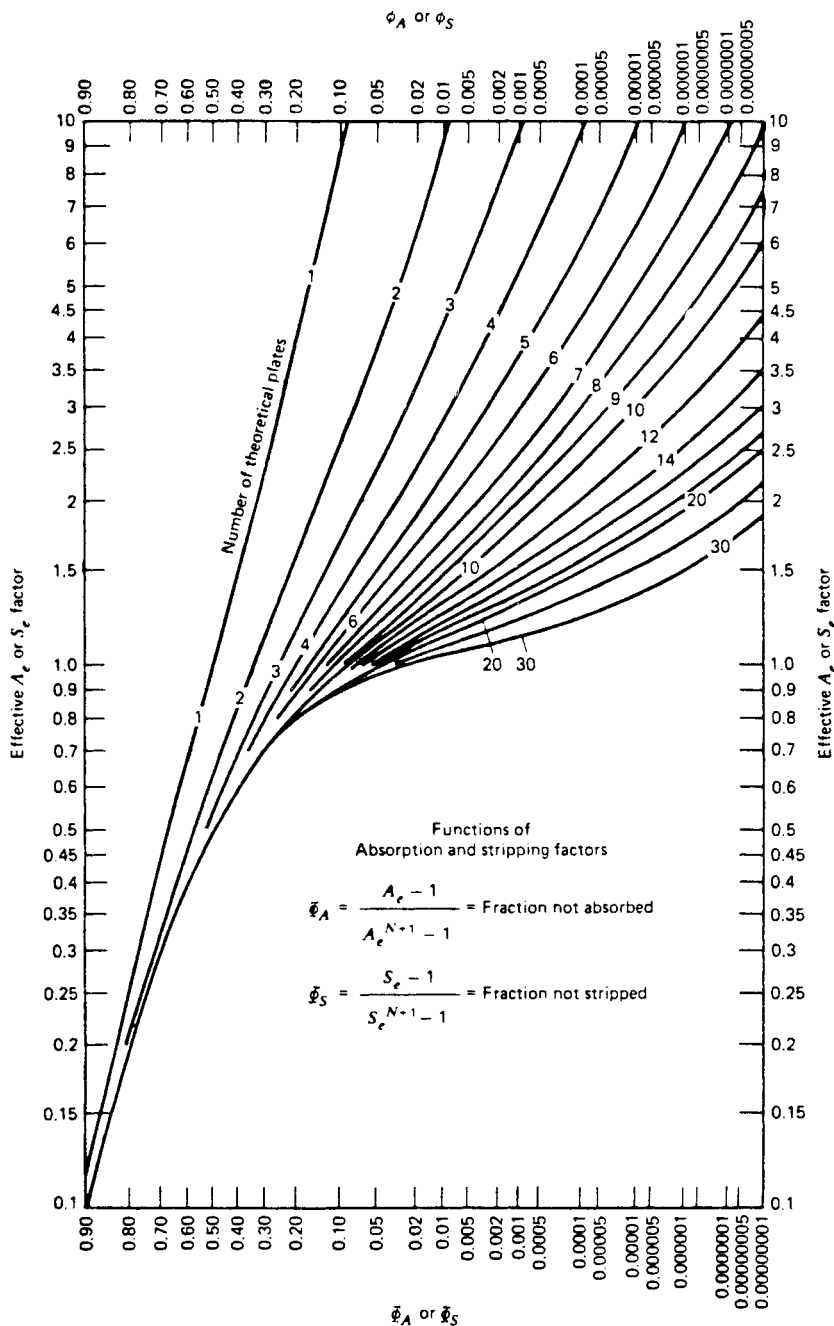


FIG. 13-34 Absorption and stripping factors. [W. C. Edmister, *AIChE J.*, 3, 165-171 (1957).]

product flow rates, and corresponding effective absorption and stripping factors were obtained by iterative calculations in using Eqs. (13-40) and (13-41) with $N=6$. Use the Kremser method to estimate component product rates if N is doubled to a value of 12.

Assume that values of A_e and S_e will not change with a change in N . Application of Eqs. (13-40), (13-41), and (13-39) gives the results in the last four

columns of Table 13-7. Because of its small value of A_e , the extent of absorption of C_1 is unchanged. For the other components, somewhat increased amounts of absorption occur. The degree of stripping of the absorber oil is essentially unchanged. Overall, only an additional 0.5 percent of absorption occurs. The greatest increase in absorption occurs for $n-C_4$, to the extent of about 4 percent.

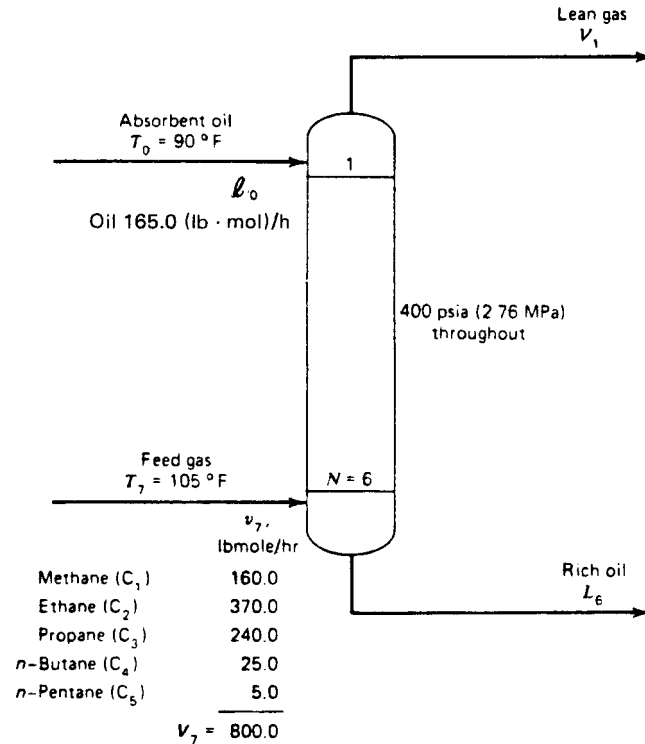


FIG. 13-35 Specifications for the absorber example.

SIMULATION OF DISTILLATION PROCESSES

Chemical engineers have been solving distillation problems by using the *equilibrium-stage model* since 1893 when Sorel outlined the concept to describe the distillation of alcohol. Since that time, it has been used to model a wide variety of distillation-like processes, including simple distillation (single-feed, two-product columns), complex distillation (multiple-feed, multiple-product columns), extractive and azeotropic distillation, petroleum distillation, absorption, liquid-liquid extraction, stripping, and supercritical extraction.

Real distillation processes, however, nearly always operate away from equilibrium. In recent years it has become possible to simulate distillation and absorption as the mass-transfer rate-based operations that they really are, using what have become known as *nonequilibrium* (NEQ) or *rate-based* models [Taylor et al., *CEP* (July 28, 2003)].

The computer simulation of distillation processes, whether done using equilibrium or nonequilibrium models, requires us to address the following topics:

- Formulation of the model equations
 - Physical property data and calculations (see Sec. 4 of this handbook)
 - Degrees-of-freedom analysis
 - Solution of large linear and strongly nonlinear systems of equations
- These are the topics we consider in what follows. We also discuss the use of simulation tools in the modeling of real distillation columns.

EQUILIBRIUM-STAGE MODELING

A schematic diagram of an equilibrium stage is shown in Fig. 13-36a. Vapor from the stage below and liquid from a stage above are brought into contact on the stage together with any fresh or recycle feeds. The

vapor and liquid streams leaving the stage are assumed to be in equilibrium with each other. A complete separation process is modeled as a sequence of these *equilibrium stages*, as shown in Fig. 13-36b.

The MESH Equations (the 2c + 3 Formulation) The equations that model equilibrium stages often are referred to as the MESH equations. The M equations are the material balance equations, E stands for equilibrium equations, S stands for mole fraction summation equations, and H refers to the heat or enthalpy balance equations.

There are two types of material balance: the total material balance

$$V_{j+1} + L_{j-1} + F_j - (1 + r_j^v)V_j - (1 + r_j^l)L_j = 0 \quad (13-47)$$

and the component material balance

$$V_{j+1}y_{i,j+1} + L_{j-1}x_{i,j-1} + F_jz_{i,j} - (1 + r_j^v)V_jy_{i,j} - (1 + r_j^l)L_jx_{i,j} = 0 \quad (13-48)$$

In the material balance equations given above, r_j is the ratio of side-stream flow to interstage flow:

$$r_j^v = \frac{U_j}{V_j} \quad r_j^l = \frac{W_j}{L_j} \quad (13-49)$$

Mole fractions must be forced to sum to unity, thus

$$\sum_{i=1}^c x_{i,j} = 1 \quad \sum_{i=1}^c y_{i,j} = 1 \quad \sum_{i=1}^c z_{i,j} = 1 \quad (13-50)$$

The enthalpy balance is given by

$$V_{j+1}H_{j+1}^v + L_{j-1}H_{j-1}^l + F_jH_j^f - (1 + r_j^v)V_jH_j^v - (1 + r_j^l)L_jH_j^l - Q_j = 0 \quad (13-51)$$

The superscripted H 's are the enthalpies of the appropriate phase.

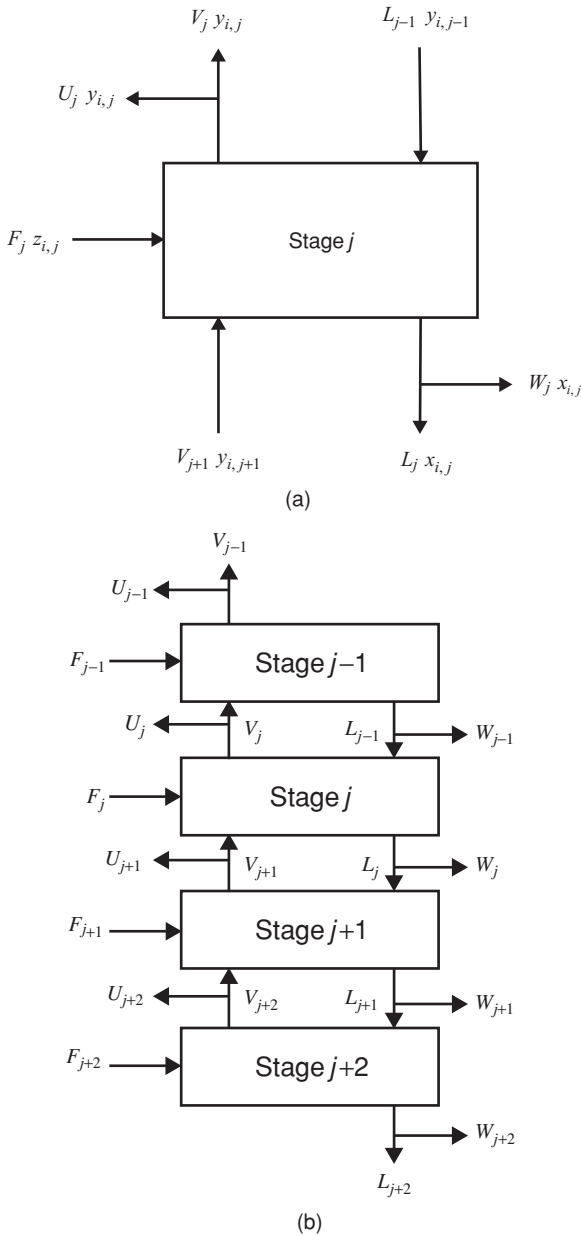


FIG. 13-36 (a) The equilibrium stage. (b) Multistage column.

To complete the model, it is usual to add equations that relate the compositions of the two streams leaving the stage. In the standard model of a distillation column, we assume that these two streams are in equilibrium with each other. Thus, the mole fractions in the exiting streams are related by the familiar equations of phase equilibrium:

$$y_{i,j} = K_{i,j} x_{i,j} \tag{13-52}$$

The $K_{i,j}$ are the equilibrium ratios or K values for species i on stage j .

Degrees-of-Freedom Analysis and Problem Formulation
 Table 13-8 summarizes the equations for a single equilibrium stage (in a sequence of stages). There are $2c + 4$ equations per stage, of which

TABLE 13-8 Equations for an Equilibrium Stage

Equation	Equation no.	Number
Total mass balance	(13-47)	1
Component mass balances	(13-48)	c
Total energy balance	(13-51)	1
Mole fraction summation equations	(13-50)	2
Equilibrium equations	(13-52)	c
		$2c + 4$

only $2c + 3$ are independent. Thus, one of these equations must be ignored in a (computer-based) method to solve the equations. In some methods we disregard the total material balance; an alternative is to combine the vapor and liquid mole fraction summation equations (as was done for flash calculations by Rachford and Rice, op. cit.). Note that the mole fraction summation equations for the feed are omitted here, as are the mole fraction summation equations for interstage vapor and liquid traffic; the latter “belong” to the equation set for adjacent stages (see, however, the subsection Degrees of Freedom below in which this topic is revisited in greater detail).

The quantities for stage j that appear in these equations are summarized in Table 13-9. The total number of variables appearing in these equations is $3c + 10$. Note that the K values and enthalpies that also appear in the MESH equations are not included in the table of variables, nor are equations for their estimation included in the list of equations. Thermodynamic properties are functions of temperature, pressure, and composition, quantities that do appear in the table of variables.

The $2c + 3$ unknown variables normally determined by solving the MESH equations are the c vapor mole fractions $y_{i,j}$; the c liquid mole fractions $x_{i,j}$; the stage temperature T_j ; and the vapor and liquid flow V_j and L_j . The remaining variables, $c + 7$ in number (the difference between the number of variables and the number of independent equations), that need to be specified are the stage pressure P_j , the feed flow rate, $c - 1$ mole fractions in the feed (the last is then computed directly from the feed mole fraction summation equation, which was not included in the equations for stage j in Table 13-8), temperature and pressure of the feed, the stage heat duty Q_j , and the sidestream flows U_j and W_j . It is important to recognize that the other flows and composition variables appearing in the MESH equations are associated with the equivalent equations for adjacent stages.

For a column of N stages, we must solve $N(2c + 3)$ equations. The table below shows how we may need to solve hundreds or even thousands of equations.

c	N	$N(2c + 3)$
2	10	70
3	20	180
5	50	650
10	30	690
40	100	8300

TABLE 13-9 Variables for an Equilibrium Stage

Variable	Symbol	Number
Vapor flow rate	V_j	1
Liquid flow rate	L_j	1
Feed flow rate	F_j	1
Vapor sidestream flow	W_j	1
Liquid sidestream flow	U_j	1
Vapor-phase mole fractions	$y_{i,j}$	c
Liquid-phase mole fractions	$x_{i,j}$	c
Feed composition	$z_{i,j}$	c
Stage temperature	T_j	1
Stage pressure	P_j	1
Feed temperature		1
Feed pressure		1
Stage heat duty	Q_j	1
		$3c + 10$

The $2c + 1$ Formulation An alternative form of the MESH equations is used in many algorithms. In this variation, we make use of the component flow defined by

$$v_{ij} = V_j y_{ij} \quad l_{ij} = L_j x_{ij} \quad f_{ij} = F_j z_{ij} \quad (13-53)$$

In terms of the component flow, the component material balance becomes

$$v_{i,j+1} + l_{i,j-1} + f_{i,j} - (1 + r_j^v) v_{i,j} - (1 + r_j^l) l_{i,j} = 0 \quad (13-54)$$

Since the total vapor and liquid flow rates are, by definition, the sum of the component flow rates of the respective phases, the summation equations and total mass balance equation are satisfied automatically. Thus, the number of equations and variables per stage has been reduced by 2 to $2c + 1$.

The $c + 3$ Formulation The number of unknown variables per stage can be reduced to only $c + 3$ if we use the equilibrium relations to eliminate the vapor-phase mole fractions from the component mass balances

$$V_{j+1} K_{i,j+1} x_{i,j+1} + L_{j-1} x_{i,j-1} + F_j z_{i,j} - (1 + r_j^v) V_j K_{i,j} x_{i,j} - (1 + r_j^l) L_j x_{i,j} = 0 \quad (13-55)$$

and from the summation equation

$$\sum_{i=1}^c K_{i,j} x_{i,j} = 1 \quad (13-56)$$

This equation is familiar to us from bubble point calculations. In this formulation of the MESH equations, the vapor-phase mole fractions no longer are independent variables but are defined by Eq. (13-52). This formulation of the MESH equations has been used in quite a number of algorithms. It is less useful if vapor-phase nonideality is important (and, therefore, the K values depend on the vapor-phase composition).

Condenser and Reboiler The MESH equations given above apply to all the interior stages of a column. In addition, any reboiler and condenser must be considered. On an actual plant, a total condenser may be followed by a reflux accumulator and a stream divider. The accumulator does not add any equations to a steady-state model (but it is important to consider in an unsteady-state model), but the stream splitter is a separate unit with its own temperature, pressure, and heat loss, and modeled by the appropriate balance equations (see the section below on Degrees of Freedom where we address this topic in greater detail). In practice the condenser and reflux splitter often are modeled as a single combined unit, and the MESH equations described above may be used to model these stages with only some minor modifications. For example, for a total condenser *and* the reflux stream splitter at the top of a distillation column, the liquid distillate is U_1 and the reflux ratio $R = 1/r_1^l$. For a partial condenser (with no stream splitter needed) the vapor product is V_1 and the reflux ratio $R = L_1/V_1$. A condenser/splitter device unit that provides both vapor and liquid products is given by a combination of these two units. Finally, for a partial reboiler at the base of a column, the bottoms flow rate is L_N . Note that an equilibrium stage with a sidestream is considered here to be a single unit in essentially the same way.

In computer-based methods for solving the MESH equations, it is common to replace the energy balance of the condenser (with or without the associated stream splitter) and reboiler with a specification equation. Possible specifications include

- The flow rate of the distillate/bottoms product stream
- The mole fraction of a component in either the distillate or bottoms product stream
- Component flow rate in either the distillate or bottoms product stream
- A reflux/reboil ratio or rate
- The temperature of the condenser or reboiler
- The heat duty to the condenser or reboiler

If the condenser and/or reboiler heat duties are not specified, it is possible to calculate them from the energy balances after all the other model equations have been solved.

For a total condenser, the vapor composition used in the equilibrium relations is that determined during a bubble point calculation based on the actual pressure and liquid compositions found in the condenser. These vapor mole fractions are not used in the component mass balances since there is no vapor stream from a total condenser. It often happens that the temperature of the reflux stream is below the bubble point temperature of the condensed liquid (subcooled condenser). In such cases it is necessary to specify either the actual temperature of the reflux stream or the difference in temperature between the reflux stream and the bubble point of the condensate.

Solution of the MESH Equations We may identify several classes of methods of solving the *equilibrium*-stage model equations:

- *Graphical methods.* These methods were developed before modern computer methods became widely adopted. Some graphical methods retain their value for a variety of reasons and were discussed at length in a prior subsection.
- *Approximate methods.* In these a great many simplifying assumptions are made to obtain solutions of the model equations. These methods were the subject of the immediately preceding subsection.
- *Computer-based methods.* Indeed, from the late 1950s to the early 1990s hardly a year passed without the publication of at least one (and usually many more than one) new algorithm for solving these equations (Seader, op. cit.). It is possible to make the case that it was the equilibrium model that brought computing into chemical engineering in the first place! One of the incentives for this activity has always been a desire to solve problems with which existing methods have trouble. The evolution of algorithms for solving the stage model equations has been influenced by, among other things, the availability (or lack) of sufficient computer storage and speed, the development of mathematical techniques that can be exploited, the complexity of physical property (K value and enthalpy) correlations, and the form of the model equations being solved. We continue with a brief discussion of computer-based methods. Readers interested in complete details of the methods discussed should consult the references cited below. In addition, many computer-based methods are discussed at length in a number of textbooks [see, e.g., Holland, op. cit.; King, op. cit.; Seader and Henley, op. cit.; Haas (in Kister op. cit. 1992)]. Seader (op. cit.) has written an interesting history of equilibrium-stage simulation.

The MESH equations form a set of nonlinear, algebraic equations (in the sense that no derivatives or integrals are involved) and must, therefore, be solved by some iterative process. There are two key steps in the development of an algorithm for solving systems of nonlinear equations:

- The selection of particular numerical methods
 - The selection of the order in which the equations are to be solved
- We may identify several classes of methods for numerically solving the MESH equations:

1. Tearing methods in which the equations are divided into groups and each group is solved separately
2. Inside-out (IO) methods
3. Simultaneous convergence (SC) methods in which all the equations are solved at the same time simultaneously by using Newton's method (or a variant thereof)
4. Relaxation methods in which the MESH equations are cast in unsteady-state form and integrated numerically until the steady-state solution has been found
5. Continuation methods
6. Collocation methods
7. Optimization methods

The methods for solving the MESH equations that are used most widely fall into categories 1 through 3 and 5—tearing methods, inside-out methods, simultaneous convergence methods, and continuation method. Following the sections on each of these three classes of method, we discuss homotopy continuation methods. For many years the older tearing methods formed the backbone of sequential modular flow sheet simulation programs; such methods have largely been replaced by the inside-out methods that now are standard in all major (and many less widely used) flow sheet simulation programs. Simultaneous convergence methods also now are available in many of these systems. Even homotopy methods (sometimes considered to belong

to the domain of specialists) are finding increasing use in commercial software.

Tearing Methods Equation tearing involves breaking a system of nonlinear equations into small groups and solving each group of equations in turn. In solving any subset of the complete set of equations, only a corresponding number of variables, the "tear" variables, can be determined. To start the calculations, therefore, it is necessary to assume values for the remaining variables. The "torn" set of equations is then solved for the "tear" variables, assuming that the values assigned to all other variables are correct. Successive groups of equations and variables are *torn* or *decoupled* from the full set of equations and variables until all the variables have been updated. At this point, the process starts over and is repeated until all the equations are satisfied simultaneously.

A great many tearing methods for solving the MESH equations have been proposed. According to Friday and Smith (1964), tearing methods may be analyzed in the following terms:

- The order in which the equations are grouped
- The order in which each group of equations is solved
- The selection of which variables are to be computed from which equation

Subsequent issues are

- The method(s) used to solve the M and E equations
- The method of calculating the new stage temperatures
- The method of calculating the new flow rates V_j and L_j

Most tearing methods are based on keeping all the equations of a given type together, e.g., the M equations or the H equations, for all the stages at once.

The classic papers by Lewis and Matheson [*Ind. Eng. Chem.*, **24**, 496 (1932)] and Thiele and Geddes [*Ind. Eng. Chem.*, **25**, 290 (1933)] represent the first attempts at solving the MESH equations for multicomponent systems numerically (the graphical methods for binary systems discussed earlier had already been developed by Ponchon, by Savarit, and by McCabe and Thiele). At that time the computer had yet to be invented, and since modeling a column could require hundreds, possibly thousands, of equations, it was necessary to divide the MESH equations into smaller subsets if hand calculations were to be feasible. Despite their essential simplicity and appeal, stage-to-stage calculation procedures are not used now as often as they used to be.

Matrix techniques were first used in separation process calculations by Amundson and Pontinen [*Ind. Eng. Chem.*, **50**, 730 (1958)] who demonstrated that the combined M + E equations (the $c + 3$ formulation) could be conveniently written in tridiagonal matrix form.

Three quite different approaches to the problem of computing the flow rates and temperatures have evolved:

1. In the bubble point (BP) method, the S + E equations are used to determine the stage temperatures from a bubble point calculation. The vapor and liquid flow rates are computed from the energy balances and total material balances. The BP method was introduced by Amundson and Pontinen (op. cit.) who used matrix inversion to solve equations. A significant improvement in the BP method was introduced by Wang and Henke [*Hydrocarbon Process.*, **45**(8), 155 (1966)] who used a form of Gaussian elimination known as the Thomas algorithm that can be used to solve a tridiagonal system very efficiently. Holland and coworkers (Holland, op. cit.) have combined some of these ideas with the "theta method" of convergence acceleration.

2. In the sum rates (SR) method, the vapor and liquid flow rates are computed directly from the summation equations and the stage temperatures determined from the energy balances. The SR algorithm was due originally to Sujata [*Hydrocarbon Process.*, **40**(12), 137 (1961)] and Friday and Smith (op. cit.). Sujata used the $2c + 1$ version of the MESH equations in his work and the tridiagonal system of combined M + E equations was written in terms of the component flow rates in the liquid phase. Birmingham and Otto [*Hydrocarbon Process.*, **46**(10), 163 (1967)] incorporated the Thomas algorithm in their implementation of the SR method. Sridhar and Lucia [*Comput. Chem. Eng.*, **14**, 901 (1990)] developed a modified SR method that is capable of solving problems involving narrow, intermediate, and wide-boiling mixtures alike.

3. In the Newton-Raphson methods, the bubble point equations and energy balances are solved simultaneously for the stage temperatures and vapor flow rates; the liquid flow rates follow from the total material balances [Tierney and coworkers, *AIChE J.*, **13**, 556 (1967); **15**, 897 (1969); Billingsley and Boynton, *AIChE J.*, **17**, 65 (1971)]. Similar methods are described by Holland (op. cit.) and by Tomich [*AIChE J.*, **16**, 229 (1970)].

Inside-Out Methods First proposed by Boston and Sullivan [*Can. J. Chem. Engr.*, **52**, 52 (1974)] and further developed by Boston and coworkers [*Comput. Chem. Engng.*, **2**, 109 (1978); *ACS Symp. Ser. No. 124*, 135 (1980); *Comput. Chem. Engng.*, **8**, 105 (1984); and *Chem. Eng. Prog.*, **86** (8), 45-54 (1990)], Jelinek [*Comput. Chem. Engng.*, **12**, 195 (1988)], and Simandl and Svrcek [*Comput. Chem. Engng.*, **15**, 337 (1991)], inside-out methods really belong in the group of tearing methods; however, their very widespread use in many commercial simulation programs demands that they be granted a category all to themselves. In these methods, complicated equilibrium and enthalpy expressions are replaced by simple models, and the iteration variables T , V , x , y are replaced by variables within the simple models that are relatively free of interactions with each other. Seader and Henley (op. cit.) provide complete details of the somewhat lengthy algorithm. Inside-out methods have replaced many of the older algorithms in commercial simulation programs, the modified version of Russell [*Chem. Eng.*, **90**, (20), 53 (1983)] being the basis for some of them.

Simultaneous Convergence Methods One drawback of some tearing methods is their relatively limited range of application. For example, the BP methods are more successful for distillation, and the SR-type methods are considered better for mixtures that exhibit a wide range of (pure-component) boiling points (see, however, our remarks above on modified BP and SR methods). Other possible drawbacks (at least in some cases) include the number of times physical properties must be evaluated (several times per outer loop iteration) if temperature- and composition-dependent physical properties are used. It is the physical properties calculations that generally dominate the computational cost of chemical process simulation problems. Other problems can arise if any of the iteration loops are hard to converge.

The development of methods for solving all the equations at the same time was tackled independently by a number of investigators. Simultaneous solution of all the MESH equations was suggested as a method of last resort by Friday and Smith (op. cit.) in a classic paper analyzing the reasons why other algorithms fail. They did not, however, implement such a technique. The two best-known papers are those of Goldstein and Stanfield [*Ind. Eng. Chem. Process Des. Dev.*, **9**, 78 (1970)] and Naphtali and Sandholm [*AIChE J.*, **17**, 148 (1971)], the latter providing more details of an application of Newton's method described by Naphtali at an AIChE meeting in May 1965. A method to solve all the MESH equations for all stages at once by using Newton's method was implemented by Whitehouse [Ph.D. Thesis, University of Manchester Institute of Science and Technology (1964)] (see Stainthorpe and Whitehouse [*I. Chem. E. Symp. Series*, **23**, 181 (1967)]). Among other things, Whitehouse's code allowed for specifications of purity, T , V , L , or Q on any stage. Interlinked systems of columns and nonideal solutions could be dealt with even though no examples of the latter type were solved by Whitehouse.

Many others have since employed Newton's method or a related method to solve the MESH equations. Such methods have become standard in commercial process simulation programs, most often for simulating systems for which tearing and inside-out methods are less successful (typically those that involve strongly nonideal mixtures). Simultaneous convergence procedures have shown themselves to be generally fast and reliable, having a locally quadratic convergence rate in the case of Newton's method, and these methods are much less sensitive to difficulties associated with nonideal solutions than are tearing methods. Seader (Sec. 13, *Perry's Chemical Engineers' Handbook*, 7th ed., 1986) discusses the design of simultaneous convergence methods.

Continuation Methods (for Really Difficult Problems) For those problems that other methods fail to solve, we may use continuation

methods. These methods begin with a known solution of a companion set of equations and follow a path to the desired solution of the set of equations to be solved. In most cases, the path exists and can be followed. We can identify the following categories of continuation method that have been used for solving the equilibrium-stage MESH equations:

1. Mathematical methods which place the MESH equations into a homotopy equation of purely mathematical origin

2. Physical continuation methods in which the nature of the equations being solved is exploited in some way
The first to use the Newton homotopy for separation process problems were Hlavacek and coworkers [*Chem. Eng. Sci.*, **36**, 1599 (1981); *Chem. Eng. Commun.*, **28**, 165 (1984)]. In papers of considerable significance Wayburn and Seader [*Comput. Chem. Engng.*, **11**, 7–25 (1987)]; *Proc. Second Intern. Conf. Foundations of Computer-Aided Process Design*, CACHE, Austin, Tex., 765–862 (1984); *AIChE Monograph Series*, AIChE, New York, **81**, No. 15 (1985)] used the Newton homotopy in their solution of the MESH equations for interlinked distillation columns. Kovach and Seider [*Comput. Chem. Engng.*, **11**, 593 (1987)] used the Newton homotopy for solving distillation problems involving highly nonideal mixtures.

In the category of physical continuation methods are the thermodynamic homotopies of Vickery and Taylor [*AIChE J.*, **32**, 547 (1986)] and a related method due to Frantz and Van Brunt (AIChE National Meeting, Miami Beach, 1986). Thermodynamic continuation has also been used to find azeotropes in multicomponent systems by Fidkowski et al. [*Comput. Chem. Engng.*, **17**, 1141 (1993)]. Parametric continuation methods may be considered to be physical continuation methods. The reflux ratio or bottoms flow rate has been used in parametric solutions of the MESH equations [Jelinek et al., *Chem. Eng. Sci.*, **28**, 1555 (1973)].

Bryne and Baird [*Comput. Chem. Engng.*, **9**, 593 (1985)] describe the use of proprietary continuation methods. Woodman (Ph.D. thesis, University of Cambridge, 1989) has combined several continuation methods to solve problems that involved nonstandard specifications and multiple liquid phases.

For detailed descriptions of homotopy methods in chemical engineering, see Seader [*Computer Modeling of Chemical Processes*, AIChE Monograph Series 15, **81**, (1985)].

Other Methods *Relaxation techniques* differ from both tearing algorithms and simultaneous convergence methods in that the relaxation techniques do not solve steady-state problems. Rather, at least one set of the MESH equations is cast in an unsteady-state form. The equations are then integrated from some initial state (guess) until successive values of the variables do not change. The appeal of the relaxation methods lies in their extreme stability. A drawback is that convergence is generally a very slow process, slowing even more as the solution is approached. For this reason, the method is used (only) for problems which are very difficult to converge or for situations in which a knowledge of how the steady state is achieved is important. Key papers are by Rose, Sweeney, and Schrodt [*Ind. Eng. Chem.*, **50**, 737 (1958)]; Ball (AIChE National Meeting, New Orleans, 1961); Verneuil and Oleson (ACS National Mtg., Los Angeles, 1971); and Ketchum [*Chem. Eng. Sci.*, **34**, 387 (1979)].

Collocation methods are widely used for solving systems of partial differential equations. Despite their considerable potential for certain types of equilibrium-stage simulation problems, collocation methods have not become part of the mainstream of equilibrium-stage simulation. Key papers are by Stewart et al. [*Chem. Eng. Sci.*, **40**, 409 (1985)]; Swartz and Stewart [*AIChE J.*, **32**, 1832 (1986)]; Cho and Joseph [*AIChE J.*, **29**, 261, 270 (1983)]; *Comput. Chem. Engng.*, **8**, 81 (1984)], and Seferlis and Hrymak [*Chem. Eng. Sci.*, **49**, 1369 (1994)]; *AIChE J.*, **40**, 813 (1994)].

Methods that have been developed for finding the optimal solution(s) to engineering models have also been used to solve difficult equilibrium-stage separation process problems. An example of a method in this category is that of Lucia and Wang [*Comput. Chem. Engng.*, **28**, 2541 (2004)].

Examples In what follows we illustrate possible column specifications by considering four examples from Seader (*Perry's Chemical Engineers' Handbook*, 7th ed., 1997). They are a simple distillation

column, a more complicated distillation column, an absorber, and a reboiled stripper. A simultaneous convergence method was used for the calculations reported below. The computer program that was used for these exercises automatically generated initial estimates of all the unknown variables (flows, temperatures, and mole fractions). In most cases the results here differ only very slightly from those obtained by Seader (almost certainly due to small differences in physical property constants).

Example 3: Simple Distillation Column Compute stage temperatures, interstage vapor and liquid flow rates and compositions, and reboiler and condenser duties for the butane-pentane splitter studied in Example 1. The specifications for this problem are summarized below and in Fig. 13-37.

The specifications made in this case are summarized below:

Variable	Number	Value
Number of stages	1	11
Feed stage location	1	6
Component flows in feed	$c = 5$	5, 15, 25, 20, 35 lb-mol/h
Feed pressure	1	120 psia
Feed vapor fraction	1	0
Pressure on each stage including condenser and reboiler	$N = 11$	$P_j = 120$ psia
Heat duty on each stage except reboilers and condensers	$N - 2 = 9$	$Q_j = 0$
Vapor flow to condenser (replaces heat duty of reboiler)	1	$V_2 = 175$ lb-mol/h
Distillate flow rate (replaces heat duty of condenser)	1	$D = 48.9$ lb-mol/h
Total	31	

In addition, we have assumed that the pressure of the reflux divider is the same as the pressure of the condenser, the heat loss from the reflux divider is zero, and the reflux temperature is the boiling point of the condensed overhead vapor.

The Peng-Robinson equation of state was used to estimate K values and enthalpy departures [as opposed to the De Priester charts used in Example 1 and by Seader (ibid.) who solved this problem by using the Thiele-Geddes (op. cit.) method].

With 11 stages and 5 components the equilibrium-stage model has 143 equations to be solved for 143 variables (the unknown flow rates, temperatures, and mole fractions). Convergence of the computer algorithm was obtained in just four iterations. Computed product flows are shown in Fig. 13-37.

A pseudobinary McCabe-Thiele diagram for this multicomponent system is shown in Fig. 13-38. For systems with more than two components, these diagrams can only be computed from the results of a computer simulation. The axes are defined by the relative mole fractions:

$$X = \frac{x_{lk}}{x_{lk} + x_{hk}} \quad Y = \frac{y_{lk}}{y_{lk} + y_{hk}}$$

where the subscripts lk and hk refer to light and heavy key, respectively. The lines in the diagram have similar significance as would be expected from our knowledge of McCabe-Thiele diagrams for binary systems discussed earlier in this section; the triangles correspond to equilibrium stages. The operating lines are not straight because of heat effects and because the feed is not in the best location.

The fact that the staircase of triangles visible in Fig. 13-38 fails to come close to the corners of the diagram where $X = Y = 1$ and $X = Y = 0$ shows that the separation is not especially sharp. It is worth asking what can be done to improve the separation obtained with this column. The parameters that have a significant effect on the separation are the numbers of stages in the sections above and below the feed, the reflux ratio, and a product flow rate (or reflux flow). Figure 13-39 shows how the mole fraction of *i*-pentane in the overhead and of *n*-butane in the bottom product changes with the reflux ratio. For the base case considered above, the reflux ratio is 2.58 (calculated from the results of the simulation). It is clear that increasing the reflux ratio has the desired effect of improving product purity. This improvement in purity is, however, accompanied by an increase in both the operating cost, indicated in Fig. 13-39 by the increase in reboiler duty, and capital cost, because a larger column would be needed to accommodate the increased internal flow. Note, however, that the curves that represent the mole fractions of the keys in the overhead and bottoms appear to flatten, showing that product purity will not increase indefinitely as the reflux ratio increases. Further improvement in product purity can best be made by changing a different specification.

Figure 13-40 shows the tradeoff in product purities when we change the specified distillate flow rate, maintaining all other specifications at the values

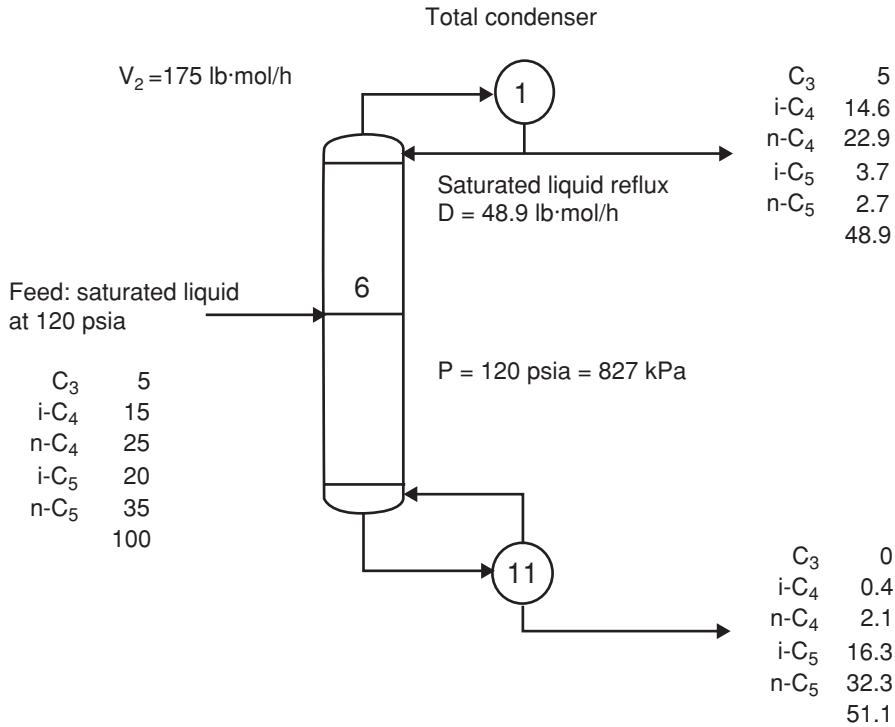


FIG. 13-37 Specifications and calculated product stream flows for butane-pentane splitter. Flows are in pound-moles per hour.

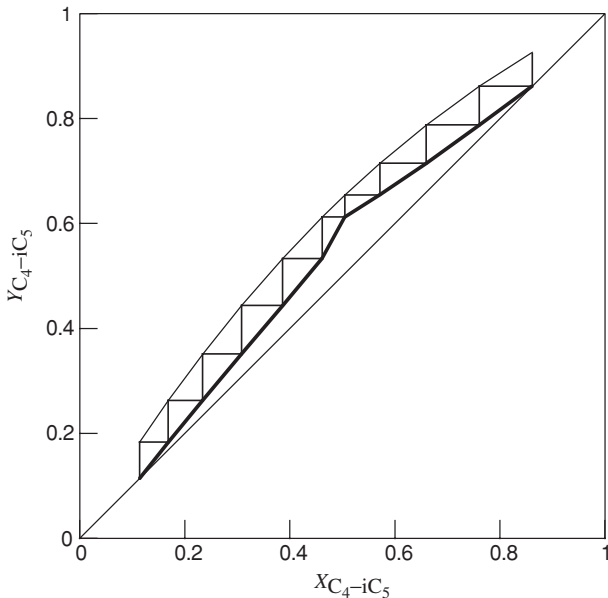


FIG. 13-38 Multicomponent McCabe-Thiele diagram for butane-pentane splitter in Fig. 13-37.

specified in the base case. At lower distillate flow rates the mole fraction of heavy key (*i*-C₅) in the distillate is small, and at higher distillate flow rates the mole fraction of light key (*n*-C₄) in the bottoms is small. Both cannot be small simultaneously. From this result we see that the “best” overall product purities are obtained when the distillate rate is in the vicinity of 45 lb-mol/h. On reflection this should not come as a surprise; the flow rate of the light key (*n*-butane) and all components with a higher volatility is 45 lb-mol/h. However, even with the distillate flow rate set to 45 lb-mol/h there remains room for improvement in the separation.

The other key design specifications here are the total number of stages and the location of the feed stage. In most cases, increasing the number of stages will improve the separation. On increasing the number of stages to 26, with the feed to stage 12, increasing the overhead vapor flow to 195 lb-mol/h, and decreasing the distillate rate to 45 lb-mol/h, we obtain the following products:

Mole flows, lb-mol/h	Feed	Top	Bottom
Propane	5.00	5.00	0.00
Isobutane	15.00	15.00	0.00
N-Butane	25.00	24.81	0.19
Isopentane	20.00	0.16	19.84
N-Pentane	35.00	0.03	34.97
Total	100.00	45.00	55.00

The McCabe-Thiele diagram for this configuration, shown in Fig. 13-41, shows that the product purities have improved significantly.

The temperature and liquid phase composition profiles for this final case are shown in Fig. 13-42. The temperature increases from top to bottom of the column. This is normally the case in distillation columns (exceptions may occur with cold feeds or feeds with boiling points significantly lower than that of the mixture on stages above the feed stage). The composition profiles also are as expected. The components more volatile than the light key (*n*-butane) are

13-36 DISTILLATION

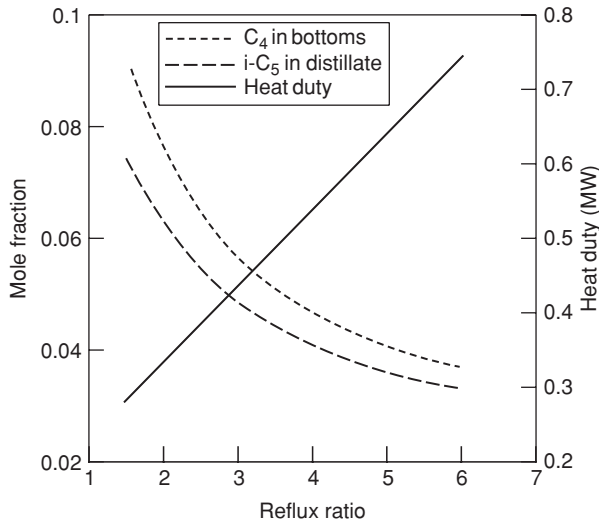


FIG. 13-39 Product mole fractions and reboiler heat duty as a function of the reflux ratio for butane-pentane splitter in Fig. 13-37.

concentrated above the feed; those compounds less volatile than the heavy key (*i*-pentane) are concentrated below the feed. The mole fractions of the two keys exhibit maxima, the light key above the feed stage and the heavy key below the feed stage. The decrease in the mole fraction of light key over the top few stages is necessary to accommodate the increase in the composition of the lighter compounds. Similar arguments pertain to the decrease in the mole fraction of the heavy key over the stages toward the bottom of the column.

Flow profiles are shown in Fig. 13-42c. Note the step change in the liquid flow rate around the feed stage. Had the feed been partially vaporized, we would have observed changes in both vapor and liquid flows around the feed stage, and a saturated vapor feed would significantly change only the vapor flow

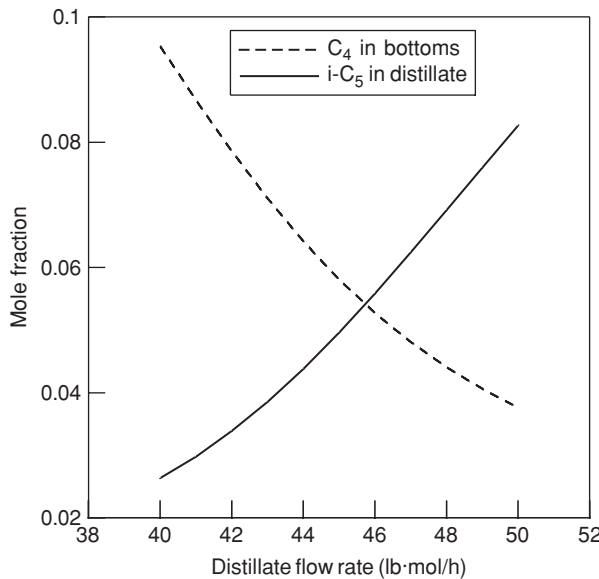


FIG. 13-40 Product mole fraction duty as a function of the distillate rate for butane-pentane splitter in Fig. 13-37.

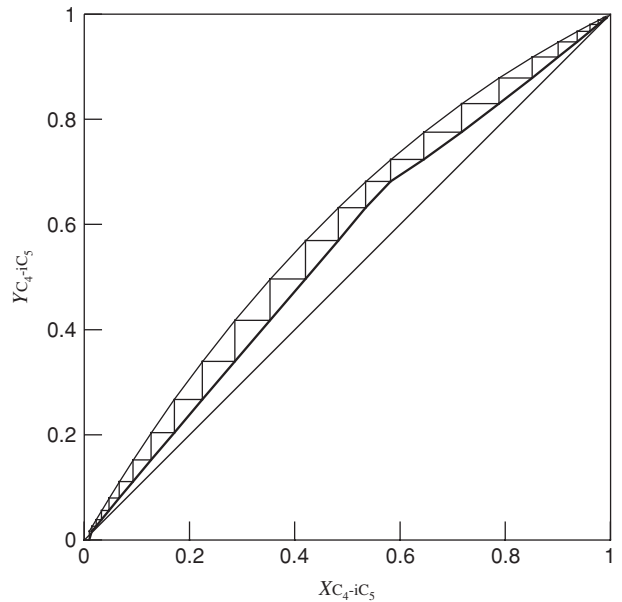


FIG. 13-41 Multicomponent McCabe-Thiele diagram for butane-pentane splitter after optimization to improve product purities.

profile. The slight (in this case) curvature in the flow profiles is due to enthalpy changes.

Example 4: Light Hydrocarbon Distillation Compute stage temperatures, interstage vapor and liquid flow rates and compositions, and reboiler and condenser duties for the light hydrocarbon distillation column shown in Fig. 13-43. How might the separation be improved?

This more complicated example features a partial condenser (with vapor product) and a vapor sidestream withdrawn from the 13th stage. The SRK equation of state may be used for estimating the *K* values and enthalpy departures for thermodynamic properties.

The specifications made in this case are summarized below:

Variable	Number	Value
Number of stages	1	17
Feed stage location	1	9
Component flows in feed	$c = 5$	3, 20, 37, 35, 5 lb·mol/h
Feed pressure	1	260 psia
Feed vapor fraction	1	0
Pressure on each stage including condenser and reboiler	$N = 17$	$P_j = 250$ psia
Heat duty on each stage except reboilers and condensers	$N - 2 = 15$	$Q_j = 0$
Reflux rate (replaces heat duty of reboiler)	1	$L_1 = 150$ lb·mol/h
Distillate flow rate (replaces heat duty of condenser)	1	$D = 23$ lb·mol/h
Sidestream stage	1	13
Sidestream flow rate and phase	2	37 lb·mol/h vapor
Total	46	

As in Example 3, we have assumed that the pressure of the reflux divider is the same as the pressure of the condenser, the heat loss from the reflux divider is zero, and the reflux temperature is the boiling point of the condensed overhead vapor.

The specifications were selected to obtain three products: a vapor distillate rich in C_2 and C_3 , a vapor sidestream rich in $n-C_4$, and a bottoms rich in $n-C_5$ and $n-C_6$, as summarized in the table below.

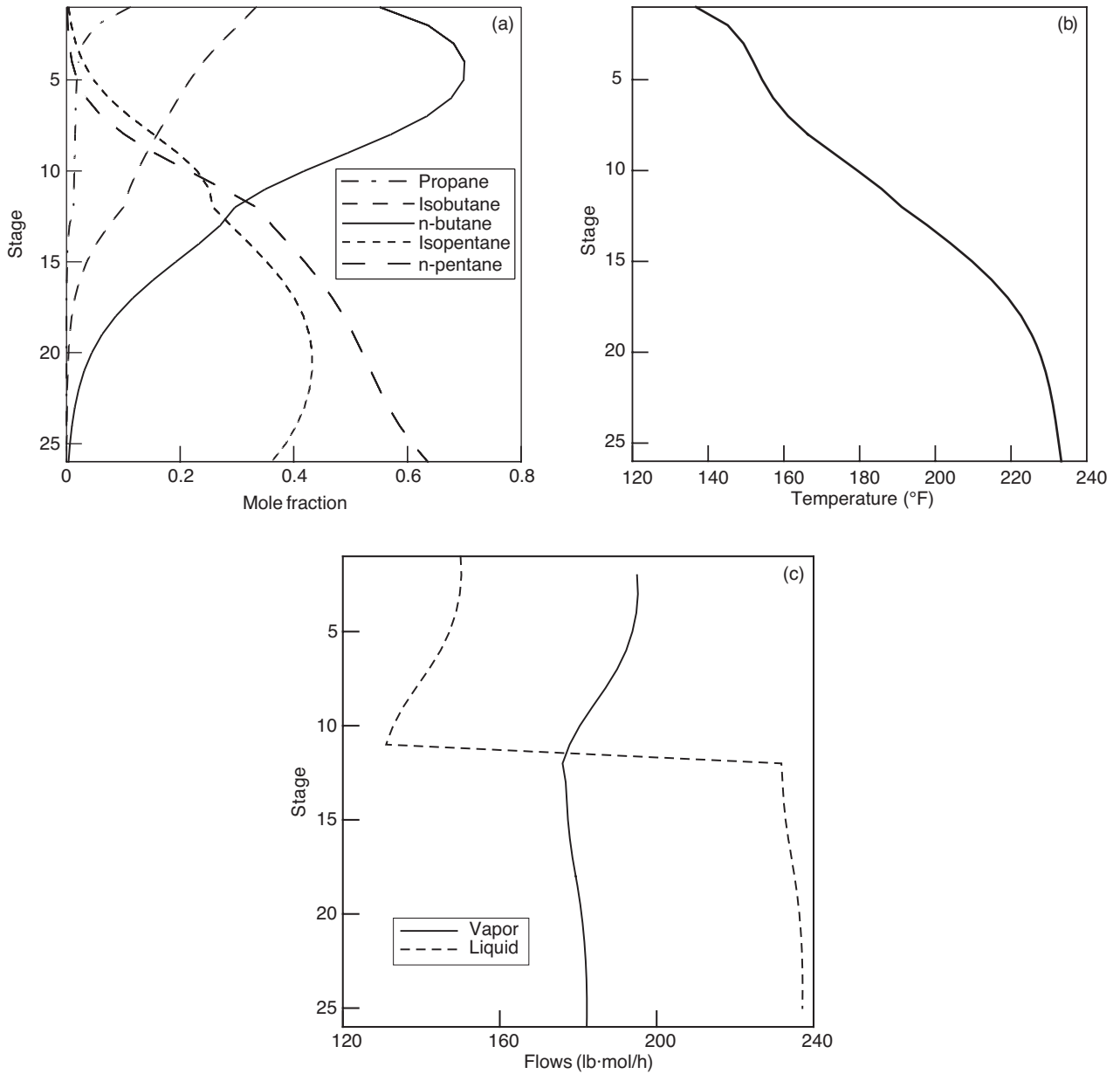


FIG. 13-42 (a) Composition, (b) temperature, and (c) flow profiles in butane-pentane splitter.

Mole flows, lb-mol/h	Feed	Top	Bottom	Sidestream
Ethane	3.00	3.00	0.0	0.0
Propane	20.00	18.3	0.0	1.6
N-Butane	37.00	1.7	9.6	25.7
N-Pentane	35.00	0.0	25.8	9.2
N-Hexane	5.00	0.0	4.5	0.5
Total molar flow	100.00	23.0	40.0	37.0

Convergence of the simultaneous convergence method was obtained in five iterations.

Further improvement in the purity of the sidestream as well as of the other two products could be obtained by increasing the reflux flow rate (or reflux ratio) and the number of stages in each section of the column. If, e.g., we increase the

number of stages to 25 (including condenser and reboiler in this total), with the feed to stage 7 and the sidestream removed from stage 17, we obtain the following:

Mole flows, lb-mol/h	Feed	Top	Bottom	Sidestream
Ethane	3.00	3.00	0.00	0.00
Propane	20.00	19.46	0.00	0.54
N-Butane	37.00	0.54	7.46	29.00
N-Pentane	35.00	0.00	27.93	7.07
N-Hexane	5.00	0.00	4.61	0.39
Total	100.0	23.0	40.0	37.00

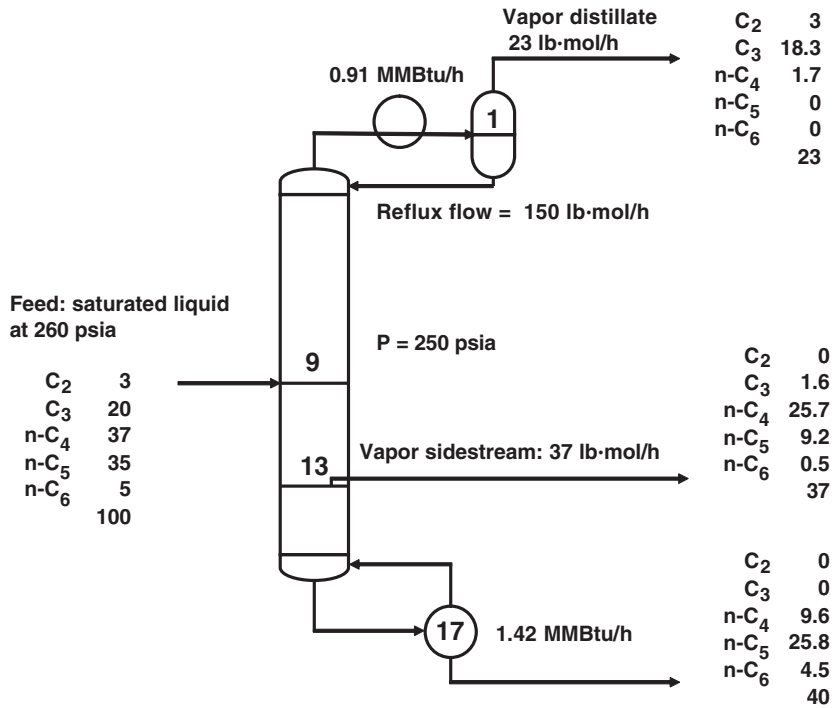


FIG. 13-43 Specifications and calculated product stream flows and heat duties for light hydrocarbon still. Flows are in pound-moles per hour.

The McCabe-Thiele diagram for this design, showing that the feed is to the optimum stage, is shown in Fig. 13-44. The flow profiles are shown in Fig. 13-45; note the step changes due to both the feed and the sidestream. As was the case in Example 3, the curvature in the flow profiles is due to enthalpy changes.

Example 5: Absorber Compute stage temperatures and interstage vapor and liquid flow rates and compositions for the absorber specifications shown in Fig. 13-46. Note that a second absorber oil feed is used in addition to the main absorber oil and that heat is withdrawn from the seventh theoretical stage. The oil may be taken to be *n*-dodecane.

The specifications made in this case are summarized below:

Variable	Number	Value(s)
Number of stages	1	8
Location of feed 1	1	1
Component flows in feed 1	$c = 6$	0, 0, 0, 0, 0, 250 lb-mol/h
Pressure of feed 1	1	400 psia
Temperature of feed 1	1	80°F
Location of feed 2	1	4
Component flows in feed 2	$c = 6$	13, 3, 4, 5, 5, 135 lb-mol/h
Pressure of feed 2	1	400 psia
Temperature of feed 2	1	80°F
Location of feed 3	1	8
Component flows in feed 3	$c = 6$	360, 40, 25, 15, 15, 10 lb-mol/h
Pressure of feed 3	1	400 psia
Temperature of feed 3	1	80°F
Pressure on each stage	$N = 8$	$P_j = 400$ psia; $j = 1, 2, \dots, 8$
Heat duty on each stage	$N = 8$	$Q_j = 0, j = 1, 2, \dots, 6, 8; Q_7 = 150,000$ Btu/h
Total	44	

The simultaneous solution method solved this example in four iterations. The Peng-Robinson equation of state was used to estimate *K* values and enthalpy

departures and by Seader (*Perry's Chemical Engineers' Handbook*, 7th ed.) who solved this problem by using the SR method.

The computed product flows are summarized below:

Mole flows, lb-mol/h	Lean oil	Secondary oil	Rich gas	Lean gas	Rich oil
Methane	0.0	13.0	360.0	303.7	69.3
Ethane	0.0	3.0	40.0	10.7	32.3
Propane	0.0	4.0	25.0	0.2	28.8
N-Butane	0.0	4.0	15.0	0.0	19.0
N-Pentane	0.0	5.0	10.0	0.0	15.0
N-Dodecane	250.0	135.0	0.0	0.0	385.0
Total molar flow	250.0	164.0	450.0	314.6	549.4

The energy withdrawn from stage 7 has the effect of slightly increasing the absorption of the more volatile species in the rich oil leaving the bottom of the column. Temperature and flow profiles are shown in Fig. 13-47. The temperature profile shows the rise in temperature toward the bottom of the column that is typical of gas absorption processes. The bottom of the column is where the bulk of the absorption takes place, and the temperature rise is a measure of the heat of absorption. The liquid flow profile exhibits a step change due to the secondary oil feed at the midpoint of the column.

Example 6: Reboiled Stripper Compute stage temperatures and interstage vapor and liquid flow rates and compositions and reboiler heat duty for the reboiled stripper shown in Fig. 13-48. Thermodynamic properties may be estimated by using the Grayson-Streed modification of the Chao-Seader method.

The specifications made in this case are summarized in Fig. 13-48 and in the table below. The specified bottoms rate is equivalent to removing most of the *n*-C₅ and *n*-C₆ in the bottoms.

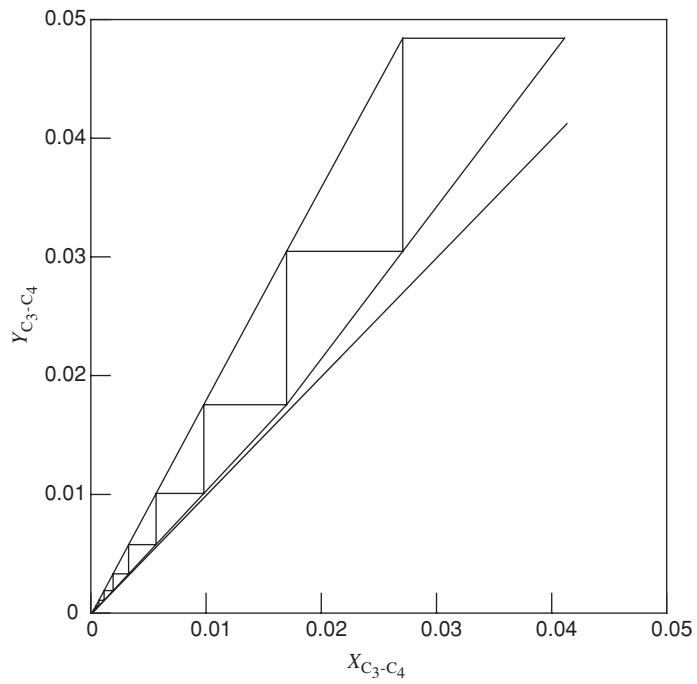
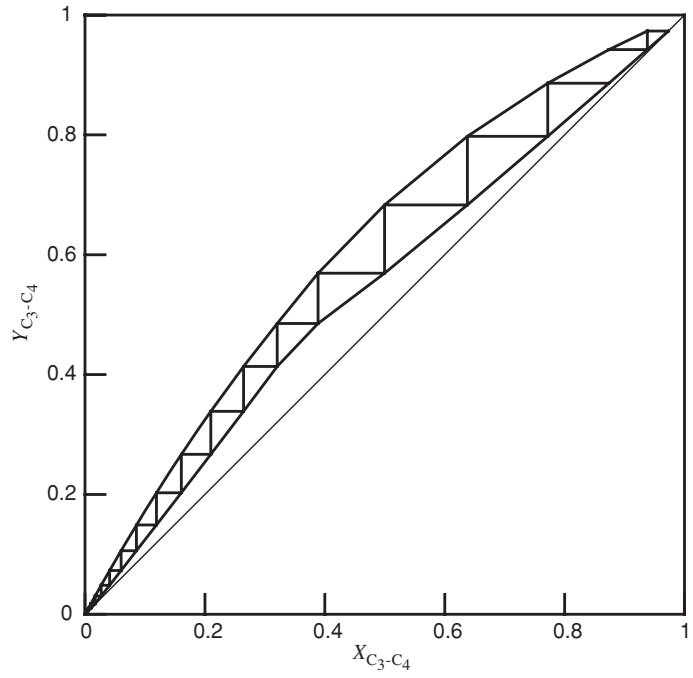


FIG. 13-44 Multicomponent McCabe-Thiele diagram for the hydrocarbon distillation in Fig. 13-43.

13-40 DISTILLATION

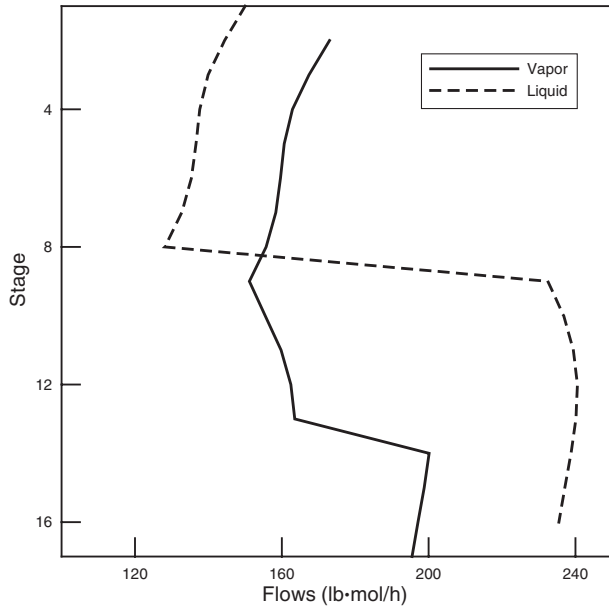


FIG. 13-45 Flow profiles in hydrocarbon distillation in Fig. 13-43.

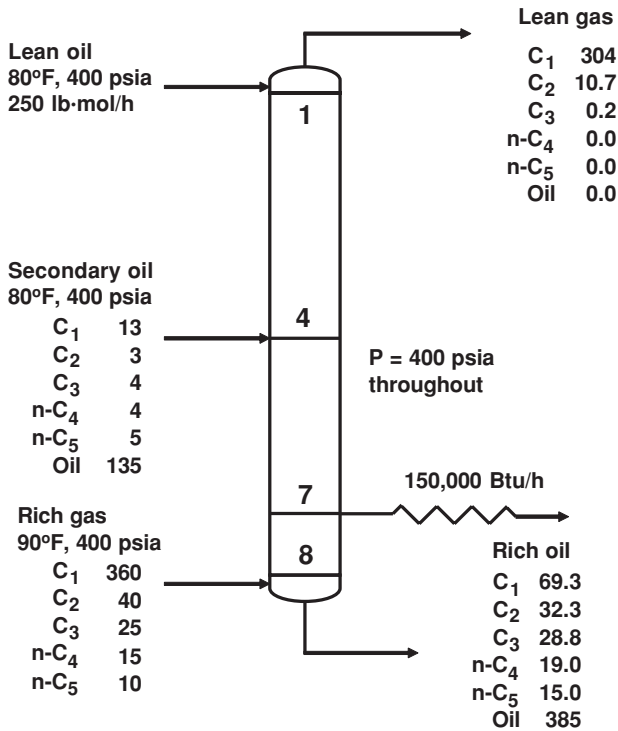
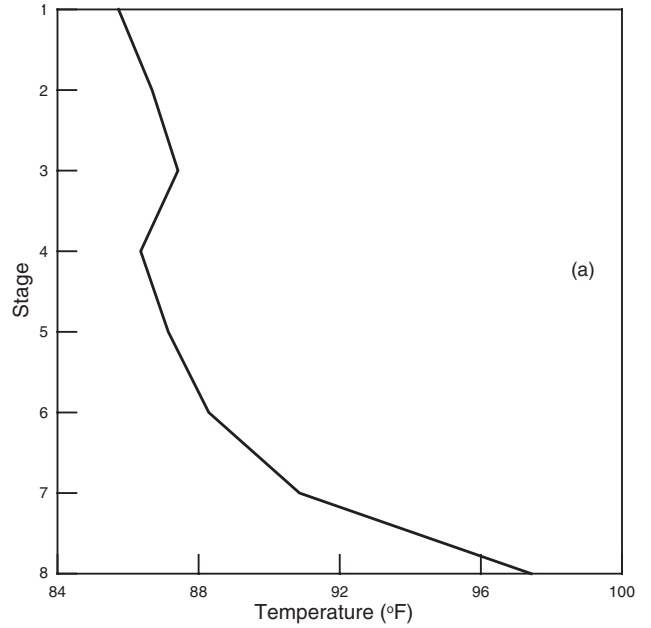


FIG. 13-46 Specifications and calculated product stream flows and heat duties for absorber. Flows are in pound-moles per hour.

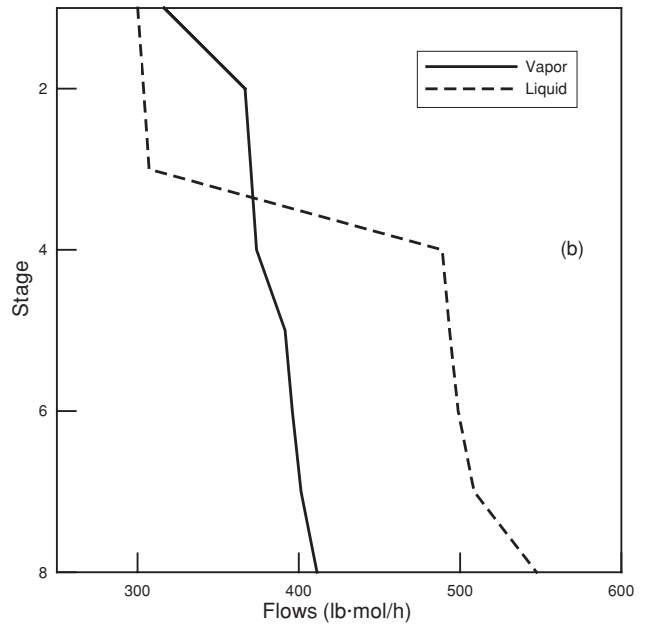


FIG. 13-47 (a) Temperature and (b) flow profiles in absorber in Fig. 13-46.

Variable	Number	Value(s)
Number of stages	1	8
Component flows in feed	$c = 7$	0.22, 59.51, 73.57, 153.2, 173.2, 58.22, 33.63 lb-mol/h
Pressure of feed	1	150 psia
Temperature of feed	1	40.8°F
Pressure on each stage	$N = 8$	$P_j = 150$ psia; $j = 1, \dots, 8$
Heat duty on each stage (except reboiler)	$N - 1 = 7$	$Q_j = 0$, $j = 1, \dots, 7$
Bottom product flow rate	$\frac{1}{26}$	99.33 lb-mol/h
Total		

Convergence in this case was obtained after four iterations. The computed product flows and reboiler duty are shown alongside the specifications in Fig. 13-48 and in the table below.

Mole flows, lb-mol/h	Feed	Overhead	Bottoms
Nitrogen	0.22	0.02	0.20
Methane	59.51	59.51	0.00
Ethane	73.57	73.57	0.00
Propane	153.22	153.16	0.06
N-Butane	173.22	150.09	23.13
N-Pentane	58.22	13.23	44.99
N-Hexane	33.63	2.69	30.94
Total	551.59	452.26	99.33

Computed temperature, flow rates, and vapor-phase mole fraction profiles, shown in Fig. 13-49, are not of the shapes that might have been expected. Vapor and liquid flow rates for n -C₄ change dramatically from stage to stage.

Example 7: An Industrial *i*-Butane/*n*-Butane Fractionator
 Klemola and Ilme [*Ind. Eng. Chem.*, **35**, 4579 (1996)] and Ilme (Ph.D. thesis, University of Lapeenranta, Finland, 1997) report data from an industrial *i*-butane/*n*-butane fractionator that is used here as the basis for this example.

The column has 74 valve trays, the design details of which can be found in Example 11. The feed was introduced onto tray 37.

To properly model an existing column, it is necessary to know all feed and product conditions (flow rate, temperature, pressure, and composition). Flows, temperatures, and pressures often are available from standard instrumentation. It may be necessary to obtain additional samples of these streams to determine

their composition. Such sampling should be scheduled as part of a plant trial to ensure that measured data are consistent. Ideally, multiple sets of plant measurements should be obtained at different operating conditions, and care should be taken to ensure that operating data are obtained at steady state since a steady-state model can only be used to describe a column at steady state. Measurements should be taken over a time interval longer than the residence time in the column and time-averaged to avoid a possible mismatch between feed and product data. Condenser and reboiler heat duties should be known (or available from the appropriate energy balance) whenever possible.

The measured compositions and flow rates of the feed and products for the C₄ splitter are summarized in the table below.

Measured Feed and Product Flows and Compositions (Mass %) for *i*-Butane/*n*-Butane Fractionator (Ilme op. cit.)

Species	Feed	Top	Bottom
Propane	1.50	5.30	0.00
Isobutane	29.4	93.5	0.30
<i>n</i> -Butane	67.7	0.20	98.1
C ₄ olefins	0.50	1.00	0.20
Neopentane	0.10	0.00	0.20
Isopentane	0.80	0.00	1.10
<i>n</i> -Pentane	0.10	0.00	0.10
Total flow, kg/h	26,234	8011	17,887

Other measured parameters are as follows:

Other Details of the *i*-Butane/*n*-Butane Fractionator

Reflux flow rate, kg/h	92,838
Reflux temperature, °C	18.5
Column top pressure, kPa	658.6
Pressure drop per tray, kPa	0.47
Feed pressure, kPa	892.67
Boiler duty, MW	10.24

Rarely, and this is a case in point, are plant data in exact material balance, and it will be necessary to reconcile errors in such measurements before continuing. The feed and product compositions, as adjusted by Ilme so that they satisfy material balance constraints, are provided below. Note how the C₄ olefins are assigned to isobutene and 1-butene.

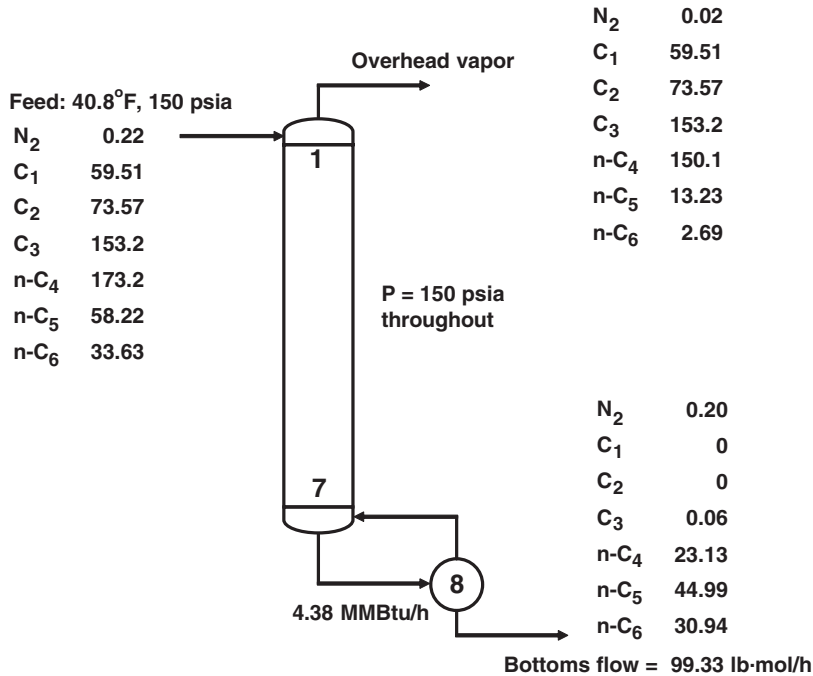


FIG. 13-48 Specifications and calculated product stream flows and reboiler heat duty for a reboiled stripper. Flows are in pound-moles per hour.

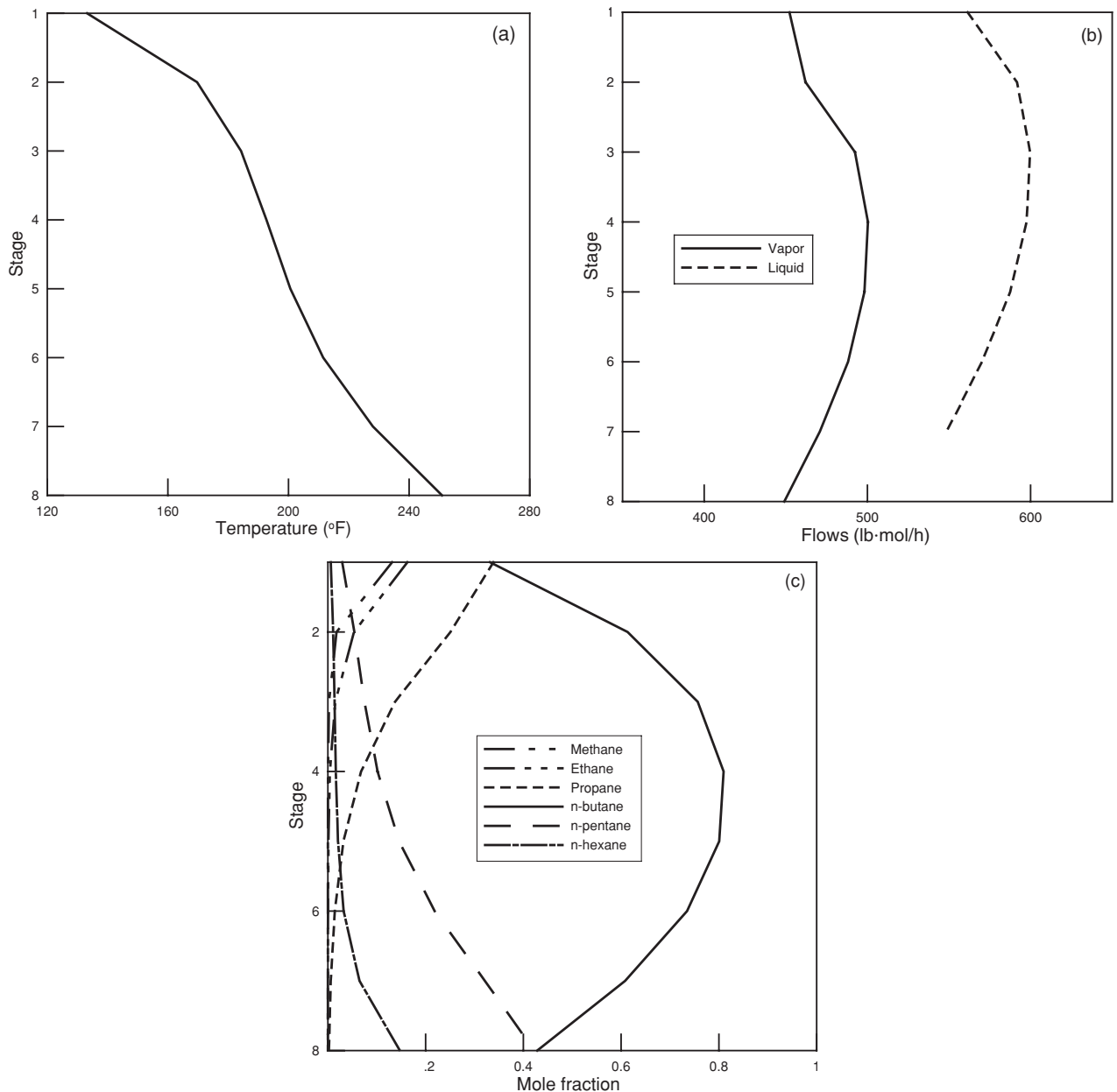


FIG. 13-49 (a) Temperature, (b) flow, and (c) vapor mole fraction profiles in reboiled stripper in Fig. 13-48.

Adjusted Feed and Product Compositions (Mass %) and Flows for *i*-Butane/*n*-Butane Fractionator (Ilme op. cit.)

Species	Feed	Top	Bottom
Propane	1.54	4.94	0.00
Isobutane	29.5	94.2	0.3
<i>n</i> -Butane	67.7	0.20	98.1
Isobutene	0.13	0.23	0.08
1-Butene	0.20	0.41	0.10
Neopentane	0.11	0.00	0.17
Isopentane	0.77	0.00	1.12
<i>n</i> -Pentane	0.08	0.00	0.11
Total flow, kg/h	26,122	8123	17,999

To proceed with building a model of this column, we specify the number of stages equal to the number of trays plus condenser and reboiler ($N = 76$). The common arrangement of locating the actual feed between stages may require modeling as two separate feeds, the liquid portion to the stage below and the vapor portion to the stage above. In this particular illustration the feed is (assumed to be) saturated liquid, and we provide just a single feed to stage 38.

Upon computing the bubble point of the overhead product, we find that the measured reflux temperature is well below the estimated boiling point. Thus, we choose the subcooled condenser model. The steady-state concept of the "subcooled" condenser often does not exist in practice. Instead, the condenser is in vapor-liquid equilibrium with the vapor augmented by a blanket of noncondensable gas (that has the effect of lowering the dew point of the overhead vapor). The subcooled condenser is a convenient work-around for steady-state models (as is needed here), but not for dynamic models. We assume a partial reboiler.

The pressure of the top stage is specified (at 658.6 kPa). The pressures of all trays below the top tray can then be fixed from the knowledge of the per-tray pressure drop (0.47 kPa). The pressure of the condenser is not known here. Thus, in the absence of further information, we make the condenser pressure equal to the top tray pressure (knowing that in practice it will be lower).

It is advisable to use the plant set points in building a model. For example, it is possible that a column simulation might involve the specification of the reflux ratio and bottoms flow rate because such specifications are (relatively) easy to converge. It is quite likely that the column may be controlled by using the temperature at some specific location (e.g., the temperature of tray 48). This specification should be used in building the model. In this case we do not know the set points used for controlling the column, but we do have sufficient information to allow us to compute the reflux ratio from plant flow data ($R = 11.6$). Finally, the bottom product flow is specified as equal to the adjusted value reported above (17,999 kg/h).

The specifications made to model this column are summarized below:

Variable	Number	Value
Number of stages	1	$N = 76$
Feed stage location	1	39
Component flows in feed	$c = 8$	See previous table
Feed pressure	1	120 psia
Feed vapor fraction	1	0
Pressure at the top of the column	1	658.6 kPa
Pressure drop per stage	$N - 1 = 75$	0.47 kPa
Heat duty on each stage except reboilers and condensers	$N - 2 = 74$	$Q_j = 0$
Reflux ratio (replaces heat duty of condenser)	1	$R = 11.588$
Bottoms flow rate (replaces heat duty of reboiler)	1	$B = 17,999$ kg/h
Temperature of reflux	1	291.65 K
Total	165	

Finally, we must select appropriate methods of estimating thermodynamic properties. Ilme (op. cit.) used the SRK equation of state to model this column, whereas Klemola and Ilme (op. cit.) had earlier used the UNIFAC model for liquid-phase activity coefficients, the Antoine equation for vapor pressures, and the SRK equation for vapor-phase fugacities only. For this exercise we used the Peng-Robinson equation of state. Computed product compositions and flow rates are shown in the table below.

Specified Feed and Computed Product Compositions (Mass %) and Flows for *i*-Butane/*n*-Butane Fractionator (Ilme op. cit.)

Compound	Feed	Top	Bottom
Propane	1.54	4.95	0.00
Isobutane	29.49	93.67	0.53
<i>n</i> -Butane	67.68	0.73	97.89
Isobutene	0.13	0.29	0.06
1-Butene	0.20	0.36	0.13
Neopentane	0.11	0.00	0.16
Isopentane	0.77	0.00	1.12
<i>n</i> -Pentane	0.08	0.00	0.12
Total flow, kg/h	26,122	8123.01	17,999

The agreement with the adjusted material balance (tabulated previously) appears to be quite good, and to a first approximation it seems that we have a good model of the column.

Note that although this column is distilling a mixture containing at least eight identifiable compounds, only two are present in significant amounts, and therefore this is essentially a binary separation. It is usually relatively straightforward to match product compositions in processes involving only two different species simply by adjusting the number of equilibrium stages. We return to this point later.

Efficiencies In actual operation the trays of a distillation column rarely, if ever, operate at equilibrium despite attempts to approach this condition by proper design and choice of operating conditions. The usual way of dealing with departures from equilibrium in multistage towers is through the use of stage and/or overall efficiencies.

The overall column efficiency is defined by

$$E_o = \frac{N_{EQ}}{N_{actual}} \quad (13-57)$$

where N_{EQ} is the number of equilibrium stages.

There are many different definitions of stage (or tray) efficiency, with that of Murphree [*Ind. Eng. Chem.*, **17**, 747–750, 960–964 (1925)] being by far the most widely used in separation process calculations:

$$E_i^{MV} = \frac{y_{ij} - y_{i,j+1}}{y_{i,j}^* - y_{i,j+1}} \quad (13-58)$$

Here E_i^{MV} is the Murphree vapor efficiency for component i on stage j , and $y_{i,j}^*$ is the composition of the vapor in equilibrium with the liquid. Other types of efficiency include that of Hausen [*Chemie Ingr. Tech.*, **25**, 595 (1953)], vaporization (see Holland, op. cit.), and generalized Hausen [Standart, *Chem. Eng. Sci.*, **20**, 611 (1965)]. There is by no means a consensus on which is best. Arguments for and against various types are presented by, among others, Standart [op. cit.; *Chem. Eng. Sci.*, **26**, 985 (1971)], Holland and McMahon [*Chem. Eng. Sci.*, **25**, 431 (1972)], and Medina et al. [*Chem. Eng. Sci.*, **33**, 331 (1978), **34**, 1105 (1979)]. Possibly the most soundly based definition, the generalized Hausen efficiency of Standart (op. cit.), is never used in industrial practice. Seader [*Chem. Eng. Progress*, **85**(10), 41 (1989)] summarizes the shortcomings of efficiencies.

The Murphree (and Hausen) efficiencies of both components in a binary mixture are equal; although they cannot be less than 0, they may be greater than 1. A table of typical values of Murphree tray efficiency can be found in Sec. 14. Also described in Sec. 14 are methods for estimating Murphree efficiencies when they are not known.

For multicomponent systems (i.e., those with more than two components) there are $c - 1$ independent component efficiencies, and there are sound theoretical reasons as well as experimental evidence for not assuming the individual component efficiencies to be alike; indeed, they may take values between plus and minus infinity. Component efficiencies are more likely to differ for strongly nonideal mixtures. While models exist for estimating efficiencies in multicomponent systems [see chapter 13 in Taylor and Krishna, (op. cit.) for a review of the literature], they are not widely used and have not (yet) been included in any of the more widely used commercial simulation programs.

The fact that component efficiencies in multicomponent systems are unbounded means that the arithmetic average of the component Murphree efficiencies is useless as a measure of the performance of a multicomponent distillation process. Taylor, Baur, and Krishna [*AIChE J.*, **50**, 3134 (2004)] proposed the following efficiency for multicomponent systems:

$$e_j = \frac{\sqrt{\sum_{i=1}^c (\Delta y_{ij})^2}}{\sqrt{\sum_{i=1}^c (\Delta y_{ij}^*)^2}} \quad (13-59)$$

This efficiency has a simple and appealing physical significance; it is the ratio of the length of the actual composition profile (in mole fraction space) to the length of the composition profile given by the equilibrium-stage model. The Taylor-Baur-Krishna (TBK) efficiency has just one value per stage regardless of the number of components in the mixture; it can never be negative. For binary systems in tray columns the TBK average efficiency simplifies to the Murphree efficiency [Taylor, Baur, and Krishna (op. cit.)].

Murphree efficiencies are easily incorporated within simultaneous convergence algorithms (something that is not always easy, or even possible, with some tearing methods). (As an aside, note that vaporization

efficiencies are very easily incorporated in all computer algorithms, a fact that has helped to prolong the use of these quantities in industrial practice despite the lack of any convenient way to relate them to the fundamental processes of heat and mass transfer. Unfortunately, it is not at all easy to include the more fundamentally sound TBK efficiencies in a computer method for equilibrium-stage simulations.)

The Murphree-stage efficiency also makes a good continuation parameter for cases that are hard to converge. For vanishingly small stage efficiencies the column performs no separation, and the streams leaving the stage have essentially the same flow rates, composition, and temperature as the combined feeds to the stage. This fact can be exploited in a simple continuation method for solving difficult equilibrium-stage separation process problems [Muller, Ph.D. Thesis in Chem. Engng., ETH Zurich, 1979; Sereno, Ph.D. Thesis in Chem. Engng., University of Porto, 1985; Vickery, Ferrari, and Taylor, *Comput. Chem. Engng.*, **12**, 99 (1988)]. These methods are very effective at solving difficult problems involving *standard specifications* (in which the reflux ratio and bottoms flow rate are specified); however, they cannot easily handle problems involving *nonstandard specifications* (e.g., when a product stream purity is specified).

Efficiencies are often used to fit actual operating data, along with the number of equilibrium stages in each section of the column (between feed and product takeoff points). The maximum number of these efficiencies is the number of independent efficiencies per stage ($c - 1$) times the number of stages—potentially a very large number, indeed. This many adjustable parameters may lead to a model that fits the data very well, but has no predictive ability (i.e., cannot describe how the column will behave when something changes). At the other extreme, the overall efficiency defined by Eq. (13-57) is just a single parameter that can improve the robustness of the model and speed of convergence, but it may be difficult to match actual temperature and/or composition profiles since there is unlikely to be a one-to-one correspondence between the model stages and actual trays. A compromise often used in practice is to use just one value for all components and all stages in a single section of a column. Efficiencies should not be used to model condensers and reboilers; it is usually safe to assume that they are equilibrium devices. It is also unwise to employ Murphree efficiencies for trays with a vapor product since any Murphree efficiency less than 1 will necessarily lead to the prediction of a subcooled vapor.

Example 8: The Industrial *i*-Butane/*n*-Butane Fractionator (Again) With the material on efficiencies in mind, we return to the model of the C_4 splitter that we developed in Example 7.

It is possible to estimate the overall efficiency for a column such as this one simply by adjusting the number of equilibrium stages in each section of the column that is needed to match the mass fractions of *i*-butane in the distillate and *n*-butane in the bottoms. Using the SRK equation of state for estimating thermodynamic properties, Ilme (op. cit.) found that 82 equilibrium stages (plus condenser and reboiler) and the feed to stage 38 were required. This corresponds to an overall column efficiency of 82/74 = 111 percent. Klemola and Ilme (op. cit.) used the UNIFAC model for liquid-phase activity coefficients, the Antoine equation for vapor pressures, and the SRK equation for vapor-phase fugacities only and found that 88 ideal stages were needed; this corresponded to an overall efficiency of 119 percent. With the Peng-Robinson equation of state for the estimation of thermodynamic properties, we find that 84 stages are needed (while maintaining the feed to the center stage as is the case here); the overall column efficiency for this model is 114 percent. The differences between these efficiencies are not large in this case, but the important point here is that efficiencies—all types—depend on the choice of model used to estimate the thermodynamic properties. Caution must therefore be exercised when one is using efficiencies determined in this way to predict column performance.

As an alternative to varying the number of stages, we may prefer to maintain a one-to-one correspondence between the number of stages and the number of actual trays, 74 in this case (plus condenser and reboiler), with the feed to tray 38. Using the Peng-Robinson equation of state and a Murphree stage efficiency of 116 percent, we find the product mass fractions that are in excellent agreement with the plant data. The McCabe-Thiele (Hengstebeck) diagram for this case, assembled from the results of the simulation, is shown in Fig. 13-50. Composition profiles computed from this model are shown in Fig. 13-51. Note that the mole fractions are shown on a logarithmic axis so that all the composition profiles can easily be seen.

It must be remembered that this is essentially a binary separation and that it is usually relatively straightforward to match product compositions in processes involving only two different species. In other cases involving a greater number

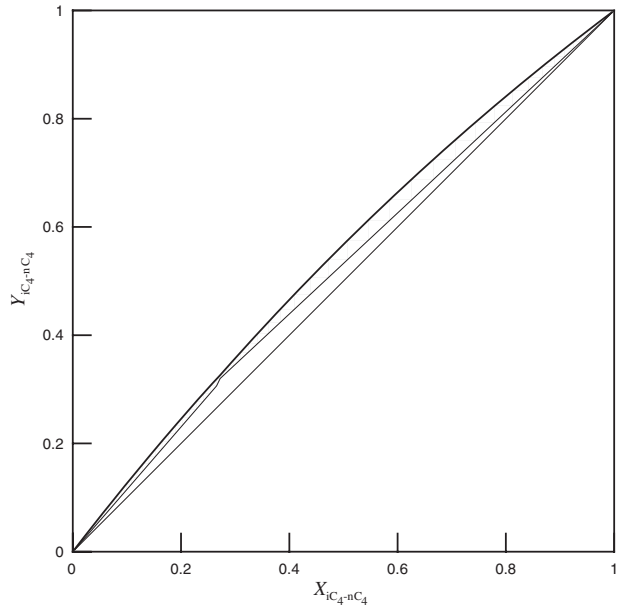


FIG. 13-50 McCabe-Thiele diagram for C_4 splitter.

of species with significant concentrations, it will likely be necessary to vary both the number of stages and the component efficiencies to match plant data. We do not recommend adjusting thermodynamic model parameters to fit plant data since this can have unfortunate consequences on the prediction of product distributions, process temperatures, and/or pressures.

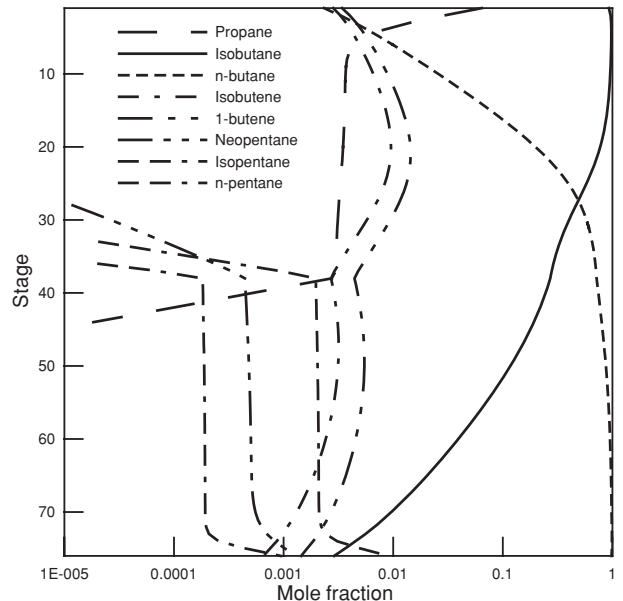


FIG. 13-51 Liquid-phase mole fraction profiles for *i*-butane/*n*-butane fractionator.

The performance of a packed column often is expressed in terms of the height equivalent to a theoretical plate (HETP) for packed columns. The HETP is related to the height of packing H by

$$\text{HETP} = \frac{H}{N_{\text{EQ}}} \quad (13-60)$$

In this case N_{EQ} is the number of equilibrium stages (theoretical plates) needed to accomplish the separation that is possible in a real packed column of height H .

Example 9: HETP of a Packed Absorber McDaniel, Bassioni, and Holland [*Chem. Engng. Sci.*, **25**, 633 (1970)] presented the results of field tests on a packed absorber in a gas plant. The packed section was 23 ft in height, and the column was 3 ft in diameter and filled with 2-in metallic Pall rings. The measured feeds are summarized in the table below.

Stream	Lean oil	Rich gas
Pressure, psia	807	807
Temperature, °F	2.9	0
Mole flows, lb-mol/h		
Carbon dioxide	0.0	14.1
Nitrogen	0.0	5.5
Methane	0.0	2655.8
Ethane	0.0	199.9
Propane	0.0	83.2
Isobutane	0.0	19.1
<i>n</i> -Butane	0.0	10.9
Isopentane	0.2	3.5
<i>n</i> -Pentane	0.2	1.5
<i>n</i> -Hexane	4.5	0.4
<i>n</i> -Heptane	17.2	0.2
<i>n</i> -Octane	54.5	0.1
<i>n</i> -Nonane	50.5	0.0
<i>n</i> -Decane	61.7	0.0
Total molar flow	188.9	2994.2

Determine the number of equilibrium stages needed to match the lean gas product flow for this column (2721.1 lb-mol/h, 93.6% methane).

As a first step, we choose an appropriate thermodynamic model that will be used to estimate K values and enthalpies. Either the Chao-Seader method or the Peng-Robinson equation of state could be considered for this system. It turns out not to be possible to match the plant data with the Chao-Seader method since even one equilibrium stage overpredicts the separation by a very significant amount. It is not even possible to match the exit flows by using the Chao-Seader model combined with a stage efficiency as low as 0.00001. With the Peng-Robinson equation of state, however, it is possible to obtain reasonable agreement with the measured overall product flows by using precisely one equilibrium stage! This suggests that the HETP for this column is 23 ft, a value much higher than any HETP ever published by a packing vendor. In this case the reason for the unrealistic estimate of the HETP has nothing to do with the packing; it is the extreme sensitivity of the simulation to the thermodynamic model, emphasizing the need for caution when one is using efficiencies and HETPs to model some absorption (and distillation) processes.

Using a Simulator to Solve Distillation Problems Computer-based methods for solving distillation (and related) column simulation problems now are reasonably reliable. Nevertheless, at times such methods fail to converge. The principal cause of convergence failures is generally a poor initial estimate of the variables being computed. Below we discuss some of the reasons that a simulation might be difficult to converge, along with suggestions on what might make the problem more amenable to solution. The key idea is to modify the problem that is difficult to solve as posed into one that is easy to solve—essentially to provide an improved initial estimate that is more likely to lead to convergence. Note that most simulators allow a calculation to be restarted from an older converged solution. The solution to the “easy” problem may then be used as a starting point for the more difficult problem whose solution is desired. By doing this we are employing a form of continuation (albeit executed manually, at least in part) to solve those problems with which the algorithm at hand may have trouble.

As a rule, the degree of difficulty increases with increasing non-ideality. Simultaneous convergence methods are often recommended for simulating strongly nonideal systems (as opposed to tearing or inside-out methods), but even SC methods can experience difficulties with strongly nonideal systems. A possible remedy is to make the system “less” nonideal. It is likely that an activity coefficient model is part of the model used to describe the thermodynamics of these systems, and the source of the convergence difficulties often encountered with such systems. First solving an equivalent

ideal system that omits entirely the activity coefficient model (i.e., using Raoult’s law) may provide a converged solution that may be an adequate starting point for the nonideal system of interest. However, since many simulators use ideal solution thermodynamic models in any self-initialization method, this technique may not be of sufficient help.

A measure of the nonideality of the system is given by the magnitude of the interaction parameters for the activity coefficient model. It is possible, therefore, to lessen the degree of nonideality by reducing the interaction parameters sufficiently to make the problem easy to solve. The parameters may then be increased in size in a series of steps until the desired values are reached, each time using the solution converged by using the previous set of parameter values as the starting point. It is essential that the parameters return to their correct values in the final step because intermediate solutions have no meaning, serving merely as an aid to convergence. Using the stage efficiency as a continuation parameter also is useful for such cases, provided that the simulation employs standard specifications (more on this topic below).

The most strongly nonideal systems are those that may exhibit two liquid phases. We have avoided detailed discussion of such systems in this section because special algorithms are needed for these cases; see, however, the section on azeotropic distillation and, for example, chapter 8 of Doherty and Malone (op. cit.) for entry points to the literature.

Large heat effects can lead to convergence difficulties. For such systems it is the enthalpies that are the source of the nonlinearity that leads to convergence failures. It is generally not straightforward to modify enthalpies in a simulator because no adjustable parameters exert their influence over the enthalpy in a way comparable to that of the interaction parameters in the activity coefficient model. Use of a constant-enthalpy model in distillation calculations, if available, will lead to constant molar flows from stage to stage (within each separate section of the column), a condition often approached in many real distillation (but not absorption) columns. Thus, if the simulator includes a constant-enthalpy model, then this can be used to obtain a converged solution that may provide a good starting point for the problem with a more realistic enthalpy model.

High pressure adds to the difficulties of converging simulation models. It is likely that an equation of state will be used to estimate fugacity coefficients and enthalpy departures in such systems. Mixtures become increasingly nonideal as the pressure is raised. In some cases the column may operate close to the critical point at which the densities of both phases approach each other. In other cases the iterations may take the estimates of temperature and composition into regions where the equation of state can provide only one mathematically real root for density or compressibility. Occurrences of this behavior often are a source of convergence difficulties. For such systems we suggest reducing the pressure until the problem becomes easy to solve. A converged solution obtained in this way may be used as the starting point for subsequent calculations at increasingly higher pressures (up to that desired).

Very large numbers of stages can pose their own kind of convergence difficulty. A possible remedy is to reduce the number of stages until a converged solution can be obtained. This solution can then be used as the starting point for a problem with more stages. Interpolation will have to be used to estimate values of the flows, temperatures, and mole fractions for any added stages, something not available in all programs.

Nonstandard specifications are very likely to be the source of convergence difficulties. It is all too easy to specify a desired product purity or component flow rate that simply cannot be attained with the specified column configuration. There is always (at least) one solution if the reflux ratio and bottoms flow rate are specified (the so-called standard specifications), which is likely to converge easily. Other specifications that can cause difficulties for similar reasons include specifying temperatures and compositions anywhere in the column and specifying condenser and/or reboiler heat duties. A way to circumvent this kind of difficulty is first to obtain a converged solution for a case involving standard specifications. Once the behavior of the column is

understood, it will be possible to make sensible nonstandard specifications, again using an old converged result as a starting point.

Columns in which temperature and/or compositions change over a wide range in a limited number of stages pose their own particular difficulties. Some highly nonideal systems exhibit this kind of behavior (see Example 11 below). For cases such as this, it is wise to limit per-iteration changes to temperature and composition. Most modern computer methods will do this as a matter of course, and problems with this cause are not the source of convergence difficulties that they once were.

This is by no means an exhaustive list of the reasons that computer-based simulations fail. Indeed, in many cases it is a combination of more than one of the above factors that leads to difficulty. In those cases it may be necessary to combine several of the strategies outlined above to solve the simulation problem. Often, however, there is no substitute for trial and error. Haas [chap. 4 in Kister (op. cit.), 1992] offers some additional insight on using simulators to solve distillation column models.

Example 10: Multiple Steady States in Distillation This example is one of the most famous in the entire literature on distillation column modeling, having been studied, in one form or another, by many investigators including Magnussen et al. [*I. Chem. E. Symp. Series*, **56** (1979)], Prokopakis and Seider [*AIChE J.*, **29**, 49 (1983)], and Venkataraman and Lucia [*Comput. Chem. Engng.*, **12**, 55 (1988)]. The column simulated here is adapted from the work of Prokopakis and Seider and shown in Fig. 13-52. The ethanol-benzene-water ternary system actually splits into two liquid phases when the overhead vapor is condensed and cooled below its bubble point. One liquid phase is sent to a second column, and the other is returned to the main column as (cold) reflux. Here, in common with others, this column is modeled by ignoring the condenser and decanter. Reflux is simulated by a feed of appropriate composition, temperature, and pressure to the top of the column. The UNIQUAC method was used for estimating the activity coefficients, with parameters given by Prokopakis and Seider. The numerical results are very sensitive to the choice of activity coefficient model and associated parameters; qualitatively, however, the behavior illustrated below is typical of many systems.

This system is considered difficult because convergence of the MESH equations can be difficult to obtain with any algorithm. In fact, for the specifications considered here, there are no less than three solutions; the composition profiles are shown in Fig. 13-53. The goal of the distillation is to recover high-purity ethanol in the bottom stream from the column by using benzene as a mass separating agent. The low-purity profile in Fig. 13-53a, containing a large amount of water in the bottom product, is easily obtained from an ideal solution starting point (but with severe restrictions on the maximum allowed temperature change per iteration). The intermediate profile in Fig. 13-53b is rather more difficult to obtain. We were able to find it by using, as a starting point, a profile that had been converged at a stage efficiency of 0.7. The high-purity solution in Fig. 13-53c, containing very little water in the bottom product, is also easily obtained from an initial profile calculated by assuming that the stage efficiency is quite low (0.3). Multiple solutions for this column have been reported by many authors (including the three cited above). In fact, with the parameters used here, the three solutions exist over a narrow range of ethanol feed flows. Taylor, Achuthan, and Lucia [*Comput. Chem. Engng.*, **20**, 93 (1996)] found complex-valued solutions to the MESH equations for values outside this range.

Multiple steady-state solutions of the MESH equations have been found for many systems, and the literature on this topic is quite extensive. An introduction to the literature is provided by Bekiaris, Guttinger, and Morari [*AIChE J.*, **46**, 955 (2000)]. Chavez, Seader, and Wayburn [*Ind. Eng. Chem. Fundam.*, **25**, 566 (1986)] used homotopy methods to find multiple solutions for some systems of interlinked columns. Parametric continuation has been used to detect multiple solutions of the MESH equations [Ellis et al., *Comput. Chem. Engng.*, **10**, 433 (1986); Kovach and Seider (op. cit.); Burton, Ph.D. Thesis in Chem. Engng., Cambridge University, 1986]. That real distillation columns can possess multiple steady states has been confirmed by the experimental work of Kienle et al. [*Chem. Engng. Sci.*, **50**, 2691 (1995)], Köggersbol et al. [*Comput. Chem. Engng.*, **20**, S835 (1996)], Gaubert et al. [*Ind. Eng. Chem. Res.*, **40**, 2914 (2001)], and others.

NONEQUILIBRIUM MODELING

Although the widely used equilibrium-stage models for distillation, described above, have proved to be quite adequate for binary and close-boiling, ideal and near-ideal multicomponent vapor-liquid mixtures,

Reflux: 298 K and 101.3 kPa

Reflux	kmol/h
Ethanol	103.2
Water	215.8
Benzene	56.3
Total	375.5

Feed: 311 K and 102.7 kPa

Feed	kmol/h
Ethanol	85.6
Water	14.4
Benzene	0.0
Total	100.0

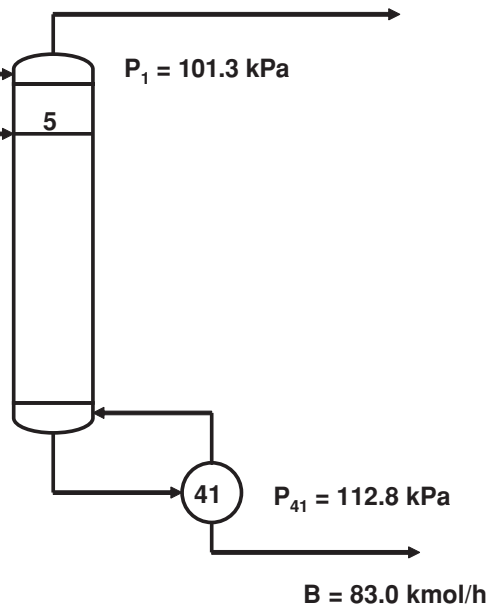


FIG. 13-52 Azeotropic distillation tower for distillation of an ethanol-water mixture using benzene as a mass separating agent. [After Prokopakis and Seider (op. cit.).]

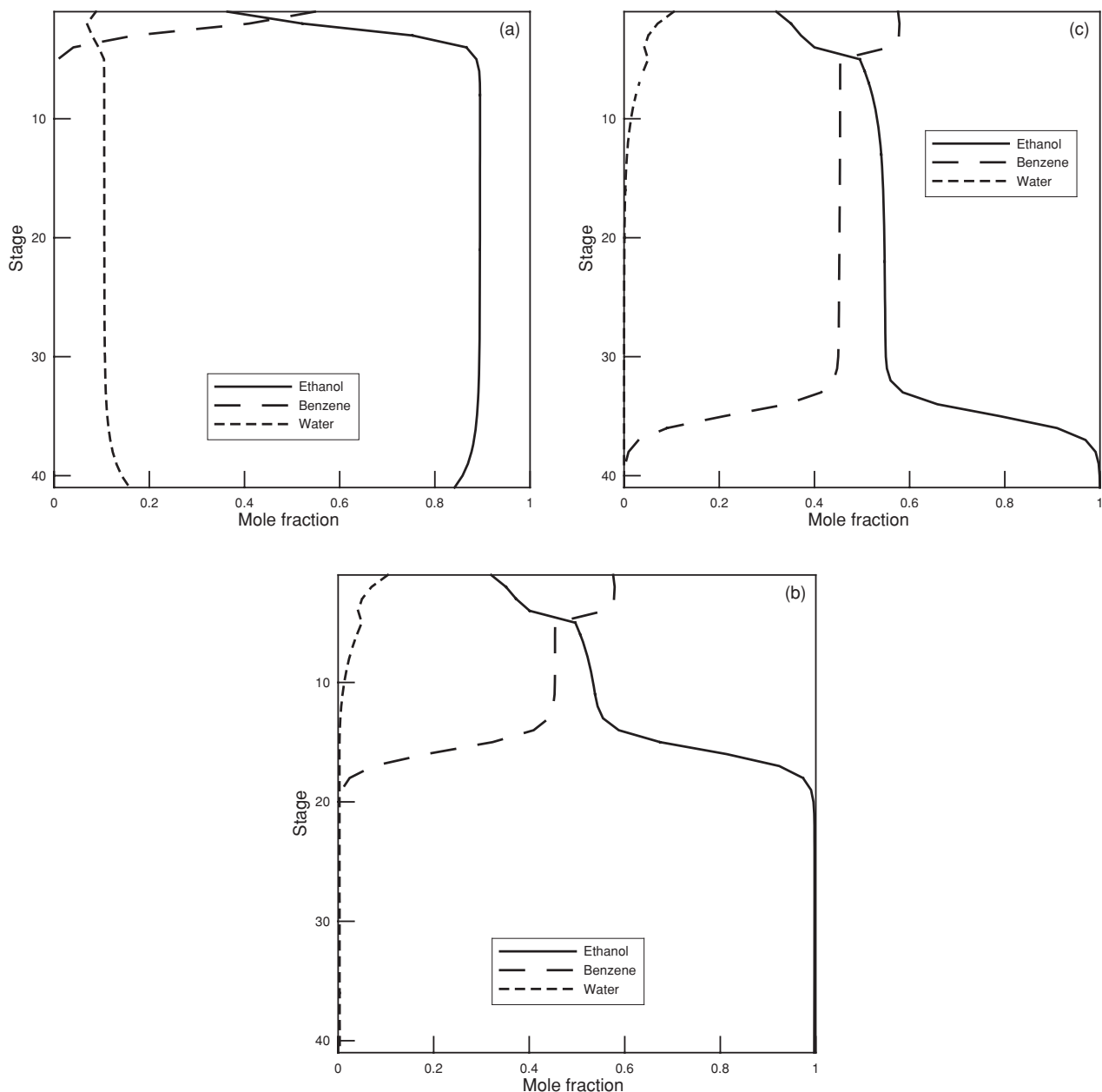


FIG. 13-53 Liquid-phase mole fraction profiles for ethanol-benzene-water distillation. (a) Low-purity profile. (b) Intermediate-purity profile. (c) High-purity profile.

their deficiencies for general multicomponent mixtures have long been recognized. Even Murphree (*op. cit.*), who formulated the widely used plate efficiencies that carry his name, pointed out clearly their deficiencies for multicomponent mixtures and when efficiencies are small. Walter and Sherwood [*Ind. Eng. Chem.*, **33**, 493 (1941)] showed that experimentally measured efficiencies could cover an enormous range, with some values less than 10 percent. Toor [*AIChE J.*, **3**, 198 (1957)] predicted that the Murphree vapor efficiencies in some multicomponent systems could cover the entire range of values from minus infinity to plus infinity, a result that was verified experimentally by others.

In recent years a new approach to the modeling of distillation and absorption processes has become available: the *nonequilibrium* or *rate-based* models. These models treat these classical separation processes as the mass-transfer rate governed processes that they really are, and avoid entirely the (a priori) use of concepts such as efficiency and HETP [Krishnamurthy and Taylor, *AIChE J.*, **31**, 449–465 (1985); Taylor, Kooijman, and Hung, *Comput. Chem. Engng.*, **18**, 205–217 (1994)].

A schematic diagram of a nonequilibrium (NEQ) stage is given in Fig. 13-54. This NEQ stage may represent (part of) the two phases on

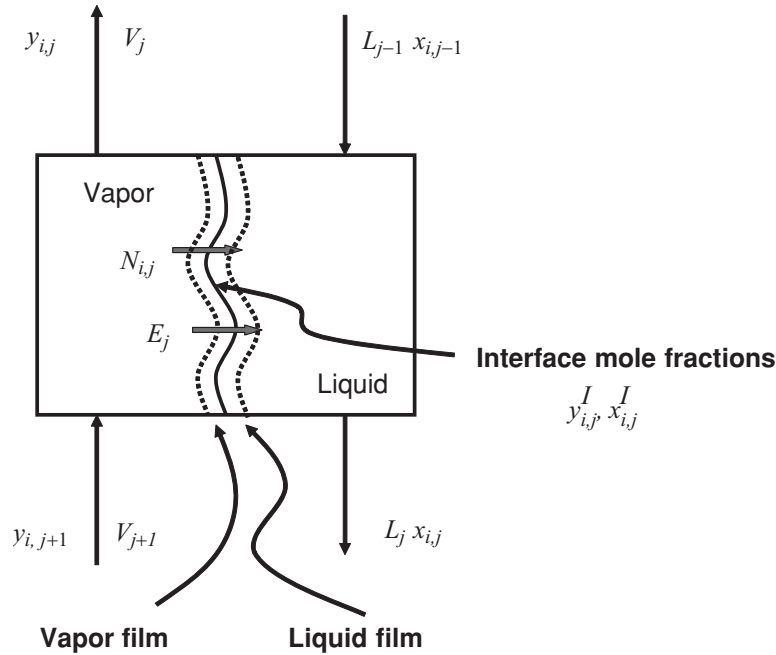


FIG. 13-54 Schematic diagram of a nonequilibrium stage.

a tray or within a section of a packed column. The wavy line in the middle of the box represents the phase interface. This illustration is intended only to aid in understanding the basic principles of nonequilibrium modeling; the actual flow patterns and the shape of the phase boundary are very complicated and depend upon, among other things, the equipment design, the column operation, and the physical properties of the system.

In a nonequilibrium model, separate balance equations are written for each distinct phase. The material balances for each species in the vapor and liquid phases on an arbitrary stage j are

$$(1 + r_j^V)V_j y_{i,j} - V_{j+1} y_{i,j+1} - f_{i,j}^V + \mathcal{N}_{i,j}^V = 0 \quad (13-61)$$

$$(1 + r_j^L)L_j x_{i,j} - L_{j-1} x_{i,j-1} - f_{i,j}^L - \mathcal{N}_{i,j}^L = 0 \quad (13-62)$$

where r_j^V and r_j^L are the ratios of sidestream to interstage flows and are defined by Eqs. (13-49); $f_{i,j}^p$ is the external feed flow rate of species i in phase p to stage j ; and $\mathcal{N}_{i,j}$ is the rate of mass transfer across the phase interface (with units of moles per second or equivalent). Formally, we may write

$$\mathcal{N}_{i,j}^p = \int N_{i,j}^p da_j \quad (13-63)$$

where $N_{i,j}^p$ is the molar flux in phase p [with units of $\text{mol}/(\text{m}^2 \cdot \text{s})$ or equivalent] at a particular point in the two-phase dispersion and da_j is the portion of interfacial area through which that flux passes. A material balance around the interface yields

$$\mathcal{N}_{i,j}^V = \mathcal{N}_{i,j}^L \quad (13-64)$$

The sum of the phase and interface balances yields the component material balance for the stage as a whole, the equation used in the equilibrium-stage model.

The energy balance is treated in a similar way, split into two parts—one for each phase, each part containing a term for the rate of energy transfer across the phase interface.

$$(1 + r_j^V)V_j H_j^V - V_{j+1} H_{j+1}^V - F_j^V H_j^{VF} + \mathcal{E}_j^V + Q_j^V = 0 \quad (13-65)$$

$$(1 + r_j^L)L_j H_j^L - L_{j-1} H_{j-1}^L - F_j^L H_j^{LF} - \mathcal{E}_j^L + Q_j^L = 0 \quad (13-66)$$

where \mathcal{E}_j^p is the rate of energy transfer across the phase interface in phase p and is defined by

$$\mathcal{E}_j^p = \int_a E_j^p da \quad (13-67)$$

where a is the interfacial area and E_j^p is the energy flux across the interface from/to phase p . An energy balance at the phase interface yields

$$\mathcal{E}_j^V = \mathcal{E}_j^L \quad (13-68)$$

In addition, we need summation equations for the mole fractions in the vapor and liquid phases.

A review of early applications of NEQ models is available in chapter 14 of Taylor and Krishna (op. cit.).

It is worth emphasizing that Eqs. (13-61) to (13-68) hold regardless of the models used to calculate the interphase transport rates $\mathcal{N}_{i,j}$ and \mathcal{E}_j^p . With a mechanistic model of sufficient complexity it is possible, at least in principle, to account for mass transfer from bubbles in the froth on a tray as well as to entrained droplets in a spray, as well as transport between the phases flowing over and through the elements of packing in a packed column. However, a completely comprehensive model for estimating mass-transfer rates in all the possible flow regimes does not exist at present, and simpler approaches are used.

The simplest approach is to say that the molar fluxes at a vapor-liquid interface may be expressed as

$$N_i^V = c_i^V k_i^V (y_i^V - y_i^I) + y_i^V N_i^V \quad (13-69)$$

with a similar expression for the liquid phase.

$$N_i^L = c_i^L k_i^L (x_i^L - x_i^I) + x_i^L N_i^L \quad (13-70)$$

In these equations c_i^V and c_i^L are the molar densities of the superscripted phases, y_i^V is the mole fraction in the bulk vapor phase, x_i^L is the mole fraction in the bulk liquid phase, and x_i^I and y_i^I are the mole fractions of species i at the phase interface. Also N_i^p is the total molar flux in phase p , and k_i^V and k_i^L are the mass-transfer coefficients for

the vapor and liquid phases (with units of velocity), respectively. Methods for estimating mass-transfer coefficients in distillation processes are discussed briefly below and at greater length in Section 5 of this handbook.

The second term on the right-hand sides of Eqs. (13-69) and (13-70) is not often important in distillation (its neglect is equivalent to the assumption of equimolar counterflows in the column), but can be quite significant in gas absorption.

The energy fluxes are related by

$$E^V = q^V + \sum_{i=1}^c N_i^V \bar{H}_i^V = E = q^L + \sum_{i=1}^c N_i^L \bar{H}_i^L = E^L \quad (13-71)$$

$$\text{with} \quad q^V = h^V(T^V - T^I) \quad q^L = h^L(T^I - T^L) \quad (13-72)$$

where h^V and h^L are the heat-transfer coefficients in the vapor and liquid phases, respectively.

The inclusion in the model of the mass and energy transport equations introduces the mole fractions and temperature at the interface. It is common in almost all treatments of mass transfer across a phase boundary to assume that the mole fractions in the vapor and liquid phases at the interface are in equilibrium with each other. We may, therefore, use the very familiar equations from phase equilibrium thermodynamics to relate the interface mole fractions

$$y_i^I = K_i x_i^I \quad (13-73)$$

where the superscript I denotes the interface compositions and K_i is the vapor-liquid equilibrium ratio (or K value) for component i . In equilibrium-stage calculations, the equilibrium equations are used to relate the composition of the streams leaving the stage, and the K values are evaluated at the composition of the two exiting streams and the stage temperature (usually assumed to be the same for both phases). In nonequilibrium models the K values are evaluated at the interface composition and temperature by using exactly the same thermodynamic property models as that used in equilibrium-stage simulations. The interface composition and temperature must, therefore, be computed during a nonequilibrium column simulation. Strictly speaking, the composition and temperature at the interface vary with position in two-phase dispersion that exists on a tray or within the confines of a packed bed. In most NEQ models, the interface state is assumed uniform on the stage; thus, the model of a single stage includes one set of mass-transfer, heat-transfer, and phase equilibrium equations.

In equilibrium-stage models, the compositions of the leaving streams are related through the assumption that they are in equilibrium (or by use of an efficiency equation). It is important to recognize that efficiencies are not used in a nonequilibrium model; they may, however, be calculated from the results obtained by solving the model equations.

Degrees of Freedom Table 13-10 summarizes the equations for a single nonequilibrium stage. There are $6c + 5$ independent equations

TABLE 13-10 Equations for a Nonequilibrium Stage

Equation	Equation no.	Number
Vapor-phase component balance	(13-61)	c
Liquid-phase component balance	(13-62)	c
Interface material balance	(13-64)	c
Vapor bulk mole fraction summation equation		1
Liquid bulk mole fraction summation equation		1
Vapor-phase energy balance	(13-65)	1
Liquid-phase energy balance	(13-66)	1
Equilibrium at the interface	(13-73)	c
Mass transfer in the vapor phase	(13-69)	$c - 1$
Mass transfer in the liquid phase	(13-70)	$c - 1$
Energy balance at phase interface	(13-71)	1
Summation equation for vapor mole fractions at phase interface		1
Summation equation for liquid mole fractions at phase interface		1
Total		$6c + 5$

TABLE 13-11 Variables for a Nonequilibrium Stage

Variable	Symbol	Number	Specified
Vapor and liquid flow rates	V_j, L_j	2	
Sidestream flow rates	U_j, W_j	2	Yes
Vapor-phase bulk composition	y_{ij}	c	
Liquid-phase bulk composition	x_{ij}	c	
Vapor interface composition	y_{ij}^I	c	
Liquid interface composition	x_{ij}^I	c	
Component feed flow rates	f_{ij}^V, f_{ij}^L	$2c$	Yes
Feed pressure and temperature		2	Yes
Vapor-phase temperature	T_j^V	1	
Liquid-phase temperature	T_j^L	1	
Interface temperature	T_j^I	1	
Stage pressure	P_j	1	Yes
Heat loss from vapor phase	Q_j^V	1	Yes
Heat loss from liquid phase	Q_j^L	1	Yes
Mass-transfer rates in the vapor phase	\mathcal{N}_{ij}^V	c	
Mass-transfer rates in the liquid phase	\mathcal{N}_{ij}^L	c	
Total		$8c + 12$	$2c + 7$

per stage. As with the equilibrium-stage model discussed above, we have not included the feed mole fraction summation equation, or those for the vapor and liquid streams coming from adjacent stages.

The variables appearing in these equations are summarized in Table 13-11.

It is important to recognize that we have not included mass- and heat-transfer coefficients in the table of variables. These quantities are considered analogous to the thermodynamic properties of the equilibrium-stage model and are functions of other variables (as discussed in greater detail below).

The $6c + 5$ variables for each stage determined during the solution of the nonequilibrium model equations are the vapor and liquid flow V_j and L_j , respectively; the bulk vapor mole fractions, y_{ij} (c in number); the bulk liquid mole fractions x_{ij} (c); the vapor and liquid temperatures T_j^V and T_j^L , respectively; the interface mole fractions and temperature y_{ij}^I (c), x_{ij}^I (c), and T_j^I ; and the mass-transfer rates \mathcal{N}_{ij}^V (c) and \mathcal{N}_{ij}^L (c). Note that the interface material balance, Eq. (13-64), means that only one set of mass-transfer rates really needs to be counted in the set of variables for this stage, say, \mathcal{N}_{ij} (this reduces the number of variables being computed). The remaining variables, $2c + 7$ in number, that need to be specified, are identified in Table 13-11. It is important to recognize that the other flows and composition variables appearing in the nonequilibrium-stage model equations are associated with the equivalent equations for adjacent stages. Although it appears that the number of degrees of freedom is higher for this more complicated model, this is misleading. The additional variables that are specified here take into account that there is one additional heat duty (one per phase) and that the feed is split into vapor and liquid fractions. In practice, the overall feed flow, pressure, temperature (or vapor fraction), and composition would be specified, and the vapor and liquid component flows in the feed determined from an adiabatic flash.

Physical Properties The only physical properties needed for an equilibrium-stage simulation are those needed to estimate K values and enthalpies; these same properties are needed for nonequilibrium models as well. Enthalpies are required for the energy balance equations; vapor-liquid equilibrium ratios are needed for the calculation of driving forces for mass and heat transfer. The need for mass- (and heat-) transfer coefficients means that nonequilibrium models are rather more demanding of physical property data than are equilibrium-stage models. These coefficients may depend on a number of other physical properties, as summarized in Table 13-12.

Methods for estimating physical and transport properties are described in Sections 4 and 5 of this handbook [see also Poling et al., *The Properties of Gases and Liquids*, McGraw-Hill, 5th ed. (2001)].

Flow Models In a real column the composition of the vapor and liquid phases changes due to flow across a tray or over and around packing. Thus, the bulk phase mole fractions that appear in the rate equations (13-69) and (13-70) vary with position and should not automatically be assumed to be equal to the average exit mole

TABLE 13-12 Physical Property Needs of Equilibrium and Nonequilibrium Models

Property	EQ model	NEQ model	Used for
K values	Yes	Yes	Driving forces
Enthalpy	Yes	Yes	Energy balances
Activity coefficient	Yes	Yes	K values, enthalpies
Fugacity coefficients	Yes	Yes	K values, enthalpies
Vapor pressure	Yes	Yes	K values
Heat capacity	Yes	Yes	Enthalpies, heat-transfer coefficient
Mass-transfer coefficients		Yes	Mass-transfer rate equations
Heat-transfer coefficients		Yes	Energy-transfer rate equation
Density		Yes	Mass-transfer coefficients
Diffusion coefficients		Yes	Mass-transfer coefficients
Viscosity		Yes	Mass-transfer coefficients
Surface tension		Yes	Mass-transfer coefficients
Thermal conductivity		Yes	Heat-transfer coefficients

fractions that appear in the material balance equations. In practice, we assume a flow pattern for the vapor and liquid phases, and this allows us to determine appropriate average mole fractions for use in the rate equations. There are three flow models in general use: mixed flow, plug flow, and dispersion flow (Lockett, op. cit.). A flow model needs to be identified for each phase. If both phases are assumed well mixed, then the average mole fractions are indeed equal to the mole fractions in the exit streams. This is the simplest (and an often used) approach that leads to the most conservative simulation (lowest mass-transfer rates, tallest column); at the opposite extreme is plug flow. The most realistic model is dispersion flow (see Lockett, op. cit.), but this model is not included in most computer implementations of NEQ models as it is quite complicated. For further discussion of the importance of flow models and the equations used to estimate average compositions, see Taylor and Krishna (op. cit.) and Kooijman and Taylor [*Chem. Engng. J.*, **57**, 177 (1995)].

Mass-Transfer Coefficients Mass-transfer coefficients (and the equally important interfacial area, a parameter with which they frequently are combined) may be computed from empirical correlations or theoretical models.

The mass-transfer performance of trays often is expressed by way of a dimensionless group called the number of transfer units [see Lockett (op. cit.), Kister (op. cit.), and Sec. 14 for additional background]. These dimensionless numbers are defined by

$$\mathbb{N}^V = k^V a' t_V = \frac{k^V a h_f}{u_s} \quad (13-74)$$

$$\mathbb{N}^L = k^L \bar{a} t_L = \frac{k^L a h_f Z}{Q_L / W} \quad (13-75)$$

where h_f = froth height, m

Z = liquid flow path length, m

W = weir length, m

$Q_L = \frac{L}{c_t^L}$ = volumetric liquid flow rate, m³/s

$u_s = \frac{V}{c_t^V A_{\text{bub}}}$ = superficial vapor velocity, m/s

A_{bub} = bubbling area of tray, m²

h_L = clear liquid height on tray, m

a' = interfacial area per unit volume of vapor, m²/m³

\bar{a} = interfacial area per unit volume of liquid, m²/m³

These areas are related to the interfacial area per unit volume of froth a by

$$a' = \frac{1}{1 - \alpha} \quad \bar{a} = \frac{\alpha}{\alpha} \quad (13-76)$$

where $\alpha = h_L/h_f$ is the relative froth density. Also t_V and t_L are the vapor- and liquid-phase residence times, defined by

$$t_V = (1 - \alpha) h_f u_s \quad (13-77)$$

$$t_L = \frac{Z}{u_L} = \frac{h_f Z W}{Q_L} \quad (13-78)$$

The *AICHE Bubble Tray Design Manual*, published in 1958 [see also Gerster et al., *Tray Efficiencies in Distillation Columns*, AIChE

(1958)], presented the first comprehensive procedure for estimating the numbers of transfer units in distillation. For many years this work represented the only such procedure available in the open literature; the work of organizations such as Fractionation Research Incorporated (FRI) was available only to member companies. Other comprehensive procedures for trays appeared in the 1980s [Zuiderweg, *Chem. Engng. Sci.*, **37**, 1441 (1982); Chan and Fair, *Ind. Engng. Chem. Proc. Des. Dev.*, **23**, 814, 820 (1984)]. Readers are referred to Kister (op. cit.), Lockett (op. cit.), Klemola and Ilme (op. cit.), and Sec. 14 of this handbook for summaries and references to what is available in the open literature.

Example 11: Mass-Transfer Coefficient in a Tray Column

Consider again the C₄ splitter that formed the basis of Examples 7 and 8. The key design parameters for the valve trays are given in the table below (from Klemola and Ilme, op. cit.).

Column height	51.8 m	Downcomer area center	0.86 m ²
Column diameter	2.9 m	Tray spacing	0.6 m
Number of trays	74	Hole diameter	39 mm
Weir length, side	1.859 m	Total hole area	0.922 m ²
Weir length, center	2.885 m	Outlet weir height	51 mm
Liquid flow path length	0.967 m	Tray thickness	2 mm
		per pass	
Active area	4.9 m ²	Number of valves per tray	772
Downcomer area, side	0.86 m ²	Free fractional hole area	18.82%

Estimate the mass-transfer coefficients for tray 7 where the flow and physical properties are estimated to be as summarized below:

	Gas/vapor	Liquid
Flow, mol/s	590	550
Density, kg/m ³	16.8	520
Viscosity, N/m ²	8.6 × 10 ⁻⁶	1.35 × 10 ⁻⁴
Molecular weight, kmol/kg	58.0	58.0
Diffusivity, m ² /s	800 × 10 ⁻⁹	1.0 × 10 ⁻⁹
Surface tension, N/m		0.014

We use the AIChE correlation to illustrate the general approach, noting that the correlation was not developed specifically for valve trays (few methods were). In this model the number of transfer units is given by

$$\mathbb{N}^V = \frac{0.776 + 4.57 h_w - 0.238 F_s + 104.8 Q_L / W}{\sqrt{Sc^V}} \quad (13-79)$$

$$\mathbb{N}^L = 19,700 \sqrt{D^L} (0.4 F_s + 0.17) t_L \quad (13-80)$$

In the expressions above h_w is the weir height (m). The vapor-phase Schmidt number Sc^V is defined by $Sc^V = \mu^V / (\rho^V D^V)$, which here takes the value $Sc^V = 0.640$.

The superficial velocity is computed next from $u_s^V = V / (c_t^V A_{\text{bub}}) = 0.42$ m/s. Here F_s is the so-called F factor and is $F_s = u_s^V \sqrt{\rho^V} = 1.7$ (kg/ms)^{1/2}. The volumetric liquid flow is $Q_L = L / c_t^L = 0.061$ m³/s.

The froth height on the tray is estimated (by using the methods in Sec. 14 of this handbook—see also Lockett, 1986; Kister, 1992) to be $h_f = 0.143$ m. The liquid-phase residence time is $t_L = h_f Z W / Q_L = 4.67$ s.

The number of transfer units follows for the vapor phase from Eq. (13-79) as $\mathbb{N}^V = 2.45$ and for the liquid phase from Eq. (13-80) as $\mathbb{N}^L = 2.33$. The products of the vapor- and liquid-phase mass-transfer coefficients and the interfacial area follow directly from the second parts of the same equations. Note that it is not possible with these correlations to separate the mass-transfer coefficient from the interfacial area. In practice this is not a concern since it is the mass-transfer rates that are needed rather than the fluxes and the product suffices for NEQ model computations.

The diffusivities used in this example were for the light key–heavy key pair of components. For systems similar to this one, the diffusion coefficients of all binary pairs in the mixture would be expected to have similar values. This will not be the case for mixtures of components that differ sharply in their fundamental properties (e.g., size, polarity). For these more highly nonideal mixtures, it is necessary to estimate the mass-transfer coefficients for each of the binary pairs.

The number of transfer units for packed columns is defined by

$$N^V = \frac{k^V a' H}{u_V} \quad (13-81)$$

$$N^L = \frac{k^L a' H}{u_L} \quad (13-82)$$

where $u_V = V/(c_V^V A_c)$ and $u_L = L/(c_V^L A_c)$ are the superficial vapor and liquid velocities, with A_c the cross-sectional area of the column; a' is the interfacial area per unit volume. The height of a transfer unit (HTU) is defined as

$$H^V = \frac{H}{N^V} = \frac{u_V}{k^V a'} \quad (13-83)$$

$$H^L = \frac{H}{N^L} = \frac{u_L}{k^L a'} \quad (13-84)$$

Methods of estimating numbers and/or heights of transfer units and mass-transfer coefficients and interfacial areas in packed columns are reviewed by Ponter and Au Yeung (in *Handbook of Heat and Mass Transfer*, Gulf Pub., 1986), by Wang et al. [*Ind. Eng. Chem. Res.*, **44**, 8715 (2005)], and in Sec. 5 of this handbook; one such method is illustrated below.

Example 12: Mass-Transfer Coefficients in a Packed Column

Estimate the mass-transfer coefficients at the top of the packed gas absorber in Example 9. The column has 23 ft of 2-in metallic Pall rings and is 3 ft in diameter. The specific surface area of this packing is 112 m²/m³. The flows and physical properties are estimated to be as summarized below.

	Gas/vapor	Liquid
Flow, mol/s	332	37
Temperature, K	267	266
Density, kg/m ³	51.2	705
Viscosity, N/m ²	1.17 × 10 ⁻⁵	2.43 × 10 ⁻⁴
Molecular weight, kmol/kg	16.8	87.9
Diffusivity, m ² /s	100 × 10 ⁻⁹	4.6 × 10 ⁻⁹
Surface tension, N/m		0.0085

We will use the well-known correlation of Onda et al. (see Sec. 14) to estimate the mass-transfer coefficients. The vapor-phase coefficient is given by

$$\frac{k^V}{a_p D^V} = A \left(\frac{\rho^V u^V}{\mu^V a_p} \right)^{0.7} \left(\frac{\mu^V}{\rho^V D^V} \right)^{0.33} (a_p d_p)^{-2} \quad (13-85)$$

where d_p is the nominal packing size (2 in = 0.0508 m), and a_p is the specific surface area of the packing. Also A is a constant that has the value 2 if nominal packing size is less than 0.012 m, otherwise, $A = 5.23$.

The liquid-phase mass-transfer coefficient is given by

$$k^L = 0.0051 \left(\frac{\rho^L}{\mu^L g} \right)^{-1/3} \left(\frac{u_L}{a' \mu^L} \right)^{2/3} \left(\frac{\mu^L}{\rho^L D^L} \right)^{1/2} (a_p d_p)^{0.4} \quad (13-86)$$

Finally, the interfacial area per unit volume is given by

$$a' = a_p \left\{ 1 - \exp \left[-1.45 \left(\frac{\sigma_c}{\sigma^L} \right)^{0.75} \left(\frac{\rho^L u_L}{a_p \mu^L} \right)^{0.1} \left(\frac{a_p \mu^L}{g} \right)^{0.05} \left(\frac{u^2 L \rho^L}{a_p \sigma^L} \right)^{0.2} \right] \right\} \quad (13-87)$$

The vapor and liquid velocities are calculated to be $u_V = V/(c_V^V A_c) = 0.42$ m/s and $u_L = L/(c_V^L A_c) = 0.0017$ m/s. Substituting the values provided above into Eqs. (13-85) to (13-87) gives $k^V = 0.0021$ m/s, $a' = 96.2$ m²/m³, and $k^L = 3.17 \times 10^{-4}$ m/s.

Solving the NEQ Model Equations In general, a nonequilibrium model of a column has many more equations than does an equivalent equilibrium-stage model. Nevertheless, we use may essentially the same computational approaches to solve the nonequilibrium model equations: simultaneous convergence (Krishnamurthy and Taylor, op. cit.) and continuation methods [Powers et al., *Comput. Chem. Engng.*, **12**, 1229 (1988)]. Convergence of a nonequilibrium model is likely to be slower than that of the equilibrium model because of the greater

number of model equations and the associated overhead in evaluating a greater number of physical properties. Finally, we note that the strategies outlined above for helping to converge equilibrium-stage simulation may prove equally useful when simulating distillation operations using the nonequilibrium models described here.

Equipment Design As we have already seen, the estimation of mass-transfer coefficients and interfacial areas from empirical correlations nearly always requires us to know something about the column design. At the very least we need to know the diameter and type of internal column (although usually we need to know more than that since most empirical correlations for mass-transfer coefficients have some dependency on equipment design parameters, e.g., weir height of trays). This need for more or less complete equipment design details suggests that nonequilibrium models cannot be used in preliminary process design (before any actual equipment design has been carried out). This is not true, however. Column design methods are available in the literature as well in most process simulation programs, and it is straightforward to carry out equipment sizing calculations at the same time as the stage equations are being solved (Taylor et al., op. cit.). This does not add significantly to the difficulty of the calculation, while providing the very significant advantage of allowing nonequilibrium or rate-based models to be used at all stages of process simulation.

Example 13: A Nonequilibrium Model of a C₄ Splitter Consider, again the C₄ splitter that formed the basis of Examples 7, 8, and 11.

When we create a nonequilibrium model of this—or any—column, we do not need to guess how many stages to use in each section of the column. The real column had 74 valve trays; the model column includes 74 model trays with the feed to tray 38 [plus a (subcooled) condenser and a reboiler, both of which are modeled as equilibrium stages, as described above]. All operating specifications are the same as for the corresponding equilibrium-stage model and are given in Examples 7 and 8. It is necessary to choose models that allow for the estimation of the rates of interphase mass transfer; that means selecting vapor and liquid flow models and correlations to estimate the mass-transfer coefficients in each phase, as discussed above. In this case the AIChE correlations were used. It is known that this method is more conservative than others (i.e., the predicted efficiencies are lower). The importance of the flow model is clear from the simulation results tabulated below. The predicted component Murphree efficiencies computed with Eq. (13-58) vary more widely from stage to stage and from component to component than might be expected for a system such as this. The TBK efficiency, on the other hand, does not change by more than a few percentage points over the height of the column; the value in the table below is an average of that computed for each tray from the simulation results using Eq. (13-59).

Vapor flow model	Liquid flow model	<i>i</i> -C ₄ in distillate, %	<i>n</i> -C ₄ in bottoms, %	TBK efficiency, %
Mixed	Mixed	90.2	96.3	63
Plug	Mixed	92.2	97.2	78
Plug	Dispersion	93.9	98.0	106

Internal vapor and/or liquid composition data rarely are available, but such data are the best possible for model discrimination and validation. It is often relatively easy to match even a simple model only to product compositions. In the absence of composition profiles, the internal temperature profile can often be as useful provided that it is known to which phase a measured temperature pertains. The table below compares the few available measured tray temperatures with those computed during the simulation. The agreement is quite good.

Tray	Temperature, °C	
	Measured	Predicted
9	47.5	48.6
65	62.2	62.5
74	63.2	63.1

A portion of the McCabe-Thiele diagram for the simulation involving plug flow of vapor and dispersion flow of the liquid is shown in Fig. 13-55. For a nonequilibrium column these diagrams can only be constructed from the results of a computer simulation. Note that the triangles that represent the stages extend beyond the curve that represents the equilibrium line; this is so because the efficiencies are greater than 100 percent.

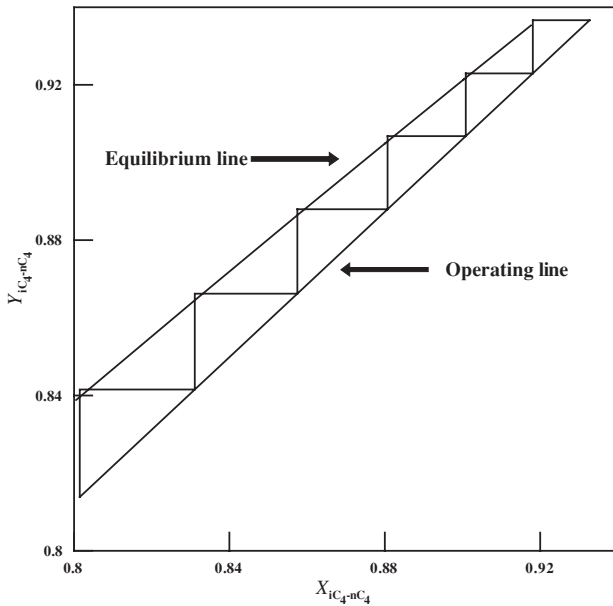


FIG. 13-55 Expanded view near upper right corner of McCabe-Thiele diagram for C_4 splitter.

In this particular case the converged composition and temperature profiles have the same shape as those obtained with the equilibrium-stage model (with specified efficiency) and, therefore, are not shown. The reason for the similarity is that, as noted above, this is basically a binary separation of very similar compounds. The important point here is that, unlike the equilibrium-stage model simulations, the nonequilibrium model predicted how the column would perform; no parameters were adjusted to provide a better fit to the plant data. That is not to say, of course, that NEQ models cannot be used to fit plant data. In principle, the mass-transfer coefficients and interfacial area (or parameters in the equations used to estimate them) can be tuned to help the model better fit plant data.

MAXWELL-STEFAN APPROACH

Strictly speaking, Eqs. (13-69) and (13-70) are valid only for describing mass transfer in binary systems under conditions where the rates of mass transfer are low. Most industrial distillation and absorption processes, however, involve more than two different chemical species. The most fundamentally sound way to model mass transfer in multi-component systems is to use the Maxwell-Stefan (MS) approach (Taylor and Krishna, op. cit.).

The MS equation for diffusion in a mixture with any number of different species can be written as

$$d_i = - \sum_{k=1}^c \frac{x_i x_k (u_i - u_k)}{\mathfrak{D}_{ik}} \quad (13-88)$$

where \mathfrak{D}_{ik} is the Maxwell-Stefan diffusion coefficient for the binary i - k pair of components. Methods for estimating these coefficients are discussed by Taylor and Krishna (op. cit.) (see also Section 5 of this handbook and Poling et al., op. cit.).

In Eq. (13-88), d_i is termed the generalized driving force. For an ideal gas mixture the driving force is related to the partial pressure gradient and the mole fraction gradient as follows:

$$d_i = \frac{1}{P} \frac{dp_i}{dz} = \frac{dx_i}{dz} \quad (13-89)$$

For a nonideal fluid, the driving force is related to the chemical potential gradient

$$d_i = \frac{x_i}{RT} \frac{d\mu_i}{dz} \quad (13-90)$$

Equations (13-88) for ideal gas mixtures may be derived by using nothing more complicated than Newton's second law: *The sum of the forces acting on the molecules of a particular species is directly proportional to the rate of change of momentum.* The rate of change of momentum between different species is proportional to the concentrations (mole fractions) of the different species and to their relative velocity [see also Taylor and Krishna (op. cit.) for a more complete derivation]. Equation (13-88) is more familiar in the form

$$d_i = - \sum_{k=1}^c \frac{x_i N_k - x_k N_i}{c_i \kappa_{i,k}} \quad (13-91)$$

where we have replaced the velocities by the molar fluxes $N_i = c_i u_i$ (see Section 5). Only $c - 1$ of Eqs. (13-91) are independent; the mole fraction of the last component is obtained by the mole fraction summation equations for both phases.

Solving the MS equations can be quite involved (see Taylor and Krishna, op. cit.). Most often a simple film model solution of Eqs. (13-91) is used, leading to a simple difference approximation to the MS equations

$$\Delta x_i = - \sum_{k=1}^c \frac{\bar{x}_i N_k - \bar{x}_k N_i}{c_i \kappa_{i,k}} \quad (13-92)$$

where $\kappa_{i,k}$ is the mass-transfer coefficient for the binary i - k pair of components. The Maxwell-Stefan mass-transfer coefficients can be estimated from existing correlations for mass-transfer coefficients using the binary MS diffusion coefficients.

For a nonideal fluid the driving force is related to the chemical potential gradient

$$d_i = \frac{x_i}{RT} \frac{d\mu_i}{dz} \quad (13-93)$$

The difference approximation of this expression is somewhat more involved since we have to include the derivative of the activity (or fugacity) coefficient in the approximation. If, as often is assumed to be the case (not always with justification), the resistance to mass transfer in the liquid phase is negligible, then the MS equations for the liquid phase can safely be replaced by

$$\Delta x_i = x_i^l - x_i^v = 0 \quad (13-94)$$

The use of the MS equations in place of the simpler Eqs. (13-69) and (13-70) does not change the number of independent model equations or the number of degrees of freedom.

Example 14: The Need for Rigorous Maxwell-Stefan-Based NEQ Models Design a distillation column to separate a feed of 20 mol/s methanol, 10 mol/s isopropanol, and 20 mol/s water. The bottom product is to contain no more than 0.5 mol % methanol, and the distillate is to contain at least 99 mol % methanol but no more than 50 ppm water.

As a first step we attempt to design the column by using the equilibrium-stage model. Following Doherty and Malone (op. cit.), the NRTL model was used for the activity coefficients and the Antoine equation for the vapor pressures. Doherty and Malone estimate the minimum reflux as 5; we used a value 50 percent higher in this example and specified the bottoms product rate at 30 mol/s; this choice provides a consistent basis for the comparison of different models. The number of stages and the location of the feed were varied until a column configuration was obtained that met the desired product purity: 80 total stages (including total condenser and partial reboiler) with the feed to stage 16.

Efficiencies of alcohol-water and alcohol-alcohol systems obtained experimentally in sieve tray columns vary from 60 to 100 percent (Sec. 14 in the seventh

edition of this handbook). After specifying an average efficiency of 80 percent, we find that 99 total stages with the feed to stage 21 were needed to get the distillate product below 50 ppm water.

If we use the nonequilibrium model to design a sieve tray column, it is found that a column with 84 trays (plus condenser and reboiler) and with the feed to tray 21 (stage 22) will produce an overhead product of the desired purity. The reflux ratio and bottoms flows were maintained at the values employed for the equilibrium-stage design. The AIChE method was used for estimating the mass-transfer coefficient–interfacial area products, and the vapor and liquid phases were assumed to be in plug flow. The pressure was assumed constant in the column (an assumption that would need to be relaxed at a later stage of the design exercise). The computer simulation also provided a preliminary tray design; that for the trays above the feed is summarized in the table below.

Column diameter, m	1.76
Total tray area, m ²	2.43
Number of flow passes	2
Tray spacing, m	0.6
Liquid flow path length, m	0.75
Active area, % total	91.4
Total hole area, % active	14
Downcomer area, % total	4.3
Hole diameter, mm	5
Hole pitch, mm	12
Weir type	Segmental
Combined weir length, m	1.55
Weir height, mm	50

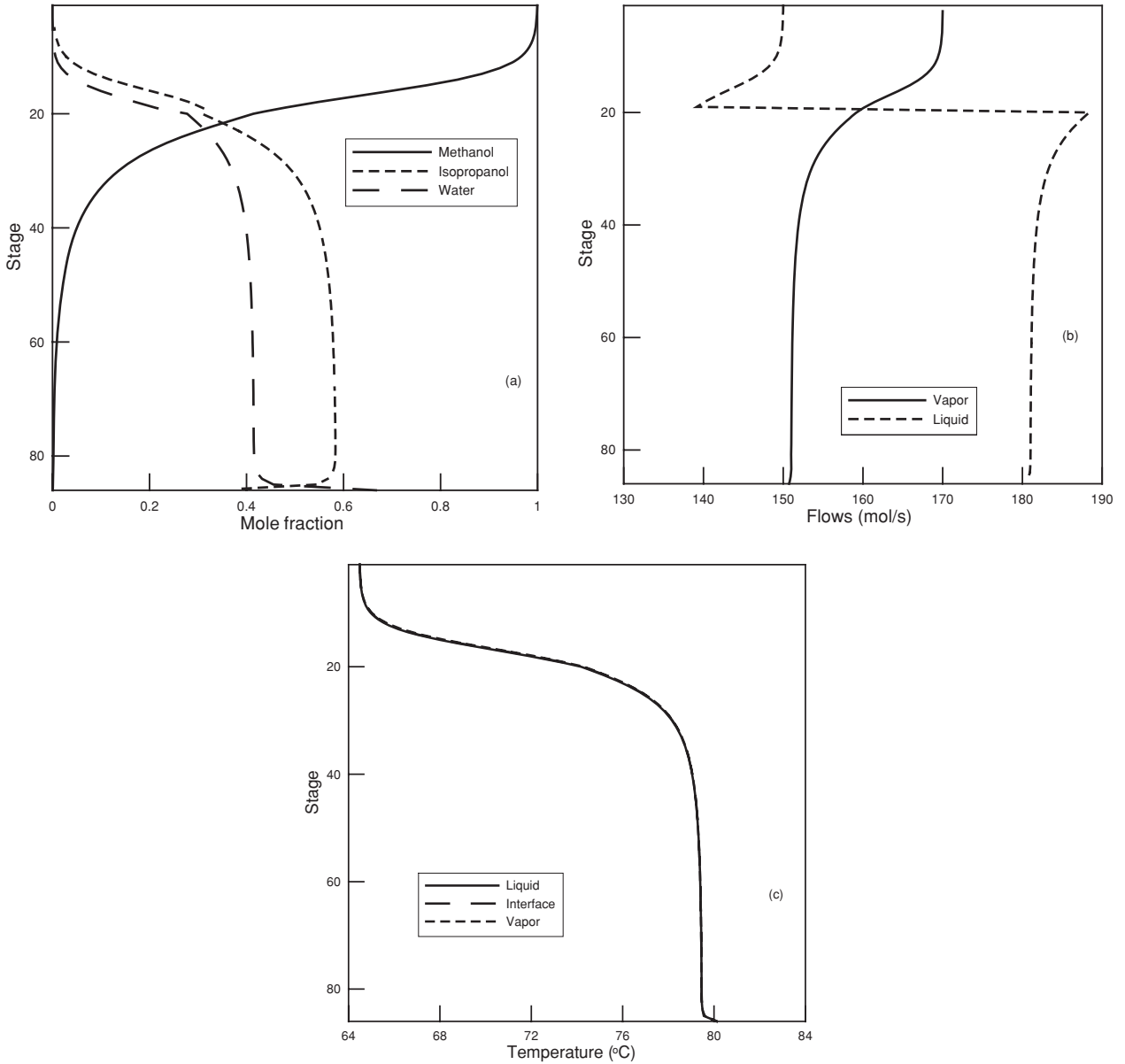


FIG. 13-56 Composition, flow, and temperature profiles in nonideal distillation process.

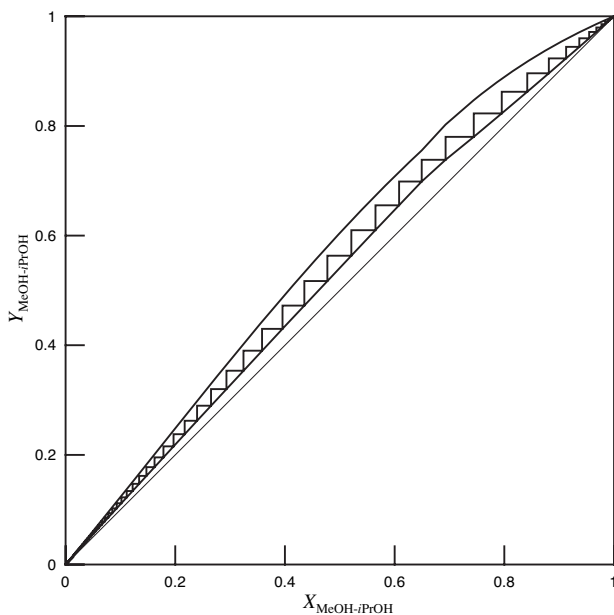


FIG. 13-57 McCabe-Thiele diagram for nonideal distillation column.

To converge the nonequilibrium model at the specified reflux ratio, it was necessary first to solve the problem at a much lower reflux ratio $R = 2$ and then increase R in steps until the desired value of 7.5 was reached.

The liquid composition, flow, and temperature profiles are shown in Fig. 13-56. In this particular system the vapor and liquid temperatures estimated by the rate-based model are quite close (as often is the case in distillation operations).

The McCabe-Thiele diagram for this column is shown in Fig. 13-57. Note that in this case the triangles that represent the stages do not touch the equilibrium line. The length of the vertical section of each step in Fig. 13-57 is a measure of the efficiency of that tray. The component Murphree efficiencies calculated from the simulation results and Eq. (13-58), as well as the TBK average efficiency defined by Eq. (13-59), are shown in Fig. 13-58. The efficiency of methanol in the stripping section is seen to be around 80 percent, that of isopropanol to be approximately 75 percent, while that of water is close to 90 percent in the bulk of the column before falling off on the bottom few trays. All component efficiencies are found to be lower in the rectifying section. The TBK average efficiency, also shown in Fig. 13-58, is close to the Murphree efficiency of methanol and varies from 60 percent in the top of the column to 78 percent. Thus, the constant value of 80 percent used above appears to be appropriate, and yet, the column designed with the constant-efficiency model required no less than 99 stages (97 trays)!

With 84 trays as opposed to 78 equilibrium stages (not counting condenser and reboiler in either case), we find an overall efficiency of 93 percent, a figure that is quite at odds with the values of the individual component efficiencies seen in Fig. 13-58. How, then, is it possible that the nonequilibrium model suggests that the column needs only 6 trays more than the number of equilibrium stages? It is, in fact, because the efficiency of water is so much higher than that of the alcohols that leads to a column design that can produce high-purity methanol while producing the 50-ppm methanol bottom product in so few extra stages. Note that nonequilibrium models will not always lead to a design with fewer trays than might be suggested by a constant-efficiency model; it is just as likely for the mass-transfer rate-based model to predict that more stages will be needed—it all depends on the differences between the component efficiencies.

Individual component efficiencies can vary as much as they do in this example only when the diffusion coefficients of the three binary pairs that exist in this system differ significantly. For ideal or nearly ideal systems, all models lead to essentially the same results. This example demonstrates the importance of mass-transfer models for nonideal systems, especially when trace components are a concern. For further discussion of this example, see Doherty and Malone (op. cit.) and Baur et al. [*AIChE J.* **51**, 854 (2005)]. It is worth noting that there exists extensive experimental evidence for mass-transfer effects for this system, and it is known that nonequilibrium models accurately describe the behavior of this system, whereas equilibrium models (and equal-efficiency models) sometime

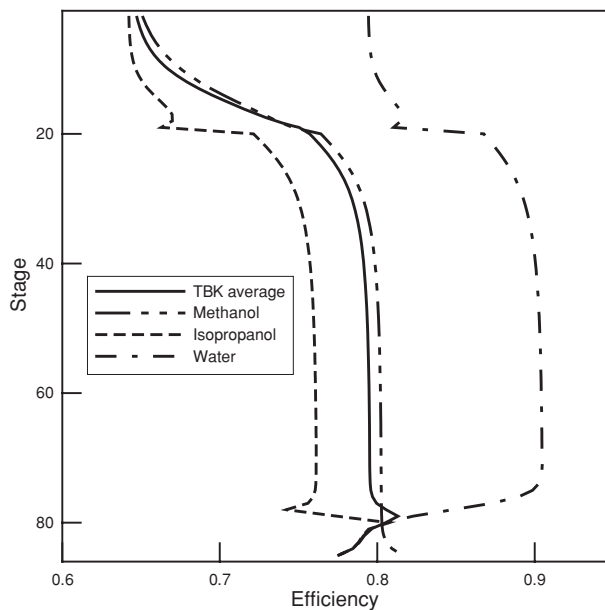


FIG. 13-58 Component Murphree efficiencies and TBK average efficiency [defined by Eq. (13-59)] for nonideal distillation.

predict completely erroneous product compositions [Pelkonen et al., *Ind. Engng. Chem. Res.*, **36**, 5392 (1997) and *Chem. Eng. Process*, **40**, 235 (2001); Baur et al., *Trans. I. Chem. E.*, **77**, 561 (1999)].

Nonequilibrium models should be preferred to equilibrium models when efficiencies are unknown, cannot be reliably predicted, and are low and/or highly variable; in nonideal systems and in processes where trace components are a concern.

There is a rapidly growing body of literature on nonequilibrium modeling of distillation and absorption processes. An extended bibliography is available at www.chemsep.org/publications. A brief review of other applications follows.

Simulation methods currently in use for three-phase systems and systems involving chemical reaction employ the equilibrium-stage model [Doherty and Malone (op. cit.)]. Three-phase distillation remains relatively poorly understood compared to conventional distillation operations involving just a single liquid phase. It is important to be able to correctly predict the location of the stages where a second liquid phase can form (e.g., to determine the appropriate location for a sidestream decanter). The limited experimental data available suggest that efficiencies are low and highly variable with between 25 percent and 50 percent being not uncommon. Clearly, a model based on the assumption of equilibrium on every stage cannot hope to be able to predict column performance. Cairns and Furzer [*Ind. Engng. Chem. Res.*, **29**, 5392 (1997)] explicitly warn against incorporating Murphree efficiencies into the equilibrium-stage model for three-phase systems, although Müller and Marquardt [*Ind. Engng. Chem. Res.*, **36**, 5410 (1997)] find that an efficiency modified EQ stage model to be perfectly adequate for their column for the dehydration of ethanol using cyclohexane.

It is possible to develop nonequilibrium models for systems with more than two phases, as shown by Lao and Taylor [*Ind. Engng. Chem. Res.*, **33**, 2367 (1994)], Eckert and Vaněk [*Comput. Chem. Eng.*, **25**, 603 (2001)], and Higler et al. [*Comput. Chem. Eng.*, **28**, 2021 (2004)]. Experimental work that can be used to evaluate these models is scarce; see, however, Cairns and Furzer (op. cit.) and Springer et al. [*Chem. Eng. Res. Design*, **81**, 413 (2003)].

There is now an extensive literature on using nonequilibrium models for reactive distillation; see, e.g., Taylor and Krishna [*Chem. Eng.*

TABLE 13-13 Selected List of Suppliers of Column Simulation Software

Supplier	Website	EQ model	NEQ model
Aspen Tech	www.aspentech.com	Yes	Yes
Bryan Research & Engineering	www.bre.com	Yes	
ChemSep	www.chemsep.com	Yes	Yes
Chemstations	www.chemstations.net	Yes	Yes
Deerhaven Technical Software	www.deerhaventech.com	Yes	
Honeywell	www.honeywell.com	Yes	Yes
Process Systems Engineering	www.psenterprise.com	Yes	Yes
ProSim	www.prosim.net	Yes	
SimSci-ESSCOR	www.simsci-esscor.com	Yes	Yes
VMG	virtualmaterials.com	Yes	

Sci., **55**, 6139 (2000)], Sundmacher and Kienle (*Reactive Distillation: Status and Future Directions*, Wiley-VCH, 2003), Noeres et al. [*Chem. Engng. Processing*, **42**, 157 (2003)], and Klöcker et al. [*Chem. Engng. Processing*, **44**, 617 (2005)]. Gas absorption accompanied by chemical reaction for a long time has been modeled by using mass-transfer rate-based concepts; see, e.g., Cornelisse et al. [*Chem. Eng. Sci.*, **35**, 1245 (1980)], Pacheco and Rochelle [*Ind. Eng. Chem. Res.*, **37**, 4107 (1998)], and a review by Kenig et al. [*Chem. Eng. Technol.*, **26**, 631 (2003)]. For such systems the chemical reaction influences the efficiencies to such an extent that the concept loses its meaning.

Even at steady state, efficiencies vary from component to component and with position in a column. Thus, if the column is not at steady state, then efficiencies also must vary with time as a result of changes to flow rates and composition inside the column. Thus, equilibrium-stage models with efficiencies should not be used to model the dynamic behavior of distillation and absorption columns. Nonequilibrium models for studying column dynamics are described by, e.g., Kooijman and Taylor [*AIChE J.*, **41**, 1852 (1995)], Baur et al. [*Chem.*

Eng. Sci., **56**, 2085 (2001)], Gunaseelan and Wankat [*Ind. Eng. Chem. Res.*, **41**, 5775 (2002)], Peng et al. [*Chem. Eng. Sci.*, **58**, 2671 (2003)], and Kenig et al. [*Chem. Eng. Sci.*, **54**, 5195 (1999)].

SOFTWARE FOR DISTILLATION COLUMN SIMULATIONS

Computer software for equilibrium-stage and nonequilibrium column models is available from a number of suppliers. Many other models have been implemented primarily for research purposes and are not available commercially.

In Table 13-13 we list several suppliers of column simulation models that are available commercially, without in any way claiming that this list is exhaustive or providing an endorsement of any particular package. We recommend that users interested in any of these (or other) packages carry out an independent evaluation that focuses on the ability of the package to tackle the simulation problems of direct interest. The simulations described in this subsection were carried out with *ChemSep*.

DEGREES OF FREEDOM AND DESIGN VARIABLES

DEFINITIONS

In the models described in previous subsections, we have determined the degrees of freedom on a case-by-case basis. We now develop a general approach to the topic.

For separation processes, a design solution is possible if the number of independent equations equals the number of unknowns

$$N_i = N_v - N_c \quad (13-95)$$

where N_v is the total number of variables (unknowns) involved in the process under consideration, N_c is the number of restricting relationships among the unknowns (independent equations), and N_i is the degrees of freedom that must be specified for there to be exactly the same number of unknowns as there are independent equations in the model. The concept of degrees of freedom in this context is similar to the same concept that appears in the Gibbs phase rule. The degrees of freedom is the number of design variables that must be specified to define one unique operation (solution) of the process.

The variables N_i with which the designer of a separation process must be concerned are

1. Stream concentrations (e.g., mole fractions)
2. Temperatures
3. Pressures
4. Stream flow rates
5. Repetition variables N_r

The first three are intensive variables. The fourth is an extensive variable that is not considered in the usual phase rule analysis. The fifth is neither an intensive nor an extensive variable but is a single degree of freedom that the designer uses in specifying how often a particular element is repeated in a unit. For example, a distillation column section is composed of a series of equilibrium stages, and when the designer specifies the number of stages that the section contains,

he or she uses the single degree of freedom represented by the repetition variable ($N_r = 1.0$). If the distillation column contains more than one section (such as above and below a feed stage), the number of stages in each section must be specified, and as many repetition variables exist as there are sections, that is, $N_r = 2$.

The various restricting relationships N_c can be classified as

1. Inherent
2. Mass balance
3. Energy balance
4. Phase distribution
5. Chemical equilibrium

The inherent restrictions are usually the result of definitions and take the form of identities. For example, the concept of the equilibrium stage involves the inherent restrictions that $T^v = T^l$ and $P^v = P^l$ where the superscripts V and L refer to the equilibrium exit streams.

The mass balance restrictions are the C balances written for the C components present in the system. (Since we will deal with only non-reactive mixtures, each chemical compound present is a phase rule component.) An alternative is to write $C - 1$ component balances and one overall mass balance.

The phase distribution restrictions reflect the requirement that $f_i^v = f_i^l$ at equilibrium where f_i is the fugacity. This may be expressed by Eq. (13-1). In vapor-liquid systems, it should always be recognized that all components appear in both phases to some extent and there will be such a restriction for each component in the system. In vapor-liquid-liquid systems, each component will have three such restrictions, but only two are independent. In general, when all components exist in all phases, the number of restricting relationships due to the distribution phenomenon will be $C(N_p - 1)$, where N_p is the number of phases present.

For the analysis here, the forms in which the restricting relationships are expressed are unimportant. Only the number of such restrictions is important.

13-56 DISTILLATION

ANALYSIS OF ELEMENTS

An *element* is defined as part of a more complex *unit*. The unit may be all or only part of an operation or the entire *process*. Our strategy will be to analyze all elements that appear in a separation process and to determine the number of design variables associated with each. The appropriate elements can then be quickly combined to form the desired units and the various units combined to form the entire process. Of course allowance must be made for the connecting streams (*interstreams*) whose variables are counted twice when elements or units are joined.

The simplest element is a *single homogeneous stream*. The variables necessary to define it are

	N_e^c
Compositions	$C - 1$
Temperature	1
Pressure	1
Flow rate	$\frac{1}{C + 2}$

There are no restricting relationships when the stream is considered only at a point. Henley and Seader (*Equilibrium-Stage Separation Operations in Chemical Engineering*, Wiley, New York, 1981) count all C compositions as variables, but then have to include as a restriction.

$$\sum_i x_i = 1 \quad \text{or} \quad \sum_i y_i = 1 \quad (13-96)$$

A stream divider simply splits a stream into two or more streams of the same composition. Consider Fig. 13-59, which shows the division of the condensed overhead liquid L_c into distillate D and reflux L_{N+1} . The divider is permitted to operate nonadiabatically if desired.

Three mass streams and one possible "energy stream" are involved, so

$$N_e^c = 3(C + 2) + 1 = 3C + 7 \quad (13-97)$$

Each mass stream contributes $C + 2$ variables, but an energy stream has only its rate q as a variable. The independent restrictions are as follows:

	N_e^c
T and P identities between L_{N+1} and D	2
Composition identities between L_{N+1} and D	$C - 1$
Mass balances	C
Energy balance	$\frac{1}{2C + 2}$

The number of design variables for the element is given by

$$N_f^c = N_e^c - N_c^c = (3C + 7) - (2C + 2) = C + 5 \quad (13-98)$$

Specification of the feed stream L_c ($C + 2$ variables), the ratio L_{N+1}/D , the "heat leak" q , and the pressure of either stream leaving the divider uses these design variables and defines one unique operation of the divider.

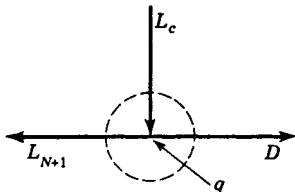


FIG. 13-59 Stream divider.

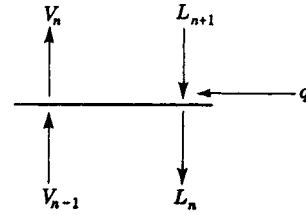


FIG. 13-60 Simple equilibrium stage.

A simple equilibrium stage (no feed or sidestreams) is depicted in Fig. 13-60. Four mass streams and a heat leak (or heat addition) stream provide the following number of variables:

$$N_e^c = 4(C + 2) + 1 = 4C + 9 \quad (13-99)$$

Vapor and liquid streams V_n and L_n , respectively, are in equilibrium with each other by definition and therefore are at the same T and P . These two inherent identities when added to C -component balances, one energy balance, and the C phase distribution relationships give

$$N_e^c = 2C + 3 \quad (13-100)$$

Then

$$N_f^c = N_e^c - N_c^c \quad (13-101)$$

$$= (4C + 9) - (2C + 3) = 2C + 6 \quad (13-102)$$

These design variables can be used as follows:

Specifications	N_f^c
Specification of L_{n+1} stream	$C + 2$
Specification of V_{n-1} stream	$C + 2$
Pressure of either leaving stream	1
Heat leak q	$\frac{1}{2C + 6}$

The results of the analyses for all the various elements commonly encountered in distillation processes are summarized in Table 13-14. Details of the analyses are given by Smith (*Design of Equilibrium Stage Processes*, McGraw-Hill, New York, 1967) and in a somewhat different form by Henley and Seader (op. cit.).

ANALYSIS OF UNITS

A *unit* is defined as a combination of elements and may or may not constitute the entire process. By definition

$$N_v^u = N_r + \sum_i N_i^c \quad (13-103)$$

and

$$N_i^u = N_v^u - N_c^c \quad (13-104)$$

TABLE 13-14 Design Variables N_i^c for Various Elements

Element	N_e^c	N_c^c	N_f^c
Homogeneous stream	$C + 2$	0	$C + 2$
Stream divider	$3C + 7$	$2C + 2$	$C + 5$
Stream mixer	$3C + 7$	$C + 1$	$2C + 6$
Pump	$2C + 5$	$C + 1$	$C + 4$
Heater	$2C + 5$	$C + 1$	$C + 4$
Cooler	$2C + 5$	$C + 1$	$C + 4$
Total condenser	$2C + 5$	$C + 1$	$C + 4$
Total reboiler	$2C + 5$	$C + 1$	$C + 4$
Partial condenser	$3C + 7$	$2C + 3$	$C + 4$
Partial reboiler	$3C + 7$	$2C + 3$	$C + 4$
Simple equilibrium stage	$4C + 9$	$2C + 3$	$2C + 6$
Feed stage	$5C + 11$	$2C + 3$	$3C + 8$
Sidestream stage	$5C + 11$	$3C + 4$	$2C + 7$
Adiabatic equilibrium flash	$3C + 6$	$2C + 3$	$C + 3$
Nonadiabatic equilibrium flash	$3C + 7$	$2C + 3$	$C + 4$

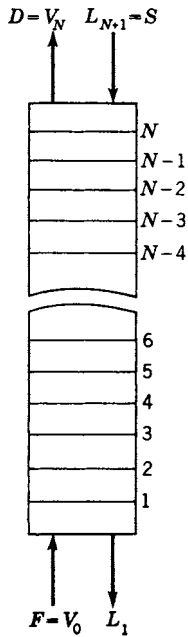


FIG. 13-61 Simple absorption column.

where N_c^u refers to *new* restricting relationships (identities) that may arise when elements are combined. Here N_c^u does not include any of the restrictions considered in calculating the N_i^e 's for the various elements. It includes only the stream identities that exist in each interstream between two elements. The interstream variables ($C + 2$) were counted in each of the two elements when their respective N_i^e 's were calculated. Therefore, $C + 2$ new restricting relationships must be counted for each interstream in the combination of elements to prevent redundancy.

The simple absorber column shown in Fig. 13-61 is analyzed here to illustrate the procedure. This unit consists of a series of simple equilibrium stages of the type in Fig. 13-60. Specification of the number of stages N uses the single repetition variable and

$$N_c^u = N_r + \sum_i N_i^e = 1 + N(2C + 6) \quad (13-105)$$

since $N_i^e = 2C + 6$ for a simple equilibrium stage in Table 13-14. There are $2(N - 1)$ interstreams, and therefore $2(N - 1)(C + 2)$ new identities (not previously counted) come into existence when elements are combined. Subtraction of these restrictions from N_c^u gives N_i^u , the design variables that must be specified.

$$N_i^u = N_c^u - N_c^r = N_r + \sum_i N_i^e - N_c^r \quad (13-106)$$

$$= [1 + N(2C + 6)] - 2[(N - 1)(C + 2)] \quad (13-107)$$

$$= 2C + 2N + 5 \quad (13-108)$$

These might be used as follows:

Specifications	N_i^u
Two feed streams	$2C + 4$
Number of stages N	1
Pressure of either stream leaving each stage	N
Heat leak for each stage	N
	$\frac{2C + 2N + 5}{}$

A more complex unit is shown in Fig. 13-62, which is a schematic diagram of a distillation column with one feed, a total condenser, and

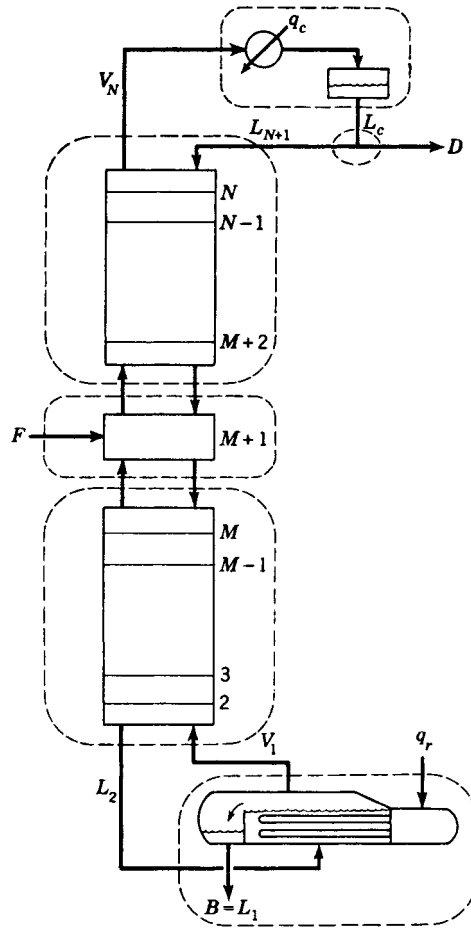


FIG. 13-62 Distillation column with one feed, a total condenser, and a partial reboiler.

a partial reboiler. Dotted lines encircle the six connected elements (or units) that constitute the distillation operation. The variables N_c^u that must be considered in the analysis of the entire process are just the sum of the N_i^e 's for these six elements since here $N_r = 0$. Using Table 13-14, we get the following:

Element (or unit)	$N_c^u = \sum_i N_i^e$
Total condenser	$C + 4$
Reflux divider	$C + 5$
$N - (M + 1)$ equilibrium stages	$2C + 2(N - M - 1) + 5$
Feed stage	$3C + 8$
$M - 1$ equilibrium stages	$2C + 2(M - 1) + 5$
Partial reboiler	$C + 4$
	$\frac{10C + 2N + 27}{}$

Here, the two units of $N - (M + 1)$ and $M - 1$ stages are treated just as elements. Nine interstreams are created by the combination of elements, so

$$N_c^u = 9(C + 2) = 9C + 18 \quad (13-109)$$

The number of design variables is

$$N_i^u = C + 2N + 9N_c^u = (10C + 2N + 27) - (9C + 18) \quad (13-110)$$

$$= C + 2N + 9 \quad (13-111)$$

13-58 DISTILLATION

One set of specifications that is particularly convenient for computer solutions is the following:

Specifications	N_i^u
Pressure of either stream leaving each stage (including reboiler)	N
Pressure of stream leaving condenser	1
Pressure of either stream leaving reflux divider	1
Heat leak for each stage (excluding reboiler)	$N - 1$
Heat leak for reflux divider	1
Feed stream	$C + 2$
Reflux temperature	1
Total number of stages N	1
Number of stages below feed M	1
Distillate rate D/F	1
Reflux ratio L_{N+1}/D	1
	$C + 2N + 9$

Other specifications often used in place of one or more of the last four listed are the fractional recovery of one component in either D or B and/or the composition of one component in either D or B .

OTHER UNITS AND COMPLEX PROCESSES

In Table 13-15, the number of design variables is summarized for several distillation-type separation operations, most of which are shown

TABLE 13-15 Design Variables N_i^u for Separation Units

Unit	N_i^u ^a
Distillation (partial reboiler-total condenser)	$C + 2N + 9$
Distillation (partial reboiler-partial condenser)	$C + 2N + 6$
Absorption	$2C + 2N + 5$
Rectification (partial condenser)	$C + 2N + 3$
Stripping	$2C + 2N + 5$
Reboiled stripping (partial reboiler)	$C + 2N + 3$
Reboiled absorption (partial reboiler)	$2C + 2N + 6$
Refluxed stripping (total condenser)	$2C + 2N + 9$
Extractive distillation (partial reboiler-total condenser)	$2C + 2N + 12$

^a N includes reboiler, but not condenser.

in Fig. 13-2. For columns not shown in Figs. 13-1 or 13-2 that involve additional feeds and/or sidestreams, add $C + 3$ degrees of freedom for each additional feed ($C + 2$ to define the feed and 1 to designate the feed stage) and 2 degrees of freedom for each sidestream (1 for the sidestream flow rate and 1 to designate the sidestream-stage location). Any number of elements or units can be combined to form complex processes. No new rules beyond those developed earlier are necessary for the analysis. Further examples are given in Henley and Seader (op. cit.). An alternative method for determining the degrees of freedom for equipment and processes is given by Pham [*Chem. Eng. Sci.*, **49**, 2507 (1994)].

DISTILLATION SYSTEMS

Distillation systems for the separation of nonazeotropic mixtures are discussed in this subsection. Many of the results extend also to azeotropic mixtures when the desired splits do not attempt to break azeotropes or cross a distillation boundary.

Whenever we desire to separate a mixture into multiple products, various combinatorial possibilities of column arrangements are feasible and the optimal (usually the least expensive) column configurations are sought. For example, there are at least two possible ways of separating a ternary mixture of components A, B, and C into pure-product streams (where A is the most volatile and C the least volatile component):

1. *Direct split*, where component A is separated from BC first (A/BC split) and then mixture BC is distilled to separate B from C
2. *Indirect split*, where C is removed first (AB/C) and then mixture AB is distilled

The difference in energy required for these splits can be assessed by simply comparing the total minimum vapor flows (summed over all the columns) for each column sequence. Example calculations were performed for a mixture with relative volatilities $\alpha_A = 4$, $\alpha_B = 2$, and $\alpha_C = 1$ containing 90 percent of A, 5 percent of B, and 5 percent of C in the feed stream. The indirect split requires 58 percent more energy than the direct split, assuming that columns are connected by a liquid stream in both cases. Moreover, the system using more energy requires bigger heat exchangers and larger column diameters, which increase the capital investment costs. Therefore, the direct split configuration would clearly be a better choice in this case.

One of the most important factors that determines the column configuration is the formulation (or goals) of the separation task with respect to the total flow sheet. Although a mixture may consist of C components, it does not mean that all C products are necessary. The components contained in streams recycled into the process (e.g., unreacted reactants recycled to the reactor) usually do not have to be separated from each other. Also separation of streams that are later mixed (blended) should be avoided, if possible. The separation system needs to be optimized together with the entire plant, either simultaneously or in a hierarchical approach, as described by Douglas (*The Conceptual Design of Chemical Processes*, McGraw-Hill, New York, 1988).

Heuristic methods have been widely used for synthesis of distillation sequences to avoid lengthy calculations. Many heuristics are intuitive, e.g., "Remove corrosive components first," "Remove most plentiful

components first," or "Remove the lightest component first." Since heuristics are just rules of thumb, they sometimes conflict with one another and may provide wrong answers even if they are not in conflict among themselves [Malone, Glinos, Marques, and Douglas, *AIChE J.*, **31**, 683 (1985)]. More exact, algorithmic synthesis methods and cost optimization should be used in practice. The total energy of separation has been identified as the major component of the total separation system cost and energy-saving distillation schemes for light hydrocarbons with high levels of flexibility and operability, were discussed by Petterson and Wells [*Chem. Engng.*, **84**, (20), 78, 1977]. Tedder and Rudd presented a three-part paper [*AIChE J.*, **24**, 303 (1978)], where they compared eight distillation systems for the separation of ternary mixtures and determined the regions of economic optimality (with respect to feed compositions and relative volatilities). They proposed several heuristics to compare various configurations. They evaluated several rank order functions that allow for comparison of various configurations without detailed cost calculations. Interestingly, one of the rank order functions used successfully to compare various systems was the total minimum vapor flow. Minimum vapor flow will also be used to compare various distillation systems presented here. Finally, in the third part of their paper, Tedder and Rudd proposed a design method for various column networks.

In other approaches, Gomez-Munoz and Seader [*Comp. & Chem. Eng.*, **9**, 311 (1985)] proposed an optimization algorithm based on maximum thermodynamic efficiency. However, Smith and Linhoff [*Chem. Eng. Res. Des.*, **66**, 195 (1988)] pointed out the importance of a simultaneous design of the separation network and the rest of the process. They developed a pinch method based on the temperature-heat duty diagram to accomplish this task. Nishida, Stephanopoulos, and Westerberg [*AIChE J.*, **27**, 321 (1981)] presented a comprehensive review of process synthesis, including distillation. Westerberg [*Comp. & Chem. Eng.*, **9**, 421 (1985)] discussed methods for synthesis of distillation systems that include sharp splits, nonsharp splits, thermal linking, and heat integration. More recently, Agrawal [*AIChE J.*, **49**, 379 (2003)] presented a method for systematic generation of distillation configurations, including conventional and complex columns—a detailed discussion of these systems is given below. Sorting through the alternatives and selecting the low-cost systems can be quite tedious and are best done with computer-aided optimization strategies such as those proposed by Caballero and Grossmann [*Ind. Eng. Chem. Res.*, **40**, 2260 (2001)].

POSSIBLE CONFIGURATIONS OF DISTILLATION COLUMNS

This subsection describes how to generate the feasible combinatorial possibilities of distillation column configurations for separation of mixtures that do not form azeotropes. Components are named A, B, C, D, . . . and they are listed in the order of decreasing volatility (or increasing boiling temperature). We limit our considerations to splits where the most volatile (lightest) component and the least volatile (heaviest) component do not distribute between the top and bottom product. For simplicity, we consider only separations where final products are relatively pure components. Systems containing simultaneously simple and complex distillation columns are considered. Simple columns are the conventional columns with one feed stream and two product streams; complex columns have multiple feeds and/or multiple product streams.

The combinatorial possibilities for separating a three-component mixture ABC into two product streams in which the most volatile component and the least volatile component do not distribute between the top and bottom product are

1. A/BC—Top product A is separated from bottom product BC.
2. AB/BC—Component B distributes between both product streams.
3. AB/C—Top product AB is separated from bottoms C.

These separations are also frequently referred to as splits; sharp splits (none of the components distribute) in cases (1) and (3), and a non-sharp split in case (2). When we add binary separations, the column configuration corresponding to split (1) is known as the direct split; the column configuration corresponding to split (2) is called the prefractionator system, and configuration (3) is called the indirect split (see Fig. 13-63). In the prefractionator system the binary columns separating components AB and BC may be stacked together, forming one column with three products A, B, and C as indicated by the dashed envelope in Fig. 13-63b. These systems are called the *basic column configurations*. Basic column configurations are configurations in which the types of interconnecting streams are not defined. The arrows on the flow sheets symbolize the net material flow, but the types of streams connecting the columns (liquid, vapor, two-phase, multiple streams) are not specified. Reboilers and condensers are deliberately not shown in Fig. 13-63, because for some types of interconnecting streams they are not necessary.

Symbolic-network representations of these separation systems, called *state-task networks* (STNs), are shown in Fig. 13-64. In this representation, the states (feeds, intermediate mixtures, and products) are represented by the nodes (ABC, AB, BC, A, B, C) in the network, and the tasks (separations) are depicted as lines (1, 2, . . . , 6) connecting the nodes, where arrows denote the net flow of material. This STN representation was used by Sargent to represent distillation systems [*Comp. & Chem. Eng.*, **22**, 31 (1998)] and has been widely used ever since. Originally STNs were introduced by Kondili, Pan-

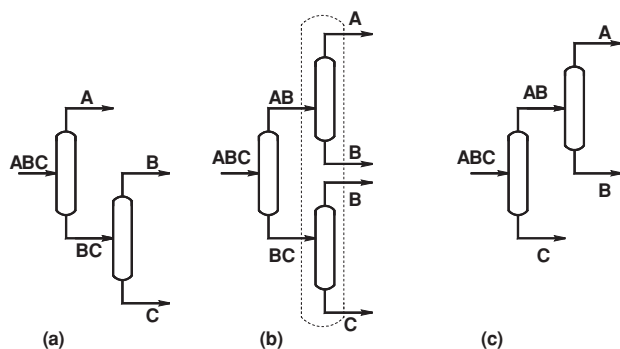


FIG. 13-63 Basic column configurations. (a) Direct split. (b) Prefractionator system. (c) Indirect split.

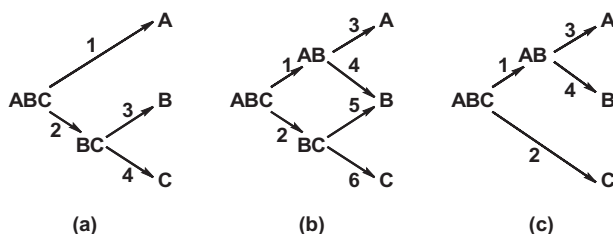


FIG. 13-64 State-task networks. (a) Direct split. (b) Prefractionator system. (c) Indirect split.

telides, and Sargent [*Comp. & Chem. Eng.*, **17**, 211 (1993)] for representing batch processes.

Interconnecting streams may be liquids, vapors, or two-phase mixtures. The total energy of separation can be minimized for the direct split if the two columns have a liquid connection; for the indirect split it is minimized if the columns have a vapor connection, and for the prefractionator system if the top connection is vapor and the bottom connection is liquid. See Fidkowski and Krolikowski [*AIChE J.*, **33**, 643 (1987); **36**, 1275 (1990)].

A complete direct split configuration, including reboilers and condensers, is shown in Fig. 13-65a. The numbers used to represent the column sections in this figure correspond to the numbers used to represent the tasks in the STN (Fig. 13-64a). By eliminating the reboiler from the first column in Fig. 13-65a and supplying the boil-up from the second column, we obtain the side rectifier arrangement, shown in Fig. 13-65b. An alternative side rectifier arrangement is seen more clearly in Fig. 13-65c, where the stripping section of the binary BC column (section 4) has been moved and lumped with the first column. Note that all these three configurations can be represented by one state-task network, shown in Fig. 13-64a. In each configuration in Fig. 13-65, feed ABC is separated in section 1 to get component A and in section 2 to get mixture BC. Then mixture BC is further separated in section 3 to give component B and in section 4 to produce C. Therefore, all these three systems are topologically equivalent to the same basic column configuration represented by the STN in Fig. 13-64a and the column arrangement in Fig. 13-63a. However, if we take into account reboilers and condensers, we see that only the two side rectifier configurations (Fig. 13-65b and c) are topologically equivalent. Side stripper configurations can be obtained from the indirect split in an analogous way (Fig. 13-66a, b, and c).

By eliminating the reboiler and condenser in the prefractionator column in Fig. 13-67a (the column containing sections 1 and 2) we obtain a *thermally coupled system*, also known as a Petlyuk system, shown in Fig. 13-67b [Petlyuk, Platonov, and Slavinskii, *Int. Chem. Eng.*, **5**, 555 (1965)]. Side stripper, side rectifier, and Petlyuk systems can also be built as divided wall columns, as explained in detail in the subsection below on thermally coupled systems.

There are many other possible ternary column systems that have different interconnecting streams between the columns. For example, if we eliminate only the reboiler (or only the condenser) from the prefractionator column in Fig. 13-67a, we obtain a partially thermally coupled system [Agrawal and Fidkowski, *AIChE J.*, **45**, 485 (1999), U.S. Patent 5,970,742]. In other instances, one may significantly increase the thermodynamic efficiency of the direct split and the indirect split if a portion of the interconnecting stream is vaporized and fed to the second column below the liquid connection [Agrawal and Fidkowski, *Ind. Eng. Chem. Res.*, **38**, 2065 (1999)].

There are six possible types of splits for a quaternary mixture. The ternary mixtures resulting from these splits may be separated in one of the three possible ternary splits, as described above. Table 13-16 summarizes the resulting number of possible basic column configurations. This number does not account for the various possible types of interconnecting streams.

This method of generating various column configurations [Fidkowski, *AIChE J.*, **52**, 2098 (2006)] is very similar to the methods

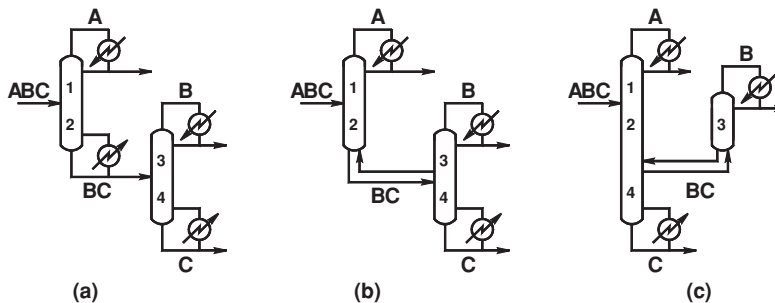


FIG. 13-65 (a) Direct split configuration. (b), (c) Side rectifier configurations.

used previously for conventional systems; see, e.g., Rathore, Van Wormer, and Powers [*AIChE J.*, **20**, 491 (1974); **20**, 940 (1974)]. The only difference is that in addition to sharp splits, the nonsharp splits are included here, which leads to unconventional systems. Similar methods were proposed by Rong et al. [Rong, Kraslawski, and Turunen, *Ind. Eng. Chem. Res.*, **42**, 1204 (2003)] to generate all the possible quaternary thermally coupled configurations.

The basic column configurations for all 22 quaternary distillation systems are shown in Fig. 13-68. Five of these configurations consist of only sharp splits; hence each species appears in only one product stream. Seventeen of the configurations have at least one nonsharp split, which results in each distributing component appearing in product streams from two different locations. Again, the interconnecting streams could be liquid, vapor, two-phase, or two-way liquid and vapor, as in thermally linked columns. There might also be several alternatives for column stacking, which increases the number of possible configurations even further. Subsequently, one can analyze possible splits for a five-component mixture, etc. These splits create quaternary and ternary products that can be further separated by one of the column configurations discussed above.

THERMALLY COUPLED SYSTEMS AND DIVIDING WALL COLUMNS

In recent years there has been significant interest in thermally coupled systems and dividing wall columns for ternary mixtures. In this subsection we discuss such column arrangements, their energy requirements, design and optimization methods, controllability and operability, experimental and industrial experience, and extension to more than three components.

Two columns are thermally coupled if a vapor (liquid) stream is sent from the first column to the second column and then a return liquid (vapor) stream is implemented between the same locations. These

streams, when introduced at the top or bottom of a column, provide (at least partial) reflux or boil-up to this column.

The development of thermally coupled systems started with attempts to find energy-saving schemes for the separation of ternary mixtures into three products. One of the first industrial applications was the side rectifier configuration for air separation. The side stripper configuration followed naturally. By combining the two we obtain the fully thermally coupled system of Petlyuk, Platonov, and Slavinskii [*Int. Chem. Eng.*, **5**, 555 (1965)]; see Fig. 13-67*b*. It consists of the prefractionator which accepts the ternary feed stream followed by the main column that produces the products (product column).

The dividing wall column was invented as a way of producing three pure products from a single column [Monro, U.S. Patent 2,134,882 (1933); Wright, U.S. Patent 2,471,134 (1949)]. In some cases it is possible to achieve high purity of the intermediate component in the sidestream of a distillation column. This is possible when the sidestream is withdrawn above the feed as a liquid or below the feed as a vapor and when relative volatilities of components differ significantly. In many applications, however, a sidestream is contaminated to an appreciable extent by either the light or the heavy component. For example, if a sidestream is withdrawn from the rectifying section, it must contain not only the intermediate component but also some of the most volatile component. This contamination problem can be eliminated by adding a dividing wall that prevents the most volatile component (and the heaviest component) from entering the zone where the intermediate component is withdrawn; see Fig. 13-69.

The dividing wall column is topologically equivalent to the fully thermally coupled system (Fig. 13-67*b*). The prefractionator and the main product column are built in one shell, separated by a dividing wall (Fig. 13-69*c*). Similarly, the side rectifier (Fig. 13-65*c*) and side stripper (Fig. 13-66*c*) configurations can be built in one shell as dividing wall columns [Agrawal, *Ind. Eng. Chem. Res.*, **40**, 4258 (2001)]. The corresponding dividing wall columns are shown in Fig. 13-69*a*

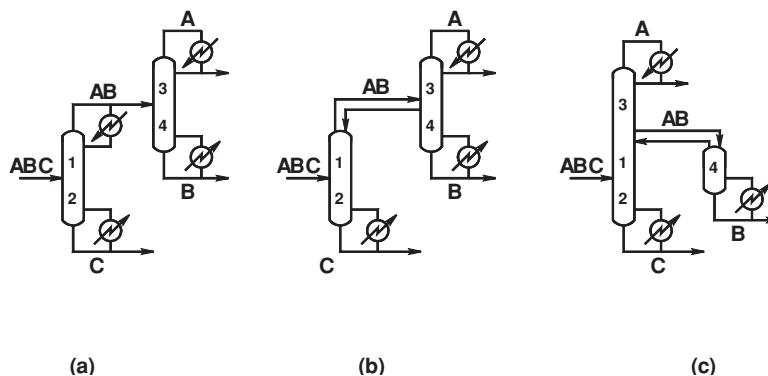


FIG. 13-66 (a) Indirect split configuration. (b), (c) Side stripper configurations.

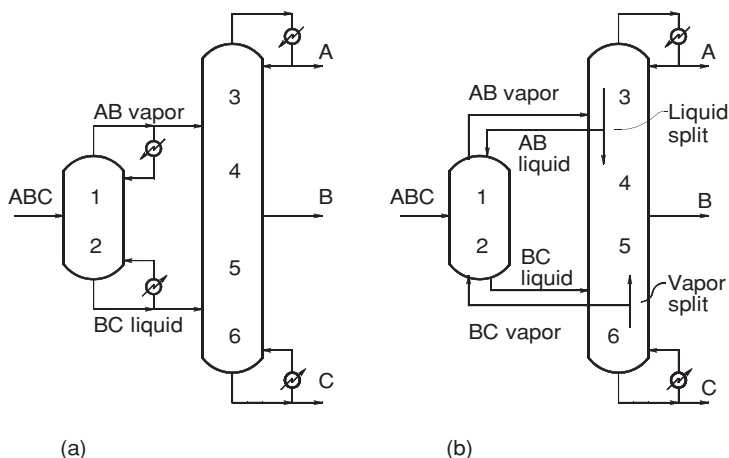


FIG. 13-67 (a) Prefractionator system. (b) Thermally coupled system.

and *b*, respectively. The corresponding sections in the thermally coupled systems and the dividing wall columns have exactly the same numbers and perform exactly the same separation tasks, indicating that the column arrangements are topologically equivalent.

Various design, simulation, and evaluation methods have been developed for the distillation systems shown in Figs. 13-65 to 13-67. These include those by Stupin and Lockhart [*Chem. Eng. Prog.*, **68**

(10), 71 (1972)]; Fidkowski and Krolikowski [*AIChE J.*, **32**, 537 (1986)]; Nikolaidis and Malone [*Ind. Eng. Chem. Res.*, **27**, 811, (1988)]; Rudd [Distillation Supplement to the Chemical Engineer, S14, (1992)]; Triantafyllou and Smith [*Trans. Inst. Chem. Eng.*, **70**, Part A, 118 (1992)]; Finn [*Gas Sep. Purif.*, **10**, 169 (1996)]; Annakou and Mizsey [*Ind. Eng. Chem. Eng.*, **35**, 1877 (1996)]; Hernandez and Jimenez [*Comp. & Chem. Eng.*, **23**, 1005 (1999)]; Dunnebier and Pantelides [*Ind. Eng. Chem. Res.*, **38**, 162 (1999)]; Watzdorf, Bausa, and Marquardt [*AIChE J.*, **45**, 1615 (1999)]; Kim [*J. Chem. Eng. Japan*, **34**, 236 (2001)]. The fully thermally coupled system uses less energy than any other ternary column configuration [Fidkowski and Krolikowski, *AIChE J.*, **33**, 643–653 (1987)]. The energy savings may be on the order of 30 to 50 percent, depending on the feed composition and volatilities of the components. Similar energy savings are possible in partially thermally coupled columns, where only one connection (top or bottom) between the columns is thermally coupled and the other is just a single liquid or vapor stream together with an associated condenser or reboiler, respectively [Agrawal and Fidkowski, *AIChE J.*, **45**, 485 (1999)]. Fidkowski and Krolikowski [*AIChE J.*, **32**, 537 (1986)]

TABLE 13-16 Number of Basic Column Configurations for Separation of a Four-Component Mixture

Split	Distillate/bottoms	Number of configurations
1	A/BCD	3
2	AB/BCD	3
3	AB/CD	1
4	ABC/BCD	$3 \times 3 = 9$
5	ABC/CD	3
6	ABC/D	3
	Total	22

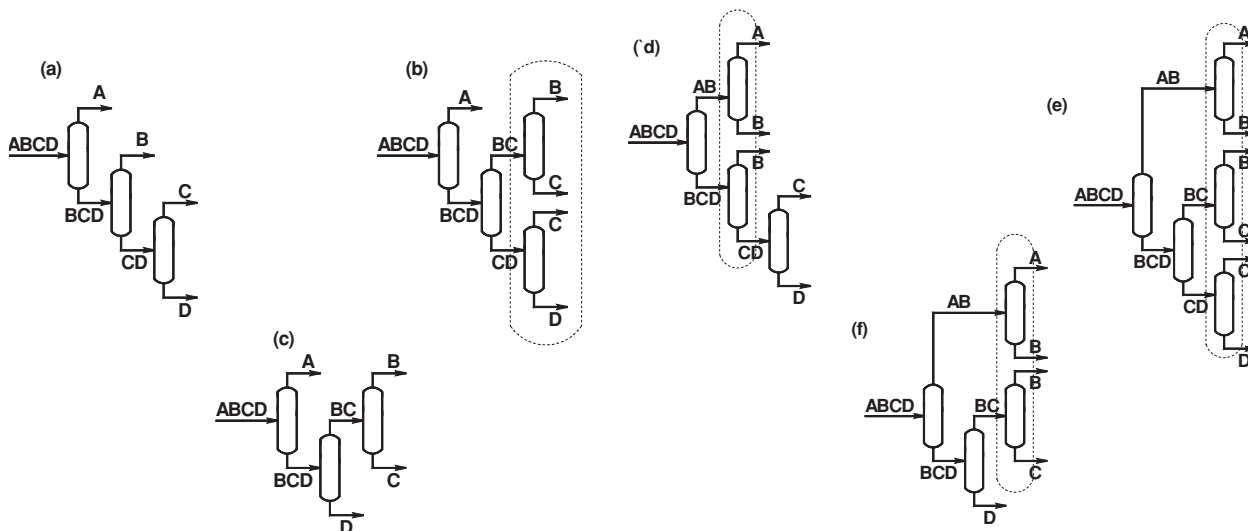


FIG. 13-68 Basic column configurations for separation of a four-component mixture.

13-62 DISTILLATION

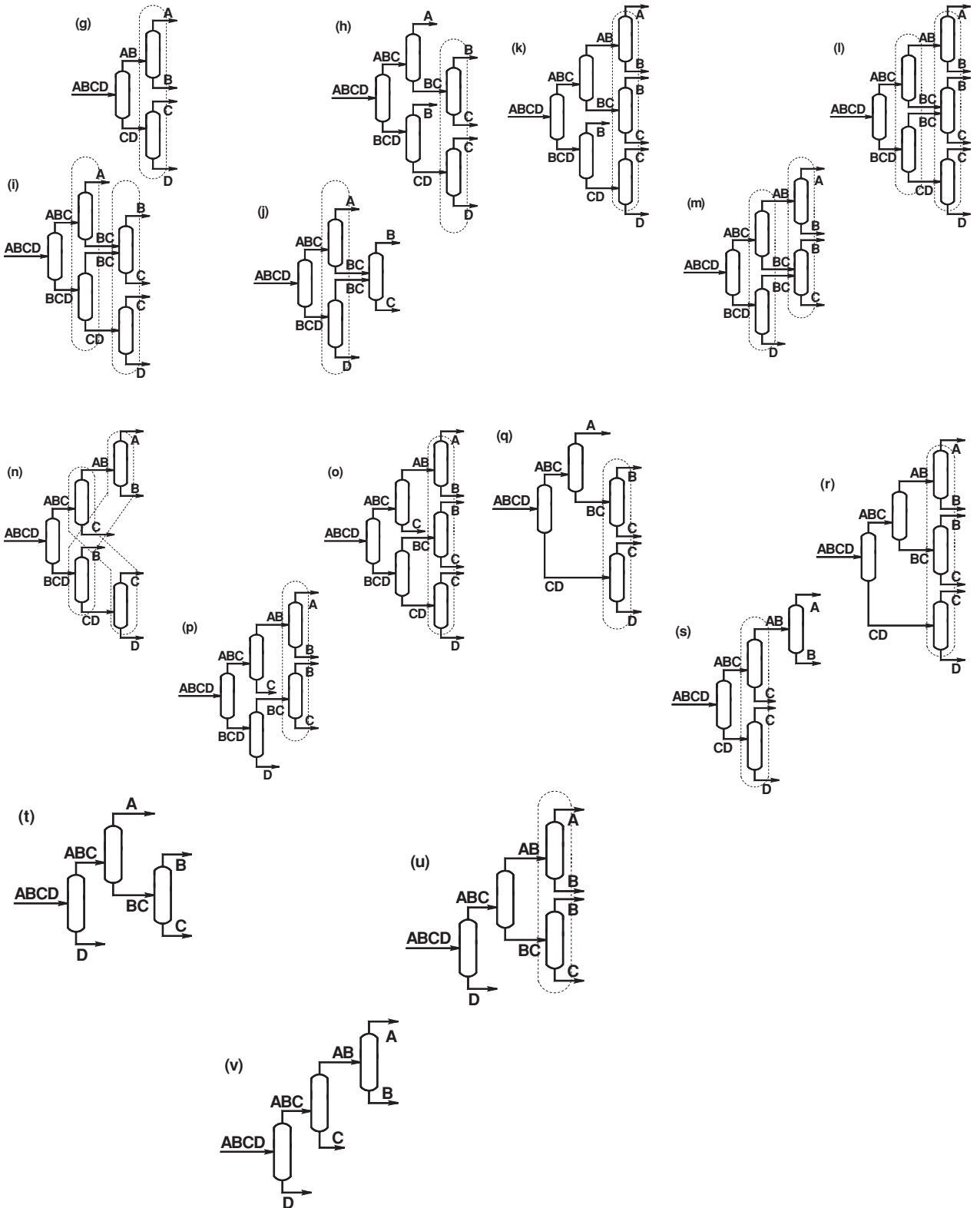


FIG. 13-68 (Continued)

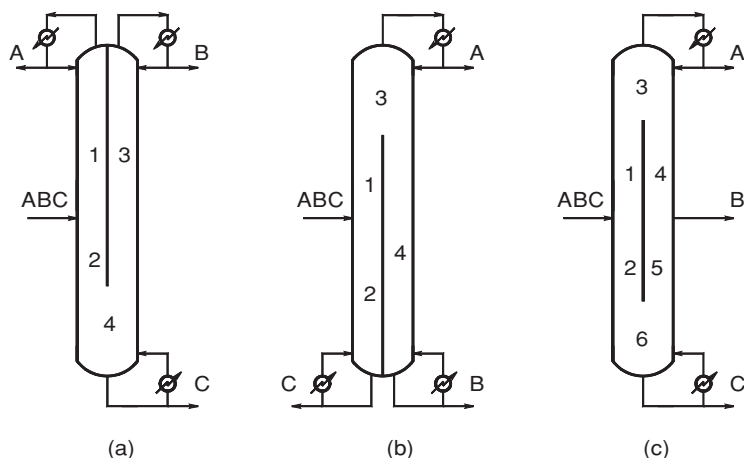


FIG. 13-69 Dividing wall columns equivalent to (a) side rectifier configuration, (b) side stripper configuration, (c) thermally coupled system.

solved analytically the optimization problem for the minimum vapor boil-up rate from the reboiler in the main column for the fully thermally coupled system (shown in Fig. 13-67b), assuming constant molar overflow and constant relative volatilities among the components. The solution depends on the splits of vapor and liquid between the main product column and the prefractionator [or between both sides of the dividing wall (Fig. 13-69c)]. The minimum vapor flow for each column in the system is shown in Fig. 13-70 as a function of β , where the parameter β is defined as the fractional recovery of the distributing component B in the top product of the prefractionator

$$\beta = \frac{V_1 y_B - L_1 x_B}{f_B} \quad (13-112)$$

where V_1 and L_1 are the vapor and liquid flows at the top of the prefractionator (section 1), y_B and x_B are corresponding mole fractions of component B, and f_B denotes the molar flow of component B in the feed stream. The lower line in Fig. 13-70 is the minimum vapor flow in the first column, the prefractionator. At $\beta = 0$ it corresponds to the A/BC split and at $\beta = 1$ to the AB/C split. There is a minimum in the minimum vapor flow in the prefractionator for $\beta = \beta_p$, the so-called transition split; β_p can be calculated as

$$\beta_p = \frac{\alpha_B - \alpha_C}{\alpha_A - \alpha_C} \quad (13-113)$$

where the α 's are relative to any reference component.

The transition split divides direct-type splits from indirect-type splits as discussed by Doherty and Malone (*Conceptual Design of Distillation Systems*, 2001, chaps. 4 and 5); also see Fidkowski, Doherty, and Malone [*AIChE J.*, **39**, 1301 (1993)]. The upper line in Fig. 13-70 is the minimum vapor flow leaving the reboiler of the main column, which also corresponds to the minimum vapor flow for the entire system since all the vapor for the total system is generated by this reboiler. For $\beta = 0$ the minimum vapor flow for the entire thermally coupled system (i.e., main column) becomes equal to the minimum vapor flow for the side rectifier system (i.e., main column of the side-rectifier system; see Fig. 13-65b or c) ($V_{SR})_{\min}$; for $\beta = 1$ it is equal to the minimum vapor flow of the entire side stripper system ($V_{SS})_{\min}$ (which is the sum of the vapor flows from both the reboilers in this system; see Fig. 13-66b or c). Coincidentally, the values of these two minimum vapor flows are always the same: $(V_{SR})_{\min} = (V_{SS})_{\min}$. For $\beta = \beta_R$ the main column is pinched at both feed locations; i.e., the minimum vapor flows for separations A/B and B/C are equal.

The minimum vapor flow for the entire thermally coupled system is flat over a wide range of β : $\beta_p \leq \beta \leq \beta_R$. This is the reason why dividing wall columns usually work well without tight control of the vapor or liquid split between both sides of the partition. The optimally designed fully thermally coupled system should operate with a fractional recovery of B in the top product of the prefractionator placed somewhere between points P and R . The transition split P is located at one end of the optimal section PR , and it is not a recommended design point for normal operation because process disturbances may move the operating point outside the optimal section PR shown in Fig. 13-70.

Although invented long ago, dividing wall columns and fully thermally coupled distillation systems were not implemented in practice until the late 1980s. The major objections concerned controllability and operability. Recently, however, several papers have shown that control of these systems is possible; see, e.g., Hernandez and Jimenez [*Ind. Eng. Chem. Res.*, **38**, 3957 (1999)]; Mutalib, Zeglam, and Smith [*Trans. Inst. Chem. Eng.*, **76**, 319 (1998)]; Halvorsen and Skogestad [*Comp. Chem. Eng.*, **21**, Suppl., S249 (1997)]. A major control problem was attributed to inability to set the vapor split between the main column and prefractionator due to conflicting pressure drop requirements between sections 6 and 2, as well as sections 1 and 3 in Fig. 13-67b. For the BC vapor to flow from section 6 to section 2, the pressure in the main column at the top of section 6 must be higher than the pressure in the prefractionator at the bottom of section 2. But the pressure at the bottom of section 3 in the main column must be lower than the pressure at the top of section 1 in the prefractionator, or else the AB vapor stream will not flow from the prefractionator to the main column. Liquid split control is easier to realize in practice, by using liquid collectors, overflows, or pumps. How much vapor flows straight up the main column and how much vapor splits off to the prefractionator depends on the pressure drops in the middle sections of the main column (sections 4 and 5 in Fig. 13-67b, between the interconnecting streams) and in the prefractionator. These pressure drops depend on the height of these sections, type of packing or stages, and liquid flows. Therefore, these pressure drops cannot be easily controlled in the configuration shown in Fig. 13-67b; moreover, they may even be such that vapor flows in the wrong direction.

Agrawal and Fidkowski [*AIChE J.*, **44**, 2565 (1998)]; U.S. Patent 6,106,674 proposed robustly operable two-column configurations that cleverly overcome this design and control problem. One is shown in Fig. 13-71. This new configuration is topologically equivalent to the original thermally coupled configuration in Fig. 13-67b and retains its energy advantage. In the new Agrawal and Fidkowski configuration, column section 6 is just shifted from the product column to the

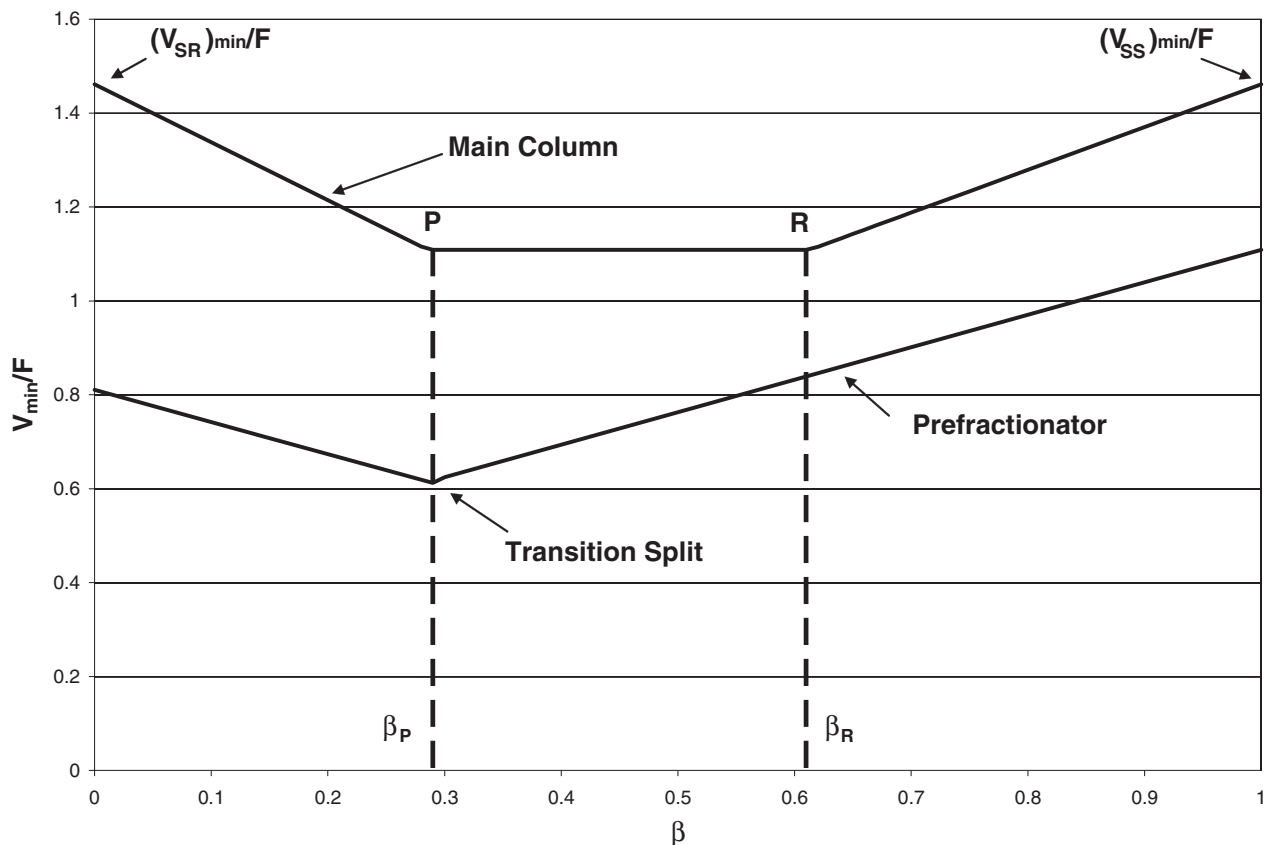


FIG. 13-70 Minimum vapor flows in the thermally coupled system; bottom curve, minimum vapor flow in prefractionator; top curve, minimum vapor flow from the reboiler of the main column (total minimum vapor flow for entire system) for $\alpha_A = 6.25$, $\alpha_B = 2.5$, $\alpha_C = 1.0$ and feed mole fractions $z_A = 0.33$, $z_B = 0.33$, and $z_C = 0.34$.

bottom of prefractionator; thus the two interconnecting vapor streams flow in the *same direction*. The first column (with sections 1, 2, and 6) in Fig. 13-71 operates at a slightly higher pressure than the second column, and the relative flows of the vapor streams can be changed by using a valve on one of them, as shown in the figure. The Agrawal and Fidkowski thermally coupled systems are expected to have higher investment cost than dividing wall columns, and the same investment cost as a Petlyuk thermally coupled system. However, for certain feed compositions and volatilities, the energy optimum in Fig. 13-70 may be narrow (i.e., the interval PR may be short) and dividing wall columns may not be able to operate at the optimum. On the other hand, the Agrawal and Fidkowski configurations are able to operate at the optimum because of better control. Also the Agrawal and Fidkowski configurations are useful in cases where high-purity products (especially B) are required. This is so because the two columns are built in separate shells which may contain more stages in one of the shells than could be accommodated in the corresponding side of the dividing wall column.

Experimental tests of dividing wall columns were carried out by Mutalib, Zeglam, and Smith [*Trans. Inst. Chem. Eng.* **76**, 319 (1998)]. Today there are about 60 dividing wall columns in operation; 42 are owned by BASF (Parkinson, CEP, p. 10, July 2005).

Thermally coupled systems can also be devised for multicomponent mixtures. Sargent and Gaminibandara (*Optimization in Action*, L. W. C. Dixon, ed., Academic Press, London, 1976, p. 267) presented a natural extension of the Petlyuk column sequence to multicomponent systems. Agrawal [*Ind. Eng. Chem. Res.*, **35**, 1059 (1996); *Trans. Inst. Chem. Eng.*, **78**, 454 (2000)] presented a method for generating an even more complete superstructure from which all the

known column configurations (including thermally coupled systems) can be derived. Fidkowski and Agrawal [*AIChE J.*, **47**, 2713 (2001)] presented a method for calculating the minimum vapor flows in multicomponent thermally coupled systems. They analyzed the quaternary fully thermally coupled system in detail (there are many equivalent column configurations, all with the minimum number of column sections, which is 10, as well as one reboiler and one condenser; one of the configurations is shown in Fig. 13-72). They showed that one of the optimum solutions (with the minimum value of the total minimum vapor flow rate from the single reboiler in the system) occurs when the quaternary feed column (far left column in Fig. 13-72) and both ternary columns (the two middle columns in Fig. 13-72) perform transition splits. They also concluded that the optimized quaternary fully coupled system always requires less energy than the five sharp-split conventional systems (where each column performs a sharp split and has one feed, two products, one reboiler, and one condenser). The basic configurations for these five sharp-split systems are shown in Fig. 13-68*a, c, g, t, and v*. Selecting the best thermally coupled column configuration can be tedious without computer-aided tools such as the disjunctive programming approach developed by Caballero and Grossmann [*Ind. Eng. Chem. Res.*, **40**, 2260 (2001)].

All the multicomponent thermally coupled configurations have a corresponding dividing wall column equivalent. Keibel [*Chem. Eng. Technol.*, **10**, 92 (1987)] has shown examples of columns with multiple dividing walls, separating three, four, and six components. Agrawal [*Ind. Eng. Chem. Res.*, **40**, 4258 (2001)] presented several examples of quaternary columns with partitions and multiple reboilers and condensers. One of these examples is shown in Fig. 13-73.

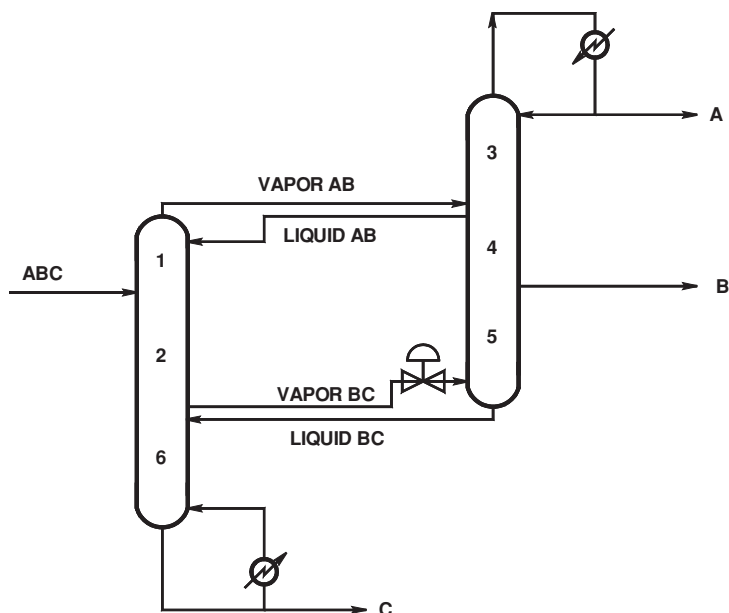


FIG. 13-71 Agrawal and Fidkowski thermally coupled system (topologically equivalent to the Petlyuk system shown in Fig. 13-67b).

THERMODYNAMIC EFFICIENCY

Thermodynamic efficiency can be a useful figure of merit (in place of total cost, or total vapor rate) for comparing alternative column configurations. This is especially true for cryogenic distillations where very low temperatures are needed and highly efficient “cold box” designs are needed for achieving them. Thermodynamic efficiency of thermally coupled and other distillation systems for the separation of ternary mixtures was analyzed by Agrawal and Fidkowski [*Ind. Eng. Chem. Res.*, **37**, 3444 (1998)]. Feed composition regions for column configurations with the highest thermodynamic efficiency are shown in Fig. 13-74. Often, the efficiency of the direct split or the indirect

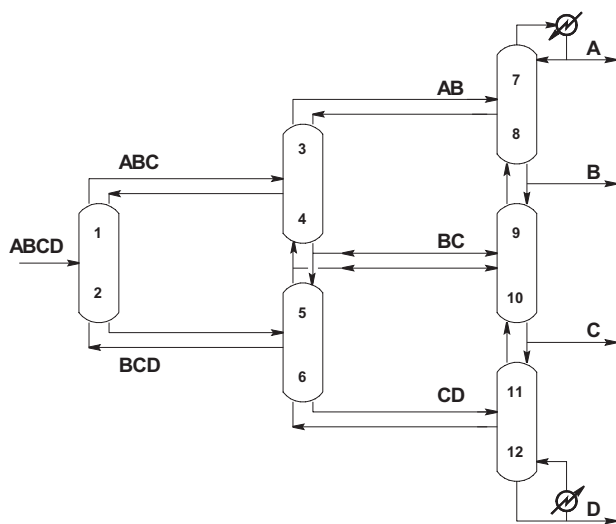


FIG. 13-72 One configuration of a fully thermally coupled system for separation of a quaternary mixture.

split is better than the efficiency of thermally coupled systems. This is primarily due to the ability of these configurations to accept or reject heat at the intermediate boiling or condensing temperatures of the binary submixtures. The fully thermally coupled system can only accept heat at the temperature of the highest-boiling component (boiling point of C) and reject heat at the lowest temperature (condensation temperature of A). This conclusion gave rise to new, more thermodynamically efficient thermally coupled configurations, as discussed by Agrawal and Fidkowski [*Ind. Eng. Chem. Res.*, **38**, 2065 (1999); U.S. Patent 6,116,051].

HEAT INTEGRATION

In this subsection we describe heat pumps, multieffect distillation of binary mixtures, synthesis of multicomponent distillation systems with heat integration, and multieffect distillation for thermally coupled configurations.

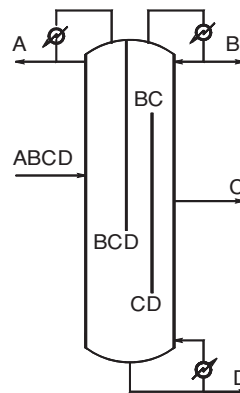


FIG. 13-73 One possible dividing wall column for separation of a quaternary mixture.

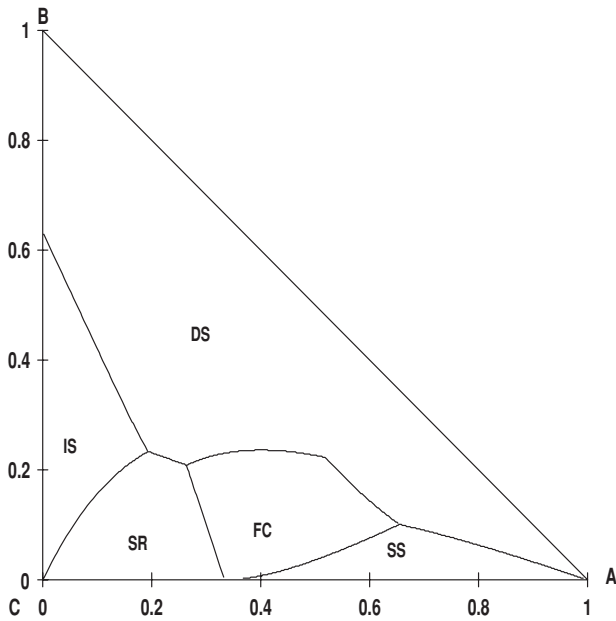


FIG. 13-74 Feed composition regions of column configurations with highest thermodynamic efficiency; DS—direct split, IS—indirect split, SR—side rectifier, SS—side stripper, FC—fully thermally coupled. Example for $\alpha_A = 4.0$, $\alpha_B = 2.0$, and $\alpha_C = 1.0$.

Two columns are heat-integrated when they exchange heat indirectly through a heat exchanger. This is different than in thermally linked configurations, where the heat exchange between columns is direct, through the material stream connecting the columns. The objective of heat integration in distillation systems is to save energy. Heat integration is realized by matching heat sources (usually condensers) with heat sinks (usually reboilers). The other heat exchangers considered for heat integration might be feed preheaters and product coolers. Typical examples of heat integration schemes are heat transfer from a condenser to a reboiler, or heat exchange between a (hot) column feed and a reboiler. If the temperature of the heat source

(condenser) is sufficiently higher than the temperature of the heat sink (reboiler), the opportunity for the match is straightforward. If the condenser temperature is too low, one may increase the condensing pressure or use a heat pump.

For example, the reboiler and condenser from the same column may be heat-integrated by using a heat pump, as discussed by Null [*Chem. Eng. Prog.*, **72**(7), 58 (1976)]. A heat pump may use an external fluid which is vaporized in the condenser, then compressed and condensed in the column reboiler (Fig. 13-75a). Another heat pump (Fig. 13-75b) uses column overhead vapor, which is compressed and condensed in the reboiler and then returned to the top of the column as reflux. A third possibility is to use the column bottoms, which is let down in pressure and vaporized in the condenser, then compressed and fed back to the bottom of the column as boil-up (Fig. 13-75c).

The entire rectifying section can be pressurized, and the heat can be transferred between any desired stages of the rectifying and stripping sections. This is called *secondary reflux and vaporization* (SRV) distillation. It reduces the consumption of both hot and cold utilities, and the sizes of the reboiler and condenser. However, capital cost is increased by additional intermediate heat exchangers; moreover, since the process is more thermodynamically reversible, it requires more stages to achieve the desired separation.

In multiple-column systems, possibilities for heat integration may be created by increasing the pressure in one of the columns, to increase the temperature of the condenser. When the temperature of the condenser becomes higher than the temperature of some other column reboiler, it is possible to heat-integrate these streams via a heat exchanger and reuse the heat rejected from the condenser. However, there are several drawbacks to this procedure. The required heat-transfer area in the integrated exchangers needs to be increased due to smaller temperature differences between the process streams than would normally exist when hot and cold external utilities are used to provide boil-up and condensation. Higher-pressure columns need hotter external heating utilities that are more expensive. Separation in higher-pressure columns is more difficult (because relative volatilities tend to decrease with increasing pressure), and more stages and energy may be required. Finally, higher-pressure column shells and piping may be more expensive, although this is not always certain, since the overall dimensions decrease with pressure.

One of the first industrial applications of heat-integrated distillation was a double column for air separation, developed by Linde in the beginning of the 20th century (Fig. 13-76). Air is compressed (typically to about 6 bar) and fed in the bottom of the high-pressure column. Nitrogen is condensed at the top of the high-pressure column.

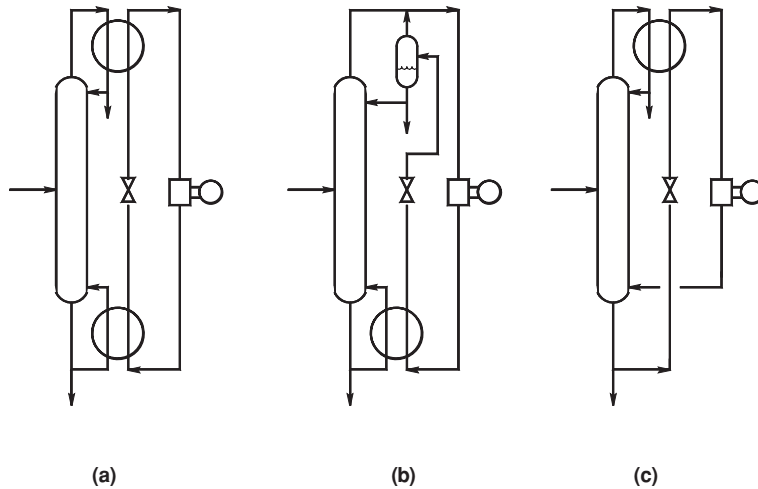


FIG. 13-75 Heat pumps transfer heat from the top to the bottom of the column. (a) External fluid heat pump. (b) Heat pump using column overhead. (c) Heat pump using column bottoms.

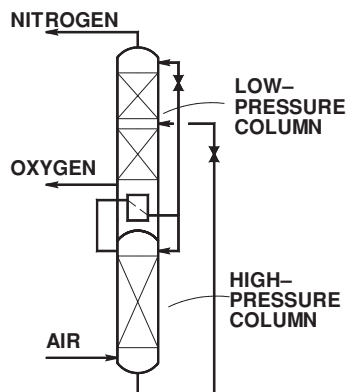


FIG. 13-76 Double-column arrangement for air separation.

The heat of condensation provides boil-up to the low-pressure column, by vaporizing oxygen in the sump located above the nitrogen condenser. Another industrial example of heat integration occurs in the large-scale methanol-water separation in the production of methanol from synthesis gas; see Siirola [*Adv. Chem. Engng.*, **23**, 1 (1996)]. Several alternative designs were evaluated, and the regions of superior cost were developed on volatility-feed composition diagrams. Three heat-integrated designs were better than a single column:

1. *Split feed configuration*, in which the feed is split between the high-pressure and the low-pressure columns

2. *Sloppy first bottom split, second column pressurized*, in which the bottoms from the first column is further separated in the high-pressure column

3. *Sloppy first bottom split, first column pressurized*, in which the bottoms from the first, high-pressure column is further separated in the low-pressure column

These heat-integrated systems were economically advantageous because of the large feed flow rate. The last configuration was built.

Design heuristics and computer-aided design methods for heat-integrated distillation systems have been developed in numerous publications. Wankat [*Ind. Eng. Chem. Res.*, **32**, 894 (1993)] analyzed 23 different multieffect distillation systems obtained by dividing a single column into two or three columns and operating them at various pressures or compositions, to obtain the temperatures necessary for heat integration. He developed heuristics to devise a feasible system. Rathore, Van Wormer, and Powers [*AIChE J.*, **20**, 491 (1974) and **20**, 940 (1974)] presented an algorithmic synthesis method for multicomponent separation systems with energy integration. The five-component separation problem was solved by decomposing it into all the possible sharp splits and then examining all the possible integrations of heat exchangers. Thermally coupled systems, however, were not considered. Umeda, Niida, and Shiriko [*AIChE J.*, **25**, 423 (1979)] published a thermodynamic approach to heat integration in distillation systems based on pinching heat source and heat sink curves on the temperature-heat duty diagram. Linhoff and coworkers (*A User Guide on Process Integration for the Efficient Use of Energy*, Institution of Chemical Engineers, Rugby, U.K., 1982) developed the very successful *pinch technology* approach, commonly used for heat exchanger synthesis and heat integration of entire plants. But, most successfully, Andrecowich and Westerberg [*AIChE J.*, **31**, 1461 (1985)] presented a simple conceptual design approach wherein temperature-enthalpy diagrams are used to select the best column stacking. This design method is the recommended starting point for heat integration studies.

Even thermally coupled systems can be heat-integrated, as discovered by Agrawal [*AIChE J.*, **46**, 2211 (2000)]. To achieve heat integration without compressors, the vapor connections between the columns must be eliminated. This is shown in Fig. 13-77a. The configuration is constructed by extending the prefractionator to a full

column with a reboiler and condenser, and adding sections 3x and 6x (analogous to sections 3 and 6 in the product column). By balancing heat duties, only liquid interconnecting streams remain, and the configuration is still thermodynamically equivalent to the original thermally coupled system (Fig. 13-67b). It is now possible to heat-integrate the columns by pressurizing one of them and allowing heat transfer from the high-pressure condenser to the low-pressure reboiler (Fig. 13-77b). The thermally coupled system and dividing wall column are equally energy-efficient. Therefore, the thermally coupled system with heat integration is even more energy-efficient than the dividing wall column.

There is a significant cost associated with heat integration (e.g., for heat pump compressors, taller columns with more stages, thicker walls of high-pressure equipment, higher cost of high-temperature utilities) which is why such configurations are not widely used. The operational flexibility of a heat-integrated system also becomes more constrained. However, heat-integrated systems can be quite economical for some applications. Typical applications where heat-integrated systems are preferred include

- Cryogenic separation, where very low-temperature cooling utilities do not exist and need to be created, which is very expensive. Therefore, it makes sense to reuse the expensive refrigeration.
- Very large-scale processes, with large feed and product flow rates. Because of the large feed rate, multiple columns may be required to process a given feed anyway. These cases have the potential to save a lot of energy due to heat integration. Also, pressurizing some equipment in these large-scale processes allows for decreased equipment sizes or increased production rate at a fixed equipment size.

IMBALANCED FEEDS

In many practical cases, feed compositions are far from equimolar, with some components present in very small amount (e.g., less than 2 percent). In these cases the top or bottom product flow rate is less than 2 percent of the feed flow rate. The design for imbalanced feeds may include

- Various column diameters
- Intermittent pumping of heavies from the reboiler
- Intermittent firing up a specially devoted column to purify the dirty product made at a small rate
- In a continuous operation an overrefluxed section (to keep the column diameter the same over the height of the column)
- Producing an impure product to be purified later or discarded

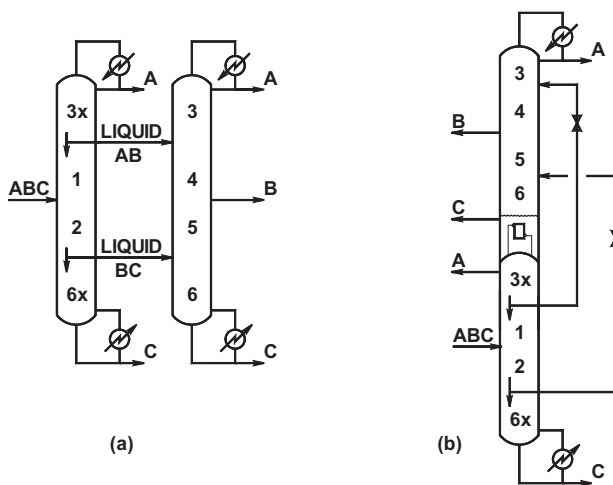


FIG. 13-77 (a) Configuration equivalent to thermally coupled system, but without vapor interconnecting streams. (b) Heat-integrated thermally coupled system.

ENHANCED DISTILLATION

In distillation operations, separation results from differences in vapor- and liquid-phase compositions arising from the partial vaporization of a liquid mixture or the partial condensation of a vapor mixture. The vapor phase becomes enriched in the more volatile components while the liquid phase is depleted of those same components. In many situations, however, the change in composition between the vapor and liquid phases in equilibrium becomes small (so-called pinched condition), and a large number of successive partial vaporizations and partial condensations are required to achieve the desired separation. Alternatively, the vapor and liquid phases may have identical compositions, because of the formation of an azeotrope, and no separation by simple distillation is possible.

Several enhanced distillation-based separation techniques have been developed for close-boiling or low-relative-volatility systems, and for systems exhibiting azeotropic behavior. All these special techniques are ultimately based on the same differences in the vapor and liquid compositions as ordinary distillation; but, in addition, they rely on some additional mechanism to further modify the vapor-liquid behavior of the key components. These enhanced techniques can be classified according to their effect on the relationship between the vapor and liquid compositions:

1. *Azeotropic distillation and pressure-swing distillation.* Methods that cause or exploit azeotrope formation or behavior to alter the boiling characteristics and separability of the mixture.
2. *Extractive distillation and salt distillation.* Methods that primarily modify liquid-phase behavior to alter the relative volatility of the components of the mixture.
3. *Reactive distillation.* Methods that use chemical reaction to modify the composition of the mixture or, alternatively, use existing vapor-liquid differences between reaction products and reactants to enhance the performance of a reaction.

AZEOTROPY

At low to moderate pressure ranges typical of most industrial applications, the fundamental composition relationship between the vapor and liquid phases in equilibrium can be expressed as a function of the total system pressure, the vapor pressure of each pure component, and the liquid-phase activity coefficient of each component i in the mixture:

$$y_i P = x_i \gamma_i P_i^{\text{sat}} \quad (13-114)$$

In systems that exhibit ideal liquid-phase behavior, the activity coefficients γ_i are equal to unity and Eq. (13-114) simplifies to Raoult's law. For nonideal liquid-phase behavior, a system is said to show negative deviations from Raoult's law if $\gamma_i < 1$ and, conversely, positive deviations from Raoult's law if $\gamma_i > 1$. In sufficiently nonideal systems, the deviations may be so large that the temperature-composition phase diagrams exhibit extrema, as shown in Figs. 13-6, 13-7, and 13-8. At such maxima or minima, the equilibrium vapor and liquid compositions are identical. Thus,

$$y_i = x_i \quad \text{for all } i = 1, \dots, c \quad (13-115)$$

and the system is said to form an azeotrope (from the Greek word meaning "to boil unchanged"). Azeotropic systems show a minimum in the T vs. x , y diagram when the deviations from Raoult's law are positive (Fig. 13-6) and a maximum in the T vs. x , y diagram when the deviations from Raoult's law are negative (Fig. 13-7). If, at these two conditions, a single liquid phase is in equilibrium with the vapor phase, the azeotrope is homogeneous. If multiple-liquid-phase behavior is exhibited at the azeotropic condition, the azeotrope is heterogeneous. For heterogeneous azeotropes, the vapor-phase composition is equal to the overall composition of the two (or more) liquid phases (Fig. 13-8). These conditions are consequences of the general definition of an azeotrope in any kind of mixture (i.e., homogeneous, heterogeneous, reactive, or in any combination), which is as follows: An *azeotropic state* is one in which mass transfer occurs between phases in a closed system while the composition of each phase remains constant, but not necessarily equal (see Prigogine and Defay, *Chemical Thermodynamics*, 4th ed., Longmans Green and Co., London, 1967;

Rowlinson, *Liquids and Liquid Mixtures*, 2d ed., Butterworths, London, 1969; Doherty and Malone, *Conceptual Design of Distillation Systems*, McGraw-Hill, 2001, chaps. 5, 8, App. C).

Mixtures with only small deviations from Raoult's law (i.e., ideal or nearly ideal mixtures) may form an azeotrope but only if the saturated vapor pressure curves of the two pure components cross each other (such a point is called a Bancroft point). In such a situation, the azeotrope occurs at the temperature and pressure where the curves cross, and perhaps also in the vicinity close to the Bancroft point [e.g., cyclohexane (n.b.p. 80.7°C) and benzene (n.b.p. 80.1°C) form an almost ideal mixture yet exhibit a minimum-boiling azeotrope with roughly equal proportions of each component]. As the boiling point difference between the components increases, the composition of the azeotrope shifts closer to one of the pure components (toward the lower-boiling pure component for minimum-boiling azeotropes, and toward the higher-boiling pure component for maximum-boiling azeotropes). For example, the minimum-boiling azeotrope between methanol (n.b.p. 64.5°C) and toluene (n.b.p. 110.6°C) occurs at ≈ 90 mol % methanol, and the minimum-boiling azeotrope between methyl acetate (n.b.p. 56.9°C) and water (n.b.p. 100°C) occurs at ≈ 90 mol % methyl acetate. Mixtures of components whose boiling points differ by more than about 50°C generally do not exhibit azeotropes distinguishable from the pure components even if large deviations from Raoult's law are present. As a qualitative guide to liquid-phase activity coefficient behavior, Robbins [*Chem. Eng. Prog.*, **76**(10), 58 (1980)] developed a matrix of chemical families, shown in Table 13-17, which indicates expected deviations from Raoult's law.

The formation of two liquid phases within some boiling temperature range is generally an indication that the system will also exhibit a minimum-boiling azeotrope, since two liquid phases may form when deviations from Raoult's law are large and positive. The fact that immiscibility does occur, however, does not guarantee that the azeotrope will be heterogeneous since the azeotropic composition may not necessarily fall within the composition range of the two-liquid phase region, as is the case for the methyl acetate–water and tetrahydrofuran–water systems. Since strong positive deviations from Raoult's law are required for liquid-liquid phase splitting, maximum-boiling azeotropes ($\gamma_i < 1$) are never heterogeneous.

Additional general information on the thermodynamics of phase equilibria and azeotropy is available in Malesinski (*Azeotropy and Other Theoretical Problems of Vapour-Liquid Equilibrium*, Interscience, London, 1965), Swietoslawski (*Azeotropy and Polyazeotropy*, Pergamon, London, 1963), Van Winkle (*Distillation*, McGraw-Hill, New York, 1967), Smith and Van Ness (*Introduction to Chemical Engineering Thermodynamics*, McGraw-Hill, New York, 1975), Wiziak [*Chem. Eng. Sci.*, **38**, 969 (1983)], and Walas (*Phase Equilibria in Chemical Engineering*, Butterworths, Boston, 1985). Horsley (*Azeotropic Data-III*, American Chemical Society, Washington, 1983) compiled an extensive list of experimental azeotropic boiling point and composition data for binary and some multicomponent mixtures. Another source for azeotropic data and activity coefficient model parameters is the multivolume *Vapor-Liquid Equilibrium Data Collection* (DECHEMA, Frankfurt, 1977), a compendium of published experimental VLE data. Most of the data have been tested for thermodynamic consistency and have been fitted to the Wilson, UNIQUAC, Van Laar, Margules, and NRTL equations. An extensive two-volume compilation of azeotropic data for 18,800 systems involving 1700 compounds, entitled *Azeotropic Data* by Gmehling et al., was published in 1994 by VCH Publishers, Deerfield Beach, Fla. A computational method for determining the temperatures and compositions of all homogeneous azeotropes of a multicomponent mixture, from liquid-phase activity coefficient correlations, by a differential arc-length homotopy continuation method is given by Fidkowski, Malone, and Doherty [*Computers and Chem. Eng.*, **17**, 1141 (1993)]. The method was generalized to determine all homogeneous and heterogeneous azeotropes by Wasylkiewicz, Doherty, and Malone [*Ind. Eng. Chem. Res.*, **38**, 4901 (1999)].

RESIDUE CURVE MAPS AND DISTILLATION REGION DIAGRAMS

The simplest form of distillation involves boiling a multicomponent liquid mixture in an open evaporation from a single-stage batch still. As the liquid is boiled, the vapor generated is removed from contact with the liquid as soon as it is formed. Because the vapor is richer in the more volatile components than the liquid, the composition and boiling temperature of the liquid remaining in the still change continuously over time and move progressively toward less volatile compositions and higher temperatures until the last drop is vaporized. This last composition may be a pure-component species, or a maximum-boiling azeotrope, and it may depend on the initial composition of the mixture charged to the still.

The trajectory of liquid compositions starting from some initial composition is called a residue curve, the collection of all such curves for a given mixture is called a residue curve map. Arrows are usually added to these curves, pointing in the direction of increasing time, which corresponds to increasing temperature, and decreasing volatility. If the liquid is well mixed and the vaporization is slow, such that the escaping vapor is in phase equilibrium with the residual liquid, then residue curve maps contain exactly the same information as the corresponding phase equilibrium diagram for the mixture, but they represent it in a way that is much more useful for understanding distillation systems. Composition changes taking place in simple batch distillation can be described mathematically by the following ordinary differential equation

$$\frac{dx_i}{d\xi} = x_i - y_i \quad \text{for all } i = 1, \dots, c \quad (13-116)$$

where ξ is a dimensionless nonlinear time scale. Normally, y_i and x_i are related by an isobaric VLE model. Integrating these equations forward in time leads to the less volatile final compositions; integrating them backward in time leads to the more volatile compositions which would produce a residue curve passing through the specified initial composition. A *residue curve map* (RCM) is generated by varying the initial composition and integrating Eq. (13-116) both forward and backward in time [Doherty and Perkins, *Chem. Eng. Sci.*, **33**, 281

(1978); Doherty and Malone, op. cit., chap. 5]. Unlike a binary y - x plot, relative-volatility information is not represented on an RCM. Therefore, it is difficult to determine the ease of separation from a residue curve map alone. The steady states of Eq. (13-116) are the constant-composition trajectories corresponding to $dx_i/d\xi = 0$ for all $i = 1, \dots, c$. The steady states therefore correspond to *all* the pure components and *all* the azeotropes in the mixture.

Residue curve maps can be constructed for mixtures of any number of components, but can be pictured graphically only up to four components. For binary mixtures, a T vs. x , y diagram or a y - x diagram suffices; the system is simple enough that vapor-phase information can be included with liquid-phase information without confusion. For ternary mixtures, liquid-phase compositions are plotted on a triangular diagram, similar to that used in liquid-liquid extraction. Four-component systems can be plotted in a three-dimensional tetrahedron. The vertices of the triangular diagram or tetrahedron represent the pure components. Any binary, ternary, and quaternary azeotropes are placed at the appropriate compositions on the edges and/or interior of the triangle and tetrahedron.

The simplest form of ternary RCM, as exemplified for the ideal normal-paraffin system of pentane-hexane-heptane, is illustrated in Fig. 13-78a, using a right-triangle diagram. Maps for all other nonazeotropic ternary mixtures are qualitatively similar. Each of the infinite number of possible residue curves originates at the pentane vertex, travels toward and then away from the hexane vertex, and terminates at the heptane vertex. The family of all residue curves that originate at one composition and terminate at another composition defines a *distillation region*. Systems that do not involve azeotropes have only one region—the entire composition space. However, for many systems, not all residue curves originate or terminate at the same two compositions. Such systems will have more than one distillation region. The residue curve that divides two distillation regions in which adjacent residue curves originate from different compositions or terminate at different compositions is called a *simple batch distillation boundary* or *separatrix*. Distillation boundaries are related to the existence of azeotropes. In the composition space for a binary system, the distillation boundary is a point (the azeotropic composition). For three components, the distillation boundary is a curve; for four components, the boundary is a surface; and so on.

TABLE 13-17 Solute-Solvent Group Interactions

Solute class	Group	Solvent class											
		1	2	3	4	5	6	7	8	9	10	11	12
H-donor													
1	Phenol	0	0	-	0	-	-	-	-	-	-	-	-
2	Acid, thiol	0	0	-	0	-	-	0	0	0	0	-	-
3	Alcohol, water	-	-	0	+	+	0	-	-	-	-	-	-
4	Active-H on multihalo paraffin	0	0	+	0	-	-	-	-	-	-	0	-
H-acceptor													
5	Ketone, amide with no H on N, sulfone, phosphine oxide	-	-	+	-	0	+	-	-	-	+	-	-
6	Tertamine	-	-	0	-	+	0	-	-	0	+	0	0
7	Secamine	-	0	-	-	+	+	0	0	0	0	0	-
8	Priamine, ammonia, amide with 2H on N	-	0	-	-	+	+	0	0	-	+	-	-
9	Ether, oxide, sulfoxide	-	0	+	-	+	0	0	-	0	+	0	-
10	Ester, aldehyde, carbonate, phosphate, nitrate, nitrite, nitrile, intramolecular bonding, e.g., <i>o</i> -nitro phenol	-	0	+	-	+	+	0	-	-	0	-	-
11	Aromatic, olefin, halogen aromatic, multihalo paraffin without active H, monohalo paraffin	+	+	+	0	+	0	0	-	0	+	0	0
Non-H-bonding													
12	Paraffin, carbon disulfide	+	+	+	+	+	0	+	+	+	+	0	0

SOURCE: Robbins, L. A., *Chem. Eng. Prog.*, **76**(10), 58-61 (1980), by permission.

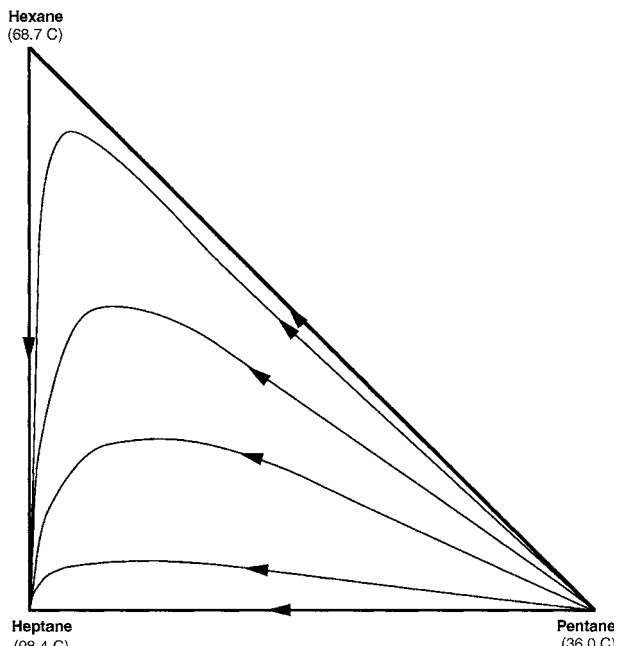


FIG. 13-78a Residue curve map: Nonazeotropic pentane-hexane-heptane system at 1 atm.

The boundaries of the composition diagram (e.g., the edges of a composition triangle) also form region boundaries since they divide physically realistic residue curves with positive compositions from unrealistic curves with negative compositions. All pure components and azeotropes in a system lie on region boundaries. Within each region, the most volatile composition on the boundary (either a pure

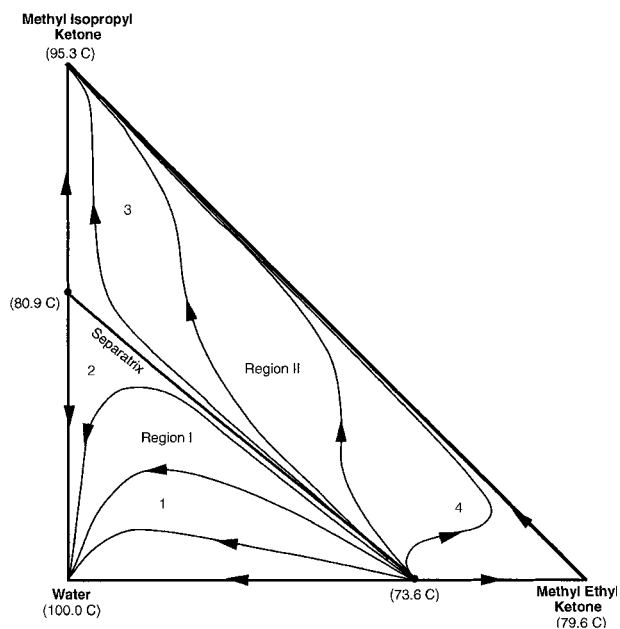


FIG. 13-78b Residue curve map: MEK-MIPK-water system at 1 atm containing two minimum-boiling binary azeotropes.

component or a minimum-boiling azeotrope, and the origin of all residue curves in that region) is called the *low-boiling node*. The least-volatile composition on the boundary (either a pure component or a maximum-boiling azeotrope, and the terminus of all residue curves in that region) is called the *high-boiling node*. All other pure components and azeotropes are called *intermediate-boiling saddles*. Adjacent regions may share some (but not all) nodes and saddles. Pure components and azeotropes are labeled as nodes and saddles as a result of the boiling points of all the components and azeotropes in a system. If one species is removed, the labeling of all remaining pure components and azeotropes, particularly those that were saddles, may change. Distillation boundaries always originate or terminate at saddle azeotropes, but never at pure component saddles—distillation boundaries can be calculated by using the method proposed by Lucia and Taylor [AIChE J., **52**, 582 (2006)]. Ternary saddle azeotropes are particularly interesting because they are more difficult to detect experimentally (being neither minimum-boiling nor maximum-boiling). However, their presence in a mixture implies the existence of distillation boundaries which may have an important impact on the design of a separation system. The first ternary saddle azeotrope to be detected experimentally was reported by Ewell and Welch [Ind. Eng. Chem., **37**, 1224 (1945)], and a particularly comprehensive set of experimental residue curves were reported by Bushmakina and Kish [J. Appl. Chem. USSR (Engl. Trans.), **30**, 205 (1957)] for a ternary mixture with a ternary saddle azeotrope (reproduced as fig. 5.9 in Doherty and Malone, op. cit.). More ternary saddle azeotropes are reported in Gmehling et al. (Azeotropic Data, 1994).

Both methylethylketone (MEK) and methylisopropylketone (MIPK) form minimum-boiling homogeneous azeotropes with water (Fig. 13-78b). In this ternary system, a distillation boundary connects the binary azeotropes and divides the RCM into two distillation regions, I and II. The high-boiling node of region I is pure water, while the low-boiling node is the MEK-water azeotrope. In region II, the high- and low-boiling nodes are MIPK and the MEK-water azeotrope, respectively. These two regions, however, have a different number of saddles—one in region I and two in region II. This leads to region I having three sides, while region II has four sides. The more complicated cyclohexane-ethanol-water system (Fig. 13-78c) has three boundaries and three regions, all of which are four-sided and share the ternary azeotrope as the low-boiling node.

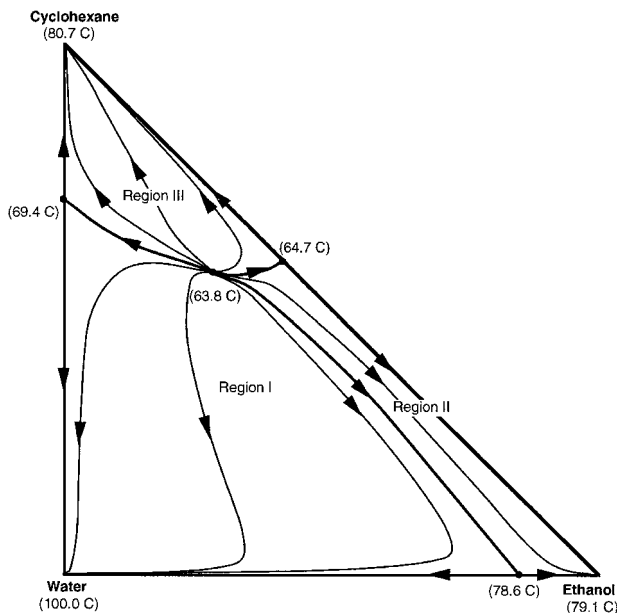


FIG. 13-78c Residue curve map: Ethanol-cyclohexane-water system at 1 atm containing four minimum-boiling azeotropes (three binary and one ternary) and three distillation regions.

The liquid composition profiles in continuous staged or packed distillation columns operating at infinite reflux and boil-up are closely approximated by simple distillation residue curves [Van Dongen and Doherty, *Ind. Eng. Chem. Fundam.*, **24**, 454 (1985)]. Residue curves are also indicative of many aspects of the general behavior of continuous columns operating at more practical reflux ratios. For example, to a first approximation, the stage-to-stage liquid compositions (along with the distillate and bottoms compositions) of a single-feed, two-product, continuous distillation column lie on the same residue curve. Therefore, for systems with distillation boundaries and multiple regions, distillation composition profiles are constrained to lie in specific regions. The precise boundaries of these distillation regions are a function of reflux ratio, but they are closely approximated by the RCM distillation boundaries. If a RCM distillation boundary exists in a system, a corresponding continuous distillation boundary will also exist. Both types of boundaries correspond exactly at all pure components and azeotropes.

Residue curves can be constructed from experimental data or can be calculated by integrating Eq. (13-116) if equation-of-state or activity-coefficient expressions are available (e.g., Wilson binary-interaction parameters, UNIFAC groups). However, considerable information on system behavior can still be deduced from a simple qualitative sketch of the RCM distillation boundaries based only on pure-component and azeotrope boiling point data and approximate azeotrope compositions. Rules for constructing such qualitative *distillation region diagrams* (DRDs) are given by Foucher et al. [*Ind. Eng. Chem. Res.*, **30**, 760, 2364 (1991)]. For ternary systems containing no more than one ternary azeotrope and no more than one binary azeotrope between each pair of components, 125 such DRDs are mathematically possible [Matsuyama and Nishimura, *J. Chem. Eng. Japan*, **10**, 181 (1977); Doherty and Calderola, *Ind. Eng. Chem. Fundam.*, **24**, 474 (1985); Peterson and Partin, *Ind. Eng. Chem. Res.*, **36**, 1799 (1997)], although only a dozen or so represent most systems commonly encountered in practice.

Figure 13-79 illustrates all the 125 possible DRDs for ternary systems [see Peterson and Partin, *Ind. Eng. Chem. Res.*, **36**, 1799 (1997)]. Azeotropes are schematically depicted generally to have equimolar composition, distillation boundaries are shown as straight lines, and the arrows on the distillation boundaries indicate increasing temperature. These DRDs are indexed in Table 13-18 according to a temperature profile sequence of position numbers, defined in a keyed triangular diagram at the bottom of the table, arranged by increasing boiling point. Positions 1, 3, and 5 are the pure components in order of decreasing volatility. Positions 2, 4, and 6 are binary azeotropes at the positions shown in the keyed triangle, and position 7 is the ternary azeotrope. Azeotrope position numbers are deleted from the temperature profile if the corresponding azeotrope is known not to exist. Note that not every conceivable temperature profile corresponds to a thermodynamically consistent system, and such combinations have been excluded from the index. As is evident from the index, some DRDs are consistent with more than one temperature profile. Also some temperature profiles are consistent with more than one DRD. In such cases, the correct diagram for a system must be determined from residue curves obtained from experimental or calculated data.

Schematic DRDs are particularly useful in determining the implications of possibly unknown ternary saddle azeotropes by postulating position 7 at interior positions in the temperature profile. Also note that some combinations of binary azeotropes require the existence of a ternary saddle azeotrope. As an example, consider the system acetone (56.4°C), chloroform (61.2°C), and methanol (64.7°C) at 1-atm pressure. Methanol forms minimum-boiling azeotropes with both acetone (54.6°C) and chloroform (53.5°C), and acetone-chloroform forms a maximum-boiling azeotrope (64.5°C). Experimentally there are no data for maximum- or minimum-boiling ternary azeotropes for this mixture. Assuming no ternary azeotrope, the temperature profile for this system is 461325, which from Table 13-18 is consistent with DRD 040 and DRD 042. However, Table 13-18 also indicates that the pure-component and binary azeotrope data are consistent with three temperature profiles involving a ternary saddle azeotrope, namely, 4671325, 4617325, and 4613725. All three of these temperature profiles correspond to DRD 107. Calculated residue curve trajectories for the acetone-chloroform-methanol system at 1-atm pressure, as

shown in Fig. 13-80, suggest the existence of a ternary saddle azeotrope and DRD 107 as the correct approximation of the distillation regions. Ewell and Welch [*Ind. Eng. Chem.*, **37**, 1224 (1945)] confirmed experimentally such a ternary saddle at 57.5°C.

APPLICATIONS OF RCM AND DRD

Residue curve maps and distillation region diagrams are very powerful tools for understanding all types of batch and continuous distillation operations, particularly when combined with other information such as liquid-liquid binodal curves. Applications include

1. *System visualization.* Location of distillation boundaries, azeotropes, distillation regions, feasible products, and liquid-liquid regions.
2. *Evaluation of laboratory data.* Location and confirmation of saddle ternary azeotropes and a thermodynamic consistency check of data.
3. *Process synthesis.* Concept development, construction of flow sheets for new processes, and redesign or modification of existing process flow sheets.
4. *Process modeling.* Identification of infeasible or problematic column specifications that could cause simulation convergence difficulties or failure, and determination of initial estimates of column parameters including feed-stage location, number of stages in the stripping and enriching sections, reflux ratio, and product compositions.
5. *Control analysis/design.* Analysis of column balances and profiles to aid in control system design and operation.

6. *Process trouble shooting.* Analysis of separation system operation and malfunction, examination of composition profiles, and tracking of trace impurities with implications for corrosion and process specifications.

Material balances for mixing or continuous separation operations are represented graphically on triangular composition diagrams such as residue curve maps or distillation region diagrams by straight lines connecting pertinent compositions. The straight lines are exact representations of the compositions due to the lever rule. Overall flow rates are found by the inverse-lever-arm rule. Distillation material balance lines are governed by two constraints:

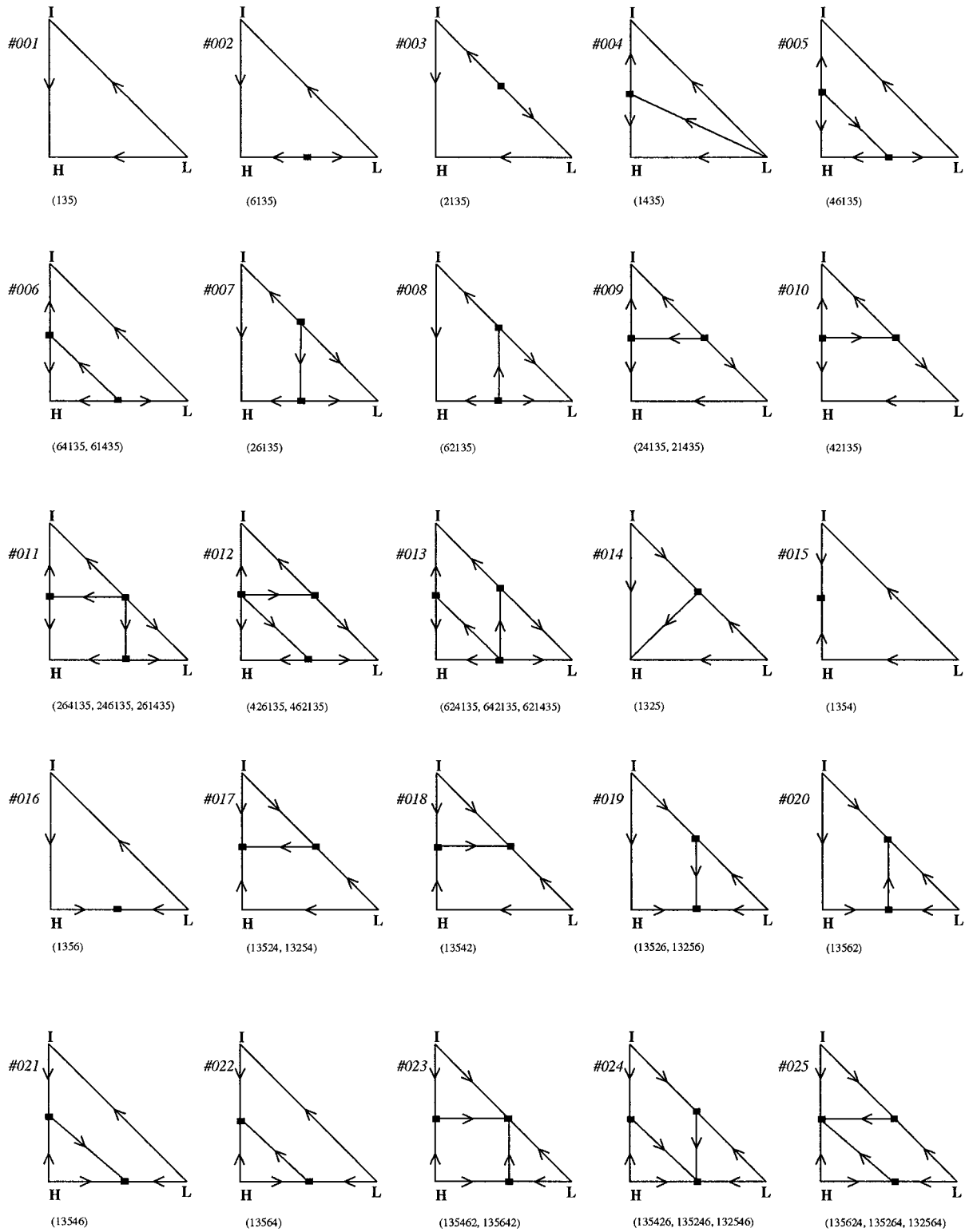
1. The bottoms, distillate, and overall feed compositions must lie on the same straight line.
2. The bottoms and distillate compositions must lie (to a very close approximation) on the same residue curve.

Since residue curves do not cross simple batch distillation boundaries, the distillate and bottoms compositions must be in the same distillation region with the mass balance line intersecting a residue curve in two places. Mass balance lines for mixing and for other separations not involving vapor-liquid equilibria, such as extraction and decantation, are of course not limited by distillation boundaries.

For a given multicomponent mixture, a single-feed, two-product distillation column (simple column) can be designed with sufficient stages, reflux, and material balance control to produce separations ranging from the *direct-split* mode of operation (low-boiling node taken as distillate) to the *indirect-split* mode (high-boiling node taken as bottoms). The bow tie shaped set of reachable product compositions for a simple distillation column is roughly bounded by the (straight) material balance lines connecting the feed composition to the sharpest direct separation and the sharpest indirect separation possible (see Fig. 13-81). A more accurate approximation involves replacing two of the straight-line segments of the bow tie with the residue curve through the feed composition [Stichlmair and Herguijuela, *AIChE J.*, **38**, 1523 (1992)]. The exact shape of the reachable product composition regions involves replacing two of the straight-line segments of the bow tie with a locus of pinch points, as explained by Wahnschafft et al. [*Ind. Eng. Chem. Res.*, **31**, 2345 (1992)] and Fidkowski, Doherty, and Malone [*AIChE J.*, **39**, 1303 (1993)]. Since residue curves are deflected by saddles, it is generally not possible to obtain a saddle product (pure component or azeotrope) from a simple distillation column.

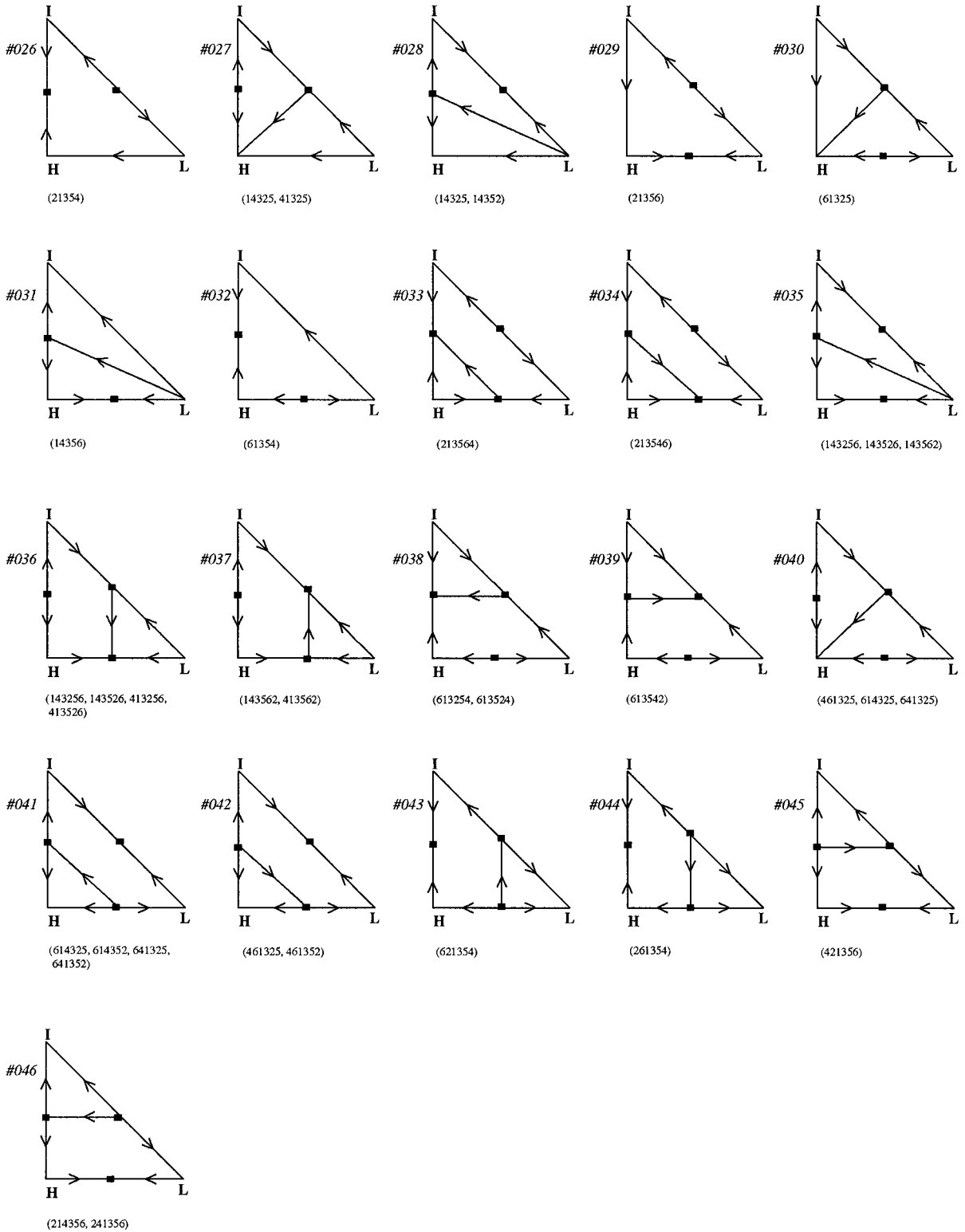
Consider the recovery of MIPK from an MEK-MIPK-water mixture. The approximate bow tie regions of product compositions for three different feeds are shown in Fig 13-81. From feed F3, which is situated in a different distillation region than the desired product, pure MIPK cannot be obtained at all. Feed F2 is more favorable, with the upper edge of the bow tie region along the MEK-MIPK (water-free) face of the composition triangle and part of the lower

13-72 DISTILLATION



(a)

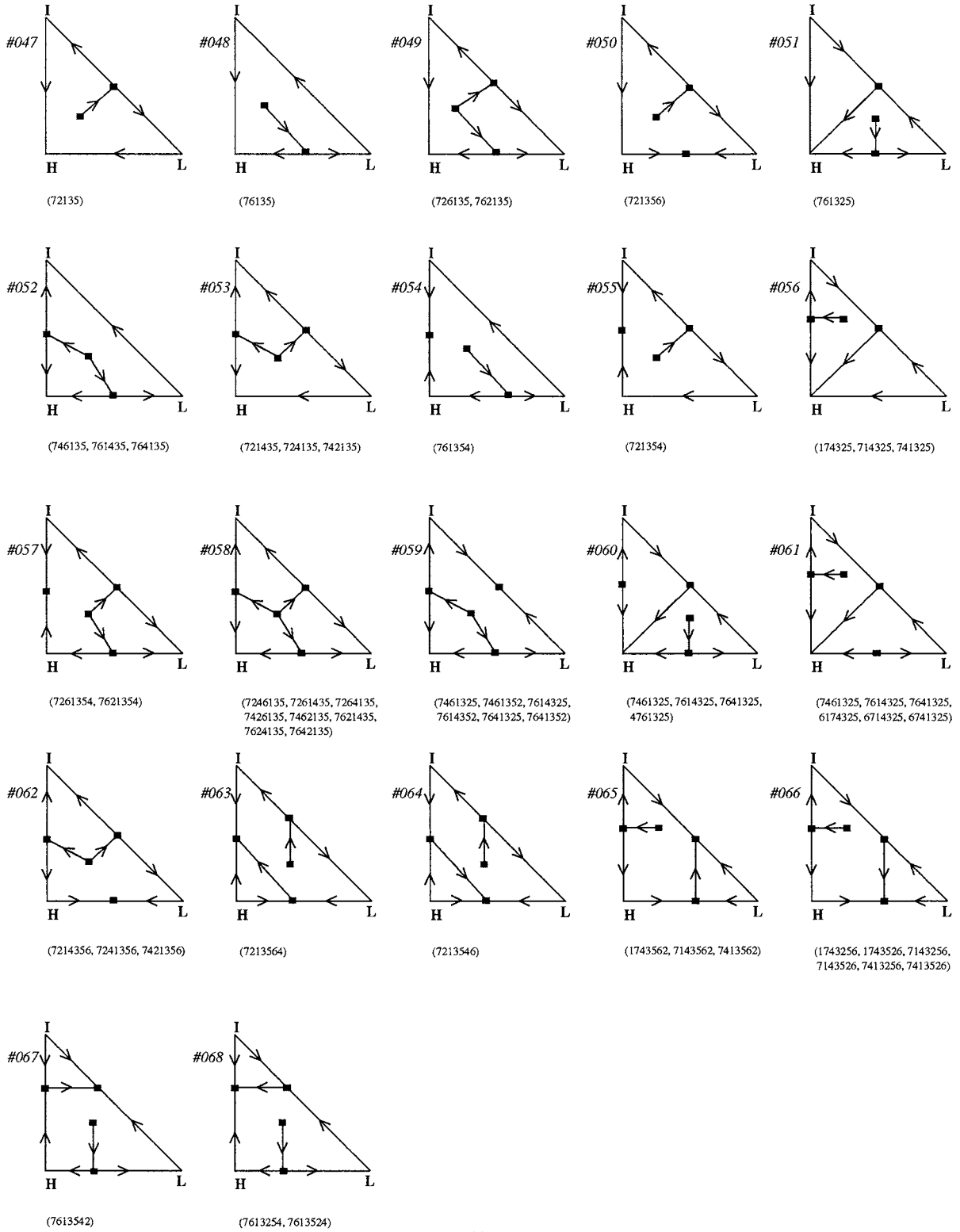
FIG. 13-79 Distillation region diagrams for ternary mixtures.



(b)

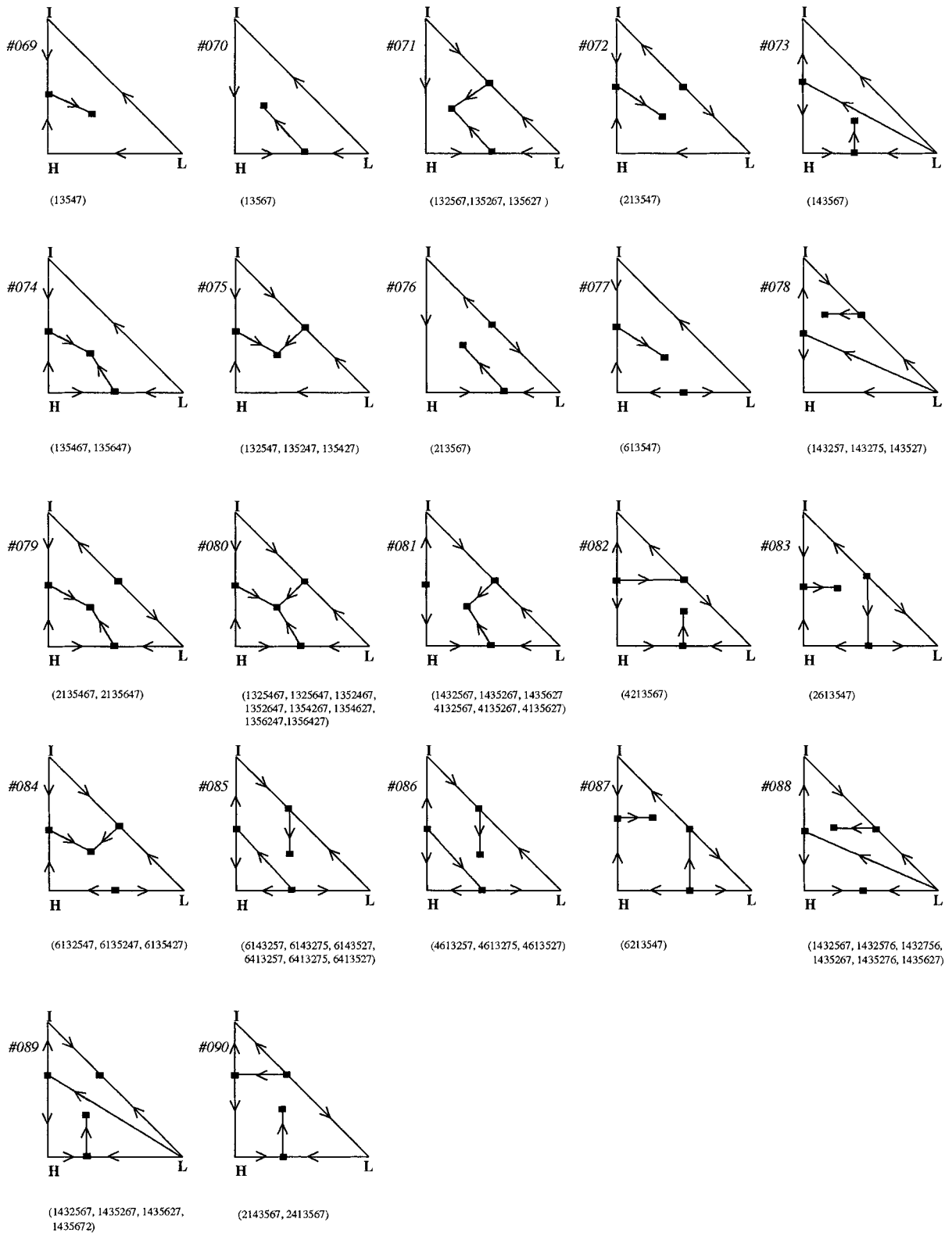
FIG. 13-79 (Continued)

13-74 DISTILLATION



(c)

FIG. 13-79 (Continued)



(d)

FIG. 13-79 (Continued)

13-76 DISTILLATION

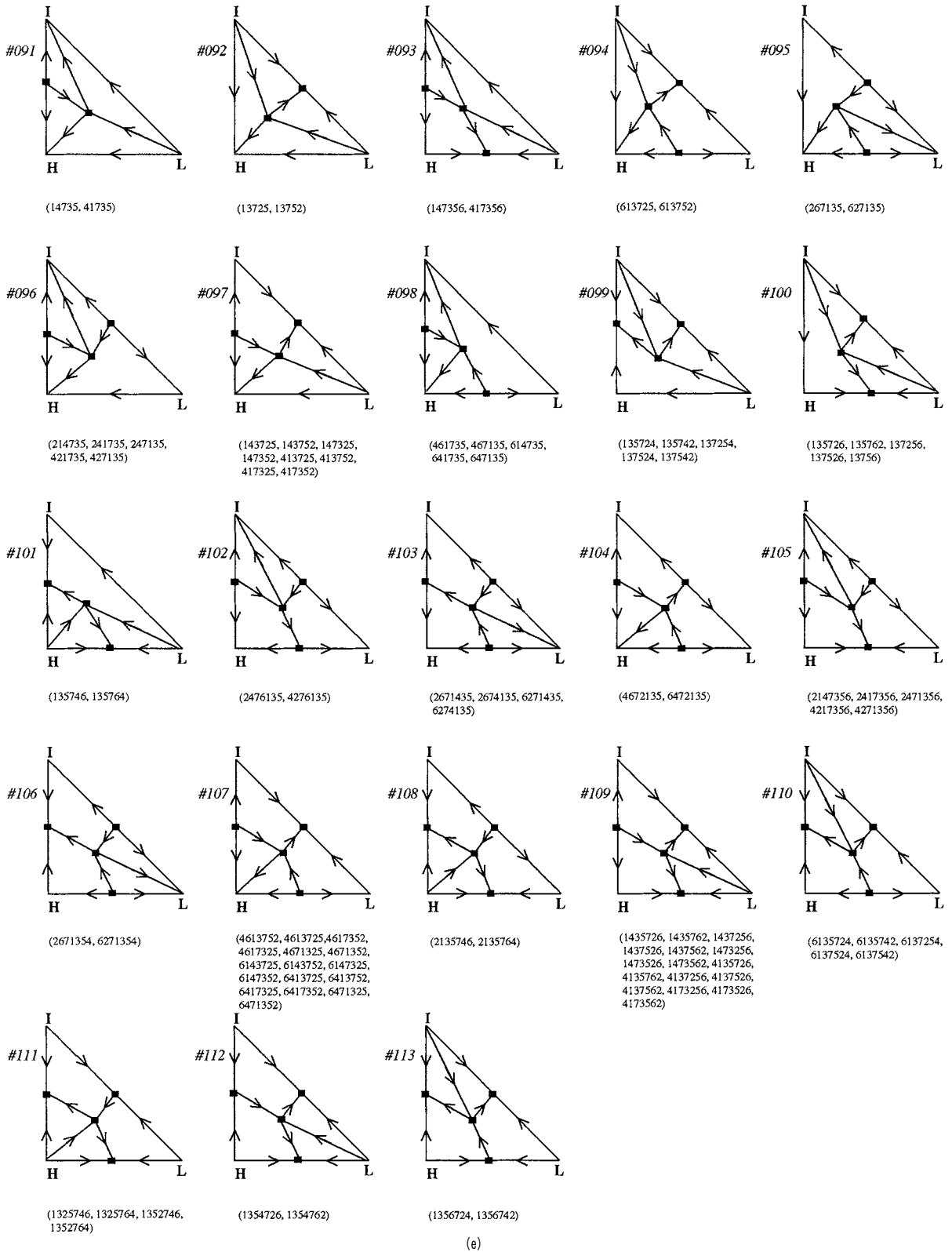


FIG. 13-79 (Continued)

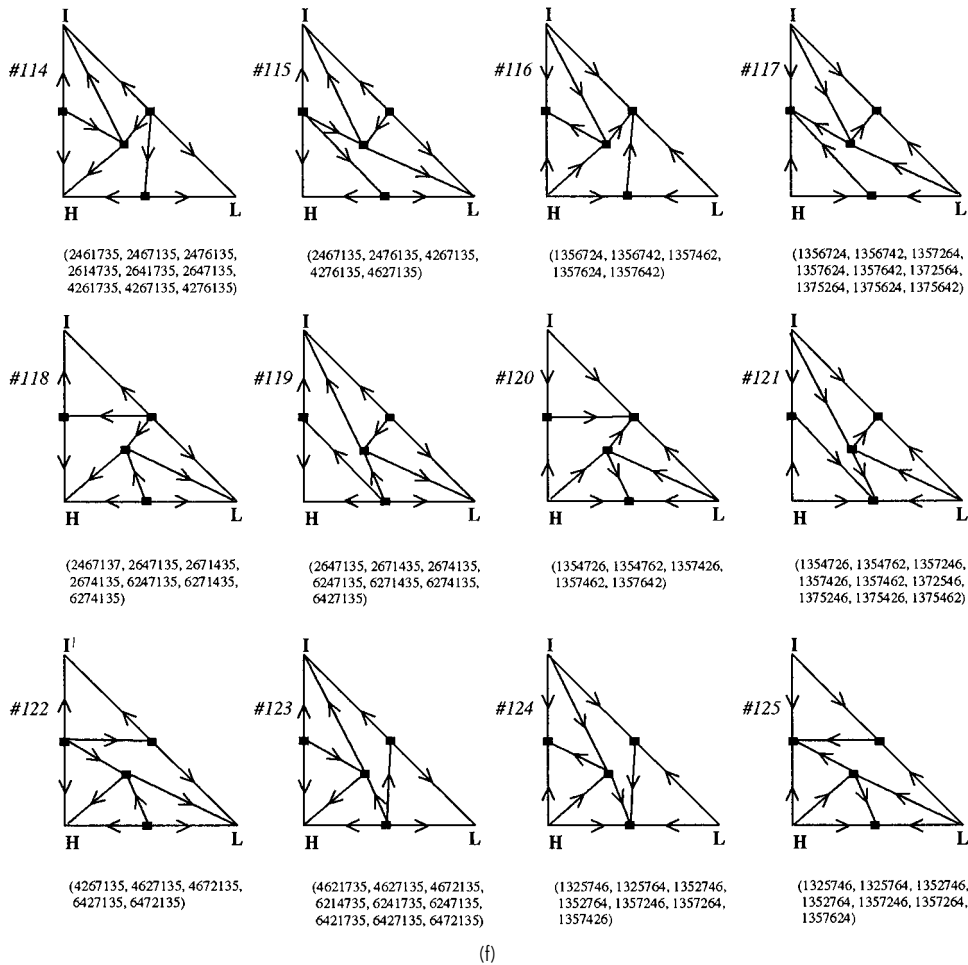


FIG. 13-79 (Continued)

edge along the MEK-water (MIPK-free) face. There are conditions under which both the water in the MIPK bottoms product can be driven to low levels (high-product purity) and MIPK in the distillate can be driven to low levels (high-product recovery), although achieving such an operation depends on having an adequate number of stages and reflux ratio.

Although feed F2 lies in the same distillation region as F1, the bow tie region for feed F2 is significantly different than that for F1, with the upper edge along the water-MIPK (MEK-free) face of the triangle and the lower edge along the distillation boundary. From this feed it is not possible to simultaneously achieve a high-purity MIPK specification while obtaining high MIPK recovery. If the column is operated to get a high purity of MIPK, then the material balance line runs into the distillation boundary. Alternatively, if the column is operated to obtain a high recovery of MIPK (by removing the MEK-water azeotrope as distillate), the material balance requires the bottoms to lie on the water-MIPK face of the triangle.

The number of saddles in a particular distillation region can have significant impact on column profile behavior, process stability, and convergence behavior in process simulation of the system. Referring to the MIPK-MEK-water system in Fig. 13-78b, region I contains one saddle (MIPK-water azeotrope), while region II contains two saddles (pure MEK and the MIPK-water azeotrope). These are three- and four-sided regions, respectively. In a three-sided region, all residue

curves track toward the solitary saddle. However, in a four- (or more) sided region with saddles on either side of a node, some residue curves will tend to track toward one saddle, while others track toward another saddle. For example, residue curve 1 in region I originates from the MEK-water azeotrope low-boiling node and travels first toward the single saddle of the region (MIPK-water azeotrope) before ending at the water high-boiling node. Likewise, residue curve 2 and all other residue curves in region I follow the same general path.

In region II, residue curve 3 originates from the MEK-water azeotrope, travels toward the MIPK-water saddle azeotrope, and ends at pure MIPK. However, residue curve 4 follows a completely different path, traveling toward the pure MEK saddle before ending at pure MIPK. Some multicomponent columns have been designed for operation in four-sided regions with the feed composition adjusted so that both the high-boiling and low-boiling nodes can be obtained simultaneously as products. However, small perturbations in feed composition or reflux can result in feasible operation on many different residue curves that originate and terminate at these product compositions. Multiple steady states and composition profiles that shift dramatically from tracking toward one saddle to the other are possible [Kovach and Seider, *AIChE J.*, **33**, 1300 (1987); Pham, Ryan, and Doherty, *AIChE J.*, **35**, 1585 (1989)]. Consider a column operating in the MIPK-MEK-water diagram. Figure 13-82 shows the composition and temperature profiles for the column operating at three different sets of

13-78 DISTILLATION

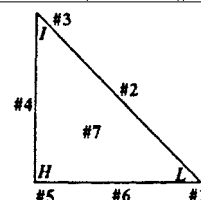
TABLE 13-18 Temperature Profile—DRD # Table*

Temp. Profile	DRD #	Temp. Profile	DRD #	Temp. Profile	DRD #	Temp. Profile	DRD #	Temp. Profile	DRD #	Temp. Profile	DRD #
135	001	137524	099	624135	013	1357462	120	2671435	103	6247135	118
1325	014	137526	100	627135	095		121		119		119
1354	015	137542	099	641325	041		116		118		123
1356	016	137562	100		040	1357624	117	2674135	118	6271354	106
1435	004	143256	035	641352	041		116		119	6271435	118
2135	003		036	641735	098		125		103		103
6135	002	143257	078	642135	013	1357642	120	4132567	081		119
13254	017	143275	078	647135	098		117	4135267	081	6274135	103
13256	019	143526	036	714325	056		116	4135627	081		118
13524	017		035	721354	055	1372546	121	4135726	109		119
13526	019	143527	078	721356	050	1372564	117	4135762	109	6413257	085
13542	018	143562	035	721435	053	1375246	121	4137256	109	6413275	085
13546	021		037	724135	053	1375264	117	4137526	109	6413527	085
13547	069	143567	073	726135	049	1375426	121	4137562	109	6413725	107
13562	020	143725	097	741325	056	1375462	121	4173256	109	6413752	107
13564	022	143752	097	742135	053	1375624	117	4173526	109	6417325	107
13567	070	147325	097	746135	052	1375642	117	4173562	109	6417352	107
13725	092	147352	097	761325	051	1432567	089	4213567	082	6421735	123
13752	092	147356	093	761354	054		088	4217356	105	6427135	122
14325	028	174325	056	761435	052		081	4261735	114		123
027		213546	034	762135	049	1432576	088	4267135	122		119
14352	028	213547	072	764135	052	1432756	088		115	6471325	107
14356	031	213564	033	1325467	080	1435267	081		114	6471352	107
14735	091	213567	076	1325647	080		089	4271356	105	6472135	104
21354	026	214356	046	1325746	111		088	4276135	114		122
21356	029	214735	096		124	1435276	088		102		123
21435	009	241356	046		125	1435627	089		115	6714325	061
24135	009	241735	096	1325764	111		081	4613257	086	6741325	061
26135	007	246135	011		124		088	4613275	086	7143256	066
41325	027	247135	096		125	1435672	089	4613527	086	7143526	066
41735	091	261354	044	1352467	080	1435726	109	4613725	107	7143562	065
42135	010	261435	011	1352647	080	1435762	109	4613752	107	7213546	064
46135	005	264135	011	1352746	125	1437256	109	4617325	107	7213564	063
61325	030	267135	095		111	1437526	109	4617352	107	7214356	062
61354	032	413256	036		124	1437562	109	4621735	123	7241356	062
61435	006	413526	036	1352764	124	1473256	109	4627135	123	7246135	058
62135	008	413562	037		111	1473526	109		115	7261354	057
64135	006	413725	097		125	1473562	109		122	7261435	058
72135	047	413752	097	1354267	080	1743256	066	4671325	107	7264135	058
76135	048	417325	097	1354627	080	1743526	066	4671352	107	7413256	066
132546	024	417352	097	1354726	120	1743562	065	4672135	104	7413526	066
132547	075	417356	093		121	2135467	079		122	7413562	065
132564	025	421356	045		112	2135647	079		123	7421356	062
132567	071	421735	096	1354762	121	2135746	108	4761325	060	7426135	058
135246	024	426135	012		120	2135764	108	6132547	084	7461325	060
135247	075	427135	096		112	2143567	090	6135247	084		059
135264	025	461325	040	1356247	080	2147356	105	6135427	084		061
135267	071		042	1356427	080	2413567	090	6135724	110	7461352	059
135426	024	461352	042	1356724	113	2417356	105	6135742	110	7462135	058
135427	075	461735	098		117	2461735	114	6137254	110	7613254	068
135462	023	462135	012		116	2467135	114	6137524	110	7613524	068
135467	074	467135	098	1356742	116		115	6137542	110	7613542	067
135624	025	613254	038		117		118	6143257	085	7614325	061
135627	071	613524	038		113	2471356	105	6143275	085		060
135642	023	613542	039	1357246	121	2476135	115	6143527	085		059
135647	074	613547	077		125		114	6143725	107	7614352	059
135724	099	613725	094		124		102	6143752	107	7621354	057
135726	100	613752	094	1357264	117	2613547	083	6147325	107	7621435	058
135742	099	614325	041		125	2614735	114	6147352	107	7624135	058
135746	101		040		124	2641735	114	6174325	061	7641325	061
135762	100	614735	098	1357426	121	2647135	118	6213547	087		060
135764	101	621354	043		120		119	6214735	123		059
137254	099	614352	041		124		114	6214735	123	7641352	059
137256	100	621435	013			2671354	106	6241735	123	7642135	058

Ternary DRD table lookup procedure:

- Classify a system by writing down each position number in ascending order of boiling points.
 - A position number is not written down if there is no azeotrope at that position.
 - The resulting sequence of numbers is known as the *temperature profile*.
 - Each temperature profile will have a minimum of three numbers and a maximum of seven numbers.
 - List multiple temperature profiles when you have incomplete azeotropic data.
 - All seven position numbers are shown on the diagram.
- Using the table, look up the temperature profile(s) to find the corresponding DRD #.

*Table 13-18 and Fig. 13-79 developed by Eric J. Peterson, Eastman Chemical Co.



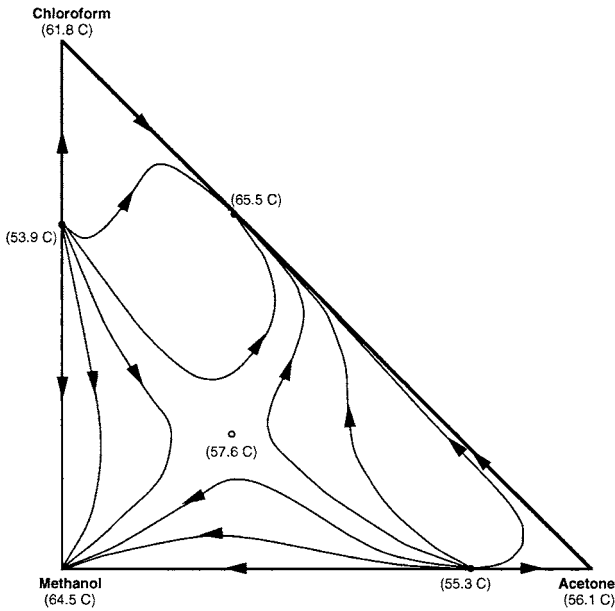


FIG. 13-80 Residue curves for acetone-chloroform-methanol system at 1-atm pressure suggesting a ternary saddle azeotrope.

operating conditions and two feed locations, as given in Table 13-19. The desired product specification is 97 mol % MIPK, no more than 3 mol % MEK, and less than 10 ppm residual water. For case A (Fig. 13-82a), the column profile tracks up the water-free side of the diagram. A pinched zone (i.e., section of little change in tray temperature and composition) occurs above the feed between the feed tray (tray 4) and tray 18. The temperature remains constant at about 93°C throughout the pinch zone. Product specifications are met.

When the feed composition becomes slightly enriched in water, as with case B, the column profile changes drastically (Fig. 13-82b). At

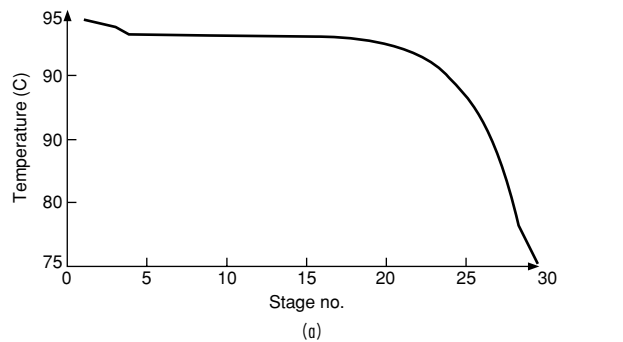
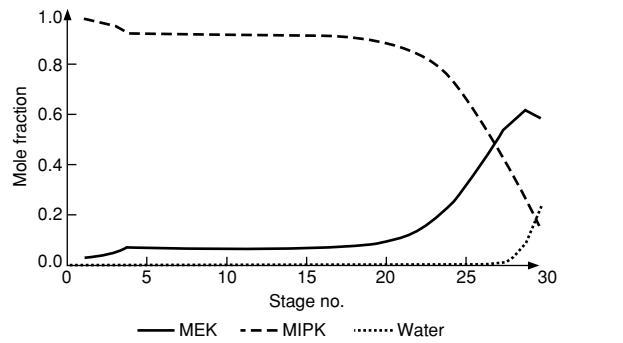
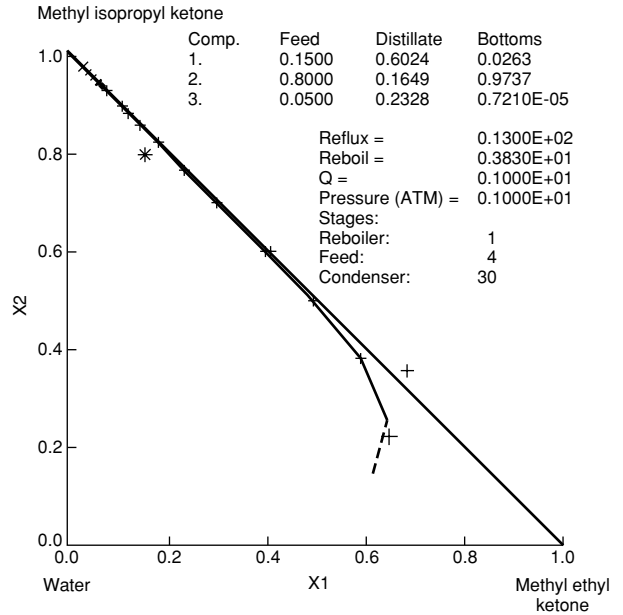


FIG. 13-82 Sensitivity of composition and temperature profiles for MEK-MIPK-water system at 1 atm.

the same reflux and boil-up, the column no longer meets specifications. The MIPK product is lean in MIPK and too rich in water. The profile now tracks generally up the left side of region II. Note also the dramatic change in the temperature profile. A pinched zone still exists above the feed between trays 4 and 18, but the tray temperature in the zone has dropped to 80°C (from 93°C). Most of the trays are required to move through the vicinity of the saddle. Typically, pinches (if they exist) occur close to saddles and nodes.

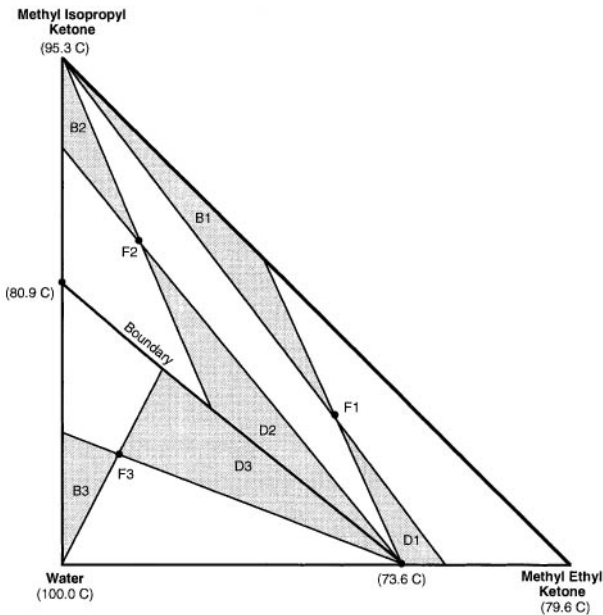


FIG. 13-81 MEK-MIPK-water system. Approximate product composition regions for a simple distillation column.

13-80 DISTILLATION

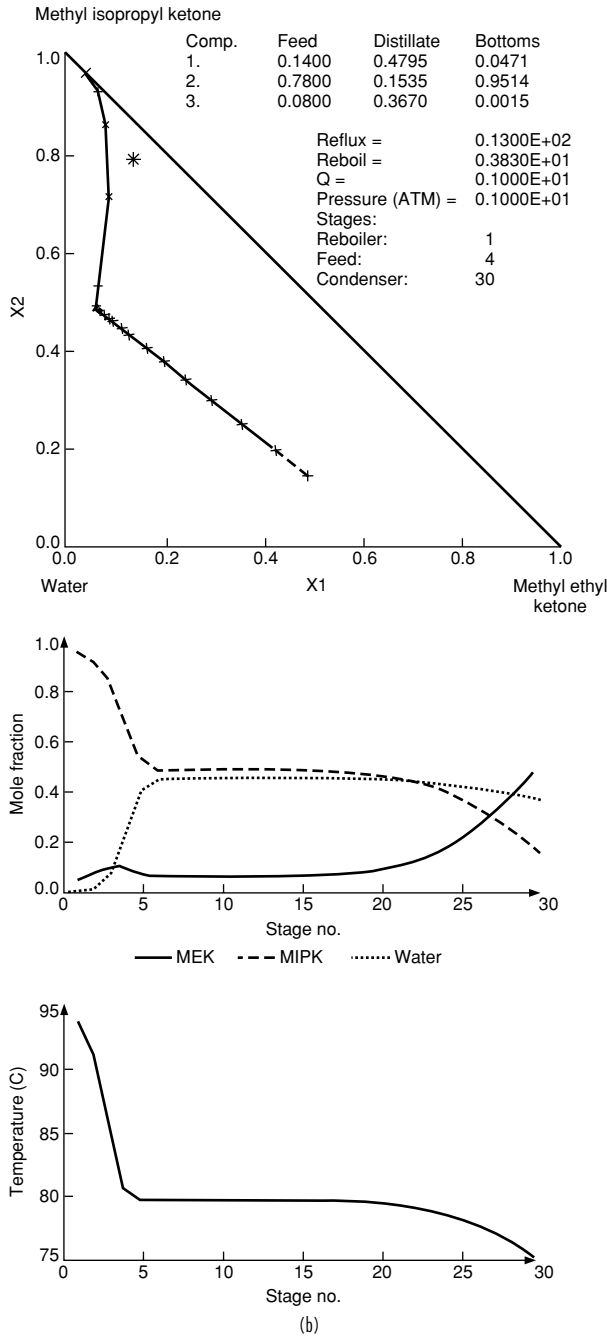


FIG. 13-82 (Continued)

In case C (Fig. 13-82c), increasing the boil-up ratio to 6 brings the MIPK product back within specifications, but the production rate and recovery have dropped off. In addition, the profile has switched back to the right side of the region; and the temperatures on trays in the pinched zone (trays 4 through 18) are back to 93°C. Such a drastic fluctuation in tray temperature with a relatively minor adjustment of the manipulated variable (boil-up in this case) can make control diffi-

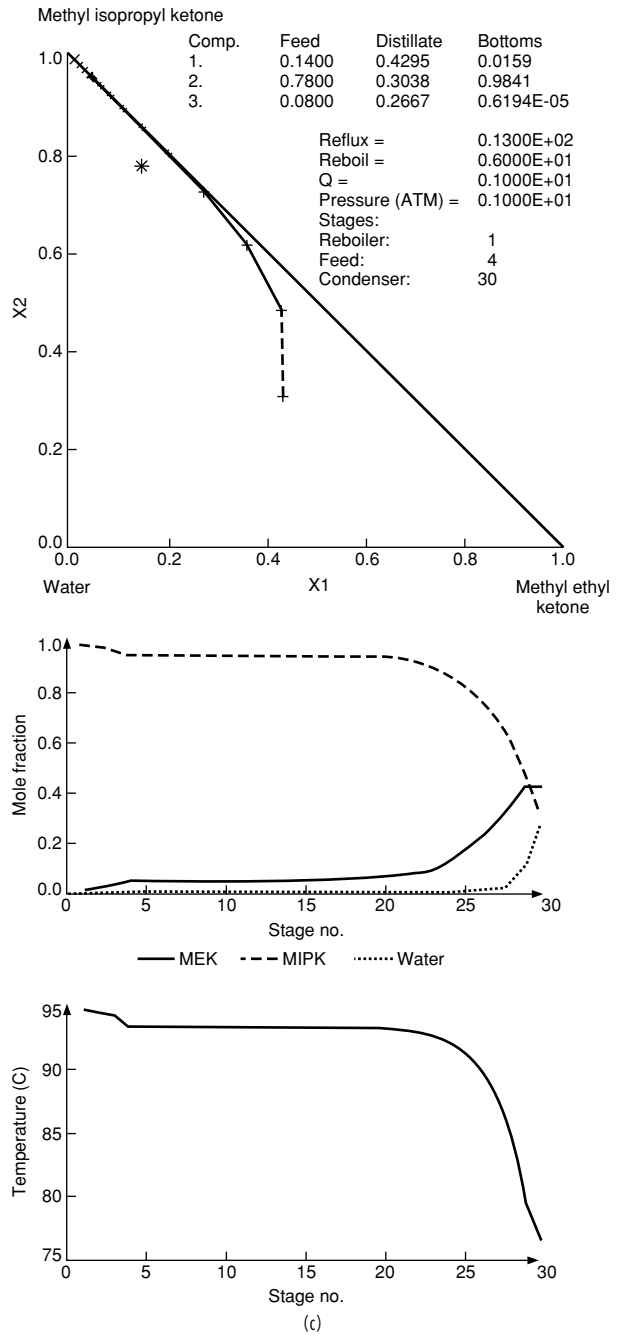


FIG. 13-82 (Continued)

cult. This is especially true if the control strategy involves maintaining a constant temperature on one of the trays between trays 4 and 18. If a tray is selected that exhibits wide temperature swings, the control system may have a difficult time compensating for disturbances. Such columns are also often difficult to model with a process simulator. Design algorithms often rely on perturbation of a variable (such as reflux or reboil) while checking for convergence of column heat and

TABLE 13-19 Sets of Operating Conditions for Fig. 13-82

Case	Reflux ratio	Reboil ratio		Feed composition	Distillate composition	Bottoms composition
A	13	3.8	MEK	0.15	0.60	0.03
			MIPK	0.80	0.16	0.97
			water	0.05	0.24	7 ppm
B	13	3.8	MEK	0.14	0.48	0.05
			MIPK	0.78	0.15	0.95
			water	0.08	0.37	20,000 ppm
C	13	6	MEK	0.14	0.43	0.02
			MIPK	0.78	0.30	0.98
			water	0.08	0.27	6.5 ppm

material balances. In situations where the column profile is altered drastically by minor changes in the perturbed variable, the simulator may be close to a feasible solution, but successive iterations may appear to be very far apart. The convergence routine may continue to oscillate between column profiles and never reach a solution. Likewise, when an attempt is made to design a column to obtain product compositions in different distillation regions, the simulation will never converge.

AZEOTROPIC DISTILLATION

The term *azeotropic distillation* has been applied to a broad class of fractional distillation-based separation techniques when specific azeotropic behavior is exploited to effect a separation. The agent that causes the specific azeotropic behavior, often called the *entrainer*, may already be present in the feed mixture (a self-entraining mixture) or may be an added mass separation agent. Azeotropic distillation techniques are used throughout the petrochemical and chemical processing industries for the separation of close-boiling, pinched, or azeotropic systems for which simple distillation is either too expensive or impossible. With an azeotropic feed mixture, presence of the azeotroping agent results in the formation of a more favorable azeotropic pattern for the desired separation. For a close-boiling or pinched feed mixture, the azeotroping agent changes the dimensionality of the system and allows separation to occur along a less pinched path. Within the general heading of azeotropic distillation techniques, several approaches have been followed in devising azeotropic distillation flow sheets including

1. Choosing an entrainer to give a residue curve map with specific distillation regions and node temperatures
2. Exploiting changes in azeotropic composition with total system pressure
3. Exploiting curvature of distillation region boundaries
4. Choosing an entrainer to cause azeotrope formation in combination with liquid-liquid immiscibility

The first three of these are solely VLE-based approaches, involving a series of simple distillation column operations and recycles. The final approach relies on distillation (VLE), but also exploits another physical phenomenon, liquid-liquid phase formation (phase splitting), to assist in entrainer recovery. This approach is the most powerful and versatile. Examples of industrial uses of azeotropic distillation grouped by method are given in Table 13-20.

The choice of the appropriate azeotropic distillation method and the resulting flow sheet for the separation of a particular mixture are strong functions of the separation objective. For example, it may be desirable to recover all constituents of the original feed mixture as pure components, or only some as pure components and others as azeotropic mixtures suitable for recycle. Not every objective may be obtainable by azeotropic distillation for a given mixture and portfolio of candidate entrainers.

Exploiting Homogeneous Azeotropes Homogeneous azeotropic distillation refers to a flow sheet structure in which azeotrope formation is exploited or avoided in order to accomplish the desired separation in one or more distillation columns. Either the azeotropes in the system

do not exhibit two-liquid-phase behavior, or the liquid-phase behavior is not or cannot be exploited in the separation sequence. The structure of a particular sequence will depend on the geometry of the residue curve map or distillation region diagram for the feed mixture-entrainer system. Two approaches are possible:

1. Selection of an entrainer such that the desired products all lie within the *same* distillation region (the products may be pure components or azeotropic mixtures)
2. Selection of an entrainer such that some type of distillation boundary-crossing mechanism is employed to separate desired products that lie in *different* regions.

As mentioned previously, ternary mixtures can be represented by 125 different residue curve maps or distillation region diagrams. However, feasible distillation sequences using the first approach can be developed for breaking homogeneous binary azeotropes by the addition of a third component only for those more restricted systems that do not have a distillation boundary connected to the azeotrope and for which one of the original components is a node. For example, from Fig. 13-79, the following eight residue curve maps are suitable for breaking homogeneous minimum-boiling azeotropes: DRD 002, 027, 030, 040, 051, 056, 060, and 061 as collected in Fig. 13-83. To produce the necessary distillation region diagrams, an entrainer must be found that is either: (1) an intermediate boiler that forms no azeotropes (DRD 002), or (2) lowest-boiling or intermediate-boiling and forms a maximum-boiling azeotrope with the lower-boiling original component (A). In these cases, the entrainer may also optionally form a minimum-boiling azeotrope with the higher boiling of the original components or a minimum-boiling ternary azeotrope. In all cases, after the addition of the entrainer, the higher-boiling original component (B) is a high-boiling node and is removed as bottoms product from a first column operated in the indirect-split mode with the lower-boiling original component recovered as distillate in a second column; see flow sheet in Fig. 13-83.

The seven residue curve maps suitable for breaking homogeneous maximum-boiling binary azeotropes (DRD 028, 031, 035, 073, 078, 088, 089) are shown in Fig. 13-84. In this case, the entrainer must form a minimum-boiling azeotrope with the higher-boiling original component and either a maximum-boiling azeotrope or no azeotrope with the lower-boiling original component. In all cases, after the addition of the entrainer, the lower-boiling original component is a low-boiling node and is removed as distillate from a first column operated in the direct-split mode with the higher-boiling original component recovered as bottoms product in a second column; see flow sheet in Fig. 13-84.

The restrictions on the boiling point and azeotrope formation of the entrainer act as efficient screening criteria for entrainer selection. Entrainers that do not show appropriate boiling point characteristics can be discarded without detailed analysis. However, the entrainers in Fig. 13-83 do suffer from serious drawbacks that limit their practical application. DRD 002 requires that the entrainer be an intermediate-boiling component that forms no azeotropes. Unfortunately these are often difficult criteria to meet, as any intermediate boiler will be closer-boiling to both of the original components and, therefore, will be more likely to be at least pinched or even form azeotropes. The remaining feasible distillation region diagrams require that the entrainer form a maximum-boiling azeotrope with the lower-boiling original component. Because maximum-boiling azeotropes are relatively rare, finding a suitable entrainer may be difficult.

For example, the dehydration of organics that form homogeneous azeotropes with water is a common industrial problem. It is extremely difficult to find an intermediate-boiling entrainer that also does not form an azeotrope with water. Furthermore, the resulting separation is likely to be close-boiling or pinched throughout most of the column, requiring a large number of stages. For example, consider the separation of valeric acid (187.0°C) and water. This system exhibits a minimum-boiling azeotrope (99.8°C) with a composition and boiling point close to those of pure water. Ignoring for the moment potentially severe corrosion problems, formic acid (100.7°C), which is an intermediate boiler and which forms a maximum-boiling azeotrope with water (107.1°C), is a candidate entrainer (DRD 030, Fig. 13-85a). In the conceptual sequence shown in Fig. 13-85b, a recycle of the formic acid-water maximum-boiling azeotrope is added to the

TABLE 13-20 Examples of Azeotropic Distillation

System	Type	Entrainer(s)	Remark
Exploitation of homogeneous azeotropes			
No known industrial examples			
Exploitation of pressure sensitivity			
THF-water Methyl acetate-methanol	Minimum-boiling azeotrope Minimum-boiling azeotrope	None None	Alternative to extractive distillation Element of recovery system for alternative to production of methyl acetate by reactive distillation; alternative to azeotropic, extractive distillation
Alcohol-ketone systems Ethanol-water	Minimum-boiling azeotropes Minimum-boiling azeotrope	None None	Alternative to extractive distillation, salt extractive distillation, heterogeneous azeotropic distillation; must reduce pressure to less than 11.5 kPa for azeotrope to disappear
Exploitation of boundary curvature			
Hydrochloric acid-water	Maximum-boiling azeotrope	Sulfuric acid	Alternative to salt extractive distillation
Nitric acid-water	Maximum-boiling azeotrope	Sulfuric acid	Alternative to salt extractive distillation
Exploitation of azeotropy and liquid phase immiscibility			
Ethanol-water	Minimum-boiling azeotrope	Cyclohexane, benzene, heptane, hexane, toluene, gasolene, diethyl ether	Alternative to extractive distillation, pressure-swing distillation
Acetic acid-water	Pinched system	Ethyl acetate, propyl acetate, diethyl ether, dichloroethane, butyl acetate	
Butanol-water Acetic acid-water-vinyl acetate Methyl acetate-methanol	Minimum-boiling azeotrope Pinched, azeotropic system Minimum-boiling azeotrope	Self-entraining Self-entraining Toluene, methyl isobutyl ketone	Element of recovery system for alternative to production of methyl acetate by reactive distillation; alternative to extractive pressure-swing distillation
Diethoxymethanol-water-ethanol Pyridine-water Hydrocarbon-water	Minimum-boiling azeotropes Minimum-boiling azeotrope Minimum-boiling azeotrope	Self-entraining Benzene Self-entraining	Alternative to extractive distillation

original valeric acid–water feed, which may be of any composition. Using the indirect-split mode of operation, the high-boiling node valeric acid is removed in high purity and high recovery as bottoms in a first column, which by mass balance produces a formic acid–water distillate. This binary mixture is fed to a second column that produces pure water as distillate and the formic acid–water azeotrope as bottoms for recycle to the first column. The inventory of formic acid is an important optimization variable in this theoretically feasible but difficult separation scheme.

Exploiting Pressure Sensitivity Breaking a homogeneous azeotrope that is part of a distillation boundary (i.e., the desired products lie in different distillation regions on either side of the boundary) requires that the boundary be “crossed” by the separation system. This may be done by mixing some external stream with the original feed stream in one region such that the resulting composition is in another region for further processing. However, the external stream must be completely regenerated, and mass balance must be preserved. For example, it is not possible to break a homogeneous binary azeotrope simply by adding one of the products to cross the azeotropic composition.

The composition of many azeotropes varies with the system pressure (Horsley, *Azeotropic Data-III*, American Chemical Society, Washington, 1983; Gmehling et al., *Azeotropic Data*, VCH Publishers, Deerfield Beach, Fla., 1994). This effect can be exploited to separate azeotropic mixtures by so-called pressure-swing distillation if at some pressure the azeotrope simply disappears, such as does the ethanol–water azeotrope at pressures below 11.5 kPa. However, pressure sensitivity can still be exploited if the azeotropic composition and related distillation boundary change sufficiently over a moderate

change in total system pressure. A composition in one distillation region under one set of conditions could be in a different region under a different set of conditions. A two-column sequence for separating a binary maximum-boiling azeotrope is shown in Fig. 13-86 for a system in which the azeotropic composition at pressure P1 is richer in component B than the azeotropic composition at pressure P2. The first column, operating at pressure P1, is fed a mixture of fresh feed plus recycle stream from the second column such that the overall composition lies on the A-rich side of the azeotropic composition at P1. Pure component A is recovered as distillate, and a mixture near the azeotropic composition is produced as bottoms. The pressure of this bottoms stream is changed to P2 and fed to the second column. This feed is on the B-rich side of the azeotropic composition at P2. Pure component B is now recovered as the distillate, and the azeotropic bottoms composition is recycled to the first column. An analogous flow sheet can be used for separating binary homogeneous minimum-boiling azeotropes. In this case the pure components are recovered as bottoms in both columns, and the distillate from each column is recycled to the other column.

For pressure-swing distillation to be practical, the azeotropic composition must vary at least 5 percent (preferably 10 percent or more) over a moderate pressure range (not more than 10 atm between the two pressures). With a very large pressure range, refrigeration may be required for condensation of the low-pressure distillate, or an impractically high reboiler temperature may result in the high-pressure column. The smaller the variation of azeotrope composition over the pressure range, the larger the recycle flow rates between the two columns. In particular, for minimum-boiling azeotropes, the pressure-swing distillation approach requires high energy usage and high capital

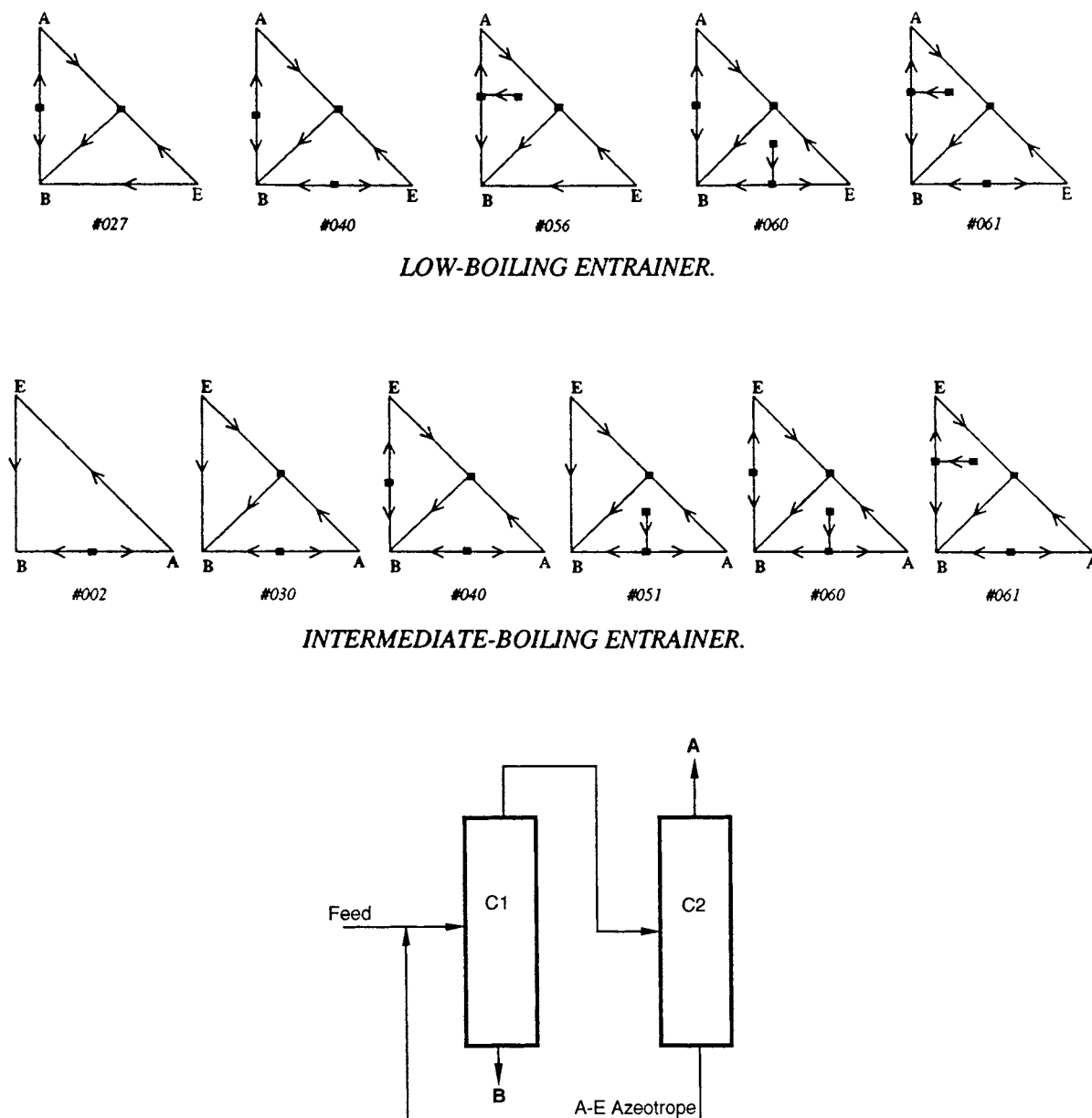


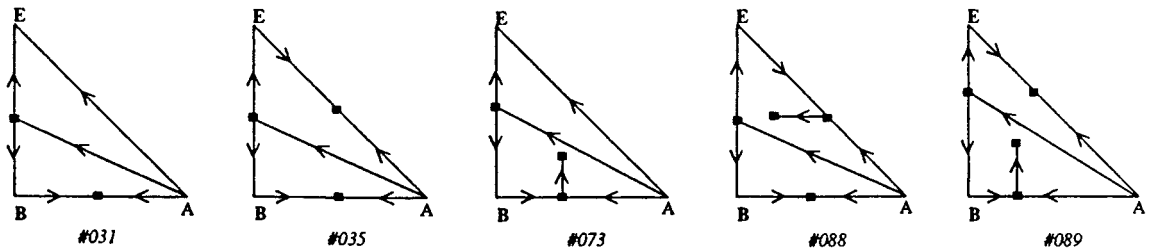
FIG. 13-83 Feasible distillation region diagrams and associated distillation system for breaking a homogeneous minimum-boiling binary azeotrope A-B. Component B boils at a higher temperature than does A.

costs (large-diameter columns) because both recycled azeotropic compositions must be taken overhead. Moreover, one lobe of an azeotropic VLE diagram is often pinched regardless of pressure; and, therefore, one of the columns will require a large number of stages to produce the corresponding pure-component product.

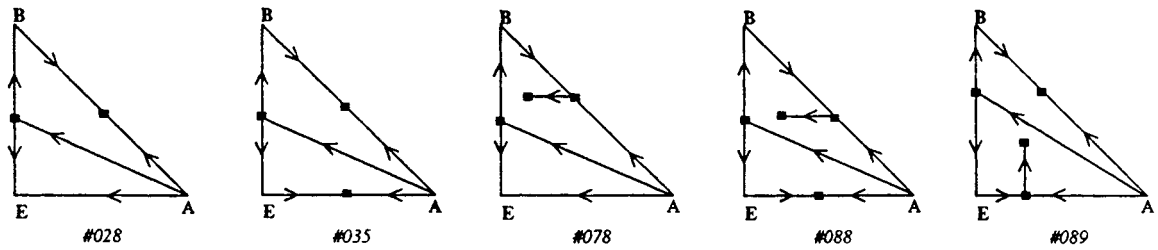
General information on pressure-swing distillation can be found in Van Winkle (*Distillation*, McGraw-Hill, New York, 1967), Wankat (*Equilibrium-Staged Separations*, Elsevier, New York, 1988), and Knapp and Doherty [*Ind. Eng. Chem. Res.*, **31**, 346 (1992)]. Only a relatively small fraction of azeotropes are sufficiently pressure-sensitive for a pressure-swing process to be economical. Some applications include the minimum-boiling azeotrope tetrahydrofuran-water [Tanabe et al.;

U.S. Patent 4,093,633 (1978)], and maximum-boiling azeotropes of hydrogen chloride-water and formic acid-water (Horsley, *Azeotropic Data-III*, American Chemical Society, Washington, 1983). Since distillation boundaries move with pressure-sensitive azeotropes, the pressure-swing principle can also be used for overcoming distillation boundaries in multicomponent azeotropic mixtures.

Exploiting Boundary Curvature A second approach to boundary crossing exploits boundary curvature to produce compositions in different distillation regions. When distillation boundaries exhibit extreme curvature, it may be possible to design a column such that the distillate and bottoms compositions are on the same residue curve in one distillation region, while the feed composition (which is not



INTERMEDIATE-BOILING ENTRAINER.



HIGH-BOILING ENTRAINER.

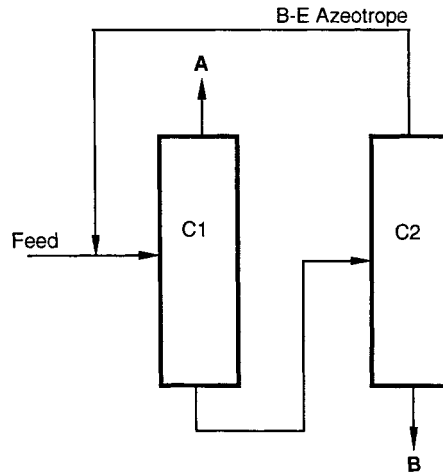
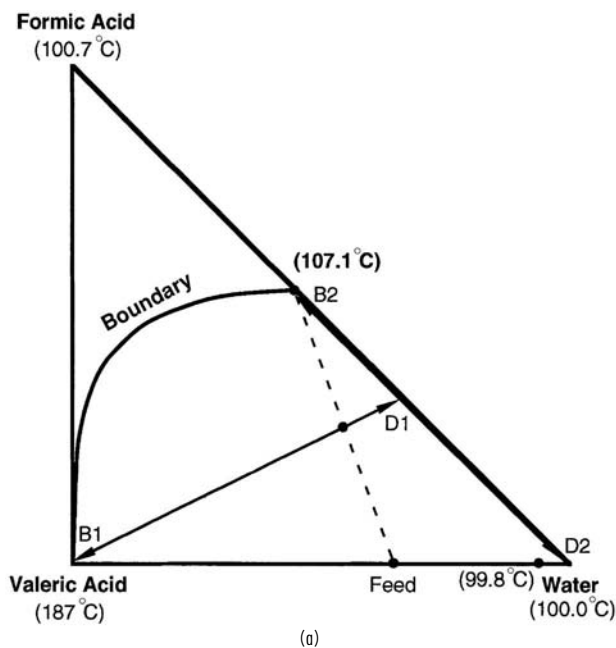


FIG. 13-84 Feasible distillation region diagrams and associated distillation system for breaking a homogeneous maximum-boiling binary azeotrope A-B. Component B boils at a higher temperature than does A.

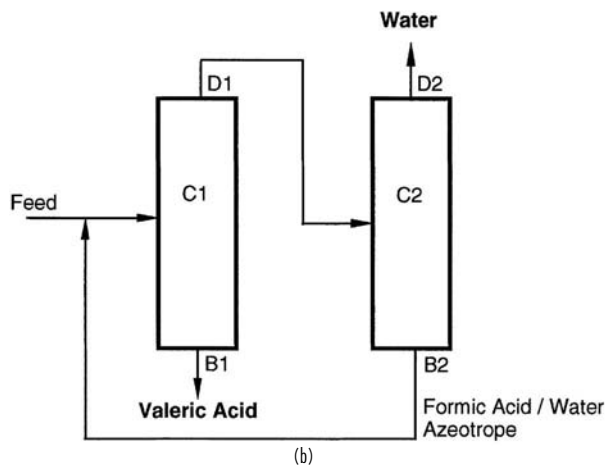
required to lie on the column composition profile) is in another distillation region. For such a column to meet material balance constraints (i.e., bottom, distillate, feed compositions on a straight line), the feed must be located in a region where the boundary is concave.

As an example, Van Dongen (Ph.D. Thesis, University of Massachusetts, 1983) considered the separation of a methanol-methyl acetate mixture, which forms a homogeneous azeotrope, using *n*-hexane as an entrainer. The distillation boundaries for this system (Fig. 13-87*a*) are somewhat curved. A separation sequence that exploits this boundary curvature is shown in Fig. 13-87*b*. Recycled methanol-methyl acetate binary azeotrope and methanol-methyl acetate-hexane ternary azeotrope are added to the original feed F0 to produce a net feed com-

position F1 for column C1 designed to lie on a line between pure methanol and the curved part of the boundary between regions I and II. Column C1 is operated in the indirect-split mode, producing the high-boiling node methanol as a bottoms product, and by mass balance, a distillate near the curved boundary. The distillate, although in region I, becomes feed F2 to column C2 which is operated in the direct-split mode entirely in region II, producing the low-boiling node ternary azeotrope as distillate and by mass balance, a methanol-methyl acetate mixture as bottoms (B2). This bottoms mixture is on the opposite side of the methanol-methyl acetate azeotrope than the original feed F0. The bottoms from C2 is finally fed to binary distillation column C3, which produces pure methyl acetate as bottoms product (B3)



(a)



(b)

FIG. 13-85 Valeric acid-water separation with formic acid. (a) Mass balances on distillation region diagram. (b) Conceptual sequence.

and the methanol–methyl acetate azeotrope as distillate (D3). The distillates from columns C2 and C3 are recycled to column C1. The distillate and bottoms compositions for column C2 lie on the same residue curve, and the composition profile lies entirely within region II, even though its feed composition is in region I. Additional information on exploiting boundary curvature, including the useful concept of a *pitchfork distillation boundary*, can be found in Doherty and Malone (*Conceptual Design of Distillation Systems*, McGraw-Hill, 2001, sec. 5.4).

Exploiting boundary curvature for breaking azeotropes is very similar to exploiting pressure sensitivity from a mass balance point of view, and suffers from the same disadvantages. Separation schemes have large recycle flows, and in the case of minimum-boiling azeotropes, the recycle streams are distillates. However, in the case of maximum-boiling azeotropes, these recycles are bottoms products, and the economics are improved. One such application, illustrated in Fig. 13-88, is the separation of the maximum-boiling nitric acid–water azeotrope by adding sulfuric acid. Recycled sulfuric acid is added to a

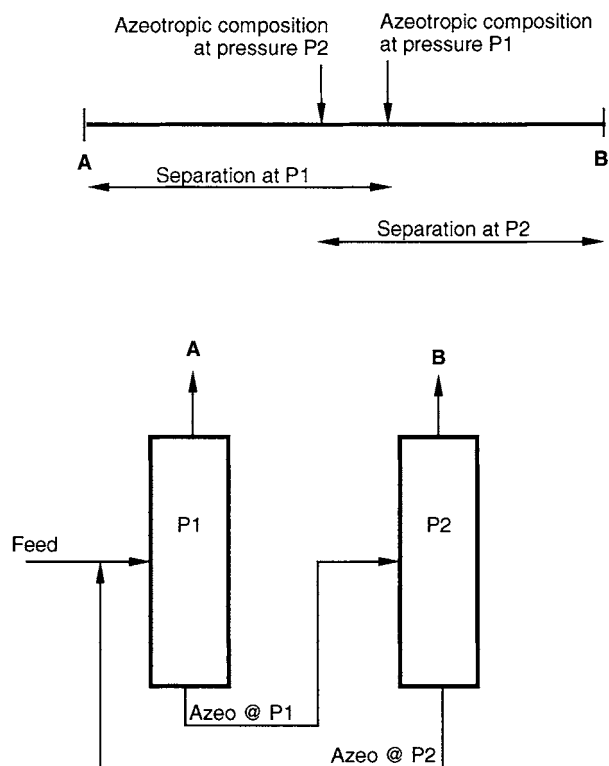


FIG. 13-86 Conceptual sequence for separating maximum-boiling binary azeotrope with pressure-swing distillation.

nitric acid–water mixture near the azeotropic composition to produce a net feed F1 in region II. The first column, operated in the direct-split mode, produces a nitric acid distillate and a bottoms product, by mass balance, near the distillation boundary. In this case, sulfuric acid associates with water so strongly and the distillation boundary is so curved and nearly tangent to the water–sulfuric acid edge of the composition diagram that the second column operating in the indirect-split mode in region I, producing sulfuric acid as bottoms product, also produces a distillate close enough to the water specification that a third column is not required [Thiemann et al., in *Ullmann's Encyclopedia of Industrial Chemistry*, 5th ed., vol. A17, VCH Verlagsgesellschaft mbH, Weinheim, (1991)].

Exploiting Azeotropy and Liquid-Phase Immiscibility One powerful and versatile separation approach exploits several physical phenomena simultaneously including nonideal vapor-liquid behavior, where possible, and liquid-liquid behavior to bypass difficult distillation separations. For example, the overall separation of close-boiling mixtures can be made easier by the addition of an entrainer that introduces liquid-liquid immiscibility and forms a heterogeneous minimum-boiling azeotrope with one (generally the lower-boiling) of the key components. Two-liquid-phase formation provides a means of breaking this azeotrope, thus simplifying the entrainer recovery and recycle process. Moreover, since liquid-liquid tie lines are unaffected by distillation boundaries (and the separate liquid phases are often located in different distillation regions), liquid-liquid phase splitting is a powerful mechanism for crossing distillation boundaries. The phase separator is usually a simple decanter, but sometimes a multistage extractor is substituted. The decanter or extractor can also be replaced by some other non-VLE-based separation technique such as membrane permeation, chromatography, adsorption, or crystallization. Also sequences may include additional separation operations (distillations or other methods) for preconcentration of the feed mixture, entrainer recovery, and final-product purification.

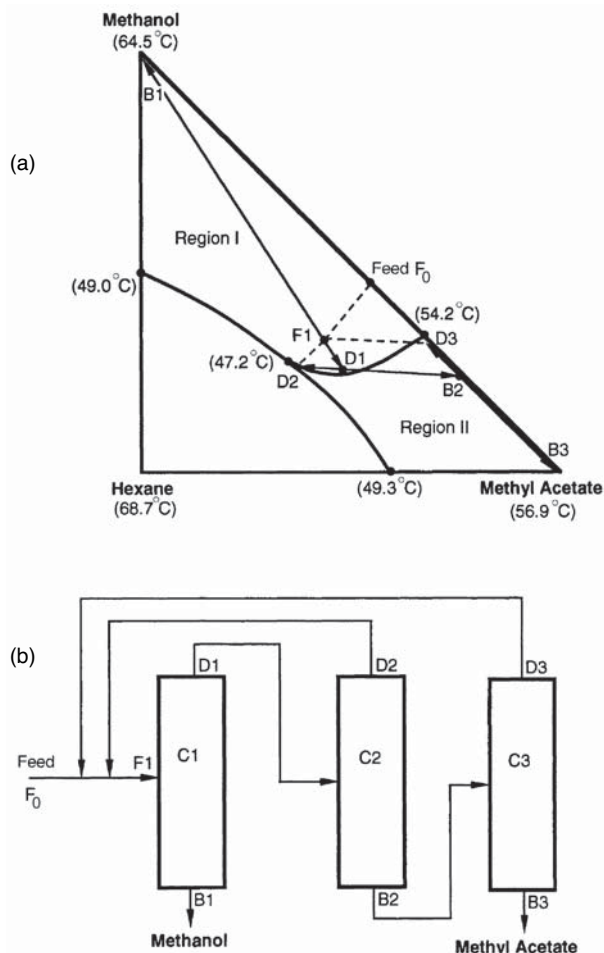


FIG. 13-87 Separation of methanol–methyl acetate by exploitation of distillation boundary curvature.

The simplest case of combining VLE and LLE is the separation of a binary heterogeneous azeotropic mixture. One example is the dehydration of 1-butanol, a self-entraining system, in which butanol (117.7°C) and water form a minimum-boiling heterogeneous azeotrope (93.0°C). As shown in Fig. 13-89, the fresh feed may be added to either column C1 or C2, depending on whether the feed is on the organic-rich side or the water-rich side of the azeotrope. The feed may also be added into the decanter directly if it does not move the overall composition of the decanter outside of the two-liquid phase region. Column C1 produces anhydrous butanol as a bottoms product and a composition close to the butanol–water azeotrope as the distillate. After condensation, the azeotrope rapidly phase-separates in the decanter. The upper layer, consisting of 78 wt % butanol, is refluxed totally to column C1 for further butanol recovery. The water layer, consisting of 92 wt % water, is fed to column C2. This column produces pure water as a bottoms product and, again, a composition close to the azeotrope as distillate for recycle to the decanter. Sparged steam may be used in C2, saving the cost of a reboiler. A similar flow sheet can be used for dehydration of hydrocarbons and other species that are largely immiscible with water.

A second example of the use of liquid–liquid immiscibilities in an azeotropic distillation sequence is the separation of the ethanol–water minimum-boiling homogeneous azeotrope. For this separation, a number of entrainers have been proposed, which are usually chosen to be immiscible with water and form a ternary minimum-boiling

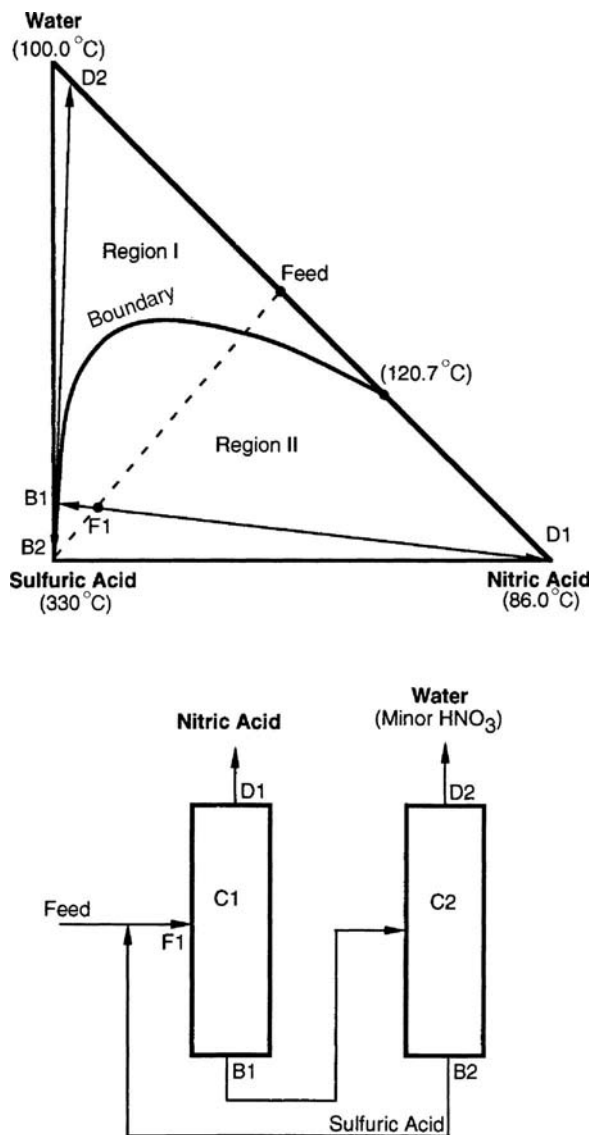


FIG. 13-88 Separation of nitric acid–water system with sulfuric acid in a two-column sequence exploiting extreme boundary curvature.

(preferably heterogeneous) azeotrope with ethanol and water (and, therefore, usually also binary minimum-boiling azeotropes with both ethanol and water). All such systems correspond to DRD 058, although the labeling of the vertices depends on whether the entrainer is lower-boiling than ethanol, intermediate-boiling, or higher-boiling than water. The residue curve map for the case of cyclohexane as entrainer was illustrated in Fig. 13-78c. One three-column distillation sequence is shown in Fig. 13-90. Other two-, three-, or four-column sequences have been described by Knapp and Doherty (*Kirk-Othmer Encyclopedia of Chemical Technology*, 5th ed., vol. 8, p. 786, Wiley, New York, 2004).

Fresh aqueous ethanol feed is first preconcentrated to nearly the azeotropic composition in column C3, while producing a water bottoms product. The distillate from C3 is sent to column C1, which is refluxed with the entire organic (entrainer-rich) layer, recycled from a decanter. Mixing of these two streams is the key to this sequence as it allows the overall feed composition to cross the distillation boundary

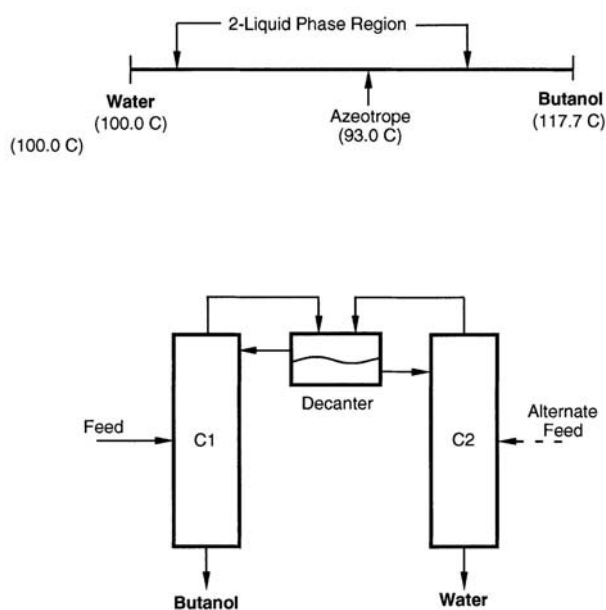


FIG. 13-89 Separation of butanol-water with heterogeneous azeotropic distillation.

into region II. Column C1 is operated to recover pure high-boiling node ethanol as a bottoms product and to produce a distillate close to the ternary azeotrope. If the ternary azeotrope is heterogeneous (as it is in this case), it is sent to the decanter for phase separation. If the ternary azeotrope is homogeneous (as it is in the alternative case of ethyl acetate as the entrainer), the distillate is first mixed with water before being sent to the decanter. The inventory of entrainer is adjusted to allow column C1 to operate essentially between two nodes, although such practice, as discussed previously, is relatively susceptible to instabilities from minor feed or reflux perturbations. Refluxing a fraction of the water-rich decanter layer results in an additional degree of freedom to mitigate against variability in the feed composition. The remaining portion of the water layer from the decanter is stripped of residual cyclohexane in column C2, which may be operated either in the direct-split mode (producing low-boiling node ternary azeotrope as distillate and, by mass balance, an ethanol-water bottoms for recycle to C3) or in the indirect-split mode (producing high-boiling node water as bottoms and, by mass balance, a ternary distillate near the distillation boundary). (The distillate may be recycled to the decanter, the top of column C1, or the C1 feed.) The indirect-split mode alternatives are discussed in greater detail by Knapp and Doherty (*Kirk-Othmer Encyclopedia of Chemical Technology*, 5th ed., vol. 8, p. 786, Wiley, New York, 2004).

Design and Operation of Azeotropic Distillation Columns
Simulation and design of azeotropic distillation columns are a difficult computational problem, but one that is readily handled, in most cases, by widely available commercial computer process simulation packages [Glasscock and Hale, *Chem. Eng.*, **101**(11), 82 (1994)]. Most simulators are capable of modeling the steady-state and dynamic behavior of both homogeneous azeotropic distillation systems and those systems involving two-liquid phase behavior within the column, if accurate thermodynamic data and activity coefficient or equation-of-state models are available. However, VLE and VLLE estimated or extrapolated from binary data or predicted from such methods as UNIFAC may not be able to accurately locate boundaries and predict the extent of liquid immiscibilities. Moreover, different activity coefficient models fit to the same experimental data often give very different results for the shape of distillation boundaries and liquid-liquid regions. Therefore the design of separation schemes relying on boundary curvature should not be attempted unless accurate, reliable experimental equilibrium data are available.

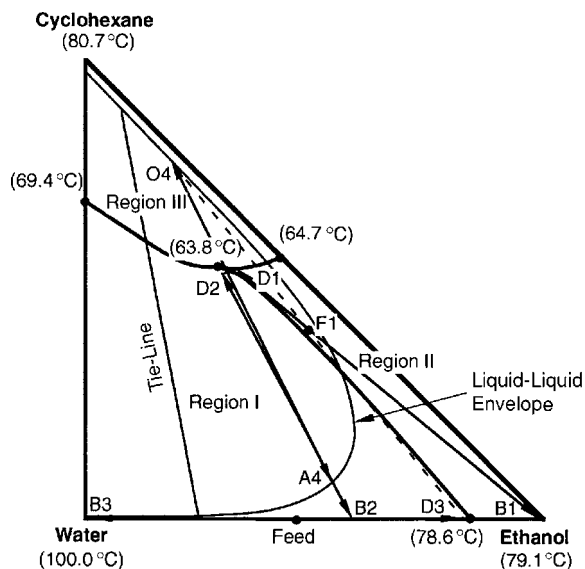


FIG. 13-90 Three-column sequence for ethanol dehydration with cyclohexane (operating column C2 in the direct-split mode).

Two liquid phases can occur within a column in the distillation of heterogeneous systems. Older references, e.g., Robinson and Gilliland (*Elements of Fractional Distillation*, McGraw-Hill, New York, 1950), state that the presence of two liquid phases in a column should be avoided as much as possible because performance may be reduced. However, more recent studies indicate that problems with two-phase flow have been overstated [Herron et al., *AIChE J.*, **34**, 1267 (1988); and Harrison, *Chem. Eng. Prog.*, **86**(11), 80 (1990)]. Based on case history data and experimental evidence, there is no reason to expect unusual capacity or pressure-drop limitations, and standard correlations for these parameters should give acceptable results. Because of the intense nature of the gas-liquid-liquid mixing on trays, mass-transfer efficiencies are relatively unaffected by liquid-liquid phase behavior. The falling-film nature of gas-liquid-liquid contact in packing, however, makes that situation more uncertain. Reduced efficiencies may be expected in systems where one of the keys distributes between the phases.

EXTRACTIVE DISTILLATION

Extractive distillation is a partial vaporization process in the presence of a miscible, high-boiling, nonvolatile mass separation agent, normally

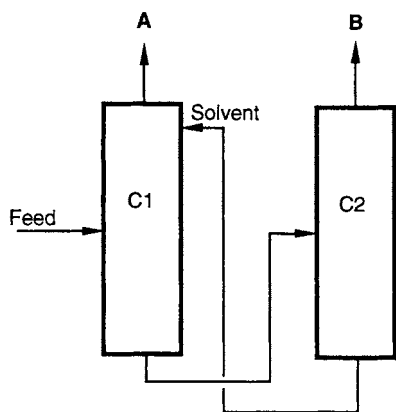


FIG. 13-91 Typical extractive distillation sequence. Component A is less associated with the solvent.

called the *solvent*, which is added to an azeotropic or nonazeotropic feed mixture to alter the volatilities of the key components without the formation of any additional azeotropes. Extractive distillation is used throughout the petrochemical and chemical processing industries for the separation of close-boiling, pinched, or azeotropic systems for which simple single-feed distillation is either too expensive or impossible. It can also be used to obtain products which are residue curve saddles, a task not generally possible with single-feed distillation.

Figure 13-91 illustrates the classical implementation of an extractive distillation process for the separation of a binary mixture. The configuration consists of a double-feed extractive column (C1) and a solvent recovery column (C2). The components A and B may have a low relative volatility or form a minimum-boiling azeotrope. The solvent is introduced into the extractive column at a high concentration a few stages below the condenser, but above the primary-feed stage. Since the solvent is chosen to be nonvolatile, it remains at a relatively high concentration in the liquid phase throughout the sections of the column below the solvent-feed stage.

One of the components, A (not necessarily the most volatile species of the original mixture), is withdrawn as an essentially pure distillate stream. Because the solvent is nonvolatile, at most a few stages above the solvent-feed stage are sufficient to rectify the solvent from the distillate. The bottoms product, consisting of B and the solvent, is sent to the recovery column. The distillate from the recovery column is pure B, and the solvent-bottoms product is recycled to the extractive column.

Extractive distillation works by the exploitation of the selective solvent-induced enhancements or moderations of the liquid-phase nonidealities of the original components to be separated. The solvent selectively alters the activity coefficients of the components being separated. To do this, a high concentration of solvent is necessary. Several features are essential:

1. The solvent must be chosen to affect the liquid-phase behavior of the key components differently; otherwise, no enhancement in separability will occur.
2. The solvent must be higher-boiling than the key components of the separation and must be relatively nonvolatile in the extractive column, in order to remain largely in the liquid phase.
3. The solvent should not form additional azeotropes with the components in the mixture to be separated.
4. The extractive column *must* be a double-feed column, with the solvent feed above the primary feed. The column must have an extractive section (middle section) between the rectifying section and the stripping section.

As a consequence of these restrictions, separation of binary mixtures by extractive distillation corresponds to only two possible three-component distillation region diagrams, depending on whether the binary mixture is pinched or close-boiling (DRD 001), or forms a minimum-boiling azeotrope (DRD 003). The addition of high-boiling solvents

can also facilitate the breaking of maximum-boiling azeotropes (DRD 014), for example, splitting the nitric acid–water azeotrope with sulfuric acid. However, as explained in the subsection on azeotropic distillation, this type of separation might better be characterized as exploiting extreme boundary curvature rather than extractive distillation, as the important liquid-phase activity coefficient modification occurs in the bottom of the column. Although many references show sulfuric acid being introduced high in the column, in fact two separate feeds are not required.

Examples of industrial uses of extractive distillation grouped by distillation region diagram type are given in Table 13-21. Achievable product compositions in double-feed extractive distillation columns are very different from the bow tie regions for single-feed columns. For a given solvent, only one of the pure components in the original binary mixture can be obtained as distillate from the extractive column (the higher-boiling of which is a saddle for close-boiling systems, and both of which are saddles for minimum-boiling azeotropic systems). However, different solvents are capable of selecting either A or B as distillate (but not both). Simple tests are available for determining which component is the distillate, as discussed below.

Extractive distillation is generally only applicable to systems in which the components to be separated contain one or more different functional groups. Extractive distillation is usually uneconomical for separating stereoisomers, homologs, or structural isomers containing the same functional groups, unless the differences in structure also contribute to significantly different polarity, dipole moment, or hydrophobic character. One such counterexample is the separation of ethanol from isopropanol, where the addition of methyl benzoate raises the relative volatility from 1.09 to 1.27 [Berg et al., *Chem. Eng. Comm.*, **66**, 1 (1988)].

Solvent Effects in Extractive Distillation In the ordinary distillation of ideal or nonazeotropic mixtures, the component with the lowest pure-component boiling point is always recovered primarily in the distillate, while the highest boiler is recovered primarily in the bottoms. The situation is not as straightforward for an extractive distillation operation. With some solvents, the key component with the lower pure-component boiling point in the original mixture will be recovered in the distillate as in ordinary distillation. For another solvent, the expected order is reversed, and the component with the higher pure-component boiling point will be recovered in the distillate. The possibility that the expected relative volatility may be reversed by the addition of solvent is entirely a function of the way the solvent interacts with and modifies the activity coefficients and, thus, the volatility of the components in the mixture.

In normal applications of extractive distillation (i.e., pinched, close-boiling, or azeotropic systems), the relative volatilities between the light and heavy key components will be unity or close to unity. Assuming an ideal vapor phase and subcritical components, the relative volatility between the light and heavy keys of the desired separation can be written as the product of the ratios of the pure-component vapor pressures and activity coefficients whether the solvent is present or not:

$$\alpha_{L,H} = \left(\frac{P_L^{\text{sat}}}{P_H^{\text{sat}}} \right) \left(\frac{\gamma_L}{\gamma_H} \right) \quad (13-117)$$

where *L* and *H* denote the lower-boiling and higher-boiling key pure component, respectively.

The addition of the solvent has an indirect effect on the vapor-pressure ratio. Because the solvent is high-boiling and is generally added at a relatively high mole ratio to the primary-feed mixture, the temperature of an extractive distillation process tends to increase over that of a simple distillation of the original mixture (unless the system pressure is lowered). The result is a corresponding increase in the vapor pressure of both key components. However, the rise in operating temperature generally *does not* result in a significant modification of the relative volatility, because the ratio of vapor pressures often remains approximately constant, unless the slopes of the vapor-pressure curves differ significantly. The ratio of the vapor pressures typically remains greater than unity, following the “natural” volatility of the system.

TABLE 13-21 Examples of Extractive Distillation, Salt Extractive Distillation

System	Type	Solvent(s)	Remark
Ethanol-water	Minimum-boiling azeotrope	Ethylene glycol, acetate salts for salt process	Alternative to azeotropic distillation, pressure swing distillation
Benzene-cyclohexane	Minimum-boiling azeotrope	Aniline	Process similar for other alcohol-ester systems
Ethyl acetate-ethanol	Minimum-boiling azeotrope	Higher esters or alcohols, aromatics	
THF-water	Minimum-boiling azeotrope	Propylene glycol	Alternative to pressure swing distillation
Acetone-methanol	Minimum-boiling azeotrope	Water, aniline, ethylene glycol	Element of recovery system for alternative to production of methyl acetate by reactive distillation; alternative to azeotropic, pressure, swing distillation
Isoprene-pentane	Minimum-boiling azeotrope	Furfural, DMF, acetonitrile	
Pyridine-water	Minimum-boiling azeotrope	Bisphenol	
Methyl acetate-methanol	Minimum-boiling azeotrope	Ethylene glycol monomethyl ether	
C4 alkenes/C4 alkanes/ C4 dienes	Close-boiling and minimum-boiling azeotropes	Furfural, DMF, acetonitrile, <i>n</i> -methylpyrrolidone	
C5 alkenes/C5 alkanes/ C5 dienes	Close-boiling and minimum-boiling azeotropes	Furfural, DMF, acetonitrile, <i>n</i> -methylpyrrolidone	
Heptane isomers-cyclohexane	Close-boiling	Aniline, phenol	
Heptane isomers-toluene	Close-boiling and minimum-boiling azeotropes	Aniline, phenol	
Vinyl acetate-ethyl acetate	Close-boiling	Phenol, aromatics	Alternative to simple distillation
Propane-propylene	Close-boiling	Acrylonitrile	
Ethanol-isopropanol	Close-boiling	Methyl benzoate	Alternative to simple distillation
Hydrochloric acid-water	Maximum-boiling azeotrope	Sulfuric acid, calcium chloride for salt process	
Nitric acid-water	Maximum-boiling azeotrope	Sulfuric acid, magnesium nitrate for salt process	Sulfuric acid process relies heavily on boundary curvature

Since activity coefficients have a strong dependence on composition, the effect of the solvent on the activity coefficients is generally more pronounced. However, the magnitude and direction of change are highly dependent on the solvent concentration as well as on the liquid-phase interactions between the solvent and the key components. The solvent acts to lessen the nonidealities of the key component whose liquid-phase behavior is similar to that of the solvent, while enhancing the nonideal behavior of the dissimilar key. The solvent and the key component that show most similar liquid-phase behavior tend to exhibit weak molecular interactions. These components form an ideal or nearly ideal liquid solution. The activity coefficient of this key approaches unity, or may even show negative deviations from Raoult's law if solvating or complexing interactions occur. On the other hand, the dissimilar key and the solvent demonstrate unfavorable molecular interactions, and the activity coefficient of this key increases. The positive deviations from Raoult's law are further enhanced by the diluting effect of the high-solvent concentration, and the value of the activity coefficient of this key may approach the infinite dilution value, often a very large number.

The natural relative volatility of the system is enhanced when the activity coefficient of the lower-boiling pure component is increased by the solvent addition (γ_L/γ_H increases and $P_L^{sat}/P_H^{sat} > 1$). In this case, the lower-boiling pure component will be recovered in the distillate as expected. For the higher-boiling pure component to be recovered in the distillate, the addition of the solvent must decrease the ratio γ_L/γ_H such that the product of γ_L/γ_H and P_L^{sat}/P_H^{sat} (that is, $\alpha_{L,H}$) in the presence of the solvent is less than unity. Generally, the latter is more difficult to achieve and requires higher solvent-to-feed ratios. It is normally better to select a solvent that forces the lower-boiling component overhead.

The effect of solvent concentration on the activity coefficients of the key components is shown in Fig. 13-92 for the system methanol-acetone with either water or methylisopropylketone (MIPK) as solvent. For an initial feed mixture of 50 mol % methanol and 50 mol % acetone (no solvent present), the ratio of activity coefficients of methanol and acetone is close to unity. With water as the solvent, the

activity coefficient of the similar key (methanol) rises slightly as the solvent concentration increases, while the coefficient of acetone approaches the relatively large infinite dilution value. With methylisopropylketone as the solvent, acetone is the similar key and its activity coefficient drops toward unity as the solvent concentration increases, while the activity coefficient of the methanol increases.

Several methods are available for determining whether the lower- or higher-boiling pure component will be recovered in the distillate. For a series of solvent concentrations, the binary y - x phase diagram for the low-boiling and high-boiling keys can be plotted on a solvent-free basis. At a particular solvent concentration (dependent on the selected solvent and keys), the azeotropic point in the binary plot disappears at one of the pure-component corners. The component corresponding to the corner where the azeotrope disappears is recovered in the distillate (Knapp and Doherty, *Kirk-Othmer Encyclopedia of Chemical Technology*, 5th ed., vol. 8, p. 786, Wiley, New York, 2004). LaRoche et al. [*Can. J. Chem. Eng.*, **69**, 1302 (1991)] present a related method in which the $\alpha_{L,H} = 1$ line is plotted on the ternary composition diagram. If this line intersects the lower-boiling pure component + solvent binary face, then the lower-boiling component will be recovered in the distillate, and vice versa if the $\alpha_{L,H} = 1$ line intersects the higher-boiling pure component + solvent face. A very simple method, if a rigorous residue curve map is available, is to examine the shape and inflection of the residue curves as they approach the pure solvent vertex. Whichever solvent-key component face the residue curves predominantly tend toward as they approach the solvent vertex is the key component that will be recovered in the bottoms with the solvent (see property 6, p. 193, in Doherty and Malone, *op. cit.*). In Fig. 13-93a, all residue curves approaching the water (solvent) vertex are inflected toward the methanol-water face, with the result that methanol will be recovered in the bottoms and acetone in the distillate. Alternatively, with MIPK as the solvent, all residue curves show inflection toward the acetone-MIPK face (Fig. 13-93b), indicating that acetone will be recovered in the bottoms and methanol in the distillate.

Extractive Distillation Design and Optimization Extractive distillation column composition profiles have a very characteristic

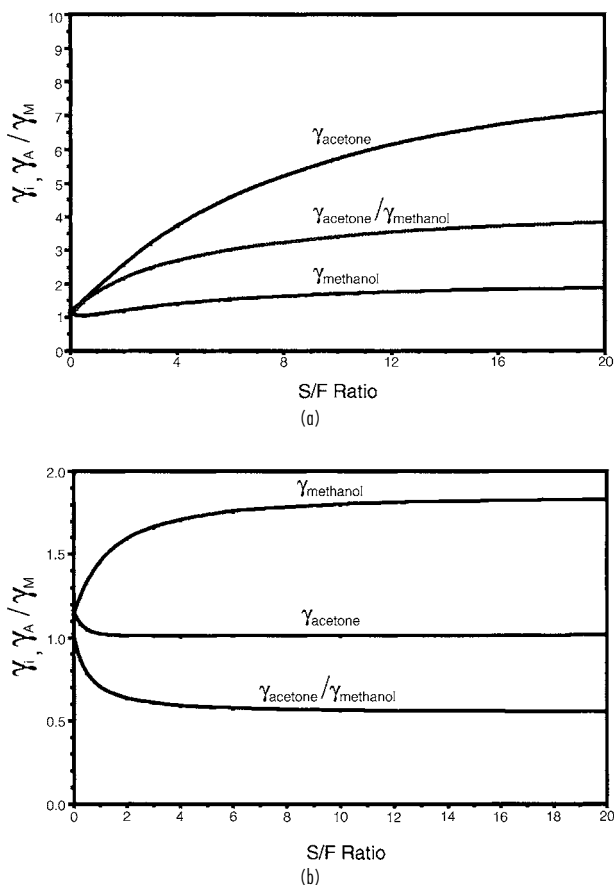


FIG. 13-92 Effect of solvent concentration on activity coefficients for acetone-methanol system. (a) Water solvent. (b) MIPK solvent.

shape on a ternary diagram. The composition profile for the separation of methanol-acetone with water is given in Fig. 13-94. Stripping and rectifying profiles start at the bottoms and distillate compositions, respectively, track generally along the faces of the composition triangle, and then turn toward the high-boiling (solvent) node and low-boiling node, respectively. For a feasible single-feed design, these profiles must cross at some point. However, in an extractive distillation they cannot cross. The extractive section profile acts at the bridge between these two sections. Most of the key component separation occurs in this section in the presence of high-solvent composition.

The variable that has the most significant impact on the economics of an extractive distillation is the solvent-to-feed flow rate ratio S/F . For close-boiling or pinched nonazeotropic mixtures, no minimum-solvent flow rate is required to effect the separation, as the separation is always theoretically possible (if not economical) in the absence of the solvent. However, the extent of enhancement of the relative volatility is largely determined by the solvent composition in the lower column sections and hence the S/F ratio. The relative volatility tends to increase as the S/F ratio increases. Thus, a given separation can be accomplished in fewer equilibrium stages. As an illustration, the total number of theoretical stages required as a function of S/F ratio is plotted in Fig. 13-95a for the separation of the nonazeotropic mixture of vinyl acetate and ethyl acetate using phenol as the solvent.

For the separation of a minimum-boiling binary azeotrope by extractive distillation, there is clearly a minimum-solvent flow rate below which the separation is impossible (due to the azeotrope). For azeotropic separations, the number of equilibrium stages is infinite at or below $(S/F)_{\text{min}}$ and decreases rapidly with increasing solvent feed

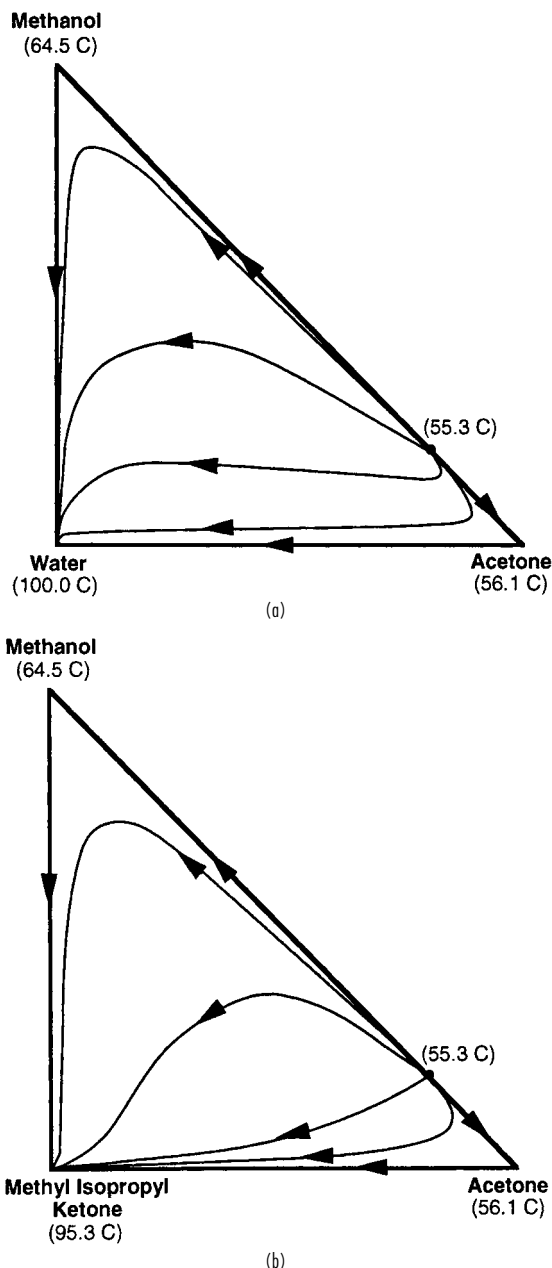


FIG. 13-93 Residue curve maps for acetone-methanol systems. (a) With water. (b) With MIPK.

flow, and then may asymptote, or rise slowly. The relationship between the total number of stages and the S/F ratio for a given purity and recovery for the azeotropic acetone-methanol system with water as solvent is shown in Fig. 13-95b. A rough idea of $(S/F)_{\text{min}}$ can be determined from a pseudobinary diagram or by plotting the $\alpha_{L,H} = 1$ line on a ternary diagram. The solvent composition at which the azeotrope disappears in a corner of the pseudobinary diagram is an indication of $(S/F)_{\text{min}}$ [LaRoche et al., *Can. J. Chem. Eng.*, **69**, 1302 (1991)]. An exact method for calculating $(S/F)_{\text{min}}$ is given by Knapp and Doherty [*AIChE J.*, **40**, 243 (1994)]. Typically, operating S/F ratios for economically acceptable solvents are between 2 and 5. Higher

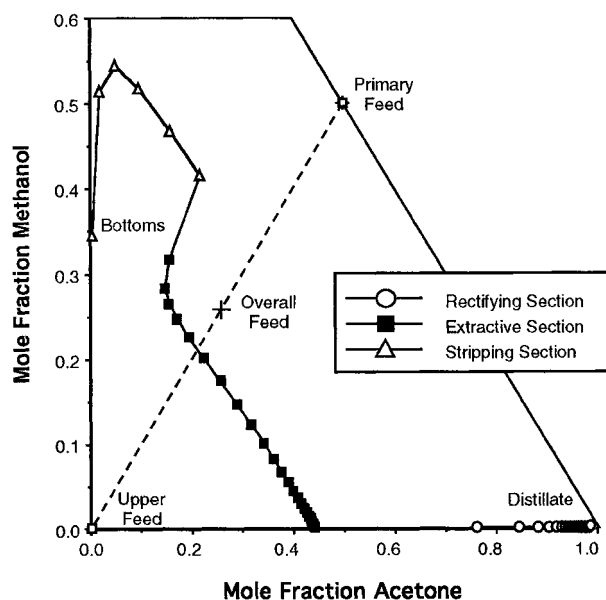


FIG. 13-94 Extractive distillation column composition profile for the separation of acetone-methanol with water.

S/F ratios tend to increase the diameter of both the extractive column and the solvent recovery columns, but reduce the required number of equilibrium stages and minimum reflux ratio. Moreover, higher S/F ratios lead to higher reboiler temperatures, resulting in the use of higher-cost utilities, higher utility usages, and greater risk of degradation.

Knight and Doherty [*Ind. Eng. Chem. Fundam.*, **28**, 564 (1989)] have published rigorous methods for computing minimum reflux for extractive distillation; they found that an operating reflux ratio of 1.2 to 1.5 times the minimum value is usually acceptable. Interestingly, unlike other forms of distillation, in extractive distillation the distillate purity or recovery does not increase monotonically with increasing reflux ratio for a given number of stages. Above a maximum reflux ratio the separation can no longer be achieved, and the distillate purity actually decreases for a given number of stages [LaRoche et al., *AIChE J.*, **38**, 1309 (1992)]. The difference between R_{\min} and R_{\max} increases as the S/F ratio increases. Large amounts of reflux lowers the solvent composition in the upper section of the column, degrading rather than enhancing column performance. Because the reflux ratio goes through a maximum, the conventional control strategy of increasing reflux to maintain purity can be detrimental rather than beneficial. However, R_{\max} generally occurs at impractically high reflux ratios and is typically not of major concern.

The thermal quality of the solvent feed has no effect on the value of S/F_{\min} , but does affect the minimum reflux to some extent, especially as the S/F ratio increases. The maximum reflux ratio R_{\max} occurs at higher values of the reflux ratio as the upper-feed quality decreases; a subcooled upper feed provides additional refluxing capacity and less external reflux is required for the same separation. It is also sometimes advantageous to introduce the primary feed to the extractive distillation column as a vapor to help maintain a higher solvent composition on the feed tray and the trays immediately below.

Robinson and Gilliland (*Elements of Fractional Distillation*, McGraw-Hill, New York, 1950), Smith (*Design of Equilibrium Stage Processes*, McGraw-Hill, New York, 1963), Van Winkle (*Distillation*, McGraw-Hill, New York, 1967), and Walas (*Chemical Process Equipment*, Butterworths, Boston, 1988) discuss rigorous stage-to-stage design techniques as well as shortcut and graphical methods for determining minimum stages, $(S/F)_{\min}$, minimum reflux, and the optimum locations of the solvent and primary feed points. Knapp and Doherty [*AIChE J.*, **40**, 243 (1994)] have published column design methods

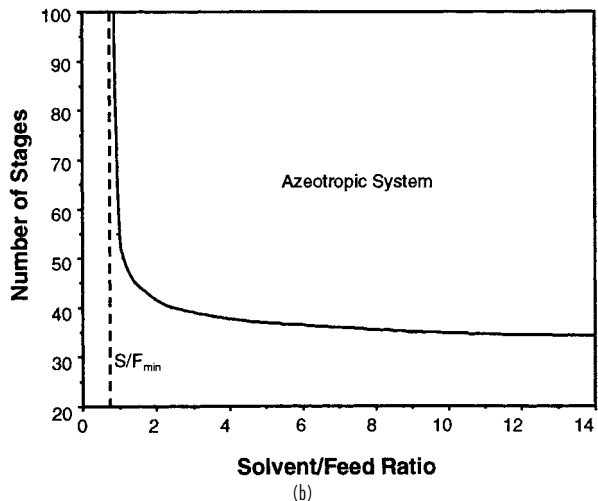
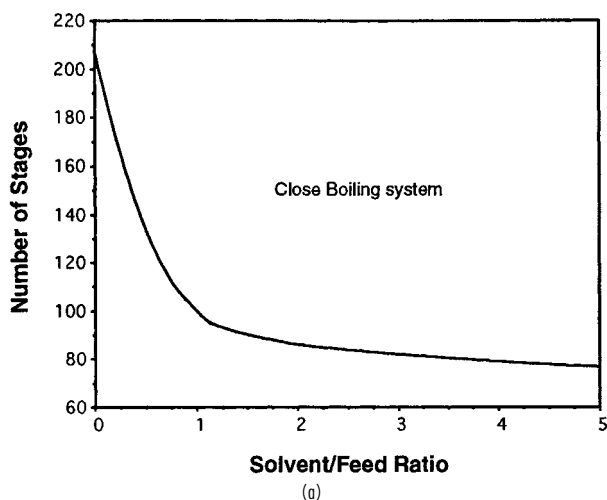


FIG. 13-95 Number of theoretical stages versus solvent-to-feed ratio for extractive distillation. (a) Close-boiling vinyl acetate-ethyl acetate system with phenol solvent. (b) Azeotropic acetone-methanol system with water solvent.

based on geometric arguments and fixed-point analysis that are capable of calculating $(S/F)_{\min}$, as well as the minimum and maximum reflux ratio. Most commercial simulators are capable of solving multiple-feed extractive distillation heat and material balances, but do not include straightforward techniques for calculating $(S/F)_{\min}$, or the minimum and maximum reflux ratio.

Solvent Screening and Selection Choosing an effective solvent can have the most profound effect on the economics of an extractive distillation process. The approach most often adopted is to first generate a short list of potential solvents by using simple qualitative screening and selection methods. Experimental verification is best undertaken only after a list of promising candidate solvents has been generated and some chance at economic viability has been demonstrated via preliminary process modeling.

Solvent selection and screening approaches can be divided into two levels of analysis. The first level focuses on identification of functional groups or chemical families that are likely to give favorable solvent-key component molecular interactions. The second level of analysis identifies and compares individual candidate solvents. The

13-92 DISTILLATION

various methods of analysis are described briefly and illustrated with an example of choosing a solvent for the methanol-acetone separation.

First Level: Broad Screening by Functional Group or Chemical Family

Homologous series. Select candidate solvents from the high-boiling homologous series of both light and heavy key components. Favor homologs of the heavy key, as this tends to enhance the natural relative volatility of the system. Homologous components tend to form ideal solutions and are unlikely to form azeotropes [Scheibel, *Chem. Eng. Prog.*, **44**(12), 927 (1948)].

Robbins chart. Select candidate solvents from groups in the Robbins chart (Table 13-17) that tend to give positive (or no) deviations from Raoult's law for the key component desired in the distillate and negative (or no) deviations for the other key.

Hydrogen-bonding characteristics. Select candidate solvents from groups that are likely to cause the formation of hydrogen bonds with the key component to be removed in the bottoms, or disruption of hydrogen bonds with the key to be removed in the distillate. Formation and disruption of hydrogen bonds are often associated with strong negative and positive deviations, respectively, from Raoult's law. Several authors have developed charts indicating expected hydrogen bonding interactions between families of compounds [Ewell et al., *Ind. Eng. Chem.*, **36**, 871 (1944); Gilmont et al., *Ind. Eng. Chem.*, **53**, 223 (1961); and Berg, *Chem. Eng. Prog.*, **65**(9), 52 (1969)]. Table 13-22 presents a hydrogen bonding classification of chemical families and a summary of deviations from Raoult's law.

fication of chemical families and a summary of deviations from Raoult's law.

Polarity characteristics. Select candidate solvents from chemical groups that tend to show higher polarity than one key component or lower polarity than the other key. Polarity effects are often cited as a factor in causing deviations from Raoult's law [Hopkins and Fritsch, *Chem. Eng. Prog.*, **51**(8), (1954); Carlson et al., *Ind. Eng. Chem.*, **46**, 350 (1954); and Prausnitz and Anderson, *AIChE J.*, **7**, 96 (1961)]. The general trend in polarity based on the functional group of a molecule is given in Table 13-23. The chart is best for molecules of similar size. A more quantitative measure of the polarity of a molecule is the polarity contribution to the three-term Hansen solubility parameter. A tabulation of calculated three-term solubility parameters is provided by Barton (*CRC Handbook of Solubility Parameters and Other Cohesion Parameters*, CRC Press, Boca Raton, Fla., 1991), along with a group contribution method for calculating the three-term solubility parameters of compounds not listed in the reference.

Second Level: Identification of Individual Candidate Solvents

Boiling point characteristics. Select only candidate solvents that boil at least 30 to 40°C above the key components to ensure that the solvent is relatively nonvolatile and remains largely in the liquid phase. With this boiling point difference, the solvent should also not form azeotropes with the other components.

Selectivity at infinite dilution. Rank candidate solvents according to their selectivity at infinite dilution. The selectivity at infinite

TABLE 13-22 Hydrogen Bonding Classification of Chemical Families

Class	Chemical family			
H-Bonding, Strongly Associative (HBSA)	Water Primary amides Secondary amides	Polyacids Dicarboxylic acids Monohydroxy acids	Polyphenols Oximes Hydroxylamines	Amino alcohols Polyols
H-Bond Acceptor-Donor (HBAD)	Phenols Aromatic acids Aromatic amines Alpha H nitriles	Imines Monocarboxylic acids Other monoacids Peracids	Alpha H nitros Azines Primary amines Secondary amines	n-alcohols Other alcohols Ether alcohols
H-Bond Acceptor (HBA)	Acyl chlorides Acyl fluorides Hetero nitrogen aromatics Hetero oxygen aromatics	Tertiary amides Tertiary amines Other nitriles Other nitros Isocyanates Peroxides	Aldehydes Anhydrides Cyclo ketones Aliphatic ketones Esters Ethers	Aromatic esters Aromatic nitriles Aromatic ethers Sulfones Sulfolanes
π -Bonding Acceptor (π -HBA)	Alkynes Alkenes	Aromatics Unsaturated esters		
H-Bond Donor (HBD)	Inorganic acids Active H chlorides	Active H fluorides Active H iodides	Active H bromides	
Non-Bonding (NB)	Paraffins Nonactive H chlorides	Nonactive H fluorides Sulfides	Nonactive H iodides Disulfides	Nonactive H bromides Thiols

Deviations from Raoult's Law

H-Bonding classes	Type of deviations	Comments
HBSA + NB HBAD + NB	Always positive dev., HBSA + NB often limited miscibility	H-bonds broken by interactions
HBA + HBD	Always negative dev.	H-bonds formed by interactions
HBSA + HBD HBAD + HBD	Always positive deviations, HBSA + HBD often limited miscibility	H-bonds broken and formed; dissociation of HBSA or HBAD liquid most important effect
HBSA + HBSA HBSA + HBAD HBSA + HBA HBAD + HBAD HBAD + HBA	Usually positive deviations; some give maximum-boiling azeotropes	H-bonds broken and formed
HBA + HBA HBA + NB HBD + HBD HBD + NB NB + NB	Ideal, quasi-ideal systems; always positive or no deviations; azeotropes, if any, minimum-boiling	No H-bonding involved

NOTE: π -HBA is enhanced version of HBA.

TABLE 13-23 Relative Polarities of Functional Groups

MOST POLAR	Water
	Organic acids
	Amines
	Polyols
	Alcohols
	Esters
	Ketones
	Aldehydes
	Ethers
	Aromatics
	Olefins
LEAST POLAR	Paraffins
Effect of branching	
MOST POLAR	Normal
	Secondary
LEAST POLAR	Tertiary

dilution is defined as the ratio of the activity coefficients at infinite dilution of the two key components in the solvent. Since solvent effects tend to increase as solvent concentration increases, the infinite-dilution selectivity gives an upper bound on the efficacy of a solvent. Infinite-dilution activity coefficients can be predicted by using such methods as UNIFAC, ASOG, MOSCED (Reid et al., *Properties of Gases and Liquids*, 4th ed., McGraw-Hill, New York, 1987). They can be found experimentally by using a rapid gas-liquid chromatography method based on relative retention times in candidate solvents (Tassios, in *Extractive and Azeotropic Distillation*, Advances in Chemistry Series 115, American Chemical Society, Washington, 1972), and they can be correlated to bubble point data [Kojima and Ochi, *J. Chem. Eng. Japan*, 7(2), 71 (1974)]. DECHEMA (*Vapor-Liquid Equilibrium Data Collection*, Frankfurt, 1977) has also published a compilation of experimental infinite-dilution activity coefficients.

Experimental measurement of relative volatility. Rank candidate solvents by the increase in relative volatility caused by the addition of the solvent. One technique is to experimentally measure the relative volatility of a fixed-composition, key component + solvent mixture (often a 1/1 ratio of each key, with a 1/1 to 3/1 solvent/key ratio) for various solvents [Carlson et al., *Ind. Eng. Chem.*, 46, 350 (1954)]. The Othmer equilibrium still is the apparatus of choice for these measurements [Zudkevitch, *Chem. Eng. Comm.*, 116, 41 (1992)].

At atmospheric pressure, methanol and acetone boil at 64.5 and 56.1°C, respectively, and form a minimum-boiling azeotrope at 55.3°C. The natural volatility of the system is acetone > methanol, so the favored solvents most likely will be those that cause acetone to be recovered in the distillate. However, for the purposes of the example, a solvent that reverses the natural volatility will also be identified. First, by examining the polarity of ketones and alcohols (Table 13-23), solvents favored for the recovery of methanol in the bottoms would come from groups more polar than methanol, such as acids, water, and polyols. Turning to the Robbins chart (Table 13-17), we see favorable groups are amines, alcohols, polyols, and water since these show expected positive deviations for acetone and zero or negative deviations for methanol. For reversing the natural volatility, solvents should be chosen that are less polar than acetone, such as ethers, hydrocarbons, and aromatics. Unfortunately, both ethers and hydrocarbons are expected to give positive deviations for both acetone and methanol, so should be discarded. Halohydrocarbons and ketones are expected to give positive deviations for methanol and either negative or no deviations for acetone. The other qualitative indicators show that both homologous series (ketones and alcohols) look promising. Thus, after discounting halohydrocarbons for environmental reasons, the best solvents will probably come from alcohols, polyols, and water for recovering methanol in the bottoms and ketones for recovering acetone in the bottoms. Table 13-24 shows the boiling points and experimental or estimated infinite-dilution activity coefficients for several candidate solvents from the aforementioned groups. Methyl ethyl ketone boils too low, as does ethanol, and also forms an azeotrope with methanol. These two candidates can be discarded. Other members of the homologous series, along with water and ethylene glycol, have acceptable

TABLE 13-24 Comparison of Candidate Solvents for Methanol/Acetone Extractive Distillation

Solvent	Boiling pt. (°C)	Azeotrope formation	$\gamma_{\text{Acetone}}^{\infty}$	$\gamma_{\text{MeOH}}^{\infty}$	$\gamma_{\text{Acetone}}^{\infty}/\gamma_{\text{MeOH}}^{\infty}$
MEK	79.6	With MeOH	1.01	1.88	0.537
MIPK	102.0	No	1.01	1.89	0.534
MIBK	115.9	No	1.06	2.05	0.517
Ethanol	78.3	No	1.85	1.04	1.78
1-Propanol	97.2	No	1.90	1.20	1.58
1-Butanol	117.8	No	1.93	1.33	1.45
Water	100.0	No	11.77	2.34	5.03
EG	197.2	No	3.71	1.25	2.97

$$\gamma_{\text{Acetone}}^{\infty} = 1.79 \text{ (in MeOH)}$$

$$\gamma_{\text{MeOH}}^{\infty} = 1.81 \text{ (in acetone)}$$

boiling points (at least 30°C higher than those of the keys). Of these, water (the solvent used industrially) clearly has the largest effect on the activity coefficients, followed by ethylene glycol. Although inferior to water or ethylene glycol, both MIPK and MIBK would probably be acceptable for reversing the natural volatility of the system.

Extractive Distillation by Salt Effects A second method of modifying the liquid-phase behavior (and thus the relative volatility) of a mixture to effect a separation is by the addition of a nonvolatile, soluble, ionic salt. The process is analogous to extractive distillation with a high-boiling liquid. In the simplest case, for the separation of a binary mixture, the salt is fed at the top of the column by dissolving it in the hot reflux stream before introduction into the column. To function effectively, the salt must be adequately soluble in both components throughout the range of compositions encountered in the column. Since the salt is completely nonvolatile, it remains in the liquid phase on each tray and alters the relative volatility throughout the length of the column. No rectification section is needed above the salt feed. The bottoms product is recovered from the salt solution by evaporation or drying, and the salt is recycled. The ions of a salt are typically capable of causing much larger and more selective effects on liquid-phase behavior than the molecules of a liquid solvent. As a result, salt-to-feed ratios of less than 0.1 are typical.

The use of a salting agent presents a number of problems not associated with a liquid solvent, such as the difficulty of transporting and metering a solid or saturated salt solution, slow mixing or dissolution rate of the salt, limits to solubility in the feed components, and potential for corrosion. However, in the limited number of systems for which an effective salt can be found, the energy usage, equipment size, capital investment, and ultimate separation cost can be significantly reduced compared to that for extractive distillation using a liquid solvent [Furter, *Chem. Eng. Commun.*, 116, 35 (1992)]. Applications of salt extractive distillation include acetate salts to produce absolute ethanol, magnesium nitrate for the production of concentrated nitric acid as an alternative to the sulfuric acid solvent process, and calcium chloride to produce anhydrous hydrogen chloride. Other examples are noted by Furter [*Can. J. Chem. Eng.*, 55, 229 (1977)].

One problem limiting the consideration of salt extractive distillation is the fact that the performance and solubility of a salt in a particular system are difficult to predict without experimental data. Some recent advances have been made in modeling the VLE behavior of organic aqueous salt solutions using modified UNIFAC, NRTL, UNIQUAC, and other approaches [Kumar, *Sep. Sci. Tech.*, 28(1), 799 (1993)].

REACTIVE DISTILLATION

Reactive distillation is a unit operation in which chemical reaction and distillation are carried out simultaneously within a fractional distillation apparatus. Reactive distillation may be advantageous for liquid-phase reaction systems when the reaction must be carried out with a large excess of one or more of the reactants, when a reaction

can be driven to completion by removal of one or more of the products as they are formed, or when the product recovery or by-product recycle scheme is complicated or made infeasible by azeotrope formation.

For consecutive reactions in which the desired product is formed in an intermediate step, excess reactant can be used to suppress additional series reactions by keeping the intermediate-species concentration low. A reactive distillation can achieve the same result by removing the desired intermediate from the reaction zone as it is formed. Similarly, if the equilibrium constant of a reversible reaction is small, high conversions of one reactant can be achieved by use of a large excess of the other reactant. Alternatively, by Le Chatelier's principle, the reaction can be driven to completion by removal of one or more of the products as they are formed. Typically, reactants can be kept much closer to stoichiometric proportions in a reactive distillation.

When a reaction mixture exhibits azeotropes, the recovery of products and recycle of excess reagents can be quite complicated and expensive. Reactive distillation can provide a means of breaking azeotropes by altering or eliminating the condition for azeotrope formation in the reaction zone through the combined effects of vaporization-condensation and consumption-production of the species in the mixture. Alternatively, a reaction may be used to convert the species to components that are more easily distilled. In each of these situations, the conversion and selectivity often can be improved markedly, with much lower reactant inventories and recycle rates, and much simpler recovery schemes. The capital savings can be quite dramatic. A list of applications of reactive distillation appearing in the literature is given in Table 13-25. Additional industrial applications are described by Sharma and Mahajani (chap. 1 in Sundmacher and Kienle, eds., *Reactive Distillation*, Wiley-VCH, 2003).

Although reactive distillation has many potential applications, it is not appropriate for all situations. Since it is in essence a distillation process, it has the same range of applicability as other distillation operations. Distillation-based equipment is not designed to effectively handle solids, supercritical components (where no separate vapor and liquid phases exist), gas-phase reactions, or high-temperature or high-pressure reactions such as hydrogenation, steam reforming, gasification, and hydrodealkylation.

Simulation, Modeling, and Design Feasibility Because reaction and separation phenomena are closely coupled in a reactive distillation process, simulation and design are significantly more complex than those of sequential reaction and separation processes. In spite of the complexity, however, most commercial computer process modeling packages offer reliable and flexible routines for simulating steady-state reactive distillation columns, with either equilibrium or kinetically controlled reaction models

[Venkataraman et al., *Chem. Eng. Prog.*, **86**(6), 45 (1990)]. As with other enhanced distillation processes, the results are very sensitive to the thermodynamic models chosen and the accuracy of the VLE data used to generate model parameters. Of equal, if not greater significance is the accuracy of data and models for reaction rate as a function of catalyst concentration, temperature, and composition. Very different conclusions can be drawn about the feasibility of a reactive distillation if the reaction is assumed to reach chemical equilibrium on each stage of the column or if the reaction is assumed to be kinetically controlled [Barbosa and Doherty, *Chem. Eng. Sci.*, **43**, 541 (1988); Chadda, Malone, and Doherty, *AIChE J.*, **47**, 590 (2001)]. Tray holdup and stage requirements are two important variables directly affected by the reaction time relative to the residence time inside the column. Unlike distillation without reaction, product feasibility can be quite sensitive to changes in tray holdup and production rate.

When an equilibrium reaction occurs in a vapor-liquid system, the phase compositions depend not only on the relative volatility of the components in the mixture, but also on the consumption (and production) of species. Thus, the condition for azeotropy in a nonreactive system ($y_i = x_i$ for all i) no longer holds true in a reactive system and must be modified to include reaction stoichiometry:

$$\frac{y_i - x_i}{v_i - v_T x_i} = \frac{y_i - x_i}{v_i - v_T x_i} \quad \text{for all } i = 1, \dots, c \quad (13-118)$$

where

$$v_T = \sum_{i=1}^c v_i$$

and v_i represents the stoichiometric coefficient of component i (negative for reactants, positive for products).

Phase compositions that satisfy Eq. (13-118) are stationary points on a phase diagram and have been labeled *reactive azeotropes* by Barbosa and Doherty [*Chem. Eng. Sci.*, **43**, 529 (1988)]. At a reactive azeotrope the mass exchange between the vapor and liquid phases and the generation (or consumption) of each species are balanced such that the composition of neither phase changes. Reactive azeotropes show the same distillation properties as ordinary azeotropes and therefore affect the achievable products. Reactive azeotropes are predicted to exist in numerous reacting mixtures and have been confirmed experimentally in the reactive boiling mixture of acetic acid + isopropanol + isopropyl acetate + water [Song et al., *Nature*, **388**, 561 (1997); Huang et al., *Chem. Eng. Sci.*, **60**, 3363 (2005)].

Reactive azeotropes are not easily visualized in conventional y - x coordinates but become apparent upon a transformation of coordinates which depends on the number of reactions, the order of each reaction (for example, $A + B \rightleftharpoons C$ or $A + B \rightleftharpoons C + D$), and the presence of nonreacting components. The general vector-matrix form of

TABLE 13-25 Applications of Reactive Distillation

Process	Reaction type	Reference
Methyl acetate from methanol and acetic acid General process for ester formation	Esterification Esterification	Agreda et al., <i>Chem. Eng. Prog.</i> , 86 (2), 40 (1990) Simons, "Esterification" in <i>Encyclopedia of Chemical Processing and Design</i> , Vol 19, Dekker, New York, 1983
Diphenyl carbonate from dimethyl carbonate and phenol	Esterification	Oyevaar et al., U.S. Patent 6,093,842 (2000)
Dibutyl phthalate from butanol and phthalic acid	Esterification	Berman et al., <i>Ind. Eng. Chem.</i> , 40 , 2139 (1948)
Ethyl acetate from ethanol and butyl acetate	Transesterification	Davies and Jeffreys, <i>Trans. Inst. Chem. Eng.</i> , 51 , 275 (1973)
Recovery of acetic acid and methanol from methyl acetate by-product of vinyl acetate production	Hydrolysis	Fuchigami, <i>J. Chem. Eng. Jap.</i> , 23 , 354 (1990)
Nylon 6,6 prepolymer from adipic acid and hexamethylenediamine	Amidation	Jaswal and Pugi, U.S. Patent 3,900,450 (1975)
MTBE from isobutene and methanol	Etherification	DeGarmo et al., <i>Chem. Eng. Prog.</i> , 88 (3), 43 (1992)
TAME from pentenes and methanol	Etherification	Brockwell et al., <i>Hyd. Proc.</i> , 70 (9), 133 (1991)
Separation of close boiling 3- and 4-picoline by complexation with organic acids	Acid-base	Duprat and Gau, <i>Can. J. Chem. Eng.</i> , 69 , 1320 (1991)
Separation of close-boiling meta and para xylenes by formation of tert-butyl meta-xylene	Transalkylation	Saito et al., <i>J. Chem. Eng. Jap.</i> , 4 , 37 (1971)
Cumene from propylene and benzene	Alkylation	Shoemaker and Jones, <i>Hyd. Proc.</i> , 67 (6), 57 (1987)
General process for the alkylation of aromatics with olefins	Alkylation	Crossland, U.S. Patent 5,043,506 (1991)
Production of specific higher and lower alkenes from butenes	Diproporation	Jung et al., U.S. Patent 4,709,115 (1987)
4-Nitrochlorobenzene from chlorobenzene and nitric acid	Nitration	Belson, <i>Ind. Eng. Chem. Res.</i> , 29 , 1562 (1990)
Production of methylal and high purity formaldehyde		Masamoto and Matsuzaki, <i>J. Chem. Eng. Jap.</i> , 27 , 1 (1994)

the transform for c reacting components, with R reactions, and I non-reacting components, has been derived by Ung and Doherty [*Chem. Eng. Sci.*, **50**, 23 (1995)]. For the transformed mole fraction of component i in the liquid phase X_i , they give

$$X_i = \left[\frac{x_i - \mathbf{v}_i^T (\mathbf{v}_{\text{Ref}})^{-1} \mathbf{x}_{\text{Ref}}}{1 - \mathbf{v}_{\text{TOT}}^T (\mathbf{v}_{\text{Ref}})^{-1} \mathbf{x}_{\text{Ref}}} \right] \quad i = 1, \dots, c - R \quad (13-119)$$

where \mathbf{v}_i^T = row vector of stoichiometric coefficients of component i for each reaction
 \mathbf{v}_{Ref} = square matrix of stoichiometric coefficients for R reference components in R reactions
 \mathbf{x}_{Ref} = column vector of mole fractions for R reference components in liquid phase
 $\mathbf{v}_{\text{TOT}}^T$ = row vector composed of sum of stoichiometric coefficients for each reaction

An equation identical to (13-119) defines the transformed mole fraction of component i in the vapor phase Y_i , where the terms in x are replaced by terms in y .

The transformed variables describe the system composition with or without reaction and sum to unity as do x_i and y_i . The condition for reactive azeotropy becomes $X_i = Y_i$. Barbosa and Doherty have shown that phase diagrams and distillation diagrams constructed by using the transformed composition coordinates have the same properties as phase and distillation diagrams for nonreactive systems and similarly can be used to assist in design feasibility and operability studies [*Chem. Eng. Sci.*, **43**, 529, 541, 1523, and 2377 (1988)]. Residue curve maps in transformed coordinates for the reactive system methanol–acetic acid–methyl acetate–water are shown in Fig. 13-96. Note that the nonreactive azeotrope between water and methyl acetate has disappeared, while the methyl acetate–methanol azeotrope remains intact. Only those azeotropes containing all the reactants or products will be altered by the reaction (water and methyl acetate can back-react to form acetic acid and methanol, whereas methanol and methyl acetate cannot further react in the absence of either water or acetic acid). This reactive system consists of only one distillation region in which the methanol–methyl acetate azeotrope is the low-boiling node and acetic acid is the high-boiling node.

The situation becomes more complicated when the reaction is kinetically controlled and does not come to complete chemical equilibrium under the conditions of temperature, liquid holdup, and rate of vaporization in the column reactor. Venimadhavan et al. [*AIChE J.*, **40**, 1814

(1994); **45**, 546 (1999)] and Rev [*Ind. Eng. Chem. Res.*, **33**, 2174 (1994)] show that the concept of a reactive azeotrope generalizes to the concept of a *reactive fixed point*, whose existence and location are a function of approach to equilibrium as well as the evaporation rate [see also Frey and Stichlmair, *Trans IChemE*, **77**, Part A, 613 (1999); Chadda, Malone, and Doherty, *AIChE J.*, **47**, 590 (2001); Chiplunkar et al., *AIChE J.*, **51**, 464 (2005)]. In the limit of simultaneous phase and reaction equilibrium, a reactive fixed point becomes identical to the thermodynamic concept of a reactive azeotrope.

These ideas have been extended to reacting systems with (1) multiple chemical reactions [Ung and Doherty, *Ind. Eng. Chem. Res.*, **34**, 3195, 2555 (1995)], (2) multiple liquid phases [Ung and Doherty, *Chem. Eng. Sci.*, **50**, 3201 (1995); Qi, Kolah, and Sundmacher, *Chem. Eng. Sci.*, **57**, 163 (2002); Qi and Sundmacher, *Comp. Chem. Eng.*, **26**, 1459 (2002)], (3) membrane separations [Huang et al., *Chem. Eng. Sci.*, **59**, 2863 (2004)], (4) finite rates of vapor-liquid mass transfer [Baur, Taylor, and Krishna, *Chem. Eng. Sci.*, **56**, 2085 (2001); Nisoli, Doherty, and Malone, *AIChE J.*, **50**, 1795 (2004)], (5) column design and multiple steady-states [Guttinger, Dorn, and Morari, *Ind. Eng. Chem. Res.*, **36**, 794 (1997); Hauan, Hertzberg, and Lien, *Comput. Chem. Eng.*, **21**, 1117 (1997); Sneesby et al., *Ind. Eng. Chem. Res.*, **36**, 1855 (1997); Bessling et al., *Chem. Eng. Technol.*, **21**, 393 (1998); Okasinski and Doherty, *Ind. Eng. Chem. Res.*, **37**, 2821 (1998); Sneesby, Tade, and Smith, *Trans IChemE*, **76**, Part A, 525 (1998); Guttinger and Morari, *Ind. Eng. Chem. Res.*, **38**, 1633, 1649 (1999); Higler, Taylor, and Krishna, *Chem. Eng. Sci.*, **54**, 1389 (1999); Mohl et al., *Chem. Eng. Sci.*, **54**, 1029 (1999); Chen et al., *Comput. Chem. Eng.*, **26**, 81 (2002)]. Much useful information is available in Taylor and Krishna [*Chem. Eng. Sci.*, **55**, 5183 (2000)] and Sundmacher and Kienle (*Reactive Distillation*, Wiley-VCH, 2003).

Mechanical Design and Implementation Issues The choice of catalyst has a significant impact on the mechanical design and operation of the reactive column. The catalyst must allow the reaction to occur at reasonable rates at the relatively low temperatures and pressures common in distillation operations (typically less than 10 atm and between 50 and 250°C). Selection of a homogeneous catalyst, such as a high-boiling mineral acid, allows the use of more traditional tray designs and internals (albeit designed with exotic materials of construction to avoid corrosion, and allowance for high-liquid holdups to achieve suitable reaction contact times). With a homogeneous catalyst, lifetime is not a problem, as it is added (and withdrawn) continuously. Alternatively, heterogeneous solid catalysts

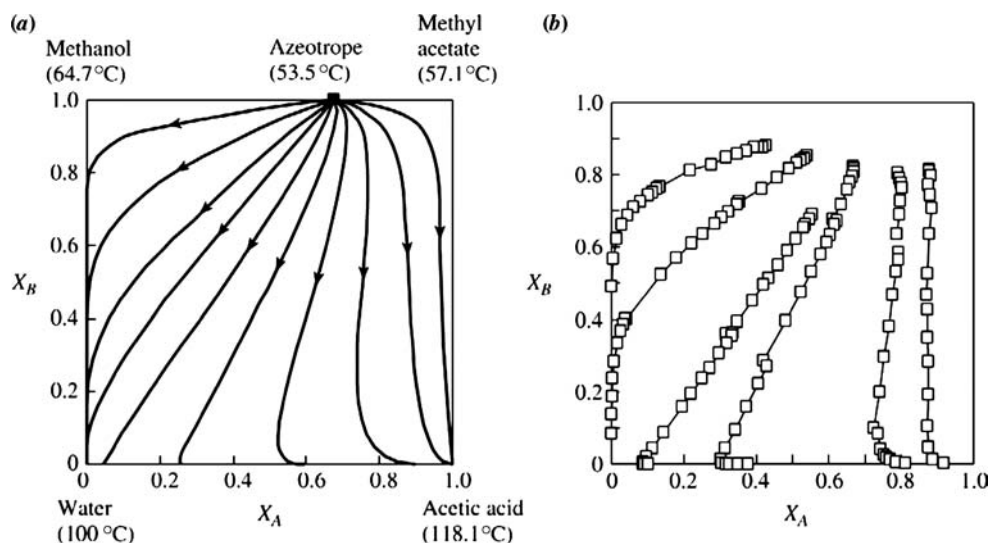


FIG. 13-96 Residue curve maps for the reactive system methanol–acetic acid–methyl acetate–water in phase and chemical equilibrium at 1-atm pressure. (a) Calculated by Barbosa and Doherty [*Chem. Eng. Sci.*, **43**, 1523 (1988)]. (b) Measured by Song et al. [*Ind. Eng. Chem. Res.*, **37**, 1917 (1998)].

TABLE 13-26 Catalyst Systems for Reactive Distillation

Description	Application	Reference
<i>Homogeneous catalysis</i>		
Liquid-phase mineral-acid catalyst added to column or reboiler	Esterifications Dibutyl phthalate Methyl acetate	Keyes, <i>Ind. Eng. Chem.</i> , 24 , 1096 (1932) Berman et al., <i>Ind. Eng. Chem.</i> , 40 , 2139 (1948) Agregda et al., U.S. Patent 4,435,595 (1984)
<i>Heterogeneous catalysis</i>		
Catalyst-resin beads placed in cloth bags attached to fiberglass strip. Strip wound around helical stainless steel mesh spacer	Etherifications Cumene	Smith et al., U.S. Patent 4,443,559 (1981) Shoemaker and Jones, <i>Hyd.</i> 57 (6), 57 (1987)
Ion exchange resin beads used as column packing	Hydrolysis of methyl acetate	Fuchigami, <i>J. Chem. Eng. Jap.</i> , 23 , 354 (1990)
Molecular sieves placed in bags or porous containers	Alkylation of aromatics	Crossland, U.S. Patent 5,043,506 (1991)
Ion exchange resins formed into Raschig rings	MTBE	Flato and Hoffman, <i>Chem. Eng. Tech.</i> , 15 , 193 (1992)
Granular catalyst resin loaded in corrugated sheet casings	Dimethyl acetals of formaldehyde	Zhang et al., Chinese Patent 1,065,412 (1992)
Trays modified to hold catalyst bed	MTBE	Sanfilippo et al., Eur. Pat. Appl. EP 470,625 (1992)
Distillation trays constructed of porous catalytically active material and reinforcing resins	None specified	Wang et al., Chinese Patent 1,060,228 (1992)
Method described for removing or replacing catalyst on trays as a liquid slurry	None specified	Jones, U.S. Patent, 5,133,942 (1992)
Catalyst bed placed in downcomer, designed to prevent vapor flow through bed	Etherifications, alkylations	Asselineau, Eur. Pat. Appl. EP 547,939 (1993)
Slotted plate for catalyst support designed with openings for vapor flow	None specified	Evans and Stark, Eur. Pat. Appl. EP 571,163 (1993)
Ion exchanger fibers (reinforced ion exchange polymer) used as solid-acid catalyst	Hydrolysis of methyl acetate	Hirata et al., Jap. Patent 05,212,290 (1993)
High-liquid holdup trays designed with catalyst bed extending below tray level, perforated for vapor-liquid contact	None specified	Yeoman et al., Int. Pat. Appl., WO 9408679 (1994)
Catalyst bed placed in downcomer, in-line withdrawal/addition system	None specified	Carland, U.S. Patent, 5,308,451 (1994)

require either complicated mechanical means for continuous replenishment or relatively long lifetimes to avoid constant maintenance. As with other multiphase reactors, use of a solid catalyst adds an additional resistance to mass transfer from the bulk liquid (or vapor) to the catalyst surface, which may be the limiting resistance. The catalyst containment system must be designed to ensure adequate liquid-solid contacting and minimize bypassing. A number of specialized column internal designs, catalyst containment methods, and catalyst replenishment systems have been proposed for both homogeneous and heterogeneous catalysts. A partial list of these methods is given in Table 13-26; see also the useful ideas presented by Krishna [*Chem. Eng. Sci.*, **57**, 1491 (2002)]; and chap. 7 in Sundmacher and Kienle, eds., *Reactive Distillation*, Wiley-VCH, 2003].

Heat management is another important consideration in the implementation of a reactive distillation process. Conventional reactors for highly exothermic or endothermic reactions are often designed as modified shell-and-tube heat exchangers for efficient heat transfer. However, a trayed or packed distillation column is a rather poor mechanical design for the management of the heat of reaction. Although heat can be removed or added in the condenser or reboiler easily, the only mechanism for heat transfer in the column proper is through vaporization (or condensation). For highly exothermic reactions, a large excess of reactants may be required as a heat sink, necessitating high-reflux rates and larger-diameter columns to return the vaporized reactants back to the reaction zone. Often a prereactor of conventional design is used to accomplish most of the reaction and heat removal before feeding to the reactive column for final conversion, as exemplified in most processes for the production of tertiary amyl methyl ether (TAME) [Brockwell et al., *Hyd. Proc.*, **70**(9), 133 (1991)]. Highly endothermic reactions may require intermediate reboilers. None of these heat management issues preclude the use of reactive distillation, but must be taken into account during the design phase. Comparison of heat of reaction and average heat of vaporization data for a system, as in Fig. 13-97, gives some indication of potential heat imbalances [Sundmacher, Rihko, and Hoffmann, *Chem. Eng. Comm.*, **127**, 151 (1994)]. The heat-neutral systems [$-\Delta H_{\text{react}} \approx \Delta H_{\text{vap}}$ (avg)]

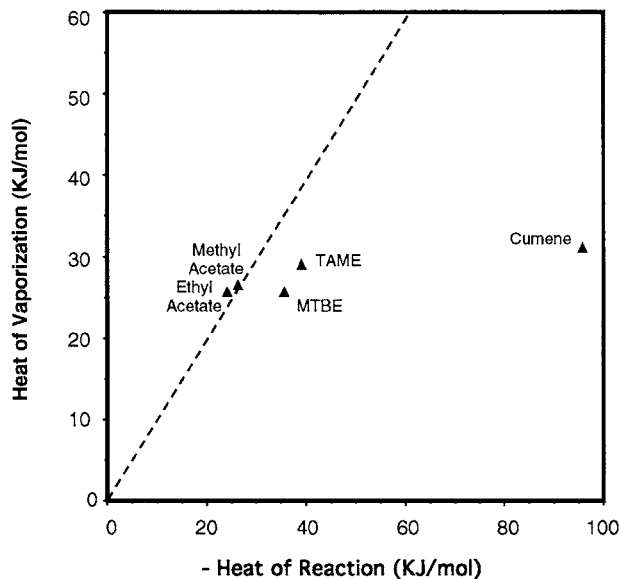


FIG. 13-97 Similarity of heats of reaction and vaporization for compounds made by reactive distillation.

such as methyl acetate and other esters can be accomplished in one reactive column, whereas the MTBE and TAME processes, with higher heats of reaction than that of vaporization, often include an additional prereactor. One exception is the catalytic distillation process for cumene production, which is accomplished without a prereactor. Three moles of benzene reactant are vaporized (and refluxed) for every mole of cumene produced. The relatively high heat of reaction is advantageous in this case as it reduces the overall

heat duty of the process by about 30 percent [Shoemaker and Jones, *Hyd. Proc.*, **57**(6), 57 (1987)].

Distillation columns with multiple conventional side reactors were first suggested by Schoenmakers and Buehler [*German Chem. Eng.*, **5**, 292 (1982)] and have the potential to accommodate gas-phase reactions, highly exo- or endothermic reactions, catalyst deactivation, and operating conditions outside the normal range suitable for distillation (e.g., short contact times, high temperature and pressure, etc). Krishna (chap. 7 in Sundmacher and Kienle, eds., *Reactive Distillation*, Wiley-VCH, 2003).

Process Applications The production of esters from alcohols and carboxylic acids illustrates many of the principles of reactive distillation as applied to equilibrium-limited systems. The true thermodynamic equilibrium constants for esterification reactions are usually in the range of 5 to 20. Large excesses of alcohols must be used to obtain acceptable yields, resulting in large recycle flow rates. In a reactive distillation scheme, the reaction is driven to completion by removal of the water of esterification. The method used for removal of the water depends on the boiling points, compositions, and liquid-phase behavior of any azeotropes formed between the products and reactants and largely dictates the structure of the reactive distillation flow sheet.

When the ester forms a binary low-boiling azeotrope with water or a ternary alcohol-ester-water azeotrope and that azeotrope is heterogeneous (or can be moved into the two-liquid phase region), the flow sheet illustrated in Fig. 13-98 can be used. Such a flow sheet works for the production of ethyl acetate and higher homologs. In this process scheme, acetic acid and the alcohol are continuously fed to the reboiler of the esterification column, along with a homogeneous strong-acid catalyst. Since the catalyst is largely nonvolatile, the reboiler acts as the primary reaction section. The alcohol is usually fed in slight excess to ensure complete reaction of the acid and to compensate for alcohol losses through distillation of the water-ester-(alcohol) azeotrope. The esterification column is operated such that the low-boiling, water-laden azeotrope is taken as the distillation product. Upon cooling, the distillate separates into two liquid phases. The aqueous layer is steam-stripped, with the organics recycled to the decanter or reactor. The ester layer from the decanter contains some water and possibly alcohol. Part of this layer may be refluxed to the esterification column. The remainder is fed to a low-boiler column where the water-ester and alcohol-ester azeotropes are removed overhead and recycled to the decanter or reactor. The dry, alcohol-free ester is then optionally taken overhead in a final refining column. Additional literature on the application of reactive distillation to ester production includes papers by Hanika, Kolenka, and Smejkal [*Chem. Eng. Sci.*, **54**, 5205 (1999)], Schwarzer and Hoffmann [*Chem. Eng. Technol.*, **25**, 975 (2002)], Steingeweg and Gmehling [*Ind. Eng.*

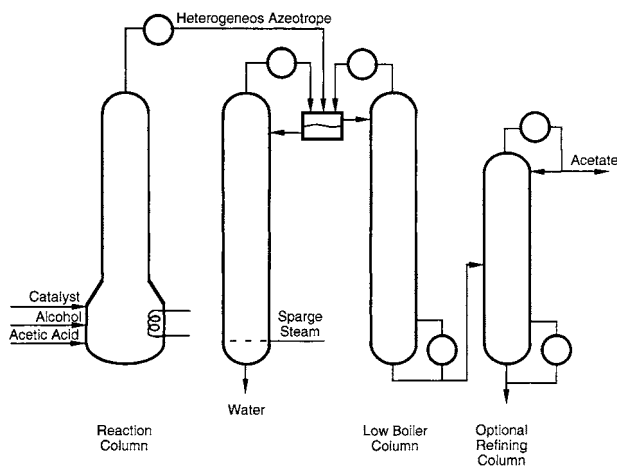


FIG. 13-98 Flow sheet for making esters which form a heterogeneous minimum-boiling azeotrope with water.

Chem. Res., **41**, 5483 (2002)], and Omata, Dimian, and Blik [*Chem. Eng. Sci.*, **58**, 3159, 3175 (2003)].

Methyl acetate cannot be produced in high purity by using the simple esterification scheme described above. The methyl acetate-methanol-water system does not exhibit a ternary minimum-boiling azeotrope, the methyl acetate-methanol azeotrope is lower-boiling than the water-methyl acetate azeotrope, a distillation boundary extends between these two binary azeotropes, and the heterogeneous region does not include either azeotrope, nor does it cross the distillation boundary. Consequently, the water of esterification cannot be removed effectively, and methyl acetate cannot be separated from the methanol and water azeotropes by a simple decantation in the same manner as outlined above. Conventional sequential reaction-separation processes rely on large excesses of acetic acid to drive the reaction to higher conversion to methyl acetate, necessitating a capital- and energy-intensive acetic acid-water separation and large recycle streams. The crude methyl acetate product, contaminated with water and methanol, can be purified by a number of enhanced distillation techniques such as pressure-swing distillation (Harrison, U.S. Patent 2,704,271, 1955), extractive distillation with ethylene glycol monomethylether as the solvent (Kumerle, German Patent 1,070,165, 1959), or azeotropic distillation with an aromatic or ketone entrainer (Yeomans, Eur. Patent Appl. 060717 and 060719, 1982). The end result is a capital- and energy-intensive process typically requiring multiple reactors and distillation columns.

The reactive distillation process in Fig. 13-99 provides a mechanism for overcoming both the limitations on conversion due to chemical

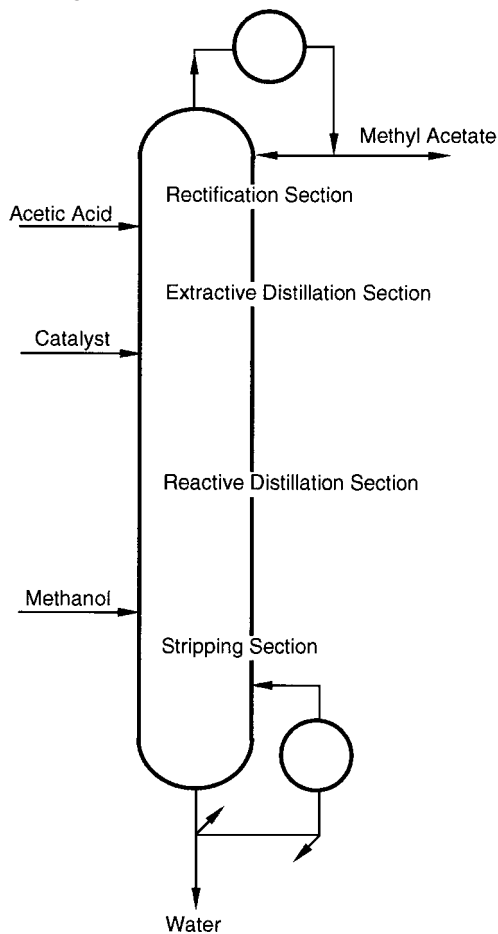


FIG. 13-99 Integrated reactive-extractive distillation column for the production of methyl acetate.

equilibrium as well as the difficulties in purification imposed by the water–methyl acetate and methanol–methyl acetate azeotropes [Agreda and Partin, U.S. Patent 4,435,595, 1984; Agreda, Partin, and Heise, *Chem. Eng. Prog.*, **86**(2), 40 (1990)]. Conceptually, this flow sheet can be thought of as four heat-integrated distillation columns (one of which is also a reactor) stacked on top of each other. The primary reaction zone consists of a series of countercurrent flashing stages in the middle of the column. Adequate residence time for the reaction is provided by high-liquid-holdup bubble cap trays with specially designed downcomer sumps to further increase tray holdup. A nonvolatile homogeneous catalyst is fed at the top of the reactive section and exits with the underflow water by-product. The extractive distillation section, immediately above the reactive section, is critical in achieving high methyl acetate purity. As shown in Fig. 13-96, simultaneous reaction and distillation eliminates the water–methyl acetate azeotrope (and the distillation boundary of the nonreactive system). However, pure methyl acetate remains a saddle in the reactive system and cannot be obtained as a pure component by simple reactive distillation. The acetic acid feed acts as a solvent in an extractive-distillation section placed above the reaction section, breaking the methanol–methyl acetate azeotrope, and yielding a pure methyl acetate distillate product. The uppermost rectification stages serve to remove any acetic acid from the methyl acetate product, and the bottommost stripping section removes any methanol and methyl acetate from the water by-product. The countercurrent flow of the reactants results in high local excesses at each end of the reactive section, even though the overall feed to the reactive column is stoichiometric. Therefore, the large excess of acetic acid at the top of the reactive section prevents methanol from reaching the distillate; similarly, methanol at the bottom of the reactive section keeps acetic acid from the water bottoms. Temperature and composition profiles for this reactive extractive distillation column are shown in Fig. 13-100*a* and *b*, respectively.

Much has been written about this reactive distillation scheme, including works by Bessling et al. [*Chem. Eng. Tech.*, **21**, 393 (1998)], Song et al., [*Ind. Eng. Chem. Res.*, **37**, 1917 (1998)], Huss et al. [*Comput. Chem. Eng.*, **27**, 1855 (2003)], Siirola (“An Industrial Perspective on Process Synthesis,” pp. 222–233 in Biegler and Doherty, eds., *Foundations of Computer-Aided Process Design*, AIChE, New York, 1995), and Krishna (chap. 7 in Sundmacher and Kienle, eds., *Reactive Distillation*, Wiley-VCH, 2003).

SYNTHESIS OF MULTICOMPONENT SEPARATION SYSTEMS

The sequencing of distillation columns and other types of equipment for the separation of multicomponent mixtures has received much attention in recent years. Although one separator of complex design can sometimes be devised to produce more than two products, more often a sequence of two-product separators is preferable. Often, the sequence includes simple distillation columns. A summary of sequencing methods, prior to 1977, that can lead to optimal or near-optimal designs, is given by Henley and Seader (op. cit.). Modern methods for distillation column sequencing are reviewed by Modi and Westerberg [*Ind. Eng. Chem. Res.*, **31**, 839 (1992)], who also present a more generally applicable method based on a marginal price that is the change in price of a separation operation when the separation is carried out in the absence of nonkey components. The synthesis of sequences that consider a wide range of separation operations in a knowledge-based approach is given by Barnicki and Fair for liquid mixtures [*Ind. Eng. Chem. Res.*, **29**, 421 (1990)] and for gas/vapor mixtures [*Ind. Eng. Chem. Res.*, **31**, 1679 (1992)]. The problem decomposition approach of Wahnschafft, Le Rudulier, and Westerberg [*Ind. Eng. Chem. Res.*, **32**, 1121 (1993)] is directed to the synthesis of complex separation sequences that involve nonsharp splits and recycle, including azeotropic distillation. The method is applied by using a computer-aided separation process designer called *SPLIT*. An expert system, called *EXSEP*, for the synthesis of solvent-based separation trains is presented by Brunet and Liu [*Ind. Eng. Chem. Res.*, **32**, 315 (1993)]. The use of ternary composition diagrams and residue curve maps is reviewed and evaluated for application to the synthesis of complex separation sequences by Fien and Liu [*Ind. Eng. Chem. Res.*, **33**, 2506 (1994)]. In recent years many optimization-based process synthesis schemes have been proposed for distillation systems. The key research groups are led by Grossmann at Carnegie Mellon University, Manousiouthakis at UCLA, and Pistikopoulos at Imperial College, London. Further information about their methods and availability of computer programs can be obtained from the principals.

Synthesis schemes for reactive distillation have been proposed by Ismail, Proios, and Pistikopoulos [*AIChE J.*, **47**, 629 (2001)], Jackson and Grossmann [*Comput. Chem. Eng.*, **25**, 1661 (2001)], Schembecker and Tlatlik [*Chem. Eng. Process.*, **42**, 179 (2003)], and Burri and Manousiouthakis [*Comput. Chem. Eng.*, **28**, 2509 (2004)].

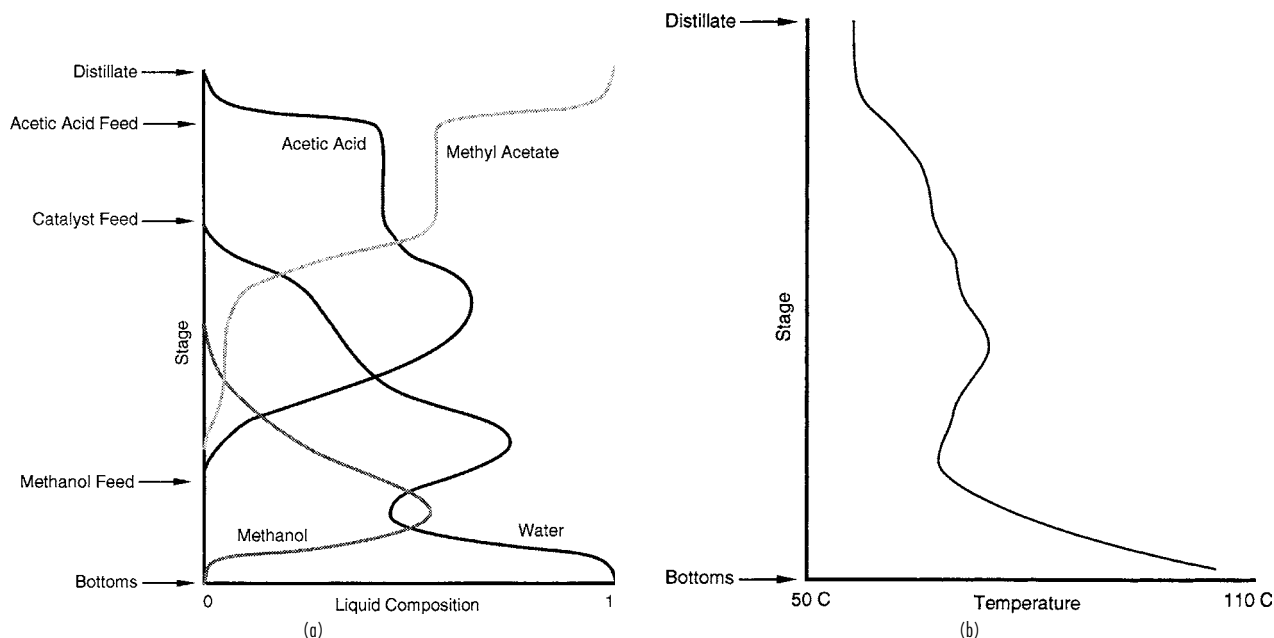


FIG. 13-100 Reactive extractive distillation for methyl acetate production. (a) Composition profile. (b) Temperature profile.

PETROLEUM AND COMPLEX-MIXTURE DISTILLATION

Although the principles of multicomponent distillation apply to petroleum, synthetic crude oil, and other complex mixtures, this subject warrants special consideration for the following reasons:

1. Such feedstocks are of exceedingly complex composition, consisting of, in the case of petroleum, many different types of hydrocarbons and perhaps of inorganic and other organic compounds. The number of carbon atoms in the components may range from 1 to more than 50, so that the compounds may exhibit atmospheric-pressure boiling points from -162°C (-259°F) to more than 538°C (1000°F). In a given boiling range, the number of different compounds that exhibit only small differences in volatility multiplies rapidly with increasing boiling point. For example, 16 of the 18 octane isomers boil within a range of only 12°C (22°F).

2. Products from the distillation of complex mixtures are in themselves complex mixtures. The character and yields of these products vary widely, depending upon the source of the feedstock. Even crude oils from the same locality may exhibit marked variations.

3. The scale of petroleum-distillation operations is generally large, and as discussed in detail by Nelson (*Petroleum Refinery Engineering*, 4th ed., McGraw-Hill, New York, 1958) and Watkins (*Petroleum Refinery Distillation*, 2d ed., Gulf, Houston, 1979), such operations are common in several petroleum refinery processes including atmospheric distillation of crude oil, vacuum distillation of bottoms residuum obtained from atmospheric distillation, main fractionation of gaseous effluent from catalytic cracking of various petroleum fractions, and main fractionation of effluent from thermal coking of various petroleum fractions. These distillation operations are conducted in large pieces of equipment that can consume large quantities of energy. Therefore, optimization of design and operation is very important and frequently leads to a relatively complex equipment configuration.

CHARACTERIZATION OF PETROLEUM AND PETROLEUM FRACTIONS

Although much progress has been made in identifying the chemical species present in petroleum, it is generally sufficient for purposes of design and analysis of plant operation of distillation to characterize petroleum and petroleum fractions by gravity, laboratory distillation curves, component analysis of light ends, and hydrocarbon-type analysis of middle and heavy ends. From such data, as discussed in the *Technical Data Book—Petroleum Refining* [American Petroleum Institute (API), Washington], five different average boiling points and an index of paraffinicity can be determined. These are then used to predict the physical properties of complex mixtures by a number of well-accepted correlations, whose use will be explained in detail and illustrated with examples. Many other characterizing properties or attributes such as sulfur content, pour point, water and sediment content, salt content, metals content, Reid vapor pressure, Saybolt Universal viscosity, aniline point, octane number, freezing point, cloud point, smoke point, diesel index, refractive index, cetane index, neutralization number, wax content, carbon content, and penetration are generally measured for a crude oil or certain of its frac-

tions according to well-specified ASTM tests. But these attributes are of much less interest here even though feedstocks and products may be required to meet certain specified values of the attributes.

Gravity of a crude oil or petroleum fraction is generally measured by the ASTM D 287 test or the equivalent ASTM D 1298 test and may be reported as specific gravity (SG) 60/60°F [measured at 60°F (15.6°C) and referred to water at 60°F (15.6°C)] or, more commonly, as API gravity, which is defined as

$$\text{API gravity} = 141.5/(\text{SG } 60/60^{\circ}\text{F}) - 131.5 \quad (13-120)$$

Water, thus, has an API gravity of 10.0, and most crude oils and petroleum fractions have values of API gravity in the range of 10 to 80. Light hydrocarbons (*n*-pentane and lighter) have values of API gravity ranging upward from 92.8.

The volatility of crude oil and petroleum fractions is characterized in terms of one or more laboratory distillation tests that are summarized in Table 13-27. The ASTM D 86 and D 1160 tests are reasonably rapid batch laboratory distillations involving the equivalent of approximately one equilibrium stage and no reflux except for that caused by heat losses. Apparatus typical of the D 86 test is shown in Fig. 13-101 and consists of a heated 100-mL or 125-mL Engler flask containing a calibrated thermometer of suitable range to measure the temperature of the vapor at the inlet to the condensing tube, an inclined brass condenser in a cooling bath using a suitable coolant, and a graduated cylinder for collecting the distillate. A stem correction is not applied to the temperature reading. Related tests using similar apparatus are the D 216 test for natural gasoline and the Engler distillation.

In the widely used ASTM D 86 test, 100 mL of sample is charged to the flask and heated at a sufficient rate to produce the first drop of distillate from the lower end of the condenser tube in 5 to 15 min, depending on the nature of the sample. The temperature of the vapor at that instant is recorded as the initial boiling point (IBP). Heating is continued at a rate such that the time from the IBP to 5 vol % recovered of the sample in the cylinder is 60 to 75 s. Again, vapor temperature is recorded. Then successive vapor temperatures are recorded for 10 to 90 percent recovered in intervals of 10, and at 95 percent recovered, with the heating rate adjusted so that 4 to 5 mL is collected per minute. At 95 percent recovered, the burner flame is increased if necessary to achieve a maximum vapor temperature, referred to as the endpoint (EP) in 3 to 5 additional min. The percent recovery is reported as the maximum percent recovered in the cylinder. Any residue remaining in the flask is reported as percent residue, and percent loss is reported as the difference between 100 mL and the sum of the percent recovery and percent residue. If the atmosphere test pressure P is other than 101.3 kPa (760 torr), temperature readings may be adjusted to that pressure by the Sidney Young equation, which for degrees Fahrenheit is

$$T_{760} = T_P + 0.00012(760 - P)(460 + T_P) \quad (13-121)$$

Another pressure correction for percent loss can also be applied, as described in the ASTM test method.

TABLE 13-27 Laboratory Distillation Tests

Test name	Reference	Main applicability
ASTM (atmospheric)	ASTM D 86	Petroleum fractions or products, including gasolines, turbine fuels, naphthas, kerosines, gas oils, distillate fuel oils, and solvents that do not tend to decompose when vaporized at 760 mmHg
ASTM [vacuum, often 10 torr (1.3 kPa)]	ASTM D 1160	Heavy petroleum fractions or products that tend to decompose in the ASTM D 86 test but can be partially or completely vaporized at a maximum liquid temperature of 750°F (400°C) at pressures down to 1 torr (0.13 kPa)
TBP [atmospheric or 10 torr (1.3 kPa)]	Nelson,* ASTM D 2892	Crude oil and petroleum fractions
Simulated TBP (gas chromatography)	ASTM D 2887	Crude oil and petroleum fractions
EFV (atmospheric, superatmospheric, or subatmospheric)	Nelson†	Crude oil and petroleum fractions

*Nelson, *Petroleum Refinery Engineering*, 4th ed., McGraw-Hill, New York, 1958, pp. 95–99.

†Ibid., pp. 104–105.

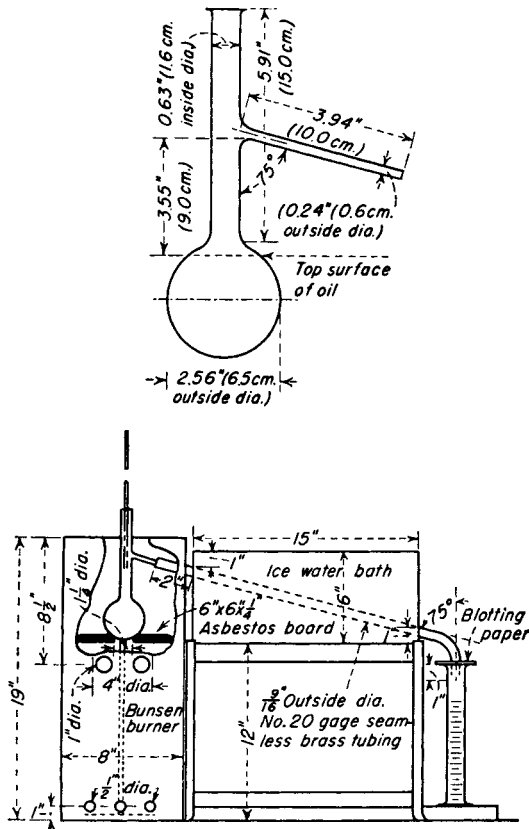


FIG. 13-101 ASTM distillation apparatus; detail of distilling flask is shown in the upper figure.

Results of a typical ASTM distillation test for an automotive gasoline are given in Table 13-28, in which temperatures have already been corrected to a pressure of 101.3 kPa (760 torr). It is generally assumed that percent loss corresponds to volatile noncondensables that are distilled off at the beginning of the test. In that case, the percent recovered values in Table 13-28 do not correspond to percent evaporated values, which are of greater scientific value. Therefore, it

TABLE 13-28 Typical ASTM D 86 Test Results for Automobile Gasoline Pressure, 760 torr (101.3 kPa)

Percent recovered basis (as measured)		Percent evaporated basis (as corrected)			
Percent recovered	T, °F	Percent evaporated	Percent evaporated	T, °F	Percent recovered
0 (IBP)	98	1.5	1.5	98	(IBP)
5	114	6.5	5	109	3.5
10	120	11.5	10	118	8.5
20	150	21.5	20	146	18.5
30	171	31.5	30	168	28.5
40	193	41.5	40	190	38.5
50	215	51.5	50	212	48.5
60	243	61.5	60	239	58.5
70	268	71.5	70	264	68.5
80	300	81.5	80	295	78.5
90	340	91.5	90	334	88.5
95	368	96.5	95	360	93.5
EP	408			408	(EP)

NOTE: Percent recovery = 97.5; percent residue = 1.0; percent loss = 1.5. To convert degrees Fahrenheit to degrees Celsius, °C = (°F - 32)/1.8.

is common to adjust the reported temperatures according to a linear interpolation procedure given in the ASTM test method to obtain corrected temperatures in terms of percent evaporated at the standard intervals as included in Table 13-28. In the example, the corrections are not large because the loss is only 1.5 vol %.

Although most crude petroleum can be heated to 600°F (316°C) without noticeable cracking, when ASTM temperatures exceed 475 °F (246°C), fumes may be evolved, indicating decomposition, which may cause thermometer readings to be low. In that case, the following correction attributed to S. T. Hadden may be applied:

$$\Delta T_{\text{corr}} = 10^{-1.587 + 0.004735T} \quad (13-122)$$

where T = measured temperature, °F
 ΔT_{corr} = correction to be added to T , °F

At 500 and 600°F (260 and 316°C), the corrections are 6 and 18°F (3.3 and 10°C), respectively.

As discussed by Nelson (op. cit.), virtually no fractionation occurs in an ASTM distillation. Thus, components in the mixture do distill one by one in the order of their boiling points but as mixtures of successively higher boiling points. The IBP, EP, and intermediate points have little theoretical significance, and, in fact, components boiling below the IBP and above the EP are present in the sample. Nevertheless, because ASTM distillations are quickly conducted, have been successfully automated, require only a small sample, and are quite reproducible, they are widely used for comparison and as a basis for specifications on a large number of petroleum intermediates and products, including many solvents and fuels. Typical ASTM curves for several such products are shown in Fig. 13-102.

Data from a true boiling point (TBP) distillation test provide a much better theoretical basis for characterization. If the sample contains compounds that have moderate differences in boiling points such as in

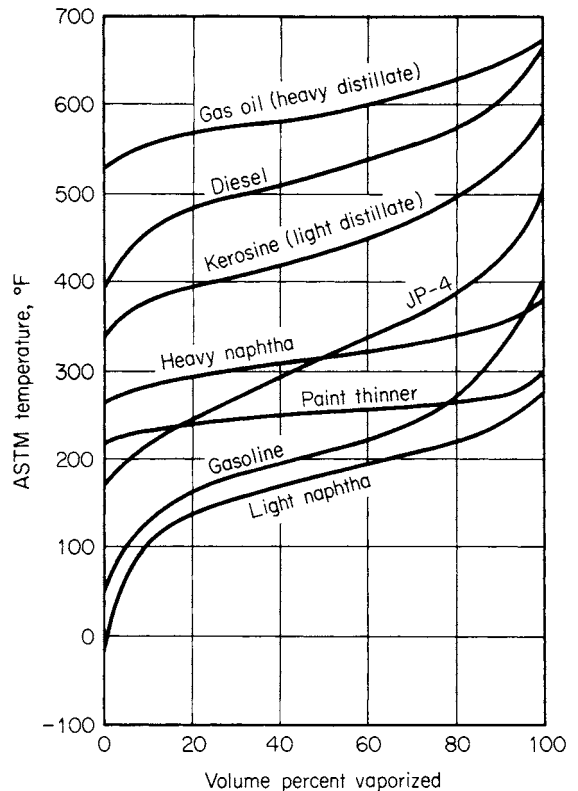


FIG. 13-102 Representative ASTM D 86 distillation curves.

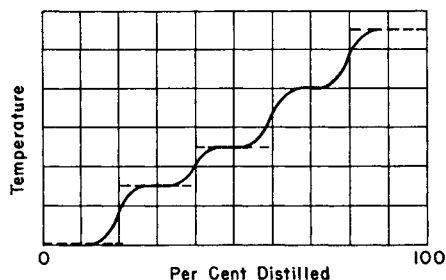


FIG. 13-103 Variation of boiling temperature with percent distilled in TBP distillation of light hydrocarbons.

a light gasoline containing light hydrocarbons (e.g., isobutane, *n*-butane, isopentane), a plot of overhead vapor distillate temperature versus percent distilled in a TBP test would appear in the form of steps as in Fig. 13-103. However, if the sample has a higher average boiling range when the number of close-boiling isomers increases, the steps become indistinct and a TBP curve such as that in Fig. 13-104 results. Because the degree of separation for a TBP distillation test is much higher than that for an ASTM distillation test, the IBP is lower and the EP is higher for the TBP method as compared with the ASTM method, as shown in Fig. 13-104.

A standard TBP laboratory distillation test method has not been well accepted. Instead, as discussed by Nelson (op. cit., pp. 95-99), batch distillation equipment that can achieve a good degree of fractionation is usually considered suitable. In general, TBP distillations are conducted in columns with 15 to 100 theoretical stages at reflux ratios of 5 or greater. Thus, the new ASTM D 2892 test method, which involves a column with 14 to 17 theoretical stages and a reflux ratio of 5, essentially meets the minimum requirements. Distillate may be collected at a constant or a variable rate. Operation may be at 101.3-kPa (760-torr) pressure or at a vacuum at the top of the column as low as 0.067 kPa (0.5 torr) for high-boiling fractions, with 1.3 kPa (10 torr) being common. Results from vacuum operation are extrapolated to 101.3 kPa (760 torr) by the vapor-pressure correlation of

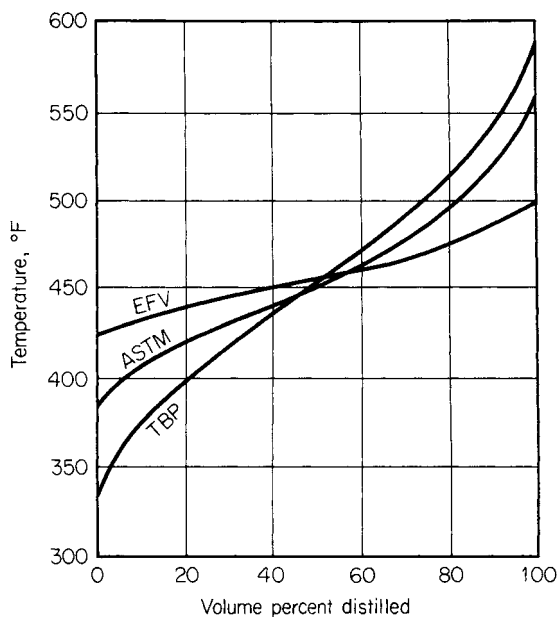


FIG. 13-104 Comparison of ASTM, TBP, and EFV distillation curves for kerosine.

Maxwell and Bonner [*Ind. Eng. Chem.*, **49**, 1187 (1957)], which is given in great detail in the *API Technical Data Book—Petroleum Refining* (op. cit.) and in the ASTM D 2892 test method. It includes a correction for the nature of the sample (paraffin, olefin, naphthene, and aromatic content) in terms of the UOP characterization factor, UOP-K, as given by

$$\frac{\text{UOP-K} = (T_B)^{1/3}}{\text{SG}} \quad (13-123)$$

where T_B is the mean average boiling point in degrees Rankine, which is the arithmetic average of the molal average boiling point and the cubic volumetric average boiling point. Values of UOP-K for *n*-hexane, 1-hexene, cyclohexene, and benzene are 12.82, 12.49, 10.99, and 9.73, respectively. Thus, paraffins with their lower values of specific gravity tend to have high values, and aromatics tend to have low values of UOP-K. A movement toward an international TBP standard is discussed by Vercier and Mouton [*Oil Gas J.*, **77**(38), 121 (1979)].

A crude oil assay always includes a whole crude API gravity and a TBP curve. As discussed by Nelson (op. cit., pp. 89-90) and as shown in Fig. 13-105, a reasonably consistent correlation (based on more than 350 distillation curves) exists between whole crude API gravity and the TBP distillation curve at 101.3 kPa (760 torr). Exceptions not correlated by Fig. 13-105 are highly paraffinic or naphthenic crude oils.

An alternative to TBP distillation is simulated distillation by gas chromatography. As described by Green, Schmauch, and Worman [*Anal. Chem.*, **36**, 1512 (1965)] and Worman and Green [*Anal. Chem.*, **37**, 1620 (1965)], the method is equivalent to a 100-theoretical-plate TBP distillation; is very rapid, reproducible, and easily automated; requires only a small microliter sample; and can better define initial and final boiling points. The ASTM D 2887 standard test method is based on such a simulated distillation and is applicable to samples having a boiling range greater than 55°C (100°F) for temperature determinations as high as 538°C (1000°F). Typically, the test is conducted with a gas chromatograph having a thermal conductivity detector, a programmed temperature capability, helium or hydrogen carrier gas, and column packing of silicone gum rubber on a crushed firebrick or diatomaceous earth support.

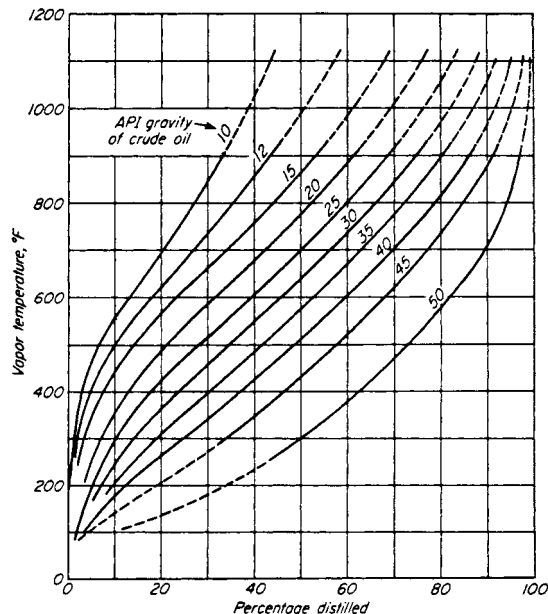


FIG. 13-105 Average true-boiling-point distillation curves of crude oils. (From W. E. Edmister, *Applied Hydrocarbon Thermodynamics*, vol. 1, 1st ed., 1961 Gulf Publishing Company, Houston, Texas, Used with permission. All rights reserved.)

It is important to note that simulated distillation does not always separate hydrocarbons in the order of their boiling points. For example, high-boiling multiple-ring-type compounds may be eluted earlier than normal paraffins (used as the calibration standard) of the same boiling point. Gas chromatography is also used in the ASTM D 2427 test method to determine quantitatively ethane through pentane hydrocarbons.

A third fundamental type of laboratory distillation, which is the most tedious to perform of the three types of laboratory distillations, is equilibrium flash vaporization (EFV), for which no standard test exists. The sample is heated in such a manner that the total vapor produced remains in contact with the total remaining liquid until the desired temperature is reached at a set pressure. The volume percent vaporized at these conditions is recorded. To determine the complete flash curve, a series of runs at a fixed pressure is conducted over a range of temperatures sufficient to cover the range of vaporization from 0 to 100 percent. As seen in Fig. 13-104, the component separation achieved by an EFV distillation is much less than that by the ASTM or TBP distillation tests. The initial and final EFV points are the bubble point and the dew point, respectively, of the sample. If desired, EFV curves can be established at a series of pressures.

Because of the time and expense involved in conducting laboratory distillation tests of all three basic types, it has become increasingly common to use empirical correlations to estimate the other two distillation curves when the ASTM, TBP, or EFV curve is available. Preferred correlations given in the *API Technical Data Book—Petroleum Refining* (op. cit.) are based on the work of Edmister and Pollock [*Chem. Eng. Prog.*, **44**, 905 (1948)], Edmister and Okamoto [*Pet. Refiner*, **38**(8), 117 (1959); **38**(9), 271 (1959)], Maxwell (*Data Book on Hydrocarbons*, Van Nostrand, Princeton, N.J., 1950), and Chu and Staffel [*J. Inst. Pet.*, **41**, 92 (1955)]. Because of the lack of sufficiently precise and consistent data on which to develop the correlations, they are, at best, first approximations and should be used with caution. Also, they do not apply to mixtures containing only a few components of widely different boiling points. Perhaps the most useful correlation of the group is Fig. 13-106 for converting between ASTM D 86 and

TBP distillations of petroleum fractions at 101.3 kPa (760 torr). The ASTM D 2889 test method, which presents a standard method for calculating EFV curves from the results of an ASTM D 86 test for a petroleum fraction having a 10 to 90 vol % boiling range of less than 55°C (100°F), is also quite useful.

APPLICATIONS OF PETROLEUM DISTILLATION

Typical equipment configurations for the distillation of crude oil and other complex hydrocarbon mixtures in a crude unit, a catalytic cracking unit, and a delayed coking unit of a petroleum refinery are shown in Figs. 13-107, 13-108, and 13-109. The initial separation of crude oil into fractions is conducted in two main columns, shown in Fig. 13-107. In the first column, called the atmospheric tower or topping still, partially vaporized crude oil, from which water, sediment, and salt have been removed, is mainly rectified, at a feed tray pressure of no more than about 276 kPa (40 psia), to yield a noncondensable light-hydrocarbon gas, a light naphtha, a heavy naphtha, a light distillate (kerosine), a heavy distillate (diesel oil), and a bottoms residual of components whose TBP exceeds approximately 427°C (800°F). Alternatively, other fractions, shown in Fig. 13-102, may be withdrawn. To control the IBP of the ASTM D 86 curves, each of the sidestreams of the atmospheric tower and the vacuum and main fractionators of Figs. 13-107, 13-108, and 13-109 may be sent to side-cut strippers, which use a partial reboiler or steam stripping. Additional stripping by steam is commonly used in the bottom of the atmospheric tower as well as in the vacuum tower and other main fractionators.

Additional distillate in the TBP range of approximately 427 to 593°C (800 to 1100°F) is recovered from bottoms residuum of the atmospheric tower by rectification in a vacuum tower, also shown in Fig. 13-107, at the minimum practical overhead condenser pressure, which is typically 1.3 kPa (10 torr). Use of special low-pressure-drop trays or column packing permits the feed tray pressure to be approximately 5.3 to 6.7 kPa (40 to 50 torr) to obtain the maximum degree of vaporization. Vacuum towers may be designed or operated to produce several different products including heavy distillates, gas-oil feedstocks for catalytic cracking, lubricating oils, bunker fuel, and bottoms residua of asphalt (5 to 8 API gravity) or pitch (0 to 5 API gravity). The catalytic cracking process of Fig. 13-108 produces a superheated vapor at approximately 538°C (1000°F) and 172 to 207 kPa (25 to 30 psia) of a TBP range that covers hydrogen to compounds with normal boiling points above 482°C (900°F). This gas is sent directly to a main fractionator for rectification to obtain products that are typically gas and naphtha [204°C (400°F) ASTM EP approximately], which are often fractionated further to produce relatively pure light hydrocarbons and gasoline; a light cycle oil [typically 204 to 371°C (400 to 700°F) ASTM D 86 range], which may be used for heating oil, hydrocracked, or recycled to the catalytic cracker; an intermediate cycle oil [typically 371 to 482°C (700 to 900°F) ASTM D 86 range], which is generally recycled to the catalytic cracker to extinction; and a heavy gas oil or bottom slurry oil.

Vacuum-column bottoms, bottoms residuum from the main fractionation of a catalytic cracker, and other residua can be further processed at approximately 510°C (950°F) and 448 kPa (65 psia) in a delayed-coker unit, as shown in Fig. 13-109, to produce petroleum coke and gas of TBP range that covers methane (with perhaps a small amount of hydrogen) to compounds with normal boiling points that may exceed 649°C (1200°F). The gas is sent directly to a main fractionator that is similar to the type used in conjunction with a catalytic cracker, except that in the delayed-coking operation the liquid to be coked first enters into and passes down through the bottom trays of the main fractionator to be preheated by and to scrub coker vapor of entrained coke particles and condensables for recycling to the delayed coker. Products produced from the main fractionator are similar to those produced in a catalytic cracking unit, except for more unsaturated cyclic compounds, and include gas and coker naphtha, which are further processed to separate out light hydrocarbons and a coker naphtha that generally needs hydrotreating; and light and heavy coker gas oils, both of which may require hydrocracking to become suitable blending stocks.

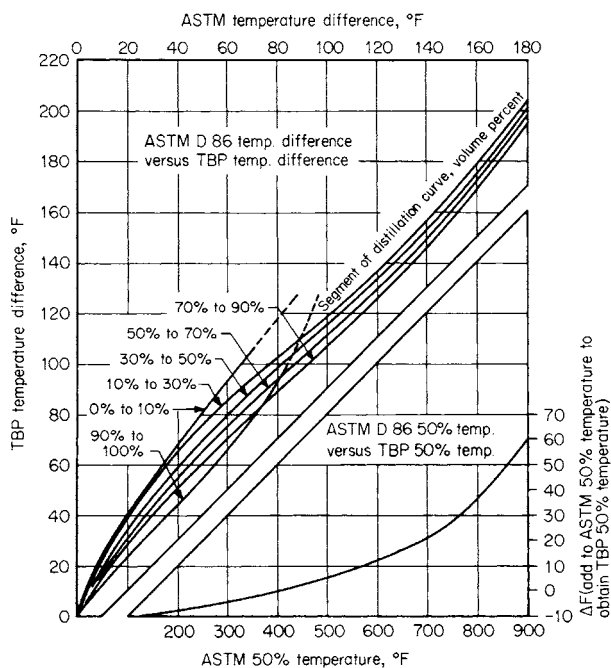


FIG. 13-106 Relationship between ASTM and TBP distillation curves. (From W. C. Edmister, *Applied Hydrocarbon Thermodynamics*, vol. 1, 1st ed., 1961 Gulf Publishing Company, Houston, Tex. Used with permission. All rights reserved.)

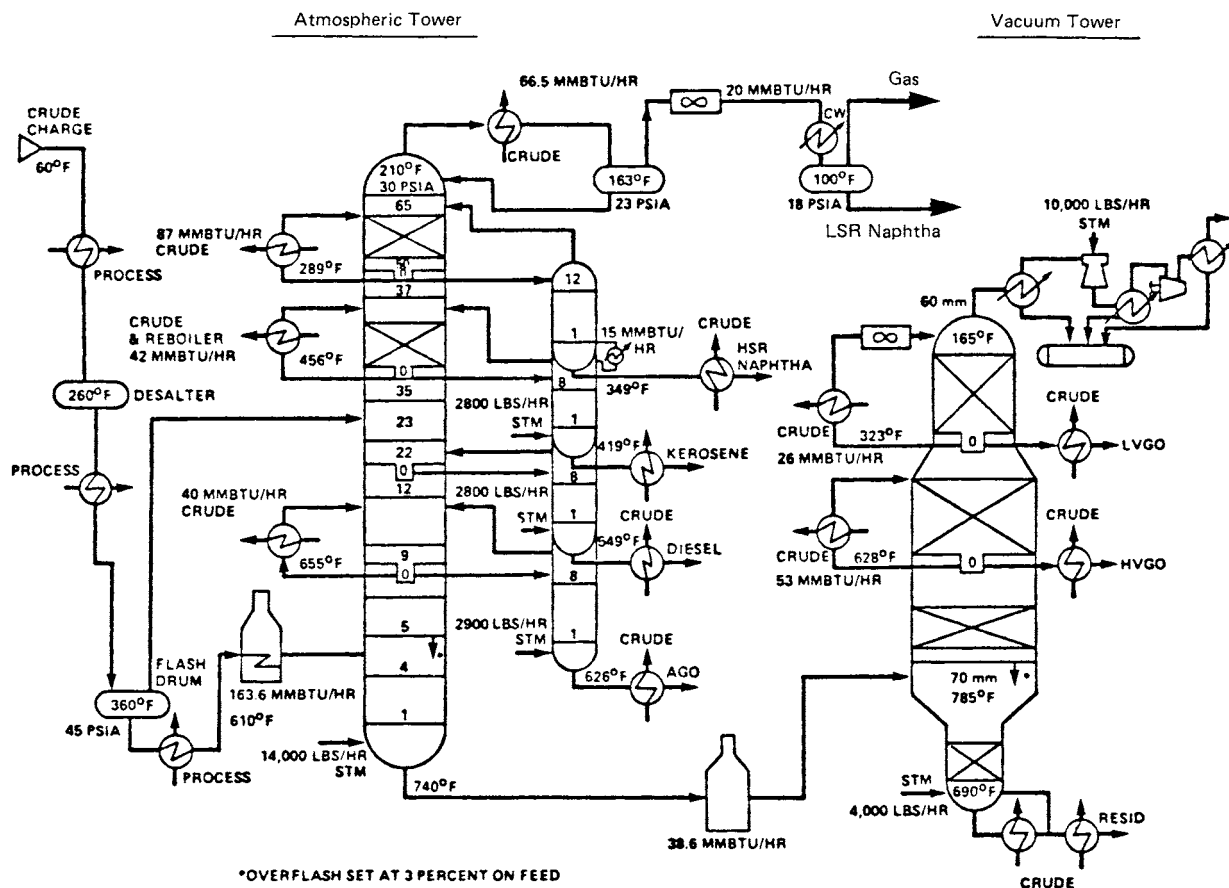


FIG. 13-107 Crude unit with atmospheric and vacuum towers. [Kleinschrodt and Hammer, Chem. Eng. Prog., 79(7), 33 (1983).]

DESIGN PROCEDURES

Two general procedures are available for designing fractionators that process petroleum, synthetic crude oils, and complex mixtures. The first, which was originally developed for crude units by Packie [*Trans. Am. Inst. Chem. Eng. J.*, **37**, 51 (1941)], extended to main fractionators by Houghland, Lemieux, and Schreiner [*Proc. API*, sec. III, *Refining*, 385 (1954)], and further elaborated and described in great detail by Watkins (op. cit.), uses material and energy balances, with empirical correlations to establish tray requirements, and is essentially a hand calculation procedure that is a valuable learning experience and is suitable for preliminary designs. Also, when backed by sufficient experience from previous designs, this procedure is adequate for final design.

In the second procedure, which is best applied with a digital computer, the complex mixture being distilled is represented by actual components at the light end and by perhaps 30 pseudocomponents (e.g., petroleum fractions) over the remaining portion of the TBP distillation curve for the column feed. Each of the pseudocomponents is characterized by a TBP range, an average normal boiling point, an average API gravity, and an average molecular weight. Rigorous material balance, energy balance, and phase equilibrium calculations are then made by an appropriate equation-tearing method, as shown by Cecchetti et al. [*Hydrocarbon Process.*, **42**(9), 159 (1963)] or a simultaneous-correction procedure as shown, e.g., by Goldstein and Stanfield [*Ind. Eng. Chem. Process Des. Dev.*, **9**, 78 (1970)] and Hess et al. [*Hydrocarbon Process.*, **56**(5), 241 (1977)]. Highly developed procedures of the latter type, suitable for preliminary or final design, are

included in most computer-aided steady-state process design and simulation programs as a special case of interlinked distillation, wherein the crude tower or fractionator is converged simultaneously with the sidecut stripper columns.

Regardless of the procedure used, certain initial steps must be taken for the determination or specification of certain product properties and yields based on the TBP distillation curve of the column feed, method of providing column reflux, column-operating pressure, type of condenser, and type of sidecut strippers and stripping requirements. These steps are developed and illustrated with several detailed examples by Watkins (op. cit.). Only one example, modified from one given by Watkins, is considered briefly here to indicate the approach taken during the initial steps.

For the atmospheric tower shown in Fig. 13-110, suppose distillation specifications are as follows:

- Feed: 50,000 bbl (at 42 U.S. gal each) per stream day (BPSD) of 31.6 API crude oil.
- Measured light-ends analysis of feed:

Component	Volume percent of crude oil
Ethane	0.04
Propane	0.37
Isobutane	0.27
<i>n</i> -Butane	0.89
Isopentane	0.77
<i>n</i> -Pentane	1.13
	3.47

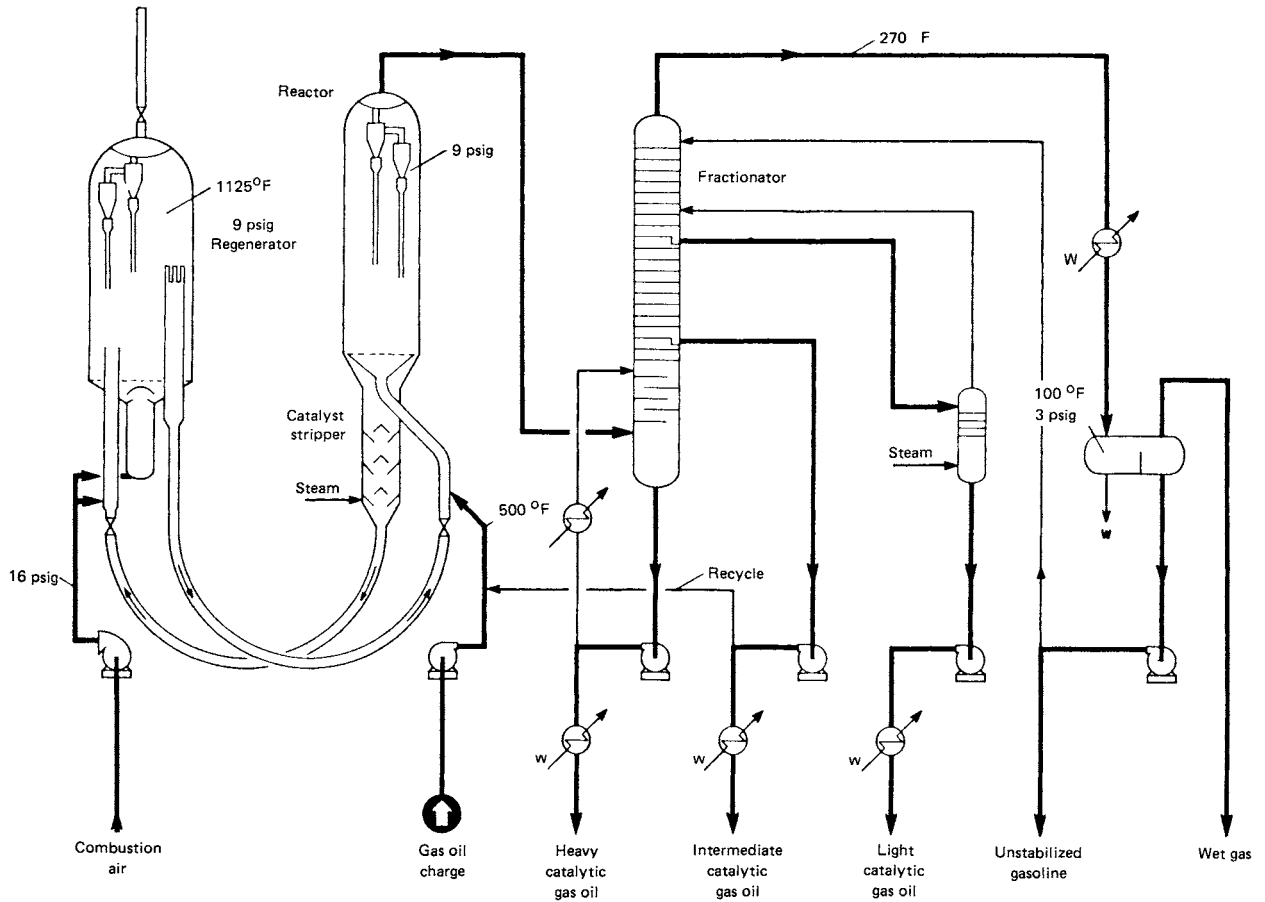


FIG. 13-108 Catalytic cracking unit. [New Horizons, Lummus Co., New York (1954)].

- Measured TBP and API gravity of feed, computed atmospheric pressure EFV (from API *Technical Data Book*), and molecular weight of feed:

Volume percent vaporized	TBP, °F	EFV, °F	°API	Molecular weight
0	-130	179		
5	148	275	75.0	91
10	213	317	61.3	106
20	327	394	50.0	137
30	430	468	41.8	177
40	534	544	36.9	223
50	639	619	30.7	273
60	747	696	26.3	327
70	867	777	22.7	392
80	1013	866	19.1	480

- Product specifications:

Desired cut	ASTM D 86, °F		
	5%	50%	95%
Overhead (OV)			253
Heavy naphtha (HN)	278	314	363
Light distillate (LD)	398	453	536
Heavy distillate (HD)	546	589	
Bottoms (B)			

NOTE: To convert degrees Fahrenheit to degrees Celsius, °C = (°F - 32)/1.8.

- TBP cut point between the heavy distillate and the bottoms = 650 °F.
- Percent overflash = 2 vol % of feed
- Furnace outlet temperature = 343°C (650 °F) maximum
- Overhead temperature in reflux drum = 49°C (120°F) minimum

From the product specifications, distillate yields are computed as follows: From Fig. 13-106 and the ASTM D 86 50 percent temperatures, TBP 50 percent temperatures of the three intermediate cuts are obtained as 155, 236, and 316°C (311, 456, and 600°F) for the HN, LD, and HD, respectively. The TBP cut points, corresponding volume fractions of crude oil, and flow rates of the four distillates are readily obtained by starting from the specified 343°C (650°F) cut point as follows, where CP is the cut point and *T* is the TBP temperature (°F):

$$\begin{aligned}
 CP_{HD,B} &= 650^\circ\text{F} \\
 CP_{HD,B} - T_{HD,50} &= 650 - 600 = 50^\circ\text{F} \\
 CP_{LD,HD} &= T_{HD,50} - 50 = 600 - 50 = 550^\circ\text{F} \\
 CP_{LD,HD} - T_{LD,50} &= 550 - 456 = 94^\circ\text{F} \\
 CP_{HN,LD} &= T_{LD,50} - 94 = 456 - 94 = 362^\circ\text{F} \\
 CP_{HN,LD} - T_{HN,50} &= 362 - 311 = 51^\circ\text{F} \\
 CP_{OV,HN} &= T_{HN,50} - 51 = 311 - 51 = 260^\circ\text{F}
 \end{aligned}$$

These cut points are shown as vertical lines on the crude oil TBP plot of Fig. 13-111, from which the following volume fractions and flow

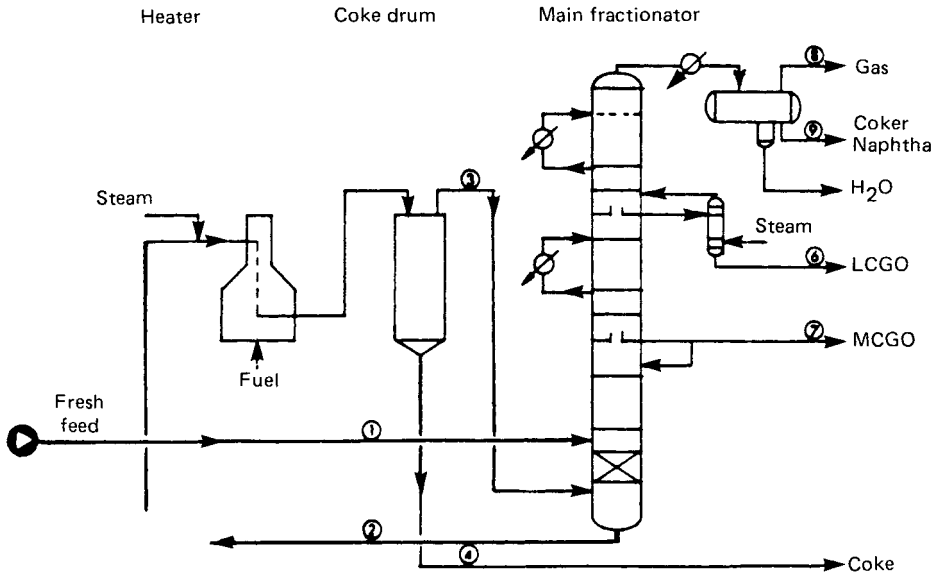


FIG. 13-109 Delayed-coking unit. (Watkins, *Petroleum Refinery Distillation*, 2d ed., Gulf, Houston, Tex., 1979).

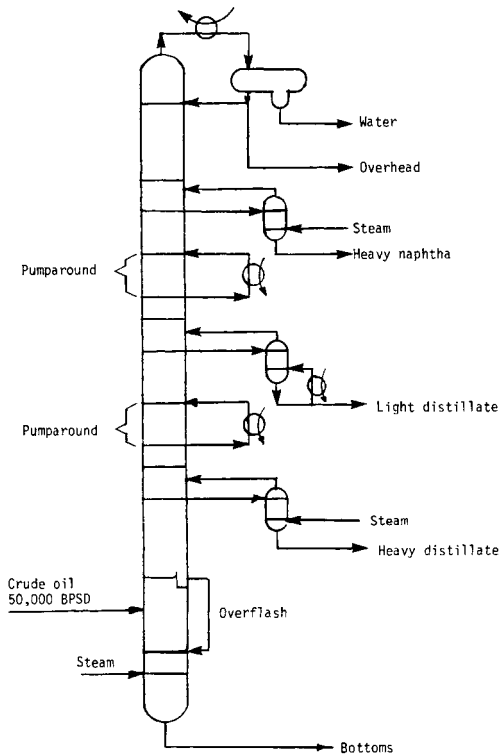


FIG. 13-110 Crude atmospheric tower.

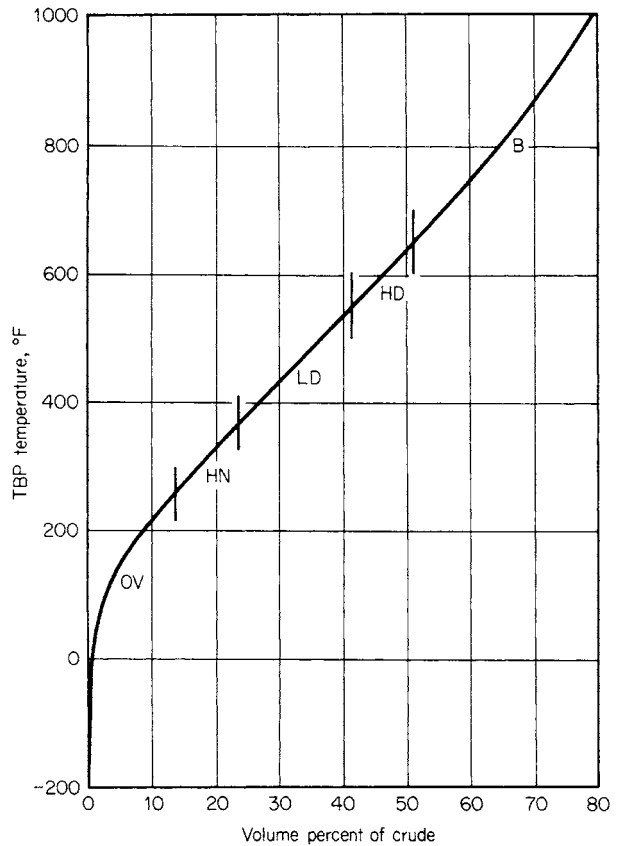


FIG. 13-111 Example of crude oil TBP cut points.

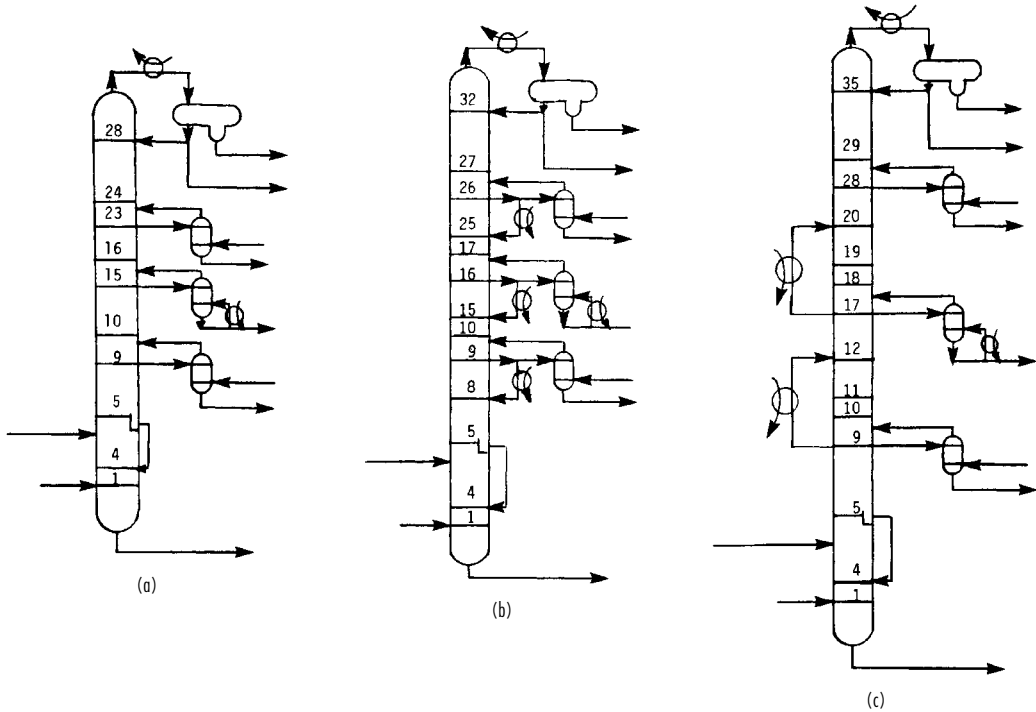


FIG. 13-112 Methods of providing reflux to crude units. (a) Top reflux. (b) Pump-back reflux. (c) Pump-around reflux.

rates of product cuts are readily obtained:

Desired cut	Volume percent of crude oil	BPSD
Overhead (OV)	13.4	6,700
Heavy naphtha (HN)	10.3	5,150
Light distillate (LD)	17.4	8,700
Heavy distillate (HD)	10.0	5,000
Bottoms (B)	48.9	24,450
	100.0	50,000

As shown in Fig. 13-112, methods of providing column reflux include (a) conventional top-tray reflux, (b) pump-back reflux from sidecut strippers, and (c) pump-around reflux. The latter two methods essentially function as intercondenser schemes that reduce the top-tray reflux requirement. As shown in Fig. 13-113 for the example being considered,

the internal-reflux flow rate decreases rapidly from the top tray to the feed-flash zone for case a. The other two cases, particularly case c, result in better balancing of the column-reflux traffic. Because of this and the opportunity provided to recover energy at a moderate- to high-temperature level, pump-around reflux is the most commonly used technique. However, not indicated in Fig. 13-113 is the fact that in cases b and c the smaller quantity of reflux present in the upper portion of the column increases the tray requirements. Furthermore, the pump-around circuits, which extend over three trays each, are believed to be equivalent for mass-transfer purposes to only one tray each. Representative tray requirements for the three cases are included in Fig. 13-112. In case c, heat-transfer rates associated with the two pump-around circuits account for approximately 40 percent of the total heat removed in the overhead condenser and from the two pump-around circuits combined.

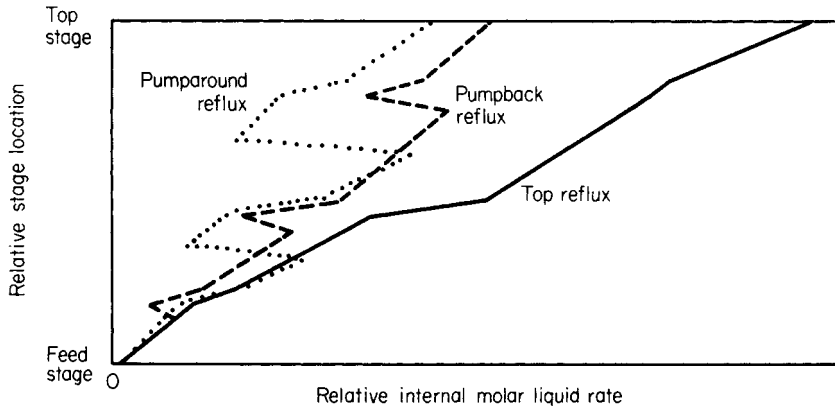


FIG. 13-113 Comparison of internal reflux rates for three methods of providing reflux.

Bottoms and three sidecut strippers remove light ends from products and may use steam or reboilers. In Fig. 13-112 a reboiled stripper is used on the light distillate, which is the largest sidecut withdrawn. Steam-stripping rates in sidecut strippers and at the bottom of the atmospheric column may vary from 0.45 to 4.5 kg (1 to 10 lb) of steam per barrel of stripped liquid, depending on the fraction of stripper feed liquid that is vaporized.

Column pressure at the reflux drum is established so as to condense totally the overhead vapor or some fraction thereof. Flash-zone pressure is approximately 69 kPa (10 psia) higher. Crude oil feed temperature at flash-zone pressure must be sufficient to vaporize the total distillates plus the overhead, which is necessary to provide reflux between the lowest sidestream-product drawoff tray and the flash zone. Calculations are made by using the crude oil EFV curve corrected for pressure. For the example being considered, percent vaporized at the flash zone must be 53.1 percent of the feed.

Tray requirements depend on internal reflux ratios and ASTM 5-95 gaps or overlaps and may be estimated by the correlation of Packie (op. cit.) for crude units and the correlation of Houghland, Lemieux, and Schreiner (op. cit.) for main fractionators.

Example 15: Simulation Calculation of an Atmospheric Tower The ability of a rigorous calculation procedure to simulate operation of an atmospheric tower with its accompanying sidecut strippers may be illustrated by comparing commercial-test data from an actual operation with results computed with the REFINE program of ChemShare Corporation, Houston, Texas. (See also DESIGN II program from WinSim, Inc., Sugar Land, Texas; <http://www.winsim.com>.) The tower configuration and plant operating conditions are shown in Fig. 13-114.

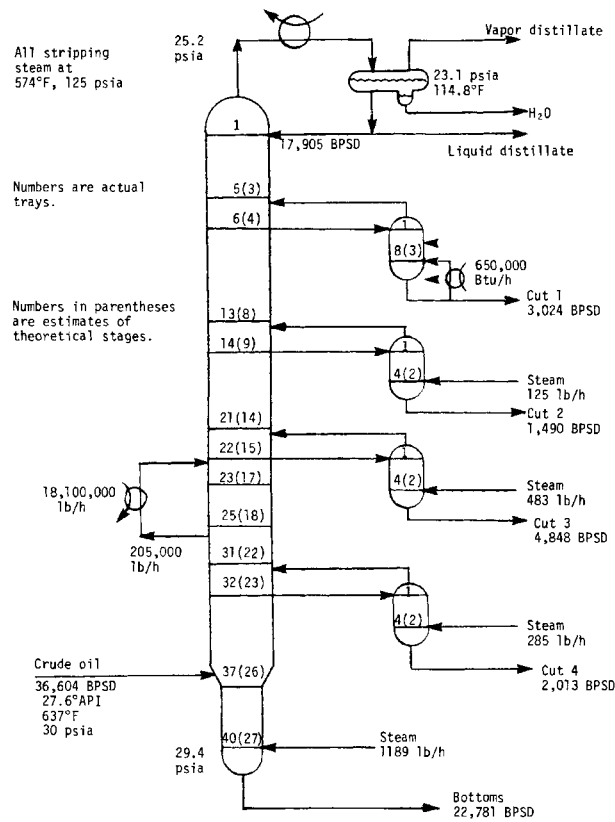


FIG. 13-114 Configuration and conditions for the simulation of the atmospheric tower of crude unit.

TABLE 13-29 Light-Component Analysis and TBP Distillation of Feed for the Atmospheric Crude Tower of Fig. 13-114

Light-component analysis		
Component	Volume percent	
Methane	0.073	
Ethane	0.388	
Propane	0.618	
n-Butane	0.817	
n-Pentane	2.05	
TBP distillation of feed		
API gravity	TBP, °F	Volume percent
80	-160.	0.1
70	155.	5.
57.5	242.	10.
45.	377.	20.
36.	499.	30.
29.	609.	40.
26.5	707.	50.
23.	805.	60.
20.5	907.	70.
17.	1054.	80.
10.	1210.	90.
-4.	1303.	95.
-22.	1467	100.

NOTE: To convert degrees Fahrenheit to degrees Celsius, °C = (°F - 32)/1.8.

TABLE 13-30 Pseudo-Component Representation of Feed for the Atmospheric Crude Tower of Fig. 13-114

No.	Component name	Molecular weight	Specific gravity	API gravity	(lb-mol)/h
1	Water	18.02	1.0000	10.0	.00
2	Methane	16.04	.3005	339.5	7.30
3	Ethane	30.07	.3561	265.8	24.54
4	Propane	44.09	.5072	147.5	37.97
5	n-Butane	58.12	.5840	110.8	43.84
6	n-Pentane	72.15	.6308	92.8	95.72
7	131 ABP	83.70	.6906	73.4	74.31
8	180 ABP	95.03	.7152	66.3	66.99
9	210 ABP	102.23	.7309	62.1	65.83
10	240 ABP	109.78	.7479	57.7	70.59
11	270 ABP	118.52	.7591	54.9	76.02
12	300 ABP	127.69	.7706	52.1	71.62
13	330 ABP	137.30	.7824	49.4	67.63
14	360 ABP	147.33	.7946	46.6	64.01
15	390 ABP	157.97	.8061	44.0	66.58
16	420 ABP	169.37	.8164	41.8	63.30
17	450 ABP	181.24	.8269	39.6	59.92
18	480 ABP	193.59	.8378	37.4	56.84
19	510 ABP	206.52	.8483	35.3	59.05
20	540 ABP	220.18	.8581	33.4	56.77
21	570 ABP	234.31	.8682	31.5	53.97
22	600 ABP	248.30	.8804	29.2	52.91
23	630 ABP	265.43	.8846	28.5	54.49
24	660 ABP	283.37	.8888	27.7	51.28
25	690 ABP	302.14	.8931	26.9	48.33
26	742 ABP	335.94	.9028	25.2	109.84
27	817 ABP	387.54	.9177	22.7	94.26
28	892 ABP	446.02	.9288	20.8	74.10
29	967 ABP	509.43	.9398	19.1	50.27
30	1055 ABP	588.46	.9531	17.0	57.12
31	1155 ABP	665.13	.9829	12.5	50.59
32	1255 ABP	668.15	1.0658	1.3	45.85
33	1355 ABP	643.79	1.1618	-9.7	29.39
34	1436 ABP	597.05	1.2533	-18.6	21.19
		246.90	.8887	27.7	1922.43

NOTE: To convert (lb-mol)/h to (kg-mol)/h, multiply by 0.454.

13-108 DISTILLATION

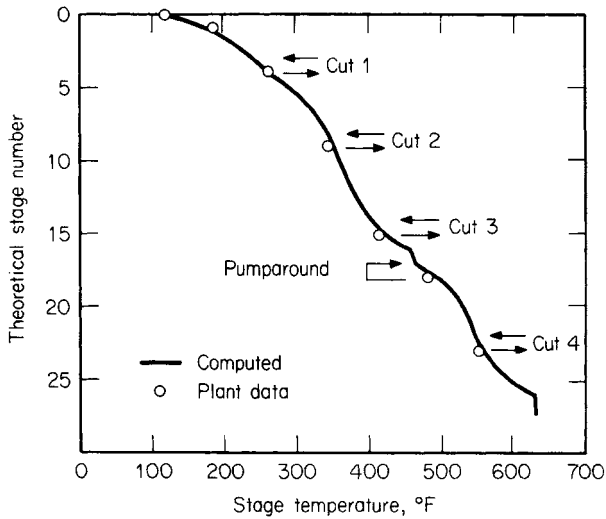


FIG. 13-115 Comparison of computed stage temperatures with plant data for the example of Fig. 13-114.

Light-component analysis and the TBP and API gravity for the feed are given in Table 13-29. Representation of this feed by pseudocomponents is given in Table 13-30 based on 16.7°C (30°F) cuts from 82 to 366°C (180 to 690°F), followed by 41.7°C (75°F) and then 55.6°C (100°F) cuts. Actual tray numbers are shown in Fig. 13-114. Corresponding theoretical-stage numbers, which were determined by trial and error to obtain a reasonable match of computed- and measured-product TBP distillation curves, are shown in parentheses. Overall tray efficiency appears to be approximately 70 percent for the tower and 25 to 50 percent for the sidestream strippers.

Results of rigorous calculations and comparison to plant data, when possible, are shown in Figs. 13-115, 13-116, and 13-117. Plant temperatures are in good agreement with computed values in Fig. 13-115. Computed sidestream-product TBP distillation curves are in reasonably good agreement with values converted from plant ASTM distillations, as shown in Fig. 13-116. Exceptions are the initial points of all four cuts and the higher-boiling end of

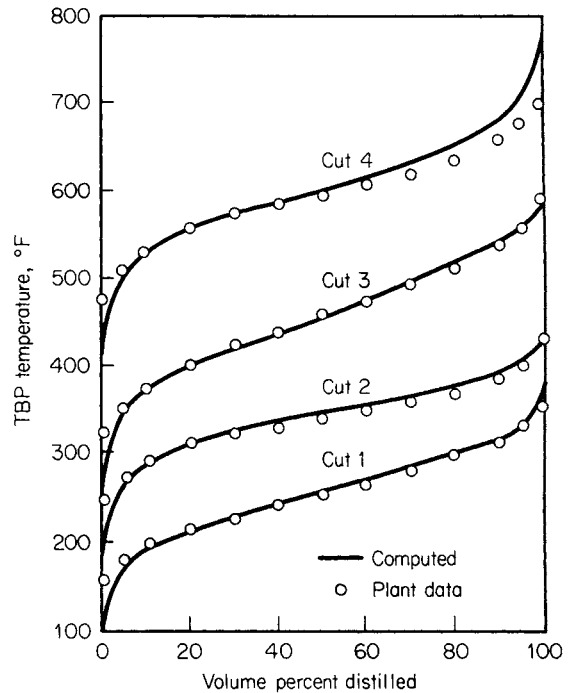


FIG. 13-116 Comparison of computed TBP curves with plant data for the example of Fig. 13-114.

the heavy-distillate curve. This would seem to indicate that more theoretical stripping stages should be added and that either the percent vaporization of the tower feed in the simulation is too high or the internal reflux rate at the lower draw-off tray is too low. The liquid-rate profile in the tower is shown in Fig. 13-117. The use of two or three pump-around circuits in Fig. 13-117. The use of two or three pump-around circuits instead of one would result in a better traffic pattern than that shown.

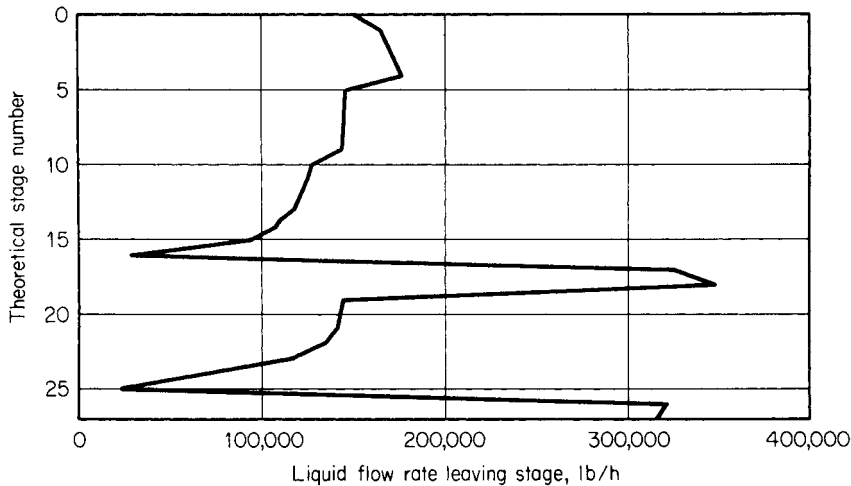


FIG. 13-117 Liquid rate profile for the example of Fig. 13-114.

BATCH DISTILLATION

Batch distillation, which is the process of separating a specific quantity (the charge) of a liquid mixture into products, is used extensively in the laboratory and in small production units that may have to serve for many mixtures. When there are C components in the feed, one batch column will often suffice where $C - 1$ simple continuous distillation columns would be required.

Many larger installations also feature a batch still. The material to be separated may be high in solids content, or it might contain tars or resins that would plug or foul a continuous unit. Use of a batch unit can keep solids separated and permit convenient removal at the termination of the process.

SIMPLE BATCH DISTILLATION

The simplest form of batch distillation consists of a heated vessel (pot or boiler), a condenser, and one or more receiving tanks. No trays or packing is provided. Feed is charged into the vessel and brought to boiling. Vapors are condensed and collected in a receiver. No reflux is returned. The rate of vaporization is sometimes limited to prevent "bumping" the charge and to avoid overloading the condenser, but other controls are minimal. This process is often referred to as a Rayleigh distillation.

If we represent the moles of vapor by V , the moles of liquid in the pot by H , the mole fraction of the more volatile component in this liquid by x , and the mole fraction of the same component in the vapor by y , a material balance yields

$$-y dV = d(Hx) \quad (13-124)$$

Since $dV = -dH$, substitution and expansion give

$$y dH = H dx + x dH \quad (13-125)$$

Rearranging and integrating give

$$\ln \frac{H_i}{H_f} = \int_{x_f}^{x_i} \frac{dx}{y-x} \quad (13-126)$$

where subscript i represents the initial condition and f the final condition of the liquid in the pot. The integration limits have been reversed to obtain a positive integral. Equation (13-126) is equivalent to an integrated form of the defining expression for residue curves in Eq. (13-116), with appropriate substitutions for the variable ξ (see below).

If phase equilibrium is assumed between liquid and vapor, the right-hand side of Eq. (13-126) may be evaluated from the area under a curve of $1/(y-x)$ versus x between the limits x_i and x_f . If the mixture is a binary system for which the relative volatility α can be approximated as a constant over the range considered, then the VLE relationship

$$y = \frac{\alpha x}{1 + (\alpha - 1)x} \quad (13-127)$$

can be substituted into Eq. (13-126) and a direct integration can be made:

$$\ln \left(\frac{H_f}{H_i} \right) = \frac{1}{\alpha - 1} \ln \left[\frac{x_f/(1-x_f)}{x_i/(1-x_i)} \right] + \ln \left(\frac{1-x_i}{1-x_f} \right) \quad (13-128)$$

For any two components A and B of a multicomponent mixture, if constant α values can be assumed for all pairs of components, then $dH_A/dH_B = y_A/y_B = \alpha_{A,B}(x_A/x_B)$. When this is integrated, we obtain

$$\ln \left(\frac{H_{A,f}}{H_{A,i}} \right) = \alpha_{A,B} \ln \left(\frac{H_{B,f}}{H_{B,i}} \right) \quad (13-129)$$

where $H_{A,i}$ and $H_{A,f}$ are the moles of component A in the pot before and after distillation and $H_{B,i}$ and $H_{B,f}$ are the corresponding moles of component B . Mixtures that cannot be accurately described by using a constant relative volatility require some form of numerical or graphical integration for the solution of Eq. (13-126).

As an example, consider the distillation of an ethanol-water mixture at 101.3 kPa (1 atm). The initial charge is 100 mol of liquid containing 18 mol % ethanol, and the mixture must be reduced to a maximum ethanol concentration in the still of 6 mol %. By using equilibrium data interpolated from Gmehling and Onken [*Vapor-Liquid Equilibrium Data Collection*, DECHEMA Chemistry Data Ser., vol. 1, Part 1, Frankfurt (1977)], we get the following:

x	y	$y-x$	$1/(y-x)$
0.18	0.517	0.337	2.97
0.16	0.502	0.342	2.91
0.14	0.485	0.345	2.90
0.12	0.464	0.344	2.90
0.10	0.438	0.338	2.97
0.08	0.405	0.325	3.08
0.06	0.353	0.293	3.41

The area under a curve of $1/(y-x)$ versus x between $x = 0.06$ and 0.18 is $0.358 = \ln(H_i/H_f)$, so that $H_f = 100/1.43 = 70.0$ mol. The liquid remaining consists of $(70.0)(0.06) = 4.2$ mol of ethanol and 65.8 mol of water. By material balance, the total accumulated distillate must contain $18.0 - 4.2 = 13.8$ mol of alcohol and $82.0 - 65.8 = 16.2$ mol of water. The total distillate is 30 mol, and the average distillate composition is $13.8/30 = 0.46$ mole fraction ethanol. The time, rate of heating, and vapor rate required to carry out the process are related by the energy balance and operating policy, which can be considered separately.

Graphical solutions of models lend significant insight, but there are many cases where such solutions are not possible or where repeated solutions are desired for different conditions. Progress in computer-based models, ranging from specialized simulation software to more general-purpose tools, now permits rapid solutions of most models. One solution of the example above using a general-purpose modeling tool Mathematica® is shown in Fig. 13-118.

The simple batch still provides only one theoretical plate of separation. Its use is usually restricted to laboratory work or preliminary manufacturing in which the products will be held for additional separation at a later time, when most of the volatile component must be removed from the batch before it is processed further, for separation of the batch from heavy undesired components.

BATCH DISTILLATION WITH RECTIFICATION

To obtain products with a narrow composition range, a batch rectifying still is commonly used. The *batch rectifier* consists of a pot (or reboiler) as in simple distillation, plus a rectifying column, a condenser, some means of accumulating and splitting off a portion of the condensed vapor (distillate) for reflux, and one or more product receivers (Fig. 13-119).

The temperature of the distillate is controlled near the bubble point, and reflux is returned at or near the upper column temperature to permit a true indication of reflux quantity and to improve the column operation. A heat exchanger is used to subcool the remainder of the distillate, which is sent to a product receiver. The column may operate at an elevated pressure or at vacuum, in which case appropriate additional devices must be included to obtain the desired pressure. Equipment design methods for batch still components, except for the pot, typically follow the same principles as those presented for continuous distillation under the assumption of conditions close to a steady state (but see the comments below on the effects of holdup). The design should be checked for each mixture if several mixtures are to be processed. The design should be checked at more than one point for each mixture, since the compositions in the pot and in the column change as the distillation proceeds. The pot design is based on the batch size and the vaporization rate, which are related to the time and rate of heating and cooling available. For existing equipment, the pot size will determine the size of the batch or at least a range of feasible sizes H_i .

In operation, a batch of liquid is charged to the pot, and the system is first brought to steady state under total reflux. A portion of the overhead condensate is then continuously withdrawn in accordance with

```

In[1]:= ydata = {{0.18, 0.517}, {0.16, 0.502}, {0.14, 0.485},
               {0.12, 0.464}, {0.10, 0.438}, {0.08, 0.405},
               {0.06, 0.353}};

In[2]:= y = Fit[ydata, {1, x, x^2}, x]

Out[2]= 0.190167 + 3.27321 x - 8.18452 x^2

In[3]:= curve = Plot[y, {x, 0.06, 0.18},
                    {DisplayFunction -> Identity}];

In[4]:= points = ListPlot[ydata,
                          {PlotStyle -> PointSize[0.025],
                           DisplayFunction -> Identity}];

In[5]:= Show [curve, points,
              {DisplayFunction -> $DisplayFunction,
               AxesOrigin -> Last[ydata],
               AxesLabel -> {"x", "y"}}];

In[6]:= Integrate[1 / {y - x}, {x, 0.06, 0.18}]

Out[6]= {{0.35856}}

```

FIG. 13-118 Solution for a simple distillation example using Mathematica,® version 5.0.1.

the established reflux policy. “Cuts” are made by switching to alternate receivers, at which time the operating conditions, e.g., reflux rate, may also be altered. The entire column operates as an enriching or rectifying section. As time proceeds, the composition of the liquid in the pot becomes less rich in the more volatile components, and distillation of a cut is stopped when the accumulated distillate attains the desired average composition.

OPERATING METHODS

A batch distillation can be operated in several ways:

1. *Constant reflux, varying overhead composition.* The reflux is set at a predetermined value at which it is maintained for the entire run. Since the pot liquid composition is changing, the instantaneous composition of the distillate also changes. The progress of the distillate and pot compositions in a particular binary separation is illustrated in Fig. 13-120. The variation of the distillate composition for a multicomponent batch distillation is shown in Fig. 13-121 (these distillate product cuts have relatively low purity). The shapes of the curves are functions of volatility, reflux ratio, and number of theoretical plates. The distillation is continued until the average distillate

composition is at the desired value. In the case of a binary mixture, the overhead is then typically diverted to another receiver, and an intermediate or “slop” cut is withdrawn until the remaining pot liquid meets the required specification. The intermediate cut is usually added to the next batch, which can therefore have a somewhat different composition from the previous batch. For a multicomponent mixture, two or more intermediate cuts may be taken between the product cuts. It is preferred to limit the size of the intermediate cuts as far as practical because they reduce the total amount of feed that can be processed.

2. *Constant overhead composition, varying reflux.* If it is desired to maintain a constant overhead composition in the case of a binary mixture, the amount of reflux returned to the column must be constantly increased throughout the run. As time proceeds, the pot is gradually depleted of the lighter component. The increase in reflux is typically gradual at first and more rapid near the end of a cut. Finally, a point is reached at which there is little of the lighter component remaining in the pot and the reflux ratio has attained a very high value. The receivers are then changed, the reflux is reduced, and an intermediate cut is taken as before. This technique can also be extended to a multicomponent mixture.

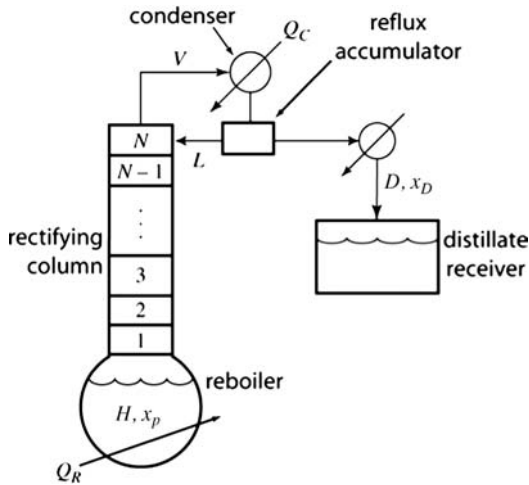


FIG. 13-119 Schematic of a batch rectifier.

3. *Other methods.* A cycling procedure can also be used for the column operation. The unit operates at total reflux until a steady state is established. The distillate is then taken as total drawoff for a short time, after which the column is returned to total reflux operation. This cycle is repeated throughout the course of distillation. Another possibility is to optimize the reflux ratio to achieve the desired separation in a minimum time. More complex operations may involve withdrawal of sidestreams, provision for intercondensers, addition of feeds to trays, and periodic feed additions to the pot.

APPROXIMATE CALCULATION PROCEDURES FOR BINARY MIXTURES

A useful analysis for a binary mixture employs the McCabe-Thiele graphical method. In addition to the usual assumptions of an adiabatic column and constant molar overflow on the trays, the following procedure assumes that the holdup of liquid on the trays, in the column,

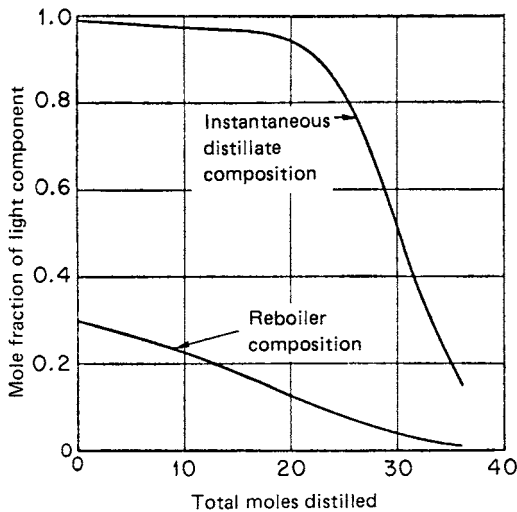


FIG. 13-120 Variation in distillate and reboiler compositions with the amount distilled in binary batch distillation at a constant reflux ratio.

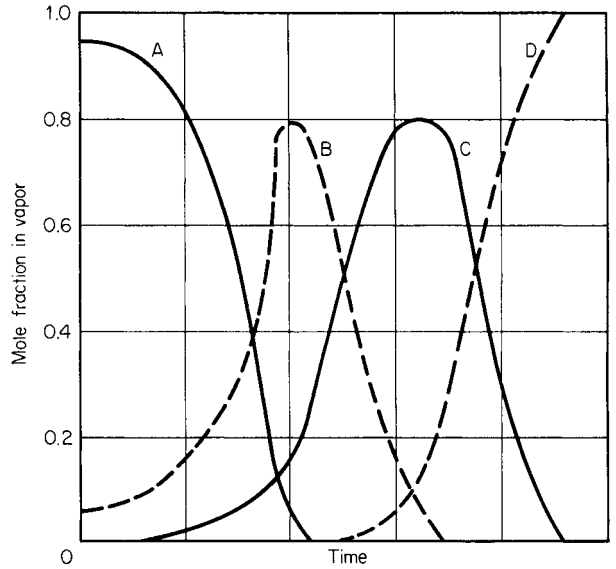


FIG. 13-121 Distillate composition for a batch distillation of a four-component mixture at a constant reflux ratio.

and in the condenser is negligible compared to the holdup in the pot. (The effects of holdup can be significant and are discussed in a later section.)

As a first step, the minimum reflux ratio should be determined. Point *D* in Fig. 13-122 represents the desired distillate composition and is located on the diagonal since a total condenser is assumed and $x_D = y_D$. Point *F* represents the initial composition in the pot x_{pi} and for the vapor entering the bottom of the rectifying column y_{pi} . The minimum internal reflux is found from the slope of the line *DF*

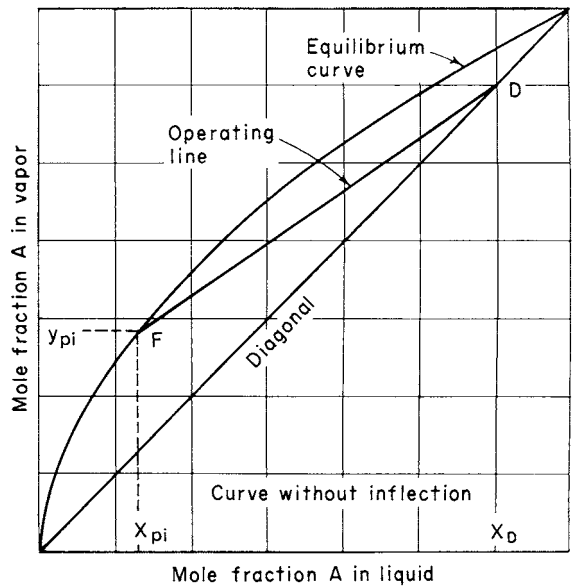


FIG. 13-122 Determination of the minimum reflux for a relatively ideal equilibrium curve.

13-112 DISTILLATION

$$\left(\frac{L}{V}\right)_{\min} = \frac{y_D - y_{pi}}{x_D - x_{pi}} \quad (13-130)$$

where L is the liquid flow rate and V is the vapor rate, both in moles per hour. Since $V = L + D$ (where D is distillate rate) and the external reflux ratio R is defined as $R = L/D$,

$$\frac{L}{V} = \frac{R}{R + 1} \quad (13-131)$$

or

$$R_{\min} = \frac{(L/V)_{\min}}{1 - (L/V)_{\min}} \quad (13-132)$$

The condition of minimum reflux for an equilibrium curve with an inflection point P is shown in Fig. 13-123. In this case the minimum internal reflux is

$$\left(\frac{L}{V}\right)_{\min} = \frac{y_D - y_P}{x_D - x_P} \quad (13-133)$$

The operating reflux ratio is usually 1.5 to 10 times the minimum. By using the ethanol-water equilibrium curve for 101.3-kPa (1-atm) pressure shown in Fig. 13-123 but extending the line to a convenient point for readability, $(L/V)_{\min} = (0.800 - 0.695)/(0.800 - 0.600) = 0.52$ and $R_{\min} = 1.083$.

Batch Rectification at Constant Reflux Using an analysis similar to the simple batch still, Smoker and Rose [*Trans. Am. Inst. Chem. Eng.*, **36**, 285 (1940)] developed the following equation:

$$\ln \frac{H_i}{H_f} = \int_{x_{pf}}^{x_{pi}} \frac{dx_p}{x_D - x_p} \quad (13-134)$$

An overall material balance on the light component gives the average or accumulated distillate composition $x_{D,avg}$

$$x_{D,avg} = \frac{H_i x_{pi} - H_f x_{pf}}{H_i - H_f} \quad (13-135)$$

If the integral on the right side of Eq. (13-134) is denoted by ξ , the time θ for distillation can be found by

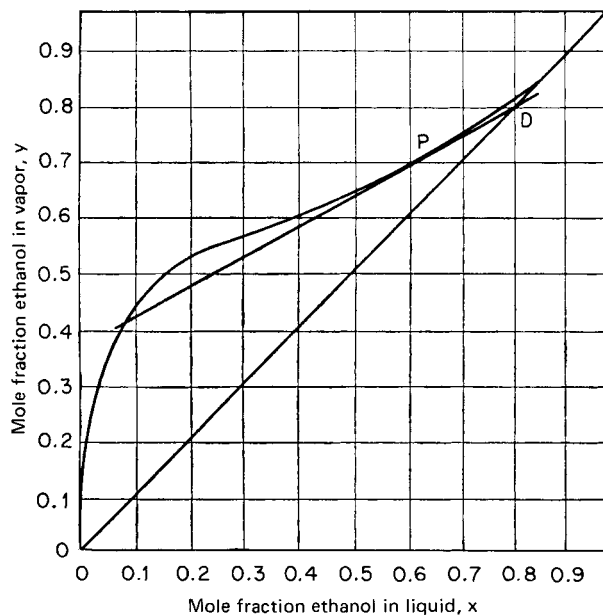


FIG. 13-123 Determination of minimum reflux for an equilibrium curve with an inflection point.

$$\theta = (R + 1) \frac{H_i(e^{\xi} - 1)}{V e^{\xi}} \quad (13-136)$$

An alternative equation is

$$\theta = \frac{R + 1}{V} (H_i - H_f) \quad (13-137)$$

Development of these equations is given by Block [*Chem. Eng.*, **68**, 88 (Feb. 6, 1961)]. The calculation process is illustrated schematically in Fig. 13-124. Operating lines are drawn with the same slope but intersecting the 45° line at different points. The number of theoretical plates under consideration is stepped off to find the corresponding bottoms composition (i.e., still pot composition) for each distillate composition. In Fig. 13-124, operating line $L-1$ with slope L/V drawn from point D_1 where the distillate composition is x_{D1} and the pot composition is x_{p1-3} for three theoretical plates, x_{D2} has a corresponding pot composition of x_{p2-3} , etc. By using these pairs of distillate and pot compositions, the right-hand side of Eq. (13-134) can be evaluated and $x_{D,avg}$ can be found from Eq. (13-135). An iterative calculation is required to find the value of H_f that corresponds to a specified $x_{D,avg}$.

To illustrate the use of these equations, consider a charge of 520 mol of an ethanol-water mixture containing 18 mol % ethanol to be distilled at 101.3 kPa (1 atm). Suppose that the vaporization rate is 75 mol/h, and the product specification is 80 mol % ethanol. Let $L/V = 0.75$, corresponding to a reflux ratio $R = 3.0$. If the column section has six theoretical plates and the pot provides an additional seventh, find how many moles of product will be obtained, what the composition of the pot residue will be, and the time that the distillation will take.

Using the vapor-liquid equilibrium data, plot a y - x diagram. Draw a number of operating lines at a slope of 0.75. Note the composition at the 45° intersection, and step off seven stages on each to find the equilibrium value of the bottoms pot composition. Some of the results are tabulated in the following table:

x_D	x_p	$x_D - x_p$	$1/(x_D - x_p)$
0.800	0.323	0.477	2.097
0.795	0.245	0.550	1.820
0.790	0.210	0.580	1.725
0.785	0.180	0.605	1.654
0.780	0.107	0.673	1.487
0.775	0.041	0.734	1.362

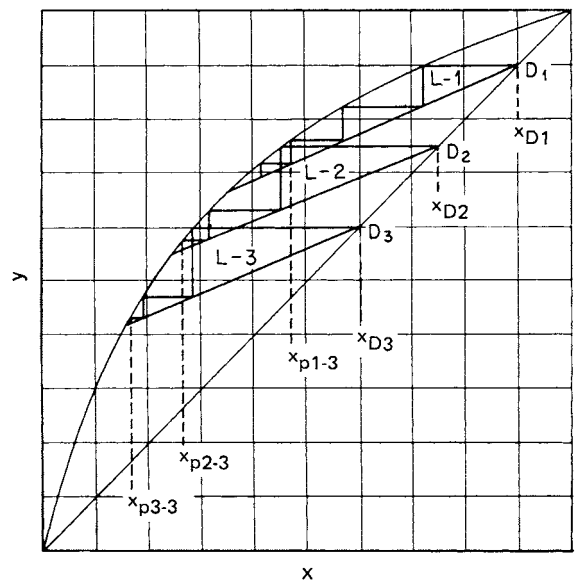


FIG. 13-124 Graphical method for constant-reflux operation.

By using an iterative procedure, integrating between x_{pi} of 0.18 and various lower limits, it is found that $x_{D,avg} = 0.80$ when $x_{pf} = 0.04$, at which time the value of the integral = $0.205 = \ln(H_i/H_f)$, so that $H_f = 424$ mol. The product collected = $H_i - H_f = 520 - 424 = 96$ mol. From Eq. (13-136),

$$\theta = \frac{(4)(520)(e^{0.205} - 1)}{75(e^{0.205})} = 5.2 \text{ h} \quad (13-138)$$

Batch Rectification at Constant Distillate Composition
Bogart [*Trans. Am. Inst. Chem. Eng.*, **33**, 139 (1937)] developed the following equation for constant distillate composition with the column holdup assumed to be negligible:

$$\theta = \frac{H_i(x_D - x_{pi})}{V} \int_{x_{pf}}^{x_{pi}} \frac{dx_p}{(1 - L/V)(x_D - x_p)^2} \quad (13-139)$$

and where the terms are defined as before. The quantity distilled can then be found by material balance once the initial and final pot compositions are known.

$$H_i - H_f = \frac{H_i(x_{pi} - x_{pf})}{x_D - x_{pf}} \quad (13-140)$$

A schematic example is shown in Fig. 13-125. The distillate composition is held constant by increasing the reflux as the pot composition becomes more dilute. Operating lines with varying slopes ($= L/V$) are drawn from the known distillate composition, and the given number of stages is stepped off to find the corresponding bottoms (still pot) compositions.

As an example, consider the same ethanol-water mixture used above to illustrate constant reflux but now with a constant distillate composition of $x_D = 0.90$. The following table is compiled:

L/V	R	x_p	$x_D - x_p$	$1/(1 - L/V)(x_D - x_p)^2$
0.600	1.50	0.654	0.147	115.7
0.700	2.33	0.453	0.348	27.5
0.750	3.00	0.318	0.483	17.2
0.800	4.00	0.143	0.658	11.5
0.850	5.67	0.054	0.747	11.9
0.900	9.00	0.021	0.780	16.4

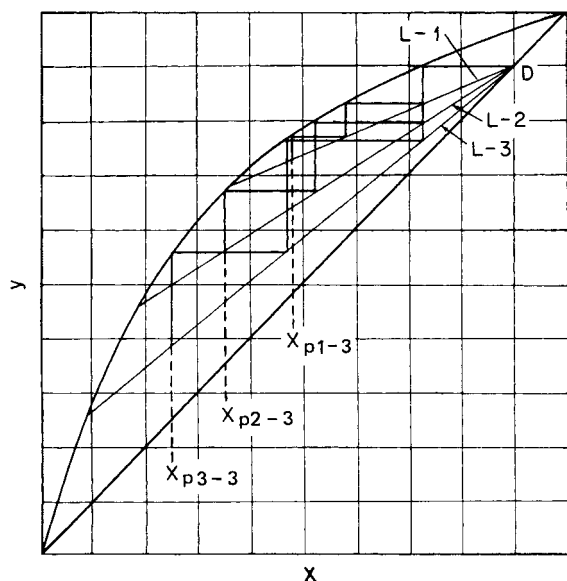


FIG. 13-125 Schematic of constant distillate composition operation.

If the right-hand side of Eq. (13-139) is integrated by using a limit for x_{pf} of 0.04, the value of the integral is 1.615 and the time is

$$\theta = \frac{(520)(0.800 - 0.180)(1.615)}{75} = 7.0 \text{ h} \quad (13-141)$$

The quantity distilled can be found from Eq. (13-140):

$$H_i - H_f = \frac{(520)(0.180 - 0.040)}{0.800 - 0.040} = 96 \text{ mol} \quad (13-142)$$

Other Operating Methods and Optimization A useful control method for difficult industrial or laboratory distillations is *cycling operation*. The most common form of cycling control is to operate the column at total reflux until steady state is established, take off the complete distillate for a short time, and then return to total reflux. An alternative scheme is to interrupt vapor flow to the column periodically by the use of a solenoid-operated butterfly valve in the vapor line from the pot. In both cases, the equations necessary to describe the system are complex, as shown by Schrodt et al. [*Chem. Eng. Sci.*, **22**, 759 (1967)]. The most reliable method for establishing the cycle relationships is by experimental trial on an operating column. Several investigators have also proposed that batch distillation be programmed to attain *time optimization* by proper variation of the reflux ratio. A comprehensive discussion was first presented by Coward [*Chem. Eng. Sci.*, **22**, 503 (1967)] and reviewed and updated by Kim and Diwekar [*Rev. Chem. Eng.*, **17**, 111 (2001)].

The *choice of operating mode* depends upon characteristics of the specific system, the product specifications, and the engineer's preference in setting up a control sequence. Probably the most direct and most common method is *constant reflux*. Operation can be regulated by a timed reflux splitter, a ratio controller, or simply a pair of flowmeters. Since composition is changing with time, some way must be found to estimate the average accumulated distillate composition in order to define the end-point. This is no problem when the specification is not critical or the change in distillate composition is sharply defined. However, when the composition of the distillate changes slowly with time, the cut point is more difficult to determine. Operating with *constant composition* (varying reflux), the specification is automatically achieved if control can be linked to composition or some composition-sensitive physical variable. The relative advantage of the two modes depends upon the materials being separated and upon the number of theoretical plates in the column. A comparison of distillation rates using the same initial and final pot composition for the system benzene-toluene is given in Fig. 13-126. Typical control instrumentation is described by Block [*Chem. Eng.*, **74**, 147 (Jan. 16, 1967)]. Control procedures for *reflux and vapor cycling* operation and for the *time-optimal* process are largely a matter of empirical trial.

Effects of Column Holdup When the holdup of liquid on the trays and in the condenser and reflux accumulator is not negligible compared with the holdup in the pot, the distillate composition at constant reflux ratio changes with time at a different rate than when the column holdup is negligible because of two separate effects.

First, with an appreciable column holdup, the composition of the charge to the pot will be higher in the light component than the pot composition at the start of the distillation. The reason is that before product takeoff begins, the column holdup must be supplied, and due to the rectification, its average composition is higher in the lighter component than that of the liquid charged as feed to the pot. Thus, when overhead takeoff begins, the pot composition is lower than it would be if there were negligible column holdup and the separation is more difficult than expected based on the composition of the feed. The second effect of column holdup is to slow the rate of exchange of the components; the holdup exerts an inertial effect, which prevents compositions from changing as rapidly as they would otherwise, and the degree of separation is usually improved.

Both these effects occur at the same time and change in importance during the course of distillation. Although a number of studies were made and approximate methods developed for predicting the effect of liquid holdup during the 1950s and 1960s (summarized in the 6th edition of *Perry's Chemical Engineers' Handbook*), it is now best to use simulation methods to determine the effect of holdup on a case-by-case basis.

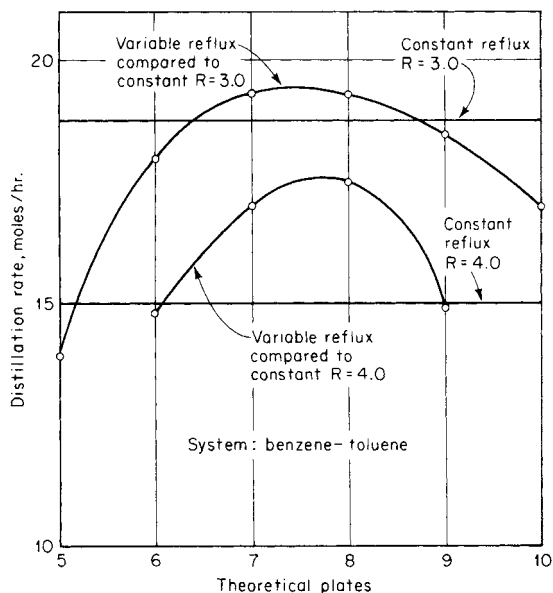


FIG. 13-126 Comparison of operating modes for a batch column.

As an example, consider a batch rectifier fed with a 1:1 mixture of ethanol and *n*-propanol. The rectifier has eight theoretical stages in the column and is operated at a reflux ratio of 19. The distillate and pot compositions are shown in Fig. 13-127 for various values of the holdups.

In Fig. 13-127a, the holdup on each stage is 0.01 percent of the initial pot holdup, and in the reflux accumulator it is 0.1 percent of the initial pot holdup (for a total of 0.108 percent). Because this model calculation does not begin with a total reflux period, there is a small initial distillate cut with relatively low ethanol purity. This is followed by a high-purity distillate cut. An intermediate cut of approximately 10 percent of the initial batch size can be collected, leaving the pot with a high purity of *n*-propanol. The column holdup for the case shown in Fig. 13-127b is 1 percent of the initial batch size on each stage while the reflux accumulator holdup remains small at 0.1 percent (for a total of 8.1 percent). In this case, both the first low-purity cut and the intermediate cut are somewhat larger for the same purity specifications. These effects are substantially larger when the reflux accumulator has a more significant holdup, as shown in Fig. 13-127c, corresponding to a holdup of 1 percent on each stage and 5 percent in the reflux accumulator (for a total of 13 percent). Similar effects are found for multicomponent mixtures. The impact of column and condenser holdup is most important when a high-purity cut is desired for a component that is present in relatively small amounts in the feed.

SHORTCUT METHODS FOR MULTICOMPONENT BATCH RECTIFICATION

For preliminary studies of batch rectification of multicomponent mixtures, shortcut methods that assume constant molar overflow and negligible vapor and liquid holdup are useful in some cases (see the discussion above concerning the effects of holdup). The method of Diwekar and Madhavan [*Ind. Eng. Chem. Res.*, **30**, 713 (1991)] can be used for constant reflux or constant overhead rate. The method of Sundaram and Evans [*Ind. Eng. Chem. Res.*, **32**, 511 (1993)] applies only to the case of constant reflux, but is easy to implement. Both methods employ the Fenske-Underwood-Gilliland (FUG) shortcut procedure at successive time steps. Thus, batch rectification is treated as a sequence of continuous, steady-state rectifications.

CALCULATION METHODS AND SIMULATION

Model predictions such as those shown in Fig. 13-126 or 13-127 are relatively straightforward to obtain by using modern simulation mod-

els and software tools. As discussed in earlier editions of this handbook, such models and algorithms for their solutions have been the subject of intensive study since the early 1960s when digital computing became practical. Detailed calculation procedures for binary and multicomponent batch distillation were initially focused on binary mixtures of constant relative volatility. For example, Huckaba and Danyl [*AIChE J.*, **6**, 335 (1960)] developed a simulation model that incorporated more details than can be included in the simple analytical models described above. They assumed constant-mass tray holdups, adiabatic tray operation, and linear enthalpy relationships, but did include energy balances around each tray and permitted the use of nonequilibrium trays by means of specified tray efficiencies. Experimental data were provided to validate the simulation. Meadows [*Chem. Eng. Prog. Symp. Ser.* **46**, 59, 48 (1963)] presented a multicomponent batch distillation model that included equations for energy, material, and volume balances around theoretical trays. The only assumptions made were perfect mixing on each tray, negligible vapor holdup, adiabatic operation, and constant-volume tray holdup. Distefano [*AIChE J.*, **14**, 190 (1968)] extended the model and developed a procedure that was used to simulate several commercial batch distillation columns successfully. Boston et al. (*Foundations of Computer-Aided Chemical Process Design*, vol. 2, Mah and Seider, eds., American Institute of Chemical Engineers, New York, 1981, p. 203) further extended the model, provided a variety of practical sets of specifications, and utilized modern numerical procedures and equation formulations to handle efficiently the nonlinear and often stiff nature of the multicomponent batch distillation problem.

It is important to note that in using computer-aided models for batch distillation, the various assumptions of the model can have a significant impact on the accuracy of the results; e.g., see the discussion of the effects of holdup above. Uncertainties in the physical and chemical parameters in the models can be addressed most effectively by a combination of sensitivity calculations using simulation tools, along with comparison to data. The mathematical treatment of stiffness in the model equations can also be very important, and there is often a substantial advantage in using simulation tools that take special account of this stiffness. (See the 7th edition of *Perry's Chemical Engineers' Handbook* for a more detailed discussion of this aspect).

The availability of detailed models and solution methods has enabled many new studies of complex, mixtures, configurations, and operating and control strategies for batch distillation.

CONSTANT-LEVEL DISTILLATION

Manipulation of the operating conditions such as reflux ratio or pressure during a batch distillation can be useful. In addition, the feed to the batch distillation may vary during the process. A common application is to replace one solvent with another in the presence of a heavy nonvolatile product, as may be encountered in pharmaceutical production. One option for switching solvents is to use simple distillation repeatedly. Initially, a portion of the first solvent is removed by boiling. Then the second solvent is added, and a simple distillation removes more of the first solvent along with some of the second. Repetition of the latter step can be used to reduce the concentration of the first solvent to very small levels.

Gentilcore [*Chem. Eng. Progr.*, **98**(1), 56 (Jan. 2002)] describes an alternative strategy of "constant-level" batch distillation where the replacement solvent is added at a rate to keep the volume of liquid in the pot constant. For simple distillation without rectification the analog of Eq. (13-126) is

$$\frac{S}{H} = \int_{x_j}^{x_i} \frac{dx}{y} \quad (13-143)$$

and the analog of Eq. (13-128) is

$$\frac{S}{H} = \frac{1}{\alpha} \ln \frac{x_i}{x_j} + \frac{\alpha - 1}{\alpha} (x_i - x_j) \quad (13-144)$$

where the mole fractions refer to the compositions of the original solvent and *S* is the amount of the second solvent added to the batch. The amount of solute, a nonvolatile heavy product, is small compared to the size of the batch (alternatively, the analysis can be done on a

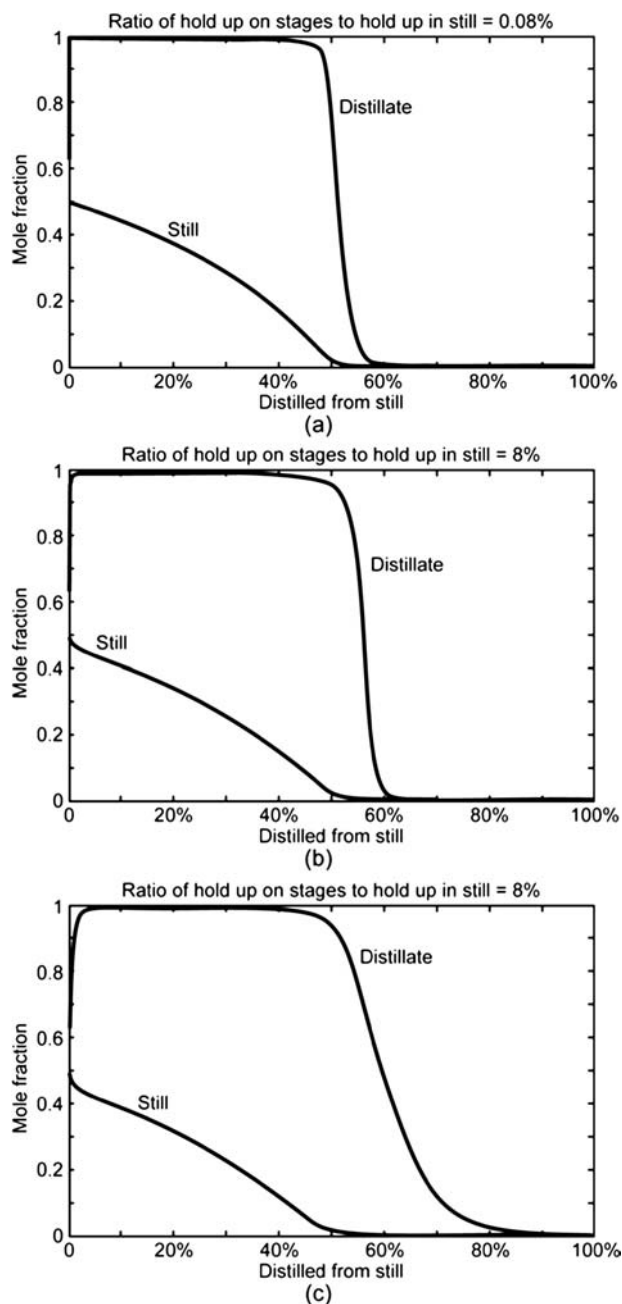


FIG. 13-127 Effects of holdup on batch rectifier.

solvent-free basis). The second solvent is assumed to be pure, and the rate of addition is manipulated to keep a constant level in the pot. Compared to the repeated application of simple distillation, this semi-batch operation can typically reduce solvent use by one-half or more depending on the volatility and the desired compositions. This is also a more efficient use of equipment at the expense of a somewhat more complex operation.

An example provided by Gentilcore considers a simple batch still that operates with an initial charge of 80 mol and a minimum of 20 mol. The original solvent use has a volatility $\alpha = 3$ relative to that of the replacement solvent. If simple distillation is used, 60 mol of the original solvent is initially boiled off and then 60 mol of the second solvent is added. A

second distillation of this mixture begins with a composition $x_i = 0.25$ of the original solvent. The solution of Eq. (13-128) by trial and error or root finding gives $x_j = 0.03$ for $H_i = 80$ and $H_j = 20$. Of the 60 mol removed as distillate in this second distillation, $20 - 0.03 = 19.97$ mol is the original solvent and $60 - 19.97 = 40.03$ mol is the replacement. An alternative constant-level batch distillation in the same equipment according to Eq. (13-144) with $H = 20$, $x_i = 0.25$, and $x_j = 0.03$ requires the addition of $S = 35.6$ mol of replacement solvent. The still contains 20 mol of the solvent; 16.2 mol is distilled compared to 40.3 mol in the simple distillation. This 60 percent savings in the use of replacement solvent arises because the distillation takes place beginning with a higher concentration of the original solvent for the second step.

ALTERNATIVE EQUIPMENT CONFIGURATIONS

The batch rectifier shown schematically in Fig. 13-119 is by far the most common configuration of equipment. Several alternative special-purpose configurations have been studied and offer potential advantages in particular applications. Also see Doherty and Malone (*Conceptual Design of Distillation Systems*, McGraw-Hill, 2001, pp. 407–409, 417–419).

For instance, a simple batch distillation can be combined with a stripping column to give the batch stripper shown in Fig. 13-128. The pot holds the batch charge and provides liquid reflux into the stripping section. The reboiler provides vapor to the column and has relatively small holdup. The product stream B in the bottom is concentrated in the higher-boiling compound, and the pot gradually becomes more concentrated in the lighter component. Multiple “cuts” can be taken as products, and the reboil rate either can be constant or can be adjusted by analogy with the reflux ratio in the batch rectifier.

For mixtures containing large concentrations of a heavy component, the batch stripper can be advantageous.

The more complex “middle vessel” column combines aspects of both the batch rectifier and the batch stripper, as shown in Fig. 13-129. The middle vessel arrangement was described qualitatively by Robinson and Gilliland (*Elements of Fractional Distillation*, McGraw-Hill, 1950, p. 388) and analyzed by Bortolini and Guirase [*Quad. Ing. Chim. Ital.*, **6**, 150 (1970)]. This configuration requires more equipment and is more complex, but can produce both distillate and bottoms product cuts simultaneously. Barolo and Botteon [*AIChE J.*, **43**, 2601 (1997)] pointed out that the middle vessel configuration at total reflux and reboil and with the appropriate collection equipment for distillate and bottoms products (not shown in Fig. 13-129) can concentrate a ternary mixture into its three pure fractions. This and analogous configurations for mixtures with more components have been studied by Hasebe et al. [*J. Chem. Eng. Japan*, **29**, 1000 (1996); *Computers Chem. Engng.*, **23**,

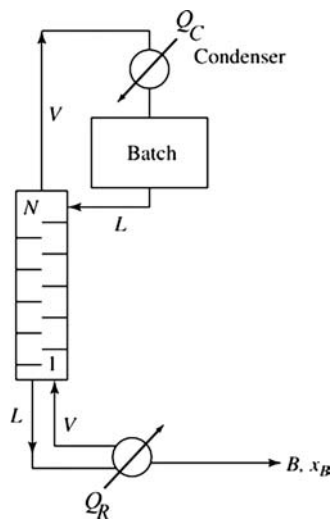


FIG. 13-128 Schematic of a batch stripper.

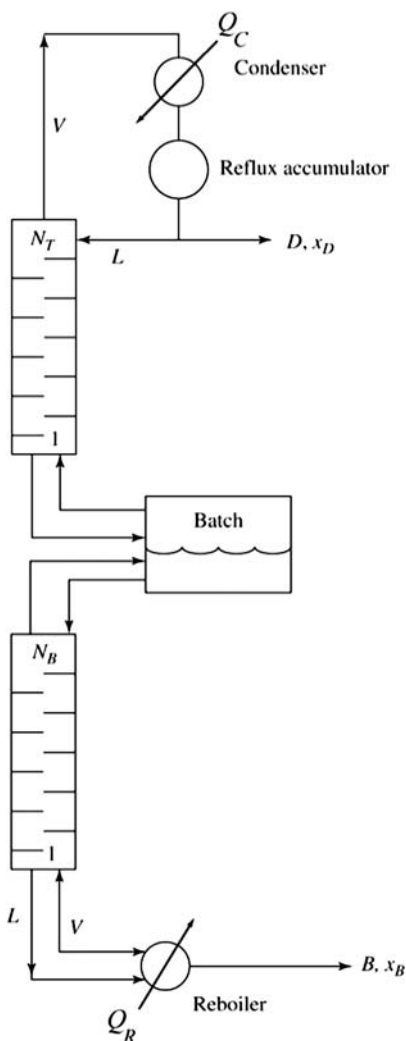


FIG. 13-129 Middle vessel batch distillation.

523 (1999)] and experimentally by Wittgens and Skogestad [*ICHEME Symp Ser.*, **142**, 239 (1997).]

The batch stripper and the middle vessel configurations provide the capability to make separations for certain azeotropic mixtures that are not possible or that cannot be done efficiently in the batch rectifier.

BATCH DISTILLATION OF AZEOTROPIC MIXTURES

Although azeotropic distillation is covered in an earlier subsection, it is appropriate to consider the application of residue curve maps to batch distillation here. (See the subsection Enhanced Distillation for a discussion of residue curve maps.) An essential point is that the sequence, number, and limiting composition of each cut from a batch distillation depend on the form of the residue curve map and the composition of the initial charge to the still. As with continuous distillation operation, the set of reachable products (cuts) for a given charge to a batch distillation is constrained by the residue curve-map distillation boundaries. Furthermore, some pure components can be produced as products from the batch stripper, but not the batch rectifier and vice versa. Doherty and Malone (*Conceptual Design of Distillation Systems*, chap. 9, McGraw-Hill, 2001) give more details, but the main points are the following.

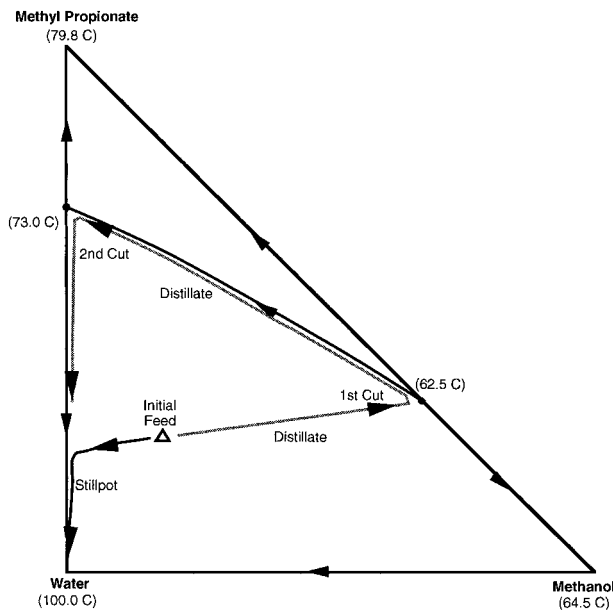


FIG. 13-130 Residue curve map and batch rectifier paths for methanol, methyl propionate, and water.

In the batch rectifier, the limiting cuts, obtainable with a sufficiently large number of stages and reflux, begin with the low-boiling node that defines the distillation region containing the feed composition. For the batch stripper, the first limiting cut is the high-boiling node. In either case, the subsequent cuts depend on the structure of the residue curve map.

For the batch rectifier, as the low-boiling component or azeotrope is removed, the still composition moves along a straight material balance line through the initial feed composition and the low-boiling node and away from the initial composition until it reaches the edge of the composition triangle or a distillation boundary. The path then follows the edge or distillation boundary to the high-boiling node of the region.

As an example, consider the residue curve map structure shown in Fig. 13-130 for a mixture of methanol, methyl propionate, and water at a pressure of 1 atm. There are two minimum-boiling binary azeotropes joined by a distillation boundary that separates the compositions into two distillation regions. Feeds in the upper and lower regions will have different distillate products. For the sample feed shown, and with a sufficient number of theoretical stages and reflux, the distillate will rapidly approach the low-boiling azeotrope of methanol and methyl propionate at 62.5°C. The still pot composition changes along the straight-line segment as shown until it is nearly free of methanol. At that point, the distillate composition changes rapidly along the distillation boundary to a composition for the second cut at or near the methyl propionate–water azeotrope. The still pot composition eventually approaches pure water. The rate of change and the precise approach to these compositions require more detailed study.

For the same feed, a batch stripper can be used to remove a bottoms product that approaches pure water. The pot composition (overhead) will contain all three components near the point of intersection of the distillation boundary with a straight line extended from the water vertex through the feed composition.

For this mixture it is not possible to isolate the pure components in a batch rectifier or batch stripper. The use of additional equipment such as a decanter to exploit liquid-liquid phase behavior or the addition of a fourth component or chemical reactions can sometimes be used to effect the separation.

The product cuts for azeotropic mixtures are also sensitive to the curvature of the distillation boundaries; see Doherty and Malone (*Conceptual Design of Distillation Systems*, McGraw-Hill, 2001; pp. 403–404) and additional references there.

SECTION 14

Equipment for
Distillation, Gas
Absorption, Phase
Dispersion, and
Phase Separation

PERRY'S CHEMICAL ENGINEERS' HANDBOOK

8TH EDITION



HENRY Z. KISTER, PAUL MATHIAS
D. E. STEINMEYER, W. R. PENNEY
B. B. CROCKER, JAMES R. FAIR

Copyright © 2008, 1997, 1984, 1973, 1963, 1950, 1941, 1934 by The McGraw-Hill Companies, Inc. All rights reserved. Manufactured in the United States of America. Except as permitted under the United States Copyright Act of 1976, no part of this publication may be reproduced or distributed in any form or by any means, or stored in a database or retrieval system, without the prior written permission of the publisher.

0-07-154221-3

The material in this eBook also appears in the print version of this title: 0-07-151137-7.

All trademarks are trademarks of their respective owners. Rather than put a trademark symbol after every occurrence of a trademarked name, we use names in an editorial fashion only, and to the benefit of the trademark owner, with no intention of infringement of the trademark. Where such designations appear in this book, they have been printed with initial caps.

McGraw-Hill eBooks are available at special quantity discounts to use as premiums and sales promotions, or for use in corporate training programs. For more information, please contact George Hoare, Special Sales, at george_hoare@mcgraw-hill.com or (212) 904-4069.

TERMS OF USE

This is a copyrighted work and The McGraw-Hill Companies, Inc. (“McGraw-Hill”) and its licensors reserve all rights in and to the work. Use of this work is subject to these terms. Except as permitted under the Copyright Act of 1976 and the right to store and retrieve one copy of the work, you may not decompile, disassemble, reverse engineer, reproduce, modify, create derivative works based upon, transmit, distribute, disseminate, sell, publish or sublicense the work or any part of it without McGraw-Hill’s prior consent. You may use the work for your own noncommercial and personal use; any other use of the work is strictly prohibited. Your right to use the work may be terminated if you fail to comply with these terms.

THE WORK IS PROVIDED “AS IS.” McGRAW-HILL AND ITS LICENSORS MAKE NO GUARANTEES OR WARRANTIES AS TO THE ACCURACY, ADEQUACY OR COMPLETENESS OF OR RESULTS TO BE OBTAINED FROM USING THE WORK, INCLUDING ANY INFORMATION THAT CAN BE ACCESSED THROUGH THE WORK VIA HYPERLINK OR OTHERWISE, AND EXPRESSLY DISCLAIM ANY WARRANTY, EXPRESS OR IMPLIED, INCLUDING BUT NOT LIMITED TO IMPLIED WARRANTIES OF MERCHANTABILITY OR FITNESS FOR A PARTICULAR PURPOSE. McGraw-Hill and its licensors do not warrant or guarantee that the functions contained in the work will meet your requirements or that its operation will be uninterrupted or error free. Neither McGraw-Hill nor its licensors shall be liable to you or anyone else for any inaccuracy, error or omission, regardless of cause, in the work or for any damages resulting therefrom. McGraw-Hill has no responsibility for the content of any information accessed through the work. Under no circumstances shall McGraw-Hill and/or its licensors be liable for any indirect, incidental, special, punitive, consequential or similar damages that result from the use of or inability to use the work, even if any of them has been advised of the possibility of such damages. This limitation of liability shall apply to any claim or cause whatsoever whether such claim or cause arises in contract, tort or otherwise.

DOI: 10.1036/0071511377

Equipment for Distillation, Gas Absorption, Phase Dispersion, and Phase Separation

Henry Z. Kister, M.E., C.Eng., C.Sc. Senior Fellow and Director of Fractionation Technology, Fluor Corporation; Fellow, American Institute of Chemical Engineers; Fellow, Institution of Chemical Engineers (UK); Member, Institute of Energy (Section Editor, Equipment for Distillation and Gas Absorption)

Paul M. Mathias, Ph.D. Technical Director, Fluor Corporation; Member, American Institute of Chemical Engineers (Design of Gas Absorption Systems)

D. E. Steinmeyer, P.E., M.A., M.S. Distinguished Fellow, Monsanto Company (retired); Fellow, American Institute of Chemical Engineers; Member, American Chemical Society (Phase Dispersion)

W. R. Penney, Ph.D., P.E. Professor of Chemical Engineering, University of Arkansas; Member, American Institute of Chemical Engineers (Gas-in-Liquid Dispersions)

B. B. Crocker, P.E., S.M. Consulting Chemical Engineer; Fellow, American Institute of Chemical Engineers; Member, Air Pollution Control Association (Phase Separation)

James R. Fair, Ph.D., P.E. Professor of Chemical Engineering, University of Texas; Fellow, American Institute of Chemical Engineers; Member, American Chemical Society, American Society for Engineering Education, National Society of Professional Engineers (Section Editor of the 7th edition and major contributor to the 5th, 6th, and 7th editions)

INTRODUCTION		
Definitions	14-6	
Equipment	14-6	
Design Procedures	14-6	
Data Sources in the Handbook	14-7	
Equilibrium Data	14-7	
DESIGN OF GAS ABSORPTION SYSTEMS		
General Design Procedure	14-7	Design of Absorber-Stripper Systems
Selection of Solvent and Nature of Solvents	14-7	Importance of Design Diagrams
Selection of Solubility Data	14-8	Packed-Tower Design
Example 1: Gas Solubility	14-9	Use of Mass-Transfer-Rate Expression
Calculation of Liquid-to-Gas Ratio	14-9	Example 2: Packed Height Requirement
Selection of Equipment	14-9	Use of Operating Curve
Column Diameter and Pressure Drop	14-9	Calculation of Transfer Units
Computation of Tower Height	14-9	Stripping Equations
Selection of Stripper Operating Conditions	14-9	Example 3: Air Stripping of VOCs from Water
		Use of HTU and $K_G a$ Data
		Use of HETP Data for Absorber Design
		Tray-Tower Design
		Graphical Design Procedure
		Algebraic Method for Dilute Gases
		Algebraic Method for Concentrated Gases
		Stripping Equations
		Tray Efficiencies in Tray Absorbers and Strippers
		Example 4: Actual Trays for Steam Stripping

14-2 EQUIPMENT FOR DISTILLATION, GAS ABSORPTION, PHASE DISPERSION, AND PHASE SEPARATION

Heat Effects in Gas Absorption	14-15	Transition between Flow Regimes	14-47
Overview	14-15	Froth-Spray	14-47
Effects of Operating Variables	14-16	Froth-Emulsion	14-48
Equipment Considerations	14-16	Valve Trays	14-48
Classical Isothermal Design Method	14-16	Tray Efficiency	14-48
Classical Adiabatic Design Method	14-17	Definitions	14-48
Rigorous Design Methods	14-17	Fundamentals	14-48
Direct Comparison of Design Methods	14-17	Factors Affecting Tray Efficiency	14-49
Example 5: Packed Absorber, Acetone into Water	14-17	Obtaining Tray Efficiency	14-50
Example 6: Solvent Rate for Absorption	14-17	Rigorous Testing	14-50
Multicomponent Systems	14-18	Scale-up from an Existing Commercial Column	14-50
Example 7: Multicomponent Absorption, Dilute Case	14-18	Scale-up from Existing Commercial Column to Different Process Conditions	14-50
Graphical Design Methods for Dilute Systems	14-18	Experience Factors	14-50
Algebraic Design Method for Dilute Systems	14-19	Scale-up from a Pilot or Bench-Scale Column	14-51
Example 8: Multicomponent Absorption, Concentrated Case	14-19	Empirical Efficiency Prediction	14-52
Absorption with Chemical Reaction	14-20	Theoretical Efficiency Prediction	14-53
Introduction	14-20	Example 12: Estimating Tray Efficiency	14-53
Recommended Overall Design Strategy	14-20		
Dominant Effects in Absorption with Chemical Reaction	14-20		
Applicability of Physical Design Methods	14-22		
Traditional Design Method	14-22		
Scaling Up from Laboratory Data	14-23		
Rigorous Computer-Based Absorber Design	14-24		
Development of Thermodynamic Model for Physical and Chemical Equilibrium	14-25		
Adoption and Use of Modeling Framework	14-25		
Parameterization of Mass Transfer and Kinetic Models	14-25		
Deployment of Rigorous Model for Process Optimization and Equipment Design	14-25		
Use of Literature for Specific Systems	14-26		
EQUIPMENT FOR DISTILLATION AND GAS ABSORPTION: TRAY COLUMNS			
Definitions	14-26		
Tray Area Definitions	14-26		
Vapor and Liquid Load Definitions	14-27		
Flow Regimes on Trays	14-27		
Primary Tray Considerations	14-29		
Number of Passes	14-29		
Tray Spacing	14-29		
Outlet Weir	14-29		
Downcomers	14-29		
Clearance under the Downcomer	14-31		
Hole Sizes	14-31		
Fractional Hole Area	14-31		
Multipass Balancing	14-32		
Tray Capacity Enhancement	14-32		
Truncated Downcomers/Forward Push Trays	14-32		
High Top to Bottom Downcomer Area and Forward Push	14-34		
Large Number of Truncated Downcomers	14-34		
Radial Trays	14-34		
Centrifugal Force Deentrainment	14-34		
Other Tray Types	14-34		
Bubble-Cap Trays	14-34		
Dual-Flow Trays	14-34		
Baffle Trays	14-34		
Flooding	14-36		
Entrainment (Jet) Flooding	14-36		
Spray Entrainment Flooding Prediction	14-36		
Example 9: Flooding of a Distillation Tray	14-38		
System Limit (Ultimate Capacity)	14-38		
Downcomer Backup Flooding	14-38		
Downcomer Choke Flooding	14-39		
Derating ("System") Factors	14-40		
Entrainment	14-40		
Effect of Gas Velocity	14-40		
Effect of Liquid Rate	14-40		
Effect of Other Variables	14-40		
Entrainment Prediction	14-41		
Example 10: Entrainment Effect on Tray Efficiency	14-42		
Pressure Drop	14-42		
Example 11: Pressure Drop, Sieve Tray	14-44		
Loss under Downcomer	14-44		
Other Hydraulic Limits	14-44		
Weeping	14-44		
Dumping	14-46		
Turndown	14-47		
Vapor Channeling	14-47		
EQUIPMENT FOR DISTILLATION AND GAS ABSORPTION: PACKED COLUMNS			
Packing Objectives	14-53		
Random Packings	14-53		
Structured Packings	14-54		
Packed-Column Flood and Pressure Drop	14-55		
Flood-Point Definition	14-56		
Flood and Pressure Drop Prediction	14-57		
Pressure Drop	14-59		
Example 13: Packed-Column Pressure Drop	14-62		
Packing Efficiency	14-63		
HETP vs. Fundamental Mass Transfer	14-63		
Factors Affecting HETP: An Overview	14-63		
HETP Prediction	14-63		
Underwetting	14-67		
Effect of Lambda	14-67		
Pressure	14-67		
Physical Properties	14-67		
Errors in VLE	14-68		
Comparison of Various Packing Efficiencies for Absorption and Stripping	14-68		
Summary	14-69		
Maldistribution and Its Effects on Packing Efficiency	14-69		
Modeling and Prediction	14-69		
Implications of Maldistribution to Packing Design Practice	14-70		
Packed-Tower Scale-up	14-72		
Diameter	14-72		
Height	14-72		
Loadings	14-73		
Wetting	14-73		
Underwetting	14-73		
Preflooding	14-73		
Sampling	14-73		
Aging	14-73		
Distributors	14-73		
Liquid Distributors	14-73		
Flashing Feed and Vapor Distributors	14-76		
Other Packing Considerations	14-76		
Liquid Holdup	14-76		
Minimum Wetting Rate	14-79		
Two Liquid Phases	14-79		
High Viscosity and Surface Tension	14-80		
OTHER TOPICS FOR DISTILLATION AND GAS ABSORPTION EQUIPMENT			
Comparing Trays and Packings	14-80		
Factors Favoring Packings	14-80		
Factors Favoring Trays	14-80		
Trays vs. Random Packings	14-81		
Trays vs. Structured Packings	14-81		
Capacity and Efficiency Comparison	14-81		
System Limit: The Ultimate Capacity of Fractionators	14-81		
Wetted-Wall Columns	14-82		
Flooding in Wetted-Wall Columns	14-85		
Column Costs	14-85		
Cost of Internals	14-85		
Cost of Column	14-86		

PHASE DISPERSION

Basics of Interfacial Contactors	14-86
Steady-State Systems: Bubbles and Droplets	14-86
Unstable Systems: Froths and Hollow Cone	
Atomizing Nozzles	14-88
Surface Tension Makes Liquid Sheets and Liquid Columns Unstable	14-88
Little Droplets and Bubbles vs. Big Droplets and Bubbles—Coalescence vs. Breakup	14-88
Empirical Design Tempered by Operating Data	14-88
Interfacial Area—Impact of Droplet or Bubble Size	14-88
Example 14: Interfacial Area for Droplets/Gas in Cocurrent Flow	14-88
Example 15: Interfacial Area for Droplets Falling in a Vessel	14-88
Example 16: Interfacial Area for Bubbles Rising in a Vessel	14-88
Rate Measures, Transfer Units, Approach to Equilibrium, and Bypassing	14-89
What Controls Mass/Heat Transfer: Liquid or Gas Transfer or Bypassing	14-89
Liquid-Controlled	14-89
Gas-Controlled	14-89
Bypassing-Controlled	14-89
Rate Measures for Interfacial Processes	14-89
Approach to Equilibrium	14-89
Example 17: Approach to Equilibrium—Perfectly Mixed, Complete Exchange	14-89
Example 18: Approach to Equilibrium—Complete Exchange but with 10 Percent Gas Bypassing	14-89
Approach to Equilibrium—Finite Contactor with No Bypassing	14-89
Example 19: Finite Exchange, No Bypassing, Short Contactor	14-89
Example 20: A Contactor That Is Twice as Long, No Bypassing	14-90
Transfer Coefficient—Impact of Droplet Size	14-90
Importance of Turbulence	14-90
Examples of Contactors	14-90
High-Velocity Pipeline Contactors	
Example 21: Doubling the Velocity in a Horizontal Pipeline Contactor—Impact on Effective Heat Transfer	14-90
Vertical Reverse Jet Contactor	14-90
Example 22: The Reverse Jet Contactor, U.S. Patent 6,339,169	14-91
Simple Spray Towers	14-91
Bypassing Limits Spray Tower Performance in Gas Cooling	14-91
Spray Towers in Liquid-Limited Systems—Hollow Cone Atomizing Nozzles	14-91
Devolatilizers	14-91
Spray Towers as Direct Contact Condensers	14-91
Converting Liquid Mass-Transfer Data to Direct Contact Heat Transfer	14-91
Example 23: Estimating Direct Contact Condensing Performance Based on $k_L a$ Mass-Transfer Data	14-91
Example 24: HCl Vent Absorber	14-91
Liquid-in-Gas Dispersions	14-91

Liquid Breakup into Droplets	14-91
Droplet Breakup—High Turbulence	14-92
Liquid-Column Breakup	14-92
Liquid-Sheet Breakup	14-92
Isolated Droplet Breakup—in a Velocity Field	14-92
Droplet Size Distribution	14-93
Atomizers	14-93
Hydraulic (Pressure) Nozzles	14-93
Effect of Physical Properties on Drop Size	14-93
Effect of Pressure Drop and Nozzle Size	14-93
Spray Angle	14-93
Two-Fluid (Pneumatic) Atomizers	14-94
Rotary Atomizers	14-95
Pipeline Contactors	14-95
Entrainment due to Gas Bubbling/Jetting through a Liquid	14-96
“Upper Limit” Flooding in Vertical Tubes	14-97
Fog Condensation—The Other Way to Make Little Droplets	14-97
Spontaneous (Homogeneous) Nucleation	14-98
Growth on Foreign Nuclei	14-98
Droplet Distribution	14-98
Gas-in-Liquid Dispersions	14-98
Objectives of Gas Dispersion	14-99
Theory of Bubble and Foam Formation	14-100
Characteristics of Dispersion	14-102
Methods of Gas Dispersion	14-104
Equipment Selection	14-106
Mass Transfer	14-108
Axial Dispersion	14-111

PHASE SEPARATION

Gas-Phase Continuous Systems	14-111
Definitions: Mist and Spray	14-112
Gas Sampling	14-112
Particle Size Analysis	14-112
Collection Mechanisms	14-113
Procedures for Design and Selection of Collection Devices	14-113
Collection Equipment	14-114
Energy Requirements for Inertial-Impaction Efficiency	14-123
Collection of Fine Mists	14-124
Fiber Mist Eliminators	14-125
Electrostatic Precipitators	14-125
Electrically Augmented Collectors	14-125
Particle Growth and Nucleation	14-126
Other Collectors	14-126
Continuous Phase Uncertain	14-126
Liquid-Phase Continuous Systems	14-126
Types of Gas-in-Liquid Dispersions	14-126
Separation of Unstable Systems	14-127
Separation of Foam	14-127
Physical Defoaming Techniques	14-128
Chemical Defoaming Techniques	14-128
Foam Prevention	14-129
Automatic Foam Control	14-129

14-4 EQUIPMENT FOR DISTILLATION, GAS ABSORPTION, PHASE DISPERSION, AND PHASE SEPARATION

Nomenclature

a, a_e	Effective interfacial area	m^2/m^3	ft^2/ft^3	E_g	Point efficiency, gas phase only, fractional	-/-	-/-
a_p	Packing surface area per unit volume	m^2/m^3	ft^2/ft^3	E_{oc}	Overall column efficiency, fractional	-/-	-/-
A	Absorption factor $L_M/(mG_M)$	-/-	-/-	E_{OG}	Overall point efficiency, gas concentrations, fractional	-/-	-/-
A	Cross-sectional area	m^2	ft^2	E_{mv}, E_{MV}	Murphree tray efficiency, gas concentrations, fractional	-/-	-/-
A_a	Active area, same as bubbling area	m^2	ft^2	E_s	Entrainment, kg entrained liquid per kg gas upflow	kg/kg	lb/lb
A_B	Bubbling (active) area	m^2	ft^2	f	Fractional approach to flood	-/-	-/-
A_D	Downcomer area (straight vertical downcomer)	m^2	ft^2	f	Liquid maldistribution fraction	-/-	-/-
A_{da}	Downcomer apron area	m^2	ft^2	f_{max}	Maximum value of f above which separation cannot be achieved	-/-	-/-
A_{DB}	Area at bottom of downcomer	m^2	ft^2	f_w	Weep fraction, Eq. (14-121)	-/-	-/-
A_{DT}	Area at top of downcomer	m^2	ft^2	F	Fraction of volume occupied by liquid phase, system limit correlation, Eq. (14-170)	-/-	-/-
A_e, A'	Effective absorption factor (Edmister)	-/-	-/-	F	F-factor for gas loading Eq. (14-76)	$m/s(kg/m^3)^{0.5}$	$ft/s(lb/ft^3)^{0.5}$
A_f	Fractional hole area	-/-	-/-	F_{LG}	Flow parameter, Eq. (14-S9) and Eq. (14-141)	-/-	-/-
A_h	Hole area	m^2	ft^2	F_p	Packing factor	m^{-1}	ft^{-1}
A_N	Net (free) area	m^2	ft^2	F_{pd}	Dry packing factor	m^{-1}	ft^{-1}
A_s	Slot area	m^2	ft^2	F_{PL}	Flow path length	m	ft
A_{SO}	Open slot area	m^2	ft^2	Fr	Froude number, clear liquid height correlation, Eq. (14-120)	-/-	-/-
A_T	Tower cross-section area	m^2	ft^2	Fr_h	Hole Froude number, Eq. (14-114)	-/-	-/-
c	Concentration	$kg\cdot mol/m^3$	$lb\cdot mol/ft^3$	E_w	Weir constriction correction factor, Fig. 14-38	-/-	-/-
c'	Stokes-Cunningham correction factor for terminal settling velocity	-/-	-/-	g	Gravitational constant	m/s^2	ft/s^2
C	C-factor for gas loading, Eq. (14-77)	m/s	ft/s	g_c	Conversion factor	$1.0\ kg\cdot m/(N\cdot s^2)$	$32.2\ lb\cdot ft/(lb\cdot s^2)$
C_1	Coefficient in regime transition correlation, Eq. (14-129)	-/-	-/-	G	Gas phase mass velocity	$kg/(s\cdot m^2)$	$lb/(hr\cdot ft^2)$
C_1, C_2	Parameters in system limit equation	m/s	ft/s	G_f	Gas loading factor in Robbins' packing pressure drop correlation	$kg/(s\cdot m^2)$	$lb/(h\cdot ft^2)$
C_3, C_4	Constants in Robbins' packing pressure drop correlation	-/-	-/-	G_M	Gas phase molar velocity	$kg\cdot mol/(s\cdot m^2)$	$lb\cdot mol/(h\cdot ft^2)$
CAF	Flood C-factor, Eq. (14-88)	m/s	ft/s	GPM	Liquid flow rate	—	gpm
CAF ₀	Uncorrected flood C-factor, Fig. 14-30	—	ft/s	h	Pressure head	mm	in
C_d	Coefficient in clear liquid height correlation, Eq. (14-116)	-/-	-/-	h'_{dc}	Froth height in downcomer	mm	in
C_G	Gas C-factor; same as C	m/s	ft/s	h_L	Pressure drop through aerated mass on tray	mm	in
C_L	Liquid loading factor, Eq. (14-144)	m/s	ft/s	h_c	Clear liquid height on tray	mm	in
C_{LG}	A constant in packing pressure drop correlation, Eq. (14-143)	$(m/s)^{0.5}$	$(ft/s)^{0.5}$	h_{cl}	Clearance under downcomer	mm	in
CP	Capacity parameter (packed towers), Eq. (14-140)	m/s	ft/s	h_{ct}	Clear liquid height at spray to froth transition	mm	in
C_{SB}, C_{sb}	C-factor at entrainment flood, Eq. (14-80)	m/s	ft/s	h_d	Dry pressure drop across tray	mm	in
C_{sbf}	Capacity parameter corrected for surface tension	m/s	ft/s	h_{da}	Head loss due to liquid flow under downcomer apron	mm	in
C_v, C_V	Discharge coefficient, Fig. 14-35	-/-	-/-	h_{dc}	Clear liquid height in downcomer	mm	in
C_w	A constant in weep rate equation, Eq. (14-123)	-/-	-/-	h_{ds}	Calculated clear liquid height, Eq. (14-108)	mm	in
C_{XY}	Coefficient in Eq. (14-159) reflecting angle of inclination	-/-	-/-	h_f	Height of froth	mm	in
d	Diameter	m	ft	h_{fwe}	Froth height over the weir, Eq. (14-117)	mm	in
d_b	Bubble diameter	m	ft	h_{hg}	Hydraulic gradient	mm	in
d_h, d_H	Hole diameter	mm	in	h_{Lo}	Packing holdup in preloading regime, fractional	-/-	-/-
d_o	Orifice diameter	m	ft	h_{Lr}	Clear liquid height at froth to spray transition, corrected for effect of weir height, Eq. (14-96)	mm	in
d_{pc}	Cut size of a particle collected in a device, 50% mass efficiency	μm	ft	h_{onc}	Height of crest over weir	mm	in
d_{psd}	Mass median size particle in the pollutant gas	μm	ft	h_T	Height of contacting	m	ft
d_{ps50}	Aerodynamic diameter of a real median size particle	μm	ft	h_t	Total pressure drop across tray	mm	in
d_w	Weir diameter, circular weirs	mm	in	h_w	Weir height	mm	in
D	Diffusion coefficient	m^2/s	ft^2/s	H	Height of a transfer unit	m	ft
D	Tube diameter (wetted-wall columns)	m	ft	H	Henry's law constant	kPa/mol fraction	atm/mol fraction
D_{32}	Sauter mean diameter	m	ft	H'	Henry's law constant	kPa/(kmol·m ³)	psi/(lb·mol·ft ³)
D_g	Diffusion coefficient	m^2/s	ft^2/h	H_C	Height of a gas phase transfer unit	m	ft
D_p	Packing particle diameter	m	ft	H_L	Height of a liquid phase transfer unit	m	ft
D_T	Tower diameter	m	ft	H_{OC}	Height of an overall transfer unit, gas phase concentrations	m	ft
D_{tube}	Tube inside diameter	m	ft	H_{OL}	Height of an overall transfer unit, liquid phase concentrations	m	ft
D_{vm}	Volume mean diameter	m	ft				
e	Absolute entrainment of liquid	$kg\cdot mol/h$	$lb\cdot mol/h$				
e	Entrainment, mass liquid/mass gas	kg/kg	lb/lb				
E	Plate or stage efficiency, fractional	-/-	-/-				
E	Power dissipation per mass	W	Btu/lb				
E_a	Murphree tray efficiency, with entrainment, gas concentrations, fractional	-/-	-/-				

Nomenclature (Continued)

H'	Henry's law coefficient	kPa/mol frac	atm/mol frac	S	Length of corrugation side, structured packing	m	ft
HETP	Height equivalent to a theoretical plate or stage	m	ft	S	Stripping factor mG_M/L_M	-/-	-/-
J_G	Dimensionless gas velocity, weep correlation, Eq. (14-124)	-/-	-/-	S	Tray spacing	mm	in
J_L	Dimensionless liquid velocity, weep correlation, Eq. (14-125)	-/-	-/-	S_e, S'	Effective stripping factor (Edmister)	-/-	-/-
k	Individual phase mass transfer coefficient	kmol/(s·m ² · mol frac)	lb·mol/(s·ft ² · mol frac)	SF	Derating (system) factor, Table 14-9	-/-	-/-
k_1	First order reaction velocity constant	1/s	1/s	t_t	Tray thickness	mm	in
k_2	Second order reaction velocity constant	m ³ /(s·kmol)	ft ³ /(h·lb·mol)	t_v	Valve thickness	mm	in
k_g	Gas mass-transfer coefficient, wetted-wall columns [see Eq. (14-171) for unique units]	kmol/(s·m ² · mol frac)	lb·mol/(s·ft ² · mol frac)	T	Absolute temperature	K	°R
k_G	gas phase mass transfer coefficient	kmol/(s·m ² · mol frac)	lb·mol/(s·ft ² · mol frac)	TS	Tray spacing; same as S	mm	in
k_L	liquid phase mass transfer coefficient	kmol/(s·m ² · mol frac)	lb·mol/(s·ft ² · mol frac)	U, u	Linear velocity of gas	m/s	ft/s
K	Constant in trays dry pressure drop equation	mm·s ² /m ²	in·s ² /ft ²	U_a	Velocity of gas through active area	m/s	ft/s
K	Vapor-liquid equilibrium ratio	-/-	-/-	U_a'	Gas velocity through active area at froth to spray transition	m/s	ft/s
K_C	Dry pressure drop constant, all valves closed	mm·s ² /m ²	in·s ² /ft ²	U_{h, u_h}	Gas hole velocity	m/s	ft/s
K_D	Orifice discharge coefficient, liquid distributor	-/-	-/-	U_L, u_L	Liquid superficial velocity based on tower cross-sectional area	m/s	ft/s
K_g	Overall mass-transfer coefficient	kg·mol/ (s·m ² ·atm)	lb·mol/ (h·ft ² ·atm)	U_n	Velocity of gas through net area	m/s	ft/s
K_O	Dry pressure drop constant, all valves open	mm·s ² /m ²	in·s ² /ft ²	U_{nf}	Gas velocity through net area at flood	-/-	-/-
K_{OG}, K_C	Overall mass transfer coefficient, gas concentrations	kmol / (s·m ² ·mol frac)	lb·mol/ (s·ft ² ·mol frac)	U_t	Superficial velocity of gas	m/s	ft/s
K_{OL}	Overall mass transfer coefficient, liquid concentrations	kmol/ (s·m ² ·mol frac)	lb·mol/ (s·ft ² ·mol frac)	v_H	Horizontal velocity in trough	m/s	ft/s
L	Liquid mass velocity	kg/(m ² ·s)	lb/ft ² ·h	V	Linear velocity	m/s	ft/s
L_f	Liquid loading factor in Robbins' packing pressure drop correlation	kg/(s·m ²)	lb/(h·ft ²)	V	Molar vapor flow rate	kg·mol/s	lb·mol/h
L_m	Molar liquid downflow rate	kg·mol/h	lb·mol/h	W	Weep rate	m ³ /s	gpm
L_M	Liquid molar mass velocity	kmol/(m ² ·s)	lb·mol/(ft ² ·h)	x	Mole fraction, liquid phase (note 1)	-/-	-/-
L_S	Liquid velocity, based on superficial tower area	m/s	ft/s	x'	Mole fraction, liquid phase, column 1 (note 1)	-/-	-/-
L_w	Weir length	m	in	x''	Mole fraction, liquid phase, column 2 (note 1)	-/-	-/-
m	An empirical constant based on Wallis' countercurrent flow limitation equation, Eqs. (14-123) and (14-143)	-/-	-/-	x^o, x^o	Liquid mole fraction at equilibrium (note 1)	-/-	-/-
m	Slope of equilibrium curve = dy^o/dx	-/-	-/-	y	Mole fraction, gas or vapor phase (note 1)	-/-	-/-
M	Molecular weight	kg/kmol	lb/(lb·mol)	y'	Mole fraction, vapor phase, column 1 (note 1)	-/-	-/-
n	Parameter in spray regime clear liquid height correlation, Eq. (14-84)	mm	in	y''	Mole fraction, vapor phase, column 2 (note 1)	-/-	-/-
n_A	Rate of solute transfer	kmol/s	lb·mol/s	y^o, y^o	Gas mole fraction at equilibrium (note 1)	-/-	-/-
n_D	Number of holes in orifice distributor	-/-	-/-	Z	Characteristic length in weep rate equation, Eq. (14-126)	m	ft
n_a	Number of actual trays	-/-	-/-	Z_p	Total packed height	m	ft
N_A, N_t	Number of theoretical stages	-/-	-/-	Greek Symbols			
N_{OG}	Number of overall gas-transfer units	-/-	-/-	α	Relative volatility	-/-	-/-
N_p	Number of tray passes	-/-	-/-	β	Tray aeration factor, Fig. (14-37)	-/-	-/-
p	Hole pitch (center-to-center hole spacing)	mm	in	ϵ	Void fraction	-/-	-/-
p	Partial pressure	kPa	atm	ϕ	Contact angle	deg	deg
P_{BM}	Logarithmic mean partial pressure of inert gas	kPa	atm	ϕ	Relative froth density	-/-	-/-
P, p_T	Total pressure	kPa	atm	γ	Activity coefficient	-/-	-/-
P^o	Vapor pressure	kPa	atm	Γ	Flow rate per length	kg/(s·m)	lb/(s·ft)
Q, q	Volumetric flow rate of liquid	m ³ /s	ft ³ /s	δ	Effective film thickness	m	ft
Q'	Liquid flow per serration of serrated weir	m ³ /s	ft ³ /s	η	Collection efficiency, fractional	-/-	-/-
Q_D	Downcomer liquid load, Eq. (14-79)	m/s	ft/s	η	Factor used in froth density correlation, Eq. (14-118)	-/-	-/-
Q_L	Weir load, Eq. (14-78)	m ³ /(h·m)	gpm/in	λ	Stripping factor = $m/(L_M/G_M)$	-/-	-/-
Q_{MW}	Minimum wetting rate	m ³ /(h·m ²)	gpm/ft ²	μ	Absolute viscosity	Pa·s	cP or lb/(ft·s)
\bar{R}	Reflux flow rate	kg·mol/h	lb·mol/h	μm	Micrometers	m	-/-
R	Gas constant	-/-	-/-	ν	Kinematic viscosity	m ² /s	cS
R_h	Hydraulic radius	m	ft	π	3.1416 . . .	-/-	-/-
R_{wc}	Ratio of valve weight with legs to valve weight without legs, Table (14-11)	-/-	-/-	θ	Residence time	s	s
				θ	Angle of serration in serrated weir	deg	deg
				ρ	Density	kg/m ³	lb/ft ³
				ρ_m	Valve metal density	kg/m ³	lb/ft ³
				σ	Surface tension	mN/m	dyn/cm
				χ	Parameter used in entrainment correlation, Eq. (14-95)	-/-	-/-
				ψ	Fractional entrainment, moles liquid entrained per mole liquid downflow	k·mol/ k·mol	lb·mol/ lb·mol
				Φ	Fractional approach to entrainment flood	-/-	-/-
				ΔP	Pressure drop per length of packed bed	mmH ₂ O/m	inH ₂ O/ft
				$\Delta \rho$	$\rho_L - \rho_G$	kg/m ³	lb/ft ³
				Subscripts			
				A	Species A		
				AB	Species A diffusing through species B		

Nomenclature (Concluded)

Subscripts		Subscripts	
B	Species B	n, N	On stage n
B	Based on the bubbling area	N	At the inlet nozzle
d	Dry	NF, nf	Based on net area at flood
da	Downcomer apron	p	Particle
dc	Downcomer	S	Superficial
dry	Uncorrected for entrainment and weeping	t	Total
e	Effective value	ult	At system limit (ultimate capacity)
f	Froth	V	Vapor
Fl	Flood	w	Water
flood	At flood	1	Tower bottom
G, g	Gas or vapor	2	Tower top
h	Based on hole area (or slot area)		
H_2O	Water		
i	Interface value		
L, l	Liquid		
m	Mean		
min	Minimum		
MOC	At maximum operational capacity		
		Dimensionless Groups	
		N_{Fr}	Froude number = $(U_L^2)/(Sg)$
		N_{Re}	Reynolds number = $(D_{tub}U_{sp}\rho_C)/(\mu_C)$
		N_{Sc}	Schmidt number = $\mu/(\rho D)$
		N_{We}	Weber number = $(U_L^2\rho_L S)/(\sigma_{gc})$

NOTE: 1. Unless otherwise specified, refers to concentration of more volatile component (distillation) or solute (absorption).

GENERAL REFERENCES: Astarita, G., *Mass Transfer with Chemical Reaction*, Elsevier, New York, 1967. Astarita, G., D. W. Savage and A. Bisio, *Gas Treating with Chemical Solvents*, Wiley, New York, 1983. Billet, R., *Distillation Engineering*, Chemical Publishing Co., New York, 1979. Billet, R., *Packed Column Analysis and Design*, Ruhr University, Bochum, Germany, 1989. Danckwerts, P. V., *Gas-Liquid Reactions*, McGraw-Hill, New York, 1970. *Distillation and Absorption 1987*, Rugby, U.K., Institution of Chemical Engineers. *Distillation and Absorption 1992*, Rugby, U.K., Institution of Chemical Engineers. *Distillation and Absorption 1997*, Rugby, U.K., Institution of Chemical Engineers. *Distillation and Absorption 2002*, Rugby, U.K., Institution of Chemical Engineers. *Distillation and Absorption 2006*, Rugby, U.K., Institution of Chemical Engineers. *Distillation Topical Conference Proceedings*, AIChE Spring Meetings (separate Proceedings Book for each Topical Conference): Houston, Texas, March 1999; Houston, Texas, April 22–26, 2001; New Orleans, La., March 10–14, 2002; New Orleans, La., March 30–April 3, 2003; Atlanta, Ga., April 10–13, 2005. Hines, A. L., and R. N. Maddox, *Mass Transfer—Fundamentals and Applications*, Prentice Hall, Englewood Cliffs, New Jersey, 1985. Hobbler,

Mass Transfer and Absorbers, Pergamon Press, Oxford, 1966. Kister, H. Z., *Distillation Operation*, McGraw-Hill, New York, 1990. Kister, H. Z., *Distillation Design*, McGraw-Hill, New York, 1992. Kister, H. Z., and G. Nalven (eds.), *Distillation and Other Industrial Separations*, Reprints from CEP, AIChE, 1998. Kister, H. Z., *Distillation Troubleshooting*, Wiley, 2006. Kohl, A. L., and R. B. Nielsen, *Gas Purification*, 5th ed., Gulf, Houston, 1997. Lockett, M. J., *Distillation Tray Fundamentals*, Cambridge, U.K., Cambridge University Press, 1986. Maćkowiak, J., "Fluiddynamik von Kolonnen mit Modernen Füllkörpern und Packungen für Gas/Flüssigkeitssysteme," Otto Salle Verlag, Frankfurt am Main und Verlag Sauerländer Aarau, Frankfurt am Main, 1991. Schweitzer, P. A. (ed.), *Handbook of Separation Techniques for Chemical Engineers*, 3d. ed., McGraw-Hill, New York, 1997. Sherwood, T. K., R. L. Pigford, C. R. Wilke, *Mass Transfer*, McGraw-Hill, New York, 1975. Stichlmair, J., and J. R. Fair, *Distillation Principles and Practices*, Wiley, New York, 1998. Strigle, R. F., Jr., *Packed Tower Design and Applications*, 2d ed., Gulf Publishing, Houston, 1994. Treybal, R. E., *Mass Transfer Operations*, McGraw-Hill, New York, 1980.

INTRODUCTION

Definitions Gas absorption is a unit operation in which soluble components of a gas mixture are dissolved in a liquid. The inverse operation, called stripping or desorption, is employed when it is desired to transfer volatile components from a liquid mixture into a gas. Both absorption and stripping, in common with distillation (Sec. 13), make use of special equipment for bringing gas and liquid phases into intimate contact. This section is concerned with the design of gas-liquid contacting equipment, as well as with the design of absorption and stripping processes.

Equipment Absorption, stripping, and distillation operations are usually carried out in vertical, cylindrical columns or towers in which devices such as plates or packing elements are placed. The gas and liquid normally flow countercurrently, and the devices serve to provide the contacting and development of interfacial surface through which mass transfer takes place. Background material on this mass transfer process is given in Sec. 5.

Design Procedures The procedures to be followed in specifying the principal dimensions of gas absorption and distillation equipment are described in this section and are supported by several worked-out examples. The experimental data required for executing the designs

are keyed to appropriate references or to other sections of the handbook.

For absorption, stripping, and distillation, there are three main steps involved in design:

1. *Data on the gas-liquid or vapor-liquid equilibrium for the system at hand.* If absorption, stripping, and distillation operations are considered equilibrium-limited processes, which is the usual approach, these data are critical for determining the maximum possible separation. In some cases, the operations are considered rate-based (see Sec. 13) but require knowledge of equilibrium at the phase interface. Other data required include physical properties such as viscosity and density and thermodynamic properties such as enthalpy. Section 2 deals with sources of such data.

2. *Information on the liquid- and gas-handling capacity of the contacting device chosen for the particular separation problem.* Such information includes pressure drop characteristics of the device, in order that an optimum balance between capital cost (column cross section) and energy requirements might be achieved. Capacity and pressure drop characteristics of the available devices are covered later in this Sec. 14.

3. *Determination of the required height of contacting zone for the separation to be made as a function of properties of the fluid mixtures and mass-transfer efficiency of the contacting device.* This determination involves the calculation of mass-transfer parameters such as heights of transfer units and plate efficiencies as well as equilibrium or rate parameters such as theoretical stages or numbers of transfer units. An additional consideration for systems in which chemical reaction occurs is the provision of adequate residence time for desired reactions to occur, or minimal residence time to prevent undesired reactions from occurring. For equilibrium-based operations, the parameters for required height are covered in the present section.

Data Sources in the Handbook Sources of data for the analysis or design of absorbers, strippers, and distillation columns are manifold, and a detailed listing of them is outside the scope of the presentation in this section. Some key sources within the handbook are shown in Table 14-1.

Equilibrium Data Finding reliable gas-liquid and vapor-liquid equilibrium data may be the most time-consuming task associated with the design of absorbers and other gas-liquid contactors, and yet it may be the most important task at hand. For gas solubility, an important data source is the set of volumes edited by Kertes et al., *Solubility Data Series*, published by Pergamon Press (1979 ff.). In the introduction to each volume, there is an excellent discussion and definition of the various methods by which gas solubility data have been reported, such as the Bunsen coefficient, the Kuenen coefficient, the Ostwald coefficient, the absorption coefficient, and the Henry's law coefficient. The fifth edition of *The Properties of Gases and Liquids* by Poling, Prausnitz, and O'Connell (McGraw-Hill, New York, 2000) provides data and recommended estimation methods for gas solubility as well as the broader area of vapor-liquid equilibrium. Finally, the Chemistry Data Series by Gmehling et al., especially the title *Vapor-Liquid Equilibrium Collection* (DECHEMA, Frankfurt, Germany, 1979 ff.), is a rich source of data evaluated

against the various models used for interpolation and extrapolation. Section 13 of this handbook presents a good discussion of equilibrium K values.

TABLE 14-1 Directory to Key Data for Absorption and Gas-Liquid Contactor Design

Type of data	Section
Phase equilibrium data	
Gas solubilities	2
Pure component vapor pressures	2
Equilibrium K values	13
Thermal data	
Heats of solution	2
Specific heats	2
Latent heats of vaporization	2
Transport property data	
Diffusion coefficients	
Liquids	2
Gases	2
Viscosities	
Liquids	2
Gases	2
Densities	
Liquids	2
Gases	2
Surface tensions	2
Packed tower data	
Pressure drop and flooding	14
Mass transfer coefficients	5
HTU, physical absorption	5
HTU with chemical reaction	14
Height equivalent to a theoretical plate (HETP)	
Plate tower data	
Pressure drop and flooding	14
Plate efficiencies	14
Costs of gas-liquid contacting equipment	14

DESIGN OF GAS ABSORPTION SYSTEMS

General Design Procedure The design engineer usually is required to determine (1) the best solvent; (2) the best gas velocity through the absorber, or, equivalently, the vessel diameter; (3) the height of the vessel and its internal members, which is the height and type of packing or the number of contacting trays; (4) the optimum solvent circulation rate through the absorber and stripper; (5) temperatures of streams entering and leaving the absorber and stripper, and the quantity of heat to be removed to account for the heat of solution and other thermal effects; (6) pressures at which the absorber and stripper will operate; and (7) mechanical design of the absorber and stripper vessels (predominantly columns or towers), including flow distributors and packing supports. This section covers these aspects.

The problem presented to the designer of a gas absorption system usually specifies the following quantities: (1) gas flow rate; (2) gas composition of the component or components to be absorbed; (3) operating pressure and allowable pressure drop across the absorber; (4) minimum recovery of one or more of the solutes; and, possibly, (5) the solvent to be employed. Items 3, 4, and 5 may be subject to economic considerations and therefore are left to the designer. For determination of the number of variables that must be specified to fix a unique solution for the absorber design, one may use the same phase-rule approach described in Sec. 13 for distillation systems.

Recovery of the solvent, occasionally by chemical means but more often by distillation, is almost always required and is considered an integral part of the absorption system process design. A more complete solvent-stripping operation normally will result in a less costly absorber because of a lower concentration of residual solute in the regenerated (lean) solvent, but this may increase the overall cost of the entire absorption system. A more detailed discussion of these and other economical considerations is presented later in this section.

The design calculations presented in this section are relatively simple and usually can be done by using a calculator or spreadsheet. In many cases, the calculations are explained through design diagrams. It is recognized that most engineers today will perform rigorous, detailed calculations using process simulators. The design procedures presented in this section are intended to be complementary to the rigorous computerized calculations by presenting approximate estimates and insight into the essential elements of absorption and stripping operations.

Selection of Solvent and Nature of Solvents When a choice is possible, preference is given to solvents with high solubilities for the target solute and high selectivity for the target solute over the other species in the gas mixture. A high solubility reduces the amount of liquid to be circulated. The solvent should have the advantages of low volatility, low cost, low corrosive tendencies, high stability, low viscosity, low tendency to foam, and low flammability. Since the exit gas normally leaves saturated with solvent, solvent loss can be costly and can cause environmental problems. The choice of the solvent is a key part of the process economic analysis and compliance with environmental regulations.

Typically, a solvent that is chemically similar to the target solute or that reacts with it will provide high solubility. Water is often used for polar and acidic solutes (e.g., HCl), oils for light hydrocarbons, and special chemical solvents for acid gases such as CO₂, SO₂, and H₂S. Solvents are classified as physical and chemical. A chemical solvent forms complexes or chemical compounds with the solute, while physical solvents have only weaker interactions with the solute. Physical and chemical solvents are compared and contrasted by examining the solubility of CO₂ in propylene carbonate (representative physical solvent) and aqueous monoethanolamine (MEA; representative chemical solvent).

Figures 14-1 and 14-2 present data for the solubility of CO₂ in the two representative solvents, each at two temperatures: 40 and 100°C.

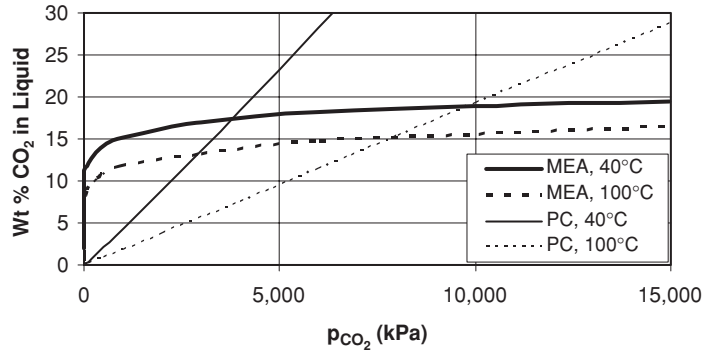


FIG. 14-1 Solubility of CO₂ in 30 wt% MEA and propylene carbonate. Linear scale.

The propylene carbonate data are from Zubchenko et al. [*Zhur. Priklad. Khim.*, **44**, 2044–2047 (1971)], and the MEA data are from Jou, Mather, and Otto [*Can. J. Chem. Eng.*, **73**, 140–147 (1995)]. The two figures have the same content, but Fig. 14-2 focuses on the low-pressure region by converting both composition and pressure to the logarithm scale. Examination of the two sets of data reveals the following characteristics and differences of physical and chemical solvents, which are summarized in the following table:

Characteristic	Physical solvent	Chemical solvent
Solubility variation with pressure	Relatively linear	Highly nonlinear
Low-pressure solubility	Low	High
High-pressure solubility	Continues to increase	Levels off
Heat of solution—related to variation of solubility with temperature at fixed pressure	Relatively low and approximately constant with loading	Relatively high and decreases somewhat with increased solute loading

Chemical solvents are usually preferred when the solute must be reduced to very low levels, when high selectivity is needed, and when the solute partial pressure is low. However, the strong absorption at low solute partial pressures and the high heat of solution are disadvantages for stripping. For chemical solvents, the strong nonlinearity of the absorption makes it necessary that accurate absorption data for the conditions of interest be available.

Selection of Solubility Data Solubility values are necessary for design because they determine the liquid rate necessary for complete or economic solute recovery. Equilibrium data generally will be found in one of three forms: (1) solubility data expressed either as weight or mole percent or as Henry's law coefficients; (2) pure-component vapor pressures; or (3) equilibrium distribution coefficients (*K* values).

Data for specific systems may be found in Sec. 2; additional references to sources of data are presented in this section.

To define completely the solubility of gas in a liquid, it is generally necessary to state the temperature, equilibrium partial pressure of the solute gas in the gas phase, and the concentration of the solute gas in the liquid phase. Strictly speaking, the total pressure of the system should also be identified, but for low pressures (less than about 507 kPa or 5 atm), the solubility for a particular partial pressure of the solute will be relatively independent of the total pressure.

For many physical systems, the equilibrium relationship between solute partial pressure and liquid-phase concentration is given by Henry's law:

$$p_A = Hx_A \tag{14-1}$$

or

$$p_A = H'c_A \tag{14-2}$$

where *H* is Henry's law coefficient expressed in kPa per mole fraction solute in liquid and *H'* is Henry's law coefficient expressed in kPa·m³/kmol.

Figure 14-1 indicates that Henry's law is valid to a good approximation for the solubility CO₂ in propylene carbonate. In general, Henry's law is a reasonable approximation for physical solvents. If Henry's law holds, the solubility is defined by knowing (or estimating) the value of the constant *H* (or *H'*).

Note that the assumption of Henry's law will lead to incorrect results for solubility of chemical systems such as CO₂-MEA (Figs. 14-1 and 14-2) and HCl-H₂O. Solubility modeling for chemical systems requires the use of a *speciation model*, as described later in this section.

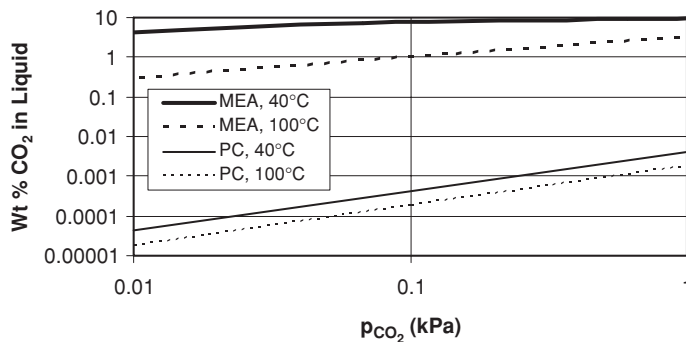


FIG. 14-2 Solubility of CO₂ in 30 wt% MEA and propylene carbonate. Logarithm scale and focus on low-pressure region.

For quite a number of physically absorbed gases, Henry's law holds very well when the partial pressure of the solute is less than about 101 kPa (1 atm). For partial pressures above 101 kPa, H may be independent of the partial pressure (Fig. 14-1), but this needs to be verified for the particular system of interest. The variation of H with temperature is a strongly nonlinear function of temperature as discussed by Poling, Prausnitz, and O'Connell (*The Properties of Gases and Liquids*, 5th ed., McGraw-Hill, New York, 2000). Consultation of this reference is recommended when temperature and pressure extrapolations of Henry's law data are needed.

The use of Henry's law constants is illustrated by the following example.

Example 1: Gas Solubility It is desired to find out how much hydrogen can be dissolved in 100 weights of water from a gas mixture when the total pressure is 101.3 kPa (760 torr; 1 atm), the partial pressure of the H_2 is 26.7 kPa (200 torr), and the temperature is 20°C. For partial pressures up to about 100 kPa the value of H is given in Sec. 3 as 6.92×10^6 kPa (6.83×10^4 atm) at 20°C. According to Henry's law,

$$x_{H_2} = p_{H_2}/H_{H_2} = 26.7/6.92 \times 10^6 = 3.86 \times 10^{-6}$$

The mole fraction x is the ratio of the number of moles of H_2 in solution to the total moles of all constituents contained. To calculate the weights of H_2 per 100 weights of H_2O , one can use the following formula, where the subscripts A and w correspond to the solute (hydrogen) and solvent (water):

$$\begin{aligned} \left(\frac{x_A}{1-x_A} \right) \frac{M_A}{M_w} 100 &= \left(\frac{3.86 \times 10^{-6}}{1-3.86 \times 10^{-6}} \right) \frac{2.02}{18.02} 100 \\ &= 4.33 \times 10^{-5} \text{ weights } H_2/100 \text{ weights } H_2O \\ &= 0.43 \text{ parts per million weight} \end{aligned}$$

Pure-component vapor pressure can be used for predicting solubilities for systems in which **Raoult's law** is valid. For such systems $p_A = p_A^0 x_A$, where p_A^0 is the pure-component vapor pressure of the solute and p_A is its partial pressure. Extreme care should be exercised when using pure-component vapor pressures to predict gas absorption behavior. Both vapor-phase and liquid-phase nonidealities can cause significant deviations from Raoult's law, and this is often the reason particular solvents are used, i.e., because they have special affinity for particular solutes. The book by Poling, Prausnitz, and O'Connell (op. cit.) provides an excellent discussion of the conditions where Raoult's law is valid. Vapor-pressure data are available in Sec. 3 for a variety of materials.

Whenever data are available for a given system under similar conditions of temperature, pressure, and composition, **equilibrium distribution coefficients** ($K = y/x$) provide a much more reliable tool for predicting vapor-liquid distributions. A detailed discussion of equilibrium K values is presented in Sec. 13.

Calculation of Liquid-to-Gas Ratio The minimum possible liquid rate is readily calculated from the composition of the entering gas and the solubility of the solute in the exit liquor, with equilibrium being assumed. It may be necessary to estimate the temperature of the exit liquid based upon the heat of solution of the solute gas. Values of latent heat and specific heat and values of heats of solution (at infinite dilution) are given in Sec. 2.

The actual liquid-to-gas ratio (solvent circulation rate) normally will be greater than the minimum by as much as 25 to 100 percent, and the estimated factor may be arrived at by economic considerations as well as judgment and experience. For example, in some packed-tower applications involving very soluble gases or vacuum operation, the minimum quantity of solvent needed to dissolve the solute may be insufficient to keep the packing surface thoroughly wet, leading to poor distribution of the liquid stream.

When the solvent concentration in the inlet gas is low and when a significant fraction of the solute is absorbed (this often the case), the approximation

$$y_1 G_M = x_1 L_M = (y_1^0/m) L_M \quad (14-3)$$

leads to the conclusion that the ratio mG_M/L_M represents the fractional approach of the exit liquid to saturation with the inlet gas, i.e.,

$$mG_M/L_M = y_1^0/y_1 \quad (14-4)$$

Optimization of the liquid-to-gas ratio in terms of total annual costs often suggests that the molar liquid-to-gas ratio L_M/G_M should be about 1.2 to 1.5 times the theoretical minimum corresponding to equilibrium at the rich end of the tower (infinite height or number of trays), provided flooding is not a problem. This, for example, would be an alternative to assuming that $L_M/G_M \approx m/0.7$.

When the exit-liquor temperature rises because of the heat of absorption of the solute, the value of m changes through the tower, and the liquid-to-gas ratio must be chosen to give reasonable values of $m_1 G_M/L_M$ and $m_2 G_M/L_M$, where the subscripts 1 and 2 refer to the bottom and top of the absorber, respectively. For this case, the value of $m_2 G_M/L_M$ will be taken to be somewhat less than 0.7, so that the value of $m_1 G_M/L_M$ will not approach unity too closely. This rule-of-thumb approach is useful only when the solute concentration is low and heat effects are negligible.

When the solute has a large heat of solution or when the feed gas contains high concentrations of the solute, one should consider the use of internal cooling coils or intermediate liquid withdrawal and cooling to remove the heat of absorption.

Selection of Equipment Trays and random packings have been extensively used for gas absorption; structured packings are less common. Compared to trays, random packings have the advantages of availability in low-cost, corrosion-resistant materials (such as plastics and ceramics), low pressure drop (which can be an advantage when the tower is in the suction of a fan or compressor), easy and economic adaptability to small-diameter (less than 0.6-m or 2-ft) columns, and excellent handling of foams. Trays are much better for handling solids and fouling applications, offer greater residence time for slow absorption reactions, can better handle high L/G ratios and intermediate cooling, give better liquid turndown, and are more robust and less prone to reliability issues such as those resulting from poor distribution. Details on the operating characteristics of tray and packed towers are given later in this section.

Column Diameter and Pressure Drop Flooding determines the minimum possible diameter of the absorber column, and the usual design is for 60 to 80 percent of the flooding velocity. In near-atmospheric applications, pressure drop usually needs to be minimized to reduce the cost of energy for compression of the feed gas. For systems having a significant tendency to foam, the maximum allowable velocity will be lower than the estimated flooding velocity. Methods for predicting flooding velocities and pressure drops are given later in this section.

Computation of Tower Height The required height of a gas absorber or stripping tower for physical solvents depends on (1) the phase equilibria involved; (2) the specified degree of removal of the solute from the gas; and (3) the mass-transfer efficiency of the device. These three considerations apply to both tray and packed towers. Items 1 and 2 dictate the required number of theoretical stages (tray tower) or transfer units (packed tower). Item 3 is derived from the tray efficiency and spacing (tray tower) or from the height of one transfer unit (packed tower). Solute removal specifications are usually derived from economic considerations.

For tray towers, the approximate design methods described below may be used in estimating the number of theoretical stages, and the tray efficiencies and spacings for the tower can be specified on the basis of the information given later. Considerations involved in the rigorous design of theoretical stages for tray towers are treated in Sec. 13.

For packed towers, the continuous differential nature of the contact between gas and liquid leads to a design procedure involving the solution of differential equations, as described in the next subsection. Note that the design procedures discussed in this section are not applicable to reboiled absorbers, which should be designed according to the procedures described in Sec. 13.

Caution is advised in distinguishing between systems involving pure physical absorption and those in which chemical reactions can significantly affect design procedures. Chemical systems require additional procedures, as described later in this section.

Selection of Stripper Operating Conditions Stripping involves the removal of one or more components from the solvent through the application of heat or contacting it with a gas such as steam, nitrogen,

or air. The operating conditions chosen for stripping normally result in a low solubility of solute (i.e., high value of m), so that the ratio mG_M/L_M will be larger than unity. A value of 1.4 may be used for rule-of-thumb calculations involving pure physical absorption. For tray-tower calculations, the stripping factor $S = KC_M/L_M$, where $K = y^0/x$ usually is specified for each tray.

When the solvent from an absorption operation must be regenerated, one may employ a "pressure-swing" or "temperature-swing" concept, or a combination of the two, in specifying the stripping operation. In pressure-swing operation, the temperature of the stripper is about the same as that of the absorber, but the stripping pressure is much lower. In temperature-swing operation, the pressures are about equal, but the stripping temperature is much higher than the absorption temperature.

In pressure-swing operation, a portion of the gas may be "sprung" from the liquid by the use of a flash drum upstream of the stripper feed point. This type of operation has been discussed by Burrows and Preece [*Trans. Inst. Chem. Eng.*, **32**, 99 (1954)] and by Langley and Haselden [*Inst. Chem. Eng. Symp. Ser. (London)*, no. 28 (1968)]. If the flashing of the liquid takes place inside the stripping tower, this effect must be accounted for in the design of the upper section in order to avoid overloading and flooding near the top of the tower.

Often the rate at which residual absorbed gas can be driven from the liquid in a stripping tower is limited by the rate of a chemical reaction, in which case the liquid-phase residence time (and hence the tower liquid holdup) becomes the most important design factor. Thus, many stripper regenerators are designed on the basis of liquid holdup rather than on the basis of mass-transfer rate.

Approximate design equations applicable only to the case of pure physical desorption are developed later in this section for both packed and tray stripping towers. A more rigorous approach using distillation concepts may be found in Sec. 13. A brief discussion of desorption with chemical reaction is given in the subsection "Absorption with Chemical Reaction."

Design of Absorber-Stripper Systems The solute-rich liquor leaving a gas absorber normally is distilled or stripped to regenerate the solvent for recirculation back to the absorber, as depicted in Fig. 14-3. It is apparent that the conditions selected for the absorption step

(e.g., temperature, pressure, L_M/G_M) will affect the design of the stripping tower, and conversely, a selection of stripping conditions will affect the absorber design. The choice of optimum operating conditions for an absorber-stripper system therefore involves a combination of economic factors and practical judgments as to the operability of the system within the context of the overall process flow sheet. In Fig. 14-3, the stripping vapor is provided by a reboiler; alternately, an extraneous stripping gas may be used.

An appropriate procedure for executing the design of an absorber-stripper system is to set up a carefully selected series of design cases and then evaluate the investment costs, the operating costs, and the operability of each case. Some of the economic factors that need to be considered in selecting the optimum absorber-stripper design are discussed later in the subsection "Economic Design of Absorption Systems."

Importance of Design Diagrams One of the first things a designer should do is to lay out a carefully constructed equilibrium curve $y^0 = F(x)$ on an xy diagram, as shown in Fig. 14-4. A horizontal line corresponding to the inlet-gas composition y_1 is then the locus of feasible outlet-liquor compositions, and a vertical line corresponding to the inlet-solvent-liquor composition x_2 is the locus of outlet-gas compositions. These lines are indicated as $y = y_1$ and $x = x_2$, respectively on Fig. 14-4.

For gas absorption, the region of feasible operating lines lies above the equilibrium curve; for stripping, the feasible region for operating lines lies below the equilibrium curve. These feasible regions are bounded by the equilibrium curve and by the lines $x = x_2$ and $y = y_1$. By inspection, one should be able to visualize those operating lines that are feasible and those that would lead to "pinch points" within the tower. Also, it is possible to determine if a particular proposed design for solute recovery falls within the feasible envelope.

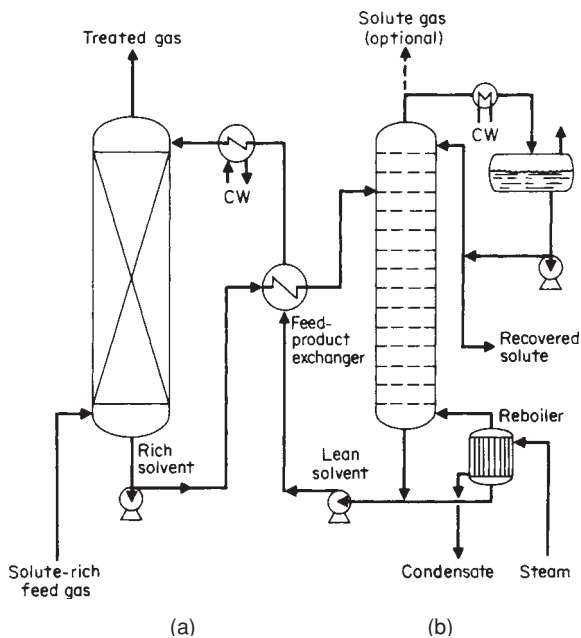


FIG. 14-3 Gas absorber using a solvent regenerated by stripping. (a) Absorber. (b) Stripper.

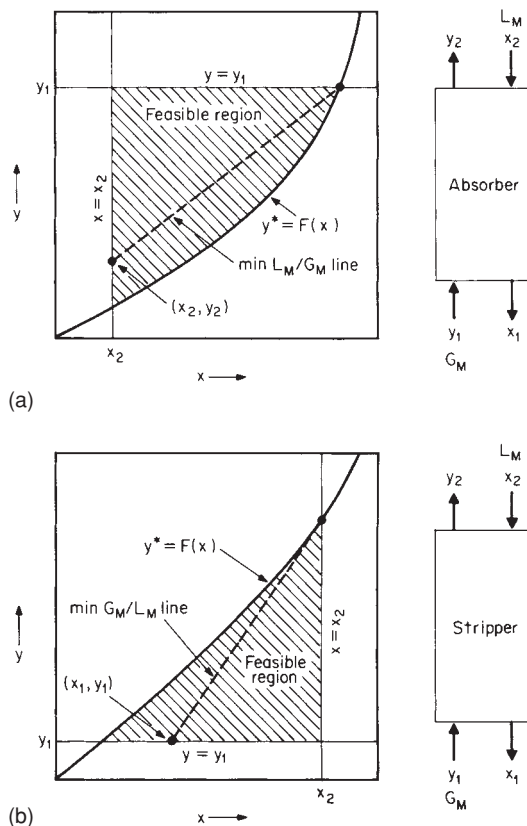


FIG. 14-4 Design diagrams for (a) absorption and (b) stripping.

Once the design recovery for an absorber has been established, the operating line can be constructed by first locating the point x_2, y_2 on the diagram. The intersection of the horizontal line corresponding to the inlet gas composition y_1 with the equilibrium curve $y^0 = F(x)$ defines the theoretical minimum liquid-to-gas ratio for systems in which there are no intermediate pinch points. This operating line which connects this point with the point x_2, y_2 corresponds to the minimum value of L_M/G_M . The actual design value of L_M/G_M should normally be around 1.2 to 1.5 times this minimum value. Thus, the actual design operating line for a gas absorber will pass through the point x_2, y_2 and will intersect the line $y = y_1$ to the left of the equilibrium curve.

For stripping one begins by using the design specification to locate the point x_1, y_1 ; then the intersection of the vertical line $x = x_2$ with the equilibrium curve $y^0 = F(x)$ defines the theoretical minimum gas-to-liquid ratio. The actual value of G_M/L_M is chosen to be about 20 to 50 percent higher than this minimum, so the actual design operating line will intersect the line $x = x_2$ at a point somewhat below the equilibrium curve.

PACKED-TOWER DESIGN

Methods for estimating the height of the active section of counterflow differential contactors such as packed towers, spray towers, and falling-film absorbers are based on rate expressions representing mass transfer at a point on the gas-liquid interface and on material balances representing the changes in bulk composition in the two phases that flow past each other. The rate expressions are based on the interphase mass-transfer principles described in Sec. 5. Combination of such expressions leads to an integral expression for the number of transfer units or to equations related closely to the number of theoretical stages. The paragraphs which follow set forth convenient methods for using such equations, first in a general case and then for cases in which simplifying assumptions are valid.

Use of Mass-Transfer-Rate Expression Figure 14-5 shows a section of a packed absorption tower together with the nomenclature that will be used in developing the equations that follow. In a differential section dh , we can equate the rate at which solute is lost from the gas phase to the rate at which it is transferred through the gas phase to the interface as follows:

$$-d(G_M y) = -G_M dy - y dG_M = N_A a dh \quad (14-5)$$

In Eq. (14-5), G_M is the gas-phase molar velocity [$\text{kmol}/(\text{s}\cdot\text{m}^2)$], N_A is the mass-transfer flux [$\text{kmol}/(\text{s}\cdot\text{m}^2)$], and a is the effective interfacial area (m^2/m^3).

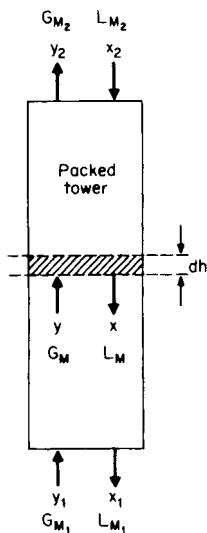


FIG. 14-5 Nomenclature for material balances in a packed-tower absorber or stripper.

When only one component is transferred,

$$dG_M = -N_A a dh \quad (14-6)$$

Substitution of this relation into Eq. (14-5) and rearranging yield

$$dh = -\frac{G_M dy}{N_A a (1-y)} \quad (14-7)$$

For this derivation we use the gas-phase rate expression $N_A = k_C(y - y_i)$ and integrate over the tower to obtain

$$h_T = \int_{y_2}^{y_1} \frac{G_M dy}{k_C a (1-y)(y - y_i)} \quad (14-8)$$

Multiplying and dividing by y_{BM} place Eq. (14-8) into the H_{G,N_C} format

$$\begin{aligned} h_T &= \int_{y_2}^{y_1} \left(\frac{G_M}{k_C a y_{BM}} \right) \frac{y_{BM} dy}{(1-y)(y - y_i)} \\ &= H_{G,av} \int_{y_2}^{y_1} \frac{y_{BM} dy}{(1-y)(y - y_i)} = H_{G,av} N_G \end{aligned} \quad (14-9)$$

The general expression given by Eq. (14-8) is more complex than normally is required, but it must be used when the mass-transfer coefficient varies from point to point, as may be the case when the gas is not dilute or when the gas velocity varies as the gas dissolves. The values of y_i to be used in Eq. (14-8) depend on the local liquid composition x_i and on the temperature. This dependency is best represented by using the operating and equilibrium lines as discussed later.

Example 2 illustrates the use of Eq. (14-8) for scrubbing chlorine from air with aqueous caustic solution. For this case one can make the simplifying assumption that y_i , the interfacial partial pressure of chlorine over the caustic solution, is zero due to the rapid and complete reaction of the chlorine after it dissolves. We note that the feed gas is not dilute.

Example 2: Packed Height Requirement Let us compute the height of packing needed to reduce the chlorine concentration of $0.537 \text{ kg}/(\text{s}\cdot\text{m}^2)$, or $396 \text{ lb}/(\text{h}\cdot\text{ft}^2)$, of a chlorine-air mixture containing 0.503 mole-fraction chlorine to 0.0403 mole fraction. On the basis of test data described by Sherwood and Pigford (*Absorption and Extraction*, McGraw-Hill, 1952, p. 121) the value of $k_{C,a y_{BM}}$ at a gas velocity equal to that at the bottom of the packing is equal to $0.1175 \text{ kmol}/(\text{s}\cdot\text{m}^3)$, or $26.4 \text{ lb}\cdot\text{mol}/(\text{h}\cdot\text{ft}^3)$. The equilibrium back pressure y_i can be assumed to be negligible.

Solution. By assuming that the mass-transfer coefficient varies as the 0.8 power of the local gas mass velocity, we can derive the following relation:

$$\hat{k}_{C,a} = k_{C,a y_{BM}} = 0.1175 \left[\frac{71y + 29(1-y)}{71y_1 + 29(1-y_1)} \left(\frac{1-y_1}{1-y} \right) \right]^{0.8}$$

where 71 and 29 are the molecular weights of chlorine and air respectively. Noting that the inert-gas (air) mass velocity is given by $G'_M = G_M(1-y) = 5.34 \times 10^{-3} \text{ kmol}/(\text{s}\cdot\text{m}^2)$, or $3.94 \text{ lb}\cdot\text{mol}/(\text{h}\cdot\text{ft}^2)$, and introducing these expressions into the integral gives

$$h_T = 1.82 \int_{0.0403}^{0.503} \left[\frac{1-y}{29+42y} \right]^{0.8} \frac{dy}{(1-y)^2 \ln [1/(1-y)]}$$

This definite integral can be evaluated numerically by the use of Simpson's rule to obtain $h_T = 0.305 \text{ m}$ (1 ft).

Use of Operating Curve Frequently, it is not possible to assume that $y_i = 0$ as in Example 2, due to diffusional resistance in the liquid phase or to the accumulation of solute in the liquid stream. When the backpressure cannot be neglected, it is necessary to supplement the equations with a material balance representing the operating line or curve. In view of the countercurrent flows into and from the differential section of packing shown in Fig. 14-5, a steady-state material balance leads to the following equivalent relations:

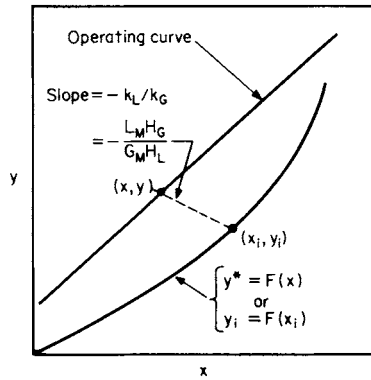


FIG. 14-6 Relationship between equilibrium curve and operating curve in a packed absorber; computation of interfacial compositions.

$$d(G_M y) = d(L_M x) \quad (14-10)$$

$$G'_M \frac{dy}{(1-y)^2} = L'_M \frac{dx}{(1-x)^2} \quad (14-11)$$

where L'_M = molar mass velocity of the inert-liquid component and G'_M = molar mass velocity of the inert gas; L_M , L'_M , G_M , and G'_M are superficial velocities based upon the total tower cross section.

Equation (14-11) is the differential equation of the operating curve, and its integral around the upper portion of the packing is the equation for the operating curve.

$$G'_M \left[\frac{y}{1-y} - \frac{y_2}{1-y_2} \right] = L'_M \left[\frac{x}{1-x} - \frac{x_2}{1-x_2} \right] \quad (14-12)$$

For dilute solutions in which the mole fractions of x and y are small, the total molar flows G_M and L_M will be nearly constant, and the operating-curve equation is

$$G_M(y - y_2) = L_M(x - x_2) \quad (14-13)$$

This equation gives the relation between the bulk compositions of the gas and liquid streams at each height in the tower for conditions in which the operating curve can be approximated as a straight line.

Figure 14-6 shows the relationship between the operating curve and the equilibrium curve $y_i = F(x_i)$ for a typical example involving solvent recovery, where y_i and x_i are the interfacial compositions (assumed to be in equilibrium). Once y is known as a function of x along the operating curve, y_i can be found at corresponding points on the equilibrium curve by

$$(y - y_i)/(x_i - x) = k_L/k_G = L_M H_G / G_M H_L \quad (14-14)$$

where L_M = molar liquid mass velocity, G_M = molar gas mass velocity, H_L = height of one transfer unit based upon liquid-phase resistance, and H_G = height of one transfer unit based upon gas-phase resistance. Using this equation, the integral in Eq. (14-8) can be evaluated.

Calculation of Transfer Units In the general case, the equations described above must be employed in calculating the height of packing required for a given separation. However, if the local mass-transfer coefficient $k_C a y_{BM}$ is approximately proportional to the first power of the local gas velocity G_M , then the height of one gas-phase transfer unit, defined as $H_G = G_M / k_C a y_{BM}$, will be constant in Eq. (14-9). Similar considerations lead to an assumption that the height of one overall gas-phase transfer unit H_{OG} may be taken as constant. The height of packing required is then calculated according to the relation

$$h_T = H_G N_G = H_{OG} N_{OG} \quad (14-15)$$

where N_G = number of gas-phase transfer units and N_{OG} = number of overall gas-phase transfer units. When H_G and H_{OG} are not constant, it

may be valid to employ averaged values between the top and bottom of the tower and the relation

$$h_T = H_{G,av} N_G = H_{OG,av} N_{OG} \quad (14-16)$$

In these equations, the terms N_G and N_{OG} are defined by Eqs. (14-17) and (14-18).

$$N_G = \int_{y_2}^{y_1} \frac{y_{BM} dy}{(1-y)(y-y_i)} \quad (14-17)$$

$$N_{OG} = \int_{y_2}^{y_1} \frac{y_{BM}^o dy}{(1-y)(y-y^o)} \quad (14-18)$$

Equation (14-18) is the more useful one in practice. It requires either actual experimental H_{OG} data or values estimated by combining individual measurements of H_G and H_L by Eq. (14-19). Correlations for H_G , H_L , and H_{OG} in nonreacting systems are presented in Sec. 5.

$$H_{OG} = \frac{y_{BM}}{y_{BM}^o} H_G + \frac{m G_M}{L_M} \frac{x_{BM}}{y_{BM}^o} H_L \quad (14-19a)$$

$$H_{OL} = \frac{x_{BM}}{x_{BM}^o} H_L + \frac{L_M}{m G_M} \frac{y_{BM}}{x_{BM}^o} H_G \quad (14-19b)$$

On occasion, the changes in gas flow and in the mole fraction of inert gas can be neglected so that inclusion of terms such as $1-y$ and y_{BM}^o can be approximated, as is shown below.

One such simplification was suggested by Wiegand [*Trans. Am. Inst. Chem. Eng.*, **36**, 679 (1940)], who pointed out that the logarithmic-mean mole fraction of inert gas y_{BM}^o (or y_{BM}) is often very nearly equal to the arithmetic mean. Thus, substitution of the relation

$$\frac{y_{BM}^o}{(1-y)} = \frac{(1-y^o) + (1-y)}{2(1-y)} = \frac{y-y^o}{2(1-y)} + 1 \quad (14-20)$$

into the equations presented above leads to the simplified forms

$$N_G = \frac{1}{2} \ln \frac{1-y_2}{1-y_1} + \int_{y_2}^{y_1} \frac{dy}{y-y_i} \quad (14-21)$$

$$N_{OG} = \frac{1}{2} \ln \frac{1-y_2}{1-y_1} + \int_{y_2}^{y_1} \frac{dy}{y-y^o} \quad (14-22)$$

The second (integral) terms represent the numbers of transfer units for an infinitely dilute gas. The first terms, usually only a small correction, give the effect of a finite level of gas concentration.

The procedure for applying Eqs. (14-21) and (14-22) involves two steps: (1) evaluation of the integrals and (2) addition of the correction corresponding to the first (logarithmic) term. The discussion that follows deals only with the evaluation of the integral term (first step).

The simplest possible case occurs when (1) both the operating and equilibrium lines are straight (i.e., the solutions are dilute); (2) Henry's law is valid ($y/x = y_i/x_i = m$); and (3) absorption heat effects are negligible. Under these conditions, the integral term in Eq. (14-21) may be computed by Colburn's equation [*Trans. Am. Inst. Chem. Eng.*, **35**, 211 (1939)]:

$$N_{OG} = \frac{1}{1 - m G_M / L_M} \ln \left[\left(1 - \frac{m G_M}{L_M} \right) \left(\frac{y_1 - m x_2}{y_2 - m x_2} \right) + \frac{m G_M}{L_M} \right] \quad (14-23)$$

Figure 14-7 is a plot of Eq. (14-23) from which the value of N_{OG} can be read directly as a function of $m G_M / L_M$ and the ratio of concentrations. This plot and Eq. (14-23) are equivalent to the use of a logarithmic mean of terminal driving forces, but they are more convenient because one does not need to compute the exit-liquor concentration x_1 .

In many practical situations involving nearly complete cleanup of the gas, an approximate result can be obtained from the equations just presented even when the simplifications are not valid, i.e., solutions are concentrated and heat effects occur. In such cases the driving forces in the upper part of the tower are very much smaller than those at the bottom, and the value of $m G_M / L_M$ used in the equations should be the ratio of the operating line L_M / G_M in the low-concentration region near the top of the tower.

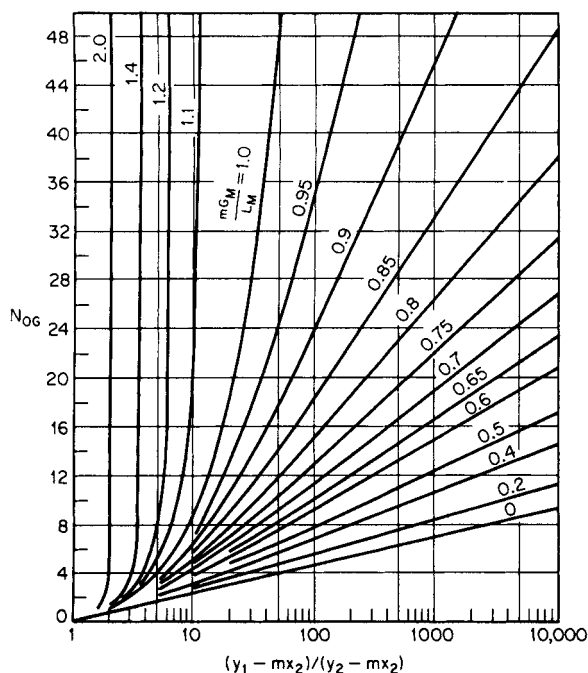


FIG. 14-7 Number of overall gas-phase mass-transfer units in a packed absorption tower for constant mG_M/L_M ; solution of Eq. (14-23). (From Sherwood and Pigford, *Absorption and Extraction*, McGraw-Hill, New York, 1952.)

Another approach is to divide the tower arbitrarily into a lean section (near the top) where approximate methods are valid, and to deal with the rich section separately. If the heat effects in the rich section are appreciable, consideration should be given to installing cooling units near the bottom of the tower. In any event, a design diagram showing the operating and equilibrium curves should be prepared to check the applicability of any simplified procedure. Figure 14-10, presented in Example 6, is one such diagram for an adiabatic absorption tower.

Stripping Equations Stripping or desorption involves the removal of a volatile component from the liquid stream by contact with an inert gas such as nitrogen or steam or the application of heat. Here the change in concentration of the liquid stream is of prime importance, and it is more convenient to formulate the rate equation analogous to Eq. (14-6) in terms of the liquid composition x . This leads to the following equations defining the number of transfer units and height of transfer units based on liquid-phase resistance:

$$h_T = H_L \int_{x_2}^{x_1} \frac{x_{BM} dx}{(1-x)(x_i-x)} = H_L N_L \quad (14-24)$$

$$h_T H_{OL} \int_{x_2}^{x_1} \frac{x_{BM}^0 dx}{(1-x)(x^0-x)} = H_{OL} N_{OL} \quad (14-25)$$

where, as before, subscripts 1 and 2 refer to the bottom and top of the tower, respectively (see Fig. 14-5).

In situations where one cannot assume that H_L and H_{OL} are constant, these terms need to be incorporated inside the integrals in Eqs. (14-24) and (14-25), and the integrals must be evaluated numerically (using Simpson's rule, for example). In the normal case involving stripping without chemical reactions, the liquid-phase resistance will dominate, making it preferable to use Eq. (14-25) together with the approximation $H_L \approx H_{OL}$.

The Weigand approximations of the above integrals, in which arithmetic means are substituted for the logarithmic means (x_{BM} and x_{BM}^0), are

$$N_L = \frac{1}{2} \ln \frac{1-x_1}{1-x_2} + \int_{x_1}^{x_2} \frac{dx}{x-x_i} \quad (14-26)$$

$$N_{OL} = \frac{1}{2} \ln \frac{1-x_1}{1-x_2} + \int_{x_1}^{x_2} \frac{dx}{x-x^0} \quad (14-27)$$

In these equations, the first term is a correction for finite liquid-phase concentrations, and the integral term represents the numbers of transfer units required for dilute solutions. In most practical stripper applications, the first (logarithmic) term is relatively small.

For dilute solutions in which both the operating and the equilibrium lines are straight and in which heat effects can be neglected, the integral term in Eq. (14-27) is

$$N_{OL} = \frac{1}{1-L_M/mG_M} \ln \left[\left(1 - \frac{L_M}{mG_M} \right) \left(\frac{x_2 - y_1/m}{x_1 - y_1/m} \right) + \frac{L_M}{mG_M} \right] \quad (14-28)$$

This equation is analogous to Eq. (14-23). Thus, Fig. 14-7 is applicable if the concentration ratio $(x_2 - y_1/m)/(x_1 - y_1/m)$ is substituted for the abscissa and the parameter on the curves is identified as L_M/mG_M .

Example 3: Air Stripping of VOCs from Water A 0.45-m diameter packed column was used by Dvorack et al. [*Environ. Sci. Tech.* **20**, 945 (1996)] for removing trichloroethylene (TCE) from wastewater by stripping with atmospheric air. The column was packed with 25-mm Pall rings, fabricated from polypropylene, to a height of 3.0 m. The TCE concentration in the entering water was 38 parts per million by weight (ppmw). A molar ratio of entering water to entering air was kept at 23.7. What degree of removal was to be expected? The temperatures of water and air were 20°C. Pressure was atmospheric.

Solution. For TCE in water, the Henry's law coefficient may be taken as 417 atm/mf at 20°C. In this low-concentration region, the coefficient is constant and equal to the slope of the equilibrium line m . The solubility of TCE in water, based on $H = 417$ atm, is 2390 ppm. Because of this low solubility, the entire resistance to mass transfer resides in the liquid phase. Thus, Eq. (14-25) may be used to obtain N_{OL} , the number of overall liquid phase transfer units.

In the equation, the ratio $x_{BM}/(1-x)$ is unity because of the very dilute solution. It is necessary to have a value of H_L for the packing used, at given flow rates of liquid and gas. Methods for estimating H_L may be found in Sec. 5. Dvorack et al. found $H_{OL} = 0.8$ m. Then, for $h_T = 3.0$ m, $N_L = N_{OL} = 3.0/0.8 = 3.75$ transfer units.

Transfer units may be calculated from Eq. 14-25, replacing mole fractions with ppm concentrations, and since the operating and equilibrium lines are straight,

$$N_{OL} = \frac{38 - (\text{ppm})_{\text{exit}}}{\ln 38/(\text{ppm})_{\text{exit}}} = 3.75$$

Solving, $(\text{ppm})_{\text{exit}} = 0.00151$. Thus, the stripped water would contain 1.51 parts per billion of TCE.

Use of HTU and $K_G a$ Data In estimating the size of a commercial gas absorber or liquid stripper it is desirable to have data on the overall mass-transfer coefficients (or heights of transfer units) for the system of interest, and at the desired conditions of temperature, pressure, solute concentration, and fluid velocities. Such data should best be obtained in an apparatus of pilot-plant or semiworks size to avoid the abnormalities of scale-up. Within the packing category, there are both random and ordered (structured) packing elements. Physical characteristics of these devices will be described later.

When no $K_G a$ or HTU data are available, their values may be estimated by means of a generalized model. A summary of useful models is given in Sec. 5. The values obtained may then be combined by use of Eq. (14-19) to obtain values of H_{OG} and H_{OL} . This simple procedure is not valid when the rate of absorption is limited by chemical reaction.

Use of HETP Data for Absorber Design Distillation design methods (see Sec. 13) normally involve determination of the number of theoretical equilibrium stages N . Thus, when packed towers are employed in distillation applications, it is common practice to rate the efficiency of tower packings in terms of the height of packing equivalent to one theoretical stage (HETP).

The HETP of a packed-tower section, valid for either distillation or dilute-gas absorption and stripping systems in which constant molal overflow can be assumed and in which no chemical reactions occur, is related to the height of one overall gas-phase mass-transfer unit H_{OC} by the equation

$$\text{HETP} = H_{OC} \frac{\ln(mG_M/L_M)}{(mG_M/L_M - 1)} \quad (14-29)$$

For gas absorption systems in which the inlet gas is concentrated, the corrected equation is

$$\text{HETP} = \left(\frac{y_{BM}^0}{1-y} \right)_{AV} H_{OC} \frac{\ln(mG_M/L_M)}{mG_M/L_M - 1} \quad (14-30)$$

where the correction term $y_{BM}^0/(1-y)$ is averaged over each individual theoretical stage. The equilibrium compositions corresponding to each theoretical stage may be estimated by the methods described in the next subsection, "Tray-Tower Design." These compositions are used in conjunction with the local values of the gas and liquid flow rates and the equilibrium slope m to obtain values for H_G , H_L , and H_{OC} corresponding to the conditions on each theoretical stage, and the local values of the HETP are then computed by Eq. (14-30). The total height of packing required for the separation is the summation of the individual HETPs computed for each theoretical stage.

TRAY-TOWER DESIGN

The design of a tray tower for gas absorption and gas-stripping operations involves many of the same principles employed in distillation calculations, such as the determination of the number of theoretical trays needed to achieve a specified composition change (see Sec. 13). Distillation differs from absorption because it involves the separation of components based upon the distribution of the various substances between a vapor phase and a liquid phase when all components are present in both phases. In distillation, the new phase is generated from the original phase by the vaporization or condensation of the volatile components, and the separation is achieved by introducing reflux to the top of the tower.

In gas absorption, the new phase consists of a relatively nonvolatile solvent (absorption) or a relatively insoluble gas (stripping), and normally no reflux is involved. This section discusses some of the considerations peculiar to gas absorption calculations for tray towers and some of the approximate design methods that can be applied (when simplifying assumptions are valid).

Graphical Design Procedure Construction of design diagrams (xy curves showing the equilibrium and operating curves) should be an integral part of any design involving the distribution of a single solute between an inert solvent and an inert gas. The number of theoretical trays can be stepped off rigorously, provided the curvatures of the operating and equilibrium lines are correctly represented in the diagram. The procedure is valid even though an inert solvent is present in the liquid phase and an inert gas is present in the vapor phase.

Figure 14-8 illustrates the graphical method for a three theoretical stage system. Note that in gas absorption the operating line is above the equilibrium curve, whereas in distillation this does not happen. In gas stripping, the operating line will be below the equilibrium curve.

On Fig. 14-8, note that the stepping-off procedure begins on the operating line. The starting point x_f, y_3 represents the compositions of the entering lean wash liquor and of the gas exiting from the top of the tower, as defined by the design specifications. After three steps one reaches the point x_1, y_f representing the compositions of the solute-rich feed gas y_f and of the solute-rich liquor leaving the bottom of the tower x_1 .

Algebraic Method for Dilute Gases By assuming that the operating and equilibrium curves are straight lines and that heat effects are negligible, Souders and Brown [*Ind. Eng. Chem.*, **24**, 519 (1932)] developed the following equation:

$$(y_1 - y_2)/(y_1 - y_2^0) = (A^{N+1} - A)/(A^{N+1} - 1) \quad (14-31)$$

where N = number of theoretical trays, y_1 = mole fraction of solute in the entering gas, y_2 = mole fraction of solute in the leaving gas, $y_2^0 = mx_2$ = mole fraction of solute in equilibrium with the incoming solvent

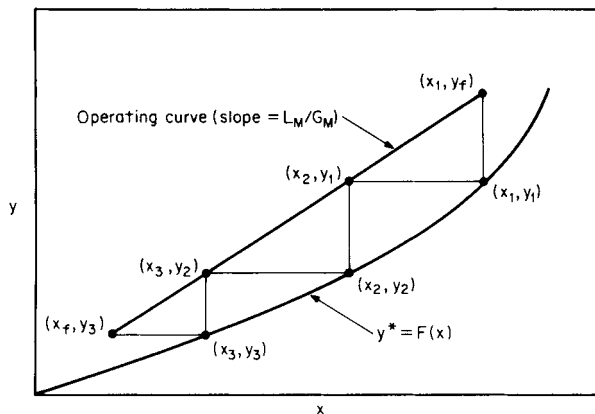


FIG. 14-8 Graphical method for a three-theoretical-plate gas-absorption tower with inlet-liquor composition x_i and inlet-gas composition y_j .

(zero for a pure solvent), and A = absorption factor = L_M/mG_M . Note that the absorption factor is the reciprocal of the expression given in Eq. (14-4) for packed columns.

Note that for the limiting case of $A = 1$, the solution is given by

$$(y_1 - y_2)/(y_1 - y_2^0) = N/(N + 1) \quad (14-32)$$

Although Eq. (14-31) is convenient for computing the composition of the exit gas as a function of the number of theoretical stages, an alternative equation derived by Colburn [*Trans. Am. Inst. Chem. Eng.*, **35**, 211 (1939)] is more useful when the number of theoretical plates is the unknown:

$$N = \frac{\ln [(1 - A^{-1})(y_1 - y_2^0)/(y_2 - y_2^0) + A^{-1}]}{\ln(A)} \quad (14-33)$$

The numerical results obtained by using either Eq. (14-31) or Eq. (14-33) are identical. Thus, the two equations may be used interchangeably as the need arises.

Comparison of Eqs. (14-33) and (14-23) shows that

$$N_{OC}/N = \ln(A)/(1 - A^{-1}) \quad (14-34)$$

thus revealing the close relationship between theoretical stages in a plate tower and mass-transfer units in a packed tower. Equations (14-23) and (14-33) are related to each other by virtue of the relation

$$h_T = H_{OC} N_{OC} = (\text{HETP})N \quad (14-35)$$

Algebraic Method for Concentrated Gases When the feed gas is concentrated, the absorption factor, which is defined in general as $A = L_M/KG_M$ and where $K = y^0/x$, can vary throughout the tower due to changes in temperature and composition. An approximate solution to this problem can be obtained by substituting the "effective" adsorption factors A_e and A' derived by Edmister [*Ind. Eng. Chem.* **35**, 837 (1943)] into the equation

$$\frac{y_1 - y_2}{y_1} = \left[1 - \frac{1}{A'} \frac{(L_M x_2)}{(G_M y_1)} \right] \frac{A_e^{N+1} - A_e}{A_e^{N+1} - 1} \quad (14-36)$$

where subscripts 1 and 2 refer to the bottom and top of the tower, respectively, and the absorption factors are defined by the equations

$$A_e = \sqrt{A_1(A_2 + 1) + 0.25} - 0.5 \quad (14-37)$$

$$A' = A_1(A_2 + 1)/(A_1 + 1) \quad (14-38)$$

This procedure has been applied to the absorption of C_5 and lighter hydrocarbon vapors into a lean oil, for example.

Stripping Equations When the liquid feed is dilute and the operating and equilibrium curves are straight lines, the stripping equations analogous to Eqs. (14-31) and (14-33) are

$$(x_2 - x_1)/(x_2 - x_1^0) = (S^{N+1} - S)/(S^{N+1} - 1) \quad (14-39)$$

where $x_1^0 = y_1/m$; $S = mG_M/L_M = A^{-1}$; and

$$N = \frac{\ln [(1-A)(x_2 - x_1^0)/(x_1 - x_1^0) + A]}{\ln(S)} \quad (14-40)$$

For systems in which the concentrations are large and the stripping factor S may vary along the tower, the following Edmister equations [Ind. Eng. Chem., **35**, 837 (1943)] are applicable:

$$\frac{x_2 - x_1}{x_2} = \left[1 - \frac{1}{S'} \frac{(G_M y)_1}{(L_M x)_2} \right] \frac{S_e^{N+1} - S_e}{S_e^{N+1} - 1} \quad (14-41)$$

$$\text{where} \quad S_e = \sqrt{S_2(S_1 + 1) + 0.25} - 0.5 \quad (14-42)$$

$$S' = S_2(S_1 + 1)/(S_2 + 1) \quad (14-43)$$

and the subscripts 1 and 2 refer to the bottom and top of the tower respectively.

Equations (14-37) and (14-42) represent two different ways of obtaining an effective factor, and a value of A_e obtained by taking the reciprocal of S_e from Eq. (14-42) will not check exactly with a value of A_e derived by substituting $A_1 = 1/S_1$ and $A_2 = 1/S_2$ into Eq. (14-37). Regardless of this fact, the equations generally give reasonable results for approximate design calculations.

It should be noted that throughout this section the subscripts 1 and 2 refer to the bottom and to the top of the apparatus respectively regardless of whether it is an absorber or a stripper. This has been done to maintain internal consistency among all the equations and to prevent the confusion created in some derivations in which the numbering system for an absorber is different from the numbering system for a stripper.

Tray Efficiencies in Tray Absorbers and Strippers Computations of the theoretical trays N assume that the liquid on each tray is completely mixed and that the vapor leaving the tray is in equilibrium with the liquid. In practice, complete equilibrium cannot exist since interphase mass transfer requires a finite driving force. This leads to the definition of an overall tray efficiency

$$E = N_{\text{theoretical}}/N_{\text{actual}} \quad (14-44)$$

which can be correlated with the system design variables.

Mass-transfer theory indicates that for trays of a given design, the factors that have the biggest influence on E in absorption and stripping towers are the physical properties of the fluids and the dimensionless ratio mG_M/L_M . Systems in which mass transfer is gas-film-controlled may be expected to have efficiencies as high as 50 to 100 percent, whereas tray efficiencies as low as 1 percent have been reported for the absorption of low-solubility (large- m) gases into solvents of high viscosity.

The fluid properties of interest are represented by the Schmidt numbers of the gas and liquid phases. For gases, the Schmidt numbers are normally close to unity and independent of temperature and pressure. Thus, gas-phase mass-transfer coefficients are relatively independent of the system.

By contrast, the liquid-phase Schmidt numbers range from about 10^2 to 10^4 and depend strongly on temperature. The temperature dependence of the liquid-phase Schmidt number derives primarily from the strong dependence of the liquid viscosity on temperature.

Consideration of the preceding discussion in connection with the relationship between mass-transfer coefficients (see Sec. 5)

$$1/K_G = 1/k_C + m/k_L \quad (14-45)$$

indicates that the variations in the overall resistance to mass transfer in absorbers and strippers are related primarily to variations in the liquid-phase viscosity μ and the slope m . O'Connell [Trans. Am. Inst. Chem. Eng., **42**, 741 (1946)] used the above findings and correlated the tray efficiency in terms of the liquid viscosity and the gas solubility. The O'Connell correlation for absorbers (Fig. 14-9) has Henry's law constant in lb-mol/(atm-ft³), the pressure in atmospheres, and the liquid viscosity in centipoise.

The best procedure for making tray efficiency corrections (which can be quite significant, as seen in Fig. 14-9) is to use experimental

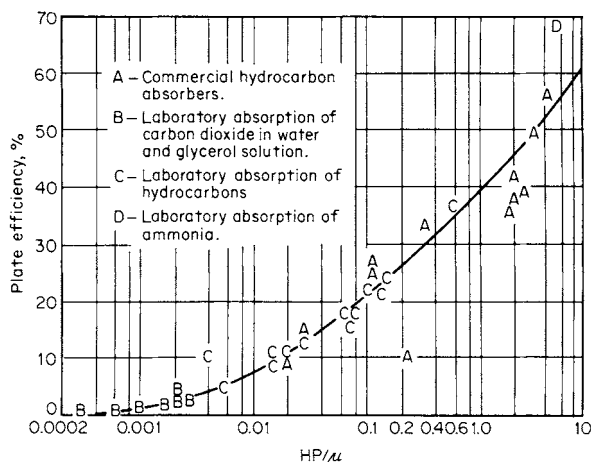


FIG. 14-9 O'Connell correlation for overall column efficiency E_{oc} for absorption. H is in lb-mol/(atm-ft³), P is in atm, and μ is in cP. To convert HP/μ in pound-moles per cubic foot-centipoise to kilogram-moles per cubic meter-pascal-second, multiply by 1.60×10^4 . [O'Connell, Trans. Am. Inst. Chem. Eng., **42**, 741 (1946).]

data from a prototype system that is large enough to be representative of the actual commercial tower.

Example 4: Actual Trays for Steam Stripping The number of actual trays required for steam-stripping an acetone-rich liquor containing 0.573 mole percent acetone in water is to be estimated. The design overhead recovery of acetone is 99.9 percent, leaving 18.5 ppm weight of acetone in the stripper bottoms. The design operating temperature and pressure are 101.3 kPa and 94°C respectively, the average liquid-phase viscosity is 0.30 cP, and the average value of $K = y^0/x$ for these conditions is 33.

By choosing a value of $mG_M/L_M = S = A^{-1} = 1.4$ and noting that the stripping medium is pure steam (i.e., $x_1^0 = 0$), the number of theoretical trays according to Eq. (14-40) is

$$N = \frac{\ln [(1 - 0.714)(1000) + 0.714]}{\ln(1.4)} = 16.8$$

The O'Connell parameter for gas absorbers is $\rho_L/KM\mu_L$, where ρ_L is the liquid density, lb/ft³; μ_L is the liquid viscosity, cP; M is the molecular weight of the liquid; and $K = y^0/x$. For the present design

$$\rho_L/KM\mu_L = 60.1/(33 \times 18 \times 0.30) = 0.337$$

and according to the O'Connell graph for absorbers (Fig. 14-7) the overall tray efficiency for this case is estimated to be 30 percent. Thus, the required number of actual trays is $16.8/0.3 = 56$ trays.

HEAT EFFECTS IN GAS ABSORPTION

Overview One of the most important considerations involved in designing gas absorption towers is to determine whether temperatures will vary along the height of the tower due to heat effects; note that the solute solubility usually depends strongly on temperature. The simplified design procedures described earlier in this section become more complicated when heat effects cannot be neglected. The role of this section is to enable understanding and design of gas absorption towers where heat effects are important and cannot be ignored.

Heat effects that cause temperatures to vary from point to point in a gas absorber are (1) the heat of solution (including heat of condensation, heat of mixing, and heat of reaction); (2) the heat of vaporization or condensation of the solvent; (3) the exchange of sensible heat between the gas and liquid phases; and (4) the loss of sensible heat from the fluids to internal or external coils.

There are a number of systems where heat effects definitely cannot be ignored. Examples include the absorption of ammonia in

water, dehumidification of air using concentrated H_2SO_4 , absorption of HCl in water, absorption of SO_3 in H_2SO_4 , and absorption of CO_2 in alkanolamines. Even for systems where the heat effects are mild, they may not be negligible; an example is the absorption of acetone in water.

Thorough and knowledgeable discussions of the problems involved in gas absorption with significant heat effects have been presented by Coggan and Bourne [*Trans. Inst. Chem. Eng.*, **47**, T96, T160 (1969)]; Bourn, von Stockar, and Coggan [*Ind. Eng. Chem. Proc. Des. Dev.*, **13**, 115, 124 (1974)]; and von Stockar and Wilke [*Ind. Eng. Chem. Fundam.*, **16**, 89 (1977)]. The first two of these references discuss tray-tower absorbers and include experimental studies of the absorption of ammonia in water. The third reference discusses the design of packed-tower absorbers and includes a shortcut design method based on a semitheoretical correlation of rigorous design calculations. All these authors demonstrate that when the solvent is volatile, the temperature inside an absorber can go through a maximum. They note that the least expensive and most common of solvents—water—is capable of exhibiting this “hot-spot” behavior.

Several approaches may be used in modeling absorption with heat effects, depending on the job at hand: (1) treat the process as isothermal by assuming a particular temperature, then add a safety factor; (2) employ the classical adiabatic method, which assumes that the heat of solution manifests itself only as sensible heat in the liquid phase and that the solvent vaporization is negligible; (3) use semitheoretical shortcut methods derived from rigorous calculations; and (4) employ rigorous methods available from a process simulator.

While simpler methods are useful for understanding the key effects involved, rigorous methods are recommended for final designs. This subsection also discusses the range of safety factors that are required if simpler methods are used.

Effects of Operating Variables Conditions that give rise to significant heat effects are (1) an appreciable heat of solution and/or (2) absorption of large amounts of solute in the liquid phase. The second condition is favored when the solute concentration in the inlet gas is large, when the liquid flow rate is relatively low (small L_M/G_M), when the solubility of the solute in the liquid is high, and/or when the operating pressure is high.

If the solute-rich gas entering the bottom of an absorber tower is cold, the liquid phase may be cooled somewhat by transfer of sensible heat to the gas. A much stronger cooling effect can occur when the solute is volatile and the entering gas is not saturated with respect to the solvent. It is possible to experience a condition in which solvent is being evaporated near the bottom of the tower and condensed near the top. Under these conditions a pinch point may develop in which the operating and equilibrium curves approach each other at a point inside the tower.

In the references previously cited, the authors discuss the influence of operating variables upon the performance of towers when large heat effects are involved. Some key observations are as follows:

Operating Pressure Raising the pressure may increase the separation effectiveness considerably. Calculations for the absorption of methanol in water from water-saturated air showed that doubling the pressure doubles the allowable concentration of methanol in the feed gas while still achieving the required concentration specification in the off gas.

Temperature of Lean Solvent The temperature of the entering (lean) solvent has surprisingly little influence upon the temperature profile in an absorber since any temperature changes are usually caused by the heat of solution or the solvent vaporization. In these cases, the temperature profile in the liquid phase is usually dictated solely by the internal-heat effects.

Temperature and Humidity of the Rich Gas Cooling and consequent dehumidification of the feed gas to an absorption tower can be very beneficial. A high humidity (or relative saturation with the solvent) limits the capacity of the gas to take up latent heat and hence is unfavorable to absorption. Thus dehumidification of the inlet gas is worth considering in the design of absorbers with large heat effects.

Liquid-to-Gas Ratio The L/G ratio can have a significant influence on the development of temperature profiles in gas

absorbers. High L/G ratios tend to result in less strongly developed temperature profiles due to the increased heat capacity of the liquid phase. As the L/G ratio is increased, the operating line moves away from the equilibrium line and more solute is absorbed per stage or packing segment. However, there is a compensating effect; since more heat is liberated in each stage or packing segment, the temperatures will rise, which causes the equilibrium line to shift up. As the L/G ratio is decreased, the concentration of solute tends to build up in the upper part of the absorber, and the point of highest temperature tends to move upward in the tower until finally the maximum temperature occurs at the top of the tower. Of course, the capacity of the liquid to absorb solute falls progressively as L/G is reduced.

Number of Stages or Packing Height When the heat effects combine to produce an extended zone in the tower where little absorption takes place (i.e., a pinch zone), the addition of trays or packing height will have no useful effect on separation efficiency. In this case, increases in absorption may be obtained by increasing solvent flow, introducing strategically placed coolers, cooling and dehumidifying the inlet gas, and/or raising the tower pressure.

Equipment Considerations When the solute has a large heat of solution and the feed gas contains a high concentration of solute, as in absorption of HCl in water, the effects of heat release during absorption may be so pronounced that the installation of heat-transfer surface to remove the heat of absorption may be as important as providing sufficient interfacial area for the mass-transfer process itself. The added heat-transfer area may consist of internal cooling coils on the trays, or the liquid may be withdrawn from the tower, cooled in an external heat exchanger, and then returned to the tower.

In many cases the rate of heat liberation is largest near the bottom of the tower, where the solute absorption is more rapid, so that cooling surfaces or intercoolers are required only at the lower part of the column. Coggan and Bourne [*Trans. Inst. Chem. Eng.*, **47**, T96, T160 (1969)] found, however, that the optimal position for a single interstage cooler does not necessarily coincide with the position of the maximum temperature of the center of the pinch. They found that in a 12-tray tower, two strategically placed interstage coolers tripled the allowable ammonia feed concentration for a given off-gas specification. For a case involving methanol absorption, it was found that greater separation was possible in a 12-stage column with two intercoolers than in a simple column with 100 stages and no intercoolers.

In the case of HCl absorption, a shell-and-tub heat exchanger often is employed as a cooled wetted-wall vertical-column absorber so that the exothermic heat of reaction can be removed continuously as it is released into a liquid film.

Installation of heat-exchange equipment to precool and dehumidify the feed gas to an absorber also deserves consideration, in order to take advantage of the cooling effects created by vaporization of solvent in the lower sections of the tower.

Classical Isothermal Design Method When the feed gas is sufficiently dilute, the exact design solution may be approximated by the isothermal one over the broad range of L/G ratios, since heat effects are generally less important when washing dilute-gas mixtures. The problem, however, is one of defining the term *sufficiently dilute* for each specific case. For a new absorption duty, the assumption of isothermal operation must be subjected to verification by the use of a rigorous design procedure.

When heat-exchange surface is being provided in the design of an absorber, the isothermal design procedure can be rendered valid by virtue of the exchanger design specification. With ample surface area and a close approach, isothermal operation can be guaranteed.

For preliminary screening and feasibility studies or for rough estimates, one may wish to employ a version of the isothermal design method which assumes that the liquid temperatures in the tower are everywhere equal to the inlet-liquid temperature. In their analysis of packed-tower designs, von Stockar and Wilke [*Ind. Eng. Chem. Fundam.*, **16**, 89 (1977)] showed that the isothermal method tended to underestimate the required height of packing by a factor of as much as

1.5 to 2. Thus, for rough estimates one may wish to employ the assumption that the absorber temperature is equal to the inlet-liquid temperature and then apply a design factor to the result.

Another instance in which the constant-temperature method is used involved the direct application of experimental K_{Ca} values obtained at the desired conditions of inlet temperatures, operating pressures, flow rates, and feed-stream compositions. The assumption here is that, regardless of any temperature profiles that may exist within the actual tower, the procedure of "working the problem in reverse" will yield a correct result. One should, however, be cautious about extrapolating such data from the original basis and be careful to use compatible equilibrium data.

Classical Adiabatic Design Method The classical adiabatic design method assumes that the heat of solution serves only to heat up the liquid stream and there is no vaporization of the solvent. This assumption makes it feasible to relate increases in the liquid-phase temperature to the solute concentration x by a simple enthalpy balance. The equilibrium curve can then be adjusted to account for the corresponding temperature rise on an xy diagram. The adjusted equilibrium curve will be concave upward as the concentration increases, tending to decrease the driving forces near the bottom of the tower, as illustrated in Fig. 14-10 in Example 6.

Colburn [*Trans. Am. Inst. Chem. Eng.*, **35**, 211 (1939)] has shown that when the equilibrium line is straight near the origin but curved slightly at its upper end, N_{OC} can be computed approximately by assuming that the equilibrium curve is a parabolic arc of slope m_2 near the origin and passing through the point x_1, K_1x_1 at the upper end. The Colburn equation for this case is

$$N_{OC} = \frac{1}{1 - m_2 G_M / L_M} \times \ln \left[\frac{(1 - m_2 G_M / L_M)^2}{1 - K_1 G_M / L_M} \left(\frac{y_1 - m_2 x_1}{y_2 - m_2 x_2} \right) + \frac{m_2 G_M}{L_M} \right] \quad (14-46)$$

Comparison by von Stockar and Wilke [*Ind. Eng. Chem. Fundam.*, **16**, 89 (1977)] between the rigorous and the classical adiabatic design methods for packed towers indicates that the simple adiabatic design methods underestimate packing heights by as much as a factor of 1.25

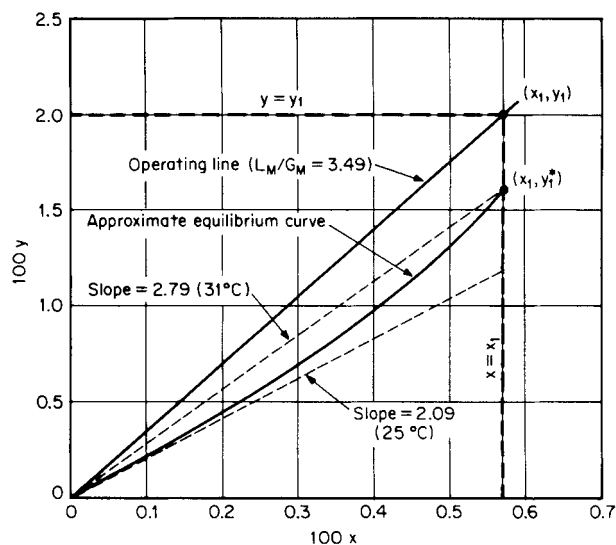


FIG. 14-10 Design diagram for adiabatic absorption of acetone in water, Example 6.

to 1.5. Thus, when using the classical adiabatic method, one should probably apply a design safety factor.

A slight variation of the above method accounts for increases in the solvent content of the gas stream between the inlet and the outlet of the tower and assumes that the evaporation of solvent tends to cool the liquid. This procedure offsets a part of the temperature rise that would have been predicted with no solvent evaporation and leads to the prediction of a shorter tower.

Rigorous Design Methods A detailed discussion of rigorous methods for the design of packed and tray absorbers when large heat effects are involved is beyond the scope of this subsection. In principle, material and energy balances may be executed under the same constraints as for rigorous distillation calculations (see Sec. 13). Further discussion on this subject is given in the subsection "Absorption with Chemical Reaction."

Direct Comparison of Design Methods The following problem, originally presented by Sherwood, Pigford, and Wilke (*Mass Transfer*, McGraw-Hill, New York, 1975, p. 616) was employed by von Stockar and Wilke (op. cit.) as the basis for a direct comparison between the isothermal, adiabatic, semitheoretical shortcut, and rigorous design methods for estimating the height of packed towers.

Example 5: Packed Absorber, Acetone into Water Inlet gas to an absorber consists of a mixture of 6 mole percent acetone in air saturated with water vapor at 15°C and 101.3 kPa (1 atm). The scrubbing liquor is pure water at 15°C, and the inlet gas and liquid rates are given as 0.080 and 0.190 kmol/s respectively. The liquid rate corresponds to 20 percent over the theoretical minimum as calculated by assuming a value of x_1 corresponding to complete equilibrium between the exit liquor and the incoming gas. H_G and H_L are given as 0.42 and 0.30 m respectively, and the acetone equilibrium data at 15°C are $p_A^s = 19.7$ kPa (147.4 torr), $\gamma_A = 6.46$, and $m_A = 6.46 \times 19.7/101.3 = 1.26$. The heat of solution of acetone is 7656 cal/gmol (32.05 kJ/gmol), and the heat of vaporization of solvent (water) is 10,755 cal/gmol (45.03 kJ/gmol). The problem calls for determining the height of packing required to achieve a 90 percent recovery of the acetone.

The following table compares the results obtained by von Stockar and Wilke (op. cit.) for the various design methods:

Design method used	N_{OC}	Packed height, m	Design safety factor
Rigorous	5.56	3.63	1.00
Shortcut rigorous	5.56	3.73	0.97
Classical adiabatic	4.01	2.38	1.53
Classical isothermal	3.30	1.96	1.85

It should be clear from this example that there is considerable room for error when approximate design methods are employed in situations involving large heat effects, even for a case in which the solute concentration in the inlet gas is only 6 mole percent.

Example 6: Solvent Rate for Absorption Let us consider the absorption of acetone from air at atmospheric pressure into a stream of pure water fed to the top of a packed absorber at 25°C. The inlet gas at 35°C contains 2 percent by volume of acetone and is 70 percent saturated with water vapor (4 percent H_2O by volume). The mole-fraction acetone in the exit gas is to be reduced to 1/400 of the inlet value, or 50 ppmv. For 100 kmol of feed-gas mixture, how many kilomoles of fresh water should be fed to provide a positive-driving force throughout the packing? How many transfer units will be needed according to the classical adiabatic method? What is the estimated height of packing required if $H_{OC} = 0.70$ m?

The latent heats at 25°C are 7656 kcal/kmol for acetone and 10,490 kcal/kmol for water, and the differential heat of solution of acetone vapor in pure water is given as 2500 kcal/kmol. The specific heat of air is 7.0 kcal/(kmol·K).

Acetone solubilities are defined by the equation

$$K = y^o/x = \gamma_a p_a / p_T \quad (14-47)$$

where the vapor pressure of pure acetone in mmHg (torr) is given by (Sherwood et al., *Mass Transfer*, McGraw-Hill, New York, 1975, p. 537):

$$p_A^s = \exp(18.1594 - 3794.06/T) \quad (14-48)$$

and the liquid-phase-activity coefficient may be approximated for low concentrations ($x \leq 0.01$) by the equation

$$\gamma_c = 6.5 \exp(2.0803 - 601.2/T) \quad (14-49)$$

Typical values of acetone solubility as a function of temperature at a total pressure of 760 mmHg are shown in the following table:

$t, ^\circ\text{C}$	25	30	35	40
γ_a	6.92	7.16	7.40	7.63
p_a, mmHg	229	283	346	422
$K = \gamma_a p_a^0 / 760$	2.09	2.66	3.37	4.23

For dry gas and liquid water at 25°C, the following enthalpies are computed for the inlet- and exit-gas streams (basis, 100 kmol of gas entering):

Entering gas:		
Acetone	2(2500 + 7656) = 20,312 kcal	
Water vapor	4(10,490) = 41,960	
Sensible heat	(100)(7.0)(35 - 25) = 7,000	
		69,272 kcal

Exit gas (assumed saturated with water at 25°C):		
Acetone	(2/400)(94/100)(2500) =	12 kcal
Water vapor	94 $\left(\frac{23.7}{760 - 23.7} \right)$ (10,490) =	31,600
		31,612 kcal

Enthalpy change of liquid = 69,272 - 31,612 = 37,660 kcal/100 kmol gas. Thus, $\Delta t = t_1 - t_2 = 37,660/18L_M$, and the relation between L_M/G_M and the liquid-phase temperature rise is

$$L_M/G_M = (37,660)/(18)(100) \Delta t = 20.92/\Delta t$$

The following table summarizes the critical values for various assumed temperature rises:

$\Delta t, ^\circ\text{C}$	L_M/G_M	K_1	$K_1 G_M/L_M$	$m_2 G_M/L_M$
0		2.09	0.	0.
2	10.46	2.31	0.221	0.200
3	6.97	2.42	0.347	0.300
4	5.23	2.54	0.486	0.400
5	4.18	2.66	0.636	0.500
6	3.49	2.79	0.799	0.599
7	2.99	2.93	0.980	0.699

Evidently a temperature rise of 7°C would not be a safe design because the equilibrium line nearly touches the operating line near the bottom of the tower, creating a pinch. A temperature rise of 6°C appears to give an operable design, and for this case $L_M = 349$ kmol per 100 kmol of feed gas.

The design diagram for this case is shown in Fig. 14-10, in which the equilibrium curve is drawn so that the slope at the origin m_2 is equal to 2.09 and passes through the point $x_1 = 0.02/3.49 = 0.00573$ at $y_1^0 = 0.00573 \times 2.79 = 0.0160$.

The number of transfer units can be calculated from the adiabatic design equation, Eq. (14-46):

$$N_{OG} = \frac{1}{1 - 0.599} \ln \left[\frac{(1 - 0.599)^2}{(1 - 0.799)} (400) + 0.599 \right] = 14.4$$

The estimated height of tower packing by assuming $H_{OG} = 0.70$ m and a design safety factor of 1.5 is

$$h_T = (14.4)(0.7)(1.5) = 15.1 \text{ m (49.6 ft)}$$

For this tower, one should consider the use of two or more shorter packed sections instead of one long section.

Another point to be noted is that this calculation would be done more easily today by using a process simulator. However, the details are presented here to help the reader gain familiarity with the key assumptions and results.

MULTICOMPONENT SYSTEMS

When no chemical reactions are involved in the absorption of more than one soluble component from an insoluble gas, the design conditions (temperature, pressure, liquid-to-gas ratio) are normally determined by the volatility or physical solubility of the least soluble component for which the recovery is specified.

The more volatile (i.e., less soluble) components will only be partially absorbed even for an infinite number of trays or transfer units. This can be seen in Fig. 14-9, in which the asymptotes become vertical for values of mG_M/L_M greater than unity. If the amount of volatile component in the fresh solvent is negligible, then the limiting value of y_1/y_2 for each of the highly volatile components is

$$y_1/y_2 = S/(S - 1) \quad (14-50)$$

where $S = mG_M/L_M$ and the subscripts 1 and 2 refer to the bottom and top of the tower, respectively.

When the gas stream is dilute, absorption of each constituent can be considered separately as if the other components were absent. The following example illustrates the use of this principle.

Example 7: Multicomponent Absorption, Dilute Case Air entering a tower contains 1 percent acetaldehyde and 2 percent acetone. The liquid-to-gas ratio for optimum acetone recovery is $L_M/G_M = 3.1$ mol/mol when the fresh-solvent temperature is 31.5°C. The value of y^0/x for acetaldehyde has been measured as 50 at the boiling point of a dilute solution, 93.5°C. What will the percentage recovery of acetaldehyde be under conditions of optimal acetone recovery?

Solution. If the heat of solution is neglected, y^0/x at 31.5°C is equal to 50(1200/7300) = 8.2, where the factor in parentheses is the ratio of pure-acetaldehyde vapor pressures at 31.5 and 93.5°C respectively. Since L_M/G_M is equal to 3.1, the value of S for the aldehyde is $S = mG_M/L_M = 8.2/3.1 = 2.64$, and $y_1/y_2 = S/(S - 1) = 2.64/1.64 = 1.61$. The acetaldehyde recovery is therefore equal to $100 \times 0.61/1.61 = 38$ percent recovery.

In concentrated systems the change in gas and liquid flow rates within the tower and the heat effects accompanying the absorption of all the components must be considered. A trial-and-error calculation from one theoretical stage to the next usually is required if accurate results are to be obtained, and in such cases calculation procedures similar to those described in Sec. 13 normally are employed. A computer procedure for multicomponent adiabatic absorber design has been described by Feintuch and Treybal [*Ind. Eng. Chem. Process Des. Dev.*, **17**, 505 (1978)]. Also see Holland, *Fundamentals and Modeling of Separation Processes*, Prentice Hall, Englewood Cliffs, N.J., 1975.

In concentrated systems, the changes in the gas and liquid flow rates within the tower and the heat effects accompanying the absorption of all components must be considered. A trial-and-error calculation from one theoretical stage to the next is usually required if accurate and reliable results are to be obtained, and in such cases calculation procedures similar to those described in Sec. 13 need to be employed.

When two or more gases are absorbed in systems involving chemical reactions, the system is much more complex. This topic is discussed later in the subsection "Absorption with Chemical Reaction."

Graphical Design Method for Dilute Systems The following notation for multicomponent absorption systems has been adapted from Sherwood, Pigford, and Wilke (*Mass Transfer*, McGraw-Hill, New York, 1975, p. 415):

L_M^S = moles of solvent per unit time

G_M^0 = moles of rich feed gas to be treated per unit time

X = moles of one solute per mole of solute-free solvent fed to top of tower

Y = moles of one solute in gas phase per mole of rich feed gas

Subscripts 1 and 2 refer to the bottom and the top of the tower, respectively, and the material balance for any one component may be written as

$$L_M^S(X - X_2) = G_M^0(Y - Y_2) \quad (14-51)$$

or else as

$$L_M^S(X_1 - X) = G_M^0(Y_1 - Y) \quad (14-52)$$

For the special case of absorption from lean gases with relatively large amounts of solvent, the equilibrium lines are defined for each component by the relation

$$Y^0 = K'X \quad (14-53)$$

Thus, the equilibrium line for each component passes through the origin with slope K' , where

$$K' = K(G_M^0/G_M^0)/(L_M/L_M^0) \quad (14-54)$$

and $K = y^0/x$. When the system is sufficiently dilute, $K' = K$.

The liquid-to-gas ratio is chosen on the basis of the least soluble component in the feed gas that must be absorbed completely. Each component will then have its own operating line with slope equal to L_M^0/G_M^0 (i.e., the operating lines for the various components will be parallel).

A typical diagram for the complete absorption of pentane and heavier components is shown in Fig. 14-11. The oil used as solvent is assumed to be solute-free (i.e., $X_2 = 0$), and the "key component," butane, was identified as that component absorbed in appreciable amounts whose equilibrium line is most nearly parallel to the operating lines (i.e., the K value for butane is approximately equal to L_M^0/G_M^0).

In Fig. 14-11, the composition of the gas with respect to components more volatile than butane will approach equilibrium with the liquid phase at the bottom of the tower. The gas compositions of the components less volatile (heavier) than butane will approach equilibrium with the oil entering the tower, and since $X_2 = 0$, the components heavier than butane will be completely absorbed.

Four theoretical trays have been stepped off for the key component (butane) on Fig. 14-11, and are seen to give a recovery of 75 percent of the butane. The operating lines for the other components have been drawn with the same slope and placed so as to give approximately the same number of theoretical trays. Figure 14-11 shows that equilibrium is easily achieved in fewer than four theoretical trays and that for the heavier components nearly complete recovery is obtained in four theoretical trays. The diagram also shows that absorption of the light components takes place in the upper part of the tower, and the final recovery of the heavier components takes place in the lower section of the tower.

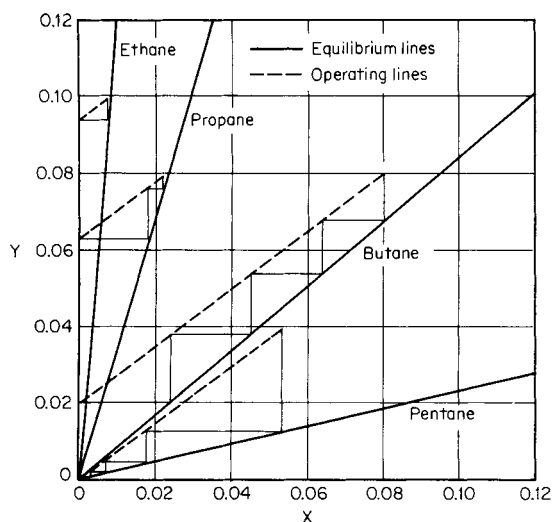


FIG. 14-11 Graphical design method for multicomponent systems; absorption of butane and heavier components in a solute-free lean oil.

Algebraic Design Method for Dilute Systems The design method described above can be performed algebraically by employing the following modified version of the Kremser formula:

$$\frac{Y_1 - Y_2}{Y_1 - mX_2} = \frac{(A^0)^{N+1} - A^0}{(A^0)^{N+1} - 1} \quad (14-55)$$

where for dilute gas absorption $A^0 = L_M^0/mG_M^0$ and $m \approx K = y^0/x$.

The left side of Eq. (14-55) represents the efficiency of absorption of any one component of the feed gas mixture. If the solvent is solute-free so that $X_2 = 0$, the left side is equal to the fractional absorption of the component from the rich feed gas. When the number of theoretical trays N and the liquid and gas feed rates L_M^0 and G_M^0 have been fixed, the fractional absorption of each component may be computed directly, and the operating lines need not be placed by trial and error as in the graphical method described above.

According to Eq. (14-55), when A^0 is less than unity and N is large,

$$(Y_1 - Y_2)/(Y_1 - mX_2) = A^0 \quad (14-56)$$

Equation (14-56) may be used to estimate the fractional absorption of more volatile components when A^0 of the component is greater than A^0 of the key component by a factor of 3 or more.

When A^0 is much larger than unity and N is large, the right side of Eq. (14-55) becomes equal to unity. This signifies that the gas will leave the top of the tower in equilibrium with the incoming oil, and when $X_2 = 0$, it corresponds to complete absorption of the component in question. Thus, the least volatile components may be assumed to be at equilibrium with the lean oil at the top of the tower.

When $A^0 = 1$, the right side of Eq. (14-56) simplifies as follows:

$$(Y_1 - Y_2)/(Y_1 - mX_2) = N/(N + 1) \quad (14-57)$$

For systems in which the absorption factor A^0 for each component is not constant throughout the tower, an effective absorption factor for use in the equations just presented can be estimated by the Edmister formula

$$A_e^0 = \sqrt{A_1^0(A_2^0 + 1) + 0.25} - 0.5 \quad (14-58)$$

This procedure is a reasonable approximation only when no pinch points exist within the tower and when the absorption factors vary in a regular manner between the bottom and the top of the tower.

Example 8: Multicomponent Absorption, Concentrated Case

A hydrocarbon feed gas is to be treated in an existing four-theoretical-tray absorber to remove butane and heavier components. The recovery specification for the key component, butane, is 75 percent. The composition of the exit gas from the absorber and the required liquid-to-gas ratio are to be estimated. The feed-gas composition and the equilibrium K values for each component at the temperature of the (solute-free) lean oil are presented in the following table:

Component	Mole %	K value
Methane	68.0	74.137
Ethane	10.0	12.000
Propane	8.0	3.429
Butane	8.0	0.833
Pentane	4.0	0.233
C_6 plus	2.0	0.065

For $N = 4$ and $Y_2/Y_1 = 0.25$, the value of A^0 for butane is found to be equal to 0.89 from Eq. (14-55) by using a trial-and-error method. The values of A^0 for the other components are then proportional to the ratios of their K values to that of butane. For example, $A^0 = 0.89(0.833/12.0) = 0.062$ for ethane. The values of A^0 for each of the other components and the exit-gas composition as computed from Eq. (14-55) are shown in the following table:

Component	A^0	Y_2 , mol/mol feed	Exit gas, mole %
Methane	0.010	67.3	79.1
Ethane	0.062	9.4	11.1
Propane	0.216	6.3	7.4
Butane	0.890	2.0	2.4
Pentane	3.182	0.027	0.03
C_6 plus	11.406	0.0012	0.0014

The molar liquid-to-gas ratio required for this separation is computed as $L_3/C_3^0 = A^0 \times K = 0.89 \times 0.833 = 0.74$.

We note that this example is the analytical solution to the graphical design problem shown in Fig. 14-11, which therefore is the design diagram for this system.

The simplified design calculations presented in this section are intended to reveal the key features of gas absorption involving multicomponent systems. It is expected that rigorous computations, based upon the methods presented in Sec. 13, will be used in design practice. Nevertheless, it is valuable to study these simplified design methods and examples since they provide insight into the key elements of multicomponent absorption.

ABSORPTION WITH CHEMICAL REACTION

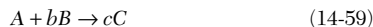
Introduction Many present-day commercial gas absorption processes involve systems in which chemical reactions take place in the liquid phase; an example of the absorption of CO_2 by MEA has been presented earlier in this section. These reactions greatly increase the capacity of the solvent and enhance the rate of absorption when compared to physical absorption systems. In addition, the selectivity of reacting solutes is greatly increased over that of nonreacting solutes. For example, MEA has a strong selectivity for CO_2 compared to chemically inert solutes such as CH_4 , CO , or N_2 . Note that the design procedures presented here are theoretically and practically related to biofiltration, which is discussed in Sec. 25 (Waste Management).

A necessary prerequisite to understanding the subject of absorption with chemical reaction is the development of a thorough understanding of the principles involved in physical absorption, as discussed earlier in this section and in Sec. 5. Excellent references on the subject of absorption with chemical reactions are the books by Dankwerts (*Gas-Liquid Reactions*, McGraw-Hill, New York, 1970) and Astarita et al. (*Gas Treating with Chemical Solvents*, Wiley, New York, 1983).

Recommended Overall Design Strategy When one is considering the design of a gas absorption system involving chemical reactions, the following procedure is recommended:

1. Consider the possibility that the physical design methods described earlier in this section may be applicable.
2. Determine whether commercial design overall $K_C a$ values are available for use in conjunction with the traditional design method, being careful to note whether the conditions under which the $K_C a$ data were obtained are essentially the same as for the new design. Contact the various tower-packing vendors for information as to whether $K_C a$ data are available for your system and conditions.
3. Consider the possibility of scaling up the design of a new system from experimental data obtained in a laboratory bench-scale or small pilot-plant unit.
4. Consider the possibility of developing for the new system a rigorous, theoretically based design procedure which will be valid over a wide range of design conditions. Note that commercial software is readily available today to develop a rigorous model in a relatively small amount of time. These topics are further discussed in the subsections that follow.

Dominant Effects in Absorption with Chemical Reaction When the solute is absorbing into a solution containing a reagent that chemically reacts with it, diffusion and reaction effects become closely coupled. It is thus important for the design engineer to understand the key effects. Figure 14-12 shows the concentration profiles that occur when solute A undergoes an irreversible second-order reaction with component B, dissolved in the liquid, to give product C.



The rate equation is

$$r_A = -k_2 C_A C_B \quad (14-60)$$

Figure 14-12 shows that the fast reaction takes place entirely in the liquid film. In such instances, the dominant mass-transfer mechanism is physical absorption, and physical design methods are applicable but the resistance to mass transfer in the liquid phase is lower due to the reaction. On the other extreme, a slow reaction occurs in the bulk of the liquid, and its rate has little dependence on the resistance to dif-

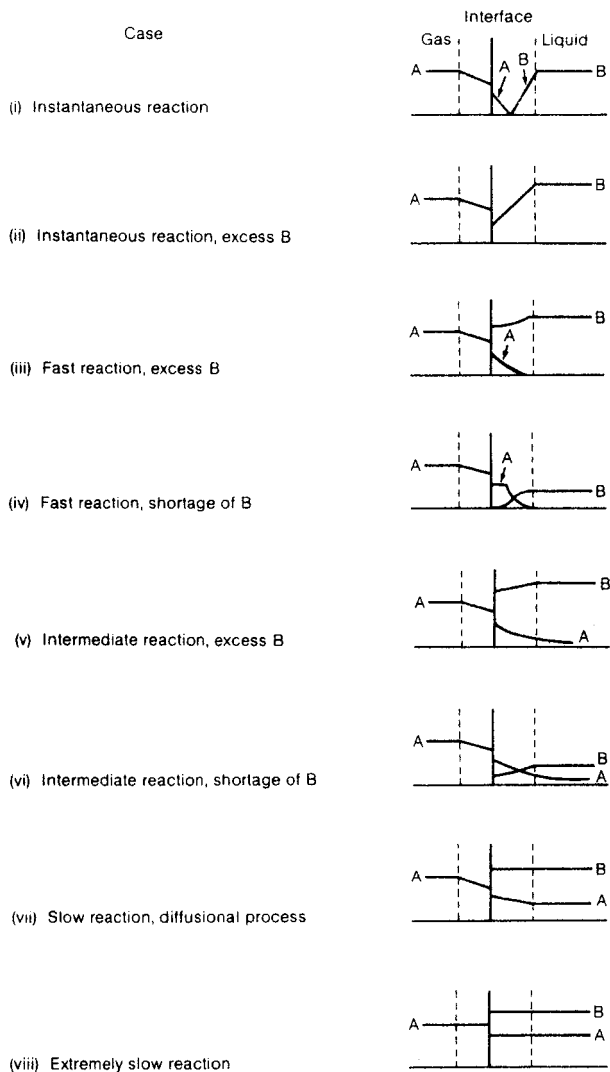


FIG. 14-12 Vapor- and liquid-phase concentration profiles near an interface for absorption with chemical reaction.

fusion in either the gas or the liquid films. Here the mass-transfer mechanism is that of chemical reaction, and holdup in the bulk liquid is the determining factor.

The Hatta number is a dimensionless group used to characterize the importance of the speed of reaction relative to the diffusion rate.

$$N_{\text{Ha}} = \frac{\sqrt{D_A k_2 C_{B0}}}{k_L^0} \quad (14-61)$$

As the Hatta number increases, the effective liquid-phase mass-transfer coefficient increases. Figure 14-13, which was first developed by Van Krevelen and Hoftzyer [*Rec. Trav. Chim.*, **67**, 563 (1948)] and later refined by Perry and Pigford and by Brian et al. [*AIChE J.*, **7**, 226 (1961)], shows how the enhancement (defined as the ratio of the effective liquid-phase mass-transfer coefficient to its physical equivalent $\phi = k_L/k_L^0$) increases with N_{Ha} for a second-order, irreversible reaction of the kind defined by Eqs. (14-60) and (14-61). The various curves in Fig. 14-13 were developed based upon penetration theory and

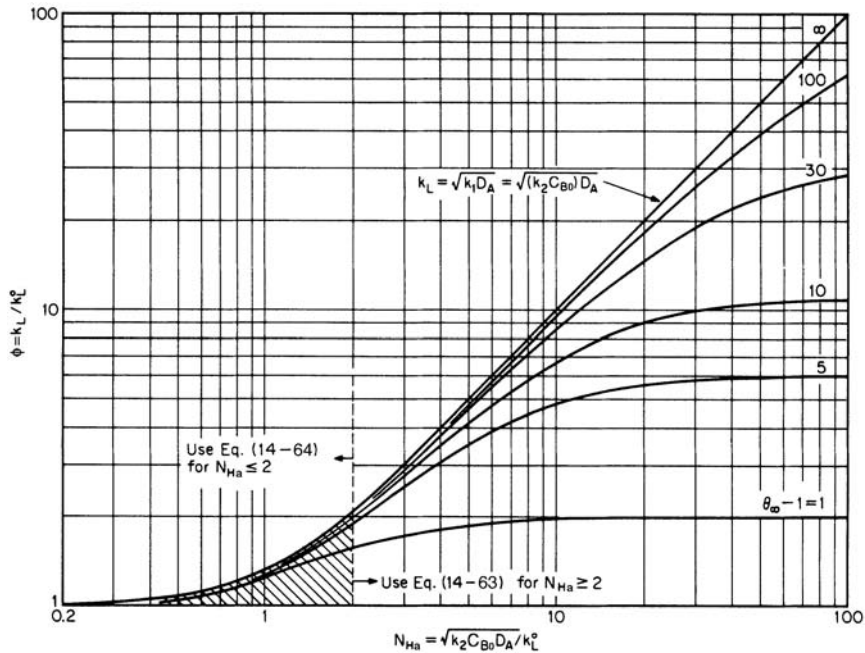


FIG. 14-13 Influence of irreversible chemical reactions on the liquid-phase mass-transfer coefficient k_L . [Adapted from Van Krevelen and Hoftyzer, *Rec. Trav. Chim.*, **67**, 563 (1948).]

depend on the parameter $\phi_\infty - 1$, which is related to the diffusion coefficients and reaction coefficients, as shown below.

$$\phi_\infty = \sqrt{\frac{D_A}{D_B}} + \sqrt{\frac{D_A}{D_B}} \left(\frac{C_B}{C_{Ab}} \right) \quad (14-62)$$

For design purposes, the entire set of curves in Fig. 14-13 may be represented by the following two equations:
For, $N_{Ha} \geq 2$:

$$k_L/k_L^0 = 1 + (\phi_\infty - 1) \{1 - \exp [-(N_{Ha} - 1)/(\phi_\infty - 1)]\} \quad (14-63)$$

For, $N_{Ha} \leq 2$:

$$k_L/k_L^0 = 1 + (\phi_\infty - 1) \{1 - \exp [-(\phi_\infty - 1)^{-1}]\} \exp [1 - 2/N_{Ha}] \quad (14-64)$$

Equation (14-64) was originally reported by Porter [*Trans. Inst. Chem. Eng.*, **44**, T25 (1966)], and Eq. (14-64) was derived by Edwards and first reported in the 6th edition of this handbook.

The Van Krevelen-Hoftyzer (Fig. 14-13) relationship was tested by Nijsing et al. [*Chem. Eng. Sci.*, **10**, 88 (1959)] for the second-order system in which CO_2 reacts with either NaOH or KOH solutions. Nijsing's results are shown in Fig. 14-14 and can be seen to be in excellent

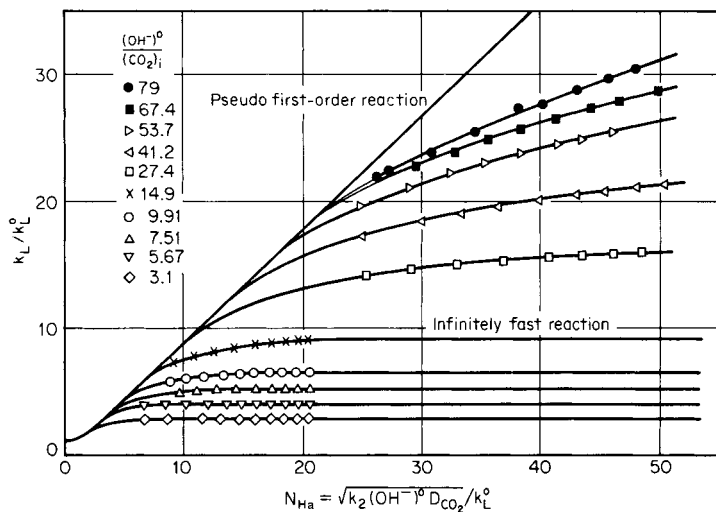


FIG. 14-14 Experimental values of k_L/k_L^0 for absorption of CO_2 into NaOH solutions at 20°C . [Data of Nijsing et al., *Chem. Eng. Sci.*, **10**, 88 (1959).]

agreement with the second-order-reaction theory. Indeed, these experimental data are well described by Eqs. (14-62) and (14-63) when values of $b = 2$ and $D_A/D_B = 0.64$ are employed in the equations.

Applicability of Physical Design Methods Physical design models such as the classical isothermal design method or the classical adiabatic design method may be applicable for systems in which chemical reactions are either extremely fast or extremely slow, or when chemical equilibrium is achieved between the gas and liquid phases.

If the chemical reaction is extremely fast and irreversible, the rate of absorption may in some cases be completely governed by gas-phase resistance. For practical design purposes, one may assume, e.g., that this gas-phase mass-transfer-limited condition will exist when the ratio y/y_1 is less than 0.05 everywhere in the apparatus.

From the basic mass-transfer flux relationship for species A (Sec. 5)

$$N_A = k_G(y - y_1) = k_L(x_i - x) \quad (14-65)$$

one can readily show that this condition on y/y_1 requires that the ratio x/x_i be negligibly small (i.e., a fast reaction) and that the ratio $mk_C/k_L = mk_C/k_L^0\phi$ be less than 0.05 everywhere in the apparatus. The ratio $mk_C/k_L^0\phi$ will be small if the equilibrium backpressure of the solute over the liquid is small (i.e., small m or high reactant solubility), or the reaction enhancement factor $\phi = k_1/k_L^0$ is very large, or both. The reaction enhancement factor ϕ will be large for all extremely fast pseudo-first-order reactions and will be large for extremely fast second-order irreversible reaction systems in which there is sufficiently large excess of liquid reagent.

Figure 14-12, case (ii), illustrates the gas-film and liquid-film concentration profiles one might find in an extremely fast (gas-phase mass-transfer-limited), second-order irreversible reaction system. The solid curve for reagent B represents the case in which there is a large excess of bulk liquid reagent B^0 . Figure 14-12, case (iv), represents the case in which the bulk concentration B^0 is not sufficiently large to prevent the depletion of B near the liquid interface.

Whenever these conditions on the ratio y/y_1 apply, the design can be based upon the physical rate coefficient k_C or upon the height of one gas-phase mass-transfer unit H_G . The gas-phase mass-transfer-limited condition is approximately valid for the following systems: absorption of NH_3 into water or acidic solutions, absorption of H_2O into concentrated sulfuric acid, absorption of SO_2 into alkali solutions, absorption of H_2S from a gas stream into a strong alkali solution, absorption of HCl into water or alkaline solutions, or absorption of Cl_2 into strong alkali solutions.

When the liquid-phase reactions are extremely slow, the gas-phase resistance can be neglected and one can assume that the rate of reaction has a predominant effect upon the rate of absorption. In this case the differential rate of transfer is given by the equation

$$dn_A = R_A f_H S dh = (k_L^0 a / \rho_L)(c_i - c) S dh \quad (14-66)$$

where n_A = rate of solute transfer, R_A = volumetric reaction rate (function of c and T), f_H = fractional liquid volume holdup in tower or apparatus, S = tower cross-sectional area, h = vertical distance, k_L^0 = liquid-phase mass-transfer coefficient for pure physical absorption, a = effective interfacial mass-transfer area per unit volume of tower or apparatus, ρ_L = average molar density of liquid phase, c_i = solute concentration in liquid at gas-liquid interface, and c = solute concentration in bulk liquid.

Although the right side of Eq. (14-66) remains valid even when chemical reactions are extremely slow, the mass-transfer driving force may become increasingly small, until finally $c \approx c_i$. For extremely slow first-order irreversible reactions, the following rate expression can be derived from Eq. (14-66):

$$R_A = k_1 c = k_1 c / (1 + k_1 \rho_L f_H / k_L^0 a) \quad (14-67)$$

where k_1 = first-order reaction rate coefficient.

For dilute systems in countercurrent absorption towers in which the equilibrium curve is a straight line (i.e., $y_i = mx_i$), the differential relation of Eq. (14-66) is formulated as

$$dn_A = -G_M S dy = k_1 c f_H S dh \quad (14-68)$$

where G_M = molar gas-phase mass velocity and y = gas-phase solute mole fraction.

Substitution of Eq. (14-67) into Eq. (14-68) and integration lead to the following relation for an extremely slow first-order reaction in an absorption tower:

$$y_2 = y_1 \exp \left[- \frac{k_1 \rho_L f_H h_T / (m G_M)}{1 + k_1 \rho_L f_H / (k_L^0 a)} \right] \quad (14-69)$$

In Eq. (14-69) subscripts 1 and 2 refer to the bottom and top of the tower, respectively.

As discussed above, the Hatta number N_{Ha} usually is employed as the criterion for determining whether a reaction can be considered extremely slow. A reasonable criterion for slow reactions is

$$N_{\text{Ha}} = \sqrt{k_1 D_A / k_L^0} \leq 0.3 \quad (14-70)$$

where D_A = liquid-phase diffusion coefficient of the solute in the solvent. Figure 14-12, cases (vii) and (viii), illustrates the concentration profiles in the gas and liquid films for the case of an extremely slow chemical reaction.

Note that when the second term in the denominator of the exponential in Eq. (14-69) is very small, the liquid holdup in the tower can have a significant influence upon the rate of absorption if an extremely slow chemical reaction is involved.

When chemical equilibrium is achieved quickly throughout the liquid phase, the problem becomes one of properly defining the physical and chemical equilibria for the system. It is sometimes possible to design a tray-type absorber by assuming chemical equilibrium relationships in conjunction with a stage efficiency factor, as is done in distillation calculations. Rivas and Prausnitz [*AIChE J.*, **25**, 975 (1979)] have presented an excellent discussion and example of the correct procedures to be followed for systems involving chemical equilibria.

Traditional Design Method The traditional procedure for designing packed-tower gas absorption systems involving chemical reactions makes use of overall mass-transfer coefficients as defined by the equation

$$K_{Ca} = n_A / (h_T S p_T \Delta y_{i_m}^0) \quad (14-71)$$

where K_{Ca} = overall volumetric mass-transfer coefficient, n_A = rate of solute transfer from the gas to the liquid phase, h_T = total height of tower packing, S = tower cross-sectional area, p_T = total system pressure, and $\Delta y_{i_m}^0$ is defined by the equation

$$\Delta y_{i_m}^0 = \frac{(y - y^0)_1 - (y - y^0)_2}{\ln [(y - y^0)_1 / (y - y^0)_2]} \quad (14-72)$$

in which subscripts 1 and 2 refer to the bottom and top of the absorption tower respectively, y = mole-fraction solute in the gas phase, and y^0 = gas-phase solute mole fraction in equilibrium with bulk-liquid-phase solute concentration x . When the equilibrium line is straight, $y^0 = mx$.

The traditional design method normally makes use of overall K_{Ca} values even when resistance to transfer lies predominantly in the liquid phase. For example, the CO_2 -NaOH system which is most commonly used for comparing K_{Ca} values of various tower packings is a liquid-phase-controlled system. When the liquid phase is controlling, extrapolation to different concentration ranges or operating conditions is not recommended since changes in the reaction mechanism can cause k_L to vary unexpectedly and the overall K_{Ca} do not capture such effects.

Overall K_{Ca} data may be obtained from tower-packing vendors for many of the established commercial gas absorption processes. Such data often are based either upon tests in large-diameter test units or upon actual commercial operating data. Since application to untried operating conditions is not recommended, the preferred procedure for applying the traditional design method is equivalent to duplicating a previously successful commercial installation. When this is not possible, a commercial demonstration at the new operating conditions may be required, or else one could consider using some of the more rigorous methods described later.

While the traditional design method is reported here because it has been used extensively in the past, it should be used with extreme

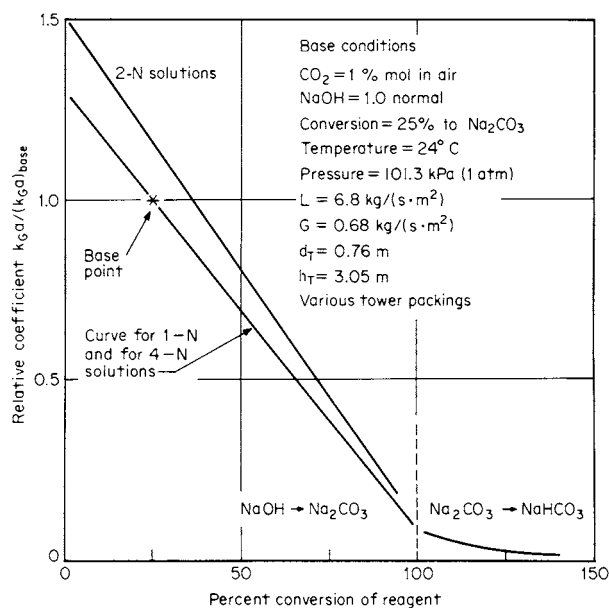


FIG. 14-15 Effects of reagent-concentration and reagent-conversion level upon the relative values of K_{Ca} in the CO_2 - NaOH - H_2O system. [Adapted from Eckert et al., *Ind. Eng. Chem.*, 59(2), 41 (1967).]

caution. In addition to the lack of an explicit liquid-phase resistance term, the method has other limitations. Equation (14-71) assumes that the system is dilute ($y_{BM} \approx 1$) and that the operating and equilibrium lines are straight, which are weak assumptions for reacting systems. Also, Eq. (14-65) is strictly valid only for the temperature and solute partial pressure at which the original test was done even though the total pressure p_T appears in the denominator.

In using Eq. (14-71), therefore, it should be understood that the numerical values of K_{Ca} will be a complex function of pressure, temperature, the type and size of packing employed, the liquid and gas mass flow rates, and the system composition (e.g., the degree of conversion of the liquid-phase reactant).

Figure 14-15 illustrates the influence of system composition and degree of reactant conversion upon the numerical values of K_{Ca} for the absorption of CO_2 into sodium hydroxide at constant conditions of temperature, pressure, and type of packing. An excellent experimental study of the influence of operating variables upon overall K_{Ca} values is that of Field et al. (*Pilot-Plant Studies of the Hot Carbonate*

Process for Removing Carbon Dioxide and Hydrogen Sulfide, U.S. Bureau of Mines Bulletin 597, 1962).

Table 14-2 illustrates the observed variations in K_{Ca} values for different packing types and sizes for the CO_2 - NaOH system at a 25 percent reactant conversion for two different liquid flow rates. The lower rate of $2.7 \text{ kg/(s}\cdot\text{m}^2)$ or $2000 \text{ lb/(h}\cdot\text{ft}^2)$ is equivalent to $4 \text{ U.S. gal/(min}\cdot\text{ft}^2)$ and is typical of the liquid rates employed in fume scrubbers. The higher rate of $13.6 \text{ kg/(s}\cdot\text{m}^2)$ or $10,000 \text{ lb/(h}\cdot\text{ft}^2)$ is equivalent to $20 \text{ U.S. gal/(min}\cdot\text{ft}^2)$ and is more typical of absorption towers such as used in CO_2 removal systems, for example. We also note that two gas velocities are represented in the table, corresponding to superficial velocities of 0.59 and 1.05 m/s (1.94 and 3.44 ft/s).

Table 14-3 presents a typical range of K_{Ca} values for chemically reacting systems. The first two entries in the table represent systems that can be designed by the use of purely physical design methods, because they are completely gas-phase mass-transfer-limited. To ensure a negligible liquid-phase resistance in these two tests, the HCl was absorbed into a solution maintained at less than $8 \text{ wt } \% \text{ HCl}$, and the NH_3 was absorbed into a water solution maintained below $\text{pH } 7$ by the addition of acid. The last two entries in Table 14-3 represent liquid-phase mass-transfer-limited systems.

Scaling Up from Laboratory Data Laboratory experimental techniques offer an efficient and cost-effective route to develop commercial absorption designs. For example, Ouwerkerk (*Hydrocarbon Process.*, April 1978, 89-94) revealed that both laboratory and small-scale pilot plant data were employed as the basis for the design of an 8.5-m (28-ft) diameter commercial Shell Claus off-gas treating (SCOT) tray-type absorber. Ouwerkerk claimed that the cost of developing comprehensive design procedures can be minimized, especially in the development of a new process, by the use of these modern techniques.

In a 1966 paper that is considered a classic, Dankwerts and Gillham [*Trans. Inst. Chem. Eng.*, 44, T42 (1966)] showed that data taken in a small stirred-cell laboratory apparatus could be used in the design of a packed-tower absorber when chemical reactions are involved. They showed that if the packed-tower mass-transfer coefficient in the absence of reaction (k_L^0) can be reproduced in the laboratory unit, then the rate of absorption in the laboratory apparatus will respond to chemical reactions in the same way as in the packed column, even though the means of agitating the liquid in the two systems may be quite different.

According to this method, it is not necessary to investigate the kinetics of the chemical reactions in detail; nor is it necessary to determine the solubilities or diffusivities of the various reactants in their unreacted forms. To use the method for scaling up, it is necessary to independently obtain data on the values of the interfacial area per unit volume a and the physical mass-transfer coefficient k_L^0 for the commercial packed tower. Once these data have been measured and tabulated, they can be used directly for scaling up the experimental laboratory data for any new chemically reacting system.

Dankwerts and Gillham did not investigate the influence of the gas-phase resistance in their study (for some processes, gas-phase resistance

TABLE 14-2 Typical Effects of Packing Type, Size, and Liquid Rate on K_{Ca} in a Chemically Reacting System, $K_{Ca} a$, $\text{kmol}/(\text{h}\cdot\text{m}^3)$

Packing size, mm	$L = 2.7 \text{ kg/(s}\cdot\text{m}^2)$				$L = 13.6 \text{ kg/(s}\cdot\text{m}^2)$			
	25	38	50	75-90	25	38	50	75-90
Berl-saddle ceramic	30	24	21		45	38	32	
Raschig-ring ceramic	27	24	21		42	34	30	
Raschig-ring metal	29	24	19		45	35	27	
Pall-ring plastic	29	27	26*	16	45	42	38*	24
Pall-ring metal	37	32	27	21*	56	51	43	27*
Intalox-saddle ceramic	34	27	22	16*	56	43	34	26*
Super-Intalox ceramic	37*		26*		59*		40*	
Intalox-saddle plastic	40*		24*	16*	56*		37*	26*
Intalox-saddle metal	43*	35*	30*		66*	58*	48*	37*
Hy-Pak metal	35	32*	27*	18*	54	50*	42*	27*

Data courtesy of the Norton Company.

Operating conditions: CO_2 , 1 percent mole in air; NaOH , 4 percent weight (1 normal); 25 percent conversion to sodium carbonate; temperature, 24°C (75°F); pressure, 98.6 kPa (0.97 atm); gas rate = $0.68 \text{ kg/(s}\cdot\text{m}^2)$ = 0.59 m/s = $500 \text{ lb/(h}\cdot\text{ft}^2)$ = 1.92 ft/s except for values with asterisks, which were run at $1.22 \text{ kg/(s}\cdot\text{m}^2)$ = 1.05 m/s = $900 \text{ lb/(h}\cdot\text{ft}^2)$ = 3.46 ft/s superficial velocity; packed height, 3.05 m (10 ft); tower diameter, 0.76 m (2.5 ft). To convert table values to units of $(\text{lb}\cdot\text{mol})/(\text{h}\cdot\text{ft}^3)$, multiply by 0.0624 .

TABLE 14-3 Typical $K_G a$ Values for Various Chemically Reacting Systems, $\text{kmol}/(\text{h}\cdot\text{m}^3)$

Gas-phase reactant	Liquid-phase reactant	$K_G a$	Special conditions
HCl	H ₂ O	353	Gas-phase limited
NH ₃	H ₂ O	337	Gas-phase limited
Cl ₂	NaOH	272	8% weight solution
SO ₂	Na ₂ CO ₃	224	11% weight solution
HF	H ₂ O	152	
Br ₂	NaOH	131	5% weight solution
HCN	H ₂ O	114	
HCHO	H ₂ O	114	Physical absorption
HBr	H ₂ O	98	
H ₂ S	NaOH	96	4% weight solution
SO ₂	H ₂ O	59	
CO ₂	NaOH	38	4% weight solution
Cl ₂	H ₂ O	8	Liquid-phase limited

Data courtesy of the Norton Company.

Operating conditions (see text): 38-mm ceramic Intalox saddles; solute gases, 0.5–1.0 percent mole; reagent conversions = 33 percent; pressure, 101 kPa (1 atm); temperature, 16–24°C; gas rate = 1.3 kg/(s·m²) = 1.1 m/s; liquid rates = 3.4 to 6.8 kg/(s·m²); packed height, 3.05 m; tower diameter, 0.76 m. Multiply table values by 0.0624 to convert to (lb·mol)/(h·ft³).

may be neglected). However, in 1975 Dankwerts and Alper [*Trans. Inst. Chem. Eng.*, 53, T42 (1975)] showed that by placing a stirrer in the gas space of the stirred-cell laboratory absorber, the gas-phase mass-transfer coefficient k_G in the laboratory unit could be made identical to that in a packed-tower absorber. When this was done, laboratory data for chemically reacting systems having a significant gas-side resistance could successfully be scaled up to predict the performance of a commercial packed-tower absorber.

If it is assumed that the values for k_G , k_L^0 , and a have been measured for the commercial tower packing to be employed, the procedure for using the laboratory stirred-cell reactor is as follows:

1. The gas-phase and liquid-phase stirring rates are adjusted so as to produce the same values of k_G and k_L^0 as will exist in the commercial tower.

2. For the reaction system under consideration, experiments are made at a series of bulk-liquid and bulk-gas compositions representing the compositions to be expected at different levels in the commercial absorber (on the basis of material balance).

3. The ratios of $r_A(C_b, B^0)$ are measured at each pair of gas and liquid compositions.

For the dilute-gas systems, one form of the equation to be solved in conjunction with these experiments is

$$h_T = \frac{G_M}{a} \int_{y_2}^{y_1} \frac{dy}{r_A} \quad (14-73)$$

where h_T = height of commercial tower packing, G_M = molar gas-phase mass velocity, a = effective mass-transfer area per unit volume in the commercial tower, y = mole fraction solute in the gas phase, and r_A = experimentally determined rate of absorption per unit of exposed interfacial area.

By using the series of experimentally measured rates of absorption, Eq. (14-73) can be integrated numerically to determine the height of packing required in the commercial tower.

A number of different types of experimental laboratory units could be used to develop design data for chemically reacting systems. Charpentier [*ACS Symp. Ser.*, 72, 223–261 (1978)] has summarized the state of the art with respect to methods of scaling up laboratory data and has tabulated typical values of the mass-transfer coefficients, interfacial areas, and contact times to be found in various commercial gas absorbers, as well as in currently available laboratory units.

The laboratory units that have been employed to date for these experiments were designed to operate at a total system pressure of about 101 kPa (1 atm) and at near-ambient temperatures. In practical situations, it may become necessary to design a laboratory absorption unit that can be operated either under vacuum or at elevated pressure

and over a range of temperatures in order to apply the Dankwerts method.

It would be desirable to reinterpret existing data for commercial tower packings to extract the individual values of the interfacial area a and the mass-transfer coefficients k_G and k_L^0 to facilitate a more general usage of methods for scaling up from laboratory experiments. Some progress has already been made, as described later in this section. In the absence of such data, it is necessary to operate a pilot plant or a commercial absorber to obtain k_G , k_L^0 , and a as described by Ouwkerk (op. cit.).

Modern techniques use rigorous modeling computer-based methods to extract fundamental parameters from laboratory-scale measurements and then apply them to the design of commercial absorption towers. These techniques are covered next.

Rigorous Computer-Based Absorber Design While the techniques described earlier in this section are very useful to gain an understanding of the key effects in commercial absorbers, current design methods used in industrial practice for chemically reactive systems are increasingly often based upon computerized rigorous methods, which are commercially available from software vendors. The advantages of these rigorous methods are as follows: (1) Approximations do not have to be made for special cases (e.g., fast chemical reactions or mass-transfer resistance dominated by the gas or liquid phase), and all effects can be simultaneously modeled. (2) Fundamental quantities such as kinetic parameters and mass-transfer coefficients can be extracted from laboratory equipment and applied to commercial absorber towers. (3) Integrated models can be developed for an entire absorption process flowsheet (e.g., the absorber-stripper system with heat integration presented in Fig. 14-3), and consequently the entire system may be optimized.

Computer programs for chemically reacting systems are available from several vendors, notably the following:

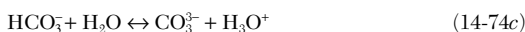
Program	Vendor	Reference
AMSIM	Schlumberger Limited	Zhang and Ng, <i>Proc. Ann. Conv.—Gas Proc. Assoc.</i> , Denver, Colo.; 1996, p. 22.
ProTreat	Sulphur Experts	Weiland and Dingman, <i>Proc. Ann. Conv., Gas Proc. Assoc.</i> , Houston, Tex., 2001, p. 80.
TSWEET	Bryan Research and Engineering	Polasek, Donnelly, and Bullin, <i>Proc. 71st GPA Annual Conv.</i> , 1992, p. 58.
RateSep	Aspen Technology	Chen et al., <i>AIChE Annual Meeting</i> , San Francisco, Nov. 12–17, 2006.

The specific approaches used to model the chemically reacting absorption system are slightly different among the different vendors. The general approach used and the benefits obtained are highlighted

by considering a specific example: removal of CO₂ from flue gases discharged by a power plant using aqueous monoethanolamine (MEA), as presented by Freguia and Rochelle [*AIChE J.*, **49**, 1676 (2003)].

The development and application of a rigorous model for a chemically reactive system typically involves four steps: (1) development of a thermodynamic model to describe the physical and chemical equilibrium; (2) adoption and use of a modeling framework to describe the mass transfer and chemical reactions; (3) parameterization of the mass-transfer and kinetic models based upon laboratory, pilot-plant, or commercial-plant data; and (4) use of the integrated model to optimize the process and perform equipment design.

Development of Thermodynamic Model for Physical and Chemical Equilibrium The first and perhaps most important step in the development of the thermodynamic model is the *speciation*, or representation of the set of chemical reactions. For CO₂ absorption in aqueous MEA solutions, the set of reactions is



In addition, a model is needed that can describe the nonideality of a system containing molecular and ionic species. Freguia and Rochelle adopted the model developed by Chen et al. [*AIChE J.*, **25**, 820 (1979)] and later modified by Mock et al. [*AIChE J.*, **32**, 1655 (1986)] for mixed-electrolyte systems. The combination of the speciation set of reactions [Eqs. (14-74a) to (14-74e)] and the nonideality model is capable of representing the solubility data, such as presented in Figs. 14-1 and 14-2, to good accuracy. In addition, the model accurately and correctly represents the actual species present in the aqueous phase, which is important for faithful description of the chemical kinetics and species mass transfer across the interface. Finally, the thermodynamic model facilitates accurate modeling of the heat effects, such as those discussed in Example 6.

Rafal et al. (Chapter 7, "Models for Electrolyte Solutions," in *Models for Thermodynamic and Phase Equilibria Calculations*, S. I. Sandler, ed., Marcel Dekker, New York, 1994, p. 686) have provided a comprehensive discussion of speciation and thermodynamic models.

Adoption and Use of Modeling Framework The rate of diffusion and species generation by chemical reaction can be described by film theory, penetration theory, or a combination of the two. The most popular description is in terms of a two-film theory, which is

diagrammed in Fig. 14-16 for absorption. Accordingly, there exists a stable interface separating the gas and the liquid. A certain distance from the interface, large fluid motions exist, and these distribute the material rapidly and equally so that no concentration gradients develop. Next to the interface, however, there are regions in which the fluid motion is slow; in these regions, termed *films*, material is transferred by diffusion alone. At the gas-liquid interface, material is transferred instantaneously, so that the gas and liquid are in physical equilibrium at the interface. The rate of diffusion in adsorption is therefore the rate of diffusion in the gas and liquid films adjacent to the interface. The model framework is completed by including terms for species generation (chemical equilibrium and chemical kinetics) in the gas and liquid film and bulk regions. Taylor, Krishna, and Kooijman (*Chem. Eng. Progress*, July 2003, p. 28) have provided an excellent discussion of rate-based models; these authors emphasize that the diffusion flux for multicomponent systems must be based upon the Maxwell-Stefan approach. The book by Taylor and Krishna (*Multicomponent Mass Transfer*, Wiley, New York, 1993) provides a detailed discussion of the Maxwell-Stefan approach. More details and discussion have been provided by the program vendors listed above.

Parameterization of Mass-Transfer and Kinetic Models The mass-transfer and chemical kinetic rates required in the rigorous model are typically obtained from the literature, but must be carefully evaluated; and fine-tuning through pilot-plant and commercial data is highly recommended.

Mass-transfer coefficient models for the vapor and liquid coefficients are of the general form

$$k_{tj}^G = a \rho_L f(D_{ij}^m, \mu_L, \rho_V, a, \text{internal characteristics}) \quad (14-75a)$$

$$k_{tj}^L = a P f(D_{ij}^m, \mu_V, \rho_V, a, \text{internal characteristics}) \quad (14-75b)$$

where a = effective interfacial area per unit volume, D_{ij}^m are the Stefan-Maxwell diffusion coefficients, P = pressure, ρ = molar density, and μ = viscosity. The functions in Eqs. (14-75a) and (14-75b) are correlations that depend on the column internals. Popular correlations in the literature are those by Onda et al. [*J. Chem. Eng. Jap.*, **1**, 56 (1968)] for random packing, Bravo and Fair [*Ind. Eng. Chem. Proc. Des. Dev.*, **21**, 162 (1982)] for structured packing, Chan and Fair [*Ind. Eng. Chem. Proc. Des. Dev.*, **23**, 814 (1984)] for sieve trays, Scheffe and Weiland [*Ind. Eng. Chem. Res.*, **26**, 228 (1987)] for valve trays, and Hughmark [*AIChE J.*, **17**, 1295 (1971)] for bubble-cap trays.

It is highly recommended that the mass-transfer correlations be tested and improved by using laboratory, pilot-plant, or commercial data for the specific application. Commercial software generally provides the capability for correction factors to adjust generalized correlations to the particular application.

Kinetic models are usually developed by replacing a subset of the speciation reactions by kinetically reversible reactions. For example, Freguia and Rochelle replaced equilibrium reactions (14-74a) and (14-74b) with kinetically reversible reactions and retained the remaining three reactions as very fast and hence effectively at equilibrium. The kinetic constants were tuned using wetted-wall column data from Dang (M.S. thesis, University of Texas, Austin, 2001) and field data from a commercial plant.

Modern commercial software provides powerful capability to deploy literature correlations and to customize models for specific applications.

Deployment of Rigorous Model for Process Optimization and Equipment Design Techniques similar to those described above may be used to develop models for the stripper as well as other pieces of plant equipment, and thus an integrated model for the entire absorption system may be produced. The value of integrated models is that they can be used to understand the combined effects of many variables that determine process performance and to rationally optimize process performance. Freguia and Rochelle have shown that the reboiler duty (the dominant source of process operating costs) may be reduced by 10 percent if the absorber height is increased by 20 percent and by 4 percent if the absorber is intercooled with a duty equal to one-third of the reboiler duty. They also show that the power plant lost work is affected by varying stripper

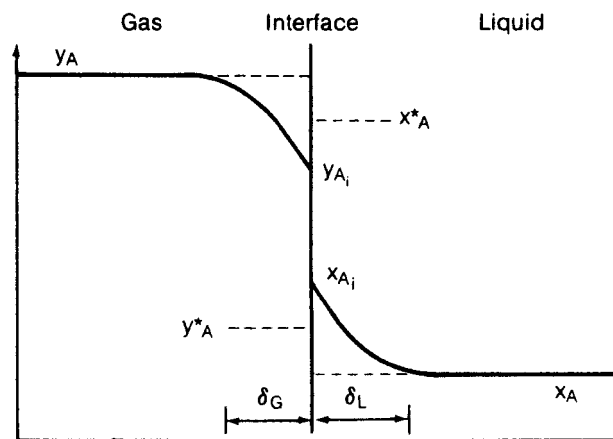


FIG. 14-16 Concentration profiles in the vapor and liquid phases near an interface.

pressure, but not significantly, so any convenient pressure can be chosen to operate the stripper.

In this section, we have used the example of CO₂ removal from flue gases using aqueous MEA to demonstrate the development and application of a rigorous model for a chemically reactive system. Modern software enables rigorous description of complex chemically reactive systems, but it is very important to carefully evaluate the models and to tune them using experimental data.

Use of Literature for Specific Systems A large body of experimental data obtained in bench-scale laboratory units and in small-diameter packed towers has been published since the early 1940s. One might wish to consider using such data for a particular chemically reacting system as the basis for scaling up to a commercial design. Extreme caution is recommended in interpreting such data for the purpose of developing commercial designs, as extrapolation of the data can lead to serious errors. Extrapolation to temperatures, pressures, or liquid-phase reagent conversions different from those that were employed by the original investigators definitely should be regarded with caution.

Bibliographies presented in the General References listed at the beginning of this section are an excellent source of information on

specific chemically reacting systems. *Gas-Liquid Reactions* by Dankwerts (McGraw-Hill, New York, 1970) contains a tabulation of references to specific chemically reactive systems. *Gas Treating with Chemical Solvents* by Astarita et al. (Wiley, New York, 1983) deals with the absorption of acid gases and includes an extensive listing of patents. *Gas Purification* by Kohl and Nielsen (Gulf Publishing, Houston, 1997) provides a practical description of techniques and processes in widespread use and typically also sufficient design and operating data for specific applications.

In searching for data on a particular system, a computerized search of *Chemical Abstracts*, *Engineering Index*, and *National Technical Information Service* (NTIS) databases is recommended. In addition, modern search engines will rapidly uncover much potentially valuable information.

The experimental data for the system CO₂-NaOH-Na₂CO₃ are unusually comprehensive and well known as the result of the work of many experimenters. A serious study of the data and theory for this system therefore is recommended as the basis for developing a good understanding of the kind and quality of experimental information needed for design purposes.

EQUIPMENT FOR DISTILLATION AND GAS ABSORPTION: TRAY COLUMNS

Distillation and gas absorption are the prime and most common gas-liquid mass-transfer operations. Other operations that are often performed in similar equipment include stripping (often considered part of distillation), direct-contact heat transfer, flashing, washing, humidification, and dehumidification.

The most common types of contactors by far used for these are tray and packed towers. These are the focus of this subsection. Other contactors used from time to time and their applications are listed in Table 14-4.

In this subsection, the terms *gas* and *vapor* are used interchangeably. *Vapor* is more precise for distillation, where the gas phase is at equilibrium. Also, the terms *tower* and *column* are used interchangeably.

A crossflow tray (Fig. 14-17) consists of the *bubbling area* and the *downcomer*. Liquid descending the downcomer from the tray above enters the bubbling area. Here, the liquid contacts gas ascending through the tray perforations, forming froth or spray. An *outlet weir* on the downstream side of the bubbling area helps maintain liquid level on the tray. Froth overflowing the weir enters the outlet downcomer. Here, gas disengages from the liquid, and the liquid descends to the tray below. The bubbling area can be fitted with numerous types of tray hardware. The most common types by far are:

Sieve trays (Fig. 14-18a) are perforated plates. The velocity of upflowing gas keeps the liquid from descending through the perforations (weeping). At low gas velocities, liquid weeps through the perforations, bypassing part of the tray and reducing tray efficiency. Because of this, sieve trays have relatively poor turndown.

Fixed valve trays (Fig. 14-18b) have the perforations covered by a fixed cover, often a section of the tray floor pushed up. Their performance is similar to that of sieve trays.

Moving valve trays (Fig. 14-18c) have the perforations covered by movable disks (valves). Each valve rises as the gas velocity increases. The upper limit of the rise is controlled by restricting legs on the bottom of the valve (Fig. 14-18c) or by a cage structure around the valve. As the gas velocity falls, some valves close completely, preventing weeping. This gives the valve tray good turndown.

Table 14-5 is a general comparison of the three main tray types, assuming proper design, installation, and operation. Sieve and valve trays are comparable in capacity, efficiency, entrainment, and pressure drop. The turndown of moving valve trays is much better than that of sieve and fixed valve trays. Sieve trays are least expensive; valve trays cost only slightly more. Maintenance, fouling tendency, and effects of corrosion are least troublesome in fixed valve and sieve trays (provided the perforations or fixed valves are large enough) and most troublesome with moving valve trays.

Fixed valve and sieve trays prevail when fouling or corrosion is expected, or if turndown is unimportant. Valve trays prevail when high turndown is required. The energy saved, even during short turndown periods, usually justifies the small additional cost of the moving valve trays.

DEFINITIONS

Tray Area Definitions Some of these are illustrated in Fig. 14-17.

Total tower cross-section area A_T The inside cross-sectional area of the empty tower (without trays or downcomers).

Net area A_N (also called *free area*) The total tower cross-sectional area A_T minus the area at the top of the downcomer A_{DT} . The

TABLE 14-4 Equipment for Liquid-Gas Systems

Equipment designation	Mode of flow	Gross mechanism	Continuous phase	Primary process applications
Tray column	Cross-flow, countercurrent	Integral	Liquid and/or gas	Distillation, absorption, stripping, DCHT, washing
Packed column	Countercurrent, cocurrent	Differential	Liquid and/or gas	Distillation, absorption, stripping, humidification, dehumidification, DCHT, washing
Wetted-wall (falling-film) column	Countercurrent, cocurrent	Differential	Liquid and/or gas	Distillation, absorption, stripping, evaporation
Spray chamber	Cocurrent, cross-flow, countercurrent	Differential	Gas	Absorption, stripping, humidification, dehumidification
Agitated vessel	Complete mixing	Integral	Liquid	Absorption
Line mixer	Cocurrent	Differential	Liquid or gas	Absorption, stripping

DCHT = direct contact heat transfer.

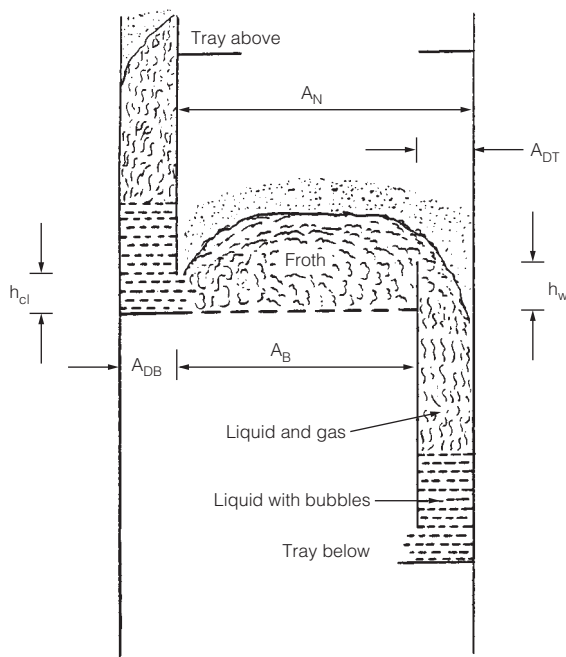


FIG. 14-17 Schematic of a tray operating in the froth regime. (Based on H. Z. Kister, *Distillation Design*, copyright © 1992 by McGraw-Hill; reprinted by permission.)

net area represents the smallest area available for vapor flow in the intertray spacing.

Bubbling area A_B (also called active area) The total tower cross-sectional area minus the sum of downcomer top area A_{DT} , downcomer seal area A_{DB} , and any other nonperforated areas on the tray. The bubbling area represents the area available for vapor flow just above the tray floor.

Hole area A_h The total area of the perforations on the tray. The hole area is the smallest area available for vapor passage on a sieve tray.

Slot area A_s The total (for all open valves) vertical curtain area through which vapor passes in a horizontal direction as it leaves the valves. It is a function of the narrowest opening of each valve and the number of valves that are open. The slot area is normally the smallest area available for vapor flow on a valve tray.

Open slot area A_{s0} The slot area when all valves are open.

Fractional hole area A_f The ratio of hole area to bubbling area (sieve trays) or slot area to bubbling area (valve trays).

Vapor and Liquid Load Definitions

F-factor F This is the square root of the kinetic energy of the gas, defined by Eq. (14-76). The velocity in Eq. (14-76) is usually (not always) based on the tower cross-sectional area A_T , the net area A_N , or the bubbling area A_B . The user should beware of any data for which the area basis is not clearly specified.

$$F = u \sqrt{\rho_G} \quad (14-76)$$

C-factor C The C-factor, defined in Eq. (14-77), is the best gas load term for comparing capacities of systems of different physical properties. It has the same units as velocity (m/s or ft/s) and is directly related to droplet entrainment. As with the F-factor, the user should beware of any data for which the area basis is not clearly specified.

$$C = u \sqrt{\frac{\rho_G}{\rho_L - \rho_G}} \quad (14-77)$$

Weir load For trays (as distinct from downcomers), liquid load is normally defined as

$$Q_L = \frac{\text{volume of liquid}}{\text{length of outlet weir}} = \frac{Q}{L_w} \quad (14-78)$$

This definition describes the flux of liquid horizontally across the tray. Units frequently used are $\text{m}^3/(\text{h}\cdot\text{m})$, $\text{m}^3/(\text{s}\cdot\text{m})$, and gpm/in .

Downcomer liquid load For downcomer design, the liquid load is usually defined as the liquid velocity at the downcomer entrance (m/s or ft/s):

$$Q_D = \frac{\text{volume of liquid}}{\text{downcomer entrance area}} = \frac{Q}{A_{DT}} \quad (14-79)$$

FLOW REGIMES ON TRAYS

Three main flow regimes exist on industrial distillation trays. These regimes may all occur on the same tray under different liquid and gas flow rates (Fig. 14-19). Excellent discussion of the fundamentals and modeling of these flow regimes was presented by Lockett (*Distillation Tray Fundamentals*, Cambridge University Press, Cambridge, 1986). An excellent overview of these as well as of less common flow regimes was given by Prince (*PACE*, June 1975, p. 31; July 1975, p. 18).

Froth regime (or mixed regime; Fig. 14-20a). This is the most common operating regime in distillation practice. Each perforation bubbles vigorously. The bubbles circulate rapidly through the liquid, are of nonuniform sizes and shapes, and travel at varying velocities. The froth surface is mobile and not level, and is generally covered by droplets. Bubbles are formed at the tray perforations and are swept away by the froth.

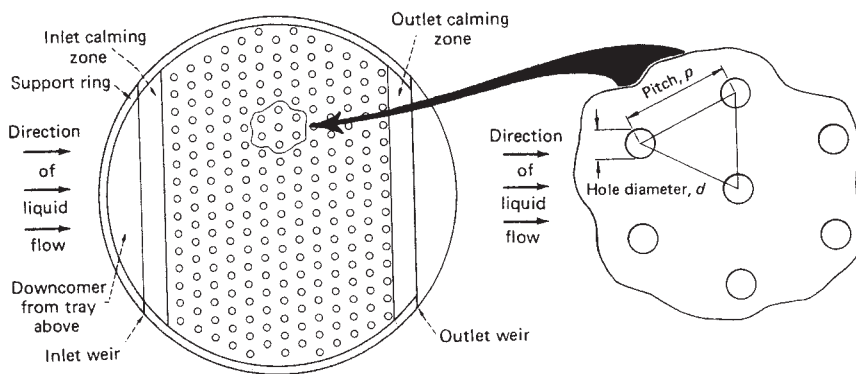
As gas load increases in the froth regime, jetting begins to replace bubbling in some holes. The fraction of holes that is jetting increases with gas velocity. When jetting becomes the dominant mechanism, the dispersion changes from froth to spray. Prado et al. [*Chemical Engineering Progr.* **83**(3), p. 32, (1987)] showed the transition from froth to spray takes place gradually as jetting replaces bubbling in 45 to 70 percent of the tray holes.

Emulsion regime (Fig. 14-20b). At high liquid loads and relatively low gas loads, the high-velocity liquid bends the swarms of gas bubbles leaving the orifices, and tears them off, so most of the gas becomes emulsified as small bubbles within the liquid. The mixture behaves as a uniform two-phase fluid, which obeys the Francis weir formula [see the subsection "Pressure Drop" and Eq. (14-109) (*Hofhuis and Zuideweg, IChemE Symp. Ser.* **56**, p. 2.2/1 (1979); *Zuideweg, Int. Chem. Eng.* **26**(1), 1 (1986))]. In industrial practice, the emulsion regime is the most common in high-pressure and high-liquid-rate operation.

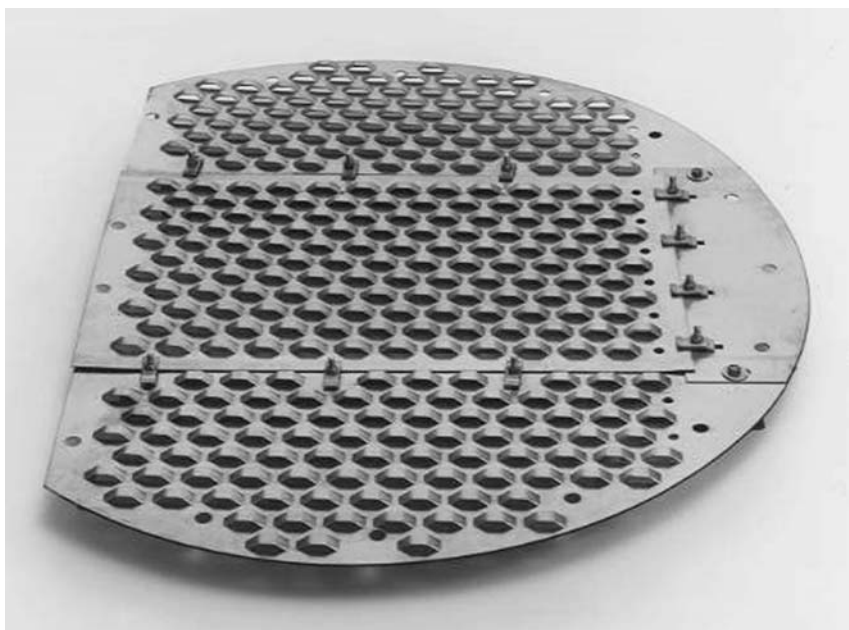
Spray regime (or drop regime; Fig. 14-20c). At high gas velocities and low liquid loads, the liquid pool on the tray floor is shallow and easily atomized by the high-velocity gas. The dispersion becomes a turbulent cloud of liquid droplets of various sizes that reside at high elevations above the tray and follow free trajectories. Some droplets are entrained to the tray above, while others fall back into the liquid pools and become reatomized. In contrast to the liquid-continuous froth and emulsion regimes, the phases are reversed in the spray regime: here the gas is the continuous phase, while the liquid is the dispersed phase.

The spray regime frequently occurs where gas velocities are high and liquid loads are low (e.g., vacuum and rectifying sections at low liquid loads).

Three-layered structure. Van Sinderen, Wijn, and Zanting [*Trans. IChemE*, **81**, Part A, p. 94 (January 2003)] postulate a tray dispersion consisting of a bottom liquid-rich layer where jets/bubbles form; an intermediate liquid-continuous froth layer where bubbles erupt, generating drops; and a top gas-continuous layer of drops. The intermediate layer that dampens the bubbles and



(a)



(b)



(c)

FIG. 14-18 Common tray types. (a) Sieve. (b) Fixed valve. (c) Moving valve with legs. [Part a, from Henry Z. Kister, *Chem. Eng.*, September 8, 1980; reprinted courtesy of Chemical Engineering. Part b, Courtesy of Sulzer Chemtech and Fractionation Research Inc. (FRI). Part c, courtesy of Koch-Glitsch LP.]

TABLE 14-5 Comparison of the Common Tray Types

	Sieve trays	Fixed valve tray	Moving valve tray
Capacity	High	High	High to very high
Efficiency	High	High	High
Turndown	About 2:1. Not generally suitable for operation under variable loads	About 2.5:1. Not generally suitable for operation under variable loads	About 4:1 to 5:1. Some special designs achieve 8:1 or more
Entrainment	Moderate	Moderate	Moderate
Pressure drop	Moderate	Moderate	Slightly higher
Cost	Low	Low	About 20 percent higher
Maintenance	Low	Low	Moderate
Fouling tendency	Low to very low	Low to very low	Moderate
Effects of corrosion	Low	Very low	Moderate
Main applications	(1) Most columns when turndown is not critical (2) High fouling and corrosion potential	(1) Most columns when turndown is not critical (2) High fouling and corrosion potential	(1) Most columns (2) Services where turndown is important

jets disappears at low liquid rates, and the drop layer approaches the tray floor, similar to the classic spray regime.

PRIMARY TRAY CONSIDERATIONS

Number of Passes Tray liquid may be split into two or more flow passes to reduce tray liquid load Q_L (Fig. 14-21). Each pass carries $1/N_p$ fraction of the total liquid load (e.g., $\frac{1}{4}$ in four-pass trays). Liquid in each pass reverses direction on alternate trays. Two-pass trays have perfect symmetry with full remixing in the center downcomers. Four-pass trays are symmetric along the centerline, but the side and central passes are nonsymmetric. Also, the center and off-center downcomers only partially remix the liquid, allowing any maldistribution to propagate. Maldistribution can cause major loss of efficiency and capacity in four-pass trays. Three-pass trays are even more prone to maldistribution due to their complete nonsymmetry. Most designers avoid three-pass trays altogether, jumping from two to four passes. Good practices for liquid and vapor balancing and for avoiding maldistribution in multipass trays were described by Pilling [*Chemical Engineering Progr.*, p. 22 (June 2005)], Bolles [*AIChE J.*, **22**(1), p. 153 (1976)], and Kister (*Distillation Operation*, McGraw-Hill, New York, 1990).

Common design practice is to minimize the number of passes, resorting to a larger number only when the liquid load exceeds 100 to 140 $\text{m}^3/(\text{h}\cdot\text{m})$ (11 to 15 gpm/in) of outlet weir length [*Davies and Gordon, Petro/Chem Eng.*, p. 228 (December 1961)]. Trays smaller than 1.5-m (5-ft) diameter seldom use more than a single pass; those with 1.5- to 3-m (5- to 10-ft) diameters seldom use more than two passes. Four-pass trays are common in high liquid services with towers larger than 5-m (16-ft) diameter.

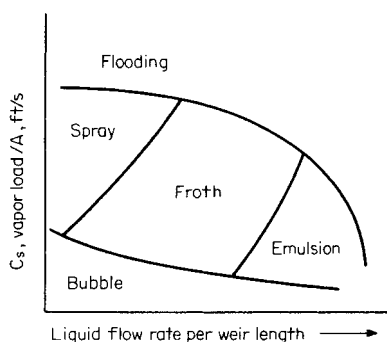


FIG. 14-19 The flow regime likely to exist on a distillation tray as a function of vapor and liquid loads. (From H. Z. Kister, *Distillation Design*, copyright ©1992 by McGraw-Hill; reprinted by permission.)

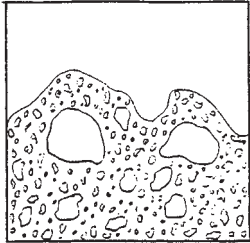
Tray Spacing Taller spacing between successive trays raises capacity, leading to a smaller tower diameter, but also raises tower height. There is an economic tradeoff between tower height and diameter. As long as the tradeoff exists, tray spacing has little effect on tower economics and is set to provide adequate access. In towers with larger than 1.5-m (5-ft) diameter, tray spacing is typically 600 mm (24 in), large enough to permit a worker to crawl between trays. In very large towers (>6-m or 20-ft diameter), tray spacings of 750 mm (30 in) are often used. In chemical towers (as distinct from petrochemical, refinery, and gas plants), 450 mm (18 in) has been a popular tray spacing. With towers smaller than 1.5 m (5 ft), tower walls are reachable from the manways, there is no need to crawl, and it becomes difficult to support thin and tall columns, so smaller tray spacing (typically 380 to 450 mm or 15 to 18 in) is favored. Towers taller than 50 m (160 ft) also favor smaller tray spacings (400 to 450 mm or 16 to 18 in). Finally, cryogenic towers enclosed in cold boxes favor very small spacings, as small as 150 to 200 mm (6 to 8 in), to minimize the size of the cold box.

More detailed considerations for setting tray spacing were discussed by Kister (*Distillation Operation*, McGraw-Hill, New York, 1990) and Mukherjee [*Chem. Eng.*, p. 53 (September 2005)].

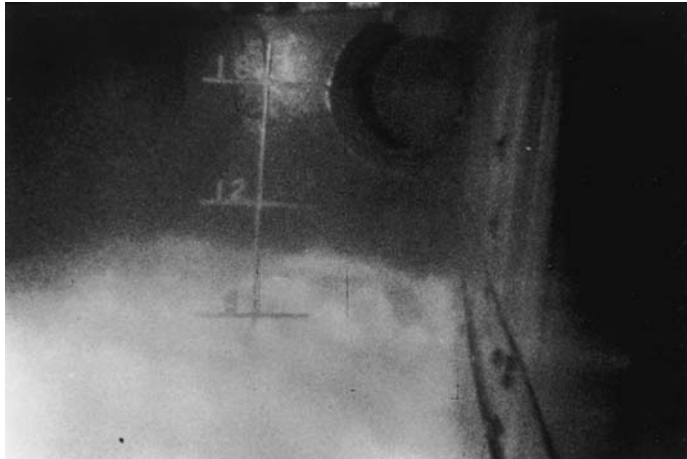
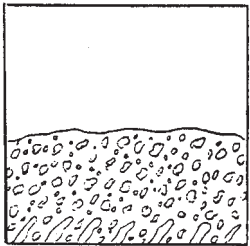
Outlet Weir The outlet weir should maintain a liquid level on the tray high enough to provide sufficient gas-liquid contact without causing excessive pressure drop, downcomer backup, or a capacity limitation. Weir heights are usually set at 40 to 80 mm (1.5 to 3 in). In this range, weir heights have little effect on distillation efficiency [Van Winkle, *Distillation*, McGraw-Hill, New York, 1967; Kreis and Raab, *ICHEME Symp. Ser.* **56**, p. 3.2/63 (1979)]. In operations where long residence times are necessary (e.g., chemical reaction, absorption, stripping) taller weirs do improve efficiency, and weirs 80 to 100 mm (3 to 4 in) are more common [Lockett, *Distillation Tray Fundamentals*, Cambridge University Press, Cambridge, England, 1986].

Adjustable weirs (Fig. 14-22a) are used to provide additional flexibility. They are uncommon with conventional trays, but are used with some proprietary trays. Swept-back weirs (Fig. 14-22b) are used to extend the effective length of side weirs, either to help balance liquid flows to nonsymmetric tray passes or/and to reduce the tray liquid loads. Picket fence weirs (Fig. 14-22c) are used to shorten the effective length of a weir, either to help balance multipass trays' liquid flows (they are used in center and off-center weirs) or to raise tray liquid load and prevent drying in low-liquid-load services. To be effective, the pickets need to be tall, typically around 300 to 400 mm (12 to 16 in) above the top of the weir. An excellent discussion of weir picketing practices was provided by Summers and Sloley (*Hydroc. Proc.*, p. 67, January 2007).

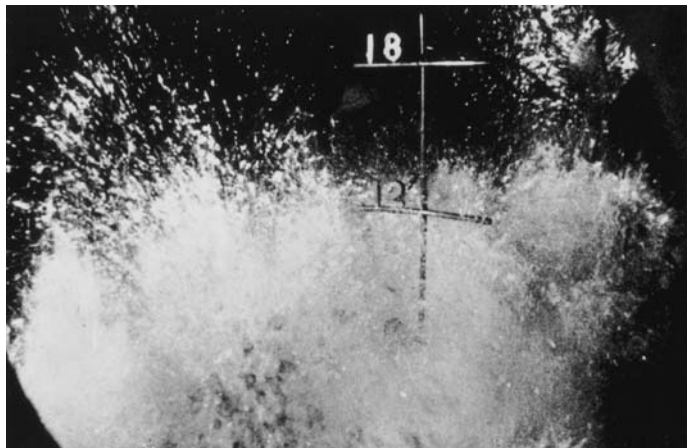
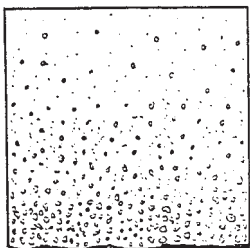
Downcomers A downcomer is the drainpipe of the tray. It conducts liquid from one tray to the tray below. The fluid entering the downcomer is far from pure liquid; it is essentially the froth on the tray, typically 20 to 30 percent liquid by volume, with the balance being gas. Due to the density difference, most of this gas disengages in the downcomer and vents back to the tray from the downcomer entrance. Some gas bubbles usually remain in the liquid even at the bottom of the downcomer, ending on the tray below [Lockett and Gharani, *ICHEME Symp. Ser.* **56**, p. 2.3/43 (1979)].



(a)



(b)



(c)

FIG. 14-20 Distillation flow regimes: schematics and photos. (a) Froth. (b) Emulsion. (c) Spray. [Schematics from H. Z. Kister, *Distillation Design*, copyright © 1992 by McGraw-Hill, Inc.; reprinted by permission. Photographs courtesy of Fractionation Research Inc. (FRI).]

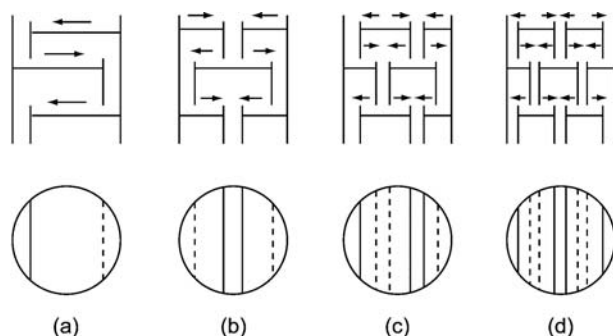


FIG. 14-21 Flow passes on trays. (a) Single-pass. (b) Two-pass. (c) Three-pass. (d) Four-pass.

The straight, segmental vertical downcomer (Fig. 14-23a) is the most common downcomer geometry. It is simple and inexpensive and gives good utilization of tower area for downflow. Circular downcomers (downpipes) (Fig. 14-23b), are cheaper, but poorly utilize tower area and are only suitable for very low liquid loads. Sloped downcomers (Fig. 14-23c, d) improve tower area utilization for downflow. They provide sufficient area and volume for gas-liquid disengagement at the top of the downcomer, gradually narrowing as the gas disengages, minimizing the loss of bubbling area at the foot of the downcomer. Sloped downcomers are invaluable when large downcomers are required such as at high liquid loads, high pressures, and foaming systems. Typical ratios of downcomer top to bottom areas are 1.5 to 2.

Antijump baffles (Fig. 14-24) are sometimes installed just above center and off-center downcomers of multipass trays to prevent liquid from one pass skipping across the downcomer onto the next pass. Such liquid jump adds to the liquid load on each pass, leading to premature flooding. These baffles are essential with proprietary trays that induce forward push (see below).

Clearance under the Downcomer Restricting the downcomer bottom opening prevents gas from the tray from rising up the downcomer and interfering with its liquid descent (*downcomer unsealing*). A common design practice makes the downcomer clearance 13 mm (0.5 in) lower than the outlet weir height (Fig. 14-25) to ensure submergence at all times [Davies and Gordon, *Petro/Chem Eng.*, p. 250 (November 1961)]. This practice is sound in the froth and emulsion regimes, where tray dispersions are liquid-continuous, but is ineffective in the spray regime where tray dispersions are gas-continuous and there is no submergence. Also, this practice can be unnecessarily restrictive at high liquid loads where high crests over the weirs sufficiently protect the downcomers from gas rise. Generally, downcomer clearances in the spray regime need to be smaller, while those in the emulsion regime can be larger, than those set by the above practice. Seal pans and inlet weirs are devices sometimes used to help with downcomer sealing while keeping downcomer clearances large. Details are in Kister's book (*Distillation Operation*, McGraw-Hill, New York, 1990).

Hole Sizes Small holes slightly enhance tray capacity when limited by entrainment flood. Reducing sieve hole diameters from 13 to 5 mm ($\frac{1}{2}$ to $\frac{3}{16}$ in) at a fixed hole area typically enhances capacity by 3 to 8 percent, more at low liquid loads. Small holes are effective for reducing entrainment and enhancing capacity in the spray regime ($Q_L < 20$ m³/hm of weir). Hole diameter has only a small effect on pressure drop, tray efficiency, and turndown.

On the debit side, the plugging tendency increases exponentially as hole diameters diminish. Smaller holes are also more prone to corrosion. While 5-mm ($\frac{3}{16}$ -in) holes easily plug even by scale and rust, 13-mm ($\frac{1}{2}$ -in) holes are quite robust and are therefore very common. The small holes are only used in clean, noncorrosive services. Holes smaller than 5 mm are usually avoided because they require drilling (larger holes are punched), which is much more expensive. For highly fouling services, 19- to 25-mm ($\frac{3}{4}$ - to 1-in) holes are preferred.

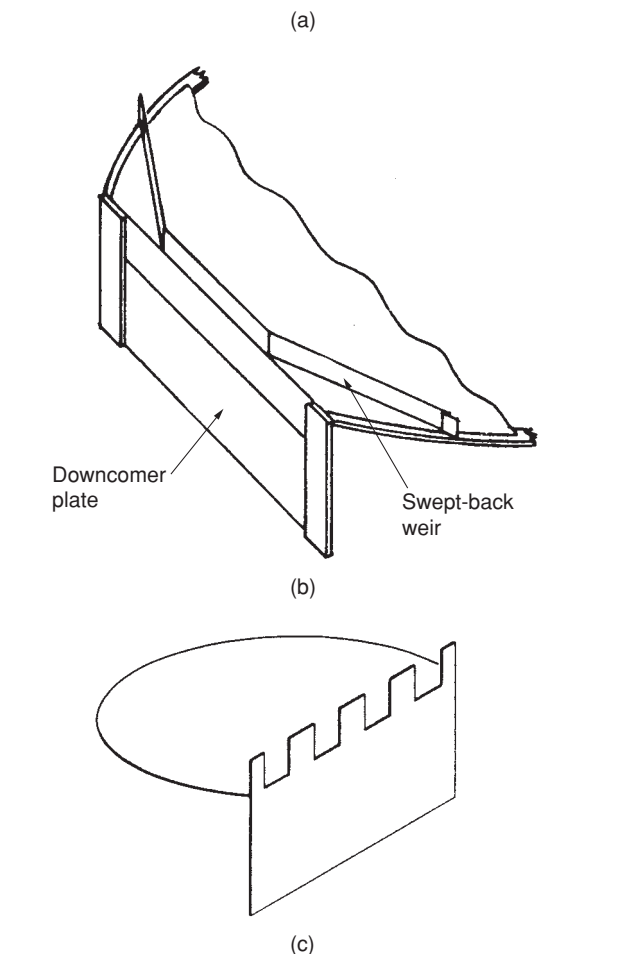
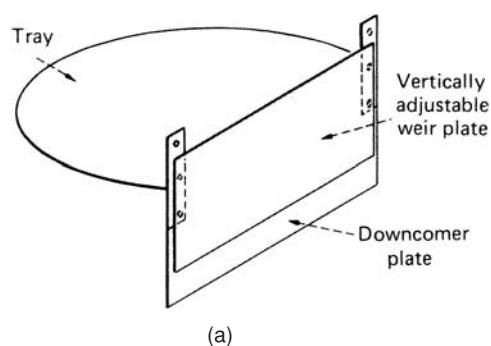


FIG. 14-22 Unique outlet weir types. (a) Adjustable. (b) Swept back. (c) Picket fence. (Parts a, c, from H. Z. Kister, *Distillation Operation*, copyright © 1990 by McGraw-Hill; reprinted by permission. Part b, courtesy of Koch-Clitsch LP.)

Similar considerations apply to fixed valves. Small fixed valves have a slight capacity advantage, but are far more prone to plugging than larger fixed valves.

For round moving valves, common orifice size is 39 mm ($1\frac{1}{2}$ in). The float opening is usually of the order of 8 to 10 mm (0.3 to 0.4 in).

In recent years there has been a trend toward minivalves, both fixed and moving. These are smaller and therefore give a slight capacity advantage while being more prone to plugging.

Fractional Hole Area Typical sieve and fixed valve tray hole areas are 8 to 12 percent of the bubbling areas. Smaller fractional hole

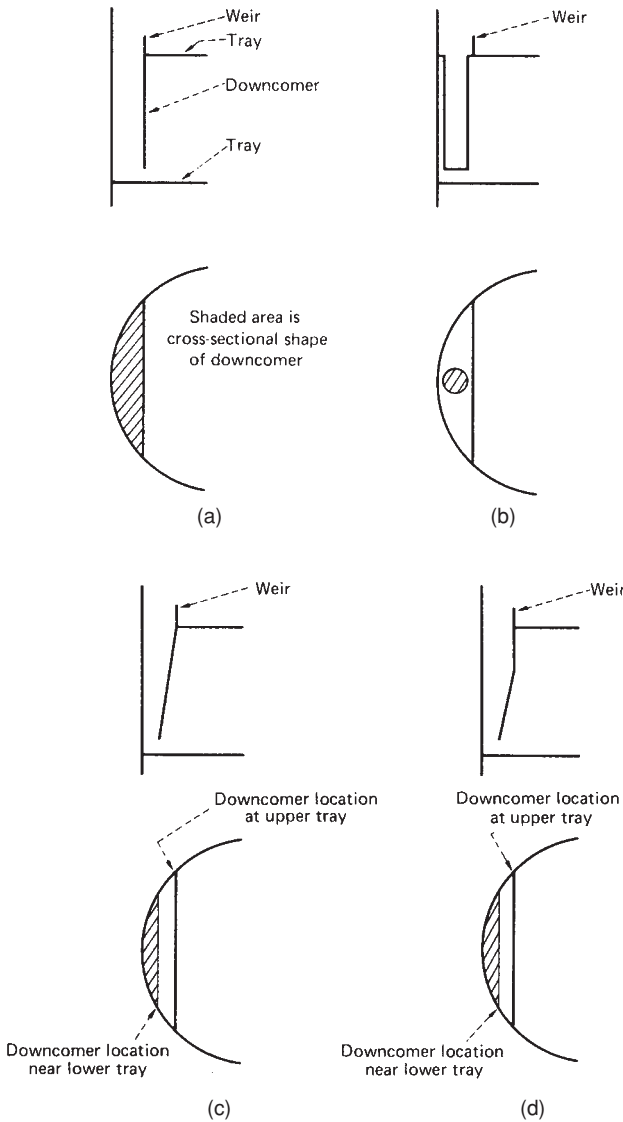


FIG. 14-23 Common downcomer types. (a) Segmental. (b) Circular. (c, d) Sloped. (From Henry Z. Kister, *Chem. Eng.*, December 29, 1980; reprinted courtesy of Chemical Engineering.)

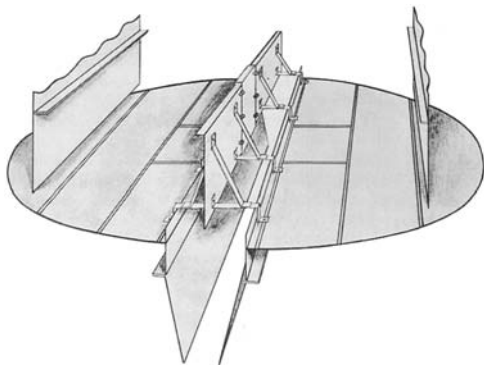


FIG. 14-24 Antijump baffle. (Reprinted courtesy of Koch-Glitsch LP.)

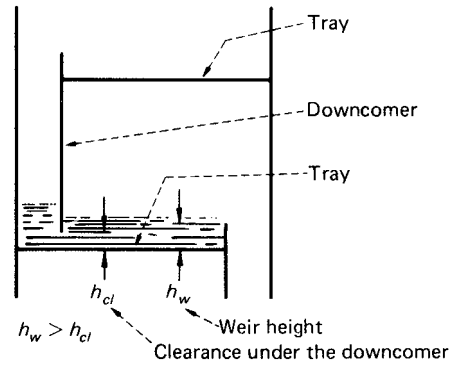


FIG. 14-25 A common design practice of ensuring a positive downcomer seal. (From Henry Z. Kister, *Chem. Eng.*, December 29, 1980; reprinted courtesy of Chemical Engineering.)

areas bring about a capacity reduction when limited by entrainment or downcomer backup flood or by excessive pressure drop. At above 12 percent of the bubbling areas, the capacity gains from higher hole areas become marginal while weeping and, at high liquid loads also channeling, escalate.

Typical open-slot areas for moving valve trays are 14 to 15 percent of the bubbling area. Here the higher hole areas can be afforded due to the high turndown of the valves.

Moving valves can have a sharp or a smooth ("venturi") orifice. The venturi valves have one-half the dry pressure drop of the sharp-orifice valves, but are far more prone to weeping and channeling than the sharp-orifice valves. Sharp orifices are almost always preferred.

Multipass Balancing There are two balancing philosophies: equal bubbling areas and equal flow path lengths. Equal bubbling areas means that all active area panels on Fig. 14-21d are of the same area, and each panel has the same hole (or open-slot) area. In a four-pass tray, one-quarter of the gas flows through each panel. To equalize the L/G ratio on each panel, the liquid needs to be split equally to each panel. Since the center weirs are longer than the side weirs, more liquid tends to flow toward the center weir. To equalize, side weirs are often swept back (Fig. 14-22b) while center weirs often contain picket fences (Fig. 14-22c).

The alternative philosophy (equal flow path lengths) provides more bubbling and perforation areas in the central panels of Fig. 14-21d and less in the side panels. To equalize the L/G ratio, less liquid needs to flow toward the sides, which is readily achieved, as the center weirs are naturally longer than the side weirs. Usually there is no need for swept-back weirs, and only minimal picket-fencing is required at the center weir.

Equal flow path panels are easier to fabricate and are cheaper, while equal bubbling areas have a robustness and reliability advantage due to the ease of equally splitting the fluids. The author had good experience with both when well-designed. Pass balancing is discussed in detail by Pilling [*Chem. Eng. Prog.*, p. 22 (June 2005)] and by Jaguste and Kelkar [*Hydroc. Proc.*, p. 85 (March 2006)].

TRAY CAPACITY ENHANCEMENT

High-capacity trays evolved from conventional trays by including one or more capacity enhancement features such as those discussed below. These features enhance not only the capacity but usually also the complexity and cost. These features have varying impact on the efficiency, turndown, plugging resistance, pressure drop, and reliability of the trays.

Truncated Downcomers/Forward Push Trays Truncated downcomers/forward push trays include the Nye™ Tray, Maxfrac™ (Fig. 14-26a), Triton™, and MVGT™. In all these, the downcomer from the tray above terminates about 100 to 150 mm (4 to 6 in) above the tray floor. Liquid from the downcomer issues via holes or slots,

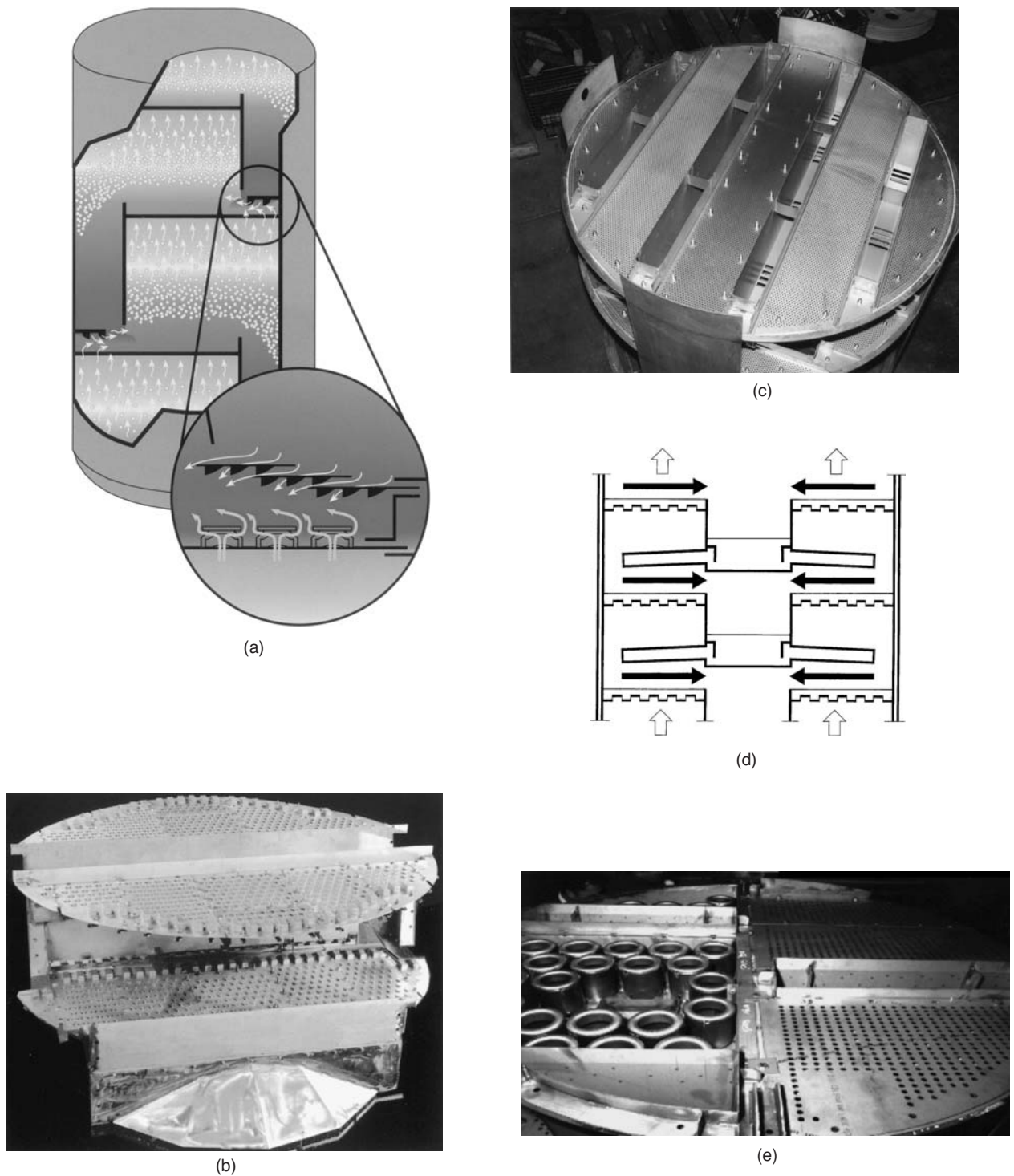


FIG. 14-26 Tray capacity enhancement. (a) Truncated downcomer/forward-push principle illustrated with a schematic of the Maxfrac™ tray. (b) High top-to-bottom area ratio illustrated with a two-pass Superfrac™ tray. Note the baffle in the front side downcomer that changes the side downcomer shape from segmental to multichordal. Also note the bubble promoters on the side of the upper tray and in the center of the lower tray, which give forward push to the tray liquid. (c) Top view of an MD™ tray with four downcomers. The decks are perforated. The holes in the downcomer lead the liquid to the active area of the tray below, which is rotated 90°. (d) Schematic of the Slit™ tray, type A, showing distribution pipes. Heavy arrows depict liquid movement; open arrows, gas movement. (e) The ConSep™ tray. The right-hand side shows sieve panels. On the left-hand side, these sieve panels were removed to permit viewing the contact cyclones that catch the liquid from the tray below. (Parts a, b, courtesy of Koch-Glitsch LP; part c, courtesy of UOP LLC; part d, courtesy of Kühni AG; part e, courtesy of Sulzer Chemtech Ltd. and Shell Global Solutions International BV.)

directed downward or in the direction of liquid flow. The tray floor under each downcomer is equipped with fixed valves or side perforations. Gas issuing in this region, typically 10 to 20 percent of the total tray gas, is deflected horizontally in the direction of liquid flow by the downcomer floor. This horizontal gas flow pushes liquid droplets toward the tower wall directly above the outlet downcomer. The tower wall catches this liquid, and directs it downward into the downcomer. This deentrains the gas space. In multipass trays, antijump baffles (Fig. 14-24), typically 300 mm or taller, are installed above center and off-center downcomers to catch the liquid and prevent its jumping from pass to pass. The rest of the tray features are similar to those of conventional trays. The tray floor may contain fixed valves, moving valves, or sieve holes.

Trays from this family are proprietary, and have been extensively used in the last two to three decades with great success. Compared to equivalent conventional trays, the truncated downcomer/forward push trays give about 8 to 12 percent more gas-handling capacity at much the same efficiency.

High Top-to-Bottom Downcomer Area and Forward Push Sloping downcomers from top to bottom raises the available tray bubbling area and, therefore, the gas-handling capacity (see "Downcomers"). As long as the ratio of top to bottom areas is not excessive, sloping does not lower downcomer capacity. Downcomer choke flood restricts the downcomer entrance, not exit, because there is much less gas at the downcomer bottom. However, a high top-to-bottom area ratio makes the downcomer bottom a very short chord, which makes distribution of liquid to the tray below difficult. To permit high top-to-bottom area ratios, some trays use a special structure (Fig. 14-26*b*) to change the downcomer shape from segmental to semiarc or multichordal. This high ratio of top to bottom areas, combined with forward push (above) imparted by bubble and directional fixed or moving valves, and sometimes directional baffles, is used in trays including Superfrac™ III (Fig. 14-26*b*) and IV and V-Grid Plus™. When the downcomer inlet areas are large, these trays typically gain 15 to 20 percent capacity compared to equivalent conventional trays at much the same efficiency. Trays from this family are proprietary, and have been used successfully for about a decade.

Large Number of Truncated Downcomers These include the MD™ (Fig. 14-26*c*) and Hi-Fi™ trays. The large number of downcomers raises the total weir length, moving tray operation toward the peak capacity point of 20 to 30 m³/hr (2 to 3 gpm/in) of outlet weir (see Fig. 14-29). The truncated downcomers extend about halfway to the tray below, discharging their liquid via holes or slots at the downcomer floor. The area directly under the downcomers is perforated or valved, and there is enough open height between the tray floor and the bottom of the downcomer for this perforated or valved area to be effective in enhancing the tray bubbling area.

Trays from this family are proprietary and have been successfully used for almost four decades. Their strength is in high-liquid-load services where reducing weir loads provides major capacity gains. Compared to conventional trays, they can gain as much as 20 to 30 percent capacity but at an efficiency loss. The efficiency loss is of the order of 10 to 20 percent due to the large reduction in flow path length (see "Efficiency"). When using these trays, the separation is maintained by either using more trays (typically at shorter spacing) or raising reflux and boilup. This lowers the net capacity gains to 10 to 20 percent above conventional trays. In some variations, forward push slots and antijump baffles are incorporated to enhance the capacity by another 10 percent.

Radial Trays These include the Slit™ tray and feature radial flow of liquid. In the efficiency-maximizing A variation (Fig. 14-26*d*), a multipipe distributor conducts liquid from each center downcomer to the periphery of the tray below, so liquid flow is from periphery to center on each tray. The capacity-maximizing B variation has central and peripheral (ring) downcomers on alternate trays, with liquid flow alternating from center-to-periphery to periphery-to-center on successive trays. The trays are arranged at small spacing (typically, 200 to 250 mm, or 8 to 10 in) and contain small fixed valves. Slit trays are used in chemical and pharmaceutical low-liquid-rate applications (<40 m³/hr or 4 gpm/in of outlet weir), typically at pressures ranging from moderate vacuum to slight superatmospheric.

Centrifugal Force Deentrainment These trays use a contact step similar to that in conventional trays, followed by a separation step that disentrains the tray dispersion by using centrifugal force. Separation of entrained liquid before the next tray allows very high gas velocities, as high as 25 percent above the system limit (see "System Limit"), to be achieved. The capacity of these trays can be 40 percent above that of conventional trays. The efficiency of these trays can be 10 to 20 percent less than that of conventional trays due to their typical short flow paths (see "Efficiency").

These trays include the Ultrafrac™, the ConSep™ (Fig. 14-26*e*), and the Swirl Tube™ trays. This technology has been sporadically used in eastern Europe for quite some time. It is just beginning to make inroads into distillation in the rest of the world, and looks very promising.

OTHER TRAY TYPES

Bubble-Cap Trays (Fig. 14-27*a*) These are flat perforated plates with risers (chimneylike pipes) around the holes, and caps in the form of inverted cups over the risers. The caps are usually (but not always) equipped with slots through which some of the gas comes out, and may be round or rectangular. Liquid and froth are trapped on the tray to a depth at least equal to the riser or weir height, giving the bubble-cap tray a unique ability to operate at very low gas and liquid rates.

The bubble-cap tray was the workhorse of distillation before the 1960s. It was superseded by the much cheaper (as much as 10 times) sieve and valve trays. Compared to the bubble-cap trays, sieve and valve trays also offer slightly higher capacity and efficiency and lower entrainment and pressure drop, and are less prone to corrosion and fouling. Today, bubble-cap trays are only used in special applications where liquid or gas rates are very low. A large amount of information on bubble-cap trays is documented in several texts (e.g., Bolles in B. D. Smith, *Design of Equilibrium Stage Processes*, McGraw-Hill, 1963; Bolles, *Pet. Proc.*, February 1956, p. 65; March 1956, p. 82; April 1956, p. 72; May 1956, p. 109; Ludwig, *Applied Process Design for Chemical and Petrochemical Plants*, 2d ed., vol. 2, Gulf Publishing, Houston, 1979).

Dual-Flow Trays These are sieve trays with no downcomers (Fig. 14-27*b*). Liquid continuously weeps through the holes, hence their low efficiency. At peak loads they are typically 5 to 10 percent less efficient than sieve or valve trays, but as the gas rate is reduced, the efficiency gap rapidly widens, giving poor turndown. The absence of downcomers gives dual-flow trays more area, and therefore greater capacity, less entrainment, and less pressure drop, than conventional trays. Their pressure drop is further reduced by their large fractional hole area (typically 18 to 30 percent of the tower area). However, this low pressure drop also renders dual-flow trays prone to gas and liquid maldistribution.

In general, gas and liquid flows pulsate, with a particular perforation passing both gas and liquid intermittently, but seldom simultaneously. In large-diameter (>2.5-m, or 8-ft) dual-flow trays, the pulsations sometimes develop into sloshing, instability, and vibrations. The Ripple Tray™ is a proprietary variation in which the tray floor is corrugated to minimize this instability.

With large holes (16 to 25 mm), these trays are some of the most fouling-resistant and corrosion-resistant devices in the industry. This defines their main application: highly fouling services, slurries, and corrosive services. Dual-flow trays are also the least expensive and easiest to install and maintain.

A wealth of information for the design and rating of dual-flow trays, much of it originating from FRI data, was published by Garcia and Fair [*Ind. Eng. Chem. Res.* **41**:1632 (2002)].

Baffle Trays Baffle trays ("shed decks," "shower decks") (Fig. 14-28*a*) are solid half-circle plates, sloped slightly in the direction of outlet flow, with weirs at the end. Gas contacts the liquid as it showers from the plate. This contact is inefficient, typically giving 30 to 40 percent of the efficiency of conventional trays. This limits their application mainly to heat-transfer and scrubbing services. The capacity is high and pressure drop is low due to the high open area (typically 50 percent of the tower cross-sectional area). Since there is not much

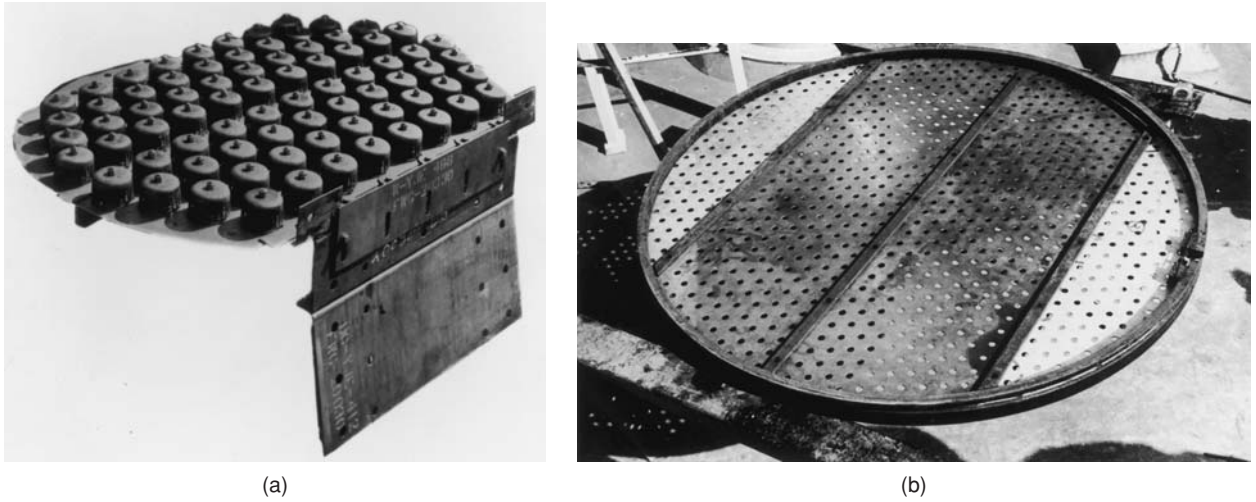


FIG. 14-27 Other trays. (a) Bubble-cap tray. (b) Dual-flow tray. [Part a, courtesy of Koch-Glitsch LP; part b, courtesy of Fractionation Research Inc. (FRI).]

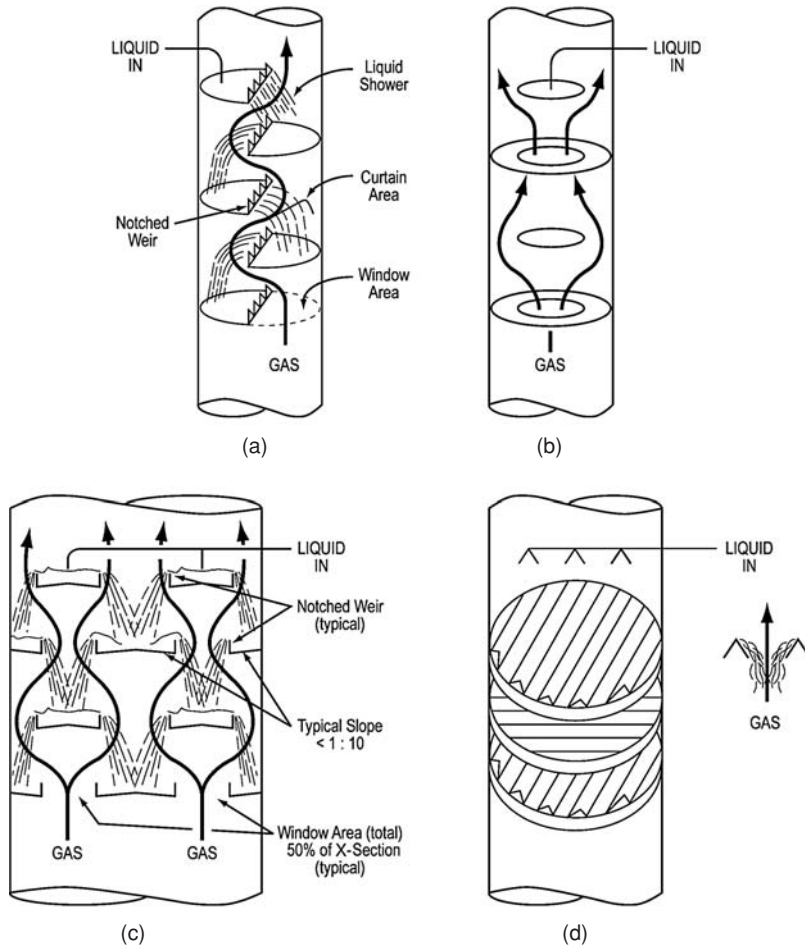


FIG. 14-28 Baffle tray variations. (a) Segmental. (b) Disk and doughnut. (c) Multipass. (d) Angle irons.

that can plug up, the baffle trays are perhaps the most fouling-resistant device in the industry, and their main application is in extremely fouling services. To be effective in these services, their liquid rate needs to exceed 20 m³/hm (2 gpm/in) of outlet weir and dead spots formed due to poor support design (Kister, *Distillation Troubleshooting*, Wiley, 2006) eliminated.

There are several geometric variations. The disk and doughnut trays (Fig. 14-28b) replace the half-circle segmental plates by alternate plates shaped as disks and doughnuts, each occupying about 50 percent of the tower cross-sectional area. In large towers, multipass baffle trays (Fig. 14-28c) are common. Another variation uses angle irons, with one layer oriented at 90° to the one below (Fig. 14-28d). Multipass baffle trays, as well as angle irons, require good liquid (and to a lesser extent, also good gas) distribution, as has been demonstrated from field heat-transfer measurements [Kister and Schwartz, *Oil & Gas J.*, p. 50 (May 20, 2002)]. Excellent overviews of the fundamentals and design of baffle trays were given by Fair and Lemieux [Fair, *Hydro. Proc.*, p. 75 (May 1993); Lemieux, *Hydroc. Proc.*, p. 106 (September 1983)]. Mass-transfer efficiency data with baffle trays by Fractionation Research Inc. (FRI) have been released and presented together with their correlation (Fair, Paper presented at the AIChE Annual Meeting, San Francisco, November 2003).

FLOODING

Flooding is by far the most common upper capacity limit of a distillation tray. Column diameter is set to ensure the column can achieve the required throughput without flooding. Towers are usually designed to operate at 80 to 90 percent of the flood limit.

Flooding is an excessive accumulation of liquid inside a column. Flood symptoms include a rapid rise in pressure drop (the accumulating liquid increases the liquid head on the trays), liquid carryover from the column top, reduction in bottom flow rate (the accumulating liquid does not reach the tower bottom), and instability (accumulation is non-steady-state). This liquid accumulation is generally induced by one of the following mechanisms.

Entrainment (Jet) Flooding Froth or spray height rises with gas velocity. As the froth or spray approaches the tray above, some of the liquid is aspirated into the tray above as entrainment. Upon a further increase in gas flow rate, massive entrainment of the froth or spray begins, causing liquid accumulation and flood on the tray above.

Entrainment flooding can be subclassified into *spray entrainment flooding* (common) and *froth entrainment flooding* (uncommon). Froth entrainment flooding occurs when the froth envelope approaches the tray above, and is therefore only encountered with small tray spacings (<450 mm or 18 in) in the froth regime. At larger (and often even lower) tray spacing, the froth breaks into spray well before the froth envelope approaches the tray above.

The entrainment flooding prediction methods described here are based primarily on spray entrainment flooding. Considerations unique to froth entrainment flooding can be found elsewhere (Kister, *Distillation Design*, McGraw-Hill, New York, 1992).

Spray Entrainment Flooding Prediction Most entrainment flooding prediction methods derive from the original work of Souders and Brown [*Ind. Eng. Chem.* **26**(1), 98 (1934)]. Souders and Brown theoretically analyzed entrainment flooding in terms of droplet settling velocity. Flooding occurs when the upward vapor velocity is high enough to suspend a liquid droplet, giving

$$C_{SB} = u_{s,\text{flood}} \sqrt{\frac{\rho_C}{\rho_L - \rho_C}} \quad (14-80)$$

The Souders and Brown constant C_{SB} is the C -factor [Eq. (14-77)] at the entrainment flood point. Most modern entrainment flooding correlations retain the Souders and Brown equation (14-80) as the basis, but depart from the notion that C_{SB} is a constant. Instead, they express C_{SB} as a weak function of several variables, which differ from one correlation to another. Depending on the correlation, C_{SB} and $u_{s,\text{flood}}$ are based on either the net area A_N or on the bubbling area A_B .

The constant C_{SB} is roughly proportional to the tray spacing to a power of 0.5 to 0.6 (Kister, *Distillation Design*, McGraw-Hill, New

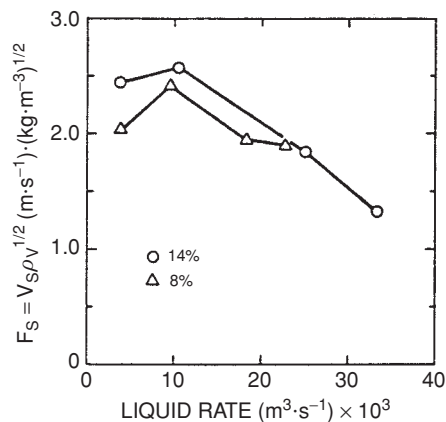


FIG. 14-29 Effect of liquid rate and fractional hole area on flood capacity. FRI sieve tray test data, cyclohexane/n-heptane, 165 kPa (24 psia), $D_T = 1.2$ m (4 ft), $S = 610$ mm (24 in), $h_w = 51$ mm (2 in), $d_H = 12.7$ mm (0.5 in), straight downcomers, $A_D/A_T = 0.13$. (From T. Yanagi and M. Sakata, *Ind. Eng. Chem. Proc. Des. Dev.* **21**, 712; copyright © 1982, American Chemical Society, reprinted by permission.)

York, 1992). Figure 14-29 demonstrates the effect of liquid rate and fractional hole area on C_{SB} . As liquid load increases, C_{SB} first increases, then peaks, and finally declines. Some interpret the peak as the transition from the froth to spray regime [Porter and Jenkins, *I. Chem. E. Symp. Ser.* **56**, Summary Paper, London (1979)]. C_{SB} increases slightly with fractional hole area at lower liquid rates, but there is little effect of fractional hole area on C_{SB} at high liquid rates. C_{SB} slightly increases as hole diameter is reduced.

For sieve trays, the entrainment flood point can be predicted by using the method by Kister and Haas [*Chem. Eng. Progr.*, **86**(9), 63 (1990)]. The method is said to reproduce a large database of measured flood points to within ± 15 percent. $C_{SB,\text{flood}}$ is based on the net area. The equation is

$$C_{SB,\text{flood}} = 0.0277(d_H^2 \sigma / \rho_L)^{0.125} (\rho_C / \rho_L)^{0.1} (TS/h_{ct})^{0.5} \quad (14-81)$$

where d_H = hole diameter, mm

σ = surface tension, mN/m (dyn/cm)

ρ_C, ρ_L = vapor and liquid densities, kg/m³

TS = tray spacing, mm

h_{ct} = clear liquid height at the froth-to-spray transition, mm; obtained from:

$$h_{ct} = h_{ct,H_2O} (996/\rho_L)^{0.5(1-n)} \quad (14-82)$$

$$h_{ct,H_2O} = \frac{0.497 A_f^{-0.791} d_H^{0.833}}{1 + 0.013 Q_L^{-0.59} A_f^{-1.79}} \quad (14-83)$$

$$n = 0.00091 d_H / A_f \quad (14-84)$$

In Eq. (14-83), Q_L = m³ liquid downflow/(h-m weir length) and A_f = fractional hole area based on active ("bubbling") area; for instance, $A_f = A_B/A_A$.

The Kister and Haas method can also be applied to valve trays, but the additional approximations reduce its data prediction accuracy for valve trays to within ± 20 percent. For valve trays, adaptations of Eqs. (14-81) to (14-84) are required:

$$d_h = \frac{4 \times (\text{area of opening of one fully open valve})}{\text{wetted perimeter of opening of one fully open valve}} \quad (14-85)$$

$$A_f = \frac{\text{no. valves} \times (\text{area of opening of one fully open valve})}{\text{active (bubbling) area}} \quad (14-86)$$

A correlation for valve tray entrainment flooding that has gained respect and popularity throughout the industry is the Glitsch "Equation 13" (Glitsch, Inc., *Ballast Tray Design Manual*, 6th ed., 1993;

available from Koch-Glitsch, Wichita, Kans.). This equation has been applied successfully for valve trays from different manufacturers, as well as for sieve trays with large fractional hole areas (12 to 15 percent). With tray spacings of 600 mm and higher, its flood prediction accuracy for valve trays has generally been within ±10 percent in the author's experience. The Glitsch correlation is

$$\frac{\% \text{ flood}}{100} = \frac{C_B}{CAF} + 1.359 \frac{Q \text{ FPL}}{A_B CAF} \tag{14-87}$$

where

$$CAF = 0.3048 CAF_0 SF \tag{14-88}$$

C_B is the operating C -factor based on the bubbling area, m/s; Q is the liquid flow rate, m³/s; A_B is the bubbling area, m²; FPL is the flow path length, m, i.e., the horizontal distance between the inlet downcomer and the outlet weir. The flow path length becomes shorter as the number of passes increases. CAF_0 and CAF are the flood C -factors. CAF_0 is obtained from Fig. 14-30 in English units (ft/s). Equation (14-88) converts CAF_0 to the metric CAF (m/s), and corrects it by using a system factor SF . Values of SF are given in Table 14-9.

The Fair correlation [*Pet/Chem Eng*, 33(10), 45 (September 1961)] for decades has been the standard of the industry for entrainment flood prediction. It uses a plot (Fig. 14-31) of surface-tension-corrected Souders and Brown flood factor C_{SB} against the dimensionless flow parameter shown in Fig. 14-31. The flow parameter represents a ratio of liquid to vapor kinetic energies:

$$F_{LG} = \frac{L}{G} \left(\frac{\rho_C}{\rho_L} \right)^{0.5} \tag{14-89}$$

Low values of F_{LG} indicate vacuum operation, high values indicate operation at higher pressures or at high liquid/vapor loadings. The liquid/gas ratio L/G is based on mass flow rates. For multipass trays, the ratio needs to be divided by the number of passes. The strength of the correlation is at the lower flow parameters. At higher flow parameters (high L/G ratios, high pressures, emulsion flow), Fig. 14-31 gives excessively conservative predictions, with the low values of C_{sb} to the right likely to result from downcomer flow restrictions rather than excessive entrainment. The curves may be expressed in equation form as [Lygeros and Magoulas, *Hydrocarbon Proc.* 65(12), 43 (1986)]:

$$C_{sbf} = 0.0105 + 8.127(10^{-4})(TS^{0.755}) \exp[-1.463 F_{LG}^{0.842}] \tag{14-90}$$

where TS = plate spacing, mm.

Figure 14-31 or Eq. (14-90) may be used for sieve, valve, or bubble-cap trays. The value of the capacity parameter (ordinate term in Fig. 14-31) may be used to calculate the maximum allowable vapor velocity through the net area of the plate:

$$U_{nf} = C_{sbf} \left(\frac{\sigma}{20} \right)^{0.2} \left(\frac{\rho_L - \rho_g}{\rho_g} \right)^{0.5} \tag{14-91}$$

where U_{nf} = gas velocity through net area at flood, m/s

C_{sbf} = capacity parameter corrected for surface tension, m/s

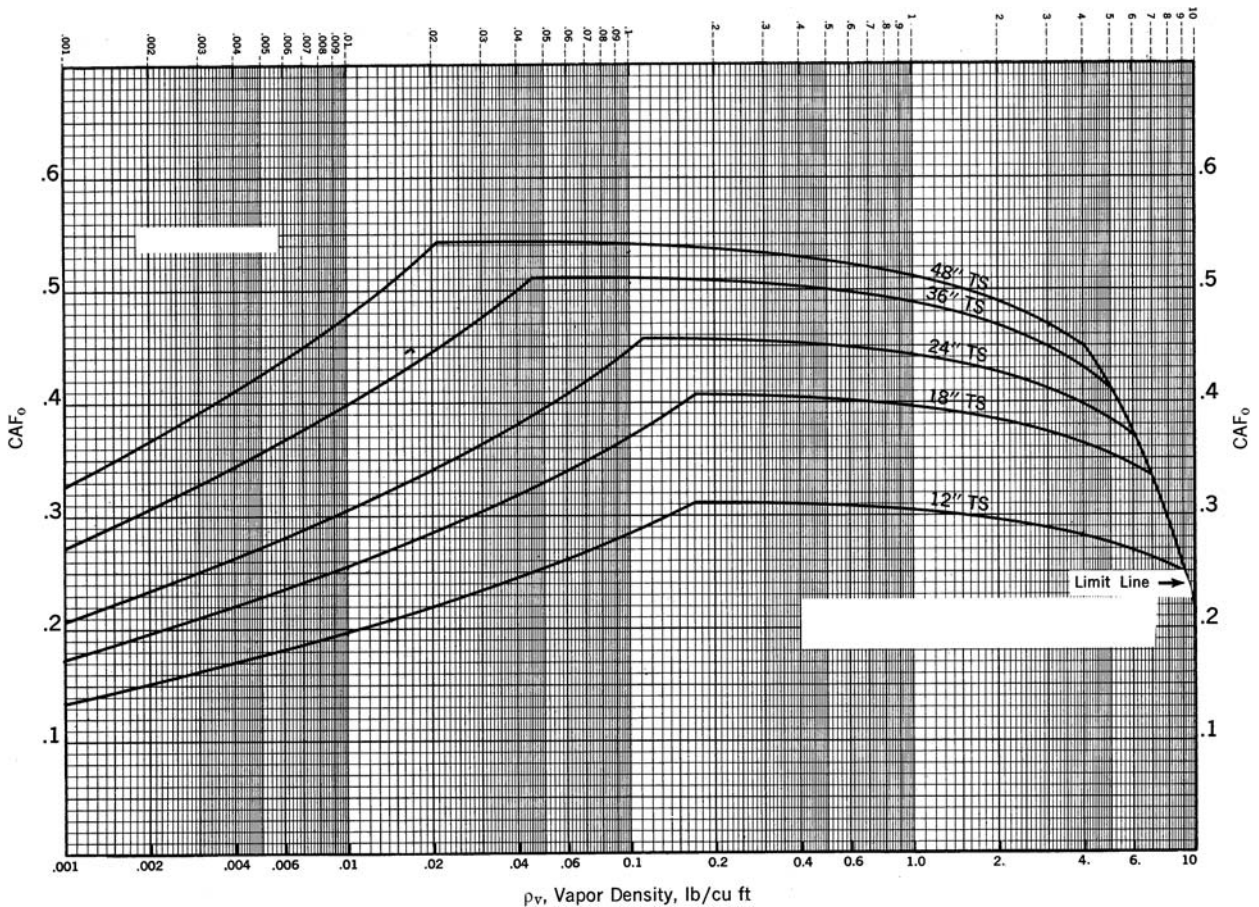


FIG. 14-30 Flood capacity of moving valve trays. (Courtesy of Koch-Glitch LP.)

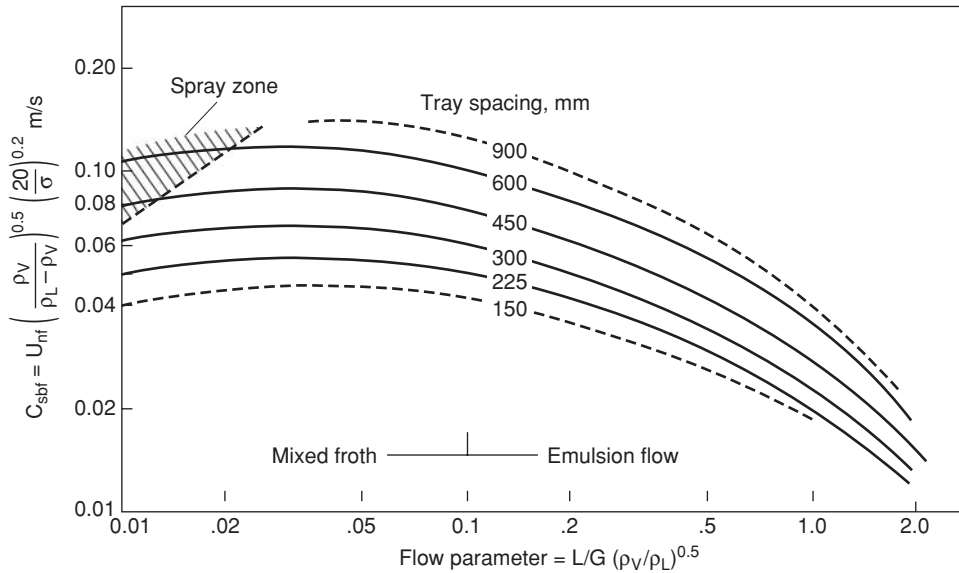


FIG. 14-31 Fair's entrainment flooding correlation for columns with crossflow trays (sieve, valve, bubble-cap). [Fair, *Pet/Chem Eng* 33(10), 45 (September 1961).]

σ = liquid surface tension, mN/m (dyn/cm)
 ρ_L = liquid density, kg/m³
 ρ_G = gas density, kg/m³

The application of the correlation is subject to the following restrictions:

1. System is low or nonfoaming.
2. Weir height is less than 15 percent of tray spacing.
3. Sieve-tray perforations are 13 mm (1/2 in) or less in diameter.
4. Ratio of slot (bubble cap), perforation (sieve), or full valve opening (valve plate) area A_h to active area A_a is 0.1 or greater. Otherwise the value of U_{nf} obtained from Fig. 14-31 should be corrected:

A_h/A_a	$U_{nf}/U_{nf, Fig. 14-31}$
0.10	1.00
0.08	0.90
0.06	0.80

where A_h = total slot, perforated, or open-valve area on tray.

Example 9: Flooding of a Distillation Tray An available sieve tray column of 2.5-m diameter is being considered for an ethylbenzene/styrene separation. An evaluation of loading at the top tray will be made. Key dimensions of the single-pass tray are:

Column cross section, m ²	4.91
Downcomer area, m ²	0.25
Net area, m ²	4.66
Active area, m ²	4.41
Hole area, m ²	0.617
Hole diameter, mm	4.76
Weir length, m	1.50
Weir height, mm	38
Tray spacing, mm	500

Conditions and properties at the top tray are:

Temperature, °C	78
Pressure, torr	100
Vapor flow, kg/h	25,500
Vapor density, kg/m ³	0.481
Liquid flow, kg/h	22,000
Liquid density, kg/m ³	841
Surface tension, mN/m	25

Solution. The method of Kister and Haas gives:

$$Q_L = \frac{22,000}{841 \times 1.50} = 17.44 \text{ m}^3/\text{h-m weir}$$

$$A_j = \frac{0.617}{4.41} = 0.14$$

By Eq. (14-83), $h_{et, H_2O} = 7.98 \text{ mm}$

$$\text{Eq. (14-84): } n = 0.0309$$

$$\text{Eq. (14-82): } h_{et} = 8.66 \text{ mm}$$

Finally, by Eq. (14-81),

$$C_{SB, flood} = 0.0277[(4.76^2)(25/841)]^{0.125} \times (0.481/841)^{0.1}(500/8.66)^{0.5} = 0.0947 \text{ m/s}$$

Alternatively, applying the Fair correlation:

The flow parameter $F_{LG} = 0.021$ [Eq. (14-89)]. From Fig. 14-31, $C_{sbf} = 0.095 \text{ m/s}$. Then, based on the net area,

$$C_{SB} = 0.095(25/20)^{0.2} = 0.0993 \text{ m/s}$$

about 5 percent higher than the answer obtained from Kister and Haas.

For the design condition, the C -factor based on the net area is

$$C = \frac{25,500}{3600(0.481)(4.66)} \sqrt{\frac{0.481}{841 - 0.481}} = 0.0756 \text{ m/s}$$

or about 80 percent of flood. The proposed column is entirely adequate for the service required.

System Limit (Ultimate Capacity) This limit is discussed later under "System Limit."

Downcomer Backup Flooding Aerated liquid backs up in the downcomer because of tray pressure drop, liquid height on the tray, and frictional losses in the downcomer apron (Fig. 14-32). All these increase with increasing liquid rate. Tray pressure drop also increases as the gas rate rises. When the backup of aerated liquid exceeds the tray spacing, liquid accumulates on the tray above, causing downcomer backup flooding.

upflow are greatly reduced. With sloped downcomers, the downcomer bottom area is normally set at 50 to 60 percent of the top downcomer area. This taper is small enough to keep the downcomer top area the prime choke variable.

There is no satisfactory published correlation for downcomer choke. The best that can be done in the absence of data or correlation is to apply the criteria for maximum velocity of clear liquid at the downcomer entrance. Kister (*Distillation Operation*, McGraw-Hill, New York, 1990) surveyed the multitude of published criteria for maximum downcomer velocity and incorporated them into a single set of guidelines (Table 14-7). The values for 30-in spacing were revised to reflect the author's recent experiences. The values given in Table 14-7 are not conservative. For a conservative design, multiply the values from Table 14-7 by a safety factor of 0.75. For very highly foaming systems, where antifoam application is undesirable, there are benefits for reducing downcomer design velocities down to 0.1 to 0.15 ft/s.

Another criterion sometimes used is to provide sufficient residence time in the downcomer to allow adequate disengagement of gas from the descending liquid, so that the liquid is relatively gas-free by the time it enters the tray below. Inadequate removal of gas from the liquid may choke the downcomer. Kister (loc. cit.) reviewed various published criteria for downcomer residence times and recommended those by Bolles (private communication, 1977) and Erbar and Maddox (Maddox, *Process Engineer's Absorption Pocket Handbook*, Gulf Publishing, Houston, 1985). Both sets of guidelines are similar and are summarized in Table 14-8. The residence times in Table 14-8 are *apparent residence times*, defined as the ratio of the total downcomer volume to the clear liquid flow in the downcomer.

As a segmental downcomer becomes smaller, its width decreases faster than its length, turning the downcomer into a long, narrow slot. This geometry increases the resistance to liquid downflow and to the upflow of disengaging gas. Small downcomers are also extremely sensitive to foaming, fouling, construction tolerances, and the introduction of debris. Generally, segmental downcomers smaller than 5 percent of the column cross-sectional area should be avoided. Additional discussion of small downcomers is available (Kister, *Distillation Operation*, McGraw-Hill, New York, 1990).

Derating ("System") Factors With certain systems, traditional flooding equations consistently give optimistic predictions. To allow for this discrepancy, an empirical derating or system factor ($SF < 1.0$) is applied. To obtain the actual or derated flood load, the flood gas load (entrainment flooding) or flood liquid load (downcomer choke) obtained from the traditional equations is multiplied by the derating factor. In the case of downcomer backup flood, the froth height from the traditional flood equation is divided by the derating factor.

Derating factors are vaguely related to the foaming tendency, but are also applied to nonfoaming systems where standard flooding equations consistently predict too high. Sometimes, derating factors are used solely as overdesign factors. Brierley (*Chem. Eng. Prog.*, July 1994, p. 68) states that some derating factors actually evolved from plant misoperation or from misinterpretation of plant data. Kister (loc. cit.) compiled the derating factors found in the literature into Table 14-9.

The application of derating factors is fraught with inconsistent practices and confusion. Caution is required. The following need to be carefully specified:

1. The flooding mechanism to which the derating factor applies (entrainment, downcomer backup, downcomer choke, or all these) must be specified.

2. Avoiding double derating. For instance, the values in Table 14-9 may apply with Eq. (14-81) because Eq. (14-81) does not take foaminess into account. However, they will double-derate a flood calculation that is made with a correlation or criteria that already take foaminess into account, such as the criteria for downcomer choke in Tables 14-7 and 14-8. Similarly, two different factors from Table 14-9 may apply to a single system; only one should be used.

3. Derating factors vary from source to source, and may depend on the correlation used as well as the system. For instance, some caustic wash applications have a track record of foaming more severely than other caustic wash applications (see note in Table 14-9). The derating factors in Table 14-9 are a useful guide, but are far from absolute.

ENTRAINMENT

Entrainment (Fig. 14-33) is liquid transported by the gas to the tray above. As the lower tray liquid is richer with the less-volatile components, entrainment counteracts the mass-transfer process, reducing tray efficiency. At times entrainment may transport nonvolatile impurities upward to contaminate the tower overhead product, or damage rotating machinery located in the path of the overhead gas.

Effect of Gas Velocity Entrainment increases with gas velocity to a high power. Generally, smaller powers, indicative of a relatively gradual change, are typical of low-pressure systems. Higher powers, which indicate a steep change, are typical of high-pressure systems.

Due to the steep change of entrainment with gas velocity at high pressure, the gas velocity at which entrainment becomes significant tends to coincide with the flood point. At low pressure, the rate of change of entrainment with gas velocity is much slower, and entrainment can be significant even if the tray is operating well below the flood point. For this reason, excessive entrainment is a common problem in low-pressure and vacuum systems, but is seldom troublesome with high-pressure systems. If encountered at high pressure, entrainment usually indicates flooding or abnormality.

Effect of Liquid Rate As the liquid rate is raised at constant gas rate, entrainment first diminishes, then passes through a minimum, and finally increases [Sakata and Yanagi, *I. Chem. E. Symp. Ser.* **56**, 3.2/21 (1979); Porter and Jenkins, *I. Chem. E. Symp. Ser.* **56**, Summary Paper, 1979; Friend, Lemieux, and Schreiner, *Chem. Eng.*, October 31, 1960, p. 101]. The entrainment minima coincide with the maxima in plots of entrainment flood F -factor against liquid load (Fig. 14-29). At the low liquid loads (spray regime), an increase in liquid load suppresses atomization, drop formation, and consequently entrainment. At higher liquid loads, an increase in liquid load reduces the effective tray spacing, thereby increasing entrainment. The entrainment minima have been interpreted by many workers as the tray dispersion change from predominantly spray to the froth regime [Porter and Jenkins, loc. cit.; Kister and Haas, *I. Chem. E. Symp. Ser.* **104**, p. A483 (1987)].

Effect of Other Variables Entrainment diminishes with higher tray spacing and increases with hole diameter [Kister and Haas, *I.*

TABLE 14-7 Maximum Downcomer Velocities

Foaming tendency	Example	Clear liquid velocity in downcomer, ft/s		
		18-in spacing	24-in spacing	30-in spacing
Low	Low-pressure (<100 psia) light hydrocarbons, stabilizers, air-water simulators	0.4-0.5	0.5-0.6	0.5-0.6*
Medium	Oil systems, crude oil distillation, absorbers, midpressure (100-300 psia) hydrocarbons	0.3-0.4	0.4-0.5	0.4-0.5*
High	Amines, glycerine, glycols, high-pressure (>300 psia) light hydrocarbons	0.2-0.25	0.2-0.25	0.2-0.3

*Revised from previous versions.

To convert from ft/s to m/s, multiply by 0.3048; from in to mm, multiply by 25.4; from psia to bar, multiply by 0.0689.

SOURCE: From H. Z. Kister, *Distillation Operation*, copyright 1990 by McGraw-Hill, Inc.; reprinted by permission.

TABLE 14-8 Recommended Minimum Residence Time in the Downcomer

Foaming tendency	Example	Residence time, s
Low	Low-molecular-weight hydrocarbons,° alcohols	3
Medium	Medium-molecular-weight hydrocarbons	4
High	Mineral oil absorbers	5
Very high	Amines and glycols	7

°The author believes that low-molecular-weight hydrocarbons refers to light hydrocarbons at atmospheric conditions or under vacuum. The foaming tendency of light-hydrocarbon distillation at medium pressure [>7 bar (100 psia)] is medium; at high pressure [>21 bar (300 psia)], it is high.

SOURCE: W. L. Bolles (Monsanto Company), private communication, 1977.

Chem. E. Symp. Ser. **104**, p. A483 (1987); *Ind. Eng. Chem. Res.* **27**, p. 2331 (1988); Lemieux and Scotti, *Chem. Eng. Prog.* **65**(3), 52 (1969)]. The hole diameter effect is large in the spray regime but small in the froth regime. In the spray regime, entrainment also increases as the fractional hole area is lowered, but this variable has little effect in the froth regime [Yanagi and Sakata, *Ind. Eng. Chem. Proc. Des. Dev.* **21**, 712 (1982); and Kister and Haas, loc. cit.].

Entrainment Prediction For spray regime entrainment, the Kister and Haas correlation was shown to give good predictions to a wide commercial and pilot-scale data bank [*I. Chem. E. Symp. Ser.* **104**, A483 (1987)]. The correlation is

$$E_s = 4.742^{(10/\bar{\sigma})^{1.54}} \chi^{(10/\bar{\sigma})} \quad (14-94)$$

$$\text{where } \chi = 872 \left(\frac{u_B h_{L1}}{\sqrt{d_H S}} \right)^4 \left(\frac{\rho_G}{Q_L \rho_L} \right) \left(\frac{\rho_L - \rho_G}{\sigma} \right)^{0.25} \quad (14-95)$$

$$\text{and } h_{L1} = \frac{h_{ct}}{1 + 0.00262 h_w} \quad (14-96)$$

The terms in Eqs. (14-94) through (14-96) are in the metric units described in the Nomenclature table at the beginning of this section.

The recommended range of application of the correlation is given in Table 14-10. The clear liquid height at the froth-to-spray transition h_{ct} is calculated using the corrected Jeronimo and Sawistowski [*Trans. Inst. Chem. Engrs.* **51**, 265 (1973)] correlation as per Eqs. (14-82) to (14-84).

For decades, the Fair correlation [*Pet/Chem. Eng.* **33**(10), 45 (September 1961)] has been used for entrainment prediction. In the spray regime the Kister and Haas correlation was shown to be more accurate [Koziol and Mackowiak, *Chem. Eng. Process.*, **27**, p. 145 (1990)]. In the froth regime, the Kister and Haas correlation does not apply, and Fair's correlation remains the standard of the industry. Fair's correlation (Fig. 14-34) predicts entrainment in terms of the flow parameter [Eq. (14-89)] and the ratio of gas velocity to entrainment flooding gas velocity. The ordinate values Ψ are fractions of gross liquid downflow, defined as follows:

$$\Psi = \frac{e}{L_m + e} \quad (14-97)$$

where e = absolute entrainment of liquid, mol/time

L_m = liquid downflow rate without entrainment, mol/time

Figure 14-34 also accepts the validity of the Colburn equation [*Ind. Eng. Chem.*, **28**, 526 (1936)] for the effect of entrainment on efficiency:

$$\frac{E_a}{E_{mc}} = \frac{1}{1 + E_{mc}[\Psi/(1 - \Psi)]} \quad (14-98)$$

where E_{mc} = Murphree vapor efficiency [see Eq. (14-134)]

E_a = Murphree vapor efficiency, corrected for recycle of liquid entrainment

The Colburn equation is based on complete mixing on the tray. For incomplete mixing, e.g., liquid approaching plug flow on the tray, Rahman and Lockett [*I. Chem. E. Symp. Ser. No. 61*, 111 (1981)] and Lockett et al. [*Chem. Eng. Sci.*, **38**, 661 (1983)] have provided corrections.

TABLE 14-9 Derating ("System") Factors

System	Factor	Reference	Notes
Nonfoaming regular systems	1.0	1-4	
High pressure ($\rho_G > 1.8$ lb/ft ³)	2.94/ $\rho_G^{0.32}$	2	Do not double-derate.
Low-foaming			
Depropanizers	0.9	4	
H ₂ S strippers	0.9	3, 4	
	0.85	2	
Fluorine systems (freon, BF ₃)	0.9	1, 4	
Hot carbonate regenerators	0.9	2, 4	
Moderate-foaming			
Deethanizers			
Absorbing type, top section	0.85	1-4	
Absorbing type, bottom section	1.0	3	
	0.85	1, 2, 4	
Refrigerated type, top section	0.85	4	
	0.8	3	
Refrigerated type, bottom section	1.0	1, 3	
	0.85	4	
Demethanizers			
Absorbing type, top section	0.85	1-3	
Absorbing type, bottom section	1.0	3	
	0.85	1, 2	
Refrigerated type, top section	0.8	3	
Refrigerated type, bottom section	1.0	3	
Oil absorbers			
Above 0°F	0.85	1-4	Ref. 2 proposes these
Below 0°F	0.95	3	for "absorbers" rather
	0.85	1, 4	than "oil absorbers."
	0.8	2	
Crude towers	1.0	3	
	0.85	4	
Crude vacuum towers	1.0	3	
	0.85	2	
Furfural refining towers	0.85	2	
	0.8	4	
Sulfolane systems	1.0	3	
	0.85	4	
Amine regenerators	0.85	1-4	
Glycol regenerators	0.85	1, 4	
	0.8	3	
	0.65	2	
Hot carbonate absorbers	0.85	1, 4	
Caustic wash	0.65	2	The author suspects that
			this low factor refers
			only to some caustic
			wash applications but
			not to others.
Heavy-foaming			
Amine absorbers	0.8	2	
	0.75	3, 4	
	0.73	1	
Glycol contactors	0.73	1	Ref. 2 recommends
	0.65	3, 4	0.65 for glycol
	0.50	2	contactors in glycol
			synthesis gas service,
			0.5 for others.
Sour water strippers	0.5-0.7	3	
	0.6	2	
Oil reclaimers	0.7	2	
MEK units	0.6	1, 4	
Stable foam			
Caustic regenerators	0.6	2	
	0.3	1, 4	
Alcohol synthesis absorbers	0.35	2, 4	

References:

- Glitsch, Inc., *Ballast Tray Design Manual*, Bulletin 4900, 6th ed., 1993. Available from Koch-Glitsch, Wichita, Kans.
 - Koch Engineering Co., Inc., *Design Manual—Flexitray*, Bulletin 960-1, Wichita, Kans., 1982.
 - Nutter Engineering, *Float Valve Design Manual*, 1976. Available from Sulzer ChemTech, Tulsa, Okla.
 - M. J. Lockett, *Distillation Tray Fundamentals*, Cambridge University Press, Cambridge, England, 1986.
- To convert lb/ft³ to kg/m³, multiply by 16.0.
SOURCE: H. Z. Kister, *Distillation Design*, copyright © 1992 by McGraw-Hill, Inc. Reprinted by permission.

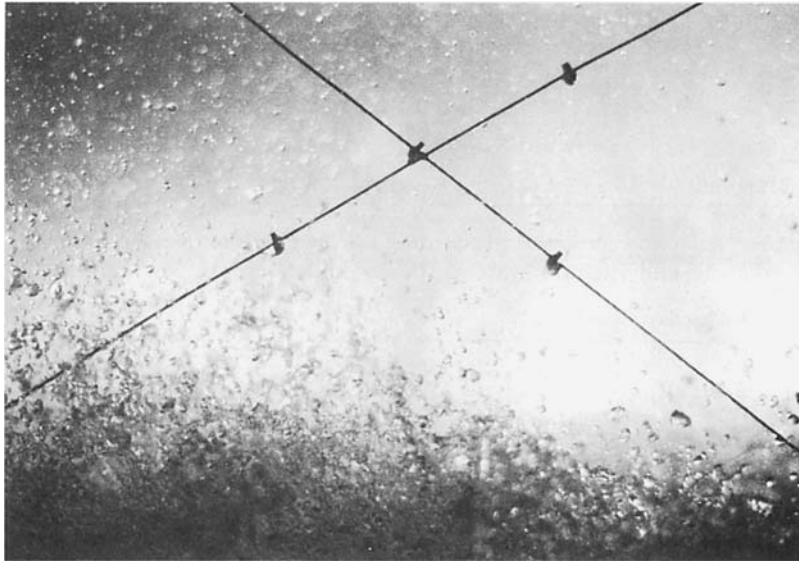


FIG. 14-33 Entrainment. [Reprinted courtesy of Fractionation Research Inc. (FRI).]

Fair (paper presented at the AIChE Annual Meeting, Chicago, Ill., November 1996) correlated data for efficiency reduction due to the rise of entrainment near entrainment flood, getting

$$\ln \psi = A + B\Phi + C\Phi^2 \quad (14-99)$$

where Φ is the fractional approach to entrainment flood and A , B , and C are constants given by

	A	B	C
Highest likely efficiency loss	-3.1898	-4.7413	7.5312
Median (most likely) efficiency loss	-3.2108	-8.9049	11.6291
Lowest likely efficiency loss	4.0992	-29.9141	25.3343

Either the Kister and Haas or the Fair method can be used to evaluate Φ . The correlation has been tested with sieve trays in the flow parameter range of 0.024 to 0.087.

Example 10: Entrainment Effect on Tray Efficiency For the column in Example 9, estimate the efficiency loss should the operation be pushed from the design 80 percent of flood to 90 percent of flood. The midrange dry Murphree tray efficiency is 70 percent.

Solution The vapor and liquid densities and LV ratio remain unchanged from Example 9, and so is the flow parameter (calculated 0.021 in Example 9). At 80 and 90 percent of flood, respectively, Fig. 14-34 gives $\psi = 0.15$ and 0.24. The respective efficiency reductions are calculated from Eq. (14-98),

TABLE 14-10 Recommended Range of Application for the Kister and Haas Spray Regime Entrainment Correlation

Flow regime	Spray only
Pressure	20–1200 kPa (3–180 psia)
Gas velocity	0.4–5 m/s (1.3–15 ft/s)
Liquid flow rate	3–40 m ³ /(m·h) (0.5–4.5 gpm/in)
Gas density	0.5–30 kg/m ³ (0.03–2 lb/ft ³)
Liquid density	450–1500 kg/m ³ (30–90 lb/ft ³)
Surface tension	5–80 mN/m
Liquid viscosity	0.05–2 cP
Tray spacing	400–900 mm (15–36 in)
Hole diameter	3–15 mm (0.125–0.75 in)
Fractional hole area	0.07–0.16
Weir height	10–80 mm (0.5–3 in)

$$\frac{E_a}{E_{mv}} = \frac{1}{1 + 0.70[0.15/(1 - 0.15)]} = 0.89$$

$$\frac{E_a}{E_{mv}} = \frac{1}{1 + 0.70[0.24/(1 - 0.24)]} = 0.82$$

signifying an efficiency loss from 62 to 57 percent.

Alternatively, at 80 and 90 percent of entrainment flood, the median value of ψ from Eq. (14-99) is

$$\ln \psi = -3.2108 - 8.9049(0.80) + 11.6291(0.80^2)$$

giving $\psi = 0.056$ and from Eq. (14-98) $E_a/E_{mv} = 0.96$

$$\ln \psi = -3.2108 - 8.9049(0.90) + 11.6291(0.90^2)$$

giving $\psi = 0.164$ and from Eq. (14-98) $E_a/E_{mv} = 0.88$

signifying an efficiency reduction from 67 to 62 percent.

PRESSURE DROP

In vacuum distillation, excessive pressure drop causes excessive bottom temperatures which, in turn, increase degradation, polymerization, coking, and fouling, and also loads up the column, vacuum system, and reboiler. In the suction of a compressor, excessive pressure drop increases the compressor size and energy usage. Such services attempt to minimize tray pressure drop. Methods for estimating pressure drops are similar for most conventional trays. The total pressure drop across a tray is given by

$$h_t = h_d + h'_L \quad (14-100)$$

where h_t = total pressure drop, mm liquid

h_d = pressure drop across the dispersion unit (dry hole for sieve trays; dry valve for valve trays), mm liquid

h'_L = pressure drop through aerated mass over and around the disperser, mm liquid

It is convenient and consistent to relate all of these pressure-drop terms to height of equivalent clear liquid (deaerated basis) on the tray, in either millimeters or inches of liquid.

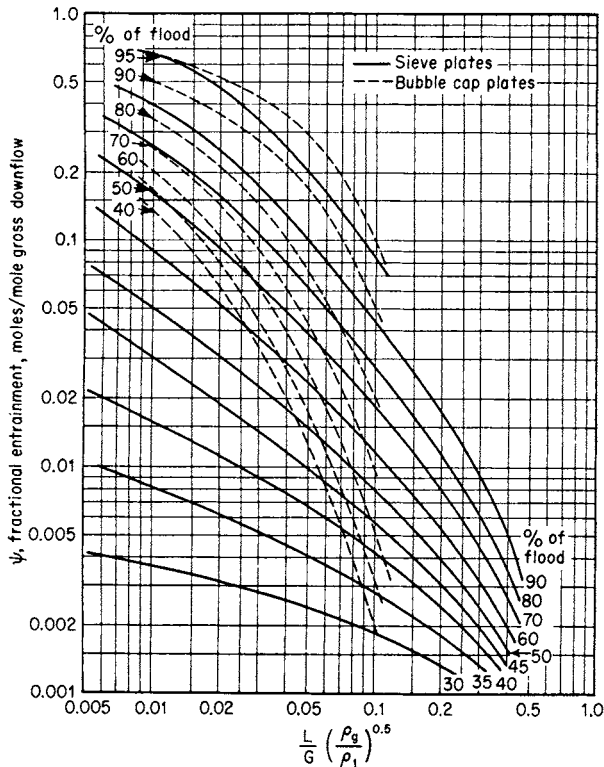


FIG. 14-34 Entrainment correlation. L/G = liquid-gas mass ratio; and ρ_l and ρ_g = liquid and gas densities. [Fair, Pet./Chem. Eng., 33(10), 45 (September 1961).]

Pressure drop across the disperser is calculated by variations of the standard orifice equation:

$$h_d = K \left(\frac{\rho_G}{\rho_L} \right) U_h^2 \tag{14-101}$$

where U_h = linear gas velocity through slots (valve trays) or perforations (sieve tray), m/s.

For sieve trays, $K = 50.8/C_v^2$. Values of C_v are taken from Fig. 14-35. Values from Fig. 14-35 may be calculated from

$$C_v = 0.74(A_h/A_a) + \exp[0.29(t/d_h) - 0.56] \tag{14-102}$$

For Sulze's fixed valve trays, Summers and van Sinderen (*Distillation 2001: Topical Conference Proceedings*, AIChE Spring National Meeting, p. 444, Houston, April 22-26, 2001) provided the following equation for K :

$$K = 58 + 386A_f \quad \text{for MVG fixed valves} \tag{14-103a}$$

$$K = 58 + 461A_f \quad \text{for SVG and LVG fixed valves} \tag{14-103b}$$

Figure 14-36 illustrates the pressure drop of a typical moving valve tray as a function of gas velocity. At low velocities, all valves are closed. Gas rises through the crevices between the valves and the tray deck, with increasing pressure drop as the gas velocity rises. Once point A, the closed balance point (CBP), is reached, some valves begin to open. Upon further increase in gas velocity, more valves open until point B, the open balance point (OBP), is reached. Between points A and B, gas flow area increases with gas velocity, keeping pressure drop constant. Further increases in gas velocity increase pressure drop similar to that in a sieve tray.

The term K in Eq. (14-101) depends on valve slot area, orifice geometry, deck thickness, and the type, shape, and weight of the valves. These are best obtained from the manufacturer's literature,

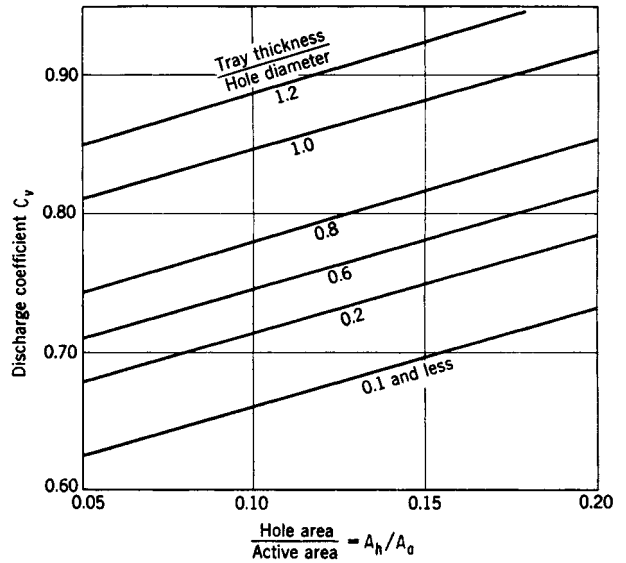


FIG. 14-35 Discharge coefficients for gas flow, sieve trays. [Liebson, Kelley, and Bullington, Pet. Refiner, 36(3), 288 (1957).]

but can also be calculated from Bolles' [*Chem. Eng. Prog.* 72(9), 43 (1976)], Lockett's (*Distillation Tray Fundamentals*, Cambridge University Press, Cambridge, England, 1986), and Klein's (*Chem. Eng.*, May 3, 1982, p. 81) methods.

For valve trays, Klein gives the following values for K (in $s^3\text{-mm/m}^2$) in Eq. (14-101), when based on the total hole area (not slot area):

	Sharp orifice	Venturi valve
All valves open (K_o)	$254.5(2.64/t)^{0.5}$	122
All valves closed (K_c)	1683	841

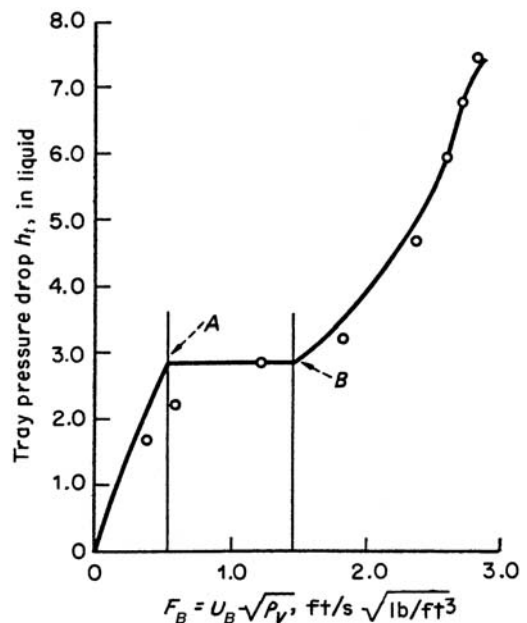


FIG. 14-36 Typical moving valve tray pressure-drop profile. (From C. F. Klein, *Chem. Eng.*, May 3, 1982, p. 81; reprinted courtesy of Chemical Engineering.)

The velocity at which the valves start to open (point A) is given by

$$U_{h,closed} = 1.14[t_v(R_{vw}/K_C)(\rho_M/\rho_C)]^{0.5} \quad (14-104)$$

where $U_{h,closed}$ = hole area at point A, m/s; t_v = valve thickness, mm; R_{vw} = ratio of valve weight with legs to valve weight without legs, given in Table 14-11; K_C = orifice coefficient with all valves closed (see above), $s^2 \cdot mm/m^2$; ρ_M = valve metal density, kg/m^3 (about 8000 kg/m^3 for steel); ρ_C = gas density, kg/m^3 .

The velocity at which all the valves are open $U_{h,open}$ can be calculated from

$$U_{h,open} = U_{h,closed}(K_C/K_O)^{0.5} \quad (14-105)$$

Pressure drop through the aerated liquid [h'_L , in Eq. (14-100)] is calculated by

$$h'_L = \beta h_{ds} \quad (14-106)$$

where β = aeration factor, dimensionless

h_{ds} = calculated height of clear liquid, mm (dynamic seal)

The aeration factor β has been determined from Fig. 14-37 for valve and sieve trays. For sieve trays, values of β in the figure may be calculated from

$$\beta = 0.0825 \ln \frac{Q}{L_w} - 0.269 \ln F_h + 1.679 \quad (14-107)$$

where L_w = weir length, m

F_h = F-factor for flow through holes, $F_h = U_h \rho_C^{0.5}$, m/s (kg/m^3)^{0.5}

For sieve and valve trays,

$$h_{ds} = h_w + h_{ow} + 0.5h_{hg} \quad (14-108)$$

where h_w = weir height, mm

h_{ow} = height of crest over weir, mm clear liquid

h_{hg} = hydraulic gradient across tray, mm clear liquid

The value of weir crest h_{ow} may be calculated from the Francis weir equation and its modifications for various weir types. For a segmental weir and for height in millimeters of clear liquid,

$$h_{ow} = 664 \left(\frac{Q}{L_w} \right)^{2/3} \quad (14-109)$$

where Q = liquid flow, m^3/s

L_w = weir length, m

For serrated weirs,

$$h_{ow} = 851 \left(\frac{Q'}{\tan \theta/2} \right)^{0.4} \quad (14-110)$$

where Q' = liquid flow, m^3/s per serration

θ = angle of serration, deg

For circular weirs,

$$h_{ow} = 44,300 \left(\frac{Q}{d_w} \right)^{0.704} \quad (14-111)$$

where q = liquid flow, m^3/s

d_w = weir diameter, mm

For most sieve and valve trays, the hydraulic gradient is small and can be dropped from Eq. (14-108). Some calculation methods are

available and are detailed in previous editions of this handbook. A rule of thumb by the author is 17 mm/m (0.2 in/ft) of flow path length. This rule only applies in the liquid-loaded froth and emulsion regimes ($Q_L > 50 m^3/hm$ or $> 5.5 gpm/in$ of outlet weir length). At lower liquid loads, the hydraulic gradient is less.

As noted, the weir crest h_{ow} is calculated on an equivalent clear-liquid basis. A more realistic approach is to recognize that in general a froth or spray flows over the outlet weir (settling can occur upstream of the weir if a large "calming zone" with no dispersers is used). Bennett et al. [AIChE J., 29, 434 (1983)] allowed for froth overflow in a comprehensive study of pressure drop across sieve trays; their correlation for residual pressure drop h'_L in Eq. (14-100) is presented in detail in the previous (seventh) edition of this handbook, including a worked example. Although more difficult to use, the method of Bennett et al. was recommended when determination of pressure drop is of critical importance.

Example 11: Pressure Drop, Sieve Tray For the conditions of Example 9, estimate the pressure drop for flow across one tray. The thickness of the tray metal is 2 mm. The superficial F-factor is 2.08 m/s(kg/m^3)^{1/2}.

Solution Equations (14-100), (14-106), and (14-107), where $h_t = h_d + \beta(h_w + h_{ow})$, are used. For $F_c = 2.08$, $F_B = 2.32$ and $F_d = 16.55$. From Example 9, $L_w = 1.50$ m and $h_w = 38$ mm. For a liquid rate of 22,000 kg/hr, $Q = 7.27(10^{-3}) m^3/s$, and $Q/L_w = 4.8(10^{-3})$. By Eq. (14-107) or Fig. 14-37, $\beta = 0.48$. From Eq. (14-102) or Fig. 14-35, $C_c = 0.75$. Then, by Eq. (14-101), $h_d = 29.0$ mm liquid. Using Eq. (14-109), $h_{ow} = 18.9$ mm. Finally, $h_t = h_d + \beta(h_w + h_{ow}) = 29.0 + 0.48(38 + 18.9) = 56.4$ mm liquid.

When straight or serrated segmental weirs are used in a column of circular cross section, a correction may be needed for the distorted pattern of flow at the ends of the weirs, depending on liquid flow rate. The correction factor F_w from Fig. 14-38 is used directly in Eq. (14-109). Even when circular downcomers are utilized, they are often fed by the overflow from a segmental weir.

Loss under Downcomer The head loss under the downcomer apron, as millimeters of liquid, may be estimated from

$$h_{da} = 165.2 \left(\frac{Q}{A_{da}} \right)^2 \quad (14-112)$$

where Q = volumetric flow of liquid, m^3/s and A_{da} = most restrictive (minimum) area of flow under the downcomer apron, m^2 . Equation (14-112) was derived from the orifice equation with an orifice coefficient of 0.6. Although the loss under the downcomer is small, the clearance is significant from the aspect of tray stability and liquid distribution.

The term A_{da} should be taken as the most restrictive area for liquid flow in the downcomer outlet. Usually, this is the area under the downcomer apron (i.e., the downcomer clearance times the length of the segmental downcomer), but not always. For instance, if an inlet weir is used and the area between the segmental downcomer and the inlet weir is smaller than the area under the downcomer apron, the smaller area should be used.

OTHER HYDRAULIC LIMITS

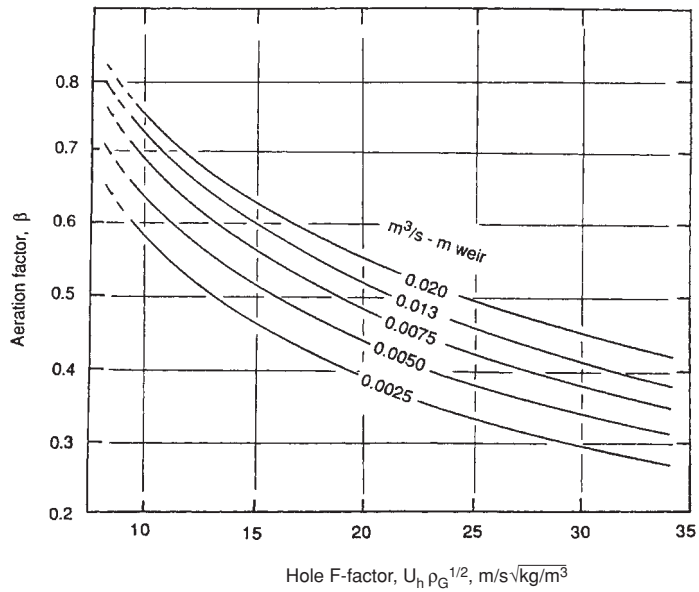
Weeping Weeping is liquid descending through the tray perforations, short-circuiting the contact zone, which lowers tray efficiency. At the tray floor, liquid static head that acts to push liquid down the perforations is counteracted by the gas pressure drop that acts to hold the liquid on the tray. When the static head overcomes the gas pressure drop, weeping occurs.

Some weeping usually takes place under all conditions due to sloshing and oscillation of the tray liquid. Generally, this weeping is too small to appreciably affect tray efficiency. The *weep point* is the gas velocity at which weeping first becomes noticeable. At this point, little efficiency is lost. As gas velocity is reduced below the weep point, the weep rate increases. When the weep rate becomes large enough to significantly reduce tray efficiency, the lower tray operating limit is reached.

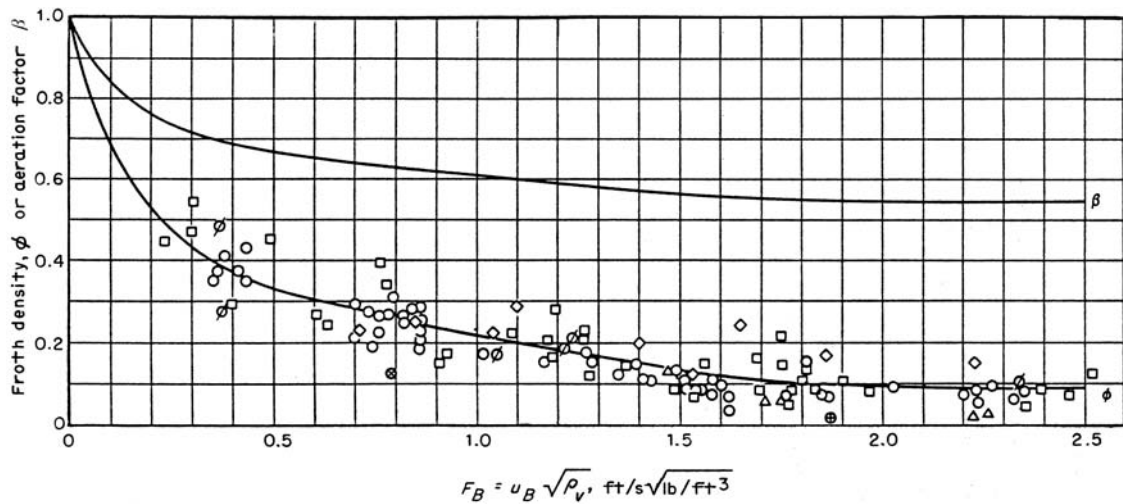
The main factor that affects weeping is the fractional hole area. The larger it is, the smaller the gas pressure drop and the greater the weeping tendency. Larger liquid rates and taller outlet weirs increase

TABLE 14-11 R_{vw} Values for Eq. (14-104)

Valve type	Sharp	Venturi
Three-leg	1.23	1.29
Four-leg	1.34	1.45
Cages (no legs)	1.00	1.00



(a)



(b)

FIG. 14-37 Aeration factor for pressure drop calculation. (a) Sieve trays. [Bolles and Fair, Encyclopedia of Chemical Processing and Design, vols. 16, 86, J. M. McKetta (ed.), Marcel Dekker, New York, 1982.] (b) Valve trays. (From G. F. Klein, Chem. Eng., May 3, 1982, p. 81; reprinted courtesy of Chemical Engineering.)

liquid heads and therefore weeping. Hole diameter has a complex effect on weeping, detailed by Lockett and Banik [*Ind. Eng. Chem. Proc. Des. Dev.* **25**, 561 (1986)].

Tests by Lockett and Banik (loc. cit.) show that weeping is often nonuniform, with some hydraulic conditions favoring weeping from the tray inlet and others from the tray outlet. Weeping from the tray inlet is particularly detrimental to tray efficiency because the weeping liquid bypasses two trays.

Weep Rate Prediction Lockett and Banik (loc. cit.) and Hsieh and McNulty (*Chem. Eng. Progr.*, July 1993, p. 71) proposed correlations for predicting weep rates from sieve trays. Colwell and O'Bara (Paper presented at the AIChE Meeting, Houston, April 1989) rec-

ommended the Lockett and Banik correlation for low pressures (<1100 kPa or 165 psia), and the Hsieh and McNulty correlation for high pressures (>1100 kPa or 165 psia). They also corrected the Lockett and Banik correlation to improve its accuracy near the weep point.

The Lockett and Banik correlation (as corrected by Colwell and O'Bara) is

$$\frac{W}{A_h} = \frac{29.45}{\sqrt{Fr_h}} - 44.18 \quad Fr_h < 0.2 \quad (14-113a)$$

$$\frac{W}{A_h} = \frac{1.841}{Fr_h^{1.533}} \quad Fr_h > 0.2 \quad (14-113b)$$

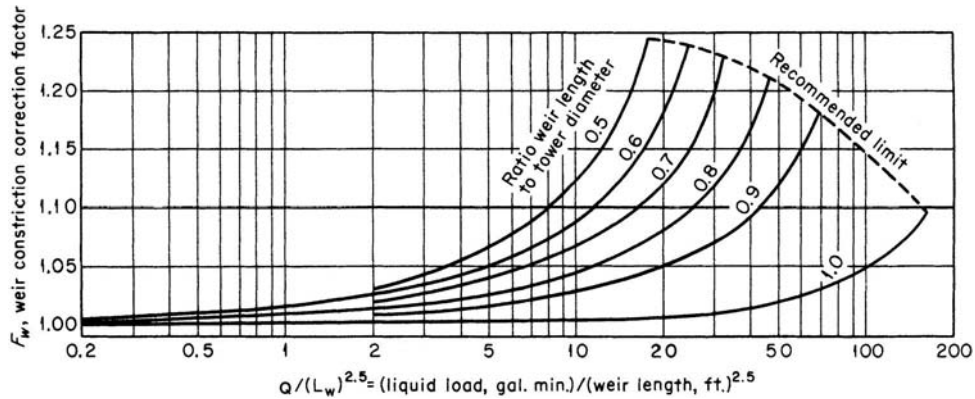


FIG. 14-38 Correction for effective weir length. To convert gallons per minute to cubic meters per second, multiply by 6.309×10^{-5} ; to convert feet to meters, multiply by 0.3048. [Bolles, *Pet. Refiner*, **25**, 613 (1946).]

where

$$Fr_h = 0.373 \frac{u_h^2}{h_c} \frac{\rho_v}{\rho_L - \rho_v} \quad (14-114)$$

Equations (14-113) and (14-114) use English units: W is the weep rate, gpm; A_h is the hole area, ft²; u_h is the hole velocity, ft/s; and h_c is the clear liquid height, in. Colwell's [*Ind. Eng. Chem. Proc. Des. Dev.* **20**(2), 298 (1981)] method below has been recommended for obtaining the clear liquid height h_c in Eq. (14-114).

$$h_c = \phi_f \left\{ 0.527 \left(\frac{Q_L(1-f_w)}{C_d \phi_f} \right)^{2/3} + h_w \right\} \quad (14-115)$$

where ϕ_f is given by Eq. (14-119) and C_d is given by Eq. (14-116)

$$\left. \begin{aligned} C_d &= 0.61 + 0.08 \frac{h_{fow}}{h_w} & \frac{h_{fow}}{h_w} < 8.135 \\ C_d &= 1.06 \left(1 + \frac{h_w}{h_{fow}} \right)^{1.5} & \frac{h_{fow}}{h_w} > 8.135 \end{aligned} \right\} \quad (14-116)$$

$$h_{fow} = h_f - h_w \quad (14-117)$$

where h_f is given by Eq. (14-122). The froth density ϕ_f is calculated from

$$\eta = 12.6 Fr^{0.4} \left(\frac{A_B}{A_h} \right)^{0.25} \quad (14-118)$$

$$\phi_f = \frac{1}{\eta + 1} \quad (14-119)$$

$$Fr = 0.37 \frac{\rho_v u_B^2}{h_c(\rho_L - \rho_v)} \quad (14-120)$$

The term f_w in Eq. (14-115) is the ratio of weep rate from the tray to the total liquid flow entering the tray, calculated as follows:

$$f_w = W/GPM \quad (14-121)$$

Some trial and error is required in this calculation because the clear liquid height h_c and the froth density ϕ_f depend on each other, and the weep fraction f_w depends on the clear liquid height h_c . Clear liquid height is related to froth height and froth density by

$$h_c = \phi_f h_f \quad (14-122)$$

The terms in Eqs. (14-115) to (14-122) are in the English units and are explained in the Nomenclature.

With large-diameter trays and low liquid loads, a small ratio of W/A_h corresponds to a large fractional weep. Under these conditions, the Lockett and Banik correlation is inaccurate. The correlation is unsuitable for trays with very small (<3-mm or $\frac{1}{8}$ -in) holes. The correlation appears to fit most data points to an accuracy of ± 15 to ± 30 percent. The Hsieh and McNulty correlation (loc. cit.) is

$$\sqrt{J_c^2} + m \sqrt{J_L^2} = C_w \quad (14-123)$$

where

$$J_c^2 = u_h \left[\frac{\rho_c}{gZ(\rho_L - \rho_c)} \right]^{0.5} \quad (14-124)$$

and

$$J_L^2 = \frac{W}{448.83A_h} \left[\frac{\rho_L}{gZ(\rho_L - \rho_c)} \right]^{0.5} \quad (14-125)$$

$$Z = h_c^{1.5} / (12d_H^{0.5}) \quad (14-126)$$

The terms in Eqs. (14-123) to (14-126) are in English units and are explained in the Nomenclature. For sieve trays, $m = 1.94$ and $C_w = 0.79$. Note that the constants are a slight revision of those presented in the original paper (C. L. Hsieh, private communication, 1991). Clear liquid height is calculated from Colwell's correlation [Eqs. (14-115) to (14-122)]. The Hsieh and McNulty correlation applies to trays with 9 percent and larger fractional hole area. For trays with smaller hole area, Hsieh and McNulty expect the weeping rate to be smaller than predicted.

Weeping from Valve Trays An analysis of weeping from valve trays [Bolles, *Chem. Eng. Progs.* **72**(9), 43 (1976)] showed that in a well-designed valve tray, the weep point is below the gas load at which the valves open; and throughout the valve opening process, the operating point remains above the weep point. In contrast, if the tray contains too many valves, or the valves are too light, excessive valve opening occurs before the gas pressure drop is high enough to counter weeping. In this case, weeping could be troublesome.

Weep point correlations for valve trays were presented by Bolles (loc. cit.) and by Klein (*Chem. Eng.*, Sept. 17, 1984, p. 128). Hsieh and McNulty (loc. cit.) gave a complex extension of their weep rate correlation to valve trays.

Dumping As gas velocity is lowered below the weep point, the fraction of liquid weeping increases until all the liquid fed to the tray weeps through the holes and none reaches the downcomer. This is the *dump point*, or the *seal point*. The dump point is well below the range of acceptable operation of distillation trays. Below the dump point, tray efficiency is slashed, and mass transfer is extremely poor. Operation below the dump point can be accompanied by severe hydraulic instability due to unsealing of downcomers.

Extensive studies on dumping were reported by Prince and Chan [*Trans. Inst. Chem. Eng.* **43**, T49 (1965)]. The Chan and Prince

dump-point correlation was recommended and is presented in detail elsewhere (Kister, *Distillation Design*, McGraw-Hill, 1992). Alternatively, the dump point can be predicted by setting the weep rate equal to 100 percent of the liquid entering the tray in the appropriate weep correlation.

Turndown The turndown ratio is the ratio of the normal operating (or design) gas throughput to the minimum allowable gas throughput. The minimum allowable throughput is usually set by excessive weeping, while normal operating throughput is a safe margin away from the relevant flooding limit.

Sieve and fixed valve trays have a poor turndown ratio (about 2:1). Their turndown can be improved by blanking some rows of tray holes, which reduces the tendency to weep, but will also reduce the tray's maximum capacity. Turndown of *moving valve trays* is normally between about 4:1 to 5:1. Special valve designs can achieve even better turndown ratios, between 6:1 and 10:1, and even more. Turndown can also be enhanced by blanking strips (which require valve removal) or valve leg crimping. Sloley and Fleming (*Chem. Eng. Progr.*, March 1994, p. 39) stress that correct implementation of turndown enhancement is central to achieving a desired turndown. When poorly implemented, turndown may be restricted by poor vapor-liquid contact rather than by weeping.

Vapor Channeling All the correlations in this section assume an evenly distributed tray vapor. When the vapor preferentially channels through a tray region, premature entrainment flood and excessive entrainment take place due to a high vapor velocity in that region. At the same time, other regions become vapor-deficient and tend to weep, which lowers tray efficiency.

Work by Davies [*Pet. Ref.* 29(8), p. 93, and 29(9), p. 121 (1950)] based on bubble-cap tray studies suggests that the vapor pressure drop of the tray (the *dry pressure drop*) counteracts channeling. The higher the dry tray pressure drop, the greater the tendency for vapor to spread uniformly over the bubbling area. If the dry tray pressure drop is too small compared with the channeling potential, channeling prevails.

Perhaps the most common vapor channeling mechanism is *vapor crossflow channeling* (VCFC, Fig. 14-39). The hydraulic gradient on the tray induces preferential vapor rise at the outlet and middle of the tray, and a vapor-deficient region near the tray inlet. The resulting high vapor velocities near the tray outlet step up entrainment, while the low vapor velocities near the tray inlet induce weeping. Interaction between adjacent trays (Fig. 14-39) accelerates both the outlet entrainment and the inlet weeping. The net result is excessive entrainment and premature flooding at the tray middle and outlet, simultaneous with weeping from the tray inlet, accompanied by a loss of efficiency and turndown.

VCFC takes place when the following four conditions exist simultaneously [Kister, Larson, and Madsen, *Chem. Eng. Progr.*, p. 86 (Nov. 1992); Kister, *The Chemical Engineer*, 544, p. 18 (June 10, 1993)]:

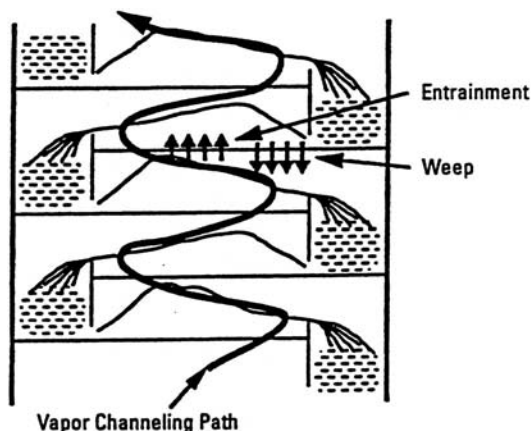


FIG. 14-39 Vapor crossflow channeling. Note entrainment near the tray middle and outlet, and weep near the tray inlet. (Kister, H. Z., K. F. Larson, and P. Madsen, *Chem. Eng. Progr.*, Nov. 1992, p. 86; reproduced with permission.)

1. Absolute pressure < 500 kPa (70 psia).
2. High liquid rates [$>50 \text{ m}^3/(\text{m}\cdot\text{h})$ or 6 gpm/in of outlet weir].
3. High ratio ($>2:1$) of flow path length to tray spacing.
4. Low dry tray pressure drop. On sieve and fixed valve trays, this means high (>11 percent) fractional hole area. On moving valve trays, this means venturi valves (smooth orifices) or long-legged valves (>15 percent slot area). On all trays, the channeling tendency and severity escalate rapidly as the dry pressure drop diminishes (e.g., as fractional hole area increases).

Hartman (*Distillation 2001: Topical Conference Proceedings*, AIChE Spring National Meeting, p. 108, Houston, Tex. (April 22–26, 2001)) reports VCFC even with conventional valve trays (14 percent slot area) at very high ratio (3.6:1) of flow path length to tray spacing and tray truss obstruction.

VCFC is usually avoided by limiting fractional hole areas, avoiding venturi valves, and using forward-push devices. Resitaris and Pappademos [Paper presented at the AIChE Annual Meeting, Reno, Nev. (November 2001)] cited tray inlet inactivity as a contributor to VCFC, and advocate inlet forward-push devices to counter it.

TRANSITION BETWEEN FLOW REGIMES

Froth-Spray Froth-spray transition has been investigated for sieve trays using a variety of techniques. The gradual nature of this transition bred a multitude of criteria for defining it, and made its correlation difficult. Excellent overviews were given by Lockett (*Distillation Tray Fundamentals*, Cambridge University Press, Cambridge, England, 1986) and Prado, Johnson, and Fair [*Chem. Eng. Progr.* 83(3), p. 32 (1987)]. Porter and Jenkins [*I. Chem. E. Symp. Ser.* 56, Summary Paper (1979)] presented a simple correlation for the froth-to-spray transition.

$$F_{LC} \frac{N_p A_B}{L_w} = 0.0191 \quad (14-127)$$

The terms of this equation are in English units and are explained in the Nomenclature. This correlation is based on the premise that froth-to-spray transition occurs when the entrainment vs. liquid load relationship passes through a minimum (see "Entrainment"). Alternatively, it was argued that the minimum represents a transition from the froth regime to a partially developed spray region (Kister, Pinczewski, and Fell, Paper presented in the 90th National AIChE Meeting, Houston, April 1981). If this alternative argument is valid, then when the correlation predicts froth, it is highly unlikely that the column operates in the spray regime; but when it predicts spray, the column may still be operating in the froth regime. Recent entrainment studies by Ohe [*Distillation 2005: Topical Conference Proceedings*, AIChE Spring National Meeting, p. 283, Atlanta (April 10–13, 2005)] argue that the entrainment minima represent minimum liquid residence times on the tray, and are unrelated to the froth-spray transition.

A second correlation is by Pinczewski and Fell [*Ind. Eng. Chem. Proc. Des. Dev.* 21, p. 774 (1982)]

$$u_B \sqrt{\rho_G} = 2.25 \left(\frac{Q_L \sqrt{\rho_L}}{100} \right)^n \quad (14-128)$$

The terms of Eq. (14-128) are in English units and are explained in the Nomenclature. The exponent n is calculated from Eq. (14-84). Equation (14-128) is based on transition data obtained from orifice jetting measurements for the air-water system and on entrainment minimum data for some hydrocarbon systems.

A third recent correlation by Johnson and Fair (loc. cit.) is

$$U_a^e = C_1 \rho_G^{-0.50} \rho_L^{0.692} \sigma^{0.06} A_f^{0.25} \left(\frac{q}{L_w} \right)^{0.05} d_h^{-0.1} \quad (14-129)$$

where U_a^e = gas velocity through active area at inversion, m/s
 ρ_G = gas density, kg/m³
 ρ_L = liquid density, kg/m³
 σ = surface tension, mN/m
 A_f = hole/active area ratio

$$\begin{aligned}
 q/L_w &= \text{liquid flow, m}^3/(\text{s}\cdot\text{m}) \text{ weir} \\
 d_h &= \text{hole diameter, mm} \\
 C_1 &= 0.0583 \text{ for 25.4-mm overflow weirs} \\
 &= 0.0568 \text{ for 50.4-mm overflow weirs} \\
 &= 0.0635 \text{ for 101.6-mm overflow weirs}
 \end{aligned}$$

Froth-Emulsion Froth-emulsion transition occurs [Hofhuis and Zuideweg, *I. Chem. E. Symp. Ser.* **56**, p. 2, 2/1 (1979)] when the aerated mass begins to obey the Francis weir formula. Using this criterion, the latest version of this transition correlation is

$$F_{LC} \frac{N_p A_B}{L_w h_c} = 0.0208 \quad (14-130)$$

The terms of this equation are in English units and are explained in the Nomenclature; h_c is calculated from the Hofhuis and Zuideweg (loc. cit.) equation.

$$h_c = 2.08 \left(F_{LC} \frac{N_p A_B}{L_w} p \right)^{0.25} h_w^{0.5} \quad (14-131)$$

An inspection of the experimental data correlated shows that this, too, is a gradual transition, which occurs over a range of values rather than at a sharp point.

Valve Trays The amount of work reported thus far on valve tray regime transition is small and entirely based on air-water tests. Correlations proposed to date require the knowledge of liquid holdup at transition, which is generally not available, and are therefore of limited application for commercial columns.

TRAY EFFICIENCY

Definitions

Overall Column Efficiency This is the ratio of the number of theoretical stages to the number of actual stages

$$E_{OC} = N_t/N_a \quad (14-132)$$

Since tray efficiencies vary from one section to another, it is best to apply Eq. (14-132) separately for the rectifying and stripping sections. In practice, efficiency data and prediction methods are often too crude to give a good breakdown between the efficiencies of different sections, and so Eq. (14-132) is applied over the entire column.

Point Efficiency This is defined by Eq. (14-133) (Fig. 14-40a):

$$E_{OC} = \left(\frac{y_n - y_{n-1}}{y_n^* - y_{n-1}} \right)_{\text{point}} \quad (14-133)$$

where y_n^* is the composition of vapor in equilibrium with the liquid at point n . The term y_n is actual vapor composition at that point. The point efficiency is the ratio of the change of composition at a point to the change that would occur on a theoretical stage. As the vapor composition at a given point cannot exceed the equilibrium composition, fractional point efficiencies are always lower than 1. If there is a composition gradient on the tray, point efficiency will vary between points on the tray.

Murphree Tray Efficiency [Ind. Eng. Chem. **17**, 747 (1925)] This is the same as point efficiency, except that it applies to the entire tray instead of to a single point (Fig. 14-40b):

$$E_{MV} = \left(\frac{y_n - y_{n-1}}{y_n^* - y_{n-1}} \right)_{\text{tray}} \quad (14-134)$$

If both liquid and vapor are perfectly mixed, liquid and vapor compositions on the tray are uniform, and the Murphree tray efficiency will coincide with the point efficiency at any point on the tray. In practice, a concentration gradient exists in the liquid, and x_n at the tray outlet is lower than x_n^* on the tray (see Fig. 14-40b). This frequently lowers y_n^* relative to y_n , thus enhancing tray efficiency [Eq. (14-134)] compared with point efficiency. The value of y_n^* may even drop below y_n . In this case, E_{MV} exceeds 100 percent [Eq. (14-134)].

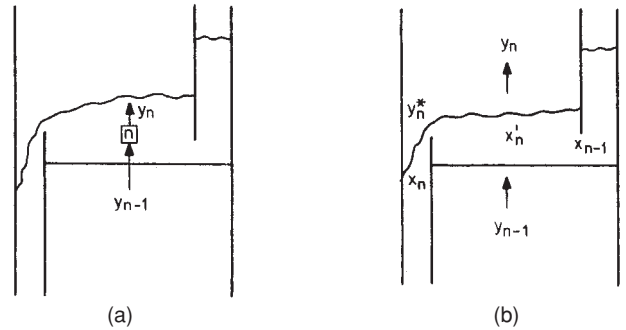


FIG. 14-40 Point and Murphree efficiencies. (a) Point. (b) Murphree. (From H. Z. Kister, *Distillation Design*, copyright © 1992 by McGraw-Hill; reprinted by permission.)

Overall column efficiency can be calculated from the Murphree tray efficiency by using the relationship developed by Lewis [Ind. Eng. Chem. **28**, 399 (1936)].

$$E_{OC} = \frac{\ln[1 + E_{MV}(\lambda - 1)]}{\ln \lambda} \quad (14-135)$$

where
$$\lambda = m \frac{G_M}{L_M} \quad (14-136)$$

Equation (14-135) is based on the assumption of constant molar overflow and a constant value of E_{MV} from tray to tray. It needs to be applied separately to each section of the column (rectifying and stripping) because G_M/L_M , and therefore λ , varies from section to section. Where molar overflow or Murphree efficiencies vary throughout a section of column, the section needs to be divided into subsections small enough to render the variations negligible.

The point and Murphree efficiency definitions above are expressed in terms of vapor concentrations. Analogous definitions can be made in terms of liquid concentrations. Further discussion is elsewhere (Lockett, *Distillation Tray Fundamentals*, Cambridge University Press, Cambridge, England, 1986).

Fundamentals Figure 14-41 shows the sequence of steps for converting phase resistances to a tray efficiency. Gas and liquid film resistances are added to give the point efficiency. Had both vapor and liquid on the tray been perfectly mixed, the Murphree tray efficiency would have equaled the point efficiency. Since the phases are not perfectly mixed, a model of the vapor and liquid mixing patterns is needed for converting point efficiency to tray efficiency. Liquid mixture patterns are plug flow, backmixing, and stagnant zones, while vapor-mixing patterns are perfect mixing and plug flow.

Lewis (loc. cit.) was the first to derive quantitative relationships between the Murphree and the point efficiency. He derived three mixing cases, assuming plug flow of liquid in all. The Lewis cases give the maximum achievable tray efficiency. In practice, efficiency is lower due to liquid and vapor nonuniformities and liquid mixing.

Most tray efficiency models are based on Lewis case 1 with vapor perfectly mixed between trays. For case 1, Lewis derived the following relationship:

$$E_{MV, \text{dry}} = \frac{\exp(\lambda E_{OC}) - 1}{\lambda} \quad (14-137)$$

The “dry” Murphree efficiency calculated thus far takes into account the vapor and liquid resistances and the vapor-liquid contact patterns, but is uncorrected for the effects of entrainment and weeping. This correction converts the dry efficiency to a “wet” or actual Murphree tray efficiency. Colburn [Eq. (14-98), under “Entrainment”] incorporated the effect of entrainment on efficiency, assuming perfect mixing of liquid on the tray.

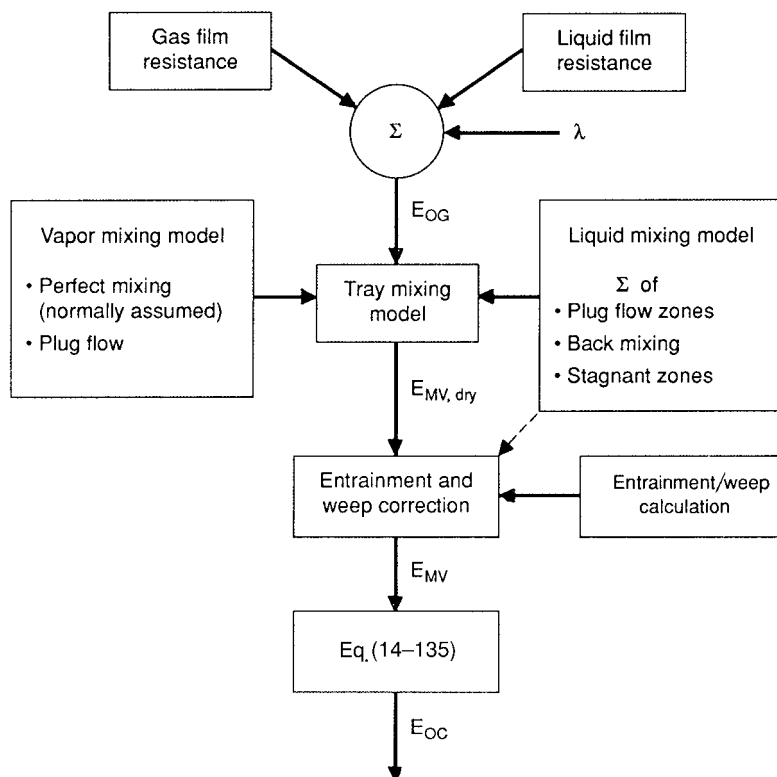


FIG. 14-41 Sequence of steps for theoretical prediction of tray efficiency. (From H. Z. Kister, *Distillation Design*, copyright © 1992 by McGraw-Hill; reprinted by permission.)

Factors Affecting Tray Efficiency Below is a summary based on the industry's experience. A detailed discussion of the fundamentals is found in Lockett's book (*Distillation Tray Fundamentals*, Cambridge University Press, Cambridge, England, 1986). A detailed discussion of the reported experience, and the basis of statements made in this section are in Kister's book (*Distillation Design*, McGraw-Hill, New York, 1992).

Errors in Vapor-Liquid Equilibrium (VLE) Errors in relative volatility are the most underrated factor affecting tray efficiency. Figure 14-42 shows the direct effect of the errors [Deibele and Brandt, *Chem. Eng. Tech.* **57**(5), p. 439 (1985); Roy P. and G. K. Hobson, *I. Chem. E. Symp. Ser.* **104**, p. A273 (1987)]. At very low relative volatilities ($\alpha < 1.2$), small errors in VLE have a huge impact on tray efficiency. For instance, at $\alpha = 1.1$, a -3 percent error gives a tray efficiency 40 to 50 percent higher than its true value (Fig. 14-42). Since VLE errors are seldom lower than ± 2 to 3 percent, tray efficiencies of low-volatility systems become meaningless unless accompanied by VLE data. Likewise, comparing efficiencies derived for a low-volatility system by different sources is misleading unless one is using identical VLE.

Figure 14-42 shows that errors in relative volatility are a problem only at low relative volatilities; for $\alpha > 1.5$ to 2.0, VLE errors have negligible direct impact on tray efficiency.

Most efficiency data reported in the literature are obtained at total reflux, and there are no indirect VLE effects. For measurements at finite reflux ratios, the indirect effects below compound the direct effect of Fig. 14-42. Consider a case where $\alpha_{\text{apparent}} < \alpha_{\text{true}}$ and test data at a finite reflux are analyzed to calculate tray efficiency. Due to the volatility difference $R_{\text{min,apparent}} > R_{\text{min,true}}$. Since the test was conducted at a fixed reflux flow rate, $(R/R_{\text{min}})_{\text{apparent}} < (R/R_{\text{min}})_{\text{true}}$. A calculation based on the apparent R/R_{min} will give more theoretical stages than a calculation based on the true R/R_{min} . This means a higher apparent efficiency than the true value.

The indirect effects add to those of Fig. 14-42, widening the gap between true and apparent efficiency. The indirect effects exponentially escalate as minimum reflux is approached. Small errors in VLE or reflux ratio measurement (this includes column material balance as well as reflux rate) alter R/R_{min} . Near minimum reflux, even small R/R_{min} errors induce huge errors in the number of stages, and therefore in tray efficiency. Efficiency data obtained near minimum reflux are therefore meaningless and potentially misleading.

Liquid Flow Patterns on Large Trays The most popular theoretical models (below) postulate that liquid crosses the tray in plug flow with superimposed backmixing, and that the vapor is perfectly mixed. Increasing tray diameter promotes liquid plug flow and suppresses backmixing.

The presence of stagnant zones on large-diameter distillation trays is well established, but the associated efficiency loss is poorly understood; in some cases, significant efficiency losses, presumably due to stagnant zones, were reported [Weiler, Kirkpatrick, and Lockett, *Chem. Eng. Progr.* **77**(1), 63 (1981)], while in other cases, no efficiency difference was observed [Yanagi and Scott, *Chem. Eng. Progr.*, **69**(10), 75 (1973)]. Several techniques are available for eliminating stagnant regions (see Kister, *Distillation Design*, McGraw-Hill, New York, 1992, for some), but their effectiveness for improving tray efficiency is uncertain.

Weir Height Taller weirs raise the liquid level on the tray in the froth and emulsion regimes. This increases interfacial area and vapor contact time, which should theoretically enhance efficiency. In the spray regime, weir height affects neither liquid level nor efficiency. In distillation systems, the improvement of tray efficiency due to taller weirs is small, often marginal.

Length of Liquid Flow Path Longer liquid flow paths enhance the liquid-vapor contact time, the significance of liquid plug flow, and therefore raise efficiency. Typically, doubling the flow path length

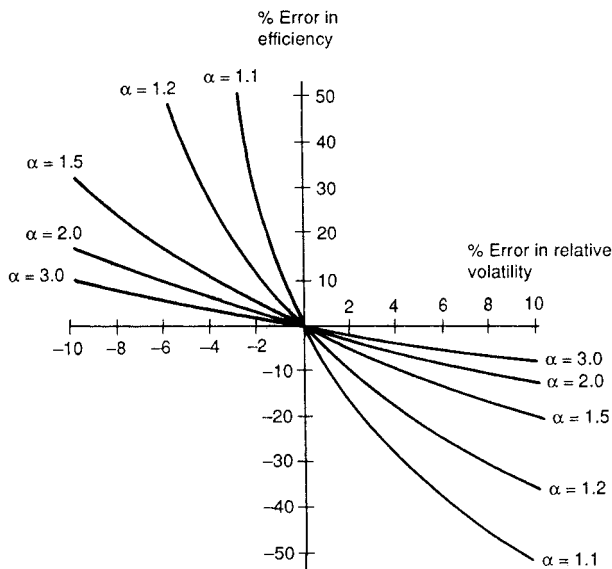


FIG. 14-42 Direct effect of errors in relative volatility on error in tray efficiency. (From H. Z. Kister, *Distillation Design*, copyright © 1992 by McGraw-Hill; reprinted by permission.)

(such as going from two-pass to one-pass trays at a constant tower diameter) raises tray efficiency by 5 to 15 percent.

Fractional Hole Area Efficiency increases with a reduction in fractional hole area. Yanagi and Sakata [*Ind. Eng. Chem. Proc. Des. Dev.* **21**, 712 (1982)] tests in commercial-scale towers show a 5 to 15 percent increase in tray efficiency when fractional hole area was lowered from 14 to 8 percent (Fig. 14-43).

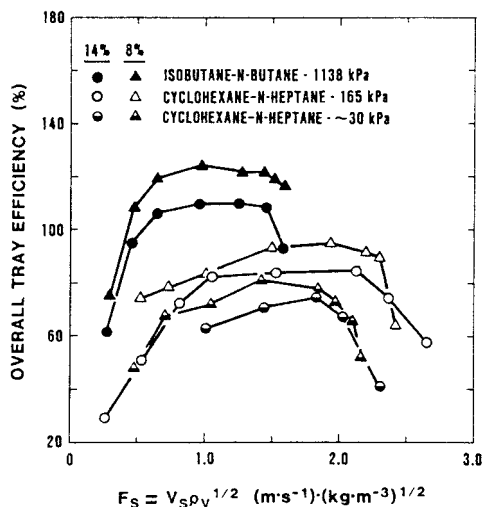


FIG. 14-43 Efficiency reduction when fractional hole area is increased, also showing little effect of vapor and liquid loads on efficiency in the normal operating range (between excessive weeping and excessive entrainment). Also shown is the small increase in efficiency with pressure. FRI data, total reflux, $D_T = 1.2$ m, $S = 610$ mm, $h_w = 50.8$ mm, $d_H = 12.7$ mm. (Reprinted with permission from T. Yanagi and M. Sakata, *Ind. Eng. Chem. Proc. Des. Dev.* **21**, 712; copyright © 1982, American Chemical Society.)

Hole Diameter The jury is out on the effect of hole diameter on tray efficiency. There is, however, a consensus that the effect of hole diameter on efficiency is small, often negligible.

Vapor-Liquid Loads and Reflux Ratio Vapor and liquid loads, as well as the reflux ratio, have a small effect on tray efficiency (Fig. 14-43) as long as no capacity or hydraulic limits (flood, weep, channeling, etc.) are violated.

Viscosity, Relative Volatility Efficiency increases as liquid viscosity and relative volatility diminish. These effects are reflected in the O'Connell correlation (below).

Surface Tension There is uncertainty regarding the effect of surface tension on tray efficiency. Often, it is difficult to divorce the surface tension effects from those of other physical properties.

Pressure Tray efficiency slightly increases with pressure (Fig. 14-43), reflecting the rise of efficiency with a reduction in liquid viscosity and in relative volatility, which generally accompany a distillation pressure increase.

At pressures exceeding 10 to 20 bar (150 to 300 psia), and especially at high liquid rates, vapor entrainment into the downcomer liquid becomes important, and tray efficiency decreases with further increases in pressure [*Zuiderveg, Int. Chem. Eng.* **26**(1), 1 (1986)].

Maldistribution Maldistribution can cause major efficiency reduction in multipass trays (>two passes). Further discussion is given under "Number of Passes."

OBTAINING TRAY EFFICIENCY

Efficiency prediction methods are listed here in decreasing order of reliability.

Rigorous Testing Rigorous testing of a plant column is generally the most reliable method of obtaining tray efficiency. Test procedures can be found elsewhere (AIChE Equipment Testing Procedures Committee, *AIChE Equipment Testing Procedure—Tray Distillation Columns*, 2d ed., 1987; Kister, *Distillation Operation*, McGraw-Hill, New York, 1990).

Scale-up from an Existing Commercial Column As long as data are for the same system under similar process conditions, loadings, and operating regime, data obtained in one column directly extend to another. Fractional hole area and the number of tray passes will have a small but significant effect on efficiency, and any changes in these parameters need to be allowed for during scale-up. The empirical information in the section "Factors Affecting Tray Efficiency" can be used to estimate the magnitude of the changes on efficiency.

Scale-up from Existing Commercial Column to Different Process Conditions During scale-up, test data are analyzed by computer simulation. The number of theoretical stages is varied until the simulated product compositions and temperature profile match the test data. Tray efficiency is determined by the ratio of theoretical stages to actual trays. In this procedure, errors in VLE are offset by compensating errors in tray efficiency. For instance, if the relative volatility calculated by the simulation is too high, fewer stages will be needed to match the measured data, i.e., "apparent" tray efficiency will be lower. Scale-up will be good as long as the VLE and efficiency errors continue to offset each other equally. This requires that process conditions (feed composition, feed temperature, reflux ratio, etc.) remain unchanged during scale-up.

When process conditions change, the VLE and efficiency errors no longer offset each other equally. If the true relative volatility is higher than simulated, then the scale-up will be conservative. If the true relative volatility is lower than simulated, scale-up will be optimistic. A detailed discussion is found in Kister, *Distillation Design*, McGraw-Hill, New York, 1992.

Experience Factors These are tabulations of efficiencies previously measured for various systems. Tray efficiency is insensitive to tray geometry (above), so in the absence of hydraulic anomalies and issues with VLE data, efficiencies measured in one tower are extensible to others distilling the same system. A small allowance to variations in tray geometry as discussed above is in order. Caution is required with mixed aqueous-organic systems, where concentration may have a marked effect on physical properties, relative volatility, and efficiency. Table 14-12 shows typical tray efficiencies reported in the literature.

TABLE 14-12 Representative Tray Efficiencies

Tray	System	Column diameter, ft	Tray spacing, in	Pressure, psia	Efficiency, %	% hole (slot) area	Ref.	
Sieve	Methanol-water	3.2	15.7	14.7	70-90	10.8	2	
	Ethanol-water	2.5	14	14.7	75-85	10.4	1	
	Methanol-water	3.2	15.7	14.7	90-100	4.8	2	
	Ethylbenzene-styrene	2.6	19.7	1.9	70	12.3	5	
	Benzene-toluene	1.5	15.7	14.7	60-75	8	10	
	Methanol- <i>n</i> propanol-sec butanol	6.0	18	18	64°		6	
	Mixed xylene + C ₈ -C ₁₀ paraffins and naphthenes	13.0	21	25	86°		4	
	Cyclohexane- <i>n</i> -heptane	4.0	24	5	60-70	14	9	
				24	80	14	9	
			4.0	24	5	70-80	8	8
				24	90	8	8	
	Isobutane- <i>n</i> -butane	4.0	24	165	110	14	9	
		4.0	24	165	120	8	8	
		4.0	24	300	110	8	8	
		4.0	24	400	100	8	8	
	<i>n</i> -Heptane-toluene	1.5	15.7	14.7	60-75	8	10	
	Methanol-water	2.0	13.6	14.7	68-72	10	11	
	Isopropanol-water	2.0	13.6	14.7	59-63		11	
	Toluene-methylcyclohexane	2.0	13.6	14.7	70-82		11	
	Toluene stripping from water	4	24	14.7	31-42	8	13	
Valve	Methanol-water	3.2	15.7	14.7	70-80	14.7	2	
	Ethanol-water	2.5	14	14.7	75-85		1	
	Ethyl benzene-styrene	2.6	19.7	1.9	75-85		3	
	Cyclohexane- <i>n</i> -heptane	4.0	24	24	70-96°		7	
	Isobutane- <i>n</i> -butane	4.0	24	165	108-121°		7	
	Cyclohexane- <i>n</i> -heptane	4.0	24	24	77-93 [†]	14.7	12	
				5	57-86 [†]	14.7	12	
	Isobutane- <i>n</i> -butane	4.0	24	165	110-123 [†]	14.7	12	
	C ₃ -C ₄ splitter	5.6	24	212	65-67 [†]	12	14	

References:

- Kirschbaum, *Distillier-Rektifizierteknik*, 4th ed., Springer-Verlag, Berlin and Heidelberg, 1969.
- Kastanek and Standart, *Sep. Sci.*, **2**, 439 (1967).
- Billet and Raichle, *Chem. Ing. Tech.*, **38**, 825 (1966); **40**, 377 (1968).
- AICHE Research Committee, *Tray Efficiency in Distillation Columns*, final report, University of Delaware, Newark, 1958.
- Billet R., *ICHEME, Symp. Ser.* **32**, p. 4:42 (1969).
- Mayfield et al., *Ind. Eng. Chem.*, **44**, 2238 (1952).
- Fractionation Research, Inc. "Report of Tests of Nutter Type B Float Valve Tray," July 2, 1964 from Sulzer Chem Tech.
- Sakata and Yanagi, *ICHEME, Eng. Symp. Ser.*, no. 56, 3.2/21 (1979).
- Yanagi and Sakata, *Ind. Eng. Chem. Process Des. Dev.*, **21**, 712 (1982).
- Zuiderweg and Van der Meer, *Chem. Tech. (Leipzig)*, **24**, 10 (1972).
- Korchinsky, *Trans. I. Chem. E.*, **72**, Part A, 472 (1994).
- Glitsch, Inc. "Glitsch Ballast Trays," Bulletin 159/160 (FRI Topical Report 15, 1958). Available from Koch-Glitsch LP, Wichita, Kans.
- Kunesh et al., Paper presented at the AIChE Spring National Meeting, Atlanta, Ga., 1994.
- Remesat, Chuang, and Svrcek, *Trans. I Chem. E.*, Vol. 83, Part A, p. 508, May 2005.

Notes:

[°]Rectangular Sulzer BDP valves.

[†]Glitsch V-1 round valves (Koch-Glitsch).

[‡]Two-pass trays, short path length.

To convert feet to meters, multiply by 0.3048; to convert inches to centimeters, multiply by 2.54; and to convert psia to kilopascals, multiply by 6.895.

Vital, Gossel and Olsen [*Hydroc. Proc.* **63**, 11, p. 147 (1984)] and Garcia and Fair [*Ind. Eng. Chem. Res.* **39**, p. 1809 (2000)] present an extensive tabulation of tray efficiency data collected from the published literature.

The *GPSA Engineering Data Book* (10th ed., Gas Processors Association, 1987) and Kaes (*Refinery Process Modeling—A Practical Guide to Steady State Modeling of Petroleum Processes Using Commercial Simulators*, Athens Printing Co., Athens, Ga., 2000) tabulate typical efficiencies in gas plant and refinery columns, respectively. Pilling (Paper presented at the 4th Topical Conference on Separations Science and Technology, November 1999, available from Sulzer Chemtech, Tulsa, Okla.) tabulated more typical efficiencies. Similar information is often available from simulation guide manuals. The quality and reliability of efficiencies from these sources vary and are generally lower than the reliability of actual measured data.

Scale-up from a Pilot- or Bench-Scale Column This is a very common scale-up. No reduction in efficiency on scale-up is expected as long as several precautions are observed. These precautions, generally relevant to pilot- or bench-scale columns, are spelled out with specific reference to the Oldershaw column.

Scale-up from Oldershaw Columns One laboratory-scale device that found wide application in efficiency investigations is the Oldershaw column [Fig. 14-44, Oldershaw, *Ind. Eng. Chem. Anal. Ed.* **13**, 265 (1941)]. This column is available from a number of laboratory supply houses and can be constructed from glass for atmospheric operation or from metal for higher pressures. Typical column diameters are 25 to 100 mm (1 to 4 in), with tray spacing the same as the column diameter.

Fair, Null, and Bolles [*Ind. Eng. Chem. Process Des. Dev.* **22**, 53 (1983)] found that efficiency measurements in Oldershaw columns closely approach the point efficiencies [Eq. (14-133)] measured in

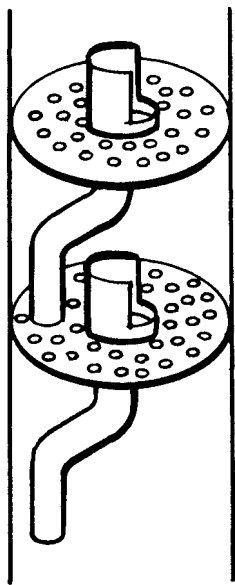


FIG. 14-44 An Oldershaw column. (From H. Z. Kister, *Distillation Design*, copyright © 1992 by McGraw-Hill; reprinted by permission.)

commercial sieve-tray columns (Fig. 14-45) providing (1) the systems being distilled are the same, (2) comparison is made at the same relative approach to the flood point, (3) operation is at total reflux, and (4) a standard Oldershaw device is used in the laboratory experimentation. Fair et al. compared several systems, utilizing as large-scale information the published efficiency studies of Fractionation Research, Inc. (FRI).

A mixing model can be used to convert the Oldershaw point efficiencies to overall column efficiencies. This enhances the commercial column efficiency estimates. A conservative approach suggested by Fair et al. is to apply the Oldershaw column efficiency as the estimate for the overall column efficiency of the commercial column, taking no credit for the greater plug-flow character upon scale-up. The author prefers this conservative approach, considering the poor reliability of mixing models.

Previous work with Oldershaw columns [Ellis, Barker, and Contractor, *Trans. Instn. Chem. Engrs.* **38**, 21 (1960)], spells an additional note of caution. Cellular (i.e., wall-supported) foam may form in pilot or Oldershaw columns, but is rare in commercial columns. For a

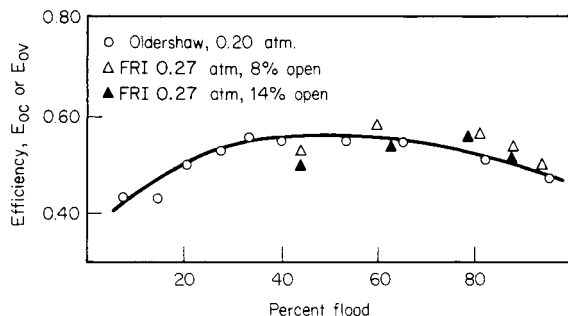


FIG. 14-45 Overall column efficiency of 25-mm Oldershaw column compared with point efficiency of 1.22-m-diameter-sieve-plate column of Fractionation Research, Inc. System = cyclohexane-*n*-heptane. [Fair, Null, and Bolles, *Ind. Eng. Chem. Process Des. Dev.*, **22**, 53 (1982).]

given system, higher Oldershaw column efficiencies were measured under cellular foam conditions than under froth conditions. For this reason, Gerster [*Chem. Eng. Progr.* **59**(3), 35 (1963)] warned that when cellular foam can form, scale-up from an Oldershaw column may be dangerous. The conclusions presented by Fair et al. do not extend to Oldershaw columns operating in the cellular foam regime. Cellular foam can be identified by lower pilot column capacity compared to a standard mixture that is visualized not to form cellular foam.

Heat losses are a major issue in pilot and Oldershaw columns and can lead to optimistic scale-up. Special precautions are needed to keep these at a minimum. Vacuum jackets with viewing ports are commonly used.

Uses of Oldershaw columns to less conventional systems and applications were described by Fair, Reeves, and Seibert [Topical Conference on Distillation, AIChE Spring Meeting, New Orleans, p. 27 (March 10–14, 2002)]. The applications described include scale-up in the absence of good VLE, steam stripping efficiencies, individual component efficiencies in multicomponent distillation, determining component behavior in azeotropic separation, and foam testing.

Empirical Efficiency Prediction Two empirical correlations which have been the standard of the industry for distillation tray efficiency prediction are the Drickamer and Bradford, in Fig. 14-46 [*Trans. Am. Inst. Chem. Eng.* **39**, 319 (1943)] and a modification of it by O'Connell [*Trans. Am. Inst. Chem. Eng.* **42**, 741 (1946)], in Fig. 14-47. The Drickamer-Bradford plot correlates efficiency as a function of liquid viscosity only, which makes it useful for petroleum cuts. O'Connell added the relative volatility to the x axis.

Lockett (*Distillation Tray Fundamentals*, Cambridge University Press, Cambridge, England, 1986) noted some theoretical sense in O'Connell's correlation. Higher viscosity usually implies lower diffusivity, and therefore greater liquid-phase resistance and lower efficiency. Higher relative volatility increases the significance of the liquid-phase resistance, thus reducing efficiency. Lockett expresses the O'Connell plot in equation form:

$$E_{OC} = 0.492(\mu_L \alpha)^{-0.245} \quad (14-138)$$

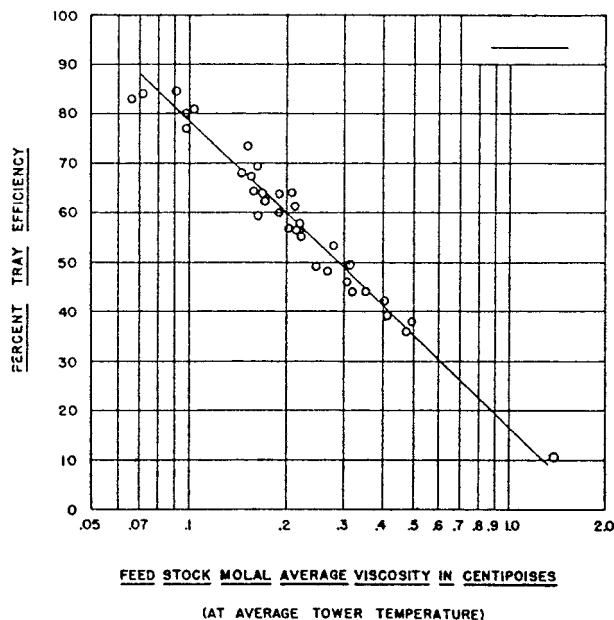


FIG. 14-46 The Drickamer and Bradford tray efficiency correlation for refinery towers. To convert centipoise to pascal-seconds, multiply by 0.0001. [From Drickamer and Bradford, *Trans. Am. Inst. Chem. Eng.* **39**, 319 (1943). Reprinted courtesy of the AIChE.]

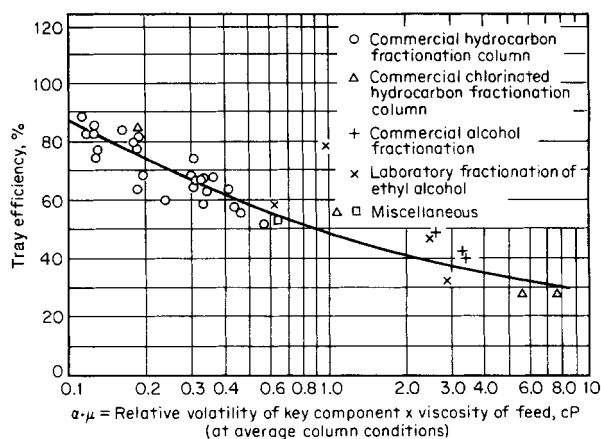


FIG. 14-47 O'Connell correlation for overall column efficiency E_{OC} for distillation. To convert centipoises to pascal-seconds, multiply by 10^{-3} . [O'Connell, *Trans. Am. Inst. Chem. Eng.*, **42**, 741 (1946).]

(The viscosity is in cP and E_{OC} is fractional.) The volatility and viscosity are evaluated at the average arithmetic temperature between the column top and bottom temperatures. The relative volatility is between the key components.

The O'Connell correlation was based on data for bubble-cap trays. For sieve and valve trays, its predictions are likely to be slightly conservative.

Theoretical Efficiency Prediction Theoretical tray efficiency prediction is based on the two-film theory and the sequence of steps in Fig. 14-41. Almost all methods evolved from the AIChE model (AIChE Research Committee, *Bubble Tray Design Manual*, New York, 1958). This model was developed over 5 years in the late 1950s in three universities. Since then, several aspects of the AIChE model have been criticized, corrected, and modified. Reviews are given by Lockett (*Distillation Tray Fundamentals*, Cambridge University Press, Cambridge, England, 1986) and Chan and Fair [*Ind. Eng. Chem. Proc.*

Des. Dev. **23**, 814 (1984)]. An improved version of the AIChE model, which alleviated several of its shortcomings and updated its hydraulic and mass-transfer relationships, was produced by Chan and Fair.

The Chan and Fair correlation generally gave good predictions when tested against a wide data bank, but its authors also observed some deviations. Its authors described it as "tentative until more data become available." The Chan and Fair correlation is considered the most reliable fundamental correlation for tray efficiency, but even this correlation has been unable to rectify several theoretical and practical limitations inherited from the AIChE correlation (see Kister, *Distillation Design*, McGraw-Hill, New York, 1992). Recently, Garcia and Fair (*Ind. Eng. Chem. Res.* **39**, 1818, 2000) proposed a more fundamental and accurate model that is also more complicated to apply.

The prime issue that appears to plague fundamental tray efficiency methods is their tendency to predict efficiencies of 80 to 100 percent for distillation columns larger than 1.2 m (4 ft) in diameter. In the real world, most columns run closer to 60 percent efficiency. Cai and Chen (*Distillation 2003: Topical Conference Proceedings*, AIChE Spring National Meeting, New Orleans, La., March 30–April 3, 2003) show that published eddy diffusivity models, which are based on small-column work, severely underestimate liquid backmixing and overestimate plug flow in commercial-scale columns, leading to optimistic efficiency predictions. Which other limitations (if any) in the theoretical methods contribute to the mismatch, and to what degree, is unknown. For this reason, the author would not recommend any currently published theoretical tray efficiency correlation for obtaining design efficiencies.

Example 12: Estimating Tray Efficiency For the column in Example 9, estimate the tray efficiency, given that at the relative volatility near the feed point is 1.3 and the viscosity is 0.25 cP.

Solution Table 14-12 presents measurements by Billet (loc. cit.) for ethylbenzene-styrene under similar pressure with sieve and valve trays. The column diameter and tray spacing in Billet's tests were close to those in Example 9. Since both have single-pass trays, the flow path lengths are similar. The fractional hole area (14 percent in Example 9) is close to that in Table 14-12 (12.3 percent for the tested sieve trays, 14 to 15 percent for standard valve trays). So the values in Table 14-12 should be directly applicable, that is, 70 to 85 percent. So a conservative estimate would be 70 percent. The actual efficiency should be about 5 to 10 percent higher.

Alternatively, using Eq. (14-138) or Fig. 14-47, $E_{OC} = 0.492(0.25 \times 1.3)^{-0.245} = 0.65$ or 65 percent. As stated, the O'Connell correlation tends to be slightly conservative. This confirms that the 70 percent above will be a good estimate.

EQUIPMENT FOR DISTILLATION AND GAS ABSORPTION: PACKED COLUMNS

Packings are generally divided into three classes:

1. *Random or dumped packings* (Figs. 14-48 and 14-49) are discrete pieces of packing, of a specific geometric shape, that are "dumped" or randomly packed into the column shell.

2. *Structured or systematically arranged packings* (Fig. 14-50) are crimped layers of corrugated sheets (usually) or wire mesh. Sections of these packings are stacked in the column.

3. *Grids*. These are also systematically arranged packings, but instead of wire mesh or corrugated sheets, these use an open-lattice structure.

Random and structured packings are common in commercial practice. The application of grids is limited primarily to heat-transfer and wash services and/or where a high fouling resistance is required. Grids are discussed in detail elsewhere (Kister, *Distillation Design*, McGraw-Hill, New York, 1992).

Figure 14-51 is an illustrative cutaway of a packed tower, depicting typical internals. This tower has a structured-packed top bed and a random-packed bottom bed. Each bed rests on a support grid or plate. The lower bed has a holddown grid at its top to restrict packing uplift. Liquid to each of the beds is supplied by a liquid distributor. An intermediate distributor, termed a *redistributor*, is used to introduce feed and/or to remix liquid at regular height intervals. The intermediate distributor in Fig. 14-51 is not self-collecting, so a chevron collector is

used to collect the liquid from the bed above. An internal pipe passes this liquid to the distributor below. The collected liquid is mixed with the fresh feed (not shown) before entering the distributor. The reboiler return enters behind a baffle above the bottom sump.

As illustrated, the packing needs to be interrupted and a distributor added at each point where a feed enters or a product leaves. A simple distillation tower with a single feed will have a minimum of two beds, a rectifying bed and a stripping bed.

Packing Objectives The objective of any packing is to maximize efficiency for a given capacity, at an economic cost. To achieve these goals, packings are shaped to

1. *Maximize the specific surface area, i.e., the surface area per unit volume.* This maximizes vapor-liquid contact area, and, therefore, efficiency. A corollary is that efficiency generally increases as the random packing size is decreased or as the space between structured packing layers is decreased.

2. *Spread the surface area uniformly.* This improves vapor-liquid contact, and, therefore, efficiency. For instance, a Raschig ring (Fig. 14-48a) and a Pall® ring (Fig. 14-48c) of an identical size have identical surface areas per unit volume, but the Pall® ring has a superior spread of surface area and therefore gives much better efficiency.

3. *Maximize the void space per unit column volume.* This minimizes resistance to gas upflow, thereby enhancing packing capacity.

A corollary is that capacity increases with random packing size or with the space between structured packing layers. Comparing with the first objective, a tradeoff exists; the ideal size of packing is a compromise between maximizing efficiency and maximizing capacity.

4. *Minimize friction.* This favors an open shape that has good aerodynamic characteristics.

5. *Minimize cost.* Packing costs, as well as the requirements for packing supports and column foundations, generally rise with the weight per unit volume of packing. A corollary is that packings become cheaper as the size increases (random packing) and as the space between layers increases (structured packing).

Random Packings Historically, there were three generations of evolution in random packings. The first generation (1907 to the 1950s) produced two basic simple shapes—the Raschig ring and the Berl saddle (Fig. 14-48*a, b*) that became the ancestors of modern random packings. These packings have been superseded by more modern packing and are seldom used in modern distillation practice.

The second generation (late 1950s to the early 1970s) produced two popular geometries—the Pall® ring, which evolved from the Raschig ring, and the Intalox® saddle (Fig. 14-48*c-f*), which evolved from the Berl saddle.

BASF developed the Pall® ring by cutting windows in the Raschig ring and bending the window tongues inward. This opened up the ring, lowering the aerodynamic resistance and dramatically enhancing capacity. The bent tongues improved area distribution around the particle, giving also better efficiency. These improvements made the first generation Raschig rings obsolete for distillation.

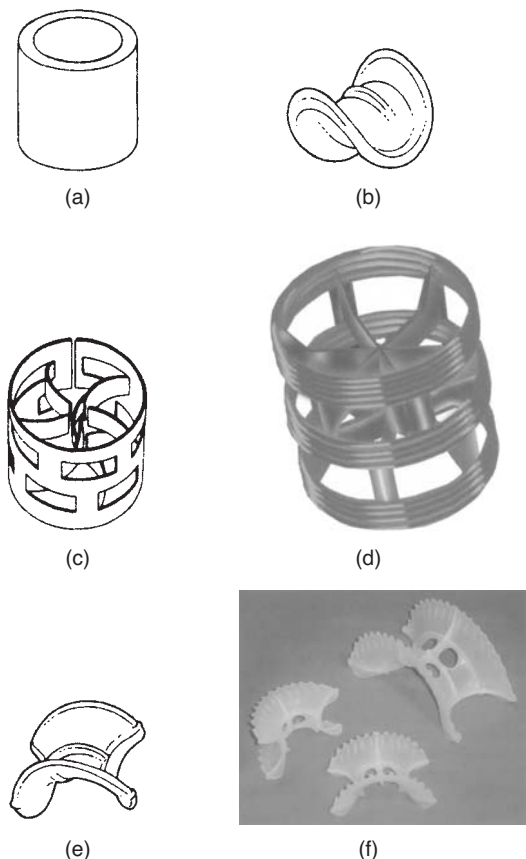


FIG. 14-48 Common first- and second-generation random packings. (a) Raschig ring (metal, plastic, ceramic). (b) Berl saddle (ceramic). (c) Pall ring (metal). (d) Pall ring (plastic). (e) Intalox saddle (ceramic). (f) Super Intalox saddle (plastic). (Parts d, f, courtesy of Koch-Glitsch LP.)

Berl saddles (ceramics) are still used due to their good breakage resistance.

The second-generation packings are still popular and extensively used in modern distillation practice. The third generation (the mid-1970s until present) has produced a multitude of popular geometries, most of which evolved from the Pall® ring and Intalox® saddle. Some are shown in Fig. 14-49. A more comprehensive description of the various packings is given elsewhere (Kister, *Distillation Design*, McGraw-Hill, New York, 1992).

The third generation of packing was a significant, yet not large, improvement over the second generation, so second-generation packings are still commonly used.

Structured Packings Structured packings have been around since as early as the 1940s. First-generation structured packings, such as Panapak, never became popular, and are seldom used nowadays.

The second generation of structured packings began in the late 1950s with high-efficiency wire-mesh packings such as Goodloe®, Hyperfil®, and the Sulzer® (wire-mesh) packings. By the early 1970s, these packings had made substantial inroads into vacuum distillation, where their low pressure drop per theoretical stage is a major advantage. In these services, they are extensively used today. Their high cost, high sensitivity to solids, and low capacity hindered their application outside vacuum distillation.

The corrugated-sheet packing, first introduced by Sulzer in the late 1970s, started a third generation of structured packings. With a high capacity, lower cost, and lower sensitivity to solids, while still retaining a high efficiency, these corrugated-sheet packings became competitive with conventional internals, especially for revamps. The 1980s saw an accelerated rise in popularity of structured packings, to the point of their becoming one of the most popular column internals in use today.

Corrugated structured packings are fabricated from thin, corrugated (crimped) metal sheets, arranged parallel to one another. The corrugated sheets are assembled into an element (Figs. 14-50*a, c* and 14-51). The sheets in each element are arranged at a fixed angle to the vertical. Table 14-14 contains geometric data for several corrugated packings.

Geometry (Fig. 14-52) The crimp size defines the opening between adjacent corrugated layers. Smaller B , h , and S yield narrower openings, more sheets (and, therefore, greater surface area) per unit volume, and more efficient packing, but higher resistance to gas upflow, lower capacity, and enhanced sensitivity to plugging and fouling.

The corrugations spread gas and liquid flow through a single element in a series of parallel planes. To spread the gas and liquid uniformly in all radial planes, adjacent elements are rotated so that sheets of one element are at a fixed angle to the layer below (Fig. 14-51). For good spread, element height s is relatively short (typically 200 to 300 mm, 8 to 12 in) and the angle of rotation is around 90°.

The surfaces of a few structured packings (especially those used in highly fouling environments) are smooth. Most structured packings have a roughened or enhanced surface that assists the lateral spread of liquid, promotes film turbulence, and enhances the area available for mass transfer. Texturing commonly employed is embossing and grooving (Fig. 14-50*a, b*).

The surfaces of most (but not all) structured packings contain holes that serve as communication channels between the upper and lower surfaces of each sheet. If the holes are too small, or nonexistent, both sides of a sheet will be wet only at low liquid rates. At high liquid rates, *sheeting* or *blanking* will cause liquid to run down the top surface with little liquid wetting the bottom surface [Chen and Chuang, *Hydroc. Proc.* 68(2), 37 (1989)], which may lower efficiency. Usually, but not always, the holes are circular (Fig. 14-50*a, b*), about 4 mm in diameter. Oluje et al. (Distillation 2003: Topical Conference Proceedings, p. 523, AIChE, 2003, Spring National Meeting, New Orleans, La.) showed that the hole diameter has a complex effect, strongly dependent on packing size, on both capacity and efficiency.

Inclination Angle In each element, corrugated sheets are most commonly inclined at about 45° to the vertical (typically indicated by the letter Y following the packing size). This angle is large enough for good drainage of liquid, avoiding stagnant pockets and regions of liquid accumulation, and small enough to prevent gas from bypassing the metal surfaces. In some packings, the inclination angle to the vertical is steepened to 30° (typically indicated by the letter X following the

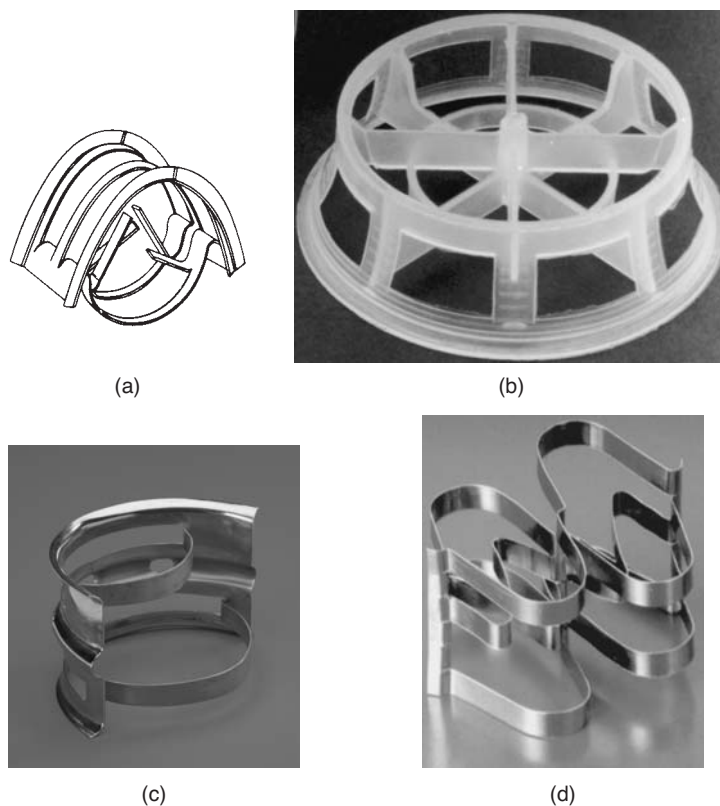


FIG. 14-49 Common third-generation random packings. (a) Intalox metal tower packing (IMTP). (b) Cascade mini-ring (CMR) (plastic). (c) Nutter ring (metal). (d) Raschig Super-Ring (metal). (Parts a, b, courtesy of Koch-Glitsch LP; part c, courtesy of Sulzer Chemtech; part d, courtesy of Raschig AG.)

packing size). This improves drainage, and therefore capacity, but at the expense of reduced gas-liquid contact, and therefore efficiency.

A recent development followed the realization that liquid drainage was restricted at the element-to-element transition rather than inside elements (Lockett and Billingham, *IChemE Symp. Ser.* **152**, London, 2006). This means that the liquid accumulation leading to flood initiates at the transition region. A fourth generation of structured packing started, in which the main body of each element has layers inclined at 45° , but the ends of each element are almost vertical to permit drainage at this end region (Fig. 14-50*d*; but keep in mind that successive elements are rotated 90° rather than continuous, as shown in Fig. 14-50*d*). These S-shaped or high-capacity packings offer greater capacity compared to equivalent 45° inclined packings with efficiency the same with some (Pilling and Haas, Topical Conference Proceedings, p. 132, AIChE Spring Meeting, New Orleans, March 10–14, 2002; McNulty and Sommerfeldt in “Distillation: Horizons for the New Millennium,” Topical Conference Proceedings, p. 89, AIChE Spring Meeting, Houston, Tex., March 1999) and lower with others [Olujić et al., *Chem. Eng. and Proc.*, **42**, p. 55 (2003)].

PACKED-COLUMN FLOOD AND PRESSURE DROP

Pressure drop of a gas flowing upward through a packing countercurrently to liquid flow is characterized graphically in Fig. 14-53. At very low liquid rates, the effective open cross section of the packing is not appreciably different from that of dry packing, and pressure drop is due to flow through a series of variable openings in the bed. Thus, pressure drop is proportional approximately to the square of the gas

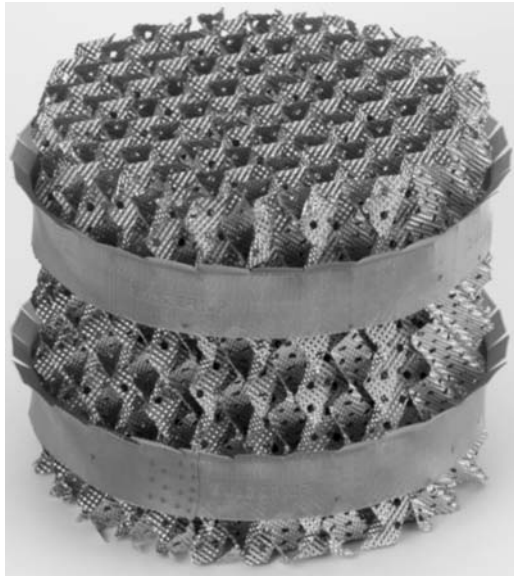
velocity, as indicated in the region *AB*. At higher liquid rates, the effective open cross section is smaller because of the presence of liquid (region *A'B'*). The pressure drop is higher, but still proportional to the square of the gas velocity.

At higher gas rates, a portion of the energy of the gas stream is used to support an increasing quantity of liquid in the column. For all liquid rates, a zone is reached where pressure drop is proportional to a gas flow rate to a power distinctly higher than 2; this zone is called the *loading zone*. The increase in pressure drop is due to the liquid accumulation in the packing voids (region *BC* or *B'C'*)

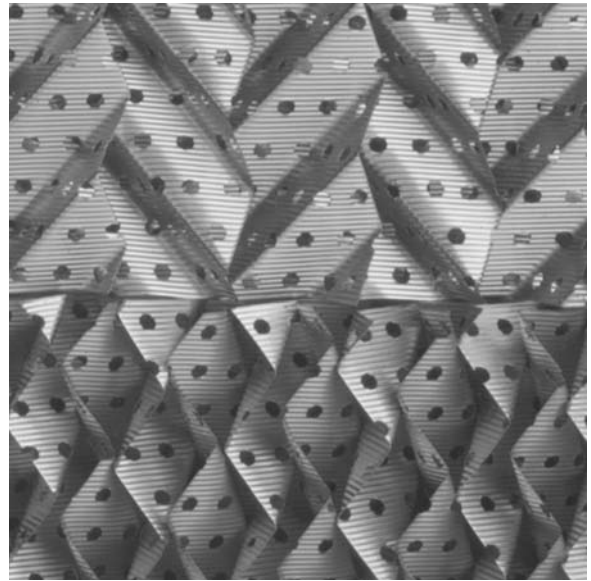
As the liquid holdup increases, the effective orifice diameter may become so small that the liquid surface becomes continuous across the cross section of the column. Column instability occurs concomitantly with a rising continuous-phase liquid body in the column. Pressure drop shoots up with only a slight change in gas rate (condition *C* or *C'*). The phenomenon is called *flooding* and is analogous to entrainment flooding in a tray column.

Alternatively, a phase inversion occurs, and gas bubbles through the liquid. The column is not unstable and can be brought back to gas-phase continuous operation by merely reducing the gas rate. A stable operating condition beyond flooding (region *CD* or *C'D'*) may form with the liquid as the continuous phase and the gas as the dispersed phase [Lerner and Grove, *Ind. Eng. Chem.* **43**, 216 (1951); Teller, *Chem. Eng.* **61**(9), 168 (1954); Leung et al., *Ind. Eng. Chem. Fund.* **14**(1), 63 (1975); Buchanan, *Ind. Eng. Chem. Fund.* **15**(1), 87 (1976)].

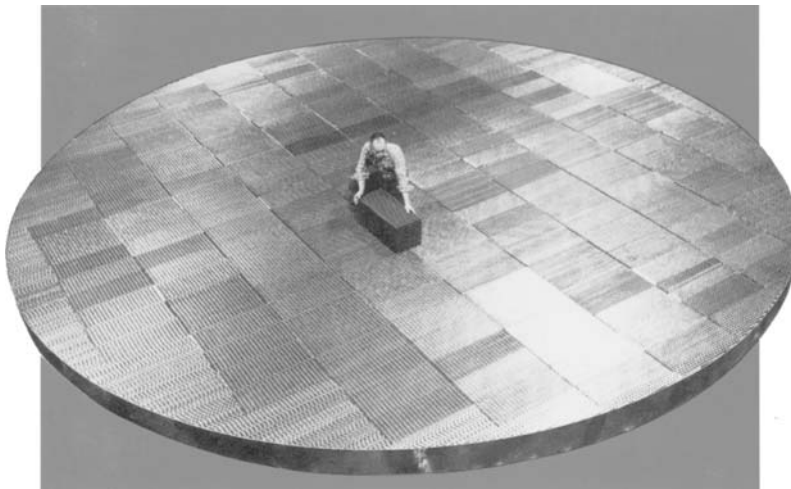
For total-reflux distillation in packed columns, regions of loading and flooding are identified by their effects on mass-transfer efficiency, as shown in Fig. 14-54. Gas and liquid rate increase together, and a



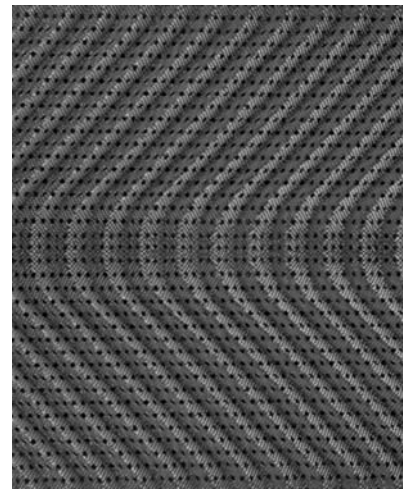
(a)



(b)



(c)



(d)

FIG. 14-50 Common structured packings. (a) A small element of Mellapak™ showing embossed surface, holes, and corrugated-sheet arrangement. (b) A closeup of the surface of Flexipac™ showing grooved surface and holes. (c) Fitting structured packing elements to a large-diameter tower. (d) Mellapak Plus™, a fourth-generation structured packing, showing a 45° inclination angle in the element and near-vertical inclination at the element-to-element transition. Note that in the tower, the successive layers will be oriented 90° to each other as in part b. (Parts a, d, courtesy of Sulzer Chemtech; parts b, c, courtesy of Koch-Glitsch LP.)

point is reached at which liquid accumulates rapidly (point B) and effective surface for mass transfer decreases rapidly.

Flood-Point Definition In 1966, Silvey and Keller [*Chem. Eng. Progr.* **62**(1), 68 (1966)] listed 10 different flood point definitions that have been used by different literature sources. A later survey (Kister and Gill, *Proceedings of Chemeca 92*, p. 185-2, Canberra, Australia, 1992) listed twice that many. As Silvey and Keller pointed out, the existence of so many definitions puts into question what constitutes flooding in a packed tower, and at what gas rate it occurs. Symptoms used to identify flood in these definitions include appearance of liquid on top of the bed, excessive entrainment, a sharp rise

in pressure drop, a sharp rise in liquid holdup, and a sharp drop in efficiency. The survey of Kister and Gill suggests that most flood point definitions describe the point of flooding initiation (*incipient flooding*; point C or C' on Figs. 14-53 and 14-54). The different incipient flooding definitions gave surprisingly little scatter of flood point data (for a given packing under similar operating conditions). It follows that any definition describing flooding initiation should be satisfactory.

The author believes that due to the variations in the predominant symptom with the system and the packing, the use of multiple symptoms is most appropriate. The author prefers the following definition

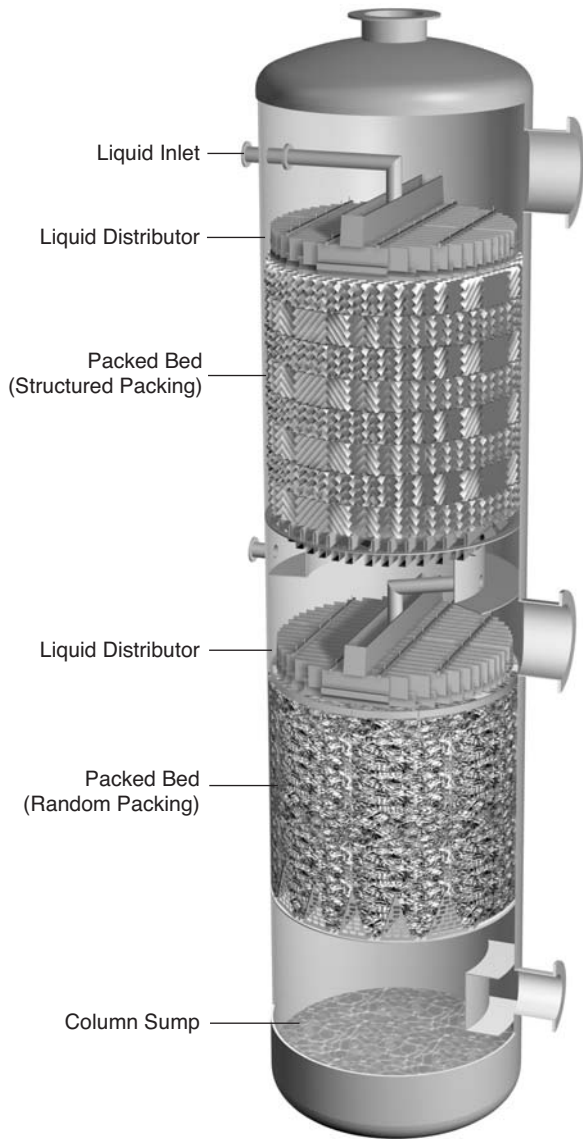


FIG. 14-51 Illustrative cutaway of a packed tower, depicting an upper bed of structured packing and a lower bed of random packing. (Courtesy of Sulzer Chemtech.)

by Fair and Bravo [*Chem. Eng. Symp. Ser.* **104**, A183 (1987)]: "A region of rapidly increasing pressure drop with simultaneous loss of mass transfer efficiency. Heavy entrainment is also recognized as a symptom of this region." An almost identical definition was presented earlier by Billet (*Distillation Engineering*, Chem. Publishing Co., New York, 1979).

The maximum operational capacity or throughput (often also referred to as maximum efficient capacity) is defined (Strigle, *Packed Tower Design and Applications*, 2d ed., Gulf Publishing, Houston, Tex., 1994) as the "Maximum vapor rate that provides normal efficiency of a packing" (i.e., point B in Fig. 14-54). The MOC is clear-cut in Fig. 14-54. On the other hand, locating the MOC in other cases is difficult and leaves a lot of room for subjectivity.

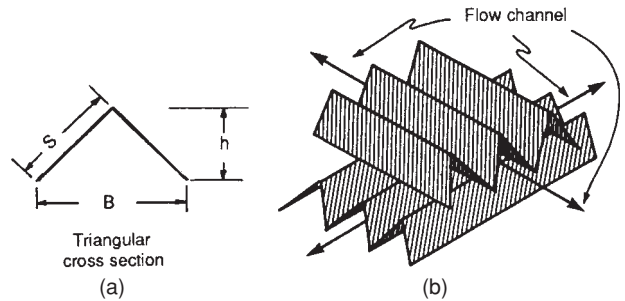


FIG. 14-52 Crimp geometry in structured packings. (a) Flow channel cross section. (b) Flow channel arrangement. (From J. R. Fair and J. L. Bravo, *Chem. Eng. Progr.*, Jan. 1990, p. 19; reproduced courtesy of the American Institute of Chemical Engineers.)

In most cases, [Kister and Gill, *Chem. Eng. Progr.* **87**(2), 32 (1991)], the velocity at which MOC is reached is related to the flood point velocity by

$$u_{s,MOC} = 0.95 u_{s,FI} \quad (14-139)$$

Flood and Pressure Drop Prediction The first generalized correlation of packed-column flood points was developed by Sherwood, Shipley, and Holloway [*Ind. Eng. Chem.*, **30**, 768 (1938)] on the basis of laboratory measurements primarily on the air-water system with random packing. Later work with air and liquids other than water led to modifications of the Sherwood correlation, first by Leva [*Chem. Eng. Progr. Symp. Ser.*, **50**(1), 51 (1954)], who also introduced the pressure drop curves, and later in a series of papers by Eckert. The generalized flooding-pressure drop chart by Eckert [*Chem. Eng. Progr.* **66**(3), 39 (1970)], included in previous editions of this handbook, was modified and simplified by Strigle (*Packed Tower Design and Applications*, 2d ed., Gulf Publishing, Houston, Tex., 1994) (Fig. 14-55). It is often called the generalized pressure drop correlation (GPDC). The ordinate is a capacity parameter [Eq. (14-140)] related to the Souders-Brown coefficient used for tray columns.

$$CP = C_s F_p^{0.5} v^{0.05} = U_s \left(\frac{\rho_G}{\rho_L - \rho_G} \right)^{0.50} F_p^{0.5} v^{0.05} \quad (14-140)$$

where U_s = superficial gas velocity, ft/s
 ρ_G , ρ_L = gas and liquid densities, lb/ft³ or kg/m³

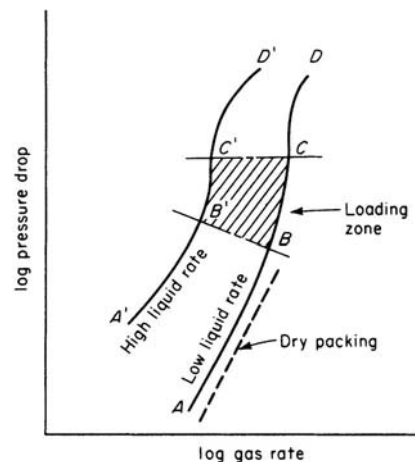


FIG. 14-53 Pressure-drop characteristics of packed columns.

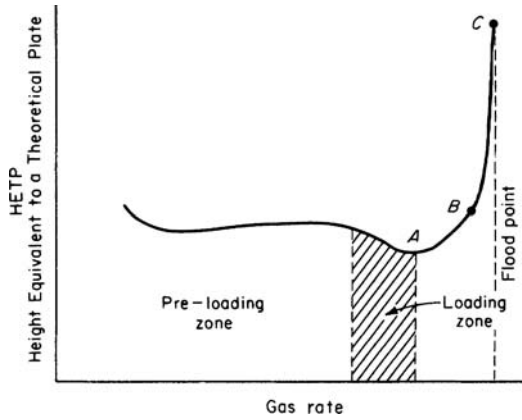


FIG. 14-54 Efficiency characteristics of packed columns (total-reflux distillation.)

- F_p = packing factor, ft^{-1}
- ν = kinematic viscosity of liquid, cS
- C_s = C-factor, Eq. (14-77), based on tower superficial cross-sectional area, ft/s
- CP = capacity factor, dimensional [units consistent with Eq. (14-140) and its symbols]

The abscissa scale term is the same flow parameter used for tray (dimensionless):

$$F_{LG} = \frac{L}{G} \left(\frac{\rho_G}{\rho_L} \right)^{0.5} \quad (14-141)$$

For structured packing, Kister and Gill [*Chem. Eng. Symp. Ser.* **128**, A109 (1992)] noticed a much steeper rise of pressure drop with flow parameter than that predicted from Fig. 14-55, and presented a modified chart (Fig. 14-56).

The GPDC charts in Figs. 14-55 and 14-56 do not contain specific flood curves. Both Strigle and Kister and Gill recommend calculating the flood point from the flood pressure drop, given by the Kister and Gill equation

$$\Delta P_{\text{flood}} = 0.12 F_p^{0.7} \quad (14-142)$$

Equation (14-142) permits finding the pressure drop curve in Fig. 14-55 or 14-56 at which incipient flooding occurs.

For low-capacity random packings, such as the small first-generation packings and those smaller than 1-in diameter ($F_p > 60 \text{ ft}^{-1}$), calculated flood pressure drops are well in excess of the upper pressure drop curve in Fig. 14-55. For these packings only, the original Eckert flood correlation [*Chem. Eng. Progr.* **66**(3), 39 (1970)] found in pre-1997 editions of this handbook and other major distillation texts is suitable.

The packing factor F_p is empirically determined for each packing type and size. Values of F_p , together with general dimensional data for individual packings, are given for random packings in Table 14-13 (to go with Fig. 14-55) and for structured packings in Table 14-14 (to go with Fig. 14-56).

Packing flood and pressure drop correlations should always be used with caution. Kister and Gill [*Chem. Eng. Progr.*, **87**(2), 32 (1991)] showed that deviations from the GPDC predictions tend to be systematic and not random. To avoid regions in which the systematic deviations lead to poor prediction, they superimposed experimental data points for each individual packing on the curves of the GPDC. Figure 14-57 is an example. This method requires a single chart for each packing type and size. It provides the highest possible accuracy as it interpolates measured data and identifies uncertain regions. A set of charts is in Chapter 10 of Kister's book (*Distillation Design*, McGraw-Hill, New York, 1992) with

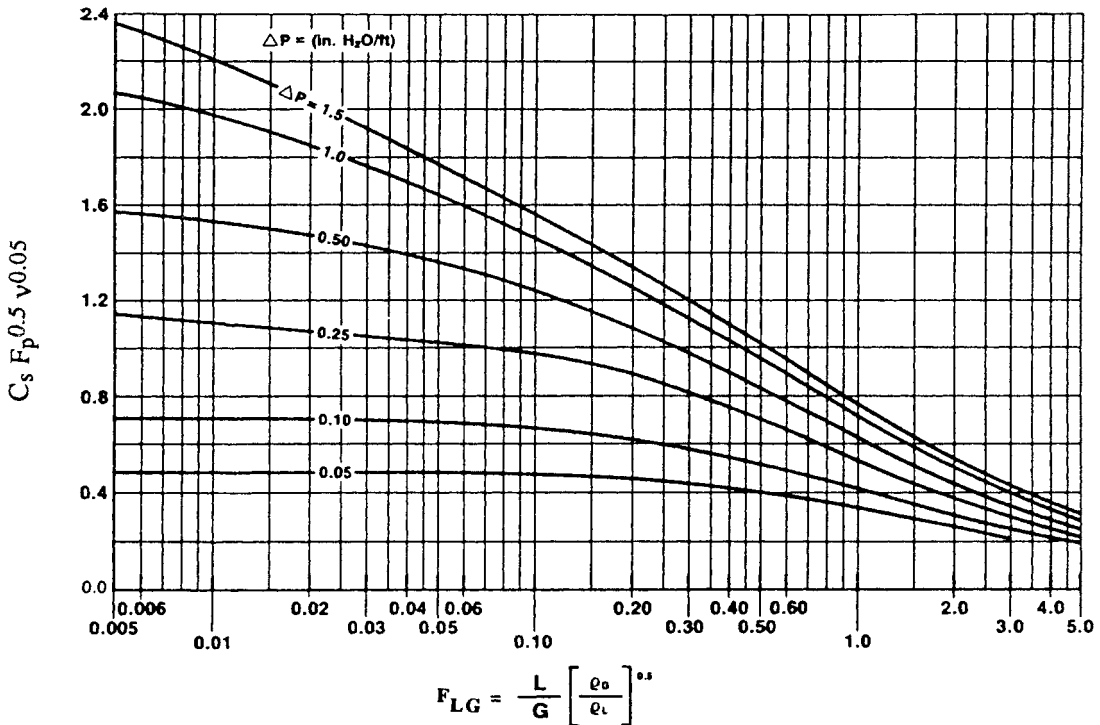


FIG. 14-55 Generalized pressure drop correlation of Eckert as modified by Strigle. To convert inches H_2O to mm H_2O , multiply by 83.31. (From *Packed Tower Design and Applications* by Ralph E. Strigle, Jr. Copyright © 1994 by Gulf Publishing Co., Houston, Texas. Used with permission. All rights reserved.)

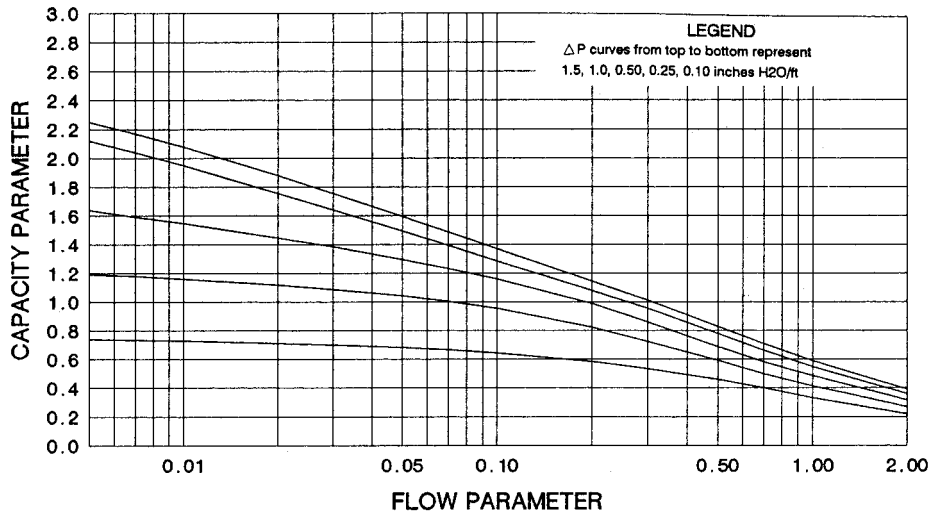


FIG. 14-56 The Kister and Gill GPDC (SP) chart for structured packings only. Abscissa and ordinate same as in Fig. 14-55. (From Kister, H. Z., and D. R. Gill, *ICHEME Symp. Ser.* 128, p. A109, 1992. Reprinted courtesy of IChemE.)

updates in Kister, Lason, and Gill, Paper presented at the AIChE Spring National Meeting, Houston, Tex., March 19–23, 1995; and in Kister, Scherffius, Afshar, and Abkar, in *Distillation 2007: Topical Conference Proceedings*, 2007 AIChE Spring National Meeting, Houston, Texas. The latter reference also discusses correct and incorrect applications of those interpolation charts.

There are many alternative methods for flood and pressure drop prediction. The Billet and Schultes [*ICHEME Symp. Ser.* 104, pp. A171 and B255 (1987)] and the Maćkowiak (“Fluiddynamik von Kolonnen mit Modernen Füllkörpern und Packungen für Gas/Flüssigkeitssysteme,” Otto Salle Verlag, Frankfurt am Main und Verlag Sauerländer Aarau, Frankfurt am Main, 1991) correlations are versions of the GPDC that take the liquid holdup into account. The Eiden and Bechtel correlation [*ICHEME Symp. Ser.* 142, p. 757 (1997)] is a version of the GPDC in which accuracy is improved by using constants representative of packing shape instead of packing factors. The Lockett and Billingham correlation (*ICHEME Symp. Ser.* 152, p. 400, London, 2006) uses a Wallis correlation

$$C_C^{0.5} + mC_L^{0.5} = C_{LC} \quad (14-143)$$

$$\text{where} \quad C_L = u_L[\rho_L/(\rho_L - \rho_G)]^{0.5} \quad (14-144)$$

and was shown to work well for high-surface-area (>400 m²/m³) structured packings. Here C_C is the gas C -factor, Eq. (14-77), based on the tower superficial cross-sectional area, and m and C_{LC} are constants, available from the cited reference for some packing.

A drawback of most of these correlations (except that of Eiden and Bechtel) is the unavailability of constants for many, often most, of the modern popular packings.

The above methods apply to nonfoaming systems. Foaming systems can be handled either by applying additional derating (system) factors to the flood correlation (see Table 14-9) or by limiting the calculated pressure drop to 0.25 in of water per foot of packing (Hausch, “Distillation Tools for the Practicing Engineer,” Topical Conference Proceedings, p. 119, AIChE Spring Meeting, New Orleans, March 10–14, 2002).

Pressure Drop The GPDC discussed above (Figs. 14-55 and 14-56) and the Kister and Gill interpolation charts provide popular methods for calculating packing pressure drops. An alternative popular method that is particularly suitable for lower liquid loads was presented by Robbins (below).

For gas flow through dry packings, pressure drop may be estimated by use of an orifice equation. For irrigated packings, pressure drop

increases because of the presence of liquid, which effectively decreases the available cross section for gas flow (Fig. 14-53). In principle, there should be a method for correcting the dry pressure drop for the presence of liquid. This approach was used by Leva [*Chem. Eng. Progr. Symp. Ser. No. 10*, 50, 51 (1954)]. A more recent method by Robbins [*Chem. Eng. Progr.*, p. 87 (May 1991)] utilizes the same approach and is described here. The total pressure drop is

$$\Delta P_t = \Delta P_d + \Delta P_L \quad (14-145)$$

where ΔP_t = total pressure drop, inches H₂O per foot of packing

$$\Delta P_d = \text{dry pressure drop} = C_3 G_f^2 10^{(C_4 L_f)} \quad (14-146)$$

$$\Delta P_L = \text{pressure drop due to liquid presence} \\ = 0.4 [L_f/20,000]^{0.1} [C_3 G_f^2 10^{(C_4 L_f)}]^4 \quad (14-147)$$

$$G_f = \text{gas loading factor} = 986 F_s (F_{pd}/20)^{0.5} \quad (14-148)$$

$$L_f = \text{liquid loading factor} = L(62.4/\rho_L)(F_{pd}/20)^{0.5} \mu_L^{0.1} \quad (14-149)$$

The term F_{pd} is a dry packing factor, specific for a given packing type and size. Values of F_{pd} are given in Tables 14-13 and 14-14. For operating pressures above atmospheric, and for certain packing sizes, L_f and G_f are calculated differently:

$$G_f = 986 F_s (F_{pd}/20)^{0.5} 10^{0.3 p_c} \quad (14-150)$$

$$L_f = L(62.4/\rho_L)(F_{pd}/20)^{0.5} \mu_L^{0.2} \quad F_{pd} > 200 \quad (14-151a)$$

$$L_f = L(62.4/\rho_L)(20/F_{pd})^{0.5} \mu_L^{0.1} \quad F_{pd} < 15 \quad (14-151b)$$

The Robbins equations require careful attention to dimensions. However, use of the equations has been simplified through the introduction of Fig. 14-58. The terms L_f and G_f are evaluated, and the ΔP_L is obtained directly from the chart. Basic nomenclature for the Robbins method follows:

$$C_3 = 7.4(10)^{-8}$$

$$C_4 = 2.7(10)^{-5}$$

$$F_{pd} = \text{dry packing factor, ft}^{-1}$$

$$F_s = \text{superficial } F\text{-factor for gas, } U_f \rho_g^{0.5}, \text{ ft/s}(\text{lb/ft}^3)^{0.5}$$

$$G = \text{gas mass velocity, lb/hr-ft}^2$$

$$G_f = \text{gas loading factor, lb/hr-ft}^2$$

$$L = \text{liquid mass velocity, lb/hr-ft}^2$$

$$L_f = \text{liquid loading factor, lb/hr-ft}^2$$

$$\Delta P = \text{pressure drop, inches H}_2\text{O/ft packing} (\times 83.3 = \text{mm H}_2\text{O/m packing})$$

TABLE 14-13 Characteristics of Random Packings

Name	Size, mm, or no. (#)	Bed density, ^o kg/m ³	Area, m ² /m ³	% voids	Packing factor, m ⁻¹		Vendor
					Normal F_p^1	Dry F_{pd}^1	
Metals							
Pall rings (also Flexi-rings, Ballast rings, P-rings)	16	510	360	92	256	262	Various
	25	325	205	94	183	174	
	38	208	130	95	131	91	
	50	198	105	96	89	79	
	90	135	66	97	59	46	
Metal Intalox (IMTP) [also I-rings, AHPP, RSMR, MSR] [§]	25	224	207	97	134	141	Koch-Glitsch [Sulzer, Amistco, Rauschert, Montz] [§]
	40	153	151	97	79	85	
	50	166	98	98	59	56	
	70	141	60	98	39	—	
Nutter rings	#0.7	177	226	98	—	128	Sulzer
	#1	179	168	98	98	89	
	#1.5	181	124	98	79	66	
	#2	144	96	98	59	56	
	#2.5	121	83	98	52	49	
	#3.0	133	66	98	43	36	
Raschig Super-ring	#0.5	275	250	98	—	—	Raschig
	#0.7	185	175	98	—	—	
	#1	220	160	98	82	—	
	#1.5	170	115	98	59	—	
	#2	155	98	99	49	—	
	#3	150	80	98	36	—	
Cascade mini-rings (CMR)	#1	389	250	96	131	102	Koch-Glitsch
	#1.5	285	190	96	95	—	
	#2	234	151	97	72	79	
	#2.5	195	121	97	62	—	
	#3	160	103	98	46	43	
	#4	125	71	98	33	32	
Fleximax	#300	—	141	98	85	—	Koch-Glitsch
	#400	—	85	98	56	—	
Jaeger Tripacks (Top-Pak)	#1	223	118	96	85	—	Raschig
	#2	170	75	98	46	—	
VSP	25	352	206	98	105 [†]	—	Raschig
	50	296	112	96	69	—	
Ralu-rings	25	310	215	98	157 [†]	—	Raschig
	38	260	135	97	92 [†]	—	
	50	200	105	98	66 [†]	—	
Hiflow	25	298	203	96	—	—	Rauschert
	50	175	92	98	52	—	
Hy-Pak, K-Pak, AIPR	#1	262	174	97	148	—	Koch-Glitsch, Amistco
	#1.5	180	118	98	95	—	
	#2	161	92	98	85	—	
	#3	181	69	98	52	—	
Raschig rings (¹ / ₁₆ in wall)	19	1500	245	80	722	—	Various
	25	1140	185	86	472	492	
	50	590	95	92	187	223	
	75	400	66	95	105	—	
Ceramics							
Berl saddles	6	900	900	60	—	2950	Various
	13	865	465	62	790	900	
	25	720	250	68	360	308	
	38	640	150	71	215	154	
	50	625	105	72	150	102	
Intalox, Flexi-saddles, Torus-saddles, Novalox	6	864	984	65	—	2720	Various
	13	736	623	71	660	613	
	25	672	256	73	302	308	
	50	608	118	76	131	121	
	75	576	92	79	72	66	
Raschig rings	6	960	710	62	—	5250	Various
	13	880	370	64	1900	1705	
	25	670	190	74	587	492	
	50	660	92	74	213	230	
	75	590	62	75	121	—	
Pall ring	25	620	220	75	350	—	Raschig
	38	540	164	78	180	—	
	50	550	121	78	142	—	
	80	520	82	78	85 [†]	—	

TABLE 14-13 Characteristics of Random Packings (Concluded)

Name	Size, mm, or no. (#)	Bed density ^a kg/m ³	Area, m ² /m ³	% voids	Packing factor, m ⁻¹		Vendor
					Normal F_p^1	Dry F_{pd}^1	
Ceramics							
Hiflow rings	38	409	108	83	121	—	Rauschert
	50	405	89	82	95	—	
	70	333	52	86	49	—	
Plastics							
Pall rings	15	95	350	87	320	348	Various
	25	71	206	90	180	180	
	40	70	131	91	131	131	
	50	60	102	92	85	82	
	90	43	85	95	56	39	
Super Intalox, Flexi-saddles, Super-Torus, Novalox	25	83	207	90	131	131	Various
	50	60	108	93	92	85	
	75	48	89	96	59	46	
Cascade mini-rings (CMR)	#1A	53	185	97	98	92	Koch-Glitsch
	#2A	46	115	97	59	—	
	#3A	40	74	98	39	33	
Raschig Super-ring	#0.6	62	205	96	105 [†]	—	Raschig
	#2	55	100	96	49	—	
Ralu-ring	15	80	320	94	230 [†]	—	Raschig
	25	56	190	94	135	—	
	38	65	150	95	80	—	
	50	60	110	95	55	—	
	90	40	75	96	38	—	
	125	30	60	97	30 [†]	—	
Snowflake	—	51	92	97	43	—	Koch-Glitsch
Nor-Pac	25	72	180	92	102	—	NSW
	38	61	144	93	69	—	
	50	53	102	94	46	—	
Tri-Packs (Hacketten)	#1	67	158	93	53 [†]	—	Raschig
	#2	53	125	95	39 [†]	43	
Ralu-Flow	#1	55	165	95	67 [†]	—	Raschig
	#2	54	100	95	38 [†]	—	
Hiflow	25	63	192	92	138	—	Rauschert
	50	59	110	93	66	—	
	90	34	65	97	30	—	
Lanpac	90	67	148	93	46	—	Lantec
Impac	#3	83	213	91	49	—	
Tellerettes	25	112	180	87	—	131	Ceilcote
	50	59	125	93	—	—	

^aValues are approximate and may not be consistent. Actual number depends on wall thickness and material.

¹Packing factor F_p from Kister, *Distillation Design*, McGraw-Hill, 1992; Kister, Larson, and Gill, paper presented at the Houston AIChE meeting, March 19–23, 1995; Strigle, *Packed Tower Design and Applications*, 2d ed., Gulf Publishing Co., Houston, Tex., 1994; Kister et al., in *Distillation 2007. Topical Conference Proceedings, 2007 AIChE Spring National Meeting*, Houston, Tex.

[†]Dry packing factor F_{pd} from Robbins, *Chem. Eng. Progr.*, **87**(1), 19 (1990).

[‡]The bracketed packings are similar to, but not the same as, the Koch-Glitsch IMTP. Some of them have holes that the IMTP do not have, and others have sizes that are different and are made by different dies.

^{††}Packing factor supplied by packing vendor.

Vendors: Koch-Glitsch LLP, Wichita, Kansas; Raschig GmbH, Ludwigshafen/Rhein, Germany; Sulzer Chemtech Ltd., Winterthur, Switzerland; Rauschert Verfahrenstechnik GmbH, Steinwiesen, Germany; Amistco Separation Products Inc., Alvin, Texas; Julius Montz GmbH, Hilden, Germany; Ceilcote Co., Berea, Ohio; NSW Corp., Roanoke, Virginia; Lantec Products Inc., Agoura Hills, California.

ρ_C = gas density, lb/ft³
 ρ_L = liquid density, lb/ft³
 μ_L = liquid viscosity, cP

The Robbins correlation applies near atmospheric pressure and under vacuum, but is not suitable above 3 bar absolute. For high (>0.3) flow parameters [Eq. (14-141)], the correlation has only been tested with air-water data.

For flood and MOC predictions, Robbins recommends his pressure drop method together with Eqs. (14-142) (flood) and (14-139) (MOC).

The GPDC and Robbins correlations are empirical. Fundamental correlations are also available. Most of these use the channel model, which attributes the pressure drop to the resistance to flow in a multitude of parallel channels. The channels may have bends, expansions, and contractions. Popular application of this approach are the Rocha et al. correlation [Rocha, Bravo, and Fair; *Ind. Eng. Chem. Res.* **32**, 641 (1993)] for structured packing and the Mackowiak ("Fluiddynamik von Kolonnen mit Modernen Füllkörpern und Packungen für Gas/Flüssigkeitssysteme," Otto Salle Verlag, Frankfurt am Main und Verlag Sauerländer Aarau, Frankfurt am Main, 1991) and Billet (*Packed Column*

TABLE 14-14 Characteristics of Structured Packings

Name	Size or number	Packing factor, m ⁻¹				Vendor
		Area, m ² /m ³	% voids ^a	Normal F _p [†]	Dry F _{pd} [‡]	
Metals, corrugated sheets						
Mellapak	125Y	125	99	33		Sulzer
	170Y	170	99	39		
	2Y	223	99	46		
	250Y	250	98	66		
	350Y	350	98	75		
	500Y	500	98	112		
	750Y	750	97			
	125X	125	99	16		
	170X	170	99	20		
	2X	223	99	23		
	250X	250	98	26		
	500X	500	98	82		
Mellapak Plus	202Y		99			Sulzer
	252Y	250	98	39		
	352Y		98			
	452Y	350	98	69		
	752Y	500	98	131		
Flexipac	700Y	710	96			Koch-Glitsch
	500Y	495	97			
	1Y	420	98	98	(105)	
	350Y	350	98			
	1.6Y	290	98	59		
	250Y	250	99			
	2Y	220	99	49	(36)	
	2.5Y	150	99			
	3.5Y	80	99	30	(15)	
	4Y	55	99	23	(10.5)	
	1X	420	98	52		
	350X	350	98			
	1.6X	290	98	33		
	250X	250	99			
	2X	220	99	23		
	2.5X	150	99			
	3X	110	99	16		
	3.5X	80	99			
	4X	55	99			
	Flexipac High-capacity	700	710	96	223	
500Z		495	97	82		
1Y		420	98			
350Y		350	98			
1.6Y		290	99	56		
250Y		250	99			
2Y	220	99	43			
Intalox	1T	310	98	66		Koch-Glitsch
	1.5T	250	99			
	2T	215	99	56		
	3T	170	99	43		

Name	Size or number	Packing factor, m ⁻¹				Vendor
		Area, m ² /m ³	% voids ^a	Normal F _p [†]	Dry F _{pd} [‡]	
Super-Pak	4T	135	99			Raschig
	5T	90	99			
	5TX	90	99			
Ralu-Pak	250	250	98	55 [§]		Raschig
	350	350	98	70 [§]		
Rhombopac	250YC	250	98	66		Raschig
	4M	151				
	6M	230		59		
Max-Pak	9M	351				Kuhni
	0.5-in	229	98	39		
Montz-Pak	B1-125	125	97			Montz
	B1-200	200				
	B1-250	250	95	66		
	B1-350	350	93			
	BSH-250 [¶]	250	95			
	BSH-500 [¶]	500	91			
	B1-250M	250		43		
	B1-350M	350				
	B1-500M	500				
Wire Mesh						
Sulzer	AX	250	95			Sulzer
	BX	492	90	69	(52.5)	
	CY	700	85			
	BX Plus					
Wire gauze	BX	495	93			Koch-Glitsch
Montz-Pak	A3-500	500	91			Montz
Goodloe	765	1010	96			Koch-Glitsch
	773	1920	95			
	779	2640	92			
Hyperfil	2300	2300	93.6	394/230 ^{§,}	460	Knit Mesh
	1900	1900	94.8	312/180 ^{§,}		
	1400	1400	96.0	180/131 ^{§,}		
Ceramic						
Flexeramic	28	260	66	131		Koch-Glitsch
	48	160	77	79		
	88	100	86	49		
Plastic						
Mellapak	125Y	125				Sulzer
	250Y	250		72		
	125X	125				
	250X	250				
Ralu-Pak	30/160	160	92			Raschig
Multifil plastics	P1500	1500	88.5			Knit Mesh

^a% voids vary with material thickness and values may not be consistent.

[†]Packing factors from Kister, *Distillation Design*, McGraw-Hill, 1992; Kister, Larson, and Gill, paper presented at the Houston AIChE Meeting, March 19–23, 1995; and Kister et al., in *Distillation 2007: Proceedings of Topical Conference*, AIChE Spring Meeting, Houston, Tex., April 22–26, 2007.

[‡]Dry packing factors from Robbins, *Chem. Eng. Prog.*, p. 87, May 1991.

[§]These packing factors supplied by the packing vendor.

[¶]These are expanded metal packings.

^{||}First figure is for hydrocarbon service, second figure for aqueous service.

Vendors: Sulzer Chemtech Ltd., Winterthur, Switzerland; Koch-Glitsch LLP, Wichita, Kansas; Raschig GmbH, Ludwigshafen/Rhein, Germany; Julius Montz GmbH, Hilden, Germany; Knit Mesh/Enhanced Separation Technologies, Houston, Texas; Kuhni Ltd., Allschwil, Switzerland.

Analysis and Design, Ruhr University, Bochum, Germany, 1989) methods. Stichlmair et al. (*Distillation Principles and Practices*, Wiley, New York, 1998; *Gas Sep. Purif.* **3**, March 1989, p. 19) present alternative correlations using the particle model, that attributes packing pressure drop to friction losses due to drag of a particle. This is similar to the Ergun model for single-phase flow [*Chem. Eng. Prog.* **48**(2), 89 (1952)].

Example 13: Packed-Column Pressure Drop Air and water are flowing countercurrently through a bed of 2-inch metal Pall rings. The air mass velocity is 2.03 kg/s·m² (1500 lbs/hr·ft²), and the liquid mass velocity is 12.20 kg/s·m² (9000 lbs/hr·ft²). Calculate the pressure drop by the generalized pressure drop (GPDC, Fig. 14-55) and the Robbins methods. Properties: ρ_G = 0.074 lbs/ft³; ρ_L = 62.4 lbs/ft³, μ_L = 1.0 cP, ν = 1.0 cS. The packing factor F_p = 27 ft⁻¹. For Robbins, F_{pd} = 24 ft⁻¹. The flow parameter F_{LG} = L/G (ρ_G/ρ_L)^{0.5} = (9000/1500) (0.074/62.4)^{0.5} = 0.207. The F-factor = F_p = U_pρ_G^{0.5} = G/(ρ_G^{0.5}3600) = 1500/[(0.074)^{0.5}(3600)] = 1.53 ft/s(lb/ft³)^{0.5}.

Using the GPDC method, the capacity parameter [by Eq. (14-140)] = $U_i[\rho_C/(\rho_L - \rho_C)]^{0.5} F_p^{0.5} v^{0.05}$, which is roughly equivalent to

$$\frac{F_i}{\rho_L^{0.5}} F_p^{0.5} v^{0.05} = \frac{1.53}{62.4^{0.5}} 27^{0.5}(1.0) \\ = 1.01$$

Referring to Fig. 14-55, the intersection of the capacity parameter and the flow parameter lines gives a pressure drop of 0.38 inches H₂O/ft packing.

Using the Robbins method, $G_f = 986F_i(F_{p,i}/20)^{0.5} = 986(1.53)(24/20)^{0.5} = 1653$. $L_f = L(62.4/\rho_L)(F_{p,i}/20)^{0.5} \mu^{0.1} = 9000(1.0)(1.095)(1.0) = 9859$. $L_f/G_f = 5.96$.

From Fig. 14-58, pressure drop = 0.40 in. H₂O/ft packing.

PACKING EFFICIENCY

HETP vs. Fundamental Mass Transfer The two-film model gives the following transfer unit relationship:

$$H_{OC} = H_G + \lambda H_L \quad (14-152)$$

where H_{OC} = height of an overall transfer unit, gas concentration basis, m

H_G = height of a gas-phase transfer unit, m

H_L = height of a liquid-phase transfer unit, m

$\lambda = m/(L_M/G_M)$ = slope of equilibrium line/slope of operating line

In design practice, a less rigorous parameter, HETP, is used to express packing efficiency. The HETP is the height of packed bed required to achieve a theoretical stage. The terms H_{OC} and HETP may be related under certain conditions:

$$\text{HETP} = H_{OC} \left[\frac{\ln \lambda}{(\lambda - 1)} \right] \quad (14-153)$$

and since $Z_p = (H_{OC})(N_{OC}) = (\text{HETP})(N_t) \quad (14-154)$

$$N_{OC} = N_t [\ln \lambda / (\lambda - 1)] \quad (14-155)$$

Equations (14-153) and (14-155) have been developed for binary mixture separations and hold for cases where the operating line and equilibrium line are straight. Thus, when there is curvature, the equations should be used for sections of the column where linearity can be assumed. When the equilibrium line and operating line have the same slope, $\text{HETP} = H_{OC}$ and $N_{OC} = N_t$ (theoretical stages).

An alternative parameter popular in Europe is the NTSM (number of theoretical stages per meter) which is simply the reciprocal of the HETP.

Factors Affecting HETP: An Overview Generally, packing efficiency increases (HETP decreases) when the following occur.

- Packing surface area per unit volume increases. Efficiency increases as the particle size decreases (random packing, Fig. 14-59) or as the channel size narrows (structured packing, Fig. 14-60).
- The packing surface is better distributed around a random packing element.
- Y structured packings (45° inclination) give better efficiencies than X structured packings (60° inclination to the horizontal) of the same surface areas (Fig. 14-60).
- For constant L/V operation in the preloading regime, generally liquid and vapor loads have little effect on random and most corrugated sheet structured packings HETP (Figs. 14-59 and 14-60). HETP increases with loadings in some wire-mesh structured packing.
- Liquid and vapor are well distributed. Both liquid and vapor maldistribution have a major detrimental effect on packing efficiency.

- Other. These include L/V ratio (λ), pressure, and physical properties. These come into play in some systems and situations, as discussed below.

HETP Prediction HETP can be predicted from mass-transfer models, rules of thumb, and data interpolation.

Mass-Transfer Models Development of a reliable mass-transfer model for packing HETP prediction has been inhibited by a lack of understanding of the complex two-phase flow that prevails in packings, by the shortage of commercial-scale efficiency data for the newer packings, and by difficulty in quantifying the surface generation in modern packings. Bennett and Ludwig (*Chem. Eng. Prog.*, p. 72, April 1994) point out that the abundant air-water data cannot be reliably used for assessing real system mass-transfer resistance due to variations in turbulence, transport properties, and interfacial areas. More important, the success and reliability of rules of thumb for predicting packing efficiency made it difficult for mass-transfer models to compete.

For random packings, the Bravo and Fair correlation [*Ind. Eng. Chem. Proc. Des. Dev.* **21**, 162 (1982)] has been one of the most popular theoretical correlations. It was shown (e.g., McDougall, *Chem SA*, p. 255, October 1985) to be better than other theoretical correlations, yet produced large discrepancies when compared to test data [Shariat and Kunesch, *Ind. Eng. Chem. Res.* **34**(4), 1273 (1995)]. For structured packings, the Bravo, Fair, and Rocha correlation [*Chem. Eng. Progr.* **86**(1), 19 (1990); *Ind. Eng. Chem. Res.* **35**, 1660 (1996)] is one of the most popular theoretical correlations. This correlation is based on the two-film theory. Interfacial areas are calculated from the packing geometry and an empirical wetting parameter.

Alternate popular theoretical correlations for random packings, structured packings, or both (e.g., Billet and Schultes, "Beitrag zur Verfahrens- und Umweltechnik," p. 88, Ruhr Universität, Bochum, Germany, 1991) are also available.

Rules of Thumb Since in most circumstances packing HETP is sensitive to only few variables, and due to the unreliability of even the best mass-transfer model, it has been the author's experience that rules of thumb for HETP are more accurate and more reliable than mass-transfer models. A similar conclusion was reached by Porter and Jenkins (*ICHEME Symp. Ser.* **56**, Summary paper, London, 1979).

The majority of published random packing rules of thumb closely agree with one another. They are based on second- and third-generation random packings and should not be applied to the obsolete first-generation packings. Porter and Jenkins's (loc. cit.), Frank's (*Chem. Eng.*, p. 40, March 14, 1977), Harrison and France's (*Chem. Eng.*, p. 121, April 1989), Chen's (*Chem. Eng.*, p. 40, March 5, 1984), and Walas' (*Chem. Eng.*, p. 75, March 16, 1987) general rules of thumb are practically the same, have been successfully tested against an extensive data bank, and are slightly conservative, and therefore suitable for design.

For small-diameter columns, the rules of thumb presented by Frank (loc. cit.), Ludwig (*Applied Process Design for Chemical and Petrochemical Plants*, vol. 2, 2d ed., Gulf Publishing, Houston, Tex., 1979), and Vital et al. [*Hydrocarbon Processing*, **63**(12), 75 (1984)] are identical. The author believes that for small columns, the more conservative value predicted from either the Porter and Jenkins or the Frank-Ludwig-Vital rule should be selected for design. Summarizing:

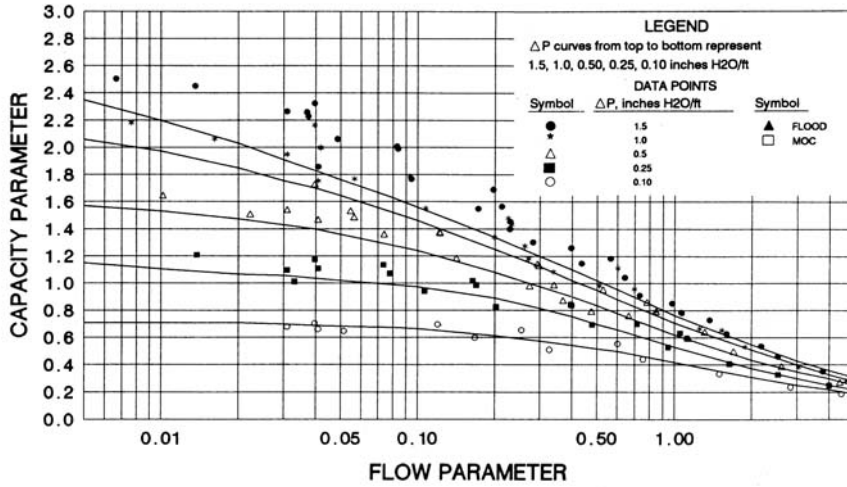
$$\text{HETP} = 18D_p \quad (14-156a)$$

$$\text{HETP} > D_T \quad \text{for } D_T < 0.67 \text{ m} \quad (14-156b)$$

where D_p and D_T are the packing and tower diameters, m, respectively, and the HETP is in meters. In high-vacuum columns (<100 mbar), and when $\lambda = mG_M/L_M$ is outside the range of 0.5 to 2.0, the above rules may be optimistic (see below).

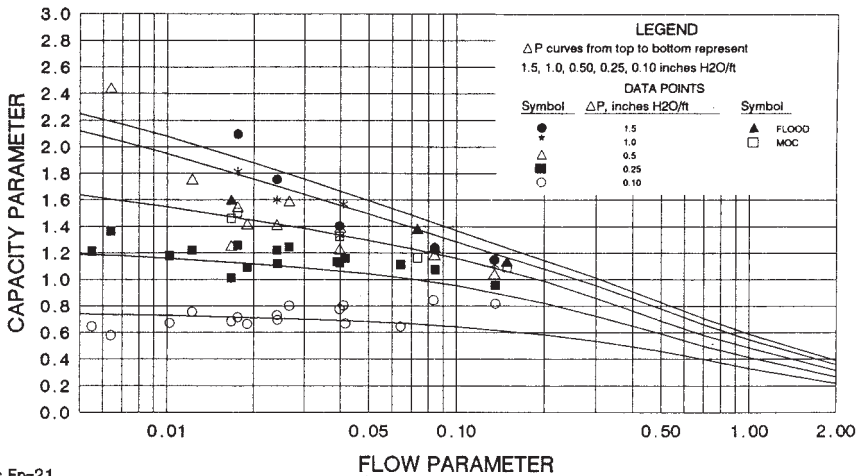
The above rules of thumb were based on experience with Pall rings. The packing diameter may be difficult to establish for some of the modern packings, especially those of saddle or flat shape. For these,

1" (M) PALL RINGS PRESSURE DROP - AQUEOUS SYSTEMS



(a)

KOCH - SULZER BX PACKING FLOOD & PRESSURE DROP



(b)

FIG. 14-57 Superimposing experimental pressure-drop data for a given packing generates a GPDC interpolation chart for this packing. (a) A random packing; chart is based on Eckert's GPDC, Fig. 14-55. (b) A structured packing; chart is based on Kister and Gill's GPDC (SP), Fig. 14-56. (From Kister, H. Z., *Distillation Design*, copyright © McGraw-Hill, 1992; used with permission.)

Kister and Larson (in Schweitzer, *Handbook of Separation Techniques for Chemical Engineers*, 3d ed., McGraw-Hill, 1997) extended Eq. (14-156a) by expressing the packing diameter in terms of the more fundamental surface area per unit volume a_p , m²/m³. For Pall rings, it can be shown that

$$a_p = 5.2/D_p \tag{14-157}$$

and Eq. (14-156a) becomes

$$\text{HETP} = 93/a_p \tag{14-158}$$

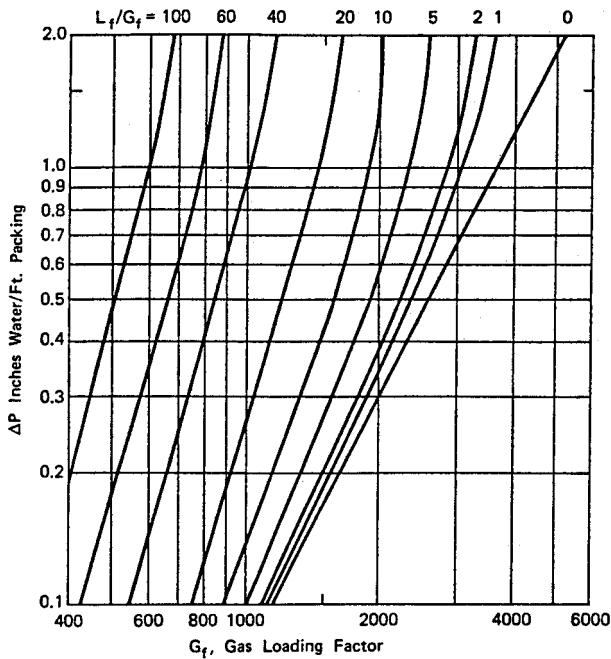


FIG. 14-58 The Robbins generalized pressure-drop correlation. (From L. A. Robbins. Chem Eng. Progr., May 1991. p. 87, reprinted courtesy of the American Institute of Chemical Engineers.)

Harrison and France (loc. cit.) presented the only published rule of thumb for structured packings efficiency as a function of packing crimp. Kister and Larson reexpressed it in terms of the surface area per unit volume to accommodate a wider range of packing geometries. The final expression is

$$\text{HETP} = 100C_{XY}/a_p + 0.10 \quad (14-159)$$

Specific surface areas are listed in Tables 14-13 and 14-14.

The above rules of thumb apply to organic and hydrocarbon systems, whose surface tensions are relatively low ($\sigma < 25$ mN/m). For higher surface tensions, the liquid does not adhere well to the packing surfaces (*underwetting*), causing higher HETPs. In a water-rich system ($\sigma = 70$ mN/m or so) HETPs obtained from Eqs. (14-156), (14-158), and (14-159) need to be doubled. For intermediate surface tension systems (some amines and glycols, whose surface tension at column conditions is 40 to 50 mN/m), HETPs obtained from Eqs. (14-156), (14-158), and (14-159) need to be multiplied by 1.5.

For random packings, Eqs. (14-156) and (14-158) apply for packings of 25-mm diameter and larger. For smaller packings, use of the a_p at 25-mm often gives a slightly conservative HETP estimate. For structured packing, C_{XY} in Eq. (14-159) reflects the effect of the inclination angle (Fig. 14-60). $C_{XY} = 1$ for Y-type, S-type, or high-capacity packings, and $C_{XY} = 1.45$ for the larger (< 300 m²/m³) X-type packings. There are insufficient data to determine C_{XY} for high specific area X-type packings, but Fig. 14-60 suggests it is somewhat lower than 1.45.

Compared to experimental data, the above rules of thumb are slightly conservative. Since packing data are usually measured with perfect distribution, a slight conservative bias is necessary to extend

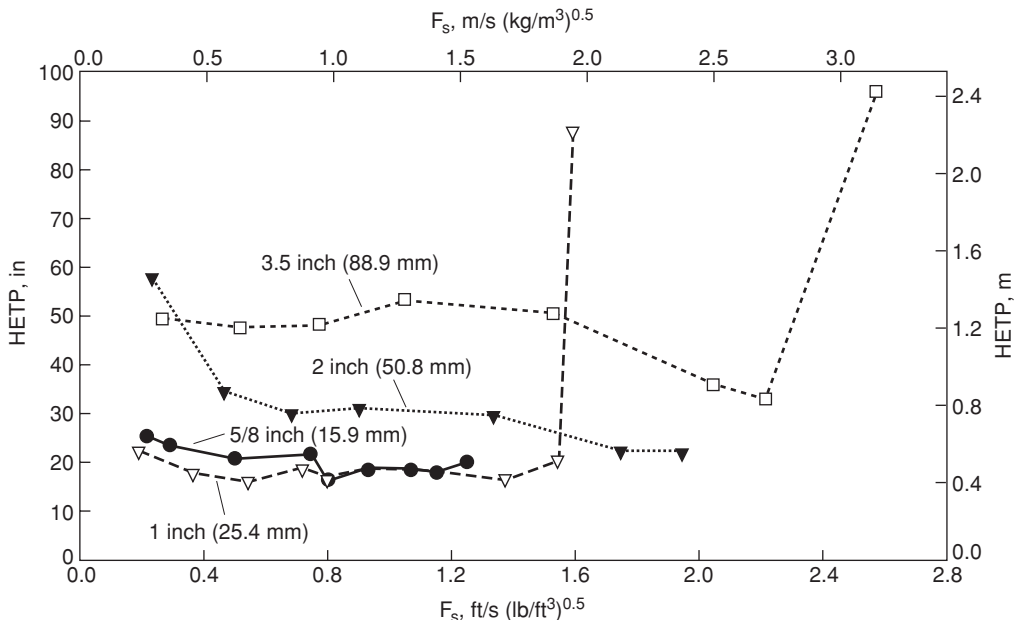


FIG. 14-59 HETP values for four sizes of metal pall rings, vacuum operation. Cyclohexane/*n*-heptane system, total reflux, 35 kPa (5.0 psia). Column diameter = 1.2 m (4.0 ft). Bed height = 3.7 m (12 ft). Distributor = tubed drip pan, 100 streams/m². [Adapted from Shariat and Kunesh, Ind. Eng. Chem. Res., 34, 1273 (1995). Reproduced with permission. Copyright © 1995 American Chemical Society.]

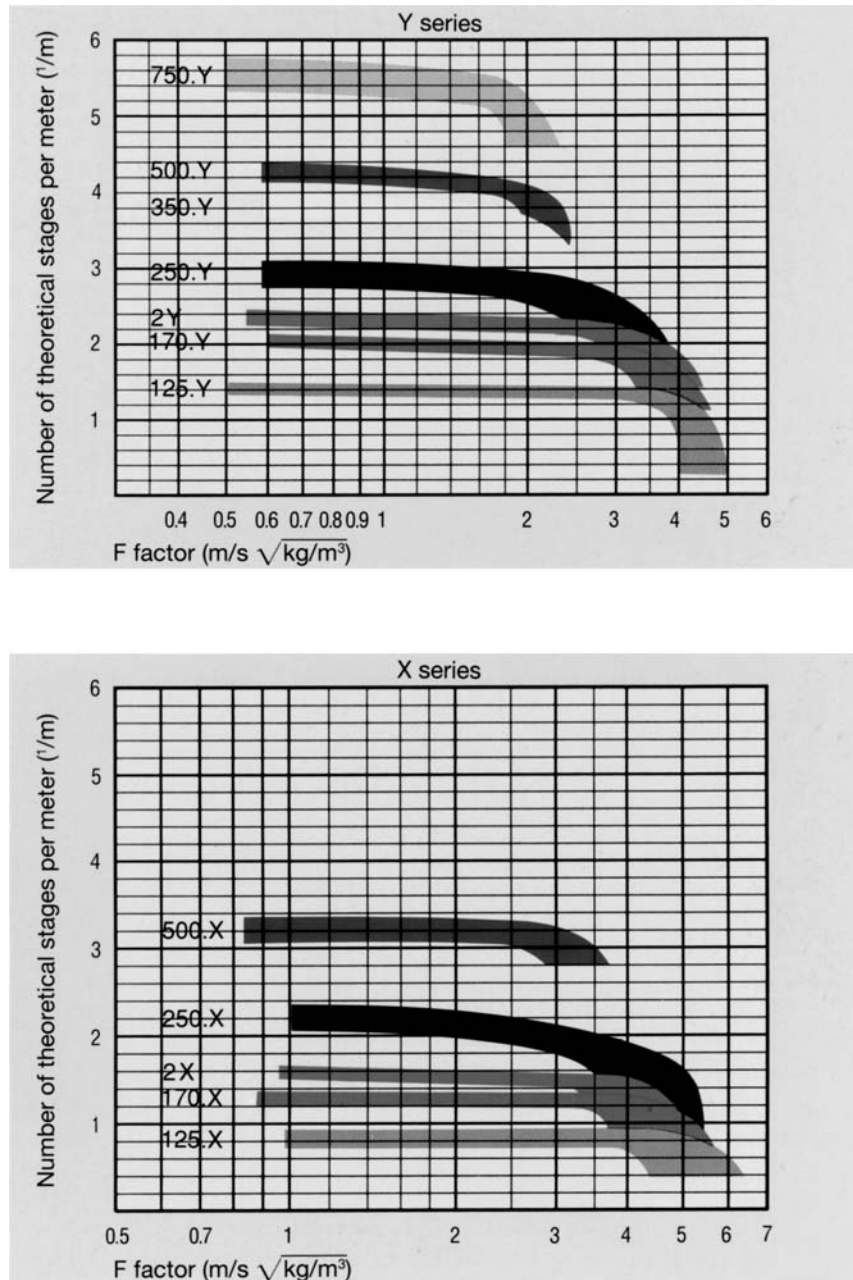


FIG. 14-60 Effect of structured packing surface areas, loads, and inclination angle on packing efficiency. Efficiency expressed as number of theoretical stages per meter, the reciprocal of HETP. Sulzer data, chlorobenzene-ethylbenzene, 100 mbar, at total reflux; 250-mm-diameter test column. (Reprinted courtesy of Sulzer Chemtech.)

these data to the good, yet imperfect, distributors used in the real world. For poor distributors, the above rules of thumb will usually predict well below the HETPs measured in the field.

Lockett (*Chem. Eng. Progr.*, p. 60, January 1998) simplified the fundamental Bravo-Fair-Rocha correlation [*Ind. Eng. Chem. Res.* **35**, p. 1660 (1996)] to derive an alternative rule of thumb for structured packing efficiency. This rule of thumb predicts HETPs under perfect distribution conditions. Lockett recommends caution when applying

this rule of thumb for aqueous systems as it does not predict the effects of underwetting (below).

Service-Oriented Rules of Thumb Strigle (*Packed Tower Design and Applications*, 2d ed., Gulf Publishing, Houston, Tex., 1994) proposed a multitude of rules of thumb as a function of the service, column pressure, and physical properties. These rules are based on the extensive experience of Strigle and the Norton Company (now merged with Koch-Glitsch LP).

Data Interpolation Interpolation of experimental HETP data is the most reliable means of obtaining design HETP values. This is hardly surprising in an area where our understanding of the theory is so poor that rules of thumb can do better than theoretical models. The author believes that it is best to derive HETP from experimental data, and to check it against a rule of thumb.

Eckert [*Chem. Eng. Progr.* **59**(5), 76 (1963)], Chen (*Chem. Eng. p.* 40, March 5, 1984), and Vital et al. [*Hydroc. Proc.* **63**(12), 75 (1984)] tabulated experimental HETP data for various random packings. Kister (*Distillation Design*, McGraw-Hill, 1992) extended these tabulations and included published HETP data and a detailed procedure for interpolating such HETP data. A prerequisite to any interpolation of packing data is thorough familiarity with the factors that affect HETP. Overlooking any of the factors listed can easily lead to poor interpolation and grossly incorrect design. In particular, it is imperative to recognize that the quality of distribution in pilot towers is generally superior to the quality of distribution in commercial towers.

Underwetting Laboratory- and pilot-scale distillation experiments with systems that exhibit large differences in surface tension along the column such as methanol-water showed a sharp drop in efficiency at the high-surface-tension end of the column [Ponter et al., *Trans. Instn. Chem. Engineers [London]*, **45**, T345 (1967)]. There appeared to be a critical methanol composition below which performance deteriorated rapidly. The poor performance at the low-methanol-concentration end appeared independent of the type and size of packing. Visual observations with disk columns attributed these effects to underwetting.

Underwetting is a packing surface phenomenon, which breaks up liquid film. The tendency of the liquid film to break (the degree of wetting) is expressed by the contact angle (Fig. 14-61). A contact angle of 0° indicates perfect wetting; an angle of 180° indicates no wetting. Mersmann and Deixler [*Chem. Ing. Tech.* **58**(1), 19 (1986)] provide a preliminary chart for estimating contact angles. The contact angle depends on both the surface and the liquid and is a strong function of composition. In systems with large surface tension gradients, both contact angles and minimum wetting rates may vary rapidly with changes of composition or surface tension. Extensive studies by Ponter et al. [loc. cit.; also, Ponter and Au-Yeung, *Chem. Ing. Tech.*, **56**(9), 701 (1984)] showed that

- Underwetting is most significant in aqueous-organic systems, and tends to occur at the high-surface-tension (aqueous) end of the composition range. Liquid viscosity may also have an effect.
- Underwetting may be alleviated by changing the material and surface roughness of the packing.
- In systems susceptible to underwetting, column efficiency can sometimes (but not always) be improved by the addition of small amounts of surfactants.

Effect of Lambda Most packed-column efficiency testing has been at total reflux. Some tests for both random and structured packings [Billet, "Packed Towers Analysis and Design," Ruhr University, Bochum, Germany, 1989; Meier, Hunkeler, and Stocker, *ICHEME Symp. Ser.* **56**, 3.3/1 (1979); Eckert and Walter, *Hydroc. Proc.* **43**(2), 107 (1964)] suggest that efficiencies at finite reflux are similar to those at total reflux when lambda ($\lambda = mG_M/L_M$, which is the ratio of the slope of the equilibrium curve to the slope of the operating line) ranges between 0.5 and 2.0. This range is typical for most distillation systems.

Koshy and Rukovena [*Hydroc. Proc.*, **65**(5), 64 (1986)], experimenting with methanol-water and water-DMF using #25 IMTP pack-

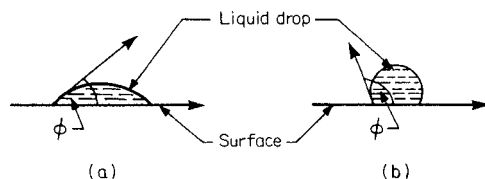


FIG. 14-61 Contact angles. (a) Acute, good wetting. (b) Obtuse, poor wetting.

ing in a pilot-scale column, observed a sharp efficiency drop when the group λ was greater than 2 or lower than 0.5. The efficiency loss escalated as λ deviated more from this range. Koshy and Rukovena recognized that surface tension gradients and underwetting may have influenced some of their findings, but argue that the lambda effect is the major cause for the efficiency differences observed in their tests. High-relative-volatility systems are those most likely to be affected by λ , because at low volatility, λ ranges from 0.5 to 2. Strigle (loc. cit.) quantified the lambda effect on HETP using the following equation:

$$\text{Actual HETP/standard HETP} = 1 + 0.278[\text{ABS}(\ln \lambda)^3] \quad (14-160)$$

For $0.5 < \lambda < 2$, Eq. (14-160) gives a ratio of less than 1.1; that is, it has a little influence on HETP.

Pressure Generally, pressure has little effect on HETP of both random and structured packing, at least above 100 mbar abs. At deep vacuum (<100 mbar), there are data to suggest that efficiency decreases as pressure is lowered for random packings [Zelvinski, Titov, and Shalygin, *Khim. Tekhnol. Topl. Masel.* **12**(10) (1966)], but most of these data can also be explained by poor wetting or maldistribution.

At high pressures (>15 to 20 bar), structured packing efficiency diminishes as pressure is raised (Fitz, Shariat, and Spiegel, Paper presented at the AIChE Spring National Meeting, Houston, Tex., March 1995). Zuiderweg and Nutter [*ICHEME Symp.* **128**, A481 (1992)] report the same phenomenon, but to a much smaller extent, also in random packings. They explain the efficiency reduction at higher pressure by vapor backmixing. Nooijen et al. [*ICHEME Symp. Ser.* **142**, 885 (1997)] concur, bringing a supporting case study in which high-pressure distillation efficiency improved by splitting a packed bed.

With structured packings (only) FRI's high-pressure (10 to 30 bar; flow parameters >0.25) distillation tests measured maxima, termed humps in the HETP vs. load plot, typically at 65 to 90 percent of flood [Fitz, Shariat, and Kunes, *ICHEME Symp. Ser.* **142**, 829 (1997); Cai et al., *Trans. ICHEME* **81**, Part A, p. 85 (2003)]. These humps (Fig. 14-62) were not observed with lower pressure distillation (flow parameters <0.2) and appeared to intensify with higher pressure. The humps did not always occur; some tests at different distributor positioning and with larger packing showed no humps. Zuiderweg et al. [*ICHEME Symp. Ser.* **142**, 865 (1997); *Trans. ICHEME* **81**, Part A, p. 85 (January 2003)] and Nooijen et al. [*ICHEME Symp. Ser.* **142**, 885 (1997)] explain the humps by two-phase backmixing. At the high liquid loads in high-pressure distillation, flow unevenness prematurely floods some of the packing channels, carrying vapor bubbles downward and recirculating liquid upward.

Physical Properties Data presented by a number of workers [e.g., Vital, Gossel, and Olsen, *Hydroc. Proc.* **63**(12), 75 (1984)] suggest that, generally, random packing HETP is relatively insensitive to system properties for nonaqueous systems. A survey of data in Chapter

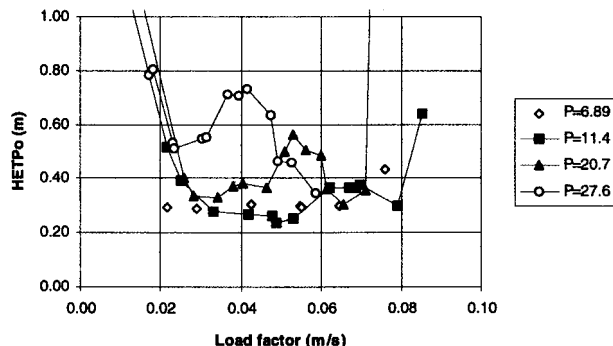


FIG. 14-62 HETP_o data as measured in the FRI column for the *iC*₄/*nC*₄ system at different pressures (bara), showing efficiency humps. (From J. L. Nooijen, K. A. Kusters, and J. J. B. Pek, *ICHEME Symp. Ser.* **142**, p. 885, 1997. Reprinted courtesy of ICHEME.)

11 of Kister's *Distillation Design* (McGraw-Hill, New York, 1992) leads to a similar conclusion for structured packings. For water-rich systems, packing HETPs tend to be much higher than for nonaqueous systems due to their high lambda or surface underwetting, as discussed above. High hydrogen concentrations (>30 percent or so in the gas) have also led to low packing efficiencies (Kister et al., *Proc. 4th Ethylene Producers Conference*, AIChE, New Orleans, La., p. 283, 1992), possibly due to the fast-moving hydrogen molecule dragging heavier molecules with it as it diffuses from a liquid film into the vapor.

Errors in VLE These affect packing HETP in the same way as they affect tray efficiency. The discussions and derivation earlier in this subsection apply equally to tray and packed towers.

Comparison of Various Packing Efficiencies for Absorption and Stripping In past editions of this handbook, extensive data on absorption/stripping systems were given. Emphasis was given to the following systems:

Ammonia-air-water	Liquid and gas phases contributing; chemical reaction contributing
Air-water	Gas phase controlling
Sulfur dioxide-air-water	Liquid and gas phase controlling
Carbon dioxide-air-water	Liquid phase controlling

The reader may refer to the data in the 5th edition. For the current work, emphasis will be given to one absorption system, carbon dioxide-air-caustic.

Carbon Dioxide-Air-Caustic System The vendors of packings have adopted this system as a "standard" for comparing the performance of different packing types and sizes for absorption/stripping. For tests, air containing 1.0 mol % CO₂ is passed countercurrently to a circulating stream of sodium hydroxide solution. The initial concentration of NaOH in water is 1.0 N (4.0 wt %), and as the circulating NaOH is converted to sodium carbonate it is necessary to make a mass-transfer correction because of reduced mass-transfer rate in the liquid phase. The procedure has been described by Eckert et al. [*Ind. Eng. Chem.*, **59**(2), 41 (1967); *Chem. Eng. Progr.*, **54**(1), 790 (1958)]. An overall coefficient is measured using gas-phase (CO₂) concentrations:

$$K_{OGa_e} = \frac{\text{moles CO}_2 \text{ absorbed}}{\text{time-bed volume-partial pressure CO}_2 \text{ driving force}} \quad (14-161)$$

The coefficients are usually corrected to a hydroxide conversion of 25 percent at 24°C. For other conversions, Fig. 14-14 may be used. Reported values of K_{OGa} for representative random packings are given in Table 14-15. The effect of liquid rate on the coefficient is shown in Fig. 14-63.

While the carbon dioxide/caustic test method has become accepted, one should use the results with caution. The chemical reaction masks

TABLE 14-15 Overall Coefficients for Representative Packings

CO ₂ -air-caustic system		
	Nominal size, mm	Overall coefficient K _{OGa} , kg-moles/(hr-m ³ -atm)
Ceramic raschig rings	25	37.0
	50	26.1
Ceramic Intalox saddles	25	45.1
	50	30.1
Metal pall rings	25	49.6
	50	34.9
Metal Intalox saddles (IMTP®)	25	54.8
	50	39.1

NOTE: Basis for reported values: CO₂ concentration in inlet gas, 1.0 vol %; 1N NaOH solution in water, 25 percent NaOH conversion; temperature = 24°C; atmospheric pressure; gas rate = 1.264 kg/(s-m²); liquid rate = 6.78 kg/(s-m²).

SOURCE: Strigle, R. L., *Packed Tower Design and Applications*, 2d ed., Gulf Publ. Co., Houston, 1994.

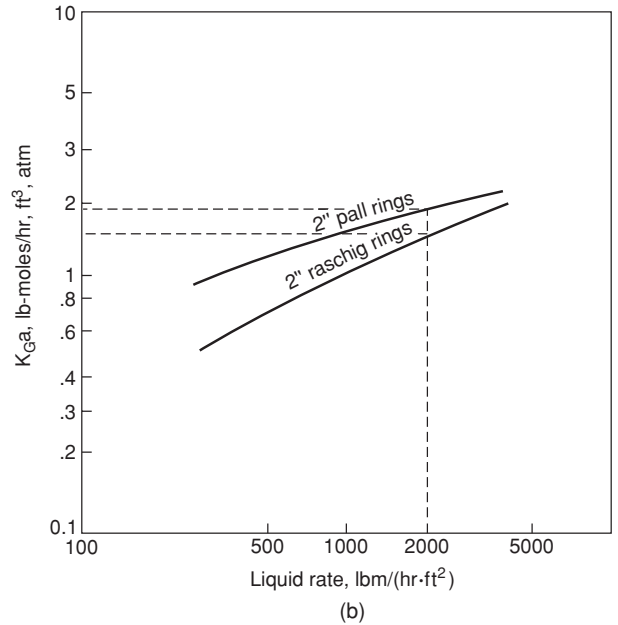
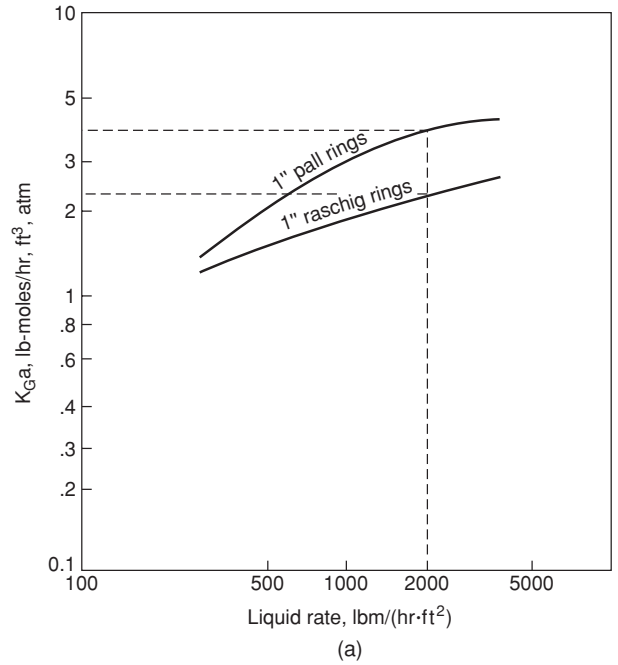


FIG. 14-63 Overall mass transfer coefficients for carbon dioxide absorbed from air by 1N caustic solution. (a) 1-in Pall rings and Raschig rings. (b) 2-in Pall rings and Raschig rings. Air rate = 0.61 kg/s-m² (450 lb/hr-ft²). To convert from lb/hr-ft² to kg/s-m², multiply by 0.00136. To convert from lb-moles/hr-ft³ atm to kg-moles/s-m³ atm, multiply by 0.0045. [Eckert et al., *Chem. Eng. Progr.*, **54**(1), 70 (1958).]

the effect of physical absorption, and the relative values in the table may not hold for other cases, where much of the resistance to mass transfer is in the gas phase. Background on this combination of physical and chemical absorption may be found earlier in the present section, under "Absorption with Chemical Reaction."

Summary In the preloading regime, packing size, type, and distribution affect HETP. With aqueous-organic systems, HETP may be sensitive to underwetting and composition. A lambda value ($\lambda = mG_d/L_d$) outside the range of 0.5 to 2.0 causes HETP to rise, and so does a high hydrogen concentration. HETP of structured packings may also be affected by pressure (at high pressure), and vapor and liquid loads.

MALDISTRIBUTION AND ITS EFFECTS ON PACKING EFFICIENCY

Modeling and Prediction Maldistribution may drastically reduce packing efficiency. HETP may increase by a factor as high as 2 or 3 due to maldistribution. Shariat and Kunesch [*Ind. Eng. Chem. Res.*, **34**(4), 1273 (1995)] provide a good demonstration.

Early models [Mullins, *Ind. Chem. Mfr.*, **33**, 408 (1957); Manning and Cannon, *Ind. Eng. Chem.*, **49**(3), 347 (1957)] expressed the effect of liquid maldistribution on packing efficiency in terms of a simple channeling model. A portion of the liquid bypasses the bed, undergoing negligible mass transfer, and then rejoins and contaminates the rest of the liquid. Huber et al. [*Chem. Ing. Tech.*, **39**, 797 (1967); *Chem. Eng. Sci.*, **21**, 819 (1966)] and Zuiderweg et al. [*ICHEME Symp. Ser.*, **104**, A217 (1987)] replaced the simple bypassing by variations in the local L/V ratios. The overirrigated parts have a high L/V ratio, the underirrigated parts a low L/V ratio. Regions with low L/V ratios experience pinching, and, therefore, produce poor separation.

Huber et al. (loc. cit.) and Yuan and Spiegel [*Chem. Ing. Tech.*, **54**, 774 (1982)] added lateral mixing to the model. Lateral deflection of liquid by the packing particles tends to homogenize the liquid, thus counteracting the channeling and pinching effect.

A third factor is the nonuniformity of the flow profile through the packing. This nonuniformity was observed as far back as 1935 [Baker, Chilton, and Vernon, *Trans. Instn. Chem. Engrs.*, **31**, 296 (1935)] and was first modeled by Cihla and Schmidt [*Coll. Czech. Chem. Commun.*, **22**, 896 (1957)]. Hoek (Ph.D. Thesis, The University of Delft, The Netherlands, 1983) combined all three factors into a single model, leading to the zone-stage model below.

The Zone-Stage Model Zuiderweg et al. [*ICHEME Symp. Ser.*, **104**, A217, A233 (1987)] extended Hoek's work combining the effects of local L/V ratio, lateral mixing, and flow profile into a model describing the effect of liquid maldistribution on packing efficiency. This work was performed at Fractionation Research Inc. (FRI) and at The University of Delft in The Netherlands. The model postulates that, in the absence of maldistribution, there is a "basic" (or "true" or "inherent") HETP which is a function of the packing and the system only. This HETP can be inferred from data for small towers, in which lateral mixing is strong enough to offset any pinching. For a given initial liquid distribution, the model uses a diffusion-type equation to characterize the splitting and recombining of liquid streams in the horizontal and vertical directions. The mass transfer is then calculated by integrating the liquid flow distribution at each elevation and the basic HETP. Kunesch et al. successfully applied the model to predict measured effects of maldistribution on packing efficiency. However, this model is difficult to use and has not gained industrywide acceptance.

Empirical Prediction Moore and Rukovena [*Chemical Plants and Processing* (European edition), p. 11, August 1987] proposed the empirical correlation in Fig. 14-64 for efficiency loss due to liquid maldistribution in packed towers containing Pall® rings or Metal Intalox® packing. This correlation was shown to work well for several case studies (Fig. 14-64), is simple to use, and is valuable, at least as a preliminary guide.

To quantify the quality of liquid irrigation, the correlation uses the distribution quality rating index. Typical indexes are 10 to 70 percent for most standard commercial distributors, 75 to 90 percent for intermediate-quality distributors, and over 90 percent for high-performance distributors. Moore and Rukovena present a method for calculating a distribution-quality rating index from distributor geometry. Their method is described in detail in their paper as well as in Kister's book (*Distillation Operation*, McGraw-Hill, New York, 1990).

Maximum Liquid Maldistribution Fraction f_{max} . To characterize the sensitivity of packed beds to maldistribution, Lockett and

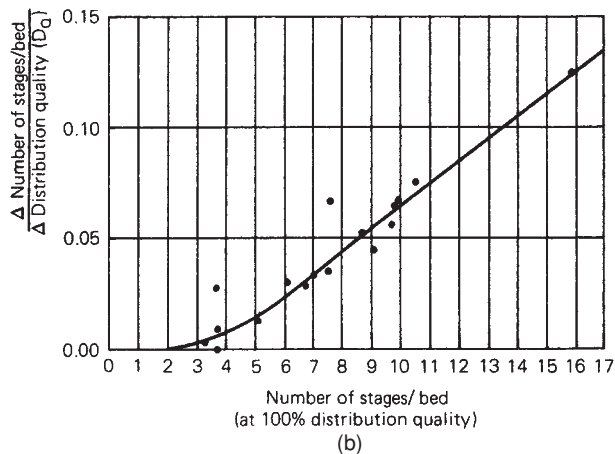
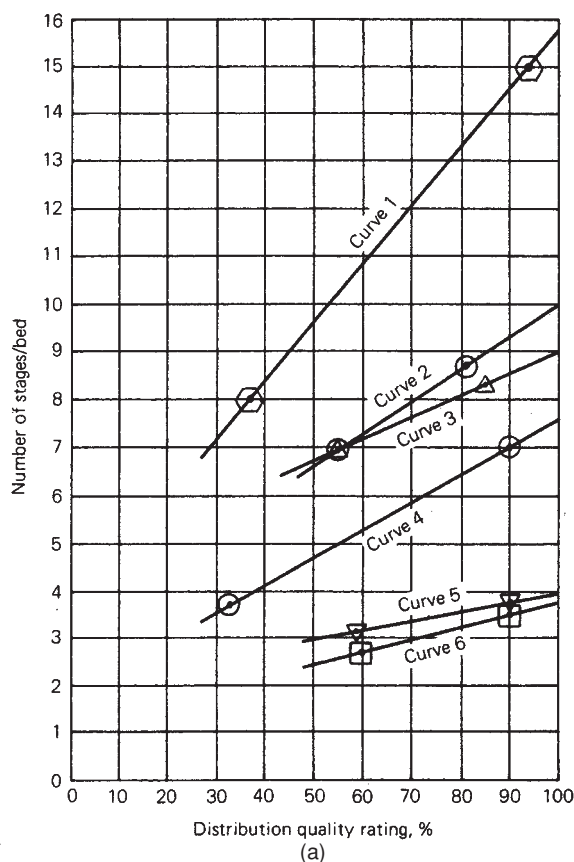


FIG. 14-64 Effect of irrigation quality on packing efficiency. (a) Case histories demonstrating efficiency enhancement with higher distribution quality rating. (b) Correlation of the effect of irrigation quality on packing efficiency. (From F. Moore and F. Rukovena, *Chemical Plants and Processing*, Europe edition, Aug. 1987; reprinted courtesy of Chemical Plants and Processing.)

Billingham (*Trans. IChemE.*, **80**, Part A, p. 373, May 2002; *Trans. IChemE.*, **81**, Part A, p. 134, January 2003) modeled maldistribution as two parallel columns, one receiving more liquid $(1 + f)L$, the other receiving less $(1 - f)L$. The vapor was assumed equally split (Fig. 14-65)

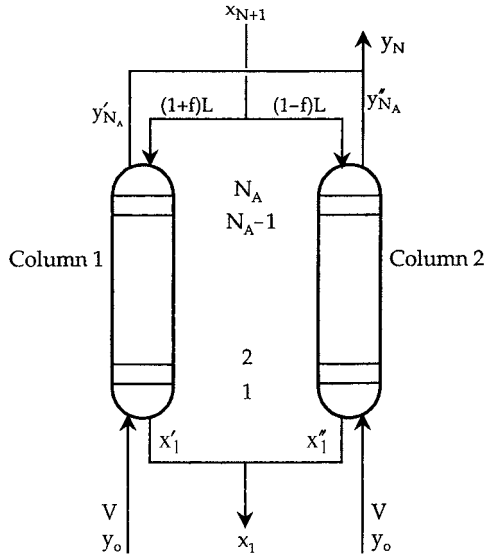


FIG. 14-65 Parallel-columns model. (From Lockett and Billingham, Trans. IChemE **80**, Part A, p. 373, May 2002; reprinted courtesy of IChemE.)

without lateral mixing. Because of the different L/V ratios, the overall separation is less than is obtained at uniform distribution. A typical calculated result (Fig. 14-66) shows the effective number of stages from the combined two-column system decreasing as the maldistribution fraction f increases. Figure 14-66a shows that the decrease is minimal in short beds (e.g., 10 theoretical stages) or when the maldistribution fraction is small. Figure 14-66a shows that there is a limiting fraction f_{\max} which characterizes the maximum maldistribution that still permits achieving the required separation. Physically, f_{\max} represents the maldistribution fraction at which one of the two parallel columns in the model becomes pinched. Figure 14-66b highlights the steep drop in packing efficiency upon the onset of this pinch. Billingham and Lockett derived the following equation for f_{\max} in a binary system:

$$f_{\max} = \frac{y_{N+1} - y_N}{y_N - y_o} + \frac{x_1 - x_o}{x_{N+1} - x_o} - \left(\frac{y_{N+1} - y_N}{y_N - y_o} \right) \left(\frac{x_1 - x_o}{x_{N+1} - x_o} \right) \quad (14-162)$$

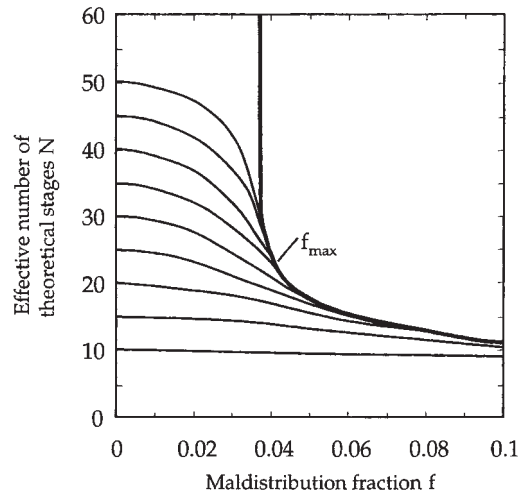
This equation can be used to calculate f_{\max} directly without the need for a parallel column model. Billingham and Lockett show that the various terms in Eq. (14-162) can be readily calculated from the output of a steady-state computer simulation. Multicomponent systems are represented as binary mixtures, either by lumping components together to form a binary mixture of pseudolight and pseudoheavy components, or by normalizing the mole fractions of the two key components. Once f_{\max} is calculated, Billingham and Lockett propose the following guidelines:

- $f_{\max} < 0.05$, extremely sensitive to maldistribution. The required separation will probably not be achieved.
- $0.05 < f_{\max} < 0.10$, sensitive to maldistribution, but separation can probably be achieved.
- $0.10 < f_{\max} < 0.20$, not particularly sensitive to maldistribution.
- $f_{\max} > 0.20$ insensitive to maldistribution.

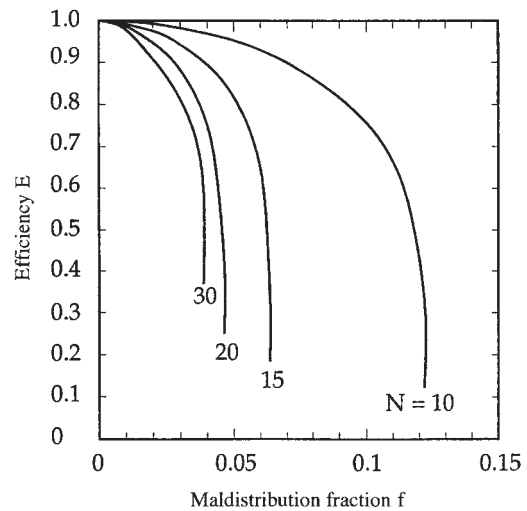
Figure 14-66b shows that shortening the bed can increase f_{\max} . Relative volatility and L/V ratio also affect f_{\max} . The bed length and L/V ratio can often be adjusted to render the bed less sensitive to maldistribution.

Implications of Maldistribution to Packing Design Practice

These are discussed at length with extensive literature citation in Kister's book *Distillation Operation*, McGraw-Hill, New York, 1990. Below are the guidelines:



(a)



(b)

FIG. 14-66 Loss of efficiency due to maldistribution as a function of maldistribution fraction f and the number of stages per bed for a given case study. (a) f_{\max} and reduction in number of stages. (b) Showing larger efficiency loss at higher number of stages per bed and higher f . The steep drops indicate pinching associated with f_{\max} . (From Lockett and Billingham, Trans. IChemE **80**, Part A, p. 373, May 2002; reprinted courtesy of IChemE.)

1. Three factors appear to set the effect of maldistribution on efficiency:

a. *Pinching*. Regional changes in L/V ratio cause regional composition pinches.

b. *Lateral mixing*. Packing particles deflect both liquid and vapor laterally. This promotes mixing of vapor and liquid and counteracts the pinching effect.

c. *Liquid nonuniformity*. Liquid flows unevenly through the packing and tends to concentrate at the wall.

2. At small tower-to-packing diameter ratios ($D_T/D_p < 10$), the lateral mixing cancels out the pinching effect, and a greater degree of maldistribution can be tolerated without a serious efficiency loss. At high ratios ($D_T/D_p > 40$), the lateral mixing becomes too small to offset

the pinching effect. The effects of maldistribution on efficiency are therefore most severe in large-diameter columns and small-diameter packings.

A good design practice is to seek a packing size that gives a D_T/D_p between 10 and 40. This is often impractical, and higher ratios are common. When D_T/D_p exceeds 100, avoiding efficiency loss due to maldistribution is difficult. Either ratios exceeding 100 should be avoided, or a special allowance should be made for loss of efficiency due to maldistribution.

3. Wall flow effects become large when D_T/D_p falls below about 10. Packing diameter should be selected such that D_T/D_p exceeds 10.

4. Columns containing less than five theoretical stages per bed are relatively insensitive to liquid maldistribution. With 10 or more stages per bed, efficiency can be extremely sensitive to maldistribution (Strigle, *Packed Tower Design and Applications*, 2d ed., Gulf Publishing, Houston, Tex., 1994) (Fig. 14-66). Beds consisting of small packings or structured packings, which develop more theoretical stages per bed, are therefore more sensitive to maldistribution than equal-depth beds of larger packings. This is clearly demonstrated by FRI's experiments [Shariat and Kunesh, *Ind. Eng. Chem. Res.* **34**(4), 1273 (1995)]. Lockett and Billingham (*Trans. IChemE*, vol. 81, Part A, p. 131, January 2003) concur with these comments when their procedure (above) indicates high sensitivity to maldistribution, but allow a higher number of stages per bed when the sensitivity is low.

5. Maldistribution tends to be a greater problem at low liquid flow rates than at high liquid flow rates [Zuiderweg, Hoek, and Lahm, *I. ChemE Symp. Ser.* **104**, A217 (1987)]. The tendency to pinch and to spread unevenly is generally higher at the lower liquid flow rates.

6. A packed column has reasonable tolerance for a uniform or smooth variation in liquid distribution and for a variation that is totally random (*small-scale maldistribution*). The impact of discontinuities or zonal flow (*large-scale maldistribution*) is much more severe [Zuiderweg et al., loc. cit.; Kunesh, *Chem. Eng.*, p. 101, Dec. 7, 1987; Kunesh, Lahm, and Yanagi, *Ind. Eng. Chem. Res.* **26**(9), 1845 (1987)]. This is so because the local pinching of small-scale maldistribution is evened out by the lateral mixing, and therefore causes few ill effects. In contrast, the lateral mixing either is powerless to rectify a large-scale maldistribution or takes considerable bed length to do so (meanwhile, efficiency is lost).

Figure 14-67 shows HETPs measured in tests that simulate various types of maldistribution in FRI's 1.2-m column containing a 3.6-m bed of 1-in Pall® rings. The y axis is the ratio of measured HETP in the maldistribution tests to the HETP obtained with an excellent distributor. Analogous measurements with structured packing were reported by Fitz, King, and Kunesh [*Trans. IChemE* **77**, Part A, p. 482 (1999)]. Generally, the response of the structured packings resembled that of the Pall® rings, except as noted below.

Figure 14-67a shows virtually no loss of efficiency when a distributor uniformly tilts, such that the ratio of highest to lowest flow is 1.25 (i.e., a "1.25 tilt"). In contrast, an 11 percent chordal blank of a level distributor causes packing HETP to rise by 50 percent.

Figure 14-67b compares continuous tilts with ratios of highest to lowest flow of 1.25 and 1.5 to a situation where one-half of the distributor passes 25 percent more liquid than the other half. The latter ("zonal") situation causes a much greater rise in HETP than a "uniform" maldistribution with twice as much variation from maximum to minimum.

Figure 14-67c shows results of tests in which flows from individual distributor drip points were varied in a gaussian pattern (maximum/mean = 2). When the pattern was randomly assigned, there was no efficiency loss. When the variations above the mean were assigned to a "high zone," and those below the mean to a "low zone," HETP rose by about 20 percent. With structured packing, both random and zonal maldistribution caused about the same loss of efficiency at the same degree of maldistribution.

7. A packed bed appears to have a "natural distribution," which is an inherent and stable property of the packings. An initial distribution which is better than natural will rapidly degrade to it, and one that is worse will finally achieve it, but sometimes at a slow rate. If the rate is extremely slow, recovery from a maldistributed pattern may not be observed in practice (Zuiderweg et al., loc. cit.). Even though the

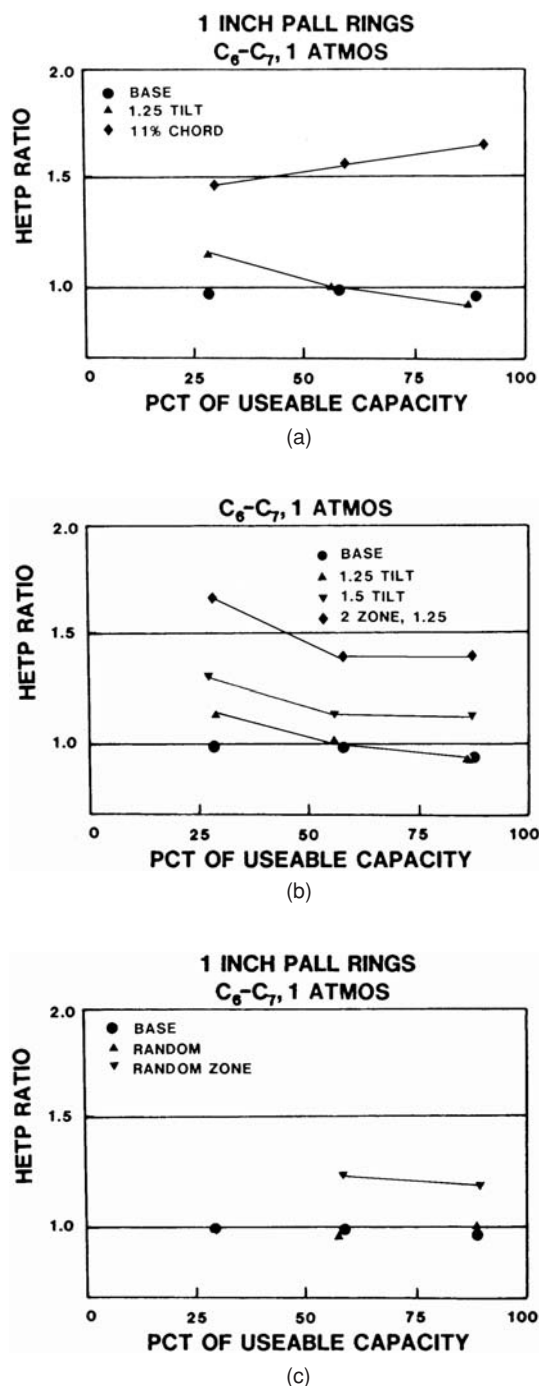


FIG. 14-67 Comparing the effects of "small-scale" and "large-scale" maldistribution on packing HETP. (a) Comparing the effect of a simulated continuous tilt (max/min flow ratio = 1.25) with the simulated effect of blanking a chordal area equal to 11 percent of the tower area. (b) Comparing the effects of simulated continuous tilts (max/min flow ratios of 1.25 and 1.5) with the effects of a situation where one-half of the distributor passes 25 percent more liquid than the other half. (c) Comparing the effects of random maldistribution with those of zonal maldistribution. (Reprinted with permission from J. G. Kunesh, L. Lahm, and T. Yahagi, *Ind. Eng. Chem. Res.*, **26**, p. 1845; copyright © 1987, American Chemical Society.)

volumetric distribution improves along the bed, the concentration profile could have already been damaged, and pinching occurs (Bonilla, *Chem. Eng. Prog.*, p. 47, March 1993).

8. Liquid maldistribution lowers packing turndown. The 2-in Pall rings curve in Fig. 14-59 shows HETP rise upon reaching the distributor turndown limit.

9. The major source of gas maldistribution is undersized gas inlet and reboiler return nozzles, leading to the entry of high-velocity gas jets into the tower. These jets persist through low-pressure-drop devices such as packings. Installing gas distributors and improving gas distributor designs, even inlet baffles, have alleviated many of these problems. Vapor distribution is most troublesome in large-diameter columns. Strigle (*Packed Tower Design and Applications*, 2d ed., Gulf Publishing, Houston, Tex., 1994) recommends considering a gas distributing device whenever the gas nozzle F -factor ($F_N = u_N \rho_N^{0.5}$) exceeds $27 \text{ m/s (kg/m}^3)^{0.5}$, or the kinetic energy of the inlet gas exceeds 8 times the pressure drop through the first foot of packing, or the pressure drop through the bed is less than 0.65 mbar/m . Gas maldistribution is best tackled at the source by paying attention to the gas inlet arrangements.

10. A poor initial liquid maldistribution may cause gas maldistribution in the loading region, i.e., at high gas rates [Stoter, Olujic, and de Graauw, *ICHEME Symp. Ser.* **128**, A201 (1992); Kouri and Sohlo, *ICHEME Symp. Ser.* **104**, B193 (1987)]. At worst, initial liquid maldistribution may induce local flooding, which would channel the gas. The segregation tends to persist down the bed. Outside the loading region, the influence of the liquid flow on gas maldistribution is small or negligible. Similarly, in high-gas-velocity situations, the liquid distribution pattern in the bottom structured packing layers is significantly influenced by a strongly maldistributed inlet gas flow [Olujic et al., *Chem. Eng. and Processing*, **43**, 465 (2004)]. Duss [*ICHEME Symp. Ser.* **152**, 418 (2006)] suggests that high liquid loads such as those experienced in high-pressure distillation also increase the susceptibility to gas maldistribution.

11. The effect of gas maldistribution on packing performance is riddled with unexplained mysteries. FRI's (Cai, Paper presented at the AIChE Annual Meeting, Reno, Nev., 2001) commercial-scale tests show little effect of gas maldistribution on both random and structured packing efficiencies. Cai et al. (*Trans ICHEME* **81**, Part A, p. 85, 2003) distillation tests in a 1.2-m-diameter tower showed that blocking the central 50 percent or the chordal 30 percent of the tower cross-sectional area beneath a 1.7-m-tall bed of $250 \text{ m}^2/\text{m}^3$ structured packing had no effect on packing efficiency, pressure drop, or capacity. The blocking did not permit gas passage but allowed collection of the descending liquid. Simulator tests with similar blocking with packing heights ranging from 0.8 to 2.4 m (Olujic et al., *Chemical Engineering and Processing*, **43**, p. 465, 2004; *Distillation 2003: Topical Conference Proceedings*, AIChE Spring National Meeting, New Orleans, La., AIChE, p. 567, 2003) differed, showing that a 50 percent chordal blank raised pressure drop, gave a poorer gas pattern, and prematurely loaded the packing. They explain the difference by the ability of liquid to drain undisturbed from the gas in the blocked segment in the FRI tests. Olujic et al. found that while gas maldistribution generated by collectors and by central blockage of 50 percent of the cross-sectional areas was smoothed after two to three layers of structured packing, a chordal blockage of 30 to 50 percent of cross-sectional area generated maldistribution that penetrated deeply into the bed.

12. Computational fluid dynamics (CFD) has been demonstrated effective for analyzing the effects of gas inlet geometry on gas maldistribution in packed beds. Using CFD, Wehrli et al. (*Trans. ICHEME* **81**, Part A, p. 116, January 2003) found that a very simple device such as the V-baffle (Fig. 14-70) gives much better distribution than a bare nozzle, while a more sophisticated vane device such as a Schoepentoeter (Fig. 14-71c) is even better. Implications of the gas inlet geometry to gas distribution in refinery vacuum towers was studied by Vaidyanathan et al. (*Distillation 2001*, Topical Conference Proceedings, AIChE Spring National Meeting, Houston, Tex., p. 287, April 22–26, 2001); Paladino et al. (*Distillation 2003: Topical Conference Proceedings*, AIChE Spring National Meeting, New Orleans, La., p. 241, 2003); Torres et al. (*ibid.*, p. 284); Waintraub et al. (*Distillation*

2005: Topical Conference Proceedings, AIChE Spring National Meeting, Atlanta, Ga., p. 79, 2005); and Wehrli et al. (*ICHEME Symp. Ser.* **152**, London, 2006). Vaidyanathan et al. and Torres et al. examined the effect of the geometry of a chimney tray (e.g., Fig. 14-72) above the inlet on gas distribution and liquid entrainment. Paladino et al. demonstrated that the presence of liquid in the feed affects the gas velocity profile, and must be accounted for in modeling. Paladino et al. and Waintraub et al. used their two-fluid model to study the velocity distributions and entrainment generated by different designs of vapor horns (e.g., Fig. 14-71). Wehrli et al. produced pilot-scale data simulating a vacuum tower inlet, which can be used in CFD model validation. Ali et al. (*Trans. ICHEME*, vol. **81**, Part A, p. 108, January 2003) found that the gas velocity profile obtained using a commercial CFD package compared well to those measured in a 1.4-m simulator equipped with structured packing together with commercial distributors and collectors. Their CFD model effectively pointed them to a collector design that minimizes gas maldistribution.

PACKED-TOWER SCALE-UP

Diameter For random packings there are many reports [Billet, *Distillation Engineering*, Chem Publishing Co., New York, 1979; Chen, *Chem. Eng.*, p. 40, March 5, 1984; Zuiderweg, Hoek, and Lahm, *ICHEME Symp. Ser.* **104**, A217 (1987)] of an increase in HETP with column diameter. Billet and Mackowiak's (Billet, *Packed Column Analysis and Design*, Ruhr University, Bochum, Germany, 1989) scale-up chart for Pall® rings implies that efficiency decreases as column diameter increases.

Practically all sources explain the increase of HETP with column diameter in terms of enhanced maldistribution or issues with the scale-up procedure. Lab-scale and pilot columns seldom operate at column-to-packing diameter ratios (D_T/D_p) larger than 20; under these conditions, lateral mixing effectively offsets loss of efficiency due to maldistribution pinch. In contrast, industrial-scale columns usually operate at D_T/D_p ratios of 30 to 100; under these conditions, lateral mixing is far less effective for offsetting maldistribution pinch.

To increase D_T/D_p , it may appear attractive to perform the bench-scale tests using a smaller packing size than will be used in the prototype. Deibele, Goedecke, and Schoenmaker [*ICHEME Symp. Ser.* **142**, 1021 (1997)], Goedecke and Alig (Paper presented at the AIChE Spring National Meeting, Atlanta, Ga., April 1994), and Gann et al. [*Chem. Ing. Tech.*, **64**(1), 6 (1992)] studied the feasibility of scaling up from 50- to 75-mm-diameter packed columns directly to industrial columns. Deibele et al. and Gann et al. provide an extensive list of factors that can affect this scale-up, including test mixture, packing pretreatment, column structure, packing installation, snug fit at the wall, column insulation and heat losses, vacuum tightness, measurement and control, liquid distribution, reflux subcooling, prewetting, sampling, analysis, adjusting the number of stages to avoid pinches and analysis issues, evaluation procedure, and more. Data from laboratory columns can be particularly sensitive to some of these factors. Goedecke and Alig show that for wire-mesh structured packing, bench-scale efficiency tends to be better than large-column efficiency, while for corrugated-sheets structured packing, the converse occurs, possibly due to excessive wall flow. For some packings, variation of efficiency with loads at bench scale completely differs from its variation in larger columns. For one structured packing, Kuhni Rom-bopak 9M, there was little load effect and there was good consistency between data obtained from different sources—at least for one test mixture. Deibele et al. present an excellent set of practical guidelines to improve scale-up reliability. So, it appears that great caution is required for packing data scale-up from bench-scale columns.

Height Experimental data for random packings show that HETP slightly increases with bed depth [Billet, *Distillation Engineering*, Chemical Publishing Co., New York, 1979; "Packed Tower Analysis and Design," Ruhr University, Bochum, Germany, 1989; Eckert and Walter, *Hydrocarbon Processing*, **43**(2), 107 (1964)].

For structured packing, some tests with Mellapak 250Y [Meier, Hunkeler, and Stöcker, *ICHEME Symp. Ser.* **56**, p. 3, 3/1 (1979)] showed no effect of bed height on packing efficiency, while others (Cai et al., *Trans ICHEME*, vol. **81**, Part A, p. 89, January 2003) did show a significant effect.

The effect of bed depth on packing HETP is attributed to liquid maldistribution. Zuiderweg et al. [*ICHEM. Symp. Ser.* **104**, A217 (1987)] suggest that the uneven irrigation generates an uneven concentration profile and localized pinching near the bottom of the beds. The tests by Martin, Bravo, and Fair (Paper presented at the National AIChE Meeting, New Orleans, La., 1988) confirm that the problem area is near the bottom. According to the zone-stage and Lockett and Billingham models (above), as well as the empirical correlation by Moore and Rukovena (Fig. 14-64), the more stages per bed, the greater is the rise in HETP with bed depth. The presence and extent of maldistribution play an important role in determining the bed-depth effect.

As the bed depth increases, end effects (i.e., mass transfer in the region of liquid introduction and in the region where liquid drips from the packing supports) become less important. Such end effects tend to lower the HETP observed in short columns, such as pilot-plant columns.

In summary, bed depth may significantly influence HETP. This adds uncertainty to scale-up. Shallow test beds should be avoided. Most investigators use beds at least 1.5 m tall, and often more than 3 m tall. The FRI sampling technique (below) can detect maldistribution along the bed height.

Loadings For many random and corrugated-sheet structured packings, HETP is independent of vapor and liquid loadings (Figs. 14-59 and 14-60). For wire-mesh and some corrugated-sheet structured packings, HETP changes with gas and liquid loads.

Wu and Chen [*ICHEM Symp. Ser.* **104**, B225 (1987)] recommend pilot testing over the entire range between the expected minimum and maximum operating rates, and taking the highest measured HETP as the basis for scale-up. The author concurs. With structured packings, the load effect may be due to liquid rather than gas loads, and the pilot tests should cover the range of liquid loads (i.e., m/s based on column cross section) that is expected in the prototype.

Wetting For operation at low liquid loads, the onset of minimum wetting can adversely affect scale-up, particularly with random packings and aqueous systems. Scale-up reliability at low liquid loads can be improved by pilot-testing at the composition range expected in the prototype, and by using identical packing materials and surface treatment in the pilot tests and in the prototype.

Underwetting At the aqueous end of aqueous-organic columns, underwetting is important. Rapid changes of concentration profiles and physical properties in organic-water separations complicate scale-up [Eiden and Kaiser, *ICHEM Symp. Ser.* **142**, 757 (1997)]. Near the onset of underwetting, HETP becomes strongly dependent on composition, packing material and surface roughness, and the presence of surfactants. Scale-up reliability can be enhanced by pilot-testing at the composition range expected in the prototype, and by using identical packing material and surface treatment in the pilot tests and in the prototype.

Preflooding For one structured packing test with an aqueous system, Billet ("Packed Column Analysis and Design," Ruhr University, Bochum, Germany, 1989) measured higher efficiency for a pre-flooded bed compared with a non-preflooded bed. Presumably, the preflooding improved either wetting or distribution. Billet recommends preflooding the packing, both in the prototype and in the pilot column, to ensure maximum efficiency.

Sampling Fractionation Research Inc. (FRI) developed a sampling technique that eliminates the influence of "end effects" and detects a maldistributed composition profile. This technique [Silvey and Keller, *ICHEM Symp. Ser.* **32**, p. 4:18 (1969)] samples the bed at frequent intervals, typically every 0.6 m or so. HETP is determined from a plot of these interbed samples rather than from the top and bottom compositions.

It is imperative that the interbed samplers catch representative samples, which are an average through the bed cross section. Caution is required when the liquid is highly aerated and turbulent (e.g., above 1300 kPa psia or above 1 m/min). The author highly recommends the FRI sampling technique for all other conditions.

Aging Billet (loc. cit.) showed that for some plastic packings in aqueous systems, the efficiency after one week's operation was almost double the efficiency of new packings. Little further change was

observed after one week. Billet explains the phenomenon by improved wetting. He recommends that data for plastic packings should only be used for scale-up after being in operation for an adequately long period.

DISTRIBUTORS

Liquid Distributors A liquid distributor (or redistributor) should be used in any location in a packed column where an external liquid stream is introduced. Liquid redistributors are also used between packed beds to avoid excessive bed lengths that may impair packing efficiency or mechanical strength. It is best to have the packing supplier also supply the distributor, with the user critically reviewing the design. The user must provide the supplier with concise information about the plugging, corrosive, and foaming tendencies of the service as well as the range of liquid flow rates that it needs to handle and the physical properties of the liquid.

Olsson (*Chem. Eng. Progr.*, p. 57, October 1999) discussed the key for successful distributor design and operation. He states that it is critical to correctly evaluate the fouling potential of the service and design for it (e.g., preventing small holes, filtering the feed, etc.); to avoid gas entry into liquid distributors (e.g., no flashing feed into a liquid distributor); to systematically check the irrigation pattern using a method such as the circle analysis of Moore and Rukovena [*Chem. Plants and Process* (European ed.), p. 11, August 1987; described in detail in Kister's *Distillation Operation*, McGraw-Hill, New York, 1990]; to water-test any liquid distributor (major suppliers have dedicated test stands that are available for those purposes at cost); to ensure correct entry of a feed into a liquid distributor; and to thoroughly inspect a distributor. Kister [*Trans. IChE*, vol. 81, Part A, p. 5 (January 2003)] found that between 80 and 90 percent of the distributor failures reported in the literature in the last 50 years could have been prevented if users and suppliers had followed Olsson's measures.

A minimum of 40 irrigation points per square meter has been recommended, with 60 to 100 per square meter being ideal [Strigle, *Packed Tower Design and Applications*, 2d ed., Gulf Publishing, Houston, Tex., 1994; Kister, *Distillation Operation*, McGraw-Hill, New York, 1990; Norton Company (now Koch-Glitsch LP), *Packed Column Internals*, Bulletin TA-80R, 1974]. Commercial-scale tests with both random and structured packings showed no improvement in packing efficiency by increasing the irrigation point density above 40 per square meter [Fitz, King, and Kunes, *Trans. IChE* **77**, Part A, p. 482 (1999)]. So going to larger numbers of irrigation points per square meter provides little improvement while leading to smaller holes which increases the plugging tendency. In orifice-type distributors, which are the most common type, the head-flow relationship is given by the orifice equation

$$Q = 3.96 \times 10^{-4} K_D n_D d_h^0.5 h^{0.5} \quad (14-163)$$

where Q is the liquid flow rate, m³/h; K_D is the orifice discharge coefficient, with a recommended value of 0.707 (Chen, *Chem. Eng.*, p. 40, March 5, 1984); n_D is the number of holes; d_h is the hole diameter, mm; and h is the liquid head, mm. Equation (14-163) shows that at a given Q , increasing n leads to either smaller d or smaller h .

Figures 14-68 and 14-69 show common distributor types used for distillation and absorption. An excellent detailed discussion of the types of distributors and their pros and cons was given by Bonilla (*Chem. Eng. Progr.*, p. 47, March 1993). The *perforated pipe* (or *ladder pipe*) distributor (Fig. 14-68a) has holes on the underside of the pipes. It is inexpensive, provides a large open area for vapor flow, and does not rely on gravity. On the debit side, it is typically designed for high velocity heads, 500 to 1000 mm of water, which is 5 to 10 times more than gravity distributors, requiring [per Eq. (14-163)] either fewer irrigation points or the use of plugging-prone smaller holes. The high hole velocities make it prone to corrosion and erosion. These disadvantages make it relatively unpopular. A gravity variation of this distributor uses a liquid drum above the distributor that gravity-feeds it.

Spray distributors (Fig. 14-68b) are pipe headers with spray nozzles fitted on the underside. The spray nozzles are typically wide-angle (often 120°) full-cone. Spray distributors are unpopular in distillation but are common in heat transfer, washing and scrubbing services

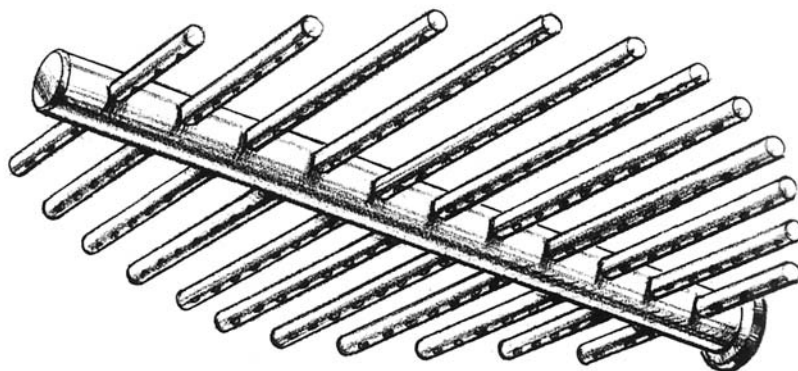
(especially in refinery towers), and in small-diameter towers where a single spray nozzle can be used. They are inexpensive and offer a large open area for vapor flow and a robustness for handling of fouling fluids when correctly designed, and the sprays themselves contribute to mass and heat transfer. On the debit side, the spray cones often generate regions of over- and underirrigation, the sprays may not be homogeneous, the spray nozzles are prone to corrosion, erosion, and damage. With highly subcooled liquids, the spray angle may collapse when pushed at high pressure drops (above 100 to 150 kPa) (Fractionation Research Inc., "A Spray Collapse Study," motion picture 919, Stillwater, Okla., 1985). The design and spray pattern are highly empirical. Sprays also generate significant entrainment to the section above [Trompiz and Fair, *Ind. Eng. Chem. Res.*, **39**(6), 1797 (2000)].

Orifice pan distributors (Fig. 14-69a) and *orifice tunnel* distributors (Fig. 14-69b) have floor holes for liquid flow and circular (Fig. 14-69a) or rectangular (Fig. 14-69b) risers for vapor passages. When they are used as redistributors, a hat is installed above each riser to prevent liquid from the bed above from dripping into the risers. Unlike the ladder pipe and spray distributors that operate by pressure drop, orifice distributors operate by gravity, and therefore use a much smaller liquid head, typically 100 to 150 mm at maximum rates. Using Eq. (14-163), the lower head translates to either more distributions points (n_D), which helps irrigation quality, or larger hole diameters, which resists plugging. However, the low liquid velocities, large residence times, and open pans (or troughs) make them more prone to plugging than the pressure distributors. A good hole pattern and avoidance of oversized risers are essential. Orifice distributors are self-collecting, a unique advantage for redistributors. Orifice distributors are one of the most popular types and are favored whenever the liquid loads are high enough to afford hole diameters large enough to resist plugging (>12 mm).

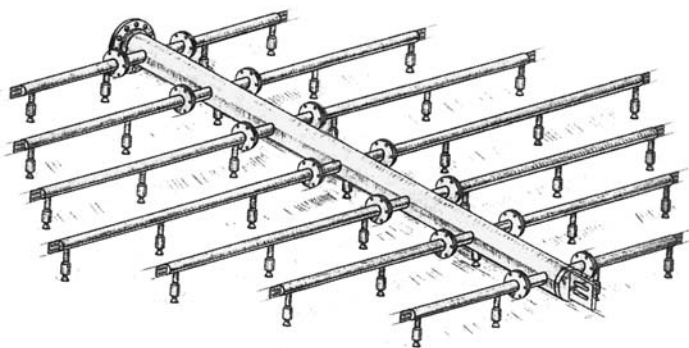
Orifice trough (or *orifice channel*) distributors (Fig. 14-69c-f) are some of the most popular types. The trough construction does away with the multitude of joints in the orifice pans, making them far more leak-resistant, a major advantage in large towers and low-liquid-rate applications. Liquid from a central parting box (Fig. 14-69c, e) or middle channel (Fig. 14-69d) is metered into each trough. The troughs can have floor holes, but elevating the holes above the floor (Fig. 14-69c-g) is preferred as it enhances plugging resistance. Tubes (Fig. 14-69c, d, f) or baffles (Fig. 14-69e) direct the liquid issuing from the elevated holes downward onto the packings. Orifice trough distributors are not self-collecting. When used for redistribution, they require a liquid collector to be installed above them.

Turndown of orifice distributors is constrained to about 2 : 1 by Eq. (14-163). For example, a 100-mm liquid head at the design drops to 25 mm when the liquid rate is halved. Lower heads give poor irrigation and high sensitivity to levelness. Turndown is often enhanced by using two rows of side tubes (in the Fig. 14-69c type) or of side holes (in the Fig. 14-69d or e types). *Perforated drip tubes* (as in Fig. 14-69d) are popular in either orifice trough or orifice pan distributors. The lower, smaller hole is active at low liquid rates, with the larger upper hole becoming active at higher liquid rates. Use of perforated drip tubes is not recommended when the vapor dew point is much higher than the liquid bubble point, because liquid may boil in the tubes, causing dryout underneath [Kister, Stupin, and Oude Lenferink, *ICHEME. Symp. Ser.* **152**, p. 409, London (2006)].

A popular type of the orifice trough distributor is the *splash plate* distributor (Fig. 14-69e). The splash plates spread the issuing liquid over their lengths, making it possible to reduce the number of irrigation points. This is a special advantage with small liquid rates, as fewer irrigation points (at a given head) translate to larger, more fouling-resistant



(a)



(b)

FIG. 14-68 Pressure liquid distributors. (a) Ladder pipe. (b) Spray. (Courtesy of Koch-Clitsch LP.)

hole diameters [Eq. (14-163)]. Lack of the drip tubes eliminates the possible in-tube boiling issue (above).

Multistage orifice trough distributors (Fig. 14-69f) also attempt to provide good irrigation at low liquid rates without resorting to plugging-prone small holes. The primary stage uses fewer irrigation points. Liquid from the primary stage is further split at the secondary stage. The secondary stage is of small size, so leveling and small flow variations are not of great concern. The secondary stage may use the same or a different liquid splitting principle as the primary stage. Even short layers of structured packings have been used as a secondary distribution stage.

Notched trough distributors (Fig. 14-69g) consist of parallel troughs with side V notches. This distributor obeys the triangular notch equation instead of the orifice equation, which makes the flow proportional to $h^{2.5}$ [instead of $h^{0.5}$ in Eq. (14-163)]. This high power renders the distributor highly sensitive to out-of-levelness and

hydraulic gradients and makes it difficult to incorporate a large number of distribution points. Since the liquid issues sideways, it is difficult to predict where the liquid will hit the packings. Baffles are sometimes used to direct the liquid downward. Overall, the quality of distribution is inferior to that of orifice distributors, making notched-trough distributors unpopular. Their strength is their insensitivity to fouling and corrosive environments and their ability to handle high liquid rates at good turndown.

With any trough distributor, and especially those with V notches, excessive hydraulic gradients must be avoided. This is often achieved by using more parting boxes.

The hydraulic gradient is highest where the liquid enters the troughs, approaching zero at the end of the trough. The hydraulic gradient (between entry point and trough end) can be calculated from [Moore and Rukovena, *Chemical Plants and Processing* (European ed.), p. 11, August 1987]

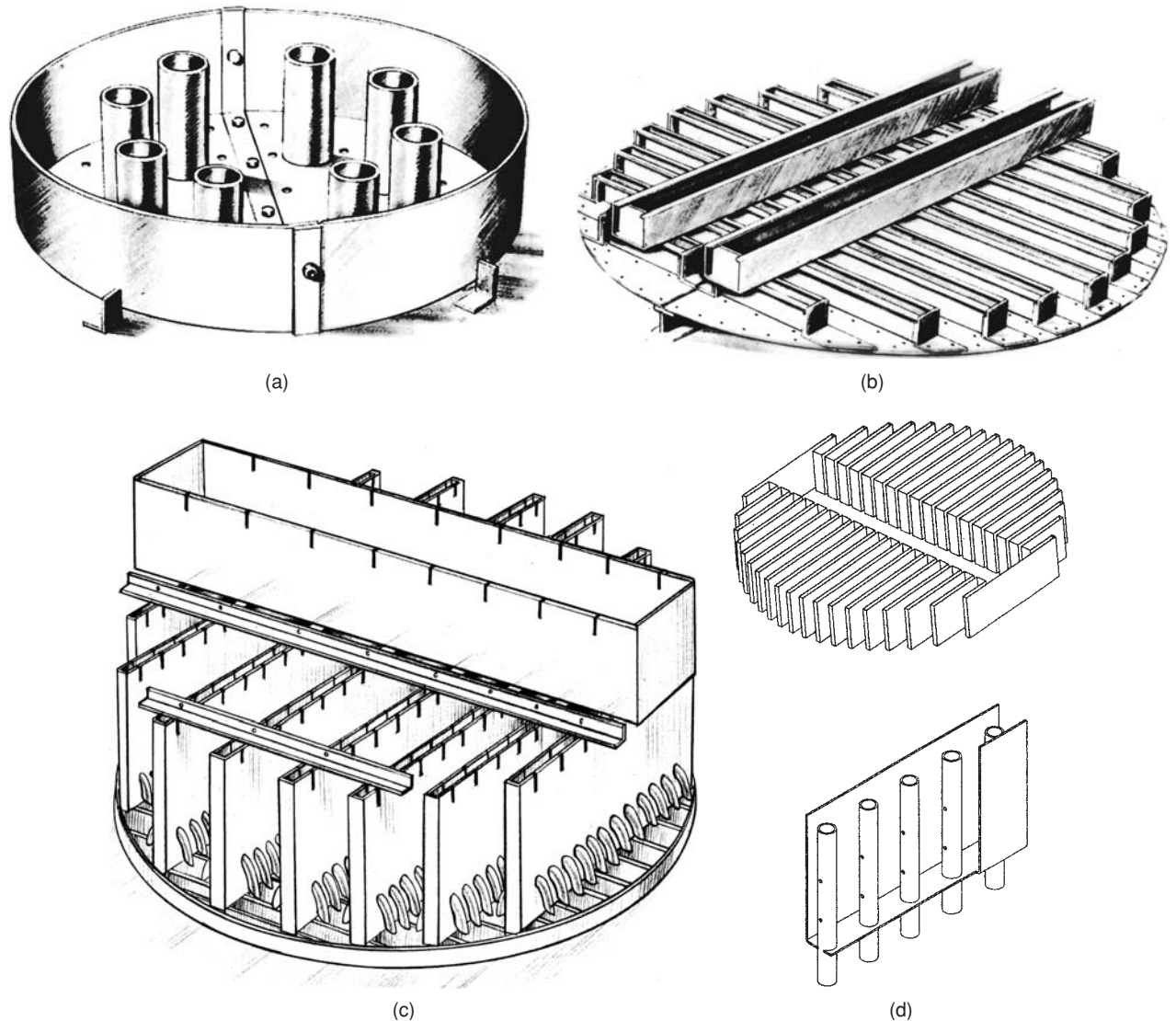


FIG. 14-69 Gravity liquid distributors. (a) Orifice pan. (b) Orifice tunnel. (c) Orifice tube, using external drip tubes. (d) Orifice trough, using internal drip tubes. (e) Splash plate orifice trough. (f) Two-stage orifice trough. (g) Notched trough. (Parts a-c, g, courtesy of Koch-Glitsch LP; parts d-f, courtesy of Sulzer Chemtech.)

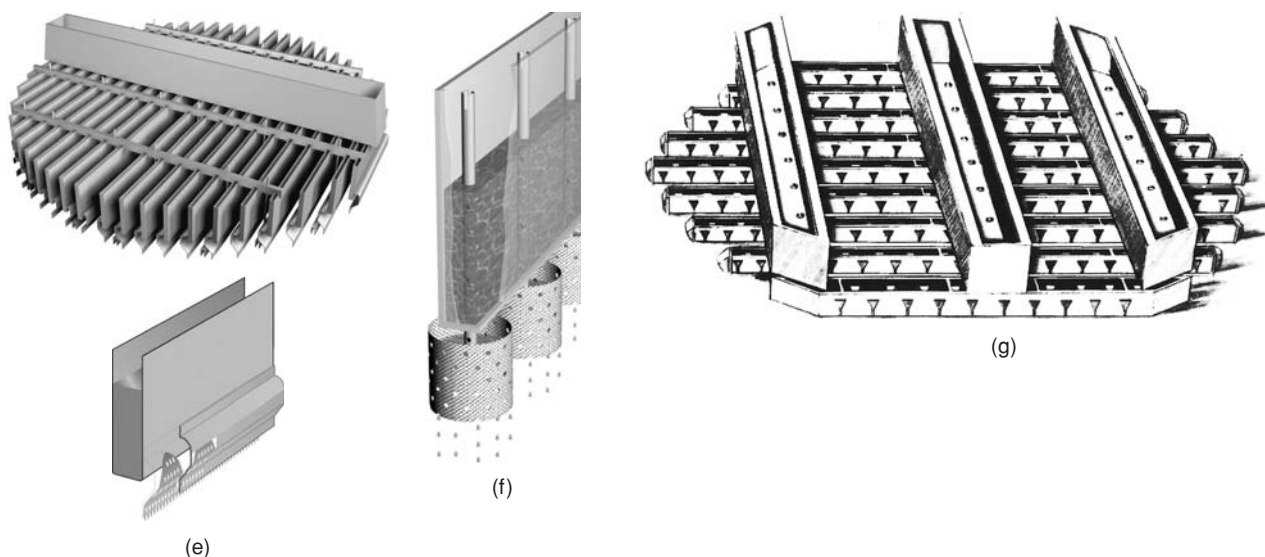


FIG. 14-69 (Continued)

$$h_{hg} = 51v_{H}^2 \quad (14-164)$$

where h_{hg} is the hydraulic gradient head, mm, and v_H is the horizontal velocity in the troughs, m/s.

Flashing Feed and Vapor Distributors When the feed or reflux is a flashing feed, the vapor must be separated out of the liquid before the liquid enters a liquid distributor. At low velocities (only), this can be achieved by a *bare nozzle* (Fig. 14-70a). A *V baffle* (Fig. 14-70b) is sometimes installed as a primitive flashing feed or vapor distributor.

For better vapor-liquid separation and distribution, with smaller-diameter towers (<1.5 m), a *flash chamber* (Fig. 14-70c) separates the liquid from the vapor, with the collected liquid descending via downpipes to a liquid distributor below. The flash chamber can be peripheral (Fig. 14-70c) or central. In larger towers, *gallery distributors* (Fig. 14-70d) are preferred. The flashing feed enters the peripheral section of the upper plate (the gallery) where vapor disengages and flows up, with liquid descending through holes (Fig. 14-70d) or down pipes onto the liquid distributor below. Alternatively, an external knockout pot is sometimes used to give separate vapor and liquid feeds.

The *vapor horn* (Fig. 14-71a) is unique for high-velocity feeds in which vapor is the continuous phase with liquid present as suspended drops in the feed vapor. This is common when the feed makes up the bulk of the vapor traffic in the tower section above. Typical examples are feeds to refinery vacuum and crude towers and rich solution feeds to hot carbonate regenerators. A tangential helical baffle or vapor horn, covered at the top, open at the bottom, and spiraling downward, is used at the feed entry. This baffle forces the vapor to follow the contour of the vessel as it expands and decreases in velocity. Liquid droplets, due to their higher mass, tend to collide with the tower wall, which deflects them downward, thus reducing upward entrainment. Large forces, generated by hurricane-force winds and vapor flashing, are absorbed by the entire tower wall rather than by a small area. A wear plate is required at the tower wall. Some designs have vane openings on the inside wall.

Alternatively, multivane triangular diffusers (Fig. 14-71b, c) such as the Schoepentoeter have been successful for high-velocity vapor-rich feeds. These are used with radial (as distinct from tangential) nozzles. The vanes knock out the liquid and direct it downward while the vapor expands to the tower diameter.

Pilot-scale tests by Fan et al. [*ICHEME Symp. Ser.* **142**, 899 (1997)] compared vapor distribution and entrainment from sparger, vapor

horns, and multivane triangular diffusers. Vapor horns gave the best overall performance considering vapor distribution, entrainment, and pressure drop, with multivane distributors doing well too. The designs of the inlets compared, however, were not optimized so the comparison could have reflected deviations from optimum rather than real differences between the devices.

Low-velocity vapor-only feeds often enter via bare nozzles or V baffles (above). At higher velocities, perforated vapor spargers are used. At high velocities, vapor horns and Schoepentoeters are often preferred. Alternatively or additionally, a vapor distributor may be mounted above the feed. The vapor distributor is a chimney tray (Fig. 14-72) where liquid is collected on the deck and flows via downcomers or is drawn out while vapor passes through the chimneys. To be effective as a vapor distributor, the pressure drop through the chimneys needs to be high enough to counter the maldistributed vapor. It was recommended to make the pressure drop through the chimneys at least equal to the velocity head at the tower inlet nozzle (Strigle, *Random Packings and Packed Towers*, Gulf Publishing, Houston, Tex., 1987), with common pressure drops ranging from 25 to 200 mm water.

OTHER PACKING CONSIDERATIONS

Liquid Holdup Liquid holdup is the liquid present in the void spaces of the packing. Reasonable liquid holdup is necessary for good mass transfer and efficient tower operation, but beyond that, it should be kept low. High holdup increases tower pressure drop, the weight of the packing, the support load at the bottom of the packing and tower, and the tower drainage time. Most important, when distilling thermally unstable materials, excessive holdup raises product degradation and fouling, and with hazardous chemicals, increases undesirable inventories.

The effect of liquid and gas rates on the operating holdup is shown in Figs. 14-73 and 14-74. In the preloading regime, holdup is essentially independent of gas velocity, but is a strong function of liquid flow rate and packing size. Smaller packings and high liquid rates tend to have greater holdup.

Holdup can be estimated by using Buchanan's correlation [*Ind. Eng. Chem. Fund.* **6**, 400 (1967)], as recommended in previous editions of this handbook. More recent correlations by Billet and Schultes [*ICHEME. Symp. Ser.* **104**, A159 (1987)], by Maćkowiak

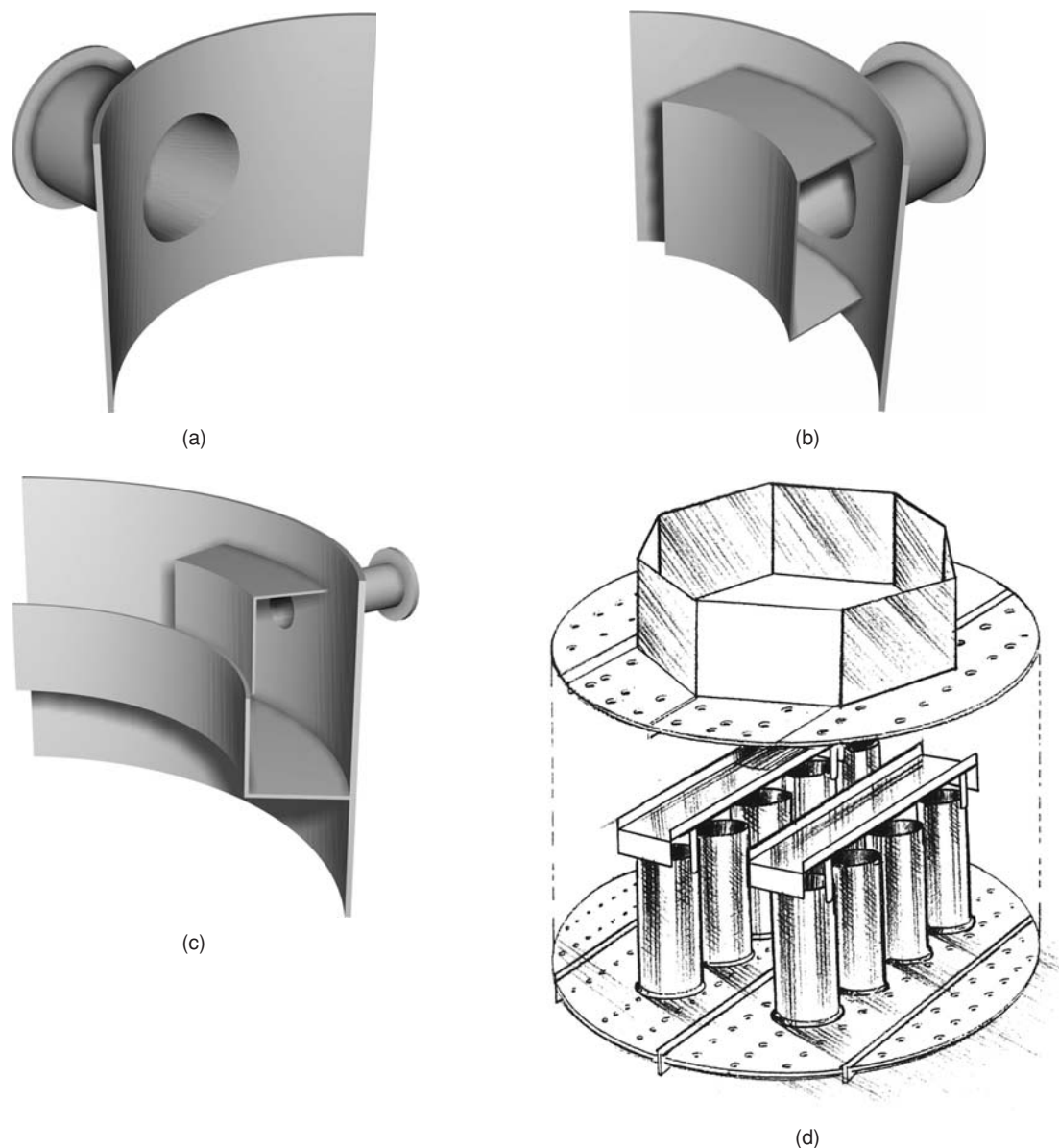


FIG. 14-70 Flashing feed and vapor distributors. (a) Bare nozzle. (b) Rounded V baffle. (c) Peripheral flash box—the box extends right around the tower wall, with the collected liquid descending via downpipes to a liquid distributor below. (d) Gallery distributor—the feed enters the gallery area (upper plate). (Parts a–c, courtesy of Sulzer Chemtech; part d, courtesy of Koch-Glitsch LP.)

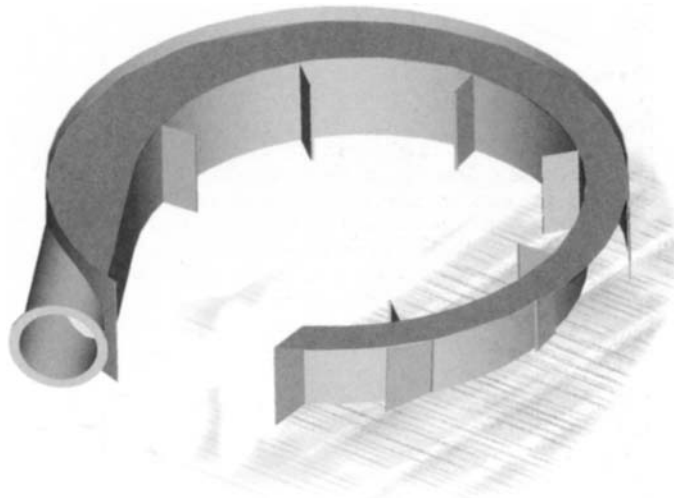
(“Fluiddynamik von Kolonnen mit Modernen Füllkörpern und Packungen für Gas/Flüssigkeitssysteme, Otto Salle Verlag, Frankfurt am Main, and Verlag Sauerländer, Aarau, 1991), and by Mersmann and Deixler [*Chem. Ing. Tech.* **58**(1), 19 (1986)] apply to second- and third-generation random packings as well as to some structured packings.

Stichlmair and Fair (*Distillation Principles and Practice*, Wiley-VCH, New York, 1998) show that liquid holdup is primarily a function of the liquid Froude number, specific surface area of the packing, and physical properties. They recommend the correction by Engel, Stichlmair, and Geipel [*Ind. Eng. Chem. Symp. Ser.* **142**, 939 (1997)].

$$h_{L0} = 0.93 \left(\frac{U_L^2 a_p}{g} \right)^{1/6} \left(\frac{\mu_L^2 a_p^3}{\rho_L^2 g} \right)^{1/10} \left(\frac{\sigma a_p^2}{1000 \rho_L g} \right)^{1/8} \quad (14-165)$$

where h_{L0} = liquid holdup, fractional
 U_L = liquid superficial velocity, m/s
 a_p = packing specific surface area, m^2/m^3
 g = acceleration due to gravity, m/s²
 μ_L = liquid viscosity, kg/(m·s)
 σ = surface tension, mN/m

The Engel, Stichlmair, and Geipel correlation applies only in the preloading regime. The packing geometry is represented in the



(a)



(b)



(c)

FIG. 14-71 High-velocity flashing feed and vapor distributors. (a) Vapor horn. (b) Radial vane distributor. (c) Schoepentoeter. (Parts a, b, courtesy of Koch-Glitsch LP; part c, courtesy of Sulzer Chemtech.)

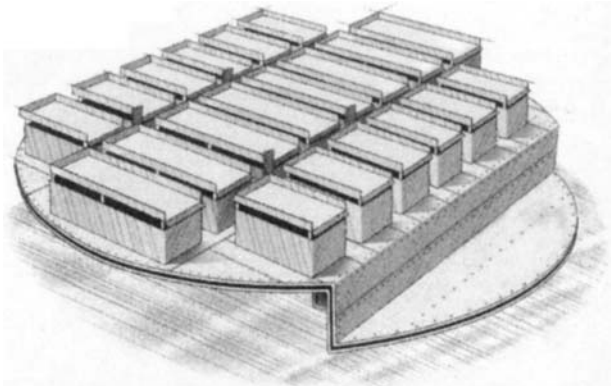


FIG. 14-72 Chimney tray vapor distributor. (Reprinted courtesy of Koch-Glitsch LP.)

correlation solely by the readily available specific surface area (Tables 14-13 and 14-14).

Minimum Wetting Rate The minimum wetting rate (MWR) is the lower stability limit of packings. Below this liquid load the liquid film on the packing surfaces breaks up and dewetting occurs. The area available for mass transfer diminishes, and efficiency drops.

Schmidt [*ICHEM E Symp. Ser.* 56, 3.1/1 (1979)] described the MWR in terms of a force balance at a dry patch along the path of a falling liquid film. While the gravity and viscous forces resist dewetting, the surface tension and vapor shear forces tend to dewet the falling film. The MWR therefore rises with an increase in surface tension and liquid density, and with a decrease in liquid viscosity. Large packing sizes and poor surface wetting characteristics also contribute to higher MWR.

Schmidt presented a fundamental correlation to predict minimum wetting for Raschig and Pall® rings. More popular have been the Glitsch rules of thumb [Table 14-16; Glitsch, Inc. (now Koch Glitsch), Bulletin 345, Dallas, Tex., 1986] for CMR® random packings with packing surface areas around 200 m²/m³. To extend these rules to other random packings, Kister (*Distillation Design*, McGraw-Hill, New York, 1992) applied Schmidt's model to give

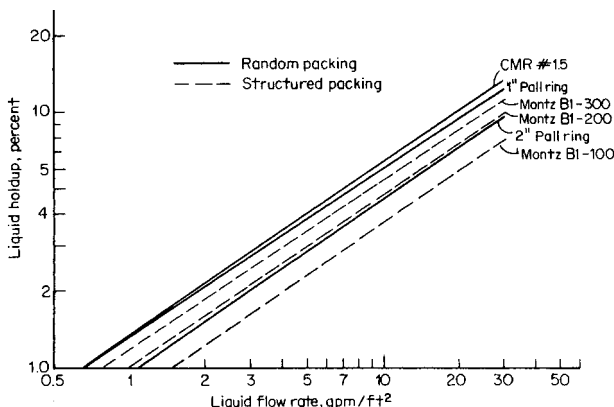


FIG. 14-73 Liquid holdup, air-water data by Billet ("Packed Column Design and Analysis," Ruhr University, Bochum, Germany), preloading regime. (From Kister, H. Z., *Distillation Design*, copyright © by McGraw-Hill; reprinted with permission.)

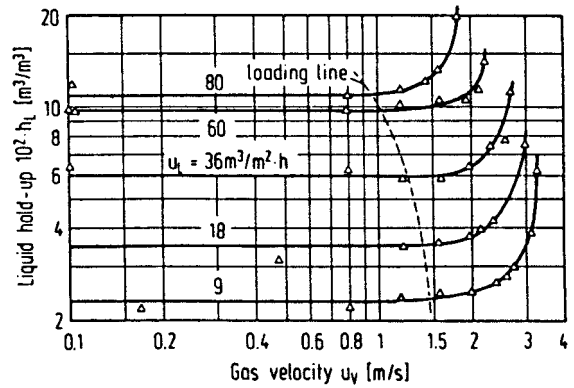


FIG. 14-74 Effect of liquid and gas rates on the operating holdup of modern random packings (25-mm NorPac®). [From R. Billet and M. Schultes, *ICHEM E Symp. Ser.* 104, p. A159, 1987. Reprinted courtesy of the Institution of Chemical Engineers (UK).]

$$Q_{MW} \approx (Q_{MW} \text{ from Table 14-16}) \times (200/a_p)^{0.5} \quad (14-166)$$

The Glitsch brochure did not state the surface tension bases of Table 14-16. The author believes that they conservatively apply to organic and hydrocarbon systems ($\sigma < 25$ mN/m). For water ($\sigma = 70$ mN/m) the author believes that double the values from Table 14-16 is reasonable.

Some surface treatments of the packing (e.g., oxidizing, sandblasting, etching) can substantially reduce the MWR. Chuang and Miller [*Can. J. Chem. Eng.* 66(6), 377 (1988)] tested a metallic random packing with an aqueous system at low liquid rates (about 0.4 m³/hm²). They used two alternative techniques for oxidizing the packing surfaces. The packings oxidized with the more effective technique gave a column efficiency twice as high as those oxidized by the others.

Superior wetting characteristics characterize structured packings. Satisfactory performance was reported down to 0.25 and 0.12 m³/hm² in corrugated-sheet and wire-mesh metal structured packings, respectively. FRI's commercial-scale tests (Fitz and Kunesh, Paper presented at the AIChE Annual Meeting, Chicago, Nov. 1996) demonstrated good efficiencies down to 0.5 m³/hm² (no lower limit reached) with good liquid and vapor distribution.

Two Liquid Phases Two liquid phases often occur in heterogeneous distillation, in steam stripping, and in solvent recovery. Harrison (*Chem. Eng. Progr.*, p. 80, November 1990) and Meier et al. [*ICHEM E Symp. Ser.* 152, 267 (2006)] saw no reason to expect unusual capacity or pressure drop limitations due to the presence of the second liquid phase, suggesting that standard correlations for these should apply.

In contrast, both expressed uncertainty in predicting packing efficiency. Harrison presented two case studies: In one, adding water to two water-insoluble organics had no effect on HETP; in another, a key

TABLE 14-16 Glitsch's Rule of Thumb for Minimum Wetting

Basis: CMR with $a_p > 150$ m²/m³

Material	Minimum wetting rate, m ³ /(m ² ·h)
Unglazed ceramic (chemical stoneware)	0.5
Oxidized metal (carbon steel, copper)	0.7
Surface-treated metal (etched stainless steel)	1.0
Glazed ceramic	2.0
Glass	2.5
Bright metal (stainless steel, tantalum, other alloys)	3.0
PVC-CPVC	3.5
Polypropylene	4.0
Fluoropolymers (PTFE type)	5.0

component was soluble in both liquid phases, and HETP was about 50 percent above normal. Harrison argued that a second liquid phase leads to lower efficiency only when it impairs diffusion of the key species. On this basis, Harrison expects efficiency loss also when an "inert" liquid or vapor represents a large fraction of the liquid or vapor phase. Meier et al. recommend obtaining efficiencies by scaling up laboratory-scale data using a similar type of packing.

Both Harrison and Meier et al. emphasize adequately distributing each liquid phase to the packing. Harrison noted that a well-designed ladder pipe distributor can maintain high velocities and low residence times that provide good mixing. With trough distributors that separate the phases and then distribute each to the packing, a light-to-heavy phase maldistribution may occur, especially when the phase ratio and separation vary. Meier et al. noted the existence of a cloudy two-liquid

layer between the clear light and heavy liquid and recommend an additional middle distribution point for this layer. They also noticed that phase separation unevenness can have a large influence on the phase ratio irrigated to the packing.

High Viscosity and Surface Tension Bravo (Paper presented at the AIChE Spring National Meeting, Houston, Tex., 1995) studied a system that had 425-cP viscosity, 350 mN/m surface tension, and a high foaming tendency. He found that efficiencies were liquid-phase-controlled and could be estimated from theoretical HTU models. Capacity was less than predicted by conventional methods which do not account for the high viscosity. Design equations for orifice distributors extended well to the system once the orifice coefficient was calculated as a function of the low Reynolds number and the surface tension head was taken into account.

OTHER TOPICS FOR DISTILLATION AND GAS ABSORPTION EQUIPMENT

COMPARING TRAYS AND PACKINGS

Most separations can be performed either with trays or with packings. The factors below represent economic pros and cons that favor each and may be overridden. For instance, column complexity is a factor favoring trays, but gas plant demethanizers that often use one or more interboilers are traditionally packed.

Factors Favoring Packings

Vacuum systems. Packing pressure drop is much lower than that of trays because the packing open area approaches the tower cross-sectional area, while the tray's open area is only 8 to 15 percent of the tower cross-sectional area. Also, the tray liquid head, which incurs substantial pressure drop (typically about 50 mm of the liquid per tray), is absent in packing. Typically, tray pressure drop is of the order of 10 mbar per theoretical stage, compared to 3 to 4 mbar per theoretical stage with random packings and about one-half of that with structured packings.

Consider a vacuum column with 10 theoretical stages, operating at 70-mbar top pressure. The bottom pressure will be 170 mbar with trays, but only 90 to 110 mbar with packings. The packed tower will have a much better relative volatility in the lower parts, thus reducing reflux and reboil requirements and bottom temperature. These translate to less product degradation, greater capacity, and smaller energy consumption, giving packings a major advantage.

Lower-pressure-drop applications. When the gas is moved by a fan through the tower, or when the tower is in the suction of a compressor, the smaller packing pressure drop is often a controlling consideration. This is particularly true for towers operating close to atmospheric pressure. Here excessive pressure drop in the tower increases the size of the fan or compressor (new plant), bottlenecks them (existing plant), and largely increases power consumption. Due to the compression ratio, pressure drop at the compressor discharge is far less important and seldom a controlling consideration.

Revamps. The pressure drop advantage is invaluable in vacuum column revamps, can be translated to a capacity gain, an energy gain, a separation improvement, or various combinations of these benefits. Likewise, for towers in the suction of compressors, replacing trays by packings reduces the compression ratio and helps debottleneck the compressor.

Packings also offer an easy tradeoff between capacity and separation. In the loaded sections of the tower, larger packings can overcome capacity bottlenecks at the expense of loss in separation. The separation loss can often be regained by retrofitting with smaller packings in sections of the tower that are not highly loaded. In tray towers, changing tray spacing gives similar results, but is more difficult to do.

Foaming (and emulsion). The low gas and liquid velocities in packing suppress foam formation. The large open area of the larger random packing promotes foam dispersal. Both attributes make

random packing excellent for handling foams. In many cases recurrent foaming was alleviated by replacing trays by random packing, especially when tray downcomers were poorly designed.

Switching from trays to structured packing can aggravate foaming. While the low gas and liquid velocities help, the solid walls restrict lateral movement of foams and give support to the foams. **Small-diameter columns.** Columns with diameter less than 1 m (3 ft) are difficult to access from inside to install and maintain the trays. "Cartridge" trays or an oversized diameter are often used. Either option is expensive. Cartridge trays also run into problems with sealing to the tower wall and matching tower to tray hardware [Sands, *Chem. Eng.*, p. 86 (April 2006)]. Packing is normally a cheaper and more desirable alternative.

Corrosive systems. The practical range of packing materials is wider. Ceramic and plastic packings are cheap and effective. Trays can be manufactured in nonmetals, but packing is usually a cheaper and more desirable alternative.

Low liquid holdup. Packings have lower liquid holdup than do trays. This is often advantageous for reducing polymerization, degradation, or the inventory of hazardous materials.

Batch distillation. Because of the smaller liquid holdup of packing, a higher percentage of the liquid can be recovered as top product.

Factors Favoring Trays

Solids. Trays handle solids much more easily than packing. Both gas and liquid velocities on trays are often an order of magnitude higher than through packing, providing a sweeping action that keeps tray openings clear. Solids tend to accumulate in packing voids. There are fewer locations on trays where solids can be deposited. Plugging in liquid distributors has been a common trouble spot. Cleaning trays is much easier than cleaning packings.

Not all trays are fouling-resistant. Floats on moving valve trays tend to "stick" to deposits on the tray deck. Fouling-resistant trays have large sieve holes or large fixed valves, and these should be used when plugging and fouling are the primary considerations.

There is much that can be done to alleviate plugging with random packing. Large, open packing with minimal pockets offers good plugging resistance. Distributors that resist plugging have large holes (> 13-mm diameter). Such large holes are readily applied with high liquid flow rates, but often not practical for small liquid flow rates.

Maldistribution. The sensitivity of packing to liquid and gas maldistribution has been a common cause of failures in packed towers. Maldistribution issues are most severe in large-diameter towers, long beds, small liquid flow rates, and smaller packing. Structured packing is generally more prone to maldistribution than random packing. While good distributor design, water testing, and inspection can eliminate most maldistribution issues, it only takes a few small details that fall through the cracks to turn success into failure. Due to maldistribution, there are far more failures experienced

with packing than in trays, and it takes more trials "to get it right" than with trays. This makes trays more robust.

Complex towers. Interboilers, intercondensers, cooling coils, and side drawoffs are more easily incorporated in trays than in packed towers. In packed towers, every complexity requires additional distribution and/or liquid collection equipment.

Feed composition variation. One way of allowing for design uncertainties and feedstock variation is by installing alternate feed points. In packed towers, every alternate feed point requires expensive distribution equipment.

Performance prediction. Due to their sensitivity to maldistribution there is greater uncertainty in predicting packed column performance.

Chemical reaction, absorption. Here the much higher liquid holdup on trays provides greater residence time for absorption or chemical reaction than does packing.

Turndown. Moving valve and bubble-cap trays normally give better turndown than packings. Unless very expensive distributors are used, packed tower turndown is usually limited by distributor turndown.

Weight. Tray towers usually weigh less than packed towers, saving on the cost of foundations, supports, and column shell.

Trays vs. Random Packings The following factors generally favor trays compared to random packings, but not compared to structured packings.

Low liquid rates. With the aid of serrated weirs, splash baffles, reverse-flow trays, and bubble-cap trays, low liquid rates can be handled better in trays. Random packings suffer from liquid dewetting and maldistribution sensitivity at low liquid rates.

Process surges. Random packings are usually more troublesome than trays in services prone to process surges (e.g., those caused by slugs of water entering a hot oil tower, relief valve lifting, compressor surges, or instability of liquid seal loops). Structured packings are usually less troublesome than trays in such services.

Trays vs. Structured Packings The following factors generally favor trays compared to structured packings, but not compared to random packings.

Packing fires. The thin sheets of structured packing (typically 0.1 mm) poorly dissipate heat away from hot spots. Also, cleaning, cooling, and washing can be difficult, especially when distributors or packing plug up. Many incidents of packing fires during turnarounds (while towers with structured packings were open to atmosphere) have been reported. Most of these fires were initiated by pyrophoric deposits, hot work (e.g., welding) above the packing, opening the tower while hot organics were still present, and packing metallurgy that was not fire-resistant. Detailed discussion can be found in Fractionation Research Inc. (FRI) Design Practices Committee, "Causes and Prevention of Packing Fires," *Chem. Eng.*, July 2007.

Materials of construction. Due to the thin sheets of structured packings, their materials of construction need to have better resistance to oxidation or corrosion. For a service in which carbon steel is usually satisfactory with trays, stainless steel is usually required with structured packings.

Column wall inspection. Due to their snug fit, structured packings are easily damaged during removal. This makes it difficult to inspect the column wall (e.g., for corrosion).

Washing and purging. Thorough removal of residual liquid, wash water, air, or process gas trapped in structured packings at start-up and shutdown is more difficult than with trays. Inadequate removal of these fluids may be hazardous.

High liquid rates. Multipass trays effectively lower the liquid load "seen" by each part of the tray. A similar trick cannot be applied with packings. The capacity of structured packings tends to rapidly fall off at high liquid rates.

Capacity and Efficiency Comparison Kister et al. [*Chem. Eng. Progr.*, **90**(2), 23 (1994)] reported a study of the relative capacity and efficiency of conventional trays, modern random packings, and conventional structured packings. They found that, for each device optimally designed for the design requirements, a rough guide could be developed on the basis of flow parameter L/G (ρ_G/ρ_L)^{0.5} (abscissa in

Figs. 14-31, 14-55, and 14-56) and the following tentative conclusions could be drawn:

Flow Parameter 0.02–0.1

1. Trays and random packings have much the same efficiency and capacity.

2. Structured packing efficiency is about 1.5 times that of trays or random packing.

3. At a parameter of 0.02, the structured packing has a 1.3–1.4 capacity advantage over random packing and trays. This advantage disappears as the parameter approaches 0.1.

Flow Parameter 0.1–0.3

1. Trays and random packings have about the same efficiency and capacity.

2. Structured packing has about the same capacity as trays and random packings.

3. The efficiency advantage of structured packing over random packings and trays decreases from 1.5 to 1.2 as the parameter increases from 0.1 to 0.3.

Flow Parameter 0.3–0.5

1. The loss of capacity of structured packing is greatest in this range.

2. The random packing appears to have the highest capacity and efficiency with conventional trays just slightly behind. Structured packing has the least capacity and efficiency.

Experience indicates that use of structured packings has capacity/efficiency disadvantages in the higher-pressure (higher-flow-parameter) region.

Zuiderveg and Nutter [*ICHEME Symp. Ser.* **128**, A481 (1992)] explain the loss of capacity/efficiency by a large degree of backmixing and vapor recycle at high flow parameters, promoted by the solid walls of the corrugated packing layers.

SYSTEM LIMIT: THE ULTIMATE CAPACITY OF FRACTIONATORS

Liquid drops of various sizes form in the gas-liquid contact zones of tray or packed towers. Small drops are easily entrained upward, but their volume is usually too small to initiate excessive liquid accumulation (flooding). When the gas velocity is high enough to initiate a massive carryover of the larger drops to the tray above, or upward in a packed bed, liquid accumulation (entrainment flooding) takes place. This flood can be alleviated by increasing the tray spacing or using more hole areas on trays or by using larger, more open packings.

Upon further increase of gas velocity, a limit is reached when the superficial gas velocity in the gas-liquid contact zone exceeds the settling velocity of large liquid drops. At gas velocities higher than this, ascending gas lifts and carries over much of the tray or packing liquid, causing the tower to flood. This flood is termed *system limit* or *ultimate capacity*. This flood cannot be debottlenecked by improving packing size or shape, tray hole area, or tray spacing. The system limit gas velocity is a function only of physical properties and liquid flow rate. Once this limit is reached, the liquid will be blown upward. This is analogous to spraying water against a strong wind and getting drenched (Yangai, *Chem. Eng.*, p. 120, November 1990). The system limit represents the ultimate capacity of the vast majority of existing trays and packings. In some applications, where very open packings (or trays) are used, such as in refinery vacuum towers, the system limit is the actual capacity limit.

The original work of Souders and Brown [*Ind. Eng. Chem.* **26**(1), 98 (1934), Eq. (14-80)] related the capacity of fractionators due to entrainment flooding to the settling velocity of drops. The concept of system limit was advanced by Fractionation Research Inc. (FRI), whose measurements and model have recently been published (Fitz and Kunes, *Distillation 2001: Proceedings of Topical Conference, AIChE Spring National Meeting, Houston, Tex., 2001*; Stupin, FRI Topical Report 34, 1965 available through Special Collection Section, Oklahoma State University Library, Stillwater, Okla.). Figure 14-75 is a plot of FRI system limit data (most derived from tests with dual-flow trays with 29 percent hole area and 1.2- to 2.4-m tray spacing) against liquid superficial velocity for a variety of systems (Stupin, loc. cit.,

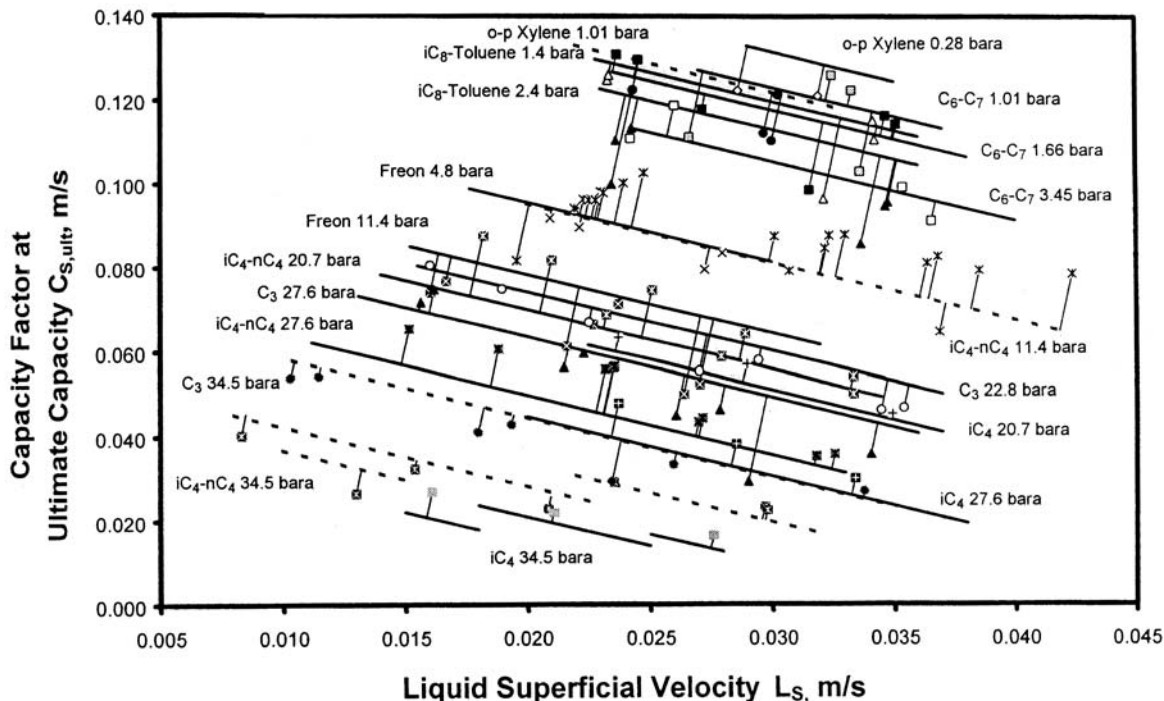


FIG. 14-75 Effect of liquid rate on ultimate capacity at higher liquid rates. (From Stupin, W. J., and H. Z. Kister, *Trans. IChemE*, vol. 81, Part A, p. 136, January 2003. Reprinted courtesy of IChemE.)

1965). The data show a constant-slope linear dependence of the system limit C -factor on the liquid load. There was a shortage of data at low liquid loads. Later data (Fig. 14-76) showed that as the liquid load was reduced, the system limit $C_{s,ult}$ stopped increasing and reached a limiting value. Based on this observation, Stupin and Kister [*Trans. IChemE* 81, Part A, p. 136 (January 2003)] empirically revised the earlier Stupin/FRI correlation to give

$$C_1 = 0.445(1 - F) \left(\frac{\sigma}{\Delta\rho} \right)^{0.25} - 1.4L_s \quad (14-167)$$

$$C_2 = 0.356(1 - F) \left(\frac{\sigma}{\Delta\rho} \right)^{0.25} \quad (14-168)$$

$$C_{s,ult} = \text{smaller of } C_1 \text{ and } C_2 \quad (14-169)$$

where

$$F = \frac{1}{1 + 1.4(\Delta\rho/\rho_G)^{1/2}} \quad (14-170)$$

In Eqs. (14-167) through (14-170), $C_{s,ult}$ is the system limit C -factor based on the tower superficial area [see Eq. (14-77) for C -factor definition]; L_s is the liquid superficial velocity, m/s; σ is the surface tension, mN/m; $\Delta\rho$ is the difference between the liquid and gas densities, kg/m³; and ρ_G is the gas density, kg/m³.

Stupin and Kister (loc. cit.) relate the flattening of the curve in Fig. 14-76 at low liquid loads to the formation of more, smaller, easier-to-entrain liquid drops when the liquid load is lowered beyond the limiting liquid load. It follows that devices that can restrict the formation of smaller drops may be able to approach the system limit capacity predicted by Stupin's original equation [Eq. (14-167)] even at low liquid loads.

The only devices capable of debottlenecking a tray system-limit device are those that introduce a new force that helps disentrain the vapor space. Devices that use centrifugal force (see "Centrifugal Force Deentrainment") are beginning to make inroads into commercial distillation and have achieved capacities as high as 25 percent above the system limit. Even the horizontal vapor push (see "Truncated Downcomers/Forward-Push Trays") can help settle the entrained drops, but to a much lesser extent. It is unknown whether the horizontal push alone can achieve capacities exceeding the system limit.

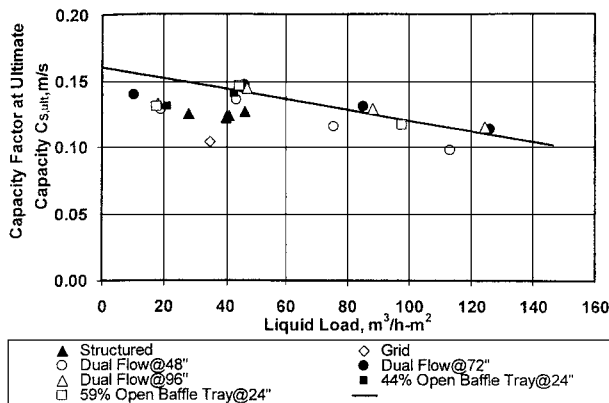


FIG. 14-76 Comparison of original ultimate capacity correlation to test data, C_6/C_7 , 1.66 bar. (From Stupin, W. J., and H. Z. Kister, *Trans. IChemE*, vol. 81, Part A, p. 136, January 2003. Reprinted courtesy of IChemE.)

WETTED-WALL COLUMNS

Wetted-wall or falling-film columns have found application in mass-transfer problems when high-heat-transfer-rate requirements are concomitant with the absorption process. Large areas of open surface

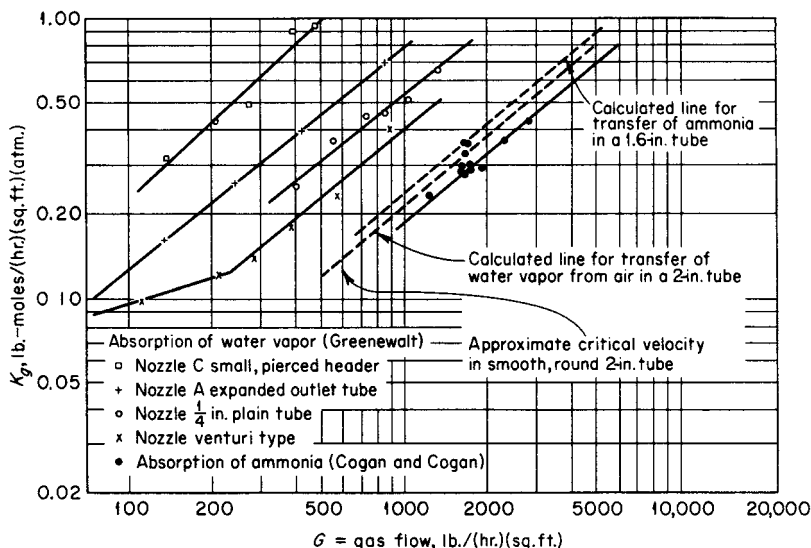


FIG. 14-77 Mass-transfer rates in wetted-wall columns having turbulence promoters. To convert pound-moles per hour-square foot-atmosphere to kilogram-moles per second-square meter-atmosphere, multiply by 0.00136; to convert pounds per hour-square foot to kilograms per second-square meter, multiply by 0.00136; and to convert inches to millimeters, multiply by 25.4. (Data of Greenewalt and Cogan and Cogan, *Sherwood, and Pigford, Absorption and Extraction, 2d ed., McGraw-Hill, New York, 1952.*)

are available for heat transfer for a given rate of mass transfer in this type of equipment because of the low mass-transfer rate inherent in wetted-wall equipment. In addition, this type of equipment lends itself to annular-type cooling devices.

Gilliland and Sherwood [*Ind. Eng. Chem.*, **26**, 516 (1934)] found that, for vaporization of pure liquids in air streams for streamline flow,

$$\frac{k_g D_{\text{tube}}}{D_g} \frac{P_{BM}}{P} = 0.023 N_{\text{Re}}^{0.83} N_{\text{Sc}}^{0.44} \quad (14-171)$$

- where D_g = diffusion coefficient, ft^2/h
- D_{tube} = inside diameter of tube, ft
- k_g = mass-transfer coefficient, gas phase, $\text{lb-mol}/(\text{h-ft}^2)$ ($\text{lb-mol}/\text{ft}^3$)
- P_{BM} = logarithmic mean partial pressure of inert gas, atm
- P = total pressure, atm
- N_{Re} = Reynolds number, gas phase
- N_{Sc} = Schmidt number, gas phase

Note that the group on the left side of Eq. (14-171) is dimensionless. When turbulence promoters are used at the inlet-gas section, an improvement in gas mass-transfer coefficient for absorption of water vapor by sulfuric acid was observed by Greenewalt [*Ind. Eng. Chem.*, **18**, 1291 (1926)]. A falling off of the rate of mass transfer below that indicated in Eq. (14-171) was observed by Cogan and Cogan (thesis, Massachusetts Institute of Technology, 1932) when a calming zone preceded the gas inlet in ammonia absorption (Fig. 14-77).

In work with the hydrogen chloride-air-water system, Dobratz, Moore, Barnard, and Meyer [*Chem. Eng. Prog.*, **49**, 611 (1953)] using a cocurrent-flow system found that $K_g \propto G^{1.5}$ (Fig. 14-78) instead of the 0.8 power as indicated by the Gilliland equation. Heat-transfer coefficients were also determined in this study. The radical increase in heat-transfer rate in the range of $G = 30 \text{ kg}/(\text{s-m}^2)$ [$20,000 \text{ lb}/(\text{h-ft}^2)$] was similar to that observed by Tepe and Mueller [*Chem. Eng. Prog.*, **43**, 267 (1947)] in condensation inside tubes.

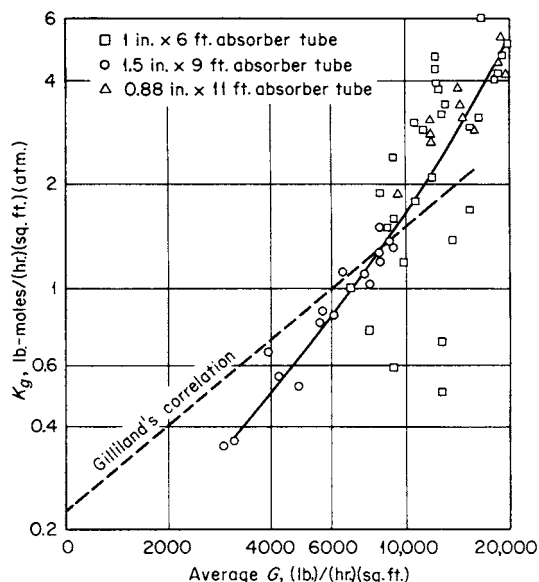


FIG. 14-78 Mass-transfer coefficients versus average gas velocity—HCl absorption, wetted-wall column. To convert pound-moles per hour-square foot-atmosphere to kilogram-moles per second-square meter-atmosphere, multiply by 0.00136; to convert pounds per hour-square foot to kilograms per second-square meter, multiply by 0.00136; to convert feet to meters, multiply by 0.305; and to convert inches to millimeters, multiply by 25.4. [Dobratz et al., *Chem. Eng. Prog.*, **49**, 611 (1953).]

Gaylord and Miranda [*Chem. Eng. Prog.*, **53**, 139M (1957)] using a multitube cocurrent-flow falling-film hydrochloric acid absorber for hydrogen chloride absorption found

$$K_g = \frac{1.66(10^{-5})}{M_m^{1.75}} \left(\frac{D_{\text{tube}} G}{\mu} \right) \quad (14.172)$$

where K_g = overall mass-transfer coefficient, (kg·mol)/(s·m²·atm)
 M_m = mean molecular weight of gas stream at inlet to tube
 D_{tube} = diameter of tube, m
 G = mass velocity of gas at inlet to tube, kg/(s·m²)
 μ = viscosity of gas, Pa·s

Note that the group $D_{\text{tube}} G / \mu$ is dimensionless. This relationship also satisfied the data obtained for this system, with a single-tube falling-film unit, by Coull, Bishop, and Gaylor [*Chem. Eng. Prog.*, **45**, 506 (1949)].

The rate of mass transfer in the liquid phase in wetted-wall columns is highly dependent on surface conditions. When laminar-flow conditions prevail without the presence of wave formation, the laminar-penetration theory prevails. When, however, ripples form at the surface, and they

may occur at a Reynolds number exceeding 4, a significant rate of surface regeneration develops, resulting in an increase in mass-transfer rate.

If no wave formations are present, analysis of behavior of the liquid-film mass transfer as developed by Hatta and Katori [*J. Soc. Chem. Ind.*, **37**, 280B (1934)] indicates that

$$k_l = 0.422 \sqrt{\frac{D_l \Gamma}{\rho B_F^2}} \quad (14.173)$$

where $B_F = (3u\Gamma/\rho^2g)^{1/3}$

D_l = liquid-phase diffusion coefficient, m²/s

ρ = liquid density, kg/m³

Z = length of surface, m

k_l = liquid-film-transfer coefficient,

(kg·mol)/[(s·m²)(kg·mol/m³)]

Γ = liquid-flow rate, kg/(s·m) based on wetted perimeter

μ = viscosity of liquid, Pa·s

g = gravity acceleration, 9.81 m/s²

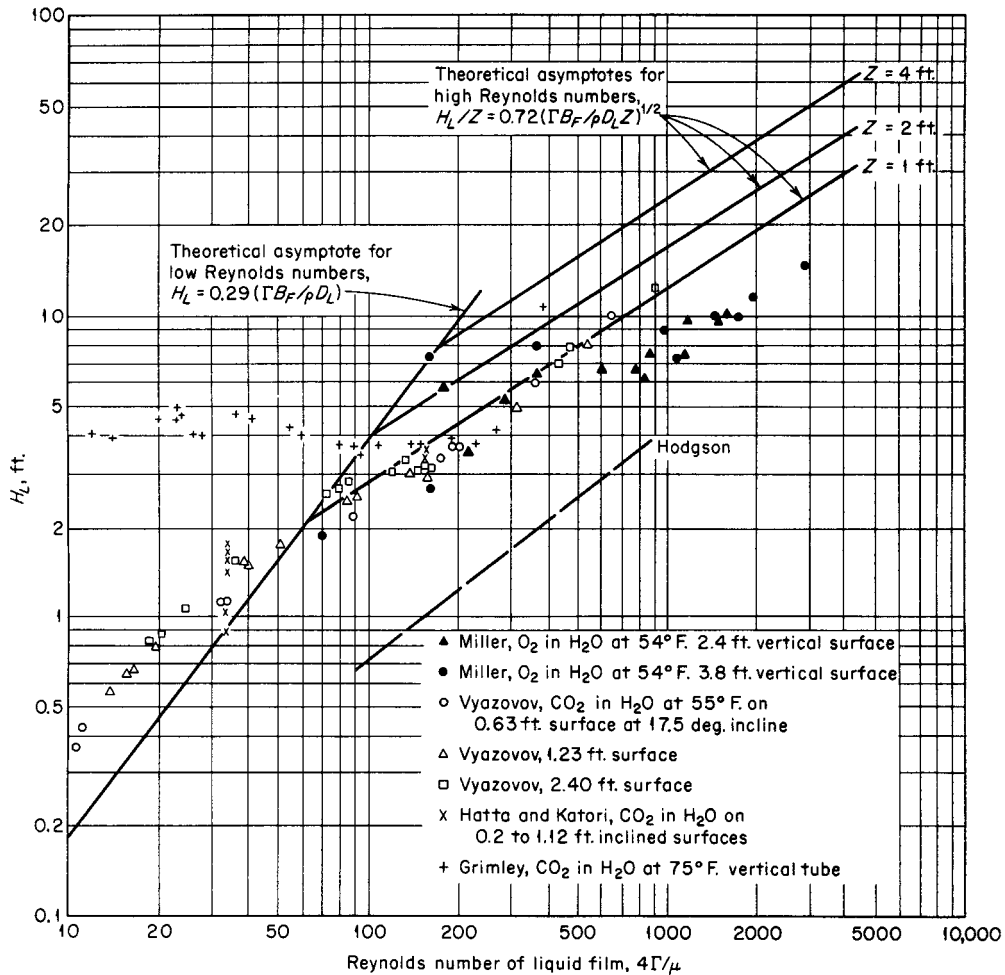


FIG. 14-79 Liquid-film resistance in absorption of gases in wetted-wall columns. Theoretical lines are calculated for oxygen absorption in water at 55°F. To convert feet to meters, multiply by 0.3048; °C = 5/9 (°F - 32). (Sherwood and Pigford, Absorption and Extraction, 2d ed., McGraw-Hill, New York, 1952.)

When Z is large or $\Gamma/\rho B_F$ is so small that liquid penetration is complete,

$$k_{\ell} = 11.800 D_{\ell}/B_F \quad (14-174)$$

and

$$H_{\ell} = 0.95 \Gamma B_F/D_{\ell} \quad (14-175)$$

A comparison of experimental data for carbon dioxide absorption obtained by Hatta and Katori (op. cit.), Grimley [*Trans. Inst. Chem. Eng.*, **23**, 228 (1945)], and Vyazov [*Zh. Tekh. Fiz.* (U.S.S.R.), **10**, 1519 (1940)] and for absorption of oxygen and hydrogen by Hodgson (S.M. thesis, Massachusetts Institute of Technology, 1949), Henley (B.S. thesis, University of Delaware, 1949), Miller (B.S. thesis, University of Delaware, 1949), and Richards (B.S. thesis, University of Delaware, 1950) was made by Sherwood and Pigford (*Absorption and Extraction*, McGraw-Hill, New York, 1952) and is indicated in Fig. 14-79.

In general, the observed mass-transfer rates are greater than those predicted by theory and may be related to the development of surface rippling, a phenomenon which increases in intensity with increasing liquid path.

Vivian and Peaceman [*Am. Inst. Chem. Eng. J.*, **2**, 437 (1956)] investigated the characteristics of the CO₂-H₂O and Cl₂-HCl, H₂O system in a wetted-wall column and found that gas rate had no effect on the liquid-phase coefficient at Reynolds numbers below 2200. Beyond this rate, the effect of the resulting rippling was to increase significantly the liquid-phase transfer rate. The authors proposed a behavior relationship based on a dimensional analysis but suggested caution in its application concomitant with the use of this type of relationship. Cognizance was taken by the authors of the effects of column length, one to induce rippling and increase of rate of transfer, one to increase time of exposure which via the penetration theory decreases the average rate of mass transfer in the liquid phase. The equation is

$$\frac{k_{\ell} h}{D_{\ell}} = 0.433 \left(\frac{\mu_{\ell}}{\rho_{\ell} D_{\ell}} \right)^{1/2} \left(\frac{\rho_{\ell}^2 g h^3}{\mu_{\ell}^2} \right)^{1/6} \left(\frac{4\Gamma}{\mu_{\ell}} \right)^{0.4} \quad (14-176)$$

where D_{ℓ} = diffusion coefficient of solute in liquid, ft²/h
 g = gravity-acceleration constant, 4.17×10^8 ft/h²
 h = length of wetted wall, ft
 k_{ℓ} = mass-transfer coefficient, liquid phase, ft/h

TABLE 14-17 Relative Fabricated Cost for Metals Used in Tray-Tower Construction*

Materials of construction	Relative cost per ft ² of tray area (based on carbon steel = 1)
Sheet-metal trays	
Steel	1
4-6% chrome—1/2 moly alloy steel	2.1
11-13% chrome type 410 alloy steel	2.6
Red brass	3
Stainless steel type 304	4.2
Stainless steel type 347	5.1
Monel	7.0
Stainless steel type 316	5.5
Inconel	8.2
Cast-iron trays	2.8

*Peters and Timmerhaus, *Plant Design and Economics for Chemical Engineers*, 4th ed., McGraw-Hill, New York, 1991. To convert cost per square foot to cost per square meter, multiply by 10.76.

Γ = mass rate of flow of liquid, lb/(h)(ft of periphery)
 μ_{ℓ} = viscosity of liquid, lb/(ft)(h)
 ρ_{ℓ} = density of liquid, lb/ft³

The equation is dimensionless.

The effect of chemical reaction in reducing the effect of variation of the liquid rate on the rate of absorption in the laminar-flow regime was illustrated by the evaluation of the rate of absorption of chlorine in ferrous chloride solutions in a wetted-wall column by Gilliland, Baddour, and White [*Am. Inst. Chem. Eng. J.*, **4**, 323 (1958)].

Flooding in Wetted-Wall Columns When gas and liquid are in counterflow in wetted-wall columns, flooding can occur at high gas rates. Methods for calculating this flood are given in "Upper Limit Flooding in Vertical Tubes." In the author's experience, Eq. (14-204) has had an excellent track record for calculating flooding in these columns.

COLUMN COSTS

Estimation of column costs for preliminary process evaluations requires consideration not only of the basic type of internals but also of their effect on overall system cost. For a distillation system, for example, the overall system can include the vessel (column), attendant structures, supports, and foundations; auxiliaries such as reboiler, condenser, feed heater, and control instruments; and connecting piping. The choice of internals influences all these costs, but other factors influence them as well. A complete optimization of the system requires a full-process simulation model that can cover all pertinent variables influencing economics.

Cost of Internals Installed costs of trays may be estimated from Fig. 14-80, with corrections for tray material taken from Table 14-17. For two-pass trays the cost is 15 to 20 percent higher. Approximate costs of random packing materials may be obtained from Table 14-18, but it should be recognized that, because of competition, there can be significant variations in these costs from vendor to vendor. Also, packings sold in very large quantities carry discounts. In 1995, costs of structured packings, made from sheet metal, averaged \$90 to \$110 per cubic foot, but the need for special distributors and redistributors can double the cost of structured-packings on a volumetric basis. Note

TABLE 14-18 Costs of Random Packings, Uninstalled, January 1990

Prices in dollars per ft³, 100 ft³ orders, f.o.b. manufacturing plant

	Size, in, \$/ft ³			
	1	1½	2	3
Raschig rings				
Chemical porcelain	12.8	10.3	9.4	7.8
Carbon steel	36.5	23.9	20.5	16.8
Stainless steel	155	117	87.8	—
Carbon	52	46.2	33.9	31.0
Intalox saddles				
Chemical stoneware	17.6	13.0	11.8	10.7
Chemical porcelain	18.8	14.1	12.9	11.8
Polypropylene	21.2	—	13.1	7.0
Berl saddles				
Chemical stoneware	27.0	21.0	—	—
Chemical porcelain	33.5	21.5	15.6	—
Pall rings				
Carbon steel	29.3	19.9	18.2	—
Stainless steel	131	99.0	86.2	—
Polypropylene	21.2	14.4	13.1	—

Peters and Timmerhaus, *Plant Design and Economics for Chemical Engineers*, 4th ed., McGraw-Hill, New York, 1991. To convert cubic feet to cubic meters, multiply by 0.0283; to convert inches to millimeters, multiply by 25.4; and to convert dollars per cubic foot to dollars per cubic meter, multiply by 35.3.

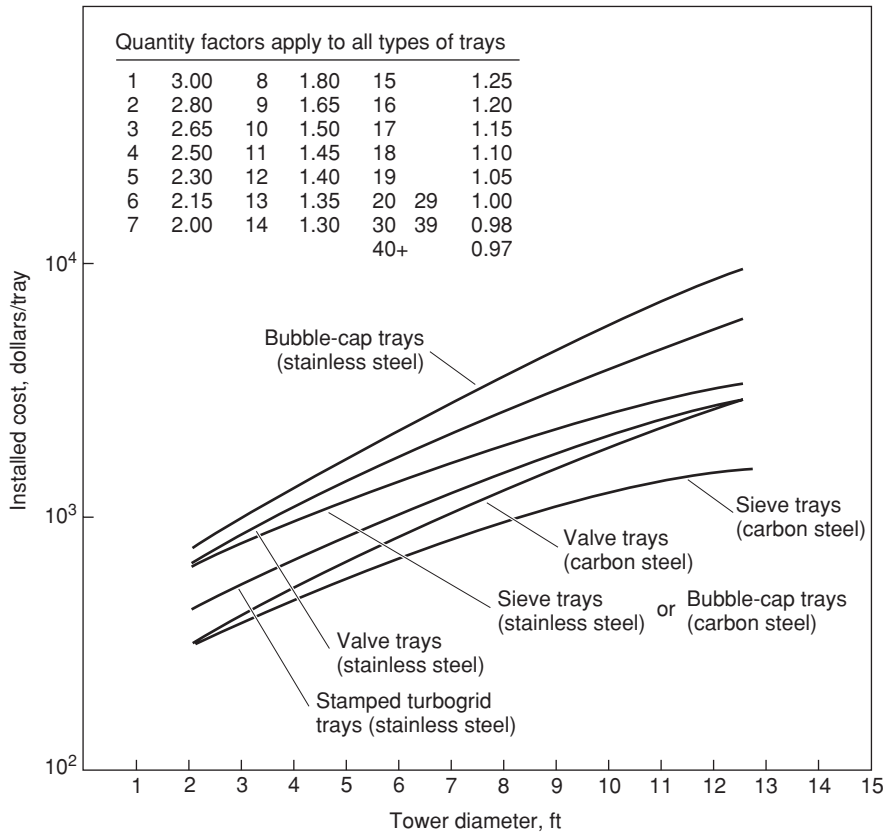


FIG. 14-80 Cost of trays. Price includes tray deck, valves, bubble caps, risers, downcomers, and structural-steel parts. The stainless steel designated is type 410 (*Peters and Timmerhaus, Plant Design and Economics for Chemical Engineers, 4th ed., McGraw-Hill, New York, 1991*).

that for Fig. 14-80 and Table 14-17, the effective cost date is January 1990, with the Marshall and Swift cost index being taken as 904.

As indicated above, packed column internals include liquid distributors, packing support plates, redistributors (as needed), and holddown plates (to prevent movement of packing under flow conditions). Costs of these internals for columns with random packing are given in Fig. 14-81, based on early 1976 prices, and a Marshall and Swift cost index of 460.

Cost of Column The cost of the vessel, including heads, skirt, nozzles, and ladderways, is usually estimated on the basis of weight. Figure 14-82 provides early 1990 cost data for the shell and heads, and Fig. 14-83 provides 1990 cost data for connections. For very approximate estimates of complete columns, including internals, Fig. 14-84 may be used. As for Figs. 14-82 and 14-83, the cost index is 904.

PHASE DISPERSION

GENERAL REFERENCES: For an overall discussion of gas-liquid breakup processes, see Brodkey, *The Phenomena of Fluid Motions*, Addison-Wesley, Reading, Massachusetts, 1967. For a discussion of atomization devices and how they work, see Masters, *Spray Drying Handbook*, 5th ed., Wiley, New York, 1991; and Lefebvre, *Atomization and Sprays*, Hemisphere, New York, 1989. A beautifully illustrated older source is Dombrowski and Munday, *Biochemical and Biological Engineering Science*, vol. 2, Academic Press, London, 1968, pp. 209-320. Steinmeyer [*Chem. Engr. Prog.*, **91**(7), 72-80 (1995)] built on Hinze's work with turbulence and showed that several atomization processes follow the common theme of breakup of large droplets due to turbulence in the gas phase. Turbulence in turn correlates with power dissipation per unit mass. In the text below, correlations referring to *power/mass* are taken from this source. For a survey on fog formation, see Amelin, *Theory of Fog Formation*, Israel Program for Scientific Translations, Jerusalem, 1967.

BASICS OF INTERFACIAL CONTACTORS

Steady-State Systems: Bubbles and Droplets Bubbles are made by injecting vapor below the liquid surface. In contrast, droplets are commonly made by atomizing nozzles that inject liquid into a vapor. Bubble and droplet systems are fundamentally different, mainly because of the enormous difference in density of the injected phase. There are situations where each is preferred. Bubble systems tend to have much higher interfacial area as shown by Example 16 contrasted with Examples 14 and 15. Because of their higher area, bubble systems will usually give a closer approach to equilibrium.

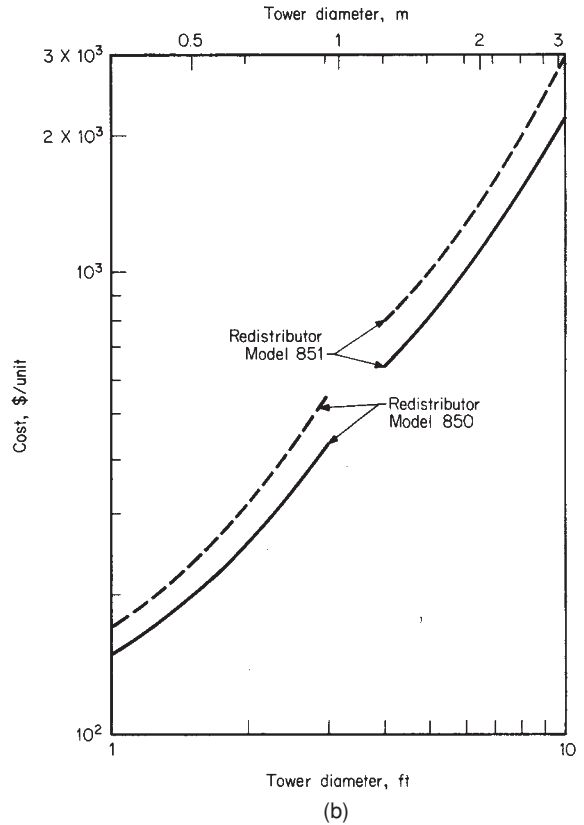
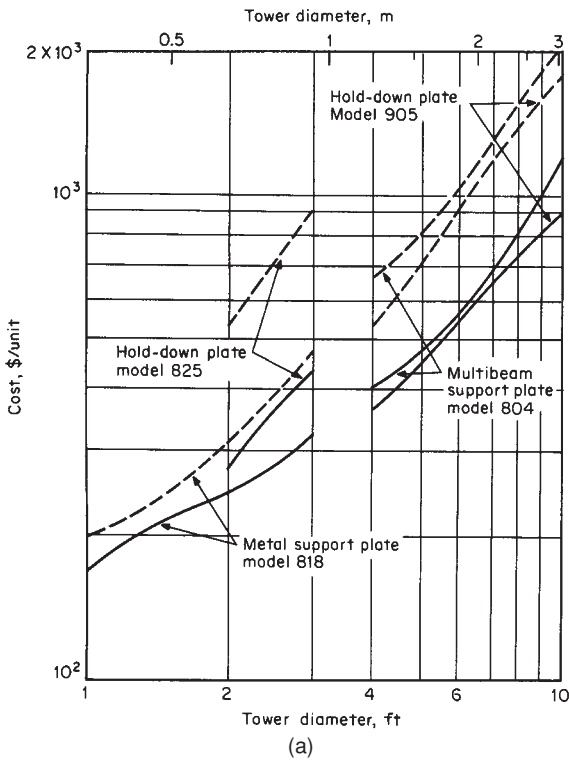


FIG. 14-81 Cost of internal devices for columns containing random packings. (a) Holddown plates and support plates. (b) Redistributors. [Pikulik and Diaz, Chem. Eng., 84(21), 106 (Oct. 10, 1977).]

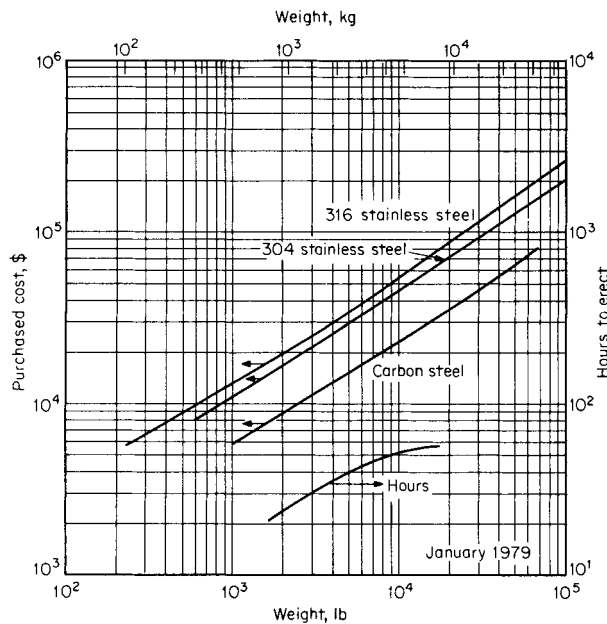


FIG. 14-82 Fabricated costs and installation time of towers. Costs are for shell with two heads and skirt, but without trays, packing, or connections. (Peters and Timmerhaus, Plant Design and Economics for Chemical Engineers, 4th ed., McGraw-Hill, New York, 1991.)

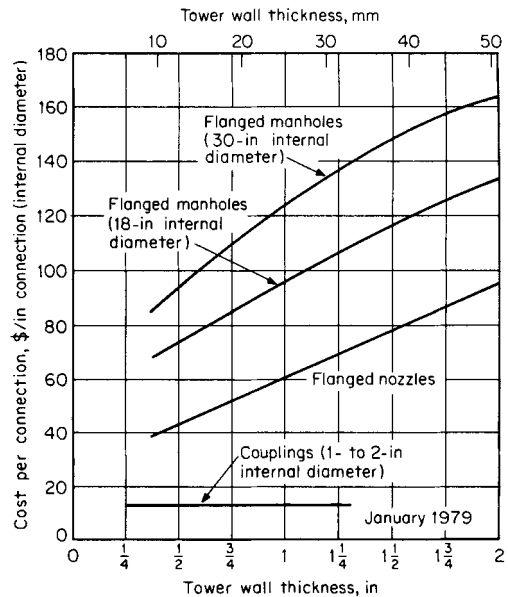


FIG. 14-83 Approximate installed cost of steel-tower connections. Values apply to 2070-kPa connections. Multiply costs by 0.9 for 1035-kPa (150-lb) connections and by 1.2 for 4140-kPa (600-lb) connections. To convert inches to millimeters, multiply by 25.4; to convert dollars per inch to dollars per centimeter, multiply by 0.394. (Peters and Timmerhaus, Plant Design and Economics for Chemical Engineers, 4th ed., New York, McGraw-Hill, 1991.)

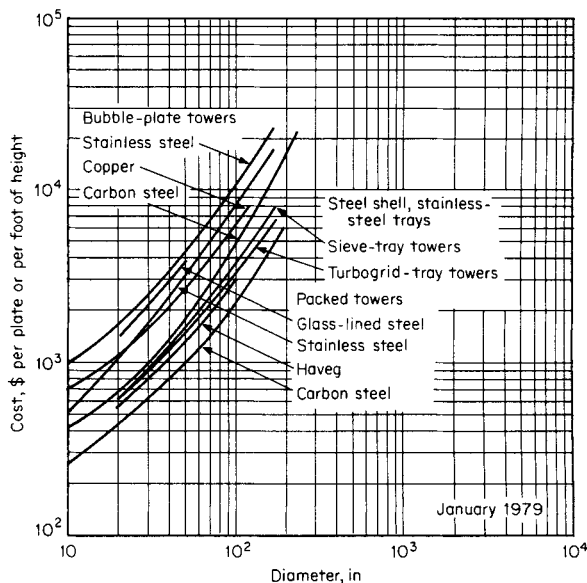


FIG. 14-84 Cost of towers including installation and auxiliaries. To convert inches to millimeters, multiply by 25.4; to convert feet to meters, multiply by 0.305; and to convert dollars per foot to dollars per meter, multiply by 3.28. (Peters and Timmerhaus, *Plant Design and Economics for Chemical Engineers*, 4th ed., McGraw-Hill, New York, 1991.)

However, droplet systems can enable much higher energy input (via gas phase pressure drop in cocurrent systems) and, as a result, dominate applications where a quick quench is needed. See Examples 21 and 22. Conversely, droplet systems can also be designed for very low pressure drop which is advantageous in applications such as vacuum condensers.

Unstable Systems: Froths and Hollow Cone Atomizing Nozzles We usually think of interfacial contact as a steady-state system of raining droplets or rising bubbles, but some of the most efficient interfacial contactors take advantage of unstable interfacial geometry. The most common is the distillation tray which operates with a wild mix of bubbles, jets, films, and droplets. The mix is often described as *froth*. Gas pressure drop provides the energy to create the froth.

A variant on the froth contact is the reverse jet contactor (Example 22), which can be considered as an upside-down distillation tray, operated above the flooding velocity in cocurrent flow of gas and liquid. It is limited to one stage.

An entirely different unstable contactor involves the thin expanding liquid film produced by a hollow cone spray nozzle. Because of fresh surface and the thinness of the film, this can give very high transfer for liquid-limited systems. Two applications are direct contact condensation and removal of volatile components from a high-boiling residual liquid.

Surface Tension Makes Liquid Sheets and Liquid Columns Unstable Surface tension is the energy required to make an increment of interfacial surface. A sheet or column of liquid has more surface than a sphere, hence surface tension converts sheets and columns to droplets. See Fig. 14-86.

There are many different atomizers, but the underlying principle of all is the same—to first generate a flat sheet or a liquid column. Liquid sheets and columns are unstable, a small surface disturbance on either will propagate, and the liquid will reshape itself into droplets. The key property in controlling this process is surface tension. Surface tension gets a high exponent in all the atomization correlations.

Little Droplets and Bubbles vs. Big Droplets and Bubbles—Coalescence vs. Breakup When big drops are subjected to shear forces, as in falling rain, the droplets are distorted; and if the distur-

tions are great enough, the big droplets break into little ones. This is why raindrops never exceed a certain size. A variant on this is breakup in highly turbulent systems such as in high-velocity quench systems or pneumatic nozzles. Here the droplets are distorted by the energy of the turbulent eddies.

But little droplets and bubbles have more surface per unit of liquid than big ones. Hence little droplets tend to coalesce into big ones, and will grow in size if given enough quiet time.

While the primary difficulty is estimating the interfacial area due to the unstable interface, a secondary problem is that freshly made, unstable surface gives higher transfer than older, more stable surface.

Empirical Design Tempered by Operating Data The net of these is that interfacial area is difficult to predict and interfacial contactors are difficult to design.

Prediction methods are given below but should always be tempered by operating experience.

INTERFACIAL AREA—IMPACT OF DROPLET OR BUBBLE SIZE

Transfer is aided by increased interfacial area. Interfacial area per unit volume a_D of a single droplet or bubble is inversely proportional to the diameter of the droplet or bubble D .

$$a_D = 6/D \quad (14-177)$$

To estimate the total interfacial area in a given volume, the a_D value is multiplied by the fractional holdup of dispersed phase in the total volume.

$$a = a_D(\Phi_D) \quad (14-178)$$

where a = interfacial area/volume and Φ_D = fraction of volume in dispersed phase = holdup. Fractional holdup in a continuous process depends on the velocities of the two phases, as if they were flowing by themselves.

$$\Phi_D = (\text{dispersed phase volume})/(\text{volume of dispersed and continuous phases})$$

Example 14: Interfacial Area for Droplets/Gas in Cocurrent Flow For equal mass flow of gas and liquid and with gas density 0.001 of liquid density, the gas velocity in cocurrent flow will be 1000 times the liquid velocity. This sets Φ_D .

$$\Phi_D = 1/(1 + 1000) = 0.00099$$

If the droplets are 500 μm in diameter, Eqs. (14-177) and (14-178) give

$$a = (6/0.0005)(0.00099) = 12 \text{ m}^2/\text{m}^3$$

If the droplets are 100 μm in diameter, Eqs. (14-177) and (14-178) give

$$a = (6/0.0001)(0.00099) = 60 \text{ m}^2/\text{m}^3$$

Example 15: Interfacial Area for Droplets Falling in a Vessel Droplet systems rarely exceed a Φ_D value of 0.01. At this low level, Φ_D in a low-velocity countercurrent contactor can be approximated by Eq. (14-179).

$$\Phi_D = U_L/(U_L - U_C) \quad (14-179)$$

where U_L = liquid superficial velocity
 U_C = terminal velocity of droplet
 U_G = gas superficial velocity

With a gas superficial velocity of 1.5 m/s, for equal mass flow of gas and liquid, with gas density 0.001 of liquid density, and with 500- μm -diameter droplets falling at a terminal settling of 2.5 m/s, Eq. (14-179) gives a fractional holdup of liquid of

$$\Phi_D = (0.001)1.5/(2.5 - 1.5) = 0.0015$$

Equations (14-177) and (14-178) then give

$$a = (6/0.0005)(0.0015) = 18 \text{ m}^2/\text{m}^3$$

Example 16: Interfacial Area for Bubbles Rising in a Vessel For bubble systems (gases dispersed in liquids) fractional holdup can approach 0.5 as shown by Fig. 14-104. However, before reaching this holdup, the bubble systems shift to an unstable mix of bubbles and vapor jets. Hence an exact

comparison to Example 14 isn't possible because at the 1.5 m/s velocity of Example 14, the system becomes a froth. But at about one-fifth the velocity of Example 14, an estimate of interfacial area is possible.

If the bubble size is 10,000 μm and fractional holdup is 0.4, Eqs. (14-177) and (14-178) give an interfacial area of

$$a = (6/0.01)(0.4) = 240 \text{ m}^2/\text{m}^3$$

Measured interfacial area in distillation trays is consistent with this high value. Note the much higher interfacial area than in the droplet systems of Examples 14 and 15. The higher interfacial area when the gas is dispersed explains why bubbling and froth systems often give better performance than droplet systems. The big difference in interfacial area stems from the much larger volume per unit of mass of gas, i.e., lower density of the gas than the liquid.

RATE MEASURES, TRANSFER UNITS, APPROACH TO EQUILIBRIUM, AND BYPASSING

What Controls Mass/Heat Transfer: Liquid or Gas Transfer or Bypassing Either gas side or liquid side of the interface can be controlling.

Liquid-Controlled In fractionation systems with high viscosity or component relative volatility that greatly exceeds 1, the liquid side will be controlling. This is clearly illustrated by Fig. 14-47 which shows a sharp decline in efficiency with either a rise in liquid viscosity or a rise in *component relative volatility*.

Note that *high component relative volatility* means the same thing as *sparingly soluble*. Oxygen dissolving in a fermentation reactor is an example of a system being liquid-controlled due to a *sparingly soluble gas*. Another application that is liquid-controlled is the removal of *high relative volatility components* out of residual oil.

Still another case where liquid controls is in condensing a pure vapor, as in Example 23, or absorbing a pure gas, as in Example 24.

Gas-Controlled The gas side dominates in gas cooling applications. An example is the quenching of a furnace effluent with a vaporizing liquid. In this application the liquid is nearly uniform in temperature. Restated, the reduction in driving force across the liquid side of the interface is unimportant.

Other applications that are gas-side-controlled include removal of a component such as NH₃ from a gas by using an acidic liquid, or removing a component such as SO₂ from a gas with a basic liquid. See Examples 19 through 22.

Bypassing-Controlled Trayed or packed columns operate with countercurrent flow and can achieve many equilibrium stages in series by good distribution of gas and liquid, and careful control of details. Other devices such as sprays are vulnerable to bypassing and are limited to one equilibrium stage.

Rate Measures for Interfacial Processes Terminology used for reporting rate data can be confusing. Normally rate data are reported on a volumetric basis with transfer rate and effective area combined. For example, *k_La* denotes mass-transfer data per unit volume. The *L* subscript means it is referenced to the molar concentration difference between the interface and the bulk liquid. This is commonly used on data involving a sparingly soluble (high relative volatility) component. Note that the lowercase *k* means the data deal only with the resistance in the liquid phase.

Less commonly, data are given as *k_{CG}a*. The *G* subscript means it is referenced to the molar concentration difference between the interface and the gas. This might be used for data on absorbing a gas such as NH₃ by a highly acidic liquid. Note that *k_{CG}a* only deals with the resistance in the gas phase.

When one is dealing with direct contact heat transfer, the corresponding terms are *h_La* and *h_{CG}a*. Here the driving force is the temperature difference. The *L* subscript means that we are dealing with a liquid-limited process such as condensing a pure liquid. How to convert *k_La* data to an *h_La* value is illustrated by Example 23.

There are ways to combine the liquid and gas resistance to get an overall transfer rate such as *K_{CG}a* (as denoted by the uppercase *K*). However, data are rarely reported in this form.

Approach to Equilibrium Although rate measures such as *k_{CG}a* and *h_{CG}a* are often cited in the literature, they are often not as useful to designers as the simpler concept of approach to equilibrium. *Approach to equilibrium* compares the transfer between liquid and gas phases to the best possible that could be achieved in a single backmixed equilibrium stage.

Approach to equilibrium is easy to understand and easy to apply. Examples 17 through 23 illustrate its use.

Example 17: Approach to Equilibrium—Perfectly Mixed, Complete Exchange This would be approximated by a very long pipeline contactor where an acidic aqueous stream is injected to cool the gas and remove NH₃.

If the adiabatic saturation temperature of the gas is 70°C, at the exit of the contactor, the gas would be cooled to 70°C.

Similarly, at the exit of the contactor, the NH₃ in the gas would be zero, regardless of the initial concentration.

Example 18: Approach to Equilibrium—Complete Exchange but with 10 Percent Gas Bypassing A spray column is used, and an acidic liquid rains down on the gas of Example 17. If the initial NH₃ is 1000 ppm and 10 percent of the gas bypasses, the NH₃ in the exit gas would be

$$0.1(1000) = 100 \text{ ppm}$$

Similarly, if the gas enters at 120°C, at the exit we would find 10 percent of the differential above the adiabatic saturation temperature. For an adiabatic saturation temperature of 70°C, the exit gas temperature would be

$$70 + 0.1(120 - 70) = 75^\circ\text{C}$$

Approach to Equilibrium—Finite Contactor with No Bypassing When there is no bypassing, the measure that sets the approach is the ratio of change to driving force. This ratio is called the *number of transfer units N_C*. It is dimensionless. For heat-transfer applications, it can be envisioned as a conventional heat exchanger where a vaporizing liquid cools a gas:

$$\text{No. of gas-phase transfer units} = \frac{T_{G,\text{out}} - T_{G,\text{in}}}{(T_G - T_{L,\text{av}})} = N_C \quad (14-180)$$

Where *T_G* = gas temperature and *T_L* = liquid temperature. The number of transfer units *N_C* can also be calculated as the capability for change divided by the thermal capacitance of the flowing streams.

$$\begin{aligned} N_C &= \frac{(\text{system volume})(h_{CG}a)}{(\text{volumetric flow rate})\rho_{CG}c_C} \\ &= \frac{(\text{gas contact time})(h_{CG}a)}{\rho_{CG}c_C} \end{aligned} \quad (14-181)$$

where *a* = interfacial area per unit volume
h_{CG} = heat-transfer coefficient from interface to gas
ρ_C = gas density
c_C = gas specific heat

Note that in the above, performance and properties all refer to the gas, which is appropriate when dealing with a gas-limited transfer process.

This leads to a way to estimate the approach to equilibrium.

$$E = 1 - e^{-N_C} \quad (14-182)$$

where *E* = "approach to equilibrium" fractional removal of NH₃ or fractional approach to adiabatic liquid temperature
N_C = number of transfer units calculated relative to gas flow

Example 19: Finite Exchange, No Bypassing, Short Contactor A short cocurrent horizontal pipeline contactor gives 86 percent removal of NH₃. There is no bypassing because of the highly turbulent gas flow and injection of liquid into the center of the pipe. What would we expect the exit gas temperature to be?

14-90 EQUIPMENT FOR DISTILLATION, GAS ABSORPTION, PHASE DISPERSION, AND PHASE SEPARATION

Equation (14-182) says that the backcalculated N_C is 2:

$$N_C = -\ln(1 - 0.86) = 2$$

For diffusing gases of similar molecular weight, the properties that control heat transfer follow the same rules as those that control mass transfer. As a result, the NH_3 scrubbing and gas cooling processes achieve similar approaches to equilibrium.

For an entry temperature of 120°C and an adiabatic saturation temperature of 70°C , the expected outlet temperature would be

$$70 + (1 - 0.86)(120 - 70) = 77^\circ\text{C}$$

This looks like a powerful concept, but its value is limited due to uncertainty in estimating $h_C a$. Both h_C and a are difficult to estimate due to dependence on power dissipation as discussed below. The primary value of the N_C concept is in estimating an expected change from baseline data as in the comparison of Example 19 with Example 20.

Example 20: A Contactor That Is Twice as Long, No Bypassing If we double the length of the pipeline contactor, double the effective contact area, and double the number of transfer units to 4, what do we expect for performance?

For $N_C = 4$,

$$E = 1 - e^{-4} = 0.982$$

The NH_3 in the exit gas would be expected to drop to

$$(1 - 0.982)(1000) = 18 \text{ ppm}$$

and the expected outlet temperature would be

$$70 + (1 - 0.982)(120 - 70) = 70.9^\circ\text{C}$$

If we double the length again, we increase the number of transfer units to 8 and achieve an approach of

$$E = 1 - e^{-8} = 0.9997$$

The outlet temperature would be

$$70 + (1 - 0.9997)(120 - 70) = 70.015^\circ\text{C}$$

Similarly the NH_3 in the exit gas would be

$$(1 - 0.9997)(1000) = 0.3 \text{ ppm}$$

Note that this approximates the exit condition of Example 17.

Transfer Coefficient—Impact of Droplet Size The transfer coefficients increase as the size of droplets decreases. This is so because the transfer process is easier if it only has to move mass or heat a shorter distance (i.e., as the bubble or droplet gets smaller).

In the limiting case of quiescent small bubbles or droplets, the transfer coefficients vary inversely with average bubble or droplet diameter. For example, in heat transfer from a droplet interface to a gas, the minimum value is

$$h_{C,\min} = \text{heat transfer coefficient from interface to gas} = 2k_C/D \quad (14-183)$$

where k_C = gas thermal conductivity and
 D = droplet diameter.

IMPORTANCE OF TURBULENCE

The designer usually has control over the size of a droplet. As discussed below, several of the correlations show that droplet diameter varies with turbulent energy dissipation. For example, Eqs. (14-190) and (14-201) suggest that in droplet systems

$$D \propto [1/(\text{gas velocity})]^{1.2}$$

and hence from Eq. (14-178)

$$a \propto 1/D \propto (\text{gas velocity})^{1.2} \quad (14-184)$$

However, just looking at the impact of velocity on droplet size underestimates the velocity impact because turbulence gives higher transfer

than Eq. (14-183) predicts. Transfer coefficients increase as the mixing adjacent to the surface increases. This mixing depends on the energy dissipated into the phases. To a first approximation this transfer from droplets increases with local power dissipation raised to the 0.2 power.

$$h_{C,\text{turbulent}} \propto (\text{power dissipated})^{0.2}$$

and since power dissipation per unit volume increases with (velocity)³,

$$h_{C,\text{turbulent}} \propto (\text{velocity})^{0.6} \quad (14-185)$$

The combined effect on interfacial area and on the transfer coefficient is that the effective transfer increases greatly with gas velocity. From Eqs. (14-178) and (14-185)

$$h_C a_{\text{turbulent}} \propto (\text{velocity})^{1.8} \quad (14-186)$$

For quenching operations, this means that even though residence time is cut as gas velocity goes up, the effective approach to equilibrium increases. Since the volume for a given length of pipe falls with (velocity)⁻¹, the expected number of transfer units N_C in a given length of pipe increases with (velocity)^{0.8}.

$$N_{C,\text{turbulent}} \propto (h_C a_{\text{turbulent}})(\text{volume}) \propto (\text{velocity})^{0.8} \quad (14-187)$$

See Example 21.

EXAMPLES OF CONTACTORS

High-Velocity Pipeline Contactors High-velocity cocurrent flow can give more power input than any other approach. This is critical when extremely high rates of reaction quenching are needed.

Example 21: Doubling the Velocity in a Horizontal Pipeline Contactor—Impact on Effective Heat Transfer Velocity in pipeline quench systems often exceeds 62 m/s (200 ft/s). Note that this is far above the flooding velocity in distillation packing, distillation trays, or gas-sparged reactors. There are few data available to validate performance even though liquid injection into high-velocity gas streams has been historically used in quenching reactor effluent systems. However, the designer knows the directional impact of parameters as given by Eq. (14-187).

For example, if a 10-ft length of pipe gives a 90 percent approach to equilibrium in a quench operation, Eq. (14-182) says that the backcalculated N_C is 2.303:

$$N_C -\ln(1 - 0.9) = 2.303$$

Equation (14-187) says if we double velocity but retain the same length, we would expect an increase of N_C to 4.0.

$$N_C = 2.303(2)^{0.8} = 4$$

and

$$E = 1 - e^{-4} = 0.982$$

Restated, the approach to equilibrium rises from 90 percent to greater than 98 percent even though the contact time is cut in half.

Vertical Reverse Jet Contactor A surprisingly effective modification of the liquid injection quench concept is to inject the liquid countercurrent *upward* into a gas flowing *downward*, with the gas velocity at some multiple of the flooding velocity defined by Eq. (14-203). The reverse jet contactor can be envisioned as an upside-down distillation tray. For large gas volumes, multiple injection nozzles are used. One advantage of this configuration is that it minimizes the chance of liquid or gas bypassing. Another advantage is that it operates in the froth region which generates greater area per unit volume than the higher-velocity cocurrent pipeline quench.

The concept was first outlined in U.S. Patent 3,803,805 (1974) and was amplified in U.S. Patent 6,339,169 (2002). The 1974 patent presents data which clarify that the key power input is from the gas stream.

A more recent article discusses use of the reverse jet in refinery offgas scrubbing for removal of both SO_2 and small particles [*Hydrocarbon*

Processing, 84,(9), 99–106 (2005)]. This article cites downward gas velocities in the range of 10 to 37 m/s and notes gas pressure drop in the range of 6 to 20 in of water. Removals of SO₂ and fine particles were both close to 99 percent. The froth produced by the contactor reverses direction, flows down, and is largely disengaged in a vessel mounted below.

Example 22: The Reverse Jet Contactor, U.S. Patent 6,339,169

This patent deals with rapid cooling and removal of NH₃ from gas exiting an acrylonitrile reactor. Liquid is injected upward. The claims suggest downward-flowing gas velocity is between 20 and 25 m/s.

Gas cooling is reported to be largely complete in 0.1 s. NH₃ removal at the exit of the contactor is reported to be greater than 99 percent. The gas is cooled by water vaporizing from the injected liquid, with total water circulated being in the range of 100 times that evaporated.

Since the gas cooling and NH₃ scrubbing move in parallel, they would be expected to achieve nearly the same approach to equilibrium as long as the pH of all the liquid stays below a key threshold. The great excess of liquid enables this.

The key is high froth interfacial area per unit volume.

Simple Spray Towers The other extreme to the pipeline and reverse jet contactors is an open vessel where spray is injected down into upflowing gas to form a rain of liquid. The advantage of simple spray towers is that they give low gas pressure drop and also tend to be nonfouling.

Even though gas velocity is well below flooding velocity, the finer droplets of the spray will be entrained. Note the wide spectrum of particle sizes shown by Fig. 14-88.

However, as shown by Examples 23 and 24, they can be extremely effective in liquid-limited systems.

Bypassing Limits Spray Tower Performance in Gas Cooling

As shown by Example 18, only modest performance is achieved in gas-limited systems. The modest efficiency is due to gas bypassing. Tall spray towers are not effective countercurrent devices. Even with nominally falling droplets, there is a great deal of backmixing because there is no stabilizing pressure drop as there would be in a column filled with packing or trays. A packet of droplets weighs more than a gas-filled space. The result is that the volume that is filled with the most droplets moves down relative to all other volumes. Similarly the gas volume that has fewest droplets moves up more quickly than other volumes. This generates bypassing of liquid and gas. The flows are driven by the rain of droplets themselves. Anything less than perfect distribution of liquid and gas will induce a dodging action between the flowing streams. Most designers limit expectations for spray contactors to some fraction of a single equilibrium stage regardless of height.

One approach that has been employed to get better distribution in spray systems is to mount a single large-capacity nozzle in the center of the vessel with radial discharge of large droplets. The droplets are discharged with enough velocity to penetrate to the vessel walls.

Spray Towers in Liquid-Limited Systems—Hollow Cone Atomizing Nozzles If we follow an element of liquid leaving a hollow cone hydraulic spray nozzle, the sequence is a rapidly thinning cone followed by wave development, followed by shedding of ligaments, followed by breakage of the ligaments into droplets. See Fig. 14-86. The sequence gives high transfer for liquid-limited systems. This results from the thin sheet of the hollow cone as well as the creation of fresh surface in the breakup process.

Devolatilizers Devolatilization systems are liquid-limited due to the combination of high liquid viscosity and removal of a component with high relative volatility. Simpson and Lynn [*AIChE J.*, 23 (5), 666–673 (1977)] reported oxygen stripping from water at 98 percent complete, in less than 1 ft of contact. The concept has been employed for residual devolatilization in refineries.

Spray Towers as Direct Contact Condensers Similarly spray contactors can be highly effective for direct contact condensers, which are also liquid-limited. The high transfer rate in the initial formation of sprays is the key. Kunesch [*Ind. Engr. Chem. Res.*, 32, 2387–2389 (1993)] reported a 97 percent approach to equilibrium in a hydrocarbon system in the 6-in space below the discharge of a row of hollow cone spray nozzles.

Other results on heat transfer in a large spray condenser are given by Waintraub et al. (“Removing Packings from Heat Transfer Sections of Vacuum Towers,” AIChE 2005 Spring National Meeting, Proceed-

ings of Topical Conference, April 10, 2005, Atlanta, p. 79). The paper highlights the importance of good gas and liquid distribution.

Converting Liquid Mass-Transfer Data to Direct Contact Heat Transfer Liquid-limited performance measures are much more commonly given for mass-transfer than for heat transfer. Often mass-transfer data are reported as $k_L a$ with units of h⁻¹. This can be converted to $h_{L,A}$ with units of Btu/(h·°F·ft³) by Eq. (14-188).

$$h_{L,A} = 187(k_L a) (c_L) (\rho_L) (\mu_L/T)^{0.5} \quad (14-188)$$

where μ_L = liquid, cP

T = temperature, °R

ρ_L = liquid density, lb/ft³

c_L = liquid specific heat, Btu/(lb·°F)

Calculation of transfer units for heat transfer is relatively simple. For a liquid

$$N_L = \frac{(\text{liquid contact time})(h_{L,A})}{\rho_L c_L} \quad (14-189)$$

where ρ_L = liquid density and c_L = liquid specific heat. [See parallel gas expression, Eq. (14-181).]

Unlike gases, the liquid properties that control mass and heat transfer differ greatly. The key term is diffusivity which for liquids drops with viscosity.

The resulting values for $h_{L,A}$ and N_L can be surprisingly large when a pure vapor such as steam is condensed. See Example 23.

Example 23: Estimating Direct Contact Condensing Performance Based on $k_L a$ Mass-Transfer Data If an aqueous system at 560°R gives a $k_L a$ of 60 h⁻¹, what does Eq. (14-188) predict for $h_{L,A}$ in a direct contact steam condenser?

For an aqueous system

$$\mu_L = 1 \text{ cP}$$

$$\rho_L = 62 \text{ lb/ft}^3$$

$$c_L = 1 \text{ Btu/(lb}\cdot\text{°F)}$$

and Eq. (14-189) predicts

$$h_{L,A} = 187(60)(1)(62)/(1/560)^{0.5} = 29,400 \text{ Btu/(h}\cdot\text{°F}\cdot\text{ft}^3)$$

When a pure gas such as HCl is absorbed by low viscosity liquid such as water, simple spray systems can also be highly effective. See Example 24.

Example 24: HCl Vent Absorber (Kister, *Distillation Troubleshooting*, Wiley, 2006, p. 95.) A 6-in-diameter, 8-ft-tall packed bed was giving major problems due to failure of the packing support. Water was the scrubbing fluid.

The liquid distributors were replaced with carefully positioned spray nozzles, and the packing was removed. HCl in the vent was removed to a level one-fortieth of the original design.

LIQUID-IN-GAS DISPERSIONS

Liquid Breakup into Droplets There are four basic mechanisms for breakup of liquid into droplets:

- Droplets in a field of high turbulence (i.e., high power dissipation per unit mass)
- Simple jets at low velocity
- Expanding sheets of liquid at relatively low velocity
- Droplets in a steady field of high relative velocity

These mechanisms coexist, and the one that gives the smallest drop size will control. The four mechanisms follow distinctly different velocity dependencies:

1. *Breakup in a highly turbulent field* (1/velocity)^{1.2}. This appears to be the dominant breakup process in distillation trays in the spray regime, pneumatic atomizers, and high-velocity pipeline contactors.

2. *Breakup of a low-velocity liquid jet* (1/velocity)⁰. This governs in special applications like prilling towers and is often an intermediate step in liquid breakup processes.

3. *Breakup of a sheet of liquid* (1/velocity)^{0.67}. This governs drop size in most hydraulic spray nozzles.

4. *Single-droplet breakup at very high velocity* $(1/\text{velocity})^2$. This governs drop size in free fall as well as breakup when droplets impinge on solid surfaces.

Droplet Breakup—High Turbulence This is the dominant breakup mechanism for many process applications. Breakup results from local variations in turbulent pressure that distort the droplet shape. Hinze [*Am. Inst. Chem. Eng. J.*, **1**, 289–295 (1953)] applied turbulence theory to obtain the form of Eq. (14-190) and took liquid-liquid data to define the coefficient:

$$D_{\max} = 0.725(\sigma/\rho_G)^{0.6}/E^{0.4} \quad (14-190)$$

where $E = (\text{power dissipated})/\text{mass length}^2/\text{time}^3$
 $\sigma = \text{surface tension}$ mass/time²
 $\rho_G = \text{gas density}$ mass/length³

Note that D_{\max} comes out with units of length. Since E typically varies with $(\text{gas velocity})^3$, this results in drop size dependence with $(1/\text{velocity})^{1.2}$.

The theoretical requirement for use of Eq. (14-190) is that the microscale of turbulence $\ll D_{\max}$. This is satisfied in most gas systems. For example, in three cases,

	(microscale of turbulence)/ D_{\max}
distillation tray in spray regime	0.007
pipeline @ 40 m/s and atmospheric pressure	0.012
two-fluid atomizer using 100 m/s air	0.03

Many applications involve a three-step process with high velocity first tearing wave crests away from liquid sheets, followed by breakup of ligaments into large droplets, followed by breakup of the large droplets. The prediction of final droplet size based on *power/mass* works surprisingly well, as shown by Eqs. (14-198), (14-201), (14-202), and (14-203).

Liquid-Column Breakup Because of increased pressure at points of reduced diameter, the liquid column is inherently unstable. As a result, it breaks into small drops with no external energy input. Ideally, it forms a series of uniform drops with the size of the drops set by the fastest-growing wave. This yields a dominant droplet diameter about 1.9 times the initial diameter of the jet as shown by

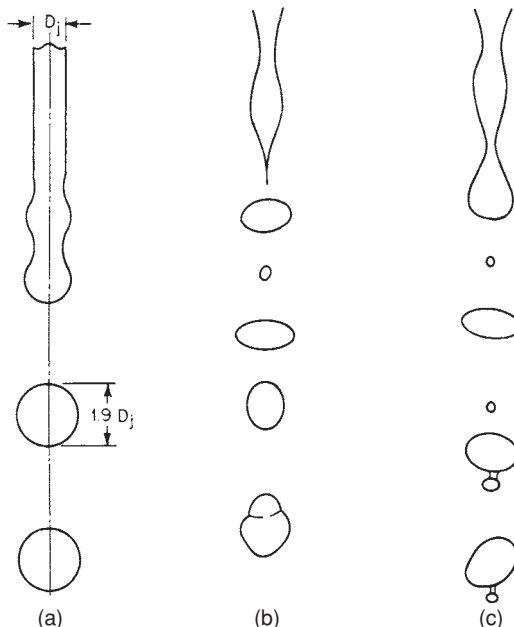


FIG. 14-85 (a) Idealized jet breakup suggesting uniform drop diameter and no satellites. (b) and (c) Actual breakup of a water jet as shown by high-speed photographs. [From W. R. Marshall, "Atomization and Spray Drying," *Chem. Eng. Prog. Monogr. Ser.*, no. 2 (1954).]

Fig. 14-85. As shown, the actual breakup is quite close to prediction, although smaller satellite drops are also formed. The prime advantage of this type of breakup is the greater uniformity of drop size.

For high-viscosity liquids, the drops are larger, as shown by Eq. (14-191):

$$D = 1.9D_j \left[1 + \frac{3\mu_L}{(\sigma\rho_L D_j)^{1/2}} \right] \quad (14-191)$$

where $D = \text{diameter of droplet}$
 $D_j = \text{diameter of jet}$
 $\mu_L = \text{viscosity of liquid}$
 $\rho_L = \text{density of liquid}$
 $\sigma = \text{surface tension of liquid}$

These units are dimensionally consistent; any set of consistent units can be used.

As the velocity of the jet is increased, the breakup process changes and ultimately becomes a mix of various competing effects, such as the capture of small drops by bigger ones in the slowing jet and the "turbulent breakup" of the bigger drops. The high-velocity jet is occasionally used in process applications because of the very narrow spray angle (5–20°) and the high penetration into a gas it can give. The focused stream also aids erosion of a surface.

Liquid-Sheet Breakup The basic principle of most hydraulic atomizers is to form a thin sheet that breaks via a variety of mechanisms to form ligaments of liquid which in turn yield chains of droplets. See Fig. 14-86.

For a typical nozzle, the drop size varies with $1/(\text{pressure drop})^{1/3}$. When $(\text{velocity})^2$ is substituted for pressure drop, droplet size is seen to vary with $(\text{velocity})^{-2/3}$.

Isolated Droplet Breakup—in a Velocity Field Much effort has focused on defining the conditions under which an isolated drop will break in a velocity field. The criterion for the largest stable drop size is the ratio of aerodynamic forces to surface-tension forces defined by the Weber number, N_{We} (dimensionless):

$$N_{We \text{ crit}} = \text{constant} = [\rho_G (\text{velocity})^2 (D_{\max}) / (\sigma)] \quad (14-192)$$

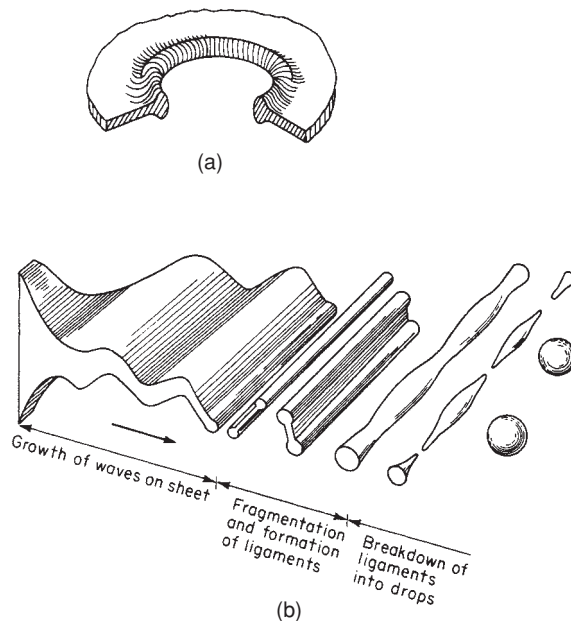


FIG. 14-86 Sheet breakup. (a) By perforation. [After Fraser et al., *Am. Inst. Chem. Eng. J.*, **8**(5), 672 (1962).] (b) By sinusoidal wave growth. [After Domrowski and Johns, *Chem. Eng. Sci.*, **18**, 203 (1963).]

$N_{We\ crit}$ for low-viscosity fluids commonly ranges from 10 to 20, with the larger value for a free-fall condition and the smaller for a sudden acceleration. High liquid viscosity also increases $N_{We\ crit}$.

Droplet breakup via impingement appears to follow a similar relationship, but much less data is available. This type of breakup can result from impingement on equipment walls or compressor blades. In general, there is less tendency to shatter on wetted surfaces.

Droplet Size Distribution Instead of the single droplet size implied by the discussion above, a spectrum of droplet sizes is produced. The most common ways to characterize this spectrum are:

- **Volume median (mass median) D_{vm} .** This has no fundamental meaning but is easy to determine since it is at the midpoint of a cumulative-volume plot.
- **Sauter mean D_{32} .** This has the same ratio of surface to volume as the total drop population. It is typically 70 to 90 percent of D_{vm} . It is frequently used in transport processes and is used here to characterize drop size.
- **Maximum D_{max} .** This is the largest-sized particle in the population. It is typically 3 to 4 times D_{32} in turbulent breakup processes, per Walzel [*International Chemical Engineering*, **33**, 46, (1993)]. It is the size directly calculated from the power/mass relationship. D_{32} is estimated from D_{max} by

$$D_{32} = 0.3 \cdot D_{max} \tag{14-193}$$

and D_{vm} is estimated from it by

$$D_{vm} = 0.4 \cdot D_{max} \tag{14-194}$$

However, any average drop size is fictitious, and none is completely satisfactory. For example, there is no way in which the high surface and transfer coefficients in small drops can be made available to the larger drops. Hence, a process calculation based on a given droplet size describes only what happens to that size and gives at best an approximation to the total mass.

There are a variety of ways to describe the droplet population. Figures 14-88 and 14-90 illustrate one of the most common methods, the plot of cumulative volume against droplet size on log-normal graph paper. This satisfies the restraint of not extrapolating to a negative drop size. Its other advantages are that it is easy to plot, the results are easy to visualize, and it yields a nearly straight line at lower drop sizes.

Cumulative volume over the range of 1 to 50 percent can also be shown to vary approximately as D^2 . This is equivalent to finding that the number of droplets of a given size is inversely proportional to the droplet area or the surface energy of the droplet.

Atomizers The common need to disperse a liquid into a gas has spawned a large variety of mechanical devices. The different designs emphasize different advantages such as freedom from plugging, pattern of spray, small droplet size, uniformity of spray, high turndown ratio, and low power consumption.

As shown in Table 14-19, most atomizers fall into three categories:

1. Pressure nozzles (hydraulic)
2. Two-fluid nozzles (pneumatic)
3. Rotary devices (spinning cups, disks, or vaned wheels)

These share certain features such as relatively low efficiency and low cost relative to most process equipment. The energy required to produce the increase in area is typically less than 0.1 percent of the total energy consumption. This is because atomization is a secondary process resulting from high interfacial shear or turbulence. As droplet sizes decrease, this efficiency drops lower.

Other types are available that use sonic energy (from gas streams), ultrasonic energy (electronic), and electrostatic energy, but they are less commonly used in process industries. See Table 14-19 for a summary of the advantages/disadvantages of the different type units. An expanded discussion is given by Masters [*Spray Drying Handbook*, Wiley, New York (1991)].

Special requirements such as size uniformity in prilling towers can dictate still other approaches to dispersion. Here plates are drilled with many holes to develop nearly uniform columns.

Commonly, the most important feature of a nozzle is the size of droplet it produces. Since the heat or mass transfer that a given dispersion can produce is often proportional to $(1/D_d)^2$, fine drops are usually favored. On the other extreme, drops that are too fine will not

settle, and a concern is the amount of liquid that will be entrained from a given spray operation. For example, if sprays are used to contact atmospheric air flowing at 1.5 m/s, drops smaller than 350 μm [terminal velocity = 1.5 m/s (4.92 ft/s)] will be entrained. Even for the relative coarse spray of the hollow-cone nozzle shown in Fig. 14-88, 7.5 percent of the total liquid mass will be entrained.

Hydraulic (Pressure) Nozzles Manufacturers' data such as shown by Fig. 14-88 are available for most nozzles for the air-water system. In Fig. 14-88, note the much coarser solid-cone spray. The coarseness results from the less uniform discharge.

Effect of Physical Properties on Drop Size Because of the extreme variety of available geometries, no attempt to encompass this variable is made here. The suggested predictive route starts with air-water droplet size data from the manufacturer at the chosen flow rate. This drop size is then corrected by Eq. (14-195) for different viscosity and surface tension:

$$\frac{D_{em, \text{system}}}{D_{em, \text{water}}} = \left(\frac{\sigma_{\text{system}}}{73} \right)^{0.25} \left(\frac{\mu_{\ell}}{1.0} \right)^{0.25} \tag{14-195}$$

where D_{em} = volume median droplet diameter
 σ = surface tension, mN/m (dyn/cm)
 μ_{ℓ} = liquid viscosity, mPa·s (cP)

The exponential dependencies in Eq. (14-195) represent averages of values reported by a number of studies with particular weight given to Lefebvre [*Atomization and Sprays*, Hemisphere, New York (1989)]. Since viscosity can vary over a much broader range than surface tension, it has much more leverage on drop size. For example, it is common to find an oil with 1000 times the viscosity of water, while most liquids fall within a factor of 3 of its surface tension. Liquid density is generally even closer to that of water, and since the data are not clear that a liquid density correction is needed, none is shown in Eq. (14-195). Vapor density also has an impact on droplet size but the impact is complex, involving conflicts of a number of effects, and vapor density is commonly omitted in atomizer droplet size correlations.

Effect of Pressure Drop and Nozzle Size For a nozzle with a developed pattern, the average drop size can be estimated to fall with rising ΔP (pressure drop) by Eq. (14-196):

$$\frac{D_1}{D_2} = \left(\frac{\Delta P_2}{\Delta P_1} \right)^{1/3} \tag{14-196}$$

For similar nozzles and constant ΔP , the drop size will increase with nozzle size as indicated by Eq. (14-197):

$$\frac{D_1}{D_2} = \left(\frac{\text{orifice diameter}_1}{\text{orifice diameter}_2} \right)^{1/2} \tag{14-197}$$

Once again, these relationships are averages of a number of reported values and are intended as rough guides.

The normal operating regime is well below turbulent breakup velocity. However the data of Kennedy [*J. of Engineering for Gas Turbines and Power*, **108**, 191 (1986)] at very high pressure drop in large nozzles shows a shift to a higher dependence on pressure drop. This data suggests that turbulent droplet breakup can also be governing with hydraulic spray nozzles, although this is unusual.

Spray Angle A shift to a smaller-angle nozzle gives slightly larger drops for a given type of nozzle because of the reduced tendency of the sheet to thin. Dietrich [*Proc. 1st Int. Conf. Liq. Atomization Spray Systems*, Tokyo (1978)] shows the following:

Angle	25°	50°	65°	80°	95°
$D_{em}, \mu\text{m}$	1459	1226	988	808	771

In calculating the impact point of spray, one should recognize that the spray angle closes in as the spray moves away from the nozzle. This is caused by loss of momentum of the spray to the gas.

14-94 EQUIPMENT FOR DISTILLATION, GAS ABSORPTION, PHASE DISPERSION, AND PHASE SEPARATION

TABLE 14-19 Atomizer Summary

Types of atomizer	Design features	Advantages	Disadvantages
Pressure.	Flow $\alpha(\Delta P/\rho_l)^{1/2}$. Only source of energy is from fluid being atomized.	Simplicity and low cost.	Limited tolerance for solids; uncertain spray with high-viscosity liquids; susceptible to erosion. Need for special designs (e.g., bypass) to achieve turndown.
1. Hollow cone.	Liquid leaves as conical sheet as a result of centrifugal motion of liquid. Air core extends into nozzle.	High atomization efficiency.	Concentrated spray pattern at cone boundaries.
<i>a.</i> Whirl chamber (see Fig. 14-87 <i>a</i>).	Centrifugal motion developed by tangential inlet in chamber upstream of orifice.	Minimum opportunity for plugging.	
<i>b.</i> Grooved core.	Centrifugal motion developed by inserts in chamber.	Smaller spray angle than <i>1a</i> and ability to handle flows smaller than <i>1a</i> .	
2. Solid cone (see Fig. 14-87 <i>b</i>).	Similar to hollow cone but with insert to provide even distribution.	More uniform spatial pattern than hollow cone.	Coarser drops for comparable flows and pressure drops. Failure to yield same pattern with different fluids.
3. Fan (flat) spray.	Liquid leaves as a flat sheet or flattened ellipse.	Flat pattern is useful for coating surfaces and for injection into streams.	Small clearances.
<i>a.</i> Oval or rectangular orifice (see Fig. 14-87 <i>c</i>). Numerous variants on cavity and groove exist.	Combination of cavity and orifice produces two streams that impinge within the nozzle.		
<i>b.</i> Deflector (see Fig. 14-87 <i>d</i>).	Liquid from plain circular orifice impinges on curved deflector.	Minimal plugging.	Coarser drops.
<i>c.</i> Impinging jets (see Fig. 14-87 <i>e</i>).	Two jets collide outside nozzle and produce a sheet perpendicular to their plane.	Different liquids are isolated until they mix outside of orifice. Can produce a flat circular sheet when jets impinge at 180°.	Extreme care needed to align jets.
4. Nozzles with wider range of turndown.			
<i>a.</i> Spill (bypass) (see Fig. 14-87 <i>f</i>).	A portion of the liquid is recirculated after going through the swirl chamber.	Achieves uniform hollow cone atomization pattern with very high turndown (50:1).	Waste of energy in bypass stream. Added piping for spill flow.
<i>b.</i> Poppet (see Fig. 14-87 <i>g</i>).	Conical sheet is developed by flow between orifice and poppet. Increased pressure causes poppet to move out and increase flow area.	Simplest control over broad range.	Difficult to maintain proper clearances.
Two-fluid (see Fig. 14-87 <i>h</i>).	Gas impinges coaxially and supplies energy for breakup.	High velocities can be achieved at lower pressures because the gas is the high-velocity stream. Liquid-flow passages can be large, and hence plugging can be minimized.	Because gas is also accelerated, efficiency is inherently lower than pressure nozzles.
Sonic.	Gas generates an intense sound field into which liquid is directed.	Similar to two-fluid but with greater tolerance for solids.	Similar to two-fluid.
Rotary wheels (see Fig. 14-87 <i>i</i>) disks, and cups.	Liquid is fed to a rotating surface and spreads in a uniform film. Flat disks, disks with vanes, and bowl-shaped cups are used. Liquid is thrown out at 90° to the axis.	The velocity that determines drop size is independent of flow. Hence these can handle a wide range of rates. They can also tolerate very viscous materials as well as slurries. Can achieve very high capacity in a single unit; does not require a high-pressure pump.	Mechanical complexity of rotating equipment. Radial discharge.
Ultrasound.	Liquid is fed over a surface vibrating at a frequency > 20 kHz.	Fine atomization, small size, and low injection velocity.	Low flow rate and need for ultrasound generator.

At some low flow, pressure nozzles do not develop their normal pattern but tend to approach solid streams. The required flow to achieve the normal pattern increases with viscosity.

Two-Fluid (Pneumatic) Atomizers This general category includes such diverse applications as venturi atomizers and reactor-effluent quench systems in addition to two-fluid spray nozzles. Depending on the manner in which the two fluids meet, several of the breakup mechanisms may be applicable, but the final one is high-level turbulent rupture.

As shown by Table 14-20, empirical correlations for two-fluid atomization show dependence on high gas velocity to supply atomizing energy, usually to a power dependence close to that for turbulent breakup. In addition, the correlations show a dependence on the ratio of gas to liquid and system dimension.

Further differences from hydraulic nozzles (controlled by sheet and ligament breakup) are the stronger increase in drop size with increasing surface tension and decreasing gas density.

The similarity of these dependencies to Eq. (14-190) led to a reformulation with two added terms that arise naturally from the theory of power dissipation per unit mass. The result is Eq. (14-198) which is labeled *power/mass* in Table 14-20.

$$D_{32} = 0.29 \left(\frac{\sigma}{\rho_G} \right)^{0.6} (1/\text{velocity})^{1.2} \left(1 + \frac{L}{G} \right)^{0.4} (D_{\text{nozzle}})^{0.4} \quad (14-198)$$

where σ = surface tension

ρ_G = gas density

L/G = mass ratio of liquid flow to gas flow

D_{nozzle} = diameter of the air discharge

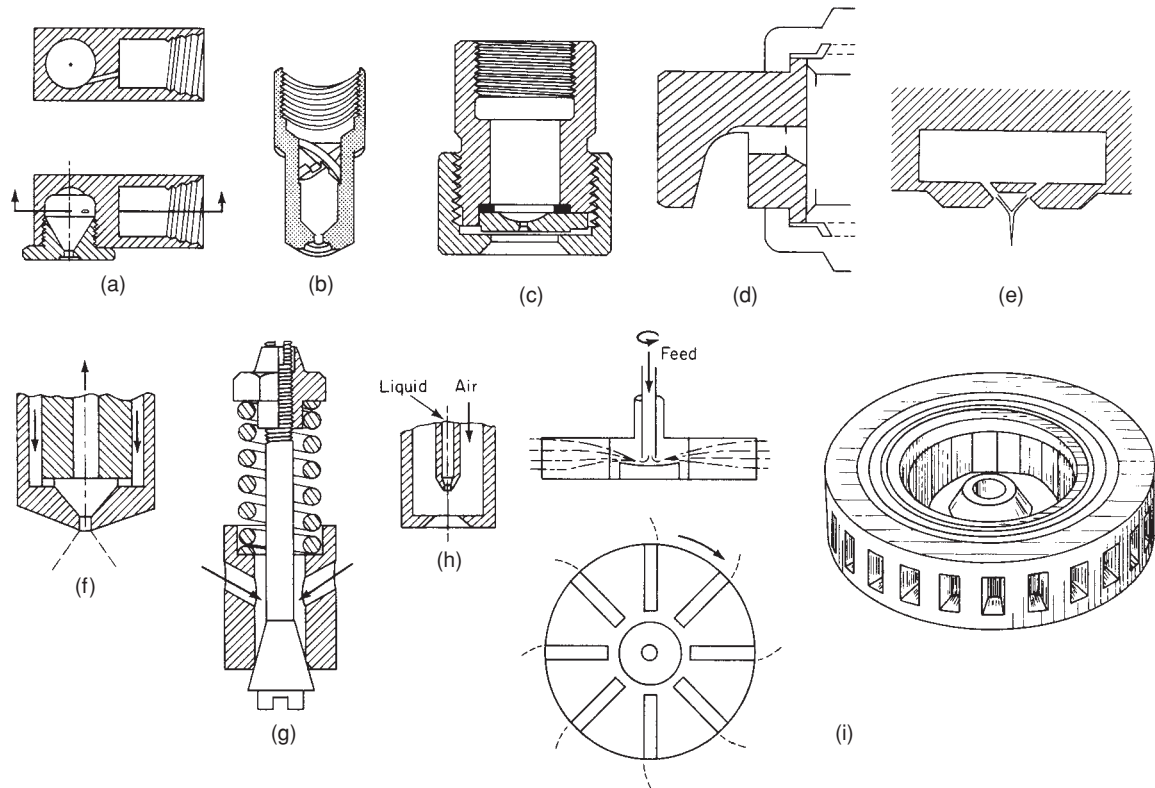


FIG. 14-87 Characteristic spray nozzles. (a) Whirl-chamber hollow cone. (b) Solid cone. (c) Oval-orifice fan. (d) Deflector jet. (e) Impinging jet. (f) Bypass. (g) Poppet. (h) Two-fluid. (i) Vaned rotating wheel.

This is remarkably similar to the empirical two-fluid atomizer relationships of El-Shanawany and Lefebvre [*J. Energy*, **4**, 184 (1980)] and Jasuja [*Trans. Am. Soc. Mech. Engr.*, **103**, 514 (1981)]. For example, El-Shanawany and Lefebvre give a relationship for a prefilming atomizer:

$$D_{32} = 0.0711(\sigma/\rho_C)^{0.6}(1/\text{velocity})^{1.2}(1 + L/G)(D_{\text{nozzle}})^{0.4}(\rho_L/\rho_C)^{0.1} + 0.015[(\mu_L)^2/(\sigma \times \rho_L)]^{0.5}(D_{\text{nozzle}})^{0.5}(1 + L/G) \quad (14-199)$$

where μ_L is liquid viscosity.

According to Jasuja,

$$D_{32} = 0.17(\sigma/\rho_C)^{0.45}(1/\text{velocity})^{0.9}(1 + L/G)^{0.5}(D_{\text{nozzle}})^{0.55} + \text{viscosity term} \quad (14-200)$$

[Eqs. (14-198), (14-199), and (14-200) are dimensionally consistent; any set of consistent units on the right-hand side yields the droplet size in units of length on the left-hand side.]

The second, additive term carrying the viscosity impact in Eq. (14-199) is small at viscosities around 1 cP but can become controlling as viscosity increases. For example, for air at atmospheric pressure atomizing water, with nozzle conditions

$$\begin{aligned} D_{\text{nozzle}} &= 0.076 \text{ m (3 in)} \\ \text{velocity} &= 100 \text{ m/s (328 ft/s)} \\ L/G &= 1 \end{aligned}$$

El-Shanawany measured 70 μm and his Eq. (14-199) predicted 76 μm . The *power/mass* correlation [Eq. (14-198)] predicts 102 μm . The agreement between both correlations and the measurement is much better than normally achieved.

Rotary Atomizers For rotating wheels, vaneless disks, and cups, there are three regimes of operation. At low rates, the liquid is shed directly as drops from the rim. At intermediate rates, the liquid leaves the rim as threads; and at the highest rate, the liquid extends from the edge as a thin sheet that breaks down similarly to a fan or hollow-cone spray nozzle. As noted in Table 14-19, rotary devices have many unique advantages such as the ability to handle high viscosity and slurries and produce small droplets without high pressures. The prime applications are in spray drying. See Masters [*Spray Drying Handbook*, Wiley, New York (1991)] for more details.

Pipeline Contactors The correlation for droplet diameter based on power/mass is similar to that for two-fluid nozzles. The dimensionless correlation is

$$D_{32} = 0.8(\sigma/\rho_C)^{0.6}(1/\text{velocity})^{1.2}(D_{\text{pipe}})^{0.4} \quad (14-201)$$

(The relation is dimensionally consistent; any set of consistent units on the right-hand side yields the droplet size in units of length on the left-hand side.)

The relationship is similar to the empirical correlation of Tatterson, Dallman, and Hanratty [*Am. Inst. Chem. Eng. J.*, **23**(1), 68 (1977)]

$$D_{32} \sim \left(\frac{\sigma}{\rho_C} \right)^{0.5} (1/\text{velocity})^1 (D_{\text{pipe}})^{0.5}$$

Predictions from Eq. (14-201) align well with the Tatterson data. For example, for a velocity of 43 m/s (140 ft/s) in a 0.05-m (1.8-inch) equivalent diameter channel, Eq. (14-201) predicts D_{32} of 490 microns, compared to the measured 460 to 480 microns.

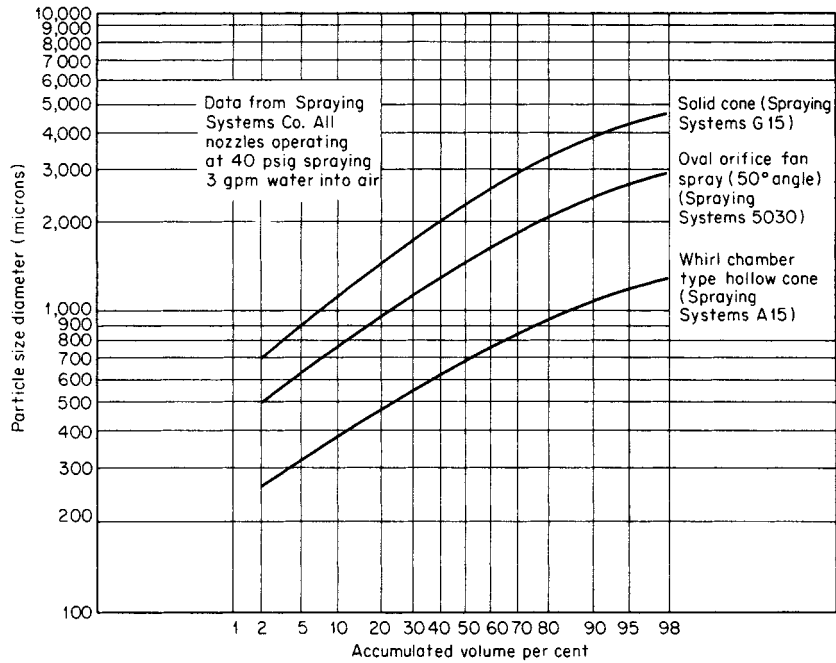


FIG. 14-88 Droplet-size distribution for three different types of nozzles. To convert pounds per square inch gauge to kilopascals, multiply by 6.89; to convert gallons per minute to cubic meters per hour, multiply by 0.227. (Spraying Systems Inc.)

Entrainment due to Gas Bubbling/Jetting through a Liquid

Entrainment generally limits the capacity of distillation trays and is commonly a concern in vaporizers and evaporators. Fortunately, it is readily controllable by simple inertial entrainment capture devices such as wire mesh pads in gravity separators.

In distillation towers, entrainment lowers the tray efficiency, and 1 pound of entrainment per 10 pounds of liquid is sometimes taken as the limit for acceptable performance. However, the impact of entrainment on distillation efficiency depends on the relative volatility of the component being considered. Entrainment has a minor impact on close separations when the difference between vapor and liquid concentration is small, but this factor can be dominant for systems where the liquid concentration is much higher than the vapor in equilibrium with it (i.e., when a component of the liquid has a very low volatility, as in an absorber).

As shown by Fig. 14-90, entrainment droplet sizes span a broad range. The reason for the much larger drop sizes of the upper curve is the short disengaging space. For this curve, over 99 percent of the entrainment has a terminal velocity greater than the vapor velocity. For contrast, in the lower curve the terminal velocity of the largest particle reported is the same as the vapor velocity. For the

settling velocity to limit the maximum drop size entrained, at least 0.8 m (30 in) disengaging space is usually required. Note that even for the lower curve, less than 10 percent of the entrainment is in drops of less than 50 μm. The coarseness results from the relatively low power dissipation per mass on distillation trays. This means that it is relatively easy to remove by a device such as a wire mesh pad. Over 50 percent is typically captured by the underside of the next higher tray or by a turn in the piping leaving an evaporator. Conversely, though small on a mass basis, the smaller drops are extremely numerous. On a number basis, more than one-half of the drops in the lower curve are under 5 μm. These can serve as nuclei for fog condensation in downstream equipment.

Entrainment *E* is inherent in the bubbling process and can stem from a variety of sources, as shown by Fig. 14-89. However, the biggest practical problem is entrainment generated by the kinetic energy of the flowing vapor rather than the bubbling process. As vapor velocity approaches the flooding limit [Eq. (14-168)], the entrainment rises approximately with (velocity)⁶.

Pinczewski and Fell [*Trans. Inst. Chem Eng.*, **55**, 46 (1977)] show that the velocity at which vapor jets onto the tray sets the droplet size, rather than the superficial tray velocity. The power/mass correlation predicts an average drop size close to that measured by Pinczewski and Fell. Combination of this prediction with the estimated fraction of the droplets entrained gave a relationship for entrainment, Eq. (14-202). The dependence of entrainment with the eighth power of velocity even approximates the observed velocity dependence, as flooding is approached.

$$E = \frac{\text{constant}(\text{velocity})^8(\rho_G)^4}{(A_j)^3(\rho_L - \rho_G)^{2.5}\sigma^{1.5}} \quad (14-202)$$

(Here *E* is the mass of entrainment per mass of vapor and *A_j* is the fractional open area on the tray.)

When flooding is defined as the condition that gives *E* of 1, the flood velocity is estimated by Eq. (14-203).

TABLE 14-20 Exponential Dependence of Drop Size on Different Parameters in Two-Fluid Atomization

	Relative velocity	Surface tension	Gas density	1 + L/G	Atomizer dimension
Jasuja (empirical for small nozzle)	-0.9	0.45	-0.45	0.5	0.55
El-Shanawany and Lefebvre (empirical for small nozzle)	-1.2	0.6	-0.7	1	0.40
Tattersson, Dallman, and Hanratty (pipe flow)	-1	0.5	-0.5		0.5
Power/mass	-1.2	0.6	-0.6	0.4	0.4

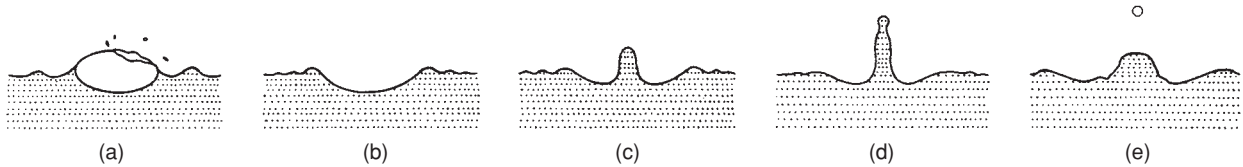


FIG. 14-89 Mechanism of the burst of an air bubble on the surface of water. [Newitt, Dombrowski, and Knellman, *Trans. Inst. Chem. Eng.*, **32**, 244 (1954).]

$$U_{\text{flood}} = \frac{1.25(A_f)^{3/8} [g(\rho_L - \rho_G)]^{0.3125} \sigma^{0.1875}}{\rho_G^{0.5}} \quad (14-203)$$

The relationship is dimensionally consistent; any set of consistent units on the right-hand side yields velocity units on the left-hand side. It is similar in form to Eq. (14-168) and provides a conceptual framework for understanding the ultimate distillation column capacity concept.

“Upper Limit” Flooding in Vertical Tubes If, instead of a gas jet being injected into a liquid as in distillation, the liquid runs down the walls and the gas moves up the center of the tube, higher velocities can be achieved than shown by Eq. (14-168) or (14-203). This application is important in the design of vertical condensers.

Maharudraya and Jayanti [*AIChE J.*, **48**(2), 212–220 (2002)] show that peak pressure drop in a 25-mm vertical tube occurs at a value close to that predicted by Eq. (14-168) or (14-203). At this velocity about 20 percent of the injected liquid is being entrained out the top of the tube. However, the condition where essentially all liquid was entrained didn’t occur until a velocity over twice the value estimated from Eq. (14-168) and Eq. (14-203).

The higher velocities at modest entrainment observed by Maharudraya and Jayanti were obtained with special smooth entry of gas (and exit of liquid) at the bottom of the tube. Hewitt (*Handbook of Heat Exchanger Design*, pp. 2.3.2-23, 1992) suggests that these values should be derated by at least 35 percent for more typical sharp heat exchanger tube entry. Similar to the smooth entry effect, other data suggest that countercurrent capacity can be increased by providing an extension of the tube below the tube sheet, with the bottom of the extension cut on a steep angle (>60°) to the horizontal. The tapered extension facilitates drainage of liquid.

An extensive data bank correlated by Dielh and Koppany [*Chem. Eng. Prog. Symp. Ser.*, **65**, 77–83 (1965)] also gave higher allowable entry velocities than Eq. (14-168) or (14-203). Dielh and Koppany’s correlation [Eq. (14-204)] is dimensional, and appears to give a much higher dependence on σ than the more recent work. However, for many fluids, $\sigma^{0.5}$ is essentially the same as the combination $\sigma^{0.1875}(\rho_L - \rho_G)^{0.3125}$ that appears in Eq. (14-203). Hence Eq. (14-204) gives a similar physical property dependence.

$$U_f = F_1 F_2 (\sigma/\rho_g)^{0.5} \quad (14-204)$$

where U_f = flooding gas velocity, m/s

- $F_1 = 1.22$ when $3.2 d_i/\sigma > 1.0$
- $= 1.22 (3.2 d_i/\sigma)^{0.4}$ when $3.2 d_i/\sigma < 1.0$
- $F_2 = (G/L)^{0.25}$
- G/L = gas-liquid mass ratio
- d_i = inside diameter of column, mm
- σ = surface tension, mN/m (dyn/cm)
- ρ_g = gas density, kg/m³

The primary reason for citing Eq. (14-204) is the large successful experience base in practical applications. Note that the reduction in allowable gas velocity for small diameters given by the F_1 factor is conceptually the same as the effect of using smaller-diameter packing in distillation. Note also that over the range of G/L between 1 and 0.1, the Maharudraya and Jayanti data show a similar reduction in allowable gas rate to the F_2 factor in Eq. (14-204). The phenomenon behind

this is that a thicker liquid film on the tube wall is more easily entrained.

While the limiting phenomenon of upper limit flooding in a vertical pipe is similar to *ultimate capacity* in distillation, there is a distinct difference. *Upper limit* in a vertical pipe applies to a design where a conscious effort should be made to minimize gas-liquid contact. Carried to extremes, it would involve separate tubes for liquid flowing down and vapor going up. In contrast, *ultimate capacity* in a distillation column corresponds to the condition where effective mass transfer disappears due to high entrainment. One could force more vapor up through the contactor, but fractionation would be poor.

Fog Condensation—The Other Way to Make Little Droplets For a variety of reasons, a gas or vapor can become supersaturated with a condensable component. Surface tension and mass transfer impose barriers on immediate condensation, so growth of fog particles lags behind what equilibrium predicts. Droplets formed by fog condensation are usually much finer (0.1 to 10 μm) than those formed by mechanical breakup and hence more difficult to collect. Sometimes fog can be a serious problem, as in the atmospheric discharge of a valuable or a hazardous material. More commonly, fog is a curiosity rather than a dominating element in chemical processing.

Fog particles grow because of excess saturation in the gas. Usually this means that the gas is supersaturated (i.e., it is below its dew point). Sometimes, fog can also grow on soluble foreign nuclei at partial pressures below saturation. Increased saturation can occur through a variety of routes:

1. Mixing of two saturated streams at different temperatures. This is commonly seen in the plume from a stack. Since vapor pressure is an exponential function of temperature, the resultant mixture of two saturated streams will be supersaturated at the mixed temperature. Uneven flow patterns and cooling in heat exchangers make this route to supersaturation difficult to prevent.
2. Increased partial pressure due to reaction. An example is the reaction of SO_3 and H_2O to yield H_2SO_4 , which has much lower vapor pressure than its components.
3. Isoentropic expansion (cooling) of a gas, as in a steam nozzle.
4. Cooling of a gas containing a condensable vapor. Here the problem is that the gas cools faster than condensable vapor can be removed by mass transfer.

These mechanisms can be observed in many common situations. For example, fog via mixing can be seen in the discharge of breath on a cold day. Fog via adiabatic expansion can be seen in the low-pressure area over the wing of an airplane landing on a humid summer day; and fog via condensation can be seen in the exhaust from an automobile air conditioner (if you follow closely enough behind another car to pick up the ions or NO molecules needed for nucleation). All of these occur at a very low supersaturation and appear to be keyed to an abundance of foreign nuclei. All of these fogs also quickly dissipate as heat or unsaturated gas is added.

The supersaturation in condensers arises for two reasons. First, the condensable vapor is generally of higher molecular weight than the noncondensable gas. This means that the molecular diffusivity of the vapor will be much less than the thermal diffusivity of the gas. Restated, the ratio of N_{S_g}/N_V is greater than 1. The result is that a condenser yields more heat-transfer units $dT_g/(T_g - T_i)$ than mass-transfer units $dY_g/(Y_g - Y_i)$. Second, both transfer processes derive their driving force from the temperature difference between the gas T_g and the interface T_i . Each incremental decrease in interface temperature

TABLE 14-21 Simulation of Three Heat Exchangers with Varying Foreign Nuclei

	1	2	3
Weight fraction, noncondensable			
Inlet	0.51	0.42	0.02
Outlet	0.80	0.80	0.32
Molecular weight			
Inert	28	29	29
Condensable	86	99	210
Temperature difference between gas and liquid interface, K			
Inlet	14	24	67
Outlet	4	10	4
Percent of liquid that leaves unit as fog			
Nuclei concentration in inlet particles/cm ³			
100	0.05	1.1	2.2
1,000	0.44	5.6	3.9
10,000	3.2	9.8	4.9
100,000	9.6	11.4	5.1
1,000,000	13.3	11.6	
10,000,000	14.7		
∞	14.7	11.8	5.1
Fog particle size based on 10,000 nuclei/cm ³ at inlet, μm	28	25	4

yields the same relative increase in temperature driving force. However, the interface vapor pressure can only approach the limit of zero. Because of this, for equal molecular and thermal diffusivities a saturated mixture will supersaturate when cooled. The tendency to supersaturate generally increases with increased molecular weight of the condensable, increased temperature differences, and reduced initial superheating. To evaluate whether a given condensing step yields fog requires rigorous treatment of the coupled heat-transfer and mass-transfer processes through the entire condensation. Steinmeyer [*Chem. Eng. Progr.*, **68**(7), 64 (1972)] illustrates this, showing the impact of foreign-nuclei concentration on calculated fog formation. See Table 14-21. Note the relatively large particles generated for cases 1 and 2 for 10,000 foreign nuclei per cm³. These are large enough to be fairly easily collected. There have been very few documented problems with industrial condensers despite the fact that most calculate to generate supersaturation along the condensing path. The explanation appears to be a limited supply of foreign nuclei.

Ryan et al. [*Chem. Eng. Progr.*, **90**(8), 83 (1994)] show that separate mass and heat transfer-rate modeling of an HCl absorber predicts 2 percent fog in the vapor. The impact is equivalent to lowering the stage efficiency to 20 percent.

Spontaneous (Homogeneous) Nucleation This process is quite difficult because of the energy barrier associated with creation of the interfacial area. It can be treated as a kinetic process with the rate a very steep function of the supersaturation ratio (S = partial pressure of condensable per vapor pressure at gas temperature). For water, an increase in S from 3.4 to 3.9 causes a 10,000-fold increase in the nucleation rate. As a result, below a critical supersaturation (S_{crit}), homogeneous nucleation is slow enough to be ignored. Generally, S_{crit} is defined as that which limits nucleation to one particle produced per cubic centimeter per second. It can be estimated roughly by traditional theory (*Theory of Fog Condensation*, Israel Program for Scientific Translations, Jerusalem, 1967) using the following equation:

$$S_{crit} = \exp \left[0.56 \frac{M}{\rho_l} \left(\frac{\sigma}{T} \right)^{3/2} \right] \quad (14-205)$$

where σ = surface tension, mN/m (dyn/cm)
 ρ_l = liquid density, g/cm³
 T = temperature, K
 M = molecular weight of condensable

Table 14-22 shows typical experimental values of S_{crit} taken from the work of Russel [*J. Chem. Phys.*, **50**, 1809 (1969)]. Since the critical supersaturation ratio for homogeneous nucleation is typically greater

TABLE 14-22 Experimental Critical Supersaturation Ratios

	Temperature, K	S_{crit}
H ₂ O	264	4.91
C ₂ H ₅ OH	275	2.13
CH ₃ OH	264	3.55
C ₆ H ₆	253	5.32
CCl ₄	247	6.5
CHCl ₃	258	3.73
C ₆ H ₅ Cl	250	9.5

than 3, it is not often reached in process equipment. However, fog formation is typically found in steam turbines. Gyarmathy [*Proc. Inst. Mech. E., Part A: J. Power and Energy* **219**(A6), 511–521 (2005)] reports fog in the range 3.5 to 5 percent of total steam flow, with average fog diameter in the range of 0.1 to 0.2 μm.

Growth on Foreign Nuclei As noted above, foreign nuclei are often present in abundance and permit fog formation at much lower supersaturation. For example,

1. **Solids.** Surveys have shown that air contains thousands of particles per cubic centimeter in the 0.1-μm to 1-μm range suitable for nuclei. The sources range from ocean-generated salt spray to combustion processes. The concentration is highest in large cities and industrial regions. When the foreign nuclei are soluble in the fog, nucleation occurs at S values very close to 1.0. This is the mechanism controlling atmospheric water condensation. Even when not soluble, a foreign particle is an effective nucleus if wet by the liquid. Thus, a 1-μm insoluble particle with zero contact angle requires an S of only 1.001 in order to serve as a condensation site for water.

2. **Ions.** Amelin [*Theory of Fog Condensation*, Israel Program for Scientific Translations, Jerusalem, (1967)] reports that ordinary air contains even higher concentrations of ions. These ions also reduce the required critical supersaturation, but by only about 10 to 20 percent, unless multiple charges are present.

3. **Entrained liquids.** Production of small droplets is inherent in the bubbling process, as shown by Fig. 14-90. Values range from near zero to 10,000/cm³ of vapor, depending on how the vapor breaks through the liquid and on the opportunity for evaporation of the small drops after entrainment.

As a result of these mechanisms, most process streams contain enough foreign nuclei to cause some fogging. While fogging has been reported in only a relatively low percent of process partial condensers, it is rarely looked for and volunteers its presence only when yield losses or pollution is intolerable.

Droplet Distribution Monodisperse (nearly uniform droplet size) fogs can be grown by providing a long retention time for growth. However, industrial fogs usually show a broad distribution, as in Fig. 14-91. Note also that for this set of data, the sizes are several orders of magnitude smaller than those shown earlier for entrainment and atomizers.

The result, as discussed in a later subsection, is a demand for different removal devices for the small particles.

While generally fog formation is a nuisance, it can occasionally be useful because of the high surface area generated by the fine drops. An example is insecticide application.

GAS-IN-LIQUID DISPERSIONS

GENERAL REFERENCES: Design methods for agitated vessels are presented by Penney in Couper et al., *Chemical Process Equipment, Selection and Design*, Chap. 10, Gulf Professional Publishing, Burlington, Mass., 2005. A comprehensive review of all industrial mixing technology is given by Paul, Atomo-Obeng, and Kresta, *Handbook of Industrial Mixing*, Wiley, Hoboken, N.J., 2004. Comprehensive treatments of bubbles or foams are given by Akers, *Foams: Symposium 1975*, Academic Press, New York, 1973; Bendure, *Tappi*, **58**, 83 (1975); Benfratello, *Energ Elettr.*, **30**, 80, 486 (1953); Berkman and Egloff, *Emulsions and Foams*, Reinhold, New York, 1941, pp. 112–152; Bikerman, *Foams*, Springer-Verlag, New York, 1975; *Kirk-Othmer Encyclopedia of Chemical Technology*, 4th ed., Wiley, New York, 1993, pp. 82–145; Haberman and Morton, *Report 802*, David W. Taylor Model Basin, Washington, 1953; Levich, *Physicochemical Hydrodynamics*, Prentice-Hall, Englewood Cliffs, NJ, 1962; and Soo, *Fluid Dynamics of Multiphase Systems*, Blaisdell, Waltham, Massachusetts,

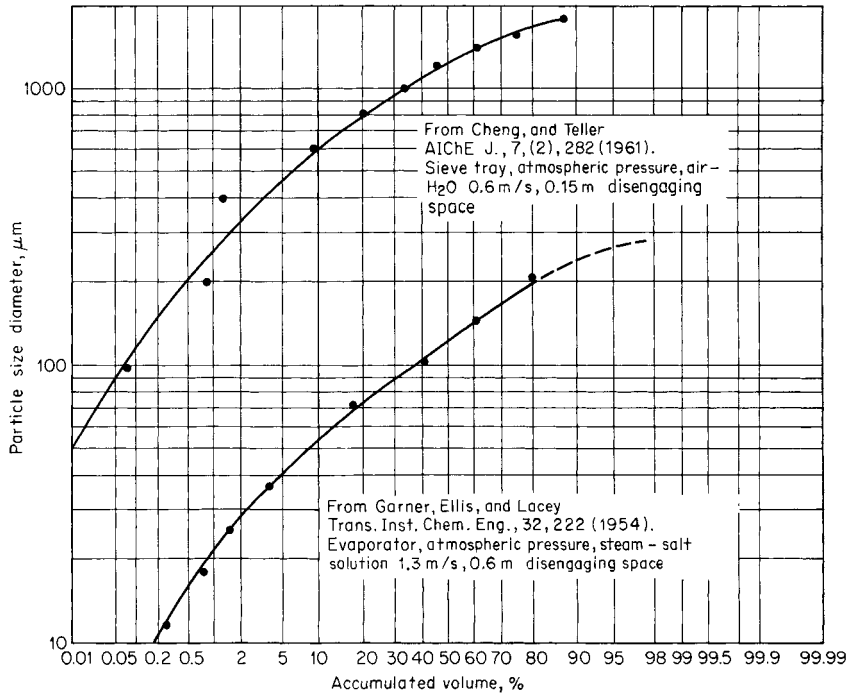


FIG. 14-90 Entrainment droplet-size distribution. To convert meters per second to feet per second, multiply by 3.28, to convert meters to feet multiply by 3.28.

1967. The formation of bubbles is comprehensively treated by Clift, Grace, and Weber, *Bubbles, Drops and Particles*, Academic, New York, 1978; Kumar and Kuloor, *Adv. Chem. Eng.*, **8**, 255-368 (1970); and Wilkinson and Van Dieren-donck, *Chem. Eng. Sci.*, **49**, 1429-1438 (1994). Design methods for units operation in bubble columns and stirred vessels are covered by Atika and Yoshida, *Ind. Eng. Chem. Process Des. Dev.*, **13**, 84 (1974); Calderbank, *The Chem. Eng.* (London), CE209 (October, 1967); and Mixing, vol. II, Academic, New York, 1967, pp. 1-111; Fair, *Chem. Eng.*, **74**, 67 (July 3, 1967); Jordan, *Chemical Process Dev.*, Interscience, New York, 1968, part I, pp. 111-175; Mersmann, *Ger. Chem. Eng.*, **1**, 1 (1978); Resnick and Gal-Or, *Adv. Chem. Eng.*, **7**, 295-395 (1968); Valentin, *Absorption in Gas-Liquid Dispersions*, E. & F. N. Spon, London, 1967; Tatter-son, *Fluid Mixing and Gas Dispersion in Agitated Tanks*, McGraw-Hill, 1991; and Deckwer and Schumpe, *Chem. Eng. Sci.*, **48**, 889-991 (1993).

Review of foam rheology is given by Herzhaft [*Oil & Gas Sci. & Technol.*, **54**, 587 (1999)] and Heller and Kuntamukkula [*Ind. Eng. Chem. Res.*, **26**, 318 (1987)]. The influence of surface-active agents on bubbles and foams is summar-ized in selected passages from Schwartz and Perry, *Surface Active Agents*, vol. 1, Interscience, New York, 1949; and from Schwartz, Perry, and Berch, *Surface Active Agents and Detergents*, vol. 2, Interscience, New York, 1958. See also Elenkov, *Theor. Found Chem. Eng.*, **1**, 1, 117 (1967); and Rubel, *Antifoaming and Defoaming Agents*, Noyes Data Corp., Park Ridge, NJ, 1972.

A review of foam stability also is given by de Vries, Meded, *Rubber Sticht. Delft*, No. 328, 1957. Foam-separation methodology is discussed by Aguyo and Lemlich, *Ind. Eng. Chem. Process Des. Dev.*, **13**, 153 (1974); and Lemlich, *Ind. Eng. Chem.*, **60**, 16 (1968). The following reviews of specific applications of gas-to-liquid dispersions are recommended: Industrial fermentations Aiba, Humphrey, and Millis, *Biochemical Engineering*, Academic, New York, 1965. Finn, *Bacteriol. Rev.*, **18**, 254 (1954). Oldshue, "Fermentation Mixing Scale-Up Techniques," in *Biotechnology and Bioengineering*, vol. 8, 1966, pp. 3-24. Aerobic oxidation of wastes: Eckenfelder and McCabe, *Advances in Biological Waste Treatment*, Macmillan, New York, 1963. Eckenfelder and O'Connor, *Biological Waste Treatment*, Pergamon, New York, 1961. McCabe and Ecken-felder, *Biological Treatment of Sewage and Industrial Wastes*, vol. 1, Reinhold, New York, 1955. Proceedings of Industrial Waste Treatment Conference, Pur-due University, annually. Zlokarnik, *Adv. Biochem. Eng.*, **11**, 158-180 (1979). *Cellular elastomers*: Fling, *Natural Rubber Latex and Its Applications: The Preparation of Latex Foam Products*, British Rubber Development Board, London, 1954. Gould, in *Symposium on Application of Synthetic Rubbers*, American Society for Testing and Materials, Philadelphia, 1944, pp. 90-103. *Firefighting foams*: Perri, in Bikerman, op. cit., Chap. 12. Ratzler, *Ind. Eng. Chem.*, **48**, 2013 (1956). *Froth-flotation methods and equipment*: Booth, in Bikerman, op. cit., Chap. 13. Gaudin, *Flotation*, McGraw-Hill, New York, 1957. Taggart, *Handbook of Mineral Dressing*, Wiley, New York, 1945, Sec. 12, pp. 52-81. Tatterson, *Fluid Mixing and Gas Dispersion in Agitated Tanks*, McGraw-Hill, New York, 1991.

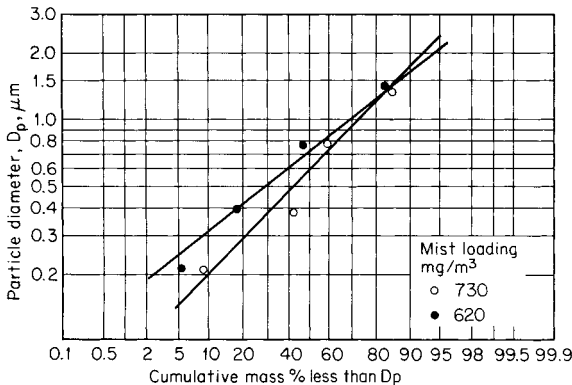


FIG. 14-91 Particle-size distribution and mist loading from absorption tower in a contact H₂SO₄ plant. [Gillespie and Johnstone, *Chem. Eng. Prog.*, **51**(2), 74 (1955).]

Objectives of Gas Dispersion The dispersion of gas as bubbles in a liquid or in a plastic mass is effected for one of the following purposes: (1) gas-liquid contacting (to promote absorption or stripping, with or without chemical reaction), (2) agitation of the liquid phase, or

(3) foam or froth production. Gas-in-liquid dispersions also may be produced or encountered inadvertently, sometimes undesirably.

Gas-Liquid Contacting Usually this is accomplished with conventional columns or with spray absorbers (see preceding subsection "Liquid-in-Gas Dispersions"). For systems containing solids or tar likely to plug columns, absorptions accomplished by strongly exothermic reactions, or treatments involving a readily soluble gas or a condensable vapor, however, bubble columns or agitated vessels may be used to advantage.

Agitation Agitation by a stream of gas bubbles (often air) rising through a liquid is often employed when the extra expense of mechanical agitation is not justified. Gas spargers may be used for simple blending operations involving a liquid of low volatility or for applications where agitator shaft sealing is difficult.

Foam Production This is important in froth-flotation separations; in the manufacture of cellular elastomers, plastics, and glass; and in certain special applications (e.g., food products, fire extinguishers). Unwanted foam can occur in process columns, in agitated vessels, and in reactors in which a gaseous product is formed; it must be avoided, destroyed, or controlled. Berkman and Egloff (*Emulsions and Foams*, Reinhold, New York, 1941, pp. 112–152) have mentioned that foam is produced only in systems possessing the proper combination of interfacial tension, viscosity, volatility, and concentration of solute or suspended solids. From the standpoint of gas comminution, foam production requires the creation of small bubbles in a liquid capable of sustaining foam.

Theory of Bubble and Foam Formation A bubble is a globule of gas or vapor surrounded by a mass or thin film of liquid. By extension, globular voids in a solid are sometimes called bubbles. Foam is a group of bubbles separated from one another by thin films, the aggregation having a finite static life. Although nontechnical dictionaries do not distinguish between foam and froth, a technical distinction is often made. A highly concentrated dispersion of bubbles in a liquid is considered a froth even if its static life is substantially nil (i.e., it must be dynamically maintained). Thus, all foams are also froths, whereas the reverse is not true. The term *lather* implies a froth that is worked up on a solid surface by mechanical agitation; it is seldom used in technical discussions. The thin walls of bubbles comprising a foam are called *laminae* or *lamellae*.

Bubbles in a liquid originate from one of three general sources: (1) They may be formed by desupersaturation of a solution of the gas or by the decomposition of a component in the liquid; (2) They may be introduced directly into the liquid by a bubbler or sparger or by mechanical entrainment; and (3) They may result from the disintegration of larger bubbles already in the liquid.

Generation Spontaneous generation of gas bubbles within a homogeneous liquid is theoretically impossible (Bikerman, *Foams: Theory and Industrial Applications*, Reinhold, New York, 1953, p. 10). The appearance of a bubble requires a gas nucleus as a void in the liquid. The nucleus may be in the form of a small bubble or of a solid carrying adsorbed gas, examples of the latter being dust particles, boiling chips, and a solid wall. A void can result from cavitation, mechanically or acoustically induced. Basu, Warriar, and Dhir [*J. Heat Transfer*, **124**, 717 (2002)] have reviewed boiling nucleation, and Blander and Katz [*AIChE J.*, **21**, 833 (1975)] have thoroughly reviewed bubble nucleation in liquids.

Theory permits the approximation of the maximum size of a bubble that can adhere to a submerged horizontal surface if the contact angle between bubble and solid (angle formed by solid-liquid and liquid-gas interfaces) is known [Wark, *J. Phys. Chem.*, **37**, 623 (1933); Jakob, *Mech. Eng.*, **58**, 643 (1936)]. Because the bubbles that actually rise from a surface are always considerably smaller than those so calculated and inasmuch as the contact angle is seldom known, the theory is not directly useful.

Formation at a Single Orifice The formation of bubbles at an orifice or capillary immersed in a liquid has been the subject of much study, both experimental and theoretical. Kulkarni and Joshi [*Ind. Eng. Chem. Res.*, **44**, 5873 (2005)] have reviewed bubble formation and rise. Bikerman (op. cit., Secs. 3 to 7), Valentin (op. cit., Chap. 2), Jackson (op. cit.), Soo (op. cit., Chap. 3), Fair (op. cit.), Kumer et al. (op. cit.), Cliff et al. (op. cit.) and Wilkinson and Van Dierendonck

[*Chem. Eng. Sci.*, **49**, 1429 (1994)] have presented reviews and analyses of this subject.

There are three regimes of bubble production (Silberman in *Proceedings of the Fifth Midwestern Conference on Fluid Mechanics*, Univ. of Michigan Press, Ann Arbor, 1957, pp. 263–284): (1) single-bubble, (2) intermediate, and (3) jet.

Single-Bubble Regime Bubbles are produced one at a time, their size being determined primarily by the orifice diameter d_o , the interfacial tension of the gas-liquid film σ , the densities of the liquid ρ_L and gas ρ_G , and the gravitational acceleration g according to the relation

$$d_b/d_o = [6\sigma/gd_o^2(\rho_L - \rho_G)]^{1/3} \quad (14-206)$$

where d_b is the bubble diameter.

$$f = Q/(\pi d_b^3/6) = Qg(\rho_L - \rho_G)/(\pi d_o \sigma) \quad (14-207)$$

where f is the frequency of bubble formation and Q is the volumetric rate of gas flow in consistent units.

Equations (14-206) and (14-207) result from a balance of bubble buoyancy against interfacial tension. They include no inertia or viscosity effects. At low bubbling rates ($<1/s$), these equations are quite satisfactory. Van Krevelen and Hoftijzer [*Chem. Eng. Prog.*, **46**, 29 (1950)], Guyer and Peterhaus [*Helv. Chim. Acta*, **26**, 1099 (1943)] and Wilkinson (op. cit.) report good agreement with Eq. (14-206) for water, transformer oil, ether, and carbon tetrachloride for vertically oriented orifices with $0.004 < D < 0.95$ cm. If the orifice diameter becomes too large, the bubble diameter will be smaller than the orifice diameter, as predicted by Eq. (14-206), and instability results; consequently, stable, stationary bubbles cannot be produced. Kulkarni et al. (op. cit.) have discussed much more detailed models for predicting bubble size; however, the models are very difficult and tedious to use in practice. These more sophisticated models need to be considered if the added accuracy warrants the extra effort.

For bubbles formed in water, the orifice diameter that permits bubbles of about its own size is calculated as 0.66 cm. Davidson and Amick [*AIChE J.*, **2**, 337 (1956)] confirmed this estimate in their observation that stable bubbles in water were formed at a 0.64-cm orifice but could not be formed at a 0.79-cm orifice.

For very thin liquids, Eqs. (14-206) and (14-207) are expected to be valid up to a gas-flow Reynolds number of 200 (Valentin, op. cit., p. 8). For liquid viscosities up to 100 cP, Datta, Napier, and Newitt [*Trans. Inst. Chem. Eng.*, **28**, 14 (1950)] and Siems and Kauffman [*Chem. Eng. Sci.*, **5**, 127 (1956)] have shown that liquid viscosity has very little effect on the bubble volume, but Davidson and Schuler [*Trans. Inst. Chem. Eng.*, **38**, 144 (1960)] and Krishnamurthi et al. [*Ind. Eng. Chem. Fundam.*, **7**, 549 (1968)] have shown that bubble size increases considerably over that predicted by Eq. (14-206) for liquid viscosities above 1000 cP. In fact, Davidson et al. (op. cit.) found that their data agreed very well with a theoretical equation obtained by equating the buoyant force to drag based on Stokes' law and the velocity of the bubble equator at break-off:

$$d_b = \left(\frac{6}{\pi}\right) \left(\frac{4\pi}{3}\right)^{1/4} \left(15 \times \frac{vQ}{2g}\right)^{3/4} \quad (14-208)$$

where v is the liquid kinematic viscosity and Q is the gas volumetric flow rate. This equation is dimensionally consistent. The relative effect of liquid viscosity can be obtained by comparing the bubble diameters calculated from Eqs. (14-206) and (14-208). If liquid viscosity appears significant, one might want to use the long and tedious method developed by Krishnamurthi et al. (op. cit.) and the review by Kulkarni et al. (op. cit.) that considers both surface-tension forces and viscous-drag forces.

Intermediate Regime This regime extends approximately from a Reynolds number of 200 to one of 2100. As the gas flow through a

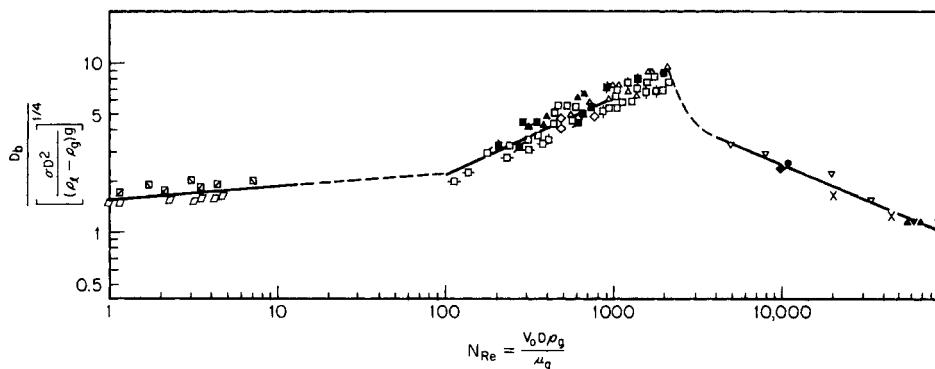


FIG. 14-92 Bubble-diameter correlation for air sparged into relatively inviscid liquids. D_b = bubble diameter, D = orifice diameter, V_o = gas velocity through sparging orifice, P = fluid density, and μ = fluid viscosity. [From *Can. J. Chem. Eng.*, **54**, 503 (1976).]

submerged orifice increases beyond the limit of the single-bubble regime, the frequency of bubble formation increases more slowly, and the bubbles begin to grow in size. Between the two regimes there may indeed be a range of gas rates over which the bubble sizes decrease with increasing rate, owing to the establishment of liquid currents that nip the bubbles off prematurely. The net result can be the occurrence of a minimum bubble diameter at some particular gas rate [Mater, *U.S. Bur. Mines Bull.* 260 (1927) and Bikerman, *op. cit.*, p. 4]. At the upper portion of this region, the frequency becomes very nearly constant with respect to gas rate, and the bubble size correspondingly increases with gas rate. The bubble size is affected primarily by (1) orifice diameter, (2) liquid-inertia effects, (3) liquid viscosity, (4) liquid density, and (5) the relationship between the constancy of gas flow and the constancy of pressure at the orifice.

Kumar et al. have done extensive experimental and theoretical work reported in *Ind. Eng. Chem. Fundam.*, **7**, 549 (1968); *Chem. Eng. Sci.*, **24**, part 1, 731; part 2, 749; part 3, 1711 (1969) and summarized in *Adv. Chem. Eng.*, **8**, 255 (1970). They, along with other investigators—Swope [*Can. J. Chem. Eng.*, **44**, 169 (1972)], Tsuge and Hibino [*J. Chem. Eng. Japan*, **11**, 307 (1972)], Pinczewski [*Chem. Eng. Sci.*, **36**, 405 (1981)], Tsuge and Hibino [*Int. Chem. Eng.*, **21**, 66 (1981)], and Takahashi and Miyahara [*ibid.*, p. 224]—have solved the equations resulting from a force balance on the forming bubble, taking into account buoyancy, surface tension, inertia, and viscous-drag forces for both conditions of constant flow through the orifice and constant pressure in the gas chamber. The design method is complex and tedious and involves the solution of algebraic and differential equations. Although Mersmann [*Ger. Chem. Eng.*, **1**, 1 (1978)] claims that the results of Kumar et al. (*loc. cit.*) well fit experimental data, Lanauze and Harn [*Chem. Eng. Sci.*, **29**, 1663 (1974)] claim differently:

Further, it has been shown that the mathematical formulation of Kumar's model, including the condition of detachment, could not adequately describe the experimental situation—Kumar's model has several fundamental weaknesses, the computational simplicity being achieved at the expense of physical reality.

In lieu of careful independent checks of predictive accuracy, the results of the comprehensive theoretical work will not be presented here. Simpler, more easily understood predictive methods, for certain important limiting cases, will be presented. As a check on the accuracy of these simpler methods, it will perhaps be prudent to calculate the bubble diameter from the graphical representation by Mersmann (*loc. cit.*) of the results of Kumar et al. (*loc. cit.*) and the review by Kulkarni et al. (*op. cit.*)

For conditions approaching constant flow through the orifice, a relationship derived by equating the buoyant force to the inertia force of the liquid [Davidson et al., *Trans. Instn. Chem. Engrs.*, **38**, 335 (1960)] (dimensionally consistent),

$$d_b = 1.378 \times \frac{6Q^{6/5}}{\pi g^{3/5}} \quad (14-209)$$

fits experimental data reasonably well. Surface tension and liquid viscosity tend to increase the bubble size—at a low Reynolds number. The effect of surface tension is greater for large orifice diameters. The magnitude of the diameter increase due to high liquid viscosity can be obtained from Eq. (14-208).

For conditions approaching constant pressure at the orifice entrance, which probably simulates most industrial applications, there is no independently verified predictive method. For air at near atmospheric pressure sparged into relatively inviscid liquids (11 ~ 100 cP), the correlation of Kumar et al. [*Can. J. Chem. Eng.*, **54**, 503 (1976)] fits experimental data well. Their correlation is presented here as Fig. 14-92.

Wilkinson et al. (*op. cit.*) make the following observation about the effect of gas density on bubble size: "The fact that the bubble size decreases slightly for higher gas densities can be explained on the basis of a force balance."

Jet Regime With further rate increases, turbulence occurs at the orifice, and the gas stream approaches the appearance of a continuous jet that breaks up 7.6 to 10.2 cm above the orifice. Actually, the stream consists of large, closely spaced, irregular bubbles with a rapid swirling motion. These bubbles disintegrate into a cloud of smaller ones of random size distribution between 0.025 cm or smaller and about 1.25 cm, with a mean size for air and water of about 0.4 cm (Leibson et al., *loc. cit.*). According to Wilkinson et al. (*op. cit.*), jetting begins when

$$N_{w,g} = \frac{\rho_g d_o U_o^2}{\sigma} \leq 2 \quad (14-210)$$

There are many contradictory reports about the jet regime, and theory, although helpful (see, for example, Siberman, *loc. cit.*), is as yet unable to describe the phenomena observed. The correlation of Kumar et al. (Fig. 14-92) is recommended for air-liquid systems.

Formation at Multiple Orifices At high velocities, coalescence of bubbles formed at individual orifices occurs; Helsby and Tuson [*Research (London)*, **8**, 270 (1955)], for example, observed the frequent coalescence of bubbles formed in pairs or in quartets at an orifice. Multiple orifices spaced by the order of magnitude of the orifice diameter increase the probability of coalescence, and when the magnitude is small (as in a sintered plate), there is invariably some. The broken lines of Fig. 14-92 presumably represent zones of increased coalescence and relatively less effective dispersion as the gas rate through porous-carbon tubes is increased. Savitskaya [*Kolloidn. Zh.*, **13**, 309 (1951)] found that the average bubble size formed at the

surface of a porous plate was such as to maintain constancy of the product of bubble specific surface and interfacial tension as the latter was varied by addition of a surfactant. König et al. [*Ger. Chem. Eng.*, **1**, 199 (1978)] produced bubble sizes varying from 0.5 to 4 mm by the use of two porous-plate spargers and one perforated-plate sparger with superficial gas velocities from 1 to 8 cm/s. The small bubble sizes were stabilized by adding up to 0.5 percent of various alcohols to water.

At high-flow rates through perforated plates such as those that occur in distillation columns, Calderbank and Rennie [*Trans. Instn. Chem. Engrs.*, **40**, T3 (1962)]; Porter et al. [*ibid.*, **45**, T265 (1967)]; Rennie and Evans [*Br. Chem. Eng.*, **7**, 498 (1962)]; and Valentin (op. cit., Chap. 3) have investigated and discussed the effect of the flow conditions through the multiple orifices on the froths and foams that occur above perforated plates.

Entrainment and Mechanical Disintegration Gas can be entrained into a liquid by a solid or a stream of liquid falling from the gas phase into the liquid, by surface ripples or waves, and by the vertical swirl of a mass of agitated liquid about the axis of a rotating agitator. Small bubbles probably form near the surface of the liquid and are caught into the path of turbulent eddies, whose velocity exceeds the terminal velocity of the bubbles. The disintegration of a submerged mass of gas takes place by the turbulent tearing of smaller bubbles away from the exterior of the larger mass or by the influence of surface tension on the mass when it is attenuated by inertial or shear forces into a cylindrical or disk form. A fluid cylinder that is greater in length than in circumference is unstable and tends to break spontaneously into two or more spheres. These effects account for the action of fluid attrition and of an agitator in the disintegration of suspended gas. Quantitative correlations for gas entrainment by liquid jets and in agitated vessels will be given later.

Foams Two excellent reviews (Shedlovsky, op. cit.; Lemlich, op. cit.; Herzhaft, op. cit.; and Heller et al., op. cit.) covering the literature pertinent to foams have been published. A foam is formed when bubbles rise to the surface of a liquid and persist for a while without coalescence with one another or without rupture into the vapor space. The formation of foam, then, consists simply of the formation, rise, and aggregation of bubbles in a liquid in which foam can exist. The life of foams varies over many magnitudes—from seconds to years—but in general is finite. Maintenance of a foam, therefore, is a dynamic phenomenon.

Gravitational force favors the separation of gas from liquid in a dispersion system, causing the bubbles to rise to the liquid surface and the liquid contained in the bubble walls to drain downward to the main body of the liquid. Interfacial tension favors the coalescence and ultimate disappearance of bubbles; indeed, it is the cause of bubble destruction upon the rupture of the laminae.

The viscosity of the liquid in a film opposes the drainage of the film and its displacement by the approach of coalescing bubbles. The higher the viscosity, the slower will be the film-thinning process; furthermore, if viscosity increases as the film grows thinner, the process becomes self-retarding. The viscosity of films appears to be greater than that of the main body of the parent liquid in many cases. Sometimes this is a simple temperature effect, the film being cooler because of evaporation; sometimes it is a concentration effect, with dissolved or fine suspended solids migrating to the interface and producing classical or anomalous increases in viscosity; at yet other times, the effect seems to occur without explanation.

If the liquid laminae of a foam system can be converted to impermeable solid membranes, the film viscosity can be regarded as having become infinite, and the resulting solid foam will be permanent. Likewise, if the laminae are composed of a gingham plastic or a thixotrope, the foam will be permanently stable for bubbles whose buoyancy does not permit exceeding the yield stress. For other non-newtonian fluids, however, and for all newtonian ones, no matter how viscous, the viscosity can only delay but never prevent foam disappearance. The popular theory, held since the days of Plateau, that foam life is proportional to surface viscosity and inversely proportional to interfacial tension, is not correct, according to Bikerman (op. cit., p. 161), who points out that it is contradicted by experiment.

The idea that foam films drain to a critical thickness at which they spontaneously burst is also rejected by Bikerman. Foam stability, rather, is keyed to the existence of a surface skin of low interfacial tension immediately overlying a solution bulk of higher tension, latent until it is exposed by rupture of the superficial layer [Maragoni, *Nuovo Cimento*, **2** (5-6), 239 (1871)]. Such a phenomenon of surface elasticity, resulting from concentration differences between bulk and surface of the liquid, accounts for the ability of bubbles to be penetrated by missiles without damage. It is conceivable that films below a certain thickness no longer carry any bulk of solution and hence have no capacity to close surface ruptures, thus becoming vulnerable to mechanical damage that will destroy them. The Maragoni phenomenon is consistent also with the observation that neither pure liquids nor saturated solutions will sustain a foam, since neither extreme will allow the necessary differences in concentration between surface and bulk of solution.

The specific ability of certain finely divided, insoluble solids to stabilize foam has long been known [Berkman and Egloff, op. cit., p. 133; and Bikerman, op. cit., Chap. 11]. Bartsch [*Kolloidchem. Beih.*, **20**, 1 (1925)] found that the presence of fine galena greatly extended the life of air foam in aqueous isoamyl alcohol, and the finer the solids, the greater the stability. Particles on the order of 50 μ m length extended the life from 17 seconds to several hours. This behavior is consistent with theory, which indicates that a solid particle of medium contact angle with the liquid will prevent the coalescence of two bubbles with which it is in simultaneous contact. Quantitative observations of this phenomenon are scanty.

Berkman and Egloff explain that some additives increase the flexibility or toughness of bubble walls, rather than their viscosity, to render them more durable. They cite as illustrations the addition of small quantities of soap to saponin solutions or of glycerin to soap solution to yield much more stable foam. The increased stability with ionic additives is probably due to electrostatic repulsion between charged, nearly parallel surfaces of the liquid film, which acts to retard draining and hence rupture.

Characteristics of Dispersion

Properties of Component Phases As discussed in the preceding subsection, dispersions of gases in liquids are affected by the viscosity of the liquid, the density of the liquid and of the gas, and the interfacial tension between the two phases. They also may be affected directly by the composition of the liquid phase. Both the formation of bubbles and their behavior during their lifetime are influenced by these quantities as well as by the mechanical aspects of their environment.

Viscosity and density of the component phases can be measured with confidence by conventional methods, as can the interfacial tension between a pure liquid and a gas. The interfacial tension of a system involving a solution or micellar dispersion becomes less satisfactory, because the interfacial free energy depends on the concentration of solute at the interface. Dynamic methods and even some of the so-called static methods involve the creation of new surfaces. Since the establishment of equilibrium between this surface and the solute in the body of the solution requires a finite amount of time, the value measured will be in error if the measurement is made more rapidly than the solute can diffuse to the fresh surface. Eckenfelder and Barnhart (*Am. Inst. Chem. Engrs.*, 42d national meeting, Repr. 30, Atlanta, 1960) found that measurements of the surface tension of sodium lauryl sulfate solutions by maximum bubble pressure were higher than those by DuNuoy tensiometer by 40 to 90 percent, the larger factor corresponding to a concentration of about 100 ppm, and the smaller to a concentration of 2500 ppm of sulfate.

Even if the interfacial tension is measured accurately, there may be doubt about its applicability to the surface of bubbles being rapidly formed in a solution of a surface-active agent, for the bubble surface may not have time to become equilibrated with the solution. Coppock and Meiklejohn [*Trans. Instn. Chem. Engrs.*, **29**, 75 (1951)] reported that bubbles formed in the single-bubble regime at an orifice in a solution of a commercial detergent had a diameter larger than that calculated in terms of the measured surface tension of the solution [Eq. (14-206)]. The disparity is probably a reflection of unequilibrated bubble laminae.

One concerned with the measurement of gas-liquid interfacial tension should consult the useful reviews of methods prepared by Harkins [in Chap. 9 of Weissberger, *Techniques of Organic Chemistry*, 2d ed., vol. 1, part 2, Interscience, New York, 1949], Schwartz and coauthors [*Surface Active Agents*, vol. 1, Interscience, New York, 1949, pp. 263-271; *Surface Active Agents and Detergents*, vol. 2, Interscience, New York, 1958, pp. 389-391, 417-418], and by Adamson [*Physical Chemistry of Surfaces*, Interscience, New York, 1960].

Dispersion Characteristics The chief characteristics of gas-liquid dispersions, like those of liquid-in-gas suspensions, are heterogeneity and instability. The composition and structure of an unstable dispersion must be observed in the dynamic situation by looking at the mixture, with or without the aid of optical devices, or by photographing it, preferably in nominal steady state; photographs usually are required for quantitative treatment. Stable foams may be examined after the fact of their creation if they are sufficiently robust or if an immobilizing technique such as freezing is employed [Chang et al., *Ind. Eng. Chem.*, **48**, 2035 (1956)].

The rate of rise of bubbles has been discussed by Kulkarni, op. cit.; Benfratello, *Energ. Elettr.*, **30**, 80 (1953); Haberman and Morton, *Report 802: David W. Taylor Model Basin*, Washington, September 1953; Jackson, loc. cit.; Valentin, op. cit., Chap. 2; Soo, op. cit., Chap. 3; Calderbank, loc. cit., p. CE220; and Levich, op. cit., Chap. 8). A comprehensive and apparently accurate predictive method has been published [Jamialahmadi et al., *Trans. ICE*, **72**, part A, 119-122 (1994)]. Small bubbles (below 0.2 mm in diameter) are essentially rigid spheres and rise at terminal velocities that place them clearly in the laminar-flow region; hence their rising velocity may be calculated from Stokes' law. As bubble size increases to about 2 mm, the spherical shape is retained, and the Reynolds number is still sufficiently small (<10) that Stokes' law should be nearly obeyed.

As bubble size increases, two effects set in, however, that alter the velocity. At about $N_{Re} = 100$, a wobble begins that can develop into a helical path if the bubbles are not liberated too closely to one another [Houghton, McLean, and Ritchie, *Chem. Eng. Sci.*, **7**, 40 (1957); and Houghton et al., *ibid.*, p. 111]. Furthermore, for bubbles in the range of 1 mm and larger (until distortion becomes serious) internal circulation can set in [Garner and Hammerton, *Chem. Eng. Sci.*, **3**, (1954); and Haberman and Morton, loc. cit.], and according to theoretical analyses by Hadamard and Rybczynski and given by Levich (op. cit.), the drag coefficient for a low-viscosity dispersed phase and a high-viscosity continuous phase will approach two-thirds of the drag coefficient for rigid spheres, namely $C_D = 16/N_{Re}$. The rise velocity of a circulating bubble or drop will thus be 1.5 times that of a rigid sphere. Redfield and Houghton [*Chem. Eng. Sci.*, **20**, 131 (1965)] have found that CO_2 bubbles rising in pure water agree with the theoretical solution for a circulating drop below $N_{Re} = 1$. Many investigators (see Valentin, op. cit.) have found that extremely small quantities of impurities can retard or stop this internal circulation. In this behavior may lie the explanation of the fact that the addition of long-chain fatty acids to water to produce a concentration of 1.5×10^{-4} molar markedly reduces the rate of rise of bubbles [Stuke, *Naturwissenschaften*, **39**, 325 (1952)].

Above diameters of about 2 mm, bubbles begin to change to ellipsoids, and above 1 cm they become lens-shaped, according to Davies and Taylor [*Proc. Roy. Soc. (London)*, **A200**, 379 (1950)]. The rising velocity in thin liquids for the size range $1 \text{ mm} < D_B < 20 \text{ mm}$ has been reported as 20 to 30 cm/s by Haberman and Morton (op. cit.) and Davenport, Richardson, and Bradshaw [*Chem. Eng. Sci.*, **22**, 1221 (1967)]. Schwerdtfeger [*ibid.*, **23**, 937 (1968)] even found the same for argon bubbles rising in mercury. Surface-active agents have no effect on the rise velocity of bubbles larger than 4 mm in thin liquids (Davenport et al., loc. cit.).

Above a Reynolds number of the order of magnitude of 1000, bubbles assume a helmet shape, with a flat bottom (Eckenfelder and Barnhart, loc. cit.; and Leibson et al., loc. cit.). After bubbles become large enough to depart from Stokes' law at their terminal velocity, behavior is generally complicated and erratic, and the reported data scatter considerably. The rise can be slowed, furthermore, by a wall effect if the diameter of the container is not greater than 10 times the diameter of the bubbles, as shown by Uno and Kintner [*AIChE J.*, **2**, 420 (1956); and Collins, *J. Fluid Mech.*, **28**(1), 97 (1967)]. Work has

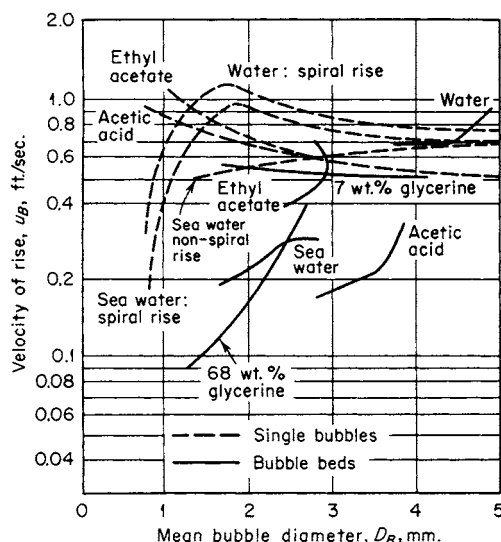


FIG. 14-93 Velocity of rising bubbles, singly and in clouds. To convert feet per second to meters per second, multiply by 0.305. [From *Chem. Eng. Sci.*, **7**, 48 (1957).]

been done to predict the rise velocity of large bubbles [Rippin and Davidson, *Chem. Eng. Sci.*, **22**, 217 (1967); Grace and Harrison, *ibid.*, 1337; Mendelson, *AIChE J.*, **13**, 250 (1967); Cole, *ibid.*; Lehrer, *J. Chem. Eng. Japan*, **9**, 237 (1976); and Lehrer, *AIChE J.*, **26**, 170 (1980)]. The works of Lehrer present correlations that accurately predict rise velocities for a wide range of system properties. Reviews of the technical literature concerning the rise of single bubbles and drops have been published by Kulkarni et al. (op. cit.) and Cliff, Grace, and Weber (*Bubbles, Drops and Particles*, Academic, New York, 1978). Mendelson has used a wave theory to predict the terminal velocity, and Cole has checked the theory with additional data. The other authors listed solved some simplified form of the Navier-Stokes equations. Jamialahmadi et al., loc. cit., have developed a single equation predictive method for bubble rise velocity, which covers the entire range of bubble diameters.

When bubbles are produced in clouds, as by a porous disperser, their behavior during rising is further complicated by interaction among themselves. In addition to the tendency for small bubbles to coalesce and large ones to disintegrate, there are two additional opposing influences on the rate of rise of bubbles of any particular size: (1) A "chimney effect" can develop in which a massive current upward appears at the axis of the bubble stream, leading to increased net bubble velocity; and (2) the proximity of the bubbles to one another can result in a hindered-settling condition, leading to reduced average bubble velocity. Figure 14-93 shows the data of Houghton et al. (op. cit.) for clouds of bubbles compared with their single-bubble data for pure water and seawater and of Peebles and Garber [*Chem. Eng. Progr.*, **49**, 88 (1953)] for acetic acid and ethyl acetate. The bubble clouds were produced with a sintered-glass plate of mean pore size (inferred from air wet-permeability data) of 81 μm .

The difference between the curves for pure water and seawater again illustrates the significance of small concentrations of solute with respect to bubble behavior. In commercial bubble columns and agitated vessels coalescence and breakup are so rapid and violent that the rise velocity of a single bubble is meaningless. The average rise velocity can, however, be readily calculated from holdup correlations that will be given later.

The quantitative examination of bubble systems is aided by the use of proper illumination and photography. The formation of bubbles at single sources often is sufficiently periodic to be stopped by stroboscopic light. Clouds of rising bubbles are more difficult to assess and

require careful technique. Satisfactory photographic methods have been developed by Vermeulen, Williams, and Langlois [*Chem. Eng. Progr.*, **51**, 85 (1955)] and by Calderbank [*Trans. Instn. Chem. Engrs.*, **36**, 443 (1958)] and are described by these authors. Calderbank's technique resulted in particularly precise measurements that permitted a good estimation of the surface area of the dispersed bubbles.

Methods of Gas Dispersion The problem of dispersing a gas in a liquid may be attacked in several ways: (1) The gas bubbles of the desired size or which grow to the desired size may be introduced directly into the liquid; (2) a volatile liquid may be vaporized by either decreasing the system pressure or increasing its temperature; (3) a chemical reaction may produce a gas; or (4) a massive bubble or stream of gas is disintegrated by fluid shear and/or turbulence in the liquid.

Spargers: Simple Bubblers The simplest method of dispersing gas in a liquid contained in a tank is to introduce the gas through an open-end standpipe, a horizontal perforated pipe, or a perforated plate at the bottom of the tank. At ordinary gassing rates (corresponding to the jet regime), relatively large bubbles will be produced regardless of the size of the orifices.

Perforated-pipe or -plate spargers usually have orifices 3 to 12 mm in diameter. Effective design methods to minimize maldistribution are presented in the fifth edition of this handbook, p. 5-47, 1973, and by Knaebel [*Chem. Eng.*, 116 (Mar. 9, 1981)]. For turbulent flow conditions into the sparger, the following relationship will allow design of a perforated-pipe sparger for a given degree of maldistribution provided $N_h > 5$ and length/diameter < 300 .

$$d_p = 0.95(N_h C_v)^{1/2} \times \left(\frac{d_h}{\Delta U_h / U_h} \right)^{1/4} \quad (14-211)$$

where d_p = pipe diameter, d_h = sparging hole diameter, N_h = number of holes in sparger, C_v = orifice coefficient for sparger hole (see *Chemical Engineers' Handbook*, 5th ed., pp. 5-13, 5-34), U_h = average velocity through sparger holes, ΔU_h = difference between maximum and minimum velocities through sparger holes, and $\Delta U_h / U_h$ = fractional maldistribution of flow through sparger holes.

Simple spargers are used as agitators for large tanks, principally in the cement and oil industries. Kauffman [*Chem. Metall. Eng.*, **37**, 178-180 (1930)] reported the following air rates for various degrees of agitation in a tank containing 2.7 m (9 ft) of liquid:

Degree of agitation	Air rate, m ³ /(m ² tank cross section, min)
Moderate	0.0033
Complete	0.0066
Violent	0.016

For a liquid depth of 0.9 m (3 ft), Kauffman recommended that the listed rates be doubled.

An air lift consisting of a sparger jetting into a draft tube with ports discharging at several heights has been recommended by Heiser [*Chem. Eng.*, **55**(1), 135 (1948)] for maintaining agitation in a heavy, coarse slurry, the level of which varies widely. The design is illustrated in Fig. 14-94.

The ability of a sparger to blend miscible liquids might be described in terms of a fictitious diffusivity. Siemes did so, reporting that the agitation produced by a stream of bubbles rising in a tube with a superficial velocity of about 8.2 cm/s corresponded to an apparent diffusion coefficient as large as 75 cm²/s [*Chem. Ing. Tech.*, **29**, 727 (1957)]. The blending rate thus is several orders of magnitude higher than it would be by natural diffusive action. These results are typical of subsequent investigations on back mixing, which will be discussed in more detail later.

Lehrer [*Ind. Eng. Chem. Process Des. Dev.*, **7**, 226 (1968)] conducted liquid-blending tests with air sparging in a 0.61-m-diameter by 0.61-m-tall vessel and found that an air volume equal to about one-half of the vessel volume gave thorough blending of inviscid liquids of equal viscosities. Using an analogy to mechanically agitated vessels in which equal tank turnovers give equal blend times, one would expect this criterion to be applicable to other vessel sizes. Liquids of unequal density would require somewhat more air.

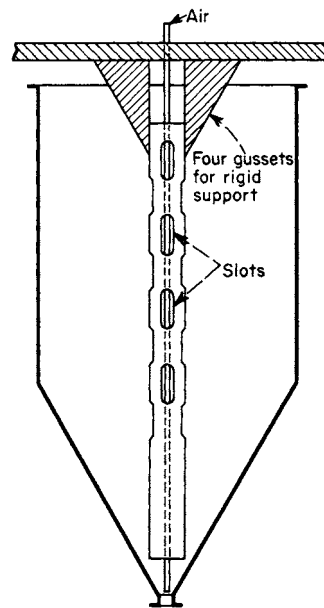


FIG. 14-94 Slotted air lift for agitation of a variable-level charge. [From *Chem. Eng.*, **55**(1), 135 (1948).]

Open-end pipes, perforated plates, and ring- or cross-style perforated-pipe spargers are used without mechanical agitation to promote mass transfer, as in chlorinators and biological sewage treatment. In the "quiescent regime" (superficial gas velocity less than 4.57 to 6.1 cm/s [0.15 to 0.2 ft/s]) the previously mentioned spargers are usually operated at orifice Reynolds numbers in excess of 6000 in order to get small bubbles so as to increase the interfacial area and thus increase mass transfer. In the "turbulent regime" (superficial gas velocity greater than 4.57 to 6.1 cm/s), sparger design is not critical because a balance between coalescence and breakup is established very quickly according to Towell et al. [*AIChE Symp. Ser. No. 10*, 97 (1965)]. However, a reasonably uniform orifice distribution over the column cross section is desirable, and according to Fair [*Chem. Eng.*, **74**, 67 (July 3, 1967); 207 (July 17, 1967)] the orifice velocity should be less than 75 to 90 m/s.

Porous Septa In the quiescent regime porous plates, tubes, disks, or other shapes that are made by bonding or sintering together carefully sized particles of carbon, ceramic, polymer, or metal are frequently used for gas dispersion, particularly in foam fractionators. The resulting septa may be used as spargers to produce much smaller bubbles than will result from a simple bubbler. Figure 14-95 shows a comparison of the bubbles emitted by a perforated-pipe sparger [0.16-cm orifices] and a porous carbon septum (120 μm pores). The gas flux through a porous septum is limited on the lower side by the requirement that, for good performance, the whole sparger surface should bubble more or less uniformly, and on the higher side by the onset of serious coalescence at the surface of the septum, resulting in poor dispersion. In the practical range of fluxes, the size of the bubbles produced depends on both the size of pores in the septum and the pressure drop imposed across it, being a direct function of both.

Table 14-23 lists typical grades of porous carbon, silica, alumina, stainless steel (type 316), and polymers commercially available.

Porous media are also manufactured from porcelain, glass, silicon carbide, and a number of metals: Monel, Inconel, nickel, bronze, Hastelloy C, Stellite L-605, gold, platinum, and many types of stainless steel. Two manufacturers of porous septa are Mott (mottcorp.com) and Pall (pall.com). The air permeabilities of Table 14-23 indicate the relative flow resistances of the various grades to homogeneous fluid but may not be used in designing a disperser for submerged

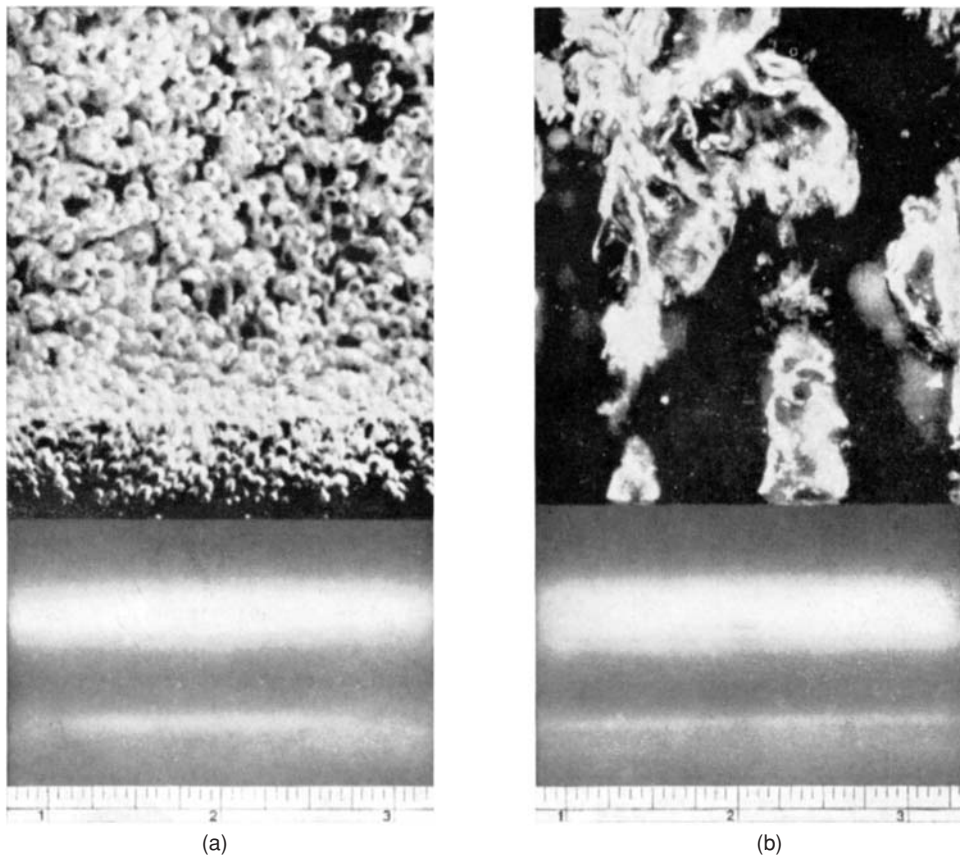


FIG. 14-95 Comparison of bubbles from a porous septum and from a perforated-pipe sparger. Air in water at 70°F. (a) Grade 25 porous-carbon diffuser operating under a pressure differential of 13.7 in. of water. (b) Karbate pipe perforated with 1/16-in. holes on 1-in. centers. To convert inches to centimeters, multiply by 2.54; °C = $\frac{5}{9}$ (°F - 32). (National Carbon Co.)

operation, for the resistance of a septum to the flow of gas increases when it is wet. The air permeabilities for water-submerged porous carbon of some of the grades listed in the table are shown in Fig. 14-96. The data were determined with septa 0.625 in thick in water at 70°F. Comparable wet-permeability data for 1-in Alundum plates of two grades of fineness are given in Table 14-24.

The gas rate at which coalescence begins to reduce the effectiveness of dispersion appears to depend not only on the pore size and pore structure of the dispersing medium but also on the liquid properties, liquid depth, agitation, and other features of the sparging environment; coalescence is strongly dependent on the concentration of surfactants capable of forming an electrical double layer and thus produce ionic bubbles, long-chain alcohols in water being excellent examples. For porous-carbon media, the manufacturer suggests that the best dispersion performance will result if the broken-line regions of Fig. 14-96 are avoided. For porous stainless-steel spargers, which extend to a lower pore size than carbon, Micro Metallic Division, Pall Corp., recommends (Release 120A, 1959) a working limit of 8 ft/min (0.044 m/s) to avoid serious coalescence. This agrees with the data reported by König et al. (loc. cit.), in which 0.08 m/s was used and bubbles as small as 1 mm were produced from a 5- μ m porous sparger.

Slabs of porous material are installed by grouting or welding together to form a diaphragm, usually horizontal. Tubes are prone to produce coalesced gas at rates high enough to cause bubbling from their lower faces, but they have the advantage of being demountable for cleaning or replacement (U.S. Patent 2,328,655). Roe [Sevage

Works J., 18, 878 (1945)] claimed that silicon carbide tubes are superior to horizontal plates, principally because of the wiping action of the liquid circulating past the tube. He reported respective maximum capacities of 2.5 and 1.5 cm³/s of gas/cm² of sparger for a horizontal tube and a horizontal plate of the same material (unspecified grade). Mounting a flat-plate porous sparger vertically instead of horizontally seriously reduces the effectiveness of the sparger for three reasons: (1) The gas is distributed over a reduced cross section; (2) at normal rates, the lower portion of the sparger may not operate because of difference in hydrostatic head; and (3) there is a marked tendency for bubbles to coalesce along the sparger surface. Bone (M.S. thesis in chemical engineering, University of Kansas, 1948) found that the oxygen sulfite solution coefficient for a 3.2- by 10-cm rectangular porous carbon sparger was 26 to 41 percent lower for vertical than for horizontal operation of the sparger, the greatest reduction occurring when the long dimension was vertical.

Precipitation and Generation Methods For a thorough understanding of the phenomena involved, bubble nucleation should be considered. A discussion of nucleation phenomena is beyond the scope of this handbook; however, a starting point with recent references is Deng, Lee, and Cheng, *J. Micromech. Microeng.*, 15, 564 (2005), and Jones, Evans, and Galvin, *Adv. Colloid and Interface Sci.* 80, 27 (1999).

Gas Dispersion—Vessel Headspace Boerma and Lankester have measured the surface aeration of a nine-bladed disk-type turbine (NOTE: A well-designed pitched-blade turbine will give equal or better performance). In a fully baffled vessel, the optimum depth to obtain maximum gas dispersion was 15 to 50 percent of the impeller diameter.

TABLE 14-23 Characteristics of Porous Septa

Grade	Avg. % porosity	Avg. pore diam.	Air-permeability data		
			Diaphragm thickness, in	Pressure differential, in water	Air flow, cu ft/(sq ft)(min)
Alundum porous alumina*					
P2220		25	1	2	0.35
P2120	36	60	1	2	2
P260	35	164	1	2	15
P236	34	240	1	2	40
P216		720	1	2	110
National porous carbon†					
60	48	33	1	2	
45	48	58	1	2	2
25	48	120	1	2	13
Filtros porous silica‡					
Extra fine	26.0	55	1.5	2	1-3
Fine	28.8	110	1.5	2	4-8
Medium fine	31.1	130	1.5	2	9-12
Medium	33.7	150	1.5	2	13-20
Medium coarse	33.8	200	1.5	2	21-30
Coarse	34.5	250	1.5	2	31-59
Extra coarse	36.5	300	1.5	2	60-100
Porous plastic§					
Teflon		9	0.125	1.38	5
Kel-F		15	0.125	1.38	13
Micro Metallic porous stainless steel¶					
H	45	5	0.125	1.38	1.8
G	50	10	0.125	1.38	3
F	50	20	0.125	1.38	5
E	50	35	0.125	1.38	18
D	50	65	0.125	1.38	60
C	55	165	0.125	27.7	990

*Data by courtesy of Norton Co., Worcester, Mass. A number of other grades between the extremes listed are available.
 †Data by courtesy of National Carbon Co., Cleveland, Ohio.
 ‡Data by courtesy of Filtros Inc., East Rochester, N.Y.
 §Data by courtesy of Pall Corp., Glen Cove, N.Y.
 ¶Similar septa made from other metals are available.

In a vessel with baffles extending only halfway to the liquid surface the optimum impeller submergence increased with agitator speed because of the vortex formed. At optimum depth, the following correlation is recommended for larger vessels:

$$Q = 0.00015(N/10)^{2.5}(D/0.1)^{4.5} \quad (14-214)$$

with Q in m^3/s , N in rps, and D in m. Thus, a typical 3-m-diameter plant-size vessel, with four-blade pitched impeller ($D = 1$ m) operating at 2 rps will give gas dispersion from the headspace into the batch of $Q = 0.00015(2/10)^{2.5}(2/0.1)^{4.5} = 1.9 m^3/s$ (4000 ft^3/min).

Borema et al. (op. cit.) recommend headspace gas dispersion with partial baffling for fatty oils hydrogenation in stirred reactors: "The hydrogen in the head-space of the closed reactor can again be brought into contact with the liquid by a stirrer under the liquid level. . . ." And Penney in Paul et al. (loc. cit.) says, "partial baffling can be very effective to produce a vortex, which can effectively drawdown gas from the headspace. . . ." However, Middleton et al. in Paul et al. (op. cit.) say, "The simplest self-inducer for an agitated vessel is an impeller located near the surface, sometimes with the upper part of the baffles removed so as to encourage the formation of a vortex. This is, however, a sensitive and unstable arrangement. It is better, although probably more expensive, to use a self-inducing impeller system in which gas is drawn down a hollow shaft to the low-pressure region behind the blades of a suitable, often shrouded impeller. . . . Various proprietary designs are available, such as the Ekato gasjet, Prasair AGR and the Frings Friborator. . . ." Figure 14-97 illustrates a gas-inducing hollow shaft/hollow impeller agitator. In many hydrogenation reactors, the impeller just

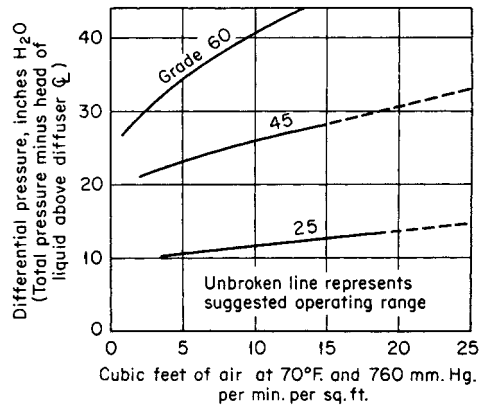


FIG. 14-96 Pressure drop across porous-carbon diffusers submerged in water at 70°F. To convert feet per minute to meters per second, multiply by 0.0051; to convert inches to millimeters, multiply by 25.4; °C = $\frac{5}{9}$ (°F - 32). (National Carbon Co.)

underneath the free surface has, without any doubt, performed admirably; consequently, one must consider this fact very carefully before using a self-inducing impeller.

Gas dispersion through the free surface by mechanical aerators is commonplace in aerobic waste-treatment lagoons. Surface aerators are generally of three types: (1) large-diameter flow-speed turbines operating just below the free surface of the liquid, often pontoon-mounted; (2) small-diameter high-speed (normally motor-speed) propellers operating in draft tubes, the units of which are always pontoon-mounted; and (3) hollow-tube turbines (Fig. 14-97). An example of the turbine type is illustrated in Fig. 14-98 and the propeller type is illustrated in Fig. 14-99. There are several other styles of the turbine type; for instance, Mixing Equipment Co., Inc., (www.light-nimixers.com), uses an unshrouded 45° axial-flow turbine [see Dykman and Michel, *Chem. Eng.*, **117** (Mar. 10, 1969)], and Infilco (www.infilcodegremon.com) makes a unit that has a large-diameter vaned disk operating just below the free surface with a smaller-diameter submerged-disk turbine for additional solids suspension.

Aeration injectors, like the one shown in Fig. 14-100 by Penberthy [a division of Houdaille Industries (penberthy-online.com/jet1.asp)], are used to provide mass transfer in gas-liquid applications, and simple impingement aerators (Fig. 14-101) are sometimes used for mass-transfer applications.

Equipment Selection Ideally, selection of equipment to produce a gas-in-liquid dispersion should be made on the basis of a complete economic analysis. The design engineer and especially the pilot-plant engineer seldom have sufficient information or time to do a complete economic analysis. In the following discussion, some

TABLE 14-24 Wet Permeability of Alundum Porous Plates 1 in Thick*

Dry permeability at 2 in of water differential, cu ft/(min)(sq ft)	Pressure differential across wet plate, in of water	Air flow through wet plate, cu ft/(min)(sq ft)
4.3	20.67	2.0
	21.77	3.0
	22.86	4.0
	23.90	5.0
55.0	4.02	1.0
	4.14	2.0
	4.22	3.0
	4.27	4.0
	4.30	5.0

*Data by courtesy of Norton Company, Worcester, Mass. To convert inches to centimeters, multiply by 2.54; to convert feet per minute to meters per second, multiply by 0.0051.

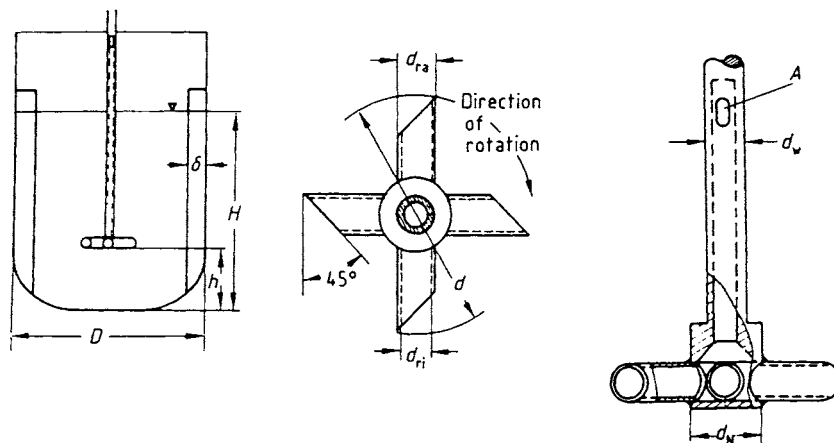


FIG. 14-97 Installation and dimensions of a tube stirrer: $h/d = 1$; $H/D = 1$; $D/\delta = 10$; $A = 1.5 d_w^2$, $D/d_N = 10$; $d/d_N = 3$; $d/d_m = 7.5$; $d/d_m = 6$. [Zlokarnik, Ullman's Encyclopedia of Industrial Chemistry, Sec. 25, VCH, Weinheim, Germany, 1988.]

guidelines are given as to what equipment might be feasible and what equipment might prove most economical.

For producing foam for foam-separation processes, perforated-plate or porous-plate spargers are normally used. Mechanical agitators are often not effective in the light foams needed in foam fractionation. Dissolved-air flotation, based on the release of a pressurized flow in which oxygen was dissolved, has been shown to be effective for particulate removal when sparged air failed because the bubbles formed upon precipitation are smaller—down to $80 \mu\text{m}$ —than bubbles possible with sparging, typically $1000 \mu\text{m}$ [Grieves and Ettelt, *AIChE J.*, **13**, 1167 (1967)]. Mechanically agitated surface aerators such as the Wemco-Fagergren flotation unit (Fig. 14-102) are used extensively for ore flotation.

To produce foam in batch processes, mechanical agitators are used almost exclusively. The gas can either be introduced through the free surface by the entraining action of the impeller or alternatively sparged beneath the impeller. In such batch operation, the liquid level gradually rises as the foam is generated; thus, squatly impellers such as turbines are rapidly covered with foam and must almost always be sparged from below. Tall impellers such as wire whips (Fig. 14-103) are especially well suited to entrain gas from the vapor space. Inter-meshing wire whips are standard kitchen utensils for producing foamed meringues, consisting of air, vegetable oil, and egg whites. For a new application, generally some experimentation with different impellers is necessary in order to get the desired fine final bubble size without getting frothing over initially. For producing foams continually, an aspirating venturi nozzle and restrictions in pipes such as baffles and metal gauzes are generally most economical.

For gas absorption, the equipment possibilities are generally packed columns; plate distillation towers, possibly with mechanical agitation on every plate; deep-bed contactors (bubble columns or sparged lagoons); and mechanically agitated vessels or lagoons. Packed towers and plate distillation columns are discussed elsewhere. Generally these

devices are used when a relatively large number of stages (more than two or three) is required to achieve the desired result practically.

The volumetric mass-transfer coefficients and heights of transfer units for bubble columns and packed towers have been compared for absorption of CO_2 into water by Houghton et al. [*Chem. Eng. Sci.*, **7**, 26 (1957)]. The bubble column will tolerate much higher vapor velocities, and in the overlapping region (superficial gas velocities of 0.9 to 1.8 cm/s), the bubble column has about three times higher mass-transfer coefficient and about 3 times greater height of transfer unit. The liquid in a bubble column is, for practical purposes, quite well mixed; thus, chemical reactions and component separations requiring significant plug flow of the liquid cannot be effected with bubble columns. Bubble columns and agitated vessels are the ideal equipment for processes in which the fraction of gas absorbed need not be great, possibly the gas can be recycled, and the liquid can or should be well mixed. The gas phase in bubble columns is not nearly so well back-mixed as the liquid, and often plug flow of the gas is a logical assumption, but in agitated vessels the gas phase is also well mixed.

The choice of a bubble column or an agitated vessel depends primarily on the solubility of the gas in the liquid, the corrosiveness of the liquid (often a gas compressor can be made of inexpensive material, whereas a mechanical agitator may have to be made of exotic, expensive materials), and the rate of chemical reaction as compared with the mass-transfer rate. Bubble columns and agitated vessels are seldom used for gas absorption except in chemical reactors. As a general rule, if the overall reaction rate is five times greater than the mass-transfer rate in a simple bubble column, a mechanical agitator will be most economical unless the mechanical agitator would have to be made from considerably more expensive material than the gas compressor.

In bubble columns and simply sparged lagoons, selecting the sparger is a very important consideration. In the turbulent regime (superficial gas velocity greater than 4.6 to 6 cm/s), inexpensive

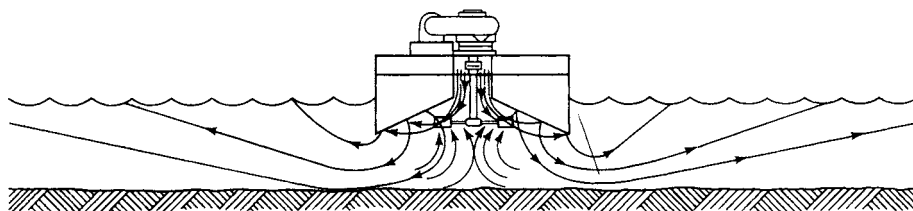


FIG. 14-98 The Cyclox surface aerator. (Cleveland Mixer Co.)

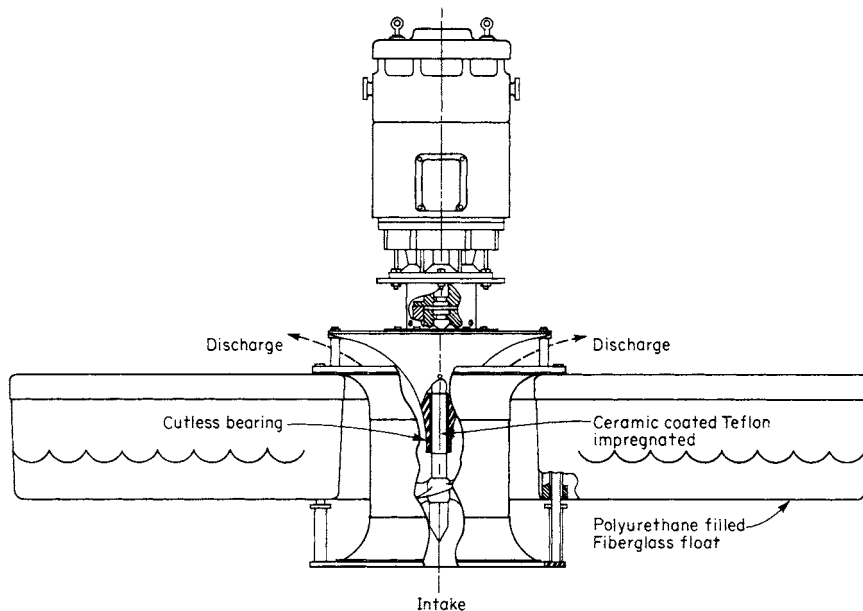


FIG. 14-99 Propeller-type surface aerator. (Ashbrook-Simon-Hartley Corp.)

perforated-pipe spargers should be used. Often the holes must be placed on the pipe bottom in order to make the sparger free-draining during operation. In the quiescent regime, porous septa will often give considerably higher overall mass-transfer coefficients than perforated plates or pipes because of the formation of tiny bubbles that do not coalesce. Chain and coworkers (*First International Symposium on Chemical Microbiology*, World Health Organization, Monograph Ser. 10, Geneva, 1952) claimed that porous disks are about twice as effective as open-pipe and ring spargers for the air oxidation of sodium sulfite. Eckenfelder [*Chem. Eng. Progr.*, **52**(7), 290 (1956)] has compared the oxygen-transfer capabilities of various devices on the basis of the operating power required to absorb a given quantity of O_2 . The installed cost of the various pieces of equipment probably would not vary sufficiently to warrant being included in an economic analysis. Surface mechanical aerators are not included in this comparison. Of the units compared, it appears that porous tubes give the most efficient power usage. Kalinske (*Adv. Biol. Waste Treatment*, 1963, p. 157) has compared submerged sparged aerators with mechanical surface aerators. He has summarized this comparison in *Water Sewage Works*, **33** (January 1968). He indicates that surface aerators are significantly more efficient than subsurface aeration, both for oxygen absorption and for gas-stripping operations.

Zlokarnik and Mann (paper at Mixing Conf., Rindge, New Hampshire, August 1975) have found the opposite of Kalinske, i.e., subsurface diffusers, subsurface sparged turbines, and surface aerators compare approximately as 4:2:1 respectively in terms of O_2 transfer efficiency; however, Zlokarnik [*Adv. Biochem. Eng.*, **11**, 157 (1979)] later indicates that the scale-up correlation used earlier might be somewhat inaccurate. When all available information is considered, it appears that with near-optimum design any of the aeration systems (diffusers, submerged turbines, or surface impellers) should give a transfer efficiency of at least 2.25 kg O_2 /kWh. Thus, the final selection should probably be made primarily on the basis of operational reliability, maintenance, and capital costs.

Mass Transfer Mass transfer in plate and packed gas-liquid contactors has been covered earlier in this subsection. Attention here will be limited to deep-bed contactors (bubble columns and agitated vessels). Theory underlying mass transfer between phases is discussed in Sec. 5 of this handbook.

To design deep-bed contactors for mass-transfer operations, one must have, in general, predictive methods for the following design parameters:

- Flooding (for both columns and agitator impellers)
- Agitator power requirements

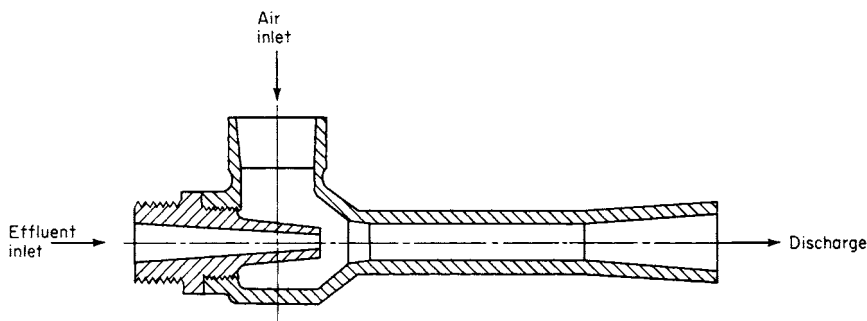


FIG. 14-100 Aeration ejector. (Penberthy, a division of Houdaille Industries, Inc.)

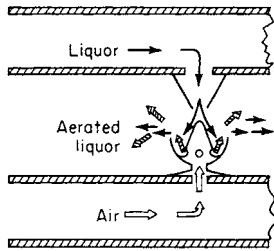


FIG. 14-101 Impingement aerator.

- Gas-phase and liquid-phase mass-transfer coefficients
- Interfacial area
- Interface resistance
- Mean concentration driving force for mass transfer

In most cases, available methods are incomplete or unreliable, and some supporting experimental work is necessary, followed by scale-up. The methods given here should allow theoretical feasibility studies, help minimize experimentation, and permit a measure of optimization in final design.

Flooding of Agitator Impellers Impeller flooding correlations for six-blade disk (6BD) Rushton turbines and six-blade disk Smith turbines (Chemineer designation: CD-6) are presented by Bakker, Myers, and Smith [*Chem. Eng.*, **101**, 98 (Dec. 1994)] and a review of impeller flooding. The Bakker et al. (loc. cit.) correlation is

$$Q/ND^3 = C_{FL}N_{Fr}(D/T)^{3.5} \quad (14-215)$$

where $C_{FL} = 30$ for a 6BD impeller and $C_{FL} = 70$ for a concave blade CD-6 impeller and $N_{Fr} = \text{Froude number} = N^2D/g$; $Q = \text{gas flow rate at flooding, m}^3/\text{s}$; $N = \text{impeller speed, rps}$; $D = \text{impeller diameter, m}$; and $T = \text{tank diameter, m}$. Note that the CD-6 impeller will handle $70/30 = 2.33$ times the gas a 6BD will handle, without flooding, at the

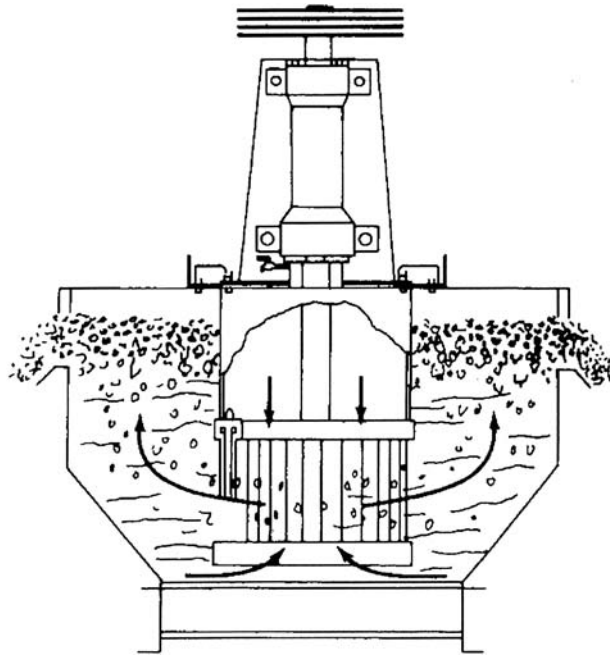


FIG. 14-102 The Wemco-Fagergren flotation machine. [From [www.tucottbus.de/BTU/Fak4/Aufbtech/pages/pbrr_N7Sep2-\(elstat-flotat\).pdf](http://www.tucottbus.de/BTU/Fak4/Aufbtech/pages/pbrr_N7Sep2-(elstat-flotat).pdf)].

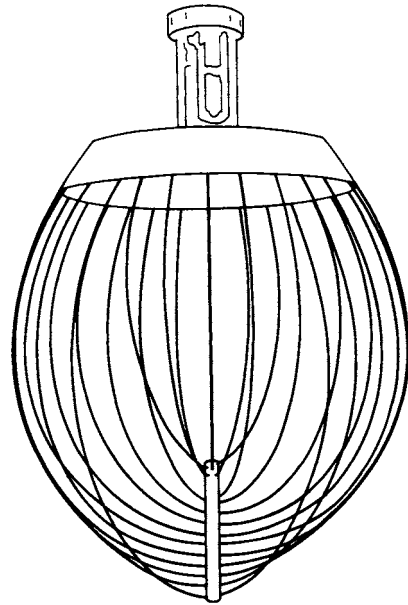


FIG. 14-103 Wire whip.

same N and D ; this is the great advantage of the CD-6 along with lower power decrease as the gas flow rate increases.

Gassed Impeller Power Bakker et al. (op. cit.) have given a gassed power correlation for the 6BD and CD-6 impellers.

$$P_g/P_u = [1 - (b - a\mu)]N_{Fr}^d \tanh(eN_A) \quad (14-216a)$$

where $P_g = \text{gassed power, W}$; $P_u = \text{ungassed power, W}$; $N_A = Q/ND^3$; and the constants of Eq. (14-216a) are given in Table 14-25.

As mentioned previously, the CD-6 suffers much less power decrease with increased gassing compared to the 6BD. For example, at $N_A = 0.15$, $P_g/P_u = 0.7$ for the CD-6 and 0.5 for the 6BD.

The ungassed power is calculated by

$$P_u = N_p \rho N^3 D^5 \quad (14-216b)$$

where the impeller power numbers N_p are given Table 14-25.

Bakker et al. (op. cit.) and Sensel et al. (op. cit.) have given correlations for gas holdup in agitated vessels. The Bakker et al. correlation is

$$\epsilon = C_\epsilon = (P_g/V)^A v_{sg}^B \quad (14-217)$$

where $C_\epsilon = 0.16$, $A = 0.33$, $B = 0.67$; $V = \text{batch volume, m}^3$; $v_{sg} = \text{superficial gas velocity} = Q/[(\pi/4)T^2]$; $T = \text{tank diameter, m}$. Equation (14-217) applies for both 6BD and CD-6.

Interfacial Area This consideration in agitated vessels has been reviewed and summarized by Tatterson (op. cit.). Predictive methods for interfacial area are not presented here because correlations are given for the overall volumetric mass transfer coefficient liquid phase controlling mass transfer.

TABLE 14-25 Constants in Eq. (14-216) and Impeller Power Numbers

Impeller type	a	b	c	d	N_p
6BD	0.72	0.72	24	0.25	3.2
CD-6	0.12	0.44	12	0.37	5.5

Overall Mass-Transfer Coefficient In systems with relatively sparingly soluble gases, where the gas-phase resistance is negligible, the mass-transfer rate can be determined by using the concept of an overall volumetric mass-transfer coefficient $k_L a$ as follows:

$$M_s = k_L a (C_s^* - C_{s,b}) \quad (14-218)$$

where M_s = solute molar mass-transfer rate, kg/mol/s; $k_L a$ = overall mass-transfer coefficient, 1/s; C_s^* = solute concentration in equilibrium with the liquid phase, kg/mol/s; and $C_{s,b}$ = solute concentration in bulk of liquid.

Bakker et al. (op. cit.) have given a correlation for $k_L a$ for aqueous systems in the absence of significant surface active agents.

$$k_L a = C_{k_L a} (P_g/V)^n v_{sg}^b \quad (14-219)$$

where $C_{k_L a} = 0.015$, 1/s; Eq. (14-219) applies for both 6BD and CD-6.

Interfacial Phenomena These can significantly affect overall mass transfer. Deckwer, *Bubble Column Reactors*, Wiley, Hoboken, N.J., 1992, has covered the effect of surfactants on mass transfer in bubble columns. In fermentation reactors, small quantities of surface-active agents (especially antifoaming agents) can drastically reduce overall oxygen transfer (Aiba et al., op. cit., pp. 153, 154), and in aerobic mechanically aerated waste-treatment lagoons, overall oxygen transfer has been found to be from 0.5 to 3 times that for pure water from tests with typical sewage streams (Eckenfelder et al., op. cit., p. 105).

One cannot quantitatively predict the effect of the various interfacial phenomena; thus, these phenomena will not be covered in detail here. The following literature gives a good general review of the effects of interfacial phenomena on mass transfer: Goodridge and Robb, *Ind. Eng. Chem. Fund.*, **4**, 49 (1965); Calderbank, *Chem. Eng. (London)*, CE 205 (1967); Gal-Or et al., *Ind. Eng. Chem.*, **61**(2), 22 (1969); Kintner, *Adv. Chem. Eng.*, **4** (1963); Resnick and Gal-Or, op. cit., p. 295; Valentin, loc. cit.; and Elenkov, loc. cit., and *Ind. Eng. Chem. Ann. Rev. Mass Transfer*, **60**(1), 67 (1968); **60**(12), 53 (1968); **62**(2), 41 (1970). In the following outline, the effects of the various interfacial phenomena on the factors that influence overall mass transfer are given. Possible effects of interfacial phenomena are tabulated below:

1. Effect on continuous-phase mass-transfer coefficient
 - a. Impurities concentrate at interface. Bubble motion produces circumferential surface-tension gradients that act to retard circulation and vibration, thereby decreasing the mass-transfer coefficient.
 - b. Large concentration gradients and large heat effects (very soluble gases) can cause interfacial turbulence (the Marangoni effect), which increases the mass-transfer coefficient.
2. Effect on interfacial area
 - a. Impurities will lower static surface tension and give smaller bubbles.
 - b. Surfactants can electrically charge the bubble surface (produce ionic bubbles) and retard coalescence (soap stabilization of an oil-water emulsion is an excellent example of this phenomenon), thereby increasing the interfacial area.
 - c. Large concentration gradients and large heat effects can cause bubble breakup.
3. Effect on mean mass-transfer driving force
 - a. Relatively insoluble impurities concentrate at the interface, giving an interfacial resistance. This phenomenon has been used in retarding evaporation from water reservoirs.
 - b. The axial concentration variation can be changed by changes in coalescence. The mean driving force for mass transfer is therefore changed.

Gas Holdup (ϵ) in Bubble Columns With coalescing systems, holdup may be estimated from a correlation by Hughmark [*Ind. Eng. Chem. Process Des. Dev.*, **6**, 218–220 (1967)] reproduced here as Fig. 14-104. For noncoalescing systems, with considerably smaller bubbles, ϵ can be as great as 0.6 at $U_{sg} = 0.05$ m/s, according to Mersmann [*Ger. Chem. Eng.*, **1**, 1 (1978)].

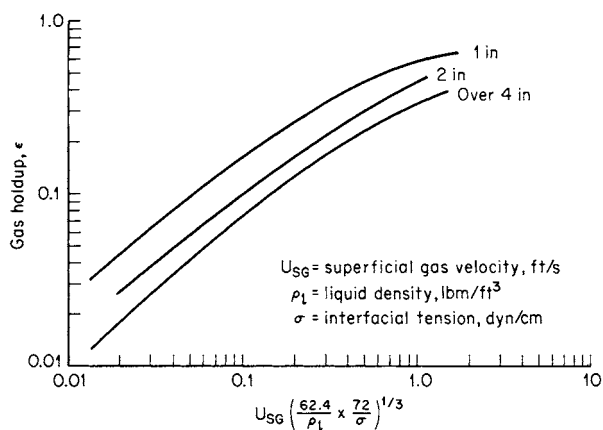


FIG. 14-104 Gas holdup correlation. [*Ind. Eng. Chem. Process Des. Dev.*, **6**, 218 (1967).]

It is often helpful to use the relationship between ϵ and superficial gas velocity (U_{sg}) and the rise velocity of a gas bubble relative to the liquid velocity ($U_r + U_L$, with U_L defined as positive upward):

$$\epsilon = \frac{U_{sg}}{U_r + U_L} \quad (14-220)$$

Rise velocities of bubbles through liquids have been discussed previously.

For a better understanding of the interactions between parameters, it is often helpful to calculate the effective bubble rise velocity U_r from measured values of ϵ ; for example, the data of Mersmann (loc. cit.) indicated $\epsilon = 0.6$ for $U_{sg} = 0.05$ m/s, giving $U_r = 0.083$ m/s, which agrees with the data reported in Fig. 14-43 for the rise velocity of bubble clouds. The rise velocity of single bubbles, for $d_b \sim 2$ mm, is about 0.3 m/s, for liquids with viscosities not too different from water. Using this value in Eq. (14-220) and comparing with Fig. 14-104, one finds that at low values of U_{sg} , the rise velocity of the bubbles is less than the rise velocity of a single bubble, especially for small-diameter tubes, but that the opposite occurs for large values of U_{sg} .

More recent literature regarding generalized correlational efforts for gas holdup is adequately reviewed by Tsuchiya and Nakanishi [*Chem. Eng. Sci.*, **47**(13/14), 3347 (1992)] and Sotelo et al. [*Int. Chem. Eng.*, **34**(1), 82–90 (1994)]. Sotelo et al. (op. cit.) have developed a dimensionless correlation for gas holdup that includes the effect of gas and liquid viscosity and density, interfacial tension, and diffuser pore diameter. For systems that deviate significantly from the waterlike liquids for which Fig. 14-104 is applicable, their correlation (the fourth numbered equation in the paper) should be used to obtain a more accurate estimate of gas holdup. Mersmann (op. cit.) and Deckwer et al. (op. cit.) should also be consulted.

Liquid-phase mass-transfer coefficients in bubble columns have been reviewed by Calderbank ("Mixing," loc. cit.), Fair (*Chem. Eng.*, loc. cit.), Mersmann [*Ger. Chem. Eng.*, **1**, 1 (1978)], *Int. Chem. Eng.*, **32**(3) 397–405 (1991)], Deckwer et al. [*Can. J. Chem. Eng.*, **58**, 190 (1980)], Hikita et al. [*Chem. Eng. J.*, **22**, 61 (1981)] and Deckwer and Schumpe [*Chem. Eng. Sci.*, **48**(5), 889–911 (1993)]. The correlation of Ozturk, Schumpe, and Deckwer [*AIChE J.*, **33**, 1473–1480 (1987)] is recommended. Deckwer et al. (op. cit.) have documented the case for using the correlation:

Ozturk et al. (1987) developed a new correlation on the basis of a modification of the Akita-Yoshida correlation suggested by Nakanoh and Yoshida (1980). In addition, the bubble diameter d_b rather than the column diameter was used as the characteristic length as the column diameter has little influence on $k_L a$. The value of d_b was assumed to be approximately constant ($d_b = 0.003$ m). The correlation was obtained by nonlinear regression is as follows:

$$\left(\frac{k_{L,a} d_B}{D_L}\right) = 0.62 \left[\frac{\mu_L}{(\rho_L D_L)} \right]^{0.5} \left(\frac{g \rho_L d_B^2}{\sigma} \right)^{0.33} \left(\frac{g \rho_L^2 d_B}{\mu_L^2} \right)^{0.29} \times \left[\frac{U_G}{(g d_B)^{0.5}} \right]^{0.68} \left(\frac{\rho_G}{\rho_L} \right)^{0.04} \quad (14-221)$$

where $k_{L,a}$ = overall mass-transfer coefficient, d_B = bubble diameter = 0.003 m, D_L = diffusivity of gas in liquid, ρ = density, μ = viscosity, σ = interfacial tension, g = gravitational acceleration.

As mentioned earlier, surfactants and ionic solutions significantly affect mass transfer. Normally, surface affects act to retard coalescence and thus increase the mass transfer. For example, Hikata *et al.* [*Chem. Eng. J.*, **22**, 61–69 (1981)] have studied the effect of KCl on mass transfer in water. As KCl concentration increased, the mass transfer increased up to about 35 percent at an ionic strength of 6 gm/l. Other investigators have found similar increases for liquid mixtures.

Axial Dispersion Backmixing in bubble columns has been extensively studied. Wiemann and Mewes [*Ind. Eng. Chem. Res.*, **44**, 4959 (2005)] and Wild *et al.* [*Int. J. Chemical Reactor Eng.*, **1**, R7 (2003)] give a long list of references pertaining to backmixing in bubble columns. An excellent review article by Shah *et al.* [*AIChE J.*, **24**, 369 (1978)] has summarized the literature prior to 1978. Works by König *et al.* [*Ger. Chem. Eng.*, **1**, 199 (1978)], Lucke *et al.* [*Trans. Inst. Chem. Eng.*, **58**, 228 (1980)], Riquarts [*Ger. Chem. Eng.*, **4**, 18 (1981)], Mersmann (*op. cit.*), Deckwer (*op. cit.*), Yang *et al.* [*Chem. Eng. Sci.*, **47**(9–11), 2859 (1992)], and Garcia-Calvo and Leton [*Chem. Eng. Sci.*, **49**(21), 3643 (1994)] are particularly useful references.

Axial dispersion occurs in both the liquid and the gas phases. The degree of axial dispersion is affected by vessel diameter, vessel internals, gas superficial velocity, and surface-active agents that retard coalescence. For systems with coalescence-retarding surfactants the initial bubble size produced by the gas sparger is also significant. The gas and liquid physical properties have only a slight effect on the degree of axial dispersion, except that liquid viscosity becomes important as the flow regime becomes laminar. With pure liquids, in the absence of coalescence-inhibiting, surface-active agents, the nature of the sparger has little effect on the axial dispersion, and experimental results are reasonably well correlated by the dispersion model. For the liquid phase the correlation recommended by Deckwer *et al.* (*op. cit.*), after the original work by Baird and Rice [*Chem. Eng. J.*, **9**, 171(1975)] is as follows:

$$\frac{E_L}{(DU_G)} = 0.35 \left(\frac{gD}{U_G^2} \right)^{1/3} \quad (14-222)$$

where E_L = liquid-phase axial dispersion coefficient, U_G = superficial velocity of the gas phase, D = vessel diameter, and g = gravitational acceleration.

The recommended correlation for the gas-phase axial-dispersion coefficient is given by Field and Davidson (*loc. cit.*):

$$E_G = 56.4 D^{1.33} \left(\frac{U_G}{\epsilon} \right)^{3.56} \quad (14-223)$$

where E_G = gas-phase axial-dispersion coefficient, m^2/s ; D = vessel diameter, m; U_G = superficial gas velocity, m/s; and ϵ = fractional gas holdup, volume fraction.

The correlations given in the preceding paragraphs are applicable to vertical cylindrical vessels with pure liquids without coalescence inhibitors. For other vessel geometries such as columns of rectangular cross section, packed columns, and coiled tubes, the work of Shah *et al.* (*loc. cit.*) should be consulted. For systems containing coalescence-inhibiting surfactants, axial dispersion can be vastly different from that in systems in which coalescence is negligible. König *et al.* (*loc. cit.*) have well demonstrated the effects of surfactants and sparger type by conducting tests with weak alcohol solutions using three different porous spargers. With pure water, the sparger—and, consequently, initial bubble size—had little effect on back mixing because coalescence produced a dynamic-equilibrium bubble size not far above the sparger. With surfactants, the average bubble size was smaller than the dynamic-equilibrium bubble size. Small bubbles produced minimal back mixing up to $\epsilon \approx 0.40$; however, above $\epsilon \approx 0.40$ backmixing increased very rapidly as U_G increased. The rapid increase in back mixing as ϵ exceeds 0.40 was postulated to occur indirectly because a bubble carries upward with it a volume of liquid equal to about 70 percent of the bubble volume, and, for $\epsilon \approx 0.40$, the bubbles carry so much liquid upward that steady, uniform bubble rise can no longer be maintained and an oscillating, slugging flow develops, which produces fluctuating pressure at the gas distributor and the formation of large eddies. The large eddies greatly increase backmixing. For the air alcohol-water system, the minimum bubble size to prevent unsteady conditions was about 1, 1.5, and 2 mm for $U_G = 1, 3,$ and 5 cm/s, respectively. Any smaller bubble size produced increased backmixing. The results of König *et al.* (*loc. cit.*) clearly indicate that the interaction of surfactants and sparger can be very complex; thus, one should proceed very cautiously in designing systems for which surfactants significantly retard coalescence. Caution is particularly important because surfactants can produce either much more or much less backmixing than surfactant-free systems, depending on the bubble size, which, in turn, depends on the sparger utilized.

PHASE SEPARATION

Gases and liquids may be intentionally contacted as in absorption and distillation, or a mixture of phases may occur unintentionally as in vapor condensation from inadvertent cooling or liquid entrainment from a film. Regardless of the origin, it is usually desirable or necessary ultimately to separate gas-liquid dispersions. While separation will usually occur naturally, the rate is often economically intolerable and separation processes are employed to accelerate the step.

GAS-PHASE CONTINUOUS SYSTEMS

Practical separation techniques for liquid particles in gases are discussed. Since gas-borne particulates include both liquid and solid particles, many devices used for dry-dust collection (discussed in Sec. 17 under "Gas-Solids Separation") can be adapted to liquid-particle separation. Also, the basic subject of particle mechanics is covered in Sec. 6. Separation of liquid particulates is frequently desirable in chemical processes such as in countercurrent-stage contacting because liquid entrainment with the gas partially reduces true countercurrency. Sep-

aration before entering another process step may be needed to prevent corrosion, to prevent yield loss, or to prevent equipment damage or malfunction. Separation before the atmospheric release of gases may be necessary to prevent environmental problems and for regulatory compliance.

GENERAL REFERENCES

- G-1. Buonicore and Davis, eds., *Air Pollution Engineering Manual*, Van Nostrand Reinhold, New York, 1992.
- G-2. Calvert and Englund, eds., *Handbook of Air Pollution Technology*, Wiley, New York, 1984.
- G-3. Cheremisinoff, ed., *Encyclopedia of Environmental Control Technology*, vol. 2, Gulf Pub., Houston, 1989.
- G-4. McKetta, *Unit Operations Handbook*, vol. 1–2, Dekker, New York, 1992.
- G-5. Wark and Warner, *Air Pollution: Its Origin and Control*, 2d ed., Harper & Row, New York, 1981.
- G-6. Hesketh, *Air Pollution Control*, 1979; *Fine Particles in Gaseous Media*, Ann Arbor Science Pubs., Ann Arbor, MI, 1977.
- G-7. Stern, *Air Pollution*, 3d ed., vols. 3–5, Academic, Orlando, FL, 1976–77.

G-8. Strauss, *Industrial Gas Cleaning*, 2d ed., Pergamon, New York, 1975.
 G-9. Theodore and Buonicore, *Air Pollution Control Equipment; Selection, Design, Operation and Maintenance*, Prentice Hall, Englewood Cliffs, NJ, 1982.
 G-10. Wang and Pereira, eds., *Handbook of Environmental Engineering*, vol. 1, Humana, Clifton, NJ 1979.
 G-11. Chermisinoff and Young, *Air Pollution Control and Design Handbook*, parts 1-2, Dekker, New York, 1977.
 G-12. Nonhebel, *Gas Purification Processes for Air Pollution Control*, Newnes-Butterworth, London, 1972.

Sampling

R-1. *Code of Federal Regulations*, 40 (CFR 40), subchapter C—Air Programs, parts 50–99. Office of the Federal Register, Washington.
 R-2. Ref. G-11, part 1, pp. 65–121.
 R-3. Cooper and Rossano, *Source Testing for Air Pollution Control*, Environmental Science Services, Wilton, Connecticut, 1970.
 R-4. Ref. G-7, vol. 3, pp. 525–587.
 R-5. *Methods of Air Sampling and Analysis*, 2d Ed., American Public Health Assoc., Washington, 1977.
 R-6. Stockham and Fochtman, *Particle Size Analysis*, Ann Arbor Science Pubs., Ann Arbor, Michigan, 1977.
 R-7. Ref. G-2, Ch. 31, pp. 785–832.
 R-8. Ref. G-8, Ch. 2, pp. 39–79.

Specific

R-9. Calvert, Goldchmid, Leith, and Mehta, NTIS Publ. PB-213016, 213017, 1972.
 R-10. Calvert, *J. Air Pollut. Control Assoc.*, **24**, 929 (1974).
 R-11. Calvert, *Chem. Eng.*, **84**(18), 54 (1977).
 R-12. Calvert, Yung, and Leung, NTIS Publ. PB-248050, 1975.
 R-13. Calvert and Lundgren, *J. Air Pollut. Control Assoc.*, **18**, 677 (1968).
 R-14. Calvert, Lundgren, and Mehta, *J. Air Pollut. Control Assoc.*, **22**, 529 (1972).
 R-15. Yung, Barbarika, and Calvert, *J. Air Pollut. Control Assoc.*, **27**, 348, (1977).
 R-16. Katz, M.S. thesis, Pennsylvania State University, 1958.
 R-17. York and Poppele, *Chem. Eng. Prog.*, **59**(6), 45 (1963).
 R-18. York, *Chem. Eng. Prog.*, **50**, 421 (1954).
 R-19. Ref. G-2, Ch. 10, pp. 215–248.
 References with the notation (R-) are cited in the text.

Definitions: Mist and Spray Little standardization has been adopted in defining gas-borne liquid particles, and this frequently leads to confusion in the selection, design, and operation of collection equipment. Aerosol applies to suspended particulate, either solid or liquid, which is slow to settle by gravity and to particles from the sub-micrometer range up to 10 to 20 μm . Mists are fine suspended liquid dispersions usually resulting from condensation and ranging upward in particle size from around 0.1 μm . Spray refers to entrained liquid droplets. The droplets may be entrained from atomizing processes previously discussed under "Liquid-in-Gas Dispersions" in this section. In such instances, size will range from the finest particles produced up to a particle whose terminal settling velocity is equal to the entraining gas velocity if some settling volume is provided. Process spray is often created unintentionally, such as by the condensation of vapors on cold duct walls and its subsequent reentrainment, or from two-phase flow in pipes, gas bubbling through liquids, and entrainment from boiling liquids. Entrainment size distribution from sieve trays has been given by Cheng and Teller [*Am. Inst. Chem. Eng. J.*, **7**(2), 282 (1961)] and evaporator spray by Garner et al. [*Trans. Inst. Chem. Eng.*, **32**, 222 (1954)]. In general, spray can range downward in particle size from 5000 μm . There can be overlapping in size between the coarsest mist particles and the finest spray particles, but some authorities have found it convenient arbitrarily to set a boundary of 10 μm between the two. Actually, considerable overlap exists in the region of 5 to 40 μm . Table 14-26 lists typical ranges of particle size created by different mechanisms. The sizes actually entrained can be influenced by the local gas velocity. Figure 14-105 compares the approximate size range of liquid particles with other particulate material and the approximate applicable size range of collection devices. Figure 17-34 gives an expanded chart by Lapple for solid particles. Mist and fog formation has been discussed previously.

Gas Sampling The sampling of gases containing mists and sprays may be necessary to obtain data for collection-device design, in which case particle-size distribution, total mass loading, and gas volume,

TABLE 14-26 Particle Sizes Produced by Various Mechanisms

Mechanism or process	Particle-size range, μm
Liquid pressure spray nozzle	100–5000
Gas-atomizing spray nozzle	1–100
Gas bubbling through liquid or boiling liquid	20–1000
Condensation processes with fogging	0.1–30
Annular two-phase flow in pipe or duct	10–2000

temperature, pressure, and composition may all be needed. Other reasons for sampling may be to determine equipment performance, measure yield loss, or determine compliance with regulations.

Location of a sample probe in the process stream is critical especially when larger particles must be sampled. Mass loading in one portion of a duct may be severalfold greater than in another portion as affected by flow patterns. Therefore, the stream should be sampled at a number of points. The U.S. Environmental Protection Agency (R-1) has specified 8 points for ducts between 0.3 and 0.6 m (12 and 24 in) and 12 points for larger ducts, provided there are no flow disturbances for eight pipe diameters upstream and two downstream from the sampling point. When only particles smaller than 3 μm are to be sampled, location and number of sample points are less critical since such particles remain reasonably well dispersed by brownian motion. However, some gravity settling of such particles and even gases of high density have been observed in long horizontal breeching. Isokinetic sampling (velocity at the probe inlet is equal to local duct velocity) is required to get a representative sample of particles larger than 3 μm (error is small for 4- to 5- μm particles). Sampling methods and procedures for mass loading have been developed (R-1 through R-8).

Particle Size Analysis Many particle-size-analysis methods suitable for dry-dust measurement are unsuitable for liquids because of coalescence and drainage after collection. Measurement of particle sizes in the flowing aerosol stream by using a cascade impactor is one

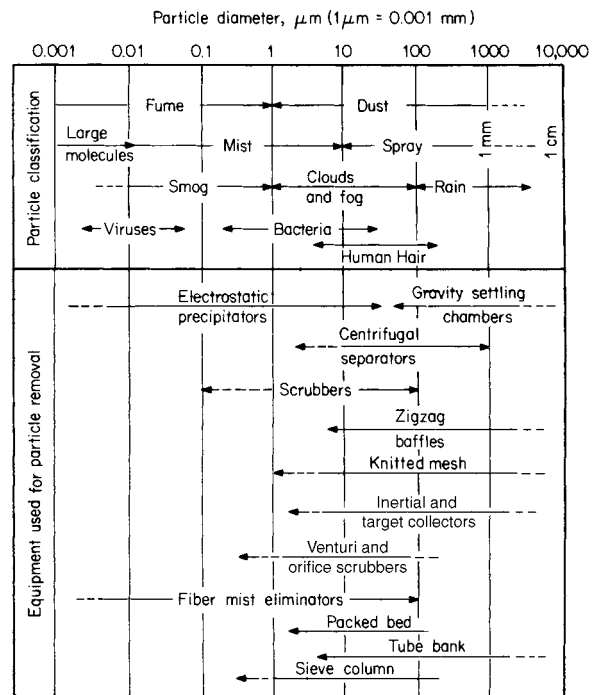


FIG. 14-105 Particle classification and useful collection equipment versus particle size.

of the better means. The impacting principle has been described by Ranz and Wong [*Ind. Eng. Chem.*, **44**, 1371 (1952)] and Gillespie and Johnstone [*Chem. Eng. Prog.*, **51**, 75F (1955)]. The Andersen, Sierra, and University of Washington impactors may be used if the sampling period is kept short so as not to saturate the collection substrate. An impactor designed specifically for collecting liquids has been described by Brink, Kennedy, and Yu [*Am. Inst. Chem. Eng. Symp. Ser.*, **70**(137), 333 (1974)].

Collection Mechanisms Mechanisms which may be used for separating liquid particles from gases are (1) gravity settling, (2) inertial (including centrifugal) impaction, (3) flow-line interception, (4) diffusional (brownian) deposition, (5) electrostatic attraction, (6) thermal precipitation, (7) flux forces (thermophoresis, diffusiophoresis, Stefan flow), and (8) particle agglomeration (nucleation) techniques. Equations and parameters for these mechanisms are given in Table 17-2. Most collection devices rarely operate solely with a single mechanism, although one mechanism may so predominate that it may be referred to, for instance, as an inertial-impaction device.

After collection, liquid particles coalesce and must be drained from the unit, preferably without reentrainment. Calvert (R-12) has studied the mechanism of reentrainment in a number of liquid-particle collectors. Four types of reentrainment were typically observed: (1) transition from separated flow of gas and liquid to a two-phase region of separated-entrained flow, (2) rupture of bubbles, (3) liquid creep on the separator surface, and (4) shattering of liquid droplets and splashing. Generally, reentrainment increased with increasing gas velocity. Unfortunately, in devices collecting primarily by centrifugal and inertial impaction, primary collection efficiency increases with gas velocity; thus overall efficiency may go through a maximum as reentrainment overtakes the incremental increase in efficiency. Prediction of collection efficiency must consider both primary collection and reentrainment.

Procedures for Design and Selection of Collection Devices Calvert and coworkers (R-9 to R-12 and R-19) have suggested useful design and selection procedures for particulate-collection devices in which direct impingement and inertial impaction are the most significant mechanisms. The concept is based on the premise that the mass median aerodynamic particle diameter d_{p50} is a significant measure of the difficulty of collection of the liquid particles and that the collection device cut size d_{pc} (defined as the aerodynamic particle diameter collected with 50 percent efficiency) is a significant measure of the capability of the collection device. The aerodynamic diameter for a particle is the diameter of a spherical particle (with an arbitrarily assigned density of 1 g/cm³) which behaves in an air stream in the same fashion as the actual particle. For real spherical particles of diameter d_p , the equivalent aerodynamic diameter d_{pa} can be obtained from the equation $d_{pa} = dp(\rho_p C')^{1/2}$, where ρ_p is the apparent particle density (mass/volume) and C' is the Stokes-Cunningham correction factor for the particle size, all in consistent units. If particle diameters are expressed in micrometers, ρ_p can be in grams per cubic centimeter and C' can be approximated by $C' = 1 + A_c(2\lambda/d_p)$, where A_c is a constant dependent upon gas composition, temperature, and pressure ($A_c = 0.88$ for atmospheric air at 20°C) and λ is the mean free path of the gas molecules ($\lambda = 0.10 \mu\text{m}$ for 20°C atmospheric air). For other temperatures or pressures, or gases other than air, calculations using these more precise equations may be made: $A_c = 1.257 + 0.4 \exp[-1.1(d_p/2\lambda)]$ and $\lambda = \mu_g/0.499\rho_g \times \mu_m$ (where μ_g is the gas viscosity, kg/m-h; ρ_g is gas density, g/cm³; and μ_m is the mean molecular speed, m/s. $\mu_m = [8R_g T/\pi M]^{0.5}$, where R_g is the universal gas constant, 8.315 kJ/kg-mol-K; T is the gas absolute temperature, K; and M is the molar mass or equivalent molecular weight of the gas. (π is the usual geometric constant.) For test purposes (air at 25°C and 1 atm), $\rho_g = 1.183 \text{ kg/m}^3$, $\mu_g = 0.0666 \text{ kg/m-h}$, $\lambda = 0.067 \mu\text{m}$, and $u_m = 467 \text{ m/s}$. For airborne liquid particles, the assumption of spherical shape is reasonably accurate, and ρ_p is approximately unity for dilute aqueous particles at ambient temperatures. C' is approximately unity at ambient conditions for such particles larger than 1 to 5 μm , so that often the actual liquid particle diameter and the equivalent aerodynamic diameter are identical.

When a distribution of particle sizes which must be collected is present, the actual size distribution must be converted to a mass dis-

tribution by aerodynamic size. Frequently the distribution can be represented or approximated by a log-normal distribution (a straight line on a log-log plot of cumulative mass percent of particles versus diameter) which can be characterized by the mass median particle diameter d_{p50} and the standard statistical deviation of particles from the median σ_g . σ_g can be obtained from the log-log plot by $\sigma_g = D_{p950}/D_{p50}$ at 15.87 percent = D_{p50} at 84.13 percent/ D_{p50} .

The grade efficiency η of most collectors can be expressed as a function of the aerodynamic particle size in the form of an exponential equation. It is simpler to write the equation in terms of the particle penetration P_t (those particles not collected), where the fractional penetration $P_t = 1 - \eta$, when η is the fractional efficiency. The typical collection equation is

$$P_t = e^{(-A_n D_{pa}^B)} \tag{14-224}$$

where A_n and B are functions of the collection device. Calvert (R-12) has determined that for many devices in which the primary collection mechanism is direct interception and inertial impaction, such as packed beds, knitted-mesh collectors, zigzag baffles, target collectors such as tube banks, sieve-plate columns, and venturi scrubbers, the value of B is approximately 2.0. For cyclonic collectors, the value of B is approximately 0.67. The overall integrated penetration \bar{P}_t for a device handling a distribution of particle sizes can be obtained by

$$\bar{P}_t = \int_0^W \left(\frac{dW}{W} \right) P_t \tag{14-225}$$

where (dW/W) is the mass of particles in a given narrow size distribution and P_t is the average penetration for that size range. When the particles to be collected are log-normally distributed and the collection device efficiency can be expressed by Eq. (14-224), the required overall integrated collection efficiency \bar{P}_t can be related to the ratio of the device aerodynamic cut size D_{pc} to the mass median aerodynamic particle size D_{p50} . This required ratio for a given distribution and collection is designated R_{rL} and these relationships are illustrated graphically in Fig. 14-106. For the many devices for which B is approximately 2.0, a simplified plot (Fig. 14-107) is obtained. From these figures, by knowing the desired overall collection efficiency and particle distribution, the value of R_{rL} can be read. Substituting the mass median particle diameter gives the aerodynamic cut size

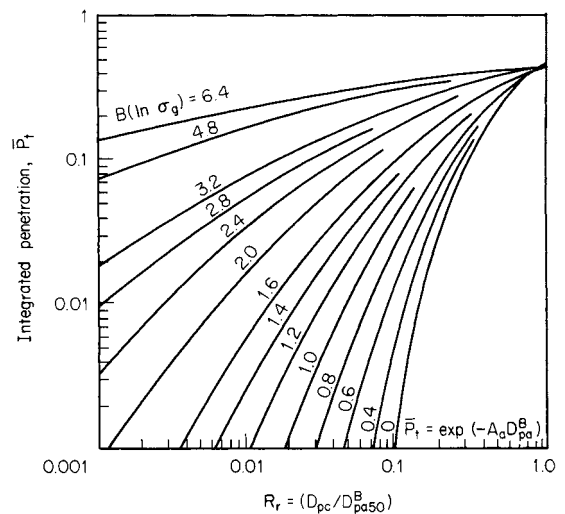


FIG. 14-106 Overall integrated penetration as a function of particle-size distribution and collector parameters. (Calvert, Yung, and Leung, NTIS Publ. PB-248050, 1975.)

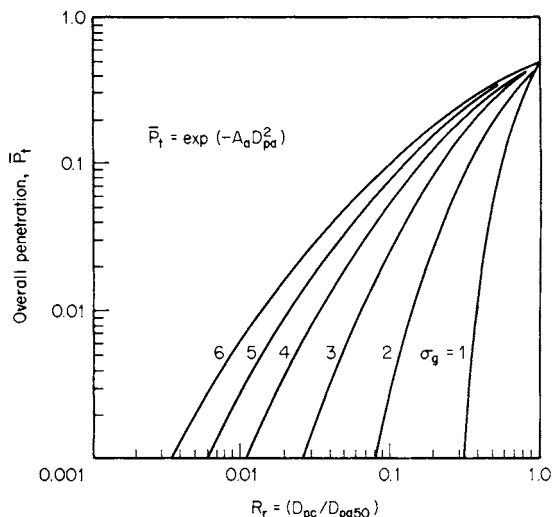


FIG. 14-107 Overall integrated penetration as a function of particle-size distribution and collector cut diameter when $B = 2$ in Eq. (14-224). (Calvert, Goldshmid, Leith, and Mehta, NTIS Publ. PB-213016, 213017, 1972.)

required from the collection device being considered. Therefore, an experimental plot of aerodynamic cut size for each collection device versus operating parameters can be used to determine the device suitability.

Collection Equipment

Gravity Settlers Gravity can act to remove larger droplets. Settling or disengaging space above aerated or boiling liquids in a tank or spray zone in a tower can be very useful. If gas velocity is kept low, all particles with terminal settling velocities (see Sec. 6) above the gas velocity will eventually settle. Increasing vessel cross section in the settling zone is helpful. Terminal velocities for particles smaller than $50\ \mu\text{m}$ are very low and generally not attractive for particle removal. Laminar flow of gas in long horizontal paths between trays or shelves on which the droplets settle is another effective means of employing gravity. Design equations are given in Sec. 17 under "Gas-Solids Separations." Settler pressure drop is very low, usually being limited to entrance and exit losses.

Centrifugal Separation Centrifugal force can be utilized to enhance particle collection to several hundredfold that of gravity. The design of cyclone separators for dust removal is treated in detail in Sec. 17 under "Gas-Solids Separations," and typical cyclone designs are shown in Fig. 17-43. Dimension ratios for one family of cyclones are given in Fig. 17-36. Cyclones, if carefully designed, can be more efficient on liquids than on solids since liquids coalesce on capture and are easy to drain from the unit. However, some precautions not needed for solid cyclones are necessary to prevent reentrainment.

Tests by Calvert (R-12) show high primary collection efficiency on droplets down to $10\ \mu\text{m}$ and in accordance with the efficiency equations of Leith and Licht [*Am. Inst. Chem. Eng. Symp. Ser.*, 68(126), 196-206 (1972)] for the specific cyclone geometry tested if entrainment is avoided. Typical entrainment points are (1) creep along the gas outlet pipe, (2) entrainment by shearing of the liquid film from the walls, and (3) vortex pickup from accumulated liquid in the bottom (Fig. 14-108a). Reentrainment from creep of liquid along the top of the cyclone and down the outlet pipe can be prevented by providing the outlet pipe with a flared conical skirt (Fig. 14-108b), which provides a point from which the liquid can drip without being caught in the outlet gas. The skirt should be slightly shorter than the gas outlet pipe but extend below the bottom of the gas inlet. The cyclone inlet gas should not impinge on this skirt. Often the bottom edge of the skirt is V-notched or serrated.

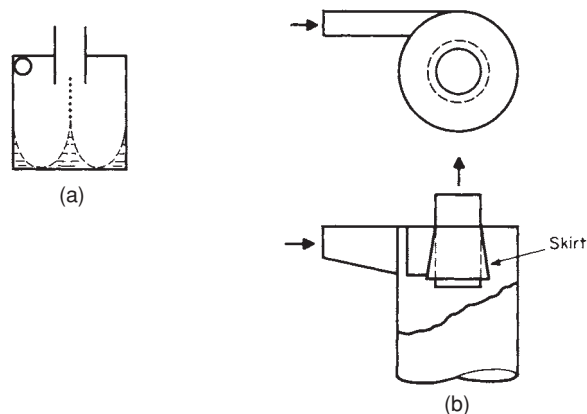


FIG. 14-108 (a) Liquid entrainment from the bottom of a vessel by centrifugal flow. (Rietema and Verver, *Cyclones in Industry*, Elsevier, Amsterdam, 1961.) (b) Gas-outlet skirt for liquid cyclones. (Stern et al., *Cyclone Dust Collectors*, American Petroleum Institute, New York, 1955.)

Reentrainment is generally reduced by lower inlet gas velocities. Calvert (R-12) reviewed the literature on predicting the onset of entrainment and found that of Chien and Ibele (ASME Pap. 62-WA170) to be the most reliable. Calvert applies their correlation to a liquid Reynolds number on the wall of the cyclone, $N_{Re,L} = 4Q_L/h_i v_L$, where Q_L is the volumetric liquid flow rate, cm^3/s ; h_i is the cyclone inlet height, cm ; and v_L is the kinematic liquid viscosity, cm^2/s . He finds that the onset of entrainment occurs at a cyclone inlet gas velocity V_{ci} , m/s , in accordance with the relationship in $V_{ci} = 6.516 - 0.2865 \ln N_{Re,L}$.

Reentrainment from the bottom of the cyclone can be prevented in several ways. If a typical long-cone dry cyclone is used and liquid is kept continually drained, vortex entrainment is unlikely. However, a vortex breaker baffle in the outlet is desirable, and perhaps a flat disk on top extending to within 2 to 5 cm (0.8 to 2 in) of the walls may be beneficial. Often liquid cyclones are built without cones and have dished bottoms. The modifications described earlier are definitely needed in such situations. Stern, Caplan, and Bush (*Cyclone Dust Collectors*, American Petroleum Institute, New York, 1955) and Rietema and Verver (in Tengbergen, *Cyclones in Industry*, Elsevier, Amsterdam, 1961, chap. 7) have discussed liquid-collecting cyclones.

As with dust cyclones, no reliable pressure-drop equations exist (see Sec. 17), although many have been published. A part of the problem is that there is no standard cyclone geometry. Calvert (R-12) experimentally obtained $\Delta P = 0.000513 \rho_g (Q_g/h_i W_i)^2 (2.8 h_i w_i/d_o^2)$, where ΔP is in cm of water; ρ_g is the gas density, g/cm^3 ; Q_g is the gas volumetric flow rate, cm^3/s ; h_i and w_i are cyclone inlet height and width respectively, cm ; and d_o is the gas outlet diameter, cm . This equation is in the same form as that proposed by Shepherd and Lapple [*Ind. Eng. Chem.*, 31, 1246 (1940)] but gives only 37 percent as much pressure drop.

Liquid cyclone efficiency can be improved somewhat by introducing a coarse spray of liquid in the cyclone inlet. Large droplets which are easily collected collide with finer particles as they sweep the gas stream in their travel to the wall. (See subsection "Wet Scrubbers" regarding optimum spray size.) Cyclones may also be operated wet to improve their operation on dry dust. Efficiency can be improved through reduction in entrainment losses since the dust particles become trapped in the water film. Collision between droplets and dust particles aids collection, and adequate irrigation can eliminate problems of wall buildup and fouling. The most effective operation is obtained by spraying countercurrently to the gas flow in the cyclone inlet duct at liquid rates of 0.7 to $2.0\ \text{L/m}^3$ of gas. There are also many proprietary designs of liquid separators using centrifugal force, some of which are illustrated in Fig. 14-109. Many of these were originally

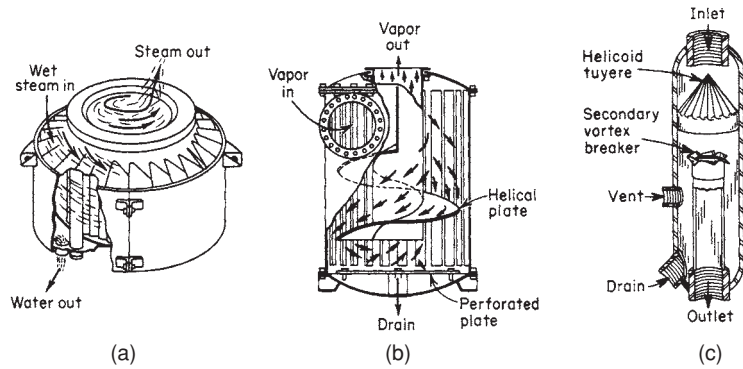


FIG. 14-109 Typical separators using impingement in addition to centrifugal force. (a) Hi-eF purifier. (V. D. Anderson Co.) (b) Flick separator. (Wurster & Sanger, Inc.) (c) Type RA line separator. (Centrifix Corp., Bull. 220.)

developed as steam separators to remove entrained condensate. In some designs, impingement on swirl baffles aids separation.

Impingement Separation Impingement separation employs direct impact and inertial forces between particles, the gas streamlines, and target bodies to provide capture. The mechanism is discussed in Sec. 17 under "Gas-Solids Separations." With liquids, droplet coalescence occurs on the target surface, and provision must be made for drainage without reentrainment. Calvert (R-12) has studied droplet collection by impingement on targets consisting of banks of tubes, zigzag baffles, and packed and mesh beds. Figure 14-110 illustrates some other types of impingement-separator designs.

In its simplest form, an impingement separator may be nothing more than a target placed in front of a flow channel such as a disk at the end of a tube. To improve collection efficiency, the gas velocity may be increased by forming the end into a nozzle (Fig. 14-110a). Particle collection as a function of size may be estimated by using the target-efficiency correlation in Fig. 17-39. Since target efficiency will be low for systems with separation numbers below 5 to 10 (small particles, low gas velocities), the mist will frequently be subjected to a number of targets in series as in Fig. 14-110c, d , and g .

The overall droplet penetration is the product of penetration for each set of targets in series. Obviously, for a distribution of particle sizes, an integration procedure is required to give overall collection efficiency. This target-efficiency method is suitable for predicting efficiency when the design effectively prevents the bypassing or short-circuiting of targets by the gas stream and provides adequate time to accelerate the liquid droplets to gas velocity. Katz (R-16) investigated a jet and target-plate entrainment separator design and found the pressure drop less than would be expected to supply the kinetic energy both for droplet acceleration and gas friction. An estimate based on his results indicates that the liquid particles on the average were being accelerated to only about 60 percent of the gas velocity. The largest droplets, which are the easiest to collect, will be accelerated less than the smaller particles. This factor has a leveling effect on collection efficiency as a function of particle size so that experimental results on such devices may not show as sharp a decrease in efficiency with particle size as predicted by calculation. Such results indicate that in many cases our lack of predicting ability results, not from imperfections in the theoretical treatment, but from our lack of knowledge of velocity distributions within the system.

Katz (R-16) also studied *wave-plate impingement separators* (Fig. 14-110b) made up of 90° formed arcs with an 11.1-mm (0.44-in) radius and a 3.8-mm (0.15-in) clearance between sheets. The pressure drop is a function of system geometry. The pressure drop for Katz's system and collection efficiency for seven waves are shown in Fig. 14-111. Katz used the Souders-Brown expression to define a design velocity for the gas between the waves:

$$U = K \sqrt{(\rho_l - \rho_g) / \rho_g} \quad (14-226)$$

K is 0.12 to give U in ms^{-1} (0.4 for ft/s), and ρ_l and ρ_g are liquid and gas densities in any consistent set of units. Katz found no change in efficiency at gas velocities from one-half to 3 times that given by the equation.

Calvert (R-12) investigated *zigzag baffles* of a design more like Fig. 14-110c. The baffles may have spaces between the changes in direction or be connected as shown. He found close to 100 per collection for water droplets of 10 μm and larger. Some designs had high efficiencies down to 5 or 8 μm . Desirable gas velocities were 2 to 3.5 m/s (6.6 to 11.5 ft/s), with a pressure drop for a six-pass baffle of 2 to 2.5 cm (0.8 to 1.0 in) of water. On the basis of turbulent mixing, an equation was developed for predicting primary collection efficiency as a function of particle size and collector geometry:

$$\eta = 1 - \exp\left[-\frac{u_{te} n W \theta}{57.3 U_g b \tan \theta}\right] \quad (14-227)$$

where η is the fractional primary collection efficiency; u_{te} is the drop terminal centrifugal velocity in the normal direction, cm/s ; U_g is the superficial gas velocity, cm/s ; n is the number of rows of baffles or bends; θ is the angle of inclination of the baffle to the flow path, °; W is the width of the baffle, cm ; and b is the spacing between baffles in the same row, cm . For conditions of low Reynolds number ($N_{Re,D} < 0.1$) where Stokes' law applies, Calvert obtains the value for drop terminal centrifugal velocity of $u_{te} = d_p^2 \rho_p a / 18 \mu_g$, where d_p and ρ_p are the drop particle diameter, cm , and particle density, g/cm^3 , respectively; μ_g is the gas viscosity, P ; and a is the acceleration due to centrifugal force. It is defined by the equation $a = 2U_g^2 \sin \theta / W \cos^3 \theta$. For situations in which Stokes' law does not apply, Calvert recommends substitution in the derivation of Eq. (14-227) for u of drag coefficients from drag-coefficient data of Foust et al. (*Principles of Unit Operations*, Toppan Co., Tokyo, 1959).

Calvert found that reentrainment from the baffles was affected by the gas velocity, the liquid-to-gas ratio, and the orientation of the baffles. Horizontal gas flow past vertical baffles provided the best drainage and lowest reentrainment. Safe operating regions with vertical baffles are shown in Fig. 14-112. Horizontal baffles gave the poorest drainage and the highest reentrainment, with inclined baffles intermediate in performance. Equation (14-228), developed by Calvert, predicts pressure drop across zigzag baffles. The indicated summation must be made over the number of rows of baffles present.

$$\Delta P = \sum_{i=1}^{i=n} 1.02 \times 10^{-3} f_D \rho_g \frac{U_g' A_p}{2A_t} \quad (14-228)$$

ΔP is the pressure drop, cm of water; ρ_g is the gas density, g/cm^3 ; A_p is the total projected area of an entire row of baffles in the direction of inlet gas flow, cm^2 ; and A_t is the duct cross-sectional area, cm^2 . The

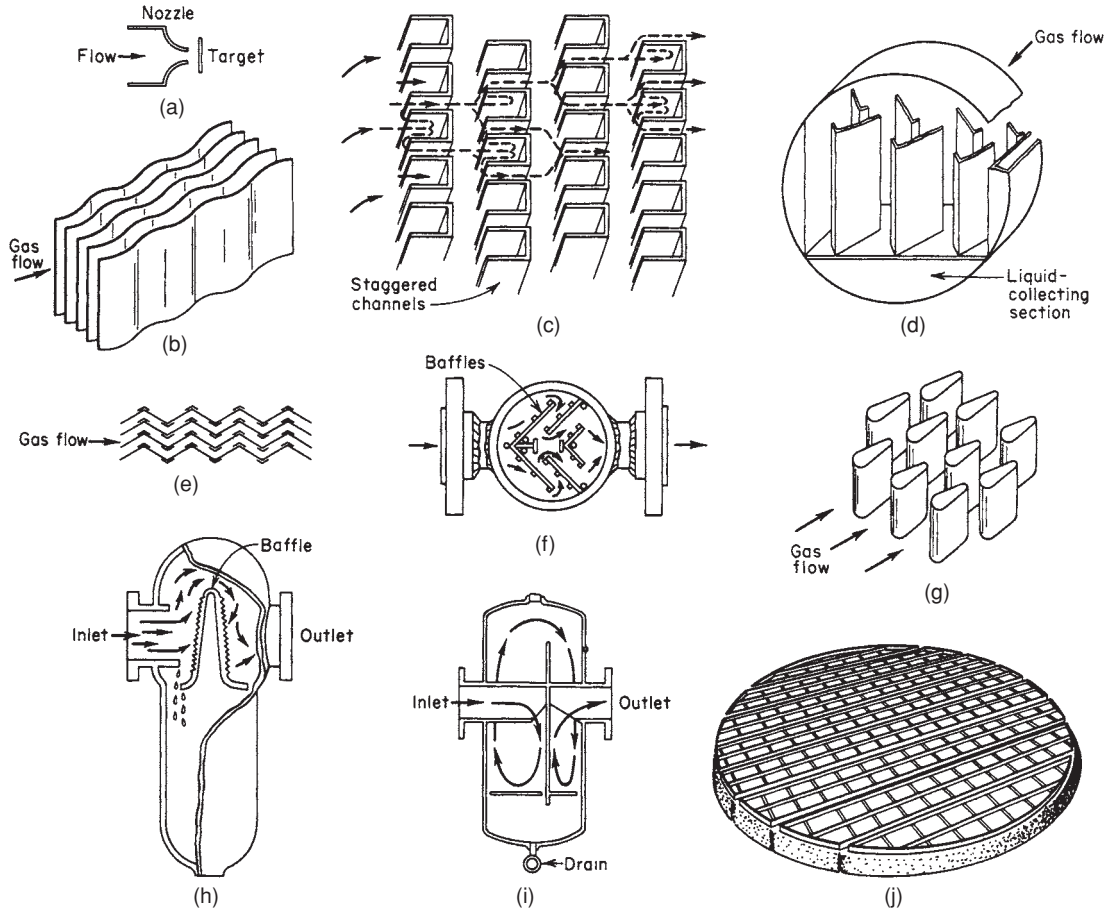


FIG. 14-110 Typical impingement separators. (a) Jet impactor. (b) Wave plate. (c) Staggered channels. (*Blaw-Knox Food & Chemical Equipment, Inc.*) (d) Vane-type mist extractor. (*Maloney-Crawford Tank and Mfg. Co.*) (e) Peerless line separator. (*Peerless Mfg. Co.*) (f) Strong separator. (*Strong Carlisle and Hammond.*) (g) Karbate line separator. (*Union Carbide Corporation*) (h) Type E horizontal separator. (*Wright-Austin Co.*) (i) PL separator. (*Ingersoll Rand.*) (j) Wire-mesh demister. (*Otto H. York Co.*)

value f_D is a drag coefficient for gas flow past inclined flat plates taken from Fig. 14-113, while U_g' is the actual gas velocity, cm/s, which is related to the superficial gas velocity U_g by $U_g' = U_g / \cos \theta$. It must be noted that the angle of incidence θ for the second and successive rows of baffles is twice the angle of incidence for the first row. Most of

Calvert's work was with 30° baffles, but the method correlates well with other data on 45° baffles.

The Karbate line separator (Fig. 14-110g) is composed of several layers of teardrop-shaped target rods of Karbate. A design flow constant K in Eq. (14-226) of 0.035 m/s (1.0 ft/s) is recommended by the

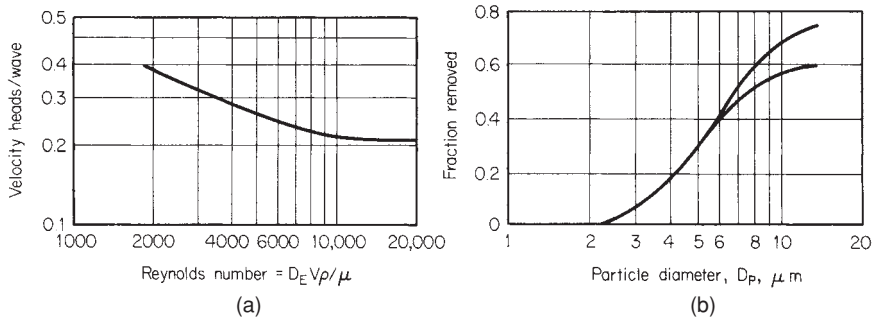


FIG. 14-111 Pressure drop and collection efficiency of a wave-plate separator. (a) Pressure drop. (b) Efficiency. D_E = clearance between sheets. (*Katz, M.S. thesis, Pennsylvania State University, 1958.*)

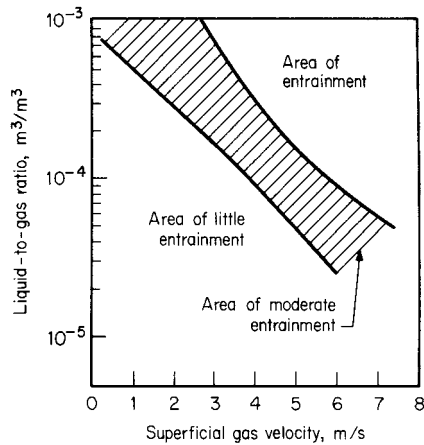


FIG. 14-112 Safe operating region to prevent reentrainment from vertical zigzag baffles with horizontal gas flow. (Calvert, Yung, and Leung, NTIS Publ. PB-248050, 1975.)

manufacturer. Pressure drop is said to be 5½ velocity heads on the basis of the superficial gas velocity. This value would probably increase at high liquid loads. Figure 14-114 gives the manufacturer's reported grade efficiency curve at the design air velocity.

The use of multiple tube banks as a droplet collector has also been studied by Calvert (R-12). He reports that collection efficiency for closely packed tubes follows equations for rectangular jet impaction which can be obtained graphically from Fig. 14-115 by using a dimensional parameter β which is based on the tube geometry; $\beta = 2l_i/b$, where b is the open distance between adjacent tubes in the row (orifice width) and l_i is the impaction length (distance between orifice and impingement plane), or approximately the distance between centerlines of successive tube rows. Note that the impaction parameter K_p is plotted to the one-half power in Fig. 14-115 and that the radius of the droplet is used rather than the diameter. Collection efficiency overall for a given size of particle is predicted for the entire tube bank by

$$\eta = 1 - (1 - \eta_b)^N \tag{14-229}$$

where η_b is the collection efficiency for a given size of particle in one stage of a rectangular jet impactor (Fig. 14-115) and N is the number of stages in the tube bank (equal to one less than the number of rows).

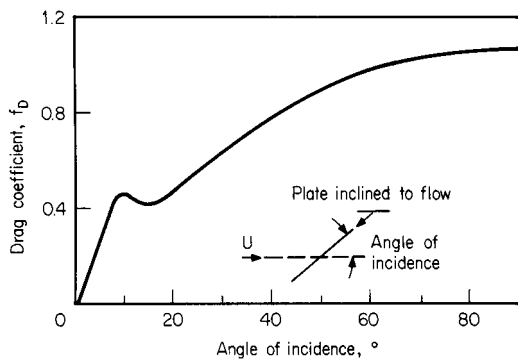


FIG. 14-113 Drag coefficient for flow past inclined flat plates for use in Eq. (14-228). [Calvert, Yung, and Leung, NTIS Publ. PB-248050; based on Fage and Johansen, Proc. R. Soc. (London), 116A, 170 (1927).]

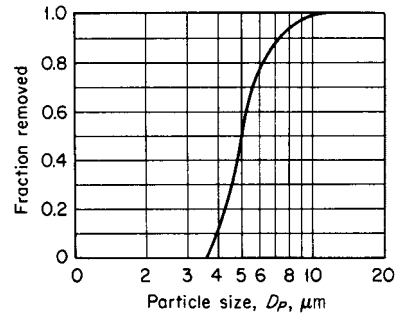


FIG. 14-114 Collection efficiency of Karbate line separator, based on particles with a specific gravity of 1.0 suspended in atmospheric air with a pressure drop of 2.5 cm water gauge. (Union Carbide Corporation Cat. Sec. S-6900, 1960.)

For widely spaced tubes, the target efficiency η_g can be calculated from Fig. 17-39 or from the impaction data of Golovin and Putnam [Ind. Eng. Chem. Fundam., 1, 264 (1962)]. The efficiency of the overall tube banks for a specific particle size can then be calculated from the equation $\eta = 1 - (1 - \eta_a/A)^n$, where a' is the cross-sectional area of all tubes in one row, A is the total flow area, and n is the number of rows of tubes.

Calvert reports pressure drop through tube banks to be largely unaffected by liquid loading and indicates that Grimison's correlations in Sec. 6 ("Tube Banks") for gas flow normal to tube banks or data for gas flow through heat-exchanger bundles can be used. However, the following equation is suggested:

$$\Delta P = 8.48 \times 10^{-3} n \rho_g U_g^2 \tag{14-230}$$

where ΔP is cm of water; n is the number of rows of tubes; ρ_g is the gas density, g/cm³; and U_g is the actual gas velocity between tubes in a row, cm/s. Calvert did find an increase in pressure drop of about 80 to 85 percent above that predicted by Eq. (14-230) in vertical upflow of gas through tube banks due to liquid holdup at gas velocities above 4 m/s.

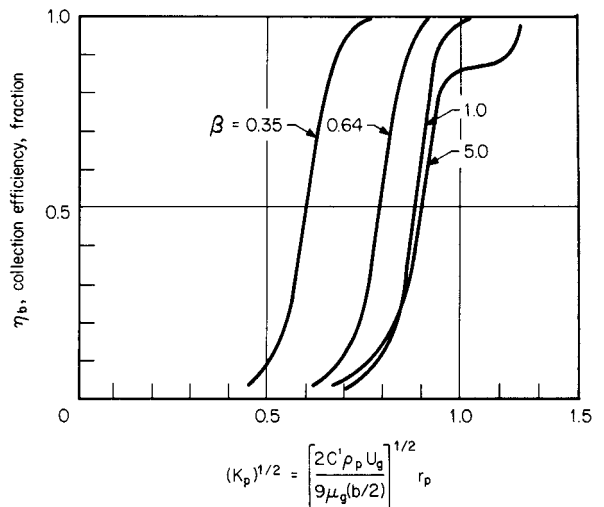


FIG. 14-115 Experimental collection efficiencies of rectangular impactors. C' is the Stokes-Cunningham correction factor; ρ_p , particle density, g/cm³; U_g , superficial gas velocity, approaching the impactor openings, cm/s; and μ_g , gas viscosity, P. [Calvert, Yung, and Leung, NTIS Publ. PB-248050; based on Mercer and Chow, J. Coll. Interface Sci., 27, 75 (1968).]

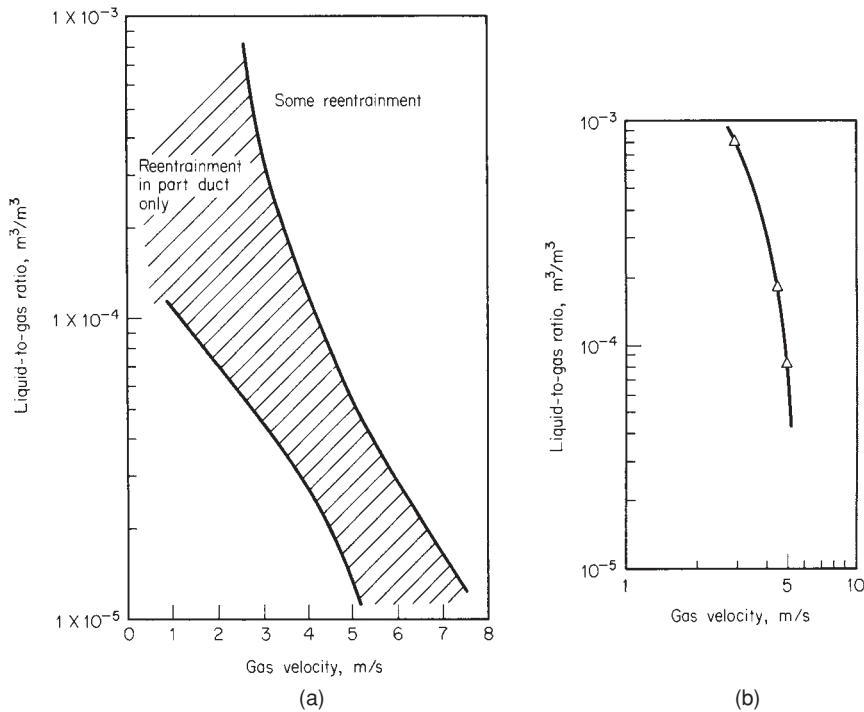


FIG. 14-116 Experimental results showing effect of gas velocity and liquid load on entrainment from (a) vertical tube banks with horizontal gas flow and (b) horizontal tube banks with upflow. To convert meters per second to feet per second, multiply by 3.281. (Calvert, Yung, and Leung, NTIS Publ. PB-248050.)

The onset of liquid reentrainment from tube banks can be predicted from Fig. 14-116. Reentrainment occurred at much lower velocities in vertical upflow than in horizontal gas flow through vertical tube banks. While the top of the cross-hatched line of Fig. 14-116a predicts reentrainment above gas velocities of 3 m/s (9.8 ft/s) at high liquid loading, most of the entrainment settled to the bottom of the duct in 1 to 2 m (3.3 to 6.6 ft), and entrainment did not carry significant distances until the gas velocity exceeded 7 m/s (23 ft/s).

Packed-Bed Collectors Many different materials, including coal, coke, broken solids of various types such as brick, tile, rock, and stone, as well as normal types of tower-packing rings, saddles, and special plastic shapes, have been used over the years in packed beds to remove entrained liquids through impaction and filtration. Separators using natural materials are not available as standard commercial units but are designed for specific applications. Coke boxes were used extensively in the years 1920 to 1940 as sulfuric acid entrainment separators (see *Chemical Engineers' Handbook*, 5th ed., p. 18-87) but have now been largely superseded by more sophisticated and efficient devices.

Jackson and Calvert [*Am. Inst. Chem. Eng. J.*, **12**, 1075 (1966)] studied the collection of fine fuel-oil-mist particles in beds of 1/2-in glass spheres, Raschig rings, and Berl and Intalox saddles. The mist had a mass median particle diameter of 6 μm and a standard deviation of 2.0. The collection efficiency as a function of particle size and gas velocity in a 355-mm- (14-in-) diameter by 152-mm- (6-in-) thick bed of Intalox saddles is given in Fig. 14-117. This and additional work have been generalized by Calvert (R-12) to predict collection efficiencies of liquid particles in any packed bed. Assumptions in the theoretical development are that the drag force on the drop is given by Stokes' law and that the number of semicircular bends to which the gas is subjected, η_1 , is related to the length of the bed, Z (cm), in the direction of gas flow, the packing diameter, d_c (cm), and the gas-flow channel width, b (cm), such that $\eta_1 = Z/(d_c + b)$. The gas velocity through the channels, U_{gb} (cm/s), is inversely proportional to the bed

free volume for gas flow such that $U_{gb} = U_g [1/(\epsilon - h_b)]$, where U_g is the gas superficial velocity, cm/s, approaching the bed, ϵ is the bed void fraction, and h_b is the fraction of the total bed volume taken up with liquid which can be obtained from data on liquid holdup in packed beds. The width of the semicircular channels b can be expressed as a fraction j of the diameter of the packing elements, such that $b = jd_c$. These assumptions (as modified by G. E. Goltz, personal communica-

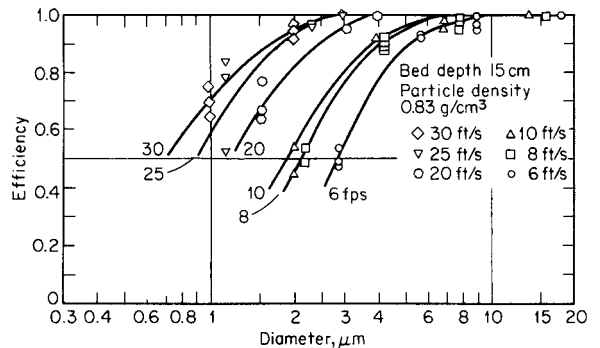


FIG. 14-117 Experimental collection efficiency, 1/2-in Intalox saddles. To convert feet per second to meters per second, multiply by 0.3048; to convert centimeters to inches, multiply by 0.394; and to convert grams per cubic centimeter to pounds per cubic foot, multiply by 62.43. [Jackson and Calvert, *Am. Inst. Chem. Eng. J.*, **12**, 1975 (1968).]

TABLE 14-27 Experimental Values for j , Channel Width in Packing as a Fraction of Packing Diameter

Packing size		Type of packing	j
cm	in		
1.27	0.5	Berl and Intalox saddles, marbles, Raschig rings	0.192
2.54	1.0	Berl and Intalox saddles, pall rings	0.190
3.8	1.5	Berl and Intalox saddles, pall rings	0.165
7.6–12.7	3–5	Coke	0.03

tion) lead to an equation for predicting the penetration of a given size of liquid particle through a packed bed:

$$P_t = \exp \left[\frac{-\pi}{2(j + j^2)(\epsilon - h_p)} \left(\frac{Z}{d_c} \right) K_p \right] \quad (14-231)$$

where

$$K_p = \frac{\rho_p d_p^2 U_g}{9 \mu_g d_c} \quad (14-232)$$

Values of ρ_p and d_p are droplet density, g/cm^3 , and droplet diameter, cm; μ_g is the gas viscosity, P. All other terms were defined previously. Table 14-27 gives values of j calculated from experimental data of Jackson and Calvert. Values of j for most manufactured packing appear to fall in the range from 0.16 to 0.19. The low value of 0.03 for coke may be due to the porosity of the coke itself.

Calvert (R-12) has tested the correlation in cross-flow packed beds, which tend to give better drainage than countercurrent beds, and has found the effect of gas-flow orientation insignificant. However, the onset of reentrainment was somewhat lower in a bed of 2.5-cm (1.0-in) pall rings with gas upflow [6 m/s (20 ft/s)] than with horizontal cross-flow of gas. The onset of reentrainment was independent of liquid loading (all beds were nonirrigated), and entrainment occurred at values somewhat above the flood point for packed beds as predicted by conventional correlations. In beds with more than 3 cm (1.2 in) of water pressure drop, the experimental drop with both vertical and horizontal gas flow was somewhat less than predicted by generalized packed-bed pressure-drop correlations. However, Calvert recommends these correlations for design as conservative.

Calvert's data indicate that packed beds irrigated only with the collected liquid can have collection efficiencies of 80 to 90 percent on mist particles down to 3 μm but have low efficiency on finer mist particles. Frequently, irrigated packed towers and towers with internals will be used with liquid having a wetting capability for the fine mist which must be collected. Tennessee Valley Authority (TVA) experiments with the collection of 1.0- μm mass median phosphoric acid mist in packed towers have shown that the strength of the circulating phosphoric acid is highly important [see Baskerville, *Am. Inst. Chem. Eng. J.*, **37**, 79 (1941); and p. 18–87, 5th ed. of the *Handbook*]. Hesketh (*J. Air Pollut. Control Assoc.*, **24**, 942 (1974)) has reported up to 50 percent improvement in collection efficiency in venturi scrubbers on fine particles with the addition of only 0.10 percent of a low-foaming nonionic surfactant to the scrubbing liquid, and others have experienced similar results in other gas-liquid-contacting devices. Calvert (R-9 and R-10) has reported on the efficiency of various gas-liquid-contacting devices for fine particles. Figure 14-118 gives the particle aerodynamic cut size for a single-sieve-plate gas scrubber as a function of sieve hole size d_h , cm; hole gas velocity u_h , m/s; and froth or foam density on the plate F , g/cm^3 . This curve is based on standard air and water properties and wettable (hydrophilic) particles. The cut diameter decreases with an increase in froth density, which must be predicted from correlations for sieve-plate behavior (see Fig. 14-32). Equation (14-231) can be used to calculate generalized design curves for collection in packed columns in the same fashion by finding parameters of packing size, bed length, and gas velocity which give collection efficiencies of 50 percent for various size particles. Figure 14-119 illustrates such a plot for three gas velocities and two sizes of packing.

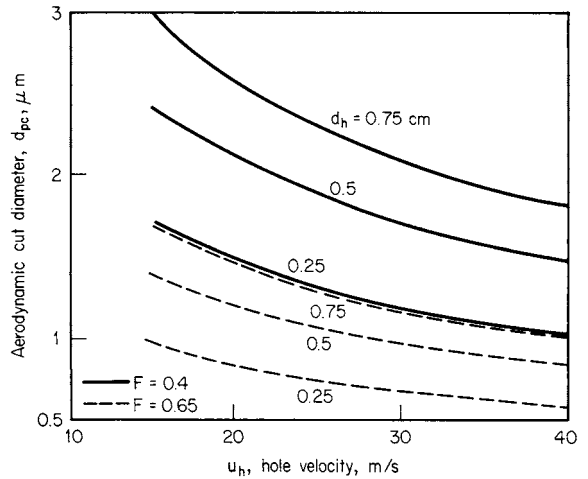


FIG. 14-118 Aerodynamic cut diameter for a single-sieve-plate scrubber as a function of hole size, hole-gas velocity, and froth density, F , g/cm^3 . To convert meters per second to feet per second, multiply by 3.281; to convert grams per cubic centimeter to pounds per cubic foot, multiply by 62.43. [Calvert, J. Air Pollut. Control Assoc., **24**, 929 (1974).]

Wire-Mesh Mist Collectors Knitted mesh of varying density and voidage is widely used for entrainment separators. Its advantage is close to 100 percent removal of drops larger than 5 μm at superficial gas velocities from about 0.2 m/s (0.6 ft/s) to 5 m/s (16.4 ft/s), depending somewhat on the design of the mesh. Pressure drop is usually no more than 2.5 cm (1 in) of water. A major disadvantage is the ease with which tars and insoluble solids plug the mesh. The separator can be made to fit vessels of any shape and can be made of any material which can be drawn into a wire. Stainless-steel and plastic fibers are most common, but other metals are sometimes used. Generally three basic types of mesh are used: (1) layers with a crimp in the same direction (each layer is actually a nested double layer); (2) layers with a crimp in

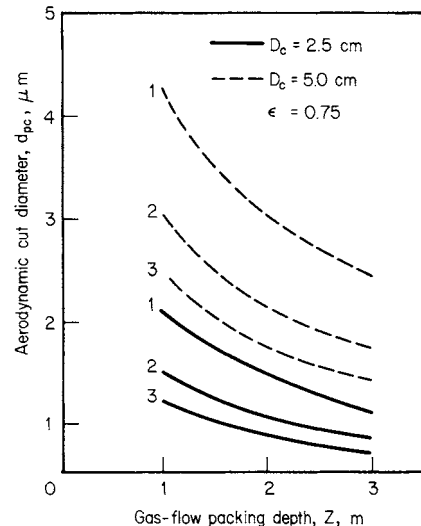


FIG. 14-119 Aerodynamic cut diameter for a typical packed-bed entrainment separator as a function of packing size, bed depth, and three gas velocities: curve 1–1.5 m/s, curve 2–3.0 m/s, and curve 3–4.5 m/s. To convert meters to feet, multiply by 3.281; to convert centimeters to inches, multiply by 0.394. [Calvert, J. Air Pollut. Control Assoc., **24**, 929 (1974).]

alternate directions, which increases voidage, reduces sheltering and increases target efficiency per layer, and gives a lower pressure drop per unit length; and (3) spiral-wound layers which reduce pressure drop by one-third, but fluid creep may lead to higher entrainment. Some small manufacturers of plastic meshes may offer other weaves claimed to be superior. The filament size can vary from about 0.15 mm (0.006 in) for fine-wire pads to 3.8 mm (0.15 in) for some plastic fibers. Typical pad thickness varies from 100 to 150 mm (4 to 6 in), but occasionally pads up to 300 mm (12 in) thick are used. A typical wire diameter for standard stainless mesh is 0.28 mm (0.011 in), with a finished mesh density of 0.15 g/cm³ (9.4 lb/ft³). A lower mesh density may be produced with standard wire to give 10 to 20 percent higher flow rates.

Figure 14-120 presents an early calculated estimate of mesh efficiency as a fraction of mist-particle size. Experiments by Calvert (R-12) confirm the accuracy of the equation of Bradie and Dickson (*Joint Symp. Proc. Inst. Mech. Eng./Yorkshire Br. Inst. Chem. Eng.*, 1969, pp. 24-25) for primary efficiency in mesh separators:

$$\eta = 1 - \exp(-2/3)\pi a l \eta_i \quad (14-232)$$

where η is the overall collection efficiency for a given-size particle; l is the thickness of the mesh, cm, in the direction of gas flow; a is the surface area of the wires per unit volume of mesh pad, cm²/cm³; and η_i , the target collection efficiency for cylindrical wire, can be calculated from Fig. 17-39 or the impaction data of Golovin and Putnam [*Ind. Eng. Chem.*, **1**, 264 (1962)]. The factor 2/3, introduced by Carpenter and Othmer [*Am. Inst. Chem. Eng. J.*, **1**, 549 (1955)], corrects for the fact that not all the wires are perpendicular to the gas flow and gives the projected perpendicular area. If the specific mesh surface area a is not available, it can be calculated from the mesh void area ϵ and the mesh wire diameter d_w in cm, $a = 4(1 - \epsilon)/d_w$.

York and Poppele (R-17) have stated that factors governing maximum allowable gas velocity through the mesh are (1) gas and liquid density, (2) liquid surface tension, (3) liquid viscosity, (4) specific wire surface area, (5) entering-liquid loading, and (6) suspended-solids content. York (R-18) has proposed application of the Souders-Brown equation [Eq. (14-226)] for correlation of maximum allowable gas velocity with values of K for most cases of 0.1067 m/s to give U in m/s (0.35 for ft/s). When liquid viscosity or inlet loading is high or the liquid is dirty, the value of K must be reduced. Schroeder (M.S. thesis, Newark College of Engineering, 1962) found lower values for K necessary when liquid surface tension is reduced such as by the presence of surfactants in water. Ludwig (*Applied Process Design for Chemical and Petrochemical Plants*, 2d ed., vol. I, Gulf, Houston, 1977, p. 157) recommends reduced K values of (0.061 m/s) under vacuum at an absolute pressure of 6.77 kPa (0.98 lbf/in²) and $K = 0.082$ m/s at 54 kPa (7.83 lbf/in²) absolute. Most manufacturers suggest setting the design velocity at three-fourths of the maximum velocity to allow for surges in gas flow.

York and Poppele (R-17) have suggested that total pressure drop through the mesh is equal to the sum of the mesh dry pressure drop

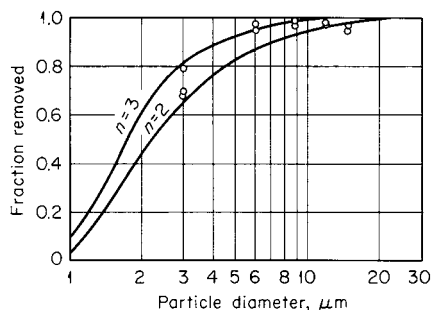


FIG. 14-120 Collection efficiency of wire-mesh separator; 6-in thickness, 98.6 percent free space, 0.006-in-diameter wire used for experiment points. Curves calculated for target area equal to 2 and 3 times the solids volume of packing. To convert inches to millimeters, multiply by 25.4.

plus an increment due to the presence of liquid. They considered the mesh to be equivalent to numerous small circular channels and used the D'Arcy formula with a modified Reynolds number to correlate friction factor (see Fig. 14-121) for Eq. (14-233) giving dry pressure drop.

$$\Delta P_{\text{dry}} = f l \rho_g U_g^2 / 981 \epsilon^3 \quad (14-233)$$

where ΔP is in cm of water; f is from Fig. (14-121); ρ_g is the gas density, g/cm³; U_g is the superficial gas velocity, cm/s; and ϵ is the mesh porosity or void fraction; l and a are as defined in Eq. (14-232). Figure 14-121 gives data of York and Poppele for mesh crimped in the same and alternating directions and also includes the data of Satsangee, of Schuring, and of Bradie and Dickson.

The incremental pressure drop for wet mesh is not available for all operating conditions or for mesh of different styles. The data of York and Poppele for wet-mesh incremental pressure drop, ΔP_L in cm of water, are shown in Fig. 14-122 or parameters of liquid velocity L/A , defined as liquid volumetric flow rate, cm³/min per unit of mesh cross-sectional area in cm²; liquid density ρ_L is in g/cm³.

York generally recommends the installation of the mesh horizontally with upflow of gas as in Fig. 14-110f; Calvert (R-12) tested the mesh horizontally with upflow and vertically with horizontal gas flow. He reports better drainage with the mesh vertical and somewhat higher permissible gas velocities without reentrainment, which is contrary to past practice. With horizontal flow through vertical mesh, he found collection efficiency to follow the predictions of Eq. (14-232) up to 4 m/s (13 ft/s) with air and water. Some reentrainment was encountered at higher velocities, but it did not appear serious until velocities exceeded 6.0 m/s (20 ft/s). With vertical upflow of gas, entrainment was encountered at velocities above and below 4.0 m/s (13 ft/s), depending on inlet liquid quantity (see Fig. 14-123). Figure 14-124 illustrates the onset of entrainment from mesh as a function of liquid loading and gas velocity and the safe operating area recommended by Calvert. Measurements of dry pressure drop by Calvert gave values only about one-third of those predicted from Eq. (14-233). He found the pressure drop to be highly affected by liquid load. The pressure drop of wet mesh could be correlated as a function of $U_g^{1.65}$ and parameters of liquid loading L/A , as shown in Fig. 14-125.

As indicated previously, mesh efficiency drops rapidly as particles decrease in size below 5 μm . An alternative is to use two mesh pads in series. The first mesh is made of fine wires and is operated beyond the

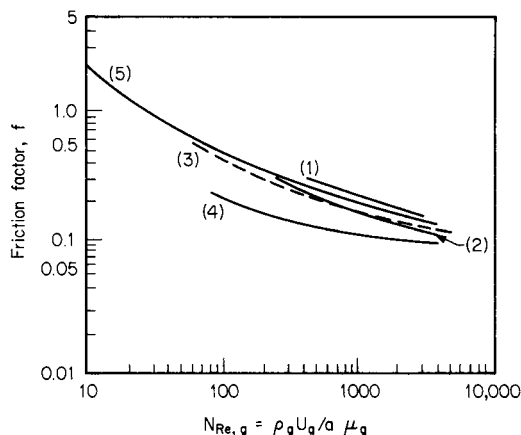


FIG. 14-121 Value of friction factor f for dry knitted mesh for Eq. (14-233). Values of York and Poppele [*Chem. Eng. Prog.*, **50**, 421 (1954)] are given in curve 1 for mesh crimped in the alternating direction and curve 2 for mesh crimped in the same direction. Data of Bradie and Dickson (*Joint Symp. Proc. Inst. Mech. Eng./Yorkshire Br. Inst. Chem. Eng.*, 1969, pp. 24-25) are given in curve 3 for layered mesh and curve 4 for spiral-wound mesh. Curve 5 is data of Satsangee (M.S. thesis, Brooklyn Polytechnic Institute, 1948) and Schurig (D.Ch.E. dissertation, Brooklyn Polytechnic Institute, 1946). (From Calvert, Yung, and Leung, NTIS Publ. PB-248050, 1975.)

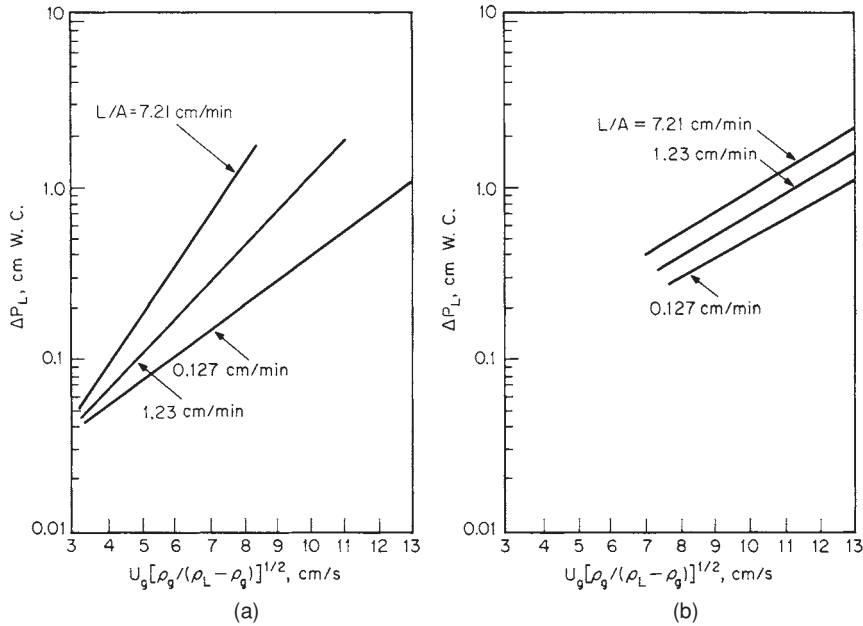


FIG. 14-122 Incremental pressure drop in knitted mesh due to the presence of liquid (a) with the mesh crimps in the same direction and (b) with crimps in the alternating direction, based on the data of York and Poppele [Chem. Eng. Prog., 50, 421 (1954)]. To convert centimeters per minute to feet per minute, multiply by 0.0328; to convert centimeters per second to feet per second, multiply by 0.0328. (From Calvert, Yung, and Leung, NTIS Publ. PB-248050, 1975.)

flood point. It results in droplet coalescence, and the second mesh, using standard wire and operated below flooding, catches entrainment from the first mesh. Coalescence and flooding in the first mesh may be assisted with water sprays or irrigation. Massey [Chem. Eng. Prog., 53(5), 114 (1959)] and Coykendall et al. [J. Air Pollut. Control Assoc., 18, 315 (1968)] have discussed such applications. Calvert (R-12) presents data on the particle size of entrained drops from mesh as a function of gas velocity which can be used for sizing the secondary collector. A major disadvantage of this approach is high pressure drop, which can be in the range from 25 cm (10 in) of water to as high as 85 cm (33 in) of water if the mist is mainly submicrometer.

Wet Scrubbers Scrubbers have not been widely used for the collection of purely liquid particulate, probably because they are generally more complex and expensive than impaction devices of the types previously discussed. Further, scrubbers are no more efficient than

the former devices for the same energy consumption. However, scrubbers of the types discussed in Sec. 17 and illustrated in Figs. 17-48 to 17-54 can be used to capture liquid particles efficiently. Their use is primarily indicated when it is desired to accomplish simultaneously another task such as gas absorption or the collection of solid and liquid particulate mixtures.

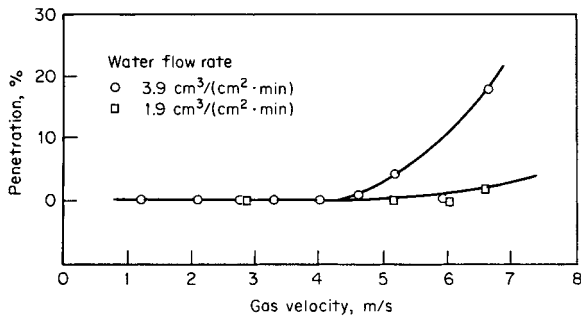


FIG. 14-123 Experimental data of Calvert with air and water in mesh with vertical upflow, showing the effect of liquid loading on efficiency and reentrainment. To convert meters per second to feet per second, multiply by 3.281; to convert cubic centimeters per square centimeter-minute to cubic feet per square foot-minute, multiply by 0.0328. (Calvert, Yung, and Leung, NTIS Publ. PB-248050, 1975.)

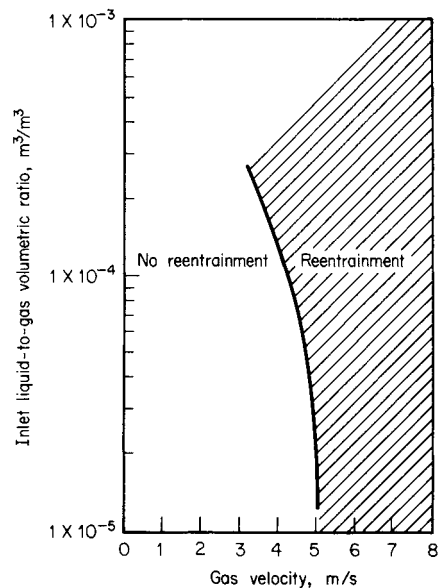


FIG. 14-124 Effect of gas and liquid rates on onset of mesh reentrainment and safe operating regions. To convert meters per second to feet per second, multiply by 3.281. (Calvert, Yung, and Leung, NTIS Publ. PB-248050, 1975.)

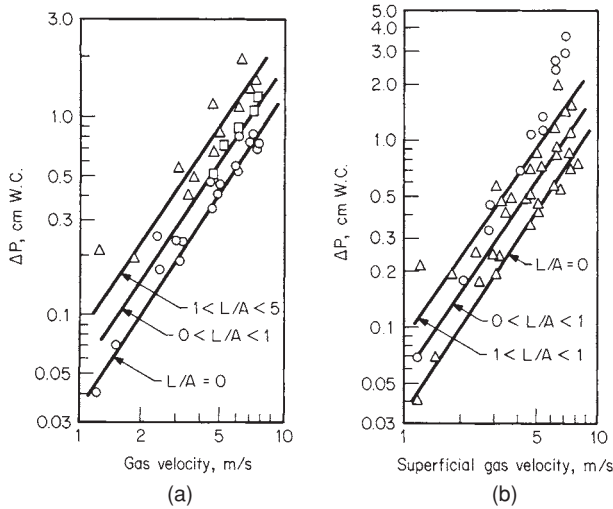


FIG. 14-125 Experimental pressure measured by Calvert as a function of gas velocity and liquid loading for (a) horizontal gas flow through vertical mesh and (b) gas upflow through horizontal mesh. Mesh thickness was 10 cm with 2.8-mm wire and void fraction of 98.2 percent, crimped in alternating directions. To convert meters per second to feet per second, multiply by 3.281; to convert centimeters to inches, multiply by 0.394. (Calvert, Yung, and Leung, NTIS Publ. PB-248050, 1975.)

Table 20-41 [Chemical Engineers' Handbook, 5th ed.], showing the minimum size of particles collectible in different types of scrubbers at reasonably high efficiencies, is a good selection guide. Cyclonic spray towers can effectively remove liquid particles down to around 2 to 3 μm . Figures 20-112 and 20-113 (Chemical Engineers' Handbook, 5th ed.), giving target efficiency between spray drop size and particle size as calculated by Stairmand or Johnstone and Roberts, should be considered in selecting spray atomization for the most efficient tower operation. Figure 14-126 gives calculated particle cut size as a function of tower height (or length) for vertical countercurrent spray towers and for horizontal-gas-flow, vertical-liquid-flow cross-current spray towers with parameters for liquid

drop size. These curves are based on physical properties of standard air and water and should be used under conditions in which these are reasonable approximations. Lack of uniform liquid distribution or liquid flowing down the walls can affect the performance, requiring empirical correction factors. Calvert (R-10) suggests that a correction factor of 0.2 be used in small-diameter scrubbers to account for the liquid on the walls, i.e., let $Q_L/Q_G = 0.2 (Q_L/Q_G)_{\text{actual}}$. Many more complicated wet scrubbers employ a combination of sprays or liquid atomization, cyclonic action, baffles, and targets. These combinations are not likely to be more efficient than similar devices previously discussed that operate at equivalent pressure drop. The vast majority of wet scrubbers operate at moderate pressure drop [8 to 15 cm (3 to 6 in) of water or 18 to 30 cm (7 to 12 in) of water] and cannot be expected to have high efficiency on particles smaller than 10 μm or 3 to 5 μm respectively. Fine and submicrometer particles can be captured efficiently only in wet scrubbers having high energy input such as venturi scrubbers, two-phase eductor scrubbers, and flux-force-condensation scrubbers.

Venturi Scrubbers One type of venturi scrubber is illustrated in Fig. 17-48. Venturi scrubbers have been used extensively for collecting fine and submicrometer solid particulate, condensing tars and mists, and mixtures of liquids and solids. To a lesser extent, they have also been used for simultaneous gas absorption, although Lundy [Ind. Eng. Chem., 50, 293 (1958)] indicates that they are generally limited to three transfer units. They have been used to collect submicrometer chemical incinerator fume and mist as well as sulfuric and phosphoric acid mists. The collection efficiency of a venturi scrubber is highly dependent on the throat velocity or pressure drop, the liquid-to-gas ratio, and the chemical nature of wettability of the particulate. Throat velocities may range from 60 to 150 m/s (200 to 500 ft/s). Liquid injection rates are typically 0.67 to 1.4 $\text{m}^3/1000 \text{ m}^3$ of gas. A liquid rate of 1.0 m^3 per 1000 m^3 of gas is usually close to optimum, but liquid rates as high as 2.7 m^3 (95 ft^3) have been used. Efficiency improves with increased liquid rate but only at the expense of higher pressure drop and energy consumption. Pressure-drop predictions for a given efficiency are hazardous without determining the nature of the particulate and the liquid-to-gas ratio. In general, particles coarser than 1 μm can be collected efficiently with pressure drops of 25 to 50 cm of water. For appreciable collection of submicrometer particles, pressure drops of 75 to 100 cm (30 to 40 in) of water are usually required. When particles are appreciably finer than 0.5 μm , pressure drops of 175 to 250 cm (70 to 100 in) of water have been used.

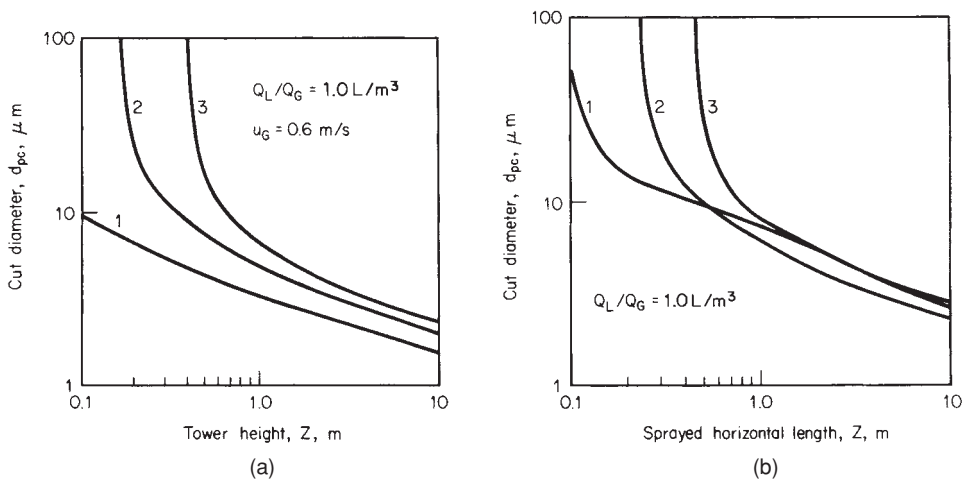


FIG. 14-126 Predicted spray-tower cut diameter as a function of sprayed length and spray droplet size for (a) vertical-countercurrent towers and (b) horizontal-cross-flow towers per Calvert [J. Air Pollut. Control Assoc., 24, 929 (1974)]. Curve 1 is for 200- μm spray droplets, curve 2 for 500- μm spray, and curve 3 for 1000- μm spray. Q_L/Q_G is the volumetric liquid-to-gas ratio, L liquid/ m^3 gas, and u_G is the superficial gas velocity in the tower. To convert liters per cubic meter to cubic feet per cubic foot, multiply by 10^{-3} .

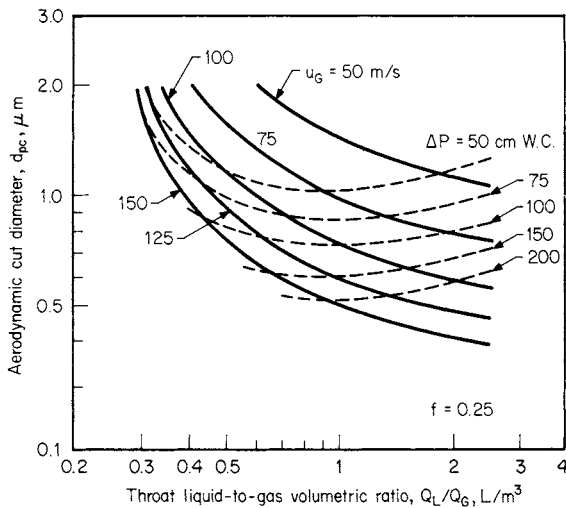


FIG. 14-127 Prediction of venturi-scrubber cut diameter for hydrophobic particles as functions of operating parameters as measured by Calvert [Calvert, Goldshmid, Leith, and Mehta, NTIS Publ. PB-213016, 213017, 1972; and Calvert, J. Air Pollut. Control Assoc., **24**, 929 (1974).] u_g is the superficial throat velocity, and ΔP is the pressure drop from converging to diverging section. To convert meters per second to feet per second, multiply by 3.281; to convert liters per cubic meter to cubic feet per cubic foot, multiply by 10^{-3} ; and to convert centimeters to inches, multiply by 0.394.

One of the problems in predicting efficiency and required pressure drop of a venturi is the chemical nature or wettability of the particulate, which on 0.5- μm -size particles can make up to a threefold difference in required pressure drop for its efficient collection. Calvert (R-9, R-10) has represented this effect by an empirical factor f , which is based on the hydrophobic ($f = 0.25$) or hydrophilic ($f = 0.50$) nature of the particles. Figure 14-127 gives the cut diameter of a venturi scrubber as a function of its operating parameters (throat velocity, pressure drop, and liquid-to-gas ratio) for hydrophobic particles. Figure 14-129 compares cut diameter as a function of pressure drop for an otherwise identically operating venturi on hydrophobic and hydrophilic particles. Calvert (R-9) gives equations which can be used for constructing cut-size curves similar to those of Fig. 14-127 for other values of the empirical factor f . Most real particles are neither completely hydrophobic nor completely hydrophilic but have f values lying between the two extremes. Phosphoric acid mist, on the basis of data of Brink and Contant [Ind. Eng. Chem., **50**, 1157 (1958)] appears to have a value of $f = 0.46$. Unfortunately, no chemical-test methods have yet been devised for determining appropriate f values for a particulate in the laboratory.

Pressure drop in a venturi scrubber is controlled by throat velocity. While some venturis have fixed throats, many are designed with variable louvers to change throat dimensions and control performance for changes in gas flow. Pressure-drop equations have been developed by Calvert (R-13, R-14, R-15), Boll [Ind. Eng. Chem. Fundam., **12**, 40 (1973)], and Hesketh [J. Air Pollut. Control Assoc., **24**, 939 (1974)]. Hollands and Goel [Ind. Eng. Chem. Fundam., **14**, 16 (1975)] have developed a generalized pressure-drop equation.

The Hesketh equation is empirical and is based upon a regression analysis of data from a number of industrial venturi scrubbers:

$$\Delta P = U_{gt}^2 \rho_g A_t^{0.155} L^{0.78} / 1270 \quad (14-234)$$

where ΔP is the pressure drop, in of water; U_{gt} is the gas velocity in the throat, ft/s; ρ_g is the gas density, lb/ft³; A_t is the throat area, ft²; and L is the liquid-to-gas ratio, gal/1000 acf.

Calvert (R-15) critiqued the many pressure-drop equations and suggested the following simplified equation as accurate to ± 10 percent:

$$\Delta P = \frac{2\rho_l U_g^2}{981g_c} \left(\frac{Q_l}{Q_g} \right) [1 - x^2 + \sqrt{(x^4 - x^2)^{0.5}}] \quad (14-235)$$

where

$$x = (3l_i C_{Di} \rho_g / 16d_l \rho_l) + 1 \quad (14-236)$$

ΔP is the pressure drop, cm of water; ρ_l and ρ_g are the density of the scrubbing liquid and gas respectively, g/cm³; U_g is the velocity of the gas at the throat inlet, cm/s; Q_l/Q_g is the volumetric ratio of liquid to gas at the throat inlet, dimensionless; l_i is the length of the throat, cm; C_{Di} is the drag coefficient, dimensionless, for the mean liquid diameter, evaluated at the throat inlet; and d_l is the Sauter mean diameter, cm, for the atomized liquid. The atomized-liquid mean diameter must be evaluated by the Nukiyama and Tanasawa [Trans. Soc. Mech. Eng. (Japan), **4**, 5, 6 (1937-1940)] equation:

$$d_l = \frac{0.0585}{U_g} \left(\frac{\sigma_l}{\rho_l} \right)^{0.5} + 0.0597 \left[\frac{\mu_l}{(\sigma_l \rho_l)^{0.5}} \right]^{0.45} \left(\frac{Q_l}{Q_g} \right)^{1.5} \quad (14-237)$$

where σ_l is the liquid surface tension, dyn/cm; and μ_l is the liquid viscosity; P . The drag coefficient C_{Di} should be evaluated by the Dickinson and Marshall [Am. Inst. Chem. Eng. J., **14**, 541 (1968)] correlation $C_{Di} = 0.22 + (24/N_{Rei})(1 + 0.15 N_{Rei}^{0.6})$. The Reynolds number, N_{Rei} , is evaluated at the throat inlet considerations as $d_l C_{Di} / \mu_g$.

All venturi scrubbers must be followed by an entrainment collector for the liquid spray. These collectors are usually centrifugal and will have an additional pressure drop of several centimeters of water, which must be added to that of the venturi itself.

Other Scrubbers A liquid-ejector venturi (Fig. 17-49), in which high-pressure water from a jet induces the flow of gas, has been used to collect mist particles in the 1- to 2- μm range, but submicrometer particles will generally pass through an eductor. Power costs for liquid pumping are high if appreciable motive force must be imparted to the gas because jet-pump efficiency is usually less than 10 percent. Harris [Chem. Eng. Prog., **42**(4), 55 (1966)] has described their application. Two-phase eductors have been considerably more successful on capture of submicrometer mist particles and could be attractive in situations in which large quantities of waste thermal energy are available. However, the equivalent energy consumption is equal to that required for high-energy venturi scrubbers, and such devices are likely to be no more attractive than venturi scrubbers when the thermal energy is priced at its proper value. Sparks [J. Air Pollut. Control Assoc., **24**, 958 (1974)] has discussed steam ejectors giving 99 percent collection of particles 0.3 to 10 μm . Energy requirements were 311,000 J/m³ (8.25 Btu/scf). Gardener [J. Air Pollut. Control Assoc., **24**, 954 (1974)] operated a liquid eductor with high-pressure (6900- to 27,600-kPa) (1000- to 4000-lbf/in²) hot water heated to 200°C (392°F) which flashed into two phases as it issued from the jet. He obtained 95 to 99 percent collection of submicrometer particulate. Figure 14-128 shows the water-to-gas ratio required as a function of particle size to achieve 99 percent collection.

Effect of Gas Saturation in Scrubbing If hot unsaturated gas is introduced into a wet scrubber, spray particles will evaporate to cool and saturate the gas. The evaporating liquid molecules moving away from the target droplets will repel particles which might collide with them. This results in the forces of diffusio-phoresis opposing particle collection. Semrau and Witham (Air Pollut. Control Assoc. Prepr. 75-30.1) investigated temperature parameters in wet scrubbing and found a definite decrease in the efficiency of evaporative scrubbers and an enhancement of efficiency when a hot saturated gas is scrubbed with cold water rather than recirculated hot water. Little improvement was experienced in cooling a hot saturated gas below a 50°C dew point.

Energy Requirements for Inertial-Impaction Efficiency Semrau [J. Air Pollut. Control Assoc., **13**, 587 (1963)] proposed a "contacting-power" principle which states that the collecting efficiency of a given size of particle is proportional to the power expended and that the smaller the particle, the greater the power required.

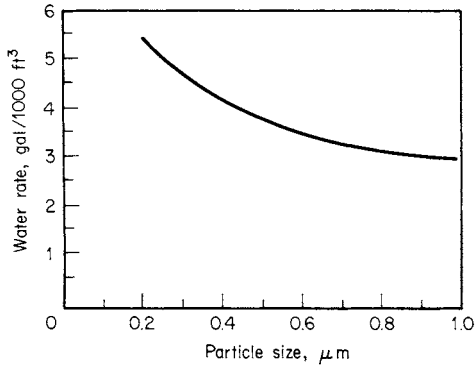


FIG. 14-128 Superheated high-pressure hot-water requirements for 99 percent collection as a function of particle size in a two-phase eductor jet scrubber. To convert gallons per 1000 cubic feet to cubic meters per 1000 cubic meters, multiply by 0.134. [Gardenier, J. Air Pollut. Control Assoc., 24, 954 (1974).]

Mathematically expressed, $N_T = \infty P_T^\gamma$, where N_T is the number of particulate transfer units achieved and P_T is the total energy expended within the collection device, including gas and liquid pressure drop and thermal and mechanical energy added in atomizers. N_T is further defined as $N_T = \ln [1/(1 - \eta)]$, where η is the overall fractional collection efficiency. This was intended as a universal principle, but the constants ∞ and γ have been found to be functions of the chemical nature of the system and the design of the control device. Others have pointed out that the principle is applicable only when the primary collection mechanism is impaction and direct interception. Calvert (R-10, R-12) has found that plotting particle cut size versus pressure drop (or power expended) as in Fig. 14-129 is a more suitable way to develop a generalized energy-requirement curve for impaction

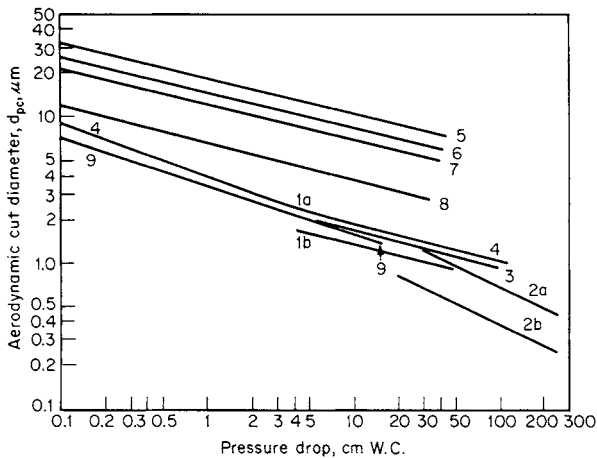


FIG. 14-129 Typical cut diameter as a function of pressure drop for various liquid-particle collectors. Curves 1a and b are single-sieve plates with froth density of 0.4 g/cm³; 1a has sieve holes of 0.5 cm and 1b holes of 0.3 cm. Curves 2a and b are for a venturi scrubber with hydrophobic particles (2a) and hydrophilic particles (2b). Curve 3 is an impingement plate, and curve 4 is a packed column with 2.5-cm-diameter packing. Curve 5 is a zigzag baffle collector with six baffles at $\theta = 30^\circ$. Curve 7 is for six rows of staggered tubes with 1-cm spacing between adjacent tube walls in a row. Curve 8 is similar, except that tube-wall spacing in the row is 0.3 cm. Curve 9 is for wire-mesh pads. To convert grams per cubic centimeter to pounds per cubic foot, multiply by 62.43; to convert centimeters to inches, multiply by 0.394. [Calvert, J. Air Pollut. Control Assoc., 24, 929 (1974); and Calvert, Yung, and Leung, NTIS Publ. PB-248050, 1975.]

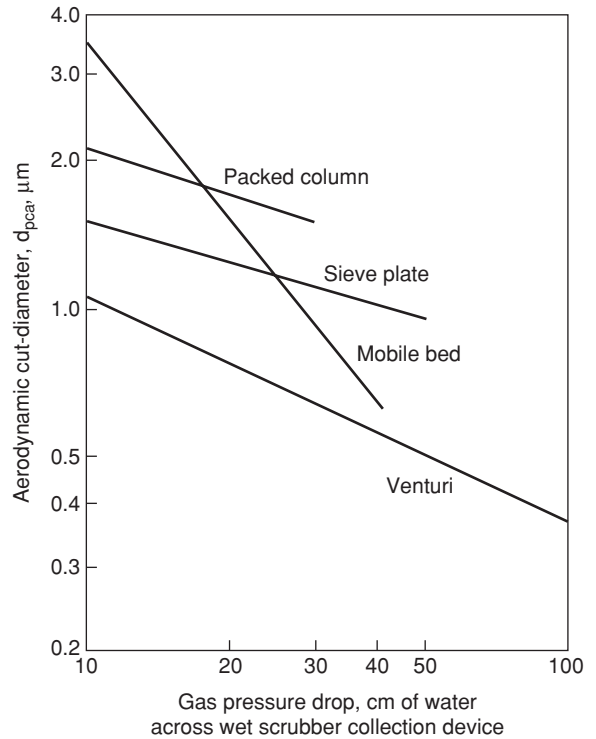


FIG. 14-130 Calvert's refined particle cut-size/power relationship for particle inertial impaction wet collectors. Ref. (R-19) by permission.

devices. The various curves fall close together and outline an imaginary curve that indicates the magnitude of pressure drop required as particle size decreases bound by the two limits of hydrophilic and hydrophobic particles. By calculating the required cut size for a given collection efficiency, Fig. 14-129 can also be used as a guide to deciding between different collection devices.

Subsequently, Calvert (R-19, p. 228) has combined mathematical modeling with performance tests on a variety of industrial scrubbers and has obtained a refinement of the power-input/cut-size relationship as shown in Fig. 14-130. He considers these relationships sufficiently reliable to use this data as a tool for selection of scrubber type and performance prediction. The power input for this figure is based solely on gas pressure drop across the device.

Collection of Fine Mists Inertial-impaction devices previously discussed give high efficiency on particles above 5 μm in size and often reasonable efficiency on particles down to 3 μm in size at moderate pressure drops. However, this mechanism becomes ineffective for particles smaller than 3 μm because of the particle gaslike mobility. Only impaction devices having extremely high energy input such as venturi scrubbers and a flooded mesh pad (the pad interstices really become miniature venturi scrubbers in parallel and in series) can give high collection efficiency on fine particles, defined as 2.5 or 3 μm and smaller, including the submicrometer range. Fine particles are subjected to brownian motion in gases, and diffusional deposition can be employed for their collection. Diffusional deposition becomes highly efficient as particles become smaller, especially below 0.2 to 0.3 μm . Table 14-28 shows typical displacement velocity of particles. Randomly oriented fiber beds having tortuous and narrow gas passages are suitable devices for utilizing this collection mechanism. (The diffusional collection mechanism is discussed in Sec. 17 under "Mechanisms of Dust Collection.") Other collection mechanisms which are efficient for fine particles are electrostatic forces and flux forces such as thermophoresis and diffusiophoresis. Particle growth and nucleation methods are also applicable. Efficient collection of fine particles

TABLE 14-28 Brownian Movement of Particles*

Particle diameter, μm	Brownian displacement of particle, $\mu\text{m/s}$
0.1	29.4
0.25	14.2
0.5	8.92
1.0	5.91
2.5	3.58
5.0	2.49
10.0	1.75

*Brink, *Can. J. Chem. Eng.*, **41**, 134 (1963). Based on spherical water particles in air at 21°C and 1 atm.

is important because particles in the range of 2.0 to around 0.2 μm are the ones which penetrate and are deposited in the lung most efficiently. Hence, particles in this range constitute the largest health hazard.

Fiber Mist Eliminators These devices are produced in various configurations. Generally, randomly oriented glass or polypropylene fibers are densely packed between reinforcing screens, producing fiber beds varying in thickness usually from 25 to 75 mm (1 to 3 in), although thicker beds can be produced. Units with efficiencies as high as 99.9 percent on fine particles have been developed (see *Chemical Engineers' Handbook*, 5th ed., p. 18-88). A combination of mechanisms interacts to provide high overall collection efficiency. Particles larger than 2 to 3 μm are collected on the fibers by inertial impaction and direct interception, while small particles are collected by brownian diffusion. When the device is designed to use this latter mechanism as the primary means, efficiency turndown problems are eliminated as collection efficiency by diffusion increases with residence time. Pressure drop through the beds increases with velocity to the first power since the gas flow is laminar. This leads to design capability trade-offs. As pressure drop is reduced and energy is conserved, capital increases because more filtering area is required for the same efficiency.

Three series of fiber mist eliminators are typically available. A spray-catcher series is designed primarily for essentially 100 percent capture of droplets larger than 3 μm . The high-velocity type is designed to give moderately high efficiency on particles down to 1.0 μm as well. Both of these types are usually produced in the form of flat panels of 25- to 50-mm (1- to 2-in) thickness. The high-efficiency type is illustrated in Fig. 14-131. As mist particles are collected, they coalesce into a liquid film which wets the fibers. Liquid is moved horizontally through the bed by the gas drag force and downward by gravity. It drains down the downstream retaining screen to the bottom of the element and is returned to the process through a liquid seal. Table 14-29 gives typical operating characteristics of the three types of collectors. The application of these devices to sulfuric acid plants and other process gases has been discussed by Brink (see *Chemical Engineers' Handbook*, 5th ed., pp. 18-89, 18-90).

Solid particulates are captured as readily as liquids in fiber beds but can rapidly plug the bed if they are insoluble. Fiber beds have frequently been used for mixtures of liquids and soluble solids and with soluble solids in condensing situations. Sufficient solvent (usually water) is atomized into the gas stream entering the collector to irrigate the fiber elements and dissolve the collected particulate. Such fiber beds have been used to collect fine fumes such as ammonium nitrate and ammonium chloride smokes, and oil mists from compressed air.

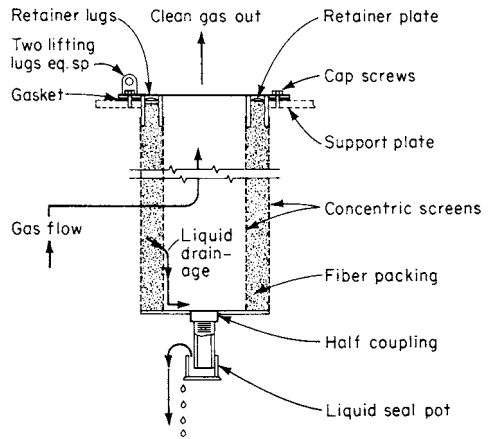


FIG. 14-131 Monsanto high-efficiency fiber-mist-eliminator element. (Monsanto Company.)

Electrostatic Precipitators The principles and operation of electrical precipitators are discussed in Sec. 17 under "Gas-Solids Separations." Precipitators are admirably suited to the collection of fine mists and mixtures of mists and solid particulates. Tube-type precipitators have been used for many years for the collection of acid mists and the removal of tar from coke-oven gas. The first practical installation of a precipitator by Cottrell was made on sulfuric acid mist in 1907. Most older installations of precipitators were tube-type rather than plate-type. However, recently two plate-type wet precipitators employing water sprays or overflowing weirs have been introduced by Mikropul Corporation [Bakke, *J. Air Pollut. Control Assoc.*, **25**, 163 (1975)] and by Fluid Ionics. Such precipitators operate on the principle of making all particles conductive when possible, which increases the particle migration velocity and collection efficiency. Under these conditions, particle dielectric strength becomes a much more important variable, and particles with a low dielectric constant such as condensed hydrocarbon mists become much more difficult to collect than water-wettable particles. Bakke (U.S.-U.S.S.R. Joint Work. Group Symp.: Fine Particle Control, San Francisco, 1974) has developed equations for particle charge and relative collection efficiency in wet precipitators that show the effect of dielectric constant. Wet precipitators can also be used to absorb soluble gases simultaneously by adjusting the pH or the chemical composition of the liquid spray. The presence of the electric field appears to enhance absorption. Wet precipitators have found their greatest usefulness to date in handling mixtures of gaseous pollutants and submicrometer particulate (either liquid or solid, or both) such as fumes from aluminum-pot lines, carbon anode baking, fiber-glass-fume control, coke-oven and metallurgical operations, chemical incineration, and phosphate-fertilizer operations. Two-stage precipitators are used increasingly for moderate-volume gas streams containing nonconductive liquid mists which will drain from the collecting plates. Their application on hydrocarbon mists has been quite successful, but careful attention must be given to fire and explosion hazards.

Electrically Augmented Collectors A new area for enhancing collection efficiency and lowering cost is the combining of electrostatic forces with devices using other collecting mechanisms such as

TABLE 14-29 Operating Characteristics of Various Types of Fiber Mist Eliminators as Used on Sulfuric Acid Plants*

	High efficiency	High velocity	Spray catcher
Controlling mechanism for mist collection	Brownian movement	Impaction	Impaction
Superficial velocity, m/s	0.075-0.20	2.0-2.5	2.0-2.5
Efficiency on particles greater than 3 μm , %	Essentially 100	Essentially 100	Essentially 100
Efficiency on particles 3 μm and smaller, %	95-99+	90-98	15-30
Pressure drop, cm H ₂ O	12-38	15-20	1.0-2.5

*Brink, Burggrabe, and Greenwell, *Chem. Eng. Prog.*, **64**(11), 82 (1968). To convert centimeters to inches, multiply by 0.394.

impaction and diffusion. Cooper (Air Pollut. Control Assoc. Prepr. 75-02.1) evaluated the magnitude of forces operating between charged and uncharged particles and concluded that electrostatic attraction is the strongest collecting force operating on particles finer than 2 μm . Nielsen and Hill [*Ind. Eng. Chem. Fundam.*, **15**, 149 (1976)] have quantified these relationships, and a number of practical devices have been demonstrated. Pilat and Meyer (NTIS Publ. PB-252653, 1976) have demonstrated up to 99 percent collection of fine particles in a two-stage spray tower in which the inlet particles and water spray are charged with opposite polarity. The principle has been applied to retrofitting existing spray towers to enhance collection.

Klugman and Sheppard (Air Pollut. Control Assoc. Prepr. 75-30.3) have developed an ionizing wet scrubber in which the charged mist particles are collected in a grounded, irrigated cross-flow bed of Tellerette packing. Particles smaller than 1 μm have been collected with 98 percent efficiency by using two units in series. Dembinsky and Vicard (Air Pollut. Control Assoc. Prepr. 78-17.6) have used an electrically augmented low-pressure [5 to 10 cm (2 to 4 in) of water] venturi scrubber to give 95 to 98 percent collection efficiency on submicrometer particles.

Particle Growth and Nucleation Fine particles may be subjected to conditions favoring the growth of particles either through condensation or through coalescence. Saturation of a hot gas stream with water, followed by condensation on the particles acting as nuclei when the gas is cooled, can increase particle size and ease of collection. Addition of steam can produce the same results. Scrubbing of the humid gas with a cold liquid can bring diffusiohoresis into play. The introduction of cold liquid drops causes a reduction in water-vapor pressure at the surface of the cold drop. The resulting vapor-pressure gradient causes a hydrodynamic flow toward the drop known as Stefan flow which enhances the movement of mist particles toward the spray drop. If the molecular mass of the diffusing vapor is different from the carrier gas, this density difference also produces a driving force, and the sum of these forces is known as diffusiohoresis. A mathematical description of these forces has been presented by Calvert (R-9) and by Sparks and Pilat [*Atmos. Environ.*, **4**, 651 (1970)]. Thermal differences between the carrier gas and the cold scrubbing droplets can further enhance collection through thermophoresis. Calvert and Jhaseri [*J. Air Pollut. Control Assoc.*, **24**, 946 (1974)]; and NTIS Publ. PB-227307, 1973)] have investigated condensation scrubbing in multiple-sieve plate towers.

Submicrometer droplets can be coagulated through brownian diffusion if given ample time. The introduction of particles 50 to 100 times larger in diameter can enhance coagulation, but the addition of a broad range of particle sizes is discouraged. Increasing turbulence will aid coagulation, so fans to stir the gas or narrow, tortuous passages such as those of a packed bed can be beneficial. Sonic energy can also produce coagulation, especially the production of standing waves in the confines of long, narrow tubes. Addition of water and oil mists can sometimes aid sonic coagulation. Sulfuric acid mist [Danser, *Chem. Eng.*, **57**(5), 158 (1950)] and carbon black [Stokes, *Chem. Eng. Prog.*, **46**, 423 (1950)] have been successfully agglomerated with sonic energy. Frequently sonic agglomeration has been unsuccessful because of the high energy requirement. Most sonic generators have very poor energy-transformation efficiency. Wegrzyn et al. (U.S. EPA Publ. EPA-600/7-79-004C, 1979, p. 233) have reviewed acoustic agglomerators. Mednikov (U.S.S.R. Akad. Soc. Moscow, 1963) suggested that the incorporation of sonic agglomeration with electrostatic precipitation could greatly reduce precipitator size.

Other Collectors Tarry particulates and other difficult-to-handle liquids have been collected on a dry, expendable phenol formaldehyde-bonded glass-fiber mat (Goldfield, *J. Air Pollut. Control Assoc.*, **20**, 466 (1970)) in roll form which is advanced intermittently into a filter frame. Superficial gas velocities are 2.5 to 3.5 m/s (8.2 to 11.5 ft/s), and pressure drop is typically 41 to 46 cm (16 to 18 in) of water. Collection efficiencies of 99 percent have been obtained on submicrometer particles. Brady [*Chem. Eng. Prog.*, **73**(8), 45 (1977)] has discussed a cleanable modification of this approach in which the gas is passed through a reticulated foam filter that is slowly rotated and solvent-cleaned.

In collecting very fine (mainly submicron) mists of a hazardous nature where one of the collectors previously discussed has been used

as the primary one (fiber-mist eliminators of the Brownian diffusion type and electrically augmented collectors are primarily recommended), there is the chance that the effluent concentration may still be too high for atmospheric release when residual concentration must be in the range of 1–2 μm . In such situations, secondary treatment may be needed. Probably removal of the residual mist by adsorption will be in order. See "Adsorption," Sec. 16. Another possibility might be treatment of the remaining gas by membrane separation. A separator having a gas-permeable membrane that is essentially nonliquid-permeable could be useful. However, if the gas-flow volumes are appreciable, the device could be expensive. Most membranes have low capacity (requiring high membrane surface area) to handle high gas-permeation capacity. See "Membrane Separation Processes," Sec. 20.

Continuous Phase Uncertain Some situations exist such as in two-phase gas-liquid flow where the volume of the liquid phase may approach being equal to the volume of the vapor phase, and where it may be difficult to be sure which phase is the continuous phase. Svrcek and Monnery [*Chem. Eng. Prog.*, **89**(10), 53–60 (Oct. 1993)] have discussed the design of two-phase separation in a tank with gas-liquid separation in the middle, mist elimination in the top, and entrained gas-bubble removal from the liquid in the bottom. Monnery and Svrcek [*Chem. Eng. Prog.*, **90**(9), 29–40 (Sept. 1994)] have expanded the separation to include multiphase flow, where the components are a vapor and two immiscible liquids and these are also separated in a tank. A design approach for sizing the gas-liquid disengaging space in the vessel is given using a tangential tank inlet nozzle, followed by a wire mesh mist eliminator in the top of the vessel for final separation of entrained mist from the vapor. Design approaches and equations are also given for sizing the lower portion of the vessel for separation of the two immiscible liquid phases by settling and separation of discontinuous liquid droplets from the continuous liquid phase.

LIQUID-PHASE CONTINUOUS SYSTEMS

Practical separation techniques for gases dispersed in liquids are discussed. Processes and methods for dispersing gas in liquid have been discussed earlier in this section, together with information for predicting the bubble size produced. Gas-in-liquid dispersions are also produced in chemical reactions and electrochemical cells in which a gas is liberated. Such dispersions are likely to be much finer than those produced by the dispersion of a gas. Dispersions may also be unintentionally created in the vaporization of a liquid.

GENERAL REFERENCES: Adamson, *Physical Chemistry of Surfaces*, 4th ed., Wiley, New York, 1982. Akers, *Foams*, Academic, New York, 1976. Bikerman, *Foams*, Springer-Verlag, New York, 1973. Bikerman, et al., *Foams: Theory and Industrial Applications*, Reinhold, New York, 1953. Cheremisinoff, ed., *Encyclopedia of Fluid Mechanics*, vol. 3, Gulf Publishing, Houston, 1986. Kerner, *Foam Control Agents*, Noyes Data Corp., Park Ridge, NJ, 1976. Rubel, *Antifoaming and Defoaming Agents*, Noyes Data Corp., Park Ridge, NJ, 1972. Rosen, *Surfactants and Interfacial Phenomena*, 2d ed., Wiley, New York, 1989. Sonntag and Strenge, *Coagulation and Stability of Disperse Systems*, Halsted-Wiley, New York, 1972. Wilson, ed., *Foams: Physics, Chemistry and Structure*, Springer-Verlag, London, 1989. "Defoamers" and "Foams", *Encyclopedia of Chemical Technology*, 4th ed., vols. 7, 11, Wiley, New York, 1993–1994.

Types of Gas-in-Liquid Dispersions Two types of dispersions exist. In one, gas bubbles produce an unstable dispersion which separates readily under the influence of gravity once the mixture has been removed from the influence of the dispersing force. Gas-liquid contacting means such as bubble towers and gas-dispersing agitators are typical examples of equipment producing such dispersions. More difficulties may result in separation when the gas is dispersed in the form of bubbles only a few micrometers in size. An example is the evolution of gas from a liquid in which it has been dissolved or released through chemical reaction such as electrolysis. Coalescence of the dispersed phase can be helpful in such circumstances.

The second type is a stable dispersion, or foam. Separation can be extremely difficult in some cases. A pure two-component system of gas and liquid cannot produce dispersions of the second type. Stable foams can be produced only when an additional substance is adsorbed

TABLE 14-30 Terminal Velocity of Standard Air Bubbles Rising in Water at 20°C*

Bubble diameter, μm	10	30	50	100	200	300
Terminal velocity, mm/s	0.061	0.488	1.433	5.486	21.95	49.38

*Calculated from Stokes' law. To convert millimeters per second to feet per second, multiply by 0.003281.

at the liquid-surface interface. The substance adsorbed may be in true solution but with a chemical tendency to concentrate in the interface such as that of a surface-active agent, or it may be a finely divided solid which concentrates in the interface because it is only poorly wetted by the liquid. Surfactants and proteins are examples of soluble materials, while dust particles and extraneous dirt including traces of nonmiscible liquids can be examples of poorly wetted materials.

Separation of gases and liquids always involves coalescence, but enhancement of the rate of coalescence may be required only in difficult separations.

Separation of Unstable Systems The buoyancy of bubbles suspended in liquid can frequently be depended upon to cause the bubbles to rise to the surface and separate. This is a special case of gravity settling. The mixture is allowed to stand at rest or is moved along a flow path in laminar flow until the bubbles have surfaced. Table 14-30 shows the calculated rate of rise of air bubbles at atmospheric pressure in water at 20°C (68°F) as a function of diameter. It will be observed that the velocity of rise for 10- μm bubbles is very low, so that long separating times would be required for gas which is more finely dispersed.

For liquids other than water, the rise velocity can be approximated from Table 14-30 by multiplying by the liquid's specific gravity and the reciprocal of its viscosity (in centipoises). For bubbles larger than 100 μm , this procedure is erroneous, but the error is less than 15 percent for bubbles up to 1000 μm . More serious is the underlying assumption of Table 14-30 that the bubbles are rigid spheres. Circulation within the bubble causes notable increases in velocity in the range of 100 μm to 1 mm, and the flattening of bubbles 1 cm and larger appreciably decreases their velocity. However, in this latter size range the velocity is so high as to make separation a trivial problem.

In design of separating chambers, static vessels or continuous-flow tanks may be used. Care must be taken to protect the flow from turbulence, which could cause back mixing of partially separated fluids or which could carry unseparated liquids rapidly to the separated-liquid outlet. Vertical baffles to protect rising bubbles from flow currents are sometimes employed. Unseparated fluids should be distributed to the separating region as uniformly and with as little velocity as possible. When the bubble rise velocity is quite low, shallow tanks or flow channels should be used to minimize the residence time required.

Quite low velocity rise of bubbles due either to small bubble size or to high liquid viscosity can cause difficult situations. With low-viscosity liquids, separation-enhancing possibilities in addition to those previously enumerated are to sparge the liquid with large-diameter gas bubbles or to atomize the mixture as a spray into a tower. Large gas bubbles rising rapidly through the liquid collide with small bubbles and aid their coalescence through capture. Atomizing of the continuous phase reduces the distance that small gas bubbles must travel to reach a gas interface. Evacuation of the spray space can also be beneficial in promoting small-bubble growth and especially in promoting gas evolution when the gas has appreciable liquid solubility. Liquid heating will also reduce solubility.

Surfaces in the settling zone for bubble coalescence such as closely spaced vertical or inclined plates or tubes are beneficial. When clean low-viscosity fluids are involved, passage of the undegassed liquid through a tightly packed pad of mesh or fine fibers at low velocity will result in efficient bubble coalescence. Problems have been experienced in degassing a water-based organic solution that has been passed through an electrolytic cell for chemical reaction in which extremely fine bubbles of hydrogen gas are produced in the liquid within the cell. Near-total removal of hydrogen gas from the liquid is needed for process safety. This is extremely difficult to achieve by gravity settling alone because of the fine bubble size and the need for a coalescing surface. Utilization of a fine fiber media is strongly recommended in such situations. A low-forward liquid flow through the

media is desirable to provide time for the bubbles to attach themselves to the fiber media through Brownian diffusion. Spielman and Goren [*Ind. Eng. Chem.*, **62**(10), (1970)] reviewed the literature on coalescence with porous media and reported their own experimental results [*Ind. Eng. Chem. Fundam.*, **11**(1), 73 (1972)] on the coalescence of oil-water liquid emulsions. The principles are applicable to a gas-in-liquid system. Glass-fiber mats composed of 3.5-, 6-, or 12- μm diameter fibers, varying in thickness from 1.3 to 3.3 mm, successfully coalesced and separated 1- to 7- μm oil droplets at superficial bed velocities of 0.02 to 1.5 cm/s (0.0067 to 0.049 ft/s).

In the deaeration of high-viscosity fluids such as polymers, the material is flowed in thin sheets along solid surfaces. Vacuum is applied to increase bubble size and hasten separation. The Versator (Cornell Machine Co.) degasses viscous liquids by spreading them into a thin film by centrifugal action as the liquids flow through an evacuated rotating bowl.

Separation of Foam Foam is a colloidal system containing relatively large volumes of dispersed gas in a relatively small volume of liquid. Foams are thermodynamically unstable with respect to separation into their components of gas and vapor, and appreciable surface energy is released in the bursting of foam bubbles. Foams are dynamic systems in which a third component produces a surface layer that is different in composition from the bulk of the liquid phase. The stabilizing effect of such components (often present only in trace amounts) can produce foams of troubling persistence in many operations. (Foams which have lasted for years when left undisturbed have been produced.) Bendure [*TAPPI*, **58**(2), 83 (1975)], Keszthelyi [*J. Paint Technol.*, **46**(11), 31 (1974)], Ahmad [*Sep. Sci.* **10**, 649 (1975)], and Shedlovsky ("Foams," *Encyclopedia of Chemical Technology*, 2d ed., Wiley, New York, 1966) have presented concise articles on the characteristics and properties of foams in addition to the general references cited at the beginning of this subsection.

Foams can be a severe problem in chemical-processing steps involving gas-liquid interaction such as distillation, absorption, evaporation, chemical reaction, and particle separation and settling. It can also be a major problem in pulp and paper manufacture, oil-well drilling fluids, production of water-based paints, utilization of lubricants and hydraulic fluids, dyeing and sizing of textiles, operation of steam boilers, fermentation operations, polymerization, wet-process phosphoric acid concentration, adhesive production, and foam control in products such as detergents, waxes, printing inks, instant coffee, and glycol antifreeze.

Foams, as freshly generated, are gas emulsions with spherical bubbles separated by liquid films up to a few millimeters in thickness. They age rapidly by liquid drainage and form polyhedrals in which three bubbles intersect at corners with angles of approximately 120°. During drainage, the lamellae become increasingly thinner, especially in the center (only a few micrometers thickness), and more brittle. This feature indicates that with some foams if a foam layer can be tolerated, it may be self-limiting, as fresh foam is added to the bottom of the layer with drained foam collapsing on the top. (A quick-breaking foam may reach its maximum life cycle in 6 s. A moderately stable foam can persist for 140 s.) During drainage, gas from small foam bubbles, which is at a high pressure, will diffuse into large bubbles so that foam micelles increase with time. As drainage proceeds, weak areas in the lamella may develop. However, the presence of a higher concentration of surfactants in the surface produces a lower surface tension. As the lamella starts to fail, exposing bulk liquid with higher surface tension, the surface is renewed and healed. This is known as the *Marangoni effect*. If drainage can occur faster than Marangoni healing, a hole may develop in the lamella. The forces involved are such that collapse will occur in milliseconds without concern for rupture propagation. However, in very stable foams, electrostatic surface forces (zeta potential) prevent complete drainage and collapse. In

some cases, stable lamella thicknesses of only two molecules have been measured.

Drainage rate is influenced by surface viscosity, which is very temperature-sensitive. At a critical temperature, which is a function of the system, a temperature change of only a few degrees can change a slow-draining foam to a fast-draining foam. This change in drainage rate can be a factor of 100 or more; thus increasing the temperature of foam can cause its destruction. An increase in temperature may also cause liquid evaporation and lamella thinning. As the lamellae become thinner, they become more brittle and fragile. Thus, mechanical deformation or pressure changes, which cause a change in gas-bubble volume, can also cause rupture.

Bendure indicates 10 ways to increase foam stability: (1) increase bulk liquid viscosity, (2) increase surface viscosity, (3) maintain thick walls (higher liquid-to-gas ratio), (4) reduce liquid surface tension, (5) increase surface elasticity, (6) increase surface concentration, (7) reduce surfactant-adsorption rate, (8) prevent liquid evaporation, (9) avoid mechanical stresses, and (10) eliminate foam inhibitors. Obviously, the reverse of each of these actions, when possible, is a way to control and break foam.

Physical Defoaming Techniques Typical physical defoaming techniques include mechanical methods for producing foam stress, thermal methods involving heating or cooling, and electrical methods. Combinations of these methods may also be employed, or they may be used in conjunction with chemical defoamers. Some methods are only moderately successful when conditions are present to reform the foam such as breaking foam on the surface of boiling liquids. In some cases it may be desirable to draw the foam off and treat it separately. Foam can always be stopped by removing the energy source creating it, but this is often impractical.

Thermal Methods Heating is often a suitable means of destroying foam. As indicated previously, raising the foam above a critical temperature (which must be determined experimentally) can greatly decrease the surface viscosity of the film and change the foam from a slow-draining to a fast-draining foam. Coupling such heating with a mechanical force such as a revolving paddle to cause foam deformation is frequently successful. Other effects of heating are expansion of the gas in the foam bubbles, which increases strain on the lamella walls as well as requiring their movement and flexing. Evaporation of solvent may occur causing thinning of the walls. At sufficiently high temperatures, desorption or decomposition of stabilizing substances may occur. Placing a high-temperature bank of steam coils at the maximum foam level is one control method. As the foam approaches or touches the coil, it collapses. The designer should consider the fact that the coil will frequently become coated with solute.

Application of radiant heat to a foam surface is also practiced. Depending on the situation, the radiant source may be electric lamps, Glowbar units, or gas-fired radiant burners. Hot gases from burners will enhance film drying of the foam. Heat may also be applied by jetting or spraying hot water on the foam. This is a combination of methods since the jetting produces mechanical shear, and the water itself provides dilution and change in foam-film composition. Newer approaches might include foam heating with the application of focused microwaves. This could be coupled with continuous or intermittent pressure fluctuations to stress lamella walls as the foam ages.

Cooling can also destroy foam if it is carried to the point of freezing since the formation of solvent crystals destroys the foam structure. Less drastic cooling such as spraying a hot foam with cold water may be effective. Cooling will reduce the gas pressure in the foam bubbles and may cause them to shrink. This is coupled with the effects of shear and dilution mentioned earlier. In general, moderate cooling will be less effective than heating since the surface viscosity is being modified in the direction of a more stable foam.

Mechanical Methods Static or rotating breaker bars or slowly revolving paddles are sometimes successful. Their application in conjunction with other methods is frequently better. As indicated in the theory of foams, they will work better if installed at a level at which the foam has had some time to age and drain. A rotating breaker works by deforming the foam, which causes rupture of the lamella walls. Rapidly moving slingers will throw the foam against the vessel wall and may cause impact on other foam outside the envelope of the

slinger. In some instances, stationary bars or closely spaced plates will limit the rise of foam. The action here is primarily one of providing surface for coalescence of the foam. Wettability of the surface, whether moving or stationary, is frequently important. Usually a surface not wetted by the liquid is superior, just as is frequently the case of porous media for foam coalescence. However, in both cases there are exceptions for which wettable surfaces are preferred. Shkodin [*Kolloidn. Zh.*, **14**, 213 (1952)] found molasses foam to be destroyed by contact with a wax-coated rod and unaffected by a clean glass rod.

Goldberg and Rubin [*Ind. Eng. Chem. Process Des. Dev.*, **6** 195 (1967)] showed in tests with a disk spinning vertically to the foam layer that most mechanical procedures, whether centrifugation, mixing, or blowing through nozzles, consist basically of the application of shear stress. Subjecting foam to an air-jet impact can also provide a source of drying and evaporation from the film, especially if the air is heated. Other effective means of destroying bubbles are to lower a frame of metal points periodically into the foam or to shower the foam with falling solid particles.

Pressure and Acoustic Vibrations These methods for rupturing foam are really special forms of mechanical treatment. Change in pressure in the vessel containing the foam stresses the lamella walls by expanding or contracting the gas inside the foam bubbles. Oscillation of the vessel pressure subjects the foam to repeated film flexing. Parlow [*Zucker*, **3**, 468 (1950)] controlled foam in sugar-sirup evaporators with high-frequency air pulses. It is by no means certain that high-frequency pulsing is necessary in all cases. Lower frequency and higher amplitude could be equally beneficial. Acoustic vibration is a similar phenomenon causing localized pressure oscillation by using sound waves. Impulses at 6 kHz have been found to break froth from coal flotation [*Sun. Min. Eng.*, **3**, 865 (1958)]. Sonntag and Strenge (*Coagulation and Stability of Disperse Systems*, Halsted-Wiley, New York, 1972, p. 121) report foam suppression with high-intensity sound waves (11 kHz, 150 dB) but indicate that the procedure is too expensive for large-scale application. The Sontrifuge (Teknika Inc., a subsidiary of Chemineer, Inc.) is a commercially available low-speed centrifuge employing sonic energy to break the foam. Walsh [*Chem. Process.*, **29**, 91 (1966)], Carlson [*Pap. Trade J.*, **151**, 38 (1967)], and Thorhildsen and Rich [*TAPPI*, **49**, 95A (1966)] have described the unit.

Electrical Methods As colloids, most foams typically have electrical double layers of charged ions which contribute to foam stability. Accordingly, foams can be broken by the influence of an external electric field. While few commercial applications have been developed, Sonntag and Strenge (op. cit., p. 114) indicate that foams can be broken by passage through devices much like electrostatic precipitators for dusts. Devices similar to two-stage precipitators having closely spaced plates of opposite polarity should be especially useful. Sonntag and Strenge, in experiments with liquid-liquid emulsions, indicate that the colloid structure can be broken at a field strength of the order of 8 to 9×10^5 V/cm.

Chemical Defoaming Techniques Sonntag and Strenge (op. cit., p. 111) indicate two chemical methods for foam breaking. One method is causing the stabilizing substances to be desorbed from the interface, such as by displacement with other more surface-active but nonstabilizing compounds. Heat may also cause desorption. The second method is to carry on chemical changes in the adsorption layer, leading to a new structure. Some defoamers may act purely by mechanical means but will be discussed in this subsection since their action is generally considered to be chemical in nature. Often chemical defoamers act in more than one way.

Chemical Defoamers The addition of chemical foam breakers is the most elegant way to break a foam. Effective defoamers cause very rapid disintegration of the foam and frequently need be present only in parts per million. The great diversity of compounds used for defoamers and the many different systems in which they are applied make a brief and orderly discussion of their selection difficult. Compounds needed to break aqueous foams may be different from those needed for aqueous-free systems. The majority of defoamers are insoluble or nonmiscible in the foam continuous phase, but some work best because of their ready solubility. Lichtman (*Defoamers*, 3d ed., Wiley, New York, 1979) has presented a concise summary of the application and use of defoamers. Rubel (*Antifoaming and Defoaming*

TABLE 14-31 Major Types and Applications of Defoamers

Classification	Examples	Applications
Silicones	Dimethyl silicone, trialkyl and tetraalkyl silanes	Lubricating oils; distillation; fermentation; jam and wine making; food processing
Aliphatic acids or esters	Mostly high-molecular-weight compounds; diethyl phthalate; lauric acid	Papermaking; wood-pulp suspensions; water-based paints; food processing
Alcohols	Moderate- to high-molecular-weight monohydric and polyhydric alcohols; octyl alcohol; C-12 to C-20 alcohols; lauryl alcohol	Distillation; fermentation; papermaking; glues and adhesives
Sulfates or sulfonates	Alkali metal salts of sulfated alcohols, sulfonic acid salts; alkyl-aryl sulfonates; sodium lauryl sulfate	Nonaqueous systems; mixed aqueous and nonaqueous systems; oil-well drilling muds; spent H ₂ SO ₄ recovery; deep-fat frying
Amines or amides	Alkyl amines (undecyloctyl and diamyl methyl amine); polyamides (acyl derivatives of piperazine)	Boiler foam; sewage foam; fermentation; dye baths
Halogenated compounds	Fluochloro hydrocarbons with 5 to 50 C atoms; chlorinated hydrocarbons	Lubrication-oil and grease distillation; vegetable-protein glues
Natural products	Vegetable oils; waxes, mineral oils plus their sulfated derivatives (including those of animal oils and fats)	Sugar extraction; glue manufacture; cutting oils
Fatty-acid soaps	Alkali, alkaline earth, and other metal soaps; sodium stearate; aluminum stearate	Gear oils; paper stock; paper sizing; glue solutions
Inorganic compounds	Monosodium phosphate mixed with boric acid and ethyl carbonate, disodium phosphate; sodium aluminate, bentonite and other solids	Distillation; instant coffee; boiler feedwater; sugar extraction
Phosphates	Alkyl-alkalene diphosphates; tributyl phosphate in isopropanol	Petroleum-oil systems; foam control in soap solutions
Hydrophobic silica	Finely divided silica in polydimethyl siloxane	Aqueous foaming systems
Sulfides or thio derivatives	Metallic derivatives of thio ethers and disulfides, usually mixed with organic phosphite esters; long-chain alkyl thienyl ketones	Lubricating oils; boiler water

Agents, Noyes Data Corp., Park Ridge, N.J., 1972) has reviewed the extensive patent literature on defoamers. Defoamers are also discussed extensively in the general references at the beginning of this subsection.

One useful method of aqueous defoaming is to add a nonfoam stabilizing surfactant which is more surface-active than the stabilizing substance in the foam. Thus a foam stabilized with an ionic surfactant can be broken by the addition of a very surface-active but nonstabilizing silicone oil. The silicone displaces the foam stabilizer from the interface by virtue of its insolubility. However, it does not stabilize the foam because its foam films have poor elasticity and rupture easily.

A major requirement for a defoamer is cost-effectiveness. Accordingly, some useful characteristics are low volatility (to prevent stripping from the system before it is dispersed and does its work), ease of dispersion and strong spreading power, and surface attraction-orientation. Chemical defoamers must also be selected in regard to their possible effect on product quality and their environmental and health suitability. For instance, silicone antifoam agents are effective in textile jet dyeing but reduce the fire retardancy of the fabric. Mineral-oil defoamers in sugar evaporation have been replaced by specifically approved materials. The tendency is no longer to use a single defoamer compound but to use a formulation specially tailored for the application comprising carriers, secondary antifoam agents, emulsifiers, and stabilizing agents in addition to the primary defoamer. Carriers, usually hydrocarbon oils or water, serve as the vehicle to support the release and spread of the primary defoamer. Secondary defoamers may provide a synergistic effect for the primary defoamer or modify its properties such as spreadability or solubility. Emulsifiers may enhance the speed of dispersion, while stabilizing agents may enhance defoamer stability or shelf life.

Hydrophobic silica defoamers work on a basis which may not be chemical at all. They are basically finely divided solid silica particles dispersed in a hydrocarbon or silicone oil which serves as a spreading vehicle. Kulkarni [*Ind. Eng. Chem. Fundam.*, **16**, 472 (1977)] theorizes that this mixture defoams by the penetration of the silica particle into the bubble and the rupture of the wall. Table 14-31 lists major types of defoamers and typical applications.

Other Chemical Methods These methods rely chiefly on destroying the foam stabilizer or neutralizing its effect through methods other than displacement and are applicable when the process will permit changing the chemical environment. Forms stabilized with alkali esters can be broken by acidification since the equivalent free

acids do not stabilize foam. Foams containing sulfated and sulfonated ionic detergents can be broken with the addition of fatty-acid soaps and calcium salts. Several theories have been proposed. One suggests that the surfactant is tied up in the foam as double calcium salts of both the sulfonate and the soap. Another suggests that calcium soaps oriented in the film render it inelastic.

Ionic surfactants adsorb at the foam interface and orient with the charged group immersed in the lamellae and their uncharged tails pointed into the gas stream. As the film drains, the charged groups, which repel each other, tend to be moved more closely together. The repulsive force between like charges hinders drainage and stabilizes the film. Addition of a salt or an electrolyte to the foam screens the repulsive effect, permits additional drainage, and can reduce foam stability.

Foam Prevention Chemical prevention of foam differs from defoaming only in that compounds or mixtures are added to a stream prior to processing to prevent the formation of foam either during processing or during customer use. Such additives, sometimes distinguished as antifoam agents, are usually in the same chemical class of materials as defoamers. However, they are usually specifically formulated for the application. Typical examples of products formulated with antifoam agents are laundry detergents (to control excess foaming), automotive antifreeze, instant coffee, and jet-aircraft fuel. Foaming in some chemical processes such as distillation or evaporation may be due to trace impurities such as surface-active agents. An alternative to antifoam agents is their removal before processing such as by treatment with activated carbon [*Pool. Chem. Process.*, **21**(9), 56 (1958)].

Automatic Foam Control In processing materials when foam can accumulate, it is often desirable to measure the height of the foam layer continuously and to dispense defoamer automatically as required to control the foam. Other corrective action can also be taken automatically. Methods of sensing the foam level have included electrodes in which the electrical circuit is completed when the foam touches the electrode [*Nelson, Ind. Eng. Chem.*, **48**, 2183 (1956); and Browne, U.S. Patent 2,981,693, 1961], floats designed to rise in a foam layer (Carter, U.S. Patent 3,154,577, 1964), and change in power input required to turn a foam-breaking impeller as the foam level rises (Yamashita, U.S. Patent 3,317,435, 1967). Timers to control the duration of defoamer addition have also been used. Browne has suggested automatic addition of defoamer through a porous wick when the foam level reaches the level of the wick. Foam control has also been discussed by Kroll [*Ind. Eng. Chem.*, **48**, 2190 (1956)].

SECTION 15

Liquid-Liquid
Extraction
and Other
Liquid-Liquid
Operations and
Equipment

PERRY'S CHEMICAL ENGINEERS' HANDBOOK

8TH EDITION



TIMOTHY C. FRANK, LISE DAHURON
BRUCE S. HOLDEN, WILLIAM D. PRINCE
A. FRANK SEIBERT, LOREN C. WILSON

Copyright © 2008, 1997, 1984, 1973, 1963, 1950, 1941, 1934 by The McGraw-Hill Companies, Inc. All rights reserved. Manufactured in the United States of America. Except as permitted under the United States Copyright Act of 1976, no part of this publication may be reproduced or distributed in any form or by any means, or stored in a database or retrieval system, without the prior written permission of the publisher.

0-07-154222-1

The material in this eBook also appears in the print version of this title: 0-07-151138-5.

All trademarks are trademarks of their respective owners. Rather than put a trademark symbol after every occurrence of a trademarked name, we use names in an editorial fashion only, and to the benefit of the trademark owner, with no intention of infringement of the trademark. Where such designations appear in this book, they have been printed with initial caps.

McGraw-Hill eBooks are available at special quantity discounts to use as premiums and sales promotions, or for use in corporate training programs. For more information, please contact George Hoare, Special Sales, at george_hoare@mcgraw-hill.com or (212) 904-4069.

TERMS OF USE

This is a copyrighted work and The McGraw-Hill Companies, Inc. (“McGraw-Hill”) and its licensors reserve all rights in and to the work. Use of this work is subject to these terms. Except as permitted under the Copyright Act of 1976 and the right to store and retrieve one copy of the work, you may not decompile, disassemble, reverse engineer, reproduce, modify, create derivative works based upon, transmit, distribute, disseminate, sell, publish or sublicense the work or any part of it without McGraw-Hill’s prior consent. You may use the work for your own noncommercial and personal use; any other use of the work is strictly prohibited. Your right to use the work may be terminated if you fail to comply with these terms.

THE WORK IS PROVIDED “AS IS.” MCGRAW-HILL AND ITS LICENSORS MAKE NO GUARANTEES OR WARRANTIES AS TO THE ACCURACY, ADEQUACY OR COMPLETENESS OF OR RESULTS TO BE OBTAINED FROM USING THE WORK, INCLUDING ANY INFORMATION THAT CAN BE ACCESSED THROUGH THE WORK VIA HYPERLINK OR OTHERWISE, AND EXPRESSLY DISCLAIM ANY WARRANTY, EXPRESS OR IMPLIED, INCLUDING BUT NOT LIMITED TO IMPLIED WARRANTIES OF MERCHANTABILITY OR FITNESS FOR A PARTICULAR PURPOSE. McGraw-Hill and its licensors do not warrant or guarantee that the functions contained in the work will meet your requirements or that its operation will be uninterrupted or error free. Neither McGraw-Hill nor its licensors shall be liable to you or anyone else for any inaccuracy, error or omission, regardless of cause, in the work or for any damages resulting therefrom. McGraw-Hill has no responsibility for the content of any information accessed through the work. Under no circumstances shall McGraw-Hill and/or its licensors be liable for any indirect, incidental, special, punitive, consequential or similar damages that result from the use of or inability to use the work, even if any of them has been advised of the possibility of such damages. This limitation of liability shall apply to any claim or cause whatsoever whether such claim or cause arises in contract, tort or otherwise.

DOI: 10.1036/0071511385

Liquid-Liquid Extraction and Other Liquid-Liquid Operations and Equipment*

Timothy C. Frank, Ph.D. *Research Scientist and Sr. Technical Leader, The Dow Chemical Company; Member, American Institute of Chemical Engineers (Section Editor, Introduction and Overview, Thermodynamic Basis for Liquid-Liquid Extraction, Solvent Screening Methods, Liquid-Liquid Dispersion Fundamentals, Process Fundamentals and Basic Calculation Methods, Dual-Solvent Fractional Extraction, Extractor Selection, Packed Columns, Agitated Extraction Columns, Mixer-Settler Equipment, Centrifugal Extractors, Process Control Considerations, Liquid-Liquid Phase Separation Equipment, Emerging Developments)*

Lise Dahuron, Ph.D. *Sr. Research Specialist, The Dow Chemical Company (Liquid Density, Viscosity, and Interfacial Tension; Liquid-Liquid Dispersion Fundamentals; Liquid-Liquid Phase Separation Equipment; Membrane-Based Processes)*

Bruce S. Holden, M.S. *Process Research Leader, The Dow Chemical Company; Member, American Institute of Chemical Engineers [Process Fundamentals and Basic Calculation Methods, Calculation Procedures, Computer-Aided Calculations (Simulations), Single-Solvent Fractional Extraction with Extract Reflux, Liquid-Liquid Phase Separation Equipment]*

William D. Prince, M.S. *Process Engineering Associate, The Dow Chemical Company; Member, American Institute of Chemical Engineers (Extractor Selection, Agitated Extraction Columns, Mixer-Settler Equipment)*

A. Frank Seibert, Ph.D., P.E. *Technical Manager, Separations Research Program, The University of Texas at Austin; Member, American Institute of Chemical Engineers (Liquid-Liquid Dispersion Fundamentals, Process Fundamentals and Basic Calculation Methods, Hydrodynamics of Column Extractors, Static Extraction Columns, Process Control Considerations, Membrane-Based Processes)*

Loren C. Wilson, B.S. *Sr. Research Specialist, The Dow Chemical Company (Liquid Density, Viscosity, and Interfacial Tension; Phase Diagrams; Liquid-Liquid Equilibrium Experimental Methods; Data Correlation Equations; Table of Selected Partition Ratio Data)*

INTRODUCTION AND OVERVIEW

Historical Perspective	15-6
Uses for Liquid-Liquid Extraction	15-7
Definitions	15-10

Desirable Solvent Properties	15-11
Commercial Process Schemes	15-13
Standard Extraction	15-13
Fractional Extraction	15-13

*Certain portions of this section are drawn from the work of Lanny A. Robbins and Roger W. Cusack, authors of Sec. 15 in the 7th edition. The input from numerous expert reviewers also is gratefully acknowledged.

15-2 LIQUID-LIQUID EXTRACTION AND OTHER LIQUID-LIQUID OPERATIONS AND EQUIPMENT

Dissociative Extraction	15-15
pH-Swing Extraction	15-16
Reaction-Enhanced Extraction	15-16
Extractive Reaction	15-16
Temperature-Swing Extraction	15-17
Reversed Micellar Extraction	15-18
Aqueous Two-Phase Extraction	15-18
Hybrid Extraction Processes	15-18
Liquid-Solid Extraction (Leaching)	15-19
Liquid-Liquid Partitioning of Fine Solids	15-19
Supercritical Fluid Extraction	15-19
Key Considerations in the Design of an Extraction Operation	15-20
Laboratory Practices	15-21

THERMODYNAMIC BASIS FOR LIQUID-LIQUID EXTRACTION

Activity Coefficients and the Partition Ratio	15-22
Extraction Factor	15-22
Separation Factor	15-23
Minimum and Maximum Solvent-to-Feed Ratios	15-23
Temperature Effect	15-23
Salting-out and Salting-in Effects for Nonionic Solutes	15-24
Effect of pH for Ionizable Organic Solutes	15-24
Phase Diagrams	15-25
Liquid-Liquid Equilibrium Experimental Methods	15-27
Data Correlation Equations	15-27
Tie Line Correlations	15-27
Thermodynamic Models	15-28
Data Quality	15-28
Table of Selected Partition Ratio Data	15-32
Phase Equilibrium Data Sources	15-32
Recommended Model Systems	15-32

SOLVENT SCREENING METHODS

Use of Activity Coefficients and Related Data	15-32
Robbins' Chart of Solute-Solvent Interactions	15-32
Activity Coefficient Prediction Methods	15-33
Methods Used to Assess Liquid-Liquid Miscibility	15-34
Computer-Aided Molecular Design	15-38
High-Throughput Experimental Methods	15-39

LIQUID DENSITY, VISCOSITY, AND INTERFACIAL TENSION

Density and Viscosity	15-39
Interfacial Tension	15-39

LIQUID-LIQUID DISPERSION FUNDAMENTALS

Holdup, Sauter Mean Diameter, and Interfacial Area	15-41
Factors Affecting Which Phase Is Dispersed	15-41
Size of Dispersed Drops	15-42
Stability of Liquid-Liquid Dispersions	15-43
Effect of Solid-Surface Wettability	15-43
Marangoni Instabilities	15-43

PROCESS FUNDAMENTALS AND BASIC CALCULATION METHODS

Theoretical (Equilibrium) Stage Calculations	15-44
McCabe-Thiele Type of Graphical Method	15-45
Kremser-Souders-Brown Theoretical Stage Equation	15-45
Stage Efficiency	15-46
Rate-Based Calculations	15-47
Solute Diffusion and Mass-Transfer Coefficients	15-47
Mass-Transfer Rate and Overall Mass-Transfer Coefficients	15-47
Mass-Transfer Units	15-48
Extraction Factor and General Performance Trends	15-49
Potential for Solute Purification Using Standard Extraction	15-50

CALCULATION PROCEDURES

Shortcut Calculations	15-51
Example 1: Shortcut Calculation, Case A	15-52

Example 2: Shortcut Calculation, Case B	15-52
Example 3: Number of Transfer Units	15-53
Computer-Aided Calculations (Simulations)	15-53
Example 4: Extraction of Phenol from Wastewater	15-54
Fractional Extraction Calculations	15-55
Dual-Solvent Fractional Extraction	15-55
Single-Solvent Fractional Extraction with Extract Reflux	15-56
Example 5: Simplified Sulfolane Process—Extraction of Toluene from <i>n</i> -Heptane	15-56

LIQUID-LIQUID EXTRACTION EQUIPMENT

Extractor Selection	15-58
Hydrodynamics of Column Extractors	15-59
Flooding Phenomena	15-59
Accounting for Axial Mixing	15-60
Liquid Distributors and Dispersers	15-63
Static Extraction Columns	15-63
Common Features and Design Concepts	15-63
Spray Columns	15-69
Packed Columns	15-70
Sieve Tray Columns	15-74
Baffle Tray Columns	15-78
Agitated Extraction Columns	15-79
Rotating-Impeller Columns	15-79
Reciprocating-Plate Columns	15-83
Rotating-Disk Contactor	15-84
Pulsed-Liquid Columns	15-85
Raining-Bucket Contactor (a Horizontal Column)	15-85
Mixer-Settler Equipment	15-86
Mass-Transfer Models	15-86
Miniplant Tests	15-87
Liquid-Liquid Mixer Design	15-87
Scale-up Criteria	15-88
Specialized Mixer-Settler Equipment	15-89
Suspended-Fiber Contactor	15-90
Centrifugal Extractors	15-91
Single-Stage Centrifugal Extractors	15-91
Centrifugal Extractors Designed for Multistage Performance	15-92

PROCESS CONTROL CONSIDERATIONS

Steady-State Process Control	15-93
Sieve Tray Column Interface Control	15-94
Controlled-Cycling Mode of Operation	15-94

LIQUID-LIQUID PHASE SEPARATION EQUIPMENT

Overall Process Considerations	15-96
Feed Characteristics	15-96
Gravity Decanters (Settlers)	15-97
Design Considerations	15-97
Vented Decanters	15-98
Decanters with Coalescing Internals	15-99
Sizing Methods	15-99
Other Types of Separators	15-101
Coalescers	15-101
Centrifuges	15-101
Hydrocyclones	15-101
Ultrafiltration Membranes	15-102
Electrotreaters	15-102

EMERGING DEVELOPMENTS

Membrane-Based Processes	15-103
Polymer Membranes	15-103
Liquid Membranes	15-104
Electrically Enhanced Extraction	15-104
Phase Transition Extraction and Tunable Solvents	15-105
Ionic Liquids	15-105

Nomenclature

A given symbol may represent more than one property. The appropriate meaning should be apparent from the context. The equations given in Sec. 15 reflect the use of the SI or cgs system of units and not ft-lb-s units, unless otherwise noted in the text. The gravitational conversion factor g_c needed to use ft-lb-s units is not included in the equations.

Symbol	Definition	SI units	U.S. Customary System units	Symbol	Definition	SI units	U.S. Customary System units
a	Interfacial area per unit volume	m^2/m^3	ft^2/ft^3	\mathcal{E}^C	Extraction factor for case C [Eq. (15-98)]	Dimensionless	Dimensionless
a_p	Specific packing surface area (area per unit volume)	m^2/m^3	ft^2/ft^3	\mathcal{E}_i	Extraction factor for component i	Dimensionless	Dimensionless
a_w	Specific wall surface area (area per unit volume)	m^2/m^3	ft^2/ft^3	\mathcal{E}_s	Stripping section extraction factor	Dimensionless	Dimensionless
b_{ij}	NRTL model regression parameter (see Table 15-10)	K	K	\mathcal{E}_{wc}	Washing section extraction factor	Dimensionless	Dimensionless
A	Envelope-style downcomer area	m^2	ft^2	f_{da}	Fractional downcomer area in Eq. (15-160)	Dimensionless	Dimensionless
A	Area between settled layers in a decanter	m^2	ft^2	f_{ha}	Fractional hole area in Eq. (15-159)	Dimensionless	Dimensionless
A_{col}	Column cross-sectional area	m^2	ft^2	F	Mass or mass flow rate of feed phase	kg or kg/s	lb or lb/h
A_{dow}	Area for flow through a downcomer (or upcomer)	m^2	ft^2	F	Force	N	lb _f
$A_{i/RT}$	van Laar binary interaction parameter	Dimensionless	Dimensionless	F'	Feed mass or mass flow rate (feed solvent only)	kg or kg/s	lb or lb/h
A_o	Cross-sectional area of a single hole	m^2	in^2	F_R	Solute reduction factor (ratio of inlet to outlet concentrations)	Dimensionless	Dimensionless
C	Concentration (mass or mol per unit volume)	kg/m^3 or $kgmol/m^3$ or $gmol/L$	lb/ft^3 or $lbmol/ft^3$	g	Gravitational acceleration	$9.807 m/s^2$	$32.17 ft/s^2$
C_A^i	Concentration of component A at the interface	kg/m^3 or $kgmol/m^3$ or $gmol/L$	lb/ft^3 or $lbmol/ft^3$	C_{ij}	NRTL model parameter	Dimensionless	Dimensionless
C°	Concentration at equilibrium	kg/m^3 or $kgmol/m^3$ or $gmol/L$	lb/ft^3 or $lbmol/ft^3$	h	Height of coalesced layer at a sieve tray	m	in
C_D	Drag coefficient	Dimensionless	Dimensionless	h	Head loss due to frictional flow	m	in
C_o	Initial concentration	kg/m^3 or $kgmol/m^3$ or $gmol/L$	lb/ft^3 or $lbmol/ft^3$	h	Height of dispersion band in batch decanter	m	in
C_t	Concentration at time t	kg/m^3 or $kgmol/m^3$ or $gmol/L$	lb/ft^3 or $lbmol/ft^3$	h_i^E	Excess enthalpy of mixing	J/gmol	Btu/lbmol or cal/gmol
d	Drop diameter	m	in	H	Dimensionless group defined by Eq. (15-123)	Dimensionless	Dimensionless
d_C	Critical packing dimension	m	in	H	Dimension of envelope-style downcomer (Fig. 15-39)	m	in or ft
d_i	Diameter of an individual drop	m	in	ΔH	Steady-state dispersion band height in a continuously fed decanter	m	in
d_m	Characteristic diameter of media in a packed bed	m	in	HDU	Height of a dispersion unit	m	in
d_o	Orifice or nozzle diameter	m	in	H_e	Height of a transfer unit due to resistance in extract phase	m	in
d_p	Sauter mean drop diameter	m	in	HETS	Height equivalent to a theoretical stage	m	in
d_{32}	Sauter mean drop diameter	m	in	H_{or}	Height of an overall mass-transfer unit based on raffinate phase	m	in
D_{col}	Column diameter	m	in or ft	H_r	Height of a transfer unit due to resistance in raffinate phase	m	in
D_{eq}	Equivalent diameter giving the same area	m	in	I	Ionic strength in Eq. (15-26)		
D_h	Equivalent hydraulic diameter	m	in	k	Individual mass-transfer coefficient	m/s or cm/s	ft/h
\mathcal{D}_i	Distribution ratio for a given chemical species including all its forms (unspecified units)			k	Mass-transfer coefficient (unspecified units)		
D_i	Impeller diameter or characteristic mixer diameter	m	in or ft	k_m	Membrane-side mass-transfer coefficient	m/s or cm/s	ft/h
D_{sm}	Static mixer diameter	m	in or ft	k_o	Overall mass-transfer coefficient	m/s or cm/s	ft/h
D_t	Tank diameter	m	ft	k_c	Continuous-phase mass-transfer coefficient	m/s or cm/s	ft/h
\mathcal{D}	Molecular diffusion coefficient (diffusivity)	m^2/s	cm^2/s	k_d	Dispersed-phase mass-transfer coefficient	m/s or cm/s	ft/h
\mathcal{D}_{AB}	Mutual diffusion coefficient for components A and B	m^2/s	cm^2/s	k_s	Setschenow constant	L/gmol	L/gmol
E	Mass or mass flow rate of extract phase	kg or kg/s	lb or lb/h	k_s	Shell-side mass-transfer coefficient	m/s or cm/s	ft/h
E'	Solvent mass or mass flow rate (in the extract phase)			k_t	Tube-side mass-transfer coefficient	m/s or cm/s	ft/h
E	Axial mixing coefficient (eddy diffusivity)	m^2/s	cm^2/s	K	Partition ratio (unspecified units)		
				K_s	Stripping section partition ratio (in Bancroft coordinates)	Mass ratio/mass ratio	Mass ratio/mass ratio

15-4 LIQUID-LIQUID EXTRACTION AND OTHER LIQUID-LIQUID OPERATIONS AND EQUIPMENT

Nomenclature (Continued)

Symbol	Definition	SI units	U.S. Customary System units	Symbol	Definition	SI units	U.S. Customary System units
K'_w	Washing section partition ratio (in Bancroft coordinates)	Mass ratio/mass ratio	Mass ratio/mass ratio	Re	Reynolds number: for pipe flow, $Vd\rho/\mu$; for an impeller, $\rho_m\omega D_i^2/\mu_m$; for drops, $V_w d_p \rho_c/\mu_c$; for flow in a packed-bed coalescer, $V d_m \rho_c/\mu$; for flow through an orifice, $V_o d_o \rho_c/\mu_o$	Dimensionless	Dimensionless
K'	Partition ratio, mass ratio basis (Bancroft coordinates)	Mass ratio/mass ratio	Mass ratio/mass ratio	Re_{Stokes}	$\rho_c \Delta p g d_p^2/18\mu_c^2$	Dimensionless	Dimensionless
K''	Partition ratio, mass fraction basis	Mass fraction/mass fraction	Mass fraction/mass fraction	S	Mass or mass flow rate of solvent phase	kg or kg/s	lb or lb/h
K^o	Partition ratio, mole fraction basis	Mole fraction/mole fraction	Mole fraction/mole fraction	S	Dimension of envelope-style downcomer (Fig. 15-39)	m	ft
K^{vol}	Partition ratio (volumetric concentration basis)	Ratio of kg/m^3 or $kgmol/m^3$ or $gmol/L$	Ratio of lb/ft^3 or $lbmol/ft^3$	S'	Solvent mass or mass flow rate (extraction solvent only)	kg or kg/s	lb or lb/h
L	Downcomer (or upcomer) length	m	in or ft	S'_s	Mass flow rate of extraction solvent within stripping section	kg/s	lb/h
L_{fp}	Length of flow path in Eq. (15-161)	m	in or ft	S'_w	Mass flow rate of extraction solvent within washing section	kg/s	lb/h
m	Local slope of equilibrium line (unspecified concentration units)			S_{ij}	Separation power for separating component i from component j [defined by Eq. (15-105)]	Dimensionless	Dimensionless
m'	Local slope of equilibrium line (in Bancroft coordinates)	Mass ratio/mass ratio	Mass ratio/mass ratio	S_{tip}	Impeller tip speed	m/s	ft/s
m_{dc}	Local slope of equilibrium line for dispersed-phase concentration plotted versus continuous-phase concentration			t_b	Batch mixing time	s or h	min or h
m_{er}	Local slope of equilibrium line for extract-phase concentration plotted versus raffinate-phase concentration			T	Temperature (absolute)	K	$^{\circ}R$
m^{vol}	Local slope of equilibrium line (volumetric concentration basis)	Ratio of kg/m^3 or $kgmol/m^3$ or $gmol/L$	Ratio of lb/ft^3 or $lbmol/ft^3$ units	u_t	Stokes' law terminal or settling velocity of a drop	m/s or cm/s	ft/s or ft/min
M	Mass or mass flow rate	kg or kg/s	lb or lb/h	u_{∞}	Unhindered settling velocity of a single drop	m/s or cm/s	ft/s or ft/min
MW	Molecular weight	kg/kgmol or g/gmol	lb/lbmol	v	Molar volume	$m^3/kgmol$ or $cm^3/gmol$	$ft^3/lbmol$
N	Number of theoretical stages	Dimensionless	Dimensionless	V	Liquid velocity (or volumetric flow per unit area)	m/s	ft/s or ft/min
N_A	Flux of component A (mass or mol/area/unit time)	(kg or kgmol)/($m^2 \cdot s$)	(lb or lbmol)/($ft^2 \cdot s$)	V'	Volume	m^3	ft^3 or gal
N_{holes}	Number of holes	Dimensionless	Dimensionless	V_{cf}	Continuous-phase flooding velocity	m/s	ft/s or ft/min
N_{or}	Number of overall mass-transfer units based on the raffinate phase	Dimensionless	Dimensionless	V_{cflow}	Cross-flow velocity of continuous phase at sieve tray	m/s	ft/s or ft/min
N_s	Number of theoretical stages in stripping section	Dimensionless	Dimensionless	V_{df}	Dispersed-phase flooding velocity	m/s	ft/s or ft/min
N_w	Number of theoretical stages in washing section	Dimensionless	Dimensionless	V_{drop}	Average velocity of a dispersed drop	m/s	ft/s or ft/min
P	Pressure	bar or Pa	atm or lb_f/in^2	V_{ic}	Interstitial velocity of continuous phase	m/s	ft/s or ft/min
P	Dimensionless group defined by Eq. (15-122)	Dimensionless	Dimensionless	$V_{o,max}$	Maximum velocity through an orifice or nozzle	m/s	ft/s or ft/min
P	Power	W or kW	HP or $ft \cdot lb_f/h$	V_s	Slip velocity	m/s	ft/s or ft/min
Pe	Péclet number Vb/E , where V is liquid velocity, E is axial mixing coefficient, and b is a characteristic equipment dimension	Dimensionless	Dimensionless	V_{so}	Slip velocity at low dispersed-phase flow rate	m/s	ft/s or ft/min
$P_{i,extract}$	Purity of solute i in extract (in wt %)	wt %	wt %	V_{sm}	Static mixer superficial liquid velocity (entrance velocity)	m/s	ft/s or ft/min
$P_{i,feed}$	Purity of solute i in feed (in wt %)	wt %	wt %	W	Mass or mass flow rate of wash solvent phase	kg or kg/s	lb or lb/h
P_o	Power number $P/(\rho_m \omega^3 D_i^5)$	Dimensionless	Dimensionless	W'_s	Mass flow rate of wash solvent within stripping section	kg/s	lb/h
ΔP_{dow}	Pressure drop for flow through a downcomer (or upcomer)	bar or Pa	atm or lb_f/in^2	W'_w	Mass flow rate of wash solvent within washing section	kg/s	lb/h
ΔP_o	Orifice pressure drop	bar or Pa	atm or lb_f/in^2	We	Weber number: for an impeller, $\rho_c \omega^2 D_i^3/\sigma$; for flow through an orifice or nozzle, $V_o^2 d_o \rho_c/\sigma$; for a static mixer, $V_{sm}^2 D_{sm} \rho_c/\sigma$	Dimensionless	Dimensionless
q	MOSCED induction parameter	Dimensionless	Dimensionless	x	Mole fraction solute in feed or raffinate	Mole fraction	Mole fraction
Q	Volumetric flow rate	m^3/s	ft^3/min	X	Concentration of solute in feed or raffinate (unspecified units)		
R	Universal gas constant	8.31 J/K/kgmol	1.99 Btu. $^{\circ}R/lbmol$	X''	Mass fraction solute in feed or raffinate	Mass fractions	Mass fractions
R	Mass or mass flow rate of raffinate phase	kg or kg/s	lb or lb/h	X'	Mass solute/mass feed solvent in feed or raffinate	Mass ratios	Mass ratios
R_A	Rate of mass-transfer (moles per unit time)	kgmol/s	lbmol/h	X_f^B	Pseudoccentration of solute in feed for case B [Eq. (15-95)]	Mass ratios	Mass ratios

Nomenclature (Concluded)

Symbol	Definition	SI units	U.S. Customary System units	Symbol	Definition	SI units	U.S. Customary System units
X_f^C	Pseudoconcentration of solute in feed for case C [Eq. (15-97)]	Mass ratios	Mass ratios	Greek Symbols			
$X_{i,extract}$	Concentration of solute i in extract	Mass fraction	Mass fraction	δ^i	Solubility parameter for component i	(J/cm ³) ^{1/2}	(cal/cm ³) ^{1/2}
$X_{i,feed}$	Concentration of solute i in feed	Mass fraction	Mass fraction	$\bar{\delta}$	Solubility parameter for mixture	(J/cm ³) ^{1/2}	(cal/cm ³) ^{1/2}
X_{ij}	Concentration of component i in the phase richest in j	Mass fraction	Mass fraction	ζ	Tortuosity factor defined by Eq. (15-147)	Dimensionless	Dimensionless
y	Mole fraction solute in solvent or extract	Mole fraction	Mole fraction	θ	Residence time for total liquid	s	s or min
Y	Concentration of solute in the solvent or extract (unspecified units)	Mass fraction	Mass fraction	θ_i	Fraction of solute i extracted from feed	Dimensionless	Dimensionless
Y''	Mass fraction solute in solvent or extract	Mass fraction	Mass fraction	λ	MOSCED dispersion parameter	(J/cm ³) ^{1/2}	(cal/cm ³) ^{1/2}
Y'	Mass solute/mass extraction solvent in solvent or extract	Mass ratio	Mass ratio	λ_m	Membrane thickness	mm	in
Y_s^B	Pseudoconcentration of solute in solvent for case B [Eq. (15-96)]	Mass ratio	Mass ratio	μ	Liquid viscosity	Pa·s	cP
z	Dimension or direction of mass transfer	m	in or ft	μ_i^I	Chemical potential of component i in phase I	J/gmol	Btu/lbmol
z	Sieve tray spacing	m	in or ft	μ_m	Mixture mean viscosity defined in Eq. (15-180)	Pa·s	cP
z	Point representing feed composition on a tie line	Dimensionless	Dimensionless	μ_w	Reference viscosity (of water)	Pa·s	cP
z_i	Number of electronic charges on an ion	Dimensionless	Dimensionless	ξ_1	MOSCED asymmetry factor	Dimensionless	Dimensionless
Z_t	Total height of extractor	m	ft	ξ_{batch}	Efficiency of a batch experiment [Eq. (15-175)]	Dimensionless	Dimensionless
Greek Symbols				$\xi_{continuous}$	Efficiency of a continuous process [Eq. (15-176)]	Dimensionless	Dimensionless
α	MOSCED hydrogen-bond acidity parameter	(J/cm ³) ^{1/2}	(cal/cm ³) ^{1/2}	ξ_m	Murphree stage efficiency	Dimensionless	Dimensionless
α	Solvatochromic hydrogen-bond acidity parameter	(J/cm ³) ^{1/2}	(cal/cm ³) ^{1/2}	ξ_{nd}	Murphree stage efficiency based on dispersed phase	Dimensionless	Dimensionless
α_j	Separation factor for solute i with respect to solute j	Dimensionless	Dimensionless	ξ_o	Overall stage efficiency	Dimensionless	Dimensionless
α_j	NRTL model parameter	Dimensionless	Dimensionless	π	Solvatochromic polarity parameter	(J/cm ³) ^{1/2}	(cal/cm ³) ^{1/2}
β	MOSCED hydrogen-bond basicity parameter	(J/cm ³) ^{1/2}	(cal/cm ³) ^{1/2}	$\Delta\pi$	Osmotic pressure gradient	bar or Pa	atm or lb _f /in ²
β	Solvatochromic hydrogen-bond basicity parameter	(J/cm ³) ^{1/2}	(cal/cm ³) ^{1/2}	ρ	Liquid density	kg/m ³	lb/ft ³
γ_{ij}	Activity coefficient of i dissolved in j	Dimensionless	Dimensionless	ρ_m	Mixture mean density defined in Eq. (15-178)	kg/m ³	lb/ft ³
γ^∞	Activity coefficient at infinite dilution	Dimensionless	Dimensionless	σ	Interfacial tension	N/m	dyn/cm
γ_i^C	Activity coefficient, combinatorial part of UNIFAC	Dimensionless	Dimensionless	τ	MOSCED polarity parameter	(J/cm ³) ^{1/2}	(cal/cm ³) ^{1/2}
γ_i^I	Activity coefficient of component i in phase I	Dimensionless	Dimensionless	$\tau_{i,j}$	NRTL model parameter	Dimensionless	Dimensionless
γ_i^R	Activity coefficient, residual part of UNIFAC	Dimensionless	Dimensionless	ϕ	Volume fraction	Dimensionless	Dimensionless
ϵ	Void fraction	Dimensionless	Dimensionless	ϕ_d	Volume fraction of dispersed phase (holdup)	Dimensionless	Dimensionless
ϵ	Fractional open area of a perforated plate	Dimensionless	Dimensionless	$\phi_{d,feed}$	Volume fraction of dispersed phase in feed	Dimensionless	Dimensionless
δ	Solvatochromic polarizability parameter	(J/cm ³) ^{1/2}	(cal/cm ³) ^{1/2}	ϕ_o	Initial dispersed-phase holdup in feed to a decanter	Dimensionless	Dimensionless
δ_d	Hansen nonpolar (dispersion) solubility parameter	(J/cm ³) ^{1/2}	(cal/cm ³) ^{1/2}	φ	Volume fraction of voids in a packed bed	Dimensionless	Dimensionless
δ_h	Hansen solubility parameter for hydrogen bonding	(J/cm ³) ^{1/2}	(cal/cm ³) ^{1/2}	Φ	Factor governing use of Eqs. (15-148) and (15-149)	Dimensionless	Dimensionless
δ_p	Hansen polar solubility parameter	(J/cm ³) ^{1/2}	(cal/cm ³) ^{1/2}	χ	Parameter in Eq. (15-41) indicating which phase is likely to be dispersed	Dimensionless	Dimensionless
				ω	Impeller speed	Rotations/s	Rotations/min
				Additional Subscripts			
				c	Continuous phase		
				d	Dispersed phase		
				e	Extract phase		
				f	Feed phase or flooding condition (when combined with d or c)		
				i	Component i		
				j	Component j		
				H	Heavy liquid		
				L	Light liquid		
				max	Maximum value		
				min	Minimum value		
				o	Orifice or nozzle		
				r	Raffinate phase		
				s	Solvent		

GENERAL REFERENCES: Wankat, *Separation Process Engineering*, 2d ed. (Prentice-Hall, 2006); Seader and Henley, *Separation Process Principles*, 2d ed. (Wiley, 2006); Seibert, "Extraction and Leaching," Chap. 14 in *Chemical Process Equipment: Selection and Design*, 2d ed., Couper et al., eds. (Elsevier, 2005); Aguilar and Cortina, *Solvent Extraction and Liquid Membranes: Fundamentals and Applications in New Materials* (Dekker, 2005); Glatz and Parker, "Enriching Liquid-Liquid Extraction," *Chem. Eng. Magazine*, **111**(11), pp. 44–48 (2004); *Solvent Extraction Principles and Practice*, 2d ed., Rydberg et al., eds. (Dekker, 2004); *Ion Exchange and Solvent Extraction*, vol. 17, Marcus and SenGupta, eds. (Dekker, 2004), and earlier volumes in the series; Leng and Calabrese, "Immiscible Liquid-Liquid Systems," Chap. 12 in *Handbook of Industrial Mixing: Science and Practice*, Paul, Atiemo-Obeng, and Kresta, eds. (Wiley, 2004); Cheremisinoff, *Industrial Solvents Handbook*, 2d ed. (Dekker, 2003); Van Brunt and Kanel, "Extraction with Reaction," Chap. 3 in *Reactive Separation Processes*, Kulprathipanja, ed. (Taylor & Francis, 2002); Mueller et al., "Liquid-Liquid Extraction" in *Ullmann's Encyclopedia of Industrial Chemistry*, 6th ed. (VCH, 2002); Benitez, *Principles and Modern Applications of Mass Transfer Operations* (Wiley, 2002); Wypych, *Handbook of Solvents* (Chemtec, 2001); Flick, *Industrial Solvents Handbook*, 5th ed. (Noyes, 1998); Robbins, "Liquid-Liquid Extraction," Sec. 1.9 in *Handbook of Separation Techniques for Chemical Engineers*, 3d ed., Schweitzer, ed. (McGraw-Hill, 1997); Lo, "Commercial Liquid-Liquid Extraction Equipment," Sec. 1.10 in *Handbook of Separation Techniques for Chemical Engineers*, 3d ed., Schweitzer, ed. (McGraw-Hill, 1997); Humphrey and Keller, "Extraction," Chap. 3 in *Separation Process Technology* (McGraw-Hill, 1997), pp. 113–151; Cusack and Glatz, "Apply Liquid-Liquid Extraction to Today's Problems," *Chem. Eng. Magazine*, **103**(7), pp. 94–103 (1996); *Liquid-Liquid Extraction Equipment*, Godfrey and Slater, eds. (Wiley, 1994); Zaslavsky, *Aqueous Two-Phase Partitioning* (Dekker, 1994); Strigle, "Liquid-Liquid Extraction," Chap. 11 in *Packed Tower Design and Applications*, 2d ed. (Gulf, 1994); Schigerl, *Solvent Extraction in Biotechnology* (Springer-Verlag, 1994); Schigerl, "Liquid-Liquid Extraction (Small Molecules)," Chap. 21 in *Biotechnology*, 2d ed., vol. 3, Stephanopoulos, ed. (VCH, 1993); Kelley and Hatton, "Protein Purification by Liquid-Liquid Extraction," Chap. 22 in *Biotechnology*, 2d ed., vol. 3, Stephanopoulos, ed. (VCH, 1993); Lo and Baird, "Extraction,

Liquid-Liquid," in *Kirk-Othmer Encyclopedia of Chemical Technology*, 4th ed., vol. 10, Kroschwitz and Howe-Grant, eds. (Wiley, 1993), pp. 125–180; *Science and Practice of Liquid-Liquid Extraction*, vol. 1, *Phase Equilibria; Mass Transfer and Interfacial Phenomena; Extractor Hydrodynamics, Selection, and Design*, and vol. 2, *Process Chemistry and Extraction Operations in the Hydrometallurgical, Nuclear, Pharmaceutical, and Food Industries*, Thornton, ed. (Oxford, 1992); Cusack, Fremeaux, and Glatz, "A Fresh Look at Liquid-Liquid Extraction," pt. 1, "Extraction Systems," *Chem. Eng. Magazine*, **98**(2), pp. 66–67 (1991); Cusack and Fremeaux, pt. 2, "Inside the Extractor," *Chem. Eng. Magazine*, **98**(3), pp. 132–138 (1991); Cusack and Karr, pt. 3, "Extractor Design and Specification," *Chem. Eng. Magazine*, **98**(4), pp. 112–120 (1991); *Methods in Enzymology*, vol. 182, *Guide to Protein Purification*, Deutscher, ed. (Academic, 1990); Wankat, *Equilibrium Staged Separations* (Prentice Hall, 1988); Blumberg, *Liquid-Liquid Extraction* (Academic, 1988); Skelland and Tedder, "Extraction—Organic Chemicals Processing," Chap. 7 in *Handbook of Separation Process Technology*, Rousseau, ed. (Wiley, 1987); Chapman, "Extraction—Metals Processing," Chap. 8 in *Handbook of Separation Process Technology*, Rousseau, ed. (Wiley, 1987); Novak, Matous, and Pick, *Liquid-Liquid Equilibria*, Studies in Modern Thermodynamics Series, vol. 7 (Elsevier, 1987); Bailes et al., "Extraction, Liquid-Liquid" in *Encyclopedia of Chemical Processing and Design*, vol. 21, McKetta and Cunningham, eds. (Dekker, 1984), pp. 19–166; *Handbook of Solvent Extraction*, Lo, Baird, and Hanson, eds. (Wiley, 1983; Krieger, 1991); Sorenson and Arlt, *Liquid-Liquid Equilibrium Data Collection*, DECHEMA, *Binary Systems*, vol. V, pt. 1, 1979, *Ternary Systems*, vol. V, pt. 2, 1980, *Ternary and Quaternary Systems*, vol. 5, pt. 3, 1980, Macedo and Rasmussen, Suppl. 1, vol. V, pt. 4, 1987; Wisniak and Tamir, *Liquid-Liquid Equilibrium and Extraction, a Literature Source Book*, vols. I and II (Elsevier, 1980–1981), Suppl. 1 (1985); Treybal, *Mass Transfer Operations*, 3d ed. (McGraw-Hill, 1980); King, *Separation Processes*, 2d ed. (McGraw-Hill, 1980); Laddha and Degaleesan, *Transport Phenomena in Liquid Extraction* (McGraw-Hill, 1978); Brian, *Staged Cascades in Chemical Processing* (Prentice-Hall, 1972); Pratt, *Countercurrent Separation Processes* (Elsevier, 1967); Treybal, "Liquid Extractor Performance," *Chem. Eng. Prog.*, **62**(9), pp. 67–75 (1966); Treybal, *Liquid Extraction*, 2d ed. (McGraw-Hill, 1963); Alders, *Liquid-Liquid Extraction*, 2d ed. (Elsevier, 1959).

INTRODUCTION AND OVERVIEW

Liquid-liquid extraction is a process for separating the components of a liquid (the feed) by contact with a second liquid phase (the solvent). The process takes advantage of differences in the chemical properties of the feed components, such as differences in polarity and hydrophobic/hydrophilic character, to separate them. Stated more precisely, the transfer of components from one phase to the other is driven by a deviation from thermodynamic equilibrium, and the equilibrium state depends on the nature of the interactions between the feed components and the solvent phase. The potential for separating the feed components is determined by differences in these interactions.

A liquid-liquid extraction process produces a solvent-rich stream called the extract that contains a portion of the feed and an extracted-feed stream called the raffinate. A commercial process almost always includes two or more auxiliary operations in addition to the extraction operation itself. These extra operations are needed to treat the extract and raffinate streams for the purposes of isolating a desired product, recovering the solvent for recycle to the extractor, and purging unwanted components from the process. A typical process includes two or more distillation operations in addition to extraction.

Liquid-liquid extraction is used to recover desired components from a crude liquid mixture or to remove unwanted contaminants. In developing a process, the project team must decide what solvent or solvent mixture to use, how to recover solvent from the extract, and how to remove solvent residues from the raffinate. The team must also decide what temperature or range of temperatures should be used for the extraction, what process scheme to employ among many possibilities, and what type of equipment to use for liquid-liquid contacting and phase separation. The variety of commercial equipment options is large and includes stirred tanks and decanters, specialized mixer-settlers, a wide variety of agitated and nonagitated extraction columns or towers, and various types of centrifuges.

Because of the availability of hundreds of commercial solvents and extractants, as well as a wide variety of established process schemes and equipment options, liquid-liquid extraction is a versatile technology with a wide range of commercial applications. It is utilized in the

processing of numerous commodity and specialty chemicals including metals and nuclear fuel (hydrometallurgy), petrochemicals, coal and wood-derived chemicals, and complex organics such as pharmaceuticals and agricultural chemicals. Liquid-liquid extraction also is an important operation in industrial wastewater treatment, food processing, and the recovery of biomolecules from fermentation broth.

HISTORICAL PERSPECTIVE

The art of solvent extraction has been practiced in one form or another since ancient times. It appears that prior to the 19th century solvent extraction was primarily used to isolate desired components such as perfumes and dyes from plant solids and other natural sources [Aftalion, *A History of the International Chemical Industry* (Univ. Penn. Press, 1991); and Taylor, *A History of Industrial Chemistry* (Abelard-Schuman, 1957)]. However, several early applications involving liquid-liquid contacting are described by Blass, Liebel, and Haerberl ["Solvent Extraction—A Historical Review," *International Solvent Extraction Conf. (ISEC) '96 Proceedings* (Univ. of Melbourne, 1996)], including the removal of pigment from oil by using water as the solvent.

The modern practice of liquid-liquid extraction has its roots in the middle to late 19th century when extraction became an important laboratory technique. The partition ratio concept describing how a solute partitions between two liquid phases at equilibrium was introduced by Berthelot and Jungfleisch [*Ann. Chim. Phys.*, **4**, p. 26 (1872)] and further defined by Nernst [*Z. Phys. Chemie*, **8**, p. 110 (1891)]. At about the same time, Gibbs published his theory of phase equilibrium (1876 and 1878). These and other advances were accompanied by a growing chemical industry. An early countercurrent extraction process utilizing ethyl acetate solvent was patented by Goering in 1883 as a method for recovering acetic acid from "pyroigneous acid" produced by pyrolysis of wood [Othmer, p. xiv in *Handbook of Solvent Extraction* (Wiley, 1983; Krieger, 1991)], and Pfeleiderer patented a stirred extraction column in 1898 [Blass, Liebel, and Haerberl, *ISEC '96 Proceedings* (Univ. of Melbourne, 1996)].

With the emergence of the chemical engineering profession in the 1890s and early 20th century, additional attention was given to process fundamentals and development of a more quantitative basis for process design. Many of the advances made in the study of distillation and absorption were readily adapted to liquid-liquid extraction, owing to its similarity as another diffusion-based operation. Examples include application of mass-transfer coefficients [Lewis, *Ind. Eng. Chem.*, **8**(9), pp. 825–833 (1916); and Lewis and Whitman, *Ind. Eng. Chem.*, **16**(12), pp. 1215–1220 (1924)], the use of graphical stagewise design methods [McCabe and Thiele, *Ind. Eng. Chem.*, **17**(6), pp. 605–611 (1925); Evans, *Ind. Eng. Chem.*, **26**(8), pp. 860–864 (1934); and Thiele, *Ind. Eng. Chem.*, **27**(4), pp. 392–396 (1935)], the use of theoretical-stage calculations [Kremser, *National Petroleum News*, **22**(21), pp. 43–49 (1930); and Souders and Brown, *Ind. Eng. Chem.*, **24**(5), pp. 519–522 (1932)], and the transfer unit concept introduced in the late 1930s by Colburn and others [Colburn, *Ind. Eng. Chem.*, **33**(4), pp. 459–467 (1941)]. Additional background is given by Hampe, Hartland, and Slater [Chap. 2 in *Liquid-Liquid Extraction Equipment*, Godfrey and Slater, eds. (Wiley, 1994)].

The number of commercial applications continued to grow, and by the 1930s liquid-liquid extraction had replaced various chemical treatment methods for refining mineral oil and coal tar products [Varteressian and Fenske, *Ind. Eng. Chem.*, **28**(8), pp. 928–933 (1936)]. It was also used to recover acetic acid from waste liquors generated in the production of cellulose acetate, and in various nitration and sulfonation processes [Hunter and Nash, *The Industrial Chemist*, **9**(102–104), pp. 245–248, 263–266, 313–316 (1933)]. The article by Hunter and Nash also describes early mixer-settler equipment, mixing jets, and various extraction columns including the spray column, baffle tray column, sieve tray column, and a packed column filled with Raschig rings or coke breeze, the material left behind when coke is burned.

Much of the liquid-liquid extraction technology in practice today was first introduced to industry during a period of vigorous innovation and growth of the chemical industry as a whole from about 1920 to 1970. The advances of this period include development of fractional extraction schemes including work described by Cornish et al., [*Ind. Eng. Chem.*, **26**(4), pp. 397–406 (1934)] and by Thiele [*Ind. Eng. Chem.*, **27**(4), pp. 392–396 (1935)]. A well-known commercial example involving the use of extract reflux is the Udex process for separating aromatic compounds from hydrocarbon mixtures using diethylene glycol, a process developed jointly by The Dow Chemical Company and Universal Oil Products in the 1940s. This period also saw the introduction of many new equipment designs including specialized mixer-settler equipment, mechanically agitated extraction columns, and centrifugal extractors as well as a great increase in the availability of different types of industrial solvents. A variety of alcohols, ketones, esters, and chlorinated hydrocarbons became available in large quantities beginning in the 1930s, as petroleum refiners and chemical companies found ways to manufacture them inexpensively using the byproducts of petroleum refining operations or natural gas. Later, a number of specialty solvents were introduced including sulfolane (tetrahydrothiophene-1,1-dioxane) and NMP (*N*-methyl-2-pyrrolidone) for improved extraction of aromatics from hydrocarbons. Specialized extractants also were developed including numerous organophosphorous extractants used to recover or purify metals dissolved in aqueous solutions.

The ready availability of numerous solvents and extractants, combined with the tremendous growth of the chemical industry, drove the development and implementation of many new industrial applications. Handbooks of chemical process technology provide a glimpse of some of these [Riegel's *Handbook of Industrial Chemistry*, 10th ed., Kent, ed. (Springer, 2003); *Chemical Processing Handbook*, McKetta, ed. (Dekker, 1993); and Austin, *Shreve's Chemical Process Industries*, 5th ed. (McGraw-Hill, 1984)], but many remain proprietary and are not widely known. The better-known examples include the separation of aromatics from aliphatics, as mentioned above, extraction of phenolic compounds from coal tars and liquors, recovery of ϵ -caprolactam for production of polyamide-6 (nylon-6), recovery of hydrogen peroxide from oxidized anthraquinone solution, plus many processes involving the washing of crude organic streams with alkaline or acidic

solutions and water, and the detoxification of industrial wastewater prior to biotreatment using steam-strippable organic solvents. The pharmaceutical and specialty chemicals industry also began using liquid-liquid extraction in the production of new synthetic drug compounds and other complex organics. In these processes, often involving multiple batch reaction steps, liquid-liquid extraction generally is used for recovery of intermediates or crude products prior to final isolation of a pure product by crystallization. In the inorganic chemical industry, extraction processes were developed for purification of phosphoric acid, purification of copper by removal of arsenic impurities, and recovery of uranium from phosphate-rock leach solutions, among other applications. Extraction processes also were developed for bioprocessing applications, including the recovery of citric acid from broth using trialkylamine extractants, the use of amyl acetate to recover antibiotics from fermentation broth, and the use of water-soluble polymers in aqueous two-phase extraction for purification of proteins.

The use of supercritical or near-supercritical fluids for extraction, a subject area normally set apart from discussions of liquid-liquid extraction, has received a great deal of attention in the R&D community since the 1970s. Some processes were developed many years before then; e.g., the propane deasphalting process used to refine lubricating oils uses propane at near-supercritical conditions, and this technology dates back to the 1930s [McHugh and Krukoni, *Supercritical Fluid Processing*, 2d ed. (Butterworth-Heinemann, 1993)]. In more recent years the use of supercritical fluids has found a number of commercial applications displacing earlier liquid-liquid extraction methods, particularly for recovery of high-value products meant for human consumption including decaffeinated coffee, flavor components from citrus oils, and vitamins from natural sources.

Significant progress continues to be made toward improving extraction technology, including the introduction of new methods to estimate solvent properties and screen candidate solvents and solvent blends, new methods for overall process conceptualization and optimization, and new methods for equipment design. Progress also is being made by applying the technology developed for a particular application in one industry to improve another application in another industry. For example, much can be learned by comparing equipment and practices used in organic chemical production with those used in the inorganic chemical industry (and vice versa), or by comparing practices used in commodity chemical processing with those used in the specialty chemicals industry. And new concepts offering potential for significant improvements continue to be described in the literature. (See "Emerging Developments.")

USES FOR LIQUID-LIQUID EXTRACTION

For many separation applications, the use of liquid-liquid extraction is an alternative to the various distillation schemes described in Sec. 13, "Distillation." In many of these cases, a distillation process is more economical largely because the extraction process requires extra operations to process the extract and raffinate streams, and these operations usually involve the use of distillation anyway. However, in certain cases the use of liquid-liquid extraction is more cost-effective than using distillation alone because it can be implemented with smaller equipment and/or lower energy consumption. In these cases, differences in chemical or molecular interactions between feed components and the solvent provide a more effective means of accomplishing the desired separation compared to differences in component volatilities.

For example, liquid-liquid extraction may be preferred when the relative volatility of key components is less than 1.3 or so, such that an unusually tall distillation tower is required or the design involves high reflux ratios and high energy consumption. In certain cases, the distillation option may involve addition of a solvent (extractive distillation) or an entrainer (azeotropic distillation) to enhance the relative volatility. Even in these cases, a liquid-liquid extraction process may offer advantages in terms of higher selectivity or lower solvent usage and lower energy consumption, depending upon the application. Extraction may be preferred when the distillation option requires operation at pressures less than about 70 mbar (about 50 mmHg) and an unusually large-diameter distillation tower is required, or when most of the

feed must be taken overhead to isolate a desired bottoms product. Extraction may also be attractive when distillation requires use of high-pressure steam for the reboiler or refrigeration for overheads condensation [Null, *Chem. Eng. Prog.*, **76**(8), pp. 42–49 (August 1980)], or when the desired product is temperature-sensitive and extraction can provide a gentler separation process.

Of course, liquid-liquid extraction also may be a useful option when the components of interest simply cannot be separated by using distillation methods. An example is the use of liquid-liquid extraction employing a steam-strippable solvent to remove nonstrippable, low-volatility contaminants from wastewater [Robbins, *Chem. Eng. Prog.*, **76**(10), pp. 58–61 (1980)]. The same process scheme often provides a cost-effective alternative to direct distillation or stripping of volatile impurities when the relative volatility of the impurity with respect to water is less than about 10 [Robbins, U.S. Patent 4,236,973 (1980); Hwang, Keller, and Olson, *Ind. Eng. Chem. Res.*, **31**, pp. 1753–1759 (1992); and Frank et al., *Ind. Eng. Chem. Res.*, **46**(11), pp. 3774–3786 (2007)].

Liquid-liquid extraction also can be an attractive alternative to separation methods, other than distillation, e.g., as an alternative to crystallization from solution to remove dissolved salts from a crude organic feed, since extraction of the salt content into water eliminates the need to filter solids from the mother liquor, often a difficult or expensive operation. Extraction also may compete with process-scale chromatography, an example being the recovery of hydroxytyrosol (3,4-dihydroxyphenylethanol), an antioxidant food additive, from olive-processing wastewaters [Guzman et al., U.S. Patent 6,849,770 (2005)].

The attractiveness of liquid-liquid extraction for a given application compared to alternative separation technologies often depends upon the concentration of solute in the feed. The recovery of acetic acid from aqueous solutions is a well-known example [Brown, *Chem. Eng. Prog.*, **59**(10), pp. 65–68 (1963)]. In this case, extraction generally is more economical than distillation when handling dilute to moderately concentrated feeds, while distillation is more economical at higher concentrations. In the treatment of water to remove trace amounts of organics, when the concentration of impurities in the feed is greater than about 20 to 50 ppm, liquid-liquid extraction may be more economical than adsorption of the impurities by using carbon beds, because the latter may require frequent and costly replacement of the adsorbent [Robbins, *Chem. Eng. Prog.*, **76**(10), pp. 58–61 (1980)]. At lower concentrations of impurities, adsorption may be the more economical option because the usable lifetime of the carbon bed is longer.

Examples of cost-effective liquid-liquid extraction processes utilizing relatively low-boiling solvents include the recovery of acetic acid from aqueous solutions using ethyl ether or ethyl acetate [King, Chap. 18.5 in *Handbook of Solvent Extraction*, Lo, Baird, and Hanson, eds. (Wiley, 1983; Krieger, 1991)] and the recovery of phenolic compounds from water by using methyl isobutyl ketone [Greminger et al., *Ind. Eng. Chem. Process Des. Dev.*, **21**(1), pp. 51–54 (1982)]. In these processes, the solvent is recovered from the extract by distillation, and dissolved solvent is removed from the raffinate by steam stripping (Fig. 15-1). The solvent circulates through the process in a closed loop.

One of the largest applications of liquid-liquid extraction in terms of total worldwide production volume involves the extraction of aromatic compounds from hydrocarbon mixtures in petrochemical operations using high-boiling polar solvents. A number of processes have been developed to recover benzene, toluene, and xylene (BTX) as feedstock for chemical manufacturing or to refine motor oils. This general technology is described in detail in “Single-Solvent Fractional Extraction with Extract Reflux” under “Calculation Procedures.” A typical flow diagram is shown in Fig. 15-2. Liquid-liquid extraction also may be used to upgrade used motor oil; an extraction process employing a relatively light polar solvent such as *N,N*-dimethylformamide or acetonitrile has been developed to remove polynuclear aromatic and sulfur-containing contaminants [Sherman, Hershberger, and Taylor, U.S. Patent 6,320,090 (2001)]. An alternative process utilizes a blend of methyl ethyl ketone + 2-propanol and small amounts of aqueous KOH [Rincón, Cañizares, and García, *Ind. Eng. Chem. Res.*, **44**(20), pp. 7854–7859 (2005)].

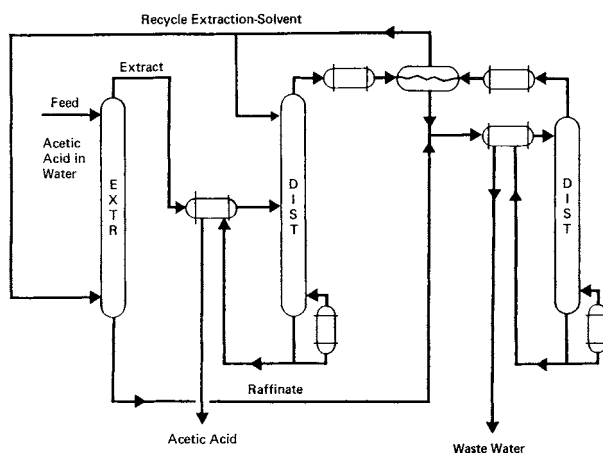


FIG. 15-1 Typical process for extraction of acetic acid from water.

Extraction also is used to remove CO_2 , H_2S , and other acidic contaminants from liquefied petroleum gases (LPGs) generated during operation of fluid catalytic crackers and cokers in petroleum refineries, and from liquefied natural gas (LNG). The acid gases are extracted from the liquefied hydrocarbons (primarily C_1 to C_3) by reversible reaction with various amine extractants. Typical amines are methyldiethanolamine (MDEA), diethanolamine (DEA), and monoethanolamine (MEA). In a typical process (Fig. 15-3), the treated hydrocarbon liquid (the raffinate) is washed with water to remove residual amine, and the loaded amine solution (the extract) is regenerated in a stripping tower for recycle back to the extractor [Nielsen et al., *Hydrocarbon Proc.*, **76**, pp. 49–59 (1997)]. The technology is similar to that used to scrub CO_2 and H_2S from gas streams [Oyenekan and Rochelle, *Ind. Eng. Chem. Res.*, **45**(8), pp. 2465–2472 (2006); and Jassim and Rochelle, *Ind. Eng. Chem. Res.*, **45**(8), pp. 2457–2464 (2006)], except that the process involves liquid-liquid contacting instead of gas-liquid contacting. Because of this, a common stripper often is used to regenerate solvent from a variety of gas absorbers and liquid-liquid extractors operated within a typical refinery. In certain applications, organic acids such as formic acid are present in low concentrations in the hydrocarbon feed. These contaminants will react with the amine extractant to form heat-stable amine salts that accumulate in the solvent loop over time, requiring periodic purging or regeneration of the solvent solution [Price and Burns, *Hydrocarbon Proc.*, **74**, pp. 140–141 (1995)]. The amine-based extraction process is an alternative to washing with caustic or the use of solid adsorbents.

A typical extraction process used in hydrometallurgical applications is outlined in Fig. 15-4. This technology involves transferring the desired element from the ore leachate liquor, an aqueous acid, into an organic solvent phase containing specialty extractants that form a complex with the metal ion. The organic phase is later contacted with an aqueous solution at a different pH and temperature to regenerate the solvent and transfer the metal into a clean solution from which it can be recovered by electrolysis or another method [Cox, Chap. 1 in *Science and Practice of Liquid-Liquid Extraction*, vol. 2, Thornton, ed. (Oxford, 1992)]. Another process technology utilizes metals complexed with various organophosphorus compounds as recyclable homogeneous catalysts; liquid-liquid extraction is used to transfer the metal complex between the reaction phase and a separate liquid phase after reaction. Different ligands having different polarities are chosen to facilitate the use of various extraction and recycle schemes [Kanel et al., U.S. Patents 6,294,700 (2001) and 6,303,829 (2001)].

Another category of useful liquid-liquid extraction applications involves the recovery of antibiotics and other complex organics from fermentation broth by using a variety of oxygenated organic solvents such as acetates and ketones. Although some of these products are unstable at the required extraction conditions (particularly if pH must

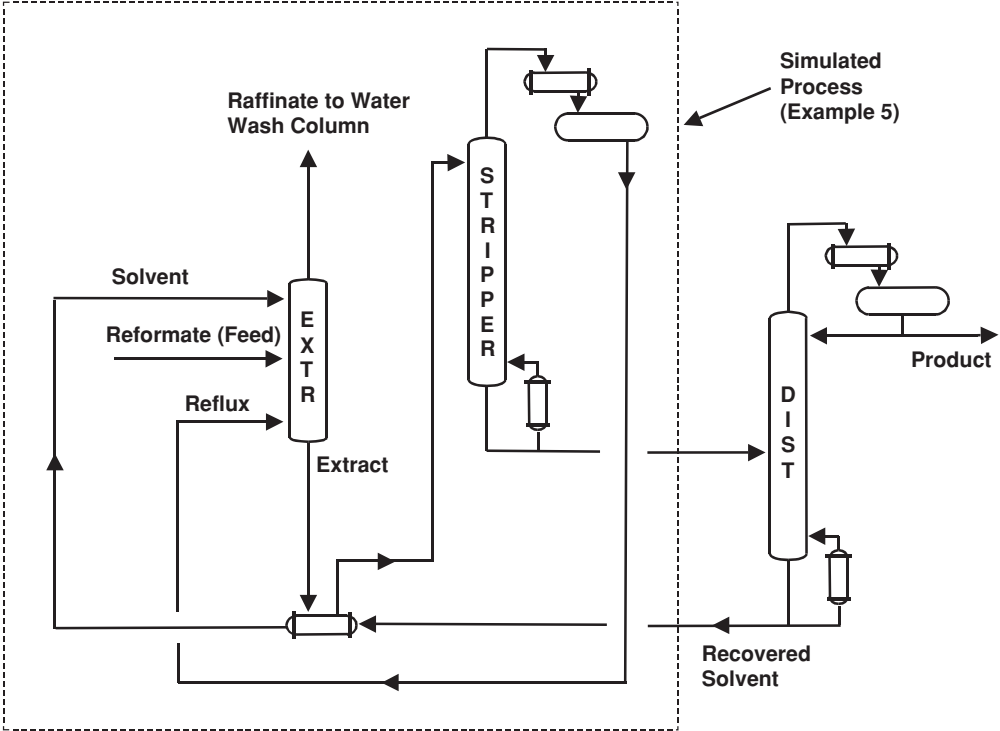


FIG. 15-2 Flow sheet of a simplified aromatic extraction process (see Example 5).

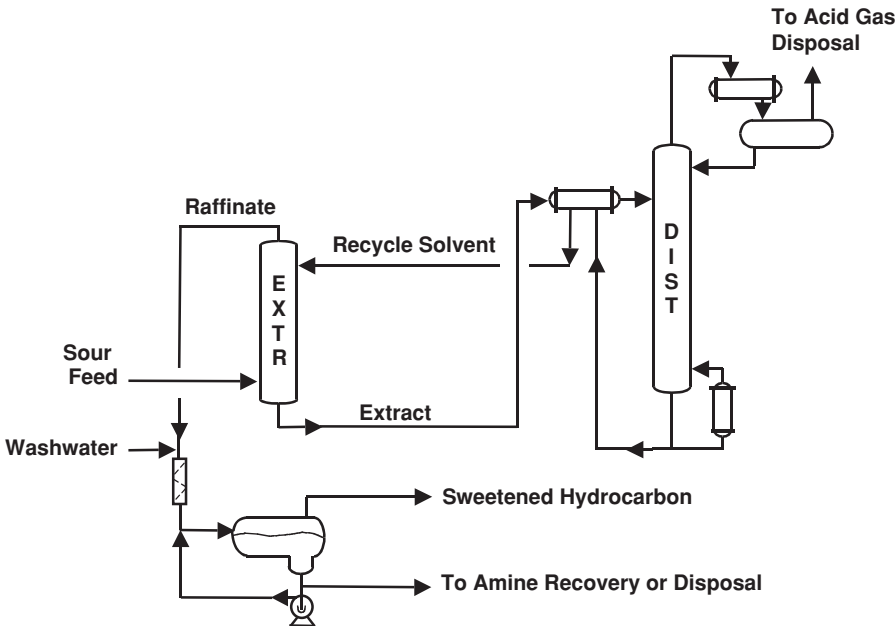


FIG. 15-3 Typical process for extracting acid gases from LPG or LNG.

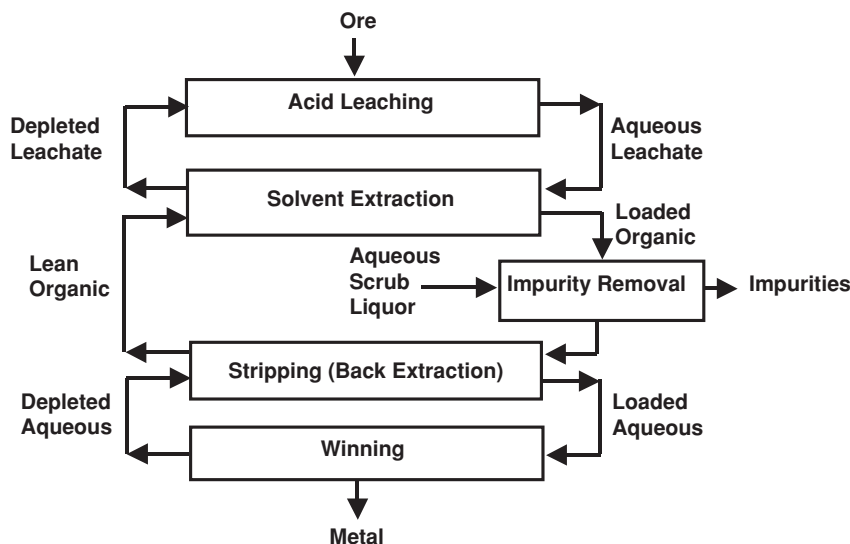


FIG. 15-4 Example process scheme used in hydrometallurgical applications. [Taken from Cox, Chap. 1 in *Science and Practice of Liquid-Liquid Extraction*, vol. 2, Thornton, ed. (Oxford, 1992), with permission. Copyright 1992 Oxford University Press.]

be low for favorable partitioning), short-contact-time centrifugal extractors may be used to minimize exposure. Centrifugal extractors also help overcome problems associated with formation of emulsions between solvent and broth. In a number of applications, the whole broth can be processed without prior removal of solids, a practice that can significantly reduce costs. For detailed information, see "The History of Penicillin Production," Elder, ed., *Chemical Engineering Progress Symposium Series No. 100*, vol. 66, pp. 37–42 (1970); Queener and Swartz, "Penicillins: Biosynthetic and Semisynthetic," in *Secondary Products of Metabolism, Economic Microbiology*, vol. 3, Rose, ed. (Academic, 1979); and Chaung et al., *J. Chinese Inst. Chem. Eng.*, **20**(3), pp. 155–161 (1989). Another well-known commercial application of liquid-liquid extraction in bioprocessing is the Baniel process for the recovery of citric acid from fermentation broth with tertiary amine extractants [Baniel, Blumberg, and Hadju, U.S. Patent 4,275,234 (1980)]. This type of process is discussed in "Reaction-Enhanced Extraction" under "Commercial Process Schemes."

DEFINITIONS

Extraction terms defined by the International Union of Pure and Applied Chemistry (IUPAC) generally are recommended. [See Rice, Irving, and Leonard, *Pure Appl. Chem.* (IUPAC), **65**(11), pp. 2673–2396 (1993); and J. Inczédy, *Pure Appl. Chem.* (IUPAC), **66**(12), pp. 2501–2512 (1994).] **Liquid-liquid extraction** is a process for separating components dissolved in a liquid feed by contact with a second liquid phase. **Solvent extraction** is a broader term that describes a process for separating the components of any matrix by contact with a liquid, and it includes liquid-solid extraction (leaching) as well as liquid-liquid extraction. The **feed** to a liquid-liquid extraction process is the solution that contains the components to be separated. The major liquid component (or components) in the feed can be referred to as the **feed solvent** or the **carrier solvent**. Minor components in solution often are referred to as **solutes**. The **extraction solvent** is the immiscible or partially miscible liquid added to the process to create a second liquid phase for the purpose of extracting one or more solutes from the feed. It is also called the **separating agent** and may be a mixture of several individual solvents (a **mixed solvent** or a **solvent blend**). The extraction solvent also may be a liquid comprised of an **extractant** dissolved in a liquid **diluent**. In this case, the extractant species is primarily responsible for extraction of solute due to a relatively strong attractive

interaction with the desired solute, forming a reversible adduct or molecular complex. The diluent itself does not contribute significantly to the extraction of solute and in this respect is not the same as a true extraction solvent. A **modifier** may be added to the diluent to increase the solubility of the extractant or otherwise enhance the effectiveness of the extractant. The phase leaving a liquid-liquid contactor rich in extraction solvent is called the **extract**. The **raffinate** is the liquid phase left from the feed after it is contacted by the extract phase. The word *raffinate* originally referred to a "refined product"; however, common usage has extended its meaning to describe the feed phase after extraction whether that phase is a product or not.

Industrial liquid-liquid extraction most often involves processing two immiscible or partially miscible liquids in the form of a **dispersion** of droplets of one liquid (the **dispersed phase**) suspended in the other liquid (the **continuous phase**). The dispersion will exhibit a distribution of drop diameters d_i often characterized by the volume to surface area average diameter or **Sauter mean drop diameter**. The term **emulsion** generally refers to a liquid-liquid dispersion with a dispersed-phase mean drop diameter on the order of 1 μm or less.

The tension that exists between two liquid phases is called the **interfacial tension**. It is a measure of the energy or work required to increase the surface area of the liquid-liquid interface, and it affects the size of dispersed drops. Its value, in units of force per unit length or energy per unit area, reflects the compatibility of the two liquids. Systems that have low compatibility (low mutual solubility) exhibit high interfacial tension. Such a system tends to form relatively large dispersed drops and low interfacial area to minimize contact between the phases. Systems that are more compatible (with higher mutual solubility) exhibit lower interfacial tension and more easily form small dispersed droplets.

A **theoretical or equilibrium stage** is a device or combination of devices that accomplishes the effect of intimately mixing two liquid phases until equilibrium concentrations are reached, then physically separating the two phases into clear layers. The **partition ratio K** is commonly defined for a given solute as the solute concentration in the extract phase divided by that in the raffinate phase after equilibrium is attained in a single stage of contacting. A variety of concentration units are used, so it is important to determine how partition ratios have been defined in the literature for a given application. The term *partition ratio* is preferred, but it also is referred to as the **distribution constant**, **distribution coefficient**, or the **K value**. It is a measure of the

thermodynamic potential of a solvent for extracting a given solute and can be a strong function of composition and temperature. In some cases, the partition ratio transitions from a value less than unity to a value greater than unity as a function of solute concentration. A system of this type is called a **solutrope** [Smith, *Ind. Eng. Chem.*, **42**(6), pp. 1206–1209 (1950)]. The term *distribution ratio*, designated by \mathcal{D}_i , is used in analytical chemistry to describe the distribution of a species that undergoes chemical reaction or dissociation, in terms of the total concentration of analyte in one phase over that in the other, regardless of its chemical form.

The **extraction factor** \mathcal{E} is a process variable that characterizes the capacity of the extract phase to carry solute relative to the feed phase. Its value largely determines the number of theoretical stages required to transfer solute from the feed to the extract. The extraction factor is analogous to the stripping factor in distillation and is the ratio of the slope of the equilibrium line to the slope of the operating line in a McCabe-Thiele type of stagewise graphical calculation. For a standard extraction process with straight equilibrium and operating lines, \mathcal{E} is constant and equal to the partition ratio for the solute of interest times the ratio of the solvent flow rate to the feed flow rate. The **separation factor** $\alpha_{i,j}$ measures the relative enrichment of solute i in the extract phase, compared to solute j , after one theoretical stage of extraction. It is equal to the ratio of K values for components i and j and is used to characterize the **selectivity** a solvent has for a given solute.

A **standard extraction** process is one in which the primary purpose is to transfer solute from the feed phase into the extract phase in a manner analogous to stripping in distillation. **Fractional extraction** refers to a process in which two or more solutes present in the feed are sharply separated from each other, one fraction leaving the extractor in the extract and the other in the raffinate. **Cross-current or cross-flow extraction** (Fig. 15-5) is a series of discrete stages in which the raffinate R from one extraction stage is contacted with additional fresh solvent S in a subsequent stage. **Countercurrent extraction** (Fig. 15-6) is an extraction scheme in which the extraction solvent enters the stage or end of the extraction farthest from where the feed F enters, and the two phases pass each other in countercurrent fashion. The objective is to transfer one or more components from the feed solution F into the extract E . Compared to cross-current operation, countercurrent operation generally allows operation with less solvent. When a **staged contactor** is used, the two phases are mixed with droplets of one phase suspended in the other, but the phases are separated before leaving each stage. A **countercurrent cascade** is a process utilizing multiple staged contactors with countercurrent flow of solvent and feed streams from stage to stage. When a **differential contactor** is used, one of the phases can remain dispersed as drops throughout the contactor as the phases pass each other in countercurrent fashion. The dispersed phase is then allowed to coalesce at the end of the device before being discharged. For these types of processes, **mass-transfer units** (or the related **mass-transfer coefficients**) often are used instead of theoretical stages to characterize separation performance. For a given phase, mass-transfer units are

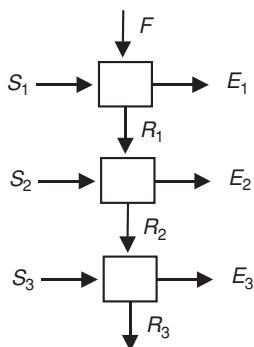


FIG. 15-5 Cross-current extraction.

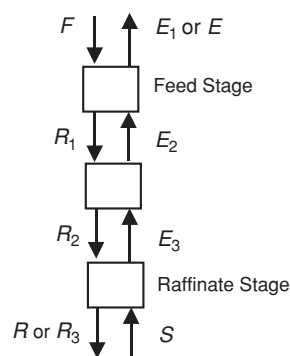


FIG. 15-6 Standard countercurrent extraction.

defined as the integral of the differential change in solute concentration divided by the deviation from equilibrium, between the limits of inlet and outlet solute concentrations. A single transfer unit represents the change in solute concentration equal to that achieved by a single theoretical stage when the extraction factor is equal to 1.0. It differs from a theoretical stage at other values of the extraction factor.

The term **flooding** generally refers to excessive breakthrough or entrainment of one liquid phase into the discharge stream of the other. The flooding characteristics of an extractor limit its hydraulic capacity. Flooding can be caused by excessive flow rates within the equipment, by **phase inversion** due to accumulation and coalescence of dispersed droplets, or by formation of stable dispersions or emulsions due to the presence of surface-active impurities or excessive agitation. The **floor point** typically refers to the specific total volumetric **throughput** in ($\text{m}^3/\text{h}/\text{m}^2$ or gpm/ft^2 of cross-sectional area (or the equivalent **phase velocity** in m/s or ft/s) at which flooding begins.

DESIRABLE SOLVENT PROPERTIES

Common industrial solvents generally are single-functionality organic solvents such as ketones, esters, alcohols, linear or branched aliphatic hydrocarbons, aromatic hydrocarbons, and so on; or water, which may be acidic or basic or mixed with water-soluble organic solvents. More complex solvents are sometimes used to obtain specific properties needed for a given application. These include compounds with multiple functional groups such as diols or triols, glycol ethers, and alkanol amines as well as heterocyclic compounds such as pine-derived solvents (terpenes), sulfolane (tetrahydrothiophene-1,1-dioxane), and NMP (*N*-methyl-2-pyrrolidinone). Solvent properties have been summarized in a number of handbooks and databases including those by Cheremisinoff, *Industrial Solvents Handbook*, 2d ed. (Dekker, 2003); Wypych, *Handbook of Solvents* (ChemTech, 2001); Wypych, *Solvents Database*, CD-ROM (ChemTec, 2001); Yaws, *Thermodynamic and Physical Property Data*, 2d ed. (Gulf, 1998); and Flick, *Industrial Solvents Handbook*, 5th ed. (Noyes, 1998). Solvents are sometimes blended to obtain specific properties, another approach to achieving a multifunctional solvent with properties tailored for a given application. Examples are discussed by Escudero, Cabezas, and Coca [*Chem. Eng. Comm.*, **173**, pp. 135–146 (1999)] and by Delden et al. [*Chem. Eng. Technol.*, **29**(10), pp. 1221–1226 (2006)]. As discussed earlier, a solvent also may be a liquid containing a dissolved extractant species, the extractant chosen because it forms a specific attractive interaction with the desired solute.

In terms of desirable properties, no single solvent or solvent blend can be best in every respect. The choice of solvent often is a compromise, and the relative weighting given to the various considerations depends on the given situation. Assessments should take into account long-term sustainability and overall cost of ownership. Normally, the factors considered in choosing a solvent include the following.

1. **Loading capacity.** This property refers to the maximum concentration of solute the extract phase can hold before two liquid phases can no longer coexist or solute precipitates as a separate phase.

If a specialized extractant is used, loading capacity may be determined by the point at which all the extractant in solution is completely occupied by solute and extractant solubility limits capacity. If loading capacity is low, a high solvent-to-feed ratio may be needed even if the partition ratio is high.

2. *Partition ratio* $K_i = Y_i/X_i$. Partition ratios on the order of $K_i = 10$ or higher are desired for an economical process because they allow operation with minimal amounts of solvent (more specifically, with a minimal solvent-to-feed ratio) and production of higher solute concentrations in the extract—unless the solute concentration in the feed already is high and a limitation in the solvent's loading capacity determines the required solvent-to-feed ratio. Since high partition ratios generally allow for low solvent use, smaller and less costly extraction equipment may be used and costs for solvent recovery and recycle are lower. In principle, partition ratios less than $K_i = 1.0$ may be accommodated by using a high solvent-to-feed ratio, but usually at much higher cost.

3. *Solute selectivity*. In certain applications, it is important not only to recover a desired solute from the feed, but also to separate it from other solutes present in the feed and thereby achieve a degree of solute purification. The selectivity of a given solvent for solute i compared to solute j is characterized by the separation factor $\alpha_{ij} = K_i/K_j$. Values must be greater than $\alpha_{ij} = 1.0$ to achieve an increase in solute purity (on a solvent-free basis). When solvent blends are used in a commercial process, often it is because the blend provides higher selectivity, and often at the expense of a somewhat lower partition ratio. The degree of purification that can be achieved also depends on the extraction scheme chosen for the process, the amount of extraction solvent, and the number of stages employed.

4. *Mutual solubility*. Low liquid-liquid mutual solubility between feed and solvent phases is desirable because it reduces the separation requirements for removing solvents from the extract and raffinate streams. Low solubility of extraction solvent in the raffinate phase often results in high relative volatility for stripping the residual solvent in a raffinate stripper, allowing low-cost desolventizing of the raffinate [Hwang, Keller, and Olson, *Ind. Eng. Chem. Res.*, **31**(7), pp. 1753–1759 (1992)]. Low solubility of feed solvent in the extract phase reduces separation requirements for recovering solvent for recycle and producing a purified product solute. In some cases, if the solubility of feed solvent in the extract is high, more than one distillation operation will be required to separate the extract phase. If mutual solubility is nil (as for aliphatic hydrocarbons dissolved in water), the need for stripping or another treatment method may be avoided as long as efficient liquid-liquid phase separation can be accomplished without entrainment of solvent droplets into the raffinate. However, very low mutual solubility normally is achieved at the expense of a lower partition ratio for extracting the desired solute—because a solvent that has very little compatibility with the feed solvent is not likely to be a good extractant for something that is dissolved in the feed solvent—and therefore has some compatibility. Mutual solubility also limits the solvent-to-feed ratios that can be used, since a point can be reached where the solvent stream is so large it dissolves the entire feed stream, or the solvent stream is so small it is dissolved by the feed, and these can be real limitations for systems with high mutual solubility.

5. *Stability*. The solvent should have little tendency to react with the product solute and form unwanted by-products, causing a loss in yield. Also it should not react with feed components or degrade to undesirable contaminants that cause development of undesirable odors or color over time, or cause difficulty achieving desired product purity, or accumulate in the process because they are difficult to purge.

6. *Density difference*. As a general rule, a difference in density between solvent and feed phases on the order of 0.1 to 0.3 g/mL is preferred. A value that is too low makes for poor or slow liquid-liquid phase separation and may require use of a centrifuge. A value that is too high makes it difficult to build high dispersed-droplet population density for good mass transfer; i.e., it is difficult to mix the two phases together and maintain high holdup of the dispersed phase within the extractor—but this depends on the viscosity of the continuous phase.

7. *Viscosity*. Low viscosity is preferred since higher viscosity generally increases mass-transfer resistance and liquid-liquid phase

separation difficulty. Sometimes an extraction process is operated at an elevated temperature where viscosity is significantly lower for better mass-transfer performance, even when this results in a lower partition ratio. Low viscosity at ambient temperatures also facilitates transfer of solvent from storage to processing equipment.

8. *Interfacial tension*. Preferred values for interfacial tension between the feed phase and the extraction solvent phase generally are in the range of 5 to 25 dyn/cm (1 dyn/cm is equivalent to 10^{-3} N/m). Systems with lower values easily emulsify. For systems with higher values, dispersed droplets tend to coalesce easily, resulting in low interfacial area and poor mass-transfer performance unless mechanical agitation is used.

9. *Recoverability*. The economical recovery of solvent from the extract and raffinate is critical to commercial success. Solvent physical properties should facilitate low-cost options for solvent recovery, recycle, and storage. For example, the use of relatively low-boiling organic solvents with low heats of vaporization generally allows cost-effective use of distillation and stripping for solvent recovery. Solvent properties also should enable low-cost methods for purging impurities from the overall process (lights and/or heavies) that may accumulate over time. One of the challenges often encountered in utilizing a high-boiling solvent or extractant involves accumulation of heavy impurities in the solvent phase and difficulty in removing them from the process. Another consideration is the ease with which solvent residues can be reduced to low levels in final extract or raffinate products, particularly for food-grade products and pharmaceuticals.

10. *Freezing point*. Solvents that are liquids at all anticipated ambient temperatures are desirable since they avoid the need for freeze protection and/or thawing of frozen solvent prior to use. Sometimes an “antifreeze” compound such as water or an aliphatic hydrocarbon can be added to the solvent, or the solvent is supplied as a mixture of related compounds instead of a single pure component—to suppress the freezing point.

11. *Safety*. Solvents with low potential for fire and reactive chemistry hazards are preferred as inherently safe solvents. In all cases, solvents must be used with a full awareness of potential hazards and in a manner consistent with measures needed to avoid hazards. For information on the safe use of solvents and their potential hazards, see Sec. 23, “Safety and Handling of Hazardous Materials.” Also see Crowl and Louvar, *Chemical Process Safety: Fundamentals with Applications* (Prentice-Hall, 2001); Yaws, *Handbook of Chemical Compound Data for Process Safety* (Elsevier, 1997); Lees, *Loss Prevention in the Process Industries* (Butterworth, 1996); and Bretherick's *Handbook of Reactive Chemical Hazards*, 6th ed., Urben and Pitt, eds. (Butterworth-Heinemann, 1999).

12. *Industrial hygiene*. Solvents with low mammalian toxicity and good warming properties are desired. Low toxicity and low dermal absorption rate reduce the potential for injury through acute exposure. A thorough review of the medical literature must be conducted to ascertain chronic toxicity issues. Measures needed to avoid unsafe exposures must be incorporated into process designs and implemented in operating procedures. See Goetsch, *Occupational Safety and Health for Technologists, Engineers, and Managers* (Prentice-Hall, 2004).

13. *Environmental requirements*. The solvent must have physical or chemical properties that allow effective control of emissions from vents and other discharge streams. Preferred properties include low aquatic toxicity and low potential for fugitive emissions from leaks or spills. It also is desirable for a solvent to have low photoreactivity in the atmosphere and be biodegradable so it does not persist in the environment. Efficient technologies for capturing solvent vapors from vents and condensing them for recycle include activated carbon adsorption with steam regeneration [Smallwood, *Solvent Recovery Handbook* (McGraw-Hill, 1993), pp. 7–14] and vacuum-swing adsorption [Pezolt et al., *Environmental Prog.*, **16**(1), pp. 16–19 (1997)]. The optimization of a process to increase the efficiency of solvent utilization is a key aspect of waste minimization and reduction of environmental impact. An opportunity may exist to reduce solvent use through application of countercurrent processing and other chemical engineering principles aimed at improving processing efficiencies. For a discussion of environmental issues in

process design, see Allen and Shonnard, *Green Engineering: Environmentally Conscious Design of Chemical Processes* (Prentice-Hall, 2002)]. Also see Sec. 22, "Waste Management."

14. *Multiple uses.* It is desirable to use as the extraction solvent a material that can serve a number of purposes in the manufacturing plant. This avoids the cost of storing and handling multiple solvents. It may be possible to use a single solvent for a number of different extraction processes practiced in the same facility, either in different equipment operated at the same time or by using the same equipment in a series of product campaigns. In other cases, the solvent used for extraction may be one of the raw materials for a reaction carried out in the same facility, or a solvent used in another operation such as a crystallization.

15. *Materials of construction.* It is desirable for a solvent to allow the use of common, relatively inexpensive materials of construction at moderate temperatures and pressures. Material compatibility and potential for corrosion are discussed in Sec. 25, "Materials of Construction."

16. *Availability and cost.* The solvent should be readily available at a reasonable cost. Considerations include the initial fill cost, the investment costs associated with maintaining a solvent inventory in the plant (particularly when expensive extractants are used), as well as the cost of makeup solvent.

COMMERCIAL PROCESS SCHEMES

For the purpose of illustrating process concepts, liquid-liquid extraction schemes typically practiced in industry may be categorized into a number of general types, as discussed below.

Standard Extraction Also called simple extraction or single-solvent extraction, standard extraction is by far the most widely practiced type of extraction operation. It can be practiced using single-stage or multistage processing, cross-current or countercurrent flow of solvent, and batch-wise or continuous operation. Figure 15-6 illustrates the contacting stages and liquid streams associated with a typical multistage, countercurrent scheme. Standard extraction is analogous to stripping in distillation because the process involves transferring or stripping components from the feed phase into another phase. Note that the feed (*F*) enters the process where the extract stream (*E*) leaves the process, analogous to feeding the top of a stripping tower. And the raffinate (*R*) leaves where the extraction solvent (*S*) enters. Standard extraction is used to remove contaminants from a crude liquid feed (product purification) or to recover valuable components from the feed (product recovery). Applications can involve very dilute feeds, such as when purifying a liquid product or detoxifying a wastewater stream, or concentrated feeds, such as when recovering a crude product from a reaction mixture. In either case, standard extraction can be used to transfer a high fraction of solute from the feed phase into the extract. Note, however, that transfer of the desired solute or solutes may be accompanied by transfer of unwanted solutes. Because of this, standard extraction normally cannot achieve satisfactory solute purity in the extract stream unless the separation factor for the desired solute with respect to unwanted solutes is at least $\alpha_{i,j} = K_i/K_j = 20$ and usually much higher. This depends on the crude feed purity and the product purity specification. (See "Potential for Solute Purification Using Standard Extraction" under "Process Fundamentals and Basic Calculation Methods.")

Fractional Extraction Fractional extraction combines solute recovery with cosolute rejection. In principle, the process can achieve high solute recovery and high solute purity even when the solute separation factor is fairly low, as low as $\alpha_{i,j} = 4$ or so (see "Dual-Solvent Fractional Extraction" under "Calculation Procedures"). Dual-solvent fractional extraction utilizes an extraction solvent (*S*) and a wash solvent (*W*) and includes a stripping section at the raffinate end of the process (for product-solute recovery) and a washing section at the extract end of the process (for cosolute rejection and product purification) (Fig. 15-7). The feed enters the process at an intermediate stage located between the extract and raffinate ends. In this respect, the process is analogous to a middle-fed fractional distillation, although the analogy is not exact since wash solvent is added to the extract end of the process instead of returning a reflux stream. The

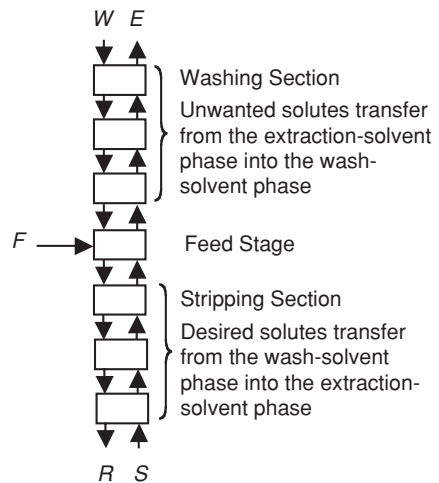


FIG. 15-7 Dual-solvent fractional extraction without reflux.

desired solutes transfer into the extraction solvent (the extract phase) within the stripping section, and unwanted solutes transfer into the wash solvent (the raffinate phase) within the washing section. Typically, the feed stream consists of feed solutes predissolved in wash solvent or extraction solvent; or, if they are liquids, they may be injected directly into the process. To maximize performance, a fractional extraction process may be operated such that the washing and stripping sections are carried out in different equipment and at different temperatures. The stripping section is sometimes called the extraction section, and the washing section is sometimes called the enriching section, the scrubbing section, or the absorbing section. A dual-solvent fractional extraction process involving reflux to the washing section is shown in Fig. 15-8.

In a special case referred to as single-solvent fractional extraction with extract reflux, the wash solvent is comprised of components that

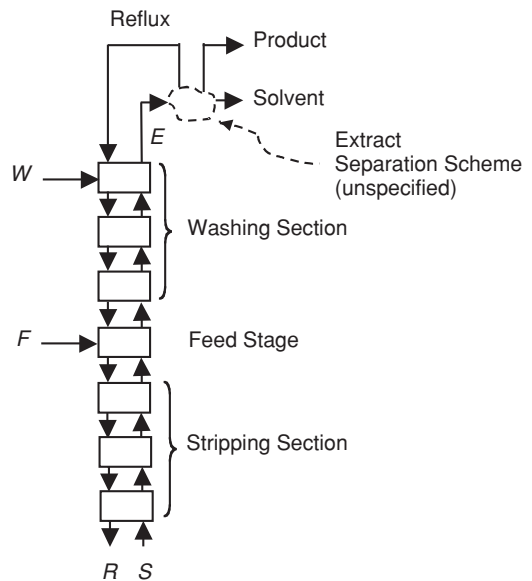


FIG. 15-8 Process concepts for dual-solvent fractional extraction with extract reflux.

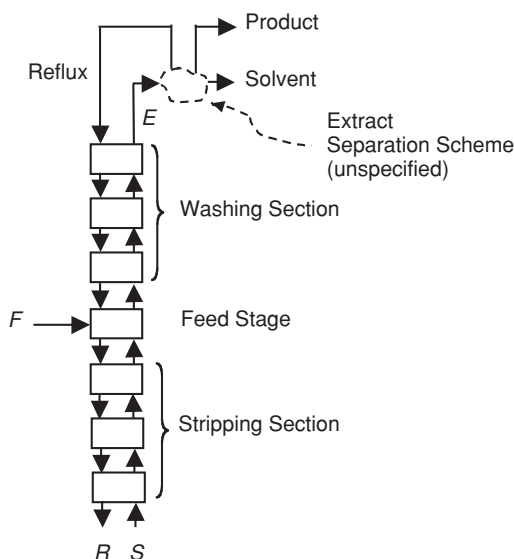


FIG. 15-9 Process concepts for single-solvent fractional extraction with extract reflux. The process flow sheet shown in Fig. 15-2 is an example of this general process scheme.

enter the overall process with the feed and return as reflux (Fig. 15-9). This is the type of extraction scheme commonly used to recover aromatic components from crude hydrocarbon mixtures using high-boiling polar solvents (as in Fig. 15-2). A reflux stream rich in light aromatics including benzene is refluxed to the washing section to serve as wash solvent. This process scheme is very similar in concept to fractional distillation. It is used only in a very limited number of applications [Stevens and Pratt, Chap. 6, in *Science and Practice of Liquid-Liquid Extraction*, vol. 1, Thornton, ed. (Oxford, 1992), pp. 379–395]. More detailed discussion is given in “Single-Solvent Fractional Extraction with Extract Reflux” under “Calculation Procedures.”

In terms of common practice, fractional extraction operations may be classified into several types: (1) standard extraction augmented by addition of a washing section utilizing a relatively small amount of feed solvent as the wash solvent; (2) full fractionation (less common); and (3) full fractionation with solute reflux (much less common). The first two categories are examples of dual-solvent fractional extraction. The third category can be practiced as dual-solvent or single-solvent fractional extraction.

In the first type of operation, a relatively small amount of feed solvent is added to a short washing section as wash solvent. (The word *short* is used here in an extraction column context, but refers in general to a relatively few theoretical stages.) This approach is useful for systems exhibiting a moderate to high solute separation factor ($\alpha_{ij} > 20$ or so) and requiring a boost in product-solute purity. An example involves recovery of an organic solute from a dilute brine feed by using a partially miscible organic solvent. In this case, the inorganic salt present in the aqueous feed stream has some solubility in the organic solvent phase because of water that saturates that phase, and the partition ratio for transfer of salt into the organic phase is small (i.e., the partition ratio for transfer of salt into wash water is high). Adding wash water to the extract end of the process has the effect of washing a portion of the soluble salt content out of the organic extract. The reduction in salt content depends on how much wash water is added and how many washing stages or transfer units are used in the design.

The second type of fractional extraction operation involves the use of stripping and washing sections without reflux (Fig. 15-7) to separate a mixture of feed solutes with close K values. In this case, the solute separation factor is low to moderate. Normally, α_{ij} must be greater than about 4 for a commercially viable process. Scheibel [*Chem. Eng. Prog.*, **44**(9), pp. 681–690 (1948); and **44**(10), pp. 771–782 (1948)] gives several

instructive examples of fractional extraction: (1) separation of ortho and para chloronitrobenzenes using heptane and 85% aqueous methanol as solvents ($\alpha_{\text{para,ortho}} \approx 1.6$ to 1.8); (2) separation of ethanol and isopropanol by using water and xylene ($\alpha_{\text{ethanol,isopropanol}} \approx 2$); and (3) separation of ethanol and methyl ethyl ketone (MEK) by using water and kerosene ($\alpha_{\text{ethanol,MEK}} \approx 10$ to 20). The first two applications demonstrate fractional extraction concepts, but a sharp separation is not achieved because the selectivity of the solvent is too low. In these kinds of applications, fractional extraction might be combined with another separation operation to complete the separation. (See “Hybrid Extraction Processes.”) In Scheibel’s third example, the selectivity is much higher and nearly complete separation is achieved by using a total of about seven theoretical stages. In another example, Venter and Nieuwoudt [*Ind. Eng. Chem. Res.*, **37**(10), pp. 4099–4106 (1998)] describe a dual-solvent extraction process using hexane and aqueous tetraethylene glycol to selectively recover *m*-cresol from coal pyrolysis liquors also containing *o*-toluonitrile. This process has been successfully implemented in industry. The separation factor for *m*-cresol with respect to *o*-toluonitrile varies from 5 to 70 depending upon solvent ratios and the resulting liquid compositions. The authors compare a standard extraction configuration (bringing the feed into the first stage) with a fractional extraction configuration (bringing the feed into the second stage of a seven theoretical-stage process).

Another example of the use of dual-solvent fractional extraction concepts involves the recovery of ϵ -caprolactam monomer (for nylon-6 production) from a two-liquid-phase reaction mixture containing ammonium sulfate plus smaller amounts of other impurities, using water and benzene as solvents [Simons and Haasen, Chap. 18.4 in *Handbook of Solvent Extraction* (Wiley, 1983; Krieger, 1991)]. In this application, the separation factor for caprolactam with respect to ammonium sulfate is high because the salt greatly favors partitioning into water; however, separation factors with respect to the other impurities are smaller. Alessi et al. [*Chem. Eng. Technol.*, **20**, pp. 445–454 (1997)] describe two process schemes used in industry. These are outlined in Fig. 15-10. The simpler scheme (Fig. 15-10a) is a straightforward dual-solvent fractional extraction process that isolates caprolactam (CPL) in a benzene extract stream and ammonium sulfate (AS) in the aqueous raffinate. The feed stage is comprised of mixer M1 and settler S1, and separate extraction columns are used for the washing and stripping sections. In Fig. 15-10a, these are denoted by C1 and C2, respectively. Minor impurity components also present in the feed must exit the process in either the extract or the raffinate. The more complex scheme (Fig. 15-10b) eliminates addition of benzene to the feed stage and adds a back-extraction section at the extract end of the process (denoted by C4) to extract CPL from the benzene phase leaving the washing section. Also, a separate fractional extractor (denoted as C1 in Fig. 15-10b) is added between the original stripping and washing sections to treat the benzene phase leaving the stripping section and recover the CPL content of the CPL-rich aqueous stream leaving the feed stage. In the C1 extractor, the CPL transfers into the benzene stream that ultimately enters the upper washing section, leaving hydrophilic impurities in an aqueous purge stream that exits at the bottom. The resulting process scheme includes two purge streams for rejecting minor impurities: a stream rich in heavy organic impurities leaving the bottom of the benzene distillation tower and the aqueous stream rich in hydrophilic impurities leaving the bottom of the C1 extractor. This sophisticated design separates the feed into four streams instead of just two, allowing separate removal of two impurity fractions to increase the purity of the two main products. The caprolactam is made to transfer into either an aqueous or a benzene-rich stream as desired, by judicious choice of solvent-to-feed ratio at the various sections in the process (perhaps aided by adjustment of temperature).

A dual-solvent fractional extraction process can provide a powerful separation scheme, as indicated by the examples given above, and some authors suggest that fractional extraction is not utilized as much as it could be. In many cases, instead of using full fractional extraction, standard extraction is used to recover solute from a crude feed; and if the solvent-to-feed ratio is less than 1.0, concentrate the solute in a smaller solute-bearing stream. Another operation such as crystallization, adsorption, or process chromatography is then used downstream for solute purification. Perhaps fractional extraction schemes should be evaluated more often as an alternative processing scheme that may have advantages.

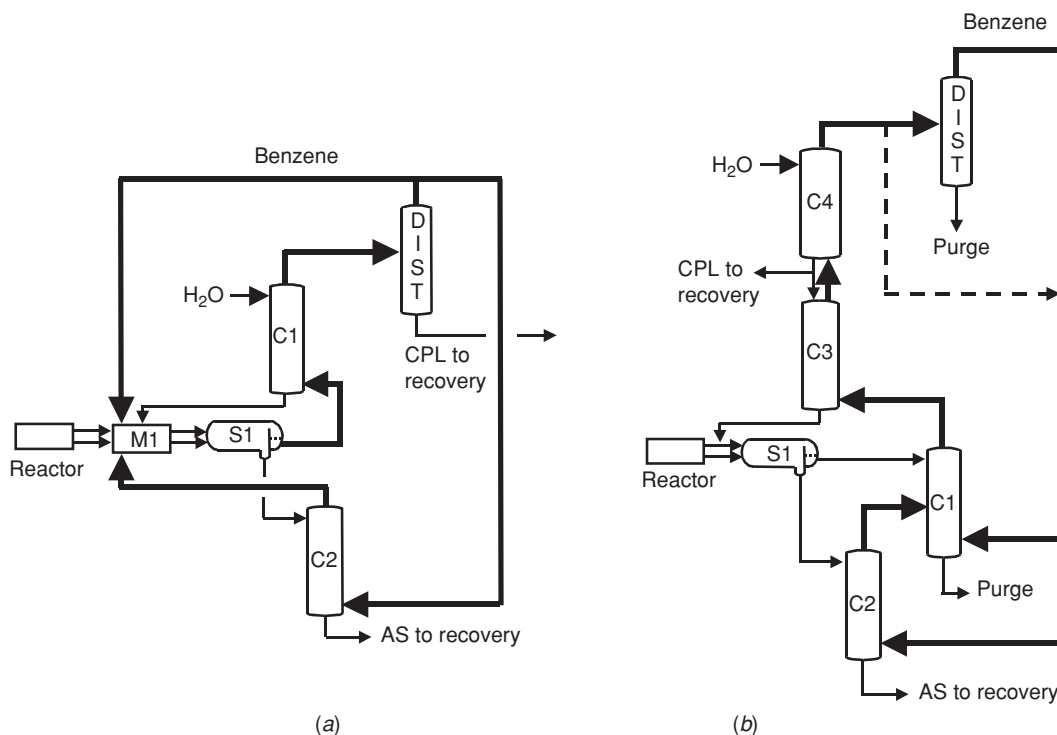


FIG. 15-10 Two industrial extraction processes for separation of caprolactam (CPL) and ammonium sulfate (AS): (a) a simpler fractional extraction scheme; (b) a more complex scheme. Heavy lines denote benzene-rich streams; light lines denote aqueous streams. [Taken from Alessi, Penzo, Slater, and Tessari, *Chem. Eng. Technol.*, **20**(7), pp. 445–454 (1997), with permission. Copyright 1997 Wiley-VCH.]

The third type of fractional extraction operation involves refluxing a portion of the extract stream back to the extract end (washing section) of the process. As mentioned earlier, this process can be practiced as a dual-solvent process (Fig. 15-8) or as a single-solvent process (Figs. 15-2 and 15-9). However, unlike in distillation, the use of reflux is not common. The reflux consists of a portion of the extract stream from which a significant amount of solvent has been removed. Injection of this solvent-lean, concentrated extract back into the washing section increases the total amount of solute and the amount of raffinate phase present in that section of the extractor. This can boost separation performance by allowing the process to operate at a more favorable location within the phase diagram, resulting in a reduction in the number of theoretical stages or transfer units needed within the washing section. This also allows the process to boost the concentration of solute in the extract phase above that in equilibrium with the feed phase. The increased amount of solute present within the process may require use of extra solvent to avoid approaching the plait point at the feed stage (the composition at which only a single liquid phase can exist at equilibrium). Because of this, utilizing reflux normally involves a tradeoff between a reduction in the number of theoretical stages and an increase in the total liquid traffic within the process equipment, requiring larger-capacity equipment and increasing the cost of solvent recovery and recycle. This tradeoff is discussed by Scheibel with regard to extraction column design [*Ind. Eng. Chem.*, **47**(11), pp. 2290–2293 (1955)]. The potential benefit that can be derived from the use of extract reflux is greatest for applications utilizing solvents with a low solute separation factor and low partition ratios (as in the example illustrated in Fig. 15-2). In these cases, reflux serves to reduce the number of required theoretical stages or transfer units to a practical number on the order of 10 or so, or reduce the solvent-to-feed ratio required for the desired separation.

The fractional extraction schemes described above are typical of those practiced in industry. A related kind of process employs a second solvent in a separate extraction operation to wash the raffinate

produced in an upstream extraction operation. This process scheme is particularly useful when the wash solvent is only slightly soluble in the raffinate and can easily be removed. An example is the use of water to remove residual amine solvent from the treated hydrocarbon stream in an acid-gas extraction process (Fig. 15-3).

A potential fourth type of fractional extraction operation involves the use of reflux at both ends of a dual-solvent process, i.e., reflux to the raffinate end of the process (the stripping section) as well as reflux to the extract end of the process (the washing section). The authors are not aware of a commercial application of this kind; however, Scheibel [*Chem. Eng. Prog.*, **62**(9), pp. 76–81 (1966)] discusses such a process scheme in light of several potential flow sheets. In the special case of single-solvent fractional extraction with extract reflux, Skelland [*Ind. Eng. Chem.*, **53**(10), pp. 799–800 (1961)] has pointed out that addition of raffinate reflux is not effective from a strictly thermodynamic point of view as it cannot reduce the required number of theoretical stages in this special case.

Dissociative Extraction This process scheme normally involves partitioning of weak organic acids or bases between water and an organic solvent. Whether the solute partitions mainly into one phase or the other depends upon whether it is in its neutral state or its charged ionic state and the ability of each phase to solvate that form of the solute. In general, water interacts much more strongly with the charged species, and the ionic form will strongly favor partitioning into the aqueous phase. The nonionic form generally will favor partitioning into the organic phase.

The pK_a is the pH at which 50 percent of the solute is in the dissociated (ionized) state. It is a function of solute concentration and normally is reported for dilute conditions. For an organic acid (RCOOH) dissolved in aqueous solution, the amount of solute in the dissociated state relative to that in the nondissociated state is $[RCOO^-]/[RCOOH] = 10^{pH-pK_a}$. Extraction of an organic acid out of an organic feed into an aqueous phase is greatly facilitated by operating at a pH

above the acid's pK_a value because the majority of the acid will be deprotonated to yield the dissociated form ($RCOO^-$). On the other hand, partitioning of the organic acid from an aqueous feed into an organic solvent is favored by operating at a pH below its pK_a to ensure most of the acid is in the protonated (nondissociated) form. Another example involves extraction of a weak base, such as a compound with amine functionality (RNH_2), out of an organic phase into water at a pH below the pK_a . This will protonate or neutralize the majority of the base, yielding the ionized form (RNH_3^+) and favoring extraction into water. It follows that extracting an organic base out of an aqueous feed into an organic solvent is favored by operating at a pH above its pK_a since this yields most of the solute in the free base (nonionized) form. For weak bases, $pK_a = 14 - pK_b$, and the relative amount of solute in the dissociated state in the aqueous phase is given by $10^{pK_a - pH}$. In principle, to obtain the maximum partition ratio for an extraction, the pH should be maintained about 2 units from the solute's pK_a value to obtain essentially complete dissociation or nondissociation, as appropriate for the extraction. In a typical continuous application, the pH of the aqueous stream leaving the process is controlled at a constant pH set point by injection of acid or base at the opposite end of the process, and a pH gradient exists within the process. The pH set point may be adjusted to optimize performance. The effect of pH on the partition ratio is discussed in "Effect of pH for Ionizable Organic Solutes" under "Thermodynamic Basis for Liquid-Liquid Extraction." Determination of the optimum pH for extraction of compounds with multiple ionizable groups and thus multiple pK_a values is discussed by Crocker, Wang, and McCauley [*Organic Process Res. Dev.*, **5**(1), pp. 77–79 (2001)].

In fractional dissociative extraction, a sharp separation of feed solutes is achieved by taking advantage of a difference in their pK_a values. If the difference in pK_a is sufficient, controlling pH at a specific value can yield high K values for one solute fraction and very low K values for another fraction, thus allowing a sharp separation. For example, a mixture of two organic bases can be separated by contacting the mixture with an aqueous acid containing less than the stoichiometric amount of acid needed to neutralize (ionize) both bases. The stronger of the two bases reacts with the acid to yield the dissociated form in the aqueous phase, while the other base remains undissociated in a separate organic phase. Buffer compounds may be used to control pH within a desired range for improved separation results [Ma and Jha, *Organic Process Res. Dev.*, **9**(6), pp. 847–852 (2005)]. Buffers are discussed by Perrin and Dempsey [*Buffers for pH and Metal Ion Control* (Chapman and Hall, 1979)]. For additional discussion, see Pratt, Chap. 21 in *Handbook of Solvent Extraction*, Lo, Baird, and Hanson, eds. (Wiley, 1983; Krieger, 1991), and Anwar, Arif, and Pritchard, *Solvent Ext. Ion Exch.*, **16**, p. 931 (1998).

pH-Swing Extraction A pH-swing extraction process utilizes dissociative extraction concepts to recover and purify ionizable organic solutes in a forward- and back-extraction scheme, each extraction operation carried out at a different pH. For example, in the forward extraction, the desired solute may be in its nonionized state so it can be extracted out of a crude aqueous feed into an organic solvent. The extract stream from this operation is then fed to a separate extraction operation where the solute is ionized by readjustment of pH and back-extracted into clean water. This scheme can achieve both high recovery and high purity if the impurity solutes are not ionizable or have pK_a values that differ greatly from those of the desired solute. A pH-swing extraction scheme commonly is used for recovery and purification of antibiotics and other complex organic solutes with some ionizable functionality. The production of high-purity food-grade phosphoric acid from lower-grade acid is another example of a pH-swing process ["Purification of Wet Phosphoric Acid" in *Ullmann's Encyclopedia of Industrial Chemistry*, 6th ed. (VCH, 2002)].

Reaction-Enhanced Extraction Reaction-enhanced extraction involves enhancement of the partition ratio for extraction through the use of a reactive extractant that forms a reversible adduct or molecular complex with the desired solute. Normally, the extractant compound is dissolved in a diluent liquid such as kerosene or another high-boiling hydrocarbon. Because reactive extractants form strong specific interactions with the solute molecule, they can provide much

higher partition ratios and generally are more selective compared to conventional solvents. Also, when used to recover relatively volatile compounds, extractants may allow significant reduction in the energy required to separate the extract phase by distillation. Extractants are successfully used at very large scales to recover metals in hydrometallurgical processing, among other applications. However, it is important to note that the use of high-boiling extractants can present severe difficulties whenever high-boiling impurities are present. A number of commercial processes have failed because there was no economical option for purging high-boiling contaminants that accumulated in the solvent phase over time, so care must be taken to address this possibility when developing a new application. The advantages and disadvantages of using high-boiling solvents or extractants versus low-boiling solvents are discussed by King in the context of acetic acid recovery [Chap. 18.5 in *Handbook of Solvent Extraction*, Lo, Baird, and Hanson, eds. (Wiley, 1983; Krieger, 1991)].

Detailed reviews of reactive extractants are given by Cox [Chap. 1 in *Science and Practice of Liquid-Liquid Extraction*, vol. 2 (Oxford, 1992), (pp. 1–27)] and by King [Chap. 15 in *Handbook of Separation Process Technology*, Rousseau, ed. (Wiley, 1987)]. Also see *Solvent Extraction Principles and Practice*, 2d ed., Rydberg et al., eds. (Dekker, 2004). Cox has classified extractants as either acidic, ion-pair-forming or solvating (nonionic) according to the mechanism of solute-solvent interaction in solution. In hydrometallurgical applications involving recovery or purification of metals dissolved in aqueous feed solutions, commercial extractants include acid chelating agents, alkyl amines, and various organophosphorous compounds including trioctylphosphine oxide (TOPO) and tri-*n*-butyl phosphate, plus quaternary ammonium salts. A well-known example is the use of TOPO to remove arsenic impurities from copper electrolyte solutions produced in copper refining operations. Another well-known class of applications involves formation of ion-pair interactions between a carboxylic acid dissolved in an aqueous feed and alkylamine extractants such as trioctylamine dissolved in a hydrocarbon diluent, as discussed by Wennersten [*J. Chem. Technol. Biotechnol.*, **33B**, pp. 85–94 (1983)], by King and others [*Ind. Eng. Chem. Res.*, **29**(7), pp. 1319–1338 (1990); and *Chemtech*, **22**, p. 285 (1992)], and by Schunk and Maurer [*Ind. Eng. Chem. Res.*, **44**(23), pp. 8837–8851 (2005)]. Extractants also may be used to facilitate extraction of other ionizable organic solutes including certain antibiotics [Pai, Doherty, and Malone, *AIChE J.*, **48**(3), pp. 514–526 (2002)]. Sometimes mixing extractants with promoter compounds (called modifiers) provides synergistic effects that dramatically enhance the partition ratio. An example is discussed by Atanassova and Dukov [*Sep. Purif. Technol.*, **40**, pp. 171–176 (2004)]. Also see the discussion of combined physical (hydrogen-bonding) and reaction-enhanced extraction by Lee [*Biotechnol. Prog.*, **22**(3), pp. 731–736 (2006)].

Extractive Reaction Extractive reaction combines reaction and separation in the same unit operation for the purpose of facilitating a desired reaction. To avoid confusion, the term *extractive reaction* is recommended for this type of process, while the term *reaction-enhanced extraction* is recommended for a process involving formation of reversible solute-extractant interactions and enhanced partition ratios for the purpose of facilitating a desired separation. The term *reactive extraction* is a more general term commonly used for both types of processes.

In general, extractive reaction involves carrying out a reaction in the presence of two liquid phases and taking advantage of the partitioning of reactants, products, and homogeneous catalyst (if used) between the two phases to improve reaction performance. The classes of reactions that can benefit from an extractive reaction scheme include chemical-equilibrium-limited reactions (such as esterifications, transesterifications, and hydrolysis reactions), where it is important to remove a product or by-product from the reaction zone to drive conversion, and consecutive or sequential reactions (such as nitrations, sulfonations, and alkylations), where the goal may be to produce only the mono- or difunctional product and minimize formation of subsequent addition products. For additional discussion, see Gorissen, *Chem Eng. Sci.*, **58**, pp. 809–814 (2003); Van Brunt and Kanel, Chap. 3, in *Reactive Separation Processes*, S. Kulprathipanja, ed. (Taylor & Francis, 2002), pp. 51–92; and Hanson, "Extractive Reaction Processes," Chap. 22 in *Handbook of Solvent*

Extraction, Lo, Baird, and Hanson, eds. (Wiley, 1983; Krieger, 1991), pp. 615–618.

The manufacture of fatty acid methyl esters (FAME) for use as biodiesel fuel, by transesterification of triglyceride oils and greases [Canakci and Van Gerpen, *ASAE Trans.*, **46**(4), pp. 945–954 (2003)], provides an example of a chemical-equilibrium-limited extractive reaction. Low-grade triglycerides are reacted with methanol to produce FAME plus glycerin as a by-product. Because glycerin is only partially miscible with the feed and the FAME product, it transfers from the reaction zone into a separate glycerin-rich liquid phase, driving further conversion of the triglycerides. In another example, Minotti, Doherty, and Malone [*Ind. Eng. Chem. Res.*, **37**(12), pp. 4748–4755 (1998)] studied the esterification of aqueous acetic acid by reaction with butanol in an extractive reaction process involving extraction of the butyl acetate product into a separate butanol-rich phase. The authors concluded that cocurrent processing is preferred over countercurrent processing in this case. Their general conclusions likely apply to other applications involving extraction of a reaction product out of the reaction phase to drive conversion. The cocurrent scheme is equivalent to a series of two-liquid-phase stirred-tank reactors approaching the performance of a plug-flow reactor. Rohde, Marr, and Siebenhofer [Paper no. 232f, AIChE Annual Meeting, Austin, Tex., Nov. 7–12, 2004] studied the esterification of acetic acid with methanol to produce methyl acetate. Their extractive reaction scheme involves selective transfer of methyl acetate into a high-boiling solvent such as *n*-nonane.

An example of a sequential-reaction extractive reaction is the manufacture of 2,4-dinitrotoluene, an important precursor to 2,4-diaminotoluene and toluene diisocyanate (TDI) polyurethanes. The reaction involves nitration of toluene by using concentrated nitric and sulfuric acids which form a separate phase. Toluene transfers into the acid phase where it reacts with nitronium ion, and the reaction product transfers back into the organic phase. Careful control of liquid-liquid contacting conditions is required to obtain high yield of the desired product and minimize formation of unwanted reaction products. A similar reaction involves nitration of benzene to mononitrobenzene, a precursor to aniline used in the manufacture of many products including methylenediphenylisocyanate (MDI) for polyurethanes [Quadros, Reis, and Baptista, *Ind. Eng. Chem. Res.*, **44**(25), pp. 9414–9421 (2005)].

Another category of extractive reaction involves the extraction of a product solute during microbial fermentation (biological reaction) to avoid microbe inhibition effects, allowing an increase in fermenter productivity. An example involving production of ethanol is discussed by Weinhhammer and Blass [*Chem. Eng. Technol.*, **17**, pp. 365–373 (1994)], and an example involving production of propionic acid is discussed by Gu, Glatz, and Glatz [*Biotechnol. and Bioeng.*, **57**(4), pp. 454–461 (1998)]. Finally, the scrubbing of reactive components from a feed liquid, by irreversible reaction with a treating solution, also may be considered an extractive reaction. An example is removal of acidic components from petroleum liquids by reaction with aqueous NaOH.

Temperature-Swing Extraction Temperature-swing processes take advantage of a change in *K* value with temperature. An extraction example is the commercial process used to recover citric acid from whole fermentation broth by using trioctylamine (TOA) extractant [Baniel et al., U.S. Patent 4,275,234 (1981); Wennersten, *J. Chem. Biotechnol.*, **33B**, pp. 85–94 (1983); and Pazouki and Panda, *Bioprocess Eng.*, **19**, pp. 435–439 (1998)]. This process involves a forward reaction-enhanced extraction carried out at 20 to 30°C in which citric acid transfers from the aqueous phase into the extract phase. Relatively pure citric acid is subsequently recovered by back extraction into clean water at 80 to 100°C, also liberating the TOA extractant for recycle. This temperature-swing process is feasible because partitioning of citric acid into the organic phase is favored at the lower temperature but not at 80 to 100°C.

Partition ratios can be particularly sensitive to temperature when solute-solvent interactions in one or both phases involve specific attractive interactions such as formation of ion-pair bonds (as in trialkylamine-carboxylic acid interactions) or hydrogen bonds, or when mutual solubility between feed and extraction solvent involves hydrogen bonding. An interesting example is the extraction of citric acid from water with 1-butoxy-2-propanol (common name propylene glycol *n*-butyl ether) as solvent (Fig. 15-11). This example illustrates how important it can be when developing and optimizing an extraction operation to understand how *K* varies with temperature, regardless of whether a temperature-swing process is contemplated. Of course, changes in other properties such as mutual solubility and viscosity also must be considered. For additional discussion, see “Temperature Effect” under “Thermodynamic Basis for Liquid-Liquid Extraction.”

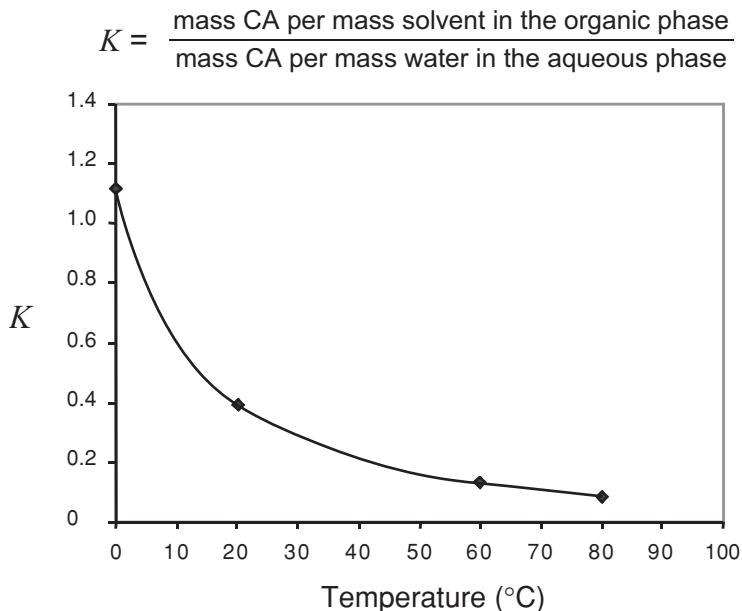


FIG. 15-11 Partition ratio as a function of temperature for recovery of citric acid (CA) from water using 1-butoxy-2-propanol (propylene glycol *n*-butyl ether). (Data generated by The Dow Chemical Company.)

Reversed Micellar Extraction This scheme involves use of microscopic water-in-oil micelles formed by surfactants and suspended within a hydrophobic organic solvent to isolate proteins from an aqueous feed. The micelles essentially are microdroplets of water having dimensions on the order of the protein to be isolated. These stabilized water droplets provide a compatible environment for the protein, allowing its recovery from a crude aqueous feed without significant loss of protein activity [Ayala et al., *Biotechnol. and Bioeng.*, **39**, pp. 806–814 (1992); and Bordier, *J. Biol. Chem.*, **256**(4), pp. 1604–1607 (February 1981)]. Also see the discussion of ultrafiltration membranes for concentrating micelles in “Liquid-Liquid Phase Separation Equipment.”

Aqueous Two-Phase Extraction Also called aqueous biphasic extraction, this technique generally involves use of two incompatible water-miscible polymers [normally polyethylene glycol (PEG) and dextran, a starch-based polymer], or a water-miscible polymer and a salt (such as PEG and Na_2SO_4), to form two immiscible aqueous phases each containing 75+% water. This technology provides mild conditions for recovery of proteins and other biomolecules from broth or other aqueous feeds with minimal loss of activity [Walter and Johansson, eds., *Aqueous Two Phase Systems, Methods in Enzymology*, vol. 228 (Academic, 1994); Zaslavsky, *Aqueous Two-Phase Partitioning* (Dekker, 1994); and Blanch and Clark, Chap. 6 in *Biochemical Engineering* (Dekker, 1997) pp. 474–482]. The effect of salts on the liquid-liquid phase equilibrium of polyethylene glycol + water mixtures has been extensively studied [Salabat, *Fluid Phase Equil.*, **187–188**, pp. 489–498 (2001)]. A typical phase diagram, for PEG 6000 + Na_2SO_4 + water, is shown in Fig. 15-12. The hydraulic characteristics of the aqueous two-phase system PEG 4000 + Na_2SO_4 + water in a countercurrent sieve plate column have been reported by Hamidi et al. [*J. Chem. Technol. Biotechnol.*, **74**, pp. 244–249 (1999)]. Two immiscible aqueous phases also may be formed by using two incompatible salts. An example is the system formed by using the hydrophilic organic salt 1-butyl-3-methylimidazolium chloride and a water-structuring (kosmotropic) salt such as K_3PO_4 [Gutowski et al., *J. Am. Chem. Soc.*, **125**, p. 6632 (2003)].

Hybrid Extraction Processes Hybrid processes employ an extraction operation in close association with another unit operation. In these processes, the individual unit operations may not be able to achieve all the separation goals, or the use of one or the other operation alone may not be as economical as the hybrid process. Common examples include the following.

Extraction-distillation An example involves the use of extraction to break the methanol + dichloromethane azeotrope. The near-azeotropic overheads from a distillation tower can be fed to an extrac-

tor where water is used to extract the methanol content and generate nearly methanol-free dichloromethane (saturated with roughly 2000 ppm water). A related type of extraction-distillation operation involves closely coupling extraction with the distillate or bottoms stream produced by a distillation tower, such that the distillation specification for that stream can be relaxed. For example, this approach has been used to facilitate distillation of aqueous acetic acid to produce acetic acid as a bottoms product, taking a mixture of acetic acid and water overhead [Gualy et al., U.S. Patent 5,492,603 (1996)]. The distillate is sent to an extraction tower to recover the acetic acid content for recycle back to the process. The hybrid process allows operation with lower energy consumption compared to distillation alone, because it allows the distillation tower to operate with a reduced requirement for recovering acetic acid in the bottoms stream, which permits relaxation of the minimum concentration of acetic acid allowed in the distillate. Another type of hybrid process involves combining liquid-liquid extraction with azeotropic or extractive distillation of the extract [Skelland and Tedder, chap. 7, in *Handbook of Separation Process Technology*, Rousseau, ed. (Wiley, 1987), pp. 449–453]. The solvent serves both as the extraction solvent for the upstream liquid-liquid extraction operation and as the entrainer for a subsequent azeotropic distillation or as the distillation solvent for a subsequent extractive distillation. (For a detailed discussion of azeotropic and extraction distillation concepts, see Sec. 13, “Distillation.”) The solvent-to-feed ratio must be optimized with regard to both the liquid-liquid extraction operation and the downstream distillation operation. An example is the use of ethyl acetate to extract acetic acid from an aqueous feed, followed by azeotropic distillation of the extract to produce a dry acetic acid bottoms product and an ethyl acetate + water overheads stream. In this example, ethyl acetate serves as the extraction solvent in the extractor and as the entrainer for removing water overhead in the distillation tower. Examples involving extractive distillation and high-boiling solvents can be seen in the various processes used to recover aromatics from aliphatic hydrocarbons, as described by Mueller et al., in *Ullmann's Encyclopedia of Industrial Chemistry*, 5th ed., vol. B3, Gerhartz, ed. (VCH, 1988), pp. 6-34 to 6-43.

Extraction-crystallization Extraction often is used in association with a crystallization operation. In the pharmaceutical and specialty chemical industries, extraction is used to recover a product compound (or remove impurities) from a crude reaction mixture, with subsequent crystallization of the product from the extract (or from the preextracted reaction mixture). In many of these applications, the product needs to be delivered as a pure crystalline solid, so crystallization is a necessary

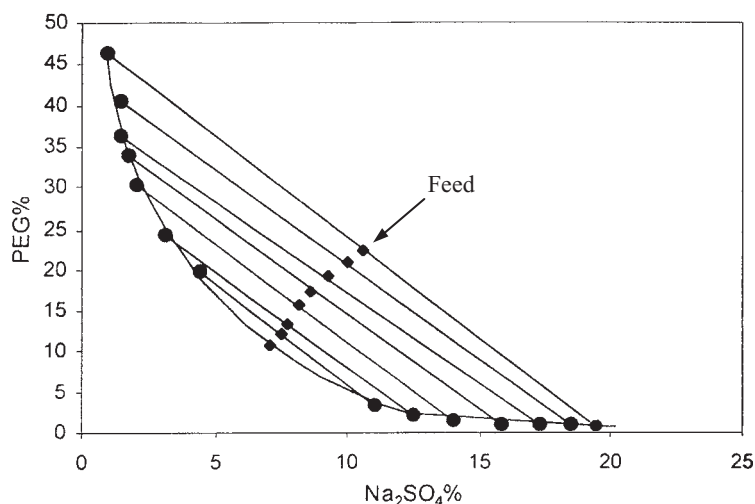


FIG. 15-12 Equilibrium phase diagram for PEG 6000 + Na_2SO_4 + water at 25°C. [Reprinted from Salabat, *Fluid Phase Equil.*, **187–188**, pp. 489–498 (2001), with permission. Copyright 2001 Elsevier B. V.]

operation. (For a detailed discussion of crystallization operations, see Sec. 18, "Liquid-Solid Operations and Equipment.") The desired solute can sometimes be crystallized directly from the reaction mixture with sufficient purity and yield, thus avoiding the cost of the extraction operation; however, direct crystallization generally is more difficult because of higher impurity concentrations. In cases where direct crystallization is feasible, deciding whether to use extraction prior to crystallization or crystallization alone involves consideration of a number of tradeoffs and ultimately depends on the relative robustness and economics of each approach [Anderson, *Organic Process Res. Dev.*, **8**(2), pp. 260–265 (2004)]. A well-known example of extraction-crystallization is the recovery of penicillin from fermentation broth by using a pH-swing forward and back extraction scheme followed by final purification using crystallization [Queener and Swartz, "Penicillins: Biosynthetic and Semisynthetic," in *Secondary Products of Metabolism, Economic Microbiology*, vol. 3, Rose, ed. (Academic, 1979)]. Extraction is used for solute recovery and initial purification, followed by crystallization for final purification and isolation as a crystalline solid. Another category of extraction-crystallization processes involves use of extraction to recover solute from the spent mother liquor leaving a crystallization operation. In yet another example, Maeda et al., [*Ind. Eng. Chem. Res.*, **38**(6), pp. 2428–2433 (1999)] describe a crystallization-extraction hybrid process for separating fatty acids (lauric and myristic acids). In comparing these process options, the potential uses of extraction should include efficient countercurrent processing schemes, since these may significantly reduce solvent usage and cost.

Neutralization-extraction A common example of neutralization-extraction involves neutralization of residual acidity (or basicity) in a crude organic feed by injection of an aqueous base (or aqueous acid) combined with washing the resulting salts into water. The neutralization and washing operations may be combined within a single extraction column as illustrated in Fig. 15-13. Also see the discussion by Koolen [*Design of Simple and Robust Process Plants* (Wiley-VCH, 2001), pp. 159–161].

Reaction-extraction This technique involves chemical modification of solutes in solution in order to more easily extract them in a subsequent extraction operation. Applications generally involve modification of impurity compounds to facilitate purification of a desired product. An example is the oxygenation of sulfur-containing aromatic impurities present in fuel oil by using H_2O_2 and acetic acid, followed by liquid-liquid extraction into an aqueous acetonitrile solution [Shiraishi and Hirai, *Energy and Fuels*, **18**(1), pp. 37–40 (2004); and Shiraishi et al., *Ind. Eng. Chem. Res.*, **41**, pp. 4362–4375 (2002)]. Another example involves esterification of aromatic alcohol impurities to facilitate their separation from apolar hydrocarbons by using an aqueous extractant solution [Kuzmanovid et al., *Ind. Eng. Chem. Res.*, **43**(23), pp. 7572–7580 (2004)].

Reverse osmosis-extraction In certain applications, reverse osmosis (RO) or nanofiltration membranes may be used to reduce the volume of an aqueous stream and increase the solute concentration, in

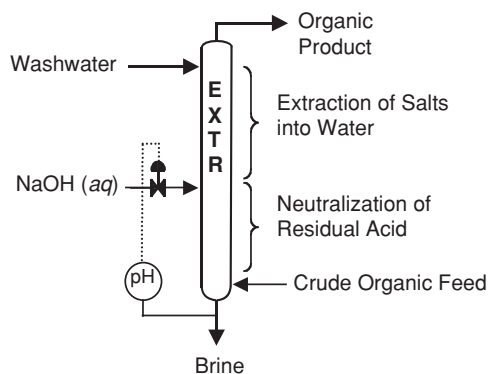


FIG. 15-13 Example of neutralization-extraction hybrid process implemented in an extraction column.

order to reduce the size of downstream extraction and solvent recovery equipment. Wytcherley, Gentry, and Gualy [U.S. Patents 5,492,625 (1996) and 5,624,566 (1997)] describe such a process for carboxylic acid solutes. Water is forced through the membrane when the operating pressure drop exceeds the natural osmotic pressure difference generated by the concentration gradient:

$$\text{Flux} = \frac{\mathcal{P}}{\lambda_m} (\Delta P - \Delta\pi) \quad (15-1)$$

where \mathcal{P} is a permeability coefficient for water, λ_m is the membrane thickness, ΔP is the operating pressure drop, and $\Delta\pi$ is the osmotic pressure gradient, a function of solute concentration on each side of the membrane. Normally the solute also will permeate the membrane to a small extent. The maximum possible concentration of solute in the concentrate is limited by that corresponding to an osmotic pressure of about 70 bar (about 1000 psig), since this is the maximum pressure rating of commercially available membrane modules (typical). For acetic acid, this maximum concentration is about 25 wt %. Depending upon whether the particular organic permeate of interest can swell or degrade the membrane material, the concentration achieved in practice may need to be reduced below this osmotic-pressure limit to avoid excessive membrane deterioration. In general, a membrane preconcentrator is considered for feeds containing on the order of 3 wt % solute or less. In these cases, a moderate membrane operating pressure may be used, and the preconcentrator can provide a large reduction in the volume of feed entering the extraction process. In these processes, the stream entering the membrane module normally must be carefully prefiltered to avoid fouling the membrane. The general application of RO and nanofiltration membranes is described in Sec. 20, "Alternative Separation Processes." The modeling of mass transfer through RO membranes, with an emphasis on cases involving solute-membrane interactions, is discussed by Mehdizadeh, Molaiee-Nejad, and Chong [*J. Membrane Sci.*, **267**, pp. 27–40 (2005)].

Liquid-Solid Extraction (Leaching) Extraction of solubles from porous solids is a form of solvent extraction that has much in common with liquid-liquid extraction [Prabhudesai, "Leaching," Sec. 5.1 in *Handbook of Separation Techniques for Chemical Engineers*, Schweitzer, ed., pp. 5-3 to 5-31 (McGraw-Hill, 1997)]. The main differences come from the need to handle solids and the fact that mass transfer of soluble components out of porous solids generally is much slower than mass transfer between liquids. Because of this, different types of contacting equipment operating at longer residence times often are required. Washing of nonporous solids is a related operation that generally exhibits faster mass-transfer rates compared to leaching. On the other hand, purification of nonporous solids or crystals by removal of impurities that reside within the bulk solid phase often is not economical or even feasible by using these methods, because the rate of mass transfer of impurities through the bulk solid is extremely slow. Liquid-solid extraction is covered in Sec. 18, "Liquid-Solid Operations and Equipment."

Liquid-Liquid Partitioning of Fine Solids This process involves separation of small-particle solids suspended in a feed liquid, by contact with a second liquid phase. Robbins describes such a process for removing ash from pulverized coal [U.S. Patent 4,575,418 (1986)]. The process involves slurrying pulverized coal fines into a hydrocarbon liquid and contacting the resulting slurry with water. The coal slurry is cleaned by preferential transfer of ash particles into the aqueous phase. The process takes advantage of differences in surface-wetting properties to separate the different types of solid particles present in the feed.

Supercritical Fluid Extraction This process generally involves the use of CO_2 or light hydrocarbons to extract components from liquids or porous solids [Brunner, *Gas Extraction: An Introduction to Fundamentals of Supercritical Fluids and the Application to Separation Processes* (Springer-Verlag, 1995); Brunner, ed., *Supercritical Fluids as Solvents and Reaction Media* (Elsevier, 2004); and McHugh and Krukoni, *Supercritical Fluid Extraction*, 2d ed. (Butterworth-Heinemann, 1993)]. Supercritical fluid extraction differs from liquid-liquid or liquid-solid extraction in that the operation is carried out at high-pressure, supercritical (or near-supercritical) conditions where the extraction fluid exhibits

physical and transport properties that are in between those of liquid and vapor phases (intermediate density, viscosity, and solute diffusivity). Most applications involve the use of CO₂ (critical pressure = 73.8 bar at 31°C) or propane (critical pressure = 42.5 bar at 97°C). Other supercritical fluids and their critical-point properties are discussed by Poling, Prausnitz, and O'Connell [*The Properties of Gas and Liquids*, 5th ed. (McGraw-Hill, 2001)].

Supercritical CO₂ extraction often is considered for extracting high-value soluble components from natural materials or for purifying low-volume specialty chemicals. For products derived from natural materials, this can involve initial processing of solids followed by further processing of the crude liquid extract. Applications include decaffeination of coffee and recovery of active ingredients from plant- and animal-derived feeds including recovery of flavor components and vitamins from natural oils. An example is the use of supercritical CO₂ fractional extraction to remove terpenes from cold-pressed bergamot oil [Kondo et al., *Ind. Eng. Chem. Res.*, **39**(12), pp. 4745–4748 (2000)]. A nonfood example involves the removal of unreacted dodecanol from nonionic surfactant mixtures and fractionation of the surfactant mixture based on polymer chain length [Eckert et al., *Ind. Eng. Chem. Res.*, **31**(4), pp. 1105–1110 (1992)]. In these applications, process advantages may be obtained because solvent residues are easily removed or are nontoxic, the process can be operated at mild temperatures that avoid product degradation, the product is easily recovered from the extract fluid, or the solute separation factor and product purity can be adjusted by making small changes in the operating temperature and pressure. Although the loading capacity of supercritical CO₂ typically is low, addition of cosolvents such as methanol, ethanol, or tributylphosphate can dramatically boost capacity and enhance selectivity [Brennecke and Eckert, *AIChE J.*, **35**(9), pp. 1409–1427 (1989)].

For processing liquid feeds, some supercritical fluid extraction processes utilize packed columns, in which the liquid feed phase wets the packing and flows through the column in film flow, with the supercritical fluid forming the continuous phase. In other applications, sieve trays give improved performance [Seibert and Moosberg, *Sep. Sci. Technol.*, **23**, p. 2049 (1988)]. In a number of these applications, concentrated solute is added back to the column as reflux to boost separation power (a form of single-solvent fractional extraction). Supercritical fluid extraction requires high-pressure equipment and may involve a high-pressure compressor. These requirements add considerable capital and operating costs. In certain cases, pumps can be used instead of compressors, to bring down the cost. The separators are run slightly below the critical point at slightly elevated pressure and reduced temperature to ensure the material is in the liquid state so it can be pumped. As a rule, supercritical fluid extraction is considerably more expensive than liquid-liquid extraction, so when the required separation can be accomplished by using a liquid solvent, liquid-liquid extraction often is more cost-effective.

Although most commercial applications of supercritical fluid extraction involve processing of high-value, low-volume products, a notable exception is the propane deasphalting process used to refine lubricating oils. This is a large-scale, commodity chemical process dating back to the 1930s. In this process and more recent versions, lube oils are extracted into propane at near-supercritical conditions. The extract phase is depressurized or cooled in stages to isolate various fractions. Compared to operation at lower pressures, operation at near-supercritical conditions minimizes the required pressure or temperature change—so the process is more efficient. For further discussion of supercritical fluid separation processes, see Sec. 20, "Alternative Separation Processes," Gironi and Maschietti, *Chem. Eng. Sci.*, **61**, pp. 5114–5126 (2006), and Fernandes et al., *AIChE J.*, **53**(4), pp. 825–837 (2007).

KEY CONSIDERATIONS IN THE DESIGN OF AN EXTRACTION OPERATION

Successful approaches to designing an extraction process begin with an appreciation of the fundamentals (basic phase equilibrium and mass-transfer principles) and generally rely on both experimental studies and mathematical models or simulations to define the commercial technology. Small-scale experiments using representative feed usually are needed to accurately quantify physical properties and phase equilibrium. Additionally, it is common practice in industry to perform

miniplant or pilot-plant tests to accurately characterize the mass-transfer capabilities of the required equipment as a function of throughput [Robbins, *Chem. Eng. Prog.*, **75**(9), pp. 45–48 (1979)]. In many cases, mass-transfer resistance changes with increasing scale of operation, so an ability to accurately scale up the data also is needed. The required scale-up know-how often comes from experience operating commercial equipment of various sizes or from running pilot-scale equipment of sufficient size to develop and validate a scale-up correlation. Mathematical models are used as a framework for planning and analyzing the experiments, for correlating the data, and for estimating performance at untested conditions by extrapolation. Increasingly, designers and researchers are utilizing computational fluid dynamics (CFD) software or other simulation tools as an aid to scale-up.

Typical steps in the work process for designing and implementing an extraction operation include the following:

1. Outline the design basis including specification of feed composition, required solute recovery or removal, product purity, and production rate.
2. Search the published literature (including patents) for information relevant to the application.
3. For dilute feeds, consider options for preconcentrating the feed to reduce the volumes of feed and solvent that must be handled by the extraction operation. Consider evaporation or distillation of a high-volatility feed solvent or the use of reverse osmosis membranes to concentrate aqueous feeds. (See "Hybrid Extraction Processes" under "Commercial Process Schemes.")
4. Generate a list of candidate solvents based on chemical knowledge and experience. Consider solvents similar to those used in analogous applications. Use one or more of the methods described in "Solvent Screening Methods" to identify additional candidates. Include consideration of solvent blends and extractants.
5. Estimate key physical properties and review desirable solvent properties. Give careful consideration to safety, industrial hygiene, and environmental requirements. Use this preliminary information to trim the list of candidate solvents to a manageable size. (See "Desirable Solvent Properties.")
6. Measure partition ratios for selected solvents at representative conditions.
7. Evaluate the potential for trace chemistry under extraction and solvent recovery conditions to determine whether solutes and candidate solvents are likely to degrade or react to produce unwanted impurities. For example, it is well known that penicillin G easily degrades at commercial extraction conditions, and short contact time is required for good results. Also under certain conditions acetate solvents may hydrolyze to form alcohols, certain alcohols and ethers can form peroxides, sulfur-containing solvents may degrade at elevated regeneration temperatures to form acids, chlorinated solvents may hydrolyze at elevated temperatures to form trace HCl with severe corrosion implications, and so on. In other cases, leakage of air into the process may cause formation of trace oxidation products. Understanding the potential for trace chemistry, the fate of potential impurities (i.e., where they go in the process), their possible effects on the process (including impact on product purity and interfacial tension) and devising means to avoid or successfully deal with impurities often are critical to a successful process design. Laboratory tests designed to probe the stability of feed and solvent mixtures may be needed.
8. Characterize mass-transfer difficulty in terms of the required number of theoretical stages or transfer units as a function of the solvent-to-feed ratio. Keep in mind that there will be a limit to the number of theoretical stages that can be achieved. For most cost-effective extraction operations, this limit will be in the range of 3 to 10 theoretical stages, although some can achieve more, depending upon the chemical system, type of equipment, and flow rate (throughput).
9. Estimate the cost of the proposed extraction operation relative to alternative separation technologies, such as extractive distillation, adsorption, and crystallization. Explore other options if they appear less expensive or offer other advantages.
10. If technical and economic feasibility looks good, determine accurate values of physical properties and phase equilibria, particularly liquid densities, mutual solubilities (miscibility), viscosities, interfacial tension, and *K* values (at feed, extract, and raffinate ends of the

proposed process), as well as data needed to evaluate solvent recycle options. Search available literature and databases. Assess data quality and generate additional data as needed. Develop the appropriate data correlations. Finalize the choice of solvent.

11. Outline an overall process flow sheet and material balance including solvent recovery and recycle. This should be done with the aid of process simulation software. [See Seider, Seader, and Lewin, *Product and Process Design Principles: Synthesis, Analysis, and Evaluation*, 2d ed. (Wiley, 2004); and Turton et al., *Analysis, Synthesis, and Design of Chemical Processes*, 2d ed. (Prentice-Hall, 2002)]. In the flow sheet include methods needed for controlling emissions and managing wastes. Carefully consider the possibility that impurities may accumulate in the recycled solvent, and devise methods for purging these impurities, if needed.

12. In some cases, especially with multiple solutes and complex phase equilibria, it may be useful to perform laboratory batch experiments to simulate a continuous, countercurrent, multistage process. These experiments can be used to test/verify calculation results and determine the correct distribution of components. For additional information, see Treybal, Chap. 9 in *Liquid Extraction*, 2d ed. (McGraw-Hill, 1963), pp. 359–393, and Baird and Lo, Chap. 17.1 in *Handbook of Solvent Extraction* (Wiley, 1983; Krieger, 1991).

13. Identify useful equipment options for liquid-liquid contacting and liquid-liquid phase separation, estimate approximate equipment size, and outline preliminary design specifications. (See “Extractor Selection” under “Liquid-Liquid Extraction Equipment.”) Where appropriate, consult with equipment vendors. Using small-scale experiments, determine whether sludgelike materials are likely to accumulate at the liquid-liquid interface (called formation of a rag layer). If so, it will be important to identify equipment options that can tolerate accumulation of a rag layer and allow the rag to be drained or otherwise purged periodically.

14. For the most promising equipment option, run miniplant or pilot-plant tests over a range of operating conditions. Utilize representative feed including all anticipated impurities, since even small concentrations of surface-active components can dramatically affect interfacial behavior. Whenever possible, the miniplant tests should be conducted by using actual material from the manufacturing plant, and should include solvent recycle to evaluate the effects of impurity accumulation or possible solvent degradation. Run the miniplant long enough that the solvent encounters numerous cycles so that recycle effects can be seen. If difficulties arise, consider alternative solvents.

15. Analyze miniplant data and update the preliminary design. Carefully evaluate loss of solvent to the raffinate, and devise methods to minimize losses as needed. Consult equipment vendors or other specialists regarding recommended scale-up methods.

16. Specify the final material balance for the overall process and carry out detailed equipment design calculations. Try to add some flexibility (depending on the cost) to allow for some adjustment of the process equipment during operation—to compensate for uncertainties in the design.

17. Install and start up the equipment in the manufacturing plant.

18. Troubleshoot and improve the operation as needed. Once a unit is operational, carefully measure the material balance and characterize mass-transfer performance. If performance does not meet expectations, look for defects in the equipment installation. If none are found, revisit the scale-up methodology and its assumptions.

LABORATORY PRACTICES

An equilibrium or theoretical stage in liquid-liquid extraction, as defined earlier, is routinely utilized in laboratory procedures. A feed solution is contacted with a solvent to remove one or more of the solutes from the feed. This can be carried out in a separating funnel or, preferably, in an agitated vessel that can produce droplets about 1 mm in diameter. After agitation has stopped and the phases separate, the two clear liquid layers are isolated by decantation. The partition ratio can then be determined directly by measuring the concentration of solute in the extract and raffinate layers. (Additional discussion is given in “Liquid-Liquid Equilibrium Experimental Meth-

ods” under “Thermodynamic Basis for Liquid-Liquid Extraction.”) When an appropriate analytical method is available only for the feed phase, the partition ratio can be determined by measuring the solute concentration in the feed and raffinate phases and calculating the partition ratio from the material balance. When the initial concentration of solute in the extraction solvent is zero (before extraction), the partition ratio expressed in terms of mass fractions is given by

$$K'' = \frac{Y_e''}{X_r''} = \frac{M_f}{M_e} \left(\frac{M_f}{M_r} \frac{X_f''}{X_r''} - 1 \right) \quad (15-2)$$

where K'' = mass fraction solute in extract divided by that in raffinate

M_f = total mass of feed added to vial

M_s = total mass of extraction solvent before extraction

M_r = mass of raffinate phase after extraction

M_e = mass of extract phase after extraction

X_f'' = mass fraction solute in feed prior to extraction

X_r'' = mass fraction solute in raffinate, at equilibrium

Y_e'' = mass fraction solute in extract, at equilibrium

For systems with low mutual solubility between phases, $K'' \approx (M_f/M_s)(X_f''/X_r'' - 1)$. An actual analysis of solute concentration in the extract and raffinate is preferred in order to understand how well the material balance closes (a check of solute accountability).

After a single stage of liquid-liquid contact, the phase remaining from the feed solution (the raffinate) can be contacted with another quantity of fresh extraction solvent. This cross-current (or cross-flow) extraction scheme is an excellent laboratory procedure because the extract and raffinate phases can be analyzed after each stage to generate equilibrium data for a range of solute concentrations. Also, the feasibility of solute removal to low levels can be demonstrated (or shown to be problematic because of the presence of “extractable” and “non-extractable” forms of a given species). The number of cross-current treatments needed for a given separation, assuming a constant K value, can be estimated from

$$N = \frac{\ln \left(\frac{X_{in} - Y_{in}/K}{X_{out} - Y_{in}/K} \right)}{\ln(KS^*/F + 1)} \quad (15-3)$$

where F is the amount of feed, the feed and solvent are presaturated, and equal amounts of solvent (denoted by S^*) are used for each treatment [Treybal, *Liquid Extraction*, 2d ed. (McGraw-Hill, 1963), pp. 209–216]. The total amount of solvent is $N \times S^*$. The variable Y_{in} is the concentration of solute in the fresh solvent, normally equal to zero. Equation (15-3) is written in a general form without specifying the units, since any consistent system of units may be used. (See “Process Fundamentals and Basic Calculation Methods.”)

A cross-current scheme, although convenient for laboratory practice, is not generally economically attractive for large commercial processes because solvent usage is high and the solute concentration in the combined extract is low. A number of batchwise countercurrent laboratory techniques have been developed and can be used to demonstrate countercurrent performance. (See item 12 in the previous subsection, “Key Considerations in the Design of an Extraction Operation.”) Several equipment vendors also make available continuously fed laboratory-scale extraction equipment. Examples include small-scale mixer-settler extraction batteries offered by Rousselet-Robatel, Normag, MEAB, and Schott/QVF. Small-diameter extraction columns also may be used, such as the $\frac{3}{8}$ -in. (16-mm-) diameter reciprocating-plate agitated column offered by Koch Modular Process Systems, and a 60-mm-diameter rotary-impeller agitated column offered by Kühni. Static mixers also may be useful for mixer-settler studies in the laboratory [Benz et al., *Chem. Eng. Technol.*, **24**(1), pp. 11–17 (2001)].

For additional discussion of laboratory techniques, see “Liquid-Liquid Equilibrium Experimental Methods” as well as “High-Throughput Experimental Methods” under “Solvent-Screening Methods.”

THERMODYNAMIC BASIS FOR LIQUID-LIQUID EXTRACTION

GENERAL REFERENCES: See Sec. 4, "Thermodynamics," as well as Sandler, *Chemical, Biochemical, and Engineering Thermodynamics* (Wiley, 2006); *Solvent Extraction Principles and Practice*, 2d ed., Rydberg et al., eds. (Dekker, 2004); Smith, Abbott, and Van Ness, *Introduction to Chemical Engineering Thermodynamics*, 7th ed. (McGraw-Hill, 2004); Schwarzenbach, Gschwend, and Imboden, *Environmental Organic Chemistry*, 2d ed. (Wiley-VCH, 2002); Elliot and Lira, *Introduction to Chemical Engineering Thermodynamics* (Prentice-Hall, 1999); Prausnitz, Lichtenthaler, and Gomez de Azevedo, *Molecular Thermodynamics of Fluid-Phase Equilibria*, 3d ed. (Prentice-Hall, 1999); Seader and Henley, Chap. 2 in *Separation Process Principles* (Wiley, 1998); Bolz et al., *Pure Appl. Chem.* (IUPAC), **70**, pp. 2233–2257 (1998); Grant and Higuchi, *Solubility Behavior of Organic Compounds*, Techniques of Chemistry Series, vol. 21 (Wiley, 1990); Abbott and Prausnitz, "Phase Equilibria," in *Handbook of Separation Process Technology*, Rousseau, ed. (Wiley, 1987), pp. 3–59; Novak, Matous, and Pick, *Liquid-Liquid Equilibria*, Studies in Modern Thermodynamics Series, vol. 7 (Elsevier, 1987); Walas, *Phase Equilibria in Chemical Engineering* (Butterworth-Heinemann, 1985); and Rowlinson and Swinton, *Liquids and Liquid Mixtures*, 3d ed. (Butterworths, 1982).

ACTIVITY COEFFICIENTS AND THE PARTITION RATIO

Two phases are at equilibrium when the total Gibbs energy for the system is at a minimum. This criterion can be restated as follows: Two nonreacting phases are at equilibrium when the chemical potential of each distributed component is the same in each phase; i.e., for equilibrium between two phases I and II containing n components

$$\mu_i = \mu_i^{\text{II}} \quad i = 1, 2, \dots, n \quad (15-4)$$

For two phases at the same temperature and pressure, Eq. (15-4) can be expressed in terms of mole fractions and activity coefficients, giving

$$y_i \gamma_i^{\text{I}} = x_i \gamma_i^{\text{II}} \quad i = 1, 2, \dots, n \quad (15-5)$$

where y_i and x_i represent mole fractions of component i in phases I and II, respectively. The equilibrium partition ratio, in units of mole fraction, is then given by

$$K_i^{\circ} = \frac{y_i}{x_i} = \frac{\gamma_i^{\text{raffinate}}}{\gamma_i^{\text{extract}}} \quad (15-6)$$

where y_i is the mole fraction in the extract phase and x_i is the mole fraction in the raffinate. Note that, in general, activity coefficients and K_i° are functions of temperature and composition. For ionic compounds that dissociate in solution, the species that form and the extent of dissociation in each phase also must be taken into account. Similarly, for extractions involving adduct formation or other chemical reactions, the reaction stoichiometry is an important factor. For discussion of these special cases, see Choppin, Chap. 3, and Rydberg et al., Chap. 4, in *Solvent Extraction Principles and Practice*, 2d ed., Rydberg et al., eds. (Dekker, 2004).

The activity coefficient for a given solute is a measure of the non-ideality of solute-solvent interactions in solution. In this context, the solvent is either the feed solvent or the extraction solvent depending on which phase is considered, and the composition of the "solvent" includes all components present in that phase. For an ideal solution, activity coefficients are unity. For solute-solvent interactions that are repulsive relative to solvent-solvent interactions, γ_i is greater than 1. This is said to correspond to a positive deviation from ideal solution behavior. For attractive interactions, γ_i is less than 1.0, corresponding to a negative deviation. Activity coefficients often are reported for binary pairs in the limit of very dilute conditions (infinite dilution) since this represents the interaction of solute completely surrounded by solvent molecules, and this normally gives the largest value of the activity coefficient (denoted as γ_i^{∞}). Normally, useful approximations of the activity coefficients at more concentrated conditions can be obtained by extrapolation from infinite dilution using an appropriate activity coefficient correlation equation. (See Sec. 4, "Thermodynamics.") Extrapolation in the reverse direction, i.e., from finite concentration to infinite dilution, often does not provide reliable results.

In units of mass fraction, the partition ratio for a nonreacting/nondissociating solute is given by

$$K_i'' \text{ (mass frac. basis)} = \frac{Y_i''}{X_i''} = K_i^{\circ} \text{ (mole frac. basis)} \\ \times \left[\frac{y_i(\text{MW}_i - \text{MW}_{\text{raffinate}}) + \text{MW}_{\text{raffinate}}}{x_i(\text{MW}_i - \text{MW}_{\text{extract}}) + \text{MW}_{\text{extract}}} \right] \quad (15-7)$$

Here, the notation MW refers to the molecular weight of solute i and the effective average molecular weights of the extract and raffinate phases, as indicated by the subscripts. For dilute systems, $K_i'' \approx K_i^{\circ}$ ($\text{MW}_{\text{raffinate}}/\text{MW}_{\text{extract}}$). For theoretical stage or transfer unit calculations, often it is useful to express the partition ratio in terms of mass ratio coordinates introduced by Bancroft [*Phys. Rev.*, **3**(1), pp. 21–33; **3**(2), pp. 114–136; and **3**(3), pp. 193–209 (1895)]:

$$K_i' = \frac{Y_i'}{X_i'} = \frac{M_{\text{solute}}/M_{\text{extraction solvent}} \text{ in extract phase}}{M_{\text{solute}}/M_{\text{feed solvent}} \text{ in raffinate phase}} \quad (15-8)$$

Partition ratios also may be expressed on a volumetric basis. In that case,

$$K_i^{\text{vol}} \text{ (mass/vol. basis)} = K_i'' \frac{\rho_{\text{extract}}}{\rho_{\text{raffinate}}} \quad (15-9)$$

$$K_i^{\text{vol}} \text{ (mole/vol. basis)} = K_i^{\circ} \left(\frac{\rho_{\text{extract}}}{\rho_{\text{raffinate}}} \right) \left(\frac{\text{MW}_{\text{raffinate}}}{\text{MW}_{\text{extract}}} \right) \quad (15-10)$$

Extraction Factor The extraction factor is defined by

$$\mathcal{E}_i = m_i \frac{S}{F} \quad (15-11)$$

where $m_i = dY_i/dX_i$, the slope of the equilibrium line, and F and S are the flow rates of the feed phase and the extraction-solvent phase, respectively. On a McCabe-Thiele type of diagram, \mathcal{E} is the slope of the equilibrium line divided by the slope of the operating line F/S . (See "McCabe-Thiele Type of Graphical Method" under "Process Fundamentals and Basic Calculation Methods.") For dilute systems with straight equilibrium lines, the slope of the equilibrium line is equal to the partition ratio $m_i = K_i$.

To illustrate the significance of the extraction factor, consider an application where K_i , S , and F are constant (or nearly so) and the extraction solvent entering the process contains no solute. When $\mathcal{E}_i = 1$, the extract stream has just enough capacity to carry all the solute present in the feed:

$$SY_{i,\text{extract}} = FX_{i,\text{feed}} \quad \text{at } \mathcal{E}_i = 1 \text{ and equilibrium conditions} \quad (15-12)$$

At $\mathcal{E}_i < 1.0$, the extract's capacity to carry solute is less than this amount, and the maximum fraction that can be extracted θ_i is numerically equal to the extraction factor:

$$(\theta_i)_{\text{max}} = \mathcal{E}_i \quad \text{when } \mathcal{E}_i < 1.0 \quad (15-13)$$

At $\mathcal{E}_i > 1.0$, the extract phase has more than sufficient carrying capacity (in principle), and the actual amount extracted depends on the extraction scheme, number of contacting stages, and mass-transfer resistance. Even a solute for which $m_i < 1.0$ (or $K_i < 1.0$) can, in principle, be extracted to a very high degree—by adjusting S/F so that $\mathcal{E}_i > 1$.

Thus, the extraction factor characterizes the relative capacity of the extract phase to carry solute present in the feed phase. Its value is a major factor determining the required number of theoretical stages or transfer units. (For further discussion, see "The Extraction Factor and

General Performance Trends.”) In general, the value of the extraction factor can vary at each point along the equilibrium curve, although in many cases it is nearly constant. Many commercial extraction processes are designed to operate with an average or overall extraction factor in the range of 1.3 to 5. Exceptions include applications where the partition ratio is very large and the solvent-to-feed ratio is set by hydraulic considerations.

Because the extraction factor is a dimensionless variable, its value should be independent of the units used in Eq. (15-11), as long as they are consistently applied. Engineering calculations often are carried out by using mole fraction, mass fraction, or mass ratio units (Bancroft coordinates). The flow rates S and F then need to be expressed in terms of total molar flow rates, total mass flow rates, or solute-free mass flow rates, respectively. In the design of extraction equipment, volume-based units often are used. Then the appropriate concentration units are mass or mole per unit volume, and flow rates are expressed in terms of the volumetric flow rate of each phase.

Separation Factor The separation factor in extraction is analogous to relative volatility in distillation. It is a dimensionless factor that measures the relative enrichment of a given component in the extract phase after one theoretical stage of extraction. For cosolutes i and j ,

$$\alpha_{i,j} = \frac{(Y_i/Y_j)_{\text{extract}}}{(X_i/X_j)_{\text{raffinate}}} = \frac{(Y_i)_{\text{extract}}/(X_i)_{\text{raffinate}}}{(Y_j)_{\text{extract}}/(X_j)_{\text{raffinate}}} = \frac{K_i}{K_j} \quad (15-14)$$

The enrichment of solute i with respect to solute j can be further increased with the use of multiple contacting stages. The solute separation factor $\alpha_{i,j}$ is used to characterize the selectivity a solvent has for extracting a desired solute from a feed containing other solutes. It can be calculated by using any consistent units. As in distillation, $\alpha_{i,j}$ must be greater than 1.0 to achieve an increase in product-solute purity (on a solvent-free basis). In practice, if solute purity is an important requirement of a given application, $\alpha_{i,j}$ must be greater than 20 for standard extraction (at least) and greater than about 4 for fractional extraction, in order to have sufficient separation power. (See “Potential for Solute Purification Using Standard Extraction” in “Process Fundamentals and Basic Calculation Methods” and “Dual-Solvent Fractional Extraction” in “Calculation Procedures.”)

The separation factor also can be evaluated for solute i with respect to the feed solvent denoted as component f . The value of $\alpha_{i,f}$ must be greater than 1.0 if the proposed separation is to be feasible, i.e., in order to be able to enrich solute i in a separate extract phase. Note that the feed may still be separated if $\alpha_{i,f} < 1.0$, but this would have to involve concentrating solute i in the feed phase by preferential transfer of component f into the extract phase. Although $\alpha_{i,f} > 1.0$ represents a minimum theoretical requirement for enriching solute i in a separate extract phase, most commercial extraction processes operate with values of $\alpha_{i,f}$ on the order of 20 or higher. There are exceptions to this rule, such as the Udex process and similar processes involving extraction of aromatics from aliphatic hydrocarbons. In these applications, $\alpha_{i,f}$ can be as low as 10 and sometimes even lower. Applications such as these involve particularly difficult design challenges because of low solute partition ratios and high mutual solubility between phases. (For more detailed discussion of these kinds of systems, see “Single Solvent Fractional Extraction with Extract Reflux” in “Fractional Extraction Calculations.”)

Minimum and Maximum Solvent-to-Feed Ratios Normally, it is possible to quickly estimate the physical constraints on solvent usage for a standard extraction application in terms of minimum and maximum solvent-to-feed ratios. As discussed above, the minimum theoretical amount of solvent needed to transfer a high fraction of solute i is the amount corresponding to $\mathcal{E}_i = 1$. In practice, the minimum practical extraction factor is about 1.3, because at lower values the required number of theoretical stages increases dramatically. This gives a minimum solvent-to-feed ratio for a practical process equal to

$$\left(\frac{S}{F}\right)_{\min} \approx \frac{1.3}{K_i} \quad (15-15)$$

Note that this minimum is achievable only if a sufficient number of contacting stages or transfer units can be used. (For additional discussion,

see “The Extraction Factor and General Performance Trends.”) It is also achievable only if the amount of solvent added to the feed is greater than the solubility limit in the feed phase (including solute); otherwise, only one liquid phase can exist. In certain cases involving fairly high mutual solubilities, this can be an important consideration when running a process using minimal solvent—because if the process operates close to the solubility limit, an upset in the solvent-to-feed ratio may cause the solvent phase to disappear.

The maximum possible solvent-to-feed ratio is obtained when the amount of extraction solvent is so large that it dissolves the feed phase. Assuming the feed entering the process does not contain extraction solvent,

$$\left(\frac{S}{F}\right)_{\max} = \frac{1}{1 - Y_s^{\text{SAT}}} \quad (15-16)$$

where Y_s^{SAT} denotes the concentration of extraction solvent in the extract phase at equilibrium after contact with the feed phase. The denominator in Eq. (15-16) represents the solubility limit on the solvent-rich side of the miscibility envelope, including the effect of the presence of solute on solubility. Normally, the solubility limits are easily measured in small-scale experiments by adding solvent until the solvent phase appears (representing the feed-rich side of the miscibility envelope) and continuing to add solvent until the feed phase disappears (the solvent-rich side). For dilute feeds containing less than about 1% solute, reasonable estimates often can be obtained by using mutual solubility data for the feed solvent + extraction solvent binary pair.

If an application proves to be technically feasible, the choice of solvent-to-feed ratio is determined by identifying the most cost-effective ratio between the minimum and maximum limits. For most applications, the maximum solvent-to-feed ratio will be much larger than the ratio chosen for the commercial process; however, the maximum ratio can be a real constraint when dealing with applications exhibiting high mutual solubility, especially for systems that involve high solute concentrations. Additional discussion is given by Seader and Henley [Chap. 8 in *Separations Process Principles* (Wiley, 1998)]. Solvent ratios are further constrained for a fractional extraction scheme, as discussed in “Fractional Extraction Calculations.”

Temperature Effect The effect of temperature on the value of the partition ratio can vary greatly from one system to another. This depends on how the activity coefficients of the components in each phase are affected by changes in temperature, including any effects due to changes in mutual solubility with temperature. For a given phase, the Gibbs-Helmholtz equation indicates that

$$\left[\frac{\partial \ln \gamma_i^\infty}{\partial (1/T)}\right]_{p,x} = \frac{h_i^{E,\infty}}{R} \quad (15-17)$$

where γ_i^∞ is the activity coefficient for solute i at infinite dilution and $h_i^{E,\infty}$ is the partial molar excess enthalpy of mixing relative to ideal solution behavior [Atik et al., *J. Chem. Eng. Data*, **49**(5), pp. 1429–1432 (2004); and Sherman et al., *J. Phys. Chem.*, **99**, pp. 11239–11247 (1995)].

Systems with specific interactions between solute and solvent, such as hydrogen bonds or ion-pair bonds, often are particularly sensitive to changes in temperature because the specific interactions are strongly temperature-dependent. In general, hydrogen bonding and ion-pair formation are disrupted by increasing temperature (increasing molecular motion), and this can dominate the overall temperature dependence of the partition ratio. An example of a temperature-sensitive hydrogen bonding system is toluene + diethylamine + water [Morello and Beckmann, *Ind. Eng. Chem.*, **42**, pp. 1079–1087 (1950)]. The partition ratio for transfer of diethylamine from water into toluene increases with increasing temperature (on a weight percent basis, $K = 0.7$ at 20°C and $K = 2.8$ at 58°C). For further discussion of the temperature dependence of K for this type of system, see Frank et al., *Ind. Eng. Chem. Res.*, **46**(11), pp. 3774–3786 (2007). An example of a temperature-sensitive system involving ion-pair formation is the commercial process used to recover citric acid from fermentation broth using trioctylamine (TOA) extractant [Pazouki and Panda, *Bioprocess*

Engineering, **19**, pp. 435–439 (1998)]. In this case, the partition ratio for transfer of citric acid into the TOA phase decreases with increasing temperature. Temperature-sensitive ion-pair interactions in the extract phase are disrupted with increasing temperature, and this appears to dominate the temperature sensitivity of the partition ratio, not the interactions between citric acid and water in the aqueous raffinate phase [Canari and Eyal, *Ind. Eng. Chem. Res.*, **43**, pp. 7608–7617 (2004)]. Also see the discussion of “Temperature-Swing Extraction” in “Commercial Extraction Schemes.”

Salting-out and Salting-in Effects for Nonionic Solutes It is well known that the presence of an inorganic salt can significantly affect the solubility of a nonionic (nonelectrolyte) organic solute dissolved in water. In most cases the inorganic salt reduces the organic solute’s solubility (salting-out effect). Here, the salt increases the organic solute’s activity coefficient in the aqueous solution. As a result, certain solutes that are not easily extracted from water may be quite easily extracted from brine, depending upon the type of solute and the salt. In principle, the deliberate addition of a salt to an aqueous feed is an option for enhancing partition ratios and reducing the mutual solubility of the two liquid phases; however, this approach complicates the overall process and normally is not cost-effective. Difficulties include the added complexity and costs associated with recovery and recycle of the salt in the overall process, or disposal of the brine after extraction and the need to purchase makeup salt. The potential use of NaCl to enhance the extraction of ethanol from fermentation broth is discussed by Gomis et al. [*Ind. Eng. Chem. Res.*, **37**(2), pp. 599–603 (1998)].

When an aqueous feed contains a salt, the effect of the dissolved salt on the partition ratio for a given organic solute may be estimated by using an expression introduced by Setschenow [*Z. Phys. Chem.*, **4**, pp. 117–128 (1889)] and commonly written in the form

$$\log \frac{\gamma_{i,\text{brine}}}{\gamma_{i,\text{water}}} = k_s C_{\text{salt}} \quad (15-18)$$

where C_{salt} is the concentration of salt in the aqueous phase in units of gmol/L and k_s is the Setschenow constant. Equation (15-18) generally is valid for dilute organic solute concentrations and low to moderate salt concentrations. In many cases, the salt has no appreciable effect on the activity coefficient in the organic phase since the salt solubility in that phase is low or negligible. Then

$$\log \frac{K_{i,\text{brine}}}{K_{i,\text{water}}} \approx \log \frac{\gamma_{i,\text{brine}}}{\gamma_{i,\text{water}}} = k_s C_{\text{salt}} \quad (15-19)$$

for extraction from the aqueous phase into an organic phase. For aromatic solutes dissolved in NaCl brine at room temperature, typical values of k_s fall within the range of 0.2 to 0.3 L/gmol. In general, k_s is found to vary with salt composition (i.e., with the type of salt) and increase with increasing organic-solute molar volume. Kojima and Davis [*Int. J. Pharm.*, **20**(1–2), pp. 203–207 (1984)] showed that partition ratio data for extraction of phenol dissolved in NaCl brine (at low concentration) using CCl_4 solvent is well fit by a Setschenow equation for salt concentrations up to 4 gmol/L (about 20 wt % NaCl). Experimental values and methods for estimating Setschenow constants are discussed by Ni and Yalkowski [*Int. J. Pharm.*, **254**(2), pp. 167–172 (2003)] and by Xie, Shiu, and MacKay [*Marine Environ. Res.*, **44**, pp. 429–444 (1997)].

In special cases, salts with large ions (such as tetramethylammonium chloride and sodium toluene sulfonate) may cause a “salting in” or “hydrotropic” effect where by the salt increases the solubility of an organic solute in water, apparently by disordering the structure of associated water molecules in solution [Sugunan and Thomas, *J. Chem. Eng. Data.*, **38**(4), pp. 520–521 (1993)]. Agrawal and Gaikar [*Sep. Technol.*, **2**, pp. 79–84 (1992)] discuss the use of hydrotropic salts to facilitate extraction processes. For additional discussion, see Ruckenstein and Shulgin, *Ind. Eng. Chem. Res.*, **41**(18), pp. 4674–4680 (2002); and Akia and Fezyi, *AIChE J.*, **52**(1), pp. 333–341 (2006).

Effect of pH for Ionizable Organic Solutes The distribution of weak acids and bases between organic and aqueous phases is dramatically affected by the pH of the aqueous phase relative to the $\text{p}K_a$ of the solute. As discussed earlier, the $\text{p}K_a$ is the pH at which 50 percent of the solute is in the ionized state. (See “Dissociative Extraction” in “Commercial Extraction Schemes.”) For a weak organic acid (RCOOH) that dissociates into RCOO^- and H^+ , the overall partition ratio for extraction into an organic phase depends upon the extent of dissociation such that

$$K_{\text{weak acid}} = K_{\text{nonionized}} \div \left(1 + \frac{[\text{RCOO}^-]_{\text{aq}}}{[\text{RCOOH}]_{\text{aq}}} \right) \quad (15-20)$$

where $K_{\text{weak acid}} = [\text{RCOOH}]_{\text{org}} / ([\text{RCOO}^-]_{\text{aq}} + [\text{RCOOH}]_{\text{aq}})$ is the partition ratio for both ionized and nonionized forms of the acid, and $K_{\text{nonionized}} = [\text{RCOOH}]_{\text{org}} / [\text{RCOOH}]_{\text{aq}}$ is the partition ratio for the nonionized form alone [Treybal, *Liquid Extraction*, 2d ed. (McGraw-Hill, 1963), pp. 38–40]. Equation (15-20) can be rewritten in terms of the $\text{p}K_a$ for a weak acid or weak base:

$$K_{\text{weak acid}} = K_{\text{nonionized}} \div (1 + 10^{\text{pH} - \text{p}K_a}) \quad (15-21)$$

$$\text{and} \quad K_{\text{weak base}} = K_{\text{nonionized}} \div (1 + 10^{\text{p}K_b - \text{pH}}) \quad (15-22)$$

For weak bases, $\text{p}K_a = 14 - \text{p}K_b$. Appropriate values for $K_{\text{nonionized}}$ may be obtained by measuring the partition ratio at sufficiently low pH (for acids) or high pH (for bases) to ensure the solute is in its nonionized form (normally at a pH at least 2 units from the $\text{p}K_a$ value). In Eqs. (15-21) and (15-22), it is assumed that concentrations are dilute, that dissociation occurs only in the aqueous phase, and that the acid does not associate (dimerize) in the organic phase. The effect of pH on the partition ratio for extraction of penicillin G, a complex organic containing a carboxylic acid group, is illustrated in Fig. 15-14. For a discussion of the effect of pH on the extraction of carboxylic acids with tertiary amines, see Yang, White, and Hsu, *Ind. Eng. Chem. Res.*, **30**(6), pp. 1335–1342 (1991). Another example is discussed by Greminger et al., [*Ind. Eng. Chem. Process Des. Dev.*, **21**(1), pp. 51–54 (1982)]; they present partition ratio data for various phenolic compounds as a function of pH.

For compounds with multiple ionizable groups, such as amino acids, the effect of pH on partitioning behavior is more complex. Amino acids are zwitterionic (dipolar) molecules with two or three ionizable groups; the $\text{p}K_a$ values corresponding to RCOOH acid groups generally are between 2 and 3, and $\text{p}K_a$ values for RNH_3^+ amino groups generally are between 9 and 10. Amino acid partitioning is discussed by Schügerl [*Solvent Extraction in Biotechnology* (Springer-Verlag, 1994); Chap. 21 in *Biotechnology*, 2d ed., vol. 3, Stephanopoulos, ed. (VCH, 1993)]; and by Gude, Meuwissen, van der Wielen, and Luyben [*Ind. Eng. Chem. Res.*, **35**, pp. 4700–4712

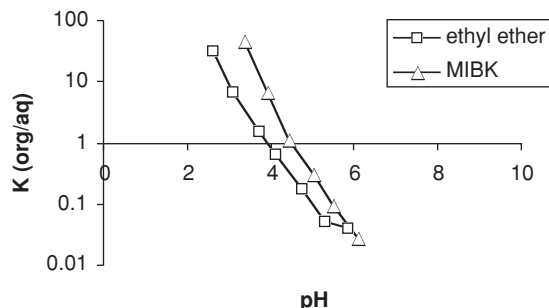


FIG. 15-14 The effect of pH on the partition ratio for extraction of penicillin G ($\text{p}K_a = 2.75$) from broth using an oxygenated organic solvent. The partition ratio is expressed in units of grams per liter in the organic phase over that in the aqueous phase. [Data from R. L. Feder, M.S. thesis (Polytechnic Institute of Brooklyn, 1947).]

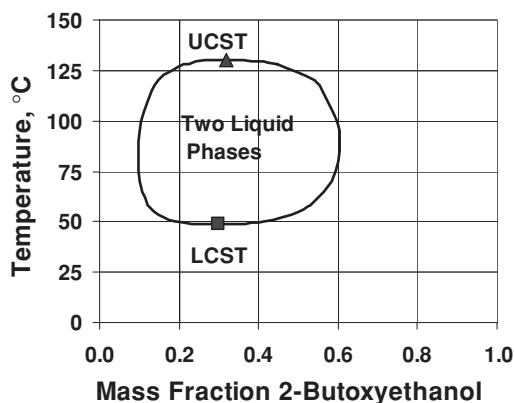


FIG. 15-15 Temperature-composition diagram for water + 2-butoxyethanol (ethylene glycol *n*-butyl ether). [Reprinted from Christensen, Donate, Frank, LaTulip, and Wilson, *J. Chem. Eng. Data*, **50**(3), pp. 869–877 (2005), with permission. Copyright 2005 American Chemical Society.]

(1996)]. The aqueous solubility of amino acids as a function of pH is discussed by Fuchs et al., *Ind. Eng. Chem. Res.*, **45**(19), pp. 6578–6584 (2006). Solution pH also has a strong effect on the solubility of proteins (complex polyaminoacids) in aqueous solution; solubility is lowest at the pH corresponding to the protein's isoelectric point (the pH at which all negative charges are balanced by all positive charges and the protein has zero net charge) [van Holde, Johnson, and Ho, *Principles of Physical Biochemistry* (Prentice-Hall, 1998)]. Partition ratios for partitioning of proteins in two-aqueous-phase systems depend upon many factors and are difficult to predict [Zaslavsky, *Aqueous Two-Phase Partitioning* (Dekker, 1994); and Kelley and Hatton, Chap. 22, "Protein Purification by Liquid-Liquid Extraction," in *Biotechnology*, 2d ed., vol. 3, Stephanopoulos, ed. (VCH, 1993)].

For general discussions of organic acid and base ionic equilibria, see Butler, *Ionic Equilibrium: Solubility and pH Calculations* (Wiley,

1998); and March, *Advanced Organic Chemistry: Reactions, Mechanisms, and Structure*, 5th ed., Chap. 8 (Wiley, 2000). The dissociation of inorganic salts is discussed in the book edited by Perrin [*Ionization Constants of Inorganic Acids and Bases in Aqueous Solution*, vol. 29 (Franklin, 1982)]. Compilations of pK_a values are given in several handbooks [Jencks and Regenstein, "Ionization Constants of Acids and Bases," in *Handbook of Biochemistry and Molecular Biology: Physical and Chemical Data*, vol. 1, 3d ed., Fasman, ed. (CRC Press, 1976), pp. 305–351; and *CRC Handbook of Chemistry and Physics*, 84th ed., Lide, ed. (CRC Press, 2003–2004)]. Also see Perrin, Dempsey, and Serjeant, *pK_a Prediction for Organic Acids and Bases* (Chapman and Hall, 1981).

PHASE DIAGRAMS

Phase diagrams are used to display liquid-liquid equilibrium data across a wide composition range. Consider the binary system of water + 2-butoxyethanol (common name ethylene glycol *n*-butyl ether) plotted in Fig. 15-15. This system exhibits both an upper critical solution temperature (UCST), also called the upper consolute temperature, and a lower critical solution temperature (LCST), or lower consolute temperature. The mixture is only partially miscible at temperatures between 48°C (the LCST) and 130°C (the UCST). Most mixtures tend to become more soluble in each other as the temperature increases; i.e., they exhibit UCST behavior. The presence of a LCST in the phase diagram is less common. Mixtures that exhibit LCST behavior include hydrogen-bonding mixtures such as an amine, a ketone, or an etheric alcohol plus water. Numerous water + glycol ether mixtures behave in this way [Christensen et al., *J. Chem. Eng. Data*, **50**(3), pp. 869–877 (2005)]. For these systems, hydrogen bonding leads to complete miscibility below the LCST. As temperature increases, hydrogen bonding is disrupted by increasing thermal (kinetic) energy, and hydrophobic interactions begin to dominate, leading to partial miscibility at temperatures above the LCST. The ethylene glycol + triethylamine system shown in Fig. 15-16 is another example.

Most of the ternary or pseudoternary systems used in extraction are of two types: one binary pair has limited miscibility (termed a type I system), or two binary pairs have limited miscibility (a type II system). The water + acetic acid + methyl isobutyl ketone (MIBK) system

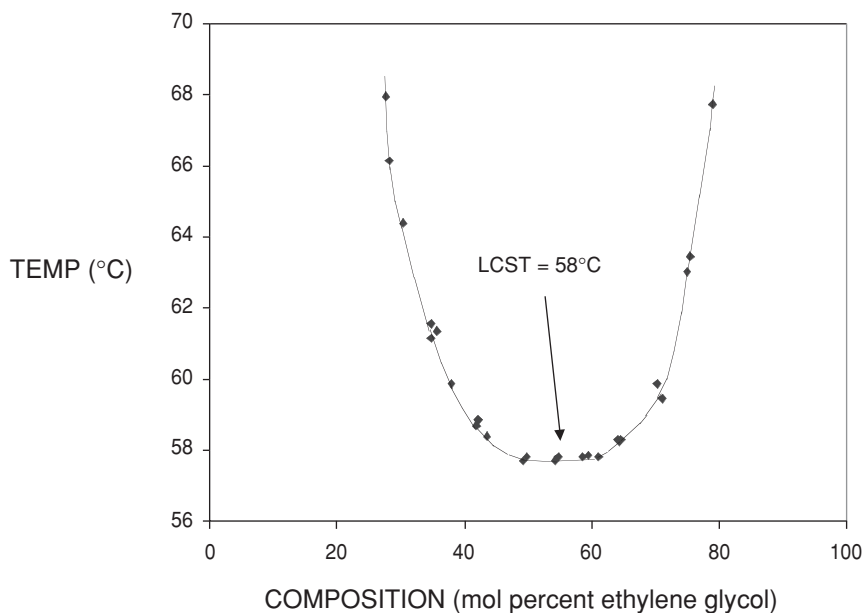


FIG. 15-16 Temperature-composition diagram for ethylene glycol + triethylamine. [Data taken from Sorenson and Arlt, *Liquid-Liquid Equilibrium Data Collection, DECHEMA, Binary Systems*, vol. V, pt. 1, 1979.]

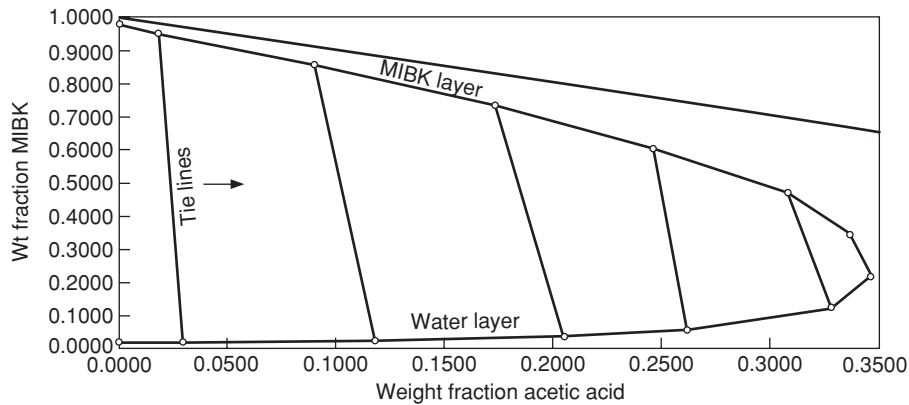


FIG. 15-17 Water + acetic acid + methyl isobutyl ketone at 25°C, a type I system.

shown in Fig. 15-17 is a type I system where only one of the binary pairs, water + MIBK, exhibits partial miscibility. The heptane + toluene + sulfolane system is another example of a type I system. In this case, only the heptane + sulfolane binary is partially miscible (Fig. 15-18). For a type II system, the solute has limited solubility in one of the liquids. An example of a type II system is MIBK + phenol + water (Fig. 15-19), where MIBK + water and phenol + water are only partially miscible. Some systems form more complicated phase diagrams. For example, the system water + dodecane + 2-butoxyethanol can form three liquid phases in equilibrium at 25°C [Lin and Chen, *J. Chem. Eng. Data*, **47**(4), pp. 992–996 (2002)]. Complex systems such as this rarely are encountered in extraction applications; however, Shen, Chang, and Liu [*Sep. Purif. Technol.*, **49**(3), pp. 217–222 (2006)] describe a single-stage, three-liquid-phase extraction process for transferring phenol and *p*-nitrophenol from wastewater in separate phases. In this process, the three-phase system consists of ethylene oxide–propylene oxide copolymer + ammonium sulfate + water + an oxygenated organic solvent such as butyl acetate or 2-octanol.

For ternary systems, a three-dimensional plot is required to represent the effects of both composition and temperature on the phase behavior. Normally, ternary phase data are plotted on isothermal, two-dimensional triangular diagrams. These can be right-triangle plots, as in Fig. 15-17, or equilateral-triangle plots, as in Figs. 15-18 and 15-19. In Fig. 15-18, the line delineating the region where two liquid phases form is called the binodal locus. The lines connecting equilibrium compositions for each phase are called tie lines, as illustrated by lines *ab* and *cd*. The tie lines converge on the plait point, the point on the binodal locus where both liquid phases attain the same composition

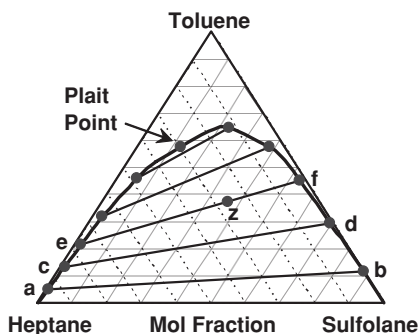


FIG. 15-18 Heptane + toluene + sulfolane at 25°C, a type I system. [Data taken from De Fre and Verhoeye, *J. Appl. Chem. Biotechnol.*, **26**, pp. 1-19 (1976).]

and the tie line length goes to zero. To calculate the relative amounts of the liquid phases, the lever rule is used. For the total feed composition z , the fraction of phase I with the composition e is equal to the ratio of the lengths of the line segments given by fz/ez in Fig. 15-18. Data often are plotted on a mass fraction basis when differences in the molecular weights of the components are large, since plotting the phase diagram on a mole basis tends to compress the data into a small region and details are hidden by the scale. This often is the case for systems involving water, for example.

An extraction application normally involves more than three components, including the key solute, the feed solvent, and extraction solvent (or solvent blend), plus impurity solutes. Usually, the minor impurity components do not have a major impact on the phase equilibrium. Phase equilibrium data for multicomponent systems may be represented by using an appropriate activity coefficient correlation. (See “Data Correlation Equations.”) However, for many dilute and moderately concentrated feeds, process design calculations are carried out as if the system were a ternary system comprised only of a single solute plus the feed solvent and extraction solvent (a pseudoternary). Partition ratios are determined for major and minor solutes by using a representative feed, and solute transfer calculations are carried out using solute *K* values as if they were completely independent of one another. This approach often is satisfactory, but its validity should be checked with a few key experiments. For industrial mixtures containing numerous impurities, a mass fraction or mass ratio basis often is used to avoid

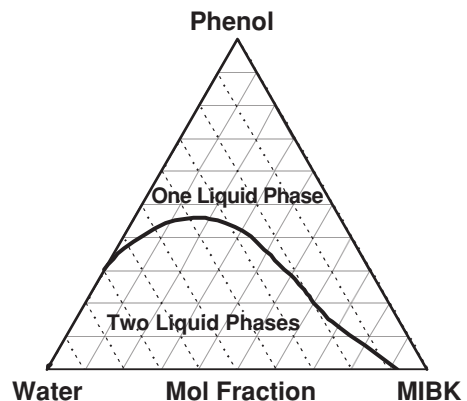


FIG. 15-19 Methyl isobutyl ketone + phenol + water at 30°C, a type II system. [Data taken from Narashinhan, Reddy, and Chari, *J. Chem. Eng. Data*, **7**, p. 457 (1962).]

difficulties accounting for impurities of unknown structure and molecular weight.

LIQUID-LIQUID EQUILIBRIUM EXPERIMENTAL METHODS

GENERAL REFERENCES: Raal, Chap. 3, "Liquid-Liquid Equilibrium Measurements," in *Vapor-Liquid Equilibria Measurements and Calculations* (Taylor & Francis, 1998); Newsham, Chap. 1 in *Science and Practice of Liquid-Liquid Extraction*, vol. 1, Thornton, ed. (Oxford, 1992); and Novak, Matous, and Pick, *Liquid-Liquid Equilibria, Studies in Modern Thermodynamics Series*, vol. 7, pp. 266–282 (Elsevier, 1987).

Three general types of experimental methods commonly are used to generate liquid-liquid equilibrium data: (1) titration with visual observation of liquid clarity or turbidity; (2) visual observation of clarity or turbidity for known compositions as a function of temperature; and (3) direct analysis of equilibrated liquids typically using GC or LC methods. In the titration method, one compound is slowly titrated into a known mass of the second compound during mixing. The titration is terminated when the mixture becomes cloudy, indicating that a second liquid phase has formed. A tie line may be determined by titrating the second compound into the first at the same temperature. This method is reasonably accurate for binary systems composed of pure materials. It also may be applied to ternaries by titrating the third component into a solution of the first and second components, at least to some extent. This method also requires the least time to perform. Since the method is visual, a trace impurity in the "titrant" that is less soluble in the second compound may cause cloudiness at a lower concentration than if pure materials were used. This method has poor precision for sparingly soluble systems. Normally, it is used at ambient temperature and pressure for systems that do not pose a significant health risk to the operator.

In the second method, several mixtures of known composition are formulated and placed in glass vials or ampoules. These are placed in a bath or oven and heated or cooled until two phases become one, or vice versa. In this way, the phase boundaries of a binary system may be determined. Again, impurities in the starting materials may affect the results, and this method does not work well for sparingly soluble systems or for systems that develop significant pressure.

To obtain tie-line data for systems that involve three or more significant components, or for systems that cannot be handled in open containers, both phases must be sampled and analyzed. This generally requires the greatest effort but gives the most accurate results and can be used over the widest range of solubilities, temperatures, and pressures. This method also may be used on multicomponent systems, which are more likely to be encountered in an industrial process. For this method, an appropriate glass vessel or autoclave is selected, based on the temperature, pressure, and compounds in the mixture. It is best to either place the vessel in an oven or submerge it in a bath to ensure there are no cold or hot spots. The mixture is introduced, thermostatted, and thoroughly mixed, and the phases are allowed to separate fully. Samples are then carefully withdrawn through lines that have the minimum dead volume feasible. The sampling should be done isothermally; otherwise the collected sample may not be exactly the same as what was in the equilibrated vessel. Adding a carefully chosen, nonreactive diluent to the sample container will prevent phase splitting, and this can be an important step to ensure accuracy in the subsequent sample workup and analysis. Take sufficient purges and at least three samples from each phase. Use the appropriate analytical method and analyze a calibration standard along with the samples. Try to minimize the time between sampling and analysis.

Rydberg and others describe automated equipment for generating tie line data, including an apparatus called AKUFVE offered by MEAB [Rydberg et al., Chap. 4 in *Solvent Extraction Principles and Practice*, 2d ed., Rydberg et al., eds. (Dekker, 2004), pp. 193–197]. The AKUFVE apparatus employs a stirred cell, a centrifuge for phase separation, and online instrumentation for rapid generation of data. As an alternative, Kuzmanović et al. [*J. Chem. Eng. Data*, **48**, pp. 1237–1244 (2003)] describe a fully automated workstation for rapid measurement of liquid-liquid equilibrium using robotics for automated sampling.

DATA CORRELATION EQUATIONS

Tie Line Correlations Useful correlations of ternary data may be obtained by using the methods of Hand [*J. Phys. Chem.*, **34**(9), pp. 1961–2000 (1930)] and Othmer and Tobias [*Ind. Eng. Chem.*, **34**(6), pp. 693–696 (1942)]. Hand showed that plotting the equilibrium line in terms of mass ratio units on a log-log scale often gave a straight line. This relationship commonly is expressed as

$$\log \frac{X_{23}}{X_{33}} = a + b \log \frac{X_{21}}{X_{11}} \quad (15-23)$$

where X_{ij} represents the mass fraction of component i dissolved in the phase richest in component j , and a and b are empirical constants. Subscript 2 denotes the solute, while subscripts 1 and 3 denote feed solvent and extraction solvent, respectively. An equivalent expression can be written by using the Bancroft coordinate notation introduced earlier: $Y' = cX'^b$, where $c = 10^a$. Othmer and Tobias proposed a similar correlation:

$$\log \frac{1 - X_{33}}{X_{33}} = d + e \log \frac{1 - X_{11}}{X_{11}} \quad (15-24)$$

where d and e are constants. Equations (15-23) and (15-24) may be used to check the consistency of tie line data, as discussed by Awwad et al. [*J. Chem. Eng. Data*, **50**(3), pp. 788–791 (2005)] and by Kirbaslar et al. [*Braz. J. Chem. Eng.*, **17**(2), pp. 191–197 (2000)].

A particularly useful diagram is obtained by plotting the solute equilibrium line on log-log scales as X_{23}/X_{33} versus X_{21}/X_{11} [from Eq. (15-23)] along with a second plot consisting of X_{23}/X_{33} versus X_{23}/X_{13} and X_{21}/X_{31} versus X_{21}/X_{11} . This second plot is termed the limiting solubility curve. The plait point may easily be found from the intersection of the solute equilibrium line with this curve, as shown by Treybal, Weber, and Daley [*Ind. Eng. Chem.*, **38**(8), pp. 817–821 (1946)]. This type of diagram also is helpful for interpolation and limited extrapolation when equilibrium data are scarce. An example diagram is shown in Fig. 15-20 for the water + acetic acid + methyl isobutyl ketone (MIBK) system. For additional discussion of various

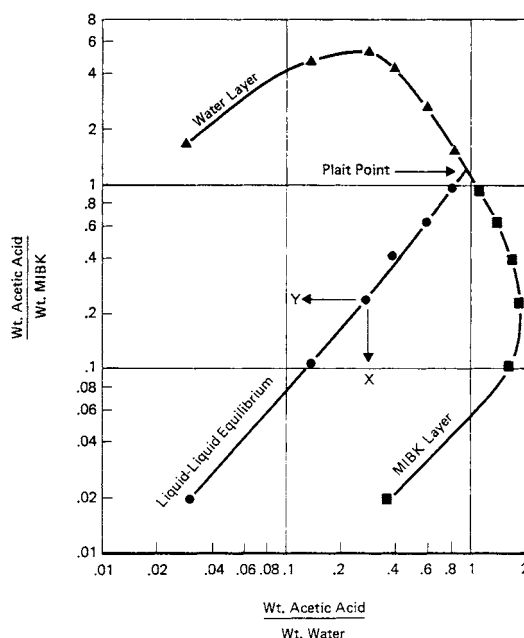


FIG. 15-20 Hand-type ternary diagram for water + acetic acid + MIBK at 25°C.

correlation methods, see Laddha and Degaleesan, *Transport Phenomena in Liquid Extraction* (McGraw-Hill, 1978), Chap. 2.

Thermodynamic Models The thermodynamic theories and equations used to model phase equilibria are reviewed in Sec. 4, "Thermodynamics." These equations provide a framework for data that can help minimize the required number of experiments. An accurate liquid-liquid equilibrium (LLE) model is particularly useful for applications involving concentrated feeds where partition ratios and mutual solubility between phases are significant functions of solute concentration. Sometimes it is difficult to model LLE behavior across the entire composition range with a high degree of accuracy, depending upon the chemical system. In that case, it is best to focus on the composition range specific to the particular application at hand—to ensure the model accurately represents the data in that region of the phase diagram for accurate design calculations. Such a model can be a powerful tool for extractor design or when used with process simulation software to conceptualize, evaluate, and optimize process options. However, whether a complete LLE model is needed will depend upon the application. For dilute applications where partition ratios do not vary much with composition, it may be satisfactory to characterize equilibrium in terms of a simple Hand-type correlation or in terms of partition ratios measured over the range of anticipated feed and raffinate compositions and fit to an empirical equation. Also, when partition ratios are always very large, on the order of 100 or larger, as can occur when washing salts from an organic phase into water, a continuous extractor is likely to operate far from equilibrium. In this case, a precise equilibrium model may not be needed because the extraction factor always is very large and solute diffusion rates dominate performance. (See "Rate-Based Calculations" under "Process Fundamentals and Basic Calculation Methods.")

LLE models for nonionic systems generally are developed by using either the NRTL or UNIQUAC correlation equations. These equations can be used to predict or correlate multicomponent mixtures using only binary parameters. The NRTL equations [Renon and Prausnitz, *AIChE J.*, **14**(1), pp. 135–144 (1968)] have the form

$$\ln \gamma_i = \frac{\sum_j \tau_{ji} G_{ji} x_j}{\sum_j G_{ji} x_j} + \sum_k \frac{G_{jk} x_j}{\sum_k G_{jk} x_k} \left(\tau_{ij} - \frac{\sum_k \tau_{kj} G_{kj} x_k}{\sum_k G_{kj} x_k} \right) \quad (15-25)$$

where τ_{ij} and $G_{ij} = \exp(-\alpha_{ij} \tau_{ij})$ are model parameters. The UNIQUAC equations [Abrams and Prausnitz, *AIChE J.*, **21**(1), pp. 116–128 (1975)] are somewhat more complex. (See Sec. 4, "Thermodynamics.") Most commercial simulation software packages include these models and allow regression of data to determine model parameters. One should refer to the process simulator's operating manual for specific details. Not all simulation software will use exactly the same equation format and parameter definitions, so parameters reported in the literature may not be appropriate for direct input to the program but need to be converted to the appropriate form. In theory, activity coefficient data from binary or ternary vapor-liquid equilibria can be used for calculating liquid-liquid equilibria. While this may provide a reasonable starting point, in practice at least some of the binary parameters will need to be determined from liquid-liquid tie line data to obtain an accurate model [Lafyatis et al., *Ind. Eng. Chem. Res.*, **28**(5), pp. 585–590 (1989)]. Detailed discussion of the application and use of NRTL and UNIQUAC is given by Walas [*Phase Equilibria in Chemical Engineering* (Butterworth-Heinemann, 1985)]. The application of NRTL in the design of a liquid-liquid extraction process is discussed by van Grieken et al. [*Ind. Eng. Chem. Res.*, **44**(21), pp. 8106–8112 (2005)], by Venter and Nieuwoudt [*Ind. Eng. Chem. Res.*, **37**(10), pp. 4099–4106 (1998)], and by Coto et al. [*Chem. Eng. Sci.*, **61**, pp. 8028–8039 (2006)]. The use of the NRTL model also is discussed in Example 5 under "Single-Solvent Fractional Extraction with Extract Reflux" in "Calculation Procedures." The application of UNIQUAC is discussed by Anderson and Prausnitz [*Ind. Eng. Chem. Process Des. Dev.*, **17**(4), pp. 561–567 (1978)].

Although the NRTL or UNIQUAC equations generally are recommended for nonionic systems, a number of alternative approaches have been introduced. Some include explicit terms for association of

molecules in solution, and these may have advantages depending upon the application. An example is the statistical associating fluid theory (SAFT) equation of state introduced by Chapman et al. [*Ind. Eng. Chem. Res.*, **29**(8), pp. 1709–1721 (1990)]. SAFT approximates molecules as chains of spheres and uses statistical mechanics to calculate the energy of the mixture [Müller and Gubbins, *Ind. Eng. Chem. Res.*, **40**(10), pp. 2193–2211 (2001)]. Yu and Chen discuss the application of SAFT to correlate data for 41 binary and 8 ternary liquid-liquid systems [*Fluid Phase Equilibria*, **94**, pp. 149–165 (1994)]. Note that at present not all commercial simulation software packages include SAFT as an option; or if it is included, the association term may be left out. The SAFT equation often is used to correlate LLE data for polymer-solvent systems [Jog et al., *Ind. Eng. Chem. Res.*, **41**(5), pp. 887–891 (2002)]. In another approach, Aspiron, Hasse, and Maurer [*Fluid Phase Equil.*, **205**, pp. 195–214 (2003)] discuss the addition of chemical theory association terms to the UNIQUAC model and other phase equilibrium models in general. With this approach, molecular association is treated as a reversible chemical reaction, and parameter values for the association terms may be determined from spectroscopic data. Another activity coefficient correlation called COSMO-SPACE is presented as an alternative to UNIQUAC [Klamt, Krooshof, and Taylor, *AIChE J.*, **48**(10), pp. 2332–2349 (2002)].

Other methods are used to describe the behavior of ionic species (electrolytes). The activity coefficient of an ion in solution may be expressed in terms of modified Debye-Hückel theory. A common expression suitable for low concentrations has the form

$$\log \gamma_i = \frac{-az_i^2 I^{1/2}}{1 + I^{1/2}} + bz_i^2 I \quad (15-26)$$

where I is ionic strength, z_i is the number of electronic charges, and a and b are parameters that depend upon temperature. Ionic strength is defined in terms of the ion molal concentration. Equation (15-26) represents the activity coefficient for a single ion. For a compound MX that dissociates into M^+ and X^- in solution, the mean ionic activity coefficient is given by $\gamma^{\pm} = (\gamma^+ \gamma^-)^{1/2}$. Activity coefficients for most electrolytes dissolved in water are less than unity because of the strong attractive interaction between water and a charged species, but this can vary depending upon the organic character of the ion and its concentration. For more detailed discussions focusing on extraction, see Marcus, Chap. 2, and Grenthe and Wanner, Chap. 6, in *Solvent Extraction Principles and Practice*, 2d ed., Rydberg et al., eds. (Dekker, 2004). For general discussions, see *Activity Coefficients in Electrolyte Solutions*, 2d ed., Pitzer, ed. (CRC Press, 1991); Zemaitis et al., *Handbook of Aqueous Electrolyte Thermodynamics* (DIPPR, AIChE, 1986); and Robinson and Stokes, *Electrolyte Solutions* (Butterworths, 1959). The concepts of molecular association have been applied to modeling electrolyte solutions with good success [Stokes and Robinson, *J. Soln. Chem.*, **2**, p. 173 (1973)].

Modeling phase equilibria for mixed-solvent electrolyte systems including nonionic organic compounds is discussed by Polka, Li, and Gmehling [*Fluid Phase Equil.*, **94**, pp. 115–127 (1994)]; Li, Lin, and Gmehling [*Ind. Eng. Chem. Res.*, **44**(5), pp. 1602–1609 (2005)]; and Wang et al. [*Fluid Phase Equil.*, **222–223**, pp. 11–17 (2004)]. Another computer program is discussed by Baes et al. [*Sep. Sci. Technol.*, **25**, p. 1675 (1990)]. Ahlem, Abdeslam-Hassen, and Mossaab [*Chem. Eng. Technol.*, **24**(12), pp. 1273–1280 (2001)] discuss two approaches to modeling metal ion extraction for purification of phosphoric acid.

Data Quality Normally, it is not possible to evaluate LLE data for thermodynamic consistency [Sorenson and Arlt, *Liquid-Liquid Equilibrium Data Collection*, Binary Systems, vol. V, pt. 1 (DECHEMA, 1979), p. 12]. The thermodynamic consistency test for VLE data involves calculating an independently measured variable from the others (usually the vapor composition from the temperature, pressure, and liquid composition) and comparing the measurement with the calculated value. Since LLE data are only very weakly affected by change in pressure, this method is not feasible for LLE. However, if the data were produced by equilibration and analysis of both phases, then at least the data can be checked to determine how well the material balance closes. This can be done by plotting the total

TABLE 15-1 Selected Partition Ratio Data

Partition ratios are listed in units of weight percent solute in the extract divided by weight percent solute in the raffinate, generally for the lowest solute concentrations given in the cited reference. The partition ratio tends to be greatest at low solute concentrations. Consult the original references for more information about a specific system.

Solute	Feed solvent	Extraction solvent	Temp. (°C)	K (wt % basis)	Reference
Ethanol	Cyclohexane	Ethanolamine	25	2.79	1
Acetone	Ethylene glycol	Amyl acetate	31	1.84	2
Acetone	Ethylene glycol	Ethyl acetate	31	1.85	2
Acetone	Ethylene glycol	Butyl acetate	31	1.94	2
Trilinolein	Furfural	Heptane	30	47.5	3
<i>o</i> -Xylene	Heptane	Tetraethylene glycol	20	0.15	4
<i>o</i> -Xylene	Heptane	Tetraethylene glycol	30	0.15	4
<i>o</i> -Xylene	Heptane	Tetraethylene glycol	40	0.16	4
Toluene	Heptane	Sulfolane	25	0.34	5
Toluene	Heptane	Sulfolane	50	0.36	5
Toluene	Heptane	Sulfolane	75	0.31	5
Toluene	Heptane	Sulfolane	100	0.33	5
Toluene	Hexane	Sulfolane	25	0.34	6
Xylene	Hexane	Sulfolane	25	0.30	6
Toluene	<i>n</i> -Hexane	Sulfolane	25	0.34	6
Xylene	<i>n</i> -Hexane	Sulfolane	25	0.30	6
Toluene	<i>n</i> -Octane	Sulfolane	25	0.35	6
Xylene	<i>n</i> -Octane	Sulfolane	25	0.25	6
Toluene	Octane	Sulfolane	25	0.35	6
Xylene	Octane	Sulfolane	25	0.25	6
1,2-Dimethoxyethane	Water	Dodecane	25	0.46	7
1,4-Dioxane	Water	Ethyl acetate	30	1.29	8
1-Butanol	Water	Benzonitrile	25	3.01	9
1-Butanol	Water	Ethyl acetate	40	5.48	10
1-Butanol	Water	Methyl <i>t</i> -butyl ether	25	7.95	11
1-Heptene	Water	1-Propanol	25	3.95	12
1-Octanol	Water	Methyl <i>t</i> -butyl ether	25	10.9	13
1-Propanol	Water	1-Heptene	25	1.36	12
1-Propanol	Water	Butyraldehyde	25	4.14	14
1-Propanol	Water	Cyclohexane	25	0.34	15
1-Propanol	Water	Di-isobutyl ketone	25	0.93	14
1-Propanol	Water	Methyl <i>tert</i> -butyl ether	25	3.79	11
2,3-Butanediol	Water	2,4-Dimethylphenol	40	1.89	16
2,3-Butanediol	Water	2-Butoxyethanol	70	1.79	17
2,3-Dichloropropene	Water	Epichlorohydrin	20	181	18
2,3-Dichloropropene	Water	Epichlorohydrin	77	69.5	18
2-Butoxyethanol	Water	Decane	22	0.45	19
2-Methoxyethanol	Water	Cyclohexanone	70	0.54	20
2-Methyl-1-propanol	Water	Benzene	25	1.18	21
2-Methyl-1-propanol	Water	Toluene	25	0.88	21
2-Propanol	Water	1-Methylcyclohexanol	20	3.66	22
2-Propanol	Water	2,2,4-Trimethylpentane	20	0.045	23
2-Propanol	Water	Carbon tetrachloride	20	1.41	24
2-Propanol	Water	Dichloromethane	20	3.56	22
2-Propanol	Water	Di-isopropyl ether	25	0.41	25
2-Propanol	Water	Di-isopropyl ether	25	0.98	26
3-Cyanopyridine	Water	Benzene	30	1.55	27
Acetaldehyde	Water	Furfural	16	0.97	28
Acetaldehyde	Water	1-Pentanol	18	1.43	28
Acetic acid	Water	1-Butanol	27	1.61	29
Acetic acid	Water	1-Hexene	25	0.0073	30
Acetic acid	Water	1-Octanol	20	0.56	31
Acetic acid	Water	20 vol % Trioctylamine + 20 vol % 1-Decanol + 60 vol % dodecane	20	0.61	32
Acetic acid	Water	2-Butanone	25	1.20	33
Acetic acid	Water	2-Ethyl-1-hexanol	20	0.58	34
Acetic acid	Water	2-Pentanol	25	1.35	35
Acetic acid	Water	2-Pentanone	25	1.00	30
Acetic acid	Water	4-Heptanone	25	0.30	30
Acetic acid	Water	70 vol % Tributylphosphate + 30 vol % dodecane	20	0.31	36
Acetic acid	Water	Cyclohexanol	27	1.33	29
Acetic acid	Water	Diethyl phthalate	20	0.22	37
Acetic acid	Water	Di-isopropyl carbinol	25	0.80	38
Acetic acid	Water	Dimethyl phthalate	20	0.34	37
Acetic acid	Water	Di- <i>n</i> -butyl ketone	25	0.38	39
Acetic acid	Water	Ethyl acetate	30	0.91	40
Acetic acid	Water	Isopropyl ether	20	0.25	41
Acetic acid	Water	Methyl cyclohexanone	25	0.93	38
Acetic acid	Water	Methylisobutyl ketone	25	0.66	42
Acetic acid	Water	Methylisobutyl ketone	25	0.76	38
Acetic acid	Water	Toluene	25	0.06	43
Acetone	Water	1-Octanol	25	0.81	44
Acetone	Water	1-Pentanol	25	4.11	44

15-30 LIQUID-LIQUID EXTRACTION AND OTHER LIQUID-LIQUID OPERATIONS AND EQUIPMENT

TABLE 15-1 Selected Partition Ratio Data (Continued)

Partition ratios are listed in units of weight percent solute in the extract divided by weight percent solute in the raffinate, generally for the lowest solute concentrations given in the cited reference. The partition ratio tends to be greatest at low solute concentrations. Consult the original references for more information about a specific system.

Solute	Feed solvent	Extraction solvent	Temp. (°C)	K (wt % basis)	Reference
Acetone	Water	1-Pentanol	30	1.14	44
Acetone	Water	2-Octanol	30	0.66	44
Acetone	Water	Chloroform	25	1.83	45
Acetone	Water	Chloroform	25	1.72	46
Acetone	Water	Dibutyl ether	25	1.94	38
Acetone	Water	Diethyl ether	30	1.00	47
Acetone	Water	Ethyl acetate	30	1.50	48
Acetone	Water	Ethyl butyrate	30	1.28	48
Acetone	Water	Methyl acetate	30	1.15	48
Acetone	Water	Methylisobutyl ketone	25	1.91	38
Acetone	Water	Hexane	25	0.34	49
Acetone	Water	Toluene	25	0.84	38
Acrylic acid	Water	89.6 wt % Kerosene/10.4 wt % trialkylphosphine oxide (C7-C9)	25	6.50	50
Aniline	Water	Methylcyclohexane	25	2.05	51
Aniline	Water	Methylcyclohexane	50	3.41	51
Aniline	Water	Heptane	25	1.43	51
Aniline	Water	Heptane	50	2.20	51
Aniline	Water	Toluene	25	12.9	52
Benzoic acid	Water	87.4 wt % Kerosene/ 12.6 wt % tributylphosphate	25	36.0	53
Benzoic acid	Water	89.6 wt % Kerosene/10.4 wt % trialkylphosphine oxide (C7-C9)	25	1.30	50
Butyric acid	Water	20 vol % Trioctylamine + 20 vol % 1-decanol + 60 vol % dodecane	20	6.16	36
Butyric acid	Water	70 vol % Tributylphosphate + 30 vol % dodecane	20	2.51	36
Butyric acid	Water	Methyl butyrate	30	6.75	54
Citric acid	Water	25 wt % Tri-isooctylamine + 75 wt % Chloroform	25	14.1	55
Citric acid	Water	26 wt % Tri-isooctylamine + 75 wt % 1-Octanol	25	41.5	55
Epichlorohydrin	Water	2,3-Dichloropropene	20	11.4	56
Epichlorohydrin	Water	2,3-Dichloropropene	77	13.4	56
Ethanol	Water	1-Octanol	25	0.66	57
Ethanol	Water	1-Octene	25	0.036	58
Ethanol	Water	2,2,4-Trimethylpentane	5	0.027	59
Ethanol	Water	2,2,4-Trimethylpentane	40	0.041	59
Ethanol	Water	3-Heptanol	25	0.78	60
Ethanol	Water	1-Butanol	20	3.00	61
Ethanol	Water	Di- <i>n</i> -propyl ketone	25	0.59	38
Ethanol	Water	1-Hexanol	28	1.00	62
Ethanol	Water	2-Octanol	28	0.83	62
Ethyl acetate	Water	1-Butanol	40	11.1	10
Ethylene glycol	Water	Furfural	25	0.32	64
Formic acid	Water	20 vol % Trioctylamine + 20 vol % 1-decanol + 60 vol % dodecane	20	1.77	36
Formic acid	Water	70 vol % Tributylphosphate + 30 vol % dodecane	20	0.37	36
Formic acid	Water	Methylisobutyl carbinol	30	1.22	65
Furfural	Water	Toluene	25	5.64	66
Glycolic acid	Water	89.6 wt % Kerosene/10.4 wt % trialkylphosphine oxide (C7-C9)	25	0.29	67
Glyoxylic acid	Water	89.6 wt % Kerosene/10.4 wt % trialkylphosphine oxide (C7-C9)	25	0.067	67
Lactic acid	Water	20 vol % Trioctylamine + 20 vol % 1-decanol + 60 vol % dodecane	20	0.65	36
Lactic acid	Water	25 wt % Tri-isooctylamine + 75 wt % chloroform	25	19.2	55
Lactic acid	Water	26 wt % Tri-isooctylamine + 75 wt % 1-octanol	25	25.9	55
Lactic acid	Water	70 vol % Tributylphosphate + 30 vol % dodecane	20	0.14	36
Lactic acid	Water	<i>iso</i> -Amyl alcohol	25	0.35	68
Malic acid	Water	25 wt % Tri-isooctylamine + 75 wt % chloroform	25	30.7	55
Malic acid	Water	25 wt % Tri-isooctylamine + 75 wt % 1-octanol	25	59.0	55
Methanol	Water	1-Octanol	25	0.28	57
Methanol	Water	Ethyl acetate	0	0.059	69
Methanol	Water	Ethyl acetate	20	0.24	69
Methanol	Water	1-Butanol	0	0.60	70
Methanol	Water	1-Hexanol	28	0.57	71
Methanol	Water	<i>p</i> -Cresol	35	0.31	72

TABLE 15-1 Selected Partition Ratio Data (Concluded)

Partition ratios are listed in units of weight percent solute in the extract divided by weight percent solute in the raffinate, generally for the lowest solute concentrations given in the cited reference. The partition ratio tends to be greatest at low solute concentrations. Consult the original references for more information about a specific system.

Solute	Feed solvent	Extraction solvent	Temp. (°C)	K (wt % basis)	Reference
Methanol	Water	Phenol	25	1.33	72
Methyl <i>t</i> -butyl ether	Water	1-Octanol	25	2.61	13
Methyl <i>t</i> -amyl ether	Water	2,2,4-Trimethylpentane	25	131	73
Methylethyl ketone	Water	1,1,2-Trichloroethane	25	3.44	74
Methylethyl ketone	Water	Hexane	25	1.78	75
1-Propanol	Water	Ethyl acetate	20	1.54	69
1-Propanol	Water	Heptane	38	0.54	76
<i>p</i> -Cresol	Water	Methylnaphthalene	35	9.89	72
Phenol	Water	Ethyl acetate	25	0.048	77
Phenol	Water	Isoamyl acetate	25	0.046	77
Phenol	Water	Isopropyl acetate	25	0.040	77
Phenol	Water	Methyl isobutyl ketone	30	39.8	78
Phenol	Water	Methylnaphthalene	25	7.06	79
Phosphoric acid	Water	4-Methyl-2-pentanone	25	0.0012	80
Propionic acid	Water	20 vol % Trioctylamine + 20 vol % 1-decanol + 60 vol % dodecane	20	2.13	36
Propionic acid	Water	70 vol % Tributylphosphate + 30 vol % dodecane	20	1.02	36
Propionic acid	Water	Ethyl acetate	30	2.77	81
Propionic acid	Water	Toluene	31	0.52	82
Pyridine	Water	Chlorobenzene	25	2.10	83
Pyridine	Water	Toluene	25	1.90	84
Pyridine	Water	Xylene	25	1.26	84
<i>t</i> -Butanol	Water	Ethyl acetate	20	1.74	69
Tetrahydrofuran	Water	1-Octanol	20	3.31	85

References:

- Harris et al., *J. Chem. Eng. Data*, **47**, pp. 781–787 (2002).
- Garner, Ellis, and Roy, *Chem. Eng. Sci.*, **2**, p. 14 (1953).
- Beech and Glasstone, *J. Chem. Soc.*, p. 67 (1938).
- Darwish et al., *J. Chem. Eng. Data*, **48**, pp. 1614–1619 (2003).
- De Fre, Thesis, University of Gent, 1976.
- Barbaudy, *Compt. Rend.*, **182**, p. 1279 (1926).
- Burgdorf, Thesis, Technische University, Berlin, 1995.
- Komatsu and Yamamoto, *Kagaku Kogaku Ronbunshu*, **22**(2), pp. 378–384 (1996).
- Grande et al., *J. Chem. Eng. Data*, **41**(4), pp. 926–928 (1996).
- De Andrade and D'Avila, Private communication to DDB, pp. 1–7 (1991).
- Letcher, Ravindran, and Radloff, *Fluid Phase Equil.*, **69**, pp. 251–260 (1991).
- Letcher et al., *J. Chem. Eng. Data*, **39**(2), pp. 320–323 (1994).
- Arce et al., *J. Chem. Thermodyn.*, **28**, pp. 3–6 (1996).
- Letcher et al., *J. Chem. Eng. Data*, **41**(4), pp. 707–712 (1996).
- Plackov and Stern, *Fluid Phase Equil.*, **71**, pp. 189–209 (1992).
- Escudero, Cabezas, and Coca, *J. Chem. Eng. Data*, **39**(4), pp. 834–839 (1994).
- Escudero, Cabezas, and Coca, *J. Chem. Eng. Data*, **41**(6), pp. 1383–1387 (1996).
- Zhang and Liu, *J. Chem. Ind. Eng. (China)*, **46**(3), pp. 365–369 (1995).
- Sazonov, *Zh. Obshch. Khim.*, **61**(1), pp. 59–64 (1991).
- Hauschild and Knapp, *J. Solution Chem.*, **23**(3), pp. 363–377 (1994).
- Stephenson, *J. Chem. Eng. Data*, **37**(1), pp. 80–95 (1992).
- Sayar, *J. Chem. Eng. Data*, **36**(1), pp. 61–65 (1991).
- Arda and Sayar, *Fluid Phase Equil.*, **73**, pp. 129–138 (1992).
- Blumberg, Čejtin, and Fuchs, *J. Appl. Chem.*, **10**, p. 407 (1960).
- Chang and Moulton, *Ind. Eng. Chem.*, **45**, p. 2350 (1953).
- Letcher, Ravindran, and Radloff, *Fluid Phase Equil.*, **71**, pp. 177–188 (1992).
- Hu, Shi, and Yun, *Shiyou Huagong*, **21**, pp. 38–42 (1992).
- Elgin and Browning, *Trans. Am. Inst. Chem. Engrs.*, **31**, p. 639 (1935).
- Griswold, Chu, and Winsauer, *Ind. Eng. Chem.*, **41**, p. 2352 (1949).
- Nakahara, Masamoto, and Arai, *Kagaku Kogaku Ronbunshu*, **19**(4), pp. 663–668 (1993).
- Ratkovics et al., *J. Chem. Thermodyn.*, **23**, pp. 859–865 (1991).
- Morales et al., *J. Chem. Eng. Data*, **48**, pp. 874–886 (2003).
- Gomis et al., *Fluid Phase Equil.*, **106**, pp. 203–211 (1995).
- Ratkovics et al., *J. Chem. Thermodyn.*, **23**, pp. 859–865 (1991).
- Al-Muhtaseb and Fahim, *Fluid Phase Equil.*, **123**, pp. 189–203 (1996).
- Morales et al., *J. Chem. Eng. Data*, **48**, pp. 874–886 (2003).
- Dramur and Tatli, *J. Chem. Eng. Data*, **38**(1), pp. 23–25 (1993).
- Fairburn, Cheney, and Chernovsky, *Chem. Eng. Progr.*, **43**, p. 280 (1947).
- Fairburn, Cheney, and Chernovsky, *Chem. Eng. Progr.*, **43**, p. 280 (1947).
- Briggs and Comings, *Ind. Eng. Chem.*, **35**, p. 411 (1943).
- Buchanan, *Ind. Eng. Chem.*, **44**, p. 2449 (1952).
- Griswold, Chew, and Klecka, *Ind. Eng. Chem.*, **42**, p. 1246 (1950).
- Johnson and Bliss, *Trans. Am. Inst. Chem. Engrs.*, **42**, p. 331 (1946).
- Tiryaki, Guruz, and Orbey, *Fluid Phase Equil.*, **94**, pp. 267–280 (1994).
- Church and Briggs, *J. Chem. Eng. Data*, **9**, p. 207 (1964).
- Baker, *Phys. Chem.*, **59**, p. 1182 (1955).
- Conway and Phillips, *Ind. Eng. Chem.*, **46**, p. 1474 (1954).
- Hixon and Bockelmann, *Trans. Am. Inst. Chem. Engrs.*, **38**, p. 891 (1942).
- Hirata and Hirose, *Kagaku Kogaku*, **27**, p. 407 (1963).
- Li et al., *J. Chem. Eng. Data*, **48**, pp. 621–624 (2003).
- Charles and Morton, *J. Appl. Chem.*, **7**, p. 39 (1957).
- Hand, *J. Phys. Chem.*, **34**, p. 1961 (1930).
- Mei, Qin, and Dai, *J. Chem. Eng. Data*, **47**, pp. 941–943 (2002).
- Durandet and Gladel, *Rev. Inst. Franc. Petrole*, **11**, p. 811 (1956).
- Davison, Smith, and Hood, *J. Chem. Eng. Data*, **11**, p. 304 (1966).
- Zhang and Liu, *J. Chem. Ind. Eng. (China)*, **46**(3), pp. 365–369 (1995).
- Arce et al., *J. Chem. Eng. Data*, **39**(2), pp. 378–380 (1994).
- Purvanto et al., *J. Chem. Eng. Data*, **41**(6), pp. 1414–1417 (1996).
- Wagner and Sandler, *J. Chem. Eng. Data*, **40**(5), pp. 1119–1123 (1995).
- Forbes and Coolidge, *J. Am. Chem. Soc.*, **41**, p. 150 (1919).
- Boobar et al., *Ind. Eng. Chem.*, **43**, p. 2922 (1951).
- Crook and Van Winkle, *Ind. Eng. Chem.*, **46**, p. 1474 (1954).
- De Andrade and D'Avila, private communication to DDB, pp. 1–7 (1991).
- Berg, Manders, and Switzer, *Chem. Eng. Progr.*, **47**, p. 11 (1951).
- Fritzsche and Stockton, *Ind. Eng. Chem.*, **38**, p. 737 (1946).
- Conway and Norton, *Ind. Eng. Chem.*, **43**, p. 1433 (1951).
- Li et al., *J. Chem. Eng. Data*, **48**, pp. 621–624 (2003).
- Jeffreys, *J. Chem. Eng. Data*, **8**, p. 320 (1963).
- Bancroft and Hubard, *J. Am. Chem. Soc.*, **64**, p. 347 (1942).
- Durandet and Gladel, *Rev. Inst. Franc. Petrole*, **9**, p. 296 (1954).
- Coull and Hope, *J. Phys. Chem.*, **39**, 967 (1935).
- Frere, *Ind. Eng. Chem.*, **41**, p. 2365, (1949).
- Peschke and Sandler, *J. Chem. Eng. Data*, **40**(1), pp. 315–320 (1995).
- Eaglesfield, Kelly, and Short, *Ind. Chemist*, **29**, pp. 147, 243 (1953).
- Henty, McManamey, and Price, *J. Appl. Chem.*, **14**, p. 148 (1964).
- Denzler, *J. Phys. Chem.*, **49**, p. 358 (1945).
- Alberty and Washburn, *J. Phys. Chem.*, **49**, p. 4 (1945).
- Narashimhan, Reddy, and Chari, *J. Chem. Eng. Data*, **7**, p. 457 (1962).
- Pruett, Wash, and Desar, *Ind. Eng. Chem.*, **42**, p. 1210 (1950).
- Feki et al., *Can. J. Chem. Eng.*, **72**, pp. 939–944 (1994).
- Gladel and Lablaude, *Rev. Inst. Franc. Petrole*, **12**, p. 1236 (1957).
- Fuoss, *J. Am. Chem. Soc.*, **62**, p. 3183 (1940).
- Fowler and Noble, *J. Appl. Chem.*, **4**, p. 546 (1954).
- Hunter and Brown, *Ind. Eng. Chem.*, **39**, p. 1343 (1947).
- Senol, Alptekin, and Sayar, *J. Chem. Thermodyn.*, **27**, pp. 525–529 (1995).

feed composition used in the experiments along with the measured tie line compositions on a ternary diagram. The feed composition should lie on the tie line. For very low solute concentrations, this plot may be unrevealing. Alternatively, a plot of Y_i''/Z_i'' versus X_i''/Z_i'' (where Y_i'' is the mass fraction of component i in the extract phase, X_i'' is the mass fraction of component i in the raffinate phase, and Z_i'' is the mass fraction of component i in the total feed) should give a straight line that passes through the point (1, 1). The tie line data also may be checked for consistency by plotting the data in the form of a Hand plot or Othmer-Tobias plot, as described in "Tie Line Correlations," and looking for outliers. Another approach is to plot the partition ratio as a function of solute concentration and look for data points that deviate significantly from otherwise smooth trends. If the NRTL equation is used, refit all the binary data sets by using the same value for model parameter α . A value of 0.3 is recommended by Walas [*Phase Equilibria in Chemical Engineering* (Butterworth-Heinemann, 1985), p. 203] for nonaqueous systems, and a higher value of 0.4 is recommended for aqueous systems. Sorensen and Arlt [*Chemistry Data Series: Liquid-Liquid Equilibrium Data Collection*, Vol. V, pt. 1 (DECHEMA, 1979), p. 14] use a value of 0.2 for all their work. The particular value chosen appears to be less important than using the same value for all binaries of the same type (aqueous or nonaqueous). Try for a reasonable fit of the overall data, but be sure to focus on achieving a good fit of the data in the region most relevant to the application at hand.

TABLE OF SELECTED PARTITION RATIO DATA

Table 15-1 summarizes typical partition ratio data for selected systems.

PHASE EQUILIBRIUM DATA SOURCES

A comprehensive collection of phase equilibrium data (including vapor-liquid, liquid-liquid, and solid-liquid data) is maintained by a group headed by Prof. Juergen Gmehling at the University of Oldenburg, Germany. This collection, known as the Dortmund Data Bank, includes LLE measurements as well as NRTL and UNIQUAC fitted parameters. The data bank also includes a compilation of infinite-dilution activity coefficients. The LLE collection is available as a series of

books [Sorensen and Arlt, *Chemistry Data Series: Liquid-Liquid Equilibrium Data Collection, Binary Systems*, vol. V, pts. 1–4 (DECHEMA, 1979–1980)], as a proprietary database including retrieval and modeling software, and online by subscription. There also is a new online database offered by FIZ-Berlin Infotherm. Other sources of thermodynamic data include the IUPAC Solubility Data Series published by Oxford University Press, and compilations prepared by the Thermodynamics Research Center (TRC) in Boulder, Colo., a part of the Physical and Chemical Properties Division of the National Institute of Standards and Technology. An older but still useful data collection is that of Stephens and Stephens [*Solubilities of Inorganic and Organic Compounds*, vol. 1, pts. 1 and 2 (Pergamon, 1960)]. Also, a database of activity coefficients is included in the supporting information submitted with the article by Lazzaroni et al. [*Ind. Eng. Chem. Res.*, **44**(11), pp. 4075–4083 (2005)] and available from the publisher. A listing of the original sources is included. Additional sources of data are discussed by Skrzecz [*Pure Appl. Chem.* (IUPAC), **69**(5), pp. 943–950 (1997)].

RECOMMENDED MODEL SYSTEMS

To facilitate the study and comparison of various types of extraction equipment, Bart et al. [Chap. 3 in Godfrey and Slater, *Liquid-Liquid Extraction Equipment* (Wiley, 1994)] recommend several model systems. These include (1) water + acetone + toluene (high interfacial tension); (2) water + acetone + butyl acetate (moderate interfacial tension); and (3) water + succinic acid + *n*-butanol (low interfacial tension). All have solute partition ratios near $K = 1.0$. Misek, Berger, and Schröter [*Standard Test Systems for Liquid Extraction* (The Instn. of Chemical Engineers, 1985)] summarize phase equilibrium, viscosities, densities, diffusion coefficients, and interfacial tensions for these systems. Note that methyl isobutyl ketone + acetic acid + water was replaced with the water + acetone + butyl acetate system because of concerns over acetic acid dimerization and Marangoni instabilities. (See "Liquid-Liquid Dispersion Fundamentals.") For test systems with a partition ratio near $K = 10$, Bart et al. recommend (1) water + methyl isopropyl ketone + toluene (high interfacial tension) and (2) water + methyl isopropyl ketone + butyl acetate (medium interfacial tension) and give references to data sources. Bart et al. also recommend a number of systems involving reactive extractants.

SOLVENT SCREENING METHODS

A variety of methods may be used to estimate solvent properties as an aid to identifying useful solvents for a new application. Many of these methods focus on thermodynamic properties; a favorable partition ratio and low mutual solubility often are necessary for an economical extraction process, so ranking candidates according to thermodynamic properties provides a useful initial screen of the more promising candidates. Keep in mind, however, that other factors also must be taken into account when selecting a solvent, as discussed in "Desirable Solvent Properties" under "Introduction and Overview." When using the following methods, also note that the level of uncertainty may be fairly high. The uncertainty depends upon how closely the chemical system of interest resembles the systems used to develop the method.

USE OF ACTIVITY COEFFICIENTS AND RELATED DATA

Compilations of infinite-dilution activity coefficients, when available for the solute of interest, may be used to rank candidate solvents. Partition ratios at finite concentrations can be estimated from these data by extrapolation from infinite dilution using a suitable correlation equation such as NRTL [Eq. (15-25)]. Examples of these kinds of calculations are given by Walas [*Phase Equilibria in Chemical Engineering* (Butterworth-Heinemann, 1985)]. Most activity coefficients available in the literature are for small organic molecules and are derived from vapor-liquid equilibrium measurements or azeotropic composition data.

Partition ratios at infinite dilution can be calculated directly from the ratio of infinite-dilution activity coefficients for solute dissolved in the extraction solvent and in the feed solution, often providing a reasonable estimate of the partition ratio for dilute concentrations. Infinite-dilution

activity coefficients often are reported in terms of a van Laar binary interaction parameter [Smallwood, *Solvent Recovery Handbook* (McGraw-Hill, 1993)] such that

$$\ln \gamma_{ij}^{\infty} = \frac{A_{ij}}{RT} \quad (15-27)$$

$$K_i^{\circ} = \frac{\gamma_i^{\circ}}{\gamma_i^{\infty}} = \frac{\exp(A_{ij}/RT)}{\exp(A^{*ij}/RT)} \quad (15-28)$$

where $*$ denotes the extraction solvent phase. For example, the partition ratio for transferring acetone from water into benzene at 25°C and dilute conditions may be estimated as follows: For acetone dissolved in benzene $A_{ij}/RT = 2.47$, and for acetone dissolved in water $A_{ij}/RT = 2.29$. Then $K_i^{\circ} = e^{2.29} e^{0.47} = 9.87/1.6 = 6.17$ (mol/mol) $\cong 1.4$ (wt/wt). Briggs and Comings [*Ind. Eng. Chem.*, **35**(4), pp. 411–417 (1943)] report experimental values that range between 1.06 and 1.39 (wt/wt).

For screening candidate solvents, comparing the magnitude of the activity coefficient for the solute of interest dissolved in the solvent phase often is a good way to rank solvents, since a smaller value of $\gamma_{i,\text{solvent}}$ indicates a higher K value. Solubility data available for a given solute dissolved in a range of solvents also can be used to rank solvents, since higher solubility in a candidate solvent indicates a more attractive interaction (a lower activity coefficient) and therefore a higher partition ratio.

ROBBINS' CHART OF SOLUTE-SOLVENT INTERACTIONS

When available data are not sufficient (the most common situation), Robbins' chart of functional group interactions (Table 15-2) is a useful

TABLE 15-2 Robbins' Chart of Solute-Solvent Interactions*

Solute class		Solvent class											
		1	2	3	4	5	6	7	8	9	10	11	12
H donor groups													
1	Phenol	0	0	-	0	-	-	-	-	-	-	+	+
2	Acid, thiol	0	0	-	0	-	-	0	0	0	0	+	+
3	Alcohol, water	-	-	0	+	+	0	-	-	+	+	+	+
4	Active H on multihalogen paraffin	0	0	+	0	-	-	-	-	-	-	0	+
H acceptor groups													
5	Ketone, amide with no H on N, sulfone, phosphine oxide	-	-	+	-	0	+	+	+	+	+	+	+
6	Tertiary amine	-	-	0	-	+	0	+	+	0	+	0	0
7	Secondary amine	-	0	-	-	+	+	0	0	0	0	0	+
8	Primary amine, ammonia, amide with 2H on N	-	0	-	-	+	+	0	0	+	+	+	+
9	Ether, oxide, sulfoxide	-	0	+	-	+	0	0	+	0	+	0	+
10	Ester, aldehyde, carbonate, phosphate, nitrate, nitrite, nitrile, intramolecular bonding, e.g., <i>o</i> -nitrophenol	-	0	+	-	+	+	0	+	+	0	+	+
11	Aromatic, olefin, halogen aromatic, multihalogen paraffin without active H, monohalogen paraffin	+	+	+	0	+	0	0	+	0	+	0	0
Non-H-bonding groups													
12	Paraffin, carbon disulfide	+	+	+	+	+	0	+	+	+	+	0	0

*From Robbins, *Chem. Eng. Prog.*, **76**(10), pp. 58–61 (1980), by permission. Copyright 1980 AIChE.

guide to ranking general classes of solvents. It is based on an evaluation of hydrogen bonding and electron donor-acceptor interactions for 900 binary systems [Robbins, *Chem. Eng. Prog.*, **76** (10), pp. 58–61 (1980)]. The chart includes 12 general classes of functional groups, divided into three main types: hydrogen-bond donors, hydrogen-bond acceptors, and non-hydrogen-bonding groups. Compounds representative of each class include (1) phenol, (2) acetic acid, (3) pentanol, (4) dichloromethane, (5) methyl isobutyl ketone, (6) triethylamine, (7) diethylamine, (8) *n*-propylamine, (9) ethyl ether, (10) ethyl acetate, (11) toluene, and (12) hexane. Robbins' chart is applicable to any process where liquid-phase activity coefficients are important, including liquid-liquid extraction, extractive distillation, azeotropic distillation, and crystallization from solution. The activity coefficient in the liquid phase is common to all these separation processes.

Robbins' chart predicts positive, negative, or zero deviations from ideal behavior for functional group interactions. For example, consider an application involving extraction of acetone from water into chloroform solvent. Acetone contains a ketone carbonyl group which is a hydrogen acceptor and a member of solute class 5 according to Table 15-2. Chloroform contains a hydrogen donor group (solvent class 4). The solute class 5 and solvent class 4 interaction in Table 15-2 is shown to give a negative deviation from ideal behavior. This indicates an attractive interaction which enhances the liquid-liquid partition ratio. Other classes of solvents shown in Table 15-2 that yield a negative deviation with a ketone (class 5) are classes 1 and 2 (phenolics and acids). Other ketones (solvent class 5) are shown to be compatible with acetone (solute class 5) and tend to give activity coefficients near 1.0, that is, nearly ideal behavior. The solvent classes 6 through 12 tend to provide repulsive interactions between these groups and acetone, and so they are not likely to exhibit partition ratios for ketones as high as the other solvent groups do.

Most of the classes in Table 15-2 are self-explanatory, but some can use additional definition. Class 4 includes halogenated solvents that have highly active hydrogens as described by Ewell, Harrison, and Berg [*Ind. Eng. Chem.*, **36**(10), pp. 871–875 (1944)]. These are molecules that have two or three halogen atoms on the same carbon as a hydrogen atom, such as dichloromethane, trichloromethane, 1,1-dichloroethane, and 1,1,2,2-tetrachloroethane. Class 4 also includes molecules that have one halogen on the same carbon atom as a hydrogen atom and one or more halogen atoms on an adjacent carbon atom, such as 1,2-dichloroethane and 1,1,2-trichloroethane.

Apparently, the halogens interact intramolecularly to leave the hydrogen atom highly active. Monohalogen paraffins such as methyl chloride and ethyl chloride are in class 11 along with multihalogen paraffins and olefins without active hydrogen, such as carbon tetrachloride and perchloroethylene. Chlorinated benzenes are also in class 11 because they do not have halogens on the same carbon as a hydrogen atom. Intramolecular bonding on aromatics is another fascinating interaction which gives a net result that behaves much as does an ester group, class 10. Examples of this include *o*-nitrophenol and *o*-hydroxybenzaldehyde (salicylaldehyde). The intramolecular hydrogen bonding is so strong between the hydrogen donor group (phenol) and the hydrogen acceptor group (nitrate or aldehyde) that the molecule acts as an ester. One result is its low solubility in hot water. By contrast, the *para* derivative is highly soluble in hot water.

ACTIVITY COEFFICIENT PREDICTION METHODS

Robbins' chart provides a useful qualitative indication of interactions between classes of molecules but does not give quantitative differences within each class. For this, a number of methods are available. Many have been implemented in commercial and university-supported software packages. Perhaps the most widely used of these is the UNIFAC group contribution method [Fredenslund et al., *Ind. Eng. Chem. Proc. Des. Dev.*, **16**(4), pp. 450–462 (1977); and Wittig et al., *Ind. Eng. Chem. Res.*, **42**(1), pp. 183–188 (2003). Also see Jakob et al., *Ind. Eng. Chem. Res.*, **45**, pp. 7924–7933 (2006)]. The use of UNIFAC for estimating LLE is discussed by Gupte and Danner [*Ind. Eng. Chem. Res.*, **26**(10), pp. 2036–2042 (1987)] and by Hooper, Michel, and Prausnitz [*Ind. Eng. Chem. Res.*, **27**(11), pp. 2182–2187 (1988)]. Vakili-Nezhand, Modarress, and Mansoori [*Chem. Eng. Technol.*, **22**(10), pp. 847–852 (1999)] discuss its use for representing a complex feed containing a large number of components for which available LLE data are incomplete.

UNIFAC calculates activity coefficients in two parts:

$$\ln \gamma_i = \ln \gamma_i^C + \ln \gamma_i^R \quad (15-29)$$

The combinatorial part $\ln \gamma_i^C$ is calculated from pure-component properties. The residual part $\ln \gamma_i^R$ is calculated by using binary interaction parameters for solute-solvent group pairs determined by fitting phase equilibrium data. Both parts are based on the UNIQUAC set

of equations. With this approach, a molecule is treated as an assembly of various groups of atoms. Compounds for which phase equilibrium already has been measured are used to regress constants for these different groups. These constants are then used in a correlation to predict properties for a new molecule. There are several UNIFAC parameter sets available. It is important to use a consistent set of parameters since the different parameter databases are not necessarily compatible.

A number of methods based on regular solution theory also are available. Only pure-component parameters are needed to make estimates, so they may be applied when UNIFAC group-interaction parameters are not available. The Hansen solubility parameter model divides the Hildebrand solubility parameter into three parts to obtain parameters δ_d , δ_p , and δ_h accounting for nonpolar (dispersion), polar, and hydrogen-bonding effects [Hansen, *J. Paint Technol.*, **39**, pp. 104–117 (1967)]. An activity coefficient may be estimated by using an equation of the form

$$\ln \gamma_i = \frac{v_i}{RT} \left\{ \left(\bar{\delta}_i - \delta_i^i \right)^2 + 0.25 \left[\left(\bar{\delta}_p - \delta_p^i \right)^2 + \left(\bar{\delta}_h - \delta_h^i \right)^2 \right] \right\} \quad (15-30)$$

where $\bar{\delta}$ is the solubility parameter for the mixture, δ^i is the solubility parameter for component i , v is molar volume, R is the universal gas constant, and T is absolute temperature [Frank, Downey, and Gupta, *Chem. Eng. Prog.*, **95**(12), pp. 41–61 (1999)]. The Hansen model has been used for many years to screen solvents and facilitate development of product formulations. Hansen parameters have been determined for more than 500 solvents [Hansen, *Hansen Solubility Parameters: A User's Handbook* (CRC, 2000); and *CRC Handbook of Solubility Parameters and Other Cohesion Parameters*, 2d ed., Barton, ed. (CRC, 1991)].

MOSCED, another modified regular solution model, utilizes two parameters to represent hydrogen bonding: one for proton donor capability (acidity) and one for proton acceptor capability (basicity) [Thomas and Eckert, *Ind. Eng. Chem. Proc. Des. Dev.*, **23**(2), pp. 194–209 (1984)]. This provides a more realistic representation of hydrogen bonding that allows more accurate modeling of a wider range of solvents, and unlike the Hansen model, MOSCED can predict negative deviations from ideal solution (activity coefficients less than 1.0). MOSCED calculates infinite-dilution activity coefficients by using an equation of the general form

$$\ln \gamma_{21}^{\infty} = \frac{v_2}{RT} \left[(\lambda_1 - \lambda_2)^2 + \frac{q_1^2 q_2^2 (\tau_1 - \tau_2)^2}{\psi_1} + \frac{(\alpha_1 - \alpha_2)(\beta_1 - \beta_2)}{\xi_1} \right] \quad (15-31)$$

There are five adjustable parameters per molecule: λ , the dispersion parameter; q , the induction parameter; τ , the polarity parameter; α , the hydrogen-bond acidity parameter; and β , the hydrogen-bond basicity parameter. The induction parameter q often is set to a value of 1.0, yielding a four-parameter model. The terms ψ_1 and ξ_1 are asymmetry factors calculated from the other parameters. A database of parameter values for 150 compounds, determined by regression of phase equilibrium data, is given by Lazzaroni et al. [*Ind. Eng. Chem. Res.*, **44**(11), pp. 4075–4083 (2005)]. An application of MOSCED in the study of liquid-liquid extraction is described by Escudero, Cabezas, and Coca [*Chem. Eng. Comm.*, **173**, pp. 135–146 (1999)]. Also see Frank et al., *Ind. Eng. Chem. Res.*, **46**, pp. 4621–4625 (2007).

Another method for estimating activity coefficients is described by Chen and Song [*Ind. Eng. Chem. Res.*, **43**(26), pp. 8354–8362 (2004); **44**(23), pp. 8909–8921 (2005)]. This method involves regression of a small data set in a manner similar to the way the Hansen and MOSCED models typically are used. The model is based on a modified NRTL framework called NRTL-SAC (for segment activity coefficient) that utilizes only pure-component parameters to represent polar, hydrophobic, and hydrophilic segments of a molecule. An electrolyte parameter may be added to characterize ion-ion and ion-molecule interactions attributed to ionized segments of species in solution. The resulting model may be used to estimate activity coefficients and related properties for mixtures of nonionic organics plus electrolytes in aqueous and nonaqueous solvents.

A method developed by Meyer and Maurer [*Ind. Eng. Chem. Res.*, **34**(1), pp. 373–381 (1995)] uses the linear solvation energy relationships (LSER) model [Taft et al., *Nature*, **313**, p. 384 (1985); and Taft et al.,

J. Pharma Sci., **74**, pp. 807–814 (1985)] to estimate infinite-dilution partition ratios for solute distributed between water and an organic solvent. The model uses 36 generalized parameters and four solvatochromic parameters to characterize a given solute. The solvatochromic parameters are α (acidity), β (basicity), π (polarity), and δ (polarizability). Another method utilizing LSER concepts is the SPACE model for estimating infinite-dilution activity coefficients [Hait et al., *Ind. Eng. Chem. Res.*, **32**(11), pp. 2905–2914 (1993)]. Also see Abraham, Ibrahim, and Zissimos, *J. Chromatography*, **1037**, pp. 29–47 (2004).

The thermodynamic methods described above glean information from available data to make estimates for other systems. As an alternative approach, quantum chemistry calculations and molecular simulation methods are finding more and more use in engineering applications [Gupta and Olson, *Ind. Eng. Chem. Res.*, **42**(25), pp. 6359–6374 (2003); and Chen and Mathias, *AIChE J.*, **48**(2), pp. 194–200 (2002)]. These methods minimize the need for data; however, the computational effort and specialized expertise required to use them generally are higher, and the accuracy of the results may not be known. An important method gaining increasing application in the chemical industry is the conductorlike screening model (COSMO) introduced by Klamt and colleagues [Klamt, *J. Phys. Chem.*, **99**, p. 2224 (1995); Klamt and Eckert, *Fluid Phase Equil.*, **172**, pp. 43–72 (2000); Eckert and Klamt, *AIChE J.*, **48**(2), pp. 369–385 (2002); and Klamt, *From Quantum Chemistry to Fluid Phase Thermodynamics and Drug Design* (Elsevier, 2005)]. Also see Grensemann and Gmehling, *Ind. Eng. Chem. Res.*, **44**(5), pp. 1610–1624 (2005). This method utilizes computational quantum mechanics to calculate a two-dimensional electron density profile to characterize a given molecule. This profile is then used to estimate phase equilibrium using statistical mechanics and solvation theory. The Klamt model is called COSMO-RS (for realistic solvation). A similar model is COSMO-SAC (segment activity coefficient) published by Lin and Sandler [*Ind. Eng. Chem. Res.*, **41**(5), pp. 899–913, 2332 (2002)]. Databases of electron density profiles (sigma profiles) are available from a number of vendors and universities. For example, a sigma-profile database of more than 1000 molecules is available from the Virginia Polytechnic Institute and State University [Mullins et al., *Ind. Eng. Chem. Res.*, **45**(12), pp. 4389–4415 (2006)]. Once determined, the profiles allow convenient calculation of phase equilibria using available software. An application of COSMO-RS to predict liquid-liquid equilibria is discussed by Banerjee et al. [*Ind. Eng. Chem. Res.*, **46**(4), pp. 1292–1304 (2007)].

METHODS USED TO ASSESS LIQUID-LIQUID MISCIBILITY

In evaluating potential solvents, it is important to determine whether a given candidate will exhibit sufficiently limited miscibility with the feed liquid. Mutual solubility data for organic-solvent + water mixtures often are listed somewhere in the literature and can be obtained through a literature search. (See “Phase Equilibrium Data Sources” under “Thermodynamic Basis for Liquid-Liquid Extraction.”) However, data often are not available for pairs of organic solvents and for multicomponent mixtures showing the effect of dissolved solutes. In these cases, estimates can provide useful guidance. Note, however, that the available estimation methods normally provide limited accuracy, so it is best to measure these properties for the more promising candidates.

Phase splitting behavior can be inferred from activity coefficients. In general, partial miscibility will not occur whenever the infinite-dilution activity coefficients of the components in solution are less than 7. This is a reliable rule but it depends upon the quality of the activity coefficient data or estimates. If γ^{∞} for any one of the components is greater than 7, then partial miscibility may occur at some finite composition. The criterion $\gamma^{\infty} > 7$ often is cited as a general rule indicating a partially miscible system, but there are many exceptions. For detailed discussion, see Prausnitz, Lichtenthaler, and Gomez de Azevedo, *Molecular Thermodynamics of Fluid-Phase Equilibria*, 3d ed. (Prentice-Hall, 1999). Solubility parameters also can be used to assess miscibility [*Handbook of Solubility Parameters and Other Cohesion Parameters*, 2d ed., Barton, ed. (CRC, 1991)].

As a complementary alternative, Godfrey's data-based method [*CHEMTECH*, **2**(6), pp. 359–363 (1972)] provides a quick way of qualitatively assessing whether an organic-solvent pair of interest is likely to

TABLE 15-3 Godfrey Miscibility Numbers

Acetal	23	Chloroform	19
Acetic acid	14	1-Chloronaphthalene	22
Acetic anhydride	12, 19	3-Chlorophenetole	15, 20
Acetol	8	2-Chlorophenol	16
Acetol acetate	10	2-Chloropropane	23
Acetol formate	9, 17	2-Chlorotoluene	20
Acetone	15, 17	Coconut oil	29
Acetonitrile	11, 17	<i>p</i> -Cresol	14
Acetophenone	15, 18	4-Cyano-2,2-dimethylbutyraldehyde	11, 18
<i>N</i> -Acetylmorpholine	11	Cyclohexane	28
Acrylonitrile	14, 18	Cyclohexanecarboxylic acid	16
Adiponitrile	8, 19	Cyclohexanol	16
Allyl alcohol	14	Cyclohexanone	17
Allyl ether	22	Cyclohexene	26
2-Allyloxyethanol	13	Cyclooctane	29
2-Aminoethanol	2	Cyclooctene	27
2-(2-Aminoethoxy) ethanol	2	<i>p</i> -Cymene	25
Aminoethylethanolamine	5	Decalin	29
1-(2-Aminoethyl) piperazine	12	Decane	29
1-Amino-2-propanol	6	1-Decanol	18
Aniline	12	1-Decene	29
Anisole	20	Diacetone alcohol	14
Benzaldehyde	15, 19	Diallyl adipate	21
Benzene	21	1,2-Dibromobutane	22
Benzonitrile	15, 19	1,4-Dibromobutane	21
Benzyl alcohol	13	Dibromoethane	19
Benzyl benzoate	15, 21	1,2-Dibromopropane	21
Bicyclohexyl	29	1,2-Dibutoxyethane	25
Bis(2-butoxyethyl) ether	23	<i>N,N</i> -Dibutylacetamide	17
Bis(2-chloroethyl) ether	20	Dibutyl ether	26
Bis(2-chloroisopropyl) ether	20	Dibutyl maleate	22
Bis(2-ethoxyethyl) ether	15	Dibutyl phthalate	22
Bis(2-hydroxyethyl) thiodipropionate	5	1,3-Dichloro-2-propanol	12
Bis(2-hydroxypropyl) maleate	6	Dichloroacetic acid	13
Bis(2-methoxyethyl) ether	15, 17	1,2-Dichlorobenzene	21
Bis(2-methoxyethyl) phthalate	11, 19	1,4-Dichlorobutane	20
Bromobenzene	21	1,1-Dichloroethane	20
1-Bromobutane	23	1,2-Dichloroethane	20
Bromocyclohexane	25	<i>cis</i> -1,2-Dichloroethylene	20
1-Bromodecane	27	<i>trans</i> -1,2-Dichloroethylene	21
1-Bromododecane	27	Dichloromethane	20
Bromoethane	21	1,2-Dichloropropane	20
1-Bromohexane	24	1,3-Dichloropropane	20
1-Bromo-3-methylbutane	24	Dicyclopentadiene	26
1-Bromooctane	26	Didecyl phthalate	26
2-Bromooctane	26	Diethanolamine	1
1-Bromotetradecane	29	Diethoxydimethylsilane	26
1,2-Butanediol	6	<i>N,N</i> -Diethylacetamide	14
1,3-Butanediol	4	Diethyl adipate	19
1,4-Butanediol	3	Diethyl carbonate	21
2,3-Butanediol	12, 17	Diethyl ketone	18
1-Butanol	15	Diethyl oxalate	14, 20
2-Butanol	16	Diethyl phthalate	13, 20
<i>t</i> -Butanol	16	Diethyl sulfate	12, 21
2-Buten-1-ol	15	Diethylene glycol	5
2-Buten-1,4-diol	3	Diethylene glycol diacetate	12, 19
2-Butoxyethanol	16	Diethylenetriamine	9
2-(2-Butoxyethoxy) ethanol	15	Diethyl ether	23
Butyl acetate	22	2,5-Dihydrofuran	17
Butyl formate	19	Di-isobutyl ketone	23
Butyl methacrylate	23	Di-isopropyl ketone	23
Butyl oleate	26	Di-isopropylbenzene	25
Butyl sulfide	26	1,2-Dimethoxyethane	17
Butylaloxime	15	<i>N,N</i> -Dimethylacetamide	13
Butyric acid	16	<i>N,N</i> -Dimethylacetoacetamide	10
Butyric anhydride	21	2-Dimethylaminoethanol	14
Butyrolactone	10	Dimethyl carbonate	14, 19
Butyronitrile	14, 19	Dimethylformamide	12
Carbon disulfide	26	Dimethyl maleate	12, 19
Carbon tetrachloride	24	Dimethyl malonate	11, 19
Castor oil	25	Dimethyl phthalate	12, 19
1-Chlorobutane	23	1,4-Dimethylpiperazine	16
2-Chloroethanol	11	2,5-Dimethylpyrazine	16
3-Chloro-1,2-propanediol	4	Dimethyl sebacate	22
1-Chloro-2-propanol	14	2,4-Dimethylsulfonate	12, 17
Chlorobenzene	21	Dimethyl sulfoxide	9
1-Chlorobutane	23	Dioctyl phthalate	24
1-Chlorodecane	27	1,4-Dioxane	17

TABLE 15-3 Godfrey Miscibility Numbers (Continued)

1,4-Dioxene	15, 19	Isobromobutane	23
Dipentene	26	2-Isobutoxyethanol	15, 17
Dipentyl ether	26	Isobutyl acetate	21
Diphenyl ether	22	Isobutyl isobutyrate	23
Diphenyl methane	21	Isobutanol	15
Dipropyl sulfone	12, 17	Isophorone	18
Dipropylene glycol	11	Isoprene	25
Dodecane	29	Isopropenyl acetate	19
1-Dodecanol	18	Isopropyl acetate	19
1-Dodecene	29	Isopropyl ether	26
Epichlorohydrin	14, 19	Isopropylbenzene	24
Epoxyethylbenzene	15, 19	Kerosene	30
Ethanesulfonic acid	5	2-Mercaptoethanol	9
Ethanol	14	Mesityl oxide	18
2-Ethoxyethanol	14	Mesitylene	24
2-(2-Ethoxy) ethanol	13	Methacrylonitrile	15, 19
2-Ethoxyethylacetate	15, 19	Methanesulfonic acid	4
Ethyl acetate	19	Methanol	12
Ethyl acetoacetate	13, 19	5-Methoxazolidinone	7
Ethyl benzene	24	Methoxyacetic acid	8
Ethyl benzoate	21	Methoxyacetoneitrile acetamide	11, 19
2-Ethylbutanol	17	3-Methoxybutanol	14
Ethyl butyrate	22	2-Methoxyethanol	13
Ethylene carbonate	6, 17	2-(2-Methoxyethoxy) ethanol	12
Ethylenediamine	9	2-Methoxyethyl acetate	14, 17
Ethylene glycol	2	2-Methoxyethyl methoxyacetate	15
Ethylene glycol bis(methoxyacetate)	9, 17	1-[2-Methoxy-1-methylethoxy]-2-propanol	15
Ethylene glycol diacetate	12, 19	3-Methoxy-1,2-propanediol	5
Ethylene glycol diformate	8, 17	1-Methoxy-2-propanol	15
Ethylene monobiscarbonate	10, 19	3-Methoxypropionitrile	11, 17
Ethylformamide	9	3-Methoxypropylamine	15
Ethyl formate	15, 19	3-Methoxypropylformamide	10
2-Ethyl-1,3-hexanediol	14, 17	Methyl acetate	15, 17
2-Ethylhexanol	17	Methylal	19
Ethyl hexoate	23	2-Methylaminoethanol	11
Ethyl lactate	14	2-Methyl-1-butene	27
N-Ethylmorpholine	16	2-Methyl-2-butene	26
Ethyl orthoformate	23	Methylchloroacetate	13, 19
Ethyl propionate	21	Methylcyanoacetate	8, 17
2-Ethylthioethanol	13	Methylcyclohexane	29
Ethyl trichloroacetate	21	1-Methylcyclohexene	27
Fluorobenzene	20	Methylcyclopentane	28
1-Fluoronaphthalene	21	Methyl ethyl ketone	17
Formamide	3	Methyl formate	14, 19
Formic acid	5	2,2'-Methyliminodiethanol	8
N-Formylmorpholine	10	Methyl isoamyl ketone	19
Furan	20	Methyl isobutyl ketone	19
Furfural	11, 17	Methyl methacrylate	20
Furfuryl alcohol	11	Methyl methoxyacetate	13
Glycerol (glycerin)	1	N-Methylmorpholine	16
Glycerol carbonate	3	1-Methylnaphthalene	22
Glycidyl phenyl ether	13, 19	Methyl oleate	26
Heptane	29	2-Methylpentane	29
1-Heptanol	17	3-Methylpentane	29
3-Heptanone	22	4-Methyl-2-pentanol	17
4-Heptanone	23	2-Methyl-2,4-pentanediol	14
1-Heptene	28	4-Methyl-1-pentene	28
Hexachlorobutadiene	26	cis-4-Methyl-2-pentene	27
Hexadecane	30	N-Methyl-2-pyrrolidinone	13
1-Hexadecene	29	Methyl stearate	26
Hexamethylphosphoramide	15	α -Methylstyrene	23
Hexane	29	3-Methylsulfolane	10, 17
2,5-Hexanediol	5	Mineral spirits	29
2,5-Hexanedione	12, 17	Morpholine	14
1,2,6-Hexanetriol	2	Nitrobenzene	14, 20
1-Hexanol	17	Nitroethane	13, 20
Hexanoic acid	17	Nitromethane	10, 19
1-Hexene	27	2-Nitropropane	15, 20
2-Hydroxyethyl carbamate	2	1-Nonanol	17
2-Hydroxyethylformamide	1	Nonylphenol	17
2-Hydroxyethylmethacrylate	12	1-Octadecene	30
1-(2-Hydroxyethoxy)-2-propanol	8	1,7-Octadiene	27
2-Hydroxypropyl carbamate	3	Octane	29
Hydroxypropyl methacrylate	14, 17	1-Octanethiol	26
Iodobenzene	22	1-Octanol	17
Iodoethane	22	2-Octanol	17
Iodomethane	21	2-Octanone	22
Isoamylbenzene	25	1-Octene	28

TABLE 15-3 Godfrey Miscibility Numbers (Concluded)

<i>cis</i> -2-Octene	27	Tetrahydrofuran	17
<i>trans</i> -2-Octene	28	Tetrahydrofurfuryl alcohol	13
3,3'-Oxydipropionitrile	6	Tetrahydrothophene	21
Paraldehyde	15, 19	Tetralin	24
Polyethylene glycol PEG-200	7	Tetramethylsilane	29
Polyethylene glycol PEG-300	8	Tetramethylurea	15
Polyethylene glycol PEG-600	8	Tetrapropylene	29
1,3-Pentadiene	25	1,1-Thiodi-2-propanol	8
Pentaethylene glycol	7	2,2'-Thiodiethanol	4
Pentaethylenehexamine	9	3,3'-Thiodipropionitrile	6, 19
Pentafluoroethanol	9	Thiophene	20
1,5-Pentanediol	3	Toluene	23
2,4-Pentanedione	12, 18	Triacetin	11, 19
1-Pentanol	17	Tributylphosphate	18
<i>t</i> -Pentanol	16	Tributylamine	28
Petrolatum (C ₁₄ -C ₁₆ alkanes)	31	1,2,4-Trichlorobenzene	24
Phenetole	20	1,1,1-Trichloroethane	22
2-Phenoxyethanol	12	1,1,2-Trichloroethane	19
1-Phenoxy-2-propanol	13, 17	Trichloroethylene	20
Phenyl acetate	23	1,1,2-Trichloro-2,2,2-trifluoroethane	27
Phenylacetonitrile	12, 19	1,2,3-Trichloropropane	20
<i>N</i> -Phenylethanolamine	10	Tricresyl phosphate	21
2-Picoline	16	Triethanolamine	2
Polypropyleneglycol PPG-1000	14, 23	Triethyl phosphate	14
Polypropyleneglycol PPG-400	14	Triethylamine	26
Propanediamine	11, 11	Triethylbenzene	25
1,2-Propanediol	4	Triethylene glycol	6
1,3-Propanediol	3	Triethylene glycol monobutyl ether	14
Propanesulfone	7, 19	Triethylene glycol monomethyl ether	13
1-Propanol	15	Triethylenetetramine	9
2-Propanol	15	Triisobutylene	29
Propionic acid	15	Trimethyl borate	16
Propionitrile	13, 17	Trimethyl nitrilotripropionate	12
Propyl acetate	19	Trimethyl phosphate	10
Propylene carbonate	9, 17	2,4,4-Trimethyl-1-pentane	27
Propylene oxide	17	2,4,4-Trimethyl-2-pentane	27
Pyridine	16	Trimethylboroxin	12, 17
2-Pyrrolidinone	10	2,2,4-Trimethylpentene	29
Styrene	22	Tripropylamine	26
Sulfolane	9, 17	Tripropylene glycol	12
1,1,2,2-Tetrabromoethane	11, 19	Vinyl acetate	20
1,1,2,2-Tetrachloroethane	19	Vinyl butyrate	22
Tetrachloroethylene	25	4-Vinylcyclohexene	26
Tetradecane	30	Naphtha	29
1-Tetradecene	29	<i>m</i> -Xylene	23
Tetraethyl orthosilicate	23	<i>o</i> -Xylene	23
Tetraethylene glycol	7	<i>p</i> -Xylene	24
Tetraethylenepentamine	9		

Reprinted from Godfrey, *CHEMTECH*, 2(6), pp. 359-363 (1972), with permission. Published 1972 by the American Chemical Society.

exhibit partial miscibility at near-ambient temperatures. Godfrey assigned miscibility numbers to approximately 400 organic solvents (Table 15-3) by observing their miscibility in a series of 31 standard solvents (Table 15-4). He then showed that the general miscibility behavior of a given solvent pair can be predicted by comparing their miscibility numbers. Godfrey's rules, slightly modified, are summarized below:

1. If $\Delta \leq 12$, where Δ is the difference in miscibility numbers, the solvents are likely to be miscible in all proportions at 25°C.
2. If $13 \leq \Delta \leq 15$, the solvents may be only partially miscible with an upper critical solution temperature (UCST) between 25 and 50°C. This is a borderline case. If the binary mixture is miscible, then adding a relatively small amount of water likely will induce phase splitting.
3. If $\Delta = 16$, the solvents are likely to exhibit a UCST between 25 and 75°C.
4. If $\Delta \geq 17$, the solvents are likely to exhibit a UCST above 75°C.

About 15 percent of the solvents in Table 15-3 have dual miscibility numbers A and B because the appropriate difference in miscibility numbers depends upon which end of the hydrophobic-lipophilic scale is being considered. If one of the solvents has dual miscibility numbers A and B and the other has a single miscibility number C , then Δ should be calculated as follows:

5. If $C > B$, then the solvent having miscibility number C is somewhat more lipophilic than the solvent having numbers A and B . At

this end of the lipophilicity scale, the number A characterizes the solvent's miscibility behavior. Apply rules 1 through 3 above, using $\Delta = C - A$.

6. If $C < A$, then the solvent having miscibility number C is somewhat less lipophilic than the solvent with numbers A and B . At this end of the lipophilicity scale, the number B characterizes the solvent's miscibility behavior. Apply rules 1 through 3, using $\Delta = B - C$.

7. If $A \leq C \leq B$, then evaluate $\Delta = C - A$ and $\Delta = B - C$ and use the larger of the Δ values in applying rules 1 through 3. Such a mixture is likely to be miscible in all proportions at 25°C.

8. If both members of a solvent pair have dual miscibility numbers, then the pair is likely to be miscible in all proportions at 25°C.

If a compound of interest is not listed in Table 15-3 or 15-4, a compound of the same type or class may help to gauge its miscibility behavior. In cases where Godfrey's rules indicate that partial miscibility is likely, whether phase splitting actually occurs depends upon the composition of the mixture and the temperature. The composition may be close to but still outside the two-liquid-phase region on a temperature-composition diagram.

Godfrey's method is a useful guide for compounds that exhibit behavior similar to the 31 standard solvents used to define miscibility numbers. The method deals with the common situation in which a mixture exhibits a UCST; i.e. solubility tends to increase with

233a, AIChE National Meeting, Austin, Tex. (2004); and Van Dyk and Nieuwoudt, *Ind. Eng. Chem. Res.*, **39**(5), pp. 1423–1429 (2000)]. Similar programs have been written to facilitate identification of alternative solvents or solvent blends as replacements for a given solvent, by attempting to identify compounds that match the physical properties of the solvent the user wishes to replace. An example is the PARIS II program developed by the U.S. Environmental Protection Agency [Cabezas, Harten, and Green, *Chem. Eng. Magazine*, pp. 107–109 (March 2000)].

HIGH-THROUGHPUT EXPERIMENTAL METHODS

In addition to the methods described above, it may be useful to devise a rapid experimental method for screening solvents and extraction conditions. High-throughput methods are designed to measure a key property and automatically carry out tens or hundreds

of experiments in a short time. An example involves automation of liquid-liquid extraction using a 96-well sample plate and a robotic liquid-handling workstation in conjunction with automated liquid chromatography for analysis [Peng et al., *Anal. Chem.*, **72**(2), pp. 261–266 (2000)]. The authors developed this method to purify libraries of compounds for accelerated discovery of active compounds (such as new pharmaceuticals); however, the same approach may prove useful for screening solvents for a particular extraction application. Another paper describes a high throughput screening method for rapid optimization of aqueous two-phase extraction applications [Bensch et al., *Chem. Eng. Sci.*, **62**, pp. 2011–2021 (2007)]. For a review of high-throughput methods in general, see Murray, *Principles and Practice of High Throughput Screening* (Blackwell, 2005). The automated methods described in “Liquid-Liquid Equilibrium Experimental Methods” under “Thermodynamic Basis for Liquid-Liquid Extraction” also may be useful for screening solvents.

LIQUID DENSITY, VISCOSITY, AND INTERFACIAL TENSION

GENERAL REFERENCES: See Sec. 2, “Prediction and Correlation of Physical Properties,” and Rosen, *Surfactants and Interfacial Phenomena*, 3d ed. (Wiley, 2004); Hartland, *Surface and Interfacial Phenomena* (Dekker, 2004); and Poling, Prausnitz, and O’Connell, *The Properties of Gases and Liquids*, 5th ed. (McGraw-Hill, 2000).

The utility of liquid-liquid extraction as a separation tool depends upon both phase equilibria and transport properties. The most important physical properties that influence transport properties are liquid-liquid interfacial tension, liquid density, and viscosity. These properties influence solute diffusion and the formation and coalescence of drops, and so are critical factors affecting the performance of liquid-liquid contactors and phase separators.

DENSITY AND VISCOSITY

Many handbooks, including this one, contain an extensive compilation of liquid density data. These same sources often include liquid viscosity data, although fewer experimental data may be available for a particular compound. Available data compilations include those by Wypych, *Handbook of Solvents* (ChemTech, 2001); Wypych, *Solvents Database*, CD-ROM (ChemTec, 2001); Yaws, *Thermodynamic and Physical Property Data*, 2d ed. (Gulf, 1998); and Flick, *Industrial Solvents Handbook*, 5th ed. (Noyes, 1998). In addition, viscosity data for C₁–C₂₈ organic compounds have been compiled by Yaws in *Handbook of Viscosity*, vols. 1–3 (Elsevier, 1994). Density and viscosity data also are available from the Thermodynamics Research Center at the National Institute of Standards and Technology (Boulder, Colo.) and from the DIPPR physical property databank of AIChE.

Methods for estimating density and viscosity are reviewed in Sec. 2, “Prediction and Correlation of Physical Properties,” and in the book by Poling, Prausnitz, and O’Connell, *The Properties of Gases and Liquids*, 5th ed. (McGraw-Hill, 2000). However, it is best to measure density and viscosity in the laboratory whenever possible. The methods used to measure viscosity are described in numerous books including *Measurement of Transport Properties of Fluids*, vol. 3, Wakeham, Nagashima, and Sengers, eds. (Blackwell, 1991); and Leblanc, Secco, and Kostic, “Viscosity Measurement,” Chap. 30 in *Measurement, Instrumentation, and Sensors Handbook*, Webster, ed. (CRC Press, 1999). A new instrument introduced by the Anton Paar Company utilizes Stabinger’s methods for simultaneous measurement of viscosity and density [American Society for Testing and Materials, ASTM D7042-04 (2005)].

INTERFACIAL TENSION

Typical values of interfacial tension are listed in Tables 15-6 and 15-7. Refer to the references listed in these tables for the full data sets and for data on other mixtures. Table 15-6 shows typical values for organic + water binary mixtures. Table 15-7 shows the strong effect of the addition of a third component. Also, Treybal’s classic plot of interfacial tension versus mutual solubility is given in Fig. 15-21. This information can be helpful in assessing whether interfacial tension is likely to be low, moderate, or high for a new application. However, for design purposes, interfacial tension should be measured by using representative feed and solvent because even small amounts of surface-active impurities can significantly impact the result.

Methods used to measure interfacial tension are reviewed by Drelich, Fang, and White [“Measurement of Interfacial Tension in Fluid-Fluid Systems,” in *Encyclopedia of Surface and Colloid Science* (Dekker, 2003), pp. 3152–3156]. Also see Megias-Alguacil, Fischer, and Windhab, *Chem. Eng. Sci.*, **61**, pp. 1386–1394 (2006). One class of methods derives interfacial tension values from measurement of the shape, contact angle, or volume of a drop suspended in a second liquid. These methods include the pendant drop method (a drop of heavy liquid hangs from a vertically mounted capillary tube immersed

TABLE 15-6 Typical Interfacial Tensions for Different Classes of Organic + Water Binary Mixtures at 20 to 25°C

Class of organic compounds	Interfacial tension, dyn/cm
Alkanes (C ₅ –C ₁₂)	45–53
Halogenated alkanes (C ₁ –C ₄)	30–40
Halogenated aromatics (single ring)	35–40
Aromatics (single ring)	30–40
Mononitro aromatics (single ring)	25–28
Ethers (C ₄ –C ₆)	10–30
Esters (C ₄ –C ₆)	10–20
Ketones (C ₄ –C ₈)	5–15
Organic acids (C ₅ –C ₁₂)	3–15
Aniline	6–7
Alcohols (C ₄ –C ₈)	2–8

References:

1. Demond and Lindner, *Environ. Sci. Technol.*, **27**(12), pp. 2318–2331 (1993).
2. Fu, Li, and Wang, *Chem. Eng. Sci.*, **41**(10), pp. 2673–2679 (1986).
3. Backes et al., *Chem. Eng. Sci.*, **45**(1), pp. 275–286 (1990).

TABLE 15-7 Example Interfacial-Tension Data for Selected Ternary Mixtures

Component 1	Component 2 in phase 1, wt %	Component 3 in phase 1, wt %	Component 2 in phase 2, wt %	Component 3 in phase 2, wt %	Interfacial tension, dyn/cm
Water	Benzene	Ethanol	Benzene	Ethanol	At 25°C
	0.2	10.8	98.6	1.2	17.2
	3.6	43.7	91.3	7.9	1.99
	21.2	52.0	79.3	18.0	0.04
Water	Benzene	Acetone	Benzene	Acetone	At 30°C
	0.1	1.9	98.1	1.8	25.9
	0.2	10.3	91.2	8.6	16.1
	0.6	23.6	81.9	17.8	9.5
	2.7	45.5	68.2	30.9	3.8
Water	Benzene	Acetic acid	Benzene	Acetic acid	At 25°C
	0.3	17.2	98.6	1.3	17.3
	1.1	45.1	92.2	7.5	7.0
	7.9	64.7	77.0	21.9	2.0
Water	Hexane	Ethanol	Hexane	Ethanol	At 20°C
	0.1	32.5	99.5	0.5	9.82
	8.2	73.0	93.9	6.0	1.5
	30.0	64.0	86.2	13.2	0.096
Hexane	Methyl ethyl ketone	Water	Methyl ethyl ketone	Water	At 25°C
	0.4	99.6	0.59	0.01	40.1
	11.7	88.3	35.56	0.09	9.0
	24.5	75.5	89.88	9.97	1.1

References:

1. Sada, Kito, and Yamashita, *J. Chem. Eng. Data*, **20**(4), pp. 376-377 (1975).
2. Pliskin and Treybal, *J. Chem. Eng. Data*, **11**(1), pp. 49-52 (1966).
3. Paul and de Chazal, *J. Chem. Eng. Data*, **12**(1), pp. 105-107 (1967).
4. Ross and Patterson, *J. Chem. Eng. Data*, **24**(2), pp. 111-115 (1979).
5. Backes et al., *Chem. Eng. Sci.*, **45**(1), pp. 275-286 (1990).

in the light liquid), the sessile drop method (a drop of heavy liquid lies on a plate immersed in the light liquid), and the spinning drop method (a drop of one liquid is suspended in a rotating tube filled with the second liquid). The sessile drop method is particularly useful for following the change in interfacial tension when surfactants or macromolecules accumulate at the surface of the drop. The spinning drop method is well suited to measuring low interfacial tensions. Another class of methods derives interfacial tension values from measurement of the force required to detach a ring of wire (Du Noüy's method), or a plate of glass or platinum foil (the Wilhelmy method), from the liquid-liquid interface. The ring or plate must be extremely clean. For the commonly used ring-pull method, the wire is usually flamed before the experiment and must be kept very horizontal and located exactly at the interface of the two liquids.

For an initial assessment, an approximate value for the interfacial tension may be obtained, at least in principle, from knowledge of the maximum size of drops that can persist in a dispersion at equilibrium and without agitation. For example, if it is possible to determine drop size from a photograph of the dispersion of interest at quiescent conditions, then an estimate of interfacial tension may be obtained from the balance between interfacial tension and buoyancy forces

$$\sigma \approx d_{\max}^2 \Delta \rho g \tag{15-32}$$

where d_{\max} is the maximum drop diameter. Antonov's rule also may be used to obtain an approximate value. This rule states that interfacial tension between two liquids is approximately equal to the difference in their liquid-air surface tensions measured at the same conditions. For an organic + water system,

$$\sigma \approx |\sigma_{w(o)} - \sigma_{o(w)}| \tag{15-33}$$

where $\sigma_{w(o)}$ represents the surface tension of the water saturated with the organic and $\sigma_{o(w)}$ represents the surface tension of organic saturated with water.

Measurements of interfacial tension are not always feasible, and calculation methods are sometimes used. The results are least reliable for interfacial tensions below about 10 dyn/cm (10^{-2} N/m). A commonly used empirical correlation of interfacial tension and mutual solubilities is given by Donahue and Bartell [*J. Phys. Chem.*, **56**, pp. 480-484 (1952)]:

$$\sigma = -3.33 - 7.21 \ln(x'_1 + x'_2) \tag{15-34}$$

where σ = interfacial tension, dyn/cm (10^{-3} N/m)
 x'_1 = mole fraction solubility of organic in aqueous phase
 x'_2 = mole fraction solubility of water in organic phase

Treybal [*Liquid Extraction*, 2d ed. (McGraw-Hill, 1963)] modified Eq. (15-36) to expand its application to ternary systems:

$$\sigma = -5.0 - 7.355 \ln[x'_1 + x'_2 + 0.5(x'_3 + x'_4)] \tag{15-35}$$

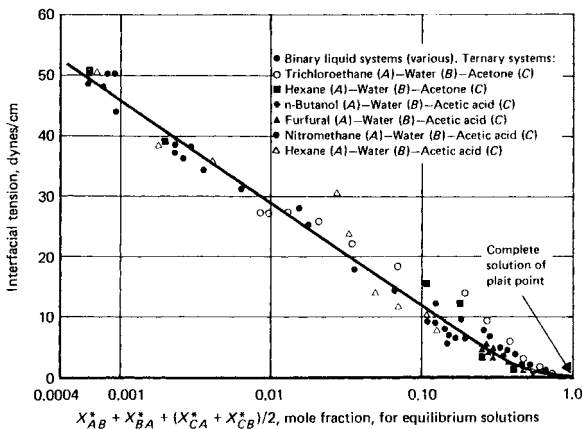


FIG. 15-21 Correlation of interfacial tension with mutual solubility for binary and ternary two-liquid-phase mixtures. [Reprinted from Treybal, *Liquid Extraction*, 2d ed. (McGraw-Hill, 1963). Copyright 1963 McGraw-Hill, Inc.]

where σ = interfacial tension, dyn/cm (10^{-3} N/m)
 x_3'' = mole fraction solute in aqueous phase
 x_3' = mole fraction solute in organic phase

The results are plotted in Fig. 15-21. More recently, Fu, Li, and Wang [*Chem. Eng. Sci.*, **41**(10), pp. 2673–2679 (1986)] derived a relationship for ternary mixtures:

$$\sigma = \frac{0.914RT\chi}{(A_o \exp \chi)(x_1''q_1 + x_2'q_2 + x_3'q_3)} \quad (15-36)$$

$$\chi = -\ln(x_1'' + x_2' + x_3') \quad (15-37)$$

where σ = interfacial tension, dyn/cm (10^{-3} N/m)
 R = ideal gas law constant

T = absolute temperature
 x_1'' = solubility of extract phase in raffinate phase (mole fraction)
 x_2' = solubility of raffinate phase in extract phase (mole fraction)
 x_3' = mole fraction of solute 3 in bulk phase richest in solute 3
 A_o = van der Waals area of standard segment (2.5×10^9 cm²/mol)
 q_i = van der Waals surface area ratio, usually calculated from UNIQUAC

For additional discussion, see Suarez, Torres-Marchal, and Rasmussen, *Chem. Eng. Sci.*, **44**(3), pp. 782–786 (1989); Wu and Zhu, *Chem. Eng. Sci.*, **54**, pp. 433–440 (1990); and Li and Fu, *Fluid Phase Equil.*, **81**, pp. 129–152 (1992).

LIQUID-LIQUID DISPERSION FUNDAMENTALS

GENERAL REFERENCES: Leng and Calabrese, Chap. 12 in *Handbook of Industrial Mixing*, Paul, Atiemo-Obeng, and Kresta, eds. (Wiley, 2004); Becher, *Emulsions: Theory and Practice*, 3d ed. (American Chemical Society, 2001); Binks, *Modern Aspects of Emulsion Science* (Royal Chemical Society, 1998); Adamson and Gast, *Physical Chemistry of Surfaces*, 6th ed. (Wiley, 1997); *Liquid-Liquid Extraction Equipment*, Godfrey and Slater, eds. (Wiley, 1994); *Encyclopedia of Emulsion Technology*, vols. 1–4, Becher, ed. (Decker, 1983–); and Laddha and Degaleesan, Chap. 4 in *Handbook of Solvent Extraction*, Lo, Hanson, and Baird, eds. (Wiley, 1983; Krieger, 1991).

HOLDUP, SAUTER MEAN DIAMETER, AND INTERFACIAL AREA

Most liquid-liquid extractors are designed to generate drops of one liquid suspended in the other rather than liquid films. The volume fraction of the dispersed phase (or holdup) within the extractor is defined as

$$\phi_d = \frac{\text{volume of dispersed phase}}{\text{total contacting volume}} \quad (15-38)$$

where the total contacting volume is the volume within the extractor minus the volume of any internals such as impellers, packing, or trays. A distribution of drop sizes will be present. The Sauter mean drop diameter d_{32} represents a volume to surface-area average diameter

$$d_{32} = \frac{\sum_{i=1}^n N_i d_i^3}{\sum_{i=1}^n N_i d_i^2} \quad (15-39)$$

where N_i is the number of drops with diameter d_i . The Sauter mean diameter often is used in the analysis and modeling of extractor performance because it is directly related to holdup and interfacial area (assuming spherical drops). It is calculated from the total dispersed volume divided by total interfacial area, and often it is expressed in the form

$$d_{32} = \frac{6\epsilon\phi_d}{a} \quad (15-40)$$

where a is interfacial area per unit volume and ϵ is the void fraction within the extractor, i.e., the fraction of internal volume not occupied by any packing, trays, and so on. In the remainder of Sec. 15, the Sauter mean diameter is denoted simply by d_p .

Much less is known about the actual distribution of drop sizes existing within liquid-liquid extractors, particularly at high holdup and as a function of agitation intensity (if agitation is used) and location within

the extractor. For a review, see Kumar and Hartland, Chap. 17 in *Liquid-Liquid Extraction Equipment*, Godfrey and Slater, eds. (Wiley, 1994). Experimental methods used to measure drop size distribution include the use of a high-speed video camera [Ribeiro, et al., *Chem. Eng. J.*, **97**, pp. 173–182 (2004)], real-time optical measurements [Ritter and Kraume, *Chem. Eng. Technol.*, **23**(7), pp. 579–581 (2000)], and phase-Doppler anemometry [Lohner, Bauchhage, and Schombacher, *Chem. Eng. Technol.*, **21**(4), pp. 337–341 (1998); and Willie, Langer, and Werner, *Chem. Eng. Technol.*, **24**(5), pp. 475–479 (2001)].

FACTORS AFFECTING WHICH PHASE IS DISPERSED

Consider mixing a batch of two liquid phases in a stirred tank. The minority phase generally will be the dispersed phase whenever the ratio of minority to majority volume fractions, or phase ratio, is less than about 0.5 (equivalent to a dispersed-phase volume fraction or holdup less than 0.33). For phase ratios between 0.5 and about 2, a region called the ambivalent range, the phase that becomes dispersed is determined in large part by the protocol used to create the dispersion. For example, pouring liquid A into a stirred tank already containing liquid B will tend to create a dispersion of A suspended in B, as long as agitation is maintained. When more of the dispersed-phase material is added to the system, the population density of dispersed drops will increase and eventually reach a point where the drops are so close together that they rapidly coalesce and the phases become inverted, i.e., the formerly dispersed phase becomes the continuous phase. In the ambivalent range, a sudden increase in the agitation intensity also can trigger phase inversion by increasing the number of drop-to-drop collisions. Once phase inversion occurs, it is not easily reversed because the new condition corresponds to a more stable configuration.

This phase behavior may be roughly correlated in terms of light and heavy phase properties including relative density and viscosity as follows:

$$\chi = \frac{\phi_L}{\phi_H} \left(\frac{\rho_L \mu_H}{\rho_H \mu_L} \right)^{0.3} = \frac{\phi_L}{1 - \phi_L} \left(\frac{\rho_L \mu_H}{\rho_H \mu_L} \right)^{0.3} \quad (15-41)$$

where $\chi < 0.3$ light phase always dispersed
 $\chi = 0.3 - 0.5$ light phase probably dispersed
 $\chi = 0.5 - 2.0$ either phase can be dispersed, and phase inversion may occur
 $\chi = 2.0 - 3.3$ heavy phase probably dispersed
 $\chi > 3.3$ heavy phase always dispersed

The symbol ϕ denotes the volume fraction of light (L) and heavy (H) phases existing within the vessel. Equation (15-41) is taken from the expression recommended by Hooper [Sec. 1.11 in *Handbook of*

Separation Techniques for Chemical Engineers, 3d ed., Schweitzer, ed. (McGraw-Hill, 1997)] and Jacobs and Penney [Chap. 3 in *Handbook of Separation Process Technology*, Rousseau, ed. (Wiley, 1987)] for design of continuous decanters. It is based on the dispersed-phase data of Selker and Sleicher [*Can. J. Chem. Eng.*, **43**, pp. 298–301 (1965)].

Equation (15-41) should apply to continuously fed extraction columns and other continuous extractors as well as batch vessels. The equation is expressed here in terms of volume fractions ϕ_L/ϕ_H existing within the vessel, not volumetric flow rates of each phase entering the vessel Q_L/Q_H . The ratio of volume fractions within a continuously fed vessel can be very different from Q_L/Q_H —primarily because buoyancy allows the dispersed-phase drops to travel rapidly through the continuous phase relative to the dispersed-phase superficial velocity. For example, a continuously fed extraction column can be designed to operate with either phase being the dispersed phase, with the main liquid-liquid interface controlled at the top of the column (for a light-phase dispersed system) or at the bottom (for a heavy-phase dispersed system). As the dispersed-to-continuous phase ratio within the column is increased, through either changes in operating variables or changes in the design of the internals, a point may be reached where the population density or holdup of dispersed drops is too large and phase inversion occurs. In the absence of stabilizing surfactants, the point of phase inversion should correspond roughly to the same general phase-ratio rules given in Eq. (15-41), with the exact conditions at which phase inversion occurs depending upon agitation intensity (if used) and the geometry of any internals (baffles, packing, trays, and so on). Certain extractors such as sieve-tray columns often are designed to disperse the majority flowing phase. In extreme cases, the ratio Q_d/Q_c (where d and c represent dispersed and continuous phases) may be as high as 50, and the continuous phase may be nearly stagnant with a superficial velocity as low as 0.02 cm/s; yet the phase ratio within the extractor can be controlled within the guidelines needed to avoid phase inversion [approximated by Eq. (15-41)].

The stability of a dispersion also can be affected by the presence of fine solids or gas bubbles as well as surfactants. For additional discussion of factors affecting which phase is dispersed, see Norato, Tsouris, and Tavlarides, *Can. J. Chem. Eng.*, **76**, pp. 486–494 (1998); and Pacek et al., *AIChE J.*, **40**(12), pp. 1940–1949 (1994). For a given application, the precise conditions that lead to phase inversion must be determined by experiment. For organic + water dispersions, experimental determination may be facilitated by measuring the conductivity of the mixture, since conductivity normally will be significantly higher when water is in the continuous phase [Gilchrist, et al., *Chem. Eng. Sci.*, **44**(10), pp. 2381–2384 (1989)]. Another method involves monitoring the dynamics of phase inversion by using a stereo microscope and video camera [Pacek et al., *AIChE J.*, **40**(12), pp. 1940–1949 (1994)].

SIZE OF DISPERSED DROPS

In nonagitated (static) extractors, drops are formed by flow through small holes in sieve plates or inlet distributor pipes. The maximum size of drops issuing from the holes is determined not by the hole size but primarily by the balance between buoyancy and interfacial tension forces acting on the stream or jet emerging from the hole. Neglecting any viscosity effects (i.e., assuming low dispersed-phase viscosity), the maximum drop size is proportional to the square root of interfacial tension σ divided by density difference $\Delta\rho$:

$$d_{\max} = \text{const} \sqrt{\frac{\sigma}{\Delta\rho g}} \quad \text{for static extractors} \quad (15-42)$$

The proportionality constant typically is close to unity [Seibert and Fair, *Ind. Eng. Chem. Res.*, **27**(3), pp. 470–481 (1988)]. Note that Eq. (15-42) indicates the maximum stable drop diameter and not the Sauter mean diameter (although the two are proportionally related and may be close in value). Smaller drops may be formed at the distributor due to jetting of the inlet liquid through the distributor holes or by mechanical pulsation of the liquid inside the distributor [Koch and Vogelpohl, *Chem. Eng. Technol.*, **24**(12), pp. 1245–1248 (2001)]. In static extractors, hydrodynamic stresses within the main body of the

extractor away from the distributor are small and normally not sufficient to cause significant drop breakage as drops flow through the extractor, although small drops may collide and coalesce into larger drops. Some authors report a small amount of drop breakage in packed columns due to collisions with packing materials [Mao, Godfrey, and Slater, *Chem. Eng. Technol.*, **18**, pp. 33–40 (1995)]. Additional discussion is given in “Static Extraction Columns” under “Liquid-Liquid Extraction Equipment.”

In agitated extractors, drop size is determined by the equilibrium established between drop breakage and coalescence rates occurring within the extractor. Breakage is due to turbulent stresses caused by the agitator, so it is mainly confined to the vicinity of the agitator. Drop coalescence, however, can happen anywhere in the vessel where drops can come into close proximity with one another. Dispersed drops will begin to break into smaller droplets when turbulent stresses exceed the stabilizing forces of interfacial tension and liquid viscosity. Kolmogorov [*Dokl. Akad. Nauk*, **66**, pp. 825–828 (1949)] and Hinze [*AIChE J.*, **1**(3), pp. 289–295 (1955)] developed expressions for the maximum size of drops in an agitated liquid-liquid dispersion. Their results can be expressed as follows:

$$d_{\max} = (\text{const}) \sigma^{3/5} \rho_c^{-1/5} \left(\frac{P}{V} \right)^{-2/5} \quad \text{for agitated extractors} \quad (15-43)$$

where P/V is the rate of mechanical energy dissipation (or power P) input to the dispersion per unit volume V . Equation (15-43) assumes dispersed-phase holdup is low. It also assumes viscous forces that resist breakage can be neglected, a valid assumption for water and typical low- to moderate-viscosity organic solvents. Wang and Calabrese discuss how to determine when viscous resistance to breakage becomes important and show that this depends upon interfacial tension as well as dispersed-phase viscosity [Wang and Calabrese, *AIChE J.*, **32**(4), pp. 667–676 (1986)]. Equation (15-43) can be restated as

$$\frac{d_{\max}}{D_i} \propto We^{-3/5} \quad (15-44)$$

where We is a dimensionless Weber number (disruptive shear stress/cohesive interfacial tension) and D_i is a characteristic diameter. For applications involving the use of rotating impellers, D_i is the impeller diameter and the appropriate Weber number is $We = \rho \omega^2 D_i^3 / \sigma$ where ω is the impeller speed (in rotations per unit time). For static mixers, $D_i = D_{sm}$ and $We = \rho V_{sm}^2 D_{sm} / \sigma$, where D_{sm} is the static mixer pipe diameter and V_{sm} is the superficial liquid velocity (entrance velocity). A variety of drop size models derived for various mixers and operating conditions have been tabulated by Leng and Calabrese [Chap. 12 in *Handbook of Industrial Mixing*, Paul, Atiemo-Obeng, and Kresta, eds. (Wiley, 2004), pp. 669–675]. Also see Naseef, Sulttan, and Stamatoudis, *Chem. Eng. Technol.*, **29**(5), pp. 583–587 (2006).

Equation (15-44) represents a limiting operating regime where the rate of drop breakage dominates performance and the coalescence rate can be neglected. Drop coalescence requires that two drops collide, and the coalescence rate increases with increasing holdup since there is greater opportunity for drop-drop collisions. For agitated systems with fast coalescence at high holdup, i.e., when drop coalescence dominates, drop size appears best correlated by an expression of the form $d_p/D \propto We^{-n}$, where n varies between 0.35 and 0.45 [Pacek, Man, and Nienow, *Chem. Eng. Sci.*, **53**(11), pp. 2005–2011 (1998); and Kraume, Gabler, and Schulze, *Chem. Eng. Technol.*, **27**(3), pp. 330–334 (2004)]. This is similar to the theoretical expression derived by Shinnar [*J. Fluid Mech.*, **10**, p. 259 (1961)].

When two drops first come into contact in the process of coalescing, a film of continuous phase becomes trapped between them. The film is compressed at the point of encounter until it drains away and the two drops can merge. Decreasing the viscosity of the continuous phase, by heating or by addition of a low-viscosity diluent, may promote drop coalescence by increasing the rate of film drainage. Surface-active impurities or surfactants, when present, also can affect the coalescence rate, by accumulating at the surface of the drop. Surfactants tend to stabilize the film and reduce coalescence rates. Fine

solid particles that are wetted by the continuous phase tend to slow film drainage, also reducing the rate of drop coalescence.

A number of semiempirical drop size data correlations have been developed for different types of extractors (static and agitated) including a term for holdup. See Kumar and Hartland, *Ind. Eng. Chem. Res.*, **35**(8), pp. 2682–2695 (1996); and Kumar and Hartland, Chap. 17 in *Liquid-Liquid Extraction Equipment*, Godfrey and Slater, eds. (Wiley, 1994). These equations predict a characteristic drop size. They do not provide information about the drop size distribution or the minimum drop size. For discussion of minimum drop size, see Zhou and Kresta, *Chem. Eng. Sci.*, **53**(11), pp. 2063–2079 (1998).

STABILITY OF LIQUID-LIQUID DISPERSIONS

In designing a liquid-liquid extraction process, normally the goal is to generate an unstable dispersion that provides reasonably high interfacial area for good mass transfer during extraction and yet is easily broken to allow rapid liquid-liquid phase separation after extraction. Given enough time, most dispersions will break on standing. Often this process occurs in two distinct periods. The first is a relatively short initial period or primary break during which an interface forms between two liquid layers, one or both of which remain cloudy or turbid. This is followed by a longer period or secondary break during which the liquid layers become clarified. During the primary break, the larger drops migrate to the interface where they accumulate and begin to coalesce. If the coalescence rate is relatively slow compared to the rate at which drops rise or fall to the interface, then a layer of coalescing drops or *dispersion band* will form at the interface. The initial interface can form within a few minutes or less for drop sizes on the order of 100 to 1000 μm (0.1 to 1 mm), as in a water + toluene system, for example. When the drop size distribution in the feed dispersion is wide, smaller droplets remain suspended in one or both phases. Longer residence times are then required to break this secondary dispersion. In extreme cases, the secondary dispersion can take days or even longer to break.

When a dispersion requires a long time to break, the presence of surfactantlike impurities may be a contributing factor. Surfactants are molecules with a hydrophobic end (such as a long hydrocarbon chain) and a hydrophilic end (such as an ionic group or oxygen-containing short chain). Surfactants stabilize droplets by forming an adsorbed film at the interface and by introducing electrical repulsions between drops [Tcholakova, Denkov, and Danner, *Langmuir*, **20**(18), pp. 7444–7458 (2004)]. Both effects can interfere with drop coalescence. Surfactants also decrease the interfacial tension of the system. As more surfactant is introduced into a solution, the concentration of free surfactant molecules in the bulk liquid increases and reaches a plateau called the critical micelle concentration. At this point, any excess molecules begin forming aggregates with other surfactant molecules at the interface of the two liquids to minimize interaction with the continuous phase. The dispersed phase is then trapped inside the micelles. As more surfactant is added to the mixture, more micelles can form and in most cases the droplets become smaller to maximize interfacial area. In theory, the maximum volume fraction of the dispersed phase should be limited to 0.74 due to the close packing density of spheres; but in practice much higher values are possible when the micelles change to other structures of different geometries such as a mix of small drops among larger ones and nonspherical shapes.

Emulsions are broken by changing conditions to promote drop coalescence, either by disrupting the film formed at the interface between adjacent drops or by interfering with the electrical forces that stabilize the drops. Water droplets are usually positively charged while oil droplets are negatively charged. Physical techniques used to break emulsions include heating (including application of microwave radiation), freezing and thawing, adsorption of surface-active compounds, filtration of fine particles that stabilize films between drops, and application of an electric field. Heating can be particularly effective for nonionic surfactants, since heating disrupts hydrogen bonding interactions that contribute to micelle stability. Chemical techniques include adding a salt to alter the charges around drops, changing the

pH of the system, and adding a deemulsifier compound (or even another type of surfactant) to interact with and alter the surfactant layer. Ionic surfactants are particularly sensitive to change in pH. Additives include bases and acids, aluminum or ferric salts, chelating agents, charged polymers (polyamines or polyacrylates), polyalcohols, silicone oils, various fatty acid esters and fatty alcohols, as well as adsorbents such as clay and lime. For further discussion, see Rajaković and Skala, *Sep. Purif. Technol.*, **49**(2), pp. 192–196 (2006); and Alther, *Chem. Eng. Magazine*, **104**(3) pp. 82–88 (1998). Chemical additives need to be used in sufficiently small concentrations so as not to interfere with other operations in the overall process or product quality. General information is available in Schramm, *Emulsions, Foams, and Suspensions* (Wiley-VCH, 2005); Becher, *Emulsions: Theory and Practice*, 3d ed. (American Chemical Society, 2001); and Binks, *Modern Aspects of Emulsion Science* (Royal Society of Chemical 1998).

EFFECT OF SOLID-SURFACE WETTABILITY

The stability of a dispersion also may depend upon the surface properties of the container or equipment used to process the dispersion, since the walls of the vessel, or more importantly, the surfaces of any internal structures, may promote drop coalescence. In a liquid-liquid extractor or a liquid-liquid phase separator, the wetting of a solid surface by a liquid is a function of the interfacial tensions of both the liquid-solid and the liquid-liquid interfaces. For dispersed drops with low liquid-solid interfacial tension, the drops tend to spread out into films when in contact with the solid surface. In general, an aqueous liquid will tend to wet a metal or ceramic surface better than an organic liquid will, and an organic liquid will tend to wet a polymer surface better than an aqueous liquid will. However, there are many exceptions. Strigle [*Packed Tower Design and Applications*, 2d ed., Chap. 11 (Gulf, 1994)] indicates that for packed extractors, metal packings may be wetted by either an aqueous or an organic solvent depending upon the initial exposure of the metal surface (whether the unit is started up filled with the aqueous phase or the organic phase). In general, however, metals tend to be preferentially wetted by an aqueous phase. Also, it is not uncommon for materials of construction to acquire different surface properties after aging in service, since the solid surface can change due to adsorption of impurities, corrosion, or fouling. This aging effect often is observed for polymer materials. Small-scale lab tests are recommended to determine these wetting effects. For detailed discussion of wettability and its characterization, see *Contact Angle, Wettability, and Adhesion*, vols. 1–3, Mittal, ed. (VSP, 1993–); or *Wettability*, Berg, ed. (Dekker, 1993).

In liquid-liquid extraction equipment, the internals generally should be preferentially wetted by the continuous phase—in order to maintain dispersed-phase drops with a high population density (high holdup). If the dispersed phase preferentially wets the internals, then drops may coalesce on contact with these surfaces, and this can result in loss of interfacial area for mass transfer and even in the formation of rivulets that flow along the internals. In an agitated extractor, this tendency may be mitigated somewhat, if needed, by increasing the agitation intensity.

MARANGONI INSTABILITIES

Numerous studies have shown that mass transfer of solute from one phase to the other can alter the behavior of a liquid-liquid dispersion—because of interfacial tension gradients that form along the surface of a dispersed drop. For example, see Sawistowski and Goltz, *Trans. Inst. Chem. Engrs.*, **41**, p. 174 (1963); Bakker, van Buytenen, and Beek, *Chem. Eng. Sci.*, **21**(11), pp. 1039–1046 (1966); Ruckenstein and Berbente, *Chem. Eng. Sci.*, **25**(3), pp. 475–482 (1970); Lode and Heideger, *Chem. Eng. Sci.*, **25**(6), pp. 1081–1090 (1970); and Takeuchi and Numata, *Int. Chem. Eng.*, **17**(3), p. 468 (1977). These interfacial tension gradients can induce interfacial turbulence and circulation within drops. These effects, known as Marangoni instabilities, have been shown to enhance mass-transfer rates in certain cases.

The direction of mass transfer also can have a significant effect upon drop-drop coalescence and the resulting drop size. Seibert and

Fair [*Ind. Eng. Chem. Res.*, **27**(3), pp. 470–481 (1988)] showed that mass transfer out of the drop will promote coalescence. Larger drop sizes were observed when transferring solute into the continuous phase (interfacial tension was increasing as the drop traveled through the extractor). Kumar and Hartland [*Ind. Eng. Chem. Res.*, **35**(8), pp. 2682–2695 (1996)] suggest that transfer of solute from the dispersed to the continuous phase ($d \rightarrow c$) tends to produce larger drops because the concentration of transferring solute in the draining film between two approaching drops is higher than that in the surrounding continuous liquid. This accelerates drainage, thus promoting drop coalescence. For mass transfer in the opposite direction

($c \rightarrow d$), smaller drops tend to form because the solute concentration in the draining film between drops is relatively low. The magnitude of these effects depends upon system properties, the surface activity of the transferring solute, and the degree of mass transfer. Unless the solute is unusually surface-active, the effect will be small. For more information, see Gourdon, Casamatta, and Muratet, Chap. 7 in *Liquid-Liquid Extraction Equipment*, Godfrey and Slater, eds. (Wiley, 1994); Perez de Ortiz, Chap. 3, “Marangoni Phenomena,” in *Science and Practice of Liquid-Liquid Extraction*, vol. 1, Thornton, ed. (Oxford, 1992); and Grahn, *Chem. Eng. Sci.*, **61**, pp. 3586–3592 (2006).

PROCESS FUNDAMENTALS AND BASIC CALCULATION METHODS

GENERAL REFERENCES: See Sec. 5, “Mass Transfer,” as well as Wankat, *Separation Process Engineering*, 2d ed. (Prentice-Hall, 2006); Seader and Henley, *Separation Process Principles* (Wiley, 1998); Godfrey and Slater, *Liquid-Liquid Extraction Equipment* (Wiley, 1994); Thornton, ed., *Science and Practice of Liquid-Liquid Extraction*, vol. 1 (Oxford, 1992); Wankat, *Equilibrium Staged Separations* (Prentice-Hall, 1988); Kirwin, Chap. 2 in *Handbook of Separation Process Technology*, Rousseau, ed. (Wiley, 1987); Skelland and Tedder, Chap. 7 in *Handbook of Separation Process Technology*, Rousseau, ed. (Wiley, 1987); Lo, Baird, and Hanson, eds., *Handbook of Solvent Extraction* (Wiley, 1983; Krieger, 1991); King, *Separation Processes*, 2d ed. (McGraw-Hill, 1980); Brian, *Staged Cascades in Chemical Processing* (Prentice-Hall, 1972); Geankoplis, *Mass Transport Phenomena* (Holt, Rinehart and Winston, 1972); and Treybal, *Liquid Extraction*, 2d ed. (McGraw-Hill, 1963).

The fundamental mechanisms for solute mass transfer in liquid-liquid extraction involve molecular diffusion driven by a deviation from equilibrium. When a liquid feed is contacted with a liquid solvent, solute transfers from the interior of the feed phase across a liquid-liquid interface into the interior of the solvent phase. Transfer of solute will continue until the solute's chemical potential is the same in both phases and equilibrium is achieved.

The calculation methods used to quantify extraction processes generally involve either the calculation of theoretical stages, with application of an operating efficiency to reflect mass-transfer resistance, or calculations based on consideration of mass-transfer rates using expressions related in some way to molecular diffusion. Theoretical-stage calculations commonly are used to characterize separation difficulty regardless of the type of extractor to be used. They are also used for extractor design purposes, although for this purpose they generally should be reserved for single-stage contactors or mixer-settler cascades involving discrete stages, or for other equipment where discrete contacting zones exist, such as in a sieve-tray column. The appropriate stage efficiency reflects how closely an actual contacting stage approaches equilibrium, and is a function of operating variables that affect drop size, population density, and contact time.

The development and application of rate-based models for analysis and design of extraction processes are becoming more common. For example, Jain, Sen, and Chopra [*ISEC '02 Proceedings*, **2**, pp. 1265–1270 (2002)] recently described a rate-based model for a lube oil extraction process. Rate-based models most often are applied to differential-type contactors that lack discrete contacting stages, to staged contactors with low stage efficiencies, or to processes with extraction factors greater than about 3, indicating a mass-transfer-limited operating regime. Differential-type contactors operating at extraction factors less than 3 also can be adequately modeled with theoretical stages since these contactors operate reasonably close to equilibrium. With either approach, appropriate values for model parameters typically are determined by fitting data generated by using laboratory or pilot-plant experiments, or by analysis of the performance of large-scale commercial units. In certain cases, parameter values have been correlated as a function of physical properties and operating conditions for specific types of equipment using model systems. The reliability of the resulting correlations is generally limited to applications very similar to those used to develop the correlations. Also, most calculation methods have been developed for

continuous steady-state operation. The dynamic modeling of extraction processes is discussed elsewhere [Mohanty, *Rev. Chem. Eng.*, **16**(3), p. 199 (2000); Weinstein, Semiat, and Lewin, *Chem. Eng. Sci.*, **53**(2), pp. 325–339 (1998); and Steiner and Hartland, Chap. 7 in *Handbook of Solvent Extraction*, Lo, Baird, and Hanson, eds. (Wiley, 1983; Krieger, 1991)].

The calculation methods used for designing extraction operations are analogous in many respects to methods used to design absorbers and strippers in vapor-liquid and gas-liquid contacting such as those described by Ortiz-Del Castillo, et al. [*Ind. Eng. Chem. Res.*, **39**(3), pp. 731–739 (2000)] and by Kohl [“Absorption and Stripping,” Chap. 6 in *Handbook of Separation Process Technology* (Wiley-Interscience, 1987)]. Unlike in stripping and absorption, however, liquid-liquid extraction always deals with highly nonideal systems; otherwise, only one liquid phase would exist. This nonideality contributes to difficulties in modeling and predicting phase equilibrium, liquid-liquid phase behavior (hydraulics), and thus mass transfer. Also, the mass-transfer efficiency of an extractor generally is much less than that observed in distillation, stripping, or absorption equipment. For example, an overall sieve tray efficiency of 70 percent is common in distillation, but it is rare when a sieve tray extractor achieves an overall efficiency greater than 30 percent. The difference arises in part because generation of interfacial area, normally by dispersing drops of one phase in the other, generally is more difficult in liquid-liquid contactors. Unlike in distillation, formation of liquid films often is purposely avoided; generation of dispersed droplets provides greater interfacial area for mass transfer per unit volume of extractor. (Film formation may be important in extraction applications involving centrifugal contactors or baffle tray extractors, but this is not generally the case.) In certain cases, mass-transfer rates also may be slower compared to those of gas-liquid contactors because the second phase is a liquid instead of a gas, and transport properties in that phase are less favorable. Although mass-transfer efficiency generally is lower, the specific throughput of liquid-liquid extraction equipment (in kilograms of feed processed per hour per unit volume) can be higher than is typical of vapor-liquid contactors, simply because liquids are much denser than vapors.

THEORETICAL (EQUILIBRIUM) STAGE CALCULATIONS

Calculating the number of theoretical stages is a convenient method used by process designers to evaluate separation difficulty and assess the compromise between the required equipment size (column height or the number of actual stages) and the ratio of solvent rate to feed rate required to achieve the desired separation. In any mass-transfer process, there can be an infinite number of combinations of flow rates, number of stages, and degrees of solute transfer. The optimum is governed by economic considerations. The cost of using a high solvent rate with relatively few stages should be carefully compared with the cost of using taller extraction equipment (or more equipment) capable of achieving more theoretical stages at a reduced solvent rate and operating cost. While the operating cost of an extractor is generally quite low, the operating cost for a solvent recovery distillation tower can be quite high. Another common objective for calculating the number of countercurrent theoretical stages is to evaluate

the performance of liquid-liquid extraction test equipment in a pilot plant or to evaluate production equipment in an industrial plant. As mentioned earlier, most liquid-liquid extraction equipment in common use can be designed to achieve the equivalent of 1 to 8 theoretical countercurrent stages, with some designed to achieve 10 to 12 stages.

McCabe-Thiele Type of Graphical Method Graphical methods may be used to determine theoretical stages for a ternary system (solute plus feed solvent and extraction solvent) or for a pseudo-ternary system with the focus placed on a key solute of interest. Although developed long ago, graphical methods are still valuable today because they help visualize the problem, clearly illustrating pinch points and other design issues not readily apparent by using other techniques. Even with computer simulations, often it is useful to plot the results for a key solute as an aid to analyzing the design. This section briefly reviews the commonly used McCabe-Thiele type of graphical method. More detailed discussions of this and other graphical methods are available elsewhere. For example, see Seibert, "Extraction and Leaching," Chap. 14 in *Chemical Process Equipment: Selection and Design*, 2d ed., Couperet et al., eds. (Elsevier, 2005); Wankat, *Separation Process Engineering* (Prentice-Hall, 2006); and King, *Separation Processes*, 2d ed. (McGraw-Hill, 1980), among others.

In distillation calculations, the McCabe-Thiele graphical method assumes constant molar vapor and liquid flow rates and allows convenient stepwise calculation with straight operating lines and a curved equilibrium line. A similar concept can be achieved in liquid-liquid extraction by using Bancroft coordinates and expressing flow rates on a solute-free basis, i.e., a constant flow rate of feed solvent F' and a constant flow rate of extraction solvent S' through the extractor [Evans, *Ind. Eng. Chem.*, **26**(8), pp. 860-864 (1934)]. The solute concentrations are then given as the mass ratio of solute to feed solvent X' and the mass ratio of solute to extraction solvent Y' . These concentrations and coordinates give a straight operating line on an $X'-Y'$ diagram for stages 2 through $r - 1$ in Fig. 15-22. The ratio of solute-free extraction solvent to solute-free feed solvent will be constant within the extractor except at the outer stages where unsaturated feed and extraction solvent enter the process. Equilibrium data using these mass ratios have been shown to follow straight-line segments on a log-log plot (see Fig. 15-20), and they will be approximately linear over some composition range on an $X'-Y'$ plot. When expressed in terms of Bancroft coordinates, the equilibrium line typically will curve upward at high solute concentrations, as shown in Fig. 15-23.

To illustrate the McCabe-Thiele method, consider the simplified case where feed and extraction solvents are immiscible; i.e., mutual solubility is nil. Then the rate of feed solvent alone in the feed stream

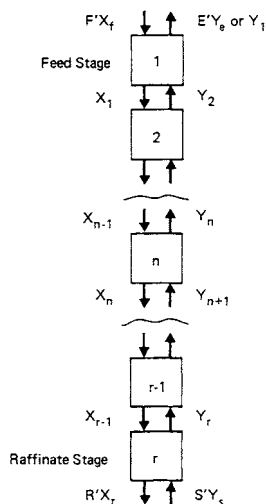


FIG. 15-22 Countercurrent extraction cascade.

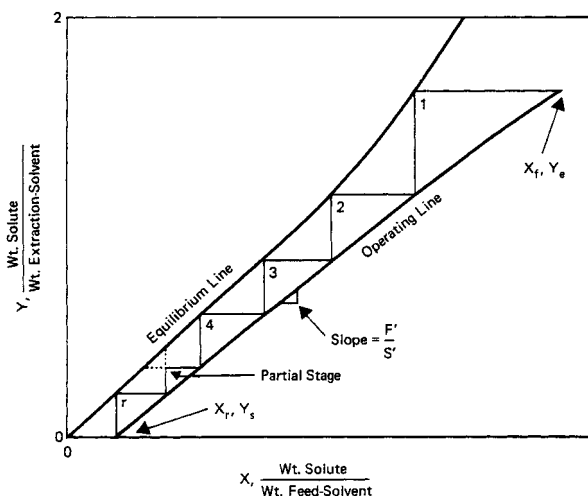


FIG. 15-23 McCabe-Thiele type of graphical stage calculation using Bancroft coordinates.

F' is the same as the rate of feed solvent alone in the raffinate stream R' . In like manner, the rate of extraction solvent alone is the same in the entering stream S' as in the leaving extract stream E' . The ratio of extraction-solvent to feed-solvent flow rates is therefore $S'/F' = E'/R'$. A material balance can be written around the feed end of the extractor down to any stage n (as shown in Fig. 15-22) and then rearranged to a McCabe-Thiele type of operating line with a slope of F'/S' :

$$Y'_{n+1} = \frac{F'}{S'} X'_n + \frac{E'Y'_e - F'X'_f}{S'} \quad (15-45)$$

Similarly, the same operating line can be derived from a material balance around the raffinate end of the extractor up to stage n :

$$Y'_n = \frac{F'}{S'} X'_{n-1} + \frac{S'Y'_s - R'X'_r}{S'} \quad (15-46)$$

The overall extractor material balance is given by

$$Y'_e = \frac{F'X'_f + S'Y'_s - R'X'_r}{E'} \quad (15-47)$$

The endpoints of the operating line on an $X'-Y'$ plot (Fig. 15-23) are the points (X'_f, Y'_e) and (X'_r, Y'_s) where X' and Y' are the mass ratios for solute in the feed phase and extract phase, respectively, and subscripts $f, r, s,$ and e denote the feed, raffinate, entering extraction solvent, and leaving extract streams. The number of theoretical stages can then be stepped off graphically as illustrated in Fig. 15-23.

Kremser-Souders-Brown Theoretical Stage Equation The Kremser-Souders-Brown (KSB) equation [Kremser, *Natl. Petrol. News*, **22**(21), pp. 43-49 (1930); and Souders and Brown, *Ind. Eng. Chem.*, **24**(5), pp. 519-522 (1932)] provides a way of calculating performance equivalent to that of a McCabe-Thiele type of graphical calculation with straight equilibrium and operating lines. In terms of Bancroft coordinates, the KSB equation may be written

$$N = \frac{\ln \left[\left(\frac{X'_f - Y'_s/m'}{X'_r - Y'_s/m'} \right) \left(1 - \frac{1}{\mathcal{E}} \right) + \frac{1}{\mathcal{E}} \right]}{\mathcal{E} - m' \frac{S'}{F'}} \quad \mathcal{E} \neq 1 \quad (15-48)$$

where N = number of theoretical stages
 X'_f = mass ratio solute to feed solvent in feed entering process (Bancroft coordinates)

- X'_f = mass ratio solute to feed solvent in raffinate leaving process
- Y'_s = mass ratio solute to extraction solvent in extraction solvent entering process
- \mathcal{E} = extraction factor
- m' = dY'/dX' , local slope of equilibrium line in Bancroft coordinates
- S' = mass flow rate of extraction solvent (solute-free basis)
- F' = mass flow rate of feed solvent (solute-free units)

Solutions to Eq. (15-48) are shown graphically in Fig. 15-24. The concentration of solute in the extract leaving the process Y'_e is determined from the material balance, as in Eq. (15-47). (Note that other systems of units also may be used in these equations, as long as they are consistently applied.)

Rearranging Eq. (15-48) yields another common form of the KSB equation:

$$\frac{X'_f - Y'_e/m'}{X'_r - Y'_e/m'} = \frac{\mathcal{E}^N - 1/\mathcal{E}}{1 - 1/\mathcal{E}} \quad \mathcal{E} \neq 1 \quad (15-49)$$

Equations (15-48) and (15-49) can be used whenever $\mathcal{E} > 1$ or $\mathcal{E} < 1$. They cannot be used when \mathcal{E} is exactly equal to unity because this would involve division by zero. When $\mathcal{E} = 1$, the number of theoretical stages is given by

$$N = \frac{X'_f - Y'_e/m'}{X'_r - Y'_e/m'} - 1 \quad \text{for } \mathcal{E} = 1 \quad (15-50)$$

Equation (15-50) may be rewritten

$$\frac{X'_f - Y'_e/m'}{X'_r - Y'_e/m'} = N + 1 \quad \text{for } \mathcal{E} = 1 \quad (15-51)$$

In the special case where $\mathcal{E} < 1$, the *maximum* performance potential is represented by

$$\left(\frac{X'_f - Y'_e/m'}{X'_r - Y'_e/m'} \right)_{\max} \approx \frac{1}{1 - \mathcal{E}} \quad \text{for } \mathcal{E} < 1 \text{ and large } N \quad (15-52)$$

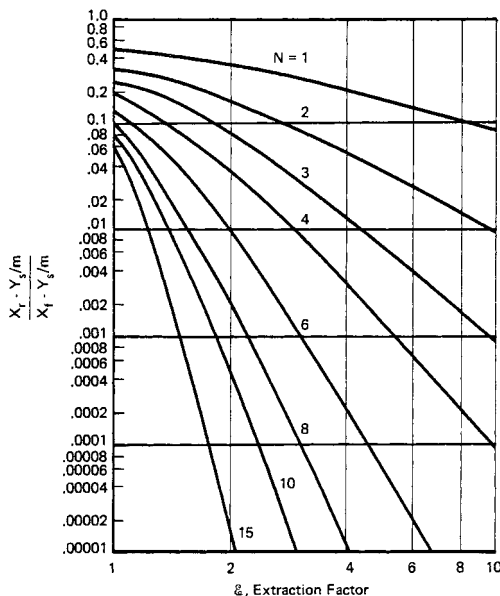


FIG. 15-24 Graphical solutions to the KSB equation [(Eq. 15-48)].

Equation (15-52) reflects the fact that the carrying capacity of the extract stream limits performance at $\mathcal{E} < 1$, as noted in earlier discussions.

In general, Eqs. (15-48) through (15-52) (and Fig. 15-24) are valid for any concentration range in which equilibrium can be represented by a linear relationship $Y = mX + b$ (written here in general form for any system of units). For applications that involve dilute feeds, the section of the equilibrium line of interest is a straight line that extends through the origin where $Y_i = 0$ at $X_i = 0$. In this case, $b = 0$ and the slope of the equilibrium line is equal to the partition ratio ($m = K$). The KSB equation also may be used to represent a linear segment of the equilibrium curve at higher solute concentrations. In this case, the linear segment is represented by a straight line that does not extend through the origin, and m is the local slope of the equilibrium line, so $b \neq 0$ and $m \neq K$. Furthermore, a series of KSB equations may be used to model a highly curved equilibrium line by dividing the analysis into linear segments and matching concentrations where the segments meet. For equilibrium lines with moderate curvature, an approximate average slope of the equilibrium line may be obtained from the geometric mean of the slopes at low and high solute concentrations:

$$m_{\text{average}} \approx m_{\text{geometric mean}} = \sqrt{m_{\text{low}} m_{\text{high}}} \quad (15-53)$$

As noted above, other systems of units such as mass fraction and total mass flow rates or mole fraction and total molar flow rates also may be used with the KSB equation; however, Bancroft coordinates and solute-free mass flow rates are recommended because then the operating line must be linear, and this normally extends the concentration range over which the KSB analysis may be used. It is important to check whether equilibrium can be adequately represented by a straight line over the concentration range of interest. The application of the KSB equation is discussed in "Shortcut Calculations" under "Calculation Procedures." Additional discussion is given by Wankat [*Equilibrium Staged Separations* (Prentice-Hall, 1988)] and by King [*Separation Processes*, 2d ed. (McGraw-Hill, 1980)]. To facilitate use of the KSB equation in computer calculations where the singularity around $\mathcal{E} = 1$ can present difficulties, Shenoy and Fraser have proposed an alternative form of the equation [*Chem. Eng. Sci.*, **58**(22) pp. 5121-5124 (2003)].

Stage Efficiency For a multistage process, the overall stage efficiency is simply the number of theoretical stages divided by the number of actual stages times 100:

$$\xi_o (\%) = \frac{\text{theoretical stages}}{\text{actual stages}} \times 100 \quad (15-54)$$

The fundamental stage efficiency is referred to as the Murphree stage efficiency ξ_m . The Murphree efficiency based on the dispersed phase is defined as

$$\xi_{md} = \frac{C_{d,n+1} - C_{d,n}}{C_{d,n+1} - C_d^*} \quad (15-55)$$

where $C_{d,n+1}$ = concentration of solute i in dispersed phase at stage $n + 1$

$C_{d,n}$ = concentration of solute i in dispersed phase at stage n

C_d^* = concentration of solute i in dispersed phase, at equilibrium

The overall stage efficiency is related to the Murphree stage efficiency and the extraction factor (\mathcal{E}):

$$\xi_o (\%) = \frac{\ln [1 + \xi_{md}(\mathcal{E} - 1)]}{\ln \mathcal{E}} \times 100 \quad (15-56)$$

For applications involving extraction of multiple solutes, sometimes the extraction rate and mass-transfer efficiency for each solute are significantly different. In these cases, individual efficiencies will need to be determined for each solute.

Stage efficiencies normally are determined by running miniplant tests to measure performance as a function of process variables such as feed rates, operating temperature, physical properties, impurities,

and agitation (if used). A number of data correlations have been developed for various types of mixing equipment. In principle, these can be used in the estimation of mass-transfer rates and stage efficiencies, but in practice reliable design generally requires generation of mini-plant data and application of mixing scale-up methods. (See "Mixer-Settler Equipment" under "Liquid-Liquid Extraction Equipment.")

The overall efficiency of an extraction column also can be expressed as the height equivalent to a theoretical stage (HETS). This is simply the total contacting height Z_t divided by the number of theoretical stages achieved.

$$\text{HETS} = \frac{Z_t}{N} \quad (15-57)$$

The HETS often is used to compare staged contactors with differential contactors.

RATE-BASED CALCULATIONS

This section reviews the basics of the mass-transfer coefficient and mass-transfer unit approaches to modeling extraction performance. These methods have been used for many years and continue to provide a useful basis for the design of extractors and extraction processes. Additional discussions of these and other rate-based methods are given in the books edited by Godfrey and Slater [*Liquid-Liquid Extraction Equipment* (Wiley, 1994)] and by Thornton [*Science and Practice of Liquid-Liquid Extraction*, vol. 1 (Oxford, 1992)]. For discussions of more mechanistic methods that include characterization of drop breakage and coalescence rates, drop size distributions, and drop population balances, see Leng and Calabrese, Chap. 12 in *Handbook of Industrial Mixing*, Paul, Atiemo-Obeng, and Kresta, eds. (Wiley, 2004); Goodson and Kraft, *Chem. Eng. Sci.*, **59**, pp. 3865–3881 (2004); Attarakih, Bart, and Faqir, *Chem. Eng. Sci.*, **61**, pp. 113–123 (2006); and Schmidt et al., *Chem. Eng. Sci.*, **61**, pp. 246–256 (2006). These methods are the subject of current research. Also see the discussion of general approaches to analyzing dispersed-phase systems given by Ramkrishna, Sathyagal, and Narsimhan [*AIChE J.*, **41**(1), pp. 35–44 (1995)]. For discussions of the effect of contaminants on mass-transfer rates, see Saïen et al., *Ind. Eng. Chem. Res.*, **45**(4), pp. 1434–1440 (2006); and Dehkordi et al., *Ind. Eng. Chem. Res.*, **46**(5), pp. 1563–1571 (2007).

Solute Diffusion and Mass-Transfer Coefficients For a binary system consisting of components A and B, the overall rate of mass transfer of component A with respect to a fixed coordinate is the sum of the rates due to diffusion and bulk flow:

$$N_A = -D_{AB} \frac{\partial C_A}{\partial z} + N_A \frac{C_A}{C} \quad (15-58)$$

where N_A = flux for component A (moles per unit area per unit time)
 D_{AB} = mutual diffusion coefficient of A into B (area/unit time)
 z = dimension or direction of mass transfer (length)
 C = total concentration of A and B (mass or mole per unit volume)
 C_A = concentration of A (mass or mole per unit volume)

Equation (15-58) is written for steady-state unidirectional diffusion in a quiescent liquid, assuming that the net transfer of component B is negligible. For transfer of component A across an interface or film between two liquids, it may be rewritten in the form

$$N_A = \frac{D_{AB}}{\Delta z(1-x_A)_m} (C_A - C_A^i) \quad (15-59)$$

where $(1-x_A)_m$ = mean mole fraction of component B
 C_A^i = concentration of component A at interface
 C_A = concentration of component A in bulk

For steady-state counter diffusion where $N_A + N_B = 0$, the flux equation simplifies to

$$N_A = \frac{D_{AB}}{\Delta z} (C_A - C_A^i) \quad (15-60)$$

The flux also may be written in terms of an individual mass-transfer coefficient k

$$N_A = k(C_A - C_A^i) \quad (15-61)$$

$$\text{where } k = \frac{D_{AB}}{\Delta z(1-x_A)_m} \quad (15-62)$$

In Eqs. (15-58) to (15-62), the flux is expressed in terms of mass or moles per unit area per unit time, and the concentration driving force is defined in terms of mass or moles per unit volume. The units of the mass-transfer coefficients are then length per unit time. Other definitions of the flux and resulting mass-transfer coefficients also are used. When mass-transfer coefficients are used, it is important to understand their definition and how they were determined; they need to be used in the same way in any subsequent calculations. Additional discussion of mass-transfer coefficients and mass-transfer rate is given in Sec. 5. Also see Laddha and Degaleesan, *Transport Phenomena in Liquid Extraction* (McGraw-Hill, 1978), Chap. 3; Skelland, *Diffusional Mass Transfer* (Krieger, 1985); Skelland and Tedder, Chap. 7 in *Handbook of Separation Process Technology*, Rousseau, ed. (Wiley, 1987); Curtiss and Bird, *Ind. Eng. Chem. Res.*, **38**(7), pp. 2515–2522 (1999); and Bird, Stewart, and Lightfoot, *Transport Phenomena*, 2d ed. (Wiley, 2002). Available correlations of molecular diffusion coefficients (diffusivities) are discussed in Sec. 5 and in Poling, Prausnitz, and O'Connell, *The Properties of Gases and Liquids*, 5th ed. (McGraw-Hill, 2000). The prediction of diffusion coefficients is discussed by Bosse and Bart, *Ind. Eng. Chem. Res.*, **45**(5), pp. 1822–1828 (2006).

Mass-Transfer Rate and Overall Mass-Transfer Coefficients

In transferring from one phase to the other, a solute must overcome certain resistances: (1) movement from the bulk of the raffinate phase to the interface; (2) movement across the interface; and (3) movement from the interface to the bulk of the extract phase, as illustrated in Fig. 15-25. The two-film theory first used to model this process [Lewis and Whitman, *Ind. Eng. Chem.*, **16**, pp. 1215–1220 (1924)] assumes that motion in the two phases is negligible near the interface such that the entire resistance to transfer is contained within two laminar films on each side of the interface, and mass transfer occurs by molecular diffusion through these films. The theory further invokes the following simplifying assumptions: (1) The rate of mass transfer within each phase is proportional to the difference in concentration in the bulk liquid and the interface; (2) mass-transfer resistance across the interface itself is negligible, and the phases are in equilibrium at the interface; and (3) steady-state diffusion occurs with negligible holdup of diffusing solute at the interface. Within a liquid-liquid extractor, the rate of steady-state mass transfer between the dispersed phase and the continuous phase (mass or moles per unit time per unit volume of extractor) is then expressed as

$$R_A = \frac{dC}{dt} = k_d a (C_{d,i} - C_d) = k_c a (C_c - C_{c,i}) \quad (15-63)$$

where C_i = concentration at interface (mass or moles per unit volume)
 C = concentration in bulk liquid (mass or moles per unit volume)
 k_c = continuous-phase mass-transfer coefficient (length per unit time)
 k_d = dispersed-phase film mass-transfer coefficient (length per unit time)
 a = interfacial area for mass transfer per unit volume of extractor (length⁻¹)

Subscripts d and c denote the dispersed and continuous phases. The concentrations at the interface normally are not known, so the rate expression is written in terms of equilibrium concentrations assuming that the rate is proportional to the deviation from equilibrium:

$$R_A = \frac{dC}{dt} = k_{oc} a (C_d^* - C_d) = k_{oc} a (C_c - C_c^*) \quad (15-64)$$

where the superscript * denotes equilibrium, and k_{oc} is an overall mass-transfer coefficient given by

$$\frac{1}{k_{oc}} = \underbrace{\frac{1}{k_c}}_{\text{Continuous phase resistance}} + \underbrace{\frac{1}{m_{dc}^* k_d}}_{\text{Dispersed phase resistance}} \quad (15-65)$$

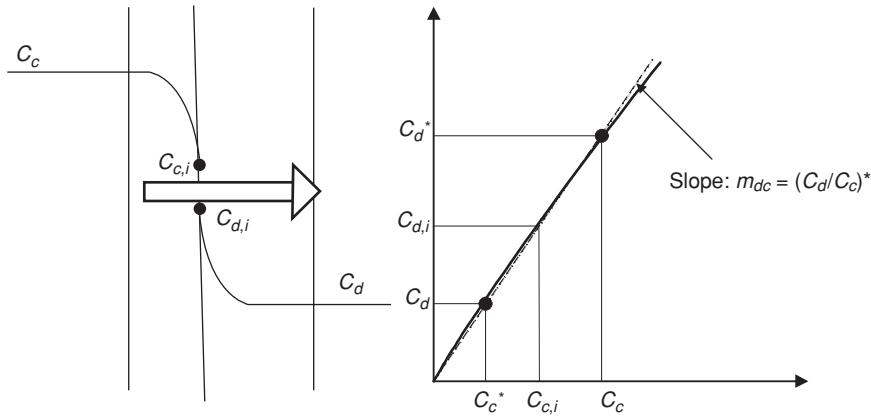


FIG. 15-25 Two-film mass transfer.

Similarly, the overall mass-transfer coefficient based on the dispersed phase is given by

$$\frac{1}{k_{od}} = \underbrace{\frac{1}{k_d}}_{\text{Dispersed phase resistance}} + \underbrace{\frac{m_{dc}^{vol}}{k_c}}_{\text{Continuous phase resistance}} \quad (15-66)$$

Assuming mass-transfer coefficients are constant over the range of conditions of interest, Eq. (15-64) may be integrated to give

$$\frac{C_c - C_c^*}{C_{c,initial} - C_c^*} = \exp(-k_{oc}a\theta) \approx \frac{C_c}{C_{c,initial}} \quad (15-67)$$

where θ is the contact time.

In Eqs. (15-65) and (15-66), $m_{dc}^{vol} = dC_d/dC_c$ is the local slope of the equilibrium line, with the equilibrium concentration of solute in the dispersed phase plotted on the ordinate (y axis), and the equilibrium concentration of solute in the continuous phase plotted on the abscissa (x axis). Note that m_{dc}^{vol} is expressed on a volumetric basis (denoted by superscript *vol*), i.e., in terms of mass or mole per unit volume, because of the way the mass-transfer coefficients are defined. The mass-transfer coefficients will not necessarily be the same for each solute being extracted, so depending upon the application, mass-transfer coefficients may need to be determined for a range of different solutes. As noted earlier, other systems of units also may be used as long as they are consistently applied.

The mass-transfer coefficient in each film is expected to depend upon molecular diffusivity, and this behavior often is represented by a power-law function $k \propto \mathcal{D}^n$. For two-film theory, $n = 1$ as discussed above [Eq. (15-62)]. Subsequent theories introduced by Higbie [Trans. AIChE, 31, p. 365 (1935)] and by Danckwerts [Ind. Eng. Chem., 43, pp. 1460–1467 (1951)] allow for surface renewal or penetration of the stagnant film. These theories indicate a 0.5 power-law relationship. Numerous models have been developed since then where $0.5 < n < 1.0$; the results depend upon such things as whether the dispersed drop is treated as a rigid sphere, as a sphere with internal circulation, or as oscillating drops. These theories are discussed by Skelland [“Interphase Mass Transfer,” Chap. 2 in *Science and Practice of Liquid-Liquid Extraction*, vol. 1, Thornton, ed. (Oxford, 1992)].

In the design of extraction equipment with complex flows, mass-transfer coefficients are determined by experiment and then correlated as a function of molecular diffusivity and system properties. The available theories provide an approximate framework for the data. The correlation constants vary depending upon the type of equipment and operating conditions. In most cases, the dominant mass-transfer resistance resides in the feed (raffinate) phase, since

the slope of the equilibrium line usually is greater than unity. In that case, the overall mass-transfer coefficient based on the raffinate phase may be written

$$\frac{1}{k_{or}} = \frac{1}{k_r} + \frac{1}{m_{dc}^{vol}k_c} \approx \frac{1}{k_r} \quad \text{for large } m_{dc}^{vol} \quad (15-68)$$

where m_{dc}^{vol} is defined by the usual convention in terms of concentration in the extract phase over that in the raffinate phase, $m_{dc}^{vol} = dC_{i,extract}/dC_{i,raffinate}$. This approximation is particularly useful when the extraction solvent is significantly less viscous than the feed liquid, so the solute diffusivity and mass-transfer coefficient in the extract phase are relatively large.

Mass-Transfer Units The mass-transfer unit concept follows directly from mass-transfer coefficients. The choice of one or the other as a basis for analyzing a given application often is one of preference. Colburn [Ind. Eng. Chem., 33(4), pp. 450–467 (1941)] provides an early review of the relationship between the height of a transfer unit and volumetric mass-transfer coefficients ($k_{or}a$). From a differential material balance and application of the flux equations, the required contacting height of an extraction column is related to the height of a transfer unit and the number of transfer units

$$Z_t = \left(\frac{V_r}{k_{or}a} \right) \int_{X_{out}}^{X_{in}} \frac{dX}{X - X^*} = H_{or} \times N_{or} \quad (15-69)$$

where V_r is the velocity of the raffinate phase, a is the interfacial area per unit volume, and the superscript * denotes the equilibrium concentration. The transfer unit model has proved to be a convenient framework for characterizing mass-transfer performance.

Thus, mass-transfer units are defined as the integral of the differential change in solute concentration divided by the deviation from equilibrium, between the limits of inlet and outlet solute concentrations:

$$N_{or} = \int_{X_{out}}^{X_{in}} \frac{dX}{X - X^*} \quad (15-70)$$

When the equilibrium and operating lines are linear, the solution to Eq. (15-70) can be expressed as

$$N_{or} = \frac{\ln \left[\left(\frac{X'_f - Y'_s/m'}{X'_r - Y'_s/m'} \right) \left(1 - \frac{1}{E} \right) + \frac{1}{E} \right]}{1 - \frac{1}{E}} \quad E = m' \frac{S'}{F'}, E \neq 1 \quad (15-71)$$

where N_{or} is the number of overall mass-transfer units based on the raffinate phase. The units are the same as those used previously for the KSB equation [(Eq. 15-48)]. Rearranging Eq. (15-71) gives

$$\frac{X'_f - Y'_f/m'}{X'_r - Y'_r/m'} = \frac{\exp[N_{or}(1 - 1/\mathcal{E})] - 1/\mathcal{E}}{1 - 1/\mathcal{E}} \quad (15-72)$$

Note that Eq. (15-71) is the same as the KSB equation except in the denominator. Comparing these equations shows that the number of overall raffinate phase transfer units is related to the number of theoretical stages by

$$N_{or} = N \times \frac{\ln \mathcal{E}}{1 - 1/\mathcal{E}} \quad (15-73)$$

The difference becomes pronounced when values of the extraction factor are high. When $\mathcal{E} = 1$, the number of mass-transfer units and number of theoretical stages are the same:

$$N_{or} = N = \frac{X'_f - Y'_f/m'}{X'_r - Y'_r/m'} - 1 \quad \text{for } \mathcal{E} = 1 \quad (15-74)$$

As with the KSB equation, in the special case where $\mathcal{E} < 1$, the maximum performance potential is represented by

$$\left(\frac{X'_f - Y'_f/m'}{X'_r - Y'_r/m'} \right)_{\max} \approx \frac{1}{1 - \mathcal{E}} \quad \text{for } \mathcal{E} < 1 \text{ and large } N_{or} \quad (15-75)$$

Equation (15-71) often is referred to as the Colburn equation. Although commonly used to represent the performance of a differential contactor, it models any steady-state, diffusion-controlled processes with straight equilibrium and operating lines. As with the KSB equation, the operating line is straight even when solute concentration changes significantly as long as Bancroft coordinates are used, and both the KSB and Colburn equations can be used to model applications involving a highly curved equilibrium line by dividing the analysis into linear segments. With these approaches, these equations often can be used for applications involving high concentrations of solute.

Solutions to the Colburn equation are shown graphically in Fig. 15-26. Note the contrast to the KSB equation solutions shown in Fig. 15-24. The KSB equations are best used to model countercurrent contact devices where the separation is primarily governed by equilibrium limitations, such as extractors involving discrete stages with high stage efficiencies. The Colburn equation, on the other hand, better represents the performance of a diffusion rate-controlled contactor because performance approaches a definite limit as the extraction factor increases beyond $\mathcal{E} = 10$ or so, corresponding to a diffusion rate limitation where addition of extra solvent has little or no effect. Note that in Eq. (15-71) the extraction factor always appears as $1/\mathcal{E}$, and this is how a finite diffusion rate is taken into account. The KSB equation can be misleading in this regard because it predicts continued improvement as the extraction factor increases without limit. Rate-based models most often are utilized for applications with no discrete stages; however, even staged equipment may be modeled best by the number of mass-transfer units when the extraction factor is higher than about 3, especially when stage efficiencies are low.

The height of an overall mass-transfer unit based on raffinate phase compositions H_{or} is the total contacting height Z_t divided by the number of transfer units achieved by the column.

$$H_{or} = \frac{Z_t}{N_{or}} \quad (15-76)$$

The value of H_{or} is the sum of contributions from the resistance to mass transfer in the raffinate phase (H_r) plus resistance to mass transfer in the extract phase (H_e) divided by the extraction factor \mathcal{E} :

$$H_{or} = H_r + \frac{H_e}{\mathcal{E}} \quad (15-77)$$

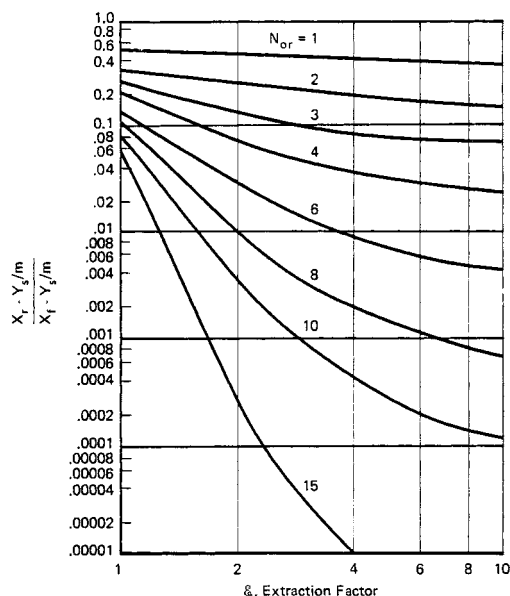


FIG. 15-26 Graphical solutions to the Colburn equation [Eq. (15-71)].

The individual transfer unit heights are given by

$$H_r = \frac{Q_r}{A_{col} k_r a} \quad (15-78)$$

$$H_e = \frac{Q_e}{A_{col} k_e a} \quad (15-79)$$

where Q = volumetric flow rate

A_{col} = column cross-sectional area

k = film mass-transfer coefficient (length per unit time)

a = interfacial mass-transfer area per unit volume of extractor

and subscripts r and e denote the raffinate and extract phases, respectively. As discussed earlier, the main resistance to mass transfer generally resides in the feed (raffinate) phase.

The lumped parameter H_{or} often is employed for design of extraction columns. Its value reflects the efficiency of the differential contactor; higher contacting efficiency is reflected in a lower value of H_{or} . It deals directly with the ultimate design criterion, the height of the column, and reliable values often can be obtained from miniplant experiments and experience with commercial units. For processes with discrete contacting stages, mass-transfer efficiency may be expressed as the number of transfer units achieved per actual stage. For applications involving transfer of multiple solutes, the value of H_{or} or N_{or} per actual stage may differ for each solute, as discussed earlier with regard to stage efficiencies and mass-transfer coefficients.

EXTRACTION FACTOR AND GENERAL PERFORMANCE TRENDS

Because of their simplicity, the KSB equation [Eq. (15-48)] and Colburn equation [Eq. (15-71)] are useful for illustrating a number of general trends in mass-transfer performance, in particular, helping to show how the extraction factor is related to process performance for different process configurations. For illustration, consider a dilute system involving immiscible liquids and zero solute concentration in the entering extraction solvent. The resulting expressions that follow are written in a general form without regard to a specific set of units.

15-50 LIQUID-LIQUID EXTRACTION AND OTHER LIQUID-LIQUID OPERATIONS AND EQUIPMENT

For a single-stage batch process or a continuous extraction process that achieves one theoretical stage, the solute reduction factor is given by

$$F_R = \frac{X_{in}}{X_{out}} = \frac{\mathcal{E} - 1/\mathcal{E}}{1 - 1/\mathcal{E}} \quad \text{for } N = 1 \quad (15-80)$$

The required solvent-to-feed ratio is then approximated by

$$\frac{S}{F} = \frac{F_R - 1}{K} \quad \text{for } N = 1 \quad (15-81)$$

After extraction, the concentration of solute in the extract, no matter what the extraction configuration, is given by

$$Y_{out} = \frac{X_{in}}{S/F} \left(1 - \frac{1}{F_R} \right) \quad \text{for } Y_{in} = 0 \quad (15-82)$$

Equation (15-82) follows from Eq. (15-47).

If the performance of a single-stage extraction is not adequate, repeated cross-current extractions can be carried out to increase solute recovery or removal. For this configuration, the reduction factor is given by

$$F_R = \left(1 + \frac{\mathcal{E}}{N} \right)^{\xi_o N} \quad \text{for cross-current operation} \quad (15-83)$$

where N is the number of repeated extractions or stages employing equal amounts of solvent, ξ_o is overall stage efficiency, and the extraction factor is expressed in terms of the total amount of solvent used by the process. Although high solute recoveries can be obtained by using cross-current processing, the required solvent usage will be high, as indicated by

$$\frac{S}{F} = \frac{N}{K} (F_R^{\xi_o N} - 1) \quad \text{for cross-current-operation} \quad (15-84)$$

where S is the total amount of solvent. The concentration of solute in the combined extract will be low, as calculated by using Eq. (15-82). Comparing the results of Eqs. (15-80) and (15-81) with Eqs. (15-83) and (15-84) will show that multistage cross-current extraction yields improved performance relative to using single-stage extraction with the same total amount of solvent, but at the cost of additional contacting steps.

Compared to single-stage or cross-current processing, multistage, countercurrent processing allows a significant reduction in solvent use or an increase in separation performance. For this type of process, the reduction factor is approximated by

$$F_R = \frac{\mathcal{E}^{\xi_o N} - 1/\mathcal{E}}{1 - 1/\mathcal{E}} \quad \text{for countercurrent operation} \quad (15-85)$$

Inspection of Eqs. (15-80) and (15-85) will show how the addition of countercurrent stages magnifies the effect of the extraction factor on performance. Note that Eq. (15-85) predicts that performance will continue to improve as the value of \mathcal{E} increases, approaching $F_R = \mathcal{E}^{\xi_o N}$ at high values of \mathcal{E} . However, stage efficiency must remain high, and this likely will require a change in some operating variable such as residence time per stage.

Multistage countercurrent processing may be practiced batchwise as well as in a continuous cascade. A batchwise countercurrent operation involves first treating a batch with extract solution as the extract leaves the process, and the last treatment is carried out by using fresh solvent as it enters the process (as in Figs. 15-6 and 15-22). A multistage, countercurrent process with discrete contacting stages (practiced either batchwise or using a continuous cascade) is well suited to applications with fairly slow rates of mass transfer because liquid-

liquid contacting is carried out stagewise in separate vessels or compartments, and long residence times can be designed into each stage.

For a countercurrent extraction column with no discrete stages (or for processes operated within a diffusion-controlled regime far from equilibrium), performance is well modeled by the Colburn equation, where

$$F_R = \frac{\exp [N_{or}(1 - 1/\mathcal{E})] - 1/\mathcal{E}}{1 - 1/\mathcal{E}} \quad \text{for countercurrent operation} \quad (15-86)$$

$$\text{and} \quad Z_t = N_{or} \times H_{or} \quad (15-87)$$

Extraction columns are most attractive for applications with fairly fast mass transfer because residence time in the column is limited. Performance becomes mass-transfer-limited at high values of \mathcal{E} , approaching $F_R = \exp N_{or}$. At this point, a significant increase in performance can be achieved only by adding transfer units (column height).

With countercurrent processing, carried out using either a multistage cascade or an extraction column, the required solvent-to-feed ratio generally can be reduced by adding more and more stages or transfer units. As discussed in "Minimum and Maximum Solvent-to-Feed Ratios," the minimum practical solvent-to-feed ratio is approximated by

$$\left(\frac{S}{F} \right)_{\min} \approx \frac{1.3}{K} \quad \text{for countercurrent processing} \quad (15-88)$$

Below this value, the required number of stages or transfer units increases rapidly. At $\mathcal{E} = 1$, the number of theoretical stages and number of transfer units are equal, and

$$F_R = N + 1 = N_{or} + 1 \quad \text{for } \mathcal{E} = 1 \quad (15-89)$$

For $\mathcal{E} < 1$, the fraction of solute removed from the feed θ_i will approach a value equal to the extraction factor. In this case,

$$(F_R)_{\max} = \frac{1}{1 - \mathcal{E}} \quad \text{for } \mathcal{E} < 1 \quad (15-90)$$

POTENTIAL FOR SOLUTE PURIFICATION USING STANDARD EXTRACTION

As noted earlier, the ability of a standard extraction process to isolate a desired solute from other solutes is limited. This can be illustrated by using the KSB equation [Eq. (15-48)] to calculate solute transfer for a dilute feed containing a desired solute i and an impurity solute j . On a solvent-free basis, the purity of solute i in the feed is given by

$$P_{i,\text{feed}} (\text{in units of wt } \%) = 100 \left(\frac{X''_{i,\text{feed}}}{X''_{i,\text{feed}} + X''_{j,\text{feed}}} \right) \quad (15-91)$$

Similarly, the purity of solute i in the extract is given by

$$P_{i,\text{extract}} (\text{wt } \%) = 100 \left(\frac{\theta_i X''_{i,\text{feed}}}{\theta_i X''_{i,\text{feed}} + \theta_j X''_{j,\text{feed}}} \right) \quad (15-92)$$

where θ_i is the fraction of solute extracted from the feed into the extract. By using the KSB equation to estimate θ for solutes i and j , the following expression is derived:

$$\begin{aligned} P_{i,\text{extract}} (\text{wt } \%) &= \frac{100}{1 + \left(\frac{\theta_j}{\theta_i} \right) \left(\frac{X''_{j,\text{feed}}}{X''_{i,\text{feed}}} \right)} \\ &= \frac{100}{1 + \left(\frac{\mathcal{E}_j^N - 1}{\mathcal{E}_i^N - 1} \right) \left(\frac{\mathcal{E}_i^N - 1/\mathcal{E}_i}{\mathcal{E}_j^N - 1/\mathcal{E}_j} \right) \left(\frac{X''_{j,\text{feed}}}{X''_{i,\text{feed}}} \right)} \quad \text{for } \mathcal{E} \neq 1.0 \end{aligned} \quad (15-93)$$

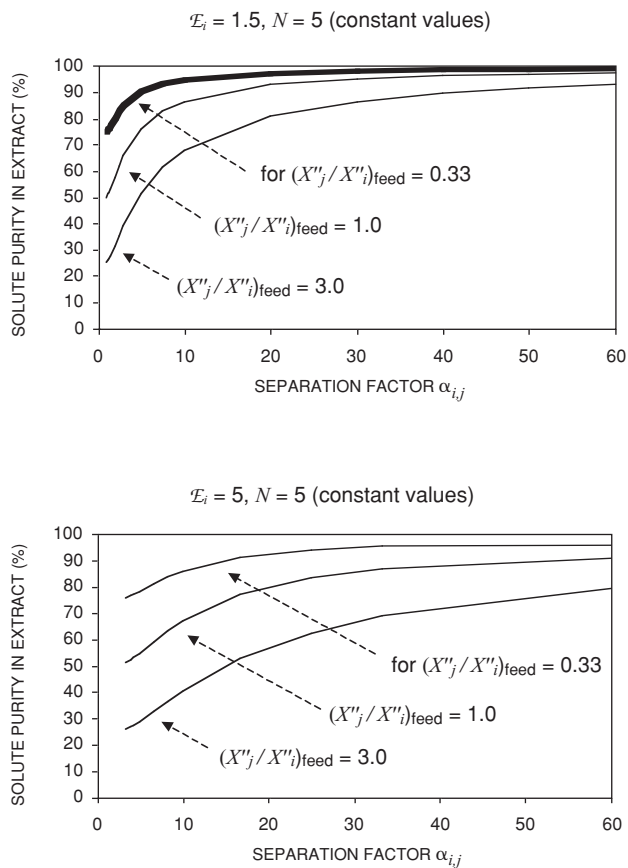


FIG. 15-27 Approximate purity of solute i in the extract ($P_{i,\text{extract}}$) versus separation factor $\alpha_{i,j}$ for standard extraction involving dilute feeds containing solutes i and j . Results obtained by using Eq. (15-93). Concentrations are in mass fraction (X'').

Equation (15-93) assumes that no solute enters the process with the extraction solvent and that \mathcal{E}_i and \mathcal{E}_j are constant. An alternative expression can be written in terms of transfer units; however, the calculated results are essentially the same as a function of the number of stages or the number of transfer units—because the models assume that both solute i and solute j experience the same mass-transfer resistance. Example results obtained by using Eq. (15-93) are shown in Fig. 15-27. Note that performance is not uniquely determined by a given value of $\alpha_{i,j} = K_i/K_j = \mathcal{E}_i/\mathcal{E}_j$, but depends upon the absolute value of \mathcal{E}_i , as well. In principle, the purity of solute i in the extract will approach a maximum value as the number of stages or transfer units

approaches infinity:

$$\text{Maximum } P_{i,\text{extract}} (\%) = 100 \div \left[1 + \frac{1}{\alpha_{i,j}} \left(\frac{X''_{j,\text{feed}}}{X''_{i,\text{feed}}} \right) \right] \quad \text{in limit as } N \rightarrow \infty \quad (15-94)$$

Of course, this theoretical maximum can never be attained in practice. Equation (15-94) follows from Eq. (15-93), noting that $\theta_j/\theta_i = 1/\alpha_{i,j}$ for $N \rightarrow \infty$ as discussed by Brian [*Staged Cascades in Chemical Processing* (Prentice-Hall, 1972), p. 50]. As noted earlier, the ability to purify a desired solute is greatly enhanced by using fractional extraction (see “Fractional Extraction Calculations”).

CALCULATION PROCEDURES

SHORTCUT CALCULATIONS

Shortcut calculations can be quite useful to the process designer or run-plant engineer; they may be used to outline process requirements (stream and equipment sizes) early in a design project, to check the output of a process simulation program for reasonableness, to help analyze or troubleshoot a unit operating in the manufacturing plant or pilot plant, or to help explain performance trends and relationships between key process variables. In some applications involving dilute

or even moderately concentrated feeds, they also may be used to specify the final design of an extraction process. In carrying out such calculations, Robbins [Sec. 1.9 in *Handbook of Separation Techniques for Chemical Engineers*, Schweitzer, ed. (McGraw-Hill, 1997)] indicates that most liquid-liquid extraction systems can be treated as having immiscible solvents (case *A*), partially miscible solvents with a low solute concentration in the extract (case *B*), or partially miscible solvents with a high solute concentration in the extract (case *C*). These cases are illustrated in Examples 1 through 3 below.

Example 1: Shortcut Calculation, Case A Consider a 100-kg/h feed stream containing 20 wt % acetic acid in water that is to be extracted with 200 kg/h of recycle MIBK that contains 0.1 wt % acetic acid and 0.01 wt % water. The aqueous raffinate is to be extracted down to 1% acetic acid. How many theoretical stages will be required and what will the extract composition be? The equilibrium data for this system are listed in Table 15-8 (in units of weight percent). The corresponding Hand plot is shown in Fig. 15-20. The Hand correlation (in mass ratio units) can be expressed as $Y' = 0.930(X')^{1.10}$, for X' between 0.03 and 0.25.

Assuming immiscible solvents, we have

$$F' = 100(1 - 0.2) = 80 \text{ kg water/h}$$

$$X'_f = \frac{0.2}{0.8} = 0.25 \text{ kg acetic acid/kg water}$$

$$X'_r = \frac{0.01}{0.99} = 0.01 \text{ kg acetic acid/kg water}$$

$$S' = 200(1 - 0.001) = 199.8 \text{ kg MIBK/h}$$

$$Y'_s = \frac{0.2}{199.8} = 0.001 \text{ kg acetic acid/kg MIBK}$$

If we assume $R' = F'$ and $E' = S'$, we can calculate Y'_e from Eq. (15-47):

$$Y'_e = \frac{80(0.25) + 199.8(0.001) - 80(0.01)}{199.8} = 0.097 \frac{\text{kg acetic acid}}{\text{kg MIBK}}$$

Calculate $X'_1 = (0.097/0.930)^{1/1.10} = 0.128$. Then

$$m'_1 = \frac{dY'}{dX'} = (0.930)(1.10)(X')^{0.1} \quad \text{for } X' \text{ between } 0.03 \text{ and } 0.25$$

$$m'_1 = 0.833 \quad \text{at } X' = 0.128$$

$$m'_r = \frac{dY'}{dX'} = K' = 0.656 \quad \text{for } X' \text{ below } 0.03$$

$$K'_r = 0.656 \quad \text{at } Y'_r = 0.001$$

$$\mathcal{E} = \sqrt{m'_1 m'_r} \frac{S'}{F'} = \frac{0.739(199.8)}{80} = 1.85$$

And N is determined from Fig. 15-24 and Eq. (15-48).

$$N = \frac{\ln \left[\frac{(0.25 - 0.001/0.656)}{(0.01 - 0.001/0.656)} \left(1 - \frac{1}{1.85} \right) + \frac{1}{1.85} \right]}{\ln 1.85} = 4.3 \text{ theoretical stages}$$

This result is very close to that obtained by using a McCabe-Thiele diagram (Fig. 15-23). From solubility data at $Y' = 0.1039$ kg acetic acid/kg MIBK (given in Table 15-8), the extract layer contains $5.4/85.7 = 0.0630$ kg water/kg MIBK, and $Y'_e = (0.097)/(1 + 0.097 + 0.063) = 0.084$ mass fraction acetic acid in the extract.

For cases B and C , Robbins developed the concept of pseudosolute concentrations for the feed and solvent streams entering the extractor that will allow the KSB equations to be used. In case B the solvents are partially miscible, and the miscibility is nearly constant through the extractor. This frequently occurs when all solute concentrations are relatively low. The feed stream is assumed to dissolve extraction solvent only in the feed stage and to retain the same amount throughout the extractor. Likewise, the extraction solvent is assumed to dissolve feed solvent only in the raffinate stage. With these assumptions the primary extraction solvent rate moving through the extractor is

assumed to be S' , and the primary feed solvent rate is assumed to be F' . The extract rate E' is less than S' , and the raffinate rate R' is less than F' because of solvent mutual solubilities.

The slope of the operating line is F'/S' , just as in Eqs. (15-45) and (15-46), but only stages 2 through $r - 1$ will fall directly on the operating line. And X'_1 must be on the equilibrium line in equilibrium with Y'_e by definition. One can also calculate a pseudofeed concentration X'_f^B that will fall on the operating line at $Y'_{r+1} = Y'_e$ as follows:

$$X'_f^B = X'_f + \frac{S' - E'}{F'} Y'_e \quad (15-95)$$

Likewise, one knows that Y'_r will be on the equilibrium line with X'_r . One can therefore calculate a pseudoconcentration of solute in the inlet extraction solvent Y'_s^B that will fall on the operating line where $X'_{r-1} = X'_r$, as follows:

$$Y'_s^B = Y'_s + \frac{F' - R'}{S'} X'_r \quad (15-96)$$

For case B , the pseudo inlet concentration X'_f^B can be used in the KSB equation with the actual value of X'_r and $\mathcal{E} = m'S'/F'$ to calculate rapidly the number of theoretical stages required. The graphical stepwise method illustrated in Fig. 15-23 also can be used. The operating line will go through points (X'_r, Y'_s) and (X'_f^B, Y'_e) with a slope of F'/S' .

Example 2: Shortcut Calculation, Case B Let us solve the problem in Example 1 by assuming case B . The solute (acetic acid) concentration is low enough in the extract that we may assume that the mutual solubilities of the solvents remain nearly constant. The material balance can be calculated by an iterative method.

From equilibrium data (Table 15-8) the extraction solvent (MIBK) loss in the raffinate will be about $0.016/0.984 = 0.0163$ kg MIBK/kg water, and the feed solvent (water) loss in the extract will be about $5.4/85.7 = 0.0630$ kg water/kg MIBK.

First iteration: Assume $R' = F' = 80$ kg water/h. Then extraction solvent in raffinate = $(0.0163)(80) = 1.30$ kg MIBK/h. Estimate $E' = 199.8 - 1.3 = 198.5$ kg MIBK/h. Then feed solvent in extract = $(0.063)(198.5) = 12.5$ kg water/h.

Second iteration: Calculate $R' = 80 - (0.063)(198.7) = 67.5$ kg water/h. And $E' = 199.8 - (0.0163)(67.5) = 198.7$ kg MIBK/h.

Third iteration: Converge $R' = 80 - (0.063)(198.7) = 67.5$ kg water/h. And Y'_e is calculated from the overall extractor material balance [(Eq. (15-47))]:

$$Y'_e = \frac{(80)(0.25) + (199.8)(0.001) - (67.5)(0.01)}{198.7} = 0.0983 \frac{\text{kg acetic acid}}{\text{kg MIBK}}$$

$$Y'_e = \frac{0.0983}{1 + 0.0983 + 0.0630} = 0.0846 \text{ mass fraction acetic acid in extract}$$

From the Hand correlation of equilibrium data,

$$Y'_e = 0.930(X')^{1.10} \quad \text{for } X' \text{ between } 0.03 \text{ and } 0.25$$

The raffinate composition leaving the feed (first stage) is

$$X'_1 = \left(\frac{0.0983}{0.930} \right)^{1/1.10} = 0.130$$

$$m'_1 = \frac{dY'}{dX'} = (0.930)(1.10)(X')^{0.1}$$

TABLE 15-8 Water + Acetic Acid + Methyl Isobutyl Ketone Equilibrium Data at 25°C

Weight percent in raffinate			X'	Weight percent in extract			Y'
Water	Acetic acid	MIBK	Acetic acid	Water	Acetic acid	MIBK	Acetic acid
98.45	0	1.55	0	2.12	0	97.88	0
95.46	2.85	1.7	0.0299	2.80	1.87	95.33	0.0196
85.8	11.7	2.5	0.1364	5.4	8.9	85.7	0.1039
75.7	20.5	3.8	0.2708	9.2	17.3	73.5	0.2354
67.8	26.2	6.0	0.3864	14.5	24.6	60.9	0.4039
55.0	32.8	12.2	0.5964	22.0	30.8	47.2	0.6525
42.9	34.6	22.5	0.8065	31.0	33.6	35.4	0.9492

SOURCE: Sherwood, Evans, and Longcor, *Ind. Eng. Chem.*, **31**(9), pp. 1144-1150 (1939).

$$\begin{aligned}
 m'_r &= \frac{dY}{dX} = K' = 0.656 \\
 m'_1 &= 0.834 \quad \text{at } X'_1 = 0.13 \\
 m'_r &= 0.656 \quad \text{at } X'_r = 0.01 \\
 K'_s &= 0.656 \quad \text{at } Y'_s = 0.001 \\
 E &= \sqrt{m'_1 m'_r} \frac{S'}{F'} = \frac{(0.740)(199.8)}{80} = 1.85
 \end{aligned}$$

And X_f^B is calculated from Eq. (15-95)

$$X_f^B = 0.25 + \frac{(199.8 - 198.7)(0.0983)}{80} = 0.251$$

and Y_s^B from Eq. (15-96):

$$Y_s^B = 0.001 + \frac{(80 - 67.5)(0.01)}{199.8} = 0.0016$$

Now N is determined from Fig. 15-24, Eq. (15-48), or the McCabe-Thiele type of plot (Fig. 15-23). For case B ,

$$N = \frac{\ln \left[\left(\frac{0.251 - 0.0016/0.656}{0.01 - 0.0016/0.656} \right) \left(1 - \frac{1}{1.85} \right) + \frac{1}{1.85} \right]}{\ln 1.85} = 4.5 \text{ theoretical stages}$$

A less frequent situation, case C , can occur when the solute concentration in the extract is so high that a large amount of feed solvent is dissolved in the extract stream in the "feed stage" but a relatively small amount of feed solvent (say one-tenth as much) is dissolved by the extract stream in the "raffinate stage." The feed stream is assumed to dissolve the extraction solvent only in the feed stage just as in case B . But the extract stream is assumed to dissolve a large amount of feed solvent leaving the feed stage and a negligible amount leaving the raffinate stage. With these assumptions the primary feed solvent rate is assumed to be R' , so the slope of the operating line for case C is R'/S' . Again the extract rate E' is less than S' , and the raffinate rate R' is less than F' .

The pseudofeed concentration for case C , X_f^C , can be calculated from

$$X_f^C = \frac{F'}{R'} X_f' + \frac{S' - E'}{R'} Y_e' \quad (15-97)$$

For case C , the value of Y'_s will fall on the operating line, and the extraction factor is given by

$$E^C = \frac{m' S'}{R'} \quad (15-98)$$

On an X' - Y' diagram for case C , the operating line will go through points (X'_r, Y'_r) and (X_f^C, Y_e') with a slope of R'/S' similar to Fig. 15-23. When the KSB equation is used for case C , use the pseudofeed concentration X_f^C from Eq. (15-97) and the extraction factor E^C from Eq. (15-98). The raffinate concentration X'_r and inlet solvent concentration Y'_s are used without modification. For more detailed discussion, see Robbins, Sec. 1.9 in *Handbook of Separation Techniques for Chemical Engineers*, Schweitzer, ed. (McGraw-Hill, 1997).

Example 3: Number of Transfer Units Let us calculate the number of transfer units required to achieve the separation in Example 1. The solution to the problem is the same as in Example 1 except that the denominator is changed. From Eq. (15-73):

$$N_{or} = 4.5 \frac{\ln 1.85}{1 - 1/1.85} = 6.0 \text{ transfers units}$$

COMPUTER-AIDED CALCULATIONS (SIMULATIONS)

A number of process simulation programs such as Aspen Plus[®] from Aspen Technology, HYSYS[®] from Honeywell, ChemCAD[®] from Chemstations, and PRO/II[®] from SimSci E&S, among others, can

facilitate rigorous calculation of the number of theoretical stages required by a given application, provided an accurate liquid-liquid equilibrium model is employed. At the time of this writing, commercially available simulation packages do not include rate-based programs specifically designed for extraction process simulation; however, the equivalent number of transfer units at each stage can be calculated from knowledge of the extraction factor by using Eq. (15-73). Process simulation programs are particularly useful for concentrated systems that exhibit highly nonlinear equilibrium and operating lines, significant change in extract and raffinate flow rates within the process due to transfer of solute from one phase to the other, significant changes in the mutual solubility of the two phases as solute concentration changes, or nonisothermal operation. They also facilitate convenient calculation for complex extraction configurations such as fractional extraction with extract reflux as well as calculations involving more than three components (more than one solute). They can also facilitate process optimization by allowing rapid evaluation of numerous design cases. These programs do not provide information about mass-transfer performance in terms of stage efficiencies or extraction column height requirements, or information about the throughput and flooding characteristics of the equipment; these factors must be determined separately by using other methods. The use of simulation software to analyze extraction processes is illustrated in Examples 4 and 5.

In using simulation software, it is important to keep in mind that the quality of the results is highly dependent upon the quality of the liquid-liquid equilibrium (LLE) model programmed into the simulation. In most cases, an experimentally validated model will be needed because UNIFAC and other estimation methods are not sufficiently accurate. It also is important to recognize, as mentioned in earlier discussions, that binary interaction parameters determined by regression of vapor-liquid equilibrium (VLE) data cannot be relied upon to accurately model the LLE behavior for the same system. On the other hand, a set of binary interaction parameters that model LLE behavior properly often will provide a reasonable VLE fit for the same system—because pure-component vapor pressures often dominate the calculation of VLE.

Commercially available simulation programs often are used in a fashion similar to the classic graphical methods. When separation of specific solutes is important, the design of a new process generally focuses on determining the optimum solvent rates and number of theoretical stages needed to comply with the separation specifications according to relative K values for solutes of interest. Calculations often are made by focusing on a "soluble" key solute with a relatively high K value, and an "insoluble" key solute, expressing the design specification in terms of the maximum concentration of soluble key left in the raffinate and the maximum concentration of insoluble key contaminating the extract (analogous to light and heavy key components in distillation design). Then solutes with K values higher than that of the soluble key will go out with the extract to a greater extent, and solutes with K values less than that of the insoluble key will go out with the raffinate. If the desired separation is not feasible using a standard extraction scheme, then fractional extraction schemes should be evaluated.

For rating an existing extractor, the designer must make an estimate of the number of theoretical stages the unit can deliver and then determine the concentrations of key solutes in extract and raffinate streams as a function of the solvent-to-feed ratio, keeping in mind the fact that the number of theoretical stages a unit can deliver can vary depending upon operating conditions.

The use of process simulation software for process design is discussed by Seider, Seader, and Lewin [*Product and Process Design Principles: Synthesis, Analysis, and Evaluation*, 2d ed. (Wiley, 2004)] and by Turton et al. [*Analysis, Synthesis, and Design of Chemical Processes*, 2d ed. (Prentice-Hall, 2002)]. Various computational procedures for extraction simulation are discussed by Steiner [Chap. 6 in *Liquid-Liquid Extraction Equipment*, Godfrey and Slater, eds. (Wiley, 1994)]. In addition, a number of authors have developed specialized methods of analysis. For example, Sanpui, Singh, and Khanna [*AIChE J.*, **50**(2), pp. 368–381 (2004)] outline a computer-based approach to rate-based, nonisothermal modeling of extraction processes. Harjo,

Ng, and Wibowo [*Ind. Eng. Chem. Res.*, **43**(14), pp. 3566–3576 (2004)] describe methods for visualization of high-dimensional liquid-liquid equilibrium phase diagrams as an aid to process conceptualization. Since in general it is not economically feasible to generate precise phase equilibrium data for the entire multicomponent phase diagram, this methodology can help focus the design effort by identifying specific composition regions where the design analysis will be particularly sensitive to uncertainties in the equilibrium behavior. The method of Minotti, Doherty, and Malone [*Ind. Eng. Chem. Res.*, **35**(8), pp. 2672–2681 (1996)] facilitates a feasibility analysis of potential solvents and process options by locating fixed points or pinches in the composition profiles determined by equilibrium and operating constraints. Marcilla et al. [*Ind. Eng. Chem., Res.*, **38**(8), pp. 3083–3095 (1999)] developed a method involving correlation of tie lines to calculate equilibrium compositions at each stage without iterations. To optimize the design and operating parameters of an extraction cascade, Reyes-Labarta and Grossmann [*AIChE J.*, **47**(10), pp. 2243–2252 (2001)] have proposed a calculation framework that employs nonlinear programming techniques to systematically evaluate a wide range of potential process configurations and interconnections. Focusing on another aspect of process design, Ravi and Rao [*Ind. Eng. Chem. Res.*, **44**(26), pp. 10016–10020 (2005)] provide an analysis of the phase rule (number of degrees of freedom) for liquid-liquid extraction processes. For discussion of reactive extraction process conceptualization methods, see Samant and Ng, *AIChE J.*, **44**(12), pp. 2689–2702 (1998); and Gorissen, *Chem. Eng. Sci.*, **58**, pp. 809–814 (2003).

Example 4: Extraction of Phenol from Wastewater The amount of 350 gpm (79.5 m³/h) of wastewater from a coke oven plant contains an average of 700 ppm phenol by weight that needs to be reduced to 1 ppm or less to meet environmental requirements [Karr and Ramanujam, *St. Louis AIChE Symp.* (March 19, 1987)]. The wastewater comes from the bottom of an ammonia stripping tower at 105°C and is to be extracted at 1.7 atm with recycle methylisobutyl ketone (MIBK) containing 5 ppm phenol. The extraction will be carried out by using a reciprocating-plate extractor (Karr column). How many theoretical stages will be required in the extractor at a solvent-to-feed ratio of 1:15, and what is the resulting extract composition?

The Aspen Plus® process simulation program is used in this example, but it should be recognized that any of a number of process simulation programs such as mentioned above may be used for this purpose. In Aspen Plus, the EXTRACT liquid-liquid extraction unit-operation block is used to model the phenol wastewater extraction. As is typical in process simulation programs, the EXTRACT block is fundamentally a rating calculation rather than a design calculation, so the determination of the required number of stages for the separation cannot be made directly. In addition, since the EXTRACT block can only handle integral numbers of theoretical stages, the fractional number of required theoretical stages must be determined by an interpolation method.

The partition ratio for transfer of phenol from water into MIBK at 105°C is $K'' = 34$ on a mass fraction basis [Greminger et al., *Ind. Eng. Chem. Process Des. Dev.*, **21**(1), pp. 51–54 (1982)]. Because the partition ratio is so high, a fairly low solvent-to-feed ratio of 1:15 can be used and still give an extraction factor of about 2. In the EXTRACT block, a property option is available that allows the user to specify liquid-liquid K value correlations (designated as “KLL Correlation” in Aspen Plus) for the components involved in the extraction rather than a complete set of binary interaction parameters to define the liquid-liquid equilibria. In this example, it is time-consuming to regress a set of liquid-liquid binary interaction parameters that results in representative partition ratios, so the option of simply specifying K values directly is highly recommended.

Because phenol will be relatively dilute in both the raffinate and extract phases, appropriate liquid-liquid K values for distribution of water and MIBK between phases at 105°C can be estimated from water-MIBK liquid-liquid equilibrium data [Rehak et al., *Collect. Czech Chem. Commun.*, **65**, pp. 1471–1486 (2000)] to yield $K''_{\text{water}} = 0.0532$ and $K''_{\text{MIBK}} = 53.8$ (mass fraction basis). It is important in Aspen Plus to specify K values for all the components in the extractor in order to properly model the liquid-liquid equilibria with this approach.

The temperatures and compositions of the wastewater and solvent feed streams, as well as the wastewater feed flow rate, are specified in the problem statement. The solvent flow rate is specified as one-fifteenth of the wastewater flow rate as described above. In the EXTRACT block, the number of stages will be manually varied from 2 to 10 to observe the effect on the raffinate and extract concentrations, and it will be specified as operating adiabatically at 1.7 atm. Water is specified as the key component in the first liquid phase, and MIBK is specified as the key component in the second liquid phase. The rest of the block parameters (convergence, report, and miscellaneous block options) are allowed to remain at their default values.

The raffinate and extract concentrations resulting from successive simulation runs for 2 through 10 theoretical stages are given in Table 15-9, and the raffinate phenol concentrations are presented graphically in Fig. 15-28. Examining the results, we can see that the number of theoretical stages required to achieve the 1 ppm phenol discharge limitation falls somewhere between 7 and 8. In addition, we can see from Fig. 15-28 that the dependence of raffinate phenol concentration on number of stages yields nearly a straight line on a semilog plot. As a result, performing a linear interpolation of the log of the raffinate concentration between 7 and 8 stages yields the number of stages required to achieve 1 ppm phenol in the raffinate:

$$N = 7 + (8 - 7) \left(\frac{\log 1.47 - \log 1}{\log 1.47 - \log 0.707} \right) = 7.53 \text{ theoretical stages}$$

From examining the extract phenol concentrations in Table 15-9, it is clear that for 5 or more stages, they varied little with number of stages, as is expected since nearly all the phenol contained in the wastewater feed was extracted in stages 1 through 4. As a result, the extract will contain 1.3 wt % phenol, 5.2% water, and 93.5% MIBK.

The simulation results can be checked by using a shortcut calculation—to provide confidence that the simulation is delivering a reasonable result. The KSB equation [Eq. (15-48)] can be used for this purpose with values taken from the problem specification and estimates of the phenol K' value (in Bancroft coordinates). Since phenol is always quite dilute in both the extract and raffinate phases, its K' value can be calculated from the component mass fraction K'' values according to the following approximation:

$$K'_{\text{PhOH}} \cong K''_{\text{PhOH}} \left[\frac{K_{\text{MIBK}} - 1}{K_{\text{MIBK}}(1 - K_{\text{H}_2\text{O}})} \right] = 34 \left[\frac{53.8 - 1}{53.8(1 - 0.0532)} \right] = 35.24$$

This value compares favorably with the value of 35.28 calculated directly from phenol mass ratios taken from extractor internal profile data in the simulation output. The extraction factor [Eq. (15-11)] is then calculated with the dilute system approximation that $m_{\text{PhOH}} \cong K_{\text{PhOH}}$ and solute-free water and MIBK feed rates of 159,841 and 10,668 lb/h taken from the simulation output:

$$E_{\text{PhOH}} = m_{\text{PhOH}} \frac{S}{F} \cong K'_{\text{PhOH}} \frac{S''}{F''} = K'_{\text{PhOH}} \frac{S'}{F'} = 35.24 \times \frac{10,668}{159,841} = 2.35$$

It is interesting to note that this value of the extraction factor, 2.35, is the same as those calculated on mole fraction, mass fraction, and Bancroft coordinate bases from extractor internal profile data in the simulation, a confirmation that the extraction factor is indeed independent of units as long as consistent values of m , S , and F are used. By substituting the above values into Eq. (15-48) along

TABLE 15-9 Simulation Results for Extraction of Phenol from Wastewater Using MIBK (Example 4)

N	Raffinate compositions			Extract compositions		
	X''_{PhOH} , ppm	$X''_{\text{H}_2\text{O}}$, mass fraction	X''_{MIBK} , mass fraction	Y''_{PhOH} , mass fraction	$Y''_{\text{H}_2\text{O}}$, mass fraction	Y''_{MIBK} , mass fraction
2	101	0.98235	0.01755	0.01146	0.05223	0.93631
3	41.8	0.98237	0.01759	0.01260	0.05223	0.93517
4	17.7	0.98238	0.01761	0.01306	0.05223	0.93471
5	7.55	0.98238	0.01761	0.01326	0.05223	0.93451
6	3.28	0.98238	0.01762	0.01334	0.05223	0.93443
7	1.47	0.98238	0.01762	0.01337	0.05223	0.93440
8	0.707	0.98238	0.01762	0.01339	0.05223	0.93438
9	0.381	0.98238	0.01762	0.01340	0.05223	0.93437
10	0.242	0.98238	0.01762	0.01340	0.05223	0.93437

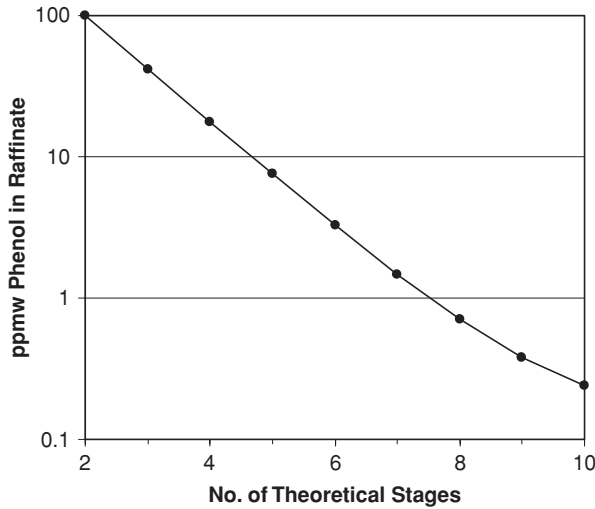


FIG. 15-28 Simulation results showing phenol concentration in the raffinate versus number of theoretical stages (Example 4).

with concentrations taken from the problem statement and Table 15-9, the required number of stages is estimated as

$$N \approx \frac{\ln \left[\frac{0.0007/0.9993 - (0.000005)/(0.999995)/35.24}{0.000001/0.9824 - (0.000005)/(0.999995)/35.24} (1 - 1/2.35) + 1/2.35 \right]}{\ln 2.35} = 7.18 \text{ theoretical stages}$$

The simulation result of 7.53 theoretical stages is close to this shortcut estimate, indicating that the simulation is indeed delivering reasonable results.

FRACTIONAL EXTRACTION CALCULATIONS

Dual-Solvent Fractional Extraction As discussed in "Commercial Process Schemes," under "Introduction and Overview," fractional extraction often may be viewed as combining product purification with product recovery by adding a washing section to the stripping section of a standard extraction process. In the stripping section, the mass transfer we focus on is the transfer of the product solute from the wash solvent into the extraction solvent. If we assume dilute conditions and use shortcut calculations for illustration, the extraction factor is given by

$$\mathcal{E}_s = K'_s \frac{S'_s}{W'_s} \quad (15-99)$$

where \mathcal{E}_s = stripping section extraction factor (dimensionless)
 K'_s = stripping section partition ratio, defined as equilibrium concentration of product solute in extraction solvent divided by that in wash solvent (Bancroft coordinates)
 S'_s = mass flow rate of extraction solvent within stripping section (solute-free basis)
 W'_s = mass flow rate of wash solvent in stripping section (solute-free basis)

The change in the concentration of product dissolved in the wash solvent, within the stripping section, can be calculated by using the KSB equation

$$\left(\frac{X'_{out}}{X'_{in}} \right)_{\text{product}} \approx \frac{1 - 1/\mathcal{E}_s}{(\mathcal{E}_s)^N - 1/\mathcal{E}_s} \quad (15-100)$$

where N_s = number of theoretical stages in stripping section
 X'_{in} = concentration of product solute in wash solvent at inlet to stripping section (feed stage)
 X'_{out} = concentration of product solute in wash solvent at outlet from stripping section (raffinate end of overall process)

In the washing section, we focus on transfer of impurity solute from the extraction solvent into the wash solvent. A washing extraction factor can be defined as

$$\mathcal{E}_w = \frac{1}{K'_w} \frac{W'_w}{S'_w} \quad (15-101)$$

where \mathcal{E}_w = washing section extraction factor (dimensionless)
 K'_w = washing section partition ratio (equilibrium concentration of impurity solute in extraction solvent divided by that in wash solvent, in Bancroft coordinates)
 S'_w = mass flow rate of extraction solvent within washing section (solute-free basis)
 W'_w = mass flow rate of wash solvent in washing section (solute-free basis)

Then the change in the concentration of impurity solute dissolved in the extraction solvent, within the washing section, is given by

$$\left(\frac{Y'_{out}}{Y'_{in}} \right)_{\text{impurities}} \approx \frac{1 - 1/\mathcal{E}_w}{(\mathcal{E}_w)^{N_w} - 1/\mathcal{E}_w} \quad (15-102)$$

where N_w = number of theoretical stages in washing section
 Y'_{in} = concentration of impurity solute in extraction solvent at inlet to washing section (feed stage)
 Y'_{out} = concentration of impurity solute in extraction solvent at outlet from washing section (extract end of overall process)

The ratio of extraction solvent to wash solvent in each section will be different if either solvent enters the process with the feed. Note that both K'_s and K'_w are defined as the ratio of the appropriate solute concentration in the *extraction* solvent to that in the *wash* solvent.

The shortcut calculations outlined above illustrate the general considerations involved in analyzing a fractional extraction process. The analysis requires locating the feed stage and matching the calculations for each section with the material balance at the feed stage, an iterative procedure. Buford and Brinkley [AIChE J., 6(3), pp. 446-450 (1960)] discuss application of the KSB equation to fractional extraction calculations including the use of reflux. Transfer unit calculations also may be used. When equilibrium and operating lines are not linear, more sophisticated calculations will be needed to take this into account. Commercially available simulation software or other computer programs often are used to carry out this procedure (see "Computer-Aided Calculations"). Note that with dual-solvent fractional extraction, solute concentrations always are highest at the feed stage. This can lead to undesired behavior such as tendencies toward emulsion formation or even formation of a single liquid phase at the plait point. The minimum amounts of solvent needed to avoid these effects can be determined in laboratory tests.

Early in a project, it may be useful to consider a simplified case in which the ratio of extraction solvent to wash solvent is constant and the same in the stripping and washing sections (i.e., the amount of solvent entering with the feed is negligible) and the extraction factors for each section are equal. For this special case, termed a *symmetric separation*, the extraction factors are

$$\mathcal{E}_s = \mathcal{E}_w = \sqrt{\alpha_{ij}} \quad (15-103)$$

and the ratio of extraction solvent to wash solvent is given by

$$\frac{S}{W} \approx \frac{1}{\sqrt{K_s K_w}} \approx \frac{1}{\sqrt{\alpha_{ij} K_w}} = \frac{\sqrt{\alpha_{ij}}}{K_s} \quad (15-104)$$

Using these relationships, we find the number of stages required for the stripping and washing sections will be about the same and the total number of stages required likely will be close to the minimum number—assuming symmetric separation requirements. The effects of the separation factor and the number of stages on the separation performance can be estimated by using expressions given by Brian [*Staged Cascades in Chemical Processing* (Prentice-Hall, 1972)]. For a process containing two solutes i and j , with the feed entering at the middle stage, it follows from Brian's analysis that

$$S_{ij} = \frac{Y_i}{X_i} \frac{1 - X_i}{1 - Y_i} \approx \alpha_{ij}^{(N+1)/2} \quad (15-105)$$

where S_{ij} is termed the *separation power* of the process. Equation (15-105) is derived by assuming that the ratio of extract phase to raffinate phase within the process is constant, and that α_{ij} is constant. Interestingly, Eq. (15-105) is very similar in its general form to the equation obtained by using the Fenske equation to calculate fractional distillation performance for a binary feed, assuming that the required number of theoretical stages is twice the minimum number obtained at total reflux. (See Sec. 13, "Distillation.")

For a proposed symmetric separation, Eqs. (15-104) and (15-105) can be used to gauge the required flow rates, number of theoretical stages, and separation factor. For example, consider a hypothetical application with the goal of transferring 99 percent of a key solute i into the extract and 99 percent of an impurity solute j into the raffinate. For illustration, let $K_i = 2.0$ and $K_j = 0.5$, so $\alpha_{ij} = 4$. From Eq. (15-104), the extraction solvent to wash solvent ratio should be about $S/W = 1.0$ for a symmetric separation. The number of theoretical stages is estimated by using Eq. (15-105): $S_{ij} = 99 \times 99 = 9801$ gives $N \approx 12$ total stages for $\alpha_{ij} = 4$. When one is evaluating candidate solvent pairs for a proposed fractional extraction process, a useful first step is to measure the equilibrium K values for product and impurity solutes and then assess process feasibility by using Eqs. (15-104) and (15-105). This can provide a quick way of assessing whether the measured separation factor is sufficiently large to achieve the separation goals, using a reasonable number of stages.

Single-Solvent Fractional Extraction with Extract Reflux As discussed earlier, single-solvent fractional extraction with extract reflux is widely practiced in the petrochemical industry to separate aromatics from crude hydrocarbon feeds. For example, a variety of extraction processes utilizing different high-boiling, polar solvents are used to separate benzene, toluene, and xylene (BTX) from aliphatic hydrocarbons and naphthenes (cycloalkanes), although processes involving extractive distillation are displacing some of the older extraction processes, depending upon the application. A typical hydrocarbon feed is a distillation cut containing mostly C_5 to C_9 components. Commercial extraction processes include the Udex process (employing diethylene and/or triethylene glycol), the AROSOLVAN process (employing *N*-methyl-2-pyrrolidone), and the Sulfolane process (employing tetrahydrothiophene-1,1-dioxane), among others. Although the flow diagrams for these processes differ, they all involve use of a liquid-liquid extractor followed by a top-fed extract stripper or extractive distillation tower. A number of different processing schemes are used to isolate the aromatics and recycle the heavy solvent. For detailed discussion, see Chaps. 18.1 to 18.3 in *Handbook of Solvent Extraction*, Lo, Baird, and Hanson, eds. (Wiley, 1983; Krieger, 1991); Mueller et al., *Ullmann's Encyclopedia of Industrial Chemistry*, 5th ed., vol. B3, Gerhartz, ed. (VCH, 1988), pp. 6-34 to 6-43; Gaile et al., *Chem. Technol. Fuels Oils*, **40**(3), pp. 131-136, and **40**(4), pp. 215-221 (2004); and Schneider, *Chem. Eng. Prog.*, **100**(7), pp. 34-39 (2004).

Consider a process scheme involving a liquid-liquid extractor followed by a top-fed extract stripper (as illustrated in Fig. 15-2). In the extractor, the feed is contacted with the polar solvent to transfer aromatics into the solvent phase. Some nonaromatics (NAs) also transfer into the solvent. In the stripper, low-boiling NAs plus some aromatics are stripped out of the extract. The overheads stream also contains some high-boiling NAs because their low solubility in the polar solvent boosts their relative volatility in the stripper. In this respect, the

stripper may be thought of as an extractive distillation tower with the high-boiling polar solvent serving as the extractive distillation solvent. The stripper overheads are then condensed and returned to the bottom of the extractor as extract reflux. As the backwash of extract reflux passes up through the extractor, the aromatics and a portion of the low-boiling NAs transfer back into the solvent phase, preferentially displacing high-boiling NAs from the extract phase because of their lower solubilities in the polar solvent. Without extract reflux, the concentration of higher-boiling NAs in the extract phase would be significantly higher, and they would be difficult to completely remove in the stripper in spite of their low solubilities in the polar solvent. In this manner, low-boiling aromatics and NAs tend to build up in the extract reflux loop to provide a sort of barrier that minimizes entry of higher-boiling NAs into the extract phase.

The use of simulation software to analyze this type of process is illustrated in Example 5, which considers a simplified ternary system for illustration. The simulation of an actual aromatics extraction process is more complex and can exhibit considerable difficulty converging on a solution; however, Example 5 illustrates the basic considerations involved in carrying out the calculations. For more detailed discussion of process simulation and optimization methods, see Seider, Seader, and Lewin, *Product and Process Design Principles: Synthesis, Analysis, and Evaluation*, 2d ed. (Wiley, 2004); and Turton et al., *Analysis, Synthesis, and Design of Chemical Processes*, 2d ed. (Prentice-Hall, 2002).

Example 5: Simplified Sulfolane Process—Extraction of Toluene from *n*-Heptane The amount of 40 metric tons (t) per hour (t/h) of distilled catalytic reformat from petroleum refining, containing 50% by weight aromatics, is to be extracted with recovered sulfolane containing 0.4 vol % aromatics in a 10-stage column contactor operating nearly adiabatically at 3 bar (gauge pressure). The extract will be fed to a 10-stage top-fed extract/paraffin stripper operating at 1 bar gauge to recover 98 percent of the aromatics with no more than 500 ppm by weight of nonaromatics. The catalytic reformat at 90°C is fed into the extractor at three stages up from the bottom, and the recovered sulfolane leaving the bottom of a solvent recovery tower at 185°C is cross-exchanged with the extract stream leaving the bottom of the extractor before being fed to the top of the extractor at 105°C. Extract reflux is returned from the paraffin stripper's condenser to the bottom of the extractor with subcooling to 105°C.

1. What solvent flow and stripper reboiler duty are required to achieve the performance specifications, and what are the extract reflux rate and composition?

2. If the required aromatics recovery is increased to 99 percent, what is the effect on solvent flow and stripper reboiler duty?

In real-world commercial catalytic reformat streams, a wide range of aromatic and nonaromatic hydrocarbons must be considered, and the liquid-liquid extraction and distillation simulation becomes quite complicated. In addition, real-world applications of sulfolane extraction normally add a few percent of water to the sulfolane to reduce its pure-component freezing point of 27 to 28°C during shipping and storage [Kosters, Chap. 18.2.3 in *Handbook of Solvent Extraction*, Lo, Baird, and Hanson, eds. (Wiley, 1983; Krieger, 1991)]. Also, in many processes, steam is injected into the bottom of the solvent recovery tower to help strip the aromatics (i.e., the tower is both steam-stripped and reboiled). This also allows operation of the recovery tower at higher pressures without incurring (excessive) solvent thermal degradation. In a real-world process, water also may be used to wash the raffinate to recover solvent. To simplify the problem for this example, however, we model the aromatics as toluene and the NAs as *n*-heptane, consider only sulfolane as the extraction solvent, and do not include water in the calculations—to reduce the problem to a simple ternary system for illustration.

As in Example 4, the EXTRACT block in the Aspen Plus process simulation program (version 12.1) is used to model this problem, but any of a number of process simulation programs such as mentioned earlier may be used for this purpose. The first task is to obtain an accurate fit of the liquid-liquid equilibrium (LLE) data with an appropriate model, realizing that liquid-liquid extraction simulations are very sensitive to the quality of the LLE data fit. The NRTL liquid activity-coefficient model [Eq. (15-27)] is utilized for this purpose since it can represent a wide range of LLE systems accurately. The regression of the NRTL binary interaction parameters is performed with the Aspen Plus Data Regression System (DRS) to ensure that the resulting parameters are consistent with the form of the NRTL model equations used within Aspen Plus.

Since the extractor operates nearly isothermally only slightly above and below 100°C, the 100°C data of De Fre and Verhoeve [*J. Appl. Chem. Biotechnol.*, **26**, pp. 1-19 (1976)] are used as the basis for the toluene + *n*-heptane + sulfolane LLE. Because of the liquid-liquid miscibility gap for the *n*-heptane + sulfolane binary, the NRTL α_{ij} parameter for this pair is given a value of 0.2. The NRTL

TABLE 15-10 NRTL Binary Interaction Parameters for Example 5

Component <i>i</i>	Component <i>j</i>	<i>b_{ij}</i> , K
<i>n</i> -Heptane	Toluene	23.2040
Toluene	<i>n</i> -Heptane	-34.3180
Toluene	Sulfolane	238.952
Sulfolane	Toluene	203.243
<i>n</i> -Heptane	Sulfolane	1476.41
Sulfolane	<i>n</i> -Heptane	719.006

$\tau_{ij} = b_{ij}/T$ (K); $\alpha_{ij} = 0.2$ for *n*-heptane + sulfolane; $\alpha_{ij} = 0.3$ for toluene + sulfolane and for *n*-heptane + sulfolane. Aspen Plus regression parameters *a_{ij}*, *d_{ij}*, *e_{ij}*, and *f_{ij}* are set to zero; *c_{ij}* = α_{ij} ; $\tau_{ii} = 0$; and *G_{ii}* = 1.

α_{ij} parameters for toluene + sulfolane and *n*-heptane + toluene are allowed to remain at the default value of 0.3 because of their low levels of nonideality. The temperature dependence of α_{ij} is set to zero (Aspen Plus parameter *d_{ij}* = 0). In Aspen Plus, the τ_{ij} parameter may be regressed as a function of temperature by using the expression $\tau_{ij} = a_{ij} + b_{ij}/T + e_{ij} \ln T + f_{ij}T$. In this example, all the regression parameters are set to zero except *b_{ij}*. The component activity coefficients are chosen as the objective function for the regression to obtain a fit that models the liquid-liquid *K* values closely, generally found to be within 5 to 10 percent in this case. The resulting *b_{ij}* binary parameters given in Table 15-10 are then entered into the properties section of the Aspen Plus flow sheet simulation. Pure-component properties were taken from the standard Aspen Plus pure-component databases supplied with the program.

The major unit operations in the sulfolane process usually include an extractor, paraffin stripper, solvent recovery tower, raffinate wash tower, solvent regenerator, and numerous heat exchangers; but for the purposes of this example, the simulation includes only the extractor, paraffin stripper, and extract/recovered solvent cross-exchanger—the portion of the flow sheet shown in Fig. 15-2 outlined by dotted lines. It should be recognized that the exclusion of the solvent recovery tower ignores the highly interactive behavior of the extractor, stripper, and recovery tower; but this is done here to simplify the analysis for the purposes of illustration. Note that the stripper's condenser is modeled as a separate Aspen Plus HEATER block rather than being included in the stripper block, because the Aspen Plus RADFRAC multistage distillation block used to model the stripper requires some distillate reflux if a condenser is included within the block, and generally none is required for the top-fed stripper in the sulfolane process. As a result, the stripper RADFRAC block is specified with no condenser. Also note that in the sulfolane process, the sulfolane solvent enters the top of the extractor since it is denser than the catalytic reformate feed stream.

The 40,000 kg/h of catalytic reformate fed to stage 7 (counting from the top according to the convention in the EXTRACT block) is modeled as 50/50 *n*-heptane/toluene on a mass basis, and the residual aromatic content of the recovered sulfolane fed to the top of the extractor is 0.4 vol % toluene as given

in the problem statement. As an initial guess, the sulfolane rate to the extractor was set at 120,000 kg/h or a solvent-to-feed ratio of 3.0 since depending on the feedstock, solvent-to-feed ratios can range from about 2.0 to 4.0 (Huggins, "Sulfolane Extraction of Aromatics," Paper 67C, AIChE, Spring National Meeting, Houston, March 1997). In the EXTRACT block, sulfolane must be specified as the key component in the first liquid phase, and *n*-heptane must be specified as the key component in the second liquid phase, since the EXTRACT block requires that the first liquid be the one exiting the bottom of the extractor. A constant-temperature profile of 105°C in the extractor is entered as an initial estimate. The rest of the block parameters (convergence, report, and miscellaneous block options) are allowed to remain at their default values.

The paraffin stripper RADFRAC block is specified with feed to the first of 10 stages, a reboiler but no condenser, a 1-bar gauge top pressure, no internal pressure drop, and a molar boil-up ratio (boil-up rate/bottoms rate) of 0.2 as an initial guess. An internal RADFRAC design specification is entered to vary the boil-up ratio from 0.10 to 0.30 to achieve a mass purity of 500 ppm *n*-heptane in the stripper bottoms on a sulfolane solvent-free basis. To aid RADFRAC convergence, the standard algorithm was changed to Petroleum/Wide-boiling (Sum-Rates) because of the large volatility difference between the hydrocarbons and the sulfolane solvent.

A separate flow sheet Design Spec block (termed a *controller* block in some other simulators) is entered to vary the solvent feed rate to the extractor to achieve the required 98 percent toluene recovery. In addition, the extract reflux stream is called out as the flow sheet tear stream in a Wegstein convergence block to provide proper block sequencing in the simulation. (This is a numerical technique used to accelerate convergence to a solution.) Since the EXTRACT block will not execute with a zero extract reflux flow to the bottom of the extractor, an initial guess is required for that stream: 10,000 kg/h of 50/50 by weight *n*-heptane/toluene at 100°C is chosen.

During simulation execution, we found that reflux tear stream convergence with the default Wegstein parameters is very oscillatory, with no convergence even with maximum iterations raised to 200. As a result, significant damping needs to be provided in the convergence block. We raised the bounds of the Wegstein *q* acceleration parameter to be between 0.75 and 1.0 for nearly full damping, after which flow sheet convergence was achieved in less than 50 iterations of every reflux tear stream loop. We also found that good initial guesses and bounds on variables needed to be set to keep the simulation from converging to an aberrant solution that was not physically valid.

With these modifications, the result is that 125,500 kg/h of sulfolane feed to the extractor is required to recover 98 percent of the toluene in the simplified reformate feed. The stage-by-stage mass fraction profile in the extractor is given in Table 15-11, from which we can see that there is very little change in concentration in either phase from the feed stage downward. This is so because in our simplified example we have only a single NA hydrocarbon component (*n*-heptane) to deal with, so the benefit of a backwash section in the extractor below the feed is not apparent. In a real-world profile, however, concentrations of higher-boiling NAs would decrease from the feed point to the bottom of the extractor. Also given in Table 15-11 are stage-by-stage *K''* values, the separation factor (toluene with respect to *n*-heptane), and the extraction factor profiles in

TABLE 15-11 Stage Profiles for 98 Percent Recovery (Example 5)

Stage	Liquid 1 profile (extract) (mass fractions)			Liquid 2 profile (raffinate) (mass fractions)		
	<i>n</i> -Heptane	Toluene	Sulfolane	<i>n</i> -Heptane	Toluene	Sulfolane
1	0.02630	0.00624	0.96746	0.97239	0.01945	0.00815
2	0.02683	0.01145	0.96171	0.95565	0.03521	0.00914
3	0.02777	0.02031	0.95192	0.92796	0.06106	0.01098
4	0.02940	0.03519	0.93542	0.88354	0.10196	0.01450
5	0.03225	0.05955	0.90821	0.81568	0.16281	0.02151
6	0.03721	0.09769	0.86510	0.71952	0.24481	0.03568
7	0.04568	0.15309	0.80123	0.59750	0.33926	0.06324
8	0.04570	0.15323	0.80107	0.59680	0.33963	0.06357
9	0.04590	0.15419	0.79991	0.59524	0.34081	0.06395
10	0.04729	0.16016	0.79255	0.58397	0.34838	0.06766
Stage	<i>K''</i> values (mass fraction basis)			α_{ij} Toluene/ <i>n</i> -heptane	<i>E</i> Toluene	
	<i>n</i> -Heptane	Toluene	Sulfolane			
1	0.0270	0.321	118.7	11.87	2.02	
2	0.0281	0.325	105.2	11.58	1.73	
3	0.0299	0.333	86.7	11.12	1.73	
4	0.0333	0.345	64.5	10.37	1.73	
5	0.0395	0.366	42.2	9.25	1.73	
6	0.0517	0.399	24.2	7.72	1.73	
7	0.0765	0.451	12.7	5.90	1.66	
8	0.0766	0.451	12.6	5.89	5.90	
9	0.0771	0.452	12.5	5.87	5.91	
10	0.0810	0.460	11.7	5.68	5.88	

TABLE 15-12 Stream Compositions and Conditions (Example 5)

	Extract	Raffinate	Reflux	Stripper bottoms
98% Recovery—125,500 kg/h required solvent flow				
Wt. fraction <i>n</i> -heptane	0.04729	0.97239	0.57717	69 ppm
Wt. fraction toluene	0.16016	0.01945	0.41273	0.13765
Wt. fraction sulfolane	0.79255	0.00815	0.01010	0.86228
Total flow, kg/h	157,817	205,578	12,914	144,903
Temperature, °C	96.4	103.7	105.0	194.1
99% Recovery—212,800 kg/h required solvent flow				
Wt. fraction <i>n</i> -heptane	0.03821	0.98258	0.62353	44 ppm
Wt. fraction toluene	0.10444	0.00982	0.36100	0.08771
Wt. fraction sulfolane	0.85736	0.00759	0.01547	0.91225
Total flow, kg/h	247,592	20,344	15,155	232,437
Temperature, °C	98.9	103.9	105.0	215.9

the extractor. From these we can see that the separation factor for toluene with respect to *n*-heptane varies from about 6 at the bottom of the extractor to 12 at the top, and that the extraction factor is about 2 above the feed and about 6 below the feed. These separation factors are somewhat higher than the value of 4 or so normally seen in real-world aromatic extraction cases; this, too, is an artifact of the simplified ternary system used to model the sulfolane process.

Another result of the simulation is that a molar boil-up ratio of 0.180 is required in the stripper to achieve the bottoms mass purity of 500 ppm *n*-heptane considering only the hydrocarbons (solvent-free basis). This boil-up ratio corresponds to a reboiler duty of 3695 kW, or roughly 6700 kg/h of 12-bar gauge steam, and results in 12,914 kg/h of extract reflux for an extractor reflux-to-feed ratio of 0.323. Compositions and rates of the extract, raffinate, reflux, and stripper bottoms streams are given in Table 15-12.

To determine the solvent flow and other conditions required to achieve 99 percent toluene recovery, we merely need to change the specification of the recovery Design Spec block from 98 to 99 percent and reconverge the simula-

tion. With this change and an additional 180 total reflux tear stream iterations, the result is that 212,800 kg/h of sulfolane feed to the extractor is required, 1.7 times the amount needed for 98 percent toluene recovery. A molar boil-up ratio of 0.158 is required in the stripper to maintain the bottoms mass purity of 500 ppm *n*-heptane on a solvent-free basis, even lower than that for the 98 percent recovery case. Likewise, only a slightly higher extract reflux rate is required, 15,155 kg/h, for an extractor reflux-to-feed ratio of 0.379. However, this boil-up ratio corresponds to a reboiler duty of 7191 kW, or roughly 13,100 kg/h of 12-bar gauge steam, about 95 percent higher than for the 98 percent recovery case. The much higher stripper reboiler duty required for 99 percent recovery results from the significantly greater sulfolane feed rate, indicating that the sizes of the extractor and stripper as well as the energy consumption would need to be significantly greater for that increased recovery, probably making it uneconomical in most applications with a 10-stage extractor and stripper. Compositions and rates of the extract, raffinate, reflux, and stripper bottoms streams for the 99 percent recovery case are also given in Table 15-12.

LIQUID-LIQUID EXTRACTION EQUIPMENT

GENERAL REFERENCES: Seibert, "Extraction and Leaching," Chap. 14 in *Chemical Process Equipment: Selection and Design*, 2d ed., Couper et al., eds. (Elsevier, 2005); Robbins, Sec. 1.9 in *Handbook of Separation Techniques for Chemical Engineers*, 3d ed., Schweitzer, ed. (McGraw-Hill, 1997); Lo, Sec. 1.10 in *Handbook of Separation Techniques for Chemical Engineers*, 3d ed., Schweitzer, ed. (McGraw-Hill, 1997); *Liquid-Liquid Extraction Equipment*, Godfrey and Slater, eds. (Wiley, 1994); *Science and Practice of Liquid-Liquid Extraction*, vol. 1, Thornton, ed. (Oxford, 1992); *Handbook of Solvent Extraction*, Lo, Baird, and Hanson, eds. (Wiley, 1983; Krieger, 1991); Laddha and Degaleesan, *Transport Phenomena in Liquid Extraction* (McGraw-Hill, 1978); and Treybal, *Liquid Extraction*, 2d ed. (McGraw-Hill, 1963).

EXTRACTOR SELECTION

The common types of commercially available extraction equipment and their general features are outlined in Table 15-13. The choice of extractor type depends upon many factors including the required number of theoretical stages or transfer units, required residence time (due to slow or fast extraction kinetics or limited solute stability), required production rate, tolerance to fouling, ease of cleaning, availability of the required materials of construction, as well as the ability to handle high or low interfacial tension, high or low density difference, and high or low viscosities. Other factors that influence the choice of extractor include familiarity and tradition (the preferences among designers and operating companies often differ), confidence in scale-up, height constraints, and, of course, the relative capital and operating costs. The flexibility of the extractor to adjust to changes in feed properties also can be an important consideration. For example, compared to a static extractor, a mechanically agitated extractor typically provides a greater turndown ratio (ability to handle a wider range of flow rates), and agitation intensity can be adjusted in the field as needed to accommodate changes in the feed over time. Other factors

that may be important include the ability to operate under pressure, to handle corrosive, highly toxic, or flammable materials, and to meet maintenance requirements, among many other possible considerations. Experience with applications similar to the current application and the use of pilot-plant testing play important roles in equipment selection. Pilot testing can address critical issues including demonstration of separation capabilities and equipment scale-up. The simplest extractor design that can meet the process requirements generally will be selected over other competing designs.

Figure 15-29 outlines the decision process recommended by Robbins [Sec. 1.9 in *Handbook of Separation Techniques for Chemical Engineers*, 3d ed., Schweitzer, ed. (McGraw-Hill, 1997)]. As an aid to decision making, Robbins recommends characterizing the feed by measuring a flooding curve using a 1-in-diameter reciprocating-plate (Karr column) miniplant extractor. This is a plot of maximum specific throughput (very close to flooding) versus agitation intensity in the Karr column. The position of the resulting curve may be used to identify the type of extractor best suited for commercial development, as illustrated in Fig. 15-30. The flooding curve results reflect the liquid-liquid dispersion behavior of the system, and so they can point to options most in line with those properties. The test typically requires 40 to 200 L of feed materials (10 to 50 gal).

A number of equipment selection guides have been published. Pratt and Hanson [Chap. 16 in *Handbook of Solvent Extraction*, Lo, Baird, and Hanson, eds. (Wiley, 1983; Krieger, 1991)] provide a detailed comparison chart for 20 equipment types considering 14 characteristics. Pratt and Stevens [Chap. 8 in *Science and Practice of Liquid-Liquid Extraction*, vol. 1, Thornton, ed. (Oxford, 1992)] modified the Pratt and Hanson selection guide to include solvent volatility and flammability design parameters. Stichlmair [*Chem. Ing. Tech.*, **52**(3) pp. 253–255 (1980)] and Holmes, Karr, and Cusack (AIChE

TABLE 15-13 Common Liquid-Liquid Extraction Equipment and Applications

Type of extractor	General features	Fields of industrial application
Static extraction columns Spray column Baffle column Packed column (random and structured packing) Sieve tray column	Deliver low to medium mass-transfer efficiency, simple construction (no internal moving parts), low capital cost, low operating and maintenance costs, best suited to systems with low to moderate interfacial tension, can handle high production rates	Petrochemical Chemical Food
Mixer-settlers Stirred-vessels with integral or external settling zones	Can deliver high stage efficiencies with long residence time, can handle high-viscosity liquids, can be adjusted in the field (good flexibility), with proper mixer-settler design can handle systems with low to high interfacial tension, can handle very high production rates	Petrochemical Nuclear Fertilizer Metallurgical
Rotary-agitated columns Rotary disc contactor (RDC) Asymmetric rotating disc (ARD) contactor Oldshue-Rushton column Scheibel column Kühni column	Can deliver moderate to high efficiency (many theoretical stages possible in a single column), moderate capital cost, low operating cost, can be adjusted in the field (good flexibility), suited to low to moderate viscosity (up to several hundred centipoise), well suited to systems with moderate to high interfacial tension, can handle moderate production rates	Petrochemical Chemical Pharmaceutical Metallurgical Fertilizer Food
Reciprocating-plate column Karr column	Can deliver moderate to high efficiency (many theoretical stages possible in a single column), moderate capital cost, low operating cost, can be adjusted in the field (good flexibility), well suited to systems with low to moderate interfacial tension including mixtures with emulsifying tendencies, can handle moderate production rates	Petrochemical Chemical Pharmaceutical Metallurgical Food
Pulsed columns Packed column Sieve tray column	No internal moving parts, can deliver moderate to high efficiency, can handle moderate production rates, well suited to highly corrosive or toxic feeds requiring a hermetically sealed system	Nuclear Petrochemical Metallurgical
Centrifugal extractors	Allow short contact time for unstable solutes, minimal space requirements (minimal footprint and height), can handle systems with low density difference or tendency to easily emulsify	Petrochemical Chemical Pharmaceutical Nuclear

Summer National Meeting, August 1987) compared performance characteristics of various equipment designs in the form of a Stichlmair plot. This is a plot of typical mass-transfer efficiency versus characteristic specific throughput (for combined feed and solvent flows) for various types of extractors. Figure 15-31 represents typical performance data generated by using various small-diameter (2- to 6-in, equal to 5- to 15-cm) extractors. This type of plot is intended for use in comparing the relative performance of different extractor types and can be very helpful in this regard. It should not be used for design purposes.

Volumetric efficiency is another characteristic used to compare the different types of extractors. It can be expressed as the product of specific throughput (including feed and extraction solvent) in total volumetric flow rate per unit area (or a characteristic liquid velocity) times the number of theoretical stages achieved per unit length of extractor. It has the units of stages per unit time, or simply reciprocal time (h^{-1}). Thus, volumetric efficiency is inversely proportional to the volume of the column needed to perform a given separation. The Karr reciprocating-plate extractor provides relatively high volumetric efficiency, as it has both a high capacity per unit area and a high number of stages per meter. The Scheibel rotary-impeller column also can provide a high number of stages per meter, but the column throughput typically is less than that of a Karr column, so volumetric efficiency is less. Thus, for a given separation a Scheibel column might be somewhat shorter than a Karr column, but it will need to have a larger diameter to process the same flow rate of feed and extraction solvent. The sieve plate extractor generally exhibits moderate to high throughput, but the number of stages per meter typically is low. The Graesser raining-bucket contactor exhibits low to moderate throughput, but is reported to have a high separating capability in certain applications.

The ability of an extractor to tolerate the presence of surface-active impurities also may be an important factor in choosing the most

appropriate design. Karr, Holmes, and Cusack [*Solvent Extraction and Ion Exchange*, 8(30), pp. 515-528 (1990)] investigated the performance of small-diameter agitated columns and found that the performance of a rotating-disk contactor (RDC) declined faster on addition of trace surface-active impurities compared to the Karr or Scheibel column. The test results indicate that care should be taken when comparing pilot tests of different types of extractors when the data were generated by using high-purity materials. The presence of surface-active impurities can lower column capacity by 20+ percent and efficiency by as much as 60 percent.

Production capacity also may be a deciding factor, since some extractors are available only in small to moderate sizes suitable for low to moderate production rates, as in specialty chemical manufacturing, while others are available in very large sizes designed to handle the very high production rates needed in the petroleum and petrochemical industries. An estimate of relative production rates (feed plus solvent) for selected extractors is given in Table 15-14. Note that the numbers are intended to represent approximate maximum values for a rough comparison. The actual values likely will vary depending upon the particular application. Keep in mind that the relative mass-transfer performance of the various designs is not represented in Table 15-14, and that very large-diameter columns are limited as to how tall they can be built.

HYDRODYNAMICS OF COLUMN EXTRACTORS

Flooding Phenomena The hydraulic capacity of a countercurrent extractor is constrained by breakthrough of one liquid phase into the discharge stream of the other, a condition called *flooding*. The point at which an extractor floods is a function of the design of the internals (as this affects the pressure drop and holdup characteristics of the extractor), the solvent-to-feed ratio and physical properties (as

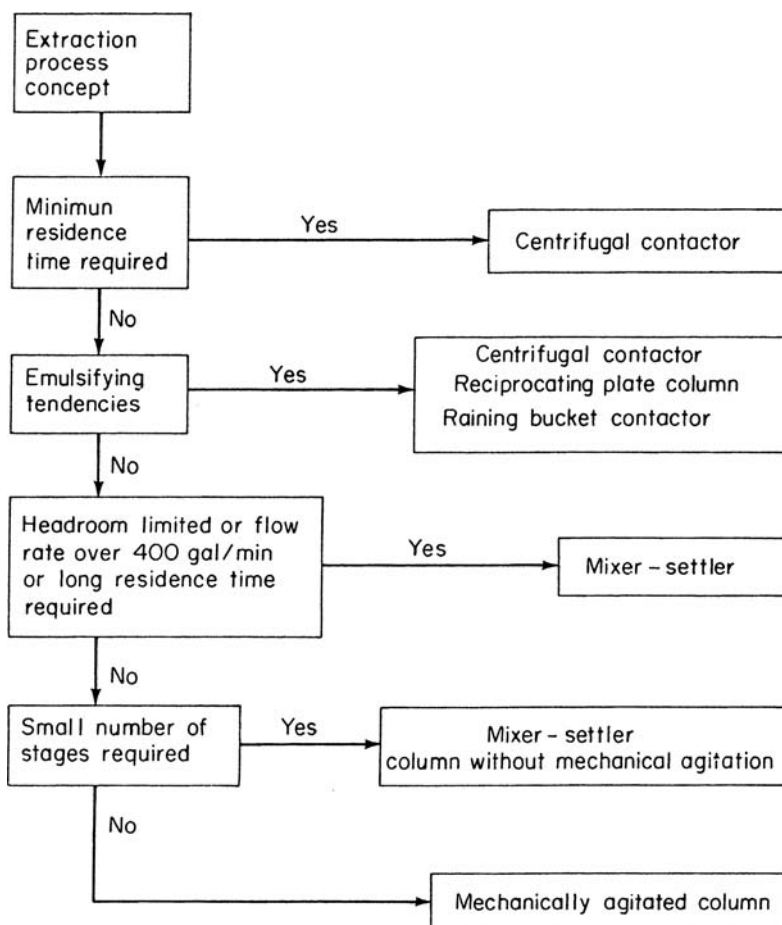


FIG. 15-29 Decision guide for extractor selection. [Reprinted from Robbins, Sec. 1.9 in Handbook of Separation Techniques for Chemical Engineers, 3d ed., Schweitzer, ed. (McGraw-Hill, 1997), with permission. Copyright 1997 McGraw-Hill, Inc.]

this affects the liquid-liquid dispersion behavior), the agitation intensity (if agitation is used), and the specific throughput. The latter often is expressed in terms of the volumetric flow rate per cross-sectional area; or, equivalently, in terms of liquid velocity. A plot of the maximum throughput that can be sustained just prior to flooding versus a key operating variable is called a flooding curve. Ideally, extractors are designed to operate near flooding to maximize productivity. In practice, however, many new column extractors are designed to operate at 40 to 60 percent of the predicted flood point because of uncertainties in the design, process impurity uncertainties, and to allow for future capacity increases. This practice varies from one type of extractor to another and one designer to another. In a static extraction column, countercurrent flow of the two liquid phases is maintained by virtue of the difference in their densities and the pressure drop through the equipment. Only one of the liquids may be pumped through the equipment at any desired flow rate or velocity; the maximum velocity of the other phase is then fixed by the flood point. If an attempt is made to exceed this hydraulic limit, the extractor will flood.

In extraction equipment, flooding may occur through a variety of mechanisms [Seibert, Bravo, and Fair, *ISEC '02 Proc.*, **2**, pp. 1328–1333 (2002)]:

1. Excessive flow rates of either dispersed-phase or continuous-phase, or high agitation intensity, cause dispersed-phase holdup or population density to exceed the volumetric capacity of the equipment.

2. Excessively high continuous-phase flow rate causes excessive entrainment of dispersed phase into the continuous-phase outlet.

3. Inadequate drop coalescence causes formation of dispersion bands or layers of uncoalesced drops that entrap continuous phase between them. The continuous phase can then be entrained into the wrong outlet.

4. Operation at a high ratio of dispersed phase to continuous phase results in phase inversion. (See "Liquid-Liquid Dispersion Fundamentals.")

5. Operating too close to the liquid-liquid phase boundary causes complete miscibility during an upset. A slight change in solvent or feed rates or an increase in solute concentration in the feed can potentially cause formation of a single phase.

6. In sieve tray columns, excessive orifice and/or downcomer pressure drop within the extractor causes formation of large coalesced layers that back up and overflow the trays.

7. Poor interface control allows the main liquid-liquid interface to leave the extractor. This may result from inadequate size of interface flow control valves, or operation with internals that provide inverse control responses such as those observed with sieve tray extractors. (See "Process-Control Considerations.")

8. Mechanical problems such as plugging of internals or outlet flow control valves can develop.

Accounting for Axial Mixing Differential-type column extractors are subject to axial (longitudinal) mixing, also called axial dispersion

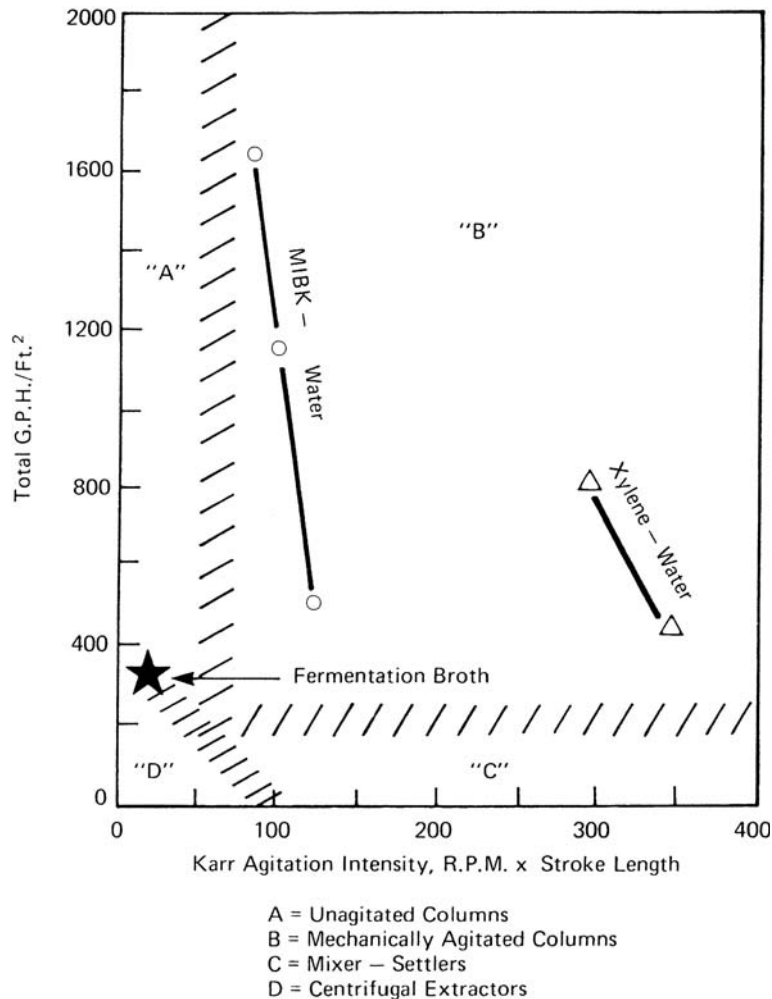


FIG. 15-30 Typical Karr column flooding characteristics. Example flooding data are shown for two applications involving MIBK + water and xylene + water (flooding occurs to the right of the indicated flooding curve). A data point for extraction of a fermentation broth is indicated by the star. Results will vary depending upon process variables including solute concentration, the presence of other solutes, and temperature. [Reprinted from Robbins, Sec. 1.9 in Handbook of Separation Techniques for Chemical Engineers, 3d ed., Schweitzer, ed. (McGraw-Hill, 1997), with permission. Copyright 1997 McGraw-Hill, Inc.]

and generally referred to as backmixing. This condition refers to a departure from uniform plug flow of the swarm of dispersed drops as drops rise or fall in the column, as well as any departure from plug flow of continuous phase in the opposite direction. As a result of axial mixing, the elements of the dispersed phase and the continuous phase exhibit a distribution of residence times within the equipment, and this decreases the effective or overall concentration driving force in the contactor. Because of this effect, the actual column must be taller than simple application of an ideal, plug flow model would indicate. When one is approaching the design of a contactor, factors that may contribute to axial mixing should be considered so that measures might be taken to reduce their effects. This may involve design of baffles to help direct the liquid traffic within the column. Also, if the transfer of solute occurs such that the continuous phase is significantly denser at the top of an extraction column than at the bottom, this may encourage circulation of continuous phase, and it may be advisable to switch the phase that is dispersed. For more information on this effect, see Holmes, Karr, and Baird, *AIChE J.*, **37**(3), pp. 360-366

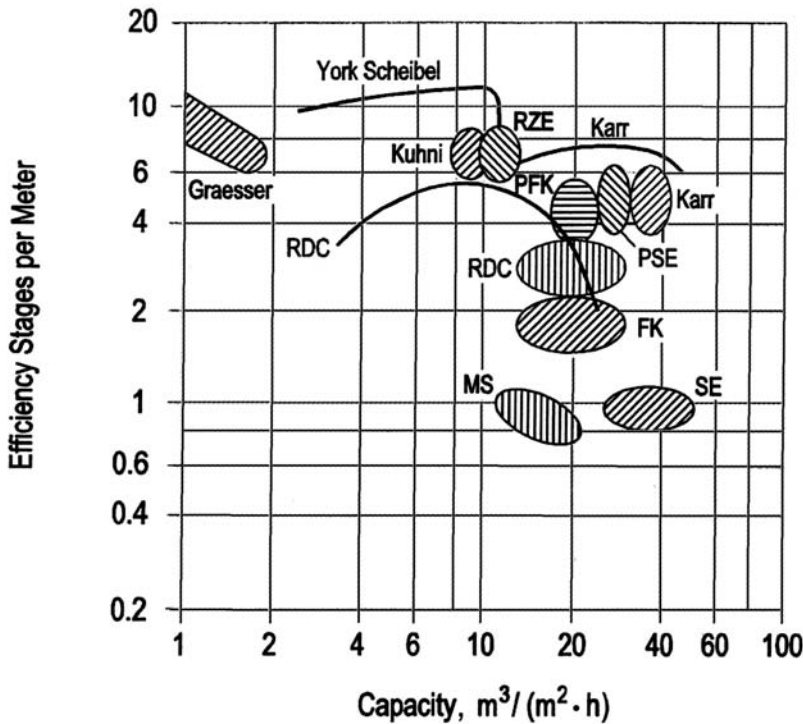
(1991); and Aravamudan and Baird, *AIChE J.*, **42**(8), pp. 2128-2140 (1996).

Axial mixing effects commonly are taken into account by using a diffusion analogy and an axial mixing coefficient E , also called the longitudinal dispersion coefficient or eddy diffusivity, to account for the spreading of the concentration profiles. At steady state, the conservation equation has the general form

$$E \frac{\partial^2 C}{\partial z^2} + V \frac{\partial C}{\partial z} + k_o a (C - C^*) = 0 \quad (15-106)$$



where V is phase velocity, k_o is an overall mass-transfer coefficient, C is solute concentration (mass or moles per unit volume), and the superscript asterisk denotes equilibrium. By using Eq. (15-106) as a foundation, the required height of extractor may be calculated from a simplified plug flow model plus application of a correction factor expressed as a function of E or a Péclet number $Pe = Vb/E$, where b is a characteristic equipment

Comparison Plot of Various Commercial Extractors



Key:

Graesser = Raining Bucket Extractor	RDC = Rotating Disc Contactor
MS = Mixer Settler	RZE = Agitated Cell Extractor
SE = Sieve Plate Extractor	Karr = Karr Reciprocating Plate Column
FK = Random Packed Column	Kuhni = Kuhni Extractor
PFK = Pulsed Packed Column	York-Scheibel = Scheibel Column
PSE = Pulsed Sieve Plate Column	

Source: Shaded Area = 
 Curves = 

(1) J. Stichlmair, University of Essen, Wiesbaden, Germany, "Performance and Cost Comparison of Various Equipment Designs for Liquid-Liquid Extraction", *Chemie-Ingenieur-Technik* 52(3), 1980

(2) T. Holmes, R. Cusack, A. Karr, The Otto H. York Company, AIChE Summer National Meeting, August 17, 1987

FIG. 15-31 Modified Stichlmair chart. (Courtesy of Koch Modular Process Systems.)

dimension. The required values of E must be determined by experiment. A variety of models and data correlations have been developed for various types of column extractors. For detailed discussion, see Sleicher, *AIChE J.*, 5(2), pp. 145-149 (1959); Vermeulen et al., *Chem. Eng. Prog.*, 62(9), pp. 95-102 (1966); and Li and Zeigler, *Ind. Eng. Chem.*, 59(3), pp. 30-36 (1967). Also see the detailed discussions in Laddha and Degaleesan, *Transport Phenomena in Liquid Extraction* (McGraw-Hill, 1978); Pratt and Baird, Chap. 6 in *Handbook of Solvent Extraction*, Lo, Baird, and Hanson, eds. (Wiley, 1983;

Krieger, 1991); and *Liquid-Liquid Extraction Equipment*, Godfrey and Slater, eds. (Wiley, 1994). The method used by Becker [*Chem. Eng. Technol.* 26(1), pp. 35-41 (2003)] is discussed in "Static Extraction Columns."

Computational fluid dynamics (CFD) simulations are beginning to be developed for certain types of extractors to better understand flow patterns in column extractors. The simulation of two-liquid-phase flows around complex internals is an active research area. For an example of this approach, see the discussion of CFD calculations for a

TABLE 15-14 Estimated Maximum Production Rate for Selected Extractors

Extractor type	Maximum ^a specific throughput		Maximum ^b diameter (typical)	Estimated maximum production rate	
	m ³ /h/m ²	gal/h/ft ²	m	m ³ /h	gal/min
Mixer-settler ^c	30	750	10	~2,400	10,000
Baffle tray column	60	1,500	5	~1,200	5,200
Sieve plate column	50	1,200	5	~1,000	4,300
Packed column	50	1,200	5	~1,000	4,300
Spray column ^d	70	1,700	4	~900	4,000
Rotating disk contactor	35	850	4	~450	1,900
Kühni rotating-impeller column ^e	40	1,000	3	~280	1,200
Karr reciprocating-plate column	40	1,000	3	~280	1,200
Scheibel rotating-impeller column	25	600	3	~200	800
Graesser raining-bucket contactor	10	250	3	~70	300

^a Typical maximum value for dispersed + continuous phase flow rates. The actual value for a given application will depend upon physical properties and may be much lower.

^b Typical value. Larger diameters may be possible.

^c Throughput and equivalent diameter are based on mixer-settler footprint.

^d Larger diameters possible but not recommended due to severe backmixing.

^e Higher throughput may be achieved by increasing the column open area.

rotating-disk contactor by Modes and Bart [*Chem. Eng. Technol.*, **24**(12), pp. 1242–1244 (2001)].

Liquid Distributors and Dispersers It should be recognized that the performance of a column extractor can be significantly affected by how uniformly the feed and solvent inlet streams are distributed to the cross section of the column. The requirements for distribution and redistribution vary depending upon the type of column internals (packing, trays, agitators, or baffles) and the impact of the internals on the flow of dispersed and continuous phases within the column. Important considerations in specifying a distributor include the number of holes and the hole pattern (geometric layout), hole size, number of downcomers or upcomers (if used) and their placement, the maximum to minimum flow rates the design can handle (turndown ratio), and resistance to fouling. Various types of liquid distributors are available, including sieve tray dispersers and ladder-type pipe distributors designed to give uniform distribution of drops across the column cross section. (See “Packed Columns” and “Sieve Tray Columns” under “Liquid-Liquid Extraction Equipment” for more information about these. The height of the coalesced layer on a disperser plate may be calculated by using the method described in “Sieve Tray Columns.”) Ring-type distributors also are used, primarily for agitated extractors. Equipment vendors should be consulted for additional information.

Typical hole sizes for distributors and dispersers are between 0.05 in (1.3 mm) and 0.25 in (6.4 mm). Small holes should be avoided in applications where the potential for plugging or fouling of the holes is a concern. For plate dispersers, the holes should be spaced no closer than about 3 hole diameters to avoid coalescence of drops emerging from adjacent holes. Design velocities for liquid exiting the holes generally are in the range of 0.5 to 1.0 ft/s (15 to 30 cm/s). Several methods have been proposed for more precisely specifying the design velocities. For detailed discussion, see Kumar and Hartland, Chap. 17 in *Liquid-Liquid Extraction Equipment*, Godfrey and Slater, eds. (Wiley, 1994), pp. 631–635; Ruff, *Chem. Ing. Tech.*, **50**(6), pp. 441–443 (1978); and Laddha and Degaleesan, *Transport Phenomena in Liquid Extraction* (McGraw-Hill, 1978), Chap. 11, pp. 307–310. These methods are relevant for the design of distributors/dispersers used in all types of column extractors. The liquid should issue from the hole as a jet that breaks up into drops. The jet should yield a drop size distribution that provides good interfacial area, with an average drop size smaller than the maximum given by $d_{\max} = [\sigma/(\Delta\rho g)]^{0.5}$, but without creating small secondary drops that cause entrainment problems or formation of an emulsion. (See “Size of Dispersed Drops” in “Liquid-

Liquid Dispersion Fundamentals.”) As a general guideline, the maximum recommended design velocity corresponds to a Weber number of about 12:

$$V_{o,\max} \approx \left(\frac{12\sigma}{d_o \rho_d} \right)^{1/2} \quad (15-107)$$

The minimum Weber number that ensures jetting in all the holes is about 2. It is common practice to specify a Weber number between 8 and 12 for a new design. For a detailed discussion of fundamentals, see Homma et al., *Chem. Eng. Sci.*, **61**, pp. 3986–3996 (2006).

It is well established that the dispersed phase must issue cleanly from the holes. This requires that the material of the pipe or disperser plate be preferentially wetted by the continuous phase (requiring the use of plastics or plastic-coated trays in some instances), or that the dispersed phase issue from nozzles projecting beyond the surface. For plate dispersers, these may be formed by punching the holes and leaving the burr in place [Mayfield and Church, *Ind. Eng. Chem.*, **44**(9), pp. 2253–2260 (1952)]. Once the design velocity is set, the number of holes is given by

$$N_{\text{holes}} = \frac{Q_d}{A_o V_o} \quad (15-108)$$

where Q_d is the total volumetric flow rate of dispersed phase and A_o is the cross-sectional area of a single hole.

STATIC EXTRACTION COLUMNS

Common Features and Design Concepts Static extractors include spray-type, packed, and trayed columns often used in the petrochemical industries (Fig. 15-32). They offer the advantages of (1) availability in large diameters for very high production rates, (2) simple operation with no moving parts and associated seals, (3) requirement for control of only one operating interface, and (4) relatively small required footprint compared to mixer-settler equipment. Their primary disadvantage is low mass-transfer efficiency compared to that of mechanically agitated extractors. This usually limits applications to those involving low viscosities (less than about 5 cP), low to moderate interfacial tensions (typically 3 to 20 dyn/cm equal to 0.003 to 0.02 N/m), and no more than three to five equilibrium stages. Although the spray column is the least efficient static extractor in terms of mass-transfer performance, due to considerable backmixing effects, it finds

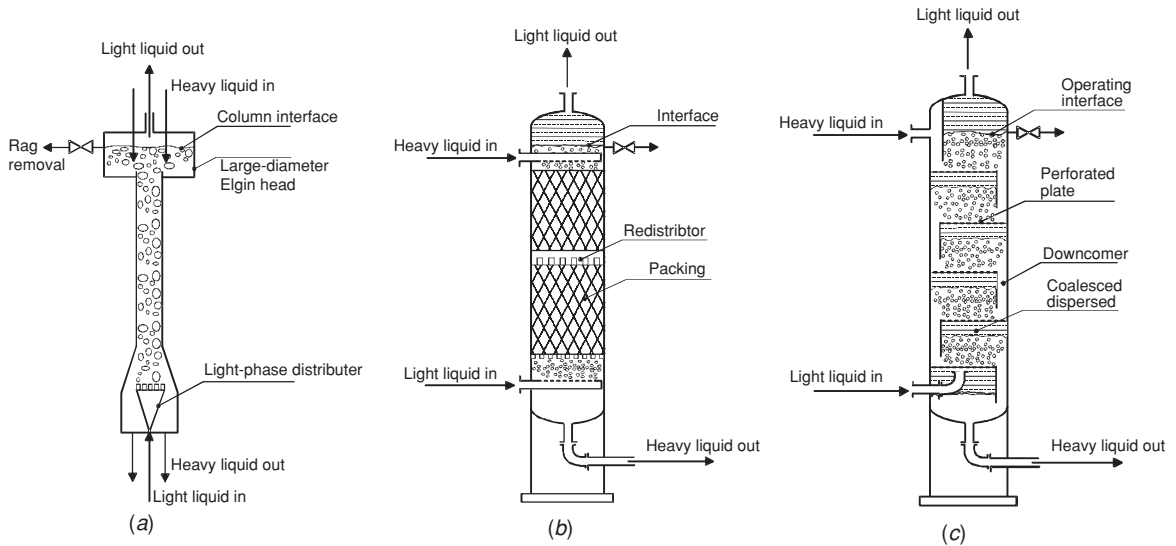


FIG. 15-32 Schematic of common static extractors. (a) Spray column. (b) Packed column. (c) Sieve tray column.

use in processing feeds that would easily foul other equipment. Packed and trayed column designs provide improved mass-transfer performance by limiting backmixing.

An understanding of the general hydraulics of a static contactor is necessary for estimating the diameter and height of the column, as this affects both capacity and mass-transfer efficiency. Accurate evaluations of characteristic drop diameter, dispersed-phase holdup, slip velocity, and flooding velocities usually are necessary. Fortunately, the relative simplicity of these devices facilitates their analysis and the approaches taken to modeling performance.

Choice of Dispersed Phase In general, formation of dispersed drops is preferred over formation of films or rivulets in order to maximize contact area and mass transfer. Static extractors generally are designed with the majority phase dispersed in order to maximize interfacial area needed for mass transfer; i.e., the phase with the greatest flow rate entering the column generally is dispersed. The choice of dispersed phase also depends upon the relative viscosity of the two phases. If one phase is particularly viscous, it may be necessary to disperse that phase.

Drop Size and Dispersed-Phase Holdup Various models used to estimate the size of dispersed drops in static extractors are listed in Table 15-15. Also see “Size of Dispersed Drops” under “Liquid-Liquid Dispersion Fundamentals.” Measurements of dispersed-phase holdup within a column-type extractor often are made by stopping all flows in and out of the extractor and measuring the change in the main interface level. This technique can be prone to significant experimental error as a result of end effects, static holdup present in small laboratory packings, inaccurate measurement of the baseline interface level, and holdup variations within a column as flooding conditions are approached. Examples of models for prediction of holdup are provided in Table 15-16. Additional models are given in *Liquid-Liquid Extraction Equipment*, Godfrey and Slater, eds. (Wiley, 1994). In general, an implicit calculation of the dispersed-phase holdup is usually encountered. One must be very careful in evaluating the roots of these equations, especially in the region of high dispersed-phase holdup ($\phi_d > 0.2$).

Interfacial Area The mass-transfer efficiency of most extraction devices is proportional to the area available for mass transfer (neglecting any axial mixing effects). As discussed in “Liquid-Liquid Dispersion Fundamentals,” for the general case where the dispersed phase travels through the column as drops, an average liquid-liquid interfacial area can be calculated from the Sauter mean drop diameter and dispersed-phase holdup:

$$a = \frac{6\epsilon\phi_d}{d_p} \quad (15-109)$$

In most cases, the drop size distribution is not known.

Drop Velocity and Slip Velocity The hydraulic characteristics of a static extractor depend upon drop diameter, liquid velocities, and physical properties. The average velocity of a dispersed-phase drop (V_{drop}) and the interstitial velocity of the continuous phase V_{ic} are given by

$$V_{drop} = \frac{V_d}{\epsilon\phi_d} \quad (15-110)$$

$$V_{ic} = \frac{V_c}{\epsilon(1 - \phi_d)} \quad (15-111)$$

where V_d = superficial velocity of dispersed phase
 V_c = superficial velocity of continuous phase
 ϕ_d = fraction of void volume occupied by dispersed phase
 ϵ = void fraction of column ($\epsilon = 1.0$ for sprays and sieve trays)

The relative velocity between the counterflowing phases is referred to as the slip velocity and defined by

$$V_s = V_{drop} + V_{ic} = \frac{V_d}{\epsilon\phi_d} + \frac{V_c}{\epsilon(1 - \phi_d)} \quad (15-112)$$

The slip velocity of a dispersed-phase drop of diameter d_p can be estimated from a balance of gravitational, buoyancy, and frictional forces:

$$F_{buoyancy} - F_{gravity} - F_{drag} = 0 \quad (15-113)$$

$$F_{buoyancy} = \rho_c \left(\frac{\pi}{6} d_p^3 \right) g \quad (15-114)$$

$$F_{gravity} = \rho_d \left(\frac{\pi}{6} d_p^3 \right) g \quad (15-115)$$

$$F_{drag} = \frac{1}{2} C_D \rho_c \left(\frac{\pi}{4} d_p^2 \right) V_{so}^2 \quad (15-116)$$

TABLE 15-15 Example Drop Diameter Models for Static Extractors

Example	Eq.	Comments	Ref.
$d_p = 1.15\eta\sqrt{\frac{\sigma}{\Delta\rho g}}$, $\eta = 1.0$ for no mass transfer and $c \rightarrow d$, $\eta = 1.4$ for $d \rightarrow c$	1	Spray, packing, and sieve tray	1
$d_p = 0.12D_h We_c^{-0.5} Re_c^{0.15}$, developed with no mass transfer, We_c and Re_c are calculated based on slip velocity	2	SMV structured packing	2
$d_p = C_p\sqrt{\frac{\sigma}{\Delta\rho g}}$, $C_p = 1$ for $\rho_d < \rho_c$, $C_p = 0.8$ for $\rho_d > \rho_c$ developed with no mass transfer	3	Packing	3
$d_p = 1.09\sqrt{\frac{\sigma}{\Delta\rho g}}\left(1 + 700\frac{V_{sl}}{\sigma}\right)$, developed with no mass transfer	4	Packing	4
$d_p = 0.74C_\psi\sqrt{\frac{\sigma}{\Delta\rho g}}\left(\frac{\Delta\rho\rho_f\sigma}{\rho_w^2\sigma_w}\right)^{-0.12}$, $C_\psi = 1$ for no mass transfer, $C_\psi = 0.84$ for $c \rightarrow d$, $C_\psi = 1.23$ for $d \rightarrow c$	5	Packing	5
$d_p = \frac{C_\psi}{(6d_o\sigma/\Delta\rho g)^{1/3} + \frac{1}{2.04(12\sigma/\rho_d V_o^2)}}$ $C_\psi = 1.0$ for $c \rightarrow d$ and no mass transfer, $C_\psi = 1.06$ for $d \rightarrow c$	6	Spray nozzles	5
$d_p = d_o E\ddot{o}_o^{-0.35}\left[0.80 + \exp\left(-2.73 \times 10^{-2}\frac{We_o}{E\ddot{o}_o}\right)\right]$ $E\ddot{o}_o = \frac{d_o^2\Delta\rho g}{\sigma}$, $We_o = \frac{\rho_d d_o V_o^2}{\sigma}$	7	Perforated plate	6

References:

- Seibert and Fair, *Ind. Eng. Chem. Res.*, **27**(3), pp. 470–481 (1988).
 - Streiff and Jancic, *Ger. Chem. Eng.*, **7**, pp. 178–183 (1984).
 - Billet, Mackowiak, and Pajak, *Chem. Eng. Process.*, **19**, pp. 39–47 (1985).
 - Lewis, Jones, and Pratt, *Trans. Instn. Chem. Engrs.*, **29**, pp. 126–148 (1951).
 - Kumar and Hartland, *Ind. Eng. Chem. Res.*, **35**(8), pp. 2682–2695 (1996).
 - Kumar and Hartland, Chap. 17 in *Liquid-Liquid Extraction Equipment*, Godfrey and Slater, eds. (Wiley, 1994), pp. 625–735.
- Refer to the original articles for details.

where V_{so} is defined as the characteristic slip velocity obtained at low dispersed-phase flow rate. Rearranging Eqs. (15-113) to (15-116) gives

$$V_{so} = \sqrt{\frac{4\Delta\rho g d_p}{3\rho_c C_D}} \quad (15-117)$$

The slip velocity at higher holdup often is estimated from $V_s \approx V_{so}(1 - \phi_d)$.

Equation (15-117) provides the basis for various methods used to predict the characteristic slip velocity. For additional discussion, see Mišek, Chap. 5 in *Liquid-Liquid Extraction Equipment*, Godfrey and Slater, eds. (Wiley, 1994). Equation (15-117) can be difficult to use for design because of difficulty estimating the drag coefficient C_D and difficulty accounting for packing resistance or drop-drop interactions. The drag coefficient can be affected by internal circulation within the drop. For good mass transfer, it is most desirable to have circulating drops traveling through a relatively nonviscous continuous phase. Particular care should be taken in utilizing models developed primarily from studies involving small laboratory packings, because the packing resistance is particularly significant in that case. Also many studies do not include low-interfacial-tension systems, even though most applications of static extractors involve low to moderate interfacial tension. Also note that surface-active impurities can reduce the characteristic

drop velocity [Garner and Skelland, *Ind. Eng. Chem.*, **48**(1), pp. 51–58 (1956); and Skelland and Caenepeel, *AIChE J.*, **18**(6), pp. 1154–1163 (1972)], which is another reason to approach these models with care.

The following method is recommended for calculating slip velocity in static extractors at low dispersed-phase holdup:

$$\text{If } Re_{\text{Stokes}} = \frac{\rho_c \Delta\rho g d_p^3}{18\mu_c^2} < 2, \text{ then } V_{so} = \frac{\Delta\rho g d_p^2}{18\mu_c} \quad (\text{Stokes' law}) \quad (15-118)$$

For $Re_{\text{Stokes}} > 2$, Seibert and coworkers [Seibert and Fair, *Ind. Eng. Chem. Res.*, **27**(3), pp. 470–481 (1988); and Seibert, Reeves, and Fair [*Ind. Eng. Chem. Res.*, **29**(9), pp. 1901–1907 (1990)] recommend the model of Grace, Wairegi, and Nguyen [*Trans. Inst. Chem. Eng.*, **54**, p. 167 (1976)]. In this case, the characteristic slip velocity may be calculated from

$$V_{so} = \frac{Re\mu_c}{d_p\rho_c} \quad (15-119)$$

TABLE 15-16 Example Hold-up Models for Static Extractors

Example	Eq.	Comments	Ref.
$\phi_d = \frac{V_d[\cos(\pi\zeta/4)]^2}{\varepsilon[V_{so}\exp(-6\phi_d/\pi) - V_c/\varepsilon(1 - \phi_d)]}, \quad \zeta = \frac{a_p d_p}{2}$	1	Spray, packing, and sieve tray V_{so} is calculated by the method of Grace et al. (1976), Eqs. (15-118) to (15-123).	1
$\frac{V_d}{\phi_d} + \frac{V_c}{1 - \phi_d} = \frac{4c_p}{3} \sqrt{\frac{d_p \Delta\rho g}{C_D \rho_c}}$	2	SMV structured packing. Drag coefficient, C_D is calculated by assuming a drop is a rigid sphere. Parameter c_p depends upon drop-drop and drop-packing interactions.	2
$\frac{V_d}{\phi_d} + \frac{V_c}{1 - \phi_d} = \varepsilon C \left(\frac{4g \Delta\rho \sigma}{\rho_c^2} \right)^{0.25} \exp(-b\phi_d)$	3	Packing. Constants C and b differ for different packings. Drag coefficient = 1.	3
$\left(\frac{V_d}{\phi_d} + \frac{V_c}{1 - \phi_d} \right) \left(\frac{a_p \rho_c}{\varepsilon^3 g \Delta\rho} \right)^{0.5} = 0.683\phi_d (1 - \phi_d)$	4	Packing	4
$\phi_d = A \left\{ 0.27 + \left[\frac{\varepsilon}{g} \left(\frac{\rho_c}{g\sigma} \right)^{0.25} \right]^{0.78} \right\} \left[V_d \left(\frac{\rho_c}{g\sigma} \right)^{0.25} \right]^{0.87} \exp(B)$ $B = 3.34 V_c \left(\frac{\rho_c}{g\sigma} \right)^{0.25}$ $A = \left(\frac{\Delta\rho}{\rho_c} \right)^{-0.58} \left(\frac{\mu_d}{\mu_w} \right)^{0.18} C \varepsilon^n \left[l \left(\frac{\rho_c g}{\sigma} \right)^{0.5} \right]^{-0.39}$	5	Unified model for packing, spray, Karr, pulsed perforated plate, Kühni, rotating disk. Constants C , n , and l depend upon type of contactor.	5

References:

1. Seibert and Fair, *Ind. Eng. Chem. Res.*, **27**(3), pp.470–481 (1988).
 2. Streiff and Jancic, *Ger. Chem. Eng.*, **7**, pp. 178–183 (1984).
 3. Billet, Mackowiak, and Pajak, *Chem. Eng. Process.*, **19**, pp. 39–47 (1985).
 4. Sitaramayya and Laddha, *Chem. Eng. Sci.*, **13**, p. 263 (1961).
 5. Kumar and Hartland *Ind. Eng. Chem. Res.*, **34**, pp. 3925–3940 (1995).
- Refer to the original articles for details.

where Re is obtained from the correlation:

$$\frac{Re}{P^{0.149}} = 0.94H^{0.757} - 0.857 \quad H \leq 59.3 \quad (15-120)$$

$$\frac{Re}{P^{0.149}} = 3.42H^{0.441} - 0.857 \quad H > 59.3 \quad (15-121)$$

And P and H are dimensionless groups defined by

$$P = \frac{\rho_c^2 \sigma^3}{\mu_w^2 g \Delta\rho} \quad (15-122)$$

$$H = \left(\frac{4d_p^2 g \Delta\rho}{3\sigma} \right) \left(\frac{\mu_w}{\mu_c} \right)^{0.14} P^{0.149} \quad (15-123)$$

and μ_w is a reference viscosity equal to 0.9 cP (9×10^{-4} Pa·s). For discussion of methods to correct slip velocity to account for the effect of high dispersed-phase holdup, see Angier, Masbernat, and Guiraud, *AIChE J.*, **49**(9), pp. 2300–2316 (2003).

Flooding Velocity Maximum flow through a countercurrent extractor is limited by the flooding velocity. See “Hydrodynamics of Column Extractors” for a general discussion of flooding mechanisms. Because of the many possible causes of flooding, published data and

models should be viewed with some caution. In addition, models developed from laboratory data can lead to problems when used for design of commercial-scale columns. For example, in packed columns a column diameter/packing diameter ratio of at least 8 is recommended to avoid channeling due to wall effects. This means that laboratory studies must utilize small packings with high specific packing surface areas (packing area/contacting volume). The high packing area will provide significant resistance to drop flow, greater than that encountered in large columns containing large commercial packings. In addition, many of the published laboratory data on flooding velocities were generated by using moderate to high-interfacial-tension systems. In this case, the packing surface area resistance controls the flooding mechanism.

Several correlations of flooding velocity have the general form

$$V_{fj} \propto C_1 \frac{C_2}{a_p^n} \quad 0 < n < 1 \quad (15-124)$$

where V_{fj} is the continuous-phase velocity at which flooding occurs, a_p is the specific packing surface area, and C_1 and C_2 are empirical constants that depend upon the specific type of packing, fluid physical properties, and flow ratio. While these types of models have excellent reported fits of data, they were primarily developed by using laboratory-scale packings. Furthermore, in the limit as the packing surface area approaches zero, the predicted flooding velocity becomes infinite, an unrealistic result. Care should be taken when extrapolating such models to a larger packing size.

Seibert, Reeves, and Fair [*Ind. Eng. Chem. Res.*, **29**(9), pp. 1901–1907 (1990)] proposed a more mechanistically consistent flooding model that is derived by assuming a tightly packed arrangement of drops at flooding and yields

$$\frac{1}{V_{cf}} = C_1 + \frac{C_2}{C_3 \cos^2(C_4 a_p)} \quad (15-125)$$

where parameters C_1 , C_2 , C_3 , and C_4 are functions of the system properties and flow ratio. An advantage of this flooding model is that as the packing surface area approaches zero, a finite flooding velocity is calculated since the $\cos 0 = 1$. In the absence of packing, Eq. (15-125) can be rewritten to predict flooding in a spray column and the ultimate capacity of a tray column. Examples of published flooding models for static extractors are given in Table 15-17. Unfortunately, very

few flooding data are available for columns greater than 30 cm (12 in) in diameter. Also, many of the available flooding data have been obtained in the absence of mass transfer. With this in mind, for new designs it is recommended that flow velocities be limited to no more than 50 percent of the calculated flooding values. The final design should be refined in miniplant or pilot-plant tests using actual feed materials.

Drop Coalescence Rate The rate of drop coalescence often is assumed to be rapid (not rate-limiting) in the design of static extractors. However, this is not necessarily the case, particularly during operation at high dispersed-phase holdup and high flow ratios of dispersed phase to continuous phase. Under these conditions, a large number of drops flow through a nearly stagnant continuous phase, and these drops must coalesce at the main operating interface located at the top or bottom of the column. Seibert, Bravo, and Fair [*ISEC '02 Proc.* **2**, pp. 1328–1333 (2002)] report that problems with coalescence are most likely when the

TABLE 15-17 Example Flooding Models for Static Extractors

Example	Eq.	Comments	Ref.
$V_{cf} = \frac{0.178\epsilon V_{so}}{1 + 0.925(V_{df}/V_{cf}) \{1/[\cos(\pi\zeta/4)]\}^2}$ $\zeta = \frac{a_p d_p}{2}$	1	Spray, packing, and ultimate capacity of sieve tray V_{so} is calculated by the method of Grace et al. (1976), Eqs. 15-118 to 15-123.	1
$V_{cf} = \sqrt{\frac{L_{dc} - A}{B(V_{df}/V_{cf})^2 + C}}$ $A = \frac{6\sigma}{d_p \Delta\rho g}$ $B = \frac{1.1\rho_d}{g \Delta\rho f_{ja}^2}$ $C = \frac{2.7\rho_c}{2g \Delta\rho f_{da}^2}$	2	Sieve tray capacity limited by coalesced layer flood	2
$V_{cf} = \epsilon C \left(\frac{4g \Delta\rho \sigma}{\rho_c^2} \right)^{1/4} (1 - \phi_{df})^2 [\exp(-b\phi_{df})] (1 - b\phi_{df})$	3	Packing	3
$\frac{V_d}{V_c} = \frac{\phi_{df}^2}{(1 - \phi_{df})^2} \frac{1 + b(1 - \phi_{df})}{1 - b\phi_{df}}$	4	Constants C and b depend on packing. Drag coefficient = 1.	
$V_{cf} = \left\{ \frac{C[(a_p/g\epsilon^3)(\rho_c/\Delta\rho)\sigma^{0.251-0.25}]^2}{1 + 0.835(\rho_d/\rho_c)^{0.25}(V_{df}/V_{cf})^{0.5}} \right\}^2$	5	Packing C is a constant for each packing.	4
$V_{cf} = \left[\left[1 + \left(\frac{V_{df}}{V_{cf}} \right)^{0.57} \right]^2 \sqrt{\frac{a_p}{g}} \right]^{-1} \alpha C_1 \epsilon^{1.54} \left(\frac{\Delta\rho}{\rho_d} \right)^{0.41} \left[\frac{1}{a_p} \left(\frac{\Delta\rho^2 g}{\mu_c^2} \right)^{1/3} \right]^{0.3} \left(\frac{\mu_c}{\sqrt{\Delta\rho \sigma a_p}} \right)^{0.15}$ <p>$\alpha = 1$ for continuous-phase wetting, $\alpha = 1.29$ for dispersed-phase wetting</p>	6	Packing C_1 is a constant that depends upon the type of packing.	5
$\frac{(V_{df} + V_{cf})d_c \rho_c}{\mu_c} = 0.30137 \left(\frac{A_{col}}{\pi d_c^2 N/4} \right)^{0.0948} A \left(\frac{\Delta\rho}{\rho_c} \right)^{0.1397} B \left(\frac{d_d^3 \rho_c^2 g}{\mu_c^2} \right)^{0.3875}$ $A = \left(\frac{V_{df}}{V_{cf}} \right)^{0.0593} \quad B = \left(\frac{\sigma \rho_d d_o}{\mu_d^2} \right)^{0.0127} \quad A_{col} = \frac{1}{1 - \frac{A_{dow}}{A_{col}}} \frac{Q_d}{f V_{dfn}}$ <p>f = fraction of flood</p>	7	Sieve tray	6

References:

- Seibert and Fair, *Ind. Eng. Chem. Res.*, **27**(3), pp. 470–481 (1988).
- Seibert and Fair, *Ind. Eng. Chem. Res.*, **32**(10), pp. 2213–2219 (1993).
- Billet, Mackowiak, and Pajak, *Chem. Eng. Process.*, **19**, pp. 39–47 (1985).
- Dell and Pratt, *Trans. Inst. Chem. Eng.*, **29**, p. 89 (1951).
- Kumar and Hartland, *Trans. Inst. Chem. Eng.*, **72**(Pt. A), pp. 89–104 (1994).
- Rocha et al., *Ind. Eng. Chem. Res.*, **28**(12), pp. 1873–1878 (1989).

Refer to the original articles for details.

superficial dispersed-phase velocity V_{d1} is greater than about 12 percent of the characteristic slip velocity given by Eqs. (15-118) to (15-123). For these systems, miniplant tests normally are needed to understand the rate of coalescence. If coalescence is slow, design rates will need to be reduced below those predicted by assuming rapid coalescence.

For slowly coalescing systems, placement of coalescing material within the column at the main interface may significantly improve performance. The height of the uncoalesced layer located at the main operating interface may be reduced by adding a high-surface-area mesh type of coalescer that is wetted by the dispersed phase. If plugging is a concern, a more open (lower-surface-area) structured packing may be preferred. It also may be useful to add a separate liquid-liquid phase separator outside the extractor to clarify the extract or raffinate streams. See "Liquid-Liquid Phase Separation Equipment."

Mass-Transfer Coefficients As described in "Rate-Based Calculations," the overall mass-transfer coefficient may be written as

$$\frac{1}{k_{od}} = \frac{1}{k_d} + \frac{m_{dc}^{vol}}{k_c} \tag{15-126}$$

where the slope of the equilibrium line m_{dc}^{vol} is expressed in volumetric concentration units. The dispersed-phase and continuous-phase film coefficients k_d and k_c generally are functions of convection and turbulence effects, as well as molecular diffusion coefficients and the thicknesses of stagnant films at the interface between drops and the continuous phase. Examples of mass-transfer coefficient models for static extractors are given in Table 15-18. For additional discussion of

TABLE 15-18 Example Mass-Transfer Coefficient Models

Example	Eq.	Comments	Ref.
$k_c = 0.698 \left(\frac{D_c}{d_p} \right) \left(\frac{d_p V_s \rho_c}{\mu_c} \right)^{0.5} \left(\frac{\mu_c}{\rho_c D_c} \right)^{0.4} (1 - \phi_d)$	1	For nonrigid drops. Spray, packing, and sieve trays.	1
$k_d = 0.023 V_s \sqrt{\frac{\rho_c D_c}{\mu_c}}$	2	Model of Laddha and Degaleesan. For nonrigid drops. Spray, packing, and sieve trays.	2 1
$k_d = \frac{0.00375 V_s}{1 + \mu_d/\mu_c}$	3	Model of Handlos and Baron. Approximate solution to series model. Independent of molecular diffusion. Use for large drops.	3
$\Phi = \frac{\sqrt{\mu_c \rho_c D_c}}{1 + \mu_d/\mu_c}$	4	Spray, packing, and sieve trays. Use Eq. (3) if $\Phi < 6$.	1
$k_d = \frac{17.9 D_d}{d_p}$	5	Laminar circulation within drops. Recommended for long contact times. For $Re < 50$.	4 5
$k_d = 1.14 \left(\frac{D_d}{d_p} \right) \left(\frac{\rho_d d_p^2 \bar{\omega}}{\mu_D} \right)^{0.56} \left(\frac{\mu_d}{\rho_d D_d} \right)^{0.5}$	6	For oscillating drops. Simplified version for assumption of $\theta = 0.2$.	6
$\bar{\omega} = \frac{1}{2\pi} \left[\frac{192\sigma b}{d_p^3(3\rho_d + 2\rho_c)} \right]^{0.5} \quad b = 0.805 d_p^{0.225}, d_p \text{ in cm}$	7		
$k_c = \frac{D_c}{d_p} \left[2 + 0.95 \left(\frac{\rho_c V_s d_p}{\mu_c} \right)^{0.5} \left(\frac{\mu_c}{\rho_c D_c} \right)^{0.33} \right]$	8	For rigid drops.	7
$k_c = 0.725 \left(\frac{D_c}{d_p} \right) \left(\frac{\rho_c V_s d_p}{\mu_c} \right)^{0.57} \left(\frac{\mu_c}{\rho_c D_c} \right)^{0.42} (1 - \phi_d)$	9	For circulating drops. Developed from correlation of spray column data.	8
$k_c = 1.4 \left(\frac{D_d}{d_p} \right) \left(\frac{\rho_c d_p^2 \bar{\omega}}{\mu_c} \right)^{0.5} \left(\frac{\mu_c}{\rho_c D_c} \right)^{0.5}$	10	For oscillating drops.	9

References:

1. Seibert and Fair, *Ind. Eng. Chem. Res.*, **27**(3), pp. 470–481 (1988).
2. Laddha and Degaleesan, *Transport Phenomena in Liquid Extraction* (McGraw-Hill, 1978).
3. Handlos and Baron, *AIChE J.*, **3**, p.127 (1957).
4. Kronig and Brink, *Appl. Sci. Res.*, **A2**, p. 142 (1950).
5. Johnson and Hamielec, *AIChE J.*, **6**, p. 145 (1960).
6. Yamaguchi, Fujimoto, and Katayama, *J. Chem. Japan*, **8**, p. 361 (1975).
7. Garner and Suckling, *AIChE J.*, **4**, p. 114 (1958).
8. Treybal, *Liquid Extraction* (McGraw-Hill, 1963).
9. Yamaguchi, Watanabe, and Katayama, *J. Chem. Japan*, **8**, p. 415 (1975).

Refer to the original articles for details.

film coefficient models, see *Liquid-Liquid Extraction Equipment*, Godfrey and Slater, eds. (Wiley, 1994).

Axial Mixing See "Accounting for Axial Mixing" under "Liquid-Liquid Extraction Equipment." Many approaches have been developed. Becker recommends the concept of the height of a dispersion unit (HDU) to correct the height of a transfer unit for axial mixing in a static contactor [Becker, *Chem. Eng. Technol.*, **26**(1), pp. 35–41 (2003); *Chem. Ing. Tech.*, **74**, pp. 59–66 (2002); and Becker and Seibert, *Chem. Ing. Tech.*, **72**, pp. 359–364 (2000)]:

$$H_{or|axial} = H_{or|plug} + HDU_o \quad (15-127)$$

where

$$HDU_o = \left(p_0 + \frac{0.8}{Z_i} \frac{\mathcal{E} \ln \mathcal{E}}{\mathcal{E} - 1} \right)^{-1} \quad (15-128)$$

$$p_0 = \frac{0.1Z_i/H_{or}^* + 1}{0.1Z_i/H_{or}^* + p_1/p_2} \cdot p_1 \quad (15-129)$$

$$\frac{1}{p_1} = \frac{1}{\mathcal{E}} HDU_r + HDU_e \quad \frac{1}{p_2} = HDU_r + \frac{1}{\mathcal{E}} HDU_e \quad (15-130)$$

For a given phase,

$$HDU = \frac{E}{V} \quad (15-131)$$

In these equations, the superscript * denotes the plug flow overall height of a transfer unit, subscript *r* denotes the raffinate phase, subscript *e* denotes the extract phase, and Z_i is the contacting height. For $\mathcal{E} = 1$, the equations reduce to

$$HDU_o = \left(\frac{1}{HDU_r + HDU_e} + \frac{0.8}{Z_i} \right)^{-1} \quad (15-132)$$

The axial mixing coefficient is correlated by

$$\frac{E_c \rho_c}{\mu_c} = (C_1 Re_c^a + C_2 Re_d^b) \left(\frac{D_{col}}{100} \right)^c \quad (15-133)$$

D_{col} = column diameter, cm

where

$$Re_c = \frac{V_{re} \rho_c}{\mu_c (a_p + a_w)} \quad (15-134)$$

$$a_w = \frac{4}{D_{col}} \quad (15-135)$$

$$Re_d = \frac{V_d \rho_c}{\mu_c} \quad (15-136)$$

In Eq. (15-135), a_w is the specific wall surface (cm^2/cm^3) and a_p is the specific packing surface (cm^2/cm^3). This term is dropped for a spray column ($C_1 = 0$). The model coefficients are summarized in Table 15-19. Most of the axial mixing data available in the literature are for the continuous phase; dispersed-phase axial mixing data are rare. Becker recommends assuming $HDU_r = HDU_e$ when dispersed-phase data are not available. Becker presents a parity plot (Fig. 15-33) based on small- and large-scale data for packed and spray columns.

Spray Columns The spray column is one of the simplest and oldest types of equipment used to contact two liquid phases in counter-current flow. Normally it consists of an empty vertical vessel with a distributor located at one end. The distributor disperses one of the liquids into drops. These drops then rise or fall against the flow of the continuous phase, collecting at the other end of the column and finally coalescing to form a layer of clear liquid that is withdrawn from the column. Because spray columns often are used when solids are present, phases often are dispersed through pipe distributors with large holes oriented in the direction of flow. In cases where the ratio of volumetric flow rates entering the column is far from unity, the liquid entering the extractor at the smaller rate generally should be dispersed to avoid excessive backmixing. Sometimes liquid distributors are used at each end to disperse both phases, with the main liquid-liquid interface located in the middle of the column (Fig. 15-34). See "Liquid Distributors and Dispersers" under "Liquid-Liquid Extraction Equipment."

Spray columns are inexpensive and easy to operate and provide high volumetric throughput. However, because the continuous phase flows freely through the column, backmixing effects generally are severe. As a result, spray columns rarely achieve more than one theoretical stage. Spray columns may be used when only one theoretical stage is required or when solid precipitation is prevalent and no other contacting device can be used because of plugging. Spray columns also are used for direct heat transfer between large immiscible liquid streams.

Drop Size, Holdup, and Interfacial Area Drop size is estimated by using one of the models listed in Table 15-15, and holdup is estimated from expressions given in Table 15-16. Interfacial area is then calculated by using Eq. (15-109).

Flooding Several empirical and mechanistic flooding models have been reported. These have been reviewed by Kumar and Hartland [Chap. 17 in *Liquid-Liquid Extraction Equipment*, Godfrey and Slater, eds. (Wiley, 1994), pp. 680–686]. Seibert, Reeves, and Fair [*Ind. Eng. Chem. Res.*, **29**(9), pp. 1901–1907 (1990)] propose an alternative model:

$$V_{of} = \frac{0.178V_{so}}{1 + 0.925(V_{df}/V_{of})} \quad (15-137)$$

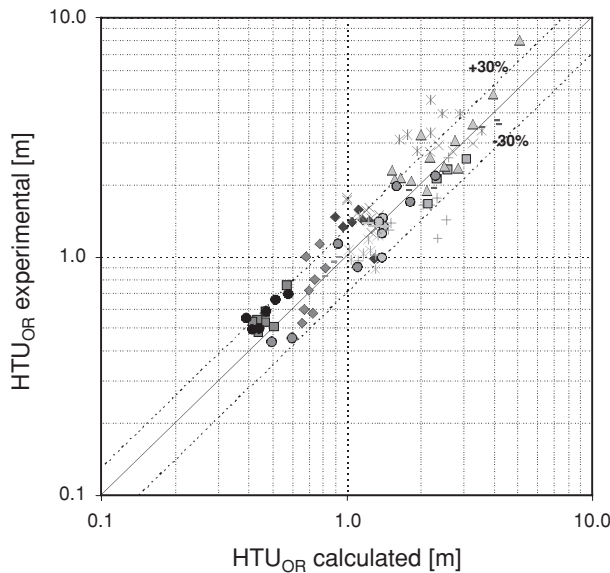
where V_{so} is the characteristic slip velocity determined by using Eqs. (15-118) to (15-123).

Mass-Transfer Efficiency As mentioned earlier, spray columns rarely develop more than one theoretical stage due to axial mixing within the column. Nevertheless, it is necessary to determine the column height that will give this theoretical stage. Cavers [Chap. 10 in

TABLE 15-19 Correlation Constants for the Becker Axial Mixing Model*

	No. of data points	C_1	a	C_2	B	c	Average relative error, %
Spray column	197	0	0	45.6	1.058	0.917	24.8
Structured packed columns and IMTP random packing	118	405.1	0.798	27.7	0.914	1.178	32.0
Structured packed columns with dual flow plates	57	284.5	0.494	35.0	0.406	0.847	18.7

*Becker, *Chem. Eng. Technol.*, **24**(12), pp. 1242–1244 (2001).



- ◆ SMVP, Hexane/Methanol/Water, 42 cm, d-c
- SMV, Hexane/Methanol/Water, 10 cm, d-c
- Spray, Hexane/Methanol/Water, 42 cm, d-c
- × Pall Rings, Hexane/Methanol/Water, 42 cm, d-c
- * IMTP®40 Random Packing, Hexane/MeOH/Water, 42 cm d-c
- SMVP, Hexane/Methanol/Water, 10 cm, d-c
- + SMV, Toluene/Acetone/Water, 10 cm, d-c
- Spray C., Toluene/Acetone/Water, 10 cm, d-c
- ◆ BX Water/Ethanol/CO₂, 6, 7 cm, d-c
- INTALOX®2T, Toluene/Acetone/Water, 42 cm, c-d
- ▲ Spray, Toluene/Acetone/Water, 42 cm, c-d
- × IMTP®40 Random Packing, Tol./Ac./Water, 42 cm, c-d
- * IMTP®25 Random Packing, Tol./Ac./Water, 42 cm, c-d
- ▲ IMTP®25 Random Packing, Tol./Ac./Water, 42 cm, c-d (Redistr.)
- SMV, Toluene/Acetone/Water, 10 cm, c-d
- SMV, Water/MIBK/BuAc, 5 cm, c-d

FIG. 15-33 Parity plot comparing spray and packed column results incorporating axial mixing model. [Reprinted from Becker, *Chemie Ing. Technik*, **74**(1–2), pp. 59–66 (2002). Copyright 2002 Wiley-VCH.]

Handbook of Solvent Extraction, Lo, Baird, and Hanson, eds. (Wiley, 1983; Krieger, 1991)] recommends the following equation from Ladha and Degaleesan [*Transport Phenomena in Liquid Extraction* (McGraw-Hill, 1978), p. 233] to estimate the overall volumetric mass-transfer coefficient:

$$k_{oc} a = m_{dc}^{vol} k_{od} a = 0.08 \times \frac{\phi_d(1 - \phi_d)(g^3 \Delta \rho^3 / \sigma \rho_c^2)^{1/4}}{(\mu_c / \rho_c \mathcal{D}_c)^{1/2} + (1/m_{dc})(\mu_d / \rho_d \mathcal{D}_d)^{1/2}} \quad (15-138)$$

Here \mathcal{D}_c and \mathcal{D}_d are the solute diffusivity coefficients in the continuous and dispersed phases, respectively. The height of a transfer unit can then be estimated from

$$H_{oc} = \frac{V_c}{k_{oc} a} \quad (15-139)$$

where H_{oc} is the height of an overall transfer unit based on the continuous phase and V_c is the superficial velocity of the continuous phase. Equation (15-138) provides only a rough approximation.

Packed Columns Packing is used in a column extractor to reduce axial mixing (backmixing). Packing also affects interfacial area and mass transfer through its impact on the holdup and flow path of dispersed drops. For reviews of packed-column extractor design, see Strigle, *Packed Tower Design and Applications*, 2d ed., Chap. 11 (Gulf, 1994); and Stevens, Chap. 8 in *Liquid-Liquid Extraction Equipment*, Godfrey and Slater, eds. (Wiley, 1994).

The packings used for liquid-liquid extraction are essentially the same as those used in distillation and absorption service, although the distributors and dispersers and many of the associated internals are not the same. Various commercially available packings offered by Koch-Glitsch and Sulzer Chemtech for liquid-liquid extraction service are listed in Table 15-20. Other manufacturers of packings include Raschig, Montz, Lantec, and Jaeger Products. It is a good idea to consult a variety of vendors before making a selection. Illustrations of various types of packings are given in Sec. 14, "Equipment for Distillation, Gas Absorption, Phase Dispersion, and Phase Separation."

Packings are classified as either random or structured. Random packings may be wet-loaded into a column by filling the column

with liquid and slowly adding the packing at the liquid surface so the packing pieces gently fall to the surface of the forming bed (typical of ceramic packings); or they may be dry-loaded by transferring them into an empty column through a chute or fabric sock (typical of metal or plastic packings). The familiar ring and saddle packings such as Raschig rings, Berl saddles, Intalox saddles, and Lessing rings are examples of ceramic packings. The more modern metal and plastic random packings such as Pall rings, Hy-Pak®, and IMTP® packings are ring or saddle shapes with internal fingers and slots in the wall. These packings are more open and provide greater access to the interior surfaces for improved capacity and mass-transfer performance. Structured packings are modular assemblies placed inside the column in a specific arrangement. Many are in the form of woven wire mesh or crimped sheets arranged in layers at specific angles. For packing made from sheets, it is not clear whether surface treatments such as perforations and embossing are important in liquid-liquid extraction, so a number of smooth-surface structured packings are marketed for extraction applications. For best performance, the packing should be preferentially wetted by the continuous phase. (See "Effect of Solid-Surface Wettability" under "Liquid-Liquid Dispersion Fundamentals.") Many older packed extractors are being refurbished with newer packings and internals to achieve higher throughput and better separation performance. As with any packing and the associated internals, installation procedures recommended by the packing vendor need to be carefully followed to ensure the packing performs as designed. In addition to mass-transfer performance and throughput, another important consideration when choosing metal packing is the packing material and wall thickness relative to corrosion rates. The packing should have sufficient wall thickness for a reasonable service life.

Liquid Distribution Good initial distribution of the dispersed phase is very important for good performance. Strigle [*Packed Tower Design and Applications*, 2d ed., Chap. 11 (Gulf, 1994)] describes typical packed-column internals for liquid-liquid contacting. When the light phase is dispersed, a combination liquid disperser/packing support is preferred because a separate support plate can adversely affect the flow of dispersed drops. An example of a disperser plate is shown in Fig. 15-35. A ladder-type pipe distributor commonly is used to distribute the dispersed-phase feed to the initial disperser plate. Other

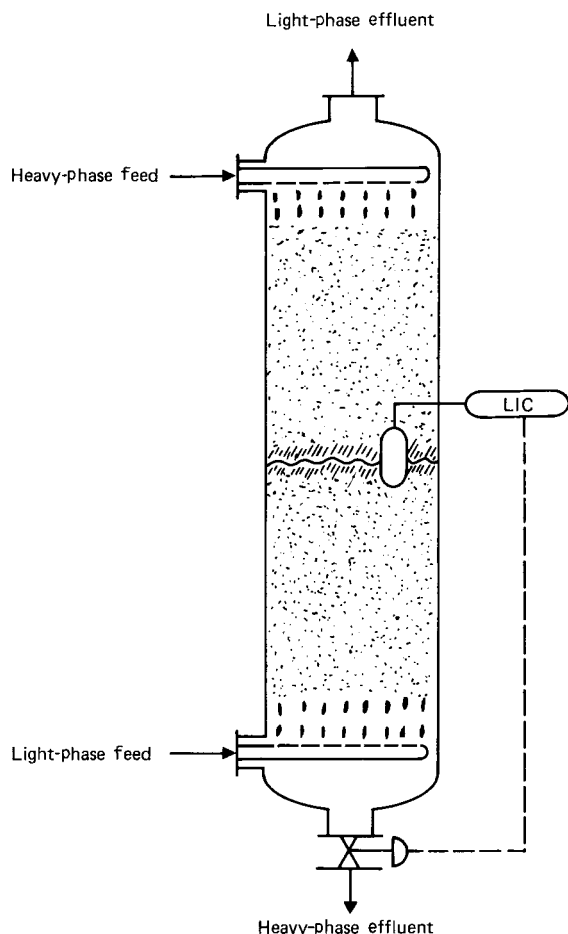


FIG. 15-34 Spray column with both phases dispersed.

distributor designs also are available. Koch and Vogelpohl [*Chem. Eng. Technol.*, **24**(7), pp. 695–698 (2001); and *Chem. Eng. Technol.*, **24**(8), pp. 795–798 (2001)] discuss a sieve plate distributor design that includes a predistributor plate. Many of the concepts concerning geometric uniformity for liquid distribution in packed gas-liquid contactors [Perry, Nutter, and Hale, *Chem. Eng. Prog.*, **86**(1), pp. 30–35 (1990)] are relevant to liquid-liquid contactors as well. See “Liquid Distributors and Dispersers” under “Liquid-Liquid Extraction Equipment.”

Redistribution Seibert, Reeves, and Fair [*Ind. Eng. Chem. Res.*, **29**(9), pp. 1901–1907 (1990)] and Nemunaitis et al. [*Chem. Eng. Prog.*, **67**(11), p. 60 (1971)] report data showing little benefit from a packed height greater than 10 ft (3 m) and recommend redistributing the dispersed phase about every 5 to 10 ft (1.5 to 3 m) to generate new droplets and constrain backmixing. A random packed column often is designed with a redistributor placed between two or more packed sections. Structured packings sometimes are installed with a dual-flow perforated plate (with no downcomer) between elements, without coalescence of dispersed drops.

Minimum Packing Size and Drop Size For a given application there will be a minimum packing size or dimension below which random packing is too small for good extraction performance [Lewis, Jones, and Pratt, *Trans. Inst. Chem. Eng.*, **29**, pp. 126–148 (1951); Gayler and Pratt, *Trans. Inst. Chem. Eng.*, **31**, pp. 69–77 (1953); and Laddha and Degaleesan, *Transport Phenomena in Liquid Extraction*

TABLE 15-20 Random and Structured Packings Used in Packed Extractors

Packing	Surface area a_p , m^2/m^3	Void fraction ^a , ϵ
Metal random packing		
Koch-Glitsch IMTP [®] 25	224	0.964
Koch-Glitsch IMTP [®] 40	151	0.980
Koch-Glitsch IMTP [®] 50	102	0.979
Koch-Glitsch IMTP [®] 60	84	0.983
Sulzer I-Ring #25	224	0.964
Sulzer I-Ring #40	151	0.980
Sulzer I-Ring #50	102	0.979
Nutter Ring [®] NR 0.7	226	0.977
Nutter Ring [®] NR 1	168	0.977
Nutter Ring [®] NR 1.5	124	0.976
Nutter Ring [®] NR 2	96	0.982
Nutter Ring [®] NR 2.5	83	0.984
HY-PAK [®] #1	172	0.965
HY-PAK [®] #1½	118	0.976
HY-PAK [®] #2	84	0.979
FLEXIRING [®] 1 in	200	0.959
FLEXIRING [®] 1½ in	128	0.974
FLEXIRING [®] 2 in	97	0.975
CMR [™] 1	246	0.973
CMR [™] 2	157	0.970
CMR [™] 3	102	0.980
BETA RING [®] #1	186	0.963
BETA RING [®] #2	136	0.973
FLEXIMAX [®] 200	189	0.973
FLEXIMAX [®] 300	148	0.979
FLEXIMAX [®] 400	92	0.983
Plastic random packing		
Super INTALOX [®] Saddles #1	204	0.896
Super INTALOX [®] Saddles #2	105	0.934
BETA RING [®] #1 in	167	0.942
BETA RING [®] #2	114	0.940
SNOWFLAKE [®]	93	0.949
FLEXIRING [®] 1 in	205	0.922
FLEXIRING [®] 1½ in	119	0.925
FLEXIRING [®] 2 in	99	0.932
Ceramic random packing		
INTALOX [®] Saddles 1 in	256	0.730
INTALOX [®] Saddles 1½ in	195	0.750
INTALOX [®] Saddles 2 in	118	0.760
Ceramic structured packing		
FLEXERAMIC [®] 28	282	0.720
FLEXERAMIC [®] 48	157	0.770
FLEXERAMIC [®] 88	102	0.850
Metal structured packing†		
Koch-Glitsch SMV-8	417	0.978
Koch-Glitsch SMV-10	292	0.985
Koch-Glitsch SMV-16	223	0.989
Koch-Glitsch SMV-32	112	0.989
Sulzer SMV 2Y	205	0.990
Sulzer SMV 250Y	256	0.988
Sulzer SMV 350Y	353	0.983
INTALOX [®] 2T	214	0.989
INTALOX [®] 3T	170	0.989
INTALOX [®] 4T	133	0.987
Plastic structured packing†		
Koch Glitsch SMV-8	330	0.802
Koch-Glitsch SMV-16	209	0.875
Koch-Glitsch SMV-32	93	0.944
Sulzer SMV 250Y	256	0.875

^aTypical value for standard wall thickness. Values will vary depending upon thickness.

†SMV structured packings also are available with horizontal dual-flow perforated plates installed between elements (typically designated SMVP packing). These plates generally reduce backmixing and improve mass-transfer performance at the expense of a reduction in the open cross-sectional area and somewhat reduced capacity.

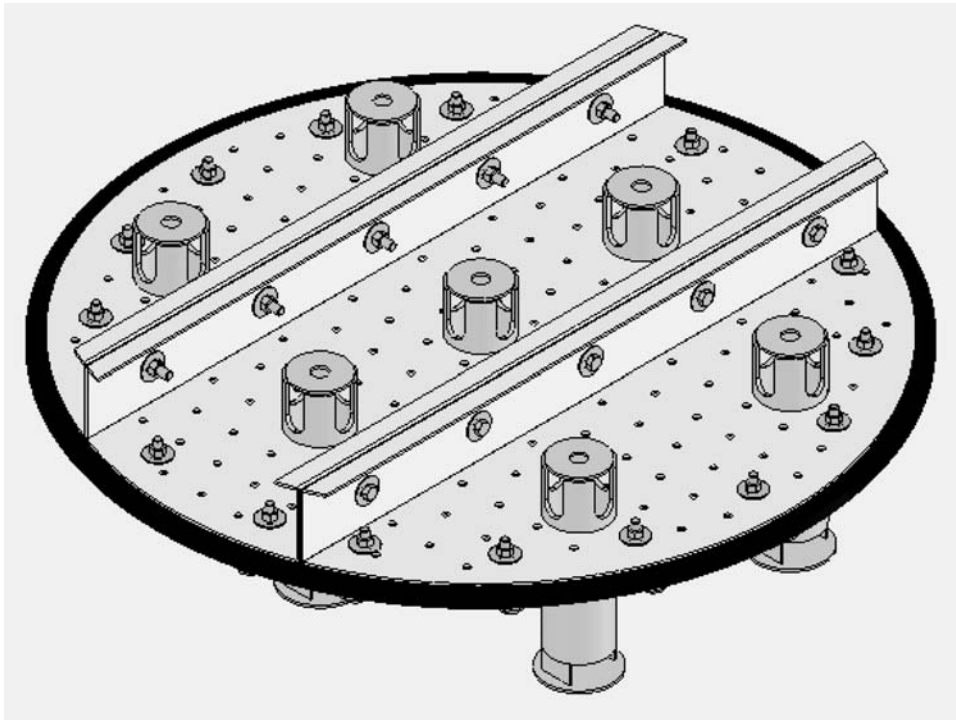


FIG. 15-35 Example of disperser plate (Sulzer Chemtech model VSX). (Courtesy of Sulzer Chemtech.)

(McGraw-Hill, 1978), Chap. 10, pp. 288–289]. The critical packing dimension is given by

$$d_c = 2.4 \sqrt{\frac{\sigma}{\Delta\rho g}} \quad (15-140)$$

In many cases, the minimum random packing size is about 0.5 in (1.3 cm). A similar effect may be seen with short-crimp-height structured sheet packings that might act as a parallel-plate type of coalescer. For packings smaller than the critical size, the packing acts to promote growth of dispersed drops somewhat as a packed-bed coalescer as drops flow through the spaces between the packing elements. (For a discussion of packed-bed coalescers, see “Coalescers” under “Liquid-Liquid Phase Separation Equipment.”) For packing sizes larger than d_c , the characteristic drop diameter is independent of packing size and may be estimated by using the models listed in Table 15-15. The choice of packing size above d_c generally involves a tradeoff; throughput increases with increasing packing size, while mass-transfer performance may decrease with increasing packing size due to an increase in backmixing effects. Typical random packings for commercial-scale columns are in the range of $\frac{3}{4}$ to 2 in (or about 2 to 5 cm). For small columns, the packing should be no larger than one-eighth the column diameter to avoid channeling at the wall. This effectively restricts the size of laboratory extractors packed with random packings to no less than 4 in (10 cm) in diameter if they are intended to generate directly scalable data.

Holdup and Interfacial Area The dispersed-phase holdup in a packed-column extractor may be placed into two categories: (1) a small portion that is held in the column for extended periods (essentially permanent) and (2) a larger portion that is free to move through the packing. This is the portion that participates in transfer of solute between phases. The total is ϕ_d which here refers to the volume of dispersed phase expressed as a fraction of the void space in the packed section. Pratt and coworkers [Trans. Inst. Chem. Eng.,

29, pp. 89–109, 110–125, 126–148 (1951); 31, pp. 57–68, 69–77, 78–93 (1953)] developed relationships between dispersed-phase velocity and holdup for packed columns. For standard commercial packings of 0.5 in (1.27 cm) and larger, they found that ϕ_d varies linearly with V_d up to values of $\phi_d = 0.10$ (for low values of V_d). With further increase of V_d , ϕ_d increases sharply up to a “lower transition point” resembling loading in gas-liquid contact. At still higher values of V_d an upper transition point occurs, the drops of dispersed phase tend to coalesce, and V_d can increase without a corresponding increase in ϕ_d . This regime ends in flooding. Below the upper transition point, Pratt and coworkers calculated dispersed-phase holdup from the expression

$$\frac{V_d}{\phi_d} + \frac{V_c}{1 - \phi_d} = \epsilon V_{so} (1 - \phi_d) \quad (15-141)$$

where V_{so} is the characteristic slip velocity at low dispersed-phase flow rate. The slip velocity may be estimated by using Eqs. (15-118) to (15-123) or alternative methods listed in Table 15-16. (See the related discussion in “Common Features and Design Concepts.”) Interfacial area is calculated from Eq. (15-109).

Flooding Numerous methods have been proposed for correlating flooding velocities in packed extractors as a function of the packing specific surface area and void volume. Most were developed by using the older-style packings such as Raschig rings and Berl saddles. For example, the well-known flooding correlation $(\sigma/\rho_c)^{0.2}(\mu/\Delta\rho)(a_p/\epsilon)^{1.5}$ versus $(V_c^{1/2} + V_d^{1/2})^2 \rho_c/(a_p \mu_c)$, developed by Crawford and Wilke [Chem. Eng. Prog., 47(8), pp. 423–431 (1951)], is plotted in Fig. 15-36. This is a dimensional correlation developed by using U.S. Customary System units, so the following units must be used: viscosity in lb/ft/h (equal to 2.42 times the value in cP), density in lb/ft³, interfacial tension in dyn/cm, specific packing surface area in ft²/ft³, and velocities in ft/h based on total column cross section. Nemunaitis et al. [Chem. Eng. Prog., 67(11),

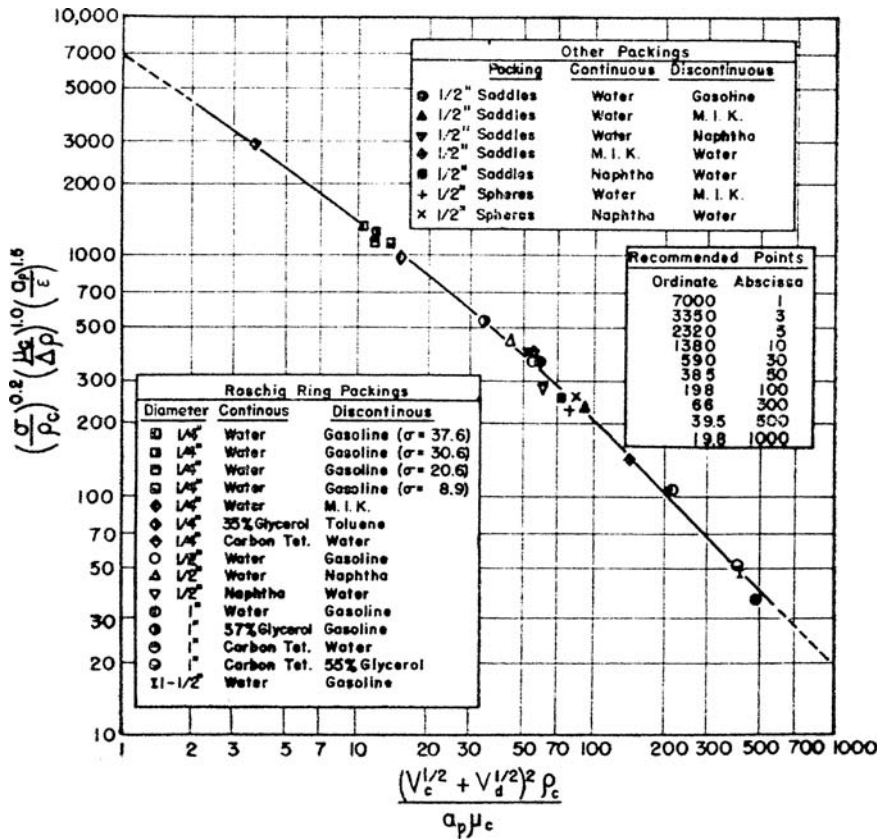


FIG. 15-36 Crawford-Wilke correlation for flooding in packed columns. Use only the units given in the text. [Reprinted from Crawford and Wilke, Chem. Eng. Prog., 47(8), pp. 423-431 (1951), with permission.]

pp. 60-67 (1971)] modified the Crawford-Wilke correlation to include packing factors for specific types of packings (including Raschig rings, Intalox® saddles, and Pall rings). Another correlation that uses packing factors is given by Sakiadis and Johnson [Ind. Eng. Chem., 46(6), pp. 1229-1239 (1954)]:

$$1 + 0.835 \left(\frac{\rho_c}{\rho_d} \right)^{1/4} \left(\frac{V_{cf}}{V_{df}} \right)^{1/2} = C_p \left[\frac{V_{cf}^2 a_p}{g \epsilon^3} \left(\frac{\rho_c}{\Delta p} \right) \sigma^{1/4} \mu_c^{1/4} \right]^{-1/4} \quad (15-142)$$

where $C_p = 0.87 \frac{\epsilon^{0.0068}}{a_p^{0.048}}$ for nonribbed Raschig rings (15-143)

$C_p = 1.2 \frac{\epsilon^{0.78}}{a_p^{0.0351}}$ for Berl saddles (15-144)

$C_p = 1.02 \frac{\epsilon^{0.0068}}{a_p^{0.048}}$ for Lessing rings (15-145)

In Eqs. (15-142) to (15-145), the units are as follows: viscosity in cP, interfacial tension in dyn/cm, and specific packing surface area in ft²/ft³. Other correlation methods are listed in Table 15-17. The generalized flooding model of Seibert, Reeves, and Fair [Ind. Eng. Chem. Res., 29(9), pp. 1901-1907 (1990)] was developed by using data for several types of packing and a range of operating scales, including data from a larger-scale column (42.5-cm inner diameter) using more modern packings: No. 25 IMTP® and No. 40 IMTP®

random packings and Intalox® Structured Packing 2T. It has the form

$$V_{cf} = \frac{0.178 \epsilon V_{so}}{1 + 0.925 (V_{df}/V_{cf}) \{1 / [\cos(\pi \zeta / 4)]\}^2} \quad (15-146)$$

$$\zeta = \frac{a_p d_p}{2} \quad (15-147)$$

where ζ is a dimensionless tortuosity factor. The quantity V_{so} is calculated by using Eqs. (15-118) to (15-123).

These correlations may be used to estimate extractor capacity for various types and sizes of packings; however, the results must be used with care due to considerable uncertainties in the calculation. This is particularly true when data for the packing of interest were not included in the data used to develop the correlation equation, and this is generally the case for the more modern packings. Nemunaitis et al. [Chem. Eng. Prog., 67(11), pp. 60-67 (1971)] recommend designing for only 20 percent of the flood point calculated by using the Crawford-Wilke correlation (or their modified version). Because of this level of uncertainty, it is recommended that some experimental data be generated for a new design. In this regard, the flooding correlations may be used to scale up the pilot plant data to a larger packing size needed for the commercial-scale unit—by calculating the expected percentage change in capacity. This extrapolation approach also may be taken to estimate the improvement that might be achieved by retrofitting an existing commercial unit with a new packing. But again, the results should be used with caution, and consultation with packing vendors is recommended.

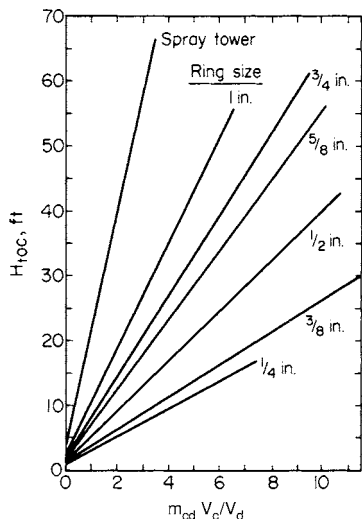


FIG. 15-37 Extraction of diethylamine from water into toluene (dispersed) in columns packed with unglazed porcelain Raschig rings. To convert feet to meters, multiply by 0.3048; to convert inches to centimeters, multiply by 2.54. [Reprinted from Leibson and Beckman, *Chem. Eng. Prog.*, **49**, p. 405 (1953), with permission.]

Pressure Drop In general, the pressure drop through a packed extractor is due to the hydrostatic head pressure. The resistance to flow caused by the packing itself normally is negligible because typical packings are large, and flooding velocities are much lower than those that would be needed to develop significant ΔP from resistance to flow between the packing elements. In some applications, solids may accumulate in the region of the packing support over time, and this may cause added pressure drop and premature flooding. For additional discussion, see Laddha and Degaleesan, *Transport Phenomena in Liquid Extraction* (McGraw-Hill, 1978), Chap. 10, pp. 271–273.

Mass Transfer Figure 15-37 plots the height of an overall transfer unit based on the raffinate phase H_{or} versus the extraction factor \mathcal{E} for a series of Raschig rings of different sizes. The data are for transfer of diethylamine from water into toluene, where toluene is the dispersed phase. The data are typical in that mass-transfer performance is shown to improve (H_{or} decreases) as the size of the packing decreases. At the same time, the pressure drop must increase and hydraulic capacity decrease, so the design problem involves finding the economic optimum for the given production rate. The system water + ethylenamine + toluene is a high-interfacial-tension system, so the H_{or} data in Fig. 15-37 are expected to be somewhat high compared to those in systems with lower interfacial tension due to larger drop size in a nonagitated extractor. Note that most extractor designs will involve extraction factors in the range of $\mathcal{E} = 1.3$ to 2.

Table 15-21 lists typical mass-transfer performance of various packing sizes, as given by Strigle [*Packed Tower Design and Applications*, 2d ed., Chap. 11 (Gulf, 1994)]. Strigle's table is based on experience

TABLE 15-21 Typical Packed Extractor Performance According to Strigle*

Transfer units per bed	Required bed depth for modern random packings, ft (m)		
	Nominal packing size of 1 in (2.5 cm)	Nominal packing size of 1.5 in (3.8 cm)	Nominal packing size of 2 in (5 cm)
1.5	4.4 (1.3)	5.3 (1.6)	6.2 (1.9)
2.0	7.2 (2.2)	8.6 (2.6)	10.1 (3.1)
2.5	9.9 (3.0)	11.9 (3.6)	14.0 (4.3)

*Taken from Strigle, Chap. 11 in *Packed Tower Design and Applications*, 2d ed. (Gulf, 1994), with permission. Copyright 1994 Gulf Publishing Company. The numbers represent typical performance achieved with good liquid distribution.

with organic aqueous systems and the use of metal slotted-ring or ceramic saddle packings, using high-performance dispersion plates for liquid distribution and redistribution between packed sections.

Figure 15-37 and Table 15-21 provide only general guidelines. To estimate mass-transfer rates in packed towers, the calculation procedure outlined by Seibert, Reeves, and Fair [*Ind. Eng. Chem. Res.*, **29**(9), pp. 1901–1907 (1990)] and corrected for axial mixing [as in Eqs. (15-127) to (15-136)] is recommended. The overall mass-transfer coefficient is obtained by using Eq. (15-126). The predictive method of Handlos and Baron [*AIChE J.*, **3**(1), pp. 127–136 (1957)] allows calculation of the dispersed-phase coefficient:

$$k_d = \frac{0.00375V_s}{1 + \mu_d/\mu_c} \quad \text{when } \Phi = \frac{(\mu_d/\rho_d \mathcal{D}_d)^{1/2}}{1 + \mu_d/\mu_c} < 6 \quad (15-148)$$

For $\Phi > 6$, the method given by Laddha and Degaleesan [*Transport Phenomena in Liquid Extraction* (McGraw-Hill, 1978)] is recommended:

$$k_d = 0.023V_s \left(\frac{\mu_d}{\rho_d \mathcal{D}_d} \right)^{-1/2} \quad (15-149)$$

The continuous-phase coefficient may be calculated from

$$\frac{k_c d_p}{\mathcal{D}_c} = 0.698 \left(\frac{\mu_c}{\rho_c \mathcal{D}_c} \right)^{0.25} \left(\frac{d_p V_s \rho_c}{\mu_c} \right)^{1/2} (1 - \phi_d) \quad (15-150)$$

where V_s is the slip velocity of the dispersed drop [Seibert and Fair, *Ind. Eng. Chem. Res.*, **27**(3), pp. 470–481 (1988)]. While this calculation procedure can provide useful estimates, it does not replace the need for good pilot tests for any new design. Table 15-22 lists selected sources of data for mass transfer in packed columns.

Sieve Tray Columns A schematic diagram of the most common design of sieve tray column (also called a sieve plate or perforated-plate column) is shown in Fig. 15-32c. The light liquid is shown as the dispersed phase. The liquid flows up through the perforations of each tray and is thereby dispersed into drops that rise up through the continuous phase. The continuous liquid flows horizontally across each tray and passes to the tray beneath through the downcomer. For dispersing the heavy phase, the same design may be used, but turned upside down. The trays serve to eliminate (or at least greatly reduce) the vertical recirculation of continuous phase. Mass-transfer rates may be enhanced by the repeated coalescence and redispersion into droplets of the dispersed phase at each tray, although in general the overall efficiency of a sieve tray is fairly low, on the order of 15 to 30 percent. The higher efficiencies generally are achieved for systems with low to moderate interfacial tension. As discussed earlier, the liquid entering the column at the larger volumetric flow rate generally should be dispersed to obtain satisfactory interfacial area for mass transfer. Example mass-transfer data are plotted in Fig. 15-38 for low values of \mathcal{E} . The advantage gained by dispersing the liquid flowing at the larger rate, which results in lower values on the x axis of Fig. 15-38 and consequently lower transfer unit heights, is clear.

Liquid Distribution Good initial distribution is not as essential in a sieve tray extractor as it is in a packed extractor, since the trays provide redistribution. While the same distributors used in packed columns are applicable, simpler devices also are used. Capped pipes with holes drilled uniformly have been found to be adequate in many cases.

Drop Size, Holdup, and Interfacial Area Drop size is estimated by using one of the models listed in Table 15-15, and holdup is estimated from expressions given in Table 15-16. Interfacial area is then calculated by using Eq. (15-109).

Sieve Tray Design Perforations usually are in the range of 0.125 to 0.25 in (0.32 to 0.64 cm) in diameter, set 0.5 to 0.75 in (1.27 to 1.81 cm) apart, on square or triangular pitch. There appears to be relatively little effect of hole size on the mass-transfer rate, except that with systems of high interfacial tension, smaller holes will produce somewhat better mass transfer. The entire hole area is normally set at 15 to 25 percent of the column cross section, although adjustments may be needed. The velocity through the holes should be such that drops do not form slowly at the holes, but rather the

TABLE 15-22 Mass-Transfer Data for Packed Columns

System	Column diameter, in	Packing	Ref.
Water-acetic acid-ethyl acetate, cyclohexane, methylcyclohexane, ethyl acetate + benzene	1	0.25-in saddles	3
Water-acetic acid-methyl isobutyl ketone	1.95	0.23-in rings	9
	3	0.375-in plastic spheres	12
		0.375-in plastic, ceramic rings	14
		0.5-in plastic, ceramic saddles	14
Water-acetic acid-toluene	6	Montz B1-300 1-in stacked Bialecki rings	2
Water-acetone-hydrocarbon	1.88	0.25- and 0.375-in rings, 6-mm beads	16
	2-4	0.5- and 0.75-in rings	1
Water-acetone-toluene	4	0.5-in rings, $\frac{5}{8}$ -in Pall rings, IMTP® 15, SMV structured, spray	18
	16.8	IMTP® 25, IMTP® 40, Intalox® 2T structured, spray	19
	6	Montz B1-300 1-in stacked Bialecki rings	2
	4	SMV	22
Water-adipic acid-ethyl ether	6	0.5- and 0.75-in rings, 0.375-in spheres	7
Water-benzoic acid-carbon tetrachloride	1.95	0.25-in rings	8
Water-benzoic acid-toluene	8.7	0.5-in saddles, 0.5-in rings	17
Water-diethylamine-toluene	3, 4, 6	0.25- to 1-in rings	11
	3	0.375-in rings	20
Water-ethyl acetate	4	0.5-in rings	5
Water-isopar(m)	16.8	IMTP® 25, IMTP® 40, Intalox® 2T structured, spray	19
Water-kerosene	4	SMV	22
Water-methyl ethyl ketone-kerosene	18	1-in rings, 1-in saddles, 1-in Pall rings, spray	13, 4
Water-methylisobutyl-carbinol	4	0.5-in rings	21
Water-methyl ethyl ketone	4	0.5-in rings	21
Water-propionic acid-methyl isobutyl ketone	1.88	0.25- and 0.375-in rings, 6-mm beads	16
Water-propionic acid-carbon tetrachloride	4	SMV	22
Water-succinic acid-1-butanol	4	0.5-in rings, $\frac{5}{8}$ -in Pall rings, IMTP® 15, SMV structured, spray	18
	4	SMV	22
Water-toluene	6	Montz B1-300 1-in stacked Bialecki rings	2
Acetone (aq)-soybean oil, linseed oil	2	0.25-in saddles, 0.5-in rings	23
Petroleum-furfural	2	0.25-in rings	6
	1.2	0.16-in rings	15
Toluene-heptane-diethylene glycol	1.4, 2.25	Glass and brass rings	10

NOTE: To convert inches to centimeters, multiply by 2.54.

References:

1. Degaleesan and Laddha, *Chem. Eng. Sci.*, **21**, p. 199 (1966); *Indian Chem. Eng.*, **8**(1), p. 6 (1966).
2. Billet and Mackowiak, *Fette-Seifen-Anstrichmittel*, **87**, pp. 205-208 (1985).
3. Eaglesfield, Kelly, and Short, *Ind. Chem.*, **29**, pp. 147, 243 (1953).
4. Eckert, *Hydrocarbon Processing*, **55**(3), pp. 117-124 (1976).
5. Gaylor and Pratt, *Trans. Inst. Chem. Eng. (London)*, **31**, p. 78 (1953).
6. Garwin and Barber, *Pet. Refiner*, **32**(1), p. 144 (1953).
7. Gier and Hougen, *Ind. Eng. Chem.*, **45**, p. 1362 (1953).
8. Guyer, Guyer, and Mauli, *Helv. Chim. Acta*, **38**, p. 790 (1955).
9. Guyer, Guyer, and Mauli, *Helv. Chim. Acta*, **38**, p. 955 (1955).
10. Kishinevskii and Mochalova, *Zh. Prikl. Khim.*, **33**, p. 2344 (1960).
11. Liebson and Beckmann, *Chem. Eng. Prog.*, **49**, pp. 405-416 (1953).
12. Moorhead and Himmelblau, *Ind. Eng. Chem. Fundam.*, **1**, p. 68 (1962).
13. Nemunaitis, Eckert, Foote and Rollison, *Chem. Eng. Prog.*, **67**(11), pp. 60-67 (1971).
14. Osmon and Himmelblau, *J. Chem. Eng. Data*, **6**, p. 551 (1961).
15. Sef and Moretu, *Nafta (Zagreb)*, **5**, p. 125 (1954).
16. Rao and Rao, *J. Chem. Eng. Data*, **6**, p. 200 (1961).
17. Row, Koffolt, and Withrow, *Trans. Am. Inst. Chem.*, **46**, p. 1229 (1954).
18. Seibert and Fair, *Ind. Chem. Eng. Res.*, **27**(3), p. 470 (1988).
19. Seibert, Reeves, and Fair, *Ind. Chem. Eng. Res.*, **29**(9), p. 1901 (1990).
20. Shih and Kraybill, *Ind. Eng. Chem. Process. Des. Dev.*, **5**, p. 260 (1966).
21. Smith and Beckmann, *Am. Inst. Chem. Eng. J.*, **4**, p. 180 (1958).
22. Streiff and Jancic, *Ger. Chem. Eng.*, **7**, pp. 178-183 (1984).
23. Young and Sullans, *J. Am. Oil Chem. Soc.*, **32**, p. 397 (1955).

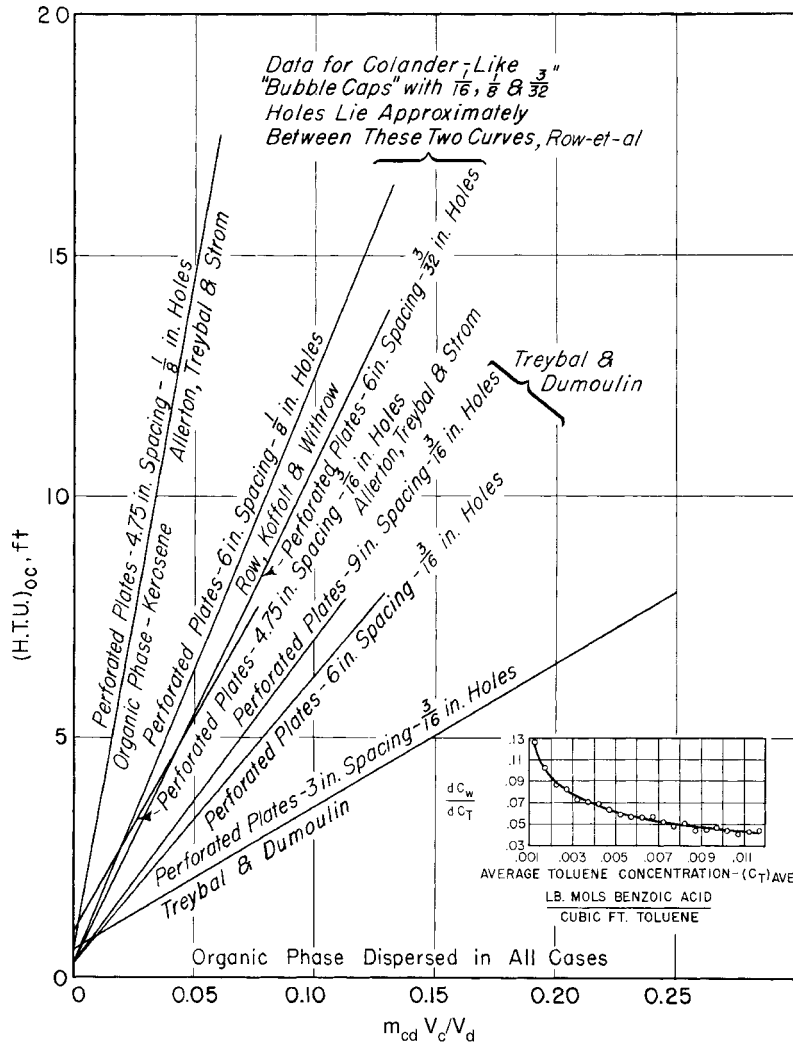


FIG. 15-38 Mass-transfer data for sieve plate and modified bubble plate columns. System: benzoic acid + water + toluene, except where noted. To convert feet to meters, multiply by 0.3048; to convert inches to centimeters, multiply by 2.54. [Data taken from Allerton, Strom, and Treybal, *Trans. AIChE*, **39**, p. 361 (1943); Row, Koffolt, and Withrow, *Trans. AIChE*, **37**, p. 559 (1941); and Treybal and Dumoulin, *Ind. Eng. Chem.*, **34**, p. 709 (1942).]

dispersed phase streams through the openings as a jet that breaks up into drops at a slight distance from the tray. It is common practice to set the velocity of liquid exiting the holes to correspond to a Weber number between 8 and 12. This normally gives velocities in the range of 0.5 to 1.0 ft/s (15 to 30 cm/s). The same general guidelines used to specify hole size and velocities for plate dispersers apply to sieve tray design. See Eqs. (15-107) and (15-108) and the related discussions in "Liquid Distributors and Dispersers" under "Liquid-Liquid Extraction Equipment."

The velocity of the continuous phase in the downcomer (or upcomer) V_{down} , which sets the downcomer cross-sectional area, should be set at a value lower than the terminal velocity of some arbitrarily small droplet of dispersed phase, say, $\frac{1}{32}$ or $\frac{1}{16}$ in (0.08 or 0.16 cm) in diameter; otherwise, recirculation of entrained dispersed phase around a tray will result in flooding. The terminal velocity of these small drops can be calculated by using Stokes' law: $u_t = (gd_p^2 \Delta\rho) / 18\mu_c$.

Downcomer area typically is in the range of 5 to 20 percent of the total cross-sectional area, depending upon the ratio of continuous- to dispersed-phase volumetric flow rates. The downcomers should extend beyond the accumulated layer of dispersed phase on the tray, and the tray area directly opposite downcomers should be kept free of perforations.

The spacing between trays should be sufficient that (1) the "streamers" of dispersed liquid from the holes break up into drops before coalescing into the layer of liquid on the next tray; (2) the cross-flow velocity of continuous-phase liquid does not cause excessive entrainment of the dispersed phase; and (3) the column may be entered through handholes or manholes in the sides for inspection and cleaning. For systems that accumulate an interface rag, provision may be made for periodic withdrawal of the rag through the side of the column between trays. For large columns, tray spacing between 18 and 24 in (45 and 60 cm) is generally recommended.

The height of the coalesced layer at each tray is given by

$$h = \frac{\Delta P_o + \Delta P_{\text{dow}} - \phi_d g \Delta \rho L}{(1 - \phi_d) g \Delta \rho} \quad (15-151)$$

where L is the downcomer length. Equation (15-151) is a slightly simplified form of the expression given by Mewes and Kunkel [*Ger. Chem. Eng.*, **1**, pp. 111–115 (1978)]. In most cases holdup is low, and Eq. (15-151) reduces to $h = (\Delta P_o + \Delta P_{\text{dow}})/(g \Delta \rho)$. The orifice pressure drop ΔP_o may be calculated by using the model of Pilhofer and Goedl [*Chem. Eng. Tech.*, **49**, p. 431 (1977)]:

$$\Delta P_o = \frac{1}{2} \left(1 - \frac{0.71}{\log \text{Re}} \right)^{-2} \rho_d V_o^2 + 3.2 \left(\frac{d_o^2 g \Delta \rho}{\sigma} \right)^{0.2} \frac{\sigma}{d_o} \quad (15-152)$$

where V_o is the velocity through the orifice, d_o is the orifice diameter, and $\text{Re} = V_o d_o \rho_d / \mu_d$. The pressure drop through the downcomer ΔP_{dow} includes losses due to (1) friction in the downcomer, which should be negligible; (2) contraction and expansion upon entering and leaving the downcomer; and (3) two abrupt changes in direction. These losses total 4.5 velocity heads:

$$\Delta P_{\text{dow}} = \frac{4.5 V_{\text{dow}}^2 \rho_c}{2} \quad (15-153)$$

For large columns, the design should be specified such that the height of the coalesced layer is at least 1 in (2.5 cm) to ensure all the holes are adequately covered, and one should allow for the trays to be slightly out of level. On the other hand, the height of the coalesced layer should not be too large, since this is unproductive column height that unnecessarily increases the total column height requirement. A typical design value is about 2 in (5 cm).

Envelope-style segmental downcomers (Fig. 15-39) often are used in commercial-scale sieve tray extractors instead of circular or pipe-style downcomers. The area of an envelope downcomer is given by

$$A = \frac{H}{6S} (3H^2 + 4S^2) \quad (15-154)$$

The distance S is determined from the column diameter. The distance H is obtained from

$$S = \left[8H \left(\frac{D_{\text{col}}}{2} - \frac{H}{2} \right) \right]^{1/2} \quad (15-155)$$

The diameter of a circular downcomer with equivalent area is given by

$$D_{\text{eq}} = \sqrt{\frac{4}{\pi} A} \quad (15-156)$$

Sieve Tray Capacity at Flooding The capacity of a sieve tray is determined by hydraulic mechanisms involved in flooding and is not

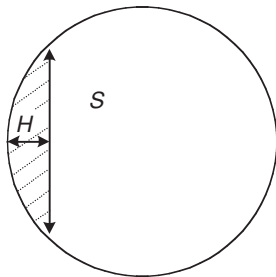


FIG. 15-39 Dimensions of an envelope-style segmental downcomer or upcomer (shaded area).

completely understood, especially for larger-diameter columns. Three studies using larger equipment have been reported by Oloidi, Jeffreys, and Mumford [*Inst. Chem. Eng. Symp. Ser.*, **103**, pp. 117–132 (1987)]; Seibert and Fair [*Ind. Eng. Chem.*, **32**, pp. 2213–2219 (1993)]; and Eldridge and Fair [*Ind. Eng. Chem.*, **38**, pp. 218–222 (1999)]. An example of sieve tray flooding data is illustrated in Fig. 15-40.

The sieve tray capacity and efficiency are strongly influenced by the height of the coalesced layer. If the height of this layer grows to the outlet of the downcomer, a sharp reduction in efficiency will result since the mass-transfer height will be significantly reduced. In this case, the downcomer area and/or total perforated area should be increased. A flooding model based on the height of the coalesced layer is given by Seibert and Fair [*Ind. Eng. Chem. Res.*, **32**(10), pp. 2213–2219 (1993)]

$$V_{\text{cf}} = \left[\frac{L - A}{B(V_d/V_{\text{cf}})^2 + C} \right]^{0.5} \quad (15-157)$$

$$A = \frac{6\sigma}{d_{\text{es}} \Delta \rho g} \quad (15-158)$$

$$B = \frac{1.11 \rho_d}{g \Delta \rho f_{\text{ha}}^2} \quad (15-159)$$

$$C = \frac{2.7 \rho_c}{2g \Delta \rho f_{\text{da}}} \quad (15-160)$$

where L is the downcomer length, f_{ha} is the fractional hole area, and f_{da} is the fractional downcomer area.

High Cross-flow of the Continuous Phase Miniplant tests of sieve tray extractors are often performed prior to the final design of a commercial-scale column. The design often is scaled up based on superficial velocities of the dispersed and continuous phases calculated from the volumetric flow rates and the column cross-sectional area. However, in scaling up one must be careful about the cross-flow velocity (V_{cflow}) of the continuous phase. A value may be estimated from

$$V_{\text{cflow}} \approx \frac{L_{\text{fp}}}{z - h} V_c \quad (15-161)$$

where L_{fp} is the length of flow path, z is the tray spacing, h is the height of coalesced layer, and V_c is the superficial continuous-phase velocity. The magnitude of the cross-flow velocity of the continuous phase can be much greater than that studied in the miniplant. Multiple downcomers or upcomers reduce the flow path length and can be utilized in new designs to reduce cross-flow velocity. Large-diameter multiple downcomer (or upcomer) trays have been reported to provide 10 to 15 percent greater capacity relative to the single-pass tray. Seibert, Bravo, and Fair [*ISEC '02 Proc.*, **2**, pp. 1328–1333 (2002)] propose a model for correcting the sieve tray capacity for high cross-flow velocity.

Mass-Transfer Data Mass-transfer data are available from the sources listed in Table 15-23. Mass-transfer performance can be expressed in terms of the number of transfer units per actual tray, or in terms of overall heights of transfer units for a given column configuration, as in Fig. 15-38. The system of Fig. 15-38 is one of high interfacial tension, so the heights of transfer units are expected to be relatively large. For systems of low interfacial tension, mass-transfer performance is likely to be much improved. Since sieve trays resemble and basically behave in the manner of stages, performance also can be expressed in terms of a stage efficiency, either as an overall ξ_o for the entire tower or, more satisfactorily, as a Murphree efficiency for each tray.

Tray Efficiency The overall efficiencies of sieve trays typically are between 10 and 30 percent. One of the earliest models for predicting the overall tray efficiency was an empirical one reported by Treybal [*Liquid Extraction*, 2d ed. (McGraw-Hill, 1963)]. Krishna, Murty, and Rao [*Ind. Eng. Chem. Process Des. Dev.*, **7**(2),

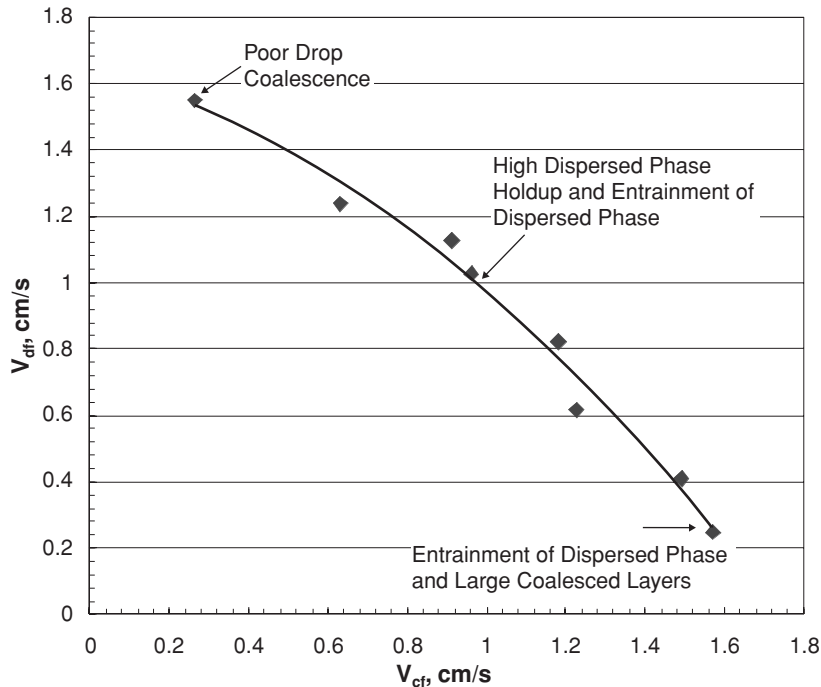


FIG. 15-40 Sieve tray flooding data. System: toluene (dispersed) + water (continuous). Tray spacing = 30.5 cm. Column diameter = 42.8 cm. [Taken from Seibert, Bravo, and Fair, ISEC '02 Proc., 2, pp. 1328–1333 (2002), with permission. Copyright 2002 South African Institute of Mining and Metallurgy.]

pp. 166–172 (1968)] modified the Treybal model to account for hole diameter:

$$\xi_o = 0.21 \left(\frac{z^{0.5}}{\sigma d_o^{0.35}} \right) \left(\frac{V_d}{V_c} \right)^{0.42} \quad (15-162)$$

where z is the tray spacing, cm; d_o is the hole diameter, cm; and σ is interfacial tension, dyn/cm. Seibert and Fair [Ind. Eng. Chem., 32(10), pp. 2213–2219 (1993)] recommend calculating the local Murphree stage efficiency based on the dispersed phase, assuming a log mean driving force and negligible mass-transfer contribution from drop formation:

$$\xi_{md} = 1 - \exp \left[- \frac{6k_{od} \phi_d (z - h)}{d_p V_d} \right] \quad (15-163)$$

The overall tray efficiency may then be estimated by using

$$\xi_o = \frac{\ln [1 + \xi_{md} (\mathcal{E} - 1)]}{\ln \mathcal{E}} \quad (15-164)$$

$$\mathcal{E} = m_{dc}^{vol} \frac{V_d}{V_c} \quad (15-165)$$

Equation (15-163) assumes plug flow of the rising or falling drop population and complete mixing of the continuous phase on the tray. Also see Eldridge and Fair, Ind. Eng. Chem. Res., 38, pp. 218–222 (1999); Rocha et al., Ind. Eng. Chem. Res., 28(12), pp. 1873–1878 (1989); and Rocha, Cárdenas, and García, Ind. Eng. Chem. Res., 28(12), pp. 1879–1883 (1989).

Baffle Tray Columns Baffle tray columns are similar to spray columns except that baffles are added to reduce backmixing. The

baffles usually are slightly sloped to drain any solids that might settle out in the column and are designed to provide a high open area. Lemieux [Hydrocarbon Proc., 62(9), pp. 106–111 (1983)] and Fair [Hydrocarbon Proc., 72(5), pp. 75–79 (1993)] report on the performance and design of these columns for gas-liquid contacting. Treybal [Liquid Extraction, 2d ed. (McGraw-Hill, 1963)] provides a brief but valuable description of a baffle tray extractor. Although no design equations or performance data are provided, Treybal indicates that commercial tray spacings should be in the range of 10 to 15 cm (4 to 6 in). Treybal also provides an interesting illustration of a baffle tray extractor in operation (Fig. 15-41). This figure shows multiple trays with a very short spacing, with the dispersed light phase moving as a layer of liquid under each tray.

Because baffle tray performance data are not widely available, the results of a pilot-scale study (Seibert, Lewis, and Fair, Paper No. 112a, AIChE National Meeting, Indianapolis, 2002) are summarized in Figs. 15-42 to 15-47. The study was carried out using a 4.0-in- (10.2-cm-) diameter column set up with 5 to 30 trays. The trays were arranged in a side-to-side horizontal arrangement, as indicated in Fig. 15-41a. The data were generated by using the toluene (dispersed) + acetone + water (continuous) and butanol (dispersed) + succinic acid + water (continuous) systems. The effects of changes in baffle spacing and tray overlap (expressed as the percentage of total tray area covered by the next tray above or below) were measured for transfer of solute from the organic to the aqueous phase.

Hydraulic Capacity The capacity of the baffle trays at flooding was found to depend strongly on system properties, as shown in Fig. 15-42. The butanol system with its lower interfacial tension provided a much lower capacity relative to the toluene system with its higher interfacial tension. The capacity was found to be independent of tray spacing, as shown in Fig. 15-43. However, capacity was strongly affected by the degree of tray overlap, as shown in Figs. 15-44 and 15-45. See Seibert, Lewis, and Fair (Paper No. 112a, AIChE National Meeting, Indianapolis, 2002) for discussion of a proposed flooding model.

TABLE 15-23 Mass-Transfer Data for Sieve Tray Columns

System	Column diameter, in	Tray spacing, in	Ref.
Benzene-acetic acid-water	1.97	3.9-6.3	25
	1.97	3.2-6.3	24
	2.2	2.8-6.3	23
	1.6 × 3.2	5.9	20
Benzene-acetone-water	3	4, 8	13
Benzene-benzoic acid-water	3	4	13
Benzene-monochloroacetic acid-water	1.97	3.9-6.3	25
Benzene-propionic acid-water	1.97	3.2-6.3	24
Carbon tetrachloride-propionic acid-water	1.97	3.9-6.3	25
Clairsol-water	17.7	13-15	14
Ethyl acetate-acetic acid-water	2	8-24	10
Ethyl ether-acetic acid-water	8.63	4-7.2	15
Gasoline-methyl ethyl ketone-water	3.75	4.5, 6	11
Isopar(M)-water	16.8	12	21
Kerosene-acetone-water	3	4, 8	13
Kerosene-benzoic acid-water	3.63	4.75	1
Kerosene-benzoic acid-water	6	6, 12	9
Isopar-H-benzyl alcohol, methyl benzyl alcohol, acetophenone-water	2 × 12	24	2
Methylisobutylcarbinol-acetic acid-water	3	6	12
Methyl isobutyl ketone-adipic acid-water	4.18	6	5
Methyl isobutyl ketone-butyric acid-water	4.8	6-23	8
Methyl isobutyl ketone-acetic acid-water	4	6-12	17
Pegasol-propionic acid-water	9.7	8-24	18, 19
	4.8	6-11	7
	8.75	6	16
	3.63	4.75	1
Toluene-benzoic acid-water	3.56	3-9	22
	3	6	12
	2.72	9	6
	2	24	10
Toluene-diethylamine-water	4.18	6	3, 4
Toluene-water	16.8	12	21
	9.7	8-24	18
	16.8	12	21
Toluene-acetone-water	9.7	8-24	19
	4	6-12	17
	3.75	4.5, 6	11

NOTE: To convert inches to centimeters, multiply by 2.54.

References:

- Allerton, Strom, and Treybal, *Trans. Am. Inst. Chem. Eng.*, **39**, p. 361 (1943).
- Angelo and Lightfoot, *Am. Inst. Chem. Eng. J.*, **14**, p. 531 (1968).
- Garner, Ellis, and Fosbury, *Trans. Inst. Chem. Eng. (London)*, **31**, p. 348 (1953).
- Garner, Ellis, and Hill, *Am. Inst. Chem. Eng. J.*, **1**, p. 185 (1955).
- Garner, Ellis, and Hill, *Trans. Inst. Chem. Eng. (London)*, **34**, p. 223 (1956).
- Goldberger and Benenati, *Ind. Eng. Chem.*, **51**, p. 641 (1959).
- Krishnamurty and Rao, *Indian J. Technol.*, **5**, p. 205 (1967).
- Krishnamurty and Rao, *Ind. Eng. Chem. Process Des. Dev.*, **7**, p. 166 (1968).
- Lodh and Rao, *Indian J. Technol.*, **4**, p. 163 (1966).
- Mayfield and Church, *Ind. Eng. Chem.*, **44**, p. 2253 (1952).
- Moulton and Walkey, *Trans. Am. Inst. Chem. Eng.*, **40**, p. 695 (1944).
- Murali and Rao, *J. Chem. Eng. Data*, **7**, p. 468 (1962).
- Nandi and Ghosh, *J. Indian Chem. Soc., Ind. News Ed.*, **13**, pp. 93, 103, 108 (1950).
- Oloidi and Mumford, *ISEC Proc.* (Munich, 1986).
- Pyle, Duffey, and Colburn, *Ind. Eng. Chem.*, **42**, p.1042 (1950).
- Row, Koffolt, and Withrow, *Trans. Am. Inst. Chem. Eng.*, **37**, p. 559 (1941).
- Rocha, Humphrey, and Fair, *Ind. Eng. Chem. Process Des.*, **25**, p. 862 (1986).
- Rocha et al., *Ind. Eng. Chem. Res.*, **28**(12), pp. 1873-1878 (1989).
- Rocha, Cardenas, and Garcia, *Ind. Eng. Chem. Res.*, **28**(12), pp. 1879-1883 (1989).
- Shirotsuka and Murakami, *Kagaku Kogaku*, **30**, p. 727 (1966).
- Seibert and Fair, *Ind. Eng. Chem. Res.*, **32**(10), pp. 2213-2219 (1993).
- Treybal and Dumoulin, *Ind. Eng. Chem.*, **34**, p. 709 (1942).
- Ueyama and Koboyashi, *Bull. Univ. Osaka Prefect.*, **A7**, p. 113 (1959).
- Zheliznyak, *Zh. Prikl. Khim.*, **40**, p. 689 (1967).
- Zheliznyak and Brounshtein, *Zh. Prikl. Khim.*, **40**, p. 584 (1967).

Baffle Tray Efficiency Baffle tray mass-transfer efficiency was observed to depend strongly on the tray spacing and system properties, as shown in Figs. 15-46 and 15-47. In these studies, a tray spacing of about 10 cm provided a minimum HETS. The data indicate that the performance of baffle trays relative to sieve trays depends upon the interfacial tension of the system. For the high-interfacial-tension system (Fig. 15-46), the baffle tray performance (in terms of capacity and mass transfer) is relatively low compared to that of a sieve tray. However, for the low-interfacial-tension system (Fig. 15-47), performance was somewhat better using 62 percent tray overlap.

AGITATED EXTRACTION COLUMNS

In certain applications, the mass-transfer efficiency of a static extraction column is quite low, especially for systems with moderate to high interfacial tension. In these cases, efficiency may be improved by

mechanically agitating the liquid-liquid dispersion within the column to better control drop size and population density (dispersed-phase holdup). Many different types of mechanically agitated extraction columns have been proposed. The more common types include various rotary-impeller columns, the reciprocating-plate column, and the rotating-disk contactor (RDC). The following is a brief review. For more detailed discussion, see *Liquid-Liquid Extraction Equipment*, Godfrey and Slater, eds. (Wiley, 1994); *Science and Practice of Liquid-Liquid Extraction*, vol. 1, Thornton, ed. (Oxford, 1992); and *Handbook of Solvent Extraction*, Lo, Baird, and Hanson, eds. (Wiley, 1983; Krieger, 1991).

Rotating-Impeller Columns A number of different rotating-impeller column extractors have been proposed and built over the years. Only the Scheibel and Kühni designs are reviewed here. For information about the Oldshue-Rushton design, see the previous edition of this handbook. Also see Oldshue, Chap. 13.4 in *Handbook of*

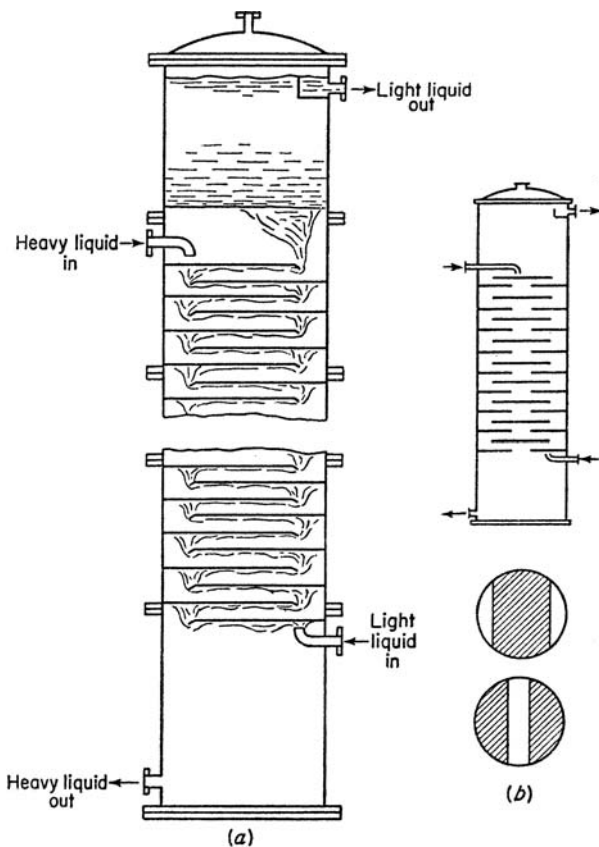


FIG. 15-41 Baffle towers. (a) Side-to-side flow at each tray. (b) Center-to-center flow (disk-and-doughnut style). (c) Center-to-side flow. [Reprinted from Treybal, *Liquid Extraction* (McGraw-Hill, 1963), with permission. Copyright 1963 McGraw-Hill, Inc.]

Solvent Extraction, Lo, Baird, and Hanson, eds. (Wiley, 1983; Krieger, 1991).

Scheibel Extraction Column The original Scheibel column design consisted of a series of knitted-wire-mesh packed sections placed within a vertical column, with a centrally located impeller placed between each section and no baffles [Scheibel and Karr, *Ind. Eng. Chem.*, **42**(6) pp. 1048–1057 (1950)]. A second-generation Scheibel design [*AIChE J.*, **2**(1), pp. 74–78 (1956); U.S. Patent 2,850,362 (1958)] added flat partitions or baffles to the ends of each packed section, and the impellers were surrounded by stationary shroud baffles to direct the flow of droplets discharged from the impeller tips. The new baffling arrangement improved efficiency, allowing design of larger-diameter columns with less power input and decreased height per theoretical stage. A third design by Scheibel [U.S. Patent 3,389,970 (1968)] eliminated the wire-mesh packing and retained the use of baffles and shrouded impellers (Fig. 15-48). The packed sections were replaced by agitated sections. This design was developed because the wire-mesh packed sections were prone to fouling (plugging) and difficult to clean. A Scheibel extractor of this type is very well suited to handling mixtures with high interfacial tension and can be designed with a large number of stages. It is not as well suited for systems that tend to emulsify easily owing to the high shear rate generated by a rotating impeller. Because of its internal baffling, which controls the mixing patterns on the stages, the Scheibel column has proved to be one of the more efficient extractors in terms of height of a theoretical stage; this makes it well suited to applications that

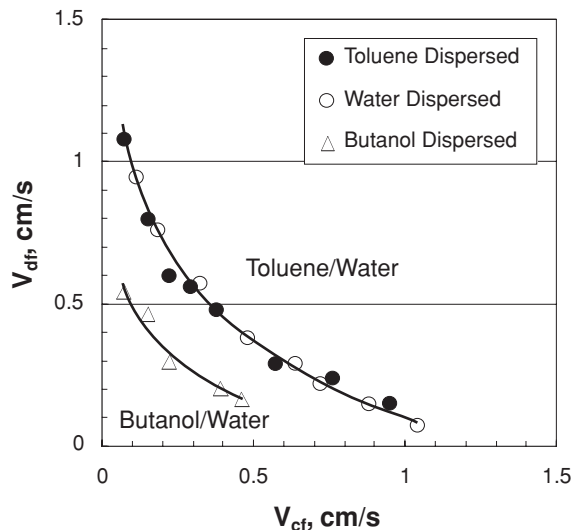


FIG. 15-42 Capacity characteristics of a baffle tray extractor. Tray overlap = 62 percent. Column diameter = 10.2 cm. [Taken from Seibert, Lewis, and Fair, Paper No. 112a, *AIChE National Meeting, Indianapolis* (November 2002), with permission. Copyright 2002 AIChE.]

require a large number of stages or are located indoors with headroom restrictions. Holmes, Karr, and Cusack [*Solvent Extraction and Ion Exchange*, **8**(3), pp. 515–528 (1990)] have published results comparing the efficiency of the Scheibel column to that of other extractors using the system toluene + acetone + water. For additional discussion, see Scheibel, Chap. 13.3 in *Handbook of Solvent Extraction*, Lo, Baird, and Hansen, eds. (Wiley, 1983; Kreiger, 1991). A related column design called the AP column consists of alternating sections of Scheibel-type agitators and structured packing [Cusack, Glatz, and Holmes, *Proc. ESEC'99, Soc. Chem. Ind.*, p. 427 (2001)]. The high open area of the packing allows for higher capacity while the agitation provides increased efficiency.

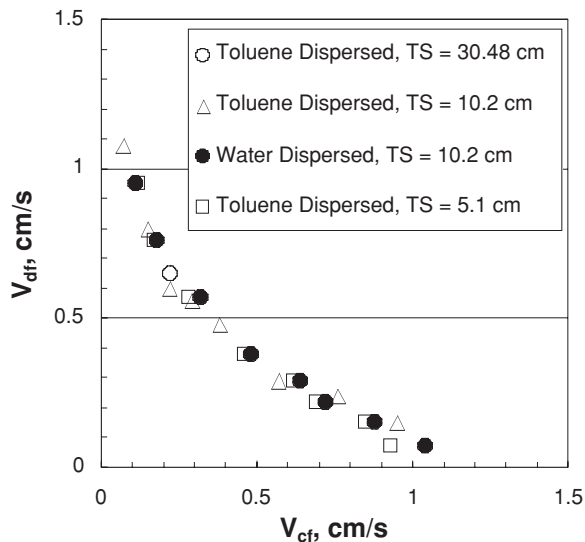


FIG. 15-43 Effect of tray spacing on baffle tray capacity. [Taken from Seibert, Lewis, and Fair, Paper No. 112a, *AIChE National Meeting, Indianapolis* (November 2002), with permission. Copyright 2002 AIChE.]

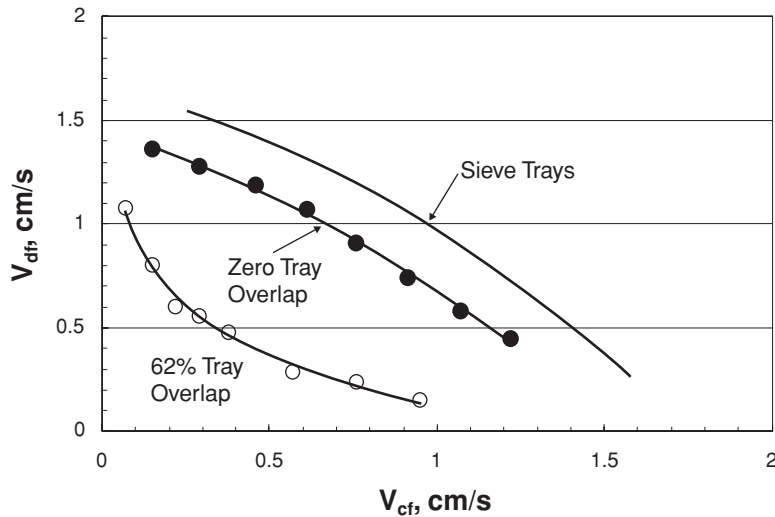


FIG. 15-44 Effect of tray overlap on baffle tray capacity. System: toluene (*d*) + acetone + water (*c*). [Taken from Seibert, Lewis, and Fair, Paper No. 112a, AIChE National Meeting, Indianapolis (November 2002), with permission. Copyright 2002 AIChE.]

As with most agitated extractors, the final design of a Scheibel column typically involves scale-up of data generated in a miniplant or pilot-plant test. The column vendor should be consulted for specific information. The key scale-up guidelines are as follows: (1) $D_i(2)/D_i(1) = [Q(2)/Q(1)]^{0.4}$; (2) $Z_i(2)/Z_i(1) = [D_i(2)/D_i(1)]^{0.70}$; (3) stage efficiency is the same for the pilot and full scale; and (4) power per unit volume is the same for each scale [Cusack and Karr, *Chem. Eng. Magazine*, pp. 112–119 (1991)]. Industrial columns up to 10 ft (3 m) in diameter and containing 90 actual stages have been designed using the following general procedures and a 3-in (75-mm) pilot column:

1. Pilot tests usually are conducted in 3-in (75-mm-) diameter columns. The column should contain a sufficient number of stages to complete the extraction. This may require several iterations on column height.

2. The column is run over a range of throughputs $V_d + V_c$ and agitation speeds. At each condition, the concentrations of solute in extract and raffinate streams are measured after steady-state operation has been achieved (usually after 3 to 5 turnovers of column volume). At each throughput, the flood point is determined by increasing the agitation until flooding is induced. A minimum of three throughput ranges are examined in this manner. Mass-transfer performance is measured at several agitation speeds up to the flood point.

3. From the above mass-transfer and flooding data, the combination of specific throughput and agitation speed that gives the optimum economic performance for the required separation can be determined. This information is used to specify the specific throughput value [$\text{gal}/(\text{h}\cdot\text{ft}^3)$ or $\text{m}^3/(\text{h}\cdot\text{m}^3)$] and agitation speed (rpm) for the commercial design. However, unlike the RDC and Karr columns, for

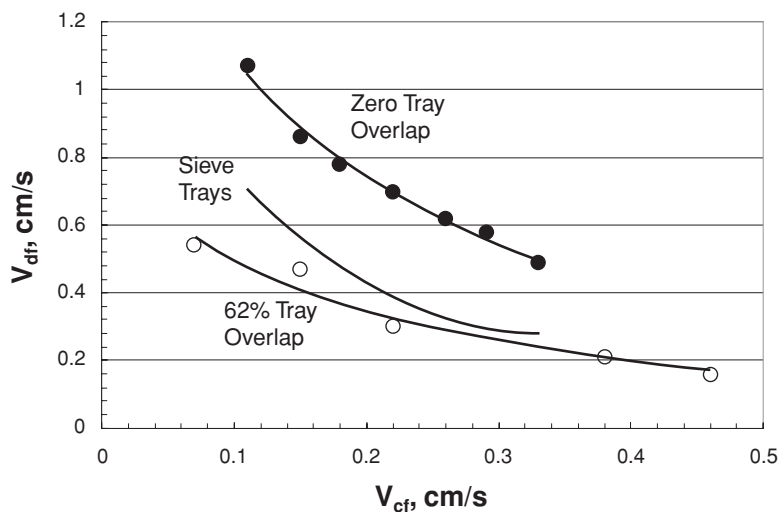


FIG. 15-45 Effect of tray overlap on baffle tray capacity. System: *n*-Butanol (*d*) + succinic acid + water (*c*). [Taken from Seibert, Lewis, and Fair, Paper No. 112a, AIChE National Meeting, Indianapolis (November 2002), with permission. Copyright 2002 AIChE.]

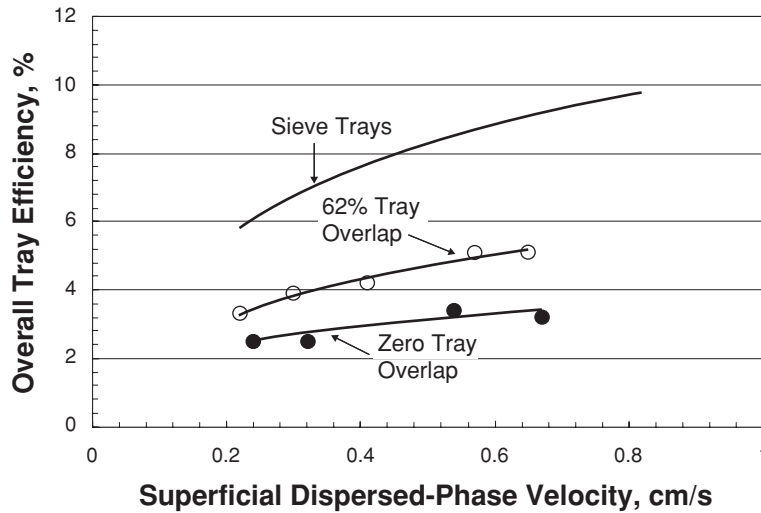


FIG. 15-46 Effect of tray overlap on baffle tray efficiency. System: toluene (*d*) + acetone + water (*c*). Tray spacing = 10.2 cm. [Taken from Seibert, Lewis, and Fair, Paper No. 112a, AIChE National Meeting, Indianapolis (November 2002), with permission. Copyright 2002 AIChE.]

which the specific throughput of the scaled-up version is the same as that of the pilot column, it is a characteristic of the Scheibel column that the throughput of the scaled-up column is on the order of 3 to 5 times greater than that achieved on the 3-in-diameter pilot column. The limited throughput of the 3-in column is due to its restrictive geometry; these restrictions are removed in the scaled-up columns.

4. Once the column diameter is determined, the stage geometry can be fixed. The geometry of a stage is a complex function of the column diameter. In the 3-in pilot column, the stage height-to-diameter ratio is on the order of 1:3. On a 10-ft- (3-m-) diameter column, it is on the order of 1:8. The recommended ratio of height to diameter is $Z_i(2)/Z_i(1) = [D_i(2)/D_i(1)]^{10.70}$.

5. The principle of the Scheibel column scale-up procedure is to maintain the same stage efficiency. Therefore, the scaled-up column

will have the same number of actual stages as the pilot column. The only difference is that the stages will be taller, to take into account the effect of axial mixing. With the agitator dimensions determined, the speed is then calculated to give the same power input per unit of throughput. Scheibel found that power input can be correlated by

$$P = 1.85\rho\omega^3 D_i^5 \tag{15-166}$$

where P is the power input per mixing stage, D_i is the impeller diameter, ρ is the average liquid density, and ω is the impeller speed (rotations per unit time).

Kühni Column Like the Scheibel column, the Kühni column uses shrouded (closed) turbine impellers as mixing elements on a central shaft (Fig. 15-49). Perforated partitions or stator plates extend

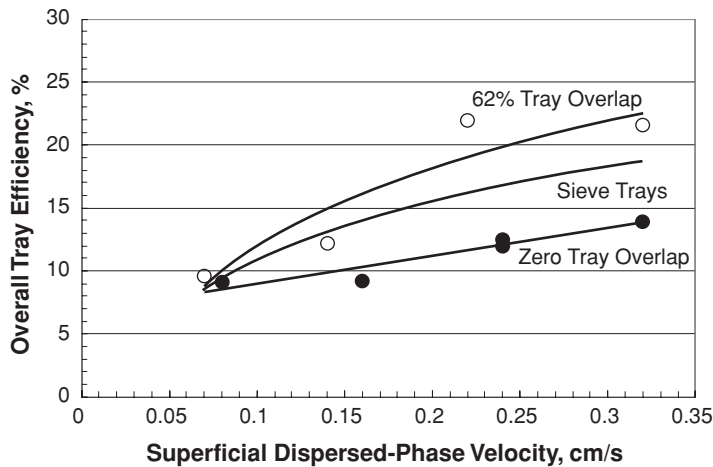


FIG. 15-47 Effect of tray overlap on baffle tray efficiency. System: *n*-butanol + succinic acid + water. Tray spacing = 10.2 cm. [Taken from Seibert, Lewis, and Fair, Paper No. 112a, AIChE National Meeting, Indianapolis (November 2002), with permission. Copyright 2002 AIChE.]

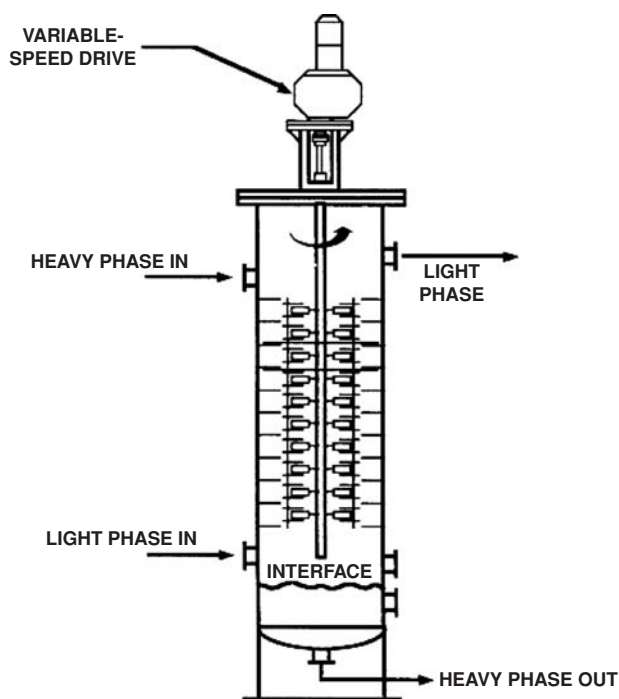


FIG. 15-48 Scheibel column extractor (third-generation design). (Courtesy of Koch Modular Process Systems.)

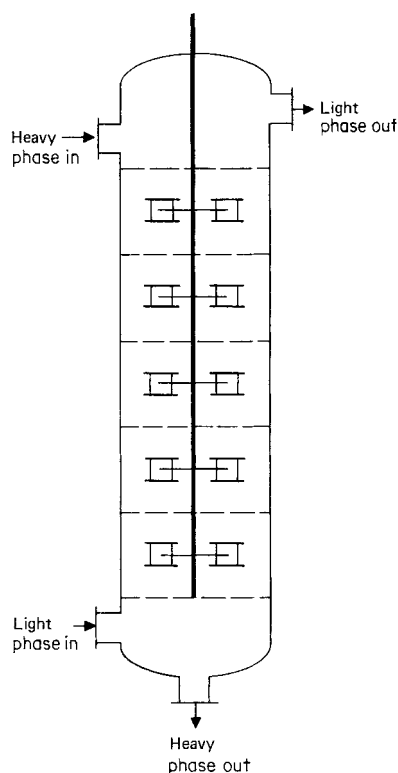


FIG. 15-49 Kühni column extractor.

over the vessel cross section to separate the extraction stages and reduce backmixing between stages. The fractional free-flow area between compartments can be adjusted by changing the free area around the rotor shaft and/or the perforations in the stator plate. As the free-flow area increases, throughput increases at the expense of increased axial mixing of the continuous phase and reduced mass-transfer performance. Throughput typically varies from $30 \text{ m}^3/(\text{h}\cdot\text{m}^2)$ [$750 \text{ gal}/(\text{h}\cdot\text{ft}^2)$] to significantly higher values depending upon the specific design factors chosen to meet the requirements of a given application.

Mögli and Bühlmann [Chap. 13.5 in *Handbook of Solvent Extraction*, Lo, Baird, and Hanson, eds. (Wiley, 1983; Krieger, 1991)] outline general considerations for specifying a commercial design from pilot data. The column vendor should be consulted for specific information. The scale-up procedures are based upon hydrodynamic and geometric similarity between the pilot-scale and plant-scale designs. Individual stage geometry (impeller size and free area of the stator plate) may be tailored for each stage, especially in cases where physical properties vary significantly along the column length. Mögli and Bühlmann suggest design options to maintain a somewhat uniform interfacial area along the column to minimize the impacts of axial mixing. Pratt and Stevens [*Science and Practice of Liquid-Liquid Extraction*, vol. 1, Thornton, ed. (Oxford, 1992), [Chap. 8, p. 541] provide recommended scale-up factors for a Kühni column as follows: $D_i/D_t = 0.33$ to 0.5 , compartment height = 0.2 to $0.3D_t$, and the fractional free area of the stator plates = 0.2 to 0.4 . The minimum recommended diameter for the pilot column is 60 mm (2.4 in) for specifying columns up to 1 m in diameter and 150 mm (6 in) for specifying larger-diameter columns.

A stage-wise computational procedure is proposed by Kumar and Hartland [*Ind. Eng. Chem. Res.*, **38**(3), pp. 1040–1056 (1999)] for design of a Kühni column. The procedure considers backflow of the continuous phase, with an attempt to estimate average drop size, drop size distribution, dispersed-phase holdup, flooding velocities, mass-transfer coefficients, and axial mixing. A design example for extraction of aniline from water is presented. This approach to design can be very useful for initial estimates, but as with all agitated extractors, some pilot testing is recommended for a final commercial design. Also see the discussion by Gomes et al. [*Ind. Eng. Chem. Res.*, **43**(4), pp. 1061–1070 (2004)].

Reciprocating-Plate Columns Another approach to agitating a dispersion within an extraction column is the use of reciprocating plates. This generally results in a more uniform drop size distribution because the shear forces are more evenly distributed over the entire cross section of the column. Reciprocating-plate extractors have a wide turndown range and are well suited to systems with moderate interfacial tension. They often can handle systems exhibiting a tendency to emulsify, and because of their high open-area design, they can handle slurries of solids, some containing as much as 30 percent solids by weight. Several types of reciprocating-plate extractors have been designed; design differences generally involve differences in the plate open area and plate spacing as well as the inclusion or omission of static baffles or downcomers. For detailed discussion of these designs, see Lo and Procházka, Chap. 12 in *Handbook of Solvent Extraction*, Lo, Baird, and Hanson, eds. (Wiley, 1983; Krieger, 1991); and Baird et al., Chap. 11 in *Liquid-Liquid Extraction Equipment*, Godfrey and Slater, eds. (Wiley, 1994).

The Karr reciprocating-plate column (Fig. 15-50) is a popular example. It uses dual-flow plates with 50 to 60 percent open area and has no downcomers [Karr, *AIChE J.*, **5**(4), pp. 446–452 (1959); Karr and Lo, *Chem. Eng. Prog.*, **72**(11), pp. 68–70 (1976); and Karr, *AIChE J.*, **31**(4), pp. 690–692 (1985)]. Because of the high open area, a Karr column may be operated with relatively high throughput compared to other types of agitated columns, up to about $1000 \text{ gal}/(\text{h}\cdot\text{ft}^2)$ [$40 \text{ m}^3/(\text{h}\cdot\text{m}^2)$] depending upon the application. The plates are mounted on a central shaft that moves up and down through a stroke length of up to 2 in (5 cm). As the diameter of the column increases, the HETS achieved by the column tends to increase due to axial mixing effects. For columns with a diameter greater than 1 ft (0.3 m), doughnut-shaped baffle plates may be added every 5 plates (typically) within the plate stack to minimize axial mixing. A Karr column also is well suited

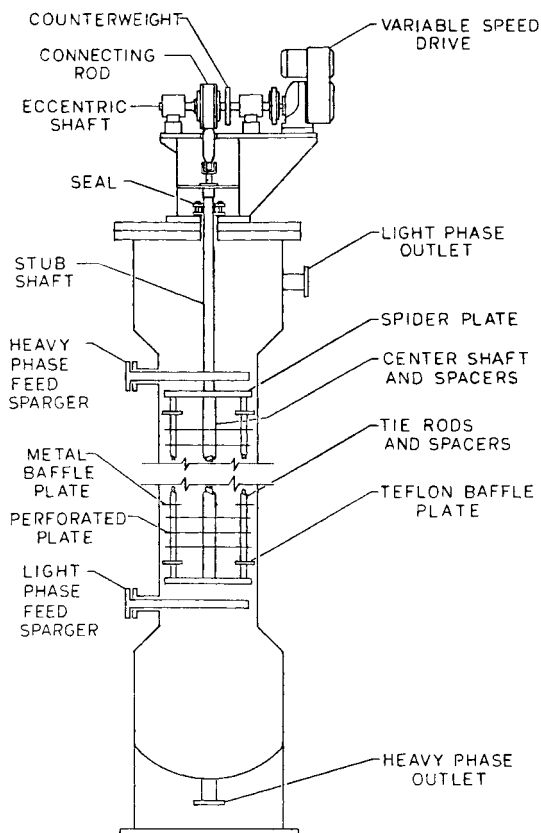


FIG. 15-50 Karr reciprocating-plate extraction column.

for corrosive systems since the plates can be fabricated from non-metallic materials. Pratt and Stevens [Chap. 8 in *Science and Practice of Liquid-Liquid Extraction*, vol. 1, Thornton, ed. (Oxford, 1992), p. 556] provide recommended geometric design and operating conditions for a Karr column as follows: reciprocation amplitude = 1 to 2 in (2.5 to 5 cm) with a 1-in amplitude being most common; reciprocation speed = 10 to 400 complete strokes (up and down) per minute; plate spacing = 2 to 6 in (5 to 15 cm); hole pitch = 0.625 to 0.75 in (1.6 to 1.9 cm); hole diameter = 0.50 to 0.625 in (1.3 to 1.6 cm); plate wall clearance = 1.25 to 2.5 in (3.2 to 6.4 cm). The plate spacing may be graduated to produce uniform drop size and population density along the length of the column, particularly for systems with high solute concentrations and depending upon how physical properties change along the column length [Karr, U.S. Patent 4,200,525 (1980)].

Baird et al. [Chap. 11 in *Liquid-Liquid Extraction Equipment*, Godfrey and Slater, eds. (Wiley, 1994)] discuss and summarize correlations for predicting holdup and flooding, mean drop diameter, axial mixing, mass transfer, and reciprocating-plate column performance. Kumar and Hartland [*Ind. Eng. Chem. Res.*, **38**(3), pp. 1040–1056 (1999)] present a correlation-based computational procedure for design of a Karr reciprocating-plate column, and they give an example for separation of acetone from water by using toluene. A backmixing model is described by Stella et al. [*Ind. Eng. Chem. Res.*, **45**(19), pp. 6555–6562 (2006)].

As with other agitated extractors, the final design of a commercial-scale Karr column is based on pilot test data. The column vendor should be consulted for specific information. The following general procedure is recommended:

1. For specifying commercial columns up to 6.5 ft (2 m) in diameter, testing in a pilot column of 1-in (25-mm) diameter is sufficient. If the anticipated scaled-up diameter is greater than 6.5 ft, then the pilot

tests should be conducted in a 2-in- (50-mm-) diameter column. The column should be tall enough to accomplish the complete extraction. This may require several iterations on column height.

2. The column is first optimized with regard to plate spacing. The plate spacing is adjusted along the length of the column to obtain the same tendency to flood everywhere in the column. If one particular section appears to flood early, limiting the throughput, then the plate spacing should be increased in this section. This will decrease the power input into that section. Similarly, in sections that appear to be undermixed because the population of drops is low, the plate spacing should be decreased.

3. Once the plate spacing is optimized, the column is run over a range of total throughputs ($V_d + V_c$) and agitation speeds. There should be a minimum of three throughput levels and at each throughput three agitation speeds. After steady state is attained at each condition (usually 3 to 5 turnovers of column volume), samples are taken and the separation is measured. At each condition the flood point also is determined. In small-scale tests, the data used for scale-up should be collected at a point very close to flooding, say, 95 percent of flooding. Scaling these data typically results in a commercial-scale unit that operates at roughly 80 or 85 percent of flooding.

4. From the data, plots are made of volumetric efficiency and agitation speed at each throughput level. From these plots the condition that gives the maximum volumetric efficiency is selected for scale-up. For additional discussion, see Lo and Prochazka, Chap. 12 in *Handbook of Solvent Extraction*, Lo, Baird, and Hanson, eds. (Wiley, 1983; Krieger, 1991).

5. For scale-up, the following parameters are kept constant: total throughput per unit area, plate spacing, and stroke length. The height and agitation speed of the scaled-up column are then calculated from the following relationships:

$$\frac{Z_i(2)}{Z_i(1)} = \left(\frac{D_{col}(2)}{D_{col}(1)} \right)^{0.38} \quad (15-167)$$

$$\frac{SPM(2)}{SPM(1)} = \left(\frac{D_{col}(1)}{D_{col}(2)} \right)^{0.14} \quad (15-168)$$

Here Z_i is the plate stack height, D_{col} is the column diameter, SPM is the reciprocating speed (complete strokes per minute), and 1 and 2 denote the pilot column and the scaled-up column, respectively.

Karr and Ramanujam [St. Louis AIChE Symposium (March 19, 1987)] propose a power per unit volume normalization factor for scale-up of the reciprocation speed if the pilot column plates have a different open area than the industrial scale plates, as follows:

$$\frac{SPM(2)}{SPM(1)} = \left(\frac{D_{col}(1)}{D_{col}(2)} \right)^{0.14} \left(\frac{\epsilon(2)^2}{1 - \epsilon(2)^2} \right) \left(\frac{1 - \epsilon(1)^2}{\epsilon(1)^2} \right) \quad (15-169)$$

where ϵ is the fractional open area of the perforated plate.

Rotating-Disk Contactor The rotary-disk contactor (RDC) is a vertical column containing an assembly of rotating disks and stationary baffles or stators. A typical design is illustrated in Fig. 15-51. The column is formed into compartments by horizontal doughnut-shaped or annular baffles, and within each compartment agitation is provided by a rotating, centrally located, horizontal disk. The rotating disk is smooth and flat and has a diameter less than that of the opening in the stationary baffles. The RDC extractor has been widely used because of its simplicity of construction, availability in relatively large diameters for high production rates, and low power consumption. For detailed reviews, see Chaps. 9 and 17 in *Liquid-Liquid Extraction Equipment*, Godfrey and Slater, eds. (Wiley, 1994); and Chaps. 13.1 and 13.2 in *Handbook of Solvent Extraction*, Lo, Baird, and Hanson, eds. (Wiley, 1983; Krieger, 1991). Also see Al-Rahawi, *Chem. Eng. Technol.*, **30**(2), pp. 184–192 (2007); Drummond and Bart, *Chem. Eng. Technol.*, **29**(11), pp. 1297–1302 (2006).

The RDC has a moderate throughput typically in the range of 20 to 35 m³/(h·m²) [500 to 850 gal/(h·ft²)], and it can be turned down to 20 to 35 percent of the design rate. However, the relatively open arrangement leads to some backmixing and results in only moderate mass-transfer performance. As a consequence, some RDC columns are being replaced by more efficient extractor designs. The RDC can be

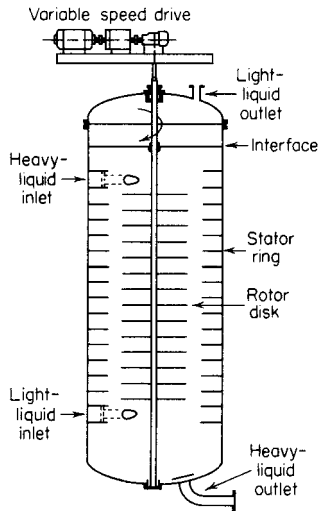


FIG. 15-51 Typical rotating-disk contactor.

used for systems with moderate viscosities up to about 100 cP and can be used for systems that tend to foul easily. The RDC also is suitable for systems with slow mass-transfer rates requiring only a few theoretical stages. An RDC can have difficulty handling feeds with emulsion formation tendencies, so it may not be suitable for some systems with low interfacial tension and low density difference.

Pulsed-Liquid Columns These are packed or tray column extractors in which a rapid reciprocating motion of relatively short amplitude is applied to the liquid contents to give improved rates of extraction (Fig. 15-52). Liquid pulsing improves the mass-transfer performance at a cost of somewhat reduced throughput. For detailed reviews of this technology, see Logsdail and Slater, Chap. 11.2 in *Handbook of Solvent Extraction*, Lo, Baird, and Hanson, eds. (Wiley, 1983; Krieger, 1991); Pratt and Stevens, Chap. 8 in *Science and Practice of Liquid-Liquid Extraction*, vol. 1, Thorton, ed. (Oxford, 1992); and Haverland and Slater, Chap. 10 in *Liquid-Liquid Extraction Equipment*, Godfrey and Slater, eds. (Wiley, 1994). Also see Bujalski et al., *Chem. Eng. Sci.*, **61**, pp. 2930–2938 (2006), for discussion of a disk and doughnut type of column extractor operated with pulsed liquid. Externally pulsing the liquid to impart mechanical agitation allows for a sealed agitated extraction column with

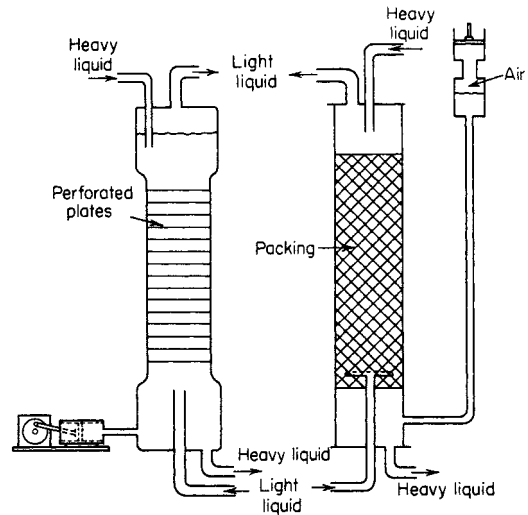


FIG. 15-52 Pulsed-liquid columns. (a) Sieve tray column with pump-type pulse generator. (b) Packed column with air pulser.

no moving parts. This feature is important for special applications involving highly corrosive or dangerously radioactive liquids, and it is the main reason why pulsed columns commonly are applied in the extraction and separation of metals from solutions in atomic energy operations. Pulsed-liquid contactors are similar to reciprocating-plate extractors in their basic operation. However, considerably more energy generally is required to move the entire column of liquid than to move the plates. For this reason, a reciprocating-plate or other type of mechanically agitated column design generally is preferred, unless special conditions require a sealed extraction column.

Raining-Bucket Contactor (a Horizontal Column) The “raining-bucket” contactor, originally developed by the Graesser Company in the United Kingdom, consists of a horizontal column or shell, as illustrated in Fig. 15-53. The shell slowly rotates about a central axis, and during operation a main liquid-liquid interface is maintained near the centerline. The light phase is continuous in the upper half of the shell, and the heavy phase is continuous in the lower half. Buckets mounted within the shell pick up continuous phase in one half and discharge it as dispersed droplets into the other half. As a result, each phase is dispersed. The raining-bucket design is intended for systems

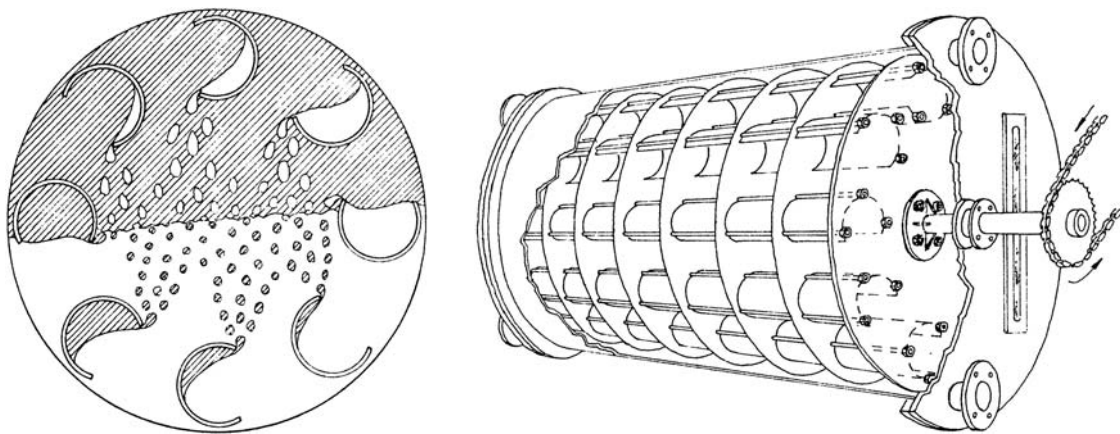


FIG. 15-53 Schematic views of a Graesser raining-bucket contactor. [Reprinted from Coleby, Chap. 13.6 in *Handbook of Solvent Extraction*, Lo, Baird, and Hanson, eds. (Wiley, 1983; Krieger, 1991), with permission.]

with low density difference and low interfacial tension, i.e., systems that tend to emulsify easily. It was originally developed for handling difficult settling systems in the coal-tar industry. A detailed review is given by Coleby [Chap. 13.6 in *Handbook of Solvent Extraction*, Lo, Baird, and Hanson, eds. (Wiley, 1983; Kreiger, 1991)]. Units currently are available through the Biotechna Company.

The rotor assembly of a raining-bucket contactor is made of a series of disks that divide the shell into a series of compartments. Each compartment contains an assembly of buckets. A small gap is maintained between the edge of the disks and the interior wall of the shell to allow for flow between compartments. The gap needs to be small to minimize backmixing. During operation, the phases are fed and removed from opposite ends of the column to produce a countercurrent flow. Throughput generally is low compared to that of other mechanically agitated extractors owing to the limited cross-sectional area available for flow. Rotational speeds are in the range of 0.25 to 40 rpm depending upon the contactor diameter and physical properties of the phases. Coleby [Chap. 13.6 in *Handbook of Solvent Extraction*, Lo, Baird, and Hanson, eds. (Wiley, 1983; Kreiger, 1991)] indicates that raining-bucket contactors can achieve up to 0.3 theoretical stage per compartment depending upon the application. Applications should not involve too high a viscosity in either phase, since dispersing drops in a high-viscosity continuous phase can result in slow liquid-liquid phase separation, and this can severely limit mass-transfer performance and the throughput of the extractor. Experience indicates that careful attention to this possibility is needed if viscosity is on the order of 30 cP or greater. A theoretical approach to estimating axial mixing and efficiency in a raining-bucket extractor is presented by Dente and Bozzano [*Ind. Eng. Chem. Res.*, **43**(16), pp. 4761–4767 (2004)]. A biotechnology application is described by Jarndilokkul, Paulsen, and Stuckey [*Biotechnol. Prog.*, **16**(6), pp. 1071–1078 (2000)].

MIXER-SETTLER EQUIPMENT

Mixer-settlers are used in hydrometallurgical processing for recovery of metals from aqueous acid solutions, and in multistep batchwise production of specialty chemicals including pharmaceuticals and agricultural chemicals, among other applications. In principle, any mixer may be coupled with any settler to obtain a complete stage. The function of a single stage within the cascade is to contact the liquids so that equilibrium is closely approached (achieving a high stage efficiency), and then to separate the liquids so they can be routed to the next stage. The design must strike a balance between contacting and settling requirements; i.e., the liquids should be mixed with sufficient intensity to suspend drops and facilitate good mass transfer, but not so intensely that drop sizes are too small and settling of the resulting dispersion is problematic.

A mixer-settler operation may be carried out batchwise or with a continuous feed. If batchwise operation is chosen, the same vessel used for mixing often is used for settling. Batchwise extraction in a stirred tank is a common operation in multistep, batchwise manufacture of complex organics. Such equipment allows flexibility to accommodate batch-to-batch variability, can ensure a single batch remains isolated from other batches throughout the manufacturing process (sometimes a regulatory requirement for pharmaceuticals), and is suitable for multipurpose plants producing a variety of products in campaigns. A batchwise process may be implemented in cocurrent, cross-current, or countercurrent multistage arrangements. A countercurrent operation is carried out as in Figs. 15-6 and 15-22, by initially treating the feed batch with extract solution as the extract leaves the process. The final treatment is carried out using fresh solvent as it enters the process. A two-stage batchwise countercurrent process scheme is common practice.

Continuously operated devices may place the mixing and settling functions in separate vessels or combine them into a single, specially designed vessel with compartments for mixing and settling. Continuous mixer-settlers are particularly attractive for applications requiring several equilibrium stages and long residence times due to slow extraction kinetics, especially for applications involving the use of reactive extractants or viscous fluids. Mixing commonly is done using rotating impellers. Impeller type, shape, size, tip speed, and position

within the mixing vessel may be adjusted to optimize the overall design. A static mixer may be a feasible alternative, but only if the required mass transfer can be accomplished in the short contacting time these devices allow, without generating a difficult-to-separate dispersion. Mixer-settlers may offer other advantages including easy start-up and operation, the ability to handle very high production rates and suspended solids, and the ability to achieve high stage efficiency with proper design. For systems that accumulate rag layers (sludges) between settled liquid layers, the rag material may easily be removed at each settler. As a potential disadvantage, difficult-to-break emulsions may be formed from the shear due to mixing and pumping liquids between tanks. Mixer-settlers also generally require large floor space, and the relatively long residence time in a mixer-settler can be a disadvantage if the desired solute is degraded over time at the required extraction conditions.

Mass-Transfer Models Because the mass-transfer coefficient and interfacial area for mass transfer of solute are complex functions of fluid properties and the operational and geometric variables of a stirred-tank extractor or mixer, the approach to design normally involves scale-up of miniplant data. The mass-transfer coefficient and interfacial area are influenced by numerous factors that are difficult to precisely quantify. These include drop coalescence and breakage rates as well as complex flow patterns that exist within the vessel (a function of impeller type, vessel geometry, and power input). Nevertheless, it is instructive to review available mass-transfer coefficient and interfacial area models for the insights they can offer.

The correlation of Skelland and Moeti [*Ind. Eng. Chem. Res.*, **29**(11), pp. 2258–2267 (1990)] for estimating individual continuous-phase mass-transfer coefficients is given by

$$\frac{k_d d_p}{\mathcal{D}_c} = 1.237 \times 10^{-5} \left(\frac{\mu_c}{\rho_c \mathcal{D}_c} \right)^{1/3} \left(\frac{D_i \omega^2}{g} \right)^{5/12} \left(\frac{D_i}{d_p} \right)^2 \times \left(\frac{d_p}{D_i} \right)^{1/2} \left(\frac{\rho_d d_p^2 g}{\sigma} \right)^{5/4} \phi_d^{-1/2} \quad (15-170)$$

where ω is impeller speed (rotations per unit time), D_i is impeller diameter, D_t is tank diameter, and \mathcal{D}_c is the solute diffusion coefficient in the continuous phase. Equation (15-170) is restricted to dispersed-phase holdup values less than $\phi_d = 0.06$. Other studies are described by Schindler and Treybal [*AIChE J.*, **14**(5), pp. 790–798 (1968)] and by Kee and Glen [*AIChE J.*, **15**(6), pp. 942–947 (1969)]. Equation (15-170) normally is used to estimate performance for applications in which the feed phase is the continuous phase and the partition ratio for transfer of solute into the raffinate phase is large. In this case, the overall resistance to mass transfer is dominated by the continuous-phase resistance. Relatively little information is available about individual dispersed-phase mass-transfer coefficients. Skelland and Xien [*Ind. Eng. Chem. Res.*, **29**(3), pp. 415–420 (1990)] offer a correlation of k_d values for batchwise extraction of solute from the dispersed phase into the continuous phase.

To use these correlation equations, it is necessary to identify which phase will be dispersed and to estimate the dispersed drop size and holdup as a function of throughput near flooding conditions. For relevant discussions, see “Factors Affecting Which Phase Is Dispersed” and “Size of Dispersed Drops” under “Liquid-Liquid Dispersion Fundamentals.” Holdup is a complex function of flow rates, impeller type, vessel geometry, and power input, as well as physical properties. For most impeller types, correlations for estimating holdup are not available. However, Weinstein and Treybal [*AIChE J.*, **19**(2), pp. 304–312; **19**(4), pp. 851–852 (1973)] offer the following correlations for estimating holdup in a vessel agitated using a six-blade disk-style flat-blade turbine (Rushton): For a baffled vessel with a gas-liquid surface:

$$\frac{\phi_d}{\phi_{d,\text{feed}}} = 0.764 \left(\frac{PQ_d \mu_c^2}{V_i \sigma^3} \right)^{0.300} \left(\frac{\mu_c^2}{Q_d \rho_c^2 \sigma} \right)^{0.178} \left(\frac{\rho_c}{\Delta \rho} \right)^{0.0741} \times \left(\frac{\sigma^2 \rho_c}{\mu_c^2 g} \right)^{0.276} \left(\frac{\mu_d}{\mu_c} \right)^{0.136} \quad (15-171)$$

For a liquid-full vessel without baffles:

$$\frac{\phi_d}{\phi_{d,\text{feed}}} = 3.39 \left(\frac{PQ_d \mu_c^2}{V_t \sigma^3} \right)^{0.247} \left(\frac{\mu_c^3}{Q_d \rho_c^2 \sigma} \right)^{0.427} \left(\frac{\rho_c}{\Delta \rho} \right)^{0.430} \times \left(\frac{\sigma^3 \rho_c}{\mu_c^4 g} \right)^{0.401} \left(\frac{\mu_d}{\mu_c} \right)^{0.0987} \quad (15-172)$$

Baffles are not needed if the vessel is operated full of liquid with no head space. In Eqs. (15-171) and (15-172), $\phi_{d,\text{feed}}$ is the volume fraction of the phase that ultimately becomes the dispersed phase, for the combined streams entering the vessel: $\phi_{d,\text{feed}} = Q_d / (Q_d + Q_c)$. If $\phi_d / \phi_{d,\text{feed}}$ is calculated to be greater than 1.0, it should be taken as 1.0. These equations are not applicable to other types of impellers.

When an estimate of ϕ_d is available, then $a \approx 6\epsilon \phi_d / d_p$ [Eq. (15-109)]. If the individual mass-transfer coefficients can be estimated with reasonable accuracy, a value for the overall coefficient k_{or} can be calculated from the individual coefficients as in Eq. (15-68). The stage efficiency for a continuous process can then be estimated from

$$\xi_{mr} = 1 - \exp\left(-\frac{k_{or} a \theta}{\phi_d}\right) \quad (15-173)$$

where ξ_{mr} is the Murphree raffinate-based stage efficiency and θ is the residence time for total liquid in the vessel [Treybal, "Liquid Extractor Performance," *Chem. Eng. Prog.*, **62**(9), pp. 67-75 (1966); and Laddha and Degaleesan, *Transport Phenomena in Liquid Extraction* (McGraw-Hill, 1978), p. 418]. Also see the discussion by Skelland and Kanel [*Ind. Eng. Chem. Res.*, **31**(3), pp. 908-920 (1992)]. These authors describe an extraction model framework that includes terms representing drop breakage and coalescence effects.

Miniplant Tests As mentioned earlier, for most liquid-liquid extraction applications involving mixer-settlers, the requirements for satisfactory performance with respect to mixing and settling are determined by using small miniplant or pilot-plant tests. For mixer design, the usual procedure is to run continuous experiments for a specific mixer geometry and type of impeller, generating performance data over a range of residence times and agitation intensities. The experimental program typically involves testing a variety of impellers and impeller locations until satisfactory results are obtained, with the ultimate goal of scaling up the miniplant design to achieve the same performance at the commercial scale. The design of settlers is discussed in the section "Liquid-Liquid Separation Equipment." With careful design, most extractions require residence times in the range of 1 to 3 min. However, for reaction-enhanced extractions having relatively slow chemical kinetics compared to mass transfer, longer times in the range of 10 to 15 min are not unusual. As noted earlier, it is important to consider the time required to settle the dispersion after mixing and to determine the optimum mixing intensity that provides good mass transfer with reasonable ease of settling.

In these tests, extraction efficiency may be expressed in terms of a Murphree efficiency as

$$\xi = \frac{C_o - C_t}{C_o - C^*} \quad (15-174)$$

where C_o is the initial concentration of solute in the feed, C_t is the concentration in the outlet for a given residence time or at time t for a batch process, and C^* is the concentration at equilibrium. Normally, the extraction efficiency is determined from continuous experiments. If batch extraction data are available for the same solvent-to-feed ratio, the efficiency of a continuous process may be estimated by fitting the batch data to a first-order rate expression

$$\xi_{\text{batch}} = 1 - \exp(-kt_b) \quad (15-175)$$

where ξ_{batch} for the batch experiment is measured as a function of t_b , the batch mixing time [Godfrey, Chap. 12 in *Liquid-Liquid Extraction Equipment*, Godfrey and Slater, eds. (Wiley, 1994)]. The efficiency of the continuous process is calculated from the expression

$$\xi_{\text{continuous}} = \frac{k\theta}{1 + k\theta} \quad (15-176)$$

where θ is the total liquid residence time for the continuous process. This approach is valid for most diffusion rate controlled processes, but may not be valid for reaction-enhanced processes in which the chemical reaction rate may be rate-limiting and not necessarily first-order.

When the ratio of phases entering a mixer-settler stage is far from unity, recycling a portion of the minority phase from the settler back to the mixer sometimes improves the settling of the dispersion by boosting the phase ratio in the settler. (See "Gravity Decanters (Settlers)" under "Liquid-Liquid Phase Separation Equipment.") The stage efficiency also may be enhanced. For example, when the extract (solvent) is the minority phase (because K is greater than unity) and mass-transfer rates are poor, recycling the settled extract phase can boost the mass-transfer efficiency [Treybal, *Ind. Eng. Chem. Fundam.*, **3**(3), pp. 185-188 (1964)].

Liquid-Liquid Mixer Design Many different types of impellers are used for liquid-liquid extraction, including flat-blade and pitched-blade turbines, marine-type propellers, and special pump-mix impellers. With pump-mix designs, the impeller serves not only to mix the fluids, but also to move the fluids through the extraction stages of a mixer-settler cascade. The agitated vessel should be baffled if the vessel is operated with a gas-liquid surface, to avoid forming a vortex. As noted earlier in reference to Eq. (15-172), baffles are not needed if the vessel is operated with the liquid full [Weinstein and Treybal, *AIChE J.*, **19**(2), pp. 304-312 (1973)].

The design of a liquid-liquid mixer includes specification of impeller type and rotational speed (or tip speed), the number of impellers required, the ratio of impeller diameter to vessel diameter D_i/D_r , and the location of impeller(s) and any baffles within the vessel. A single impeller generally can be used for vessels with a height-to-diameter ratio less than 1.2 and liquid density ratios within the range of $0.9 < \rho_d/\rho_c < 1.1$. Multiple impeller designs are used to improve circulation and power distribution in tall vessels. For detailed discussions of liquid-liquid mixer design, see Leng and Calabrese, Chap. 12 in *Handbook of Industrial Mixing, Science and Practice*, Paul, Atiemo-Obeng, and Kresta, eds. (Wiley, 2004); and Edwards and Baker, Chap. 7, and Edwards, Baker, and Godfrey, Chap. 8, in *Mixing in the Process Industries*, 2d ed., Hamby, Edwards, and Nienow, eds. (Butterworth-Heinemann, 1992). Also see Daglas and Stamatoudis, *Chem. Eng. Technol.*, **23**(5), pp. 437-440 (2000), for discussion of the effect of impeller vertical position on drop size; and Willie, Langer, and Werner, *Chem. Eng. Technol.*, **24**(5), pp. 475-479 (2001), for discussion of the influence of power input on drop size distribution for a variety of impeller types.

The mixing power per unit volume P/V is a function of impeller rotational speed ω , impeller diameter D_i , and the Power number (P_o) for the type of impeller and vessel geometry:

$$\frac{P}{V} = P_o \left(\frac{\rho_m \omega^3 D_i^5}{V_{\text{tank}}} \right) \quad (15-177)$$

In Eq. (15-177), the mixture mean density is given by

$$\rho_m = \phi_d \rho_d + (1 - \phi_d) \rho_c \quad (15-178)$$

Power numbers for different impeller types depend upon the impeller Reynolds number. Representative relationships of Power number versus Reynolds number for several types of impellers are given in Fig. 15-54. For additional information on a variety of impellers, see Sec. 6 and Hemrajani and Tatterson, Chap. 6 in *Handbook of Industrial Mixing, Science and Practice*, Paul, Atiemo-Obeng, and Kresta, eds. (Wiley, 2004).

The power P in Eq. (15-177) does not include losses associated with the motor and drive unit. These losses can contribute as much as 30 to 40 percent to the overall power requirement. The drive supplier should be consulted for specific information. For pump-mix impellers, knowledge of the power characteristics for pumping is required in addition to that for mixing. For a discussion of these special cases, see Godfrey,

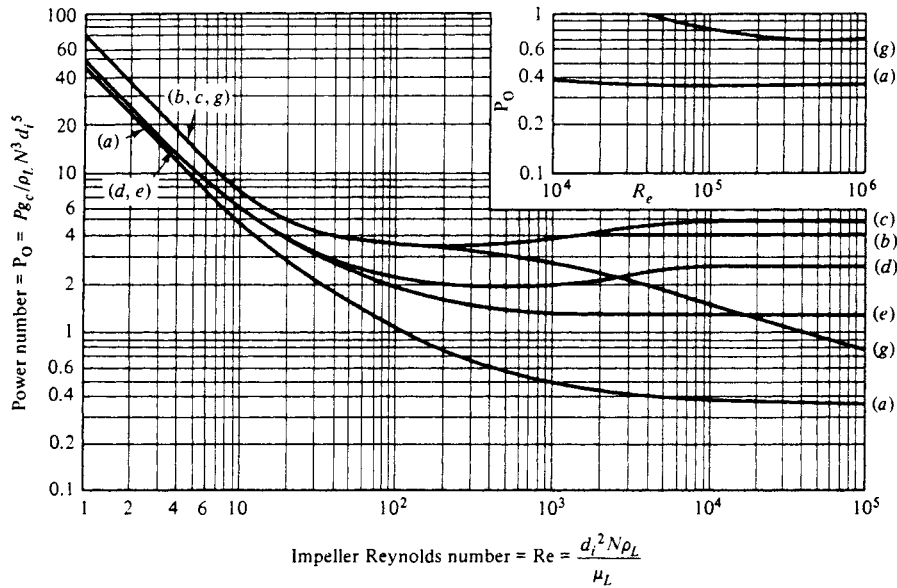


FIG. 15-54 Power for agitation impellers immersed in single-phase liquids, baffled vessels with a gas-liquid surface (except curves c and g). Curves correspond to (a) marine impellers; (b) flat-blade turbines, width = $D/5$; (c) disk flat-blade turbines (Rushton) with or without a gas-liquid surface; (d) curved blade turbines; (e) pitched blade turbines; (g) flat-blade turbines, no baffles, no gas-liquid interface, no vortex.

Notes on Fig. 15-54:

1. All the curves are for axial impeller shafts, with liquid depth equal to the tank diameter D .
2. Curves a to e are for open vessels, with a gas-liquid surface, fitted with four baffles, baffle width = $D/10$ to $D/12$. The impeller is set at a distance $C = D_i$ or greater from the bottom of the vessel.
3. Curve a is for marine propellers, $D_i/D_i \approx \frac{1}{3}$. The effect of changing D_i/D_i is apparently felt only at very high Reynolds numbers.
4. Curves b to e are for turbines. For disk flat-blade (Rushton) turbines, curve c, the effect of changing D_i/D_i is negligible in the range $0.15 < D_i/D_i < 0.50$. For open types (without the disk), curve b, the effect of D_i/D_i may be strong.
5. Curve g is for disk flat-blade turbines operated in unbaffled vessels filled with liquid and covered, so that no vortex forms. If baffles are present, the power characteristics at high Reynolds numbers are essentially the same as curve b for baffled open vessels, with only a slight increase in power.
6. For very deep tanks, two impellers normally are mounted on the same shaft, one above the other. For all flat-blade turbines, at a spacing of $1.5D$, or greater, the combined power for both will approximate that for a single turbine.

SOURCE: Treybal, *Mass-Transfer Operations* (McGraw-Hill, 1980), p. 152. For more detailed information, consult *Handbook of Industrial Mixing*, Paul, Atiemo-Obeng, and Kresta, eds. (Wiley, 2004).

Chap. 12 in *Liquid-Liquid Extraction Equipment*, Godfrey and Slater, eds. (Wiley, 1994); and Singh et al., *Ind. Eng. Chem. Res.*, **46**(7), pp. 2180–2190 (2007).

Skelland and Ramsay [*Ind. Eng. Chem. Res.*, **26**(1), pp. 77–81 (1987)] correlated the minimum impeller speed needed to completely disperse one liquid in another in an agitated vessel with standard baffles as follows:

$$\frac{\omega_{\min}^2 \rho_m D_i}{g \Delta \rho} = C^2 \left(\frac{D_i}{D_i} \right)^{2\alpha} \phi^{0.106} \left(\frac{\mu_m^2 \sigma}{D_i^2 \rho_m g^2 \Delta \rho^2} \right)^{0.084} \quad (15-179)$$

The mixture mean density is given by Eq. (15-178), and the mixture mean viscosity is given by

$$\mu_m = \frac{\mu_c}{1 - \phi_d} \left(1 + \frac{1.5 \mu_d \phi_d}{\mu_d + \mu_c} \right) \quad (15-180)$$

The authors determined correlation constants C and α for five common types of impellers (two axial-flow impellers and three radial-flow impellers) and four impeller locations within a standard tank configuration. The specific power requirement can then be estimated by using Eq. (15-177). The power required to disperse one liquid phase

into another typically is in the range of 0.2 to 0.8 kW/m³ (1 to 4 hp/1000 gal) [Edwards, Baker, and Godfrey, Chap. 8 in *Mixing in the Process Industries*, 2d ed., Harnby, Edwards, and Nienow, eds. (Butterworth-Heinemann, 1992), p. 144].

Scale-up Criteria It is common practice to scale up a miniplant design on the basis of equal residence time, constant power per unit volume, and geometric similarity such that the ratio D_i/D_i is held constant and the same types of impeller, tank geometry, and baffling are used. Treybal [*Chem. Eng. Prog.*, **62**(9), pp. 67–75 (1966)] indicates that in using this criterion, stage efficiency for liquid-liquid extraction is likely to increase on scale-up, so it is expected to yield a conservative design. With this approach, P/D_i^3 is constant and proportional to $P_0 \omega^3 D_i^3 / D_i^3 = P_0 \omega^3 D_i^2$. Assuming that the Power number is independent of scale, this yields the relationship

$$\frac{\omega(2)}{\omega(1)} = \left(\frac{D_i(1)}{D_i(2)} \right)^{2/3} = \left(\frac{D_i(1)}{D_i(2)} \right)^{2/3} \quad (15-181)$$

Skelland and Ramsay [*Ind. Eng. Chem. Res.*, **26**(1), pp. 77–81 (1987)] indicate that Eq. (15-181) is somewhat conservative, in general agreement with Treybal. Based on an analysis of mixing data generated at low holdup, they indicate that the exponent $\frac{2}{3}$ may be replaced with 0.71 as

a scale-up rule. Skelland and Ramsay also discuss the criteria for scale-up to a tank design involving a different ratio of D_2/D_1 at the large scale.

Leng and Calabrese [Chap. 12 in *Handbook of Industrial Mixing: Science and Practice*, Paul, Atiemo-Obeng, and Kresta, eds. (Wiley, 2004), p. 732] show that constant power per unit volume also yields the following relationship if a change in drop size is desired (again, for applications with low holdup):

$$\frac{d_{\max}(1)}{d_{\max}(2)} \approx \frac{\omega(2)^{6/5} D_1(2)^{4/5}}{\omega(1)^{6/5} D_1(1)^{4/5}} \quad \text{for } \text{Re} = \frac{\rho_m \omega D_i^2}{\mu_m} > 10^4 \quad (15-182)$$

Equation (15-182) reduces to Eq. (15-181) when $d_{\max}(1)$ is set equal to $d_{\max}(2)$.

The constant power per unit volume scale-up criterion is equivalent to scaling the impeller tip speed ($S_{\text{tip}} = \pi D_i \omega$) by the ratio $S_{\text{tip}}(2)/S_{\text{tip}}(1) = [D(2)/D(1)]^{1/3}$. It follows that when the tank diameter is doubled, the impeller tip speed must increase by a factor of 1.26 to maintain constant power per unit volume. If the Skelland and Ramsay exponent of 0.71 is applied in Eq. (15-181) instead of $\frac{2}{3}$, then tip speed scales as $S_{\text{tip}}(2)/S_{\text{tip}}(1) = [D(2)/D(1)]^{0.29}$ and doubling the tank diameter involves increasing the tip speed by a factor of 1.22.

Podgórska and Bałdyga [*Chem. Eng. Sci.*, **56**, pp. 741–746 (2001)] present a model of drop breakage and coalescence and compare four scale-up criteria for agitated liquid-liquid dispersions:

- I. Equal power per unit volume and geometric similarity
- II. Equal average circulation time and geometric similarity
- III. Equal power per unit volume and equal average circulation time ($D_2/D_1 \neq \text{constant}$)
- IV. Equal tip speed and geometric similarity

For slow-coalescing systems and systems at low holdup, the rate of drop breakage dominates. In this case, according to the analysis of Podgórska

and Bałdyga, criteria I and II yield smaller drops on scale-up, and criteria III and IV yield larger drops. For fast-coalescing systems, the rate of drop coalescence begins to dominate breakage. In this case, the authors indicate that I and III yield almost constant drop size with scale-up, II yields much smaller drops, and IV yields larger drops. Podgórska and Bałdyga recommend III for fast-coalescing systems, although they point out a limitation in terms of the maximum size of tank that this criterion will allow. See Leng and Calabrese, Chap. 12 in *Handbook of Industrial Mixing: Science and Practice*, Paul, Atiemo-Obeng, and Kresta, eds. (Wiley, 2004), pp. 682–687, for detailed discussion of factors influencing coalescence and their impact on scale-up difficulty.

Based on the analyses described above, taken together, it appears that scaling according to constant power per unit volume and geometric similarity generally will give satisfactory results, although the resulting design may not be optimal. For a new design, generally it is advisable to specify a variable-speed drive that can operate within a range of tip speeds. This provides flexibility for further adjustment and optimization of the process in the plant, and it also allows flexibility to accommodate variability in feed composition (a likely scenario in an industrial process).

Specialized Mixer-Settler Equipment As mentioned earlier, any mixer and settler can be combined to produce a stage, and the stages in turn arranged in a multistage cascade. A great many specialized designs have been developed in an effort to reduce costs, e.g., by minimizing or eliminating interstage pumping or by combining the various stages into a single vessel. With proper design, these devices generally can achieve overall stage efficiencies in excess of 80 percent, with many providing 90 to 95 percent stage efficiency. Only a few of the more commonly used types are mentioned here. For more detailed discussions, see Chaps. 9.1 to 9.5 in *Handbook of Solvent Extraction*, Lo, Baird, and Hanson, eds. (Wiley, 1983; Krieger, 1991).

Several pump-mix combinations have been developed by industry to simplify overall plant layout and minimize the number of pumps, at the expense of more expensive mixer design or complexity. The IMI axial pump-mix and draft tube (Fig. 15-55a) has the pumping

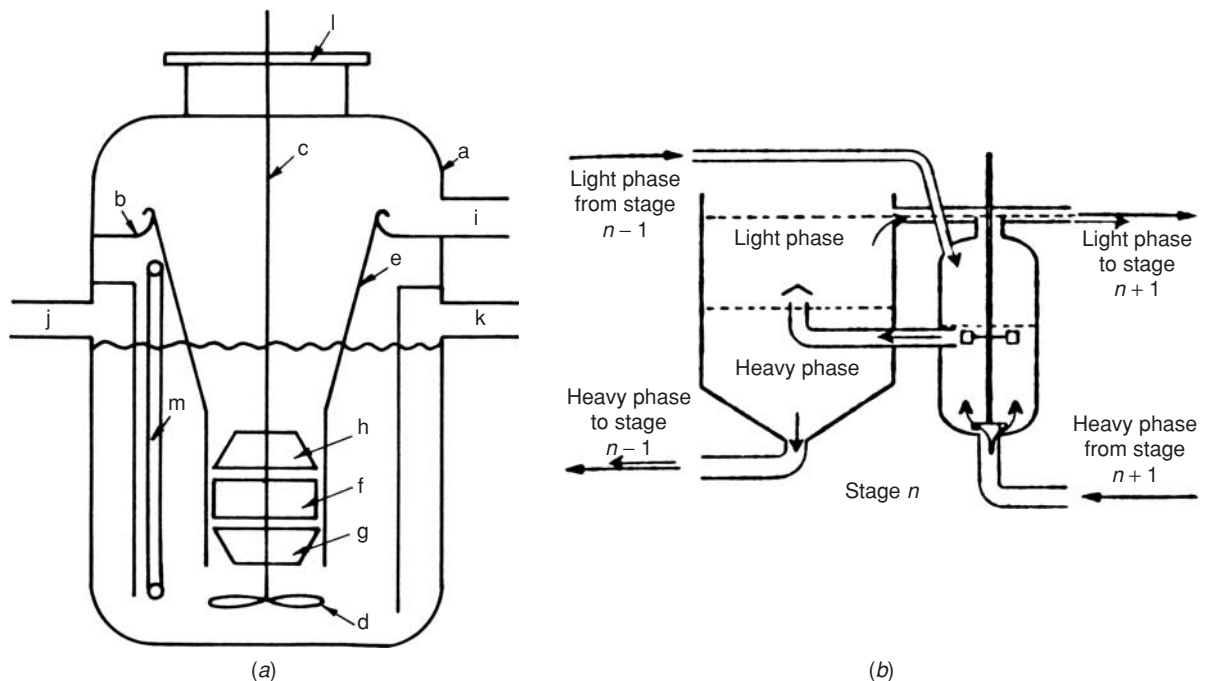


FIG. 15-55 Types of pump-mix arrangements for mixer-settler extractors. (a) IMI pump mix with mixing and pumping impellers (a, vessel; b, internal deck; c, shaft; d, mixing impeller; e, draft tube; f, pumping impeller; g and h, guide vanes; i, dispersion discharge; j, light-phase feed; k, heavy-phase feed; l, mounting flange; m, sight glass). (b) Kemira mixer-settler. [Figure 15-55a taken from *Handbook of Solvent Extraction*, Lo, Baird, and Hanson, eds. (Wiley, 1983; Krieger, 1991), with permission. Figure 15-55b taken from Mattila, ISEC '74 Proc., London, 1974, with permission.]

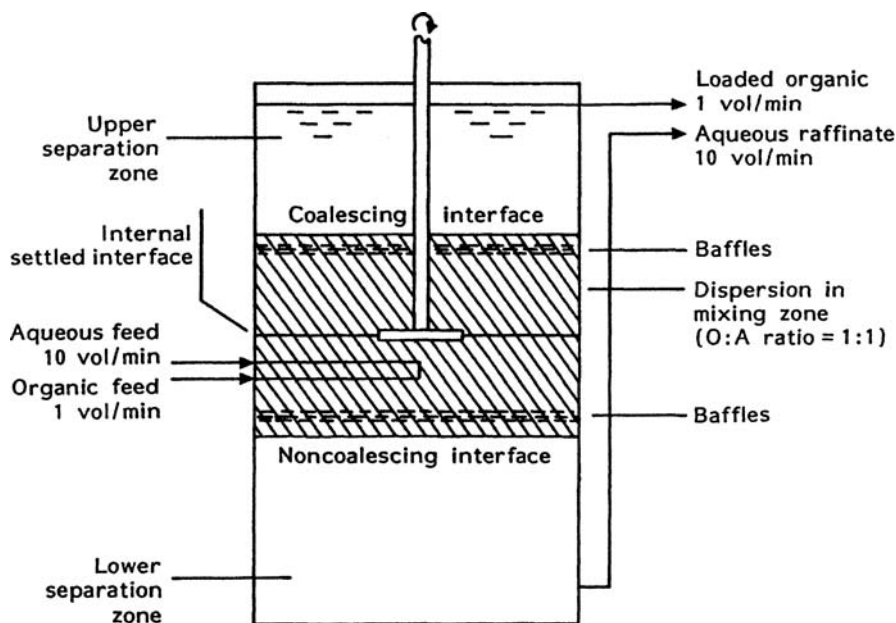


FIG. 15-56 Davy CMS extractor with pump-mix impeller and phase separation zones. [Reprinted from *Liquid-Liquid Extraction Equipment*, Godfrey and Slater, eds. (Wiley, 1994), with permission. Copyright 1994 John Wiley & Sons Ltd.]

and mixing impellers on the same shaft. The upper part of the tank contains the draft tube and the mixing-impeller. The pumping-impeller for transferring the dispersion to the settler is in the lower part of the tank. There is a potential disadvantage of forming smaller and hard to separate drops when pumping a dispersion versus pumping a single phase. The Kemira design (Fig. 15-55b) uses a pumping-impeller located near the bottom of the tank along with a mixing-impeller located near the central zone of the tank. The draft tube is eliminated and a dispersion is not pumped in this design. The Davy CMS design (Fig. 15-56) uses a pump-mix impeller in a large tank that provides both mixing and settling capability over a wide range of phase flow ratios. The dispersion occurs in the central section of the tank, and the separation occurs in the upper and lower separation zones.

A compact alternating arrangement of mixers and settlers has been adopted in many of the "box-type" extractors developed originally for processing radioactive solutions. These designs are used for many other processes, with literally dozens of modifications. An example is the pump-mix mixer-settler (Fig. 15-57), in which adjacent stages have common walls [Coplan, Davidson, and Zebroski, *Chem. Eng. Prog.*, **50**(8), pp. 403-408 (1954)]. In this case, the impellers pump as well as mix by drawing the heavy liquid upward through the hollow impeller shaft and discharging it at a higher level through the hollow impeller. Rectangular tanks are not ideal for good mixing; however, the compromise in mixing and settling performance is offset by the compact and economical design.

Vertical arrangement of the stages is desirable, since then a single drive may be used for agitators and the floor space requirement of a cascade is reduced to that of a single stage. The Lurgi extractor configuration has the mixer and settlers in separate vertical shells interconnected with piping [Guccione, *Chem. Eng. Magazine*, **73**(4), pp. 78-80 (1966)]. A great many other designs are known. For example, the Fenske and Long extractor [Fenske and Long, *Chem. Eng. Prog.*, **51**(4), pp. 194-198 (1955); Long and Fenske, *Ind. Eng. Chem.*, **53**(10), pp. 791-798 (1961); Long, *Ind. Eng. Chem. Fundam.*, **1**, p. 152 (1962)] is a vertical stack of mixer-settler stages. This

design employs a reciprocating plate at each stage to mix the two phases.

Suspended-Fiber Contactor The Merichem Fiber-Film® contactor is used in petroleum refining operations to wash hydrocarbon streams with caustic or other treating solutions [Suarez, U.S. Patent 5,997,731 (1999)]. The hydrocarbon feed and wash fluid are brought together within a vertical pipe or wash column containing fibers suspended from the top, as shown in Fig. 15-58. The two liquids flow cocurrently down the column through the bed of fibers. The fibers are attached at the top of the column but not at the bottom. Liquid-liquid contacting is facilitated through capillary and surface-wetting effects. This arrangement avoids (or minimizes) formation of small dispersed

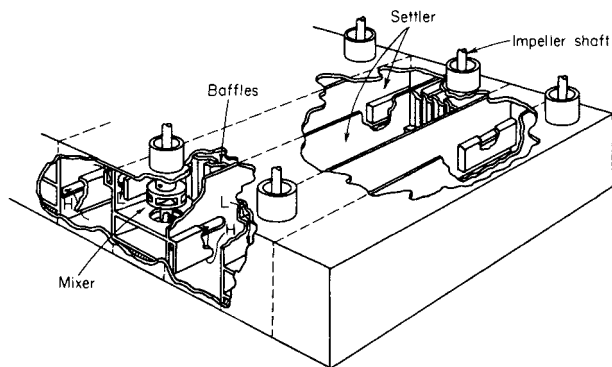


FIG. 15-57 Pump-mix box-type mixer-settler. [Taken from Coplan, Davidson, and Zebroski, *Chem. Eng. Prog.*, **50**, p. 403 (1954), with permission.]

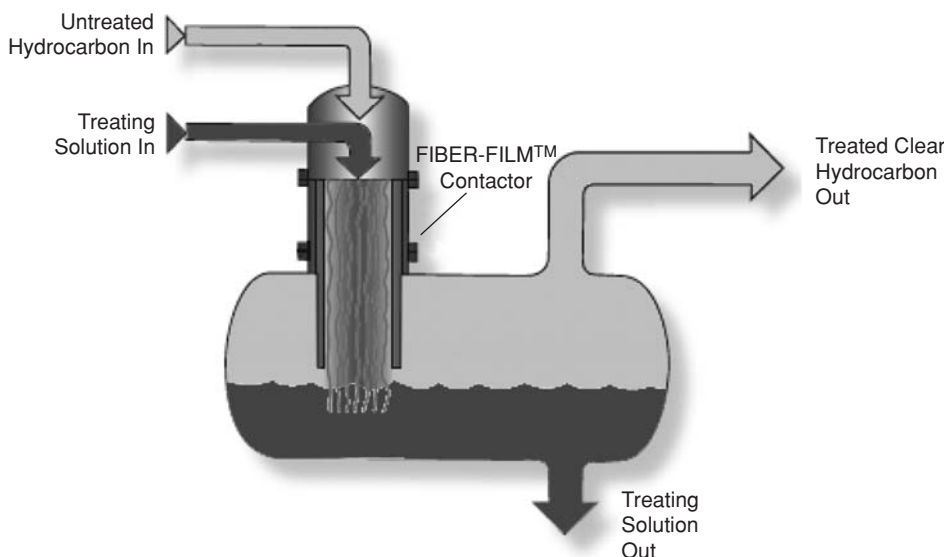


FIG. 15-58 Merichem Fiber-Film™ contactor. (Courtesy of Merichem Chemicals and Refinery Services, LLC.)

drops, and this helps to minimize entrainment of aqueous phase into the hydrocarbon outlet. Little information about the mass-transfer performance and design requirements for this type of contactor has been published.

CENTRIFUGAL EXTRACTORS

A centrifugal extractor multiplies the force of gravity acting on two liquid phases. Centrifugal extractors can facilitate a liquid-liquid extraction process by reducing diffusion path lengths and increasing the driving force for liquid-liquid phase separation. They can achieve very high specific throughput with very low liquid residence time. A wide variety of machine types are available, ranging from relatively simple devices used primarily for phase separation or for single-stage liquid-liquid contacting with separation to more complex machines designed to provide the equivalent of multistage liquid-liquid contacting within a single unit. Some machines are designed to handle feeds containing solids such as whole fermentation broth. This section provides a brief overview with a description of several machines for illustration. More detailed descriptions of centrifuge design and performance are available from equipment vendors. For additional discussion, see Janoske and Piesche, *Chem. Eng. Technol.*, **22**(3), pp. 213–216 (1999); Leonard, Chamberlain, and Conner, *Sep. Sci. Tech.*, **32**(1–4), pp. 193–210 (1997); Blass, Chap. 14 in *Liquid-Liquid Extraction Equipment*, Godfrey and Slater, eds. (Wiley, 1994); Schügerl, *Solvent Extraction in Biotechnology* (Springer-Verlag, 1994); Ollinger and Blass, “Mass Transfer in Centrifugal Extractors,” *Chem. Eng. Technol.*, **11**, pp. 312–320 (1988); and Hafez, Chap. 15 in *Handbook of Solvent Extraction*, Lo, Baird, and Hanson, eds. (Wiley, 1983; Krieger, 1991).

Centrifugal extractors can be beneficial when the liquid density difference is small, when short contact time is needed to avoid product degradation, when feed and solvent easily emulsify, or in cases where high specific throughput is needed due to limitations in available floor space or ceiling height. Centrifugal extractors also can provide flexibility in operation in cases where feed variability is high, by allowing adjustment of feed rate and rotational speed as needed to obtain satisfactory performance. Potential disadvantages generally derive from difficulties associated with maintaining high-speed rotating machinery, relatively high purchase prices compared to those of some other types of extractors, and limitations as to the number of theoretical stages that can be achieved per machine (generally < 1 or up to 5 or 6

theoretical stages depending upon throughput and the type of machine). Another consideration for some machines with close internal clearances is the potential for plugging if any solids are present in the feed; however, as noted above, some machines are specifically designed to handle and discharge solids.

Commercial-scale centrifuges almost always are continuously fed machines, unless the scale of the operation is very low, as in some low-volume bioprocessing operations where very-high-*g* operation and long processing times are needed. A continuously fed centrifugal extractor can deliver high multiples of *g*, but at much lower residence time (given by holdup volume of the feed phase divided by volumetric feed rate) compared to a batch process. The maximum hydraulic capacity (or nominal capacity) of a continuously operated machine often is not realized in commercial applications, because the feed rate needs to be turned down in order to have sufficient residence time for good extraction and phase separation performance.

In evaluating options, it generally is not possible to accurately predict performance because of the complexity of the hydrodynamics within a centrifuge. While high-*g* operation can promote good performance, in certain cases the extremely rapid acceleration generated within the machine also can promote backmixing or emulsification. Miniplant tests using small units generally are needed, and vendors often offer testing services.

Single-Stage Centrifugal Extractors The types of centrifuges used in extraction operations are quite varied. Differences include vertical versus horizontal configuration, fluid-filled versus operation with an air core, pressurized or unpressurized operation, generation of low to extremely high multiples of gravitational acceleration (500 up to 20,000 × *g* or higher), as well as differences in the liquid holdup volume, design of internals, internal clearances, and purchase price. The simpler machines, such as the CINC separator from CINC Processing Equipment, Inc. (Fig. 15-59) and the Rousselet-Robatel model BXP, have relatively large internal clearances. An air core is maintained within the machine, and liquid layers decant over internal weirs. Flow restrictions in the overflow piping need to be minimized to avoid any pressure imbalance between light- and heavy-liquid overflow lines, since this can affect the location of the liquid-liquid interface and the liquid overflow/underflow split. These machines often are used for washing operations and other extraction applications with high *K* values requiring few theoretical stages. They often serve as the separator in a mixer-settler stage, such that solvent and

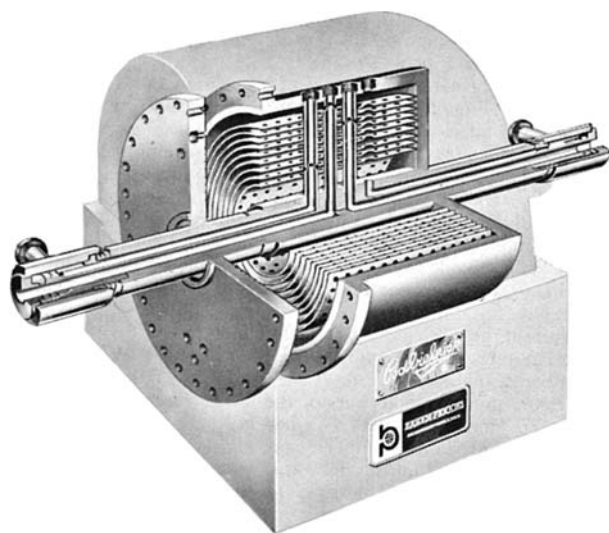


FIG. 15-60 Podbielniak centrifugal extractor. (Courtesy of Baker Perkins, Inc.)

depending upon operating conditions, with some authors claiming as many as 7 or 8 stages.

The classic machine of this type is the Podbielniak extractor available from Baker-Perkins (Fig. 15-60). The body of the extractor is a horizontal cylindrical drum containing concentric perforated cylinders. The liquids are introduced through the horizontal rotating shaft with the help of special mechanical seals; the light liquid is fed internally to the drum periphery and the heavy liquid to the axis of the drum. Rapid rotation (up to several thousand revolutions per minute, depending on size) causes radial counterflow of the liquids, which then flow out through the shaft. Materials of construction include steel, stainless steel, Hastelloy, and other corrosion-resistant alloys. The Podbielniak design provides extremely low holdup of liquid per stage, and this led to its extensive use in the extraction of antibiotics, such as penicillin and the like, for which multistage extraction and phase separation must be done rapidly to avoid chemical destruction of the product under conditions of extraction

[Podbielniak, Kaiser, and Ziegenhorn, Chap. VI in *Chemical Engineering Progress Symposium Series No. 100*, vol. 66, pp. 43-50 (1970)]. Podbielniak extractors have been used in all phases of pharmaceutical manufacturing, in petroleum processing (both solvent refining and acid treating), in extraction of uranium from ore leach liquors, and for clarification and phase separation work. Jacobsen and Beyer [*AIChE J.*, 2(3), pp. 283-289 (1956)] describe operating characteristics and the number of theoretical stages achieved for a specific application.

The Quadronics (Liquid Dynamics) extractor is a horizontally rotated device, a variant of the Podbielniak extractor, in which either fixed or adjustable orifices may be inserted radially as a package. These permit control of the mixing intensity as the liquids pass radially through the extractor. Flow capacities, depending on machine size, range from 0.34 to 340 m³/h (1.5 to 1500 gal/min).

The Luwesta (Centriwesta) extractor is a development from Coutour [Eisenlohr, *Ind. Chem.*, 27, p. 271 (1951)]. This centrifuge revolves about a vertical axis and contains three actual stages. It operates at 3800 rotations per minute and handles approximately 5 m³/h (1300 gal/h) total liquid flow at 12-kW power requirement. Provision is made in the machine for the accumulation of solids separated from the liquids, for periodic removal. It is used, more extensively in Europe than in the United States, for the extraction of acetic acid, pharmaceuticals, and similar products.

The de Laval extractor contains a number of perforated cylinders revolving about a vertical shaft [Palmqvist and Beskow, U.S. Patent 3,108,953 (1959)]. The liquids follow a spiral path about 25 m (82 ft) long, in countercurrent fashion radially, and mix when passing through the perforations. There are no published performance data.

The Rousselet-Robatel LX multistage centrifugal extractor is designed with up to 7 internal mixing/separation stages. Each stage consists of a mixing chamber where the two phases are mixed by means of a stationary agitation disk mounted on a central drum. The high relative speed between the stationary disk and the rotating walls of the mixing chamber creates a liquid-liquid dispersion with high interfacial area to facilitate rapid mass transfer. The agitation disk and the mixing chamber's inlet and outlet channels form a pump which draws the two phases from the adjacent stages and transfers the dispersion to a settling chamber, where it is separated by centrifugal force. The manufacturer claims that high stage efficiencies can be achieved. Extract and raffinate phases are removed from the machine by gravity discharge, or an internal centripetal pump can be employed to discharge these streams under pressure. Nominal flow rates range from 25 L/h up to 80 m³/h.

PROCESS CONTROL CONSIDERATIONS

GENERAL REFERENCES: Wilkinson and Ingham, Chap. 27.2, and S. Plonsky, Chap. 27.3, in *Handbook of Solvent Extraction*, Lo, Baird, and Hanson, eds. (Wiley, 1983; Krieger, 1991).

STEADY-STATE PROCESS CONTROL

Control of a continuous liquid-liquid extraction process generally refers to maintaining satisfactory dispersion of one phase in another for good mass-transfer performance while also maintaining the required production rate. This must be done without entering a flooding condition. It is common practice to set up a continuously fed extractor to handle a range of feed rates while maintaining other operating variables at constant preset values. These include the solvent flow rate, temperatures, and mechanical variables (if agitation or centrifugation is employed). For extraction processes that experience large swings in feed flow rate, the solvent flow rate may be manipulated to maintain a constant solvent-to-feed ratio, in order to reduce the volume of extract that needs to be processed. In this case, the extractor must be able to operate within a fairly wide range of volumetric throughput.

A common cause of upsets in operation is contamination of the feed by trace amounts of impurities that affect interfacial tension, so it is

important to control upstream operations to avoid contamination. Upsets or deviations from desired performance also can be caused by changes in the purity of solvent entering from solvent recovery equipment, so adequate control of closely coupled auxiliary operations is needed to ensure good extractor performance. Periodic monitoring of the interfacial tension of light and heavy phases at the feed location (where interfacial tension is likely to be lowest due to higher solute concentration) may be useful for understanding the range of values that can be tolerated, and trends in the data may provide warning of an impending flooding or coalescence problem.

Steady-state control of a continuously fed extraction column requires maintenance of the location of the liquid-liquid interface at one end of the column. The main interface will appear at the top of the column when the light phase is dispersed and at the bottom of the column when the heavy phase is dispersed. If needed, extraction columns can be designed with an expanded-diameter settling zone to facilitate liquid-liquid phase separation by reducing liquid velocities. If sufficient clarification of the phases cannot be achieved, then it may be necessary to add an external device such as a gravity decanter or centrifuge. (See "Liquid-Liquid Phase Separation Equipment.") Sometimes a column is built with expanded ends at

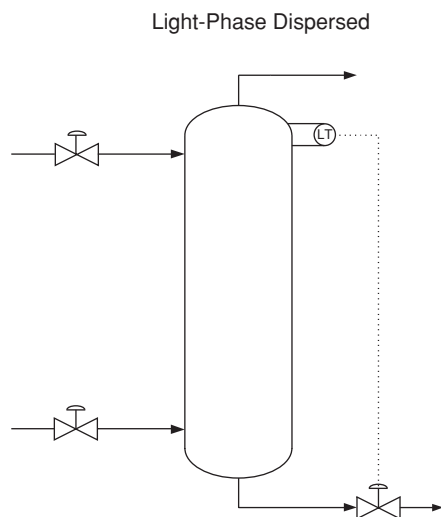


FIG. 15-61 Typical interface control for a light-phase dispersed process (with the main interface located at the top of the column). The same basic arrangement can be used for the heavy-phase dispersed case, but the level transmitter would be located differently to reflect the location of the main interface at the bottom of the column.

both top and bottom to allow the option of operating with either phase dispersed.

The position of the main operating interface in an extraction column, whether located at the top or the bottom, generally is controlled by adjusting the outlet flow of the heavy phase; the heavy-phase outlet valve opens to lower the interface and closes to raise the interface, and the light phase is allowed to overflow the top of the column. The location of the interface often can be maintained at a set position by measuring the differential pressure (if density difference is sufficiently large) or the capacitance of the liquid across the settling zone (for aqueous/organic systems) and manipulating the control valve in the bottom outlet stream to control a set point. Another technique uses a float that rests at the position of the interface. The general concept is illustrated in Fig. 15-61. Weinstein, Semiat, and Lewin [*Chem. Eng. Sci.*, **53**(2), pp. 325–339 (1998)] studied the light-phase dispersed case (with the main interface maintained at the top of the column) and recommend controlling the main interface level by manipulating the continuous-phase feed flow rate instead of the continuous-phase outlet flow rate. The authors developed a dynamic model of the hydrodynamics and mass transfer in a countercurrent liquid-liquid extraction column, and the simulation results indicate faster dynamic response using their alternative scheme.

When a continuous extraction column begins to flood, often one of the first indications is the appearance of an interface at the wrong end of the column; so adding instrumentation that can detect such an interface (such as one or more conductivity probes when phase inversion involves formation of a continuous aqueous phase) may help identify a flooding condition in time to take corrective action. Sometimes a rag layer will accumulate at the liquid-liquid interface, and it is necessary to provide a means for periodically draining the rag to avoid entrainment into the extract or raffinate. It may be useful to add instrumentation that can detect the rag at high positions to warn an operator before breakthrough occurs; however, often the approach taken is to drain the interface region on a predetermined schedule. Installing sensors to detect a rag layer can be problematic because they are easily fouled.

For a continuous extraction column, it is important to control the holdup of each phase within the column to obtain high interfacial area for good mass transfer. For nonagitated extraction columns, this is set by proper design of the internals and maintaining flow rates during operation within a fairly narrow range of values needed for good performance. Agitated columns allow greater flexibility in this regard,

because agitation intensity can be adjusted in the plant to maintain good performance over a wider range of flow rates and as the properties of the feed change. In industrial practice, agitation intensity normally is set at a constant rate or manually adjusted at infrequent intervals in response to a significant change in feed characteristics. Model-based control schemes offer potential for automatic adjustment of agitation intensity and other variables for faster response [Mjalli, *Chem. Eng. Sci.*, **60**(1), pp. 239–253 (2005); and Mjalli, Abdel-Jabbar, and Fletcher, *Chem. Eng. Processing*, **44**, pp. 531–542 and 543–555 (2005)]. Careful programming will be needed to avoid inappropriate control actions when sensors are out of calibration. Real-time measurement of dispersed-phase holdup also may be helpful; Chen et al. [*Ind. Eng. Chem. Res.*, **41**(7), pp. 1868–1872 (2002)] report a method for a pulsed-liquid column. They studied a system consisting of 30% trialkyl(C_{6-s}) phosphine oxide in kerosene + nitric acid solution, with the acid phase dispersed.

For some extraction operations, particularly fractional extractions, it may be useful to control a temperature profile across the process. In extraction columns, this is normally done by controlling the temperature of entering feed and solvent streams. Heating jackets generally are not effective because of insufficient heat-transfer area. Internal heating or cooling coils are problematic because they are difficult and expensive to install and can interfere with other column internals and liquid-liquid traffic within the column. For fractional extraction, the stripping and washing operations may be carried out in separate equipment with external heating or cooling of the streams entering the equipment.

For startup of column extractors, it generally is best to start from dilute-solute conditions to avoid unstable operation. For example, when starting a column in which the feed is the continuous phase, first fill the column with solute-lean feed liquid before starting the flow of solvent and actual feed. This way, the solvent quickly becomes dispersed and mass transfer approaches steady state from dilute conditions, promoting faster and more stable startup.

SIEVE TRAY COLUMN INTERFACE CONTROL

Control of the main liquid-liquid interface for a sieve tray column can be counterintuitive because of complexity caused by the presence of multiple interfaces within the column. For example, if the interface level is too high, the usual control response is to allow the heavy phase to flow out the bottom of the column for a time until the desired level is reached (using the scheme outlined in Fig. 15-61). Ideally, this should lower the interface level, as shown in Fig. 15-62a. This is a typical response for most differential contactors such as packed or spray columns. However, for the sieve tray column the initial response can actually be a rise in the interface level for a short time, as shown in Fig. 15-62b. In some cases, this can result in entrainment of heavy phase out the top of the tower.

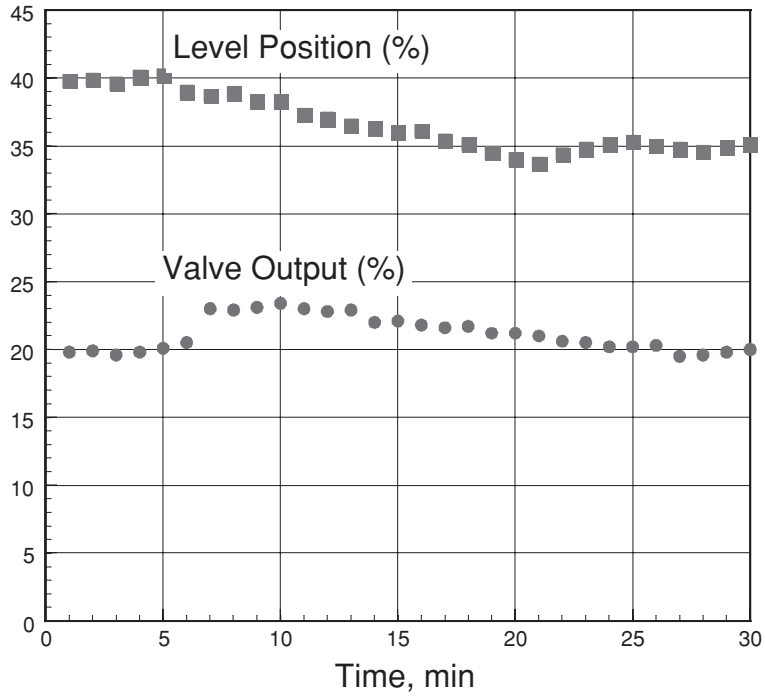
The inverse response is caused by changes in the coalesced layer heights at each tray. Neglecting any correction for dispersed-phase holdup, the height of the coalesced layer is affected by the pressure drop through the sieve holes and downcomer:

$$h = \frac{\Delta P_o + \Delta P_{dow}}{\Delta \rho g} = \frac{C_1 V_o^2 + C_2 V_{dow}^2}{\Delta \rho g} \quad (15-183)$$

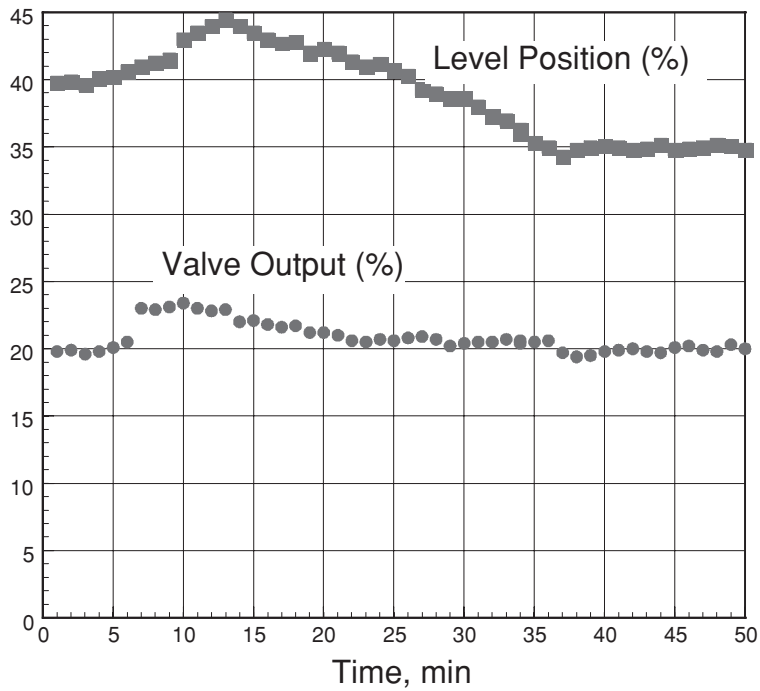
where h is the coalesced layer height, ΔP_o is the pressure drop through perforations, ΔP_{dow} is the pressure drop through the downcomer, V_o is the average velocity through a perforation (orifice), V_{dow} is the average velocity through the downcomer, and C_1 and C_2 are constants related to tray geometry and physical properties. Tray designs often vary as to which contribution, orifice or downcomer pressure drop, controls the height of the coalesced layer. The inverse response can cause significant control problems if the downcomer pressure drop is much greater than the orifice pressure drop, and this issue should be addressed during design.

CONTROLLED-CYCLING MODE OF OPERATION

Extraction columns usually are operated in a steady-state continuous-flow mode of operation with one liquid dispersed in the other. Mass transfer is then promoted by using various fixed or moving elements (various types of packings, trays, or agitators). These elements are



(a)



(b)

FIG. 15-62 Dynamic response to a change in heavy-phase flow rate. (a) Normal dynamic response to increasing outlet heavy-phase flow (packing). (b) Dynamic response to increasing outlet heavy-phase flow rate (sieve trays).

designed to strike a balance between throughput capacity and mass-transfer efficiency. An alternative mode of operation is the controlled-cycling mode in which light and heavy phases are alternately dispersed and coalesced. Flow is stopped periodically so the phases can switch roles (dispersed versus continuous phase) for the next portion of the cycle. While these coalescing periods reduce the net throughput, the overall mass-transfer effectiveness can be enhanced.

The concept of controlled cycling of phase contactors in general was introduced in the early 1950s by Cannon [*Oil Gas J.*, **51**(12), p. 268 (1952); *Oil Gas J.*, **55**(38), p. 68 (1956); and *Ind. Eng. Chem.*, **53**(8), p. 629 (1961)]. When applied to extraction, it normally involves the use of perforated tray columns, where both phases can flow through the same openings. Since only one phase flows at a time, downcomers are not necessary, and dual-flow trays generally are used. A cycle is completed by the following sequence of events: (1) A light-phase flow period, during which the heavy phase does not flow; (2) a coalescing period, during which neither phase flows; (3) a heavy-phase flow period, during which the light phase does not flow; and (4) a repeat of the coalescing period. The net result can be an increase in overall stage efficiency, roughly doubling the number of theoretical stages the column can achieve, provided the total holdup of each phase is dis-

placed during each cycle. Robinson and Engel [*Ind. Eng. Chem.*, **59**(3), pp. 22–29 (1967)] provide a theoretical analysis for describing the advantages of controlled cycling, and Lövlund [*Ind. Eng. Chem. Proc. Des. Dev.*, **7**(1), pp. 65–67 (1968)] discussed a graphical method for determining the number of theoretical stages.

Belter and Speaker [*Ind. Eng. Chem. Proc. Des. Dev.*, **6**(1), pp. 36–42 (1967)] reported studies using a 6-in-diameter column and the system cyclohexane + ethyl acetate + ethanol + water, a low-interfacial-tension system (1.2 dyn/cm, equal to 1.2×10^{-3} N/m). Excellent stage efficiencies were reported in the range of 50 to 75 percent. Darsi and Feick [*Can. J. Chem. Eng.*, **49**(2), p. 95 (1971)] determined the effects of hole size, direction of solute transfer, and throughput using a 4-in-diameter extractor and a MIBK + acetic acid + water test mixture. They reported that smaller holes and transfer from the organic phase enhanced mass transfer. Stage efficiencies ranged up to 50 percent. Seibert, Humphrey, and Fair [*Solvent Extraction and Ion Exchange*, **4**(5), p. 1049 (1986)] observed that the volume of phase transferred within a cycle should be less than the total holdup volume per stage to minimize backmixing. They also showed that the capacity of a controlled cyclic extractor, while lower than that of a conventional sieve tray extractor, could be higher than that of a pulsed sieve tray extractor.

LIQUID-LIQUID PHASE SEPARATION EQUIPMENT

GENERAL REFERENCES: Sinnott, Coulson and Richardson's *Chemical Engineering*, vol. 6, 4th ed. (Butterworth-Heinemann, 2005); Mueller et al., "Liquid-Liquid Extraction," in *Ullmann's Encyclopedia of Industrial Chemistry*, 6th ed. (VCH, 2002); Hooper, Sec. 1.11 in *Handbook of Separation Techniques for Chemical Engineers*, 3d ed., Schweitzer, ed. (McGraw-Hill, 1997); Hartland and Jeelani, Chap. 13 in *Liquid-Liquid Extraction Equipment*, Godfrey and Slater, eds. (Wiley, 1994); Monnery and Srceek, *Chem. Eng. Prog.*, **90**(9), pp. 29–40 (1994); and Jacobs and Penney, Chap. 3 in *Handbook of Separation Process Technology*, Rousseau, ed. (Wiley, 1987).

OVERALL PROCESS CONSIDERATIONS

The ability to separate a mixture of two liquid phases is critical to the successful operation of many chemical and petrochemical processes. Besides its obvious importance to liquid-liquid extraction and washing operations, liquid-liquid phase separation can be a critical factor in other operations including two-liquid-phase reaction, azeotropic distillation, and industrial wastewater treatment. Sometimes the required phase separation can be accomplished within the main process equipment, such as in using an extraction column or a batchwise, stirred-tank reactor; but in many cases a stand-alone separator is used. These include many types of gravity decanters, filter-type coalescers, coalescers filled with granular media, centrifuges, and hydrocyclones.

The path that a liquid-liquid mixture takes through a chemical process on its way to the separator often has a dramatic impact on separation difficulty once the mixture arrives. For this reason, the first steps toward designing a decanter or other type of liquid-liquid phase separator should include a study of the overall process flow sheet to determine whether changes in upstream processing conditions can make for an easier and more robust separation. For example, if the main stream entering the separator is produced by mixing a number of smaller streams, look for opportunities to remove fine solids that contaminate the main stream by filtering solids from one or more small streams before they enter the larger stream. Also, standard centrifugal pumps are notorious for producing stable dispersions. If this type of pump is used, determine whether the turbulence caused by the pump is contributing to phase separation difficulty; and if so, consider using gravity flow (if possible) or replacing a high-shear pump and piping system with a lower-shear design. If a dispersion proves to be particularly difficult to separate, it may be due to the presence of some contaminant acting as a surfactant. Contaminants may be oxidation products produced in trace amounts owing to leakage of air into

the process, or they may be the products of corrosion of upstream equipment. They also may be materials that are intentionally added upstream to solve a problem there, such as cleaning agents and antifouling agents, but their presence, even in very small concentration, may cause unintended phase separation difficulties downstream.

FEED CHARACTERISTICS

Traditionally, the guidelines for selection and design of a gravity decanter or other type of separator focus on the size of dispersed drops. However, drop diameter often cannot be accurately predicted during the design of a new process, especially the size of the smaller drops in the distribution of drop sizes, and often this information is not available for an existing process because of sampling difficulties. Furthermore, knowledge of drop size alone is not sufficient because it says nothing about the rate of drop coalescence. In light of this, it is recommended instead to characterize the feed material in terms of the results of simple shake tests, as indicated in Table 15-24. This basic information can be very helpful in identifying an appropriate separator.

In Table 15-24, feed materials are classified into four main types according to the results of a shake test. Typical values of interfacial tension, density difference, and viscosity also are listed. The shake test can be as simple as vigorously shaking a representative feed by hand in a sealed graduated cylinder (about an inch in diameter) for 30 s or 1 min. The graduated cylinder is then placed on the bench, the time is recorded, and the progress of the separation is observed. For systems with drops that coalesce quickly, a sharp interface will quickly form between two settling liquid layers, and the rate at which drops fall or rise to the interface will determine the rate of phase separation or clarification of the layers. For many other systems, however, drops will accumulate at the interface forming a dispersion band, i.e., a layer of slowly coalescing drops, and the rate at which the drops coalesce determines the rate of phase separation. Whether a system is fast-coalescing or slow-coalescing is an important question that is easily answered by performing a simple shake test. Figure 15-63 illustrates the details of a batch settling profile. Once the dispersion band has disappeared, one or both of the phases may remain cloudy. If so, this typically indicates the presence of droplets on the order of 100 μm in diameter or smaller. For additional discussion of dispersion properties, see "Liquid-Liquid Dispersion Fundamentals."

TABLE 15-24 Shake Test Characterizations

Type	Shake test observations	Interfacial tension ^a	Density difference ^a	Viscosity of each phase ^a	Presence of fine solids or surfactants ^a
I	Dispersion band collapses within 5 min with crystal-clear liquids on top and bottom	Moderate to high, 10 dyn/cm or higher	$\Delta\rho > 0.1 \text{ g/cm}^3$	$\mu < 5 \text{ cP}$	Negligible
II	Dispersion band collapses within 10 to 20 min with clear liquids on top and bottom	Moderate, ~10 dyn/cm	$\Delta\rho > 0.1 \text{ g/cm}^3$	$\mu < 20 \text{ cP}$	Negligible
III	Dispersion band collapses within 20 min but one or more phases remain cloudy	Low to moderate, 3–10 dyn/cm	$\Delta\rho > 0.05 \text{ g/cm}^3$	$\mu < 100 \text{ cP}$	Might be present in low concentration
IVa	Stable dispersion is formed (dispersion band does not collapse within an hour or longer)—high viscosity	Low to high	$\Delta\rho > 0.1 \text{ g/cm}^3$	$\mu > 100 \text{ cP}$ in one of the phases	Negligible
IVb	Stable dispersion is formed—low interfacial tension	< 3 dyn/cm	$\Delta\rho > 0.1 \text{ g/cm}^3$	$\mu < 100 \text{ cP}$	Negligible
IVc	Stable dispersion is formed—low density difference	Low to high	$\Delta\rho < 0.05 \text{ g/cm}^3$	$\mu < 100 \text{ cP}$	Negligible
IVd	Stable dispersion is formed—stabilized by surface-active components or solids	Low	$\Delta\rho > 0.1 \text{ g/cm}^3$	$\mu < 100 \text{ cP}$	Enough surfactant/solids to keep emulsion stable

^aTypical physical properties. Behavior also depends upon the shear history of the fluid. For this test, a sample is characterized by the results of the shake test (second column), not its physical properties. Physical properties are listed only as typical values.

GRAVITY DECANTERS (SETTLERS)

Gravity decanters or settlers are simple vessels designed to allow time for two liquid phases to settle into separate layers (Fig. 15-64). Ideally, clear top and bottom layers form above and below a sharp interface or dispersion band. The top and bottom layers serve as clarifying zones. The height of the dispersion band, if present, generally remains constant during steady-state operation, although it may vary with position. The choice of where to locate the phase boundary within the vessel depends on whether more or less height is needed in the upper or lower clarification zones to obtain the desired clarity in the discharge streams. It can also depend on whether the inventory of one particular layer within the vessel should be minimized, as when handling reactive fluids such as monomers. Gravity decanters are well suited for separating type I feeds defined in Table 15-24 and, in most cases, type II feeds as well. It is common for coalescence to be the limiting factor in the separation of type II mixtures, so the design and sizing of the decanter will differ from those of the fast-coalescing systems.

Design Considerations Gravity decanters normally are specified as horizontal vessels with a length-to-diameter ratio greater than 2 (and often greater than 4) to maximize the phase boundary (cross-sectional area) between the two settled layers. This provides more effective utilization of the vessel volume compared to vertical decanters, although vertical decanters may be more practical for low-flow applications or when space requirements limit the footprint of the vessel.

The volume fraction of the minority phase is an important parameter in the operation of a decanter. Vessels handling less than 10 to 20 percent dispersed phase typically contain a wider distribution of droplet diameters with a long tail in the small size range [Barnea and Mizrahi, *Trans. Instn. Chem. Engrs.*, **53**, pp. 61–69 (1975)]. These decanters have a smaller capacity than when they contain more-concentrated dispersions. If one of the phases has a concentration lower than 20 percent in the feed mixture, it might be worthwhile to recycle the low-concentration phase to the feed point to boost the phase ratio within the separator vessel. Also, in certain cases increasing the operating temperature increases the drop coalescence rate. The result is a reduction in the dispersion band height for a given throughput, allowing an increase in the capacity of the settler. This behavior often can be attributed to a reduction in the continuous-phase viscosity.

Numerous methods are used to control the location of the interface inside the decanter. A boot or sump sometimes is included in the design to increase the path traveled by the heavy phase before exiting the vessel, to maximize the clarification zone for the light phase, or to minimize the inventory of heavy phase within the vessel. The interface can even be located inside the boot for one of these reasons. When a rag layer forms at the interface between settled layers, adding one or more nozzles in the vicinity of the interface will allow periodic draining of the rag (Fig. 15-65). Instruments such as differential pressure cells, conductance probes, or density meters are commonly used to control the location of the interface in a decanter. These instruments can be prone to fouling, and their operation can be compromised by the presence of a dispersion band or a rag layer. In that case, an alternative is to use an overflow leg or seal loop as illustrated in Figs. 15-64 and 15-65. The following expression can be used to specify the loop dimensions [Bocangel, *Chem. Eng. Magazine*, **93**(2), pp. 133–135 (1986); and Aerstn and Street, *Applied Chemical Process Design* (Plenum, 1982)]:

$$Z_2 = \frac{(h_L + Z_1 - Z_3)\rho_L}{\rho_H} + Z_3 - h_H \quad (15-184)$$

where Z_1 , Z_2 , and Z_3 are the heights shown in Fig. 15-65 and h_L and h_H are the head losses in the light- and heavy-liquid discharge piping. An overflow leg can work reasonably well, provided that the densities of the two phases and the height of the dispersion band do not change significantly in operation (as in an upset). The light phase also may be removed through a takeoff tube entering the vessel from the bottom. This design provides added flexibility by allowing adjustment of the pipe length in the field without altering the vessel itself. Care should be taken to avoid the possibility of inducing a swirling motion as liquid enters the top of the weir. Swirling motions may be avoided or minimized by adding vanes or slots at the entrance.

To allow the phases to settle and remain calm, any form of turbulence or vortexing inside the decanter should be avoided. Introduction of the feed stream into the decanter should be located close to the interface to facilitate phase separation. Turbulence can arise from the inlet liquid entering the vessel at too high a velocity, forming a jet that disturbs the liquid layers. To counter these flow patterns, the feed into the gravity settler should enter the vessel at a velocity of less than

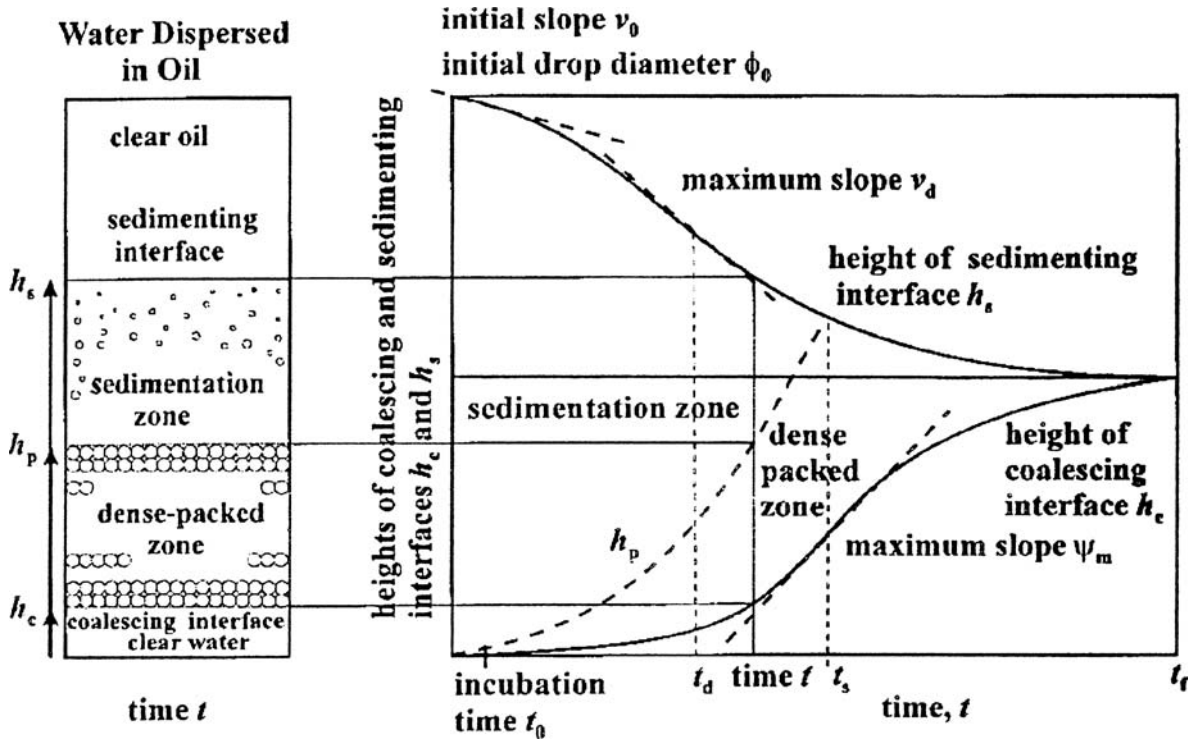


FIG. 15-63 Batch settling profile showing four regions: a top clarified phase, a sedimentation zone, a dense-packed dispersion zone, and a bottom clarified phase. [Reprinted from Jeelani, Panoussopoulos, and Hartland, *Ind. Eng. Chem. Res.*, 38(2), pp. 493-501 (1999), with permission. Copyright 1999 American Chemical Society.] Consult the original article for a detailed description.

about 1 m/s (3 ft/s) as a general rule. This can be achieved by enlarging the feed line in the last 1 to 2 m (3 to 6 ft) leading to the vessel, to slow down the feed velocity at the inlet nozzle. In addition, a quiet feed zone may be created by installing a baffle plate in front of the feed pipe or a cap at the end of the feed line, with slots machined into the side of the pipe. Some designers are now using computational fluid dynamics (CFD) methods to analyze general flow patterns as an aid to specifying decanter designs.

Vented Decanters When the liquid-liquid stream to be decanted also contains a gas or vapor, provisions for venting the decanter must be included. This often is the case when decanting overheads condensate from an azeotropic distillation tower operating under vacuum, since

some amount of air leakage is virtually unavoidable, or when decanting liquids from an extractor operating at a higher pressure. A common design used for this service when the amount of gas is low is shown in Fig. 15-66. The feed enters the vessel at a point below the liquid level, so any gas must flow up through the liquid before disengaging in the vapor head space. An alternative design is illustrated in Fig. 15-67. With this design, the feed is introduced to the top of the vessel in the vapor head-space so that gases can be freely discharged and disengaged with no back-pressure. One drawback to this approach is that the feed liquids are dropped onto the light liquid surface, and significant quantities of heavy liquid may be carried over to the light liquid draw-off nozzle owing to the resulting turbulence. To mitigate this effect, a quiescent zone may be

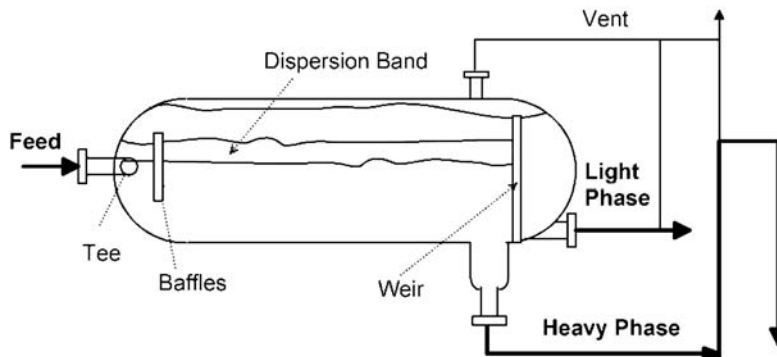


FIG. 15-64 Typical horizontal gravity decanter design.

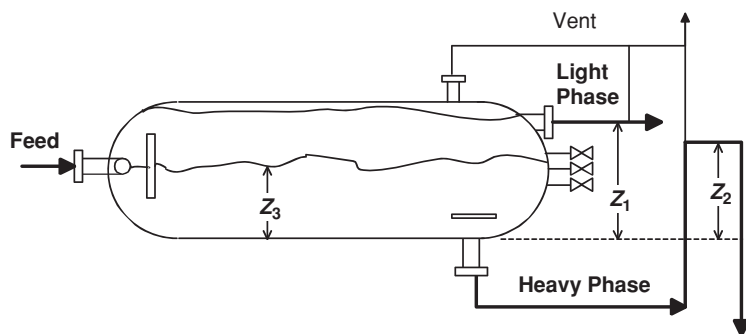


FIG. 15-65 Overflow loop for the control of the main interface in a decanter.

provided immediately below the top feed nozzle by means of a perforated baffle, as shown in Fig. 15-67. The baffle separates the disturbance caused by the entering feed from a calm separation zone where the two liquid phases can coalesce and disengage prior to draw-off.

Decanters with Coalescing Internals Adding coalescing internals may improve decanter performance by promoting the growth of drops and may reduce the size of vessel required to handle dispersions with slow coalescence (as in type II systems in Table 15-24). A wide variety of internals have been used including wire mesh, knitted wire or fibers, and flat or corrugated plates. When plates are used, the coalescer is sometimes referred to as a lamella-type coalescer. Plates typically are arranged in packets installed at a slight angle with respect to horizontal. The plates shorten the distance that drops must rise or fall to a coalescing surface and guide the flow of the resulting coalesced film [Menon, Rommel, and Blass, *Chem. Eng. Sci.*, **48**(1), pp. 159–168 (1993); and Menon and Blass, *Chem. Eng. Technol.*, **14**, pp. 11–19 (1991)]. Arranging the plates in packets of opposite slopes promotes flow reversal, and this may lead to more frequent drop-drop collisions [Berger, *Int. Chem. Eng.*, **29**(3), pp. 377–387 (1989)]. The Merichem Fiber-Film® contactor described earlier in “Suspended-Fiber Contactor” under “Mixer-Settler Equipment” also may be used

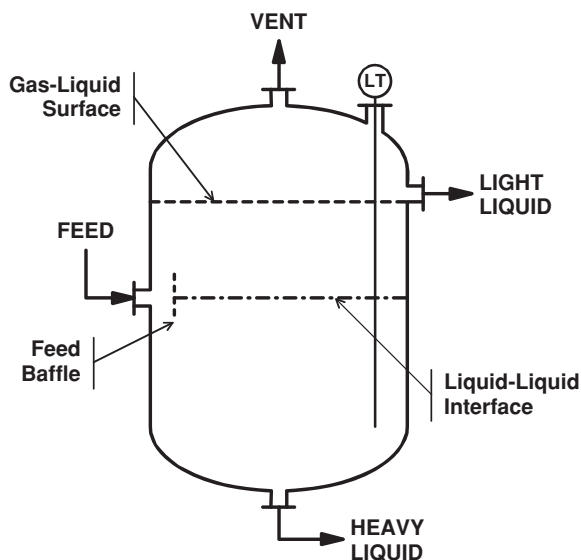


FIG. 15-66 Vertical decanter with submerged feed.

to promote growth of dispersed drops in a stream feeding a gravity decanter. In any case, the dispersed phase normally must preferentially wet the coalescence media for the media to be effective. If the feed contains solids, the potential for plugging the internals should be carefully evaluated. In certain cases, it may be necessary to allow access to the vessel internals for thorough cleaning. For more information, see Mueller et al., “Liquid-Liquid Extraction,” *Ullmann’s Encyclopedia of Industrial Chemistry*, 6th ed. (Wiley-VCH, 2002).

Sizing Methods Sizing a decanter involves quantifying the relationship between the velocity of liquid to the phase boundary between settled layers and the average height of a dispersion band formed at the boundary. For fast-coalescing systems, the height of the dispersion band is negligible. Performance is determined solely by the rate of droplet rise or fall to the interface compared with the rate of flow through the decanter. In this case, design methods based on Stokes’ law may be used to size the decanter, and residence time in the vessel becomes a key parameter. In many cases, however, coalescence is slow and the shake tests show a coalescence band that requires a fair amount of time to disappear. Then performance is determined by the volumetric flow rate of liquid to the boundary between the two settled layers, the boundary area available for coalescence, and the steady-state height of the dispersion band. For these systems, residence time is not a useful parameter for characterizing performance requirements.

Stokes’ Law Design Method This method is described by Hooper [Sec. 1.11 in *Handbook of Separation Techniques for Chemical Engineers*, 3d ed., Schweitzer, ed. (McGraw-Hill, 1997)]; and by Jacobs and Penney [Chap. 3 in *Handbook of Separation Process Technology*, Rousseau, ed. (Wiley, 1987)]. It assumes that the drop coalescence rate is rapid and relies on knowledge of drop size. The terminal settling velocity of a drop is computed by using Stokes’ law

$$u_t = \frac{gd^2\Delta\rho}{18\mu_c} \quad (15-185)$$

where d is a characteristic minimum drop diameter. (See Sec. 6 for detailed discussion of terminal settling velocity.) Note that which phase is continuous and which is dispersed can make a significant difference, since only the continuous-phase viscosity appears in Eq. (15-185). The decanter size is then specified such that

$$\frac{Q_c}{A} < u_t \quad (15-186)$$

where Q_c is the volumetric flow rate of the continuous phase and A is the cross-sectional area between the settled layers. This analysis assumes no effect of swirling or other deviation from quiescent flow, so a safety factor of 20 percent often is applied. Hooper and Jacobs indicate that designing for a Reynolds number $Re = VD_h\rho_c/\mu_c$ less than 5000 or so should provide sufficiently quiescent conditions, where V is the continuous-phase cross-flow velocity and D_h is the

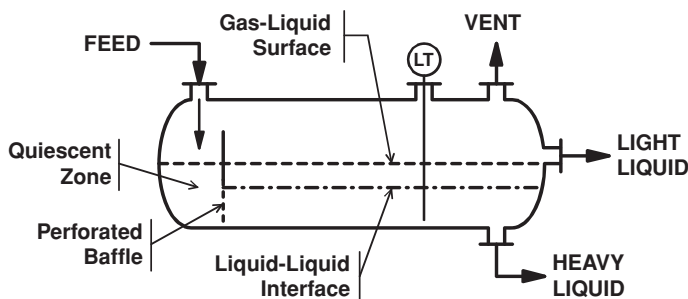


FIG. 15-67 Horizontal decanter with feed entering from the top and a baffled quiescent zone.

hydraulic diameter of the continuous-phase layer (given by 4 times the flow area divided by the perimeter of the flow channel including the interface). Decanter design methods based on Stokes' law generally assume a minimum droplet size of 150 μm , and this appears to be a reasonably conservative value for many chemical process applications. For separating secondary dispersions, it is common to assume a drop size in the range 70 to 100 μm . For more detailed discussion, see Hartland and Jeelani, Chap. 13, pp. 509–516, in *Liquid-Liquid Extraction Equipment*, Godfrey and Slater, eds. (Wiley, 1994).

The method described above neglects any reduction in settling velocity due to the presence of neighboring drops at high population density (hindered settling). For best results, experimental data showing the relationship between settling velocity and initial dispersed-phase holdup should be generated. A simplified expression that neglects any drop coalescence during settling may be suitable for approximate design purposes

$$u_i \approx u_{t\infty}(1 - \phi_0) \frac{\mu_c}{\mu_d} \quad (15-187)$$

where u_i is an average settling velocity used to specify the decanter design, $u_{t\infty}$ is the velocity of an isolated drop calculated from Eq. (15-185), and ϕ_0 is the initial holdup. For more detailed discussion, see Ishii and Zuber, *AIChE J.*, **25**, pp. 843–855 (1979); and Das, *Chem. Eng. Technol.*, **20**, pp. 475–477 (1997).

Design Methods for Systems with Slow Coalescence For slow-coalescing systems, simple Stokes' law calculations will not provide a reliable design. Instead, it is necessary to understand the height of the dispersion band as a function of throughput. Jeelani and Hartland [*AIChE J.*, **31**, pp. 711–720 (1985)] recommend correlating decanter performance by using an expression of the form

$$\frac{1}{Q/A} = \frac{1}{k_1 \Delta H} + \frac{1}{k_2} \quad (15-188)$$

where ΔH is an average steady-state dispersion band height, Q is total volumetric throughput, and k_1 and k_2 are empirical constants. The general relationship between ΔH and Q/A also may be expressed in terms of a power law equation of the form

$$\Delta H \propto \left(\frac{Q}{A}\right)^a \propto \left(\frac{Q_c}{A}\right)^a \propto \left(\frac{Q_d}{A}\right)^a \quad (15-189)$$

Equations (15-188) and (15-189) represent decanter performance for a given feed with constant properties, i.e., a constant composition and phase ratio. Note that the analysis can be done in terms of total flow Q or the flow of continuous phase Q_c or dispersed phase Q_d . Typically, the value of the exponent a is greater than 2.5 [Barnea and Mizrahi, *Trans. Inst. Chem. Eng.*, **53**, pp. 61–91 (1975); and Golob and Modic,

Trans. Inst. Chem. Eng., **55**, pp. 207–211 (1977)]. The required size of a commercial-scale decanter may be determined by operating a small miniplant decanter to obtain values for the constants in Eqs. (15-188) and (15-189), since scale-up to the larger size generally follows the same relationship as long as the phase ratio and other operating variables are maintained constant. A commercial-scale decanter normally is designed for a throughput Q/A that yields a value of ΔH no larger than 15 percent of the total decanter height. Designs specifying taller dispersion bands are avoided because a sudden change in feed rate can trigger a dramatic increase in the height of the dispersion band that quickly floods the vessel. The dynamic response of ΔH has been studied by Jeelani and Hartland [*AIChE J.*, **34**(2), pp. 335–340 (1988)].

In certain cases, batch experiments may be used to size a continuous decanter [Jeelani and Hartland, *AIChE J.*, **31**, pp. 711–720 (1985)]. In a batch experiment similar to the simple shake test described earlier, the change in the height of the dispersion band with time may follow a relationship given by

$$\frac{1}{-dh/dt} = \frac{1}{k_1 h} + \frac{1}{k_2} \quad (15-190)$$

where h is the height of the batch dispersion band varying with time t . The constants k_1 and k_2 in Eq. (15-190) are the same as those used in the steady-state equation [Eq. (15-188)], assuming the batch test conditions (phase ratio and turbulence) are the same. Jeelani and Hartland have derived a number of models for systems with different coalescence behaviors [Jeelani and Hartland, *Chem. Eng. Sci.*, **42**(8), pp. 1927–1938 (1987)]. The most appropriate coalescence model is determined in batch tests and then is used to estimate ΔH versus throughput Q/A for a continuous decanter. For additional information, see Hartland and Jeelani, Chap. 13 in *Liquid-Liquid Extraction Equipment*, Godfrey and Slater, eds. (Wiley, 1994); Nadiv and Semiat, *Ind. Eng. Chem. Res.*, **34**(7), pp. 2427–2435 (1995); Jeelani and Hartland, *Ind. Eng. Chem. Res.*, **37**(2), pp. 547–554 (1998); Jeelani, Panoussopoulos, and Hartland, *Ind. Eng. Chem. Res.*, **38**(2), pp. 493–501 (1999); and Yu and Mao, *Chem. Eng. Technol.*, **27**(4), pp. 407–413 (2004). Development of design methods for specifying continuous decanters with coalescing internals using batch test data is a current area of research [Hülswitt and Pfennig, *ISEC '05*, Beijing, China (September 2005)].

Several authors have derived correlations relating the height of the dispersion band to the density of each phase, the density difference, the viscosities, and the interfacial tension of aqueous/organic or aqueous/organic two-phase systems [Golob and Modic, *Trans. Inst. Chem. Eng.*, **55**, pp. 207–211 (1977); and Asenjo et al., *Biotech. and Bioeng.*, **79**(2), pp. 217–223 (2002)]. These correlations can provide useful estimates, but the results are generally valid only for the systems used to develop the correlations and should be used with caution. For new applications, some experimental work will be needed for reliable design.

OTHER TYPES OF SEPARATORS

Coalescers As noted earlier, adding coalescing internals to a decanter can improve decanter performance by promoting growth of small drops. The same concept can be applied in a separate coalescer vessel to treat the stream feeding the decanter. Systems of type III or type IV (Table 15-24) in particular may benefit, i.e., applications involving a need to break a secondary dispersion. Coalescers typically are packed with a granular material, a mesh made of metal wire or polymer filaments (or both), or fine fibers in woven or nonwoven composite sheets. The typical flow configuration is upflow if the light phase is dispersed and downflow if the heavy phase is dispersed. Coalescers containing fairly large media such as beds of granules or wire mesh may be able to tolerate a feed containing some fine solids. Coalescers containing fine granules or fine fibers require that the feed be free of solids to avoid plugging, so prefiltration may be necessary. For more detailed information, see Li and Gu, *Sep. and Purif. Tech.*, **42**, pp. 1–13 (2005); Shin and Chase, *AIChE J.*, **50**(2), pp. 343–350 (2004); Wines and Brown, *Chem. Eng. Magazine*, **104**(12), pp. 104–109 (1997); Hennessey et al., *Hydrocarbon Proc.*, **74**, pp. 107–124 (1995); Madia et al., *Env. Sci. Technol.*, **10**(10), pp. 1044–1046 (1976); Davies, Jeffreys, and Azfal, *Brit. Chem. Eng. Proc. Tech.*, **17**(9), pp. 709–712 (1972); and Hazlett, *Ind. Eng. Chem. Fund.*, **8**(4), pp. 625–632 (1969).

In most applications, the packing material should be wetted by the dispersed phase to some degree for best performance; however, this will depend on the size of dispersed droplets. For very fine droplets on the order of 10 μm or smaller, surface wetting is not the primary coalescence mechanism [Davies and Jeffreys, *Filtration and Separation*, pp. 349–354 (July/August 1969)]. In these cases, the packing promotes coalescence by providing a tortuous path that holds dispersed drops in close contact, facilitating drop-drop collisions. In other cases involving larger drops, a drop interception and wettability mechanism becomes important; i.e., the media provide a target for drop–solid surface collisions, and the surface becomes wetted with drops that merge together and leave the media as larger drops. In this case, an intermediate (optimum) wettability may be needed to most effectively promote the growth and dislodging of drops from the media [Shin and Chase, *AIChE J.*, **50**(2), pp. 343–350 (2004)]. In general, the degree to which flow path/collision mechanisms and/or surface wettability are important for good performance depends on the drop size distribution and dispersed-phase holdup in the feed, as well as system physical properties and whether surfactants or fine particulates are present. (See “Stability of Liquid-Liquid Dispersions” under “Liquid-Liquid Dispersion Fundamentals.”) All this affects the choice of media, media size and porosity, and coalescer dimensions as a function of throughput. For a given application, some experimental work generally will be needed to sort this out and identify an effective and reliable design.

In cases where wettability is important, various types of sand, zeolites, glass fibers, and other inorganic materials may be used to facilitate coalescence of aqueous drops dispersed in organic feeds. Carbon granules, polymer beads, or polymer fibers may be useful in coalescing organic drops dispersed in water. The packing material should resist disarming by impurities, meaning that impurities should not become adsorbed and degrade the surface wettability characteristics over time. This can happen with charged or surfactantlike impurities; Paria and Yuet [*Ind. Eng. Chem. Res.*, **45**(2), pp. 712–718 (2006)] describe the adsorption of cationic surfactants at sand-water interfaces, a phenomenon that can alter surface wettability. In a few cases, the packing needs to age in service to develop its most effective surface properties.

Madia et al. [*Env. Sci. Technol.*, **10**(10), pp. 1044–1046 (1976)] describe a chromatography method for screening potential media with regard to surface wettability. The method involves measuring the retention times of water and heptane (or other components of interest) by using columns filled with the packing materials of interest (reduced in size if needed); the longer the relative retention time, the greater is the wettability of the packing for that component. The authors used gas chromatography of water and heptane to characterize coalescence for an oil-in-water dispersion; but it should be possible to characterize other systems by using this approach, and liquid chromatography methods might be used for components with low volatility.

For granular bed coalescers, typical granule sizes include 12 \times 16 Tyler screen mesh (between 1.4 and 1 mm) and 24 \times 48 Tyler mesh (0.7 to 0.3 mm). Smaller sizes sometimes are used as well. Typical bed heights range from 8 in to 4 ft (0.2 to 1.2 m), with the taller beds used with the larger granules. Layered beds may be used. For example, the front of the coalescer may contain a thin layer of fine media with low porosity and high tortuosity characteristics to facilitate drop-drop collisions of very small droplets, followed by a layer of coarser media having the wetting characteristics needed to further grow and shed larger drops.

For fine-fiber coalescers, the coalescing media normally are arranged in the form of a filter cartridge. Wines and Brown [*Chem. Eng. Magazine*, **104**(12), pp. 104–109 (1997)] describe a coalescing mechanism in which a drop (on the order of 0.2 to 50 μm) becomes adsorbed onto a fiber and then moves along the fiber with the bulk liquid flow until colliding with another adsorbed drop at the intersection where two fibers cross. Fiber diameter and wettability are important properties as they affect porosity (tortuous path) and wettable surface area. Like a packed-bed coalescer, a filter-type coalescer may be constructed in layers: an initial prefilter zone to remove particulates and minimize fouling, a primary coalescence zone where small droplets grow to larger ones, and a secondary coalescence zone with greater porosity and having surface-wetting characteristics optimized to grow the larger drops.

Pressure drop, an important consideration in the design of any coalescer, depends upon media size and shape, bed height or filter thickness, and throughput. Methods for calculating pressure drop through packed beds and porous media are described in Sec. 6. For approximately spherical media, the pressure drop due to frictional losses, assuming incompressible media, may be estimated from

$$\frac{\Delta P}{L} = \frac{150(1-\phi)^2\mu V}{d_m^2\phi^3} + \frac{1.75\rho_c V^2}{d_m\phi^3} \quad \text{Re}_{\text{particle}} = \frac{V\rho_c d_m}{\mu} \leq 10 \quad (15-191)$$

where L is the length of the packed section, V is the superficial velocity of the total liquid flow, d_m is an equivalent spherical diameter of the media particles (given by 6 times the mean ratio of particle volume to particle surface area), and ϕ is the volume fraction of voids (flow channels) within the bed [Ergun, *Chem. Eng. Prog.*, **48**(2), pp. 89–94 (1952)]. Also see Leva, *Chem. Eng. Magazine*, **56**(5), pp. 115–117 (1949), or Leva, *Fluidization* (McGraw-Hill, 1959). The minimum value of ϕ for a tightly ordered bed of uniform spherical particles is 0.26, but of course for real media this will vary depending upon the particle size distribution and particle shape. The second term in Eq. (15-191) often is neglected at $\text{Re}_{\text{particle}} \leq 1$. For fiber media, d_m can be thought of as a characteristic fiber dimension. For discussion of pressure drop through fiber beds, see Shin and Chase, *AIChE J.*, **50**(2), pp. 343–350 (2004); and Li and Gu, *Sep. and Purif. Tech.*, **42**, pp. 1–13 (2005). In practice, pressure drop data may be correlated by using an equation of the same form as Eq. (15-191), $\Delta P/L = aV + bV^2$, where a and b are empirically determined constants. Media and equipment suppliers generally will have some experimental data showing $\Delta P/L$ versus flow rate.

Centrifuges A stacked-disk centrifuge or other type of centrifuge may be a cost-effective option for liquid-liquid phase separation whenever use of a gravity decanter/coalescer proves to be impractical because rates of drop settling or coalescence are too low. This may be the case for type III and type IV systems (Table 15-24) in particular. Factors involved in specifying a centrifuge are discussed in “Centrifugal Extractors” under “Liquid-Liquid Extraction Equipment.”

Hydrocyclones Liquid-liquid hydrocyclones, like centrifuges, utilize centrifugal force to facilitate the separation of two liquid phases [*Hydrocyclones: Analysis and Applications*, Svarovsky and Thew, eds. (Kluwer, 1992); and Bradley, *The Hydrocyclone* (Pergamon, 1965)]. Instead of using rotating internals, as in a centrifuge, a hydrocyclone

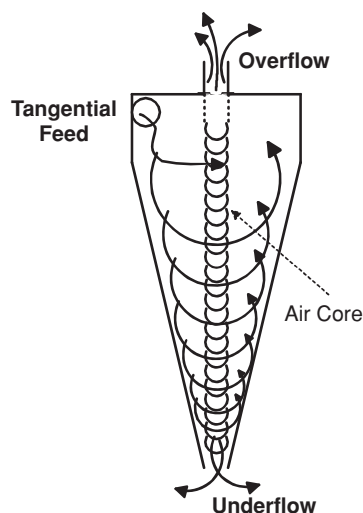


FIG. 15-68 Flow patterns in a hydrocyclone.

generates centrifugal force through fluid pressure to create rotational fluid motion (Fig. 15-68). Feed enters the hydrocyclone through a tangential-entry nozzle. A primary vortex rich in the heavy phase forms along the inner wall, and a secondary vortex rich in the light phase forms near the centerline. The underflow stream (heavy phase) exits the cyclone through the apex of the cone (underflow nozzle). The overflow stream (light phase) exits through the vortex finder, a tube extending from the cylinder roof into the interior. The feed split can be adjusted by changing the relative diameters of the vortex finder and underflow nozzle. A hydrocyclone is not completely filled with liquid; an air core exists at the centerline. A commercial-scale hydrocyclone multiplies the force of gravity by a factor of 100 to 1000 or so, depending on the diameter and operating pressure. Hydrocyclones traditionally have been used for liquid-solid separations, but by adjusting their design (cone angle and length, vortex finder length, and so on) they can be applied to liquid-liquid separations [Mozley, *Filtration and Sep.*, pp. 474–477 (Nov./Dec. 1983)].

Since the fluid flow is turbulent at the top of the unit and the rotation of liquid within the device produces a high shear field, mixtures with low interfacial tension tend to emulsify or create foam within a hydrocyclone. However, hydrocyclones may be well suited for type I or possibly type II mixtures containing some solids, especially if only a rough cut is needed. The flow pattern established within a hydrocyclone normally requires that a considerable part of the feed leave in the overflow outlet. For this reason, hydrocyclones are generally more efficient for feeds containing only a small fraction of heavy phase, although some authors indicate they can be effective for feeds with a small fraction of light phase through careful specification of hydrocyclone geometry.

The main operating variables for a hydrocyclone are the feed pressure, the feed flow rate, and the split ratio, i.e., the relative amounts of fluid exiting top and bottom. The split ratio may be adjusted by specifying the size of the underflow and overflow nozzles. Choosing a material of construction wetted by the heavy phase for the cone may improve the effectiveness of the device. Experimental work is needed to determine the efficiency of the separation as a function of the split ratio for a series of flow rates and hydrocyclone geometries [Sheng, *Sep. and Purif. Methods*, **6**(1), pp. 89–127 (1977); and Colman and Thew, *Chem. Eng. Res. Des.*, **61**(7), pp. 233–240 (1983)]. If testing indicates satisfactory performance, hydrocyclones can be relatively inexpensive and simple-to-operate units (no moving parts). Because sufficient centrifugal force cannot be generated in large-diameter units, scale-up consists of connecting multiple small units in parallel.

Units are sometimes placed in series to provide multiple stages of separation. Hydrocyclones are used on ships and drilling platforms for removing oil from water [Bednarski and Listewnik, *Filtration and Sep.*, pp. 92–97 (March/April 1988)]. Numerical simulations of hydrocyclone performance and flow profiles are described by Bai and Wang [*Chem. Eng. Technol.*, **29**(10), pp. 1161–1166 (2006)] and by Murphy et al. [*Chem. Eng. Sci.*, **62**, pp. 1619–1635 (2007)].

Ultrafiltration Membranes These are microporous membranes with pore sizes in the range of 0.1 and 0.001 μm [Porter, “Ultrafiltration,” in *Handbook of Industrial Membrane Technology* (Noyes, 1990)]. In this size range, the pores may be used to “filter out” and concentrate micelles from a liquid feed without disrupting (breaking) the micellar structure. Such a membrane may also be used to remove micrometer size droplets from a dilute dispersion. However, if the dispersed-phase content is too high, the membrane may become fouled owing to deposition of a coalesced layer that obstructs the pores. This can be a particular problem when removing oil droplets for an oil-in-water dispersion using a polymeric membrane.

The feed solution is fed to the membrane module under pressure (normally less than 6 bar). The majority of the continuous phase flows through the pores of the membranes by pressure difference and collects on the permeate side as a clarified solution. The micelles or microdroplets are rejected and flow with the remaining continuous phase, tangentially along the membrane surface, to the retentate outlet of the membrane module [Voges, Wu, and Dalan, *Chem. Processing*, pp. 40–43 (April 2001)]. The shear at the surface of the membrane should be high enough to stop the micelles from aggregating on the polymeric surface of the membrane, but low enough to avoid breaking the colloidal particles.

Ultrafiltration membranes can be very efficient at removing colloidal particles of an emulsion but normally will not stop dissolved oil from permeating. Since most membranes are polymeric, they are more stable in the presence of water, so they are best suited for aqueous systems. Since they produce only one well-clarified phase (the permeate), they should be applied to processes with stable micelles where clear continuous phase is required and where losses of continuous phase with the micellar phase can be tolerated. The use of ultrafiltration membranes in an extractive ultrafiltration process for recovery of carboxylic acids is discussed by Rodríguez et al. [*J. Membrane Sci.*, **274**(1–2), pp. 209–218 (2006)].

Selecting the membrane best suited for a given application is best accomplished experimentally. The membrane material must be compatible with the feed, and the module should exhibit high permeation flow while maintaining good micelle rejection. The pore size and the molecular weight cutoff reported by the manufacturer are good indications of membrane performance; but since other factors such as membrane/solute interaction and fouling impact the separation, this information is only a starting point. Key operating parameters include temperature, feed flow rate, and permeate-to-feed ratio. Scale-up consists of adding membrane modules to handle the required production rate [Eykamp and Steen, Chap. 18 in *Handbook of Separation Process Technology*, Rousseau, ed. (Wiley, 1987)].

Electrotreaters In an electrostatic coalescer, an electric field is applied to a dispersion to induce dipoles or net charges on the suspended drops. The drops are then attracted to one another, facilitating their coalescence [Waterman, *Chem. Eng. Prog.*, **61**(10), pp. 51–57 (1965); and Yamaguchi, Chap. 16 in *Liquid-Liquid Extraction Equipment*, Godfrey and Slater, eds. (Wiley, 1994)]. This technology is applicable only to a nonconductive continuous phase and an aqueous dispersed phase. Once the water drops are sufficiently large, they settle to the bottom of the vessel while the clarified oil phase migrates to the top. The top and bottom zones are kept quiet and out of the electric field. In cases where inlet salt content is high, a multistage, countercurrent desalting system can be used. Units with ac or dc voltage are available.

Electrostatic separators are high-voltage electrostatic devices that can arc under certain conditions. For this reason, a careful review of safety considerations is needed, especially for applications involving flammable liquids. Evaluating feasibility and generating design data normally involve close consultation with the equipment vendors. This technology is applied on a very large scale in the petroleum industry for crude oil desalting.

EMERGING DEVELOPMENTS

MEMBRANE-BASED PROCESSES

Polymer Membranes Extraction processes employing polymer membranes are sometimes referred to as nondispersive or pertraction operations. The use of membranes in extraction offers a number of potential advantages including (1) constant well-defined mass-transfer area; (2) the ability to operate at very low solvent-to-feed ratios independent of other operating variables; (3) very low holdup of solvent and product within the extractor, thus providing low residence time similar to a centrifugal extractor; (4) dispersion-free liquid-liquid contacting that eliminates the need for liquid-liquid interface control and phase separation; (5) no requirement for a difference in density between liquid phases; and (6) linear scale-up by addition of extra modules, so performance at large scale can be determined directly from small-scale tests using a single module. This last point suggests, however, that the economy of scale may not be as large as it is for extractors that are scaled up as a single larger unit.

The most important advantages that membranes can offer to the process designer are those that overcome an inherent limitation of another type of extractor, as in the ability to handle liquids with close or even equal densities and the ability to operate at extremely low solvent-to-feed ratios. Thus, the types of applications where membranes are likely to be most attractive include applications with close densities and/or a K value greater than 50 or so. In principle, $K > 50$ would allow operation using a solvent-to-feed ratio of 1 : 25 or less (for an extraction factor of 2), something that can be difficult to accomplish by using conventional extractors. To take full advantage, the feed would have to be sufficiently dilute that the loading capacity of the solvent is not exceeded. The primary disadvantages of membrane-based extractors are the added mass-transfer resistance across the membrane, limited fiber-side or tube-side throughput, and concerns about fouling and limited membrane life in industrial service. Applications are limited to feeds that are free of solid particles (or can be cost effectively prefiltered); otherwise, the membranes are easily fouled. The useful life of a membrane module also is a critical factor since the frequency with which membrane modules must be replaced has a dramatic impact on overall cost.

The use of nonporous polymer membranes for liquid-liquid extraction suffers from very slow permeation of solute through the membrane, although this approach has been developed for a special case

involving reaction-enhanced extraction of an aromatic acid from wastewater through a nonporous silicone membrane into a caustic solution [Ferreira et al., *Desalination*, **148**(1-3), pp. 267-273 (2002)]. For most liquid-liquid extraction applications, however, a porous membrane is used and extraction involves transfer through a liquid-liquid meniscus maintained within the pores. One of the most promising contactors for this type of extraction is the microporous hollow-fiber (MHF) contactor (Fig. 15-69). The MHF contactor resembles a shell-and-tube heat exchanger in which the tube walls are porous and are capable of immobilizing a liquid-liquid interface within the pores. For a hydrophobic polymeric membrane, the aqueous phase normally is fed to the interior of the fiber (the fiber-bore side), while the organic phase is fed to the shell side. In this configuration, the aqueous fluid is maintained at a higher pressure relative to the organic phase, to immobilize the liquid-liquid interface within each pore. Care must be taken to avoid too high an aqueous pressure, or else breakthrough of the aqueous phase can occur. This breakthrough pressure is a function of the interfacial tension and pore size. Earlier versions of MHF contactors provided a parallel-flow design, but this design suffered from shell-side bypassing [Seibert et al., *Sep. Sci. Technol.*, **28**(1-3), p. 343 (1993)]. An improved design that incorporates a central baffle and uniform fiber spacing is currently available (Fig. 15-69). The dimensions are listed in Table 15-25.

In the baffled design, the shell-side fluid is fed through a central perforated distributor. It flows radially through the fiber bundle, around a baffle located in the middle of the module, and leaves the module through the central distributor. As in conventional extraction, the mass transfer of solute occurs across a liquid-liquid interface. However, unlike in conventional extraction, the interface is maintained at micrometer-size pores, and three mass-transfer resistances are present: tube-side (k_t), shell-side (k_s), and pore or membrane-side (k_m). The overall mass-transfer coefficient based on the tube-side liquid k_{ot} is given by

$$\frac{1}{k_{ot}} = \frac{1}{k_t} + \frac{m^{vol}}{k_s} + \frac{1}{k_m} \quad (15-192)$$

where m^{vol} is the local slope of the equilibrium line for the solute of interest, with the equilibrium concentration of solute in the tube-side

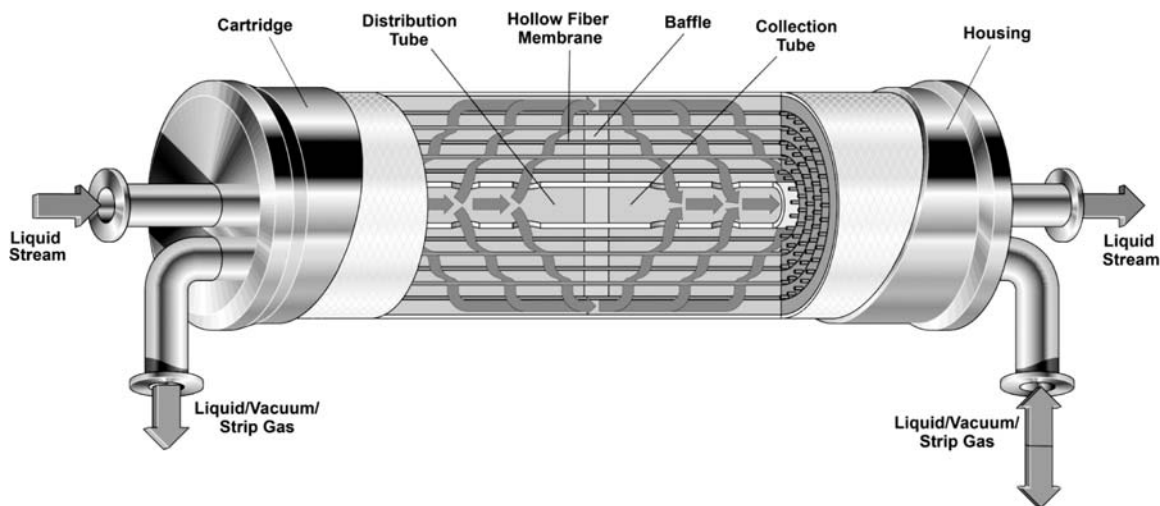


FIG. 15-69 Schematic of the Liqui-Cel Membrane Contactor. (Courtesy of Membrana-Charlotte. Liqui-Cel is a registered trademark of Membrana-Charlotte, a division of Celgard, LLC.)

TABLE 15-25 Baffled MHF Contactor Geometric Characteristics

Baffles per module	1
Module diameter, cm	9.8
Module length, cm	71
Effective fiber length, cm	63.5
Fiber outside diameter, μm	300
Fiber inside diameter, μm	240
Porosity of fiber	0.3
Number of fibers per module	30,000
Contact area per module, cm^2	81,830
Interfacial area, cm^2/cm^3	27
Tortuosity	2.6

Reprinted from Seibert and Fair, *Sep. Sci. Technol.*, **32**(1-4), pp. 573-583 (1997), with permission. Copyright 1997 Taylor & Francis.

liquid plotted on the y axis and the equilibrium concentration of solute in the shell-side liquid plotted on the x axis. Equation (15-192) assumes the tube-side fluid wets the pores.

The mass-transfer efficiencies of various MHF contactors have been studied by many researchers. Dahuron and Cussler [*AIChE J.*, **34**(1), pp. 130-136 (1988)] developed a membrane mass-transfer coefficient model (k_m); Yang and Cussler [*AIChE J.*, **32**(11), pp. 1910-1916 (1986)] developed a shell-side mass-transfer coefficient model (k_s) for flow directed radially into the fibers; and Prasad and Sirkar [*AIChE J.*, **34**(2), pp. 177-188 (1988)] developed a tube-side mass-transfer coefficient model (k_t). Additional studies have been published by Prasad and Sirkar ["Membrane-Based Solvent Extraction," in *Membrane Handbook*, Ho and Sirkar, eds. (Chapman & Hall, 1992)]; by Reed, Semmens, and Cussler ["Membrane Contactors," *Membrane Separations Technology: Principles and Applications*, Noble and Stern, eds. (Elsevier, 1995)]; by Qin and Cabral [*AIChE J.*, **43**(8), pp. 1975-1988 (1997)]; by Baudot, Floury, and Smorenburg [*AIChE J.*, **47**(8), pp. 1780-1793 (2001)]; by González-Muñoz et al. [*J. Membrane Sci.*, **213**(1-2), pp. 181-193 (2003) and *J. Membrane Sci.*, **255**(1-2), pp. 133-140 (2005)]; by Saikia, Dutta, and Dass [*J. Membrane Sci.*, **225**(1-2), pp. 1-13 (2003)]; by Bocquet et al. [*AIChE J.*, **51**(4), pp. 1067-1079 (2005)]; and by Schlosser, Kertesz, and Martak [*Sep. Purif. Technol.*, **41**, p. 237 (2005)]. A review of mass-transfer correlations for hollow-fiber membrane modules is given by Liang and Long [*Ind. Eng. Chem. Res.*, **44**(20), pp. 7835-7843 (2005)]. Eksangri, Habaki, and Kawasaki [*Sep. Purif. Technol.*, **46**, pp. 63-71 (2005)] discuss the effect of hydrophobic versus hydrophilic membranes for a specific application involving transfer of solute from an aqueous feed to an organic solvent. Karabelas and Asimakopoulou [*J. Membrane Sci.*, **272**(1-2), pp. 78-92 (2006)] discuss process and equipment design considerations.

In general, researchers have treated MHF contactors as differential contacting devices. However, Seibert and Fair [*Sep. Sci. Technol.*, **32**(1-4), pp. 573-583 (1997)] and Seibert et al. [*ISEC '96 Proc.*, **2**, p. 1137 (1996)] suggest that the baffled MHF contactor can be treated as a staged countercurrent contactor. Their recommendations are based on studies using a commercial-scale skid-mounted extraction system. Their semi-work-scale study demonstrated the performance advantages of the MHF contactor relative to a column filled with structured packing for a system with a high partition ratio. Seibert et al. [*ISEC '96 Proc.*, **2**, p. 1137 (1996)] also provide limited economic data for the extraction of *n*-hexanol from water by using *n*-octanol. Also see the discussion by Yeh [*J. Membrane Sci.*, **269**(1-2), pp. 133-141 (2006)] regarding the use of internal reflux in a cross-flow membrane configuration to boost liquid velocities for enhanced performance.

Liquid Membranes Emulsion liquid-membrane (ELM) extraction involves intentional formation of an emulsion between two immiscible liquid phases followed by suspension of the emulsion in a third liquid that forms an outer continuous phase. The encapsulated liquid and the continuous phase are miscible. The liquid-membrane phase is immiscible with the other phases and normally must be stabi-

lized by using surfactants. If the continuous phase is aqueous, the suspended phase is a water-in-oil emulsion. If the continuous phase is organic, the emulsion is the oil-in-water type. This technology differs from traditional liquid-liquid extraction processes in that it allows transfer of solute between miscible liquids by introducing an immiscible liquid membrane between them. A typical process involves first forming a stable emulsion and contacting it with the continuous phase to transfer solute between the encapsulated phase and the continuous phase, followed by steps for separating the emulsion and continuous phases and breaking the emulsion. The emulsion must be sufficiently stable to remain intact during processing, but not so stable that it cannot be broken after processing, and this may present a challenge for commercial implementation. The technology is described by Frankendorf and Li [Chap. 19 in *Handbook of Separation Process Technology*, Rousseau, ed. (Wiley, 1987)].

Potential applications of ELM extraction include separation of aromatic and aliphatic hydrocarbons [Chakraborty and Bart, *Chem. Eng. Technol.*, **28**(12), pp. 1518-1524 (2005)], separation and concentration of amino acids [Thien, Hatton, and Wang, *Biotech. and Bioeng.*, **32**(5), pp. 604-615 (1988)], and recovery of penicillin G from fermentation broth [Lee, Lee, and Lee, *J. Chem. Technol. Biotechnol.*, **59**(4), pp. 365-370, 371-376 (1994)]; Lee et al. [*J. Membrane Sci.*, **124**, pp. 43-51 (1997)]; and Lee and Yeo, *J. Ind. Eng. Chem.*, **8**(2), p. 114 (2002)]. The latter application involves transfer of the penicillin G solute ($\text{p}K_a = 2.7$) from the continuous phase (consisting of a filtered broth adjusted to a pH of about 3) into the membrane phase (typically *n*-lauryltrialkylmethyl amine extractant dissolved in kerosene) and then into the interior aqueous phase (clean water at a pH of about 8). Lee et al. [*J. Membrane Sci.*, **124**, pp. 43-51 (1997)] show that the operation can be carried out in a continuous countercurrent extraction column. The product is later obtained by separating the emulsion droplets from the continuous phase by using filtration, and this is followed by breaking the emulsion and isolating the interior aqueous phase from the amine extractant phase. A polyamine surfactant is used to stabilize the emulsion during extraction.

Supported liquid-membrane (SLM) processes involve introduction of a microporous solid membrane to serve as a support for the liquid-membrane phase. The microporous membrane provides well-defined interfacial area and eliminates the need for a surfactant. As in the penicillin ELM application described above, SLM applications often employ an extractant solution as the liquid-membrane phase to enable a facilitated transport mechanism. The extractant species interacts with the desired solute at the feed side and then carries the solute across the membrane to the other side, where solute transfers into a stripping solution. Such a process, whether using a surfactant-stabilized emulsion or a supported liquid membrane, allows forward and back extraction (or stripping) in a single operation. Ho and Wang [*Ind. Eng. Chem. Res.*, **41**(3), pp. 381-388 (2002)] discuss the application of SLM technology to remove radioactive strontium, Sr-90, from contaminated waters. Other examples involve extraction of metal ions from water [Canet and Seta, *Pure Appl. Chem. (IUPAC)*, **73**(12), pp. 2039-2046 (2001)] and recovery of aromatic acids or bases from wastewater [Dastgir et al., *Ind. Eng. Chem. Res.*, **44**(20), pp. 7659-7667 (2005)]. One of the challenges encountered in using supported liquid membranes is the difficulty in controlling trans-membrane pressure drop and maintaining the liquid membrane on the support; it may become dislodged and entrained into the flowing phases. Various approaches to stabilizing the supported liquid have been proposed. These are discussed by Dastgir et al. [*Ind. Eng. Chem. Res.*, **44**(20), pp. 7659-7667 (2005)].

ELECTRICALLY ENHANCED EXTRACTION

An electric field may be used to enhance the performance of an aqueous-organic liquid-liquid contactor, by promoting either drop breakup or drop coalescence, depending upon the operating conditions and how the field is applied. The technology normally involves dispersing an electrically conductive phase (the aqueous phase) within a continuous nonconductive phase, applying a high-voltage electric field (either ac or dc) across the continuous phase, and taking advantage of the effect of the electric field

on the shape, size, and motion of the dispersed drops. The potential advantages of this technology include more precise control of drop size and motion for improved control of mass transfer and phase separation within an extractor. Potential disadvantages include the requirement for more complex equipment, difficulties in scaling up the technology to handle large production rates, and safety hazards involved in processing flammable liquids in high-voltage equipment.

A number of different equipment configurations and operating concepts have been proposed. Yamaguchi [Chap. 16 in *Liquid-Liquid Extraction Equipment*, Godfrey and Slater, eds. (Wiley, 1994)] classifies the proposed equipment into three general types: perforated-plate and spray columns, mixed contactors, and liquid-film contactors. For example, Yamaguchi and Kanno [*AIChE J.*, **42**(9), pp. 2683–2686 (1996)] describe an apparatus in which a dc voltage is applied between two electrodes in the presence of a nitrogen gas interface. Aqueous drops form in the presence of the electric field, and they are first attracted to the gas-liquid interface. Once the drops contact the interface, the charge on the drops is reversed, and the drops fall back to coalesce at the bottom of the vessel. Bailes and Stitt [U.S. Patent 4,747,921 (1988)] describe a rotating-impeller extraction column containing alternating zones of high voltage (to promote dispersed drop coalescence) and high-intensity mixing (to promote redispersion of drops). In this design, the electric field serves to promote drop coalescence so that dispersed drops experience alternating drop breakup and growth as they move through the agitated column. Scott and Wham [*Ind. Eng. Chem. Res.*, **28**(1), pp. 94–97 (1989)] and Scott, DePaoli, and Sisson [*Ind. Eng. Chem. Res.*, **33**(5), pp. 1237–1244 (1994)] describe a nonagitated apparatus called an emulsion-phase contactor. This device employs an electric field to induce formation of a stable emulsion or dispersion band, with clear organic and aqueous layers above and below. The aqueous phase is fed to the middle or top of the dispersion band; it flows down through the band and is removed from a clarified aqueous zone maintained at the bottom. The lighter organic phase is fed to the bottom; it moves up through the dispersion band and is removed from the top. The net result is countercurrent contacting with very high interfacial area and significantly improved mass transfer in terms of the number of transfer units achieved for a given contactor height.

Another approach involves electrostatically spraying aqueous solutions into a continuous organic phase to create dispersed drops within a spray column contactor [Weatherley et al., *J. Chem. Technol. Biotechnol.*, **48**(4), pp. 427–438 (1990)]. A high voltage is applied between electrodes, one connected to a nozzle where dispersed drops are formed and the other placed within the continuous organic phase. Petera et al. [*Chem. Eng. Sci.*, **60**, pp. 135–149 (2005)] discuss the modeling of drop size and motion within such a device. For additional discussion, see Tsouris et al. [*Ind. Eng. Chem. Res.*, **34**(4), pp. 1394–1403 (1995)], Tsouris et al. [*AIChE J.*, **40**(11), pp. 1920–1923 (1994)], Gneist and Bart [*Chem. Eng. Technol.*, **25**(2), pp. 129–133 (2002)], Gneist and Bart [*Chem. Eng. Technol.*, **25**(9), pp. 899–904 (2002)], and Elperin and Fominykh [*Chem. Eng. Technol.*, **29**(4), pp. 507–511 (2006)].

PHASE TRANSITION EXTRACTION AND TUNABLE SOLVENTS

Phase transition extraction (PTE) involves transitioning between single-liquid-phase and two-liquid-phase states to facilitate a desired separation. Ullmann, Ludmer, and Shinnar [*AIChE J.*, **41**(3), pp. 488–500 (1995)] showed that extraction of an antibiotic from fermentation broth into an organic solvent could be improved by transitioning across a UCST phase boundary using heating and cooling. The results showed much higher stage efficiency compared to a standard extraction technique without phase transition and much faster phase separation. The phase transition may be induced by a change in temperature or a change in composition through addition and/or removal of organic solvents or antisolvents [Gupta, Mauri, and Shinnar, *Ind. Eng. Chem. Res.*, **35**(7), pp. 2360–2368 (1996)]. Alizadeh and Ashtari describe a temperature-induced phase transition process for extracting silver(I) from aqueous solution using dinitrile solvents [*Sep. Purification*

Technol., **44**, pp. 79–84 (2005)]. Another process that exploits a phase transition to facilitate separation and recycle of solvent after extraction utilizes ethylene oxide-propylene oxide copolymers in aqueous two-phase extraction of proteins [Persson et al., *J. Chem. Technol. Biotechnol.*, **74**, pp. 238–243 (1999)]. After extraction, the polymer-rich extract phase is heated above its LCST to form two layers: an aqueous layer containing the majority of protein and a polymer-rich layer that can be decanted and recycled to the extraction.

Another approach utilizes pressurized CO₂ to control phase splitting and tune partition ratios in organic-water mixtures. Addition of pressurized CO₂ yields an organic phase rich in CO₂ (the gas-expanded phase) and an aqueous phase containing little CO₂. Adrian, Freitag, and Maurer [*Chem. Eng. Technol.*, **23**(10), pp. 857–860 (2000)] report data demonstrating the ability to induce phase splitting in the completely miscible 1-propanol + water system by pressurization with CO₂ at near-critical pressures above 74 bar (about 1100 psia). The authors also show that the partition ratio for transfer of methyl anthranilate from the aqueous phase to the organic phase can be varied between 1 and about 13 by adjusting pressure and temperature. Jie Lu et al. [*Ind. Eng. Chem. Res.*, **43**(7), pp. 1586–1590 (2004)] demonstrate a reduction in the lower critical solution temperature for the partially miscible THF + water system by addition of CO₂ at more moderate pressures (on the order of 10 bar, or about 145 psia). The authors show that the partition ratio for transfer of a water-soluble dye from the organic phase to the aqueous phase can be increased dramatically by increasing CO₂ pressure. For more detailed discussion of gas-expanded-liquid techniques used to facilitate various reaction and extraction processes, see Eckert et al., *J. Phys. Chem. B*, **108**(47), pp. 18108–18118 (2004).

IONIC LIQUIDS

The potential use of ionic liquids for liquid-liquid extraction is gaining considerable attention [Parkinson, *Chem. Eng. Prog.*, **100**(9), pp. 7–9 (2004)]. Ionic liquids are low-melting organic salts that form highly polar liquids at or near ambient temperature [Rogers and Seddon, *Science*, **302**, p. 792 (2003)]. The potential use of ionic liquids to extract metal ions from aqueous solution is discussed by Visser et al. [*Sep. Sci. Technol.*, **36**(5–6), pp. 785–804 (2001)] and by Nakashima et al. [*Ind. Eng. Chem. Res.*, **44**(12), pp. 4368–4372 (2005)]. In another example, phenolic impurities are extracted from an organic reaction mixture using an acidic ionic liquid such as methylimidazolium chloride [BASF promotional literature (2005)]. After extraction, the extract phase is separated by evaporation of the phenolic content, and the raffinate containing the desired product is washed with water to remove small amounts of ionic liquid that saturate that phase. Other potential applications are described in *Ionic Liquids IIIB: Fundamentals, Challenges, and Opportunities*, Rogers and Seddon, eds. (Oxford, 2005). The possibility of switching a solvent system from ionic to nonionic states also is being investigated [Jessop et al., *Nature*, **436**, p. 1102 (2005)]. The authors report that a 50/50 blend of 1-hexanol and 1,8-diazabicyclo[5.4.0]undec-7-ene (DBU) becomes ionic when CO₂ is bubbled through the solution. The CO₂ reacts to form a mixture of 1-hexylcarbonate anion and DBUH⁺ cation, a viscous ionic liquid. The reaction can be reversed by using N₂ to strip the weakly bound CO₂ from solution. This returns the solution to its less viscous, nonionic state and provides a basis for a switchable solvent system.

The challenges involved in using ionic liquids for extraction appear similar to those encountered using nonvolatile extractants dissolved in a diluent, including difficulty dealing with buildup of heavy impurities in the solvent phase over time. Additionally, solvent stability and recovery need to be very high for the process to be economical due to the high cost of makeup solvent. Potential advantages include the possibility of obtaining higher *K* values, allowing use of lower solvent-to-feed ratios, and simplification of extract and raffinate separation requirements. For example, volatile components may easily be removed from the ionic liquid by using evaporation under vacuum instead of multistage distillation; and, in certain cases, the solubility of ionic liquid in the raffinate may be very low.

SECTION 16

Adsorption and
Ion Exchange

PERRY'S CHEMICAL ENGINEERS' HANDBOOK

8TH EDITION



M. DOUGLAS LEVAN
GIORGIO CARTA

Copyright © 2008, 1997, 1984, 1973, 1963, 1950, 1941, 1934 by The McGraw-Hill Companies, Inc. All rights reserved. Manufactured in the United States of America. Except as permitted under the United States Copyright Act of 1976, no part of this publication may be reproduced or distributed in any form or by any means, or stored in a database or retrieval system, without the prior written permission of the publisher.

0-07-154223-X

The material in this eBook also appears in the print version of this title: 0-07-151139-3.

All trademarks are trademarks of their respective owners. Rather than put a trademark symbol after every occurrence of a trademarked name, we use names in an editorial fashion only, and to the benefit of the trademark owner, with no intention of infringement of the trademark. Where such designations appear in this book, they have been printed with initial caps.

McGraw-Hill eBooks are available at special quantity discounts to use as premiums and sales promotions, or for use in corporate training programs. For more information, please contact George Hoare, Special Sales, at george_hoare@mcgraw-hill.com or (212) 904-4069.

TERMS OF USE

This is a copyrighted work and The McGraw-Hill Companies, Inc. (“McGraw-Hill”) and its licensors reserve all rights in and to the work. Use of this work is subject to these terms. Except as permitted under the Copyright Act of 1976 and the right to store and retrieve one copy of the work, you may not decompile, disassemble, reverse engineer, reproduce, modify, create derivative works based upon, transmit, distribute, disseminate, sell, publish or sublicense the work or any part of it without McGraw-Hill’s prior consent. You may use the work for your own noncommercial and personal use; any other use of the work is strictly prohibited. Your right to use the work may be terminated if you fail to comply with these terms.

THE WORK IS PROVIDED “AS IS.” McGRAW-HILL AND ITS LICENSORS MAKE NO GUARANTEES OR WARRANTIES AS TO THE ACCURACY, ADEQUACY OR COMPLETENESS OF OR RESULTS TO BE OBTAINED FROM USING THE WORK, INCLUDING ANY INFORMATION THAT CAN BE ACCESSED THROUGH THE WORK VIA HYPERLINK OR OTHERWISE, AND EXPRESSLY DISCLAIM ANY WARRANTY, EXPRESS OR IMPLIED, INCLUDING BUT NOT LIMITED TO IMPLIED WARRANTIES OF MERCHANTABILITY OR FITNESS FOR A PARTICULAR PURPOSE. McGraw-Hill and its licensors do not warrant or guarantee that the functions contained in the work will meet your requirements or that its operation will be uninterrupted or error free. Neither McGraw-Hill nor its licensors shall be liable to you or anyone else for any inaccuracy, error or omission, regardless of cause, in the work or for any damages resulting therefrom. McGraw-Hill has no responsibility for the content of any information accessed through the work. Under no circumstances shall McGraw-Hill and/or its licensors be liable for any indirect, incidental, special, punitive, consequential or similar damages that result from the use of or inability to use the work, even if any of them has been advised of the possibility of such damages. This limitation of liability shall apply to any claim or cause whatsoever whether such claim or cause arises in contract, tort or otherwise.

DOI: 10.1036/0071511393

Adsorption and Ion Exchange*

M. Douglas LeVan, Ph.D. *J. Lawrence Wilson Professor of Engineering, Department of Chemical Engineering, Vanderbilt University; Member, American Institute of Chemical Engineers, American Chemical Society, International Adsorption Society (Section Coeditor)*

Giorgio Carta, Ph.D. *Professor, Department of Chemical Engineering, University of Virginia; Member, American Institute of Chemical Engineers, American Chemical Society, International Adsorption Society (Section Coeditor)*

DESIGN CONCEPTS		
Introduction	16-4	
Example 1: Surface Area and Pore Volume of Adsorbent	16-5	
Design Strategy	16-5	
Characterization of Equilibria	16-5	
Example 2: Calculation of Variance	16-5	
Adsorbent/Ion Exchanger Selection	16-5	
Fixed-Bed Behavior	16-6	
Cycles	16-7	
Practical Aspects	16-7	
ADSORBENTS AND ION EXCHANGERS		
Classifications and Characterizations	16-8	
Adsorbents	16-8	
Ion Exchangers	16-8	
Physical Properties	16-9	
SORPTION EQUILIBRIUM		
General Considerations	16-11	
Forces	16-11	
Surface Excess	16-12	
Classification of Isotherms by Shape	16-12	
Categorization of Equilibrium Models	16-12	
Heterogeneity	16-12	
Isothermic Heat of Adsorption	16-12	
Experiments	16-13	
Dimensionless Concentration Variables	16-13	
Single Component or Exchange	16-13	
Flat-Surface Isotherm Equations	16-13	
Pore-Filling Isotherm Equations	16-14	
Ion Exchange	16-14	
Example 3: Calculation of Useful Ion-Exchange Capacity	16-14	
Donnan Uptake	16-14	
Separation Factor	16-14	
Example 4: Application of Isotherms	16-15	
Multiple Components or Exchanges	16-16	
Adsorbed-Solution Theory	16-16	
Example 5: Application of Ideal Adsorbed-Solution Theory	16-16	
Langmuir-Type Relations	16-16	
Example 6: Comparison of Binary Langmuir Isotherms	16-16	
Freundlich-Type Relations	16-16	
Equations of State	16-16	
Ion Exchange—Stoichiometry	16-16	
Mass Action	16-17	
Constant Separation-Factor Treatment	16-17	
CONSERVATION EQUATIONS		
Material Balances	16-17	
Energy Balance	16-18	
RATE AND DISPERSION FACTORS		
Transport and Dispersion Mechanisms	16-18	
Intraparticle Transport Mechanisms	16-18	
Extraparticle Transport and Dispersion Mechanisms	16-19	
Heat Transfer	16-19	
Intraparticle Mass Transfer	16-19	
Pore Diffusion	16-19	
Solid Diffusion	16-20	
Combined Pore and Solid Diffusion	16-21	
External Mass Transfer	16-21	
Axial Dispersion in Packed Beds	16-21	
Rate Equations	16-22	
General Component Balance	16-22	
Linear Driving Force Approximation	16-22	
Combined Intraparticle Resistances	16-23	
Overall Resistance	16-24	
Axial Dispersion Effects	16-25	
Rapid Adsorption-Desorption Cycles	16-25	
Determination of Controlling Rate Factor	16-25	

*The contributions of Carmen M. Yon (retired), UOP, to material retained from the seventh edition in the "Process Cycles" and "Equipment" subsections are gratefully acknowledged.

16-2 ADSORPTION AND ION EXCHANGE

Example 7: Estimation of Rate Coefficient for Gas Adsorption	16-26	Prediction of Chromatographic Behavior	16-42
Example 8: Estimation of Rate Coefficient for Ion Exchange	16-26	Isocratic Elution	16-42
Example 9: Estimation of Rate Coefficient for Protein Adsorption	16-26	Concentration Profiles	16-44
BATCH ADSORPTION			
External Mass-Transfer Control	16-27	Linear Gradient Elution	16-44
Solid Diffusion Control	16-27	Displacement Development	16-45
Pore Diffusion Control	16-29	Example 14: Calculation of Band Profiles in	
Combined Resistances	16-30	Displacement Chromatography	16-46
Parallel Pore and Solid Diffusion Control	16-30	Design for Trace Solute Separations	16-48
External Mass Transfer and Intraparticle Diffusion Control	16-30	PROCESS CYCLES	
Bidispersed Particles	16-30	General Concepts	16-49
FIXED-BED TRANSITIONS			
Dimensionless System	16-31	Temperature Swing Adsorption	16-49
Local Equilibrium Theory	16-31	Other Cycle Steps	16-50
Single Transition System	16-32	Applications	16-50
Example 10: Transition Types	16-32	Pressure-Swing Adsorption	16-50
Multiple Transition System	16-32	Other Cycle Steps	16-51
Extensions	16-33	Applications	16-51
Example 11: Two-Component Isothermol Adsorption	16-33	Purge/Concentration Swing Adsorption	16-52
Example 12: Adiabatic Adsorption and Thermal Regeneration	16-33	Inert Purge	16-52
Constant Pattern Behavior for Favorable Isotherms	16-34	Displacement Purge	16-53
Asymptotic Solution	16-35	Chromatography	16-53
Example 13: Estimation of Breakthrough Time	16-36	Ion Exchange	16-54
Breakthrough Behavior for Axial Dispersion	16-36	Parametric Pumping	16-55
Extensions	16-36	Temperature	16-55
Square Root Spreading for Linear Isotherms	16-37	Pressure	16-55
Complete Solution for Reaction Kinetics	16-38	Simulated Moving Bed Systems	16-56
Numerical Methods and Characterization of Wave Shape	16-38	Complete Design and Extensions	16-57
CHROMATOGRAPHY			
Classification	16-38	Other Adsorption Cycles	16-58
Modes of Operation	16-38	Hybrid Recycle Systems	16-58
Elution Chromatography	16-38	Steam Regeneration	16-58
Frontal Analysis	16-39	Energy Applications	16-58
Displacement Development	16-39	Energy Conservation Techniques	16-60
Characterization of Experimental Chromatograms	16-40	Process Selection	16-60
Method of Moments	16-40	EQUIPMENT	
Approximate Methods	16-40	Adsorption	16-61
Tailing Peaks	16-41	General Design	16-61
Resolution	16-41	Adsorber Vessel	16-61
		Regeneration Equipment	16-63
		Cycle Control	16-64
		Continuous Countercurrent Systems	16-64
		Cross-Flow Systems	16-64
		Ion Exchange	16-67

Nomenclature and Units

a	Specific external surface area per unit bed volume, m^2/m^3	t_R	Chromatographic retention time, s
a_c	Surface area per unit particle volume, m^2/m^3 particle	T	Absolute temperature, K
A	Surface area of solid, m^2/kg	u	Superficial velocity, m/s
A_s	Chromatography peak asymmetry factor (Fig. 16-32)	u_s	Adsorbent velocity in TMB or SMB systems, $\text{kg}/(\text{m}^2\cdot\text{s})$
b	Correction factor for resistances in series (Fig. 16-12)	u_f	Fluid-phase internal energy, J/mol
c	Fluid-phase concentration, mol/m^3 fluid	u_s, u_{sol}	Stationary-phase and sorbent solid internal energy, J/kg
c_p	Pore fluid-phase concentration, mol/m^3	v	Interstitial velocity, m/s
c^s	Fluid-phase concentration at particle surface, mol/m^3	V_f	Extraparticle fluid volume, m^3
C_{pf}°	Ideal gas heat capacity, $\text{J}/(\text{mol}\cdot\text{K})$	W	Volume adsorbed as liquid, m^3 ; baseline width of chromatographic peak, s (Fig. 16-31)
C_s	Heat capacity of sorbent solid, $\text{J}/(\text{kg}\cdot\text{K})$	x	Adsorbed-phase mole fraction; particle coordinate, m
d_p	Particle diameter, m	y	Fluid-phase mole fraction
D	Fluid-phase diffusion coefficient, m^2/s	z	Bed axial coordinate, m; ionic valence
D_e	Effective pore diffusion coefficient, m^2/s [Eq. (16-77)]		
D_L	Axial dispersion coefficient, m^2/s [Eq. (16-79)]	Greek Letters	
D_p	Pore diffusion coefficient, m^2/s [Eqs. (16-66), (16-67), (16-69)]	α	Separation factor
D_s	Adsorbed-phase (solid, surface, particle, or micropore) diffusion coefficient, m^2/s [Eqs. (16-70), (16-71)]	β	Scaling factor in Polanyi-based models; slope in gradient elution chromatography [Eq. (16-190)]
D_0	Diffusion coefficient corrected for thermodynamic driving force, m^2/s [Eq. (16-71)]	Δ	Peak width at half height, s (Fig. 16-31)
\bar{D}	Ionic self-diffusion coefficient, m^2/s [Eqs. (16-73), (16-74)]	ε	Void fraction of packing (extraparticle); adsorption potential in Polanyi model, J/mol
F	Fractional approach to equilibrium	ε_p	Particle porosity (intraparticle void fraction)
F_e	Volumetric flow rate, m^3/s	ε_b	Total bed voidage (inside and outside particles) [(Eq. 16-4)]
h	Enthalpy, J/mol ; reduced height equivalent to theoretical plate [Eq. (16-183)]	γ	Activity coefficient
htu	Reduced height equivalent to a transfer unit [Fig. (16-13)]	Γ	Surface excess, mol/m^2 (Fig. 16-4)
HETP	Height equivalent to theoretical plate, m [Eq. (16-158)]	κ	Boltzmann constant
HTU	Height equivalent to a transfer unit, m [Eq. (16-92)]	λ	Isosteric heat of adsorption, J/mol [Eq. (16-7)]
J	Mass-transfer flux relative to molar average velocity, $\text{mol}/(\text{m}^2\cdot\text{s})$; J function [Eq. (16-148)]	Λ	Partition ratio [Eq. (16-125)]
k	Rate coefficient, s^{-1} [Eq. (16-83)]	Λ^∞	Ultimate fraction of solute adsorbed in batch
k_a	Forward rate constant for reaction kinetics, $\text{m}^3/(\text{mol}\cdot\text{s})$	μ	Fluid viscosity, $\text{kg}/(\text{m}\cdot\text{s})$
k_c	Rate coefficient based on fluid-phase concentration driving force, $\text{m}^3/(\text{kg}\cdot\text{s})$ (Table 16-12)	μ_0	Zero moment, $\text{mol}\cdot\text{s}/\text{m}^3$ [Eq. (16-153)]
k_f	External mass-transfer coefficient, m/s [Eq. (16-78)]	μ_1	First moment, s [Eq. (16-154)]
k_n	Rate coefficient based on adsorbed-phase concentration driving force, s^{-1} (Table 16-12)	ν	Kinematic viscosity, m^2/s
k'	Retention factor [Eq. (16-156)]	Ω	Cycle-time dependent LDF coefficient [Eq. (16-91)]
K	Isotherm parameter	ω	Parameter defined by Eq. (16-185b)
K^c	Molar selectivity coefficient	φ	Volume fraction or mobile-phase modulator concentration, mol/m^3
K'	Rational selectivity coefficient	π	Spreading pressure, N/m [(Eq. (16-20)]
L	Bed length, m	Ψ	LDF correction factor (Table 16-12)
m	Isotherm exponent; flow ratio in TMB or SMB systems [Eq. (16-207)]	Ψ	Mechanism parameter for combined resistances (Fig. 16-12)
M_r	Molecular mass, kg/kmol	ρ	Subparticle radial coordinate, m
M_a	Mass of adsorbent, kg	ρ_b	Bulk density of packed bed, kg/m^3
n	Adsorbed-phase concentration, mol/kg adsorbent	ρ_p	Particle density, kg/m^3 [Eq. (16-1)]
n^e	Ion-exchange capacity, $\text{g-equiv}/\text{kg}$	ρ_s	Skeletal particle density, kg/m^3 [Eq. (16-2)]
N	Number of transfer or reaction units; $k_f a L / (\varepsilon v^{ref})$ for external mass transfer; $15(1 - \varepsilon) \varepsilon_p D_p L / (\varepsilon v^{ref} r_p^2)$ for pore diffusion; $15AD_s L / (\varepsilon v^{ref} r_p^2)$ for solid diffusion; $k_n AL / (\varepsilon v^{ref})$ for linear driving-force approximation; $k_c c_{ref} AL / [(1 - R) \varepsilon v^{ref}]$ for reaction kinetics (Table 16-13)	σ^2	Second central moment, s^2 [Eq. (16-155)]
N_p	Number of theoretical plates [Eq. (16-157)]	τ	Dimensionless time [Eq. (16-120)]
N_{Pe}	$v^{ref} L / D_L$, bed Peclet number (number of dispersion units)	τ_1	Dimensionless time [Eq. (16-127) or (16-129)]
p	Partial pressure, Pa; cycle time, s	τ_p	Tortuosity factor [Eq. (16-65)]
P	Pressure, Pa	ξ	Particle dimensionless radial coordinate (r/r_p)
Pe	Particle-based Peclet number, $d_p v / D_L$	ζ	Dimensionless bed axial coordinate (z/L)
Q_i	Amount of component i injected with feed, mol	Subscripts	
r, R	Separation factor [Eqs. (16-30), (16-32)]; particle radial coordinate, m	a	Adsorbed phase
r_c	Column internal radius, m	f	Fluid phase
r_m	Stokes-Einstein radius of molecule, m [Eq. (16-68)]	i, j	Component index
r_p	Particle radius, m	tot	Total
r_{pore}	Pore radius, m	Superscripts	
r_s	Radius of subparticles, m	–	An averaged concentration
\mathfrak{R}	Gas constant, $\text{Pa}\cdot\text{m}^3/(\text{mol}\cdot\text{K})$	\wedge	A combination of averaged concentrations
Re	Reynolds number based on particle diameter, $d_p \varepsilon v / \nu$	\circ	Dimensionless concentration variable
Sc	Schmidt number, ν/D	e	Equilibrium
Sh	Sherwood number, $k_f d_p / D$	ref	Reference (indicates feed or initial values)
t	Time, s	s	Saturation
t_c	Cycle time, s	SM	Service mark
t_f	Feed time, s	TM	Trademark
		0	Initial fluid concentration in batch
		0'	Initial adsorbed-phase concentration in batch
		∞	Final state approached in batch

GENERAL REFERENCES

1. Adamson, *Physical Chemistry of Surfaces*, Wiley, New York, 1990.
2. Barrer, *Zeolites and Clay Minerals as Adsorbents and Molecular Sieves*, Academic Press, New York, 1978.
3. Breck, D. W., *Zeolite Molecular Sieves*, Wiley, New York, 1974.
4. Cheremisinoff and Ellerbusch, *Carbon Adsorption Handbook*, Ann Arbor Science, Ann Arbor, 1978.
5. Cooney, *Adsorption Design for Wastewater Treatment*, CRC Press, Boca Raton, Fla., 1998.
6. Do, *Adsorption Analysis: Equilibria and Kinetics*, Imperial College, London, 1998.
7. Dorfner (ed.), *Ion Exchangers*, W. deGruyter, Berlin, 1991.
8. Dyer, *An Introduction to Zeolite Molecular Sieves*, Wiley, New York, 1988.
9. EPA, *Process Design Manual for Carbon Adsorption*, U.S. Envir. Protect. Agency., Cincinnati, 1973.
10. Gembicki, Oroskar, and Johnson, "Adsorption, Liquid Separation" in *Kirk-Othmer Encyclopedia of Chemical Technology*, 4th ed., Wiley, 1991.
11. Guiochon, Felinger-Shirazi, and Katti, *Fundamentals of Preparative and Nonlinear Chromatography*, Elsevier, 2006.
12. Gregg and Sing, *Adsorption, Surface Area and Porosity*, Academic Press, New York, 1982.
13. Helfferich, *Ion Exchange*, McGraw-Hill, New York, 1962; reprinted by University Microfilms International, Ann Arbor, Michigan.
14. Helfferich and Klein, *Multicomponent Chromatography*, Marcel Dekker, New York, 1970.
15. Jaroniec and Madey, *Physical Adsorption on Heterogeneous Solids*, Elsevier, New York, 1988.
16. Kärger and Ruthven, *Diffusion in Zeolites and Other Microporous Solids*, Wiley, New York, 1992.
17. Keller, Anderson, and Yon, "Adsorption" in Rousseau (ed.), *Handbook of Separation Process Technology*, Wiley-Interscience, New York, 1987.
18. Keller and Staudt, *Gas Adsorption Equilibria: Experimental Methods and Adsorption Isotherms*, Springer, New York, 2005.
19. Ladisch, *Bioseparations Engineering: Principles, Practice, and Economics*, Wiley, New York, 2001.
20. Rhee, Aris, and Amundson, *First-Order Partial Differential Equations: Volume 1. Theory and Application of Single Equations; Volume 2. Theory and Application of Hyperbolic Systems of Quasi-Linear Equations*, Prentice Hall, Englewood Cliffs, New Jersey, 1986, 1989.
21. Rodrigues, LeVan, and Tondeur (eds.), *Adsorption: Science and Technology*, Kluwer Academic Publishers, Dordrecht, The Netherlands, 1989.
22. Rudzinski and Everett, *Adsorption of Gases on Heterogeneous Surfaces*, Academic Press, San Diego, 1992.
23. Ruthven, *Principles of Adsorption and Adsorption Processes*, Wiley, New York, 1984.
24. Ruthven, Farooq, and Knaebel, *Pressure Swing Adsorption*, VCH Publishers, New York, 1994.
25. Seader and Henley, *Separation Process Principles*, 2d ed., Wiley, New York, 2006.
26. Sherman and Yon, "Adsorption, Gas Separation" in *Kirk-Othmer Encyclopedia of Chemical Technology*, 4th ed., Wiley, 1991.
27. Streat and Cloete, "Ion Exchange," in Rousseau (ed.), *Handbook of Separation Process Technology*, Wiley, New York, 1987.
28. Suzuki, *Adsorption Engineering*, Elsevier, Amsterdam, 1990.
29. Thomas and Crittenden, *Adsorption Technology and Design*, Butterworth-Heinemann, Oxford, U.K., 1998.
30. Tien, *Adsorption Calculations and Modeling*, Butterworth-Heinemann, Newton, Massachusetts, 1994.
31. Valenzuela and Myers, *Adsorption Equilibrium Data Handbook*, Prentice Hall, Englewood Cliffs, New Jersey, 1989.
32. Vermeulen, LeVan, Hiester, and Klein, "Adsorption and Ion Exchange" in Perry, R. H. and Green, D. W. (eds.), *Perry's Chemical Engineers' Handbook* (6th ed.), McGraw-Hill, New York, 1984.
33. Wankat, *Large-Scale Adsorption and Chromatography*, CRC Press, Boca Raton, Florida, 1986.
34. Yang, *Adsorbents: Fundamentals and Applications*, Wiley, Hoboken, N.J., 2003.
35. Yang, *Gas Separation by Adsorption Processes*, Butterworth, Stoneham, Mass., 1987.
36. Young and Crowell, *Physical Adsorption of Gases*, Butterworths, London, 1962.

DESIGN CONCEPTS

INTRODUCTION

Adsorption and ion exchange share so many common features in regard to application in batch and fixed-bed processes that they can be grouped together as sorption for a unified treatment. These processes involve the transfer and resulting distribution of one or more solutes between a fluid phase and particles. The partitioning of a single solute between fluid and sorbed phases or the selectivity of a sorbent toward multiple solutes makes it possible to separate solutes from a bulk fluid phase or from one another.

This section treats batch and fixed-bed operations and reviews process cycles and equipment. As the processes indicate, fixed-bed operation with the sorbent in granule, bead, or pellet form is the predominant way of conducting sorption separations and purifications. Although the fixed-bed mode is highly useful, its analysis is complex. Therefore, fixed beds including chromatographic separations are given primary attention here with respect to both interpretation and prediction.

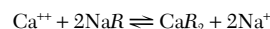
Adsorption involves, in general, the accumulation (or depletion) of solute molecules at an interface (including gas-liquid interfaces, as in foam fractionation, and liquid-liquid interfaces, as in detergency). Here we consider only gas-solid and liquid-solid interfaces, with solute distributed selectively between the fluid and solid phases. The accumulation per unit surface area is small; thus, highly porous solids with very large internal area per unit volume are preferred. Adsorbent surfaces are often physically and/or chemically heterogeneous, and bonding energies may vary widely from one site to another. We seek to promote physical adsorption or *physisorption*, which involves van der Waals forces (as in vapor condensation), and retard chemical adsorption or *chemisorption*, which involves chemical bonding (and often dissociation, as in catalysis). The former is well suited for a regenerable process, while the latter generally destroys the capacity of the adsorbent.

Adsorbents are natural or synthetic materials of amorphous or microcrystalline structure. Those used on a large scale, in order of sales volume, are activated carbon, molecular sieves, silica gel, and activated alumina [Keller et al., gen. refs.].

Ion exchange usually occurs throughout a polymeric solid, the solid being of gel-type, which dissolves some fluid-phase solvent, or truly porous. In ion exchange, ions of positive charge in some cases (cations) and negative charge in others (anions) from the fluid (usually an aqueous solution) replace dissimilar ions of the same charge initially in the solid. The ion exchanger contains permanently bound functional groups of opposite charge-type (or, in special cases, notably weak-base exchangers act as if they do). Cation-exchange resins generally contain bound sulfonic acid groups; less commonly, these groups are carboxylic, phosphonic, phosphinic, and so on. Anionic resins involve quaternary ammonium groups (strongly basic) or other amino groups (weakly basic).

Most ion exchangers in large-scale use are based on synthetic resins—either preformed and then chemically reacted, as for polystyrene, or formed from active monomers (olefinic acids, amines, or phenols). Natural zeolites were the first ion exchangers, and both natural and synthetic zeolites are in use today.

Ion exchange may be thought of as a reversible reaction involving chemically equivalent quantities. A common example for cation exchange is the familiar water-softening reaction



where *R* represents a stationary univalent anionic site in the polyelectrolyte network of the exchanger phase.

Table 16-1 classifies sorption operations by the type of interaction and the basis for the separation. In addition to the normal sorption operations of adsorption and ion exchange, some other similar separations are included. Applications are discussed in this section in "Process Cycles."

TABLE 16-1 Classification of Sorptive Separations

Type of interaction	Basis for separation	Examples
Adsorption	Equilibrium	Numerous purification and recovery processes for gases and liquids Activated carbon-based applications Desiccation using silica gels, aluminas, and zeolites Oxygen from air by PSA using LiX and 5A zeolites
	Rate	Nitrogen from air by PSA using carbon molecular sieve Nitrogen and methane using titanosilicate ETS-4
	Molecular sieving	Separation on <i>n</i> - and <i>iso</i> -paraffins using 5A zeolite Separation of xylenes using zeolite
Ion exchange (electrostatic)	Equilibrium	Deionization Water softening Rare earth separations Recovery and separation of pharmaceuticals (e.g., amino acids, proteins)
Ligand exchange	Equilibrium	Chromatographic separation of glucose-fructose mixtures with Ca-form resins Removal of heavy metals with chelating resins Affinity chromatography
Solubility	Equilibrium	Partition chromatography
None (purely steric)	Equilibrium partitioning in pores	Size exclusion or gel permeation chromatography

Example 1: Surface Area and Pore Volume of Adsorbent A simple example will show the extent of internal area in a typical granular adsorbent. A fixed bed is packed with particles of a porous adsorbent material. The bulk density of the packing is 500 kg/m^3 , and the interparticle void fraction is 0.40. The intraparticle porosity is 0.50, with two-thirds of this in cylindrical pores of diameter 1.4 nm and the rest in much larger pores. Find the surface area of the adsorbent and, if solute has formed a complete monomolecular layer 0.3 nm thick inside the pores, determine the percent of the particle volume and the percent of the total bed volume filled with adsorbate.

From surface area to volume ratio considerations, the internal area is practically all in the small pores. One gram of the adsorbent occupies 2 cm^3 as packed and has 0.4 cm^3 in small pores, which gives a surface area of $1150 \text{ m}^2/\text{g}$ (or about 1 mi^2 per 5 lb or $6.3 \text{ mi}^2/\text{ft}^3$ of packing). Based on the area of the annular region filled with adsorbate, the solute occupies 22.5 percent of the internal pore volume and 13.5 percent of the total packed-bed volume.

DESIGN STRATEGY

The design of sorption systems is based on a few underlying principles. First, knowledge of *sorption equilibrium* is required. This equilibrium, between solutes in the fluid phase and the solute-enriched phase of the solid, supplants what in most chemical engineering separations is a fluid-fluid equilibrium. The selection of the sorbent material with an understanding of its equilibrium properties (i.e., capacity and selectivity as a function of temperature and component concentrations) is of primary importance. Second, because sorption operations take place in batch, in fixed beds, or in simulated moving beds, the processes have *dynamical character*. Such operations generally do not run at steady state, although such operation may be approached in a simulated moving bed. Fixed-bed processes often approach a periodic condition called a periodic state or cyclic steady state, with several different feed steps constituting a cycle. Thus, some knowledge of how transitions travel through a bed is required. This introduces both time and space into the analysis, in contrast to many chemical engineering operations that can be analyzed at steady state with only a spatial dependence. For good design, it is crucial to understand fixed-bed performance in relation to adsorption equilibrium and rate behavior. Finally, many *practical aspects* must be included in design so that a process starts up and continues to perform well, and that it is not so overdesigned that it is wasteful. While these aspects are process-specific, they include an understanding of dispersive phenomena at the bed scale and, for regenerative processes, knowledge of aging characteristics of the sorbent material, with consequent changes in sorption equilibrium.

Characterization of Equilibria Phase equilibrium between fluid and sorbed phases for one or many components in adsorption or two or more species in ion exchange is usually the single most

important factor affecting process performance. In most processes, it is much more important than mass and heat transfer rates; a doubling of the stoichiometric capacity of a sorbent or a significant change in the shape of an isotherm would almost always have a greater impact on process performance than a doubling of transfer rates.

A difference between adsorption and ion exchange with completely ionized resins is indicated in the *variance* of the systems. In adsorption, part of the solid surface or pore volume is vacant. This diminishes as the fluid-phase concentration of solute increases. In contrast, for ion exchange the sorbent has a fixed total capacity and merely exchanges solutes while conserving charge. Variance is defined as the number of independent variables in a sorption system at equilibrium—that is, variables that one can change separately and thereby control the values of all others. Thus, it also equals the difference between the total number of variables and the number of independent relations connecting them. Numerous cases arise in which ion exchange is accompanied by chemical reaction (neutralization or precipitation, in particular), or adsorption is accompanied by evolution of sensible heat. The concept of variance helps greatly to assure correct interpretations and predictions.

The working capacity of a sorbent depends on fluid concentrations and temperatures. Graphical depiction of sorption equilibrium for single component adsorption or binary ion exchange (monovariance) is usually in the form of isotherms [$n_i = n_i(c_i)$ or $n_i(p_i)$ at constant T] or isosteres [$p_i = p_i(T)$ at constant n_i]. Representative forms are shown in Fig. 16-1. An important dimensionless group dependent on adsorption equilibrium is the **partition ratio** [see Eq. (16-125)], which is a measure of the relative affinities of the sorbed and fluid phases for solute.

Historically, isotherms have been classified as *favorable* (concave downward) or *unfavorable* (concave upward). These terms refer to the spreading tendencies of transitions in fixed beds. A favorable isotherm gives a compact transition, whereas an unfavorable isotherm leads to a broad one.

Example 2: Calculation of Variance In mixed-bed deionization of a solution of a single salt, there are 8 concentration variables: 2 each for cation, anion, hydrogen, and hydroxide. There are 6 connecting relations: 2 for ion exchange and 1 for neutralization equilibrium, and 2 ion-exchanger and 1 solution electroneutrality relations. The variance is therefore $8 - 6 = 2$.

Adsorbent/Ion Exchanger Selection Guidelines for sorbent selection are different for regenerative and nonregenerative systems. For a nonregenerative system, one generally wants a high capacity and a strongly favorable isotherm for a purification and additionally high selectivity for a separation. For a regenerative

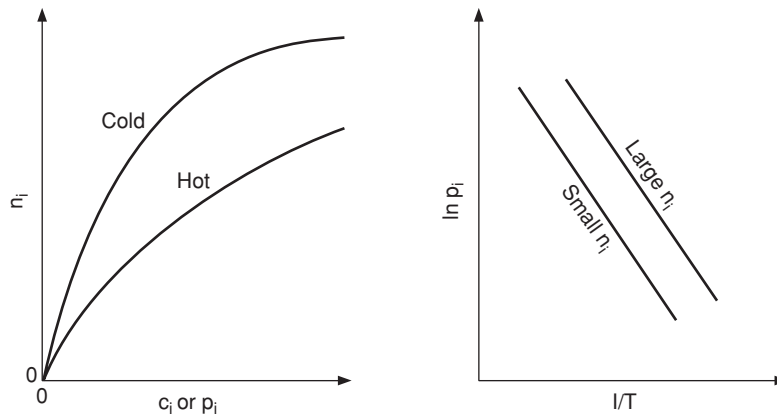


FIG. 16-1 Isotherms (left) and isosteres (right). Isosteres plotted using these coordinates are nearly straight parallel lines, with deviations caused by the dependence of the isosteric heat of adsorption on temperature and loading.

system, high overall capacity and selectivity are again desired, but needs for cost-effective regeneration leading to a reasonable working capacity influence what is sought after in terms of isotherm shape. For separations by pressure swing adsorption (or vacuum pressure swing adsorption), generally one wants a linear to slightly favorable isotherm (although purifications can operate economically with more strongly favorable isotherms). Temperature-swing adsorption usually operates with moderately to strongly favorable isotherms, in part because one is typically dealing with heavier solutes and these are adsorbed fairly strongly (e.g., organic solvents on activated carbon and water vapor on zeolites). Exceptions exist, however; for example, water is adsorbed on silica gel and activated alumina only moderately favorably, with some isotherms showing unfavorable sections. Equilibria for ion exchange separations generally vary from moderately favorable to moderately unfavorable; depending on feed concentrations, the alternates often exist for the different steps of a regenerative cycle. Other factors in sorbent selection are mechanical and chemical stability, mass transfer characteristics, and cost.

Fixed-Bed Behavior The number of transitions occurring in a fixed bed of initially uniform composition before it becomes saturated by a constant composition feed stream is generally equal to the variance of the system. This introductory discussion will be limited to single transition systems.

Methods for analysis of fixed-bed transitions are shown in Table 16-2. Local equilibrium theory is based solely of stoichiometric concerns and system nonlinearities. A transition becomes a “simple wave” (a gradual transition), a “shock” (an abrupt transition), or a combination of the two. In other methods, mass-transfer resistances are incorporated.

The asymptotic behavior of transitions under the influence of mass-transfer resistances in long, “deep” beds is important. The three basic asymptotic forms are shown in Fig. 16-2. With an unfavorable isotherm, the breadth of the transition becomes proportional to the depth of bed it has passed through. For the linear isotherm, the breadth becomes proportional to the square root of the depth. For the favorable isotherm, the transition approaches a constant breadth called a *constant pattern*.

Design of nonregenerative sorption systems and many regenerative ones often relies on the concept of the mass-transfer zone or MTZ, which closely resembles the constant pattern [Collins, *Chem. Eng. Prog. Symp. Ser. No. 74*, **63**, 31 (1974); Keller et al., gen. refs.]. The length of this zone (depicted in Fig. 16-3) together with stoichiometry can be used to predict accurately how long a bed can be utilized prior to breakthrough. Upstream of the mass-transfer zone, the adsorbent is in equilibrium with the feed. Downstream, the adsorbent is in its initial state. Within the mass-transfer zone, the fluid-phase concentration drops from the feed value to the initial, presaturation state.

TABLE 16-2 Methods of Analysis of Fixed-Bed Transitions

Method	Purpose	Approximations
Local equilibrium theory	Shows wave character—simple waves and shocks Usually indicates best possible performance Better understanding	Mass and heat transfer very rapid Dispersion usually neglected If nonisothermal, then adiabatic
Mass-transfer zone	Design based on stoichiometry and experience	Isothermal MTZ length largely empirical Regeneration often empirical
Constant pattern and related analyses	Gives asymptotic transition shapes and upper bound on MTZ	Deep bed with fully developed transition
Full rate modeling	Accurate description of transitions Appropriate for shallow beds, with incomplete wave development General numerical solutions by finite difference or collocation methods	Various to few

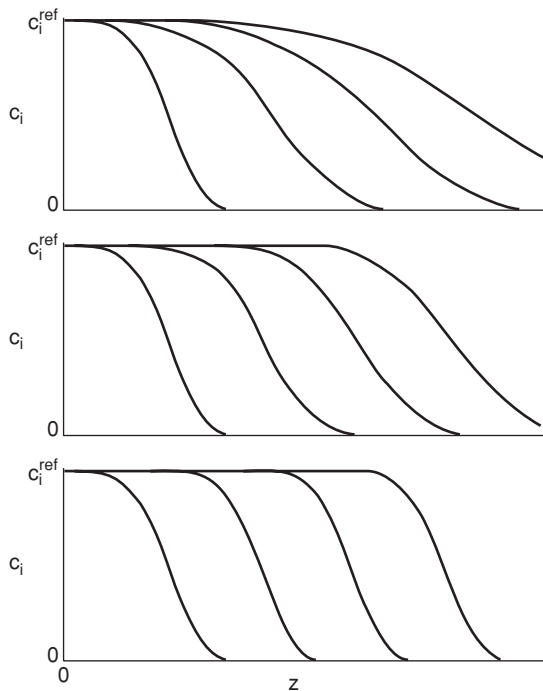


FIG. 16-2 Limiting fixed-bed behavior: simple wave for unfavorable isotherm (top), square-root spreading for linear isotherm (middle), and constant pattern for favorable isotherm (bottom). [From LeVan in Rodrigues et al. (eds.), *Adsorption: Science and Technology*, Kluwer Academic Publishers, Dordrecht, The Netherlands, 1989; reprinted with permission.]

Equilibrium with the feed is not attained in this region. As a result, because an adsorption bed must typically be removed from service shortly after breakthrough begins, the full capacity of the bed is not utilized. Obviously, the broader that the mass-transfer zone is, the greater will be the extent of unused capacity. Also shown in the figure is the length of the equivalent equilibrium section (LES) and the length of equivalent unused bed (LUB). The length of the MTZ is divided between these two.

Adsorption with strongly favorable isotherms and ion exchange between strong electrolytes can usually be carried out until most of the stoichiometric capacity of the sorbent has been utilized, corresponding to a thin MTZ. Consequently, the total capacity of the bed is practically constant regardless of the composition of the solution being treated.

The effluent concentration history is the breakthrough curve, also shown in Fig. 16-3. The effluent concentration stays at or near zero or a low residual concentration until the transition reaches the column outlet. The effluent concentration then rises until it becomes unacceptable, this time being called the breakthrough time. The feed step must stop and, for a regenerative system, the regeneration step begins.

Two dimensionless variables play key roles in the analysis of single transition systems (and some multiple transition systems). These are the **throughput parameter** [see Eq. (16-129)] and the **number of transfer units** (see Table 16-13). The former is time made dimensionless so that it is equal to unity at the stoichiometric center of a breakthrough curve. The latter is, as in packed tower calculations, a measure of mass-transfer resistance.

Cycles Design methods for cycles rely on mathematical modeling (or empiricism) and often extensive pilot plant experiments. Many

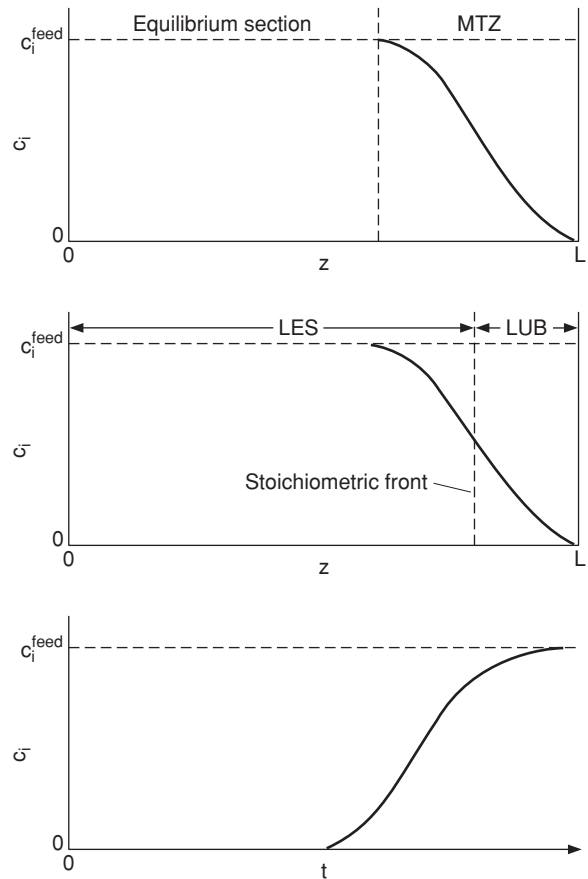


FIG. 16-3 Bed profiles (top and middle) and breakthrough curve (bottom). The bed profiles show the mass-transfer zone (MTZ) and equilibrium section at breakthrough. The stoichiometric front divides the MTZ into two parts with contributions to the length of equivalent equilibrium section (LES) and the length of equivalent unused bed (LUB).

cycles can be easily analyzed using the methods described above applied to the collection of steps. In some cycles, however, especially those operated with short cycle times or in shallow beds, transitions may not be very fully developed, even at a periodic state, and the complexity may be compounded by multiple sorbates.

A wide variety of complex process cycles have been developed. Systems with many beds incorporating multiple sorbents, possibly in layered beds, are in use. Mathematical models constructed to analyze such cycles can be complex. With a large number of variables and nonlinear equilibria involved, it is usually not beneficial to make all variables in such models dimensionless; doing so does not help appreciably in making comparisons with other largely dissimilar systems. If dimensionless variables are used, these usually begin with a dimensionless bed length and a dimensionless time, which is often different from the throughput parameter.

Practical Aspects There are a number of process-specific concerns that are accounted for in good design. In regenerable systems, sorbents age, losing capacity because of fouling by heavy contaminants, loss of surface area or crystallinity, oxidation, and the like. Mass-transfer resistances may increase over time. Because of particle shape, size distribution, or column packing method,

dispersion may be more pronounced than would normally be expected. The humidity of an entering stream will usually impact a solvent recovery application. Safety, including the possibility of a fire, may be a concern. For gas-phase adsorption, scale-up from an isothermal laboratory column to a nonisothermal pilot plant col-

umn to a largely adiabatic process column requires careful judgment. If the MTZ concept is utilized, the length of the MTZ cannot be reliably determined solely from knowledge on other systems. Experience plays the key role in accounting for these and other such factors.

ADSORBENTS AND ION EXCHANGERS

CLASSIFICATIONS AND CHARACTERIZATIONS

Adsorbents Table 16-3 classifies common adsorbents by structure type and water adsorption characteristics. Structured adsorbents take advantage of their crystalline structure (zeolites and silicalite) and/or their molecular sieving properties. The hydrophobic (nonpolar surface) or hydrophilic (polar surface) character may vary depending on the competing adsorbate. A large number of zeolites have been identified, and these include both synthetic and naturally occurring (e.g., mordenite and chabazite) varieties.

TABLE 16-3 Classification of Common Adsorbents

	Amorphous	Structured
Hydrophobic	Activated carbon Polymers	Carbon molecular sieves Silicalite
Hydrophilic	Silica gel Activated alumina	Common zeolites: 3A (KA), 4A (NaA), 5A (CaA), 13X (NaX), Mordenite, Chabazite, etc.

The classifications in Table 16-3 are intended only as a rough guide. For example, a carbon molecular sieve is truly amorphous but has been manufactured to have certain structural, rate-selective properties. Similarly, the extent of hydrophobicity of an activated carbon will depend on its ash content and its level of surface oxidation.

Zeolites are crystalline aluminosilicates. Zeolitic adsorbents have had their water of hydration removed by calcination to create a structure with well-defined openings into crystalline cages. The molecular sieving properties of zeolites are based on the size of these openings. Two crystal types are common: type A (with openings formed by 4 sodalite cages) and type X or Y (with openings formed by 6 sodalite cages). Cations balancing charge and their locations determine the size of opening into a crystal unit cell. Nominal opening sizes for the most common synthetic zeolites are 0.3 nm for KA, 0.4 nm for NaA, 0.5 nm for CaA, and 1.0 nm for NaX. Further details, including effective molecular diameters, are widely available [Barrer; Breck; Ruthven; Yang 1987, gen. refs.].

Many adsorbents, particularly the amorphous adsorbents, are characterized by their pore size distribution. The distribution of small pores is usually determined by analysis, using one of several available methods, of a cryogenic nitrogen adsorption isotherm, although other probe molecules are also used. The distribution of large pores is usually determined by mercury porosimetry [Gregg and Sing, gen. refs.].

Table 16-4 shows the IUPAC classification of pores by size. Micropores are small enough that a molecule is attracted to both of the opposing walls forming the pore. The potential energy functions for these walls superimpose to create a deep well, and strong adsorption results. Hysteresis is generally not observed. (However, water vapor adsorbed in the micropores of activated carbon shows a large hysteresis loop, and the desorption branch is sometimes used with the Kelvin equation to determine the pore size distribution.) Capillary condensation occurs in mesopores and a hysteresis loop is typically found. Macropores form important paths for molecules to diffuse into a par-

ticule; for gas-phase adsorption, they do not fill with adsorbate until the gas phase becomes saturated.

New adsorbents and ion-exchange materials are constantly under development. The class of microporous crystalline materials with molecular sieving properties is extensive and includes many metal silicates and phosphates, with the zeolites (aluminosilicates) being the most broadly useful. The titanosilicate ETS-4 is currently being implemented for separation of CH₄ and N₂. Metal organic framework (MOF) materials are currently in the research stage but appear to have great potential for adsorbing light gases and specific adsorbates. Among other classes of materials, the recently developed π -complexation sorbents are particularly promising; these use weak chemical bonds instead of purely physical interaction as the basis for separation (Yang, 2003, gen. refs.). Two other adsorbent materials of considerable research interest, but which have not been implemented for commercial separations, are carbon nanotubes and the mesoporous silica MCM-41.

Ion Exchangers Ion exchangers are classified according to (1) their functionality and (2) the physical properties of the support matrix. Cation and anion exchangers are classified in terms of their ability to exchange positively or negatively charged species. Strongly acidic and strongly basic ion exchangers are ionized and thus are effective at nearly all pH values (pH 0–14). Weakly acidic exchangers are typically effective in the range of pH 5–14. Weakly basic resins are effective in the range of pH 0–9. Weakly acidic and weakly basic exchangers are often easier to regenerate, but leakage due to incomplete exchange may occur. Chelating resins containing iminodiacetic acid form specific metal complexes with metal ions with complex stability constants that follow the same order as those for EDTA. However, depending on pH, they also function as weak cation exchangers. The achievable ion-exchange capacity depends on the concentration of ionogenic groups and their availability as an exchange site. The latter is a function of the support matrix.

Polymer-based, synthetic ion-exchangers known as resins are available commercially in gel type or truly porous forms. Gel-type resins are not porous in the usual sense of the word, since their structure depends upon swelling in the solvent in which they are immersed. Removal of the solvent usually results in a collapse of the three-dimensional structure, and no significant surface area or pore diameter can be defined by the ordinary techniques available for truly porous materials. In their swollen state, gel-type resins approximate a true molecular-scale solution. Thus, we can identify an internal porosity ϵ_p only in terms of the equilibrium uptake of water or other liquid. When crosslinked polymers are used as the support matrix, the internal porosity so defined varies in inverse proportion to the degree of crosslinking, with swelling and therefore

TABLE 16-4 Classification of Pore Sizes

Type	Slit width* (<i>w</i>)	Characteristic
Micropore†	$w < 2$ nm	Superimposed wall potentials
Mesopore	$2 \text{ nm} < w < 50$ nm	Capillary condensation
Macropore	$w > 50$ nm	Effectively flat walled until $p \rightarrow P^*$

*Or pore diameter.

†Further subdivided into ultramicropores and supermicropores (Gregg and Sing, gen. refs.).

porosity typically being more pronounced in solvents with a high dielectric constant. The ion held by the exchanger also influences the resin swelling. Thus, the size of the resin particles changes during the ion-exchange process as the resin is changed from one form to another, and this effect is more dramatic for resins with a lower degree of crosslinking. The choice of degree of crosslinking is dependent on several factors including: the extent of swelling, the exchange capacity, the intraparticle diffusivity, the ease of regeneration, and the physical and chemical stability of the exchanger under chosen operating conditions. The concentration of ionogenic groups determines the capacity of the resin. Although the capacity per unit mass of dry resin is insensitive to the degree of crosslinking, except for very highly crosslinked resins, the exchange capacity per unit volume of swollen resin increases significantly with degree of crosslinking, so long as the mesh size of the polymer network allows the ions free access to functional groups within the interior of the resin. The degree of crosslinking also affects the rate of ion exchange. The intraparticle diffusivity decreases nearly exponentially with the mesh size of the matrix. As a result, resins with a lower degree of crosslinking are normally required for the exchange of bulky species, such as organic ions with molecular weight in excess of 100. The regeneration efficiency is typically greater for resins with a lower degree of crosslinking. Finally, the degree of crosslinking also affects the long-term stability of the resin. Strongly acidic and strongly basic resins are subject to irreversible oxidative degradation of the polymer and thermal and oxidative decomposition of functional groups. Generally, more highly crosslinked resins are less prone to irreversible chemical degradation but they may be subject to osmotic breakage caused by volume changes that occur during cyclic operations. In general, experience shows that an intermediate degree of crosslinking is often preferred. However, readers are referred to manufacturers' specifications for resin stability data at different operating conditions.

Truly porous, synthetic ion exchangers are also available. These materials retain their porosity even after removal of the solvent and have measurable surface areas and pore size. The term macroporous is commonly used for resins prepared from a phase separation technique, where the polymer matrix is prepared with the addition of a liquid that is a good solvent for the monomers, but in which the polymer is insoluble. Matrices prepared in this way usually have the appearance of a conglomerate of gel-type microspheres held together to form an interconnected porous network. Macroporous resins possessing a more continuous cellular structure interlaced with a pore network have also been obtained with different techniques and are commercially available. Since higher degrees of crosslinking are typically used to produce truly porous ion-exchange resins, these materials tend to be more stable under highly oxidative conditions, more attrition-resistant, and more resistant to breakage due to osmotic shock than their gel-type counterparts. Moreover, since their porosity does not depend entirely on swelling, they can be used in solvents with low dielectric constant where gel-type resins can be ineffective. In general, compared to gel-type resins, truly porous resins typically have somewhat lower capacities and can be more expensive. Thus, for ordinary ion-exchange applications involving small ions under nonharsh conditions, gel-type resins are usually preferred.

Adsorbents for biomacromolecules such as proteins have special properties. First, they need to have large pore sizes. A ratio of pore radius to molecule radius larger than 5 is desirable to prevent excessive diffusional hindrance (see "Intraparticle Mass Transfer" in this section). Thus, for typical proteins, pore radii need to be in excess of 10–15 nm. Second, functional groups for interactions with the protein are usually attached to the adsorbent backbone via a spacer arm to provide accessibility. Third, adsorbents based on hydrophilic structures are preferred to limit nonspecific interactions with the adsorbent backbone and prevent global unfolding or denaturation of the protein. Thus, if hydrophobic supports are used, their surfaces are usually rendered hydrophilic by incorporating hydrophilic coatings such as dextran or polyvinyl alcohol. Finally, materials stable in sodium hydroxide solutions (used for clean-in-place) are

preferred. Support matrices for protein adsorption can be classified into the following four broad groups: hydrophilic gels, including cross-linked agarose, cross-linked dextran, cross-linked polyacrylamide, and cellulose; rigid macroporous media, including silica/ceramic, alumina, polystyrene-DVB, and polymethacrylate; composite media including agarose-dextran and ceramic-polyacrylamide; and monoliths, including polystyrene-DVB, polymethacrylate, and silica-based materials. Monoliths for biomacromolecule adsorption are generally synthesized in place in a column, resulting in a continuous random structure of linked, generally nonporous microparticles intercalated by a network of flow-through pores. The continuous structure allows independent control of microparticle size and flow-through pore sizes resulting in rapid adsorption and moderate pressure drop. Although the adsorption capacity for proteins is smaller than for porous-particle-based adsorbents, they offer significant advantages for rapid high-resolution separations and for adsorption of very large bioparticles such as plasmid DNA and viruses [see Josic et al., *J. Chrom. B.*, **752**, 191 (2001)].

Functional groups or ligands incorporated in materials for biomacromolecule adsorption can be classified in the following four broad groups: cation exchange, including sulfopropyl (SP), methyl sulfonate (S), and carboxymethyl (CM); anion exchange, including quaternary ammonium ion (Q), quaternary aminoethyl (QAE), and diethylamino ethyl (DEAE); hydrophobic interaction, including ether, isopropyl, butyl, octyl, and phenyl ligands in order of increasing hydrophobicity; and biospecific interaction, including amino acids, dyes, and proteins covalently bound to the adsorbent through coupling ligands and transition metals supported via complexing ligands. Polystyrene-based particles and silica particles functionalized with hydrocarbon chains from C2 to C18 in length are also used for reversed-phase chromatographic separations. However, because of the limited stability of biomacromolecules, their process applications are limited. Inert, hydrophilic porous matrices and gels are used extensively for size exclusion chromatography (SEC). A useful general reference is Janson and Ryden, *Protein Purification: Principles, High-Resolution Methods, and Applications*, Wiley-Liss, 1998.

PHYSICAL PROPERTIES

Selected data on some commercially available adsorbents and ion exchangers are given in Tables 16-5 and 16-6. The purpose of the tables is twofold: to assist the engineer or scientist in identifying materials suitable for a needed application, and to supply typical physical property values.

In addition to the particulate adsorbents listed in Table 16-5, some adsorbents are available in structured form for specific applications. Monoliths, papers, and paint formulations have been developed for zeolites, with these driven by the development of wheels (Fig. 16-60), adsorptive refrigeration, etc. Carbon monoliths are also available as are activated carbon fibers, created from polymeric materials, and sold in the forms of fabrics, mats, felts, and papers for use in various applications including in pleated form in filters. Zeolitic and carbon membranes are also available, with the latter developed for separation by "selective surface flow" [Rao and Sircar, *J. Membrane Sci.*, **85**, 253 (1993)].

Excellent sources of information on the characteristics of adsorbents or ion exchange products for specific applications are the manufacturers themselves. Additional information on adsorbents and ion exchangers is available in many of the general references and in several articles in *Kirk-Othmer Encyclopedia of Chemical Technology*. A comprehensive summary of commercial ion-exchangers, including manufacturing methods, properties, and applications, is given by Dorfner (*Ion Exchangers*, de Gruyter, New York, 1991).

Several densities and void fractions are commonly used. For adsorbents, usually the **bulk density** ρ_b , the weight of clean material per unit bulk volume as packed in a column, is reported. The **dry particle density** ρ_p is related to the (external) **void fraction of**

16-10 ADSORPTION AND ION EXCHANGE

TABLE 16-5 Physical Properties of Adsorbents

Material and uses	Shape* of particles	Size range, U.S. standard mesh†	Internal porosity, %	Bulk dry density, kg/L	Average pore diameter, nm	Surface area, km ² /kg	Sorptive capacity, kg/kg (dry)
Aluminas							
Low-porosity (fluoride sorbent)	G, S	8–14, etc.	40	0.70	~7	0.32	0.20
High-porosity (drying, separations)	G	Various	57	0.85	4–14	0.25–0.36	0.25–0.33
Desiccant, CaCl ₂ -coated	G	3–8, etc.	30	0.91	4.5	0.2	0.22
Activated bauxite	G	8–20, etc.	35	0.85	5		0.1–0.2
Chromatographic alumina	G, P, S	80–200, etc.	30	0.93			~0.14
Silicates and aluminosilicates							
Molecular sieves	S, C, P	Various					
Type 3A (dehydration)			~30	0.62–0.68	0.3	~0.7	0.21–0.23
Type 4A (dehydration)			~32	0.61–0.67	0.4	~0.7	0.22–0.26
Type 5A (separations)			~34	0.60–0.66	0.5	~0.7	0.23–0.28
Type 13X (purification)			~38	0.58–0.64	1.0	~0.6	0.25–0.36
Silicalite (hydrocarbons)	S, C, P	Various		0.64–0.70	0.6	~0.4	0.12–0.16
Dealuminated Y (hydrocarbons)	S, C, P	Various		0.48–0.53	0.8	0.5–0.8	0.28–0.42
Mordenite (acid drying)				0.88	0.3–0.8		0.12
Chabazite (acid drying)				0.72	0.4–0.5		0.20
LiX (air separation)	S	14–40		0.61	1.0		
Titanosilicate ETS-4 (N ₂ /CH ₄)	S	Various	25–30	1.0	0.37		
Silica gel (drying, separations)	G, P	Various	38–48	0.70–0.82	2–5	0.6–0.8	0.35–0.50
Magnesium silicate (decolorizing)	G, P	Various	~33	~0.50		0.18–0.30	
Calcium silicate (fatty-acid removal)	P		75–80	~0.20		~0.1	
Clay, acid-treated (refining of petroleum, food products)	G	4–8		0.85			
Fuller's earth (same)	G, P	<200		0.80			
Diatomaceous earth	G	Various		0.44–0.50		~0.002	
Carbons							
Shell-based	G	Various	60	0.45–0.55	2	0.8–1.6	0.40
Wood-based	G	Various	~80	0.25–0.30		0.8–1.8	~0.70
Petroleum-based	G, C	Various	~80	0.45–0.55	2	0.9–1.3	0.3–0.4
Peat-based	G, C, P	Various	~55	0.30–0.50	1–4	0.8–1.6	0.5
Lignite-based	G, P	Various	70–85	0.40–0.70	3	0.4–0.7	0.3
Bituminous-coal-based	G, P	8–30, 12–40	60–80	0.40–0.60	2–4	0.9–1.2	0.4
Synthetic-polymer-based (pyrolyzed)	S	20–100	40–70	0.49–0.60		0.1–1.1	
Carbon molecular sieve (air separation)	C	Various	35–50	0.5–0.7	0.3–0.6		0.5–0.20
Organic polymers							
Polystyrene (removal of organics, e.g., phenol; antibiotics recovery)	S	20–60	40–60	0.64	4–20	0.3–0.7	
Polyacrylic ester (purification of pulping wastewaters; antibiotics recovery)	G, S	20–60	50–55	0.65–0.70	10–25	0.15–0.4	
Phenolic (also phenolic amine) resin (decolorizing and deodorizing of solutions)	G	16–50	45	0.42		0.08–0.12	0.45–0.55

*Shapes: C, cylindrical pellets; F, fibrous flakes; G, granules; P, powder; S, spheres.

†U.S. Standard sieve sizes (given in parentheses) correspond to the following diameters in millimeters: (3) 6.73, (4) 4.76, (8) 2.98, (12) 1.68, (14) 1.41, (16) 1.19, (20) 0.841, (30) 0.595, (40) 0.420, (50) 0.297, (60) 0.250, (80) 0.177, (200) 0.074.

packing ϵ by

$$\rho_p = \frac{\rho_b}{1 - \epsilon} \quad (16-1)$$

The **skeletal density** ρ_s of a particle (or crystalline density for a pure chemical compound) is given in terms of **internal porosity** ϵ_p by

$$\rho_s = \frac{\rho_p}{1 - \epsilon_p} \quad (16-2)$$

For an adsorbent or ion exchanger, the **wet density** ρ_w of a particle is related to these factors and to the liquid density ρ_f by

$$\rho_w = \rho_p + \epsilon_p \rho_f \quad (16-3)$$

The **total voidage** ϵ_b in a packed bed (outside and inside particles) is

$$\epsilon_b = \epsilon + (1 - \epsilon)\epsilon_p \quad (16-4)$$

TABLE 16-6 Physical Properties of Ion-Exchange Materials

Material	Shape ^a of particles	Bulk wet density (drained), kg/L	Moisture content (drained), % by weight	Swelling due to exchange, %	Maximum operating temperature, † °C	Operating pH range	Exchange capacity	
							Dry, equivalent/kg	Wet, equivalent/L
Cation exchangers: strongly acidic								
Polystyrene sulfonate								
Homogeneous (gel) resin	S				120–150	0–14		
4% cross-linked		0.75–0.85	64–70	10–12			5.0–5.5	1.2–1.6
6% cross-linked		0.76–0.86	58–65	8–10			4.8–5.4	1.3–1.8
8–10% cross-linked		0.77–0.87	48–60	6–8			4.6–5.2	1.4–1.9
12% cross-linked		0.78–0.88	44–48	5			4.4–4.9	1.5–2.0
16% cross-linked		0.79–0.89	42–46	4			4.2–4.6	1.7–2.1
20% cross-linked		0.80–0.90	40–45	3			3.9–4.2	1.8–2.0
Porous structure								
12–20% cross-linked	S	0.81	50–55	4–6	120–150	0–14	4.5–5.0	1.5–1.9
Cation exchangers: weakly acidic								
Acrylic (pK 5) or methacrylic (pK 6)								
Homogeneous (gel) resin								
Macroporous	S	0.70–0.75	45–50	20–80	120	4–14	8.3–10	3.3–4.0
	S	0.67–0.74	50–55	10–100	120		~8.0	2.5–3.5
Polystyrene phosphonate	G, S	0.74	50–70	<40	120	3–14	6.6	3.0
Polystyrene iminodiacetate	S	0.75	68–75	<100	75	3–14	2.9	0.7
Polystyrene amidoxime	S	~0.75	58	10	50	1–11	2.8	0.8–0.9
Zeolite (Al silicate)	G	0.85–0.95	40–45	0	60	6–8	1.4	0.75
Zirconium tungstate	G	1.15–1.25	~5	0	>150	2–10	1.2	1.0
Anion exchangers: strongly basic								
Polystyrene-based								
Trimethyl ammonium (type I)								
Homogeneous, 8% CL	S	0.70	46–50	~20	60–80	0–14	3.4–3.8	1.3–1.5
Porous, 11% CL	S	0.67	57–60	15–20	60–80	0–14	3.4	1.0
Dimethyl hydroxyethyl ammonium (type II)								
Homogeneous, 8% CL	S	0.71	~42	15–20	40–80	0–14	3.8–4.0	1.2
Porous, 10% CL	S	0.67	~55	12–15	40–80	0–14	3.8	1.1
Acrylic-based								
Homogeneous (gel)	S	0.72	~70	~15	40–80	0–14	~5.0	1.0–1.2
Porous	S	0.67	~60	~12	40–80	0–14	3.0–3.3	0.8–0.9
Anion exchangers: intermediately basic (pK 11)								
Polystyrene-based								
Epoxy-polyamine	S	0.75	~50	15–25	65	0–10	4.8	1.8
Anion exchangers: weakly basic (pK 9)								
Aminopolystyrene								
Homogeneous (gel)	S	0.67	~45	8–12	100	0–7	5.5	1.8
Porous	S	0.61	55–60	~25	100	0–9	4.9	1.2
Acrylic-based amine								
Homogeneous (gel)	S	0.72	~63	8–10	80	0–7	6.5	1.7
Porous	S	0.72	~68	12–15	60	0–9	5.0	1.1

^aShapes: C, cylindrical pellets; G, granules; P, powder; S, spheres.

†When two temperatures are shown, the first applies to H form for cation, or OH form for anion, exchanger; the second, to salt ion.

SORPTION EQUILIBRIUM

The quantity of a solute adsorbed can be given conveniently in terms of moles or volume (for adsorption) or ion-equivalents (for ion exchange) per unit mass or volume (dry or wet) of sorbent. Common units for adsorption are mol/(m³ of fluid) for the fluid-phase concentration c_i and mol/(kg of clean adsorbent) for adsorbed-phase concentration n_i . For gases, partial pressure may replace concentration.

Many models have been proposed for adsorption and ion exchange equilibria. The most important factor in selecting a model from an engineering standpoint is to have an accurate mathematical description over the entire range of process conditions. It is usually fairly easy to obtain correct capacities at selected points, but isotherm shape over the entire range is often a critical concern for a regenerable process.

GENERAL CONSIDERATIONS

Forces Molecules are attracted to surfaces as the result of two types of forces: dispersion-repulsion forces (also called London or van der Waals forces) such as described by the Lennard-Jones potential for molecule-molecule interactions; and electrostatic forces, which exist as the result of a molecule or surface group having a permanent electric dipole or quadrupole moment or net electric charge.

Dispersion forces are always present and in the absence of any stronger force will determine equilibrium behavior, as with adsorption of molecules with no dipole or quadrupole moment on nonoxidized carbons and silicalite.

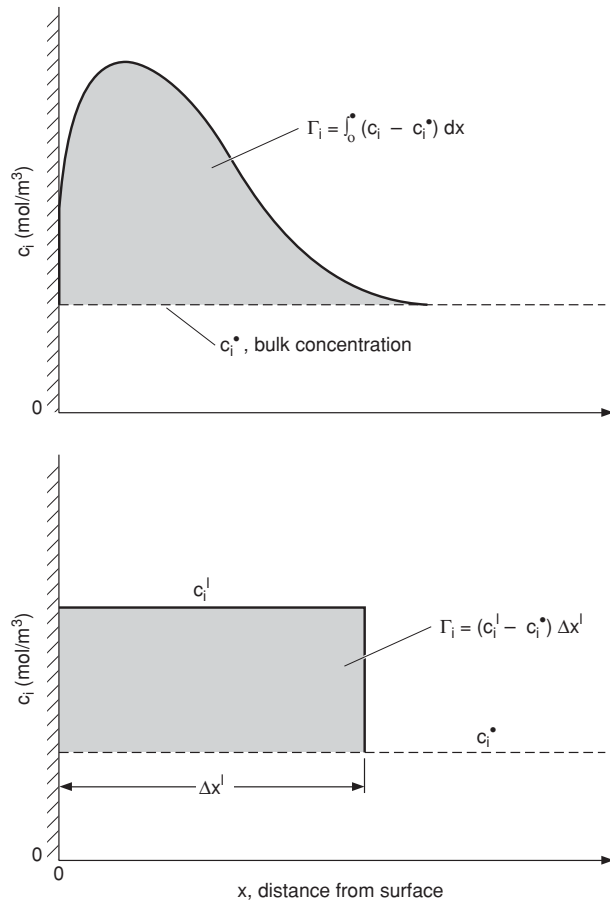


FIG. 16-4 Depictions of surface excess Γ_i . *Top*: The force field of the solid concentrates component i near the surface; the concentration c_i is low at the surface because of short-range repulsive forces between adsorbate and surface. *Bottom*: Surface excess for an imagined homogeneous surface layer of thickness $\Delta x'$.

If a surface is polar, its resulting electric field will induce a dipole moment in a molecule with no permanent dipole and, through this polarization, increase the extent of adsorption. Similarly, a molecule with a permanent dipole moment will polarize an otherwise nonpolar surface, thereby increasing the attraction.

For a polar surface and molecules with permanent dipole moments, attraction is strong, as for water adsorption on a hydrophilic adsorbent. Similarly, for a polar surface, a molecule with a permanent quadrupole moment will be attracted more strongly than a similar molecule with a weaker moment; for example, nitrogen is adsorbed more strongly than oxygen on zeolites (Sherman and Yon, gen. refs.).

Surface Excess With a Gibbs dividing surface placed at the surface of the solid, the surface excess of component i , Γ_i (mol/m²), is the amount per unit area of solid contained in the region near the surface, above that contained at the fluid-phase concentration far from the surface. This is depicted in two ways in Fig. 16-4. The quantity adsorbed per unit mass of adsorbent is

$$n_i = \Gamma_i A \quad (16-5)$$

where A (m²/kg) is the surface area of the solid.

For a porous adsorbent, the amount adsorbed in the pore structure per unit mass of adsorbent, based on surface excess, is obtained by the difference

$$n_i = n_i^{\text{tot}} - V_p c_i^{\infty} \quad (16-6)$$

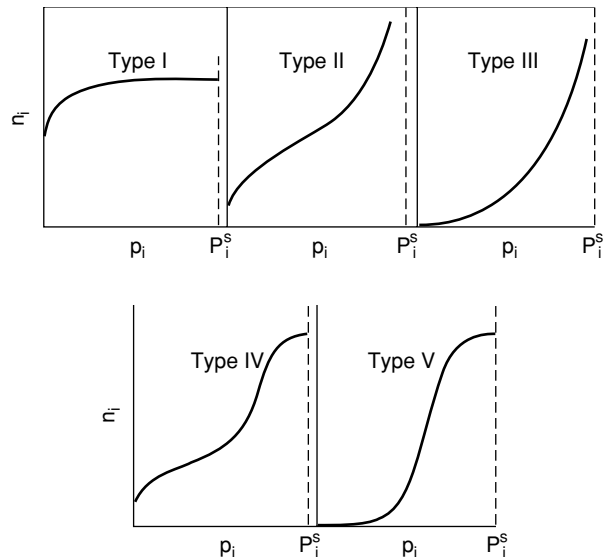


FIG. 16-5 Representative isotherm types. p_i and P_i^s are pressure and vapor pressure of the solute. [Brunauer, J. Am. Chem. Soc., **62**, 1723 (1940); reprinted with permission.]

where n_i^{tot} (mol/kg) is the total amount of component i contained within the particle's pore volume V_p (m³/kg), and c_i^{∞} is the concentration outside of the particle. If n_i differs significantly from n_i^{tot} (as it will for weakly adsorbed species), then it is important to consider adsorbed-phase quantities in terms of surface excesses.

Classification of Isotherms by Shape Representative isotherms are shown in Fig. 16-5, as classified by Brunauer and coworkers. Curves that are concave downward throughout (type I) have historically been designated as "favorable," while those that are concave upward throughout (type III) are "unfavorable." Other isotherms (types II, IV, and V) have one or more inflection points. The designations "favorable" and "unfavorable" refer to fixed-bed behavior for the uptake step, with a favorable isotherm maintaining a compact wave shape. A favorable isotherm for uptake is unfavorable for the discharge step. This becomes particularly important for a regenerative process, in which a favorable isotherm may be too favorable for regeneration to occur effectively.

Categorization of Equilibrium Models Historically, sorption equilibrium has been approached from different viewpoints. For adsorption, many models for flat surfaces have been used to develop explicit equations and equations of state for pure components and mixtures, and many of the resulting equations are routinely applied to porous materials. Explicit equations for pore filling have also been proposed, generally based on the Polanyi potential theory. Ion exchange adds to these approaches concepts of adsorption or dissolution (adsorption) and exchange reactions. Statistical mechanics and molecular dynamics contribute to our understanding of all of these approaches (Steele, *The Interaction of Gases with Solid Surfaces*, Pergamon, Oxford, 1974; Nicholson and Parsonage, *Computer Simulation and the Statistical Mechanics of Adsorption*, Academic Press, New York, 1982). Mixture models are often based on the adsorbed solution theory, which uses thermodynamic equations from vapor-liquid equilibria with volume replaced by surface area and pressure replaced by a two-dimensional spreading pressure. Other approaches include lattice theories and mass-action exchange equilibrium.

Heterogeneity Adsorbents and ion exchangers can be physically and chemically heterogeneous. Although exceptions exist, solutes generally compete for the same sites. Models for adsorbent heterogeneity have been developed for both discrete and continuous distributions of energies [Ross and Olivier, *On Physical Adsorption*, Interscience, New York, 1964; Jaroniec and Madey, Rudzinski and Everett, gen. refs.].

Isosteric Heat of Adsorption The most useful heat of adsorption for fixed-bed calculations is the *isosteric heat of adsorption*, which

is given by the Clausius-Clapeyron type relation

$$\lambda_i = \mathfrak{R}T^2 \left. \frac{\partial \ln p_i}{\partial T} \right|_{n_i, n_j} \quad (16-7)$$

where the n_j can be dropped for single-component adsorption. λ_i is positive by convention. If isosteres are straight lines when plotted as $\ln p_i$ versus T^{-1} (see Fig. 16-1), then Eq. (16-7) can be integrated to give

$$\ln p_i = f(n_i) - \frac{\lambda_i}{\mathfrak{R}T} \quad (16-8)$$

where $f(n_i)$ is an arbitrary function dependent only on n_i . Many other heats of adsorption have been defined and their utility depends on the application (Ross and Olivier; Young and Crowell, gen. refs.).

From Eq. (16-8), if a single isotherm is known in the pressure explicit form $p_i = p_i(n_i, T)$ and if λ_i is known at least approximately, then equilibria can be estimated over a narrow temperature range using

$$\ln \frac{p_i}{p_i^{\text{ref}}} = \frac{\lambda_i}{\mathfrak{R}} \left(\frac{1}{T^{\text{ref}}} - \frac{1}{T} \right) \quad (\text{const } n_i) \quad (16-9)$$

Similarly, Eq. (16-9) is used to calculate the isosteric heat of adsorption from two isotherms.

Experiments Sorption equilibria are measured using apparatuses and methods classified as volumetric, gravimetric, flow-through (frontal analysis), and chromatographic. Apparatuses are discussed elsewhere [Yang 1987; Keller and Staudt (gen. refs.)]. Heats of adsorption can be determined from isotherms measured at different temperatures or measured independently by calorimetric methods.

Dimensionless Concentration Variables Where appropriate, isotherms will be written here using the dimensionless system variables

$$c_i^\circ = \frac{c_i}{c_i^{\text{ref}}} \quad n_i^\circ = \frac{n_i}{n_i^{\text{ref}}} \quad (16-10)$$

where the best choice of reference values depends on the operation.

In some cases, to allow for some preloading of the adsorbent, it will be more convenient to use the dimensionless transition variables

$$c_i^\circ = \frac{c_i - c_i'}{c_i'' - c_i'} \quad n_i^\circ = \frac{n_i - n_i'}{n_i'' - n_i'} \quad (16-11)$$

where single and double primes indicate initial and final concentrations, respectively. Figure 16-6 shows n_i° plotted versus c_i° for a sample system. Superimposed are an upward transition (loading) and a downward transition (unloading), shown by the respective positions of (c_i', n_i') and (c_i'', n_i'') .

SINGLE COMPONENT OR EXCHANGE

The simplest relationship between solid-phase and fluid-phase concentrations is the **linear isotherm**

$$n_i = K_i c_i \quad \text{or} \quad n_i = K_i' p_i \quad (16-12)$$

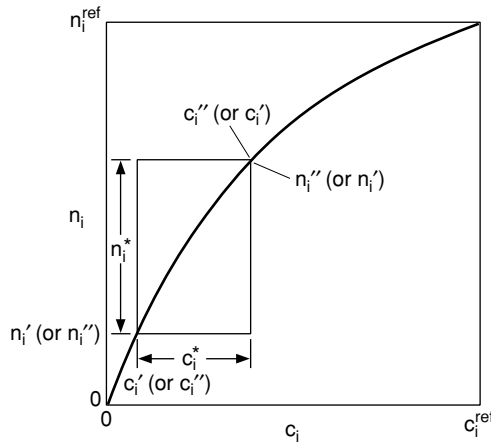


FIG. 16-6 Isotherm showing concentration variables for a transition from (c_i', n_i') to (c_i'', n_i'') .

Thermodynamics requires that a linear limit be approached in the Henry's law region for all isotherm equations.

Flat-Surface Isotherm Equations The classification of isotherm equations into two broad categories for flat surfaces and pore filling reflects their origin. It does not restrict equations developed for flat surfaces from being applied successfully to describe data for porous adsorbents.

The classical isotherm for a homogeneous flat surface, and most popular of all nonlinear isotherms, is the **Langmuir isotherm**

$$n_i = \frac{n_i^* K_i c_i}{1 + K_i c_i} \quad (16-13)$$

where n_i^* is the monolayer capacity approached at large concentrations and K_i is an equilibrium constant. These parameters are often determined by plotting $1/n_i$ versus $1/c_i$. The derivation of the isotherm assumes negligible interaction between adsorbed molecules. For temperature-dependent adsorption equilibrium and a constant isosteric heat of adsorption, K_i is given by

$$K_i = K_i^0 \exp(\lambda_i / \mathfrak{R}T) \quad (16-14)$$

where K_i^0 is a constant. A variation on Eq. (16-13) is the multisite Langmuir isotherm, which is [Nitta et al., *J. Chem. Eng. Japan*, **17**, 39 (1984)]

$$K_i p_i = \frac{n_i / n_i^*}{(1 - n_i / n_i^*)^{a_i}} \quad (16-15)$$

where a_i is a constant.

The classical isotherm for multilayer adsorption on a homogeneous, flat surface is the **BET isotherm** [Brunauer, Emmett, and Teller, *J. Am. Chem. Soc.*, **60**, 309 (1938)]

$$n_i = \frac{n_i^* K_i p_i}{[1 + K_i p_i - (p_i / P_i^s)][1 - (p_i / P_i^s)]} \quad (16-16)$$

where p_i is the pressure of the adsorbable component and P_i^s is its vapor pressure. It is useful for gas-solid systems in which condensation is approached, fitting type-II behavior.

For a heterogeneous flat surface, a classical isotherm is the **Freundlich isotherm**

$$n_i = K_i c_i^{m_i} \quad (16-17)$$

where m_i is positive and generally not an integer. The isotherm corresponds approximately to an exponential distribution of heats of adsorption. Although it lacks the required linear behavior in the Henry's law region, it can often be used to correlate data on heterogeneous adsorbents over wide ranges of concentration.

Several isotherms combine aspects of both the Langmuir and Freundlich equations. One that has been shown to be effective in describing data mathematically for heterogeneous adsorbents is the **Toth isotherm** [*Acta Chim. Acad. Sci. Hung.*, **69**, 311 (1971)]

$$n_i = \frac{n_i^* p_i}{[(1/K_i) + p_i^{m_i}]^{1/m_i}} \quad (16-18)$$

This three-parameter equation behaves linearly in the Henry's law region and reduces to the Langmuir isotherm for $m = 1$. Other well-known isotherms include the **Langmuir-Freundlich isotherm** or **Sips isotherm** [Sips, *J. Chem. Phys.*, **16**, 490 (1948); Koble and Corrigan, *Ind. Eng. Chem.*, **44**, 383 (1952)] or **loading ratio correlation** with prescribed temperature dependence [Yon and Turnock, *AIChE Symp. Ser.*, **67**(117), 75 (1971)]

$$n_i = \frac{n_i^* (K_i p_i)^m}{1 + (K_i p_i)^m} \quad (16-19)$$

Equations of state are also used. Given such an equation written in terms of the two-dimensional spreading pressure π , the corresponding isotherm is easily determined, as described later for mixtures [see Eq. (16-43)]. The two-dimensional equivalent of an ideal gas is an ideal surface gas, which is described by

$$\pi A = n_i \mathfrak{R}T \quad (16-20)$$

which readily gives the linear isotherm, Eq. (16-12). Many more complicated equations of state are available, including two-dimensional analogs of the virial equation and equations of van der Waals, Redlich-Kwong, Peng-Robinson, etc. [Adamson, gen. refs.; Patrykiewicz et al., *Chem. Eng. J.*, **15**, 147 (1978); Haydel and Kobayashi, *Ind. Eng. Chem. Fundam.*, **6**, 546 (1967)].

Pore-Filling Isotherm Equations Most pore-filling models are grounded in the **Polanyi potential theory**. In Polanyi's model, an attracting potential energy field is assumed to exist adjacent to the surface of the adsorbent and concentrates vapors there. Adsorption takes place wherever the strength of the field, independent of temperature, is great enough to compress the solute to a partial pressure greater than its vapor pressure. The last molecules to adsorb form an equipotential surface containing the adsorbed volume. The strength of this field, called the adsorption potential ϵ (J/mol), was defined by Polanyi to be equal to the work required to compress the solute from its partial pressure to its vapor pressure

$$\epsilon = \mathcal{R}T \ln \left(\frac{P_i}{p_i} \right) \quad (16-21)$$

The same result is obtained by considering the change in chemical potential. In the basic theory, W (m³/kg), the volume adsorbed as saturated liquid at the adsorption temperature, is plotted versus ϵ to give a characteristic curve. Data measured at different temperatures for the same solute-adsorbent pair should fall on this curve. Using the method, it is possible to use data measured at a single temperature to predict isotherms at other temperatures. Data for additional, homologous solutes can be collapsed into a single "correlation curve" by defining a scaling factor β , the most useful of which has been V/V^{ref} , the adsorbate molar volume as saturated liquid at the adsorption temperature divided by that for a reference compound. Thus, by plotting W versus ϵ/β or ϵ/\bar{V} for data measured at various temperatures for various similar solutes and a single adsorbent, a single curve should be obtained. Variations of the theory are often used to evaluate properties for components near or above their critical points [Grant and Manes, *Ind. Eng. Chem. Fund.*, **5**, 490 (1966)].

The most popular equations used to describe the shape of a characteristic curve or a correlation curve are the two-parameter **Dubinin-Radushkevich** (DR) equation

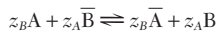
$$\frac{W}{W_0} = \exp \left[-k \left(\frac{\epsilon}{\beta} \right)^2 \right] \quad (16-22)$$

and the three-parameter **Dubinin-Astakhov** (DA) equation

$$\frac{W}{W_0} = \exp \left[-k \left(\frac{\epsilon}{\beta} \right)^m \right] \quad (16-23)$$

where W_0 is micropore volume and m is related to the pore size distribution [Gregg and Sing, gen. refs.]. Neither of these equations has correct limiting behavior in the Henry's law regime.

Ion Exchange A useful tool is provided by the **mass action law** for describing the general exchange equilibrium in fully ionized exchanger systems as



where overbars indicate the ionic species in the ion exchanger phase and z_A and z_B are the valences of ions A and B. The associated equilibrium relation is of the form

$$K_{A,B} = K_{A,B} \left(\frac{\gamma_A}{\gamma_B} \right)^{z_B} \left(\frac{\gamma_B}{\gamma_A} \right)^{z_A} = \left(\frac{n_A}{c_A} \right)^{z_B} \left(\frac{c_B}{n_B} \right)^{z_A} \quad (16-24)$$

where $K'_{A,B}$ is the apparent equilibrium constant or molar selectivity coefficient, $K_{A,B}$ is the thermodynamic equilibrium constant based on activities, and the γ s are activity coefficients. Often it is desirable to represent concentrations in terms of equivalent ionic fractions based on solution normality c_{tot} and fixed exchanger capacity n^s as $c_i^o = z_i c_i / c_{\text{tot}}$ and $n_i^o = z_i n_i / m_{\text{tot}}$, where $c_{\text{tot}} = \sum z_i c_i$ and $n_{\text{tot}} = \sum z_i n_i = n^s$ with the summations extended to all counter-ion species. A rational selectivity coefficient is then defined as

$$K'_{A,B} = K_{A,B} \left(\frac{n_{\text{tot}}}{c_{\text{tot}}} \right)^{z_A - z_B} = \left(\frac{n_A^o}{c_A^o} \right)^{z_B} \left(\frac{c_B^o}{n_B^o} \right)^{z_A} \quad (16-25)$$

For the exchange of ions of equal valence ($z_A = z_B$), $K'_{A,B}$ and $K_{A,B}$ are

coincident and, to a first approximation, independent of concentration. When $z_A > z_B$, $K'_{A,B}$ decreases with solution normality. This reflects the fact that ion exchangers exhibit an increasing affinity for ions of lower valence as the solution normality increases.

An alternate form of Eq. (16-25) is

$$n_A^o = K_{A,B}^c \left(\frac{n_{\text{tot}}}{c_{\text{tot}}} \right)^{(z_A - z_B)/z_B} \left(\frac{1 - n_A^o}{1 - c_A^o} \right)^{z_A/z_B} c_A^o \quad (16-26)$$

When B is in excess ($c_A^o, n_A^o \rightarrow 0$), this reduces to

$$n_A^o = K_{A,B}^c \left(\frac{n_{\text{tot}}}{c_{\text{tot}}} \right)^{(z_A - z_B)/z_B} c_A^o = K_A c_A^o \quad (16-27)$$

where the linear equilibrium constant $K_A = K_{A,B}^c (n_{\text{tot}}/c_{\text{tot}})^{(z_A/z_B)-1}$ decreases with solution normality c_{tot} when $z_A > z_B$ or increases when $z_A < z_B$.

Table 16-7 gives equilibrium constants for crosslinked cation and anion exchangers for a variety of counterions. The values given for cation exchangers are based on ion A replacing Li⁺, and those given for anion exchangers are based on ion A replacing Cl⁻. The selectivity for a particular ion generally increases with decreasing hydrated ion size and increasing degree of crosslinking. The selectivity coefficient for any two ions A and D can be obtained from Table 16-7 from values of $K_{A,B}$ and $K_{D,B}$ as

$$K_{A,D} = K_{A,B}/K_{D,B} \quad (16-28)$$

The values given in this table are only approximate, but they are adequate for process screening purposes with Eqs. (16-24) and (16-25). Rigorous calculations generally require that activity coefficients be accounted for. However, for the exchange between ions of the same valence at solution concentrations of 0.1 N or less, or between any ions at 0.01 N or less, the solution-phase activity coefficients will be similar enough that they can be omitted.

Models for ion exchange equilibria based on the mass-action law taking into account solution and exchanger-phase nonidealities with equations similar to those for liquid mixtures have been developed by several authors [see Smith and Woodburn, *AIChE J.*, **24**, 577 (1978); Mehablia et al., *Chem. Eng. Sci.*, **49**, 2277 (1994)]. Thermodynamics-based approaches are also available [Soldatov in Dorfner, gen. refs.; Novosad and Myers, *Can J. Chem. Eng.*, **60**, 500 (1982); Myers and Byington in Rodrigues, ed., *Ion Exchange Science and Technology*, NATO ASI Series, No. 107, Nijhoff, Dordrecht, 1986, pp. 119-145] as well as approaches for the exchange of macromolecules, taking into account steric-hindrance effects [Brooks and Cramer, *AIChE J.*, **38**, 12 (1992)].

Example 3: Calculation of Useful Ion-Exchange Capacity An 8 percent crosslinked sulfonated resin is used to remove calcium from a solution containing 0.0007 mol/l Ca²⁺ and 0.01 mol/l Na⁺. The resin capacity is 2.0 equiv/l. Estimate the resin capacity for calcium removal.

From Table 16-7, we obtain $K_{Ca,Na} = 5.16/1.98 = 2.6$. Since $n_{\text{tot}} = 2$ equiv/l and $c_{\text{tot}} = 2 \times 0.0007 + 0.01 = 0.0114$ equiv/l, $K'_{Ca,Na} = 2.6 \times 2/0.011 = 470$. Thus, with $c_{Ca}^o = 2 \times 0.0007/0.011 = 0.13$, Eq. (16-25) gives $470 = (n_{Ca}^o/0.13)/[(1 - 0.13)/(1 - n_{Na}^o)]^2$ or $n_{Ca}^o = 0.9$. The available capacity for calcium is $n_{Ca} = 0.9 \times 2/0.2 = 0.9$ mol/l.

Donnan Uptake The uptake of an electrolyte as a neutral ion pair of a salt is called Donnan uptake. It is generally negligible at low ionic concentrations. Above 0.5 g-equiv/l with strongly ionized exchangers (or at lower concentrations with those more weakly ionized), the resin's fixed ion-exchange capacity is measurably exceeded as a result of electrolyte invasion. With only one coion species Y (matching the charge sign of the fixed groups in the resin), its uptake n_Y equals the total excess uptake of the counterion. Equilibrium is described by the mass-action law. For the case of a resin in A-form in equilibrium with a salt AY, the excess counterion uptake is given by [Helfferich, gen. refs., pp. 133-147]

$$z_Y n_Y = \left[\frac{n^s}{4} + (z_Y c_Y)^2 \left(\frac{\gamma_{AY}}{\gamma_{AY}} \right)^2 \left(\frac{a_w}{a_w} \right)^{\delta_{AY}/\delta_w} \right]^{1/2} - \frac{n^s}{2} \quad (16-29)$$

where γ s are activity coefficients, a_w water activities, and v_s partial molar volumes. For dilute conditions, Eq. (16-29) predicts a squared dependence of n_Y on c_Y . Thus, the electrolyte sorption isotherm has a strong positive curvature. Donnan uptake is more pronounced for resins of lower degree of crosslinking and for counterions of low valence.

Separation Factor By analogy with the mass-action case and appropriate for both adsorption and ion exchange, a **separation factor** r

TABLE 16-7 Equilibrium Constants for Polystyrene DVB Cation and Anion Exchangers

Strong acid sulfonated cation exchangers (Li ⁺ reference ion)							
Counter-ion	Degree of crosslinking			Counter-ion	Degree of crosslinking		
	4% DVB	8% DVB	16% DVB		4% DVB	8% DVB	16% DVB
Li ⁺	1.00	1.00	1.00	Mg ⁺⁺	2.95	3.29	3.51
H ⁺	1.32	1.27	1.47	Zn ⁺⁺	3.13	3.47	3.78
Na ⁺	1.58	1.98	2.37	Co ⁺⁺	3.23	3.74	3.81
NH ₄ ⁺	1.90	2.55	3.34	Cu ⁺⁺	3.29	3.85	4.46
K ⁺	2.27	2.90	4.50	Cd ⁺⁺	3.37	3.88	4.95
Rb ⁺	2.46	3.16	4.62	Ni ⁺⁺	3.45	3.93	4.06
Cs ⁺	2.67	3.25	4.66	Ca ⁺⁺	4.15	5.16	7.27
Ag ⁺	4.73	8.51	22.9	Pb ⁺⁺	6.56	9.91	18.0
Tl ⁺	6.71	12.4	28.5	Ba ⁺⁺	7.47	11.5	20.8

Strong base anion exchangers, 8% DVB (Cl ⁻ reference ion)					
Counterion	Type I resin ^o	Type II resin [†]	Counterion	Type I resin ^o	Type II resin [†]
Salicylate	32	28	Cyanide	1.6	1.3
Iodide	8.7	7.3	Chloride	1.0	1.0
Phenoxide	5.2	8.7	Hydroxide	0.05-0.07	0.65
Nitrate	3.8	3.3	Bicarbonate	0.3	0.5
Bromide	2.8	2.3	Formate	0.2	0.2
Nitrite	1.2	1.3	Acetate	0.2	0.2
Bisulfite	1.3	1.3	Fluoride	0.09	0.1
Cyanide	1.6	1.3	Sulfate	0.15	0.15

^oTrimethylamine.

[†]Dimethyl-hydroxyethylamine.

Data from Bonner and Smith, *J. Phys. Chem.*, **61**, 326 (1957) and Wheaton and Bauman, *Ind. Eng. Chem.*, **45**, 1088 (1951).

can be defined based on dimensionless system variables [Eq. (16-10)] by

$$r = \frac{c_i^o(1 - n_i^o)}{n_i^o(1 - c_i^o)} \quad \text{or} \quad r = \frac{n_B^o/c_B^o}{n_A^o/c_A^o} \quad (16-30)$$

This term is analogous to relative volatility or its reciprocal (or to an equilibrium selectivity). Similarly, the assumption of a constant separation factor is a useful assumption in many sorptive operations. [It is constant for the Langmuir isotherm, as described below, and for mass-action equilibrium with $z_a = z_b$ in Eq. (16-24).] This gives the constant separation factor isotherm

$$n_i^o = \frac{c_i^o}{r + (1 - r)c_i^o} \quad (16-31)$$

The separation factor r identifies the equilibrium increase in n_i^o from 0 to 1, which accompanies an increase in c_i^o from 0 to 1. For a concentration change over only part of the isotherm, a separation factor R can be defined for the dimensionless transition variables [Eq. (16-11)]. This separation factor is

$$R = \frac{n_i''/c_i''}{n_i'/c_i'} = \frac{c_i^o(1 - n_i^o)}{n_i^o(1 - c_i^o)} \quad (16-32)$$

and gives an equation identical to Eq. (16-31) with R replacing r .

Figure 16-7 shows constant separation factor isotherms for a range of r (or R) values. The isotherm is linear for $r = 1$, favorable for $r < 1$, rectangular (or irreversible) for $r = 0$, and unfavorable for $r > 1$. As a result of symmetry properties, if r is defined for adsorption of component i or exchange of ion A for B, then the reverse process is described by $1/r$.

The Langmuir isotherm, Eq. (16-13), corresponds to the constant separation factor isotherm with

$$r = 1/(1 + K_i c_i^{\text{ref}}) \quad (16-33)$$

for system variables Eq. (16-10) or

$$R = \frac{r + (1 - r)(c_i'/c_i^{\text{ref}})}{r + (1 - r)(c_i''/c_i^{\text{ref}})} \quad (16-34)$$

for transition variables [Eq. (16-11)]. Vermeulen et al. [gen. refs.] give additional properties of constant separation factor isotherms.

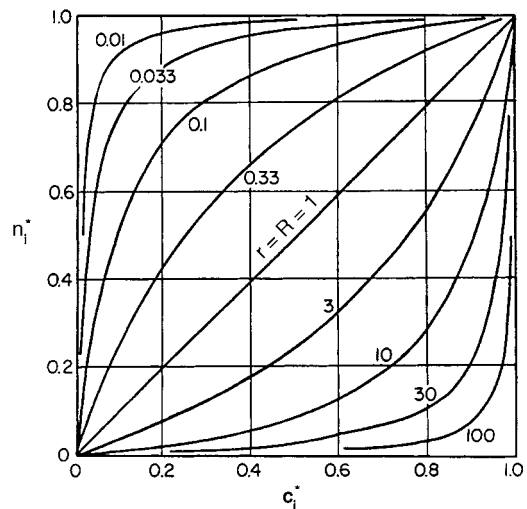


FIG. 16-7 Constant separation factor isotherm as a function of the separation factor r (or interchangeably R). Each isotherm is symmetric about the perpendicular line connecting (0,1) and (1,0). Isotherms for r and $1/r$ are symmetric about the 45° line.

Example 4: Application of Isotherms Thomas [*Ann. N.Y. Acad. Sci.*, **49**, 161 (1948)] provides the following Langmuir isotherm for the adsorption of anthracene from cyclohexane onto alumina:

$$n_i = \frac{22c_i}{1 + 375c_i}$$

with n_i in mol anthracene/kg alumina and c_i in mol anthracene/l liquid.

a. What are the values of K_i and n_i^o according to Eq. (16-13)?

$$K_i = 375 \text{ l/mol}$$

$$n_i^o = \frac{22}{K_i} = 0.0587 \text{ mol/kg}$$

16-16 ADSORPTION AND ION EXCHANGE

b. For a feed concentration of 8.11×10^{-4} mol/l, what is the value of r ?

$$r = \frac{1}{1 + K_i(8.11 \times 10^{-4})} = 0.766 \quad [\text{from Eq. (16-33)}]$$

c. If the alumina is presaturated with liquid containing 2.35×10^{-4} mol/l and the feed concentration is 8.11×10^{-4} mol/l, what is the value of R ?

$$R = 0.834 \quad [\text{from Eq. (16-32) or (16-34)}]$$

MULTIPLE COMPONENTS OR EXCHANGES

When more than one adsorbed species or more than two ion-exchanged species interact in some manner, equilibrium becomes more complicated. Usually, thermodynamics provides a sound basis for prediction.

Adsorbed-Solution Theory The common thermodynamic approach to multicomponent adsorption treats adsorption equilibrium in a way analogous to fluid-fluid equilibrium. The theory has as its basis the Gibbs adsorption isotherm [Young and Crowell, gen. refs.], which is

$$Ad\pi = \sum_i n_i d\mu_i \quad (\text{const } T) \quad (16-35)$$

where μ is chemical potential. For an ideal gas ($d\mu = \mathcal{R}T d \ln p_i$), if it is assumed that an adsorbed solution is defined with a pure-component standard state (as is common for a liquid solution), then Eq. (16-35) can be integrated to give [Rudisill and LeVan, *Chem. Eng. Sci.*, **47**, 1239 (1992)]

$$p_i = \gamma_i x_i P_i^{\text{ref}}(T, \pi) \quad (16-36)$$

where γ_i and x_i are the adsorbed-phase activity coefficient and mole fraction of component i and P_i^{ref} is the standard state, specified to be at the temperature and spreading pressure of the mixture.

Equation (16-36) with $\gamma_i = 1$ provides the basis for the ideal adsorbed-solution theory [Myers and Prausnitz, *AIChE J.*, **11**, 121 (1965)]. The spreading pressure for a pure component is determined by integrating Eq. (16-35) for a pure component to obtain

$$\frac{\pi A}{\mathcal{R}T} = \int_0^{p_i^{\text{ref}}} \frac{n_i}{p_i} dp_i \quad (16-37)$$

where n_i is given by the pure-component isotherm. Also, since $\sum x_i = 1$, Eq. (16-36) with $\gamma_i = 1$ gives $\sum (p_i/P_i^{\text{ref}}) = 1$. With no area change on mixing for the ideal solution, the total number of moles adsorbed per unit weight of adsorbent is determined using a two-dimensional form of Amagat's law:

$$\frac{1}{n_{\text{tot}}} = \sum \frac{x_i}{n_i^{\text{ref}}} \quad (16-38)$$

where $n_{\text{tot}} = \sum n_i$ and n_i^{ref} is given by the pure-component isotherm at P_i^{ref} . Adsorbed-phase concentrations are calculated using $n_i = x_i n_{\text{tot}}$. Generally, different values of π [or $\pi A/(\mathcal{R}T)$] must be tried until the one is found that satisfies Eq. (16-37) and $\sum x_i = 1$.

Example 5: Application of Ideal Adsorbed-Solution Theory

Consider a binary adsorbed mixture for which each pure component obeys the Langmuir equation, Eq. (16-13). Let $n_1^s = 4$ mol/kg, $n_2^s = 3$ mol/kg, $K_1 p_1 = K_2 p_2 = 1$. Use the ideal adsorbed-solution theory to determine n_1 and n_2 .

Substituting the pure component Langmuir isotherm

$$n_i = \frac{n_i^s K_i p_i}{1 + K_i p_i}$$

into Eq. (16-37) and integrating gives

$$\frac{\pi A}{\mathcal{R}T} = n_1^s \ln(1 + K_1 P_i^{\text{ref}})$$

which can be solved explicitly for $K_i P_i^{\text{ref}}$. Values are guessed for $\pi A/(\mathcal{R}T)$, values of $K_i P_i^{\text{ref}}$ are calculated from the equation above, and $\sum x_i = \sum K_i p_i / (K_i P_i^{\text{ref}}) = 1$ is checked to see if it is satisfied. Trial and error gives $\pi A/(\mathcal{R}T) = 3.8530$ mol/kg, $K_1 P_1^{\text{ref}} = 1.6202$, $K_2 P_2^{\text{ref}} = 2.6123$, and $x_1 = 0.61720$. Evaluating the pure-component isotherms at the reference pressures and using Eq. (16-38) gives $n_{\text{tot}} = 2.3475$ mol/kg, and finally $n_i = x_i n_{\text{tot}}$ gives $n_1 = 1.4489$ mol/kg and $n_2 = 0.8986$ mol/kg.

Other approaches to account for various effects have been developed. Negative deviations from Raoult's law (i.e., $\gamma_i < 1$) are frequently found due to adsorbent heterogeneity [e.g., Myers, *AIChE J.*, **29**, 691

(1983)]. Thus, contributions include accounting for adsorbent heterogeneity [Valenzuela et al., *AIChE J.*, **34**, 397 (1988)] and excluded pore-volume effects [Myers, in Rodrigues et al., gen. refs.]. Several activity coefficient models have been developed to account for non-ideal adsorbate-adsorbate interactions including a spreading pressure-dependent activity coefficient model [e.g., Talu and Zwiebel, *AIChE J.*, **32**, 1263 (1986)] and a vacancy solution theory [Suwanayuen and Danner, *AIChE J.*, **26**, 68, 76 (1980)].

Langmuir-Type Relations For systems composed of solutes that individually follow Langmuir isotherms, the traditional multicomponent Langmuir equation, obtained via a kinetic derivation, is

$$n_i = \frac{n_i^s K_i p_i}{1 + \sum_j K_j p_j} \quad (16-39)$$

where j is summed over all components. This equation has been criticized on thermodynamic grounds because it does not satisfy the Gibbs adsorption isotherm unless all monolayer capacities n_i^s are equal.

To satisfy the Gibbs adsorption isotherm for unequal monolayer capacities, explicit isotherms can be obtained in the form of a series expansion [LeVan and Vermeulen, *J. Phys. Chem.*, **85**, 3247 (1981)]. A two-term form is

$$n_1 = \frac{(n_1^s + n_2^s) K_1 p_1}{2(1 + K_1 p_1 + K_2 p_2)} + \frac{(n_1^s - n_2^s) K_1 p_1 K_2 p_2}{(K_1 p_1 + K_2 p_2)^2} \ln(1 + K_1 p_1 + K_2 p_2) \quad (16-40)$$

where the subscripts may be interchanged. Multicomponent forms are also available [Frey and Rodrigues, *AIChE J.*, **40**, 182 (1994)].

A variation on the multicomponent Langmuir isotherm for application to heterogeneous surfaces with sites of various energies involves summing terms given by the right-hand side of Eq. (16-39) to give the multipatch Langmuir isotherm

$$n_i = \sum_k \frac{n_{i,k}^s K_{i,k} p_i}{1 + \sum_j K_{j,k} p_j} \quad (16-41)$$

where k is summed over all patches.

Example 6: Comparison of Binary Langmuir Isotherms Use the numerical values in Example 5 to evaluate the binary Langmuir isotherms given by Eqs. (16-39) and (16-40) and compare results with the exact answers given in Example 5.

Equation (16-39) gives $n_1 = 1.3333$ mol/kg and $n_2 = 1.0000$ mol/kg for an average deviation from the exact values of approximately 10 percent. Equation (16-40) gives $n_1 = 1.4413$ mol/kg and $n_2 = 0.8990$ mol/kg for an average deviation of about 0.6 percent.

Freundlich-Type Relations A binary Freundlich isotherm, obtained from the ideal adsorbed solution theory in loading-explicit closed form [Crittenden et al., *Environ. Sci. Technol.*, **19**, 1037 (1985)], is

$$c_i = \frac{n_i}{\sum_{j=1}^N n_j} \left(\frac{\sum_{j=1}^N (n_j/m_j)}{K_i/m_i} \right)^{1/m_i} \quad (16-42)$$

Equations of State If an equation of state is specified for a multicomponent adsorbed phase of the form $\pi A/(\mathcal{R}T) = f(n_1, n_2, \dots)$, then the isotherms are determined using [Van Ness, *Ind. Eng. Chem. Fundam.*, **8**, 464-473 (1969)]

$$\ln \left(\frac{K_i p_i}{n_i/M_s} \right) = \int_A^\infty \left[\frac{\partial [\pi A/(\mathcal{R}T)]}{\partial n_i} \right]_{T,A,n_j} - 1 \Bigg] \frac{dA}{A} \quad (16-43)$$

where, because integration is over A , M_s is mass of adsorbent, units for n and A are mol and m^2 (rather than mol/kg and m^2/kg), and $K_i p_i / (n_i/M_s) = 1$ is the linear lower limit approached for the ideal surface gas [see Eqs. (16-12) and (16-20)].

Ion Exchange—Stoichiometry In most applications, except for some weak-electrolyte and some concentrated-solution cases, the following summations apply:

$$\sum_i z_i c_i = c_{\text{tot}} = \text{const} \quad \sum_i z_i n_i = n_{\text{tot}} = \text{const} \quad (16-44a)$$

In equivalent-fraction terms, the sums become

$$\sum_i c_i^* = 1 \quad \sum_i n_i^* = 1 \quad (16-44b)$$

Mass Action Here the equilibrium relations, consistent with Eq. (16-25), are

$$K'_{ij} = \left(\frac{n_i^*}{c_i^*} \right)^{z_j} \left(\frac{c_j^*}{n_j^*} \right)^{z_i} \quad (16-45)$$

For an N -species system, with N c^* 's (or n^* 's) known, the N n^* 's (or c^* 's) can be found by simultaneous solution of the $N - 1$ independent i, j combinations for Eq. (16-45) using Eq. (16-44a); one n_j^*/c_j^* is assumed, the other values can be calculated using Eq. (16-45), and the sum of the trial n^* 's (or c^* 's) is compared with Eq. (16-44b).

Because an N -component system has $N - 1$ independent concentrations, a three-component equilibrium can be plotted in a plane and a four-component equilibrium in a three-dimensional space. Figure 16-8 shows a triangular plot of c^* contours in equilibrium with the corresponding n^* coordinates.

Improved models for ion-exchange equilibria are in Smith and Woodburn [*AIChE J.*, **24**, 577 (1978)]; Mehablia et al. [*Chem. Eng. Sci.*, **49**, 2277 (1994)]; Soldatov [in Dorfner, gen. refs.]; Novosad and Myers, [*Can J. Chem. Eng.*, **60**, 500 (1982)]; and Myers and Byington [in Rodrigues, ed., *Ion Exchange: Science and Technology*, NATO ASI Series, No. 107, Nijhoff, Dordrecht, 1986, pp. 119-145].

Constant Separation-Factor Treatment If the valences of all species are equal, the separation factor α_{ij} applies, where

$$\alpha_{ij} = K_{ij} = \frac{n_i^* c_j^*}{c_i^* n_j^*} \quad (16-46)$$

For a binary system, $r = \alpha_{BA} = 1/\alpha_{AB}$. The symbol r applies primarily to the process, while α is oriented toward interactions between pairs of solute species. For each binary pair, $r_{ij} = \alpha_{ij} = 1/\alpha_{ji}$. Equilibrium then is given explicitly by

$$n_i^* = \frac{c_i^*}{\sum_j \alpha_{ji} c_j^*} = \frac{\alpha_{iN} c_i^*}{\sum_j \alpha_{jN} c_j^*} \quad (16-47)$$

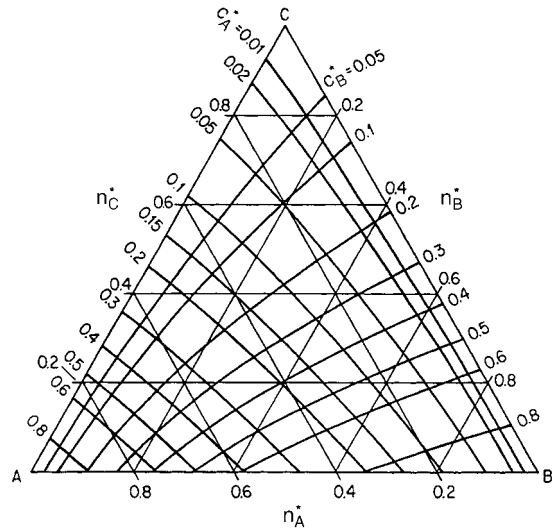


FIG. 16-8 Ideal mass-action equilibrium for three-component ion exchange with unequal valences. $K'_{A,C} = 8.06$; $K'_{B,C} = 3.87$. Duolite C-20 polystyrenesulfonate resin, with Ca as A, Mg as B, and Na as C. [*Klein et al.*, *Ind. Eng. Chem. Fund.*, **6**, 339 (1967); reprinted with permission.]

and

$$c_i^* = \frac{n_i^*}{\sum_j \alpha_{ij} n_j^*} = \frac{\alpha_{Ni} n_i^*}{\sum_j \alpha_{Nj} n_j^*} \quad (16-48)$$

For the constant separation factor case, the c^* contours in a plot like Fig. 16-8 are linear.

CONSERVATION EQUATIONS

Material balances, often an energy balance, and occasionally a momentum balance are needed to describe an adsorption process. These are written in various forms depending on the specific application and desire for simplicity or rigor. Reasonably general material balances for various processes are given below. An energy balance is developed for a fixed bed for gas-phase application and simplified for liquid-phase application. Momentum balances for pressure drop in packed beds are given in Sec. 6.

MATERIAL BALANCES

At a microscale, a sorbable component exists at three locations—in a sorbed phase, in pore fluid, and in fluid outside particles. As a consequence, in material balances time derivatives must be included of terms involving n_i , c_{pi} (the pore concentration), and c_i (the extraparticle concentration). Let \bar{n}_i represent n_i averaged over particle volume, and let \bar{c}_{pi} represent c_{pi} averaged over pore fluid volume.

For batch or stirred tank processes, in terms of the mass of adsorbent M_s (kg), extraparticle volume of fluid V_f (m^3), and volumetric flow rates F_v (m^3/s) in and out of a tank, the material balance on component i is

$$M_s \frac{d\hat{n}_i}{dt} + \frac{d(V_f c_i)}{dt} = F_{v,in} c_{i,in} - F_{v,out} c_i \quad (16-49)$$

with

$$\hat{n}_i = \bar{n}_i + (\epsilon_p/\rho_p) \bar{c}_{pi} = \bar{n}_i + [(1 - \epsilon)\epsilon_p/\rho_b] \bar{c}_{pi} \quad (16-50)$$

where ρ_p and ρ_b are particle and bulk densities, and ϵ and ϵ_p are void fraction (extra particle volume fraction) and particle porosity, respectively.

For a fixed-bed process, the material balance for component i is

$$\rho_b \frac{\partial \hat{n}_i}{\partial t} + \epsilon \frac{\partial c_i}{\partial t} + \epsilon \frac{\partial(v c_i)}{\partial z} = \epsilon D_L \frac{\partial}{\partial z} \left(c \frac{\partial y_i}{\partial z} \right) \quad (16-51)$$

where v is interstitial fluid velocity, D_L is a Fickian axial dispersion coefficient, and $y_i = c_i/c$ is the fluid-phase mole fraction of component i . In certain applications such as adsorption of biological molecules in gels, where the density of the adsorbent material is not known, the group $\rho_b \hat{n}_i$ in the first term of Eq. (16-51) can be replaced by $(1 - \epsilon) q_i$, where q_i has units of $\text{mol}/(\text{m}^3 \text{ of adsorbent})$. An alternative form, grouping together fluid-phase concentrations rather than intraparticle concentrations, is

$$\rho_b \frac{\partial \bar{n}_i}{\partial t} + \epsilon_b \frac{\partial c_i}{\partial t} + \epsilon \frac{\partial(v c_i)}{\partial z} = \epsilon D_L \frac{\partial}{\partial z} \left(c \frac{\partial y_i}{\partial z} \right) \quad (16-52)$$

16-18 ADSORPTION AND ION EXCHANGE

where, noting Eq. (16-4), \hat{c}_i is defined by

$$\varepsilon_b \hat{c}_i = \varepsilon c_i + (1 - \varepsilon) \varepsilon_p \bar{c}_{pi} \quad (16-53)$$

For moving-bed processes, we add a term to Eq. (16-51) to obtain

$$\rho_b \left[\frac{\partial \hat{n}_i}{\partial t} + v_s \frac{\partial \hat{n}_i}{\partial z} \right] + \varepsilon \left[\frac{\partial c_i}{\partial t} + \frac{\partial (vc_i)}{\partial z} - D_L \frac{\partial}{\partial z} \left(c \frac{\partial y_i}{\partial z} \right) \right] = 0 \quad (16-54)$$

where v_s is the solid-phase velocity (opposite in sign to v for a countercurrent process).

ENERGY BALANCE

Many different forms of the energy balance have been used in fixed-bed adsorption studies. The form chosen for a particular study depends on the process considered (e.g., temperature swing adsorption or pressure swing adsorption) and on the degree of approximation that is appropriate [see Walton and LeVan, *Ind. Eng. Chem. Research*, **42**, 6938 (2003); **44**, 7474 (2005)].

An energy balance for a fixed-bed process, ignoring dispersion, is

$$\rho_b \frac{\partial u_s}{\partial t} + \frac{\partial (\varepsilon_b \hat{c}_i u_{fi})}{\partial t} + \frac{\partial (\varepsilon v c h_f)}{\partial z} = - \frac{2h_w(T - T_w)}{r_c} \quad (16-55)$$

where h_w is a heat transfer coefficient for energy transfer with the column wall and r_c is the radius of the column. The second term of Eq. (16-55) combines contributions from both pore and extraparticle fluid.

Thermodynamic paths are necessary to evaluate the enthalpy (or internal energy) of the fluid phase and the internal energy of the stationary phase. For gas-phase processes at low and modest pressures, the enthalpy departure function for pressure changes can be ignored and a reference state for each pure component chosen to be ideal gas at temperature T^{ref} , and a reference state for the stationary phase (adsorbent plus adsorbate) chosen to be adsorbate-free solid at T^{ref} . Thus, for the gas phase we have

$$h_f = \sum_i y_i h_{fi} = \sum_i y_i \left[h_{fi}^{\text{ref}} + \int_{T^{\text{ref}}}^T C_{pfi}^{\circ} dT \right] \quad (16-56)$$

$$u_f = h_f - P/c \quad (16-57)$$

and for the stationary phase

$$u_s = u_{\text{sol}} + nu_a \approx u_{\text{sol}} + nh_a \quad (16-58)$$

$$u_{\text{sol}} = u_{\text{sol}}^{\text{ref}} + \int_{T^{\text{ref}}}^T C_s dT \quad (16-59)$$

The enthalpy of the adsorbed phase h_a is evaluated along a path for which the gas-phase components undergo temperature change from T^{ref} to T and then are adsorbed isothermally, giving

$$h_a = \sum_i x_i h_{pi} - \left(\frac{1}{n} \right) \sum_i \int_0^{n_i} q_i^{\text{st}}(n_i, n_j, T) dn_i \quad (16-60)$$

The isosteric heat of adsorption q_i^{st} is composition-dependent, and the sum of integrals in Eq. (16-60) is difficult to evaluate for multicomponent adsorption if the isosteric heats indeed depend on loading. Because each isosteric heat depends on the loadings of all components, the sum must be evaluated for a path beginning with clean adsorbent and ending with the proper loadings of all components. If the isosteric heat of adsorption is constant, as is commonly assumed, then the energy balance [Eq. (16-55)] becomes

$$\left[\rho_b \left(C_s + \sum_i n_i C_{pfi}^{\circ} \right) + \varepsilon_b c C_{pff}^{\circ} \right] \frac{\partial T}{\partial t} - \rho_b \sum_i q_i^{\text{st}} \frac{\partial n_i}{\partial t} - \frac{\partial (\varepsilon_b P)}{\partial t} + \varepsilon v c C_{pff}^{\circ} \frac{\partial T}{\partial z} = - \frac{2h_w(T - T_w)}{r_c} \quad (16-61)$$

where Eq. (16-52) with $D_L = 0$ has been used. Equation (16-61) is a popular form of the energy balance for fixed-bed adsorption calculations. Often the first summation on the left-hand side, which involves gas-phase heat capacities, is neglected, or the gas-phase heat capacities are replaced by adsorbed-phase heat capacities. It is also possible to estimate the adsorbed-phase heat capacities from thermodynamic paths given gas-phase heat capacities and temperature-dependent adsorption equilibrium [Walton and LeVan, *Ind. Eng. Chem. Research*, **44**, 178 (2005)].

Nonisothermal liquid-phase processes may be driven by changes in feed temperature or heat addition or withdrawal through a column wall. For these, heats of adsorption and pressure effects are generally of less concern. For this case a suitable energy balance is

$$(\rho_b C_s + \varepsilon_b c C_{pff}^{\circ}) \frac{\partial T}{\partial t} + \varepsilon v c C_{pff}^{\circ} \frac{\partial T}{\partial z} = - \frac{2h_w(T - T_w)}{r_c} \quad (16-62)$$

RATE AND DISPERSION FACTORS

The performance of adsorption processes results in general from the combined effects of thermodynamic and rate factors. It is convenient to consider first thermodynamic factors. These determine the process performance in a limit where the system behaves ideally; i.e. without mass transfer and kinetic limitations and with the fluid phase in perfect piston flow. **Rate factors** determine the efficiency of the real process in relation to the ideal process performance. Rate factors include heat- and mass-transfer limitations, reaction kinetic limitations, and hydrodynamic dispersion resulting from the velocity distribution across the bed and from mixing and diffusion in the interparticle void space.

TRANSPORT AND DISPERSION MECHANISMS

Figure 16-9 depicts porous adsorbent particles in an adsorption bed with sufficient generality to illustrate the nature and location of individual transport and dispersion mechanisms. Each mechanism involves a different driving force and, in general, gives rise to a different form of mathematical result.

Intraparticle Transport Mechanisms Intraparticle transport may be limited by *pore diffusion*, *solid diffusion*, *reaction kinetics* at phase boundaries, or two or more of these mechanisms together.

1. *Pore diffusion in fluid-filled pores.* These pores are sufficiently large that the adsorbing molecule escapes the force field of the adsorbent surface. Thus, this process is often referred to as *macropore diffusion*. The driving force for such a diffusion process can be approximated by the gradient in mole fraction or, if the molar concentration is constant, by the gradient in concentration of the diffusing species within the pores.

2. *Solid diffusion in the adsorbed phase.* Diffusion in pores sufficiently small that the diffusing molecule never escapes the force field of the adsorbent surface. In this case, transport may occur by an activated process involving jumps between adsorption sites. Such a process is often called *surface diffusion* or, in the case of zeolites, *micropore* or *intracrystalline* diffusion. The driving force for the process can thus be approximated by the gradient in concentration of the species in its adsorbed state. Phenomenologically, the process is not distinguishable from that of homogeneous diffusion that occurs inside a sorbent gel or in a pore-filling fluid that is immiscible with the external fluid. The generic term *solid diffusion* is used here to encompass the general traits of these physically different systems.

3. *Reaction kinetics at phase boundaries.* Rates of adsorption and desorption in porous adsorbents are generally controlled by mass

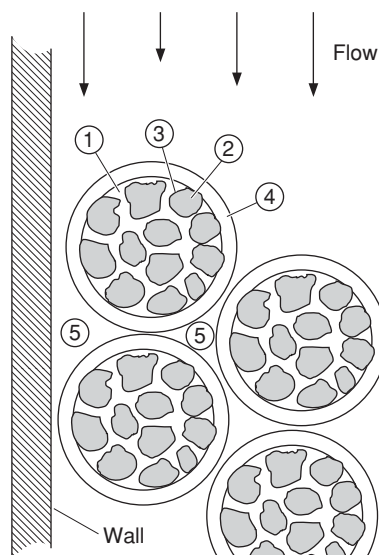


FIG. 16-9 General scheme of adsorbent particles in a packed bed showing the locations of mass transfer and dispersive mechanisms. Numerals correspond to numbered paragraphs in the text: 1, pore diffusion; 2, solid diffusion; 3, reaction kinetics at phase boundary; 4, external mass transfer; 5, fluid mixing.

transfer within the pore network rather than by the kinetics of sorption at the surface. Exceptions are the cases of chemisorption and affinity-adsorption systems used for biological separations, where the kinetics of bond formation can be exceedingly slow.

Intraparticle convection can also occur in packed beds when the adsorbent particles have very large and well-connected pores. Although, in general, bulk flow through the pores of the adsorbent particles is only a small fraction of the total flow, intraparticle convection can affect the transport of very slowly diffusing species such as macromolecules. The driving force for convection, in this case, is the pressure drop across each particle that is generated by the frictional resistance to flow experienced by the fluid as this flows through the packed bed [Rodrigues et al., *Chem. Eng. Sci.*, **46**, 2765 (1991); Carta et al., *Sep. Technol.*, **2**, 62 (1992); Frey et al., *Biotechnol. Progr.*, **9**, 273 (1993); Liapis and McCoy, *J. Chromatogr.*, **599**, 87 (1992)]. Intraparticle convection can also be significant when there is a total pressure difference between the center of the particle and the outside, such as is experienced in pressurization and depressurization steps of pressure swing adsorption or when more gas is drawn into an adsorbent to equalize pressure as adsorption occurs from the gas phase within a porous particle [Lu et al., *AIChE J.*, **38**, 857 (1992); Lu et al., *Gas Sep. Purif.*, **6**, 89 (1992); Taqvi et al., *Adsorption*, **3**, 127 (1997)].

Extraparticle Transport and Dispersive Mechanisms Extraparticle mechanisms are affected by the design of the contacting device and depend on the hydrodynamic conditions outside the particles.

4. *External mass transfer* between the external surfaces of the adsorbent particles and the surrounding fluid phase. The driving force is the concentration difference across the boundary layer that surrounds each particle, and the latter is affected by the hydrodynamic conditions outside the particles.

5. *Mixing*, or lack of mixing, between different parts of the contacting equipment. This may occur through the existence of a velocity distribution or dead zones in a packed bed or through inefficient mixing in an agitated contactor. In packed-bed adsorbers, mixing is often described in terms of an axial dispersion coefficient whereby all mechanisms contributing to axial mixing are lumped together in a single effective coefficient.

Heat Transfer Since adsorption is generally accompanied by the evolution of heat, the rate of heat transfer between the adsorbent

particles and the fluid phase may be important. In addition, heat transfer can occur across the column wall in small diameter beds and is important in energy applications of adsorption. In gas adsorption systems, even with highly porous particles, the controlling heat transfer resistance is generally associated with extraparticle transport [Lee and Ruthven, *Can. J. Chem. Eng.*, **57**, 65 (1979)], so that the temperature within the particles is essentially uniform. In liquid-phase adsorption, intraparticle and extraparticle heat transfer resistances are generally comparable. However, in this case the heat capacity of the fluid phase is sufficiently high that temperature effects may be negligible except in extreme cases. General discussions of heat-transfer effects in adsorbents and adsorption beds are found in Suzuki (gen. refs., pp. 187–208 and pp. 275–290) and in Ruthven (gen. refs., pp. 189–198 and pp. 215–219).

INTRAPARTICLE MASS TRANSFER

The phenomenological aspects of diffusional mass transfer in adsorption systems can be described in terms of Fick's law:

$$J_i = -D_i(c_i) \frac{\partial c_i}{\partial x} \quad (16-63)$$

This expression can be used to describe both pore and solid diffusion so long as the driving force is expressed in terms of the appropriate concentrations. Although the driving force should be more correctly expressed in terms of chemical potentials, Eq. (16-63) provides a qualitatively and quantitatively correct representation of adsorption systems so long as the diffusivity is allowed to be a function of the adsorbate concentration. The diffusivity will be constant only for a thermodynamically ideal system, which is an adequate approximation for only a limited number of adsorption systems.

Pore Diffusion When fluid transport through a network of fluid-filled pores inside the particles provides access for solute adsorption sites, the diffusion flux can be expressed in terms of a pore diffusion coefficient D_{pi} as:

$$J_i = -\epsilon_p D_{pi} \frac{\partial c_{pi}}{\partial r} \quad (16-64)$$

D_{pi} is smaller than the diffusivity in a straight cylindrical pore as a result of the random orientation of the pores, which gives a longer diffusion path, and the variation in the pore diameter. Both effects are commonly accounted for by a tortuosity factor τ_p such that $D_{pi} = D_i/\tau_p$. In principle, predictions of the tortuosity factor can be made if the pore structure, pore size, and shape distributions are known (see Dullien, *Porous Media: Fluid Transport and Pore Structure*, Academic Press, NY, 1979). In some cases, approximate prediction can be obtained from the following equations.

Mackie and Meares, *Proc. Roy. Soc.*, **A232**, 498 (1955):

$$\tau_p = \frac{(2 - \epsilon_p)^2}{\epsilon_p} \quad (16-65a)$$

Wakao and Smith, *Chem. Eng. Sci.*, **17**, 825 (1962):

$$\tau_p = \frac{1}{\epsilon_p} \quad (16-65b)$$

Suzuki and Smith, *Chem. Eng. J.*, **3**, 256 (1972):

$$\tau_p = \epsilon_p + 1.5(1 - \epsilon_p) \quad (16-65c)$$

In practice, however, the predictive value of these equations is rather uncertain, and vastly different results are obtained from each. All of them, on the other hand, predict that τ_p increases as the porosity decreases.

For catalyst particles, Satterfield (*Heterogeneous Catalysis in Practice*, McGraw-Hill, 1980) recommends the use of a value of $\tau_p = 4$ when no other information is available, and this can be used for many adsorbents. In general, however, it is more reliable to treat the tortuosity as an empirical constant that is determined experimentally for any particular adsorbent.

For adsorbent materials, experimental tortuosity factors generally fall in the range 2–6 and generally decrease as the particle porosity is

increased. Higher apparent values may be obtained when the experimental measurements are affected by other resistances, while values much lower than 2 generally indicate that surface or solid diffusion occurs in parallel to pore diffusion.

Ruthven (gen. refs.) summarizes methods for the measurement of effective pore diffusivities that can be used to obtain tortuosity factors by comparison with the estimated pore diffusion coefficient of the adsorbate. Molecular diffusivities can be estimated with the methods in Sec. 6.

For gas-phase diffusion in small pores at low pressure, the molecular mean free path may be larger than the pore diameter, giving rise to Knudsen diffusion. Satterfield (*Mass Transfer in Heterogeneous Catalysis*, MIT, Cambridge, MA, 1970, p. 43) gives the following expression for the pore diffusivity:

$$D_{pi} = \frac{1}{\tau_p} \left[\frac{3}{4r_{\text{pore}}} \left(\frac{\pi M_{ri}}{2RT} \right)^{1/2} + \frac{1}{D_i} \right]^{-1} \quad (16-66)$$

where r_{pore} is the average pore radius, T the absolute temperature, and M_{ri} the molecular weight.

For liquid-phase diffusion of large adsorbate molecules, when the ratio $\lambda_m = r_m/r_{\text{pore}}$ of the molecule radius r_m to the pore radius is significantly greater than zero, the pore diffusivity is reduced by steric interactions with the pore wall and hydrodynamic resistance. When $\lambda_m < 0.2$, the following expressions derived by Brenner and Gaydos [*J. Coll. Int. Sci.*, **58**, 312 (1977)] for a hard sphere molecule (a particle) diffusing in a long cylindrical pore, can be used

$$D_{pi} = \frac{D_i}{\tau_p} (1 - \lambda_m)^{-2} \left[1 + \frac{9}{8} \lambda_m \ln \lambda_m - 1.539 \lambda_m \right] \quad (16-67)$$

r_m is the Stokes-Einstein radius of the solute that can be determined from the free diffusivity as

$$r_m = \frac{\kappa T}{6\pi\mu D_i} \quad (16-68)$$

where κ is the Boltzmann constant. When $\lambda_m > 0.2$, the centerline approximation [Anderson and Quinn, *Biophys. J.*, **14**, 130, (1974)] can be used instead of Eq. (16-67)

$$D_{pi} = \frac{D_i}{\tau_p} (1 - 2.1044\lambda_m + 2.089\lambda_m^3 - 0.984\lambda_m^5) \times 0.865 \quad (16-69)$$

The 0.865 factor is used to match this equation to the Brenner and Gaydos expression for $\lambda_m = 0.2$. In these cases, the pore concentration C_{pi} is related to the external concentration C_i by the partition ratio $(1 - \lambda_m)^2$.

Solid Diffusion In the case of pore diffusion discussed above, transport occurs within the fluid phase contained inside the particle; here the solute concentration is generally similar in magnitude to the external fluid concentration. A solute molecule transported by pore diffusion may attach to the sorbent and detach many times along its path. In other cases, attachment can be essentially permanent, but in both cases, only detached molecules undergo transport. In contrast, the following four instances illustrate cases where diffusion of adsorbate molecules occurs in their adsorbed state within phases that are distinct from the pore fluid:

1. Movement of mobile adsorbed solute molecules along pore surfaces, without detaching
2. Transport in a homogeneously dissolved state, as for a neutral molecule inside a sorbent gel or in a pore filled with a liquid which is immiscible with the external fluid
3. Ion transport in charged ion-exchange resins
4. Advance of an adsorbate molecule from one cage to another within a zeolite crystal

In these cases, the diffusion flux may be written in terms of the adsorbed solute concentration as

$$J_i = -\rho_p D_{si} \frac{\partial n_i}{\partial r} \quad (16-70)$$

The diffusion coefficient in these phases D_{si} is usually considerably smaller than that in fluid-filled pores; however, the adsorbate concentration is often much larger. Thus, the diffusion rate can be smaller or

larger than can be expected for pore diffusion, depending on the magnitude of the fluid/solid partition coefficient.

Numerical values for solid diffusivities D_{si} in adsorbents are sparse and vary greatly. Moreover, they may be strongly dependent on the adsorbed phase concentration of solute. Hence, locally conducted experiments and interpretation must be used to a great extent. Summaries of available data for surface diffusivities in activated carbon and other adsorbent materials and for micropore diffusivities in zeolites are given in Ruthven, Yang (1987), Suzuki, and Karger and Ruthven (gen. refs.).

Surface diffusivities are generally strongly dependent on the fractional surface coverage and increase rapidly at surface coverage greater than 80 percent [see, for example, Yang et al., *AIChE J.*, **19**, 1052 (1973)]. For estimation purposes, the correlation of Sladek et al. [*Ind. Eng. Chem. Fundam.*, **13**, 100 (1974)] can be used to predict surface diffusivities for gas-phase adsorption on a variety of adsorbents.

Zeolite crystallite diffusivities for sorbed gases range from 10^{-7} to 10^{-14} cm²/s. These diffusivities generally show a strong increase with the adsorbate concentration that is accounted for by the Darken thermodynamic correction factor

$$D_{si} = D_{oi} \frac{d \ln a_i}{d \ln n_i} \quad (16-71)$$

where D_{oi} is the corrected diffusivity and a_i the thermodynamic activity of the species in the adsorbed phase. Corrected diffusivities D_{oi} calculated according to this equation are often found to be essentially independent of concentration. If the adsorption equilibrium isotherm obeys the Langmuir equation [Eq. (16-13)], Eq. (16-71) yields:

$$D_{si} = D_{oi} \left(1 - \frac{n_i}{n_i^s} \right)^{-1} \quad (16-72)$$

The effect of temperature on diffusivities in zeolite crystals can be expressed in terms of the Eyring equation (see Ruthven, gen. refs.).

In ion-exchange resins, diffusion is further complicated by electrical coupling effects. In a system with M counterions, diffusion rates are described by the Nernst-Planck equations (Helfferich, gen. refs.). Assuming complete Donnan exclusion, these equations can be written as:

$$J_i = -\rho_p \frac{1}{z_i} \sum_{j=1}^{M-1} \bar{D}_{i,j} \frac{\partial z_j n_j}{\partial r} \quad (16-73)$$

$$\text{with } \bar{D}_{i,j} = -\frac{\bar{D}_i(\bar{D}_j - \bar{D}_M)z_i^2 n_i}{\sum_{k=1}^M \bar{D}_k z_k^2 n_k} \quad (16-74a)$$

$$\bar{D}_{i,i} = \bar{D}_i - \frac{\bar{D}_i(\bar{D}_i - \bar{D}_M)z_i^2 n_i}{\sum_{k=1}^M \bar{D}_k z_k^2 n_k} \quad (16-74b)$$

which are dependent on the **ionic self diffusivities** \bar{D}_i of the individual species. As a qualitative rule, ionic diffusivities of inorganic species in crosslinked polystyrene-DVB ion-exchange resins compared with those in water are 1:10 for monovalent ions, 1:100 for divalent ions, and 1:1000 for trivalent ions. Table 16-8 shows typical ionic diffusivities of inorganic ions in cation and anion exchange resins; larger organic ions, however, can have ionic diffusivities much smaller than inorganic ions of the same valence [see, for example, Jones and Carta, *Ind. Eng. Chem. Research*, **32**, 117 (1993)].

For mixtures of unlike ions (the usual case), the apparent diffusivity will be intermediate between these values because of the electrical coupling effect. For a system with two counterions A and B, with charge z_A and z_B , Eqs. (16-73) and (16-74) reduce to:

$$J_A = -\rho_p \bar{D}_{A,B} \frac{\partial n_A}{\partial r} = -\rho_p \frac{\bar{D}_A \bar{D}_B [z_A^2 n_A + z_B^2 n_B]}{z_A^2 \bar{D}_A n_A + z_B^2 \bar{D}_B n_B} \frac{\partial n_A}{\partial r} \quad (16-75)$$

which shows that the apparent diffusivity $\bar{D}_{A,B}$ varies between \bar{D}_A when the ionic fraction of species A in the resin is very small and \bar{D}_B when the ionic fraction of A in the resin approaches unity, indicating that the ion present in smaller concentration has the stronger effect on the local interdiffusion rate.

TABLE 16-8 Self Diffusion Coefficients in Polystyrene-Divinylbenzene Ion Exchangers (Units of 10⁻⁷ cm²/s)*

Temperature	0.3 °C					25 °C				
Crosslinking, %	4	6	8	12	16	4	6	8	12	16
Cation exchangers (sulfonated): Dowex 50										
Na ⁺	6.7		3.4	1.15	0.66	14.1		9.44		2.40
Cs ⁺			6.6		1.11			13.7		3.10
Ag ⁺			2.62		1.00			6.42		2.75
Zn ²⁺			0.21		0.03			0.63		0.14
La ³⁺	0.30		0.03		0.002			0.092		0.005
Anion exchangers (dimethyl hydroxyethylamine): Dowex 2										
Cl ⁻		1.25					3.54			
Br ⁻	(1.8)	1.50	0.63		0.06	(4.3)	3.87	2.04		0.26
I ⁻		0.35					1.33			
BrO ₃ ⁻		1.76					4.55			
WO ₄ ²⁻		0.60					1.80			
PO ₄ ³⁻		0.16					0.57			

*Data from Boyd and Soldano, *J. Am. Chem. Soc.*, **75**, 6091 (1953).

Combined Pore and Solid Diffusion In porous adsorbents and ion-exchange resins, intraparticle transport can occur with pore and solid diffusion in parallel. The dominant transport process is the faster one, and this depends on the relative diffusivities and concentrations in the pore fluid and in the adsorbed phase. Often, equilibrium between the pore fluid and the solid phase can be assumed to exist locally at each point within a particle. In this case, the mass-transfer flux is expressed by:

$$J_i = - \left[\epsilon_p D_{pi} + \rho_p D_{si} \frac{dn_i^e}{dc_i} \right] \frac{\partial c_{pi}}{\partial r} = -D_{ei}(c_{pi}) \frac{\partial c_{pi}}{\partial r} \quad (16-76)$$

where dn_i^e/dc_i is the derivative of the adsorption isotherm and it has been assumed that at equilibrium $c_{pi} = c_i$. This equation suggests that in such an adsorbent, pore and solid diffusivities can be obtained by determining the apparent diffusivity D_{ei} for conditions of no adsorption ($dn_i^e/dc_i = 0$) and for conditions of strong adsorption, where dn_i^e/dc_i is large. If the adsorption isotherm is linear over the range of experimental measurement:

$$D_{ei} = \epsilon_p D_{pi} + \rho_p K_i D_{si} \quad (16-77)$$

Thus, a plot of the apparent diffusivity versus the linear adsorption equilibrium constant should be linear so long as D_{pi} and D_{si} remain constant.

In a particle having a **bidispersed pore structure** comprising spherical adsorptive subparticles of radius r_s , forming a macroporous aggregate, separate flux equations can be written for the macroporous network in terms of Eq. (16-64) and for the subparticles themselves in terms of Eq. (16-70) if solid diffusion occurs.

EXTERNAL MASS TRANSFER

Because of the complexities encountered with a rigorous treatment of the hydrodynamics around particles in industrial contactors, mass transfer to and from the adsorbent is described in terms of a mass-transfer coefficient k_f . The flux at the particle surface is:

$$N_i = k_f(c_i - c_i^s) \quad (16-78)$$

where c_i and c_i^s are the solute concentrations in the bulk fluid and at the particle surface, respectively. k_f can be estimated from available correlations in terms of the Sherwood number $Sh = k_f d_p / D_i$ and the Schmidt number $Sc = \nu / D_i$. For packed-bed operations, the correlations in Table 16-9 are recommended. A plot of these equations is given in Fig. 16-10 for representative ranges of Re and Sc with $\epsilon = 0.4$.

External mass-transfer coefficients for particles suspended in agitated contactors can be estimated from equations in Levins and Glasstonbury [*Trans. Instn. Chem. Eng.*, **50**, 132 (1972)] and Armenante and Kirwan [*Chem. Eng. Sci.*, **44**, 2871 (1989)].

AXIAL DISPERSION IN PACKED BEDS

The axial dispersion coefficient [cf. Eq. (16-51)] lumps together all mechanisms leading to axial mixing in packed beds. Thus, the axial dispersion coefficient must account not only for molecular diffusion and convective mixing but also for nonuniformities in the fluid velocity across the packed bed. As such, the axial dispersion coefficient is best determined experimentally for each specific contactor.

The effects of **flow nonuniformities**, in particular, can be severe in gas systems when the ratio of bed-to-particle diameters is small; in liquid systems when viscous fingering occurs as a result of large

TABLE 16-9 Recommended Correlations for External Mass Transfer Coefficients in Adsorption Beds ($Re = \epsilon v d_p / \nu$, $Sc = \nu / D$)

Equation	Re	Phase	Ref.
$Sh = 1.15 \left(\frac{Re}{\epsilon} \right)^{0.5} Sc^{0.33}$	$Re > 1$	Gas/liquid	Carberry, <i>AIChE J.</i> , 6 , 460 (1960)
$Sh = 2.0 + 1.1 Re^{0.6} Sc^{0.33}$	$3 < Re < 10^4$	Gas/liquid	Wakao and Funazkri, <i>Chem. Eng. Sci.</i> , 33 , 1375 (1978)
$Sh = 1.85 \left(\frac{1 - \epsilon}{\epsilon} \right)^{0.33} Re^{0.33} Sc^{0.33}$	$Re < 40$	Liquid	Kataoka et al., <i>J. Chem. Eng. Japan</i> , 5 , 132 (1972)
$Sh = \frac{1.09}{\epsilon} Re^{0.33} Sc^{0.33}$	$0.0015 < Re < 55$	Liquid	Wilson and Geankoplis, <i>Ind. Eng. Chem. Fundam.</i> , 5 , 9 (1966)
$Sh = \frac{0.25}{\epsilon} Re^{0.69} Sc^{0.33}$	$55 < Re < 1050$	Liquid	Wilson and Geankoplis, <i>Ind. Eng. Chem. Fundam.</i> , 5 , 9 (1966)

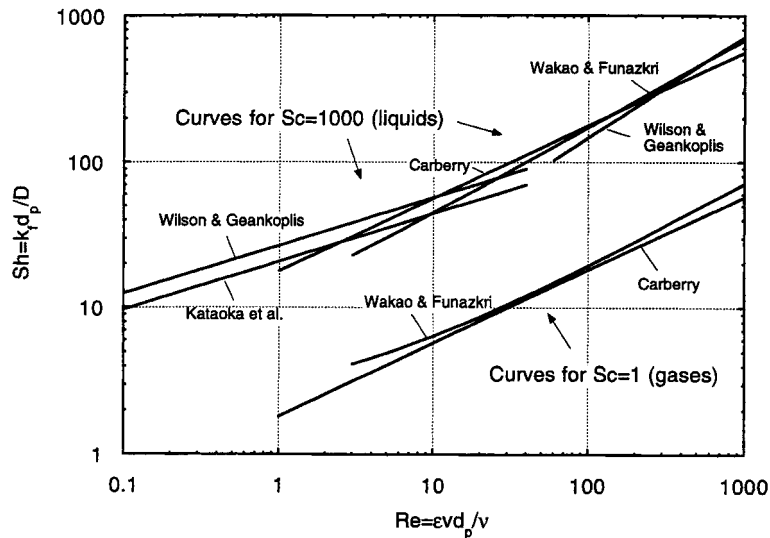


FIG. 16-10 Sherwood number correlations for external mass-transfer coefficients in packed beds for $\epsilon = 0.4$. (Adapted from Suzuki, *gen. refs.*)

viscosity gradients in the adsorption bed; when very small particles ($<50 \mu\text{m}$) are used, such as in high performance liquid chromatography systems; and in large-diameter beds. A lower bound of the axial dispersion coefficient can be estimated for well-packed beds from correlations that follow.

Neglecting flow nonuniformities, the contributions of molecular diffusion and turbulent mixing arising from stream splitting and recombination around the sorbent particles can be considered additive [Langer et al., *Int. J. Heat and Mass Transfer*, **21**, 751 (1978)]; thus, the axial dispersion coefficient D_L is given by:

$$\frac{D_L}{D_i} = \gamma_1 + \gamma_2 \frac{d_p v}{D_i} = \gamma_1 + \gamma_2 \frac{(Re)(Sc)}{\epsilon} \quad (16-79)$$

or, in terms of a particle-based Peclet number ($Pe = d_p v / D_L$), by:

$$\frac{1}{Pe} = \frac{\gamma_1 \epsilon}{(Re)(Sc)} + \gamma_2 \quad (16-80)$$

The first term in Eqs. (16-79) and (16-80) accounts for molecular diffusion, and the second term accounts for mixing. For the first term, Wicke [Ber. Bunsenges, **77**, 160 (1973)] has suggested:

$$\gamma_1 = 0.45 + 0.55\epsilon \quad (16-81)$$

which, for typical void fractions, $\epsilon = 0.35 - 0.5$ gives $\gamma_1 = 0.64 - 0.73$ (Ruthven, *gen. refs.*). Expressions for the axial mixing term, γ_2 in Eq. (16-79) are given in Table 16-10. The expression of Wakao and Funazkri includes an axial diffusion term, γ_1 , that varies from 0.7 for nonporous particles to $20/\epsilon$, depending on the intraparticle mass-transfer mechanism. For strongly adsorbed species, Wakao and Funazkri suggest that the effective axial dispersion coefficient is much larger than that predicted on the basis of nonporous, nonadsorbing particles. The Gunn expression includes a term σ_v^2 accounting for deviations from plug flow. σ_v^2 is defined as the dimensionless variance of the distribution of the ratio of velocity to average velocity over the cross section of the bed. The parameter values included in this equation are valid for spherical particles. Values for nonspherical particles can be found in the original reference.

Figure 16-11 compares predicted values of D_L/D_i for $\sigma_v = 0$ and $\epsilon = 0.4$ with $Sc = 1$ (gases at low pressure), and $Sc = 1000$ (liquids), based on the equations in Table 16-10.

Correlations for axial dispersion in beds packed with very small particles ($<50 \mu\text{m}$) that take into account the holdup of liquid in a bed are discussed by Horvath and Lin [*J. Chromatogr.*, **126**, 401 (1976)].

RATE EQUATIONS

Rate equations are used to describe interphase mass transfer in batch systems, packed beds, and other contacting devices for sorptive processes and are formulated in terms of fundamental transport properties of adsorbent and adsorbate.

General Component Balance For a spherical adsorbent particle:

$$\epsilon_p \frac{\partial c_{pi}}{\partial t} + \rho_p \frac{\partial n_i}{\partial t} = \frac{1}{r^2} \frac{\partial}{\partial r} (-r^2 N_i) \quad (16-82)$$

For particles that have no macropores, such as gel-type ion-exchange resins, or when the solute holdup in the pore fluid is small, ϵ_p may be taken as zero. Ignoring bulk flow terms, the fluxes N_i and J_i are equal. In this case, coupling the component balance with the flux expressions previously introduced gives the rate equations in Table 16-11. Typical boundary conditions are also included in this table. Generally, these equations apply to particles that can be approximated as spherical and of a uniform size and properties. An appropriately chosen mean particle size must be used in these equations when dealing with adsorbents having a broad particle size distribution. The appropriate average depends on the controlling mass-transfer mechanism. For intraparticle mass-transfer mechanisms, the volume or mass-average particle size usually provides the best prediction.

Linear Driving Force Approximation Simplified expressions can also be used for an approximate description of adsorption in terms of rate coefficients for both extraparticle and intraparticle mass transfer controlling. As an approximation, the rate of adsorption on a particle can be written as:

$$\frac{\partial \hat{n}_i}{\partial t} = k f(n_i, c_i) \quad (16-83)$$

where k is a rate coefficient, and the function $f(n_i, c_i)$ is a driving force relationship. The variables k_c and k_n are used to denote rate coefficients based on fluid-phase and adsorbed-phase concentration driving forces, respectively.

TABLE 16-10 Coefficients for Axial Dispersion Correlations in Packed Beds Based on Eq. (16-79)

γ_1	γ_2	Ref.
0.73	$0.5 \left(1 + \frac{13\gamma_1\epsilon}{ReSc} \right)^{-1}$	Edwards and Richardson, <i>Chem. Eng. Sci.</i> , 23 , 109 (1968)
Nonporous particles: 0.7 Porous particles: $\leq 20/\epsilon$	0.5	Wakao and Funazkri, <i>Chem. Eng. Sci.</i> , 33 , 1375 (1978)
1	$\frac{3}{4}\epsilon + \frac{\pi^2\epsilon(1-\epsilon)}{6} \ln(ReSc)$	Koch and Brady, <i>J. Fluid Mech.</i> , 154 , 399 (1985)
0.714	$\frac{\sigma_v^2}{2} + (1 + \sigma_v^2) \left\{ \gamma(1-p)^2 + \gamma^2 p(1-p)^3 \left[e^{-\frac{1}{\gamma p(1-p)}} - 1 \right] \right\}$ with $\gamma = 0.043 ReSc/(1-\epsilon)$ $p = 0.33 \exp(-24/Re) + 0.17$	Gunn, <i>Chem. Eng. Sci.</i> , 2 , 363 (1987)

Commonly used forms of this rate equation are given in Table 16-12, where $\Lambda = \rho_p n_1^{ref}/c_1^{ref}$ is the partition ratio based on the feed concentration as a reference [cf. Eq. (16-125)]. For adsorption bed calculations with constant separation factor systems, somewhat improved predictions are obtained using correction factors ψ_s and ψ_p defined in Table 16-12.

The linear driving force (LDF) approximation is obtained when the driving force is expressed as a concentration difference. It was originally developed to describe packed-bed dynamics under linear equilibrium conditions [Glueckauf, *Trans. Far. Soc.*, **51**, 1540 (1955)]. This form is exact for a nonlinear isotherm only when external mass transfer is controlling. However, it can also be used for nonlinear systems with pore or solid diffusion mechanisms as an approximation, since it provides qualitatively correct results.

Alternate driving force approximations, item 2B in Table 16-12 for solid diffusion, and item 3B in Table 16-12 for pore diffusion, provide somewhat more accurate results in constant pattern packed-bed calculations with pore or solid diffusion controlling for constant separation factor systems.

The reaction kinetics approximation is mechanically correct for systems where the reaction step at pore surfaces or other fluid-solid interfaces is controlling. This may occur in the case of chemisorption on porous catalysts and in affinity adsorbents that involve very slow binding steps. In these cases, the mass-transfer parameter k is replaced

by a second-order reaction rate constant k_a . The driving force is written for a constant separation factor isotherm (column 4 in Table 16-12). When diffusion steps control the process, it is still possible to describe the system by its apparent second-order kinetic behavior, since it usually provides a good approximation to a more complex exact form for single transition systems (see "Fixed Bed Transitions").

Combined Intraparticle Resistances When solid diffusion and pore diffusion operate in parallel, the effective rate is the sum of these two rates. When solid diffusion predominates, mass transfer can be represented approximately in terms of the LDF approximation, replacing k_n in column 2 of Table 16-12 with

$$k_n^c = \frac{15\psi_s D_{si}}{r_p^2} + \frac{15(1-\epsilon)\psi_p \epsilon_p D_{pi}}{\Lambda r_p^2} \quad (16-84)$$

When pore diffusion predominates, use of column 3 in Table 16-12 is preferable, with k_n^c replacing k_n .

For particles with a **bidispersed pore structure**, the mass-transfer parameter k_n in the LDF approximation (column 2 in Table 16-12) can be approximated by the series-combination of resistances as:

$$\frac{1}{k_n} = \frac{1}{b_s} \left[\frac{\Lambda r_p^2}{15(1-\epsilon)\psi_p \epsilon_p D_{pi}} + \frac{r_s^2}{15\psi_s D_{si}} \right] \quad (16-85)$$

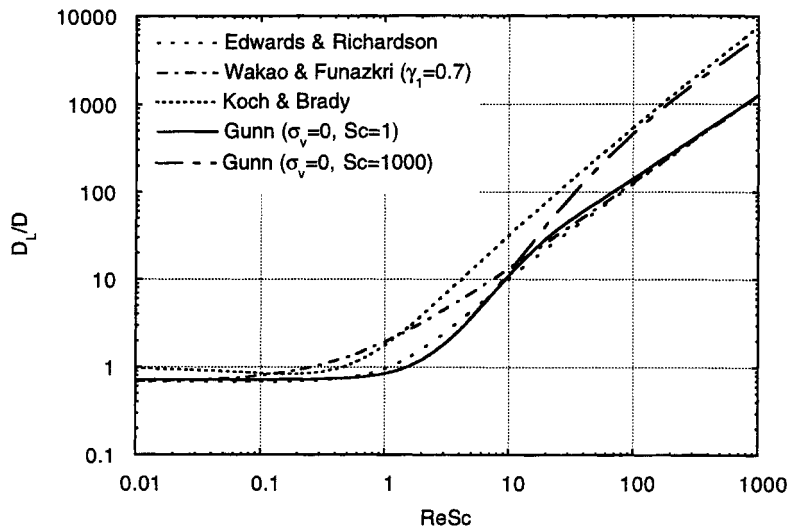


FIG. 16-11 Axial dispersion coefficient correlations for well-packed beds for $\epsilon = 0.4$.

16-24 ADSORPTION AND ION EXCHANGE

TABLE 16-11 Rate Equations for Description of Mass Transfer in Spherical Adsorbent Particles

Mechanism	Flux equation	Rate equation
A. Pore diffusion	16-64	$\epsilon_p \frac{\partial c_{pi}}{\partial t} + \rho_p \frac{\partial n_i}{\partial t} = \frac{1}{r^2} \frac{\partial}{\partial r} \left(\epsilon_p D_{pi} r^2 \frac{\partial c_{pi}}{\partial r} \right)$ $(\partial c_{pi} / \partial r)_{r=0} = 0, (\epsilon_p D_{pi} \partial c_{pi} / \partial r)_{r=r_p} = k_f (c_i - c_{pi _{r=r_p}})$ or $(c_{pi})_{r=r_p} = c_i$ for no external resistance
B. Solid diffusion	16-70	$\frac{\partial n_i}{\partial t} = \frac{1}{r^2} \frac{\partial}{\partial r} \left(D_{si} r^2 \frac{\partial n_i}{\partial r} \right)$ $(\partial n_i / \partial r)_{r=0} = 0, (\rho_p D_{si} \partial n_i / \partial r)_{r=r_p} = k_f (c_i - c_i^s)$ or $(n_i)_{r=r_p} = n_i^s (c_i)$ for no external resistance
C. Parallel pore and solid diffusion (local equilibrium between pore and adsorbed phase)	16-76	$\left(\epsilon_p + \rho_p \frac{dn_i^s}{dc_i} \right) \frac{\partial c_{pi}}{\partial t} = \frac{1}{r^2} \frac{\partial}{\partial r} \left[r^2 \left(\epsilon_p D_{pi} + \rho_p D_{si} \frac{dn_i^s}{dc_i} \right) \frac{\partial c_{pi}}{\partial r} \right]$ $(\partial c_{pi} / \partial r)_{r=0} = 0, [(\epsilon_p D_{pi} + \rho_p D_{si} \frac{dn_i^s}{dc_i}) \partial c_{pi} / \partial r]_{r=r_p} = k_f (c_i - c_{pi _{r=r_p}})$ or $(c_{pi})_{r=r_p} = c_i$ for no external resistance
D. Diffusion in bidispersed particles (no external resistance)	16-64 and 16-70	$\frac{\partial n_i}{\partial t} = \frac{1}{\rho^2} \frac{\partial}{\partial \rho} \left(D_{si} \rho^2 \frac{\partial n_i}{\partial \rho} \right), (\partial n_i / \partial \rho)_{\rho=0} = 0, (n_i)_{\rho=r_p} = n_i^s(c_{pi})$ $\bar{n}_i(r, t) = \frac{3}{r^3} \int_0^r \rho^2 n_i d\rho$ $\epsilon_p \frac{\partial c_{pi}}{\partial t} + \rho_p \frac{\partial \bar{n}_i}{\partial t} = \frac{1}{r^2} \frac{\partial}{\partial r} \left(\epsilon_p D_{pi} r^2 \frac{\partial c_{pi}}{\partial r} \right), (\partial c_{pi} / \partial r)_{r=0} = 0, (c_{pi})_{r=r_p} = c_i$

where b_s is a correction to the driving force that is described below. In the limiting cases where the controlling resistance is diffusion through the particle pores or diffusion within the subparticles, the rate coefficients $k_n = 15(1 - \epsilon)\psi_p \epsilon_p D_{pi} / \Lambda r_p^2$ and $k_n = 15\psi_s D_{si} / r_s^2$ are obtained.

Overall Resistance With a linear isotherm ($R = 1$), the overall mass transfer resistance is the sum of intraparticle and extraparticle resistances. Thus, the overall LDF coefficient for use with a particle-side

driving force (column 2 in Table 16-12) is:

$$\frac{1}{k_n^o} = \frac{\Lambda r_p}{3(1 - \epsilon)k_f} + \frac{1}{k_n^c} \quad (16-86)$$

or

$$\frac{1}{k_c^o} = \frac{\rho_b r_p}{3(1 - \epsilon)k_f} + \frac{\rho_b}{\Lambda k_n^c} \quad (16-87)$$

for use with a fluid-phase driving force (column 1 in Table 16-12).

TABLE 16-12 Expressions for Rate Coefficient k and Driving Force Relationships for Eq. (16-83)

Mechanism	1. External film	2. Solid diffusion	3. Pore diffusion	4. Reaction kinetics
Expression for rate coefficient, k	$k_c = \frac{k_f a}{\rho_b} = \frac{3(1 - \epsilon)k_f}{\rho_b r_p}$	$k_n = \frac{15\psi_s D_{si}}{r_p^2}$	$k_n = \frac{15\psi_p (1 - \epsilon)\epsilon_p D_{pi}}{\Lambda r_p^2}$	k_a
A. Linear driving force (LDF)	$c - c_i^e$	$n_i^e - \bar{n}_i$	$n_i^e - \bar{n}_i$	—
LDF for constant R	$c_i - \frac{Rc^{\text{ref}} \bar{n}_i / n_i^{\text{ref}}}{1 - (R - 1)\bar{n}_i / n_i^{\text{ref}}}$	$\frac{n_i^{\text{ref}} c_i / c_i^{\text{ref}}}{R + (R - 1)c_i / c_i^{\text{ref}}} - \bar{n}_i$	$\frac{n_i^{\text{ref}} c_i / c_i^{\text{ref}}}{R + (R - 1)c_i / c_i^{\text{ref}}} - \bar{n}_i$	—
Correction factors ψ for constant R	—	$\frac{0.894}{1 - 0.106R^{0.5}}$	$\frac{0.775}{1 - 0.225R^{0.5}}$	—
B. Alternate driving force for constant R	—	$\frac{n_i^{e2} - \bar{n}_i^2}{2\bar{n}_i}$	$\frac{n_i^e - \bar{n}_i}{[1 - (R - 1)\bar{n}_i / n_i^{\text{ref}}]^{0.5}}$	—
Correction factors ψ for alternate driving force	—	$\frac{0.590}{1 - 0.410R^{0.5}}$	$\frac{0.548}{1 - 0.452R^{0.5}}$	—
C. Reaction kinetics for constant R	—	—	—	$\frac{c_i(n_i^{\text{ref}} - \bar{n}_i) - R\bar{n}_i(c_i^{\text{ref}} - c_i)}{1 - R}$

References: 1A. Beaton and Fumas, *Ind. Eng. Chem.*, **33**, 1500 (1941); Michaels, *Ind. Eng. Chem.*, **44**, 1922 (1952)
 2A,3A. Glueckauf and Coates, *J. Chem. Soc.*, 1315 (1947); *Trans. Faraday Soc.*, **51**, 1540 (1955); Hall et al., *Ind. Eng. Chem. Fundam.*, **5**, 212 (1966)
 2B. Vermeulen, *Ind. Eng. Chem.*, **45**, 1664 (1953)
 3B. Vermeulen and Quilici, *Ind. Eng. Chem. Fundam.*, **9**, 179 (1970)
 4C. Hiester and Vermeulen, *Chem. Eng. Progr.*, **48**, 505 (1952)

In either equation, k_c^e is given by Eq. (16-84) for parallel pore and surface diffusion or by Eq. (16-85) for a bidispersed particle. For nearly linear isotherms ($0.7 < R < 1.5$), the same linear addition of resistance can be used as a good approximation to predict the adsorption behavior of packed beds, since solutions for all mechanisms are nearly identical. With a highly favorable isotherm ($R \rightarrow 0$), however, the rate at each point is controlled by the resistance that is locally greater, and the principle of additivity of resistances breaks down. For approximate calculations with intermediate values of R , an overall transport parameter for use with the LDF approximation can be calculated from the following relationship for solid diffusion and film resistance in series:

$$\frac{\Lambda r_p}{3(1-\epsilon)k_f} + \frac{r_p^2}{15\Psi_s D_{si}} = \frac{b_s}{k_n} = \frac{b_f \Lambda}{\rho_b k_c^o} \quad (16-88)$$

b_s and b_f are correction factors that are given by Fig. 16-12 as a function of the separation factor R and the mechanism parameter

$$\Psi = \frac{10\Psi_s D_{si} \Lambda}{D_i} \frac{1}{Sh} \quad (16-89)$$

Axial Dispersion Effects In adsorption bed calculations, axial dispersion effects are typically accounted for by the axial diffusion-like term in the bed conservation equations [Eqs. (16-51) and (16-52)]. For nearly linear isotherms ($0.5 < R < 1.5$), the combined effects of axial dispersion and mass-transfer resistances on the adsorption behavior of packed beds can be expressed approximately in terms of an apparent rate coefficient k_c for use with a fluid-phase driving force (column 1, Table 16-12):

$$\frac{1}{k_c} = \frac{\rho_b}{\epsilon} \frac{D_L}{v^2} + \frac{1}{k_c^o} \quad (16-90)$$

which extends the linear addition principle to combined axial dispersion and mass-transfer resistances. Even for a highly nonlinear isotherm ($R = 0.33$), the linear addition principle expressed by this equation provides a useful approximation except in the extreme case

of low mass-transfer resistance and large axial dispersion, when $D_L \rho_b k_c^o / v^2 \epsilon \gg 5$ [Garg and Ruthven, *Chem. Eng. Sci.*, **30**, 1192 (1975)]. However, when the isotherm is irreversible ($R \rightarrow 0$), the linear addition principle breaks down and axial dispersion has to be taken into account by explicit models (see "Fixed Bed Transitions").

Rapid Adsorption-Desorption Cycles For rapid cycles with particle diffusion controlling, when the cycle time t_c is much smaller than the time constant for intraparticle transport, the LDF approximation becomes inaccurate. The generalized expression

$$\frac{\partial \hat{n}_i}{\partial t} = \Omega k_n (n_i^e - \bar{n}_i) \quad (16-91)$$

can be used for packed-bed calculations when the parameter Ω is defined to be a function of the cycle time such that the amount of solute adsorbed and desorbed during a cycle is equal to that obtained by solution of the complete particle diffusion equations. Graphical and analytical expressions for Ω in the case of a single particle, usable for very short beds, are given by Nakao and Suzuki [*J. Chem. Eng. Japan*, **16**, 114 (1983)] and Carta [*Chem. Eng. Sci.*, **48**, 622 (1993)]. With equal adsorption and desorption times, $t_a = t_d = t_c/2$, Ω approaches the value $\pi^2/15$ for long cycle times and the asymptote $\Omega = 1.877/\sqrt{t_c k_n}$ for short cycle times [Alpay and Scott, *Chem. Eng. Sci.*, **47**, 499 (1992)]. However, other results by Raghavan et al. [*Chem. Eng. Sci.*, **41**, 2787 (1986)] indicate that a limiting constant value of Ω (larger than 1) is obtained for very short cycles, when calculations are carried out for beds of finite length.

Determination of Controlling Rate Factor The most important physical variables determining the controlling dispersion factor are particle size and structure, flow rate, fluid- and solid-phase diffusivities, partition ratio, and fluid viscosity. When multiple resistances and axial dispersion can potentially affect the rate, the spreading of a concentration wave in a fixed bed can be represented approximately in terms of the single rate parameter k . In customary separation-process calculations, the height of an adsorption bed can be calculated approximately as the product of the number of transfer units times the height of one fluid-phase transfer unit (HTU). The HTU is related to the LDF rate parameters k_c and k_n by:

$$HTU = \frac{\epsilon v}{\rho_b k_c} = \frac{\epsilon v}{\Lambda k_n} \quad (16-92)$$

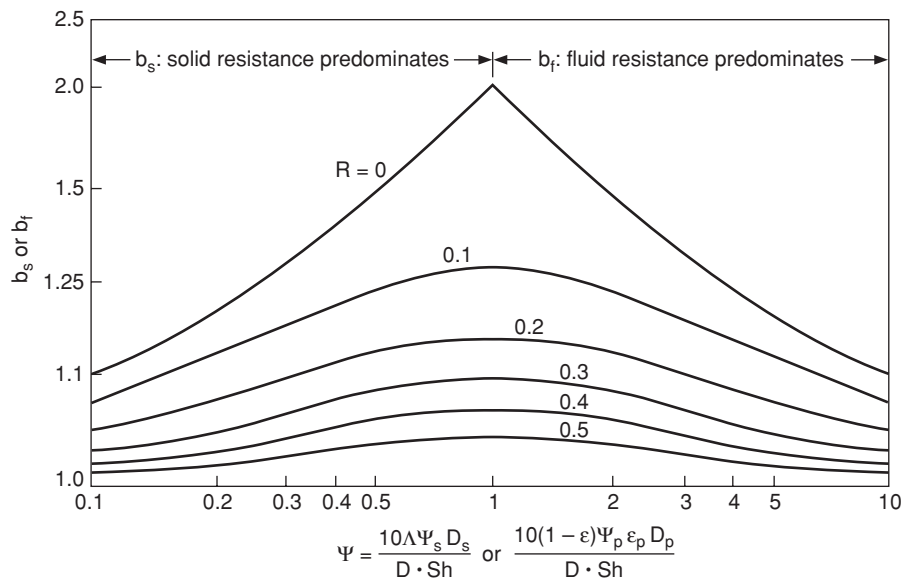


FIG. 16-12 Correction factors for addition of mass-transfer resistances, relative to effective overall solid phase or fluid phase rates, as a function of the mechanism parameter. Each curve corresponds to both b_s and b_f over its entire range.

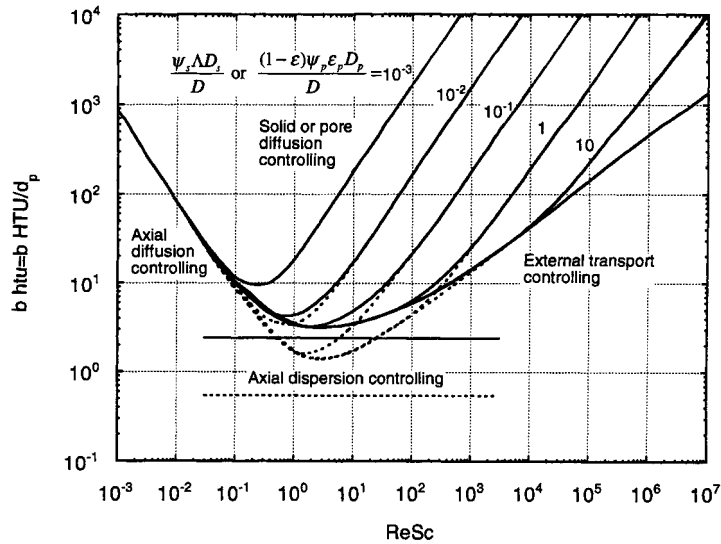


FIG. 16-13 Effect of $ReSc$ group, distribution ratio, and diffusivity ratio on height of a transfer unit. Dotted lines for gas and solid lines for liquid-phase systems.

Figure 16-13 is a plot of the dimensionless HTU ($htu = HTU/d_p$) multiplied times the correction factor b_f (between 1 and 2) as a function of the dimensionless velocity $(Re)(Sc) = \epsilon v d_p / D$ and a ratio of the controlling diffusivity to the fluid-phase diffusivity, generated on the basis of results of Vermeulen et al. (gen. ref.) using typical values of the individual physical factors likely to be found in adsorption beds. This figure can be used to determine the controlling rate factor from a knowledge of individual physical parameters. If fluid-side effects control (dotted for gas and solid for liquid-phase systems). If particle-side diffusivities control, the dimensionless HTU is given by a point above the lower envelope on the appropriate diffusional contour (through the ψ_s , the contour value depends slightly on the separation factor R). If pore and solid diffusion occur in parallel, the reciprocal of the HTU is the sum of the reciprocals of the HTU values for the two mechanisms. Near the intersections of the diffusional contours with the envelope, the dimensionless HTU is the sum of the HTU values for fluid-side and particle-side resistances.

Example 7: Estimation of Rate Coefficient for Gas Adsorption

An adsorption bed is used to remove methane from a methane-hydrogen mixture at 10 atm (abs.) (10.1 bar) and 25°C (298 K), containing 10 mol % methane. Activated carbon particles having a mean diameter $d_p = 0.17$ cm, a surface area $A = 1.1 \times 10^7$ cm²/g, a bulk density $\rho_b = 0.509$ g/cm³, a particle density $\rho_p = 0.777$ g/cm³, and a skeletal density $\rho_s = 2.178$ g/cm³ is used as the adsorbent. Based on data of Grant et al. [AIChE J., 8, 403 (1962)], adsorption equilibrium is represented by $n = 2.0 \times 10^{-3} K_{sp} p / (1 + K_{sp} p)$ mol/g adsorbent, with $K_A = 0.346$ atm⁻¹. Estimate the rate coefficient and determine the controlling rate factor for a superficial velocity of 30 cm/s.

1. The intraparticle void fraction is $\epsilon_p = (0.777^{-1} - 2.178^{-1}) / (0.777^{-1}) = 0.643$ and the extraparticle void fraction is $\epsilon = (0.509^{-1} - 0.777^{-1}) / (0.509^{-1}) = 0.345$. The pore radius is estimated from $r_p = 2\epsilon_p / (A \rho_p) = 1.5 \times 10^{-7}$ cm.
2. The fluid phase diffusivity is $D = 0.0742$ cm²/s. The pore diffusivity is estimated from Eq. (16-66) with a tortuosity factor $\tau_p = 4$; $D_p = 1.45 \times 10^{-3}$ cm²/s.
3. The fluid-side mass transfer coefficient is estimated from Fig. 16-10. For these conditions, $v = 0.108$ cm/s, $Re = 30 \times 0.17/0.108 = 47$, and $Sc = 0.108/0.0742 = 1.5$. From Fig. 16-10 or equations in Table 16-9, $Sh = 13$.
4. The isotherm parameters based on the feed concentration are $R = 1 / (1 + K_{sp} p) = 0.4$ and $\Lambda = 0.509 \times 7.68 \times 10^{-4} / 4.09 \times 10^{-5} = 9.56$. For pore diffusion, $\psi_p = 0.961$ from item 3A in Table 16-12. Thus, $(1 - \epsilon) \psi_p \epsilon_p D_p / D = (1 - 0.345) \times 0.961 \times 0.643 \times 1.45 \times 10^{-3} / 0.0742 = 7.9 \times 10^{-3}$. From Fig. 16-13 at $ReSc = 69$, $b htu = 150$. b is found from Fig. 16-12. However, since the mechanism parameter Ψ is very small, $b \sim 1$. Thus, $k_a = \epsilon v / (htu d_p \Lambda) = 0.12$ s⁻¹. This value applies to the driving force $n_i^* - n_i$. Since pore diffusion is dominant, this

value is very close to the value $k_a = 15(1 - \epsilon) \psi_p \epsilon_p D_p / (r_p^2 \Lambda) = 0.13$ s⁻¹ obtained directly from Table 16-12. It should be noted that surface diffusion is neglected in this estimation. Its occurrence could significantly affect the overall mass transfer rate (see Suzuki, gen. refs., pp. 70-85).

Example 8: Estimation of Rate Coefficient for Ion Exchange

Estimate the rate coefficient for flow of a 0.01-M water solution of NaCl through a bed of cation exchange particles in hydrogen form with $\epsilon = 0.4$. The superficial velocity is 0.2 cm/s and the temperature is 25°C. The particles are 600 μ m in diameter, and the diffusion coefficient of sodium ion is 1.2×10^{-5} cm²/s in solution and 9.4×10^{-7} cm²/s inside the particles (cf. Table 16-8). The bulk density is 0.7 g dry resin/cm³ of bed, and the capacity of the resin is 4.9 mequiv/g dry resin. The mass action equilibrium constant is 1.5.

1. Estimate the fluid-side mass transfer coefficient; $Re = \epsilon v d_p / \nu = 0.2 \times 0.06/0.00913 = 1.3$, $Sc = v/D = 0.00913/1.2 \times 10^{-5} = 761$. From Fig. 16-10 or Table 16-9, $Sh = 23$. Thus, $k_f = D Sh/d_p = 4.5 \times 10^{-3}$ cm/s.
2. From the equilibrium constant, $R = 1/K_{Na,H} = 0.67$. Thus, from Table 16-12, item 2A, $\psi_s = 0.979$. Using $n_i^{ref} = 4.9$ mequiv/g and $c_i^{ref} = 0.01$ mmole/cm³, $\Lambda = \rho_p n_i^{ref} / c_i^{ref} = 343$. Thus, $\psi_s D_s \Lambda / D = 26$ and the external mass-transfer resistance is controlling (cf. Fig. 16-13).
3. The rate coefficient for use with a fluid-phase driving force is $k_c = 3(1 - \epsilon) k_f / (\rho_p r_p) = 0.39$ cm³/(g·s).

Example 9: Estimation of Rate Coefficient for Protein Adsorption

Estimate the rate coefficient for the adsorption of an antibody ($M_r = 150,000$) from a 1 mg/cm³ aqueous solution ($\mu = 1$ cP) in a column with $\epsilon = 0.4$ operated at 0.05 cm/s and 25°C. The adsorbent particles have diameter $d_p = 100$ μ m, porosity $\epsilon_p = 0.5$, and pore radius $r_{pore} = 30$ nm. The adsorption isotherm is $n = 500c / (1 + 9.0c)$, where n is in mg/cm³ particle volume and c is in mg/cm³.

1. Estimate k_f . $Re = \epsilon v d_p / \nu = 0.05 \times 100 \times 10^{-4} / 0.01 = 0.05$. For a 150,000 molecular mass globular protein in water $D = 4 \times 10^{-7}$ cm²/s [Tyn and Gusek, *Biotechnol. Bioeng.*, 35, 327 (1990)], $Sc = v/D = 25,000$. From Table 16-9, $Sh = (1.09/0.4)(0.05)^{0.33}(25,000)^{0.33} = 29$. Thus, $k_f = D Sh/d_p = 1.1 \times 10^{-3}$ cm/s.
2. Determine the controlling resistance. From the isotherm, $n_i^{ref} = (500 \times 1) / (1 + 9.0 \times 1) = 50$ mg/cm³ particle. Thus, $\Lambda = (1 - \epsilon) n_i^{ref} / c_i^{ref} = (1 - 0.4) \times 50/1 = 30$ and $R = 1 / (1 + 9.0 \times 1) = 0.1$ [cf. Eqs. (16-33) and (16-34)]. From Eq. (16-68), $r_m = \kappa T / 6\pi \mu D = (1.38 \times 10^{-16} \times 298) / (6\pi \times 0.01 \times 4 \times 10^{-7}) = 5.5$ nm. Thus, $\lambda_m = r_m / r_{pore} = 5.5/30 = 0.18$. From Eq. (16-67) with $\tau_p = 4$ obtain $D_p = 5.8 \times 10^{-8}$ cm²/s. From Table 16-12, item 3A, $\psi_p = 0.83$, giving $10(1 - \epsilon) \psi_p \epsilon_p D_p / (D \cdot Sh) = 0.012$. Thus, from Fig. 16-13, the intraparticle pore diffusion resistance is dominant. For these conditions, from Table 16-12 we have $k_a = 15 \psi_p (1 - \epsilon) \epsilon_p D_p / (r_p^2 \Lambda) = 2.8 \times 10^{-4}$ s⁻¹. A similar approximate result is obtained directly from Fig. 16-13 with $(Re)(Sc) = 0.05 \times 25,000 = 1250$ and $(1 - \epsilon) \psi_p \epsilon_p D_p / D \sim 0.04$, giving $HTU/d_p \sim 1,000$. $k_a \sim 2 \times 10^{-4}$ s⁻¹ is obtained by using the HTU value in Eq. (16-92). These calculations assume that intraparticle transport is by pore diffusion alone, typically limiting for protein adsorption in porous adsorbents.

BATCH ADSORPTION

In this section, we consider the transient adsorption of a solute from a dilute solution in a constant-volume, well-mixed batch system or, equivalently, adsorption of a pure gas. The solutions provided can approximate the response of a stirred vessel containing suspended adsorbent particles, or that of a very short adsorption bed. Uniform, spherical particles of radius r_p , are assumed. These particles, initially of uniform adsorbate concentration, are assumed to be exposed to a step change in concentration of the external fluid.

In general, solutions are obtained by coupling the basic conservation equation for the batch system, Eq. (16-49) with the appropriate rate equation. Rate equations are summarized in Tables 16-11 and 16-12 for different controlling mechanisms.

Solutions are provided for external mass-transfer control, intraparticle diffusion control, and mixed resistances for the case of constant V_f and $F_{v, in} = F_{v, out} = 0$. The results are in terms of the fractional approach to equilibrium $F = (\hat{n}_i - \hat{n}_i^o) / (\hat{n}_i^\infty - \hat{n}_i^o)$, where \hat{n}_i^o and \hat{n}_i^∞ are the initial and ultimate solute concentrations in the adsorbent. The solution concentration is related to the amount adsorbed by the material balance $c_i = c_i^o - (\hat{n}_i - \hat{n}_i^o)M_s/V_f$.

Two general cases are considered: (1) adsorption under conditions of constant or nearly constant external solution concentration (equivalent to infinite fluid volume); and (2) adsorption in a batch with finite volume. In the latter case, the fluid concentration varies from c_i^o to c_i^∞ when equilibrium is eventually attained. $\Lambda^\infty = (c_i^o - c_i^\infty)/c_i^o = M_s(\hat{n}_i^\infty - \hat{n}_i^o)/(V_f c_i^o)$ is a partition ratio that represents the fraction of adsorbate that is ultimately adsorbed. It determines which general case should be considered in the analysis of experimental systems. Generally, when $\Lambda^\infty \geq 0.1$, solutions for the second case are required.

EXTERNAL MASS-TRANSFER CONTROL

The intraparticle concentration is uniform, and the rate equation is given by column 1 in Table 16-12.

For a **Langmuir isotherm** with negligible solute accumulation in the particle pores, the solution for an infinite fluid volume:

$$(1 - R)(1 - n_i^o/n_i^o)F - R \ln(1 - F) = (3k_f t/r_p)(c_i^o/\rho_p n_i^o) \quad (16-93)$$

where $n_i^o = n_i^\infty = n_i^o K_i c_i^o / (1 + K_i c_i^o)$ is the adsorbate concentration in the particle at equilibrium with the fluid concentration. The predicted behavior is shown in Fig. 16-14 for $n_i^o = 0$. In the **irreversible limit**

($R = 0$), F increases linearly with time; and in the **linear limit** ($R = 1$), $1 - F$ decreases exponentially with time.

For a finite fluid volume ($\Lambda^\infty > 0$), the fractional approach to equilibrium is given by:

$$\left[1 - \frac{b'(1 - R^\infty)}{2c'} \right] \frac{1}{q'} \ln \frac{(2c'F - b' - q')(-b' + q')}{(2c'F - b' + q')(-b' - q')} - \frac{1 - R^\infty}{2c'} \ln(1 - b'F + c'F^2) = \frac{3k_f t}{r_p} \frac{c_i^o}{\rho_p n_i^\infty} \quad (16-94)$$

where

$$b' = \frac{1 - R^\infty}{1 - R^0} + \Lambda^\infty \quad (16-95a)$$

$$c' = \Lambda^\infty(1 - R^\infty) \quad (16-95b)$$

$$q' = (b'^2 - 4c')^{0.5} \quad (16-95c)$$

$$R^0 = \frac{1}{1 + K_i c_i^o} \quad (16-95d)$$

$$R^\infty = \frac{1}{1 + K_i c_i^\infty} \quad (16-95e)$$

The predicted behavior is shown in Fig. 16-15 for $R^0 = 0.5$ with different values of Λ^∞ .

SOLID DIFFUSION CONTROL

For a constant diffusivity and an infinite fluid volume the solution is:

$$F = 1 - \frac{6}{\pi^2} \sum_{n=1}^{\infty} \frac{1}{n^2} \exp\left(-\frac{n^2 \pi^2 D_{st} t}{r_p^2}\right) \quad (16-96)$$

For short times, this equation does not converge rapidly. The following approximations can be used instead (Helfferich and Hwang, in Dorfner, gen. refs., pp. 1277-1309):

$$F = \frac{6}{r_p} \left(\frac{D_{st} t}{\pi}\right)^{0.5} \quad F < 0.2 \quad (16-97)$$

$$F = \frac{6}{r_p} \left(\frac{D_{st} t}{\pi}\right)^{0.5} - \frac{3D_{st} t}{r_p^2} \quad F < 0.8 \quad (16-98)$$

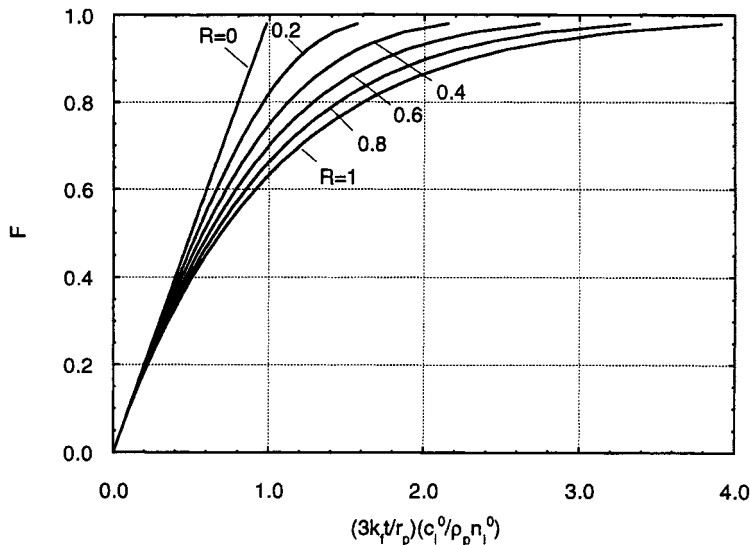


FIG. 16-14 Constant separation factor batch adsorption curves for external mass-transfer control with an infinite fluid volume and $n_i^o = 0$.

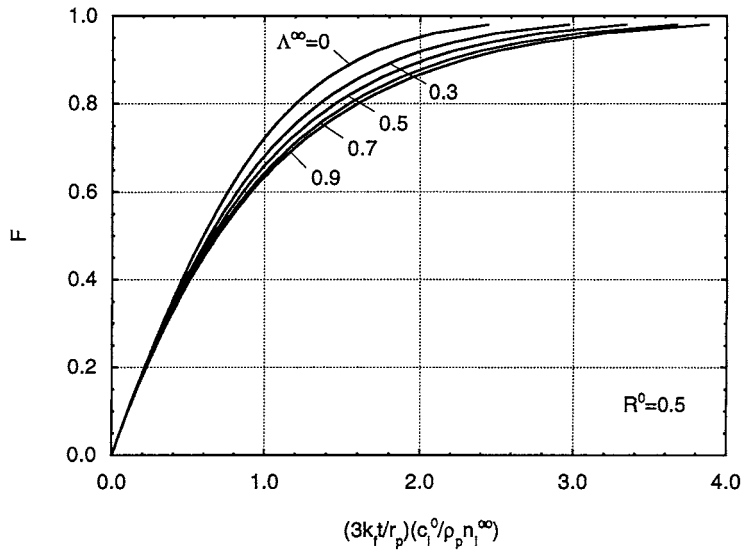


FIG. 16-15 Constant separation factor batch adsorption curves for external mass-transfer control with a finite fluid volume, $n_1^0 = 0$ and $R^0 = 0.5$.

For values of $F > 0.8$, the first term ($n = 1$) in Eq. (16-96) is generally sufficient. If the controlling resistance is diffusion in the subparticles of a bidispersed adsorbent, Eq. (16-96) applies with r_s replacing r_p .

For a finite fluid volume the solution is:

$$F = 1 - 6 \sum_{n=1}^{\infty} \frac{\exp(-p_n^2 D_s t / r_p^2)}{9\Lambda^\infty / (1 - \Lambda^\infty) + (1 - \Lambda^\infty) p_n^2} \quad (16-99)$$

where the p_n s are the positive roots of

$$\frac{\tan p_n}{p_n} = \frac{3}{3 + (1/\Lambda^\infty - 1)p_n^2} \quad (16-100)$$

The predicted behavior is shown in Fig. 16-16. F is calculated from Eq. (16-96) for $\Lambda^\infty = 0$ and from Eq. (16-99) for $\Lambda^\infty > 0$. Significant deviations from the $\Lambda^\infty = 0$ curve exist for $\Lambda^\infty > 0.1$.

For nonconstant diffusivity, a numerical solution of the conservation equations is generally required. In molecular sieve zeolites, when equilibrium is described by the Langmuir isotherm, the concentration dependence of the intracrystalline diffusivity can often be approximated by Eq. (16-72). The relevant rate equation is:

$$\frac{\partial n_i}{\partial t} = \frac{D_{0i}}{r^2} \frac{\partial}{\partial r} \left(\frac{r^2}{1 - n_i/n_i^s} \frac{\partial n_i}{\partial r} \right) \quad (16-101)$$

A numerical solution of this equation for a constant surface concentration (infinite fluid volume) is given by Garg and Ruthven [*Chem.*

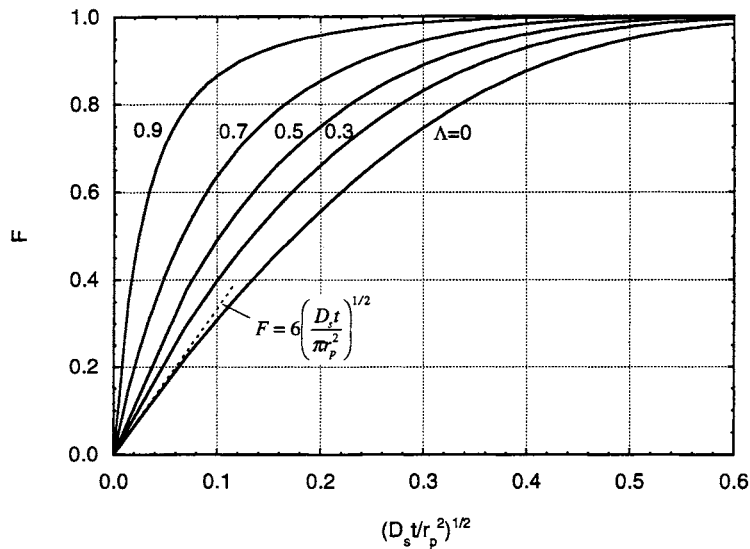


FIG. 16-16 Batch adsorption curves for solid diffusion control. The curve for $\Lambda^\infty = 0$ corresponds to an infinite fluid volume. (Adapted from Ruthven, *gen. refs.*, with permission.)

Eng. Sci., **27**, 417 (1972)]. The solution depends on the value of $\lambda = (n_i^0 - n_i^s)/(n_i^s - n_i^0)$. Because of the effect of adsorbate concentration on the effective diffusivity, for large concentration steps adsorption is faster than desorption, while for small concentration steps, when D_s can be taken to be essentially constant, adsorption and desorption curves are mirror images of each other as predicted by Eq. (16-96); see Ruthven, gen. refs., p. 175.

In binary ion-exchange, intraparticle mass transfer is described by Eq. (16-75) and is dependent on the ionic self diffusivities of the exchanging counterions. A numerical solution of the corresponding conservation equation for spherical particles with an infinite fluid volume is given by Helfferich and Plesset [*J. Chem. Phys.*, **66**, 28, 418 (1958)]. The numerical results for the case of two counterions of equal valence where a resin bead, initially partially saturated with A, is completely converted to the B form, is expressed by:

$$F = [1 - \exp \{ \pi^2 (f_1(\alpha')\tau_D + f_2(\alpha')\tau_D^2 + f_3(\alpha')\tau_D^3) \}]^{1/2} \quad (16-102)$$

$$\text{with } f_1(\alpha') = -(0.570 + 0.430\alpha'^{0.775})^{-1} \quad (16-103a)$$

$$f_2(\alpha') = (0.260 + 0.782\alpha')^{-1} \quad (16-103b)$$

$$f_3(\alpha') = -(0.165 + 0.177\alpha')^{-1} \quad (16-103c)$$

where $\tau_D = \bar{D}_A t / r_p^2$ and $\alpha' = 1 + (\bar{D}_A / \bar{D}_B - 1)n_A^0 / n^s$ for $0.1 \leq \alpha' \leq 10$. The predicted behavior is shown in Fig. 16-17. When $\alpha' = 1$ (equal ion diffusivities or $n_A^0 \sim 0$), the solution coincides with Eq. (16-96). For $\alpha' \neq 1$, the exchange rate is faster or slower depending on which counterion is initially present in the ion exchanger and on the initial level of saturation.

For an initially fully saturated particle, the exchange rate is faster when the faster counterion is initially in the resin, with the difference in rate becoming more important as conversion from one form to the other progresses. Helfferich (gen. refs., pp. 270-271) gives explicit expressions for the exchange of ions of unequal valence.

PORE DIFFUSION CONTROL

The rate equation is given by item A in Table 16-11. With pore fluid and adsorbent at equilibrium at each point within the particle and for a constant diffusivity, the rate equation can be written as:

$$\frac{\partial c_{pi}}{\partial t} = \frac{\epsilon_p D_{pi}}{\epsilon_p + \rho_p} \frac{1}{dn_i^s/dc_i} \frac{1}{r^2} \frac{\partial}{\partial r} \left(r^2 \frac{\partial c_{pi}}{\partial r} \right) \quad (16-104)$$

For a **linear isotherm** ($n_i = K_i c_i$), this equation is identical to the conservation equation for solid diffusion, except that the solid diffusivity D_{si} is replaced by the equivalent diffusivity $D_{ei} = \epsilon_p D_{pi} / (\epsilon_p + \rho_p K_i)$. Thus, Eqs. (16-96) and (16-99) can be used for pore diffusion control with infinite and finite fluid volumes simply by replacing D_{si} with D_{ei} .

When the adsorption isotherm is nonlinear, a numerical solution is generally required. For a **Langmuir system** with negligible solute holdup in the pore fluid, item A in Table 16-11 gives:

$$\frac{\partial n_i}{\partial t} = \frac{\epsilon_p D_{pi}}{\rho_p n_i^s K_i} \frac{1}{r^2} \frac{\partial}{\partial r} \left[\frac{r^2}{(1 - n_i/n_i^s)^2} \frac{\partial n_i}{\partial r} \right] \quad (16-105)$$

This equation has the same form as that obtained for solid diffusion control with D_{si} replaced by the equivalent concentration-dependent diffusivity $D_{ei} = \epsilon_p D_{pi} / [\rho_p n_i^s K_i (1 - n_i/n_i^s)^2]$. Numerical results for the case of adsorption on an initially clean particle are given in Fig. 16-18 for different values of $\lambda = n_i^0/n_i^s = 1 - R$. The uptake curves become increasingly steeper, as the nonlinearity of the isotherm, measured by the parameter λ , increases. The desorption curve shown for a particle with $n_i^0/n_i^s = 0.9$ shows that for the same step in concentration, adsorption occurs much more quickly than desorption. This difference, however, becomes smaller as the value of λ is reduced, and in the linear region of the adsorption isotherm ($\lambda \rightarrow 0$), adsorption and desorption curves are mirror images. The solution in Fig. 16-18 is applicable to a nonzero initial adsorbent loading by redefining λ as $(n_i^0 - n_i^s)/(n_i^s - n_i^0)$ and the dimensionless time variable as $[\epsilon_p D_{pi} t / \rho_p (1 - n_i^0/n_i^s)^2 n_i^s K_i r_p^2]^{1/2}$ (Ruthven, gen. refs.).

In the **irreversible limit** ($R < 0.1$), the adsorption front within the particle approaches a shock transition separating an inner core into which the adsorbate has not yet penetrated from an outer layer in which the adsorbed phase concentration is uniform at the saturation value. The dynamics of this process is described approximately by the shrinking-core model [Yagi and Kunii, *Chem. Eng. (Japan)*, **19**, 500 (1955)]. For an infinite fluid volume, the solution is:

$$\frac{\epsilon_p D_{pi} t}{r_p^2} \frac{c_i^0}{\rho_p n_i^s} = \frac{1}{2} - \frac{1}{3} F - \frac{1}{2} (1 - F)^{2/3} \quad (16-106)$$

or, in explicit form [Brauch and Schlunder, *Chem. Eng. Sci.*, **30**, 540 (1975)]:

$$F = 1 - \left\{ \frac{1}{2} + \cos \left[\frac{\pi}{3} + \frac{1}{3} \cos^{-1} \left(1 - \frac{12 \epsilon_p D_{pi} t}{r_p^2} \frac{c_i^0}{\rho_p n_i^s} \right) \right] \right\}^3 \quad (16-107)$$

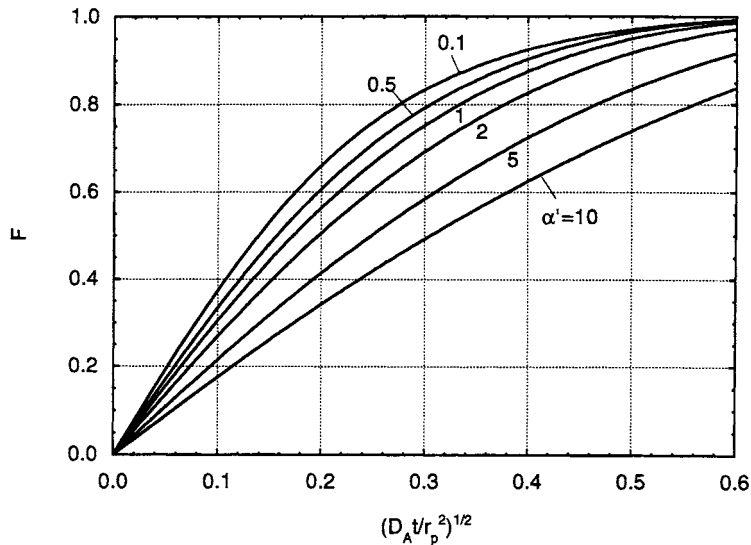


FIG. 16-17 Batch ion exchange for two equal-valence counterions. The exchanger is initially uniformly loaded with ion A in concentration n_A^0 and is completely converted to the B form. $\alpha' = 1 + (\bar{D}_A / \bar{D}_B - 1)n_A^0 / n^s$.

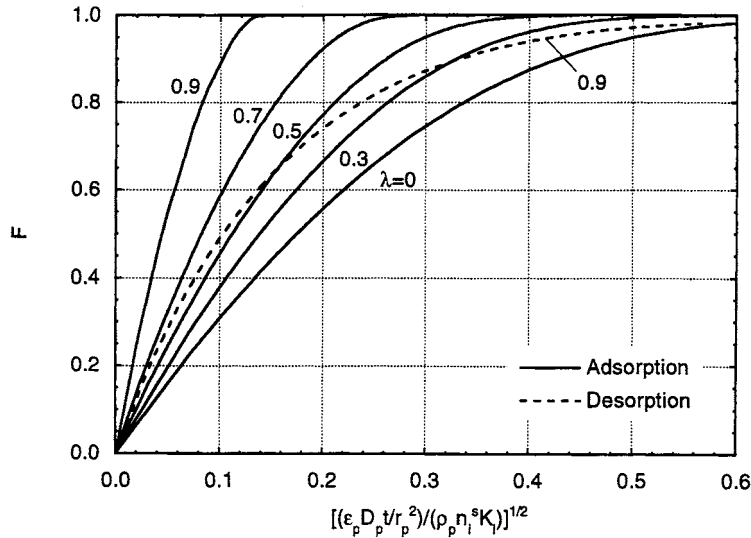


FIG. 16-18 Constant separation factor batch adsorption curves for pore diffusion control with an infinite fluid volume. λ is defined in the text.

For a finite fluid volume with $0 < \Lambda^\infty \leq 1$, the solution is [Teo and Ruthven, *Ind. Eng. Chem. Process Des. Dev.*, **25**, 17 (1986)]:

$$\frac{\varepsilon_p D_{pi} t}{r_p^2} \frac{c_i^0}{\rho_p n_i^s} = I_2 - I_1 \quad (16-108)$$

where

$$I_1 = \frac{1}{\lambda' \Lambda^\infty \sqrt{3}} \left[\tan^{-1} \frac{2\eta - \lambda'}{\lambda' \sqrt{3}} - \tan^{-1} \frac{2 - \lambda'}{\lambda' \sqrt{3}} \right] + \frac{1}{6\lambda' \Lambda^\infty} \ln \left[\frac{\lambda'^3 + \eta^3}{\lambda'^3 + 1} \left(\frac{\lambda' + 1}{\lambda' + \eta} \right)^3 \right] \quad (16-109a)$$

$$I_2 = \frac{1}{3\Lambda^\infty} \ln \frac{\lambda'^3 + \eta^3}{\lambda'^3 + 1} \quad (16-109b)$$

$$\eta = (1 - F)^{1/3} \quad (16-109c)$$

$$\lambda' = \left(\frac{1}{\Lambda^\infty} - 1 \right)^{1/3} \quad (16-109d)$$

COMBINED RESISTANCES

In general, exact analytic solutions are available only for the linear ($R = 1$) and irreversible limits ($R \rightarrow 0$). Intermediate cases require numerical solution or use of approximate driving force expressions (see "Rate and Dispersion Factors").

Parallel Pore and Solid Diffusion Control With a **linear isotherm**, assuming equilibrium between the pore fluid and the solid adsorbent, batch adsorption can be represented in terms of an equivalent solid diffusivity $\bar{D}_{ei} = (\varepsilon_p D_{pi} + \rho_p D_{si}) / (\varepsilon_p + \rho_p K_i)$. Thus, Eqs. (16-96) and (16-99) can be used for this case with D_{si} replaced by \bar{D}_{ei} .

External Mass Transfer and Intraparticle Diffusion Control With a **linear isotherm**, the solution for combined external mass transfer and pore diffusion control with an infinite fluid volume is (Crank, *Mathematics of Diffusion*, 2d ed., Clarendon Press, 1975):

$$F = 1 - \sum_{n=1}^{\infty} \frac{6Bi^2 \exp[-(p_n^2 \varepsilon_p D_{pi} t / r_p^2) / (\varepsilon_p + \rho_p K_i)]}{p_n^2 [p_n^2 + Bi(Bi - 1)]} \quad (16-110)$$

where $Bi = k_f r_p / \varepsilon_p D_{pi}$ is the **Biot number** and the p_n s are the positive roots of

$$p_n \cot p_n = 1 - Bi \quad (16-111)$$

For a finite fluid volume the solution is:

$$F = 1 - 6 \sum_{n=1}^{\infty} \frac{\exp[-(p_n^2 \varepsilon_p D_{pi} t / r_p^2) / (\varepsilon_p + \rho_p K_i)]}{\frac{9\Lambda^\infty}{1 - \Lambda^\infty} + (1 - \Lambda^\infty) p_n^2 - (5\Lambda^\infty + 1) \frac{p_n^2}{Bi} + (1 - \Lambda^\infty) \frac{p_n^4}{Bi^2}} \quad (16-112)$$

where the p_n s are the positive roots of

$$\tan p_n = \frac{3 - \frac{1 - \Lambda^\infty}{\Lambda^\infty} \frac{p_n^2}{Bi}}{3 + \frac{1 - \Lambda^\infty}{\Lambda^\infty} \frac{(Bi - 1) p_n^2}{Bi}} \quad (16-113)$$

These expressions can also be used for the case of external mass transfer and solid diffusion control by substituting D_{si} for $\varepsilon_p D_{pi} / (\varepsilon_p + \rho_p K_i)$ and $k_f r_p / (\rho_p K_i D_{si})$ for the Biot number.

In the **irreversible limit**, the solution for combined external resistance and pore diffusion with infinite fluid volume is (Yagi and Kunii):

$$\frac{\varepsilon_p D_{pi} t}{r_p^2} \frac{c_i^0}{\rho_p n_i^s} = \frac{1}{2} - \frac{1}{3} \left(1 - \frac{1}{Bi} \right) F - \frac{1}{2} (1 - F)^{2/3} \quad (16-114)$$

For a finite fluid volume the solution is (Teo and Ruthven):

$$\frac{\varepsilon_p D_{pi} t}{r_p^2} \frac{c_i^0}{\rho_p n_i^s} = \left(1 - \frac{1}{Bi} \right) I_2 - I_1 \quad (16-115)$$

where I_1 and I_2 are given by Eqs. (16-109a) and (16-109b).

Bidispersed Particles For particles of radius r_p comprising adsorptive subparticles of radius r_s that define a macropore network, conservation equations are needed to describe transport both within the macropores and within the subparticles and are given in Table 16-11, item D. Detailed equations and solutions for a linear isotherm are given in Ruthven (gen. refs., p. 183) and Ruckenstein et al. [*Chem. Eng. Sci.*, **26**, 1306 (1971)]. The solution for a **linear isotherm** with no external resistance and an infinite fluid volume is:

$$F = 1 - \frac{18}{\beta + 3\alpha} \sum_{m=1}^{\infty} \sum_{n=1}^{\infty} \left(\frac{n^2 \pi^2}{p_{n,m}^4} \right) \times \frac{\exp(-p_{n,m}^2 D_{si} t / r_s^2)}{\alpha + \frac{\beta}{2} \left[1 + \frac{\cot p_{n,m}}{p_{n,m}} (p_{n,m} \cot p_{n,m} - 1) \right]} \quad (16-116)$$

where the $p_{n,m}$ values are the roots of the equation

$$\alpha p_{n,m}^2 - n^2 \pi^2 = \beta (\rho_{n,m} \cot p_{n,m} - 1) \quad (16-117)$$

and

$$\alpha = \frac{D_{si}/r_s^2}{D_{pi}/r_p^2} \quad (16-118a)$$

$$\beta = \frac{3\alpha \rho_p K_i}{\varepsilon_p} \quad (16-118b)$$

In these equations, D_{si} is the diffusivity in the subparticles, and D_{pi} is the diffusivity in the pore network formed by the subparticles.

For large K_i values, the uptake curve depends only upon the value of the parameter β representing the ratio of characteristic time constants for diffusion in the pores and in the subparticles. For small β values, diffusion in the subparticles is controlling and the solution coincides with Eq. (16-96) with r_s replacing r_p . For large β values, pore diffusion is controlling, and the solution coincides with Eq. (16-96) with $\varepsilon_p D_{pi}/(\varepsilon_p + \rho_p K_i)$ replacing D_{si} .

Lee [AICHE J., 24, 531 (1978)] gives the solution for batch adsorption with bidispersed particles for the case of a finite fluid volume.

FIXED-BED TRANSITIONS

As discussed in "Design Concepts," a large fraction of adsorption and ion-exchange processes takes place in fixed beds. Two classical methods for analyzing fixed-bed transitions are described here. First, local equilibrium theory is presented. In this, all mass-transfer resistances are ignored to focus on the often dominating role of isotherm shape. Second, results of constant pattern analysis are presented. This gives the maximum breadth to which a mass-transfer zone will spread for various rate mechanisms. It is therefore conservative for design purposes. Both of these methods pertain to behavior in deep beds. For shallow beds, the equations given below must be solved for the particular case of interest.

DIMENSIONLESS SYSTEM

For the methods, we consider Eq. (16-52), the material balance for a fixed bed, written in the form

$$\rho_b \frac{\partial \bar{n}_i}{\partial t} + \varepsilon_b \frac{\partial c_i}{\partial t} + \varepsilon \frac{\partial (vc_i)}{\partial z} = \varepsilon D_L \frac{\partial}{\partial z} \left(c \frac{\partial y_i}{\partial z} \right) \quad (16-119)$$

where it has been assumed that D_L is constant and that $\hat{c}_i \approx c_i$ (or that the second term in the balance is small compared to the first—usually a good assumption).

Dimensionless variables can be defined for time, the axial coordinate, and velocity:

$$\tau = \frac{\varepsilon v^{\text{ref}} t}{L} \quad (16-120)$$

$$\zeta = \frac{z}{L} \quad (16-121)$$

$$v^\circ = \frac{v}{v^{\text{ref}}} \quad (16-122)$$

where L is bed length, v^{ref} is the interstitial velocity at the bed inlet, and τ is equal to the number of empty bed volumes of feed passed into the bed. The material balance becomes

$$\rho_b \frac{\partial \bar{n}_i}{\partial \tau} + \varepsilon_b \frac{\partial c_i}{\partial \tau} + \frac{\partial (v^\circ c_i)}{\partial \zeta} = \frac{1}{N_{Pe}} \frac{\partial}{\partial \zeta} \left(c \frac{\partial y_i}{\partial \zeta} \right) \quad (16-123)$$

where $N_{Pe} = v^{\text{ref}} L / D_L$ is a Peclet number for the bed or a **number of dispersion units**. Equation (16-123) or a similar equation is often the material balance used in nonisothermal problems, in problems involving adsorption of nontrace components, and in calculations of cycles.

For a trace, isothermal system, we have $v^\circ = 1$, and using the dimensionless system variables for concentrations [Eq. (16-10)], Eq. (16-123) becomes

$$\Lambda \frac{\partial \bar{n}_i^\circ}{\partial \tau} + \varepsilon_b \frac{\partial c_i^\circ}{\partial \tau} + \frac{\partial c_i^\circ}{\partial \zeta} = \frac{1}{N_{Pe}} \frac{\partial^2 c_i^\circ}{\partial \zeta^2} \quad (16-124)$$

where Λ is the **partition ratio** defined by

$$\Lambda = \frac{\rho_b n_i^{\text{ref}}}{c_i^{\text{ref}}} \quad (16-125)$$

This important dimensionless group is the volumetric capacity of the bed for the sorbable component divided by the concentration of the sorbable component in the feed. The stoichiometric capacity of the bed for solute is exactly equal to Λ empty bed volumes of feed (to saturate the sorbent at the feed concentration) plus a fraction of a bed volume of feed to fill the voids outside and inside the particles. Alternatively, we also obtain Eq. (16-124) using the dimensionless transition variables for concentrations [Eq. (16-11)], but now the partition ratio in the first term of Eq. (16-124) pertains to the transition and is given by

$$\Lambda = \rho_b \frac{n_i'' - n_i'}{c_i'' - c_i'} \quad (16-126)$$

Equation (16-124) is a commonly used form of material balance for a fixed-bed adsorber.

If the system under consideration involves use of the sorbent for only a single feed step or reuse after uniform regeneration, as in many applications with activated carbons and ion exchangers, then one of two paths is often followed at this point to simplify Eq. (16-124) further. The second term on the left-hand side of the equation is often assumed to be negligibly small (usually a good assumption), and time is redefined as

$$\tau_1 = \frac{\tau}{\Lambda} \quad (16-127)$$

to give
$$\frac{\partial \bar{n}_i^\circ}{\partial \tau_1} + \frac{\partial c_i^\circ}{\partial \zeta} = \frac{1}{N_{Pe}} \frac{\partial^2 c_i^\circ}{\partial \zeta^2} \quad (16-128)$$

Alternatively, in the absence of axial dispersion, a variable of the form

$$\tau_1 = \frac{\tau - \varepsilon_b \zeta}{\Lambda} \quad (16-129)$$

can be defined to reduce Eq. (16-124) directly to

$$\frac{\partial \bar{n}_i^\circ}{\partial \tau_1} + \frac{\partial c_i^\circ}{\partial \zeta} = 0 \quad (16-130)$$

The variable τ_1 defined by Eq. (16-127) or (16-129) is a **throughput parameter**, equal to unity (hence, the "1" subscript) at the time when the stoichiometric center of the concentration wave leaves the bed. This important group, in essence a dimensionless time variable, determines the location of the stoichiometric center of the transition in the bed at any time.

LOCAL EQUILIBRIUM THEORY

In local equilibrium theory, fluid and sorbed phases are assumed to be in local equilibrium with one another at every axial position in the bed. Thus, because of uniform concentrations, the overbar on n_i° is not necessary and we have $\hat{c}_i \approx c_i$ [note Eqs. (16-52) and (16-119)].

Single Transition System For a system described by a single material balance, Eq. (16-130) gives

$$\frac{d\tau_1}{d\zeta} = -\frac{\partial c_i^*/\partial \zeta}{\partial c_i^*/\partial \tau_1} = \frac{dn_i^*}{dc_i^*} \quad (16-131)$$

where $d\tau_1/d\zeta$ is the reciprocal of a concentration velocity. Equation (16-131) is the equation for a **simple wave** (or gradual transition or proportionate pattern). If a bed is initially uniformly saturated, then $d\tau_1/d\zeta = \tau_1/\zeta$. Thus, for the dimensionless system, the reciprocal of the velocity of a concentration is equal to the slope of the isotherm at that concentration. Furthermore, from Eq. (16-131), the depth of penetration of a given concentration into the bed is directly proportional to time, so the breadth of a simple wave increases in direct proportion to the depth of its penetration into the bed (or to time). Thus, for the simple wave, the length of the MTZ is proportional to the depth of the bed through which the wave has passed. Consideration of isotherm shape indicates that a simple wave occurs for an unfavorable dimensionless isotherm ($d^2n_i^*/dc_i^{*2} > 0$), for which low concentrations will go faster than high concentrations. Equation (16-131) also pertains to a linear isotherm, in which case the wave is called a **contact discontinuity**, because it has neither a tendency to spread nor sharpen. If a mass-transfer resistance is added to the consideration of wave character for unfavorable isotherms, the wave will still asymptotically approach the simple wave result given by Eq. (16-131).

For a favorable isotherm ($d^2n_i^*/dc_i^{*2} < 0$), Eq. (16-131) gives the impossible result that three concentrations can coexist at one point in the bed (see example below). The correct solution is a **shock** (or abrupt transition) and not a simple wave. Mathematical theory has been developed for this case to give "weak solutions" to conservation laws. The form of the solution is

$$\text{Shock speed} = \frac{\text{change in flux}}{\text{change in accumulated quantity}}$$

where the changes are jump discontinuities across the shock. The reciprocal of this equation, using Eq. (16-130), is

$$\frac{d\tau_1}{d\zeta} = \frac{\Delta n_i^*}{\Delta c_i^*} \quad (16-132)$$

where the differences are taken across the shock.

It is also possible to have a **combined wave**, which has both gradual and abrupt parts. The general rule for an isothermal, trace system is that in passing from the initial condition to the feed point in the isotherm plane, the slope of the path must not decrease. If it does, then a shock chord is taken for part of the path. Referring to Fig. 16-19, for

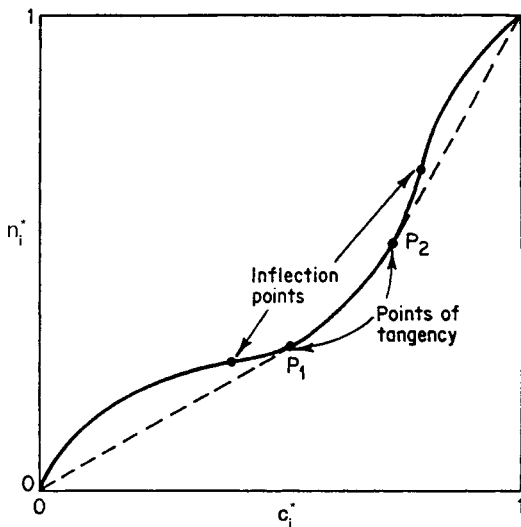


FIG. 16-19 Path in isotherm plane for a combined wave. (After Tudge.)

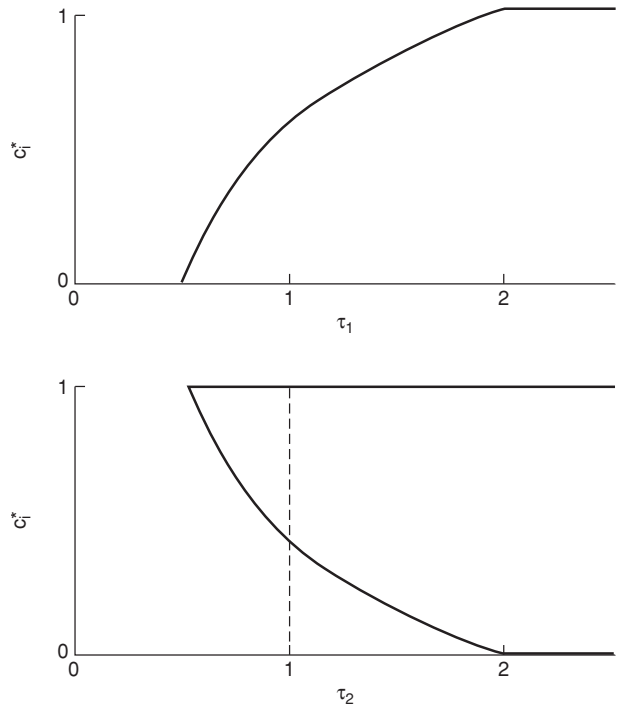


FIG. 16-20 Breakthrough curves for $r=2$ (top) and $r=0.5$ (bottom) for Example 9.

a transition from (0,0) to (1,1), the dashes indicate shock parts, which are connected by a simple wave part between points P_1 and P_2 .

Example 10: Transition Types For the constant separation-factor isotherm given by Eq. (16-31), determine breakthrough curves for $r=2$ and $r=0.5$ for transitions from $c_i^* = 0$ to $c_i^* = 1$.

Using Eq. (16-131), we obtain

$$\frac{\tau_1}{\zeta} = \frac{r}{[r + (1-r)c_i^*]^2}$$

This equation, evaluated at $\zeta = 1$, is plotted for $r=2$ and $r=0.5$ in Fig. 16-20. Clearly, the solution for $r=0.5$ is not physically correct. Equation (16-132), with $d\tau_1/d\zeta = \tau_1/\zeta$, is applied to this case to give the shock indicated by the dashed line. Alternatively, we could have obtained bed profiles by evaluating equations at $\tau_1 = \text{const}$.

Multiple Transition System Local equilibrium theory for multiple transitions begins with some combination of material and energy balances, written

$$\rho_b \frac{\partial n_i}{\partial \tau} + \epsilon_b \frac{\partial c_i}{\partial \tau} + \frac{\partial(v^*c_i)}{\partial \zeta} = 0 \quad (i = 1, 2, \dots) \quad (16-133)$$

$$\rho_b \frac{\partial u_s}{\partial \tau} + \epsilon_b \frac{\partial(cu_f)}{\partial \tau} + \frac{\partial(v^*ch_f)}{\partial \zeta} = 0 \quad (16-134)$$

which are Eq. (16-123) written with no dispersion and Eq. (16-55) written for an adiabatic bed.

For a simple wave, application of the method of characteristics (hodograph transformation) gives

$$\frac{d\tau}{d\zeta} = \frac{d(\rho_b n_1 + \epsilon_b c_1)}{d(v^*c_1)} = \frac{d(\rho_b n_2 + \epsilon_b c_2)}{d(v^*c_2)} = \dots = \frac{d(\rho_b u_s + \epsilon_b cu_f)}{d(v^*ch_f)} \quad (16-135)$$

where the derivatives are taken along the path of a transition (i.e., directional derivatives).

If a simple wave is not possible on physical grounds, then it (or part of it) is replaced by a shock, given by

$$\frac{d\tau}{d\zeta} = \frac{\Delta(\rho_b n_1 + \epsilon_b c_1)}{\Delta(v^* c_1)} = \frac{\Delta(\rho_b n_2 + \epsilon_b c_2)}{\Delta(v^* c_2)} = \dots = \frac{\Delta(\rho_b u_s + \epsilon_b c u_f)}{\Delta(v^* c u_f)} \quad (16-136)$$

Extensions When more than two conservation equations are to be solved simultaneously, matrix methods for eigenvalues and left eigenvectors are efficient [Jeffrey and Taniuti, *Nonlinear Wave Propagation*, Academic Press, New York, 1964; Jacob and Tondeur, *Chem. Eng. J.*, **22**, 187 (1981), **26**, 41 (1983); Davis and LeVan, *AIChE J.*, **33**, 470 (1987); Rhee et al., gen. refs.].

Nontrace isothermal systems give the “adsorption effect” (i.e., significant change in fluid velocity because of loss or gain of solute). Criteria for the existence of simple waves, contact discontinuities, and shocks are changed somewhat [Peterson and Helfferich, *J. Phys. Chem.*, **69**, 1283 (1965); LeVan et al., *AIChE J.*, **34**, 996 (1988); Frey, *AIChE J.*, **38**, 1649 (1992)].

Local equilibrium theory also pertains to adsorption with axial dispersion, since this mechanism does not disallow existence of equilibrium between stationary and fluid phases across the cross section of the bed [Rhee et al., *Chem. Eng. Sci.*, **26**, 1571 (1971)]. It is discussed below in further detail from the standpoint of the constant pattern.

Example 11: Two-Component Isothermal Adsorption Two components present at low mole fractions are adsorbed isothermally from an inert fluid in an initially clean bed. The system is described by $\rho_b = 500 \text{ kg/m}^3$, $\epsilon_b = 0.7$, and the binary Langmuir isotherm

$$n_i = \frac{n_i^s K_i c_i}{1 + K_i c_i + K_2 c_2} \quad (i = 1, 2)$$

with $n_1^s = n_2^s = 6 \text{ mol/kg}$, $K_1 = 40 \text{ m}^3/\text{mol}$, and $K_2 = 20 \text{ m}^3/\text{mol}$. The feed is $c_1 = c_2 = 0.5 \text{ mol/m}^3$. Find the bed profile.

Using the isotherm to calculate loadings in equilibrium with the feed gives $n_1 = 3.87 \text{ mol/kg}$ and $n_2 = 1.94 \text{ mol/kg}$. An attempt to find a simple wave solution for this problem fails because of the favorable isotherms (see the next example for the general solution method). To obtain the two shocks, Eq. (16-136) is written

$$\frac{d\tau}{d\zeta} = \frac{\Delta(\rho_b n_1 + \epsilon_b c_1)}{\Delta c_1} = \frac{\Delta(\rho_b n_2 + \epsilon_b c_2)}{\Delta c_2}$$

The concentration of one of the components will drop to zero in the shock nearest the bed inlet. If it is component 1, then using feed values and the equation above, that shock would be at

$$\frac{\tau}{\zeta} = \frac{\rho_b n_1 + \epsilon_b c_1}{c_1} \approx \frac{\rho_b n_1}{c_1} = 3870$$

Similarly, if the second component were to disappear in the first shock, we would have $\tau/\zeta = 1940$. Material balance considerations require that we accept the shorter distance, so component 1 disappears in the first shock.

The concentrations of component 2 on the plateau downstream of the first shock are then calculated from

$$\frac{\tau}{\zeta} = \frac{\Delta(\rho_b n_2 + \epsilon_b c_2)}{\Delta c_2} \approx \frac{\rho_b \Delta n_2}{\Delta c_2} = 3870$$

and its pure component isotherm, giving $c_2 = 0.987 \text{ mol/m}^3$ and $n_2 = 5.71 \text{ mol/kg}$. The location of this shock is determined using these concentrations and

$$\frac{\tau}{\zeta} = \frac{\rho_b n_2 + \epsilon_b c_2}{c_2} \approx \frac{\rho_b n_2}{c_2}$$

which gives $\tau/\zeta = 2890$. The bed profile is plotted in Fig. 16-21 using ζ/τ as the abscissa. (This example can also be worked with the h -transformation described in this section under chromatography.)

Example 12: Adiabatic Adsorption and Thermal Regeneration

An initially clean activated carbon bed at 320 K is fed a vapor of benzene in nitrogen at a total pressure of 1 MPa. The concentration of benzene in the feed is 6 mol/m^3 . After the bed is uniformly saturated with feed, it is regenerated using benzene-free nitrogen at 400 K and 1 MPa. Solve for both steps. For simplicity, neglect fluid-phase accumulation terms and assume constant mean heat capacities for stationary and fluid phases and a constant velocity. The system is described by

$$\rho_b n_1 = \frac{\rho_b n_1^s K_1 c_1}{1 + K_1 c_1}$$

$$\rho_b n_1^s = 2750 \text{ mol/m}^3$$

$$K_1 = 3.88 \times 10^{-8} \sqrt{T} \exp [q_1^s / (RT)] \text{ m}^3/(\text{mol K}^{1/2})$$

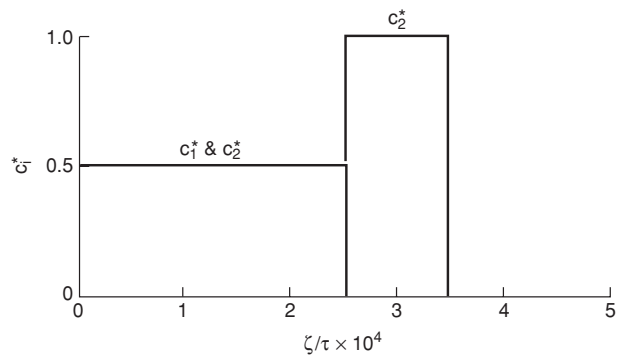


FIG. 16-21 Bed profiles for two-component isothermal adsorption, Example 10.

$$\rho_b C_{sm} = 850 \text{ kJ}/(\text{m}^3 \text{ K})$$

$$c C_{pfm} = 11.3 \text{ kJ}/(\text{m}^3 \text{ K})$$

$$q_1^s = 43.5 \text{ kJ/mol}$$

$$T^{\text{ref}} = 320 \text{ K}$$

Extensive analysis has been made of this system [Rhee et al., *Chem. Eng. J.*, **1**, 241 (1970) and gen. refs.; LeVan, in Rodrigues et al., gen. refs.].

To obtain the concentration and temperature profiles, the two transitions are first assumed to be gradual. Equation (16-135) is written in the form

$$\frac{\tau}{\zeta} = \rho_b \frac{dn_1}{dc_1} = \rho_b \frac{du_s}{d(ch_f)}$$

where, from Eqs. (16-56) to (16-60),

$$\rho_b u_s = \rho_b C_{sm}(T - T^{\text{ref}}) - \rho_b n_1 q_1^s$$

$$ch_f = c C_{pfm}(T - T^{\text{ref}})$$

This equation is expanded in terms of c_1 and T to obtain

$$\frac{\tau}{\zeta} = \rho_b \left(\frac{\partial n_1}{\partial c_1} + \frac{\partial n_1}{\partial T} \frac{dT}{dc_1} \right) = \frac{\rho_b C_{sm}}{c C_{pfm}} - \frac{\rho_b q_1^s}{c C_{pfm}} \left(\frac{\partial n_1}{\partial T} + \frac{\partial n_1}{\partial c_1} \frac{dc_1}{dT} \right)$$

Solving the rightmost equality for the directional derivative using the quadratic formula gives

$$\frac{dc_1}{dT} = \frac{-b \pm \sqrt{b^2 - 4ad}}{2a}$$

with

$$a = \left[\frac{\rho_b q_1^s}{c C_{pfm}} \right] \frac{\partial n_1}{\partial c_1}$$

$$b = \left[\frac{\rho_b q_1^s}{c C_{pfm}} \right] \frac{\partial n_1}{\partial T} - \frac{\rho_b C_{sm}}{c C_{pfm}} + \frac{\rho_b \partial n_1}{\partial c_1}$$

$$d = \frac{\rho_b \partial n_1}{\partial T}$$

The plus sign corresponds to the downstream transition and the minus sign to the upstream one. This equation is solved along each path beginning at the respective end points—the initial condition of the bed for the downstream transition and the feed condition for the upstream transition. If either path fails to evolve continuously in the expected direction, the difference form, from Eq. (16-136),

$$\frac{d\tau}{d\zeta} = \rho_b \frac{\Delta n_1}{\Delta c_1} = \rho_b \frac{\Delta u_s}{\Delta(ch_f)}$$

is used for that path (or part thereof, if appropriate); two solutions of this equation pass through each composition point, and care must be taken to ensure that the correct path is taken. The two correct paths found intersect to give the composition and temperature of an intermediate plateau region.

Letting $c_1^{\text{ref}} = 6 \text{ mol/m}^3$, the isotherm gives $\rho_b n_1^{\text{ref}} = 2700 \text{ mol/m}^3$, and the partition ratio is $\Lambda = 450$.

In the figures, $\Gamma(k)$ and $\Sigma(k)$ symbolize simple waves and shocks, respectively, with $k = 1$ downstream and $k = 2$ upstream.

Adiabatic Adsorption The construction is shown in Figs. 16-22 and 16-23. The first path begins at the initial condition, point A ($T = 320 \text{ K}$, $c_1 = 0 \text{ mol/m}^3$). Since $\partial n_1 / \partial T = 0$ there, we obtain $dc_1/dT = 0$ and $\tau/\zeta = \rho_b C_{sm} / (c C_{pfm}) = 75.2$ (or

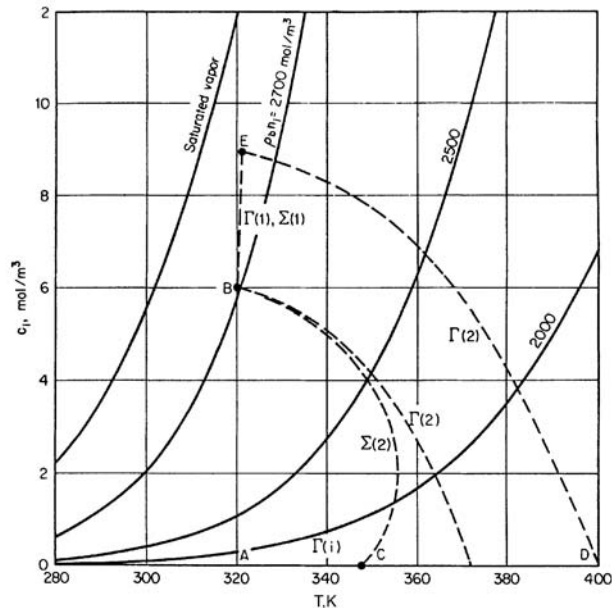


FIG. 16-22 Transition paths in c_1, T plane for adiabatic adsorption and thermal regeneration.

$\tau/\Lambda = 0.167$ at $\zeta = 1$, corresponding to a pure thermal wave along the $c_1 = 0$ axis of Fig. 16-22. The second path begins at the feed condition, point B ($T = 320$ K, $c_1 = 6$ mol/m³). A $\Gamma(2)$ fails, so a $\Sigma(2)$ is calculated and plotted in the two figures. The $\Gamma(1)$ and $\Sigma(2)$ intersect at point C ($T = 348$ K, $c_1 = 0$ mol/m³). Breakthrough curves of temperature and concentration are shown in Fig. 16-24.

Thermal Regeneration The bed, initially at point B, is fed with pure nitrogen. The feed, at point D ($T = 400$ K, $c_1 = 0$ mol/m³), provides a successful $\Gamma(2)$. The $\Gamma(1)$ from point B fails, so a $\Sigma(1)$, which differs imperceptibly from $\Gamma(1)$, is determined. The $\Sigma(1)$ and $\Gamma(2)$ meet at point E ($T = 320.8$ K, $c_1 = 8.93$ mol/m³),

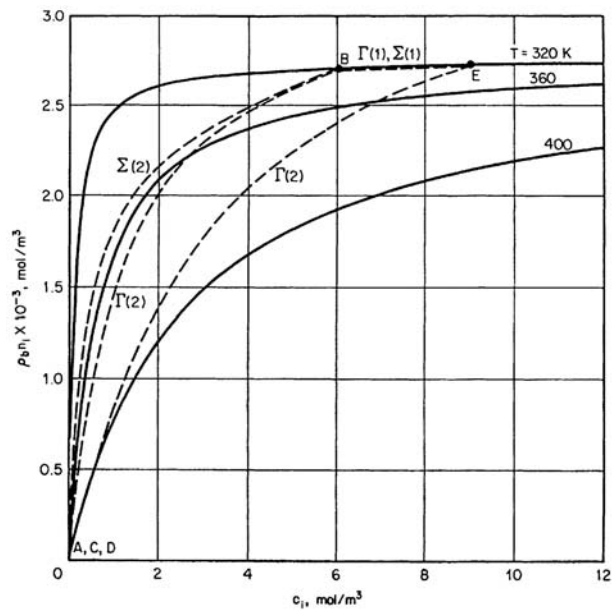


FIG. 16-23 Transition paths in isotherm plane for adiabatic adsorption and thermal regeneration.

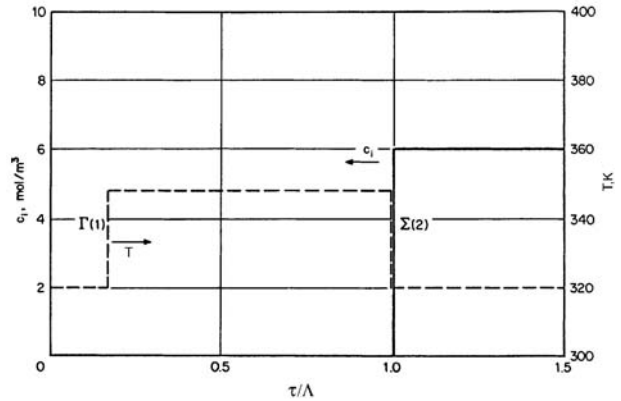


FIG. 16-24 Breakthrough curves for adiabatic adsorption.

where $\rho_B n_1 = 2716$ mol/m³, which is greater than the initial loading, indicating “roll-up,” a term attributed to Basmadjian et al. [*Ind. Eng. Chem. Process Des. Dev.*, **14**, 328 (1975)], of the adsorbed-phase concentration. Breakthrough curves are shown in Fig. 16-25. The $\Sigma(1)$ leaves the bed at $\tau/\Lambda = 0.011$. The $\Gamma(2)$ begins to emerge at $\tau/\Lambda = 0.169$, but regeneration is not complete until $\tau/\Lambda = 2.38$.

It is possible (with lower initial bed temperature, higher initial loading, or higher regeneration temperature or pressure) for the transition paths to contact the saturated vapor curve in Fig. 16-22 rather than intersect beneath it. For this case, liquid benzene condenses in the bed, and the effluent vapor is saturated during part of regeneration [Friday and LeVan, *AIChE J.*, **30**, 679 (1984)].

CONSTANT PATTERN BEHAVIOR FOR FAVORABLE ISOTHERMS

With a favorable isotherm and a mass-transfer resistance or axial dispersion, a transition approaches a **constant pattern**, which is an asymptotic shape beyond which the wave will not spread. The wave is said to be “self-sharpening.” (If a wave is initially broader than the constant pattern, it will sharpen to approach the constant pattern.) Thus, for an initially uniformly loaded bed, the constant pattern gives the maximum breadth of the MTZ. As bed length is increased, the constant pattern will occupy an increasingly smaller fraction of the bed. (Square-root spreading for a linear isotherm gives this same qualitative result.)

The treatment here is restricted to the Langmuir or constant separation factor isotherm, single-component adsorption, dilute systems, isothermal behavior, and mass-transfer resistances acting alone. References to extensions are given below. Different isotherms have been considered, and the theory is well understood for general isotherms.

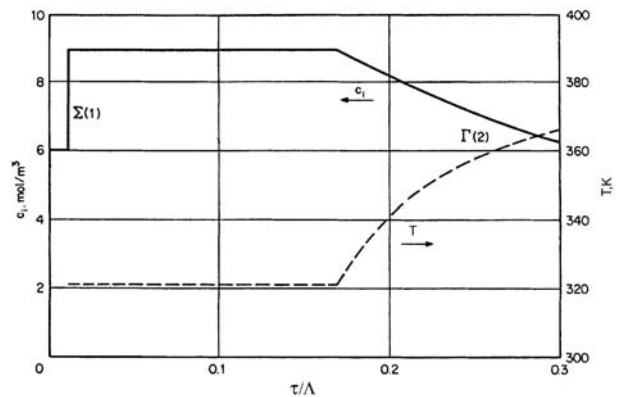


FIG. 16-25 Breakthrough curves for thermal regeneration.

TABLE 16-13 Constant Pattern Solutions for Constant Separation Factor Isotherm ($R < 1$)

Mechanism	N	Dimensionless rate equation ¹	Constant pattern	Refs.
Pore diffusion	$\frac{15(1-\epsilon)\epsilon_p D_p L}{\epsilon v^{\text{ref}} r_p^2}$	$\frac{\partial n_i^*}{\partial \tau_1} = \frac{N}{15} \frac{1}{\xi^2} \frac{\partial}{\partial \xi} \left(\xi^2 \frac{\partial c_i^*}{\partial \xi} \right)$	Numerical for $0 < R < 1$ Analytical for $R = 0$	A B
Solid diffusion	$\frac{15\Delta D_s L}{\epsilon v^{\text{ref}} r_p^2}$	$\frac{\partial n_i^*}{\partial \tau_1} = \frac{N}{15} \frac{1}{\xi^2} \frac{\partial}{\partial \xi} \left(\xi^2 \frac{\partial n_i^*}{\partial \xi} \right)$	Numerical for $0 < R < 1$ Analytical for $R = 0$	C D
External mass transfer	$\frac{k_f a L}{\epsilon v^{\text{ref}}}$	$\frac{\partial \bar{n}_i^*}{\partial \tau_1} = N (c_i^* - c_i^{\text{e}})$	$\frac{1}{1-R} \ln \left[\frac{(1-c_i^{\text{e}})^R}{c_i^{\text{e}}} \right] - 1 = N (\zeta - \tau_1)$	E
Linear driving force	$\frac{k_n \Delta L}{\epsilon v^{\text{ref}}}$	$\frac{\partial \bar{n}_i^*}{\partial \tau_1} = N (n_i^{\text{e}} - \bar{n}_i^*)$	$\frac{1}{1-R} \ln \left[\frac{1-c_i^{\text{e}}}{c_i^{\text{e}R}} \right] + 1 = N (\zeta - \tau_1)$	F
Reaction kinetics	$\frac{k_r c^{\text{ref}} \Delta L}{(1-R)\epsilon v^{\text{ref}}}$	$\frac{\partial \bar{n}_i^*}{\partial \tau_1} = N [(1 - \bar{n}_i^*)c_i^{\text{e}} - R\bar{n}_i^*(1 - c_i^{\text{e}})]$	$\frac{1}{1-R} \ln \left[\frac{1-c_i^{\text{e}}}{c_i^{\text{e}}} \right] = N (\zeta - \tau_1)$	G
Axial dispersion	$\frac{v^{\text{ref}} L}{D_L}$	Eq. (16-128)	$\frac{1}{1-R} \ln \left[\frac{1-c_i^{\text{e}}}{c_i^{\text{e}R}} \right] = N (\zeta - \tau_1)$	H

1: Dimensional rate equations are given in Tables 16-11 and 16-12.

A: Hall et al., *Ind. Eng. Chem. Fundam.*, **5**, 212 (1966).

B: Hall et al., *Ind. Eng. Chem. Fundam.*, **5**, 212 (1966); Cooper and Liberman, *Ind. Eng. Chem. Fundam.*, **9**, 620 (1970). Analytical solution for $R = 0$ is

$$\frac{15}{2} \ln [1 + (1 - c_i^{\text{e}})^{1/3} + (1 - c_i^{\text{e}})^{2/3}] - \frac{15}{\sqrt{3}} \tan^{-1} \left[\frac{2(1 - c_i^{\text{e}})^{1/3} + 1}{\sqrt{3}} \right] + \frac{5\pi}{2\sqrt{3}} - \frac{5}{2} = N(\zeta - \tau_1)$$

C: Hall et al., *Ind. Eng. Chem. Fundam.*, **5**, 212 (1966); Garg and Ruthven, *Chem. Eng. Sci.*, **28**, 791, 799 (1973).

D: Hall et al., *Ind. Eng. Chem. Fundam.*, **5**, 212 (1966) [see also Cooper, *Ind. Eng. Chem. Fundam.*, **4**, 308 (1965); Ruthven (gen. refs.)]. Analytical solution for $R = 0$ is

$$c_i^* = 1 - \frac{6}{\pi^2} \sum_{n=0}^{\infty} \frac{1}{n^2} \exp \left\{ -n^2 \left[\left(\frac{\pi^2}{15} \right) N(\tau_1 - \zeta) + 0.64 \right] \right\}$$

E: Michaels, *Ind. Eng. Chem.*, **44**, 1922 (1952); Miura and Hashimoto, *J. Chem. Eng. Japan*, **10**, 490 (1977).

F: Glueckauf Coates, *J. Chem. Soc.*, **1947**, 1315 (1947); Vermeulen, *Advances in Chemical Engineering*, **2**, 147 (1958); Hall et al., *Ind. Eng. Chem. Fundam.*, **5**, 212 (1966); Miura and Hashimoto, *J. Chem. Eng. Japan*, **10**, 490 (1977).

G: Walter, *J. Chem. Phys.*, **13**, 229 (1945); Hiester and Vermeulen, *Chem. Eng. Progress*, **48**, 505 (1952).

H: Acrivos, *Chem. Eng. Sci.*, **13**, 1 (1960); Coppola and LeVan, *Chem. Eng. Sci.*, **36**, 967 (1981).

Asymptotic Solution Rate equations for the various mass-transfer mechanisms are written in dimensionless form in Table 16-13 in terms of a number of transfer units, $N = L/\text{HTU}$, for particle-scale mass-transfer resistances, a number of reaction units for the reaction kinetics mechanism, and a number of dispersion units, N_{pe} , for axial dispersion. For pore and solid diffusion, $\xi = r/r_p$ is a dimensionless radial coordinate, where r_p is the radius of the particle. If a particle is bidisperse, then r_p can be replaced by r_s , the radius of a subparticle. For preliminary calculations, Fig. 16-13 can be used to estimate N for use with the LDF approximation when more than one resistance is important.

In constant pattern analysis, equations are transformed into a new coordinate system that moves with the wave. Variables are changed from (ζ, τ_1) to $(\zeta - \tau_1, \tau_1)$. The new variable $\zeta - \tau_1$ is equal to zero at the stoichiometric center of the wave. Equation (16-130) for a bed with no axial dispersion, when transformed to the $(\zeta - \tau_1, \tau_1)$ coordinate system, becomes

$$-\frac{\partial \bar{n}_i^*}{\partial (\zeta - \tau_1)} + \frac{\partial \bar{n}_i^*}{\partial \tau_1} + \frac{\partial c_i^*}{\partial (\zeta - \tau_1)} = 0 \quad (16-137)$$

The constant pattern is approached as the τ_1 dependence in this equation disappears. Thus, discarding the derivative with respect to τ_1 and integrating, using the condition that \bar{n}_i^* and c_i^* approach zero as $N(\zeta - \tau_1) \rightarrow \infty$ [or approach unity as $N(\zeta - \tau_1) \rightarrow -\infty$], gives simply

$$\bar{n}_i^* = c_i^* \quad (16-138)$$

For adsorption with axial dispersion, the material balance transforms to

$$-\frac{\partial n_i^*}{\partial (\zeta - \tau_1)} + \frac{\partial n_i^*}{\partial \tau_1} + \frac{\partial c_i^*}{\partial (\zeta - \tau_1)} = \frac{1}{N_{pe}} \frac{\partial^2 c_i^*}{\partial (\zeta - \tau_1)^2} \quad (16-139)$$

The partial derivative with respect to τ_1 is discarded and the resulting equation integrated once to give

$$-n_i^* + c_i^* = \frac{1}{N_{pe}} \frac{dc_i^*}{d(\zeta - \tau_1)} \quad (16-140)$$

After eliminating n_i^* or c_i^* using the adsorption isotherm, Eq. (16-140) can be integrated directly to obtain the constant pattern.

For other mechanisms, the particle-scale equation must be integrated. Equation (16-138) is used to advantage. For example, for external mass transfer acting alone, the dimensionless rate equation in Table 16-13 would be transformed into the $(\zeta - \tau_1, \tau_1)$ coordinate system and derivatives with respect to τ_1 discarded. Equation (16-138) is then used to replace c_i^* with \bar{n}_i^* in the transformed equation. Furthermore, for this case there are assumed to be no gradients within the particles, so we have $\bar{n}_i^* = n_i^*$. After making this substitution, the transformed equation can be rearranged to

$$-\frac{dn_i^*}{n_i^* - c_i^*} = d(\zeta - \tau_1) \quad (16-141)$$

Since n_i^* and c_i^* are related by the adsorption isotherm, Eq. (16-141) can be integrated.

The integration of Eq. (16-140) or (16-141) as an indefinite integral will give an integration constant that must be evaluated to center the transition properly. The material balance depicted in Fig. 16-26 is used. The two shaded regions must be of equal area if the stoichiometric center of the transition is located where the throughput parameter is unity. Thus, we have

$$\int_{-\infty}^0 (1 - n_i^*) d(\zeta - \tau_1) = \int_0^{\infty} n_i^* d(\zeta - \tau_1) \quad (16-142)$$

Integrating Eq. (16-142) by parts gives

$$\int_0^1 (\zeta - \tau_1) dn_i^* = 0 \quad (16-143)$$

For all mechanisms except axial dispersion, the transition can be centered just as well using c_i^* , because of Eq. (16-138). For axial dispersion, the transition should be centered using n_i^* , provided the fluid-phase accumulation term in the material balance, Eq. (16-124), can be neglected. If fluid-phase accumulation is important, then the

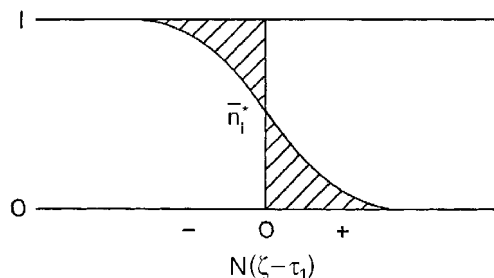


FIG. 16-26 Material balance for centering profile. [From LeVan in Rodrigues et al. (eds), *Adsorption: Science and Technology*, Kluwer Academic Publishers, Dordrecht, The Netherlands, 1989; reprinted with permission.]

transition for axial dispersion can be centered by taking into account the relative quantities of solute held in the fluid and adsorbed phases.

Constant pattern solutions for the individual mechanisms and constant separation factor isotherm are given in Table 16-13. The solutions all have the expected dependence on R —the more favorable the isotherm, the sharper the profile.

Figure 16-27 compares the various constant pattern solutions for $R = 0.5$. The curves are of a similar shape. The solution for reaction kinetics is perfectly symmetrical. The curves for the axial dispersion fluid-phase concentration profile and the linear driving force approximation are identical except that the latter occurs one transfer unit further down the bed. The curve for external mass transfer is exactly that for the linear driving force approximation turned upside down [i.e., rotated 180° about $c_i^* = n_i^* = 0.5$, $N(\zeta - \tau_1) = 0$]. The linear driving force

approximation provides a good approximation for both pore diffusion and surface diffusion.

Because of the close similarity in shape of the profiles shown in Fig. 16-27 (as well as likely variations in parameters; e.g., concentration-dependent surface diffusion coefficient), a controlling mechanism cannot be reliably determined from transition shape. If reliable correlations are not available and rate parameters cannot be measured in independent experiments, then particle diameters, velocities, and other factors should be varied and the observed impact considered in relation to the definitions of the numbers of transfer units.

Example 13: Estimation of Breakthrough Time With reference to Example 9, determine the 10 percent breakthrough time and the column dynamic binding capacity if the column is 20 cm long.

1. From Example 9, $\Lambda = 30$, $R = 0.1$, and $D_p = 5.8 \times 10^{-8}$ cm²/s. For pore diffusion control (Table 16-13, item A), $N = 15(1 - \epsilon)\epsilon_p D_p L / (\epsilon V \cdot r_p^2) = 4.2$. Based on the numerical solution of Hall et al., $N(1 - \tau_1) = 1.3$ with $c_i^* = 0.1$, giving $\tau_1 = 0.69$. The corresponding time is $t = (L/\epsilon v)(\epsilon + \Lambda\tau_1) = (20/0.05)(0.4 + 30 \times 0.69) = 8,400$ s. The column dynamic binding capacity (DBC_{10%}) is the amount of adsorbate retained in the column per unit column volume when the outlet concentration reaches 10 percent of the feed. As a fraction of equilibrium capacity, DBC_{10%} is equal to τ_1 , neglecting the adsorbate held in the pore volume and the leakage prior to 10 percent of breakthrough.

2. From Example 9, the rate coefficient for the linear driving-force approximation (Table 16-13, item E) is $k_n = 2.8 \times 10^{-4}$ s⁻¹. Thus, $N = k_n \Lambda L / \epsilon v = 2.8 \times 10^{-4} \times 30 \times 20 / 0.05 = 3.4$ and

$$N(1 - \tau_1) = \frac{1}{1 - 0.1} \ln \left(\frac{1 - 0.1}{0.1} \right) + 1 = 1.1$$

with $c_i^* = 0.1$, giving $\tau_1 = 0.67$. The corresponding breakthrough time is $t = 8,200$ s.

3. If the isotherm is approximated as irreversible ($R = 0$), from Table 16-13, item B, we obtain $N(1 - \tau_1) = 1.03$ with $c_i^* = 0.1$, giving $\tau_1 = 0.75$ with a corresponding breakthrough time $t = 9,100$ s.

Breakthrough Behavior for Axial Dispersion Breakthrough behavior for adsorption with axial dispersion in a deep bed is not adequately described by the constant pattern profile for this mechanism. Equation (16-128), the partial differential equation of the second order Fickian model, requires two boundary conditions for its solution. The constant pattern pertains to a bed of infinite depth—in obtaining the solution we apply the downstream boundary condition $c_i^* \rightarrow 0$ as $N_{pe}\zeta \rightarrow \infty$. Breakthrough behavior presumes the existence of a bed outlet, and a boundary condition must be applied there.

The full mathematical model for this problem is Eq. (16-128) with boundary conditions

$$c_i^* - \frac{1}{N_{pe}} \frac{\partial c_i^*}{\partial \zeta} = 1 \quad \text{at} \quad \zeta = 0 \quad (16-144)$$

$$\frac{\partial c_i^*}{\partial \zeta} = 0 \quad \text{at} \quad \zeta = 1 \quad (16-145)$$

and an initial condition. Equation (16-144) specifies a constant flux at the bed inlet, and Eq. (16-145), the Danckwerts-type boundary condition at the bed outlet, is appropriate for fixed-bed adsorption, provided that the partition ratio is large.

The solution to this model for a deep bed indicates an increase in velocity of the fluid-phase concentration wave during breakthrough. This is most dramatic for the rectangular isotherm—the instant the bed becomes saturated, the fluid-phase profile jumps in velocity from that of the adsorption transition to that of the fluid, and a near shock-like breakthrough curve is observed [Coppola and LeVan, *Chem. Eng. Sci.*, **36**, 967 (1981)].

Extensions Existence, uniqueness, and stability criteria have been developed for the constant pattern [Cooney and Lightfoot, *Ind. Eng. Chem. Fundam.*, **4**, 233 (1965); Rhee et al., *Chem. Eng. Sci.*, **26**, 1571 (1971); Rhee and Amundson, *Chem. Eng. Sci.*, **26**, 1571 (1971), **27**, 199 (1972), **29**, 2049 (1974)].

The rectangular isotherm has received special attention. For this, many of the constant patterns are developed fully at the bed inlet, as shown for external mass transfer [Klotz, *Chem. Revs.*, **39**, 241 (1946)], pore diffusion [Vermeulen, *Adv. Chem. Eng.*, **2**, 147 (1958); Hall et al., *Ind. Eng. Chem. Fundam.*, **5**, 212 (1966)], pore diffusion with film resistance in series [Weber and Chakraborti, *AIChE J.*, **20**, 228 (1974)], the

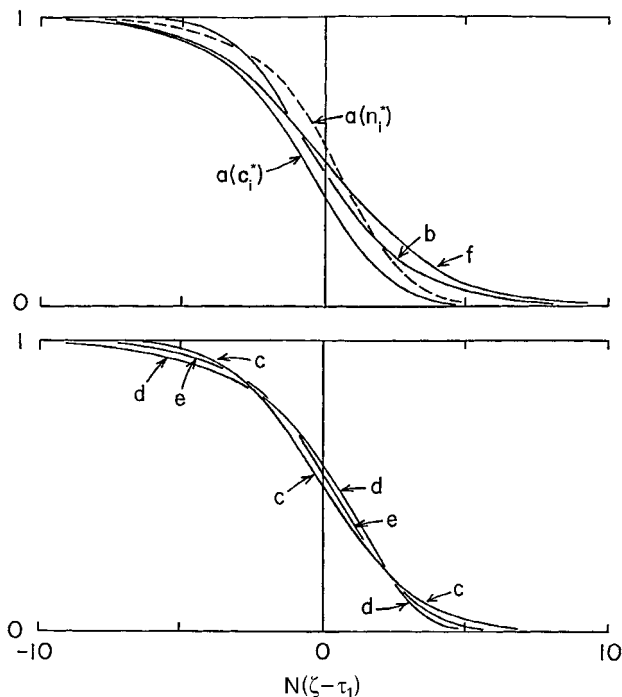


FIG. 16-27 Constant pattern solutions for $R = 0.5$. Ordinate is c_i^* or n_i^* except for axial dispersion for which individual curves are labeled: a, axial dispersion; b, external mass transfer; c, pore diffusion (spherical particles); d, surface diffusion (spherical particles); e, linear driving force approximation; f, reaction kinetics. [From LeVan in Rodrigues et al. (eds.), *Adsorption: Science and Technology*, Kluwer Academic Publishers, Dordrecht, The Netherlands, 1989; reprinted with permission.]

linear driving force approximation [Cooper, *Ind. Eng. Chem. Fundam.*, **4**, 308 (1965)], reaction kinetics [Hiester and Vermeulen, *Chem. Eng. Progress*, **48**, 505 (1952); Bohart and Adams, *J. Amer. Chem. Soc.*, **42**, 523 (1920)], and axial dispersion [Coppola and LeVan, *Chem. Eng. Sci.*, **38**, 991 (1983)].

Multiple mass-transfer resistances have been considered in many studies [Vermeulen, *Adv. in Chem. Eng.*, **2**, 147 (1958); Vermeulen et al., Ruthven, gen. refs.; Fleck et al., *Ind. Eng. Chem. Fundam.*, **12**, 95 (1973); Yoshida et al., *Chem. Eng. Sci.*, **39**, 1489 (1984)].

Treatments of constant pattern behavior have been carried out for multicomponent adsorption [Vermeulen, *Adv. in Chem. Eng.*, **2**, 147 (1958); Vermeulen et al., Ruthven, gen. refs.; Rhee and Amundson, *Chem. Eng. Sci.*, **29**, 2049 (1974); Cooney and Lightfoot, *Ind. Eng. Chem. Fundam.*, **5**, 25 (1966); Cooney and Strusi, *Ind. Eng. Chem. Fundam.*, **11**, 123 (1972); Bradley and Sweed, *AIChE Symp. Ser. No. 152*, **71**, 59 (1975)]. The behavior is such that coexisting compositions advance through the bed together at a uniform rate; this is the *coherence* concept of Helfferich and coworkers [gen. refs.].

Nontrace systems have been considered [Sircar and Kumar, *Ind. Eng. Chem. Proc. Des. Dev.*, **22**, 271 (1983)].

Constant patterns have been developed for adiabatic adsorption [Pan and Basmadjian, *Chem. Eng. Sci.*, **22**, 285 (1967); Ruthven et al., *Chem. Eng. Sci.*, **30**, 803 (1975); Kagueli et al., *Chem. Eng. Sci.*, **42**, 2964 (1987)].

The constant pattern concept has also been extended to circumstances with nonplug flows, with various degrees of rigor, including flow profiles in tubes [Sartory, *Ind. Eng. Chem. Fundam.*, **17**, 97 (1978); Tereck et al., *Ind. Eng. Chem. Res.*, **26**, 1222 (1987)], wall effects [Vortmeyer and Michael, *Chem. Eng. Sci.*, **40**, 2135 (1985)], channelling [LeVan and Vermeulen in Myers and Belfort (eds.), *Fundamentals of Adsorption*, Engineering Foundation, New York (1984), pp. 305-314, *AIChE Symp. Ser. No. 233*, **80**, 34 (1984)], networks [Avilés and LeVan, *Chem. Eng. Sci.*, **46**, 1935 (1991)], and general structures of constant cross section [Rudisill and LeVan, *Ind. Eng. Chem. Res.*, **29**, 1054 (1991)].

SQUARE ROOT SPREADING FOR LINEAR ISOTHERMS

The simplest isotherm is $n_i^* = c_i^*$, corresponding to $R = 1$. For this isotherm, the rate equation for external mass transfer, the linear driving force approximation, or reaction kinetics, can be combined with Eq. (16-130) to obtain

$$\frac{\partial \bar{n}_i^*}{\partial \tau_1} = - \frac{\partial c_i^*}{\partial \zeta} = N(c_i^* - \bar{n}_i^*) \tag{16-146}$$

The solution to this equation, with initial condition $n_i^* = 0$ at $\tau_1 = 0$ and boundary condition $c_i^* = 1$ at $\zeta = 0$, originally obtained for an analogous heat transfer case [Anzelius, *Z. Angew. Math. Mech.*, **6**, 291 (1926); Schumann, *J. Franklin Inst.*, **208**, 405 (1929)], is

$$c_i^* = J(N\zeta, N\tau_1) \quad n_i^* = 1 - J(N\tau_1, N\zeta) \tag{16-147}$$

where the J function is [Hiester and Vermeulen, *Chem. Eng. Prog.*, **48**, 505 (1952)]

$$J(s, t) = 1 - \int_0^s e^{-t-\xi} I_0(2\sqrt{t\xi}) d\xi \tag{16-148}$$

where I_0 is the modified Bessel function of the first kind of order zero. This linear isotherm result can be generalized to remove the assumption that $\bar{c}_i^* \approx c_i^*$ if the throughput parameter is redefined as

$$\tau_1 = \frac{\tau - \varepsilon\zeta}{(1 - \varepsilon)(\rho_p K_i + \varepsilon_p)}$$

The J function is plotted in Fig. 16-28 and tables are available (e.g., Sherwood et al., *Mass Transfer*, McGraw-Hill, New York, 1975). Vermeulen et al. (gen. refs.) discuss several approximations of the J function; see also Eq. (16-185). For large arguments J approaches

$$J(s, t) = \frac{1}{2} \operatorname{erfc} [\sqrt{s} - \sqrt{t}] \tag{16-149}$$

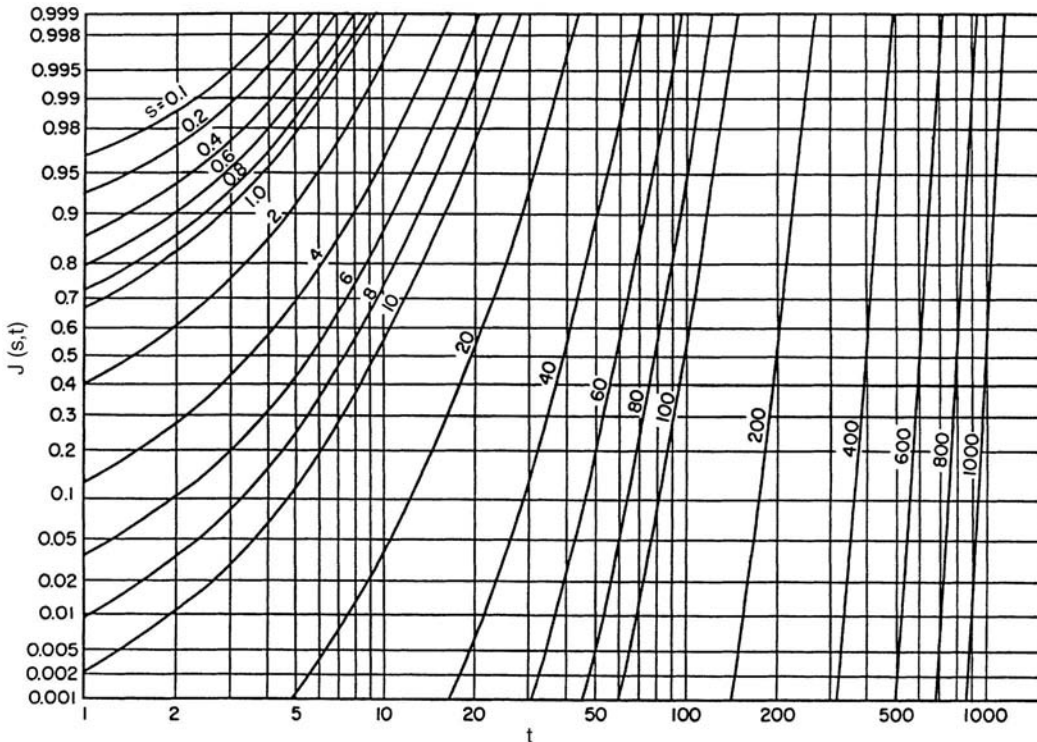


FIG. 16-28 Plot of the function $J(s, t)$ defined by Eq. (16-148).

A derivation for particle-phase diffusion accompanied by fluid-side mass transfer has been carried out by Rosen [*J. Chem. Phys.*, **18**, 1587 (1950); *ibid.*, **20**, 387 (1952); *Ind. Eng. Chem.*, **46**, 1590 (1954)] with a limiting form at $N > 50$ of

$$c_i^* = \frac{1}{2} \operatorname{erfc} \left[\frac{\sqrt{N}}{2} (\zeta - \tau_1) \right] \quad (16-150)$$

For axial dispersion in a semi-infinite bed with a linear isotherm, the complete solution has been obtained for a constant flux inlet boundary condition [Lapidus and Amundson, *J. Phys. Chem.*, **56**, 984 (1952); Brenner, *Chem. Eng. Sci.*, **17**, 229 (1962); Coates and Smith, *Soc. Petrol. Engrs. J.*, **4**, 73 (1964)]. For large N , the leading term is

$$c_i^* = \frac{1}{2} \operatorname{erfc} \left[\frac{\sqrt{N}}{2\sqrt{\tau_1}} (\zeta - \tau_1) \right] \quad (16-151)$$

All of these solutions are very similar and show, for large N , a wave with breadth proportional to the square root of the bed depth through which it has passed.

COMPLETE SOLUTION FOR REACTION KINETICS

In general, full time-dependent analytical solutions to differential equation-based models of the above mechanisms have not been obtained for nonlinear isotherms. Only for reaction kinetics with the constant separation factor isotherm has a full solution been found [Thomas, *J. Amer. Chem. Soc.*, **66**, 1664 (1944)]. Referred to as the *Thomas solution*, it has been extensively studied [Amundson, *J. Phys. Colloid Chem.*, **54**, 812 (1950); Hiester and Vermeulen, *Chem. Eng. Progress*, **48**, 505 (1952); Gilliland and Baddour, *Ind. Eng. Chem.*, **45**, 330 (1953); Vermeulen, *Adv. in Chem. Eng.*, **2**, 147 (1958)]. The solution to Eq. (16-130) for item 4C in Table 16-12 for the same initial and boundary conditions as Eq. (16-146) is

$$\begin{aligned} c_i^* &= \frac{J(RN\zeta, N\tau_1)}{J(RN\zeta, N\tau_1) + e^{-(R-1)N(\zeta-\tau_1)} [1 - J(N\zeta, RN\tau_1)]} \\ n_i^* &= \frac{1 - J(N\tau_1, RN\zeta)}{J(RN\zeta, N\tau_1) + e^{-(R-1)N(\zeta-\tau_1)} [1 - J(N\zeta, RN\tau_1)]} \end{aligned} \quad (16-152)$$

The solution gives all of the expected asymptotic behaviors for large N —the proportionate pattern spreading of the simple wave if $R > 1$, the constant pattern if $R < 1$, and square root spreading for $R = 1$.

NUMERICAL METHODS AND CHARACTERIZATION OF WAVE SHAPE

For the solution of sophisticated mathematical models of adsorption cycles incorporating complex multicomponent equilibrium and rate expressions, two numerical methods are popular, including implementations in commercially available software packages. These are finite difference and weighted residual methods. The former vary in the manner in which distance variables are discretized, ranging from simple backward difference stage models (akin to the plate theory of chromatography) to more involved schemes exhibiting little numerical dispersion. The weighted residual method of orthogonal collocation is often thought to be faster computationally, but oscillations in the polynomial trial function can be a problem. The choice of best method is often the preference of the user.

For both the finite difference and weighted residual methods a set of coupled ordinary differential equations results which are integrated forward in time using the method of lines. Various software packages implementing Gear's method are popular.

The development of mathematical models is described in several of the general references [Guiochon et al., Rhee et al., Ruthven, Ruthven et al., Suzuki, Tien, Wankat, and Yang]. See also Finlayson [*Numerical Methods for Problems with Moving Fronts*, Ravenna Park, Washington, 1992; Holland and Liapis, *Computer Methods for Solving Dynamic Separation Problems*, McGraw-Hill, New York, 1982; Villadsen and Michelsen, *Solution of Differential Equation Models by Polynomial Approximation*, Prentice Hall, Englewood Cliffs, N.J., 1978].

For the characterization of wave shape and breakthrough curves, three methods are popular. The MTZ method [Michaels, *Ind. Eng. Chem.*, **44**, 1922 (1952)] measures the breadth of a wave between two chosen concentrations (e.g., $c_i^* = 0.05$ and 0.95 or $c_i^* = 0.01$ and 0.99). Outside of a laboratory, the measurement of full breakthrough curves is rare, so the breadth of the MTZ is often estimated from an independently determined stoichiometric capacity and a measured small concentration in the "toe" of the breakthrough curve. A second method for characterizing wave shape is by the slope of the breakthrough curve at its midheight (i.e., $c_i^* = 0.5$ [Vermeulen et al., *gen. refs.*]). The use of moments of the slope of breakthrough curves is a third means for characterization. They can often be used to extract numerical values for rate coefficients for linear systems [Ruthven, Suzuki, *gen. refs.*; Nauman and Buffham, *Mixing in Continuous Flow Systems*, Wiley-Interscience, New York, 1983]. The method of moments is discussed further in the following part of this section.

CHROMATOGRAPHY

CLASSIFICATION

Chromatography is a sorptive separation process where a portion of a solute mixture (feed) is introduced at the inlet of a column containing a selective adsorbent (stationary phase) and separated over the length of the column by the action of a carrier fluid (mobile phase) that is continually supplied to the column following introduction of the feed. The mobile phase is generally free of the feed components, but may contain various other species introduced to modulate the chromatographic separation. The separation occurs as a result of the different partitioning of the feed solutes between the stationary phase; the separated solutes are recovered at different times in the effluent from the column. Chromatography is used both in analysis of mixtures and in preparative and process-scale applications. It can be used for both trace-level and for bulk separations both in the gas and the liquid phase.

Modes of Operation The classical modes of operation of chromatography as enunciated by Tiselius [*Kolloid Z.*, **105**, 101 (1943)] are: elution chromatography, frontal analysis, and displacement development. Basic features of these techniques are illustrated in Fig. 16-29. Often, each of the different modes can be implemented with the same equipment and stationary phase. The results are, however, quite different in the three cases.

Elution Chromatography The components of the mobile phase supplied to the column after feed introduction have less affinity for the stationary phase than any of the feed solutes. Under trace conditions, the feed solutes travel through the column as bands or zones at different velocities that depend only on the composition of the mobile phase and the operating temperature and that exit from the column at different times.

Two variations of the technique exists: **isocratic elution**, when the mobile phase composition is kept constant, and **gradient elution**, when the mobile phase composition is varied during the separation. Isocratic elution is often the method of choice for analysis and in process applications when the retention characteristics of the solutes to be separated are similar and not dramatically sensitive to very small changes in operating conditions. Isocratic elution is also generally practical for systems where the equilibrium isotherm is linear or nearly linear. In all cases, isocratic elution results in a dilution of the separated products.

In **gradient elution**, the eluting strength of the mobile phase is gradually increased after supplying the feed to the column. In liquid chromatography, this is accomplished by changing the mobile phase composition. The gradient in eluting strength of the mobile phase that is generated in the column is used to modulate the separation allowing control of the retention time of weakly and strongly retained

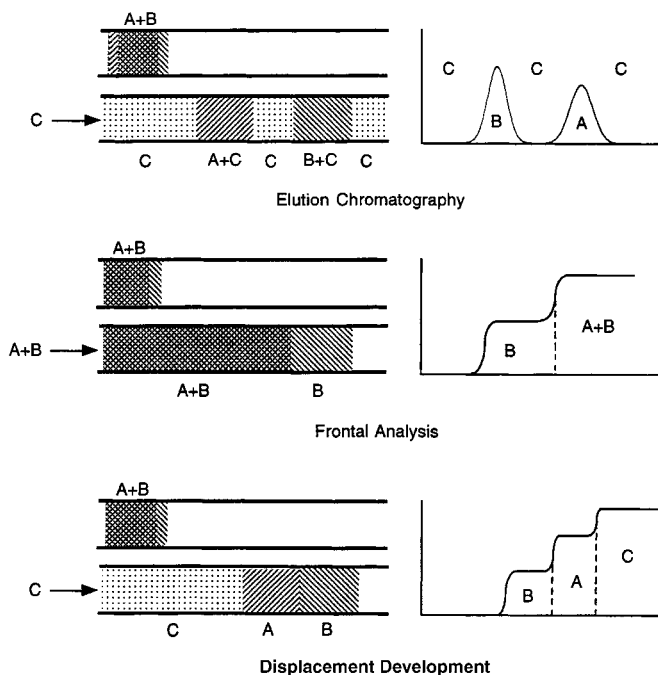


FIG. 16-29 Modes of operation of chromatography for the separation of a mixture of two components A and B. Figures on the left represent a schematic of the column with sample passing through it. Top diagrams show column at end of feed step. Figures on the right show the corresponding effluent concentrations as might be seen by a non-specific detector. C is either the eluent or the displacer. (Adapted from *Ettré*, 1980.)

components. A similar effect can be obtained in gas chromatography by modulating the column temperature. In either case, the column has to be brought back to the initial conditions before the next cycle is commenced.

Generally, gradient elution is best suited for the separation of complex mixtures that contain both species that interact weakly with the stationary phase and species that interact strongly. Since the eluting strength of the mobile phase is adjusted continuously, weakly retained components of a mixture are separated in the initial phase when the relative elution strength of the mobile phase is low, while strongly retained components are separated later in the gradient when the elution strength is high. In addition, the technique is used to obtain reproducible chromatographic separations when the solute retention characteristics are extremely sensitive to the operating conditions, as in the case of the chromatography of biopolymers, such as proteins. These molecules are often found to be very strongly retained in an extremely small range of mobile phase compositions and completely unretained elsewhere, making it practically impossible to obtain reproducible isocratic separations.

Frontal Analysis The feed mixture to be separated is continuously supplied to the column where the mixture components are competitively retained by the stationary phase. These solutes are partially separated in a series of fronts, preceded downstream by the least strongly retained species forming a pure component band, and upstream by the feed mixture. The technique is best suited for the removal of strongly adsorbed impurities present in trace amounts from an unretained or weakly retained product of interest. In this case, a large amount of feed can be processed before the impurities begin to break through. When this point is reached, the bed is washed to remove any desired product from the interstitial voids, and the adsorbent is regenerated. The method can only provide a single component in pure form, but avoids product dilution completely. Multicomponent

separations require a series of processing steps; either a series of frontal analysis separations, or a combination of elution and displacement separations. Example 11 illustrates bed concentration profiles for the frontal analysis separation of two components.

Displacement Development The column is partially loaded with the feed mixture as in frontal analysis, usually for conditions where all solutes of interest are strongly and competitively retained by the stationary phase. The feed supply is then stopped and a mobile phase containing the **displacer**, a component that has an affinity for the stationary phase stronger than any of the feed components, is fed to the column. The advancement of the displacer front through the column causes desorption of the feed components and their competitive readsorption downstream of the displacer front. As in frontal chromatography, the less strongly retained species tends to migrate faster down the column concentrating in a band farthest from the displacer front, while the most strongly adsorbed solute tends to move more slowly concentrating in a band adjacent to the displacer front. If the column is sufficiently long, all feed components eventually become distributed into a pattern of adjacent pure component bands where each upstream component acts as a displacer for each downstream species located in the band immediately downstream. When this occurs, all bands in the displacement train move at the same velocity which is equal to the velocity of the displacer front and the bed concentration profile is called an **isotachic pattern**.

The various operational steps of a displacement development separation are shown in Fig. 16-30. Ideally, the separated species exit the column as adjacent rectangular bands in order of increasing affinity for the stationary phase as shown in this figure. In practice, dispersion effects result in a partial mixing of adjacent bands requiring recycling of portions of the effluent that do not meet purity requirements. Following separation, the displacer has to be removed from the column with a suitable regenerant and the initial conditions of the column restored

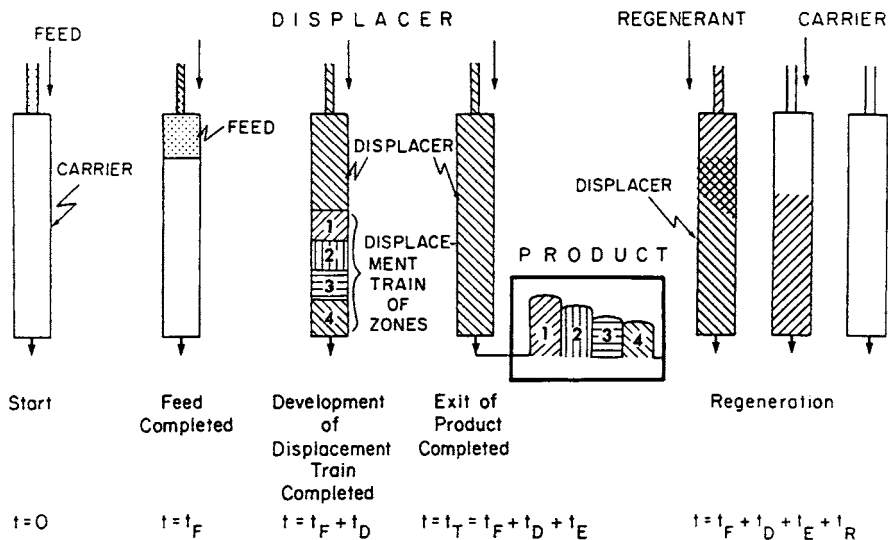


FIG. 16-30 Operational steps in displacement chromatography. The column, initially equilibrated with a carrier solvent at time 0, is loaded with feed until time t_F and supplied with displacer for a time $t_D + t_E$. Development of the displacement train occurs during the time t_D and elution of the separated products ends at time t_E . t_R is the time required to remove the displacer from the column and restore the initial conditions. Components are numbered in order of decreasing affinity for the stationary phase. [Reference: Horvath et al., *J. Chromatogr.*, **218**, 365 (1981). Reprinted with permission of *J. Chromatogr.*]

before the next cycle. Column regeneration may consume a significant portion of the cycle, when removal of the displacer is difficult.

Displacement chromatography is suitable for the separation of multicomponent bulk mixtures. For dilute multicomponent mixtures it allows a simultaneous separation and concentration. Thus, it permits the separation of compounds with extremely low separation factors without the excessive dilution that would be obtained in elution techniques.

Other modes of operation, including recycle and flow reversal schemes and continuous chromatography, are discussed in Ganetsos and Barker (*Preparative and Production Scale Chromatography*, Marcel Dekker, New York, 1993).

CHARACTERIZATION OF EXPERIMENTAL CHROMATOGRAMS

Method of Moments The first step in the analysis of chromatographic systems is often a characterization of the column response to small pulse injections of a solute under trace conditions in the Henry's law limit. For such conditions, the statistical moments of the response peak are used to characterize the chromatographic behavior. Such an approach is generally preferable to other descriptions of peak properties which are specific to Gaussian behavior, since the statistical moments are directly correlated to equilibrium and dispersion parameters. Useful references are Schneider and Smith [*AIChE J.*, **14**, 762 (1968)], Suzuki and Smith [*Chem. Eng. Sci.*, **26**, 221 (1971)], and Carbonell et al. [*Chem. Eng. Sci.*, **9**, 115 (1975); **16**, 221 (1978)].

The relevant moments are:

$$\mu_0 = \int_0^{\infty} c_i dt \quad (16-153)$$

$$\mu_1 = \frac{1}{\mu_0} \int_0^{\infty} c_i t dt \quad (16-154)$$

$$\sigma^2 = \frac{1}{\mu_0} \int_0^{\infty} c_i (t - \mu_1)^2 dt \quad (16-155)$$

where c_i is the peak profile, μ_0 represents the area, μ_1 the mean residence time, and σ^2 the variance of the response peak. Moments can be calculated by numerical integration of experimental profiles.

The **retention factor** is defined as a dimensionless peak locator as:

$$k'_i = \frac{\mu_1 - \mu_1^0}{\mu_1^0} \quad (16-156)$$

where μ_1^0 is the first moment obtained for an inert tracer which is excluded from the stationary phase. k'_i is a partition ratio representing the equilibrium ratio of the amount of solute in the stationary phase (including any pores) and the amount in the external mobile phase. Another commonly used definition of the retention factor uses as a reference the first moment of an inert that has access to all the pores.

The number of plates, N_p , and the height equivalent to a theoretical plate, HETP, are defined as measures of dispersion effects as:

$$N_p = \frac{L}{\text{HETP}} = \frac{\mu_1^2}{\sigma^2} \quad (16-157)$$

$$\text{HETP} = \frac{\sigma^2 L}{\mu_1^2} \quad (16-158)$$

A high number of plates and a low HETP indicate a high column efficiency.

Higher moments can also be computed and used to define the skewness of the response peak. However, difficulties often arise in such computations as a result of drifting of the detection system.

In practice, experimental peaks can be affected by extracolumn retention and dispersion factors associated with the injector, connections, and any detector. For linear chromatography conditions, the apparent response parameters are related to their corresponding true column value by

$$\mu_1^{app} = \mu_1 + \mu_1^{inj} + \mu_1^{conn} + \mu_1^{det} \quad (16-159)$$

$$\sigma^{2app} = \sigma^2 + \sigma^{2inj} + \sigma^{2conn} + \sigma^{2det} \quad (16-160)$$

Approximate Methods For certain conditions, symmetrical, Gaussian-like peaks are obtained experimentally. Such peaks may be

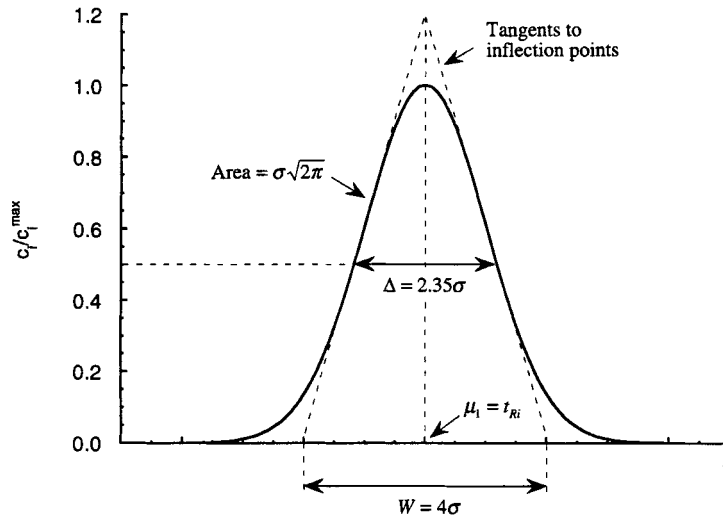


FIG. 16-31 Properties of a Gaussian peak. c_i^{\max} is the peak height; t_{Ri} , the peak apex time; σ , the standard deviation; Δ , the peak width at midheight; and W , the distance between the baseline intercepts of the tangents to the peak.

empirically described by:

$$c_i = \frac{Q_i/F_v}{\sigma\sqrt{2\pi}} \exp\left[-\left(\frac{t-t_{Ri}}{\sigma\sqrt{2}}\right)^2\right] = \frac{Q_i/F_v}{t_{Ri}} \sqrt{\frac{N_p}{2\pi}} \exp\left[-\frac{N_p}{2}\left(\frac{t}{t_{Ri}}-1\right)^2\right] \quad (16-161)$$

where Q_i is the amount of solute injected, F_v is the volumetric flow rate, and t_{Ri} is the peak apex time. The relationships between the moments and other properties of such peaks are shown in Fig. 16-31. For such peaks, approximate calculations of the number of plates can be done with the following equations:

$$N_p = 5.54 \left(\frac{t_{Ri}}{\Delta}\right)^2 \quad (16-162)$$

$$N_p = 16 \left(\frac{t_{Ri}}{W}\right)^2 \quad (16-163)$$

$$N_p = 2\pi \left(\frac{c_i^{\max} t_{Ri}}{\mu_0}\right)^2 \quad (16-164)$$

where Δ is the peak width at half peak height and W is the distance between the baseline intercepts of the tangents to the inflection points of the peak.

In general, Gaussian behavior can be tested by plotting the cumulative fractional recovery $\int_0^t c_i dt/\mu_0$ versus time on probability-linear coordinates; if the plot is linear, Gaussian behavior is confirmed. For nearly Gaussian peaks, calculations of N_p based on Eqs. (16-162) to (16-164) provide results close to those obtained with a rigorous calculation of moments. When deviations from Gaussian behavior are significant, however, large errors can be obtained using these expressions.

Tailing Peaks Tailing peaks can be obtained experimentally when the column efficiency is very low, when there are large extracolumn dispersion effects, when the stationary phase is heterogeneous (in the sense that it contains different adsorption sites), or when the adsorption equilibrium deviates from the Henry's law limit. Asymmetrical tailing peaks can sometimes be described empirically by an exponentially modified Gaussian (EMG) defined as the convolute integral of a Gaussian constituent with mean time t_C and standard deviation σ_C and an exponential decay with time constant τ_C [Grushka, *Anal. Chem.*, **44**, 1733 (1972)]:

$$c_i = \frac{Q_i/F_v}{\sigma_C \tau_C \sqrt{2\pi}} \int_0^\infty \exp\left[-\left(\frac{t-t_C-t'}{\sigma_C\sqrt{2}}\right)^2 - \frac{t'}{\tau_C}\right] dt' \quad (16-165)$$

Although a numerical integration is required to compute the peak profile, the moments are calculated directly as $\mu_1 = t_C + \tau_C$ and $\sigma^2 = \sigma_C^2 + \tau_C^2$ and the **peak skew** as:

$$\text{Peak skew} = \frac{1}{\mu_0 \sigma^3} \int_0^\infty c_i (t - \mu_1)^3 dt \sim \frac{2(\tau_C/\sigma_C)^3}{[1 + (\tau_C/\sigma_C)^2]^{3/2}} \quad (16-166)$$

For EMG peaks, peak skew increases with the ratio τ_C/σ_C . Figure 16-32 illustrates the characteristics of such a peak calculated for $\tau_C/\sigma_C = 1.5$. In general, with $\tau_C/\sigma_C > 1$ (peak skew > 0.7), a direct calculation of the moments is required to obtain a good approximation of the true value of N_p , since other methods give a large error (Yau et al., *Moderns Size-Exclusion Liquid Chromatography*, Wiley, New York, 1979). Alternatively, Eq. (16-165) can be fitted to experimental peaks to determine the optimum values of t_C , σ_C , and τ_C .

In practice, the calculation of peak skew for highly tailing peaks is rendered difficult by baseline errors in the calculation of third moments. The **peak asymmetry factor**, $A_s = b/a$, at 10 percent of peak height (see Fig. 16-32) is thus frequently used. An approximate relationship between peak skew and A_s for tailing peaks, based on data in Yau et al. is: Peak skew = $[0.51 + 0.19/(A_s - 1)]^{-1}$. Values of $A_s < 1.25$ (corresponding to peak skew < 0.7) are generally desirable for an efficient chromatographic separation.

Resolution The chromatographic separation of two components, A and B, under trace conditions with small feed injections can be characterized in terms of the resolution, R_s . For nearly Gaussian peaks:

$$R_s = \frac{2(t_{R,A} - t_{R,B})}{W_A + W_B} = \frac{\Delta t_R}{4\sigma_{AB}} \quad (16-167)$$

where Δt_R is the difference in retention time of the two peaks and $\sigma_{AB} = (\sigma_A + \sigma_B)/2$ is the average of their standard deviations. When Eq. (16-161) is applicable, the resolution for two closely spaced peaks is approximated by:

$$R_s = \frac{1}{2} \frac{\alpha - 1}{\alpha + 1} \frac{\bar{k}'_i}{1 + \bar{k}'_i} \sqrt{N_p} \\ \sim \frac{\alpha - 1}{4} \frac{k'_A}{1 + k'_A} \sqrt{N_p} \quad \text{for } \alpha \sim 1 \quad (16-168)$$

where $\alpha = k'_A/k'_B$ and $\bar{k}' = (k'_A + k'_B)/2$.

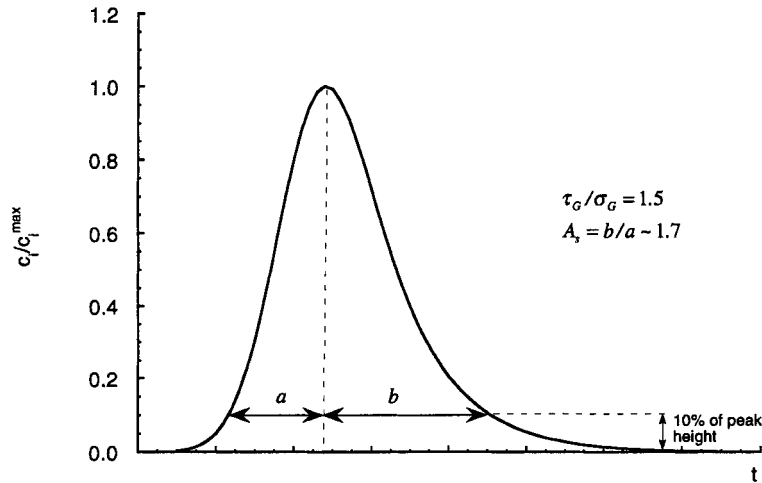


FIG. 16-32 Exponentially modified Gaussian peak with $\tau_G/\sigma_G = 1.5$. The graph also shows the definition of the peak asymmetry factor A_s at 10 percent of peak height.

Equation (16-168) shows that the resolution is the result of independent effects of the separation selectivity (α), column efficiency (N_p), and capacity (\bar{K}). Generally, peaks are essentially completely resolved when $R_s = 1.5$ (>99.5 percent separation). In practice, values of $R_s \sim 1$, corresponding to 98 percent separation, are often considered adequate.

The preceding equations are accurate to within about 10 percent for feed injections that do not exceed 40 percent of the final peak width. For large, rectangular feed injections, the baseline width of the response peak is approximated by:

$$W \sim 4\sigma + t_F \quad (16-169)$$

where 4σ is the baseline width obtained with a small pulse injection and t_F is the duration of feed injection. In this case, the resolution is defined as (see Ruthven, gen. refs., pp. 324–331):

$$R_s = \frac{t_{R,A} - t_{R,B} - t_F}{4\sigma_{AB}} \quad (16-170)$$

For strongly retained components ($\bar{K} \gg 1$), the number of plates required to obtain a given resolution with a finite feed injection is approximated by:

$$N_p = 4R_s^2 \left(\frac{\alpha + 1}{\alpha - 1} \right)^2 \left(1 + \frac{t_F}{4\sigma_{AB}R_s} \right)^2 \quad (16-171)$$

PREDICTION OF CHROMATOGRAPHIC BEHAVIOR

The conservation equations and the rate models described in the “Rate and Dispersion Factors” can normally be used for a quantitative description of chromatographic separations. Alternatively, **plate models** can be used for an approximate prediction, lumping together all dispersion contributions into a single parameter, the HETP or the number of plates [Sherwood et al., *Mass Transfer*, McGraw-Hill, New York, 1975, p. 576; Dondi and Guiochon, *Theoretical Advancements in Chromatography and Related Techniques*, NATO-ASI, Series C: Mathematical and Physical Sciences, vol. 383, Kluwer, Dordrecht, 1992, pp. 1–61]. Exact analytic solutions are generally available for linear isocratic elution under trace conditions (see Dondi and Guiochon, *ibid.*, Ruthven [gen. refs., pp. 324–335], Suzuki [gen. refs., pp. 224–243]). Other cases generally require numerical solution (see Guiochon et al., gen. refs.) or approximate treatments with simplified rate models.

Isocratic Elution In the simplest case, feed with concentration c_i^f is applied to the column for a time t_F followed by the pure carrier fluid. Under trace conditions, for a linear isotherm with external mass-transfer control, the linear driving force approximation or reaction kinetics (see Table 16-12), solution of Eq. (16-146) gives the following expression for the dimensionless solute concentration at the column outlet:

$$c_i^e = J(N, N\tau_1) - J(N, N\tau_1') \quad (16-172)$$

where N is the number of transfer units given in Table 16-13 and $\tau_1 = (\epsilon vt/L - \epsilon)/[(1 - \epsilon)(\rho_p K_i + \epsilon_p)]$ the throughput parameter (see “Square Root Spreading for Linear Isotherms” in “Fixed Bed Transitions”). τ_1' represents the value of τ_1 with time measured from the end of the feed step. Thus, the column effluent profile is obtained as the difference between a breakthrough profile for a feed started at $t = 0$ and another for a feed started at $t = t_F$.

The behavior predicted by this equation is illustrated in Fig. 16-33 with $N = 80$. $\tau_F = (\epsilon vt_F/L)/[(1 - \epsilon)(\rho_p K_i + \epsilon_p)]$ is the dimensionless duration of the feed step and is equal to the amount of solute fed to the column divided by the sorption capacity. Thus, at $\tau_F = 1$, the column has been supplied with an amount of solute equal to the stationary phase capacity. The graph shows the transition from a case where complete saturation of the bed occurs before elution ($\tau_F = 1$) to incomplete saturation as τ_F is progressively reduced. The lower curves with $\tau_F \leq 0.4$ are seen to be nearly Gaussian and centered at a dimensionless time $\tau_m \sim (1 - \tau_F/2)$. Thus, as $\tau_F \rightarrow 0$, the response curve approaches a Gaussian centered at $\tau_1 = 1$.

When τ_F is small ($\ll 0.4$), the solution for a feed pulse represented by a Dirac’s delta function at $\zeta = 0$ can be used in lieu of Eq. (16-172). In terms of the dimensionless concentration $c_i^e = c_i/c_i^f$ (Sherwood et al., *ibid.*, pp. 571–577):

$$c_i^e = \frac{\tau_F N}{\sqrt{\tau_1}} e^{-N} e^{-N\tau_1} I_1(2N\sqrt{\tau_1}) \quad (16-173)$$

where I_1 is the Bessel function of imaginary argument. When N is larger than 5, this equation is approximated by:

$$c_i^e = \frac{\tau_F}{2\sqrt{\pi}} \sqrt{\frac{N}{\tau_1}} \frac{\exp[-N(\sqrt{\tau_1} - 1)^2]}{(\tau_1)^{1/4}} \quad (16-174)$$

The behavior predicted by Eq. (16-174) is shown in Fig. 16-34 as $c_i^e/(\tau_F\sqrt{N})$ versus τ_1 for different values of N . For $N > 50$, the response peak is symmetrical, the peak apex occurs at $\tau_1 = 1$, and the

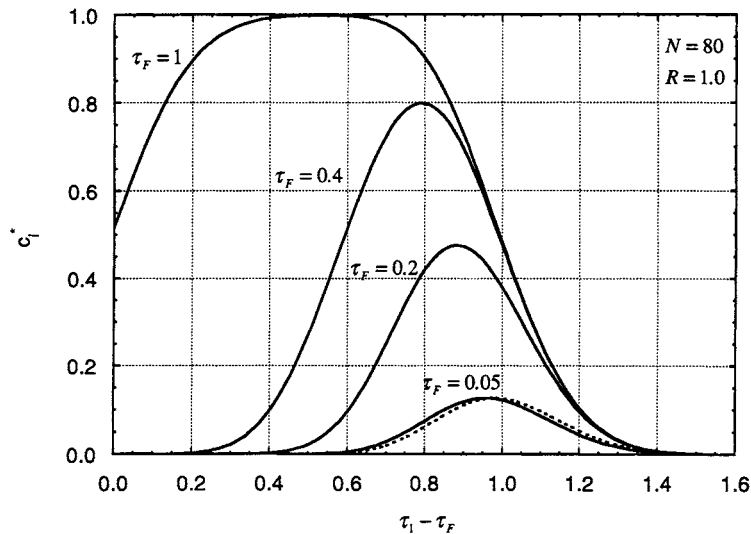


FIG. 16-33 Elution curves under trace linear equilibrium conditions for different feed loading periods and $N = 80$. Solid lines, Eq. (16-172); dashed line, Eq. (16-174) for $\tau_F = 0.05$.

dimensionless peak height is $c_i^{o\max} = \tau_F \sqrt{N/4\pi}$. A comparison of this equation with Eq. (16-172) with $N = 80$ is shown in Fig. 16-33 for $\tau_F = 0.05$.

The moments of the response peak predicted by Eq. (16-173) are

$$\mu_1 = \frac{L}{v} \left[1 + \frac{1-\epsilon}{\epsilon} (\epsilon_p + \rho_p K_i) \right] = \frac{L}{v} (1 + k'_i) \quad (16-175)$$

$$\sigma^2 = \frac{2\mu_1^2}{N} \left(\frac{k'_i}{1+k'_i} \right)^2 \quad (16-176)$$

where $k'_i = (1-\epsilon)(\epsilon_p + \rho_p K_i)/\epsilon$. Correspondingly, the number of plates and the HETP are:

$$N_p = \frac{N}{2} \left(\frac{1+k'_i}{k'_i} \right)^2 \quad (16-177)$$

$$\text{HETP} = \frac{2L}{N} \left(\frac{k'_i}{1+k'_i} \right)^2 \quad (16-178)$$

Since the term $(1+k'_i)/k'_i$ approaches unity for large k' -value, the number of plates is equal to one half the number of transfer units for a strongly retained component. For these conditions, when $N_p = N/2$, Eq. (16-174) and Eq. (16-161) produce the same peak retention time, peak spreading, and predict essentially the same peak profile.

In the general case of axially dispersed plug flow with bidispersed particles, the first and second moment of the pulse response are [Haynes and Sarma, *AIChE J.*, **19**, 1043 (1973)]:

$$\mu_1 = \frac{L}{v} \left[1 + \frac{1-\epsilon}{\epsilon} (\epsilon_p + \rho_p K_i) \right] = \frac{L}{v} (1 + k'_i) \quad (16-179)$$

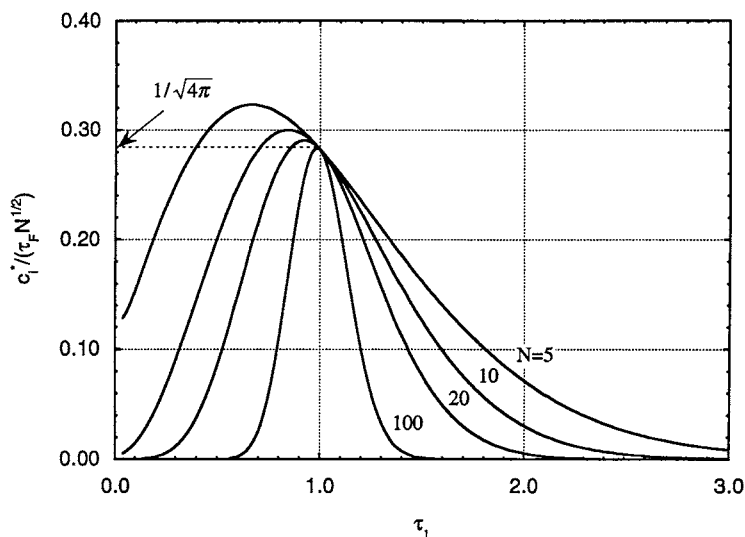


FIG. 16-34 Elution curves under trace linear equilibrium conditions with a pulse feed from Eq. (16-174).

$$\sigma^2 = \frac{2LD_L}{v^3} (1 + k_i')^2 + 2 \frac{L}{v} \frac{\epsilon k_i'^2}{1 - \epsilon} \left[\frac{r_p}{3k_f} + \frac{r_p^2}{15\epsilon_p D_{pi}} + \frac{\rho_p K_i}{(\epsilon_p + \rho_p K_i)^2} \frac{r_s^2}{15D_{si}} \right] \quad (16-180)$$

Correspondingly, the number of plates and the plate height are:

$$N_p = \left\{ \frac{2D_L}{vL} + \frac{2\epsilon}{1 - \epsilon} \frac{v}{L} \left(\frac{k_i'}{1 + k_i'} \right)^2 \times \left[\frac{r_p}{3k_f} + \frac{r_p^2}{15\epsilon_p D_{pi}} + \frac{\rho_p K_i}{(\epsilon_p + \rho_p K_i)^2} \frac{r_s^2}{15D_{si}} \right] \right\}^{-1} \quad (16-181)$$

$$\text{HETP} = \frac{2D_L}{v} + \frac{2\epsilon v}{1 - \epsilon} \left(\frac{k_i'}{1 + k_i'} \right)^2 \times \left[\frac{r_p}{3k_f} + \frac{r_p^2}{15\epsilon_p D_{pi}} + \frac{\rho_p K_i}{(\epsilon_p + \rho_p K_i)^2} \frac{r_s^2}{15D_{si}} \right] \quad (16-182)$$

In dimensionless form, a **reduced HETP**, $h = \text{HETP}/d_p$, analogous to the reduced HTU (cf. Fig. 16-13), is obtained as a function of the dimensionless velocity $ReSc$:

$$h = \frac{b}{ReSc} + a + cReSc \quad (16-183)$$

where $b = 2\epsilon\gamma_1$ (16-184a)

$$a = 2\gamma_2 \quad (16-184b)$$

$$c = \frac{1}{30} \frac{1}{1 - \epsilon} \left(\frac{k_i'}{1 + k_i'} \right)^2 \left[\frac{10}{Sh} + \frac{\tau_p}{\epsilon_p} + \frac{\rho_p K_i}{(\epsilon_p + \rho_p K_i)^2} \frac{r_s^2}{D_{si}} \frac{D_{pi}}{r_p^2} \right] \quad (16-184c)$$

Equation (16-183) is qualitatively the same as the **van Deemter equation** [van Deemter and Zuidervog, *Chem. Eng. Sci.*, **5**, 271 (1956)] and is equivalent to other empirical reduced HETP expressions such as the **Knox equation** [Knox, *J. Chromatogr. Sci.*, **15**, 352 (1977)].

The Sherwood number, Sh , is estimated from Table 16-9, and the dispersion parameters γ_1 and γ_2 from Table 16-10 for well-packed columns. Typical values are $a = 1-4$ and $b = 0.5-1$. Since $\text{HETP} \sim 2\text{HTU}$, Fig. 16-13 can also be used for approximate calculations.

Concentration Profiles In the general case but with a linear isotherm, the concentration profile can be found by numerical inversion of the Laplace-domain solution of Haynes and Sarma [see Lenhoff, *J. Chromatogr.*, **384**, 285 (1987)] or by direct numerical solution of the conservation and rate equations. For the special case of no axial dispersion, an explicit time-domain solution is also available in the cyclic steady state for repeated injections of arbitrary duration t_F followed by an elution period t_E with cycle time $t_C = t_F + t_E$ [Carta, *Chem. Eng. Sci.*, **43**, 2877 (1988)]. For the linear driving force mechanism, the solution is

$$c_i^o = \phi + \frac{2}{\pi} \sum_{j=1}^{\infty} \left\{ \frac{1}{j} \exp \left(- \frac{j^2 N}{j^2 + \omega^2} \right) \sin(j\pi\phi) \times \cos \left[\frac{2j\pi}{t_C} \left(t - \frac{t_F}{2} - \frac{L}{v} \right) - \frac{j\omega N}{j^2 + \omega^2} \right] \right\} \quad (16-185)$$

where

$$\phi = \frac{t_F}{t_C} \quad (16-185a)$$

$$\omega = \frac{N\epsilon v c/L}{2\pi(1 - \epsilon)(\rho_p K_i + \epsilon_p)} \quad (16-185b)$$

The average effluent concentration in a product cut between times t_1 and t_2 can be calculated directly from

$$\bar{c}_i^o = \frac{\int_{t_1}^{t_2} c_i^o dt}{t_2 - t_1} \phi + \frac{t_C}{t_2 - t_1} \frac{2}{\pi^2}$$

$$\times \sum_{j=1}^{\infty} \left\{ \frac{1}{j^2} \exp \left(- \frac{j^2 N}{j^2 + \omega^2} \right) \sin(j\pi\phi) \sin \left[j\pi \frac{t_2 - t_1}{t_C} \right] \times \cos \left[\frac{2j\pi}{t_C} \left(\frac{t_1 + t_2 - t_F}{2} - \frac{L}{v} \right) - \frac{j\omega N}{j^2 + \omega^2} \right] \right\} \quad (16-186)$$

The same equations can also be used as a good approximation for other rate mechanisms with N calculated according to Table 16-13. When t_C is large, Eq. (16-185) describes a single feed injection and approaches the results of Eqs. (16-173) and (16-148) for small and large values of ϕ , respectively. See Seader and Henley (gen. refs.), and Carta, op. cit., for sample calculations.

When the adsorption equilibrium is nonlinear, skewed peaks are obtained, even when N is large. For a constant separation-factor isotherm with $R < 1$ (favorable), the leading edge of the chromatographic peak is steeper than the trailing edge. When $R > 1$ (unfavorable), the opposite is true.

Figure 16-35 portrays numerically calculated chromatographic peaks for a constant separation factor system showing the effect of feed loading on the elution profile with $R = 0.5$ ($\tau_1 - \tau_F = [\epsilon v(t - t_F)/L - \epsilon]/\Lambda$). When the dimensionless feed time $\tau_F = 1$, the elution curve comprises a sharp leading profile reaching the feed concentration followed by a gradual decline to zero. As τ_F is reduced, breakthrough of the leading edge occurs at later times, while the trailing edge, past the peak apex, continues to follow the same profile. As the amount of feed injected approaches zero, mass-transfer resistance reduces the solute concentration to values that fall in the Henry's law limit of the isotherm, and the peak retention time gradually approaches the value predicted in the infinite dilution limit for a linear isotherm.

For high feed loads, the shape of the diffuse trailing profile and the location of the leading front can be predicted from local equilibrium theory (see "Fixed Bed Transitions"). This is illustrated in Fig. 16-35 for $\tau_F = 0.4$. For the diffuse profile (a "simple wave"), Eq. (16-131) gives:

$$c_i^o = \frac{R}{1 - R} \left[\left(\frac{1}{R(\tau_1 - \tau_F)} \right)^{1/2} - 1 \right] \quad (16-187)$$

Thus, the effluent concentration becomes zero at $\tau_1 - \tau_F = 1/R$. The position of the leading edge (a "shock front") is determined from Eq. (16-132):

$$\tau_{1s} = \tau_F + \frac{1}{R} [1 - \sqrt{(1 - R)\tau_F}]^2 \quad (16-188)$$

and the peak highest concentration by [Golshan-Shirazi and Guiochon, *Anal. Chem.*, **60**, 2364 (1988)]:

$$c_i^{o \max} = \frac{R}{1 - R} \frac{\sqrt{(1 - R)\tau_F}}{1 - \sqrt{(1 - R)\tau_F}} \quad (16-189)$$

The local equilibrium curve is in approximate agreement with the numerically calculated profiles except at very low concentrations when the isotherm becomes linear and near the peak apex. This occurs because band-spreading, in this case, is dominated by adsorption equilibrium, even if the number of transfer units is not very high. A similar treatment based on local equilibrium for a two-component mixture is given by Golshan-Shirazi and Guiochon [*J. Phys. Chem.*, **93**, 4143 (1989)].

Prediction of multicomponent nonlinear chromatography accounting for rate factors requires numerical solution (see Guiochon et al., gen. refs., and "Numerical Methods and Characterization of Wave Shape" in "Fixed Bed Transitions").

Linear Gradient Elution Analytical solutions are available for special cases under trace conditions with a linear isotherm. Other situations normally require a numerical solution. General references are Snyder [in Horvath (ed.), *High Performance Liquid Chromatography: Advances and Perspectives*, vol. 1, Academic Press, 1980, p. 208], Antia and Horvath [*J. Chromatogr.*, **484**, 1 (1989)], Yamamoto et al. [*Ion Exchange Chromatography of Proteins*, Marcel Dekker, 1988], and Guiochon et al. (gen. refs.).

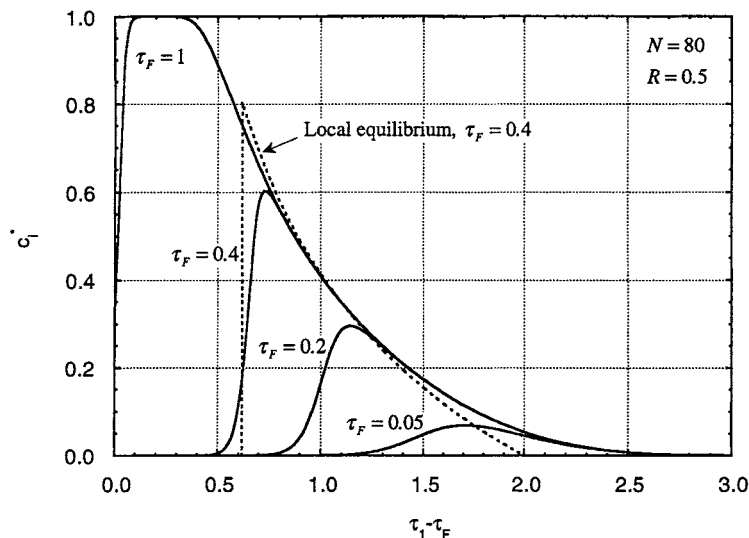


FIG. 16-35 Elution curves under trace conditions with a constant separation factor isotherm for different feed loadings and $N = 80$. Solid lines, rate model; dashed line, local equilibrium theory for $\tau_F = 0.4$.

The most commonly used gradients are linear gradients where the starting solvent is gradually mixed with a second gradient-forming solvent at the column entrance to yield a volume fraction φ of the mobile phase modulator that increases linearly with time:

$$\varphi = \varphi_0 + \beta t \quad (16-190)$$

When the mobile phase modulator is a dilute solute in a solvent, as when the modulator is a salt, φ indicates molar concentration.

Under *trace conditions*, the retention of the modulator in the column is independent of the presence of any solutes. The modulator concentration at the column exit is approximated by

$$\varphi = \varphi_0 + \beta \left[t - \frac{L}{v} (1 + k'_M) \right] \quad (16-191)$$

where k'_M is the retention factor of the modulator.

For a small feed injection, the modulator concentration φ_R at which a feed solute is eluted from the column is obtained from the following integral relationship

$$G(\varphi_R) = \frac{\beta L}{v} = \int_{\varphi_0}^{\varphi_R} \frac{d\varphi}{k'_i(\varphi) - k'_M} \quad (16-192)$$

where $k'_i(\varphi)$ is the solute retention factor as a function of the mobile phase modulator concentration. Note that the solute retention time in the column is affected by the steepness of the gradient at the column entrance.

$k'_i(\varphi)$ can be obtained experimentally from isocratic elution experiments at different φ values, or from linear gradient elution experiments where the ratio $G = \beta L/v$ is varied. In the latter case, the retention factor is obtained by differentiation of Eq. (16-192) from $k'_i(\varphi_R) = k'_M + (dG/d\varphi_R)^{-1}$.

Table 16-14 gives explicit expressions for chromatographic peak properties in isocratic elution and linear gradient elution for two cases.

In **reversed-phase chromatography** (RPC), the mobile phase modulator is typically a water-miscible organic solvent, and the stationary phase is a hydrophobic adsorbent. In this case, the logarithm of solute retention factor is commonly found to be linearly related to the volume fraction of the organic solvent.

In **ion-exchange chromatography** (IEC), the mobile phase modulator is typically a salt in aqueous solution, and the stationary phase is an ion-exchanger. For dilute conditions, the solute retention factor is commonly found to be a power-law function of the salt normality [cf. Eq. (16-27) for ion-exchange equilibrium].

Band broadening is also affected by the gradient steepness. This effect is expressed in Table 16-14 by a **band compression factor** C , which is a function of the gradient steepness and of equilibrium parameters. Since $C < 1$, gradient elution yields peaks that are sharper than those that would be obtained in isocratic elution at $\varphi = \varphi_R$.

Other cases, involving an arbitrary relationship between the solute retention factor and the modulator concentration can be handled analytically using the approaches of Frey [*Biotechnol. Bioeng.*, **35**, 1055 (1990)] and Carta and Stringfield [*J. Chromatogr.*, **605**, 151 (1992)].

Displacement Development A complete prediction of displacement chromatography accounting for rate factors requires a numerical solution since the adsorption equilibrium is nonlinear and intrinsically competitive. When the column efficiency is high, however, useful predictions can be obtained with the local equilibrium theory (see "Fixed Bed Transitions").

For constant-separation factor systems, the ***h*-transformation** of Helfferich and Klein (gen. refs.) or the method of Rhee et al. [*AIChE J.*, **28**, 423 (1982)] can be used [see also Helfferich, *Chem. Eng. Sci.*, **46**, 3320 (1991)]. The equations that follow are adapted from Frenz and Horvath [*AIChE J.*, **31**, 400 (1985)] and are based on the *h*-transformation. They refer to the separation of a mixture of $M - 1$ components with a displacer (component 1) that is more strongly adsorbed than any of the feed solutes. The **multicomponent Langmuir isotherm** [Eq. (16-39)] is assumed valid with equal monolayer capacities, and components are ranked numerically in order of decreasing affinity for the stationary phase (i.e., $K_1 > K_2 > \dots > K_M$).

The development of component bands is predicted by mapping the trajectories of the ***h*-function roots** h_i , which are obtained from the solution of

$$\sum_{i=1}^M \frac{K_i c_i}{h \alpha_{i,1} - 1} = 1 \quad (16-193)$$

where $\alpha_{i,j} = K_i/K_j$.

Trivial roots also exist for each component with zero concentration. In displacement chromatography, for each of the transitions at the column entrance, a new set of M roots is generated. These roots are given in Table 16-15. The change from the initial solvent (carrier) to feed changes $M - 1$ roots, generating $M - 1$ boundaries or transitions that move through the column. These boundaries are all self-sharpening, characterized by upstream h'_i values larger than the corresponding downstream h'_i values.

TABLE 16-14 Expressions for Predictions of Chromatographic Peak Properties in Linear Gradient Elution Chromatography under Trace Conditions with a Small Feed Injection and Inlet Gradient Described by $\varphi = \varphi_0 + \beta t$ (Adapted from Refs. A and B)

Parameter	Isocratic	Gradient elution—RPC (Ref. A)	Gradient elution—IEC (Ref. B)
Dependence of retention factor on modulator concentration	—	$k' - k'_M = \alpha_s e^{-S\varphi}$	$k' - k'_M = \alpha_s \varphi^{-z}$
Retention time	$t_R = \frac{L}{v} (1 + k'_o)$	$t_R = \frac{L}{v} (1 + k'_M) + \frac{1}{S\beta} \ln \left[\frac{S\beta L}{v} (k'_o - k'_M) + 1 \right]$	$t_R = \frac{L}{v} (1 + k'_M) + \frac{1}{\beta} \left[\frac{\alpha_z \beta L}{v} (Z + 1) + \varphi_0^{Z+1} \right]^{1/(Z+1)} - \frac{\varphi_0}{\beta}$
Mobile phase composition at column exit	$\varphi_R = \varphi_0$	$\varphi_R = \varphi_0 + \beta \left[t_R - \frac{L}{v} (1 + k'_M) \right]$	$\varphi_R = \varphi_0 + \beta \left[t_R - \frac{L}{v} (1 + k'_M) \right]$
Retention factor at peak elution	$k'_R = k'_o$	$k'_R = \frac{k'_o + (k'_o - k'_M) S\beta L/v}{1 + (k'_o - k'_M) S\beta L/v}$	$k'_R = \alpha_z \left[\frac{\alpha_z \beta L}{v} (Z + 1) + \varphi_0^{Z+1} \right]^{-z/(Z+1)} + k'_M$
Peak standard deviation	$\sigma = \frac{L/v}{\sqrt{N_P}} (1 + k'_o)$	$\sigma = C \frac{L/v}{\sqrt{N_{PR}}} (1 + k'_R)$	$\sigma = C \frac{L/v}{\sqrt{N_{PR}}} (1 + k'_R)$
Band compression factor	—	$C = \frac{(1 + p + p^2/3)^{1/2}}{1 + p}$ $p = \frac{(k'_o - k'_M)(1 + k'_M) S\beta L/v}{1 + k'_o}$	$C = \begin{cases} \sqrt{M'} & \text{for } M' < 0.25 \\ \frac{3.22M'}{1 + 3.13M'} & \text{for } 0.25 < M' < 0.25 \\ 1 & \text{for } M' > 120.25 \end{cases}$ $M' = \frac{1}{2} \frac{1 + k'_R}{1 + k'_M} \frac{Z + 1}{Z}$

References: A. Snyder in Horvath (ed.), *High Performance Liquid Chromatography: Advances and Perspectives*, vol. 1, Academic Press, 1980, p. 208.
 B. Yamamoto, *Biotechnol. Bioeng.*, **48**, 444 (1995).
 Solute equilibrium parameters: α_s, S for RPC and α_z, Z for IEC
 Solute retention factor for initial mobile phase: k'_o
 Retention factor of mobile phase modulator: k'_M
 Plate number obtained for $k' = k'_R$: N_{PR}

The switch from feed to displacer changes M roots, generating M boundaries. All of these boundaries are self-sharpening, except the boundary associated with the transition from h_{MF} to $\alpha_{1,M+1}$ that can be self-sharpening or diffuse depending on the relative value of these roots. Note that only one root changes value across a particular boundary.

The **adjusted propagation velocity** of each self-sharpening boundary is:

$$u_{si} = \frac{d\zeta}{d\tau_1} = h'_i h'_i P_i \tag{16-194}$$

$$P_i = \prod_{j=1}^{i-1} h'_j \prod_{j=i+1}^M h''_j \prod_{j=1}^{M+1} \alpha_{j,i} \tag{16-195}$$

and that of each diffuse boundary:

$$u_{di} = h_i^2 P_i \tag{16-196}$$

where $\zeta = z/L$ and $\tau_1 = (\epsilon vt/L - \epsilon_i \zeta)/\Lambda$ with $\Lambda = \rho_i n_i^0/c_i^0$ equal to the partition ratio for the displacer.

The root trajectories are mapped as follows on the ζ - τ_1 plane:

1. The starting points are the beginning and end of the feed step. From these points trajectories are traced according to Eqs. (16-194) and (16-196).

2. At the points of intersection of trajectories, a change in boundary velocity occurs: When two boundaries associated with a change in the same root number intersect, they combine into a single boundary with velocity given by Eq. (16-194) or (16-196), intermediate in value between those of the intersecting trajectories. When two trajectories associated with different root numbers intersect, they both continue beyond the point of intersection with new velocities calculated from Eqs. (16-194) and (16-196), reflecting any change in root values.

3. After constructing the trajectories, the following equation is used to calculate the band profiles

$$c_j = \frac{\prod_{i=1}^M (h_i \alpha_{i,j} - 1)}{K_j \prod_{i=1}^M (\alpha_{j,i} - 1)} \tag{16-197}$$

Example 14: Calculation of Band Profiles in Displacement Chromatography An equimolar mixture of two components (concentrations $c_2^f = c_3^f = 1$ arbitrary unit) is separated with a displacer with concentration $c_1^f = 2$. The equilibrium isotherm is:

$$n_i = \frac{n^* K_i c_i}{1 + K_1 c_1 + K_2 c_2 + K_3 c_3} \quad (i = 1, 2, 3)$$

with $K_1 = 2$, $K_2 = 1$, and $K_3 = 0.667$. The dimensionless feed time is $\tau_f = 0.2$. The separation factors used for calculating the trivial roots are $\alpha_{1,1} = 1$, $\alpha_{1,2} = 2$, $\alpha_{1,3} = 3$, $\alpha_{1,4} = 1 + K_1 c_1^f = 5$. The remaining h -function roots are calculated by solving Eq. (16-193) for the carrier, feed, and displacer concentrations. The results are summarized in Table 16-16.

TABLE 16-15 Concentrations and h -Function Roots for Displacement Chromatography of a Mixture of $M - 1$ Components Numbered in Order of Decreasing Affinity for the Stationary Phase (Adapted from Frenz and Horvath, 1985)

Solution	$c_i = 0$		$c_i > 0$	
	i	h_i	i	h_i
Carrier	1, 2, ..., M	$\alpha_{1,1}, \dots, \alpha_{1,M}$	—	—
Feed	1	$\alpha_{1,1}$	2, ..., M	h_{2f}, \dots, h_{Mf}^0
Displacer	2, 3, ..., M	$\alpha_{1,2}, \dots, \alpha_{1,M}$	1	$\alpha_{1,M+1} = 1 + K_1 c_1^f$

⁰Roots calculated from the solution of Eq. (16-193).

TABLE 16-16 Values of h -Roots for Example 14

State	h_1	h_2	h_3
Carrier	1	2	3
Feed	1	2.44	6.56
Displacer	2	3	5

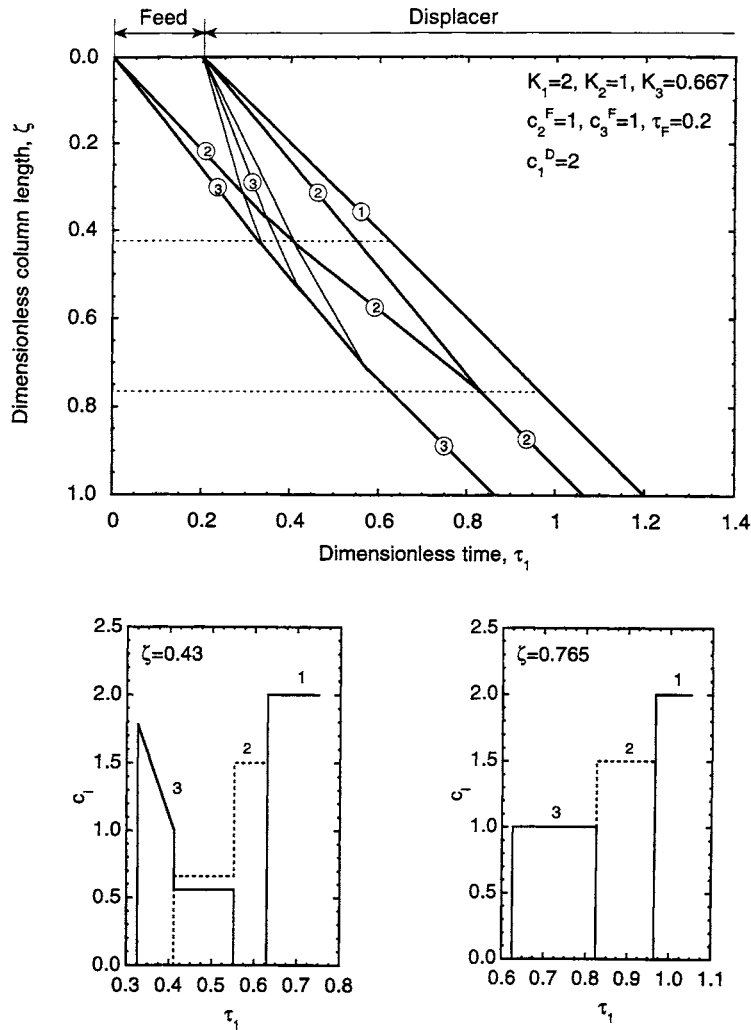


FIG. 16-36 Dimensionless time-distance plot for the displacement chromatography of a binary mixture. The darker lines indicate self-sharpening boundaries and the thinner lines diffuse boundaries. Circled numerals indicate the root number. Concentration profiles are shown at intermediate dimensionless column lengths $\zeta = 0.43$ and $\zeta = 0.765$. The profiles remain unchanged for longer column lengths.

The switch from carrier to feed generates self-sharpening boundaries, since the h'_s 's (upstream) are larger than the h'_s 's (downstream). The switch from feed to displacer generates two self-sharpening boundaries (corresponding to h_1 and h_2) and a diffuse boundary (corresponding to h_3) since $h_3^s < h_3^f$. The velocity of each boundary is calculated from Eq. (16-194) for self-sharpening boundaries and from Eq. (16-196) for diffuse boundaries. The root trajectories are shown in Fig. 16-36 (top). From one boundary to the next, the root values change one at a time from the values corresponding to the carrier to the values corresponding to the displacer. Concentration profiles calculated from Eq. (16-197) are shown in Fig. 16-36 (bottom) for two different values of ζ . The concentrations in the z and t coordinates are easily reconstructed from the definitions of τ_1 and ζ .

In general, for a constant separation factor system, complete separation is obtained when:

$$c_1^D > \frac{1}{K_1} (\alpha_{1,M} - 1) \quad (16-198)$$

Then, band profiles eventually develop into the **isotachic pattern** of pure component bands moving at the velocity of the displacer front. In Example 16-14, this occurs at $\zeta = 0.765$.

The **isotachic concentrations** c_j^I in the fully developed train are calculated directly from the single component isotherms using:

$$\frac{n_1^I}{c_1^I} = \frac{n_2^I}{c_2^I} = \dots = \frac{n_M^I}{c_M^I} \quad (16-199)$$

or

$$c_j^I = c_1^D - \frac{1}{K_j} (1 - \alpha_{j,1}) \quad (16-200)$$

The graphical interpretation of Eq. (16-199) is shown in Fig. 16-37 for the conditions of Example 16-14. An operating line is drawn from the origin to the point of the pure displacer isotherm at $c_1 = c_1^D$. For displacement to occur, the operating line must cross the pure component isotherms of the feed solutes. The product concentrations in the isotachic train are found where the operating line crosses the isotherms.

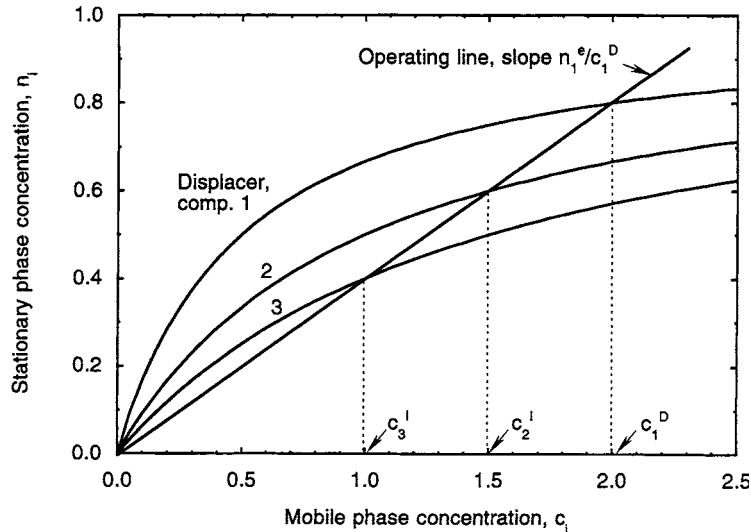


FIG. 16-37 Schematic showing the intersection of the operating line with the pure-component isotherms in displacement chromatography. Conditions are the same as in Fig. 16-36.

When this condition is met, the feed concentrations do not affect the final product concentrations.

Analyses of displacement chromatography by the method of characteristics with non-Langmuirian systems is discussed by Antia and Horvath [*J. Chromatogr.*, **556**, 199 (1991)] and Carta and Dinerman [*AIChE J.*, **40**, 1618 (1994)]. Optimization studies and analyses by computer simulations are discussed by Jen and Pinto [*J. Chromatogr.*, **590**, 47 (1992)], Katti and Guiochon [*J. Chromatogr.*, **449**, 24 (1988)], and Phillips et al. [*J. Chromatogr.*, **54**, 1 (1988)].

DESIGN FOR TRACE SOLUTE SEPARATIONS

The design objectives of the analyst and the production line engineer are generally quite different. For analysis the primary concern is typically resolution. Hence operating conditions near the minimum value of the HETP or the HTU are desirable (see Fig. 16-13).

In preparative chromatography, however, it is generally desirable to reduce capital costs by maximizing the **productivity**, or the amount of feed processed per unit column volume, subject to specified purity requirements. This reduction, however, must be balanced against operating costs that are determined mainly by the mobile phase flow rate and the pressure drop. In practice, preparative chromatography is often carried out under **overload conditions**, i.e., in the nonlinear region of the adsorption isotherm. Optimization under these conditions is discussed in Guiochon et al. (gen. refs.). General guidelines for trace-level, isocratic binary separations, in the Henry's law limit of the isotherm are:

1. The stationary phase is selected to provide the maximum selectivity. Where possible, the retention factor is adjusted (by varying the mobile phase composition, temperature, or pressure) to an optimum value that generally falls between 2 and 10. Resolution is adversely affected when $k' \ll 2$, while product dilution and separation time increase greatly when $k' \gg 10$. When this is not possible for all feed components and large differences exist among the k' -values of the different solutes, gradient elution should be considered.

2. The average feed mixture charging rate, molar or volumetric, is fixed by the raw material supply or the demand for finished product.

3. The value of N_p required to achieve a desired resolution is determined by Eq. (16-168) or (16-171). Since $N = L/HTU \sim 2N_p =$

$2L/HETP$, Fig. 16-13 or Eq. (16-183) can be used to determine the range of the dimensionless velocity $ReSc$ that maximizes N_p for a given particle diameter and column length.

4. The allowable pressure drop influences the choice of the particle size and helps determine the column length. Equations for estimating the pressure drop in packed beds are given in Section 6.

5. When only a few solutes are separated, they may occupy only a small portion of the total column volume at any given instant. In such cases, the productivity is improved by cyclic feed injections, timed so that the most strongly retained component from an injection elutes just before the least strongly retained component from the following injection (see Fig. 16-57). For a mixture of two components with $\bar{k}' > 1$, when the same resolution is maintained between bands of the same injections and bands of successive injections, the cycle time t_C and the plate number requirement are:

$$t_C = 2(t_{RA} - t_{RB}) = \frac{2L}{v} (k'_A - k'_B) \quad (16-201)$$

$$N_p = 4R_s^2 \left(\frac{\alpha + 1}{\alpha - 1} \right)^2 (1 - 2\phi)^{-2} \quad (16-202)$$

where $\phi = t_f/t_C$ is the fraction of the cycle time during which feed is supplied to the column. The productivity, $P = \text{volume of feed}/(\text{time} \times \text{bed volume})$, is:

$$\begin{aligned} P &= \frac{1}{4R_s^2} \left(\frac{\alpha - 1}{\alpha + 1} \right)^2 \frac{\epsilon v}{HETP} \phi(1 - 2\phi)^2 \\ &= \frac{1}{4R_s^2} \left(\frac{\alpha - 1}{\alpha + 1} \right)^2 \frac{D_i}{d_p^2} \left(\frac{ReSc}{b/ReSc + a + cReSc} \right) \phi(1 - 2\phi)^2 \end{aligned} \quad (16-203)$$

For a given resolution, P is maximized when $\phi = 1/6$ (i.e., feed is supplied for one sixth of the cycle time), and by the use of small particle sizes. The function $ReSc/(b/ReSc + a + cReSc)$ generally increases with $ReSc$, so that productivity generally increases with the mobile phase velocity. For typical columns, however, this function is within about 10 percent of its maximum value ($\sim 1/c$) when $ReSc$ is in the range 30–100. Thus, increasing the velocity above this range must be balanced against the costs associated with the higher pressure drop. Similar results are predicted with Eq. (16-185).

PROCESS CYCLES

GENERAL CONCEPTS

Some applications of adsorption and ion exchange can be achieved by sorbent-fluid contact in batch equipment. Batch methods are well adapted to laboratory use and have also been applied on a larger scale in several specific instances. In a batch run for either adsorption or ion exchange, a sorbent is added to a fluid, completely mixed, and subsequently separated. Batch treatment is adopted when the capacity and equilibrium of the sorbent are large enough to give nearly complete sorption in a single step, as in purifying and decoloration of laboratory preparations with carbons and clays. Batch runs are useful in the measurement of equilibrium isotherms and also of adsorptive diffusion rate. Batch tests or measurements are often conducted in portions of adsorbent or ion-exchange material intended for larger-scale use. For example, either the equilibrium sorption of a solid and/or its ultimate sorption capacity can be determined in this way. The solid is first equilibrated with a fluid at the concentration of interest; after separating the phases, gravimetric and chemical analyses can be used to determine the sorbed amount and composition.

Like the laboratory batch use, some commercial applications use the adsorbent on a throwaway basis. Reasons for using sorption non-regeneratively are usually: (1) low cost of the sorbent, (2) high value of the product, (3) very low dosage (sorbent-to-fluid ratio), and (4) difficulty in desorbing the sorbates. Magnesium perchlorate and barium oxide are used for drying, iron sponge (hydrated iron oxide on wood chips) is used to remove hydrogen sulfide, and sodium or potassium hydroxide is applied to removal of sulfur compounds or carbon dioxide. In wastewater treatment, powdered activated carbon (PAC) is added to enhance biological treatment but is not regenerated; instead, it remains with the sludge. Silica gel is used as a desiccant in packaging. Activated carbon is used in packaging and storage to adsorb other chemicals for preventing the tarnishing of silver, retarding the ripening or spoiling of fruits, "gettering" (scavenging) out-gassed solvents from electronic components, and removing odors. Synthetic zeolites, or blends of zeolites with silica gel, are used in dual-pane windows to adsorb water during initial dry-down and any in-leakage and to adsorb organic solvents emitted from the sealants during their cure; this prevents fogging between the sealed panes that could result from the condensation of water or the solvents [Ausikaitis, *Glass Digest*, **61**, 69-78 (1982)]. Activated carbon is used to treat recirculated air in office buildings, apartments, and manufacturing plants using thin

filter-like frames to treat the large volumes of air with low pressure drop. On a smaller scale, activated carbon filters are in kitchen hoods, air conditioners, and electronic air purifiers. On the smallest scale, gas masks containing carbon or carbon impregnated with promoters are used to protect individual wearers from industrial odors, toxic chemicals, and gas-warfare chemicals. Activated carbon fibers have been formed into fabrics for clothing to protect against vesicant and percutaneous chemical vapors [Macnair and Arons in Chermisinoff and Ellerbusch (eds.), gen. refs.].

Ion exchangers are sometimes used on a throwaway basis also. In the laboratory, ion exchangers are used to produce deionized water, purify reagents, and prepare inorganic sols. In medicine, they are used as antacid, for sodium reduction, for the sustained release of drugs, in skin-care preparations, and in toxin removal.

Although there are many practical applications for which the sorbent is discarded after one use, most applications of interest to chemical engineers involve the removal of adsorbates from the sorbent (i.e., regeneration). This allows the adsorbent to be reused and the adsorbates to be recovered.

The maximum efficiency that a cyclic adsorption process can approach for any given set of operating conditions is defined by the adsorptive loading in equilibrium with the feed fluid. There are several factors that reduce the practical (or "operating") adsorption: mass-transfer resistance (see above), deactivation (see above), and incomplete regeneration (or *desorption*). The severity of regeneration influences how closely the dynamic capacity of an adsorbent resembles that of fresh, virgin material. Regeneration, or reversal of the adsorption process, requires a reduction in the driving force for adsorption. This is accomplished by increasing the equilibrium driving force for the adsorbed species to desorb from the solid to the surrounding fluid.

TEMPERATURE SWING ADSORPTION

A temperature-swing, or thermal-swing, adsorption (TSA) process cycle is one in which desorption takes place at a temperature much higher than adsorption. The elevation of temperature is used to shift the adsorption equilibrium and affect regeneration of the adsorbent. Figure 16-38 depicts a simplified (and ideal) TSA cycle. The feed fluid containing an adsorbate at a partial pressure of p_1 is passed through an

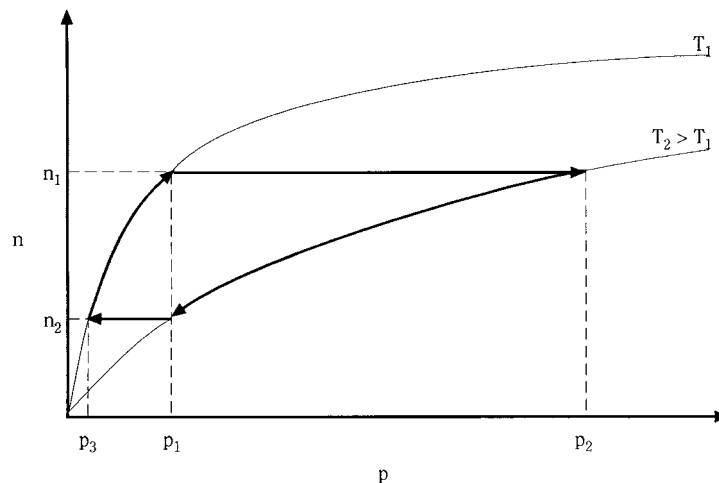


FIG. 16-38 Ideal temperature swing cycle. (Reprinted with permission of UOP.)

adsorbent at temperature T_1 . This adsorption step continues until the equilibrium loading n_1 is achieved with p_1 . Next the adsorbent temperature is raised to T_2 (heating step) so that the partial pressure in equilibrium with n_1 is increased to p_2 , creating a partial pressure driving force for desorption into any fluid containing less than p_2 of the adsorbate. By means of passing a purge fluid across the adsorbent, adsorbate is swept away, and the equilibrium proceeds down the isotherm to some point such as p_1, n_2 . (This point need not coincide with the feed partial pressure; it is selected for illustrative purposes. Also, in some applications, roll-up of the adsorbed-phase concentration can occur during heating such that in some regions of the bed p_2 reaches the condensation pressure of the component, causing a condensed liquid phase to form temporarily in particles [Friday and LeVan, *AIChE J.*, **31**, 1322 (1985)].) During a cooling step, the adsorbent temperature is returned to T_1 . The new equilibrium p_3, n_2 represents the best-quality product that can be produced from the adsorbent at a regenerated loading of n_2 in the simplest cycle. The adsorption step is now repeated. The differential loading, $n_1 - n_2$, is the maximum loading that can be achieved for a TSA cycle operating between a feed containing p_1 at temperature T_1 , regeneration at T_2 , and a product containing a partial pressure p_3 of the adsorbate. The regeneration fluid will contain an average partial pressure between p_2 and p_1 and will therefore have accomplished a concentration of the adsorbate in the regenerant fluid. For liquid-phase adsorption, the partial pressure can be replaced by the fugacity of the adsorbate. Then, the entire discussion above is applicable whether the regeneration is by a fluid in the gas or liquid phase.

In a TSA cycle, the heating step must provide the thermal energy necessary to raise the adsorbate, adsorbent, and adsorber temperatures, to desorb the adsorbate, and to make up for heat losses. TSA regeneration is classified as (1) heating-limited (or stoichiometric-limited) when transfer of energy to the system is limiting, or (2) stripping-limited (or equilibrium-limited) when transferring adsorbate away is limiting. Heating is accomplished by either direct contact of the adsorbent by the heating medium (external heat exchange to a purge gas) or indirect means (heating elements, coils, or panels inside the adsorber). Direct heating is the most commonly used, especially for stripping-limited heating. Indirect heating can be considered for stripping-limited heating, but the complexity of indirect heating limits its practicality to heating-limited regeneration where purge gas is in short supply. Microwave fields [Benchanaa, Lallemand, Simonet-Grange, and Bertrand, *Thermochim. Acta*, **152**, 43–51 (1989)] and dielectric fields [Burkholder, Fanslow, and Bluhm, *Ind. Eng. Chem. Fundam.*, **25**, 414–416 (1986)] are also used to supply indirect heating.

Because high temperatures can be used, resulting in thorough desorption, TSA cycles are characterized by low residual loadings and thus high operating loadings. These high capacities at low concentrations allow long cycle times for reasonably sized adsorbers (hours to days). Long cycle time is needed because particles of adsorbent respond slowly to changes in gas temperature. Most applications of TSA are for systems in which adsorbates are present at low concentration (purification), such as drying, and in which species are strongly adsorbed, such as sweetening, CO_2 removal, and pollution control.

Other Cycle Steps Besides the necessary adsorption and heating steps, TSA cycles may employ additional steps. A purge or sweep gas removes the thermally desorbed components from the adsorbent, and cooling returns it to adsorption temperature. Although the cooling is normally accomplished as a separate step after the heating, sometimes adsorption is started on a hot bed. If certain criteria are met [Basmadjian, *Can. J. Chem. Eng.*, **53**, 234–238 (1975)], the dynamic adsorption efficiency is not significantly affected by the lack of a cooling step.

For liquid-phase adsorption cycles when the unit is to treat a product of significant value, there must be a step to remove the liquid from the adsorbent and one to displace any liquid regenerant thoroughly before filling with the valuable fluid. Because adsorbents and ion exchangers are porous, some retention of the product is unavoidable but needs to be minimized to maximize recovery. When regeneration is by a gas, removal and recovery is accomplished by a drain (or pressure-assisted drain) step using the gas to help displace liquid from the sorbent before heating. When the regenerant is another liquid, the

feed or product can be displaced out of the adsorbent. When heating and cooling are complete, liquid feed must be introduced again to the adsorbent with a corresponding displacement of the gas or liquid regenerant. In ion exchange, these steps for draining and filling are commonly referred to as “sweetening off” and “sweetening on,” respectively.

Applications Drying is the most common gas-phase application for TSA. The natural gas, chemical, and cryogenics industries all use adsorbents to dry streams. Zeolites, activated alumina, and silica gel are used for drying pipeline natural gas. Alumina and silica gel are used because they have higher equilibrium capacity and are more easily regenerated with waste-level heat [Crittenden, *Chem. Engr.*, **452**, 21–24 (1988); Goodboy and Fleming, *Chem. Eng. Progr.*, **80**, 63–68 (1984); Ruthven, *Chem. Eng. Progr.*, **84**, 42–50 (1988)]. The low dew-point that can be achieved with zeolites is especially important when drying cryogenic-process feed-streams to prevent freeze-up. Zeolites dry natural gas before liquefaction to liquefied natural gas (LNG) and before ethane recovery utilizing the cryogenic turboexpander process [Anderson in Katzer (ed.), *Molecular Sieves—II*, *Am. Chem. Soc. Symp. Ser.*, **40**, 637–649 (1977); Brooking and Walton, *The Chem. Engr.*, **257**, 13–17 (1972)]. The feed air to be cryogenically separated into N_2 , O_2 , and argon is purified of both water and CO_2 with 13X zeolites using TSA cycles. Zeolites, silica gel, and activated alumina are used to dry synthesis gas, inert gas, hydrocracker gas, rare gases, and reformer recycle H_2 . Because 3A and pore-closed 4A zeolites size-selectively adsorb water but exclude hydrocarbons, they are used extensively to dry reactive streams such as cracked gas in order to prevent coke formation on the adsorbent. This molecular sieving increases the recovery of hydrocarbons by reducing the coadsorption that would otherwise cause them to be desorbed and lost with the water.

Another area of application for TSA processes is in sweetening, H_2S , mercaptans, organic sulfides and disulfides, and carbonyl sulfide all must be removed from natural gas, H_2 , biogas, and refinery streams in order to prevent corrosion and catalyst poisoning. Natural gas feed to steam methane reforming is sweetened in order to protect the sulfur-sensitive, low-temperature shift catalyst. Well-head natural gas is treated by TSA to prevent pipeline corrosion using 4A zeolites to remove sulfur compounds without the coadsorption of CO_2 that would cause shrinkage. Sweetening and drying of refinery hydrogen streams are needed to prevent poisoning of reformer catalysts. Adsorption can be used to dry and sweeten these in the same unit operation.

TSA processes are applied to the removal of many inorganic pollutants. CO_2 is removed from base-load and peak-shaving natural-gas liquefaction facilities using 4A zeolite in a TSA cycle. The Sulfacid and Hitachi fixed-bed processes, the Sumitomo and BF moving-bed processes, and the Westvaco fluidized-bed process all use activated carbon adsorbents to remove SO_2 from flue gases and sulfuric acid plant tail gases [Juentgen, *Carbon*, **15**, 273–283 (1977)]. Activated carbon with a catalyst is used by the Unitaka process to remove NO , by reacting with ammonia, and activated carbon has been used to convert NO to NO_2 , which is removed by scrubbing. Mercury vapor from air and other gas streams is removed and recovered by activated carbon impregnated with elemental sulfur; the Hg is then recovered by thermal oxidation in a retort [Lovett and Cunniff, *Chem. Eng. Progr.*, **70**, 43–47 (1974)]. Applications for HCl removal from Cl_2 , chlorinated hydrocarbons, and reformer catalyst gas streams use TSA with mordenite and clinoptilolite zeolites [Dyer, gen. refs., pp. 102–105]. Activated aluminas are also used for HCl adsorption as well as fluorine and boron-fluorine compounds from alkylation processes [Crittenden, *ibid.*].

PRESSURE-SWING ADSORPTION

A pressure-swing adsorption (PSA) process cycle is one in which desorption takes place at a pressure much lower than adsorption. Reduction of pressure is used to shift the adsorption equilibrium and affect regeneration of the adsorbent. Figure 16-39 depicts a simplified pressure-swing cycle. Feed fluid containing an adsorbate at a molar concentration of $y_1 = p_1/P_1$ is passed through an adsorbent at conditions

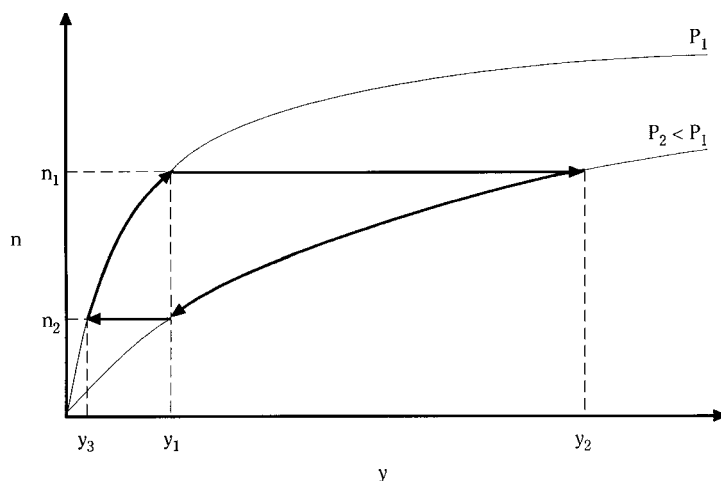


FIG. 16-39 Ideal pressure swing cycle. (Reprinted with permission of UOP.)

T_1 , P_1 , and the adsorption step continues until the equilibrium loading n_1 is achieved with y_1 . Next, the total pressure is reduced to P_2 during the depressurization (or blowdown) step. Now, although the partial pressure in equilibrium with n_1 is still p_1 , there is a concentration driving force of $y_2 = p_1/P_2 > y_1$ for desorption into any fluid containing less than y_2 . By passing a fluid across the adsorbent in a purge step, adsorbate is swept away, and the equilibrium proceeds down the isotherm to some point such as y_1 , n_2 . (The choice of y_1 is arbitrary and need not coincide with feed composition.) At this time, the adsorbent is repressurized to P_1 . The new equilibrium y_3 , n_2 represents the best quality product that can be produced from the adsorbent at a regenerated loading of n_2 . The adsorption step is now repeated. The differential loading, $n_1 - n_2$, is the maximum loading that can be achieved for a pressure-swing cycle operating between a feed containing y_1 and a product containing a molar concentration y_3 of the adsorbate. The regeneration fluid will contain an average concentration between y_2 and y_1 and will therefore have accomplished a concentration of the adsorbate in the regenerant gas. There is no analog for a liquid-phase PSA process cycle.

Thus, in a PSA process cycle, regeneration is achieved by a depressurization that must reduce the partial pressure of the adsorbates to allow desorption. These cycles operate at constant temperature, requiring no heating or cooling steps. Rather, they use the exothermic heat of adsorption remaining in the adsorbent to supply the endothermic heat needed for desorption. Pressure-swing cycles are classified as: (1) PSA, which, although used broadly, usually swings between a high superatmospheric and a low superatmospheric pressure; (2) VSA (vacuum-swing adsorption), which swings from a superatmospheric pressure to a subatmospheric pressure; and (3) PSPP (pressure-swing parametric pumping) and RPSA (rapid pressure-swing adsorption), which operate at very fast cycle times such that significant pressure gradients develop in the adsorbent bed (see the subsection on parametric pumping). Otherwise, the broad principles remain the same.

Low pressure is not as effective in totally reversing adsorption as is temperature elevation unless very high feed to purge pressure ratios are applied (e.g., deep vacuum). Therefore, most PSA cycles are characterized by high residual loadings and thus low operating loadings. These low capacities at high concentrations require that cycle times be short for reasonably sized beds (seconds to minutes). These short cycle times are attainable because particles of adsorbent respond quickly to changes in pressure. Major uses for PSA processes include purification as well as applications where contaminants are present at high concentration (bulk separations).

Other Cycle Steps A PSA cycle may have several other steps in addition to the basic adsorption, depressurization, and repressurization.

Cocurrent depressurization, purge, and pressure-equalization steps are normally added to increase efficiency of separation and recovery of product. At the end of the adsorption step, the more weakly adsorbed species have been recovered as product, but there is still a significant amount held up in the bed in the inter- and intraparticle void spaces. A cocurrent depressurization step can be added before the blowdown step, which is countercurrent to adsorption. This increases the amount of product produced each cycle. In some applications, the purity of the more strongly adsorbed components has also been shown to be heavily dependent on the cocurrent depressurization step [Cen and Yang, *Ind. Eng. Chem. Fundam.*, **25**, 758-767 (1986)]. This cocurrent blowdown is optional because there is always a countercurrent one. Skarstrom developed criteria to determine when the use of both is justified [Skarstrom in Li, *Recent Developments in Separation Science*, vol. II, CRC Press, Boca Raton, pp. 95-106 (1975)].

Additional stripping of the adsorbates from the adsorbent and purging of them from the voids can be accomplished by the addition of a purge step. The purge can begin toward the end of the depressurization or immediately afterward. Purging is accomplished with a flow of product countercurrent to adsorption to provide a lower residual at the product effluent end of the bed.

The repressurization step that returns the adsorber to feed pressure and completes the steps of a PSA cycle should be completed with pressure equalization steps to conserve gas and compression energy. Portions of the effluent gas during depressurization, blowdown, and enrichment purge can be used for repressurization to reduce the quantity of feed or product gas needed to pressurize the beds. The most efficient cycle is one that most closely matches available pressures and adsorbate concentration to the appropriate portion of the bed at the proper point in the cycle.

A dual reflux PSA cycle with both stripping and enriching has been proposed to obtain high enrichment and recovery. The separation is much better than that obtainable by normal PSA and suggests that it is possible to obtain two nearly pure products from a dilute feed stream [see McIntire et al., *Ind. Eng. Chem. Res.*, **41**, 3499 (2002)].

Applications PSA cycles are used primarily for purification of wet gases and of hydrogen. One of the earliest applications was the original Skarstrom two-bed cycle (adsorption, countercurrent blowdown, countercurrent purge, and cocurrent repressurization) to dry air stream to less than 1 ppm H_2O [Skarstrom, *ibid.*]. Instrument-air dryers still use a PSA cycle similar to Skarstrom's with activated alumina or silica gel [Armond, in Townsend, *The Properties and Applications of Zeolites*, The Chemical Society, London, pp. 92-102 (1980)].

The hydrocarbon exclusion by small-pore zeolites allows PSA to achieve a 10 to 30 K dewpoint depression in air-brake compressors,

even at high discharge air temperatures in the presence of compressor oil [Ausikaitis, in Katzer, *Molecular Sieves—II, Am. Chem. Soc. Symp. Ser.*, **40**, pp. 681–695 (1977)]. The high-purity hydrogen employed in processes such as hydrogenation, hydrocracking, and ammonia and methanol production is produced by PSA cycles with adsorbent beds compounded of activated carbon, zeolites, and carbon molecular sieves [Martin, Gotzmann, Notaro, and Stewart, *Adv. Cryog. Eng.*, **31**, 1071–1086 (1986)]. The impurities to be removed include ammonia, carbon oxides, nitrogen, oxygen, methane, and heavier hydrocarbons. In order to be able to produce purities as high as 99.9999 percent, systems such as a UOP™ Polybed™ separation unit use six to ten adsorbents with complex cycles (see below) [Fuderer and Rudelstorfer, U.S. Patent 3,986,849 (1976)].

Air separation, methane enrichment, and iso/normal separations are the major bulk separations utilizing PSA; recovery of CO and CO₂ are also growing uses. PSA process cycles are used to produce oxygen and/or nitrogen from air. Synthetic zeolites, clinoptilolite, mordenite, and carbon molecular sieves are all used in various PSA, VSA, and RPSA cycles. The 85 to 95 percent purity oxygen produced is employed for electric furnace steel, waste water treating, solid waste combustion, and kilns [Martin et al., *ibid.*]. Small PSA oxygen units are used for patients requiring inhalation therapy in the hospital and at home [Cassidy and Holmes, *AIChE Symp. Ser.*, **80** (1984), pp. 68–75] and for pilots on board aircraft [Tedor, Horch, and Dangieri, *SAFE J.*, **12**, 4–9 (1982)]. Lower purity oxygen (25 to 55 percent) can be produced to enhance combustion, chemical reactions, and ozone production [Sircar, in Rodrigues et al., *gen. refs.*, pp. 285–321]. High purity nitrogen (up to 99.99 percent) for inert blanketing is produced in PSA and VSA processes using zeolites and carbon molecular sieves [Kawai and Kaneko, *Gas Sep. & Purif.*, **3**, 2–6 (1989); Ruthven, *ibid.*]. Methane is upgraded to natural gas pipeline quality by another PSA process. The methane is recovered from fermentation gases of landfills and wastewater purification plants and from poor-quality natural gas wells and tertiary oil recovery. Carbon dioxide is the major bulk contaminant but the gases contain water and other “garbage” components such as sulfur and halogen compounds, alkanes, and aromatics [Kumar and VanSloun, *Chem. Eng. Progr.*, **85**, 34–40 (1989)]. These impurities are removed by TSA using activated carbon or carbon molecular sieves and then the CO₂ is adsorbed using a PSA cycle. The cycle can use zeolites or silica gel in an equilibrium-selective separation or carbon molecular sieve in a rate-selective separation [Kapoor and Yang, *Chem. Eng. Sci.*, **44**, 1723–1733 (1989); Richter, Erdoel Kohle, Erdgas, *Petrochem.*, **40**, 432–438 (1987)]. The pore-size selectivity of zeolite 5A is employed to adsorb straight-chain molecules while excluding

branched and cyclic species in the UOP IsoSivSM process. This PSA process separates C₅ to C₉ range hydrocarbons into a normal-hydrocarbon fraction of better than 95 percent purity, and a higher-octane isomer fraction with less than 2 percent normals [Cassidy and Holmes, *ibid.*].

PURGE/CONCENTRATION SWING ADSORPTION

A purge-swing adsorption cycle is usually considered to be one in which desorption takes place at the same temperature and total pressure as adsorption. Desorption is accomplished either by partial-pressure reduction using an inert gas purge or by adsorbate displacement with another adsorbable component. Purge cycles operate adiabatically at nearly constant inlet temperature and require no heating or cooling steps. As with PSA, they utilize the heat of adsorption remaining in the adsorbent to supply the heat of desorption. Purge processes are classified as (1) inert or (2) displacement.

Inert Purge In inert-purge desorption cycles, *inert* refers to the fact that the purge is not adsorbable at the cycle conditions. Inert purging desorbs the adsorbate solely by partial pressure reduction. Regeneration of the adsorbent can be achieved while maintaining the same temperature and pressure by the introduction of an inert purge fluid. Figure 16-40 depicts a simplified inert-purge swing cycle utilizing a nonadsorbing purge fluid. As before, the feed stream containing an adsorbate at a partial pressure of p_1 is passed through an adsorbent at temperature T_1 , and the adsorption step continues until equilibrium n_1 is achieved. Next the nonadsorbing fluid is introduced to reduce the partial pressure below p_1 by dilution. Therefore, there is a partial pressure driving force for desorption into the purge fluid, and the equilibrium proceeds down the isotherm to the point p_2, n_2 , where p_2 represents the best quality product that can be produced from the adsorbent at a regenerated loading of n_2 . The adsorption step is now repeated, and the differential loading is $n_1 - n_2$. The regeneration fluid will contain an average partial pressure between p_2 and p_1 , and the cycle will therefore not have accomplished a concentration of the adsorbate in the regenerant fluid. But it will have transferred the adsorbates to a fluid from which it may be more easily separated by means such as distillation.

Like PSA cycles, inert-purge processes are characterized by high residual loadings, low operating loadings, and short cycle times (minutes). Bulk separations of contaminants not easily separable at high concentration and of weakly adsorbed components are especially suited to inert-purge-swing adsorption. Another version of UOP's

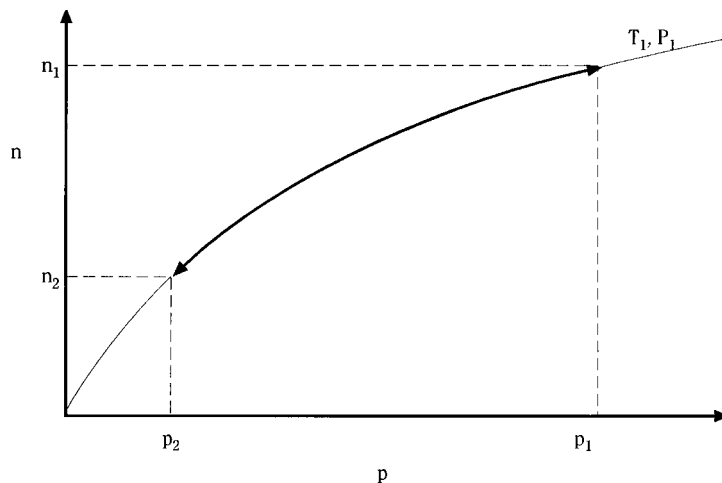


FIG. 16-40 Ideal inert-purge swing cycle. (Reprinted with permission of UOP.)

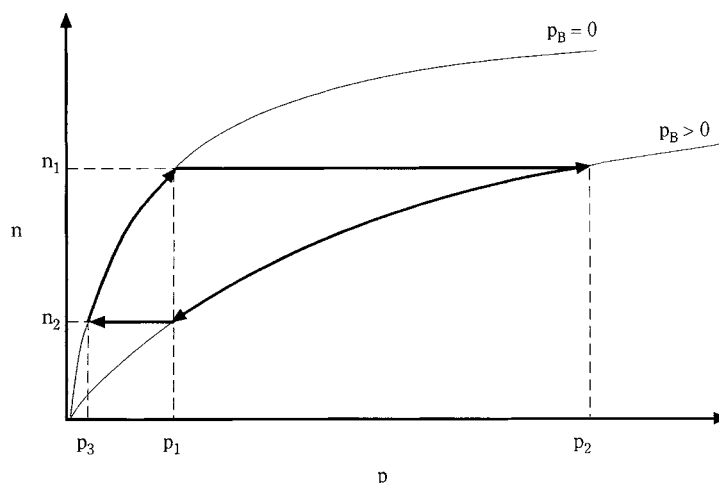


FIG. 16-41 Ideal displacement-purge swing cycle. (Reprinted with permission of UOP.)

IsoSiv process employs H_2 in an inert-purge cycle for separating C_3 to C_9 naphtha by adsorbing straight-chain molecules and excluding branched and cyclic species on size selective 5A zeolite [Cassidy and Holmes, *ibid.*]. Automobiles made in the United States have canisters of activated carbon to adsorb gasoline vapors lost from the carburetor or the gas tank during running, from the tank during diurnal cycling, and from carburetor hot-soak losses; the vapors are desorbed by an inert purge of air that is drawn into the carburetor as fuel when the engine is running [Clarke, Gerrard, Skarstrom, Vardi and Wade, *S.A.E. Trans.*, **76**, 824–842 (1968)]. UOP's Adsorptive Heat Recovery drying system has been commercialized for drying azeotropic ethanol to be blended with gasoline into gasohol; the process uses a closed loop of N_2 as the inert purge to desorb the water [Garg and Yon, *Chem. Eng. Progr.*, **82**, 54–60 (1986)].

Displacement Purge Isothermal, isobaric regeneration of the adsorbent can also be accomplished by using a purge fluid that can adsorb. In displacement-purge stripping, *displacement* refers to the displacing action of the purge fluid caused by its ability to adsorb at the cycle conditions. Figure 16-41 depicts a simplified displacement-purge cycle utilizing an adsorbable purge. Again, the feed stream containing an adsorbate at a partial pressure of p_1 is passed through an adsorbent at temperature T_1 , and the adsorption step continues until equilibrium n_1 is achieved. Next the displacement fluid, B, is introduced. The presence of another adsorbable species reduces the adsorptivity of the key adsorbate, A. Therefore, there exists a partial pressure driving force for desorption into the purge fluid, and the equilibrium proceeds down the isotherm to some point such as p_1, n_2 (again arbitrary.) Next the adsorbent is recharged with a fluid that contains no component B, shifting the effective isotherm to that where the equilibrium of component A is p_3 . The new equilibrium p_3, n_2 represents the best quality product that can be produced from the adsorbent at a regenerated loading of n_2 . The adsorption step is now repeated. The differential loading $(n_1 - n_2)$ is the maximum loading that can be achieved for a pressure-swing cycle operating between a feed containing y_1 and a product containing a partial pressure p_3 of the adsorbate. The regeneration fluid will contain an average partial pressure between p_2 and p_1 and will therefore have accomplished a concentration of the adsorbate in the regenerant gas. Displacement-purge cycles are not as dependent on the heat of adsorption remaining on the adsorbent, because the adsorption of purge releases most or all of the energy needed to desorb the adsorbate. It is best if the adsorbate is more selectively adsorbed than the displacement purge, so that the adsorbates can easily desorb the purge fluid during adsorption. The displacement purge must be carefully selected, because it

contaminates both the product stream and the recovered adsorbate, and requires separation for recovery (e.g., distillation).

Displacement-purge processes are more efficient for less selective adsorbate/adsorbent systems, while systems with high equilibrium loading of adsorbate will require more purging [Sircar and Kumar, *Ind. Eng. Chem. Proc. Des. Dev.*, **24**, 358–364 (1985)]. Several displacement-purge-swing processes have been commercialized for the separation of branched and cyclic C_{10} – C_{18} from normals using the molecular-size selectivity of 5A zeolite: Exxon's Ensorb, UOP's IsoSiv, Texaco Selective Finishing (TSF), Leuna Werke's Parex, and the Shell Process [Ruthven, *ibid.*]. All use a purge of normal paraffin or light naphtha with a carbon number of two to four less than the feed stream except for Ensorb, which uses ammonia [Yang, *gen. refs.*]. UOP has also developed a similar process, OlefinSiv, which separates isobutylene from normal butenes with displacement purge and a size-selective zeolite [Adler and Johnson, *Chem. Eng. Progr.*, **75**, 77–79 (1979)]. Solvent extraction to regenerate activated carbon is another example of a displacement-purge cycle; the adsorbent is then usually steamed to remove the purge fluid [Martin and Ng, *Water Res.*, **18**, 59–73 (1984)]. The best use of solvent regeneration is for water phase adsorption where the separation of water from carbon would use too much steam and where purge and water are easily separated; and for vapor-phase where the adsorbate is highly nonvolatile but soluble. Air Products has developed a process for separating ethanol/water on activated carbon using acetone as a displacement agent and adding a water rinse to improve the recovery of two products [Sircar, U.S. Patent 5,026,482 (1991)].

Displacement-purge forms the basis for most simulated continuous countercurrent systems (see hereafter) such as the UOP SorbexSM processes. UOP has licensed close to one hundred Sorbex units for its family of processes: ParexSM to separate *p*-xylene from C_8 aromatics, MolexSM for *n*-paraffin from branched and cyclic hydrocarbons, OlexSM for olefins from paraffin, SarexSM for fructose from dextrose plus polysaccharides, CymexSM for *p*- or *m*-cymene from cymene isomers, and CresexSM for *p*- or *m*-cresol from cresol isomers. Toray Industries' AromaxSM process is another for the production of *p*-xylene [Otani, *Chem. Eng.*, **80**(9), 106–107, (1973)]. Illinois Water Treatment [Making Waves in Liquid Processing, Illinois Water Treatment Company, IWT Adsep System, Rockford, IL, **6**(1), (1984)] and Mitsubishi [Ishikawa, Tanabe, and Usui, U.S. Patent 4,182,633 (1980)] have also commercialized displacement-purge processes for the separation of fructose from dextrose.

Chromatography Chromatography is a sorptive separation technique that allows multicomponent separations in both gas and liquid

phase. As a preparative tool, it is often used as a displacement-purge process, although many applications employ an inert-displacement mode, especially for use in analysis. General characteristics and operating modes are discussed in a separate part of this section.

ION EXCHANGE

Except in very small-scale applications, ion-exchangers are used in cyclic operations involving sorption and desorption steps. A typical ion-exchange cycle used in water-treatment applications involves (a) *backwash*—used to remove accumulated solids obtained by an upflow of water to expand (50–80 percent expansion is typical) and fluidize the exchanger bed; (b) *regeneration*—a regenerant is passed slowly through the used to restore the original ionic form of the exchanger; (c) *rinse*—water is passed through the bed to remove regenerant from the void volume and, in the case of porous exchangers, from the resin pores; (d) *loading*—the fresh solution to be treated is passed through the bed until leakage begins to occur. Water softening is practiced in this way with a cation exchange column in sodium form. At the low ionic strength used in the loading step, calcium and magnesium are strongly preferred over sodium, allowing nearly complete removal. Since the selectivity for divalent cations decreases sharply with ionic concentration, regeneration is carried out effectively with a concentrated sodium chloride solution. Removal of sulfates from boiler feed water is done by similar means with anion exchangers in chloride form.

Many ion-exchange columns operate downflow and are regenerated in the same direction (Fig. 16-42a). However, a better regeneration and lower leakage during loading can be achieved by passing the regenerant countercurrently to the loading flow. Specialized equipment is available to perform countercurrent regeneration (see "Equipment" in this section). One approach (Fig. 16-42b) is to apply a vacuum to remove the regenerant at the top of the bed.

Complete deionization with ion-exchange columns is the classical method of producing ultrapure water for boiler feed, in electronics manufacture, and for other general uses in the chemical and allied industries. Deionization requires use of two exchangers with opposite functionality to remove both cations and anions. These can be in separate columns, packed in adjacent layers in the same column, or, more frequently, in a mixed bed. In the latter case, the two exchangers are intimately mixed during the loading step. For regeneration, backwashing separates the usually lighter anion exchanger from the usually denser cation exchanger. The column typically has a screened distributor at the interface between the two exchangers, so that they may be separately regenerated without removing them from the column. The most common cycle (Fig. 16-43) permits sequential regeneration of the two exchangers, first with alkali flowing downward through the anion exchanger to the interface distributor and then acid flowing

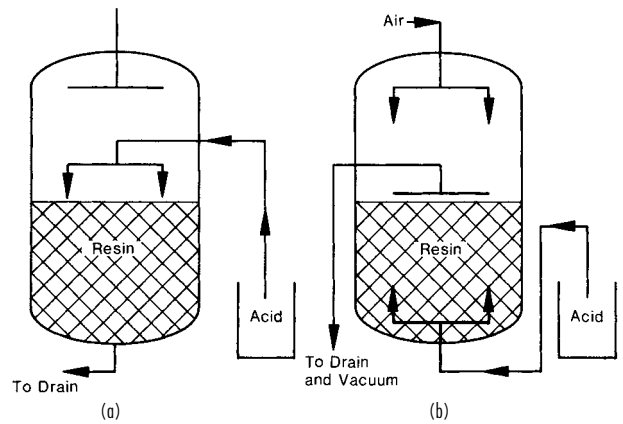


FIG. 16-42 Ion-exchanger regeneration. (a) Conventional. Acid is passed downflow through the cation-exchange resin bed. (b) Counterflow. Regenerant solution is introduced upflow with the resin bed held in place by a dry layer of resin.

downward from the interface distributor through the cation exchanger. After regeneration and rinsing, the exchangers are remixed by compressed air. To alleviate the problem of intermixing of the two different exchangers and chemical penetration through the wrong one, an inert material of intermediate density can be used to provide a buffer zone between layers of cation and anion exchangers.

When recovery of the sorbed solute is of interest, the cycle is modified to include a displacement step. In the manufacture of pharmaceuticals, ion-exchangers are used extensively in recovery and separation. Many of these compounds are amphoteric and are positively or negatively charged depending on the solution pH. Thus using, for example, a cation exchanger, loading can be carried out at a low pH and displacement at a high pH. Differences in selectivity for different species can be used to carry out separations during the displacement [Carta et al., *AIChE Symp. Ser.*, **84**, 54-61 (1988)]. Multibed cycles are also used to facilitate integration with other chemical process operations. Figure 16-44 shows a two-bed ion-exchange system using both cation and anion exchangers to treat and recover chromate from rinse water in plating operations. The cation exchanger removes trivalent chromium, while the anion exchanger removes hexavalent chromium as an anion. Regeneration of the cation exchanger with sulfuric acid produces a concentrated solution of trivalent chromium as the sulfate salt. The hexavalent chromium is eluted from the anion exchanger with sodium hydroxide in a concentrated solution. This solution is recycled

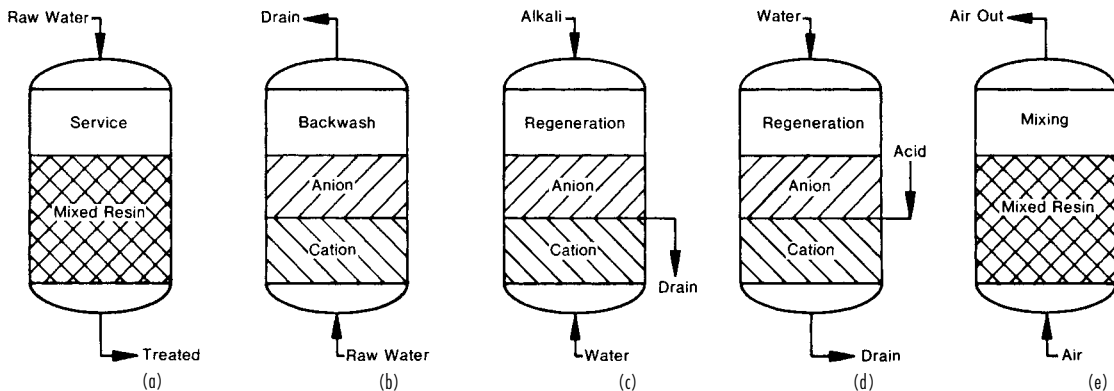


FIG. 16-43 Principles of mixed-bed ion exchange. (a) Service period (loading). (b) Backwash period. (c) Caustic regeneration. (d) Acid regeneration. (e) Resin mixing.

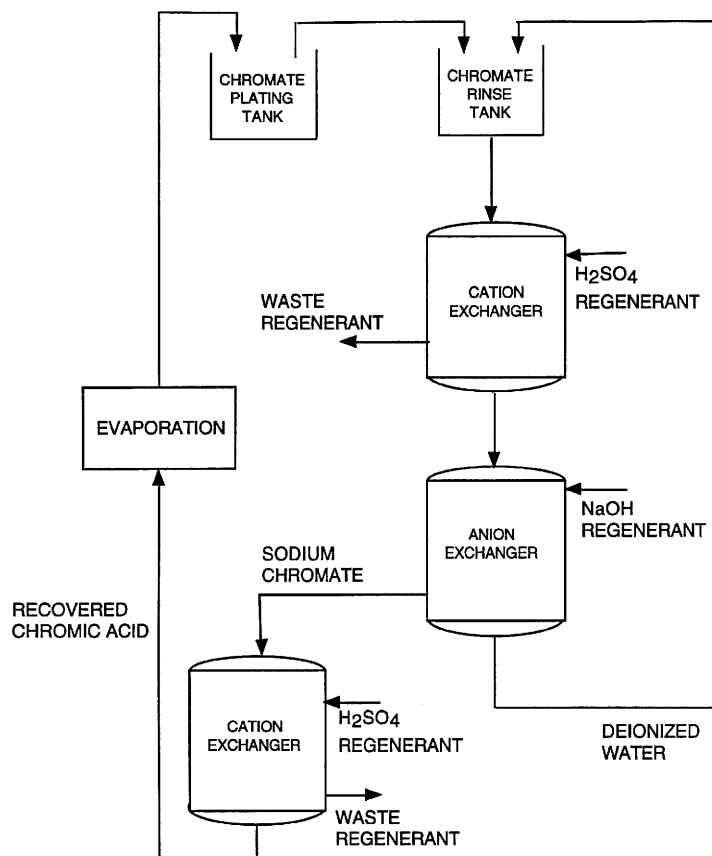


FIG. 16-44 Multicomponent ion-exchange process for chromate recovery from plating rinse water. (Adapted from Rhom & Haas with permission.)

to the plating tank by passing it through a second cation exchange column in hydrogen form to convert the sodium chromate to a dilute chromic acid solution that is concentrated by evaporation.

PARAMETRIC PUMPING

The term *parametric pumping* was coined by Wilhelm et al. [Wilhelm, Rice, and Bendelius, *Ind. Eng. Chem. Fundam.*, **5**, 141–144 (1966)] to describe a liquid-phase adsorption process in which separation is achieved by periodically reversing not only flow but also an intensive thermodynamic property such as temperature, which influences adsorptivity. Moreover, they considered the concurrent cycling of pressure, pH, and electrical and magnetic fields. A lot of research and development has been conducted on thermal, pressure, and pH driven cycles, but to date only gas-phase pressure-swing parametric pumping has found much commercial acceptance.

Temperature Two modes of temperature parametric-pumping cycles have been defined—direct and recuperative. In direct mode, an adsorbent column is heated and cooled while the fluid feed is pumped forward and backward through the bed from reservoirs at each end. When the feed is a binary fluid, one component will concentrate in one reservoir and one in the other. In recuperative mode, the heating and cooling takes place outside the adsorbent column. Parametric pumping, thermal and pH modes, have been widely studied for separation of liquid mixtures. However, the primary success for separating gas mixtures in thermal mode has been the separation of propane/ethane on activated carbon [Jencziewski and Myers, *Ind. Eng. Chem. Fundam.*, **9**, 216–221 (1970)] and of air/SO₂ on silica gel

[Patrick, Schrod, and Kermode, *Sep. Sci.*, **7**, 331–343 (1972)]. The difficulty with applying the thermal mode to gas separation is that in a fixed volume gas pressure increases during the hot step, which defeats the desorption purpose of this step. No thermal parametric-pumping cycle has yet been practiced commercially.

Pressure Another approach to parametric pumping is accomplished by pressure cycling of an adsorbent. An adsorbent bed is alternately pressurized with forward flow and depressurized with backward flow through the column from reservoirs at each end. Like TSA parametric pumping, one component concentrates in one reservoir and one in the other. The pressure mode of parametric pumping has been called pressure-swing parametric pumping (PSPP) and rapid pressure swing adsorption (RPSA). It was developed to minimize process complexity and investment at the expense of product recovery. RPSA is practiced in single-bed [Keller and Jones in Flank, *Adsorption and Ion Exchange with Synthetic Zeolites*, **135** (1980), pp. 275–286] and multiple-bed [Earls and Long, U.S. Patent number 4,194,892, 1980] implementations. Adsorbents are short (about 0.3 to 1.3 m), and particle sizes are very small (about 150 to 400 μm). The total cycle time including adsorption, dead time, countercurrent purge, and sometimes a second dead time, ranges from a few to about 30 seconds. The feature of RPSA that differentiates it from traditional PSA is the existence of axial pressure profiles throughout the cycle much as temperature gradients are present in TSA parametric-pumping. Whereas PSA processes have essentially constant pressure through the bed at any given time, the flow resistance of the very small adsorbent particles produce substantial pressure drops in the bed. These pressure dynamics are key to the attainment of separation

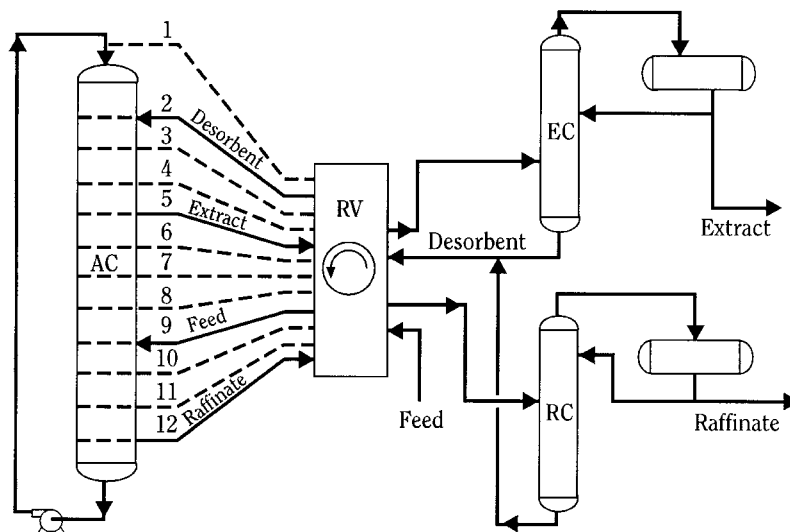


FIG. 16-45 UOP Sorbex process. (Reprinted with permission of John Wiley & Sons, Inc. Reference: Gembicki, Oroskar, and Johnson, "Adsorption, Liquid Separation," in Kirk-Othmer Encyclopedia of Chemical Technology, 4th ed., John Wiley & Sons, Inc., New York, 1991.)

performance. RPSA has been commercialized for the production of oxygen and for the recovery of ethylene and chlorocarbons (the selectively adsorbed species) in an ethylene-chlorination process while purging nitrogen (the less selectively adsorbed specie).

SIMULATED MOVING BED SYSTEMS

The concept of a simulated moving bed (SMB) system was originally used in a process developed and licensed under the name UOP Sorbex process [Broughton et al., *Pet. Int. (Milan)*, **23**(3), 91 (1976); **23**(5), 26 (1976)]. The basic process, used for separating a binary mixture, is illustrated in Fig. 16-45. As shown, the process employs a stack of packed beds connected to a rotary valve (RV) that allows the introduction of feed and desorbent and the collection of extract and raffinate streams at different junctions. Feed and withdrawal points are switched periodically as shown, resulting in a periodic counterflow of adsorbent. Even with a small number of packed beds, the periodic countercurrent action closely simulates the behavior of a true countercurrent system without the complexities associated with particle flows. Distillation columns are shown in Fig. 16-45 integrated with the adsorption system to recover and recycle the desorbent. Although the Sorbex process was originally applied to hydrocarbon separations, extensive industrial applications have been developed for sugars, amino acids, and fine chemicals, especially chiral separations. Practical operation is not restricted to rotary valves. Using multiple individual valves to control the distribution of flows is often more practical, especially on a smaller scale.

The basic principle of operation is illustrated in Fig. 16-46 by reference to an equivalent true countercurrent moving bed (TMB) system comprising four idealized moving bed columns or "zones." The feed containing components A and B is supplied between zones II and III. The least strongly adsorbed species, A, is recovered between zones III and IV, while the more strongly adsorbed species, B, is recovered between zones I and II. The adsorbent is recirculated from the bottom of zone I to the top of zone IV. A desorbent or eluent makeup stream is added to the fluid recycled from zone IV, and the combined stream is fed to the bottom of zone I. The main purpose of each zone is as follows. Zone III adsorbs B while letting A pass through. Zone II desorbs A while adsorbing B. Zone I desorbs B, allowing recycle of the adsorbent. Zone IV adsorbs A. Proper selection of operating conditions is needed to obtain the desired separation. The ensuing analysis is based on local equilibrium and plug flow conditions and assumes

linear isotherms with a nonadsorbable desorbent. In the following u^j [$\text{m}^3/(\text{m}^2\cdot\text{s})$] represents the fluid-phase velocity in zone j and u_s [$\text{kg}/(\text{m}^2\cdot\text{s})$] the adsorbent velocity, with both velocities defined based on the column cross-sectional area. Net upward transport of each component is determined by the component velocity

$$u^i = u^j - u_s \left(\frac{\epsilon_p}{\rho_p} + \frac{n_i}{c_i} \right) \quad (16-204)$$

The following inequalities must be met to obtain the desired separation:

$$u_B^I > 0 \quad (16-205a)$$

$$u_A^{II} > 0, \quad u_B^{II} < 0 \quad (16-205b)$$

$$u_A^{III} > 0, \quad u_B^{III} < 0 \quad (16-205c)$$

$$u_A^{IV} < 0 \quad (16-205d)$$

Accordingly, A moves downward in zone IV and upward in zone III and is recovered between these two zones. Similarly, B moves upward in zone I and downward in zone II and is recovered between these two zones. Combining Eqs. (16-204) and (16-205) yields the following constraints:

$$m^I > K_B \quad (16-206a)$$

$$K_B > m^{II} > K_A \quad (16-206b)$$

$$K_B > m^{III} > K_A \quad (16-206c)$$

$$m^{IV} < K_A \quad (16-206d)$$

where K_i is the linear isotherm slope [cf. Eq. (16-12)] and

$$m^j = \frac{u^j - u_s \epsilon_p / \rho_p}{u_s} \quad (16-207)$$

is a flow ratio (m^3/kg). Inequalities (16-205b) and (16-205c) determine whether separation will occur and can be represented on the $m^{III} - m^{II}$ plane in Fig. 16-47. Since $m^{III} > m^{II}$, only the region above the 45° line is valid. Values of m^{II} and m^{III} below K_A or above K_B result in incomplete separation. Thus, complete separation requires operation within the shaded triangular region. The vertex of this triangle represents the point of maximum productivity under ideal conditions. In practice, mass-transfer resistances and deviations from plug flow will result in

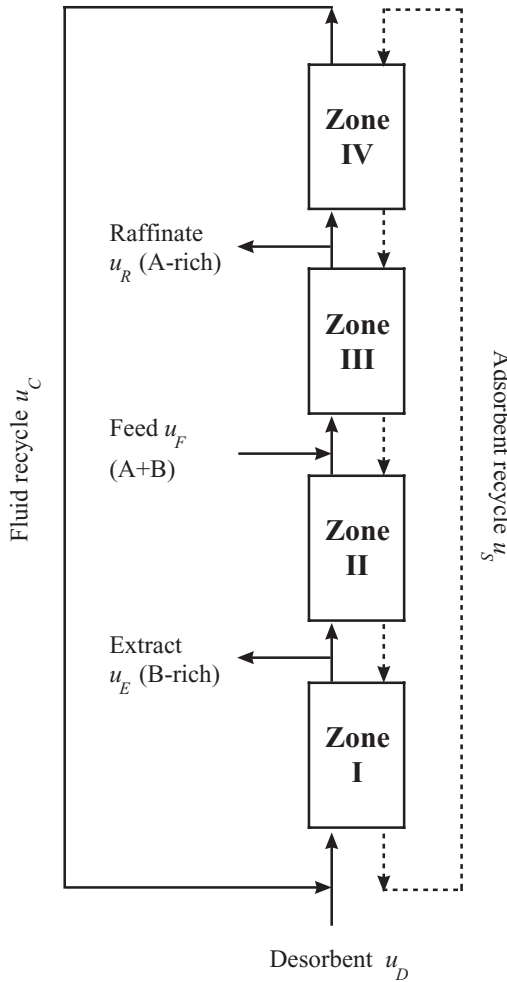


FIG. 16-46 General scheme of a true moving bed (TMB) adsorption system for binary separations. A is less strongly retained than B.

imperfect separation even within the shaded region. As a result, operating away from the vertex and closer to the 45° line is usually needed at the expense of lower productivity. By introducing a safety margin $\beta \geq 1$ (Seader and Henley, gen. refs.), Eqs. (16-206) are transformed to

$$m^I = K_B \beta \tag{16-208a}$$

$$m^{II} = K_A \beta \tag{16-208b}$$

$$m^{III} = K_B / \beta \tag{16-208c}$$

$$m^{IV} = K_A / \beta \tag{16-208d}$$

$\beta = 1$ yields maximum productivity under ideal conditions, while larger values provide a more robust design up to the maximum $\beta = \sqrt{K_B/K_A}$. For a given β , external and internal flow velocities are calculated from

$$u_S = u_F / (K_B / \beta - K_A \beta) \tag{16-209a}$$

$$u_E = u_S (K_B - K_A) \beta \tag{16-209b}$$

$$u_R = u_S (K_B - K_A) / \beta \tag{16-209c}$$

$$u_D = u_E + u_R - u_F \tag{16-209d}$$

$$u^I = u_S (K_B \beta + \epsilon_p / \rho_p) \tag{16-209e}$$

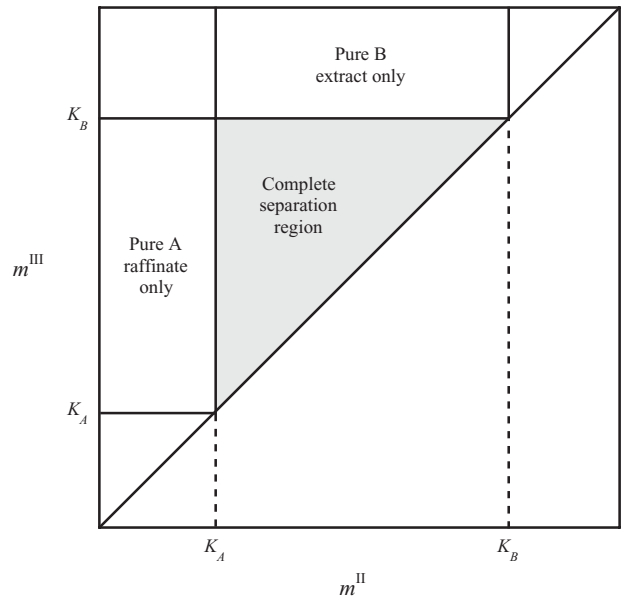


FIG. 16-47 m^{III} - m^{II} plane showing regions of complete and incomplete separation. Area below the 45° line is invalid.

$$u^{II} = u^I - u_E \tag{16-209f}$$

$$u^{III} = u^{II} + u_F \tag{16-209g}$$

$$u^{IV} = u^{III} - u_R \tag{16-209h}$$

$$u_C = u^I - u_D \tag{16-209i}$$

Analogous relationships are derived for SMB systems where each zone comprises a number of fixed beds operated in a merry-go-round sequence, as shown in Fig. 16-48. External flow velocities are calculated from Eqs. (16-209a) to (16-209d), replacing u_S with

$$u_{S,SMB} = \frac{\rho_b L}{p} \tag{16-210}$$

where L is the length of a single bed and p is the switching period. Internal flow velocities equivalent to the TMB operation are increased from the values calculated from Eqs. (16-209e) to (16-209i) to compensate for the extraparticle fluid carried along in each bed at each switch according to

$$u_{SMB}^j = u^j + \frac{\epsilon L}{p} \tag{16-211}$$

In practice, a small number of beds in series in each zone provide a close approach to the performance of ideal, true countercurrent system. Industrial SMB systems normally use 2 to 3 beds per zone.

Complete Design and Extensions Complete design of SMB systems requires a full description of equilibrium and rate factors. For an existing SMB unit, initial stream flow rates and switching period can be selected based on Eqs. (16-209) to (16-211) so that the operating point lies within the desired separation region. Column length design requires a dynamic adsorption model including a description of mass-transfer rates, adsorption kinetics, and axial dispersion. Operation with a nonlinear isotherm is analyzed in a similar manner. In this case, the right triangle defining the complete separation region in Fig. 16-47 is distorted, acquiring one or more curved sides and further restricting the range of conditions leading to complete separation. As is evident from the analysis above, only binary separations are achievable with a four-zone system. Multicomponent separations require multiple SMB units or integrated units comprising more than four zones. Useful references covering SMB design for linear and nonlinear isotherms are

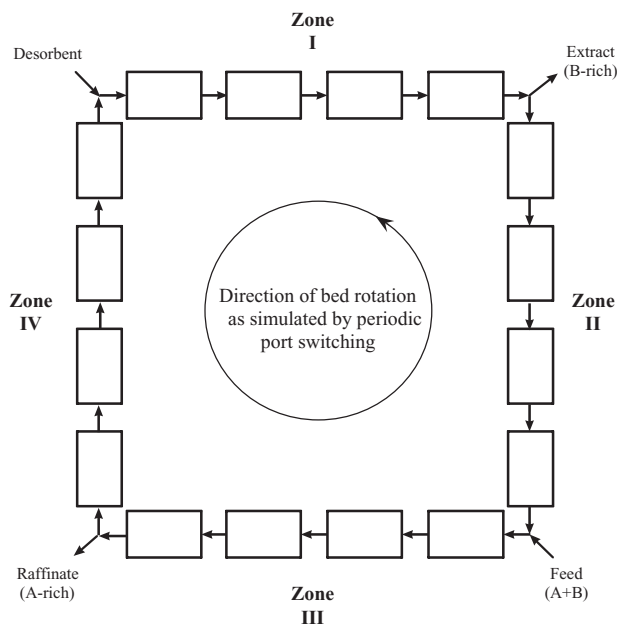


FIG. 16-48 General scheme of a simulated moving bed (SMB) adsorption system. Bed rotation is simulated by periodic switching of ports in the direction of fluid flow. A is less strongly retained than B.

by Ruthven and Ching, *Chem. Eng. Sci.*, **44**, 1011 (1989); Storti et al., *Chem. Eng. Sci.*, **44**, 1329 (1989); Zhong and Guiochon, *Chem. Eng. Sci.*, **51**, 4307 (1996); Mazzotti et al., *J. Chromatogr. A*, **769**, 3 (1997); Mazzotti et al., *AIChE J.*, **40**, 1825 (1994); and Minceva and Rodrigues, *Ind. Eng. Chem. Res.*, **41**, 3454 (2002).

OTHER ADSORPTION CYCLES

Hybrid Recycle Systems Liquid chromatography has been used commercially to separate glucose from fructose and other sugar isomers, for recovery of nucleic acids, and for other uses. A patent to Sanmatsu Kogyo Co., Ltd. (Yoritomi, Kezuka, and Moriya, U.S. Patent number 4,267,054, 1981) presents an improved chromatographic process that is simpler to build and operate than simulated moving-bed processes. Figure 16-49 (Keller et al., gen. refs.) diagrams its use for a binary separation. It is a displacement-purge cycle where pure component cuts are recovered, while cuts that contain both components are recycled to the feed end of the column.

The UOP CyclesorbSM is another adsorptive separation process with semicontinuous recycle. It utilizes a series of chromatographic columns to separate fructose from glucose. A series of internal recycle streams of impure and dilute portions of the chromatograph are used to improve the efficiency (Gerhold, U.S. Patent numbers 4,402,832, 1983; and 4,478,721, 1984). A schematic diagram of a six-vessel UOP Cyclesorb process is shown in Fig. 16-50 (Gembicki et al., gen. refs., p. 595). The process has four external streams and four internal recycles: Dilute raffinate and impure extract are like displacement steps; and impure raffinate and dilute extract are recycled from the bottom of an adsorber to its top. Feed and desorbent are fed to the top of each column in a predetermined sequence. The switching of the feed and desorbent are accomplished by the same rotary valve used for Sorbex switching (see hereafter). A chromatographic profile is established in each column that is moving from top to bottom, and all portions of an adsorber are performing a useful function at any time.

Steam Regeneration When steam is used for regeneration of activated carbon, it is desorbing by a combination thermal swing and displacement purge (described earlier in this section). The exothermic heat released when the steam is adsorbed supplies the thermal energy much more efficiently than is possible with heated gas purging. Slightly superheated steam at about 130°C is introduced into the bed counter-

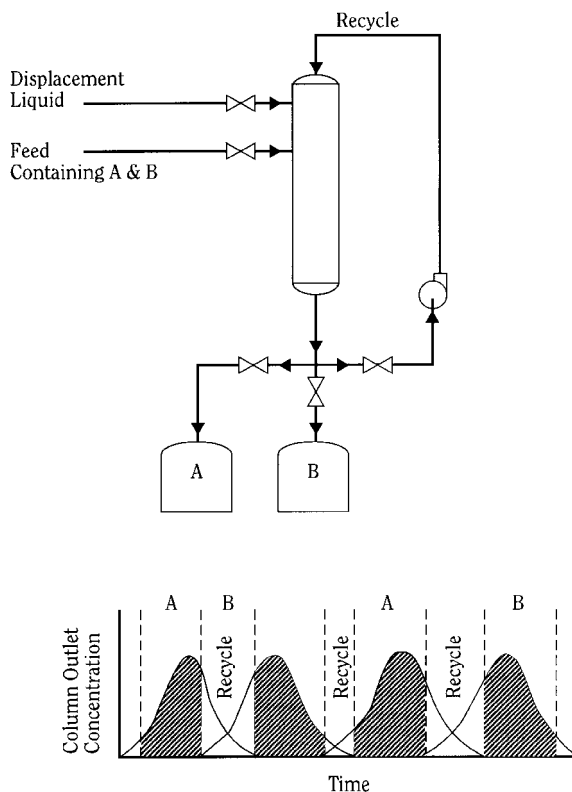


FIG. 16-49 Sanmatsu Kogyo chromatographic process. (Reprinted with permission of Wiley. Reference: Keller, Anderson, and Yon, Chap. 12 in Rousseau, Handbook of Separation Process Technology, John Wiley & Sons, Inc., New York, 1987.)

current to adsorption; for adsorbates with high boiling points, the steam temperature must be higher. Adsorbates are desorbed and purged out of the bed with the steam. Steam and desorbates then go to a condenser for subsequent separation. The water phase can be further cleaned by air stripping, and the sorbate-laden air from that stripper can be recycled with the feed to the adsorption bed.

Steam regeneration is most commonly applied to activated carbon that has been used in the removal and/or recovery of solvents from gases. At volatile organic compound (VOC) concentration levels from 500 to 15,000 ppm, recovery of the VOC from the stream used for regeneration is economically justified. Below about 500 ppm, recovery is not economically justifiable, but environmental concerns often dictate adsorption followed by destruction. While activated carbon is also used to remove similar chemicals from water and wastewater, regeneration by steam is not usual. The reason is that the water-treatment carbon contains 1 to 5 kg of water per kg of adsorbent that must be removed by drying before regeneration or an excessive amount of superheated steam will be needed. In water treatment, there can also be significant amounts of nonvolatile compounds that do not desorb during steam regeneration and that residual will reduce the adsorption working capacity. There is a growing use of reticulated styrene-type polymeric resins for VOC removal from air [Beckett, Wood, and Dixon, *Environ. Technol.*, **13**, 1129–1140 (1992); Heinegaard, *Chem.-Ing.-Tech.*, **60**, 907–908 (1988)]. LeVan and Schweiger [in Mersmann and Scholl (eds.), *Fundamentals of Adsorption*, United Engineering Trustees, New York (1991), pp. 487–496] tabulate reported steam utilizations (kg steam/kg adsorbate recovered) for a number of processes.

Energy Applications Desiccant cooling is a means for more efficiently providing air conditioning for enclosures such as supermarkets, ice rinks, hotels, and hospitals. Adsorbents are integrated with evaporative and electric vapor compression cooling equipment into an overall

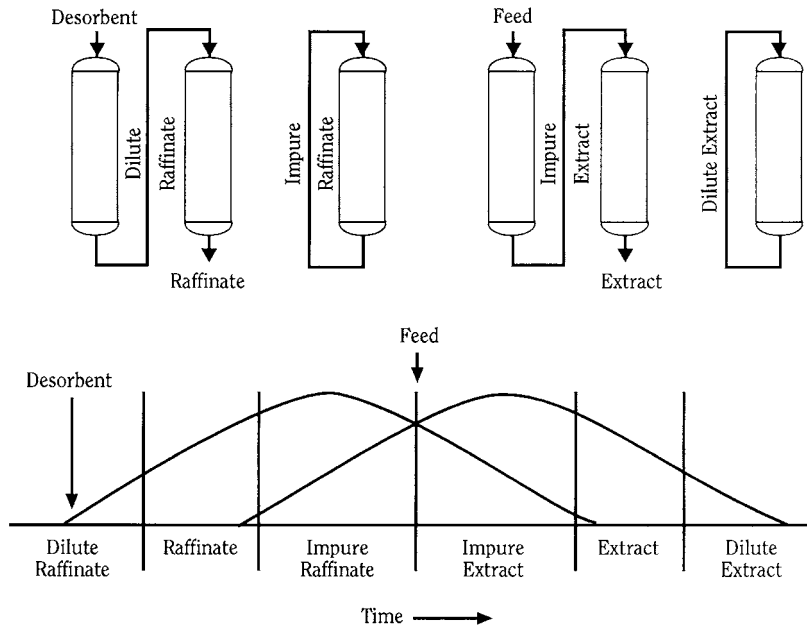


FIG. 16-50 UOP Cyclesorb process. (Reprinted with permission of John Wiley & Sons, Inc. Reference: Gembicki, Oroskar, and Johnson, "Adsorption, Liquid Separation," in Kirk-Othmer Encyclopedia of Chemical Technology, 4th ed., Wiley, New York, 1991.)

air handling system. Air conditioning is comprised of two cooling loads, latent heat for water removal and sensible heat for temperature reduction. The energy savings derive from shifting the latent heat load from expensive compression cooling (chilling) to cooling tower load. Early desiccant cooling used adsorption wheels (see hereafter) impregnated with the hygroscopic salt, LiCl. More recently, these wheels are being fabricated with zeolite and/or silica gel. They are then incorporated into a system such as the example shown in Fig. 16-51 [Collier, Cohen, and Slosberg, in Harriman, *Desiccant Cooling and Dehumidification*,

ASHRAE, Atlanta (1992)]. Process air stream 6, to be conditioned, passes through the adsorbent wheel, where it is dried. This is a non-isothermal process due to the release of heat of adsorption and transfer of heat from a wheel that may be above ambient temperature. The dry but heated air (7) is cooled in a heat exchanger that can be a thermal wheel. This stream (8) is further cooled, and the humidity adjusted back up to a comfort range by direct contact evaporative cooling to provide supply air. Regeneration air stream 1, which can be ambient air or exhausted air, is evaporatively cooled to provide a heat sink for the hot,

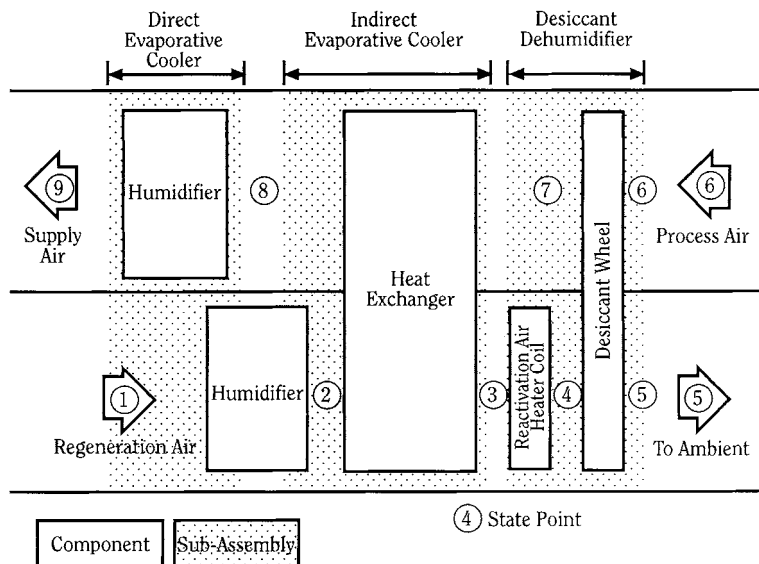


FIG. 16-51 Flow diagram of desiccant cooling cycle. [Reprinted with permission of American Society of Heating, Refrigeration and Air Conditioning Engineers, Inc. (ASHRAE). Reference: Collier, Cohen, and Slosberg in Harriman, *Desiccant Cooling and Dehumidification*, ASHRAE, Atlanta, 1992.]

dry air. This warmed air (3) is heated to the desired temperature for regeneration of the adsorbent wheel and exhausted to the atmosphere. Many other combinations of drying and cooling are used to accomplish desiccant cooling [Belding, in *Proceedings of AFEAS Refrigeration and Air Conditioning Workshop*, Breckenridge, CO (June 23–25, 1993)].

Heat pumps are another developing application of adsorbents. Zeolite/water systems have been evaluated as a means for transferring heat from a low temperature to a higher, more valuable level. Both natural (chabazite and clinoptilolite) and synthetic (NaX and high silica NaY) zeolites have favorable properties for sorption heat pumps. Data have demonstrated that hydrothermally stable Na-mordenite and dealuminated NaY can be used with water in chemical heat pumps to upgrade 100°C heat sources by 50 to 80°C using a 20°C heat sink [Fujiwara, Suzuki, Shin, and Sato, *J. Chem. Eng. Japan*, **23**, 738–743 (1990)]. Other work has shown that integration of two adsorber beds can achieve heating coefficients of performance of 1.56 for the system NaX/water, upgrading 150°C heat to 200°C with a 50°C sink [Douss, Meunier, and Sun, *Ind. Eng. Chem. Res.*, **27**, 310–316 (1988)].

Gas storage of onboard vehicular fuel is important to provide alternatives to gasoline and diesel fuel. Natural gas is cleaner-burning, and hydrogen would burn essentially pollution-free. Onboard storage of natural gas is typically as a high-pressure compressed gas. Adsorbed natural gas systems are a desirable solution because they could operate at lower pressures while maintaining the same capacities. The major problem currently impeding commercialization is the development of adsorbent materials with desirable isotherm capacities and shapes. Also, the exothermic nature of physical adsorption has a negative impact on charge and discharge in a gas storage cycle. Heat released during adsorption will increase the temperature of the adsorbent, thereby lowering the total amount of gas that can be stored. The vessel will cool during the discharge step, decreasing the amount of gas that can be delivered. Technological solutions are being developed and should appear in coming years [Chang and Talu, *Appl. Therm. Eng.*, **16**, 359 (1996); Mota, *AIChE J.*, **45**, 986 (1999)].

Energy Conservation Techniques The major use of energy in an adsorption cycle is associated with the regeneration step, whether it is thermal energy for TSA or compression energy for PSA. Since the regeneration energy per pound of adsorbent tends to be constant, the first step in minimizing consumption is to maximize the operating loading. When the mass-transfer zone (MTZ) is a large portion of the adsorber relative to the equilibrium section, the fraction of the bed being fully utilized is small. Most fixed-bed adsorption systems have two adsorbers so that one is on stream while the other is being regenerated. One means of improving adsorbent utilization is to use a lead/trim (or cascade, or merry-go-round) cycle. Two (or more) adsorbent beds in series treat the feed. The feed enters the lead bed first and then the trim bed. The trim bed is the one that has most recently been regenerated. The MTZ is allowed to proceed through the lead beds but not to break through the trim bed. In this way the lead bed can be almost totally utilized before being regenerated. When a lead bed is taken out of service, the trim bed is placed in lead position, and a regenerated bed is placed in the trim position.

TABLE 16-17 Process Descriptors

Number	Statement
1	Feed is a vaporized liquid or a gas.
2	Feed is a liquid that can be fully vaporized at less than about 200°C.
3	Feed is a liquid that cannot be fully vaporized at 200°C.
4	Adsorbate concentration in the feed is less than about 3 wt %.
5	Adsorbate concentration in the feed is between about 3 and 10 wt %.
6	Adsorbate concentration in the feed is greater than about 10 wt %.
7	Adsorbate must be recovered in high purity (> than 90–99% rejection of nonadsorbed material).
8	Adsorbate can be desorbed by thermal regeneration.
9	Practical purge or displacement agents cannot be easily separated from the adsorbate.

Keller, Anderson, and Yon in Rousseau (ed.), *Handbook of Separation Process Technology*, John Wiley & Sons, Inc., New York, 1987; reprinted with permission.

A thermal pulse cycle is a means of conserving thermal energy in heating-limited desorption. A process cycle that is heat-limited needs only a very small time (dwell) at temperature to achieve satisfactory desorption. If the entire bed is heated before the cooling is begun, every part of the bed will dwell at temperature for the entire time it takes the cooling front to traverse the bed. Thus, much of the heat in the bed at the start of cooling would be swept from the bed. Instead, cooling is begun before any heat front has exited the bed, creating a thermal pulse that moves through the bed. The pulse expends its thermal energy for desorption so that only a small temperature peak remains at the end of the regeneration and no excess heat has been wasted. If the heating step is stripping-limited, a thermal pulse is not applicable.

A series cool/heat cycle is another way in which the heat that is purged from the bed during cooling can be conserved. Sometimes the outlet fluid is passed to a heat sink where energy is stored to be reused to preheat heating fluid, or cross exchanged against the purge fluid to recover energy. However, there is also a process cycle that accomplishes the same effect. Three adsorbers are used, with one on adsorption, one on heating, and one on cooling. The regeneration fluid flows in series, first to cool the bed just heated and then to heat the bed to be desorbed. Thus all of the heat swept from the adsorber during heating can be reused to reduce the heating requirement. Unlike thermal pulse, this cycle is applicable to both heat- and stripping-limited heating.

Process Selection The preceding sections present many process cycles and their variations. It is important to have some guidelines for design engineers to narrow their choice of cycles to the most economical for a particular separation. Keller and coworkers [Keller et al., gen. refs.] have presented a method for choosing appropriate adsorption processes. Their procedure considers the economics of capital, energy, labor, and other costs. Although these costs can vary from site to site, the procedure is robust enough to include most scenarios. In Table 16-17, nine statements are made about the character of the separation being considered. The numbers of the statements that are true (i.e., applicable) are used in the matrix in Table 16-18. A “no” for any true statement under a given

TABLE 16-18 Process Selection Matrix

Statement number, Table 16-17	Gas- or vapor-phase processes					Liquid-phase processes		
	Temperature swing	Inert purge	Displacement purge	Pressure swing	Chromatography	Temperature swing ^a	Simulated moving bed	Chromatography
1	Yes	Yes	Yes	Yes	Yes	No	No	No
2	Not likely	Yes	Yes	Yes	Yes	Yes	Yes	Yes
3	No	No	No	No	No	Yes	Yes	Yes
4	Yes	Yes	Not likely	Not likely	Not likely	Yes	Not likely	Maybe
5	Yes	Yes	Yes	Yes	Yes	No	Yes	Yes
6	No	Yes	Yes	Yes	Yes	No	Yes	Yes
7	Yes	Yes	Yes	Maybe†	Yes	Yes	Yes	Yes
8	Yes	No	No	No	No	Yes‡	No	No
9	Maybe§	Not likely	Not likely	N/A	Not likely	Maybe§	Not likely	Not likely

^aIncludes powdered, fixed-bed, and moving-bed processes.

†Very high ratio of feed to desorption pressure (>10:1) will be required. Vacuum desorption will probably be necessary.

‡If adsorbate concentration in the feed is very low, it may be practical to discard the loaded adsorbent or reprocess off-site.

§If it is not necessary to recover the adsorbate, these processes are satisfactory.

Keller, Anderson, and Yon in Rousseau (ed.), *Handbook of Separation Process Technology*, John Wiley & Sons, Inc., New York, 1987; reprinted with permission.

process should remove that process from further consideration. Any process having all “yes” answers for true statements deserves strong

consideration. Entries other than “yes” or “no” provide a means of prioritizing processes when more than one cycle is satisfactory.

EQUIPMENT

ADSORPTION

General Design Adsorbents are used in adsorbers with fixed inventory, with intermittent solids flow, or with continuous-moving solids flow. The most common are fixed beds operating as batch units or as beds of adsorbent through which the feed fluid passes, with periodic interruption for regeneration. Total systems consist of pressure vessels or open tanks along with the associated piping, valves, controls, and auxiliary equipment needed to accomplish regeneration of the adsorbent. Gas treating equipment includes blowers or compressors with a multiplicity of paths to prevent dead-heading. Liquid treating equipment includes pumps with surge vessels as needed to assure continuous flow.

Adsorber Vessel The most frequently used method of fluid-solid contact for adsorption operations is in cylindrical, vertical vessels, with the adsorbent particles in a fixed and closely but randomly packed arrangement. The adsorbers must be designed with consideration for pressure drop and must contain a means of supporting the adsorbent and a means of assuring that the incoming fluid is evenly distributed to the face of the bed. There are additional design considerations for adsorbers when the streams are liquid and for high-performance separation applications using very small particles (<0.05 mm) such as in HPLC.

For most large-scale processes, adsorbent particle size varies from 0.06 to 6 mm (0.0025 to 0.25 in), but the adsorbent packed in a fixed bed will have a fairly narrow particle size range. Pressure drop in adsorbers can be changed by changing the diameter to bed depth ratio and by changing the particle size (see Sec. 5). Adsorbent size also determines separation performance of adsorbent columns—increasing efficiency with decreasing particle size. In liquid-phase processing, total cost of the adsorption step can sometimes be reduced by designing for overall pressure drops as large as 300 to 600 kPa (45 to 90 psi) because pumping is not the major utility cost. In special, high-resolution applications (HPLC), pressure drops as high as 5000–25,000 kPa (800–4000 psi) are sometimes used requiring special pumping and column hardware [Colin in Ganetsos and Barker, *Preparative and Production Scale Chromatography*, Marcel Dekker, New York, 1993, pp. 11–45]. However, the cost of compressing gases is significant. Since blowers are limited to about 5 kPa (20 in wc) of lift, atmospheric gas applications are typically designed with adsorbent pressure drops of 1 to 4 kPa (4 to 16 in wc). To keep compression ratio low, compressed gas adsorption pressure drops are 5 to 100 kPa (0.7 to 15 psi) depending on the pressure level.

Besides influencing how much pressure drop is allowable, the operating pressure determines other design features. When adsorption and/or regeneration is to be performed at pressures above atmospheric, the adsorber vessels are designed like process pressure vessels (Fig. 16-52 [EPA, gen. refs.]). Their flow distributors can consume more gas momentum at higher pressure. On the other hand, for applications near atmospheric pressure, any pressure drop can be costly, and most design choices are made in the direction of minimizing head loss. Beds have large face areas and shallow depth. Many times, the choice is to fabricate a horizontal (horizontal axis) vessel where flows are radial rather than axial as in conventional vertical beds. Figure 16-53 [Leatherdale in Cheremisnoff and Ellerbusch, gen. refs.] depicts how a rectangular, shallow adsorber bed is oriented in a horizontal vessel. Flow distributors, especially for large units, are often elaborate in order to evenly divide the flow rather than consume precious head.

There are two types of support systems used for fixed beds of adsorbent. The first is a progressive series of grid- and screen-layers. In this system, each higher layer screen has successively smaller openings,

with the last small enough to prevent particles from passing through. Each lower layer has greater strength. A series of I-beams can be used to support a layer of subway grating that, in turn, supports several layers of screening. In other cases, special support grills such as Johnson™ screens may rest on the I-beams or on clips at the vessel wall and thus directly support the adsorbent. The topmost screen must retain the original size particles and some reasonable size of broken particles. The second type of support is a graded system of particles such as ceramic balls or gravel that rests directly on the bottom of the adsorber. A typical system might consist of 100 mm (4 in) of 50 mm (2 in) diameter material, covered by succeeding layers of 25, 12, and 6 mm (1, ½, ¼ in) of support material for a 3 mm (¼ in) adsorbent. In water treatment, the support may actually start with filter blocks and have an upper layer of sand (see Fig. 16-54 [EPA, gen. refs.]).

If flow is not evenly distributed throughout the bed of adsorbent, there will be less than maximum utilization of the adsorbent during adsorption and of the desorption fluid during regeneration. Incoming fluids from the nozzles is at a much higher velocity than the average through the bed and may have asymmetric momentum components due to the piping manifold. The simplest means of allowing flow to redistribute across the face of the bed is to employ ample plenum space above and below the fixed bed. A much more cost-effective method is to install simple baffle plates with symmetrically placed inlet and outlet nozzles. The solid, or perforated, baffles are designed to break the momentum of the incoming fluid and redistribute it to prevent direct impingement on the adsorbent. When graded bed support is installed at the bottom, the baffles should be covered by screening to restrain the particles. An alternative to screened baffles is slotted metal or Johnson™ screen distributors. Shallow horizontal beds often have such a large flow area that multiple inlet and outlet nozzles are required. These nozzle headers must be carefully designed to assure balanced flow to each nozzle. In liquid systems, a single inlet may enter the vessel and branch into several pipes that are often perforated along their length (Fig. 16-52). Such “spiders” and “Christmas trees” often have holes that are not uniformly spaced and sized but are distributed to provide equal flow per bed area.

Although allowable pressure loss with liquids is not a restricting factor, there are special considerations for liquid treating systems. Activated carbon adsorbers used in water and wastewater treatment are designed and constructed using the same considerations used for turbidity removal by sand or multilayer filters. A typical carbon bed is shown in Fig. 16-54. Such contactors for liquids at ambient pressure are often nothing more than open tanks or concrete basins with flow distribution simply an overflow weir. In liquid treating, the adsorbers must be designed with a means for liquid draining and filling occasionally or during every cycle when a gas is used for regeneration. Draining is by gravity, sometimes assisted by a 70–140 kPa (10–20 psig) pressure pad. Even with time to drain, there will be significant liquid holdup to recover. As much as 40 cc of liquid per 100 g of adsorbent is retained in the micro- and macropores and bridged between particles. When drain is cocurrent to adsorption, the drained liquid can be recovered as treated product. When drain is countercurrent, drained fluid must be returned to feed surge. Minimizing other holdup in dead volume is especially important for liquid separation processes such as chromatography, because it adversely affects product recovery and regeneration efficiency. In filling an adsorber, there must be sufficient time for any gas trapped in the pores to escape. The fill step is preferably upflow to sweep the vapor out and to prevent gas pockets that could cause product contamination, bed lifting, or flow maldistribution. In liquid upflow, the buoyancy force of the liquid plus the pressure drop must not exceed the gravitational forces if bed lifting is to be prevented. Because there is very little increase in pressure

16-62 ADSORPTION AND ION EXCHANGE

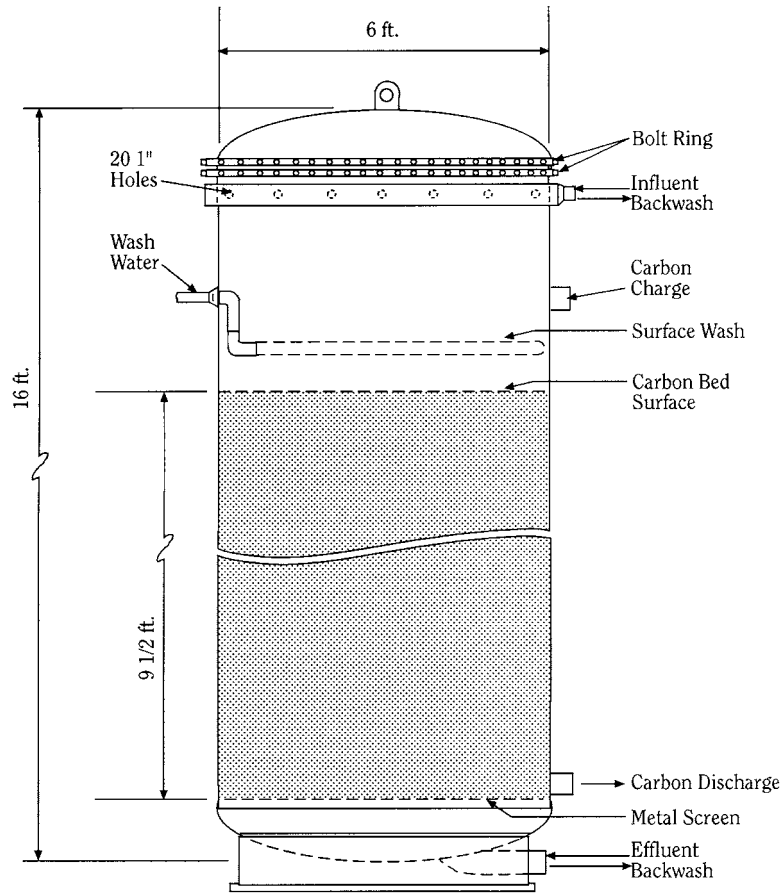


FIG. 16-52 Pressurized adsorber vessel. (Reprinted with permission of EPA. Reference: EPA, Process Design Manual for Carbon Adsorption, U.S. Envir. Protect. Agency., Cincinnati, 1973.)

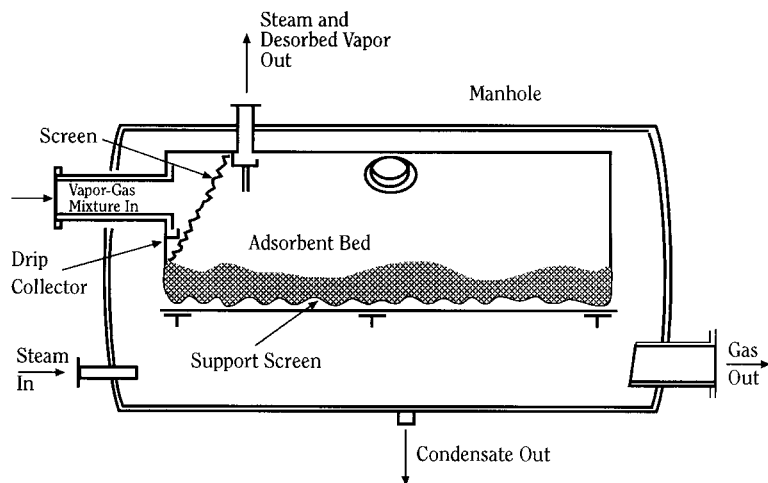


FIG. 16-53 Ambient pressure adsorber vessel. (Reprinted with permission of Ann Arbor Science. Reference: Leatherdale in Chermisinoff and Ellerbusch, Carbon Adsorption Handbook, Ann Arbor Science, Ann Arbor, 1978.)

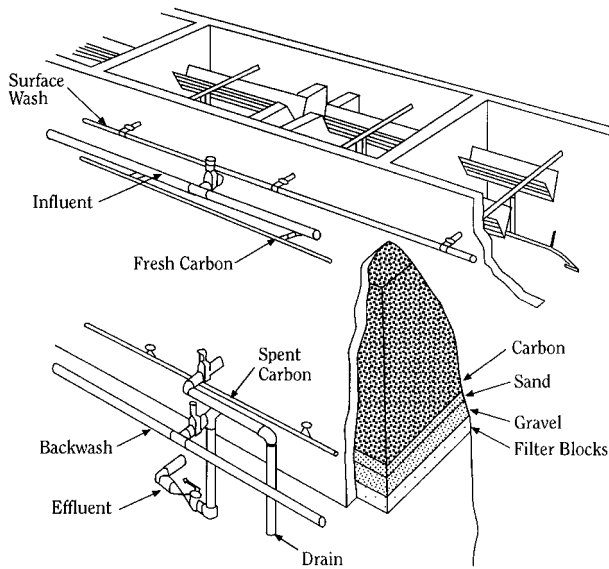


FIG. 16-54 Adsorber vessel with graded support system. (Reprinted with permission of EPA. Reference: EPA, Process Design Manual for Carbon Adsorption, U.S. Envir. Protect. Agency., Cincinnati, 1973.)

drop beyond the lifting (or fluidization) velocity, some liquid systems are designed with bed expansion to limit pressure drop. Upflow-adsorption expanded-beds are also preferred when the liquid contains any suspended solids, so that the bed does not act as a filter and become plugged. Since increased expansion causes the adsorbent to become increasingly well mixed, with accompanying drop in removal efficiency, expansion is usually limited to about 10 percent. Higher velocities also tend to cause too much particle turbulence, abrasion, attrition, and erosion.

Regeneration Equipment Sometimes it is economically justified to remove the adsorbent from the adsorber when it is exhausted and have an outside contractor regenerate it rather than install on-site regeneration equipment. This is feasible only if the adsorbent can treat feed for weeks or months rather than only hours or days. In other cases, the process conditions during regeneration are so much more severe than those for adsorption that a single regenerator with materials of construction capable of handling the conditions is more cost-effective than to make all adsorbents the expensive material. This is true for most water and wastewater treatment with thermally reactivated carbon. Otherwise, desorption is conducted in situ with any additional equipment connected to the adsorbers.

Figure 16-55 [Engineering Data Book, 10th ed., Gas Processors Suppliers Association, Tulsa, 1988, Sec. 20, p. 22] depicts the flow scheme for a typical two-bed TSA dryer system showing the auxiliary equipment associated with regeneration. Some of the dry product gas is externally heated and used countercurrently to heat and desorb water from the adsorber not currently drying feed. The wet, spent regeneration gas is cooled; the water is condensed out; and the gas is recycled for recovery.

The thermal reactivation of spent activated carbon may require the same high temperatures and reaction conditions used for its manufacture. Although the exact conditions to be used for reactivation depend on the type of carbon and the adsorbates to be removed, the objective is to remove the adsorbed material without altering the carbon structure. This occurs in four stages: (a) drying, (b) desorption, (c) pyrolysis and carbonization, and (d) burnoff. Each of these steps is associated with a particular temperature range and is carried out in a multiple hearth furnace such as that depicted in Fig. 16-56. This six-hearth system is a typical configuration for water treatment carbons. The gas temperature ranges from 100°C on the top hearth to 950°C at the bottom. The rotating rabble arms rake the carbon from hearth to hearth. Wet, spent carbon is fed to the top, where it is dried by the top two hearths. Pyrolysis (desorption and decomposition) is accomplished on the next hearth. The bottom four hearths are for reactivation. Varying amounts of air, steam, and/or fuel are added to the different hearths to maintain the conditions established for the particular reactivation. A hearth area requirement of 0.1 m²/kg/hr (0.5 ft²/lb/hr) is adequate for cost estimating, but there are also detailed design procedures available [von Dreusche in Cheremisinoff and Ellerbusch, gen. refs.].

In addition to the multiple-hearth furnace, the reactivation system is comprised of additional equipment to transport, store, dewater, and quench the carbon.

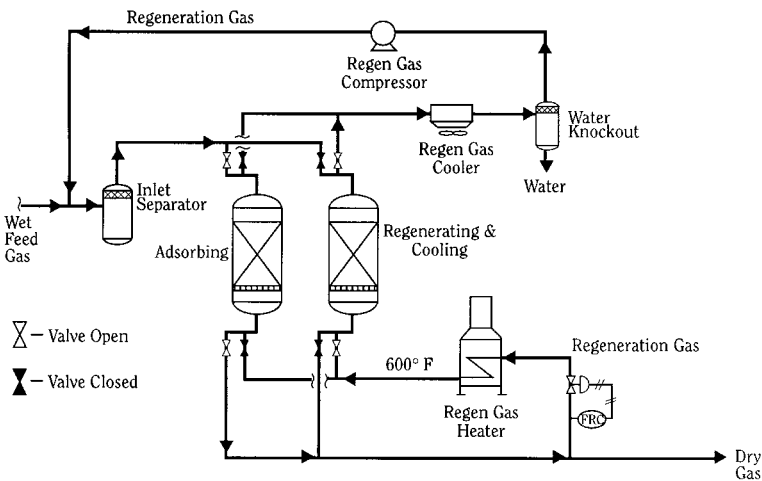


FIG. 16-55 Two-bed TSA system with regeneration equipment. (Reprinted with permission of GPSA. Reference: Engineering Data Book, 10th ed., Gas Processors Suppliers Association, Tulsa, 1988, Sec. 20, p. 22.)

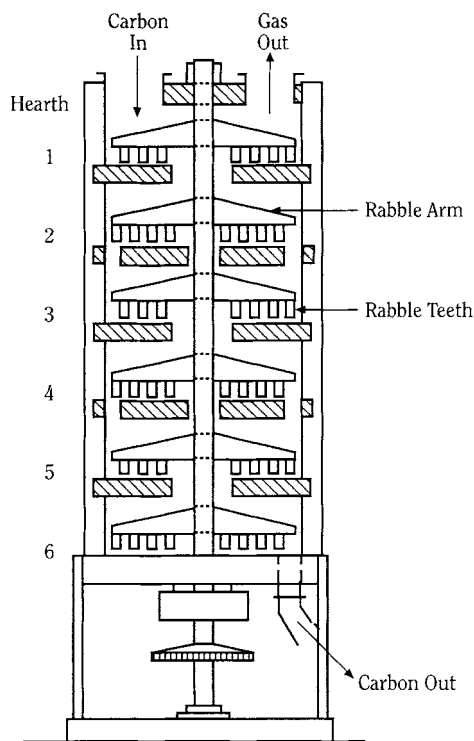


FIG. 16-56 Multiple hearth furnace for carbon reactivation. (Reprinted with permission of EPA. Reference: EPA, Process Design Manual for Carbon Adsorption, U.S. Envir. Protect. Agency., Cincinnati, 1973.)

A typical two-bed PSA dryer process flow scheme is very similar to Fig. 16-55 without the regeneration gas heater. A portion of the dry product gas is used countercurrently to purge the water from the adsorber not currently drying feed. Again, the wet, spent purge gas is cooled, and the water is condensed out and recycled to feed for recovery. If the cycle is VSA, then instead of the regeneration gas compressor, there is a vacuum compressor at the purge outlet upstream of the regeneration cooler. Some PSA cycles such as in air-brake dryers operate with one adsorber, a surge volume, and a three-way valve to switch between pressurizing and countercurrent blowdown. The other extreme of complexity is demonstrated by the UOP nine-bed Polybed PSA H₂ unit shown in Fig. 16-57 [Fuderer and Rudelstorfer, U.S. Patent number 3,986,849, 1976]. This cycle requires nine adsorbers sequenced by 55 valves to maximize purity and recovery.

Cycle Control Valves are the heart of cycle control for cyclic adsorption systems. These on/off valves switch flows among beds so that external to the system it appears as if operation is continuous. In general, one valve is needed for each bed at each end for each step that is performed (e.g., for a two-bed system with an adsorption step plus heating and cooling step [carried out in the same direction and during the same step], only $2 \times 2 \times 2 = 8$ valves would be needed [see Fig. 16-55]). In some cycles such as pressure-swing systems, it may be possible to use valves for more than one function (e.g., repressurization with feed gas using the same manifold as adsorption feed). Without multiple use, the cycle in Fig. 16-57 would need $9 \times 2 \times 5 = 90$ valves instead of 55 to accommodate the five steps of adsorption, purge to product, blowdown, purge, and feed repressurization (even without the equalization). For some applications, 3- and 4-way valves can replace two and four valves, respectively. The ultimate integration of switching valves is the UOP rotary valve discussed below. For long step times (8 hours or more) it is possible for the valves to be manually switched by operators. For most systems, it is

advantageous for the opening and closing of the valves be controlled by automatic timers. The same controller can be responsible for maintaining flows and pressure, logic for proceeding only on completion of events, and safety bypass or shutdown. Automatic control can provide for a period of parallel flow paths to assure transitions. In some applications, process analyzers can interface with the controller to initiate bed-switching when adsorbate is detected breaking through into the effluent.

Continuous Countercurrent Systems Most adsorption systems use fixed-bed adsorbers. However, if the fluid to be separated and that used for desorption can be countercurrently contacted by a moving bed of the adsorbent, there are significant efficiencies to be realized. Because the adsorbent leaves the adsorption section essentially in equilibrium with the feed composition, the inefficiency of the mass-transfer zone is eliminated. The adsorption section only needs to contain a MTZ length of adsorbent compared to a MTZ plus an equilibrium section in a fixed bed. Likewise, countercurrent regeneration is more efficient. Since the adsorbent is moved from an adsorption chamber to another chamber for regeneration, only the regeneration section is designed for the often more severe conditions. Countercurrent adsorption can take advantage of an exceptionally favorable equilibrium in water softening; and the regeneration step can be made favorable by the use of relatively concentrated eluent. Continuous units generally require more headroom but much less footprint. The foremost problems to be overcome in the design and operation of continuous countercurrent sorption operations are the mechanical complexity of equipment and the attrition of the sorbent.

An early example of a commercial countercurrent adsorption processes is the hypersorption process developed by Union Oil Company for the recovery of propane and heavier components from natural gas [Berg, *Chem. Eng. Progr.*, **47**, 585-590 (1951)]. Hypersorption used an activated carbon adsorbent moving as a dense bed continuously downward through a rising gas stream (Fig. 16-58 [Berg, *ibid.*]). However, this process proved to be less economical than cryogenic distillation and had excessive carbon losses resulting from attrition. The commercialization by Kureha Chemical Co. of Japan of a new, highly attrition-resistant, activated-carbon adsorbent, allowed development of a process employing fluidized-bed adsorption and moving bed desorption for removal of VOC compounds from air. The process has been marketed as GASTAKSM in Japan and as PuraSivSM HR (Fig. 16-59 [Anon., *Chem. Eng.*, **84**(18), 39-40 (1977)]) in the United States, and now as SOLDACS by Daikin Industries, Ltd. A similar process using beaded polymeric resin is offered by Chematur [Heinegaard, *Chem.-Ing.-Tech.*, **60**, 907-908 (1988)]. The recent discovery [Acharya and BeVier, U.S. Patent number 4,526,877, 1985] that the graphite coating of zeolites can dramatically improve attrition resistance without significantly impairing adsorption performance could allow the extension of moving-bed technology to other separations. A good review of continuous ion-exchange applications is presented by Wankat [gen. refs.].

Cross-Flow Systems There are at least three implementations of moving-bed adsorption that are cross flow rather than fixed beds or countercurrent flow: (1) panel beds, (2) adsorbent wheels, and (3) rotating annular beds. By *cross flow* is meant that the adsorbent is moving in a direction perpendicular to the fluid flow. All of these employ moving adsorbent—the first, a down-flowing solid; and the others, a constrained solid. Panel beds of activated carbon have been applied to odor control [Lovett and Cunniff, *Chem. Eng. Progr.*, **70**(5), 43-47 (1974)] and to the desulfurization of waste gas [Richter, Knoblauch, and Juntgen, *Verfahrenstechnik (Mainz)*, **14**, 338-342 (1980)]. The spent solid falls from the bottom panel into a load-out bin, and fresh regenerated carbon is added to the top; gas flows across the panel.

The heart of an adsorbent wheel system is a rotating cylinder containing the adsorbent. Figure 16-60 illustrates two types: horizontal and vertical. In some adsorbent wheels, the adsorbent particles are placed in basket segments (a multitude of fixed beds) to form a horizontal wheel that rotates around a vertical axis. In other instances, the adsorbent is integral to the monolithic wheel or coated onto a metal, paper, or ceramic honeycomb substrate. These monolithic or

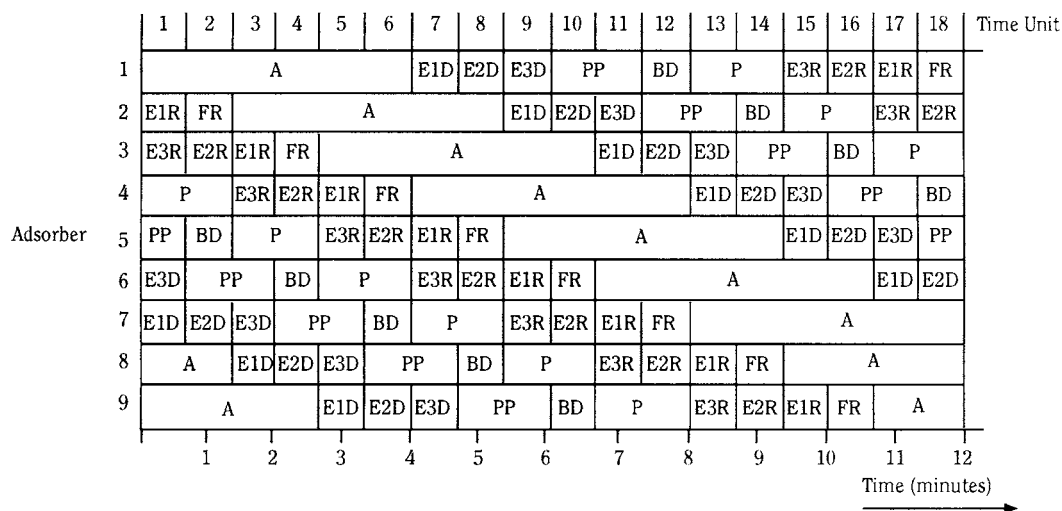
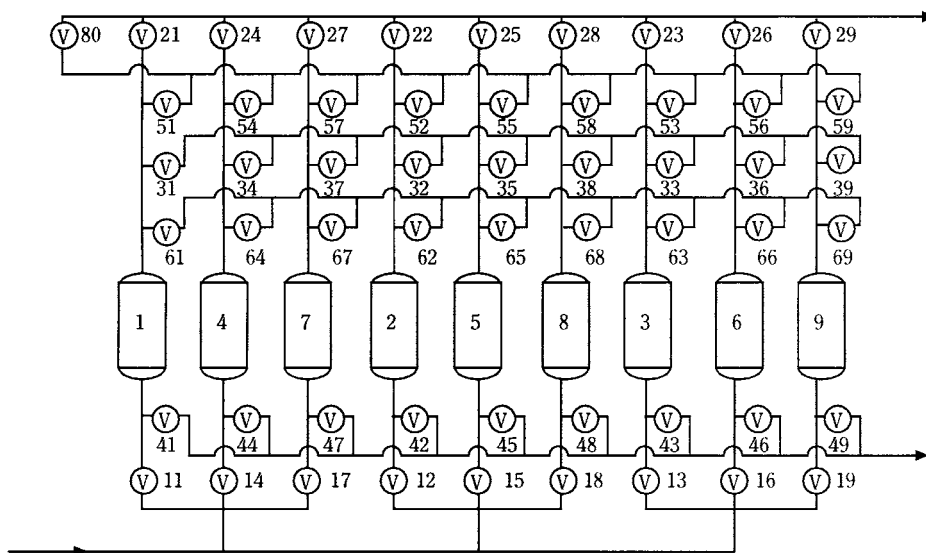


FIG. 16-57 UOP nine-bed polybed PSA H₂ unit: (a) flow scheme; (b) cycle diagram. (Reference: Fuderer and Rudelstorfer, U.S. Patent number 3,986,849, 1976.)

honeycomb structures rotate around either a vertical or a horizontal axis. The gas to be treated usually flows through the wheel parallel to the axis of rotation, although some implementations use radial flow configurations. Most of the wheel is removing adsorbates. The remaining (smaller) portion of the wheel is undergoing thermal regeneration—usually countercurrently. The wheel constantly rotates to provide a continuous treated stream and a steady concentrated stream. Adsorbent wheels are most often used to treat ambient air because they have very low pressure drop. One application of wheels is the removal of VOC where the regeneration stream is usually sent to an incinerator for destruction of VOC. Another use is in desiccant cooling (see previously). They do suffer from low efficiency due to the short contact time, mechanical leakage at seals,

and the tendency to allow the wheel to exceed breakthrough in order to get better adsorbent utilization. Some adsorbent wheels are operated in an intermittent manner such that the wheel periodically indexes to a new position; this is particularly true of radial flow wheels.

The rotating annular bed system for liquid chromatographic separation (two-dimensional chromatography) is analogous to the horizontal adsorbent wheel for gases. Feed to be separated flows to a portion of the top face of an annular bed of sorbent. A displacement purge in the form of a solvent or carrier gas flows to the rest of the annulus. The less strongly adsorbed components travel downward through the sorbent at a higher rate. Thus, they will exit at the bottom of the annulus at a smaller angular distance from the feed sector. The more strongly adsorbed species will exit at a greater angle. The mechanical and

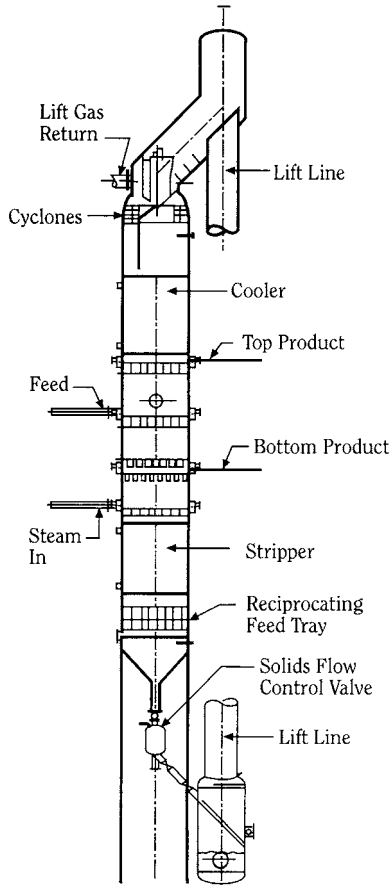


FIG. 16-58 Hypersorption adsorber vessel. [Reprinted with permission of AIChE. Reference: Berg, Chem. Eng. Progr., 47, 585-590 (1951).]

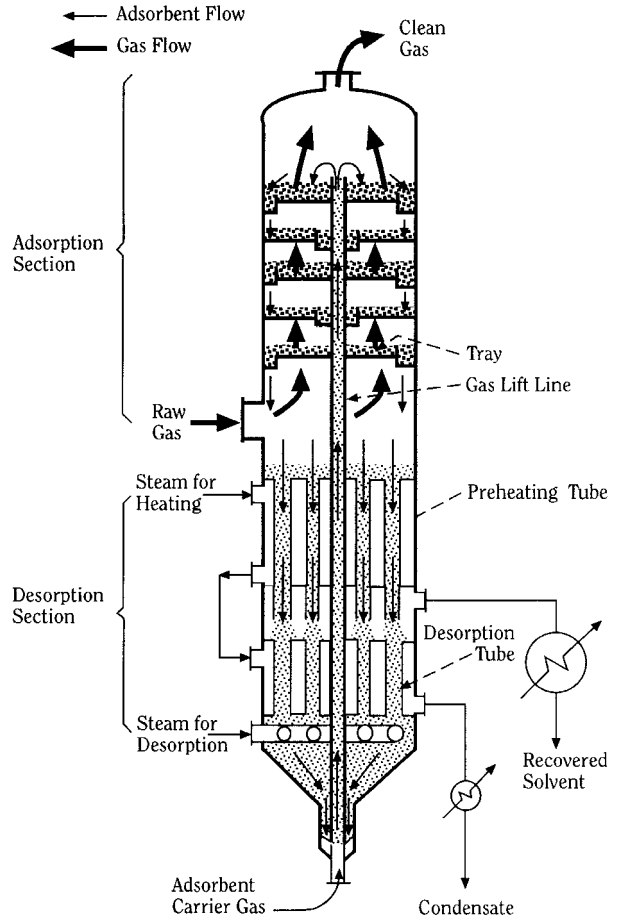


FIG. 16-59 PuraSiv HR adsorber vessel. [Reprinted with permission of Chemical Engineering. Reference: Anon., Chem. Eng., 84(18), 39-40 (1977).]

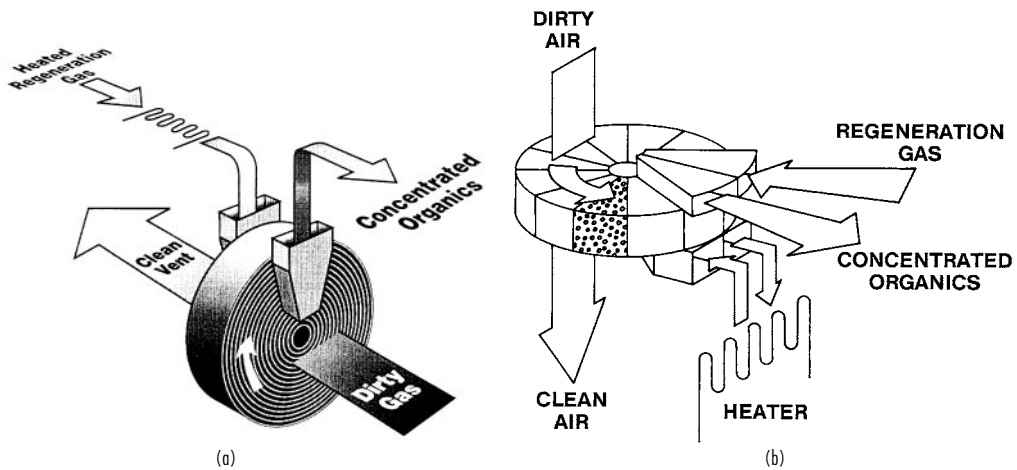


FIG. 16-60 Adsorbent wheels for gas separation: (a) horizontal with fixed beds; (b) vertical monolith. (Reprinted with permission of UOP.)

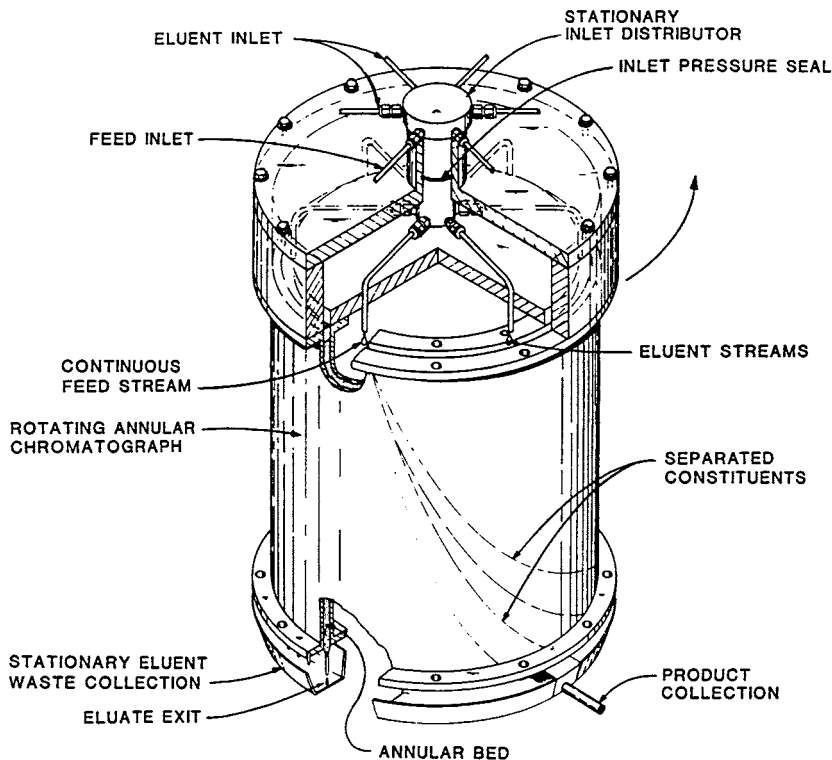


FIG. 16-61 Annular bed for liquid separation. [Reprinted with permission of Marcel Dekker. Reference: Canon, Begovich, and Sisson, *Sep. Sci. Technol.*, **15**, 655-678 (1980).]

packing complexities of such an apparatus have been overcome for a pressurized system by workers at the Oak Ridge National Laboratory shown in Fig. 16-61 [Canon, Begovich, and Sisson, *Sep. Sci. Technol.*, **15**, 655-678 (1980)]. Several potential applications are reviewed by Carta and Byers [*Chromatographic and Membrane Processes in Biotechnology*, NATO ASI Proceeding, Kluwer, 1991].

ION EXCHANGE

A typical fixed-bed ion exchanger consists of a vertical cylindrical vessel of lined steel or stainless steel. Linings are usually of natural or synthetic rubber. Spargers are provided at the top and bottom, and frequently a separate distributor is used for the regenerant solution. The resin bed, consisting of a meter or more of ion-exchange particles, is supported by the screen of the bottom distributor. Externally, the unit is provided with a valve manifold to permit downflow loading, upflow backwash, regeneration, and rinsing. For deionization, a two-exchanger assembly comprising a cation and an anion exchanger, is a common configuration (Fig. 16-62).

Column hardware designed to allow countercurrent, upflow regeneration of ion-exchange resins is available. An example is given in Fig. 16-63. During upflow of the regenerant, bed expansion is prevented by withdrawing the effluent through the application of vacuum. A layer of drained particles is formed at the top of the bed while the rest of the column functions in the usual way.

Typical design data for fixed-bed ion-exchange columns are given in Table 16-19. These should be used for preliminary evaluation purposes only. Characteristic design calculations are presented and illustrated by Applebaum [*Deminceralization by Ion Exchange*, Academic, New York, 1968]. Large amounts of data are available in published literature and in bulletins of manufacturers of ion exchangers. In general, however, laboratory testing and pilot-plant work is advisable

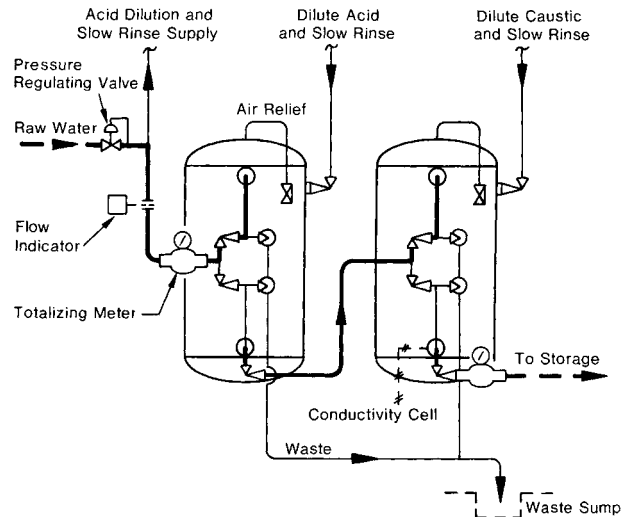


FIG. 16-62 Typical two-bed deionizing system. (Infilco Degremont Inc.)

TABLE 16-19 Design Data for Fixed-Bed Ion Exchanger*

Type of resin	Maximum and minimum flow, m ³ /h [gal/(min-ft ²)]	Minimum bed depth, m (in)	Maximum operating temperatures, °C (°F)	Usable capacity, g-equivalent/L†	Regenerant, g/L resin‡
Weak acid cation	20 max. (8) 3 min. (1)	0.6 (24)	120 (248)	0.5–2.0	110% theoretical (HCl or H ₂ SO ₄)
Strong acid cation	30 max. (12) 3 min. (1)	0.6 (24)	120 (248)	0.8–1.5 0.5–1.0 0.7–1.4	80–250 NaCl 35–200 66° Bé. H ₂ SO ₄ 80–500 20° Bé. HCl 35–70 NaOH
Weak and intermediate base anions	17 max. (7) 3 min. (1)	0.75 (30)	40 (104)	0.8–1.4	
Strong-base anions	17 max. (7) 3 min. (1)	0.75 (30)	50 (122)	0.35–0.7	70–140 NaOH
Mixed cation and strong-base anion (chemical-equivalent mixture)	40 max. (16)	1.2 (47)	50 (122)	0.2–0.35 (based on mixture)	Same as cation and anion individually

*These figures represent the usual ranges of design for water-treatment applications. For chemical-process applications, allowable flow rates are generally somewhat lower than the maximums shown, and bed depths are usually somewhat greater.

†To convert to capacity in terms of kilograms of CaCO₃ per cubic foot of resin, multiply by 21.8.

‡To convert to pounds of regenerant per cubic foot of resin, multiply by 0.0625.

to determine usable exchanger capacities, regenerant quantities, exchanger life, and quality of product for any application not already thoroughly proven in other plants for similar conditions. Firms that manufacture ion exchangers and ion-exchange equipment will often cooperate in such tests.

For larger-scale applications, a number of continuous or semicontinuous ion-exchange units are also available. The Higgins contactor (Fig. 16-64) was originally developed to recover uranium from leach slurries at the Oak Ridge National Laboratory. More recently, it has been adapted to a wide variety of applications, including large-volume water softening.

The Asahi process (Fig. 16-65) is used principally for high-volume water treatment. The liquid to be treated is passed upward through a resin bed in the adsorption tank. The upward flow at 30–40 m/h [12–16 gal/(min ft²)] keeps the bed packed against the top. After a preset time, 10 to 60 min, the flow is interrupted for about 30 s,

allowing the entire bed to drop. A small portion (10 percent or less) of the ion-exchange resin is removed from the bottom of the adsorption tank and transferred hydraulically to the hopper feeding the regeneration tank. The process is then resumed. Meanwhile, regeneration is occurring by a similar flow system in the regeneration tank, from which the regenerated ion exchanger is transferred periodically to the hopper above the water-rinse tank. In the latter, the resin particles are fluidized to flush away fines and accumulated foreign matter before the resin is returned to the adsorption tank.

Another continuous ion-exchange system is described by Himsley and Farkas (see Fig. 16-66). Such a system is used to treat 1590 m³/h (7000 gal/min) of uranium-bearing copper leach liquor using fiberglass-construction columns 3.7 m (12 ft) in diameter. The adsorption column is divided vertically into stages. Continuous transfer of batches of resin occurs from stage to stage without any interruption of flow. This is accomplished by pumping solution from one stage (A) to the stage (B) immediately above by means of external pumping in such a manner that the net flow through stage B is downward, carrying with it all of the resin in that stage B. When transfer of the ion exchanger is complete, the resin in stage C above is transferred downward in a similar manner. The process

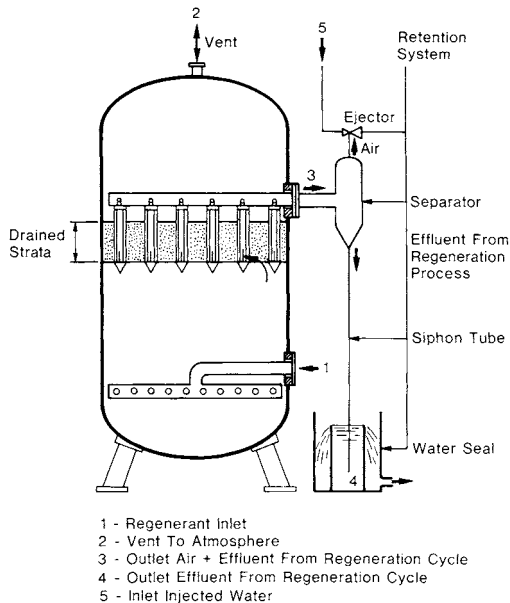


FIG. 16-63 Internals of an upflow regenerated unit. (Infilco Degremont Inc.)

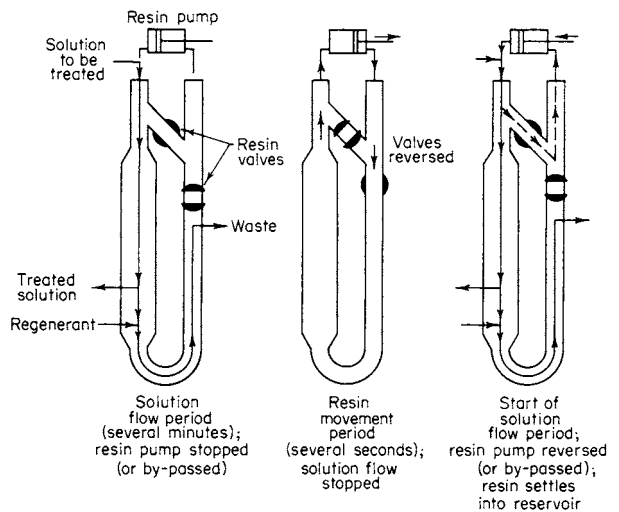


FIG. 16-64 Mode of operation of the Higgins contactor. (ORNL-LR-Dwg. 27857R.)

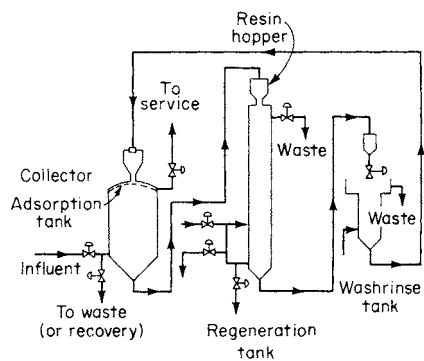


FIG. 16-65 Asahi countercurrent ion-exchange process. [Gilwood, *Chem. Eng.*, 74(26), 86 (1967); copyright 1967 by McGraw-Hill, Inc., New York. Excerpted with special permission of McGraw-Hill.]

continues until the last stage (F) is empty. The regenerated resin is then transferred from the elution column to the empty stage (F). Elution of the sorbed product is carried out in the elution column in a moving packed bed mode. The countercurrent contact achieved in this column yields a concentrated eluate with a minimum consumption of regenerant.

Disadvantages of these continuous countercurrent systems are associated primarily with the complexity of the equipment required and with the attrition resulting from the transport of the ion exchanger. An effective alternative for intermediate scale processes is the use of merry-go-round systems and SMB units employing only packed-beds with no movement of the ion-exchanger.

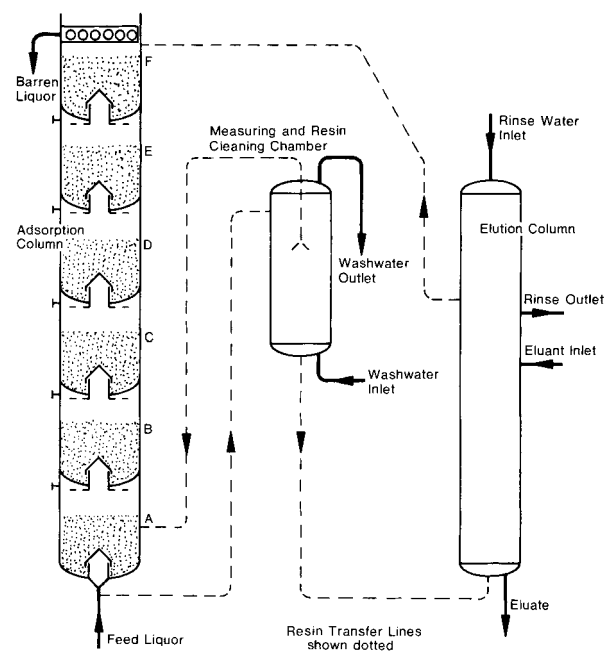


FIG. 16-66 Himsley continuous ion-exchange system. (Himsley and Farkas, "Operating and Design Details of a Truly Continuous Ion Exchange System," *Soc. Chem. Ind. Conf.*, Cambridge, England, July 1976. Used by permission of the Society of Chemical Industry.)

SECTION 17

Gas-Solid
Operations and
Equipment

PERRY'S CHEMICAL ENGINEERS' HANDBOOK

8TH EDITION



MEL PELL, JAMES B. DUNSON
TED M. KNOWLTON

Copyright © 2008, 1997, 1984, 1973, 1963, 1950, 1941, 1934 by The McGraw-Hill Companies, Inc. All rights reserved. Manufactured in the United States of America. Except as permitted under the United States Copyright Act of 1976, no part of this publication may be reproduced or distributed in any form or by any means, or stored in a database or retrieval system, without the prior written permission of the publisher.

0-07-154224-8

The material in this eBook also appears in the print version of this title: 0-07-151140-7.

All trademarks are trademarks of their respective owners. Rather than put a trademark symbol after every occurrence of a trademarked name, we use names in an editorial fashion only, and to the benefit of the trademark owner, with no intention of infringement of the trademark. Where such designations appear in this book, they have been printed with initial caps.

McGraw-Hill eBooks are available at special quantity discounts to use as premiums and sales promotions, or for use in corporate training programs. For more information, please contact George Hoare, Special Sales, at george_hoare@mcgraw-hill.com or (212) 904-4069.

TERMS OF USE

This is a copyrighted work and The McGraw-Hill Companies, Inc. (“McGraw-Hill”) and its licensors reserve all rights in and to the work. Use of this work is subject to these terms. Except as permitted under the Copyright Act of 1976 and the right to store and retrieve one copy of the work, you may not decompile, disassemble, reverse engineer, reproduce, modify, create derivative works based upon, transmit, distribute, disseminate, sell, publish or sublicense the work or any part of it without McGraw-Hill’s prior consent. You may use the work for your own noncommercial and personal use; any other use of the work is strictly prohibited. Your right to use the work may be terminated if you fail to comply with these terms.

THE WORK IS PROVIDED “AS IS.” McGRAW-HILL AND ITS LICENSORS MAKE NO GUARANTEES OR WARRANTIES AS TO THE ACCURACY, ADEQUACY OR COMPLETENESS OF OR RESULTS TO BE OBTAINED FROM USING THE WORK, INCLUDING ANY INFORMATION THAT CAN BE ACCESSED THROUGH THE WORK VIA HYPERLINK OR OTHERWISE, AND EXPRESSLY DISCLAIM ANY WARRANTY, EXPRESS OR IMPLIED, INCLUDING BUT NOT LIMITED TO IMPLIED WARRANTIES OF MERCHANTABILITY OR FITNESS FOR A PARTICULAR PURPOSE. McGraw-Hill and its licensors do not warrant or guarantee that the functions contained in the work will meet your requirements or that its operation will be uninterrupted or error free. Neither McGraw-Hill nor its licensors shall be liable to you or anyone else for any inaccuracy, error or omission, regardless of cause, in the work or for any damages resulting therefrom. McGraw-Hill has no responsibility for the content of any information accessed through the work. Under no circumstances shall McGraw-Hill and/or its licensors be liable for any indirect, incidental, special, punitive, consequential or similar damages that result from the use of or inability to use the work, even if any of them has been advised of the possibility of such damages. This limitation of liability shall apply to any claim or cause whatsoever whether such claim or cause arises in contract, tort or otherwise.

DOI: 10.1036/0071511407

Gas-Solid Operations and Equipment

Mel Pell, Ph.D. *President, ESD Consulting Services; Fellow, American Institute of Chemical Engineers; Registered Professional Engineer (Delaware) (Section Editor, Fluidized-Bed Systems)*

James B. Dunson, M.S. *Principal Division Consultant (retired), E. I. duPont de Nemours & Co.; Member, American Institute of Chemical Engineers; Registered Professional Engineer (Delaware) (Gas-Solids Separations)*

Ted M. Knowlton, Ph.D. *Technical Director, Particulate Solid Research, Inc.; Member, American Institute of Chemical Engineers (Fluidized-Bed Systems)*

FLUIDIZED-BED SYSTEMS

Gas-Solid Systems	17-2
Types of Solids	17-2
Two-Phase Theory of Fluidization	17-2
Phase Diagram (Zenz and Othmer)	17-3
Phase Diagram (Grace)	17-3
Regime Diagram (Grace)	17-3
Solids Concentration versus Height	17-5
Equipment Types	17-5
Minimum Fluidizing Velocity	17-5
Particulate Fluidization	17-6
Vibrofluidization	17-6
Design of Fluidized-Bed Systems	17-6
Fluidization Vessel	17-6
Scale-up	17-9
Heat Transfer	17-11
Temperature Control	17-12
Solids Mixing	17-12
Gas Mixing	17-12
Size Enlargement	17-12
Size Reduction	17-12
Standpipes, Solids Feeders, and Solids Flow Control	17-12
Solids Discharge	17-13
Dust Separation	17-14
Example 1: Length of Seal Leg	17-15
Instrumentation	17-15

Uses of Fluidized Beds	17-16
Chemical Reactions	17-16
Physical Contacting	17-20

GAS-SOLIDS SEPARATIONS

Nomenclature	17-21
Purpose of Dust Collection	17-24
Properties of Particle Dispersoids	17-24
Particle Measurements	17-24
Atmospheric-Pollution Measurements	17-24
Process-Gas Sampling	17-24
Particle-Size Analysis	17-24
Mechanisms of Dust Collection	17-26
Performance of Dust Collectors	17-27
Dust-Collector Design	17-27
Dust-Collection Equipment	17-28
Gravity Settling Chambers	17-28
Impingement Separators	17-28
Cyclone Separators	17-28
Mechanical Centrifugal Separators	17-36
Particulate Scrubbers	17-36
Dry Scrubbing	17-43
Fabric Filters	17-46
Granular-Bed Filters	17-51
Air Filters	17-52
Electrical Precipitators	17-55

FLUIDIZED-BED SYSTEMS

Consider a bed of particles in a column that is supported by a distributor plate with small holes in it. If gas is passed through the plate so that the gas is evenly distributed across the column, the drag force on the particles produced by the gas flowing through the particles increases as the gas flow through the bed is increased. When the gas flow through the bed causes the drag forces on the particles to equal the weight of the particles in the bed, the particles are fully supported and the bed is said to be fluidized. Further increases in gas flow through the bed cause bubbles to form in the bed, much as in a fluid, and early researchers noted that this resembled a fluid and called this a fluidized state.

When fluidized, the particles are suspended in the gas, and the fluidized mass (called a fluidized bed) has many properties of a liquid. Like a liquid, the fluidized particles seek their own level and assume the shape of the containing vessel. Large, heavy objects sink when added to the bed, and light particles float.

Fluidized beds are used successfully in many processes, both catalytic and noncatalytic. Among the catalytic processes are fluid catalytic cracking and reforming, oxidation of naphthalene to phthalic anhydride, the production of polyethylene and ammoxidation of propylene to acrylonitrile. Some of the noncatalytic uses of fluidized beds are in the roasting of sulfide ores, coking of petroleum residues, calcination of ores, combustion of coal, incineration of sewage sludge, and drying and classification.

Although it is possible to fluidize particles as small as about 1 μm and as large as 4 cm, the range of the average size of solid particles which are more commonly fluidized is about 30 μm to over 2 cm. Particle size affects the operation of a fluidized bed more than particle density or particle shape. Particles with an average particle size of about 40 to 150 μm fluidize smoothly because bubble sizes are relatively small in this size range. Larger particles (150 μm and larger) produce larger bubbles when fluidized. The larger bubbles result in a less homogeneous fluidized bed, which can manifest itself in large pressure fluctuations. If the bubble size in a bed approaches approximately one-half to two-thirds the diameter of the bed, the bed will slug. A slugging bed is characterized by large pressure fluctuations that can result in instability and severe vibrations in the system. Small particles (smaller than 30 μm in diameter) have large interparticle forces (generally van der Waals forces) that cause the particles to stick together, as flour particles do. These type of solids fluidize poorly because of the agglomerations caused by the cohesion. At velocities that would normally fluidize larger particles, channels, or spouts, form in the bed of these small particles, resulting in severe gas bypassing. To fluidize these small particles, it is generally necessary to operate at very high gas velocities so that the shear forces are larger than the cohesive forces of the particles. Adding finer-sized particles to a coarse bed, or coarser-sized particles to a bed of cohesive material (i.e., increasing the particle size range of a material), usually results in better (smoother) fluidization.

Gas velocities in fluidized beds generally range from 0.1 to 3 m/s (0.33 to 9.9 ft/s). The gas velocities referred to in fluidized beds are superficial gas velocities—the volumetric flow through the bed divided by the bed area. More detailed discussions of fluidized beds can be found in Kunii and Levenspiel, *Fluidization Engineering*, 2d ed., Butterworth Heinemann, Boston, 1991; Pell, *Gas Fluidization*, Elsevier, New York, 1990; Geldart (ed.), *Gas Fluidization Technology*, Wiley, New York, 1986; Yang (ed.), *Handbook of Fluidization and Fluid Particle Systems*, Marcel Dekker, New York, 2003; and papers published in periodicals, transcripts of symposia, and the American Institute of Chemical Engineers symposium series.

GAS-SOLID SYSTEMS

Researchers in the fluidization field have long recognized that particles of different size behave differently in fluidized beds, and several have tried to define these differences. Some of these characterizations are described below.

Types of Solids Perhaps the most widely used categorization of particles is that of Geldart [*Powder Technol.* 7: 285–292 (1973)].

Geldart categorized solids into four different groups (groups A, B, C, and D) that exhibited different properties when fluidized with a gas. He classified the four groups in his famous plot, shown in Fig. 17-1. This plot defines the four groups as a function of average particle size d_{sv} , μm , and density difference $\rho_s - \rho_f$, g/cm^3 , where ρ_s = particle density, ρ_f = fluid density, and d_{sv} = surface volume diameter of the particles. Generally d_{sv} is the preferred average particle size for fluid-bed applications, because it is based on the surface area of the particle. The drag force used to generate the pressure drop used to fluidize the bed is proportional to the surface area of the particles. Another widely used average particle size is the median particle size $d_{p,50}$.

When the gas velocity through a bed of group A, B, C, or D particles increases, the pressure drop through the bed also increases. The pressure drop increases until it equals the weight of the bed divided by the cross-sectional area of the column. The gas velocity at which this occurs is called the minimum fluidizing velocity U_{mf} . After minimum fluidization is achieved, increases in velocity for a bed of group A (generally in the particle size range between 30 and 100 μm) particles will result in a uniform expansion of the particles without bubbling until at some higher gas velocity the gas bubbles form at a velocity called the minimum bubbling velocity U_{mb} . For Geldart group B (between 100 and about 1000 μm) and group D (1000 μm and larger) particles, bubbles start to form immediately after U_{mf} is achieved, so that U_{mf} and U_{mb} are essentially equal for these two Geldart groups. Group C (generally smaller than 30 μm) particles are termed cohesive particles and clump together in particle agglomerates because of interparticle forces (generally van der Waals forces). When gas is passed through beds of cohesive solids, the gas tends to channel or “rathole” through the bed. Instead of fluidizing the particles, the gas opens channels that extend from the gas distributor to the surface of the bed. At higher gas velocities where the shear forces are great enough to overcome the interparticle forces, or with mechanical agitation or vibration, cohesive particles will fluidize but with larger clumps or clusters of particles formed in the bed.

Two-Phase Theory of Fluidization The two-phase theory of fluidization assumes that all gas in excess of the minimum bubbling velocity passes through the bed as bubbles [Toomey and Johnstone, *Chem. Eng. Prog.* 48: 220 (1952)]. In this view of the fluidized bed, the gas flowing through the emulsion phase in the bed is at the minimum bubbling velocity, while the gas flow above U_{mb} is in the bubble phase. This view of the bed is an approximation, but it is a helpful way

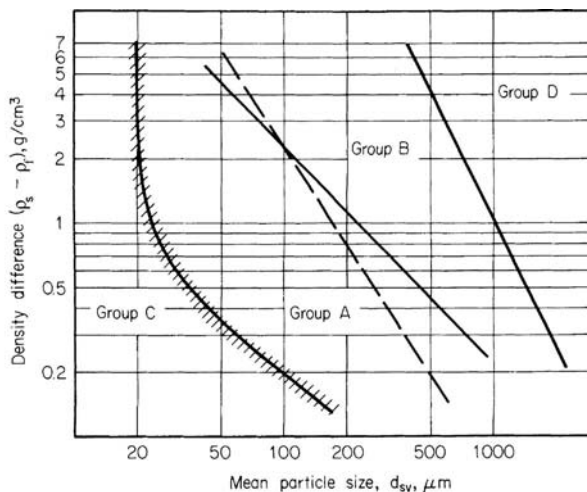


FIG. 17-1 Powder-classification diagram for fluidization by air (ambient conditions). [From Geldart, *Powder Technol.*, 7, 285–292 (1973).]

of understanding what happens as the gas velocity is increased through a fluidized bed. As the gas velocity is increased above U_{mb} , more and larger bubbles are formed in the bed. As more bubbles are produced in the bed, the bed expands and the bed density decreases.

For all Geldart groups (A, B, C, and D), as the gas velocity is increased, the fluidized-bed density is decreased and the turbulence of the bed is increased. In smaller-diameter beds, especially with group B and D powders, slugging will occur as the bubbles increase in size to greater than one-half to two-thirds of the bed diameter. Bubbles grow by vertical and lateral merging and increase in size as the gas velocity is increased [Whitehead, in Davidson and Harrison (eds.), *Fluidization*, Academic, London and New York, 1971]. As the gas velocity is increased further, the stable bubbles break down into unstable voids. When unstable voids characterize the gas phase in fluidized beds, the bed is not in the bubbling regime anymore, but is said to be in the turbulent regime. The turbulent regime is characterized by higher heat- and mass-transfer rates than bubbling fluidized beds, and the pressure fluctuations in the bed are reduced relative to bubbling beds. As the gas velocity is increased above the turbulent fluidized regime, the turbulent bed gradually changes into the pneumatic conveying regime.

Phase Diagram (Zenz and Othmer) As shown in Fig. 17-2, Zenz and Othmer, (*Fluidization and Fluid Particle Systems*, Reinhold, New York, 1960) developed a gas-solid phase diagram for systems in which gas flows upward, as a function of pressure drop per unit length versus gas velocity with solids mass flux as a parameter. Line OAB in Fig. 17-2 is the pressure drop versus gas velocity curve for a packed bed, and line BD is the curve for a fluidized bed with no net solids flow through it. Zenz indicated that there was an instability between points D and H because with no solids flow, all the particles will be

entrained from the bed. However, if solids are added to replace those entrained, system IJ (generally known as the pneumatic conveying region) prevails. The area DHIJ will be discussed in greater detail later.

Phase Diagram (Grace) Grace [*Can. J. Chem. Eng.*, **64**: 353-363 (1986); Fig. 17-3] has correlated the various types of gas-solid systems in which the gas is flowing vertically upward in a status graph using the parameters of the Archimedes number Ar for the particle size and a nondimensional velocity U^* for the gas effects. By means of this plot, the fluidization regime for various operating systems can be approximated. This plot is a good guide to estimate the fluidization regime for various particle sizes and operating conditions. However, it should not be substituted for more exact methods of determining the actual fluidization operating regime.

Regime Diagram (Grace) Grace [*Can. J. Chem. Eng.*, **64**, 353-363 (1986)] approximated the appearance of the different regimes of fluidization in the schematic drawing of Fig. 17-4. This drawing shows the fluidization regimes that occur as superficial gas velocity is increased from the low-velocity packed bed regime to the pneumatic conveying transport regime. As the gas velocity is increased from the moving packed bed regime, the velocity increases to a value U_{mf} such that the drag forces on the particles equal the weight of the bed particles, and the bed is fluidized. If the particles are group A particles, then a "bubbleless" particulate fluidization regime is formed. At a higher gas velocity U_{mb} , bubbles start to form in the bed. For Geldart group B and D particles, the particulate fluidization regime does not form, but the bed passes directly from a packed bed to a bubbling fluidized bed. As the gas velocity is increased above U_{mb} , the bubbles in the bed grow in size. In small laboratory beds, if the bubble size grows to a value equal to approximately one-half to two-thirds the diameter

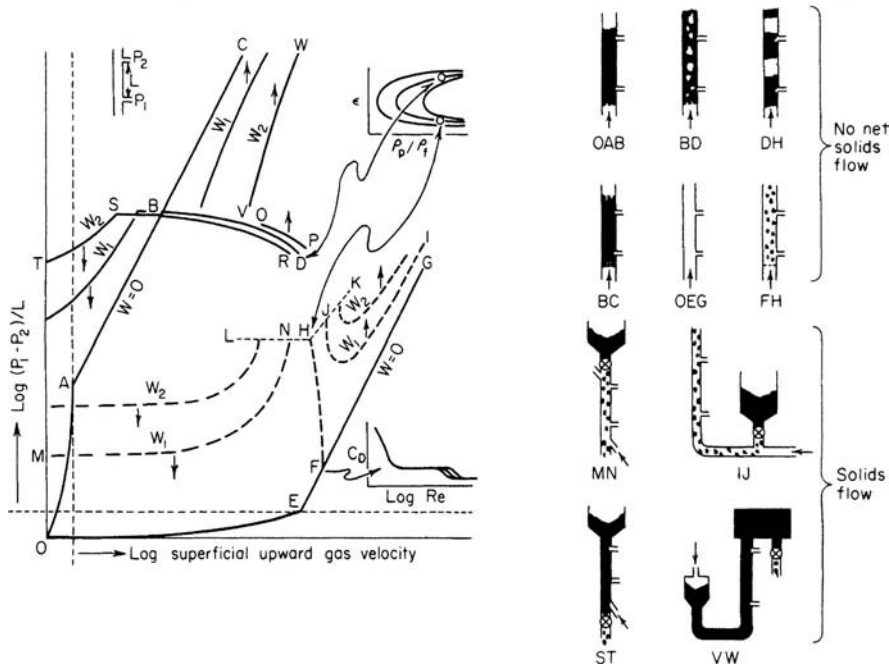


FIG. 17-2 Schematic phase diagram in the region of upward gas flow. W = mass flow solids, lb/(h · ft²); ϵ = fraction voids; ρ_p = particle density, lb/ft³; ρ_f = fluid density, lb/ft³; C_D = drag coefficient; Re = modified Reynolds number. (Zenz and Othmer, *Fluidization and Fluid Particle Systems*, Reinhold, New York, 1960.)

Key:

- | | | | |
|--------------------|----------------------------------------|-------------------------------------|-----------------------------------------|
| OAB = packed bed | IJ = cocurrent flow (dilute phase) | AC = packed bed (restrained at top) | FH = dilute phase |
| BD = fluidized bed | ST = countercurrent flow (dense phase) | OEG = fluid only (no solids) | MN = countercurrent flow (dilute phase) |
| DH = slugging bed | | | VW = cocurrent flow (dense phase) |

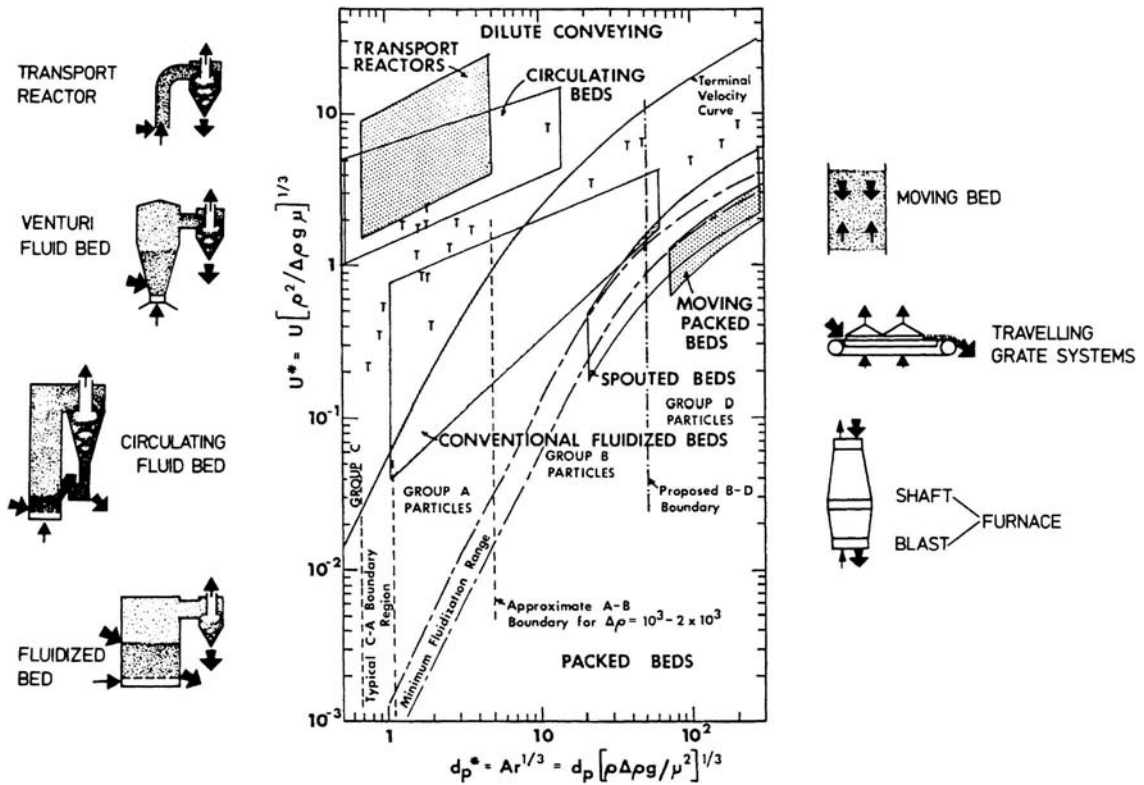


FIG. 17-3 Simplified fluid-bed status graph. [From Grace, Can. J. Chem. Eng., 64, 353-363 (1986); sketches from Reh, Ger. Chem. Eng., 1, 319-329 (1978).]

of the fluidization column, the bed will slug. The slugging fluidized bed is characterized by severe pressure fluctuations and limited solids mixing. It only occurs with small-diameter fluidization columns. Commercial fluidized beds are too large for bubbles to grow to the size where slugging will occur.

At high gas velocities in the bed, the stable bubbles break down into unstable voids that continuously disintegrate and reform. This type of bed is said to be operating in the turbulent fluidized-bed regime, and is characterized by higher heat- and mass-transfer rates than in the bubbling bed. As the gas velocity is increased further, the

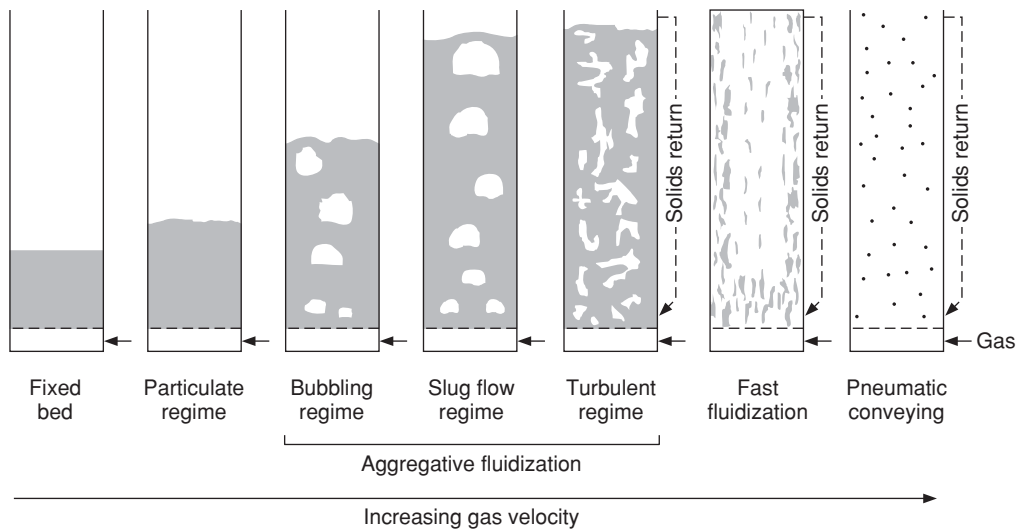


FIG. 17-4 Fluidization regimes. [Adapted from Grace, Can. J. Chem. Eng., 64, 353-363 (1986).]

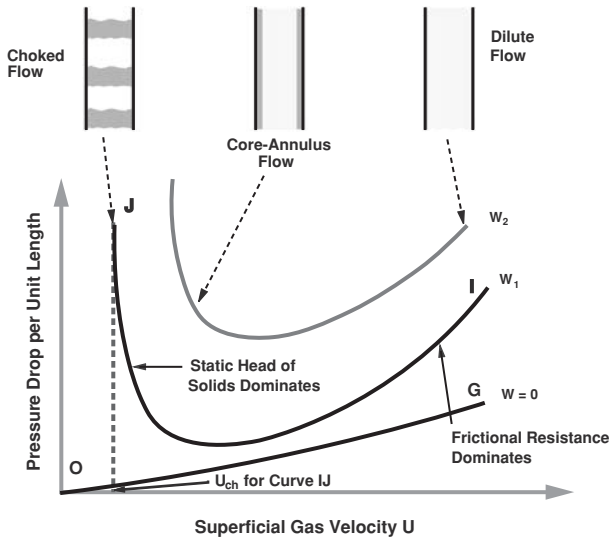


FIG. 17-5 Total transport regime. (Courtesy of PSRI, Chicago, Ill.)

bed transitions from the turbulent bed into the dilute-phase transport regime. This pneumatic conveying regime is composed of two basic regions: the lower-velocity fast fluidized-bed regime and the higher-velocity transport regime (often called the pneumatic conveying regime). The total transport regime is a very important regime, and is defined by the line *IJ* for the constant solids flow rate W_1 in Fig. 17-2. A more detailed drawing of this regime is shown in Fig. 17-5. In this figure, it can be seen that as the gas velocity is decreased from point *J*, the pressure drop per unit length begins to decrease. This occurs because the total pressure drop in the transport regime is composed of two types of terms—a term composed of frictional pressure drops (gas/wall friction, solid/wall friction, and gas/solids friction) and a term required to support the solids in the vertical line (the static head of solids term). At high gas velocities the frictional terms dominate; and as the gas velocity is decreased from point *J*, the frictional terms begin to decrease in magnitude. As this occurs, the concentration of solids in the line starts to increase. At some gas velocity, the static head of solids term and the frictional pressure drop term are equal (the minimum point on the curve). As the gas velocity is decreased below the minimum point, the static head of solids term begins to dominate as the concentration of solids in the line increases. This pressure drop increases until it is no longer possible for the gas to fully support the solids in the line. The gas velocity at which the solids cannot be supported at solids flow rate W_1 is known as the choking velocity for solids flow rate W_1 . Because beds in the turbulent and the transport regimes operate above the terminal velocity of some of or all the particles, a solids collection and return system is necessary to maintain a stable fluidized bed with these regimes.

Solids Concentration versus Height From the foregoing it is apparent that there are several regimes of fluidization. These are, in order of increasing gas velocity, particulate fluidization (Geldart group A), bubbling (aggregative), turbulent, fast, and transport. Each of these regimes has a characteristic solids concentration profile as shown in Fig. 17-6.

Equipment Types Fluidized-bed systems take many forms. Figure 17-7 shows some of the more prevalent concepts with approximate ranges of gas velocities.

Minimum Fluidizing Velocity U_{mf} , the minimum fluidizing velocity, is frequently used in fluid-bed calculations and in quantifying one of the particle properties. This parameter is best measured in small-scale equipment at ambient conditions. The correlation by Wen and Yu [A.I.Ch.E.J., 610–612 (1966)] given below can then be used to back calculate d_p . This gives a particle size that takes into account

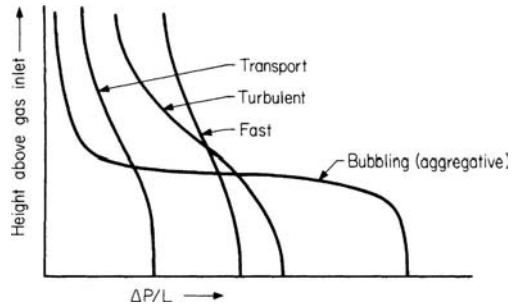


FIG. 17-6 Solids concentration versus height above distributor for regimes of fluidization.

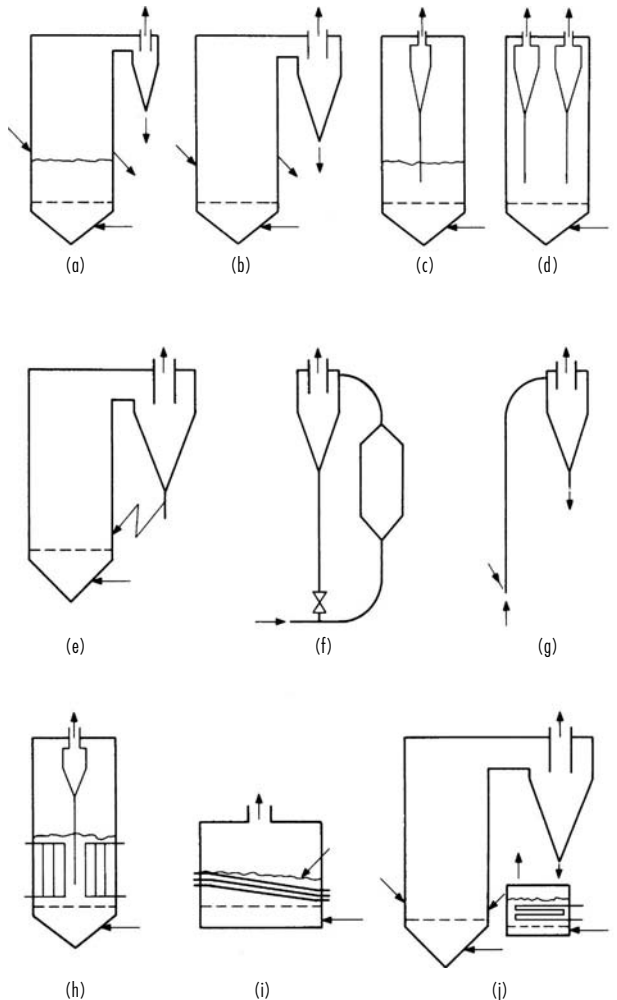


FIG. 17-7 Fluidized-bed systems. (a) Bubbling bed, external cyclone, $U < 20 \times U_{mf}$. (b) Turbulent bed, external cyclone, $20 \times U_{mf} < U < 200 \times U_{mf}$. (c) Bubbling bed, internal cyclones, $U < 20 \times U_{mf}$. (d) Turbulent bed, internal cyclones, $20 \times U_{mf} < U < 200 \times U_{mf}$. (e) Circulating (fast) bed, external cyclones, $U > 200 \times U_{mf}$. (f) Circulating bed, $U > 200 \times U_{mf}$. (g) Transport, $U > U_T$. (h) Bubbling or turbulent bed with internal heat transfer, $2 \times U_{mf} < U < 200 \times U_{mf}$. (i) Bubbling or turbulent bed with internal heat transfer, $2 \times U_{mf} < U < 100 \times U_{mf}$. (j) Circulating bed with external heat transfer, $U > 200 \times U_{mf}$.

17-6 GAS-SOLID OPERATIONS AND EQUIPMENT

effects of size distribution and particle shape, or sphericity. The correlation can then be used to estimate U_{mf} at process conditions. If U_{mf} cannot be determined experimentally, use the expression below directly.

$$Re_{mf} = (1135.7 + 0.0408Ar)^{0.5} - 33.7$$

where $Re_{mf} = d_{sv}\rho_f U_{mf}/\mu$
 $Ar = d_{sv}\rho_f(\rho_s - \rho_f)g/\mu^2$
 $d_{sv} = 1/\sum (x_i/d_{pi})$

The flow required to maintain a complete homogeneous bed of solids in which coarse or heavy particles will not segregate from the fluidized portion is very different from the minimum fluidizing velocity. See Nienow and Chiba, *Fluidization*, 2d ed., Wiley, 1985, pp. 357–382, for a discussion of segregation or mixing mechanism as well as the means of predicting this flow; also see Baeyens and Geldart, *Gas Fluidization Technology*, Wiley, 1986, 97–122.

Particulate Fluidization Fluid beds of Geldart group A powders that are operated at gas velocities above the minimum fluidizing velocity (U_{mf}) but below the minimum bubbling velocity (U_{mb}) are said to be particulate fluidized. As the gas velocity is increased above U_{mf} , the bed further expands. Decreasing $(\rho_s - \rho_f)$, d_p , and/or increasing μ_f increases the spread between U_{mf} and U_{mb} . Richardson and Zaki [*Trans. Inst. Chem. Eng.*, **32**, 35 (1954)] showed that $U/U_i = \epsilon^n$, where n is a function of system properties, ϵ = void fraction, U = superficial fluid velocity, and U_i = theoretical superficial velocity from the Richardson and Zaki plot when $\epsilon = 1$.

Vibrofluidization It is possible to fluidize a bed mechanically by imposing vibration to throw the particles upward cyclically. This enables the bed to operate with either no gas upward velocity or reduced gas flow. Entrainment can also be greatly reduced compared to unaided fluidization. The technique is used commercially in drying and other applications [Mujumdar and Erdesz, *Drying Tech.*, **6**, 255–274 (1988)], and chemical reaction applications are possible. See Sec. 12 for more on drying applications of vibrofluidization.

DESIGN OF FLUIDIZED-BED SYSTEMS

The use of the fluidization technique requires in almost all cases the employment of a fluidized-bed system rather than an isolated piece of equipment. Figure 17-8 illustrates the arrangement of components of a system.

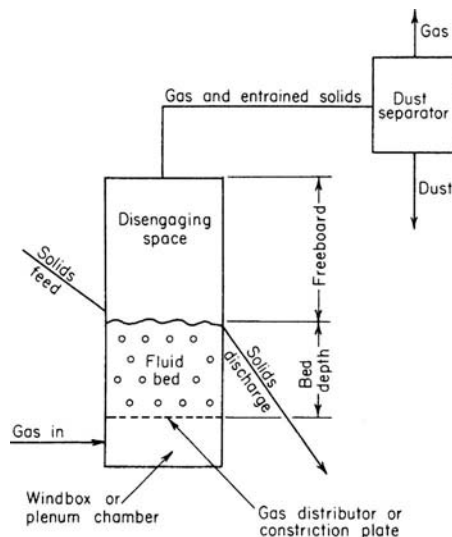


FIG. 17-8 Noncatalytic fluidized-bed system.

The major parts of a fluidized-bed system can be listed as follows:

1. Fluidization vessel
 - a. Fluidized-bed portion
 - b. Disengaging space or freeboard
 - c. Gas distributor
2. Solids feeder or flow control
3. Solids discharge
4. Dust separator for the exit gases
5. Instrumentation
6. Gas supply

Fluidization Vessel The most common shape is a vertical cylinder. Just as for a vessel designed for boiling a liquid, space must be provided for vertical expansion of the solids and for disengaging splashed and entrained material. The volume above the bed is called the disengaging space. The cross-sectional area is determined by the volumetric flow of gas and the allowable or required fluidizing velocity of the gas at operating conditions. In some cases the lowest permissible velocity of gas is used, and in others the greatest permissible velocity is used. The maximum flow is generally determined by the carry-over or entrainment of solids, and this is related to the dimensions of the disengaging space (cross-sectional area and height).

Bed Bed height is determined by a number of factors, either individually or collectively, such as:

1. Gas-contact time
2. L/D ratio required to provide staging
3. Space required for internal heat exchangers
4. Solids-retention time

Generally, bed heights are not less than 0.3 m (12 in) or more than 16 m (50 ft).

Although the reactor is usually a vertical cylinder, generally there is no real limitation on shape. The specific design features vary with operating conditions, available space, and use. The lack of moving parts lends toward simple, clean design.

Many fluidized-bed units operate at elevated temperatures. For this use, refractory-lined steel is the most economical design. The refractory serves two main purposes: (1) it insulates the metal shell from the elevated temperatures, and (2) it protects the metal shell from abrasion by the bed and particularly the splashing solids at the top of the bed resulting from bursting bubbles. Depending on specific conditions, several different refractory linings are used [Van Dyck, *Chem. Eng. Prog.*, 46–51 (December 1979)]. Generally, for the moderate temperatures encountered in catalytic cracking of petroleum, a reinforced-gunnite lining has been found to be satisfactory. This also permits the construction of larger units than would be permissible if self-supporting ceramic domes were to be used for the roof of the reactor.

When heavier refractories are required because of operating conditions, insulating brick is installed next to the shell and firebrick is installed to protect the insulating brick. Industrial experience in many fields of application has demonstrated that such a lining will successfully withstand the abrasive conditions in the bed for many years without replacement. Most serious refractory wear occurs with coarse particles at high gas velocities and is usually most pronounced near the operating level of the fluidized bed.

Gas leakage behind the refractory has plagued a number of units. Care should be taken in the design and installation of the refractory to reduce the possibility of the formation of "chimneys" in the refractories. A small flow of solids and gas can quickly erode large passages in soft insulating brick or even in dense refractory. Gas stops are frequently attached to the shell and project into the refractory lining. Care in design and installation of openings in shell and lining is also required.

In many cases, cold spots on the reactor shell will result in condensation and high corrosion rates. Sufficient insulation to maintain the shell and appurtenances above the dew point of the reaction gases is necessary. Hot spots can occur where refractory cracks allow heat to permeate to the shell. These can sometimes be repaired by pumping castable refractory into the hot area from the outside.

The violent motion of a fluidized bed requires an ample foundation and a sturdy supporting structure for the reactor. Even a relatively small differential movement of the reactor shell with the lining will materially shorten refractory life. The lining and shell must be designed as a unit. Structural steel should not be supported from a vessel that is subject to severe vibration.

Freeboard and Entrainment The freeboard or disengaging height is the distance between the top of the fluid bed and the gas-exit nozzle in bubbling- or turbulent-bed units. The distinction between bed and freeboard is difficult to determine in fast and transport units (see Fig. 17-6).

At least two actions can take place in the freeboard: classification of solids and reaction of solids and gases.

As a bubble reaches the upper surface of a fluidized bed, the bubble breaks through the thin upper envelope composed of solid particles entraining some of these particles. The crater-shaped void formed is rapidly filled by flowing solids. When these solids meet at the center of the void, solids are geysered upward. The downward pull of gravity and the upward pull of the drag force of the upward-flowing gas act on the particles. The larger and denser particles return to the top of the bed, and the finer and lighter particles are carried upward. The distance above the bed at which the entrainment becomes constant is the transport disengaging height, TDH. Cyclones and vessel gas outlets are usually located above TDH. Figure 17-9 graphically estimates TDH as a function of velocity and bed size.

The higher the concentration of an entrainable component in the bed, the greater its rate of entrainment. Finer particles have a greater rate of entrainment than coarse ones. These principles are embodied in the method of Geldart (*Gas Fluidization Tech.*, Wiley, 1986, pp. 123–153) via the equation, $E(i) = K^\circ(i)x(i)$, where $E(i)$ = entrainment rate for size i , $\text{kg/m}^2 \text{ s}$; $K^\circ(i)$ = entrainment rate constant for particle size i ; and $x(i)$ = weight fraction for particle size i . K° is a function of operating conditions given by $K^\circ(i)/(P_j u) = 23.7 \exp [-5.4 U_r(i)/U]$. The composition and the total entrainment are calculated by summing over the entrainable fractions. An alternative is to use the method of Zenz as reproduced by Pell (*Gas Fluidization*, Elsevier, 1990, pp. 69–72).

In batch classification, the removal of fines (particles less than any arbitrary size) can be correlated by treating as a second-order reaction $K = (F/\theta)[1/x(x - F)]$, where K = rate constant, F = fines removed in time θ , and x = original concentration of fines.

Gas Distributor The gas distributor (also often called the grid of a fluidized bed) has a considerable effect on proper operation of the

fluidized bed. For good fluidized-bed operation, it is absolutely necessary to have a properly designed gas distributor. Gas distributors can be used both when the gas is clean and when the gas contains solids. The primary purpose of the gas distributor is to cause uniform gas distribution across the entire bed cross-section. It should operate for years without plugging or breaking, minimize sifting of solids back into the gas inlet to the distributor, and minimize the attrition of the bed material. When the gas is clean, the gas distributor is often designed to prevent backflow of solids during normal operation, and in many cases it is designed to prevent backflow during shutdown. To provide good gas distribution, it is necessary to have a sufficient pressure drop across the grid. This pressure drop should be at least one-third the pressure drop across the fluidized bed for gas upflow distributors, and one-tenth to one-fifth the pressure drop across the fluidized bed for downflow gas distributors. If the pressure drop across the bed is not sufficient, gas maldistribution can result, with the bed being fluidized in one area and not fluidized in another. In units with shallow beds such as dryers or where gas distribution is less crucial, lower gas distributor pressure drops can be used.

When both solids and gas pass through the distributor, such as in some catalytic cracking units, a number of different gas distributor designs have been used. Because the inlet gas contains solids, it is much more erosive than gas alone, and care has to be taken to minimize the erosion of the grid openings as the solids flow through them. Generally, this is done by decreasing the inlet gas/solids velocity so that erosion of the grid openings is low. Some examples of grids that have been used with both solids and gases in the inlet gas are concentric rings in the same plane, with the annuli open (Fig. 17-10a); concentric rings in the form of a cone (Fig. 17-10b); grids of T bars or other structural shapes (Fig. 17-10c); flat metal perforated plates supported or reinforced with structural members (Fig. 17-10d); dished and perforated plates concave both upward and downward (Fig. 17-10e and f). Figure 17-10d, e, and f also uses no solids in the gas to the distributor. The curved distributors of Fig. 17-10d and e are often used because they minimize thermal expansion effects.

There are three basic types of clean inlet gas distributors: (1) a perforated plate distributor, (2) a bubble cap type of distributor, and (3) a sparger or pipe-grid type of gas distributor. The perforated plate distributor (Fig. 17-10d) is the simplest type of gas distributor and consists of a flat or curved plate containing a series of vertical holes. The gas flows upward into the bed from a chamber below the bed called a plenum. This type of distributor is easy and economical to construct. However, when the gas is shut off, the solids can sift downward into

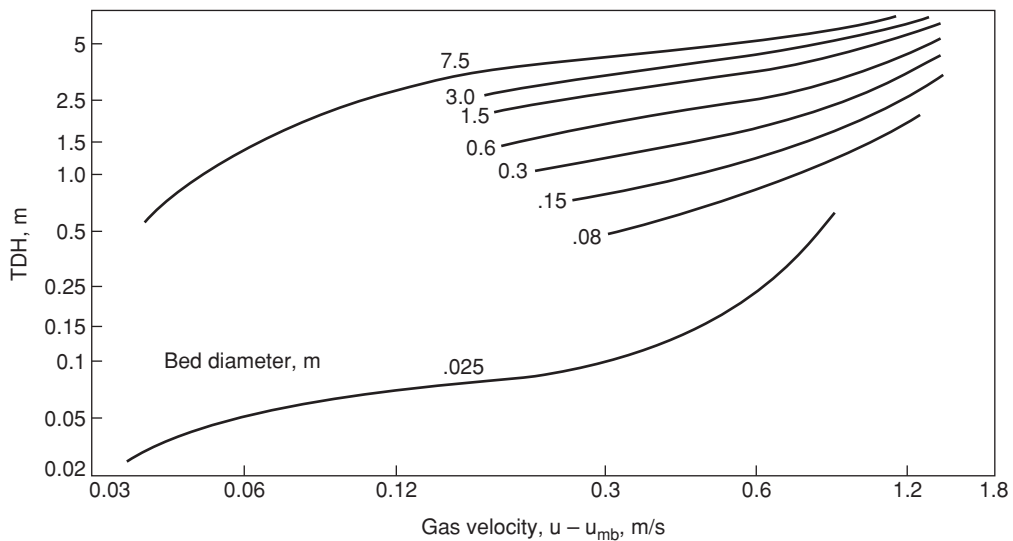


FIG. 17-9 Estimating transport disengaging height (TDH).

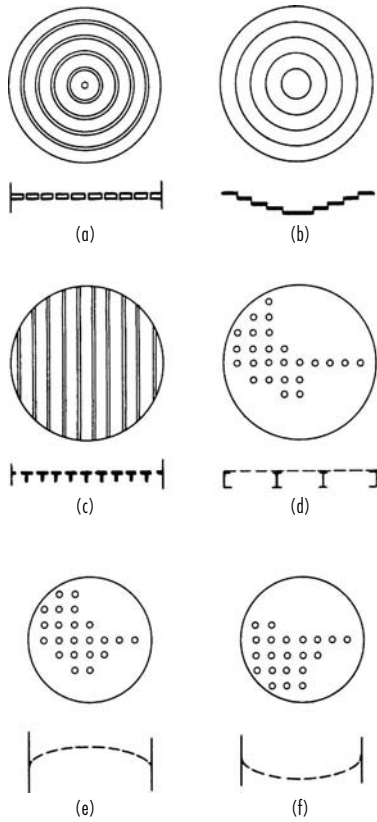


FIG. 17-10 Gas distributors for gases containing solids.

the plenum and may cause erosion of the holes when the bed is started up again. The bubble cap type of distributor is designed to prevent backflow of solids into the plenum chamber or inlet line of the gas distributor on start-up. The cap or tuyere type of distributor generally consists of a vertical pipe containing several small horizontal holes or holes angled downward from 30° to 45° from the horizontal (Fig. 17-11a and b). It is difficult for the solids to flow back through such a configuration when the fluidizing gas is shut off.

The pipe distributor (often called a sparger) differs from the other two distributor types because it consists of pipes with distribution holes in them that are inserted into the bed. This type of distributor will have solids below it that are not fluidized. If this is not acceptable for a process, then this type of distributor cannot be used. However, the pipe distributor has certain advantages. It does not require a large plenum, the holes in the pipe can be positioned at any angle, and it can be used in cases when multiple gas injections are required in a process. A common type of pipe distributor is the multiple-pipe (manifold sparger) grid shown in Fig. 17-12.

To generate a sufficient pressure drop for good gas distribution, a high velocity through the grid openings may be required. It is best to limit this velocity to less than 60 m/s to minimize attrition of the bed material. The maximum hole velocity allowable may be even lower for very soft materials that attrite easily. The pressure drop and the gas velocity through the hole in the gas distributor are related by the equation

$$\Delta P = \frac{u^2 \rho_f}{2c^2 g_c} \quad \text{for fps units}$$

$$\Delta P = \frac{u^2 \rho_f}{2c^2} \quad \text{for SI units}$$

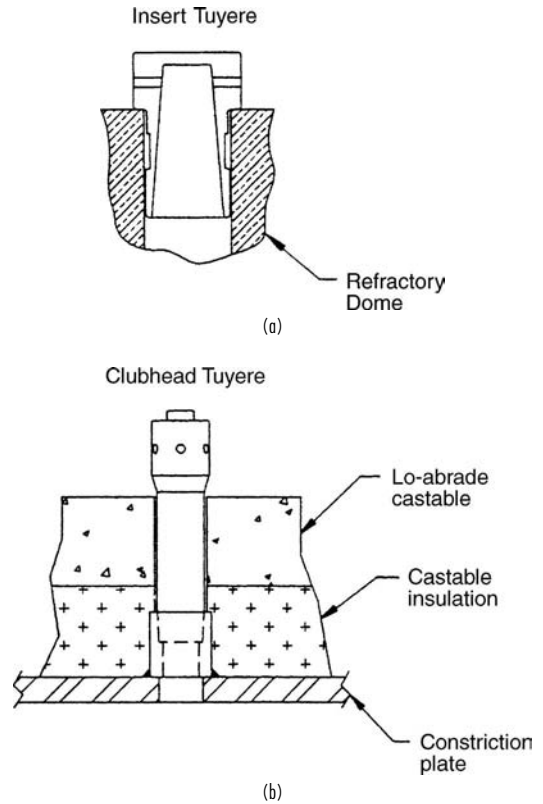


FIG. 17-11 Gas inlets designed to prevent backflow of solids. (a) Insert tuyere; (b) clubhead tuyere. (Dorr-Oliver, Inc.)

where u = velocity in hole at inlet conditions
 ρ_f = fluid density in hole at conditions in inlet to hole
 ΔP = pressure drop in consistent units, kPa or lb/ft²
 c = orifice constant, dimensionless (typically 0.8 for gas distributors)
 g_c = gravitational conversion constant, ft·lbm/(s²·lbf)

Due to the pressure drop requirements across the gas distributor for good gas distribution, the velocity through the grid hole may be higher than desired in order to minimize or limit particle attrition. Therefore, it is common industrial practice to place a length of pipe (called a

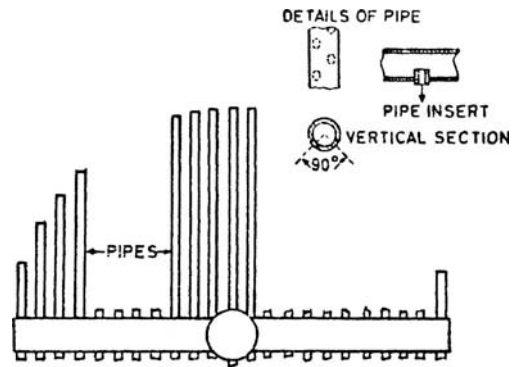


FIG. 17-12 Multiple-pipe gas distributor. [From Sternering, de Groot, and Kuypers, Soc. Chem. Ind. J. Symp. Fluidization Proc., 35-46, London (1963).]

shroud) over the gas distributor hole such that the diameter of the pipe is larger than the diameter of the distributor hole. This technique effectively allows a smaller hole to give the required pressure drop, but the larger hole diameter of the shroud reduces the exit gas velocity into the bed so that particle attrition at the grid will be minimized. This technique is applied to both plate and pipe spargers.

Experience has shown that a concave-downward (Fig. 17-10f) gas distributor is a better arrangement than a concave-upward (Fig. 17-10e) gas distributor, as it tends to increase the flow of gases in the outer portion of the bed. This counteracts the normal tendency of the gas to flow into the center of the bed after it exits the gas distributor. In addition, the concave-downward type of gas distributor tends to assist the general solids flow pattern in the bed, which is up in the center and down near the walls. The concave-upward gas distributor tends to have a slow-moving region at the bottom near the wall. If solids are large (or if they are slightly cohesive), they can build up in this region.

Structurally, distributors must withstand the differential pressure across the restriction during normal and abnormal flow. In addition, during a shutdown, all or a portion of the bed will be supported by the distributor until sufficient backflow of the solids has occurred into the plenum to reduce the weight of solids above the distributor and to support some of this remaining weight by transmitting the force to the walls and bottom of the reactor. During start-up, a considerable upward thrust can be exerted against the distributor as the settled solids under the distributor are carried up into the normal reactor bed.

When the feed gas is devoid of or contains only small quantities of fine solids, more sophisticated designs of gas distributors can be used to effect economies in initial cost and maintenance. This is most pronounced when the inlet gas is cold and noncorrosive. When this is the case, the plenum chamber gas distributor and distributor supports can be fabricated of mild steel by using normal temperature design factors. The first commercial fluidized-bed ore roaster [Mathews, *Trans. Can. Inst. Min. Metall.* **L11:97** (1949)], supplied by the Dorr Co. (now Dorr-Oliver Inc.) in 1947 to Cochenour-Willans, Red Lake, Ontario, was designed with a mild-steel constriction plate covered with castable refractory to insulate the plate from the calcine and to provide cones in which refractory balls were placed to act as ball checks. The balls eroded unevenly, and the castable cracked. However, when the unit was shut down by closing the air control valve, the runback of solids was negligible because of bridging. If, however, the unit were shut down by deenergizing the centrifugal blower motor, the higher pressure in the reactor would relieve through the blower and fluidizing gas plus solids would run back through the constriction plate. Figure 17-11 illustrates two designs of gas inlets which have been successfully used to prevent flowback of solids. For best results, irrespective of the design, the gas flow should be stopped and the pressure relieved from the bottom upward through the bed. Some units have been built and successfully operated with simple slot-type distributors made of heat-resistant steel. This requires a heat-resistant plenum chamber but eliminates the frequently encountered problem of corrosion caused by condensation of acids and water vapor on the cold metal of the distributor. When the inlet gas is hot, such as in dryers or in the upper distributors of multibed units, ceramic arches or heat-resistant metal grates are generally used. Self-supporting ceramic domes have been in successful use for many years as gas distributors when temperatures range up to 1100°C. Some of these domes are fitted with alloy-steel orifices to regulate air distribution. However, the ceramic arch presents the same problem as the dished head positioned concave upward. Either the holes in the center must be smaller, so that the sum of the pressure drops through the distributor plus the bed is constant across the entire cross section, or the top of the arch must be flattened so that the bed depths in the center and outside are equal. This is especially important when shallow beds are used.

It is important to consider thermal effects in the design of the grid-to-shell seal. Bypassing the grid at the seal point is a common problem caused by situations such as uneven expansion of metal and ceramic parts, a cold plenum and hot solids in contact with the grid plate at the same time, and start-up and shutdown scenarios. When the atmosphere in the bed is sufficiently benign, a sparger-type

distributor may be used (Fig. 17-12). In some cases, it is impractical to use a plenum chamber under the constriction plate. This condition arises when a flammable or explosive mixture of gases is being introduced to the reactor. One solution is to pipe the gases to a multitude of individual gas inlets in the floor of the reactor. In this way it may be possible to maintain the gas velocities in the pipes above the flame velocity or to reduce the volume of gas in each pipe to the point at which an explosion can be safely contained. Another solution is to provide separate inlets for the different gases and to rely on the rapid axial mixing of the fluidized bed. The inlets should be fairly close to one another, as lateral gas mixing in fluidized beds is poor.

Much attention has been paid to the effect of gas distribution on bubble growth in the bed and the effect of this on catalyst utilization, space-time yield, etc., in catalytic systems. It would appear that the best gas distributor would be a porous membrane because of its even distribution. However, this type of distributor is seldom practical for commercial units because of structural limitations and the fact that it requires absolutely clean gas. Practically, the limitations on hole spacing in a gas distributor are dependent on the particle size of the solids, materials of construction, and type of distributor. If easily worked metals are used, then punching, drilling, and welding are not expensive operations and permit the use of large numbers of holes. The use of tuyeres or bubble caps permits horizontal distribution of the gas so that a smaller number of gas inlet ports can still achieve good gas distribution. If a ceramic arch is used, generally only one hole per brick is permissible and brick dimensions must be reasonable.

Scale-up

Bubbling or Turbulent Beds Scale-up of noncatalytic fluidized beds when the reaction is fast, as in roasting or calcination, is straightforward and is usually carried out on an area basis. Small-scale tests are made to determine physical limitations such as sintering, agglomeration, solids-holdup time required, etc. Slower ($k < 1/s$) catalytic or more complex reactions in which several gas interchanges are required are usually scaled up in several steps, from laboratory to commercial size. The hydrodynamics of gas-solids flow and contacting is quite different in small-diameter high- L/D fluid beds as compared with large-diameter moderate- L/D beds. In small-diameter beds, bubbles tend to be small and cannot grow larger than the vessel diameter. In larger, deeper units, bubbles can grow very large. The large bubbles have less surface for mass transfer to the solids than the same volume of small bubbles. The large bubbles also rise through the bed more quickly.

The size of a bubble as a function of height was given by Darton et al. [*Trans. Inst. Chem. Eng.*, **55**, 274-280 (1977)] as

$$d_b = \frac{0.54(u - u_{mb})^{0.4}(h + 4\sqrt{A_r/N_o})^{0.8}}{g^{0.2}}$$

where d_b = bubble diameter, m
 h = height above the grid, m
 A_r/N_o = grid area per hole

Bubble growth in fluidized beds will be limited by the diameter of the containing vessel and bubble hydrodynamic stability. Bubbles in group B systems can grow to over 1 m in diameter if the gas velocity and the bed height are both high enough. Bubbles in group A materials with high percentage of fines (material less than 44 μm in size) may reach a maximum stable bubble size in a range of about 5 to 15 cm. Furthermore, solids and gas backmixing are much less in high- L/D beds (whether they are slugging or bubbling) compared with low- L/D beds. Thus, the conversion or yield in large, unstaged reactors is sometimes considerably lower than in small high- L/D units. To overcome some of the problems of scale-up, staged units are used (Fig. 17-13). It is generally concluded that an unstaged 1-m (40-in-) diameter unit will achieve about the same conversion as a large industrial unit. The validity of this conclusion is dependent on many variables, including bed depth, particle size, size distribution, temperature, and system pressure. A brief history of fluidization, fluidized-bed scale-up, and modeling will illustrate the problems.

17-10 GAS-SOLID OPERATIONS AND EQUIPMENT

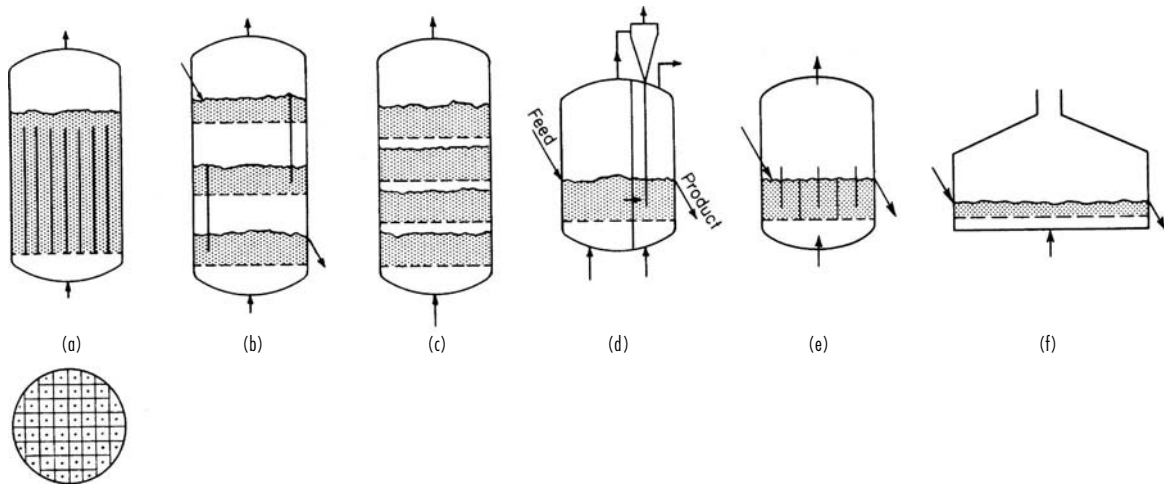


FIG. 17-13 Methods of providing staging in fluidized beds.

Fluidized beds were used in Europe in the 1920s to gasify coal. Scale-up problems either were insignificant or were not publicized. During World War II, catalytic cracking of oil to produce gasoline was successfully commercialized by scaling up from pilot-plant size (a few centimeters in diameter) to commercial size (several meters in diameter). It is fortunate that the kinetics of the cracking reactions are fast, that the ratio of crude oil to catalyst is determined by thermal balance and the required catalyst circulation rates, and that the crude feed point was in the plug-flow riser. The first experience of problems with scale-up was associated with the production of gasoline from natural gas by using the Fischer-Tropsch process. Some 0.10-m- (4-in-), 0.20-m- (8-in-), and 0.30-m- (12-in-) diameter pilot-plant results were scaled to a 7-m-diameter commercial unit, where the yield was only about 50 percent of that achieved in the pilot units. The Fischer-Tropsch synthesis is a relatively slow reaction; therefore, gas-solid contacting is very important. Since this unfortunate experience or perhaps because of it, much effort has been given to the scale-up of fluidized beds. Many models have been developed; these basically are of two types, the two-phase model [May, *Chem. Eng. Prog.*, **55**, 12, 5, 49–55 (1959); and Van Deemter, *Chem. Eng. Sci.*, **13**, 143–154 (1961)] and the bubble model (Kunii and Levenspiel, *Fluidization Engineering*, Wiley, New York, 1969). The two-phase model according to May and Van Deemter is shown in Fig. 17-14. In these models all or most of the gas passes through the bed in plug flow in the bubbles which do not contain solids (catalyst). The solids form a dense

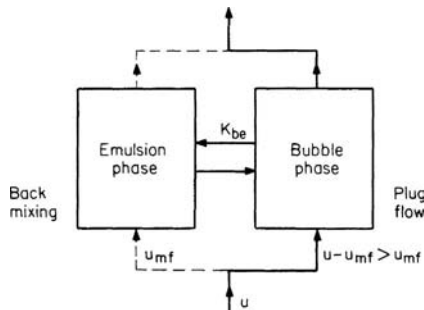


FIG. 17-14 Two-phase model according to May [*Chem. Eng. Prog.*, **55**, 12, 5, 49–55 (1959)] and Van Deemter [*Chem. Eng. Sci.*, **13**, 143–154 (1961)]. U = superficial velocity, U_{mf} = minimum fluidizing velocity, E = axial dispersion coefficient, and K_{bc} = mass-transfer coefficient.

suspension-emulsion phase in which gas and solids mix according to an axial dispersion coefficient (E). Cross flow between the two phases is predicted by a mass-transfer coefficient.

Conversion of a gaseous reactant can be given by $C/C_0 = \exp[-Na \times Nr/(Na + Nr)]$ where C = the exit concentration, C_0 = the inlet concentration, Na = diffusional driving force and Nr = reaction driving force. Conversion is determined by both reaction and diffusional terms. It is possible for reaction to dominate in a lab unit with small bubbles and for diffusion to dominate in a plant size unit. It is this change of limiting regime that makes scale-up so difficult. Refinements of the basic model and predictions of mass-transfer and axial-dispersion coefficients are the subject of many papers [Van Deemter, *Proc. Symp. Fluidization*, Eindhoven (1967); de Groot, *ibid.*; Van Swaaij and Zuidweg, *Proc. 5th Eur. Symp. React. Eng., Amsterdam*, B9–25 (1972); DeVries, Van Swaaij, Mantovani, and Heijkoop, *ibid.*, B9–59 (1972); Werther, *Ger. Chem. Eng.*, **1**, 243–251 (1978); and Pell, *Gas Fluidization*, Elsevier, 75–81 (1990)].

The bubble model (Kunii and Levenspiel, *Fluidization Engineering*, Wiley, New York, 1969; Fig. 17-15) assumes constant-sized bubbles (effective bubble size d_b) rising through the suspension phase. Gas is transferred from the bubble void to the cloud and wake at mass-transfer coefficient K_{bc} and from the mantle and wake to the emulsion

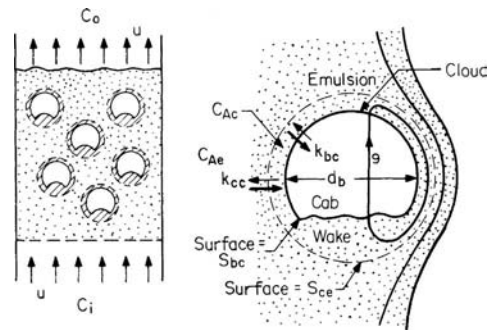


FIG. 17-15 Bubbling-bed model of Kunii and Levenspiel. d_b = effective bubble diameter, C_{Ab} = concentration of A in bubble, C_{Ac} = concentration of A in cloud, C_{Ae} = concentration of A in emulsion, q = volumetric gas flow into or out of bubble, k_{bc} = mass-transfer coefficient between bubble and cloud, and k_{cc} = mass-transfer coefficient between cloud and emulsion. (From Kunii and Levenspiel, *Fluidization Engineering*, Wiley, New York, 1969, and Krieger, Malabar, Fla., 1977.)

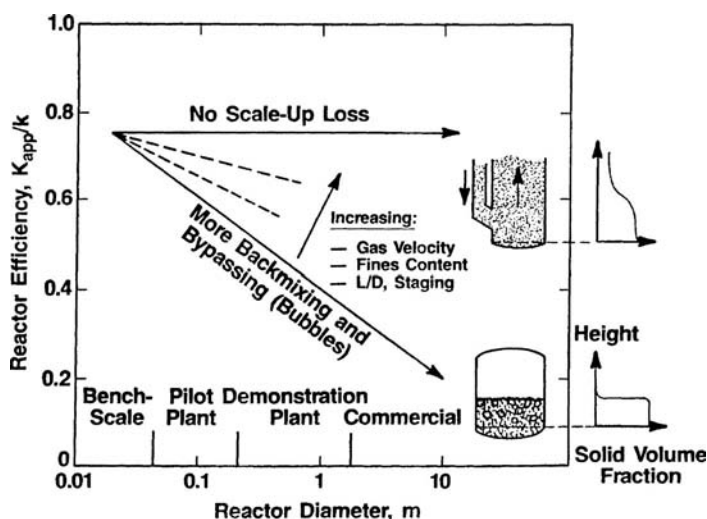


FIG. 17-16 Reducing scale-up loss. (From Krambeck, Avidan, Lee, and Lo, *A.I.Ch.E.J.*, 1727-1734, 1987.)

phase at mass-transfer coefficient K_g . Experimental results have been fitted to theory by means of adjusting the effective bubble size. As mentioned previously, bubble size changes from the bottom to the top of the bed, and thus this model is not realistic though of considerable use in evaluating reactor performance. Several bubble models using bubbles of increasing size from the distributor to the top of the bed and gas interchange between the bubbles and the emulsion phase according to Kunii and Levenspiel have been proposed [Kato and Wen, *Chem. Eng. Sci.*, **24**, 1351-1369 (1969); and Fryer and Potter, in Keairns (ed.), *Fluidization Technology*, vol. I, Hemisphere, Washington, 1975, pp. 171-178].

There are several methods available to reduce scale-up loss. These are summarized in Fig. 17-16. The efficiency of a fluid bed reactor usually decreases as the size of the reactor increases. This can be minimized by the use of high velocity, fine solids, staging methods, and a high L/D . High velocity maintains the reactor in the turbulent mode, where bubble breakup is frequent and backmixing is infrequent. A fine catalyst leads to smaller maximum bubble sizes by promoting instability of large bubbles. Maintaining high L/D minimizes backmixing, as does the use of baffles in the reactor. By these techniques, Mobil was able to scale up its methanol to gasoline technology with little difficulty [Krambeck, Avidan, Lee, and Lo, *A.I.Ch.E.J.*, 1727-1734 (1987)].

Another way to examine scale-up of hydrodynamics is to build a cold or hot scale model of the commercial design. Validated scaling criteria have been developed and are particularly effective for group *B* and *D* materials [Glicksman, Hyre, and Woloshun, *Powder Tech.*, 177-199 (1993)].

Circulating or Fast Fluidized Beds The circulating or fast fluidized bed is actually a misnomer in that it is not an extension of the turbulent bed, but is actually a part of the transport regime, as discussed above. However, the fast fluidized bed operates in that part of the transport regime that is dominated by the static head of solids pressure drop term (the part of the regime where the solids concentration is the highest). The solids may constitute up to 10 percent of the volume of the system in this regime. There are no bubbles, mass-transfer rates are high, and there is little gas backmixing in the system. The high velocity in the system results in a high gas throughput which minimizes reactor cost. Because there are no bubbles, scale-up is also less of a problem than with bubbling beds.

Many circulating systems are characterized by an external cyclone return system that usually has as large a footprint as the reactor itself. The axial solids density profile is relatively flat, as indicated in Fig. 17-6. There is a parabolic radial solids density profile that is termed core

annular flow. In the center of the reactor, the gas velocity and the solids velocity may be double the average. The solids in the center of the column (often termed a riser) are in dilute flow, traveling at their expected slip velocity $U_g - U_s$. Near the wall in the annulus, the solids are close to their fluidized-bed density. The solids at the wall can flow either upward or downward. Whether they do so is determined primarily by the velocity used in the system. In circulating fluidized-bed combustor systems, the gas velocity in the rectangular riser is generally in the range of 4 to 6 m/s, and the solids flow down at the wall. In fluid catalytic cracking, the velocity in the riser is typically in the range of 12 to 20 m/s, and the solids flow upward at the wall. Engineering methods for evaluating the hydrodynamics of the circulating bed are given by Kunii and Levenspiel (*Fluidization Engineering*, 2d ed., Butterworth, 1991, pp. 195-209), Werther (*Circulating Fluid Bed Technology IV*, 1994), and Avidan, Grace, and Knowlton (eds.), (*Circulating Fluidized Beds*, Blackie Academic, New York, 1997).

Pneumatic Conveying Pneumatic conveying systems can generally be scaled up on the principles of dilute-phase transport. Mass and heat transfer can be predicted on both the slip velocity during acceleration and the slip velocity at full acceleration. The slip velocity increases as the solids concentration is increased.

Heat Transfer Heat-exchange surfaces have been used to provide the means of removing or adding heat to fluidized beds. Usually, these surfaces are provided in the form of vertical or horizontal tubes manifolded at the tops and bottom or in a trombone shape manifolded exterior to the vessel. Horizontal tubes are extremely common as heat-transfer tubes. In any such installation, adequate provision must be made for abrasion of the exchanger surface by the bed. The prediction of the heat-transfer coefficient for fluidized beds is covered in Secs. 5 and 11.

Normally, the heat-transfer rate is between 5 and 25 times that for the gas alone. Bed-to-surface-heat transfer coefficients vary according to the type of solids in the bed. Group *A* solids have bed-to-surface heat-transfer coefficients of approximately $300 \text{ J}/(\text{m}^2 \cdot \text{s} \cdot \text{K})$ [$150 \text{ Btu}/(\text{h} \cdot \text{ft}^2 \cdot ^\circ\text{F})$]. Group *B* solids have bed-to-surface heat-transfer coefficients of approximately $100 \text{ J}/(\text{m}^2 \cdot \text{s} \cdot \text{K})$ [$50 \text{ Btu}/(\text{h} \cdot \text{ft}^2 \cdot ^\circ\text{F})$], while group *D* solids have bed-to-surface heat-transfer coefficients of $60 \text{ J}/(\text{m}^2 \cdot \text{s} \cdot \text{K})$ [$30 \text{ Btu}/(\text{h} \cdot \text{ft}^2 \cdot ^\circ\text{F})$].

The large area of the solids per cubic foot of bed, $5000 \text{ m}^2/\text{m}^3$ ($15,000 \text{ ft}^2/\text{ft}^3$) for 60- μm particles of about $600 \text{ kg}/\text{m}^3$ ($40 \text{ lb}/\text{ft}^3$) bulk density, results in the rapid approach of gas and solids temperatures near the bottom of the bed. Equalization of gas and solids temperatures generally occurs within 2 to 10 cm (1 to 4 in) of the top of the distributor.

Bed thermal conductivities in the vertical direction have been measured in the laboratory in the range of 40 to 60 kJ/(m²·s·K) [20,000 to 30,000 Btu/(h·ft²·°F·ft)]. Horizontal conductivities for 3-mm (0.12-in) particles in the range of 2 kJ/(m²·s·K) [1000 Btu/(h·ft²·°F·ft)] have been measured in large-scale experiments. Except for extreme *L/D* ratios, the temperature in the fluidized bed is uniform—with the temperature at any point in the bed generally being within 5 K (10°F) of any other point.

Temperature Control Because of the rapid equalization of temperatures in fluidized beds, temperature control can be accomplished in a number of ways.

1. *Adiabatic.* Control gas flow and/or solids feed rate so that the heat of reaction is removed as sensible heat in off gases and solids or heat supplied by gases or solids.
2. *Solids circulation.* Remove or add heat by circulating solids.
3. *Gas circulation.* Recycle gas through heat exchangers to cool or heat.
4. *Liquid injection.* Add volatile liquid so that the latent heat of vaporization equals excess energy.
5. *Cooling or heating surfaces in bed.*

Solids Mixing Solids are mixed in fluidized beds by means of solids entrained in the lower portion of bubbles, and the shedding of these solids from the wake of the bubble (Rowe and Patridge, "Particle Movement Caused by Bubbles in a Fluidized Bed," Third Congress of European Federation of Chemical Engineering, London, 1962). Thus, no mixing will occur at incipient fluidization, and mixing increases as the gas rate is increased. Naturally, particles brought to the top of the bed must displace particles toward the bottom of the bed. Generally, solids upflow is upward in the center of the bed and downward at the wall.

At high ratios of fluidizing velocity to minimum fluidizing velocity, tremendous solids circulation from top to bottom of the bed assures rapid mixing of the solids. For all practical purposes, beds with *L/D* ratios of from 4 to 0.1 can be considered to be completely mixed continuous-reaction vessels insofar as the solids are concerned.

Batch mixing using fluidization has been successfully employed in many industries. In this case there is practically no limitation to vessel dimensions.

All the foregoing pertains to solids of approximately the same physical characteristics. There is evidence that solids of widely different characteristics will classify one from the other at certain gas flow rates [Geldart, Baeyens, Pope, and van de Wijer, *Powder Technol.*, **30**(2), 195 (1981)]. Two fluidized beds, one on top of the other, may be formed, or a lower static bed with a fluidized bed above may result. The latter frequently occurs when agglomeration takes place because of either fusion in the bed or poor dispersion of sticky feed solids. Increased gas flows sometimes overcome the problem; however, improved feeding techniques or a change in operating conditions may be required. Another solution is to remove agglomerates either continuously or periodically from the bottom of the bed.

Gas Mixing The mixing of gases as they pass vertically up through the bed has never been considered a problem. However, horizontal mixing is very poor and requires effective distributors if two gases are to be mixed in the fluidized bed.

In bubbling beds operated at velocities of less than about 5 to 11 times U_{mf} the gases will flow upward in both the emulsion and the bubble phases. At velocities greater than about 5 to 11 times U_{mf} the downward velocity of the emulsion phase is sufficient to carry the contained gas downward. The back mixing of gases increases as U/U_{mf} is increased until the circulating or fast regime is reached where the back mixing decreases as the velocity is further increased.

Size Enlargement Under proper conditions, solid particles can be caused to increase in size in the bed. This can be advantageous or disadvantageous. Particle growth is usually associated with the melting or softening of some portion of the bed material (i.e., addition of soda ash to calcium carbonate feed in lime reburning, tars in fluidized-bed coking, or lead or zinc roasting causes agglomeration of dry particles in much the same way as binders act in rotary pelletizers). The motion of the particles, one against the other, in the bed results in spherical pellets. If the size of these particles is not controlled, rapid agglomeration and segregation of the large particles from the bed will

occur. Control of agglomeration can be achieved by crushing a portion of the bed product and recycling it to form nuclei for new growth. Often, liquids or slurries are fed via a spray nozzle into the bed to cause particles to grow. In drying solutions or slurries of solutions, the location of the feed injection nozzle (spray nozzle) has a great effect on the size of particle that is formed in the bed. Also of importance are the operating temperature, relative humidity of the off-gas, and gas velocity in the bed. Particle growth can occur as agglomeration (two or more particles sticking together) or by the particle growing in layers, often called *onion skinning*.

Size Reduction *Attrition* is the term describing particle reduction in the fluidized bed. Three major attrition mechanisms occur in the fluidized bed: particle fragmentation, particle fracture, and particle thermal decrepitation. Particle fragmentation occurs when the protruding edges on individual particles are broken off in the bed. These particle fragments are very small—usually on the order of 2 to 10 μm . Particle fracture occurs when particle interaction is severe enough to cause the particles to break up into large individual pieces.

Because of the random motion of the solids, some abrasion of the surface occurs in the bed. However, this abrasion is very small relative to the particle breakup caused by the high-velocity jets at the distributor. Typically, particle abrasion (fragmentation) will amount to about 0.25 to 1 percent of the solids per day. In the area of high gas velocities at the distributor, greater rates of attrition will occur because of fracture of the particles by impact. As mentioned above, particle fracture of the grid is reduced by adding shrouds to the gas distributor.

Generally, particle attrition is unwanted. However, at times controlled attrition is desirable. For example, in coking units where agglomeration due to wet particles is frequent, jets are used to attrit particles to control particle size [Dunlop, Griffin, and Moser, *J. Chem. Eng. Prog.* **54**:39–43 (1958)].

Thermal decrepitation occurs frequently when crystals are rearranged because of transition from one form to another, or when new compounds are formed (i.e., calcination of limestone). Sometimes the stresses on particles in cases such as this are sufficient to reduce the particle to the basic crystal size. All these mechanisms will cause completion of fractures that were started before the introduction of the solids into the fluidized bed.

Standpipes, Solids Feeders, and Solids Flow Control In a fluid catalytic cracking (FCC) unit, hot catalyst is added to aspirated crude oil feed in a riser to crack the feed oil into gasoline and other light and heavy hydrocarbons. The catalyst activity is reduced by this contact as carbon is deposited on the catalyst. The catalyst is then passed through a steam stripper to remove the gas product in the interstices of the catalyst and is transported to a regenerator. The carbon on the catalyst is burned off in the fluidized-bed regenerator, and then the regenerated, hot catalyst is transported back to the bottom of the riser to crack the feed oil. Large FCC units have to control solids flow rates from 10 to 80 tons/min. The units require makeup catalyst to be added to replace solids losses due to attrition, etc. The amount of catalyst makeup is small, and need not be continuous. Therefore, the makeup catalyst is fed into the commercial unit from pressurized hoppers into one of the conveying lines. However, the primary solids flow control problem in this FCC unit is to maintain the correct temperature in the riser reactor by controlling the flow of hot regenerated catalyst around the test unit. This is done by using large, 1.2-m (4-ft)-diameter slide valves (also known as knife-gate valves) located in standpipes to control the flow rates of catalyst.

In the FCC process, the solids are transferred out of the fluidized-bed regenerator into the bottom of the riser via a standpipe. The purpose of a standpipe is to transfer solids from a low-pressure region to a high-pressure region. The point of removal of the solids from the regenerator bed is at a lower pressure than the point of feed introduction into the riser. Therefore, the transfer of solids from the regenerator bed to the bottom of the riser is accomplished with a standpipe. The standpipes in FCC units can be as large as 1.5 m (5 ft) in diameter and as long as about 30 m (100 ft). They can be either vertical or angled (generally approximately 60° from the horizontal). The pressure is higher at the bottom of a standpipe due to the relative flow of gas counter to the solids flow. The gas in the standpipe may be flowing either downward relative to the pipe wall but more slowly than the

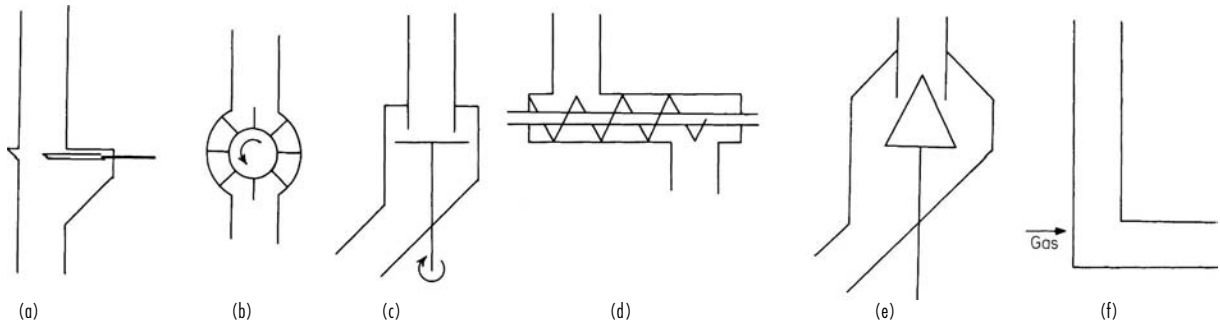


FIG. 17-17 Solids flow control devices. (a) Slide valve. (b) Rotary valve. (c) Table feeder. (d) Screw feeder. (e) Cone valve. (f) L Valve.

solids (the most common occurrence) or upward. The standpipe may be fluidized, or the solids may be in moving packed bed flow.

Fluidized standpipes can accommodate a much higher solids flow rate than moving packed bed standpipes because the friction of the solids flow on the wall of the standpipe is much less in fluidized standpipes. In longer standpipes, the pressure gain over the length of the standpipe is so great that it compresses the gas relative to the conditions at the standpipe inlet. This gas "shrinkage" can cause the gas in and around the particles to compress, which can result in defluidization of the solids in the standpipe unless aeration gas is added to the standpipe to replace the gas volume lost via compression. If the solids defluidize, the flow regime will revert to a moving packed bed with a lower pressure gain across the standpipe. In standpipes operating with group B solids, aeration is added to replace the compressed volume approximately every 1.5 m along the standpipe. In standpipes operating with group A solids, it has been found that aeration is only required at the bottom of the standpipe. Typically, the pressure drop across the solids control valve in the standpipe should be designed for a minimum of approximately 2 psi (14 kPa) for good control. A maximum of no more than 10 to 12 psi (70 to 84 kPa) is recommended to prevent excessive erosion of the valve at high pressure drops [Zenz, *Powder Technol.* pp. 105-113 (1986)].

Several designs of valves for solids flow control are used. These should be chosen with care to suit the specific conditions. Usually, block valves are used in conjunction with the control valves. Figure 17-17 shows schematically some of the devices used for solids flow control. Not shown in Fig. 17-17 is the flow-control arrangement used in the Exxon Research & Engineering Co. model IV catalytic-cracking units. This device consists of a U bend. A variable portion of regenerating air is injected into the riser leg. Changes in air-injection rate change the fluid density in the riser and thereby achieve control of the solids flow rate. Catalyst circulation rates of 1200 kg/s (70 tons/min) have been reported.

When the solid is one of the reactants, such as in ore roasting, the flow must be continuous and precise in order to maintain constant conditions in the reactor. Feeding of free-flowing granular solids into a fluidized bed is not difficult. Standard commercially available solids-weighing and -conveying equipment can be used to control the rate and deliver the solids to the feeder. Screw conveyors, dip pipes, seal legs, and injectors are used to introduce the solids into the reactor proper (Fig. 17-17). Difficulties arise and special techniques must be used when the solids are not free-flowing, such as is the case with most filter cakes. One solution to this problem was developed at Cochenour-Willans. After much difficulty in attempting to feed a wet and sometimes frozen filter cake into the reactor by means of a screw feeder, experimental feeding of a water slurry of flotation concentrates was attempted. This trial was successful, and this method has been used in almost all cases in which the heat balance, particle size of solids, and other considerations have permitted. Gilfillan et al. (*J. Chem. Metall. Min. Soc. S. Afr.*, May 1954) and Soloman and Beal (*Uranium in South Africa, 1946-56*) present complete details on the use of this system for feeding.

When slurry feeding is impractical, recycling of solids product to mix with the feed, both to dry and to achieve a better-handling

material, has been used successfully. Also, the use of a rotary table feeder mounted on top of the reactor, discharging through a mechanical disintegrator, has been successful. The wet solids generally must be broken up into discrete particles of very fine agglomerates either by mechanical action before entering the bed or by rapidly vaporizing water. If lumps of dry or semidry solids are fed, the agglomerates do not break up but tend to fuse together. As the size of the agglomerate is many times the size of the largest individual particle, these agglomerates will segregate out of the bed, and in time the whole of the fluidized bed may be replaced with a static bed of agglomerates.

Solids Discharge The type of discharge mechanism utilized is dependent upon the necessity of sealing the atmosphere inside the fluidized-bed reactor and the subsequent treatment of the solids. The simplest solids discharge is an overflow weir. This can be used only when the escape of fluidizing gas does not present any hazards due to nature or dust content or when the leakage of gas into the fluidized-bed chamber from the atmosphere into which the bed is discharged is permitted. Solids will overflow from a fluidized bed through a port even though the pressure above the bed is maintained at a slightly lower pressure than the exterior pressure. When it is necessary to restrict the flow of gas through the opening, a simple flap valve is frequently used. Overflow to combination seal and quench tanks (Fig. 17-18) is used when it is permissible to wet the solids and when disposal or subsequent treatment of the solids in slurry form is desirable. The FluoSeal is a simple and effective way of sealing and purging gas from the solids when an overflow-type discharge is used (Fig. 17-19).

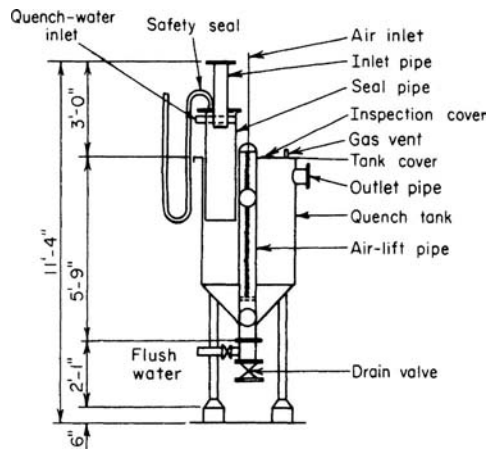


FIG. 17-18 Quench tank for overflow or cyclone solids discharge. [Gilfillan et al., "The FluoSolids Reactor as a Source of Sulphur Dioxide," *J. Chem. Metall. Min. Soc. S. Afr.* (May 1954).]

17-14 GAS-SOLID OPERATIONS AND EQUIPMENT

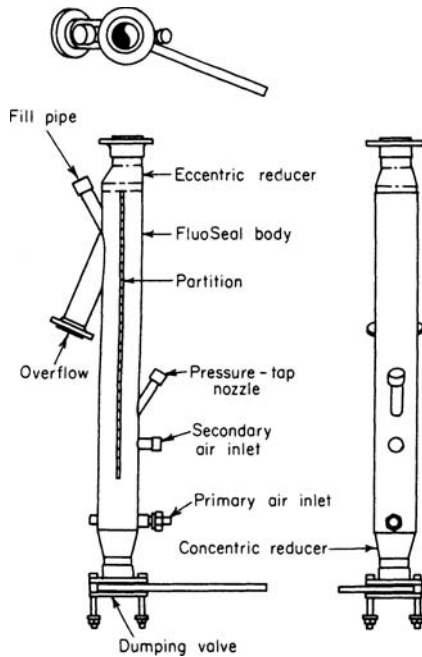


FIG. 17-19 Dorcco FluoSeal, type UA. (Dorr-Oliver Inc.)

Either trickle (flapper) or star (rotary) valves are effective sealing devices for solids discharge. Each functions with a head of solids above it. Bottom of the bed discharge is also acceptable via a slide valve with a head of solids.

Seal legs are frequently used in conjunction with solids-flow-control valves to equalize pressures and to strip trapped or adsorbed gases from the solids. The operation of a seal leg is shown schematically in Fig. 17-20. The solids settle by gravity from the fluidized bed into the seal leg or standpipe. Seal and/or stripping gas is introduced near the bottom of the leg. This gas flows both upward and downward. Pressures indicated in the illustration have no absolute value but are only relative. The legs are designed for either fluidized or settled solids.

The L valve is shown schematically in Fig. 17-21. It can act as a seal and as a solids-flow control valve. However, control of solids rate is only practical for solids that deaerate quickly (Geldart *B* and *D* solids). The height at which aeration is added in Fig. 17-21 is usually one exit pipe diameter above the centerline of the exit pipe. For L-valve design equations, see Yang and Knowlton [*Powder Tech.*, **77**, 49-54 (1993)].

In the sealing mode, the leg is usually fluidized. Gas introduced below the normal solids level and above the discharge port will flow upward and downward. The relative flow in each direction is self-adjusting, depending upon the differential pressure between the point of solids feed and discharge and the level of solids in the leg. The length and diameter of the discharge spout are selected so that the undisturbed angle of repose of the solids will prevent discharge of the solids. As solids are fed into the leg, height H of solids increases. This in turn reduces the flow of gas in an upward direction and increases the flow of gas in a downward direction. When the flow of gas downward and through the solids-discharge port reaches a given rate, the angle of repose of the solids is upset and solids discharge commences. Usually, the level of solids above the point of gas introduction will float. When used as a flow controller, the vertical leg is best run in the packed bed mode. The solids flow rate is controlled by varying the aeration gas flow.

In most catalytic-reactor systems, no solids removal is necessary as the catalyst is retained in the system and solids loss is in the form of fines that are not collected by the dust-recovery system.

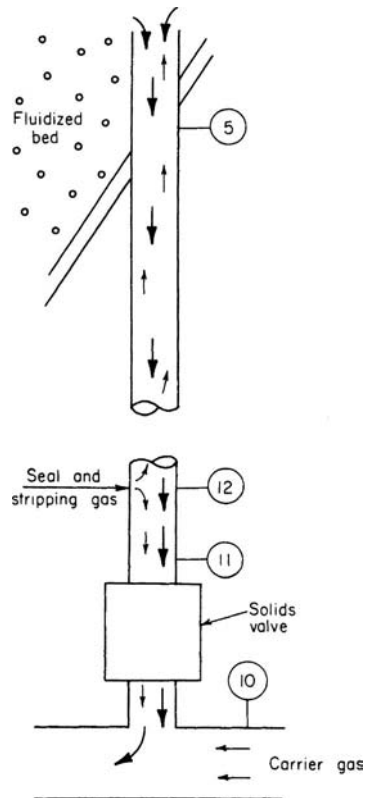


FIG. 17-20 Fluidized-bed seal leg.

Dust Separation It is usually necessary to recover the solids carried by the gas leaving the disengaging space or freeboard of the fluidized bed. Generally, cyclones are used to remove the major portion of these solids (see "Gas-Solids Separation"). However, in a few cases, usually on small-scale units, filters are employed without the use of cyclones to reduce the loading of solids in the gas. For high-temperature usage, either porous ceramic or sintered metal filters have been employed. Multiple units must be provided so that one unit can be blown back with clean gas while one or more are filtering.

Cyclones are arranged generally in any one of the arrangements shown in Fig. 17-22. The effect of cyclone arrangement on the height of the vessel and the overall height of the system is apparent. Details regarding cyclone design and collection efficiencies are to be found in another part of this section.

Discharging of the cyclone into the fluidized bed requires some care. It is necessary to seal the bottom of the cyclone so that the collection efficiency of the cyclone will not be impaired by the passage of

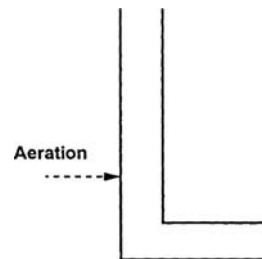


FIG. 17-21 L valve.

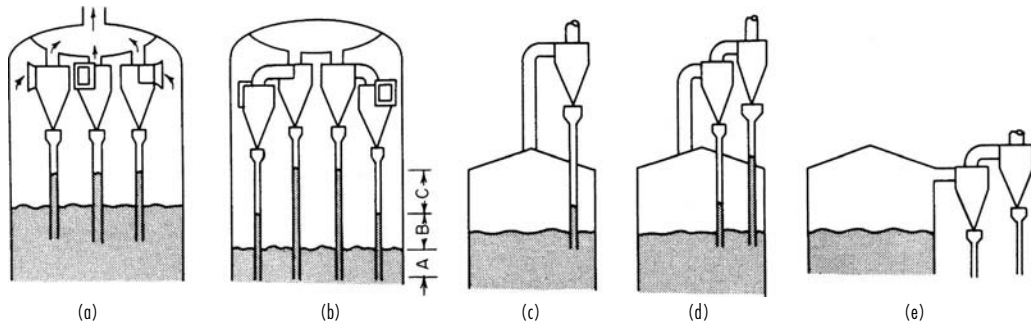


FIG. 17-22 Fluidized-bed cyclone arrangements. (a) Single-stage internal cyclone. (b) Two-stage internal cyclone. (c) Single-stage external cyclone; dust returned to bed. (d) Two-stage external cyclone; dust returned to bed. (e) Two-stage external cyclone; dust collected externally.

appreciable quantities of gas up through the bottom of the dipleg. This is usually done by (1) sealing the dipleg in the fluid bed, or (2) adding a trickle or flapper valve to the bottom of the dipleg if the dipleg is terminated in the freeboard of the fluidized bed. Experience has shown, particularly in the case of deep beds, that the bottom of the dipleg pipe must be protected from the action of large gas bubbles which, if allowed to pass up the leg, would carry quantities of fine solids up into the cyclone and cause momentarily high losses. This is accomplished by attaching a horizontal plate larger in diameter than the pipe to the bottom of the dipleg (see Fig. 17-23e). Care must be taken to ensure that the horizontal plate is located far enough away from the dipleg outlet that the solids discharge from the dipleg is not affected.

Example 1: Length of Seal Leg The length of the seal leg can be estimated as shown.

Given: Fluid density of bed at 0.3-m/s (1-ft/s) superficial gas velocity = 1100 kg/m³ (70 lb/ft³).

Fluid density of cyclone product at 0.15 m/s (0.5 ft/s) = 650 kg/m³ (40 lb/ft³).

Settled bed depth = 1.8 m (6 ft)

Fluidized-bed depth = 2.4 m (8 ft)

Pressure drop through cyclone = 1.4 kPa (0.2 lbf/in²)

In order to assure seal at start-up, the bottom of the seal leg is 1.5 m (5 ft) above the constriction plate or submerged 0.9 m (3 ft) in the fluidized bed.

The pressure at the solids outlet of a gas cyclone is usually about 0.7 kPa (0.1 lbf/in²) lower than the pressure at the discharge of the leg. Total pressure to be balanced by the fluid leg in the cyclone dipleg is

$$(0.9 \times 1100 \times 9.81) / 1000 + 1.4 + 0.7 = 11.8 \text{ kPa}$$

$$[(3 \times 70) / 144 + 0.2 + 0.1 = 1.7 \text{ lb/in}^2]$$

Height of solids in dipleg = $(11.8 \times 1000) / (650 \times 9.81) = 1.9 \text{ m}$ [$(1.7 \times 144) / 40 = 6.1 \text{ ft}$]; therefore, the bottom of the separator pot on the cyclone must be at least 1.9 + 1.5 or 3.4 m (6.1 + 5 or 11.1 ft) above the gas distributor. To allow for upsets, changes in size distribution, etc., use 4.6 m (15 ft).

In addition to the open dipleg, various other devices have been used to seal cyclone solids returns, especially for second-stage cyclones. A number of these are shown in Fig. 17-23. One of the most frequently used is the trickle valve (Fig. 17-23a). There is no general agreement as to whether this valve should discharge below the bed level or in the freeboard. In any event, the legs must be large enough to carry momentarily high rates of solids and must provide seals to overcome cyclone pressure drops as well as to allow for differences in fluid density of bed and cyclone products. It has been reported that, in the case of catalytic-cracking catalysts, the fluid density of the solids collected by the primary cyclone is essentially the same as that in the fluidized bed because the particles in the bed are so small, nearly all are entrained. However, as a general rule the fluidized density of solids collected by the second-stage cyclone is less than the fluidized density of the bed. Each succeeding cyclone collects finer and less dense solids.

As cyclones are less effective as the particle size decreases, secondary collection units are frequently required, i.e., filters, electrostatic precipitators, and scrubbers. When dry collection is not required, elimination of cyclones is possible if allowance is made for heavy solids loads in the scrubber (see "Gas-Solids Separations"; see also Sec. 14).

Instrumentation

Temperature Measurement This is usually simple, and standard temperature-sensing elements are adequate for continuous use. Because of the high abrasion wear on horizontal protection tubes, vertical installations are frequently used. In highly corrosive atmospheres in which metallic protection tubes cannot be used, short, heavy ceramic tubes have been used successfully.

Pressure Measurement Although successful pressure measurement probes or taps have been fabricated by using porous materials, the most universally accepted pressure tap consists of a purged tube

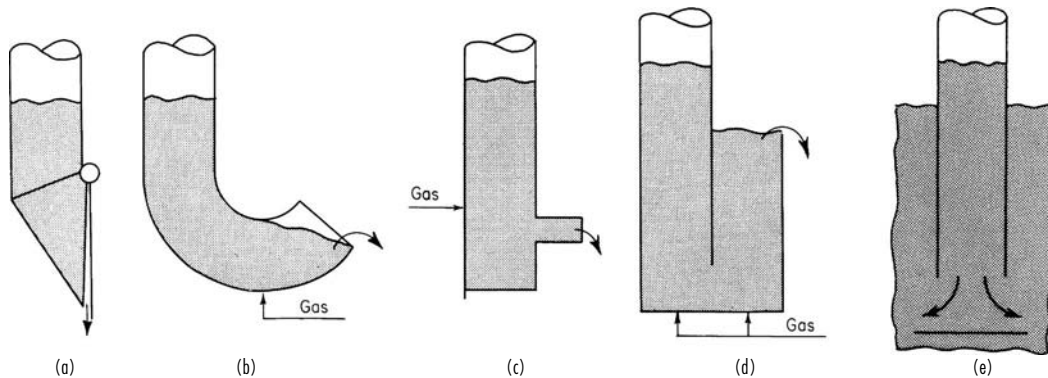


FIG. 17-23 Cyclone solids-return seals. (a) Trickle valve (Ducon Co., Inc.). (b) J valve. (c) L valve. (d) Fluid-seal pot. (e) "Dollar" plate. a, b, c, and d may be used above the bed; a and e are used below the bed.

projecting into the bed. Minimum internal diameters of the tube are 0.6 to 1.2 cm (0.25 to 0.5 in.). A purge rate of at least 1.5 m/s (5 ft/s) is usually required to prevent solids from plugging the signal lines. Bed density is determined directly from $\Delta P/L$, the pressure drop inside the bed itself ($\Delta P/L$ in units of weight/area $\times 1/L$). The overall bed weight is obtained from ΔP taken between a point just above the gas distributor and a point in the freeboard. Nominal bed height is determined by dividing the ΔP across the entire bed and dividing it by the $\Delta P/L$ over a section of the bed length. Splashing of the solids by bubbles bursting at the bed surface will eject solids well above the nominal bed height in most cases. The pressure drop signal from fluidized beds fluctuates due to bubble effects and the generally statistical nature of fluid-bed flow parameters. A fast Fourier transform of the pressure drop signal transforms the perturbations to a frequency versus amplitude plot with a maximum at about 3 to 5 Hz and frequencies generally tailing off above 20 Hz. Changes in frequency and amplitude are associated with changes in the quality of the fluidization. Experienced operators of fluidized beds can frequently predict what is happening in the bed from changes in the ΔP signal.

Flow Measurements Measurement of flow rates of clean gases presents no problem. Flow measurement of gas streams containing solids is almost always avoided. The flow of solids is usually controlled but not measured except solids flows added to or taken from the system. Solids flows in the system are usually adjusted on an inferential basis (temperature, pressure level, catalyst activity, gas analysis, heat balance, etc.). In many roasting operations, the color of the calcine discharge material indicates whether the solids feed rate is too high or too low.

USES OF FLUIDIZED BEDS

There are many uses of fluidized beds. A number of applications have become commercial successes; others are in the pilot-plant stage, and others in bench-scale stage. Generally, the fluidized bed is used for gas-solids contacting; however, in some instances the presence of the gas or solid is used only to provide a fluidized bed to accomplish the end result. Uses or special characteristics follow:

- I. Chemical reactions
 - A. Catalytic
 - B. Noncatalytic
 1. Homogeneous
 2. Heterogeneous
- II. Physical contacting
 - A. Heat transfer
 1. To and from fluidized bed
 2. Between gases and solids
 3. Temperature control
 4. Between points in bed
 - B. Solids mixing
 - C. Gas mixing
 - D. Drying
 1. Solids
 2. Gases
 - E. Size enlargement
 - F. Size reduction
 - G. Classification
 1. Removal of fines from solids
 2. Removal of fines from gas
 - H. Adsorption-desorption
 - I. Heat treatment
 - J. Coating

Chemical Reactions

Catalytic Reactions This use has provided the greatest impetus for use, development, and research in the field of fluidized solids. Some of the details pertaining to this use are to be found in the preceding pages of this section. Reference should also be made to Sec. 21.

Cracking The evolution of fluidized catalytic cracking since the early 1940s has resulted in several fluidized-bed process configurations.

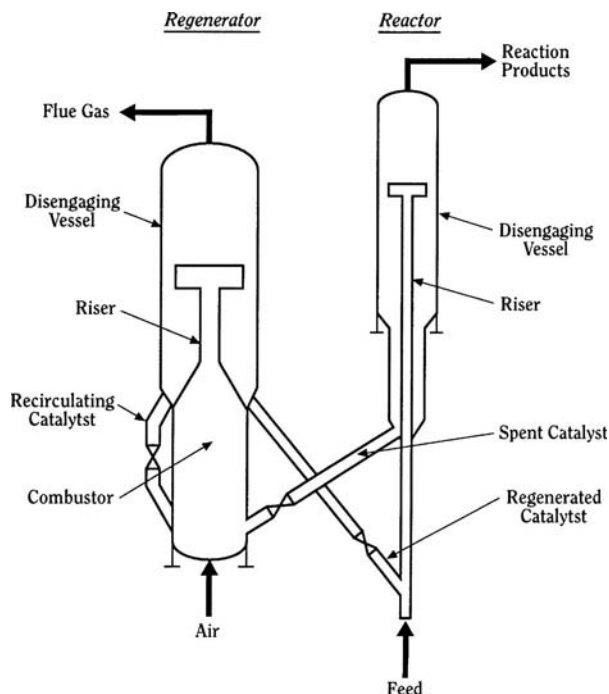


FIG. 17-24 UOP fluid cracking unit. (Reprinted with permission of UOP.)

The high rate of solids transfer between the fluidized-bed regenerator and the riser reactor in this process permits a balancing of the exothermic burning of carbon and tars in the regenerator and the endothermic cracking of petroleum in the reactor. Therefore, the temperature in both units can usually be controlled without resorting to auxiliary heat control mechanisms. The high rate of catalyst circulation also permits the maintenance of the catalyst at a constantly high activity. The original fluidized-bed regenerators were considered to be completely backmixed units. Newer systems have staged regenerators to improve conversion (see Fig. 17-24). The use of the riser reactor operating in the fast fluid-bed mode results in much lower gas and solids backmixing due to the more plug-flow nature of the riser.

The first fluid catalytic cracking unit (called Model I) was placed in operation in Baytown, Texas, in 1942. This was a low-pressure, 14- to 21-kPa (2- to 3-psig) unit operating in what is now called the turbulent fluidized-bed mode with a gas velocity of 1.2 to 1.8 m/s (4 to 6 ft/s). Before the start-up of the Model I cracker, it was realized that by lowering the gas velocity in the bed, a dense, bubbling or turbulent fluidized bed, with a bed density of 300 to 400 kg/m³ (20 to 25 lb/ft³), would be formed. The increased gas/solids contacting time in the denser bed allowed completion of the cracking reaction and catalyst regeneration. System pressure was eventually increased to 140 to 210 kPa (20 to 30 psig).

In the 1970s more-active zeolite catalysts were developed so that the cracking reaction could be conducted in the transport riser. Recently, heavier crude feedstocks have resulted in higher coke production in the cracker. The extra coke causes higher temperatures in the regenerator than are desired. This has resulted in the addition of catalyst cooling to the regeneration step, as shown in Fig. 17-25.

Many companies have participated in the development of the fluid catalytic cracker, including ExxonMobil Research & Engineering Co., UOP, Kellogg Brown and Root, ChevronTexaco, Gulf Research Development Co., and Shell Oil Company. Many of the companies provide designs and/or licenses to operate to others. For further details, see Luckenbach et al., "Cracking, Catalytic," in McKetta (ed.), *Encyclopedia of Chemical Processing and Design*, vol. 13, Marcel Dekker, New York, 1981, pp. 1-132.

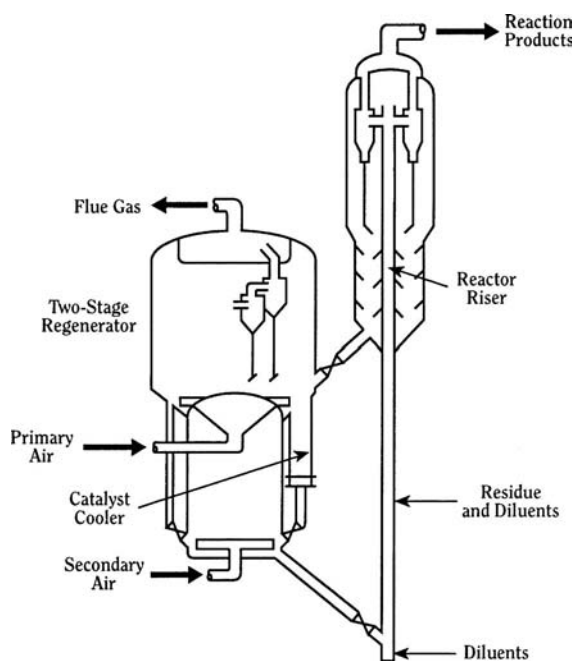


FIG. 17-25 Modern FCC unit configured for high-efficiency regeneration and extra catalyst cooling. (Reprinted with permission of UOP. FCC is a service mark of Ashland Oil Inc.)

Alkyl chloride Olefins are chlorinated to alkyl chlorides in a single fluidized bed. In this process, HCl reacts with O_2 over a copper chloride catalyst to form chlorine. The chlorine reacts with the olefin to form alkyl chloride. The process was developed by Shell Development Co. and uses a recycle of catalyst fines in aqueous HCl to control the temperature [Chem. Proc. **16**:42 (1953)].

Phthalic anhydride Naphthalene is oxidized by air to phthalic anhydride in a bubbling fluidized reactor. Even though the naphthalene feed is in liquid form, the reaction is highly exothermic. Temperature control is achieved by removing heat through vertical tubes in the bed to raise steam [Graham and Way, Chem. Eng. Prog. **58**:96 (January 1962)].

Acrylonitrile Acrylonitrile is produced by reacting propylene, ammonia, and oxygen (air) in a single fluidized bed of a complex catalyst. Known as the SOHIO process, this process was first operated commercially in 1960. In addition to acrylonitrile, significant quantities of HCN and acetonitrile are produced. This process is also exothermic, and temperature control is achieved by raising steam inside vertical tubes immersed in the bed [Veatch, Hydrocarbon Process. Pet. Refiner **41**:18 (November 1962)].

Fischer-Tropsch synthesis The early scale-up of a bubbling bed reactor to produce gasoline from CO and H_2 was unsuccessful (see "Design of Fluidized-Bed Systems: Scale-up"). However, Kellogg Co. later developed a successful Fischer-Tropsch synthesis reactor based on a dilute-phase transport-reactor concept. Kellogg, in its design, prevented gas bypassing by using the transport reactor and maintained temperature control of the exothermic reaction by inserting heat exchangers in the transport line. This process has been very successful and repeatedly improved upon at the South African Synthetic Oil Limited (SASOL) plant in the Republic of South Africa, where politics and economics favor the conversion of coal to gasoline and other hydrocarbons. Refer to Jewell and Johnson, U.S. Patent 2,543,974, Mar. 6, 1951. Recently, the process has been modified to a simpler, less expensive turbulent bed catalytic reactor system (Silverman et al., Fluidization V, Engineering Foundation, 1986, pp. 441-448).

Polyethylene The first commercial fluidized-bed polyethylene plant was constructed by Union Carbide in 1968. Modern units operate at a temperature of approximately $100^\circ C$ and a pressure of

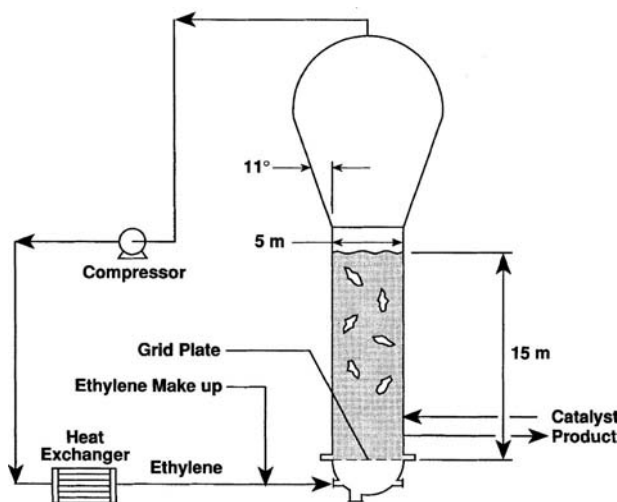


FIG. 17-26 High-pressure polyethylene reactor.

2100 kPa (300 psig). The bed is fluidized with ethylene at about 0.5 to 0.7 m/s (1.65 to 2.3 ft/s) and operates in the turbulent fluidization regime. Small catalyst is added to the bed, and the ethylene polymerizes on the catalyst to form polyethylene particles of approximately 600- to 1000- μm average size, depending on the type of polyethylene product being produced. The excellent mixing provided by the fluidized bed is necessary to prevent hot spots, since the unit is operated near the melting point of the product. A model of the reactor (Fig. 17-26) that couples kinetics to the hydrodynamics was given by Choi and Ray, Chem. Eng. Sci. **40**: 2261 (1985).

Additional catalytic processes Nitrobenzene is hydrogenated to aniline (U.S. Patent 2,891,094). Melamine and isophthalonitrile are produced in catalytic fluidized-bed reactors. Badger developed a process to produce maleic anhydride by the partial oxidation of butane (Schaffel, Chen, and Graham, "Fluidized Bed Catalytic Oxidation of Butane to Maleic Anhydride," presented at Chemical Engineering World Congress, Montreal, Canada, 1981). Dupont developed a circulating bed process for production of maleic anhydride (Contractor, Circulating Fluidized Bed Tech. II, Pergamon, 1988, pp. 467-474). Mobil developed a commercial process to convert methanol to gasoline (Grimmer et al., Methane Conversion, Elsevier, 1988, pp. 273-291).

Noncatalytic Reactions

Homogeneous reactions Homogeneous noncatalytic reactions are normally carried out in a fluidized bed to achieve mixing of the gases and temperature control. The solids of the bed act as a heat sink or source and facilitate heat transfer from or to the gas or from or to heat-exchange surfaces. Reactions of this type include chlorination of hydrocarbons or oxidation of gaseous fuels.

Heterogeneous reactions This category covers the greatest commercial use of fluidized beds other than fluid catalytic cracking. Roasting of ores in fluidized beds is very common. Roasting of sulfide, arsenical, and/or antimonial ores to facilitate the release of gold or silver values; the roasting of pyrite, pyrrhotite, or naturally occurring sulfur ores to provide SO_2 for sulfuric acid manufacture; and the roasting of copper, cobalt, and zinc sulfide ores to solubilize the metals are the major metallurgical uses. Figure 17-27 shows the basic items in the roasting process.

Thermally efficient calcination of lime, dolomite, and clay can be carried out in a multicompartiment fluidized bed (Fig. 17-28). Fuels are burned in a fluidized bed of the product to produce the required heat. Bunker C oil, natural gas, and coal are used in commercial units as the fuel. Temperature control is accurate enough to permit production of lime of very high quality with close control of slaking characteristics. Also, half calcination of dolomite is an accepted practice in fluidized

17-18 GAS-SOLID OPERATIONS AND EQUIPMENT

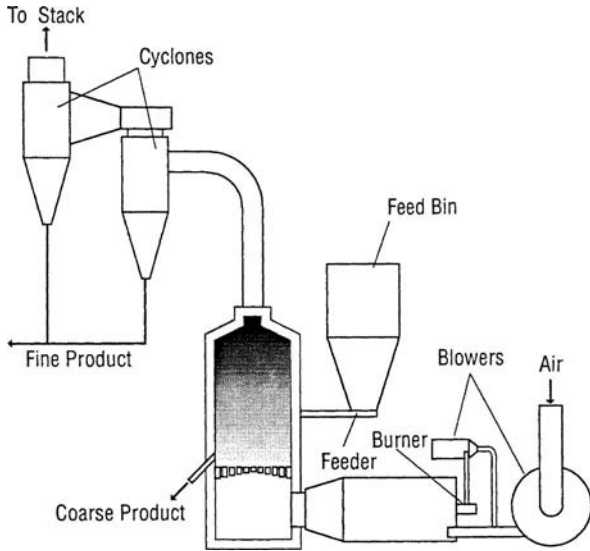


FIG. 17-27 Single-stage FluoSolids roaster or dryer. (Dorr-Oliver, Inc.)

beds. The requirement of large crystal size for the limestone limits application. Small crystals in the limestone result in low yields due to high dust losses from the fluidized bed.

Phosphate rock is calcined to remove carbonaceous material before being digested with sulfuric acid. Several different fluidized-bed processes have been commercialized for the direct reduction of hematite to high-iron, low-oxide products. Foundry sand is also calcined to remove organic binders and release fines. The calcination of $Al(OH)_3$ to Al_2O_3 in a circulating fluidized process produces a high-grade product. The process combines the use of circulating, bubbling, and transport beds to achieve high thermal efficiency. See Fig. 17-29.

An interesting feature of these high-temperature-calcination applications is the direct injection of heavy oil, natural gas, or fine coal into the fluidized bed. Combustion takes place at well below flame temperatures without atomization. Considerable care in the design of the fuel and air supply system is necessary to take full advantage of the fluidized bed, which serves to mix the air and fuel.

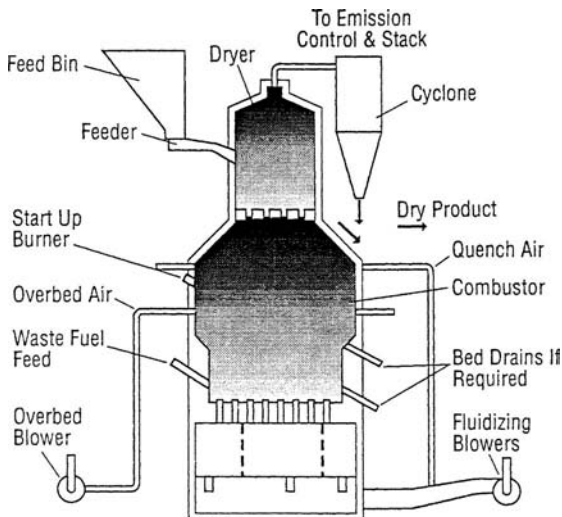


FIG. 17-28 FluoSolids multicompartiment fluidized bed. (Dorr-Oliver, Inc.)

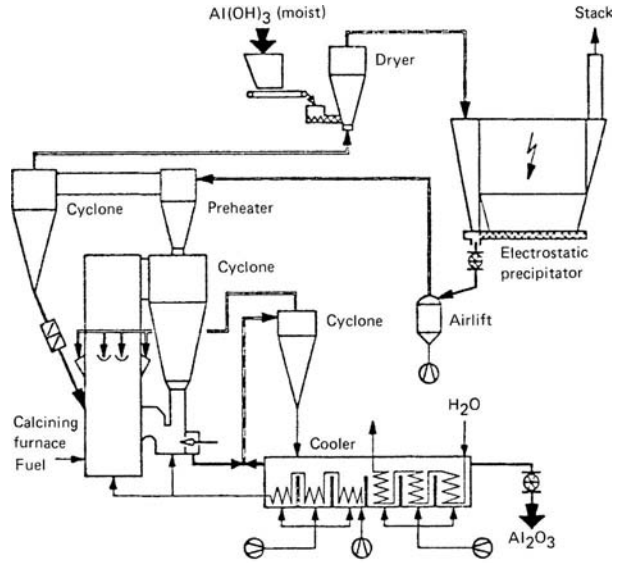


FIG. 17-29 Circulating fluid-bed calciner. (Lurgi Corp.)

Coal can be burned in fluidized beds in an environmentally acceptable manner by adding limestone or dolomite to the bed to react with the SO_2 to form $CaSO_4$. Because of moderate combustion temperatures, about 800 to 900°C, NO_x formation, which results from the oxidation of nitrogen compounds contained in the coal, is kept at a low level. NO_x is increased by higher temperatures and higher excess oxygen contents. Two-stage air addition reduces NO_x . Several concepts of fluidized-bed combustion have been or are being developed. Atmospheric fluidized-bed combustion (AFBC), in which most of the heat-exchange tubes are located in the bed, is illustrated in Fig. 17-30.

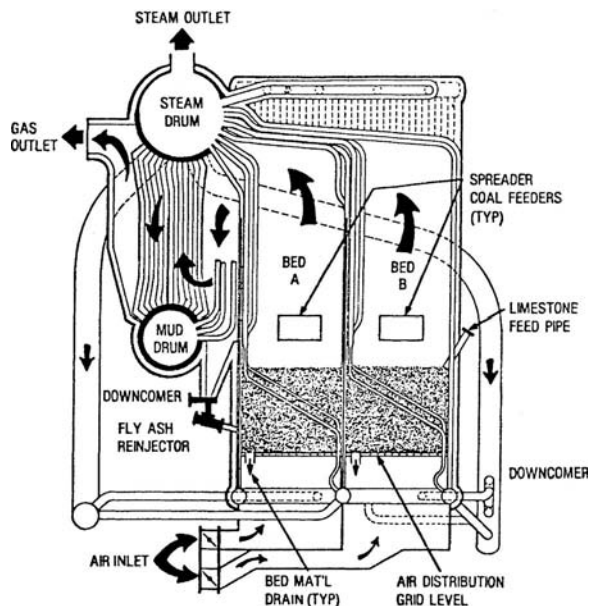


FIG. 17-30 Fluidized-bed steam generator at Georgetown University; 12.6-kg/s (100,000-lb/h) steam at 4.75-MPa (675-psig) pressure. (From Georgetown Univ. Q. Tech. Prog. Rep. METC/DOE/10381/135, July–September 1980.)

This type of unit is most commonly used for industrial applications up to about 50 t/h of steam generation. Larger units are generally of the circulating bed type, as shown in Fig. 17-30. **Circulating fluidized-bed combustors** have many advantages. The gas velocity is significantly higher than in bubbling or turbulent beds, which results in greater throughput. Since all the solids are recycled, fine limestone and coal can be fed to the combustor, which gives better limestone utilization and greater latitude in specifying coal sizing. Because of erosion due to high-velocity coarse solids, heat-transfer surface is usually not designed into the bottom of the combustion zone.

Pressurized fluidized-bed combustion (PFBC) is, as the name implies, operated at above atmospheric pressures. The beds and

heat-transfer surface are stacked to conserve space and to reduce the size of the pressure vessel. This type of unit is usually conceived as a cogeneration unit. Steam raised in the boilers is employed to drive turbines or for other uses. The hot pressurized gases after cleaning are let down through an expander coupled to a compressor to supply the compressed combustion air and/or electric generator. A 71-MWe PFBC unit is shown in Fig. 17-31. Also see Sec. 24, "Energy Resources, Conversion, and Utilization."

Incineration The majority of over 400 units in operation are used for the incineration of biological sludges. These units can be designed to operate autogenously with wet sludges containing as little as 6 MJ/kg (2600 Btu/lb) heating value (Fig. 17-32). Depending

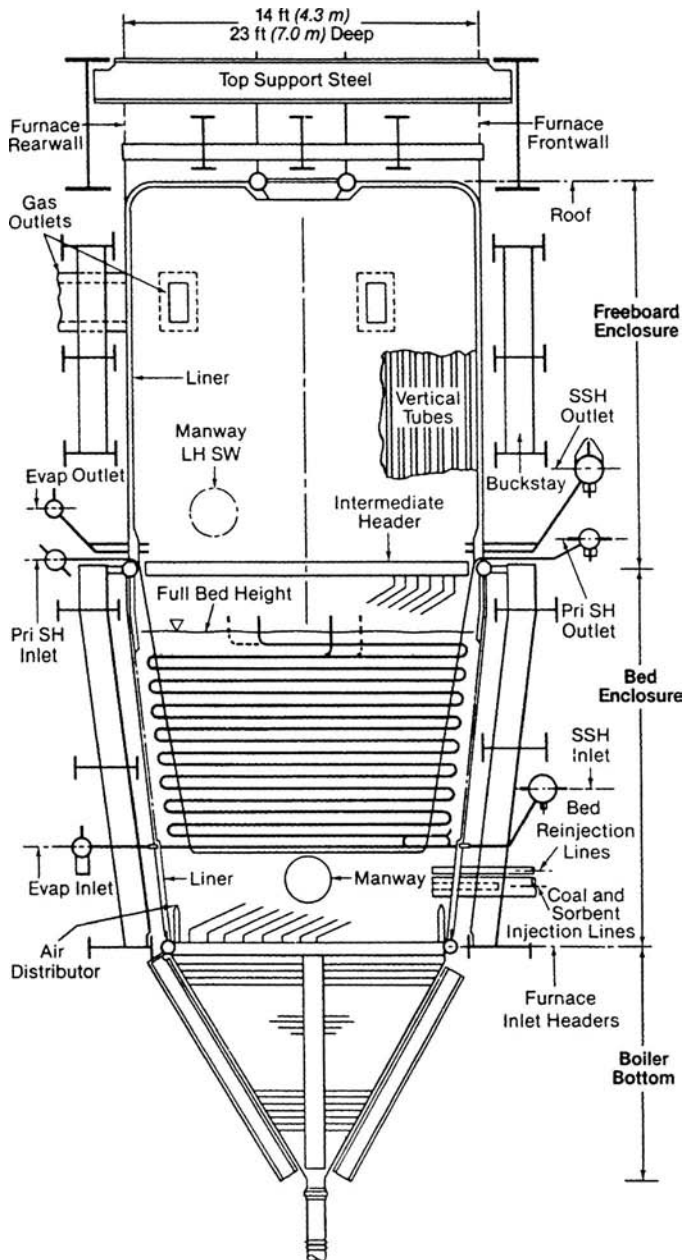


FIG. 17-31 71 MWe PFBC unit. (From Steam, 40th ed., 29-9, Babcock & Wilcox, 1992).

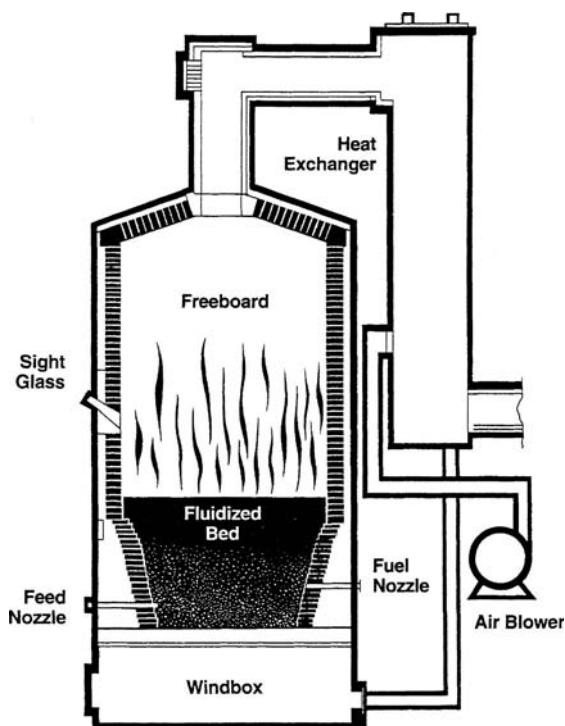


FIG. 17-32 Hot windbox incinerator/reactor with air preheating. (Dorr-Oliver, Inc.)

on the calorific value of the feed, heat can be recovered as steam either by means of waste heat boilers or by a combination of waste heat boilers and the heat-exchange surface in the fluid bed. Several units are used for sulfite papermill waste liquor disposal. Several units are used for oil refinery wastes, which sometimes include a mixture of liquid sludges, emulsions, and caustic waste [Flood and Kernel, *Chem. Proc.* (Sept. 8, 1973)]. Miscellaneous uses include the incineration of sawdust, carbon-black waste, pharmaceutical waste, grease from domestic sewage, spent coffee grounds, and domestic garbage.

Toxic or hazardous wastes can be disposed of in fluidized beds by either chemical capture or complete destruction. In the former case, bed material, such as limestone, will react with halides, sulfides, metals, etc., to form stable compounds which can be landfilled. Contact times of up to 5 or 10 s at 1200 K (900°C) to 1300 K (1000°C) ensure complete destruction of most compounds.

Physical Contacting

Drying Fluidized-bed units for drying solids, particularly coal, cement, rock, and limestone, are in wide use. Economic considerations make these units particularly attractive when large tonnages of solids are to be handled. Fuel requirements are 3.3 to 4.2 MJ/kg (1500 to 1900 Btu/lb of water removed), and total power for blowers, feeders, etc., is about 0.08 kWh/kg of water removed. The maximum feed size is approximately 6 cm (2.4 in) \times 0 coal. One of the major advantages of this type of dryer is the close control of conditions so that a predetermined amount of free moisture may be left with the solids to prevent dusting of the product during subsequent material handling operations. The fluidized-bed dryer is also used as a classifier so that drying and classification operations are accomplished simultaneously. Wall and Ash [*Ind. Eng. Chem.* **41**: 1247 (1949)] state that in drying 4.8-mm (-4-mesh) dolomite with combustion gases at a superficial

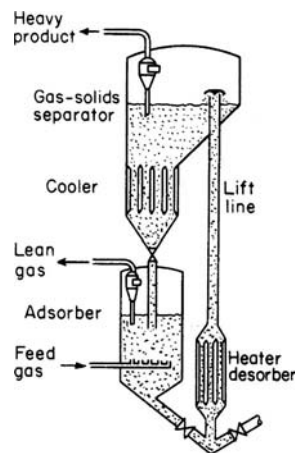


FIG. 17-33 Fluidized bed for gas fractionation. [Sittig, *Chem. Eng.* (May 1953).]

velocity of 1.2 m/s (4 ft/s), the following removals of fines were achieved:

Particle size	% removed
-65 + 100 mesh	60
-100 + 150 mesh	79
-150 + 200 mesh	85
-200 + 325 mesh	89
-325 mesh	89

Classification The separation of fine particles from coarse can be effected by use of a fluidized bed (see "Drying"). However, for economic reasons (i.e., initial cost, power requirements for compression of fluidizing gas, etc.), it is doubtful except in special cases if a fluidized-bed classifier would be built for this purpose alone.

It has been proposed that fluidized beds be used to remove fine solids from a gas stream. This is possible under special conditions.

Adsorption-Desorption An arrangement for gas fractionation is shown in Fig. 17-33.

The effects of adsorption and desorption on the performance of fluidized beds are discussed elsewhere. Adsorption of carbon disulfide vapors from air streams as great as 300 m³/s (540,000 ft³/min) in a 17-m- (53-ft-) diameter unit has been reported by Avery and Tracey ("The Application of Fluidized Beds of Activated Carbon to Recover Solvent from Air or Gas Streams," Tripartate Chemical Engineering Conference, Montreal, Sept. 24, 1968).

Heat Treatment Heat treatment can be divided into two types, treatment of fluidizable solids and treatment of large, usually metallic objects in a fluid bed. The former is generally accomplished in multi-compartment units to conserve heat (Fig. 17-28). The heat treatment of large metallic objects is accomplished in long, narrow heated beds. The objects are conveyed through the beds by an overhead conveyor system. Fluid beds are used because of the high heat-transfer rate and uniform temperature. See Reindl, "Fluid Bed Technology," *American Society for Metals*, Cincinnati, Sept. 23, 1981; Fennell, *Ind. Heat.*, **48**, 9, 36 (September 1981).

Coating Fluidized beds of thermoplastic resins have been used to facilitate the coating of metallic parts. A properly prepared, heated metal part is dipped into the fluidized bed, which permits complete immersion in the dry solids. The heated metal fuses the thermoplastic, forming a continuous uniform coating.

GAS-SOLIDS SEPARATIONS

This subsection is concerned with the application of particle mechanics (see Sec. 5, "Fluid and Particle Mechanics") to the design and application of dust-collection systems. It includes wet collectors, or

scrubbers, for particle collection. Scrubbers designed for purposes of mass transfer are discussed in Secs. 14 and 18. Equipment for removing entrained liquid mist from gases is described in Sec. 18.

Nomenclature

Except where otherwise noted here or in the text, either consistent system of units (SI or U.S. customary) may be used. Only SI units may be used for electrical quantities, since no comparable electrical units exist in the U.S. customary system. When special units are used, they are noted at the point of use.

Symbols	Definition	SI units	U.S. customary units	Special units
B_c	Width of rectangular cyclone inlet duct	m	ft	
B_e	Spacing between wire and plate, or between rod and curtain, or between parallel plates in electrical precipitators	m	ft	
B_s	Width of gravity settling chamber	m	ft	
C°	Dry scrubber pollutant gas equilibrium concentration over sorbent			
C_1	Dry scrubber pollutant gas inlet concentration			
C_2	Dry scrubber pollutant gas outlet concentration			
c_d	Dust concentration in gas stream	g/m ³		grains/ft ³
c_h	Specific heat of gas	J/(kg·K)	Btu/(lbm·°F)	
c_{hb}	Specific heat of collecting body	J/(kg·K)	Btu/(lbm·°F)	
c_{hp}	Specific heat of particle	J/(kg·K)	Btu/(lbm·°F)	
D_b	Diameter or other representative dimension of collector body or device	m	ft	
D_{b1}, D_{b2}	Other characteristic dimensions of collector body or device	m	ft	
D_c	Cyclone diameter	m	ft	
D_d	Outside diameter of wire or discharge electrode of concentric-cylinder type of electrical precipitator	m	ft	
D_e	Diameter of cyclone gas exit duct	m	ft	
D_o	Volume/surface-mean-drop diameter			μm
D_p	Diameter of particle	m	ft	μm
D_{pth}	Cut diameter, diameter of particles of which 50% of those present are collected	m	ft	μm
d_p	Particle diameter of fraction number c'	m	ft	
D_i	Inside diameter of collecting tube of concentric-cylinder type of electrical precipitator	m	ft	
D_c	Diffusion coefficient for particle	m ² /s	ft ² /s	
DI	Decontamination index = $\log_{10}[1/(1 - \eta)]$	Dimensionless	Dimensionless	
e	Natural (napierian) logarithmic base	2.718 . . .	2.718 . . .	
E	Potential difference	V		
E_c	Potential difference required for corona discharge to commence	V		
E_d	Voltage across dust layer	V		
E_s	Potential difference required for sparking to commence	V		
E_L	Cyclone collection efficiency at actual loading			
E_O	Cyclone collection efficiency at low loading			
F_E	Effective friction loss across wetted equipment in scrubber	kPa		in water
F_k	Packed bed friction loss			
g_c	Conversion factor		32.17 (lbm/lbf)(ft/s ²)	
g_L	Local acceleration due to gravity	m/s ²	ft/s ²	
H_c	Height of rectangular cyclone inlet duct	m	ft	
H_s	Height of gravity settling chamber	m	ft	
I	Electrical current per unit of electrode length	A/m		
j	Corona current density at dust layer	A/m ²		
k_p	Density of gas relative to its density at 0°C, 1 atm	Dimensionless	Dimensionless	Dimensionless
k_t	Thermal conductivity of gas	W/(m·K)	Btu/(s·ft·°F)	
k_{tb}	Thermal conductivity of collecting body	W/(m·K)	Btu/(s·ft·°F)	
k_{tp}	Thermal conductivity of particle	W/(m·K)	Btu/(s·ft·°F)	
K	Empirical proportionality constant for cyclone pressure drop or friction loss	Dimensionless	Dimensionless	
K_1	Resistance coefficient of "conditioned" filter fabric	kPa/(m/min)	in water/(ft/min)	
K_2	Resistance coefficient of dust cake on filter fabric	$\frac{\text{kPa}}{(\text{m/min})(\text{g/m}^2)}$	$\frac{\text{in water}}{(\text{ft/min})(\text{lbm/ft}^2)}$	

17-22 GAS-SOLID OPERATIONS AND EQUIPMENT

Nomenclature (Concluded)

Symbols	Definition	SI units	U.S. customary units	Special units
K_a	Proportionality constant, for target efficiency of a single fiber in a bed of fibers	Dimensionless	Dimensionless	
K_c	Resistance coefficient for "conditioned" filter fabric			$\frac{\text{in water}}{(\text{ft}/\text{min})(\text{cP})}$
K_d	Resistance coefficient for dust cake on filter fabric		$\frac{\text{in water}}{(\text{ft}/\text{min})(\text{gr}/\text{ft}^2)(\text{cP})}$	
K_e	Electrical-precipitator constant	s/m	s/ft	
K_F	Resistance coefficient for clean filter cloth			$\frac{\text{in water}}{(\text{ft}/\text{min})(\text{cP})}$
K_v	"Energy-distance" constant for electrical discharge in gases	m		
K_m	Stokes-Cunningham correction factor	Dimensionless	Dimensionless	Dimensionless
L	Thickness of fibrous filter or of dust layer on surface filter	m	ft	
L_c	Length of collecting electrode in direction of gas flow	m	ft	
L_s	Length of gravity settling chamber in direction of gas flow	m	ft	
\ln	Natural logarithm (logarithm to the base e)	Dimensionless	Dimensionless	Dimensionless
M	Molecular weight	kg/mol	lbm/mol	
n	Exponent	Dimensionless	Dimensionless	Dimensionless
N_{Kn}	Knudsen number = λ_m/D_b	Dimensionless	Dimensionless	
N_{Ma}	Mach number	Dimensionless	Dimensionless	
N_o	Number of elementary electrical charges acquired by a particle	Dimensionless	Dimensionless	
N_{Re}	Reynolds number = $(D_p \rho V_c / \mu)$ or $(D_p \rho u_c / \mu)$	Dimensionless	Dimensionless	
N_{sc}	Interaction number = $18 \mu / K_m \rho_p D_c$	Dimensionless	Dimensionless	
N_{sd}	Diffusional separation number	Dimensionless	Dimensionless	
N_{sec}	Electrostatic-attraction separation number	Dimensionless	Dimensionless	
N_{sei}	Electrostatic-induction separation number	Dimensionless	Dimensionless	
N_{sf}	Flow-line separation number	Dimensionless	Dimensionless	
N_{sg}	Gravitational separation number	Dimensionless	Dimensionless	
N_{si}	Inertial separation number	Dimensionless	Dimensionless	
N_{st}	Thermal separation number	Dimensionless	Dimensionless	
N_t	Number of transfer units = $\ln [1/(1 - \eta)]$	Dimensionless	Dimensionless	
N_s	Number of turns made by gas stream in a cyclone separator	Dimensionless	Dimensionless	
Δp	Gas pressure drop	kPa	lbf/ft ²	in water
Δp_i	Gas pressure drop in cyclone or filter			in water
p_F	Gauge pressure of water fed to scrubber	kPa		lbf/in ²
P_G	Gas-phase contacting power	MJ/1000 m ³		hp/(1000 ft ³ /min)
P_L	Liquid-phase contacting power	MJ/1000 m ³		hp/(1000 ft ³ /min)
P_M	Mechanical contacting power	MJ/1000 m ³		hp/(1000 ft ³ /min)
P_T	Total contacting power	MJ/1000 m ³		hp/(1000 ft ³ /min)
q	Gas flow rate	m ³ /s	ft ³ /s	
Q_G	Gas flow rate		ft ³ /s	ft ³ /min
Q_L	Liquid flow rate		ft ³ /s	gal/min
Q_p	Electrical charge on particle	C		
r	Radius; distance from centerline of cyclone separator; distance from centerline of concentric-cylinder electrical precipitator	m	ft	
t_m	Time			min
T	Absolute gas temperature	K	°R	
T_b	Absolute temperature of collecting body	K	°R	
u_s	Velocity of migration of particle toward collecting electrode	m/s	ft/s	
u_t	Terminal settling velocity of particle under action of gravity	m/s	ft/s	ft/s
v_m	Average cyclone inlet velocity, based on area A_c	m/s	ft/s	ft/s
v_p	Actual particle velocity	m/s	ft/s	
V_f	Filtration velocity (superficial gas velocity through filter)	m/min		ft/min
V_o	Gas velocity	m/s	ft/s	
V_s	Average gas velocity in gravity settling	m/s	ft/s	
V_{ct}	Tangential component of gas velocity in cyclone	m/s	ft/s	
w	Loading of collected dust on filter	g/m ²	lbm/ft ²	gr/ft ²

Nomenclature (Concluded)

Symbols	Definition	SI units	U.S. customary units	Special units
Greek symbols				
α	Empirical constant in equation of scrubber performance curve	$\left[\frac{\text{MJ}}{1000 \text{ m}^3} \right]^{-\gamma}$		$\left[\frac{\text{hp}}{100 \text{ ft}^3/\text{min}} \right]^{-\gamma}$
γ	Empirical constant in equation of scrubber performance curve	Dimensionless		Dimensionless
δ	Dielectric constant	Dimensionless		
δ_g	Dielectric constant at 0°C, 1 atm	Dimensionless		
δ_0	Permittivity of free space	F/m		
δ_b	Dielectric constant of collecting body	Dimensionless		
δ_p	Dielectric constant of particle	Dimensionless		
Δ	Fractional free area (for screens, perforated plates, grids)	Dimensionless	Dimensionless	
ϵ	Elementary electrical charge	$1.60210 \times 10^{-19} \text{ C}$		
ϵ_b	Characteristics potential gradient at collecting surface	V/m		
ϵ_c	Fraction voids in bed of solids	Dimensionless	Dimensionless	Dimensionless
ζ	$= 1 + 2 \frac{\delta - 1}{\delta + 2}$ ranges from a value of 1 for materials with a dielectric constant of 1 to 3 for conductors	Dimensionless		
η	Collection efficiency, weight fraction of entering dispersoid collected	Dimensionless	Dimensionless	Dimensionless
η_0	Target efficiency of an isolated collecting body, fraction of dispersoid in swept volume collected on body	Dimensionless	Dimensionless	Dimensionless
η_f	Target efficiency of a single collecting body in an array of collecting bodies, fraction of dispersoid in swept volume collected on body	Dimensionless	Dimensionless	Dimensionless
λ_i	Ionic mobility of gas	(m/s)/(V/m)		
λ_p	Particle mobility = $u_c/f\mathcal{E}$	(m/s)/(V/m)		
μ	Gas viscosity	Pa·s	lbm/(s·ft)	cP
μ_L	Liquid viscosity			cP
ρ	Gas density	g/m^3	lb/ft ³	
ρ_d	Resistivity of dust layer	$\Omega\text{-m}$		
ρ_L	Liquid density		lbm/ft ³	lbm/ft ³
ρ_s	True (not bulk) density of solids or liquid drops	kg/m^3	lbm/ft ³	lbm/ft ³
ρ'	Density of gas relative to its density at 25°C, 1 atm	Dimensionless	Dimensionless	Dimensionless
σ	Ion density	Number/m ³		
σ_{avg}	Average ion density	Number/m ³		
σ_L	Liquid surface tension			dyn/cm
ϕ_s	Particle shape factor = (surface of sphere)/(surface of particle of same volume)	Dimensionless	Dimensionless	Dimensionless
Script symbols				
\mathcal{E}	Potential gradient	V/m		
\mathcal{E}_c	Potential gradient required for corona discharge to commence	V/m		
\mathcal{E}_i	Average potential gradient in ionization stage	V/m		
\mathcal{E}_o	Electrical breakdown constant for gas	V/m		
\mathcal{E}_p	Average potential gradient in collection stage	V/m		
\mathcal{E}_s	Potential gradient required for sparking to commence	V/m		

GENERAL REFERENCES: Burchsted, Kahn, and Fuller, *Nuclear Air Cleaning Handbook*, ERDA 76-21, Oak Ridge, Tenn., 1976. Cadle, *The Measurement of Airborne Particles*, Wiley, New York, 1975. Davies, *Aerosol Science*, Academic, New York, 1966. Davies, *Air Filtration*, Academic, New York, 1973. Dennis, *Handbook on Aerosols*, ERDA TID-26608, Oak Ridge, Tenn., 1976. Drinker and Hatch, *Industrial Dust*, 2d ed., McGraw-Hill, New York, 1954. Friedlander, *Smoke, Dust, and Haze*, Wiley, New York, 1977. Fuchs, *The Mechanics of Aerosols*, Pergamon, Oxford, 1964. Green and Lane, *Particulate Clouds: Dusts, Smokes, and Mists*, Van Nostrand, New York, 1964. Lapple, *Fluid and Particle Mechanics*, University of Delaware, Newark, 1951. Licht, *Air Pollution Control Engineering—Basic Calculations for Particle Collection*, Marcel Dekker, New York, 1980. Liu, *Fine Particles—Aerosol Generation, Measurement, Sampling, and Analysis*, Academic, New York, 1976. Lunde and Lapple, *Chem. Eng. Prog.*,

53, 385 (1957). Lundgren et al., *Aerosol Measurement*, University of Florida, Gainesville, 1979. Mercer, *Aerosol Technology in Hazard Evaluation*, Academic, New York, 1973. Nonhebel, *Processes for Air Pollution Control*, CRC Press, Cleveland, 1972. Shaw, *Fundamentals of Aerosol Science*, Wiley, New York, 1978. Stern, *Air Pollution: A Comprehensive Treatise*, vols. 3 and 4, Academic, New York, 1977. Strauss, *Industrial Gas Cleaning*, 2d ed., Pergamon, New York, 1975. Theodore and Buonicore, *Air Pollution Control Equipment: Selection, Design, Operation, and Maintenance*, Prentice-Hall, Englewood Cliffs, N.J., 1982. White, *Industrial Electrostatic Precipitation*, Addison-Wesley, Reading, Mass., 1963. White and Smith, *High-Efficiency Air Filtration*, Butterworth, Washington, 1964. ASME Research Committee on Industrial and Municipal Wastes, *Combustion Fundamentals for Waste Incineration*, American Society of Mechanical Engineers, 1974. Buonicore and Davis (eds.), *Air Pollution Engineering*

Manual, Air & Waste Management Association, Van Nostrand Reinhold, 1992. Burchsted, Fuller, and Kahn, *Nuclear Air Cleaning Handbook*, ORNL for the U.S. Energy Research and Development Administration, NTIS Report ERDA 76-21, 1976. Dennis (ed.), *Handbook on Aerosols*, GCA for the U.S. Energy Research and Development Administration, NTIS Report TID-26608, 1976. Stern, *Air Pollution*, 3d ed., Academic Press, 1977 (supplement 1986).

PURPOSE OF DUST COLLECTION

Dust collection is concerned with the removal or collection of solid dispersoids in gases for purposes of:

1. Air-pollution control, as in fly-ash removal from power-plant flue gases
2. Equipment-maintenance reduction, as in filtration of engine-intake air or pyrites furnace-gas treatment prior to its entry to a contact sulfuric acid plant
3. Safety- or health-hazard elimination, as in collection of siliceous and metallic dusts around grinding and drilling equipment and in some metallurgical operations and flour dusts from milling or bagging operations
4. Product-quality improvement, as in air cleaning in the production of pharmaceutical products and photographic film
5. Recovery of a valuable product, as in collection of dusts from dryers and smelters
6. Powdered-product collection, as in pneumatic conveying; the spray drying of milk, eggs, and soap; and the manufacture of high-purity zinc oxide and carbon black

PROPERTIES OF PARTICLE DISPERSOIDS

An understanding of the fundamental properties and characteristics of gas dispersoids is essential to the design of industrial dust-control equipment. Figure 17-34 shows characteristics of dispersoids and other particles together with the types of gas-cleaning equipment that are applicable to their control. Two types of solid dispersoids are shown: (1) dust, which is composed of particles larger than 1 μm ; and (2) fume, which consists of particles generally smaller than 1 μm . Dusts usually result from mechanical disintegration of matter. They may be redispersed from the settled, or bulk, condition by an air blast. Fumes are submicrometer dispersoids formed by processes such as combustion, sublimation, and condensation. Once collected, they cannot be redispersed from the settled condition to their original state of dispersion by air blasts or mechanical dispersion equipment.

The primary distinguishing characteristic of gas dispersoids is particle size. The generally accepted unit of particle size is the micrometer, μm . (Prior to the adoption of the SI system, the same unit was known as the micron and was designated by μ .) The particle size of a gas dispersoid is usually taken as the diameter of a sphere having the same mass and density as the particle in question. Another common method is to designate the screen mesh that has an aperture corresponding to the particle diameter; the screen scale used must also be specified to avoid confusion.

From the standpoint of collector design and performance, the most important size-related property of a dust particle is its dynamic behavior. Particles larger than 100 μm are readily collectible by simple inertial or gravitational methods. For particles under 100 μm , the range of principal difficulty in dust collection, the resistance to motion in a gas is viscous (see Sec. 6, "Fluid and Particle Dynamics"), and for such particles, the most useful size specification is commonly the Stokes settling diameter, which is the diameter of the spherical particle of the same density that has the same terminal velocity in viscous flow as the particle in question. It is yet more convenient in many circumstances to use the "aerodynamic diameter," which is the diameter of the particle of unit density (1 g/cm^3) that has the same terminal settling velocity. Use of the aerodynamic diameter permits direct comparisons of the dynamic behavior of particles that are actually of different sizes, shapes, and densities [Raabe, *J. Air Pollut. Control Assoc.*, **26**, 856 (1976)].

When the size of a particle approaches the same order of magnitude as the mean free path of the gas molecules, the settling velocity is greater than predicted by Stokes' law because of molecular slip. The slip-flow correction is appreciable for particles smaller than 1 μm and is allowed for by the Cunningham correction for Stokes' law (Lapple, *op. cit.*; Licht, *op. cit.*). The Cunningham correction is applied in

calculations of the aerodynamic diameters of particles that are in the appropriate size range.

Although solid fume particles may range in size down to perhaps 0.001 μm , fine particles effectively smaller than about 0.1 μm are not of much significance in industrial dust and fume sources because their aggregate mass is only a very small fraction of the total mass emission. At the concentrations present in such sources (e.g., production of carbon black) the coagulation, or flocculation, rate of the ultrafine particles is extremely high, and the particles speedily grow to sizes of 0.1 μm or greater. The most difficult collection problems are thus concerned with particles in the range of about 0.1 to 2 μm , in which forces for deposition by inertia are small. For collection of particles under 0.1 μm , diffusional deposition becomes increasingly important as the particle size decreases.

In a gas stream carrying dust or fume, some degree of particle flocculation will exist, so that both discrete particles and clusters of adhering particles will be present. The discrete particles composing the clusters may be only loosely attached to each other, as by van der Waals forces [Lapple, *Chem. Eng.*, **75**(11), 149 (1968)]. Flocculation tends to increase with increases in particle concentration and may strongly influence collector performance.

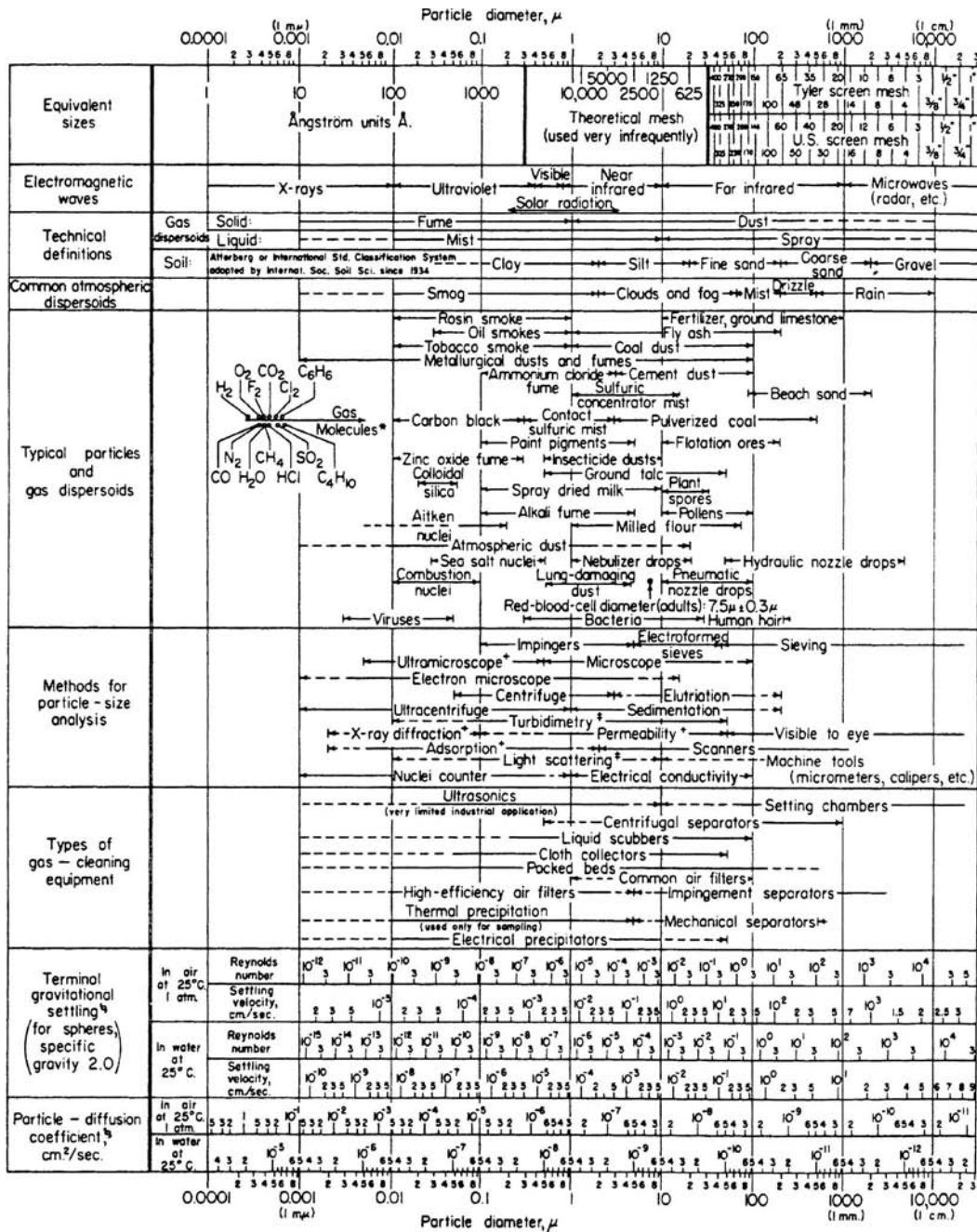
PARTICLE MEASUREMENTS

Measurements of the concentrations and characteristics of dust dispersed in air or other gases may be necessary (1) to determine the need for control measures, (2) to establish compliance with legal requirements, (3) to obtain information for collector design, and (4) to determine collector performance.

Atmospheric-Pollution Measurements The dust-fall measurement is one of the common methods for obtaining a relative long-period evaluation of particulate air pollution. Stack-smoke densities are often graded visually by means of the Ringelmann chart. Plume opacity may be continuously monitored and recorded by a photoelectric device which measures the amount of light transmitted through a stack plume. Equipment for local atmospheric-dust-concentration measurements fall into five general types: (1) the impinger, (2) the hot-wire or thermal precipitator, (3) the electrostatic precipitator, (4) the filter, and (5) impactors and cyclones. The filter is the most widely used, in the form of either a continuous tape, or a number of filter disks arranged in an automatic sequencing device, or a single, short-term, high-volume sampler. Samplers such as these are commonly used to obtain mass emission and particle-size distribution. Impactors and small cyclones are commonly used as size-discriminating samplers and are usually followed by filters for the determination of the finest fraction of the dust (Lundgren et al., *Aerosol Measurement*, University of Florida, Gainesville, 1979; and Dennis, *Handbook on Aerosols*, U.S. ERDA TID-26608, Oak Ridge, Tenn., 1976).

Process-Gas Sampling In sampling process gases either to determine dust concentration or to obtain a representative dust sample, it is necessary to take special precautions to avoid inertial segregation of the particles. To prevent such classification, a traverse of the duct may be required, and at each point the sampling nozzle must face directly into the gas stream with the velocity in the mouth of the nozzle equal to the local gas velocity at that point. This is called "isokinetic sampling." If the sampling velocity is too high, the dust sample will contain a lower concentration of dust than the mainstream, with a greater percentage of fine particles; if the sampling velocity is too low, the dust sample will contain a higher concentration of dust with a greater percentage of coarse particles [Lapple, *Heat. Piping Air Cond.*, **16**, 578 (1944); *Manual of Disposal of Refinery Wastes*, vol. V, American Petroleum Institute, New York, 1954; and Dennis, *op. cit.*].

Particle-Size Analysis Methods for particle-size analysis are shown in Fig. 17-34, and examples of size-analysis methods are given in Table 17-1. More detailed information may be found in Lapple, *Chem. Eng.*, **75**(11), 140 (1968); Lapple, "Particle-Size Analysis," in *Encyclopedia of Science and Technology*, 5th ed., McGraw-Hill, New York, 1982; Cadle, *The Measurement of Airborne Particles*, Wiley, New York, 1975; Lowell, *Introduction to Powder Surface Area*, 2d ed., Wiley, New York, 1993; and Allen, *Particle Size Measurement*, 4th ed., Chapman and Hall, London, 1990. Particle-size distribution may be presented on either a frequency or a cumulative basis; the various methods are discussed in



* Molecular diameters calculated from viscosity data at 0°C.
 † Furnishes average particle diameter but no size distribution.
 ‡ Size distribution may be obtained by special calibration.
 § Stokes-Cunningham factor included in values given for air but not included for water.

FIG. 17-34 Characteristics of particles and particle dispersoids. (Courtesy of the Stanford Research Institute; prepared by C. E. Lapple.)

the references just cited. The most common method presents a plot of particle size versus the cumulative weight percent of material larger or smaller than the indicated size, on logarithmic-probability graph paper. For determination of the aerodynamic diameters of particles, the most commonly applicable methods for particle-size analysis are those

based on inertia: aerosol centrifuges, cyclones, and inertial impactors (Lundgren et al., *Aerosol Measurement*, University of Florida, Gainesville, 1979; and Liu, *Fine Particles—Aerosol Generation, Measurement, Sampling, and Analysis*, Academic, New York, 1976). Impactors are the most commonly used. Nevertheless, impactor

TABLE 17-1 Particle Size Analysis Methods and Equipment

Method	Brand names	Size range	Sample size, g
Quantitative image analysis	American Innovation Videometric, Analytical Measuring Systems Quickstep & Optomax, Artec Omnicon Automatrix, Boeckeler, Buehler Omnimat, Compix Imaging Systems, Data Translation—Global Lab, Image, Hamamatsu C-1000, Hitech Olympus Cue-3, Joyce-Loebl Magiscan, Leco AMF System, Leico Quantimet, LeMont Oasys, Millipore_MC, Nacht 1500, Nikon Microphot, Oncor Instrument System, Optomax V, Outokumpu Imagist, Shapspere Juliet, Tracor Northern, Carl Zeiss Videoplan	1–1000 μm	0.001
Sieves:		4–100 mm	500
Punched Plate	Many		
Woven wire	Many	20 μm –125 mm	25–200
Micromesh	Buckbee Mears, Veco, Endecottes	5–500+ μm	1–5
Sieving machines (Air jet, sonic wet and dry)	Alpine, ATM, Gilson, Gradex, Hosokawa, Retsch, Seishin		
Sedimentation	<i>Pipette</i> —Gilson, <i>Photosedimentometer—gravitational</i> , Paar; <i>centrifugal</i> , Joyce Loebl, Brookhaven, Horiba, Seishin, Shimadzu; <i>x-ray absorption—gravitational</i> , Quantachrome, Micromeretics; <i>centrifugal</i> , Brookhaven	Gravitational 1–100 μm Centrifugal 0.05–5 mm	0.1–5+ g
Classification	Air-Bahco, Water-Warman Cyclosizer	5–500 μm	5–100 g
Field scanning (light)	Cilas, Coulter, Insitex, Fritsch, Horiba, Leeds & Northrup (Microtrac), Malvern, Nitto, Seishin, Shimadzu, Sympatec	0.04–3500 μm	<1 g (wet) >20 g (on-line) On-line
Field scanning (ultrasonics)	Sympatec OPUS, Pen-Kem		
Stream scanning	Brinkmann, Climet, Coulter, Dantec, Erldco, Faley, Flowvision, Hiac/Royco, Kowa, Lasentec, Malvern, Met One, Particle Measuring Systems, Polytec, Proceadyne, Rion, Spectrex	0.2–10,000 μm	0.1–10 g (also on-line)
Zeta potential	Zeta Plus, Micromeretics, Zeta sizer	0.001–30 μm	0.1–1 μm
Photon correlation Spectroscopy	Malvern, Nicomp, Brookhaven, Coulter, Photol		

NOTE: This table was compiled with the assistance of T. Allen, DuPont Particle Science and Technology, and is not intended to be comprehensive. Many other fine suppliers of particle analysis equipment are available.

measurements are subject to numerous errors [Rao and Whitby, *Am. Ind. Hyg. Assoc. J.*, **38**, 174 (1977); Marple and Willeke, "Inertial Impactors," in Lundgren et al., *Aerosol Measurement*; and Fuchs, "Aerosol Impactors," in Shaw, *Fundamentals of Aerosol Science*, Wiley, New York, 1978]. Reentrainment due to particle bouncing and blowoff of deposited particles makes a dust appear finer than it actually is, as does the breakup of flocculated particles. Processing cascade-impactor data also presents possibilities for substantial errors (Fuchs, *The Mechanics of Aerosols*, Pergamon, Oxford, 1964) and is laborious as well. Lawless (Rep. No. EPA-600/7-78-189, U.S. EPA, 1978) discusses problems in analyzing and fitting cascade-impactor data to obtain dust-collector efficiencies for discrete particle sizes.

The measured diameters of particles should as nearly as possible represent the effective particle size of a dust as it exists in the gas stream. When significant flocculation exists, it is sometimes possible to use measurement methods based on gravity settling.

For dust-control work, it is recommended that a preliminary qualitative examination of the dust first be made without a detailed particle count. A visual estimate of particle-size distribution will often provide sufficient guidance for a preliminary assessment of requirements for collection equipment.

MECHANISMS OF DUST COLLECTION

The basic operations in dust collection by any device are (1) separation of the gas-borne particles from the gas stream by deposition on a collecting surface; (2) retention of the deposit on the surface; and (3) removal of the deposit from the surface for recovery or disposal. The separation step requires (1) application of a force that produces a differential motion of a particle relative to the gas and (2) a gas retention time sufficient for the particle to migrate to the collecting surface. The principal mechanisms of aerosol deposition that are applied in dust collectors are (1) gravitational deposition, (2) flow-line interception, (3) inertial deposition, (4) diffusional deposition, and (5) electrostatic deposition.

Thermal deposition is only a minor factor in practical dust-collection equipment because the thermophoretic force is small. Table 17-2 lists these six mechanisms and presents the characteristic parameters of their operation [Lunde and Lapple, *Chem. Eng. Prog.*, **53**, 385 (1957)]. The actions of the inertial-deposition, flow-line-interception, and diffusional-deposition mechanisms are illustrated in Fig. 17-35 for the case of a collecting body immersed in a particle-laden gas stream.

Two other deposition mechanisms, in addition to the six listed, may be in operation under particular circumstances. Some dust particles may be collected on filters by sieving when the pore diameter is less than the particle diameter. Except in small membrane filters, the sieving mechanism is probably limited to surface-type filters, in which a layer of collected dust is itself the principal filter medium.

The other mechanism appears in scrubbers. When water vapor diffuses from a gas stream to a cold surface and condenses, there is a net hydrodynamic flow of the noncondensable gas directed toward the surface. This flow, termed the Stefan flow, carries aerosol particles to the condensing surface (Goldsmith and May, in Davies, *Aerosol Science*, Academic, New York, 1966) and can substantially improve the performance of a scrubber. However, there is a corresponding Stefan flow directed away from a surface at which water is evaporating, and this will tend to repel aerosol particles from the surface.

In addition to the deposition mechanisms themselves, methods for preliminary conditioning of aerosols may be used to increase the effectiveness of the deposition mechanisms subsequently applied. One such conditioning method consists of imposing on the gas high-intensity acoustic vibrations to cause collisions and flocculation of the aerosol particles, producing large particles that can be separated by simple inertial devices such as cyclones. This process, termed "sonic (or acoustic) agglomeration," has attained only limited commercial acceptance.

Another conditioning method, adaptable to scrubber systems, consists of inducing condensation of water vapor on the aerosol particles as nuclei, increasing the size of the particles and making them more susceptible to collection by inertial deposition.

TABLE 17-2 Summary of Mechanisms and Parameters in Aerosol Deposition

Deposition	Origin of force field	Deposition mechanism measurable in terms of		System parameters
		Basic parameter	Specific modifying parameters	
Flow-line interception ^o	Physical gradient ^o	$N_{jf} = \left(\frac{D_p}{D_b} \right)$	$N_{sc} = \left(\frac{N_{jf}^2}{N_{at} N_{df}} \right)$ $= \left(\frac{18\mu}{K_m \rho_p D_c} \right)^\dagger$	Geometry: $(D_{b1}/D_b), (D_{b2}/D_b), \text{ etc.}$ ϵ_p Δ
Inertial deposition	Velocity gradient	$N_{at} = \left(\frac{K_m \rho_s D_p^2 V_o}{18\mu D_b} \right)$		
Diffusional deposition	Concentration gradient	$N_{df} = \left(\frac{D_c}{V_o D_b} \right)$		
Gravity settling	Elevation gradient	$N_{sg} = \left(\frac{u_t}{V_o} \right)$		Flow pattern: N_{Re}^\ddagger N_{Ma} N_{Kn}
Electrostatic precipitation	Electric-field gradient \S	$N_{sec} = \left(\frac{K_{eo} Q_p \epsilon_b}{\mu D_p V_o} \right)$	$\delta_p, \delta_b \P$	Surface accommodation
	a. Attraction b. Induction	$N_{sei} = \left(\frac{\delta_p - 1}{\delta_p + 2} \right) \left(\frac{K_m D_p^2 \delta_o \epsilon_b 2}{\mu D_b V_o} \right)$		
Thermal precipitation	Temperature gradient	$N_{st} = \left(\frac{T - T_b}{T} \right) \left(\frac{\mu}{K_m \rho D_b V_o} \right) \left(\frac{k_t}{2k_t + k_{tp}} \right)$	$(T_b/T), (T_p/T), \ddagger (N_{Pr}), (k_{tp}/k_t), (k_{tb}/k_t), \P (c_{tp}/c_b), (c_{tb}/c_b) \P$	

SOURCE: Lunde and Lapple, *Chem. Eng. Prog.*, **53**, 385 (1957).

^oThis has also commonly been termed "direct interception" and in conventional analysis would constitute a physical boundary condition imposed upon the particle path induced by action of other forces. By itself it reflects deposition that might result with a hypothetical particle having finite size but no mass or elasticity.

\ddagger This parameter is an alternative to N_{jf}, N_{at} , or N_{df} and is useful as a measure of the interactive effect of one of these on the other two. It is comparable with the Schmidt number.

\S When applied to the inertial deposition mechanism, a convenient alternative is $(K_m \rho_s / 18\mu) = N_{at} / (N_{jf}^2 N_{Re})$.

\P In cases in which the body charge distribution is fixed and known, ϵ_b may be replaced with Q_{be} / δ_o .

\P Not likely to be significant contributions.

Most forms of dust-collection equipment use more than one of the collection mechanisms, and in some instances the controlling mechanism may change when the collector is operated over a wide range of conditions. Consequently, collectors are most conveniently classified by type rather than according to the underlying mechanisms that may be operating.

PERFORMANCE OF DUST COLLECTORS

The performance of a dust collector is most commonly expressed as the collection efficiency η , the weight ratio of the dust collected to the dust entering the apparatus. However, the collection efficiency is usually related exponentially to the properties of the dust and gas and the operating conditions of most types of collectors and hence is an insensitive function of the collector operating conditions as its value approaches 1.0. Performance in the high-efficiency range is better expressed by the penetration $1 - \eta$, the weight ratio of the dust escaping to the dust entering. Particularly in reference to collection of radioactive aerosols, it is common to express performance in terms of the reciprocal of the penetration $1/(1 - \eta)$, which is termed the *decontamination index* (DI). The number of transfer units N_t , which is equal to $\ln [1/(1 - \eta)]$ in the case of dust collection, was first proposed for use by Lapple (Wright, Stasny, and Lapple, "High Velocity Air Filters," WADC Tech. Rep. 55-457, ASTIA No. AD-142075, October 1957) and is more commonly used than the DI. Because of the exponential form of the relationship between efficiency and process variables for most dust collectors, the use of N_t (or DI) is particularly suitable for correlating collector performance data.

In comparing alternative collectors for a given service, a figure of merit is desirable for ranking the different devices. Since power consumption is one of the most important characteristics of a collector, the ratio of N_t to power consumption is a useful criterion. Another is the ratio of N_t to capital investment.

DUST-COLLECTOR DESIGN

In dust-collection equipment, most or all of the collection mechanisms may be operating simultaneously, their relative importance being determined by the particle and gas characteristics, the geometry of the equipment, and the fluid-flow pattern. Although the general case is exceedingly complex, it is usually possible in specific instances to determine which mechanism or mechanisms may be controlling. Nevertheless, the difficulty of theoretical treatment of dust-collection phenomena has made necessary simplifying assumptions, with the introduction of corresponding uncertainties. Theoretical studies have been hampered by a lack of adequate experimental techniques for verification of predictions. Although theoretical treatment of collector performance has been greatly expanded in the period since 1960, few of the resulting performance models have received adequate experimental confirmation because of experimental limitations.

The best-established models of collector performance are those for fibrous filters and fixed-bed granular filters, in which the structures and fluid-flow patterns are reasonably well defined. These devices are also adapted to small-scale testing under controlled laboratory conditions. Realistic modeling of full-scale electrostatic precipitators and scrubbers is incomparably more difficult. Confirmation of the models has been further limited by a lack of monodisperse aerosols that can be generated on a scale suitable for testing equipment of substantial sizes. When a polydisperse test dust is used, the particle-size distributions of the dust both entering and leaving a collector must be determined with extreme precision to avoid serious errors in the determination of the collection efficiency for a given particle size.

The design of industrial-scale collectors still rests essentially on empirical or semiempirical methods, although it is increasingly guided by concepts derived from theory. Existing theoretical models frequently embody constants that must be evaluated by experiment and that may actually compensate for deficiencies in the models.

DUST-COLLECTION EQUIPMENT

Gravity Settling Chambers The gravity settling chamber is probably the simplest and earliest type of dust-collection equipment, consisting of a chamber in which the gas velocity is reduced to enable dust to settle out by the action of gravity. Its simplicity lends it to almost any type of construction. Practically, however, its industrial utility is limited to removing particles larger than 325 mesh (43- μm diameter). For removing smaller particles, the required chamber size is generally excessive.

Gravity collectors are generally built in the form of long, empty, horizontal, rectangular chambers with an inlet at one end and an outlet at the side or top of the other end. By assuming a low degree of turbulence relative to the settling velocity of the dust particle in question, the performance of a gravity settling chamber is given by

$$\eta = \frac{u_t L_s}{H V_s} = \frac{u_t B_s L_s}{q} \quad (\text{for } \eta \leq 1.0) \quad (17-1)$$

where V_s = average gas velocity. Expressing u_t in terms of particle size (equivalent spherical diameter), the smallest particle that can be completely separated out corresponds to $\eta = 1.0$ and, assuming Stokes' law, is given by

$$D_{p,\min} = \sqrt{\frac{18\mu H_s V_s}{g L_s (\rho_s - \rho)}} \\ = \sqrt{\frac{18\mu q}{g L_s B_s (\rho_s - \rho)}} \quad (17-2)$$

where ρ = gas density and ρ_s = particle density. For a given volumetric air-flow rate, collection efficiency depends on the total plan cross section of the chamber and is independent of the height. The height need be made only large enough so that the gas velocity V_s in the chamber is not so high as to cause reentrainment of separated dust. Generally V_s should not exceed about 3 m/s (10 ft/s).

Horizontal plates arranged as shelves within the chamber will give a marked improvement in collection. This arrangement is known as the Howard dust chamber (Fume Arrester, U.S. Patent 896,111, 1908). The disadvantage of the unit is the difficulty of cleaning owing to the close shelf spacing and warpage at elevated temperatures.

The pressure drop through a settling chamber is small, consisting primarily of entrance and exit losses. Because low gas velocities are used, the chamber is not subject to abrasion and may therefore be used as a precleaner to remove very coarse particles and thus minimize abrasion on subsequent equipment.

Impingement Separators Impingement separators are a class of inertial separators in which particles are separated from the gas by inertial impingement on collecting bodies arrayed across the path of the gas stream, as shown on Fig. 17-35. Fibrous-pad inertial impingement separators for the collection of wet particles are the main application in current technology, as is described in Sec. 14, "Impingement Separation." With the growing need for very high performance dust collectors, there is little application anymore for dry impingement collectors.

Cyclone Separators The most widely used type of dust-collection equipment is the cyclone, in which dust-laden gas enters a cylindrical or conical chamber tangentially at one or more points and

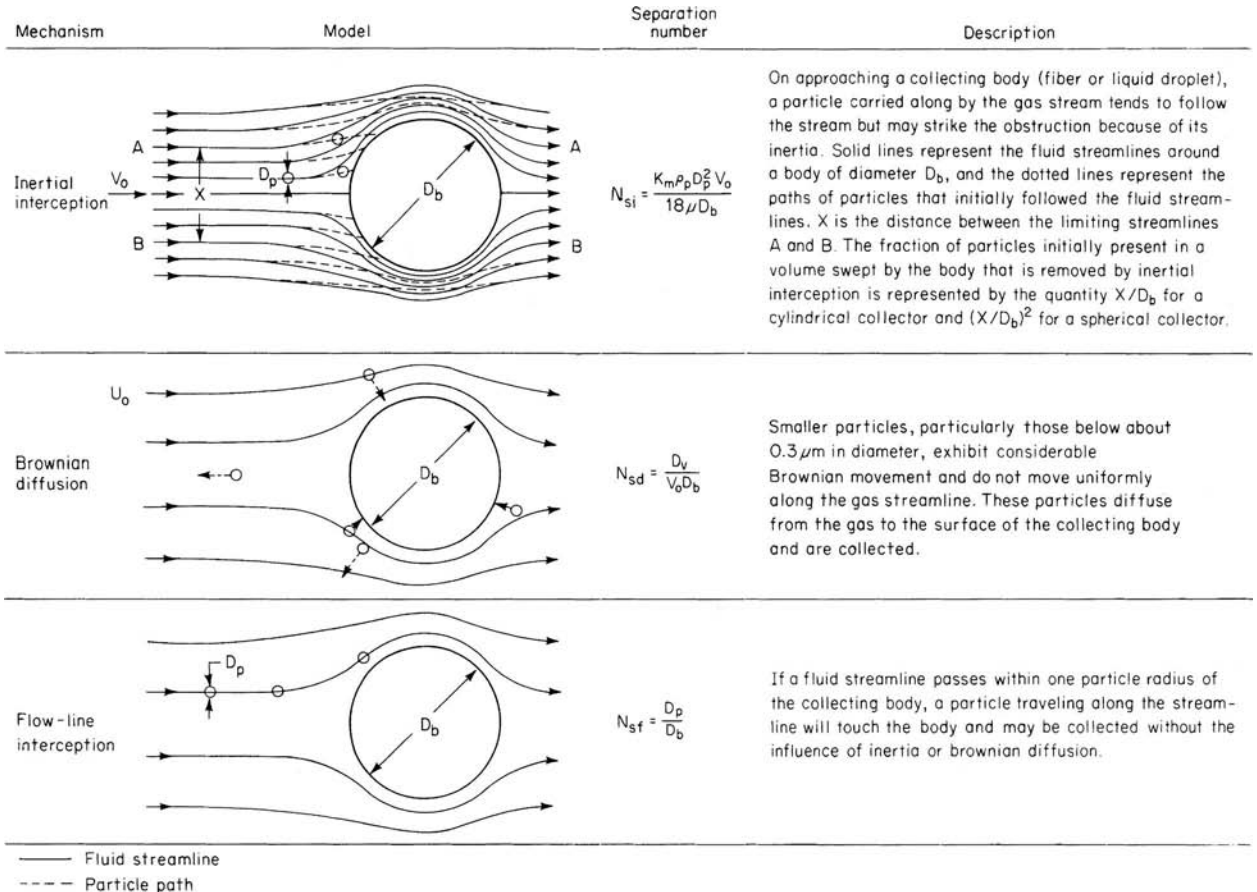


FIG. 17-35 Particle deposition on collector bodies.

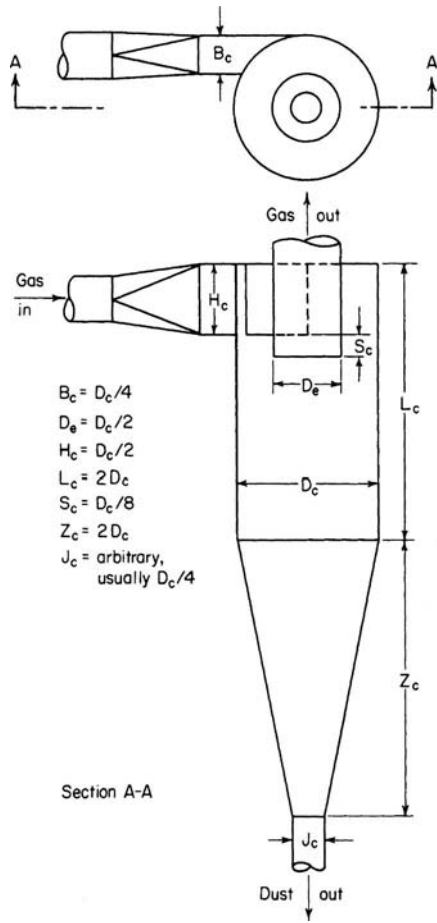


FIG. 17-36 Cyclone-separator proportions.

leaves through a central opening (Fig. 17-36). The dust particles, by virtue of their inertia, will tend to move toward the outside separator wall, from which they are led into a receiver. A cyclone is essentially a settling chamber in which gravitational acceleration is replaced by centrifugal acceleration. At operating conditions commonly employed, the centrifugal separating force or acceleration may range from 5 times gravity in very large diameter, low-resistance cyclones, to 2500 times gravity in very small, high-resistance units. The immediate entrance to a cyclone is usually rectangular.

Fields of Application Within the range of their performance capabilities, cyclone collectors offer one of the least expensive means of dust collection from the standpoint of both investment and operation. Their major limitation is that their efficiency is low for collection of particles smaller than 5 to 10 μm . Although cyclones may be used to collect particles larger than 200 μm , gravity settling chambers or simple inertial separators (such as gas-reversal chambers) are usually satisfactory for this size of particle and are less subject to abrasion. In special cases in which the dust is highly agglomerated or in high dust concentrations (over 230 g/m^3 , or 100 gr/ft^3) are encountered, cyclones will remove dusts having small particle sizes. In certain instances, efficiencies as high as 98 percent have been attained on dusts having ultimate particle sizes of 0.1 to 2.0 μm because of the predominant effect of particle agglomeration due to high interparticle forces. Cyclones are used to remove both solids and liquids from gases and have been operated at temperatures as high as 1200°C and pressures as high as 50,700 kPa (500 atm).

Cyclones can be very small or very large. The smallest cyclones range from approximately 1 to 2 cm in diameter and the largest up to about 10 m in diameter. The number of cyclones used for a single fluidized bed can vary from 1 to up to 22 sets of first-stage and second-stage cyclones (44 cyclones total).

Flow Pattern In a cyclone, the gas moves in a double vortex with the gas initially spiraling downward at the outside after it enters the inlet; then, the gas flows upward in the center of the cyclone before it exits. When the gas enters the cyclone, its velocity undergoes a redistribution so that the tangential component of velocity increases with decreasing radius, as expressed by $V_{ct} \sim r^{-n}$. The tangential velocity in a cyclone may reach a value several times the average inlet gas velocity. Theoretical considerations indicate that n should be equal to 1.0 in the absence of wall friction. Actual measurements [Shepherd and Lapple, *Ind. Eng. Chem.* **31**: 972 (1939); **32**: 1246 (1940)], however, indicate that n may range from 0.5 to 0.7 over a large portion of the cyclone radius. Ter Linden [*Inst. Mech. Eng. J.* **160**: 235 (1949)] found n to be 0.52 for tangential velocities measured in the cylindrical portion of the cyclone at positions ranging from the radius of the gas outlet pipe to the radius of the outer wall. Although the velocity approaches zero at the wall, the boundary layer is sufficiently thin that pitot-tube measurements show relatively high tangential velocities there, as shown in Fig. 17-37. The radial velocity V_r is directed toward the center throughout most of the cyclone, except at the center, where it is directed outward. Superimposed on the “double spiral,” there may be a “double eddy” [Van Tongran, *Mech. Eng.* **57**: 753 (1935); and Wellmann, *Feuerungstechnik* **26**: 137 (1938)] similar to that encountered in pipe coils. Measurements on cyclones of the type shown in Fig. 17-36 indicate, however, that such double-eddy velocities are small compared with the tangential velocity (Shepherd and Lapple, *op. cit.*). Recent analyses of flow patterns can be found in Hoffman et al., *Powder Technol.* **70**: 83 (1992); and Trefz and Muschelknautz, *Chem. Eng. Technol.* **16**: 153 (1993).

The inner vortex (often called the core of the vortex) rotates at a much higher velocity than the outer vortex. In the absence of solids, the radius of this inner vortex has been measured to be 0.4 to 0.8 r . With axial inlet cyclones, the inner core vortex is aligned with the axis of the gas outlet tube. With tangential or volute cyclone inlets, however, the vortex is not exactly aligned with the axis. The non-symmetric entry of the tangential or volute inlet causes the axis of the vortex to be slightly eccentric from the axis of the cyclone. This means that the bottom of the vortex is displaced some distance from the axis and can “pluck off” and reentrain dust from the solids

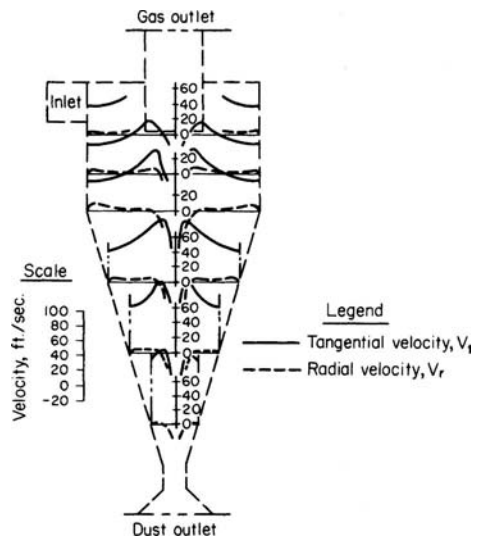


FIG. 17-37 Variation of tangential velocity and radial velocity at different points in a cyclone. [Ter Linden, *Inst. Mech. Eng. J.*, **160**, 235 (1949).]

sliding down the cyclone cone if the vortex gets too close to the wall of the cyclone cone.

At the bottom of the vortex, there is substantial turbulence as the gas flow reverses and flows up the middle of the cyclone into the gas outlet tube. As indicated above, if this region is too close to the wall of the cone, substantial reentrainment of the separated solids can occur. Therefore, it is very important that cyclone design take this into account.

The vortex of a cyclone will precess (or wobble) about the center axis of the cyclone. This motion can bring the vortex into close proximity to the wall of the cone of the cyclone and "pluck" off and reentrain the collected solids flowing down along the wall of the cone. The vortex may also cause erosion of the cone if it touches the cone wall. Sometimes an inverted cone or a similar device is added to the bottom of the cyclone in the vicinity of the cone and dipleg to stabilize and "fix" the vortex. If it is placed correctly, the vortex will attach to the cone and the vortex movement will be stabilized, thus minimizing the efficiency loss due to plucking the solids off the wall and erosion of the cyclone cone.

Hugi and Reh [*Chem. Eng. Technol.* 21(9): 716-719 (1998)] have reported that (at high solids loadings) enhanced cyclone efficiency occurs when the solids form a coherent, stable strand at the entrance to a cyclone. The formation of such a strand is dependent upon several factors. They reported a higher cyclone efficiency for smaller ($d_{p,50} = 40 \mu\text{m}$) solids than for larger solids ($d_{p,50} = 125 \mu\text{m}$). This is not what theory would predict. However, they also found that the smaller particles formed coherent, stable strands more readily than the larger particles, which explained the reason for the apparent discrepancy.

Cyclone Efficiency The methods described below for pressure drop and efficiency calculations were given by Zenz in *Manual on Disposal of Refinery Wastes—Atmospheric Emissions*, chap. 11 (1975), American Petroleum Institute Publ. 931 and improved by Particulate Solid Research Inc. (PSRI), Chicago. Cyclones work by using centrifugal force to increase the gravity field experienced by the solids. They then move to the wall under the influence of their effectively increased weight. Movement to the wall is improved as the path the solids traverse under centrifugal flow is increased. This path is equated with the number of spirals the solids make in the cyclone barrel. Figure 17-38 gives the number of spirals N_s as a function of the maximum velocity in the cyclone. The maximum velocity may be either the inlet or the outlet velocity depending on the design. The equation for D_{pth} , the theoretical size particle removed by the cyclone at 50 percent collection efficiency, is

$$D_{pth} = \sqrt{\frac{9\mu_g B_c}{\pi N_s v_{max} (\rho_p - \rho_g)}}$$

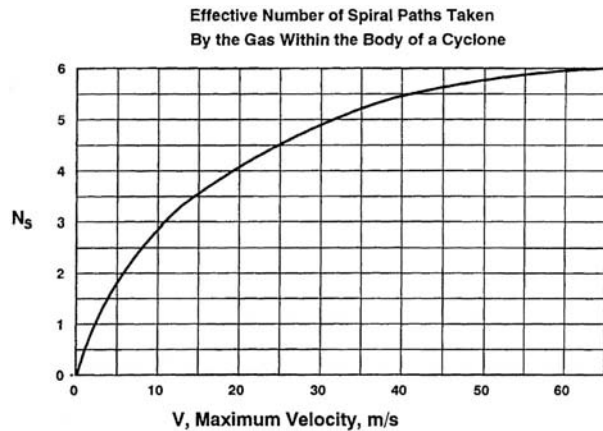


FIG. 17-38 N_s versus velocity—where the larger of either the inlet or outlet velocity is used.

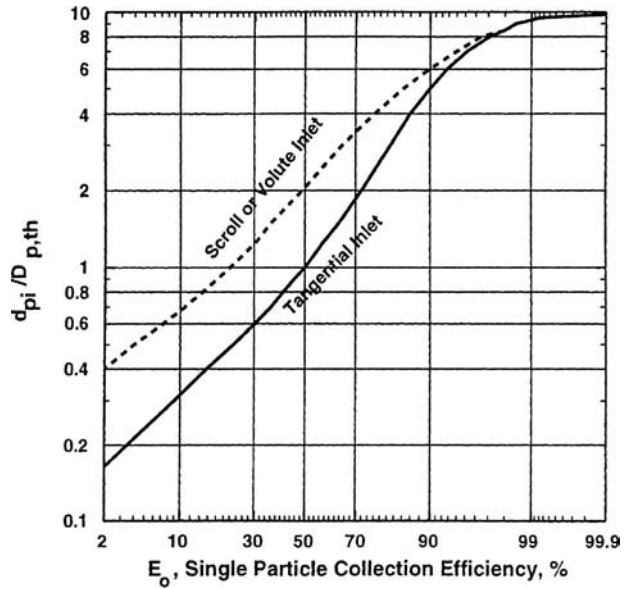


FIG. 17-39 Single particle collection efficiency curve. (Courtesy of PSRI, Chicago.)

This equation is a result of the residence time theory of particle collection. In this theory, the time that it takes for a particle to reach the wall is balanced by the time that a particle spends in the cyclone. The particle size that makes it to the wall by the time that it exits the cyclone is the particle size collected at 50 percent collection efficiency, D_{pth} .

When consistent units are used, the particle size calculated by the above equation will be in either meters or feet. The equation contains effects of cyclone size, gas velocity, gas viscosity, gas density, and particle density of the solids. In practice, a design curve such as given in Fig. 17-39 uses D_{pth} as the size at which 50 percent of solids of a given size are collected by the cyclone. The material entering the cyclone is divided into fractional sizes, and the collection efficiency for each size is determined. The total efficiency of collection is the sum of the collection efficiencies of the cuts.

The above applies for very dilute systems, usually on the order of 1 gr/ft³, or 2.3 g/m³ where 1 gr = (1/7000) lb. When denser flows of solids are present in the inlet gas, cyclone efficiency increases dramatically. This is thought to be due to the coarse particles colliding with fines as they move to the wall, which carry a large percentage of the finer particles along with them. Other explanations are that the solids have a lower drag coefficient or tend to agglomerate in multiparticle environments, thus effectively becoming larger particles. At very high inlet solids loadings, it is believed the gas simply cannot hold that much solid material in suspension at high centrifugal forces, and the bulk of the solids simply "condense" out of the gas stream.

The phenomenon of increasing efficiency with increasing loading is represented by Figs. 17-40 and 17-41 for Geldart group A and B solids, respectively (see beginning of Sec. 17). The initial efficiency of a particle size cut is found on the chart, and the parametric line is followed to the proper overall solids loading. The efficiency for that cut size is then read from the graph.

A single cyclone can sometimes give sufficient gas-solids separation for a particular process or application. However, solids collection efficiency can usually be enhanced by placing cyclones in series. Cyclones in series are typically necessary for most processes to minimize particulate emissions or to minimize the loss of expensive solid reactant or catalyst. Two cyclones in series are most common, but sometimes three cyclones in series are used. Series cyclones can be very efficient. In fluidized catalytic cracking regenerators, two stages of cyclones can give efficiencies of up to and even greater than 99.999 percent.

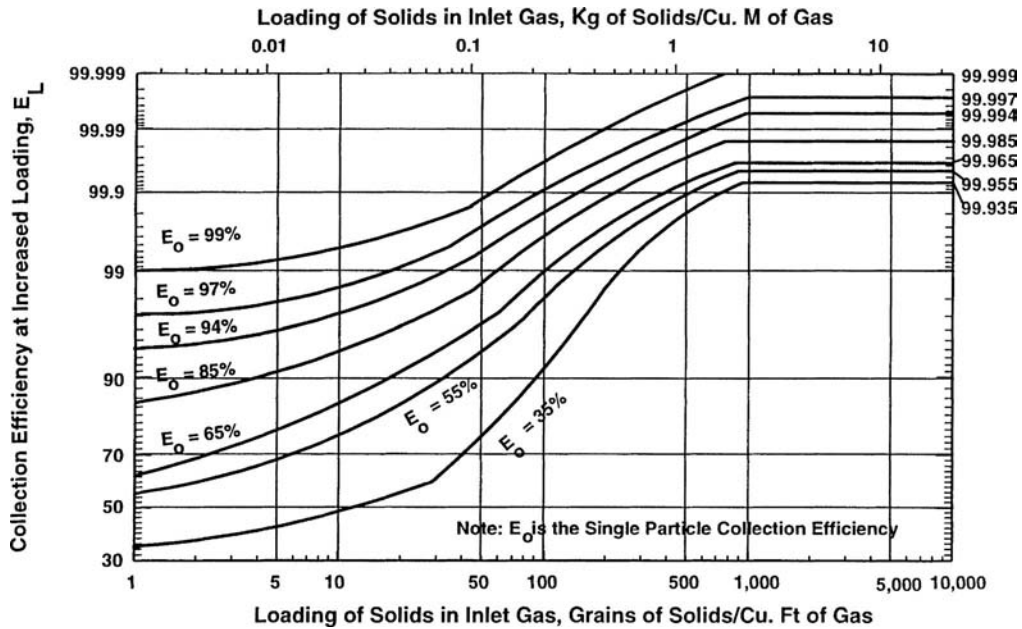


FIG. 17-40 Effect of inlet loading on collection efficiency for Geldart group A and group C particles. (Courtesy of PSRI, Chicago.)

Typically, first-stage cyclones will have an inlet gas velocity less than that of second-stage cyclones. The lower inlet velocity of first-stage cyclones results in lower particle attrition rates and lower wall erosion rates. After most of the solids are collected in the first stage, a higher velocity is generally used in second-stage cyclones to increase the centrifugal force on the solids and increase collection efficiency. Inlet erosion rates are generally low in the second stage because of the vastly reduced flux of solids into the second-stage cyclone. However, cone erosion rates in second-stage cyclones are much greater than in first-stage cyclones.

Pressure Drop Pressure drop is first determined by summing five pressure drop components associated with the cyclone.

1. *Inlet contraction*

$$\Delta P = 0.5\rho_g(v_{in}^2 - v_{vessel}^2 + Kv_{in}^2)$$

where K is taken from Table 17-3. Using SI units gives the pressure drop in Pa. In English units, the factor of 32.2 for g must be included. This loss is primarily associated with cyclones located in the freeboard of a fluidized bed. If the cyclone is located external to a vessel and the

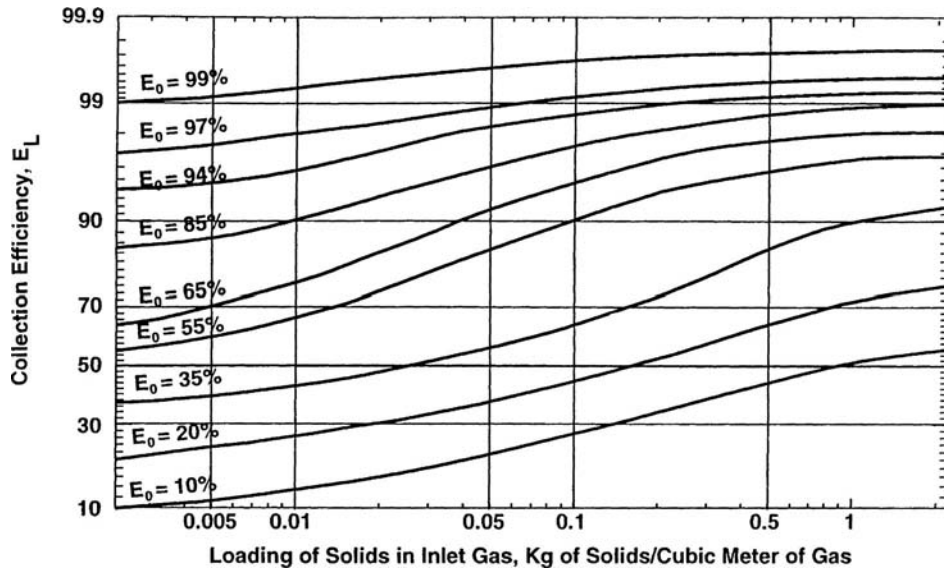


FIG. 17-41 Effect of inlet loading on collection efficiency (Geldart group B and group D) particles. (Courtesy of PSRI, Chicago.)

TABLE 17-3 K versus Area Ratio

Area ratio	K
0	0.50
0.1	0.47
0.2	0.43
0.3	0.395
0.4	0.35

high-pressure tap used to measure the cyclone pressure drop is in the inlet pipe before the cyclone, the measured pressure drop will not include this pressure loss, and this term should not be used to calculate total cyclone pressure drop. However, if the high-pressure tap to measure the cyclone pressure drop is located in the freeboard of the bed, this component will be included in the measured pressure drop, and it should be included in the calculation of the total cyclone pressure drop.

2. Particle acceleration

$$\Delta P = Lv_{in}(v_{pin} - v_{pessel})$$

For small particles, the velocity is taken as equal to the gas velocity and *L* is the solids loading, kg/m³.

3. Barrel friction The inlet diameter *d_{in}* is taken as 4 × (inlet area)/inlet perimeter. Then

$$\Delta P = \frac{2f\rho_g v_{in}^2 \pi D_c N_s}{d_{in}}$$

where the Reynolds number for determining the friction factor *f* is based on the inlet area.

4. Gas flow reversal

$$\Delta P = \frac{\rho_g v_{in}^2}{2}$$

5. Exit contraction

$$\Delta P = 0.5\rho_g(v_{exit}^2 - v_c^2 + Kv_{exit}^2)$$

where *K* is determined from Table 17-3 based on the area ratio of barrel and exit tube of the cyclone.

The total pressure drop is the sum of the five individual pressure drops.

However, the actual pressure drop observed turns out to be a function of the solids loading. The pressure drop is high when the gas is free of solids and then *decreases* as the solids loading increases up to about 3 kg/m³ (0.2 lb/ft³). The cyclone ΔP then begins to increase with loading. The cause of the initial decline is that the presence of solids decreases the tangential velocity of the gas [Yuu, *Chem. Eng. Sci.*, **33**, 1573 (1978)]. Figure 17-42 gives the actual pressure drop based on the loading. When solids are absent, the observed pressure drop can be 2.5 times the calculated pressure drop with solids present.

Cyclone Design Factors Cyclones are sometimes designed to meet specified pressure drop limitations. For ordinary installations, operating at approximately atmospheric pressure, fan limitations generally dictate a maximum allowable pressure drop corresponding to a cyclone inlet velocity in the range of 8 to 30 m/s (25 to 100 ft/s). Consequently, cyclones are usually designed for an inlet velocity of 15 to 20 m/s (50 to 65 ft/s), although this need not be strictly adhered to.

Because of the relatively high gas velocities at the inlet of cyclones, particle attrition in fluidized-bed systems is generally dominated by the attrition produced in the cyclone. In some catalytic systems with very expensive catalysts, the economics of the process can be dependent on low attrition losses. In such cases, reducing the inlet velocity of the cyclone will significantly reduce the attrition losses in the process. To compensate for the reduction in inlet velocity, the exit gas velocity will generally be increased (by reducing the diameter of the outlet tube) in order to maintain high cyclone efficiencies. Reducing the outlet tube diameter increases the outlet gas velocity and increases the velocity in the vortex of the cyclone—increasing collection efficiency. However, as the vortex velocity is increased, its length is also increased. Therefore, care must be taken to ensure that the cyclone is long enough to contain the increased vortex length. If it is not, the vortex can extend far into the cone and can entrain solids flowing on the sides of the cone as it comes near them.

Cyclone Roughness Large weld beads, etc., can also reduce cyclone efficiency. If the solids flow along the wall of a cyclone encounters a large protuberance such as a weld bead, the weld bead acts as a type of “ski jump” and causes the solids to be deflected farther into the center of the cyclone, where they can be thrown into the vortex and carried out of the cyclone. In small pilot or research cyclones, this is especially common, because the distance between the wall of the cyclone and the vortex tube is very small. Because of their

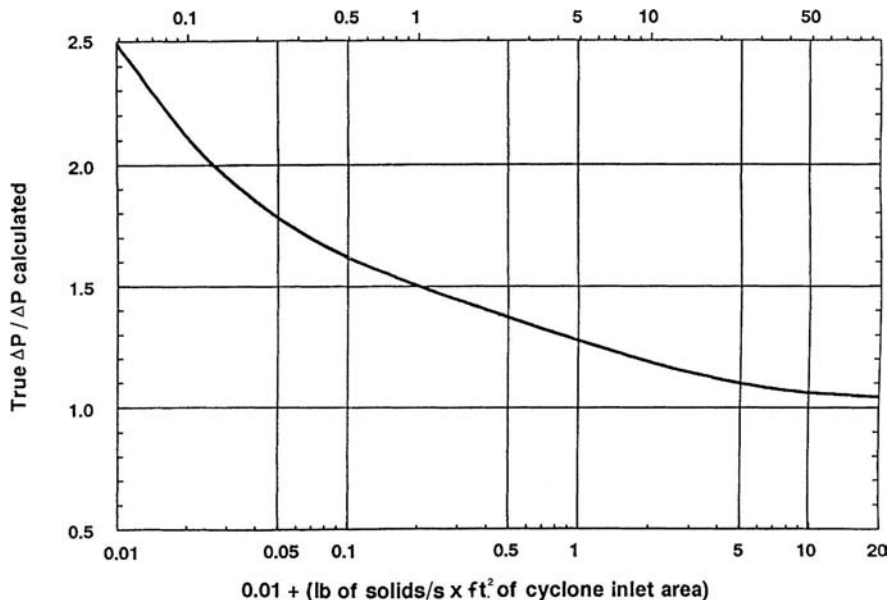


FIG. 17-42 Effect of cyclone inlet loading on pressure drop. (Courtesy of PSRI, Chicago.)

detrimental effect on cyclone efficiency, weld beads should be ground off to make the cyclone inner wall smooth.

In high-temperature processes, cyclones are often lined with refractory to both minimize heat loss and protect the metal surfaces from abrasion. These refractory surfaces are not as smooth as metal, but after a few days of operation, the refractory becomes smoother because of the abrasive action of the solids.

With very small laboratory or pilot cyclones, some solids (large polymer beads, spherical particles, etc.) can sometimes bounce off the cyclone wall immediately across from the cyclone inlet and be deflected into the vortex. Very large particles can be found in the gas outlet stream of the cyclone with these very small cyclones and with particles that bounce. To increase cyclone efficiency with these types of solids, the cyclone barrel diameter can be increased. This increases the distance between the cyclone vortex and the wall and prevents most of the solids from bouncing back into the vortex.

Theoretically, a primary design factor that can be utilized to control collection efficiency is the cyclone diameter. A smaller-diameter unit operating at a fixed pressure drop has a higher efficiency than a larger-diameter cyclone [Anderson, *Chem. Metall.* **40**: 525 (1933); Drijver, *Wärme* **60**: 333 (1937); and Whiton, *Power* **75**: 344 (1932); *Chem. Metall.* **39**: 150 (1932)]. In addition, smaller-diameter cyclones have a much smaller overall length. Small-diameter cyclones, however, will require multiple units in parallel to give the same capacity as a large cyclone. In such cases, the smaller cyclones generally discharge the dust into a common receiving hopper [Whiton, *Trans. Am. Soc. Mech. Eng.* **63**: 213 (1941)]. However, when cyclones discharge into a common hopper, there is a tendency of the gas to produce "cross-talk." This occurs when the gas exiting from one small cyclone passes up the exit of an adjoining cyclone, thus reducing efficiency. Various types of mechanical devices are generally added to the bottom of these small cyclones in parallel to reduce the cross-talk. The final cyclone design involves a compromise between collection efficiency and the complexity of equipment. It is customary to design systems for a single cyclone for a given capacity, resorting to multiple parallel units only if the predicted collection efficiency is inadequate for a single unit or single units in series.

Reducing the gas outlet diameter should increase both collection efficiency and pressure drop. To exit the cyclone, gas must enter the cyclonic flow associated with the outlet tube. If the outlet diameter is reduced, the outlet vortex increases in length to compensate. Therefore, when the outlet area is less than the inlet area, the length of the cyclone must increase. Too short a cyclone is associated with erosion of the cone and reentrainment of solids into the exit flow. Table 17-4 gives the required increase in cyclone length as a function of outlet-to-inlet area. The cyclone length is measured centrally along a cylinder 10 cm larger than the inner diameter of the outlet tube to prevent interference with the cone. If the cone interferes with this "extended vortex," the barrel must be lengthened.

As discussed above, theoretically a smaller-diameter cyclone should be able to collect smaller particles because it can develop a higher centrifugal force. However, using smaller cyclones generally means that many have to be used in parallel to accommodate large gas flows. The problem with parallel cyclones (as indicated above) is that it is difficult to get even distribution of solids into all the cyclones. If maldistribution occurs, this can cause inefficiencies that can negate the natural advantage of the smaller cyclones.

Cyclone diameters can be very large. Perhaps the largest cyclones are those used in circulating fluidized-bed combustors, where cyclone diameters approach 10 m. Large-diameter cyclones also result in very long cyclones, and so these large-diameter, long-length cyclones are

really not feasible as internal cyclones in fluidized beds (they make the vessel too tall).

The minimum cone angle of the cyclone should be 60°. It is generally greater, with steeper cone angles appropriate to materials that are more cohesive. The cyclone inlet is usually rectangular (more efficient at getting material to the wall), but in some cases has been circular. In either case, projection of the inlet flow path should never cause interference with the outlet tube. This generally means that the inlet width of a cyclone should always be less than the distance between the wall and the outside diameter of the outlet tube. If a very heavy solids loading is anticipated, the barrel diameter should be increased slightly to minimize interference with the outlet gas tube.

Collection efficiency is normally increased by increasing the gas throughput (Drijver, op. cit.). However, if the entering dust is agglomerated, high gas velocities may cause breakup of the agglomerated solids in the cyclone, so that efficiency remains the same or actually decreases. Also, variations in design proportions that result in increased collection efficiency with dispersed dusts may be detrimental with agglomerated dusts. Kalen and Zenz [*Am. Inst. Chem. Eng. Symp. Ser.* **70**(137): 388 (1974)] report that collection efficiency increases with increasing gas inlet velocity up to a minimum tangential velocity at which dust is either reentrained or not deposited because of saltation. Koch and Licht [*Chem. Eng.* **84**(24): 80 (1977)] estimate that for typical cyclones the saltation velocity is consistent with cyclone inlet velocities in the range of 15 to 27 m/s (50 to 90 ft/s). Lapple (private communication) reports that in cyclone tests with talc dust, collection efficiency increased steadily as the inlet velocity was increased up to a maximum of 52 m/s (170 ft/s). With ilmenite dust, which was much more strongly flocculated, efficiency decreased over the same inlet velocity range. In later experiments with well-dispersed talc dust, collection efficiency continued to increase at inlet velocities up to the maximum used, 82 m/s (270 ft/s).

Another effect of increasing the cyclone inlet gas velocity is that friable materials may disintegrate (or attrit) as they hit the cyclone wall at high velocity. Thus, the increase in efficiency associated with increased velocity may be more than lost due to generation of fine attrited material that the cyclone cannot contain.

Cyclones can be either placed in the freeboard above the fluidized bed or located outside of the fluidized-bed vessel. There are advantages and disadvantages to each type of placement, and the optimum type of placement depends on what is best for a particular process.

Internal cyclones have the advantages that they require no inlet piping (their inlets can be open to the freeboard) and no high-pressure shell, and they have straight cyclone diplegs. Internal cyclones are generally smaller in diameter than external cyclones because their size is limited by the headspace available in the freeboard above the fluidized bed. These size limitations result in using several smaller cyclones in parallel instead of one large cyclone. In addition, it is difficult to aerate second-stage cyclone diplegs (generally an advantageous technique) when internal cyclones are used. Aerating secondary cyclone diplegs can improve the operation of the diplegs significantly.

The advantages of external cyclones are that (1) they can be much larger than internal cyclones, (2) they are more accessible than internal cyclones, and (3) their diplegs can be aerated more easily. The disadvantages of external cyclones are that (1) they require a pressure shell and (2) external cyclone diplegs generally require a section with an angled or a horizontal pipe to return the solids to the bed. The angled or horizontal dipleg sections can result in poor dipleg operation, if not designed correctly.

Cyclones in series may be justified under the following circumstances:

1. The dust has a broad size distribution, including particles under 10 to 15 μm as well as larger and possibly abrasive particles. A large low-velocity cyclone may be used to remove the coarse particles ahead of a unit with small-diameter multiple tubes.
2. The dust is composed of fine particles but is highly flocculated or tends to flocculate in preceding equipment and in the cyclones themselves. Efficiencies predicted on the basis of ultimate particle size will be highly conservative.
3. The dust is relatively uniform, and the efficiency of the second-stage cyclone is not greatly lower than that of the first stage.

TABLE 17-4 Required Cyclone Length as a Function of Area Ratio

A_{out}/A_{in}	Length below outlet tube/ D_o
>1.0	2.0
0.8	2.2
0.6	2.6
0.4	3.2

4. Dependable operation is critical. Second-stage or even third-stage cyclones may be used as backup.

Cyclone Inlets The design of the cyclone inlet can greatly affect cyclone performance. It is generally desired to have the width of the inlet B_c as narrow as possible so that the entering solids will be as close as possible to the cyclone wall where they can be collected. However, narrow inlet widths require that the height of the inlet H be very long in order to give an inlet area required for the desired inlet gas velocities. Therefore, a balance between narrow inlet widths and the length of the inlet height has to be struck. Typically, low-loading cyclones (cyclones with inlet loadings less than approximately 2 to 5 kg/m³) have height/width ratios H/B_c of between 2.5 and 3.0. For high-loading cyclones, this inlet aspect ratio can be increased to as high as 7 or so with the correct design. Such high inlet aspect ratios require that the cyclone barrel length increase.

A common cyclone inlet is a rectangular tangential inlet with a constant area along its length. This type of inlet is satisfactory for many cyclones, especially those operating at low solids loadings. However, a better type of inlet is one in which the inner wall of the inlet is angled toward the outer cyclone wall at the cyclone inlet. This induces solids momentum toward the outer wall of the cyclone. The bottom wall of the inlet is angled downward so that the area decrease along the inlet flow path is not too rapid and acceleration is controlled. In addition, the entire inlet can be angled slightly downward to give enhanced efficiencies. This type of inlet is superior to the constant-area tangential inlet, especially for higher solids loadings (greater than 2 to 5 kg/m³).

Hugi and Reh [*Chem. Eng. Technol.* **21**(9):716–719 (1998)] report that continuous acceleration of the solids throughout the inlet is desired for improved efficiency and that the angled inlet described above achieves this. If the momentum of the solids is sufficient and the solids are continuously accelerating along the length of the inlet, the stable, coherent strand important for high collection efficiencies is produced.

The best inlet for high solids loadings is the volute cyclone inlet. At high inlet loadings (above approximately 2 to 3 kg/m³) in a tangential cyclone inlet, the gas-solids stream expands rapidly from its minimum width at the point of contact. This rapid expansion disturbs the laminar gas flow around the gas outlet tube and causes flow separation around the tube. At some loadings, the inlet stream can expand to such an extent that the solids can impact the gas outlet tube. Both effects result in lowered cyclone efficiency. However, when a volute inlet is used, the expanding solids stream is farther from the gas outlet tube and enters at an angle so that the solids do not induce as much flow separation or asymmetric flow around the gas outlet tube. Therefore, cyclone efficiency is not affected to as great a degree. If a tangential cyclone is used at high solids loadings, an extra distance between the gas outlet tube and the cyclone wall should be designed into the cyclone to prevent the solids from impacting on the gas outlet tube. At low solid loadings, the impacting on the gas outlet tube does not occur. Because tangential cyclone inlets are less expensive than volute inlets, the tangential cyclone is typically utilized for low loadings—and the volute inlet cyclone is used for high loadings.

The nature of the gas solids flow in the inlet ducting to the cyclone can affect cyclone efficiency significantly. If the solids in the inlet salt out on the bottom and result in dune formation and the resulting unsteady or pulsing flow, cyclone efficiency is adversely affected. To minimize the possibility of this occurring, it is recommended that the inlet line to the cyclone operate above the saltation velocity [Gauthier et al., in *Circulating Fluidized Bed Technology III*, Basu, Horio, and Hasatani (eds.), 1990, pp. 639–644], which will prevent the solids from operating in the dune or pulsing flow regime. If this is not possible, then the inlet line can be angled downward (approximately 15° to 20°) to let gravity assist in the flow of the solids. Keeping the inlet line as short as possible can also minimize any pulsing of the solids flow.

A cyclone will operate equally well on the suction or pressure side of a fan if the dust receiver is airtight. Probably the greatest single cause of poor cyclone performance, however, is the leakage of air into the dust outlet of the cyclone. A slight air leak at this point can result in a tremendous drop in collection efficiency, particularly with fine dusts. For a cyclone operating under pressure, air leakage at this point is objectionable primarily because of the local dust nuisance created.

For batch operation, an airtight hopper or receiver may be used. For continuous withdrawal of collected dust, a rotary star valve, a double-lock valve, or a screw conveyor may be used, the latter only with fine dusts. A collapsible open-ended rubber tube can be used for cyclones operating under slight negative pressure. Mechanical trickle and flapper valves at the end of cyclone diplegs can also be used for continuous withdrawal into fluidized beds or into the freeboard of fluidized beds. Open diplegs simply immersed in a fluidized bed can be used in cases where start-up losses are not excessive and are the simplest type of discharge system returning solids to a fluidized bed (see “Fluidized-Bed Systems: Solids Discharge”). Special pneumatic unloading devices can also be used with dusts. In any case it is essential that sufficient unloading and receiving capacity be provided to prevent collected material from accumulating in the cyclone.

Solids Loading Cyclones can collect solids over a wide range of loadings. Traditionally, solids loadings have been reported as either kilograms of solids per cubic meter of gas (kg/m³), or as kilograms of solids per kilogram of gas (kg/kg_g). However, loading based on mass is probably not the best way to report solids loadings for cyclones. This is so because the volume of solids processed by a cyclone at the same mass loading can vary greatly, depending on the density of the solids. For example, many polymers have a bulk density of approximately 400 kg/m³, and iron ore has a bulk density of approximately 2400 kg/m³. This is a factor of 6. Therefore, a cyclone operating with polymer would have to process 6 times the volume of solids that a cyclone operating with iron ore would process at the same mass loading. If the cyclone operating with the polymer were designed to operate at high loadings on a mass basis, it would probably plug. In addition, the diplegs below the cyclone operating with the polymer may experience operational problems because of the high volumetric loading.

At ambient conditions, cyclones have been operated at solids loadings as low as 0.02 kg/m³ (0.0125 kg/kg) and as high as 64 kg/m³ (50 kg/kg_g) or more. This is a factor of 3200. In general, cyclone efficiency increases with increasing solids loading. This is so because at higher loadings, very fine particles are trapped in the interstices of the larger particles, and this entrapment increases the collection efficiency of the small particles. Even though collection efficiencies are increased with increased loading, cyclone loss rates are also increased as loading is increased. This is so because the cyclone efficiency increase is almost always less than the increase in the solids loading.

Generally cone-and-disk baffles, helical guide vanes, etc., placed inside a cyclone, will have a detrimental effect on performance. However, a few of these devices do have some merit under special circumstances. Although an inlet vane will reduce pressure drop (and may result in significant erosion), it generally causes a correspondingly greater reduction in collection efficiency. Its use is recommended only when collection efficiency is normally so high as to be a secondary consideration, and when it is desired to decrease the resistance of an existing cyclone system for purposes of increased air handling capacity or when floorspace or headroom requirements are controlling factors. If an inlet vane is used, it is advantageous to increase the gas exit duct length inside the cyclone chamber.

A disk or cone baffle located beneath the gas outlet duct may be beneficial if air in-leakage at the dust outlet cannot be avoided. A heavy chain suspended from the gas outlet duct has been found beneficial to minimize dust buildup on the cyclone walls in certain circumstances. Such a chain should be suspended from a swivel so that it is free to rotate without twisting. Substantially all devices that have been reported to reduce pressure drop do so by reducing spiral velocities in the cyclone chamber and consequently result in reduced collection efficiency.

At low dust loadings, the pressure in the dust receiver of a single cyclone will generally be lower than in the gas outlet duct. Increased dust loadings will increase the pressure in the dust receiver. Such devices as cones, disks, and inlet vanes will generally cause the pressure in the dust receiver to exceed that in the gas outlet duct. A cyclone will operate as well in a horizontal position as in a vertical position. However, departure from the normal vertical position results in an increasing tendency to plug the dust outlet. If the dust outlet becomes plugged, collection efficiency will, of course, be low. If the

cyclone exit duct must be reduced to tie in with proposed duct sizes, the transition should be made at least five diameters downstream from the cyclone and preferably after a bend. In the event that the transition must be made closer to the cyclone, a Greek cross should be installed in the transition piece to avoid excessive pressure drop.

Cyclone Length As described above, the cyclone length should be great enough to contain the vortex below the gas outlet tube. It is generally advisable to have the cyclone somewhat longer than required so that modifications to the gas outlet tube can be made if required. Either the barrel or the cone can be increased in length to contain the vortex. However, cyclone barrels can be made too long. If the barrel is too long, the rotating spiral of solids along the wall can lose its momentum. When this happens, the solids along the wall can be reentrained into the rotating gas in the barrel, and cyclone efficiency will be reduced.

Hoffman et al. [*AIChE J.* 47(11): 2452–2460 (2001)] studied the effect of cyclone length on cyclone efficiency and showed that the efficiency of a cyclone increases with length. However, they also found that after a certain length, cyclone efficiency decreased. They reported that cyclone efficiency suddenly decreased after a certain cyclone length, which in their cyclone was at a length/diameter ratio of 5.65.

(Although many researchers employ this length/diameter ratio as a correlating parameter to make the length parameter dimensionless, it is likely that it is the actual length of the cyclone that is important.) Hoffman et al. stated that the probable reason for the sudden decrease in cyclone efficiency was the central vortex touching and turning on the cyclone cone. When this occurred, the efficiency collapsed, causing increased solids reentrainment.

Hoffman et al. also reported that cyclone pressure drop decreased with increasing cyclone length. This probably occurs for the same reason that cyclone pressure drop decreases with increasing cyclone loading. For long cyclones, the increased length of the cyclone wall results in a longer path for the gas to travel. This creates greater resistance to the flow of the gas in the cyclone (much as a longer pipe produces greater resistance to gas flow than a shorter pipe) that results in reducing the tangential velocity in the cyclone and, therefore, the cyclone pressure drop.

Commercial Equipment and Operations Simple cyclones are available in a wide variety of shapes ranging from long, slender units to short, large-diameter units. The body may be conical or cylindrical, and entrances may be involute or tangential and round or rectangular.

Some of the special types of commercial cyclones are shown in Fig. 17-43. In the Multiclone, a spiral motion is imparted to the gas by

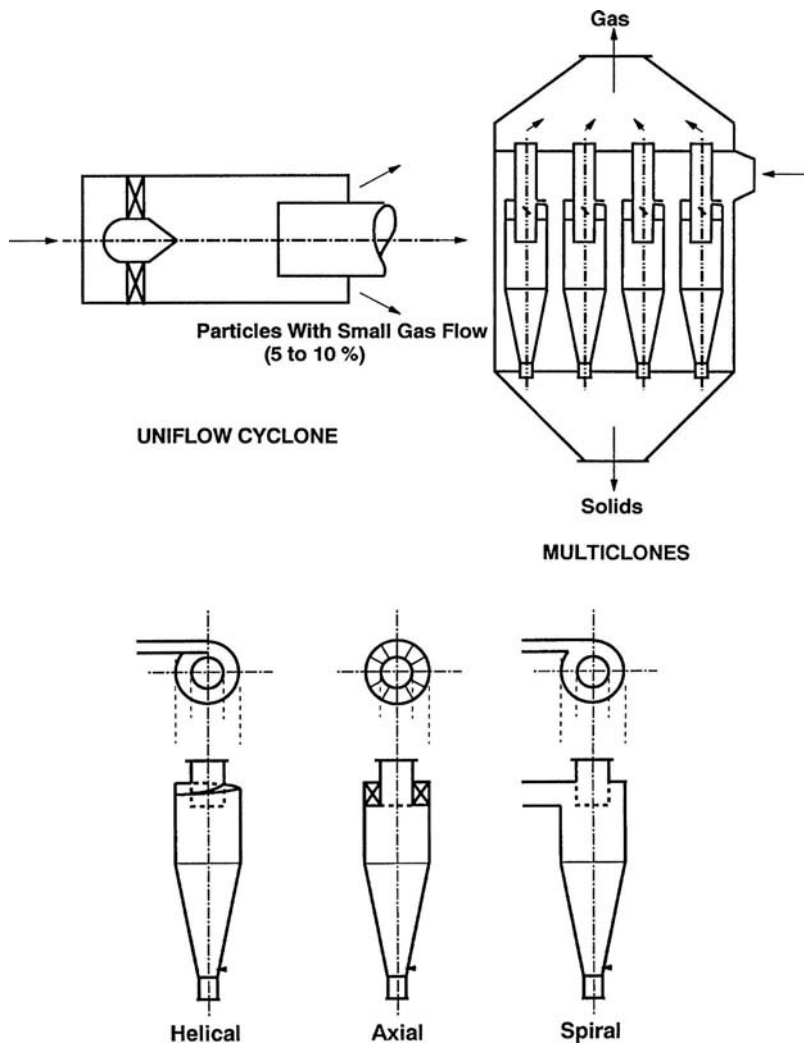


FIG. 17-43 Some commercial cyclone design alternatives. (Courtesy of PSRI, Chicago.)

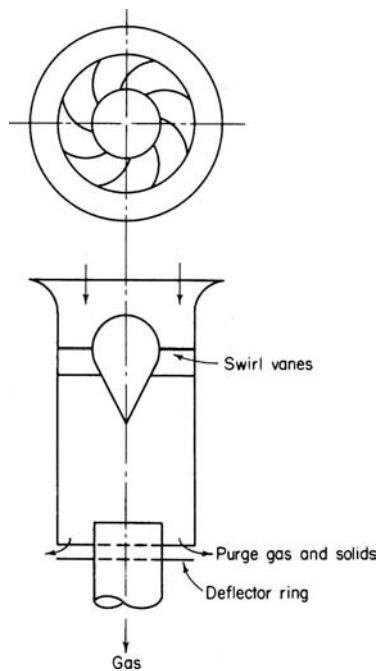


FIG. 17-44 Uniflow cyclone. [Ter Linden, *Inst. Mech. Eng. J.*, **160**, 233 (1949).]

annular vanes, and it is furnished in multiple units of 15.2- and 22.9-cm (6- and 9-in) diameter. Its largest field of application has been in the collection of fly ash from steam boilers. The tubes are commonly constructed of cast iron and other abrasion-resistant alloys. In addition to the conventional reverse-flow cyclones, some use is made of uniflow, or straight-through, cyclones, in which the gas and solids discharge at the same end (Fig. 17-44). These devices generally act as concentrators; the concentrated dust, together with the inlet gas, is discharged at the periphery, while the clean gas passes out through the center tube. The purge gas and concentrated dust enter a conventional cyclone for final separation. The straight-through cyclones are usually designed into multiple-tube units, or they can be used to try to minimize the residence time of the gas and solids to minimize unwanted reactions.

Most processes operate at high temperatures and/or high pressures. Therefore, it is important to know how cyclones operate at these conditions. Efficient cyclones are able to collect very small particles sizes. Therefore, cyclone efficiency is proportional to $1/D_{pth}$.

$$E_o \propto \frac{1}{D_{pth}} = \sqrt{\frac{\pi N_s U (\rho_p - \rho_g)}{9 \mu B_c}}$$

The effects of temperature and pressure manifest themselves in how they affect the gas density and gas viscosity. From the equation above, it can be seen that cyclone efficiency is theoretically related to gas density and gas viscosity as

$$E_o \propto \sqrt{\frac{\rho_p - \rho_g}{\mu}}$$

As pressure is increased, gas density will increase. However, the term $\rho_p - \rho_g$ does not change with increases in gas density because particle density is so much greater than the gas density (typically about 2000 kg/m³ versus approximately 20 kg/m³ at high pressure) that it dominates this term. Therefore, it is expected that gas density would have little or no effect on cyclone efficiency. Conversely, cyclone efficiency would be expected to decrease with system temperature because gas viscosity increases with increasing pressure.

Knowlton and Bachovchin [*Coal Processing Technol.* **4**:122–127 (1978)] studied the effect of pressure on cyclone performance and

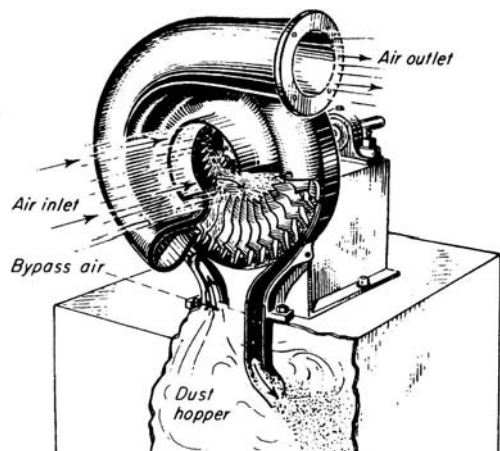


FIG. 17-45 Typical mechanical centrifugal separator. Type D Rotoclone (cut-away view). (American Air Filter Co., Inc.)

found little change in overall cyclone efficiency with pressure over a pressure range from 0 to 55 barg. However, fractional efficiency curves from the same study showed that cyclone efficiency decreased with pressure for particle sizes less than about 20 to 25 μm . For particle sizes greater than about 25 μm there was no effect of pressure on cyclone efficiency.

The effect of temperature on cyclone efficiency was studied by both Parker et al. [*J. Environ. Sci. and Technol.* **15** (4):451 (1981)] and Patterson and Munz [*Canadian J. Chem. Eng.* **67**:321 (1989)]. Both studies showed that cyclone efficiency decreased with increasing gas viscosity. As with the studies at high pressure, Patterson and Munz (1989) reported that only the collection efficiency of particles less than about 10 μm was reduced because of operation at high temperature.

Mechanical Centrifugal Separators A number of collectors in which the centrifugal field is supplied by a rotating member are commercially available. In the typical unit shown in Fig. 17-45, the exhaustor or fan and dust collector are combined as a single unit. The blades are especially shaped to direct the separated dust into an annular slot leading to the collection hopper while the cleaned gas continues to the scroll.

Although no comparative data are available, the collection efficiency of units of this type is probably comparable with that of the single-unit high-pressure-drop-cyclone installation. The clearances are smaller and the centrifugal fields higher than in a cyclone, but these advantages are probably compensated for by the shorter gas path and the greater degree of turbulence with its inherent reentrainment tendency. The chief advantage of these units lies in their compactness, which may be a prime consideration for large installations or plants requiring a large number of individual collectors. Caution should be exercised when attempting to apply this type of unit to a dust that shows a marked tendency to build up on solid surfaces, because of the high maintenance costs that may be encountered from plugging and rotor unbalancing.

Particulate Scrubbers Wet collectors, or scrubbers, form a class of devices in which a liquid (usually water) is used to assist or accomplish the collection of dusts or mists. Such devices have been in use for well over 100 years, and innumerable designs have been or are offered commercially or constructed by users. Wet-film collectors logically form a separate subcategory of devices. They comprise inertial collectors in which a film of liquid flows over the interior surfaces, preventing reentrainment of dust particles and flushing away the deposited dust. Wetted-wall cyclones are an example [Stairmand, *Trans. Inst. Chem. Eng.* **29**, 356 (1951)]. Wet-film collectors have not been studied systematically but can probably be expected to perform much as do equivalent dry inertial collectors, except for the benefit of reduced reentrainment.

In particulate scrubbers, the liquid is dispersed into the gas as a spray, and the liquid droplets are the principal collectors for the dust particles. Depending on their design and operating conditions, particulate scrubbers can be adapted to collecting fine as well as coarse particles. Collection of particles by the drops follows the same principles illustrated in Fig. 17-35. Various investigations of the relative contributions of the various mechanisms have led to the conclusion that the predominant mechanism is inertial deposition. Flow-line interception is only a minor mechanism in the collection of the finer dust particles by liquid droplets of the sizes encountered in scrubbers. Diffusion is indicated to be a relatively minor mechanism for the particles larger than $0.1 \mu\text{m}$ that are of principal concern. Thermal deposition is negligible. Gravitational settling is ineffective because of the high gas velocities and short residence times used in scrubbers. Electrostatic deposition is unlikely to be important except in cases in which the dust particles or the water, or both, are being deliberately charged from an external power source to enhance collection. Deposition produced by Stefan flow can be significant when water vapor is condensing in a scrubber.

Despite numerous claims or speculations that wetting of dust particles by the scrubbing liquid plays a major role in the collection process, there is no unequivocal evidence that this is the case. The issue is whether wetting is an important factor in the adherence of a particle to a collecting droplet upon impact. From the body of general experience, it can be inferred that wettable particles probably are not collected much, if any, more readily than nonwetable particles of the same size. However, the available experimental techniques have not been adequate to permit any direct test to resolve the question. Changing from a wettable to a nonwetable test aerosol or from one scrubbing liquid to another is virtually certain to introduce other (and possibly unknown) factors into the scrubbing process. The most informative experimental studies appear to be some by Weber [Staub, English trans., **28**, 37 (November 1968); **29**, 12 (July 1969)], who bombarded single drops of various liquids with dust particles at different velocities and studied the behavior at impact by means of high-speed photography. Dust particles hitting the drops were invariably retained by the latter, regardless of their wettability by the liquid used.

The use of wetting agents in scrubbing water is equally controversial, and there has been no clear demonstration that it is beneficial.

A particulate scrubber may be considered as consisting of two parts: (1) a contactor stage, in which a spray is generated and the dust-laden gas stream is brought into contact with it; and (2) an entrainment separation stage, in which the spray and deposited dust particles are separated from the cleaned gas. These two stages may be separate or physically combined. The contactor stage may be of any form intended to bring about effective contacting of the gas and spray. The spray may be generated by the flow of the gas itself in contact with the liquid, by spray nozzles (pressure-atomizing or pneumatic-atomizing), by a motor-driven mechanical spray generator, or by a motor-driven rotor through which both gas and liquid pass.

Entrainment separation is accomplished with inertial separators, which are usually cyclones or impingement separators of various forms. If properly designed, these devices can remove virtually all droplets of the sizes produced in scrubbers. However, reentrainment of liquid can take place in poorly designed or overloaded separators.

Scrubber Types and Performance The diversity of particulate scrubber designs is so great as to defy any detailed and self-consistent system of classification based on configuration or principle of operation. However, it is convenient to characterize scrubbers loosely according to prominent constructional features, even though the modes of operation of different devices in a group may vary widely.

A relationship of power consumption to collection efficiency is characteristic of all particulate scrubbers. Attaining increased efficiency requires increased power consumption, and the power consumption required to attain a given efficiency increases as the particle size of the dust decreases. Experience generally indicates that the power consumption required to provide a specific efficiency on a given dust does not vary widely even with markedly different devices. The extent to which this generalization holds true has not been fully explored, but the known extent is sufficient to suggest that the underlying collection mechanism may be essentially the same in all types of particulate scrubbers.

Since some relationship of power consumption to performance appears to be a universal characteristic of particulate scrubbers, it is useful to characterize such devices broadly according to the source from which the energy is supplied to the gas-liquid contacting process. The energy may be drawn from (1) the gas stream itself, (2) the liquid stream, or (3) a motor driving a rotor. For convenience, devices in these classes may be termed, respectively, (1) gas-atomized spray scrubbers, (2) spray, or preformed-spray, scrubbers, and (3) mechanical scrubbers. In the spray scrubbers, all the energy may be supplied from the liquid, using a pressure nozzle, but some or all may be provided by compressed air or steam in a two-fluid nozzle or by a motor driving a spray generator.

Particulate scrubbers may also be classed broadly into low-energy and high-energy scrubbers. The distinction between the two classes is arbitrary, since the devices are not basically different and the same device may fall into either class depending on the amount of power it consumes. However, some differences in configuration are sometimes necessary to adapt a device for high-energy service. No specific level of power consumption is commonly agreed upon as the boundary between the two classes, but high-energy scrubbers may be regarded as those using sufficient power to give substantial efficiencies on sub-micrometer particles.

Scrubber Performance Models A number of investigators have made theoretical studies of the performance of venturi scrubbers and have sought to produce performance models, based on first principles, that can be used to design a unit for a given duty without recourse to experimental data other than the particle size and size distribution of the dust. Among these workers are Calvert [*Am. Inst. Chem. Eng. J.*, **16**, 392 (1970); *J. Air Pollut. Control Assoc.*, **24**, 929 (1974)], Boll [*Ind. Eng. Chem. Fundam.*, **12**, 40 (1973)], Goel and Hollands [*Atmos. Environ.*, **11**, 837 (1977)], and Yung et al. [*Environ. Sci. Technol.*, **12**, 456 (1978)]. Comparatively few efforts have been made to model the performance of scrubbers of types other than the venturi, but a number of such models are summarized by Yung and Calvert (U.S. EPA-600/8-78-005b, 1978).

The various venturi-scrubber models embody a variety of assumptions and approximations. The solutions of the equations for particulate collection must in general be determined numerically, although Calvert et al. [*J. Air Pollut. Control Assoc.*, **22**, 529 (1972)] obtained an explicit equation by making some simplifying assumptions and incorporating an empirical constant that must be evaluated experimentally; the constant may absorb some of the deficiencies in the model. Although other models avoid direct incorporation of empirical constants, use of empirical relationships is necessary to obtain specific estimates of scrubber collection efficiency. One of the areas of greatest uncertainty is the estimation of droplet size.

Most of the investigators have assumed the effective drop size of the spray to be the Sauter (surface-mean) diameter and have used the empirical equation of Nukiyama and Tanasawa [*Trans. Soc. Mech. Eng., Japan*, **5**, 63 (1939)] to estimate the Sauter diameter:

$$D_o = \frac{1920\sqrt{\sigma_L}}{V_o\sqrt{\rho_L/62.3}} + 75.4 \left(\frac{\mu_L}{\sqrt{\sigma_L\rho_L/62.3}} \right)^{0.45} \left(\frac{1000Q_L}{Q_C} \right)^{1.5} \quad (17-3)$$

where D_o = drop diameter, μm ; V_o = gas velocity, ft/s; σ_L = liquid surface tension, dyn/cm; ρ_L = liquid density, lb/ft³; μ_L = liquid viscosity, cP; Q_L = liquid flow rate, ft³/s; and Q_C = gas flow rate, ft³/s.

The Nukiyama-Tanasawa equation, which is not dimensionally homogeneous, was derived from experiments with small, internal-mix pneumatic atomizing nozzles with concentric feed of air and liquid (Lapple et al., "Atomization: A Survey and Critique of the Literature," Stanford Res. Inst. Tech. Rep. No. 6, AD 821-314, 1967; Lapple, "Atomization," in *McGraw-Hill Encyclopedia of Science and Technology*, 5th ed., vol. 1, McGraw-Hill, New York, 1982, p. 858). The effect of nozzle size on the drop size is undefined. Even within the range of parameters for which the relationship was derived, the drop sizes reported by various investigators have varied by twofold to threefold from those predicted by the equation (Boll, op. cit.). The Nukiyama-Tanasawa equation has, nevertheless, been applied to large venturi and orifice scrubbers with configurations radically different from those of the atomizing nozzles for which the equation was originally developed.

Primarily because of the lack of adequate experimental techniques (particularly, the production of appropriate monodisperse aerosols), there has been no comprehensive experimental test of any of the venturi-scrubber models over wide ranges of design and operating variables. The models for other types of scrubbers appear to be essentially untested.

Contacting Power Correlation A scrubber design method that has achieved wide acceptance and use is based on correlation of the collection efficiency with the power dissipated in the gas-liquid contacting process, which is termed "contacting power." The method originated from an investigation by Lapple and Kamack [*Chem. Eng. Prog.*, **51**, 110 (1955)] and has been extended and refined in a series of papers by Semrau and coworkers [*Ind. Eng. Chem.*, **50**, 1615 (1958); *J. Air Pollut. Control Assoc.*, **10**, 200 (1960); **13**, 587 (1963); U.S. EPA-650/2-74-108, 1974; U.S. EPA-600/2-77-234, 1977; *Chem. Eng.*, **84**(20), 87 (1977); and "Performance of Particulate Scrubbers as Influenced by Gas-Liquid Contactor Design and by Dust Flocculation," EPA-600/9-82-005c, 1982, p. 43]. Other workers have made evidence independent studies of the correlation method [Walker and Hall, *J. Air Pollut. Control Assoc.*, **18**, 319 (1968)], and numerous studies of narrower scope have been made. The major conclusion from these studies is that the collection efficiency of a scrubber on a given dust is essentially dependent only on the contacting power and is affected to only a minor degree by the size or geometry of the scrubber or by the way in which the contacting power is applied. This contacting-power rule is strictly empirical, and the full extent of its validity has still not been explored. It has been best verified for the class of gas-atomized spray scrubbers, in which the contacting power is derived from the gas stream and takes the form of gas pressure drop. Tests of the equivalence of contacting power supplied from the liquid stream in pressure spray nozzles have been far less extensive and are strongly indicative but not yet conclusive. Evidence for the equivalence of contacting power from mechanically driven devices is also indicative but extremely limited in quantity.

Contacting power is defined as the power per unit of volumetric gas flow rate that is dissipated in gas-liquid contacting and is ultimately converted to heat. In the simplest case, in which all the energy is obtained from the gas stream in the form of pressure drop, the contacting power is equivalent to the friction loss across the wetted equipment, which is termed "effective friction loss," F_E . The pressure drop may reflect kinetic-energy changes rather than energy dissipation, and pressure drops that result solely from kinetic-energy changes in the gas stream do not correlate with performance. Likewise, any friction losses taking place across equipment that is operating dry do not contribute to gas-liquid contacting and do not correlate with performance. The gross power input to a scrubber includes losses in motors, drive shafts, fans, and pumps that obviously should be unrelated to scrubber performance.

The effective friction loss, or "gas-phase contacting power," is easily determined by direct measurements. However, the "liquid-phase contacting power," supplied from the stream of scrubbing liquid, and the "mechanical contacting power," supplied by a mechanically driven rotor, are not directly measurable; the theoretical power inputs can be estimated, but the portions of these quantities effectively converted to contacting power can only be inferred from comparison with gas-phase contacting power. Such data as are available indicate that the contributions of contacting power from different sources are directly additive in their relation to scrubber performance.

Contacting power is variously expressed in units of MJ/1000 m³ (SI), kWh/1000 m³ (meter-kilogram-second system), and hp/(1000 ft³/min) (U.S. customary). Relationships for conversion to SI units are

$$1.0 \text{ kWh}/1000 \text{ m}^3 = 3.60 \text{ MJ}/1000 \text{ m}^3$$

$$1.0 \text{ hp}/(1000 \text{ ft}^3/\text{min}) = 1.58 \text{ MJ}/1000 \text{ m}^3$$

The gas-phase contacting power P_C may be calculated from the effective friction loss by the following relationships:

SI units:

$$P_C = 1.0F_E \quad (17-4)$$

where $F_E = \text{kPa}$.

U.S. customary units:

$$P_C = 0.1575F_E \quad (17-5)$$

where $F_E = \text{in of water}$.

The power input from a liquid stream injected with a hydraulic spray nozzle may usually be taken as approximately equal to the product of the nozzle feed pressure p_F and the volumetric liquid rate. The liquid-phase contacting power P_L may then be calculated from the following formulas:

SI units:

$$P_L = 1.0p_F(Q_L/Q_C) \quad (17-6)$$

where $p_F = \text{kPa gauge}$, and Q_L and $Q_C = \text{m}^3/\text{s}$.

U.S. customary units:

$$P_L = 0.583p_F(Q_L/Q_C) \quad (17-7)$$

where $p_F = \text{lbf/in}^2 \text{ gauge}$, $Q_L = \text{gal/min}$, and $Q_C = \text{ft}^3/\text{min}$.

The correlation of efficiency data is based on the total contacting power P_T , which is the sum of P_C , P_L , and any power P_M that may be supplied mechanically by a power-driven rotor.

In general, the liquid-to-gas ratio does not have an influence independent of contacting power on the collection efficiency of scrubbers of the venturi type. This is true at least of operation with liquid-to-gas ratios above some critical lower value. However, several investigations [Semrau and Lunn, "Performance of Particulate Scrubbers as Influenced by Gas-Liquid Contactor Design and by Dust Flocculation," EPA-600/9-82-005c, 1982, p. 43; and Muir et al., *Filtr. Sep.*, **15**, 332 (1978)] have shown that at low liquid-to-gas ratios relatively poor efficiencies may be obtained at a given contacting power. Such regions of operation are obviously to be avoided.

It has sometimes been asserted that multiple gas-liquid contactors in series will give higher efficiencies at a given contacting power than will a single contacting stage. However, there is little experimental evidence to support this contention. Lapple and Kamack (op. cit.) obtained slightly higher efficiencies with a venturi and an orifice in series than they did with a venturi alone. Muir and Mihisei [*Atmos. Environ.*, **13**, 1187 (1979)] obtained somewhat higher efficiencies on two redispersed dusts when using two venturis in series rather than one. The improvement obtained with two-stage scrubbing was greatest with the coarser of the two dusts and was relatively small with the finer dust. Flocculation or deflocculation of the dusts may have been responsible for some of the behavior encountered. Semrau et al. (EPA-600/2-77-234, 1977) compared the performance of a four-stage multiple-orifice contactor with that of a single-orifice contactor, using well-dispersed aerosols generated from ammonium fluorescein. The multiple-orifice contactor gave about the same efficiency as the single-orifice in the upper range of contacting power but lower efficiencies in the lower range. The deviations in performance in this case were probably characteristic of the particular multiple-orifice contactor rather than of multistage contacting as such.

Most scrubbers actually incorporate more than one stage of gas-liquid contacting even though these may not be identical (e.g., the contactor and the entrainment separator). The preponderance of evidence indicates that multiple-stage contacting is not inherently either more or less efficient than single-stage contacting. However, two-stage contacting may have practical benefits in dealing with abrasive or flocculated dusts.

Some investigators have proposed, mostly on the basis of mathematical modeling, to optimize the design of scrubbers to obtain a given efficiency with a minimum power consumption (e.g., Goel and Hollands, op. cit.). In fact, no optimum in performance appears to exist; so long as increased entrainment is prevented increased contacting power yields increased efficiency.

Scrubber Performance Curves The scrubber performance curve, which shows the relationship of scrubber efficiency to the contacting power, has been found to take the form

$$N_i = \alpha P_T^\gamma \quad (17-8)$$

where α and γ are empirical constants that depend primarily on the aerosol (dust or mist) collected. In a log-log plot of N_i versus P_T , γ is the slope of the performance curve and α is the intercept at $P_T = 1$.

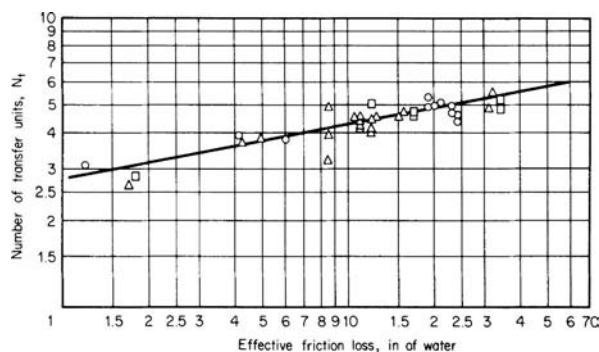


FIG. 17-46 Performance of pilot-plant venturi scrubber on fly ash. Liquid-to-gas ratio, gal/1000 ft³: ○, 10; △, 15; □, 20. (Raben, United States-U.S.S.R. Symposium on Fine-Particulate Emissions from Industrial Sources, San Francisco, 1974.)

Figure 17-46 shows such a performance curve for the collection of coal fly ash by a pilot-plant venturi scrubber (Raben "Use of Scrubbers for Control of Emissions from Power Boilers," United States-U.S.S.R. Symposium on Control of Fine-Particulate Emissions from Industrial Sources, San Francisco, 1974). The scatter in the data reflects not merely experimental errors but actual variations in the particle-size characteristics of the dust. Because the characteristics of an industrial dust vary with time, the scrubber performance curve necessarily must represent an average material, and the scatter in the data is frequently greater than is shown in Fig. 17-46. For best definition, the curve should cover as wide a range of contacting power as possible. Obtaining the data thus requires pilot-plant equipment with the flexibility to operate over a wide range of conditions. Because scrubber performance is not greatly affected by the size of the unit, it is feasible to conduct the tests with a unit handling no more than 170 m³/h (100 ft³/min) of gas.

A clear interpretation of γ , the slope of the curve, is still lacking. Presumably, it should be related to the particle-size distribution of the dust. Because scrubbing preferentially removes the coarser particles, the fraction of the dust removed (or the increment of N_t) per unit of contacting power should decrease as the contacting power and efficiency increase, so that the value of γ should be less than unity. In fact, the value of γ has been less than unity for most dusts. Nevertheless, some data in the literature have displayed values of γ greater than unity when plotted on the transfer-unit basis, indicating that the residual fraction of dust became more readily collectible as contacting power and efficiency increased. More recent studies by Semrau et al. (EPA-650/2-74-108 and EPA-600/2-77-237) have revealed performance curves having two branches (typified by Fig. 17-47), the lower having a slope greater than unity and the upper a slope less than unity. This suggests that had the earlier tests been extended into higher contacting-power ranges, performance curves with flatter slopes might have appeared in those ranges.

Among the aerosols that gave performance curves with $\gamma > 1$, the only obvious common characteristic was that a large fraction of each was composed of submicrometer particles.

Cut-Power Correlation Another design method, also based on scrubber power consumption, is the cut-power method of Calvert [*J. Air Pollut. Control Assoc.*, **24**, 929 (1974); *Chem. Eng.*, **84**(18), 54 (1977)]. In this approach, the cut diameter (the particle diameter for which the collection efficiency is 50 percent) is given as a function of the gas pressure drop or of the power input per unit of volumetric gas flow rate. The functional relationship is presented as a log-log plot of the cut diameter versus the pressure drop (or power input). In principle, the function could be constructed by experimentally determining scrubber performance curves for discrete particle sizes and then plotting the particle sizes against the corresponding pressure drops necessary to give efficiencies of 50 percent. In practice, Calvert and coworkers evidently have in most cases constructed the cut-power functions for various scrubbers by modeling (Yung and Calvert, U.S. EPA-600/8-78-005b, 1978). They show a variety of curves, whereas empirical studies have

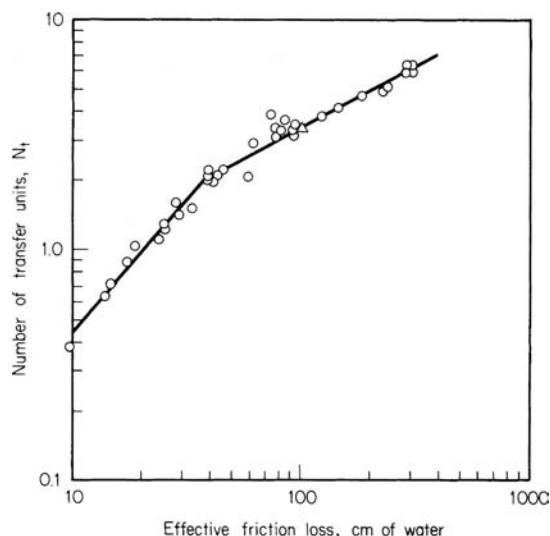


FIG. 17-47 Performance curve for orifice scrubber collecting ammonium fluorescein aerosol. (Semrau et al., EPA 600/2-77-237, 1977.)

indicated that different types of scrubbers generally have about the same performance at a given level of power consumption.

Condensation Scrubbing The collection efficiency of scrubbing can be increased by the simultaneous condensation of water vapor from the gas stream. Water-vapor condensation assists in particle removal by two entirely different mechanisms. One is the deposition of particles on cold-water droplets or other surfaces as the result of Stefan flow. The other is the condensation of water vapor on particles as nuclei, which enlarges the particles and makes them more readily collected by inertial deposition on droplets. Both mechanisms can operate simultaneously. However, for the buildup of particles by condensation to be effective, there must be adequate time for the particles to grow substantially before the principal gas-liquid-contacting operation takes place. Hence, if particle buildup is to be sought, the scrubber should be preceded by an appropriate gas-conditioning section. On the other hand, particle collection by Stefan flow can be induced simply by scrubbing the hot, humid gas with sufficient cold water to bring the gas below its initial dew point. Any practical method of inducing condensation on the dust particles will incidentally afford opportunities for the operation of the Stefan-flow mechanism. The hot gas stream must, of course, have a high initial moisture content, since the magnitude of the effects obtained is related to the quantity of water vapor condensed.

Although there is a considerable body of literature on particle collection by condensation mechanisms, most of it is either theoretical or, if experimental, treats basic phenomena in simplified cases. Few studies have been made to determine what performance may be expected from condensation scrubbing under practical conditions in industrial applications. In a series of studies, Calvert and coworkers investigated several types of equipment for condensation scrubbing, generally emphasizing the use of the condensation center effect to build up the particles for collection by inertial deposition (Calvert and Parker, EPA-600/8-78-005c, 1978). From early estimates, they predicted that a condensation scrubber would require only about one-third or less of the power required by a conventional high-energy scrubber. A subsequent demonstration-plant scrubber system consisted of a direct-contact condensing tower fed with cold water followed by a venturi scrubber fed with recirculated water (Chmielewski and Calvert, EPA-600/7-81-148, 1981). The condensation and particle buildup took place in the cooling tower. In operation on humidified iron-foundry-cupola gas, this system still required about 65 percent as much power as for conventional high-energy scrubbing.

Semrau and coworkers [*Ind. Eng. Chem.*, **50**, 1615 (1958); *J. Air Pollut. Control Assoc.*, **13**, 587 (1963); EPA-650/2-74-108, 1974] investigated

condensation scrubbing in pilot-plant studies in the field and, later, under laboratory conditions. Hot, humid gases were scrubbed directly with cold water under conditions that were favorable for the Stefan-flow mechanism but offered little or no opportunity for particle buildup. Some of the field studies indicated a contacting-power saving of as much as 50 percent for condensation scrubbing of Kraft-recovery-furnace fume. Laboratory tests on a predominantly submicrometer synthetic aerosol showed contacting-power savings of up to 40 percent with condensation scrubbing.

In the scrubbing of hot gases with high water content, condensation reduces contacting power and affords a direct power saving through the reduction of the gas volume by cooling and water-vapor condensation, but it incurs other costs for power and equipment for heat transfer and water cooling. However, condensation scrubbing may offer a net economic advantage if recovery of low-level heat is practical. It should also be advantageous when a hot gas must be not only cleaned but cooled and dehumidified as well; examples are the cleaning of blast-furnace gas for use as fuel and of SO₂-bearing waste gases for feed to a sulfuric acid plant.

Entrainment Separation The entrainment separator is a critical element of a scrubber, since the collection efficiency of the scrubber depends on essentially total removal of the spray from the gas stream. The sprays generated in scrubbers are generally large enough in droplet size that they can be readily removed by properly designed inertial separators. Primary collection of the spray is seldom the critical limitation on separator performance, but reentrainment is a common problem. In dust scrubbers it is essential that the entrainment separator not be of a form readily subject to blockage by solids deposits and that it be readily cleared of deposits if they should occur. Cyclone separators are advantageous in this respect and are widely used with venturi contactors. However, they cannot readily be made integral with scrubbers of some other configurations, which can be more conveniently fitted with various forms of impingement separators. Although separator design can be important, the most common cause of reentrainment is simply the use of excessive gas velocities, and few data are available on the gas-handling

capacities of separators. In the absence of good data, there is a frequent tendency to underdesign separators in an effort to reduce costs.

Venturi Scrubbers The venturi scrubber is one of the most widely used types of particulate scrubbers. The designs have become generally standardized, and units are manufactured by a large number of companies. Venturi scrubbers may be used as either high- or low-energy devices but are most commonly employed as high-energy units. The units originally studied and used were designed to the proportions of the classical venturis used for metering, but since it was discovered that these proportions have no special merits, simpler and more practical designs have been adopted. Most "venturi" contactors in current use are in fact not venturis but variable orifices of one form or another. Any of a wide range of devices can be used, including a simple pipeline contactor. Although the venturi scrubber is not inherently more efficient at a given contacting power than other types of devices, its simplicity and flexibility favor its use. It is also useful as a gas absorber for relatively soluble gases, but because it is a cocurrent contactor, it is not well suited to absorption of gases having low solubilities.

Current designs for venturi scrubbers generally use the vertical downflow of gas through the venturi contactor and incorporate three features: (1) a "wet-approach" or "flooded-wall" entry section, to avoid dust buildup at a wet-dry junction; (2) an adjustable throat for the venturi (or orifice), to provide for adjustment of the pressure drop; and (3) a "flooded elbow" located below the venturi and ahead of the entrainment separator, to reduce wear by abrasive particles. The venturi throat is sometimes fitted with a refractory lining to resist abrasion by dust particles. The entrainment separator is commonly, but not invariably, of the cyclone type. An example of the "standard form" of venturi scrubber is shown in Fig. 17-48. The wet-approach

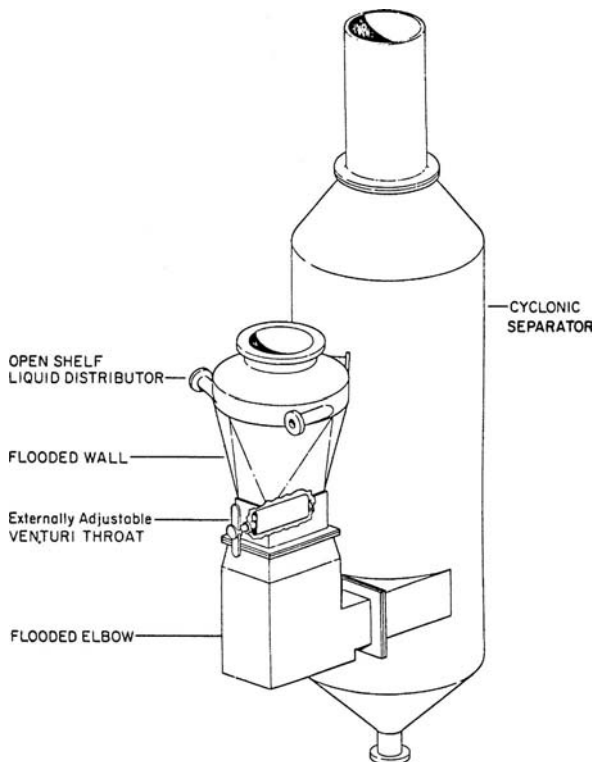


FIG. 17-48 Venturi scrubber. (Neptune AirPol.)

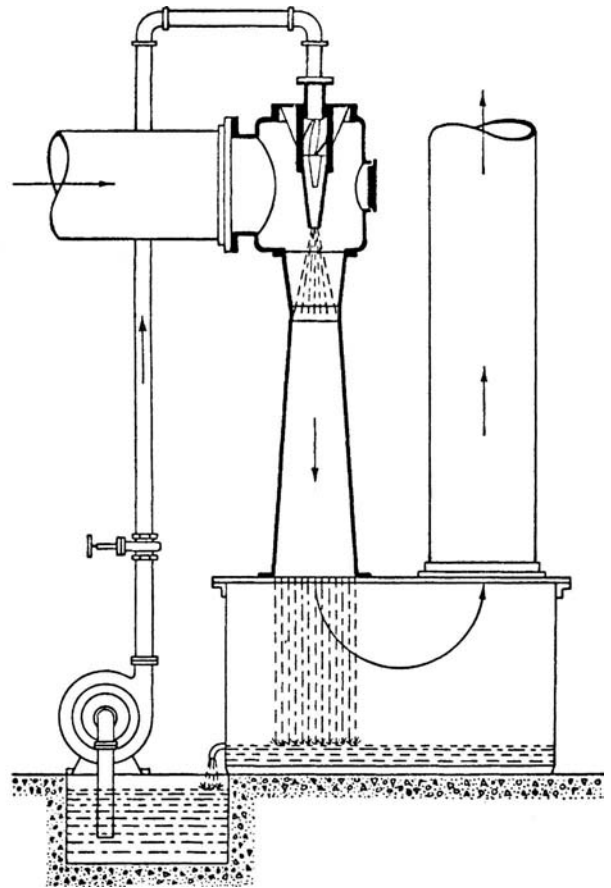


FIG. 17-49 Ejector-venturi scrubber. (Schutte & Koerting Division, Amtek, Inc.)

entry section has made practical the recirculation of slurries. Various forms of adjustable throats, which may be under manual or automatic control, permit maintaining a constant pressure drop and constant efficiency under conditions of varying gas flow.

Ejector-Venturi Scrubbers In the ejector-venturi scrubber (Fig. 17-49) the cocurrent water jet from a spray nozzle serves both to scrub the gas and to provide the draft for moving the gas. No fan is required, but the equivalent power must be supplied to the pump that delivers water to the ejector nozzle. The water must be supplied in sufficient volume and at high enough pressure to provide both adequate draft and enough contacting power for the required scrubbing operation. Considered as a gas pump, the ejector is not a very efficient device, but the dissipated energy that is not effective in pumping does serve in gas-liquid contacting. The energy equivalent to any gas pressure rise across the scrubber is not part of the contacting power (Semrau et al., EPA-600/2-77-234, 1974).

The ejector-venturi scrubber is widely used as a gas absorber, but the combinations of water pressure and flow rate that are sufficient to provide the required draft usually do not also yield enough contacting power to give high collection efficiency on submicrometer particles. Other types of ejectors have been employed to provide higher contacting-power levels. In one, superheated water is discharged through the nozzle, and part flashes to steam, increasing the mechanical energy available for scrubbing [Gardenier, *J. Air Pollut. Control Assoc.*, **24**, 954 (1974)]. Some units use two-fluid nozzles, with either compressed air or steam as the compressible fluid [Sparks, *J. Air Pollut. Control Assoc.*, **24**, 958 (1974)]. Most of the energy for gas movement and for atomizing the liquid and scrubbing the gas is derived from the compressed air or steam. In some ejector-venturi-scrubbers installations, part of the draft is supplied by a fan [Williams and Fuller, *TAPPI*, **60**(1), 108 (1977)].

Self-Induced Spray Scrubbers Self-induced spray scrubbers form a category of gas-atomized spray scrubbers in which a tube or a

duct of some other shape forms the gas-liquid-contacting zone. The gas stream flowing at high velocity through the contactor atomizes the liquid in essentially the same manner as in a venturi scrubber. However, the liquid is fed into the contactor and later recirculated from the entrainment separator section by gravity instead of being circulated by a pump as in venturi scrubbers. The scheme is well illustrated in Fig. 17-50a. A great many such devices using contactor ducts of various shapes, as in Fig. 17-50b, are offered commercially. Although self-induced spray scrubbers can be built as high-energy units and sometimes are, most such devices are designed for only low-energy service.

The principal advantage of self-induced spray scrubbers is the elimination of a pump for recirculation of the scrubbing liquid. However, the designs for high-energy service are somewhat more complex and less flexible than those for venturi scrubbers.

Spray Scrubbers Spray scrubbers consist of empty chambers of some simple form in which the gas stream is contacted with liquid droplets generated by spray nozzles. A common form is a spray tower, in which the gas flows upward through a bank or successive banks of spray nozzles. Similar arrangements are sometimes used in spray chambers with horizontal gas flow. Such devices have very low gas pressure drops, and all but a small part of the contacting power is derived from the liquid stream. The required contacting power is obtained from an appropriate combination of liquid pressure and flow rate. Most spray scrubbers are low-energy units. Collection of fine particles is possible but may require very high liquid-to-gas ratios, liquid feed pressures, or both. Plugging of small nozzles can be a persistent maintenance problem. Entrainment separators are necessary to prevent carryover of spray into the exit gas.

Nonatomizing reverse-jet froth scrubbers using large pluggage-resistant open nozzles allow effective use of higher contacting power to efficiently collect finer dust particles, as described in U.S. Patents 3,803,805, 4,056,371, and 4,057,404. Such scrubbers are provided by

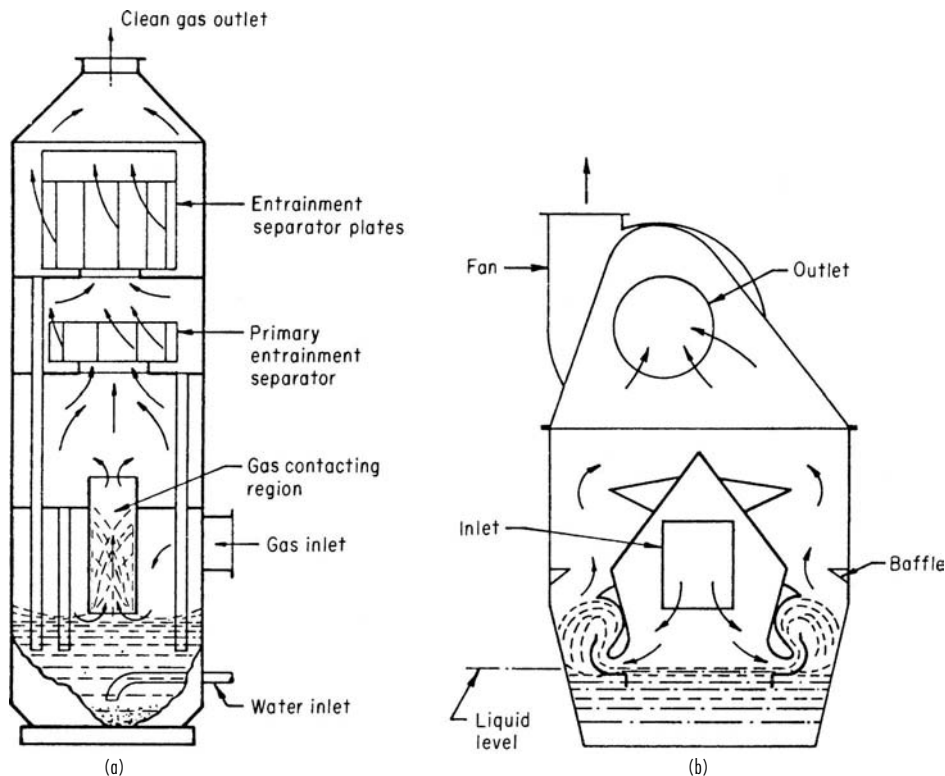


FIG. 17-50 Self-induced spray scrubbers. (a) Blaw-Knox Food & Chemical Equipment, Inc. (b) American Air Filter Co., Inc.

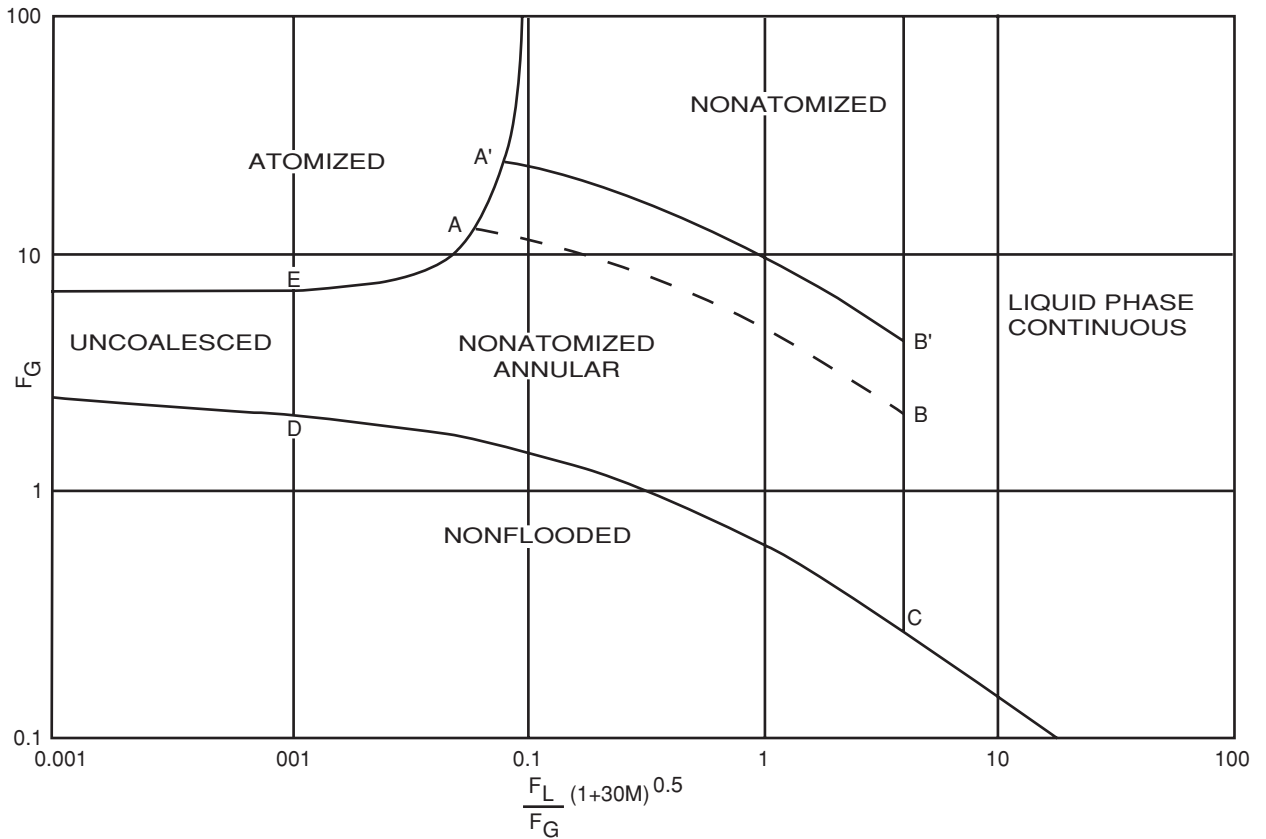


FIG. 17-51 Spray scrubbing flow regime map. (U.S. Patent 4,057,404.)

Monsanto Enviro-Chem under the Dyna-Wave® trademark; case histories can be downloaded from a web site (<http://www.enviro-chem.com/airpol/common/rjstop.html>). Nonatomizing froth scrubbing is described in those patents as occurring within defining boundaries on a new dimensionless velocity versus dimensionless liquid/gas ratio two-phase flow regime map, shown here as Fig. 17-51.

Cyclone Scrubbers The vessels of cyclone scrubbers are all in the form of cyclones, which provide for compact integral entrainment separation. The gas-liquid contacting section normally uses some sort of spray generator to disperse liquid throughout the gas. Performance is similar to other spray scrubbers.

Plate Towers Plate (tray) towers are countercurrent gas-atomized spray scrubbers using one or more plates for gas-liquid contacting. They are essentially the same as, if not identical to, the devices used for gas absorption and are frequently employed in applications in which gases are to be absorbed simultaneously with the removal of dust. Except possibly in cases in which condensation effects are involved, countercurrent operation is not significantly beneficial in dust collection.

The plates may be any of several types, including sieve, bubble-cap, and valve trays. Valve trays constitute multiple self-adjusting orifices that provide nearly constant gas pressure drop over considerable ranges of variation in gas flow. The gas pressure drop that can be taken across a single plate is necessarily limited, so that units designed for high contacting power must use multiple plates.

Plate towers are more subject to plugging and fouling than venturi-type scrubbers that have large passages for gas and liquid.

Packed-Bed Scrubbers Packed-bed scrubbers using gas-absorption-type tower packing may also be used for collecting soluble solids, but are not irrigated intensively enough to avoid plugging by deposits of

insoluble solids. Mobile-bed and fiber-bed scrubbers can be self-cleaning if they are adequately flushed.

Mobile-Bed Scrubbers Mobile-bed scrubbers (Fig. 17-52) are constructed with one or more beds of low-density spheres that are free to move between upper and lower retaining grids. The spheres are

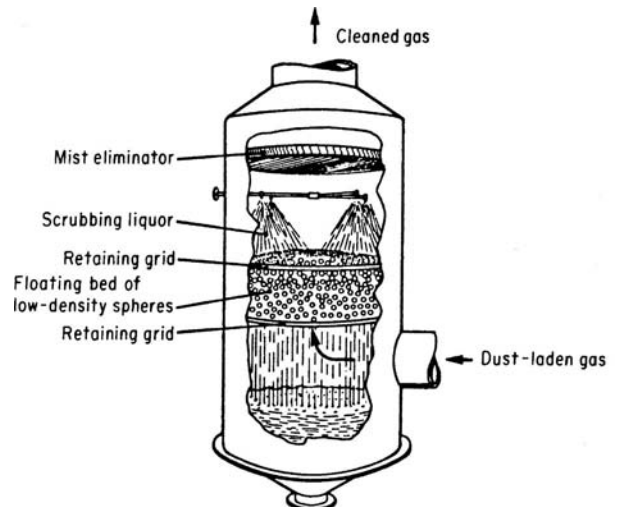


FIG. 17-52 Mobile-bed scrubber. (Air Correction Division, UOP.)

commonly 1.0 in (2.5 cm) or more in diameter and made from rubber or a plastic such as polypropylene. The plastic spheres may be solid or hollow. Gas and liquid flows are countercurrent, and the spherical packings are fluidized by the upward-flowing gas. The movement of the packings is intended to minimize fouling and plugging of the bed. Mobile-bed scrubbers were first developed for absorbing gases from gas streams that also carry solid or semisolid particles.

The spherical packings are too large to serve as effective targets for the deposition of fine dust particles. In dust-collection service, the packings actually serve as turbulence promoters, while the dust particles are collected primarily by the liquid droplets.

The gas pressure drop through the scrubber may be increased by increasing the gas velocity, the liquid-to-gas ratio, the depth of the bed, the density of the packings, and the number of beds in series. In an experimental study, Yung et al. (EPA-600/7-79-071, 1979) determined that the collection efficiency of a mobile-bed scrubber was dependent only on the gas pressure drop and was not influenced independently by the gas velocity, the liquid-to-gas ratio, or the number of beds except as these factors affected the pressure drop. Yung et al. also reported that the mobile-bed scrubber was less efficient at a given pressure drop than scrubbers of the venturi type, but without offering comparable experimental supporting evidence.

Fiber-Bed Scrubbers Fibrous-bed structures are sometimes used as gas-liquid contactors, with cocurrent flow of the gas and liquid streams. In such contactors, both scrubbing (particle deposition on droplets) and filtration (particle deposition on fibers) may take place. If only mists are to be collected, small fibers may be used, but if solid particles are present, the use of fiber beds is limited by the tendency of the beds to plug. For dust-collection service, the fiber bed must be composed of coarse fibers and have a high void fraction, so as to minimize the tendency to plug. The fiber bed may be made from metal or plastic fibers in the form of knitted structures, multiple layers of screens, or random-packed fibers. However, the bed must have sufficient dimensional stability so that it will not be compacted during operation.

Lucas and Porter (U.S. Patent 3,370,401, 1967) developed a fiber-bed scrubber in which the gas and scrubbing liquid flow vertically upward through a fiber bed (Fig. 17-53). The beds tested were composed of knitted structures made from fibers with diameters ranging from 89 to 406 μm . Lucas and Porter reported that the

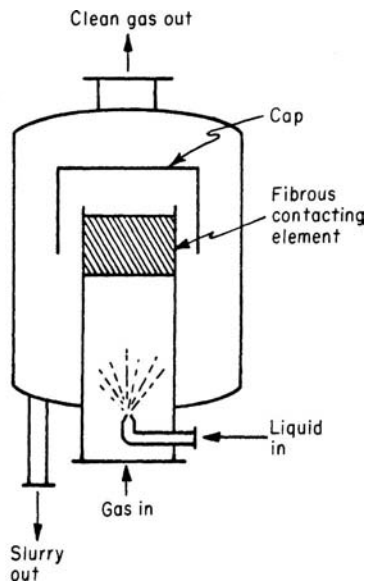


FIG. 17-53 Fibrous-bed scrubber. (Lucas and Porter, U.S. Patent 3,370,401, 1967.)

fiber-bed scrubber gave substantially higher efficiencies than did venturi-type scrubbers tested with the same dust at the same gas pressure drop. In similar experiments, Semrau (Semrau and Lunn, op. cit.) also found that a fiber-bed contactor made with random-packed steel-wool fibers gave higher efficiencies than an orifice contactor. However, there were indications that the fiber bed would have little advantage in the collection of submicrometer particles, presumably because of the large fiber size feasible for dust-collection service.

Alliger (U.S. Patents 3,659,402, 1972, and 3,905,788, 1975) describes fiber-bed structures which are not random, but are rather built up from flat mesh sheets offset angularly from one layer to the next and then compressed and bonded. Such bonded beds of relatively coarse hydrophobic fibers both are remarkably flushable, to prevent fouling by insoluble solids, and have surprisingly high collection efficiency per unit pressure drop for submicrometer particles, approaching that of irrigated fine hydrophobic fiber filters such as described by Fair (U.S. Patent 3,135,592, 1964) and Vosseller (U.S. Patent 3,250,059, 1966).

Electrically Augmented Scrubbers In some types of wet collectors, attempts are made to apply the electrostatic-deposition mechanism by charging the dust particles, the water droplets, or both. The objective is to combine in a scrubber high efficiency in collecting fine particles and the moderate power consumption characteristic of an electrical precipitator. Successful devices of this type have been essentially wet electrical precipitators and should properly be discussed in that category (see "Electrical Precipitators"). So far, there has been no clear demonstration of a device that combines the small size, compactness, and high efficiency of a high-energy scrubber with the relatively low power consumption of an electrical precipitator.

Mechanical Scrubbers Mechanical scrubbers comprise those devices in which a power-driven rotor produces the fine spray and the contacting of gas and liquid. As in other types of scrubbers, it is the droplets that are the principal collecting bodies for the dust particles. The rotor acts as a turbulence producer. An entrainment separator must be used to prevent carry-over of spray. Among potential maintenance problems are unbalancing of the rotor by buildup of dust deposits and abrasion by coarse particles.

The simplest commercial devices of this type are essentially fans upon which water is sprayed. The unit shown in Fig. 17-54 is adapted to light duty, and heavy dust loads are avoided to minimize buildup on the rotor.

Dry Scrubbing *Dry scrubbing* is an umbrella term used to associate several different unit operations and types of hardware that can

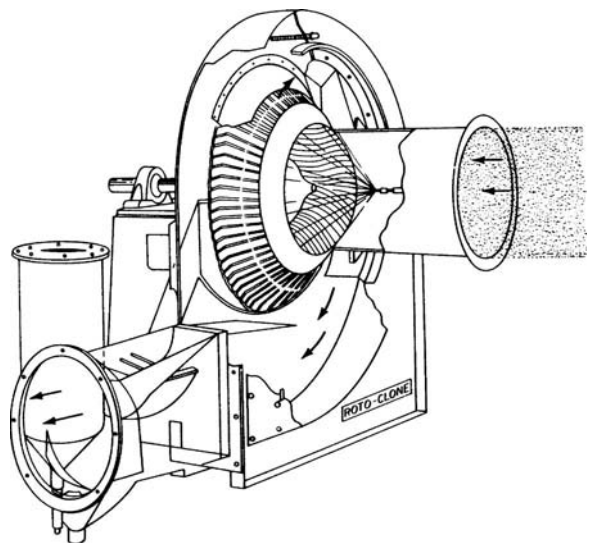


FIG. 17-54 Mechanical scrubber. (American Air Filter Co., Inc.)

be used in combinations to accomplish the unit process of dry scrubbing. They all utilize scrubbing, in which mass transfer takes place between the gas phase and an active liquidlike surface, and they all discharge the resulting products separately as a gas and a solidlike "dry" product for reuse or disposal.

It is helpful to recognize three phases in the development of systems using dry scrubbing. The first phase used mainly good contactors and relatively expensive sorbents, which were tailored to catch targeted compounds with high efficiency (>99 percent). The second phase used mainly minimal contactors and cheap sorbents in order to get enough sulfur dioxide capture (>60 percent) to justify using cheaper higher sulfur coal. The third phase is ongoing; it uses mainly better contactors, sorbents, and fabric filters in order to get not only high SO₂ capture (>90 percent), but also substantial capture of other regulated emissions such as metals and dioxins.

The principle of dry scrubbing was first recognized by Lamb and Wilson [*I&EC*, **11**(5), 420 (1919)] and Wilson [*I&EC*, **12**(10), 1000 (1920)] at MIT during their World War I program to develop better media for military gas masks. The preferred medium turned out to be a mixture of granular activated carbon with a new kind of porous granular hydrated lime, which they dubbed *activated soda-lime*. What activated it was a small but critical amount of sodium hydroxide, which was enough to maintain in use on French battlefields an equilibrium moisture film a few molecules thick on the surface of pores within lime particles. That film enhanced surface hydrolysis, diffusion, and neutralization of acid gases such as Cl₂ and SO₂, to the point that their removal became controlled by fast external gas-film diffusion, up to substantial utilization of the potential stoichiometric capacity. The better varieties of army activated soda-lime used in gas masks captured more than 99 percent of Cl₂ or SO₂ even after using up more than 10 percent of alkalinity. Gas-mask-canister sorbent beds typically used 8 × 14 mesh granules 10 cm deep, and tests were run with 1 percent acid gas at space velocities of 3000 to 7400 l/hr. Carbon dioxide was tested to higher penetrations; its capture was more than 50 percent even after using up more than 50 percent of available alkalinity.

With good dry scrubbing sorbents, the controlling resistance for gas cleaning is external turbulent diffusion, which also depends on energy dissipated by viscous and by inertial mechanisms. It turns out to be possible to correlate mass-transfer rate as a function of the friction factor [Ergun, *CEP* **48**(2):89 and **48**(5):227(1952)].

It turns out that packed beds much less than a hundred particles thick behave as if they were well-stirred due to the entrance effect. Although it may seem odd that a packed bed can behave as if well-stirred, it typically takes at least a 100-particle bed depth in order for a plug-flow concentration wave to develop.

Integration of the Ergun equation for well-stirred flow gives

$$\frac{C_2 - C_1}{C^\circ - C_2} = F_k \frac{\rho D_v (1 - \epsilon_v) L}{\mu \epsilon_v D_p} \quad (17-9)$$

Recognition of dry scrubbing as a mechanism useful in treating large gas flows first came in the 1960s as regulations were tightening on fly ash emissions from utility boilers. Dry scrubbing turns out to be the appropriate way to describe the interactions of sulfuric acid vapor with fly ash from pulverized coal combustion. On one hand, powdered sodium bicarbonate was added to some flue gases in order to protect fabric filter bags from attack by sulfuric acid films on ash from high sulfur coal combustion. On the other hand, sulfur trioxide was added to other flue gases in order to generate sulfuric acid films that would improve the performance of electrostatic precipitators collecting inherently high resistivity ash from low sulfur coal. From Eq. (17-9), it is readily apparent that the way to get more gas cleaning per unit pressure drop is to optimize the particle size and void fraction, and use relatively fewer particles operating at higher velocity. Such an arrangement runs out of stoichiometric capacity quickly, which leads naturally to transported bed contactors fed with fresh sorbent.

The actual name "dry scrubbing" was first publicized by Teller [U.S. Patent no. 3,721,066 (1973)]. He worked both with classical Army-type soda-lime and with his patented water-activated form of the alkaline feldspar nepheline syenite as a flow agent and feedstock sorbent for HF and SO₂ in hot, sticky fumes from glass melting furnaces. He

claimed capture of more than 99 percent of 180 ppm HF and SO₂ for more than 20 hours in a packed bed of 200 × 325 mesh hydrated nepheline syenite at 42,000/hr.

Teller [U.S. Patent no. 3,997,652 (1976)] also patented a number of "chromatographic sorbents" using semivolatiles liquid coatings similar to mobile phases used in capillary columns for gas chromatographs. For simple acid gases, Teller generally used a flash-drying-type venturi injector and pneumatic transport system to disperse fresh sorbent into hot gas to be treated and to provide time for turbulent mixing. He then typically used a baghouse to collect the loaded sorbent for inclusion with other feeds into the glass melting system.

Aluminum producers were also early users of another type of dry scrubbing for the difficult cleaning problem of acid gases in hot, sticky fumes from aluminum reduction potlines. Bazhenov et al. [*Isvetn. Met.—Russia*, (6) 44 (1975)] described the use of a fluidized bed of feedstock aluminum oxide to clean potline offgas in an arrangement where there was an integral freeboard baghouse. Loaded sorbent was purged from the bed for feed into the aluminum reduction system. In that anhydrous system there was no water film as such inside the pores, but there was high specific surface, having liquidlike mobile active sites with a strong affinity for binding fluoride. The potential for achieving significant gas cleaning at very high space velocities led to dry scrubbing being applied both for incremental desulfurization of flue gases from coal-fired utility boilers and for removal of trace acid gases from solid waste incineration. A number of different hardware arrangements were tested all the way to full scale in order to determine accurately the various effects that must be optimized in order to achieve minimum net cost to be carried by the rate-paying public.

It was apparent from the very earliest tests that control of thin moisture films on the surface of reactive particles was the key to success. The main three competing arrangements, as compared by Statnick et al. [4th Annual Pitt. Coal Conf. (1987)] involved slurry spray dryers, where lime and water were injected together, versus systems where the gas was humidified by water injection before or after injection of lime dry powder reagents. It turns out that there are tradeoffs among the costs of hardware, reagent, and water dispersion and reagent purchase and disposal. Systems where water evaporates in the presence of active particles are usually less expensive overall.

The evaporation lifetimes of pure water droplets are described by Marshall and Seltzer [*CEP*, **46**(10), 501 and **46**(11), 575 (1950)] and by Duffie and Marshall [*CEP*, **49**(8), 417 (1953) and **49**(9), 480 (1953)]. Figure 17-55 is easy to use to estimate the necessary spray dispersion. For typical humidifier conditions of 300°F gas inlet temperature and a 20°F approach to adiabatic saturation at the outlet, a 60-μm droplet will require about 0.9 s to evaporate, while a 110-μm droplet will require about 3 s. If the time available for drying is no more than 3 s, it therefore follows that the largest droplets in a humidifier spray should be no larger than 100 μm. If the material being dried contains solids, droplet top size will need to be smaller due to slower evaporation rates. Droplets this small not only require considerable expensive power to generate, but since they have inherent penetration distances of less than a meter, they require expensive dispersion arrangements to get good mixing into large gas flows without allowing damp, sticky particles to reach walls.

The economics seem to be better for systems where dry powdered fresh lime plus ground recycled lime is injected along with a relatively coarse spray which impinges on and dries out from the reagent, as described by Stouffer et al. [*I&EC Res.*, **28**(1):20 (1989)]. Withum et al. [9th Ann. Pitt. Coal Prep. Util. Env. Control Contractors Conf. (1993)] describes an advanced version of that system that has been further optimized to the point that it is competitive with wet limestone scrubbing for >90 percent flue gas desulfurization.

The most popular dry scrubbing systems for incinerators have involved the spray drying of lime slurries, followed by dry collection in electrostatic precipitators or fabric filters. Moller and Christiansen [Air Poll. Cont. Assoc. 84-9.5 (1984)] published data on early European technology. Moller et al. [U.S. Patent no. 4,889,698 (1989)] describe the newer extension of that technology to include both spray-dryer absorption and dry scrubbing with powdered, activated carbon injection. They claim greatly improved removal of mercury, dioxins, and NO_x.

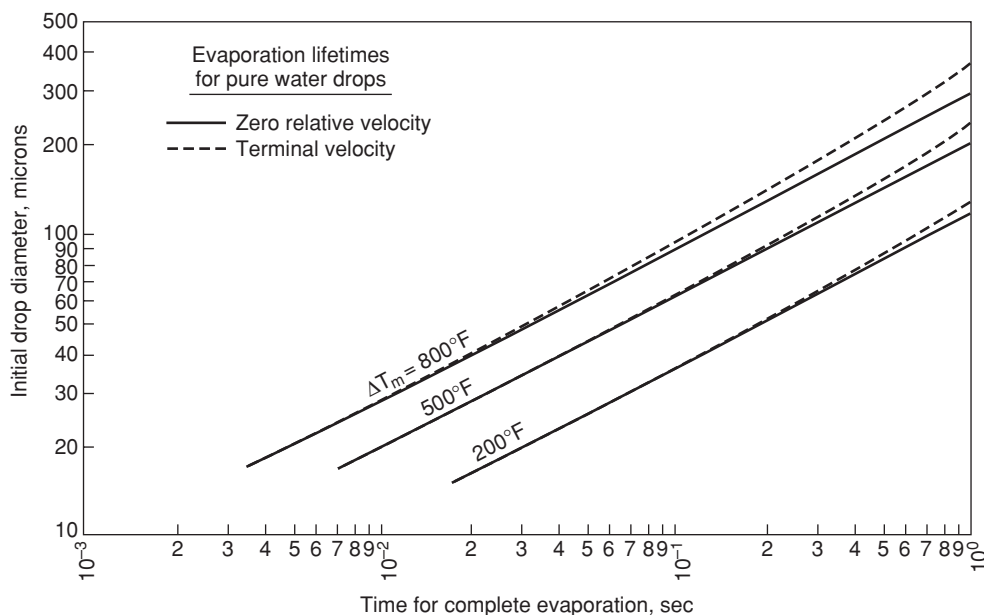


FIG. 17-55 Effect of drop diameter on time for complete evaporation of water drops.

Optimized modern dry scrubbing systems for incinerator gas cleaning are much more effective (and expensive) than their counterparts used so far for utility boiler flue gas cleaning. Brinckman and Maresca [ASME Med. Waste Symp. (1992)] describe the use of dry hydrated lime or sodium bicarbonate injection followed by membrane filtration as preferred treatment technology for control of acid gas and particulate matter emissions from modular medical waste incinerators, which have especially high dioxin emissions.

Kreindl and Brinckman [Air Waste Man. Assoc., paper 93-RP-154.04 (1993)] describe the three conventional flue-gas cleaning-process concepts (standard dry scrubbing, quasi-dry scrubbing, and wet scrubbing) as being inherently inadequate to meet the emerging European incinerator metal and organic emissions limits. Standard dry scrubbing can be upgraded by using powdered carbon along with lime, and switching to membrane filter media. Quasi-dry scrubbing can be upgraded by using powdered carbon along with lime spray drying [as also described by Moller (1989)], and switching to membrane filter media. Wet scrubbing can be upgraded by post-treatment following the wet scrubber with a circulating fluidized bed of granular activated carbon, again followed by a membrane filter.

Control of metal and organic emissions by dry scrubbing involves more than the simple acid gas neutralization discussed so far. Capture of metals other than mercury is mainly a matter of using a fabric filter having the capability of retaining unagglomerated submicron particles that are relatively enriched in toxic metals such as cadmium. Use of membrane-coated filter media is almost essential to do that well. Capture of mercury and dioxins is mainly achieved with activated carbon, which is more effective when used in combination with inhibitors for chlorine formation by the Deacon reaction. Karasek [U.S. Patent no. 4,793,270 (1988)] describes the inhibiting effects of sulfur compounds, which is why dioxins are rarely a problem in flue gases from coal-fired combustion. Naikwadi and Karasek [*Chemosphere*, 27(1-3), 335 (1993)] describe the potent inhibiting effect of amines. That is presumably why German experience is finding that dioxins are rarely a problem in flue gases that have undergone some form of ammonia deNO_x treatment, as described by Hahn [*Chemosphere*, 25(1-2), 57 (1992)]. Hahn, like Kreindl and Brinckman, also argues that classical wet scrubbers will need to be upgraded with modern dry scrubbers and fabric filters.

Maerker Sorbalit® (<http://www.maerker-umwelttechnik.de/englisch/Produkt.htm>) pioneered the use as a filter aid or precoat lime hydrated with activated carbon so as to adsorb heavy semivolatile polynuclear aromatic hydrocarbons under conditions which prevent their gradual chlorination to dioxins. The material is free-flowing and easy to disperse, and the little dust is nonflammable, unlike that of some plain activated carbons. Donau Carbon also produces an equivalent Desomix® material which is effective in entrained flow or precoat reactors (<http://www.dcffm.de/englisch/programm/flugstromverfahren.html>). Such filter precoat greatly decrease dioxin emissions and can capture mercury when impregnated with sulfur. A different approach also depending on sorption is to adsorb the heavy semivolatile polynuclear aromatic hydrocarbons onto an active oxidation catalyst where they can be destroyed in situ. Promoted catalysts similar to those used for ammonia deNO_x are generally effective. Such catalysts may be used either in traditional pellet beds following a baghouse or within a baghouse dispersed in a porous felted PTFE membrane filter fabric, e.g., W. L. Gore's Remedia® (U.S. Patent 5,620,669).

Emission control of heavy semivolatile polynuclear organic hydrocarbon soot from diesel engines is becoming required in many jurisdictions. That is generally accomplished by passing exhaust gases through a regenerable porous ceramic foam or fiber filter, so as to capture organics during cool smoky operation and then to burn them off during hotter clean operation. A typical porous wall tube array is shown in Fig. 17-56. Size distribution of soot in cool exhaust gas typically has a log-mean mobility diameter of 50 nm with a geometric standard deviation of 1.7. Given the small particle size and the short filter transit time, collection is clearly by diffusion, but it is not totally clear whether particles are yet fully agglomerated. There is very active ongoing research in this area, and the technology undoubtedly has not yet stabilized. Hardware which is already in use in Europe is summarized in the "VERT Filter List" of particle-trap systems which have been tested and approved for retrofitting diesel engines by the Swiss Agency for the Environment Forests and Landscape (SAEFL). The current list is available for download (http://www.umwelt-schweiz.ch/imperia/md/content/luft/fachgebiet/e/industrie/filterliste_01_03_04_e.pdf). The underlying technology is publicized by vendors and summarized by Mayer in many ongoing publications, such as his encyclopaedic article http://www.akpf.org/pub/2003_particle_traps.pdf.

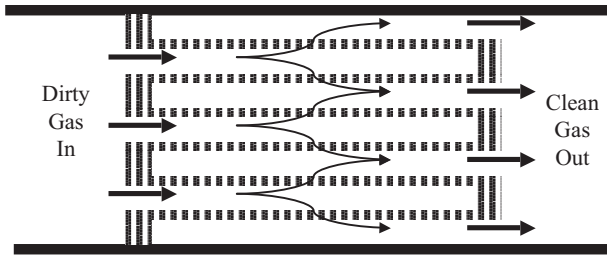


FIG. 17-56 Typical porous wall tube array diesel particulate filter.

Fabric Filters Fabric filters, commonly termed “bag filters” or “baghouses,” are collectors in which dust is removed from the gas stream by passing the dust-laden gas through a fabric of some type (e.g., woven cloth, felt, or porous membrane). These devices are “surface” filters in that dust collects in a layer on the surface of the filter medium, and the dust layer itself becomes the effective filter medium. The pores in the medium (particularly in woven cloth) are usually many times the size of the dust particles, so that collection efficiency is low until sufficient particles have been collected to build up a “precoat” in the fabric pores (Billings and Wilder, *Handbook of Fabric Filter Technology*, vol. I, EPA No. APTD-0690, NTIS No. PB-200648, 1979). During this initial period, particle deposition takes place mainly by inertial and flow-line interception, diffusion, and gravity. Once the dust layer has been fully established, sieving is probably the dominant deposition mechanism, penetration is usually extremely low except during the fabric-cleaning cycle, and only limited additional means remain for influencing collection efficiency by filter design. Filter design is related mainly to choices of gas filtration velocities and pressure drops and of fabric-cleaning cycles.

Because of their inherently high efficiency on dusts in all particle-size ranges, fabric filters have been used for collection of fine dusts and fumes for over 100 years. The greatest limitation on filter application has been imposed by the temperature limits of available fabric materials. The upper limit for natural fibers is about 90°C (200°F). The major new developments in filter technology that have been made since 1945 have followed the development of fabrics made from glass and synthetic fibers, which has extended the temperature limits to about 230 to 260°C (450 to 500°F). The capabilities of available fibers to resist high temperatures are still among the most severe limitations on the possible applications of fabric filters.

Gas Pressure Drops The filtration, or superficial face, velocities used in fabric filters are generally in the range of 0.3 to 3 m/min (1 to 10 ft/min), depending on the types of fabric, fabric supports, and cleaning methods used. In this range, gas pressure drops conform to Darcy’s law for streamline flow in porous media, in which the pressure drop is directly proportional to the flow rate. The pressure drop across the fabric and the collected dust layer may be expressed (Billings and Wilder, *op. cit.*) by

$$\Delta p = K_1 V_f + K_2 w V_f \tag{17-10}$$

where $\Delta p = kPa$, or in of water; $V_f =$ superficial velocity through filter, m/min, or ft/min; $w =$ dust loading on filter, g/m^2 , or lbm/ft^2 ; and K_1 and K_2 are resistance coefficients for the “conditioned” fabric and the dust layer, respectively. The conditioned fabric is that fabric in which a relatively consistent dust load remains deposited in depth following cycles of filtration and cleaning. K_1 , expressed in units of $kPa/(m/min)$ or in $water/(ft/min)$, may be more than 10 times the value of the resistance coefficient for the original clean fabric. If the depth of the dust layer on the fabric is greater than about 0.2 cm ($1/16$ in), corresponding to a fabric dust loading on the order of $200 g/m^2$ ($0.04 lbm/ft^2$), the pressure drop across the fabric (including the dust in the pores) is usually negligible relative to that across the dust layer.

The specific resistance coefficient for the dust layer K_2 was originally defined by Williams et al. [*Heat. Piping Air Cond.*, **12**, 259

TABLE 17-5 Specific Resistance Coefficients for Certain Dusts*

Dust	K_2 † for particle size less than						
	20 mesh	140 mesh	375 mesh	90 μm	45 μm	20 μm	2 μm
Granite	1.58	2.20				19.8	
Foundry	0.62	1.58	3.78				
Gypsum			6.30				
Feldspar			6.30				
Stone	0.96			6.30			
Lampblack							47.2
Zinc oxide							15.7‡
Wood				6.30			
Resin (cold)		0.62				25.2	
Oats	1.58			9.60	11.0		
Corn	0.62		1.58	3.78	8.80		

*Data from Williams et al., *Heat. Piping Air Cond.*, **12**, 259–263 (1940).

$$\dagger K_2 = \frac{\Delta p_i}{V_f w} \frac{\text{in water}}{(\text{ft}/\text{min})(\text{lbm}/\text{ft}^2)}$$

NOTE: These data were obtained when filtering air at ambient conditions. For gases other than atmospheric air, the Δp_i values predicted from Table 17-5 should be multiplied by the actual gas viscosity divided by the viscosity of atmospheric air.

‡Flocculated material not dispersed; size actually larger.

(1940)], who proposed estimating values of the coefficient by use of the Kozeny-Carman equation [Carman, *Trans. Inst. Chem. Eng. (London)*, **15**, 150 (1937)]. In practice, K_1 and K_2 are measured directly in filtration experiments. The K_1 and K_2 values can be corrected for temperature by multiplying by the ratio of the gas viscosity at the desired condition to the gas viscosity at the original experimental conditions. Values of K_2 determined for certain dusts by Williams et al. (*op. cit.*) are presented in Table 17-5.

Lapple (in Perry, *Chemical Engineers’ Handbook*, 3d ed., McGraw-Hill, New York, 1950) presents an alternative form of Eq. (17-10) in which the gas-viscosity term is explicit instead of being incorporated into the resistance coefficients:

$$\Delta p_i = K_c \mu V_f + K_d \mu w V_f \tag{17-11}$$

where $\Delta p_i =$ in water, $\mu = cP$, $V_f = ft/min$, $w = gr/ft^2$, $K_c =$ cloth resistance coefficient = (in water)/(cP)(ft/min), and $K_d =$ dust-layer resistance coefficient = (in water)/(cP)(gr/ft²)(ft/min). K_d may be expressed in the same units, using the Kozeny-Carman equation:

$$K_d = \frac{160.0(1 - \epsilon_s)}{\phi_s^2 D_p^2 \rho_s \epsilon_s^3} \tag{17-12}$$

where $D_p = \mu m$ and $\rho_s = lbm/ft^3$.

Data sufficient to permit reasonable predictions of K_d from Eq. (17-12) are seldom available. The range in the values of K_d that may be encountered in practice is illustrated in Fig. 17-57 in which available experimental determinations of K_d reported in the literature for a variety of dusts are plotted against particle size. In most cases no accurate particle-size data were reported, and the curves represent the estimated range of particle size involved. The data of Williams et al. (*op. cit.*) are related to a wide variety of dusts, and only the approximate limits enclosing these data are shown. Also included are curves predicted from Eq. (17-12) for specific values of ϕ_s , ρ_s , and ϵ_s . It is apparent from these curves that smaller particles tend toward higher values of ϵ_s , which is consistent with the observation that fine dusts (particularly those smaller than 10 μm) have lower bulk densities than coarser fractions, apparently because of the effects of surface forces. For coarse dusts, K_d varies approximately inversely as the square of the particle diameter, which implies that the void fraction (or bulk density) does not change with particle size. However, for particles finer than 10 μm , the value of K_d appears to become constant, increased voids compensating for the reduction in size. In addition to the increased voidages encountered with small particles, slip flow also contributes to the relative constancy of the experimental values of K_d for particle sizes under 5 μm .

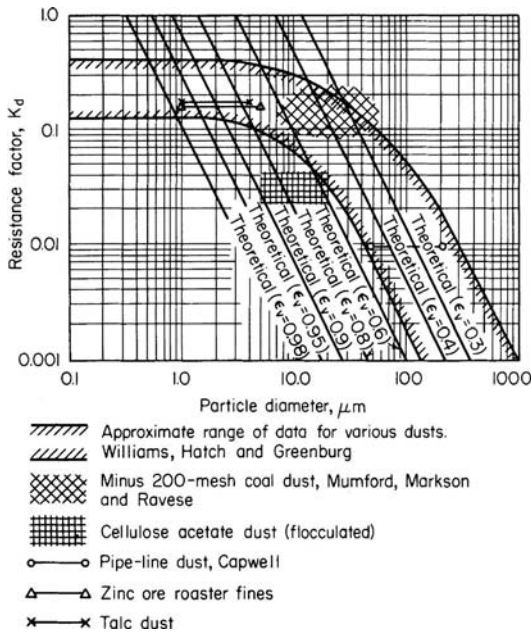


FIG. 17-57 Resistance factors for dust layers. Theoretical curves given are based on Eq. (20-78) for a shape factor of 0.5 and a true particle specific gravity of 2.0. [Williams, Hatch, and Greenburg, *Heat. Piping Air. Cond.*, **12**, 259 (1940); Mumford, Markson, and Ravese, *Trans. Am. Soc. Mech. Eng.*, **62**, 271 (1940); Capwell, *Gas*, **15**, 31 (August 1939)].

Because of the assumptions underlying its derivation, the Kozeny-Carman equation is not valid at void fractions greater than 0.7 to 0.8 (Billings and Wilder, *op. cit.*). In addition, *in situ* measurement of the void fraction of a dust layer on a filter fabric is extremely difficult and has seldom even been attempted. The structure of the layer is dependent on the character of the fabric surface as well as on the characteristics of the dust, whereas the application of Eq. (17-12) implicitly assumes that K_2 is dependent only on the properties of the dust. A smooth fabric surface permits the dust to become closely packed, leading to a relatively high value of K_2 . If the surface is napped or has numerous extended fibrils, the dust cake formed will be more porous and have a lower value of K_2 [Billings and Wilder, *op. cit.*; Snyder and Pring, *Ind. Eng. Chem.*, **47**, 960 (1955); and K. T. Semrau, unpublished data, SRI International, Menlo Park, Calif., 1952-1953].

Equation (17-10) indicates that for filtration at a given velocity the pressure drop is a linear function of the fabric dust loading w . In some cases, particularly with smooth-surfaced fabrics, this is at least approximately the case, but in other instances the function displays an upward curvature with increases in w , indicating compression of the dust layer, the fabric, or both, and a consequent increase in K_2 (Snyder and Pring, *op. cit.*; Semrau, *op. cit.*). Several investigations have shown K_2 to be increased by increases in the filtration velocity [Billings and Wilder, *op. cit.*; Spaite and Walsh, *Am. Ind. Hyg. Assoc. J.*, **24**, 357 (1968)]. However, the various investigators do not agree on the magnitude of the velocity effects. Billings and Wilder suggest assuming as an approximation that K_2 is directly proportional to the filtration velocity, but the actual relationship is probably dependent on the nature of the fabric and fabric surface, the characteristics of the dust, the dust loading on the fabric, and the pressure drop.

Clearly, the factors determining K_2 are far more complex than is indicated by a simple application of the Kozeny-Carman equation, and when possible, filter design should be based on experimental determinations made under conditions approximating those expected in the planned installation.

Types of Filters Current fabric-filter designs fall into three types, depending on the method of cleaning used: (1) shaker-cleaned,

(2) reverse-flow-cleaned, and (3) reverse-pulse-cleaned. The shaker-cleaned filter is the earliest form of bag filter (Fig. 17-58). The open lower ends of the bags are fastened over openings in the tube sheet that separates the lower dirty-gas inlet chamber from the upper clean-gas chamber. The bag supports from which the bags are suspended are connected to a shaking mechanism. The dirty gas flows upward into the filter bags, and the dust collects on the inside surfaces of the bags. When the gas pressure drop rises to a chosen upper limit as the result of dust accumulation, the gas flow is stopped and the shaker is operated, giving a whipping motion to the bags. The dislodged dust falls into the dust hopper located below the tube sheet. If the filter is to be operated continuously, it must be constructed with multiple compartments, so that the individual compartments can be sequentially taken off line for cleaning while the other compartments continue in operation (Fig. 17-59).

Shaker-cleaned filters are available as standard commercial units, although large baghouses for heavy-duty service are commonly custom-designed and -fabricated. The oval or round bags used in the standard units are usually 12 to 20 cm (5 to 8 in) in diameter and 2.5 to 5 m (8 to 17 ft) long. The large, heavy-duty baghouses may use bags up to 30 cm (12 in) in diameter and 9 m (30 ft) long. The bags must be made of woven fabrics to withstand the flexing and stretching involved in shaking. The fabrics may be made from natural fibers (cotton or wool) or synthetic fibers. Fabrics of glass or mineral fibers are generally too fragile to be cleaned by shaking and are usually used in reverse-flow-cleaned filters.

Large units (other than custom units) are usually built up of standardized rectangular sections in parallel. Each section contains on the order of 1000 to 2000 ft^2 of cloth, and the sections are assembled in the field to form a single filter housing. In this manner, the filter can be partitioned so that one or more sections at a time can be cut out of service for shaking or general maintenance.

Ordinary shaker-cleaned filters may be shaken every $\frac{1}{4}$ to 8 h, depending on the service. A manometer connected across the filter is useful in determining when the filter should be shaken. Fully automatic filters may be shaken as frequently as every 2 min, but bag maintenance will be greatly reduced if the time between shakings can be increased to 15 or 20 min without developing excessive pressure drop. Cleaning may be actuated automatically by a differential-pressure switch. It is essential that the gas flow through the filter be stopped when shaking in order to permit the dust to fall off. With very fine dust, it may even be necessary to equalize the pressure across the cloth [Mumford, Markson, and Ravese, *Trans. Am. Soc. Mech. Eng.*, **62**, 271 (1940)]. In practice this can be accomplished without interrupting the operation by cutting one section out of service at a time, as shown in Fig. 17-59. In automatic filters this operation involves closing the dampers, shaking the filter units either pneumatically or mechanically, sometimes with the addition of a reverse flow of cleaned gas through the filter, and lastly reopening the dampers. For compressed-air-operated automatic filters, this entire operation may take only 2 to 10 s. For ordinary mechanical filters equipped for automatic control, the operation may take as long as 3 min.

Equation (17-11) may be rewritten as

$$\Delta p_i = K_d \mu c_d V_f^2 t_m \tag{17-13}$$

where c_d = dust concentration in dirty gas, gr/ft^3 ; and t_m = filtration time, min. This shows that the pressure drop due to dust accumulation varies as the square of the gas velocity through the filter. (The actual effect of velocity on pressure drop may be even greater in some instances.) Greater cloth area and reduced filtration velocity therefore afford substantial reductions in shaking frequency and in bag wear. Consequently, it is generally economical to be conservative in specifying cloth area. Shaker-cleaned filters are generally operated at filtration velocities of 0.3 to 2.5 m/min (1 to 8 ft/min) and at pressure drops of 0.5 to 1.5 kPa (2 to 6 in water). For very fine dusts or high dust concentrations, filtration velocities should not exceed 1 m/min (3 ft/min). For fine fumes and dusts in heavy-duty installations, filtration velocities of 0.3 to 0.6 m/min (1 to 2 ft/min) have long been accepted on the basis of operating experience.

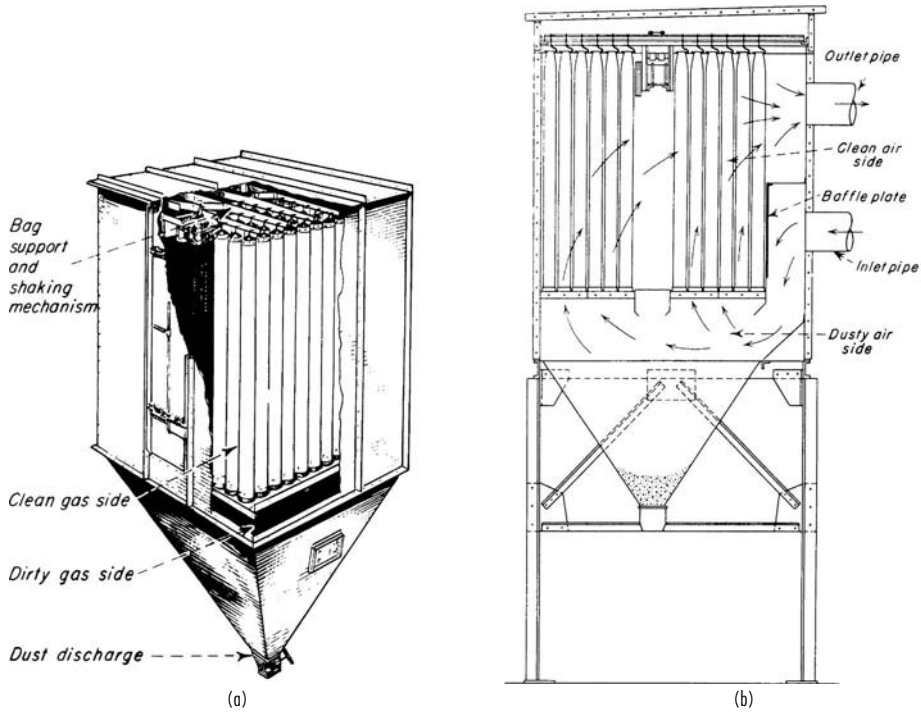


FIG. 17-58 Typical shaker-type fabric filters. (a) Buell Norblo (cutaway view). (b) Wheelabrator-Frye Inc. (sectional view).

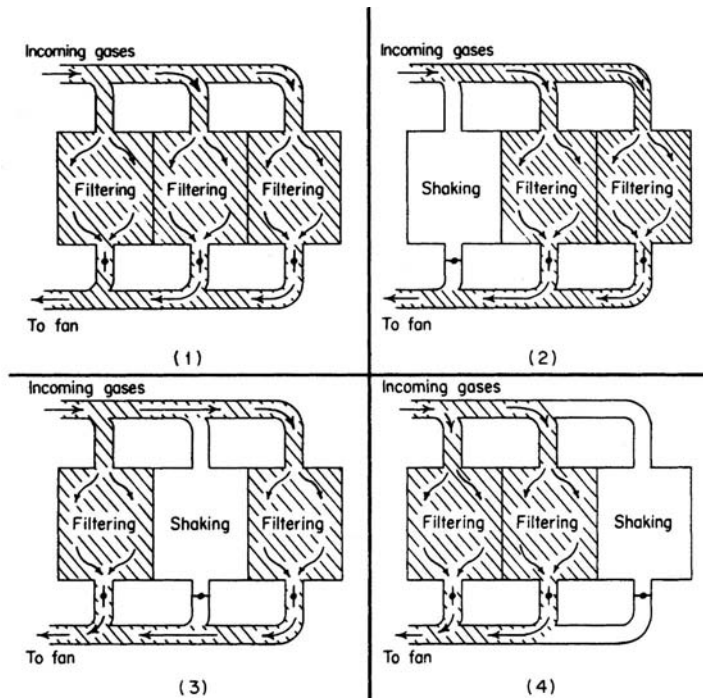


FIG. 17-59 Three-compartment bag filter at various stages in the cleaning cycle. (Wheelabrator-Frye Inc.)

Cyclone precleaners are sometimes used to reduce the dust load on the filter or to remove large hot cinders or other materials that might damage the bags. However, reducing the dust load on the filter by this means may not reduce the pressure drop, since the increase in K_2 produced by the reduction in average particle size may compensate for the decrease in the fabric dust loading.

In filter operation, it is essential that the gas be kept above its dew point to avoid water-vapor condensation on the bags and resulting plugging of the bag pores. However, fabric filters have been used successfully in steam atmospheres, such as those encountered in vacuum dryers. In such cases, the housing is generally steam-traced.

Reverse-flow-cleaned filters are generally similar to the shaker-cleaned filters except for the elimination of the shaker. After the flow of dirty gas has stopped, a fan is used to force clean gas through the bags from the clean-gas side. This flow of gas partly collapses the bags and dislodges the collected dust, which falls to the dust hopper. Rings are usually sewn into the bags at intervals along the length to prevent complete collapse, which would obstruct the fall of the dislodged dust. The principal applications of reverse-flow cleaning are in units using fiberglass fabric bags for dust collection at temperatures above 150°C (300°F). Collapsing and reinflation of the bags can be made sufficiently gentle to avoid putting excessive stresses on the fiberglass fabrics [Perkins and Imbalzano, "Factors Affecting the Bag Life Performance in Coal-Fired Boilers," 3d APCA Specialty Conference on the User and Fabric Filtration Equipment, Niagara Falls, N.Y., 1978; and Miller, *Power*, **125**(8), 78 (1981)]. As with shaker-cleaned filters, compartments of the baghouse are taken off line sequentially for bag cleaning. The gas for reverse-flow cleaning is commonly supplied in an amount necessary to give a superficial velocity through the bags of 0.5 to 0.6 m/min (1.5 to 2.0 ft/min), which is the same range as the filtration velocities frequently used.

In the reverse-pulse filter (frequently termed a reverse-jet filter), the filter bag forms a sleeve that is drawn over a wire cage, which is usually cylindrical (Fig. 17-60). The cage supports the fabric on the clean-gas side, and the dust is collected on the outside of the bag. A venturi nozzle is located in the clean-gas outlet from the bag. For cleaning, a jet of high-velocity air is directed through the venturi nozzle and into the bag, inducing a flow of cleaned gas to enter the bag and flow through the fabric to the dirty-gas side. The high-velocity jet is released in a sudden, short pulse (typical duration 100 ms or less) from a compressed-air line by a solenoid valve. The pulse of air and clean gas expands the bag and dislodges the collected dust. Rows of bags are cleaned in a timed sequence by programmed operation of the

solenoid valves. The pressure of the pulse is sufficient to dislodge the dust without cessation of the gas flow through the filter unit.

It has been a common practice to clean the bags on line (i.e., without stopping the flow of dirty gas into the filter), and reverse-pulse bag filters have been built without division into multiple compartments. However, investigations [Leith et al., *J. Air Pollut. Control Assoc.*, **27**, 636 (1977)] and experience have shown that, with online cleaning of reverse-pulse filters, a large fraction of the dust dislodged from the bag being cleaned may redeposit on neighboring bags rather than fall to the dust hopper. As a result, there is a growing trend to off-line cleaning of reverse-pulse filters. The baghouse is sectionalized so that the outlet-gas plenum serving the bags in a section can be closed off from the clean-gas exhaust, thereby stopping the flow of inlet gas through the bags. On the dirty-gas side of the tube sheet, the bags of the section are separated by partitions from the neighboring sections, where filtration is continuing. Sections of the filter are cleaned in rotation, as in shaker and reverse-flow filters.

Some manufacturers are using relatively low-pressure air (100 kPa, or 15 lbf/in², instead of 690 kPa, or 100 lbf/in²) and are eliminating the venturi tubes for clean-gas induction. Others have eliminated the separate jet nozzles located at the individual bags and use a single jet to inject a pulse into the outlet-gas plenum.

Reverse-pulse filters are typically operated at higher filtration velocities (air-to-cloth ratios) than shaker or reverse-flow filters designed for the same duty. Filtration velocities may range from 1 to 4.5 m/min (3 to 15 ft/min), depending on the dust being collected, but for most dusts the commonly used range is about 1.2 to 2.5 m/min (4 to 8 ft/min). The frequency of cleaning is also dependent on the nature and concentration of the dust, with the intervals between pulses varying from about 2 to 15 min.

The cleaning action of the pulse is so effective that the dust layer may be completely removed from the surface of the fabric. Consequently, the fabric itself must serve as the principal filter medium for at least a substantial part of the filtration cycle. Woven fabrics are unsuitable for such service, and felts of various types must be used. The bulk of the dust is still removed in a surface layer, but the felt ensures that an adequate collection efficiency is maintained until the dust layer has formed.

Filter Fabrics The cost of the filter bags represents a substantial part of the erected cost of a bag filter—typically 5 to 20 percent, depending on the bag material [Reigel and Bundy, *Power*, **121**(1), 68 (1977)]. The cost of bag repair and replacement is the largest component of the cost of bag-filter maintenance. Consequently, the proper choice of filter fabric is critical to both the technical performance and the economics of operating a filter. With the advent of synthetic fibers, it has become possible to produce fabrics having a wide range of properties. However, demonstrating the acceptability of a fabric still depends on experience with prolonged operation under the actual or simulated conditions of the proposed application. The choice of a fabric material for a given service is necessarily a compromise, since no single material possesses all the properties that may be desired. Following the choice of material, the type of fabric construction is critical.

Two principal types of fabric are adaptable to filter use: woven fabrics, which are used in shaker and reverse-flow filters; and felts, which are used in reverse-pulse filters. The felts made from synthetic fibers are needle felts (i.e., felted on a needle loom) and are normally reinforced with a woven insert. The physical properties and air permeabilities of some typical woven and felt filter fabrics are presented in Tables 17-6 and 17-7. The "air permeability" of a filter fabric is defined as the flow rate of air in cubic feet per minute (at 70°F, 1 atm) that will pass through 1 ft² of clean fabric under an applied differential pressure of ½ in. water. The resistance coefficient K_f of the clean fabric is defined by the equation in Table 17-6, which may be used to calculate the value of K_f from the air permeability. If Δp_i is taken as 0.5 in. water, μ as 0.0181 cP (the viscosity of air at 70°F and 1 atm), and V_f as the air permeability, then $K_f = 27.8/\text{air permeability}$.

Collection Efficiency The inherent collection efficiency of fabric filters is usually so high that, for practical purposes, the precise level has not commonly been the subject of much concern. Furthermore, for collection of a given dust, the efficiency is usually fixed by the choices of filter fabric, filtration velocity, method of cleaning, and

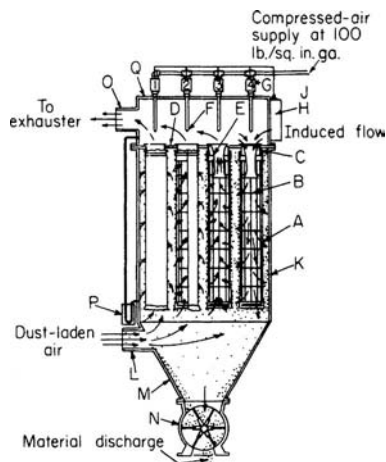


FIG. 17-60 Reverse-pulse fabric filter: (a) filter cylinders; (b) wire retainers; (c) collars; (d) tube sheet; (e) venturi nozzle; (f) nozzle or orifice; (g) solenoid valve; (h) timer; (j) air manifold; (k) collector housing; (l) inlet; (m) hopper; (n) air lock; (o) upper plenum. (Mikropul Division, U.S. Filter Corp.)

17-50 GAS-SOLID OPERATIONS AND EQUIPMENT

TABLE 17-6 Resistance Factors and Air Permeabilities for Typical Woven Fabrics

Cloth	Pore size, ^a in	Threads/in	Weight, oz/yd ²	Thread ^a diameter, in	K_F [†]	Air permeability, (ft ³ /min)/ft ² at $\Delta p_i = \frac{1}{2}$ in H ₂ O
Osnaburg cotton	0.01	32 × 28		0.02	0.51	55
Osnaburg cotton (soiled) [‡]		32 × 28			4.80	5.8
Drill cotton	0.01	65 × 40	5.28	0.01	0.093	300
Cotton [§]		46 × 56			1.39	20
Cotton [§]		104 × 68			1.54	18
Cotton sateen (unnapped)	0.007	96 × 56	6.88	0.009	0.27	103
Cotton sateen (unnapped)	0.005	96 × 64	8.23	0.01	0.88	32
Cotton sateen (unnapped)		96 × 60		0.012	1.63	17
Cotton sateen (unnapped)	0.004	96 × 56	10.2	0.011	1.12	25
Wool					0.25	111
Wool		40 × 50	11.5	0.014	0.33	84
Wool, white [§]		36 × 32			0.15	185
Wool, black [§]		28 × 30			0.25	110
Wool [§]		30 × 26			0.51	55
Vinyon [§]		37 × 37			0.12	23
Nylon tackle twill		72 × 196		0.010	0.66	42
Nylon sailcloth		130 × 130		0.007	1.66	17
Nylon [§]		37 × 37			1.74	16
Nylon [§]					3.71	7.5
Asbestos [§]					0.56	50
Orlon [§]		72 × 72			0.66	42
Orlon [§]		74 × 38			0.75	37
Orlon [§]					1.16	24
Orlon [§]					1.98	14
Smoothtex nickel screen		(300 mesh)			0.16	174
Glass		32 × 28		0.03	1.60	17
Dacron		60 × 40	5.8		0.84	33
Dacron		76 × 48	13.4		0.29	9.5
Teflon		76 × 70	8.7		1.39	20

^aEstimates based on microscopic examination.

[†]Measured with atmospheric air. This value will be constant only for streamline flow, which is the case for values of $\rho V_f/\mu$ of less than approximately 100.

$$K_F = \Delta p_i / \mu V_f$$

where Δp_i = pressure drop, in water; μ = gas viscosity, cP; V_f = superficial gas velocity through cloth, ft/min; and ρ = gas density, lb/ft³.

[‡]Cloth, similar to previous one, that had been in service and contained dust in pores although free of surface accumulation.

[§]Data from Pring, *Air Pollution*, McGraw-Hill, New York, 1952, p. 280.

cleaning cycle, leaving few if any controllable variables by which efficiency can be further influenced. Inefficiency usually results from bags that are poorly installed, torn, or stretched from excessive dust loading and pressure drop. Of course, certain types of fabrics may simply be unsuited for filtration of a particular dust, but usually this will soon become obvious.

Few basic studies of the efficiency of bag filters have been made. Increased dust penetration immediately following cleaning has been readily observed while the dust layer is being reestablished. However, field and laboratory studies have indicated that during the rest of the filtration cycle the effluent-dust concentration tends to remain

constant regardless of the inlet concentration [Dennis, *J. Air Pollut. Control Assoc.*, **24**, 1156 (1974)]. In addition, there has been little indication that the penetration is strongly related to dust-particle size, except possibly in the low-submicrometer range. These observations appear to be generally consistent with sieving being the principal collection mechanism.

Leith and First [*J. Air Pollut. Control Assoc.*, **27**, 534 (1977); **27**, 754 (1977)] studied the collection efficiency of reverse-pulse filters and concluded that once the dust cake has been established, "straight-through" penetration by dust particles that pass through the filter without being stopped is negligible by comparison with penetration by dust

TABLE 17-7 Physical Properties of Selected Felts for Reverse-Pulse Filters

Fiber	Weight, oz/yd ²	Thickness, in	Breaking strength, lbf/in width	Elongation, % to rupture	Air permeability, (ft ³ /min)/ft ² at $\Delta p_i = \frac{1}{2}$ in water	K_F
Wool	23.1	0.135			27.1	1.03
Wool	21.2	0.129			29.8	0.93
Orlon [°]	10.9	0.045	65	18	20–25	1.11–1.39
Orlon [°]	17.9	0.088	85	18	15–20	1.39–1.85
Orlon [°]	24	0.125	110	60	10–20	1.39–2.78
Acrlan [°]	17.9	0.075	100	22	15–20	1.39–1.85
Dynel [°]	24	0.125	60	80	30–40	0.70–0.93
Dacron [°]	17.9	0.080	125	22	15–20	1.39–1.85
Dacron [°]	9.9	0.250	20	150	200–225	0.11–0.14
Dacron [°]	24	0.125	175	80	20–30	0.93–1.39
Nylon [°]	24	0.125	100	100	30–40	0.70–0.93
Amel [°]	24	0.125	60	80	30–40	0.70–0.93
Teflon	15.6	0.053			82.5	0.34
Teflon	43.5	0.119			21.6	1.29

[°]These data courtesy of American Felt Co.

that actually deposits initially and then "seeps" through the fabric to be reentrained into the exit air stream. They also noted that "pinholes" may form in the dust cake, particularly over pores between yarns in a woven fabric, and that particles may subsequently penetrate straight through at the pinholes. The formation of pinholes, or "cake puncture," had been observed earlier by Stephan et al. [*Am. Ind. Hyg. Assoc. J.*, **21**, 1 (1960)], but without measurement of the associated loss of collection efficiency. When a supported flat filter medium with extremely fine pores (e.g., glass-fiber paper, membrane filter) was used, no cake puncture took place even with very high pressure differentials across the cake. However, puncture did occur when a cotton-sateen filter fabric was used as the cake support. The formation of pinholes with certain combinations of dusts, fabrics, and filtration conditions was also observed by Kosciowski et al. (EPA-600/7-78-056, 1978). Evidently puncture occurs when the local cake structure is not strong enough to maintain a bridge over the aperture represented by a large pore and the portion of the cake covering the pore is blown through the fabric. This suggests that formation of pinholes will be highly dependent on the strength of the surface forces between particles that produce flocculation of dusts. The seepage of a dust through a filter is probably also closely related to the strength of the surface forces.

Surface pores can be greatly reduced in size by coating what will become the dusty side of the filter fabric with a thin microporous membrane that is supported by the underlying fabric. That has the effect of decreasing the effective penetration, both by eliminating cake pinholes, and by preventing the seepage of dust that is dragged through the fabric by successive cleanings. A variety of different membrane-forming polymers can be used in compatible service. The most versatile and effective surface filtration membranes are microfibrillar Teflon as already described by Brinckman and Maresca [*ASME Med. Waste Symp.* (1992)] in the section on dry scrubbing.

Granular-Bed Filters Granular-bed filters may be classified as "depth" filters, since dust particles deposit in depth within the bed of granules. The granules themselves present targets for the deposition of particles by inertia, diffusion, flow-line interception, gravity, and electrostatic attraction, depending on the dust and filter characteristics and the operating conditions. Other deposition mechanisms are minor at most. Although it is physically possible under some circumstances for a dust layer to form on the inlet face of the filter, the practical limits of gas pressure drop will normally have been reached long before a surface dust layer can be established.

Granular-bed filters may be divided into three classes:

1. *Fixed-bed, or packed-bed, filters.* These units are not cleaned when they become plugged with deposited dust particles but are broken up for disposal or simply abandoned. If they are constructed from fine granules (e.g., sand particles), they may be designed to give high collection efficiencies on fine dust particles. However, if such a filter is to have a reasonable operating life, it can be used only on a gas containing a low concentration of dust particles.

2. *Cleanable granular-bed filters.* In these devices provisions are made to separate the collected dust from the granules either continuously or periodically, so that the units can operate continuously on gases containing moderate to high dust concentrations. The necessity for cleaning and recycling the granules generally restricts the practical lower granule size to about 3 to 10 mm. This in turn makes it difficult to attain high collection efficiencies on fine particles with granule beds of reasonable depth and gas pressure drop.

3. *Fluidized-bed filters.* Fluidized beds of granules have received considerable study on theoretical and experimental levels but have not been applied on a practical commercial scale.

Fixed Granular-Bed Filters Fixed-bed filters composed of granules have received considerable theoretical and experimental study [Thomas and Yoder, *AMA Arch. Ind. Health*, **13**, 545 (1956); **13**, 550 (1956); Knetting and Beeckmans, *Can. J. Chem. Eng.*, **52**, 703 (1974); Schmidt et al., *J. Air Pollut. Control Assoc.*, **28**, 143 (1978); Tardos et al., *J. Air Pollut. Control Assoc.*, **28**, 354 (1978); and Gutfinger and Tardos, *Atmos. Environ.*, **13**, 853 (1979)]. The theoretical approach is the same as that used in the treatment of deep-bed fibrous filters.

Fibers for filter applications can be produced with diameters smaller than it is practical to obtain with granules. Consequently, most concern with filtration of fine particles has been focused on fibrous-

bed rather than granular-bed filters. However, for certain specialized applications granular beds have shown some superior properties, such as greater dimensional stability. Granular-bed filters of special design (deep-bed sand filters) have been used since 1948 for removing radioactive particles from waste air and gas streams in atomic energy plants (Lapple, "Interim Report—200 Area Stack Contamination," U.S. AEC Rep. HDC-743, Oct. 11, 1948; Juvinall et al., "Sand-Bed Filtration of Aerosols: A Review of Published Information," U.S. AEC Rep. ANL-7683, 1970; and Burchsted et al., *Nuclear Air Cleaning Handbook*, U.S. ERDA 76-21, 1976). The filter characteristics needed included high collection efficiency on fine particles, large dust-holding capacity to give long operating life, and low maintenance requirements. The sand filters are as much as 2.7 m (9 ft) in depth and are constructed in graded layers with about a 2:1 variation in the granule size from one layer to the next. The air-flow direction is upward, and the granules decrease in size in the direction of the air flow. The bottom layer is composed of rocks about 5 to 7.5 cm (2 to 3 in) in diameter, and granule sizes in successive layers decrease to 0.3 to 0.6 mm (50 to 30 mesh) in the finest layer. With superficial face velocities of about 1.5 m/min (5 ft/min), gas pressure drops of clean filters have ranged from 1.7 to 2.8 kPa (7 to 11 in water). Collection efficiencies of up to 99.98 percent with a polydisperse dioctyl phthalate aerosol of 0.7- μ m mean diameter have been reported (Juvinall et al., op. cit.). Operating lives of 5 years or more have been attained.

Cleanable Granular-Bed Filters The principal objective in the development of cleanable granular-bed filters is to produce a device that can operate at temperatures above the range that can be tolerated with fabric filters. In some of the devices, the granules are circulated continuously through the unit, then are cleaned of the collected dust and returned to the filter bed. In others, the granular bed remains in place but is periodically taken out of service and cleaned by some means, such as backflushing with air.

A number of moving-bed granular filters have used cross-flow designs. One form of cross-flow moving-granular-bed filter, produced by the Combustion Power Company (Fig. 17-61), is currently in commercial use in some applications. The granular filter medium consists of 1/8- to 1/4-in (3- to 6-mm) pea gravel. Gas face velocities range from 30 to 46 m/min (100 to 150 ft/min), and reported gas pressure drops are in the range of 0.5 to 3 kPa (2 to 12 in water). The original form of the device [Reese, TAPPI, **60**(3), 109 (1977)] did not incorporate electrical augmentation. Collection efficiencies for submicrometer particles were low, and the electrical augmentation was added to correct the deficiency (Parquet, "The Electroscrubber Filter: Applications and Particulate Collection Performance," EPA-600/9-82-005c, 1982, p. 363). The electrostatic grid immersed in the bed of granules is charged to a potential of 20,000 to 30,000 V, producing an electric field between the grid and the inlet and outlet louvers that enclose the bed. No ionizing electrode is used to charge particles in the incoming gas; reliance is placed on the existence of natural charges on the dust particles. Individual dust particles commonly carry positive or negative charges even though the net charge on the dust as a whole is normally neutral. Depending on their charges, dust particles are attracted or repelled by the electrical field and are therefore caused to deposit on the rocks in the bed.

Self et al. ("Electrical Augmentation of Granular Bed Filters," EPA-600/9-80-039c, 1980, p. 309) demonstrated in theoretical studies and laboratory experiments that such an augmentation system should yield substantial increases in the collection efficiency for fine particles if the particles carry significant charges. Significant improvements in the performance of the Combustion Power units with electrical augmentation have been reported by the manufacturer (Parquet, op. cit.).

Another type of gravel-bed filter, developed by GFE in Germany, has had limited commercial application in the United States [Schueler, *Rock Prod.*, **76**(7), 66 (1973); **77**(11), 39 (1974)]. After precleaning in a cyclone, the gas flows downward through a stationary horizontal filter bed of gravel. When the bed becomes loaded with dust, the gas flow is cut off, and the bed is backflushed with air while being stirred with a double-armed rake that is rotated by a gear motor. The backflush air also flows backward through the cyclone, which then acts as a dropout chamber. Multiple filter units are constructed in parallel so that individual units can be taken off the line for cleaning. The dust dislodged

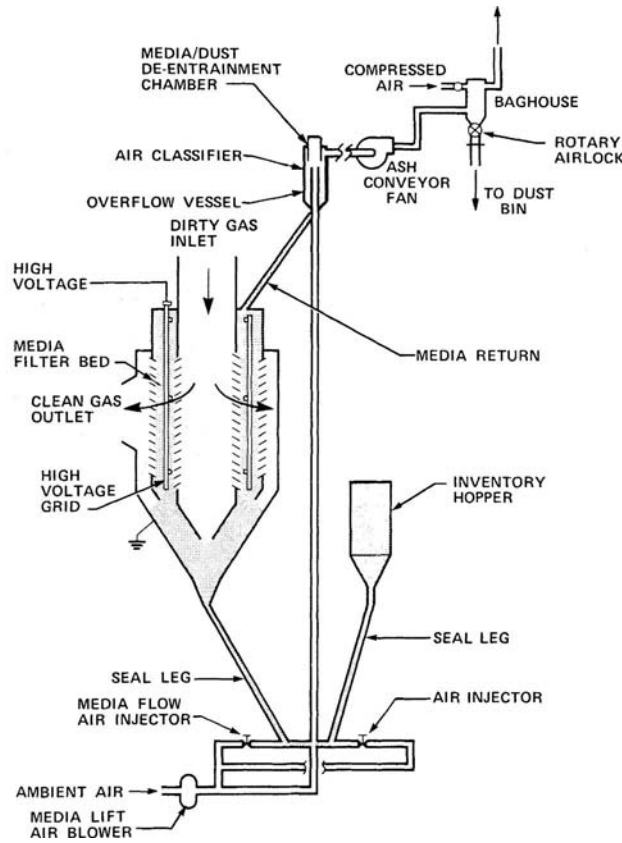


FIG. 17-61 Electrically augmented granular-bed filter. (Combustion Power Company.)

from the bed and carried by the backflush air is flocculated, and part is collected in the cyclone. The backflush air with the remaining suspended dust is cleaned in the other gravel-bed filter units that are operating on line. Performance tests made on one installation for the U.S. Environmental Protection Agency (EPA-600/7-78-093, 1978) did not give clear results but indicated that collection efficiencies were low on particles under 2 μm and that some of the dust in the backflush air was redispersed sufficiently to penetrate the operating filter units.

Air Filters The types of equipment previously described are intended primarily for the collection of process dusts, whereas air filters comprise a variety of filtration devices designed for the collection of particulate matter at low concentrations, usually atmospheric dust. The difference in the two categories of equipment is not in the principles of operation but in the adaptations required to deal with the different quantities of dust. Process-dust concentrations may run as high as several hundred grams per cubic meter (or grains per cubic foot) but usually do not exceed 45 g/m³ (20 gr/ft³). Atmospheric-dust concentrations that may be expected in various types of locations are shown in Table 17-8 and are generally below 12 mg/m³ (5 gr/1000 ft³).

The most frequent application of air filters is in cleaning atmospheric air for building ventilation, which usually requires only moderately high collection-efficiency levels. However, a variety of industrial operations developed mostly since the 1940s require air of extreme cleanliness, sometimes for pressurizing enclosures such as clean rooms and sometimes for use in a process itself. Examples of applications include the manufacture of antibiotics and other pharmaceuticals, the production of photographic film, and the manufacture and assembly of semiconductors and other electronic devices. Air cleaning at the necessary efficiency levels is accomplished by the use of high-efficiency fibrous filters that have been developed since the 1940s.

TABLE 17-8 Average Atmospheric-Dust Concentrations*

1 gr/1000 ft³ = 2.3 mg/m³

Location	Dust concentration, gr/1000 ft ³
Rural and suburban districts	0.02–0.2
Metropolitan districts	0.04–0.4
Industrial districts	0.1–2.0
Ordinary factories or workrooms	0.2–4.0
Excessive dusty factories or mines	4.0–400

*Heating Ventilating Air Conditioning Guide, American Society of Heating, Refrigerating and Air-Conditioning Engineers, New York, 1960, p. 77.

Air filters are also used to protect internal-combustion engines and gas turbines by cleaning the intake air. In some locations and applications, the atmospheric-dust concentrations encountered are much higher than those normally encountered in air-conditioning service.

High-efficiency air filters are sometimes used for emission control when particulate contaminants are low in concentration but present special hazards; cleaning of ventilation air and other gas streams exhausted from nuclear plant operations is an example.

Air-Filtration Theory Current high-efficiency air- and gas-filtration methods and equipment have resulted largely from the development of filtration theory since about 1930 and particularly since the 1940s. Much of the theoretical advance was originally encouraged by the requirements of the military and atomic energy programs. The fibrous filter has served both as a practical device and as a model for theoretical and experimental investigation. Extensive reviews and new treatments of air-filtration theory and experience have been presented by Chen [*Chem. Rev.*, **55**, 595 (1955)], Dorman ("Filtration," in Davies, *Aerosol Science*, Academic, New York, 1966), Pich (*Theory of Aerosol Filtration by Fibrous and Membrane Filters*, in *ibid.*), Davies (*Air Filtration*, Academic, New York, 1973), and Kirsch and Stechkina ("The Theory of Aerosol Filtration with Fibrous Filters," in Shaw, *Fundamentals of Aerosol Science*, Wiley, New York, 1978). The theoretical treatment of filtration starts with the processes of dust-particle deposition on collecting bodies, as outlined in Fig. 17-35 and Table 17-2. All the mechanisms shown in Table 17-2 may come into play, but inertial deposition, flow-line interception, and diffusional deposition are usually dominant. Electrostatic precipitation may become a major mechanism if the collecting body, the dust particle, or both, are charged. Gravitational settling is a minor influence for particles in the size range of usual interest. Thermal precipitation is nil in the absence of significant temperature gradients. Sieving is a possible mechanism only when the pores in the filter medium are smaller than or approximately equal to the particle size and will not be encountered in fibrous filters unless they are loaded sufficiently for a surface dust layer to form.

The theoretical prediction of the efficiency of collection of dust particles by a fibrous filter consists of three steps (Chen, *op. cit.*):

1. Calculation of the target efficiency η_0 of an isolated fiber in an air stream having a superficial velocity the same as that in the filter
2. Determining the difference between the target efficiency of the isolated fiber and that of an individual fiber in the filter array η_i
3. Determining the collection efficiency of the filter η from the target efficiency of the individual fibers

The results of computations of η_0 for an isolated fiber are illustrated in Figs. 17-62 and 17-63. The target efficiency η_0 of an individual fiber in a filter differs from η_0 for two main reasons (Pich, *op. cit.*): (1) the average gas velocity is higher in the filter, and (2) the velocity field around the individual fibers is influenced by the proximity of neighboring fibers. The interference effect is difficult to determine on a purely theoretical basis and is usually evaluated experimentally. Chen (*op. cit.*) expressed the effect with an empirical equation:

$$\eta_i = \eta_0 [1 + K_a(1 - \epsilon_v)] \quad (17-14)$$

This indicates that the target efficiency of the fiber is increased by the proximity of other fibers. The value of K_a averaged 4.5 for values of the void fraction ϵ_v , ranging from 0.90 to 0.99. Extending use of the equation to values of ϵ_v lower than 0.90 may result in large errors.

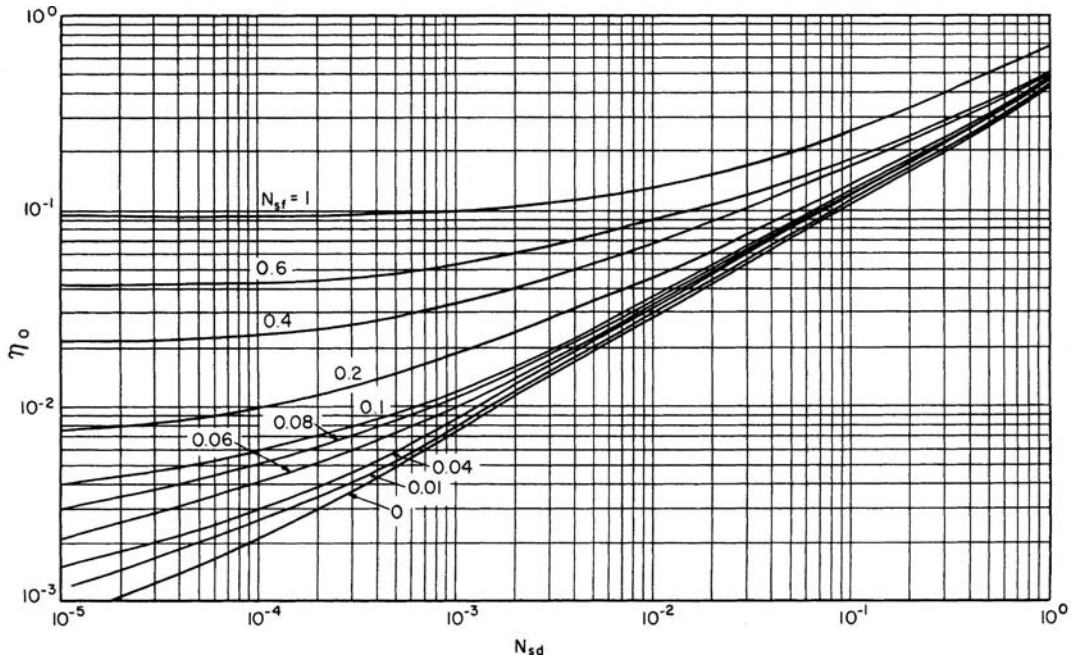


FIG. 17-62 Isolated fiber efficiency for combined diffusion and interception mechanism at $N_{Re} = 10^{-2}$. [Chen, Chem. Rev., 55, 595 (1955).]

The collection efficiency of the filter may be calculated from the fiber target efficiency and other physical characteristics of the filter (Chen, op. cit.):

$$N_t = \frac{4\eta_t L(1 - \epsilon_v)}{\pi D_b \epsilon_v} \quad (17-15)$$

where D_b = fiber diameter and L = filter thickness. The derivation of Eq. (17-15) assumes that (1) η_t is the same throughout the filter, (2) all fibers are of the same diameter D_b , are cylindrical and are normal to the direction of the gas flow, (3) the fraction of the particles deposited in any one layer of fiber is small, and (4) the gas passing through the filter is essentially completely remixed after it leaves one layer of the filter and before it enters the next. The first assumption requires that Eq. (17-15) apply only for particles of a single size for which there are corresponding values of η_t , η , and N_t .

For filters of high porosity, ϵ_v approaches unity and Eq. (17-15) reduces to the expression used by Wong et al. [J. Appl. Phys., 27, 161 (1956)] and Thomas and Lapple [Am. Inst. Chem. Eng. J., 7, 203 (1961)]:

$$N_t = \frac{4\eta_t L(1 - \epsilon_v)}{\pi D_b} \quad (17-16)$$

The foregoing procedure is commonly employed in reverse to determine or confirm fiber target efficiencies from the experimentally determined efficiencies of fibrous filter pads.

Filtration theory assumes that a dust particle that touches a collector body adheres to it. This assumption appears to be valid in most cases, but evidence of nonadherence, or particle bouncing, has appeared in some instances. Wright et al. ("High Velocity Air Filters," WADC TR 55-457, ASTIA Doc. AD-142075, 1957) investigated the performance of fibrous filters at filtration velocities of 0.091 to 3.05 m/s (0.3 to 10 ft/s), using 0.3- μ m and 1.4- μ m supercooled liquid aerosols and a 1.2- μ m solid aerosol. The collection efficiencies agreed well with theoretical predictions for the liquid aerosols and apparently also for the solid aerosol at filtration velocities under 0.3 m/s (1 ft/s). But at filtration velocities above 0.3 m/s some of the solid particles failed to adhere. With a filter composed of 30- μ m glass fibers and a filtration velocity of 9.1 m/s (30 ft/s), there were indications that 90 percent of the solid aerosol particles striking a fiber bounced off.

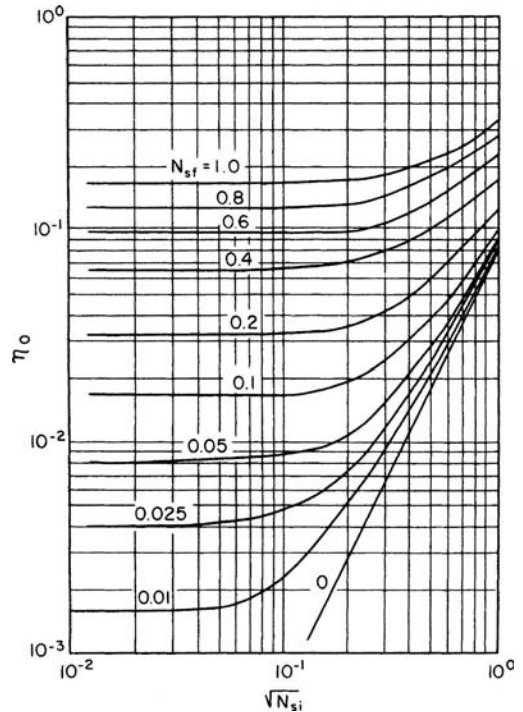


FIG. 17-63 Isolated fiber efficiency for combined inertia and interception mechanisms at $N_{Re} = 0.2$. [Chen, Chem. Rev., 55, 595 (1955).]

Bouncing may be regarded as a defect in the particle-deposition process. However, particles that have been deposited in filters may subsequently be blown off and reentrained into the air stream (Corn, "Adhesion of Particles," in Davies, *Aerosol Science*, Academic, New York, 1966; and Davies, op. cit.).

The theories of filtration by a fibrous filter relate only to the initial efficiency of the clean filter in the "static" period of filtration before the deposition of any appreciable quantity of dust particles. The deposition of particles in a filter increases the number of targets available to intercept particles, so that collection efficiency increases as the filter loads. At the same time, the filter undergoes clogging and the pressure drop increases. No theory is available for dealing with the "dynamic" period of filtration in which collection efficiency and pressure drop vary with the loading of collected dust. The theoretical treatment of this filtration period is incomparably more complex than that for the "static" period. Investigators have noted that both the increase in collection efficiency and the increase in pressure drop are exponential functions of the loading of collected dust or are at least roughly so (Davies, op. cit.). Some empirical relationships have been derived for correlating data in particular instances.

The dust particles collected by a fibrous filter do not deposit in uniform layers on fibers but tend to deposit preferentially on previously deposited particles (Billings, "Effect of Particle Accumulation in Aerosol Filtration," Ph.D. dissertation, California Institute of Technology, Pasadena, 1966), forming chainlike agglomerates termed "dendrites." The growth of dendritic deposits on fibers has been studied experimentally [Billings, op. cit.; Bhutra and Payatakes, *J. Aerosol Sci.*, **10**, 445 (1979)], and Payatakes and coworkers [Payatakes and Tien, *J. Aerosol Sci.*, **7**, 85 (1976); Payatakes, *Am. Inst. Chem. Eng. J.*, **23**, 192 (1977); and Payatakes and Gradon, *Chem. Eng. Sci.*, **35**, 1083 (1980)] have attempted to model the growth of dendrites and its influence on filter efficiency and pressure drop.

Air-Filter Types Air filters may be broadly divided into two classes: (1) panel, or unit, filters; and (2) automatic, or continuous, filters. Panel filters are constructed in units of convenient size (commonly 20- by 20-in or 24- by 24-in face area) to facilitate installation, maintenance, and cleaning. Each unit consists of a cleanable or replaceable cell or filter pad in a substantial frame that may be bolted to the frames of similar units to form an airtight partition between the source of the dusty air and the destination of the cleaned air.

Panel filters may use either viscous or dry filter media. Viscous filters are so called because the filter medium is coated with a tacky liquid of high viscosity (e.g., mineral oil and adhesives) to retain the dust. The filter pad consists of an assembly of coarse fibers (now usually metal, glass, or plastic). Because the fibers are coarse and the media are highly porous, resistance to air flow is low and high filtration velocities can be used.

Dry filters are usually deeper than viscous filters. The dry filter media use finer fibers and have much smaller pores than the viscous media and need not rely on an oil coating to retain collected dust. Because of their greater resistance to air flow, dry filters must use lower filtration velocities to avoid excessive pressure drops. Hence, dry media must have larger surface areas and are usually pleated or arranged in the form of pockets (Fig. 17-64), generally sheets of cellulose pulp, cotton, felt, or spun glass.

Automatic filters are made with either viscous-coated or dry filter media. However, the cleaning or disposal of the loaded medium is essentially continuous and automatic. In most such devices the air passes horizontally through a movable filter curtain. As the filter loads with dust, the curtain is continuously or intermittently advanced to expose clean media to the air flow and to clean or dispose of the loaded medium. Movement of the curtain can be provided by a hand crank or a motor drive. Movement of a motor-driven curtain can be actuated automatically by a differential-pressure switch connected across the filter.

High-Efficiency Air Cleaning Air-filter systems for nuclear facilities and for other applications demanding extremely high standards of air purity require filtration efficiencies well beyond those attainable with the equipment described above. The *Nuclear Air Cleaning Handbook* (Burchsted et al., op. cit.) presents an extensive treatment of the requirements for and the design of such air-cleaning

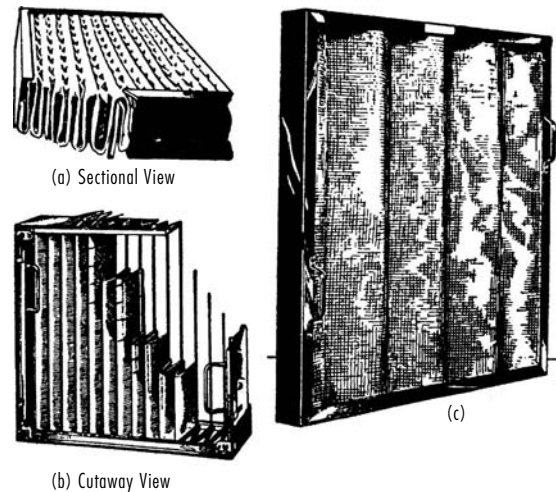


FIG. 17-64 Typical dry filters. (a) Throwaway type, Airplex (Davies Air Filter Corporation). (b) Replaceable medium type, Airmat PL-24, cutaway view (American Air Filter Co., Inc.). (c) Cleanable type, Amirglass sawtooth (Amirton Company).

facilities. Much of the material is pertinent to high-efficiency air-filter systems for applications to other than nuclear facilities.

HEPA (high-efficiency particulate air) filters were originally developed for nuclear and military applications but are now widely used and are manufactured by numerous companies. By definition, an HEPA filter is a "throwaway, extended-medium dry-type" filter having (1) a minimum particle-removal efficiency of not less than 99.97 percent for 0.3- μm particles, (2) a maximum resistance, when clean, of 1.0 in water when operated at rated air-flow capacity, and (3) a rigid casing extending the full depth of the medium (Burchsted et al., op. cit.). The filter medium is a paper made of submicrometer glass fibers in a matrix of larger-diameter (1- to 4- μm) glass fibers. An organic binder is added during the papermaking process to hold the fibers and give the paper added tensile strength. Filter units are made in several standard sizes (Table 17-9).

Because HEPA filters are designed primarily for high efficiency, their dust-loading capacities are limited, and it is common practice to use prefilters to extend their operating lives. In general, HEPA filters should be protected from (1) lint, (2) particles larger than 1 to 2 μm in diameter, and (3) dust concentrations greater than 23 mg/m^3 (10 $\text{gr}/1000 \text{ ft}^3$). Air filters used in nuclear facilities as prefilters and building-supply air filters are classified as shown in Table 17-10. The standard of the American Society of Heating, Refrigerating and Air-Conditioning Engineers (*Method of Testing Air Cleaning Devices Used in General Ventilation for Removing Particulate Matter*, ASHRAE 52-68, 1968) requires both a dust-spot (dust-stain) efficiency test made with atmospheric dust and a weight-arrestance test made with a synthetic test dust. A more precise comparison of the different groups of filters, based on removal efficiencies for particles of specific sizes, is presented in Table 17-11.

TABLE 17-9 Standard HEPA Filters*

Face dimensions, in	Depth, less gaskets, in	Design air-flow capacity at clean-filter resistance of 1.0 in water (standard ft^3/min)
24 × 24	11½	1000
24 × 24	5½	500
12 × 12	5½	125
8 × 8	5½	20
8 × 8	3¼	25

*Burchsted et al., *Nuclear Air Cleaning Handbook*, ERDA 76-21, Oak Ridge, Tenn., 1976.

TABLE 17-10 Classification of Common Air Filters*

Group	Efficiency	Filter type	Stain test efficiency, %	Arrestance, %
I	Low	Viscous impingement, panel type	<20†	40–80†
II	Moderate	Extended medium, dry type	20–60†	80–96†
III	High	Extended medium, dry type	60–98‡	96–99†
HEPA	Extreme	Extended medium, dry type	100§	100†

*Burchsted et al., *Nuclear Air Cleaning Handbook*, ERDA 76-21, Oak Ridge, Tenn., 1976.

†Test using synthetic dust.

‡Stain test using atmospheric dust.

§ASHRAE/52-68, American Society of Heating, Refrigerating and Air-Conditioning Engineers.

Table 17-12 presents the relative performance of Group I, II, and III filters with respect to air-flow capacity, resistance, and dust-holding capacity. The dust-holding capacities correspond to the manufacturers' recommended maximum allowable increases in air-flow resistance. The values for dust-holding capacity are based on tests with a synthetic dust and hence are relative. The actual dust-holding capacity in a specific application will depend on the characteristics of the dust encountered. In some instances it may be appropriate to use two or more stages of precleaning in air-filter systems to achieve a desired combination of operating life and efficiency. In very dusty locations, inertial devices such as multiple small cyclones may be used as first-stage separators.

Electrical Precipitators When particles suspended in a gas are exposed to gas ions in an electrostatic field, they will become charged and migrate under the action of the field. The functional mechanisms of electrical precipitation may be listed as follows:

1. Gas ionization
2. Particle collection
 - a. Production of electrostatic field to cause charging and migration of dust particles
 - b. Gas retention to permit particle migration to a collection surface
 - c. Prevention of reentrainment of collected particles
 - d. Removal of collected particles from the equipment

There are two general classes of electrical precipitators: (1) single-stage, in which ionization and collection are combined; (2) two-stage, in which ionization is achieved in one portion of the equipment, followed by collection in another. Various types in each class differ essentially in the details by which each function is accomplished.

The underlying theory presented in the following paragraphs assumes that the dust concentration is small, since only very incomplete evaluations for conditions of high dust concentration have been made.

Field Strength Whereas the applied potential or voltage is the quantity commonly known, it is the field strength that determines behavior in an electrostatic field. When the current flow is low (i.e., before the onset of spark or corona discharge), these are related by the following equations for two common forms of electrodes:

TABLE 17-11 Comparison of Air Filters by Percent Removal Efficiency for Various Particle Sizes*

Group	Efficiency	Removal efficiency, %, for particle size of			
		0.3 μm	1.0 μm	5.0 μm	10.0 μm
I	Low	0–2	10–30	40–70	90–98
II	Moderate	10–40	40–70	85–95	98–99
III	High	45–85	75–99	99–99.9	99.9
HEPA	Extreme	99.97 min	99.99	100	100

*Burchsted et al., *Nuclear Air Cleaning Handbook*, ERDA 76-21, Oak Ridge, Tenn., 1976.

TABLE 17-12 Air-Flow Capacity, Resistance, and Dust-Holding Capacity of Air Filters*

Group	Efficiency	Air-flow capacity, ft ³ /(min·ft ² of frontal area)	Resistance, in water		Dust-holding capacity, g/(1000 ft ³ ·min of air-flow capacity)
			Clean filter	Used filter	
I	Low	300–500	0.05–0.1	0.3–0.5	50–1000
II	Moderate	250–750	0.1–0.5	0.5–1.0	100–500
III	High	250–750	0.20–0.5	0.6–1.4	50–200

*Burchsted et al., *Nuclear Air Cleaning Handbook*, ERDA 76-21, Oak Ridge, Tenn., 1976.

Parallel plates:

$$\mathcal{E} = E/B_e \tag{17-17}$$

Concentric cylinders (wire-in-cylinder):

$$\mathcal{E} = \frac{E}{r \ln(D_i/D_d)} \tag{17-18}$$

The field strength is uniform between parallel plates, whereas it varies in the space between concentric cylinders, being highest at the surface of the central cylinder. After corona sets in, the current flow will become appreciable. The field strength near the center electrode will be less than given by Eq. (17-18) and that in the major portion of the clearance space will be greater and more uniform [see Eqs. (17-23) and (17-24)].

Potential and Ionization In order to obtain gas ionization it is necessary to exceed, at least locally, the electrical breakdown strength of the gas. Corona is the name applied to such a local discharge that fails to propagate itself. Sparking is essentially an advanced stage of corona in which complete breakdown of the gas occurs along a given path. Since corona represents a local breakdown, it can occur only in a nonuniform electrical field (Whitehead, *Dielectric Phenomena—Electrical Discharge in Gases*, Van Nostrand, Princeton, N.J., 1927, p. 40). Consequently, for parallel plates, only sparking occurs at a field strength or potential difference given by the empirical expressions

$$\mathcal{E}_s = \mathcal{E}_o k_p \left[1 + \left(\frac{K_o}{k_p B_e} \right) \right] \tag{17-19}$$

$$E_s = \mathcal{E}_o k_p B_e + K_o \mathcal{E}_o \tag{17-20}$$

For air in the range of $k_p B_e$ from 0.1 to 2, $\mathcal{E}_o = 111.2$ and $K_o = 0.048$. Thornton [*Phil. Mag.*, **28**(7), 666 (1939)] gives values for other gases. For concentric cylinders (Loeb, *Fundamental Processes of Electrical Discharge in Gases*, Wiley, New York, 1939; Peek, *Dielectric Phenomena in High-Voltage Engineering*, McGraw-Hill, New York, 1929; and Whitehead, op. cit.), corona sets in at the central wire when

$$\mathcal{E}_c = \mathcal{E}_o k_p \left(1 + \sqrt{\frac{K_o}{k_p D_d}} \right) \tag{17-21}$$

$$E_c = \left(\frac{\mathcal{E}_o k_p D_d}{2} \right) \left(1 + \sqrt{\frac{K_o}{k_p D_d}} \right) \ln \left(\frac{D_i}{D_d} \right) \tag{17-22}$$

For air approximate values are $\mathcal{E}_o = 110$, $K_o = 0.18$. Corona, however, will set in only if $(D_i/D_d) > 2.718$. If this ratio is less than 2.718, no corona occurs, and only sparking will result, following the laws given by Eqs. (17-21) and (17-22) (Peek, op. cit.).

In practice, precipitators are usually operated at the highest voltage practicable without sparking, since this increases both the particle charge and the electrical precipitating field. The sparking potential is generally higher with a negative charge on the discharge electrode and is less erratic in behavior than a positive corona discharge. It is the consensus, however, that ozone formation with a positive discharge is considerably less than with a negative discharge. For these reasons negative discharge is generally used in industrial precipitators, and a

TABLE 17-13 Sparking Potentials* (Small Wire Concentric in Pipe)

Pipe diameter, in	Sparking potential, † volts	
	Peak	Root mean square
4	59,000	45,000
6	76,000	58,000
9	90,000	69,000
12	100,000	77,000

*Data reported by Anderson in Perry, *Chemical Engineers' Handbook*, 2d ed., p. 1873, McGraw-Hill, New York, 1941.

†For gases at atmospheric pressure, 100°F, containing water vapor, air, CO₂, and mist, and negative-discharge-electrode polarity.

positive discharge is utilized in air-conditioning applications. In Table 17-13 are given some typical values for the sparking potential for the case of small wires in pipes of various sizes. The sparking potential varies approximately directly as the density of the gas but is very sensitive to the character of any material collected on the electrodes. Even small amounts of poorly conducting material on the electrodes may markedly lower the sparking voltage. For positive polarity of the discharge electrode, the sparking voltage will be very much lower. The sparking voltage is greatly affected by the temperature and humidity of the gas, as shown in Fig. 17-65.

Current Flow Corona discharge is accompanied by a relatively small flow of electric current, typically 0.1 to 0.5 mA/m² of collecting-electrode area (projected, rather than actual area). Sparking usually involves a considerably larger flow of current which cannot be tolerated except for occasional periods of a fraction of a second duration, and then only when suitable electrical controls are provided to limit the current. However, when suitable controls are provided, precipitators have been operated continuously with a small amount of sparking to ensure that the voltage is in the correct range to ensure corona. Besides disruptive effects on the electrical equipment and electrodes, sparking will result in low collection efficiency because of reduction in applied voltage, redispersion of collected dust, and current channeling. Although an exact calculation can be made for the current flow for a direct-current potential applied between concentric cylinders, the following simpler expression, based on the assumption of a constant space charge or ion density, gives a good approximation of corona current [Ladenburg, *Ann. Phys.*, **4**(5), 863 (1930)]:

$$I = \frac{8\lambda_e E(E - E_c)}{D_i^2 \ln(D_i/D_d)} \quad (17-23)$$

and the average space charge is given by (Whitehead, op. cit.)

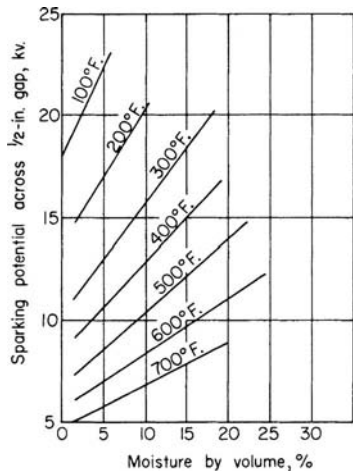


FIG. 17-65 Sparking potential for negative point-to-plane 1/2-in. (1.3-cm) gap as a function of moisture content and temperature of air at 1-atm (101.3-kPa) pressure. [Sproull and Nakada, *Ind. Eng. Chem.*, **43**, 1356 (1951).]

$$\sigma_{\text{avg}} = \frac{4(E - E_c)}{\pi D_i^2 \epsilon} \quad (17-24)$$

In the space outside the immediate vicinity of corona discharge, the field strength is sensibly constant, and an average value is given by

$$\mathcal{E} = \sqrt{2I/\lambda_i} \quad (17-25)$$

which applies if the potential difference is above the critical potential required for corona discharge so that an appreciable current flows.

Ionic mobilities are given by Loeb (*International Critical Tables*, vol. 6, McGraw-Hill, New York, 1929, p. 107). For air at 0°C, 760 mmHg, $\lambda_i = 624$ (cm/s)/(statV/cm) for negative ions. Positive ions usually have a slightly lower mobility. Loeb (*Basic Processes of Gaseous Electronics*, University of California Press, Berkeley and Los Angeles, 1955, p. 53) gives a theoretical expression for ionic mobility of gases which is probably good to within ± 50 percent:

$$\lambda_i = \frac{100.0}{k_p \sqrt{(\delta_g - 1)M}} \quad (17-26)$$

In general, ionic mobilities are inversely proportional to gas density. Ionic velocities in the usual electrostatic precipitator are on the order of 30.5 m/s (100 ft/s).

Electric Wind By virtue of the momentum transfer from gas ions moving in the electrical field to the surrounding gas molecules, a gas circulation, known as the "electric" or "ionic" wind, is set up between the electrodes. For conditions encountered in electrical precipitators, the velocity of this circulation is on the order of 0.6 m/s (2 ft/s). Also, as a result of this momentum transfer, the pressure at the collecting electrode is slightly higher than at the discharge electrode (Whitehead, op. cit., p. 167).

Charging of Particles [Deutsch, *Ann. Phys.*, **68**(4), 335 (1922); **9**(5), 249 (1931); **10**(5), 847 (1931); Ladenburg, op. cit.; and Mierdel, *Z. Tech. Phys.*, **13**, 564 (1932).] Three forces act on a gas ion in the vicinity of a particle: attractive forces due to the field strength and the ionic image; and repulsive forces due to the Coulomb effect. For spherical particles larger than 1- μ m diameter, the ionic image effect is negligible, and charging will continue until the other two forces balance according to the equation

$$N_o = \left(\frac{\zeta \mathcal{E} D_p^2}{4\epsilon} \right) \left(\frac{\pi \sigma \epsilon t \lambda_i}{1 + \pi \sigma \epsilon \lambda_i t} \right) \quad (17-27)$$

The ultimate charge acquired by the particle is given by

$$N_o = \zeta \mathcal{E} D_p^2 / 4\epsilon \quad (17-28)$$

and is very nearly attained in a fraction of a second. For particles smaller than 1- μ m diameter, the initial charging will occur according to Eq. (17-27). However, owing to the ionic-image effect, the ultimate charge will be considerably greater because of penetration resulting from the kinetic energy of the gas ions. For charging times of the order encountered in electrical precipitation, the ultimate charge acquired by spherical particles smaller than about 1- μ m diameter may be approximated (± 30 percent) by the empirical expression

$$N_o = 3.4 \times 10^3 D_p T \quad (17-29)$$

Values of N_o for various sized particles are listed in Table 17-14 for 70°F, $\zeta = 2$, and $\mathcal{E} = 10$ statV/cm.

Particle Mobility By equating the electrical force acting on a particle to the resistance due to air friction, as expressed by Stokes' law, the particle velocity or mobility may be expressed by

1. For particles larger than 1- μ m diameter:

$$\lambda_p = \left(\frac{u_c}{\mathcal{E}_p} \right) = \frac{\zeta D_p \mathcal{E}_i K_m}{12\pi\mu} \quad (17-30)$$

2. For particles smaller than 1- μ m diameter:

$$\lambda_p = \left(\frac{u_c}{\mathcal{E}_p} \right) = \frac{360 K_m \epsilon T}{\mu} \quad (17-31)$$

For single-stage precipitators, \mathcal{E}_i and \mathcal{E}_p may be considered as essentially equal. It is apparent from Eq. (17-31) that the mobility in an electric field will be almost the same for all particles smaller than

TABLE 17-14 Charge and Motion of Spherical Particles in an Electric Field

For $\zeta = 2$, and $\epsilon = \epsilon_i = \epsilon_r = 10$ statV/cm

Particle diam., μ	Number of elementary electrical charges, N_0	Particle migration velocity,* u_e , ft/sec
0.1	10	0.27
.25	25	.15
.5	50	.12
1.0	105	.11
2.5	655	.26
5.0	2,620	.50
10.0	10,470	.98
25.0	65,500	2.40

NOTE: To convert feet per second to meters per second, multiply by 0.3048.

about 1- μ m diameter, and hence, in the absence of reentrainment, collection efficiency should be almost independent of particle size in this range. Very small particles will actually have a greater mobility because of the Stokes-Cunningham correction factor. Values of u_e are listed in Table 17-14 for 70°F, $\zeta = 2$, and $\mathcal{E} = \mathcal{E}_i = \mathcal{E}_r = 10$ statV/cm.

Collection Efficiency Although actual particle mobilities may be considerably greater than would be calculated on the basis given in the preceding paragraph because of the action of the electric wind in single-stage precipitators, the latter acts in a compensating fashion, and the overall effect of the electric wind is probably to provide an equalization of particle concentration between the electrodes similar to the action of normal turbulence (Mierdel, op. cit.). On this basis Deutsch (op. cit.) has derived the following equations for collection efficiency, the form of which had previously been suggested by Anderson on the basis of experimental data:

$$\eta = 1 - e^{-(u_e A/q)} = 1 - e^{-K_e t} \quad (17-32)$$

For the concentric-cylinder (or wire-in-cylinder) type of precipitator, $K_e = 4L_e/D_i V_e$; for rod-curtain or wire-plate types, $K_e = L_e/B_e V_e$. Strictly speaking, Eq. (17-32) applies only for a given particle size, and the overall efficiency must be obtained by an integration process for a specific dust distribution, as described in the subsection "Cyclone Separators." However, over limited ranges of performance conditions, Eq. (17-32) has been found to give a good approximation of overall collection efficiency, with the term for particle migration velocity representing an empirical average value. Such values, calculated from overall collection-efficiency measurements, are given in Table 17-15 for specific installations.

For two-stage precipitators with close collecting-plate spacings (Fig. 17-76), the gas flow is substantially streamline, and no electric wind exists. Consequently, with reentrainment neglected, collection efficiency may be expressed as [Penny, *Electr. Eng.* **56**, 159 (1937)]

$$\eta = u_e L_e / V_e B_e \quad (17-33)$$

TABLE 17-15 Performance Data on Typical Single-Stage Electrical Precipitator Installations*

Type of precipitator	Type of dust	Gas volume, cu ft/min	Average gas velocity, ft/sec	Collecting electrode area, sq ft	Over-all collection efficiency, %	Average particle migration velocity, ft/sec
Rod curtain	Smelter fume	180,000	6	44,400	85	0.13
Tulip type	Gypsum from kiln	25,000	3.5	3,800	99.7	.64
Perforated plate	Fly ash	108,000	6	10,900	91	.40
Rod curtain	Cement	204,000	9.5	26,000	91	.31

*Research-Cottrell, Inc. To convert cubic feet per minute to cubic meters per second, multiply by 0.00047; to convert feet per second to meters per second, multiply by 0.3048; and to convert square feet to square meters, multiply by 0.0929.

which holds for values of $\eta \leq 1.0$. In practice, however, extraneous factors may cause the actual efficiency to approach a relationship of the type given by Eq. (17-32).

Application The theoretical considerations that have been expounded should be used only for order-of-magnitude estimates, since a number of extraneous factors may enter into actual performance. In actual installations rectified alternating current is employed. Hence the electric field is not fixed but varies continuously, depending on the waveform of the rectifier, although Schmidt and Anderson [*Electr. Eng.*, **57**, 332 (1938)] report that the waveform is not a critical factor. Allowances for high dust concentrations have not been fully studied, although Deutsch (op. cit.) has presented a theoretical approach. In addition, irregularities on the discharge electrode will result in local discharges. Such irregularities can readily result from dust incrustation on the discharge electrodes due to charging of particles with opposite polarity within the thin but appreciable flow or ionization layer surrounding this electrode. Very high dust loadings increase the potential difference required for corona and reduce the current due to the space charge of the particles. This tends to reduce the average particle charge and reduces collection efficiency. This can be compensated for by increasing the potential difference when high dust loadings are involved.

Several investigators have attempted to modify the basic Deutsch equation so that it would more nearly describe precipitator performance. Cooperman ("A New Theory of Precipitator Efficiency," Pap. 69-4, APCA meeting, New York, 1969) introduced correction factors for diffusional forces arising from variations in particle concentration along the precipitator length and also perpendicular to the collecting surface. Robinson [*Atmos. Environ.* **1**(3), 193 (1967)] derived an equation for collection efficiency in which two erosion or reentrainment terms are introduced.

An analysis of precipitator performance based on theoretical considerations was undertaken by the Southern Research Institute for the National Air Pollution Control Administration (Nichols and Oglesby, "Electrostatic Precipitator Systems Analysis," AIChE annual meeting, 1970). A mathematical model was developed for calculating the particle charge, electric field, and collection efficiency based on the Deutsch-Anderson equation. The system diagram is shown in Fig. 17-66. This system-analysis method, using high-speed computers, makes it possible to analyze what takes place in each increment of precipitator length. Collection efficiency versus particle size is computed for each 1 ft (0.3 m) of gas travel, and the inlet particle-size distribution is modified accordingly. Computed overall efficiencies compare well with measured values on three precipitators. The model assumes that field charging is the only charging mechanism. The authors considered the addition of several refinements to the program: the influence of diffusion charging; reentrainment effects due to rapping and erosion; and loss of efficiency due to maldistribution of gas, dust resistivity, and gas-property effects. The modeling technique appeared promising, but much more work was needed before it could be used for design. The same authors prepared a general treatise (Oglesby and Nichols, *A Manual of Electrostatic Precipitator Technology*, parts I and II, Southern Research Institute, Birmingham, Ala., U.S. Government Publications PB196360, 196381, 1970).

High-Pressure-High-Temperature Electrostatic Precipitation

In general, increased pressure increases precipitation efficiency, although a somewhat higher potential is required, because it reduces ion mobility and hence increases the potential required for corona and sparking. Increased temperature reduces collection efficiency because ion mobility is increased, lowering critical potentials, and because gas viscosity is increased, reducing migration velocities.

Precipitators have been operated at pressures up to 5.5 MPa (800 psig) and temperatures to 800°C.

The effect of increasing gas density on sparkover voltage has been investigated by Robinson [*J. Appl. Phys.*, **40**, 5107 (1969); *Air Pollution Control*, part 1, Wiley-Interscience, New York, 1971, chap. 5]. Figure 17-67 shows the effect of gas density on corona-starting and sparkover voltages for positive and negative corona in a pipe precipitator. The sparkover voltages are experimental and are given by the solid points. Experimental corona-starting voltages are given by the hollow points. The solid lines are corona-starting voltage curves

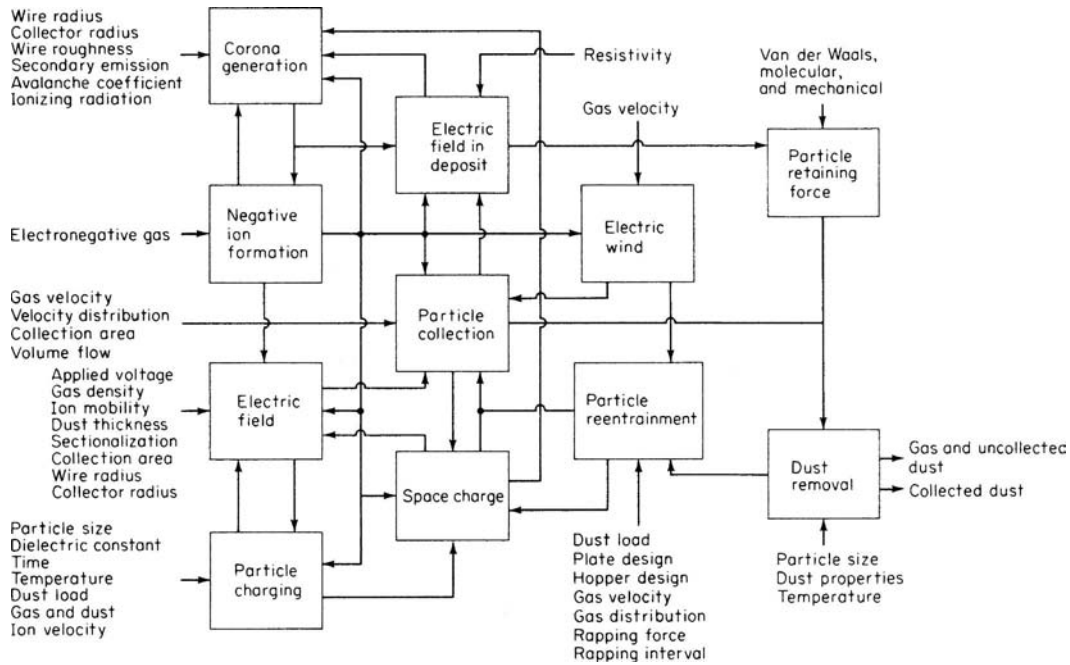


FIG. 17-66 Electrostatic-precipitator-system model. (Nichols and Oglesby, "Electrostatic Precipitator Systems Analysis," AIChE annual meeting, 1970.)

calculated from Eq. (17-33). This is an empirical relationship developed by Robinson.

$$\frac{E_c}{\rho'} = A \frac{B}{\sqrt{D_d \rho' / 2}} \quad (17-34)$$

E_c is the corona-starting field, kV/cm. ρ' is the relative gas density, equal to the actual gas density divided by the density of air at 25°C, 1 atm. D_d is the diameter of the ionizing wire, cm. A and B are constants which are characteristics of the gas. In dry air, $A = 32.2$ kV/cm and $B = 8.46$

kV/cm^{1/2}. Agreement between experimental and calculated starting voltages is good for the case of positive corona, but in the case of negative corona the calculated line serves as an upper limit for the data. This lower-than-expected starting-voltage characteristic of negative corona is confirmed by Hall et al. [*Oil Gas J.*, **66**, 109 (1968)] in a report of an electrostatic precipitator which removes lubricating-oil mist from natural gas at 5.5 MPa (800 psig) and 38°C (100°F). The use of electrostatic precipitators at elevated pressure is expected to increase, because the method requires very low pressure drop [approximately 69 Pa (0.1

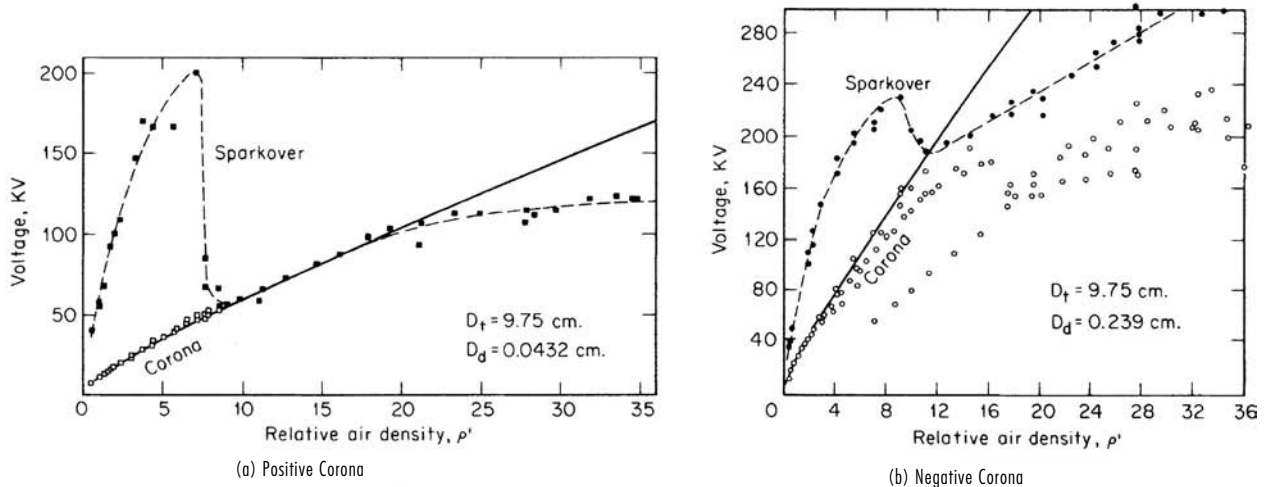


FIG. 17-67 Corona-starting and sparkover voltages for coaxial wire-pipe electrodes in air (25°C). D_t and D_d are the respective pipe and wire diameters. The voltage is unvarying direct current. (Robinson, *Air Pollution Control, part 1*, Wiley-Interscience, New York, 1971, chap. 5.)

lb/in²]. This results from the fact that the electric separation forces are applied directly to the particles themselves rather than to the entire mass of the gas, as in inertial separators. The use of electrostatic precipitators at temperatures up to 400°C is well developed for the power-house fly-ash application, but in the range of 600 to 800°C they are still in the experimental phase. The U.S. Bureau of Mines has tested a pilot-scale tubular precipitator for fly ash. See Shale [Air Pollut. Control Assoc. J., 17, 159 (1967)] and Shale and Fasching (Operating Characteristics of a High-Temperature Electrostatic Precipitator; U.S. Bur. Mines Rep. 7276, 1969). It operated over a temperature range of 27 to 816°C (80 to 1500°F) and a pressure range of 552 kPa (35 to 80 psig). Initial collection efficiencies ranged from 90 to 98 percent at 793°C (1460°F), 552 kPa (80 psig), but continuous operation was not achieved because of excessive thermal expansion of internal parts.

Resistivity Problems Optimum performance of electrostatic precipitators is achieved when the electrical resistivity of the collected dust is sufficiently high to result in electrostatic pinning of the particles to the collecting surface, but not so high that dielectric breakdown of the dust layer occurs as the corona current passes through it. The optimum resistivity range is generally considered to be from 10^9 to 10^{10} Ω-cm, measured at operating conditions. As the dust builds up on the collecting electrode, it impedes the flow of current, so that a voltage drop is developed across the dust layer:

$$E_d = j\rho_d L_d \quad (17-35)$$

If E_d/L_d exceeds the dielectric strength of the dust layer, sparks occur in the deposit and form back-corona craters. Ions of both polarities are formed. Positive ions formed in the craters are attracted to the negatively charged particles in the gas stream, whose charge level is reduced so that collection efficiency decreases. Some of the positive ions neutralize part of the negative-space-charge cloud normally present near the wire, thereby increasing total current. Collection efficiency under these conditions will not correlate with total power input (Owens, E. I. du Pont de Nemours & Co. internal communication, 1971). Under normal conditions, collection efficiency is an exponential function of corona power (White, *Industrial Electrostatic Precipitation*, Addison-Wesley, Reading, Mass., 1963). With typical ion density in the range of 10^9 /cm³, overall voltage gradient would be about 4000 V/cm, and current about 1 μA/cm². Dielectric breakdown of the dust layer (at about 10,000 V/cm) would therefore be expected for dusts with resistivities above 10^{10} Ω-cm.

Problems due to high resistivity are of great concern in fly-ash precipitation because air-pollution regulations require that coals have low (<1 percent) sulfur content. Figure 17-68 shows that the resistivity of low-sulfur coal ash exceeds the threshold of 10^{10} Ω-cm at common operating temperatures. This has resulted in the installation of a number of precipitators which have failed to meet guaranteed performance. This has occurred to an alarming extent in the United States but has also been encountered in Australia, where the sulfur content is typically 0.3 to 0.6 percent. Maartmann (Pap. EN-34F, 2d International Clean Air Congress, Washington, 1970) reports the installation of a number of precipitators which performed below guarantees, so that the Electricity Commission of New South Wales decided that each manufacturer wishing to bid on a new station must first make pilot tests to prove performance on the actual coal to be burned in that station. Problems of back corona and excessive sparking with low-sulfur coal usually require that the operating voltage be reduced. This reduces the migration velocity and leads to larger precipitators. Ramsdell (*Design Criteria for Precipitators for Modern Central Station Power Plants*, American Power Conference, Chicago, 1968) developed the curves in Fig. 17-69. They show the results of extensive field tests by the Consolidated Edison Co. In another paper ("Anti-pollution Program of Consolidated Edison Co. of New York," ASCE, May 13-17, 1968), Ramsdell traces the remarkable growth in the size of precipitators required for high efficiency on low-sulfur coals. The culmination of this work was the precipitator at boiler 30 at Ravenswood Station, New York. Resistivity problems were avoided by operating at high temperature [343°C (650°F)]. The mechanical (cyclone) collector was installed after the precipitator to clean up puffs due to rapping.

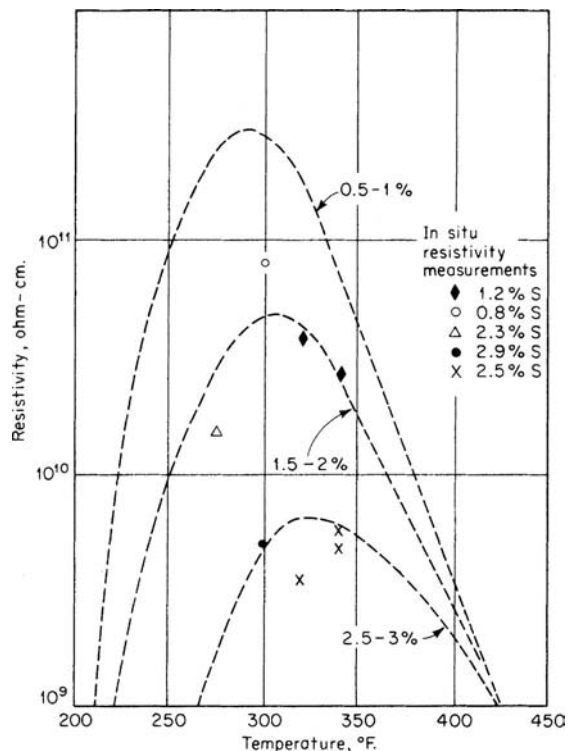


FIG. 17-68 Trends in resistivity of fly ash with variations in flue-gas temperature and coal sulfur content. °C = (°F - 32) × 5/9. (Oglesby and Nichols, A Manual of Electrostatic Precipitator Technology, part II, Southern Research Institute, Birmingham, Ala., 1970.)

Maartmann (op. cit.) agrees that sulfur content is important but feels that it should not be the sole criterion for the determination of collecting surface. He points to specific collecting-surface requirements as high as 500 ft²/(1000 ft³-min) for 95 percent collection efficiency with high-resistivity Australian ash.

Schmidt and Anderson (op. cit.) and Anderson [*Physics*, 3, 23 (July 1932)] claim that resistivity of the collected dust may be a controlling factor which is very sensitive to moisture. They state that an increase in relative humidity of 5 percent may double the precipitation rate because of its effect on the conductivity of the collected dust layer.

Conditioning agents have been added to the flue gas to alter dust resistivity. Steam, sodium chloride, sulfur trioxide, and ammonia have all been successfully used. Research by Chittum and others [Schmidt, *Ind. Eng. Chem.*, 41, 2428 (1949)] led to a theory of conditioning by alteration of the moisture-adsorption properties of dust surfaces. Chittum proposed that an intermediate chemical-adsorption film, which was strongly bound to the particle and which in turn strongly adsorbed water, would be an effective conditioner. This explains how acid conditioners, such as SO₃, help resistivity problems associated with basic dusts, such as many types of fly ash, whereas ammonia is a good additive for acidic dusts such as alumina. Moisture alone can be used as a conditioning agent. This is shown in Fig. 17-65. Moisture is beneficial in two ways: it reduces the electrical resistivity of most dusts (an exception is powdered sulfur, which apparently does not absorb water), and it increases the voltage which may safely be employed without sparking, as shown in Fig. 17-65.

Low resistivity can sometimes be a problem. If the resistivity is below 10^4 Ω-cm, the collected particles are so conductive that their charges leak to ground faster than they are replenished by the corona. The particles are no longer electrostatically pinned to the plate, and they may then be swept away and reentrained in the exit gas. The particles may even pick up positive charges from the collecting plate and

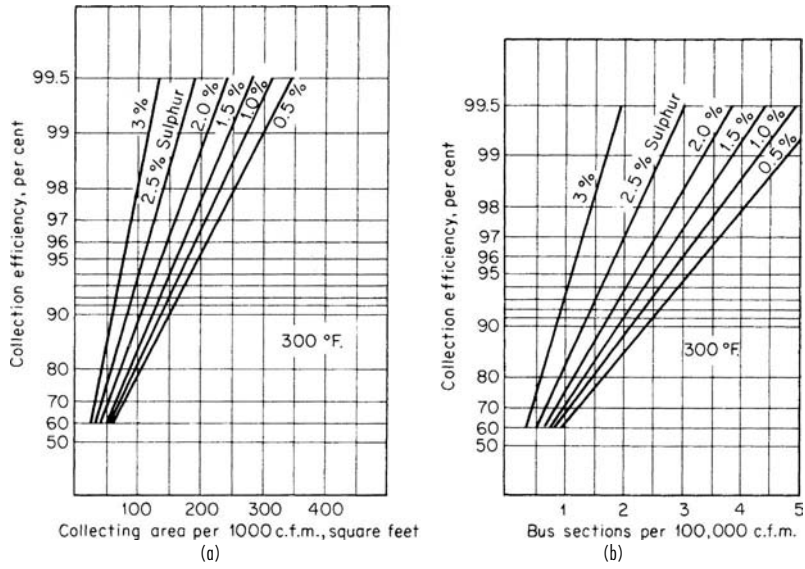


FIG. 17-69 Design curves for electrostatic precipitators for fly ash. Collection efficiency for various levels of percent sulfur in coal versus (a) specific collecting surface, and (b) bus sections per 100,000 ft³/min (4.7 m³/s). °C = (°F - 32) × 5/9. (Ramsdell, Design Criteria for Precipitators for Modern Central Station Power Plants, American Power Conference, Chicago, Ill., 1968.)

then be repelled. Low-resistivity problems are common with dusts of high carbon content and may also occur in fly-ash precipitators which handle the ash from high-sulfur coal and operate at low gas temperatures. Low resistivity in this case results from excessive condensation of electrically conductive sulfuric acid.

Single-Stage Precipitators The single-stage type of unit, commonly known as a Cottrell precipitator, is most generally used for dust or mist collection from industrial-process gases. The corona discharge is maintained throughout the precipitator and, besides providing initial ionization, serves to prevent redispersion of precipitated dust and recharges neutralized or discharged particle ions. Cottrell precipitators may be divided into two main classes, the so-called plate type (Fig. 17-70), in which the collecting electrodes consist of parallel plates, screens, or rows of rods, chains, or wires; and the pipe type (Fig. 17-71), in which the collecting electrodes consist of a nest of parallel pipes which may be square, round, or of any other shape. The discharge or precipitating electrodes in each case are wires or rods, either round or edged, which are placed midway between the collecting electrodes or in the center of the pipes and may be either parallel or perpendicular to the gas flow in the case of plate precipitators. When the collecting electrodes are screens or rows of rods or wires,

the gases are usually passed parallel to the plane of each but may also be passed through it. In pipe precipitators, the gas flow is generally vertical up through the pipe, although downflow is not unusual. The pipe-type precipitator is usually used for the removal of liquid particles and volatilized fumes [Beaver, op. cit.; and Cree, *Am. Gas J.*, **162**, 27 (March 1945)], and the plate type is used mainly on dusts. In the pipe type, the discharge electrodes are usually suspended from an insulated support and kept taut by a weight at the bottom. Cree (op. cit.) discusses the application of electrical precipitators to tar removal in the gas industry.

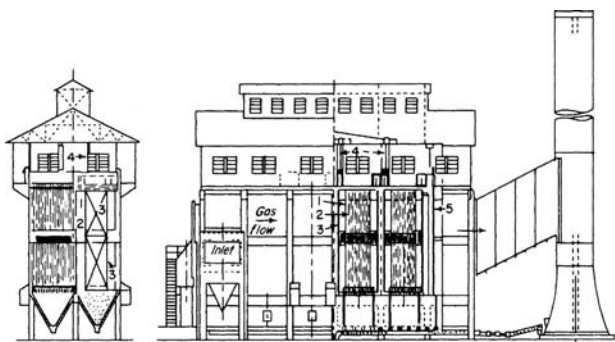


FIG. 17-70 Horizontal-flow plate precipitator used in a cement plant. (Western Precipitation Division, Joy Manufacturing Company.)

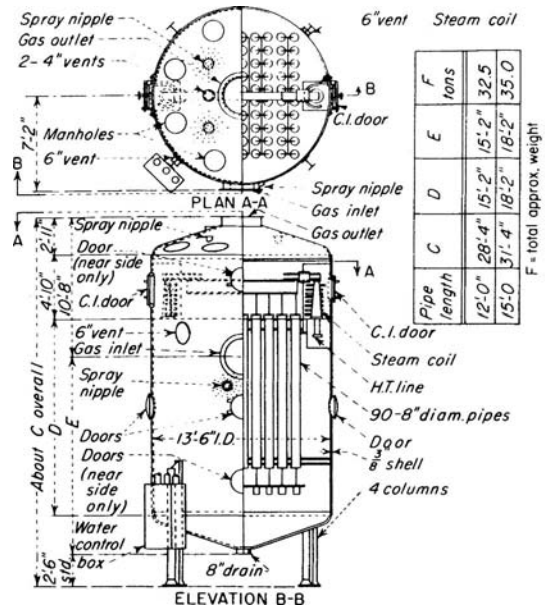


FIG. 17-71 Blast-furnace pipe precipitator. (Research-Cottrell, Inc.)

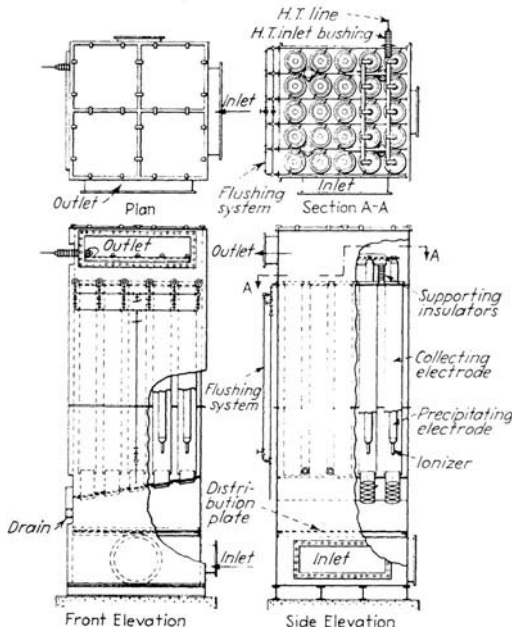


FIG. 17-72 Two-stage water-film pipe precipitator. (Western Precipitation Division, Joy Manufacturing Company.)

Rapping Except when liquid dispersoids are being collected or, in the case of film precipitators, when a liquid is circulated over the collecting-electrode surface (Fig. 17-72), thus continuously removing the precipitated material, the collected dust is dislodged from the

electrodes either periodically or continuously by mechanical rapping or scraping, which may be performed automatically or manually. Automatic rapping with either impact-type or vibrator-type rappers is common practice. White (op. cit.) recommends fairly continuous rapping with magnetic-impulse rappers. Rapping with excessive force leads to dust reentrainment and possible mechanical failure of the plates, while insufficient rapping leads to excessive dust buildup with poor electrical operation and reduced collection efficiency. Intermittent rapping at intervals of an hour or more causes heavy puffs of reentrained dust. Sproull [Air Pollut. Control Assoc. J., 15, 50 (1965)] reports the importance of electrode acceleration and shows that it varies with the type of dust, whether the electrode is rapped perpendicularly (normally) to the plate or parallel to it. Figure 17-73 shows the accelerations required for rapping normally to the plate. Difficult dusts may require as much as 100 G acceleration for 90 percent removal, and even higher accelerations are required when the vibrating force is applied in the plane of the plate.

Perforated-plate or rod-curtain precipitators are frequently rapped without shutting off the gas flow and with the electrodes energized. This procedure, however, results in a tendency for reentrainment of collected dust. Sectional or composite-plate collecting electrodes (sometimes known as hollow, pocket, or tulip electrodes) are used to minimize this tendency in the continuous removal of the precipitated material, provided that it is free-flowing. These are generally designed for vertical gas flow and comprise a collecting electrode containing a dead air space and provided with horizontal protruding slots that guide the dust into this space (see Fig. 17-74), although some types use horizontal flow.

The choice of size, shape, and type of electrode is based on economic considerations and is usually determined by the characteristics of the gas and suspended matter and by mechanical considerations such as flue arrangement, the available space, and previous experience with the electrodes on similar problems. The spacing between collecting electrodes in plate-type precipitators and the pipe diameter in pipe-type precipitators usually ranges from 15 to 38 cm (6 to 15 in). The smaller the spacing, the lower the necessary voltage and overall

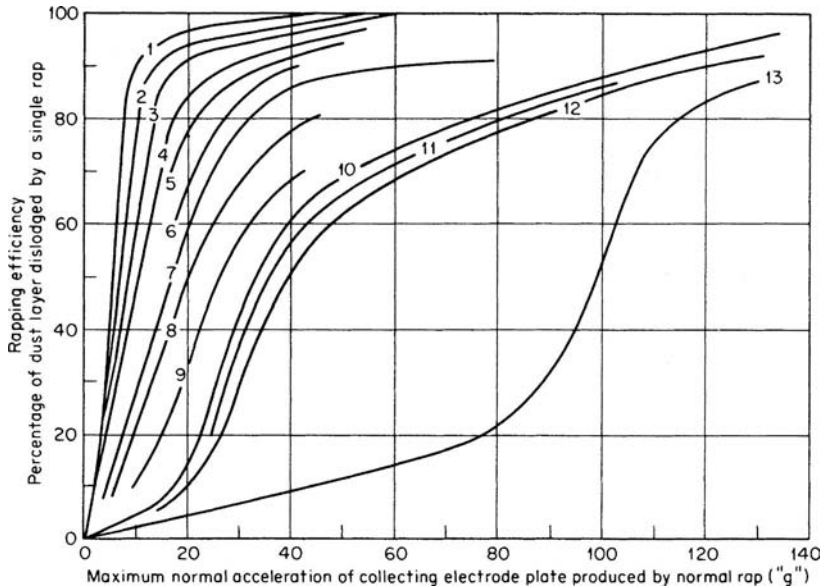


FIG. 17-73 Normal (perpendicular) rapping efficiency for various precipitated dust layers having about 0.03 g dust/cm² (0.2 g dust/in²) as a function of maximum acceleration in multiples of g. Curve 1, fly ash, 200 or 300°F, power off. Curve 2, fly ash, 70°F, power off; also 200 or 300°F, power on. Curve 3, fly ash, 70°F, power on. Curve 4, cement-kiln feed, 300°F, power off. Curve 5, cement dust, 300°F, power off. Curve 6, same as 5, except power on. Curve 7, cement-kiln feed, 300°F, power on. Curve 8, cement dust, 200°F, power off. Curve 9, same as 8, except power on. Curve 10, cement-kiln feed, 200°F, power off. Curve 11, same as 10, except at 70°F. Curve 12, cement-kiln feed, 200°F, power on. Curve 13, cement-kiln feed, 70°F, power on. °C = (°F - 32) × 5/9. [Sproull, Air Pollut. Control Assoc. J., 15, 50 (1965).]

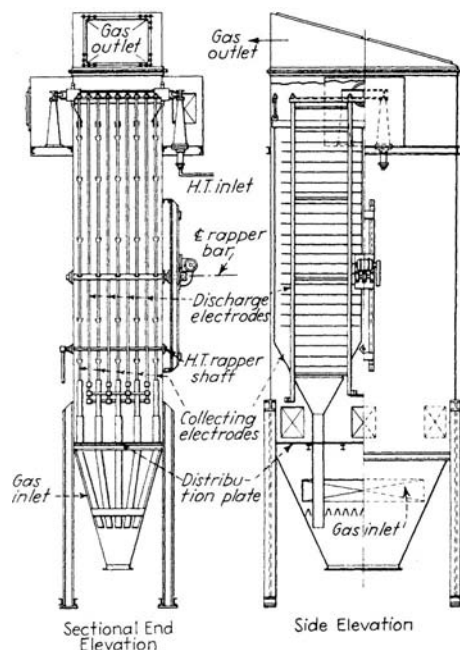


FIG. 17-74 Vertical-flow heavy-duty plate precipitator. (Western Precipitation Division, Joy Manufacturing Company.)

equipment size, but the greater the difficulties involved in maintaining proper alignment and resulting from disturbances due to collected material. Large spacings are usually associated with high dust concentration in order to minimize sparkover due to dust buildup. For very high dust concentrations, such as those encountered in fluid-catalyst plants, it is advantageous to use greater spacings in the first half of the precipitator than in the second half. Precipitators, especially of the plate type, are frequently built with groups of collecting electrodes in series in a common housing. Collecting electrodes are generally on the order of 0.9 to 1.8 m (3 to 6 ft) wide and 3 to 5.5 m (10 to 18 ft) high in plate-type precipitators and 1.8 to 4.6 m (6 to 15 ft) high in pipe types. It is essential for good collection efficiency that the gas be evenly distributed across the various electrode elements. Although this can be achieved by proper gas-inlet transitions and guide vanes, perforated plates or screens located on the upstream side of the electrodes are generally used for distribution. Perforated plates or screens located on the downstream side may be used in special cases.

Electrical precipitators are generally designed for collection efficiency in the range of 90 to 99.9 percent. It is essential, however, that the units be properly maintained in order to achieve the required collection efficiency. Electric power consumption is generally 0.2 to 0.6 kW/(1000 ft³-min) of gas handled, and the pressure drop across the precipitator unit is usually less than 124 Pa (0.5 in water), ranging from 62 to 248 Pa (¼ to 1 in) and representing primarily distributor and entrance-exit losses. Applied potentials range from 30,000 to 100,000 V. Gas velocities and retention times are generally in the range of 0.9 to 3 m/s (3 to 10 ft/s) and 1 to 15 s, respectively. Velocities are kept low in conventional precipitators to avoid reentrainment of dust. There are, however, precipitator installations on carbon black in which the precipitator acts to flocculate the dust so that it may be subsequently collected in multiple small-diameter cyclone collectors. By not attempting to collect the particles in the precipitator, higher velocities may be used with a correspondingly lower investment cost.

Power Supply Electrical precipitators are generally energized by rectified alternating current of commercial frequency. The voltage is stepped up to the required value by means of a transformer and then rectified. The rectifying equipment has undergone an evolution which began with the synchronous mechanical rectifier in 1904 and was

followed by mercury-vapor rectifiers in the 1920s; the first solid-state selenium rectifiers were introduced about 1939. Silicon rectifiers are the latest and most widely used type, since they provide high efficiency and reliability. Automatic controls commonly are tied to voltage, current, spark rate, or some combination of these parameters. Modern precipitators use control circuits similar to those on Fig. 17-75. A high-voltage silicon rectifier is used together with a saturable reactor and means for limiting current and controlling voltage and/or spark rate. One popular method adjusts the voltage to give a specified sparking frequency (typically 50 to 150 sparks per minute per bus section). Half-wave rectification is sometimes used because of its lower equipment requirements and power consumption. It also has the advantage of longer decay periods for sparks to extinguish between current pulses.

Electrode **insulators** must also be designed for a particular service. The properties of the dust or mist and gas determine their design as well as the physical details of the installation. Conducting mists require special allowances such as oil seals, energized shielding cups, or air bleeds. With saturated gas, steam coils are frequently used to prevent condensation on the electrodes.

Typical applications in the chemical field (Beaver, op. cit.) include detarring of manufactured gas, removal of acid mist and impurities in contact sulfuric acid plants, recovery of phosphoric acid mists, removal of dusts in gases from roasters, sintering machines, calciners, cement and lime kilns, blast furnaces, carbon-black furnaces, regenerators on fluid-catalyst units, chemical-recovery furnaces in soda and sulfate pulp mills, and gypsum kettles. Figure 17-74 shows a vertical-flow steel-plate-type precipitator similar to a type used for catalyst-dust collection in certain fluid-catalyst plants.

A development of interest to the chemical industry is the tubular precipitator of reinforced-plastic construction (Wanner, *Gas Cleaning Plant after TiO₂ Rotary Kilns*, technical bulletin, Lurgi Corp., Frankfurt, Germany, 1971). Tubes made of polyvinyl chloride plastic are reinforced on the outside with polyester-fiber glass. The use of modern economical materials of construction to replace high-maintenance materials such as lead has been long awaited for corrosive applications.

Electrical precipitators are probably the most versatile of all types of dust collectors. Very high collection efficiencies can be obtained regardless of the fineness of the dust, provided that the precipitators are given proper maintenance. The chief disadvantages are the high initial cost and, in some cases, high maintenance costs. Furthermore, caution must be exercised with dusts that are combustible in the carrier gas.

Two-Stage Precipitators In two-stage precipitators, corona discharge takes place in the first stage between two electrodes having a nonuniform field (see Fig. 17-76). This is generally obtained by a fine-wire discharge electrode and a large-diameter receiving electrode. In this stage the potential difference must be above that required for corona discharge. The second stage involves a relatively uniform electrostatic field in which charged particles are caused to migrate to a collecting surface. This stage usually consists of either alternately charged parallel plates or concentric cylinders with relatively close clearances compared with their diameters. The only voltage requirement in this stage is that no sparking occur, though higher voltages will result in increased collection efficiency. Since collection occurs in the absence of corona discharge, there is no way of recharging reentrained and discharged particles. Consequently, some means must be provided for avoiding reentrainment of particles from the collecting surface. It is also essential that there be sufficient time and mixing between the first and second stages to secure distribution of gas ions across the gas stream and proper charging of the dust particles.

A unit is available in which electrostatic precipitation is combined with a dry-air filter of the type shown in Fig. 17-64*b*. In another unit an electrostatic field is superimposed on an automatic filter. In this case the ionizer wires are located on the leading face of the unit, and the collecting electrodes consist of alternate stationary and rotating parallel plates. Cleaning in this case is automatic and continuous.

Although intended primarily for air-conditioning applications, these units have been successfully applied to the collection of relatively non-conducting mists such as oil. However, other process applications have been limited largely to experimental installations. The large cost advantage of these units over the Cottrell precipitator lies in the

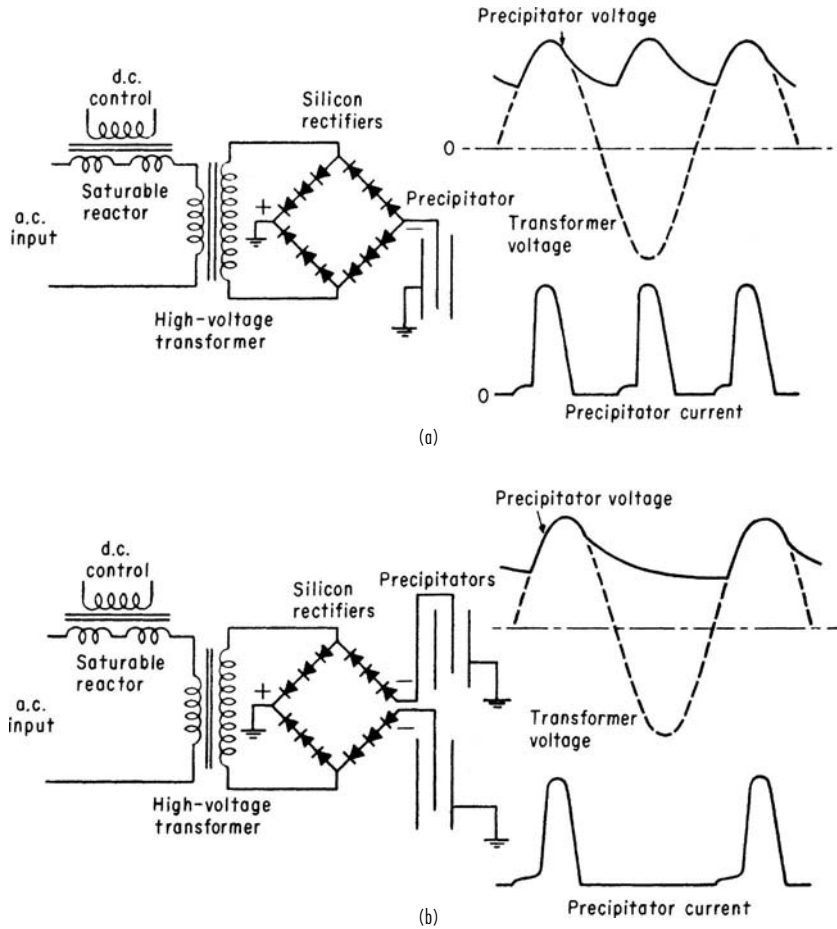


FIG. 17-75 Schematic circuits for silicon rectifier sets with saturable reactor control. (a) Full-wave silicon rectifier. (b) Half-wave silicon rectifier. (White, Industrial Electrostatic Precipitation, Addison-Wesley, Reading, Mass., 1963.)

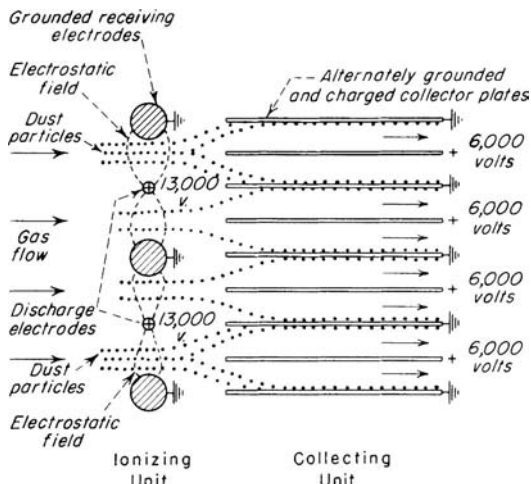


FIG. 17-76 Two-stage electrical-precipitation principle.

smaller equipment size made possible by the close plate spacing, in the lower power consumption due to the two-stage operation, and primarily in the mass production of standardized units. In process applications, the close plate spacing is objectionable because of the relatively high dust concentrations involved. Special material or weight requirements for the structural members may eliminate the mass-production advantage except for individual wide applications.

Alternating-Current Precipitators High-voltage alternating current may be employed for electrical precipitation. Corona discharge will result in a net rectification, provided that no spark gaps are used in series with the precipitator. However, the equipment capacity for a given efficiency is considerably lower than for direct current. In addition, difficulties due to induced high-frequency currents may be encountered. The simplicity of an ac system, on the other hand, has permitted very satisfactory adaptation for laboratory and sampling purposes [Drinker, Thomson, and Fitchet, *J. Ind. Hyg.*, **5**, 162 (September 1923)].

Some promising work with alternating current has been undertaken at the University of Karlsruhe. Lau [Staub, English ed., **29**, 10 (1969)] and coworkers found that ac precipitators operated at 50 Hz were more effective than dc precipitators for dusts with resistivities higher than $10^{11} \Omega\text{-cm}$. An insulating screen covering the collecting electrode permitted higher-voltage operation without sparkover.

SECTION 18

Liquid-Solid
Operations and
Equipment

PERRY'S CHEMICAL ENGINEERS' HANDBOOK

8TH EDITION



WAYNE J. GENCK, DAVID S. DICKEY, FRANK A. BACZEK
DANIEL C. BEDELL, KENT BROWN, WU CHEN
DANIEL E. ELLIS, PETER HARRIOTT, WENPING LI
JAMES K. MCGILLICUDDY, TERENCE P. MCNULTY
JAMES Y. OLDSHUE, FRED SCHOENBRUNN
JULIAN C. SMITH, DONALD C. TAYLOR, DANIEL R. WELLS

Copyright © 2008, 1997, 1984, 1973, 1963, 1950, 1941, 1934 by The McGraw-Hill Companies, Inc. All rights reserved. Manufactured in the United States of America. Except as permitted under the United States Copyright Act of 1976, no part of this publication may be reproduced or distributed in any form or by any means, or stored in a database or retrieval system, without the prior written permission of the publisher.

0-07-154225-6

The material in this eBook also appears in the print version of this title: 0-07-151141-5.

All trademarks are trademarks of their respective owners. Rather than put a trademark symbol after every occurrence of a trademarked name, we use names in an editorial fashion only, and to the benefit of the trademark owner, with no intention of infringement of the trademark. Where such designations appear in this book, they have been printed with initial caps.

McGraw-Hill eBooks are available at special quantity discounts to use as premiums and sales promotions, or for use in corporate training programs. For more information, please contact George Hoare, Special Sales, at george_hoare@mcgraw-hill.com or (212) 904-4069.

TERMS OF USE

This is a copyrighted work and The McGraw-Hill Companies, Inc. (“McGraw-Hill”) and its licensors reserve all rights in and to the work. Use of this work is subject to these terms. Except as permitted under the Copyright Act of 1976 and the right to store and retrieve one copy of the work, you may not decompile, disassemble, reverse engineer, reproduce, modify, create derivative works based upon, transmit, distribute, disseminate, sell, publish or sublicense the work or any part of it without McGraw-Hill’s prior consent. You may use the work for your own noncommercial and personal use; any other use of the work is strictly prohibited. Your right to use the work may be terminated if you fail to comply with these terms.

THE WORK IS PROVIDED “AS IS.” MCGRAW-HILL AND ITS LICENSORS MAKE NO GUARANTEES OR WARRANTIES AS TO THE ACCURACY, ADEQUACY OR COMPLETENESS OF OR RESULTS TO BE OBTAINED FROM USING THE WORK, INCLUDING ANY INFORMATION THAT CAN BE ACCESSED THROUGH THE WORK VIA HYPERLINK OR OTHERWISE, AND EXPRESSLY DISCLAIM ANY WARRANTY, EXPRESS OR IMPLIED, INCLUDING BUT NOT LIMITED TO IMPLIED WARRANTIES OF MERCHANTABILITY OR FITNESS FOR A PARTICULAR PURPOSE. McGraw-Hill and its licensors do not warrant or guarantee that the functions contained in the work will meet your requirements or that its operation will be uninterrupted or error free. Neither McGraw-Hill nor its licensors shall be liable to you or anyone else for any inaccuracy, error or omission, regardless of cause, in the work or for any damages resulting therefrom. McGraw-Hill has no responsibility for the content of any information accessed through the work. Under no circumstances shall McGraw-Hill and/or its licensors be liable for any indirect, incidental, special, punitive, consequential or similar damages that result from the use of or inability to use the work, even if any of them has been advised of the possibility of such damages. This limitation of liability shall apply to any claim or cause whatsoever whether such claim or cause arises in contract, tort or otherwise.

DOI: 10.1036/0071511415

Liquid-Solid Operations and Equipment*

Wayne J. Genck, Ph.D. *President, Genck International; consultant on crystallization and precipitation; Member, American Chemical Society, American Institute of Chemical Engineers, Association for Crystallization Technology, International Society of Pharmaceutical Engineers (ISPE) (Section Editor, Crystallization)*

David S. Dickey, Ph.D. *Senior Consultant, MixTech, Inc.; Fellow, American Institute of Chemical Engineers; Member, North American Mixing Forum (NAMF); Member, American Chemical Society; Member, American Society of Mechanical Engineers (Mixing of Viscous Fluids, Pastes, and Doughs)*

Frank A. Baczek, B.S.Ch.E.&Chem. *Manager, Paste and Sedimentation Technology, Dorr-Oliver EIMCO; Member, Society of Metallurgical and Exploration Engineers of the American Institute of Mining, Metallurgical, and Petroleum Engineers (Gravity Sedimentation Operations)*

Daniel C. Bedell, B.S.Ch.E. *Global Market Manager E-CAT & Sedimentation, Dorr-Oliver EIMCO; Member, Society of Metallurgical and Exploration Engineers of the American Institute of Mining, Metallurgical, and Petroleum Engineers (Gravity Sedimentation Operations)*

Kent Brown, B.S.Civ.E. *Sedimentation Product Manager N.A., Dorr-Oliver EIMCO (Gravity Sedimentation Operations)*

Wu Chen, Ph.D. *Fluid/Particle Specialist, Dow Chemical Company; Member, American Filtration and Separations Society, American Institute of Chemical Engineers (Expression)*

Daniel E. Ellis, B.S.Ch.E. *Product Manager, Sedimentation Centrifuges and Belt Presses, Krauss Maffei Process Technology, Inc. (Centrifuges)*

Peter Harriott, Ph.D. *Professor Emeritus, School of Chemical Engineering, Cornell University; Member, American Institute of Chemical Engineers, American Chemical Society (Selection of a Solids-Liquid Separator)*

Tim J. Laros, M.S. *Senior Process Consultant, Dorr-Oliver EIMCO; Member, Society for Mining, Metallurgy, and Exploration (Filtration)*

Wenping Li, Ph.D. *R&D Manager, Agrilectric Research Company; Member, American Filtration and Separations Society, American Institute of Chemical Engineers (Expression)*

James K. McGillicuddy, B.S.M.E. *Product Manager, Filtration Centrifuges and Filters, Krauss Maffei Process Technology, Inc.; Member, American Institute of Chemical Engineers (Centrifuges)*

Terence P. McNulty, Ph.D. *President, T. P. McNulty and Associates, Inc.; Member, National Academy of Engineering; Member, American Institute of Mining, Metallurgical, and Petroleum Engineers; Member, Society for Mining, Metallurgy, and Exploration (Leaching)*

*The contributions of Donald A. Dahlstrom (Section Editor) and Robert C. Emmett, Jr. (Gravity Sedimentation Operations), authors for this section in the Seventh Edition, are acknowledged.

18-2 LIQUID-SOLID OPERATIONS AND EQUIPMENT

James Y. Oldshue, Ph.D. *Deceased; President, Oldshue Technologies International, Inc.; Adjunct Professor of Chemical Engineering at Beijing Institute of Chemical Technology, Beijing, China; Member, National Academy of Engineering, American Chemical Society, American Institute of Chemical Engineers, Traveler Century Club; Member of Executive Committee on the Transfer of Appropriate Technology for the World Federation of Engineering Organizations (Agitation of Low-Viscosity Particle Suspensions)**

Fred Schoenbrunn, B.S.Ch.E. *Product Manager for Minerals Sedimentation, Dorr-Oliver EIMCO; Member, Society of Metallurgical and Exploration Engineers of the American Institute of Mining, Metallurgical, and Petroleum Engineers; Registered Professional Engineer (Gravity Sedimentation Operations)*

Julian C. Smith, B.Chem.&Ch.E. *Professor Emeritus, School of Chemical Engineering, Cornell University; Member, American Chemical Society, American Institute of Chemical Engineers (Selection of a Solids-Liquid Separator)*

Donald C. Taylor, B.S.Eng.Geol., M.S.Civ.E. *Process Manager Industrial Water & Wastewater Technology, Dorr-Oliver EIMCO; Member, Water Environment Federation; Registered Professional Engineer (Gravity Sedimentation Operations)*

Daniel R. Wells, B.S.Ind.E., MBA *Product Manager Sedimentation Products, Dorr-Oliver EIMCO (Gravity Sedimentation Operations)*

Todd W. Wisdom, M.S.Ch.E. *Global Filtration Product Manager, Dorr-Oliver EIMCO; Member, American Institute of Chemical Engineers (Filtration)*

PHASE CONTACTING AND LIQUID-SOLID PROCESSING: AGITATION OF LOW-VISCOSITY PARTICLE SUSPENSIONS

Fluid Mixing Technology	18-6
Introductory Fluid Mechanics	18-7
Scale-up/Scale-down	18-7
Mixing Equipment	18-9
Small Tanks	18-9
Close-Clearance Impellers	18-9
Axial-Flow Impellers	18-9
Radial-Flow Impellers	18-10
Close-Clearance Stirrers	18-10
Unbaffled Tanks	18-10
Baffled Tanks	18-11
Fluid Behavior in Mixing Vessels	18-12
Impeller Reynolds Number	18-12
Relationship between Fluid Motion and Process Performance	18-12
Turbulent Flow in Stirred Vessels	18-12
Fluid Velocities in Mixing Equipment	18-12
Impeller Discharge Rate and Fluid Head for Turbulent Flow	18-12
Laminar Fluid Motion in Vessels	18-13
Vortex Depth	18-13
Power Consumption of Impellers	18-13
Design of Agitation Equipment	18-14
Selection of Equipment	18-14
Blending	18-14
High-Viscosity Systems	18-15
Chemical Reactions	18-16
Solid-Liquid Systems	18-16
Some Observations on the Use of N_{js}	18-16
Solid Dispersion	18-17
Solid-Liquid Mass Transfer	18-17
Leaching and Extraction of Mineral Values from High Concentration of Solids	18-18
Gas-Liquid Systems	18-18
Gas-Liquid Dispersion	18-18
Gas-Liquid Mass Transfer	18-19
Liquid-Gas-Solid Systems	18-19
Loop Reactors	18-20
Liquid-Liquid Contacting	18-20
Emulsions	18-20
Stagewise Equipment: Mixer-Settlers	18-20
Introduction	18-20

Objectives	18-20
Mixer-Settler Equipment	18-21
Flow or Line Mixers	18-21
Mixing in Agitated Vessels	18-23
Liquid-Liquid Extraction	18-24
Liquid-Liquid-Solid Systems	18-24
Fluid Motion	18-24
Pumping	18-24
Heat Transfer	18-25
Jackets and Coils of Agitated Vessels	18-25
Liquid-Liquid-Gas-Solid Systems	18-26
Computational Fluid Dynamics	18-26

MIXING OF VISCOUS FLUIDS, PASTES, AND DOUGHS

Introduction	18-27
Batch Mixers	18-28
Anchor Mixers	18-28
Helical Ribbon Mixers	18-28
Example 1: Calculate the Power for a Helix Impeller	18-29
Planetary Mixers	18-30
Double- and Triple-Shaft Mixers	18-31
Double-Arm Kneading Mixers	18-31
Screw-Discharge Batch Mixers	18-32
Intensive Mixers	18-32
Banbury Mixers	18-32
High-Intensity Mixers	18-33
Roll Mills	18-33
Miscellaneous Batch Mixers	18-33
Continuous Mixers	18-34
Single-Screw Extruders	18-34
Twin-Screw Extruders	18-34
Farrel Continuous Mixer	18-35
Miscellaneous Continuous Mixers	18-35
Process Design Considerations	18-37
Scale-up of Batch Mixers	18-37
Scale-up of Continuous Mixers	18-38
Heating and Cooling Mixers	18-38
Heat Transfer	18-38
Heating Methods	18-38
Cooling Methods	18-38
Equipment Selection	18-38
Preparation and Addition of Materials	18-39

*The contribution of the late Dr. J. Y. Oldshue, who authored part of this and many editions, is acknowledged.

CRYSTALLIZATION FROM SOLUTION

Principles of Crystallization 18-39
 Crystals 18-39
 Solubility and Phase Diagrams 18-39
 Heat Effects in a Crystallization Process 18-40
 Yield of a Crystallization Process 18-40
 Example 2: Yield from a Crystallization Process 18-41
 Fractional Crystallization 18-41
 Example 3: Yield from Evaporative Cooling 18-41
 Crystal Formation 18-41
 Geometry of Crystal Growth 18-42
 Purity of the Product 18-42
 Coefficient of Variation 18-44
 Crystal Nucleation and Growth 18-44
 Example 4: Population, Density, Growth and Nucleation Rate 18-47
 Crystallization Equipment 18-50
 Mixed-Suspension, Mixed-Product-Removal Crystallizers 18-50
 Reaction-Type Crystallizers 18-51
 Mixed-Suspension, Classified-Product-Removal Crystallizers 18-52
 Classified-Suspension Crystallizer 18-52
 Scraped-Surface Crystallizer 18-52
 Batch Crystallization 18-53
 Recompression Evaporation-Crystallization 18-55
 Information Required to Specify a Crystallizer 18-57
 Crystallizer Operation 18-58
 Crystallizer Costs 18-58

LEACHING

Definition 18-59
 Mechanism 18-60
 Methods of Operation 18-60
 Leaching Equipment 18-60
 Percolation 18-60
 Dispersed-Solids Leaching 18-61
 Screw-Conveyor Extractors 18-63
 Tray Classifier 18-64
 Selection or Design of a Leaching Process 18-64
 Process and Operating Conditions 18-64
 Extractor-Sizing Calculations 18-65

GRAVITY SEDIMENTATION OPERATIONS

Classification of Settleable Solids and the Nature of Sedimentation 18-66
 Sedimentation Testing 18-67
 Testing Common to Clarifiers and Thickeners 18-67
 Feed Characterization 18-67
 Coagulant and/or Flocculant Selection 18-67
 Testing Specific to Clarification 18-68
 Detention Test 18-68
 Bulk Settling Test 18-68
 Clarification with Solids Recycle 18-68
 Detention Efficiency 18-68
 Testing Specific to Thickening 18-68
 Optimization of Flocculation Conditions 18-68
 Determination of Thickener Basin Area 18-69
 Thickener-Basin Depth 18-70
 Scale-up Factors 18-70
 Torque Requirements 18-70
 Underflow Pump Requirements 18-71
 Thickeners 18-71
 Thickener Types 18-72
 Design Features 18-73
 Operation 18-73
 Clarifiers 18-74
 Rectangular Clarifiers 18-74
 Circular Clarifiers 18-74
 Clarifier-Thickener 18-74
 Industrial Waste Secondary Clarifiers 18-74
 Inclined-Plate Clarifiers 18-74
 Solids-Contact Clarifiers 18-75
 Components and Accessories for Sedimentation Units 18-75
 Tanks 18-75
 Drive-Support Structures 18-75
 Drive Assemblies 18-75
 Feedwell 18-77
 Overflow Arrangements 18-77
 Underflow Arrangements 18-78
 Instrumentation 18-78

Thickener 18-78
 Clarifiers 18-79
 Instrumentation and Controls 18-79
 Torque 18-79
 Rake Height 18-79
 Bed Level 18-79
 Bed Pressure 18-81
 Flow Rate 18-81
 Density 18-81
 Settling Rate 18-81
 Overflow Turbidity 18-81
 Continuous Countercurrent Decantation 18-81
 Flow-Sheet Design 18-81
 Equipment 18-81
 Underflow Pumping 18-81
 Overflow Pumps 18-81
 Interstage Mixing Efficiencies 18-81
 Thickener Costs 18-82
 Equipment 18-82
 Operating Costs 18-82

FILTRATION

Definitions and Classification 18-82
 Filtration Theory 18-83
 Continuous Filtration 18-83
 Factors Influencing Small-Scale Testing 18-83
 Vacuum or Pressure 18-83
 Cake Discharge 18-83
 Feed Slurry Temperature 18-83
 Cake Thickness Control 18-84
 Filter Cycle 18-84
 Representative Samples 18-84
 Feed Solids Concentration 18-84
 Pretreatment Chemicals 18-84
 Cloth Blinding 18-85
 Homogeneous Cake 18-85
 Agitation of Sample 18-85
 Use of Steam or Hot Air 18-85
 Small-Scale Test Procedures 18-85
 Apparatus 18-85
 Test Program 18-87
 Bottom-Feed Procedure 18-88
 Top-Feed Procedure 18-88
 Precoat Procedure 18-88
 Data Correlation 18-89
 Dry Cake Weight vs. Thickness 18-89
 Dry Solids or Filtrate Rate 18-89
 Effect of Time on Flocculated Slurries 18-90
 Cake Moisture 18-91
 Cake Washing 18-92
 Wash Time 18-92
 Air Rate 18-92
 Scale-up Factors 18-93
 Scale-up on Rate 18-93
 Scale-up on Cake Discharge 18-93
 Scale-up on Actual Area 18-94
 Overall Scale-up Factor 18-94
 Full-Scale Filter Performance Evaluation 18-94
 Filter Sizing Examples 18-94
 Example 5: Sizing a Disc Filter 18-94
 Example 6: Sizing a Drum Belt Filter with Washing 18-94
 Horizontal Belt Filter 18-95
 Batch Filtration 18-95
 Constant-Pressure Filtration 18-95
 Constant-Rate Filtration 18-95
 Variable-Pressure, Variable-Rate Filtration 18-96
 Pressure Tests 18-96
 Compression-Permeability Tests 18-96
 Scaling Up Test Results 18-97
 Filter Media 18-97
 Fabrics of Woven Fibers 18-97
 Metal Fabrics or Screens 18-97
 Pressed Felts and Cotton Batting 18-97
 Filter Papers 18-97
 Rigid Porous Media 18-98
 Polymer Membranes 18-98
 Granular Beds of Particulate Solids 18-98
 Filter Aids 18-98
 Diatomaceous Earth 18-99
 Perlite 18-99

18-4 LIQUID-SOLID OPERATIONS AND EQUIPMENT

Filtration Equipment	18-99
Cake Filters	18-99
Batch Cake Filters	18-99
Continuous Cake Filters	18-105
Rotary Drum Filters	18-105
Disc Filters	18-106
Horizontal Vacuum Filters	18-108
Filter Thickeners	18-109
Clarifying Filters	18-109
Selection of Filtration Equipment	18-112
Filter Prices	18-114

CENTRIFUGES

Introduction	18-115
General Principles	18-115
Centripetal and Centrifugal Acceleration	18-115
Solid-Body Rotation	18-115
G-Level	18-115
Coriolis Acceleration	18-115
Effect of Fluid Viscosity and Inertia	18-115
Sedimenting and Filtering Centrifuges	18-115
Performance Criteria	18-116
Stress in the Centrifuge Rotor	18-117
G-Force vs. Throughput	18-117
Critical Speeds	18-117
Sedimentation Centrifuges	18-118
Laboratory Tests	18-118
Transient Centrifugation Theory	18-120
Tubular-Bowl Centrifuges	18-120
Multichamber Centrifuges	18-120
Knife-Discharge Centrifugal Clarifiers	18-120
Disc Centrifuges	18-121
Decanter Centrifuges	18-122
Three-Phase Decanter (Tricanter) Centrifuges	18-125
Specialty Decanter Centrifuges	18-125
Screenbowl Centrifuges	18-125
Continuous Centrifugal Sedimentation Theory	18-126
Filtering Centrifuges	18-127
Batch Filtering Centrifuges	18-127
Vertical Basket Centrifuge—Operating Method and Mechanical Design	18-128
Bottom Unloading Vertical Basket Centrifuges	18-128
Top Suspended Vertical Centrifuges	18-128
Horizontal Peeler Centrifuge—Operating Method and Mechanical Design	18-129

Siphon Peeler Centrifuge	18-131
Pressurized Siphon Peeler Centrifuge	18-132
Pharma Peeler Centrifuge	18-132
Inverting Filter Centrifuge	18-133
Continuous-Filtering Centrifuges	18-133
Conical-Screen Centrifuges	18-135
Pusher Centrifuges—Operating Method and Mechanical Design	18-135
Single-Stage versus Multistage	18-136
Single-Stage	18-136
Two-Stage	18-136
Three- and Four-Stage	18-137
Cylindrical/Conical	18-138
Theory of Centrifugal Filtration	18-138
Selection of Centrifuges	18-140
Sedimentation Centrifuges	18-140
Filtering Centrifuges	18-140
Costs	18-140
Purchase Price	18-140
Installation Costs	18-141
Maintenance Costs	18-142
Operating Labor	18-142
Expression	18-143
Fundamentals of Expression	18-143
Definition	18-143
Filtration and Expression of Compactible Filter Cakes	18-143
Fundamental Theory	18-143
Factors Affecting Expression Operations	18-144
Expression Equipment	18-144
Batch Expression Equipment	18-144
Continuous Expression Equipment	18-146

SELECTION OF A SOLIDS-LIQUID SEPARATOR

Preliminary Definition and Selection	18-149
Problem Definition	18-149
Preliminary Selections	18-149
Samples and Tests	18-150
Establishing Process Conditions	18-150
Representative Samples	18-150
Simple Tests	18-150
Modification of Process Conditions	18-151
Consulting the Manufacturer	18-151

Nomenclature

Symbol	Definition	SI units	U.S. customary units
c	Specific heat	J/(kg·k)	Btu/(lb·°F)
C	Constant		
C_o	Orifice coefficient	Dimensionless	Dimensionless
d_o	Orifice diameter	m	in
d_p	Drop diameter	m	ft
d_p, \max			
d_i	Pipe diameter	m	in
d_t	Tube diameter	m	ft
D	Impeller diameter	m	ft
D_a	Impeller diameter	m	ft
D_j	Diameter of jacketed vessel	m	ft
D_T	Tank diameter	m	ft
g	Acceleration	m/s ²	ft/s ²
g_c	Dimensional constant	$g_c = 1$ when using SI units	32.2 (ft·lb)/(lb·s ²)
h	Local individual coefficient of heat transfer, equals $dq/(dA)(\Delta T)$	J/(m ² ·s·K)	Btu/(h·ft ² ·°F)
H	Velocity head	m	ft
k	Thermal conductivity	J/(m·s·K)	(Btu·ft)/(h·ft ² ·°F)
L_p	Diameter of agitator blade	m	ft
N	Agitator rotational speed	s ⁻¹ , (r/s)	s ⁻¹ , (r/s)
N_{js}	Agitator speed for just suspension	s ⁻¹	s ⁻¹
N_{re}	$D_a^2 N_p / \mu$ impeller Reynolds number	Dimensionless	Dimensionless
N_p	Power number = $(g_c P) / \rho N^3 D_a^5$	Dimensionless	Dimensionless
N_Q	Impeller pumping coefficient = Q / ND_a^3	Dimensionless	Dimensionless
N_r	Impeller speed	s ⁻¹	s ⁻¹
N_i	Impeller speed	s ⁻¹	s ⁻¹
P	Power	(N·m/s)	ft·lb _f /s
Q	Impeller flow rate	m ³ /s	ft ³ /s
T	Tank diameter	m	ft
v	Average fluid velocity	m/s	ft/s
v'	Fluid velocity fluctuation	m/s	ft/s
V	Bulk average velocity	m/s	ft/s
Z	Liquid level in tank	m	ft
Greek Symbols			
γ	Rate of shear	s ⁻¹	s ⁻¹
Δp	Pressure drop across orifice		lb _f /ft ²
μ	Viscosity of liquid at tank temperature	Pa·s	lb/(ft·s)
μ	Stirred liquid viscosity	Pa·s	lb/(ft·s)
μ_b	Viscosity of fluid at bulk temperature	Pa·s	lb/(ft·s)
μ_c	Viscosity, continuous phase	Pa·s	lb/(ft·s)
μ_D	Viscosity of dispersed phase	Pa·s	lb/(ft·s)
μ_f	Viscosity of liquid at mean film temperature	Pa·s	lb/(ft·s)
μ_{wt}	Viscosity at wall temperature	Pa·s	lb/(ft·s)
ρ	Stirred liquid density	g/m ³	lb/ft ³
ρ	Density of fluid	kg/m ³	lb/ft ³
ρ_{av}	Density of dispersed phase	kg/m ³	lb/ft ³
ρ_c	Density	kg/m ³	lb/ft ³
σ	Interfacial tension	N/m	lb _f /ft
Φ_D	Average volume fraction of discontinuous phase	Dimensionless	Dimensionless

PHASE CONTACTING AND LIQUID-SOLID PROCESSING: AGITATION OF LOW-VISCOSITY PARTICLE SUSPENSIONS

GENERAL REFERENCES: Hamby, N., M. F. Edwards, and A. W. Neinow (eds.), *Mixing in the Process Industries*, Butterworth, Stoneham, Mass., 1986. Lo, T. C., M. H. I. Baird, and C. Hanson, *Handbook of Solvent Extraction*, Wiley, New York, 1983. Nagata, S., *Mixing: Principles and Applications*, Kodansha Ltd., Tokyo, Wiley, New York, 1975. Oldshue, J. Y., *Fluid Mixing Technology*, McGraw-Hill, New York, 1983. Tatterson, G. B., *Fluid Mixing and Gas Dispersion in Agitated Tanks*, McGraw-Hill, New York, 1991. Uhl, V. W., and J. B. Gray (eds.), *Mixing*, vols. I and II, Academic Press, New York, 1966; vol. III, Academic Press, Orlando, Fla., 1992. Ulbrecht, J. J., and G. K. Paterson (eds.), *Mixing of Liquids by Mechanical Agitation*, Gordon & Breach Science Publishers, New York, 1985.

PROCEEDINGS: *Fluid Mixing*, vol. I, Inst. Chem. Eng. Symp., Ser. No. 64 (Bradford, England), The Institute of Chemical Engineers, Rugby, England, 1984. *Mixing—Theory Related to Practice*, AIChE, Inst. Chem. Eng. Symp. Ser. No. 10 (London), AIChE and The Institute of Chemical Engineers, London, 1965. *Proc. First (1974), Second (1977), Third (1979), Fourth (1982), Fifth (1985), and Sixth (1988) European Conf. on Mixing*, N. G. Coles (ed.), (Cambridge, England) BHRA Fluid Eng., Cranfield, England. *Process Mixing, Chemical and Biochemical Applications*, G. B. Tatterson, and R. V. Calabrese (eds.), AIChE Symp. Ser. No. 286, 1992.

FLUID MIXING TECHNOLOGY

Fluid mixers cut across almost every processing industry including the chemical process industry; minerals, pulp, and paper; waste and water treating and almost every individual process sector. The engineer working with the application and design of mixers for a given process has three basic sources for information. One is published literature, consisting of several thousand published articles and several currently available books, and brochures from equipment vendors. In addition, there may be a variety of in-house experience which may or may not be cataloged, categorized, or usefully available for the process application at hand. Also, short courses are currently available in selected locations and with various course objectives, and a large body of experience and information lies in the hands of equipment vendors.

In the United States, it is customary to design and purchase a mixer from a mixing vendor and purchase the vessel from another supplier. In many other countries, it is more common to purchase the vessel and mixer as a package from one supplier.

In any event, the users of the mixer can issue a mechanical specification and determine the speed, diameter of an impeller, and power with in-house expertise. Or they may issue a process specification which describes the engineering purpose of the mixing operation and the vendor will supply a description of the mixer process performance as well as prepare a mechanical design.

This section describes fluid mixing technology and is referred to in other sections in this handbook which discuss the use of fluid mixing equipment in their various operating disciplines. This section does not describe paste and dough mixing, which may require planetary and extruder-type mixers, nor the area of dry solid-solid mixing.

It is convenient to divide mixing into five pairs (plus three triplets and one quadruplicate combination) of materials, as shown in Table 18-1. These five pairs are blending (miscible liquids), liquid-solid, liquid-gas, liquid-liquid (immiscible liquids), and fluid motion. There are also four other categories that occur, involving three or four phases. One concept that differentiates mixing requirements is the difference between physical criteria listed on the left side of Table 18-1, in which some degree of sampling can be used to determine the character of the mixture in various parts in the tank, and various definitions of mixing requirements can be based on these physical

descriptions. The other category on the right side of Table 18-1 involves chemical and mass-transfer criteria in which rates of mass transfer or chemical reaction are of interest and have many more complexities in expressing the mixing requirements.

The first five classes have their own mixing technologies. Each of these 10 areas has its own mixing technology. There are relationships for the optimum geometry of impeller types, D/T ratios, and tank geometry. They each often have general, overall mixing requirements and different scale-up relationships based on process definitions. In addition, there are many subclassifications, some of which are based on the viscosity of fluids. In the case of blending, we have blending in the viscous region, the transition region, and the turbulent region. Since any given mixer designed for a process may be required to do several different parts of these 10 categories, it must be a compromise of the geometry and other requirements for the total process result and may not optimize any one particular process component. If it turns out that one particular process requirement is so predominant that all the other requirements are satisfied as a consequence, then it is possible to optimize that particular process step. Often, the only process requirement is in one of these 10 areas, and the mixer can be designed and optimized for that one step only.

As an example of the complexity of fluid mixing, many batch processes involve adding many different materials and varying the liquid level over wide ranges in the tank, have different temperatures and shear rate requirements, and obviously need experience and expert attention to all of the requirements. Superimposing the requirements for sound mechanical design, including drives, fluid seals, and rotating shafts, means that the concepts presented here are merely a beginning to the overall, final design.

A few general principles are helpful at this point before proceeding to the examination of equipment and process details. For any given impeller geometry, speed, and diameter, the impeller draws a certain amount of power. This power is 100 percent converted to heat. In low-viscosity mixing (defined later), this power is used to generate a macro-scale regime in which one typically has the visual observation of flow pattern, swirls, and other surface phenomena. However, these flow patterns are primarily energy transfer agents that transfer the power down to the micro scale. The macro-scale regime involves the pumping capacity of the impeller as well as the total circulating capacity throughout the tank and it is an important part of the overall mixer design. The micro-scale area in which the power is dissipated does not care much which impeller is used to generate the energy dissipation. In contrast, in high-viscosity processes, there is a continual progress of energy dissipation from the macro scale down to the micro scale.

There is a wide variety of impellers using *fluidfoil principles*, which are used when flow from the impeller is predominant in the process requirement and macro- or micro-scale shear rates are a subordinate issue.

TABLE 18-1 Classification System for Mixing Processes

Physical	Components	Chemical, mass transfer
Blending	Blending	Chemical reactions
Suspension	Solid-liquid	Dissolving, precipitation
Dispersion	Gas-liquid	Gas absorption
	Solid-liquid-gas	
Emulsions	Liquid-liquid	Extraction
	Liquid-liquid-solid	
	Gas-liquid-liquid	
	Gas-liquid-liquid-solid	
Pumping	Fluid motion	Heat transfer

Scale-up involves selecting mixing variables to give the desired performance in both pilot and full scale. This is often difficult (sometimes impossible) using geometric similarity, so that the use of nongeometric impellers in the pilot plant compared to the impellers used in the plant often allows closer modeling of the mixing requirements to be achieved.

Computational fluid mixing allows the modeling of flow patterns in mixing vessels and some of the principles on which this is based in current techniques are included.

INTRODUCTORY FLUID MECHANICS

The fluid mixing process involves three different areas of viscosity which affect flow patterns and scale-up, and two different scales within the fluid itself: macro scale and micro scale. Design questions come up when looking at the design and performance of mixing processes in a given volume. Considerations must be given to proper impeller and tank geometry as well as the proper speed and power for the impeller. Similar considerations come up when it is desired to scale up or scale down, and this involves another set of mixing considerations.

If the fluid discharge from an impeller is measured with a device that has a high-frequency response, one can track the velocity of the fluid as a function of time. The velocity at a given point in time can then be expressed as an average velocity v plus fluctuating component v' . Average velocities can be integrated across the discharge of the impeller, and the pumping capacity normal to an arbitrary discharge plane can be calculated. This arbitrary discharge plane is often defined as the plane bounded by the boundaries of the impeller blade diameter and height. Because there is no casing, however, an additional 10 to 20 percent of flow typically can be considered as the primary flow from an impeller.

The velocity gradients between the average velocities operate only on larger particles. Typically, these larger-size particles are greater than 1000 μm . This is not a proven definition, but it does give a feel for the magnitudes involved. This defines macro-scale mixing. In the turbulent region, these macro-scale fluctuations can also arise from the finite number of impeller blades. These set up velocity fluctuations that can also operate on the macro scale.

Smaller particles see primarily only the fluctuating velocity component. When the particle size is much less than 100 μm , the turbulent properties of the fluid become important. This is the definition of the physical size for micro-scale mixing.

All of the power applied by a mixer to a fluid through the impeller appears as heat. The conversion of power to heat is through viscous shear and is approximately 2542 Btu/h/hp. Viscous shear is present in turbulent flow only at the micro-scale level. As a result, the power per unit volume is a major component of the phenomena of micro-scale mixing. At a 1- μm level, in fact, it doesn't matter what specific impeller design is used to supply the power.

Numerous experiments show that power per unit volume in the zone of the impeller (which is about 5 percent of the total tank volume) is about 100 times higher than the power per unit volume in the rest of the vessel. Making some reasonable assumptions about the fluid mechanics parameters, the root-mean-square (rms) velocity fluctuation in the zone of the impeller appears to be approximately 5 to 10 times higher than in the rest of the vessel. This conclusion has been verified by experimental measurements.

The ratio of the rms velocity fluctuation to the average velocity in the impeller zone is about 50 percent with many open impellers. If the rms velocity fluctuation is divided by the average velocity in the rest of the vessel, however, the ratio is on the order of 5 percent. This is also the level of rms velocity fluctuation to the mean velocity in pipeline flow. There are phenomena in micro-scale mixing that can occur in mixing tanks that do not occur in pipeline reactors. Whether this is good or bad depends upon the process requirements.

Figure 18-1 shows velocity versus time for three different impellers. The differences between the impellers are quite significant and can be important for mixing processes.

All three impellers are calculated for the same impeller flow Q and the same diameter. The A310 (Fig. 18-2) draws the least power and has the least velocity fluctuations. This gives the lowest micro-scale turbulence and shear rate. The A200 (Fig. 18-3) shows increased velocity

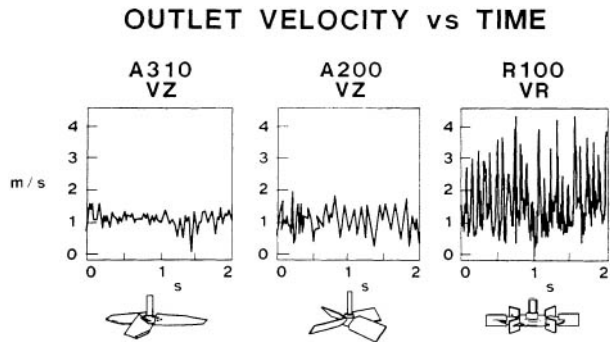


FIG. 18-1 Velocity fluctuations versus time for equal total pumping capacity from three different impellers.

fluctuations and draws more power. The R100 (Fig. 18-4) draws the most power and has the highest micro-scale shear rate. The proper impeller should be used for each individual process requirement.

Scale-up/Scale-down Two aspects of scale-up frequently arise. One is building a model based on pilot-plant studies that develop an understanding of the process variables for an existing full-scale mixing installation. The other is taking a new process and studying it in the pilot plant in such a way that pertinent scale-up variables are worked out for a new mixing installation.

There are a few principles of scale-up that can indicate which approach to take in either case. Using geometric similarity, the macro-scale variables can be summarized as follows:

- Blend and circulation times in the large tank will be much longer than in the small tank.



FIG. 18-2 An A310 impeller.

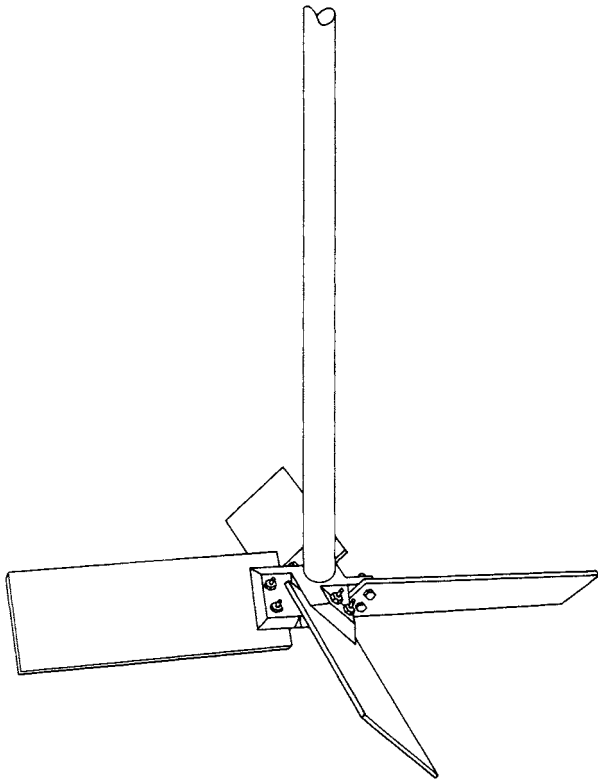


FIG. 18-3 Pitched-blade turbine.

- Maximum impeller zone shear rate will be higher in the larger tank, but the average impeller zone shear rate will be lower; therefore, there will be a much greater variation in shear rates in a full-scale tank than in a pilot unit.
- Reynolds numbers in the large tank will be higher, typically on the order of 5 to 25 times higher than those in a small tank.
- Large tanks tend to develop a recirculation pattern from the impeller through the tank back to the impeller. This results in a behavior similar to that for a number of tanks in a series. The net result is that the mean circulation time is increased over what would be predicted from the impeller pumping capacity. This also

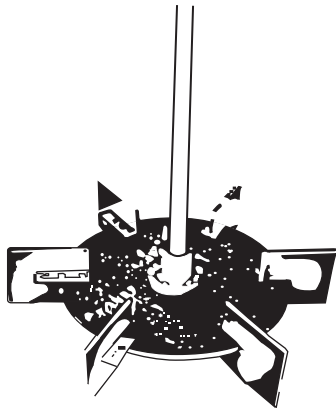


FIG. 18-4 Flat-blade turbine.

increases the standard deviation of the circulation times around the mean.

- Heat transfer is normally much more demanding on a large scale. The introduction of helical coils, vertical tubes, or other heat-transfer devices causes an increased tendency for areas of low recirculation to exist.
- In gas-liquid systems, the tendency for an increase in the gas superficial velocity upon scale-up can further increase the overall circulation time.

What about the micro-scale phenomena? These are dependent primarily on the energy dissipation per unit volume, although one must also be concerned about the energy spectra. In general, the energy dissipation per unit volume around the impeller is approximately 100 times higher than in the rest of the tank. This results in an rms velocity fluctuation ratio to the average velocity on the order of 10:1 between the impeller zone and the rest of the tank.

Because there are thousands of specific processes each year that involve mixing, there will be at least hundreds of different situations requiring a somewhat different pilot-plant approach. Unfortunately, no set of rules states how to carry out studies for any specific program, but here are a few guidelines that can help one carry out a pilot-plant program.

- For any given process, one takes a qualitative look at the possible role of fluid shear stresses. Then one tries to consider pathways related to fluid shear stress that may affect the process. If there are none, then this extremely complex phenomenon can be dismissed and the process design can be based on such things as uniformity, circulation time, blend time, or velocity specifications. This is often the case in the blending of miscible fluids and the suspension of solids.
- If fluid shear stresses are likely to be involved in obtaining a process result, then one must qualitatively look at the scale at which the shear stresses influence the result. If the particles, bubbles, droplets, or fluid clumps are on the order of 1000 μm or larger, the variables are macro scale and average velocities at a point are the predominant variable.

When macro-scale variables are involved, every geometric design variable can affect the role of shear stresses. They can include such items as power, impeller speed, impeller diameter, impeller blade shape, impeller blade width or height, thickness of the material used to make the impeller, number of blades, impeller location, baffle location, and number of impellers.

Micro-scale variables are involved when the particles, droplets, baffles, or fluid clumps are on the order of 100 μm or less. In this case, the critical parameters usually are power per unit volume, distribution of power per unit volume between the impeller and the rest of the tank, rms velocity fluctuation, energy spectra, dissipation length, the smallest micro-scale eddy size for the particular power level, and viscosity of the fluid.

- The overall circulating pattern, including the circulation time and the deviation of the circulation times, can never be neglected. No matter what else a mixer does, it must be able to circulate fluid throughout an entire vessel appropriately. If it cannot, then that mixer is not suited for the task being considered.

Qualitative and, hopefully, quantitative estimates of how the process result will be measured must be made in advance. The evaluations must allow one to establish the importance of the different steps in a process, such as gas-liquid mass transfer, chemical reaction rate, or heat transfer.

- It is seldom possible, either economically or timewise, to study every potential mixing variable or to compare the performance of many impeller types. In many cases, a process needs a specific fluid regime that is relatively independent of the impeller type used to generate it. Because different impellers may require different geometries to achieve an optimum process combination, a random choice of only one diameter of each of two or more impeller types may not tell what is appropriate for the fluid regime ultimately required.
- Often, a pilot plant will operate in the viscous region while the commercial unit will operate in the transition region, or alternatively, the pilot plant may be in the transition region and the commercial unit in the turbulent region. Some experience is required to estimate the difference in performance to be expected upon scale-up.
- In general, it is not necessary to model Z/T ratios between pilot and commercial units.

- In order to make the pilot unit more like a commercial unit in macro-scale characteristics, the pilot unit impeller must be designed to lengthen the blend time and to increase the maximum impeller zone shear rate. This will result in a greater range of shear rates than is normally found in a pilot unit.

MIXING EQUIPMENT

There are three types of mixing flow patterns that are markedly different. The so-called axial-flow turbines (Fig. 18-3) actually give a flow coming off the impeller of approximately 45°, and therefore have a recirculation pattern coming back into the impeller at the hub region of the blades. This flow pattern exists to an approximate Reynolds number of 200 to 600 and then becomes radial as the Reynolds number decreases. Both the R100 and A200 impellers normally require four baffles for an effective flow pattern. These baffles typically are 1/2 of the tank diameter and width.

Radial-flow impellers include the flat-blade disc turbine, Fig. 18-4, which is labeled an R100. This generates a radial flow pattern at all Reynolds numbers. Figure 18-17 is the diagram of Reynolds number/power number curve, which allows one to calculate the power knowing the speed and diameter of the impeller. The impeller shown in Fig. 18-4 typically gives high shear rates and relatively low pumping capacity.

The current design of fluidfoil impellers includes the A310 (Fig. 18-2), as well as several other impellers of that type commonly referred to as *high-efficiency impellers*, *hydrofoil*, and other descriptive names to illustrate that they are designed to maximize flow and minimize shear rate. These impellers typically require two baffles, but are normally used with three, since three gives a more stable flow pattern. Since most industrial mixing processes involve pumping capacity and, to a lesser degree, fluid shear rate, the fluidfoil impellers are now used on the majority of the mixer installations. There is now an additional family of these fluidfoil impellers, which depend upon different solidity ratios to operate in various kinds of fluid mixing systems. Figure 18-5 illustrates four of these impellers. The solidity ratio is the ratio of total blade area to a circle circumscribing the impeller and, as viscosity increases, higher values of the solidity ratios are more effective in providing an axial flow pattern rather than a radial flow pattern. Also the A315-type provides an effective area of preventing gas bypassing through the hub of the impeller by having exceptionally wide blades. Another impeller of that type is the Prochem Maxflo T.

Small Tanks For tanks less than 1.8 m in diameter, the clamp or flanged mounted angular, off-center axial-flow impeller without baffles should be used for a wide range of process requirements (refer to Fig. 18-14). The impellers currently used are the fluidfoil type. Since small impellers typically operate at low Reynolds numbers, often in the transition region, the fluidfoil impeller should be designed to give good flow characteristics over a range of Reynolds numbers, probably on the order of 50 to 500. The *Z/T* ratio should be 0.75 to 1.5. The volume of liquid should not exceed 4 m³.

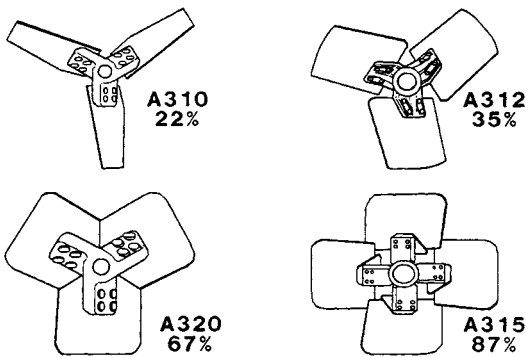


FIG. 18-5 The solidity ratio for four different impellers of the axial-flow fluidfoil type.

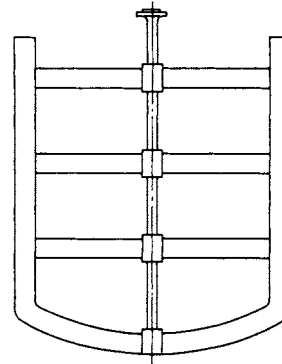


FIG. 18-6 Anchor impeller.

Close-Clearance Impellers There are two close-clearance impellers. They are the *anchor impeller* (Fig. 18-6) and the *helical impeller* (Fig. 18-7), which operate near the tank wall and are particularly effective in pseudoplastic fluids in which it is desirable to have the mixing energy concentrated out near the tank wall where the flow pattern is more effective than with the open impellers that were covered earlier.

Axial-Flow Impellers Axial-flow impellers include all impellers in which the blade makes an angle of less than 90° with the plane of

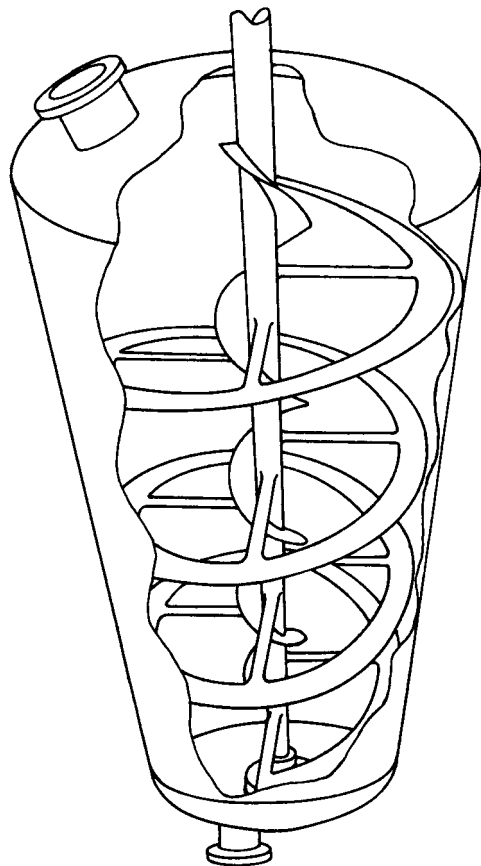


FIG. 18-7 Helical mixer for high-viscosity fluid.

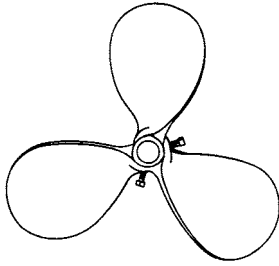


FIG. 18-8 Marine-type mixing impeller.

rotation. Propellers and pitched-blade turbines, as illustrated in Figs. 18-8 and 18-3, are representative axial-flow impellers.

Portable mixers may be clamped on the side of an open vessel in the angular, off-center position shown in Fig. 18-14 or bolted to a flange or plate on the top of a closed vessel with the shaft in the same angular, off-center position. This mounting results in a strong top-to-bottom circulation.

Two basic speed ranges are available: 1150 or 1750 r/min with direct drive and 350 or 420 r/min with a gear drive. The high-speed units produce higher velocities and shear rates (Fig. 18-9) in the impeller discharge stream and a lower circulation rate throughout the vessel than the low-speed units. For suspension of solids, it is common to use the gear-driven units, while for rapid dispersion or fast reactions the high-speed units are more appropriate.

Axial-flow impellers may also be mounted near the bottom of the cylindrical wall of a vessel as shown in Fig. 18-10. Such side-entering agitators are used to blend low-viscosity fluids [<0.1 Pa-s (100 cP)] or to keep slowly settling sediment suspended in tanks as large as some 4000 m³ (10⁶ gal). Mixing of paper pulp is often carried out by side-entering propellers.

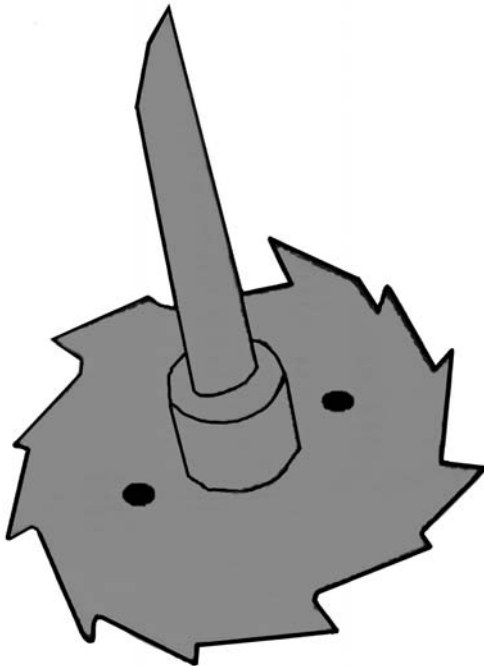


FIG. 18-9 High-shear-rate-impeller.

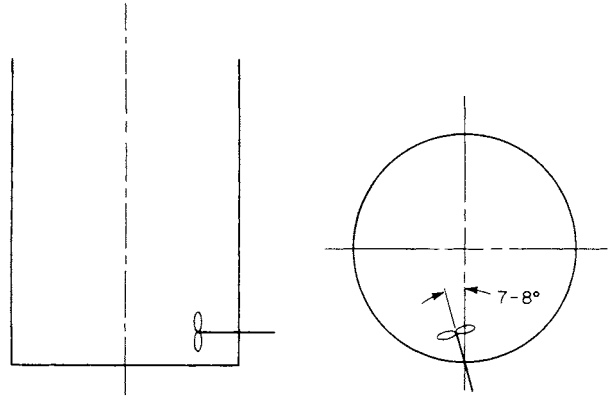


FIG. 18-10 Side-entering propeller mixer.

Pitched-blade turbines (Fig. 18-3) are used on top-entering agitator shafts instead of propellers when a high axial circulation rate is desired and the power consumption is more than 2.2 kW (3 hp). A pitched-blade turbine near the upper surface of liquid in a vessel is effective for rapid submergence of floating particulate solids.

Radial-Flow Impellers Radial-flow impellers have blades which are parallel to the axis of the drive shaft. The smaller multiblade ones are known as *turbines*; larger, slower-speed impellers, with two or four blades, are often called *paddles*. The diameter of a turbine is normally between 0.3 and 0.6 of the tank diameter. Turbine impellers come in a variety of types, such as curved-blade and flat-blade, as illustrated in Fig. 18-4. Curved blades aid in starting an impeller in settled solids.

For processes in which corrosion of commonly used metals is a problem, glass-coated impellers may be economical. A typical modified curved-blade turbine of this type is shown in Fig. 18-11.

Close-Clearance Stirrers For some pseudoplastic fluid systems stagnant fluid may be found next to the vessel walls in parts remote from propeller or turbine impellers. In such cases, an "anchor" impeller may be used (Fig. 18-6). The fluid flow is principally circular or helical (see Fig. 18-7) in the direction of rotation of the anchor. Whether substantial axial or radial fluid motion also occurs depends on the fluid viscosity and the design of the upper blade-supporting spokes. Anchor agitators are used particularly to obtain improved heat transfer in high-consistency fluids.

Unbaffled Tanks If a low-viscosity liquid is stirred in an unbaffled tank by an axially mounted agitator, there is a tendency for a swirling

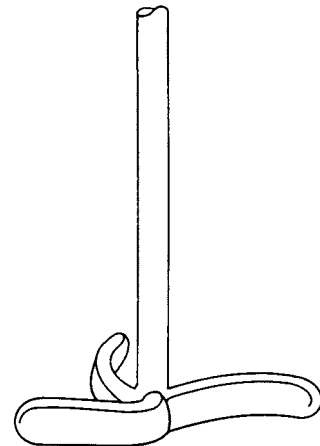


FIG. 18-11 Glass-steel impeller. (The Pfaudler Company.)

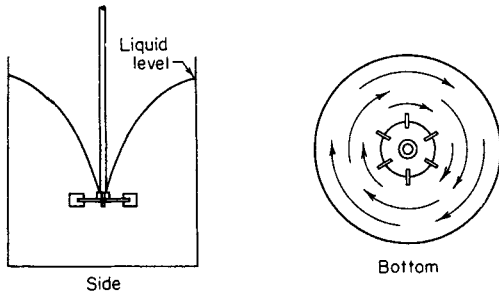


FIG. 18-12 Typical flow pattern for either axial- or radial-flow impellers in an unbaffled tank.

flow pattern to develop regardless of the type of impeller. Figure 18-12 shows a typical flow pattern. A vortex is produced owing to centrifugal force acting on the rotating liquid. In spite of the presence of a vortex, satisfactory process results often can be obtained in an unbaffled vessel. However, there is a limit to the rotational speed that may be used, since once the vortex reaches the impeller, severe air entrainment may occur. In addition, the swirling mass of liquid often generates an oscillating surge in the tank, which coupled with the deep vortex may create a large fluctuating force acting on the mixer shaft.

Vertical velocities in a vortexing low-viscosity liquid are low relative to circumferential velocities in the vessel. Increased vertical circulation rates may be obtained by mounting the impeller off center, as illustrated in Fig. 18-13. This position may be used with either turbines or propellers. The position is critical, since too far or too little off center in one direction or the other will cause greater swirling, erratic vortexing, and dangerously high shaft stresses. Changes in viscosity and tank size also affect the flow pattern in such vessels. Off-center mountings have been particularly effective in the suspension of paper pulp.

With axial-flow impellers, an angular off-center position may be used. The impeller is mounted approximately 15° from the vertical, as shown in Fig. 18-14.

The angular off-center position used with fluidfoil units is usually limited to impellers delivering 2.2 kW (3 hp) or less. The unbalanced fluid forces generated by this mounting can become severe with higher power.

Baffled Tanks For vigorous agitation of thin suspensions, the tank is provided with baffles which are flat vertical strips set radially along the tank wall, as illustrated in Figs. 18-15 and 18-16. Four baffles are almost always adequate. A common baffle width is one-tenth to one-twelfth of the tank diameter (radial dimension). For agitating

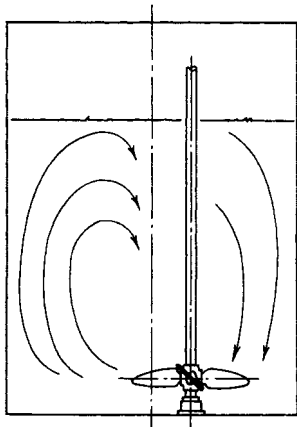


FIG. 18-13 Flow pattern with a paper-stock propeller, unbaffled; vertical off-center position.

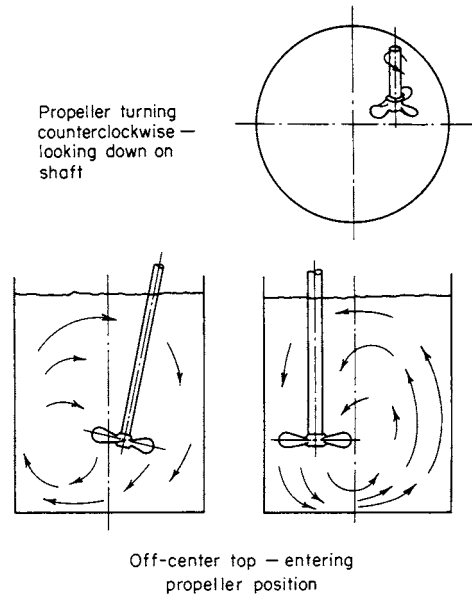


FIG. 18-14 Typical flow pattern with a propeller in angular off-center position without baffles.

slurries, the baffles often are located one-half of their width from the vessel wall to minimize accumulation of solids on or behind them.

For Reynolds numbers greater than 2000 baffles are commonly used with turbine impellers and with on-centerline axial-flow impellers. The flow patterns illustrated in Figs. 18-15 and 18-16 are quite different, but in both cases the use of baffles results in a large top-to-bottom circulation without vortexing or severely unbalanced fluid forces on the impeller shaft.

In the transition region [Reynolds numbers, Eq. (18-1), from 10 to 10,000], the width of the baffle may be reduced, often to one-half of standard width. If the circulation pattern is satisfactory when the tank is unbaffled but a vortex creates a problem, partial-length baffles may be used. These are standard-width and extend downward from the surface into about one-third of the liquid volume.

In the region of laminar flow ($N_{Re} < 10$), the same power is consumed by the impeller whether baffles are present or not, and they are seldom required. The flow pattern may be affected by the baffles, but not always advantageously. When they are needed, the baffles are usually placed one or two widths radially off the tank wall, to allow fluid to circulate behind them and at the same time produce some axial deflection of flow.

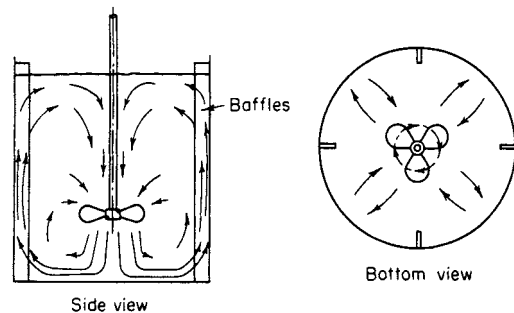


FIG. 18-15 Typical flow pattern in a baffled tank with a propeller or an axial-flow turbine positioned on center.

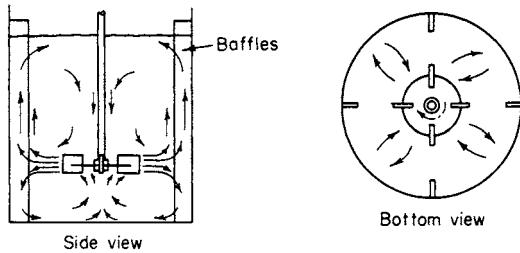


FIG. 18-16 Typical flow pattern in a baffled tank with a turbine positioned on center.

FLUID BEHAVIOR IN MIXING VESSELS

Impeller Reynolds Number The presence or absence of turbulence in an impeller-stirred vessel can be correlated with an impeller Reynolds number defined

$$N_{Re} = \frac{D_a^2 N \rho}{\mu} \quad (18-1)$$

where N = rotational speed, r/s ; D_a = impeller diameter, m (ft); ρ = fluid density, kg/m^3 (lb/ft^3); and μ = viscosity, $Pa \cdot s$ [$lb/(ft \cdot s)$]. Flow in the tank is turbulent when $N_{Re} > 10,000$. Thus viscosity alone is not a valid indication of the type of flow to be expected. Between Reynolds numbers of 10,000 and approximately 10 is a transition range in which flow is turbulent at the impeller and laminar in remote parts of the vessel; when $N_{Re} < 10$, flow is laminar only.

Not only is the type of flow related to the impeller Reynolds number, but also such process performance characteristics as mixing time, impeller pumping rate, impeller power consumption, and heat- and mass-transfer coefficients can be correlated with this dimensionless group.

Relationship between Fluid Motion and Process Performance Several phenomena which can be used to promote various processing objectives occur during fluid motion in a vessel.

1. Shear stresses are developed in a fluid when a layer of fluid moves faster or slower than a nearby layer of fluid or a solid surface. In laminar flow, the shear stress is equal to the product of fluid viscosity and velocity gradient or rate of shear. Under laminar-flow conditions, shear forces are larger than inertial forces in the fluid.

With turbulent flow, shear stress also results from the behavior of transient random eddies, including large-scale eddies which decay to small eddies or fluctuations. The scale of the large eddies depends on equipment size. On the other hand, the scale of small eddies, which dissipate energy primarily through viscous shear, is almost independent of agitator and tank size.

The shear stress in the fluid is much higher near the impeller than it is near the tank wall. The difference is greater in large tanks than in small ones.

2. Inertial forces are developed when the velocity of a fluid changes direction or magnitude. In turbulent flow, inertia forces are larger than viscous forces. Fluid in motion tends to continue in motion until it meets a solid surface or other fluid moving in a different direction. Forces are developed during the momentum transfer that takes place. The forces acting on the impeller blades fluctuate in a random manner related to the scale and intensity of turbulence at the impeller.

3. The interfacial area between gases and liquids, immiscible liquids, and solids and liquids may be enlarged or reduced by these viscous and inertia forces when interacting with interfacial forces such as surface tension.

4. Concentration and temperature differences are reduced by bulk flow or circulation in a vessel. Fluid regions of different composition or temperature are reduced in thickness by bulk motion in which velocity gradients exist. This process is called bulk diffusion or Taylor diffusion (Brodkey, in Uhl and Gray, op. cit., vol. 1, p. 48). The turbulent and molecular diffusion reduces the difference between these regions. In laminar flow, Taylor diffusion and molecular diffusion are the mechanisms of concentration- and temperature-difference reduction.

5. Equilibrium concentrations which tend to develop at solid-liquid, gas-liquid, or liquid-liquid interfaces are displaced or changed by molecular and turbulent diffusion between bulk fluid and fluid adjacent to the interface. Bulk motion (Taylor diffusion) aids in this mass-transfer mechanism also.

Turbulent Flow in Stirred Vessels Turbulence parameters such as intensity and scale of turbulence, correlation coefficients, and energy spectra have been measured in stirred vessels. However, these characteristics are not used directly in the design of stirred vessels.

Fluid Velocities in Mixing Equipment Fluid velocities have been measured for various turbines in baffled and unbaffled vessels. Typical data are summarized in Uhl and Gray, op. cit., vol. 1, chap. 4. Velocity data have been used for calculating impeller discharge and circulation rates but are not employed directly in the design of mixing equipment.

Impeller Discharge Rate and Fluid Head for Turbulent Flow When fluid viscosity is low and flow is turbulent, an impeller moves fluids by an increase in momentum from the blades which exert a force on the fluid. The blades of rotating propellers and turbines change the direction and increase the velocity of the fluids.

The pumping rate or discharge rate of an impeller is the flow rate perpendicular to the impeller discharge area. The fluid passing through this area has velocities proportional to the impeller peripheral velocity and velocity heads proportional to the square of these velocities at each point in the impeller discharge stream under turbulent-flow conditions. The following equations relate velocity head, pumping rate, and power for geometrically similar impellers under turbulent-flow conditions:

$$Q = N_D N D_a^3 \quad (18-2)$$

$$H = \frac{N_p N^2 D_a^2}{N_Q g} \quad (18-3)$$

$$P = N_p \rho N^3 \left(\frac{D_a^5}{g_c} \right) \quad (18-4)$$

$$P = \frac{\rho H Q g}{g_c} \quad (18-5)$$

where Q = impeller discharge rate, m^3/s (ft^3/s); N_D = discharge coefficient, dimensionless; H = velocity head, m (ft); N_p = power number, dimensionless; P = power, $(N \cdot m)/s$ [$(ft \cdot lb)/s$]; g_c = dimensional constant, $32.2 (ft \cdot lb)/(lb \cdot s^2)$ ($g_c = 1$ when using SI units); and g = gravitational acceleration, m/s^2 (ft/s^2).

The discharge rate Q has been measured for several types of impellers, and discharge coefficients have been calculated. The data of a number of investigators are reviewed by Uhl and Gray (op. cit., vol. 1, chap. 4). N_D is 0.4 to 0.5 for a propeller with pitch equal to diameter at $N_{Re} = 10^5$. For turbines, N_D ranges from 0.7 to 2.9, depending on the number of blades, blade-height-to-impeller-diameter ratio, and impeller-to-vessel-diameter ratio. The effects of these geometric variables are not well defined.

Power consumption has also been measured and correlated with impeller Reynolds numbers. The velocity head for a mixing impeller can be calculated, then, from flow and power data, by Eq. (18-3) or Eq. (18-5).

The velocity head of the impeller discharge stream is a measure of the maximum force that this fluid can exert when its velocity is changed. Such inertia forces are higher in streams with higher discharge velocities. Shear rates and shear stresses are also higher under these conditions in the smallest eddies. If a higher discharge velocity is desired at the same power consumption, a smaller-diameter impeller must be used at a higher rotational speed. According to Eq. (18-4), at a given power level $N \propto D_a^{-5/3}$ and $N D_a \propto D_a^{-2/3}$. Then, $H \propto D_a^{-4/3}$ and $Q \propto D_a^{4/3}$.

An impeller with a high fluid head is one with high peripheral velocity and discharge velocity. Such impellers are useful for (1) rapid reduction of concentration differences in the impeller discharge stream (rapid mixing), (2) production of large interfacial area and

small droplets in gas-liquid and immiscible-liquid systems, (3) solids deagglomeration, and (4) promotion of mass transfer between phases.

The impeller discharge rate can be increased at the same power consumption by increasing impeller diameter and decreasing rotational speed and peripheral velocity so that $N^2 D_a^5$ is a constant (Eq. 18-4). Flow goes up, velocity head and peripheral velocity go down, but impeller torque T_Q goes up. At the same torque, $N^2 D_a^5$ is constant, $P \propto D_a^{-5/2}$, and $Q \propto D_a^{1/2}$. Therefore, increasing impeller diameter at constant torque increases discharge rate at lower power consumption. At the same discharge rate, ND_a^3 is constant, $P \propto D_a^{-4}$, and $T_Q \propto D_a^{-1}$. Therefore, power and torque decrease as impeller diameter is increased at constant Q .

A large-diameter impeller with a high discharge rate is used for (1) short times to complete mixing of miscible liquid throughout a vessel, (2) promotion of heat transfer, (3) reduction of concentration and temperature differences in all parts of vessels used for constant-environment reactors and continuous averaging, and (4) suspension of particles of relatively low settling rate.

Laminar Fluid Motion in Vessels When the impeller Reynolds number is less than 10, the flow induced by the impeller is laminar. Under these conditions, the impeller drags fluid with it in a predominantly circular pattern. If the impeller blades curve back, there is a viscous drag flow toward the tips of these blades. Under moderate-viscosity conditions in laminar flow, centrifugal force acting on the fluid layer dragged in a circular path by the rotating impeller will move fluid in a radial direction. This centrifugal effect causes any gas accumulated behind a rotating blade to move to the axis of impeller rotation. Such radial-velocity components are small relative to tangential velocity.

For turbines at Reynolds numbers less than 100, toroidal stagnant zones exist above and below the turbine periphery. Interchange of liquid between these regions and the rest of the vessel is principally by molecular diffusion.

Suspensions of fine solids may have pseudoplastic or plastic-flow properties. When they are in laminar flow in a stirred vessel, motion in remote parts of the vessel where shear rates are low may become negligible or cease completely. To compensate for this behavior of slurries, large-diameter impellers or paddles are used, with $(D_a/D_T) > 0.6$, where D_T is the tank diameter. In some cases, for example, with some anchors, $D_a > 0.95 D_T$. Two or more paddles may be used in deep tanks to avoid stagnant regions in slurries.

In laminar flow ($N_{Re} < 10$), $N_p \propto 1/N_{Re}$ and $P \propto \mu N^2 D_a^3$. Since shear stress is proportional to rotational speed, shear stress can be increased at the same power consumption by increasing N proportionally to $D_a^{-3/2}$ as impeller diameter D_a is decreased.

Fluid circulation probably can be increased at the same power consumption and viscosity in laminar flow by increasing impeller diameter and decreasing rotational speed, but the relationship between Q , N , and D_a for laminar flow from turbines has not been determined.

As in the case of turbulent flow, then, small-diameter impellers ($D_a < D_T/3$) are useful for (1) rapid mixing of dry particles into liquids, (2) gas dispersion in slurries, (3) solid-particle deagglomeration, and (4) promoting mass transfer between solid and liquid phases. If stagnant regions are a problem, large impellers must be used and rotational speed and power increased to obtain the required results. Small continuous-processing equipment may be more economical than batch equipment in such cases.

Likewise, large-diameter impellers ($D_a > D_T/2$) are useful for (1) avoiding stagnant regions in slurries, (2) short mixing times to obtain uniformity throughout a vessel, (3) promotion of heat transfer, and (4) laminar continuous averaging of slurries.

Vortex Depth In an unbaffled vessel with an impeller rotating in the center, centrifugal force acting on the fluid raises the fluid level at the wall and lowers the level at the shaft. The depth and shape of such a vortex [Rieger, Dittl, and Novak, *Chem. Eng. Sci.*, **34**, 397 (1978)] depend on impeller and vessel dimensions as well as rotational speed.

Power Consumption of Impellers Power consumption is related to fluid density, fluid viscosity, rotational speed, and impeller diameter by plots of power number ($g_c P/\rho N^3 D_a^5$) versus Reynolds number ($D_a^2 N \rho/\mu$). Typical correlation lines for frequently used impellers operating in newtonian liquids contained in baffled cylindrical vessels are presented in Fig. 18-17. These curves may be used also

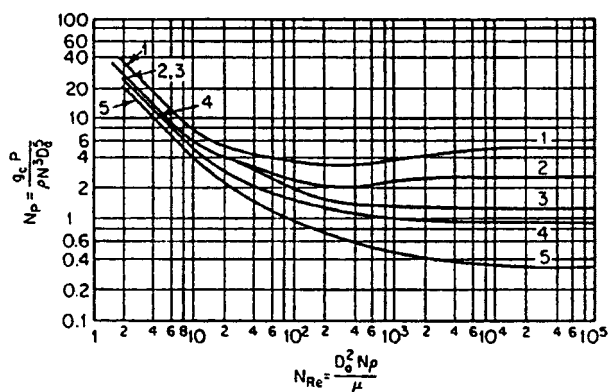


FIG. 18-17 Impeller power correlations: curve 1, six-blade turbine, $D_a/W_i = 5$, like Fig. 18-4 but with six blades, four baffles, each $D_T/12$; curve 2, vertical-blade, open turbine with six straight blades, $D_a/W_i = 8$, four baffles each $D_T/12$; curve 3, 45° pitched-blade turbine like Fig. 18-3 but with six blades, $D_a/W_i = 8$, four baffles, each $D_T/12$; curve 4, propeller, pitch equal to $2D_a$, four baffles, each $0.1D_T$, also same propeller in angular off-center position with no baffles; curve 5, propeller, pitch equal to D_a , four baffles each $0.1D_T$, also same propeller in angular off-center position as in Fig. 18-14 with no baffles. D_a = impeller diameter, D_T = tank diameter, g_c = gravitational conversion factor, N = impeller rotational speed, P = power transmitted by impeller shaft, W_i = impeller blade height, μ = viscosity of stirred liquid, and ρ = density of stirred mixture. Any set of consistent units may be used, but N must be rotations (rather than radians) per unit time. In the SI system, g_c is dimensionless and unity. [Curves 4 and 5 from Rushton, Costich, and Everett, *Chem. Eng. Prog.*, **46**, 395, 467 (1950), by permission; curves 2 and 3 from Bates, Fondy, and Corpstein, *Ind. Eng. Chem. Process Des. Dev.*, **2**, 310 (1963), by permission of the copyright owner, the American Chemical Society.]

for operation of the respective impellers in unbaffled tanks when the Reynolds number is 300 or less. When N_{Re} is greater than 300, however, the power consumption is lower in an unbaffled vessel than indicated in Fig. 18-17. For example, for a six-blade disc turbine with $D_T/D_a = 3$ and $D_a/W_i = 5$, $N_p = 1.2$ when $N_{Re} = 10^4$. This is only about one-fifth of the value of N_p when baffles are present.

Additional power data for other impeller types such as anchors, curved-blade turbines, and paddles in baffled and unbaffled vessels are available in the following references: Holland and Chapman, op. cit., chaps. 2, 4, Reinhold, New York, 1966; and Bates, Fondy, and Fenic, in Uhl and Gray, op. cit., vol. 1, chap. 3.

Power consumption for impellers in pseudoplastic, Bingham plastic, and dilatant non-newtonian fluids may be calculated by using the correlating lines of Fig. 18-17 if viscosity is obtained from viscosity-shear rate curves as described here. For a pseudoplastic fluid, viscosity decreases as shear rate increases. A Bingham plastic is similar to a pseudoplastic fluid but requires that a minimum shear stress be exceeded for any flow to occur. For a dilatant fluid, viscosity increases as shear rate increases.

The appropriate shear rate to use in calculating viscosity is given by one of the following equations when a propeller or a turbine is used (Bates et al., in Uhl and Gray, op. cit., vol. 1, p. 149):

For dilatant liquids,

$$\dot{\gamma} = 13N \left(\frac{D_a}{D_T} \right)^{0.5} \quad (18-6)$$

For pseudoplastic and Bingham plastic fluids,

$$\dot{\gamma} = 10N \quad (18-7)$$

where $\dot{\gamma}$ = average shear rate, s^{-1} .

The shear rate calculated from impeller rotational speed is used to identify a viscosity from a plot of viscosity versus shear rate determined with a capillary or rotational viscometer. Next N_{Re} is calculated, and N_p is read from a plot like Fig. 18-17.

DESIGN OF AGITATION EQUIPMENT

Selection of Equipment The principal factors which influence mixing-equipment choice are (1) the process requirements, (2) the flow properties of the process fluids, (3) equipment costs, and (4) construction materials required.

Ideally, the equipment chosen should be that of the lowest total cost which meets all process requirements. The total cost includes depreciation on investment, operating cost such as power, and maintenance costs. Rarely is any more than a superficial evaluation based on this principle justified, however, because the cost of such an evaluation often exceeds the potential savings that can be realized. Usually optimization is based on experience with similar mixing operations. Often the process requirements can be matched with those of a similar operation, but sometimes tests are necessary to identify a satisfactory design and to find the minimum rotational speed and power.

There are no satisfactory specific guides for selecting mixing equipment because the ranges of application of the various types of equipment overlap and the effects of flow properties on process performance have not been adequately defined. Nevertheless, what is frequently done in selecting equipment is described in the following paragraphs.

Top-Entering Impellers For vessels less than 1.8 m (6 ft) in diameter, a clamp- or flange-mounted, angular, off-center fluidfoil impeller with no baffles should be the initial choice for meeting a wide range of process requirements (Fig. 18-14). The vessel straight-side-height-to-diameter ratio should be 0.75 to 1.5, and the volume of stirred liquid should not exceed 4 m^3 (about 1000 gal).

For suspension of free-settling particles, circulation of pseudoplastic slurries, and heat transfer or mixing of miscible liquids to obtain uniformity, a speed of 350 or 420 r/min should be stipulated. For dispersion of dry particles in liquids or for rapid initial mixing of liquid reactants in a vessel, an 1150- or 1750- r/min propeller should be used at a distance $D_T/4$ above the vessel bottom. A second propeller can be added to the shaft at a depth D_a below the liquid surface if the submergence of floating liquids or particulate solids is otherwise inadequate. Such propeller mixers are readily available up to 2.2 kW (3 hp) for off-center sloped-shaft mounting.

Propeller size, pitch, and rotational speed may be selected by model tests, by experience with similar operations, or, in a few cases, by published correlations of performance data such as mixing time or heat transfer. The propeller diameter and motor power should be the minimum that meets process requirements.

If agitation is required for a vessel less than 1.8 m (6 ft) in diameter and the same operations will be scaled up to a larger vessel ultimately, the equipment type should be the same as that expected in the larger vessel.

Axial-Flow Fluidfoil Impellers For vessel volumes of 4 to 200 m^3 (1000 to 50,000 gal), a turbine mixer mounted coaxially within the vessel with four or more baffles should be the initial choice. Here also the vessel straight-side-height-to-diameter ratio should be 0.75 to 1.5. Four vertical baffles should be fastened perpendicularly to the vessel wall with a gap between baffle and wall equal to $D_T/24$ and a radial baffle width equal to $D_T/12$.

For suspension of rapidly settling particles, the impeller turbine diameter should be $D_T/3$ to $D_T/2$. A clearance of less than one-seventh of the fluid depth in the vessel should be used between the lower edge of the turbine blade tips and the vessel bottom. As the viscosity of a suspension increases, the impeller diameter should be increased. This diameter may be increased to $0.6 D_T$ and a second impeller added to avoid stagnant regions in pseudoplastic slurries. Moving the baffles halfway between the impeller periphery and the vessel wall will also help avoid stagnant fluid near the baffles.

As has been shown, power consumption is decreased and turbine discharge rate is increased as impeller diameter is increased at constant torque (in the completely turbulent regime). This means that for a stipulated discharge rate, more efficient operation is obtained (lower power and torque) with a relatively large impeller operating at a relatively low speed ($N \propto D_a^{-3}$). Conversely, if power is held constant, decreasing impeller diameter results in increasing peripheral velocity and decreasing torque. Thus at a stipulated power level the rapid, effi-

cient initial mixing of reactants identified with high peripheral velocity can be achieved by a relatively small impeller operating at a relatively high speed ($N \propto D_a^{-3}$).

For circulation and mixing to obtain uniformity, the impeller should be located at one-third of the liquid depth above the vessel bottom unless rapidly settling material or a need to stir a nearly empty vessel requires a lower impeller location.

Side-Entering Impellers For vessels greater than 4 m^3 (1000 gal), a side-entering propeller agitator (Fig. 18-9) may be more economical than a top-mounted impeller on a centered vertical shaft. For vessels greater than 38 m^3 (10,000 gal), the economic attractiveness of side-entering impellers increases. For vessels larger than 380 m^3 (100,000 gal), units may be as large as 56 kW (75 hp), and two or even three may be installed in one tank. For the suspension of slow-settling particles or the maintenance of uniformity in a viscous slurry of small particles, the diameter and rotational speed of a side-entering agitator must be selected on the basis of model tests or experience with similar operations.

When abrasive solid particles must be suspended, maintenance costs for the submerged shaft seal of a side-entering propeller may become high enough to make this type of mixer an uneconomical choice.

Jet Mixers Continuous recycle of the contents of a tank through an external pump so arranged that the pump discharge stream appropriately reenters the vessel can result in a flow pattern in the tank which will produce a slow mixing action [Fossett, *Trans. Inst. Chem. Eng.*, **29**, 322 (1951)].

Large Tanks Most large vessels (over 4 m^3) require a heavy-duty drive. About two-thirds of the mixing requirements industrially involve flow, circulation, and other types of pumping capacity requirements, including such applications as blending and solid suspension. There often is no requirement for any marked level of shear rate, so the use of the fluidfoil impellers is most common. If additional shear rate is required over what can be provided by the fluidfoil impeller, the axial-flow turbine (Fig. 18-3) is often used, and if extremely high shear rates are required, the flat-blade turbine (Rushton turbine) (Fig. 18-4) is required. For still higher shear rates, there is an entire variety of high-shear-rate impellers, typified by that shown in Fig. 18-10 that are used.

The fluidfoil impellers in large tanks require only two baffles, but three are usually used to provide better flow pattern asymmetry. These fluidfoil impellers provide a true axial flow pattern, almost as though there was a draft tube around the impeller. Two or three or more impellers are used if tanks with high D/T ratios are involved. The fluidfoil impellers do not vortex vigorously even at relatively low coverage so that if gases or solids are to be incorporated at the surface, the axial-flow turbine is often required and can be used in combination with the fluidfoil impellers also on the same shaft.

BLENDING

If the blending process is between two or more fluids with relatively low viscosity such that the blending is not affected by fluid shear rates, then the difference in blend time and circulation between small and large tanks is the only factor involved. However, if the blending involves wide disparities in the density of viscosity and surface tension between the various phases, then a certain level of shear rate may be required before blending can proceed to the required degree of uniformity.

The role of viscosity is a major factor in going from the turbulent regime, through the transition region, into the viscous regime and the change in the role of energy dissipation discussed previously. The role of non-newtonian viscosities comes into the picture very strongly since that tends to markedly change the type of influence of impellers and determines the appropriate geometry that is involved.

There is the possibility of misinterpretation of the difference between circulation time and blend time. Circulation time is primarily a function of the pumping capacity of the impeller. For axial-flow impellers, a convenient parameter, but not particularly physically accurate, is to divide the pumping capacity of the impeller by the cross-sectional area of the tank to give a superficial liquid velocity.

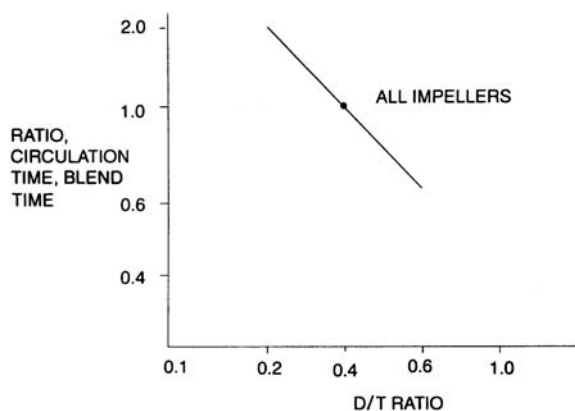


FIG. 18-18 Effect of D/T ratio on any impeller on the circulation time and the blend time.

This is sometimes used by using the total volume of flow from the impeller including entrainment of the tank to obtain a superficial liquid velocity.

As the flow from an impeller is increased from a given power level, there will be a higher fluid velocity and therefore a shorter circulation time. This holds true when dealing with any given impeller. This is shown in Fig. 18-18, which shows that circulation time versus D/T decreases. A major consideration is when increasing D/T becomes too large and actually causes the curve to reverse. This occurs somewhere around $0.45, \pm 0.05$, so that using impellers of D/T ratios of 0.6 to 0.8 is often counterproductive for circulation time. They may be useful for the blending or motion of pseudoplastic fluids.

When comparing different impeller types, an entirely different phenomenon is important. In terms of circulation time, the phenomena shown in Figs. 18-18 and 18-19 still apply with the different impellers shown in Fig. 18-5. When it comes to blending another factor enters the picture. When particles A and B meet each other as a result of shear rates, there has to be sufficient shear stress to cause A and B to blend, react, or otherwise participate in the process.

It turns out that in low-viscosity blending the actual result does depend upon the measuring technique used to measure blend time. Two common techniques, which do not exhaust the possibilities in reported studies, are to use an acid-base indicator and inject an acid or base into the system that will result in a color change. One can also put a dye into the tank and measure the time for color to arrive at uniformity. Another system is to put in a conductivity probe and inject a salt

or other electrolyte into the system. With any given impeller type at constant power, the circulation time will increase with the D/T ratio of the impeller. Figure 18-18 shows that both circulation time and blend time decrease as D/T increases. The same is true for impeller speed. As impeller speed is increased with any impeller, blend time and circulation time are decreased (Fig. 18-19).

However, when comparing different impeller types at the same power level, it turns out that impellers that have a higher pumping capacity will give decreased circulation time, but all the impellers, regardless of their pumping efficiency, give the same blend time at the same power level and same diameter. This means that circulation time must be combined with shear rate to carry out a blending experiment which involves chemical reactions or interparticle mixing (Fig. 18-20).

For other situations in low-viscosity blending, the fluid in tanks may become stratified. There are few studies on that situation, but Oldshue (op. cit.) indicates the relationship between some of the variables. The important difference is that blend time is inversely proportional to power, not impeller flow, so that the exponents are quite different for a stratified tank. This situation occurs more frequently in the petroleum industry, where large petroleum storage tanks become stratified either by filling techniques or by temperature fluctuations.

There is a lot of common usage of the terms *blend time*, *mixing time*, and *circulation time*. There are differences in concept and interpretation of these different "times." For any given experiment, one must pick a definition of *blend time* to be used. As an example, if one is measuring the fluctuation of concentration after an addition of material to the tank, then one can pick an arbitrary definition of blending such as reducing the fluctuations below a certain level. This often is chosen as a fluctuation equal to 5% of the original fluctuation when the feed material is added. This obviously is a function of the size of the probe used to measure these fluctuations, which often is on the order of 500 to 1000 μm .

At the micro-scale level, there really is no way to measure concentration fluctuations. Resort must be made to other qualitative interpretation of results for either a process or a chemical reaction study.

High-Viscosity Systems All axial-flow impellers become radial flow as Reynolds numbers approach the viscous region. Blending in the transition and low-viscosity system is largely a measure of fluid motion throughout the tank. For close-clearance impellers, the anchor and helical impellers provide blending by having an effective action at the tank wall, which is particularly suitable for pseudoplastic fluids.

Figure 18-21 gives some data on the circulation time of the helical impeller. It has been observed that it takes about three circulation times to get one blend time being the visual uniformity of a dye added to the material. This is a macro-scale blending definition.

Axial-flow turbines are often used in blending pseudoplastic materials, and they are often used at relatively large D/T ratios, from 0.5 to 0.7, to adequately provide shear rate in the majority of the batch particularly in pseudoplastic material. These impellers develop a flow

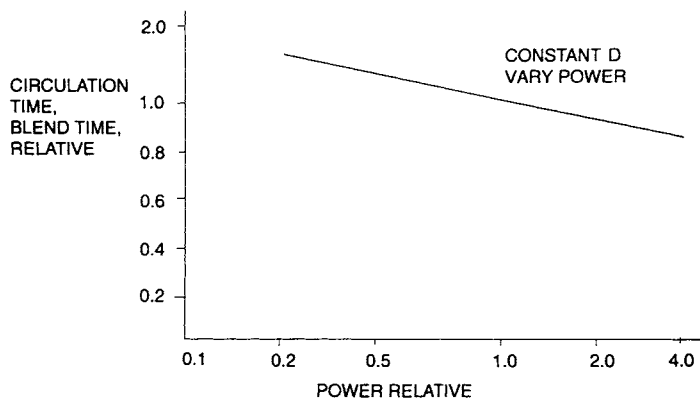


FIG. 18-19 Effect of impeller power for the same diameter on circulation time and blend time for a particular impeller.

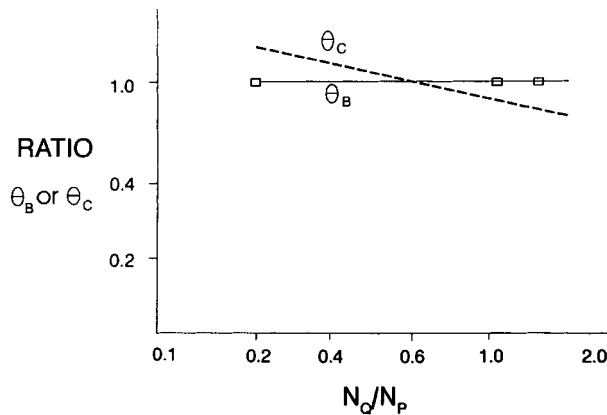


FIG. 18-20 At constant power and constant impeller diameter, three different impellers give the same blend time but different circulation times.

pattern which may or may not encompass an entire tank, and these areas of motion are sometimes referred to as *caverns*. Several papers describe the size of these caverns relative to various types of mixing phenomena. An effective procedure for the blending of pseudoplastic fluids is given in Oldshue (op. cit.).

Chemical Reactions Chemical reactions are influenced by the uniformity of concentration both at the feed point and in the rest of the tank and can be markedly affected by the change in overall blend time and circulation time as well as the micro-scale environment. It is possible to keep the ratio between the power per unit volume at the impeller and in the rest of the tank relatively similar on scale-up, but many details need to be considered when talking about the reaction conditions, particularly where they involve selectivity. This means that reactions can take different paths depending upon chemistry and fluid mechanics, which is a major consideration in what should be examined. The method of introducing the reagent stream can be projected in several different ways depending upon the geometry of the impeller and feed system.

Chemical reactions normally occur in the micro-scale range. In turbulent flow, almost all of the power dissipation occurs eventually in the micro-scale regime because that is the only place where the scale of the fluid fluctuations is small enough that viscous shear stress exists. At approximately 100 μm , the fluid does not know what type of impeller is used to generate the power; continuing down to 10 μm and, even further, to chemical reactions, the actual impeller type is not a major vari-

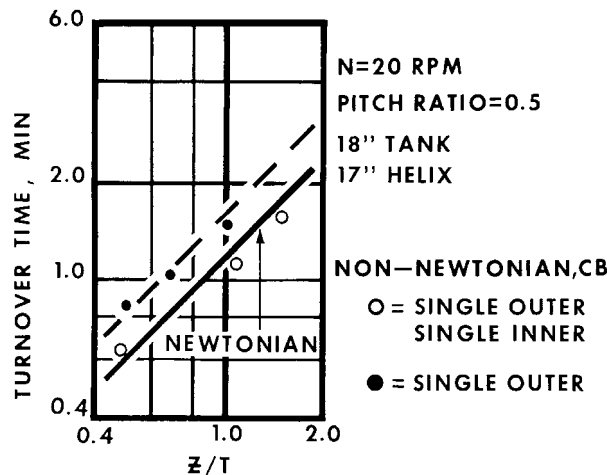


FIG. 18-21 Effect of impeller speed on circulation time for a helical impeller in the Reynolds number arranged less than 10.

able as long as the proper macro-scale regime has been provided throughout the entire tank. The intensity of the mixing environment in the micro-scale regime can be related to a series of variables in an increasing order of complexity. Since all of the power is ultimately dissipated in the micro-scale regime, the power per unit volume throughout the tank is one measure of the overall measure of micro-scale mixing and the power dissipation at individual volumes in the tank is another way of expressing the influence. In general, the power per unit volume dissipated around an impeller zone can be 100 times higher than the power dissipated throughout the remainder of the tank.

The next level of complexity is to look at the rms velocity fluctuation, which is typically 50 percent of the mean velocity around the impeller zone and about 5 percent of the mean velocity in the rest of the vessel. This means that the feed introduction point for either a single reactant or several reactants can be of extreme importance. It seems that the selectivity of competing or consecutive chemical reactions can be a function of the rms velocity fluctuations in the feed point if the chemical reactants remain constant and involve an appropriate relationship to the time between the rms velocity fluctuations. There are three common ways of introducing reagents into a mixing vessel. One is to let them drip on the surface. The second is to use some type of introduction pipe to bring the material into various parts of the vessel. The third is to purposely bring them in and around the impeller zone. Generally, all three methods have to be tried before determining the effect of feed location.

Since chemical reactions are on a scale much below 1 μm , and it appears that the Komolgoroff scale of isotropic turbulence turns out to be somewhere between 10 and 30 μm , other mechanisms must play a role in getting materials in and out of reaction zones and reactants in and out of those zones. One cannot really assign a shear rate magnitude to the area around a micro-scale zone, and it is primarily an environment that particles and reactants witness in this area.

The next level of complexity looks at the kinetic energy of turbulence. There are several models that are used to study the fluid mechanics, such as the K ϵ model. One can also put the velocity measurements through a spectrum analyzer to look at the energy at various wave numbers.

In the viscous regime, chemical reactants become associated with each other through viscous shear stresses. These shear stresses exist at all scales (macro to micro) and until the power is dissipated continuously through the entire spectrum. This gives a different relationship for power dissipation than in the case of turbulent flow.

SOLID-LIQUID SYSTEMS

The most-used technique to study solid suspension, as documented in hundreds of papers in the literature, is called the *speed for just suspension*, N_{js} . The original work was done in 1958 by Zwietering and this is still the most extensive range of variables, although other investigators have added to it considerably.

This particular technique is suitable only for laboratory investigation using tanks that are transparent and well illuminated. It does not lend itself to evaluation of the opaque tanks, nor is it used in any study of large-scale tanks in the field. It is a very minimal requirement for uniformity, and definitions suggested earlier are recommended for use in industrial design.

Some Observations on the Use of N_{js} With D/T ratios of less than 0.4, uniformity throughout the rest of the tank is minimal. In D/T ratios greater than 0.4, the rest of the tank has a very vigorous fluid motion with a marked approach to complete uniformity before N_{js} is reached.

Much of the variation in N_{js} can be reduced by using P_{js} , which is the power in the just-suspended state. This also gives a better feel for the comparison of various impellers based on the energy requirement rather than speed, which has no economic relevance.

The overall superficial fluid velocity, mentioned earlier, should be proportional to the settling velocity of the solids if that were the main mechanism for solid suspension. If this were the case, the requirement for power if the settling velocity were doubled should be eight times. Experimentally, it is found that the increase in power is more nearly four times, so that some effect of the shear rate in macro-scale turbulence is effective in providing uplift and motion in the system.

Picking up the solids at the bottom of the tank depends upon the eddies and velocity fluctuations in the lower part of the tank and is a different criterion from the flow pattern required to keep particles suspended and moving in various velocity patterns throughout the remainder of the vessel. This leads to the variables in the design equation and a relationship that is quite different when these same variables are studied in relation to complete uniformity throughout the mixing vessel.

Another concern is the effect of multiple particle sizes. In general, the presence of fine particles will affect the requirements of suspension of larger particles. The fine particles act largely as a potential viscosity-increasing agent and give a similar result to what would happen if the viscosity of the continuous phase were increased.

Another phenomenon is the increase in power required with percent solids, which makes a dramatic change at approximately 40 percent by volume, and then dramatically changes again as we approach the ultimate weight percent of settled solids. This phenomenon is covered by Oldshue (op. cit.), who describes conditions required for mixing slurries in the 80 to 100 percent range of the ultimate weight percent of settled solids.

Solids suspension in general is not usually affected by blend time or shear-rate changes in the relatively low to medium solids concentration in the range from 0 to 40 percent by weight. However, as solids become more concentrated, the effect of solids concentration on power required gives a change in criterion from the settling velocity of the individual particles in the mixture to the apparent viscosity of the more concentrated slurry. This means that we enter into an area where the blending of non-newtonian fluid regions affects the shear rates and plays a marked role.

The suspension of a single solid particle should depend primarily on the upward velocity at a given point and also should be affected by the uniformity of this velocity profile across the entire tank cross section. There are upward velocities in the tank and there also must be corresponding downward velocities.

In addition to the effect of the upward velocity on a settling particle, there is also the random motion of the micro-scale environment, which does not affect large particles very much but is a major factor in the concentration and uniformity of particles in the transition and micro-scale size range.

Using a draft tube in the tank for solids suspension introduces another, different set of variables. There are other relationships that are very much affected by scale-up in this type of process, as shown in Fig. 18-22. Different scale-up problems exist whether the impeller is pumping up or down within the draft tube.

Solid Dispersion If the process involves the dispersion of solids in a liquid, then we may either be involved with breaking up agglomerates or possibly physically breaking or shattering particles that have a low cohe-

sive force between their components. Normally, we do not think of breaking up ionic bonds with the shear rates available in mixing machinery.

If we know the shear stress required to break up a particle, we can then determine the shear rate required from the machinery by various viscosities with the equation:

$$\text{Shear stress} = \text{viscosity} (\text{shear rate})$$

The shear rate available from various types of mixing and dispersion devices is known approximately and also the range of viscosities in which they can operate. This makes the selection of the mixing equipment subject to calculation of the shear stress required for the viscosity to be used.

In the equation referred to above, it is assumed that there is 100 percent transmission of the shear rate in the shear stress. However, with the slurry viscosity determined essentially by the properties of the slurry, at high concentrations of slurries there is a slippage factor. Internal motion of particles in the fluids over and around each other can reduce the effective transmission of viscosity efficiencies from 100 percent to as low as 30 percent.

Animal cells in biotechnology do not normally have tough skins like those of fungal cells and they are very sensitive to mixing effects. Many approaches have been and are being tried to minimize the effect of increased shear rates on scale-up. These include encapsulating the organism in or on microparticles and/or conditioning cells selectively to shear rates. In addition, traditional fermentation processes have maximum shear-rate requirements in which cells become progressively more and more damaged until they become motile.

Solid-Liquid Mass Transfer There is potentially a major effect of both shear rate and circulation time in these processes. The solids can either be fragile or rugged. We are looking at the slip velocity of the particle and also whether we can break up agglomerates of particles which may enhance the mass transfer. When the particles become small enough, they tend to follow the flow pattern, so the slip velocity necessary to affect the mass transfer becomes less and less available.

What this shows is that, from the definition of off-bottom motion to complete uniformity, the effect of mixer power is much less than from going to on-bottom motion to off-bottom suspension. The initial increase in power causes more and more solids to be in active communication with the liquid and has a much greater mass-transfer rate than that occurring above the power level for off-bottom suspension, in which slip velocity between the particles of fluid is the major contributor (Fig. 18-23).

Since there may well be chemical or biological reactions happening on or in the solid phase, depending upon the size of the process participants, macro- or micro-scale effects may or may not be appropriate to consider.

In the case of living organisms, their access to dissolved oxygen throughout the tank is of great concern. Large tanks in the fermentation industry often have a Z/T ratio of 2:1 to 4:1; thus, top-to-bottom blending can be a major factor. Some biological particles are facultative and can adapt and reestablish their metabolisms at different dissolved-oxygen levels. Other organisms are irreversibly destroyed by sufficient exposure to low dissolved-oxygen levels.

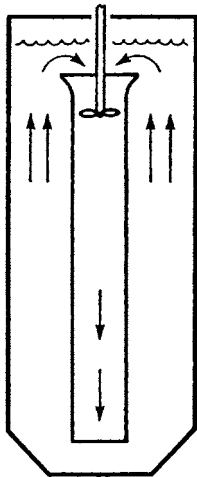


FIG. 18-22 Typical draft tube circulator, shown here for down-pumping mode for the impeller in the draft tube.

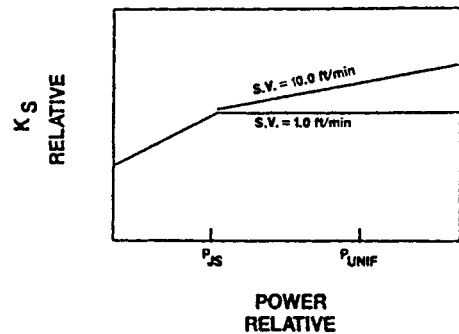


FIG. 18-23 Relative change in solid-liquid mass-transfer ratio with three different suspension levels, i.e., on-bottom motion, off-bottom motion, and complete uniformity.

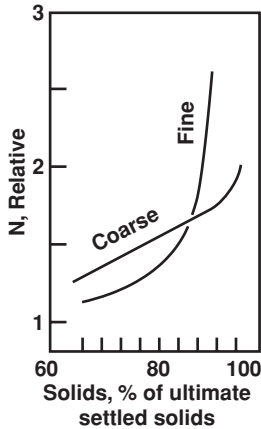


FIG. 18-24 Effect of percent solids on speed required for complete motion throughout the tank on two different grind sizes.

Leaching and Extraction of Mineral Values from High Concentration of Solids A uranium plant had 10 large slurry tanks for leaching and extraction (approximately 14 m in diameter and 14 m high). They had about 14,000-m³ capacity.

In a study designed to modify the leaching operation, it was desired to look at two different grind sizes of ore, one labeled fine grind and the other labeled coarse grind. Also, the effect of various mixer designs and power levels on the extraction efficiency to arrive at the overall economic optimum was examined. Figure 18-24 shows the results of a pilot study in which the impeller speed for a given impeller and tank geometry was measured for complete overall motion throughout the slurry for both the fine and coarse grinds at various weight percent solids. As can be seen in the figure, the fine material required lower horsepower at low weight percent solids while the coarse grind required less horsepower up near the ultimate settled solids weight percentage.

The interpretation is that at lower percent solids, the viscosity of the fine grind aided suspension whereas at higher percent solids, the higher viscosity of the fine material was detrimental to fluid mixing.

A mixing viscosimeter was used to measure the viscosity of the slurry. Figure 18-25 shows the viscosity of the fine and coarse slurries.

By combining the data from Figs. 18-24 and 18-25 into Fig. 18-26, it is seen that there is a correlation between the impeller speed required and the viscosity of the slurry regardless of whether the

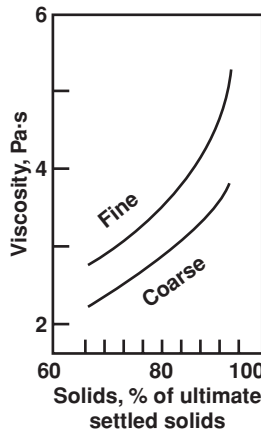


FIG. 18-25 Viscosity of fine grind and coarse grind at various weight percent solids.

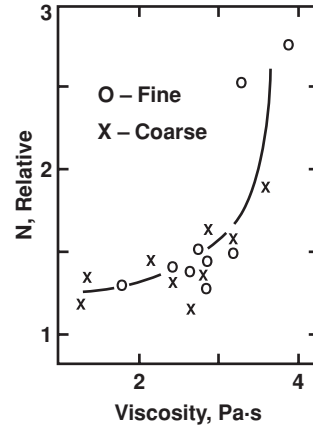


FIG. 18-26 Correlation of impeller speed vs. viscosity of the pulp including both fine and coarse grind experimental data points.

material was finely or coarsely ground. This illustrates that viscosity is a key parameter in the process design for solid-liquid slurries.

The overall process economics examined the extraction rate as a function of power, residence time, and grind size. The full-scale design possibilities were represented in the form of Table 18-2, which were accompanied by other charts that gave different heights of suspension in the tank for the three different particle size fractions: fine, medium, and coarse. These various combinations of power levels also gave various blending efficiencies and had different values of the effective residence time used in a system.

By calculating the residence times of the various solids in the tank and relating them to their corresponding extraction curves, the total uranium extraction for the entire train of mixers was estimated. The cost of the various mixer options, the production efficiency net result, and the cost of the installation and tank design could be combined to yield the economic optimum for the plant.

GAS-LIQUID SYSTEMS

Gas-Liquid Dispersion This involves physical dispersion of gas bubbles by the impeller, and the effect of gas flow on the impeller.

The observation of the physical appearance of a tank undergoing gas-liquid mass transfer can be helpful but is not a substitute for mass-transfer data on the actual process. The mixing vessel can have four regimes of visual comparisons between gas bubbles and flow patterns. A helpful parameter is the ratio between the power given up by the gas phase and the power introduced by the mixing impeller. In general, if the power in the gas stream (calculated as the expansion energy from the gas expanding from the sparging area to the top of the tank, shown in Fig. 18-27) is greater, there will be considerable blurring and entrainment of liquid drops by a very violent explosion of gas bubbles at the surface. If the power level is more than the expanding gas energy, then the surface action will normally be very coalescent and uniform by comparison, and the gas will be reasonably well distributed throughout the remainder of the tank. With power levels up to 10 to 100 times the

TABLE 18-2 Four Different Selections of Mixers with Different Mixing Characteristics on 14,000 ft³ of Leach Tanks

Process factor	Proposal for Revised Installation		
	Relative torque	Motor kW	D/T (dual)
1.2	1.0	300	0.5
1.0	1.0	250	0.5
0.8	0.9	200	0.5
0.7	1.0	150	0.6

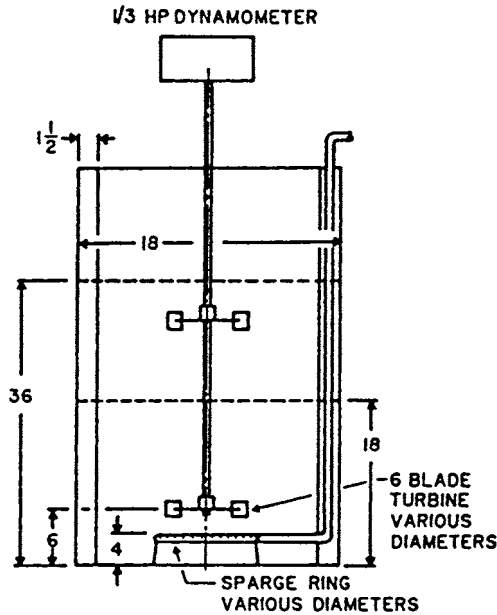


FIG. 18-27 Typical arrangement of Rushton radial-flow R100 flat-blade turbine with typical sparge ring for gas-liquid mass transfer.

gas energy, the impeller will cause a more uniform and vigorous dispersion of the gas bubbles and smaller gas bubbles in the vessel.

In the 1960s and before, most gas-liquid operations were conducted using flat-blade turbines as shown in Fig. 18-4. These impellers required input of approximately three times the energy in the gas stream before they completely control the flow pattern. This was usually the case, and the mass-transfer characteristics were comparable to what would be expected. One disadvantage of the radial-flow impeller is that it is a very poor blending device so blend time is very long compared to that in pilot-scale experiments and compared to the fluidfoil impeller types often used currently. Using curvature of the blades to modify the tendency of gas bubbles to streamline the back of the flat-blade turbine gives a different characteristic to the power drawn by the impeller at a given gas rate compared to no gas rate, but it seems to give quite similar mass transfer at power levels similar to those of the flat-blade design. In order to improve the blending and solid-suspension characteristics, fluidfoil impellers (typified by the A315, Fig. 18-28) have been introduced in recent years and they have many of the advantages and some of the disadvantages of the flat-blade turbine. These impellers typically have a very high solidity ratio, on the order of 0.85 or more, and produce a strong axial downflow at low gas rate. As the gas rate increases, the flow pattern becomes more radial due to the upflow of the gas counteracting the downward flow of the impeller.

Mass-transfer characteristics on large-scale equipment seem to be quite similar, but the fluidfoil impellers tend to release a larger-diameter bubble than is common with the radial-flow turbines. The blend time is one-half or one-third as long, and solid-suspension characteristics are better so that there have been notable improved process results with these impellers. This is particularly true if the process requires better blending and there is solid suspension. If this is not the case, the results from these impellers can be negative compared to radial-flow turbines.

It is very difficult to test these impellers on a small scale, since they provide better blending on a pilot scale where blending is already very effective compared to the large scale. Caution is recommended if it is desirable to study these impellers in pilot-scale equipment.

Gas-Liquid Mass Transfer Gas-liquid mass transfer normally is correlated by means of the mass-transfer coefficient $K_g a$ versus power level at various superficial gas velocities. The superficial gas velocity is



FIG. 18-28 An impeller designed for gas-liquid dispersion and mass transfer of the fluidfoil type, i.e., A315.

the volume of gas at the average temperature and pressure at the mid-point in the tank divided by the area of the vessel. In order to obtain the partial-pressure driving force, an assumption must be made of the partial pressure in equilibrium with the concentration of gas in the liquid. Many times this must be assumed, but if Fig. 18-29 is obtained in the pilot plant and the same assumption principle is used in evaluating the mixer in the full-scale tank, the error from the assumption is limited.

In the plant-size unit, Fig. 18-29 must be translated into a mass-transfer-rate curve for the particular tank volume and operating condition selected. Every time a new physical condition is selected, a different curve similar to that of Fig. 18-30 is obtained.

Typical exponents on the effect of power and gas rate on $K_g a$ tend to be around 0.5 for each variable, ± 0.1 .

Viscosity markedly changes the picture and, usually, increasing viscosity lowers the mass-transfer coefficient. For the common application of waste treating and for some of the published data on biological slurries, data for $k_L a$ (shown in Fig. 18-31) is obtained in the literature. For a completely new gas or liquid of a liquid slurry system, Fig. 18-29 must be obtained by an actual experiment.

Liquid-Gas-Solid Systems Many gas-liquid systems contain solids that may be the ultimate recipient of the liquid-gas-solid mass transfer entering into the process result. Examples are biological

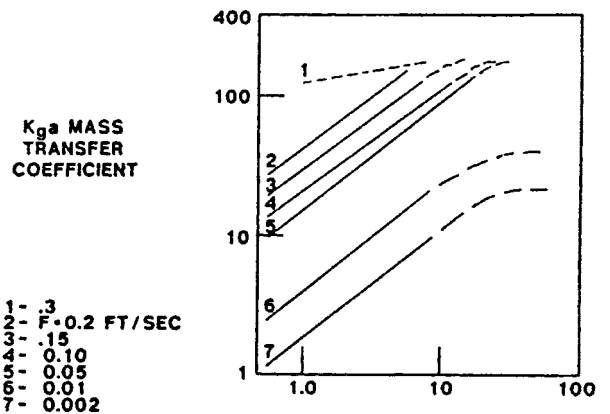


FIG. 18-29 Typical curve for mass transfer coefficient $K_g a$ as a function of mixer power and superficial gas velocity.

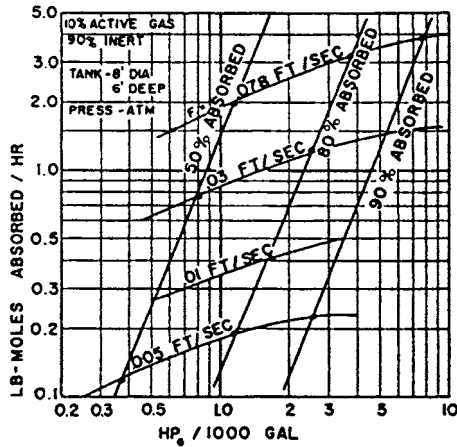


FIG. 18-30 Example of a specific chart to analyze the total mass-transfer rate in a particular tank under a process condition obtained from basic $K_L a$ data shown in Fig. 18-28.

processes in which the biological solids are the user of the mass transfer of the mixing-flow patterns, various types of slurries reactors in which the solids either are being reactive or there may be extraction or dissolving taking place, or there may be polymerization or precipitation of solids occurring.

Normally there must be a way of determining whether the mass-transfer rate with the solids is the key controlling parameter or the gas-liquid mass transfer rate.

In general, introduction of a gas stream to a fluid will increase the blend time because the gas-flow patterns are counterproductive to the typical mixer-flow patterns. In a similar vein, the introduction of a gas stream to a liquid-solid suspension will decrease the suspension uniformity because the gas-flow pattern is normally counterproductive to the mixer-flow pattern. Many times the power needed for the gas-liquid mass transfer is higher than the power needed for solid suspension, and the effect of the gas flow on the solid suspensions are of little concern. On the other hand, if power levels are relatively low and solid-suspension characteristics are critical—examples being the case of activated sludge reactors in the waste-treating field or biological solid reactors in the hydrometallurgical field—then the effect of the gas-flow pattern of the mixing system can be quite critical to the overall design.

Another common situation is batch hydrogenation, in which pure hydrogen is introduced to a relatively high pressure reactor and a decision must be made to recycle the unabsorbed gas stream from the top of the reactor or use a vortexing mode for an upper impeller to incorporate the gas from the surface.

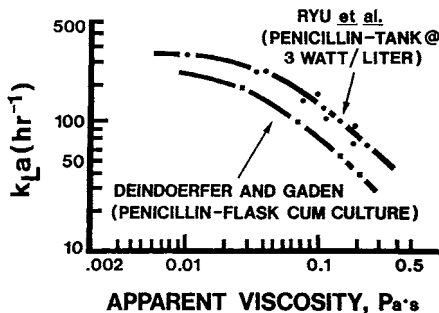


FIG. 18-31 Usually, the gas-liquid mass-transfer coefficient, $K_L a$, is reduced with increased viscosity. This shows the effect of increased concentration of microbial cells in a fermentation process.

Loop Reactors For some gas-liquid-solid processes, a recirculating loop can be an effective reactor. These involve a relatively high horsepower pumping system and various kinds of nozzles, baffles, and turbulence generators in the loop system. These have power levels anywhere from 1 to 10 times higher than the power level in a typical mixing reactor, and may allow the retention time to be less by a factor of 1 to 10.

LIQUID-LIQUID CONTACTING

Emulsions Almost every shear rate parameter affects liquid-liquid emulsion formation. Some of the effects are dependent upon whether the emulsion is both dispersing and coalescing in the tank, or whether there are sufficient stabilizers present to maintain the smallest droplet size produced for long periods of time. Blend time and the standard deviation of circulation times affect the length of time it takes for a particle to be exposed to the various levels of shear work and thus the time it takes to achieve the ultimate small particle size desired.

The prediction of drop sizes in liquid-liquid systems is difficult. Most of the studies have used very pure fluids as two of the immiscible liquids, and in industrial practice there almost always are other chemicals that are surface-active to some degree and make the prediction of absolute drop sizes very difficult. In addition, techniques to measure drop sizes in experimental studies have all types of experimental and interpretation variations and difficulties so that many of the equations and correlations in the literature give contradictory results under similar conditions. Experimental difficulties include dispersion and coalescence effects, difficulty of measuring actual drop size, the effect of visual or photographic studies on where in the tank you can make these observations, and the difficulty of using probes that measure bubble size or bubble area by light or other sample transmission techniques which are very sensitive to the concentration of the dispersed phase and often are used in very dilute solutions.

It is seldom possible to specify an initial mixer design requirement for an absolute bubble size prediction, particularly if coalescence and dispersion are involved. However, if data are available on the actual system, then many of these correlations could be used to predict relative changes in drop size conditions with changes in fluid properties or impeller variables.

STAGewise EQUIPMENT: MIXER-SETTLERS

Introduction Insoluble liquids may be brought into direct contact to cause transfer of dissolved substances, to allow transfer of heat, and to promote chemical reaction. This subsection concerns the design and selection of equipment used for conducting this type of liquid-liquid contact operation.

Objectives There are four principal purposes of operations involving the direct contact of immiscible liquids. The purpose of a particular contact operation may involve any one or any combination of the following objectives:

1. *Separation of components in solution.* This includes the ordinary objectives of liquid extraction, in which the constituents of a solution are separated by causing their unequal distribution between two insoluble liquids, the washing of a liquid with another to remove small amounts of a dissolved impurity, and the like. The theoretical principles governing the phase relationships, material balances, and number of ideal stages or transfer units required to bring about the desired changes are to be found in Sec. 15. Design of equipment is based on the quantities of liquids and the efficiency and operating characteristics of the type of equipment selected.
2. *Chemical reaction.* The reactants may be the liquids themselves, or they may be dissolved in the insoluble liquids. The kinetics of this type of reaction are treated in Sec. 4.
3. *Cooling or heating a liquid by direct contact with another.* Although liquid-liquid-contact operations have not been used widely for heat transfer alone, this technique is one of increasing interest. Applications also include cases in which chemical reaction or liquid extraction occurs simultaneously.
4. *Creating permanent emulsions.* The objective is to disperse one liquid within another in such finely divided form that separation

by settling either does not occur or occurs extremely slowly. The purpose is to prepare the emulsion. Neither extraction nor chemical reaction between the liquids is ordinarily sought.

Liquid-liquid contacting equipment may be generally classified into two categories: **stagewise** and **continuous (differential)** contact.

The function of a stage is to contact the liquids, allow equilibrium to be approached, and to make a mechanical separation of the liquids. The contacting and separating correspond to mixing the liquids, and settling the resulting dispersion; so these devices are usually called **mixer-settlers**. The operation may be carried out in batch fashion or with continuous flow. If batch, it is likely that the same vessel will serve for both mixing and settling, whereas if continuous, separate vessels are usually but not always used.

Mixer-Settler Equipment The equipment for extraction or chemical reaction may be classified as follows:

- I. Mixers
 - A. Flow or line mixers
 1. Mechanical agitation
 2. No mechanical agitation
 - B. Agitated vessels
 1. Mechanical agitation
 2. Gas agitation
- II. Settlers
 - A. Nonmechanical
 1. Gravity
 2. Centrifugal (cyclones)
 - B. Mechanical (centrifuges)
 - C. Settler auxiliaries
 1. Coalescers
 2. Separator membranes
 3. Electrostatic equipment

In principle, at least, any mixer may be coupled with any settler to provide the complete stage. There are several combinations which are especially popular. Continuously operated devices usually, but not always, place the mixing and settling functions in separate vessels. Batch-operated devices may use the same vessel alternately for the separate functions.

Flow or Line Mixers

Definition Flow or line mixers are devices through which the liquids to be contacted are passed, characterized principally by the very small time of contact for the liquids. They are used only for continuous operations or semibatch (in which one liquid flows continuously and the other is continuously recycled). If holding time is required for extraction or reaction, it must be provided by passing the mixed liquids through a vessel of the necessary volume. This may be a long pipe of large diameter, sometimes fitted with segmental baffles, but frequently the settler which follows the mixer serves. The energy for mixing and dispersing usually comes from pressure drop resulting from flow.

There are many types, and only the most important can be mentioned here. [See also Hunter, in Dunstan (ed.), *Science of Petroleum*, vol. 3, Oxford, New York, 1938, pp. 1779–1797.] They are used fairly extensively in treating petroleum distillates, in vegetable-oil refining, in extraction of phenol-bearing coke-oven liquors, in some metal extractions, and the like. Kalichevsky and Kobe (*Petroleum Refining with Chemicals*, Elsevier, New York, 1956) discuss detailed application in the refining of petroleum.

Jet Mixers These depend upon impingement of one liquid on the other to obtain a dispersion, and one of the liquids is pumped through a small nozzle or orifice into a flowing stream of the other. Both liquids are pumped. They can be used successfully only for liquids of low interfacial tension. See Fig. 18-32 and also Hunter and Nash [*Ind. Chem.*, **9**, 245, 263, 317 (1933)]. Treybal (*Liquid Extraction*, 2d ed., McGraw-Hill, New York, 1963) describes a more elaborate device. For a study of the extraction of antibiotics with jet mixers, see Anneskova and Boiko, *Med. Prom. SSSR*, **13**(5), 26 (1959). Insonation with ultrasound of a toluene-water mixture during methanol extraction with a simple jet mixer improves the rate of mass transfer, but the energy requirements for significant improvement are large [Woodle and Vilbrandt, *Am. Inst. Chem. Eng. J.*, **6**, 296 (1960)].

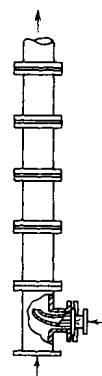


FIG. 18-32 Elbow jet mixer.

Injectors The flow of one liquid is induced by the flow of the other, with only the majority liquid being pumped at relatively high velocity. Figure 18-33 shows a typical device used in semibatch fashion for washing oil with a recirculated wash liquid. It is installed directly in the settling drum. See also Hampton (U.S. Patent 2,091,709, 1933), Sheldon (U.S. Patent 2,009,347, 1935), and Ng (U.S. Patent 2,665,975, 1954). Folsom [*Chem. Eng. Prog.*, **44**, 765 (1948)] gives a good review of basic principles. The most thorough study for extraction is provided by Kafarov and Zhukovskaya [*Zh. Prikl. Khim.*, **31**, 376 (1958)], who used very small injectors. With an injector measuring 73 mm from throat to exit, with 2.48-mm throat diameter, they extracted benzoic acid and acetic acid from water with carbon tetrachloride at the rate of 58 to 106 L/h, to obtain a stage efficiency $E = 0.8$ to 1.0. Data on flow characteristics are also given. Boyadzhiiev and Elenkov [*Collect. Czech. Chem. Commun.*, **31**, 4072 (1966)] point out that the presence of surface-active agents exerts a profound influence on drop size in such devices.

Orifices and Mixing Nozzles Both liquids are pumped through constrictions in a pipe, the pressure drop of which is partly utilized to create the dispersion (see Fig. 18-34). Single nozzles or several in series may be used. For the orifice mixers, as many as 20 orifice plates

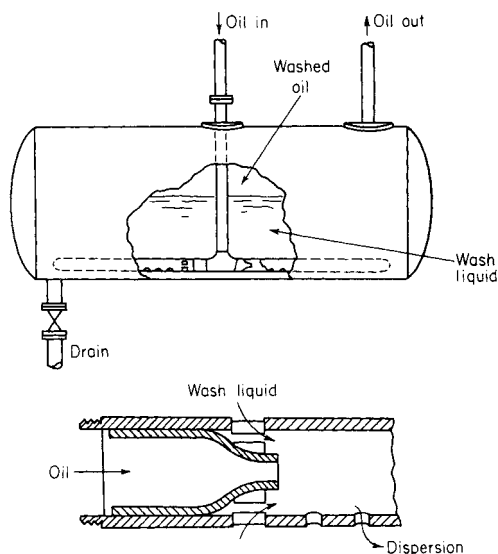


FIG. 18-33 Injector mixer. (Ayles, U.S. Patent 2,531,547, 1950.)

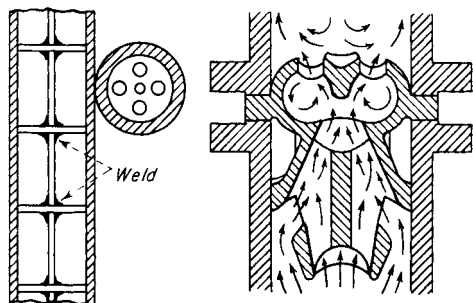


FIG. 18-34 Orifice mixer and nozzle mixer.

each with 13.8-kPa (2-lb/in²) pressure drop may be used in series [Morell and Bergman, *Chem. Metall. Eng.*, **35**, 211 (1928)]. In the Dualayer process for removal of mercaptans from gasoline, 258 m³/h (39,000 bbl/day) of oil and treating solution are contacted with 68.9-kPa (10-lb/in²) pressure drop per stage [Greek et al., *Ind. Eng. Chem.*, **49**, 1938 (1957)]. Holland et al. [*Am. Inst. Chem. Eng. J.*, **4**, 346 (1958); **6**, 615 (1960)] report on the interfacial area produced between two immiscible liquids entering a pipe (diameter 0.8 to 2.0 in) from an orifice, $\gamma_D = 0.02$ to 0.20, at flow rates of 0.23 to 4.1 m³/h (1 to 18 gal/min). At a distance 17.8 cm (7 in) downstream from the orifice,

$$a_{av} = \frac{0.179}{\sigma g_c} (C_O^2 \Delta p)^{0.75} \left(\frac{\sigma \sqrt{g_c \rho_{av}}}{\mu_D} \right)^{0.158} \left[\left(\frac{d_t}{d_o} \right)^4 - 1 \right] \gamma_D^{0.578} \quad (18-8)$$

where a_{av} = interfacial surface, cm²/cm³; C_O = orifice coefficient, dimensionless; d_t = pipe diameter, in; d_o = orifice diameter, in; g_c = gravitational conversion factor, (32.2 lbm-ft)/(lbf-s²); Δp = pressure drop across orifice, lbf/ft²; μ_D = viscosity of dispersed phase, lbm/(ft-s); ρ_{av} = density of dispersed phase, lbm/ft³; and σ = interfacial tension, lbf/ft. See also Shirotzuka et al. [*Kagaku Kogaku*, **25**, 109 (1961)].

Valves Valves may be considered to be adjustable orifice mixers. In desalting crude petroleum by mixing with water, Hayes et al. [*Chem. Eng. Prog.*, **45**, 235 (1949)] used a globe-valve mixer operating at 110- to 221-kPa (16- to 32-lb/in²) pressure drop for mixing 66 m³/h (416 bbl/h) oil with 8 m³/h (50 bbl/h) water, with best results at the lowest value. Simkin and Olney [*Am. Inst. Chem. Eng. J.*, **2**, 545 (1956)] mixed kerosine and white oil with water, using 0.35- to 0.62-kPa (0.05- to 0.09-lb/in²) pressure drop across a 1-in gate valve, at 22-m³/h (10-gal/min) flow rate for optimum separating conditions in a cyclone, but higher pressure drops were required to give good extractor efficiencies.

Pumps Centrifugal pumps, in which the two liquids are fed to the suction side of the pump, have been used fairly extensively, and they offer the advantage of providing interstage pumping at the same time. They have been commonly used in the extraction of phenols from coke-oven liquors with light oil [Gollmar, *Ind. Eng. Chem.*, **39**, 596, 1947]; Carbone, *Sewage Ind. Wastes*, **22**, 200 (1950)], but the intense shearing action causes emulsions with this low-interfacial-tension system. Modern plants use other types of extractors. Pumps are useful in the extraction of slurries, as in the extraction of uranyl nitrate from acid-uranium-ore slurries [*Chem. Eng.*, **66**, 30 (Nov. 2, 1959)]. Shaw and Long [*Chem. Eng.*, **64**(11), 251 (1957)] obtain a stage efficiency of 100 percent ($E = 1.0$) in a uranium-ore-slurry extraction with an open impeller pump. In order to avoid emulsification difficulties in these extractions, it is necessary to maintain the organic phase continuous, if necessary by recycling a portion of the settled organic liquid to the mixer.

Agitated Line Mixer See Fig. 18-35. This device, which combines the features of orifice mixers and agitators, is used extensively in treating petroleum and vegetable oils. It is available in sizes to fit ½- to 10-in pipe. The device of Fig. 18-36, with two impellers in separate stages, is available in sizes to fit 4- to 20-in pipe.

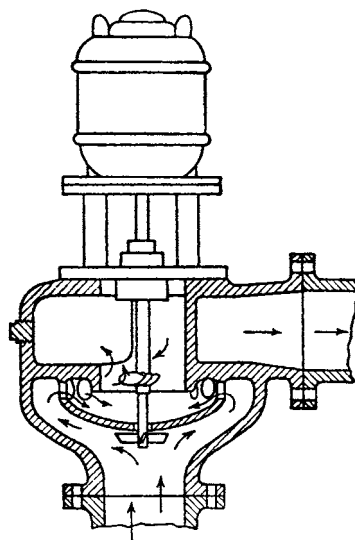


FIG. 18-35 Nettek Corp. Flomix.

Packed Tubes Cocurrent flow of immiscible liquids through a packed tube produces a one-stage contact, characteristic of line mixers. For flow of isobutanol-water* through a 0.5-in diameter tube packed with 6 in of 3-mm glass beads, Leacock and Churchill [*Am. Inst. Chem. Eng. J.*, **7**, 196 (1961)] find

$$k_C a_{av} = c_1 L_C^{0.5} L_D \quad (18-9)$$

$$k_D a_{av} = c_2 L_C^{0.75} L_D^{0.75} \quad (18-10)$$

where $c_1 = 0.00178$ using SI units and 0.00032 using U.S. customary units; and $c_2 = 0.0037$ using SI units and 0.00057 using U.S. customary units. These indicate a stage efficiency approaching 100 percent. Organic-phase holdup and pressure drop for larger pipes similarly packed are also available [Rigg and Churchill, *ibid.*, **10**, 810 (1964)].

* Isobutanol dispersed: $L_D = 3500$ to 27,000; water continuous; $L_C = 6000$ to 32,000 in pounds-mass per hour-square foot (to convert to kilograms per second-square meter, multiply by 1.36×10^{-3}).

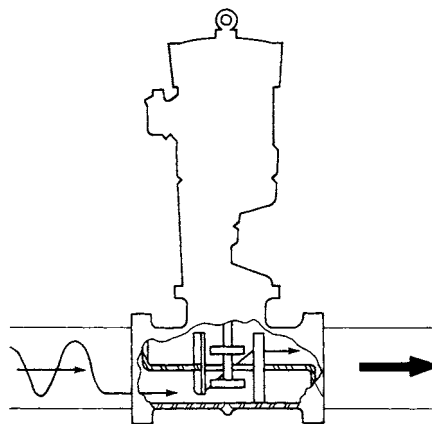


FIG. 18-36 Lightnin line blender. (Mixing Equipment Co., Inc., with permission.)

Pipe Lines The principal interest here will be for flow in which one liquid is dispersed in another as they flow cocurrently through a pipe (stratified flow produces too little interfacial area for use in liquid extraction or chemical reaction between liquids). Drop size of dispersed phase, if initially very fine at high concentrations, increases as the distance downstream increases, owing to coalescence [see Holland, loc. cit.; Ward and Knudsen, *Am. Inst. Chem. Eng. J.*, **13**, 356 (1967)]; or if initially large, decreases by breakup in regions of high shear [Sleicher, *ibid.*, **8**, 471 (1962); *Chem. Eng. Sci.*, **20**, 57 (1965)]. The maximum drop size is given by (Sleicher, loc. cit.)

$$\frac{d_{p,\max} \rho_c V^2}{\sigma_{g_c}} \sqrt{\frac{\mu_c V}{\sigma_{g_c}}} = C \left[1 + 0.7 \left(\frac{\mu_D V}{\sigma_{g_c}} \right)^{0.7} \right] \quad (18-11)$$

where $C = 43$ ($d_t = 0.013$ m or 0.0417 ft) or 38 ($d_t = 0.038$ m or 0.125 ft), with $d_{p,av} = d_{p,\max}/4$ for high flow rates and $d_{p,\max}/13$ for low velocities.

Extensive measurements of the rate of mass transfer between *n*-butanol and water flowing in a 0.008-m (0.314-in) ID horizontal pipe are reported by Watkinson and Cavers [*Can. J. Chem. Eng.*, **45**, 258 (1967)] in a series of graphs not readily reproduced here. Length of a transfer unit for either phase is strongly dependent upon flow rate and passes through a pronounced maximum at an organic-water phase ratio of 0.5. In energy (pressure-drop) requirements and volume, the pipe line compared favorably with other types of extractors. Boyadzhiev and Elenkov [*Chem. Eng. Sci.*, **21**, 955 (1966)] concluded that, for the extraction of iodine between carbon tetrachloride and water in turbulent flow, drop coalescence and breakup did not influence the extraction rate. Yoshida et al. [*Coal Tar* (Japan), **8**, 107 (1956)] provide details of the treatment of crude benzene with sulfuric acid in a 1-in diameter pipe, $N_{Re} = 37,000$ to 50,000. Fernandes and Sharma [*Chem. Eng. Sci.*, **23**, 9 (1968)] used cocurrent flow downward of two liquids in a pipe, agitated with an upward current of air.

The pipe has also been used for the transfer of heat between two immiscible liquids in cocurrent flow. For hydrocarbon oil-water, the heat-transfer coefficient is given by

$$\frac{U_{av} d_t^2}{vk_{to}} = \frac{\gamma_D N_{We,t}^{0.65}}{\frac{k_{to}}{0.415k_{tC}} + \frac{k_{to}}{0.173k_{tD}}} \quad (18-12)$$

for $\gamma_D = 0$ to 0.2. Additional data for $\gamma_D = 0.4$ to 0.8 are also given. Data for stratified flow are given by Wilke et al. [*Chem. Eng. Prog.*, **59**, 69 (1963)] and Grover and Knudsen [*Chem. Eng. Prog.*, **51**, *Symp. Ser.* **17**, 71 (1955)].

Mixing in Agitated Vessels Agitated vessels may frequently be used for either batch or continuous service and for the latter may be sized to provide any holding time desired. They are useful for liquids of any viscosity up to 750 Pa·s (750,000 cP), although in contacting two liquids for reaction or extraction purposes viscosities in excess of 0.1 Pa·s (100 cP) are only rarely encountered.

Mechanical Agitation This type of agitation utilizes a rotating impeller immersed in the liquid to accomplish the mixing and dispersion. There are literally hundreds of devices using this principle, the major variations being found when chemical reactions are being carried out. The basic requirements regarding shape and arrangement of the vessel, type and arrangement of the impeller, and the like are essentially the same as those for dispersing finely divided solids in liquids, which are fully discussed in Sec. 18.

The following summary of operating characteristics of mechanically agitated vessels is confined to the data available on liquid-liquid contacting.

Phase Dispersed There is an ill-defined upper limit to the volume fraction of dispersed liquid which may be maintained in an agitated dispersion. For dispersions of organic liquids in water [Quinn and Sigloh, *Can. J. Chem. Eng.*, **41**, 15 (1963)],

$$\gamma_{D,\max} = \gamma' + \left(\frac{C}{N^3} \right) \quad (18-13)$$

where γ' is a constant, asymptotic value, and C is a constant, both depending in an unestablished manner upon the systems' physical properties and geometry. Thus, inversion of a dispersion may occur if the agitator speed is increased. With systems of low interfacial tension ($\sigma' = 2$ to 3 mN/m or 2 to 3 dyn/cm), γ_D as high as 0.8 can be maintained. Selker and Sleicher [*Can. J. Chem. Eng.*, **43**, 298 (1965)] and Yeh et al. [*Am. Inst. Chem. Eng. J.*, **10**, 260 (1964)] feel that the viscosity ratio of the liquids alone is important. Within the limits in which either phase can be dispersed, for *batch operation* of baffled vessels, that phase in which the impeller is immersed when at rest will normally be continuous [Rodger, Trice, and Rushton, *Chem. Eng. Prog.*, **52**, 515 (1956); Laity and Treybal, *Am. Inst. Chem. Eng. J.*, **3**, 176 (1957)]. With water dispersed, *dual emulsions* (continuous phase found as small droplets within larger drops of dispersed phase) are possible. In *continuous operation*, the vessel is first filled with the liquid to be continuous, and agitation is then begun, after which the liquid to be dispersed is introduced.

Uniformity of Mixing This refers to the gross uniformity throughout the vessel and not to the size of the droplets produced. For *unbaffled vessels, batch, with an air-liquid interface*, Miller and Mann [*Trans. Am. Inst. Chem. Eng.*, **40**, 709 (1944)] mixed water with several organic liquids, measuring uniformity of mixing by sampling the tank at various places, comparing the percentage of dispersed phase found with that in the tank as a whole. A power application of 200 to 400 W/m³ [(250 to 500 ft-lb)/(min-ft³)] gave maximum and nearly uniform performance for all. See also Nagata et al. [*Chem. Eng. (Japan)*, **15**, 59 (1951)].

For *baffled vessels operated continuously, no air-liquid interface*, flow upward, light liquid dispersed [Treybal, *Am. Inst. Chem. Eng. J.*, **4**, 202 (1958)], the average fraction of dispersed phase in the vessel $\gamma_{D,av}$ is less than the fraction of the dispersed liquid in the feed mixture, unless the impeller speed is above a certain critical value which depends upon vessel geometry and liquid properties. Thornton and Bouyatiotis [*Ind. Chem.*, **39**, 298 (1963); *Inst. Chem. Eng. Symp. Liquid Extraction*, Newcastle-upon-Tyne, April 1967] have presented correlations of data for a 17.8-cm (7-in) vessel, but these do not agree with observations on 15.2- and 30.5-cm (6- and 12-in) vessels in Treybal's laboratory. See also Kovalev and Kagan [*Zh. Prikl. Khim.*, **39**, 1513 (1966)] and Trambouze [*Chem. Eng. Sci.*, **14**, 161 (1961)]. Stemerding et al. [*Can. J. Chem. Eng.*, **43**, 153 (1965)] present data on a large mixing tank [15 m³ (530 ft³)] fitted with a marine-type propeller and a draft tube.

Drop Size and Interfacial Area The drops produced have a size range [Sullivan and Lindsey, *Ind. Eng. Chem. Fundam.*, **1**, 87 (1962); Sprow, *Chem. Eng. Sci.*, **22**, 435 (1967); and Chen and Middleman, *Am. Inst. Chem. Eng. J.*, **13**, 989 (1967)]. The average drop size may be expressed as

$$d_{p,av} = \frac{\sum n_i d_{pi}^3}{\sum n_i d_{pi}^2} \quad (18-14)$$

and if the drops are spherical,

$$a_{av} = \frac{6\gamma_{D,av}}{d_{p,av}} \quad (18-15)$$

The drop size varies locally with location in the vessel, being smallest at the impeller and largest in regions farthest removed from the impeller owing to coalescence in regions of relatively low turbulence intensity [Schindler and Treybal, *Am. Inst. Chem. Eng. J.*, **14**, 790 (1968); Vanderveen, U.S. AEC UCRL-8733, 1960]. Interfacial area and hence average drop size have been measured by light transmittance, light scattering, direct photography, and other means. Typical of the resulting correlations is that of Thornton and Bouyatiotis [*Inst. Chem. Eng. Symp. Liquid Extraction*, Newcastle-upon-Tyne, April 1967] for a 17.8-cm- (7-in-) diameter baffled vessel, six-bladed flat-blade turbine, $d_t = 6.85$ cm (0.225 ft), operated full, for organic liquids

($\sigma' = 8.5$ to 34 , $\rho_D = 43.1$ to 56.4 , $\mu_D = 1.18$ to 1.81) dispersed in water, in the absence of mass transfer, and under conditions giving nearly the vessel-average $d_{p,av}$:

$$\frac{d_{p,av}}{d_p^0} = 1 + 1.18\phi_D \left(\frac{\sigma^2 g_c^2}{d_p^0 \mu_c^2 g} \right) \left(\frac{\mu_c^4 g}{\Delta\rho \sigma^3 g_c^3} \right)^{0.62} \left(\frac{\Delta\rho}{\rho_c} \right)^{0.05} \quad (18-16)$$

where d_p^0 is given by

$$\frac{(d_p^0)^3 \rho_c^2 g}{\mu_c^2} = 29.0 \left(\frac{P^3 g_c^3}{v^3 \rho_c^2 \mu_c g^4} \right)^{-0.32} \left(\frac{\rho_c \sigma^3 g_c^3}{\mu_c^4 g} \right)^{0.14} \quad (18-17)$$

Caution is needed in using such correlations, since those available do not generally agree with each other. For example, Eq. (21-28) gives $d_{p,av} = 4.78(10^{-4})$ ft for a liquid pair of properties $a' = 30$, $\rho_c = 62.0$, $\rho_D = 52.0$, $\mu_c = 2.42$, $\mu_D = 1.94$, $\gamma_{D,av} = 0.20$ in a vessel $T = Z = 0.75$, a turbine impeller $d_t = 0.25$ turning at 400 r/min. Other correlations provide $3.28(10^{-4})$ [Thornton and Bouyatiotis, *Ind. Chem.*, **39**, 298 (1963)], $8.58(10^{-4})$ [Calderbank, *Trans. Inst. Chem. Eng. (London)*, **36**, 443 (1958)], $6.1(10^{-4})$ [Kafarov and Babinov, *Zh. Prikl. Khim.*, **32**, 789 (1959)], and $2.68(10^{-3})$ (Rushton and Love, paper at AIChE, Mexico City, September 1967). See also Vermeulen et al. [*Chem. Eng. Prog.*, **51**, 85F (1955)], Rodgers et al. [*ibid.*, **52**, 515 (1956)]; U.S. AEC ANL-5575 (1956), Rodrigues et al. [*Am. Inst. Chem. Eng. J.*, **7**, 663 (1961)], Sharma et al. [*Chem. Eng. Sci.*, **21**, 707 (1966); **22**, 1267 (1967)], and Kagan and Kovalev [*Khim. Prom.*, **42**, 192 (1966)]. For the effect of absence of baffles, see Fick et al. (U.S. AEC UCRL-2545, 1954) and Schindler and Treybal [*Am. Inst. Chem. Eng. J.*, **14**, 790 (1968)]. The latter have observations during mass transfer.

Coalescence Rates The droplets coalesce and redisperse at rates that depend upon the vessel geometry, N , $\gamma_{D,av}$, and liquid properties. The few measurements available, made with a variety of techniques, do not as yet permit quantitative estimates of the coalescence frequency v . Madden and Damarell [*Am. Inst. Chem. Eng. J.*, **8**, 233 (1962)] found for baffled vessels that v varied as $N^{2.2} \gamma_{D,av}^{0.57}$, and this has generally been confirmed by Groothuis and Zuiderweg [*Chem. Eng. Sci.*, **19**, 63 (1964)], Miller et al. [*Am. Inst. Chem. Eng. J.*, **9**, 196 (1963)], and Howarth [*ibid.*, **13**, 1007 (1967)], although absolute values of v in the various studies are not well related. Hillestad and Rushton (paper at AIChE, Columbus, Ohio, May 1966), on the other hand, find v to vary as $N^{0.73} \gamma_{D,av}$ for impeller Weber numbers $N_{We,i}$ below a certain critical value and as $N^{-3.5} \gamma_{D,av}^{1.58}$ for higher Weber numbers. The influence of liquid properties is strong. There is clear evidence [Groothuis and Zuiderweg, loc. cit.; *Chem. Eng. Sci.*, **12**, 288 (1960)] that coalescence rates are enhanced by mass transfer from a drop to the surrounding continuum and retarded by transfer in the reverse direction. See also Howarth [*Chem. Eng. Sci.*, **19**, 33 (1964)]. For a theoretical treatment of drop breakage and coalescence and their effects, see Valentas and Amundsen [*Ind. Eng. Chem. Fundam.*, **5**, 271, 533 (1966); **7**, 66 (1968)], Gal-Or and Walatka [*Am. Inst. Chem. Eng. J.*, **13**, 650 (1967)], and Curl [*ibid.*, **9**, 175 (1963)].

In calculating the power required for mixers, a reasonable estimate of the average density and viscosity for a two-phase system is satisfactory.

Solids are often present in liquid streams either as a part of the processing system or as impurities that come along and have to be handled in the process. One advantage of mixers in differential contact equipment is the fact that they can handle slurries in one or both phases. In many industrial leaching systems, particularly in the minerals processing industry, coming out of the leach circuit is a slurry with a desired material involved in the liquid but a large amount of solids contained in the stream. Typically, the solids must be separated out by filtration or centrifugation, but there has always been a desire to try a direct liquid-liquid extraction with an immiscible liquid contact with this often highly concentrated slurry leach solution. The major problem with this approach is loss of organic material going out with the highly concentrated liquid slurry.

Data are not currently available on the dispersion with the newer fluidfoil impellers, but they are often used in industrial mixer-settler systems to maintain dispersion when additional resonance time holdup is required, after an initial dispersion is made by a radial- or axial-flow turbine.

Recent data by Calabrese⁵ indicates that the sauter mean drop diameter can be correlated by equation and is useful to compare with other predictions indicated previously.

As an aside, when a large liquid droplet is broken up by shear stress, it tends initially to elongate into a dumbbell shape, which determines the particle size of the two large droplets formed. Then, the neck in the center between the ends of the dumbbell may explode or shatter. This would give a debris of particle sizes which can be quite different than the two major particles produced.

Liquid-Liquid Extraction The actual configuration of mixers in multistage mixer-settlers and/or multistage columns is summarized in Section 15. A general handbook on this subject is *Handbook of Solvent Extraction* by Lowe, Beard, and Hanson. This handbook gives a comprehensive review of this entire operation as well.

In the liquid-liquid extraction area, in the mining industry, coming out of the leach tanks is normally a slurry, in which the desired mineral is dissolved in the liquid phase. To save the expense of separation, usually by filtration or centrifugation, attempts have been made to use a resident pump extraction system in which the organic material is contacted directly with the slurry. The main economic disadvantage to this proposed system is the fact that considerable amounts of organic liquid are entrained in the aqueous slurry system, which, after the extraction is complete, are discarded. In many systems this has caused an economic loss of solvent into this waste stream.

LIQUID-LIQUID-SOLID SYSTEMS

Many times solids are present in one or more phases of a solid-liquid system. They add a certain level of complexity in the process, especially if they tend to be a part of both phases, as they normally will do. Approximate methods need to be worked out to estimate the density of the emulsion and determine the overall velocity of the flow pattern so that proper evaluation of the suspension requirements can be made. In general, the solids will behave as though they were a fluid of a particular average density and viscosity and won't care much that there is a two-phase dispersion going on in the system. However, if solids are being dissolved or precipitated by participating in one phase and not the other, then they will be affected by which phase is dispersed or continuous, and the process will behave somewhat differently than if the solids migrate independently between the two phases within the process.

FLUID MOTION

Pumping Some mixing applications can be specified by the pumping capacity desired from the impeller with a certain specified geometry in the vessel. As mentioned earlier, this sometimes is used to describe a blending requirement, but circulation and blending are two different things. The major area where this occurs is in draft tube circulators or pump-mix mixer settler. In draft tube circulators (shown in Fig. 18-22), the circulation occurs through the draft tube and around the annulus and for a given geometry, the velocity head required can be calculated with reference to various formulas for geometric shapes. What is needed is a curve for head versus flow for the impeller, and then the system curve can be matched to the impeller curve. Adding to the complexity of this system is the fact that solids may settle out and change the character of the head curve so that the impeller can get involved in an unstable condition which has various degrees of erratic behavior depending upon the sophistication of the impeller and inlet and outlet vanes involved. These draft tube circulators often involve solids, and applications are often for precipitation or crystallization in these units. Draft tube circulators can either have the impeller pump up in the draft tube and flow down the annulus

or just the reverse. If the flow is down the annulus, then the flow has to make a 180° turn where it comes back at the bottom of the tank into the draft tube again. This is a very sensitive area, and special baffles must be used to carefully determine how the fluid will make this turn since many areas of constriction are involved in making this change in direction.

When pumping down the draft tube, flow normally makes a more troublefree velocity change to a flow going up the annulus. Since the area of the draft tube is markedly less than the area of the annulus, pumping up the draft tube requires less flow to suspend solids of a given settling velocity than does pumping down the draft tube.

Another example is to eliminate the interstage pump between mixing and settling stages in the countercurrent mixer-settler system. The radial-flow impeller typically used is placed very close to an orifice at the bottom of the mixing tank and can develop heads from 12 to 18 in. All the head-loss terms in the mixer and settler circuit have to be carefully calculated because they come very close to that 12- to 18-in range when the passages are very carefully designed and streamlined. If the mixing tank gets much above 10 ft in depth, then the heads have to be higher than the 12- to 18-in range and special designs have to be worked on which have the potential liability of increasing the shear rate acting on the dispersed phase to cause more entrainment and longer settling times. In these cases, it is sometimes desirable to put the mixer system outside the actual mixer tank and have it operate in a single phase or to use multiple impellers, each one of which can develop a portion of the total head required.

Heat Transfer In general, the fluid mechanics of the film on the mixer side of the heat transfer surface is a function of what happens at that surface rather than the fluid mechanics going on around the impeller zone. The impeller largely provides flow across and adjacent to the heat-transfer surface and that is the major consideration of the heat-transfer result obtained. Many of the correlations are in terms of traditional dimensionless groups in heat transfer, while the impeller performance is often expressed as the impeller Reynolds number.

The fluidfoil impellers (shown in Fig. 18-2) usually give more flow for a given power level than the traditional axial- or radial-flow turbines. This is also thought to be an advantage since the heat-transfer surface itself generates the turbulence to provide the film coefficient and more flow should be helpful. This is true to a limited degree in jacketed tanks (Fig. 18-37), but in helical coils (Fig. 18-38), the

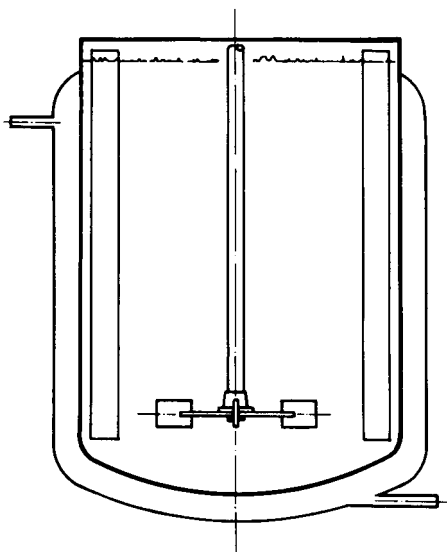


FIG. 18-37 Typical jacket arrangement for heat transfer.

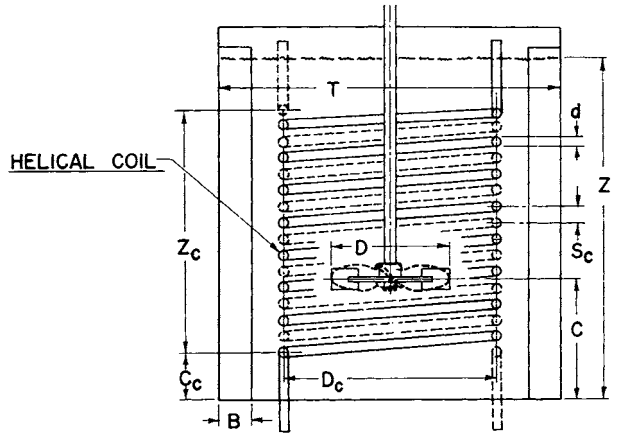


FIG. 18-38 Typical arrangement of helical coil at mixing vessel for heat transfer.

extreme axial flow of these impellers tends to have the first or second turn in the coil at the bottom of the tank blank off the flow from the turns above it in a way that (at the same power level) the increased flow from the fluidfoil impeller is not helpful. It best gives the same coefficient as with the other impellers and on occasion can cause a 5 to 10 percent reduction in the heat-transfer coefficient over the entire coil.

JACKETS AND COILS OF AGITATED VESSELS

Most of the correlations for heat transfer from the agitated liquid contents of vessels to jacketed walls have been of the form:

$$\frac{hD_j}{k} = a \left(\frac{L_p^2 N_i \rho}{\mu} \right)^b \left(\frac{c\mu}{k} \right)^{1/3} \left(\frac{\mu_b}{\mu_w} \right)^m \tag{18-18}$$

The film coefficient *h* is for the inner wall; *D_j* is the inside diameter of the mixing vessel. The term $L_p^2 N_i \rho / \mu$ is the Reynolds number for mixing in which *L_p* is the diameter and *N_i* the speed of the agitator. Recommended values of the constants *a*, *b*, and *m* are given in Table 18-3.

A wide variety of configurations exists for coils in agitated vessels. Correlations of data for heat transfer to helical coils have been of two forms, of which the following are representative:

$$\frac{hD_j}{k} = 0.87 \left(\frac{L_p^2 N_i \rho}{\mu} \right)^{0.62} \left(\frac{c\mu}{k} \right)^{1/3} \left(\frac{\mu_b}{\mu_w} \right)^{0.14} \tag{18-19}$$

TABLE 18-3 Values of Constants for Use in Eq. (18-18)

Agitator	<i>a</i>	<i>b</i>	<i>m</i>	Range of Reynolds number
Paddle ^a	0.36	2/3	0.21	300–3 × 10 ⁵
Pitched-blade turbine ^b	0.53	2/3	0.24	80–200
Disc, flat-blade turbine ^c	0.54	2/3	0.14	40–3 × 10 ⁵
Propeller ^d	0.54	2/3	0.14	2 × 10 ³ (one point)
Anchor ^b	1.0	1/2	0.18	10–300
Anchor ^b	0.36	2/3	0.18	300–40,000
Helical ribbon ^e	0.633	1/2	0.18	8–10 ⁵

^aChilton, Drew, and Jebens, *Ind. Eng. Chem.*, **36**, 510 (1944), with constant *m* modified by Uhl.

^bUhl, *Chem. Eng. Progr., Symp. Ser.* **17**, **51**, 93 (1955).

^cBrooks and Su, *Chem. Eng. Progr.*, **55**(10), 54 (1959).

^dBrown et al., *Trans. Inst. Chem. Engrs. (London)*, **25**, 181 (1947).

^eGluz and Pavlushenko, *J. Appl. Chem. U.S.S.R.*, **39**, 2323 (1966).

18-26 LIQUID-SOLID OPERATIONS AND EQUIPMENT

where the agitator is a paddle, the Reynolds number range is 300 to 4×10^5 [Chilton, Drew, and Jebens, *Ind. Eng. Chem.*, **36**, 510 (1944)], and

$$\frac{hD_o}{k} = 0.17 \left(\frac{L_p^2 N_f \rho}{\mu} \right)^{0.67} \left(\frac{c\mu}{k} \right)^{0.37} \left(\frac{L_p}{D_j} \right)^{0.1} \left(\frac{D_o}{D_j} \right)^{0.5} \quad (18-20)$$

where the agitator is a disc flat-blade turbine, and the Reynolds number range is 400 to $(2)(10^5)$ [Oldshue and Gretton, *Chem. Eng. Prog.*, **50**, 615 (1954)]. The term D_o is the outside diameter of the coil tube.

The most comprehensive correlation for heat transfer to vertical baffle-type coils is for a disc flat-blade turbine over the Reynolds number range 10^3 to $(2)(10^6)$:

$$\frac{hD_o}{k} = 0.09 \left(\frac{L_p^2 N_f \rho}{\mu} \right)^{0.65} \left(\frac{c\mu}{k} \right)^{1/3} \left(\frac{L_p}{D_j} \right)^{1/3} \left(\frac{2}{n_b} \right)^{0.2} \left(\frac{\mu}{\mu_f} \right)^{0.4} \quad (18-21)$$

where n_b is the number of baffle-type coils and μ_f is the fluid viscosity at the mean film temperature [Dunlop and Rushton, *Chem. Eng. Prog. Symp. Ser.* **5**, **49**, 137 (1953)].

Chapman and Holland (*Liquid Mixing and Processing in Stirred Tanks*, Reinhold, New York, 1966) review heat transfer to low-viscosity fluids in agitated vessels. Uhl ["Mechanically Aided Heat Transfer," in Uhl and Gray (eds.), *Mixing: Theory and Practice*, vol. I, Academic, New York, 1966, chap. V] surveys heat transfer to low- and high-viscosity agitated fluid systems. This review includes scraped-wall units and heat transfer on the jacket and coil side for agitated vessels.

LIQUID-LIQUID-GAS-SOLID SYSTEMS

This is a relatively unusual combination, and one of the more common times it exists is in the fermentation of hydrocarbons with aerobic microorganisms in an aqueous phase. The solid phase is a microorganism which is normally in the aqueous phase and is using the organic phase for food. Gas is supplied to the system to make the fermentation aerobic. Usually the viscosities are quite low, percent solids is also modest, and there are no special design conditions required when this particular gas-liquid-liquid-solid combination occurs. Normally, average properties for the density or viscosity of the liquid phase are used. In considering that the role the solids play in the system is adequate, there are cases of other processes which consist of four phases, each of which involves looking at the particular properties of the phases to see whether there are any problems of dispersion, suspension, or emulsification.

COMPUTATIONAL FLUID DYNAMICS

There are several software programs that are available to model flow patterns of mixing tanks. They allow the prediction of flow patterns based on certain boundary conditions. The most reliable models use accurate fluid mechanics data generated for the impellers in question and a reasonable number of modeling cells to give the overall tank flow pattern. These flow patterns can give velocities, streamlines, and localized kinetic energy values for the systems. Their main use at the present time is to look at the effect of making changes in mixing variables based on doing certain things to the mixing process. These programs can model velocity, shear rates, and kinetic energy, but probably cannot adapt to the actual chemistry of diffusion or mass-transfer kinetics of actual industrial process at the present time.

Relatively uncomplicated transparent tank studies with tracer fluids or particles can give a similar feel for the overall flow pattern. It is important that a careful balance be made between the time and expense of calculating these flow patterns with computational fluid dynamics compared to their applicability to an actual industrial process. The future of computational fluid dynamics appears very encouraging and a

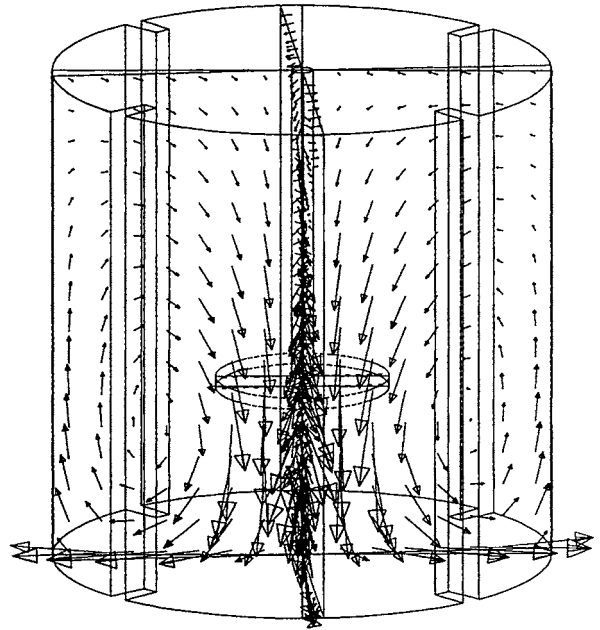


FIG. 18-39 Laser scan.

reasonable amount of time and effort put forth in this regard can yield immediate results as well as potential for future process evaluation.

Figures 18-39, 18-40, and 18-41 show some approaches. Figure 18-39 shows velocity vectors for an A310 impeller. Figure 18-40 shows contours of kinetic energy of turbulence. Figure 18-41 uses a particle trajectory approach with neutral buoyancy particles.

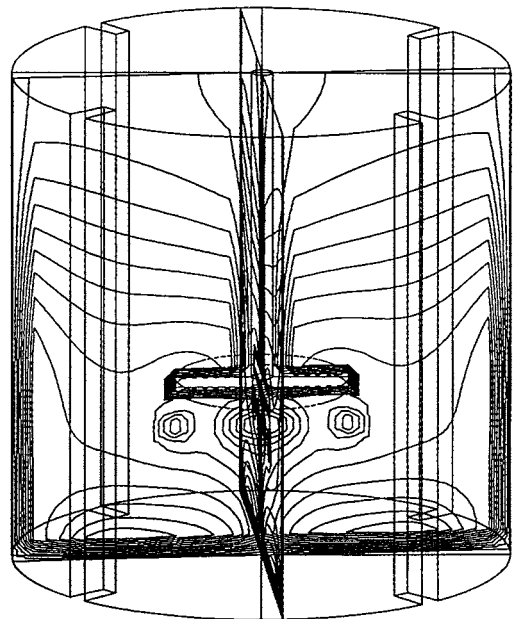


FIG. 18-40 Laser scan.

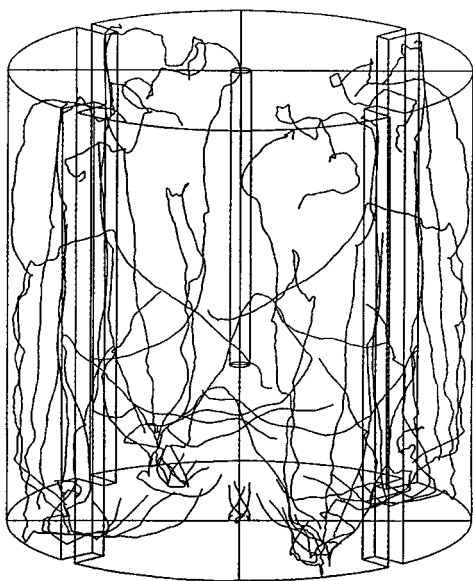


FIG. 18-41 Laser scan.

Numerical fluid mechanics can define many of the fluid mechanics parameters for an overall reactor system. Many of the models break up the mixing tank into small microcells. Suitable material and mass-transfer balances between these cells throughout the reactor are then made. This can involve long and massive computational requirements. Programs are available that can give reasonably acceptable models of experimental data taken in mixing vessels. Modeling the three-dimensional aspect of a flow pattern in a mixing tank can require a large amount of computing power.

Most modeling codes are a time-averaging technique. Depending upon the process, a time-dependent technique may be more suitable. Time-dependent modeling requires much more computing power than does time averaging.

GENERAL REFERENCES

1. J. Y. Oldshue, "Mixing '89," *Chemical Engineering Progress*, **85**(5): 33-42 (1989).
2. J. C. Middleton, *Proc. 3d European Conf. on Mixing*, 4/89, BHRA, pp. 15-36.
3. J. Y. Oldshue, T. A. Post, R. J. Weetman, "Comparison of Mass Transfer Characteristics of Radial and Axial Flow Impellers," *BHRA Proc. 6th European Conf. on Mixing*, 5/88.
4. A. W. Neimow, B. Buckland, R. J. Weetman, *Mixing XII Research Conference*, Potosi, Mo., 8/89.
5. R. Calabrese et al., *AIChE J.* **32**: 657, 677 (1986).
6. T. N. Zwietering, *Chemical Engineering Science*, **8**(3): 244-253 (1958).
7. J. Y. Oldshue, *Chemical Engineering Progress*, "Mixing of Slurries Near the Ultimate Settled Solids Concentration," **77**(5): 95-98 (1981).

MIXING OF VISCOUS FLUIDS, PASTES, AND DOUGHS

GENERAL REFERENCES: Paul, E. L., V. A. Atiemo-Obeng, and S. M. Kresta (eds.), *Handbook of Industrial Mixing, Science and Practice*, Wiley, Hoboken, N.J., 2004. Harnby, N., M. F. Edwards, and A. W. Nienow (eds.), *Mixing in the Process Industries*, 2d ed., Butterworth-Heinemann, Boston, 1992. Oldshue, J. Y., *Fluid Mixing Technology*, McGraw-Hill, New York, 1983. Ottino, J. M., *The Kinematics of Mixing: Stretching, Chaos, and Transport*, Cambridge University Press, New York, 1999. Tatterson, G. B., *Fluid Mixing and Gas Dispersion in Agitated Tanks*, McGraw-Hill, New York, 1991. Zlokarnik, M., *Stirring, Theory and Practice*, Wiley-VCH, New York, 2001.

INTRODUCTION

Even the definition of mixing for viscous fluids, pastes, and doughs is complicated. While mixing can be defined simply as increasing or maintaining uniformity, the devices that cause mixing to take place may also accomplish deagglomeration, dispersion, extrusion, heat transfer, or other process objectives. Fluids with viscosities greater than 10 Pa·s (10,000 cP) can be considered *viscous*. However, non-newtonian fluid properties are often as important in establishing mixing requirements. Viscous fluids can be polymer melts, polymer solutions, and a variety of other high-molecular-weight or low-temperature materials. Many polymeric fluids are shear thinning. Pastes are typically formed when particulate materials are wetted by a fluid to the extent that particle-particle interactions create flow characteristics similar to those of viscous fluids. The particle-particle interactions may cause shear thickening effects. Doughs have the added characteristic of elasticity. Viscous materials often exhibit a combination of other non-newtonian characteristics, such as a yield stress.

One common connection between viscous fluids, pastes, and doughs is the types of equipment used to mix or process them. While often designed for a specific process objective or a certain fluid characteristic, most types of viscous mixing equipment have some common characteristics. The nature of all viscous materials is their resistance to flow. This resistance is usually overcome by a mixer that will eventually contact or directly influence all the material in a container, particularly material near the walls or in corners. Small clearances between rotating and stationary parts of a mixer create regions

of high local shear. Intermeshing blades or stators prevent material from rotating as a solid mass. Such equipment provides greater control of fluid motion than equipment used for low-viscosity fluids, but typically at greater cost and complexity.

The one failure common to all mixing equipment is any region of stagnant material. With a shear thinning material, the relative motion between a rotating mixer blade and adjacent fluid will reduce the local viscosity. However, away from the mixer blade, shear will decrease and the viscosity will increase, leading to the possibility of stagnation. With a shear thickening material, high shear near a mixer blade will result in high viscosity, which may reduce either local relative motion or the surrounding bulk motion. Yield stress requires some minimum shear stress to accomplish any motion at all. Viscoelastic characteristics cause motion normal to the applied stresses. Thus all major non-newtonian characteristics reduce effective mixing and increase the possibility of local stagnation.

Blade shape and mixing action can have significant impacts on the mixing process. A scraping action is often necessary to promote heat transfer or prevent adhesion to equipment surfaces. A smearing action can improve dispersion. A combination of actions is necessary to accomplish the random or complicated pattern necessary for complete mixing. No one mixing effect or equipment design is ideal for all applications.

Because of high viscosity, the mixing Reynolds number ($N_{Re} = D^2 N \rho / \mu$, where D is impeller diameter, N is rotational speed, ρ is density, and μ is viscosity) may be less than 100. At such viscous conditions, mixing occurs because of laminar shearing and stretching. Turbulence is not a factor, and complicated motion is a direct result of the mixer action. The relative motion between moving parts of the mixer and the walls of the container or other mixer parts creates both shear and bulk motion. The shear effectively creates thinner layers of nonuniform material, which diminishes striations or breaks agglomerates to increase homogeneity. Bulk motion redistributes the effects of the stretching processes throughout the container.

Often as important as or more important than the primary viscosity is the relative viscosity of fluids being mixed. When a high-viscosity material is added to a low-viscosity material, the shear created by the

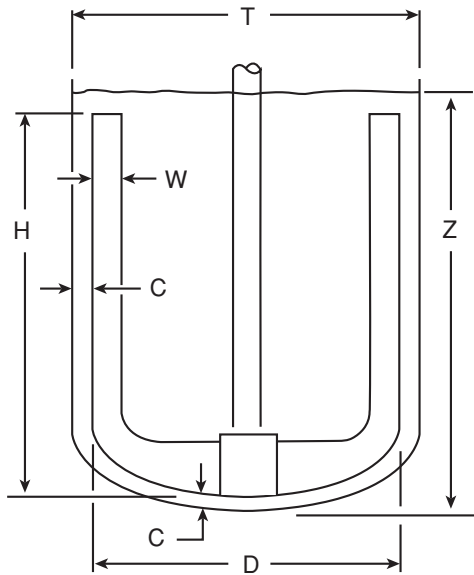


FIG. 18-42 Anchor impeller with nomenclature.

low-viscosity material may not be sufficient to stretch and interact with the high-viscosity material. When a low-viscosity material is added to a high-viscosity material, the low-viscosity material may act as a lubricant, thus allowing slippage between the high-viscosity material and the mixer surfaces. Viscosity differences can be orders of magnitude different. Density differences are smaller and typically less of a problem in viscous mixing.

Besides mixing fluids, pastes, and doughs, the same equipment may be used to create those materials. Viscous fluids such as polymers can be created by reaction from low-viscosity monomers in the same equipment described for viscous mixing. Pastes may be created by either the addition of powders to liquids or the removal of liquids from slurries, again using the same type of equipment as for bulk mixing. Doughs are usually created by the addition of a powder to liquid and the subsequent hydration of the powder. The addition process itself becomes a mixer application, which may fall somewhere between low-viscosity and high-viscosity mixing, but often including both types of mixing.

BATCH MIXERS

Anchor Mixers Anchor mixers are the simplest and one of the more common types of high-viscosity mixers (Fig. 18-42). The diameter of the anchor D is typically 90 to 95 percent of the tank diameter T . The result is a small clearance C between the rotating impeller and the tank wall. Within this gap the fluid is sheared by the relative motion between the rotating blade and the stationary tank wall. The shear near the wall typically reduces the buildup of stagnant material and promotes heat transfer. To reduce buildups further, flexible or spring-loaded scrapers, typically made of polymeric material, can be mounted on the rotating blades to move material physically away from the wall.

The benefits of an anchor mixer are limited by the fact that the vertical blades provide very little fluid motion between the top and bottom of the tank. Ingredient additions at the surface of the fluid may make many rotations before gradually being spread and circulated to the bottom of the tank. To promote top-to-bottom fluid motion, angled blades on the anchor or helical ribbon blades, described in the next subsection, make better mixers for uniform blending. Significant viscosity differences between fluids may extend mixing times to unacceptable limits with the basic anchor.

Anchor mixers may be used in combination with other types of mixers, such as turbine mixers, high-shear mixers, or rotor-stator mixers, which were described in the previous subsection. Such mixers can be placed on a vertical shaft midway between the anchor shaft and blade. A secondary mixer can promote top-to-bottom motion and also limit bulk rotation of the fluid. A stationary baffle is sometimes placed between the anchor shaft and rotating blade to limit fluid rotation and enhance shear.

A dimensionless group called the power number is commonly used to predict the power required to rotate a mixing impeller. The *power number* is defined as $P/(\rho N^3 D^5)$, where P is power, ρ is fluid density, N is rotational speed, and D is impeller diameter. To be dimensionless, the units of the variables must be coherent, such as SI metric; otherwise appropriate conversion factors must be used. The conversion factor for common engineering units gives the following expression for power number:

$$N_p = \frac{1.524 \times 10^{13} P}{\text{sp gr } N^3 D^5} \quad (18-22)$$

where P is power in horsepower, sp gr is fluid specific gravity based on water, N is rotational speed in rpm, and D is impeller diameter in inches. The power number is an empirically measured value that describes geometrically similar impellers. Power number is a function of Reynolds number, which accounts for the effects of fluid properties. Impeller Reynolds number, as defined earlier, is another dimensionless group. A conversion factor is needed for common engineering units:

$$N_{\text{Re}} = \frac{10.4D^2 N \text{ sp gr}}{\mu} \quad (18-23)$$

where D is the impeller diameter in inches, N is rotational speed in rpm, sp gr is specific gravity based on water, and μ is viscosity in centipoise.

Power can be calculated by rearranging the definition of power number; see the following example. A value for the appropriate power number must be obtained from empirically derived data for geometrically similar impellers. Power number correlations for anchor impellers are shown in Fig. 18-43. The typical anchor impellers have two vertical arms with a blade width W equal to one-tenth of the impeller diameter D , and the arm height H equal to the impeller diameter D . Correlations are shown for typical impellers 95 and 90 percent of the tank diameter. The clearance C is one-half of the difference between the impeller diameter and the tank diameter, or 2.5 and 5.0 percent of the tank diameter for the respective correlations. An additional correlation is shown for an anchor with three vertical arms and a diameter equal to 95 percent of the tank diameter. The correlation for a three-arm impeller which anchors 90 percent of the tank diameter is the same as that for the typical anchor 95 percent of the tank diameter.

The power number and corresponding power of an anchor impeller are proportional to the height of the vertical arm. Thus, an anchor with a height H equal to 75 percent of the impeller diameter would have a power number equal to 75 percent of the typical values shown in Fig. 18-43. Similarly, a partially filled tank with a liquid level Z that covers only 75 percent of the vertical arm will also have a power number that is 75 percent of the typical correlation value. The addition of scrapers will increase the power requirement for an anchor impeller, but the effect depends on the clearance at the wall, design of the scrapers, processed material, and many other factors. Correlations are not practical or available.

Unfortunately, the power number only provides a relationship between impeller size, rotational speed, and fluid properties. The power number does not tell whether a mixer will work for an application. Successful operating characteristics for an anchor mixer usually depend on experience with a similar process or experimentation in a pilot plant. Scale-up of pilot-plant experience is most often done for a geometrically similar impeller and equal tip (peripheral) speed.

Helical Ribbon Mixers Helical ribbon mixers (Fig. 18-44), or simply helix mixers, have major advantages over the anchor mixer, because they force strong top-to-bottom motion even with viscous

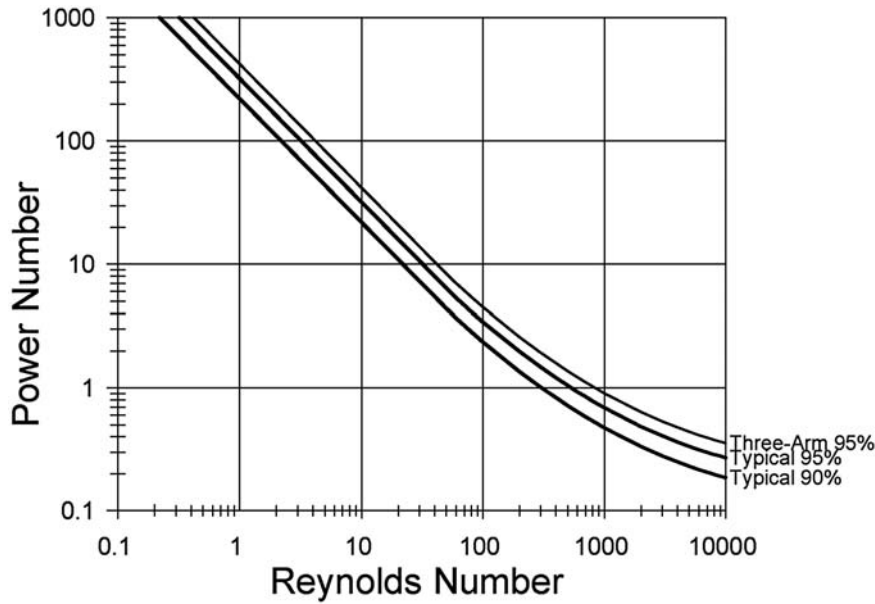


FIG. 18-43 Power numbers for anchor impellers: typical two-arm impeller anchors 95 percent of tank diameter T and 90 percent of T ; three-arm impeller anchors 95 percent of T ; and three-arm impeller anchors 90 percent of T , similar to two-arm impeller that anchors 95 percent of T .

materials. These impellers are some of the most versatile mixing impellers, but also some of the most expensive. Besides having a formed helical shape, the blades must be rolled the hard way with the thick dimension normal to the direction of the circular rolled shape. Helical ribbon mixers will work with most viscous fluids up to the lim-

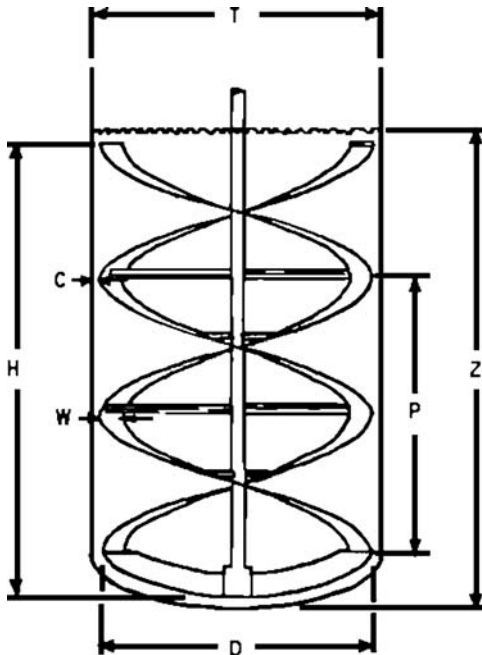


FIG. 18-44 Helical ribbon impeller with nomenclature.

its of a flowable material, as high as 4,000,000 cP or more depending on non-newtonian characteristics. While not cost-effective for low-viscosity materials, they will adequately mix, and even suspend solids, in low-viscosity liquids. These characteristics make helical ribbon mixers effective for batch processes, such as polymerization or other processes beginning with low-viscosity materials and changing to high-viscosity products. Helical ribbon mixers will even work with heavy pastes and flowable powders. Usually the helix pumps down at the tank wall with fluids and up at the wall with pastes or powders.

The helical ribbon power numbers are a function of Reynolds number similar to the correlations for anchor impellers. Figure 18-45 shows correlations for some typical helical ribbon power numbers. The upper curve is for a double-flight helix with the blade width W equal to one-tenth the impeller diameter D , the pitch P equal to the impeller diameter, and the impeller diameter at 95 percent of the tank diameter T . The height H for this typical helix is equal to the impeller diameter and pitch, not 15 times the pitch, as shown in Fig. 18-45. A second curve shows the power number correlation for a helical ribbon impeller that is 90 percent of the tank diameter. The curve marked "Single 90%" is for a single flight helix, 90 percent of the tank diameter. Each ribbon beginning at the bottom of the impeller and spiraling around the axis of the impeller is called a flight. Single-flight helices are theoretically more efficient, but a partially filled tank can cause imbalanced forces on the impeller. The correlation for a 95 percent diameter single-flight helix is the same as the correlation for the double-flight 90 percent diameter helix.

Example 1: Calculate the Power for a Helix Impeller Calculate the power required to rotate a double-flight helix impeller that is 57 in in diameter, 57 in high, with a 57-in pitch operating at 30 rpm in a 60-in-diameter tank. The tank is filled 85 percent full with a 100,000-cP fluid, having a 1.05 specific gravity.

$$N_{re} = \frac{10.4 D^2 N \text{ sp gr}}{\mu} = \frac{10.4(57)^2(30)(1.05)}{100,000} = 10.6$$

Referring to Fig. 18-45, the power number N_p for the full-height helix impeller is 27.5 at $N_{re} = 10.6$. At 85 percent full, the power number is $0.85 \times 27.5 = 23.4$. Power can be calculated by rearranging Eq. (18-22).

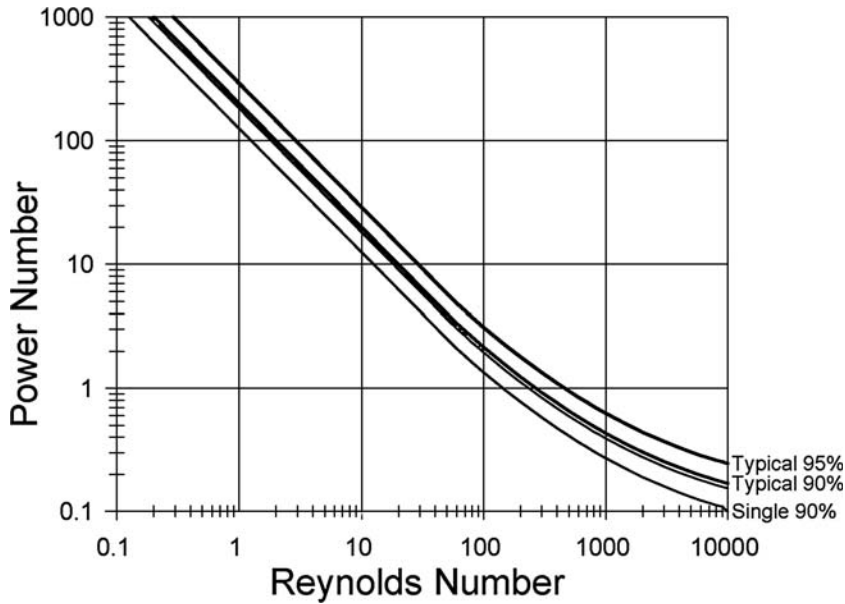


FIG. 18-45 Power numbers for helical-ribbon impeller: typical double-flight helixes 95 percent of tank diameter T and 90 percent of T ; single-flight helix 90 percent of T ; single-flight 95 percent of T similar to double-flight 90 percent of T .

$$P = \frac{N_{Fsp} \text{ gr } N^3 D^5}{1.524 \times 10^{13}} = \frac{23.4(1.05)(30)^3(57)^5}{1.524 \times 10^{13}} = 26.2 \text{ hp}$$

Helical ribbon mixers can also be formed to fit in conical bottom tanks. While not as effective at mixing as in a cylindrical tank, the conical bottom mixer can force material to the bottom discharge. By more effectively discharging, a higher yield of the product can be obtained.

Planetary Mixers A variation on the single anchor mixer is essentially a double anchor mixer with the impellers moving in a planetary pattern. Each anchor impeller rotates on its own axis, while the pair of intermeshing anchors also rotates on the central axis of the tank. The intermeshing pattern of the two impellers gives a kneading action with blades alternately wiping each other. The rotation around the central axis also creates a scraping action at the tank wall and across the bottom. With successive rotations of the impellers, all the tank contents can be contacted directly. A typical planetary mixer is shown in Fig. 18-46.

The intimate mixing provided by the planetary motion means that the materials need not actively flow from one location in the tank to another. The rotating blades cut through the material, creating local shear and stretching. Even thick pastes and viscoelastic and high-viscosity fluids can be mixed with planetary mixers. The disadvantage of poor top-to-bottom motion still exists with conventional planetary mixers. However, some new designs offer blades with a twisted shape to increase vertical motion.

To provide added flexibility and reduce batch-to-batch turnaround or cross-contamination, a change-can feature is often available with planetary and other multishaft mixers. The container (can) in a change-can mixer is a separate part that can be rapidly exchanged between batches. Batch ingredients can even be put in the can before it is placed under the mixing head. Once the mixing or processing is accomplished, the container can be removed from the mixer and taken to another location for packaging and cleaning. After one container is removed from the mixer and the blades of the impeller are cleaned, another batch can begin processing. Because the cans are relatively inexpensive compared with the cost of the mixer head, a change-can mixer can be better utilized and processing costs can be reduced.



FIG. 18-46 Planetary mixer. (Charles Ross & Son Company.)

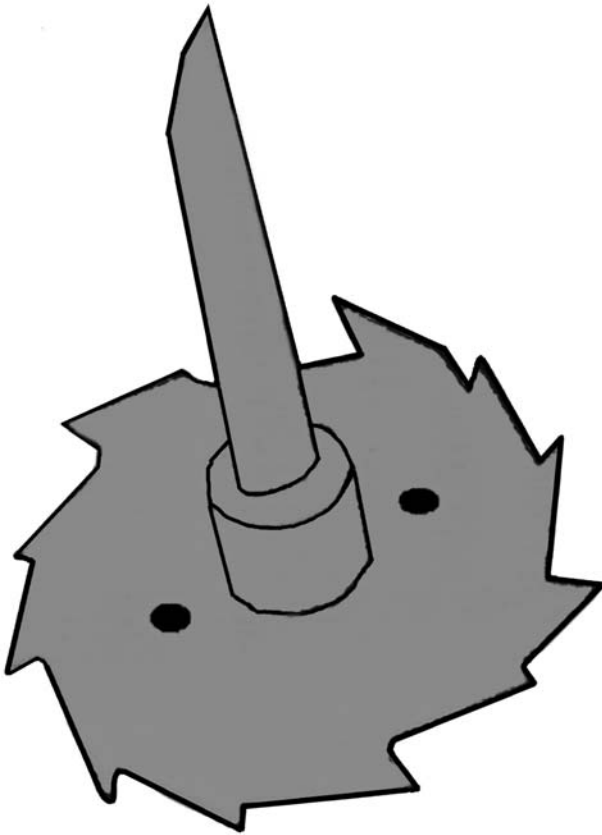


FIG. 18-47 High-shear impeller.

Double- and Triple-Shaft Mixers The planetary mixer is an example of a double shaft mixer. However, many different combinations of mixing actions can be achieved with multi-shaft mixers. One variation on planetary motion involves replacing one anchor-style impeller with a high-shear impeller similar to the one shown in Fig. 18-47. The high-shear mixer can be used to incorporate powdered material effectively or create a stable emulsion leading to a final batch of viscous paste or fluid.

Many types of multishaft mixers do not require planetary motion. Instead the mixers rely on an anchor-style impeller to move and shear material near the tank wall, while another mixer provides a different type of mixing. The second or third mixer shafts may have a pitched-blade turbine, hydrofoil impeller, high-shear blade, rotor-stator mixer, or other type of mixer. The combination of multiple impeller types adds to the flexibility of the total mixer. Many batch processes involve different types of mixing over a range of viscosities. Some mixer types provide the top-to-bottom motion that is missing from the anchor impeller alone.

Double-Arm Kneading Mixers A double-arm kneader consists of two counter-rotating blades in a rectangular trough with the bottom formed like two overlapping or adjacent half-cylinders (Fig. 18-48). The blades are driven by gearing at one or both ends. The older-style kneaders emptied through a door or valve at the bottom. Those mixers are still used where complete discharge or thorough cleaning between batches is not essential. More commonly, double-arm kneaders are tilted for discharge. The tilting mechanism may be manual, mechanical, or hydraulic, depending on the size of the mixer and weight of the material.

A variety of blade shapes have evolved for different applications. The mixing action is a combination of bulk movement, shearing,

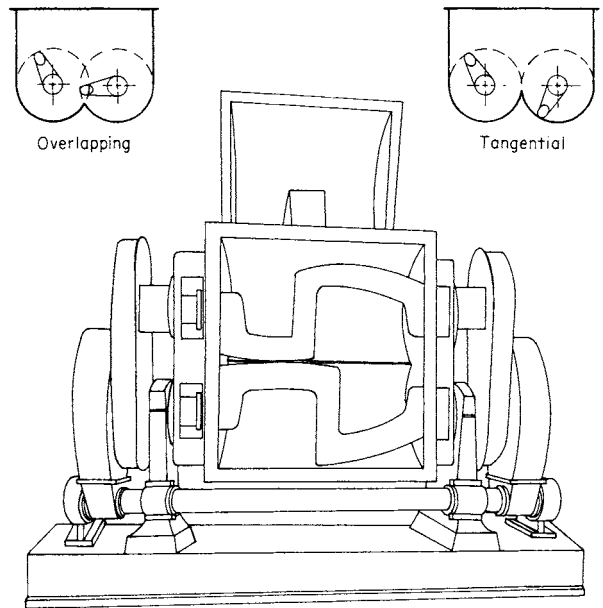


FIG. 18-48 Double-arm kneader. (APV Baker Incensys.)

stretching, folding, dividing, and recombining. The material being mixed is also squeezed and stretched against the blades, bottom, and sidewalls of the mixer. Clearances may be as close as 1 mm (0.04 in). Rotation is usually such that the material is drawn down in the center between the blades and up at the sidewalls of the trough. Most of the blades are pitched to cause end-to-end motion.

The blades can be tangential or overlapping. Tangential blades can run at different speeds with the advantages of faster mixing caused by changes in the relative position of the blades, greater heat-transfer surface area per unit volume, and less tendency for the material to ride above the blades. Overlapping blades can reduce the buildup of material sticking to the blades.

Because the materials most commonly mixed in kneaders are very viscous, often elastic or rubbery materials, a large amount of energy must be applied to the mixer blades. All that energy is converted to heat within the material. Often the material begins as a semisolid mass, with liquid or powder additives, and the blending process both combines the materials and heats them to create uniform bulk properties.

The blade design most commonly used is the sigma blade (Fig. 18-49a). The sigma-blade mixer can start and operate with either liquids or solids, or a combination of both. Modifications to the blade faces have been introduced to increase particular effects, such as shredding or wiping. The sigma blades can handle elastic materials and readily discharge materials that do not stick to the blades. The sigma blades are easy to clean, even with sticky materials.

The dispersion blade in Fig. 18-49b was developed to provide higher compressive shear than the standard sigma blade. The blade shape forces material against the trough surface. The compressive action is especially good for dispersing fine particles in a viscous material. Rubbery materials have a tendency to ride the blades, and a dispersion blade is frequently used to keep the material in the mixing zone.

Multiwiping overlapping (MWOL) blades (Fig. 18-49c), are commonly used for mixtures that start tough and rubberlike. The blade shape initially cuts the material into small pieces before plasticating it.

The single-curve blade (Fig. 18-49d), was developed for incorporating fiber reinforcement into plastics. In this application the individual fibers, e.g., glass, must be wetted with the polymer without undue fiber breakage.

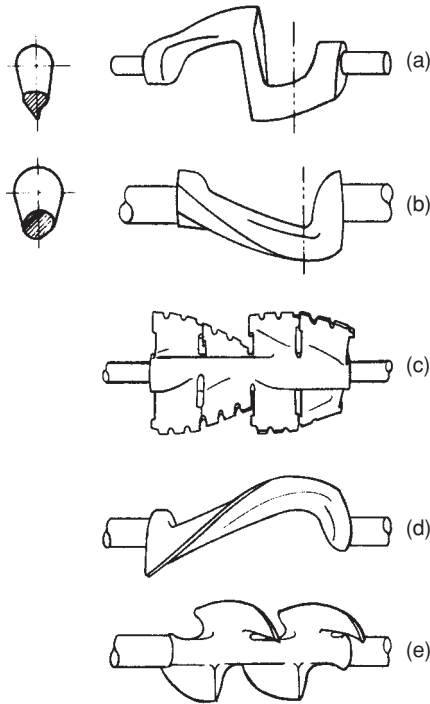


FIG. 18-49 Agitator blades for double-arm kneader: (a) Sigma; (b) dispersion; (c) multiwiping; (d) single-curve; (e) double-naben. (APV Baker Incensys.)

Many other designs have been developed for specific applications. The double-naben blade (Fig. 18-49e), is good for mixtures which "ride," meaning they form a lump that bridges across the sigma blade.

Figure 18-50 provides a guide for some typical applications of double-arm mixers. Individual formulations may require more power.

Screw-Discharge Batch Mixers A variant of the sigma-blade mixer has an extrusion-discharge screw located at the center of the

Character of Material	Material and Blade Type	Blade interaction	
		Tangential	Overlapping
Semi-solid	Enamel (dispersion)	X	X
	Floor tile (sigma)	X	XX
	Flush colors (sigma)	X	X
	Brake lining (sigma)	X	X
	Adhesive (sigma)	X	X
Plastic mass	Toothpaste (dispersion)	X	X
	Molding (mod. sigma)	X	X
	Cookie dough (sigma)	X	X
Paste	Epoxy resin (sigma)	X	X
	Dog food (sigma)	X	X
	Gravy base (sigma)	X	X

FIG. 18-50 Typical application and power for double-arm kneaders. To convert horsepower per gallon to kilowatts per cubic meter, multiply by 197.3. [Parker, Chem. Eng. 72(18): 125 (1965); excerpted by special permission of the copyright owner, McGraw-Hill, Inc.]

trough, just below the rotating blades. During the mixing cycle the screw moves the material within the reach of the mixing blades, thus accelerating the mixing process. At discharge time, the screw extrudes the finished material through a die opening in the end of the machine. The discharge screw is driven independently of the mixer blades.

INTENSIVE MIXERS

Banbury Mixers The dominant high-intensity mixer, with power input up to 6000 kW/m³ (30 hp/gal), is the Banbury mixer made by Farrel Co. (Fig. 18-51). It is used primarily in the plastics and rubber industries. The batch charge of material is forced into the mixing chamber by an air-operated ram at the top of the mixer. The clearance between the rotors and the walls is extremely small. The mixing action takes place in that small gap. The rotors of the Banbury mixer operate at different speeds, so one rotor can drag material against the rear of the other and thus clean ingredients from behind and between the rotors.

The extremely high power consumption of these machines, which operate at speeds of 40 rpm or less, requires large-diameter shafts. The combination of heavy shafts, stubby blades, close clearances, and

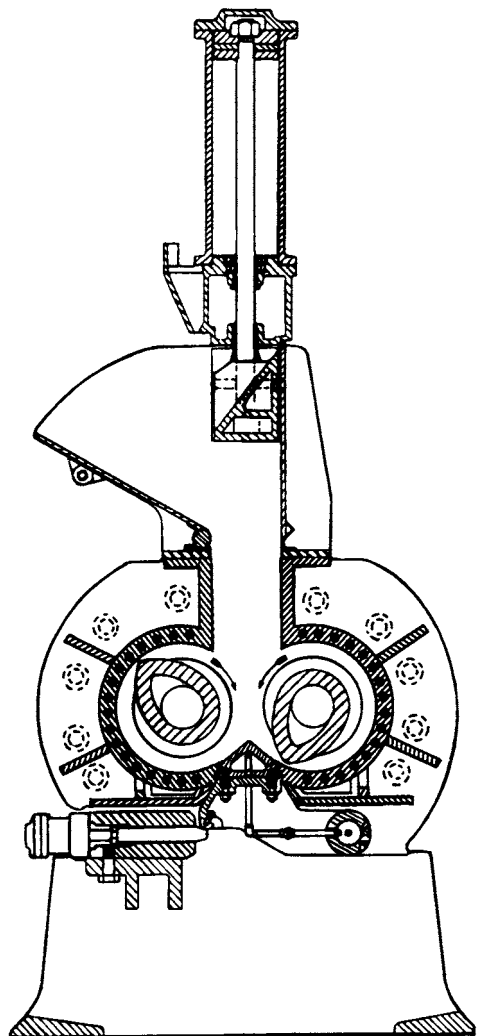


FIG. 18-51 Banbury mixer. (Farrel Co.)

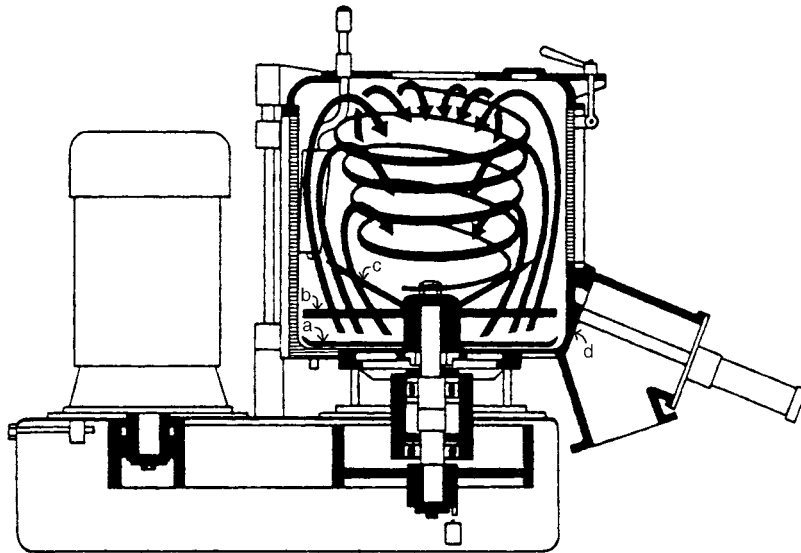


FIG. 18-52 High-intensity mixer: (a) bottom scraper; (b) fluidizing tool; (c) horn tool; (d) flush-mounted discharge valve. (Henschel Mixers America, Inc.)

a confined charge limits the Banbury mixer to small batches. The production rate is increased as much as possible by using powerful drives and rotating the blades at the highest speed that the material can tolerate without degradation. The heat added by the high-power input often limits operating conditions because of temperature limits on the material being mixed. Equipment is available from laboratory size to a mixer that can handle a 450-kg (1000-lb) charge and applying 2240 kW (3000 hp).

High-Intensity Mixers Mixers, such as the one shown in Fig. 18-52, combine a high-shear zone with a fluidized vortex for mixing of pastes and powders. Blades at the bottom of the vessel scoop the material upward with peripheral speeds of about 40 m/s (130 ft/s). The high-shear stresses between the blade and the bowl, along with blade impact, easily reduce agglomerates and create an intimate dispersion of powders and liquids. Because the energy input is high, 200 kW/m³ (8 hp/ft³), even powdery material can heat rapidly.

These mixers are particularly suited for the rapid mixing of powders and granules with liquids, for dissolving resins or solids in liquids, or for removal of volatiles from pastes under a vacuum. Scale-up is usually based on constant peripheral speed of the impeller.

Roll Mills Roll mills can provide extremely high localized shear while retaining extended surface area for temperature control. A typical roll mill has two parallel rolls mounted in a heavy frame with provisions for accurately regulating the pressure and distance between the rolls. Since one pass between the rolls does only a little blending, the mills are usually used as a series of mixers. Only a small amount of material is in the high-shear zone at a time, thus allowing time and exposure for cooling.

To increase the shearing action, the rolls are usually operated at different speeds. The material passing between the rolls can be returned to the feed by the rotation of the rolls. If the rolls are at different temperatures, the material will usually stick to the hotter roll and return to the feed point as a thick layer.

At the end of a period of batch mixing, heavy materials may be discharged by simply dropping from between the rolls. Thin, lighter mixes may be removed by a scraper bar pressing against the descending surface of one of the rolls. Roll mixers are used primarily for preparing color pastes for inks, paints, and coatings. A few applications in heavy-duty blending of rubber stocks use corrugated rolls for masticating the material.

Miscellaneous Batch Mixers Many mixers used for solids blending (Sec. 19 of seventh edition) are suitable for liquid-solids blending.

Some solids processing applications involve the addition of liquids, and the same blenders may transition from dry powders to cohesive pastes.

Ribbon blenders typically have multiple helical ribbons with opposing pitches operating in a horizontal trough with a half-cylinder bottom. These mixers can be used for wetting or coating a powder. The final product may have a paste consistency, but must remain at least partially flowable for removal from the blender.

Plowshare mixers have plow-shaped blades mounted at the ends of arms on a horizontal rotating shaft in a cylindrical chamber. The shaft rotates at a sufficient speed to toss the material into the free space in the vessel. The angled surfaces of the plow-shaped blades provide additional intermixing and blending in the bed of solids. High-speed (3600-rpm) chopper blades mounted in the lower side of the mixing chamber can disperse fine particles or break agglomerates. Mixers are available in sizes from 0.03- to 30-m³ (1.0- to 1000-ft³) working capacity. Plowshare mixers can be used for either batch or continuous processing.

Conical mixers are also known as Nauta mixers (Fig. 18-53). Material placed in the conical bin is lifted by the rotation of the helical screw, which in turn is rotated around the wall of the cone. The lifting actions of the screw combined with motion around the cone provide bulk mixing for flowable dry powders, paste materials, and even viscous fluids. The specific energy input is relatively small, and the large volume of the mixers can even provide storage capacity. The mixers may have multiple screws, tapered screws, and high-speed dispersers for different applications. At constant speed, both the mixing time and power scale up with the square root of volume. Sizes from 0.1 to 20 m³ (3.3 to 700 ft³) are available.

Pan mullers are the modern industrial equivalent of the traditional mortar and pestle. Typical mullers have two broad wheels (M1 and M2) on an axle (Fig. 18-54). The mixer rotates about the approximate midpoint of the axle, so that the wheels both rotate and skid over the bottom of the mixing chamber (A). Plow blades (P1 and P2), which rotate with the mixer, push material from the center (T) and walls (C) of the mixing chamber into the path of the rollers. The mixing action combines both crushing and shearing to break lumps or agglomerates and evenly distribute moisture.

Mullers can be used if the paste is not too fluid or sticky. The main application of muller mixers is now in the foundry industry to mix small amounts of moisture and binder with sand for both core and molding sand. Muller mixers also handle such diverse materials as



FIG. 18-53 Day Nauta conical mixer. (Littleford Day, Inc.)

clay, storage-battery paste, welding-rod coatings, and chocolate coatings. Standard muller mixers range in capacity from 0.01 to 1.7 m³ (0.4 to 60 ft³), with power requirements from 0.2 to 56 kW (1/3 to 75 hp).

A continuous muller design employs two intersecting and communicating chambers, each with its own mullers and plows. At the point of intersection of the two chambers, the outside plows give an approximately equal exchange of material from one chamber to the other. Material builds in the first chamber until the feed rate and the discharge rate of the material are equal. The quantity of material in the muller is regulated by adjusting the outlet gate.

CONTINUOUS MIXERS

Some batch mixers previously described can be modified for continuous processing. Product uniformity may be limited because of broad residence time distributions. If ingredients can be accurately metered,

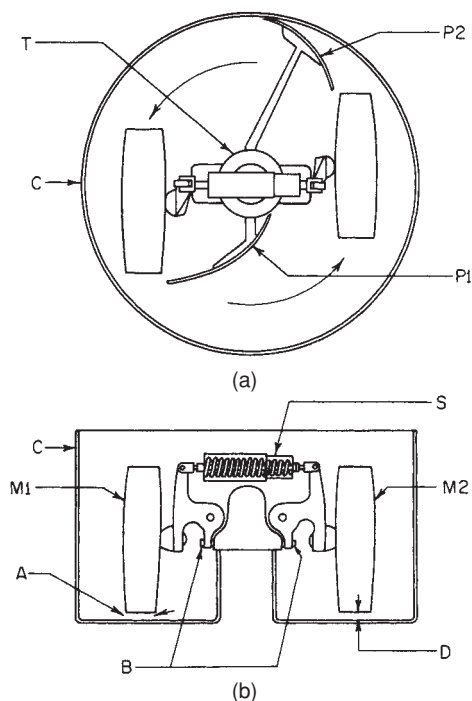


FIG. 18-54 Pan muller: (a) plan view; (b) sectional elevation. [Bullock, Chem. Eng. Prog. 51: 243 (1955); by permission.]

which can be a problem with powdered or viscous materials, several continuous mixers are available. Continuous mixers often consist of a closely fitting agitator element rotating within a stationary housing.

Single-Screw Extruders The use of extruders, like the one shown in Fig. 18-55, is widespread in the plastic industries. The quality and utility of the product often depend on the uniformity of additives, stabilizers, fillers, etc. A typical extruder combines the process functions of melting the base resin, mixing in additives, and developing the pressure required for shaping the product into pellets, sheet, or profiles. Dry ingredients, sometimes premixed in a batch blender, are fed into the feed throat where the channel depth is deepest. As the root diameter of the screw is increased, the plastic is melted by a combination of friction and heat transfer from the barrel. Shear forces can be very high, especially in the melting zone. The mixing is primarily a laminar shear action.

Single-screw extruders can be built with a long length-to-diameter ratio to permit sufficient space and residence time for a sequence of process operations. Capacity is determined by diameter, length, and power. Most extruders are in the 25- to 200-mm-diameter range. Larger units have been made for specific applications, such as polyethylene homogenization. Mixing enhancers (Fig. 18-56) are used to provide both elongation and shearing action to enhance dispersive (axial) and distributive (radial) mixing.

The maximum power (P in kilowatts) supplied for single-screw extruders varies with the screw diameter (D in millimeters) approximately as

$$P = 5.3 \times 10^{-3} D^{2.25} \quad (18-24)$$

The energy required for most polymer mixing applications is from 0.15 to 0.30 kWh/kg (230 to 460 Btu/lb).

Twin-Screw Extruders Two screws in a figure-eight barrel have the advantage of interaction between the screws plus action between the screws and the barrel. Twin-screw extruders are used to melt continuously, mix, and homogenize different polymers and additives. Twin-screw extruders can also be used to provide the intimate

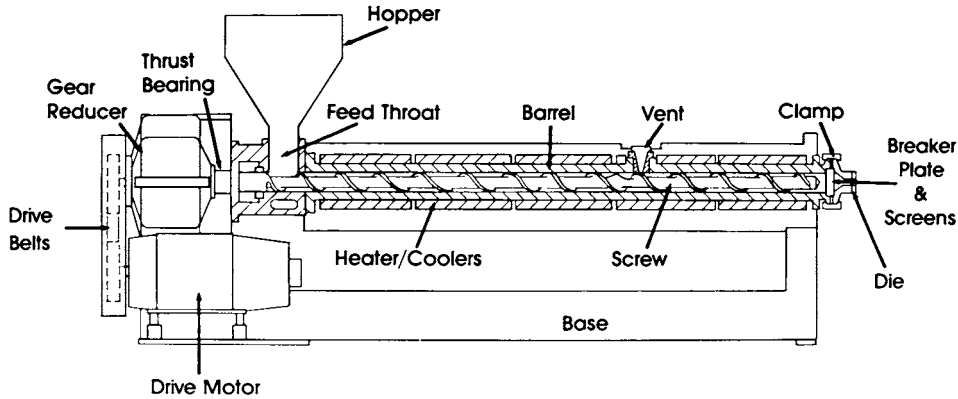


FIG. 18-55 Single-screw extruder. (Davis Standard.)

mixing needed to carry out chemical reactions in high-viscosity materials. The screws can be either tangential or intermeshing, with the latter either corotating or counterrotating. Tangential designs allow variability in the channel depth and permit longer lengths.

The most common twin-screw extruder is the counterrotating intermeshing type. The counterrotating intermeshing screws provide a dispersive milling action between the screws and the ability to generate pressure efficiently. The two keyed or splined shafts are fitted with pairs of slip-on kneading or conveying elements, as shown in Fig. 18-57. Each pair of kneading paddles causes an alternating compression and expansion effect that massages the contents and provides a combination of shearing and elongational mixing actions. The arrays of elements can

be varied to provide a wide range of mixing effects. The barrel sections are also segmented to allow for optimum positioning of feed ports, vents, barrel valves, etc. The barrels may be heated electrically or with oil or steam and cooled with air or water.

Counterrotating twin-screw extruders are available in diameters ranging from 15 to 300 mm (0.5 to 12 in), with length-to-diameter ratios up to 50 and throughput capacities to 7 kg/s (55,000 lb/h). Screw speeds can be as high as 8 r/s (500 rpm) in small production extruders. Residence times for melting are usually less than 120 s (2 min).

Farrel Continuous Mixer The Farrel mixer (Fig. 18-58) consists of rotors similar in cross section to the Banbury batch mixer. The first section of the rotor acts as a screw conveyor, moving the feed ingredients into the mixing section. The mixing action is a combination of intensive shear between the rotor and chamber wall, kneading between the rotors, and a rolling action within the material itself. The amount and quality of mixing are controlled by adjustment of speed, feed rate, and discharge orifice opening. Mixers are available with chamber volumes up to 0.12 m³ (4.2 ft³). With speeds to 3.3 r/s (200 rpm), the power range is from 5 to 2200 kW (7.5 to 3000 hp).

Miscellaneous Continuous Mixers Because of the diversity of material properties and process applications involving viscous fluids, pastes, and doughs, the types of mixers are almost as diverse.

Trough-and-screw mixers usually consist of a single rotor or twin rotors that continually turn the feed material over as it progresses toward the discharge end of the mixer. Some mixers have been designed with extensive heat-transfer surface area. The continuous-screw, **Holo-Flite processor** (Fig. 18-59) is used primarily for heat transfer, since the hollow screws provide extended surfaces without creating much shear. Two or four screws may be used.

Another type of trough-and-screw mixer is the **AP Conti paste mixer**, shown in Fig. 18-60. These self-cleaning mixers are particularly appropriate when the product being handled goes through a sticky stage, which could plug the mixer or foul the heat-transfer surfaces.

Pug mills have one or two shafts fitted with short heavy paddles, mounted in a cylinder or trough holding the material to be processed. In the two-shaft mills the shafts are parallel and may be either horizontal or vertical. The paddles may or may not intermesh. Clearances are wide, so considerable mass mixing takes place. Unmixed or partially mixed ingredients are fed at one end of the machine, which is usually totally enclosed. Liquid may be added to the material entering the mixer. The paddles push the material forward as they cut through it. The action of the paddles carries the material toward the discharge end of the mixer. The product may discharge through one or two open ports or through extrusion nozzles. The nozzles create roughly shaped continuous strips of material. Automatic cutters may be used to make blocks or pellets from the strips. Pug mills are most often used for mixing mineral or clay products.

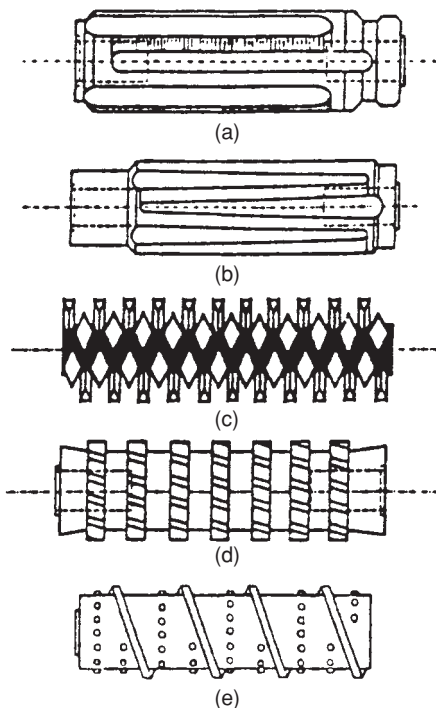


FIG. 18-56 Mixing enhancers for single-screw extruders: (a) Maddock, straight; (b) Maddock, tapered; (c) pineapple; (d) gear; (e) pin.

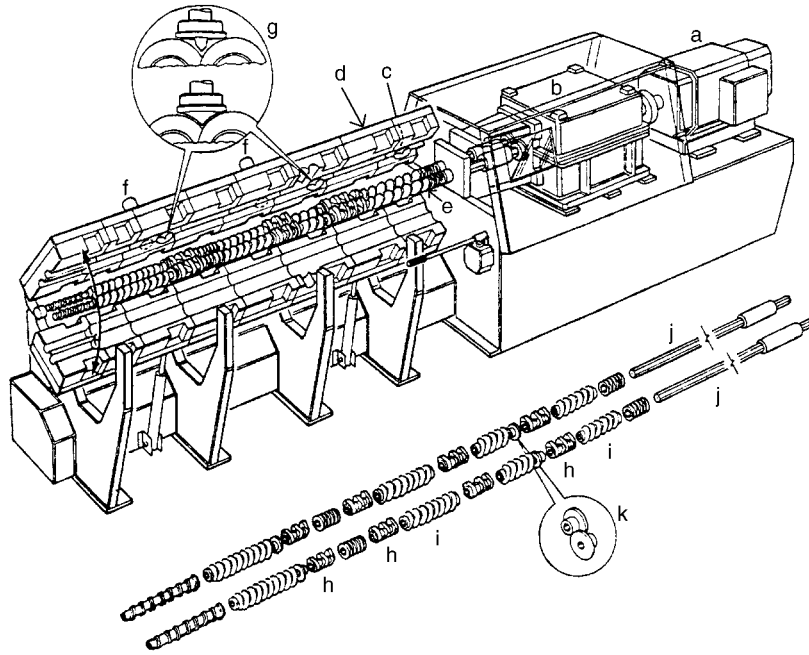


FIG. 18-57 Intermeshing corotating twin-screw extruder: (a) drive motor; (b) gearbox; (c) feed port; (d) barrel; (e) assembled rotors; (f) vent; (g) barrel valve; (h) kneading paddles; (i) conveying screws; (j) splined shafts; (k) blister rings. (APV Chemical Machinery, Inc.)

Motionless mixers are an alternative to rotating impeller mixers. Motionless or static mixers use stationary shaped elements inside pipes or conduits to divide, divert, twist, and recombine flowing material. The dividing, stretching, and recombining processes lead to thinner and thinner striations in viscous materials to achieve uniformity.

The twisted-element mixers, such as the **Kenics static mixer** (Fig. 18-61), create 2^n layers in n divisions. Each element twists the flow, moving material from the center to the wall and from the wall to the center. The twisting also stretches striations having different properties and reorients the material before the next division. The following element

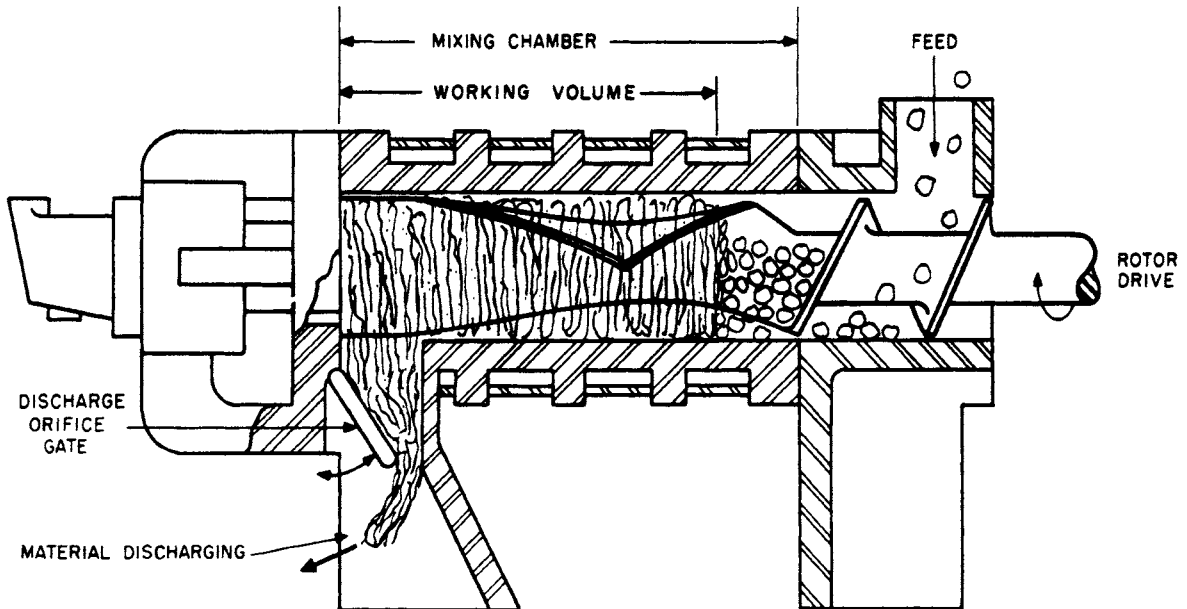


FIG. 18-58 Farrel continuous mixer. (Farrel Co.)

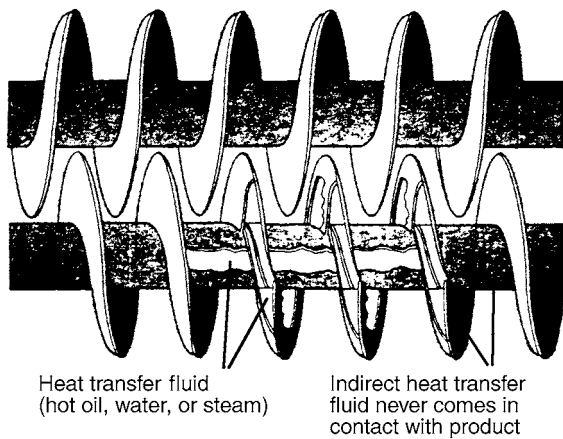


FIG. 18-59 Holo-Flite Processor. (Metso Minerals.)

twists the divided material in the opposite direction. The more viscous the material, the more mixing elements are required for uniformity.

Other motionless designs, such as the **Sulzer static mixer** (Fig. 18-62), accomplish mixing by making multiple divisions at each element transition. The flowing material follows a wavy path to stretch and distort the striations. The number of divisions and distorted paths causes more rapid mixing, but at the expense of a greater pressure drop per unit length of the mixer.

The power required to accomplish mixing in a motionless mixer is provided by the pump used to force the fluid through the mixer. The pressure drop through a motionless mixer is usually expressed as a multiplier K of the open pipe loss or as a valve coefficient C_V . The value of the multiplier is strongly dependent on the detail geometry of the mixer, but is usually available through information from the supplier. Fluid properties are taken into account by the value of the Reynolds

number for the open pipe. Motionless mixers are usually sized to match the diameter of the connecting pipe. Pumping adjustments are made when necessary to handle the increased pressure drop.

Because motionless mixers continuously interchange fluid between the walls and the center of the conduit, they also provide good heat transfer, especially with the twisted-element style of mixers. Sometimes, high-viscosity heat exchange is best accomplished with a static mixer.

Distributive (radial) mixing is usually excellent; dispersive (axial) mixing is often poor. The result can be a good plug-flow mixer or reactor, with corresponding benefits and limitations.

PROCESS DESIGN CONSIDERATIONS

Scale-up of Batch Mixers While a desirable objective of scale-up might be equal blending uniformity in equal time, practicality dictates that times for blending are longer with larger batches. Scale-up of many processes and applications can be successfully done by holding constant the peripheral speed of the rotating element in the mixer. Equal peripheral speed, often called *equal tip speed*, essentially means that the maximum velocity in the mixer remains constant.

Perhaps one of the most difficult concepts to grasp about viscous mixing is that, unlike in turbulent mixing, greater mixer speed does not always translate to better mixing results. If a rotating mixer blade cuts through a viscous fluid or heavy paste too quickly, the stretching process that reduces striation thickness does not take place throughout the material. At high rotational speeds, rapid shearing between a blade tip and the wall or housing may take place, but flow to create bulk motion may not have time to occur. Thus, slower speeds may actually give better mixing results.

With geometric similarity, equal tip speed means that velocity gradients are reduced and blend times become longer. However, power per volume is also reduced, and viscous heating problems are likely to be more controllable. With any geometric scale-up, the surface-to-volume ratio is reduced, which means that any internal heating, whether by viscous dissipation or chemical reaction, becomes more difficult to remove through the surface of the vessel.

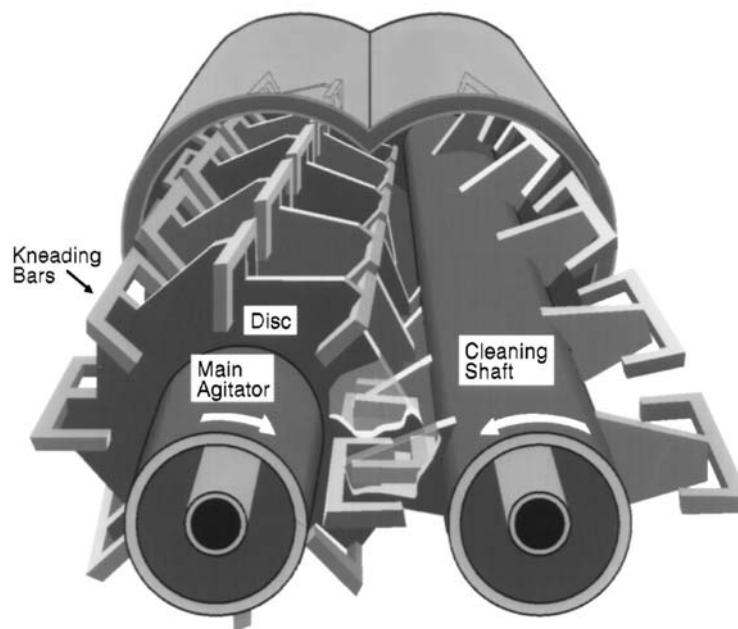


FIG. 18-60 AP Conti paste mixer. (LIST, Inc.)



FIG. 18-61 Kenics static mixer. (Chemineer, Inc.)

In many applications the blend time is closely related to the actual number of revolutions made by the mixing device. Thus if mixing were successfully accomplished in 5 min at 60 rpm in a small mixer, the same uniformity could be achieved in 10 min at 30 rpm in a larger mixer. Other factors, such as the rate of heating, could limit scale-up and mixing times.

The physical properties of a paste are difficult to define because a combination of yield stress, shear dependence, time dependence, and even elasticity may be present. Further, many process applications involve the formation or modification of the physical properties. To relate accurately specific material properties to mixing characteristics or power requirements can be extremely difficult. Actual observation and measurement in small-scale equipment or comparison with similar existing processes may be the only practical way of predicting successful operating conditions. Power measurements in small-scale equipment are often essential to predict large-scale conditions and may form the basis for operating production equipment.

Scale-up of Continuous Mixers While geometric similarity may be practical for most batch mixers, changes in the length-to-diameter ratio or other geometry may be necessary with continuous mixers. The most common problem is heat generation by friction and heat removal by surface transfer.

In single-screw extruders, e.g., Fig. 18-55, channel depth in the flights cannot be increased in proportion to the screw diameter because the distribution of heat generated by friction at the barrel wall requires more time as the channel depth becomes greater. With constant retention time, therefore, a nonhomogeneous product would be discharged from a geometrically similar large-scale extruder.

As the result of the departure from geometric similarity, the throughput rate of single-screw extruders scales up with the diameter to 2.0 to 2.5 power, instead of the diameter cubed, at constant length-to-diameter and screw speed. The throughput rates of twin-screw extruders (Fig. 18-57) and the Farrel continuous mixer (Fig. 18-58) are scaled up with the diameter to about the 2.6 power.

The extent of axial dispersion through a continuous mixer can be characterized either by an axial diffusion coefficient or by analogy to a number of well-mixed stages in series. Retention time can control the performance of a mixing system. As the number of apparent stages increases, the greater is the assurance that all the material will have the required residence time. Under conditions requiring uniform retention time, the feed streams must enter at the correct ratio on a time scale much shorter than the average residence time of the mixer. Otherwise, variations in the feed will appear as changes in the product. Different types of continuous mixers have different degrees of axial dispersion. Thus, appropriate feed conditions must be considered. Single-screw extruders have an equivalent number of stages equal to approximately one-half the length-to-diameter ratio.

HEATING AND COOLING MIXERS

Heat Transfer Pastes and viscous fluids are often heated or cooled by heat transfer through the walls of the mixing container or hollow mixing arms. A uniform temperature throughout the bulk material is almost as important for good heat transfer as a large heat-transfer surface to mixer volume ratio. Bulk temperature uniformity

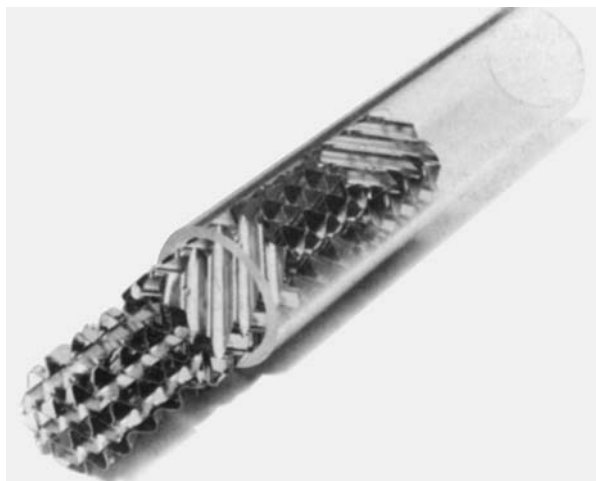


FIG. 18-62 Sulzer static mixer. (Sulzer Chemtech.)

will maximize the temperature-difference driving force for heat transfer. Surface area is a direct factor in overall heat transfer. Effective motion near the surface promotes convection over conduction for better heat transfer. Most mixers for pastes or viscous fluids have some sort of scraper or close-clearance device to move stagnant material away from heat-transfer surfaces.

Typical overall heat-transfer coefficients are between 20 and 200 $J/(m^2 \cdot s \cdot K)$ [4 to 35 $Btu/(h \cdot ft^2 \cdot ^\circ F)$].

Heating Methods Steam heating is widely used because it is economical, safe, and easily controlled. The mixer shell must be designed to withstand both the positive pressure of steam and a vacuum caused when the steam condenses. Transfer liquid heating, using water, oil, special organic liquids, or molten salts, permits good temperature control and provides insurance against overheating the process material. Jackets for transfer liquids are usually baffled to provide good circulation. Higher temperatures can be achieved without the heavy vessel construction required by steam pressures.

Electric heating requires that the elements be electrically insulated from the vessel, while still providing good thermal contact. The heaters must be designed for uniform heating to avoid creating hot spots. Temperature control can be precise, maintenance costs low, but utility costs can be very high for large mixers. Electrical heating may be excluded when flammable vapors or dusts are present.

Friction or viscous heating develops rapidly in some mixers, such as a Banbury mixer. The first temperature rise may be beneficial in softening the materials and accelerating chemical reactions. Because energy inputs can be high, higher temperatures detrimental to the products may develop rapidly. So cooling may be required during other portions of a process.

Cooling Methods Air cooling with air blown over external surfaces or external fins may be sufficient for some mixers. Evaporation of excess water or solvent under a vacuum or ambient pressure provides good cooling. A small amount of evaporation produces a large amount of cooling. However, removing too much solvent may damage the product. Some mixers are cooled by circulation of water or refrigerants through jackets or hollow agitators. With viscous fluids, lower temperatures near the cooled surfaces increase viscosity and make heat transfer more difficult.

EQUIPMENT SELECTION

The most common and sometimes the only available approach is by analogy. Many companies manufacture similar products, either of their own or those of competitors. With similar products, both good and bad features of existing or typical mixing equipment need to be considered carefully. Some types of mixing equipment are commonly

used throughout certain industries. Sometimes existing equipment can be adapted to a new process. Otherwise, new equipment will be needed.

If new equipment is needed, laboratory or pilot-plant studies are recommended. Often unique product features involve unusual or special fluid properties, which makes prediction of mixer performance almost impossible. The objective is to find potentially suitable equipment and test available mixers. Most equipment vendors have equipment to rent or a demonstration laboratory to test their mixers.

The following list provides some characteristics of a new process that must be considered:

1. List all materials in the process and describe their characteristics.
 - a. Method of delivery to the mixer: bags, drums, tote sacks, bulk, pipeline, etc.
 - b. Storage and/or weighing requirements at the mixer
 - c. Physical form of the material
 - d. Specific gravity and bulk characteristics
 - e. Particle size or size range
 - f. Viscosity
 - g. Melting, boiling, or degradation point
 - h. Corrosive properties
 - i. Abrasive characteristics
 - j. Toxicity
 - k. Fire or explosion hazards
 - l. Irritant characteristics, to skin, eyes, or lungs
 - m. Sensitivity of materials when exposed to air, moisture, or heat
2. List pertinent information related to production.
 - a. Quantity to be produced per batch
 - b. Formulation and order of addition
 - c. Analysis required
 - d. Cleaning requirements between batches or products
 - e. Preceding and/or following process steps
 - f. Any changes in physical state during process

- g. Any chemical reactions—exothermic or endothermic
 - h. Temperature requirements
 - i. Physical form of final product
 - j. Removal of product from mixer—pumping or gravity flow through piping, chute, or dumping
3. Describe the controlling features of the finished product.
 - a. Degree of uniformity: solution, aggregates, particle size, etc.
 - b. Stability of emulsion or dispersion
 - c. Ultimate color requirements
 - d. Uniformity of active ingredients, as in a pharmaceutical product
 - e. Degree of moisture content control

Preparation and Addition of Materials To ensure product quality and productivity, ingredient preparation is important. Order of addition, method and rate of addition, and even preprocessing must be considered.

Some finely powdered materials, such as carbon black or silica, contain a lot of air. If possible, such materials should be compacted, wetted, or agglomerated before addition to the mixture. Air bubbles can be extremely difficult to remove from viscous materials. Holding the product under a vacuum may help release some air or trapped gases. The presence of air in the product may make packaging difficult and may even cause eventual degradation of the product.

Critical ingredients, such as vulcanizers, antioxidants, surfactants, and active agents, are often present in small proportions. If these materials form lumps or aggregates, milling or screening of the materials may be necessary to ensure a uniform product. If small ingredients are soluble in liquid ingredients, adding them as a solution may improve blending. Master batching small quantities of an ingredient into part of a major ingredient often simplifies mixing and makes a more uniform product.

Additional considerations, such as automatic weighing, feed control, liquid metering, and automatic control, may be essential for continuous processes.

CRYSTALLIZATION FROM SOLUTION

GENERAL REFERENCES: *AICHE Testing Procedures: Crystallizers*, American Institute of Chemical Engineers, New York, 1970; *Evaporators*, 1961. Bennett, *Chem. Eng. Prog.*, **58**(9), 76 (1962). Buckley, *Crystal Growth*, Wiley, New York, 1951. Campbell and Smith, *Phase Rule*, Dover, New York, 1951. De Jong and Jancic (eds.), *Industrial Crystallization*, North-Holland Publishing Company, Amsterdam, 1979. "Crystallization from Solution: Factors Influencing Size Distribution," *Chem. Eng. Prog. Symp. Ser.*, **67**(110), (1971). Mullin (ed.), *Industrial Crystallization*, 4th ed., Butterworth-Heinemann, Boston, 2001. Mersmann (ed.), *Crystallization Technology Handbook*, Marcel Dekker, New York, 1995. Jancic and Grootsholten, *Industrial Crystallization*, D. Reidel Publishing, Boston, 1984. Jones, *Crystallization Process Systems*, Butterworth-Heinemann, Boston, 2002. Genck, *Chem. Eng. Prog.* **100**(10), 26 (2004). Newman and Bennett, *Chem. Eng. Prog.*, **55**(3), 65 (1959). Palermo and Larson (eds.), "Crystallization from Solutions and Melts," *Chem. Eng. Prog. Symp. Ser.*, **65**(95), (1969). Randolph (ed.), "Design, Control and Analysis of Crystallization Processes," *Am. Inst. Chem. Eng. Symp. Ser.*, **76**(193), (1980). Randolph and Larson, *Theory of Particulate Processes*, Academic, New York, 2d ed., 1988. Seidell, *Solubilities of Inorganic and Metal Organic Compounds*, American Chemical Society, Washington, 1965.

Crystallization is important as an industrial process because of the number of materials that are and can be marketed in the form of crystals. Its wide use is due to the highly purified and favorable form of a chemical solid which can be obtained from relatively impure solutions in a single processing step. In terms of energy requirements, crystallization requires much less energy for separation than do distillation and other commonly used methods of purification. In addition, it can be performed at relatively low temperatures and on a scale which varies from a few grams up to thousands of tons per day.

Crystallization may be carried out from a vapor, from a melt, or from a solution. Most of the industrial applications of the operation involve crystallization from solutions. Nevertheless, crystal solidification of metals is basically a crystallization process, and much theory has been developed in relation to metal crystallization. This topic is highly specialized, and is outside the scope of this subsection, which is limited to crystallization from solution.

PRINCIPLES OF CRYSTALLIZATION

Crystals A crystal may be defined as a solid composed of atoms or molecules arranged in an orderly, repetitive array. The interatomic distances in a crystal of any definite material are constant and are characteristic of that material. Because the pattern or arrangement of the atoms or molecules is repeated in all directions, there are definite restrictions on the kinds of symmetry that crystals can possess.

There are five main types of crystals, and these types have been arranged into seven crystallographic systems based on the crystal interfacial angles and the relative length of its axes. The treatment of the description and arrangement of the atomic structure of crystals is the science of **crystallography**. The material in this discussion will be limited to a treatment of the growth and production of crystals as a unit operation.

Solubility and Phase Diagrams Equilibrium relations for crystallization systems are expressed in the form of solubility data which are plotted as phase diagrams or solubility curves. Solubility data are ordinarily given as parts by weight of anhydrous material per 100 parts by weight of total solvent. In some cases these data are reported as parts by weight of anhydrous material per 100 parts of solution. If water of crystallization is present in the crystals, this is indicated as a separate phase. The concentration is normally plotted as a function of temperature and has no general shape or slope. It can also be reported as a function of pressure, but for most materials the change in solubility with change in pressure is very small. If there are two components in solution, it is common to plot the concentration of these two components on the X and Y axes and represent the solubility by isotherms. When three or more components are present, there are various techniques for depicting the solubility and phase relations in both three-dimension and two-dimension models. For a description of these techniques, refer to Campbell and Smith (loc. cit.). Shown in Fig. 18-63 is a phase diagram for magnesium sulfate in water. The line p - a

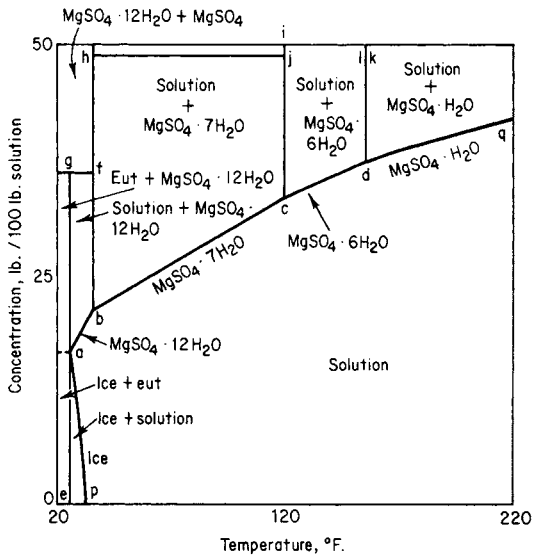


FIG. 18-63 Phase diagram. MgSO₄·H₂O. To convert pounds to kilograms, divide by 2.2; K = (°F + 459.7)/1.8.

represents the freezing points of ice (water) from solutions of magnesium sulfate. Point *a* is the eutectic, and the line *a-b-c-d-q* is the solubility curve of the various hydrates. Line *a-b* is the solubility curve for MgSO₄·12H₂O, *b-c* is the solubility curve for MgSO₄·7H₂O, *c-d* is the solubility curve for MgSO₄·6H₂O, and *d-q* is the portion of the solubility curve for MgSO₄·H₂O.

As shown in Fig. 18-64, the mutual solubility of two salts can be plotted on the X and Y axes with temperatures as isotherm lines. In the example shown, all the solution compositions corresponding to 100°C with solid-phase sodium chloride present are shown on the line *DE*. All the solution compositions at equilibrium with solid-phase KCl at 100°C are shown by the line *EF*. If both solid-phase KCl and NaCl are present, the solution composition at equilibrium can only be represented by point *E*, which is the invariant point (at constant pressure). Connecting all the invariant points results in the mixed-salt line. The locus of this line is an important consideration in making phase separations.

There are numerous solubility data in the literature; the standard reference is by Seidell (loc. cit.). Valuable as they are, they nevertheless must be used with caution because the solubility of compounds

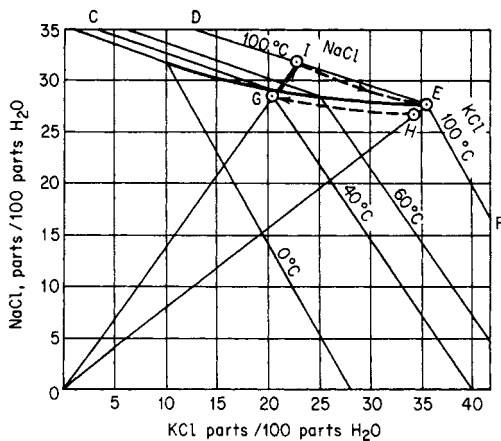


FIG. 18-64 Phase diagram, KCl - NaCl - H₂O. K = °C + 273.2.

is often influenced by pH and/or the presence of other soluble impurities which usually tend to depress the solubility of the major constituents. While exact values for any system are frequently best determined by actual composition measurements, the difficulty of reproducing these solubility diagrams should not be underestimated. To obtain data which are readily reproducible, elaborate pains must be taken to be sure the system sampled is at equilibrium, and often this means holding a sample at constant temperature for a period of from 1 to 100 h. While the published curves may not be exact for actual solutions of interest, they generally will be indicative of the shape of the solubility curve and will show the presence of hydrates or double salts.

Heat Effects in a Crystallization Process The heat effects in a crystallization process can be computed by two methods: (1) a heat balance can be made in which individual heat effects such as sensible heats, latent heats, and the heat of crystallization can be combined into an equation for total heat effects; or (2) an enthalpy balance can be made in which the total enthalpy of all leaving streams minus the total enthalpy of all entering streams is equal to the heat absorbed from external sources by the process. In using the heat-balance method, it is necessary to make a corresponding mass balance, since the heat effects are related to the quantities of solids produced through the heat of crystallization. The advantage of the enthalpy-concentration-diagram method is that both heat and mass effects are taken into account simultaneously. This method has limited use because of the difficulty in obtaining enthalpy-concentration data. This information has been published for only a few systems.

With compounds whose solubility increases with increasing temperature there is an absorption of heat when the compound dissolves. In compounds with decreasing solubility as the temperature increases, there is an evolution of heat when solution occurs. When there is no change in solubility with temperature, there is no heat effect. The solubility curve will be continuous as long as the solid substance of a given phase is in contact with the solution, and any sudden change in the slope of the curve will be accompanied by a change in the heat of solution and a change in the solid phase. Heats of solution are generally reported as the change in enthalpy associated with the dissolution of a large quantity of solute in an excess of pure solvent. Tables showing the heats of solution for various compounds are given in Sec. 2.

At equilibrium the heat of crystallization is equal and opposite in sign to the heat of solution. Using the heat of solution at infinite dilution as equal but opposite in sign to the heat of crystallization is equivalent to neglecting the heat of dilution. With many materials the heat of dilution is small in comparison with the heat of solution and the approximation is justified; however, there are exceptions. Relatively large heat effects are usually found in the crystallization of hydrated salts. In such cases the total heat released by this effect may be a substantial portion of the total heat effects in a cooling-type crystallizer. In evaporative-type crystallizers the heat of crystallization is usually negligible when compared with the heat of vaporizing the solvent.

Yield of a Crystallization Process In most cases the process of crystallization is slow, and the final mother liquor is in contact with a sufficiently large crystal surface so that the concentration of the mother liquor is substantially that of a saturated solution at the final temperature in the process. In such cases it is normal to calculate the yield from the initial solution composition and the solubility of the material at the final temperature. If evaporative crystallization is involved, the solvent removed must be taken into account in determining the final yield. If the crystals removed from solution are hydrated, account must be taken of the water of crystallization in the crystals, since this water is not available for retaining the solute in solution. The yield is also influenced in most plants by the removal of some mother liquor with the crystals being separated from the process. Typically, with a product separated on a centrifuge or filter, the adhering mother liquor would be in the range of 2 to 10 percent of the weight of the crystals.

The actual yield may be obtained from algebraic calculations or trial-and-error calculations when the heat effects in the process and any resultant evaporation are used to correct the initial assumptions on calculated yield. When calculations are made by hand, it is generally

preferable to use the trial-and-error system, since it permits easy adjustments for relatively small deviations found in practice, such as the addition of wash water, or instrument and purge water additions. The following calculations are typical of an evaporative crystallizer precipitating a hydrated salt. If SI units are desired, kilograms = pounds \times 0.454; $K = (^{\circ}F + 459.7)/1.8$.

Example 2: Yield from a Crystallization Process A 10,000-lb batch of a 32.5 percent $MgSO_4$ solution at $120^{\circ}F$ is cooled without appreciable evaporation to $70^{\circ}F$. What weight of $MgSO_4 \cdot 7H_2O$ crystals will be formed (if it is assumed that the mother liquor leaving is saturated)?

From the solubility diagram in Fig. 18-56 at $70^{\circ}F$ the concentration of solids is 26.3 lb $MgSO_4$ per 100-lb solution.

The mole weight of $MgSO_4$ is 120.38.

The mole weight of $MgSO_4 \cdot 7H_2O$ is 246.49.

For calculations involving hydrated salts, it is convenient to make the calculations based on the hydrated solute and the "free water."

$$0.325 \text{ weight fraction} \times \frac{246.94}{120.38} = 0.6655 \text{ } MgSO_4 \cdot 7H_2O \text{ in the feed solution}$$

$$0.263 \times \frac{246.94}{120.38} = 0.5385 \text{ } MgSO_4 \cdot 7H_2O \text{ in the mother liquor}$$

Since the free water remains constant (except when there is evaporation), the final amount of soluble $MgSO_4 \cdot 7H_2O$ is calculated by the ratio of $\frac{0.538 \text{ lb } MgSO_4 \cdot 7H_2O}{(1 - 0.538) \text{ lb free water}}$

	Total	$MgSO_4 \cdot 7H_2O$	Free water	$\frac{MgSO_4 \cdot 7H_2O}{\text{Free water}}$
Feed	10,000	6655	3345	1.989
Mother liquor	7249	3904*	3345	1.167
Yield	2751	2751		

$$*3345 \times (0.538/0.462) = 3904$$

A formula method for calculation is sometimes used where

$$P = R \frac{100W_0 - S(H_0 - E)}{100 - S(R - 1)}$$

where P = weight of crystals in final magma, lb
 R = mole weight of hydrate/mole weight of anhydrous = 2.04759
 S = solubility at mother-liquor temperature (anhydrous basis) in lb per 100 lb solvent. $[0.263/(1 - 0.263)] \times 100 = 35.68521$
 W_0 = weight of anhydrous solute in the original batch. $10,000(0.325) = 3250$ lb
 H_0 = total weight of solvent at the beginning of the batch. $10,000 - 3250 = 6750$ lb
 E = evaporation = 0
 $P = 2.04 \frac{(100)(3250) - 35.7(6750)}{100 - 35.7(2.04 - 1)} = 2751$ lb

Note that taking the difference between large numbers in this method can increase the chance for error.

Fractional Crystallization When two or more solutes are dissolved in a solvent, it is often possible to (1) separate these into the pure components or (2) separate one and leave the other in the solution. Whether or not this can be done depends on the solubility and phase relations of the system under consideration. Normally alternative 2 is successful only when one of the components has a much more rapid change in solubility with temperature than does the other. A typical example which is practiced on a large scale is the separation of KCl and NaCl from water solution. A phase diagram for this system is shown in Fig. 18-64. In this case the solubility of NaCl is plotted on the Y axis in parts per 100 parts of water, and the solubility of KCl is plotted on the X axis. The isotherms show a marked decrease in solubility for each component as the amount of the other is increased. This is typical for most inorganic salts. As explained earlier, the mixed-salt line is CE , and to make a separation of the solutes into the pure components it is necessary to be on one side of this line or the other. Normally a 95 to 98 percent approach to this line is possible. When evaporation occurs during a cooling or concentration process, this can be represented by movement away from the origin on a straight line through the origin. Dilution by water is represented by movement in the opposite direction.

A typical separation might be represented as follows: Starting at E with a saturated brine at $100^{\circ}C$ a small amount of water is added to dissolve any traces of solid phase present and to make sure the solids precipitated initially are KCl. Evaporative cooling along line HG results in the precipitation of KCl. During this evaporative cooling, part of the water evaporated must be added back to the solution to prevent the coprecipitation of NaCl. The final composition at G can be calculated by the NaCl/KCl/ H_2O ratios and the known amount of NaCl in the incoming solution at E . The solution at point G may be concentrated by evaporation at $100^{\circ}C$. During this process the solution will increase in concentration with respect to both components until point I is reached. Then NaCl will precipitate, and the solution will become more concentrated in KCl, as indicated by the line IE , until the original point E is reached. If concentration is carried beyond point E , a mixture of KCl and NaCl will precipitate.

Example 3: Yield from Evaporative Cooling Starting with 1000 lb of water in a solution at H on the solubility diagram in Fig. 18-64, calculate the yield on evaporative cooling and concentrate the solution back to point H so the cycle can be repeated, indicating the amount of NaCl precipitated and the evaporation and dilution required at the different steps in the process.

In solving problems of this type, it is convenient to list the material balance and the solubility ratios. The various points on the material balance are calculated by multiplying the quantity of the component which does not precipitate from solution during the transition from one point to another (normally the NaCl in cooling or the KCl in the evaporative step) by the solubility ratio at the next step, illustrated as follows:

Basis. 1000 lb of water at the initial conditions.

Solution component	KCl	NaCl	Water	Solubility ratios		
				KCl	NaCl	Water
H	343	270	1000	34.3	27.0	100
$G(a)$	194	270	950	20.4	28.4	100
KCl yield	149					
Net evaporation			50			
$I(b)$	194	270	860	22.6	31.4	100
$E(c)$	194	153	554	35.0	27.5	100
NaCl yield		117				
Evaporation			306			
Dilution			11			
H'	194	153	565	34.3	27.0	-100

The calculations for these steps are:

- a. 270 lb NaCl (100 lb water/28.4 lb NaCl) = 950 lb water
 950 lb water (20.4 lb KCl/100 lb water) = 194 lb KCl
- b. 270 lb NaCl (100 lb water/31.4 lb NaCl) = 860 lb water
 860 lb water (22.6 lb KCl/100 lb water) = 194 lb KCl
- c. 194 lb KCl (100 lb water/35.0 lb KCl) = 554 lb water
 554 lb water (27.5 lb NaCl/100 lb water) = 153 lb NaCl

Note that during the cooling step the maximum amount of evaporation which is permitted by the material balance is 50 lb for the step shown. In an evaporative-cooling step, however, the actual evaporation which results from adiabatic cooling is more than this. Therefore, water must be added back to prevent the NaCl concentration from rising too high; otherwise, coprecipitation of NaCl will occur.

Inasmuch as only mass ratios are involved in these calculations, kilograms or any other unit of mass may be substituted for pounds without affecting the validity of the example.

Although the figures given are for a step-by-step process, it is obvious that the same techniques will apply to a continuous system if the fresh feed containing KCl and NaCl is added at an appropriate part of the cycle, such as between steps G and I for the case of dilute feed solutions.

Another method of fractional crystallization, in which advantage is taken of different crystallization rates, is sometimes used. Thus, a solution saturated with borax and potassium chloride will, in the absence of borax seed crystals, precipitate only potassium chloride on rapid cooling. The borax remains behind as a supersaturated solution, and the potassium chloride crystals can be removed before the slower borax crystallization starts.

Crystal Formation There are two steps involved in the preparation of crystal matter from a solution. The crystals must first form and

then grow. The formation of a new solid phase either on an inert particle in the solution or in the solution itself is called **nucleation**. The increase in size of this nucleus with a layer-by-layer addition of solute is called **growth**. The growth process involves two steps, diffusion of the solute to the crystal interface followed by incorporation of the same into the lattice. One of these will control depending on factors such as the degree of agitation and temperature. Nucleation can be classified as primary or secondary. The former usually occurs at high supersaturation and does not involve product crystals. Secondary nucleation involves nuclei generation from product crystals by contact with the agitator, with the crystallizer internals and with one another. Each system has a metastable zone where growth is encouraged in the presence of supersaturation. Secondary nucleation can occur within the zone. Both nucleation and crystal growth have supersaturation as a common driving force. Unless a solution is supersaturated, crystals can neither form nor grow. Supersaturation refers to the quantity of solute present in solution compared with the quantity which would be present if the solution were kept for a very long period of time with solid phase in contact with the solution. The latter value is the equilibrium solubility at the temperature and pressure under consideration. The supersaturation coefficient can be expressed

$$S = \frac{\text{parts solute}/100 \text{ parts solvent}}{\text{parts solute at equilibrium}/100 \text{ parts solvent}} \geq 1.0 \quad (18-25)$$

Solutions vary greatly in their ability to sustain measurable amounts of supersaturation. With some materials, such as sucrose, it is possible to develop a supersaturation coefficient of 1.4 to 2.0 with little danger of nucleation. With some common inorganic solutions such as sodium chloride in water, the amount of supersaturation which can be generated stably is so small that it is difficult or impossible to measure.

Certain qualitative facts in connection with supersaturation, growth, and the yield in a crystallization process are readily apparent. If the concentration of the initial solution and the final mother liquor are fixed, the total weight of the crystalline crop is also fixed if equilibrium is obtained. The particle-size distribution of this weight, however, will depend on the relationship between the two processes of nucleation and growth. Considering a given quantity of solution cooled through a fixed range, if there is considerable nucleation initially during the cooling process, the yield will consist of many small crystals. If only a few nuclei form at the start of the crystallization (or seeds are added) and the resulting yield occurs uniformly on these nuclei or seeds without significant secondary nucleation, a crop of large uniform crystals will result. Obviously, many intermediate cases of varying nucleation rates and growth rates can also occur, depending on the nature of the materials being handled, the rate of cooling, agitation, and other factors.

When a process is continuous, nucleation frequently occurs in the presence of a seeded solution by the combined effects of mechanical stimulus and nucleation caused by supersaturation (heterogeneous nucleation). If such a system is completely and uniformly mixed (i.e., the product stream represents the typical magma circulated within the system) and if the system is operating at steady state, the particle-size distribution has definite limits which can be predicted mathematically with a high degree of accuracy, as will be shown later in this section.

Geometry of Crystal Growth Geometrically a crystal is a solid bounded by planes. The shape and size of such a solid are functions of the interfacial angles and of the linear dimension of the faces. As the result of the constancy of its interfacial angles, each face of a growing or dissolving crystal, as it moves away from or toward the center of the crystal, is always parallel to its original position. This concept is known as the "principle of the parallel displacement of faces." The rate at which a face moves in a direction perpendicular to its original position is called the translation velocity of that face or the rate of growth of that face.

From the industrial point of view, the term **crystal habit** or **crystal morphology** refers to the relative sizes of the faces of a crystal. The crystal habit is determined by the internal structure and external influences on the crystal such as the growth rate, solvent used, and impurities present during the crystallization growth period. The crystal habit of commercial products is of very great importance. Long,

needlelike crystals tend to be easily broken during centrifugation and drying. Flat, platelike crystals are very difficult to wash during filtration or centrifugation and result in relatively low filtration rates. Complex or twinned crystals tend to be more easily broken in transport than chunky, compact crystal habits. Rounded or spherical crystals (caused generally by attrition during growth and handling) tend to give considerably less difficulty with caking than do cubical or other compact shapes.

Internal structure (unit cell) can be different in crystals that are chemically identical. This is called **polymorphism**. Polymorphs can vary substantially in physical and chemical properties such as bioavailability and solubility. They can be identified by analytical techniques such as X-ray diffraction, infrared, Raman spectro, and microscopic techniques. For the same internal structure, very small amounts of foreign substances will often completely change the crystal habit. The selective adsorption of dyes by different faces of a crystal or the change from an alkaline to an acidic environment will often produce pronounced changes in the crystal habit. The presence of other soluble anions and cations often has a similar influence. In the crystallization of ammonium sulfate, the reduction in soluble iron to below 50 ppm of ferric ion is sufficient to cause significant change in the habit of an ammonium sulfate crystal from a long, narrow form to a relatively chunky and compact form. Additional information is available in the patent literature and Table 18-4 lists some of the better-known additives and their influences.

Since the relative sizes of the individual faces of a crystal vary between wide limits, it follows that different faces must have different translational velocities. A geometric law of crystal growth known as the **overlapping principle** is based on those velocity differences: in growing a crystal, only those faces having the lowest translational velocities survive; and in dissolving a crystal, only those faces having the highest translational velocities survive.

For example, consider the cross sections of a growing crystal as in Fig. 18-65. The polygons shown in the figure represent varying stages in the growth of the crystal. The faces marked *A* are slow-growing faces (low translational velocities), and the faces marked *B* are fast-growing (high translational velocities). It is apparent from Fig. 18-65 that the faster *B* faces tend to disappear as they are overlapped by the slower *A* faces.

It has been predicted that crystal habit or crystal morphology was related to the internal structure based on energy considerations and speculated that it should be possible to predict the growth shape of crystals from the slice energy of different flat faces. One can predict the calculated attachment energy for various crystal species. Recently computer programs have been developed that predict crystal morphology from attachment energies. These techniques are particularly useful in dealing with organic or molecular crystals and rapid progress in this area is being made by companies such as Molecular Simulations of Cambridge, England.

Purity of the Product If a crystal is produced in a region of the phase diagram where a single-crystal composition precipitates, the crystal itself will normally be pure provided that it is grown at relatively low rates and constant conditions. With many products these purities approach a value of about 99.5 to 99.8 percent. The difference between this and a purity of 100 percent is generally the result of small pockets of mother liquor called inclusions trapped within the crystal. Although frequently large enough to be seen with an ordinary microscope, these inclusions can be submicroscopic and represent dislocations within the structure of the crystal. They can be caused by either attrition or breakage during the growth process or by slip planes within the crystal structure caused by interference between screw-type dislocations and the remainder of the crystal faces. To increase the purity of the crystal beyond the point where such inclusions are normally expected (about 0.1 to 0.5 percent by volume), it is generally necessary to reduce the impurities in the mother liquor itself to an acceptably low level so that the mother liquor contained within these pockets will not contain sufficient impurities to cause an impure product to be formed. It is normally necessary to recrystallize material from a solution which is relatively pure to surmount this type of purity problem.

In addition to the impurities within the crystal structure itself, there is normally an adhering mother-liquid film left on the surface of the

TABLE 18-4 Some Impurities Known to Be Habit Modifiers

Material crystallized	Additive(s)	Effect	Concentration	References
Ba(NO ₃) ₂	Mg, Te ⁴⁺	Helps growth	—	1
CaSO ₄ ·2H ₂ O	Citric, succinic, tartaric acids	Helps growth	Low	—
	Sodium citrate	Forms prisms	—	5
CuSO ₄ ·5H ₂ O	H ₂ SO ₄	Chunky crystals	0.3%	5
KCl	K ₄ Fe(CN) ₆	Inhibits growth, dendrites	1000 ppm	4
	Pb, Bi, Sn ⁺² , Ti, Zr, Th, Cd, Fe, Hg, Mg	Helps growth	Low	1
KClO ₄	Congo red (dye)	Modifies the 102 face	50 ppm	6
K ₂ CrO ₄	Acid magenta (dye)	Modifies the 010 face	50 ppm	6
KH ₂ PO ₄	Na ₂ B ₄ O ₇	Aids growth	—	1
KNO ₂	Fe	Helps growth	Low	1
KNO ₃	Acid magenta (dye)	Tabular crystals	—	7
	Pb, Th, Bi	Helps growth	Low	1
K ₂ SO ₄	Acid magenta (dye)	Forms plates	2000 ppm	6
	Cl, Mn, Mg, Bi, Cu, Al, Fe	Helps growth	Low	1
	Cl ₃	Reduces growth rate	1000 ppm	4
	(NH ₄) ₃ Ce(NO ₃) ₆	Reduces growth rate	1000 ppm	4
LiCl·H ₂ O	Cr-Mn ⁺² , Sn ⁺² , Co, Ni, Fe ⁺³	Helps growth	Low	1
MgSO ₄ ·7H ₂ O	Borax	Aids growth	5%	1
Na ₂ B ₄ O ₇ ·10H ₂ O	Sodium oleate	Reduces growth & nuc.	5 ppm	—
	Casein, gelatin	Promotes flat crystals	—	2, 5
	NaOH, Na ₂ CO ₃	Promotes chunky crystals	—	—
Na ₂ CO ₃ ·H ₂ O	SO ₄ ²⁻	Reduces L/D ratio	0.1–1.0%	Canadian Patent 812,685
	Ca ⁺² and Mg ⁺²	Increase bulk density	400 ppm	U.S. Patent 3,459,497
NaCO ₃ ·NaHCO ₃ ·2H ₂ O	D-40 detergent	Aids growth	20 ppm	U.S. Patent 3,233,983
NaCl	Na ₄ Fe(CN) ₆ , CdBr	Forms dendrites	100 ppm	4
	Pb, Mn ⁺² , Bi, Sn ⁺² , Ti, Fe, Hg	Helps growth	Low	1
	Urea, formamide	Forms octahedra	Low	2
	Tetraalkyl ammon. salts	Helps growth & hardness	1–100 ppm	U.S. Patent 3,095,281
	Polyethylene-oxy compounds	Helps growth & hardness	—	U.S. Patent 3,000,708
NaClO ₃	Na ₂ SO ₄ , NaClO ₄	Tetrahedrons	—	3
NaNO ₃	Acid green (dye)	Flattened rhombahedra	—	7
Na ₂ SO ₄	NH ₄ SO ₄ @ pH 6.5	Large single crystals	Low	—
	CdCl ₂	Inhibits growth	1000 ppm	4
	Alkyl aryl sulfonates	Aids growth	—	2
	Calgon	Aids growth	100 ppm	—
NH ₄ Cl	Mn, Fe, Cu, Co, Ni, Cr	Aid growth	Low	1
	Urea	Forms octahedra	—	5
NH ₄ ClO ₄	Azurine (dye)	Modifies the 102 face	22 ppm	6
NH ₄ F	Ca	Helps growth	Low	1
(NH ₄)NO ₃	Acid magenta (dye)	Forms 010 face plates	1%	6
(NH ₄) ₂ HPO ₄	H ₂ SO ₄	Reduces L/D ratio	7%	—
NH ₄ H ₂ PO ₄	Fe ⁺³ , Cr, Al, Sn	Helps growth	Traces	1
(NH ₄) ₂ SO ₄	Cr ⁺³ , Fe ⁺³ , Al ⁺³	Promotes needles	50 ppm	—
	H ₂ SO ₄	Promotes needles	2–6%	U.S. Patent 2,092,073
	Oxalic acid, citric acid	Promotes chunky crystals	1000 ppm	U.S. Patent 2,228,742
	H ₃ PO ₄ , SO ₂	Promotes chunky crystals	1000 ppm	—
ZnSO ₄ ·7H ₂ O	Borax	Aids growth	—	1
Adipic acid	Surfactant-SDBS	Aids growth	50–100 ppm	2
Fructose	Glucose, difructose	Affects growth	—	8
L-asparagine	L-glutamic acid	Affects growth	—	8
Naphthalene	Cyclohexane (solvent)	Forms needles	—	2
	Methanol (solvent)	Forms plates	—	—
Pentaerythritol	Sucrose	Aids growth	—	1
	Acetone (solvent)	Forms plates	—	2
Sodium glutamate	Lysine, CaO	Affects growth	—	8
Sucrose	Raffinose, KCl, NaBr	Modify growth rate	—	—
Urea	Biuret	Reduces L/D & aids growth	2–7%	—
	NH ₄ Cl	Reduces L/D & aids growth	5–10%	—

1. Gillman, *The Art and Science of Growing Crystals*, Wiley, New York, 1963.
2. Mullin, *Crystallization*, Butterworth, London, 1961.
3. Buckley, *Crystal Growth*, Wiley, New York, 1961.
4. Phoenix, L., *British Chemical Engineering*, vol. II, no. 1 (Jan. 1966), pp. 34–38.
5. Garrett, D. E., *British Chemical Engineering*, vol. I, no. 12 (Dec. 1959), pp. 673–677.
6. Buckley, *Crystal Growth*, (Faraday Soc.) Butterworths, 1949, p. 249.
7. Butchart and Whetstone, *Crystal Growth*, (Faraday Soc.) Butterworths, 1949, p. 259.
8. Nyvlt, J., *Industrial Crystallization*, Verlag Chemie Publishers, New York, 1978, pp. 26–31.

crystal after separation in a centrifuge or on a filter. Typically a centrifuge may leave about 2 to 10 percent of the weight of the crystals as adhering mother liquor on the surface. This varies greatly with the size and shape or habit of the crystals. Large, uniform crystals from low-viscosity mother liquors will retain small quantities of mother liquor, while nonuniform or small crystals crystallized from viscous solutions will retain a considerably larger proportion. Comparable

statements apply to the filtration of crystals, although normally the amounts of mother liquor adhering to the crystals are considerably larger. It is common practice when crystallizing materials from solutions which contain appreciable quantities of impurities to wash the crystals on the centrifuge or filter with either fresh solvent or feed solution. In principle, such washing can reduce the impurities quite substantially. It is also possible in many cases to reslurry the crystals in

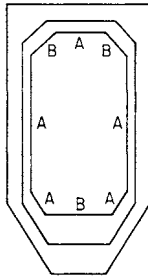


FIG. 18-65 Overlapping principle.

fresh solvent and recentrifuge the product in an effort to obtain a longer residence time during the washing operation and better mixing of the wash liquors with the crystals. Mother liquor inclusions and residual moisture after drying can present caking problems.

Coefficient of Variation One of the problems confronting any user or designer of crystallization equipment is the expected particle-size distribution of the solids leaving the system and how this distribution may be adequately described. Most crystalline-product distributions plotted on arithmetic-probability paper will exhibit a straight line for a considerable portion of the plotted distribution. In this type of plot the particle diameter should be plotted as the ordinate and the cumulative percent on the log-probability scale as the abscissa.

It is common practice to use a parameter characterizing crystal-size distribution called the coefficient of variation. This is defined as follows:

$$CV = 100 \frac{PD_{16\%} - PD_{84\%}}{2PD_{50\%}} \quad (18-26)$$

where CV = coefficient of variation, as a percentage
 PD = particle diameter from intercept on ordinate axis at percent indicated

In order to be consistent with normal usage, the particle-size distribution when this parameter is used should be a straight line between approximately 10 percent cumulative weight and 90 percent cumulative weight. By giving the coefficient of variation and the mean particle diameter, a description of the particle-size distribution is obtained which is normally satisfactory for most industrial purposes. If the product is removed from a mixed-suspension crystallizer, this coefficient of variation should have a value of approximately 50 percent (Randolph and Larson, op. cit., chap. 2).

Crystal Nucleation and Growth

Rate of Growth Crystal growth is a layer-by-layer process, and since growth can occur only at the face of the crystal, material must be transported to that face from the bulk of the solution. Diffusional resistance to the movement of molecules (or ions) to the growing crystal face, as well as the resistance to integration of those molecules into the face, must be considered. As discussed earlier, different faces can have different rates of growth, and these can be selectively altered by the addition or elimination of impurities.

If L is a characteristic dimension of a crystal of selected material and shape, the rate of growth of a crystal face that is perpendicular to L is, by definition,

$$G \equiv \lim_{\Delta L \rightarrow 0} \frac{\Delta L}{\Delta t} = \frac{dL}{dt} \quad (18-27)$$

where G is the growth rate over time interval t . It is customary to measure G in the practical units of millimeters per hour. It should be noted that growth rates so measured are actually twice the facial growth rate.

The delta L law. It has been shown by McCabe [Ind. Eng. Chem., 21, 30, 112 (1929)] that all geometrically similar crystals of the same

material suspended in the same solution grow at the same rate if growth rate is defined as in Eq. (18-27). The rate is independent of crystal size, provided that all crystals in the suspension are treated alike. This generalization is known as the delta L law. Although there are some well-known exceptions, they usually occur when the crystals are very large or when movement of the crystals in the solution is so rapid that substantial changes occur in diffusion-limited growth of the faces.

It is emphasized that the delta L law does not apply when similar crystals are given preferential treatment based on size. It fails also when surface defects or dislocations significantly alter the growth rate of a crystal face. Nevertheless, it is a reasonably accurate generalization for a surprising number of industrial cases. When it is, it is important because it simplifies the mathematical treatment in modeling real crystallizers and is useful in predicting crystal-size distribution in many types of industrial crystallization equipment.

Important exceptions to McCabe's growth-rate model have been noted by Bramson, by Randolph, and by Abegg. These are discussed by Canning and Randolph, *Am. Inst. Chem. Eng. J.*, 13, 5 (1967).

Nucleation The mechanism of crystal nucleation from solution has been studied by many scientists, and their work suggests that—in commercial crystallization equipment, at least—the nucleation rate is the sum of contributions by (1) primary nucleation and (2) nucleation due to contact between crystals and (a) other crystals, (b) the walls of the container, and (c) the impeller. If B^0 is the net number of new crystals formed in a unit volume of solution per unit of time,

$$B^0 = B_{ss} + B_{cc} + B_{ci} \quad (18-28)$$

where B_{ci} is the rate of nucleation due to crystal-impeller contacts, B_{cc} is that due to crystal-crystal contacts, and B_{ss} is the primary nucleation rate due to the supersaturation driving force. The mechanism of the last-named is not precisely known, although it is obvious that molecules forming a nucleus not only have to coagulate, resisting the tendency to redissolve, but also must become oriented into a fixed lattice. The number of atoms or molecules required to form a stable crystal nucleus has been variously estimated at from 80 to 100 (with ice), and the probability that a stable nucleus will result depends on many factors such as activation energies and supersaturation. In commercial crystallization equipment, in which supersaturation is low and agitation is employed to keep the growing crystals suspended, the predominant mechanism is contact nucleation or, in extreme cases, attrition.

In order to treat crystallization systems both dynamically and continuously, a mathematical model has been developed which can correlate the nucleation rate to the level of supersaturation and/or the growth rate. Because the growth rate is more easily determined and because nucleation is sharply nonlinear in the regions normally encountered in industrial crystallization, it has been common to assume

$$B^0 = ks^b \quad (18-29)$$

where s , the supersaturation, is defined as $(C - C_s)$, C being the concentration of the solute and C_s its saturation concentration; and the exponent b and dimensional coefficient k are values characteristic of the material.

While Eq. (18-29) has been popular among those attempting correlations between nucleation rate and supersaturation, it has become common to use a derived relationship between nucleation rate and growth rate by assuming that

$$G = k's^g \quad (18-30)$$

whence, in consideration of Eq. (18-29),

$$B^0 = k''G^i \quad (18-31)$$

where the dimensional coefficient k' and exponent g are characteristic of the material and the conditions of crystallization and $k'' = k/(k')^i$ with $i = b/g$, a measure of the relative dependence of B^0 and G on supersaturation. Feeling that a model in which nucleation depends only on supersaturation or growth rate is simplistically deficient, some have proposed that contact nucleation rate is also a power function of slurry density and that

$$B^0 = k_n G^i M_T^j \quad (18-32)$$

where M_T is the density of the crystal slurry, g/L .

Although Eqs. (18-31) and (18-32) have been adopted by many as a matter of convenience, they are oversimplifications of the very complex relationship that is suggested by Eq. (18-28); Eq. (18-32) implicitly and quite arbitrarily combines the effects of homogeneous nucleation and those due to contact nucleation. They should be used only with caution.

In work pioneered by Clontz and McCabe [*Chem. Eng. Prog. Symp. Ser.*, **67**(110), 6 (1971)] and subsequently extended by others, contact nucleation rate was found to be proportional to the input of energy of contact, frequency of contact, as well as being a function of contact area and supersaturation. This observation is important to the scaling up of crystallizers. At the laboratory or bench scale, particle contact frequency with the agitator is high while in commercial equipment the contact energy input is higher at the impeller but the contact frequency is less. Scale-up modeling of a crystallizer, therefore, must include its mechanical characteristics as well as the physiochemical driving force.

Nucleation and Growth From the preceding, it is clear that no analysis of a crystallizing system can be truly meaningful unless the simultaneous effects of nucleation rate, growth rate, heat balance, and material balance are considered. The most comprehensive treatment of this subject is by Randolph and Larson (op. cit.), who developed a mathematical model for continuous crystallizers of the mixed-suspension or circulating-magma type [*Am. Inst. Chem. Eng. J.*, **8**, 639 (1962)] and subsequently examined variations of this model that include most of the aberrations found in commercial equipment. Randolph and Larson showed that when the total number of crystals in a given volume of suspension from a crystallizer is plotted as a function of the characteristic length as in Fig. 18-66, the slope of the line is usefully identified as the crystal population density, n :

$$n = \lim_{\Delta L \rightarrow 0} \frac{\Delta N}{\Delta L} = \frac{dN}{dL} \quad (18-33)$$

where N = total number of crystals up to size L per unit volume of magma. The population density thus defined is useful because it characterizes the nucleation-growth performance of a particular crystallization process or crystallizer.

The data for a plot like Fig. 18-67 are easily obtained from a screen analysis of the total crystal content of a known volume (e.g., a liter) of magma. The analysis is made with a closely spaced set of testing sieves (or intervals for a particle counter), the cumulative number of particles smaller than each sieve in the nest being plotted against the aperture dimension of that sieve. The fraction retained on each sieve is weighed, and the mass is converted to the equivalent number of particles by dividing by the calculated mass of a particle whose dimension is the arithmetic mean of the mesh sizes of the sieve on which it is retained and the sieve immediately above it.

In industrial practice, the size-distribution curve usually is not actually constructed. Instead, a mean value of the population density for any sieve fraction of interest (in essence, the population density of the

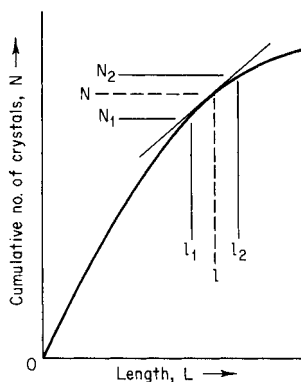


FIG. 18-66 Determination of the population density of crystals.

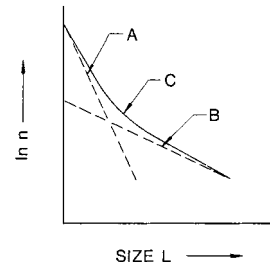


FIG. 18-67 Population density of crystals resulting from Bujacian behavior.

particle of average dimension in that fraction) is determined directly as $\Delta N/\Delta L$, ΔN being the number of particles retained on the sieve and ΔL being the difference between the mesh sizes of the retaining sieve and its immediate predecessor. It is common to employ the units of $(\text{mm}\cdot\text{L})^{-1}$ for n .

For a steady-state crystallizer receiving solids-free feed and containing a well-mixed suspension of crystals experiencing negligible breakage, a material-balance statement yields negligible agglomeration and breakage to a particle balance (the Randolph-Larson general-population balance); in turn, it simplifies to

$$\frac{dn}{dL} + \frac{n}{Gt} = 0 \quad (18-34)$$

if the delta L law applies (i.e., G is independent of L) and the draw-down (or retention) time is assumed to be invariant and calculated as $t = V/Q$. Integrated between the limits n^0 , the population density of nuclei (for which L is assumed to be zero), and n , that of any chosen crystal size L , Eq. (18-34) becomes

$$\int_{n^0}^n \frac{dn}{n} = - \int_0^L \frac{dL}{Gt} \quad (18-35)$$

$$\ln n = \frac{-L}{Gt} + \ln n^0 \quad (18-36a)$$

or

$$n = n^0 e^{-L/Gt} \quad (18-36b)$$

It can be shown that

$$B^0 = n^0 G \quad (18-36c)$$

A plot of $\ln n$ versus L is a straight line whose intercept is $\ln n^0$ and whose slope is $-1/Gt$. (For plots on base-10 log paper, the appropriate slope correction must be made.) Thus, from a given product sample of known slurry density and retention time it is possible to obtain the nucleation rate and growth rate for the conditions tested if the sample satisfies the assumptions of the derivation and yields a straight line. A number of derived relations which describe the nucleation rate, size distribution, and average properties are summarized in Table 18-5.

If a straight line does not result (Fig. 18-67), at least part of the explanation may be violation of the delta L law (Canning and Randolph, loc. cit.). The best current theory about what causes size-dependent growth suggests what has been called growth dispersion or "Bujacian behavior" [Mullen (ed.), op. cit., p. 254]. In the same environment different crystals of the same size can grow at different rates owing to differences in dislocations or other surface effects. The graphs of "slow" growers (Fig. 18-67, curve A) and "fast" growers (curve B) sum to a resultant line (curve C), concave upward, that is described by Eq. (18-37) (Randolph, in deJong and Jancic, op. cit., p. 254):

$$n = \sum \frac{B_i^0}{G_i} e^{(-L/G_i t)} \quad (18-37)$$

Equation (18-34) contains no information about the crystallizer's influence on the nucleation rate. If the crystallizer is of a mixed-suspension, mixed-product-removal (MSMPR) type, satisfying the criteria for Eq. (18-34), and if the model of Clontz and McCabe is valid, the contribution to the nucleation rate by the circulating pump

TABLE 18-5 Common Equations for Population-Balance Calculations

Name	Symbol	Units	Systems without fines removal	Systems with fines removal		References
				Fines stream	Product stream	
Drawdown time (retention time)	t	h	$t = V/Q$	$t_F = V_{\text{liquid}}/Q_F$	$t = V/Q$	
Growth rate	G	mm/h	$G = dL/dt$	$G = dL/dt$	$G = dL/dt$	
Volume coefficient	K_c	1/no. (crystals)	$K_c = \frac{\text{volume of one crystal}}{L^3}$	$K_c = \frac{\text{volume of one crystal}}{L^3}$	$K_c = \frac{\text{volume of one crystal}}{L^3}$	
Population density	n	No. (crystals)/mm	$n = dN/dL$	$n = dN/dL$	$n = dN/dL$	1
Nuclei population density	n^o	No. (crystals)/mm	$n^o = K_M M^i C^j - 1$			2
Population density	n	No. (crystals)/mm	$n = n^o e^{-L/Gt}$	$n_F = n^o e^{-L/Gt_F}$	$n = n^o e^{-L_e/Gt} e^{-L/Gt}$	1, 3
Nucleation rate	B_0	No. (crystals)/h	$B_0 = G n^o = K_M M^i C^j$	$B_0 = G_n^o$		4
Dimensionless length	x	None	$x = \frac{L}{Gt}$	$x_F = \frac{L}{Gt_F}, L_0 \rightarrow L_f$	$x = \frac{L}{Gt}, L_f \rightarrow L$	1
Mass/unit volume (slurry density)	M_T	g/L	$M_T = K_c \rho \int_0^\infty n L^3 dL$ $M_T = K_c \rho_6 n^o (Gt)^4$	$M_{T_F} = K_c \rho \int_0^{L_f} n^o e^{-L/Gt_F} L^3 dL$	$M_T = K_c \rho \int_{L_f}^\infty n^o e^{-L/Gt} e^{-L/Gt} L^3 dL$	1
Cumulative mass to x Total mass	W_x	None	$W_x = 1 - e^{-x} \left(\frac{x^3}{6} + \frac{x^2}{2} + x + 1 \right)$	$W_F = \frac{e^{-x}(x^3 + 3x^2 + 6x + 6) - 6}{e^{-x_c}(x_c^3 + 3x_c^2 + 6x_c + 6) - 6}$	$W = \frac{6K_c \rho n^o e^{-L_e/Gt} Gt^4 \left[1 - e^{-x} \left(\frac{x^3}{6} + \frac{x^2}{2} + x + 1 \right) \right]}{\text{Slurry density } M, g/L}$ when $L_e \approx 0$, compared with L_a	5
Dominant particle	L_d	mm	$L_d = 3Gt$			
Average particle, weight	L_a	mm	$L_a = 3.67Gt$			6
Total number of crystals	N_T	No./L	$N_T = \int_0^\infty n dL$	$N_F = \int_0^{L_f} n_F dL$	$N_T = \int_{L_f}^\infty n dL$	1, 3

1. Randolph and Larson, *Am. Inst. Chem. Eng. J.*, **8**, 639 (1962).
2. Timm and Larson, *Am. Inst. Chem. Eng. J.*, **14**, 452 (1968).
3. Larson, private communication.
4. Larson, Timm, and Wolff, *Am. Inst. Chem. Eng. J.*, **14**, 448 (1968).
5. Larson and Randolph, *Chem. Eng. Prog. Symp. Ser.*, **65**(95), 1 (1969).
6. Schoen, *Ind. Eng. Chem.*, **53**, 607 (1961).

can be calculated [Bennett, Fiedelman, and Randolph, *Chem. Eng. Prog.*, **69**(7), 86 (1973)]:

$$B_e = K_c \left(\frac{I^2}{P} \right) \rho G \int_0^\infty nL^4 dL \quad (18-38)$$

where I = tip speed of the propeller or impeller, m/s
 ρ = crystal density, g/cm³
 P = volume of crystallizer/circulation rate (turnover), m³/(m³/s) = s

Since the integral term is the fourth moment of the distribution (m_4), Eq. (18-38) becomes

$$B_e = K_c \rho G \left(\frac{I^2}{P} \right) m_4 \quad (18-39)$$

Equation (18-39) is the general expression for impeller-induced nucleation. In a fixed-geometry system in which only the speed of the circulating pump is changed and in which the flow is roughly proportional to the pump speed, Eq. (18-39) may be satisfactorily replaced with

$$B_e = K'_c \rho G (S_R)^3 m_4 \quad (18-40)$$

where S_R = rotation rate of impeller, r/min. If the maximum crystal-impeller impact stress is a nonlinear function of the kinetic energy, shown to be the case in at least some systems, Eq. (18-40) no longer applies.

In the specific case of an MSMPR exponential distribution, the fourth moment of the distribution may be calculated as

$$m_4 = 4! n^0 (Gt)^5 \quad (18-41)$$

Substitution of this expression into Eq. (18-39) gives

$$B_e = kn^0 G (S_R)^3 L_D^5 \quad (18-42)$$

where $L_D = 3Gt$, the dominant crystal (mode) size.

Equation (18-42) displays the competing factors that stabilize secondary nucleation in an operating crystallizer when nucleation is due mostly to impeller-crystal contact. Any increase in particle size produces a fifth-power increase in nucleation rate, tending to counteract the direction of the change and thereby stabilizing the crystal-size distribution. From dimensional argument alone the size produced in a mixed crystallizer for a (fixed) nucleation rate varies as $(B^0)^{1/3}$. Thus, this fifth-order response of contact nucleation does not wildly upset the crystal size distribution but instead acts as a stabilizing feedback effect.

Nucleation due to crystal-to-crystal contact is greater for equal striking energies than crystal-to-metal contact. However, the viscous drag of the liquid on particle sizes normally encountered limits the velocity of impact to extremely low values. The assumption that only the largest crystal sizes contribute significantly to the nucleation rate by crystal-to-crystal contact permits a simple computation of the rate:

$$B_e = K_c \rho G m_f^2 \quad (18-43)$$

where m_f = the fourth, fifth, sixth, or higher moments of the distribution.

A number of different crystallizing systems have been investigated by using the Randolph-Larson technique, and some of the published growth rates and nucleation rates are included in Table 18-6. Although the usefulness of these data is limited to the conditions tested, the table gives a range of values which may be expected, and it permits resolution of the information gained from a simple screen analysis into the fundamental factors of growth rate and nucleation rate. Experiments may then be conducted to determine the independent effects of operation and equipment design on these parameters.

Although this procedure requires laborious calculations because of the number of samples normally needed, these computations and the determination of the best straight-line fit to the data are readily programmed for digital computers.

Example 4: Population Density, Growth, and Nucleation Rate

Calculate the population density, growth, and nucleation rates for a crystal sample of urea for which there is the following information. These data are from Bennett and Van Buren [*Chem. Eng. Prog. Symp. Ser.*, **65**(95), 44 (1969)].

- Slurry density = 450 g/L
- Crystal density = 1.335 g/cm³
- Drawdown time $t = 3.38$ h

Shape factor $k_c = 1.00$

Product size:

-14 mesh, +20 mesh	4.4 percent
-20 mesh, +28 mesh	14.4 percent
-28 mesh, +35 mesh	24.2 percent
-35 mesh, +48 mesh	31.6 percent
-48 mesh, +65 mesh	15.5 percent
-65 mesh, +100 mesh	7.4 percent
-100 mesh	2.5 percent

n = number of particles per liter of volume

14 mesh = 1.168 mm, 20 mesh = 0.833 mm, average opening 1.00 mm

Size span = 0.335 mm = ΔL

$$n_{20} = \frac{(450 \text{ g/L})(0.044)}{(1.335/1000) \text{ g/mm}^3 (1.00^3 \text{ mm}^3/\text{particle})(0.335 \text{ mm})(1.0)}$$

$$n_{20} = 44,270$$

$$\ln n_{20} = 10,698$$

Repeating for each screen increment:

Screen size	Weight, %	k_c	$\ln n$	L , average diameter, mm
100	7.4	1.0	18.099	0.178
65	15.5	1.0	17.452	0.251
48	31.6	1.0	16.778	0.356
35	24.2	1.0	15.131	0.503
28	14.4	1.0	13.224	0.711
20	4.4	1.0	10.698	1.000

Plotting $\ln n$ versus L as shown in Fig. 18-68, a straight line having an intercept at zero length of 19.781 and a slope of -9.127 results. As mentioned in discussing Eq. (18-27), the growth rate can then be found.

$$\text{Slope} = -1/Gt \text{ or } -9.127 = -1/[G(3.38)]$$

or

$$G = 0.0324 \text{ mm/h}$$

and

$$B_0 = Cn^0 = (0.0324)(e^{19.781}) = 12.65 \times 10^6 \frac{n^0}{L \cdot h}$$

and

$$L_n = 3.67(0.0324)(3.38) = 0.40 \text{ mm}$$

An additional check can be made of the accuracy of the data by the relation

$$M_T = 6k_c \rho n^0 (Gt)^4 = 450 \text{ g/L}$$

$$M_T = (6)(1.0) \frac{1.335 \text{ g/cm}^3}{1000 \text{ mm}^3/\text{cm}^3} e^{19.781} [(0.0324)(3.38)]^4$$

$$M_T = 455 \text{ g/L} \approx 450 \text{ g/L}$$

Had only the growth rate been known, the size distribution of the solids could have been calculated from the equation

$$W_f = 1 - e^{-x} \left(\frac{x^3}{6} + \frac{x^2}{2} + x + 1 \right)$$

where W_f is the weight fraction up to size L and $x = L/Gt$.

$$x = \frac{L}{(0.0324)(3.38)} = \frac{L}{0.1095}$$

Screen size	L , mm	x	W_f^0	Cumulative % retained 100 (1 - W_f)	Measured cumulative % retained
20	0.833	7.70	0.944	5.6	4.4
28	0.589	5.38	0.784	21.6	18.8
35	0.417	3.80	0.526	47.4	43.0
48	0.295	2.70	0.286	71.4	74.6
65	0.208	1.90	0.125	87.5	90.1
100	0.147	1.34	0.048	95.2	97.5

*Values of W_f as a function of x may be obtained from a table of Wick's functions.

Note that the calculated distribution shows some deviation from the measured values because of the small departure of the actual sample from the theoretical coefficient of variation (i.e., 47.5 versus 50 percent).

The critical value of i , which is defined in Eq. (18-31) as the ratio of b/g or the relative dependence of nucleation and growth on supersaturation, can be determined by a few extra experiments. This is done by varying the residence time of the crystals (changing feed rate) while maintaining everything else constant. The

TABLE 18-6 Growth Rates and Kinetic Equations for Some Industrial Crystallized Products

Material crystallized	G, m/s × 10 ⁸	Range t, h	Range M _T , g/L	Temp., °C	Scale °	Kinetic equation for B ₀ no./L·s	References†
(NH ₄) ₂ SO ₄	1.67	3.83	150	70	P	B ₀ = 6.62 × 10 ⁻²⁵ G ^{0.82} ρ ^{-0.92} m ₂ ^{3.05}	Bennett and Wolf, <i>AIChE</i> , SFC, 1979.
(NH ₄) ₂ SO ₄	0.20	0.25	38	18	B	B ₀ = 2.94(10 ¹⁰)G ^{1.03}	Larsen and Mullen, <i>J. Crystal Growth</i> 20 : 183 (1973).
(NH ₄) ₂ SO ₄	—	0.20	—	34	B	B ₀ = 6.14(10 ⁻¹¹)S _R ^{7.84} M _T ^{0.98} G ^{1.22}	Youngquist and Randolph, <i>AIChE J.</i> 18 : 421 (1972).
MgSO ₄ ·7H ₂ O	3.0–7.0	—	—	25	B	B ₀ = 9.65(10 ¹²)M _T ^{0.67} G ^{1.24}	Sikdar and Randolph, <i>AIChE J.</i> 22 : 110 (1976).
MgSO ₄ ·7H ₂ O	—	—	Low	29	B	B ₀ = f(N, L ⁴ , N ^{4.2} , S ^{2.5})	Ness and White, <i>AIChE Symposium Series</i> 153, vol. 72, p. 64.
KCl	2–12	—	200	32	P	B ₀ = 7.12(10 ³⁹)M _T ^{0.14} G ^{4.99}	Randolph et al., <i>AIChE J.</i> 23 : 500 (1977).
KCl	3.3	1–2	100	37	B	B ₀ = 5.16(10 ²³)M _T ^{0.91} G ^{2.77}	Randolph et al., <i>Ind. Eng. Chem. Proc. Design Dev.</i> 20 : 496 (1981).
KCl	0.3–0.45	—	50–147	25–68	B	B ₀ = 5 × 10 ⁻³ G ^{2.78} (M _T TIP ²) ^{1.2}	Qian et al., <i>AIChE J.</i> 33 (10): 1690 (1987).
KCr ₂ O ₇	1.2–9.1	0.25–1	14–42	—	B	B ₀ = 7.33(10 ⁴)M _T ^{0.6} G ^{0.5}	Desari et al., <i>AIChE J.</i> 20 : 43 (1974).
KCr ₂ O ₇	2.6–10	0.15–0.5	20–100	26–40	B	B ₀ = 1.59(10 ⁻³)S _R ³ M _T G ^{0.48}	Janse, Ph.D. thesis, Delft Technical University, 1977.
KNO ₃	8.13	0.25–0.050	10–40	20	B	B ₀ = 3.85(10 ¹⁶)M _T ^{0.5} G ^{2.06}	Juraszek and Larson, <i>AIChE J.</i> 23 : 460 (1977).
K ₂ SO ₄	—	0.03–0.17	1–7	30	B	B ₀ = 2.62(10 ³)S _R ^{2.5} M _T ^{0.5} G ^{0.54}	Randolph and Sikdar, <i>Ind. Eng. Chem. Fund.</i> 15 : 64 (1976).
K ₂ SO ₄	2–6	0.25–1	2–20	10–50	B	B ₀ = 4.09(10 ⁶) exp($\frac{10900}{RT}$)M _T G ^{0.5}	Jones, Budz, and Mullin, <i>AIChE J.</i> 33 : 12 (1986).
K ₂ SO ₄	0.8–1.6	—	—	—	B	$\frac{G}{G_0} = 1 + 2L^{2/3}$ (L in μm)	White, Bendig, and Larson, <i>AIChE Mtg.</i> , Washington, D.C., Dec. 1974.
NaCl	4–13	0.2–1	25–200	50	B	B ₀ = 1.92(10 ¹⁰)S _R ² M _T G ²	Asselbergs, Ph.D. thesis, Delft Technical University, 1978.
NaCl	—	0.6	35–70	55	P	B ₀ = 8 × 10 ¹⁰ N ² G ² M _T	Grootscholten et al., <i>Chem. Eng. Design</i> 62 : 179 (1984).
NaCl	0.5	1–2.5	70–190	72	P	B ₀ = 1.47(10 ²) $(\frac{I^2}{P})^{0.84}$ m ₄ ^{0.54} G ^{0.98}	Bennett et al., <i>Chem. Eng. Prog.</i> 69 (7): 86 (1973).
Citric acid	1.1–3.7	—	—	16–24	B	B ₀ = 1.09(10 ¹⁰)m ₄ ^{0.084} G ^{0.84}	Sikdar and Randolph, <i>AIChE J.</i> 22 : 110 (1976).
Fructose	0.1–0.25	—	—	50	B	—	Shiau and Berglund, <i>AIChE J.</i> 33 : 6 (1987).
Sucrose	—	—	—	80	B	B ₀ = 5 × 10 ⁶ N ^{0.7} M _T ^{0.3} G ^{0.4}	Berglund and deJong, <i>Separations Technology</i> 1 : 38 (1990).
Sugar	2.5–5	0.375	50	45	B	B ₀ = 4.38(10 ⁶)M _T ^{1.01} (ΔC – 0.5) ^{1.42}	Hart et al., <i>AIChE Symposium Series</i> 193, vol. 76, 1980.
Urea	0.4–4.2	2.5–6.8	350–510	55	P	B ₀ = 5.48(10 ⁻¹)M _T ^{3.87} G ^{1.66}	Bennett and Van Buren, <i>Chem. Eng. Prog. Symposium Series</i> 95 (7): 65 (1973).
Urea	—	—	—	3–16	B	B ₀ = 1.49(10 ⁻³¹)S _R ^{2.3} M _T ^{1.07} G ^{-3.54}	Lodaya et al., <i>Ind. Eng. Chem. Proc. Design Dev.</i> 16 : 294 (1977).

°B = bench scale; P = pilot plant.

†Additional data on many components are in Garside and Shah, *Ind. Eng. Chem. Proc. Design Dev.*, **19**, 509 (1980).

B⁰ and G values are determined at each residence time, and a plot of ln B⁰ versus ln G should yield a straight line of slope i. High values of i indicate a propensity to nucleate versus grow and dictate the need to ensure low values of supersaturation.

Had sufficient data indicating a change in n⁰ for various values of M_T at constant G been available, a plot of ln n⁰ versus ln M_T at corresponding G's would permit determination of the power j.

Crystallizers with Fines Removal In Example 4, the product was from a forced-circulation crystallizer of the MSMPR type. In many cases, the product produced by such machines is too small for commercial use; therefore, a separation baffle is added within the crystallizer to permit the removal of unwanted fine crystalline material from the magma, thereby controlling the population density in the machine so as to produce a coarser crystal product. When this is done, the product sample plots on a graph of ln n versus L as shown in line P, Fig. 18-69. The line of steepest slope, line E, represents the particle-size distribution of the fine material, and samples which show this distribution can be taken from the liquid leaving the fines-separation baffle. The prod-

uct crystals have a slope of lower value, and typically there should be little material present smaller than L_f, the size which the baffle is designed to separate. However, this is not to imply that there are no fines in the product stream. The effective nucleation rate for the product material is the intersection of the extension of line P to zero size.

As long as the largest particle separated by the fines-destruction baffle is small compared with the mean particle size of the product, the seed for the product may be thought of as the particle-size distribution corresponding to the fine material which ranges in length from zero to L_f, the largest size separated by the baffle.

The product discharged from the crystallizer is characterized by the integral of the distribution from size L_f to infinity:

$$M_T = k_v \rho \int_{L_f}^{\infty} n^0 \exp(-L_f/Gt_f) \exp(L/GT) L^3 dL \quad (18-44)$$

The integrated form of this equation is shown in Table 18-5.

For a given set of assumptions it is possible to calculate the characteristic curves for the product from the crystallizer when it is operated

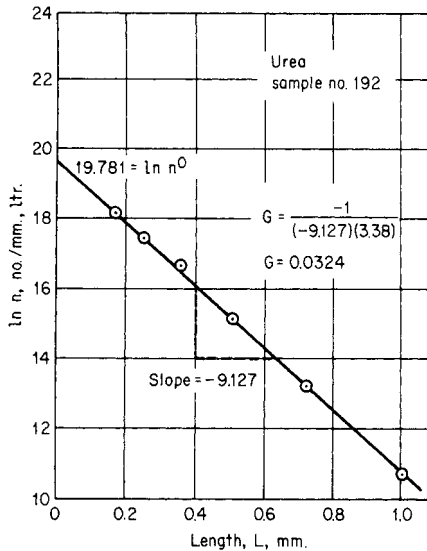


FIG. 18-68 Population density plot for Example 4.

at various levels of fines removal as characterized by L_f . This has been done for an ammonium sulfate crystallizer in Fig. 18-70. Also shown in that figure is the actual size distribution obtained. In calculating theoretical size distributions in accordance with the Eq. (18-44), it is assumed that the growth rate is a constant, whereas in fact larger values of L_f will interact with the system driving force to raise the growth rate and the nucleation rate. Nevertheless, Fig. 18-70 illus-

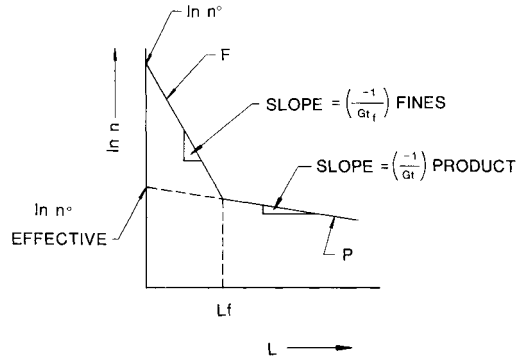


FIG. 18-69 Plot of Log N against L for a crystallizer with fines removal.

trates clearly the empirical result of the operation of such equipment, demonstrating that the most significant variable in changing the particle-size distribution of the product is the size removed by the baffle. Conversely, changes in retention time for a given particle-removal size L_f make a relatively small change in the product-size distribution. Jancic and Grootsholten (op. cit., p. 318) have found that the size enlargement is dependent on the fines size, the relative kinetic order i , and the rate of flow to the fines circuit versus product flow.

It is implicit that increasing the value of L_f will raise the supersaturation and growth rate to levels at which mass nucleation can occur, thereby leading to periodic upsets of the system or cycling [Randolph, Beer, and Keener, *Am. Inst. Chem. Eng. J.*, **19**, 1140 (1973)]. That this could actually happen was demonstrated experimentally by Randolph, Beckman, and Kraljevich [*Am. Inst. Chem. Eng. J.*, **23**, 500 (1977)], and that it could be controlled dynamically by regulating the

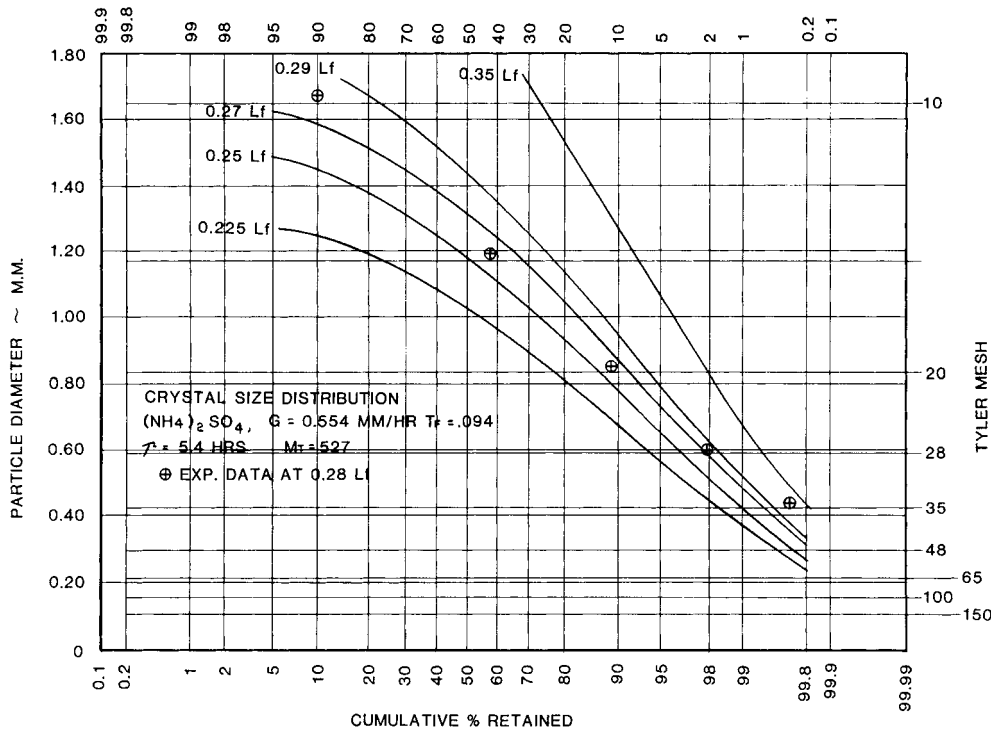


FIG. 18-70 Calculated product-size distribution for a crystallizer operation at different fine-crystal-separation sizes.

finest-destroyer system was shown by Beckman and Randolph [ibid., (1977)]. Dynamic control of a crystallizer with a fines-destruction baffle and fine-particle-detection equipment employing a light-scattering (laser) particle-size-measurement instrument is described in U.S. Patent, 4,263,010 and 5,124,265.

CRYSTALLIZATION EQUIPMENT

Whether a vessel is called an evaporator or a crystallizer depends primarily on the criteria used in arriving at its sizing. In an evaporator of the salting-out type, sizing is done on the basis of vapor release. In a crystallizer, sizing is normally done on the basis of the volume required for crystallization or for special features required to obtain the proper product size. In external appearance, the vessels could be identical. Evaporators are discussed in Sec. 11. Genck (loc. cit., 2004) provides a detailed discussion of guidelines for crystallizer selection and operation.

In the discussion which follows, crystallization equipment has been classified according to the means of suspending the growing product. This technique reduces the number of major classifications and segregates those to which Eq. (18-34) applies.

Mixed-Suspension, Mixed-Product-Removal Crystallizers

This type of equipment, sometimes called the circulating-magma crystallizer, is by far the most important in use today. In most commercial equipment of this type, the uniformity of suspension of product solids within the crystallizer body is sufficient for the theory [Eqs. (18-34) to (18-36c)] to apply. Although a number of different varieties and features are included within this classification, the equipment operating with the highest capacity is the kind in which the vaporization of a solvent, usually water, occurs.

Although surface-cooled types of MSMPR crystallizers are available, most users prefer crystallizers employing vaporization of solvents or of refrigerants. The primary reason for this preference is that heat transferred through the critical supersaturating step is through a boiling-liquid-gas surface, avoiding the troublesome solid deposits that can form on a metal heat-transfer surface. In this case very low LMTDs are required to stay within the metastable zone to promote growth and reduce scaling. The result is multipass, large-surface-area heat exchangers.

Forced-Circulation Evaporator-Crystallizer This crystallizer is shown in Fig. 18-71. Slurry leaving the body is pumped through a circulating pipe and through a tube-and-shell heat exchanger, where its temperature increases by about 2 to 6°C (3 to 10°F). Since this heating is done without vaporization, materials of normal solubility should produce no deposition on the tubes. The heated slurry, returned to the body by a recirculation line, mixes with the body slurry and raises its temperature locally near the point of entry, which causes boiling at the liquid surface. During the consequent cooling and vaporization to achieve equilibrium between liquid and vapor, the supersaturation which is created causes growth on the swirling body of suspended crystals until they again leave via the circulating pipe. Severe vortexing must be eliminated to ensure that the supersaturation is relieved. The quantity and the velocity of the recirculation, the size of the body, and the type and speed of the circulating pump are critical design items if predictable results are to be achieved. A further discussion of the parameters affecting this type of equipment is given by Bennett, Newman, and Van Buren [*Chem. Eng. Prog.*, **55**(3), 65 (1959); *Chem. Eng. Prog. Symp. Ser.*, **65**(95), 34, 44 (1969)].

If the crystallizer is not of the evaporative type but relies only on *adiabatic evaporative cooling* to achieve the yield, the heating element is omitted. The feed is admitted into the circulating line after withdrawal of the slurry, at a point sufficiently below the free-liquid surface to prevent flashing during the mixing process.

FC units typically range from 2 to 20 ft in diameter. They are especially useful for high evaporation loads. For example, a unit used to evaporate water at 380 mmHg can typically be designed to handle 250 to 300 lb/(h·ft²). Other than allowing one to adjust the residence time or slurry density, the FC affords little opportunity to change the size distribution.

Draft-Tube-Baffle (DTB) Evaporator-Crystallizer Because mechanical circulation greatly influences the level of nucleation within the crystallizer, a number of designs have been developed that

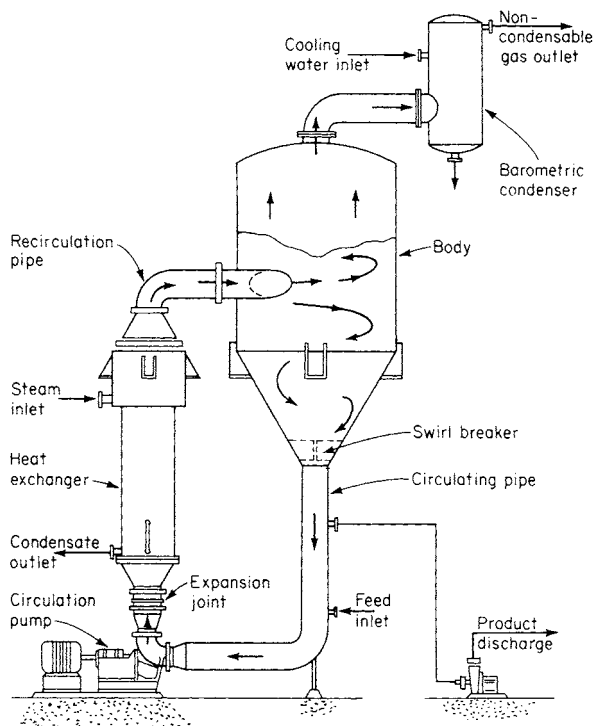


FIG. 18-71 Forced-circulation (evaporative) crystallizer. (Swenson Process Equipment, Inc.)

use circulators located within the body of the crystallizer, thereby reducing the head against which the circulator must pump. This technique reduces the power input and circulator tip speed and therefore the rate of nucleation. A typical example is the draft-tube-baffle (DTB) evaporator-crystallizer (Swenson Process Equipment, Inc.) shown in Fig. 18-72. The suspension of product crystals is maintained by a large, slow-moving propeller surrounded by a draft tube within the body. The propeller directs the slurry to the liquid surface so as to prevent solids from short-circuiting the zone of the most intense supersaturation. Slurry which has been cooled is returned to the bottom of the vessel and recirculated through the propeller. At the propeller, heated solution is mixed with the recirculating slurry.

The design of Fig. 18-72 contains a fines-destruction feature comprising the settling zone surrounding the crystallizer body, the circulating pump, and the heating element. The heating element supplies sufficient heat to meet the evaporation requirements and to raise the temperature of the solution removed from the settler so as to destroy any small crystalline particles withdrawn. Coarse crystals are separated from the fines in the settling zone by gravitational sedimentation, and therefore this fines-destruction feature is applicable only to systems in which there is a substantial density difference between crystals and mother liquor.

This type of equipment can also be used for applications in which the only heat removed is that required for adiabatic cooling of the incoming feed solution. When this is done and the fines-destruction feature is to be employed, a stream of liquid must be withdrawn from the settling zone of the crystallizer and the fine crystals must be separated or destroyed by some means other than heat addition—for example, either dilution or thickening and physical separation.

In some crystallization applications it is desirable to increase the solids content of the slurry within the body above the natural make, which is that developed by equilibrium cooling of the incoming feed solution to the final temperature. This can be done by withdrawing a stream of mother liquor from the baffle zone, thereby thickening the

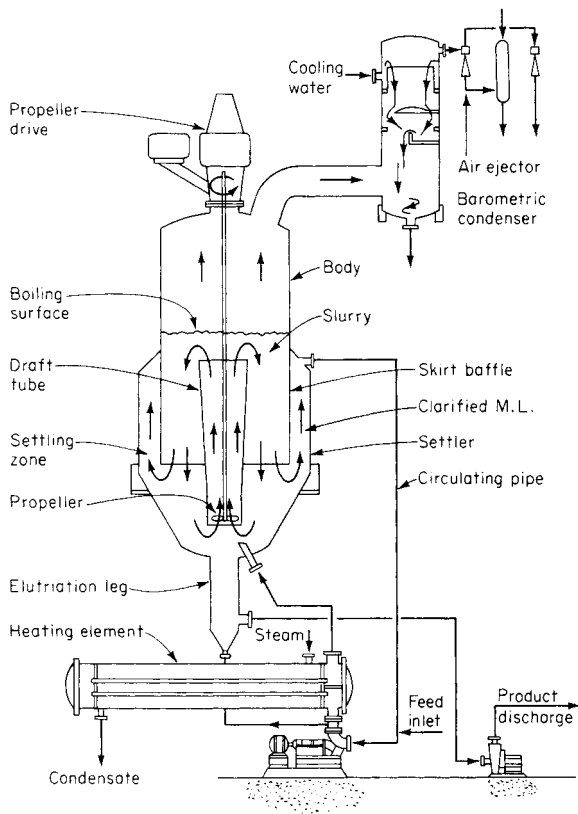


FIG. 18-72 Draft-tube-baffle (DTB) crystallizer. (Swenson Process Equipment, Inc.)

slurry within the growing zone of the crystallizer. This mother liquor is also available for removal of fine crystals for size control of the product.

Draft-Tube (DT) Crystallizer This crystallizer may be employed in systems in which fines destruction is not needed or wanted. In such cases the baffle is omitted, and the internal circulator is sized to have the minimum nucleating influence on the suspension.

In DTB and DT crystallizers the circulation rate achieved is generally much greater than that available in a similar forced-circulation crystallizer. The equipment therefore finds application when it is necessary to circulate large quantities of slurry to minimize supersaturation levels within the equipment. In general, this approach is required to obtain long operating cycles with material capable of growing on the walls of the crystallizer. The draft-tube and draft-tube-baffle designs are commonly used in the production of granular materials such as ammonium sulfate, potassium chloride, photographic hypo, and other inorganic and organic crystals for which product in the range 8 to 30 mesh is required.

Surface-Cooled Crystallizer For some materials, such as sodium chlorate, it is possible to use a forced-circulation tube-and-shell exchanger in direct combination with a draft-tube-crystallizer body, as shown in Fig. 18-73. Careful attention must be paid to the temperature difference between the cooling medium and the slurry circulated through the exchanger tubes. In addition, the path and rate of slurry flow within the crystallizer body must be such that the volume contained in the body is "active." That is to say, crystals must be so suspended within the body by the turbulence that they are effective in relieving supersaturation created by the reduction in temperature of the slurry as it passes through the exchanger. Obviously, the circulating pump is part of the crystallizing system, and careful attention must be paid to its type and its operating parameters to avoid undue nucleating influences.

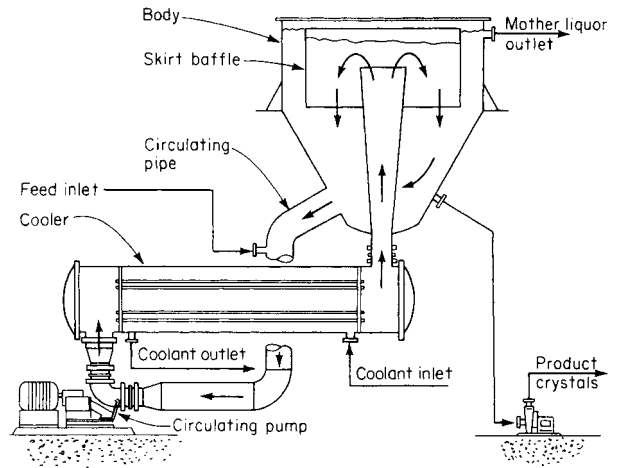


FIG. 18-73 Forced-circulation baffle surface-cooled crystallizer. (Swenson Process Equipment, Inc.)

The use of the internal baffle permits operation of the crystallizer at a slurry consistency other than that naturally obtained by the cooling of the feed from the initial temperature to the final mother-liquor temperature. The baffle also permits fines removal and destruction.

With most inorganic materials this type of equipment produces crystals in the range 30 to 100 mesh. The design is based on the allowable rates of heat exchange and the retention required to grow the product crystals.

Direct-Contact-Refrigeration Crystallizer For some applications, such as the freezing of ice from seawater, it is necessary to go to such low temperatures that cooling by the use of refrigerants is the only economical solution. In such systems it is sometimes impractical to employ surface-cooled equipment because the allowable temperature difference is so small (under 3°C) that the heat-exchanger surface becomes excessive or because the viscosity is so high that the mechanical energy put in by the circulation system requires a heat-removal rate greater than can be obtained at reasonable temperature differences. In such systems, it is convenient to admix the refrigerant with the slurry being cooled in the crystallizer, as shown in Fig. 18-74, so that the heat of vaporization of the refrigerant cools the slurry by direct contact. The successful application of such systems requires that the refrigerant be relatively immiscible with the mother liquor and be capable of separation, compression, condensation, and subsequent recycle into the crystallizing system. The operating pressures and temperatures chosen have a large bearing on power consumption.

This technique has been very successful in reducing the problems associated with buildup of solids on a cooling surface. The use of direct-contact refrigeration also reduces overall process-energy requirements, since in a refrigeration process involving two fluids a greater temperature difference is required on an overall basis when the refrigerant must first cool some intermediate solution, such as calcium chloride brine, and that solution in turn cools the mother liquor in the crystallizer.

Equipment of this type has been successfully operated at temperatures as low as -59°C (-75°F).

Reaction-Type Crystallizers In chemical reactions in which the end product is a solid-phase material such as a crystal or an amorphous solid the type of equipment described in the preceding subsections or shown in Fig. 18-75 may be used. By mixing the reactants in a large circulated stream of mother liquor containing suspended solids of the equilibrium phase, it is possible to minimize the driving force created during their reaction and remove the heat of reaction through the vaporization of a solvent, normally water. Depending on the final particle size required, it is possible to incorporate a fines-destruction baffle as shown in Fig. 18-75 and take advantage of the control over particle size afforded by this technique. In the case of ammonium sulfate crystallization from ammonia gas and concentrated sulfuric acid, it is necessary to vaporize water to remove the heat of reaction, and this water so

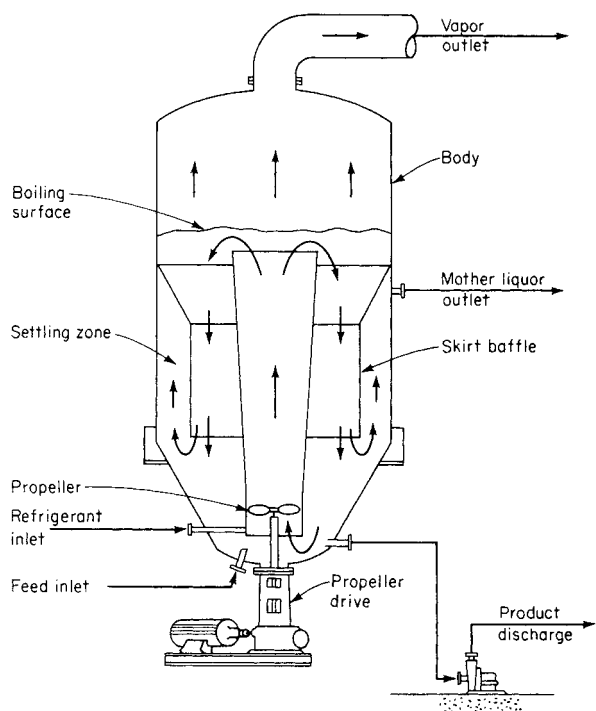


FIG. 18-74 Direct-contact-refrigeration crystallizer (DTB type). (Svenson Process Equipment, Inc.)

removed can be reinjected after condensation into the fines-destruction stream to afford a very large amount of dissolving capability.

Other examples of this technique are where a solid material is to be decomposed by mixing it with a mother liquor of a different composition, as shown in Fig. 18-76. Carnallite ore ($\text{KCl} \cdot \text{MgCl}_2 \cdot 4\text{H}_2\text{O}$) can be added to a mother liquor into which water is also added so that decomposition of the ore into potassium chloride (KCl) crystals and magnesium chloride-rich mother liquor takes place. Circulated slurry in the draft tube suspends the product crystals as well as the incoming ore particles until the ore can decompose into potassium chloride crystals and mother liquor. By taking advantage of the fact that water must be added to the process, the fines-bearing mother liquor can be removed behind the baffle and then water added so that the finest particles are dissolved before being returned to the crystallizer body.

Other examples of this technique involve neutralization reactions such as the neutralization of sulfuric acid with calcium chloride to result in the precipitation of gypsum.

Mixed-Suspension, Classified-Product-Removal Crystallizers Many of the crystallizers just described can be designed for classified-product discharge. Classification of the product is normally done by means of an elutriation leg suspended beneath the crystallizing body as shown in Fig. 18-72. Introduction of clarified mother liquor to the lower portion of the leg fluidizes the particles prior to discharge and selectively returns the finest crystals to the body for further growth. A relatively wide distribution of material is usually produced unless the elutriation leg is extremely long. Inlet conditions at the leg are critical if good classifying action or washing action is to be achieved.

If an elutriation leg or other product-classifying device is added to a crystallizer of the MSMPR type, the plot of the population density versus L is changed in the region of largest sizes. Also the incorporation of an elutriation leg destabilizes the crystal-size distribution and under some conditions can lead to cycling. To reduce cycling, fines destruction is usually coupled with classified product removal. The theoretical treatment of both the crystallizer model and the cycling relations is discussed by Randolph, Beer, and Keener (*loc. cit.*).

Although such a feature can be included on many types of classified-suspension or mixed-suspension crystallizers, it is most common to use this feature with the forced-circulation evaporative-crystallizer and the DTB crystallizer.

Classified-Suspension Crystallizer This equipment is also known as the **growth or Oslo crystallizer** and is characterized by the production of supersaturation in a circulating stream of liquor. Supersaturation is developed in one part of the system by evaporative cooling or by cooling in a heat exchanger, and it is relieved by passing the liquor through a fluidized bed of crystals. The fluidized bed may be contained in a simple tank or in a more sophisticated vessel arranged for a pronounced classification of the crystal sizes. Ideally this equipment operates within the metastable supersaturation field described by Miers and Isaac, *J. Chem. Soc.*, **1906**, 413.

In the **evaporative crystallizer** of Fig. 18-77, solution leaving the vaporization chamber at B is supersaturated slightly within the metastable zone so that new nuclei will not form. The liquor contacting the bed at E relieves its supersaturation on the growing crystals and leaves through the circulating pipe F . In a cooling-type crystallization hot feed is introduced at G , and the mixed liquor flashes when it reaches the vaporization chamber at A . If further evaporation is required to produce the driving force, a heat exchanger is installed between the circulating pump and the vaporization chamber to supply the heat for the required rate of vaporization.

The transfer of supersaturated liquor from the vaporizer (point B , Fig. 18-77) can cause salt buildup in the piping and reduction of the operating cycle in equipment of this type. The rate of buildup can be reduced by circulating a thin suspension of solids through the vaporizing chamber; however, the presence of such small seed crystals tends to rob the supersaturation developed in the vaporizer, thereby lowering the efficiency of the recirculation system.

The decrease in temperature due to flashing is typically less than 4 to 6°F, and the increase in solute concentration in the circulating liquor is often around 1 to 3 g/L solvent. Care must be taken to ensure that the liquid velocities in the tapered cross-section of the lower body allow classification of the solids. One must know the settling rates and morphologies of the crystals for proper design and operation. An unclassified operation will perform as an FC unit.

The Oslo crystallizer is best suited for use with compounds with high settling velocities such as greater than 20 to 40 mm/s. If the crystals have high settling rates, the larger particles will settle out quickly. Crystals with low settling velocities require large cross-sectional areas which implies large crystallizers and low crystal production rates.

The suggested productivities for concentration driving forces depend on the settling velocities of the crystals. For a given ΔC , the higher the settling velocity, the higher the allowable crystallizer productivity. For example, for a change in concentration of 2 g/L, the recommended productivity increases from 125 to 250 kg/(h·m³) as the settling rate increases from 20 to 30 mm/s.

An **Oslo surface-cooled crystallizer** is illustrated in Fig. 18-78. Supersaturation is developed in the circulated liquor by chilling in the cooler H . This supersaturated liquor is contacted with the suspension of crystals in the suspension chamber at E . At the top of the suspension chamber a stream of mother liquor D can be removed to be used for fines removal and destruction. This feature can be added on either type of equipment. Fine crystals withdrawn from the top of the suspension are destroyed, thereby reducing the overall number of crystals in the system and increasing the particle size of the remaining product crystals.

Scraped-Surface Crystallizer A number of crystallizer designs employing direct heat exchange between the slurry and a jacket or double wall containing a cooling medium have been developed. The heat-transfer surface is scraped or agitated in such a way that the deposits cannot build up. The scraped-surface crystallizer provides an effective and inexpensive method of producing slurry in equipment which does not require expensive installation or supporting structures. At times these units are employed to provide auxiliary cooling capacity for existing units.

Double-Pipe Scraped-Surface Crystallizer This type of equipment consists of a double-pipe heat exchanger with an internal agitator fitted with spring-loaded scrapers that wipe the wall of the inner pipe.

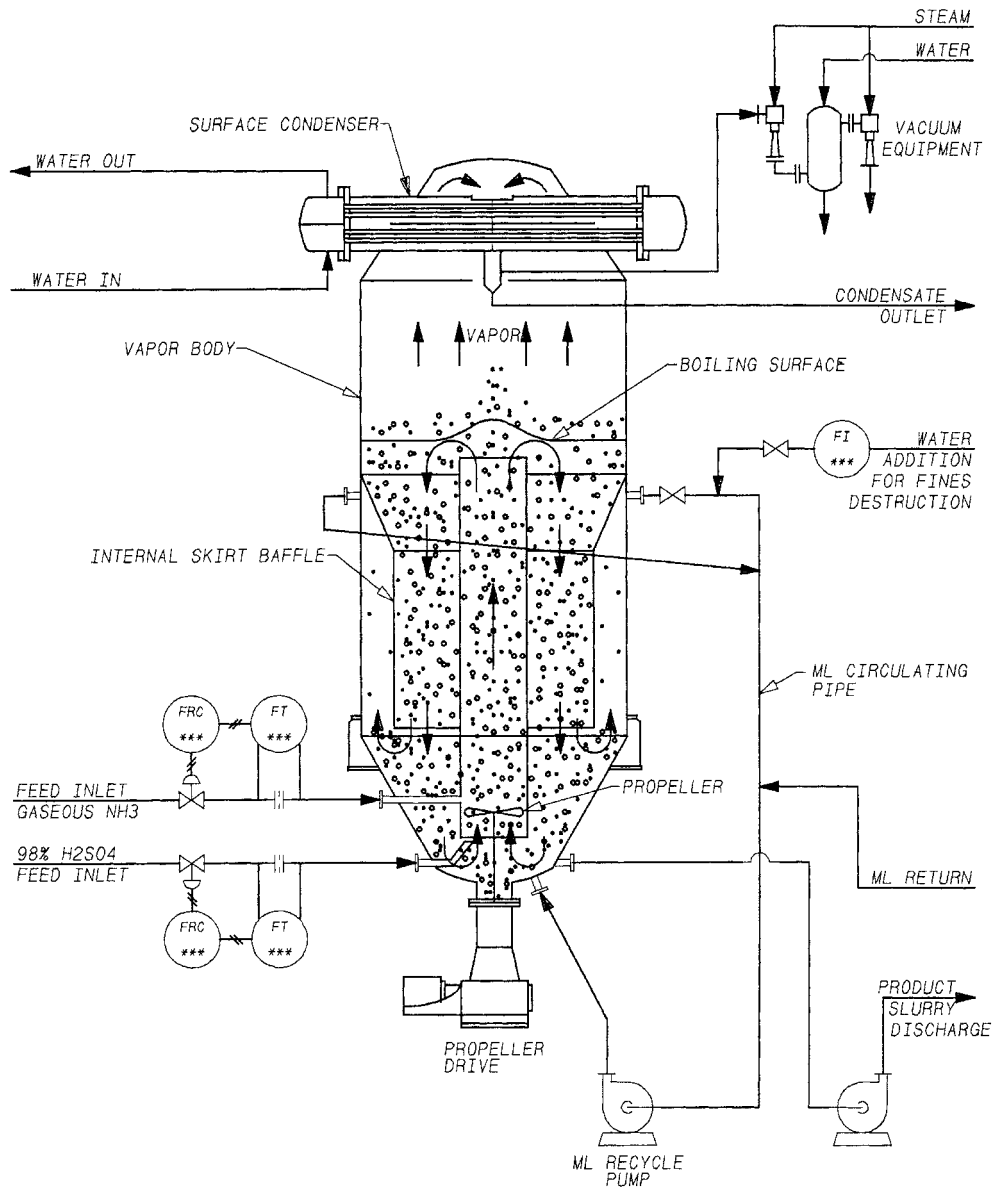


FIG. 18-75 Swenson reaction type DTB crystallizer. (Swenson Process Equipment, Inc.)

The cooling liquid passes between the pipes, this annulus being dimensioned to permit reasonable shell-side velocities. The scrapers prevent the buildup of solids and maintain a good film coefficient of heat transfer. Crystal growth is in the bulk of the liquid. The equipment can be operated in a continuous or in a recirculating batch manner.

Such units are generally built in lengths to above 12 m (40 ft). They can be arranged in parallel or in series to give the necessary liquid velocities for various capacities. Heat-transfer coefficients have been reported in the range of 170 to 850 $W/(m^2 \cdot K)$ [30 to 150 $Btu/(h \cdot ft^2 \cdot ^\circ F)$] at temperature differentials of $17^\circ C$ ($30^\circ F$) and higher [Garrett and Rosenbaum, *Chem. Eng.*, **65**(16), 127 (1958)]. Equipment of this type is marketed as the **Votator** and the **Armstrong crystallizer**.

Batch Crystallization Batch crystallization has been practiced longer than any other form of crystallization in both atmospheric

tanks, which are either static or agitated, as well as in vacuum or pressure vessels. It is widely practiced in the pharmaceutical and fine chemical industry or in those applications where the capacity is very small. This supersaturation can be generated by a number of modes including antisolvent addition, cooling, evaporation, pH adjustment, and chemical reaction.

A typical batch process involves charging the crystallizer with concentrated or near-saturated solution, producing supersaturation by means of a cooling temperature profile or evaporation profile and seeding the batch in the metastable zone or by allowing spontaneous nucleation to occur. The final mother liquor temperature and concentration is achieved by a time-dependent profile and the batch is then held for ripening followed by transferring the same to downstream processing such as centrifuging, filtration, and drying.

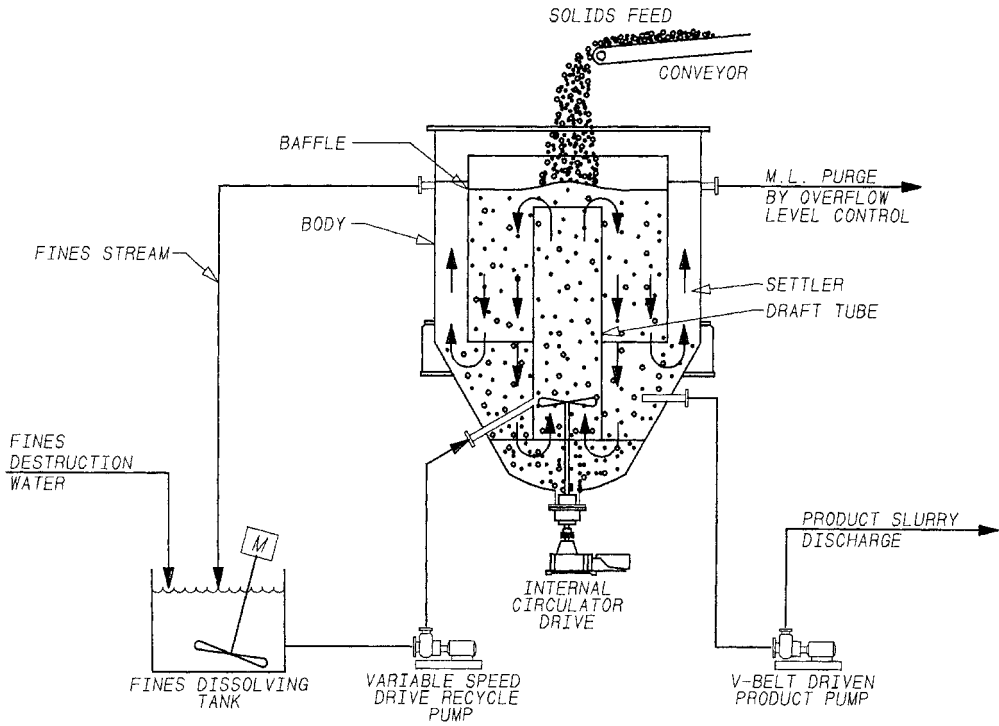


FIG. 18-76 Swenson atmospheric reaction-type DTB crystallizer. (Swenson Process Equipment, Inc.)

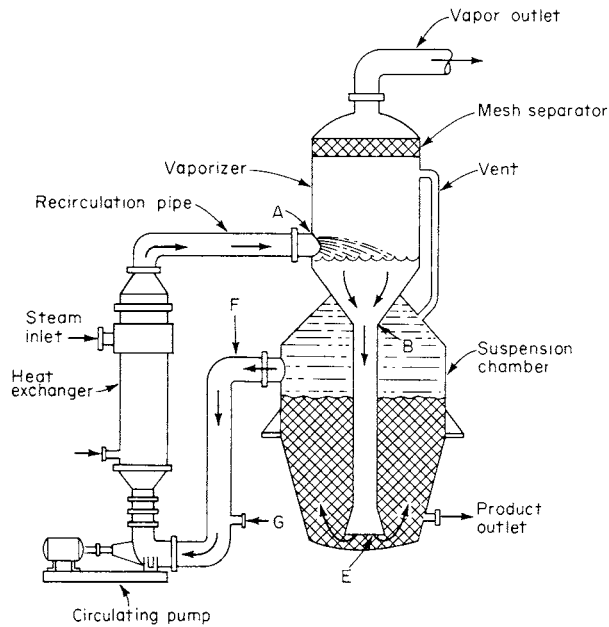


FIG. 18-77 OSLO evaporative crystallizer.

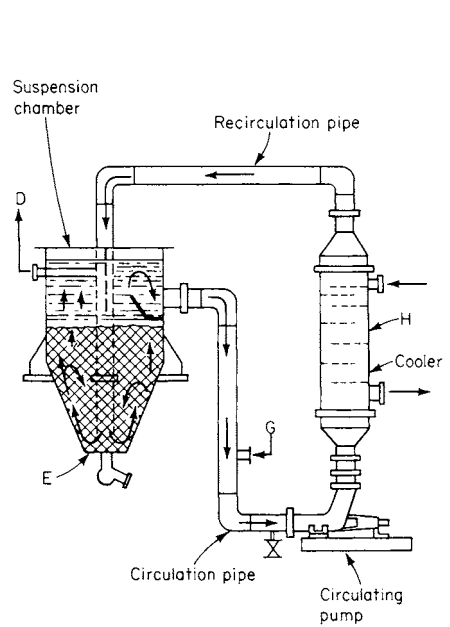


FIG. 18-78 OSLO surface-cooled crystallizer.

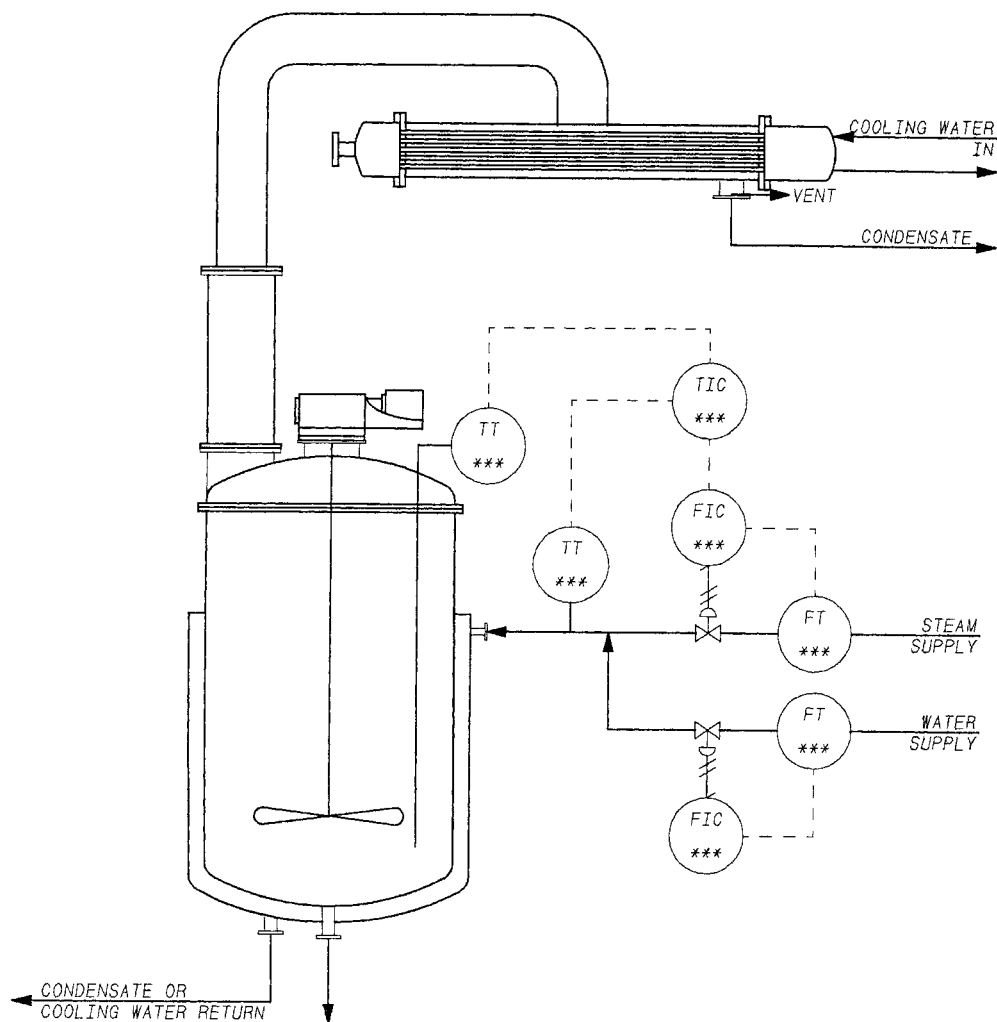


FIG. 18-79 Typical agitated batch crystallizer. (Swenson Process Equipment, Inc.)

Control of a batch crystallizer is critical to achieve the desired size distribution. It is necessary to have some means for determining when the initial solution is supersaturated so that seed of the appropriate size, quantity, and habit may be introduced into the batch. Following seeding, it is necessary to limit the cooling or evaporation in the batch to that which permits the generated supersaturation to be relieved on the seed crystals. This means that the first cooling or evaporation following seeding must be at a very slow rate, which is increased nonlinearly in order to achieve the optimum batch cycle and product properties. Frequently, such controls are operated by cycle timers or computers so as to achieve the required conditions. Shown in Fig. 18-79 is a typical batch crystallizer comprising a jacketed closed tank with top-mounted agitator and feed connections. The tank is equipped with a short distillation column and surface condenser so that volatile materials may be retained in the tank and solvent recycled to maintain the batch integrity. Provisions are included so that the vessel may be heated with steam addition to the shell or cooling solution circulated through the jacket so as to control the temperature. Tanks of this type are intended to be operated with

a wide variety of chemicals under both cooling and solvent evaporation conditions.

A detailed discussion of crystallization practice is provided by Genck in the following articles: Genck, *Chem. Eng.*, **104**(11), 94 (1997); Genck, *Chem. Eng.*, **107**(8), 90 (2000), and Genck, *Chem. Eng. Progress*, **99**(6), 36 (2003).

Recompression Evaporation-Crystallization In all types of crystallization equipment wherein water or some other solvent is vaporized to produce supersaturation and/or cooling, attention should be given to the use of mechanical vapor recompression, which by its nature permits substitution of electrical energy for evaporation and solvent removal rather than requiring the direct utilization of heat energy in the form of steam or electricity. A typical recompression crystallizer flowsheet is shown in Fig. 18-80, which shows a single-stage evaporative crystallizer operating at approximately atmospheric pressure. The amount of heat energy necessary to remove 1 kg of water to produce the equivalent in crystal product is approximately 550 kilocalories. If the water evaporated is compressed by a mechanical compressor of high efficiency

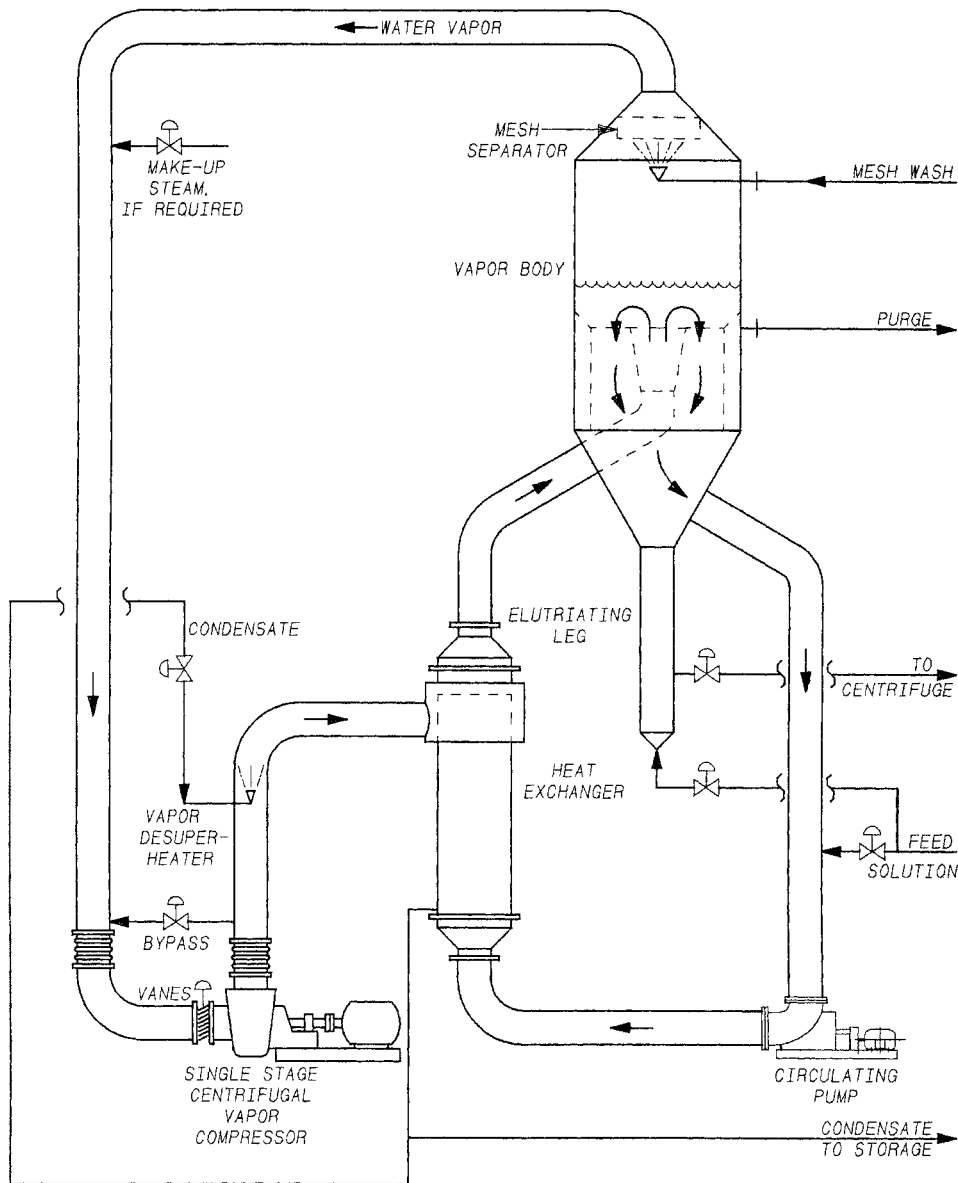


FIG. 18-80 Swenson single-stage recompression evaporator. (Swenson Process Equipment, Inc.)

to a pressure where it can be condensed in the heat exchanger of the crystallizer, it can thereby supply the energy needed to sustain the process. Then the equivalent power for this compression is about 44 kilocalories (Bennett, *Chem. Eng. Progress*, 1978, pp. 67-70).

Although this technique is limited economically to those large-scale cases where the materials handled have a relatively low boiling point elevation and in those cases where a significant amount of heat is required to produce the evaporation for the crystallization step, it nevertheless offers an attractive technique for reducing the use of heat energy and substituting mechanical energy or electrical energy in those cases where there is a cost advantage for doing so. This technique finds many applications in the crystallization of sodium sulfate,

sodium carbonate monohydrate, and sodium chloride. Shown in Fig. 18-81 is the amount of vapor compressed per kilowatt-hour for water vapor at 100°C and various ΔT s. The amount of water vapor compressed per horsepower decreases rapidly with increasing ΔT and, therefore, normal design considerations dictate that the recompression evaporators have a relatively large amount of heat-transfer surface so as to minimize the power cost. Often this technique is utilized only with the initial stages of evaporation where concentration of the solids is relatively low and, therefore, the boiling-point elevation is negligible. In order to maintain adequate tube velocity for heat transfer and suspension of crystals, the increased surface requires a large internal recirculation within the crystallizer body, which consequently lowers the supersaturation in the fluid pumped through the tubes.

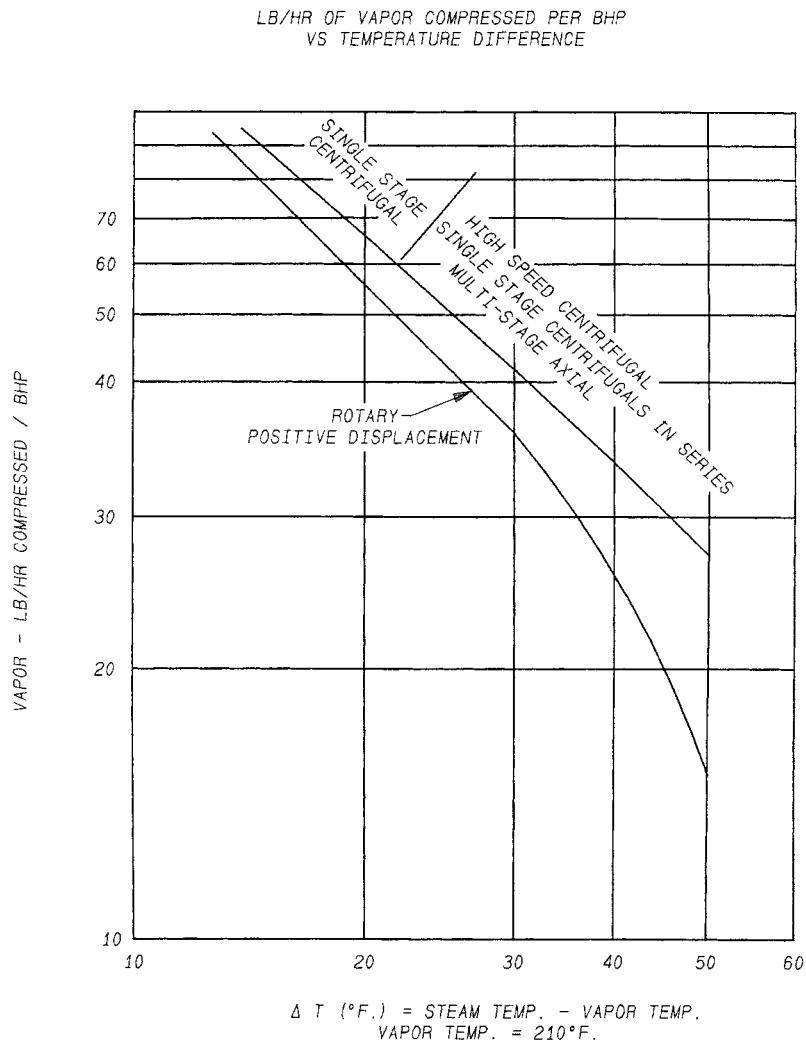


FIG. 18-81 Recompression evaporator horsepower as a function of overall ΔT .

One benefit of this design is that with materials of flat or inverted solubility, the use of recompression complements the need to maintain low ΔT 's to prevent fouling of the heat-transfer surface.

INFORMATION REQUIRED TO SPECIFY A CRYSTALLIZER

The following information regarding the product, properties of the feed solution, and required materials of construction must be available before a crystallizer application can be properly evaluated and the appropriate equipment options identified. Is the crystalline material being produced a hydrated or an anhydrous material? What is the solubility of the compound in water or in other solvents under consideration, and how does this change with temperature? Are other compounds in solution which coprecipitate with the product being crystallized, or do these remain in solution, increasing in concentration until some change in product phase occurs? What will be the influence of impurities in the solution on the crystal habit, growth, and nucleation rates? What are the physical prop-

erties of the solution and its tendency to foam? What is the heat of crystallization of the product crystal? What is the production rate, and what is the basis on which this production rate is computed? What is the tendency of the material to grow on the walls of the crystallizer? What materials of construction can be used in contact with the solution at various temperatures? What utilities will be available at the crystallizer location, and what are the costs associated with the use of these utilities? Is the final product to be blended or mixed with other crystalline materials or solids? What size of product and what shape of product are required to meet these requirements? How can the crystalline material be separated from the mother liquor and dried? Are there temperature requirements or wash requirements which must be met? How can these solids or mixtures of solids be handled and stored without undue breakage and caking? Is polymorphism an issue?

Another basic consideration is whether crystallization is best carried out on a batch basis or on a continuous basis. The present tendency in most processing plants is to use continuous equipment

whenever possible. Continuous equipment permits adjusting of the operating variables to a relatively fine degree in order to achieve the best results in terms of energy usage and product characteristics. It allows the use of a smaller labor force and results in a continuous utility demand, which minimizes the size of boilers, cooling towers, and power-generation facilities. It also minimizes the capital investment required in the crystallizer and in the feed-storage and product-liquor-storage facilities.

Materials that have a tendency to grow readily on the walls of the crystallizer require periodic washout, and therefore an otherwise continuous operation would be interrupted once or even twice a week for the removal of these deposits. The impact that this contingency may have on the processing-equipment train ahead of the crystallizer must be considered.

A batch operation usually has economic application only on small scale, or when multiple products are produced in common facilities.

CRYSTALLIZER OPERATION

Crystal growth is a layer-by-layer process, and the retention time required in most commercial equipment to produce crystals of the size normally desired is often on the order of 2 to 6 h. Growth rates are usually limited to less than 1 to 2 $\mu\text{m}/\text{min}$. On the other hand, nucleation in a supersaturated solution can be generated in a fraction of a second. The influence of any upsets in operating conditions, in terms of the excess nuclei produced, is very short-term in comparison with the total growth period of the product removed from the crystallizer. A worst-case scenario for batch or continuous operation occurs when the explosion of nuclei is so severe that it is impossible to grow an acceptable crystal size distribution, requiring redissolution or washout of the system. In a practical sense, this means that steadiness of operation is much more important in crystallization equipment than it is in many other types of process equipment.

It is to be expected that six to nine retention periods will pass before the effects of an upset will be damped out. Thus, the recovery period may last from 12 to 54 h.

The **rate of nuclei formation** required to sustain a given product size decreases exponentially with increasing size of the product. Although when crystals in the range of 100 to 50 mesh are produced, the system may react quickly, the system response when generating large crystals in the 14-mesh size range is quite slow. This is because a single pound of 150-mesh seed crystals is sufficient to provide the total number of particles in a ton of 14-mesh product crystals. In any system producing relatively large crystals, nucleation must be carefully controlled with respect to all internal and external sources. Particular attention must be paid to preventing seed crystals from entering with the incoming feed stream or being returned to the crystallizer with recycle streams of mother liquor coming back from the filter or centrifuge.

Experience has shown that in any given body operating at a given production rate, control of the magma (slurry) density is important to the control of crystal size. Although in some systems a change in slurry density does not result in a change in the rate nucleation, the more general case is that an increase in the magma density increases the product size through reduction in nucleation and increased retention time of the crystals in the growing bed. The reduction in supersaturation at longer retention times together with the increased surface area at higher percent solids appears to be responsible for the larger product.

A reduction in the magma density will generally increase nucleation and decrease the particle size. This technique has the disadvantage that crystal formation on the equipment surfaces increases because lower slurry densities create higher levels of supersaturation within the equipment, particularly at the critical boiling surface in a vaporization-type crystallizer.

High levels of supersaturation at the liquid surface or at the tube walls in a surface-cooled crystallizer are the dominant cause of wall salting. Although some types of crystallizers can operate for several months continuously when crystallizing KCl or $(\text{NH}_4)_2\text{SO}_4$, most

machines have much shorter operating cycles. Second only to control of particle size, the extension of operating cycles is the most difficult operating problem to be solved in most installations.

In the forced-circulation-type crystallizer (Fig. 19-71) primary control over particle size is exercised by the designer in selecting the circulating system and volume of the body. From the operating standpoint there is little that can be done to an existing unit other than supply external seed, classify the discharge crystals, or control the slurry density. Nevertheless, machines of this type are frequently carefully controlled by these techniques and produce a predictable and desirable product-size distribution.

When crystals cannot be grown sufficiently large in forced-circulation equipment to meet product-size requirements, it is common to employ one of the designs that allow some influence to be exercised over the population density of the finer crystals. In the DTB design (Fig. 18-76) this is done by regulating the flow in the circulating pipe so as to withdraw a portion of the fines in the body in the amount of about 0.05 to 0.5 percent by settled volume. The exact quantity of solids depends on the size of the product crystals and on the capacity of the fines-dissolving system. If the machine is not operating stably, this quantity of solids will appear and then disappear, indicating changes in the nucleation rate within the circuit. At steady-state operation, the quantity of solids overflowing will remain relatively constant, with some solids appearing at all times. Should the slurry density of product crystals circulated within the machine rise to a value higher than about 50 percent settled volume, large quantities of product crystals will appear in the overflow system, disabling the fines-destruction equipment. Too high a circulating rate through the fines trap will produce this same result. Too low a flow through the fines circuit will remove insufficient particles and result in a smaller product-size crystal. To operate effectively, a crystallizer of the type employing fines-destruction techniques requires more sophisticated control than does operation of the simpler forced-circulation equipment.

The classifying crystallizer (Fig. 18-77) requires approximately the same control of the fines-removal stream and, in addition, requires control of the fluidizing flow circulated by the main pump. This flow must be adjusted to achieve the proper degree of fluidization in the suspension chamber, and this quantity of flow varies as the crystal size varies between start-up operation and normal operation. As with the draft-tube-baffle machine, a considerably higher degree of skill is required for operation of this equipment than of the forced-circulation type.

While most of the industrial designs in use today are built to reduce the problems due to excess nucleation, it is true that in some crystallizing systems a deficiency of seed crystals is produced and the product crystals are larger than are wanted or required. In such systems nucleation can be increased by increasing the mechanical stimulus created by the circulating devices or by seeding through the addition of fine crystals from some external source.

CRYSTALLIZER COSTS

Because crystallizers can come with such a wide variety of attachments, capacities, materials of construction, and designs, it is very difficult to present an accurate picture of the costs for any except certain specific types of equipment, crystallizing specific compounds. This is illustrated in Fig. 18-82, which shows the prices of equipment for crystallizing two different compounds at various production rates, one of the compounds being produced in two alternative crystallizer modes. Installed cost (including cost of equipment and accessories, foundations and supporting steel, utility piping, process piping and pumps, electrical switchgear, instrumentation, and labor, but excluding cost of a building) will be approximately twice these price figures.

Most crystallization equipment is custom-designed, and costs for a particular application may vary greatly from those illustrated in Fig. 18-82. Realistic estimation of installation costs also requires reference to local labor rates, site-specific factors, and other case specifics.

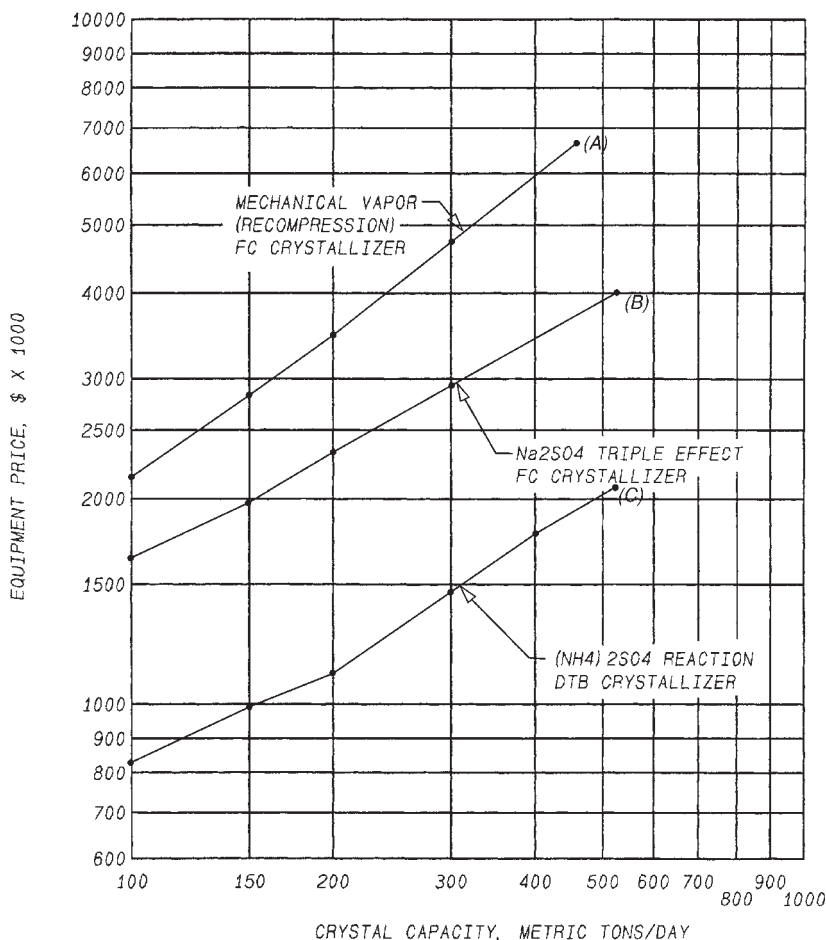


FIG. 18-82 Equipment prices, FOB point of fabrication, for typical crystallizer systems. Prices are for crystallizer plus accessories including vacuum equipment (2005). (A), (B) Na₂SO₄ production from Glauber's salt. Melting tank included. (C) Reaction of NH₃ + H₂SO₄ to make (NH₄)₂SO₄.

LEACHING

GENERAL REFERENCES: Coulson and Richardson, *Chemical Engineering*, 5th ed., vol. 2, Butterworth-Heinemann Publisher, 2002, chap. 10, "Leaching," pp. 502–541. Prabhudesai in Schweitzer, *Handbook of Separation Techniques for Chemical Engineers*, 3d ed., McGraw-Hill, New York, 1996, sec. 5.1. Wilkes, *Fluid Mechanics for Chemical Engineers*, Prentice-Hall, 1999. Wakeman, "Extraction (Liquid-Solid)" in *Kirk-Othmer Encyclopedia of Chemical Technology*, 4th ed., vol. 10, Wiley, New York, 1993, p. 186. McCabe, Smith, and Harriott, *Unit Operations of Chemical Engineering*, 7th ed., McGraw-Hill, New York, 2005. Harriott, *Chemical Reactor Design*, Marcel Dekker, 2003, pp. 89–99. Mular, Halbe, and Barratt, *Mineral Processing Plant Design, Practice, and Control*, vols. 1 and 2, Society for Mining, Metallurgy, and Exploration, Inc., 2002. Section on reactors in annual issues of *Chemical Engineering Buyers' Guide*.

DEFINITION

Leaching is the removal of a soluble fraction, in the form of a solution, from an insoluble, usually permeable, solid phase with which it

is associated. Leaching generally involves selective dissolution with or without diffusion; in the extreme case of simple washing, it requires only displacement (with some mixing) of one interstitial liquid by another with which it is miscible. The soluble constituent may be solid or liquid, and it may be incorporated within, chemically combined with, adsorbed upon, or bound mechanically in the pore structure of the insoluble material. Sometimes, the insoluble phase may be massive and porous, but usually it is particulate; the particles may be openly porous, cellular with selectively permeable cell walls, or surface-activated.

By convention, elution of a surface-adsorbed solute is treated as a special case of adsorption, rather than leaching. The washing of filter cakes is also excluded.

Due to its great breadth of application and its importance to some ancient processes, leaching is known by many names including *extraction*, *solid-liquid extraction*, *lixiviation*, *percolation*, *infusion*, *washing*,

and *decantation-settling*. If the stream of solids being leached is densified by settling, it is often called *underflow* and hydrometallurgists may refer to it as *pulp*. Oil seed processors may refer to the solids as *marc*. The liquid stream containing the leached solute is called *overflow*, *extract*, *solution*, *lixiviate*, *leachate*, or *miscella*.

Mechanism Leaching may simply result from the solubility of a substance in a liquid, or it may be enabled by a chemical reaction. The rate of transport of solvent into the mass to be leached, or of the soluble fraction into the solvent, or of extract solution out of the insoluble material, or of some combination of these rates may influence overall leaching kinetics, as may an interfacial resistance or a chemical reaction rate.

Inasmuch as the overflow and underflow streams are not immiscible phases but streams based on the same solvent, the concept of equilibrium for leaching is not the one applied in other mass-transfer separations. If the solute is not adsorbed on the inert solid, true equilibrium is reached only when all the solute is dissolved and distributed uniformly throughout the solvent in both underflow and overflow (or when the solvent is uniformly saturated with the solute, a condition never encountered in a properly designed extractor). The practical interpretation of leaching equilibrium is the state in which the overflow and underflow liquids are of the same composition; on a y - x diagram, the equilibrium line will be a straight line through the origin with a slope of unity. It is customary to calculate the number of ideal (equilibrium) stages required for a given leaching task and to adjust the number by applying a stage efficiency factor, although local efficiencies, if known, can be applied stage by stage.

Usually, however, it is not feasible to establish a stage or overall efficiency or a leaching rate index (e.g., overall coefficient) without testing small-scale models of likely apparatus. In fact, the results of such tests may have to be scaled up empirically, without explicit evaluation of rate or quasi-equilibrium indices.

Methods of Operation Leaching systems are distinguished by operating cycle (batch, continuous, or multibatch intermittent); by direction of streams (cocurrent, countercurrent, or hybrid flow); by staging (single-stage, multistage, or differential-stage); and by method of contacting (sprayed percolation, immersed percolation, or solids dispersion). In general, descriptors from all four categories must be assigned to stipulate a leaching system completely (e.g., the Bollman-type extractor is a continuous hybrid-flow multistage sprayed percolator).

Whatever the mechanism and the method of operation, it is clear that the leaching process will be favored by increased surface per unit volume of solids to be leached and by decreased radial distances that must be traversed within the solids, both of which are favored by decreased particle size. Fine solids, on the other hand, cause slow percolation rate, difficult solids separation, and possible poor quality of solid product. The basis for an optimum particle size is established by these characteristics.

LEACHING EQUIPMENT

There are two primary categories of contacting method according to which leaching equipment is classified: (1) leaching may be accomplished by percolation and (2) the particulate solids may be dispersed into a liquid phase and then separated from it. Each may be operated in a batch or continuous manner. Materials that disintegrate during leaching are treated in the second class of equipment. An important exception to this classification is in-situ leaching, as discussed below.

Percolation *Heap leaching*, as shown in Fig. 18-83 (see Mular et al. pp. 1571–1630, loc. cit.) is very widely applied to the ores of copper and precious metals, but percolation is also conducted on a smaller scale in batch tanks or vats and in continuous or dump extractors. In the heap leaching of low-grade oxidized gold ores, for instance, a dilute alkaline solution of sodium cyanide is distributed over a heap of ore that typically has been crushed finer than 1 in and the fines agglomerated with the addition of Portland cement at conveyor transfer points. Heap leaching of very low-grade gold ores and many oxide copper ores is conducted on run-of-mine material. Heap leaching is the least expensive form of leaching. In virtually all cases, an impervious polymeric membrane is installed before the heap is constructed.

In situ leaching, depicted in Fig. 18-84, depends on the existing permeability of a subsurface deposit containing minerals or compounds that are to be dissolved and extracted. Holes (“wells”) are drilled into the rock or soil surrounding the deposit and are lined with tubing that is perforated at appropriate depth intervals. The leaching solution is pumped down the injection wells and flows through the deposit or “formation,” and the “pregnant” solution is extracted from production wells, treated for solute recovery, reconstituted, and reinjected. In situ leaching is used for extraction of halite (NaCl) and uranium, as well as for the removal of toxic or hazardous constituents from contaminated soil or groundwater.

Batch Percolators The **batch tank** is not unlike a big nutsche filter; it is a large circular or rectangular tank with a false bottom. The solids to be leached are dumped into the tank to a uniform depth. They are sprayed with solvent until their solute content is reduced to an economic minimum and are then excavated. Countercurrent flow of the solvent through a series of tanks is common, with fresh solvent entering the tank containing most nearly exhausted material. So-called *vat leaching* was practiced in oxide copper ore processing prior to 1980, and the vats were typically 53 by 20 by 5.5 m (175 by 67 by 18 ft) and extracted about 8200 Mg (9000 U.S. tons) of ore on a 13-day cycle. Some tanks operate under pressure, to contain volatile solvents or increase the percolation rate. A series of pressure tanks operating with countercurrent solvent flow is called a **diffusion battery**.

Continuous Percolators Coarse solids are also leached by percolation in moving-bed equipment, including single-deck and multideck

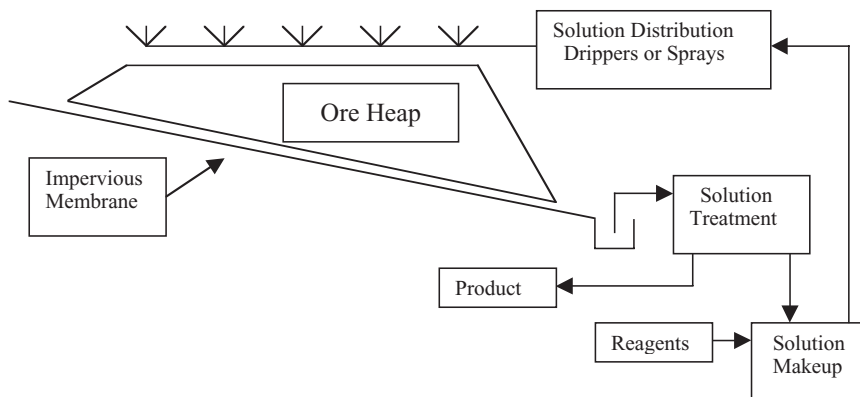


FIG. 18-83 Heap leaching for copper or precious metals.

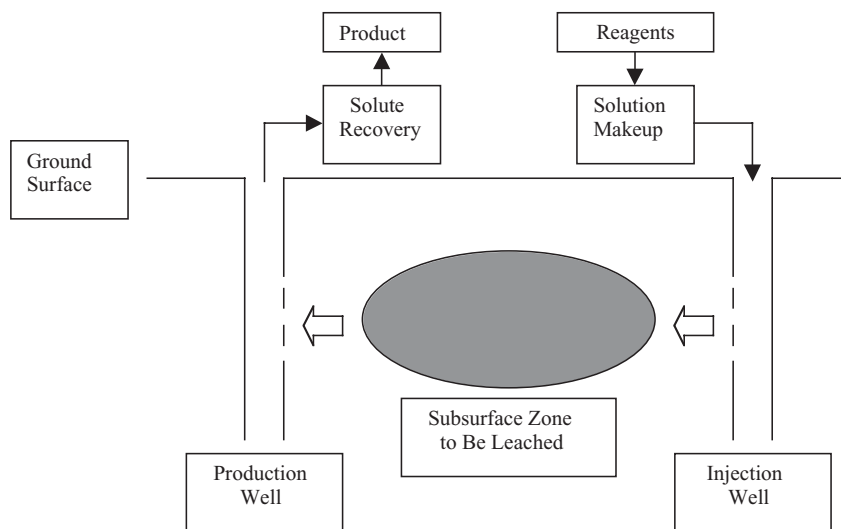


FIG. 18-84 In situ leaching.

rake classifiers, bucket-elevator contactors, and horizontal-belt conveyors.

The **Bollman-type extractor** shown in Fig. 18-85 is a bucket-elevator unit designed to handle about 2000 to 20,000 kg/h (50 to 500 U.S. tons/day) of flaky solids (e.g., soybeans). Buckets with perforated bottoms are held on an endless moving belt. Dry flakes, fed into the descending buckets, are sprayed with partially enriched solvent ("half miscella") pumped from the bottom of the column of ascending buckets. As the buckets rise on the other side of the unit, the solids are sprayed with a countercurrent stream of pure solvent. Exhausted flakes are dumped from the buckets at the top of the unit into a pad-

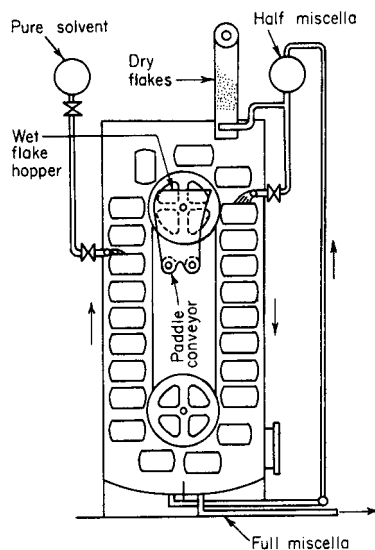


FIG. 18-85 Bollman-type extractor. (McCabe, Smith, and Harriott, *Unit Operations of Chemical Engineering*, 5th ed., p. 616. Copyright 1993 by McGraw-Hill, Inc. and used with permission.)

dle conveyor; enriched solvent, the "full miscella," is pumped from the bottom of the casing. Because the solids are unagitated and because the final miscella moves cocurrently, the Bollman extractor permits the use of thin flakes while producing extract of good clarity. It is only partially a countercurrent device, however, and it sometimes permits channeling and consequent low stage efficiency. Perhaps for this reason, it is being displaced in the oil extraction industry by horizontal basket, pan, or belt percolators (Schwartzberg, loc. cit.).

In the **horizontal-basket design**, illustrated by the **Rotocel extractor** (Fig. 18-86), walled compartments in the form of annular sectors with liquid-permeable floors revolve about a central axis. The compartments successively pass a feed point, a number of solvent sprays, a drainage section, and a discharge station (where the floor opens to discharge the extracted solids). The discharge station is circumferentially contiguous to the feed point. Countercurrent extraction is achieved by feeding fresh solvent only to the last compartment before dumping occurs and by washing the solids in each preceding compartment with the effluent from the succeeding one. The Rotocel is simple and inexpensive, and it requires little headroom. This type of equipment is made by a number of manufacturers. Horizontal table and tilting-pan vacuum filters, of which it is the gravity counterpart, are used as extractors for leaching processes involving difficult solution-residue separation. Detailed descriptions of the Bollman-type and Rotocel extractors are presented on pp. 765 and 766 of McCabe, et al., 7th ed., loc. cit.

The **endless-belt percolator** (Wakeman, loc. cit.) is similar in principle, but the successive feed, solvent spray, drainage, and dumping stations are linearly rather than circularly disposed. Examples are the **de Smet belt extractor** (uncompartmented) and the **Lurgi frame belt** (compartmented), the latter being a kind of linear equivalent of the Rotocel. Horizontal-belt vacuum filters, which resemble endless-belt extractors, are sometimes used for leaching.

The **Kennedy extractor** (Fig. 18-87), also requiring little headroom, operates substantially as a percolator that moves the bed of solids through the solvent rather than the conventional opposite. It comprises a nearly horizontal line of chambers through each of which in succession the solids being leached are moved by a slow impeller enclosed in that section. There is an opportunity for drainage between stages when the impeller lifts solids above the liquid level before dumping them into the next chamber. Solvent flows countercurrently from chamber to chamber. Because the solids are subjected to mechanical action somewhat more intense than in other types of

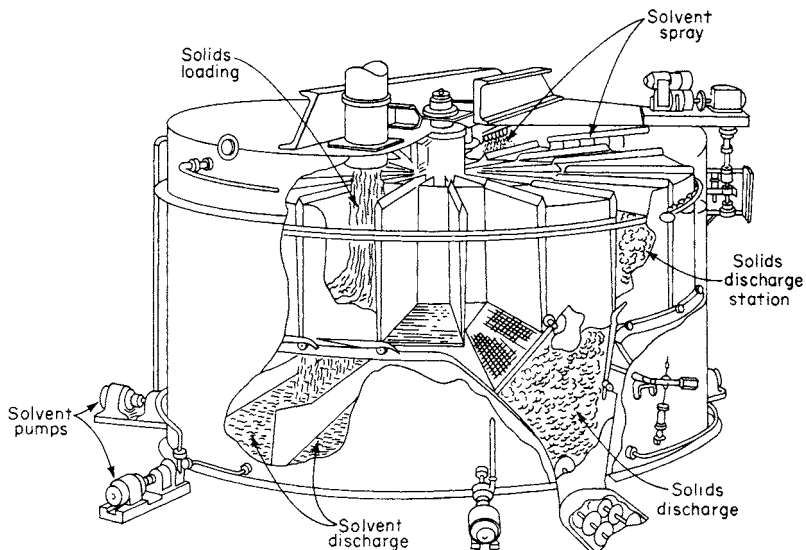


FIG. 18-86 Rotocel extractor. [Rickles, Chem. Eng. 72(6): 164 (1965). Used with permission of McGraw-Hill, Inc.]

continuous percolator, the Kennedy extractor is now little used for fragile materials such as flaked oil seeds.

Dispersed-Solids Leaching Equipment for batch leaching of fine solids in a liquid suspension is now confined mainly to batch tanks with rotating impellers. For a detailed discussion of all aspects of the suspension of solid particles in fluids, refer to agitation of particle suspensions at the beginning of this subsection.

Batch Stirred Tanks Tanks agitated by coaxial impellers (turbines, paddles, or propellers) are commonly used for batch dissolution of solids in liquids and may be used for leaching fine solids. Insofar as the controlling rate in the mass transfer is the rate of transfer of material into or from the interior of the solid particles rather than the rate of transfer to or from the surface of particles, the main function of the agitator is to supply unexhausted solvent to the particles while they reside in the tank long enough for the diffusive process to be completed. The agitator does this most efficiently if it just gently circulates the solids across the tank bottom or barely suspends them above the bottom. However, if the slurry contains particles having significantly different settling velocities, it is usually necessary to introduce sufficient mixing power to ensure full suspension of all particles. Failure to do so will result in an accumulation of the larger or denser particles unless provision is made to drain the settled material continuously.

The leached solids must be separated from the extract by settling and decantation or by external filters, centrifuges, or thickeners, all of which are treated elsewhere in Sec. 18. The difficulty of solids-extract

separation and the fact that a batch stirred tank provides only a single equilibrium stage are its major disadvantages.

Pachuca Tanks Air-agitated Pachuca tanks were widely used in mineral processing until the 1960s when the industry concluded that mechanical agitation was more economical and more effective for solids suspension. A description of Pachuca tanks can be found in previous editions of *Perry's Handbook*.

Impeller-agitated ("Stirred") tanks Often called continuous stirred-tank reactors (CSTRs), they can be operated singly or in series. Figure 18-89 illustrates three tanks in series, each with a mechanical agitator. Nearly all stirred tanks are equipped with vertical baffles to prevent swirling and ineffective energy utilization by the agitator. Advancing of slurry from one stage to the next may be by overflow if successive stages are lower, or interstage pumps may be used.

Autoclaves Autoclaves, as shown in Fig. 18-90, are closed, usually multi-compartmented, vessels often designed for operation at pressures in excess of 600 psig (40 bar) and temperatures of 600°F or higher. The purpose of some autoclaves is simply to effect aqueous oxidation, e.g., of organic wastes or sulfide minerals. In the latter case, an example is oxidation of pyrite, followed by cyanide leaching of precious metals under ambient conditions. Other autoclaves are designed to effect leaching, as in the case of sulfuric acid leaching of nickel and cobalt from lateritic ores. The feed stream is preheated by steam from the flash cooling tower(s) and delivered to the autoclave by one or

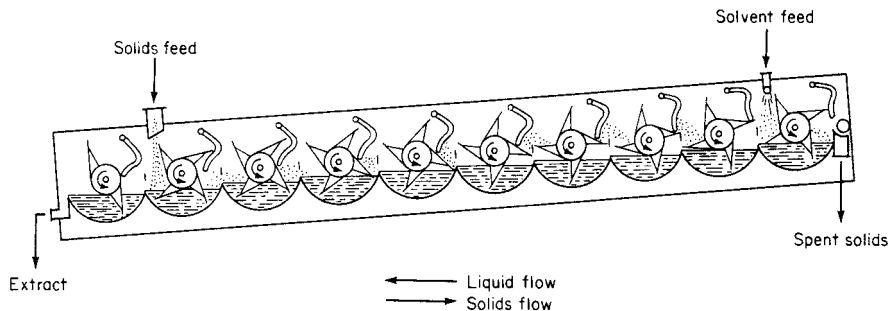


FIG. 18-87 Kennedy extractor. (Vulcan Cincinnati, Inc.)

more positive displacement pumps, usually of the piston diaphragm type. If oxidation is required, oxygen may be used instead of air to reduce operating pressure or to improve kinetics. Flash cooling of the autoclave product is usually accomplished in one or more pressure reduction vessels with abrasion-resistant nozzles and targets.

Continuous Dispersed-Solids Leaching

Vertical-plate extractor. Exemplified by the **Bonotto extractor** (Fig. 18-88), this consists of a column divided into cylindrical compartments by equispaced horizontal plates. Each plate has a radial opening staggered 180° from the openings of the plates immediately above and below it, and each is wiped by a rotating radial blade. Alternatively, the plates may be mounted on a coaxial shaft and rotated past stationary blades. The solids, fed to the top plate, thus are caused to fall to each lower plate in succession. The solids fall as a curtain into solvent which flows upward through the tower. They are discharged by a screw conveyor and compactor. Like the Bollman extractor, the Bonotto has been virtually displaced by horizontal belt or tray percolators for the extraction of oil seeds.

Gravity sedimentation tanks. Operated as thickeners, these tanks can serve as continuous contacting and separating devices in which fine solids may be leached continuously. A series of such units properly connected permit true continuous countercurrent washing of fine solids. If appropriate, a mixing tank may be associated with each thickener to improve the contact between the solids and liquid being fed to that stage. Gravity sedimentation thickeners are described under "Gravity Sedimentation Operations." Of all continuous leaching equipment, gravity thickeners require the most area, and they are limited to relatively fine solids.

Impeller-agitated ("stirred") tanks. Often called continuous stirred-tank reactors (CSTR), they can be operated singly or in series. Figure 18-89 illustrates three tanks in series, each with a mechanical agitator. Nearly all stirred tanks are equipped with vertical baffles to prevent swirling and ineffective energy utilization by the agitator. Advancing of slurry from one stage to the next may be by overflow if successive stages are lower, or interstage pumps may be used.

Autoclaves. Autoclaves, as shown in Fig. 18-90, are closed, usually multicompartimented, vessels often designed for operation at pressures in excess of 600 psig (40 bars) and temperatures of 600°F or higher. The purpose of some autoclaves is simply to effect aqueous oxidation, e.g., of organic wastes or sulfide minerals. In the latter case, an example is oxidation of pyrite, followed by cyanide leaching of precious metals under ambient conditions. Other autoclaves are designed to effect leaching, as in the case of sulfuric acid leaching of nickel and cobalt from lateritic ores. The feed stream is preheated by steam from the flash cooling tower(s) and delivered to the autoclave by one or more

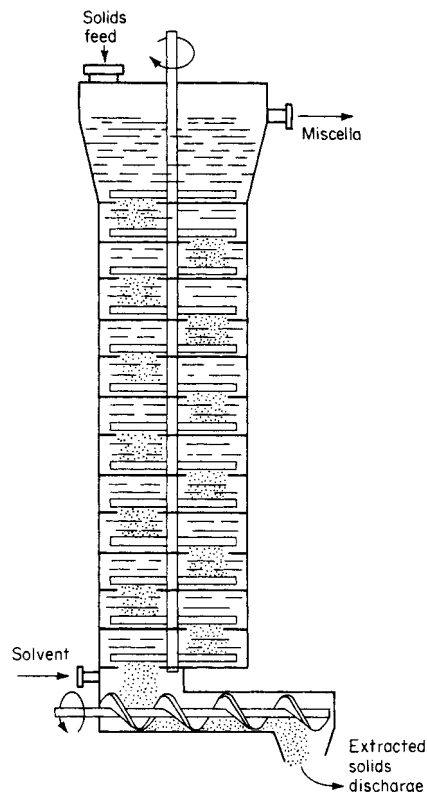


FIG. 18-88 Bonotto extractor. [Rickles, *Chem. Eng.* 72(6): 163 (1965); copyright 1965 by McGraw-Hill, Inc., New York. Excerpted with special permission of McGraw-Hill.]

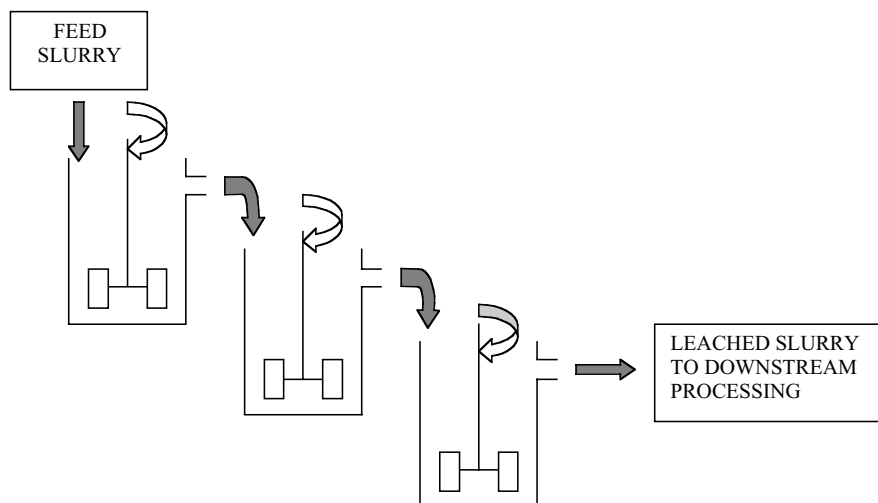


FIG. 18-89 Stirred tanks, three in series, with gravity overflow.

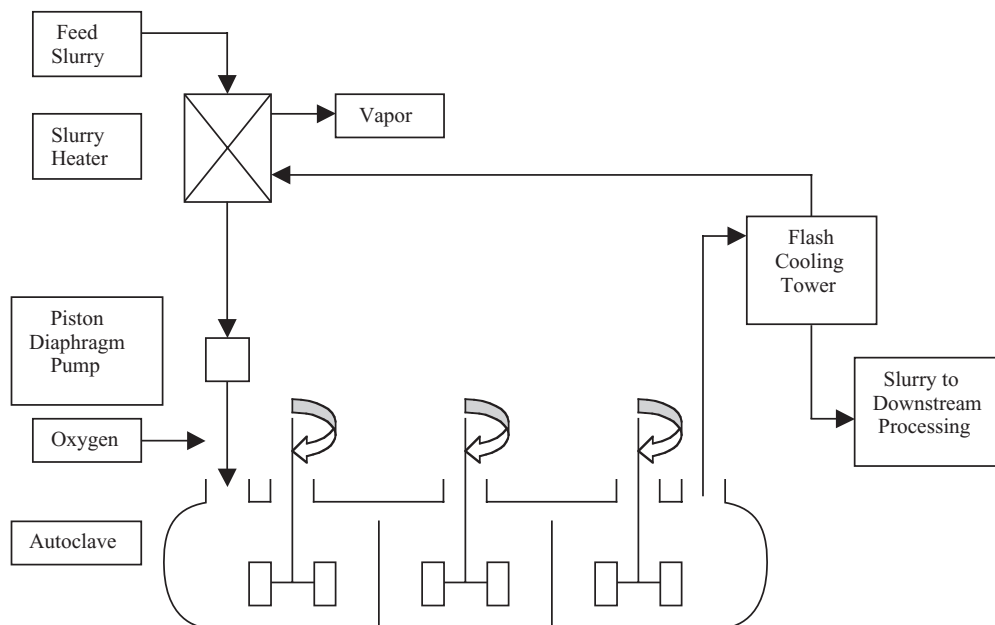


FIG. 18-90 Three-compartment autoclave.

positive displacement pumps, usually of the piston diaphragm type. If oxidation is required, oxygen may be used instead of air to reduce operating pressure or to improve kinetics. Flash cooling of the autoclave product is usually accomplished in one or more pressure-reduction vessels with abrasion-resistant nozzles and targets.

Screw-Conveyor Extractors One type of continuous leaching equipment, employing the screw-conveyor principle, is strictly speaking neither a percolator nor a dispersed-solids extractor. Although it is often classed with percolators, there can be sufficient agitation of the

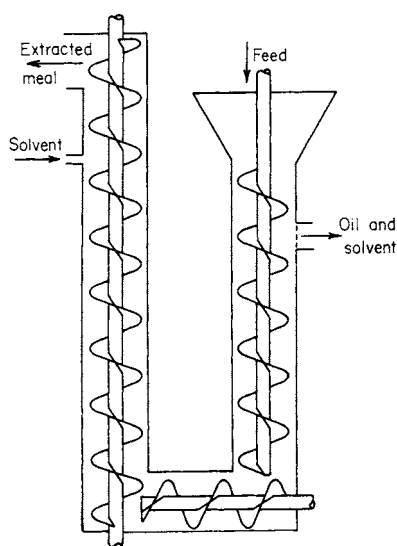


FIG. 18-91 Hildebrandt extractor. (McCabe, Smith, and Harriott, *Unit Operations of Chemical Engineering*, 5th ed., p. 616. Copyright 1993 by McGraw-Hill, Inc. and used with permission.)

solids during their conveyance by the screw that the action differs from an orthodox percolation.

The **Hildebrandt total-immersion extractor** is shown schematically in Fig. 18-91. The helix surface is perforated so that solvent can pass through countercurrently. The screws are so designed to compact the solids during their passage through the unit. The design offers the obvious advantages of countercurrent action and continuous solids compaction, but there are possibilities of some solvent loss and feed overflow, and successful operation is limited to light, permeable solids.

A somewhat similar but simpler design uses a horizontal screw section for leaching and a second screw in an inclined section for washing, draining, and discharging the extracted solids.

In the **De Danske Sukkerfabriker**, the axis of the extractor is tilted to about 10° from the horizontal, eliminating the necessity of two screws at different angles of inclination.

Sugar-beet cossettes are successfully extracted while being transported upward in a vertical tower by an arrangement of inclined plates or wings attached to an axial shaft. The action is assisted by staggered guide plates on the tower wall. The shell is filled with water that passes downward as the beets travel upward. This configuration is employed in the **BMA diffusion tower** (Wakeman, loc. cit.).

Schwartzberg (loc. cit.) reports that screw-conveyor extractors, once widely employed to extract flaked oil seeds, have fallen into disuse for this application because of their destructive action on the fragile seed flakes.

Tray Classifier A hybrid like the screw-conveyor classifier, the tray classifier rakes pulp up the sloping bottom of a tank while solvent flows in the opposite direction. The solvent is forced by a baffle to the bottom of the tank at the lower end before it overflows. The solids must be rugged enough to stand the stress of raking.

SELECTION OR DESIGN OF A LEACHING PROCESS*

At the heart of a leaching plant design at any level—conceptual, preliminary, firm engineering, or whatever—is unit-operations and process design of the extraction unit or line. The major aspects that are particular for the leaching operation are the selection of process

*Portions of this subsection are adaptations from the still-pertinent article by Rickles (loc. cit.).

and operating conditions and the sizing of the extraction equipment.

Process and Operating Conditions The major parameters that must be fixed or identified are the solvent to be used, the temperature, the terminal stream compositions and quantities, leaching cycle (batch or continuous), contact method, and specific extractor choice.

Choice of Solvent The solvent selected will offer the best balance of a number of desirable characteristics: high saturation limit and selectivity for the solute to be extracted, capability to produce extracted material of quality unimpaired by the solvent, chemical stability under process conditions, low viscosity, low vapor pressure, low toxicity and flammability, low density, low surface tension, ease and economy of recovery from the extract stream, and price. These factors are listed in an approximate order of decreasing importance, but the specifics of each application determine their interaction and relative significance, and any one can control the decision under the right combination of process conditions.

Temperature The temperature of the extraction should be chosen for the best balance of solubility, solvent-vapor pressure, solute diffusivity, solvent selectivity, and sensitivity of product. In some cases, temperature sensitivity of materials of construction to corrosion or erosion attack may be significant.

Terminal Stream Compositions and Quantities These are basically linked to an arbitrary given: the production capacity of the leaching plant (rate of extract production or rate of raw-material purification by extraction). When options are permitted, the degree of solute removal and the concentration of the extract stream chosen are those that maximize process economy while sustaining conformance to regulatory standards.

Leaching Cycle and Contact Method As is true generally, the choice between continuous and intermittent operation is largely a matter of the size and nature of the process of which the extraction is a part. The choice of a percolation or solids-dispersion technique depends principally on the amenability of the extraction to effective, sufficiently rapid percolation.

Type of Reactor The specific type of reactor that is most compatible (or least incompatible) with the chosen combination of the preceding parameters seldom is clearly and unequivocally perceived without difficulty, if at all. In the end, however, that remains the objective. As is always true, the ultimate criteria are reliability and profitability.

Extractor-Sizing Calculations For any given throughput rate (which fixes the cross-sectional area and/or the number of extractors), the size of the units boils down to the number of stages required, actual or equivalent. In calculation, this resolves into determination of the number of ideal stages required and application of appropriate stage efficiencies. The methods of calculation resemble those for other mass-transfer operations (see Secs. 13, 14, and 15), involving equilibrium data and contact conditions, and based on material balances. They are discussed briefly here with reference to countercurrent contacting.

Software Packages Since the late 1990s, increasing use has been made of software developed for modeling and simulation of all types of unit operations, including leaching. Packages currently available for mineral processing applications can be found, for instance, in Mular et al., loc. cit., pp. 479 and 495. Monthly issues of *Chemical Engineering Progress (CEP)* usually contain a page entitled *Software* that announces new packages for various applications, and the same publication usually contains a summary each year of all packages of use to chemical engineers and mineral processors.

Composition Diagrams In its elemental form, a leaching system consists of three components: inert, insoluble solids; a single non-adsorbed solute, which may be liquid or solid; and a single solvent.* Thus, it is a ternary system, albeit an unusual one, as already mentioned, by virtue of the total mutual "insolubility" of two of the phases and the simple nature of equilibrium.

The composition of a typical system is satisfactorily presented in the form of a diagram. Those diagrams most frequently employed are a right-triangular plot of mass fraction of solvent against mass fraction of solute (Fig. 18-92a) and a plot suggestive of a Ponchon-Savarit dia-

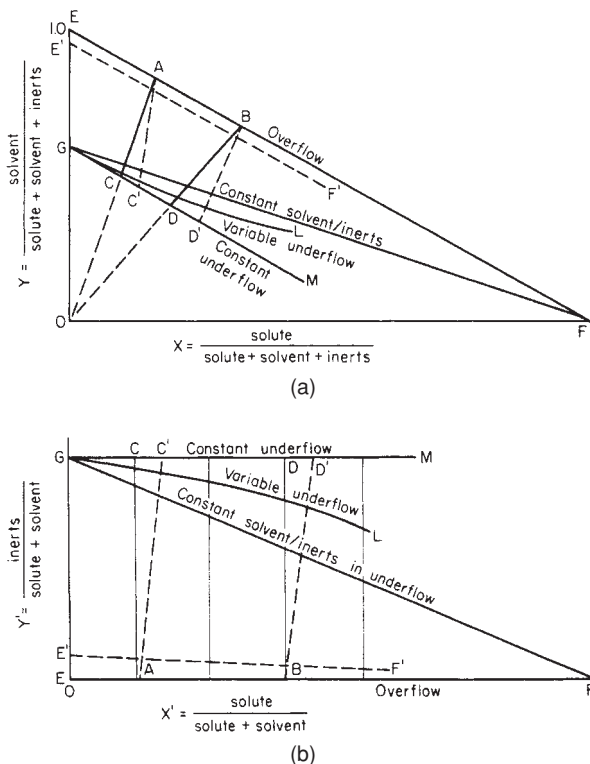


FIG. 18-92 Composition diagrams for leaching calculations: (a) right-triangular diagram; (b) modified Ponchon-Savarit diagram.

gram, with inerts taking the place of enthalpy (Fig. 18-92b). A third diagram, less frequently used, is a modified McCabe-Thiele plot in which the overflow solution (inerts-free) and the underflow solution (traveling out of a stage with the inerts) are treated as pseudo phases, the mass fraction of solute in overflow, y , being plotted against the mass fraction of solute in underflow, x . (An additional representation, the equilateral-triangular diagram frequently employed for liquid-liquid ternary systems, is seldom used because the field of leaching data is confined to a small portion of the triangle.)

With reference to Fig. 18-92 (both graphs), EF represents the locus of overflow compositions for the case in which the overflow stream contains no inert solids. $E'F'$ represents the overflow streams containing some inert solids, either by entrainment or by partial solubility in the overflow solution. Lines GF , GL , and GM represent the loci of underflow compositions for the three different conditions indicated on the diagram. In Fig. 18-92a, the constant underflow line GM is parallel to EF , the hypotenuse of the triangle, whereas GF passes through the right-hand vertex representing 100 percent solute. In Fig. 18-92b, underflow line GM is parallel to the abscissa, and GF passes through the point on the abscissa representing the composition of the clear solution adhering to the inert solids.

Compositions of overflow and underflow streams leaving the same stage are represented by the intersection of the composition lines for those streams with a tie line (AC , AC' , BD , BD'). Equilibrium tie lines (AC , BD) pass through the origin (representing 100 percent inerts) in Fig. 18-92a, and are vertical (representing the same inert-free solution composition in both streams) in Fig. 18-92b. For nonequilibrium conditions with or without adsorption or for equilibrium conditions with selective adsorption, the tie lines are displaced, such as AC' and BD' . Point C' is to the right of C if the solute concentration in the overflow solution is less than that in the underflow solution adhering to the solids. Unequal concentrations in the two solutions indicate insufficient contact time and/or preferential adsorption of one of the components on the inert solids. Tie lines such as AC' may be considered as

*The solubility of the inert, adsorption of solute on the inert, and complexity of solvent and extracted material can be taken into account if necessary. Their consideration is beyond the scope of this treatment.

“practical tie lines” (i.e., they represent actual rather than ideal stages) if data on underflow and overflow composition have been obtained experimentally under conditions simulating actual operation, particularly with respect to contact time, agitation, and particle size of solids.

The illustrative construction lines of Fig. 18-92 have been made with the assumption of constant underflow. In the more realistic case of variable underflow, the points C, C', D, D' would lie along line GL . Like the practical tie lines, GL is a representation of experimental data.

Algebraic Computation This method starts with calculation of the quantities and compositions of all the terminal streams, using a convenient quantity of one of the streams as the basis of calculation. Material balance and stream compositions are then computed for a terminal ideal stage at either end of an extraction battery (i.e., at point A or point B in Fig. 18-92), using equilibrium and solution-retention data. Calculations are repeated for each successive ideal stage from one end of the system to the other until an ideal stage which corresponds to the desired conditions is obtained. Any solid-liquid extraction problem can be solved by this method.

For certain simplified cases it is possible to calculate directly the number of stages required to attain a desired product composition for a given set of feed conditions. For example, if equilibrium is attained in all stages and if the underflow mass rate is constant, both the equilibrium and operating lines on a modified McCabe-Thiele diagram are straight, and it is possible to calculate directly the number of ideal stages required to accommodate any rational set of terminal flows and compositions (McCabe, Smith, and Harriott, op. cit.):

$$N = \frac{\log [(y_b - x_b)/(y_a - x_a)]}{\log [(y_b - y_a)/(x_b - x_a)]} \quad (18-45)$$

Even when the conditions of equilibrium in each stage and constant underflow obtain, Eq. (18-45) normally is not valid for the first stage because the unextracted solids entering that stage usually are not premixed with solution to produce the underflow mass that will leave. This is easily rectified by calculating the exit streams for the first stage and using those values in Eq. (18-45) to calculate the number of stages required after stage 1.

Graphical Method This method of calculation is simply a diagrammatic representation of all the possible compositions in a leaching system, including equilibrium values, on which material balances across ideal (or, in some cases, nonideal) stages can be evaluated in the graphical equivalent of the stage-by-stage algebraic computation. It normally is simpler than the hand calculation of the algebraic solution, and it is viewed by many as helpful because it permits visualization of the process variables and their effect on the operation. Any of the four types of composition diagrams described above can be used, but modified Ponchon-Savarit or right-triangular plots (Fig. 18-92) are most convenient for leaching calculations.

The techniques of graphical solution, in fact, are not unlike those for distillation and absorption (binary) problems using McCabe-Thiele, Ponchon-Savarit, and right-triangular diagrams and are similar to those described in Sec. 15 for solvent-extraction (ternary) systems. More detailed explanations of the application of the several graphical conventions to leaching are presented by: Coulson and Richardson, right triangle; Rickles, modified Ponchon-Savarit; McCabe, Smith, and Harriott, modified McCabe-Thiele; and Schwartzberg, equilateral ternary diagram; all in the publications cited as general references. (See also Treybal, *Mass Transfer Operations*, 3d ed., McGraw-Hill, New York, 1980.)

GRAVITY SEDIMENTATION OPERATIONS

GENERAL REFERENCES: Albertson, *Fluid/Particle Sep. J.*, 7, 1S (1994). Jewell, Fourie, and Lord, *Paste and Thickened Tailings—A Guide*, pp. 49–79, Australian Centre for Geomechanics, 2002. Mular, Halbe, and Barratt, *Mineral Processing Plant Design, Practice, and Control*, vol. 2, pp. 1295–1312 and 2164–2173, SME, 2002. Sankey and Payne, *Chemical Reagents in the Mineral Processing Industry*, p. 245, SME, 1985. Schweitzer, *Handbook of Separation Techniques for Chemical Engineers*, 2d ed., pp. 4-121 to 4-147, McGraw-Hill, 1988. Wilhelm and Naide, *Min. Eng.* (Littleton, Colo.), 1710 (1981).

Sedimentation is the partial separation or concentration of suspended solid particles from a liquid by gravity settling. This field may be divided into the functional operations of thickening and clarification. The primary purpose of thickening is to increase the concentration of suspended solids in a feed stream, while that of clarification is to remove a relatively small quantity of suspended particles and produce a clear effluent. These two functions are similar and occur simultaneously, and the terminology merely makes a distinction between the primary process results desired. Generally, thickener mechanisms are designed for the heavier-duty requirements imposed by a large quantity of relatively concentrated pulp, while clarifiers usually will include features that ensure essentially complete suspended-solids removal, such as greater depth, special provision for coagulation or flocculation of the feed suspension, and greater overflow-weir length.

CLASSIFICATION OF SETTLEABLE SOLIDS AND THE NATURE OF SEDIMENTATION

The types of sedimentation encountered in process technology will be greatly affected not only by the obvious factors—particle size, liquid viscosity, solid and solution densities—but also by the characteristics of the particles within the slurry. These properties, as well as the process requirements, will help determine both the type of equipment which will achieve the desired ends most effectively and the testing methods to be used to select the equipment.

Figure 18-93 illustrates the relationship between solids concentration, interparticle cohesiveness, and the type of sedimentation that may exist. “Totally discrete” particles include many mineral particles (usually greater in diameter than 20 μm), salt crystals, and similar substances that have little tendency to cohere. “Flocculent” particles generally will include those smaller than 20 μm (unless present in a dispersed state owing to surface charges), metal hydroxides, many chemical precipitates, and most organic substances other than true colloids.

At low concentrations, the type of sedimentation encountered is called

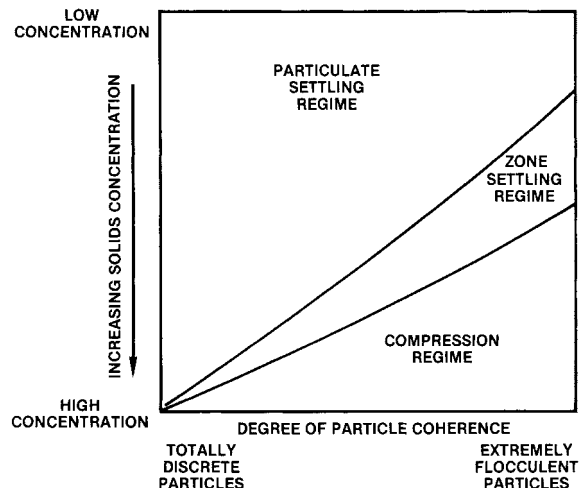


FIG. 18-93 Combined effect of particle coherence and solids concentration on the settling characteristics of a suspension.

particulate settling. Regardless of their nature, particles are sufficiently far apart to settle freely. Faster-settling particles may collide with slower-settling ones and, if they do not cohere, continue downward at their own specific rate. Those that do cohere will form flocules of a larger diameter that will settle at a rate greater than that of the individual particles.

There is a gradual transition from particulate settling into the zone-settling regime, where the particles are constrained to settle as a mass. The principal characteristic of this zone is that the settling rate of the mass, as observed in batch tests, will be a function of its solids concentration (for any particular condition of flocculation, particle density, etc.).

The solids concentration ultimately will reach a level at which particle descent is restrained not only by hydrodynamic forces but also partially by mechanical support from the particles below; therefore, the weight of particles in mutual contact can influence the rate of sedimentation of those at lower levels. This compression, as it is termed, will result in further solids concentration because of compaction of the individual flocules and partial filling of the interfloc voids by the deformed flocules. Accordingly, the rate of sedimentation in the compression regime is a function of both the solids concentration and the depth of pulp in this particular zone. As indicated in Fig. 18-93, granular, nonfloculent particles may reach their ultimate solids concentration without passing through this regime.

As an illustration, coarse-size (45 μm) the aluminum oxide trihydrate particles produced in the Bayer process would be located near the extreme left of Fig. 18-93. These solids settle in a particulate manner, passing through a zone-settling regime only briefly, and reach a terminal density or ultimate solids concentration without any significant compressive effects. At this point, the solids concentration may be as much as 80 percent by weight. The same compound, but of the gelatinous nature it has when precipitated in water treatment as aluminum hydroxide, would be on the extreme right-hand side of the figure. This flocculent material enters into a zone-settling regime at a low concentration (relative to the ultimate concentration it can reach) and gradually thickens. With sufficient pulp depth present, preferably aided by gentle stirring or vibration, the compression-zone effect will occur; this is essential for the sludge to attain its maximum solids concentration, around 10 percent. Certain fine-size (1- to 2- μm) precipitates of this compound will possess characteristics intermediate between the two extremes.

A feed stream to be clarified or thickened can exist at any state represented within this diagram. As it becomes concentrated owing to sedimentation, it may pass through all the regimes, and the settling rate in any one may be the size-determining factor for the required equipment.

Sedimentation Testing To design and size sedimentation equipment, reference information from similar applications is preferred. Data from full-scale sedimentation equipment, operating in the application under consideration, are always a first choice for sizing new equipment. However, quite often the application under question deviates sufficiently from reference installations. The characteristics of the feed stream for the new application (i.e., solids characteristics, particle size, viscosities, pH, use of flocculants, etc.) must be identical to the existing application. It is also necessary to know how close to "capacity" the existing equipment is operating. If the feed characteristics and operating conditions are different for the application under question, bench- or pilot-scale testing is recommended to size and design a new sedimentation unit.

To properly design and size sedimentation equipment, several pieces of information are required. Some information is unique to the job site (application, feed rate, etc.), while other data are supplied from similar references or from test work. Site-specific information from the plant site includes

- Application – objectives (underflow, TSS, hardness, etc.)
- Feed rate—design and maximum
- Feed characteristics—solids concentration, chemistry
- Site-specific requirements: seismic zone, weather-related specifications, local mechanical design codes, and the user's preferred design specifications
- Local operating practices

In the event testing is required to design either a thickener or a clarifier, the testing must be structured to produce all or some of the following information:

- Feed stream characteristics
- Chemical treatment (type, solution concentration, dose, etc.): coagulants and flocculants (organic or inorganic); acid/base for treatment and pH correction
- Coagulation and flocculation (mixing time, energy requirements, solids concentration)
- Expected sedimentation objectives: underflow slurry density or concentration; overflow solids concentration (suspended solids and/or turbidity); chemical treatment for soluble components (i.e., hardness, metals, anions, pH, etc.)
- Vessel area and depth
- Settled solids rheology (for raking mechanism design and drive torque specification)

There are three basic approaches to testing for sedimentation equipment:

- **Batch bench-scale settling tests** The most common procedure requires a relatively small amount of sample tested in a controlled environment using laboratory equipment under static conditions.
- **Semicontinuous bench-scale tests** Laboratory pumps are used which pump feed slurry and chemicals into settling cylinders from which overflow liquor and underflow slurry are continuously collected.
- **Continuous piloting** A small-diameter thickener or clarifier of the same design as the full-scale equipment being considered is used.

TESTING COMMON TO CLARIFIERS AND THICKENERS

Feed Characterization Sample characterization is necessary for both thickening and clarification testing. Without these data included in the basis of design, the sizing and predicted performance cannot be validated for the specified feed stream. Characterization requires the following measurements as a minimum:

- General chemical makeup of the solids and liquor phases
- Feed solids concentration
- Particle size distribution—include coarse (+100 μm) and fine (–20 μm) particle diameters
- Particle specific gravity
- Liquid specific gravity
- Liquid-phase dissolved materials concentration
- Temperature
- pH

Coagulant and/or Flocculant Selection Coagulants and flocculants are widely used to enhance the settling rate which reduces thickener and clarifier size and improves overflow clarity and/or underflow slurry density. The terms *coagulation* and *flocculation* are sometimes used interchangeably; however, each term describes separate functions in the particle agglomeration process.

Coagulation is a preconditioning step that may be required to destabilize the solids suspension to allow complete flocculation to occur in clarification applications. Flocculation is the bridging and binding of destabilized solids into larger particles. As particle size increases, settling rate generally increases. The science of flocculation is not discussed here but can be found in numerous texts and literature which are readily available from flocculant vendors.

Both coagulation and flocculation are typically considered in designing clarifiers, whereas flocculation is normally the only step in designing thickeners.

Coagulants may be either organic such as polyelectrolytes or inorganic such as alum. Coagulants can be used alone or in conjunction with flocculants to improve the performance of the flocculant or reduce the quantity of the flocculant required. In some systems, where a flocculant has been used in an upstream process, a coagulant may be needed to allow additional flocculant to be effective.

There are two primary types of flocculants:

- **Natural flocculants** Starch, guar, and other natural materials have historically been used for sedimentation flocculation, but have been replaced by more effective synthetic polymers.
- **Synthetic polymeric flocculants** There are hundreds of synthetic polymers available developed for specific applications.

Because of the many available flocculants, a screening program is necessary to choose an effective flocculant. The choice of flocculant can be narrowed by considering the following:

- Prior experience with flocculants on the feed stream under evaluation is always a good source of data.
- Test one each of the major types of flocculant charge: anionic, non-ionic, and cationic.
- Test one each of the synthetic polymer length: long chain, short chain.

The purpose of the screening test is to select a coagulant or flocculant whose generic type will most likely be effective in plant operation, and therefore, suitable for clarifier or thickener testing. Although a thickener or clarifier may be started up on the flocculant selected in the testing, it is very common to conduct further tests on the full-scale machine to further optimize dosage or flocculant type. The flocculant manufacturer can be a source of great assistance in both the testing and the full-scale optimization of flocculant use.

Coagulant or flocculant solutions should be made up according to the manufacturer's instructions and used within the shelf life recommended. The solution concentration recommended for testing is typically more dilute than the "neat" concentration so that the viscosity is lower to make dispersion more rapid during testing.

In the screen tests, each coagulant or flocculant is added to the beaker samples of representative slurry or liquor in a dropwise fashion, while the sample is mixed with a spatula, stirrer, or 3-6 jar stirrer mechanism. The amount of coagulant or flocculant required to initiate floc particle formation is noted along with relevant notes as to the size of the floc, capture of fines, resultant liquor clarity, and stability of the floc structure. The dosage is typically noted in g/t solids if the sample is primarily solids (thickener design), or in mg/L liquor if the sample is primarily for clarification and the solids concentration is low.

TESTING SPECIFIC TO CLARIFICATION

Detention Test This test utilizes a 1- to 4-L beaker or similar vessel. The sample is placed in the container, flocculated by suitable means if required, and allowed to settle. Small samples for suspended-solids analysis are withdrawn from a point approximately midway between liquid surface and settled solids interface, taken with sufficient care that settled solids are not resuspended. Sampling times may be at consecutively longer intervals, such as 5, 10, 20, 40, and 80 min.

The suspended-solids concentration can be plotted on log-log paper as a function of the sampling (detention) time. A straight line usually will result, and the required static detention time t to achieve a certain suspended-solids concentration C in the overflow of an ideal basin can be taken directly from the graph. If the plot is a straight line, the data are described by the equation

$$C = Kt^m \quad (18-46)$$

where the coefficient K and exponent m are characteristic of the particular suspension.

Should the suspension contain a fraction of solids which can be considered "unsettleable," the data are more easily represented by using the so-called second-order procedure. This depends on the data being reasonably represented by the equation

$$Kt = \frac{1}{C - C_\infty} - \frac{1}{C_0 - C_\infty} \quad (18-47)$$

where C_∞ is the unsettleable-solids concentration and C_0 is the concentration of suspended solids in the unsettled (feed) sample. The residual-solids concentration remaining in suspension after a sufficiently long detention time (C_∞) must be determined first, and the data then plotted on linear paper as the reciprocal concentration function $1/(C - C_\infty)$ versus time.

Bulk Settling Test After the detention test is completed, a bulk settling test is done to determine the maximum overflow rate. This is done by carrying out a settling test in which the solids are first concentrated to a level at which zone settling just begins. This is usually marked by a very diffuse interface during initial settling. Its rate of descent is measured with a graduated cylinder of suitable size, preferably at least 1 L, and the initial straight-line portion of the settling curve is used for specifying a bulk-settling rate. The design overflow rate generally should not exceed half of the bulk settling rate. From the two clarifier tests, detention time and bulk settling rate, the more

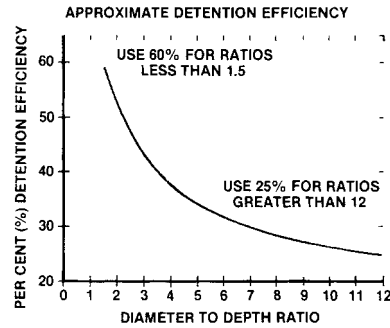


FIG. 18-94 Efficiency curve for scale-up of batch clarification data to determine nominal detention time in a continuous clarifier.

conservative results will govern the size of the clarifier.

Clarification with Solids Recycle In many instances, the rate of clarification is enhanced by increasing the solids concentration in the flocculation zone of the clarifier. This is done in a full-scale operation by internally or externally recycling previously settled solids into the flocculation zone where they are mixed with fresh, coagulated feed. The higher population of solids improves the flocculation efficiency and clarification rate.

To conduct these tests, a sample of feed is first treated at the chemical dosages and mixing intensity determined in the screening tests and flocculated according to the screening test. The solids are allowed to settle, and the supernatant is carefully decanted. The settled solids are then transferred to a new fresh sample, and tests are conducted again, using the same chemical dosages and mixing intensity. Recycle can continue with subsequent tests until the suspended solids in the sample can have concentrations of 1, 2, 3, and 5 g/L. Bulk settling rate, suspended solids, and other effluent parameters are measured with each test until an optimal treatment scenario is found.

In some suspensions, very fine colloidal solids are present and are very difficult to coagulate. In these cases, it is typically necessary to adjust for coagulation mixing intensity and time to obtain coagulated solids that are more amenable to flocculation.

Detention Efficiency Conversion from the ideal basin sized by detention-time procedures to an actual clarifier requires the inclusion of an efficiency factor to account for the effects of turbulence and nonuniform flow. Efficiencies vary greatly, being dependent not only on the relative dimensions of the clarifier and the means of feeding but also on the characteristics of the particles. The curve shown in Fig. 18-94 can be used to scale up laboratory data in sizing circular clarifiers. The static detention time determined from a test to produce a specific effluent solids concentration is divided by the efficiency (expressed as a fraction) to determine the nominal detention time, which represents the volume of the clarifier above the settled pulp interface divided by the overflow rate. Different diameter-depth combinations are considered by using the corresponding efficiency factor. In most cases, area may be determined by factors other than the bulk-settling rate, such as practical tank-depth limitations.

TESTING SPECIFIC TO THICKENING

Optimization of Flocculation Conditions After a flocculant type is selected, the next step is to conduct a range of tests using the selected flocculant, to gather data on the effects of feed slurry solids concentrations on flocculant dosage and settling rate. There are a range of solids concentrations for which flocculation effectiveness is maximized, resulting in improved settling characteristics. Operating within this feed solids range results in smaller equipment sizes, higher underflow slurry densities, better overflow liquor clarity, and lower flocculant dosages.

The tests are conducted using a series of samples prepared at solids concentrations decreasing incrementally in concentration from the expected thickener feed concentration. Typically, the samples are prepared in 250- to 500-mL graduated cylinders which give some distance

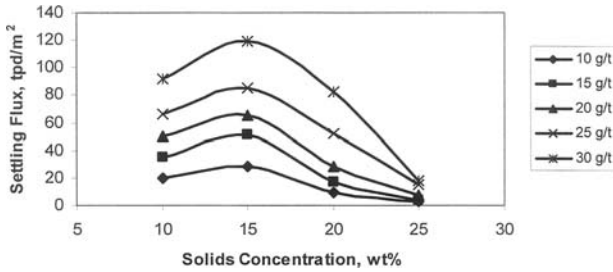


FIG. 18-95 Data showing that slurry solids concentration affects flocculation efficiency, thus improving solids settling flux.

to measure the settling rate more accurately. For some very fine solids samples (e.g., alumina red mud, clays, leached nickel laterites, etc.), it is recommended to also check a sample diluted to 2 to 3 wt % solids. Begin adding the flocculant solution dropwise; make notes on the dosage at which flocculation begins and the settling velocity. Continue adding flocculant incrementally and noting the floc structure, fines capture, liquor clarity, and settling velocity. Once the settling velocity remains constant for a few tests, sample testing can be stopped. From the tests, the plot shown in Fig. 18-95 can be drawn and the results used to set conditions for the larger and final tests for sizing the thickening equipment. The test procedure for the design tests should be structured to span the optimum solids concentration and two points slightly higher and lower. The flocculant dosage should be checked at the optimum and at dosages slightly higher and slightly lower than that determined in the above tests.

Determination of Thickener Basin Area The area requirements for thickeners frequently are based on the solids flux rates measured in the zone-settling regime. Theory holds that, for any specific sedimentation condition, a critical concentration will exist in the thickener which will limit the solids throughput rate. As the concentration in this critical zone represents a steady-state condition, its depth in the settling bed of solids may vary, responding to changes in the feed rate, underflow withdrawal rate, or flocculant dosage. In thickeners operating at relatively high solids retention times and/or low throughput rates, this zone generally does not exist.

Many batch-test methods which are based on determining the solids flux rate at this critical concentration have been developed. Most methods recognize that as the solids enter compression, thickening behavior is no longer a function only of solids concentration. Hence, these methods attempt to utilize the "critical" point dividing these two zones and size the area on the basis of the settling rate of a layer of pulp at this concentration. The difficulty lies in discerning where this point is located on the settling curve.

Many procedures have been developed, but two have been more widely used: the Coe and Clevenger approach and the Kynch method as defined by Talmage and Fitch (op. cit.).

The former requires measurement of the initial settling rate of a pulp at different solids concentrations varying from feed to final underflow value. The area requirement for each solids concentration tested is calculated by equating the net overflow rate to the corresponding interfacial settling rate, as represented by the following equation for the unit area:

$$\text{Unit area} = \frac{1/C_i - 1/C_u}{v_i} \quad (18-48)$$

where C_i is the solids concentration at the interfacial settling velocity v_i and C_u is the underflow concentration, both concentrations being expressed in terms of mass of solids per unit volume of slurry. Using kg/L for the concentrations and m/day for the settling velocity yields a unit area value in $\text{m}^2/(\text{ton}/\text{day})$.

These unit area values, plotted as a function of the feed concentration, will describe a maximum value that can be used to specify the thickener design unit area for the particular underflow concentration C_u employed in Eq. (18-48).

The method is applicable for *unfloculated* pulps or those in which the ionic characteristics of the solution produce a flocculent structure. If polymeric flocculants are used, an approach based on the Kynch theory is preferred. In this method, the test is carried out at the optimum feed solids and flocculant dose (as determined in tests described earlier) and continued until underflow concentration is achieved in the cylinder. The flocculant solution should be added to the slurry under conditions which promote rapid dispersion and uniform, complete mixing with a minimum of shear. In cylinder tests, this is accomplished by simultaneously injecting and mixing flocculant with the slurry, using an apparatus consisting of a syringe, a tube, and an inverted rubber stopper. The rubber stopper, having a diameter approximately 75 percent that of the cylinder diameter, provides sufficient turbulence as it is moved gently up and down through the slurry to cause good blending of the flocculant and pulp. To determine the unit area, Talmage and Fitch (op. cit.) proposed an equation derived from a relationship equivalent to that shown in Eq. (18-49):

$$\text{Unit area} = \frac{t_u}{C_0 H_0} \quad (18-49)$$

where t_u is the time, days; C_0 is the initial solids concentration in the feed, t/m^3 ; and H_0 is the initial height of the slurry in the test cylinder, m. The term t_u is taken from the intersection of a tangent to the curve at the critical point and a horizontal line representing the depth of pulp at underflow concentration. There are various means for selecting this critical point, all of them empirical, and the unit area value determined cannot be considered precise. The review by Pearse (op. cit.) presents many of the different procedures used in applying this approach to laboratory settling test data.

Two other approaches avoid using the critical point by computing the area requirements from the settling conditions existing at the underflow concentration. The Wilhelm and Naide procedure (op. cit.) applies zone-settling theory (Kynch) to the entire thickening regime. Tangents drawn to the settling curve are used to calculate the settling velocity at all concentrations obtained in the test. This permits construction of a plot (Fig. 18-96) showing unit area as a function of underflow concentration.

A second, "direct" approach which yields a similar result, since it also takes compression into account, utilizes the value of settling time t_s taken from the settling curve at a particular underflow concentration. This value is used to solve the Talmage and Fitch equation (18-49) for unit area.

Compression bed depth will have a significant effect on the overall settling rate (increasing compression zone depth reduces unit area). Therefore, in applying either of these two procedures it is necessary to run the test in a vessel having an average bed depth close to that expected in a full-scale thickener. This requires a very large sample, and it is more convenient to carry out the test in a cylinder having a volume of 1 to 4 liters. The calculated unit area value from this test can be extrapolated to full-scale depth by carrying out similar tests at

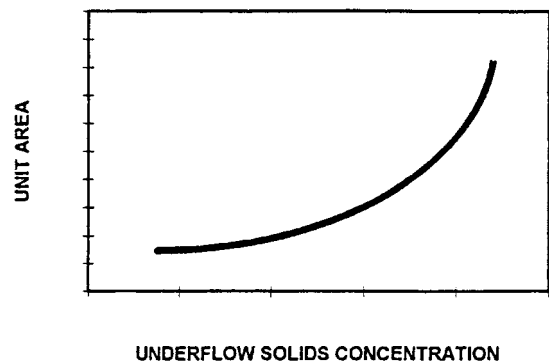


FIG. 18-96 Characteristic relationship between thickener unit area and underflow solids concentration (fixed flocculant dosage and pulp depth).

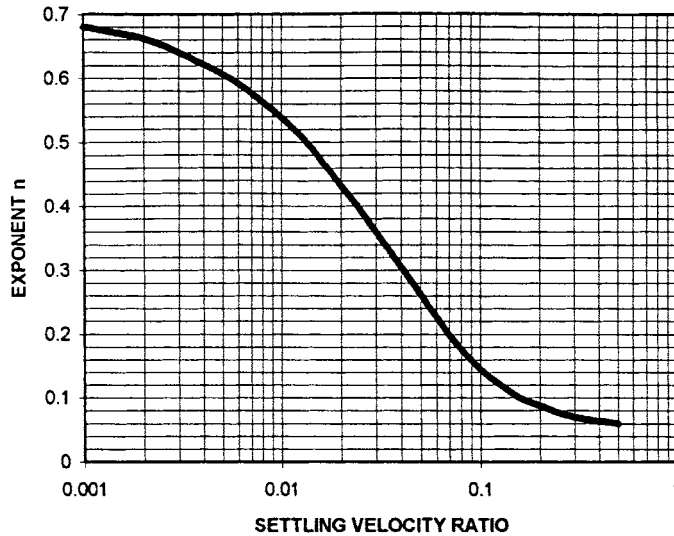


FIG. 18-97 Depth correction factor to be applied to unit areas determined by Wilhelm-Naide and "direct" methods. Velocity ratio calculated using tangents to settling curve at a particular settled solids concentration and at start of test.

different depths to determine the effect on unit area. Alternatively, an empirical relationship can be used which is effective in applying a depth correction to laboratory cylinder data over normal operating ranges. The unit area calculated by either the Wilhelm and Naide approach or the direct method is multiplied by a factor equal to $(h/H)^n$, where h is the average depth of the pulp in the cylinder, H is the expected full-scale compression zone depth, usually taken as 1 m, and n is the exponent calculated from Fig. 18-97. For conservative design purposes, the minimum value of this factor that should be used is 0.25.

It is essential to use a slow-speed (approximately 0.1 r/min) picket rake in all cylinder tests to prevent particle bridging and allow the sample to attain the underflow density which is obtainable in a full-scale thickener.

Continuously operated, small-scale or pilot-plant thickeners, ranging from 75 mm diameter by 400 mm depth to several meters in diameter, are also effectively used for sizing full-scale equipment. This approach requires a significantly greater volume of sample, such as would be available in an operating installation or a pilot plant. Continuous units and batch cylinders will produce equivalent results if proper procedures are followed with either system.

Thickener-Basin Depth The pulp depth required in the thickener will be greatly affected by the role that compression plays in determining the rate of sedimentation. If the zone-settling conditions define the area needed, then depth of pulp will be unimportant and can be largely ignored, as the "normal" depth found in the thickener will be sufficient. On the other hand, with the compression zone controlling, depth of pulp will be significant, and it is essential to measure the sedimentation rate under these conditions. This is true for the new deep-bed, high-density thickeners.

To determine the compression-zone requirement in a thickener, a test should be run in a deep cylinder in which the average settling pulp depth approximates the depth anticipated in the full-scale basin. The average density of the pulp in compression is calculated and used in Eq. (18-50) to determine the required compression-zone volume:

$$V = \frac{\theta_c(\rho_s - \rho_l)}{\rho_s(\rho_s - \rho_l)} \quad (18-50)$$

where V is the volume, m^3 , required per ton of solids per day; θ_c is the compression time, days, required in the test to reach underflow concentration; and ρ_s , ρ_l , ρ_{sl} , are the densities of the solids, liquid, and

slurry (average), respectively, ton/m^3 . This value divided by the average depth of the pulp during the period represents the unit area defined by compression requirements. If it exceeds the value determined from the zone-settling tests, it is the quantity to be used.

The side depth of the thickener is determined as the sum of the depths needed for the compression zone and for the clear zone. Normally, 1.5 to 2 m of clear liquid depth above the expected pulp level in a thickener will be sufficient for stable, effective operation. When the location of the pulp level cannot be predicted in advance or it is expected to be relatively low, a thickener sidewall depth of 2 to 3 m is usually safe. Greater depth may be used in order to provide better clarity, although in most thickener applications the improvement obtained by this means will be marginal.

Scale-up Factors Factors used in thickening will vary, but, typically, a 1.2 to 1.3 multiplier applied to the unit area calculated from laboratory data is sufficient if proper testing procedures have been followed and the samples are representative.

Torque Requirements Sufficient torque must be available in the raking mechanism of a full-scale thickener to allow it to move through the slurry and assist solids movement to the underflow outlet. Granular, particulate solids that settle rapidly and reach a terminal solids concentration without going through any apparent compression or zone-settling region require a maximum raking capability, as they must be moved to the outlet solely by the mechanism. At the other end of the spectrum, extremely fine materials, such as clays and precipitates, require a minimum of raking, for most of the solids may reach the underflow outlet hydrodynamically. The rakes prevent a gradual buildup of some solids on the bottom, however, and the gentle stirring action from the rake arm often aids the thickening process. As the underflow concentration approaches its ultimate limit, the consistency will increase greatly, resulting in a higher raking requirement and an increase in torque.

For most materials, the particle size lies somewhere between these two extremes, and the torques required in two properly designed thickeners of the same size but in distinct applications can differ greatly. Unfortunately, test methods to specify torque from small-scale tests are of questionable value, since it is difficult to duplicate actual conditions. Manufacturers of sedimentation equipment select torque ratings from experience with similar substances and will recommend a torque capability on this basis. Definitions of *operating torque* vary with the manufacturer, and the user should ask the supplier to specify the *B-10 life* for bearings and to reference appropriate mechanical

standards for continuous operation of the selected gear set at specific torque levels. This will provide guidelines for plant operators and help avoid premature failure of the mechanism. Abnormal conditions above the normal operating torque are inevitable, and a thickener should be provided with sufficient torque capability for short-term operation at higher levels in order to ensure continuous performance.

Underflow Pump Requirements Many suspensions will thicken to a concentration higher than that which can be handled by conventional slurry pumps. Thickening tests should be performed with this in mind, for, in general, the unit area to produce the maximum concentration that can be pumped is the usual design basis. Determination of this ultimate pumpable concentration is largely a judgmental decision requiring some experience with slurry pumping; however, the behavior of the thickened suspension can be used as an approximate guide to pumpability. The supernatant should be decanted following a

test and the settled solids repulped in the cylinder to a uniform consistency. Repulping is done easily with a rubber stopper fastened to the end of a rigid rod. If the bulk of the repulped slurry can be poured from the cylinder when it is tilted 10 to 30° above the horizontal, the corresponding thickener underflow can be handled by most types of slurry pumps. But if the slurry requires cylinder shaking or other mechanical means for its removal, it should be diluted to a more fluid condition, if conventional pump systems are to be employed. The best suggestion is to consult with pump experts and suppliers who have amassed large databases for a wide range of materials.

THICKENERS

The primary function of a continuous thickener is to concentrate suspended solids by gravity settling so that a steady-state material balance

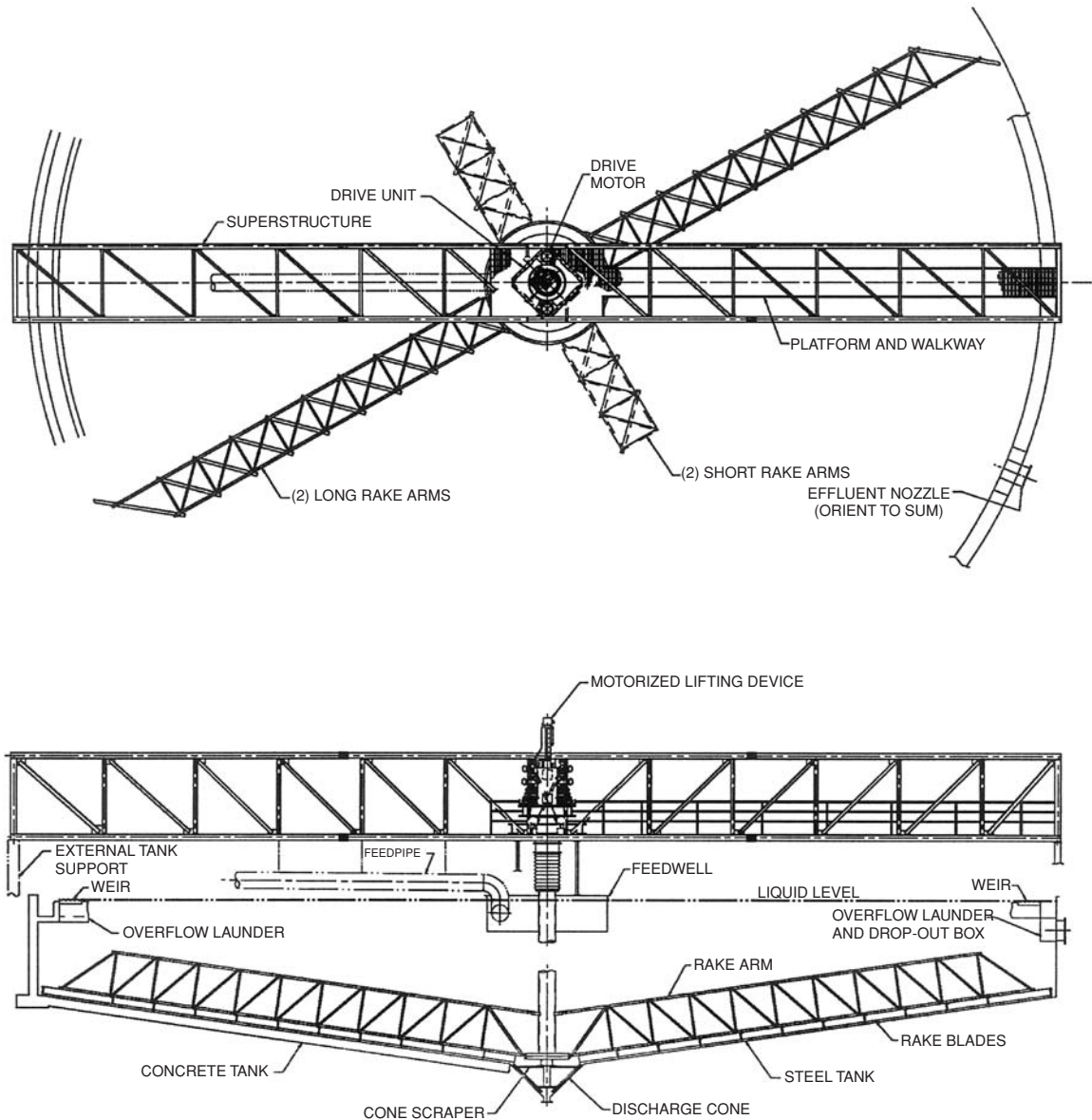


FIG. 18-98 Unit thickener bridge-mounted mechanism. (Dorr-Oliver EIMCO.)

is achieved, solids being withdrawn continuously in the underflow at the rate they are supplied in the feed. Normally, an inventory of pulp is maintained in order to achieve the desired concentration. This volume will vary somewhat as operating conditions change; on occasion, this inventory can be used for storage of solids when feed and underflow rates are reduced or temporarily suspended.

A thickener has several basic components: a tank to contain the slurry, feed piping and a feedwell to allow the feed stream to enter the tank, a rake mechanism to assist in moving the concentrated solids to the withdrawal points, an underflow solids-withdrawal system, and an overflow launder. The basic design of a bridge-supported thickener mechanism is illustrated in Fig. 18-98.

Thickener Types Flocculants are commonly used in thickeners, and this practice has resulted in thickener classifications as *conventional*, *high-rate*, *ultrahigh-rate*, or *high-density*. These designations can be confusing in that they imply sharp distinction between each type, which is *not* the case.

High-Rate Thickeners The greater capacity expected from a high-rate thickener is due solely to the effective use of flocculant to maximize throughput. In most applications there is a threshold dosage and feed solids concentration at which a noticeable increase in capacity begins to occur, as shown in Fig. 18-99. This effect will continue up to a limit, at which point the capacity will be a maximum unless a lower underflow solids concentration is accepted, as illustrated in Fig. 18-95. Since flocculant is usually added to a thickener in either the feed line or the feedwell, there are a number of proprietary feedwell designs which are used in high-rate thickeners to help optimize flocculation. Deaeration systems may be included in some cases to avoid air entrainment in the flocculated slurry. The other components of these units are not materially different from those of a conventional thickener.

Ultrahigh-Rate Thickeners This type of thickener uses a tall, deep tank with a steep bottom cone and may be used with or without a raking mechanism. This combines the functions of a thickener (to

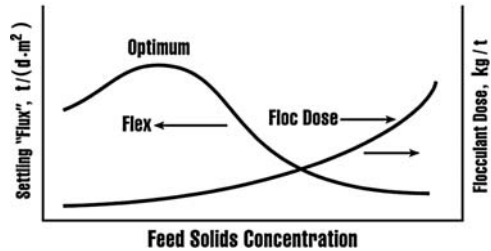


FIG. 18-99 Settling flux curve.

provide a dense underflow) and a clarifier (to provide a clear overflow or supernatant) but is considerably taller. It is generally one-half to one-third the diameter of a conventional or high-rate thickener. Figure 18-100 illustrates the internals of these units, showing the use of dewatering cones, whose function is similar to that of the lamella inclined plates of the tilted-plate thickeners.

High-Density Thickeners Thickeners can be designed to produce underflows having very high apparent viscosity, permitting disposal of waste slurries at a concentration that avoids segregation of fines and coarse particles or formation of a free-liquid pond on the surface of the deposit. This practice is applied in *dry-stacking* systems and underground *paste-fill* operations for disposal of mine tailings and similar materials. The thickener mechanism generally will require a special rake design and provide a torque capability much higher than normal for that particular diameter thickener (Fig. 18-101). Underflow slurries will be at a higher concentration than for conventional or high-rate thickeners, being 5 to 10 percent lower than vacuum filter cake from the same material. Special pumping requirements are necessary if the slurry is to be

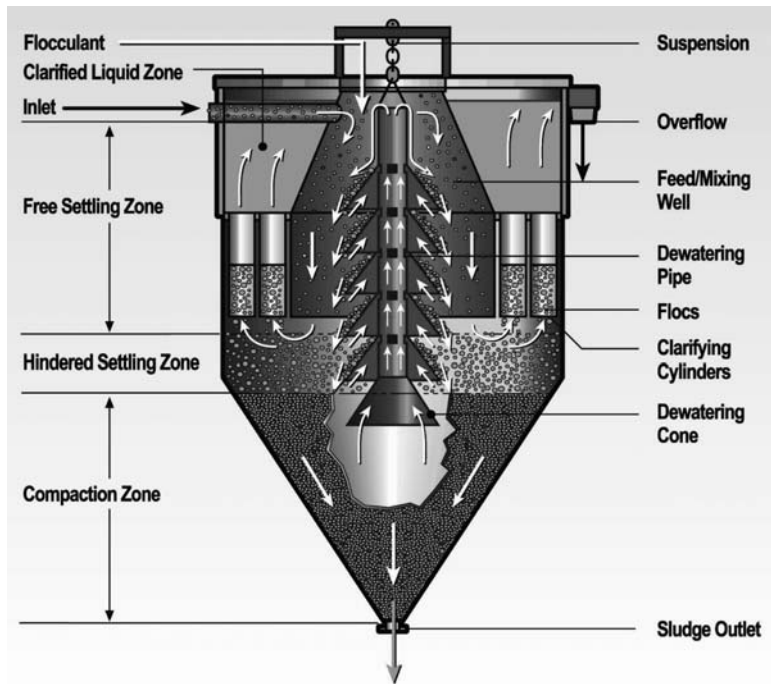


FIG. 18-100 Ultrahigh-rate thickener. (Dorr-Oliver EIMCO.)

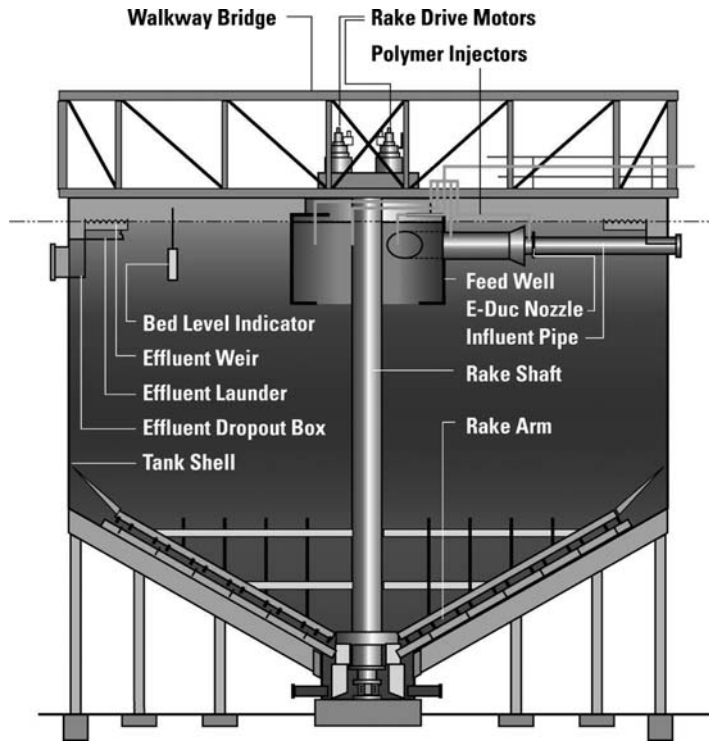


FIG. 18-101 Deep Cone™ paste thickener. (Courtesy of Dorr-Oliver EIMCO.)

transported a significant distance, with line pressure drop typically in the range of 3 to 4 kPa/m of pipeline.

Design Features There are four classes of thickeners, each differentiated by its drive mechanism: (1) bridge-supported, (2) center-column supported, (3) traction drives, and (4) without drives. The diameter of the tank will range from 2 to 150 m (6.5 to 492 ft), and the support structure often is related to the size required. These classes are described in detail in the subsection “Components and Accessories for Sedimentation Units.”

Operation When operated correctly, thickeners require a minimum of attention and, if the feed characteristics do not change radically, can be expected to maintain design performance consistently. In this regard, it is usually desirable to monitor feed and underflow rates and solids concentrations, flocculant dosage rate, and pulp interface level, preferably with dependable instrumentation systems. Process variations are then easily handled by changing the principal operating controls—underflow rate and flocculant dose—to maintain stability.

Starting up a thickener is usually the most difficult part of the operation, and there is more potential for mechanical damage to the mechanism at this stage than at any other time. In general, two conditions require special attention at this point: underflow pumping and mechanism torque. If possible, the underflow pump should be in operation as soon as feed enters the system, recirculating underflow slurry at a reduced rate if the material is relatively fine or advancing it to the next process step (or disposal) if the feed contains a considerable quantity of coarse solids, e.g., more than 20 percent + 75 μm particles. At this stage of the operation, coarse solids separate from the pulp and produce a difficult raking and pumping situation. Torque can rise rapidly if this material accumulates faster than it is removed. If the torque reaches a point where the automatic control system raises the rakes, it is usually preferable to reduce or cut off the feed completely until the torque drops and the rakes are returned to the lowest position. As the fine fraction of the feed slurry begins to thicken and accumulate in the basin, providing both buoyancy and fluidity, torque will drop and

normal feeding can be continued. This applies whether the thickener tank is empty at start-up or filled with liquid. The latter approach contributes to coarse-solids raking problems but at the same time provides conditions more suited to good flocculation, with the result that the thickener will reach stable operation much sooner.

As the solids inventory in the thickener reaches a normal level—usually about 0.5 to 1.0 m below the feedwell outlet—with underflow slurry at the desired concentration, the torque will reach a normal operating range. Special note should be made of the torque reading at this time. Subsequent higher torque levels while operating conditions remain unchanged can almost always be attributed to island formation, and corrective action can be taken early, before serious problems develop. *Island* is the name given to a mass of semisolidified solids that have accumulated on or in front of the rakes, often as a result of excessive flocculant use. This mass usually will continue to grow in size, eventually producing a torque spike that can shut down the thickener and often resulting in lower underflow densities than would otherwise be achievable.

An island is easily detected, usually by the higher-than-normal, gradually increasing torque reading. Probing the rake arms near the thickener center with a rigid rod will confirm this condition—the mass is easily distinguished by its cohesive, claylike consistency. At an early stage, the island is readily removed by raising the rakes until the torque drops to a minimum value. The rakes are then lowered gradually, a few centimeters at a time, so as to shave off the mass of solids and discharge this gelled material through the underflow. This operation can take several hours, and if island formation is a frequent occurrence, the procedure should be carried out on a regular basis, typically once a day, preferably with an automatic system to control the entire operation.

Stable thickener performance can be maintained by carefully monitoring operating conditions, particularly the pulp interface level and the underflow rate and concentration. As process changes occur, the pulp level can vary; regulation of the underflow pumping rate will

keep the level within the desired range. If the underflow varies in concentration, this can be corrected by adjusting the flocculant dosage. Response will not be immediate, of course, and care should be taken to make only small step changes at any one time. Procedures for use of automatic control are described in the section on instrumentation.

CLARIFIERS

Continuous clarifiers generally are employed with dilute suspensions, principally industrial process streams and domestic municipal wastes, and their primary purpose is to produce a relatively clear overflow. They are basically identical to thickeners in design and layout except that they employ a mechanism of lighter construction and a drive head with a lower torque capability. These differences are permitted in clarification applications because the thickened pulp produced is smaller in volume and appreciably lower in suspended solids concentration, owing in part to the large percentage of relatively fine (smaller than 10 μm) solids. The installed cost of a clarifier, therefore, is approximately 5 to 10 percent less than that of a thickener of equal tank size, as given in Fig. 18-106.

Rectangular Clarifiers Rectangular clarifiers are employed primarily in municipal water and waste treatment plants, as well as in certain industrial plants, also for waste streams. The raking mechanism employed in many designs consists of a chain-type drag, although suction systems are used for light-duty applications. The drag moves the deposited pulp to a sludge hopper located on one end by means of scrapers fixed to endless chains. During their return to the sludge raking position, the flights may travel near the water level and thus act as skimming devices for removal of surface scum. Rectangular clarifiers are available in widths of 2 to 10 m (6 to 33 ft). The length is generally 3 to 5 times the width. The larger widths have multiple raking mechanisms, each with a separate drive.

This type of clarifier is used in applications such as preliminary oil-water separations in refineries and clarification of waste streams in steel mills. When multiple units are employed, common walls are possible, reducing construction costs and saving on floor space. Overflow clarifiers, however, generally are not as good as with circular clarifiers, due primarily to reduced overflow weir length for equivalent areas.

Circular Clarifiers Circular units are available in the same three basic types as single-compartment thickeners: bridge, center-column, and peripheral-traction. Because of economic considerations, the bridge-supported type is limited generally to tanks less than 40 m in diameter.

A circular clarifier often is equipped with a surface-skimming device, which includes a rotating skimmer, scum baffle, and scum-box assembly. In sewage and organic-waste applications, squeegees normally are provided for the rake-arm blades, as it is desirable that the bottom be scraped clean to preclude accumulation of organic solids, with resultant septicity and flotation of decomposing material.

Center-drive mechanisms are also installed in square tanks. This mechanism differs from the standard circular mechanism in that a hinged corner blade is provided to sweep the corners which lie outside the path of the main mechanism.

Clarifier-Thickener Clarifiers can serve as thickeners, achieving additional densification in a deep sludge sump adjacent to the center that extends a short distance radially and provides adequate retention time and pulp depth to compact the solids to a high density. Drive mechanisms on this type of clarifier usually must have higher torque capability than would be supplied on a standard clarifier.

Industrial Waste Secondary Clarifiers Many plants which formerly discharged organic wastes to the sewer have turned to using their own treatment facilities in order to reduce municipal treatment plant charges. For organic wastes, the waste-activated sludge process is a preferred approach, using an aeration basin for the bio-oxidation step and a secondary clarifier to produce a clear effluent and to concentrate the biomass for recycling to the basin. To produce an acceptable effluent and achieve sufficient concentration of the low-density solids that make up the biomass, certain design criteria must be followed. Typical design parameters include the following:

Feed pipe velocity: ≤ 1.2 m/s.

Energy-dissipating feed entry velocity (tangential): ≤ 0.5 m/s.

Downward velocity from feedwell: $\leq 0.5\text{--}0.75$ (peak) m/min.

Feedwell depth: Entry port depth $+1\text{--}3$ m.

Tank depth: typically 3–5 m.

Radial velocity below feedwell: $\leq 90\%$ of downward velocity.

Overflow rate can range between 0.68 and 2.0 m/h depending on the application. Consult an equipment supplier and manual of practices for recommended overflow rates for specific applications.

Inclined-Plate Clarifiers Lamella or inclined-plate separators have achieved increased use for clarification. They contain a multiplicity of plates inclined at 45 to 60° from the horizontal. Various feed methods are employed so that the influent passes into each inclined channel. The geometry of the plates results in the solids having to settle only a short distance in each channel before sliding down the base to the collection zone beneath the plates. The clarified liquid passes in the opposite direction beneath the ceiling of each channel to the overflow connection.

The area that is theoretically available for separation is equal to the sum of the projected areas or all channels on the horizontal plane. Figure 18-102 shows the horizontally projected area A_s of a single channel in a clarifier of unit width. For a settling length L and width W , inclined at angle α , the horizontally projected area A_s can be calculated as

$$A_s = LW \cos \alpha \quad (18-51)$$

Multiply this area by the total number of plates in the clarifier to calculate the total clarification area available. However, α must be larger than the angle of repose of the sludge so that it will slide down the plate, and the most common range is 55 to 60°. Plate spacing must be large enough to accommodate the opposite flows of liquid and sludge while reducing interference and preventing plugging and to provide enough residence time for the solids to settle to the bottom plate. Usual X values are 50 to 75 mm (2 to 3 in).

Many different designs are available, the major difference among them being in feed-distribution methods and plate configurations. Operating capacities range from 0.2 to 1.2 gpm/ft^2 projected horizontal area.

The principal advantage of the inclined-plate clarifier is the increased solids recirculation capacity per unit of plane area. Major disadvantages are an underflow solids concentration that generally is lower than in other gravity clarifiers and difficulty of cleaning when scaling or deposition occurs. The lower underflow composition is due primarily to the reduced compression-zone volume relative to the large settling area. When flocculants are employed, flocculating equipment and tankage preceding the separator are required, as the design does not permit internal flocculation.

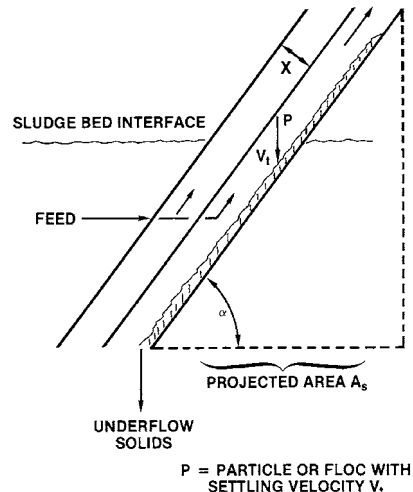


FIG. 18-102 Basic concept of the inclined-plate type of clarifier.

The **ultrahigh-rate** (rakeless) thickener uses internal cones to achieve the tilted-plate effect. The design allows internal flocculation. The tank is tall, with a 60° bottom cone, providing sludge compression height and volume, resulting in a high-density underflow.

Solids-Contact Clarifiers When desirable, mixing, flocculation, and sedimentation all may be accomplished in a single tank. Of the various designs available, those employing mechanically assisted mixing in the reaction zone are the most efficient. They generally permit the highest overflow rate at a minimum chemical dosage while producing the best effluent quality. The unit illustrated in Fig. 18-103a consists of a combination dual drive which has a low-speed rake mechanism and a high-rate low-shear turbine located in the top portion of the center well for internal solids recirculation. The influent, dosed with chemicals, is contacted with previously settled solids in a recirculation draft tube within the reaction well by means of the pumping action of the turbine. Owing to the higher concentration of solids being recirculated, chemical reactions are more rapid, and flocculation is improved. Outside of the feed well the flocculated particles settle to the bottom and are raked to the center to be used again in the recirculation process. When particles are too heavy to be circulated up through the draft tube (as in the case of metallurgical pulps), a modified design (see Fig. 18-103) using external recirculation of a portion of the thickened underflow is chosen. These units employ a special mixing impeller in a feed well with a controlled outlet.

Solids-contact clarifiers are advantageous for clarifying turbid waters or slurries that require coagulation and flocculation for the removal of bacteria, suspended solids, or color. Applications include softening water by lime addition; clarifying industrial-process streams, sewage, and industrial wastewaters; tertiary treatment for removal of phosphates, BOD₅, and turbidity; and silica removal from produce water, cooling tower make-up, and geothermal brines.

COMPONENTS AND ACCESSORIES FOR SEDIMENTATION UNITS

Sedimentation systems consist of a collection of components, each of which can be supplied in a number of variations. The basic components are the same, whether the system is for thickening or clarifying: tank, drive-support structure, drive unit and lifting device, rake structure, feedwell, overflow arrangement, underflow arrangement, instrumentation, and flocculation facilities.

Tanks Tanks or basins are constructed of such materials as steel, concrete, wood, compacted earth, plastic sheeting, and soil cement. The selection of the materials of construction is based on environmental cost, availability, topography, water table, ground conditions, climate, operating temperature, and chemical-corrosion resistance. Typically, industrial tanks up to 30 m (100 ft) in diameter are made of steel. Concrete generally is used in municipal applications and in larger industrial applications. Extremely large units employing earthen basins with impermeable liners have proved to be economical.

Drive-Support Structures There are three basic drive mechanisms. These are (1) the bridge-supported mechanism, (2) the center-column-supported mechanism, and (3) the traction-drive thickener containing a center-column-supported mechanism with the driving arm attached to a motorized carriage at the tank periphery.

Bridge-Supported Thickeners These thickeners (Fig. 18-98) are common in diameters up to 30 m, the maximum being about 45 m (150 ft). They offer the following advantages over a center-column-supported design: (1) ability to transfer loads to the tank periphery; (2) ability to give a denser and more consistent underflow concentration with the single draw-off point; (3) a less complicated lifting device; (4) fewer structural members subject to mud accumulation; (5) access to the drive from both ends of the bridge; and (6) lower cost for units smaller than 30 m in diameter.

Center-Column-Supported Thickeners These thickeners are usually 20 m (65 ft) or more in diameter. The mechanism is supported by a stationary steel or concrete center column, and the raking arms are attached to a driving cage which rotates around the center column.

Traction Thickeners These thickeners are most adaptable to tanks larger than 60 m (200 ft) in diameter. Maintenance generally is

less difficult than with other types of thickeners, which is an advantage in remote locations. The drive may be supported on the concrete wall (the wall would be a structural member) or supported outside the wall on the ground (a standard tank wall could be used). Disadvantages of the traction thickener are that (1) no practical lifting device can be used, (2) operation may be difficult in climates where snow and ice are common, and (3) the driving-torque effort must be transmitted from the tank periphery to the center, where the heaviest raking conditions occur.

The rakeless ultrahigh-rate thickeners use elevated tanks up to 20-m diameter. Advantages are no drive, high throughput rate, and the small footprint. Disadvantages are the height of the elevated tank.

Drive Assemblies The drive assembly is the key component of a sedimentation unit. The drive assembly provides (1) the force to move the rakes through the thickened pulp and to move settled solids to the point of discharge, (2) the support for the mechanism which permits it to rotate, (3) adequate reserve capacity to withstand upsets and temporary overloads, and (4) a reliable control which protects the mechanism from damage when a major overload occurs.

Drives usually have steel or iron main spur gears mounted on bearings, alloy-steel pinions, or a planetary gear. Direct-drive hydraulic systems are also employed. The gearing components preferably are enclosed for maximum service life. The drive typically includes a torque-measuring system with torque indicated on the mechanism and often transmitted to a remote indicator. If the torque becomes excessive, it can automatically activate such safeguards against structural damage as sounding an alarm, raising the rakes, and stopping the drive.

Rake-Lifting Mechanisms These should be provided when abnormal thickener operation is probable. Abnormal thickener operation or excessive torque may result from insufficient underflow pumping, surges in the solids feed rate, excessive amounts of large particles, sloughing of solids accumulated between the rakes and the bottom of the tank or on structural members of the rake mechanism, or miscellaneous obstructions falling into the thickener. The lifting mechanism may be set to raise the rakes automatically when a specific torque level (e.g., 40 percent of design) is encountered, continuing to lift until the torque returns to normal or until the maximum lift height is reached. Generally, corrective action must be taken to eliminate the cause of the upset. Once the torque returns to normal, the rake mechanism is lowered slowly to "plow" gradually through the excess accumulated solids until these are removed from the tank.

Motorized rake-lifting devices typically are designed to allow for a vertical lift of the rake mechanism of up to 90 cm (3 ft).

The cable arm design uses cables attached to a truss above or near the liquid surface to move the rake arms, which are hinged to the drive structure, allowing the rakes to raise when excessive torque is encountered. A major advantage of this design is the relatively small surface area of the raking mechanism, which reduces the solids accumulation and downtime in applications in which scaling or island formation can occur.

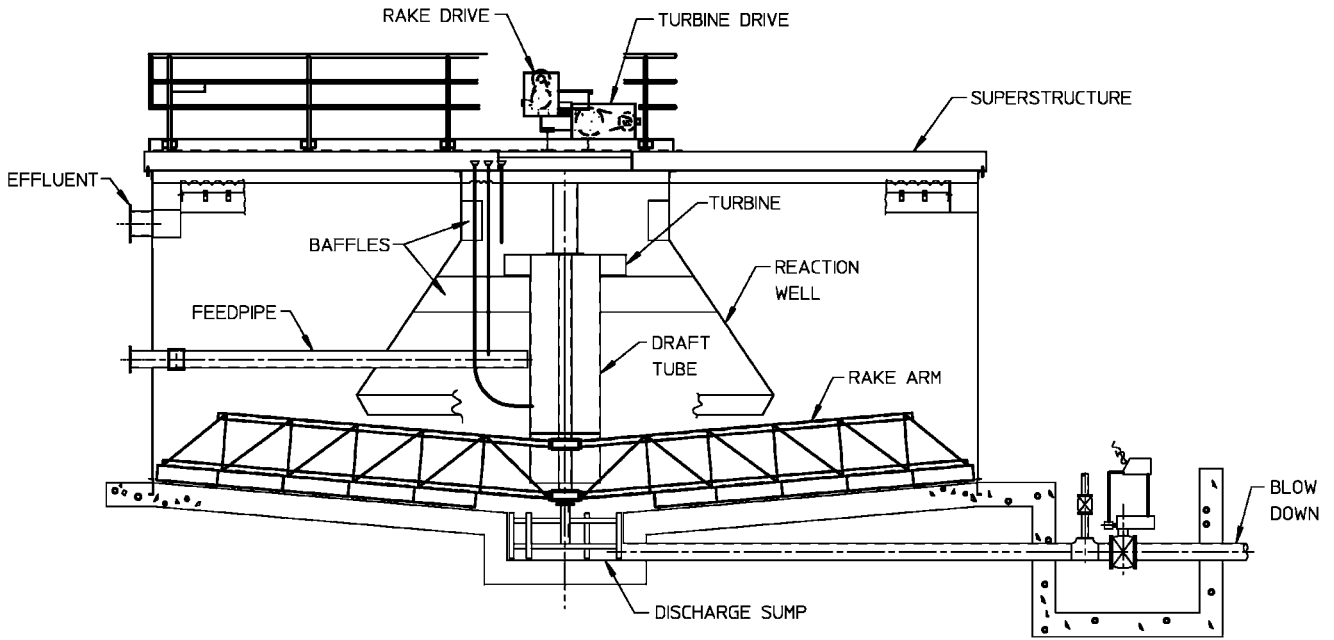
One disadvantage of this or any hinged-arm or other self-lifting design is that there is very little lift at the center, where the overload usually occurs. A further disadvantage is the difficulty of returning the rakes to the lowered position in settlers containing solids that compact firmly.

Rake Mechanism The rake mechanism assists in moving the settled solids to the point of discharge. It also aids in thickening the pulp by disrupting bridged floccules, permitting trapped fluid to escape and allowing the floccules to become more consolidated. Rake mechanisms are designed for specific applications, usually having two long rake arms with an option for two short rake arms for bridge-supported and center-column-supported units. Traction units usually have one long arm, two short arms, and one intermediate arm.

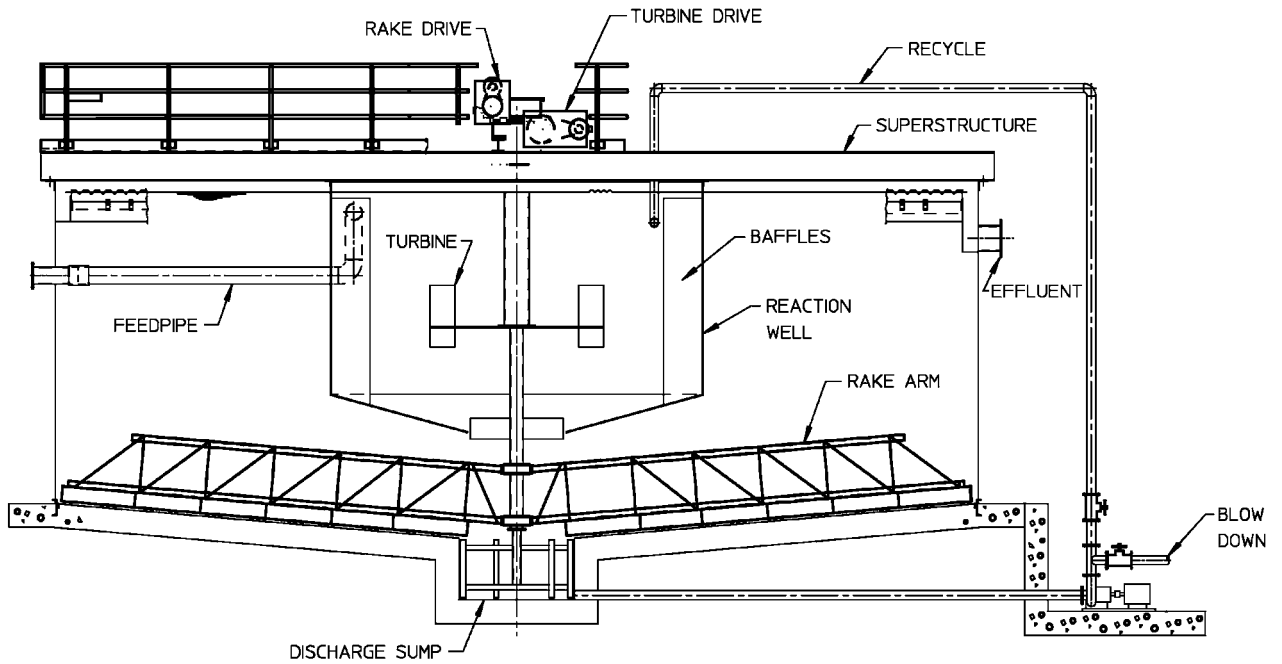
Figure 18-104 illustrates types of rake-arm designs. The conventional design typically is used in bridge-supported units, while the dual-slope design is used for units of larger diameter.

Rake blades can have attached spikes or serrated bottoms to cut into solids that have a tendency to compact. Lifting devices typically are used with these applications.

Rake-speed requirements depend on the type of solids entering the thickener. Peripheral speed ranges used are, for slow-settling solids, 3 to 8 m/min (10 to 25 ft/min); for fast-settling solids, 8 to 12 m/min



(a)



(b)

FIG. 18-103 Solids-contact reactor clarifiers. (Dorr-Oliver EIMCO.)

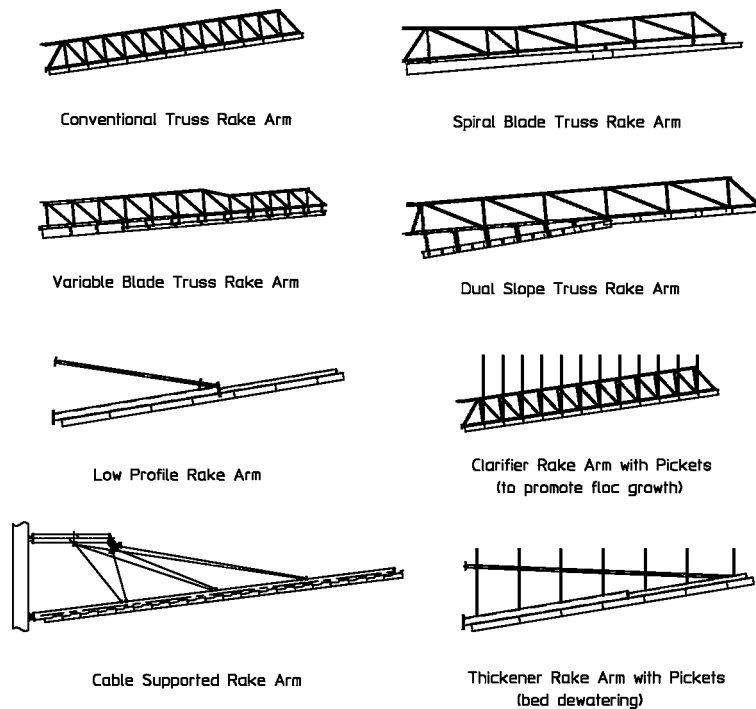


FIG. 18-104 Rake-mechanism designs for specific applications and duties. (Dorr-Oliver EIMCO.)

(25 to 40 ft/min); and for coarse solids or crystalline materials, 12 to 30 m/min (40 to 100 ft/min).

Feedwell The feedwell is designed to allow the feed to enter the thickener with minimum turbulence and uniform distribution while dissipating most of its kinetic energy. Feed slurry enters the feedwell, which is usually located in the center of the thickener, through a pipe or launder suspended from the bridge. To avoid excess velocity, an open launder normally has a slope no greater than 1 to 2 percent. Pulp should enter the launder at a velocity that prevents sanding at the inlet. With nonsanding pulps, the feed may also enter upward through the center column from a pipeline installed beneath the tank.

The standard feedwell for a thickener is designed for a maximum vertical outlet velocity of about 1.5 m/min (5 ft/min). High turbidity caused by short-circuiting the feed to the overflow can be reduced by increasing the depth of the feedwell. When overflow clarity is important or the solids specific gravity is close to the liquid specific gravity, deep feedwells of large diameter are used, and measures are taken to reduce the velocity of the entering feed slurry.

Shallow feedwells may be used when overflow clarity is not important, the overflow rate is low, and/or solids density is appreciably greater than that of water. Some special feedwell designs used to dissipate entrance velocity and create quiescent settling conditions split the feed stream and allow it to enter the feedwell tangentially on opposite sides. The two streams shear or collide with one another to dissipate kinetic energy.

When flocculants are used, often it will be found that the optimum solids concentration for flocculation is considerably less than the normal concentration, and significant savings in reagent cost will be made possible by dilution of the feed prior to flocculation. This can be achieved by recycling overflow or more efficiently by feedwell modifications, including openings in the feedwell rim. These will allow supernatant to enter the feedwell, and flocculant can be added at this point or injected below the surface of the pulp in the feedwell. Another effective means of achieving this dilution prior to flocculant

addition is illustrated in Fig. 18-105. This approach utilizes the energy available in the incoming feed stream to achieve the dilution by momentum transfer and requires no additional energy expenditure to dilute this slurry by as much as three to four times.

Overflow Arrangements Clarified effluent typically is removed in a peripheral launder located inside or outside the tank. The effluent enters the launder by overflowing a V-notch or level flat weir, or through submerged orifices in the bottom of the launder. Uneven overflow rates caused by wind blowing across the liquid surface in large thickeners can be better controlled when submerged orifices or V-notch weirs are used. Radial launders are used when uniform upward liquid flow is desired in order to improve clarifier detention efficiency. This arrangement provides an additional benefit in reducing the effect of wind, which can seriously impair clarity in applications that employ basins of large diameter.

The hydraulic capacity of a launder must be sufficient to prevent flooding, which can cause short-circuiting of the feed and deterioration of overflow clarity. Standards are occasionally imposed on weir overflow rates for clarifiers used in municipal applications; typical rates are 3.5 to 15 m³/(h·m) [7000 to 30,000 gal/(day·ft)], and they are highly dependent on clarifier side-water depth. Industrial clarifiers may have higher overflow rates, depending on the application and the desired overflow clarity. Launders can be arranged in a variety of configurations to achieve the desired overflow rate. Several alternatives to improve clarity include an annular launder inside the tank (the liquid overflows both sides), radial launders connected to the peripheral launder (providing the very long weir that may be needed when abnormally high overflow rates are encountered and overflow clarity is important), and Stamford baffles, which are located below the launder to direct flow currents back toward the center of the clarifier.

In many thickener applications, on the other hand, complete peripheral launders are not required, and no difference in either overflow clarity or underflow concentration will result through the use of launders extending over only a fraction (e.g., one-fifth) of the perimeter.

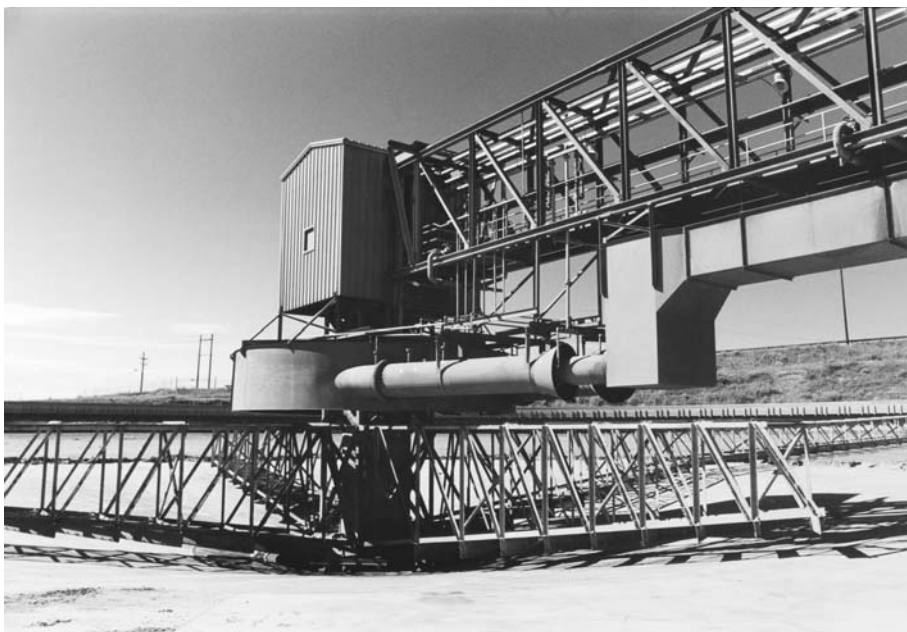


FIG. 18-105 E-Duc® Feed dilution system installed on a 122-m diameter thickener. (Dorr-Oliver EIMCO.)

For design purposes, a weir-loading rate in the range of 7.5 to 30.0 m³/(h·m) [10 to 40 gpm/ft] can be used, the higher values being employed with well-flocculated, rapidly settling slurries. The overflow launder required may occupy only a single section of the perimeter rather than consisting of multiple, shorter segments spaced uniformly around the tank.

Underflow Arrangements Concentrated solids are removed from the thickener by use of centrifugal or positive displacement pumps or, particularly with large-volume flows, by gravity discharge through a flow control valve or orifice suitable for slurry applications. Due to the risk to the thickener operation of a plugged underflow pipe, it is recommended that duplicate underflow pipes and pumps be installed in all thickening applications. Provision to recycle underflow slurry back to the feedwell is also useful, particularly if solids are to be stored in the thickener.

There are three basic underflow arrangements: (1) the underflow pump adjacent to the thickener sidewall with buried piping from the discharge cone, (2) the underflow pump under the thickeners or adjacent to the sidewall with the piping from the discharge cone in a tunnel, and (3) the underflow pump located in the center of the thickener on the bridge, or using piping up through the center column.

Pump Adjacent to Thickener with Buried Piping This arrangement of buried piping from the discharge cone is the least expensive system but the most susceptible to plugging. It is used only when the solids do not compact to an unpumpable slurry and can be easily backflushed if plugging occurs. Typically, two or more underflow pipes are installed from the discharge cone to the underflow pump so that solids removal can continue if one of the lines plugs. Valves should be installed to permit flushing with water and compressed air in both directions to remove blockages.

Tunnel A tunnel may be constructed under the thickener to provide access to the discharge cone when underflow slurries are difficult to pump and have characteristics that cause plugging. The underflow pump may be installed underneath the thickener or at the perimeter. Occasionally thickeners are installed on legs or piers, making tunneling for access to the center unnecessary. A tunnel or an elevated thickener is more expensive than the other underflow arrangements, but

there are certain operational and maintenance advantages. Of course, the hazards of working in a tunnel (flooding and interrupted ventilation, for example) and related safety regulations must be considered.

Center-Column Pumping This arrangement may be used instead of a tunnel. Several designs are available. One is a bridge-mounted pump with a suction line through a wet or dry center column. The pump selection may be limiting, requiring special attention to priming, net positive suction head, and the maximum density that the pump can handle. Another design has the underflow pump located in a room under the thickener mechanism and connected to openings in the column. Access is through the drive gear at the top of the column.

INSTRUMENTATION

Thickener Thickener control philosophies are usually based on the idea that the underflow density obtained is the most important performance criterion. The overflow clarity is also a consideration, but this is generally not as critical. Additional factors which must be considered are optimization of flocculant usage and protection of the raking mechanism.

Automated control schemes employ one or more sets of controls, which will fit into three categories: (1) control loops which are used to regulate the addition of flocculant, (2) control loops to regulate the withdrawal of underflow, and (3) rake drive controls. Frequently, the feed to a thickener is not controlled and most control systems have been designed with some flexibility to deal with changes in feed characteristics.

Flocculant addition rate can be regulated in proportion to the thickener volumetric feed rate or solids mass flow in a feed-forward mode, or in a feed-back mode on either rake torque, underflow density, settling solids (sludge) bed level, or solids settling rate.

Underflow is usually withdrawn continuously on the bases of bed level, rake torque, or underflow solids concentration in a feedback mode. Some installations incorporate two or more of these parameters in their underflow withdrawal control philosophy. For example, the

continuous withdrawal may be based on underflow solids density with an override to increase the withdrawal rate if either the rake torque or the bed level reaches a preset value. In some cases, underflow withdrawal has been regulated in a feed-forward mode on the basis of thickener feed solids mass flow rate. Any automated underflow pumping scheme should incorporate a lower limit on volumetric flow rate as a safeguard against line pluggage.

It is also important to consider the level of the sludge bed in the thickener. Although this can be allowed to increase or decrease within moderate limits, it must be controlled enough to prevent solids from overflowing the thickener or from falling so low that the underflow density becomes too dilute. The settling slurry within the sludge bed is normally free flowing and will disperse to a consistent level across the thickener diameter.

Rake drive controls protect the drive mechanism from damage and usually incorporate an alarm to indicate high torque with an interlock to shut down the drive at a higher torque level. They can have an automated rake raising and lowering feature with a device to indicate the elevation of the rakes.

A complete automated control scheme incorporates controls from each of the three categories. It is important to consider the interaction of the various controls, especially of the flocculant addition and underflow withdrawal control loops, when designing a system. The lag and dead times of any feedback loops as well as the actual response of the system to changes in manipulated variables must be considered. For example, in some applications it is possible that excessive flocculant addition may produce an increase in the rake torque (due to island formation or viscosity increase) without a corresponding increase in underflow density. Additionally, sludge bed level sensors generally require periodic cleaning to produce a reliable signal. In many cases, it has not been possible to effectively maintain the sludge bed level sensors, requiring a change in the thickener control logic after start-up. Some manufacturers offer complete thickener control packages.

Clarifiers Control philosophies for clarifiers are based on the idea that the overflow is the most important performance criterion. Underflow density or suspended solids content is a consideration, as is optimal use of flocculation and pH control reagents. Automated controls are of three basic types: (1) control loops that optimize coagulant, flocculant, and pH control reagent additions; (2) those that regulate underflow removal; and (3) rake drive controls. Equalization of the feed is provided in some installations, but the clarifier feed is usually not a controlled variable with respect to the clarifier operation.

Automated controls for flocculating reagents can use a feed-forward mode based on feed turbidity and feed volumetric rate, or a feed-back mode incorporating a streaming current detector on the flocculated feed. Attempts to control coagulant addition on the basis of overflow turbidity generally have been less successful. Control for pH has been accomplished by feed-forward modes on the feed pH and by feed-back modes on the basis of clarifier feedwell or external reaction tank pH. Control loops based on measurement of feedwell pH are useful for control in applications in which flocculated solids are internally recirculated within the clarifier feedwell.

Automated sludge withdrawal controls are usually based on the sludge bed level or pressure. These can operate in on-off or continuous modes and can use either single-point or continuous sludge level indication sensors. In many applications, automated control of underflow withdrawal does not provide an advantage, since so few settled solids are produced that it is only necessary to remove sludge for a short interval once a day, or even less frequently. In applications in which the underflow is recirculated internally within the feedwell, it is necessary to maintain sufficient sludge inventory for the recirculation turbine to pull from. This can be handled in an automated system with a single-point *low sludge* bed level sensor in conjunction with a low-level alarm or pump shutoff solenoid. Some applications require continuous external recirculation of the underflow direct to the feedwell or external reaction tanks, and an automated control loop can be used to maintain recirculation based on flow measurement, with a manually adjusted setpoint.

Control philosophies applied to continuous countercurrent decantation (CCD) thickeners are similar to those used for thickeners in

other applications, but have emphasis on maintaining the CCD circuit in balance. It is important to prevent any one of the thickeners from pumping out too fast, otherwise an upstream unit could be starved of wash liquor while at the same time too much underflow could be placed in a downstream unit, disrupting the operation of both units as well as reducing the circuit washing efficiency. Several control configurations have been attempted, and the more successful schemes have linked the solids mass flow rate of underflow pumping to that of the upstream unit or to the CCD circuit solids mass feed rate. Wide variations in the solids feed rate to a CCD circuit will require some means of dampening these fluctuations if design wash efficiency is to be maintained.

The following types of devices are commonly applied to measure the various operational parameters of thickeners and clarifiers. They have been used in conjunction with automatic valves and variable-speed pumps to achieve automatic operation as well as to simply provide local or remote indications.

INSTRUMENTATION AND CONTROLS

Torque Rake torque is an indication of the force necessary to rotate the rakes. Higher rake torque is an indication of higher underflow density or viscosity, deeper mud bed, higher fraction of coarse material, island formation, or heavy scale buildup on the rake arms.

Rake torque measurement is usually provided by the thickener manufacturer as part of the rake drive mechanism. Typical methods involve load cells, motor power measurement, hydraulic pressure, or mechanical displacement against a spring. Torque-measuring devices are designed to produce a signal that may be utilized for alarming or control.

Rake Height Rake lifting devices are used to minimize the torque on the arms by lifting them out of heavy bed solids and enable the rake to continue running during upset conditions. It is desirable to prevent the rake drives from running for extended periods at torques above 50 to 60 percent, to prevent accelerated wear on the drive. Lifting the rakes a small distance is usually effective in relieving the pressure on the rakes, thus reducing the torque. Because of this, in using "torque indication" in a control strategy one must also consider the rake height to effectively control the thickener. The two most common rake height indicators are the ultrasonic or potentiometer type with a reeling cable. Lifting of the rakes allows a short period of time to make corrections before one is forced to shut down the thickener.

Bed Level There are several general types of bed level detection instruments: ultrasonic, nuclear, float and rod, and reeling (with various sensors). Each has advantages and disadvantages, which are discussed below. There is not a standard bed level sensor that is recommended for all applications.

- **Ultrasonic** bed level sensors work by sending a pulse down from just under the surface, which bounces off the bed and back to the receiver. Elapsed time is used to calculate the distance. Advantages are noninterfering location, measurement over a large span, and relatively low cost. The downside is that they do not work on all applications. If the overflow is cloudy, it can interfere with the transmission or cause too much reflection to give a reliable signal. Sealing affects accuracy and can cause drifting or loss of signal. Using them on concentrate thickeners has proved to be particularly troublesome.
- **Nuclear** bed level sensors work by sensing either the background radiation level or attenuation between a source and detector, depending on whether the solids have a natural background radiation level. The sensor is comprised of a long rod that extends down into the bed with radiation detectors spaced along the length. If the ore changes from not having radiation to having it, there will be problems. The advantages are that it is relatively reliable when properly applied. The downside is that it measures over a limited range, may interfere with rakes (a hinged version that will swing out of the way when the rakes pass by is available), and is relatively expensive.
- **Float and rod** types work with a ball with a hollow sleeve that slides up and down on a rod that extends down into the bed. The ball weight can be adjusted to float on top of the bed of solids.

TABLE 18-7 Typical Thickener and Clarifier Design Criteria and Operating Conditions

	Percent solids		Unit area, m ² /(t/d)*†	Overflow rate, m ³ /(m ² ·h) ^o
	Feed	Underflow		
Alumina Bayer process				
Red mud, primary	3–4	10–25	2–5	
Red mud, washers	6–8	15–35	1–4	
Hydrate, fine or seed	1–10	20–50	1.2–3	0.07–0.12
Brine purification	0.2–2.0	8–15		0.5–1.2
Coal, refuse	0.5–6	20–40	0.5–1	0.7–1.7
Coal, heavy-media (magnetic)	20–30	60–70	0.05–0.1	
Cyanide, leached-ore	16–33	40–60	0.3–1.3	
Flue dust, blast-furnace	0.2–2.0	40–60		1.5–3.7
Flue dust, BOF	0.2–2.0	30–70		1–3.7
Flue-gas desulfurization sludge	3–12	20–45	0.3–3†	
High-density paste thickeners				
Red mud, washers [†]	3–4	45–50	0.05–0.08	
Coal, refuse [†]	6–8	50–54	0.08–0.1	
Cyanide, leached ore [†]	10–15	65–70	0.05–0.08	
Copper tailings [†]	10–20	50–75	0.07–0.15	
Tailings (magnetic) [†]	10–20	60–75	0.07–0.1	
Tailings (nonmagnetic) [†]	10–20	60–70	0.07–0.1	
Magnesium hydroxide from brine	8–10	25–40	5–10	
Magnesium hydroxide from seawater	1–4	15–20	3–10	0.5–0.8
Metallurgical				
Copper concentrates	14–50	40–75	0.2–2	
Copper tailings	10–30	45–65	0.4–1	
Iron ore				
Concentrate (magnetic)	20–35	50–70	0.01–0.08	
Concentrate (nonmagnetic), coarse: 40–65% –325	25–40	60–75	0.02–0.1	
Concentrate (nonmagnetic), fine: 65–100% –325	15–30	60–70	0.15–0.4	
Tailings (magnetic)	2–5	45–60	0.6–1.5	1.2–2.4
Tailings (nonmagnetic)	2–10	45–50	0.8–3	0.7–1.2
Lead concentrates	20–25	60–80	0.5–1	
Molybdenum concentrates	10–35	50–60	0.2–0.4	
Nickel, (NH ₄) ₂ CO ₃ leach residue	15–25	45–60	0.3–0.5	
Nickel, acid leach residue	20	60	0.8	
Zinc concentrates	10–20	50–60	0.3–0.7	
Zinc leach residue	5–10	25–40	0.8–1.5	
Municipal waste				
Primary clarifier	0.02–0.05	0.5–1.5		1–1.7
Thickening				
Primary sludge	1–3	5–10	8	
Waste-activated sludge	0.2–1.5	2–3	33	
Anaerobically digested sludge	4–8	6–12	10	
Phosphate slimes	1–3	5–15	1.2–18	
Pickle liquor and rinse water	1–8	9–18	3.5–5	
Plating waste	2–5	5–30		1.2
Potash slimes	1–5	6–25	4–12	
Potato-processing waste	0.3–0.5	5–6		1
Pulp and paper				
Green-liquor clarifier	0.2	5		0.8
White-liquor clarifier	8	35–45	0.8–1.6	
Kraft waste	0.01–0.05	2–5		0.8–1.2
Deinking waste	0.01–0.05	4–7		1–1.2
Paper-mill waste	0.01–0.05	2–8		1.2–2.2
Sugarcane defecation			0.5‡	
Sugar-beet carbonation	2–5	15–20	0.03–0.07‡	
Uranium				
Acid-leached ore	10–30	25–65	0.02–1	
Alkaline-leached ore	20	60	1	
Uranium precipitate	1–2	10–25	5–12.5	
Water treatment				
Clarification (after 30-min flocculation)				1–1.3
Softening lime-soda (high-rate, solids-contact clarifiers)				3.7
Softening lime-sludge	5–10	20–45	0.6–2.5	

^o m³/(t/d) × 9.76 = ft³/(short ton/day); m³/(m²·h) × 0.41 = gal/(ft²·min); 1 t = 1 metric ton.

† High-rate thickeners using required flocculant dosages operate at 10 to 50 percent of these unit areas.

‡ Typical design using high Density/Paste thickeners. Feed per cent solids are that diluted for flocculation.

§ Basis: 1 t of cane or beets.

These are subject to fouling and sticking, and can be installed and measured only in the area above the rakes; however, they are relatively inexpensive.

- **Reeling devices** work by dropping a sensor down on a cable and sensing the bed level by optical or conductivity sensors. In theory they are nonfouling and get out of the way of the rakes, but in

practice, they frequently become entangled with the rakes. The price is mid-range. Freezing wind and cold temperatures can lead to icing problems.

- **Vibrating or tuning fork sensors** are designed to sense a difference in the vibrating frequency in different masses of solids. These are used in Europe and Africa.

- **Bubble tube or differential pressure** is an old, but tried and true, method of bed level detection. There may be some plugging or fouling of the tube over time.
- **External density** through sample ports. Slurry samples are taken from nozzles on the side of the tank and pass through a density meter to determine the presence of solids. This system can be set up with automated valves to measure several different sample points. This system requires external piping and disposal of the sample stream. Line pluggage is often a problem.

Bed Pressure Because thickeners maintain a constant liquid level, the pressure at the bottom of the thickener is an indication of the overall specific gravity in the tank. If the liquor specific gravity is constant, the overall specific gravity is an indication of the amount of solids in the tank and can be converted to a rough solids inventory. This can be a very effective tool for thickener control. Because of relative height-to-diameter ratios, it is considered less useful for large-diameter thickeners.

Differential pressure sensors are used to measure the bed pressure, leaving one leg open to the atmosphere to compensate for barometric pressure variations. Care must be taken in the installation to minimize the plugging with solids. This is normally done by tilting the tank nozzle on which the DP cell is mounted downward from the sensor, so the solids tend to settle away from the sensor surface. A shutoff valve and washer flush tap are recommended to allow easy maintenance.

Flow Rate Flow rates for feed and underflow lines are useful, particularly when combined with density measurements to generate solids mass flow rates. Since flocculant is usually dosed on a solids mass basis, knowing the mass flow rate is very useful for flocculant control, providing a fast response system. Flow rate measurement is an absolute necessity for the newer generation of ultrahigh-rate and ultrahigh-density thickeners. The streams being measured are usually slurries, and the flow rate is usually measured by either magnetic flowmeters or Doppler-type flowmeters. As long as these instruments are properly installed in suitable full straight pipe sections, avoiding air if possible, they are accurate and reliable. If the feed stream is in an open launder, flow measurement is more difficult but can be accomplished using ultrasonic devices.

Density Nuclear gauges are the norm for density measurement. Nuclear density instruments require nuclear handling permits in most countries. Note that there are now some types that use very low level sources that do not require nuclear licensing. Density gauges should be recalibrated regularly as they are subject to drifting. Small flow applications may be able to use a coriolis meter to measure both mass and percent solids with one instrument.

Settling Rate The settling rate in the feed well is a good indication of the degree of flocculation, and it can be used to maintain consistent flocculation over widely varying feed conditions. A settleometer is a device that automatically pulls a sample from the feed well and measures the settling rate. The flocculant can then be adjusted to maintain a constant settling rate.

Overflow Turbidity Overflow turbidity can be used to control flocculant or coagulant. There may be some significant lag time between the actual flocculation process and when the clarified liquor reaches the overflow discharge point where the sensor is typically positioned. These sensors and meters are generally used as alarms or for trim only.

Note: It is critical that all instruments be well maintained and serviced on a regular basis in order to get the best results.

CONTINUOUS COUNTERCURRENT DECANTATION

The system of separation of solid-phase material from an associated solution by repeated stages of dilution and gravity sedimentation is adapted for many industrial-processing applications through an operation known as continuous countercurrent decantation (CCD). The flow of solids proceeds in a direction countercurrent to the flow of solution diluent (water, usually), with each stage composed of a mixing step followed by settling of the solids from the suspension. The number of stages ranges from 2 to as many as 10, depending on the degree of separation required, the amount of wash fluid added

(which influences the final solute concentration in the first-stage overflow), and the underflow solids concentration attainable. Applications include processes in which the solution is the valuable component (as in alumina extraction), or in which purified solids are sought (magnesium hydroxide from seawater), or both (as frequently encountered in the chemical-processing industry and in base-metal hydrometallurgy).

The factors which may make CCD a preferred choice over other separation systems include the following: rapidly settling solids, assisted by flocculation; relatively high ratio of solids concentration between underflow and feed; moderately high wash ratios allowable (2 to 4 times the volume of liquor in the thickened underflows); large quantity of solids to be processed; and the presence of fine-size solids that are difficult to concentrate by other means. A technical feasibility and economic study is desirable in order to make the optimum choice.

Flow-Sheet Design Thickener-sizing tests, as described earlier, will determine unit areas, flocculant dosages, and underflow densities for the various stages. For most cases, unit areas will not vary significantly throughout the circuit; similarly, underflow concentrations should be relatively constant. In practice, the same unit area is generally used for all thickeners in the circuit to simplify construction. Serious consideration should be given to the design underflow density since operating at the higher, manageable densities will offer the benefits of improved wash efficiency. Many CCD installations, alumina in particular, have installed paste thickeners and reduced the number of stages or lowered the required volume of wash water.

Equipment The equipment selected for CCD circuits may consist of multiple-compartment washing-tray thickeners or a train of individual unit thickeners. The washing-tray thickener consists of a vertical array of coaxial trays connected in series, contained in a single tank. The advantages of this design are smaller floor-area requirements, less pumping equipment and piping, and reduced heat losses in circuits operating at elevated temperatures. However, operation is generally more difficult, and user preference has shifted toward ultrahigh-rate and ultrahigh-density thickeners.

Underflow Pumping Diaphragm pumps with open discharge are employed in some low-volume cases, primarily because underflow densities are readily controlled with these units. Disadvantages include the generally higher maintenance and initial costs than for other types and their inability to transfer the slurry any great distance. Large flows often are best handled with variable-speed, rubber-lined centrifugal pumps, utilizing automatic control to maintain the underflow rate and density.

Overflow Pumps These can be omitted if the thickeners are located at increasing elevations from first to last so that overflows are transferred by gravity or if the mixture of underflow and overflow is to be pumped. Overflow pumps are necessary, however, when maximum flexibility and control are sought.

Interstage Mixing Efficiencies Mixing or stage efficiencies rarely achieve the ideal 100 percent, in which solute concentrations in overflow and underflow liquor from each thickener are identical. Part of the deficiency is due to insufficient blending of the two streams, and attaining equilibrium will be hampered further by heavily flocculated solids. In systems in which flocculants are used, interstage efficiencies often will drop gradually from first to last thickener, and typical values will range from 98 percent to as low as 70 percent. In some cases, operators will add the flocculant to an overflow solution which is to be blended with the corresponding underflow. While this is very effective for good flocculation, it can result in reflocculation of the solids before the entrained liquor has had a chance to blend completely with the overflow liquor. The preferable procedure is to recycle a portion of the overflow back to the feed line of the same thickener, adding the reagent to this liquor.

The usual method of interstage mixing consists of a relatively simple arrangement in which the flows from preceding and succeeding stages are added to a feed box at the thickener periphery. A nominal detention time in this mixing tank of 30 to 60 s and sufficient energy input to avoid solids settling will ensure interstage efficiencies greater than 95 percent.

The performance of a CCD circuit can be estimated through use of the following equations, which assume 100 percent stage efficiency:

$$R = \frac{O/U[(O/U)^N - 1]}{[(O/U)^{N+1} - 1]} \quad (18-52)$$

$$R = 1 - \left(\frac{U}{O'}\right)^N \quad (18-53)$$

for O/U and $U/O' \neq 1$. R is the fraction of dissolved value in the feed which is recovered in the overflow liquor from the first thickener, O and U are the overflow and underflow liquor volumes per unit weight of underflow solids, and N is the number of stages. Equation (18-49) applies to a system in which the circuit receives dry solids with which the second-stage thickener overflow is mixed to extract the soluble component. In this instance, O' refers to the overflow volume from the thickeners following the first stage.

For more precise values, computer programs can be used to calculate soluble recovery as well as solution compositions for conditions that are typical of a CCD circuit, with varying underflow concentrations, stage efficiencies, and solution densities in each of the stages. The calculation sequence is easily performed by utilizing material-balance equations around each thickener.

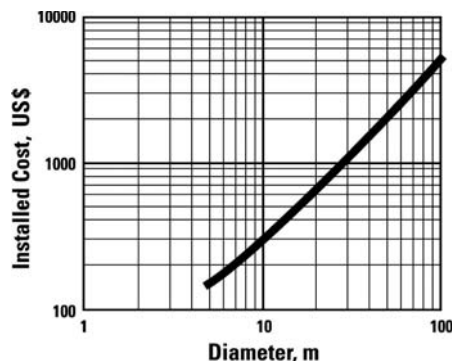


FIG. 18-106 Approximate installed cost of single-compartment thickeners (2005 US \$).

DESIGN SIZING CRITERIA

Table 18-7 has the typical design sizing criteria and operating conditions for a number of applications. It is presented for purposes of illustration or preliminary estimate. Actual thickening and classification performance is dependent on particle-size distribution, specific gravity, sludge bed compaction characteristics, and other factors. Final design should be based on bench scale tests.

THICKENER COSTS

Equipment Costs vary widely for a given diameter because of the many types of construction. As a general rule, the total installed cost will be about 3 to 4 times the cost of the raking mechanism (including drivehead and lift), plus walkways and bridge or centerpier cage, railings, and overflow launders. Figure 18-106 shows the approximate installed costs of thickeners up to 107 m (350 ft) in diameter. These costs are to be used only as a guide. They include the erection of mechanism and tank plus normal uncomplicated site preparation, excavation, reinforcing bar placement, backfill, and sur-

veying. The price does not include any electrical work, pumps, piping, instrumentation, walkways, or lifting mechanisms. Special design modifications, which are not in the price, could include elevated tanks (for underflow handling); special feedwell designs to control dilution, entrance velocity, and turbulence; electrical and drive enclosures required because of climatic conditions; and mechanism designs required because of scale buildup tendencies.

Operating Costs Power cost for a continuous thickener is an almost insignificant item. For example, a unit thickener 60 m (200 ft) in diameter with a torque rating of 1.0 MN·m (8.8 Mlbf·in) will normally require 12 kW (16 hp). The low power consumption is due to the very slow rotative speeds. Normally, a mechanism will be designed for a peripheral speed of about 9 m/min (0.5 ft/s), which corresponds to only 3 r/h for a 60-m (200-ft) unit. This low speed also means very low maintenance costs. Operating labor is low because little attention is normally required after initial operation has balanced the feed and underflow. If chemicals are required for flocculation, the chemical cost frequently dwarfs all other operating costs.

FILTRATION

GENERAL REFERENCES: Moir, *Chem. Eng.*, **89**(15), 46 (1982). Brown, *ibid.*, 58; also published as McGraw-Hill Repr. A078. Chermisinoff and Azbel, *Liquid Filtration*, Ann Arbor Science, Woburn, Mass., 1983. Orr (ed.), *Filtration: Principles and Practice*, part I, Marcel Dekker, New York, 1977; part II, 1979. Purchas (ed.), *Solid/Liquid Separation Equipment Scale-Up*, Uplands Press, Croydon, England, 1977. Schweitzer (ed.), *Handbook of Separation Techniques for Chemical Engineers*, part 4, McGraw-Hill, New York, 1979. Shoemaker (ed.), "What the Filter Man Needs to Know about Filtration," *Am. Inst. Chem. Eng. Symp. Ser.*, **73**(171), (1977). Talcott et al., in *Kirk-Othmer Encyclopedia of Chemical Technology*, 3d ed., vol. 10, Wiley, New York, 1980, p. 284. Tiller et al., *Chem. Eng.*, **81**(9), 116-136 (1974); also published as McGraw-Hill Repr. R203.

DEFINITIONS AND CLASSIFICATION

Filtration is the separation of a fluid-solids mixture involving passage of most of the fluid through a porous barrier which retains most of the solid particulates contained in the mixture. This subsection deals only with the filtration of solids from liquids; gas filtration is treated in Sec. 17. **Filtration** is the term for the unit operation. A filter is a piece of unit-operations

equipment by which filtration is performed. The **filter medium** or **septum** is the barrier that lets the liquid pass while retaining most of the solids; it may be a screen, cloth, paper, or bed of solids. The liquid that passes through the filter medium is called the **filtrate**.

Filtration and filters can be classified several ways:

1. **By driving force.** The filtrate is induced to flow through the filter medium by hydrostatic head (gravity), pressure applied upstream of the filter medium, vacuum or reduced pressure applied downstream of the filter medium, or centrifugal force across the medium. Centrifugal filtration is closely related to centrifugal sedimentation, and both are discussed later under "Centrifuges."

2. **By filtration mechanism.** Although the mechanism for separation and accumulation of solids is not clearly understood, two models are generally considered and are the basis for the application of theory to the filtration process. When solids are stopped at the surface of a filter medium and pile upon one another to form a cake of increasing thickness, the separation is called **cake filtration**. When solids are trapped within the pores or body of the medium, it is termed **depth, filter-medium, or clarifying filtration**.

3. *By objective.* The process goal of filtration may be dry solids (the cake is the product of value), clarified liquid (the filtrate is the product of value), or both. Good solids recovery is best obtained by cake filtration, while clarification of the liquid is accomplished by either depth or cake filtration.

4. *By operating cycle.* Filtration may be intermittent (batch) or continuous. Batch filters may be operated with constant-pressure driving force, at constant rate, or in cycles that are variable with respect to both pressure and rate. Batch cycle can vary greatly, depending on filter area and solids loading.

5. *By nature of the solids.* Cake filtration may involve an accumulation of solids that is compressible or substantially incompressible, corresponding roughly in filter-medium filtration to particles that are deformable and to those that are rigid. The particle or particle-aggregate size may be of the same order of magnitude as the minimum pore size of most filter media (1 to 10 μm and greater), or may be smaller (1 μm down to the dimension of bacteria and even large molecules). Most filtrations involve solids of the former size range; those of the latter range can be filtered, if at all, only by filter-medium-type filtration or by ultrafiltration unless they are converted to the former range by aggregation prior to filtration.

These methods of classification are not mutually exclusive. Thus filters usually are divided first into the two groups of cake and clarifying equipment, then into groups of machines using the same kind of driving force, then further into batch and continuous classes. This is the scheme of classification underlying the discussion of filters of this subsection. Within it, the other aspects of operating cycle, the nature of the solids, and additional factors (e.g., types and classification of filter media) will be treated explicitly or implicitly.

FILTRATION THEORY

While research has developed a significant and detailed filtration theory, it is still so difficult to define a given liquid-solid system that it is both faster and more accurate to determine filter requirements by performing small-scale tests. Filtration theory does, however, show how the test data can best be correlated, and extrapolated when necessary, for use in scale-up calculations.

In cake or surface filtration, there are two primary areas of consideration: continuous filtration, in which the resistance of the filter cake (deposited process solids) is very large with respect to that of the filter media and filtrate drainage, and batch pressure filtration, in which the resistance of the filter cake is not very large with respect to that of the filter media and filtrate drainage. Batch pressure filters are generally fitted with heavy, tight filter cloths plus a layer of precoat and these represent a significant resistance that must be taken into account. Continuous filters, except for precoats, use relatively open cloths that offer little resistance compared to that of the filter cake.

Simplified theory for both batch and continuous filtration is based on the time-honored Hagen-Poiseuille equation:

$$\frac{1}{A} \frac{dV}{d\Theta} = \frac{P}{\mu(\alpha wV/A + r)} \tag{18-54}$$

where *V* is the volume of filtrate collected, Θ is the filtration time, *A* is the filter area, *P* is the total pressure across the system, *w* is the weight of cake solids/unit volume of filtrate, μ is the filtrate viscosity, α is the cake-specific resistance, and *r* is the resistance of the filter cloth plus the drainage system.

CONTINUOUS FILTRATION

Since testing and scale-up are different for batch and continuous filtration, discussion in this section will be limited to continuous filtration.

It is both convenient and reasonable in continuous filtration, except for precoat filters, to assume that the resistance of the filter cloth plus filtrate drainage is negligible compared to the resistance of the filter cake and to assume that both pressure drop and specific cake resistance remain constant throughout the filter cycle. Equation (18-54), integrated under these conditions, may then be manipulated to give the following relationships:

$$W = \sqrt{\frac{2wP\Theta_f}{\mu(\alpha wV/A + r)}} \tag{18-55}$$

$$V_f = \sqrt{\frac{2P\Theta_f}{\mu\alpha w}} \tag{18-56}$$

$$\Theta_w = \frac{WV_w\mu\alpha}{P_w} \tag{18-57}$$

$$\Theta_w \propto NW^2 \tag{18-58}$$

$$\frac{\Theta_w}{\Theta_f} = 2 \frac{V_w}{V_f} \tag{18-59}$$

where *W* is the weight of dry filter cake solids/unit area, *V_f* is the volume of cake formation filtrate/unit area, *V_w* is the volume of cake wash filtrate/unit area, Θ_f is the cake formation time, Θ_w is the cake wash time, and *N* is the wash ratio, the volume of cake wash/volume of liquid in the discharged cake.

As long as the suspended solids concentration in the feed remains constant, these equations lead to the following convenient correlations:

$$\log W \text{ vs. } \log \Theta_f \tag{18-60}$$

$$\log V_f \text{ vs. } \log \Theta_f \tag{18-61}$$

$$\Theta_w \text{ vs. } WV_w \tag{18-62}$$

$$\Theta_w \text{ vs. } NW^2 \tag{18-63}$$

$$\Theta_{w/f} \text{ vs. } V_w/V_f \tag{18-64}$$

There are two other useful empirical correlations as follows:

$$W \text{ vs. cake thickness} \tag{18-65}$$

$$\log R \text{ vs. } N \tag{18-66}$$

where *R* is percent remaining—the percent of solute in the unwashed cake that remains after washing.

FACTORS INFLUENCING SMALL-SCALE TESTING

[Purchas (ed.), *Solid/Liquid Separation Equipment Scale-Up*, Uplands Press, Croydon, England, 1977.]

Vacuum or Pressure The vast majority of all continuous filters use vacuum to provide the driving force for filtration. However, if the feed slurry contains a highly volatile liquid phase, or if it is hot, saturated, and/or near the atmospheric pressure boiling point, the use of pressure for the driving force may be required. Pressure filtration might also be used where the required cake moisture content is lower than that obtainable with vacuum.

The objective of most continuous filters is to produce a dry or handleable cake. Most vacuum filters easily discharge a “dry” consolidated cake as they are usually operated in an open or semiopen environment. However, whenever the filter must operate under pressure or within a vapor-tight enclosure, either because of the need for a greater driving force or because of the vapor pressure of the liquid phase, a dry cake discharge becomes difficult. The problem of removing a dry cake from a pressurized enclosure has precluded the use of continuous-pressure filters in many cases where this is a requirement. Applications which do discharge dry cake from a “sealed” enclosure are restricted to relatively dry, friable cakes that will “flow” through double valves which form a “vapor lock.”

Cake Discharge For any filter application to be practical, it must be possible to produce a cake thick enough to discharge. Table 18-8 tabulates the minimum acceptable cake thickness required for discharge for various types of filters and discharge mechanisms. The experimenter, when running small-scale tests, should decide early in the test program which type of discharge is applicable and then tailor the data collected to fit the physical requirements of that type of unit. Note, however, that the data correlations recommended later are sufficiently general in nature to apply to most equipment types.

TABLE 18-8 Minimum Cake Thickness for Discharge

Filter type	Minimum design thickness	
	mm	in
Drum		
Belt	3-5	$\frac{1}{8}$ - $\frac{3}{16}$
Roll discharge	1	$\frac{1}{32}$
Std. scraper	6	$\frac{1}{4}$
Coil	3-5	$\frac{1}{8}$ - $\frac{3}{16}$
String discharge	6	$\frac{1}{4}$
Precoat	0-3 max.	0- $\frac{1}{8}$ max.
Horizontal belt	3-5	$\frac{1}{8}$ - $\frac{3}{16}$
Horizontal table	20	$\frac{3}{4}$
Tilting pan	20-25	$\frac{3}{4}$ -1
Disc	10-13	$\frac{3}{8}$ - $\frac{1}{2}$

Feed Slurry Temperature Temperature can be both an aid and a limitation. As temperature of the feed slurry is increased, the viscosity of the liquid phase is decreased, causing an increase in filtration rate and a decrease in cake moisture content. The limit to the benefits of increased temperature occurs when the vapor pressure of the liquid phase starts to materially reduce the allowable vacuum. If the liquid phase is permitted to flash within the filter internals, various undesired results may ensue: disruption in cake formation adjacent to the medium, scale deposit on the filter internals, a sharp rise in pressure drop within the filter drainage passages due to increased vapor flow, or decreased vacuum pump capacity. In most cases, the vacuum system should be designed so that the liquid phase does not boil.

In some special cases, steam filtration can be used to gain the advantages of temperature without having to heat the feed slurry. Where applicable, dry steam is passed through the deliquored cake to raise the temperature of the residual moisture, reduce its viscosity, and lower its content. The final drying or cooling period which follows steam filtration uses the residual heat left in the cake to evaporate some additional moisture.

Cake Thickness Control Sometimes the rate of cake formation with bottom feed-type filters is rapid enough to create a cake too thick for subsequent operations. Cake thickness may be controlled by adjusting the bridge-blocks in the filter valve to decrease the effective submergence, by reducing the slurry level in the vat, and by reducing the vacuum level in the cake formation portion of the filter valve. If these measures are inadequate, it may be necessary to use a top-loading filter.

Cake thickness must frequently be restricted when cake washing is required or the final cake moisture content is critical. Where the time required for cake washing is the rate-controlling step in the filter cycle, maximum filtration rate will be obtained when using the minimum cake thickness that gives good cake discharge. Where minimum cake moisture content is the controlling factor, there is usually some leeway with respect to cake thickness, although the minimum required for cake discharge is controlling in some cases. Since a relatively constant quantity of moisture is transferred from the medium to the filter cake when the vacuum is released prior to cake discharge, very thin cakes will sometimes be wetter than thicker cakes.

The effect of an increase in cake thickness on the time required for washing is easy to see if one considers what happens when the cake thickness is doubled. Assume that two cakes have the same permeability and that the quantity of washing fluid to cake solids is to remain constant. Doubling of the cake thickness doubles the resistance to flow of the washing fluid through the cake. At the same time, the quantity of washing fluid per unit area is also doubled. Thus, the time required for the washing fluid to pass through the cake is increased by the square of the ratio of the cake thicknesses. In this particular example, the washing time would be increased by a factor of four, while cake production would only be doubled.

Filter Cycle Each filter cycle is composed of cake formation plus one or more of the following operations: deliquoring (dewatering or drying), washing, thermal drying, steam drying, and cake discharge. The number of these operations required by a given filtration operation depends upon the process flowsheet. It is neither possible nor necessary to consider all of these operations at once. The basic testing program is designed to look at each operation individually. The requirements for each of the steps are then fit into a single filter cycle.

All filters utilizing a rotary filter valve have their areas divided into a number of sections, sectors, or segments (see Fig. 18-134). When a drainage port passes from one portion of the filter valve to another, the change at the filter medium does not occur instantaneously nor does it occur at some precise location on the filter surface. The change is relatively gradual and occurs over an area, as the drainage port at the filter valve first closes by passing onto a stationary bridge-block and then opens as it passes off that bridge-block on the other side.

On a horizontal belt filter, the equivalent sections extend across the filter in narrow strips. Therefore, changes in vacuum do occur rapidly and may be considered as happening at a particular point along the length of the filter.

Representative Samples The results which are obtained in any bench-scale testing program can be only as good as the sample which is tested. It is absolutely essential that the sample used be representative of the slurry in the full-scale plant and that it be tested under the conditions that prevail in the process. If there is to be some significant time between taking or producing the sample and commencing the test program, due consideration must be given to what effect this time lapse may have on the characteristics of the slurry. If the slurry is at a temperature different from ambient, the subsequent heating and/or cooling could change the particle size distribution. Even sample age itself may exert a significant influence on particle size. If there is likely to be an effect, the bench-scale testing program should be carried out at the plant or laboratory site on fresh material.

Whenever a sample is to be held for some time or shipped to a distant laboratory for testing, some type of characterizing filtration test should be run on the fresh sample and then duplicated at the time of the test program. A comparison of the results of the two tests will indicate how much of a change there has been in the sample. If the change is too great, there would be no point in proceeding with the tests, and it would be necessary to make arrangements to work on a fresh sample. Any shipped sample, especially during the winter months, must be protected from freezing, as freezing can substantially change the filtration characteristics of a slurry, particularly hydrated materials.

The slurry should always be defined as completely as possible by noting suspended solids concentration, particle size distribution, viscosity, density of solids and liquid, temperature, chemical composition, and so on.

Feed Solids Concentration Feed slurries that are so dilute that they settle rapidly usually yield reduced solids filtration rates and produce stratified cakes with higher moisture contents than would normally be obtained with a homogeneous cake. It is well known that an increase in feed solids concentration is generally an effective means of increasing solids filtration rate, assisting in forming a homogeneous suspension and thereby minimizing cake moisture content, and so on. Equipment required to concentrate a slurry sample and the tests needed to predict how far a slurry will thicken are discussed elsewhere in this section.

Pretreatment Chemicals Even though the suspended solids concentration of the slurry to be tested may be correct, it is frequently necessary to modify the slurry in order to provide an acceptable filtration rate, washing rate, or final cake moisture content. The most common treatment, and one which may provide improvement in all three of these categories, is the addition of flocculating agents, either inorganic chemicals or natural or synthetic polymers. The main task at this point is to determine which is the most effective chemical and the quantity of chemical which should be used.

It is usually difficult to observe visually a change in floc structure in a concentrated slurry. The two best indications that an effective quantity of chemical has been added is a sudden thickening or increase in viscosity of the slurry and the formation of *riverlets* on the surface of a spatula when treated slurry is shaken from it. It is generally necessary to exceed a threshold quantity of chemical before there is a measurable improvement. The proper dosage becomes an economic balance between the cost of additional chemicals and the savings resulting from a reduction in filter area.

Screening tests are used to determine the best chemical and its approximate dosage. It is usually convenient to use small, graduated beakers and sample quantities in the range of 50 to 150 mL. The chemical may be added with a syringe or medicine dropper and a note made of the quantity used, together with the results. The experimenter should filter and wash the flocculated sample on any convenient, small,

top-loading filter with good filtrate drainage. The cake formation and wash times obtained from these micro tests are not intended to provide sizing data, but they do provide an excellent indication of the relative effectiveness of various chemicals and treatment levels.

With any chemical treatment system, the main task is one of getting the chemical thoroughly mixed with the solids without degrading the flocs which are formed. For those slurries that are relatively fluid, the chemical can frequently be added and mixed satisfactorily using a relatively wide spatula. However, for those thick, relatively viscous slurries, a power mixer will be required. In this case, the mixer should be stopped about one second after the last of the flocculant is added. Should this approach be required, it means that a suitably designed addition system must be supplied with the full-scale installation in order to do an effective job of flocculation.

While the volume of chemical used should be minimized, the experimenter must use good judgment based on the viscosities of both the slurry to be treated and the chemical used. If both are relatively viscous, use of a power mixer is indicated.

There are a number of commercially available surfactants that can be employed as an aid in filter cake moisture reduction. These reagents can be added to the filter feed slurry or to the filter cake wash water, if washing is used. Since these reagents have a dispersing effect, flocculation may be required subsequently. Typical moisture reductions of 2 to 4 percentage points are obtained at reagent dosages of 200 to 500 g/m² of solids.

Cloth Blinding Continuous filters, except for precoat, generally use some type of medium to effect the separation of the solid and filtrate phases. Since the medium is in contact with the process solids, there is always the danger, and almost invariably the actual occurrence, of medium blinding. The term **blinding** refers to blockage of the fabric itself, either by the wedging of process solids or by solids precipitated in and around the yarn.

The filter medium chosen should be as open as possible yet still able to maintain the required filtrate clarity. Those fabrics which will produce a clear filtrate and yet do not have rapid blinding tendencies are frequently light in weight (woven from thin filaments or yarn) and will not wear as long as some of the heavier, more open fabrics (woven from heavy filaments or yarn). Whenever the filter follows a gravity thickening or clarification step, it is advisable to return the filtrate to the thickener or clarifier so that the filtrate clarity requirements may be relaxed in favor of using a heavier, more open cloth with reduced blinding tendencies. Excessively dirty filtrates should be avoided as the solids may be abrasive and detrimental to the internals of the filter or perhaps may cut the fabric yarn.

It should be noted at this point that an **absolutely** clear filtrate can rarely be obtained on a cloth-covered continuous filter. The passages through the medium are invariably larger than some of the solids in the slurry, and there will be some amount of solids passing through the medium. Once the pores of the fabric have been bridged, the solids themselves form the septum for the remaining particles, and the filtrate becomes clear. It is this bridging action of the solids that permits the use of a relatively open filter medium, while at the same time maintaining a reasonably clear filtrate.

Filters with media in the form of an endless belt have greatly reduced the concern about blinding. Most synthetic fabrics can be successfully cleaned of process solids by washing the medium after cake discharge, and the rate of blinding due to chemical precipitation also can be drastically reduced. Current practice suggests that the belt-type filter with continuous-medium washing be the first choice unless experience has shown that medium blinding is not a factor or if the belt-type system cannot be successfully applied.

Sealing of the belt along the edges of the filter drum is never perfect, and some leakage should be expected. If good clarity is essential, it may be preferable to use a drum filter with the cloth caulked in place and design the system to contend with the effects of blinding.

The one exception to the points noted above is the continuous precoat filter. Here the purpose of the filter medium is to act as a support for the sacrificial bed of precoat material. Thus, the medium should be tight enough to retain the precoat solids and prevent bleeding of the precoat solids through the filter medium during operation, yet open enough to permit easy cleaning at the end of each cycle. Light-weight felt media work well in these respects.

Homogeneous Cake Accurate test results and optimum filter performance require the formation of a homogeneous cake and thus the maintenance of a similarly homogeneous suspension. Settling in the sample container during a bottom-feed test program can usually be detected by comparing the back-calculated feed solids concentration (based on filtrate, wet cake, and dry cake weights) with the slurry solids concentration as prepared. It is normal to find that the back-calculated concentration is slightly lower than the prepared concentration. This difference is normally within 2 percentage points and should never be greater than 5 percentage points. Since this difference does exist, it means that the slurry sample will concentrate to some extent as the tests continue. Adding fresh slurry to the sample container after each test can counteract this condition, as the system will reach an equilibrium similar to that found in a full-scale machine.

If a more positive check is required on the quality of the filter cake, particle size analyses may be run and compared with the sample as prepared.

In a top-feed filter test, the filter cake will contain all of the solids, provided they are all emptied from the sample container. The danger in this type of test is that the solids will stratify, particularly if the cake formation time is prolonged. Close examination of the filter cake will indicate whether or not this has happened. If there has been significant stratification, the feed slurry should be modified by thickening and/or flocculation in order to increase the dry solids filtration rate and permit formation of a homogeneous cake. Another possibility, but not necessarily the best, is to use a thinner, but still dischargeable, cake to avoid stratification.

Agitation of Sample All slurries used in bottom-feed tests must be agitated by hand (if slurry characteristics permit) to check whether or not the solids are settling out around the edges of the container and to determine the degree of agitation required to maintain the solids in suspension. Generally speaking, if the solids can be maintained in suspension by hand agitation, the slurry can be processed by a bottom-feed-type filter.

Agitation by a wide spatula may be substituted for hand agitation, but only after it has been determined by feel that the spatula will provide the needed agitation. If this cannot be done, then confirmation of proper agitation must be based on back-calculated feed solids concentrations and/or particle size analyses of the filter cakes.

If it is not possible to maintain a uniform suspension, the sample should be thickened and the flowsheet modified to provide the required thickening.

Mechanical agitation of a sample is very difficult to use effectively. Generally speaking, if enough room is left in the sample container for the leaf and the agitator, the agitation is not sufficient to prevent settling out in the corners of the container. If sufficient agitation is used to maintain suspension in all parts of the container, then it is highly probable that the velocity of the slurry across the face of the test leaf will wash the solids from the leaf and give very erroneous results. Furthermore, the tendency is to leave the agitator running continuously, or at least for so long a period of time that there is attrition of the solids and, therefore, inaccurate results. Mechanical agitation during testing can generally be justified only in a most unusual and exceptional circumstance.

Use of Steam or Hot Air It was indicated earlier that the cycle might include steam filtration or thermal drying using hot air. While effective use is made of both steam and hot air, the applications are rather limited, and testing procedures are difficult and specialized. As a general rule, steam application will reduce cake moisture 2 to 4 percentage points. Hot-air drying can produce a bone-dry cake, but generally it is practical only if the air rate is high, greater than about 1800 m³/m²-h (98 cfm/ft²). Both systems require a suitable hood which must contact the dam on the leaf during the drying cycle, allowing the steam or hot air to pass through the cake without dilution by cold air. The end of the operation can be determined by a noticeable increase in the temperature of the gas leaving the leaf.

SMALL-SCALE TEST PROCEDURES

[Purchas (ed.), *Solid/Liquid Separation Equipment Scale-Up*, Uplands Press, Croydon, England, 1977.]

Apparatus There are several variations of the bench-scale test leaf that may be used, but they all have features similar to the one discussed below.

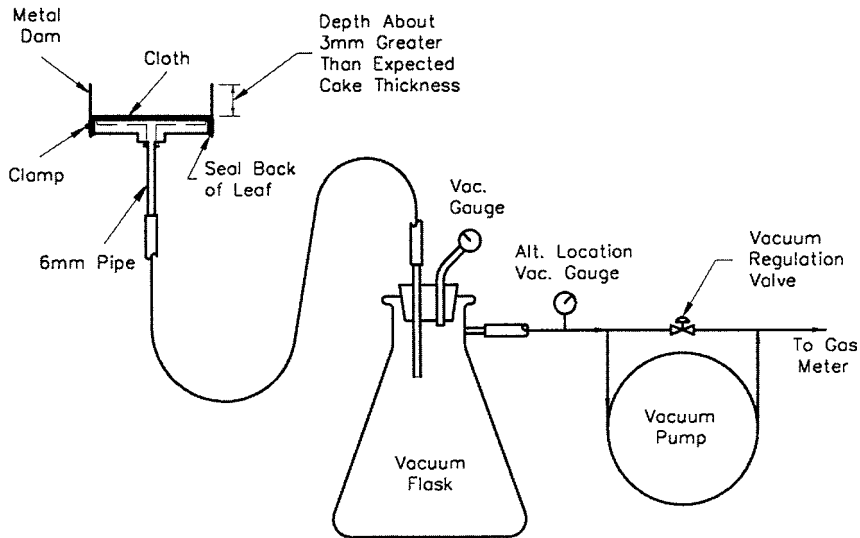


FIG. 18-107 Typical bottom-feed leaf test setup.

One typical test leaf is a circular disc with a plane area of 92.9 cm^2 (0.1 ft^2). One face of the leaf is grooved to provide large filtrate drainage passages and a support for the filter medium. A threaded drainage connection is provided on the center of the other face of the leaf. The test leaf is fitted with a filter medium and a dam, and the assembly clamped together as shown in Fig. 18-107. The depth of the dam for bottom-feed tests should be no greater than the depth of the maximum cake thickness, except where cake washing tests are to be performed. In this case, the dam depth should be about 3 mm ($\frac{1}{8}$ in) greater than the maximum expected cake thickness. Excessive dam depth will interfere with slurry agitation and can result in the formation of a nonhomogeneous cake.

It is absolutely necessary that a dam be used in all cases, except for roll discharge applications which do not involve cake washing or

where the maximum cake thickness is on the order of 2 mm or less. If a dam is not used, filter cake will form past the edge of the leaf in the general shape of a mushroom. When this happens, the total filter area is some unknown value, greater than the area of the leaf, that constantly increases with time during cake formation.

The back of the leaf assembly and the joint where the dam overlaps must be sealed with some suitable material so that the filtrate volume collected accurately represents the liquid associated with the deposited cake solids.

Figure 18-108 also contains a schematic layout of the equipment which is required for all bottom-feed leaf tests. Note that there are no valves in the drainage line between the test leaf and the filtrate receiver, nor between the filtrate receiver and the vacuum pump.

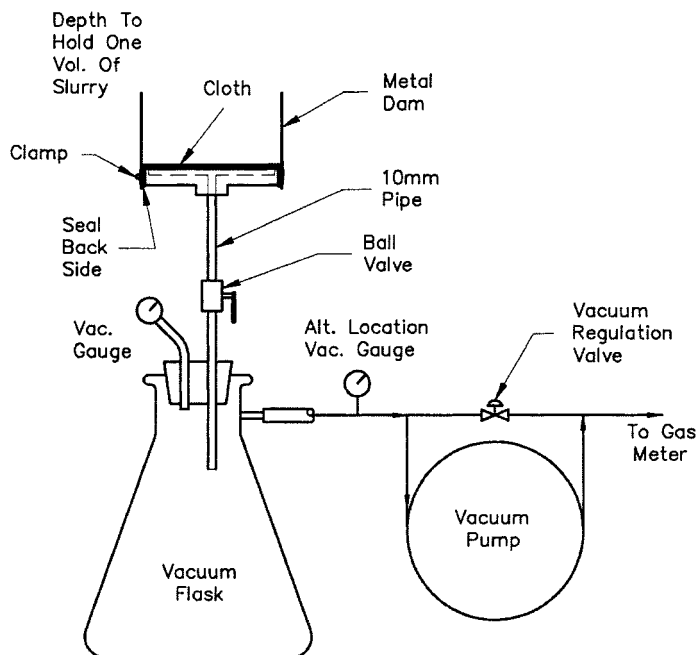


FIG. 18-108 Typical top-feed leaf test setup.

At the start of the leaf test run, the hose between the test leaf and filtrate receiver should be crimped by hand to bring the filtrate receiver to the operating vacuum level. The use of a valve at this point is not only less convenient but very frequently results in a hydraulic restriction. The net result, then, is a measurement of flow through the valve rather than the rate at which the filter cake is capable of forming. Hydraulic restriction is something which should always be kept in mind. If the filtrate runs at a high and full pipe flow rate into the filtrate receiver, it is quite likely that there is some degree of hydraulic restriction, and larger tubing and piping should be considered. When very high air flow rates are obtained, the experimenter must be satisfied that the rates being measured are limited by cake resistance and not by pressure drop through the equipment.

There will be many times when the quantity of sample is limited. While it is best to use the 92.9 cm² (0.1 ft²) area leaf in order to minimize edge effects and improve accuracy, when the sample volume is limited it is much better to have several data points with a smaller leaf than only one or two using the larger leaf. Data from leaves as small as 23.2 cm² (0.025 ft²) are reasonably accurate and can be used to scale up to commercially sized units. However, it is usually prudent to employ a more conservative scale-up factor.

For top-feed applications, the most convenient assembly is that shown in Fig. 18-108. The depth of the dam must, of course, be suffi-

cient to contain the total quantity of feed slurry required for the test. Since the test leaf is mounted on top of the vacuum receiver, it is necessary to provide a valve between the test leaf and the receiver so that the desired operating vacuum may be obtained in the receiver before the start of a test run. It is imperative, however, that there be no restriction in this valve. The preferred choice is a ball valve with the full bore of the drainage piping.

Test Program Figure 18-109 is a suggested data sheet which contains spaces for most of the information which should be taken during a leaf test program, together with space for certain calculated values. Additional data which may be required include variations in air flow rate through the cake during each dewatering period and chemical and physical data for those tests involving cake washing.

It is difficult to plan a filtration leaf test program until one test has been run. In the case of a bottom-feed test, the first run is normally started with the intention of using a 30-s cake formation time. However, if the filtrate rate is very high, it is usually wise to terminate the run at the end of 15 s. Should the filtrate rate be very low, the initial form period should be extended to at least 1 min. If cake washing is to be employed, it is useful to apply a quantity of wash water to measure its rate of passage through the cake. The results of this first run will give the experimenter an approximation of cake formation rate, cake washing rate, and the type of cake discharge that must be used. The

FILTRATION LEAF TEST DATA SHEET – VACUUM AND PRESSURE

Company _____ Mat'l as Received: Date _____ Test No. _____
 Address _____ Solids: _____ % Date Tested _____
 _____ Analysis _____ By _____
 _____ Liquid: _____ % Location _____
 Filter Type _____ Leaf Size _____ Ft.² Analysis _____
 Used Shim: No _____ Yes _____ Precoat Forming Liquid _____ Temp. _____ °F/°C

Run No.	Filter Module and/or Precoat Type	Feed Temp., °F/°C	% Solids in Food		Vacuum = in. Hg. Pressure = PSI.			TIME, MIN.				Air Flow (1)	Filtrate		Precoat Penetration	Wash		Cake/Precoat Thickness, In.	Dia. of Shared Area, In.	Cake Weights			Dish No.		
			As Prepared	Back Calculated	Form	Wash	Dry	After Cake Cracks	Form	Dewater	Wash	Dry	To Crack or Gas Breakthrough After Form/Wash	Temp., °F/°C		ML.	Clarity			ML.	Temp., °F/°C	Tare GMS.		Wet & Tare GMS.	Dry & Tare GMS.

CAKE DISCHARGE		REAGENT TREATMENT	
RUNS	COMMENT	RUNS	COMMENT

REMARKS: (1) Record Basis of Observation in Space Provided.

FIG. 18-109 Sample data sheet.

rest of the leaf test program can then be planned accordingly.

In any leaf test program there is always a question as to what vacuum level should be used. With very porous materials, a vacuum in the range of 0.1 to 0.3 bar (3 to 9 in Hg) should be used, and, except for thermal-drying applications using hot air, the vacuum level should be adjusted to give an air rate in the range of 450 to 900 m³/m²·h (30 to 40 cfm/ft²) measured at the vacuum.

For materials of moderate to low porosity, a good starting vacuum level is 0.6 to 0.7 bar (18 to 21 in Hg), as the capacity of most vacuum pumps starts to fall off rapidly at vacuum levels higher than 0.67 bar (20 in Hg). Unless there is a critical moisture content which requires the use of higher vacuums, or unless the deposited cake is so impervious that the air rate is extremely low, process economics will favor operation at vacuums below this level. When test work is carried out at an elevation above sea level different than that of the plant, the elevation at the plant should be taken into account when determining the vacuum system capacity for high vacuum levels (>0.5 bar).

Generalized correlations are available for each of the operations which make up the full filter cycle. This means that simulated operating conditions can be varied to obtain a maximum of information without requiring an excessive number of test runs. The minimum number of test runs required for a given feed will, of course, vary with the expertise of the experimenter and the number of operations performed during the filter cycle. If, for example, the operation involves only the dewatering of a slurry which forms a cake of relatively low to moderate porosity, frequently sufficient data can be obtained in as little as six runs. For more difficult tests, more runs are usually advisable, and the novice certainly should make a larger number of runs as there is likely to be more data scatter.

Bottom-Feed Test Procedure The procedure for collecting data using bottom-feed leaf test techniques is as follows:

1. Fit the test leaf with a filter cloth expected to give reasonable results and seal the back of the leaf and side of the dam with silicone or other suitable material.

2. Hand-crimp the hose in back of the test leaf, and then turn on the vacuum pump and regulate the bypass valve on the pump to give the desired vacuum level in the receiver.

3. Agitate the slurry by hand or with a wide spatula to maintain a homogeneous suspension. Immerse the test leaf face downward to approximately one-half the depth of the slurry.

4. Simultaneously start the timer and release the crimped hose to begin cake formation. Maintain agitation during cake formation and move the leaf as may be required to ensure that solids do not settle out in any part of the container. It is not necessary to try to simulate the velocity with which the full-scale unit's filtration surface passes through the slurry in the filter tank.

5. Remove the leaf from the slurry at the end of the cake-formation period and note the time. If the slurry is particularly thick and viscous, the leaf may be gently shaken to remove excess slurry and prevent the dam from scooping up extra material. Maintain the leaf in an upright position (cake surface on top) and elevated so that liquid within the drainage passages may pass to the receiver. Tilt and rotate the leaf to help the filtrate reach the drain outlet. Continue this dewatering period until:
 - a. the preselected time has elapsed, or
 - b. the cake cracks.

6. If the cake is to be washed, apply a measured quantity of wash fluid and note the time required for free fluid to disappear from the surface of the cake. Pour the wash fluid onto a deflecting baffle, such as a bent spatula, to prevent the cake from being gouged. Washing must begin before cake cracking occurs. In particular, observe that there is no crack along the edge between the cake and the dam.

7. Continue with the various operations in the predetermined sequence.

8. During each of the operations record all pertinent information such as vacuum level, temperature, time required for the cake to crack, filtrate foaming characteristics, air flow rate during the drying periods, etc.

9. At the end of the run, measure and record the filtrate volume (and weight, if appropriate), cake thickness, final cake temperature (if appropriate), wet cake weight, and note the cake discharge characteristics (roll, sticks to media, etc.).

10. For runs involving cake dewatering only, it is usually convenient to dry the total cake sample, if the associated solution contains little or no dissolved solids.

11. When cake washing is involved, it is usually convenient to weigh the wet cake and then repulp it in a known quantity of distilled water or in water at the same pH as the filtrate, if precipitation of solute could occur in distilled water. The resultant slurry is then filtered using a clean dry filter and flask and a sample of the clear liquid analyzed for the reference constituent.

Should the mother liquor contain a significant quantity of dissolved solids, the filter cake should be thoroughly washed (after the sample for analysis has been taken) so that the final dry weight of the cake will represent suspended solids only. The quantity of reference constituent in the final washed cake can be readily calculated from the wet and dry cake weights and the known amount of distilled water used for repulping.

In cake-washing tests, it is important that the feed slurry liquid be analyzed for total dissolved solids and density as well as the reference constituent.

Top-Feed Test Procedure The sequence of operations with a top-feed leaf test is the same as in a bottom-feed test, except that the leaf is not immersed in the slurry. The best method for transferring the slurry to the top-feed leaf is, of course, a function of the characteristics of the slurry. If the particles in the slurry do not settle rapidly, the feed can usually be transferred to the leaf from a beaker. If, however, the particles settle very rapidly, it is virtually impossible to pour the slurry out of a beaker satisfactorily. In this case, the best method is to make use of an Erlenmeyer flask, preferably one made of plastic. The slurry is swirled in the flask until it is completely suspended and then abruptly inverted over the leaf. This technique will ensure that all of the solids are transferred to the leaf.

When the solids involved are coarse and fast settling, the vacuum should be applied an instant after the slurry reaches the surface of the filter medium.

Precoat Test Procedure Precoat filtration tests are run in exactly the same manner as bottom-feed tests except that the leaf must first be precoated with a bed of diatomaceous earth, perlite, or other shaveable inert solids. Some trial and error is involved in selecting a grade of precoat material which will retain the filtered solids to be removed on the surface of the bed without any significant penetration. During this selection process, relatively thin precoat beds of 1 to 2 cm are satisfactory. After a grade has been selected, bench-scale tests should be run using precoat beds of the same thickness as expected on the full-scale unit.

Where the resistance of the precoat bed is significant in comparison to the resistance of the deposited solids, the thickness of the precoat bed effectively controls the filtration rate. In some instances, the resistance of the deposited solids is very large with respect to even a thick precoat bed. In this case, variations in thickness through the life of the precoat bed have relatively little effect on filtration rate. This type of information readily becomes apparent when the filtration rate data are correlated.

The depth of cut involved in precoat filtration is a very important economic factor. There is some disagreement as to the method required to accurately predict the minimum permissible depth of cut. Some investigators maintain that the depth of cut can be evaluated only in a qualitative manner during bench-scale tests by judging whether the process solids remain on the surface of the precoat bed. This being so, they indicate that it is necessary to run a continuous pilot-plant test to determine the minimum permissible depth of cut. The use of a continuous pilot-plant filter is a very desirable approach and will provide accurate information under a variety of operating conditions.

However, it is not always possible to run a pilot-plant test in order to determine the depth of cut. A well-accepted alternative approach makes use of the more sophisticated test leaf illustrated in Fig. 18-110. This test leaf is designed so that the cake and precoat are extruded axially out the open end of the leaf. The top of the retaining wall on this end of the leaf is a machined surface which serves as a support for a sharp discharge knife. This approach permits variable and known depths of cut to be made so that the minimum depth of cut may be determined. Test units are available from Betts Advanced Metal, hompoc, Calif., (805) 735-5130.

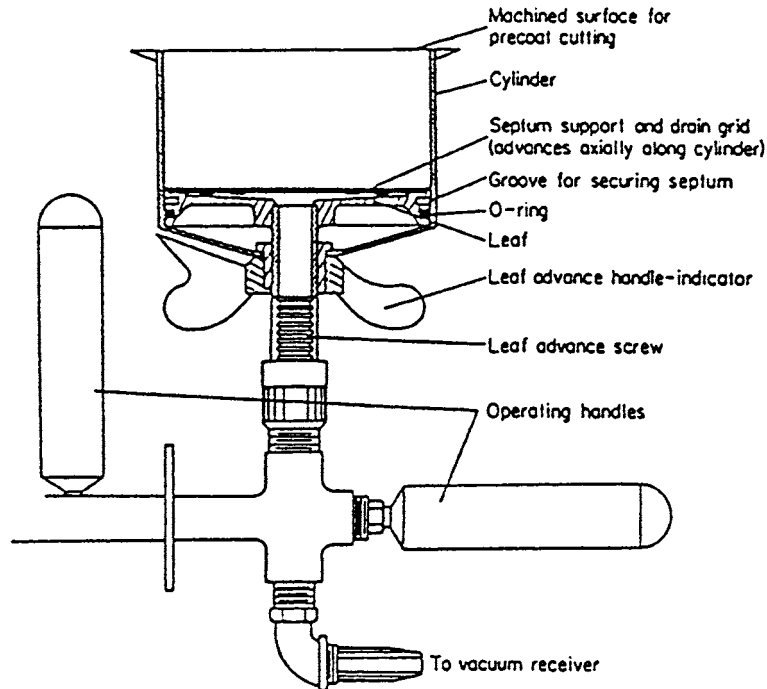


FIG. 18-110 Special test leaf for precoat filtration.

Lacking the above-described actual data, it is possible to estimate precoat consumption by using these values: nonpenetrating solids, 0.06-mm cut/drum revolution (0.0024 in); visible penetration, 0.15- to 0.20-mm cut/drum revolution (0.006 to 0.008 in); precoat bed density, 4.2 kg/m²-cm of bed depth (2.2 lb/ft²-in) for diatomaceous earth or 2.1 to 3.0 kg/m²-cm (1.1 to 1.6 lb/ft²-in) for perlite.

DATA CORRELATION

[Purchas (ed.), *Solid/Liquid Separation Equipment Scale-Up*, Uplands Press, Croydon, England, 1977.]

The correlations used are based partly on theoretical consideration and partly on empirical observations. The basic filtration data are correlated by application of the classic cake-filtration equation, aided by various simplifying assumptions which are sufficiently valid for many (but not all) situations. Washing and drying correlations are of a more empirical nature but with strong experimental justification. If steam or thermal drying is being examined, additional correlations are required beyond those summarized below; for such applications, it is advisable to consult an equipment manufacturer or refer to published technical papers for guidance.

Dry Cake Weight vs. Thickness It is convenient to convert the test dry cake weight to the weight of dry cake per unit area per cycle (*W*), and plot these values as a function of cake thickness (Fig. 18-111). Cake weight is measured quite accurately, while cake thickness measurements are subject to some variation. By plotting the data, variations in thickness measurements are averaged. The data usually give a straight line passing through the origin. However, with compressible material, sometimes a slightly curved line best represents the data, since thinner cakes are usually compressed more than thicker cakes.

Dry Solids or Filtrate Rate Filtration rate, expressed either in terms of dry solids or filtrate volume, may be plotted as a function of time on log-log paper. However, it is more convenient to delay the rate calculation until the complete cycle of operations has been defined.

It is most useful to plot either dry cake weight (weight of dry solids/unit area/cycle) or filtrate volume (volume/unit area/cycle) as a function of time on log-log paper. These data should give straight-line plots for constant operating conditions in accordance with Eqs. (18-55) and (18-56). The expected slope of the resultant rate/time plots is +0.50, as in Fig. 18-112. In practice, the vast majority of slopes range from +0.50 to +0.35. Slopes steeper than +0.5 indicate that there is some significant resistance other than that of the cake solids,

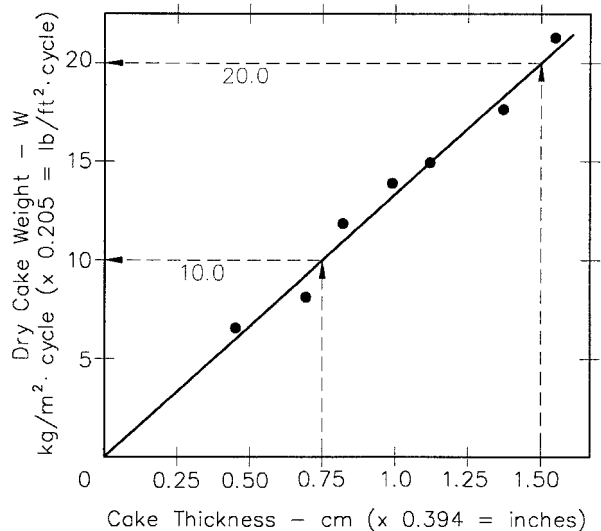


FIG. 18-111 Dry cake weight vs. cake thickness.

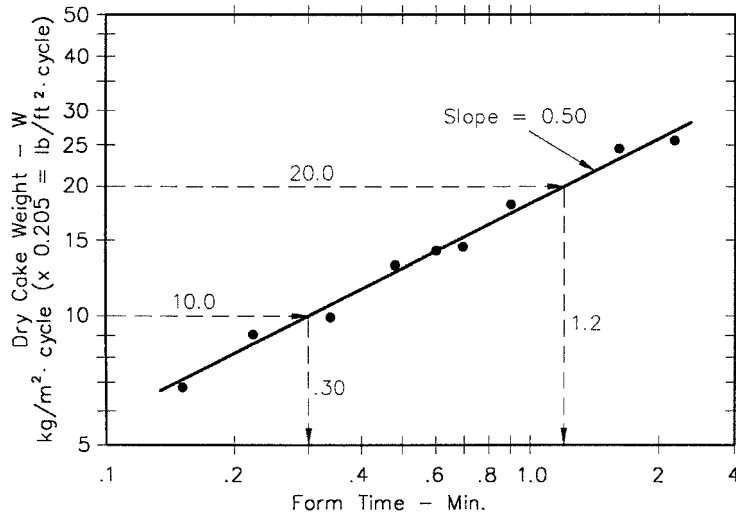


FIG. 18-112 Dry cake weight vs. form time.

such as a hydraulic restriction in the equipment or an exceptionally tight filter cloth.

Data from precoat tests, however, generally produce filtrate curves with much steeper slopes. The precoat bed has a greater resistance than most filter fabrics, and the particles which are separated on a continuous precoat usually form a cake which has a relatively low resistance when compared to that of the precoat bed. Once the thickness of the deposited solids becomes significant, their resistance increases. Thus, at very short form times, the slope of the filtrate curve may be close to 1.0, but as form time increases, the slope of the curve will decrease and will approach +0.5 (Fig. 18-113).

There are some solids, however, which form a less permeable cake, even in very thin layers. With these solids, the resistance of the

deposited cake will be very high when compared to that of the precoat bed, and the slope of the filtrate curve will be +0.5 for all values of form time.

Effect of Time on Flocculated Slurries Flocculated slurries usually show significant decreases in filterability with time (Fig. 18-114). The rate of degradation may be established by running a series of repetitive leaf tests at frequent intervals on a flocculated slurry, starting as soon as practical after the addition of the flocculant. If there is little change in the filtration rate, this factor need be given no more consideration. However, it is usually found that there is significant degradation.

When a flocculated feed is added to a filter tank, there is a definite time lag before this material reaches the surface of the filter medium.

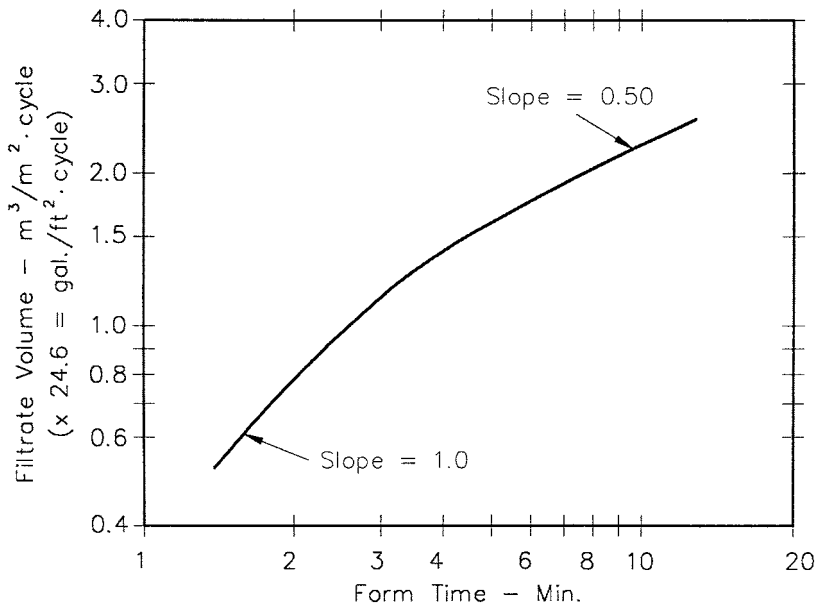


FIG. 18-113 Filtrate volume per cycle vs. form time.

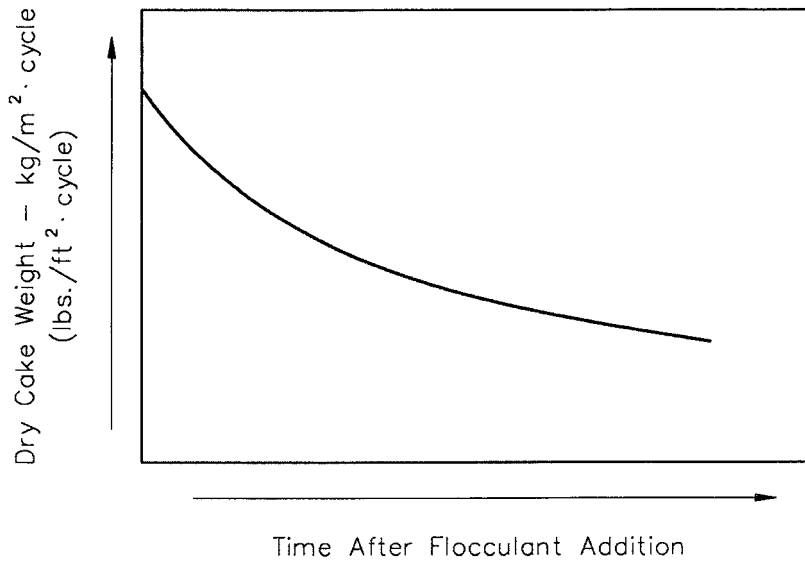


FIG. 18-114 Degradation of flocculation with time.

Since this lag time is not known at the time of testing, a lag time of 8 to 10 minutes should be allowed before starting the first leaf test on a flocculated slurry. Two, or perhaps three, tests can be run before the elapsed time exceeds the probable retention time in the full-scale filter tank. With knowledge of the elapsed time after flocculation and data relating to the rate of degradation, the rates obtained on the leaf test runs can be adjusted to some constant lag time consistent with the anticipated full-scale design.

Cake Moisture Results on a wide variety of materials have shown that the following factor is very useful for correlating cake moisture content data:

$$\text{Correlating factor} = (\text{m}^3/\text{m}^2 \cdot \text{h})(P_c/W)(\Theta_D/\mu), \quad (18-67)$$

where $\text{m}^3/\text{m}^2 \cdot \text{h}$ = air rate through filter cake measured at downstream pressure or vacuum

- P_c = pressure drop across cake
- W = dry cake weight/unit area/cycle
- Θ_D = dry time per cycle
- μ = viscosity of liquid phase

For a more rigorous discussion of cake moisture correlation, the reader is referred to an earlier article by Nelson and Dahlstrom [*Chem. Eng. Progress*, **53**, 7, 1957]. Figure 18-115 shows the general shape of the curve obtained when using the cake moisture correlating factor. The value of the correlating factor chosen for design should be somewhere past the knee of the curve. Values at and to the left of the knee are in an unstable range where a small change in operating conditions can result in a relatively large change in cake moisture content.

It is not always necessary to use all of the terms in the correlating factor, and those conditions which are held constant throughout

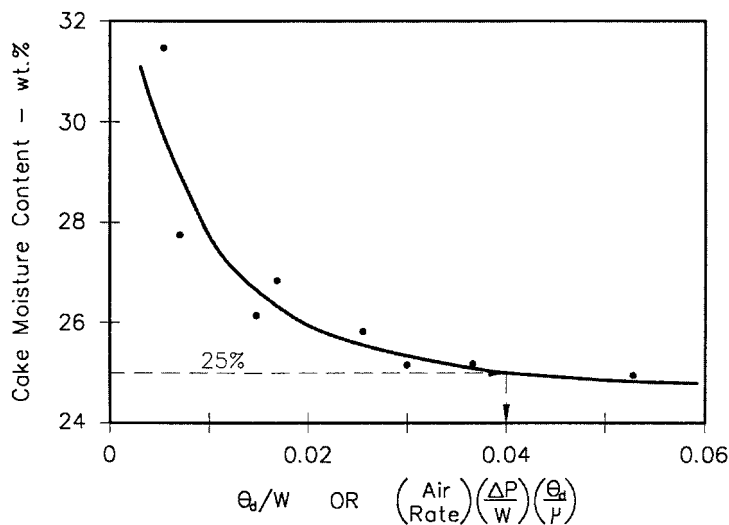


FIG. 18-115 Cake moisture correlation.

the testing may be dropped from the correlating factor. Many times, air rate data are not available and reasonable correlations can be obtained without this information, particularly if the cakes are relatively low in permeability. By dropping these terms, the correlating factor is reduced to the simplified version, Θ_D/W , involving only drying time and cake weight per unit area per revolution. While this is a very convenient factor to use, care must be taken in its application, as it is no longer a generalized factor, and there will be a tendency for the data to produce different curves for changes in operating conditions such as vacuum level and cake thickness.

Cake Washing Wash efficiency data are most conveniently represented by a semilog plot of percent remaining R as a function of wash ratio N as shown in Fig. 18-116. Percent remaining refers to that portion of the solute in the dewatered but unwashed cake which is left in the washed and dewatered cake. Since a cake-washing operation involves the displacement of one volume of liquid by another volume, the removal of solute is related to the ratio of the volume of washing fluid divided by the volume of liquid in the cake. This ratio is defined as wash ratio N .

Practical experience has shown that the most convenient and best means of expressing R is in terms of the solute concentrations in the washed cake liquid, the feed liquid (or unwashed cake liquid), and the cake wash liquid. Furthermore, the wash ratio N may also be expressed either as a volume or weight ratio.

Percent remaining is defined as follows:

$$\frac{R}{100} = \frac{C_2 - C_w}{C_1 - C_w} \tag{18-68}$$

where R = % solute remaining after washing
 C_2 = solute concentration in washed cake liquid
 C_1 = solute concentration in unwashed cake liquid
 C_w = solute concentration in wash liquid

If the cake is washed with solute-free liquid, percent remaining is readily calculated by dividing the solute concentration in the liquid remaining in the washed cake by the solute concentration in the liquid in the original feed.

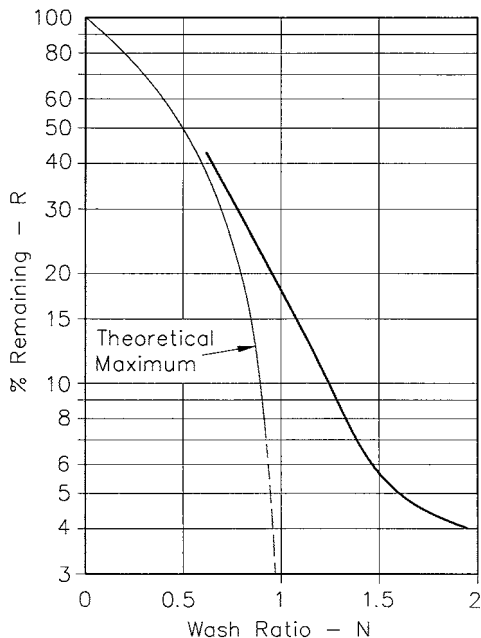


FIG. 18-116 Wash effectiveness.

The residence time of the cake-washing fluid within the cake is relatively short and is not normally considered useful for any kind of leaching operation. Therefore, it is assumed that all of the solute is in solution.

If it were possible to obtain a perfect slug displacement wash, the fraction remaining would be numerically equal to 1 minus the wash ratio. This ideal condition is represented by the maximum theoretical line as shown in Fig. 18-116. Since it represents the best that can be done, no data point should fall to the left of this curve. Most, but not all, cake-washing curves tend to fall along the heavy solid line shown. In the absence of actual data, one may estimate washing results by using this curve.

The quantity of wash water to be used in a given operation is dictated by flowsheet considerations and the required solute content of the washed cake. Generally speaking, the maximum wash water quantity should be equivalent to a wash ratio of 1.5 to 2.5. Where high solute removals are required, it is frequently necessary to use a two-stage filtration system with intermediate repulping. These two stages may involve countercurrent flow of wash water, or fresh wash water may be used on both filters and for the intermediate repulping step.

Wash Time Cake-washing time is the most difficult of the filtration variables to correlate. It is obviously desirable to use one which provides a single curve for all of the data. Filtration theory suggests three possible correlations [Eqs. (18-62) to (18-64)]. These are listed below, beginning with the easiest to use:

1. Wash time vs. WV_w
2. Wash time vs. NW^2
3. Wash time/form time vs. wash volume/form volume

where W = weight dry cake/unit area/cycle
 V_w = volume of cake wash/unit area/cycle
 N = wash ratio
 = volume of wash/volume of liquid in discharged cake

Fortunately, the easiest correlation to use usually gives satisfactory results. This curve is usually a straight line passing through the origin, but frequently falls off as the volume of wash water increases (Fig. 18-117). If for some reason this correlation is not satisfactory, one of the other two should be tried.

Air Rate Air rate through the cake, and thus vacuum pump capacity, can be determined from measurements of the air flow for various lengths of dry time. Figure 18-118 represents instantaneous air rate data. The total volume of gas passing through the cake during a dry period is determined by integrating under the curve.

Note that the air rate at the beginning of each drying or dewatering period within a given cycle starts at zero and then increases with time.

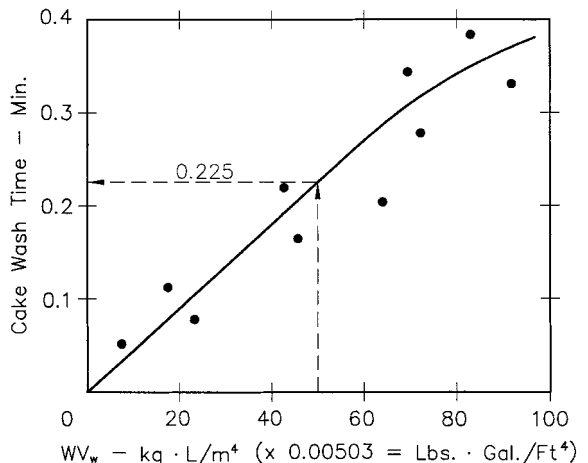


FIG. 18-117 Cake wash time correlation.

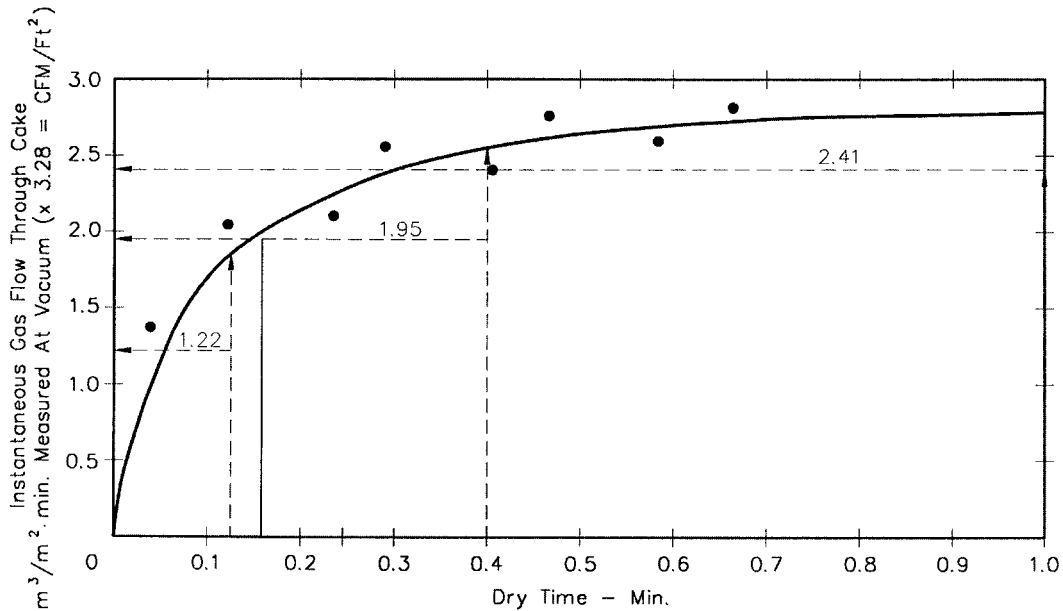


FIG. 18-118 Airflow through cake.

The shape of this curve will be a function of the permeability of the deposited cake.

Vacuum pump capacity is conventionally based on the total cycle and expressed as m³/h·m² (cfm/ft²) of filter area measured at pump inlet conditions. Thus, the gas volumes per unit area passing during each dry period in the cycle are totaled and divided by the cycle time to arrive at the design air rate. Since air rate measurements in the test program are based on pressure drop across the cake and filter medium only, allowance must be made for additional expansion due to pressure drop within the filter and auxiliary piping system in arriving at vacuum pump inlet conditions.

Air rate measurements made during a leaf test program account only for gas flow through the cake. An operating filter has drainage passages that must also be evacuated. The extra air flow may be conveniently accounted for in most cases by multiplying the leaf test rate by 1.10. With horizontal belt filters, one must also add for the leakage that occurs along the sliding seal and, depending upon the type of filter cloth used, edge leakage due to lateral permeability of the cloth. Typically, the total leakage can be significant, amounting to about 35 to 50 m³/h·m² (2 to 3 cfm/ft²).

Adjustment may also be required for differences in altitude between the test site and the commercial installation. In general terms, if the plant elevation is higher, the vacuum pump size must be increased, and conversely.

Darcy's law has been used to derive an expression which reflects not only the effect of a change in elevation, but also provides a means for estimating changes in air rate resulting from changes in vacuum level and cake thickness (or cake weight per unit area). In order for this relationship to hold for changes in vacuum and cake thickness, it must be assumed that both cakes have the same specific resistance.

The generalized equation is as follows:

$$(Air\ rate)_{b2} = (air\ rate)_{a2} \frac{(W_a)}{(W_b)} \frac{(P_{b1}^2 - P_{b2}^2)}{(P_{a1}^2 - P_{a2}^2)} \frac{(P_{a2})}{(P_{b2})} \quad (18-69)$$

where P_1 = inlet absolute pressure
 P_2 = outlet absolute pressure
 a = base condition
 b = revised condition
 W = weight of dry cake solids/unit area/cycle

SCALE-UP FACTORS

[Purchas (ed.), *Solid/Liquid Separation Equipment Scale-Up*, Uplands Press, Croydon, England, 1977.]

The overall scale-up factor used to convert a rate calculated from bench-scale data to a design rate for a commercial installation must incorporate separate factors for each of the following:

- Scale-up on rate
- Scale-up on cake discharge
- Scale-up on actual area

Special note should be made that these scale-up factors are *not* safety factors to allow for additional plant capacity at some future date. Their purpose is to account for differences in scale, including such things as minor deviations in the plant slurry from the sample tested, edge effects due to the size of the test equipment, close control of operating conditions during the leaf test program, and long-term medium blinding.

Scale-up on Rate Filtration rates calculated from bench-scale data should be multiplied by a factor of 0.8 for all types of commercial units which do not employ continuous washing of the filter medium and on which there is a possibility of filter-medium blinding. For those units which employ continuous filter-medium washing, belt-type drum and horizontal units, the scale-up factor may be increased to 0.9.

The use of this scale-up factor assumes the following:

- Complete cake discharge
- Nominal filter area approximately equal to actual area
- A representative sample
- Suitable choice of filter medium
- Operating conditions equal to those used in testing
- Normal cloth conditioning during testing and operation

The scale-up factor on rate specifically does not allow for:

- Changes in slurry filterability
- Changes in feed rate
- Changes in operating conditions
- Cloth blinding

Where there is any doubt about some of the conditions listed above (except for cake discharge and actual area which should be handled separately) a more conservative scale-up factor should be used.

Scale-up on Cake Discharge When a filter is selected for a particular application, it is intended that the unit be capable of discharging essentially 100 percent of the cake which is formed. There are,

however, many applications which are marginal, regardless of the type of discharge mechanism used. In these cases, the experimenter must judge the percent of cake discharge to be expected and factor the design rate accordingly.

Scale-up on Actual Area The nominal area of a filter as used by equipment manufacturers is based upon the overall dimensions of the filtering surface. The fraction of this total area that is active in filtration is a function of the filterability of the material being handled and any special treatment which the surface may receive.

The filtering surface is divided into a number of sections by division strips, radial rods, or some other impervious separator. Material which forms a thin, rather impervious cake will not form across the dividers, and thus the actual area is somewhat less than the nominal. Where relatively thick cakes of at least 1.5 cm are formed, the cake tends to form across the dividers due to cross-drainage in both the filter cake and the filter medium. In this case, the effective area is relatively close to the nominal area.

For most applications, the actual area of a drum filter will generally be no less than 94 to 97 percent of the nominal area, depending upon the size and number of sections. This variation is generally not accounted for separately and is assumed to be taken care of in the scale-up factor on filtration rate.

There are, however, certain special applications where the filter medium around the edge of the section may be deliberately blinded by painting in order to improve cake discharge. This technique is most frequently used on disc filters, with the result that the actual area may be only 75 to 85 percent of the nominal area. This is a significant deviation from the nominal area and must be considered separately.

Overall Scale-up Factor The final design filtration rate is determined by multiplying the bench-scale filtration rate by each of the scale-up factors discussed above. While this approach may seem to be ultraconservative, one must realize that the experimenter maintains careful control over the various steps during the filter cycle while running a bench-scale test, whereas a commercial filter operates with a minimum of attendance and at average conditions which are chosen to provide a satisfactory result in a production context.

FULL-SCALE FILTER PERFORMANCE EVALUATION

The correlations which have been presented for the evaluation of bench-scale data are the same correlations which should be used to evaluate the performance of a commercial installation.

A few random samples taken from a commercial installation most probably will not provide enough insight to determine that the filter is performing as expected. However, by making use of reasonable variations in the most important parameters, the desired correlations can be developed. Bench-scale tests should be run on representative feed samples taken at the same time test runs are made on the commercial unit. The bench-scale tests can be varied over a much wider range to provide a sound basis for both the location and shape of the appropriate correlation. A comparison of these results with the data taken from the commercial installation provides a good measure for efficiency of the commercial unit and a basis for identifying problem areas on the full-scale unit.

FILTER SIZING EXAMPLES

[Purchas (ed.), *Solid/Liquid Separation Equipment Scale-Up*, Uplands Press, Croydon, England, 1977.]

The examples which follow show how data from the correlations just presented and a knowledge of the physical characteristics of a particular filter are used to determine a filtration cycle and, subsequently, the size of the filter itself. The three examples which follow involve a disc, a drum belt, and a horizontal belt filter.

Example 5: Sizing a Disc Filter Equipment physical factors, selected from Table 18-9: Maximum effective submergence = 28%; maximum portion of filter cycle available for dewatering = 45%. (High submergence versions require trunion seals, and their use is limited to specific applications.)

Scale-up factors: On rate = 0.8; On area = 0.8; On discharge = 0.9. (Scale-up on discharge may be increased to 0.97 if based on previous experience or to 0.95 if the total filter area is based on the measured effective area of the disc.)

Objective: Determine the filter size and vacuum system capacity required to dewater 15 mtpH (metric tons per hour) of dry solids and produce a cake containing an average moisture content of 25 wt %.

Calculation procedure:

1. Choose cake thickness = 1.5 cm, slightly thicker than minimum value listed in Table 18-8.
2. From Fig. 18-111, $W = 20.0$ kg dry cake/(m² × rev.).
3. From Fig. 18-112, form time, $\gamma = 1.20$ min.
4. Use simplified moisture content correlating factor in Fig. 18-115. Choose $d/W = 0.04$ at avg. moisture content of 25 wt %.
Dry time = $d = 0.04 \times 20.0 = 0.80$ min.
5. Calculate cycle time CT both on the basis of form time and dry time to determine which is controlling:
 $CT_{form} = 1.20 / .28 = 4.29$ mpr (min/rev.).
 $CT_{dry} = 0.80 / .45 = 1.78$ mpr.

Therefore, cake formation rate is controlling and a cycle time of 4.29 mpr must be used.

6. Overall scale-up factor based on the factors presented previously = $0.8 \times 0.8 \times 0.9 = 0.58$

7. Design filtration rate = $(20.0/4.29)(60 \times 0.58) = 162$ kg/h × m²

8. Area required to filter 15 metric tons of dry solids per hour = $15 \times 1000/162 = 92.6$ m². The practical choice would then be the nearest commercial size of filter corresponding to this calculated area.

9. Dry time = 45% of CT = $0.45 \times 4.29 = 1.93$ min. This is a much longer dry time than required. Therefore, reduce the dry time to 1.00 min by proper bridging in the filter valve.

10. From Fig. 18-118, the average gas flow rate during the 1.00 min drying period was found by graphical integration to be 2.41 m³/m² × min.

11. Total volume of air flowing during dry period = $2.41 \times 1.00 = 2.41$ m³ per m² per cycle. Add 10% to allow for evacuation of drainage passages. Total flow = 2.65 m³/m² × cycle.

12. Required vacuum pump capacity = $2.65/4.29 = 0.62$ m³/min × m² of total filter area. Allow for pressure drop within system when specifying the vacuum pump. See next example.

Example 6: Sizing a Drum Belt Filter with Washing Equipment physical factors, selected from Table 18-9: Maximum effective submergence = 30%; max. apparent subm. = 35%; max. arc for washing = 29%; portion of cycle under vacuum = 75%.

Scale-up factors: On rate = 0.9; On area = 1.0; On discharge = 1.0.

Process data: Sp. gr. of feed liquid = 1.0; TDS (total dissolved solids) in feed liquid = 4.0 wt %; fresh water used for washing; vacuum level = 18 in Hg; final cake liquid content = 25 wt %.

TABLE 18-9 Typical Equipment Factors for Cycle Design

Filter type	Submergence		Total under active vac. or pres.	Max. for washing	Max. for dewatering only	Req'd. for cake discharge
	Apparent	Max. effective				
Drum						
Standard scraper	35	30	80	29	50-60	20
Roll discharge	35	30	80	29	50-60	20
Belt	35	30	75	29	45-50	25
Coil or string	35	30	75	29	45-50	25
Precoat	35,55	35,55	93	30	60,40	5
Horizontal belt	As req'd.	As req'd.	Lengthen as req'd.	As req'd.	As req'd.	0
Horizontal table	As req'd.	As req'd.	80	As req'd.	As req'd.	20
Tilting pan	As req'd.	As req'd.	75	As req'd.	As req'd.	25
Disc	35	28	75	None	45	25

Objective: Determine the filter size and vacuum capacity required to dewater and wash 15 mtpd of dry solids while producing a final washed cake with a moisture content of 25 wt % and containing 0.10 wt % TDS based on dry cake solids.

Calculation procedure:

1. Choose cake thickness = 0.75 cm, slightly thicker than the minimum in Table 18-8.

2. From Fig. 18-111, $W = 10 \text{ kg/m}^2 \times \text{cycle}$.
3. From Fig. 18-112, form time = 0.30 min.
4. From Fig. 18-115, $d/W = 0.04$ for 25 wt % residual moisture.
5. Dry time = $d = W \times 0.04 = 10.0 \times 0.04 = 0.40 \text{ min}$.
6. Determine required wash quantity:

Calculated TDS concentration in washed cake liquor:
 Liquid in final cake = $10 \times 0.25/0.75 = 3.33 \text{ kg/m}^2 \times \text{cycle}$.
 TDS in dry washed solids = $10 \times 0.001/0.999 = 0.010 \text{ kg/m}^2 \times \text{cycle}$.
 TDS in final washed cake liquor = $(0.010/3.33)100 = 0.300 \text{ wt } \%$.
 Percent remaining, $R = ((C_2 - C_w)/(C_1 - C_w))100$.

Since $C_w = 0$,
 Required percent remaining, $R = (C_2/C_1)100 = (0.300/4.00)100 = 7.5\%$.

From Fig. 18-116, required wash ratio $N = 1.35$.

For design, add 10% $\rightarrow N = 1.35 \times 1.1 = 1.49$.

Wash vol. = $V_w = 1.49 \times 3.33/1.00 = 4.96 \text{ L/m}^2 \times \text{cycle}$.

7. Determine wash time:
 $WV_w = 10.0 \times 4.96 = 49.6 \text{ kgL/m}^2$.
 From Fig. 18-117, wash time = $w = 0.225 \text{ min}$.
8. Summary of minimum times for each operation:
 Form (step 3) = 0.30 min.
 Wash (step 6) = 0.225 min.
 Final dry (step 5) = 0.40 min.

9. Maximum washing arc = horizontal centerline to 15° past top dead center, or 29% of total cycle. Minimum percent of cycle between end of form and earliest start of wash = area between horizontal centerline and maximum apparent submergence = $(50\% - 35\%)/2 = 7.5\%$.

10. Maximum percentage of cycle for wash + final dry = $75 - 30 - 7.5 = 37.5\%$.

11. Determine cycle time based on the rate-controlling operation:
 - a. $CT_{\text{form}} = 0.30/30 = 1.00 \text{ mpr}$.
 - b. $CT_{\text{wash}} = 0.225/.29 = 0.77 \text{ mpr}$.
 - c. $CT_{\text{wash} + \text{dry}} = (0.225 + 0.40)/.375 = 1.67 \text{ mpr}$.

Therefore, the cake wash + final dry rate is controlling and a cycle time of 1.67 mpr must be used.

12. Since (c) is larger than (a) in the previous step, too thick a cake will be formed and it will not wash or dry adequately unless the effective submergence is artificially restricted to yield the design cake thickness. This may be accomplished by proper bridge-block adjustment or by vacuum regulation within the form zone of the filter valve.

13. The required washing arc of $(0.225/1.67)360 = 48.5^\circ$ is assumed to start at the horizontal center line. Careful control of the wash sprays will be required to minimize runback into the slurry in the vat.

14. Overall scale-up factor = $0.9 \times 1.0 \times 1.0 = 0.9$.

15. Design filtration rate = $(10.0/1.67)/(60 \times 0.9) = 323.3 \text{ kg/h} \times \text{m}^2$.

16. Total filter area required = $15 \times 1000/323.3 = 46.4 \text{ m}^2$.
 Nearest commercial size for a single unit could be a 10 ft dia. \times 16 ft long with a total area of 502 ft² = 46.7 m².

17. Determine required vacuum capacity:
 Initial dry time = $1.67 \times 0.075 = 0.125 \text{ min}$.
 Calculate gas vol. through cake using data from Fig. 18-118:
 Initial dry = $0.125 \times 1.22 = 0.153 \text{ m}^3/\text{m}^2 \times \text{rev}$.
 Final dry = $0.40 \times 1.95 = 0.780 \text{ m}^3/\text{m}^2 \times \text{rev}$.
 Total, including 10% for evacuation of drainage passages = $0.933 \times 1.10 = 1.03 \text{ m}^3/\text{m}^2 \times \text{rev}$.

Air rate based on total cycle = $1.03/1.67 = 0.62 \text{ m}^3/\text{min} \times \text{m}^2$ measured at 18 in Hg vacuum.

If pressure drop through system = 1.0 in Hg and barometric pressure = 30 in Hg, design air rate = $0.62 \times 12/11 = 0.68 \text{ m}^3/\text{min} \times \text{m}^2$ measured at 19 in Hg vacuum.

Horizontal Belt Filter Since the total cycle of a horizontal belt filter occurs on a single, long horizontal surface, there is no restriction with respect to the relative portions of the cycle. Otherwise, scale-up procedures are similar.

BATCH FILTRATION

Since most batch-type filters operate under pressure rather than vacuum, the following discussion will apply primarily to pressure filtration and the various types of pressure filters.

To use Eq. (18-54) one must know the pattern of the filtration process, i.e., the variation of the flow rate and pressure with time. Generally the pumping mechanism determines the filtration flow

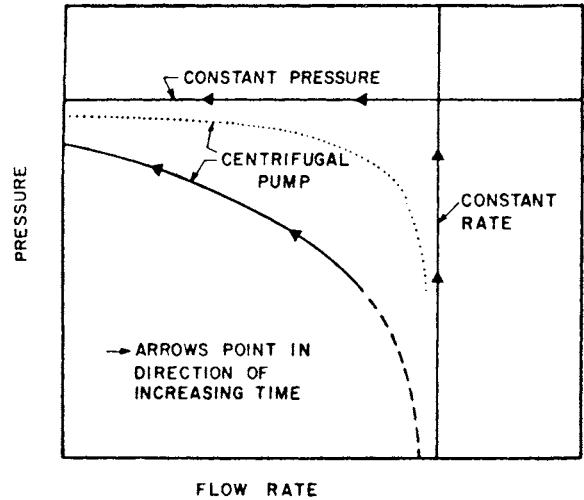


FIG. 18-119 Typical filtration cycles. [Tiller and Crump, Chem. Eng. Prog. 73(10), 72(1977), by permission.]

characteristics and serves as a basis for the following three categories° [Tiller and Crump, Chem. Eng. Prog., 73(10), 65 (1977)]:

1. *Constant-pressure filtration.* The actuating mechanism is compressed gas maintained at a constant pressure.
2. *Constant-rate filtration.* Positive-displacement pumps of various types are employed.
3. *Variable-pressure, variable-rate filtration.* The use of a centrifugal pump results in this pattern: the discharge rate decreases with increasing back pressure.

Flow rate and pressure behavior for the three types of filtration are shown in Fig. 18-119. Depending on the characteristics of the centrifugal pump, widely differing curves may be encountered, as suggested by the figure.

Constant-Pressure Filtration For constant-pressure filtration Eq. (18-54) can be integrated to give the following relationships between total time and filtrate measurements:

$$\frac{\theta}{V/A} = \frac{\mu\alpha}{2P} \frac{W}{A} + \frac{\mu r}{P} \tag{18-70}$$

$$\frac{\theta}{V/A} = \frac{\mu\alpha w}{2P} \frac{V}{A} + \frac{\mu r}{P} \tag{18-71}$$

$$\frac{\theta}{V/A} = \frac{\mu\alpha pc}{2P(1 - mc)} \frac{V}{A} + \frac{\mu r}{P} \tag{18-72}$$

For a given constant-pressure filtration, these may be simplified to

$$\frac{\theta}{V/A} = K_p \frac{W}{A} + C = K'_p \frac{V}{A} + C \tag{18-73}$$

where K_p , K'_p , and C are constants for the conditions employed. It should be noted that K_p , K'_p , and C depend on filtering pressure not only in the obvious explicit way but also in the implicit sense that α , m , and r are generally dependent on P .

Constant-Rate Filtration For substantially incompressible cakes, Eq. (18-54) may be integrated for a constant rate of slurry feed to the filter to give the following equations, in which filter-medium resistance is treated as the equivalent constant-pressure component to be deducted from the rising total pressure drop to give the variable pressure through the filter cake [Ruth, Ind. Eng. Chem., 27, 717 (1935)]:

° A combination of category 2 followed by category 1 as parts of the same filtration cycle is considered by some as a fourth category. For a method of combining the constant-rate and constant-pressure equations for such a cycle, see Brown, loc. cit.

$$\frac{\theta}{V/A} = \frac{1}{\text{rate per unit area}} = \frac{\mu\alpha}{P - P_1} \frac{W}{A} \quad (18-74)$$

which may also be written

$$\frac{\theta}{V/A} = \frac{\mu\alpha w}{P - P_1} \frac{V}{A} = \frac{\mu\alpha r c}{(P - P_1)(1 - mc)} \frac{V}{A} \quad (18-75)$$

In these equations P_1 is the pressure drop through the filter medium.

$$P_1 = \mu r (V/A\theta)$$

For a given constant-rate run, the equations may be simplified to

$$V/A = P/K_r + C' \quad (18-76)$$

where K_r and C' are constants for the given conditions.

Variable-Pressure, Variable-Rate Filtration The pattern of this category complicates the use of the basic rate equation. The method of Tiller and Crump (loc. cit.) can be used to integrate the equation when the characteristic curve of the feed pump is available.

In the filtration of small amounts of fine particles from liquid by means of bulky filter media (such as absorbent cotton or felt) it has been found that the preceding equations based upon the resistance of a cake of solids do not hold, since no cake is formed. For these cases, in which filtration takes place on the surface or within the interstices of a medium, analogous equations have been developed [Hermans and Bredée, *J. Soc. Chem. Ind.*, **55T**, 1 (1936)]. These are usefully summarized, for both constant-pressure and constant-rate conditions, by Grace [*Am. Inst. Chem. Eng. J.*, **2**, 323 (1956)]. These equations often apply to the clarification of such materials as sugar solutions, viscose and other spinning solutions, and film-casting dopes.

If a **constant-pressure test** is run on a slurry, care being taken that not only the pressure but also the temperature and the solid content remain constant throughout the run and that time readings begin at the exact start of filtration, one can observe values of filtrate volume or weight and corresponding elapsed time. With the use of the known filtering area, values of $\theta/(V/A)$ can be calculated for various values of V/A which, when plotted with $\theta/(V/A)$ as the ordinate and V/A as the abscissa (Fig. 18-120a), result in a straight line having the slope $\mu\alpha w/2P$ and an intercept on the vertical axis of $\mu r/P$. Since μ , w , and P are known, α and r can be calculated from

$$\alpha = 2P/\mu w \times (\text{slope})$$

and

$$r = P/\mu \times (\text{vertical intercept})$$

The effect of the change of any variable not affecting α or r can now be estimated. It should be remembered that α and r usually depend on P and may be affected by w .

The symbol α represents the average specific cake resistance, which is a constant for the particular cake in its immediate condition. In the usual range of operating conditions it is related to the pressure by the expression

$$\alpha = \alpha' P^s \quad (18-77)$$

where α' is a constant determined largely by the size of the particles forming the cake; s is the cake compressibility, varying from 0 for rigid, incompressible cakes, such as fine sand and diatomite, to 1.0 for very highly compressible cakes. For most industrial slurries, s lies between 0.1 and 0.8. The symbol r represents the resistance of unit area of filter

medium but includes other losses (besides those across the cake and the medium) in the system across which P is the pressure drop.

It should be noted also that the intercept is difficult to determine accurately because of large potential experimental error in observing the time of the start of filtration and the time-volume correspondence during the first moments when the filtration rate is high. The value of r calculated from the intercept may vary appreciably from test to test, and will almost always be different from the value measured with clean medium in a permeability test.

To determine the effect of a change in pressure, it is necessary to run tests at three or more pressures, preferably spanning the range of interest. Plotting α or r against P on log-log paper (or $\log \alpha$ or $\log r$ against the $\log P$ on cartesian coordinates) results in an approximate straight line (Fig. 18-120b) from which one may estimate values of α or r at interpolated or reasonably extrapolated magnitudes of P . The slope of the line is the index of a power relationship between α and P or r and P .

Not uncommonly r is found to be only slightly dependent on pressure. When this is true and especially when the filter-medium resistance is, as it should be, relatively small, an average value may be used for all pressures.

It is advisable to start a constant-pressure filtration test, like a comparable plant operation, at a low pressure, and smoothly increase the pressure to the desired operating level. In such cases, time and filtrate-quantity data should not be taken until the constant operating pressure is realized. The value of r calculated from the extrapolated intercept then reflects the resistance of both the filter medium and that part of the cake deposited during the pressure-buildup period. When only the total mass of dry cake is measured for the total cycle time, as is usually true in vacuum leaf tests, at least three runs of different lengths should be made to permit a reliable plot of θ/V against W . If rectification of the resulting three points is dubious, additional runs should be made.

Pressure Tests

Leaf Tests A bomb filter is used for small-scale leaf tests to simulate the performance of pressure-leaf (leaf-in-shell) filters. The equipment used is a small [50.8- by 50.8-mm (2- by 2-in)] leaf, covered with appropriate filter medium, suspended in a cell large enough to contain sufficient slurry to form the desired cake (Fig. 18-121). The slurry may be agitated gently, for example, by an air sparger.

Although incremental time and filtrate volume may be taken during a cake-forming cycle at a selected pressure to permit a plot like Fig. 18-120a from a single run, it may be more satisfactory to make several successive quick runs at the same pressure but for different lengths of time, recording only the terminal values of filtrate volume, time, and cake mass. Operation of the commercial unit should be kept in mind when the test cycles are planned. Displacement washing and air blowing of the cake should be tried if appropriate. Wet discharge can be simulated by opening the cell and playing a jet of water on the cake; dry discharge, by applying a gentle air blast to the filtrate-discharge tube. Tests at several pressures must be conducted to determine the compressibility of the cake solids.

Plate-and-Frame Tests These tests should be conducted if the use of a filter press in the plant is anticipated; at least a few confirming tests are advisable after preliminary leaf tests, unless the slurry is very rapidly filtering. A laboratory-size filter press consisting of two plates and a single frame may be used. It will permit the observation of solids-settling, cake-packing, and washing behavior, which may be quite different for a frame than for a leaf.

Compression-Permeability Tests Instead of model leaf tests, compression-permeability experiments may be substituted with advantage for appreciably compressible solids. As in the case of constant-rate filtration, a single run provides data equivalent to those obtained from a series of constant-pressure runs, but it avoids the data-treatment complexity of constant-rate tests.

The equipment consists of a cylindrical cell with a permeable bottom and an open top, into which is fitted a close-clearance, hollow, cylindrical piston with a permeable bottom. Slurry is poured into the cell, and a cake is formed by applying gentle vacuum to the filtrate discharge line. The cell is then filled with filtrate, and the counterweighted piston is allowed to descend to the cake level. Successive

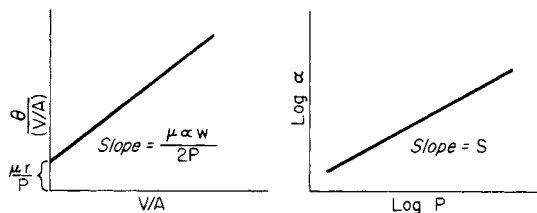


FIG. 18-120 Typical plots of filtration data.

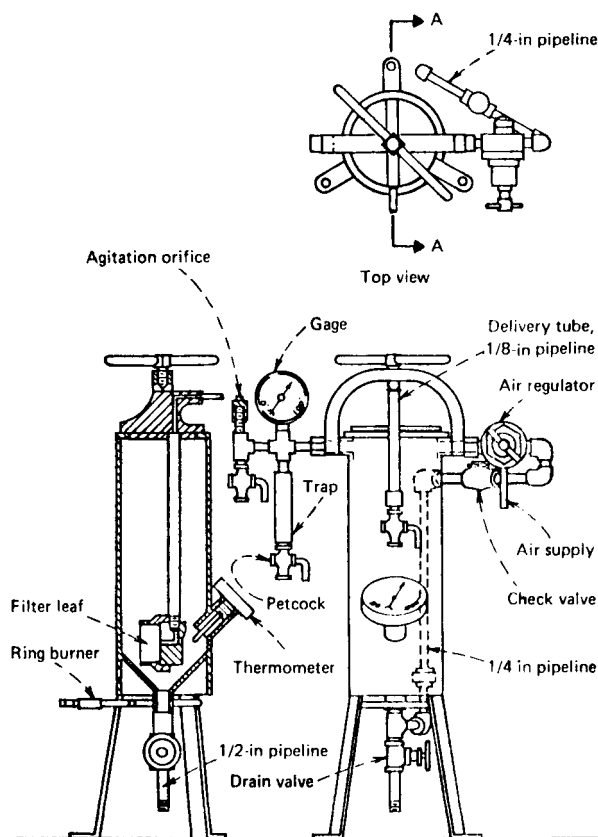


FIG. 18-121 Bomb filter for small-scale pressure filtration tests. [Silverblatt *et al.*, *Chem. Eng.*, 81(9), 132 (1974), by permission.]

increments of mechanical stress are applied to the solids, at each of which the permeability of the cake is determined by passing filtrate through the piston under low head.

The experimental procedure and method of treatment of compression-permeability data have been explained by Grace [*Chem. Eng. Prog.*, 49, 303, 427 (1953)], who showed that the values of α measured in such a cell and in a pressure filter were the same, and by Tiller [*Filtr. Sep.*, 12, 386 (1975)].

Scaling Up Test Results The results of small-scale tests are determined as dry weight of solids or volume of filtrate per unit of area per cycle. This quantity multiplied by the number of cycles per day permits the calculation of either the filter area required for a stipulated daily capacity or the daily capacity of a specified plant filter. The scaled-up filtration area should be increased by 25 percent as a factor of uncertainty. In the calculation of cycle length, proper account must be made of the downtime of a batch filter.

FILTER MEDIA

All filters require a filter medium to retain solids, whether the filter is for cake filtration or for filter-medium or depth filtration. Specification of a medium is based on retention of some minimum particle size at good removal efficiency and on acceptable life of the medium in the environment of the filter. The selection of the type of filter medium is often the most important decision in success of the operation. For cake filtration, medium selection involves an optimization of the following factors:

1. Ability to bridge solids across its pores quickly after the feed is started (i.e., minimum propensity to bleed)

2. Low rate of entrapment of solids within its interstices (i.e., minimum propensity to blind)
3. Minimum resistance to filtrate flow (i.e., high production rate)
4. Resistance to chemical attack
5. Sufficient strength to support the filtering pressure
6. Acceptable resistance to mechanical wear
7. Ability to discharge cake easily and cleanly
8. Ability to conform mechanically to the kind of filter with which it will be used
9. Minimum cost

For filter-medium filtration, attributes 3, 4, 5, 8, and 9 of the preceding list apply and must be added to them (a) ability to retain the solids required, (b) freedom from discharge of lint or other adulterant into the filtrate, and (c) ability to plug slowly (i.e., long life).

Filter-medium selection embraces many types of construction: fabrics of woven fibers, felts, and nonwoven fibers, porous or sintered solids, polymer membranes, or particulate solids in the form of a permeable bed. Media of all types are available in a wide choice of materials.

Fabrics of Woven Fibers For cake filtration these fabrics are the most common type of medium. A wide variety of materials are available; some popular examples are listed in Table 18-10, with ratings for chemical and temperature resistance. In addition to the material of the fibers, a number of construction characteristics describe the filter cloth: (1) weave, (2) style number, (3) weight, (4) count, (5) ply, and (6) yarn number. Of the many types of weaves available, only four are extensively used as filter media: plain (square) weave, twill, chain weave, and satin.

All these weaves may be made from any textile fiber, natural or synthetic. They may be woven from spun staple yarns, multifilament continuous yarns, or monofilament yarns. The performance of the filter cloth depends on the weave and the type of yarn.

A recently developed medium known as a double weave incorporates different yarns in warp and fill in order to combine the specific advantages of each type. An example of this is Style 99FS, made by Madison Filtration, in which multifilament warp yarns provide good cake release properties and spun staple fill yarns contribute to greater retentivity.

Metal Fabrics or Screens These are available in several types of weave in nickel, copper, brass, bronze, aluminum, steel, stainless steel, Monel, and other alloys. In the plain weave, 400 mesh is the closest wire spacing available, thus limiting use to coarse crystalline slurries, pulps, and the like. The "Dutch weaves" employing relatively large, widely spaced, straight warp wires and relatively small crimped filling wires can be woven much more closely, providing a good medium for filtering fine crystals and pulps. This type of weave tends to plug readily when soft or amorphous particles are filtered and makes the use of filter aid desirable. Good corrosion and high temperature resistance of properly selected metals makes filtrations with metal media desirable for long-life applications. This is attractive for handling toxic materials in closed filters to which minimum exposure by maintenance personnel is desirable.

Pressed Felts and Cotton Batting These materials are used to filter gelatinous particles from paints, spinning solutions, and other viscous liquids. Filtration occurs by deposition of the particles in and on the fibers throughout the mat.

Nonwoven media consist of web or sheet structures which are composed primarily of fibers or filaments bonded together by thermal, chemical, or mechanical (such as needlepunching) means. Needled felts are the most commonly used nonwoven fabric for liquid filtration. Additional strength often is provided by including a scrim of woven fabric encapsulated within the nonwoven material. The surface of the medium can be calendered to improve particle retention and assist in filter cake release. Weights range from 270 to 2700 gm/m² (8 to 80 oz/yd²). Because of their good retentivity, high strength, moderate cost, and resistance to blinding, nonwoven media have found wide acceptance in filter press use, particularly in mineral concentrate filtration applications. They are used frequently on horizontal belt filters where their dimensional stability reduces or eliminates wrinkling and biasing problems often encountered with woven felts.

Filter Papers These papers come in a wide range of permeability, thickness, and strength. As a class of material, they have low strength, however, and require a perforated backup plate for support.

TABLE 18-10 Characteristics of Filter-Fabric Materials*

Generic name and description	Breaking tenacity, g/denier	Abrasion resistance	Resistance to acids	Resistance to alkalis	Resistance to oxidizing agents	Resistance to solvents	Specific gravity	Maximum operating temperature, °F†
Acetate—cellulose acetate. When not less than 92% of the hydroxyl groups are acetylated, "triacetate" may be used as a generic description.	1.2–1.5	G	F	P	G	G	1.33	210
Acrylic—any long-chain synthetic polymer composed of at least 85% by weight of acrylonitrile units.	2.0–4.8	G	G	F	G	E	1.18	300
Glass—fiber-forming substance is glass.	3.0–7.2	P	E	P	E	E	2.54	600
Metallic—composed of metal, metal-coated plastic, plastic-coated metal, or a core completely covered by metal.	—	G						
Modacrylic—fiber-forming substance is any long-chain synthetic polymer composed of less than 85% but at least 35% by weight of acrylonitrile units.	2.5–3.0	G	G	G	G	G	1.30	180
Nylon—any long-chain synthetic polyamide having recurring amide groups as an integral part of the polymer chain.	3.8–9.2	E	F–P	G	F–P	G	1.14	225
Polyester—any long-chain synthetic polymer composed of at least 85% by weight of an ester of a dihydric alcohol and terephthalic acid (<i>p</i> -HOOC—C ₆ H ₄ —COOH).	2.2–7.8	E–G	G	G–F	G	G	1.38	300
Polyethylene—long-chain synthetic polymer composed of at least 85% weight of ethylene.	1.0–7.0	G	G	G	F	G	0.92	165‡
Polypropylene—long-chain synthetic polymer composed of at least 85% by weight of propylene.	4.8–8.5	G	E	E	G	G	0.90	250§
Cotton—natural fibers.	3.3–6.4	G	P	F	G	E–G	1.55	210
Fluorocarbon—long-chain synthetic polymer composed of tetrafluoroethylene units.	1.0–2.0	F	E	E	E	G	2.30	550¶

*Adapted from Mais, *Chem. Eng.*, **78**(4), 51 (1971). Symbols have the following meaning: E = excellent, G = good, F = fair, P = poor.

†°C = (°F – 32)/1.8; K = (°F + 459.7)/1.8.

‡Low-density polymer. Up to 230°F for high-density.

§Heat-set fabric; otherwise lower.

¶Requires ventilation because of release of toxic gases above 400°F.

Rigid Porous Media These are available in sheets or plates and tubes. Materials used include sintered stainless steel and other metals, graphite, aluminum oxide, silica, porcelain, and some plastics—a gamut that allows a wide range of chemical and temperature resistance. Most applications are for clarification.

Polymer Membranes These are used in filtration applications for fine-particle separations such as microfiltration and ultrafiltration (clarification involving the removal of 1- μ m and smaller particles). The membranes are made from a variety of materials, the commonest being cellulose acetates and polyamides. Membrane filtration, discussed in Sec. 22, has been well covered by Porter (in Schweitzer, op. cit., sec. 2.1).

Media made from woven or nonwoven fabrics coated with a polymeric film, such as Primapor, and Primapor II made by Madison Filtration, Gore-Tex, made by W. L. Gore and Associates, and Tetratex, made by Donaldson Company, combine the high retentivity characteristics of a membrane with the strength and durability of a thick filter cloth. These media are used on both continuous and batch filters where excellent filtrate clarity is required.

Granular Beds of Particulate Solids Beds of solids like sand or coal are used as filter media to clarify water or chemical solutions containing small quantities of suspended particles. Filter-grade grains of desired particle size can be purchased. Frequently beds will be constructed of layers of different materials and different particle sizes.

Various types of filter media and the materials of which they are constructed are surveyed extensively by Purchas (*Industrial Filtration of Liquids*, CRC Press, Cleveland, 1967, chap. 3), and characterizing measurements (e.g., pore size, permeability) are reviewed in detail by Rushton and Griffiths (in Orr, op. cit., chap. 3). Briefer summaries of classification of media and of practical criteria for the selection of a filter medium are presented by Shoemaker (op. cit., p. 26) and Purchas [*Filtr. Sep.*, **17**, 253, 372 (1980)].

FILTER AIDS

Use of filter aids is a technique frequently applied for filtrations in which problems of slow filtration rate, rapid medium blinding, or unsatisfactory filtrate clarity arise. Filter aids are granular or fibrous solids capable of forming a highly permeable filter cake in which very fine solids or slimy, deformable flocs may be trapped. Application of filter aids may allow the use of a much more permeable filter medium than the clarification would require to produce filtrate of the same quality by depth filtration.

Filter aids should have low bulk density to minimize settling and aid good distribution on a filter-medium surface that may not be horizontal. They should also be porous and capable of forming a porous cake to minimize flow resistance, and they must be chemically inert to the filtrate. These characteristics are all found in the two most popular

commercial filter aids: diatomaceous earth (also called diatomite), which is an almost pure silica prepared from deposits of diatom skeletons; and expanded perlite, particles of "puffed" lava that are principally aluminum alkali silicate. Cellulosic fibers (ground wood pulp) are sometimes used when siliceous materials cannot be used but are much more compressible. The use of other less effective aids (e.g., carbon and gypsum) may be justified in special cases. Sometimes a combination of carbon and diatomaceous earth permits adsorption in addition to filter-aid performance. Various other materials, such as salt, fine sand, starch, and precipitated calcium carbonate, are employed in specific industries where they represent either waste material or inexpensive alternatives to conventional filter aids.

Diatomaceous Earth Filter aids of diatomaceous earth have a dry bulk density of 128 to 320 kg/m³ (8 to 20 lb/ft³), contain particles mostly smaller than 50 μm, and produce a cake with porosity in the range of 0.9 (volume of voids/total filter-cake volume). The high porosity (compared with a porosity of 0.38 for randomly packed uniform spheres and 0.2 to 0.3 for a typical filter cake) is indicative of its filter-aid ability. Different methods of processing the crude diatomite result in a series of filter aids having a wide range of permeability.

Perlite Perlite filter aids are somewhat lower in bulk density (48 to 96 kg/m³, or 3 to 6 lb/ft³) than diatomaceous silica and contain a higher fraction of particles in the 50- to 150-μm range. Perlite is also available in a number of grades of differing permeability and cost, the grades being roughly comparable to those of diatomaceous earth. Diatomaceous earth will withstand slightly more extreme pH levels than perlite, and it is said to be somewhat less compressible.

Filter aids are used in two ways: (1) as a precoat and (2) mixed with the slurry as a "body feed." Precoat filtration, employing a thin layer of about 0.5 to 1.0 kg/m² (0.1 to 0.2 lb/ft²) deposited on the filter medium prior to beginning feed to the filter, is in wide use to protect the filter medium from fouling by trapping solids before they reach the medium. It also provides a finer matrix to trap fine solids and assure filtrate clarity. Body-feed application is the continuous addition of filter aid to the filter feed to increase the porosity of the cake. The amount of addition must be determined by trial, but in general, the quantity added should at least equal the amount of solids to be removed. For solids loadings greater than 1000 ppm this may become a significant cost factor. An acceptable alternative might be to use a rotary vacuum precoat filter [Smith, *Chem. Eng.*, **83**(4), 84 (1976)]. Further details of filter-aid filtration are set forth by Cain (in Schweitzer, op. cit., sec. 4.2) and Hutto [*Am. Inst. Chem. Eng. Symp. Ser.*, **73**(171), 50 (1977)]. Figure 18-122 shows a flow sheet indicating arrangements for both precoat and body-feed applications. Most filter aid is used on a one-time basis, although some techniques have been demonstrated to reuse precoat filter aid on vertical-tube pressure filters.

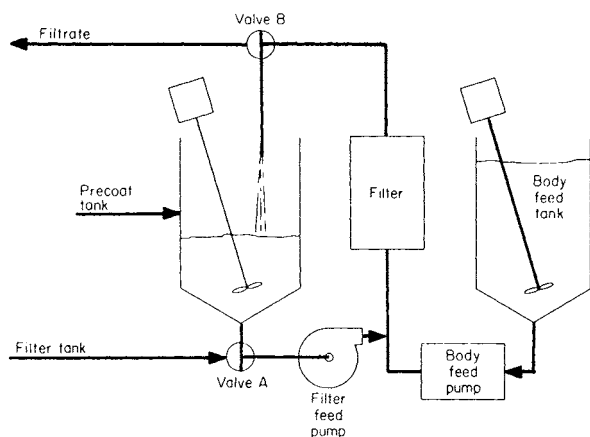


FIG. 18-122 Filter-aid filtration system for precoat or body feed. (Schweitzer, Handbook of Separation Techniques for Chemical Engineers, p. 4-12. Copyright 1979 by McGraw-Hill, Inc. and used with permission.)

FILTRATION EQUIPMENT

Cake Filters Filters that accumulate appreciable visible quantities of solids on the surface of a filter medium are called cake filters. The slurry feed may have a solids concentration from about 1 percent to greater than 40 percent. The filter medium on which the cake forms is relatively open to minimize flow resistance, since once the cake forms, it becomes the effective filter medium. The initial filtrate therefore may contain unacceptable solids concentration until the cake is formed. This situation may be made tolerable by recycling the filtrate until acceptable clarity is obtained or by using a downstream polishing filter (clarifying type).

Cake filters are used when the desired product of the operation is the solids, the filtrate, or both. When the filtrate is the product, the degree of removal from the cake by washing or blowing with air or gas becomes an economic optimization. When the cake is the desired product, the incentive is to obtain the desired degree of cake purity by washing, blowing, and sometimes mechanical expression of residual liquid.

Implicit in cake filtration is the removal and handling of solids, since the cake is usually relatively dry and compacted. Cakes can be sticky and difficult to handle; therefore, the ability of a filter to discharge the cake cleanly is an important equipment-selection criterion.

In the operational sense, some filters are batch devices, whereas others are continuous. This difference provides the principal basis for classifying cake filters in the discussion that follows. The driving force by which the filter functions—hydrostatic head ("gravity"), pressure imposed by a pump or a gas blanket, or atmospheric pressure ("vacuum")—will be used as a secondary criterion.

Batch Cake Filters

Nutsche Filters A nutsche is one of the simplest batch filters. It is a tank with a false bottom, perforated or porous, which may either support a filter medium or act as the filter medium. The slurry is fed into the filter vessel, and separation occurs by gravity flow, gas pressure, vacuum, or a combination of these forces. The term "nutsche" comes from the German term for sucking, and vacuum is the common operating mode.

The design of most nutsche filters is very simple, and they are often fabricated by the user at low cost. The filter is very frequently used in laboratory, pilot-plant, or small-plant operation. For large-scale processing, however, the excessive floor area encumbered per unit of filtration area and the awkwardness of cake removal are strong deterrents. For small-scale operations, cake is manually removed. For large-scale applications, cake may be further processed by reslurrying or redissolving; or it may be removed manually (by shovel) or by mechanical discharge arrangements such as a movable filter medium belt.

Thorough displacement washing is possible in a nutsche if the wash solvent is added before the cake begins to be exposed to air displacement of filtrate. If washing needs to be more effective, an agitator can be provided in the nutsche vessel to reslurry the cake to allow adequate diffusion of solute from the solids.

Horizontal Plate Filter The horizontal multiple-plate pressure filter consists of a number of horizontal circular drainage plates and guides placed in a stack in a cylindrical shell (Fig. 18-123). In normal practice the filtering pressure is limited to 345 kPa (50 psig), although special filters have been designed for shell pressures of 2.1 MPa (300 psig) or higher.

Filter Press The filter press, one of the most frequently used filters in the early years of the chemical industry, is still widely employed. Often referred to generically (in error) as the plate-and-frame filter, it has probably over 100 design variations. Two basic popular designs are the flush-plate, or plate-and-frame, design and the recessed-plate press. Both are available in a wide range of materials: metals, coated metals, plastics, or wood.

Plate-and-frame press. This press is an alternate assembly of plates covered on both sides with a filter medium, usually a cloth, and hollow frames that provide space for cake accumulation during filtration. The frames have feed and wash manifold ports, while the plates have filtrate drainage ports. The plates and frames usually are

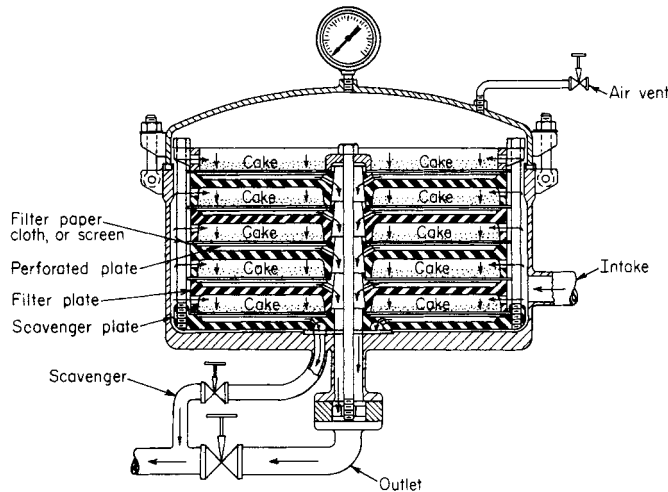


FIG. 18-123 Elevation section of a Sparkler horizontal plate filter. (Sparkler Filters, Inc.)

rectangular, although circles and other shapes also are used (Fig. 18-124). They are hung on a pair of horizontal support bars and pressed together during filtration to form a watertight closure between two end plates, one of which is stationary. The press may be closed manually, hydraulically, or by a motor drive. Several feed and filtrate discharge arrangements are possible. In the most popular, the feed and discharge of the several elements of the press are manifolded via some of the holes that are in the four corners of each plate and frame (and filter cloth) to form continuous longitudinal channels from the stationary end plate to the other end of the press. Alternatively, the filtrate may be drained from each plate by an individual valve and spigot (for open discharge) or tubing (for closed). Top feed to and bottom discharge from the chambers provide maximum recovery of filtrate and maximum mean cake dryness. This arrangement is especially suitable for heavy fast-settling solids. For most slurries, bottom feed and top filtrate discharge allow quick air displacement and produce a more uniform cake.

Two wash techniques are used in plate-and-frame filter presses, illustrated in Fig. 18-125. In simple washing, the wash liquor follows the same path as the filtrate. If the cake is not extremely uniform and highly permeable, this type of washing is ineffective in a well-filled

press. A better technique is thorough washing, in which the wash is introduced to the faces of alternate plates (with their discharge channels valved off). The wash passes through the entire cake and exits through the faces of the other plates. This improved technique requires a special design and the assembly of the plates in proper order. Thorough washing should be used only when the frames are well filled, since an incomplete fill of cake will allow cake collapse during the wash entry. The remainder of the wash flow will bypass through cracks or channels opened in the cake.

Filter presses are made in plate sizes from 10 by 10 cm (4 by 4 in) to 2.4 by 2.4 m (94 by 94 in). Frame thickness ranges from 0.3 to 20 cm (0.125 to 8 in). Operating pressures up to 689 kPa (100 psig) are common, with some presses designed for 6.9 MPa (1000 psig). Some metal units have cored plates for steam or refrigerant. Maximum pressure for wood or plastic frames is 410 to 480 kPa (60 to 70 psig).

The filter press has the advantage of simplicity, low capital cost, flexibility, and ability to operate at high pressure in either a cake-filter or a clarifying-filter application. Floor-space and headroom needs per unit of filter area are small, and capacity can be adjusted by adding or removing plates and frames. Filter presses are cleaned easily, and the filter medium is easily replaced. With proper operation a denser, drier cake compared with that of most other filters is obtained.

There are several serious disadvantages, including imperfect washing due to variable cake density, relatively short filter-cloth life due to the mechanical wear of emptying and cleaning the press (often involving scraping the cloth), and high labor requirements. Presses frequently drip or leak and thereby create housekeeping problems, but the biggest problem arises from the requirement to open the filter for cake discharge. The operator is thus exposed routinely to the contents of the filter, and this is becoming an increasingly severe disadvantage as more and more materials once believed safe are given restricted exposure limits.

Recessed-plate filter press. This press is similar to the plate-and-frame press in appearance but consists only of plates (Fig. 18-126). Both faces of each plate are hollowed to form a chamber for cake accumulation between adjacent plates. This design has the advantage of about half as many joints as a plate-and-frame press, making a tight closure more certain. Figure 18-127 shows some of the features of one type of recessed-plate filter which has a gasket to further minimize leaks. Air can be introduced behind the cloth on both sides of each plate to assist cake removal.

Some interesting variations of standard designs include the ability to roll the filter to change from a bottom to a top inlet or outlet and the

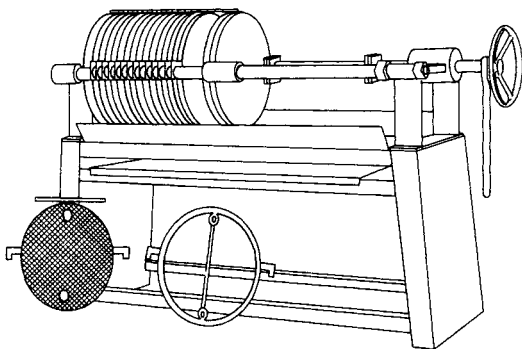


FIG. 18-124 Circular-plate fabricated-metal filter press. (Star Systems Filtration Division.)

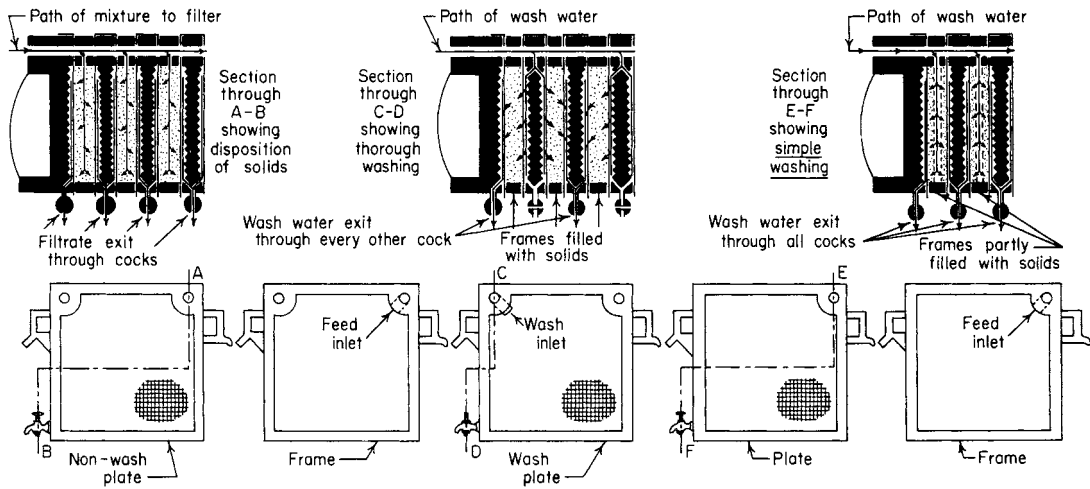


FIG. 18-125 Filling and washing flow patterns in a filter press. (D. R. Sperry & Co.)

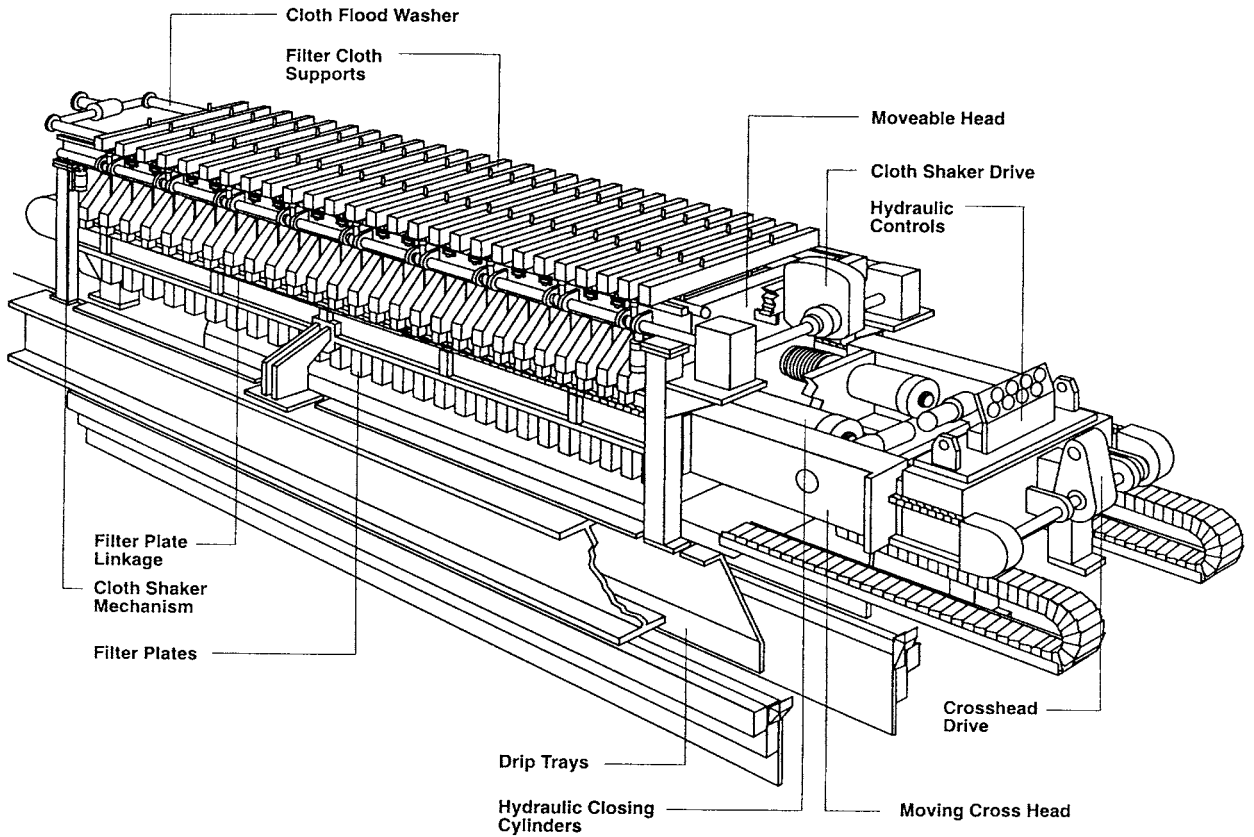


FIG. 18-126 Automated recessed-plate filter press used in mineral applications. (Dorr-Oliver EIMCO.)

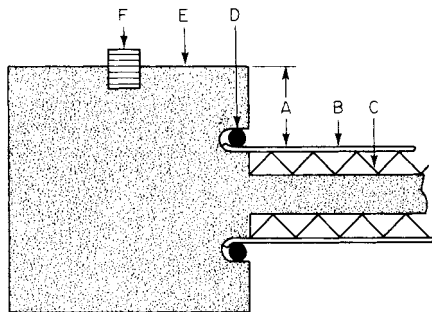


FIG. 18-127 Section detail of a caulked-gasketed-recessed filter plate: (a) cake recess; (b) filter cloth; (c) drainage surface of plate; (d) caulking strip; (e) plate joint; (f) sealing gasket. (Dorr-Oliver EIMCO)

ability to add blank dividers to convert a press to a multistage press for further clarification of the filtrate or to do two separate filtrations simultaneously in the same press. Some designs have rubber membranes between plates which can be expanded when filtration is finished to squeeze out additional moisture. Some designs feature automated opening and cake-discharge operations to reduce labor requirements. Examples of this type of pressure filter include Larox, Vertipress, and Oberlin.

Internal Cake Tube Filters or Liquid Bag Filters This type of filter, such as manufactured by Industrial Filter and Pump Mfg. Co., Rosedale, Illinois, and many others, utilizes one or more perforated tubes supported by a tube sheet or by the lip of the pressure vessel. A cylindrical filter bag sealed at one end is inserted into the perforated tube. The open end of the filter bag generally has a flange or special seal ring to prevent leakage.

Slurry under pressure is admitted to the chamber between the head of the shell and the tube sheet, whence it enters and fills the tubes. Filtration occurs as the filtrate passes radially outward through the filter medium and the wall of each tube into the shell and on out the filtrate discharge line, depositing cake on the medium. The filtration cycle is ended when the tubes have filled with cake or when the media have become plugged. The cake can be washed (if it has not been allowed to fill the tubes completely) and air-blown. The filter has a removable head to provide easy access to the tube sheet and mouth of the tubes; thus "sausages" of cake can be removed by taking out the filter bags or each tube and bag assembly together. The tubes themselves are easily removed for inspection and cleaning.

The advantages of the tubular filter are that it uses an easily replaced filter medium, its filtration cycle can be interrupted and the shell can be emptied of prefiltrate at any time without loss of the cake, the cake is readily recoverable in dry form, and the inside of the filter is conveniently accessible. There is also no unfiltered heel. Disadvantages are the necessity and attendant labor requirements of emptying by hand and replacing the filter media and the tendency for heavy solids to settle out in the header chamber. Applications are as a scavenger filter to remove fines not removed in a prior-filtration stage with a different kind of equipment, to handle the runoff from other filters, and in semiworks and small-plant operations in which the filter's size, versatility, and cleanliness recommend it.

External-Cake Tubular Filters Several filter designs are available with vertical tubes supported by a filtrate-chamber tube sheet in a vertical cylindrical vessel (Fig. 18-128). The tubes may be made of wire cloth; porous ceramic, carbon, plastic, or metal; or closely wound wire. The tubes may have a filter cloth on the outside. Frequently a filter-aid precoat will be applied to the tubes. The prefiltrate slurry is fed near the bottom of the vertical vessel. The filtrate passes from the outside to the inside of the tubes and into a filtrate chamber at the top or the bottom of the vessel. The solids form a cake on the outside of the tubes with the filter area actually increasing as the cake builds up, partially compensating for the increased flow resistance of the thicker cake. The filtration cycle continues until the differential pressure reaches a specified level, or until about 25 mm (1 in) of cake thickness is obtained.

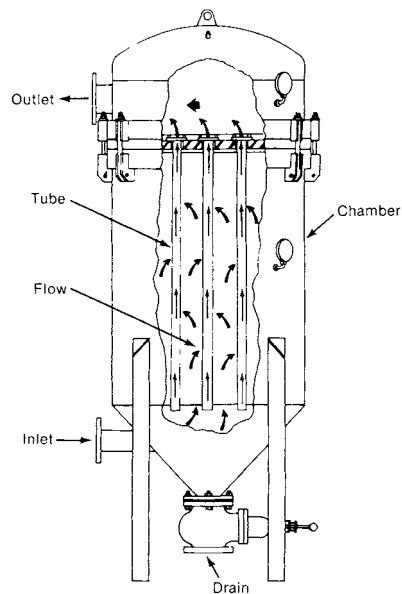


FIG. 18-128 Top-outlet tubular filter. (Industrial Filter & Pump Mfg. Co.)

Cake-discharge methods are the chief distinguishing feature among the various designs. That of the Industrial Filter & Pump Hydra-Shoc, for example, removes cake from the tubes by filtrate backflushing assisted by the "shocking" action of a compressed-gas pocket formed in the filtrate chamber at the top of the vertical vessel. Closing the filtrate outlet valve while continuing to feed the filter causes compression of the gas volume trapped in the dome of the vessel until, at the desired gas pressure, quick-acting valves stop the feed and open a bottom drain. The compressed gas rapidly expands, forcing a rush of filtrate back across the filter medium and dislodging the cake, which drains out the bottom with the flush liquid. Of course, this technique may be used only when wet-cake discharge is permitted.

Dry cake discharge can be achieved with a Fundabac candle-type filter manufactured by DrM, Dr. Müller, AG, of Switzerland. This filter uses a candle made up of six small-diameter tubes around a central filtrate delivery tube. This design allows the filter cloth to be flexed outward upon blowback, easily achieving an effective dry cake discharge (Fig. 18-129).

Pressure Leaf Filters Sometimes called tank filters, they consist of flat filtering elements (leaves) supported in a pressure shell. The leaves are circular, arc-sided, or rectangular, and they have filtering surfaces on both faces. The shell is a cylindrical or conical tank. Its axis may be horizontal or vertical, and the filter type is described by its shell axis orientation.

A filter leaf consists of a heavy screen or grooved plate over which a filter medium of woven fabric or fine wire cloth may be fitted. Textile fabrics are more commonly used for chemical service and are usually applied as bags that may be sewed, zippered, stapled, or snapped. Wire-screen cloth is frequently used for filter-aid filtrations, particularly if a precoat is applied. It may be attached by welding, riveting, bolting, or caulking or by the clamped engagement of two 180° bends in the wire cloth under tension, as in Multi Metal's Rim-Lok leaf. Leaves may also be of all-plastic construction. The filter medium, regardless of material, should be as taut as possible to minimize sagging when it is loaded with a cake; excessive sag can cause cake cracking or dropping. Leaves may be supported at top, bottom, or center and may discharge filtrate from any of these locations. Figure 18-130 shows the elevation section of a precoated bottom-support wire leaf.

Pressure leaf filters are operated batchwise. The shell is locked, and the prefiltrate slurry is admitted from a pressure source. The slurry enters in such a way as to minimize settling of the suspended solids. The shell

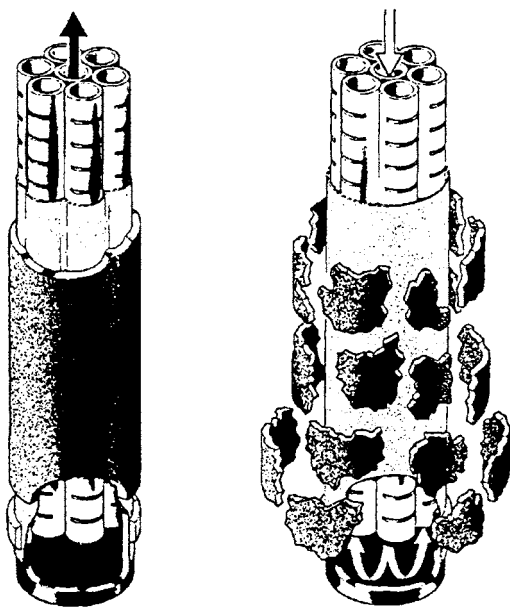


FIG. 18-129 Cake formation and discharge with the Fundabac filter element. (Dr.M, Dr. Müller AG, Switzerland.)

is filled, and filtration occurs on the leaf surfaces, the filtrate discharging through an individual delivery line or into an internal manifold, as the filter design dictates. Filtration is allowed to proceed only until a cake of the desired thickness has formed, since to overflow will cause cake consolidation with consequent difficulty in washing and discharge. The decision of when to end the filtering cycle is largely a matter of experience, guided roughly by the rate in a constant-pressure filter or pressure drop in a constant-rate filter. This judgment may be supplanted by the use of a detector which "feels" the thickness of cake on a representative leaf.

If the cake is to be washed, the slurry heel can be blown from the filter and wash liquor can be introduced to refill the shell. If the cake tends to crack during air blowing, it may be necessary to displace the slurry heel with wash gradually so as never to allow the cake to dry. Upon the completion of filtration and washing, the cake is discharged by one of several methods, depending on the shell and leaf configuration.

Horizontal pressure leaf filters. In these filters the leaves may be rectangular leaves which run parallel to the axis and are of varying sizes since they form chords of the shell; or they may be circular or square elements parallel to the head of the shell, and all of the same dimension. The leaves may be supported in the shell from an independent rack, individually from the shell, or from a filtrate manifold. Horizontal filters are particularly suited to dry-cake discharge.

Most of the currently available commercial horizontal pressure filters have leaves parallel to the shell head. Cake discharge may be wet or dry; it can be accomplished by sluicing with liquid sprays, vibration of the leaves, or leaf rotation against a knife, wire, or brush. If a wet-cake discharge is allowable, the filters will probably be sluiced with high-pressure liquid. If the filter has a top or bottom filtrate manifold, the leaves are usually in a fixed position, and the spray header is rotated to contact all filter surfaces. If the filtrate header is center-mounted, the leaves are generally rotated at about 3 r/min and the spray header is fixed. Some units may be wet-cake-discharged by mechanical vibration of the leaves with the filter filled with liquid. Dry-cake discharge normally will be accomplished by vibration if leaves are top- or bottom-manifolded and by rotation of the leaves against a cutting knife, wire, or brush if they are center-manifolded.

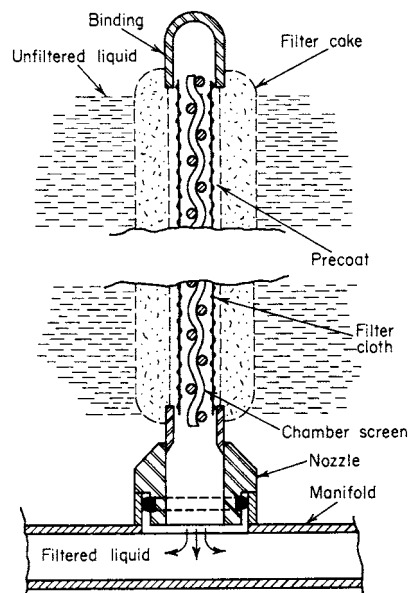


FIG. 18-130 Section of precoated wire filter leaf.

In many designs the filter is opened for cake discharge, and the leaf assembly is separated from the shell by moving one or the other on rails (Fig. 18-131). For processes involving toxic or flammable materials, a closed filter system can be maintained by sloping the bottom of the horizontal cylinder to the drain nozzle for wet discharge or by using a screw conveyor in the bottom of the shell for dry discharge.

Vertical pressure leaf filters. These filters have vertical, parallel, rectangular leaves mounted in an upright cylindrical pressure tank. The leaves usually are of such different widths as to allow them to conform to the curvature of the tank and to fill it without waste space. The leaves often rest on a filtrate manifold, the connection being sealed by an O ring, so that they can be lifted individually from the top of the filter for inspection and repair. A scavenger leaf frequently is installed in the bottom of the shell to allow virtually complete filtration of the slurry heel at the end of a cycle.

Vertical filters are not convenient for the removal of dry cake, although they can be used in this service if they have a bottom that can be retracted to permit the cake to fall into a bin or hopper below. They are adapted rather to wet-solids discharge, a process that may be assisted by leaf vibration, air or steam sparging of a filter full of water, sluicing from fixed, oscillating, or traveling nozzles, and blowback. They are made by many companies, and they enjoy their widest use for filter-aid precoat filtration.

Advantages and uses. The advantages of pressure leaf filters are their considerable flexibility (up to the permissible maximum, cakes of various thickness can be formed successfully), their low labor charges, particularly when the cake may be sluiced off or the dry cake discharged cleanly by blowback, the basic simplicity of many of the designs, and their adaptability to quite effective displacement washing. Their disadvantages are the requirement of exceptionally intelligent and watchful supervision to avoid cake consolidation or dropping, their inability to form as dry a cake as a filter press, their tendency to classify vertically during filtration and to form misshapen nonuniform cakes when the leaves rotate, and the restriction of most models to 610 kPa (75 psig) or less.

Pressure leaf filters are used to separate much the same kinds of slurries as are filter presses and are used much more extensively than filter presses for filter-aid filtrations. They should be seriously considered whenever uniformity of production permits long-time operation

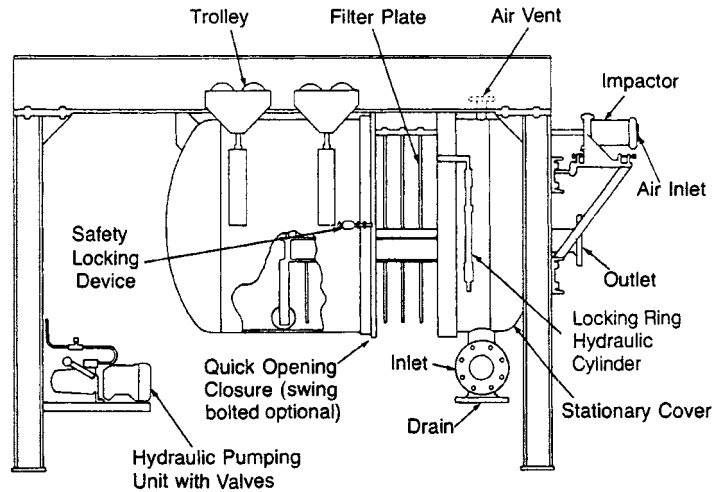


FIG. 18-131 Horizontal-tank pressure leaf filter designed for dry cake discharge. (Sparkler Filter, Inc.)

under essentially constant filtration conditions, when thorough washing with a minimum of liquor is desired, or when vapors or fumes make closed construction desirable. Under such conditions, if the filter medium does not require frequent changing, they may show a considerable advantage in cycle and labor economy over a filter press, which has a lower initial cost, and advantages of economy and flexibility over continuous vacuum filters, which have a higher first cost.

Pressure leaf filters are available with filtering areas of 930 cm^2 (1 ft^2) (laboratory size) up to about 440 m^2 (4734 ft^2) for vertical filters and 158 m^2 (1700 ft^2) for horizontal ones. Leaf spacings range from 5 to 15 cm (2 to 6 in) but are seldom less than 7.5 cm (3 in) since 1.3 to 2.5 cm (0.5 to 1 in) should be left open between surfaces.

Centrifugal-Discharge Filter Horizontal top-surface filter plates may be mounted on a hollow motor-connected shaft that serves both as a filtrate-discharge manifold and as a drive shaft to permit centrifugal removal of the cake. An example is the Funda filter (marketed in the United States by Steri Technologies), illustrated schematically in Fig. 18-132. The filtering surface may be a textile fabric or a wire screen, and the use of a precoat is optional. The Funda filter is driven from the top, leaving the bottom unobstructed for inlet and drainage lines; a somewhat similar machine that employs a bottom drive,

providing a lower center of mass and ground-level access to the drive system, is the German-made **Schenk filter** (marketed in the United States by Pall Seitz Schenk Filtersystems).

During filtration, the vessel that coaxially contains the assembly of filter plates is filled with prefiltrate under pressure, the filtrate passes through the plates and out the hollow shaft, and cake is formed on the top surfaces of the plates. After filtration, the vessel is drained, or the heel may be filtered by recirculation through a cascade ring at the top of the filter. The cake may be washed—or it may be extracted, steamed, air-blown, or dried by hot gas. It is discharged, wet or dry, by rotation of the shaft at sufficiently high speed to sling away the solids. If flushing is permitted, the discharge is assisted by a backwash of appropriate liquid.

The operating advantages of the centrifugal-discharge filter are those of a horizontal-plate filter and, further, its ability to discharge cake without being opened. It is characterized by low labor demand, easy adaptability to automatic control, and amenability to the processing of hazardous, noxious, or sterile materials. Its disadvantages are its complexity and maintenance (stuffing boxes, high-speed drive) and its cost. The Funda filter is made in sizes that cover the filtering area range of 1 to 50 m^2 (11 to 537 ft^2). The largest Schenk filter provides 100 m^2 (1075 ft^2) of area.

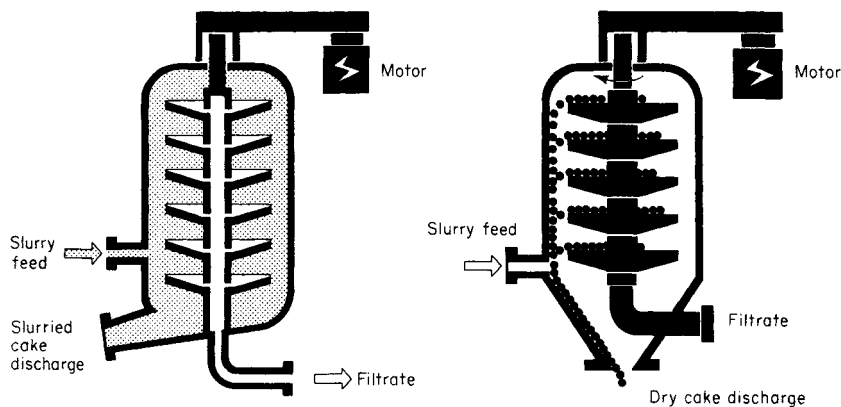


FIG. 18-132 Schematic of a centrifugal-discharge filter. (Steri Technologies.)

Continuous Cake Filters Continuous cake filters are applicable when cake formation is fairly rapid, as in situations in which slurry flow is greater than about 5 L/min (1 to 2 gal/min), slurry concentration is greater than 1 percent, and particles are greater than 0.5 μm in diameter. Liquid viscosity below 0.1 Pa·s (100 cP) is usually required for maintaining rapid liquid flow through the cake. Some designs of continuous filters can compromise some of these guidelines by sacrificial use of filter aid when the cake is not the desired product.

Rotary Drum Filters The rotary drum filter is the most widely used of the continuous filters. There are many design variations, including operation as either a pressure filter or a vacuum filter. The major difference between designs is in the technique for cake discharge, to be discussed later. All the alternatives are characterized by a horizontal-axis drum covered on the cylindrical portion by filter medium over a grid support structure to allow drainage to manifolds. Basic materials of construction may be metals or plastics. Sizes (in terms of filter areas) range from 0.37 to 186 m^2 (4 to 2000 ft^2).

All drum filters (except the single-compartment filter) utilize a rotary-valve arrangement in the drum-axis support trunnion to facilitate removal of filtrate and wash liquid and to allow introduction of air or gas for cake blowback if needed. The valve controls the relative duration of each cycle as well as providing "dead" portions of the cycle through the use of bridge blocks. A typical valve design is shown in Fig. 18-133. Internal piping manifolds connect the valve with various sections of the drum.

Most drum filters are fed by operating the drum with about 35 percent of its circumference submerged in a slurry trough, although submergence can be set for any desired amount between zero and almost total. Some units contain an oscillating rake agitator in the trough to aid solids suspension. Others use propellers, paddles, or no agitator.

Slurries of free-filtering solids that are difficult to suspend are sometimes filtered on a top-feed drum filter or filter-dryer. An example application is in the production of table salt. An alternative for slurries of extremely coarse, dense solids is the internal drum filter. In the chemical-process industry both top-feed and internal drums (which are described briefly by Emmett in Schweitzer, *op. cit.*, p. 4-41) have largely been displaced by the horizontal vacuum filter (q.v.).

Most drum filters operate at a rotation speed in the range of 0.1 to 10 r/min. Variable-speed drives are usually provided to allow adjustment for changing cake-formation and drainage rates.

Drum filters commonly are classified according to the feeding arrangement and the cake-discharge technique. They are so treated in this subsection. The characteristics of the slurry and the filter cake usually dictate the cake-discharge method.

Scraper-Discharge Filter The filter medium is usually caulked into grooves in the drum grid, with cake removal facilitated by a scraper

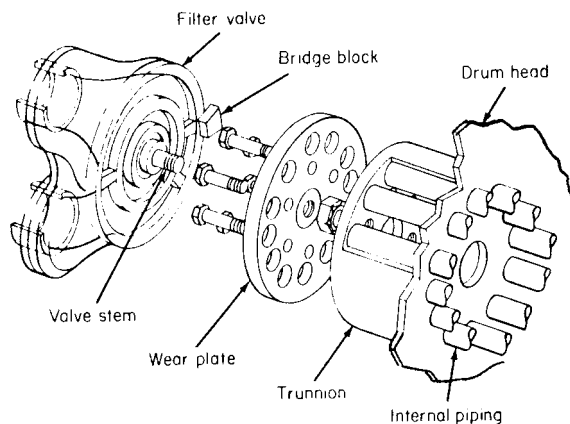


FIG. 18-133 Component arrangement of a continuous-filter valve. (Dorr-Oliver EIMCO.)

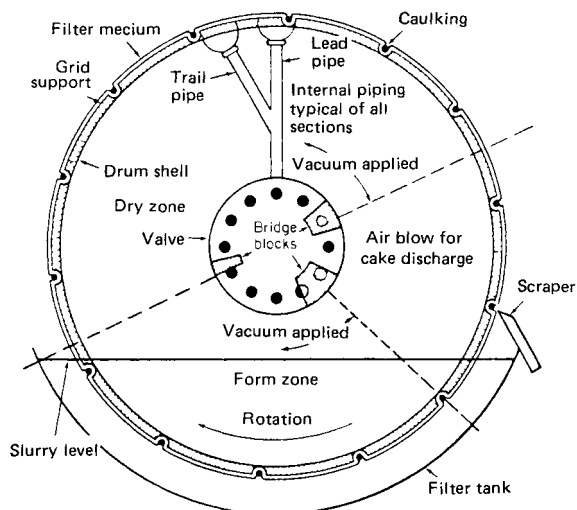


FIG. 18-134 Schematic of a rotary-drum vacuum filter with scraper discharge, showing operating zones. (Schweitzer, *Handbook of Separation Techniques for Chemical Engineers*, p. 4-38. Copyright 1979 by McGraw-Hill, Inc. and used with permission.)

blade just prior to the resubmergence of the drum (Fig. 18-134). The scraper serves mainly as a deflector to direct the cake, dislodged by an air blowback, into the discharge chute, since actual contact with the medium would cause rapid wear. In some cases the filter medium is held by circumferentially wound wires spaced 50 mm (2 in) apart, and a flexible scraper blade may rest lightly against the wire winding. A taut wire in place of the scraper blade may be used in some applications in which physical dislodging of sticky, cohesive cakes is needed.

For a given slurry, the maximum filtration rate is determined by the minimum cake thickness which can be removed—the thinner the cake, the less the flow resistance and the higher the rate. The minimum thickness is about 6 mm (0.25 in) for relatively rigid or cohesive cakes of materials such as mineral concentrates or coarse precipitates like gypsum or calcium citrate. Solids that form friable cakes composed of less cohesive materials such as salts or coal will usually require a cake thickness of 13 mm (0.5 in) or more. Filter cakes composed of fine precipitates such as pigments and magnesium hydroxide, which often produce cakes that crack or adhere to the medium, usually need a thickness of at least 10 mm (0.38 in).

String-Discharge Filter A system of endless strings or wires spaced about 13 mm (0.5 in) apart pass around the filter drum but are separated tangentially from the drum at the point of cake discharge, lifting the cake off as they leave contact with the drum. The strings return to the drum surface guided by two rollers, the cake separating from the strings as they pass over the rollers. If it has the required body, a thinner cake (5 mm or about $\frac{3}{16}$ in) than can be handled by drum filters is feasible, allowing more difficult materials to be filtered. This is done at the expense of greater dead area on the drum. Success depends on the ability of the cake to be removed with the strings and must be determined experimentally. Applications are mainly in the starch and pharmaceutical industries, with some in the metallurgical field.

Removable-Medium Filters Some drum filters provide for the filter medium to be removed and reapplied as the drum rotates. This feature permits the complete discharge of thin or sticky cake and provides the regenerative washing of the medium to reduce blinding. Higher filtration rates are possible because of the thinner cake and clean medium, but this is compromised by a less pure filtrate than normally produced by a nonremovable medium.

Belt-discharge filter. This is a drum filter carrying a fabric that is removed, passed over rollers, washed, and returned to the drum. Figure 18-135 shows the path of the medium while it is off the drum.

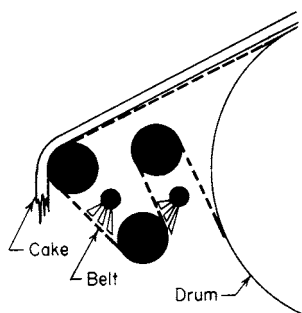


FIG. 18-135 Cake discharge and medium washing on an EIMCO belt filter. (Dorr-Oliver EIMCO.)

A special aligning device keeps the medium wrinkle-free and in proper line during its travel. Thin cakes of difficult solids which may be slightly soluble are good applications. When acceptable, a sluice discharge makes cakes as thin as 1.5 to 2 mm (about $\frac{1}{16}$ in) feasible. Several manufacturers offer belt-discharge filters.

Coilfilter. The **Coilfilter** (Komline-Sanderson Engineering Corp.) is a drum filter with a medium consisting of one or two layers of stainless-steel helically coiled springs, about 10 mm (0.4 in) in diameter, placed in a corduroy pattern around the drum. The springs follow the drum during filtration with cake forming the coils. They are separated from the drum to discharge the cake and undergo washing; if two layers are used, the coils of each layer are further separated from those of the other, passing over different sets of rolls. The use of stainless steel in spring form provides a relatively permanent medium that is readily cleaned by washing and flexing. Filtrate clarity is poorer than with most other media, and a relatively large vacuum pump is needed to handle greater air leakage than is characteristic of fabric media. Material forming a slimy, matlike cake (e.g., raw sewage) is the typical application.

Roll-Discharge Filters A roll in close proximity to the drum at the point of cake discharge rotates in the opposite direction at a peripheral speed equal to or slightly faster than that of the drum (Fig. 18-136). If the cake on the drum is adequately tacky and cohesive for this discharge technique, it adheres to cake on the smaller roll and separates from the drum. A blade or taut wire removes the material from the discharge roll. This design is especially good for thin, sticky cakes. If necessary, a slight air blow may be provided to help release the cake from the drum. Typical cake thickness is 1 to 10 mm (0.04 to 0.4 in).

Single-Compartment Drum Filter

Bird-Young filter. This filter (Bird Machine Co.) differs from most drum filters in that the drum is not compartmented and there is no internal piping or rotary valve. The entire inside of the drum is subjected to vacuum, with its surface perforated to pass the filtrate. Cake is discharged by an air blowback applied through a "shoe" that covers a narrow discharge zone on the inside surface of the drum to interrupt the vacuum, as illustrated in Fig. 18-137. The internal drum surface must be machined to provide close clearance of the shoe to avoid leakage. The filter is designed for high filtration rates with thin cakes. Rotation speeds to 40 r/min are possible with cakes typically 3 to 6 mm (0.12 to 0.24 in) thick. Filter sizes range from 930 cm² to 19 m² (1 to 207 ft²) with 93 percent of the area active. The slurry is fed into a conical feed tank designed to prevent solids from settling without the use of mechanical agitators. The proper liquid level is maintained by overflow, and submergence ranges from 5 to 70 percent of the drum circumference.

The perforated drum cylinder is divided into sections about 50 to 60 mm (2 to 2.5 in) wide. The filter medium is positioned into tubes between the sections and locked into place by round rods. No caulking, wires, or other fasteners are needed.

Wash sprays may be applied to the cake, with collection troughs or pans inserted inside the drum to keep the wash separate from the filtrate. Filtrate is removed from the lower section of the drum by a pipe passing through the trunnions.

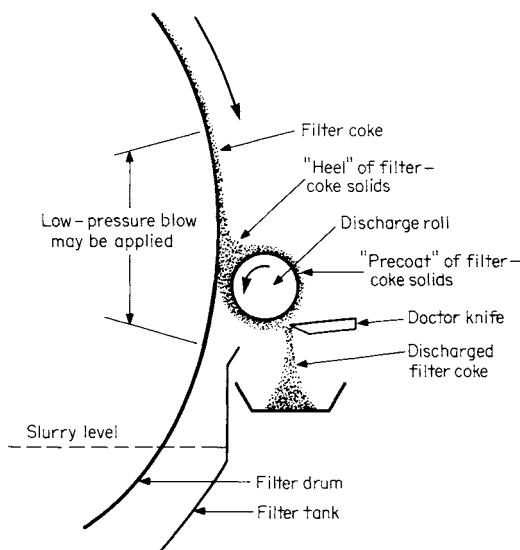


FIG. 18-136 Operating principles of a roll-discharge mechanism. (Schweitzer, Handbook of Separation Techniques for Chemical Engineers, p. 4-40. Copyright 1979 by McGraw-Hill, Inc. and used with permission.)

The major advantages of the Bird-Young filter are its ability to handle thin cakes and operate at high speeds, its washing effectiveness, and its low internal resistance to air and filtrate flow. An additional advantage is the possibility of construction as a pressure filter with up to 1.14-MPa (150-psig) operating pressure to handle volatile liquids. The chief disadvantages are its high cost and the limited flexibility imposed by not having an adjustable rotary valve. Best applications are on free-draining nonblinding materials such as paper pulp or crystallized salts.

Continuous Pressure Filters These filters consist of conventional drum or disc filters totally enclosed in pressure vessels. Filtration takes place with the vessel pressurized up to 6 bar and the filtrate discharging either at atmospheric pressure or into a receiver maintained at a suitable backpressure. Cake discharge is facilitated through a dual valve and lock-hopper arrangement in order to maintain vessel pressure. Alternatively, the discharged filter cake can be reslurried within the filter or in an adjoining pressure vessel and removed through a control valve.

One variation in design, the Ceramec, offered by Outokumpu Mintec, employs "gasless" ceramic media instead of traditional filter fabrics, relying partly on capillary action to achieve low moistures. This results in a significant drop in power consumption by greatly reducing the compressed air requirements.

Continuous Precoat Filters These filters may be operated as either pressure or vacuum filters, although vacuum operation is the prevailing one. The filters are really not continuous but have an extremely long batch cycle (1 to 10 days). Applications are for continuous clarification of liquids from slurries containing 50 to 5000 ppm of solids when only very thin unacceptable cakes would form on other filters and where "perfect" clarity is required.

Construction is similar to that of other drum filters, except that vacuum is applied to the entire rotation. Before feeding slurry a precoat layer of filter aid or other suitable solids, 75 to 125 mm (3 to 5 in) thick, is applied. The feed slurry is introduced and trapped in the outer surface of the precoat, where it is removed by a progressively advancing doctor knife which trims a thin layer of solids plus precoat (Fig. 18-138). The blade advances 0.05 to 0.2 mm (0.002 to 0.008 in) per revolution of the drum. When the precoat has been cut to a pre-defined minimum thickness, the filter is taken out of service, washed, and freshly pre-coated. This turnaround time may be 1 to 3 h.

Disc Filters A disc filter is a vacuum filter consisting of a number of vertical discs attached at intervals on a continuously rotating

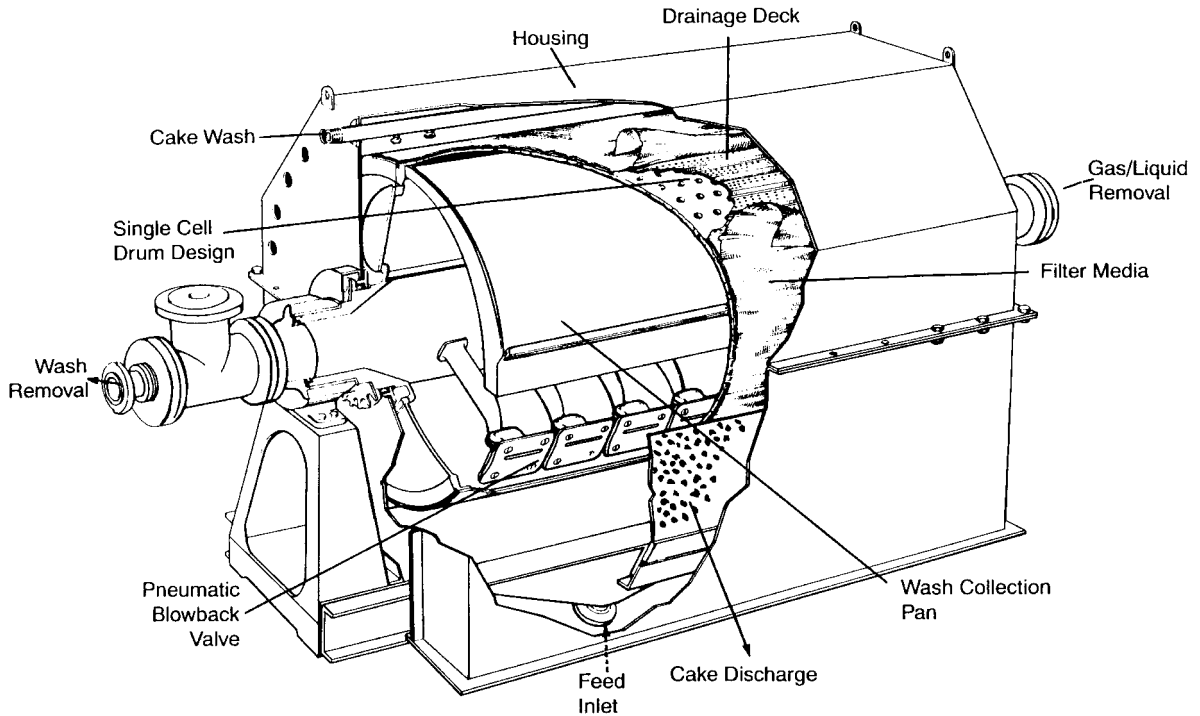


FIG. 18-137 Cutaway of the single-compartment drum filter. (Andritz Bird.)

horizontal hollow central shaft (Fig. 18-139). Rotation is by a gear drive. Each disc consists of 10 to 30 sectors of metal, plastic, or wood, ribbed on both sides to support a filter cloth and provide drainage via an outlet nipple into the central shaft. Each sector may be replaced individually. The filter medium is usually a cloth bag slipped over the sectors and sealed to the discharge nipple. For some heavy-duty applications on ores, stainless-steel screens may be used.

The discs are typically 30 to 50 percent submerged in a troughlike vessel containing the slurry. Another horizontal shaft running beneath the discs may contain agitator paddles to maintain suspension of the solids, as in the EIMCO **Agidisc filter**. In some designs, feed is distributed through nozzles below each disc. Vacuum is supplied to the sectors as they rotate into the liquid to allow cake formation. Vacuum is maintained as the sectors emerge from the liquid and are exposed to

air. Wash may be applied with sprays, but most applications are for dewatering only. As the sectors rotate to the discharge point, the vacuum is cut off, and a slight air blast is used to loosen the cake. This allows scraper blades to direct the cake into discharge chutes positioned between the discs. Vacuum and air blowback is controlled by an automatic valve as in rotary-drum filters.

Of all continuous filters, the vacuum disc is the lowest in cost per unit area of filter when mild steel, cast iron, or similar materials of construction may be used. It provides a large filtering area with minimum floor space, and it is used mostly in high-tonnage dewatering applications in sizes up to about 300 m² (3300 ft²) of filter area.

The main disadvantages are the inadaptability to have effective wash and the difficulty of totally enclosing the filter for hazardous-material operations.

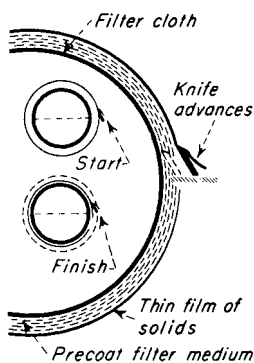


FIG. 18-138 Operating method of a vacuum precoat filter. (Dorr-Oliver EIMCO.)

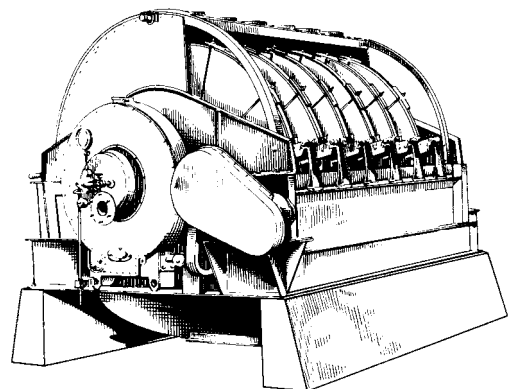


FIG. 18-139 Rotary disc filter. (Dorr-Oliver EIMCO.)

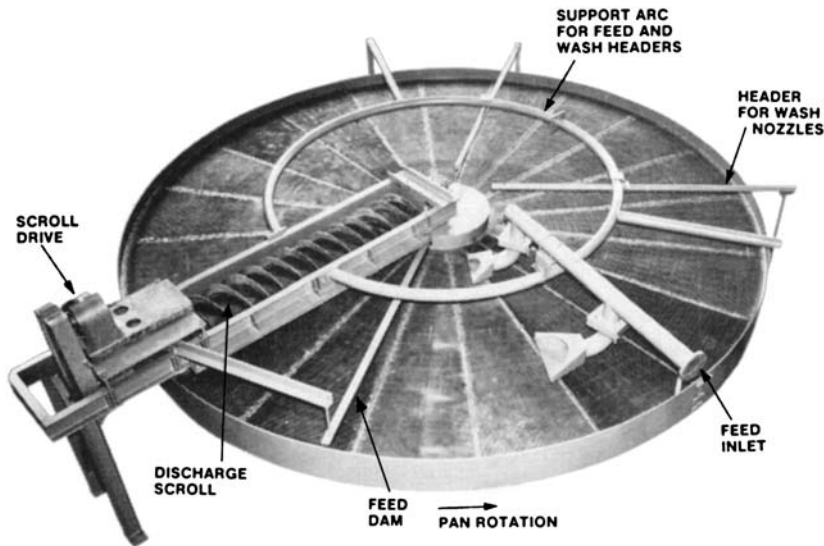


FIG. 18-140 Continuous horizontal vacuum table filter. (Dorr-Oliver EIMCO.)

Horizontal Vacuum Filters These filters are generally classified into two broad classes: rotary circular and belt-type units. Regardless of geometry, they have similar advantages and limitations. They provide flexibility of choice of cake thickness, washing time, and drying cycle. They effectively handle heavy, dense solids, allow flooding of the cake with wash liquor, and are easily designed for true counter-current leaching or washing. The disadvantages are they are more expensive to build than drum or disc filters, they use a large amount of floor space per filter area, and they are difficult to enclose for hazardous applications.

Horizontal-Table, Scroll-Discharge, and Pan Filters These are all basically revolving annular tables with the top surface a filter medium (Fig. 18-140). The table is divided into sectors, each of which is a separate compartment. Vacuum is applied through a drainage chamber beneath the table that leads to a large rotary valve. Slurry is fed at one point, and cake is removed after completing more than three-fourths of the circle, by a horizontal scroll conveyor which elevates the cake over the rim of the filter. A clearance of about 10 mm (0.4 in) is maintained between the scroll and the filter medium to prevent damage to the medium. Residual cake on the medium may be loosened by an air blow from below or with high-velocity liquid sprays from above. This residual cake is a disadvantage peculiar to this type of filter. With material that can cause blinding, frequent shutdowns for thorough cleaning may be needed. Unit sizes range from about 0.9 to 9 m (3 to 30 ft) in diameter, with about 80 percent of the surface available for filtration.

Tilting-Pan Filter This is a modification of the table or pan filter in which each of the sectors is an individual pan pivoted on a radial axis to allow its inversion for cake discharge, usually assisted by an air blast. Filter-cake thicknesses of 50 to 100 mm (2 to 4 in) are common. Most applications involve free-draining inorganic-salt dewatering. In addition to the advantages and disadvantages common to all horizontal continuous filters, tilting-pan filters have the relative advantages of complete wash containment per sector, good cake discharge, filter-medium washing, and feasibility of construction in very large sizes, up to about 25 m (80 ft) in diameter, with about 75 percent of the area usable. Relative disadvantages are high capital cost (especially in smaller sizes) and mechanical complexity leading to higher maintenance costs.

Horizontal-Belt Filter This filter consists of a slotted or perforated elastomer drainage belt driven as a conveyor belt carrying a filter fabric belt (Fig. 18-141). Both belts are supported by and pass across a lubricated support deck. A vacuum pan, aligned with the slots in the elastomer belt, forms a continuous vacuum surface which may include multiple zones for cake formation, washing and final dewater-

ing. Several manufacturers provide horizontal-belt filters, the major differences among which lie in the construction of the drainage belt, the method of retaining the slurry/cake on the belt, and the method of maintaining the alignment of the filter medium. The filters are rated according to the available active filtration area. *Indexing horizontal-belt filters* do away with the elastomer drainage belt of the original design in favor of large drainage pans directly beneath the filter medium. Either the pans or the filter medium is indexed to provide a pseudo-continuous filtration operation. The applied vacuum is cycled with the indexing operation to minimize wear to the sliding surfaces. As a result the indexing filter must be de-rated for the indexing cycle. The indexing horizontal-belt filter avoids the problem of process compatibility with the elastomer drainage belt. The major differences among the indexing machines of several manufacturers lie in the method of indexing and the method of cycling the applied vacuum.

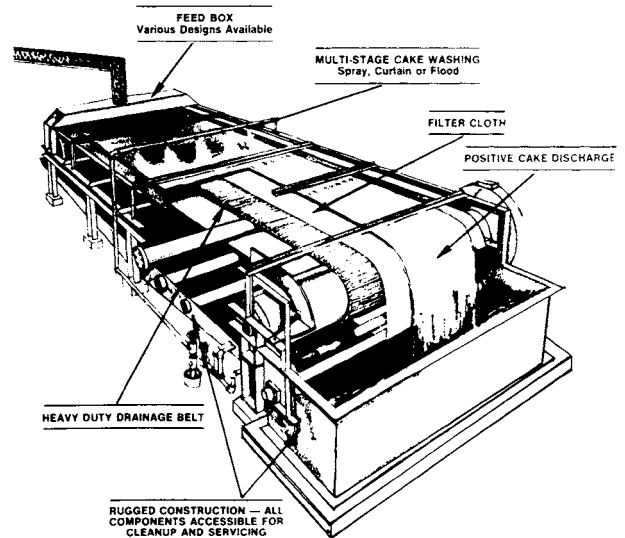


FIG. 18-141 Horizontal-belt filter. (Dorr-Oliver EIMCO.)

The method of feeding, washing, dewatering and discharging is essentially the same with all horizontal-belt filters. Slurry is fed at one end by overflow weirs or a fantail chute; wash liquor, if required, is applied by sprays or weirs at one or more locations as the formed cake moves along the filter. Wiping dams and separations in the drainage pan(s) provide controlled wash application. The cake is discharged as the filter-medium belt passes over the end pulley after separation from the drainage surface. Separating the filter-medium from the drainage surface allows thorough spray cleaning of the filter-medium belt. The duration of the filtration cycle is controlled by belt speed which may be as high as 1 m/s (3.3 ft/s) and is typically variable. The minimum possible cake thickness, at a given solids loading, which can be effectively discharged limits the belt speed from a process point of view. The maximum cake thickness is dependent on the method used to retain the slurry during cake formation and can be 100 to 150 mm (4 to 6 in) with fast draining materials.

Some of the advantages of horizontal-belt filters are the precise control of the filtration cycle including the capability for countercurrent washing of the cake, effective cake discharge and thorough cleaning of the filter medium belt. The horizontal-belt filter's primary disadvantage is that at least half of the filtration medium is always idle during the return loop. This contributes to a significantly higher capital cost which can be two to four times that of a drum or disc filter with equal area. Horizontal-belt filters with active filtration area ranging from 0.18 m² to 150 m² (2 ft² to 1600 ft²) on a single machine have been installed.

Additional equipment is sometimes integrated with horizontal-belt filters to further dewater the cake through expression. The addition of such equipment shouldn't be confused with expression equipment that utilizes filter medium belts. Belt type expression equipment is described later in the "Expression" subsection.

Filter Thickeners Thickeners are devices which remove a portion of the liquid from a slurry to increase the concentration of solids in suspension. Thickening is done to prepare a dilute slurry for more economical filtration or to change the consistency or concentration of the slurry for process reasons. The commonest method of thickening is by gravity sedimentation, discussed earlier in this section. Occasions may arise, however, in which a filter may be called upon for thickening service. Many of the filters previously discussed as cake filters can be operated as thickeners: the filter press with special plates containing flow channels that keep velocity high enough to prevent cake buildup, cycloned tube or candle filters with the cake discharge into the filter tank, and continuous leaf filters which use rotating elements adjacent to the filtering surfaces to limit filter cake buildup. Examples of these filters include the Shriver Thickener, the Industrial Hydra-Shoc Filter employing Back Pulse Technology, the DrM, Dr. Müller AG, Contibac Thickener, and the Ingersoll Rand Continuous Pressure Filter.

Clarifying Filters Clarifying filters are used to separate liquid mixtures which contain only very small quantities of solids. When the solids are finely divided enough to be observed only as a haze, the filter which removes them is sometimes called a polishing filter. The prefiltr slurry generally contains no more than 0.10 percent solids, the size of which may vary widely (0.01 to 100 μm). The filter usually produces no visible cake, sometimes because the amount of solids removed is so small, sometimes because the particles are removed by being entrapped within rather than upon the filter medium. Compared with cake filters, clarifying filters are of minor importance to pure chemical-process work, their greatest use being in the fields of beverage and water polishing, pharmaceutical filtration, fuel- and lubricating-oil clarification, electroplating-solution conditioning, and dry-cleaning-solvent recovery. They are essential, however, to the processes of fiber spinning and film extrusion; the spinning solution or dope must be free of particles above a certain size to maintain product quality and to prevent the clogging of spinnerets.

Most cake filters can be so operated as to function as clarifiers, although not necessarily with efficiency. On the other hand, a number of clarifying filters which can be used for no purpose other than clarifying or straining have been developed. In general, clarifying filters are less expensive than cake filters. Clarifying filters may be classified as disc and plate presses, cartridge clarifiers, precoat pressure filters, deep-bed filters, and miscellaneous types. Membrane filters constitute a special class of plate presses and cartridge filters. Simple strainers sometimes are

used as clarifiers of liquids containing very large particles. Because they more closely resemble wet screens than filters and because they have little primary process application, they are not discussed here.

Disc Filters and Plate Presses Filters employing asbestos-pulp discs, cakes of cotton fibers (filtermasse), or sheets of paper or other media are used widely for the polishing of beverages, plating solutions, and other low-viscosity liquids containing small quantities of suspended matter. The term **disc filter** is applied to assemblies of pulp discs made of asbestos and cellulose fibers and sealed into a pressure case. The discs may be preassembled into a self-supporting unit (Fig. 18-142), or each disc may rest on an individual screen or plate against which it is sealed as the filter is closed (Fig. 18-143). The liquid flows through the discs, and into a central or peripheral discharge manifold. Flow rates are on the order of 122 L/(min·m²) [3 gal/(min·ft²)], and the operating pressure does not normally exceed 345 kPa (50 psig) (usually it is less). Disc filters are almost always operated as pressure filters. Individual units deliver up to 378 L/min (6000 gal/h) of low-viscosity liquid.

Disc-and-plate assemblies somewhat resemble horizontal-plate pressure filters, which, in fact, may be used for polishing. In one design (**Sparkler VR filter**) both sides of each plate are used as filtering surfaces, having paper or other media clamped against them.

Pulp filters. These filters employ one or more packs of filter-masse (cellulose fibers compressed to a compact cylinder) stacked into a pressure case. The packs are sometimes supported in individual trays which provide drainage channels and sometimes rest on one another with a loose spacer plate between each two packs and with a drainage screen buried in the center of each pack. The liquid being clarified flows under a pressure of 345 kPa (50 psig) or less through the pulp packs and into a drainage manifold. Flow rates are somewhat less than for disc filters, on the order of 20 L/(min·m²) [0.5 gal/(min·ft²)]. Pulp filters are used chiefly to polish beverages. The filtermasse may be washed in special washers and re-formed into new cakes.

Plate presses. Sometimes called sheet filters, these are assemblies of plates, sheets of filter media, and sometimes screens or frames. They are essentially modified filter presses with practically no cake-holding capacity. A press may consist of many plates or of a single filter sheet between two plates, the plates may be rectangular or circular, and the sheets may lie in a horizontal or vertical plane. The operation is similar to that of a filter press, and the flow rates are about the same as for disc filters. The operating pressure usually does not exceed 138 kPa (20 psig). The presses are used most frequently for low-viscosity liquids, but an ordinary filter press with thin frames is commonly used as a clarifier for 100-Pas (1000-P) rayon-spinning solution. Here the filtration pressure may be 6900 kPa (1000 psig).

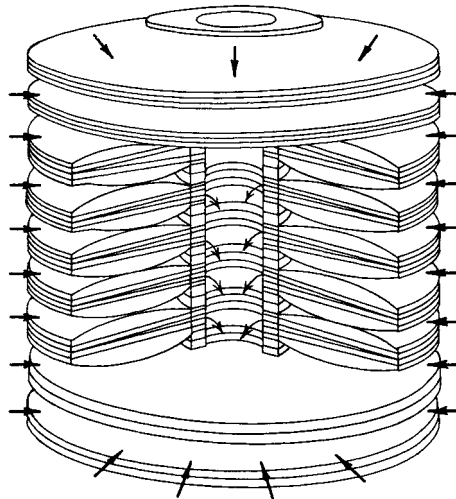


FIG. 18-142 Preassembled pack of clarifying-filter discs. (Ertel Alsop.)

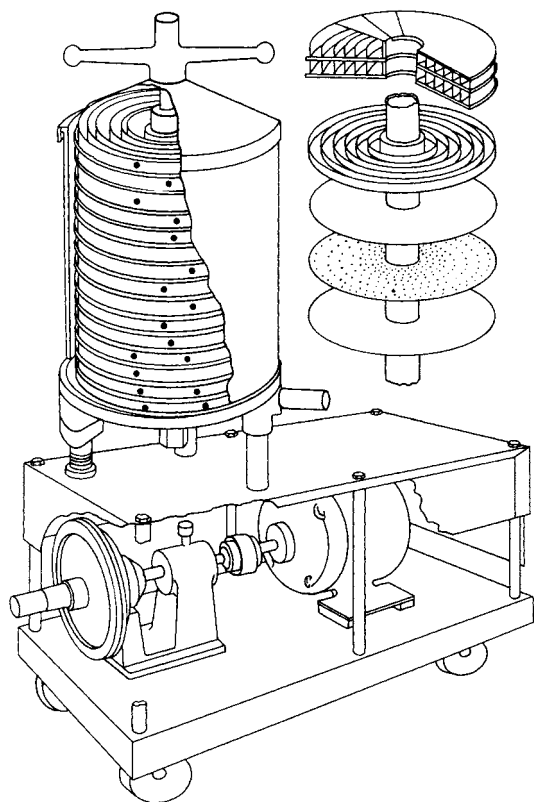


FIG. 18-143 Disc-and-plate clarifying-filter assembly. (Ertel Alsop.)

Disc, pulp, and sheet filters accomplish extreme clarification. Not infrequently their mission is complete removal of particles above a stipulated cut size, which may be much less than $1\ \mu\text{m}$. They operate over a particle-size range of four to five orders of magnitude, contrasting with two orders of magnitude for most other filters. It is not surprising, therefore, that they involve a variety of kinds and grades of filter media, often in successive stages. In addition to packs or discs of cellulosic, polymeric, or asbestos fiber, sheets of pulp, paper, asbestos, carded fiber, woven fabrics, and porous cellophane or polymer are employed. Sandwich-pack composites of several materials have been used for viscous-dope filtration.

The use of asbestos has been greatly diminished because of its identification with health hazards. There have been proposed replacement materials such as the **Zeta Plus** filter media from the AMF Cuno Division, consisting of a composite of cellulose and inorganic filter aids that have a positive charge and provide an electrokinetic attraction to hold colloids (usually negatively charged). These media therefore provide both mechanical straining and electrokinetic adsorption.

Cartridge Clarifiers Cartridge clarifiers are units which consist of or use one or more replaceable or renewable cartridges containing the active filter element. The unit usually is placed in a line carrying the liquid to be clarified; clarification thus occurs while the liquid is in transit.

Mechanical or edge filters. These consist of stacks of discs separated to precise intervals by spacer plates, or a wire wound on a cage in grooves of a precise pitch, or a combination of the two. The liquid to be filtered flows radially between the discs, wires, or layers of paper, and particles larger than the spacing are screened out. Edge filters can remove particles down to 0.001 in ($25\ \mu\text{m}$) but more often have a minimum spacing of twice this value. They have small solids-retaining capacity and hence must be cleaned often to avoid plugging. Continuous cleaning is provided in some filters. For example, the Cuno **Auto-Clean**, a wire-wound unit, employs a slowly rotating scraper that fits

into the interdisc slots to comb away accumulated solids. In either case, the dislodged solids fall into a sump that may be drained at intervals.

Micronic clarifiers. The greatest number of cartridge clarifiers are of the micronic class, with elements of fiber, resin-impregnated filter paper, porous stone, or porous stainless steel of controlled porosity. Other rustless metals are also available. The elements may be chosen to remove particles larger than a fraction of a micrometer, although many are made to pass $10\text{-}\mu\text{m}$ solids and smaller. By proper choice of multiple-cylinder cartridges or multiple cartridges in parallel any desired flow rate can be obtained at a reasonable pressure drop, often less than $138\ \text{kPa}$ ($20\ \text{psig}$).

When the pressure rises to the permissible maximum, the cartridge must be opened and the element replaced. Micronic elements of the fiber type cannot be cleaned and are so priced that they can be discarded or the filter medium replaced economically. Stone elements usually must be cleaned, a process best accomplished by the manufacturer of the porous ceramic or in accordance with the manufacturer's directions. The user can clean stainless-steel elements by chemical treatment.

Flexibility. Cartridge filters are flexible: cartridges of different ratings and materials of construction can be interchanged, permitting ready accommodation to shifting conditions. They have the disadvantage of very limited solid-handling capability so that the maximum solid concentrations in the feed are limited to about 0.01 percent solids. The biggest limitation for modern process-plant operation is the need to open the filter to replace cartridges, which makes their use for the processing of hazardous materials undesirable. Some manufacturers—for example, the Hydraulic Research Division of Textron Inc. and the Fluid Dynamics Division of Brunswick Corp.—have designed cartridges of bonded metal fibers that can be back-flushed or chemically cleaned without opening the unit. These filters, which can operate at temperatures to 482°C (900°F) and at pressures of $33\ \text{MPa}$ ($325\ \text{atm}$) or greater, are particularly useful for filtering polymers.

Granular Media Filters Many types of granular media filters are used for clarification, operating either as gravity or pressure filters. Gravity filters rely on a difference in elevation between inlet and outlet to provide the driving force necessary to force the liquid through the granular media. Pressure filters employ enclosed vessels operating at relatively low pressure differentials, in the order of 50 to $70\ \text{kPa}$ (7 to $10\ \text{psig}$), which may function in either an upflow or a downflow mode.

The media may be a single material, such as sand, but more often will consist of two or even three layers of different materials, such as anthracite coal in the top layer and sand in the lower one. Solids are captured throughout the bed depth, rather than on the surface, and the gradient in void size provides substantially more solids-holding capacity. The anthracite layer, typically employing 1-mm grain size, serves as a roughing filter and also provides a flocculating action which helps the finer sand, $\sim 0.5\text{-mm}$ particle size, to serve as an effective polishing zone. Media depths vary, but 0.7 to $1.0\ \text{m}$ is typical of a dual media installation. Deeper beds of up to $2.5\ \text{m}$ ($8\ \text{ft}$) are employed in some cases involving special applications where greater solids-holding capacity is desired.

Filtrate is collected in the underdrain system, which may be as simple as a network of perforated pipes covered by graded gravel or a complex structure with slotted nozzles or conduits that will retain the finest sand media while maintaining high flow rates. This latter design allows the use of both air and liquid for the backwashing and cleaning operations.

Backwashing usually is carried out when a limiting pressure drop is reached and before the bed becomes nearly filled with solids, which would lead to a deterioration in filtrate clarity. Cleaning the media is greatly aided by the use of an air scour which helps break loose the trapped solids and provides efficient removal of this material in the subsequent backflushing step. The filtration action tends to agglomerate the filtered solids and, as a result, these generally will settle out readily from the backwash fluid. If the filter is handling a clarifier overflow, usually it is possible to discharge the backwash liquid into the clarifier without risk of these solids returning to the filter. Filter media consumption is low, with normal replacement usually being less than 5 percent per year.

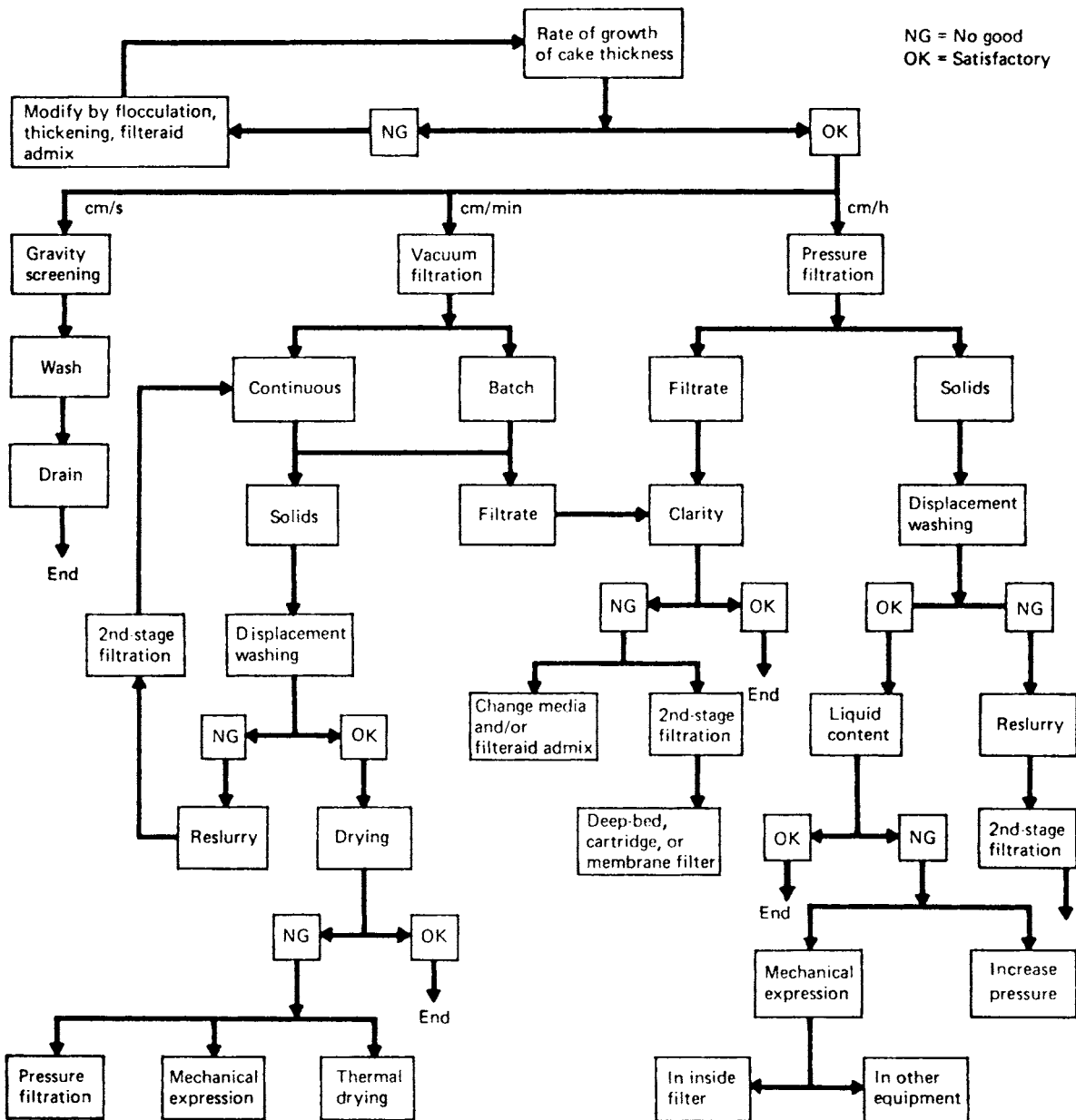


FIG. 18-144 Decision pattern for solving a filtration problem. [Tiller, Chem. Eng., 81(9), 118 (1974), by permission.]

These filters are best applied on relatively dilute suspensions, <150 mg/L suspended solids, allowing operation at relatively high rates, 7.5 to 15.0 m³/m²/h (3 to 6 gpm/ft²). Solids capture will range from 90 to 98 percent in a well-designed system. Typical operating cycles range from 8 to 24 h of filtration (and up to 48 h in municipal water treatment), followed by a backwash interval of 15 to 30 min. Applications are principally in municipal and wastewater treatment, but granular media filters also have been employed in industrial uses such as pulp and paper plant inlet water treatment; removal of oil, grease, and scale from steelmaking process wastewater; and clarification of electrolyte in copper electro-winning operations.

United States Filter Corp. Maxi-Flo Filter. The **Maxi-Flo Filter** is an example of the upflow closed-vessel design. Filtration rates to 0.0081 m³/

(m²·s) [12 gal/(ft²·min)] and filter cross-section areas up to 10.5 m² (113 ft²) are possible. Deep-bed filtration has been reviewed by Tien and Payatakes [*Am. Inst. Chem. Eng. J.*, 25, 737 (1970)] and by Oulman and Baumann [*Am. Inst. Chem. Eng. Symp. Ser.*, 73(171), 76 (1977)].

Dyna Sand Filter. A filter that avoids batch backwashing for cleaning, the **Dyna Sand Filter** is available from Parkson Corporation. The bed is continuously cleaned and regenerated by recycling solids internally through an air-lift pipe and a sand washer. Thus a constant pressure drop is maintained across the bed, and the need for parallel filters to allow continued on-stream operation, as with conventional designs, is avoided.

Miscellaneous Clarifiers Various types of filters such as cartridge, magnetic, and bag filters are widely used in polishing operations,

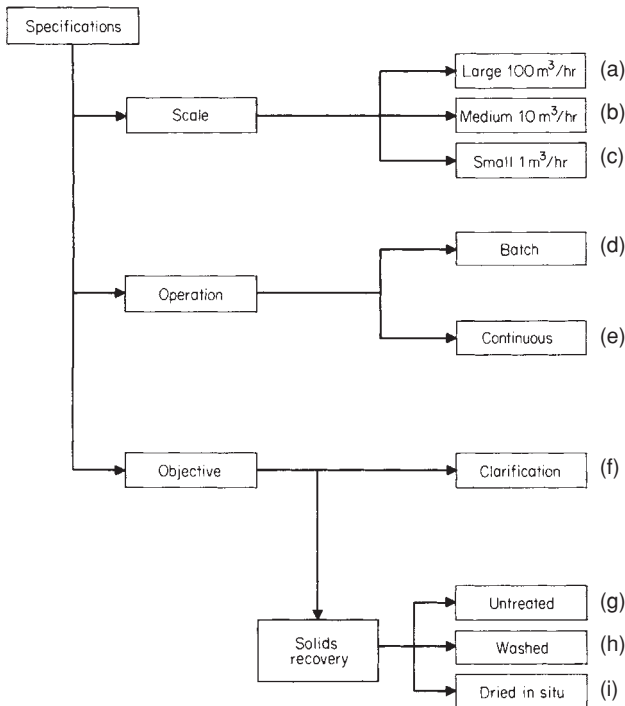


FIG. 18-145 Coding the problem specification. (*Purchas, Solid/Liquid Separation Equipment Scale-Up, Uplands Press, Croydon, England, 1977, p. 10, by permission.*)

generally to remove trace amounts of suspended solids remaining from prior unit operations. A thorough discussion of cartridge and felt strainer bag filters is available in Schweitzer, op. cit., Section 4.6 (Nickolaus) and Section 4.7 (Wrotnowski).

SELECTION OF FILTRATION EQUIPMENT

If a process developer who must provide the mechanical separation of solids from a liquid has cleared the first decision hurdle by determining that filtration is the way to get the job done (see the final subsection of Sec. 18, "Selection of a Solids-Liquid Separator")—or that it

must remain in the running until some of the details of equipment choice have been settled—choosing the right filter and right filtration conditions may still be difficult. Much as in the broader determination of which unit operation to employ, the selection of filtration equipment involves the balancing of process specifications and objectives against capabilities and characteristics of the various equipment choices (including filter media) available. The important process-related factors are slurry character, production throughput, process conditions, performance requirements, and permissible materials of construction. The important equipment-related factors are type of cycle (batch or continuous), driving force, production rates of the largest and smallest units, separation sharpness, washing capability, dependability, feasible materials of construction, and cost. The estimated cost must account for installed cost, equipment life, operating labor, maintenance, replacement filter media, and costs associated with product-yield loss (if any). In between the process and equipment factors are considerations of slurry preconditioning and use of filter aids.

Slurry characteristics determine whether a clarifying or a cake filter is appropriate; and if the latter, they determine the rate of formation and nature of the cake. They affect the choice of driving force and cycle as well as specific design of machine.

There are no absolute selection techniques available to come up with the "best" choice since there are so many factors involved, many of them difficult to make quantitative and, not uncommonly, some contradictory in their demands. However, there are some published general suggestions to guide the thinking of the engineer who faces the selection of filtration equipment. Figure 18-144 is a decision tree designed by Tiller [*Chem. Eng.*, **81**(9), 118 (1974)] to show the steps to be followed in solving a filtration problem. It is erected on the premise that rate of cake formation is the most important guide to equipment selection. A filter-selection process proposed by Purchas (op. cit., pp. 10-14) employs additional criteria and is based on a combination of process specifications and the results of simple tests. The application is coded by use of Figs. 18-145, 18-146, and 18-147, and the resulting codes are matched against Table 18-11 to identify possible filters. Information needed for Fig. 18-148 can be obtained by observing the settling of a slurry sample (Purchas suggests 1 L) in a graduated cylinder. Filter-cake-growth rate (Fig. 18-148) is determined by small-scale leaf or funnel tests as described earlier.

Almost all types of continuous filters can be adapted for cake washing. The effectiveness of washing is a function of the number of wash displacements applied, and this, in turn, is influenced by the ratio of wash time to cake-formation time. Countercurrent washing, particularly with three or more stages, is usually limited to horizontal filters, although a two-stage countercurrent wash sometimes can be applied on a drum filter handling freely filtering material, such as crystallized

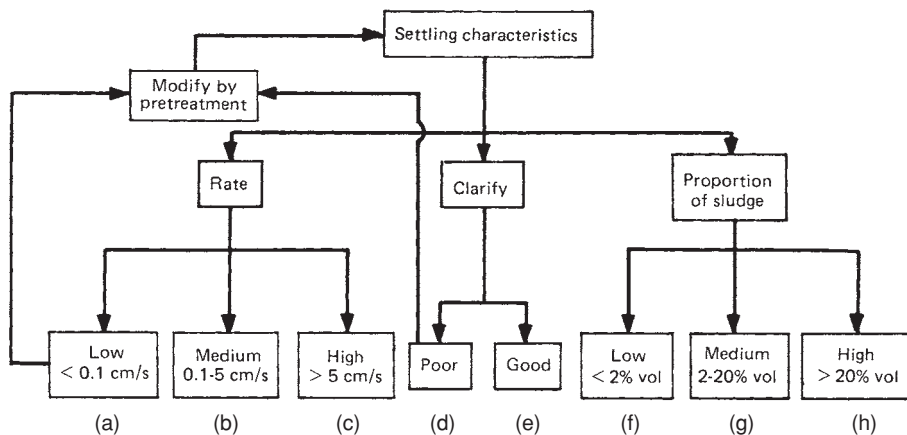


FIG. 18-146 Coding the settling characteristics of a slurry. (*Purchas, Solid/Liquid Separation Equipment Scale-Up, Uplands Press, Croydon, England, 1977, p. 11, by permission.*)

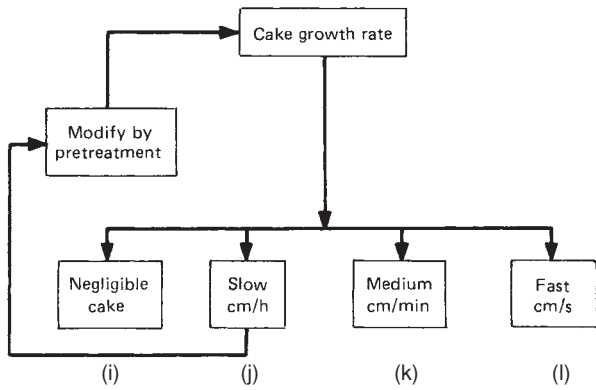


FIG. 18-147 Coding the filtration characteristics of a slurry. (Purchas, Solid/Liquid Separation Equipment Scale-Up, Uplands Press, Croydon, England, 1977, p. 12, by permission.)

salts. Cake washing on batch filters is commonly done, although, generally, a greater number of wash displacements may be required in order to achieve the same degree of washing obtainable on a continuous filter.

Continuous filters are most attractive when the process application is a steady-state continuous one, but the rate at which cake forms and the magnitude of production rate are sometimes overriding factors. A rotary vacuum filter, for example, is a dubious choice if a 3-mm (0.12-in) cake will not form under normal vacuum in less than 5 min and if less than 1.4 m³/h (50 ft³/h) of wet cake is produced. Upper production-rate limits to the practicality of batch units are harder to establish, but any operation above 5.7 m³/h (200 ft³/h) of wet cake should be considered for continuous filtration if it is at all feasible. Again, however, other factors such as the desire for flexibility or the need for high pressure may dictate batch equipment.

For estimating filtration rate (therefore, operating pressure and size of the filter), washing characteristics, and other important features,

TABLE 18-11 Classification of Filters according to Duty and Slurry-Separation Characteristics*

Type of equipment	Suitable for duty specification†	Required slurry-separation characteristics‡	
		Slurry-settling characteristics	Slurry-filtering characteristics
Deep-bed filters	a or b e f	A D F	T
Cartridges	b or c d f	A or B D or E F	
Batch filters			
Pressure vessel with vertical elements	a, b, or c d f, g, h, or i	A or B D or E F or G	I or J
Pressure vessel with horizontal elements	b or c d g or h	A or B D or E F or G	J or K
Filter presses	a, b, or c d f, g, h, or i	A or B D or E F, G, or H	I or J
Variable-volume filters	a, b, or c d or e g (or h)	A (or B) D or E G or H	J or K
Continuous filters			
Bottom-fed drum or belt drum	a, b, or c e f, g, h, or i	A or B D or E F, G, or H	I, J, K, or L
Top-fed drum	a, b, or c e g, i (or h)	C E G or H	L
Disc	a, b, or c e g	A or B D or E G or H	J or K
Horizontal belt, pan, or table	a, b, or c d or e g or h	A, B, or C D or E F, G, or H	J, K, or L

*Adapted from Purchas, Solid/Liquid Separation Equipment Scale-Up, Uplands Press, Croydon, England, 1977, p. 13, by permission.

†Symbols are identified in Fig. 18-135.

‡Symbols are identified in Figs. 18-136 and 18-137.

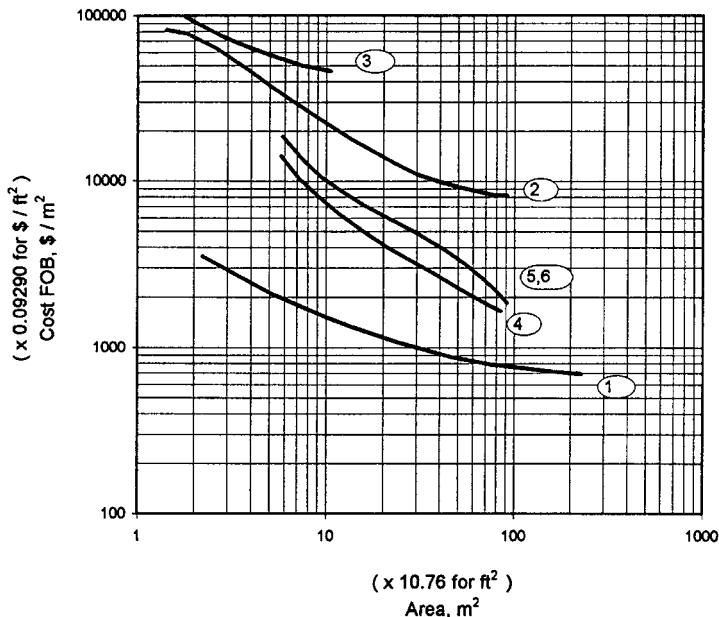


FIG. 18-148 Price of filters installed, FOB point of manufacture. (EIMCO Process Equipment Co.)

small-scale tests such as the leaf or pressure bomb tests described earlier are usually essential. In the conduct and interpretation of such tests, and for advice on labor requirements, maintenance schedule, and selection of accessory equipment the assistance of a dependable equipment vendor is advisable.

FILTER PRICES

As indicated, one of the factors affecting the selection of a filter is total cost of carrying out the separation with the selected machine. An important component of this cost item is the installed cost of the filter, which starts with the purchase price.

From a survey of early 1982, prices of a number of widely used types of process filter were collated by Hall and coworkers [*Chem. Eng.*, **89**(7), 80 (1982)]. These data are drawn together in Fig. 18-148, updated to 1995 prices. They have a claimed accuracy of ±10 percent, but they should be used confidently only with study-level cost estimations (±25 percent) at best. Cost of delivery to the plant can be approximated as 3 percent of the FOB price [Pikulik and Diaz, *Chem. Eng.*, **84**(21), 106 (1977)].

The cost of the filter station includes not only the installed cost of the filter itself but also that of all the accessories dedicated to the filtration operation. Examples are feed pumps and storage facilities, precoat tanks, vacuum systems (often a major cost factor for a vacuum filter station), and compressed-air systems. The delivered cost of the accessories plus the cost of installation of filter and accessories generally is of the same order of magnitude as the delivered filter cost and commonly is several times as large. Installation costs, of course, must be estimated with reference to local labor costs and site-specific considerations.

The relatively high prices of pulp and paper filters reflect the construction features that accommodate the very high hydraulic capacity that is required. The absence of data for some common types of filters, in particular the filter press, is explained by Hall as due to the complex variety of individual features and materials of construction. For information about missing filters and for firmer estimates for those types presented, vendors should be consulted. In all cases of serious interest, consultation should take place early in the evaluation procedure so that it can yield timely advice on testing, selection, and price.

CENTRIFUGES

GENERAL REFERENCES: Ambler, in McKetta, *Encyclopedia of Chemical Processing and Design*, vol. 7, Marcel Dekker, New York, 1978; also in Schweitzer, *Handbook of Separation Techniques for Chemical Engineers*, McGraw-Hill, New York, 1979, sec. 4. Ambler and Keith, in Perry and Weissberger, *Separation and Purification Techniques of Chemistry*, 3d ed., vol. 12, Wiley, New York, 1978. Flood, Porter, and Rennie, *Chem. Eng.*, **73**(13), 190 (1966). Greenspan, *J. of Fluid Mech.*, **127**(9), 91 (1983). Hultsch and Wilkesmann, in Purchas, *Solid/Liquid Separation Equipment Scale-Up*, Uplands Press, Croydon, England, 2d ed., 1986, chap. 12. Gerl, Stadager, and Stahl, *Chemical Eng. Progress*, **91**, 48-54, (May 1995). Leung, *Chem. Eng.* (1990). Leung, *Fluid-Particle Sep. J.*, **5**(1), 44 (1992). Leung, *10th Pittsburgh Coal Conf. Proceed.* (1993). Leung and Shapiro, *Filtration and Separation Journal*, Sept. and Oct. 1996. Leung and Shapiro, U.S. Patents 5,520,605 (May 28, 1996), 5,380,266 (Jan. 10, 1995), and 5,401,423 (March 28 1995). Mayer and Stahl, *Aufbereitungs-Technik*, **11**, 619 (1988). Moyers, *Chem. Eng.*, **73**(13), 182 (1966). Records, in Purchas, op. cit., chap. 6. Smith, *Ind. Eng. Chem.*, **43**, 439 (1961). Sullivan and Erikson, *ibid.*, p. 434. Svarovsky, in *Solid-Liquid Separation*, 3d ed., Butterworths, 1990, chap. 7. Tiller, *AIChE J.*, **33**(1), (1987). Zeitsch, in Svarovsky, op. cit., chap. 14. Dr. Andreas Karolis, *The Technology of Solid-Bowl Scroll Centrifuges*. McGillicuddy, *Chem. Process. Mag.*, **59** (12), 54-59 (Dec. 1996).

Nomenclature

Symbol	Definition	SI units	U.S. customary units
<i>a</i>	Acceleration	m/s ²	ft/s ²
<i>B_b</i>	Bond number	Dimensionless	Dimensionless
<i>b</i>	Basket axial length	m	ft
<i>C_f</i>	Frictional coefficient	Dimensionless	Dimensionless
<i>D</i>	Bowl/basket diameter	m	in
<i>d</i>	Particle diameter	m	ft
<i>Ek</i>	Ekman number	Dimensionless	Dimensionless
<i>F</i>	Cumulative fraction	Dimensionless	Dimensionless
<i>G</i>	Centrifugal gravity	m/s ²	ft/s ²
<i>g</i>	Earth gravity	m/s ²	ft/s ²
<i>h</i>	Cake height	m	ft
<i>K</i>	Cake permeability	m ²	ft ²
<i>L</i>	Length	m	ft
<i>M</i>	Mass	kg	lb
<i>m</i>	Bulk mass rate	kg/s	lb/h
<i>N_c</i>	Capillary number	Dimensionless	Dimensionless
<i>P</i>	Power	kw	hp
<i>Q</i>	Flow rate	L/s	gpm
<i>R_m</i>	Filter media resistance	m ⁻¹	ft ⁻¹
<i>Ro</i>	Rosby number	Dimensionless	Dimensionless
<i>r</i>	Radius	m	ft
Rec	Solids recovery	Dimensionless	Dimensionless
<i>S</i>	Liquid saturation in cake (=volume of liquid/volume cake void)	Dimensionless	Dimensionless

Nomenclature (Concluded)

Symbol	Definition	SI units	U.S. customary units
<i>sg</i>	Specific gravity	Dimensionless	Dimensionless
<i>t</i>	Time	s	s
<i>t_d</i>	Time	Dimensionless	Dimensionless
<i>u</i>	Velocity	m/s	ft/s
<i>Vθ</i>	Circumferential velocity	m/s	ft/s
<i>V_c</i>	Bulk cake volume	m ³	ft ³
<i>V</i>	Velocity	m/s	ft/s
<i>W</i>	Weight fraction of solids	Dimensionless	Dimensionless
<i>Y</i>	Yield	Dimensionless	Dimensionless
<i>Z</i>	Capture efficiency	Dimensionless	Dimensionless
Greek symbols			
<i>ε</i>	Cake void volume fraction	Dimensionless	Dimensionless
<i>ε_s</i>	Cake solids volume fraction	Dimensionless	Dimensionless
<i>μ</i>	Liquid viscosity	Pa·s	P
<i>ρ_s</i>	Solid density	kg/m ³	lb/ft ³
<i>ρ_L</i>	Liquid density	kg/m ³	lb/ft ³
<i>σ</i>	Surface tension	N/m	lb/ft
<i>σ_h</i>	Hoop stress	Pa	psi
<i>θ</i>	Angle	Radian	degree
<i>Σ</i>	Scale-up factor (equivalent sedimentation area)	m ²	ft ²
<i>ξ</i>	Time	Dimensionless	Dimensionless
<i>φ</i>	Feed solids volume fraction	Dimensionless	Dimensionless
<i>τ_y</i>	Yield stress	Pa	psi
<i>Δ</i>	Differential speed	1/s	r/min
<i>Ω</i>	Angular speed	1/s	r/min
Subscripts			
<i>b</i>	Bowl or basket		
<i>c</i>	Cake		
<i>e</i>	Centrate		
<i>f</i>	Feed		
<i>f</i>	Filtrate		
<i>acc</i>	Acceleration		
<i>p</i>	Pool		
<i>con</i>	Conveyance		
<i>t</i>	Tangential		
<i>L</i>	Liquid		
<i>s</i>	Solid		

INTRODUCTION

Centrifuges for the separation of solids from liquids are of two general types: (1) sedimentation centrifuges, which require a difference in density between the two or three phases present (solid-liquid or liquid-liquid or liquid-liquid-solid or solid-liquid-solid) and (2) filtering centrifuges (for solid-liquid separation), in which the solid phase is retained by the filter medium through which the liquid phase is free to pass. The following discussion is focused on solid-liquid separation for both types of centrifuges; however, a dispersed liquid phase in another continuous liquid phase as used in sedimenting centrifuges exhibits similar behavior as solid in liquid, and therefore the results developed are generally applicable. The use of centrifuges covers a broad range of applications, from separation of fine calcium carbonate particles of less than 10 μm to coarse coal of 0.013 m ($\frac{1}{2}$ in.).

GENERAL PRINCIPLES

Centripetal and Centrifugal Acceleration A centripetal body force is required to sustain a body of mass moving along a curve trajectory. The force acts perpendicular to the direction of motion and is directed radially inward. The centripetal acceleration, which follows the same direction as the force, is given by the kinematic relationship:

$$a = \frac{V_0^2}{r} \quad (18-78)$$

where V_0 is the tangential velocity at a given point on the trajectory and r is the radius of curvature at that point. This analysis holds for the motion of a body in an inertial reference frame, for example, a stationary laboratory. It is most desirable to consider the process in a centrifuge, and the dynamics associated with such, in a noninertial reference frame such as in a frame rotating at the same angular speed as the centrifuge. Here, additional forces and accelerations arise, some of which are absent in the inertial frame. Analogous to centripetal acceleration, an observer in the rotating frame experiences a centrifugal acceleration directed radially outward from the axis of rotation with magnitude:

$$a = \Omega^2 r \quad (18-79)$$

where Ω is the angular speed of the rotating frame and r is the radius from the axis of rotation.

Solid-Body Rotation When a body of fluid rotates in a solid-body mode, the tangential or circumferential velocity is linearly proportional to radius:

$$V_0 = \Omega r \quad (18-80)$$

as with a system of particles in a rigid body. Under this condition, the magnitude of the centripetal acceleration, Eq. (18-78), equals that of the centrifugal acceleration, Eq. (18-79), despite the fact that these accelerations are considered in two different reference frames. Hereafter, the rotating frame attached to the centrifuge is adopted. Therefore, centrifugal acceleration is exclusively used.

G-Level Centrifugal acceleration G is measured in multiples of earth gravity g :

$$\frac{G}{g} = \frac{\Omega^2 r}{g} \quad (18-81)$$

With the speed of the centrifuge Ω in r/min and D the diameter of the bowl,

$$\frac{G}{g} = 0.000559\Omega^2 D, D(m) \quad (18-82)$$

With D in inches, the constant in Eq. (18-82) is 0.0000142. G can be as low as 100g for slow-speed, large basket units to as much as 10,000g for high-speed, small decanter centrifuges and 15,000g for disc centrifuges. Because G is usually very much greater than g , the effect due to earth's gravity is negligible. In analytical ultracentrifuges used to

process small samples, G can be as much as 500,000g to effectively separate two phases with very small density difference.

Coriolis Acceleration The Coriolis acceleration arises in a rotating frame, which has no parallel in an inertial frame. When a body moves at a linear velocity u in a rotating frame with angular speed Ω , it experiences a Coriolis acceleration with magnitude:

$$a = 2\Omega u \quad (18-83)$$

The Coriolis vector lies in the same plane as the velocity vector and is perpendicular to the rotation vector. If the rotation of the reference frame is anticlockwise, then the Coriolis acceleration is directed 90° clockwise from the velocity vector, and vice versa when the frame rotates clockwise. The Coriolis acceleration distorts the trajectory of the body as it moves rectilinearly in the rotating frame.

Effect of Fluid Viscosity and Inertia The dynamic effect of viscosity on a rotating liquid slurry as found in a sedimenting centrifuge is confined in very thin fluid layers, known as **Ekman layers**. These layers are adjacent to rotating surfaces which are perpendicular to the axis of rotation, such as bowl heads, flanges, and conveyor blades, etc. The thickness of the Ekman layer δ is of the order

$$\delta = \sqrt{\frac{\mu/\rho}{\Omega}} \quad (18-84)$$

where μ/ρ is the kinematic viscosity of the liquid. For example with water at room temperature, μ/ρ is 1×10^{-6} m²/s and for a surface rotating at $\Omega = 3000$ r/min, δ is 0.05 mm! These layers are very thin; nevertheless, they are responsible for transfer of angular momentum between the rotating surfaces to the fluid during acceleration and deceleration. They worked together with the larger-scale inviscid bulk flow transferring momentum in a rather complicated way. This is demonstrated by the teacup example in which the content of the cup is brought to speed when it is stirred and it is brought to a halt after undergoing solid-body rotation. The viscous effect is characterized by the dimensionless Ekman number:

$$\text{Ek} = \frac{\mu/\rho}{\Omega L^2} \quad (18-85)$$

where L is a characteristics length. It measures the scale of the viscous effect to that of the bulk flow.

The effect of fluid inertia manifests during abrupt change in velocity of the fluid mass. It is quantified by the Rossby number:

$$\text{Ro} = \frac{u}{\Omega L} \quad (18-86)$$

Typically, Ro is small to the order of 1 with the high end of the range showing possible effect due to inertia, whereas the Ek number is usually very small, 10^{-6} or smaller. Therefore, the viscous effect is confined to thin boundary layers with thickness $\text{Ek}^{1/2}L$.

Sedimenting and Filtering Centrifuges Under centrifugal force, the solid phase assumed to be denser than the liquid phase settles out to the bowl wall—sedimentation. Concurrently, the lighter, more buoyant liquid phase is displaced toward the smaller diameter—flotation. This is illustrated in Fig. 18-149a. Some centrifuges run with an air core, i.e., with free surface, whereas others run with slurry filled to the center hub or even to the axis in which pressure can be sustained.

In a sedimenting centrifuge, the separation can be in the form of **clarification**, wherein solids are separated from the liquid phase in which clarity of the liquid phase is of prime concern. For biological sludge, polymers are used to agglomerate fine solids to facilitate clarification. Separation can also be in the form of **classification** and **dewatering** at which separation is effected by means of particle size and density. Typically, the finer solids (such as kaolin) of smaller size and/or density in the feed slurry are separated in the centrate stream as product (for example 90 percent of particles less than 1 μm , etc.), whereas the larger and/or denser solids are captured in cake as reject. Furthermore, separation can be in the form of **thickening**, where solids settle under centrifugal force to form a stream with concentrated solids. In

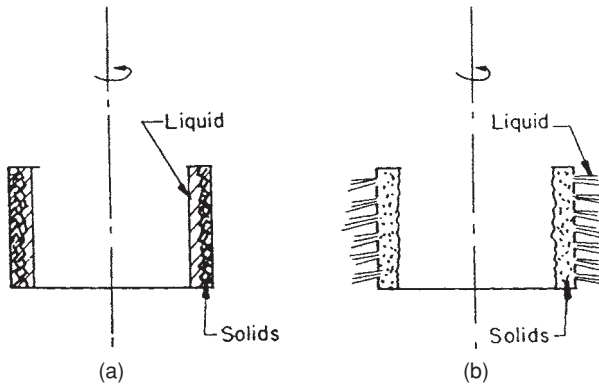


FIG. 18-149 Principles of centrifugal separation and filtration: (a) sedimentation in rotating imperforate bowl; (b) filtration in rotating perforate basket.

dewatering or deliquoring, the objective is to produce dry cake with high solids consistency by centrifugation.

In a filtering centrifuge, separating solids from liquid does not require a density difference between the two phases. Should a density difference exist between the two phases, sedimentation is usually at a much more rapid rate compared to filtration. In both cases, the solid and liquid phases move toward the bowl under centrifugal force. The solids are retained by the filter medium, while the liquid flows through the cake solids and the filter. This is illustrated in Fig. 18-149b.

Performance Criteria Separation of a given solid-liquid slurry is usually measured by the purity of the separated liquid phase in the centrate (or liquid effluent) in sedimenting mode or filtrate in filtering mode, and the separated solids in the cake. In addition, there are other important considerations. Generally, a selected subset of the following criteria are used, depending on the objectives of the process:

- Cake dryness or moisture content
- Total solids recovery
- Polymer dosage
- Size recovery and yield
- Volumetric and solids throughput
- Solid purity and wash ratio
- Power consumption

Cake Dryness In dewatering, usually the cake needs to be as dry as possible. Cake dryness is commonly measured by the solids fraction by weight W or by volume ϵ_s . The moisture content is measured by the complement of W or ϵ_s . The volume fraction of the pores and void in the wet cake is measured by the cake porosity $\epsilon(=1-\epsilon_s)$; whereas the volume fraction of the liquid in the pores of the cake is measured by the saturation S . For well-defined solids in the cake with solid density (bone dry) ρ_s and liquid density ρ_L , and given that the cake volume \dot{V}_c and the mass of solids in the cake w_s are known, the cake porosity is determined by

$$\epsilon = 1 - \frac{w_s}{\rho_s \dot{V}_c} \quad (18-87)$$

For undersaturated cake with $S < 1$, saturation can be inferred from the weight fraction of solids and the porosity of the cake, together with the solid and liquid densities:

$$S = \left(\frac{1-W}{W} \right) \left(\frac{1-\epsilon}{\epsilon} \right) \frac{\rho_s}{\rho_L} \quad (18-88)$$

When the cake is saturated $S = 1$, the cake porosity can be determined from Eq. (18-89) as

$$\epsilon = \left(1 + \frac{\rho_L}{\rho_s} \frac{W}{1-W} \right)^{-1} \quad (18-89)$$

Cake dewatering by compression and rearrangement of the solids in the cake matrix reduce ϵ , yet the cake is still saturated with $S = 1$. (Assuming cake solids are ideal spheres of uniform size, the maximum packing, in rhombohedral arrangement, is such that $\epsilon_s = 74$ percent or $\epsilon = 26$ percent.) Drainage of liquid within the cake by centrifugation further reduces S to be less than 1. There is a lower limit on S which is determined by the cake height, dewatering time, centrifugal force as compared to the capillary and surface forces, as well as the surface roughness and porosity of the particles.

Total Solids Recovery In clarification, the clarity of the effluent is measured indirectly by the total solids recovered in the cake as

$$\text{Rec} = \frac{m_c W_c}{m_f W_f} \quad (18-90)$$

where subscripts c and f denote, respectively, the cake and the feed. m is the bulk mass flow rate in kg/s (lb/h).

Under steady state, the mass balance on both solids and liquid yield, respectively:

$$m_f W_f = m_c W_c + m_e W_e \quad (18-91)$$

$$m_f = m_c + m_e \quad (18-92)$$

From the above, it follows that

$$\text{Rec} = \frac{1 - (W_e/W_f)}{1 - (W_e/W_c)} \quad (18-93)$$

where subscript e represents liquid centrate. Stringent requirements on centrate quality or capture of valuable solid product often require the recovery to exceed 90 percent and, in some cases, 99+ percent. In such cases, the centrate solids are typically measured in ppm.

Polymer Dosage Cationic and anionic polymers have been commonly used to coagulate and flocculate fine particles in the slurry. This is especially pertinent to biological materials such as are found in wastewater treatment. In the latter, cationic polymers are often used to neutralize the negative-charge ions left on the surface of the colloidal particles. Polymer dosage is measured by kg of dry polymer/1000 kg of dry solids cake (lbm of dry polymer/ton of dry solids cake). With liquid polymers, the equivalent (active) dry solid polymer is used to calculate the dosage. There is a minimum polymer dosage to agglomerate and capture the fines in the cake. Overdose can be undesirable to recovery and cake dryness. The range of optimal dosage is dictated by the type of solids in the slurry, slurry physical properties such as pH, ionic strength, etc., and the operating condition and characteristics of the centrifuge. It is known that flocculated particles or flocs obtained from certain polymers may be more sensitive to shear than others, especially during feed acceleration in the centrifuges. A more gentle feed accelerator is beneficial for this type of polymer. Also, polymers can be introduced to the feed at various locations either within or external to the centrifuge.

Size Recovery and Yield Centrifuges have been applied to classify polydispersed fine particles. The size distribution of the particles is quantified by the cumulative weight fraction F less than a given particle size d for both the feed and the centrate streams. It is measured by a particle size counter which operates based on principles such as sedimentation or optical scattering.

In kaolin classification, the product is typically measured with a certain percentage less than a given size (example 90 percent or 95 percent less than 1 or 2 μm). Each combination of percent and size cut represents a condition by which the centrifuge would have to tune to yield the product specification.

The yield Y is defined as the fraction of feed particles of a given size below which they report to the centrate product. Thus,

$$Y = \frac{m_c W_c F_c}{m_f W_f F_f} \quad (18-94)$$

From material balance, the particle size distribution of the feed and centrate, as well as the total solids recovery, determine the yield,

$$Y(d) = \frac{F_c(d)}{F_f(d)} (1 - \text{Rec}) \quad (18-95)$$

The complementary is the cumulative capture efficiency $Z (= 1 - Y)$, which is defined as the feed particles of a given size and smaller which are captured in the cake, which in most dewatering applications is the product stream.

Volumetric and Solids Throughput The maximum volumetric and solids throughput to a centrifuge are dictated by one or several governing factors, the most common ones are the centrate solids, cake dryness, and capacity (torque and power) of drive/gear unit. The solids throughput is also governed by other factors such as solids conveyance and discharge mechanisms for continuous and batch centrifuges. The settling rate, as may be significantly reduced by increasing feed solids concentration, also becomes crucial to solids throughput, especially if it has to meet a certain specification on centrate quality.

Solid Purity and Wash Ratio Cake washing in a centrifuge is used to remove dissolved impurities on the solids particle surface. It is most effective in filtering centrifuges—typically with a wash ratio of 0.05 to 0.3 kg wash/kg solids in continuous centrifuges, although higher ratios can be achieved with derated capacities to provide sufficient residence time. Batch filtering centrifuges are unlimited in the wash quantity that can be applied. Solid soluble impurities generally cannot be washed out in situ due to insufficient contact time, in which case repulp washing may be more effective. Repulp is often utilized with sedimenting centrifuges where wash is required.

Power Consumption Power is consumed to overcome windage and bearing (and seal) friction, to accelerate feed stream from zero speed to full tangential speed at the pool so as to establish the required G -force for separation, and to convey and discharge cake. The power to overcome windage and bearing friction is usually established through tests for a given centrifuge geometry at different rotation speeds. It is proportional to the mass of the centrifuge, to the first power of the speed for the bearing friction, and to the second power of speed for windage. It is also related to the bearing diameter. The seal friction is usually small.

The horsepower for feed acceleration is given by

$$P_{acc} = 5.984(10^{-10})sgQ(\Omega r_p)^2 \quad (18-96)$$

where sg is the specific gravity of the feed slurry, Q the volumetric flow rate of feed in $\text{gpm}/(\text{l/s})$, Ω the speed in r/min , r_p in meters corresponds to the radius of the pool surface for sedimenting centrifuge, or to the radius of the cake surface for filtering centrifuge. *Note:* To convert horsepower to kilowatts, multiply by 0.746.

The horsepower for cake conveyance for scroll centrifuge is

$$P_{con} = 1.587 (10^{-5}) T\Delta \quad (18-97)$$

where Δ is the differential speed in r/min (s^{-1}) between the scroll conveyor and the bowl, and T is the conveyance torque in $\text{in}\cdot\text{lb}_f$ ($\text{N}\cdot\text{m}$). For centrifuge where cake is discharged differently, the conveyance power is simply

$$P_{con} = MGC_fV \quad (18-98)$$

where M is the mass of the cake, G the centrifugal acceleration, C_f is the coefficient of friction, and V is the cake velocity. Comparing Eqs. (18-97) and (18-98) the conveyance torque is inversely related to the differential speed and directly proportional to the G acceleration, cake velocity, and cake mass.

Stress in the Centrifuge Rotor The stress in the centrifuge rotor is quite complex. Analytical methods, such as the finite element method, are used to analyze the mechanical integrity of a given rotor design. Without getting into an involved analysis, some useful knowledge can be gained from a simple analysis of the hoop stress of a rotating bowl under load. At equilibrium, the tensile hoop stress σ_h of the cylindrical bowl wall with thickness t is balanced by the centrifugal body force due to the mass of the bowl wall with density ρ_m and its contents (cake or slurry or liquid) with equivalent density ρ_L . Consider a circular wall segment with radius r , unit subtended angle, and unit axial length. A force balance requires

$$\sigma_h = \rho_m V_t^2 \left[1 + 0.5 \frac{\rho_L}{\rho_m} \left(1 - \frac{r_s^2}{r_b^2} \right) \frac{r_b}{t} \right] \quad (18-99)$$

$V_t = \Omega r_b$ is the tip speed of the bowl. The term in the bracket is typically of order 1. If the maximum allowed σ_h is designed to be no more than 60 percent of the yield stress of the bowl material, which for steel is about $2.07(10^8) \text{ Nm}^{-2}$ ($30,000 \text{ lb}_f/\text{in}^2$). Given that the ρ_m of stainless steel is 7867 kg/m^3 (0.284 lbm/in^3), and there is no liquid load, then $(V_t)_{max} = \{\sigma_h/\rho_m\}^{1/2} = 126 \text{ m/s}$ (412 ft/s). With additional liquid load, $\rho_L = 1000 \text{ kg/m}^3$ (0.0361 lbm/in^3), $r_b/t = 10$, and further assuming the worst case with liquid filling to the axis, the term in the curly bracket is 1.636. Using Eq. (18-99), $(V_t)_{max} = \{\sigma_h/\rho_m/1.636\}^{1/2} = 98 \text{ m/s}$ (322 ft/s). Indeed, almost all centrifuges are designed with top rim speed about 91 m/s (300 ft/s). With special construction materials for the rotor, such as Duplex Ferritic/Austenitic stainless steel, with higher yield stress, the maximum rim speed under full load can be over 122 m/s (400 ft/s).

G-Force vs. Throughput The G -acceleration can be expressed as

$$G = \Omega^2 r_b = \frac{(V_t)_{max}^2}{r_b} \quad (18-100)$$

Figure 18-150 shows the range of diameter of commercial centrifuges and the range of maximum G developed in each type. It demonstrates an inverse relationship between G and r_b at $V_t = (V_t)_{max}$, which is constant for a given material. Figure 18-151 shows a log-log plot of G versus Ω for various bowl diameters, [Eq. (18-100)]. Also, the limiting conditions as delineated by $G = \Omega^2 R = \Omega^2 (V_t)_{max}$ with various $(V_t)_{max}$ are superimposed on these curves. These two sets of curves dictate the operable speed and G for a given diameter and a given construction material for the bowl. The throughput capacity of a machine, depending on the process need, is roughly proportional to the n th power of the bowl radius,

$$Q = C_1 r_b^n \quad (18-101)$$

where n is normally between 2 to 3, depending on clarification, classification, thickening, or dewatering. Thus,

$$G = c_2 (V_t)_{max}^2 Q^{1/n} \quad (18-102)$$

where c_1 and c_2 are constants. It follows that large centrifuges can deliver high flow rate but separation is at lower G -force; vice versa, smaller centrifuges can deliver lower flow rate but separation is at higher G -force. Also, using higher-strength material for construction of the rotating assembly permits higher maximum tip speed, thus allowing higher G -force for separation at a given feed rate.

Centrifuge bowls are made of almost every machinable alloy of reasonably high strength. Preference is given to those alloys having 1 percent elongation to minimize the risk of cracking at stress-concentration points. Typically the list includes (in increasing cost) rubber-lined carbon steel, SS316L, SS317LMN, duplex SS (SAF2205), Alloy 904L, AL6 XN, Inconel, Hastelloy C22, Hastelloy B, nickel, and titanium Gr. 2. Most coatings (Halar, PTFE, etc.) cause problems with stressed components such as baskets, but can be utilized for static components such as housings. Vertical-basket centrifuges are frequently constructed of carbon steel or stainless steel coated with rubber, neoprene, Penton, or Kynar. Casings and feed, rinse, and discharge lines that are stationary and lightly stressed may be constructed of any suitable rigid corrosion-resistant material. Wear-resistant materials—tungsten and cermaic carbide, hard-facing, and others—are often used to protect the bare metal surfaces in high-wear areas such as the blade tips of the decanter centrifuge.

Critical Speeds In the design of any high-speed rotating machinery, attention must be paid to the phenomenon of critical speed. This is the speed at which the frequency of rotation matches the natural frequency of the rotating part. At this speed, any vibration induced by slight unbalance in the rotor is strongly reinforced, resulting in large deflections, high stresses, and even failure of the equipment. Speeds corresponding to harmonics of the natural frequency are also critical speeds but give relatively small deflections and are much less troublesome than the fundamental frequency. The critical speed of simple shapes may be calculated from the moment of inertia; with complex elements such as a loaded centrifuge bowl, it is best found by tests.

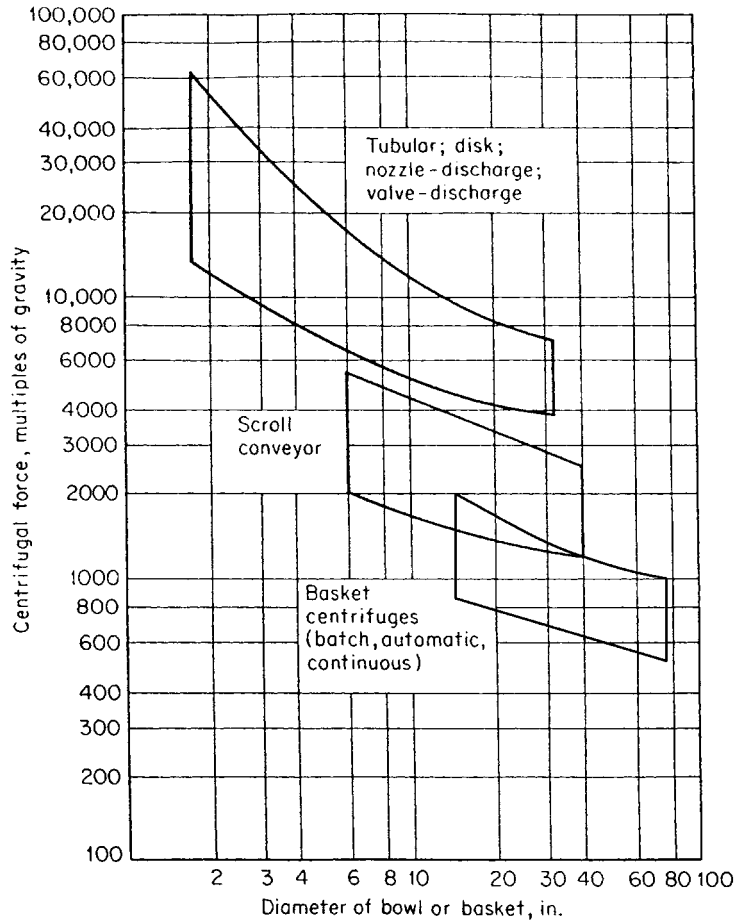


FIG. 18-150 Variation of centrifugal force with diameter in industrial centrifuges.

Nearly all centrifuges operate at speeds well above the primary critical speed and therefore must pass through this speed during acceleration and deceleration. To permit them to do so safely, some degree of damping in their mounting must be provided. This may result from the design of the spindle or driveshaft alone, spring-loading of the spindle bearing nearest the rotor, elastic loading of the suspension, or a combination of these. Smaller and medium-sized centrifuges of the cream-separator and bottle-centrifuge design are frequently mounted on elastic cushions. Horizontal decanter centrifuges are mounted on isolators with dampers to reduce vibration transmitted to the foundation.

SEDIMENTATION CENTRIFUGES

When a spherical particle of diameter d settles in a viscous liquid under earth gravity g , the terminal velocity V_s is determined by the weight of the particle-balancing buoyancy and the viscous drag on the particle in accordance to Stokes' law. In a rotating flow, Stokes' law is modified by the "centrifugal gravity" $G = \Omega^2 r$; thus

$$V_s = \frac{1}{18\mu} \Omega^2 r (\rho_s - \rho_L) d^2 \quad (18-103)$$

In order to have good separation or high settling velocity, a combination of the following conditions is generally sufficient:

1. High centrifuge speed
2. Large particle size

3. Large density difference between solid and liquid
4. Large separation radius
5. Low liquor viscosity

Among the five parameters, the settling velocity is very sensitive to change in speed and particle size. It varies as the square of both parameters. The maximum achievable rotational speed of a centrifuge is normally dictated by the stresses exerted by the processing medium on the bowl and the stresses of the bowl on periphery equipment, most notably the drive system, which consists of a gear unit or hydraulic pump. If the particles in the feed slurry are too small to be separated in the existing G -field, coagulation and flocculation by polymers are effective ways to create larger agglomerated particles for settling. Unlike separation under a constant gravitational field, the settling velocity under a centrifugal field increases linearly with the radius. The greater the radius at which the separation takes place in a given centrifuge at a given rotational speed, the better the separation. Sedimentation of particles is favorable in a less viscous liquid. Some processes are run under elevated temperature where liquid viscosity drops to a fraction of its original value at room temperature.

Laboratory Tests

Spin-Tube Tests The objective of the spin-tube test is to check the settleability of solids in a slurry under centrifugation. The clarity of the supernatant liquid and the solid concentration in the sediment can also be evaluated. A small and equal amount of feed is introduced into two diametrically opposite test tubes (typically plastic tubes in a stainless

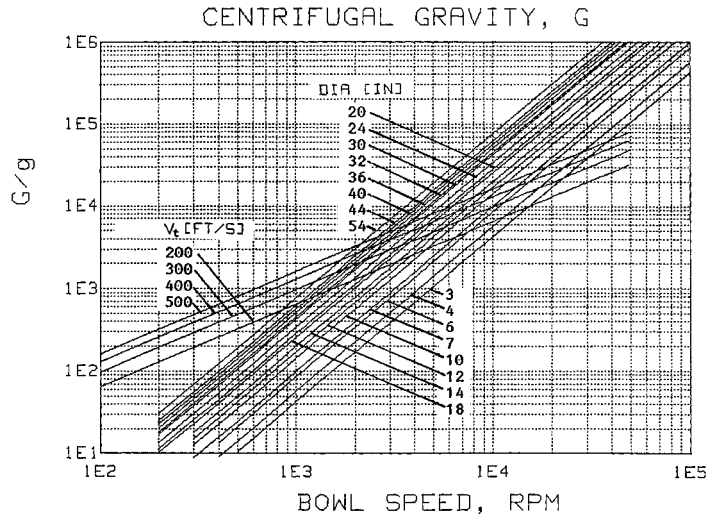


FIG. 18-151 Variation of centrifugal force with r/min.

steel holder) with a volume of 15 to 50 mL. The samples are centrifuged at a given G and for a period of time t . The supernatant liquid is decanted off from the spin tubes from which the clarity (in the form of turbidity or any measurable solids, dissolved and suspended) is measured. The integrity—more precisely, the yield stress—of the cake can be determined approximately by the amount of penetration of a rod into the cake under its weight and accounting for the buoyancy effect due to the wet cake. It is further assumed that the rod does not lean on the sides of the tube. The yield stress τ_y of the centrifuged cake can be determined from:

$$\tau_y = \frac{1}{2} \left(\frac{\rho_r L}{h} - \rho_L \right) g r_d \quad (18-104)$$

where r_d and L are, respectively, the radius and length of the solid circular rod; ρ_r is the density of the rod; and h is the penetration of the rod into the cake. By using rods of various sizes and densities, yield stress which is indicative of cake handling and integrity can be measured for a wide range of conditions.

The solids recovery in the cake can be inferred from measurements using Eq. (18-93). It is shown as a function of G -seconds for different feed solids concentration in Fig. 18-152; see also theory discussed below.

Imperforate Bowl Tests The amount of supernatant liquid from spin tubes is usually too small to warrant accurate gravimetric analysis. A fixed amount of slurry is introduced at a controlled rate into a rotating imperforate bowl to simulate a continuous sedimentation centrifuge. The liquid is collected as it overflows the ring weir. The test is

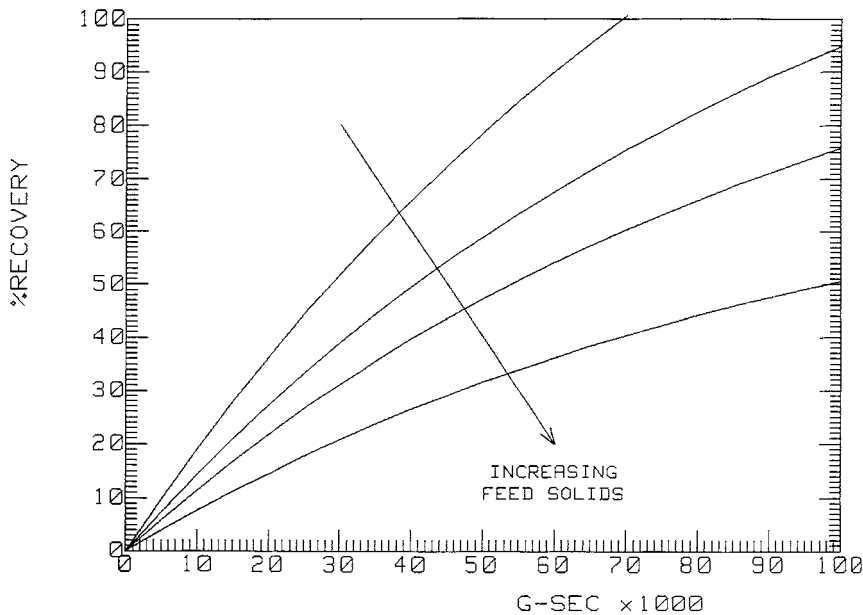


FIG. 18-152 Recovery as a function of G -seconds for centrifugal sedimentation.

stopped when the solids in the bowl build up to a thickness which affects centrate quality. The solid concentration of the centrate is determined similarly to that of the spin tube.

Transient Centrifugation Theory As in gravitational sedimentation, there are three layers which exist during batch settling of a slurry in a centrifuge: a clarified liquid layer closest to the axis, a middle feed slurry layer with suspended solids, and a cake layer adjacent to the bowl wall with concentrated solids. Unlike with constant gravity g , the centrifugal gravity G increases linearly with radius. It is highest near the bowl and is zero at the axis of rotation. Also, the cylindrical surface area through which the particle has to settle increases linearly with radius. Both of these effects give rise to some rather unexpected results.

Consider the simple initial condition $t = 0$ where the solid concentration ϕ_{so} is constant across the entire slurry domain $r_L \leq r \leq r_b$ where r_L and r_b are, respectively, the radii of the slurry surface and the bowl. At a later time $t > 0$, three layers coexist: the top clarified layer, a middle slurry layer, and a bottom sediment layer. The air-liquid interface remains stationary at radius r_L , while the liquid-slurry interface with radius r_s expands radially outward, with t with r_s given by:

$$\frac{r_s}{r_L} = \sqrt{\frac{\phi_{so}}{\phi_s}} \tag{18-105}$$

Eq. (18-105) can be derived from conservation of angular momentum as applied to the liquid-slurry interface.

Interestingly, the solid concentration in the slurry layer ϕ_s does not remain constant with time as in gravitational sedimentation. Instead, ϕ_s decreases with time uniformly in the entire slurry layer in accordance to:

$$\frac{\phi_s}{\phi_{smax}} = 1 - \left[1 - \left(\frac{\phi_{so}}{\phi_{smax}} \right) \right] e^{2\xi} \tag{18-106}$$

where ξ is a dimensionless time variable:

$$\xi = \left(\frac{V_{go}t}{r_b} \right) \left(\frac{G}{g} \right) \tag{18-107}$$

In Eqs. (18-106) and (18-107), under hindered settling and $1g$, the solids flux $\phi_s V_s$ is assumed to be a linear function of ϕ_s , decreasing at a rate of V_{go} . Also, the solids flux is taken to be zero at the "maximum" solids concentration ϕ_{smax} . As $G/g \gg 1$, this solids flux behavior based on $1g$ is assumed to be ratioed by G/g .

Concurrent with the liquid-slurry interface moving radially outward, the cake layer builds up with the cake-slurry interface moving radially inward, with radial position given by:

$$\frac{r_c}{r_b} = \sqrt{\frac{(\epsilon_s - \phi_{so})}{(\epsilon_s - \phi_s)}} \tag{18-108}$$

where ϵ_s is a constant cake solids concentration. Sedimentation stops when the growing cake-slurry interface meets the decreasing slurry-liquid interface with $r_c = r_s$. This point is reached at $\phi_s = \phi_s^o$ and $t = t^o$ when

$$\frac{1}{\phi_s^o} = \frac{1}{\epsilon_s} + \left(\frac{r_b}{r_L} \right)^2 \left(\frac{1}{\phi_{so}} - \frac{1}{\epsilon_s} \right) \tag{18-109}$$

$$t^o = \frac{1}{2} \left(\frac{gr_b}{GV_{go}} \right) \ln \left(\frac{\phi_{smax} - \phi_s^o}{\phi_{smax} - \phi_{so}} \right) \tag{18-110}$$

Example

Calcium carbonate-water slurry
 $C/g = 2667$
 $V_{go} = 1.31 \times 10^{-6} \text{ m/s } (5.16 \times 10^{-5} \text{ in/s})$
 $\phi_{smax} = 0.26$ (with $\phi_s V_s = 0$)
 $\phi_{so} = 0.13$
 $r_L = 0.0508 \text{ m } (2 \text{ in})$

$$r_b = 0.1016 \text{ m } (4 \text{ in})$$

$$\xi = 2667 (1.31 \times 10^{-6}) (1/0.1016) = 0.0344$$

$$\epsilon_s = 0.52$$

t (s)	ξ	ϕ_s/ϕ_{smax}	r_s (m)	r_c (m)
0.0	0	0.50	0.051	0.102
1.0	0.034	0.46	0.053	0.100
5.0	0.173	0.29	0.067	0.095
7.6	0.261	0.16	0.091	0.091

There are six types of industrial sedimenting centrifuges:

- Tubular-bowl centrifuges
- Multichamber centrifuges
- Skimmer pipe/knife-discharge centrifuges
- Disc centrifuges
- Decanter centrifuges
- Screenbowl centrifuges

The first three types, including the manual-discharge disc, are batch-feed centrifuges, whereas the latter three, including the intermittent and nozzle-discharge discs, are continuous centrifuges.

Tubular-Bowl Centrifuges The tubular-bowl centrifuge is widely employed for purifying used lubricating and other industrial oils and in the food, biochemical, and pharmaceutical industries. Industrial models have bowls 102 to 127 mm (4 to 5 in) in diameter and 762 mm (30 in) long (Table 18-12). It is capable of delivering up to 18,000g. The smallest size, 44 mm \times 229 mm (1.75 in \times 9 in bowl), is a laboratory model capable of developing up to 65,000g. It is also used for separating difficult-to-separate biological solids with very small density difference, such as cells and virus.

The bowl is suspended from an upper bearing and drive (electric or turbine motor) assembly through a flexible-drive spindle with a loose guide in a controlled damping assembly at the bottom. The unit finds its axis of rotation if it becomes slightly unbalanced due to process load.

The feed slurry is introduced into the lower portion of the bowl through a small orifice. Immediately downstream of the orifice is a distributor and a baffle assembly which distribute and accelerate the feed to circumferential speed. The centrate discharges from the top end of the bowl by overflowing a ring weir. Solids that have sedimented against the bowl wall are removed manually from the centrifuge when the buildup of solids inside the bowl is sufficient to affect the centrate clarity.

The liquid-handling capacity of the tubular-bowl centrifuge varies with use. The low end shown in Table 18-11 corresponds to stripping small bacteria from a culture medium. The high end corresponds to purifying transformer oil and restoring its dielectric value. The solids-handling capacity of this centrifuge is limited to 4.5 kg (10 lb) or less. Typically, the feed stream solids should be less than 1 percent in practice.

Multichamber Centrifuges While the tubular has a high aspect ratio (i.e., length-to-diameter ratio) of 5 to 7, the multichamber centrifuges have aspect ratios of 1 or less. The bowl driven from below consists of a series of short tubular sections of increasing diameter nested to form a continuous tubular passage of stepwise increasing diameter for the liquid flow. The feed is introduced at the center tube and gradually finds its way to tubes with larger diameters. The larger and denser particles settle out in the smaller-diameter tube, while the smaller and lighter particles settle out in the larger-diameter tubes. Classification of particles can be conveniently carried out. Clarification may be significantly improved by spacing especially the outer tubes more closely together to reduce the settling distance, a concept which is fully exploited by the disc-centrifuge design. This also serves to maintain a constant velocity of flow between adjacent tubes. As much as six chambers can be accommodated. The maximum solids-holding capacity is 0.064 m³ (17 gal). The most common use is for clarifying fruit juices, wort, and beer. For these services it is equipped with a centripetal pump at effluent discharge to minimize foaming and contact with air.

Knife-Discharge Centrifugal Clarifiers Knife-discharge centrifuges with solid instead of perforated bowls are used as sedimenting centrifuges. The liquid flow is usually continuous until the settled solids start to interfere with the effluent liquid. The feed enters the

TABLE 18-12 Specifications and Performance Characteristics of Typical Sedimenting Centrifuges

Type	Bowl diameter	Speed, r/min	Maximum centrifugal force × gravity	Throughput		Typical motor size, hp
				Liquid, gal/min	Solids, tons/h	
Tubular	1.75	50,000*	62,400	0.05–0.25		°
	4.125	15,000	13,200	0.1–10		2
	5	15,000	15,900	0.2–20		3
Disc	7	12,000	14,300	0.1–10		½
	13	7,500	10,400	5–50		6
	24	4,000	5,500	20–200		7½
Nozzle discharge	10	10,000	14,200	10–40	0.1–1	20
	16	6,250	8,900	25–150	0.4–4	40
	27	4,200	6,750	40–400	1–11	125
	30	3,300	4,600	40–400	1–11	125
Scroll conveyor	6	8,000	5,500	To 20	0.03–0.25	5
	14	4,000	3,180	To 75	0.5–1.5	20
	18	3,500	3,130	To 100	1–3	50
	24	3,000	3,070	To 250	2.5–12	125
	30	2,700	3,105	To 350	3–15	200
	36	2,250	2,590	To 600	10–25	300
	44	1,600	1,600	To 700	10–25	400
	54	1,000	770	To 750	20–60	250
Knife discharge	20	1,800	920	†	1.0‡	20
	36	1,200	740	†	4.1‡	30
	68	900	780	†	20.5‡	40

*Turbine drive, 100 lb/h (45 kg/h) of steam at 40 lbf/in² gauge (372 KPa) or equivalent compressed air.

†Widely variable.

‡Maximum volume of solids that the bowl can contain, ft³.

NOTE: To convert inches to millimeters, multiply by 25.4; to convert revolutions per minute to radians per second, multiply by 0.105; to convert gallons per minute to liters per second, multiply by 0.063; to convert tons per hour to kilograms per second, multiply by 0.253; and to convert horsepower to kilowatts, multiply by 0.746.

hub end and is accelerated to speed before introducing to the separation pool. The solids settle out to the bowl wall and the clarified liquid overflows the ring weir or discharges through a skimmer pipe. In some designs, internal baffles in the bowl are required to stop wave action primarily along the axial direction. When sufficient thick solid layer has built up inside the bowl, the supernatant liquid is skimmed off by moving the opening of the skimmer pipe radially inward. After the liquid is sucked out, the solids are knifed out as with centrifugal filters. However, unlike centrifugal filters, the cake is always fully saturated with liquid, $S = 100\%$. These centrifuges are used for coarse, fast-settled solids. When greater clarification effectiveness is required, the operation may be totally batchwise with prolonged spinning of each batch. If the solids content in the feed is low, several batches may be successively charged and the resulting supernatant liquor skimmed off before unloading of the accumulated solids.

Commercial centrifuges of this type have bowl diameters ranging from 0.3 to 2.4 m (12 to 96 in). The large sizes are used on heavy-duty applications such as coal dewatering and are limited by stress considerations to operate at 300g. The intermediate sizes for chemical process service develop up to 1000g (see Table 18-10).

Disc Stack Centrifuges One of the most common types of commercially utilized centrifuges is a vertically mounted disc machine, one type of which is shown in Fig. 18-153. Feed is introduced proximate to the axis of the bowl, accelerated to speed typically by a radial vane assembly, and flows through a stack of closely spaced conical discs in the form of truncated cones. Generally 50 to 150 discs are used. They are spaced 0.4 to 3 mm (0.015 to 0.125 in) apart to reduce the distance for solid/liquid separation. The angle made by conical discs with the horizontal is typically between 40 to 55° to facilitate solids conveyance. Under centrifugal force the solids settle against the underside of the disc surface and move down to the large end of the conical disc and subsequently to the bowl wall. Concurrently, the clarified liquid phase moves up the conical channel. Each disc carries several holes spaced uniformly around the circumference. When the disc stack is assembled, the holes provide a continuous upward passage for the lighter clarified liquid released from each conical channel. The liquid collects at the top of the disc stack and discharges through overflow ports. To recover the

kinetic energy and avoid foaming due to discharging of a high-velocity jet against a stationary casing, the rotating liquid is diverted to a stationary impeller from which the kinetic energy of the stream is converted to hydrostatic pressure. Unlike most centrifuges operating with a slurry pool in contact with a free surface, disc centrifuges with a rotary seal arrangement can operate under high pressure. The settled solids at the bowl wall are discharged in different forms, depending on the type of disc centrifuges.

Manual Discharge Disc Stack Centrifuges In the simplest design shown in Fig. 18-154a, the accumulated solids must be removed manually on a periodic basis, similar to that for the tubular-bowl centrifuge. This requires stopping and disassembling the bowl and removing the disc stack. Although the individual discs rarely require cleaning, manual removal of solids is economical only when the fraction of solids in the feed is very small.

Self-Cleaning Disc Centrifuges More commonly known as clarifiers (two-phase) and separators (three-phase), these centrifuges, which also contain a conical disc stack inside the bowl, automatically discharge accumulated solids on a timed cycle while the bowl is at full speed. Feed is introduced into the bowl via a nonrotating feed pipe and into a distributor which evenly distributes the slurry to the appropriate disc stack channels. Slurry is forced up through the disc stack where solids accumulate on the underside of the discs and slide down the discs, where they are forced to the sludge holding area just inside the maximum diameter of the double cone-shaped bowl, as shown in Fig. 18-153. When the solids chamber is full, the bottom of the bowl, which is held closed to the top portion hydraulically, drops by evacuating the hydraulic operating fluid. The solids are discharged at full speed in a very short time into an outer housing where they are diverted out of the machine. The liquid or liquids (in a three-phase separator) are normally discharged via stationary impellers under pressure. These types of centrifuges are commonly used in the clarification of beverages and the purification of mineral and edible oils.

Disc Nozzle Centrifuges In the nozzle-discharge disc centrifuge, solids are discharged continuously, along with a portion of the liquid phase, through nozzles spaced around the periphery of the bowl, which are tapered radially outward, providing a space for solids

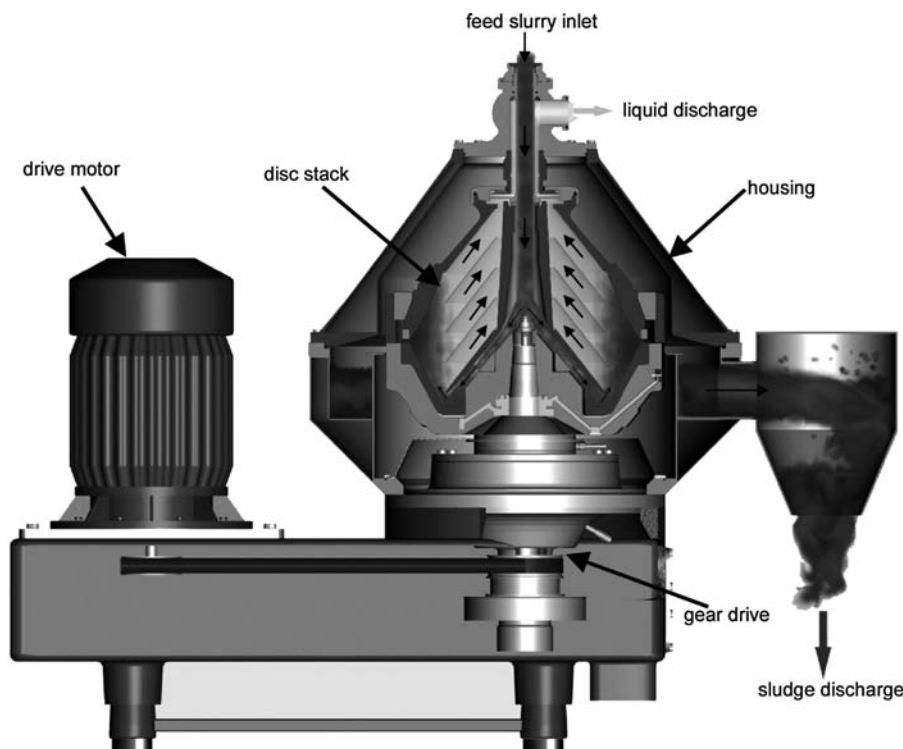


FIG. 18-153 Disc Stack Centrifuge. (Flottweg Separation Technology.)

storage (see Fig. 18-154*b*). The angle of repose of the sedimented solids determines the slope of the bowl walls for satisfactory operation. Clarification efficiency is seriously impaired if the buildup of solids between nozzles reaches into the disc stack. The nozzle diameter should be at least twice the diameter of the largest particle to be processed, and prescreening is recommended of extraneous solids. Typically, nozzle diameters range from 0.6 to 3 mm (0.25 to 0.125 in). Large disc centrifuges may have as much as 24 nozzles spaced out at the bowl.

For clarification of a single liquid phase with controlled concentration of the discharged slurry, a centrifuge which provides recirculation is used (see Fig. 18-154*b*). A fraction of the sludge discharged out of the machine is returned to the bowl to the area adjacent to the nozzles through lines external to the machine as well as built-in annular passages at the periphery of the bowl. This has the effect of preloading the nozzles with sludge which has already been separated and reduces the net flow of liquid with the newly sedimented solids from the feed. Increased concentration can be obtained alternatively by recycling a portion of the sludge to the feed, but this increases solids loading at the disc stack, with a corresponding sacrifice in the effluent clarity for a given feed rate.

With proper rotary seals, the pressure in the machine can be contained up to 1.1 MPa (150 psig) or higher. Also, operating temperature can be as high as 315°C (about 600°F). The rotating parts are made of stainless steel with the high-wear nozzles made of tungsten carbide. The bowls may be underdriven or suspended and range from several centimeters to over 1 m (3.3 ft) in outer diameter. The largest size capable of clarifying up to 1920 L/m (500 gpm) requires 112 kW (150 hp). These types of centrifuges are commonly used in applications including corn wet milling (starch separation, gluten thickening), the classification of kaolin clay particles, washing of terephthalic acid crystals, and dewaxing of lube oils.

Decanter Centrifuges The decanter centrifuge (also known as the solid-bowl or scroll centrifuge) consists of a solid exterior bowl with

an internal screw or scroll conveyor (see Fig. 18-155). Both the bowl and the conveyor rotate at a high speed, yet there is a difference in speed between the two, which is responsible for conveying the sediment along the machine from the cylinder to the conical discharge end. The rotating assembly is commonly mounted horizontally with bearings on each end. Some centrifuges are vertically mounted with the weight of the rotating assembly supported by a single bearing at the bottom or with the entire machine suspended from the top. With the former configuration, the weight of the rotating assembly provides a good sealing surface at the bearing for high-pressure applications. The bowl may be conical in shape or, in most instances, it has combined conical and cylindrical sections (see Fig. 18-155).

Slurry is fed through a stationary pipe into the feed zone located near the center of the scroll. The product is then accelerated circumferentially and passes through distribution ports into the bowl. The bowl has a cylindrical/conical shape and rotates at a preset speed optimal for the application. The slurry rotates with the bowl at the operating speed and forms a concentric layer at the bowl wall, as shown in Fig. 18-156*a*. In the separation pool or pond, under centrifugal gravity the solids which are heavier compared to the liquid settle toward the bowl wall, while the clarified liquid moves radially toward the pool surface. Subsequently, the liquid flows along the helical channel (or channels, if the screw conveyor has multiple leads) formed by adjacent blades of the conveyor to the liquid bowl head, from which it discharges over the weirs. The annular pool/pond height can be changed by adjusting the radial position of the weir openings, which take the form of circular holes or crescent-shaped slots or by adjusting a stationary impeller, which will discharge the liquid under pressure (see Fig. 18-156*b*).

The solids contained in the slurry are deposited against the bowl wall by centrifugal force. The length of the cylindrical bowl section and the cone angle are selected to meet the specific requirements of an application. The scroll conveyor rotates at a slightly different speed from the bowl, and conveys the deposited solids toward the conical

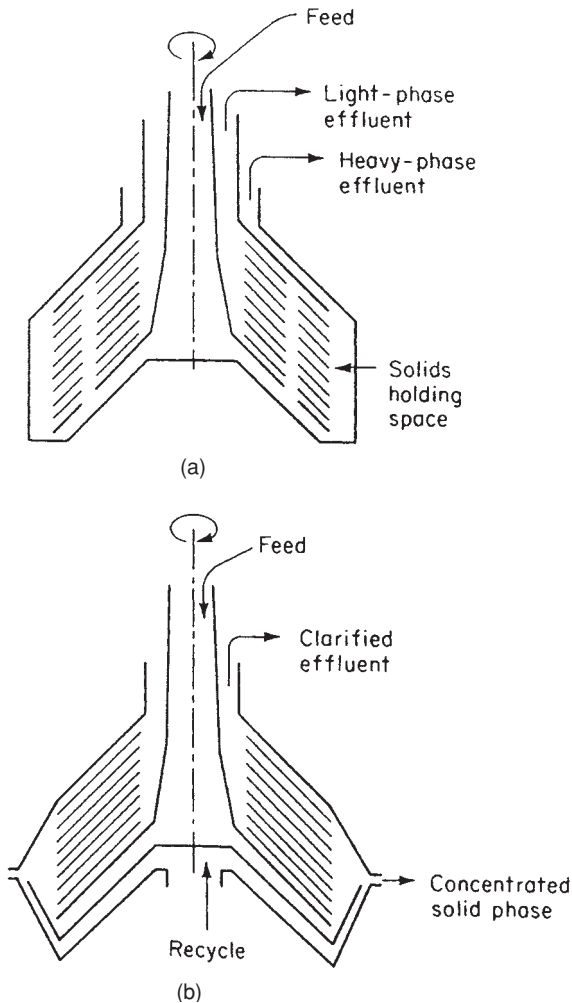


FIG. 18-154 Disc stack-centrifuge bowls: (a) separator, solid wall; (b) recycle clarifier, nozzle discharge.

end of the bowl, also known as the beach. The half cone angle ranges between 5° and 20°. The cake is submerged in the pool when it is in the cylinder and at the beginning of the beach. In this region, liquid buoyancy helps to reduce the effective weight of the cake under centrifugal gravity, resulting in lower conveyance torque. Farther up the

beach, the cake emerges above the pool and moves along the “dry beach,” where buoyancy force is absent, resulting in more difficult conveyance and higher torque. But it is also in this section that the cake is dewatered, with expressed liquid returned back to the pool. The centrifugal force helps to dewater, yet at the same time hinders the transport of the cake in the dry beach. Therefore, a balance in cake conveyance and cake dewatering is the key in setting the pool and the G-force for a given application. Also, clarification is important in dictating this decision.

The cylindrical section provides clarification under high centrifugal gravity. In some cases, the pool should be shallow to maximize the G-force for separation. In other cases, when the cake layer is too thick inside the cylinder, the settled solids—especially the finer particles at the cake surface—entrain into the fast-moving liquid stream above, which eventually ends up in the centrate. A slightly deeper pool becomes beneficial in these cases because there is a thicker buffer liquid layer to ensure settling of resuspended solids. This can be at the expense of cake dryness due to reduction of the dry beach. Consequently, there is again a compromise between centrate clarity and cake dryness. Another reason for the tradeoff of centrate clarity with cake dryness is that, in losing fine solids to the centrate (i.e., classification), the cake with larger particles, having less surface-to-volume ratio, can dewater more effectively, resulting in drier cake. It is best to determine the optimal pool for a given application through tests.

The speed with which the cake transports is controlled by the differential speed. High differential speed facilitates high solids throughput where the cake thickness is kept to a minimum so as not to impair centrate quality due to entrainment of fine solids. Also, cake dewatering is improved due to a reduction in the drainage path with smaller cake height; however, this is offset by the fact that higher differential speed also reduces cake residence time, especially in the dry beach. The opposite holds for low differential speed. Therefore, an optimal differential speed is required to balance centrate clarity and cake dryness. The desirable differential speed is usually maintained using a two-stage planetary gearbox, the housing of which rotates with the bowl speed, with a fixed first-stage pinion shaft. In some applications, the pinion is driven by an electrical backdrive (dc or ac), hydraulic backdrive, or braked by an eddy-current device at a fixed rotation speed. The differential speed is then the difference in speed between the bowl and the pinion divided by the gear ratio. This also applies to the case when the pinion arm is held stationary, in which the pinion speed is zero. The torque at the spline of the conveyor, conveyance torque, is equal to the product of the pinion torque and the gear ratio. Higher gear ratio gives lower differential speed, and vice versa; lower gear ratio gives higher differential for higher solids capacity. The torque at the pinion shaft has been used to control the feed rate or to signal an overload condition by shearing of a safety pin. Under this condition, both the bowl and the conveyor are bound to rotate at the same speed (zero differential) with no conveyance torque and no load at the pinion.

Soft solids, most of which are biological waste such as sewage, are difficult to convey up the beach. Annular baffles or dams have been commonly used to provide a pool-level difference wherein the pool is

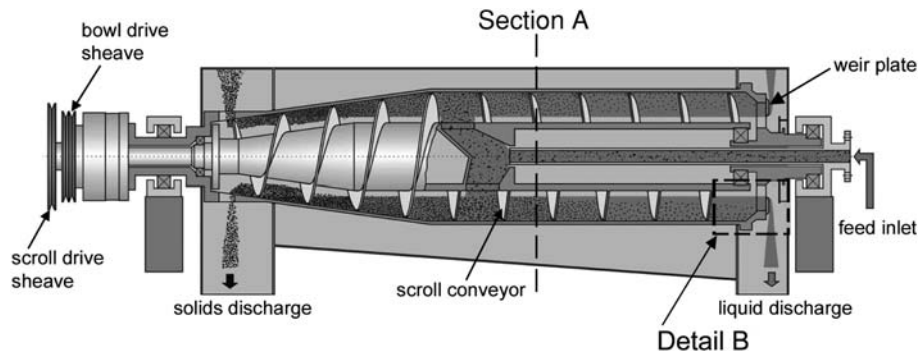


FIG. 18-155 Two-phase decanter centrifuge—gravity liquid discharge. (Flottweg Separation Technology.)

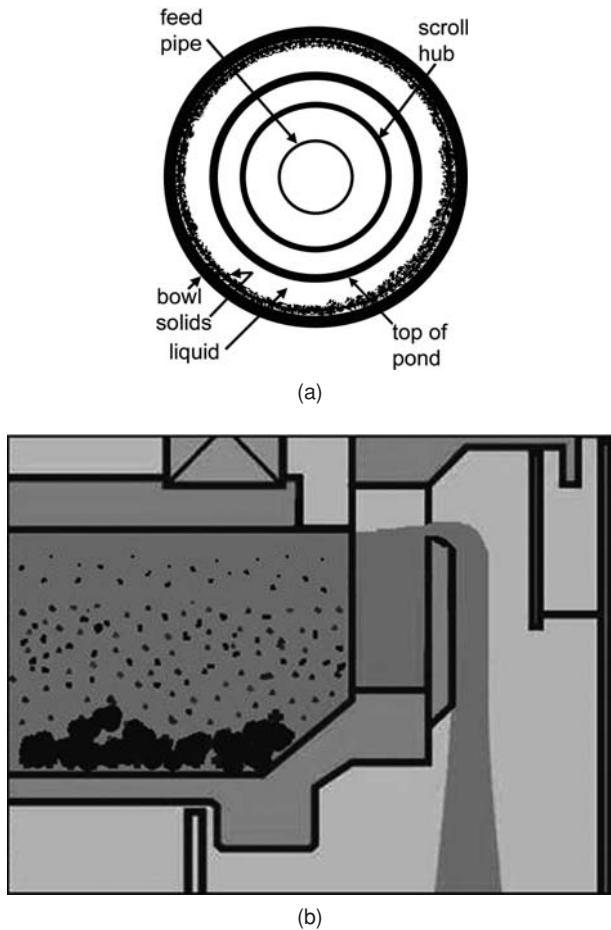


FIG. 18-156 (a) Section A from Fig. 18-155. (b) Detail B from Fig. 18-155. (Flottweg Separation Technology.)

deeper upstream of the baffle toward the clarifier and lower downstream of the baffle toward the beach. The pool-level difference across the baffle, together with the differential speed, provide the driving force to convey the compressible sludge up the beach. This has been used effectively in thickening of waste-activated sludge and in some cases of fine clay with dilatant characteristics.

High solids decanter centrifuges have been used to dewater mixed raw sewage sludge (with volume ratio of primary to waste-activated

sludge such as 50 percent to 50 percent or 40 percent to 60 percent, etc.), aerobically digested sludge, and anaerobically digested sludge. Cake solids as dry as 28 percent to 35 percent by weight are obtained for raw mixed sludge and 20 percent to 28 percent for the digested sludges, with the aerobic sludge at the lower end of the range. The typical characteristics of high-solids applications are: low differential speed (0.5 to 3 r/min), high conveyance torque, high polymer dosage (10 to 30 lb dry polymer/ton dry solids, depending on the feed sewage), and slightly lower volumetric throughput rate. An electrical (dc or ac with variable-frequency drive) or hydraulic backdrive on the conveyor with high torque capacity is essential to operate these conditions at steady state.

The horizontal decanter centrifuge is operated below its critical speed. The bowl is mounted between fixed bearings anchored to a rigid frame. The gearbox is cantilevered outboard of one of these bearings, and the feed pipe enters the rotating assembly through the other end. The frame is isolated from the support structure by spring-type or rubber vibration isolators. In the vertical configuration, the bowl and the gearbox are suspended from the drive head, which is connected to the frame and casing through vibration isolators. A clearance bushing at the bottom limits the excursion of the bowl during start-up and shutdown but does not provide the radial constraint of a bearing under normal operating conditions.

Decanter centrifuges with mechanical shaft-to-casing seals are available for pressure containment up to 1.1 MPa (150 psig), similar to the nozzle-disc centrifuge. They can be built to operate at temperatures from -87 to $+260^{\circ}\text{C}$ (-125 to $+500^{\circ}\text{F}$).

When abrasive solids are processed, the points of wear are protected with replaceable inserts/tiles made from silica carbide, tungsten carbide, ceramic, or other abrasive-resistant materials. These high-wear areas include the feed zone including feed ports; the conveyor blade tip, especially the pressure or pushing face; the conical beach; and the solids discharge ports. Transport of solids is encouraged in some applications by longitudinal strips or grooves at the inner diameter of the bowl, especially at the beach, to enhance the frictional characteristics between the sediment and the bowl surface, and by polished conveyor faces to reduce frictional drag. For fluidlike sediment cake, by using the strips in the beach, a much tighter gap between the conveyor blade tip and the bowl surface is possible with a cake heel layer trapped by the strips. This reduces leakage of the fluid sediment flowing through an otherwise larger gap opening to the pool. Gypsum coating on the bowl wall at the beach section has been used to achieve the same objective.

Various bowl configurations with a wide range of aspect ratios—i.e., length-to-diameter ratio—from less than 1 to 4 are available for specific applications, depending on whether the major objective is maximum clarification, classification, or solids dryness. Generally, the movement of liquid and solids is in countercurrent directions, but in the cocurrent design the movement of liquid is in the same direction as that of the solids. In this design, the feed is introduced at the large end of the machine and the centrate is taken by a skimmer at the beach-cylinder junction. The settled solids transverse the entire machine and discharge at the beach exit. Compound angle beaches are used in

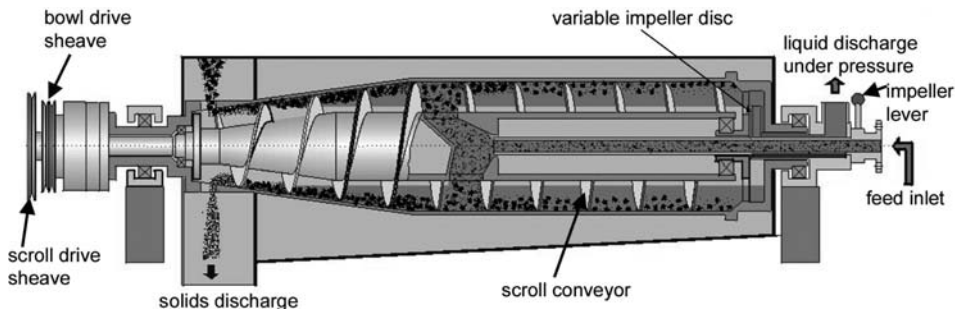


FIG. 18-157 Two-phase decanter centrifuge—pressurized liquid discharge. (Flottweg Separation Technology.)

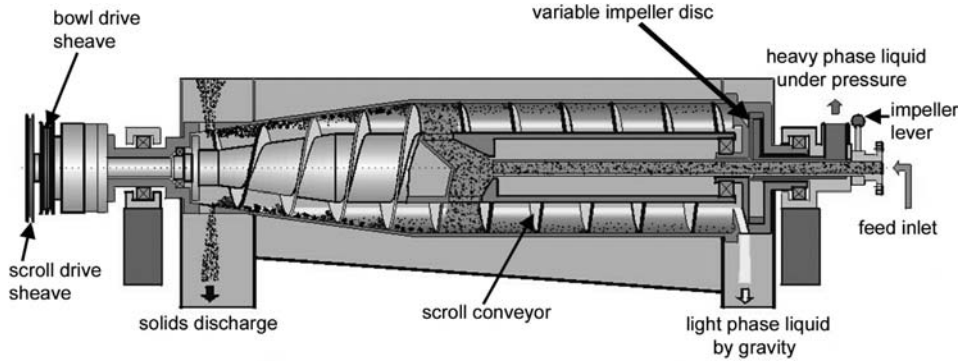


FIG. 18-158 Three-phase decanter centrifuge. (Flottweg Separation Technology.)

specific applications such as washing and drying of polystyrene beads. The pool level is located at the intersection of the two angles at the beach, the steeper angle being under the pool and the shallower angle above the pool (i.e., dry beach), allowing a longer dewatering time. The wash is applied at the pool side of the beach-angle intersection and functions as a continuously replenished annulus of wash liquid through which the solids are conveyed. The size of decanter centrifuge ranges from 6 in diameter to 54 in. The larger is the machine, the slower is the speed, and less is the G-force (Fig. 18-129). However, it provides a much higher throughput capacity, which cannot be accommodated with smaller machines (see Table 18-10). Decanter centrifuges are utilized in a broad range of industries and applications where a large amount of solids separation from liquids is required on a continuous basis. These industries include but are not limited to food, beverage including dairy, chemical, pharmaceutical, oil, edible oil, industrial, and municipal wastewater.

Three-Phase Decanter (Tricanter) Centrifuges Tricanter centrifuges are similar in principle to decanter centrifuges (see Fig. 18-158), but separate three phases that contain two immiscible liquids and one sedimenting/suspended solids phase. The sedimenting solids that collect on the bowl wall are conveyed out of the centrifuge and discharged similarly to a decanter centrifuge. The two liquid phases are discharged either via gravity over two sets of adjustable weir plates or rings or via a dual discharge system where the heavy liquid phase (typically water) is discharged via a stationary impeller under pressure and the light liquid phase (typically fat or oil) is discharged via gravity over a ring dam. The benefit of the dual discharge system is that the liquid interface zone (and ultimately the pool/pond height) is adjustable while the machine is operating at full speed. These types of centrifuges are commonly used in the fish, animal by-products, oil sludge, and edible oil (i.e., olive and palm) industries.

Specialty Decanter Centrifuges Decanter technology has evolved over the past 10 years to include machines suitable for separation applications normally not effective in standard decanter centrifuges. These specialty decanters/tricanters utilize the same basic premise of solids discharge via an internal scroll, but with specific machine geometries that allow for specialty separations. These specialty decanters include the Sedicanter (shown in Fig. 18-159) and Sorticanter (shown in Fig. 18-160). The Sedicanter, which has a double-cone cocurrent bowl design and specialized scroll geometry, is capable of achieving higher rotational speeds (up to 7750 rpm and 10,000G) and can, therefore, increase clarification efficiency and effectively discharge fine, pasty solids where a normal decanter is inefficient and ineffective. The Sedicanter is commonly used in certain biotechnology, vitamin, soy, and yeast separations.

The Sorticanter has a scroll with reversing pitch on one side, which skims a floating solids layer off the top of the carrier liquid, usually an aqueous brine of intermediate density. Sinking solids are scrolled out similarly to normal decanter centrifuges, and liquid is discharged under pressure via a stationary but variable impeller. The Sorticanter is utilized in the plastics recycling industry.

Screenbowl Centrifuges The screenbowl centrifuge consists of a solid-bowl decanter to which, at the smaller conical end, a cylindrical screen has been added (see Fig. 18-161). The scroll spans the entire bowl, conforming to the profile of the bowl. It combines a sedimenting centrifuge together with a filtering centrifuge. Therefore, the solids which are processed are typically larger than 23 to 44 μm .

As in a decanter, an accelerated feed is introduced to the separation pool. The denser solids settle toward the bowl wall and the effluent escapes through the ports at the large end of the machine. The sediment is scrolled toward the beach, typically with a steeper angle compared to the decanter centrifuge. As the solids are conveyed to the

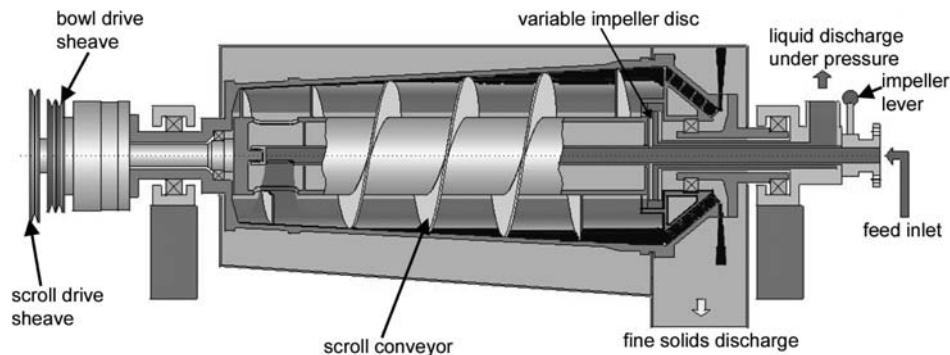


FIG. 18-159 Sedicanter centrifuge. (Flottweg Separation Technology.)

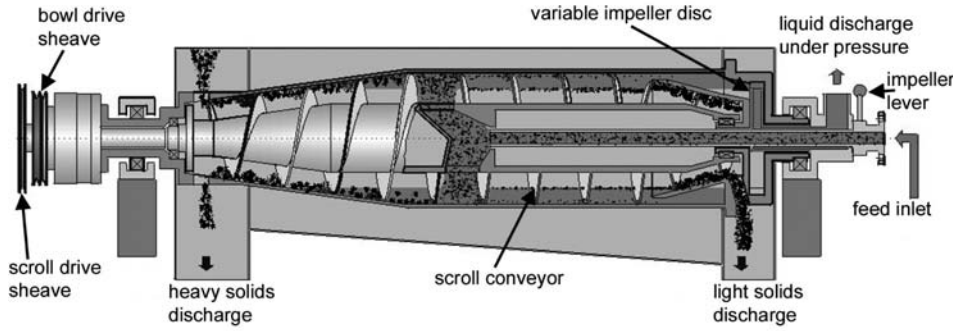


FIG. 18-160 Sorticanter centrifuge. (Flottweg Separation Technology.)

screen section, the liquid in the sediment cake further drains through the screen, resulting in drier cake. Washing of the sediment in the first half of the screen section is very effective in removing impurities, with the second half of the screen section reserved for dewatering of mother liquor and wash liquid.

The screen is typically constructed of a wedge-bar with an aperture between adjacent bars, which opens up to a larger radius. This prevents solids from blinding the screen as well as reduces conveyance torque. For abrasive materials such as coal, the screens are made of wear-resistant materials such as tungsten carbide.

Continuous Centrifugal Sedimentation Theory The Stokes settling velocity of a spherical particle under centrifugal field is given by Eq. (18-103). Useful relationships have been established on continuous sedimentation by studying the kinematics of settling of a spherical particle of diameter d in an annular rotating pool. Equating the time rate of change in a radial position to the settling velocity, and the rate of change in an axial position to bulk-flow velocity, thus gives

$$\frac{dr}{dt} = crd^2 \quad (18-111)$$

$$\frac{dx}{dt} = \frac{Q}{\pi(r_b^2 - r_p^2)} \quad (18-112)$$

where $c = (\rho_s - \rho_L) \Omega^2 / 18\mu$, x is distance along the axis of the bowl, Q is the volumetric feed rate, r_b and r_p are, respectively, the bowl and pool surface radii. For a particle located at one end of the bowl at radius r with $r_p < r < r_b$, after transverse the full bowl length, it set-

les out and is captured by the bowl wall. Solving the above equations with these boundary conditions, the limiting trajectory is:

$$\frac{r}{r_b} = \exp \left[\frac{-\pi c L (r_b^2 - r_p^2) d^2}{Q} \right] \quad (18-113)$$

If the same size particle d is located at an initial starting radius less than r given by Eq. (18-113) it is assumed to escape from being captured by the bowl, whereas it would have been captured if it had been at an initial radius greater than r . Assuming that the number of particles with size d is uniformly distributed across the annular pool, the recovery Rec_d (known also as **grade efficiency**) is the differential of the cumulative recovery $Z = 1 - Y$, with Y given in Eq. (18-95) for particles with size d , as the ratio of the two annular areas:

$$Rec_d = \frac{r_b^2 - r^2}{r_b^2 - r_p^2} \quad (18-114)$$

Combining Eqs. (18-113) and (18-114), the maximum Q to the centrifuge, so as to meet a given recovery Rec_d of particles with diameter d , is

$$\frac{Q_d}{2V_{gd}} = \left(\frac{\pi \Omega^2 L}{g} \right) \left(\frac{r_b^2 - r_p^2}{\ln [1 - Rec_d [1 - (r_p/r_b)^2]]} \right) = \Sigma_{Rec_d} \quad (18-115)$$

Note in Eq. (18-115) that V_{gd} is the settling rate under $1g$, and it is a function of the particle size and density and fluid properties. The ratio $Q_d/2V_{gd}$ is then related only to the operating speed and geometry of

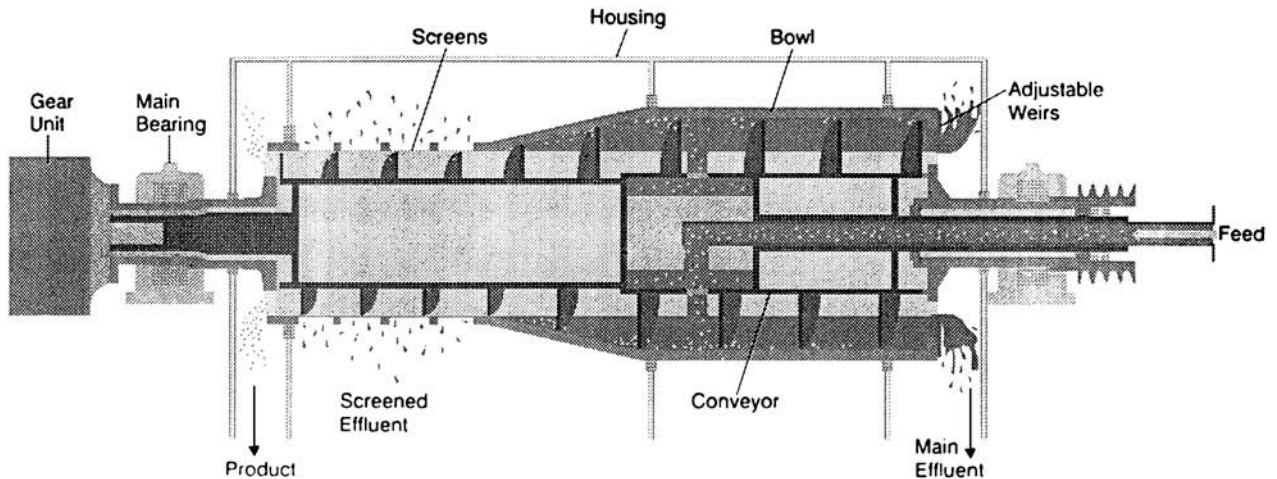


FIG. 18-161 Cylindrical-conical screen-bowl centrifuge. (Bird Machine Co.)

the centrifuge, as well as to the size recovery. It measures the *required* surface area for settling under centrifugal gravity to meet a specified Rec_d . When the size recovery Rec_d is set at 50 percent, the general result, Eq. (18-115), reduces to the special case, which is the well-known Ambler's Sigma factor, which for a straight rotating bowl (applicable to bottle centrifuge, decanter centrifuge, etc.) is:

$$\Sigma = \left[\frac{\pi \Omega^2 L}{g} \right] \left[\frac{r_b^2 - r_p^2}{\ln [2r_b^2 / (r_b^2 + r_p^2)]} \right] \tag{18-116}$$

It can be simplified to:

$$\Sigma = \pi \Omega^2 L \frac{(3r_b^2 + r_p^2)}{2g} \tag{18-117}$$

For a disc centrifuge, a similar derivation results in

$$\Sigma = \frac{2\pi \Omega^2 (N - 1) (r_2^3 - r_1^3)}{3g \tan \theta} \tag{18-118}$$

where N is the number of discs in the stack, r_1 and r_2 are the outer and inner radii of the disc stack, and θ is the conical half-angle.

Typical Σ factors for the three types of sedimenting centrifuges are given in Table 18-13. In scale-up from laboratory tests, sedimentation performance should be the same if the value of \dot{Q}/Σ is the same for the two machines. This is a widely used criterion for the comparison of centrifuges of similar geometry and liquid-flow patterns developing approximately the same G ; however, it should be used with caution when comparing centrifuges of different configurations. In general, the shortcomings of the theory are due to the oversimplified assumptions being made, such as (1) there is an idealized plug-flow pattern; (2) sedimentation abides by Stokes law as extended to many g 's; (3) feed solids are uniformly distributed across the surface of the bowl head at one end of the clarifier and capture implies that the particles' trajectory intersect the bowl wall; (4) the feed reaches full tangential speed as it is introduced to the pool; (5) the recovery of given-size particles is at 50 percent; (6) this does not account for possible entrainment of already settled particles in the liquid stream; (7) there is absence of entrance and exit effects.

Experience in using the Σ concept has demonstrated that the calculated Σ factor should be modified by an efficiency factor to account for

some of the aforementioned effects which are absent in the theory and, as such, this factor depends on the type of centrifuge. It is nearly 100 percent for simple spin-tube bottle centrifuge, 80 percent for tubular centrifuge, and less than 55 percent for disc centrifuges. The efficiency varies widely for decanter centrifuges, depending on cake conveyability and other factors.

FILTERING CENTRIFUGES

Filtering centrifuges are broadly categorized as continuous operating and batch operating. Both continuous and batch filtering centrifuges use some type of filtration media fitted against the basket (bowl) wall. As the solid-liquid mixture is introduced, the liquid filters through the solids, through the filter media, and typically through perforations in the basket shell (except with rotational siphon designs, discussed later). Filtering centrifuges are primarily chosen over sedimenting types where high cake purity through cake washing is a requirement, or where minimal residual cake moisture is desired. Typical solids retention times range from 5 to 45 s for continuous operating filtering centrifuges and 5 to 180 min for batch operating filtering centrifuges.

Usually, the solids phase is of a higher specific gravity than the liquid; but unlike with sedimenting centrifuges, this is not an absolute requirement. In the nontypical case where the opposite is true, then filtration, be it centrifugal, vacuum, or pressure, is the only option for solid-liquid separation. However, for batch filtering centrifuges with the solids phase lighter than the liquid, care must be taken that liquid is not allowed to build in the basket during the feed step, or else buoyancy forces may float the settled solids, resulting in uneven filtration and high vibration. This is not of concern for continuous filtering centrifuges since the filtration rate must inherently exceed the liquid feed rate for stable operation. Refer to Table 18-14 for typical operating ranges of filtering centrifuges.

BATCH FILTERING CENTRIFUGES

Although continuous centrifuges are often preferred for reasons of lowest capital cost, high unit capacity, and ease of integration into continuous upstream and downstream processes, batch filtering centrifuges with cyclic operation will always have a role in the CPI for reasons of highest possible product purity, lowest possible cake moisture, and highest product recovery. The slurry's physical properties such as particle size distribution or liquid viscosity may require long

TABLE 18-13 Scale-up Factors for Sedimenting Centrifuges

Type of centrifuge	Inside diameter, in	Disc diameter, in/number of discs	Speed, r/min	Σ value, units of 10 ⁴ ft ²	Recommended scale-up factors ^a
Tubular	1.75	—	23,000	0.32	1†
Tubular	4.125	—	15,000	2.7	21
Tubular	4.90	—	15,000	4.2	33
Disc	—	4.1/33	10,000	1.1	1
Disc	—	9.5/107	6,500	21.5	15
Disc	—	12.4/98	6,250	42.5	30
Disc	—	13.7/132	4,650	39.3	25
Disc	—	19.5/144	4,240	105	73
Scroll conveyor	6	—	6,000	0.27	1
Scroll conveyor	14	—	4,000	1.34	5
Scroll conveyor	14‡	—	4,000	3.0	10
Scroll conveyor	18	—	3,450	3.7	12.0
Scroll conveyor	20	—	3,350	4.0	13.3
Scroll conveyor	25	—	3,000	6.1	22
Scroll conveyor	25	—	2,700	8.6	31

^aThese scale-up factors are relative capacities of centrifuges of the same type but different sizes when performing at the same level of separation achievement (e.g., same degree of clarification). These factors must not be used to compare the capacities of different types of centrifuges.

†Approaches 2.5 at rates below mL/min.

‡Long bowl configuration.

NOTE: To convert inches to millimeters, multiply by 25.4; to convert revolutions per minute to radians per second, multiply by 0.105; and to convert 10⁴ square feet to square meters, multiply by 929.

TABLE 18-14 Operating Range of Filtering Centrifuges

Type of centrifuge	G/g	Minimum feed solids concentration by wt.	Minimum mean particle size, μm	Minimum $V_{f_{90}}$, m/s
Vibratory	30–120	50	300	5×10^{-4}
Tumbler	50–300	50	200	2×10^{-4}
Screen scroll	500–2000	35	75	1×10^{-5}
Pusher	300–800	40	120	5×10^{-5}
Screen bowl	500–2000	20	45	2×10^{-6}
Peeler	300–2000	5	10	2×10^{-7}
Vertical	200–1000	5	5	1×10^{-7}
Inverting filter	300–1000	5	2	5×10^{-8}

retention time and drive the selection from continuous to batch. Generally, when the value of the product is high, batch operating centrifuges are often preferred.

A development over the last 10 to 20 years is the introduction of true cGMP designs suitable for high-purity fine chemicals and pharmaceutical applications. Requirements in this sector usually favor batch operation due to demands for batch identity; typical properties of the slurry dictate batch operation, high wash requirements, cleanability and inspectability, avoidance of cross-contamination for multipurpose applications, and elimination of operator exposure to the process.

Most modern batch filtering centrifuges are provided with a variable-frequency drives (VFDs) for speed variation, often with power regenerative braking. Even in the case of peeler centrifuges which are capable of constant-speed operation throughout the cycle, in most cases they are still fitted with VFDs to meet starting requirements (accelerating a high inertial load), operating flexibility, and regenerative braking in hazardous areas. However, there are still units available that use either a two-speed motor (generally considered obsolete) or hydraulic drive.

The main subcategories of batch filtering centrifuges are vertical basket centrifuges (both top unloading and bottom unloading of various configurations), horizontal peeler centrifuges, and horizontal inverting filter centrifuges.

Vertical Basket Centrifuge—Operating Method and Mechanical Design The vertical basket centrifuge is equipped with a cylindrical basket rotating about the vertical axis. The basket shell is normally perforated and lined with filtration media consisting of filter cloth, and backing screens to provide liquid drainage paths to the basket holes. Securing the filter cloth may be by hook and loop attachment or with snap-in retainers.

Feed slurry is introduced into the basket through either single or multiple feed pipes, or by other means such as rotating feed cone to help distribute the solids on the basket wall. In most cases, feed slurry is introduced at an intermediate speed, although in some applications (FGD gypsum, for one), feeding is done at full speed. There are several methods available to control the feed and cake level such as mechanical, paddle-type feelers, capacitance probes, ultrasonic sensors, feed totalizer, or load cells.

The solids distribution profile may tend to be parabolic with thicker cakes near the bottom of the basket, tapering down toward the top, since the G-field is perpendicular to the force of gravity. This is especially true with fast-sedimenting solids that will settle toward the basket bottom before the slurry is fully accelerated by the basket. The coarser solids can settle toward the basket bottom, while the finer solids deposit preferentially toward the top. This can result in uneven filtration resistance in the cake, affecting the wash pattern and efficiency of the wash. In cases where this is a concern, a rotating feed cone may be better for even distribution, or a horizontal peeler centrifuge may be better suited to the application.

During and after feeding, filtrate passes through the cake, filter media, and out through the basket shell and is collected in a housing surrounding the basket and discharged through a tangential nozzle. The solids build up on the basket wall during the feed step until the desired loading is achieved.

After a spin time to filter the mother liquor through the solids, wash liquor is commonly applied in either a single step or various combinations, typically via a wash pipe with nozzles. The cake is spun for a

time at high speed, then the machine ramps down to discharge. Solids removal can be accomplished by one of several methods.

Top Unloading Vertical Basket Centrifuges This is one of the oldest types of centrifuges, dating back to about 1900 or even earlier. With this design, the perforated basket is fitted with either a filter cloth or a filter bag. The basket has a solid bottom. After the dry spin portion of the cycle is completed, the machine is stopped. Solids removal is either by manually digging out the cake or by removing (lifting) the filter bag from the top of the unit. Except for small pilot-scale units and some specialty applications, this design is no longer commonly marketed or desired due to labor intensiveness, incompatibility with solvent wet or toxic products (operator exposure), and overall inefficiency of operation. See Fig. 18-162.

One modern top unloading design is used for bulk pharmaceutical processing as part of a complete closed-loop dewatering and drying system including heaters, blowers, and sterile filters. This involves a two-motion discharge “mouth” to pneumatically remove thin layers of cake while blowing sterile, dehumidified hot nitrogen into the housing and into the discharge pipe. This method both pneumatically conveys and flash-dries the solids en route to the waiting conical mixer/dryer for subsequent vacuum drying.

Bottom Unloading Vertical Basket Centrifuges Most common for modern machines is the bottom discharge design, incorporating a swiveling scraper mechanism, typically cutting the cake in a single motion, or with a two-motion, oscillating scraper in the case of finer or stickier cakes or pharmaceuticals. In every case, solids discharge must be at low speed, which necessitates ramping the machine up and down every cycle. After discharge, a thin cake layer or heel remains on the filter cloth. See Fig. 18-163.

Heel removal can be automated by dissolving the heel, flushing the heel out the solids discharge chute with subsequent downstream diverting away from solids handling equipment, or pneumatically removing the heel with blowoff nozzles, discharging it out the solids discharge. Pneumatic heel removal can be accomplished either from within the basket (often incorporated with the knife) or from the outside of the basket.

There are different cover arrangements to access the interior, such as hinged or pivoting manway, half or full opening covers. Filter cloth maintenance or component adjustments usually require entering the unit in any case, except for small sizes. See Fig. 18-164.

Isolation of the load imbalances from the structure has historically been by link, or three-column suspension. This system is relatively inefficient and transmits substantial dynamic forces to the building foundation, limiting operating speeds and performance. In response to the common shortcomings of this design, some manufacturers redesigned the suspension/isolation system to a massive inertial base-plate and housing supported on tuned coil springs and dampers at each corner. This greatly improved the dynamic force attenuation and stability of the machine. This system has allowed designing very large machines (1600-mm-diameter by 1250-mm-high baskets) processing materials with high solids density such as wallboard-grade gypsum from FGD systems with a unit capacity in excess of 10 Mtons/h.

Top Suspended Vertical Centrifuges A special type of top suspended centrifuge is widely used in sugar processing and is shown in Fig. 18-165. Conventionally, the drive is suspended from a horizontal bar supported at both ends from two A-frames. The drive head, which is connected to the motor or a driven pulley through a flexible coupling, carries the thrust and radial bearings that support the basket,

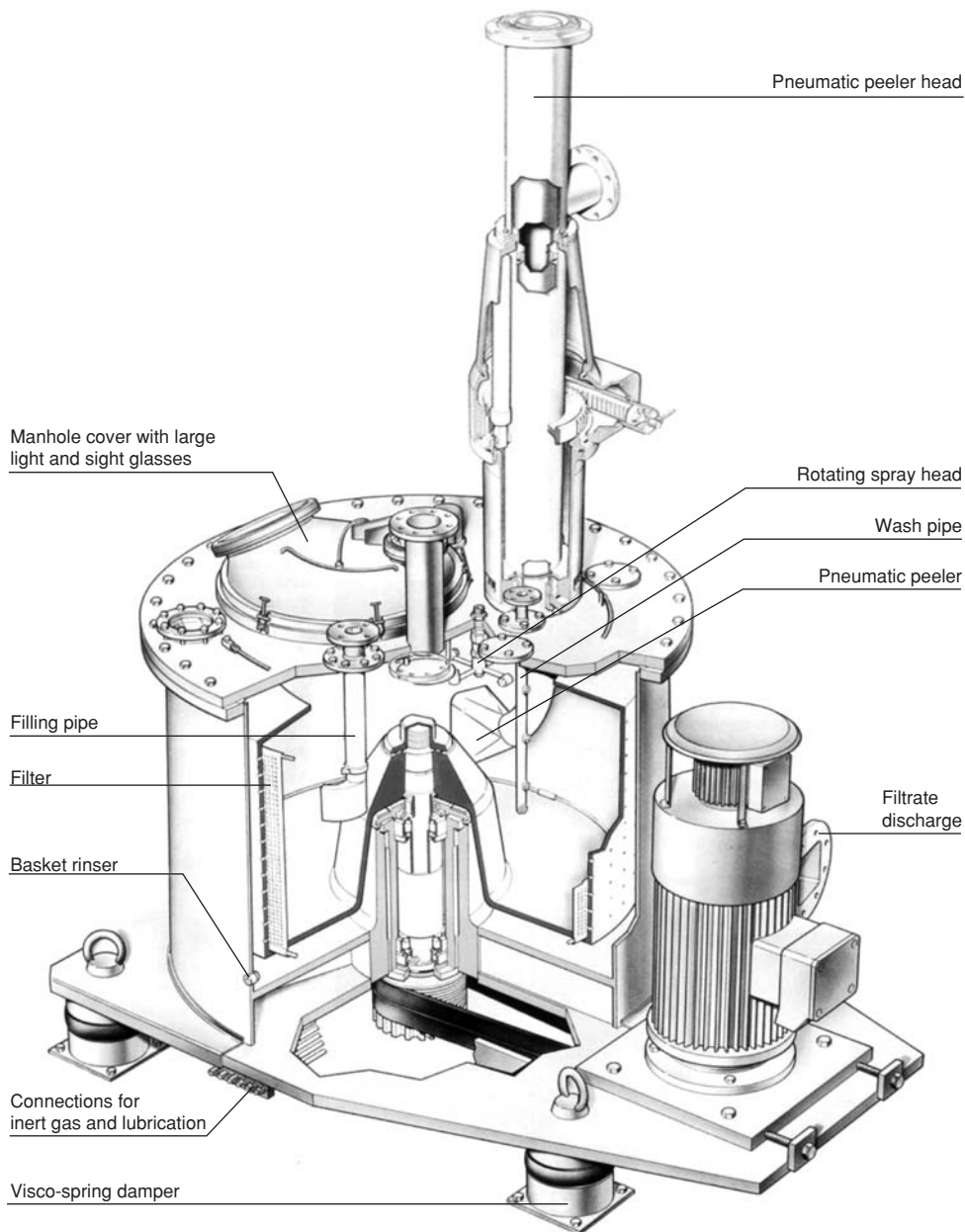


FIG. 18-162 Top unloading vertical basket centrifuge. (Krauss Maffei Process Technology.)

shaft, and load. These units can be equipped with large 112-kW (150-hp) drive motors, and on white sugar can process about 350 kg/cycle with 24 cycles/h.

Horizontal Peeler Centrifuge—Operating Method and Mechanical Design The chemical design peeler centrifuge was developed in the 1920s and has wide areas of application (Fig. 18-166). Like the vertical basket, it has a rotating filtration basket, except that it rotates about the horizontal axis. Early machines supported the basket from both ends, but virtually all modern machines are cantilever-supported for purposes of accessibility to the basket and internal components. Some machines are equipped with a full opening door which swings away with internal components, while other designs

incorporate a full opening housing that also provides access to the basket exterior. This unit has an extremely rugged construction compared to vertical baskets, required due to the full-speed feeding and discharge capability of the peeler centrifuge. It is often provided with high-power ac VFD drives for accelerating the feed slurry at full speed and for optimum operating flexibility. Gastight construction to 400-mm (16-in) water column is usually standard, and higher pressure ratings can easily be accomplished.

By reorienting the axis to horizontal, many advantages become possible such as superior wash capability with the more uniform solids distribution compared to the vertical basket, with the potential for uneven, parabolic cake profile resulting in uneven wash penetration.

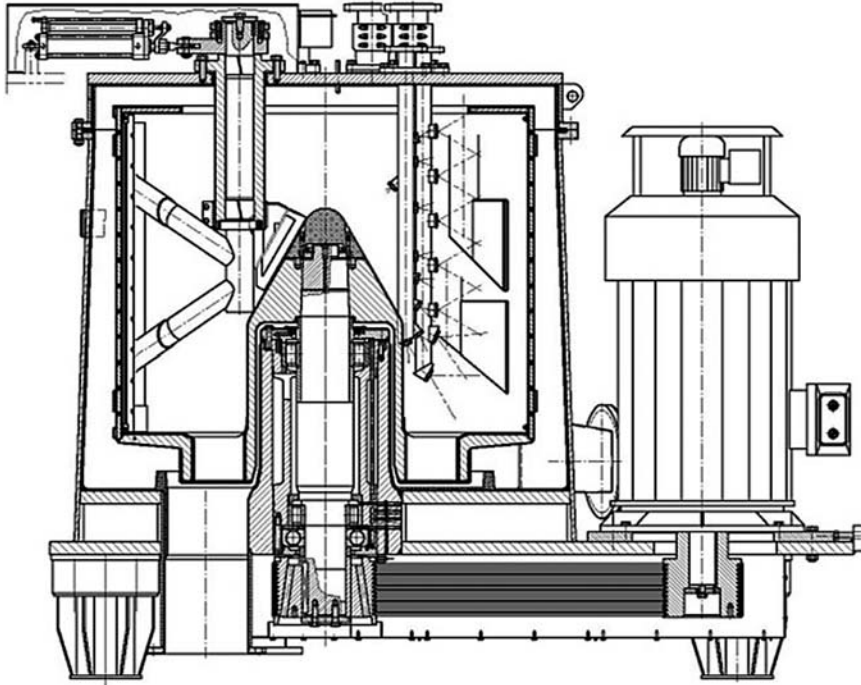


FIG. 18-163 Typical bottom unloading vertical basket centrifuge. (Krauss Maffei Process Technology.)

The peeler centrifuge costs more than a comparable basket size vertical machine, although often a smaller peeler centrifuge can outperform a larger vertical basket. In addition, the higher capital cost is offset by numerous process and mechanical advantages, such as these:

- Full opening door contains the feed, wash, feed control, and solids discharge components. Easily swung open, it then provides complete

access to the basket interior and all internal components mounted on the door. Filter cloth exchange does not require vessel entry.

- Isolation of dynamic forces is far superior with horizontal machines compared to vertical.
- The peeler centrifuge will distribute the solids more evenly since it is not feeding perpendicular to gravity as is the vertical basket. This

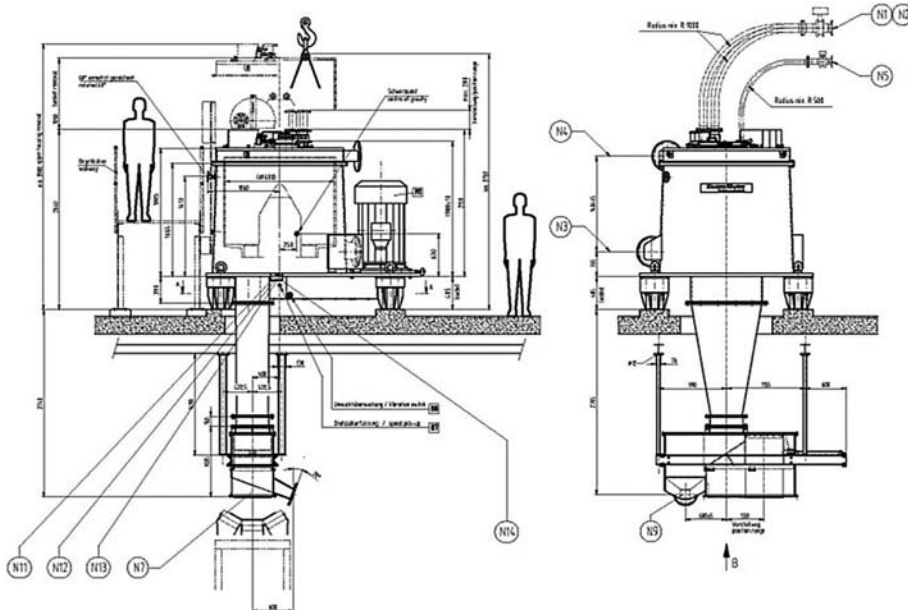


FIG. 18-164 Typical vertical basket centrifuge installation. (Krauss Maffei Process Technology.)

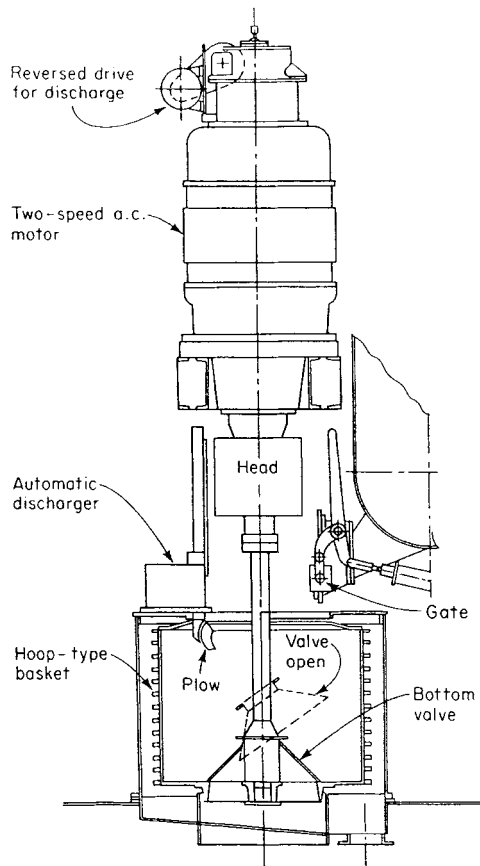


FIG. 18-165 Top-suspended vertical centrifuge. (Western States Machine Co.)

provides smoother operation, better wash effect, and an ability to handle faster-draining materials.

- Ability to discharge at high speed eliminates or minimizes dead cycle time required for acceleration and braking for higher capacity, lower power consumption, and lower wear and tear. The cycle time savings is particularly beneficial with short-cycle (fast-filtering) requirements.
- The peeler centrifuge can provide higher centrifugal forces than can vertical baskets, for increased performance and flexibility.
- Peeler centrifuges are available in larger sizes than vertical centrifuges—up to 2100-mm (83-in) diameter.
- The peeler centrifuge is also capable of automatic heel removal by several methods: dissolving the heel, reslurrying and discharging the heel wet and diverting downstream, or dry heel removal pneumatically. Pneumatic heel removal can be accomplished either from within the basket or from outside the basket.

Siphon Peeler Centrifuge The siphon peeler centrifuge (Fig. 18-167) was developed and patented by Krauss-Maffei in the 1970s. Instead of utilizing only centrifugal pressure as the driving force, as do all perforated units both vertical and horizontal, the rotational siphon centrifuge provides an increased pressure gradient by reducing the pressure behind the filter media and thereby increasing the driving force for filtration.

As in the perforated basket design, the liquid filters through the cake and filter media, but instead of discharging through perforations in the basket shell, the basket wall is solid and the liquid flows axially to the basket rear and into a separate chamber. At this point, the filtrate is skimmed out with a radially adjustable skimmer.

In perforated baskets, the driving force for filtration is approximately the hydrostatic pressure established by the liquid column. The driving force diminishes as the liquid column height decreases, often causing a wet layer near the base of the cake due to capillary pressure balancing the centrifugal pressure. In siphon baskets, in addition to the centrifugal pressure, by skimming at a radius greater than the filter cloth, a rotational siphon is established. Due to the gravitational field in which it is working, a height difference Δh of only 20 to 30 mm is sufficient to lower the pressure behind the cloth to the vapor pressure of the liquid. This additional vacuum remains in place until all the interstitial liquid is drawn through the cake, and will overcome the cake capillary pressure, thus preventing this wet layer. Once the supernatant and interstitial

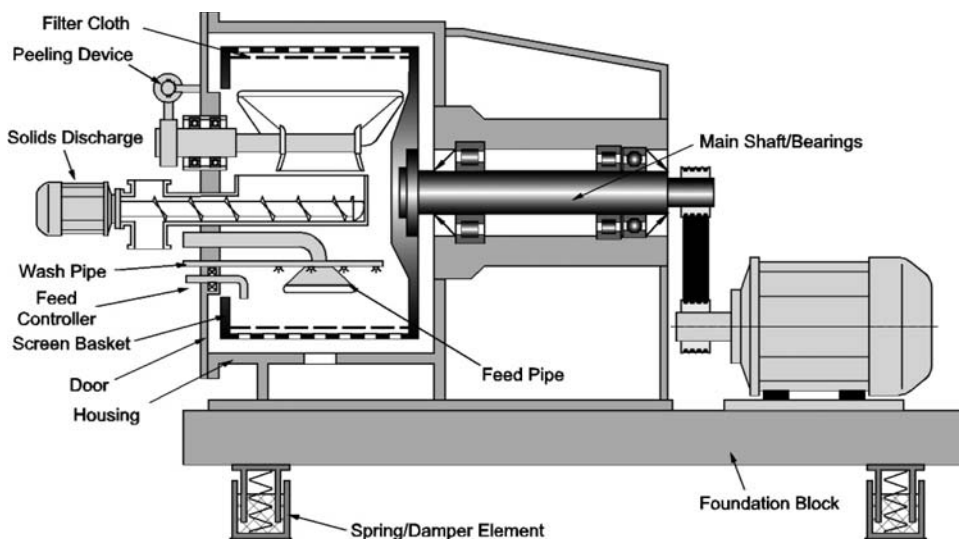


FIG. 18-166 Peeler centrifuge cross section. (Krauss Maffei Process Technology.)

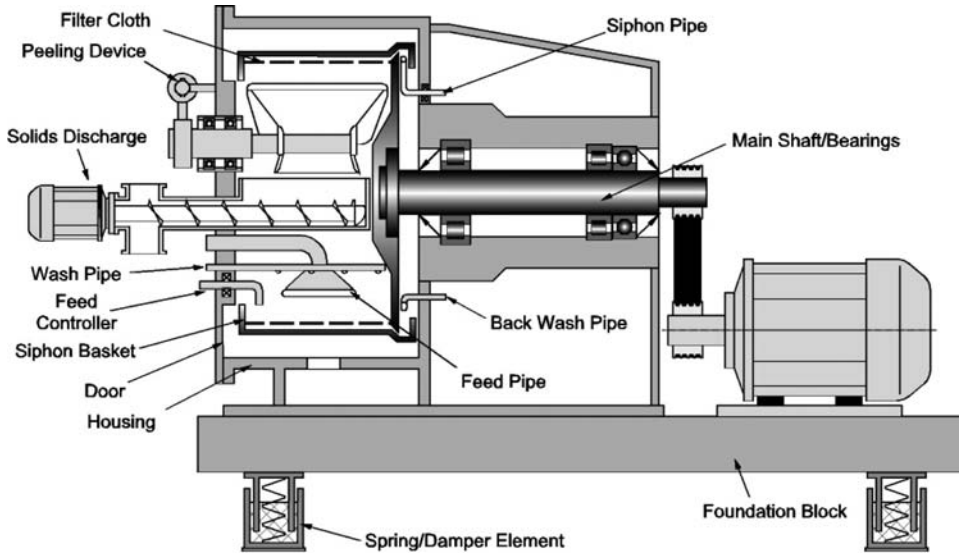


FIG. 18-167 Siphon peeler centrifuge cross section. (Krauss Maffei Process Technology.)

liquid drains from the cake, the siphon chamber behind the cloth drains and filtration characteristics are like those of a perforated basket. See Fig. 18-168.

To reestablish the siphon for the next cycle, a priming step precedes feeding where the siphon skimmer is pivoted inward near the rim of the siphon chamber, and liquid is introduced into the siphon chamber that backflows up through the heel cake, displacing gas from the chamber. Feeding then begins with the heel submerged. After a time delay, the siphon swivels downward to the working position (δh of +20 to 30 mm) where it remains for the remainder of the cycle. Besides increased driving force for filtration, other benefits of the rotational siphon include:

- Accurate control of the filtration rate is useful during feed and wash. For fast-filtering products, filtration rates can be throttled, ensuring even solids distribution.
- Backwashing the residual heel between each cycle rejuvenates the heel to maintain good permeability. Heel life is often extended.
- Feeding into a liquid bath helps lay down a more porous heel layer since the larger particles sediment faster than finer particles.

- Separate discharge of filtrate from splash/overflow provides better product yield.
- Deep siphon chambers with cake backwashing capability have been successfully utilized to completely submerge the cake and indefinitely increase wash contact time.

Pressurized Siphon Peeler Centrifuge Theoretically, the same principle can further increase driving force with overpressure in the process housing; for example, 3-bar overpressure would produce up to 4-bar pressure gradient across the cake. In practice, to date this has not been utilized due to the complexity of the installation.

Pharma Peeler Centrifuge For applications requiring hygienic operation, a special type of peeler centrifuge was developed in the 1990s (Fig. 18-169).

Primary applications for this type of machine are in fine chemicals and pharmaceuticals, often in multipurpose use where cross-contamination must be avoided. It provides for ease of cleanability and inspectability with automatic CIP/SIP, access to every wetted surface, pressure-tight construction suitable for steam sterilization, automatic heel removal, and separation of mechanical components from the

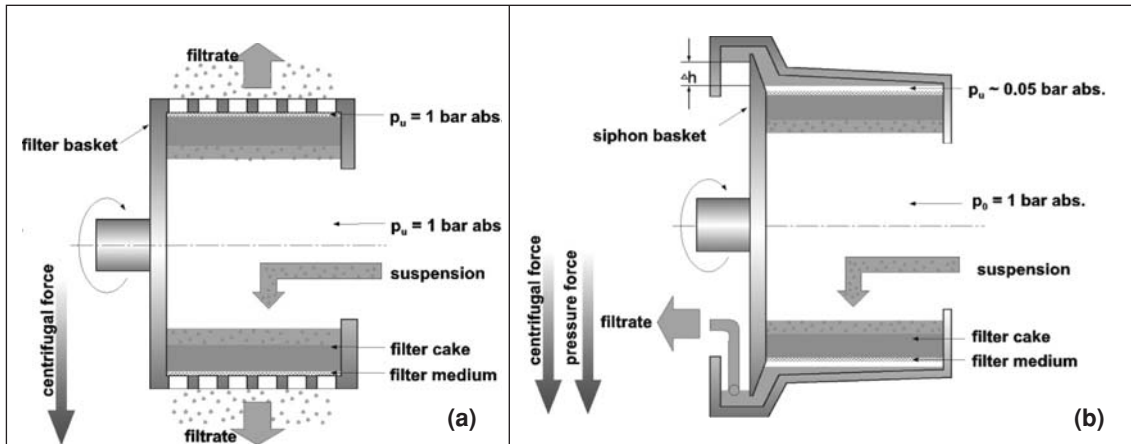


FIG. 18-168 Schematic representation of (a) perforate versus (b) siphon centrifuge. (Krauss Maffei Process Technology.)



FIG. 18-169 Pharma peeler centrifuge. (Krauss Maffei Process Technology.)

process end, making it suitable for through-the-wall clean-room installation. Operation is contained, thereby eliminating operator exposure.

Inverting Filter Centrifuge The inverting filter centrifuge was introduced in the late 1970s to provide a means of ensuring that all the filter cake is discharged from the filter medium. By turning the cloth inside out to achieve solids discharge, the problems of operator exposure and variable product quality associated with manual cake removal or residual-heel blinding were largely eliminated. By the late 1980s, this style of centrifuge had found widespread application in

pharmaceutical and agricultural chemical production. See Figs. 18-170 to 18-172.

The inverting filter design comprises a horizontal axis shaft with a two-part bowl attached. The perforated cylindrical bowl remains in a fixed axial position throughout the operation, while a bowl insert is able to move along the horizontal axis. The filter cloth is attached at one end to the axially fixed bowl and at the other to the axially movable bowl insert. Therefore, moving the bowl insert causes the filter cloth to turn inside out. In the filtering position, the bowl insert sits inside the bowl, with the filter cloth covering perforations. As with other filtering centrifuges, the cake builds up on the cloth during filling. It is washed using a true positive-displacement, plug-flow wash, and cake dewatering can be achieved simply by spinning (often at the maximum speed) for a time.

As this cake-discharging mechanism involves little or no risk of cloth blinding, inverting filter centrifuges usually operate at optimum conditions with relatively thin cakes and frequent discharges. (Cake thicknesses are typically 1 to 3 in, and cycle times are typically 8 to 14 min.) This style of operation is particularly effective with compressible materials where the filtration rate drops off dramatically with increasing cake thickness. By operating with thin cakes and short cycle times, the average filtration flux throughout the batch operation is maximized for these difficult applications.

Inverting filter centrifuges come in bowl diameters ranging from 300 to 1300 mm and achieve g -forces of 3000 – 900 \times gravity.

CONTINUOUS FILTERING CENTRIFUGES

Where processing conditions and objectives allow, continuous filtering centrifuges offer the combination of high processing capacities and good wash capabilities. Inherently they are less flexible than batch filtering centrifuges, primarily constrained by much shorter retention time, and in some cases liquid handling capacity requires upstream

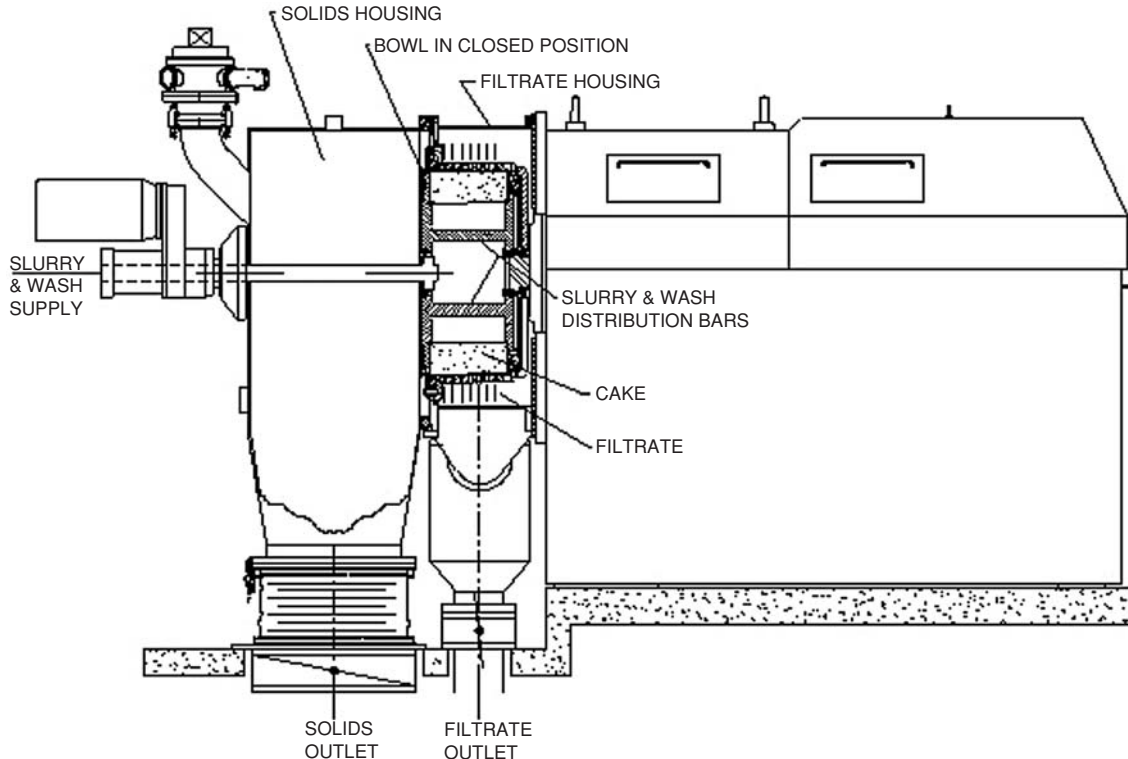


FIG. 18-170 Inverting filter centrifuge. (Heinkel USA.)

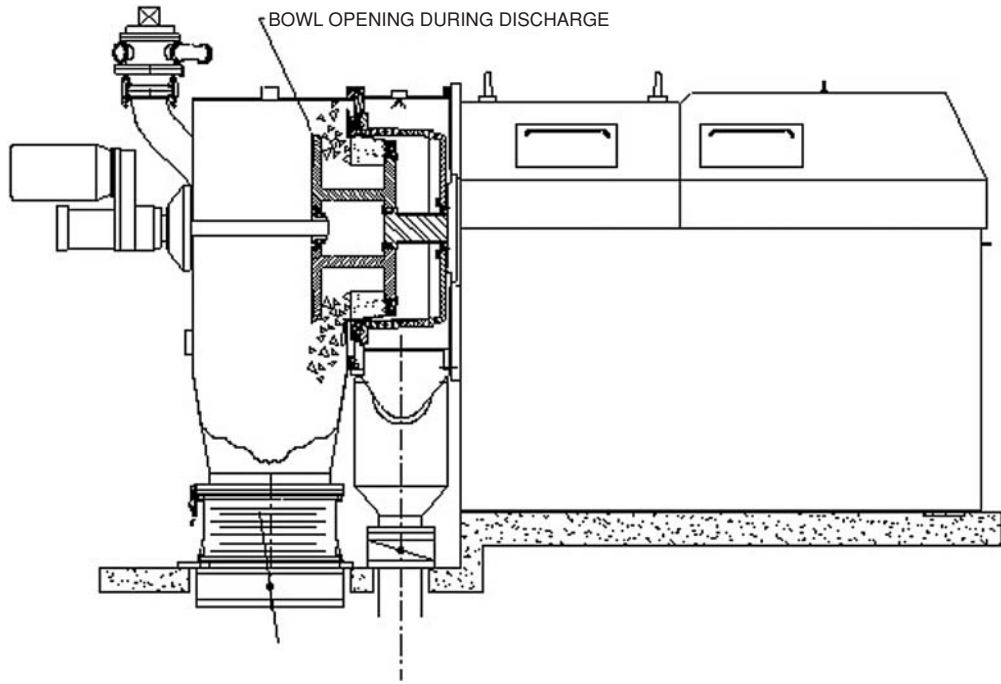


FIG. 18-171 Inverting filter centrifuge. (Heinkel USA.)

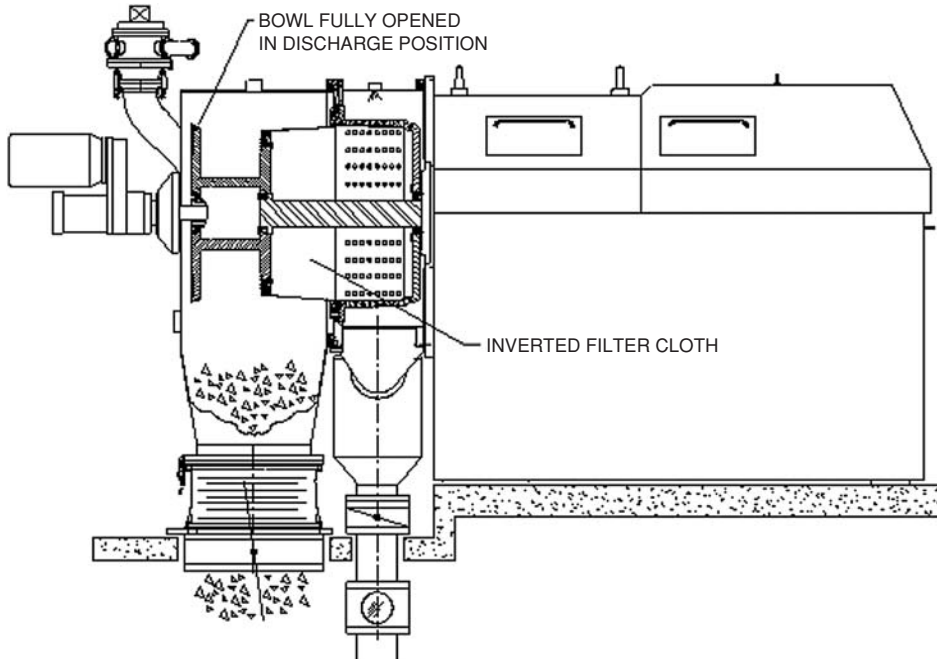


FIG. 18-172 Inverting filter centrifuge. (Heinkel USA.)

preconcentration of the slurry. Fines loss to the filtrate is also greater with continuous designs compared to batch.

Conical-Screen Centrifuges When a conical screen in the form of a frustum is rotated about its axis, the component of the centrifugal force normal to the screen surface impels the liquid to filter through the cake and the screen, whereas the component of the centrifugal force parallel to the screen in the longitudinal direction conveys the cake to the screen at a larger diameter. The sliding of the solids on the cone is favored by smooth perforated plates or wedge-wire sections with slots parallel to the axis of rotation, rather than woven wire mesh.

Wide-angle conical screen centrifuges. If the half-angle of the cone screen is greater than the angle of repose of the solids, the solids will slide across it with a velocity which depends on frictional properties of the cake but not on feed rate. The frictional property of the cake depends on the solid property, such as shape and size, as well as on moisture content. If the half-angle of the cone greatly exceeds the angle of repose, the cake slides across the screen at a high velocity, thereby reducing the retention time for dewatering. The angle selected is therefore highly critical with respect to performance on a specific application. Wide-angle and compound-angle centrifuges are used to dewater coarse coal and rubber crumb and to dewater and wash crude sugar and vegetable fibers such as from corn and potatoes.

Shallow-angle conical screen centrifuges. By selecting a half-angle for the conical screen that is less than the angle of repose of the cake and providing supplementary means for the controlled conveyance of the cake across the conical screen from the small to large diameter, longer retention time is available for cake dewatering. Three methods are in common use for cake conveyance:

1. **Vibrational conveyance.** This is referred as the vibratory centrifuge. A relatively high frequency force is superimposed on the rotating assembly. This can be either in-line with the axis of rotation or torsional, around the driveshaft. In either case, the cake under inertial force from the vibration is partly "fluidized" and propelled down the screen under a somewhat steady pace toward the large end, where it is discharged.

2. **Oscillating or "tumbling" conveyance.** This is commonly known as the tumbling centrifuge. The driveshaft is supported at its lower end on a pivot point. A supplementary power source causes the shaft and the rotating bracket it carries to gyrate about the pivot at a controlled amplitude and at a frequency lower than the rate of rotation of the basket. The inertia force generated also provides partial

fluidization of the bed of solids in the basket, causing the cake to convey toward the large end, as in the vibrational conveyance.

3. **Scroll conveyance.** Another type of continuous filtering centrifuge is the scroll screen centrifuge, as shown in Fig. 18-173. The scroll screen centrifuges are also sometimes called worm screen centrifuges. The design consists of a fixed-angle rotating basket and a concentric screw conveyor to control the transport and discharge of solids. Common applications include crystal, fiber, and mineral separations.

Scroll screen centrifuges are typically used for continuous feeds of slurries of at least 10 percent solids by volume, of materials with an average size of 100 μm or greater. This design offers some residency to process variation and typically removes the bulk of surface moisture.

The scroll and the screen are rotating in the same direction with a small differential speed of typically less than 100 rpm. The feed is deposited into the acceleration cone of the scroll, then passes through the feed openings of the scroll. The solids are retained on the screen; as the liquid migrates through, the cake passes the screen media and the basket. The discharge housing collects the liquid, and the solids are conveyed to the large diameter of the rotating basket and are continuously discharged.

An internal product wash is also available in the scroll screen centrifuges. Wash liquid is added in a chamber midway along the basket, and the wash liquid migrates through the cake prior to final drying and discharge.

The rotating basket is used to retain the screen media. Wedge-wire as well as sheet metal screens are available, but are typically limited to a minimum opening size of 70 μm or larger. Common basket designs include 10, 15 and 20 degrees.

The scroll acts as a screw conveyor and discharges the solids. The typical solids retention time in the centrifuge ranges from 0.5 to 6 s. A close tolerance, 0.3 to 1 mm, is common between the scroll and screen; therefore little material remains on the screen. This minimizes the potential for imbalances.

Pusher Centrifuges—Operating Method and Mechanical Design Pusher centrifuges (Fig. 18-174) are continuous filtering centrifuges used for dewatering and washing free-draining bulk crystalline, polymer, or fibrous materials. Where suited, they provide the best washing characteristics of any continuous centrifuge due to control of retention time, uniform cake bed, and essentially

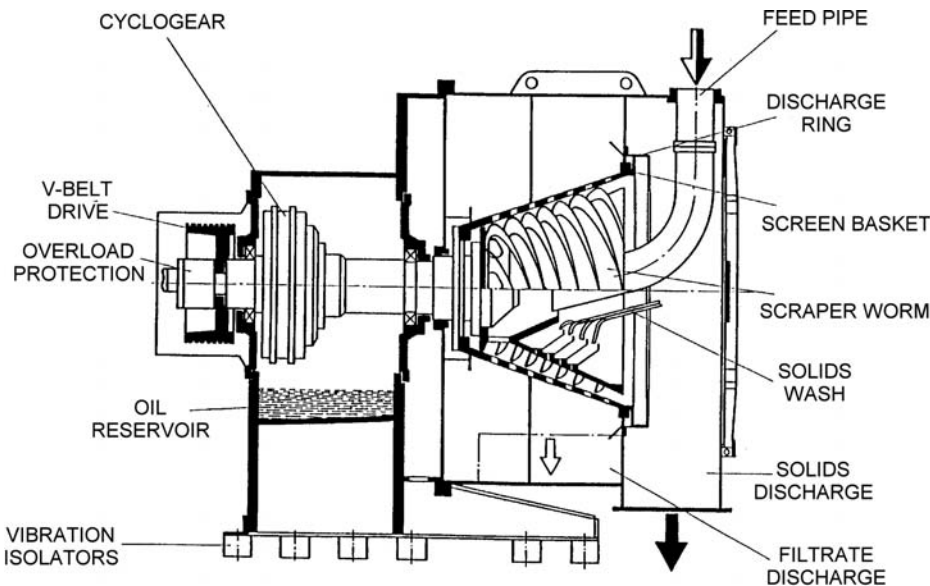


FIG. 18-173 Scroll screen centrifuge. (TEMA Systems, Inc.)

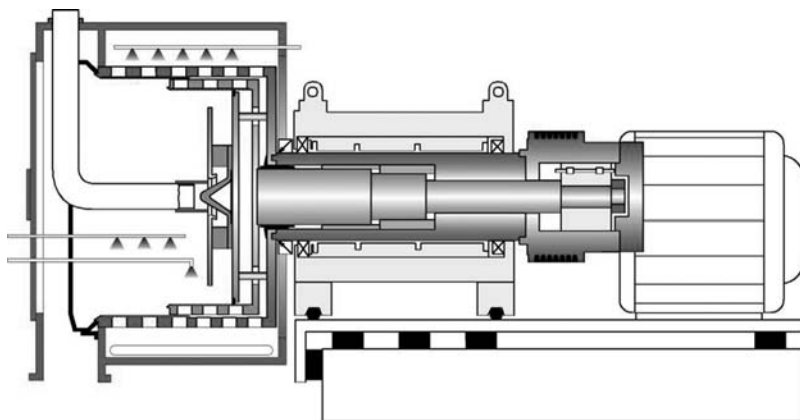


FIG. 18-174 Pusher centrifuge cross section. (Krauss Maffei Process Technology.)

plug flow of solids through the unit. For a typical application such as salt, they range in capacity from about 1 ton/h for small (250-mm-diameter) units up to about 120 tons/h or more in the largest units (1250-mm-diameter). They are generally applied where the mean particle size is at least 150 μm . Typical solids retention time is between 10 and 30 s. Normally the machine is fed by a feed pipe, but it can also be used as posttreatment of a prior dewatering step such as a vacuum filter. In this case it is fed by a feed screw. Due to the gentle handling of the product, pusher centrifuges are better suited for fragile crystals than are other types of continuous filtering centrifuges.

Generally there are three limitations to capacity in pusher centrifuges: (1) solids volumetric throughput, (2) liquid filtration capacity, and (3) retention time necessary to achieve desired objectives regarding cake purity and residual cake moisture. In most cases (2) dictates; therefore to optimize capacity and performance, pre-concentrating the feed slurry as high as possible is desired. Some designs have a short conical section at the feed end for prethickening within the unit, but generally it is preferable to thicken ahead of the centrifuge with gravity settlers, hydrocyclones, or inclined screens.

As depicted schematically in Fig. 18-174, the rotating assembly consists of a belt-driven outer rotor that rotates at constant speed. The outer shaft (hollow shaft) is fixed to the main or outer basket. Within the hollow shaft is the pusher shaft which is keyed together with the hollow shaft but also oscillates. The reciprocal motion is provided by a mechanical gearbox for smaller units (400-mm-diameter and less) or hydraulically in larger units. The depicted schematic is of a two-stage design in which the pusher shaft is fixed to the inner basket and the pusher plate is attached to the outer basket by posts. The stroke length is between 30 and 85 mm depending on machine size, and stroke frequency is usually between 45 and 90 strokes per minute.

The feed slurry enters through a stationary central pipe into a feed accelerator/distributor, then is introduced onto the (in this case) oscillating inner basket just in front of the pusher plate. In the feed zone, most of the liquid is drained, forming a cake sufficiently stiff to transfer the push force through the bed of solids and transport the cake without shearing. This is why it requires fast-draining materials and is liquid-limited, since it must form a cake within the period of one stroke.

With designs that use a simple feed cone or plate for feed distribution, most of the slurry acceleration takes place on the screen surface, with lower effective slurry speed and driving force for filtration. More advanced designs utilize an impeller-type feed accelerator that largely preaccelerates the slurry prior to introduction on the screen for higher capacity and lower screen wear.

With each stroke of the pusher, the material in the feed zone is pushed up to a certain height primarily depending on the friction coefficient between the solids and the screen and the screen deck

length, and secondarily depending on G -force and loading. Once the cake in the feed zone is compressed and has formed a ring with this height, it transmits the push force to the stationary bed of cake in the basket which begins to move the cake bed forward until the forward end of the stroke. This cake height is often referred to as the natural cake height. The schematic in Fig. 18-175 shows what is taking place in the feed zone.

The distance the cake ring moves forward divided by the stroke length is defined as the *push efficiency*. The push efficiency varies with solids volumetric loading, resulting in a self-compensating control of varying rates. Depending on the cake properties, primarily compressibility, up to about 90 percent push efficiency is achievable. In some cases volumetric throughput can be further increased beyond the volumetric push capacity at the natural cake height, in which case the push efficiency remains almost constant and the cake height increases with increasing load, commonly referred to as the forced cake height. This realm of operation is usually only possible with multistage designs.

As the cake bed is transported through the basket, it passes through the various process steps shown in Fig. 18-176 with product moisture gradient as shown in Fig. 18-177.

Usually, cake wash ratios of about 0.1 to 0.3 kg wash/kg solids are possible within the normal residence time of the wash zone. This usually can displace at least 95 percent of the mother liquor and impurities. In some cases higher wash ratios or even multistage countercurrent washes are utilized, in which case sufficient residence time via throughput reduction must be considered.

Single-Stage versus Multistage Pusher centrifuges can be single-stage configuration with a single long basket and screen, two-stage (as shown schematically in Fig. 18-177), three-, or four-stage designs. Cake height and push force are primarily influenced by screen deck length and cake friction coefficient.

Single-Stage Where single-stage units are appropriate (ammonium sulfate is one example due to very large crystal size and good cake shear strength), the solids volumetric capacity can be maximized. However, because the push force requirement increases with screen length, cake shear or buckling can be the result with unstable operation. Because the average cake thickness in the feed zone is higher, filtration capacity may be slightly less than with multistage units. Fines losses can be slightly less with single-stage units since a smaller proportion of the cake bed is in contact with the slotted screen and there is no reorientation of crystals between stages. These units are often limited to low-speed operation for stability.

Two-Stage The majority of pusher centrifuges sold today are of this type. It provides greater flexibility compared to single stages in terms of greater filtration capacity, lower tendency for cake shear, and higher speed capability. When it is possible to operate with a forced cake, capacities can approach those of single-stage designs. Wash typically is applied on the latter portion of the first stage and through the

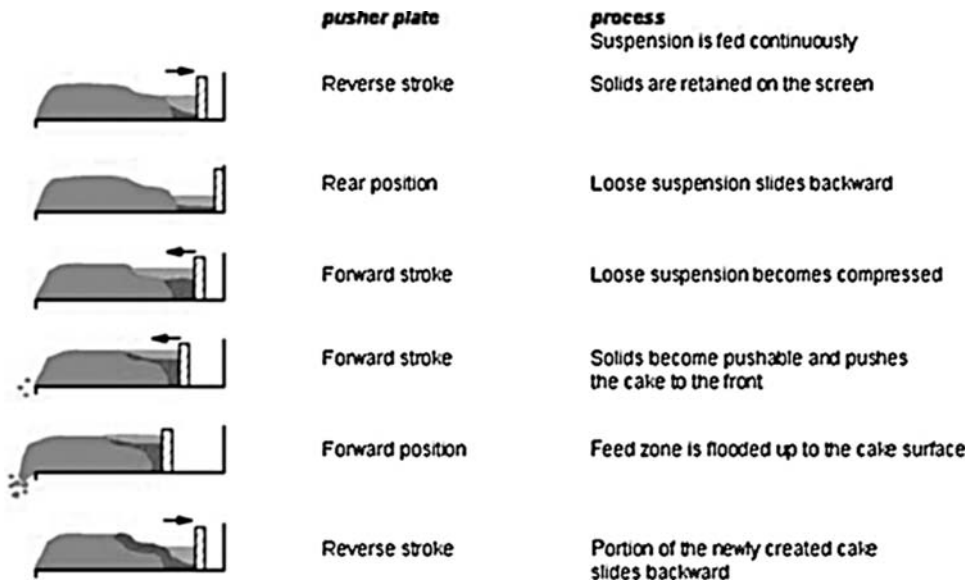


FIG. 18-175 Pusher centrifuge solids transport. (Krauss Maffei Process Technology.)

transition onto the second stage. During this transition the crystals are reoriented and the capillaries opened, which can enhance the wash effect. With even stage units, the feed acceleration system is not oscillating relative to the feed pipe. Some advanced designs of feed acceleration systems incorporating impellers benefit from this constant relationship.

Three- and Four-Stage These designs are generally reserved for the largest sizes that have long baskets that need to be subdivided

into reasonable-length stages as well as for very special applications with very high friction coefficients, low internal cake shear strength, or fairly high compressibility. For example, in processing high rubber ABS, four-stage units have been utilized; but the deck lengths are so short, with the corresponding thin cakes and short retention time, that capacity and performance are severely reduced. Other types of machine (such as peeler centrifuges or cylindrical conical pushers discussed below) can be better suited.

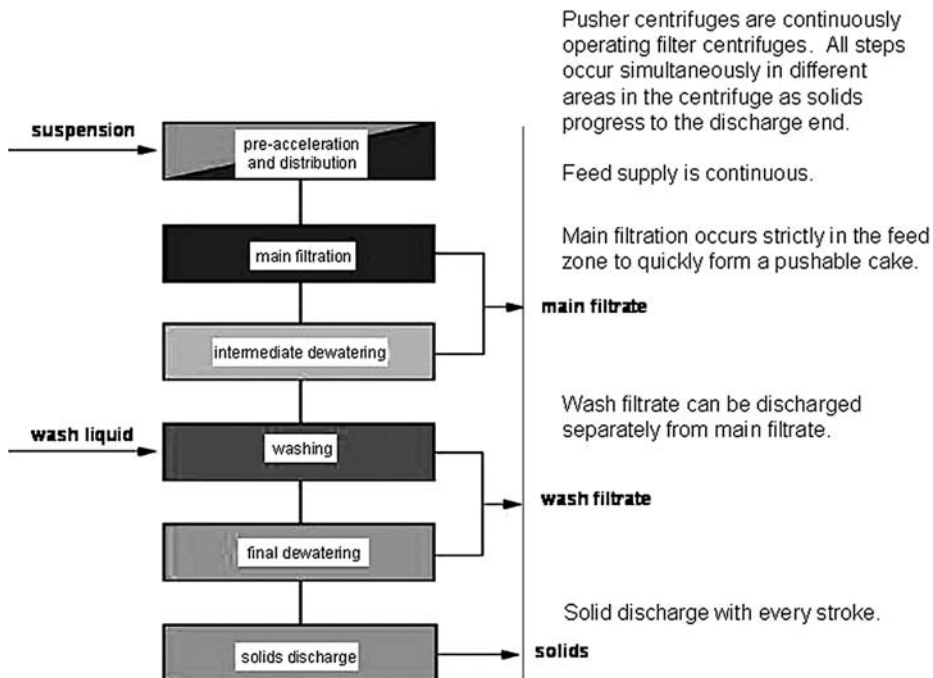


FIG. 18-176 Pusher centrifuge process steps. (Krauss Maffei Process Technology.)

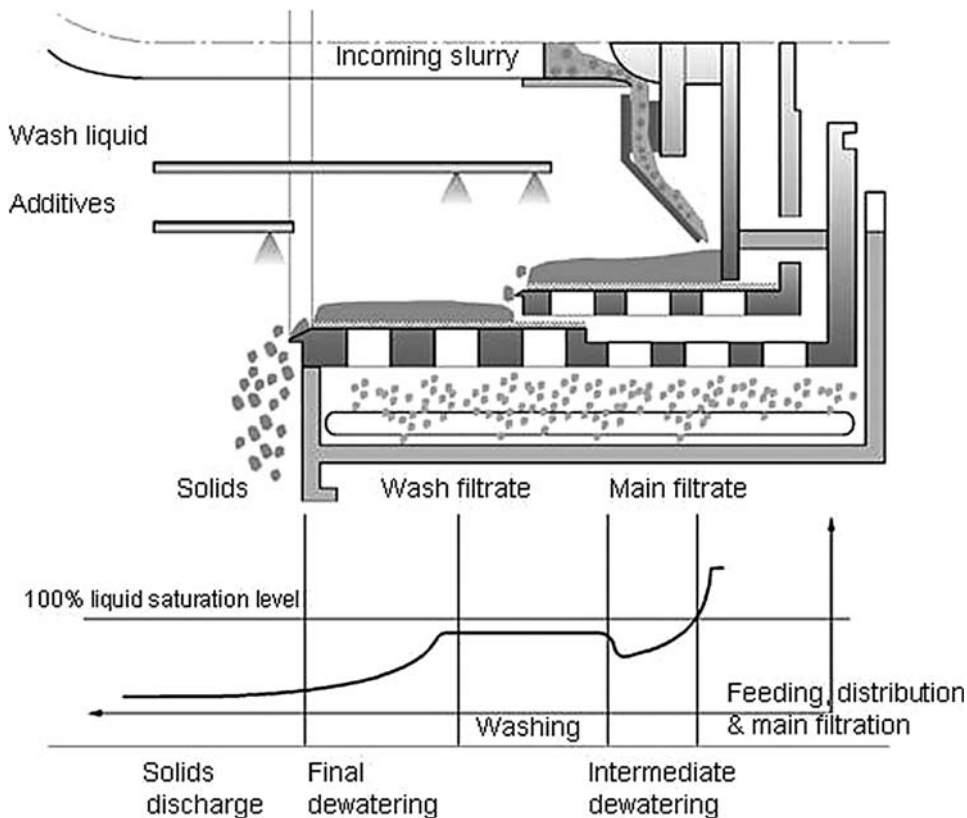


FIG. 18-177 Pusher centrifuge product moisture gradient. (Krauss Maffei Process Technology.)

Cylindrical/Conical A variation of single- and two-stage designs utilizes a cylindrical section or stage at the feed end followed by a conical section or stage sloping outward to the discharge end. The benefit of this design is that the axial component of force in the conical end assists with solids transport. Care must be taken that the cone angle not exceed the sliding friction angle of the cake, or else the cake will short-circuit the zone, resulting in poor performance and high vibration. Fabrication costs of the baskets are higher than those of cylindrical designs, and slotted screen construction is complicated with high replacement costs.

Theory of Centrifugal Filtration Theoretical predictions of the behavior of solid-liquid mixtures in a filtering centrifuge are more difficult compared to pressure and gravity filtration. The area of flow and driving force are both proportional to the radius, and the specific resistance and porosity may also change markedly within the cake. Filtering centrifuges are nearly always selected by scale-up from lab tests on materials to be processed, such as using bucket centrifuges where a wide range of test conditions (cake thickness, time, and G -force) can be controlled. Although tests with the bucket centrifuge provide some quantitative data to scale-up, the results include wall effect from buckets, which are not representative of actual cylindrical basket geometry, bucket centrifuges are not useful in quantifying filtration rates. A modified version of the buckets or even a cylindrical perforated basket can be used. In the latter, there is less control of cake depth and circumferential uniformity. The desired quantities to measure are filtration rate, washing rate, spinning time, and residual moisture. Also, with filtering centrifuges such as the screen-bowl centrifuge, screen-scroll centrifuge, and to some extent in multistage pushers, the cake is constantly disturbed by the scroll conveyor or conveyance mechanism; liquid saturation due to capillary rise as measured in bucket tests is absent. While bucket centrifuge tests are

very useful for first-look feasibility, it is always recommended to follow with pilot-scale testing of the actual equipment type being considered.

Filtration Rate When the centrifuge cake is submerged in a pool of liquid, as in the case of a fast-sedimenting, solids-forming cake almost instantly, and the rate of filtration becomes limiting, the bulk filtration rate Q for a basket with axial length b is:

$$Q = \frac{\pi b \rho K \Omega^2 (r_b^2 - r_c^2)}{\mu \left(\ln \left[\frac{r_b}{r_c} \right] + \frac{K R_m}{r_b} \right)} \quad (18-119a)$$

where μ and ρ are, respectively, the viscosity and density of the liquid; Ω is the angular speed; K is the average permeability of the cake and is related to the specific resistance α by the relationship $\alpha K \rho_s = 1$, with ρ_s being the solids density; r_b , r_c , and r_b are, respectively, the radius of the liquid pool surface, the cake surface, and the filter medium adjacent to the perforated bowl. Here, the pressure drop across the filter medium, which also includes that from the cake heel, is $\Delta p_m = \mu R_m (Q/A)$ with R_m being the combined resistance. The permeability K has a unit m^2 , α m/kg , and R_m m^{-1} . The driving force is due to the hydrostatic pressure difference across the bowl wall and the pool surface—i.e., the numerator of Eq. (18-119a), and the resistance is due to the cake layer and the filter medium—i.e., denominator of Eq. (18-119a). Fig. 18-178 shows the pressure distribution in the cake and the liquid layer above. The pressure (gauge) rises from zero to a maximum at the cake surface; thereafter, it drops monotonically within the cake in overcoming resistance to flow. There is a further pressure drop across the filter medium, the magnitude dependent on the combined resistance of the medium and the heel at a given flow rate. This

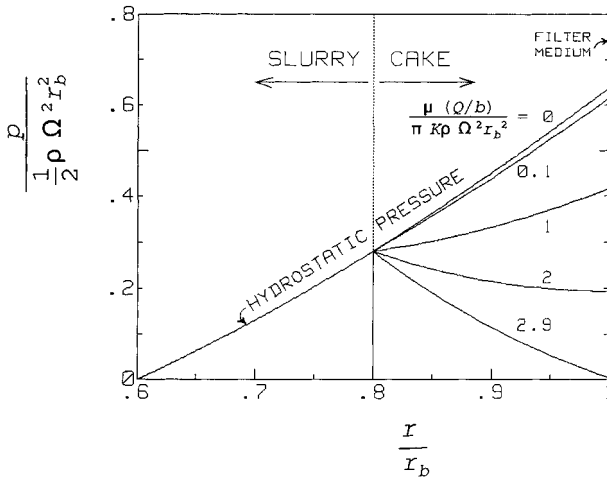


FIG. 18-178 Pressure distribution in a basket centrifuge under bulk filtration.

scenario holds, in general, for incompressible as well as for compressible cake. For the latter, the pressure distribution also depends on the compressibility of the cake.

For incompressible cake, the pressure distribution and the rate depend on the resistance of the filter medium and the permeability of the cake. Figure 18-178 shows several possible pressure profiles in the cake with increasing filtration rates through the cake. It is assumed that $r_c/r_b = 0.8$ and $r_p/r_b = 0.6$. The pressure at $r = r_b$ corresponds to pressure drop across the filter medium Δp_m with the ambient pressure taken to be zero. The filtration rate as well as the pressure distribution depend on the medium resistance and that of the cake. High medium resistance or blinding of the medium results in greater penalty on filtration rate.

In most filtering centrifuges, especially the continuous-feed ones, the liquid pool above the cake surface should be minimum to avoid liquid running over the cake. Setting $r_p = r_c$ in Eq. (18-119a), the dimensionless filtration flux is plotted in Fig. 18-179 against r_c/r_b for different ratios of filter-medium resistance to cake resistance, KR_m/r_b . For negligible medium resistance, the flux is a monotonic decreasing function with increasing cake thickness, i.e., smaller r_c . With finite medium resistance, the flux curve for a range of different cake thicknesses has a

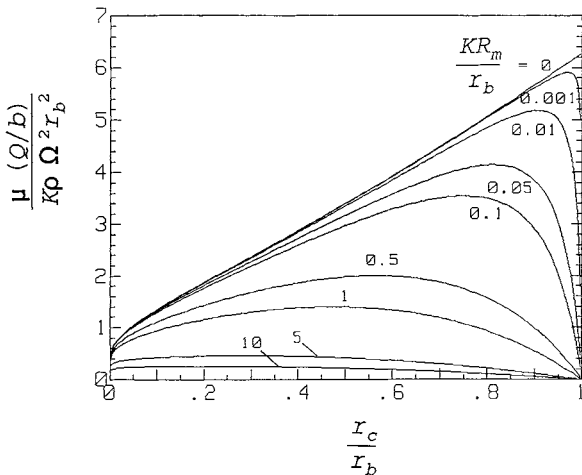


FIG. 18-179 Centrifugal filtration rate as a function of both cake and medium resistance.

maximum. This is because for thin cake the driving liquid head is small and the medium resistance plays a dominating role, resulting in lower flux. For very thick cake, despite the increased driving liquid head, the resistance of the cake becomes dominant; therefore, the flux decreases again. The medium resistance to cake resistance should be small, with $KR_m/r_b < 5$ percent. However, the cake thickness, which is directly proportional to the throughput, should not be too small, despite the fact that the machine may have to operate at somewhat less than the maximum flux condition.

It is known that the specific resistance for centrifuge cake, especially for compressible cake, is greater than that of the pressure or vacuum filter. Therefore, the specific resistance has to be measured from centrifuge tests for different cake thicknesses so as to scale up accurately for centrifuge performance. It cannot be extrapolated from pressure and vacuum filtration data. For cake thickness that is much smaller compared to the basket radius, Eq. (18-119a) can be approximated by

$$V_f = V_{f0} \left(\frac{h}{h_c} \right) \tag{18-119b}$$

where $h = r_b - r_p$ is the liquid depth, $h_c = r_b - r_c$ is the cake thickness, and $v_{f0} = (\rho g K/\mu)$ is a characteristic filtration velocity. Table 18-14 shows some common filtering centrifuges and the application with respect to the G -level, minimum feed-solids concentration, minimum mean particle size, and typical filtration velocity. The vibratory and tumbler centrifuges have the largest filtration rate of 5×10^{-4} m/s (0.02 in/s) for processing 200- μ m or larger particles, whereas the pendulum has the lowest filtration rate of 1×10^{-7} m/s (4×10^{-6} in/s) for processing 5- μ m particles with increased cycle time. The screen-scroll, pusher, screen-bowl, and peeler centrifuges are in between.

Film Drainage and Residual Moisture Content Desaturation of the liquid cake ($S < 1$) begins as the bulk filtration ends, at which point the liquid level starts to recede below the cake surface. Liquids are trapped in: (1) cake pores between particles that can be drained with time (free liquid), (2) particle contact points (pendular liquid), (3) fine pores forming continuous capillaries (capillary rise), (4) particle pores or they are bound by particles (bound liquid). Numbers (1) to (3) can be removed by centrifugation, and, as such, each of these components depends on G to a different extent. Only desaturation of the free liquid, and to a much lesser extent the liquid at contact points, is a function of time. The wet cake starts from a state of being fully saturated, $S = 1$, to a point where $S < 1$, depending on the dewatering time. At a very large amount of time, it approaches an equilibrium point S_∞ , which is a function of G , capillary force, and the amount of bound liquid trapped inside or externally attached to the particles.

The following equations, which have been tested in centrifugal dewatering of granular solids, prove useful:

Total saturation:

$$S_{total} = S_\infty + S_T(t) \tag{18-120}$$

Equilibrium component:

$$S_\infty = S_c + (1 - S_c)(S_p + S_z) \tag{18-121}$$

Transient component:

$$S_T(t) = (1 - S_c)(1 - S_p - S_z)S(t) \tag{18-122}$$

The details of the mathematical model of these four components are given below.

Drainage of free liquid in thin film:

$$S_f(t) = \left(\frac{4}{3} \right) \left(\frac{1}{t_d^n} \right), \quad t_d > 0 \tag{18-123}$$

where for smooth-surface particles, $n = 0.5$, and for particles with rough surfaces, n can be as low as 0.25.

Bound liquid saturation:

$$S_p = \text{function}(\text{particle characteristics}) \tag{18-124}$$

Pendular saturation:

$$S_z = 0.075, \quad N_c \leq 5 \quad (18-125a)$$

$$S_z = \frac{5}{(40 + 6N_c)}, \quad 5 \leq N_c \leq 10 \quad (18-125b)$$

$$S = \frac{0.5}{N_c}, \quad N_c \geq 10 \quad (18-125c)$$

Frequently when $N_c < 10$, S_p and S_z are combined for convenience, the sum of which is typically 0.075 for smooth particles and can be as high as 0.35 for rough-surface particles. This has to be determined from tests.

Saturation due to capillary rise:

$$S_c = \frac{4}{B_o} \quad (18-126)$$

where the dimensionless time t_d , capillary number N_c , and Bond number B_o are, respectively:

$$t_d = \frac{\rho G d_h^2 t}{\mu H} \quad (18-127)$$

$$N_c = \frac{\rho G d_h^2}{\sigma \cos \theta} \quad (18-128)$$

$$B_o = \frac{\rho G H d_h}{\sigma \cos \theta} \quad (18-129)$$

where ρ and μ are, respectively, the density and viscosity of the liquid; θ is the wetting angle of the liquid on the solid particles; σ is the interfacial tension; H is the cake height; d is the mean particle size; and t is the dewatering time. The hydraulic diameter of the particles can be approximated by either $d_h = 0.667 \epsilon d / (1 - \epsilon)$ or $d_h = 7.2(1 - \epsilon)K^{1/2} / \epsilon^{3/2}$, where ϵ is the cake porosity.

Example

Given: $\rho = 1000 \text{ kg/m}^3$, $\rho_s = 1200 \text{ kg/m}^3$, $\mu = 0.004 \text{ N}\cdot\text{s/m}^2$, $\sigma \cos \theta = 0.068 \text{ N/m}$, $H = 0.0254 \text{ m}$, $d = 0.0001 \text{ m}$, $\epsilon = 0.4$, $G/g = 2000$, $t = 2 \text{ s}$, $S_p = 0.03$.

Calculate: $d_h = 4.4 \times 10^{-5} \text{ m}$, $t_d = 748$, $N_c = 0.56$, $B_o = 322$, $S_f = 0.048$, $S_z = 0.075$, $S_c = 0.012$, $S_w = 0.116$, $S_T = 0.043$, $S_{\text{total}} = 0.158$, $W = 0.919$.

Note that W is the solids fraction by weight and is determined indirectly from Eq. (18-89). The moisture weight fraction is 0.081.

The transient component depends not only on G , cake height, and cake properties, but also on dewatering time, which ties to solids throughput for a continuous centrifuge and cycle time for batch centrifuge. If the throughput is too high or the dewatering cycle is too short, the liquid saturation can be high and becomes limiting. Given that time is not the limiting factor, dewatering of the liquid lens at particle contact points requires a much higher G -force. The residual saturation depends on the G -force to the capillary force, as measured by N_c , the maximum of which is about 7.5%, which is quite significant. If the cake is not disturbed (scrolled and tumbled) during conveyance and dewatering, liquid can be further trapped in fine capillaries due to liquid rise, the amount of which is a function of B_o , which weighs the G -force to the capillary force. This amount of liquid saturation is usually smaller as compared to capillary force associated with liquid-lens (also known as pendular) saturation. Lastly, liquid can be trapped by chemical force at the particle surface or physical capillary or interfacial force in the pores within the particles. Because the required desaturating force is extremely high, this portion of moisture cannot be removed by mechanical centrifugation. Fortunately, for most applications it is a small percentage, if it exists.

SELECTION OF CENTRIFUGES

Table 18-15 summarizes the several types of commercial centrifuges, their manner of liquid and solids discharge, their unloading speed, and their relative volumetric capacity. When either the liquid or the solids discharge is not continuous, the operation is said to be cyclic. Cyclic or batch centrifuges are often used in continuous processes by providing appropriate upstream and downstream surge capacity.

Sedimentation Centrifuges These centrifuges frequently are selected on the basis of tests on tubular, disc, or helical-conveyor centrifuges of small size. The centrifuge should be of a configuration similar to that of the commercial centrifuge it is proposed to be used for. The results in terms of capacity for a given performance (effluent clarity and solids concentration) may be scaled up by using the sigma concept of Eqs. (18-117) to (18-119). Spin-tube tests may be used for information on systems containing well-dispersed solids. Such tests are totally unreliable on systems containing a dispersed phase that agglomerates or flocculates during the time of centrifugation.

Filtering Centrifuges These filters often can be selected on the basis of batch tests on a laboratory unit, preferably one at least 12 in (305 mm) in diameter. A bucket centrifuge test would be helpful to study the effect of G , cake height, and dewatering time, but not filtration rates. It is always recommended to follow bucket tests with pilot-scale testing of the actual equipment type being considered. Caution has to be taken in correcting for capillary saturation, which may be absent in large continuous centrifuges with scrolling conveyances.

Unless operating data on similar material are available from other sources, continuous centrifuges should be selected and sized only after tests on a centrifuge of identical configuration.

It seems needless to state but is frequently overlooked that test results are valid only to the extent that the slurry and the test conditions duplicate what will exist in the operating plant. This may involve testing on a small scale (or even on a large one) with a slipstream from an existing unit, but the dependability of the data is often worth the extra effort involved. Most centrifuge manufacturers provide testing services and demonstration facilities in their own plants and maintain a supply of equipment for field-testing in the customer's plant, such as with a pilot centrifuge module with associated peripheral equipment. Larger-scale pilot equipment provides better scale-up accuracy, e.g., in evaluating the effect of cake thickness in batch filtering centrifuges.

COSTS

Neither the investment cost nor the operating cost of a centrifuge can be directly correlated with any single characteristic of a given type of centrifuge. The costs depend on the features of the centrifuge tailored toward the physical and chemical nature of the materials being separated, the degree and difficulty of separation, the flexibility and capability of the centrifuge and its auxiliary equipment, the environment in which the centrifuge is located, and many other nontechnical factors, including market competition. The cost figures presented herewith represent centrifuges only for use in the process industries as of 2004. In any particular installations, the costs may be somewhat less or much greater than those presented here. The prices presented herewith are for rough guidance only. Substantial variations will be found due to volatility of currency exchange and material costs.

The useful parameter for value analysis is the installed cost of the number of centrifuges required to produce the demanded separative effect (end product) at the specified capacity of the plant. The possible benefits of adjustments in the upstream and downstream components of the plant and the process should be carefully examined in order to minimize the total overall plant costs; the systems approach should be used.

Purchase Price Typical purchase prices, including drive motors, of tubular and disc sedimenting centrifuges are given in Table 18-16. The price will vary upward with the use of more exotic materials of construction, the need for explosion-proof electrical gear, the type of enclosure required for vapor containment, and the degree of portability, and this holds for all types of centrifuges.

The average purchase prices of continuous-feed, solid-bowl centrifuges made, respectively, of 316 stainless steel and steel are shown in

TABLE 18-15 Characteristics of Commercial Centrifuges

Method of separation	Rotor type	Centrifuge type	Manner of liquid discharge	Manner of solids discharge or removal	Centrifuge speed for solids discharge	Capacity ^o
Sedimentation	Batch	Ultracentrifuge	Batch	Batch manual	Zero	1 mL
	Tubular	Laboratory, clinical	Continuous†	Batch manual	Zero	To 6 L
		Supercentrifuge	Continuous†	Batch manual	Zero	To 1,200 gal/h
	Disc	Multipass clarifier	Continuous†	Batch manual	Zero	To 3,000 gal/h
		Solid wall	Continuous†	Batch manual	Zero	To 30,000 gal/h
Light-phase skimmer		Continuous	Continuous for light-phase solids	Full	To 1,200 gal/h	
Solid bowl (scroll conveyor)	Peripheral nozzles	Continuous	Continuous	Continuous	Full	To 24,000 gal/h
	Peripheral valves	Continuous	Continuous	Intermittent	Full	To 3,000 gal/h
	Peripheral annulus	Continuous	Continuous	Intermittent	Full	To 12,000 gal/h
	Constant-speed horizontal	Continuous†	Cyclic	Cyclic	Full (usually)	To 60 ft ³
	Variable-speed vertical	Continuous†	Cyclic	Cyclic	Zero or reduced	To 16 ft ³
	Continuous decanter	Continuous	Continuous screw conveyor	Continuous screw conveyor	Zero or reduced	To 54,000 gal/h
					Full	To 100 tons/h solids
Sedimentation and filtration		Screen-bowl decanter	Continuous	Continuous	Full	To 60,000 gal/h
						To 125 tons/h solids
Filtration	Conical screen	Wide-angle screen	Continuous	Continuous	Full	To 40 tons/h solids
		Differential conveyor	Continuous	Continuous	Full	To 80 tons/h solids
		Vibrating, oscillating, and tumbling screens	Continuous	Essentially continuous	Full	To 250 tons/h solids
	Cylindrical screen	Reciprocating pusher	Continuous	Essentially continuous	Full	Limited data
		Reciprocating pusher, single and multistage	Continuous	Essentially continuous	Full	To 100 tons/h solids
Horizontal		Cyclic	Intermittent, automatic	Full (usually)	To 25 tons/h solids	
Vertical, underdriven	Cyclic	Intermittent, automatic, or manual	Zero or reduced	To 10 tons/h solids		
	Vertical, suspended	Cyclic	Intermittent, automatic, or manual	Zero or reduced	To 10 tons/h solids	

^oTo convert gallons per hour to liters per second, multiply by 0.00105; to convert tons per hour to kilograms per second, multiply by 0.253; and to convert cubic feet to cubic meters, multiply by 0.0283.

†Feed and liquid discharge interrupted while solids are unloaded.

Fig. 18-180. The average purchase prices of continuous-feed filtering centrifuges are shown in Fig. 18-181. This chart includes a comparison of prices on screen-bowl, pusher, screen-scroll, and oscillating conical baskets. On average, the screen bowl is approximately 10 percent higher in price than the solid bowl of the same diameter and length. This incremental cost results from the added complexity of the screen section, bowl configuration, and casing differences. Prices for both the solid-bowl and the filtering centrifuges do not include the drive motor, which typically adds another 5 to 25 percent to the cost. The higher end of this range represents a variable-speed-type drive. If a variable-speed backdrive is used instead of the gear unit, the incremental cost is about another 10 to 15 percent, depending on the capability.

The average prices of the batch centrifuge are shown in Fig. 18-182. All the models include the drive motor and control. In Fig. 18-182, the inverting filter, horizontal peeler, and the advanced vertical peeler are the premium baskets especially used for specialty chemicals and pharmaceuticals. Control versatility with the use of programmable

logic control (PLC), automation, and cake-heel removal are the key features which are responsible for the higher price. The underdriven, top-driven, and pendulum baskets are less expensive with fewer features.

Installation Costs Installation costs of centrifuges vary over an extremely wide range, depending on the type of centrifuge, on the area and kind of structure in which it is installed, and on the details of installation. Some centrifuges, such as portable tubular and disc oil purifiers, are shipped as package units and require no foundation and a minimum of connecting piping and electrical wiring. Others, such as large batch automatic and continuous scroll-type centrifuges, may require substantial foundations and even building reinforcement, extensive interconnecting piping with required flexibility, auxiliary feed and discharge tanks and pumps and other facilities, and elaborate electrical and process-control equipment. Minimum installation costs, covering a simple foundation and minimum piping and wiring, are about 5 to 10 percent of purchase price for tubular and disc centrifuges;

TABLE 18-16 Typical Purchase Prices, Including Drive Motors, of Tubular and Disc Sedimenting Centrifuges, 2004

Type	Bowl diameter, in (mm)	Approximate Σ value, units of 10 ⁴ ft ² (10 ³ m ²)	Designation	Purchase price, 2004 \$
Tubular	4 (102)	2.7 (2.5)	Oil purifier	60,000–80,000
	4 (102)	2.7 (2.5)	Chemical separation	60,000–80,000
	5 (127)	4.2 (3.9)	Blood fractionation	100,000–140,000
Manual discharge disc	13.5 (343)	21 (20)	Hermetic	100,000–130,000
	24 (610)	95 (88)	Centripetal pump	150,000–300,000
Continuous nozzle-discharge disc	12 (305)	12 (11)	Clarifier	100,000–130,000
	18 (457)	25 (23)	Separator	150,000–200,000
	30 (762)	100 (93)	Recycle clarifier	270,000–300,000
Self-cleaning disc	14 (356)	13 (12)	Centripetal pump	130,000–150,000
	18 (457)	22 (20)	Centripetal pump	170,000–200,000
	24 (610)	38 (35)	Centripetal pump	250,000–300,000

^oNOTE: All prices quoted are for stainless steel construction with the exception of the oil purifier noted.

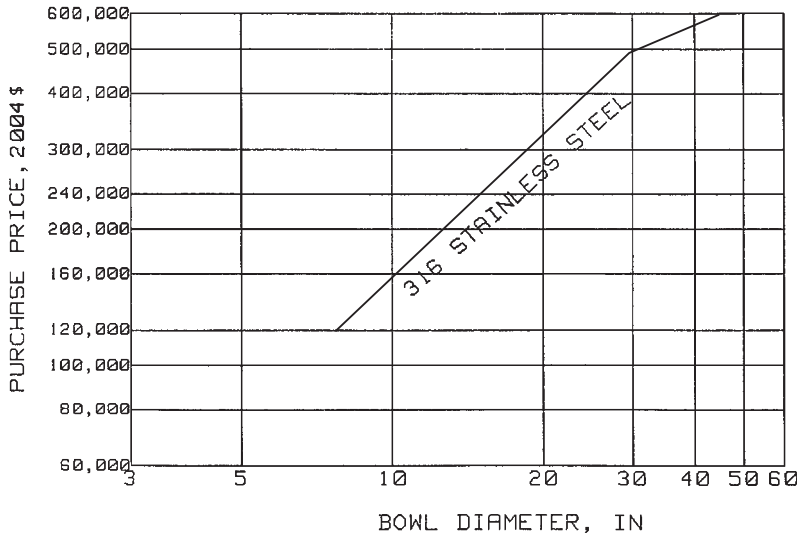


FIG. 18-180 Costs of continuous-feed solid-bowl.

10 to 25 percent for bottom drive, batch automatic, and continuous-scroll centrifuges; and up to 30 percent for top-suspended basket centrifuges. If the cost of all auxiliaries—special foundations, tanks, pumps, conveyors, electrical and control equipment, etc.—is included, the installation cost may well range from 1 to 2 times the purchase price of the centrifuge itself.

Maintenance Costs Because of the care with which centrifuges are designed and built, their maintenance costs are in line with those of other slower-speed separation equipment, averaging in the range of 1 to 4 percent for batch machines, 3 to 8 percent for pusher centrifuges, and 5 to 10 percent for decanters and disc centrifuges per year of the purchase price for centrifuges in light to moderate duty. For centrifuges in severe service and on highly corrosive fluids, the maintenance cost may be several times this value. Maintenance costs

are likely to vary from year to year, with lower costs for general maintenance and periodic large expenses for major overhaul. Centrifuges are subject to erosion from abrasive solids such as sand, minerals, and grits. When these solids are present in the feed, the centrifuge components are subject to wear. Feed and solids discharge ports, unloader knives, helical scroll blade tips, etc., should be protected with replaceable wear-resistant materials. Excessive out-of-balance forces strongly contribute to maintenance requirements and should be avoided.

Operating Labor Centrifuges run the gamut from completely manual control to fully automated operation. For the former, one operator can run several centrifuges, depending on their type and the application. Fully automatic centrifuges usually require little direct operation attention. In most production environments, PLC- or DCS-based automatic controls are the norm.

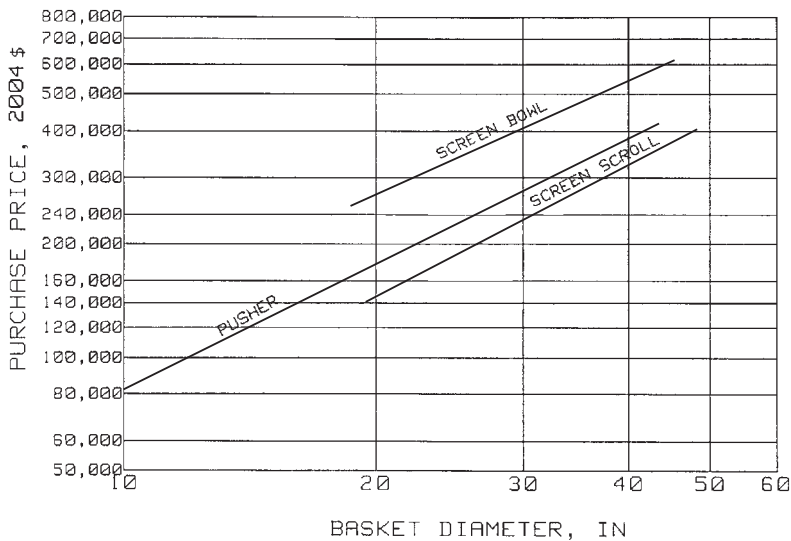


FIG. 18-181 Costs of continuous baskets (316 stainless steel).

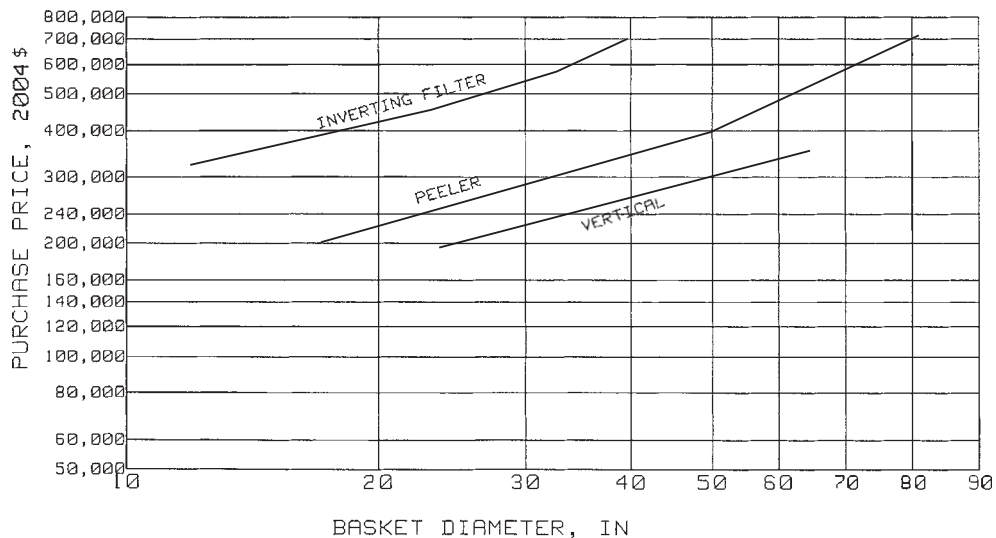


FIG. 18-182 Costs of batch baskets (316 stainless steel).

EXPRESSION

GENERAL REFERENCES: F. M. Tiller and L. L. Horng, "Hydraulic Deliquoring of Compressible Filter Cakes," *AIChE J.*, **29** (2) (1983). F. M. Tiller and C. S. Yeh, "The Role of Porosity in Filtration VI: Filtration Followed by Expression," *AIChE J.*, **33** (1987). F. M. Tiller and W. Li, "Dangers of Lab-Plant Scaleup for Solid/Liquid Separation Systems," *Chem. Eng. Commun.*, **190** (1) (2003). F. M. Tiller and T. C. Green, "Role of Porosity in Filtration IX: Skin Effect with Highly Compressible Materials," *AIChE J.*, **19** (1973). F. M. Tiller and W. Li, "Determination of the Critical Pressure Drop for Filtration of Supercompactible Cakes," *Water Sci. and Technol.*, **44** (10) (2001). M. Shirato, T. Murase, and T. Aragaki, "Slurry Deliquoring by Expression," *Progress in Filtration*, vol. 4, Elsevier, 1986. M. Shirato et al., "Internal Flow Mechanism in Filter Cakes," *AIChE J.*, **15** (1969). M. Shirato et al., "Analysis of Consolidation Process in Filter Cake Dewatering by Use of Difficult to Filter Slurries," *J. Chem. Eng. Japan*, **19** (6) (1986). F. M. Tiller and W. F. Leu, "Basic Data Fitting in Filtration," *J. Chinese Inst. Chem. Engr.*, **11** (1980). W. Chen, F. J. Parma and W. Schabel, "Testing Methods for Belt Press Biosludge Dewatering," *Filtration J.*, **5** (1) (2005).

FUNDAMENTALS OF EXPRESSION

Definition Deliquoring of filter cakes is one of the last stages of solid-liquid separations. It has been widely applied in a variety of fields, e.g., in food industries to increase product yield, in wastewater treatment plants to reduce transportation and disposal cost by decreasing sewage sludge moisture content, and in chemical processes to eliminate liquid content in the solid product prior to drying. The energy required to express liquid from solid-liquid mixtures is negligible compared to that of any thermal method. Deliquoring operations include hydraulic expression, mechanical expression, air or gas blowing, and gravity or centrifugal drainage. Hydraulic expression is provided by direct pump pressure or reversed or right-angled flow of liquid at the end of filtration (Tiller and Horng, 1983). The term *expression* used in this presentation refers to mechanical compression of a solid-liquid mixture by applying diaphragms, rolls, pistons, or screw presses on the surface of cakes.

Filtration and Expression of Compactible Filter Cakes

Filtration A filter cake can be incompactible, moderately compactible, highly compactible, or supercompactible (Tiller and Li, 2003). Tiller and Green (1973) showed that porosity or solidosity (volume fraction of cake solids ϵ_s , solidosity + porosity = 1) is not uniformly distributed in a compactible cake, and a skin cake of high resistance to

liquid flow is developed next to the filter medium, as shown in Fig. 18-183 (Tiller and Li, 2001). The skin deters frictional forces necessary to consolidate the cake and increase solidosity in a large portion of the cake. As a result, as illustrated by Fig. 18-184, increasing filtration pressure on highly compactible filter cakes cannot attain substantial deliquoring (floculated latex) while increasing filtration pressure does help to make a dryer cake on a less compactible material (Kaolin Flat D).

Expression Mechanical expression applies pressure directly on filter cakes rather than relying on flow frictions generated by hydraulic pressure drop to deliquor the cake. The effects of stress distribution in a compactible filter cake by these two different mechanisms are shown in Fig. 18-185. The stress distribution of an expression is more uniform than that of a pressure filtration, leading to a more uniform filter cake. Expression is therefore a better choice for deliquoring of compactible filter cakes.

Fundamental Theory A theoretical model was developed by Shirato (1969, 1986) based on Terzaghi's and Voigt's consolidation model in

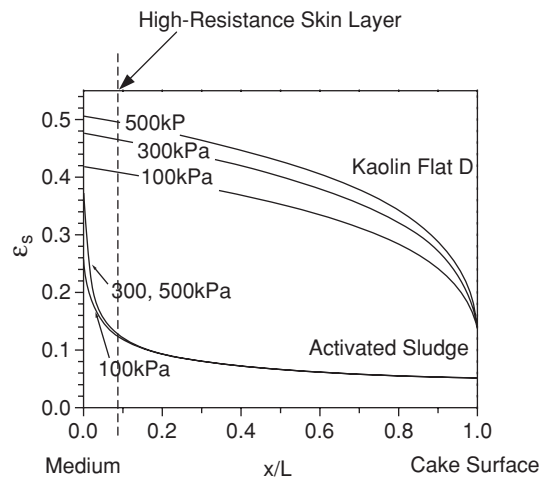


FIG. 18-183 Solidosity ϵ_s variations as a function of fractional distance throughout filter cake thicknesses.

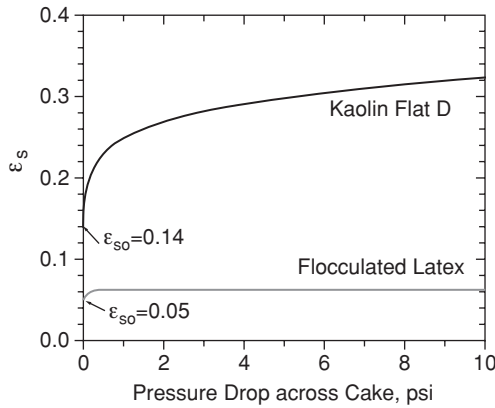


FIG. 18-184 Effect of filtration pressure on average solidosity ϵ_s .

soil mechanics. Shirato's expression theory includes a filtration stage followed by a consolidation. Average consolidation ratio U_c is given as a function of consolidation time θ_c and other characteristic parameters of an expression process including true solids density, liquid density, liquid viscosity, specific resistance (or permeability) versus pressure, porosity versus pressure, and frictional stress on solids throughout cake thickness versus applied pressure (Shirato et al., 1986). The relationships of specific resistance, and porosity versus pressure, and local frictional stress on solids throughout cake thickness during the primary consolidation stage are given by empirical constitutive equations (Tiller and Leu, 1980), and can be determined by a compression-permeability cell test (Tiller, 1977, 1980), as shown in Fig. 18-186.

Factors Affecting Expression Operations Based on fundamental theory, variables affecting expression include characteristics of suspending particles, properties of liquid, properties of filter cake, and expression operation conditions as summarized in Fig. 18-187. Expression efficiency is determined by the properties of the filter cake, which very much depend on characteristics of the suspending particle, properties of liquid, and operation conditions. Interrelationships of the above parameters are described by empirical equations covering restrictive ranges.

EXPRESSION EQUIPMENT

This type of equipment uses mechanical expression rather than pump pressure for cake compression. Dryer cakes and faster cycle rate can

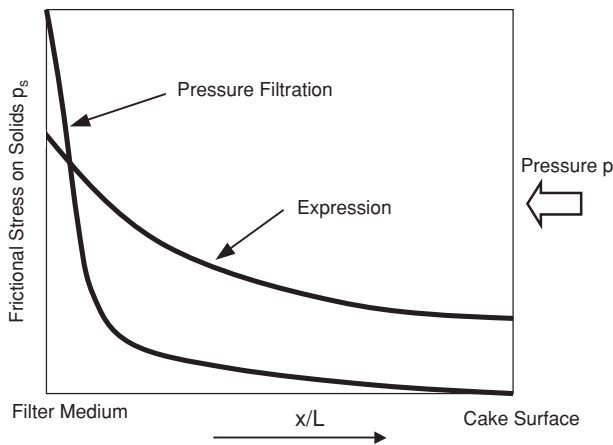


FIG. 18-185 Comparisons of frictional stress distributions in expression and pressure filtration.

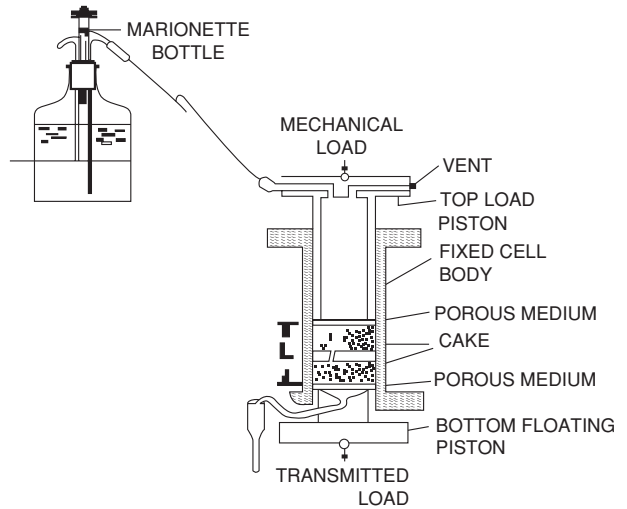


FIG. 18-186 Compression-permeability (C-P) cell.

be achieved compared to pressure filters. Low- to high-pressure (up to 2000 psi) units are available for expression equipment. They can be divided into two categories, batch expression equipment, which allows higher compression pressure and has lower slurry handling capacity, and continuous expression equipment, which uses lower compression pressure but offers higher slurry handling capacities.

Batch Expression Equipment In batch expression equipment, the cake is initially formed by pressure filtration just as in other pressure filters. After the filtration stage, a squeezing device such as a diaphragm is inflated with gas or liquid to compress the cake. Batch expression equipment allows longer compression time and higher compression pressure. The cake can be very dry.

Diaphragm Presses Diaphragm presses, also called membrane presses, are derived from filter presses, which were described in the pressure filtration section. In a diaphragm press, a diaphragm (Fig. 18-188a) is attached to the recessed chamber plate. The operation of a diaphragm press is the same as that of a chamber press during the filtration step. At the end of filtration, the diaphragm is inflated (Fig. 18-188b) to squeeze the filter cake to achieve the mechanical expression. After the squeezing, the diaphragm is deflated and the filter chamber opened to discharge the cake.

The diaphragm can be made of polypropylene or rubber, but polypropylene is most often used today. Both air and water can be used as the inflating medium for the diaphragm. As the inflating medium needs to be brought into the filter plates by hoses, a dangerous condition can exist if a hose is broken with air flowing in it. Therefore, hydraulic fluid (mostly water) is used to inflate the diaphragm to squeeze the cake. Air is only used occasionally in small pilot units.

As in filter presses, one disadvantage of the diaphragm press is the manual operation for filter cake discharge. With recent development, automatic cake discharge devices are available from most filter manufacturers. However, the reliability of an automatic cake discharge device needs to be verified by actual field operation. Normally, automatic cake discharge has a better chance of success in diaphragm presses than filter presses as the cakes are normally dryer in diaphragm presses.

The cake deliquoring is primarily done during the expression step so the cake formation period is normally carried out under low pressure and a high-pressure slurry pump is not necessary; it helps to reduce floc damage during pumping. The normal expression pressure used in a diaphragm press is 110 or 220 psi; in some designs pressure up to 800 psi can be used.

Diaphragm presses are superior to filter presses in deliquoring compactible cakes (such as biological sludge, pulps, or highly flocculated materials). As a diaphragm press is more expensive than a regular filter press, the use of a diaphragm press may not be advantageous

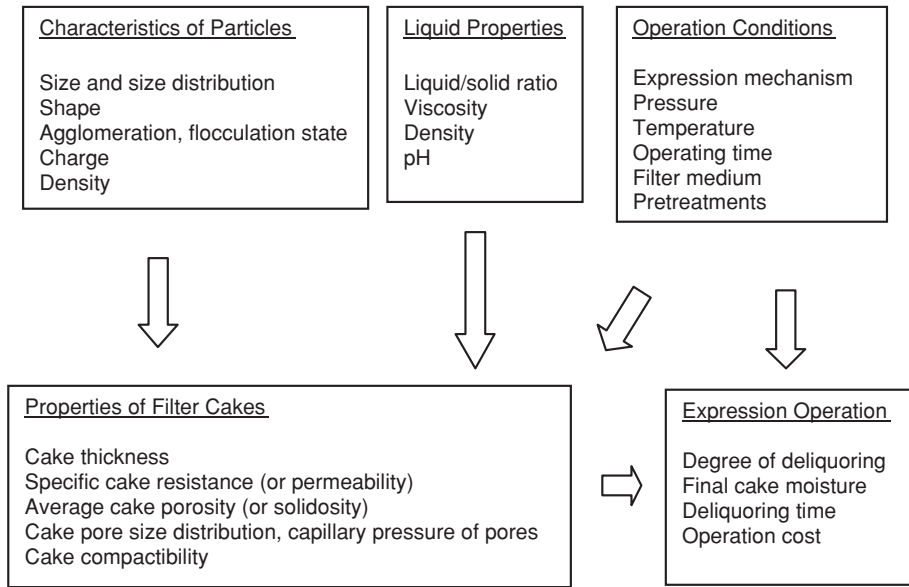


FIG. 18-187 Variables affecting expression.

if solids are not very compactible. There are laboratory and pilot tests available to determine the need for a diaphragm press.

The best way to evaluate diaphragm presses for an application is to run tests with a small pilot unit. Although smaller test units are available, pilot units with 1-ft² filter plate area are more common and are recommended.

A laboratory pressure filter (Fig. 18-189) equipped with a piston can provide a simple feasibility test. In this kind of device, the suspension is poured into the filter cylinder, and the first stage of the test is just like a pressure filtration test. After the filtration, compressed air or water is used to push the piston down to squeeze the filter cake. The filtration rate, final cake thickness and dryness are recorded for evaluation and comparison with the same test without the compression by the piston.

Horizontal Diaphragm Presses This is similar to the diaphragm press except the filter plates lay horizontally (while in diaphragm press, the filter plates are operated vertically). The press can be a single-chamber unit, or multiple chambers can be stacked to achieve greater filtration area.

In each filter plate, the filter medium is attached to a moving belt (Fig. 18-190). An elastomer seal is used at the edge of the filter chamber. The slurry is fed into the filter chamber, and the operation starts as a pressure filtration. After filtration, the diaphragm is inflated to squeeze on the

cake. At the end of expression, the filter chamber opens and the belt moves the cake out of the filter chamber for discharging. The filter chamber is then closed and ready for the next filtration cycle. Permanent filter belt or disposable medium can be used as filter media. The disposable media are especially useful when handling particles which have high tendency to foul the filter media. With the moving belt, the press operation is fully automatic and is another advantage of this equipment.

The testing for evaluating the horizontal diaphragm press is the same as that described above for the (vertical) diaphragm presses. To ensure automatic operation, the cake solids should not stick to the seal of the filter chamber and need to be carefully evaluated during testing.

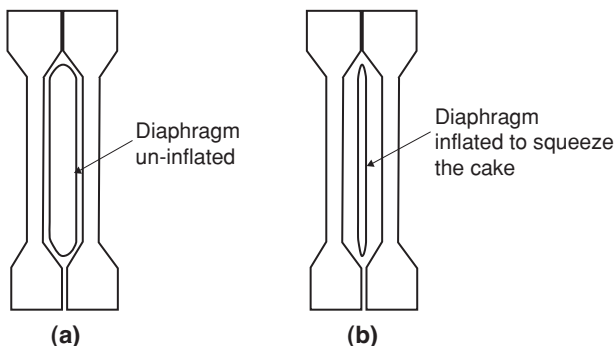


FIG. 18-188 Diaphragm press plate.

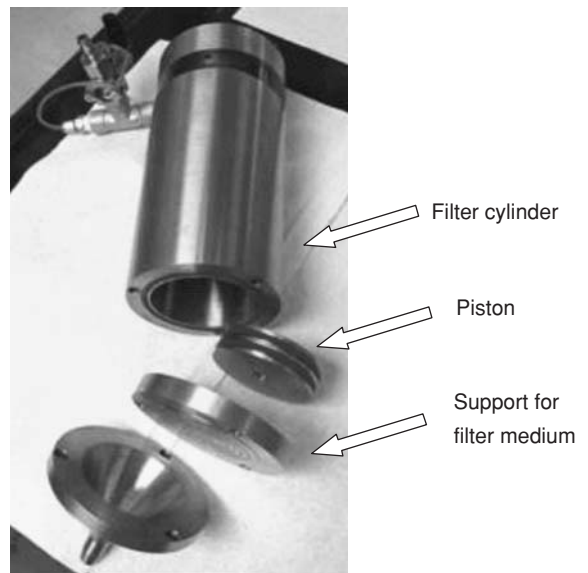


FIG. 18-189 Laboratory pressure filter with a piston to compress the cake.

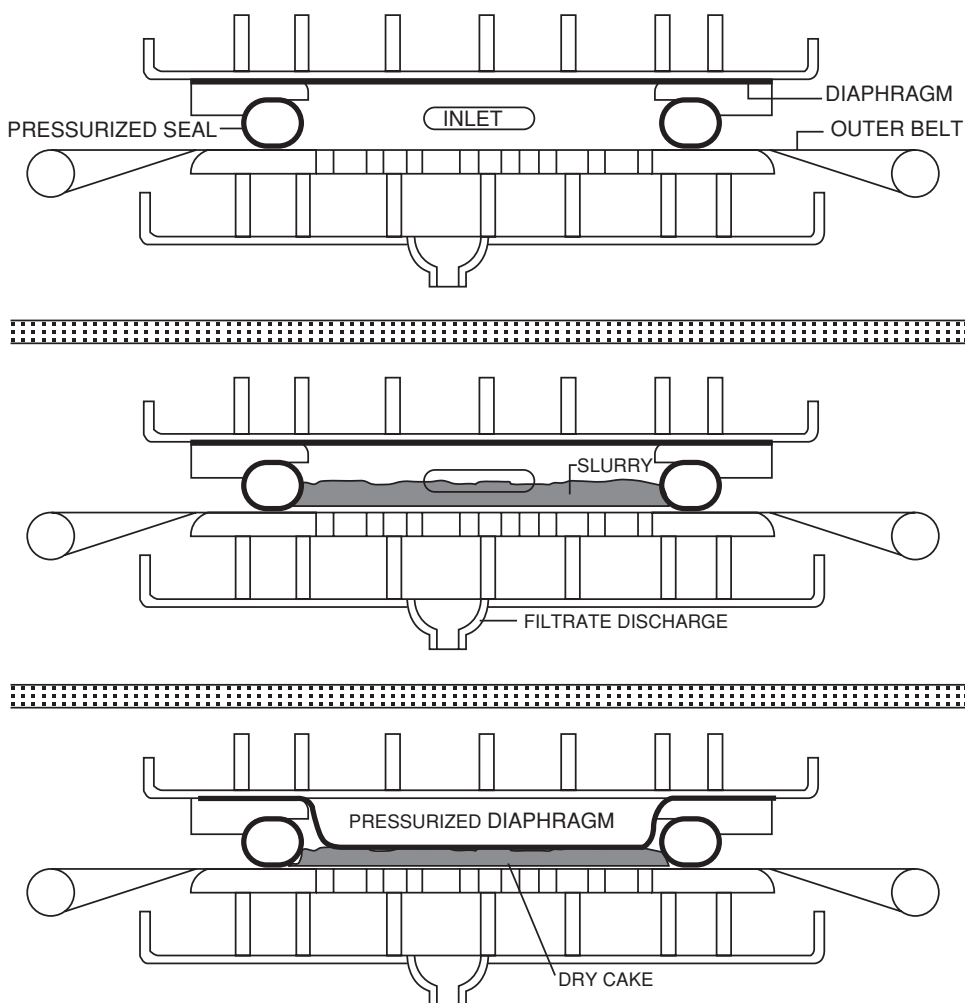


FIG. 18-190 A horizontal diaphragm press. (Courtesy of Filtra Systems.)

Tower Presses This press is similar to the stacked horizontal diaphragm presses, but only one filter belt is used (Fig. 18-191). The operation is also fully automatic. The primary applications are in chemical, mineral and pharmaceutical industries. The testing method is the same as the diaphragm presses. One important factor in designing a tower press is the solids need to be able to be cleared from the chamber seal, otherwise leakage will occur in the following filtration cycle.

Tubular Presses As the name implies, this press is composed of a candle filter inside a cylindrical hydraulic casing (Fig. 18-192). The filter cloth is wrapped around the filter candle, and a diaphragm is attached to the inner side of the outer casing. During the filtration step, the space in between two cylinders is filled with slurry, and pressure filtration is conducted. At the end of the filtration step, the diaphragm is inflated to squeeze the cake around the filter candle. At the end of expression, the bottom of the hydraulic casing tube is opened and the filter assembly is lowered. Air is then introduced to pulse the cake off the candle. After the cake is discharged, the inner filter candle moves back, and the bottom is closed for the next filtration cycle.

Tubular presses use the highest pressures among all expression equipment. The pressure can be as high as 1500 psi. With the high pressure, the cake can be very dry (> 95 percent dryness). This type of equipment normally has low capacity so multiple units are used.

Typical applications of tubular presses are for fine particle dewatering including minerals, talc, and CaCO_3 .

The same laboratory testing equipment as in the diaphragm press can be used but with a higher pressure. A commercially available piston press can also be used.

Continuous Expression Equipment Continuous expression equipment has the advantage of large capacity and automatic operation. Compared to batch expression equipment, lower pressure is used to squeeze the cake in the continuous expression equipment. As a result, the cakes are not as dry as those from the batch expression devices.

Belt Filter Presses Belt presses (Fig. 18-193) have two filter belts that move around rollers of different sizes to dewater the slurry. A typical belt press may have one or more of the following stages: a preconditioning zone, a gravity drainage zone, a linear compression zone (low pressure), and a roller compression zone (high pressure).

The conditioned slurry is fed into the belt press at the preconditioning zone (a tank or pipe), where coagulant and flocculant are added to condition the slurry. The slurry then goes to a horizontal section where the slurry is thickened by gravity drainage. At the end of the gravity drainage section, the thickened slurry (or dilute cake) drops into a wedge section where the wet cake starts to be squeezed by both belts under pressure. At the end of the wedge section, both

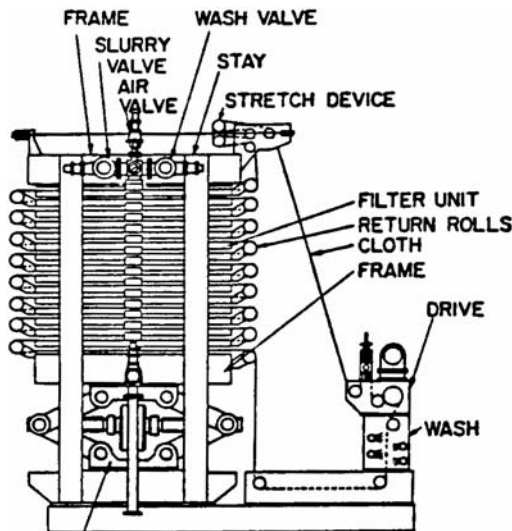


FIG. 18-191 Tower press. (Courtesy of Larox.)

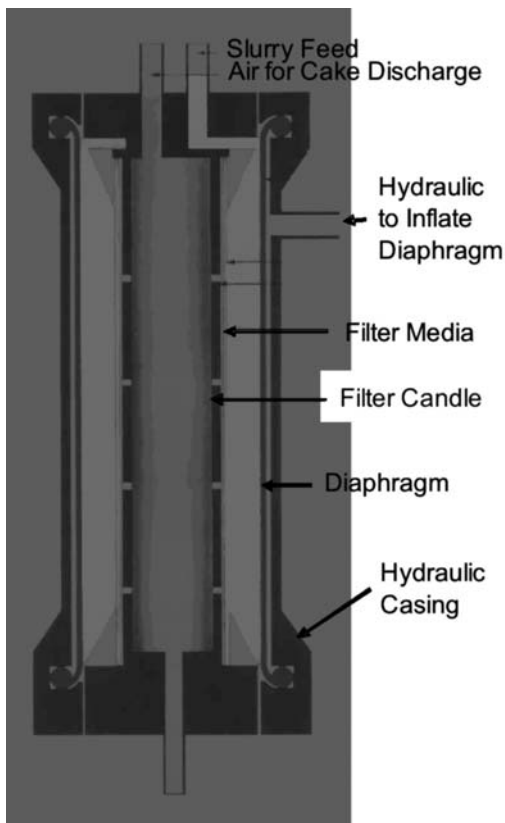


FIG. 18-192 Tubular press. (Courtesy of Metso Minerals.)

belts come together with the cake sandwiched in between and move through a series of rollers. The final dewatering is accomplished by moving the cake through these rollers in the order of decreasing roller diameters. While the roller diameter gets smaller, the pressure exerted on the cake gets higher. After the final roller, the two belts are separated to release the cake. Each belt goes through some washing nozzles to clean off any remaining solids on the belt.

It is important to condition the slurry by coagulation and/or flocculation before it is fed into the belt press. An insufficiently flocculated slurry will not dewater properly, and the cake might be squeezed out through the belts or from the side (both sides of a belt press are open). Good conditioned flocs look like cottage cheese, and it is a good field indication for troubleshooting. Most of the challenges in operating a belt press are in the slurry conditioning and the optimization of flocculant dosage. Flocculant consumption can contribute to a significant operation cost if proper control strategy is not used.

The pressure applied on the cake in a belt press operation is low compared to that in other compression filters. The applied pressures are commonly expressed in pli (pound per linear inch) which is not straightforward in translating to a commonly recognized pressure unit. As a rough comparison, the pressures used in belt presses are around 10 to 20 psi. This pressure can be controlled by the belt and roller tension but seldom is adjusted by operators in the field.

Belt presses have the advantage of large capacity and automatic operation. The initial capital cost is also low. They were originally developed in the pulp and paper industry. Any slurry with fibers will do well in a belt press, and high-fiber material can be added to the slurry as a filter aid for belt press operation. Today, in addition to pulp dewatering, the belt press is widely used in wastewater sludge dewatering.

Due to the relatively low pressure used, the final cakes are not very dry. The dryness of biological sludge cakes from a belt press ranges from 10 to 20 wt %. As fiber content goes up, the cake can be as dry as 40 wt % in dryness.

Testing for applications in belt presses is most commonly done by flocculation in beakers and visual observation of the size and strength of the formed flocs. The conditioned slurry can be poured into a filter for a gravity drainage test. These tests can be useful for an experienced person to evaluate if a slurry can be used in belt presses and to optimize an existing belt press. However, the simulation of the final cake dryness is not

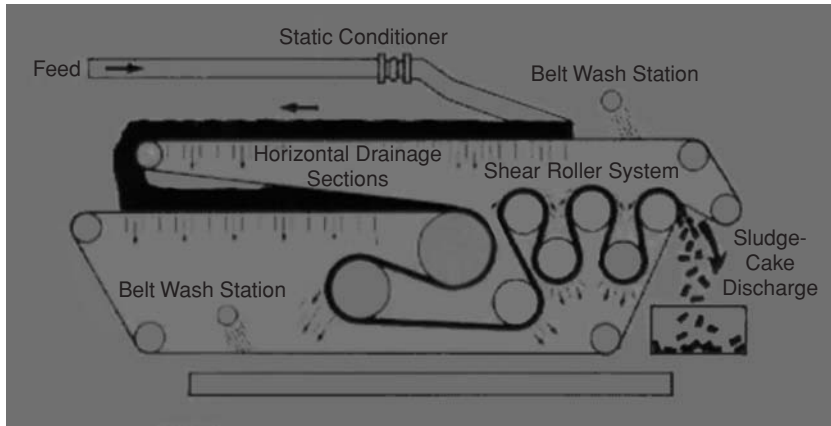


FIG. 18-193 A belt filter press. (Courtesy of Ashbrook.)

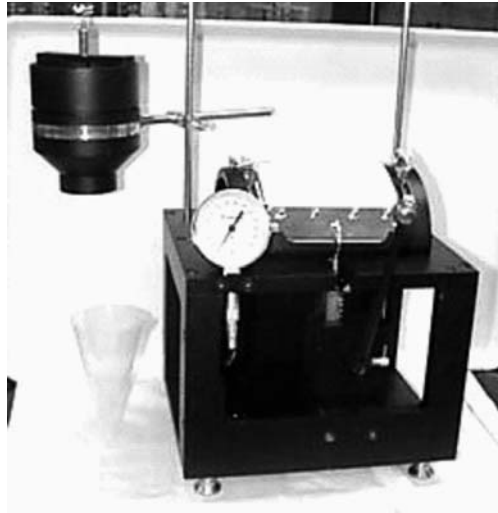


FIG. 18-194 The crown press.

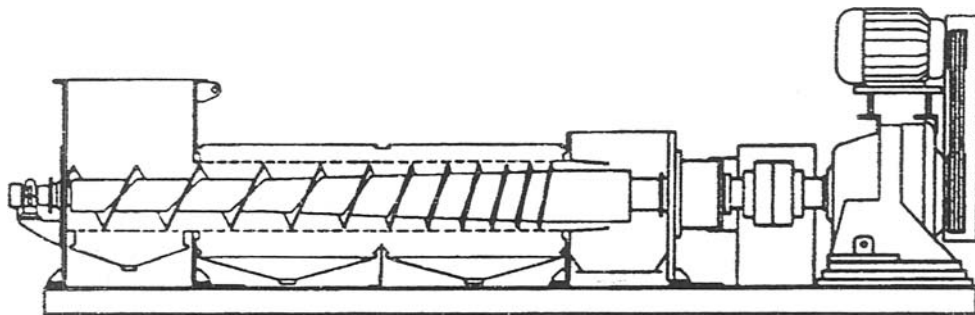


FIG. 18-195 A screw press.

possible with the above methods. The most effective testing is done with a commercially available apparatus called the crown press (Fig. 18-194). This device can simulate the roller actions on the actual belt press and can provide very accurate cake dryness predictions.

Screw Presses A typical screw press is shown in Fig. 18-195, where the slurry is fed into the feed tank at the left-hand side. The core of a screw press is a screw conveyor turning inside a perforated or slotted cylinder. The screw has a smaller diameter at the feed end, and the diameter gradually increases and the screw pitch is shortened toward the discharge end. This design allows gradually decreasing space for slurry/cake and also increasing squeezing pressure on the

cake. As the cake moves toward the outlet, the water is squeezed out through the perforated cylinder.

Screw presses also have the advantage of continuous and automatic operation. Screw presses are primarily used in the pulp and paper, citrus, and dairy industries. Applications also exist in many other industries such as dewatering of synthetic rubbers and wastewater sludge. Three pressure (high, medium, and low) ranges are used. High-pressure screw presses are used for vegetable and animal oil; the capacities are relatively smaller. Medium-pressure units are used to dewater deformable particles (such as plastic pellet and synthetic rubber) and paper pulp. Wastewater sludge applications normally use low-pressure options.

SELECTION OF A SOLIDS-LIQUID SEPARATOR

A good solids-liquid separator performs well in service, both initially and over time. It operates reliably day after day, with enough flexibility to accommodate to normal fluctuations in process conditions, and does not require frequent maintenance and repair. Selection of such a separator begins with a preliminary listing of a number of possible devices, which may solve the problem at hand, and usually ends with the purchase and installation of one or more commercially available machines of a specific type, size, and material of construction. Rarely is it worthwhile to develop a new kind of separator to fill a particular need.

In selecting a solids-liquid separator, it is important to keep in mind the capabilities and limitations of commercially available devices. Among the multiplicity of types on the market, many are designed for fairly specific applications, and unthinking attempts to apply them to other situations are likely to meet with failure. The danger is the more insidious because failure often is not of the clean no-go type; rather it is likely to be in the character of underproduction, subspecification product, or excessively costly operation—the kinds of limping failure that may be slowly detected and difficult to analyze for cause. In addition, it should be recognized that the performance of mechanical separators—more, perhaps, than most chemical-processing equipment—strongly depends on preceding steps in the process. A relatively minor upstream process change, one that might be inadvertent, can alter the optimal separator choice.

PRELIMINARY DEFINITION AND SELECTION

The steps in solving a solids-liquid separation problem, in general, are:

1. Define the overall problem, with expert assistance if necessary.
2. Establish process conditions.
3. Identify appropriate separator types; make preliminary selections.
4. Develop a test program.
5. Take representative samples.
6. Make simple tests.
7. Modify process conditions if necessary.
8. Consult equipment manufacturers.
9. Make final selection; obtain quotations.

Problem Definition Intelligent selection of a separator requires a careful and complete statement of the nature of the separation problem. Focusing narrowly on the specific problem, however, is not sufficient, especially if the separation is to be one of the steps in a new process. Instead, the problem must be defined as broadly as possible, beginning with the chemical reactor or other source of material to be separated and ending with the separated materials in their desired final form. In this way the influence of preceding and subsequent process steps on the separation step will be illuminated. Sometimes, of course, the new separator is proposed to replace an existing unit; the new separator must then fit into the current process and accept feed materials of more or less fixed characteristics. At other times the separator is only one item in a train of new equipment, all parts of which must work in harmony if the separator is to be effective.

Assistance in problem definition and in developing a test program should be sought from persons experienced in the field. If your organization has a consultant in separations of this kind, by all means make

use of the expertise available. If not, it may be wise to employ an outside consultant, whose special knowledge and guidance can save time, money, and headaches. It is important to do this early; after the separation equipment has been installed, there is little a consultant can do to remedy the sometimes disastrous effects of a poor selection. Often it is best to work with established equipment manufacturers throughout the selection process, unless the problem is unusually sensitive or confidential. Their experience with problems similar to yours may be most helpful and avoid many false starts.

Preliminary Selections Assembling background information permits tentative selection of promising equipment and rules out clearly unsuitable types. If the material to be processed is a slurry or pumpable suspension of solids in a liquid, several methods of mechanical separation may be suitable, and these are classified into settling and filtration methods as shown in Fig. 18-196. If the material is a wet solid, removal of liquid by various methods of expression should be considered.

Settling does not give a complete separation: one product is a concentrated suspension and the other is a liquid which may contain fine particles of suspended solids. However, settling is often the best way to process very large volumes of a dilute suspension and remove most of the liquid. The concentrated suspension can then be filtered with smaller equipment than would be needed to filter the original dilute suspension, and the cloudy liquid can be clarified if necessary. Settlers can also be used for classifying particles by size or density, which is usually not possible with filtration.

Screens may sometimes be used to separate suspensions of coarse particles, but are not widely applicable. For separating fine solids from liquids, cake filtration or the newer systems of crossflow filtration should be considered. Crossflow filtration includes ultrafiltration, where the solids are macromolecules or very fine solids ($D_p \leq 0.1 \mu\text{m}$), and microfiltration, where the particle size generally ranges from 0.1 to 5 μm . In microfiltration a suspension is passed at high velocity of 1 to 3 m/s (3 to 10 ft/s) and moderate pressure (10 to 30 lb/in² gauge) parallel to a semipermeable membrane in sheet or tubular form. Organic membranes are made of various polymers including cellulose acetate, polysulfone, and polyamide; and they are usually asymmetric, with a thin selective skin supported on a thicker layer that has larger pores. Inorganic membranes of sintered metal or porous alumina are also available in various shapes, with a range of average pore sizes and permeabilities. Most membranes have a wide distribution of pore sizes and do not give complete rejection unless the average pore size is much smaller than the average particle size in the suspension.

In microfiltration, particles too large to enter the pores of the membrane accumulate at the membrane surface as the liquid passes through. They form a layer of increasing thickness that may have appreciable hydraulic resistance and cause a gradual decrease in permeate flow. A decline in liquid flow may also result from small particles becoming embedded in the membrane or plugging some of the pore mouths. The particle layer may reach a steady-state thickness because of shear-induced migration of particles back into the mainstream, or the liquid flux may continue to decline, requiring frequent backwashing or other cleaning procedures. Because of the high velocities the change in solids concentration per pass is small, and the suspension is either recycled to the feed tank or sent through several

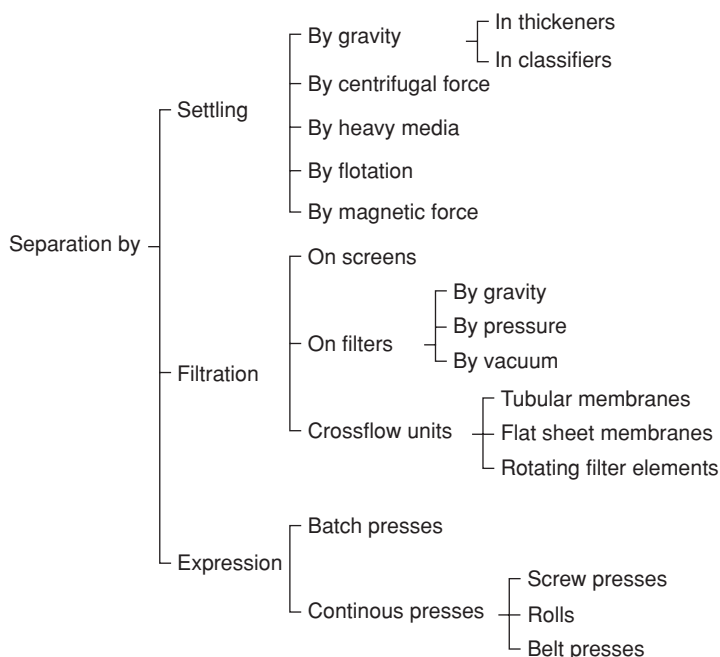


FIG. 18-196 Main paths to solids-liquid separation.

units in series to achieve the desired concentration. The products are a clear liquid and a concentrated suspension similar to those produced in a settling device, but the microfiltration equipment is much smaller for the same production rate.

SAMPLES AND TESTS

Once the initial choice of promising separator types is made, representative liquid-solid samples should be obtained for preliminary tests. At this point, a detailed test program should be developed, preferably with the advice of a specialist.

Establishing Process Conditions Step 2 is taken by defining the problem in detail. Properties of the materials to be separated, the quantities of feed and products required, the range of operating variables, and any restrictions on materials of construction must be accurately fixed, or reasonable assumptions must be made. Accurate data on the concentration of solids, the average particle size or size distribution, the solids and liquid densities, and the suspension viscosity should be obtained *before* selection is made, not after an installed separator fails to perform. The required quantity of the liquid and solid may also influence separator selection. If the solid is the valuable product and crystal size and appearance are important, separators that minimize particle breakage and permit nearly complete removal of fluid may be required. If the liquid is the more valuable product, can minor amounts of solid be tolerated, or must the liquid be sparkling clear? In some cases, partial or incomplete separation is acceptable and can be accomplished simply by settling or by crossflow filtration. Where clarity of the liquid is a key requirement, the liquid may have to be passed through a cartridge-type clarifying filter after most of the solid has been removed by the primary separator.

Table 18-17 lists the pertinent background information that should be assembled. It is typical of data requested by manufacturers when they are asked to recommend and quote on a solid-liquid separator. The more accurately and thoroughly these questions can be answered, the better the final choice is likely to be.

Representative Samples For meaningful results, tests must be run on representative samples. In liquid-solids systems good samples

are hard to get. Frequently a liquid-solid mixture from a chemical process varies significantly from hour to hour, from batch to batch, or from week to week. A well-thought-out sampling program over a prolonged period, with samples spaced randomly and sufficiently far apart, under the most widely varying process conditions possible, should be formulated. Samples should be taken from all shifts in a continuous process and from many successive batches in a batch process. The influence of variations in raw materials on the separating characteristics should be investigated, as should the effect of reactor or crystallizer temperature, intensity of agitation, or other process variables.

Once samples are taken, they must be preserved unchanged until tested. Unfortunately, cooling or heating the samples or the addition of preservatives may markedly change the ease with which solids may be separated from the liquid. Sometimes they make the separation easier, sometimes harder; in either case, tests made on deteriorated samples give a false picture of the capabilities of separation equipment. Even shipping of the samples can have a significant effect. Often it is so difficult to preserve liquid-solids samples without deterioration that accurate results can be obtained only by incorporating a test separation unit directly in the process stream.

Simple Tests It is usually profitable, however, to make simple preliminary tests, recognizing that the results may require confirmation through subsequent large-scale studies.

Preliminary gravity settling tests are made in a large graduated cylinder in which a well-stirred sample of slurry is allowed to settle, the height of the interface between clear supernatant liquid and concentrated slurry being recorded as a function of settling time. Centrifugal settling tests are normally made in a bottle centrifuge in which the slurry sample is spun at various speeds for various periods of time, and the volume and consistency of the settled solids are noted. In gravity settling tests in particular, it is important to evaluate the effects of flocculating agents on settling rates.

Preliminary filtration tests may be made with a Büchner funnel or a small filter leaf, covered with canvas or other appropriate medium and connected to a vacuum system. Usually the suspension is poured carefully into the vacuum-connected funnel, whereas the leaf is immersed

TABLE 18-17 Data for Selecting a Solids-Liquid Separator*

1. Process
 - a. Describe the process briefly. Make up a flowsheet showing places where liquid-solid separators are needed.
 - b. What are the objections to the present process?
 - c. Briefly, what results are expected of the separator?
 - d. Is the process batch or continuous?
 - e. Number the following objectives in order of importance in your problem: (a) separation of two different solids _____; (b) removal of solids to recover valuable liquor as overflow _____; (c) removal of solids to recover the solids as thickened underflow _____ or as "dry" cake _____; (d) washing of solids _____; (e) classification of solids _____; (f) clarification or "polishing" of liquid _____; (g) concentration of solids _____.
 - f. List the available power and current characteristics.
2. Feed
 - a. Quantity of feed:
 - Continuous process: _____ gal/min; _____ h/day; _____ lb/h of dry solids.
 - Batch process: volume of batch: _____; total batch cycle: _____ h.
 - b. Feed properties: temp. _____; pH _____; viscosity _____.
 - c. What maximum feed temperature is allowable?
 - d. Chemical analysis and specific gravity of carrying liquid.
 - e. Chemical analysis and specific gravity of solids.
 - f. Percentage of solids in feed slurry.
 - g. Screen analysis of solids: wet _____ dry _____
 - h. Chemical analysis and concentration of solubles in feed.
 - i. Impurities: form and probable effect on separation.
 - j. Is there a volatile component in the feed? _____ Should the separator be vapor-tight? _____ Must it be under pressure? _____ If so, how much? _____
3. Filtration and settling rates
 - a. Filtration rate on Büchner funnel: _____ gal/(min)(ft²) of filter area under a vacuum of _____ in Hg. Time required to form a cake _____ in thick: _____ s.
 - b. At what rate do the solids settle by gravity?
 - c. What percentage of the total feed volume do the settled solids occupy after settling is complete? After how long?
4. Feed preparation
 - a. If the feed tends to foam, can antifoaming agents be used? If so, what type?
 - b. Can flocculating agents be used? If so, what agents?
 - c. Can a filter aid be used?
 - d. What are the process steps immediately preceding the separation? Can they be modified to make the separation easier?
 - e. Could another carrying liquid be used?
5. Washing
 - a. Is washing necessary?
 - b. What are the chemical analysis and specific gravity of wash liquid?
 - c. Purpose of wash liquid: to displace residual mother liquor or to dissolve soluble material from the solids?
 - d. Temperature of wash liquid.
 - e. Quantity of wash allowable, in lb/lb of solids.
6. Separated solids
 - a. What percentage of solids is desired in the cake or thickened underflow?
 - b. Is particle breakage important?
 - c. Amount of residual solubles allowable in solids.
 - d. What further processing will have to be carried out on the solids?
7. Separated liquids
 - a. Clarity of liquor: what percentage of solids is permissible?
 - b. Must the filtrate and spent wash liquid be kept separate?
 - c. What further processing will be carried out on the filtrate and/or spent wash?
8. Materials of construction
 - a. What metals look most promising?
 - b. What metals must not be used?
 - c. What gasket and packing materials are suitable?

*U.S. customary engineering units have been retained in this data form. The following SI or modified-SI units might be used instead: centimeters = inches \times 2.54; kilograms per kilogram = pounds per pound \times 1.0; kilograms per hour = pounds per hour \times 0.454; liters per minute = gallons per minute \times 3.785; liters per second-square meter = gallons per minute-square foot \times 0.679; and pascals = inches mercury \times 3377.

in a sample of the slurry and vacuum is applied to pull filtrate into a collecting flask. The time required to form each of several cakes in the range of 3 to 25 mm ($\frac{1}{8}$ to 1 in) thick under a given vacuum is noted, as is the volume of the collected filtrate. Properly conducted tests with a Büchner or a vacuum leaf closely simulate the action of rotary vacuum filters of the top- and bottom-feed variety, respectively, and may give the experienced observer enough information for complete specification of a plant-size filter. Alternatively, they may point to pressure-filter tests or, indeed, to a search for an alternative to filtration. Centrifugal filter tests are made in a perforated basket centrifugal filter 254 or 305 mm (10 or 12 in) in diameter lined with a suitable filter medium. Slurry is poured into the rotating basket until an appropriately thick cake—say, 25 mm (1 in)—is formed. Filtrate is recycled to the basket at such a rate that a thin layer of liquid is just visible on the surface of the cake. The discharge rate of the liquor under these conditions is the draining rate. The test is repeated with cakes of other thicknesses to establish the productive capacity of the centrifugal filter.

Batch tests of microfiltration may be carried out in small pressurized cells with a porous membrane at the bottom and a magnetic stirrer to provide high shear at the membrane surface. These tests may quickly show what type of membrane, if any, gives satisfactory separation, but scaling up to large production units is difficult. Small modules with hollow-fiber, tubular, or spiral-wound membranes are available from equipment vendors, so that tests can be made with continuous flow at pressures and velocities likely to be used for large-scale operation. The permeate flux should be measured as a function of time for different slurry concentrations, pressure drops, and solution velocities or Reynolds numbers. Often a limiting flux will be reached as the pressure drop is increased, but operation at a lower pressure drop is often desirable since the flux decline may not be as great and the average permeation rate over a batch cycle may be greater.

More detailed descriptions of small-scale sedimentation and filtration tests are presented in other parts of this section. Interpretation of the results and their conversion into preliminary estimates of such quantities as thickener size, centrifuge capacity, filter area, sludge density, cake dryness, and wash requirements also are discussed. Both the tests and the data treatment must be in experienced hands if error is to be avoided.

Modification of Process Conditions Relatively small changes in process conditions often markedly affect the performance of specific solids-liquid separators, making possible their application when initial test results indicated otherwise or vice versa. Flocculating agents are an example; many gravity settling operations are economically feasible only when flocculants are added to the process stream. Changes in precipitation or crystallization steps may greatly enhance or diminish filtration rates and hence filter capacity. Changes in the temperature of the process stream, the solute content, or the chemical nature of the suspending liquid also influence solids-settling rates. Occasionally it is desirable to add a heavy, finely divided solid to form a pseudo-liquid suspending medium in which the particles of the desired solid will rise to the surface. Attachment of air bubbles to solid particles in a flotation cell, using a suitable flotation agent, is another way of changing the relative densities of liquid and solid.

Consulting the Manufacturer Early in the selection campaign—certainly no later than the time at which the preliminary tests are completed—manufacturers of the more promising separators should be asked for assistance. Additional tests may be made at a manufacturer's test center; again a major problem is to obtain and preserve representative samples. As much process information as tolerable should be shared with the manufacturers to make full use of their experience with their particular equipment. Full-scale plant tests, although expensive, may well be justified before final selection is made. Such tests demonstrate operation on truly representative feed, show up long-term operating problems, and give valuable operating experience.

In summary, separator selection calls for clear problem definition, in broad terms; thorough cataloging of process information; and preliminary and tentative equipment selection, followed by refinement of the initial selections through tests on an increasingly larger scale. Reliability, flexibility of operation, and ease of maintenance should be weighed heavily in the final economic evaluation; rarely is purchase price, by itself, a governing factor in determining the suitability of a liquid-solids separator.

SECTION 19

Reactors

PERRY'S CHEMICAL ENGINEERS' HANDBOOK

8TH EDITION



CARMO J. PEREIRA
TIBERIU M. LEIB

Copyright © 2008, 1997, 1984, 1973, 1963, 1950, 1941, 1934 by The McGraw-Hill Companies, Inc. All rights reserved. Manufactured in the United States of America. Except as permitted under the United States Copyright Act of 1976, no part of this publication may be reproduced or distributed in any form or by any means, or stored in a database or retrieval system, without the prior written permission of the publisher.

0-07-154226-4

The material in this eBook also appears in the print version of this title: 0-07-151142-3.

All trademarks are trademarks of their respective owners. Rather than put a trademark symbol after every occurrence of a trademarked name, we use names in an editorial fashion only, and to the benefit of the trademark owner, with no intention of infringement of the trademark. Where such designations appear in this book, they have been printed with initial caps.

McGraw-Hill eBooks are available at special quantity discounts to use as premiums and sales promotions, or for use in corporate training programs. For more information, please contact George Hoare, Special Sales, at george_hoare@mcgraw-hill.com or (212) 904-4069.

TERMS OF USE

This is a copyrighted work and The McGraw-Hill Companies, Inc. (“McGraw-Hill”) and its licensors reserve all rights in and to the work. Use of this work is subject to these terms. Except as permitted under the Copyright Act of 1976 and the right to store and retrieve one copy of the work, you may not decompile, disassemble, reverse engineer, reproduce, modify, create derivative works based upon, transmit, distribute, disseminate, sell, publish or sublicense the work or any part of it without McGraw-Hill’s prior consent. You may use the work for your own noncommercial and personal use; any other use of the work is strictly prohibited. Your right to use the work may be terminated if you fail to comply with these terms.

THE WORK IS PROVIDED “AS IS.” McGRAW-HILL AND ITS LICENSORS MAKE NO GUARANTEES OR WARRANTIES AS TO THE ACCURACY, ADEQUACY OR COMPLETENESS OF OR RESULTS TO BE OBTAINED FROM USING THE WORK, INCLUDING ANY INFORMATION THAT CAN BE ACCESSED THROUGH THE WORK VIA HYPERLINK OR OTHERWISE, AND EXPRESSLY DISCLAIM ANY WARRANTY, EXPRESS OR IMPLIED, INCLUDING BUT NOT LIMITED TO IMPLIED WARRANTIES OF MERCHANTABILITY OR FITNESS FOR A PARTICULAR PURPOSE. McGraw-Hill and its licensors do not warrant or guarantee that the functions contained in the work will meet your requirements or that its operation will be uninterrupted or error free. Neither McGraw-Hill nor its licensors shall be liable to you or anyone else for any inaccuracy, error or omission, regardless of cause, in the work or for any damages resulting therefrom. McGraw-Hill has no responsibility for the content of any information accessed through the work. Under no circumstances shall McGraw-Hill and/or its licensors be liable for any indirect, incidental, special, punitive, consequential or similar damages that result from the use of or inability to use the work, even if any of them has been advised of the possibility of such damages. This limitation of liability shall apply to any claim or cause whatsoever whether such claim or cause arises in contract, tort or otherwise.

DOI: 10.1036/0071511423

Reactors*

Carmo J. Pereira, Ph.D., MBA *DuPont Fellow, DuPont Engineering Research and Technology, E. I. du Pont de Nemours and Company; Fellow, American Institute of Chemical Engineers*

Tiberiu M. Leib, Ph.D. *Principal Consultant, DuPont Engineering Research and Technology, E. I. du Pont de Nemours and Company; Fellow, American Institute of Chemical Engineers*

REACTOR CONCEPTS		SINGLE-PHASE REACTORS	
Reactor Types	19-4	Liquid Phase	19-20
Classification by Mode of Operation	19-4	Homogeneous Catalysis	19-20
Classification by End Use	19-7	Gas Phase	19-21
Classification by Phase	19-7	Supercritical Conditions	19-21
Reactor Modeling	19-7	Polymerization Reactors	19-21
Modeling Considerations	19-7		
Chemical Kinetics	19-9	FLUID-SOLID REACTORS	
Pressure Drop, Mass and Heat Transfer	19-10	Heterogeneous Catalysts	19-25
Reactor Dynamics	19-11	Catalytic Reactors	19-27
Reactor Models	19-13	Wire Gauzes	19-27
		Monolith Catalysts	19-27
RESIDENCE TIME DISTRIBUTION AND MIXING		Fixed Beds	19-30
Tracers	19-14	Moving Beds	19-33
Inputs	19-15	Fluidized Beds	19-33
Types of Responses	19-15	Slurry Reactors	19-36
Reactor Tracer Responses	19-15	Transport Reactors	19-36
Understanding Reactor Flow Patterns	19-16	Multifunctional Reactors	19-36
Connecting RTD to Conversion	19-17	Noncatalytic Reactors	19-36
Segregated Flow	19-18	Rotary Kilns	19-36
Early versus Late Mixing—Maximum Mixedness	19-18	Vertical Kilns	19-36
Reaction and Mixing Times	19-20		

*The contributions of Stanley M. Walas, Ph.D., Professor Emeritus, Department of Chemical and Petroleum Engineering, University of Kansas (Fellow, American Institute of Chemical Engineers), author of this section in the seventh edition, are acknowledged.

The authors of the present section would like to thank Dennie T. Mah, M.S.Ch.E., Senior Consultant, DuPont Engineering Research and Technology, E. I. du Pont de Nemours and Company (Senior Member, American Institute of Chemical Engineers; Member, Industrial Electrolysis and Electrochemical Engineering; Member, The Electrochemical Society), for his contributions to the "Electrochemical Reactors" subsection; and John Villadsen, Ph.D., Senior Professor, Department of Chemical Engineering, Technical University of Denmark, for his contributions to the "Bioreactors" subsection. We acknowledge comments from Peter Harriott, Ph.D., Fred H. Rhodes Professor of Chemical Engineering (retired), School of Chemical and Biomolecular Engineering, Cornell University, on our original outline and on the subject of heat transfer in packed-bed reactors. The authors also are grateful to the following colleagues for reading the manuscript and for thoughtful comments: Thomas R. Keane, DuPont Fellow (retired), DuPont Engineering Research and Technology, E. I. du Pont de Nemours and Company (Senior Member, American Institute of Chemical Engineers); Güray Tosun, Ph.D., Senior Consultant, DuPont Engineering Research and Technology, E. I. du Pont de Nemours and Company (Senior Member, American Institute of Chemical Engineers); and Nitin H. Kolhapure, Ph.D., Senior Consulting Engineer, DuPont Engineering Research and Technology, E. I. du Pont de Nemours and Company (Senior Member, American Institute of Chemical Engineers).

19-2 REACTORS

FLUID-FLUID REACTORS

Gas-Liquid Reactors	19-38
Liquid-Liquid Reactors	19-41
Reactor Types	19-42
Agitated Stirred Tanks	19-42
Bubble Columns	19-44
Tubular Reactors	19-46
Packed, Tray, and Spray Towers	19-46

SOLIDS REACTORS

Thermal Decomposition	19-48
Solid-Solid Reactions	19-48
Self-Propagating High-Temperature Synthesis (SHS)	19-49

MULTIPHASE REACTORS

Bioreactors	19-49
Electrochemical Reactors	19-50
Reactor Types	19-53
Agitated Slurry Reactors	19-53
Slurry Bubble Column Reactors	19-56
Fluidized Gas-Liquid-Solid Reactors	19-57
Trickle Bed Reactors	19-57
Packed Bubble Columns (Cocurrent Upflow)	19-60
Countercurrent Flow	19-60

SOME CASE STUDIES

Nomenclature and Units

In this section, the concentration is represented by C . Mass balance accounting in terms of the number of moles and the fractional conversion is discussed in Sec. 7 and can be very useful. The rate of reaction is r ; the flow rate in moles is N_a ; the volumetric flow rate is V' ; reactor volume is V_r . Several equations are presented without specification of units. Use of any consistent unit set is appropriate.

Following is a listing of typical nomenclature expressed in SI and U.S. Customary System units. Specific definitions and units are stated at the place of application in this section.

Symbol	Definition	SI units	U.S. Customary System Units	Symbol	Definition	SI units	U.S. Customary System Units
a	Surface area per volume	1/m	1/ft	V'	Volumetric flow rate	m ³ /s	ft ³ /s
A_k	Heat-transfer area	m ²	ft ²	V_r	Volume of reactor	m ³	ft ³
C	Concentration of substance	kg·mol/m ³	lb·mol/ft ³	w	Catalyst loading		
C_0	Initial mean concentration	kg·mol/m ³	lb·mol/ft ³	x	Axial position in a reactor, conversion		
c_p	Heat capacity at constant pressure	kJ/(kg·K)	Btu/(lbm·°F)	Greek letters			
CSTR	Ideal continuous stirred tank reactor			α	Fraction of feed that bypasses reactor		
d	Diameter	m	ft	β	Fraction of reactor volume that is stagnant, Prater number		
D	Diameter, diffusivity			$\delta(\tau)$	Unit impulse input, Dirac delta function		
D_{eff}	Effective diffusion coefficient	m ² /s	ft ² /s	δ_L	Distance or film thickness	m	ft
D_e	Effective dispersion coefficient	m ² /s	ft ² /s	ϵ	Void fraction in a packed bed, particle porosity		
E	Activation energy	kJ/(kg·mol)	Btu/(lb·mol)	η	Effectiveness factor of porous catalyst		
$E(t)$	Residence time distribution			λ	Thermal conductivity	kJ/(s·m·°C)	Btu/(h·ft·°F)
$E(t_r)$	Normalized residence time distribution			$\Lambda(t)$	Intensity function		
f_a	Fraction of A remaining unconverted, C_a/C_{a0} or n_a/n_{a0}			μ	Viscosity	Pa·s	lbm/(ft·s)
$F(t)$	Age function of tracer			ν	Kinematic viscosity, μ/ρ	m ² /s	ft ² /s
h	Heat-transfer coefficient	kJ/(s·m ² ·°C)	Btu/(h·ft ² ·°F)	ρ	Density	kg/m ³	lbm/ft ³
H	Height of tank	m	ft	$\sigma^2(\tau)$	Variance		
H_e	Henry constant	Pa·m ³ /(kg·mol)	atm·ft ³ /(lb·mol)	$\sigma^2(t_r)$	Normalized variance		
ΔH_r	Heat of reaction	kJ/(kg·mol)	Btu/(lb·mol)	ξ	Fractional conversion		
k	Specific rate constant for first-order reaction	1/s	1/s	τ	Tortuosity		
k_m	Mass-transfer coefficient	m/s	ft/s	ϕ	Thiele modulus		
L	Length of path in reactor	m	ft	ϕ_α	Shape factor		
m	Magnitude of impulse	kg·mol	lb·mol	ϕ_E	Local rate of energy dissipation		
n	Number of stages in a CSTR battery or parameter of Erlang or gamma distribution			Subscripts			
Nu	Nusselt number			a	Agitator, axial, species A		
N	Speed of agitator	rpm	rpm	b	Bed, species B		
Ha	Hatta number			c	Critical value, catalyst, coolant, continuous phase		
p_a	Partial pressure of substance A	Pa	psi	cir	Circulation		
P	Total pressure	Pa	psi	d	Dispersed phase		
Pe	Peclet number for dispersion			f	Fluid, feed		
PFR	Plug flow reactor			G	Gas phase		
q	Heat flux, reaction order, or impeller-induced flow			i	Interface		
Q	Volumetric flow rate	m ³ /s	ft ³ /s	L	Liquid		
r	Rate of reaction per unit volume, radius			ma	Macro		
R	Radius	m	ft	me	Meso		
Re	Reynolds number			mi	Micro		
Sc	Schmidt number			p	Pellet		
Sh	Sherwood number			r	Reaction, reduced		
t	Time	s	s	R	Reactor		
\bar{t}	Mean residence time	s	s	s	Surface		
t_r	Reduced time, t/\bar{t}			t	Tank		
T	Temperature	°C	°F	u	Step function		
TFR	Tubular flow reactor			w	Wall		
u	Linear velocity	m/s	ft/s	0	Inlet		
$u(t)$	Unit step input			δ	Delta function		
U	Overall heat-transfer coefficient	kJ/(s·m ² ·°C)	Btu/(h·ft ² ·°F)	Superscripts			
v	Volumetric flow rate during semibatch operation	m ³ /s	ft ³ /s	0	Initial condition		
v_{ij}	Stoichiometric coefficients						

GENERAL REFERENCES: The General References listed in Sec. 7 are applicable for Sec. 19. References to specific topics are made throughout this section.

A chemical reactor is a controlled volume in which a chemical reaction can occur in a safe and controllable manner. A reactor typically is a piece of equipment; however, it can also be a product (such as a coating or a protective film). One or more reactants may react together at a desired set of operating conditions, such as temperature and pressure. There may be a need for appropriate mixing, control of flow distribution and residence time, contacting between the reactants (sometimes in the presence of a catalyst or biocatalyst), removal (or addition) of heat, and integration of the reactor with the rest of the downstream process. Depending on the nature of the rate-limiting step(s), a reactor may serve primarily as a holding tank, a heat exchanger, or a mass-transfer device. Chemical reactions generate desired products and also by-products that have to be separated and disposed. A successful commercial unit is an economic balance of all these factors. A variety of reactor types are used in the chemical, petrochemical, and pharmaceutical industries. Some of these reactors are listed in Table 19-1. They include gas, liquid, or multiphase batch reactors, stirred tank reactors, and tubular reactors.

There are a number of textbooks on chemical reaction engineering. Davis and Davis (*Fundamentals of Chemical Reaction Engineering*, McGraw-Hill, 2003) provide a lucid discussion of kinetics and principles. A more comprehensive treatment together with access to

CD-ROM and web resources is in the text by Fogler (*Elements of Chemical Reaction Engineering*, 3d ed., Prentice-Hall, 1999). A chemistry-oriented perspective is provided by Schmidt (*The Engineering of Chemical Reactions*, Oxford University Press, 1999). The book by Froment and Bischoff provides a thorough discussion of reactor analysis and design. A practical manual on reactor design and scale-up is by Harriott (*Chemical Reactor Design*, Marcel Dekker, 2003). Levenspiel (*Chemical Reaction Engineering*, 3d ed., Wiley, 1999) was among the first to present a phenomenological discussion of fundamentals. The mathematical underpinnings of reactor modeling are covered by Bird et al. (*Transport Phenomena*, 2d ed., Wiley, 2002). This section contains a number of illustrations and sketches from books by Walas (*Chemical Process Equipment Selection and Design*, Butterworths, 1990) and Ullmann [*Encyclopedia of Chemical Technology* (in German), vol. 3, Verlag Chemie, 1973, pp. 321–518].

Mathematical models may be used to design reactors and analyze their performance. Detailed models have mainly been developed for large-scale commercial processes. A number of software tools are now available. This chapter will discuss some of the reactors used commercially together with how mathematical models may be used. For additional details, a number of books on reactor analysis cited in this section are available. The discussion will indicate that logical choices aimed at maximizing reaction rate and selectivity for a given set of kinetics can lead to rational reactor selection. While there has been progress in recent years, reactor design and modeling are largely an art.

REACTOR CONCEPTS

Since a primary purpose of a reactor is to provide desirable conditions for reaction, the *reaction rate per unit volume* of reactor is important in analyzing or sizing a reactor. For a given production rate, it determines the reactor volume required to effect the desired transformation. The residence time in a reactor is inversely related to the term *space velocity* (defined as volumetric feed rate/reactor volume). The fraction of reactants converted to products and by-products is the *conversion*. The fraction of desired product in the material converted on a molar basis is referred to as *selectivity*. The product of conversion and the fractional selectivity provides a measure of the fraction of reactants converted to product, known as *yield*. The product yield provides a direct measure of the level of (atom) utilization of the raw materials and may be an important component of operating cost. A measure of reactor utilization called *space time yield (STY)* is the ratio of product generation rate to reactor volume. When a catalyst is used, the reactor has to make product without major process interruptions. The catalyst may be homogeneous or heterogeneous, and the latter can be a living biological cell. A key aspect of catalyst performance is the *durability* of the active site. Since a chemical or biochemical process has a number of unit operations around the reactor, it is often beneficial to minimize the variability of reactant and product flows. This typically means that the reactor is operated at a *steady state*. Interactions between kinetics, fluid flow, transport resistances, and heat effects sometimes result in *multiple steady states* and *transient (dynamic) behavior*. Reactor dynamics can also result in *runaway behavior*, where reactor temperature continues to increase until the reactants are depleted, or *wrong-way behavior*, where reducing inlet temperature (or reactant flow rate) can result in temperature increases farther downstream and a possible runaway. Since such behavior can result in large perturbations in the process and possibly safety issues, a reactor *control strategy* has to be implemented. The need to operate safely under all conditions calls for a thorough analysis to ensure that the reactor is *inherently safe* and that all possible unsafe outcomes have been considered and addressed. Since various solvents may be used in chemical processes and reactors generate both products and by-products, solvent and by-product emissions can cause *emission* and *environmental footprint* issues that must be considered.

Reactor design is often discussed in terms of independent and dependent variables. Independent variables are choices such as reactor type and internals, catalyst type, inlet temperature, pressure, and fresh feed composition. Dependent variables result from independent variable selection. They may be constrained or unconstrained. Con-

strained dependent variables often include pressure drop (limited due to compressor cost), feed composition (dictated by the composition of the recycle streams), temperature rise (or decline), and local and effluent composition. The reactor design problem is often aimed at optimizing independent variables (within constraints) to maximize an objective function (such as conversion and selectivity).

Since the reactor feed may contain inert species (e.g., nitrogen and solvents) and since there may be unconverted feed and by-products in the reactor effluent, a number of unit operations (distillation, filtration, etc.) may be required to produce the desired product(s). In practice, the flow of mass and energy through the process is captured by a process flow sheet. The flow sheet may require recycle (of unconverted feed, solvents, etc.) and purging that may affect reaction chemistry. Reactor design and operation influence the process and vice versa.

REACTOR TYPES

Reactors may be classified according to the mode of operation, the end-use application, the number of phases present, whether (or not) a catalyst is used, and whether some other function (e.g., heat transfer, separations, etc.) is conducted in addition to the reaction.

Classification by Mode of Operation

Batch Reactors A “batch” of reactants is introduced into the reactor operated at the desired conditions until the target conversion is reached. Batch reactors are typically tanks in which stirring of the reactants is achieved using internal impellers, gas bubbles, or a pump-around loop where a fraction of the reactants is removed and externally recirculated back to the reactor. Temperature is regulated via internal cooling surfaces (such as coils or tubes), jackets, reflux condensers, or pump-around loop that passes through an exchanger. Batch processes are suited to small production rates, to long reaction times, to achieve desired selectivity, and for flexibility in campaigning different products.

Continuous Reactors Reactants are added and products removed continuously at a constant mass flow rate. Large daily production rates are mostly conducted in continuous equipment.

A *continuous stirred tank reactor (CSTR)* is a vessel to which reactants are added and products removed while the contents within the vessel are vigorously stirred using internal agitation or by internally (or externally) recycling the contents. CSTRs may be employed in series or in parallel. An approach to employing CSTRs in series is to have a large

TABLE 19-1 Residence Times and/or Space Velocities in Industrial Chemical Reactors*

Product (raw materials)	Type	Reactor phase	Catalyst	<i>T</i> , °C	<i>P</i> , atm	Residence time or space velocity	Source and page†
Acetaldehyde (ethylene, air)	FB	L	Cu and Pd chlorides	50–100	8	6–40 min	[2] 1, [7] 3
Acetic anhydride (acetic acid)	TO	L	Triethylphosphate	700–800	0.3	0.25–5 s	[2]
Acetone (<i>i</i> -propanol)	MT	LG	Ni	300	1	2.5 h	[1] 1 314
Acrolein (formaldehyde, acetaldehyde)	FL	G	MnO, silica gel	280–320	1	0.6 s	[1] 1 384, [7] 33
Acrylonitrile (air, propylene, ammonia)	FL	G	Bi phosphomolybdate	400	1	4.3 s	[3] 684, [2] 47
Adipic acid (nitration of cyclohexanol)	TO	L	Co naphthenate	125–160	4–20	2 h	[2] 51, [7] 49
Adiponitrile (adipic acid)	FB	G	H ₃ BO ₃	370–410	1	3.5–5 s	[1] 2 152,
Alkylate (<i>i</i> -C ₄ , butenes)	CST	L	H ₃ PO ₄	5–10	2–3	350–500 GHSV	[7] 52
Alkylate (<i>i</i> -C ₄ , butenes)	CST	L	HF	25–38	8–11	5–40 min	[4] 223
Allyl chloride (propylene, Cl ₂)	TO	G	NA	500	3	0.3–1.5 s	[1] 2 416, [7] 67
Ammonia (H ₂ , N ₂)	FB	G	Fe	450	150	28 s	[6] 61
Ammonia (H ₂ , N ₂)	FB	G	Fe	450	225	33 s	[6] 61
Ammonia oxidation	Flame	G	Pt gauze	900	8	10,000 GHSV	[6] 115
Aniline (nitrobenzene, H ₂)	B	L	FeCl ₂ in H ₂ O	95–100	1	0.0026 s	[1] 3 289
Aniline (nitrobenzene, H ₂)	FB	G	Cu on silica	250–300	1	8 h	[7] 82
Aspirin (salicylic acid, acetic anhydride)	B	L	None	90	1	0.5–100 s	[7] 89
Benzene (toluene)	TU	G	None	740	38	>1 h	[6] 36,
Benzene (toluene)	TU	G	None	650	35	48 s	[9] 109
Benzoic acid (toluene, air)	SCST	LG	None	125–175	9–13	815 GHSV	[1] 4 183, [7] 98
Butadiene (butane)	FB	G	Cr ₂ O ₃ , Al ₂ O ₃	750	1	128 s	[7] 101
Butadiene (1-butene)	FB	G	None	600	0.25	0.2–2 h	[7] 118
Butadiene sulfone (butadiene, SO ₂)	CST	L	<i>t</i> -Butyl catechol	34	12	0.1–1 s	[3] 572
<i>i</i> -Butane (<i>n</i> -butane)	FB	L	AlCl ₃ on bauxite	40–120	18–36	34,000 GHSV	[1] 5 192
<i>i</i> -Butane (<i>n</i> -butane)	FB	L	Ni	370–500	20–50	0.2 LHSV	[4] 239, [7] 683
Butanols (propylene hydroformylation)	FB	L	PH ₂ -modified Co carbonyls	150–200	1,000	1–6 WHSV	[1] 5 373
Butanols (propylene hydroformylation)	FB	L	Fe pentacarbonyl	110	10	100 g L-h	[7] 125
Calcium stearate	B	L	None	180	5	1 h	[7] 135
Caprolactam (cyclohexane oxime)	CST	L	Polyphosphoric acid	80–110	1	1–2 h	[1] 6 73, [7] 139
Carbon disulfide (methane, sulfur)	Furn.	G	None	500–700	1	0.25–2 h	[1] 6 322, [7] 144
Carbon monoxide oxidation (shift)	TU	G	Cu-Zn or Fe ₂ O ₃	390–220	26	1.0 s	[6] 44
Portland cement	Kiln	S		1,400–1,700	1	4.5 s	[11]
Chloral (Cl ₂ , acetaldehyde)	CST	LG	None	20–90	1	7,000 GHSV	[1] 10 h
Chlorobenzenes (benzene, Cl ₂)	SCST	LG	Fe	40	1	140 h	[7] 158
Coking, delayed (heater)	TU	LG	None	490–500	15–4	24 h	[1] 8 122
Coking, delayed (drum, 100 ft max height)	B	LG	None	500–440	4	250 s	[1] 10 8
Cracking, fluid catalytic	Riser	G	Zeolite	520–540	2–3	0.3–0.5 ft/s vapor	(14) 353
Cracking, hydro (gas oils)	FB	LG	Ni, SiO ₂ , Al ₂ O ₃	350–420	100–150	2–4 s	[11]
Cracking (visbreaking residual oils)	TU	LG	None	470–495	10–30	1–2 LHSV	[11]
Cumene (benzene, propylene)	FB	G	H ₃ PO ₄	260	35	450 s, 8 LHSV	[11]
Cumene hydroperoxide (cumene, air)	CST	L	Metal porphyrins	95–120	2–15	23 LHSV	[11]
Cyclohexane (benzene, H ₂)	FB	G	Ni on Al ₂ O ₃	150–250	25–55	1–3 h	[7] 191
Cyclohexanol (cyclohexane, air)	SCST	LG	None	185–200	48	0.75–2 LHSV	[7] 201
Cyclohexanone (cyclohexanol)	CST	L	N.A.	107	1	2–10 min	[7] 203
Cyclohexanone (cyclohexanol)	MT	G	Cu on pumice	250–350	1	0.75 h	[8] (1963)
Cyclopentadiene (dicyclopentadiene)	TJ	G	None	220–300	1–2	4–12 s	[8] (1963)
DDT (chloral, chlorobenzene)	B	L	Oleum	0–15	1	0.1–0.5 LHSV	[7] 212
Dextrose (starch)	CST	L	H ₂ SO ₄	165	1	8 h	[7] 233
Dextrose (starch)	CST	L	Enzyme	60	1	20 min	[8] (1951)
Dibutylphthalate (phthalic anhydride, butanol)	B	L	H ₂ SO ₄	150–200	1	100 min	[7] 217
Diethylketone (ethylene, CO)	TO	L	Co oleate	150–300	200–500	1–3 h	[7] 227
Dimethylsulfide (methanol, CS ₂)	FB	G	Al ₂ O ₃	375–535	5	0.1–10 h	[7] 243
Diphenyl (benzene)	MT	G	None	730	2	150 GHSV	[7] 266
Dodecylbenzene (benzene, propylene tetramer)	CST	L	AlCl ₃	15–20	1	0.6 s	[7] 275,
Ethanol (ethylene, H ₂ O)	FB	G	H ₃ PO ₄	300	82	3.3 LHSV	[8] (1938)
Ethyl acetate (ethanol, acetic acid)	TU, CST	L	H ₂ SO ₄	100	1	1–30 min	[7] 283
Ethyl chloride (ethylene, HCl)	TO	G	ZnCl ₂	150–250	6–20	1,800 GHSV	[2] 356, [7] 297
Ethylene (ethane)	TU	G	None	860	2	0.5–0.8 LHSV	[10] 45, 52, 58
Ethylene (naphtha)	TU	G	None	550–750	2–7	2 s	[7] 305
Ethylene, propylene chlorohydrins (Cl ₂ , H ₂ O)	CST	LG	None	30–40	3–10	1.03 s	[3] 411,
Ethylene glycol (ethylene oxide, H ₂ O)	TO	LG	1% H ₂ SO ₄	50–70	1	1,880 GHSV	[6] 13
Ethylene glycol (ethylene oxide, H ₂ O)	TO	LG	None	195	13	0.5–3 s	[7] 254
Ethylene oxide (ethylene, air)	FL	G	Ag	270–290	1	0.5–5 min	[7] 310, 580
Ethyl ether (ethanol)	FB	G	WO ₃	120–375	2–100	30 min	[2] 398
Fatty alcohols (coconut oil)	B	L	Na, solvent	142	1	1 h	[2] 398
Formaldehyde (methanol, air)	FB	G	Ag gauze	450–600	1	1 s	[2] 409, [7] 322
Glycerol (allyl alcohol, H ₂ O ₂)	CST	L	H ₂ WO ₄	40–60	1	30 min	[7] 326
						2 h	[8] (1953)
						0.01 s	[2] 423
						3 h	[7] 347

TABLE 19-1 Residence Times and/or Space Velocities in Industrial Chemical Reactors (Concluded)

Product (raw materials)	Type	Reactor phase	Catalyst	$T, ^\circ\text{C}$	P, atm	Residence time or space velocity	Source and page†
Hydrogen (methane, steam)	MT	G	Ni	790	13	5.4 s	[6] 133
Hydrodesulfurization of naphtha	TO	LG	Co-MO	315–500	20–70	3,000 GHSV 1.5–8 LHSV 125 WHSV	[4] 285, [6] 179, [9] 201
Hydrogenation of cottonseed oil	SCST	LG	Ni	130	5	6 h	[6] 161
Isoprene (<i>i</i> -butene, formaldehyde)	FB	G	HCl, silica gel	250–350	1	1 h	[7] 389
Maleic anhydride (butenes, air)	FL	G	V_2O_5	300–450	2–10	0.1–5 s	[7] 406
Melamine (urea)	B	L	None	340–400	40–150	5–60 min	[7] 410
Methanol (CO, H_2)	FB	G	$\text{ZnO}, \text{Cr}_2\text{O}_3$	350–400	340	5,000 GHSV	[7] 421
Methanol (CO, H_2)	FB	G	$\text{ZnO}, \text{Cr}_2\text{O}_3$	350–400	254	28,000 GHSV	[3] 562
<i>o</i> -Methyl benzoic acid (xylene, air)	CST	L	None	160	14	0.32 h	[3] 732
Methyl chloride (methanol, Cl_2)	FB	G	Al_2O_3 gel	340–350	1	3.1 LHSV	[2] 533
Methyl ethyl ketone (2-butanol)	FB	G	ZnO	425–475	2–4	275 GHSV	[7] 437
Methyl ethyl ketone (2-butanol)	FB	G	Brass spheres	450	5	0.5–10 min 2.1 s 13 LHSV	[10] 284
Nitrobenzene (benzene, HNO_3)	CST	L	H_2SO_4	45–95	1	3–40 min	[7] 468
Nitromethane (methane, HNO_3)	TO	G	None	450–700	5–40	0.07–0.35 s	[7] 474
Nylon-6 (caprolactam)	TU	L	Na	260	1	12 h	[7] 480
Phenol (cumene hydroperoxide)	CST	L	SO_2	45–65	2–3	15 min	[7] 520
Phenol (chlorobenzene, steam)	FB	G	Cu, Ca phosphate	430–450	1–2	2 WHSV	[7] 522
Phosgene (CO, Cl_2)	MT	G	Activated carbon	50	5–10	16 s	[11]
Phthalic anhydride (<i>o</i> -xylene, air)	MT	G	V_2O_5	350	1	900 GHSV 1.5 s	[3] 482, 539, [7] 529
Phthalic anhydride (naphthalene, air)	FL	G	V_2O_5	350	1	5 s	[9] 136, [10] 335
Polycarbonate resin (bisphenol-A, phosgene)	B	L	Benzyltriethylammonium chloride	30–40	1	0.25–4 h	[7] 452
Polyethylene	TU	L	Organic peroxides	150–200	1,000–1,700	0.5–50 min	[7] 547
Polyethylene	TU	L	$\text{Cr}_2\text{O}_3, \text{Al}_2\text{O}_3, \text{SiO}_2$	70–200	20–50	0.1–1,000 s	[7] 549
Polypropylene	TO	L	$\text{R}_2\text{AlCl}, \text{TiCl}_4$	15–65	10–20	15–100 min	[7] 559
Polyvinyl chloride	B	L	Organic peroxides	60	10	5.3–10 h	[6] 139
<i>i</i> -Propanol (propylene, H_2O)	TO	L	H_2SO_4	70–110	2–14	0.5–4 h	[7] 393
Propionitrile (propylene, NH_3)	TU	G	CoO	350–425	70–200	0.3–2 LHSV	[7] 578
Reforming of naphtha (H_2 /hydrocarbon = 6)	FB	G	Pt	490	30–35	3 LHSV 8,000 GHSV	[6] 99
Starch (corn, H_2O)	B	L	SO_2	25–60	1	18–72 h	[7] 607
Styrene (ethylbenzene)	MT	G	Metal oxides	600–650	1	0.2 s 7,500 GHSV	[5] 424
Sulfur dioxide oxidation	FB	G	V_2O_5	475	1	2.4 s 700 GHSV	[6] 86
<i>t</i> -Butyl methacrylate (methacrylic acid, <i>i</i> -butene)	CST	L	H_2SO_4	25	3	0.3 LHSV	[1] 5 328
Thiophene (butane, S)	TU	G	None	600–700	1	0.01–1 s	[7] 652
Toluene diisocyanate (toluene diamine, phosgene)	B	LG	None	200–210	1	7 h	[7] 657
Toluene diamine (dinitrotoluene, H_2)	B	LG	Pd	80	6	10 h	[7] 656
Tricresyl phosphate (cresyl, POCl_3)	TO	L	MgCl_2	150–300	1	0.5–2.5 h	[2] 850, [7] 673
Vinyl chloride (ethylene, Cl_2)	FL	G	None	450–550	2–10	0.5–5 s	[7] 699
Aldehydes (diisobutene, CO)	CST	LG	Co Carbonyl	150	200	1.7 h	[12] 173
Allyl alcohol (propylene oxide)	FB	G	Li phosphate	250	1	1.0 LHSV	[15] 23
Automobile exhaust	FB	G	Pt-Pd: 1–2 g/unit	400–600+	1		
Gasoline (methanol)	FB	G	Zeolite	400	20	2 WHSV	[13] 383
Hydrogen cyanide (NH_3, CH_4)	FB	G	Pt-Rh	1150	1	0.005 s	[15] 211
Isoprene, polymer	B	L	$\text{Al}(\text{i-Bu})_3\text{TiCl}_4$	20–50	1–5	1.5–4 h	[15] 82
NO_x pollutant (with NH_3)	FB	G	$\text{V}_2\text{O}_5\text{-TiO}_2$	300–400	1–10		[14] 332
Automobile emission control	M	G	Pt/Rh/Pd/ Al_2O_3	350–500	1	20,000 GHSV	[16] 69
Nitrogen oxide emission control	M	G	$\text{V}_2\text{O}_5\text{-WO}_3\text{/TiO}_2$	300–400	1	4–10,000 GHSV	[16] 306
Carbon monoxide and hydrocarbon emission control	M	G	Pt-Pd/ Al_2O_3	500–600	1	80–120,000 GHSV	[16] 334
Ozone control from aircraft cabins	M	G	Pd/ Al_2O_3	130–170	1	$\sim 10^6$ GHSV	[16] 263
Vinyl acetate (ethylene + CO)	MT	LG	Cu-Pd	130	30	1 h L, 10 s G	[12] 140

*Abbreviations: reactors: batch (B), continuous stirred tank (CST), fixed bed of catalyst (FB), fluidized bed of catalyst (FL), furnace (Furn.), monolith (M), multi-tubular (MT), semicontinuous stirred tank (SCST), tower (TO), tubular (TU). Phases: liquid (L), gas (G), both (LG). Space velocities (hourly): gas (GHSV), liquid (LHSV), weight (WHSV). Not available, NA. To convert atm to kPa, multiply by 101.3.

†1. J. J. McKetta, ed., *Encyclopedia of Chemical Processing and Design*, Marcel Dekker, 1976 to date (referenced by volume).

2. W. L. Faith, D. B. Keyes, and R. L. Clark, *Industrial Chemicals*, revised by F. A. Lowenstein and M. K. Moran, John Wiley & Sons, 1975.

3. G. F. Froment and K. B. Bischoff, *Chemical Reactor Analysis and Design*, John Wiley & Sons, 1979.

4. R. J. Hengstebek, *Petroleum Processing*, McGraw-Hill, New York, 1959.

5. V. G. Jenson and G. V. Jeffreys, *Mathematical Methods in Chemical Engineering*, 2d ed., Academic Press, 1977.

6. H. F. Rase, *Chemical Reactor Design for Process Plants*, Vol. 2: Case Studies, John Wiley & Sons, 1977.

7. M. Sittig, *Organic Chemical Process Encyclopedia*, Noyes, 1969 (patent literature exclusively).

8. Student Contest Problems, published annually by AIChE, New York (referenced by year).

9. M. O. Tarhan, *Catalytic Reactor Design*, McGraw-Hill, 1983.

10. K. R. Westerterp, W. P. M. van Swaaij, and A. A. C. M. Beenackers, *Chemical Reactor Design and Operation*, John Wiley & Sons, 1984.

11. Personal communication (Walas, 1985).

12. B. C. Gates, J. R. Katzer, and G. C. A. Schuit, *Chemistry of Catalytic Processes*, McGraw-Hill, 1979.

13. B. E. Leach, ed., *Applied Industrial Catalysts*, 3 vols., Academic Press, 1983.

14. C. N. Satterfield, *Heterogeneous Catalysis in Industrial Practice*, McGraw-Hill, 1991.

15. C. L. Thomas, *Catalytic Processes and Proven Catalysts*, Academic Press, 1970.

16. Heck, Farrauto, and Gulati, *Catalytic Air Pollution Control: Commercial Technology*, Wiley-Interscience, 2002.

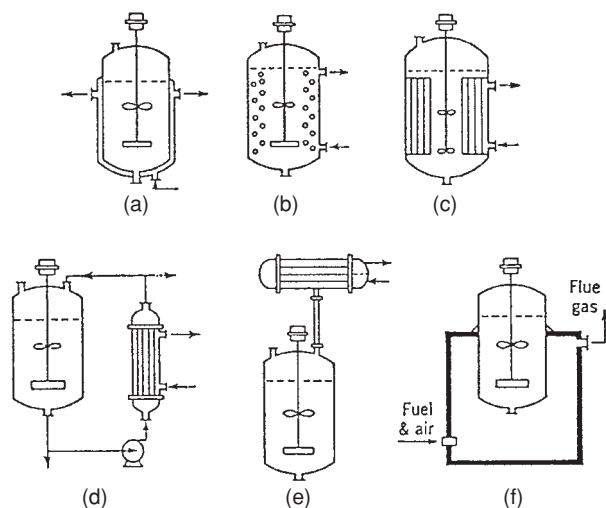


FIG. 19-1 Stirred tank reactors with heat transfer. (a) Jacket. (b) Internal coils. (c) Internal tubes. (d) External heat exchanger. (e) External reflux condenser. (f) Fired heater. (Wallas, Reaction Kinetics for Chemical Engineers, McGraw-Hill, 1959.)

cylindrical tank with partitions: feed enters the first compartment and over (or under) flows to the next compartment, and so on. The composition is maintained as uniform as possible in each individual compartment; however, a stepped concentration gradient exists from one CSTR to the next. When the reactants have limited solubility (miscibility) and a density difference, the vertical staged reactor with counter-current operation may be used. Alternatively, each CSTR in a series or parallel configuration can be an independent vessel. Examples of stirred tank reactors with heat transfer are shown in Fig. 19-1.

A *tubular flow reactor* (TFR) is a tube (or pipe) through which reactants flow and are converted to product. The TFR may have a varying diameter along the flow path. In such a reactor, there is a continuous gradient (in contrast to the stepped gradient characteristic of a CSTR-in-series battery) of concentration in the direction of flow. Several tubular reactors in series or in parallel may also be used. Both horizontal and vertical orientations are common. When heat transfer is needed, individual tubes are jacketed or a shell-and-tube construction is used. The reaction side may be filled with solid catalyst or internals such as static mixers (to improve interphase contact in heterogeneous reactions or to improve heat transfer by turbulence). Tubes that have 3- to 4-in diameter and are several miles long may be used in polymerization service. Large-diameter vessels, with packing (or trays) used to regulate the residence time in the reactor, may also be used. Some of the configurations in use are axial flow, radial flow, multishell with built-in heat exchangers, and so on.

A reaction battery of CSTRs in series, although both mechanically and operationally more complex and expensive than a tubular reactor, provides flexibility. Relatively slow reactions are best conducted in a stirred tank reactor battery. A tubular reactor is used when heat transfer is needed, where high pressures and/or high (or low) temperatures occur, and when relatively short reaction times suffice.

Semibatch Reactors Some of the reactants are loaded into the reactor, and the rest of the reactants are fed gradually. Alternatively, one reactant is loaded into the reactor, and the other reactant is fed continuously. Once the reactor is full, it may be operated in a batch mode to complete the reaction. Semibatch reactors are especially favored when there are large heat effects and heat-transfer capability is limited. Exothermic reactions may be slowed down and endothermic reactions controlled by limiting reactant concentration. In bioreactors, the reactant concentration may be limited to minimize toxicity. Other situations that may call for semibatch reactors include control of undesirable by-products or when one of the reactants is a gas of limited solubility that is fed continuously at the dissolution rate.

Classification by End Use *Chemical reactors* are typically used for the synthesis of chemical intermediates for a variety of specialty (e.g., agricultural, pharmaceutical) or commodity (e.g., raw materials for polymers) applications. *Polymerization reactors* convert raw materials to polymers having a specific molecular weight and functionality. The difference between polymerization and chemical reactors is artificially based on the size of the molecule produced. *Bioreactors* utilize (often genetically manipulated) organisms to catalyze biotransformations either aerobically (in the presence of air) or anaerobically (without air present). *Electrochemical reactors* use electricity to drive desired reactions. Examples include synthesis of Na metal from NaCl and Al from bauxite ore. A variety of reactor types are employed for specialty materials synthesis applications (e.g., electronic, defense, and other).

Classification by Phase Despite the generic classification by operating mode, reactors are designed to accommodate the reactant phases and provide optimal conditions for reaction. Reactants may be fluid(s) or solid(s), and as such, several reactor types have been developed. *Single-phase* reactors are typically gas- (or plasma-) or liquid-phase reactors. *Two-phase* reactors may be gas-liquid, liquid-liquid, gas-solid, or liquid-solid reactors. *Multiphase* reactors typically have more than two phases present. The most common type of multiphase reactor is a gas-liquid-solid reactor; however, liquid-liquid-solid reactors are also used. The classification by phases will be used to develop the contents of this section.

In addition, a reactor may perform a function other than reaction alone. *Multifunctional* reactors may provide both reaction and mass transfer (e.g., reactive distillation, reactive crystallization, reactive membranes, etc.), or reaction and heat transfer. This coupling of functions within the reactor inevitably leads to additional operating constraints on one or the other function. Multifunctional reactors are often discussed in the context of process intensification. The primary driver for multifunctional reactors is functional synergy and equipment cost savings.

REACTOR MODELING

As discussed in Sec. 7, chemical kinetics may be mathematically described by rate equations. Reactor performance is also amenable to quantitative analysis. The quantitative analysis of reaction systems is dealt with in the field of chemical reaction engineering.

The level of mathematical detail that can be included in the analysis depends on the level of understanding of the physical and chemical processes that occur in a reactor. As a practical matter, engineering data needed to build a detailed model for some new chemistry typically are unavailable early in the design phase. Reactor designers may use similarity principles (e.g., dimensionless groups), rules of thumb, trend analysis, design of experiments (DOE), and principal-component analysis (PCA) to scale up laboratory reactors. For hazardous systems in which compositional measurements are difficult, surrogate indicators such as pressure or temperature may be used. As more knowledge becomes available, however, a greater level of detail may be included in a mathematical model. A detailed reactor model may contain information on vessel configuration, stoichiometric relationships, kinetic rate equations, correlations for thermodynamic and transport properties, contacting efficiency, residence time distribution, and so on.

Models may be used for analyzing data, estimating performance, reactor scale-up, simulating start-up and shutdown behavior, and control. The level of detail in a model depends on the need, and this is often a balance between value and cost. Very elaborate models are justifiable and have been developed for certain widely practiced and large-scale processes, or for processes where operating conditions are especially critical.

Modeling Considerations A useful reactor model allows the user to predict performance or to explore uncertainties not easily or cost-effectively investigated through experimentation. Uncertainties that may be explored through modeling may include scale-up options, explosion hazards, runaway reactions, environmental emissions, reactor internals design, and so on. As such, the model must contain an optimal level of detail (principle of *optimal sloppiness*) required to meet the desired objective(s). For example, if mixing is critical to performance, the model must include flow equations that reflect the role of mixing. If heat effects are small, an isothermal model may be used.

19-8 REACTORS

A key aspect of modeling is to derive the appropriate momentum, mass, or energy conservation equations for the reactor. These balances may be used in lumped systems or derived over a differential volume within the reactor and then integrated over the reactor volume. Mass conservation equations have the following general form:

$$\left[\begin{array}{c} \text{Amount of A} \\ \text{introduced} \\ \text{per unit time} \end{array} \right] - \left[\begin{array}{c} \text{Amount of A} \\ \text{leaving per unit} \\ \text{time} \end{array} \right] - \left[\begin{array}{c} \text{Amount of A} \\ \text{converted per} \\ \text{unit time} \end{array} \right] = \left[\begin{array}{c} \text{Amount of A} \\ \text{accumulated} \\ \text{per unit time} \end{array} \right] \quad (19-1)$$

The general form for the energy balance equation is

$$\left[\begin{array}{c} \text{Amount of} \\ \text{energy added} \\ \text{per unit time} \end{array} \right] - \left[\begin{array}{c} \text{Amount of} \\ \text{energy removed} \\ \text{per unit time} \end{array} \right] - \left[\begin{array}{c} \text{Energy} \\ \text{generated per} \\ \text{unit time} \end{array} \right] = \left[\begin{array}{c} \text{Accumulation} \\ \text{of energy} \\ \text{per unit time} \end{array} \right] \quad (19-2)$$

The model defines each of these terms. Solving the set of equations provides outputs that can be validated against experimental observations and then used for predictive purposes. Mathematical models for ideal reactors that are generally useful in estimating reactor performance will be presented. Additional information on these reactors is available also in Sec. 7.

Batch Reactor Since there is no addition or removal of reactants, the mass and energy conservation equations for a batch reactor with a constant reactor volume are

$$V_r r(C, T) + V_r \frac{dC}{dt} = 0 \quad (19-3)$$

$$-qA_k - V_r (-\Delta H_r) r(C, T) + V_r \rho c_p \frac{dT}{dt} = 0 \quad (19-4)$$

where qA_k is the addition (or removal) of heat from the reactor. Mean values of physical properties are used in Eqs. (19-3) and (19-4). For an isothermal first-order reaction $r(C, T) = kC$, the mass and energy equations can be combined and the solution is

$$C = C_0 e^{-kt} \quad (19-5)$$

Typically batch reactors may have complex kinetics, mixing, and heat-transfer issues. In such cases, detailed momentum, mass, and energy balance equations will be required.

Semibatch Reactor Feed is added for a fixed time, and the reaction proceeds as the feed is added. The reactor equations governing the feed addition portion of the process are

$$V_r r(C, T) + \frac{d(V_r C)}{dt} = V_r r(C, T) + C \frac{dV_r}{dt} + V_r \frac{dC}{dt} = 0 \quad (19-6)$$

$$-qA_k - V_r (-\Delta H_r) r(C, T) + \rho c_p \frac{d(V_r T)}{dt} = 0 \quad (19-7)$$

For a constant reactant flow rate v_0 ,

$$\frac{dV_r}{dt} = v_0 \quad (19-8)$$

Given an initial condition $V_r = V_r^0$ at $t = 0$,

$$V_r(t) = V_r^0 + v_0 t \quad (19-9)$$

For an isothermal first-order reaction, substitution of this relationship in Eq. (19-6) yields

$$C = \frac{C_0 v_0}{k(V_r^0 + v_0 t)} (1 - e^{-kt}) \quad (19-10)$$

After feed addition is completed, the reactor may be operated in a batch mode. In this case, Eqs. (19-3) and (19-4) may be used with the

concentration at the end of feed addition serving as the initial concentration for the batch reactor.

Ideal Continuous Stirred Tank Reactor In an ideal CSTR, reactants are fed into and removed from an ideally mixed tank. As a result, the concentration within the tank is uniform and identical to the concentration of the effluent. The mass and energy conservation equations for an ideal constant-volume or constant-density CSTR with constant volumetric feed rate V' may be written as

$$V' C_0 = V' C + V_r r(C, T) + V_r \frac{dC}{dt} \quad (19-11)$$

$$V' \rho c_p T_0 = -Q(T) + V' \rho c_p T - V_r (-\Delta H_r) r(C, T) + V_r \rho c_p \frac{dT}{dt} \quad (19-12)$$

where $Q(T)$ represents any addition or removal of heat from the reactor and mean values of physical properties are used. For example, if heat is transferred through the reactor wall, $Q(T) = A_k U (T_c - T)$, where A_k is the heat-transfer area, U is the overall heat-transfer coefficient, and T_c is the temperature of the heat-transfer fluid.

The above *ordinary differential equations* (ODEs), Eqs. (19-11) and (19-12), can be solved with an initial condition. For an isothermal first-order reaction and an initial condition, $C(0) = 0$, the linear ODE may be solved analytically. At steady state, the accumulation term is zero, and the solution for the effluent concentration becomes

$$\frac{C}{C_0} = \frac{1}{1 + kV_r/V'} = \frac{1}{1 + kt} \quad (19-13)$$

Since the contents of an ideal CSTR are perfectly mixed, the dispersion within the reactor is infinite. In practice, CSTRs may not be ideally mixed. In such cases, the reactor may be modeled as having a fraction of the feed α in bypass and a fraction β of the reactor volume stagnant. The material balance is

$$C = \alpha C_0 + (1 - \alpha) C_1 \quad (19-14)$$

$$(1 - \alpha) V' C_0 = (1 - \alpha) V' C_1 + (1 - \beta) k V_r C_1^2 \quad (19-15)$$

where C_1 is the concentration leaving the active zone of the tank. Elimination of C_1 will relate the input and overall output concentrations. For a first-order reaction,

$$\frac{C_0}{C} = 1 + \frac{kV_r(1 - \beta)}{V'(1 - \alpha)} \quad (19-16)$$

The two parameters α and β may be expected to depend on reactor internals and the amount of agitation.

Plug Flow Reactor A plug flow reactor (PFR) is an idealized tubular reactor in which each reactant molecule enters and travels through the reactor as a "plug," i.e., each molecule enters the reactor at the same velocity and has exactly the same residence time. As a result, the concentration of every molecule at a given distance downstream of the inlet is the same. The mass and energy balance for a differential volume between position V_r and $V_r + dV_r$ from the inlet may be written as *partial differential equations* (PDEs) for a constant-density system:

$$V' \frac{\partial C}{\partial V_r} + r(C, T) + \frac{\partial C}{\partial t} = 0 \quad (19-17)$$

$$\frac{-Q(T)}{V_r} + V' c_p \rho \frac{\partial T}{\partial V_r} - (-\Delta H_r) r(C, T) + c_p \rho \frac{\partial T}{\partial t} = 0 \quad (19-18)$$

where $Q(T)$ represents any addition of heat to (or removal from) the reactor wall and mean values of physical properties are used. The above PDEs can be solved with an initial condition, e.g., $C(x, 0) = C_{I=0}(x)$, and a boundary condition, e.g., $C(0, t) = C_0(t)$, which is the concentration at the inlet. At steady state, the accumulation term above is zero, and the solution for an isothermal first-order reaction is the same as that for a batch reactor, Eq. (19-5):

$$C = C_0 \exp\left(-k \frac{V_r}{V'}\right) = C_0 e^{-kt} \quad (19-19)$$

A tubular reactor will likely deviate from plug flow in most practical cases, e.g., due to backmixing in the direction of flow, reactor internals, etc. A way of simulating axial backmixing is to represent the reactor volume as a series of n stirred tanks in series. The steady-state solution for a single ideal CSTR may be extended to find the effluent concentration after two ideal CSTRs and then to n ideal stages as

$$\frac{C_n}{C_0} = \frac{1}{(1 + kV_r/V')^n} \quad (19-20)$$

In this case, V_r is the volume of each individual reactor in the battery. In modeling a reactor, n is empirically determined based on the extent of reactor backmixing obtained from tracer studies or other experimental data. In general, the number of stages n required to approach an ideal PFR depends on the rate of reaction (e.g., the magnitude of the specific rate constant k for the first-order reaction above). As a practical matter, the conversion for a series of stirred tanks approaches a PFR for $n > 6$.

An alternate way of generating backmixing is to recycle a fraction of the product from a PFR back to the inlet. This reactor, known as a recycle reactor, has been described in Sec. 7 of the Handbook. As the recycle ratio (i.e., recycle flow to product flow) is increased, the effective dispersion is increased and the recycle reactor approaches an ideal CSTR.

Tubular Reactor with Dispersion An alternative approach to describe deviation from ideal plug flow due to backmixing is to include a term that allows for axial dispersion D_e in the plug flow reactor equations. The reactor mass balance equation now becomes

$$V' \frac{\partial C}{\partial V_r} - D_e \frac{\partial^2 C}{\partial V_r^2} + r(C, T) + \frac{\partial C}{\partial t} = 0 \quad (19-21)$$

The model is referred to as a *dispersion model*, and the value of the dispersion coefficient D_e is determined empirically based on correlations or experimental data. In a case where Eq. (19-21) is converted to dimensionless variables, the coefficient of the second derivative is referred to as the Peclet number ($Pe = uL/D_e$), where L is the reactor length and u is the linear velocity. For plug flow, $D_e = 0$ ($Pe \Rightarrow \infty$) while for a CSTR, $D_e = \infty$ ($Pe = 0$). To solve Eq. (19-21), one initial condition and two boundary conditions are needed. The “closed-ends” boundary conditions are $uC_0 = (uC - D_e \partial C/\partial L)_{L=0}$ and $(\partial C/\partial L)_{L=L} = 0$ (e.g., see Wen and Fan, *Models for Flow Systems in Chemical Reactors*, Marcel Dekker, 1975). Figure 19-2 shows the performance of a tubular reactor with dispersion compared to that of a plug flow reactor.

Ideal chemical reactors typically may be modeled using a combination of ideal CSTR, PFR, and dispersion model equations. In the case of a single phase, the approach is relatively straightforward. In the case of two-phase flow, a bubble column (fluidized-bed) reactor may be modeled as containing an ideal CSTR liquid (emulsion) phase and a plug flow (with dispersion) gas phase containing bubbles. Given inlet gas conditions, the concentration in the liquid (emulsion) may be calculated using mass-transfer correlations from the bubbles to the liquid (emulsion) along with reaction in the liquid (emulsion) phase along the length of the reactor. In flooded gas-liquid reactors where the gas and liquid are countercurrent to each other, a plug flow (with dispersion) model may be used for both phases. The concentration of reactant in a phase at each end of the reactor is known. The concentration of the other phase is assumed at one end, and mass-transfer correlations and reaction kinetics are used together with a plug flow (with dispersion) model to get to the other exit. The iterative process continues until the concentrations at each end match the feed conditions.

Reactor Selection Ideal CSTR and PFR models are extreme cases of complete axial dispersion ($D_e = \infty$) and no axial dispersion ($D_e = 0$), respectively. As discussed earlier, staged ideal CSTRs may be used to represent intermediate axial dispersion. Alternatively, within the context of a PFR, the dispersion (or a PFR with recycle) model may be used to represent increased dispersion. Real reactors inevitably have a level of dispersion in between that for a PFR or an ideal CSTR. The level of dispersion may depend on fluid properties (e.g., is the fluid newtonian),

fluid flow (e.g., the level of mixing), transport properties (e.g., the diffusivity of reactants in the fluid), and reactor geometry. The effect of dispersion in a real reactor is discussed within the context of an ideal CSTR and PFR model in Fig. 19-2.

Figure 19-2a shows the effect of dispersion on the reactor volume required to achieve a certain exit concentration (or conversion). As Pe number increases (i.e., dispersion decreases), the reactor begins to approach plug flow and the reactor volume required to achieve a certain conversion approaches the volume for a PFR. At lower Pe numbers, reactor performance approaches that of an ideal CSTR and the reactor volume required to achieve a certain concentration is much higher than that of a PFR. This behavior can be observed in Fig. 19-2b that shows the effect of exit concentration on reaction rate. At a given rate, an ideal CSTR has the highest exit concentration (lowest conversion) and a PFR has the lowest exit concentration (highest conversion). As Fig. 19-2c shows, since the concentration in an ideal CSTR is the same as the exit concentration, there is a sharp drop in concentration from the inlet to the bulk concentration. In contrast, the concentration in the reactor drops continuously from the inlet to the outlet for a PFR. At intermediate values of Pe, the “closed-ends” boundary condition in the dispersion model causes a drop in concentration to levels lower than for an ideal CSTR.

As discussed in Fig. 19-2, for a given conversion, the reactor residence time (or reactor volume required) for a positive order reaction with dispersion will be greater than that of a PFR. This need for a longer residence time is illustrated for a first-order isothermal reaction in a PFR versus an ideal CSTR using Eqs. (19-13) and (19-19).

$$\frac{t_{\text{ideal CSTR}}}{t_{\text{PFR}}} = \frac{C/C_0 - 1}{(C/C_0) \ln(C/C_0)} \quad (19-22)$$

Equation (19-22) indicates that, for a nominal 90 percent conversion, an ideal CSTR will need nearly 4 times the residence time (or volume) of a PFR. This result is also worth bearing in mind when batch reactor experiments are converted to a battery of ideal CSTRs in series in the field. The performance of a completely mixed batch reactor and a steady-state PFR having the same residence time is the same [Eqs. (19-5) and (19-19)]. At a given residence time, if a batch reactor provides a nominal 90 percent conversion for a first-order reaction, a single ideal CSTR will only provide a conversion of 70 percent. The above discussion addresses conversion. Product selectivity in complex reaction networks may be profoundly affected by dispersion. This aspect has been addressed from the standpoint of parallel and consecutive reaction networks in Sec. 7.

Reactors may contain one or more fluid phases. The level of dispersion in each phase may be represented mathematically by using some of the above thinking.

In industrial practice, the laboratory equipment used in chemical synthesis can influence reaction selection. As issues relating to kinetics, mass transfer, heat transfer, and thermodynamics are addressed, reactor design evolves to commercially viable equipment. Often, more than one type of reactor may be suitable for a given reaction. For example, in the partial oxidation of butane to maleic anhydride over a vanadium pyrophosphate catalyst, heat-transfer considerations dictate reactor selection and choices may include fluidized beds or multi-tubular reactors. Both types of reactors have been commercialized. Often, experience with a particular type of reactor within the organization can play an important part in selection.

There are several books on reactor analysis and modeling including those by Froment and Bischoff (*Chemical Reactor Analysis and Design*, Wiley, 1990), Fogler (*Elements of Chemical Reaction Engineering*, Prentice-Hall International Series, 2005), Levenspiel (*Chemical Reaction Engineering*, Wiley, 1999), and Walas (*Modeling with Differential Equations in Chemical Engineering*, Butterworth-Heinemann, 1991).

Chemical Kinetics Reactor models include chemical kinetics in the mass and energy conservation equations. The two basic laws of kinetics are the *law of mass action* for the rate of a reaction and the *Arrhenius equation* for its dependence on temperature. Both of these strictly apply to elementary reactions. More often, laboratory data are

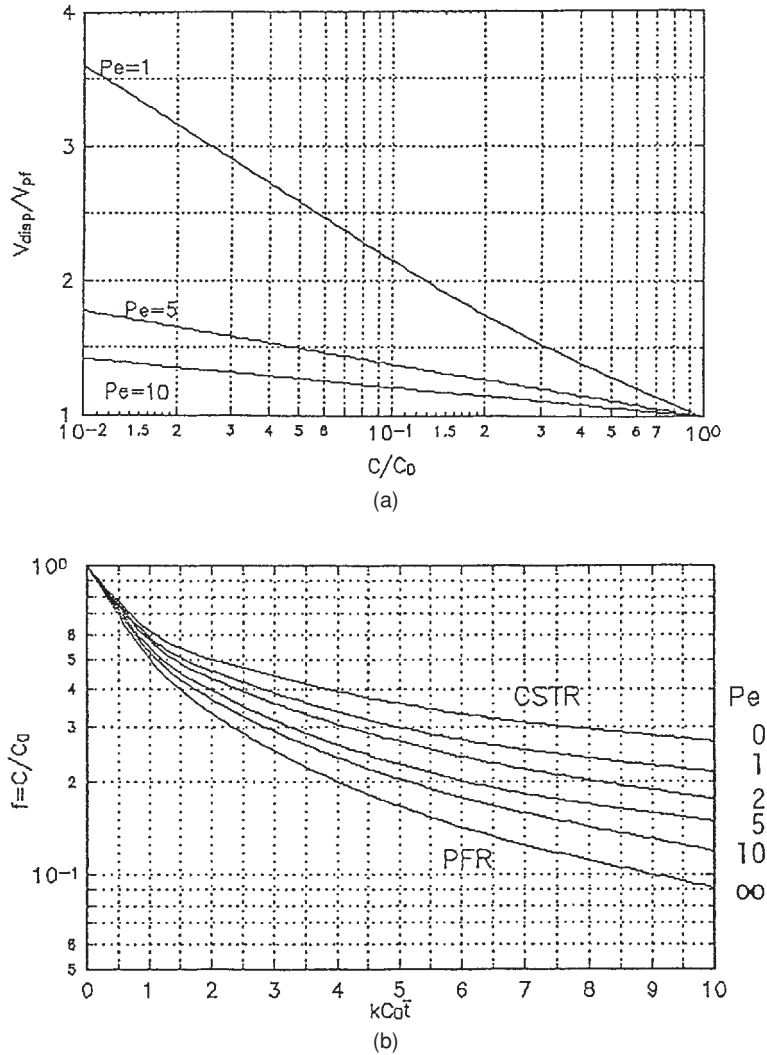


FIG. 19-2 Chemical conversion by the dispersion model. (a) Volume relative to plug flow against residual concentration ratio for a first-order reaction. (b) Residual concentration ratio against kC_0t for a second-order reaction. (c) Concentration profile at the inlet of a closed-end vessel with dispersion for a second-order reaction with $kC_0t = 5$.

to develop mathematical relationships that describe reaction rates that are then used. These relationships require analysis of the laboratory reactor data, as discussed in Sec. 7. Reactor models will require that kinetic rate information be expressed on a unit reactor volume basis. Two-phase or multiphase reactors will require a level of detail (e.g., heat and mass transport between phases) to capture the relevant physical and chemical processes that affect rate.

Pressure Drop, Mass and Heat Transfer Pressure drop is more important in reactor design than in analysis or simulation. The size of the compressor is dictated by pressure drop across the reactor, especially in the case of gas recycle. Compressor costs can be significant and can influence the aspect ratio of a packed or trickle bed reactor. Pressure drop correlations often may depend on the geometry, the scale, and the fluids used in data generation. Prior to using literature correlations, it often is advisable to validate the correlation with measurements on a similar system at a relevant scale.

Depending on the type of reactor, appropriate mass-transfer correlations may have to be used to connect intrinsic chemical kinetics to

the reaction rate per unit reactor volume. A number of these correlations have already been discussed in Sec. 5 of the Handbook, "Heat and Mass Transfer." The determination of intrinsic kinetics has already been discussed in Sec. 7 of the Handbook. In the absence of a correlation validated for a specific use, the analogy between momentum, heat and mass transfer may often be invoked.

The local reactor temperature affects the rates of reaction, equilibrium conversion, and catalyst deactivation. As such, the local temperature has to be controlled to maximize reaction rate and to minimize deactivation. In the case of an exothermic (endothermic) reaction, higher (lower) local temperatures can cause suboptimal local concentrations. Heat will have to be removed (added) to maintain more uniform temperature conditions. The mode of heat removal (addition) will depend on the application and on the required heat-transfer rate.

Examples of stirred tank reactors with heat transfer are shown in Fig. 19-1. If the heat of reaction is not significant, an adiabatic reactor may be used. For modest heat addition (removal), a jacketed stirred tank is adequate (Fig. 19-1a). As the heat exchange requirements

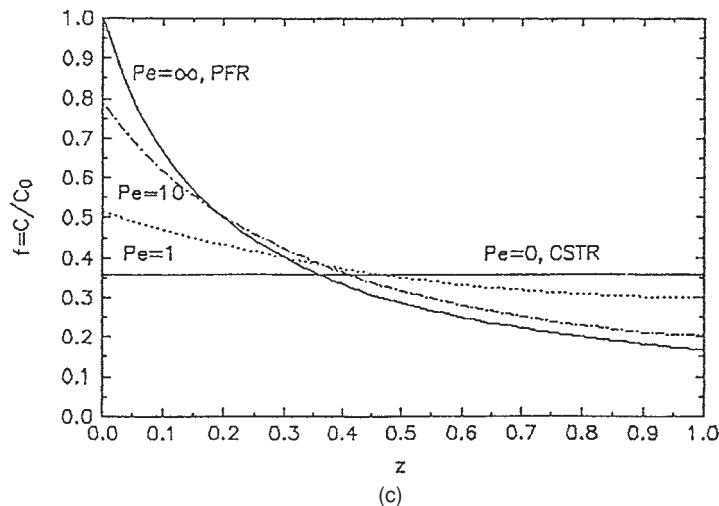


FIG. 19-2 (Continued)

increase, internal coils or internal tubes that contain a heat-transfer fluid may be required (Fig. 19-1*b* and *c*). In special cases, where the peak temperature has to be tightly controlled (e.g., in bioreactors) or where fouling may be an issue, the liquid may be withdrawn, circulated through an external heat exchanger, and returned to the reactor (Fig. 19-1*d*). In some cases, the vapor above the liquid may be passed through an external reflux condenser and returned to the reactor (Fig. 19-1*e*). In highly endothermic reactors, the entire reactor may be placed inside a fired heater (Fig. 19-1*f*), or the reactor shell may be heated to high temperatures by using induction heat.

Several of the heat-transfer options for packed beds are illustrated in Fig. 19-3. Again, if heat requirements are modest, an adiabatic reactor is adequate (Fig. 19-3*a*). If pressure drop through the reactor is an issue, a radial flow reactor may be used (Fig. 19-3*b*). There are few examples of radial flow reactors in industry. Potential problems include gas distribution in the case of catalyst attrition or settling. A common way of dealing with more exothermic (endothermic) reactions is to split the reactor into several beds and then provide interbed heat exchange (Fig. 19-3*c*). For highly exothermic (endothermic) reactors, a shell-and-tube multitubular reactor concept may be utilized (Fig. 19-3*d*). The reactor now begins to look more like a heat exchanger. If multiple beds are needed, rather than using interbed heat exchangers, cold feed may be injected (also called cold shot) in between beds (Fig. 19-3*e*). In some cases, the heat exchanger may be outside the reactor (Fig. 19-3*f*). The concept of a reactor as a heat exchanger may be extended to an autothermal multitubular reactor in which, for example, the reactants are preheated on the shell side with reaction occurring in the tubes (Fig. 19-3*g*). Such reactors can have control issues and are not widely used. A common approach is to have multiple adiabatic reactors with cooling in between reactors (Fig. 19-3*h*). If the reaction is endothermic, heat may be added by passing the effluents from each reactor through tubes placed inside a common process heater (as is the case for a petroleum reforming reactor shown in Fig. 19-3*i*). For highly endothermic reactions, a fuel-air mixture or raw combustion gases may be introduced into the reactor. In an extreme situation, the entire reactor may be housed within a furnace (as in the case of steam reforming for hydrogen synthesis or ethane cracking for ethylene production).

At times, the reaction may be exothermic with conversion being limited by thermodynamic equilibrium. In such cases, packed beds in series with interstage cooling may be used as well. The performance enhancement associated with this approach is shown for two cases in Table 19-2. Such units can take advantage of initial high rates at high temperatures and higher equilibrium conversions at lower tempera-

tures. For SO_2 oxidation, the conversion attained in the fourth bed is 97.5 percent, compared with an adiabatic single-bed value of 74.8 percent. With the three-bed ammonia reactor, final ammonia concentration is 18.0 percent, compared with the one-stage adiabatic value of 15.4 percent.

Since reactors come in a variety of configurations, use a variety of operating modes, and may handle mixed phases, design provisions for temperature control may draw on a large body of heat-transfer theory and data. These extensive topics are treated in other sections of this Handbook and in other references. Some of the high points pertinent to reactors are covered by Rase (*Chemical Reactor Design for Process Plants*, Wiley, 1977). Two encyclopedic references, *Heat Exchanger Design Handbook* (5 vols., Begell House, 1983–1998) and Chermisnoff (ed.) (*Handbook of Heat and Mass Transfer*, 4 vols., Gulf, 1986–1990), have several articles addressed specifically to reactors.

Reactor Dynamics Continuous reactors are designed to operate at or near a steady state by controlling the operating conditions. In addition, process control systems are designed to minimize fluctuations from the target conditions and for safety. Batch and semibatch reactors are designed to operate under predefined protocols based on the best understanding of the process. However, the potential for large and unexpected deviations from steady state as a result of process variable fluctuations is significant due to the complexity and nonlinearity of reaction kinetics and of the relevant mass- and heat-transfer processes. For a set of operating conditions (pressure, temperature, composition, and phases present), more than one steady state can exist. Which steady state is actually reached depends on the initial condition. Not all steady states are stable states, and only those that are stable can be reached without special control schemes. More complex behavior such as self-sustained oscillations and chaotic behavior has also been observed with reacting systems. Further, during start-up, shutdown, and abrupt changes in process conditions, the reactor dynamics may result in conditions that exceed reactor design limits (e.g., of temperature, pressure, materials of construction, etc.) and can result in a temperature runaway, reactor blowout, and even an explosion (or detonation). Parametric sensitivity deals with the analysis of reactor dynamics in response to abrupt changes.

Steady-State Multiplicity and Stability A simple example of *steady-state multiplicity* is due to the interaction between kinetics and heat transport in an adiabatic CSTR. For a first-order reaction at steady state, Eq. (19-13) gives

$$r(C, T) = kC = \frac{kC_f}{1 + k\bar{t}} = \frac{C_f \exp(a + b/T)}{1 + \bar{t} \exp(a + b/T)} \quad (19-23)$$

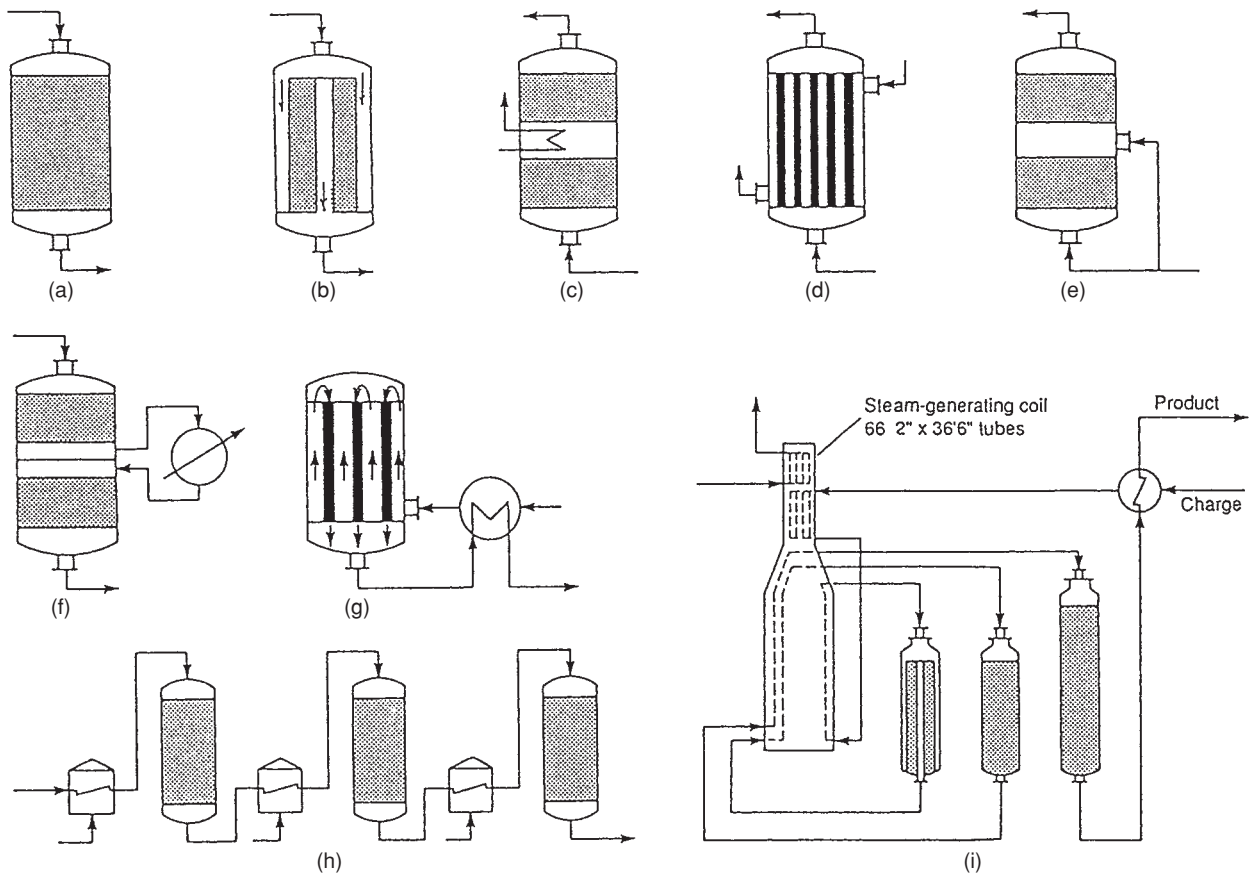


FIG. 19-3 Fixed-bed reactors with heat exchange. (a) Adiabatic downflow. (b) Adiabatic radial flow, low ΔP . (c) Built-in interbed exchanger. (d) Shell and tube. (e) Interbed cold-shot injection. (f) External interbed exchanger. (g) Autothermal shell, outside influent/effluent heat exchanger. (h) Multibed adiabatic reactors with interstage heaters. (i) Platinum catalyst, fixed-bed reformer for 5000 BPSD charge rates reactors 1 and 2 are 5.5 by 9.5 ft and reactor 3 is 6.5 by 12.0 ft; temperatures $502 \Rightarrow 433$, $502 \Rightarrow 471$, $502 \Rightarrow 496^\circ\text{C}$. To convert feet to meters, multiply by 0.3048; BPSD to m^3/h , multiply by 0.00662.

where C_f is the feed concentration and a and b are constants related to Arrhenius rate expression. The energy balance equation at steady state is given by

$$Q_C(T) = -\Delta H_r V_f r(C, T) = V_f \rho C_p (T - T_f) = Q_H(T) \quad (19-24)$$

where Q_C is the heat generation by reaction, Q_H is the heat removal by flow, T is the reactor temperature at steady state, and T_f is the feed temperature. Plotting the heat generation and heat removal terms versus temperature gives the result shown in Fig. 19-4. As shown, as many as three steady states are possible at the intersection of Q_C and Q_H .

Another example of multiplicity is shown in Fig. 19-15 for an adiabatic catalyst pellet, indicating that three effectiveness factor values can be obtained for a given Thiele modulus for a range of Prater numbers and Thiele modulus values, leading to three potential steady states. Multiple steady states can occur in different reactor types, including isothermal systems with complex nonlinear kinetics and systems with interphase transfer, the main requirement being the existence of a feedback mechanism—hence, a homogeneous PFR (without backmixing) will not exhibit multiplicity. Depending on the various physical and chemical interactions in a reactor, oscillatory and chaotic behavior can also occur.

There is a voluminous literature on steady-state multiplicity, oscillations (and chaos), and derivation of bifurcation points that define the conditions that lead to onset of these phenomena. For example, see Morbidelli et al. ["Reactor Steady-State Multiplicity and Stability," in *Chemical Reaction and Reactor Engineering*, Carberry and Varma (eds), Marcel Dekker, 1987], Luss ["Steady State Multiplicity and Uniqueness

Criteria for Chemically Reacting Systems," in *Dynamics and Modeling of Reactive Systems*, Stewart et al. (eds.), Academic Press, 1980], Schmitz [*Adv. Chem. Ser.*, **148**: 156, ACS (1975)], and Razon and Schmitz [*Chem. Eng. Sci.*, **42** (1987)]. However, many of these criteria for specific reaction and reactor systems have not been validated experimentally.

Linearized or asymptotic stability analysis examines the stability of a steady state to small perturbations from that state. For example, when heat generation is greater than heat removal (as at points A- and B+ in Fig. 19-4), the temperature will rise until the next stable steady-state temperature is reached (for A- it is A, for B+ it is C). In contrast, when heat generation is less than heat removal (as at points A+ and B- in Fig. 19-4), the temperature will fall to the next-lower stable steady-state temperature (for A+ and B- it is A). A similar analysis can be done around steady-state C, and the result indicates that A and C are stable steady states since small perturbations from the vicinity of these return the system to the corresponding stable points. Point B is an unstable steady state, since a small perturbation moves the system away to either A or C, depending on the direction of the perturbation. Similarly, at conditions where a unique steady state exists, this steady state is always stable for the adiabatic CSTR. Hence, for the adiabatic CSTR considered in Fig. 19-4, the slope condition $dQ_H/dT > dQ_C/dT$ is a necessary and sufficient condition for asymptotic stability of a steady state. In general (e.g., for an externally cooled CSTR), however, the slope condition is a necessary but not a sufficient condition for stability; i.e., violation of this condition leads to asymptotic instability, but its satisfaction does not ensure asymptotic stability. For example, in select reactor systems even

TABLE 19-2 Multibed Reactors, Adiabatic Temperature Rises and Approaches to Equilibrium*

 Oxidation of SO₂ at atmospheric pressure in a four-bed reactor. Feed 6.26% SO₂, 8.3% O₂, 5.74% CO₂, and 79.7% N₂.

°C		Conversion, %	
In	Out	Plant	Equilibrium
463.9	592.8	68.7	74.8
455.0	495.0	91.8	93.4
458.9	465.0	96.0	96.1
435.0	437.2	97.5	97.7

 Ammonia synthesis in a three bed reactor at 225 atm. Feed 22% N₂, 66% H₂, 12% inerts.

°C		Ammonia, %	
In	Out	Calculated	Equilibrium
399	518.9	13.0	15.4
427	488.9	16.0	19.0
427	470.0	18.0	21.7

*To convert atm to kPa multiply by 101.3.

 SOURCE: Plant data and calculated design values from Rase, *Chemical Reactor Design for Process Plants*, Wiley, 1977.

a unique steady state can become unstable, leading to oscillatory or chaotic behavior.

Local asymptotic stability criteria may be obtained by first solving the steady-state equations to obtain steady states and then linearizing the transient mass and energy balance equations in terms of deviations of variables around each steady state. The determinant (or slope) and trace conditions derived from the matrix A in the set of equations obtained are necessary and sufficient for asymptotic stability.

$$\frac{d}{dt} \begin{pmatrix} x \\ y \end{pmatrix} = A \begin{pmatrix} x \\ y \end{pmatrix} \quad x = C - C_{ss} \quad y = T - T_{ss}$$

$$\Delta = \det(A) > 0 \quad \sigma = \text{trace}(A) < 0 \quad (19-25)$$

where x and y are the deviation variables around the steady state (C_{ss} , T_{ss}). The approach may be extended to systems with multiple concentrations and complex nonlinear kinetics. For additional references on asymptotic stability analysis, see Denn (*Process Modeling*, Longman, 1986) and Morbidelli et al. ["Reactor Steady-State Multiplicity and Stability," in *Chemical Reaction and Reactor Engineering*, Carberry and Varma (eds.), Marcel Dekker, 1987].

Parametric Sensitivity and Dynamics The global stability and sensitivity to abrupt changes in parameters cannot be determined from an asymptotic analysis. For instance, for the simple CSTR, a key question is whether the temperature can run away from a lower stable

steady state to a higher one. The critical temperature difference ΔT_c is useful in designing for globally stable operation:

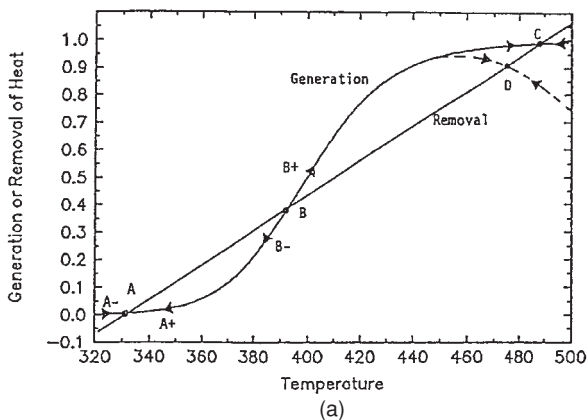
$$T - T_j < \Delta T_c = \left(\frac{RT^2}{E} \right) \quad (19-26)$$

where T is the reactor temperature, T_j is the cooling jacket temperature, E is the activation energy, and R is the universal gas constant. Similarly, for a jacketed PFR, a conservative criterion for stability is $T_{\max} - T_j < \Delta T_c$, where T_{\max} is the temperature of the hot spot.

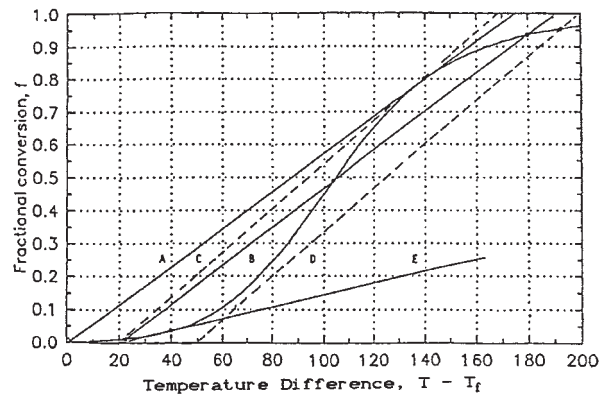
Another example of sensitivity to abrupt changes is the *wrong-way effect*, exhibited, for instance, in packed-bed reactors, where an abrupt reduction in feed rate or in feed temperature results in a dramatic increase in reactor peak temperature for exothermic reactions. Either the reactor may eventually return to the original steady state or, if a higher-temperature steady state exists, the reactor may establish a temperature profile corresponding to the new high steady state. Such a dynamic excursion can result in an increase of undesirable by-products concentration, catalyst deactivation, permanent reactor damage, and safety issues; e.g., see work by Luss and coworkers ["Wrong-Way Behavior of Packed-Bed Reactors: I. The Pseudo-homogeneous Model," *AIChE J.* **27**: 234–246 (1981)]. For more complex systems, the transient model equations are solved numerically. A more detailed discussion of parametric sensitivity is provided by Varma et al. (*Parametric Sensitivity in Chemical Systems*, Cambridge University Press, 1999).

Reactor Models As discussed earlier, reactor models attempt to strike a balance between the level of detail included and the usefulness of the model. Too many details in the model may require a larger number of adjustable model parameters, increase computational requirements, and limit how widely the model may be used. Too few details, on the other hand, increase ease of implementation but may compromise the predictive or design capabilities of the model. Figure 19-5 is a schematic of the inherent tradeoff between ease of implementation and the insight that may be obtained from the model.

Increases in computational power are allowing a more cost-effective inclusion of a greater number of details. Computational fluid dynamics (CFD) models provide detailed flow information by solving the Navier-Stokes transport equations for mass, momentum, and heat balances. The user will, however, need to be familiar with the basic elements of the software and may need a license. A typical numerical solution of the governing transport equations is obtained within the eulerian framework, using a large number of computational cells (or finite volumes that represent reactor geometry). Current capabilities in commercial CFD software can be used to resolve the flow, concentration, and temperature patterns in a single phase with sufficient detail and reasonable accuracy for all length and time scales. The ability to visualize flow, concentration, and temperature inside a reactor is useful in understanding performance and in designing reactor internals.



(a)



(b)

FIG. 19-4 Multiple steady states of CSTRs, stable and unstable, adiabatic. (a) First-order reaction, A and C stable, B unstable, the dashed line is for a reversible reaction. (b) One, two, or three steady states depending on the combination (C_f , T_j).

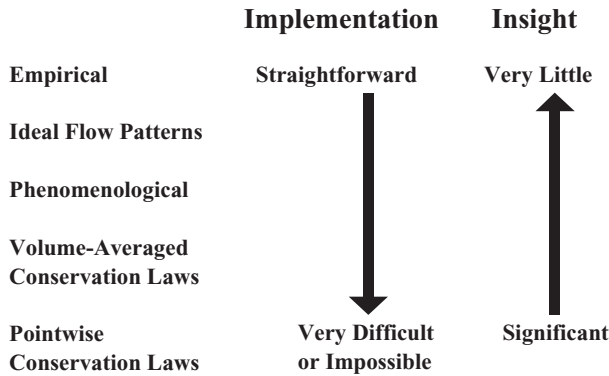


FIG. 19-5 Hierarchy of reactor models.

Addition of transport properties and more than one phase (as is the case with solid catalysts) within a CFD framework complicates the problem in that the other phase(s) also may have to be included in the calculations. This may require additional transport equations to address a range of complexities associated with the dynamics and physics of each phase, the interaction between and within phases, sub-grid-scale heterogeneities (such as size distributions within each phase), and coupling with kinetics at the molecular level. For example, one needs the bubble size distribution in a bubble column reactor to correctly model interfacial area and local mass-transfer coefficients, which can further affect the chemical kinetics. Although phenomenological models describing such physical effects have greatly improved over the years, this area still lacks reliable multiphase turbulence closures, or experimentally validated intraphase and interphase transport models. Mathematical modeling in industrial practice will continue to involve compromises between computational complexity, experimental data needs, ability to validate the model, cost, and the time frame in which the work may be useful to the organization.

RESIDENCE TIME DISTRIBUTION AND MIXING

The time spent by reactants and intermediates at reaction conditions determines conversion (and perhaps selectivity). It is therefore often important to understand the residence time distribution (RTD) of reaction species in the reactor. This RTD could be considerably different from what is expected. Reasons for the deviation could be channeling of fluid, recycling of fluid, or creation of stagnant regions in the reactor, as illustrated in Fig. 19-6.

This section introduces how tracers are used to establish the RTD in a reactor and to contrast against RTDs of ideal reactors. The section

ends with a discussion of how reactor performance may be connected to RTD information.

TRACERS

Tracers are typically nonreactive substances used in small concentration that can be easily detected. The tracer is injected at the inlet of the reactor along with the feed or by using a carrier fluid, according to some definite time sequence. The inlet and outlet concentrations of the tracer

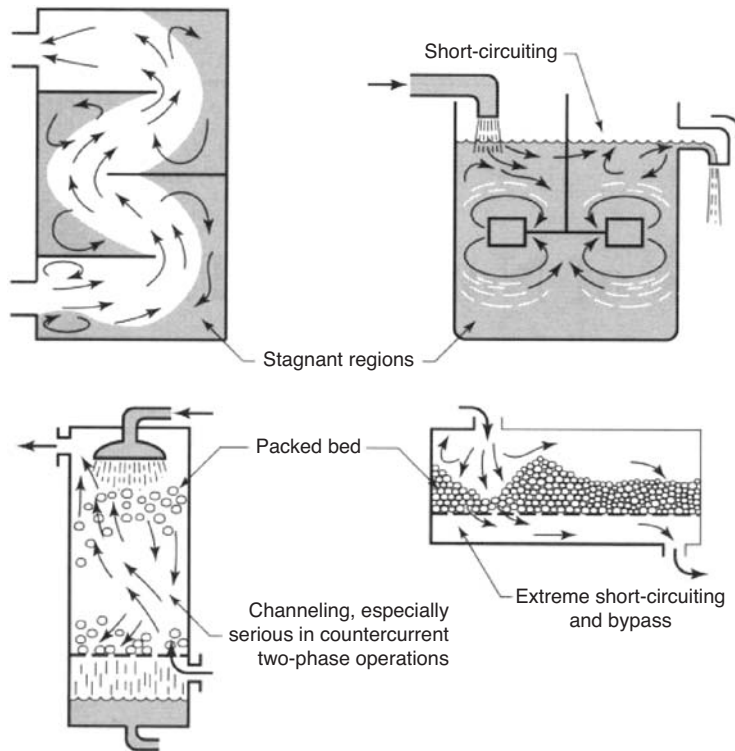


FIG. 19-6 Some examples of nonideal flow in reactors. (Fig. 11.1 in *Levenspiel, Chemical Reaction Engineering, John Wiley & Sons, 1999.*)

are recorded as a function of time. These data are converted to a residence time distribution of feed in the reactor vessel. Tracer studies may be used to detect and define regions of nonideal behavior, develop phenomenological zone models, calculate reactor performance (conversion, selectivity), and synthesize optimal reactor configurations for a given process. The RTD does not represent the mixing behavior in a vessel uniquely. Several arrangements of reactors or internals within a vessel may provide the same tracer response. For example, any series arrangement of the same number of CSTR and plug flow reactor elements will provide the same RTD. This lack of uniqueness may limit direct application of tracer studies to first-order reactions with constant specific rates. For other reactions, the tracer curve may determine the upper and lower limits of reactor performance. When this range is not too broad, or when the purpose of the tracer test is to diagnose maldistribution or bypassing in the reactor, the result can be useful. Tracer data also may be taken at several representative positions in the vessel in order to develop a better understanding for the flow behavior.

Inputs Although some arbitrary variation of input concentration with time may be employed, five mathematically simple tracer input signals meet most needs. These are *impulse*, *step*, *square pulse* (started at time a , kept constant for an interval, then reduced to the original value), *ramp* (increased at a constant rate for a period of interest), and *sinusoidal*. Sinusoidal inputs are difficult to generate experimentally.

Types of Responses The key relationships associated with tracers are provided in Table 19-3. Effluent concentrations resulting from impulse and step inputs are designated C_δ and C_u , respectively. The mean concentration resulting from an impulse of magnitude m into a vessel of volume V_r is $C^0 = m/V_r$. The mean residence time is the ratio of the vessel volume to the volumetric flow rate:

$$\bar{t} = \frac{V_r}{V'} \quad \text{or} \quad \bar{t} = \frac{\int_0^\infty t C_\delta dt}{\int_0^\infty C_\delta dt} \quad (19-27)$$

The reduced time is $t_r = t/\bar{t}$. Residence time distributions are used in two forms: normalized, $E(t_r) = C_\delta/C^0$; or plain, $E(t) = C_\delta/\int_0^\infty C_\delta dt$. The area under either RTD is unity: $\int_0^\infty E(t_r) dt_r = \int_0^\infty E(t) dt = 1$, and the relation between them is $E(t_r) = \bar{t}E(t)$. The area between the ordinates at t_1 and t_2 is the fraction of the total effluent that has spent the period between those times in the vessel. The age function is defined in terms of the step input as

$$F(t) = \frac{C_u}{C_f} = \int_0^t E(t) dt \quad (19-28)$$

Reactor Tracer Responses

Continuous Stirred Tank Reactor (CSTR) With a step input of magnitude C_f , the unsteady material balance of tracer

$$V_r \frac{dC}{dt} + V'C = V'C_f \quad (19-29)$$

can be integrated to yield

$$\frac{C}{C_f} = F(t_r) = 1 - \exp(-t_r) \quad (19-30)$$

With an impulse input of magnitude m or an initial mean concentration $C^0 = m/V_r$, the material balance is

$$\frac{dC}{dt_r} + C = 0 \quad \text{with} \quad C = C^0, t = 0 \quad (19-31)$$

And integration gives

$$\frac{C}{C^0} = E(t_r) = \exp(-t_r) \quad (19-32)$$

These results show that

$$E(t_r) = \frac{dF(t_r)}{dt_r} \quad (19-33)$$

TABLE 19-3 Tracer Response Functions

Mean residence time:

$$\bar{t} = \frac{\int_0^\infty t C_\delta dt}{\int_0^\infty C_\delta dt} = \frac{\int_0^{C_{u\infty}} t dC_u}{C_{u\infty}}$$

Initial mean concentration with impulse input,

$$C^0 = \frac{m}{V_r} = \left(\frac{V'}{V_r}\right) \int_0^\infty C_\delta dt = \frac{\int_0^\infty C_\delta dt}{\bar{t}}$$

Reduced time: $t_r = \frac{t}{\bar{t}}$

Residence time distribution:

$$E(t) = \frac{C_\delta}{\int_0^\infty C_\delta dt} = \frac{E(t_r)}{\bar{t}} = \frac{dF(t)}{dt}$$

Residence time distribution, normalized,

$$E(t_r) = \frac{\text{impulse output}}{\text{initial mean concentration}} \\ = \frac{C_\delta}{C^0} = \frac{\bar{t}C_\delta}{\int_0^\infty C_\delta dt} = \bar{t} E(t) = \frac{dF(t)}{dt}$$

Age: $F(t) = \frac{\text{step output}}{\text{step input}}$

$$= \frac{C_u}{C_f} = \frac{\int_0^t C_\delta dt}{\int_0^\infty C_\delta dt} = F(t_r)$$

Internal age: $I(t) = 1 - F(t)$

Intensity: $\Lambda(t) = \frac{E(t)}{1 - F(t)} = \frac{E(t)}{I(t)}$

Variance:

$$\sigma^2(t) = \int_0^\infty (t - \bar{t})^2 E(t) dt = -\bar{t}^2 + \frac{\int_0^\infty t^2 C_\delta dt}{\int_0^\infty C_\delta dt}$$

Variance, normalized:

$$\sigma^2(t_r) = \frac{\sigma^2(t)}{\bar{t}^2} = -1 + \frac{\int_0^\infty t^2 C_\delta dt}{\int_0^\infty C_\delta dt} \\ = \int_0^1 (t_r - 1)^2 dF(t_r)$$

Skewness, third moment:

$$\gamma^3(t_r) = \int_0^\infty (t_r - 1)^3 E(t_r) dt_r$$

Multistage CSTR Since tubular reactor performance can be simulated by a series of CSTRs, multistage CSTR tracer models are useful in analyzing data from empty tubular and packed-bed reactors. The solution for a tracer through n CSTRs in series is found by induction from the solution of one stage, two stages, and so on.

$$E(t_r) = \frac{C_n}{C^0} = \frac{n^n}{(n-1)!} t_r^{n-1} \exp(-nt_r) \quad (19-34)$$

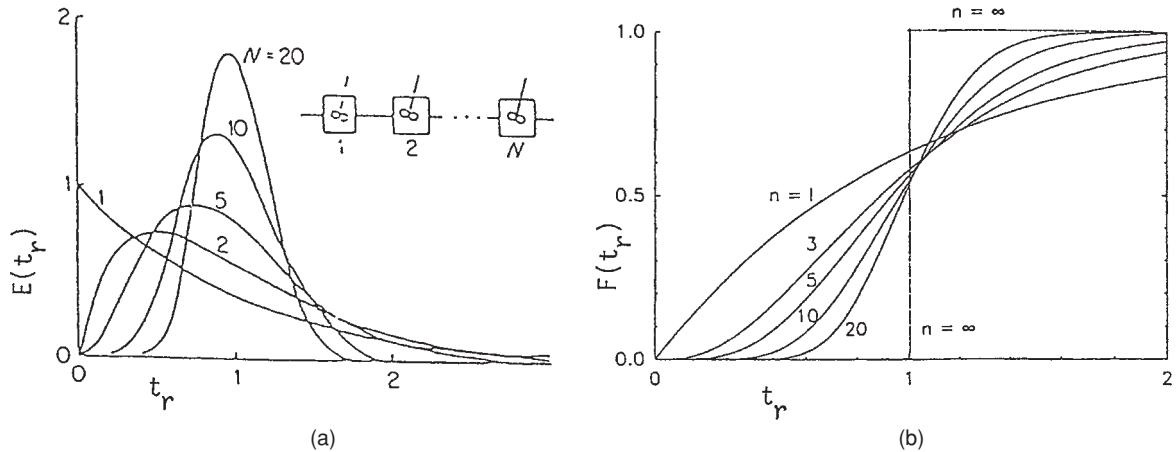


FIG. 19-7 Tracer responses to n -stage continuous stirred tanks in series: (a) Impulse inputs. (b) Step input.

The solution for a step response can be obtained by integration

$$F(t_r) = \int_0^{t_r} E(t_r) dt = 1 - \exp(-nt_r) \sum_{j=0}^{n-1} \frac{(nt_r)^j}{j!} \quad (19-35)$$

where $E(t_r)$ and $F(t_r)$ for various values of n are shown in Fig. 19-7.

The theoretical RTD responses in Fig. 19-7a are similar in shape to the experimental responses from pilot and commercial reactors shown in Fig. 19-8. The value of n in Fig. 19-8 represents the number of CSTRs in series that provide a similar RTD to that observed commercially. Although not shown in the figure, a commercial reactor having a similar space velocity as a pilot reactor and a longer length typically has a higher n value than a pilot reactor due to greater linear velocity.

The variance of the RTD of a series of CSTRs, σ^2 , is the inverse of n .

$$\sigma^2 = \int_0^{\infty} (t_r - 1)^2 E(t_r) dt_r = \frac{1}{n} \quad (19-36)$$

Plug Flow Reactor The tracer material balance over a differential reactor volume dV_r is

$$\frac{\partial C}{\partial t} + V' \frac{\partial C}{\partial V_r} = 0 \quad (19-37)$$

With step input $u(t)$, the initial and boundary conditions are

$$C(0, t) = C_f u(t) \quad \text{and} \quad C(V_r, 0) = 0 \quad (19-38)$$

The solution is

$$\frac{C}{C_f} = F(t) = u(t - \bar{t}) = \begin{cases} 0 & \text{when } t \leq \bar{t} \\ 1 & \text{when } t > \bar{t} \end{cases} \quad (19-39)$$

As discussed earlier, the response to an impulse input is the derivative of $F(t)$.

$$\frac{C}{C_\delta} = E(t) = \delta(t_r - 1) \quad (19-40)$$

The effluent RTD is an impulse that is delayed from the input impulse by $t_r = 1$, or $t = \bar{t}$.

Tubular Reactor with Dispersion As discussed earlier, a multi-stage CSTR model can be used to simulate the RTD in pilot and commercial reactors. The *dispersion model*, similar to Fick's molecular diffusion law with an empirical dispersion coefficient D_e replacing the diffusion coefficient, may also be used.

$$\frac{\partial C}{\partial t} + V' \frac{\partial C}{\partial V_r} - D_e \frac{\partial^2 C}{\partial V_r^2} = 0 \quad (19-41)$$

The above equation is often converted to dimensionless variables and solved. The solution of this partial differential equation is recorded in the literature [Otake and Kunigata, *Kagaku Kogaku*, **22**: 144 (1958)]. The plots of $E(t_r)$ versus t_r are bell-shaped, similar to the response for a series of n CSTRs model (Fig. 19-7). A relation between $\sigma^2(t_r)$, n , and Pe (for the closed-ends condition) is

$$\sigma^2(t_r) = \frac{2[Pe - 1 + \exp(-Pe)]}{Pe^2} = \frac{1}{n} \quad (19-42)$$

Examples of values of Pe are provided in Fig. 19-8. When Pe is large, $n \Rightarrow Pe/2$ and the dispersion model reduces to the PFR model. For small values of Pe , the above equation breaks down since the lower limit on n is $n = 1$ for a single CSTR. To better represent dispersion behavior, a series of CSTRs with backmixing may be used; e.g., see Froment and Bischoff (*Chemical Reactor Analysis and Design*, Wiley, 1990). A model analogous to the dispersion model may be used when there are velocity profiles across the reactor cross-section (e.g., for laminar flow). In this case, the equation above will contain terms associated with the radial position in the reactor.

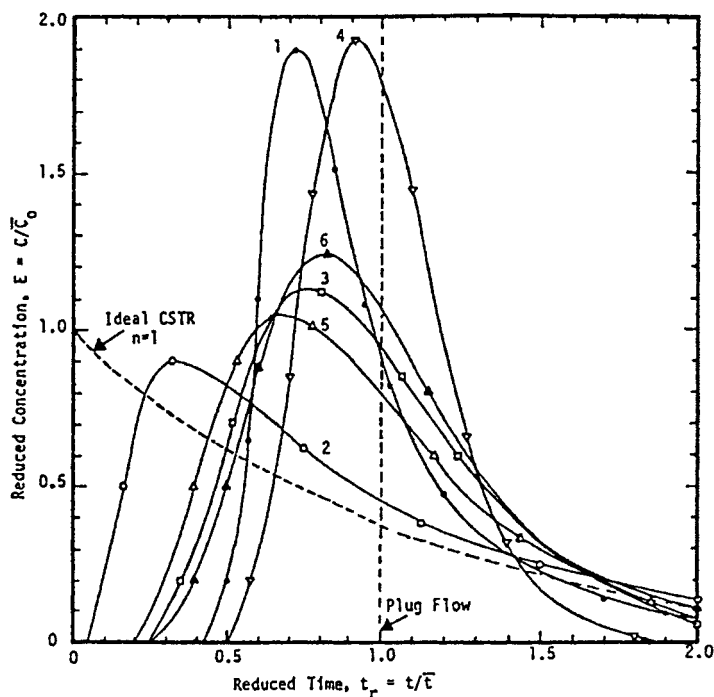
Understanding Reactor Flow Patterns As discussed above, a RTD obtained using a nonreactive tracer may not uniquely represent the flow behavior within a reactor. For diagnostic and simulation purposes, however, tracer results may be explained by combining the expected tracer responses of ideal reactors combined in series, in parallel, or both, to provide an RTD that matches the observed reactor response. The most commonly used ideal models for matching an actual RTD are PRF and CSTR models. Figure 19-9 illustrates the responses of CSTRs and PFRs to impulse or step inputs of tracers.

Since the tracer equations are linear differential equations, a Laplace transform $L\{f(t)\} = \int_0^{\infty} f(t)e^{-st} dt$ may be used to relate tracer inputs to responses. The concept of a transfer function facilitates the combination of linear elements.

$$\bar{C}_{\text{output}}(s) = (\text{transfer function}) \bar{C}_{\text{input}}(s) = G(s) \bar{C}_{\text{input}}(s) \quad (19-43)$$

Some common Laplace transfer functions are listed in Table 19-4.

The Laplace transform may be inverted to provide a tracer response in the time domain. In many cases, the overall transfer function cannot be analytically inverted. Even in this case, moments of the RTD may be derived from the overall transfer function. For instance, if G'_0 and G''_0 are the limits of the first and



No.	Code	Process	σ^2	n	Pe
1	○	Aldolization of butyraldehyde	0.050	20.0	39.0
2	●	Olefin oxonation pilot plant	0.663	1.5	1.4
3	□	Hydrodesulfurization pilot plant	0.181	5.5	9.9
4	▽	Low-temp hydroisomerization pilot	0.046	21.6	42.2
5	△	Commercial hydrofiner	0.251	4.0	6.8
6	▲	Pilot plant hydrofiner	0.140	7.2	13.2

FIG. 19-8 Residence time distributions of pilot and commercial reactors. σ^2 = variance of the residence time distribution, n = number of stirred tanks with the same variance, Pe = Peclet number. (Walas, Chemical Process Equipment, Butterworths, 1990.)

second derivatives of the transfer function $G(s)$ as $s \Rightarrow 0$, the mean residence time and variance are

$$\bar{t} = G'_0 \quad \text{and} \quad \sigma^2(t) = G''_0 - (G'_0)^2 \quad (19-44)$$

In addition to understanding the flow distribution, tracer experiments may be conducted to predict or explain reactor performance based on a particular RTD. To do this, a mathematical expression for the RTD is needed. A PFR, or a dispersion model with a small value of the dispersion coefficient, may be used to simulate an empty tubular reactor. Stirred tank performance often is nearly completely mixed (CSTR). In some cases, to fit the measured RTD, the model may have to be modified by taking account of bypass zones, stagnant zones, or other parameters associated with the geometry and operation of the reactor. Sometimes the vessel can be visualized as a zone of complete mixing in the vicinity of impellers followed by plug flow zones elsewhere, e.g., CSTRs followed by PFRs. Packed beds usually deviate substantially from plug flow. The dispersion model and some combination of PFRs and CSTRs or multiple CSTRs in series may approximate their behavior. Fluidized beds in small sizes approximate CSTR behavior, but large ones exhibit bypassing, stagnancy, nonhomogeneous regions, and several varieties of contact between particles and fluid. The additional parameters required to simulate such mixing behavior can increase the mathematical complexity of the model.

The characteristic bell shape of many RTDs can be fit to well-known statistical distributions. Hahn and Shapiro (*Statistical Models in Engineering*, Wiley, 1967) discuss many of the standard distributions and conditions for their use. The most useful distributions are the gamma (or Erlang) and the gaussian together with its Gram-Charlier extension. These distributions are represented by only a few parameters that can be used to determine, for instance, the mean and the variance.

Qualitative inspection of the tracer response can go a long way toward identifying flow distribution problems. Additional references on tracers are Wen and Fan (*Models for Flow Systems in Chemical Reactors*, Marcel Dekker, 1975) and Levenspiel (*Chemical Reaction Engineering*, 3d ed., Wiley, 1999).

CONNECTING RTD TO CONVERSION

When the flow pattern is known, the conversion for a given reaction mechanism may be evaluated from the appropriate material and energy balances. When only the RTD is known (or can be calculated from tracer response data), however, different networks of reactor elements can match the observed RTD. In reality, reactor performance for a given reactor network will be unique. The conversion obtained by matching the RTD is, however, unique only for linear kinetics. For nonlinear kinetics, two additional factors have to be

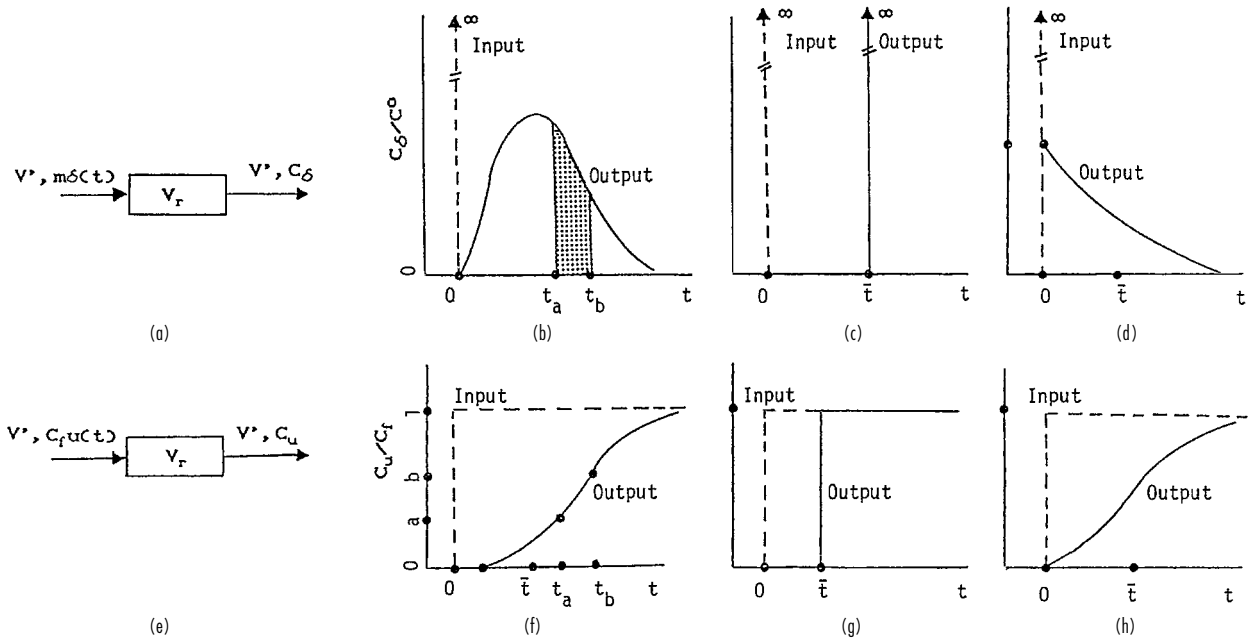


FIG. 19-9 Tracer inputs and responses for PFR and CSTR. (a) Experiment with impulse input of tracer. (b) Generic behavior; area between ordinates at t_a and t_b equals the fraction of the tracer with residence time in that range. (c) Plug flow behavior. (d) Completely mixed vessel. (e) Experiment with step input of tracer. (f) Generic behavior; fraction with ages between t_a and t_b equals the difference between the ordinates, $b - a$. (g) Plug flow behavior. (h) Completely mixed behavior.

accounted for to fully describe the contacting or flow pattern: the degree of segregation of the fluid and the earliness of mixing of the reactants.

Segregated Flow The degree of segregation relates to the tendency of fluid particles to move together as aggregates or clumps (e.g., bubbles in gas-liquid reactors, particle clumps in fluidized beds, polymer striations in high-viscosity polymerization reactors) rather than each molecule behaving independently (e.g., homogeneous gas, low-viscosity liquid). A system with no aggregates may be called a microfluid, and the system with aggregates a macrofluid (e.g., see Levenspiel, *Chemical Reaction Engineering*, 3d ed., Wiley, 1999). In an ideal plug flow or in an ideal batch reactor, the segregated particles in each clump spend an equal time in the reactor and therefore the behavior is no different from that of a microfluid that has individual molecules acting independently. The reactor performance is therefore unaffected by the degree of segregation, and the PFR or ideal batch model equations may be used to estimate performance. As shown below, however, this is not the case for a CSTR where the performance equation for a microfluid is the same as that of an ideal CSTR, while that of a CSTR with segregated flow is not.

In segregated flow the molecules travel as distinct groups. All molecules that enter the vessel together leave together. The groups are small enough that the RTD of the whole system is represented by a

smooth curve. Each group of molecules reacts independently of any other group, that is, as a batch reactor. For a batch reactor with a power law kinetics,

$$\left(\frac{C}{C_0}\right)_{\text{batch}} = \begin{cases} \exp(-kt) = \exp(-k\bar{t}t_r) & \text{first order} \\ \left[\frac{1}{1 + (q-1)kC^{q-1}\bar{t}t_r}\right]^{1/(q-1)} & \text{order } q \end{cases} \quad (19-45)$$

For other rate equations a numerical solution may be needed. The mean conversion of all the groups is the sum of the products of the individual conversions and their volume fractions of the total flow. Since the groups are small, the sum may be replaced by an integral. Thus,

$$\left(\frac{C}{C_0}\right)_{\text{segregated}} = \int_0^\infty \left(\frac{C}{C_0}\right)_{\text{batch}} E(t) dt = \int_0^\infty \left(\frac{C}{C_0}\right)_{\text{batch}} E(t_r) dt_r \quad (19-46)$$

When a conversion and an RTD are known, a value of k may be estimated by trial and error so the segregated integral is equal to the known value. If a series of conversions are known at several residence times, the order of the reaction that matches the data may be estimated by trial and error. One has to realize, however, that the RTD may change with residence time. Alternatively, for known intrinsic kinetics, a combination of ideal reactors that reasonably match both RTD and performance may be considered.

Early versus Late Mixing—Maximum Mixedness The concept of early versus late mixing may be illustrated using a plug flow reactor and an ideal CSTR in series. In one case, the ideal CSTR precedes the plug flow reactor, a case of early mixing. In the other case, the plug flow reactor precedes the CSTR, and this is a case of late mixing. Each of the two arrangements has the same RTD.

In maximum mixedness (or earliest possible mixing), the feed is intimately mixed with elements of fluid of different ages, for instance, using multiple side *inlets* at various points along a plug flow reactor. The

TABLE 19-4 Some Common Laplace Transform Functions

Element	Transfer function $G(s)$
Ideal CSTR	$\frac{1}{1 + ts}$
PFR	$\exp(-\bar{t}s)$
n -stage CSTR (Erlang)	$\frac{1}{(1 + ts)^n}$
Erlang with time delay	$\frac{\exp(-\bar{t}s)}{(1 + ts)^n}$

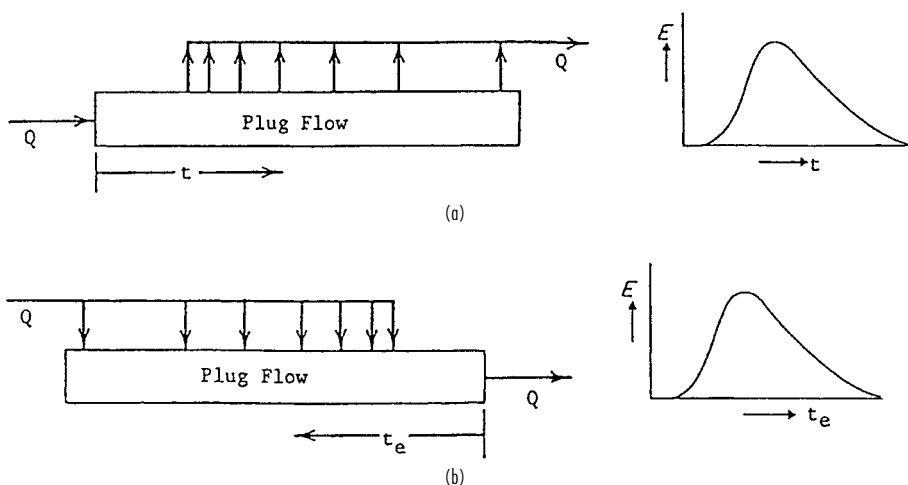


FIG. 19-10 Two limiting flow patterns with the same RTD. (a) Segregated flow. (b) Maximum mixedness flow.

amount and location of the inlet flows match the RTD. This means that each portion of fresh material is mixed with all the material that has the same life expectation, regardless of the actual residence time in the vessel up to the time of mixing. The life expectation under plug flow conditions is related to the distance remaining to be traveled before leaving the vessel. The concept of maximum mixedness and completely segregated flow is illustrated in Fig. 19-10. Segregated flow is represented as a plug flow reactor with multiple side outlets and has the same RTD.

In contrast to segregated flow, in which the mixing occurs only after each side stream leaves the vessel, under maximum mixedness flow, mixing of all molecules having a certain life expectancy occurs at the time of introduction of fresh material. These two mixing extremes—as late as possible and as soon as possible, both having the same RTD—correspond to extremes of reactor performance.

The mathematical model for maximum mixedness has been provided by Zwietering [*Chem. Eng. Sci.* **11**: 1 (1959)].

$$\frac{dC}{dt} = r_c - \frac{E(t)}{1-F(t)}(C_0 - C) \quad (19-47)$$

where r_c is the chemical reaction rate; e.g., for an order q , $r_c = kC^q$. The above differential equation in dimensionless variable form (where $f = C/C_0$ and $t_r = t/t$) becomes

$$\frac{df}{dt_r} = k\bar{t}C_0^{q-1}f^q - \frac{E(t_r)}{1-F(t_r)}(1-f) \quad (19-48)$$

with boundary condition

$$\frac{df}{dt_r} = 0 \quad \text{for } t_r \Rightarrow \infty \quad (19-49)$$

which makes

$$k\bar{t}C_0^{q-1}f_\infty^q - \frac{E(\infty)}{1-F(\infty)}(1-f_\infty) = 0 \quad (19-50)$$

The conversion achieved in the vessel is obtained by the solution of the differential equation at the exit of the vessel where the life expectation is $t = 0$. The starting point for the integration is (f_∞, t_∞) . When integrating numerically, however, the RTD becomes essentially 0 by the time t_r approaches 3 or 4. Accordingly, the integration interval is from $(f_\infty, t_r \leq 3$ or 4) to $(f_{\text{effluent}}, t_r = 0)$ with f_∞ obtained from Eq. (19-50).

The conversion is a maximum in *segregated flow* and a minimum under *maximum mixedness* conditions, for a given RTD and reaction orders >1 . A few comparisons are made in Fig. 19-11. In some ranges of the parameters n or r_c , the differences in reactor volume for a given conversion, when segregated or maximum mixedness flow is assumed,

are substantial. If only the RTD is known, these two extremes bracket reactor performance. As a general trend, for reaction orders >1 , conversion increases as maximum mixedness $<$ late mixing of microfluids $<$ segregated flow (and the opposite is the case for orders <1). Increased deviation from ideal plug flow increases the effect of segregation on conversion. At low conversion, the conversion is insensitive to the RTD and to the extent of segregation.

Novosad and Thyn [*Coll. Czech. Chem. Comm.* **31**: 3,710–3,720 (1966)] solved the maximum mixedness and segregated flow equations (fit with the Erlang model) numerically. There are few experimental confirmations of these mixing extremes. One study with a

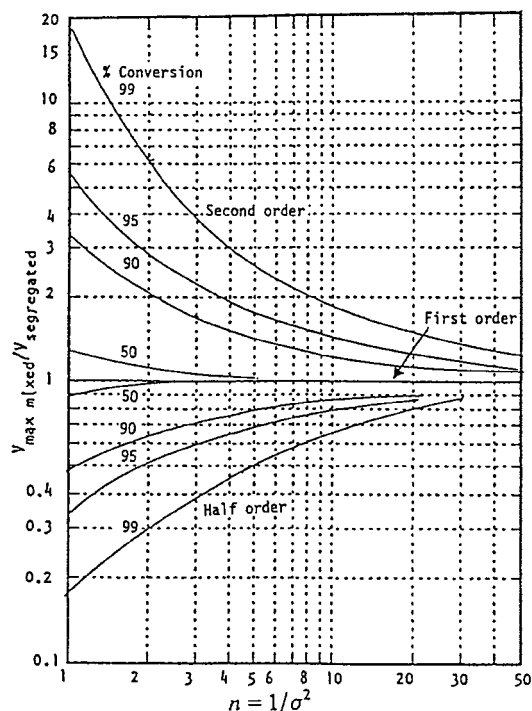


FIG. 19-11 Ratio of reactor volume for maximum mixedness and segregated flow models as a function of the variance (or n), for several reaction orders.

19-20 REACTORS

50-gal stirred tank reactor found segregation at low agitation and was able to correlate complete mixing and maximum mixedness in terms of the power input and recirculation within the vessel [Worrell and Eagleton, *Can. J. Chem. Eng.* pp. 254–258 (Dec. 1964)].

REACTION AND MIXING TIMES

Reactants may be premixed or fed directly into the reactor. To the extent that the kinetics are limiting (i.e., reaction rate is slow), the rate of mixing plays a minor role in determining conversion or selectivity. If the time to mix reactants is comparable to the reaction rate, however, mixing can have a significant impact.

The characteristic chemical reaction time t_r or characteristic time scale of the chemistry may be calculated from the reaction rate expression. For a single reaction,

$$t_r = \frac{C_0}{r(C_0, T_0)} \quad (19-51)$$

where C_0 is a reference concentration of the limiting reactant and T_0 is a reference temperature. For a first-order reaction, $t_r = 1/k$, where k (s^{-1}) is the rate constant.

Mixing may occur on several scales: on the reactor scale (macro), on the scale of dispersion from a feed nozzle or pipe (meso), and on a molecular level (micro). Examples of reactions where mixing is important include fast consecutive-parallel reactions where reactant concentrations at the boundaries between zones rich in one or the other reactant being mixed can determine selectivity.

Much of the literature around mixing times has been developed around the mixing of two liquids in agitated stirred tanks. The macromixing time t_{ma} can be defined as the time for the concentration to settle within, say, ± 2 percent of its final value (98 percent homogeneity). With a standard turbine in a baffled tank and $Re (= nD_a^2 \rho/\mu) > 5000$,

$$t_{ma} \cong \frac{4}{n} \left(\frac{D_t}{D_a} \right)^2 \left(\frac{H}{D_t} \right) \quad (19-52)$$

where n is the stirrer speed, D_t is the tank diameter, D_a is the agitator diameter, and H is the height of the tank; t_{ma} varies inversely with the stirrer speed. In a case of a tank with an aspect ratio of unity and $D_a/D_t = \frac{1}{3}$, $nt_{ma} \cong 36$. For a stirrer speed of 120 rpm, the macromixing time is 18 s.

The circulation time t_{cir} is the time to circulate the reactor contents once:

$$t_{cir} = \frac{V_r}{q} \quad (19-53)$$

where q is the flow induced by the impeller. The induced flow is about 2 times the direct discharge from the turbine, creating uncertainty in estimating q ; t_{cir} is roughly one-fourth of the macromixing time.

The micromixing time t_{mi} is the time required for equilibration of the smallest eddies by molecular diffusion, engulfment, and stretching. For liquid-liquid mixing, stretching and engulfment are limiting factors and t_{mi} depends on the kinematic viscosity (μ/ρ) and the local rate of energy dissipation $\phi\bar{\epsilon}$:

$$t_{mi} = 17 \left(\frac{\mu/\rho}{\phi\bar{\epsilon}} \right)^{1/2} \quad (19-54)$$

For a kinematic viscosity of 10^{-6} m²/s and an energy dissipation of 1.0 W/kg, $t_{mi} = 0.017$ s. The local energy dissipation will vary greatly with position in the tank with its greatest value near the tip of the impeller. Injection of reactant at the point of greatest turbulence minimizes t_{mi} .

The mesomixing time t_{me} is the time for “significant mixing” of an incoming jet of feed liquid with the surrounding fluid. A formula for estimating t_{me} is the time for turbulent diffusion to transport liquid over a distance equal to the feed pipe diameter d_0 .

$$t_{me} \cong \frac{5.3d_0^2}{(\phi\bar{\epsilon})^{1/3}D_a^{4/3}} \quad (19-55)$$

If the diameter of the pipe is proportional to the agitator diameter, t_{me} increases as $d_0^{2/3}$. Since t_{me} depends on the local energy dissipation, it is sensitive to location. Typically, $t_{me} (> t_{mi})$ is a fraction of a second or so.

A parameter used to diagnose mixing issues for reactive systems is the *Damköhler number* Da which is the ratio of the mixing time to the reaction time, $Da = t_{mixing}/t_r$. Small Da numbers ($Da \ll 1$) indicate relatively rapid mixing compared to the reaction, so mixing is less important. In contrast, large Da numbers ($Da \gg 1$) indicate a need to consider mixing issues. A more complete discussion of the topic is provided in the appropriate section of the Handbook, in Baldyga and Bourne (*Turbulent Mixing and Chemical Reactions*, Wiley, 1998), and in Harriott (*Chemical Reactor Design*, Marcel Dekker, 2003).

SINGLE-PHASE REACTORS

Section 7 of this Handbook presents the theory of reaction kinetics that deals with homogeneous reactions in batch and continuous equipment. Single-phase reactors typically contain a liquid or a gas with (or without) a homogeneous catalyst that is processed in a reactor at conditions required to complete the desired chemical transformation.

LIQUID PHASE

Batch reactions of single or miscible liquids are often done in stirred or pump-around tanks. The agitation is needed to mix multiple feeds and to enhance heat exchange with cooling (or heating media) during the process. Topics that acquire special importance on an industrial scale are the quality of mixing in tanks and the residence time distribution in vessels where plug flow may be the goal. A special case is that of laminar and related flow distributions characteristic of nonnewtonian fluids, which often occurs in polymerization reactors. The information about agitation and heat transfer in tanks is described in the relevant Handbook section.

Homogeneous Catalysis A catalyst is a substance, usually used in small amounts relative to the reactants, that increases the rate of a reaction without being consumed in the process. Liquid-phase reactions are often conducted in the presence of homogeneous catalysts. Typically, homogeneous catalysts are ions or metal coordination

complexes or enzymes in aqueous solution. The specific action of a particular metal complex can be altered by varying the ligands (or coordination number) of the complex or the oxidation state of the central metal atom. Some examples of homogeneous catalysts in industrial practice include hydrolysis of esters by hydronium (H_3O^+) or hydroxyl (OH^-) ions, hydroformylation of olefins using Rh or Co carbonyls, decomposition of hydrogen peroxide by ferrous ions, decomposition of nitramides catalyzed by acetate ion, inversion of sucrose by HCl, halogenation of acetone by H^+ and OH^- , and hydration of isobutene by acids. A characteristic of homogeneous catalysis is that, compared to solid catalysis, the reaction(s) proceeds under relatively mild conditions. A key issue associated with homogeneous catalysis is the difficulty of separating product and catalyst.

In stirred tanks, the power input to agitate the tank will depend on the physical properties of the liquid. In tubular reactors, the axial dispersion in empty tubes may be estimated [e.g., Wen in Petho and Noble (eds.), *Residence Time Distribution Theory in Chemical Engineering*, Verlag Chemie, 1982] as

$$\frac{1}{Pe} = \frac{1}{(Re)(Sc)} + \frac{(Re)(Sc)}{192} \quad 1 \leq Re \leq 2000 \quad \text{and} \quad 0.2 \leq Sc \leq 1000 \quad (19-56)$$

$$\frac{1}{Pe} = \frac{3 \times 10^7}{(Re)^{2.1}} + \frac{1.35}{(Re)^{0.125}} \quad Re \geq 2000$$

In a general case, the velocity may also be a function of radius. One such case is that of laminar flow which is characterized by a parabolic velocity profile. The velocity at the wall is zero while that at the centerline is twice the average velocity. In such cases, a momentum balance equation is solved along with the equations for heat and mass transfer, and each equation contains terms for the radial contribution. Laminar flow can be avoided by mixing over the cross-section. For this purpose, *in-line* static mixers can be provided. For very viscous materials and pastes, screws of the type used for pumping and extrusion are used as reactors. When the temperature of the reactants changes during the course of the reaction (due to either the heat of reaction or the work required to keep the contents well mixed), material and energy balance equations have to be solved simultaneously.

Examples

- Crude oil is heated to temperatures at which it thermally cracks into gasoline and distillate products and lower-molecular-weight gases. This liquid cracking process is referred to as visbreaking. A schematic of the process and the effect of operating variables on performance is shown in Fig. 19-12.
- The Wacker process for the oxidation of ethylene to acetaldehyde with $PdCl_2/CuCl_2$ at $100^\circ C$ ($212^\circ F$) with 95 percent yield and 95 to 99 percent conversion per pass.
- The OXO process for higher alcohols: $CO + H_2 + C_3H_6 \Rightarrow n\text{-butanal} \Rightarrow$ further processing. The catalyst is a rhodium triphenylphosphine coordination compound at $100^\circ C$ ($212^\circ F$), 30 atm (441 psi).
- Acetic acid from methanol by the Monsanto process, $CH_3OH + CO \Rightarrow CH_3COOH$, rhodium iodide catalyst, 3 atm (44 psi), $150^\circ C$ ($302^\circ F$), 99 percent selectivity.

See a review of industrial processes that employ homogeneous catalysts by Jennings (ed.), *Selected Developments in Catalysis*, Blackwell Scientific, 1985.

GAS PHASE

There are few examples of industrial processes with pure gas-phase reactions. The most common and oldest example is combustion. Although termed *homogeneous*, most gas-phase reactions take place in contact with solids, either the vessel wall or particles as heat carriers. With inert solids, the only complication is with heat transfer. Several of these reactions are listed in Table 19-1. Whenever possible, liquefaction of gas-phase systems is considered to take advantage of the higher rates of liquid reactions, to utilize liquid homogeneous catalysts, or to keep equipment size down.

The specific type of equipment used for gas-phase reactions depends on the conditions required for undertaking the reaction. Examples of noncatalytic gas-phase reactions are shown in Fig. 19-13. In general, mixing of feed gases and temperature control are major process requirements. Gases are usually mixed by injecting one of the streams into the rest of the gases using a high-speed nozzle, as in the flame reactor (Fig. 19-13d).

Examples

- In the cracking of light hydrocarbons and naphtha to olefins, heat is supplied from combustion gases through tubes in fired heaters at $800^\circ C$ ($1472^\circ F$) and sufficiently above atmospheric pressure to overcome pressure drop. Superheated steam is injected to bring the temperature up quickly and retard coke deposition. The reaction time is 0.5 to 3.0 s, followed by rapid quenching. The total tube length of an industrial furnace may be more than 1000 m. Some other important gas-phase cracking processes include conversion of toluene to benzene, diphenyl to benzene, dicyclopentadiene to cyclopentadiene, and 1-butene to butadiene. Figure 19-13a shows a cracking furnace.
- The Wulf process for acetylene by pyrolysis of natural gas utilizes a heated brick checkerwork on a 4-min cycle of heating and reacting. Heat is transferred by direct contact with solids that have been pre-

heated by combustion gases. The process is a cycle of alternate heating and reacting periods. The temperature play is $15^\circ C$ ($27^\circ F$), peak temperature is $1200^\circ C$ ($2192^\circ F$), residence time is 0.1 s of which 0.03 s is near the peak (Faith, Keyes, and Clark, *Industrial Chemicals*, vol. 27, Wiley, 1975).

- The Wisconsin process for the fixation of nitrogen from air operates at $2200^\circ C$ ($3992^\circ F$), followed by extremely rapid quenching to freeze the small equilibrium content of nitrogen oxide that is made [Ermenc, *Chem. Eng. Prog.* **52**: 149 (1956)]. A pebble heater recirculates refractory pebbles continuously through heating and reaction zones. Such moving-bed units have been proposed for cracking to olefins but have been obsolesced like most moving-bed reactors.
- Acetylene may be produced from light hydrocarbons and naphthas by injecting inert combustion gases directly into the reacting stream in a flame reactor. Figure 19-13a and d shows two such devices; Fig. 19-13e shows a temperature profile (with reaction times in milliseconds).
- Oxidative pyrolysis of light hydrocarbons to acetylene is conducted in a special burner, at 0.001- to 0.01-s reaction time, peak at $1400^\circ C$ ($2552^\circ F$), followed by rapid quenching with oil or water. A portion of a combustible reactant is burned by adding a small amount of air or oxygen to generate the reaction temperatures needed.
- Chlorination reactions of methane and other hydrocarbons typically result in a mixture of products whose relative amounts can be controlled by varying the Cl/hydrocarbon ratio and recycling unwanted derivatives. For example, one can recycle the mono and di derivatives when only the tri and tetra derivatives are of value or keep the chlorine ratio low when emphasizing the lower derivatives. Temperatures are normally kept in the range of 230 to $400^\circ C$ (446 to $752^\circ F$) to limit carbon formation but may be raised to $500^\circ C$ ($932^\circ F$) when favoring CCl_4 . Exothermic processes utilize cooling through heat-transfer surfaces or cold shots. Shell-and-tube reactors with small-diameter tubes, towers with internal recirculation of gases, or multiple stages with intercooling may be used for these reactions.

SUPERCRITICAL CONDITIONS

At near-critical or supercritical conditions, a heterogeneous reaction mixture (e.g., of water, organic compounds, and oxygen) becomes homogeneous and has some liquid and gaseous properties. The rate of reaction may be considerably accelerated because of (1) the higher gas-phase diffusivity, (2) increase of concentration due to liquidlike density, (3) enhanced solubility, and (4) increase of the specific rate of reaction by pressure. The mole fraction solubility of naphthalene in ethylene at $35^\circ C$ ($95^\circ F$) goes from 0.004 at 20 atm (294 psi) to 0.02 at 100 atm (1470 psi) and 0.05 at 300 atm (4410 psi). High destructive efficiencies (above 99.99 percent) of complex organic pollutant compounds in water can be achieved with residence times of under 5 min at near-critical conditions. The critical properties of water are $374^\circ C$ ($705^\circ F$) and 218 atm (3205 psi).

We are not aware of any industrial implementation of supercritical conditions in reactors. Two areas of potential interest are wastewater treatment (for instance, removal of phenol or organic compounds) and reduction of coke on refining catalysts by keeping heavy oil decomposition products in solution. A pertinent reference is by Kohnstam ("The Kinetic Effects of Pressure," in *Progress in Reaction Kinetics*, Pergamon, 1970). More recent reviews of research progress are by Bruno and Ely (eds.), *Supercritical Fluid Technology*, CRC Press, 1991; Kiran and Brennecke (eds.), *Supercritical Engineering Science*, ACS, 1992.

POLYMERIZATION REACTORS

Polymerization reactors contain one or more phases. There are examples using solvents in which the reactants and products are in the liquid phase, the reactants are fed as a liquid (gas) but the products are solid, or the reactants are a slurry and the products are soluble. Phase transformations can occur, and polymers that form from the liquid phase may remain dissolved in the remaining monomer or solvent, or they may precipitate. Sometimes beads are

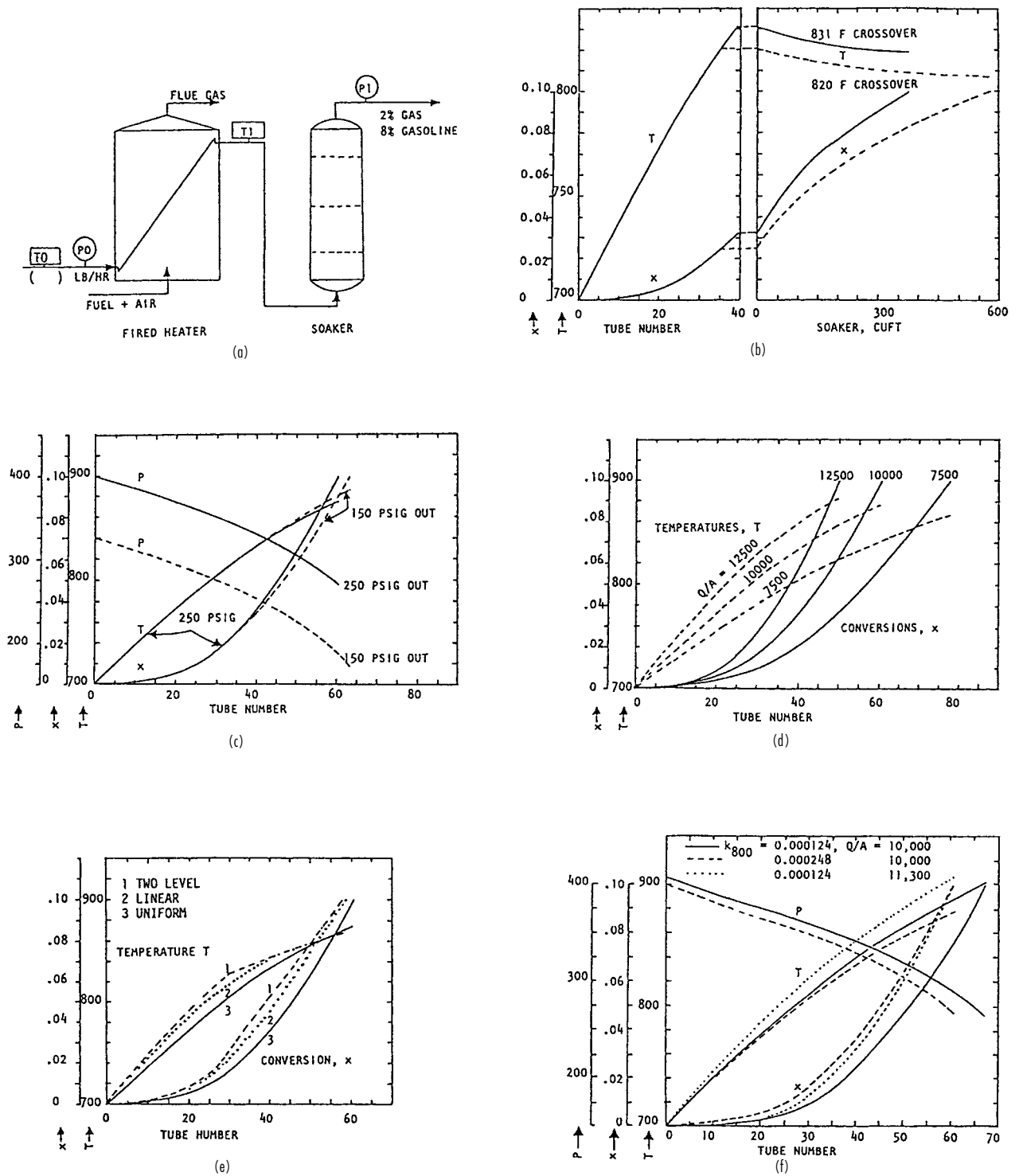


FIG. 19-12 (a) Visbreaking flow sketch, feed 160,000 lbm/h, $k_{800} = 0.000248/s$, tubes 5.05-in ID by 40 ft. (b) $Q/A = 10,000$ Btu/(ft²-h), $P_{out} = 250$ psig. (c) $Q/A = 10,000$ Btu/(ft²-h), $P_{out} = 150$ or 250 psig. (d) Three different heat fluxes, $P_{out} = 250$ psig. (e) Variation of heat flux, average 10,000 Btu/(ft²-h), $P_{out} = 250$ psig. (f) Halving the specific rate. T in °F. To convert psi to kPa, multiply by 6.895; ft to m, multiply by 0.3048; in to cm, multiply by 2.54.

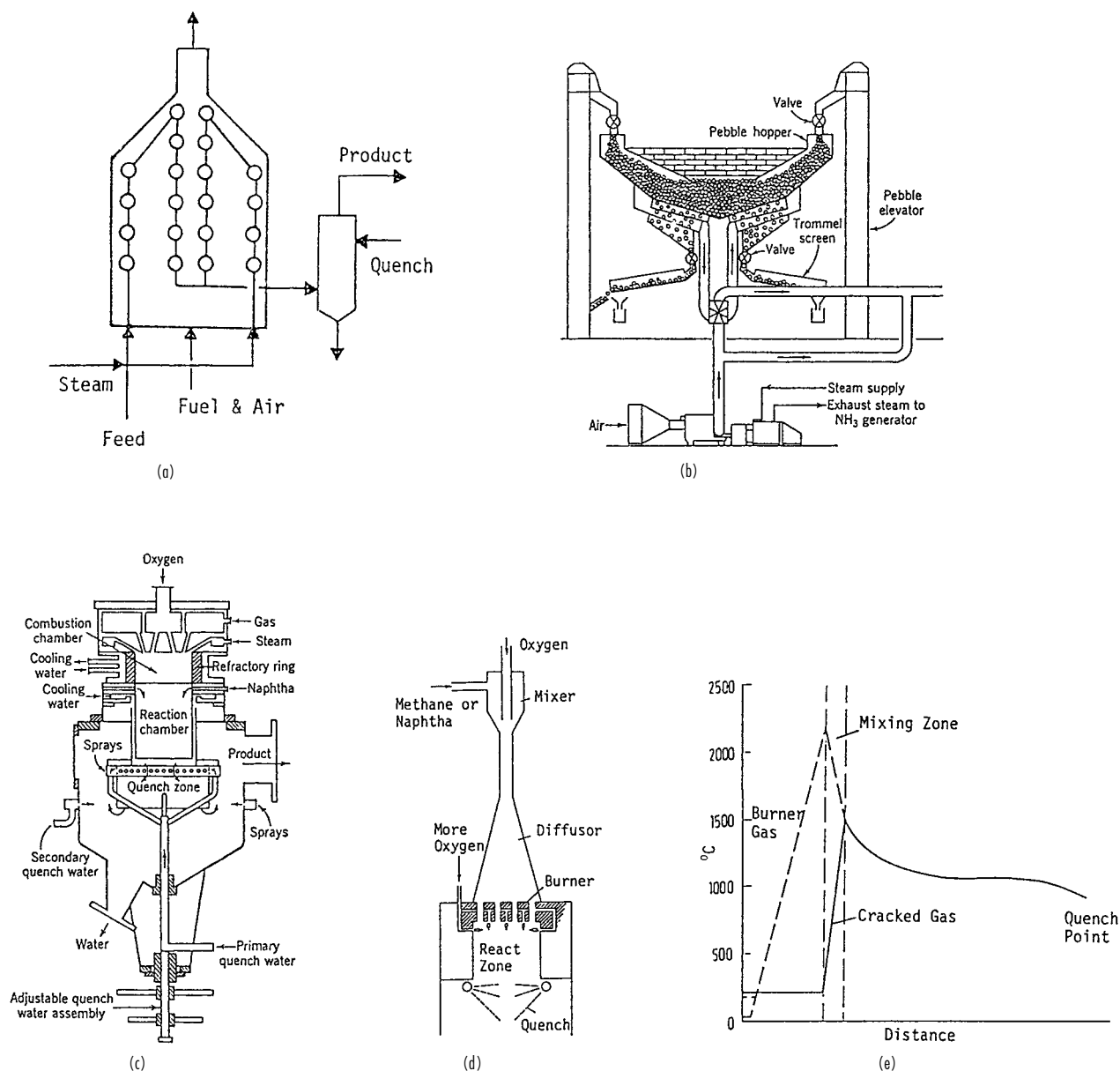


FIG. 19-13 Noncatalytic gas-phase reactions. (a) Steam cracking of light hydrocarbons in a tubular fired heater. (b) Pebble heater for the fixation of nitrogen from air. (c) Flame reactor for the production of acetylene from hydrocarbon gases or naphthas. [Patton, Grubb, and Stephenson, *Pet. Ref.* **37**(11): 180 (1958).] (d) Flame reactor for acetylene from light hydrocarbons (BASF). (e) Temperature profiles in a flame reactor for acetylene (Ullmann *Encyclopaedie der Technischen Chemie*, vol. 3, Verlag Chemie, 1973, p. 335).

formed and remain in suspension; sometimes emulsions form. In some processes, solid polymers precipitate from a gas phase into a fluidized bed containing product solids. Polymers are thought of as organic materials; however, inorganic polymers may be also synthesized (e.g., using crystallization and precipitation). Examples of inorganic polymers are zeolites.

The structure of the polymer determines its physical properties, e.g., crystallinity, refractive index, tensile strength, glass transition temperature (at which the specific volume changes slope), and processability. The average molecular weight can cover a wide range between 10^4 to 10^7 . Given the change in molecular weight, the viscosity can change dramatically as conversion increases. For example,

in styrene polymerization, the viscosity increases by a factor of 10^6 as conversion increases from 0 to 60 percent. Initiators of chain polymerization reactions have concentration as low as 10^{-8} g-mol/L so they are highly sensitive to small concentrations of poisons and impurities. The reaction time can also vary. Reaction times for butadiene-styrene rubbers are 8 to 12 h; polyethylene molecules continue to grow for 30 min, whereas ethyl acrylate in 20 percent emulsion reacts in less than 1 min, so monomer must be added gradually to keep the temperature within limits. In some cases, the adiabatic temperature rise may be very high. For example, in polymerization of ethylene, a high adiabatic temperature rise may lead to reactor safety issues by initiating runaway ethylene decomposition reactions. The reactor

19-24 REACTORS

operating conditions have to be controlled such that the possibility of *ethylene decomposition* is eliminated.

Since it is impractical to fractionate the products and reformulate them into desirable ranges of molecular weights, immediate attainment of desired properties must be achieved through the correct choice of reactor type and operating conditions, notably of distributions of residence time and temperature. Reactor selection may be made on rational grounds, for historical reasons, or to obtain a proprietary position.

Each reactor is designed based on the need for mass transfer, heat transfer, and reaction. Stirred batch (autoclave) and continuous tubular reactors are widely used because of their flexibility. In stirred tanks, ideal mixing is typically not achieved, wide variations in temperatures may result, and stagnant zones and bypassing may exist. Devices that counteract these unfavorable characteristics include inserts that cause radial mixing, scraping impellers, screw feeders, hollow-shaft impellers (with coolant flow through them), recirculation using internal and external draft tubes, and so on. The high viscosity of bulk and melt polymerization

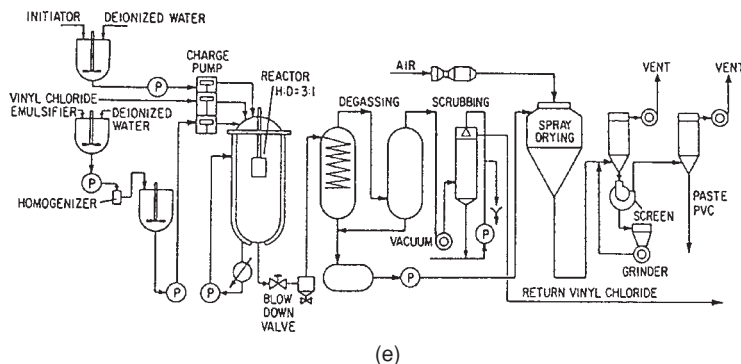
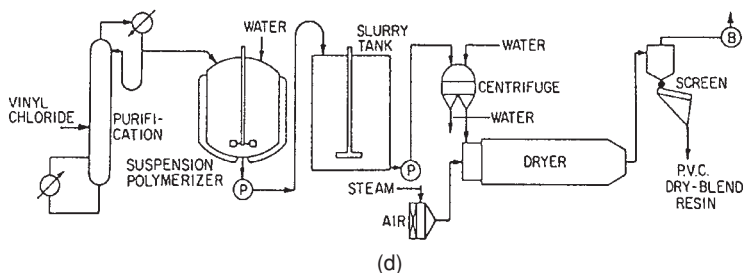
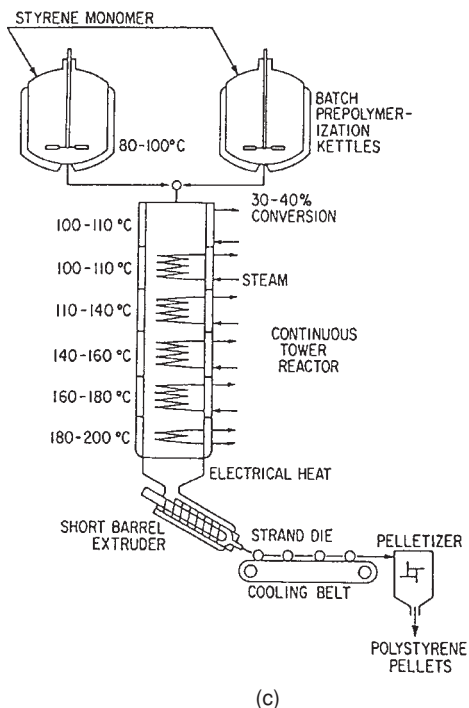
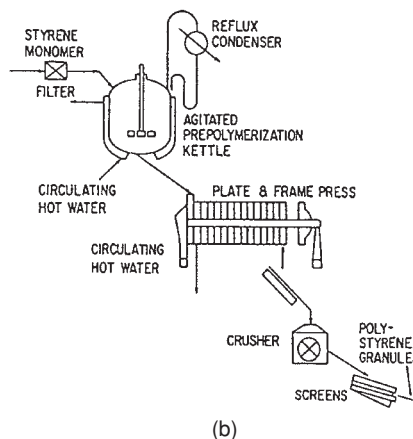
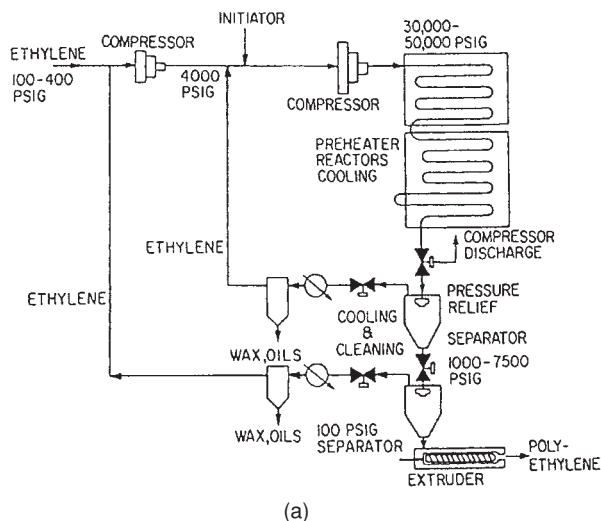


FIG. 19-14 Batch and continuous polymerizations. (a) Polyethylene in a tubular flow reactor, up to 2 km long by 6.4-cm ID. (b) Batch process for polystyrene. (c) Batch-continuous process for polystyrene. (d) Suspension (bead) process for polyvinylchloride. (e) Emulsion process for polyvinylchloride. (Ray and Laurence, in Lapidus and Amundson (eds.), *Chemical Reactor Theory Review*, Prentice-Hall, 1977.)

reactions is avoided with solution, bead, or emulsion polymerization, and more favorable RTDs are obtained. In tubular reactors, such as for low-density polyethylene production, there are strong temperature gradients in the radial direction and cooling may become an issue. These reactors are operated in a single phase, often with multiple catalyst injection points, and the reactor can be several miles in length. Examples of polymerization reactors are illustrated in Fig. 19-14.

FLUID-SOLID REACTORS

A number of industrial reactors involve contact between a fluid (either a gas or a liquid) and solids. In these reactors, the fluid phase contacts the solid catalyst which may be either stationary (in a fixed bed) or in motion (particles in a fluidized bed, moving bed, or a slurry). The solids may be a catalyst or a reactant (product). Catalyst and reactor selection and design largely depend upon issues related to heat transfer, pressure drop and contacting of the phases. In many cases, continuous regeneration or periodic replacement of deteriorated or deactivated catalyst may be needed.

HETEROGENEOUS CATALYSTS

Solid catalysts may have a homogeneous catalyst (or enzyme) or catalytic ingredients dispersed on a support. The support may be organic or inorganic in nature. For example, a catalyst metal atom may be anchored to the polymer (e.g., polystyrene) through a group that is chemically bound to the polymer with a coordinating site such as $-P(C_6H_5)_2$ or $-C_5H_4$ (cyclopentadienyl). Immobilized catalysts have applications in hydrogenation, hydroformylation, and polymerization reactions [Lieto and Gates, *ChemTech*, pp. 46–53 (Jan. 1983)]. Metal or mixed metal oxides may be dispersed on amorphous materials (such as carbon, silica, or alumina) or exchanged into the cages of a zeolite. Expensive catalytic metal ingredients, such as Pt or Pd, may be <1 percent of catalyst weight. Catalysts may be shaped as monoliths, shaped pellets, spheres, or powders. Some exceptions are bulk catalysts such as platinum gauzes for the oxidation of ammonia and synthesis of hydrogen cyanide, which are in the form of several layers of fine-mesh catalyst gauze.

The catalyst support may either be inert or play a role in catalysis. Supports typically have a high internal surface area. Special shapes (e.g., trilobed particles) are often used to maximize the geometric surface area of the catalyst per reactor volume (and thereby increase the reaction rate per unit volume for diffusion-limited reactions) or to minimize pressure drop. Smaller particles may be used instead of shaped catalysts; however, the pressure drop increases and compressor costs become an issue. For fixed beds, the catalyst size range is 1 to 5 mm (0.04 to 0.197 in). In reactors where pressure drop is not an issue, such as fluidized and transport reactors, particle diameters can average less than 0.1 mm (0.0039 in). Smaller particles improve fluidization; however, they are entrained and have to be recovered. In slurry beds the diameters can be from about 1.0 mm (0.039 in) down to 10 μ m or less.

The support has an internal pore structure (i.e., pore volume and pore size distribution) that facilitates transport of reactants (products) into (out of) the particle. Low pore volume and small pores limit the accessibility of the internal surface because of increased diffusion resistance. Diffusion of products outward also is decreased, and this may cause product degradation or catalyst fouling within the catalyst particle. As discussed in Sec. 7, the effectiveness factor η is the ratio of the actual reaction rate to the rate in the absence of any diffusion limitations. When the rate of reaction greatly exceeds the rate of diffusion, the effectiveness factor is low and the internal volume of the catalyst pellet is not utilized for catalysis. In such cases, expensive catalytic metals are best placed as a shell around the pellet. The rate of diffusion may be increased by optimizing the pore structure to provide larger pores (or macropores) that transport the reactants (products) into (out of) the pellet and smaller pores (micropores) that provide the internal surface area needed for effective catalyst dispersion. Micropores typically have volume-averaged diameters of 50 to

200 \AA with macropore diameters of 1000 to 5000 \AA . The pore volume and the pore size distribution within a porous support determine its surface area. The surface area of supports can range from 0.06 m^2/mL (18,300 ft^2/ft^3) to 600 m^2/mL (1.83×10^8 ft^2/ft^3) and above. Higher pore volume catalysts have higher diffusion rate at the expense of reduced crush strength and increased particle attrition.

The effective diffusion coefficient D_{eff} determines the rate of diffusion and therefore the volume of the catalyst utilized. The coefficient is determined by the nature of the diffusing species and the pore structure of the catalyst. It has been found to be directly proportional to the product of diffusivity and porosity ϵ and inversely proportional to the tortuosity τ (that is empirically determined). In large pores of >1000 \AA , where molecules collide with one another and the interaction with the pore walls is minimal, molecular (or bulk) diffusion is important. For pore diameters in the range of 50 to 200 \AA , collision with the pore walls becomes more important, and this regime is called the Knudsen diffusion regime. In an extreme case where the size of the molecule is comparable to the size of the pore, the size and configuration of the pores themselves affect diffusivity. This happens when the diffusing molecule is very large (as in transporting large organometallic molecules through catalyst pores in heavy oil hydrotreating) or the pore is very small (as in diffusion in zeolites), or both (e.g., see Sec. 7 for diffusion regimes). ϵ ranges from 0.1 to 0.5 and τ ranges from 1 to 7. In the absence of other information, a τ value of 3 to 4 may be used; however, it is best measured for the catalyst of interest. Expressions for estimating the effective diffusion coefficient are available in textbooks such as Satterfield (*Heterogeneous Catalysis in Practice*, McGraw-Hill, 1991).

The effectiveness factor η is the ratio of the rate of reaction in a porous catalyst to the rate in the absence of diffusion (i.e., under bulk conditions). The theoretical basis for η in a porous catalyst has been discussed in Sec. 7. For example, for an isothermal first-order reaction

$$r_c = k\eta C_i \quad (19-57)$$

where C_i is the bulk concentration of the reactant. As discussed previously, η is a function of the ratio of the rate of reaction to diffusion, also called the Thiele modulus ϕ . As the rate constant increases, η decreases and eventually reaches an asymptotic value (that depends on ϕ). Under these conditions, $k\eta$ increases as $k^{1/2}$. The role of diffusion and reaction in porous catalysts, however, is more complicated in a case where heat effects are present. In addition to the mass conservation equation around the pellet, an energy balance equation is required. Two additional dimensionless parameters are needed for estimating an effectiveness factor:

$$\beta = -\frac{\Delta H_r D_{\text{eff}} C_0}{\lambda T_s} \quad \text{and} \quad \gamma = \frac{E}{RT_s} \quad (19-58)$$

where ΔH_r is the heat of reaction, λ is the thermal conductivity of the catalyst, E is the activation energy, and R is the universal gas constant. The dimensionless parameter β , known as the Prater number, is the ratio of the heat generation to heat conduction within the pellet and is a measure of the intra-particle temperature increase; γ is the dimensionless activation energy for the reaction. For an exothermic reaction, the temperature inside the catalyst pellet is greater than or equal to the surface temperature. The maximum steady-state temperature inside the pellet is $T_s(1 + \beta)$. Figure 19-15 is one of several cases examined by Weisz and Hicks for a first-order reaction in an adiabatic

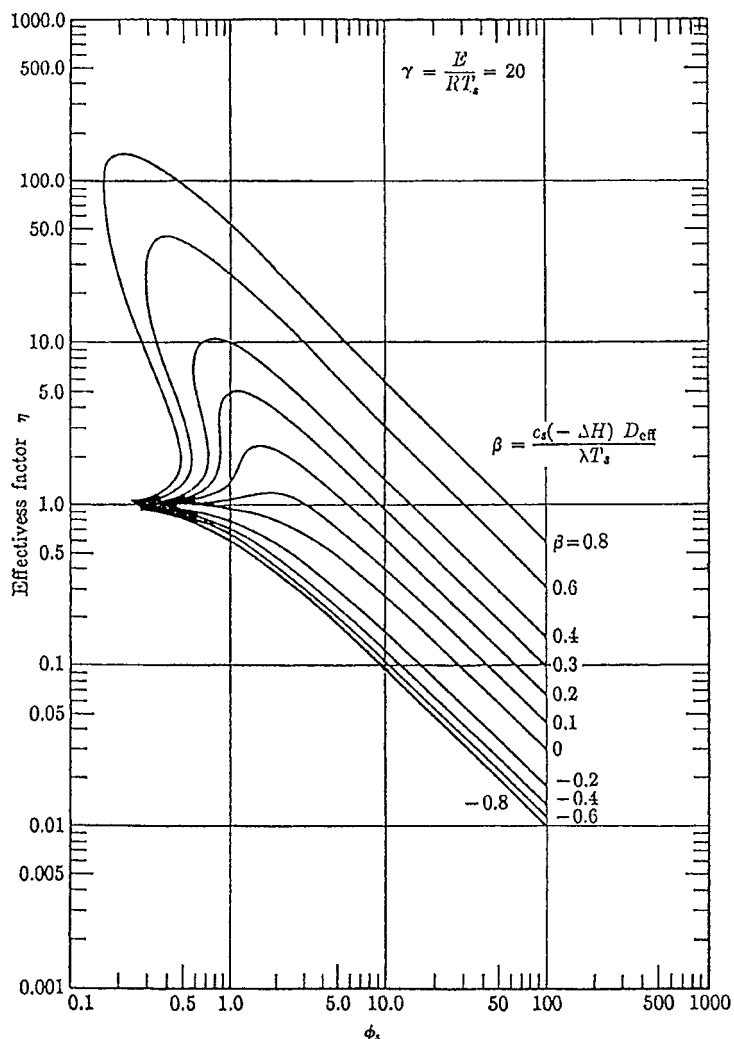


FIG. 19-15 Effectiveness factors versus Thiele modulus for a first-order reaction in spheres under adiabatic conditions. [Weisz and Hicks, *Chem. Eng. Sci.*, **17**: 265 (1962).]

catalyst pellet [*Chem. Eng. Sci.* **17**: 263 (1962)]. Although this predicts some very large values of η in some ranges of the parameters, these values are often not realized in commercial reactors (see Table 19-5). The modified Lewis number defined as $Lw' = \lambda_w/\rho_s C_{ps} D_{\text{eff}}$ can determine the transient temperature inside the pellet, which can be much larger than the steady-state temperature.

The concept of an effectiveness factor is useful in estimating the reaction rate per catalyst pellet (volume or mass). It is, however, mainly useful for simple reactions and simple kinetics. When there are complex reaction pathways, the concept of effectiveness factor is no longer easily applicable, and species and energy balance equations inside the particle may have to be solved to obtain the reaction rates per unit volume of

TABLE 19-5 Parameters of Some Exothermic Catalytic Reactions

Reaction	β	γ	$\gamma\beta$	Lw'	ϕ
NH ₃ synthesis	0.000061	29.4	0.0018	0.00026	1.2
Synthesis of higher alcohols from CO and H ₂	0.00085	28.4	0.024	0.00020	—
Oxidation of CH ₃ OH to CH ₂ O	0.0109	16.0	0.175	0.0015	1.1
Synthesis of vinyl chloride from acetylene and HCl	0.25	6.5	1.65	0.1	0.27
Hydrogenation of ethylene	0.066	23–27	2.7–1	0.11	0.2–2.8
Oxidation of H ₂	0.10	6.75–7.52	0.21–2.3	0.036	0.8–2.0
Oxidation of ethylene to ethyleneoxide	0.13	13.4	1.76	0.065	0.08
Dissociation of N ₂ O	0.64	22.0	1.0–2.0	—	1–5
Hydrogenation of benzene	0.12	14–16	1.7–2.0	0.006	0.05–1.9
Oxidation of SO ₂	0.012	14.8	0.175	0.0415	0.9

SOURCE: After Hlavacek, Kubicek, and Marek, *J. Catal.*, **15**, 17, 31 (1969).

catalyst. Dumesic et al. (*The Microkinetics of Heterogeneous Catalysis*, American Chemical Society, 1993) use microkinetic analysis to elucidate reaction pathways of several commercial catalysts.

Another complication is the fact that Fig. 19-15 was developed for the constant-concentration boundary condition, $C|_{r=R} = C_0$. In a more general case, external mass-transfer limitations will need to be included.

$$k_m a(C_0 - C_i) = r_c(C_i) = \kappa \eta C_i \quad (19-59)$$

where k_m is the external mass-transfer coefficient obtained from literature correlations and a is the external surface area per unit pellet volume. The above equation will have to be solved for C_i , the concentration of the reactant on the external surface of the catalyst, so that the rate per pellet can be obtained. The reaction rate per unit reactor volume then becomes $r_c(1 - \epsilon_b)$, where ϵ_b is the bed void fraction.

A further complication is that catalyst activity declines with time. Catalysts may deactivate chemically (via poisons and masking agents), thermally (via support sintering), or mechanically (through attrition). Commercial catalyst life can range from a second to several years. For example, in refinery fluid catalytic cracking, the catalyst may lose most of its activity in less than 10 s, and a transport bed reactor coupled with a fluidized-bed regenerator is used to circulate catalyst. In contrast, a refinery hydroprocessing catalyst deactivates very slowly and a fixed-bed reactor may be used without catalyst replacement for one or more years. The deactivation rate expression may often be inferred from aging experiments undertaken under pilot-plant conditions of constant temperature or conversion. Since accelerated-aging experiments are often difficult (especially when the concentration of reactant or products affects the deactivation rate), reactor designs where the catalyst charge provides the required performance between regeneration cycles is typically based on good basic data and experience. The literature describes approaches aimed at managing deactivation. In the case of platinum reforming with fixed beds, a large recycle of hydrogen prevents coke deposition while a high temperature compensates for the retarding effect of hydrogen on this essentially dehydrogenating process. Fluidized beds are largely isothermal and can be designed for continuous regeneration; however, they are more difficult to operate, require provisions for dust recovery, suffer from backmixing, and are more expensive. Catalyst deactivation mechanisms and kinetics are discussed in detail in Sec. 7 of the Handbook.

A catalyst for a particular chemical transformation is selected using knowledge of similar chemistry and some level of empirical experimentation. Solid catalysts are widely used due to lower cost and ease of separation from the reaction medium. Their drawbacks include a possible lack of specificity and deactivation that can require reactor shutdown for catalyst regeneration or replacement.

There are number of useful books on catalysis. Information on catalysts and processes is presented by Thomas (*Catalytic Processes and Proven Catalysts*, Academic Press, 1970), Pines (*Chemistry of Catalytic Conversions of Hydrocarbons*, Academic Press, 1981), Gates et al. (*Chemistry of Catalytic Processes*, McGraw-Hill, 1979), Matar et al. (*Catalysis in Petrochemical Processes*, Kluwer Academic Publishers, 1989), and Satterfield (*Heterogeneous Catalysis in Industrial Practice*, McGraw-Hill, 1991). The books by Thomas (*Catalytic Processes and Proven Catalysts*, Academic Press, 1970), Butt and Petersen (*Activation, Deactivation and Poisoning of Catalyst*, Academic Press, 1988), and Delmon and Froment (*Catalyst Deactivation*, Elsevier, 1980) provide several examples of catalyst deactivation. Catalyst design is discussed by Trimm (*Design of Industrial Catalysts*, Elsevier, 1980), Hegedus et al. (*Catalyst Design Progress and Perspectives*, Wiley, 1987), and Becker and Pereira (*Catalyst Design*, Marcel Dekker, 1993). A thorough review of catalytic reactions and catalysts arranged according to the periodic table is in a series by Roiter (ed.) (*Handbook of Catalytic Properties of Substances*, in Russian, 1968). Stiles (*Catalyst Manufacture*, Dekker, 1983) discusses catalyst manufacture.

CATALYTIC REACTORS

Due to the considerations noted above, reactor selection will depend on the type of catalyst chosen and its activity, selectivity, and deactiva-

tion behavior. Some reactors with solid catalysts are represented in Fig. 19-16.

Wire Gauzes Wire screens are used for very fast catalytic reactions or reactions that require a bulk noble metal surface for reaction and must be quenched rapidly. The nature and morphology of the gauze or the finely divided catalyst are important in reactor design. Reaction temperatures are typically high, and the residence times are on the order of milliseconds.

Since noble metals are expensive, the catalyst cost is typically high. The physical properties of the gauze pack are important to determine performance, selectivity, and catalyst replacement strategy. The gauze is typically mounted over the top of a heat exchanger tube sheet or over porous ceramic bricks that are laid over the tube sheet. The gauze pack may be covered with a ceramic blanket to minimize radiation losses. From a modeling standpoint, the external surface area per gauze volume and the external mass-transfer coefficient for each component are important parameters, and the reaction rate per unit volume of catalyst may be limited by the rate of external mass transfer. The reaction rate can then be included into a corresponding PFR or dispersion model to obtain estimates of conversion and selectivity.

Examples

- In ammonia oxidation, a 10 percent NH_3 concentration in air is oxidized by flow through a fine-gauze catalyst made of 2 to 10 percent Rh in Pt, 10 to 30 layers, 0.075-mm-diameter (0.0030-in) wire. Contact time is 0.0003 s at 750°C (1382°F) and 7 atm (103 psi) followed by rapid quenching.
- In hydrogen cyanide synthesis using the Andrussov process, air, methane, and ammonia are fed over 15 to 50 layers of noble metal gauze at 1050 to 1150°C at near atmospheric pressure.

Monolith Catalysts For fast reactions that may require a slightly higher residence time than gauzes or that do not benefit from the bulk noble metal gauze structure, monoliths may be used. Most often, the monolith catalyst is an extruded ceramic honeycomb structure that has discrete channels that traverse its length. The catalytic ingredients may be dispersed on a high surface area support and coated on an inert honeycomb. In some cases, the catalyst paste itself may be extruded into a monolith catalyst. Monoliths may also be made of metallic supports. Stainless steel plates (or wire mesh) with ridges may be coated with catalysts and stacked one against the other in a reactor. Corrugated stainless steel layers may alternate in between flat sheets to form the structure. A variant is a stainless steel sheet that is corrugated in a herringbone pattern, coated with catalyst and then rolled (or folded back and forth onto itself) into a reactor module. Examples of cross-sections of the types of monoliths used in industry are shown in Fig. 19-17.

The thickness of monolith walls is adjusted according to the materials of construction (ceramic honeycombs have thicker walls to provide mechanical strength). The size of the channels is selected according to the application. For example, for particulate-laden gases, a larger channel size ceramic monolith and a higher linear velocity allow the particles to pass through the catalyst without plugging the channel. In contrast, for feed that does not contain particles, smaller channel monoliths may be used. The cell density of the monolith may vary between 9 and 600 cells per square inch.

A monolith catalyst has a much higher void fraction (between 65 and 91 percent) than does a packed bed (which is between 36 and 45 percent). In the case of small channels, monoliths have a high geometric surface area per unit volume and may be preferred for mass-transfer-limited reactions. The higher void fraction provides the monolith catalyst with a pressure drop advantage compared to fixed beds.

A schematic of a monolith catalyst is shown in Fig. 19-18a. In cases where pressure drop is limiting, such as for CO oxidation in cogeneration power plant exhausts, monolith catalyst panels may be stacked to form a thin (3- to 4-in-thick) wall. The other dimensions of the wall can be on the order of 35 × 40 ft. CO conversion is over 90 percent with a pressure drop across the catalyst of 1.5 in of water. Alternatively, the monolith may be used as a catalyst and filter, as is the case for a diesel particulate filter. In this case, monolith channels are blocked and the exhaust gases from a diesel truck are forced through the walls (Fig. 19-18b). The filter is a critical component in a continuous regenerable trap. NO in the exhaust

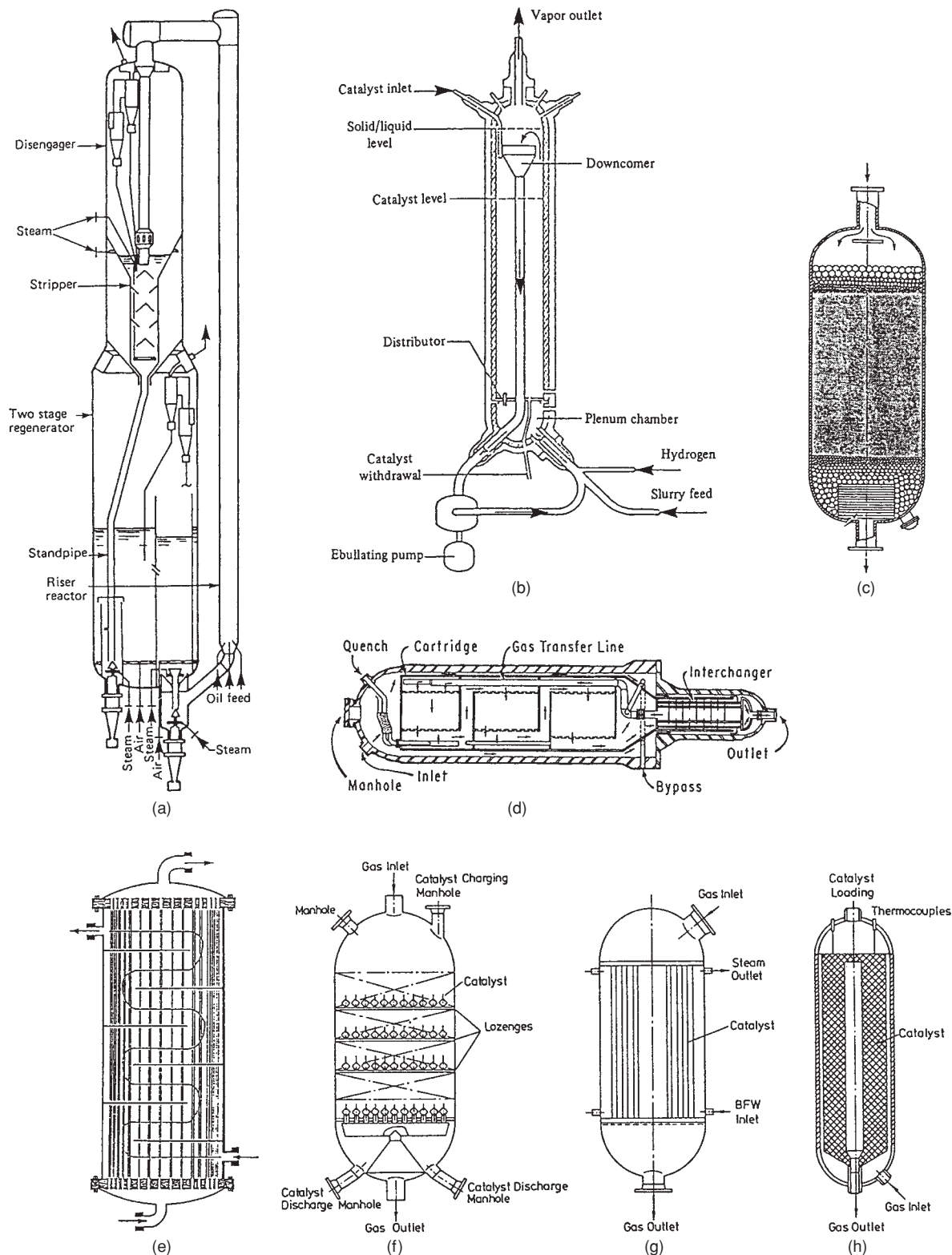


FIG. 19-16 Reactors with solid catalysts. (a) Fluid catalytic cracking riser-regenerator with fluidized zeolite catalyst, 540°C. (b) Ebullating fluidized bed for conversion of heavy stocks to gas and light oils. (c) Fixed-bed unit with support and hold-down zones of larger spheres. (d) Horizontal ammonia synthesizer, 26 m long without the exchanger (*M W Kellogg Co.*). (e) Shell-and-tube vessel for hydrogenation of crotonaldehyde has 4000 packed tubes, 30-mm ID, 10.7 m long (after Berty, in Leach (ed.), *Applied Industrial Catalysis*, vol. 1, Academic Press, 1983, p. 51). (f), (g), (h) Methanol synthesizers, 50 to 100 atm, 230 to 300°C, Cu catalyst; ICI quench type, Lurgi tubular, Haldor Topsoe radial flow (*Marschner and Moeller*, in Leach, loc. cit.). To convert atm to kPa, multiply by 101.3.

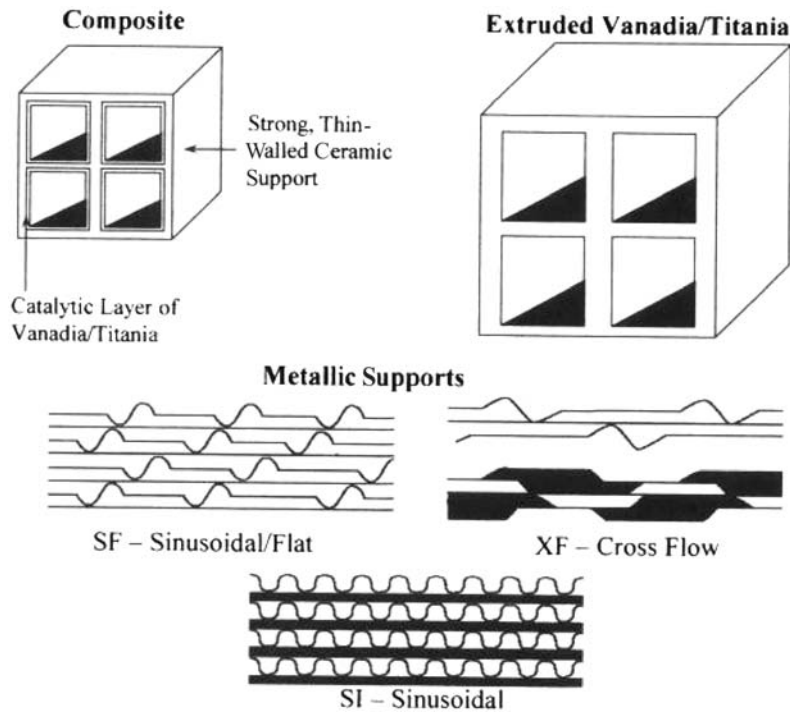


FIG. 19-17 Types of monolith catalysts. (Fig. 12.9 in Heck, Farrauto, and Gulati, *Catalytic Air Pollution Control: Commercial Technology*, Wiley-Interscience, 2002.)

gases is oxidized into NO_2 that reacts with the soot trapped in the walls of the filter to regenerate it in situ.

Modeling considerations for monoliths are similar to those of gauze catalysts; however, since the flow and temperature in each channel may be assumed to be identical to those in the next channel, the solution for a single channel may reflect the performance of the reactor. For an application in which the reaction rate is mass-transfer-limited, the reactant concentration at the wall of the catalyst is much lower than in the bulk and may be neglected. In such a case, the fractional conversion ξ is

$$\xi = 1 - e^{-k_a a t} = 1 - \exp\left(-\frac{\text{Sh } aL}{\text{Sc Re}}\right) \quad (19-60)$$

where $\text{Sh} (= k_m d_{ch}/D)$ is the Sherwood number, $\text{Sc} (= \mu/\rho D)$ is the Schmidt number, and $\text{Re} (= u d_{ch} \rho/\mu)$ is the channel Reynolds number; a is the geometric surface area per unit volume of monolith. A number of correlations for Sh are available for various types of monoliths. For example, in the case of extruded ceramic monoliths, a correlation for estimating the external mass-transfer coefficient is provided by Uberoi and Pereira (*Ind. Eng. Chem. Res.* **35**: 113–116 (1996)):

$$\text{Sh} = 2.696 \left(1 + 0.139 \text{Sc Re} \frac{d}{L}\right)^{0.81} \quad (19-61)$$

Since typical monolith catalysts have a thin coating of catalytic ingredients on the channel walls, they can be susceptible to poisoning,

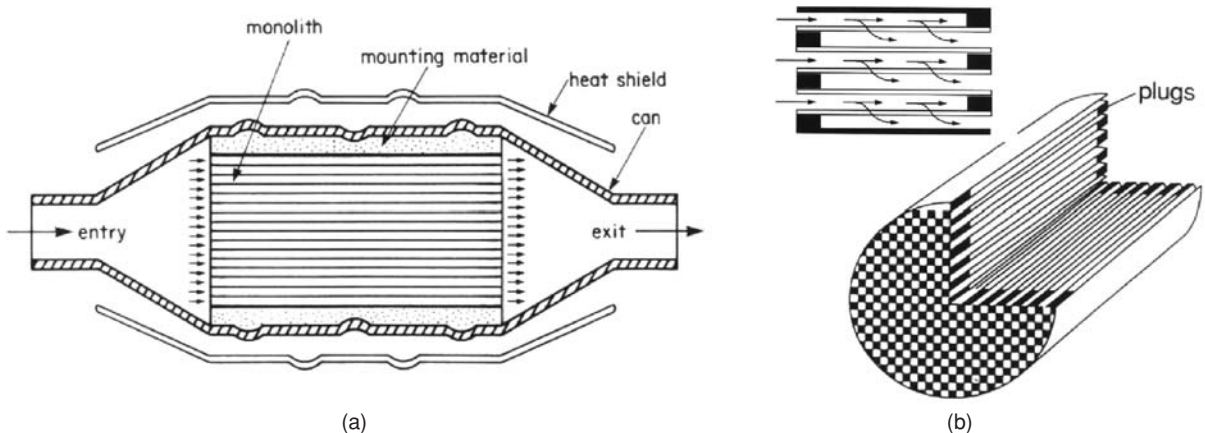


FIG. 19-18 Monolith catalysts. (a) Schematic of an automobile catalytic converter for the three-way removal of CO, hydrocarbons, and NO_x . (b) Schematic of a diesel trap. (Figs. 7.10 and 9.6 in Heck, Farrauto, and Gulati, *Catalytic Air Pollution Control: Commercial Technology*, Wiley-Interscience, 2002.)

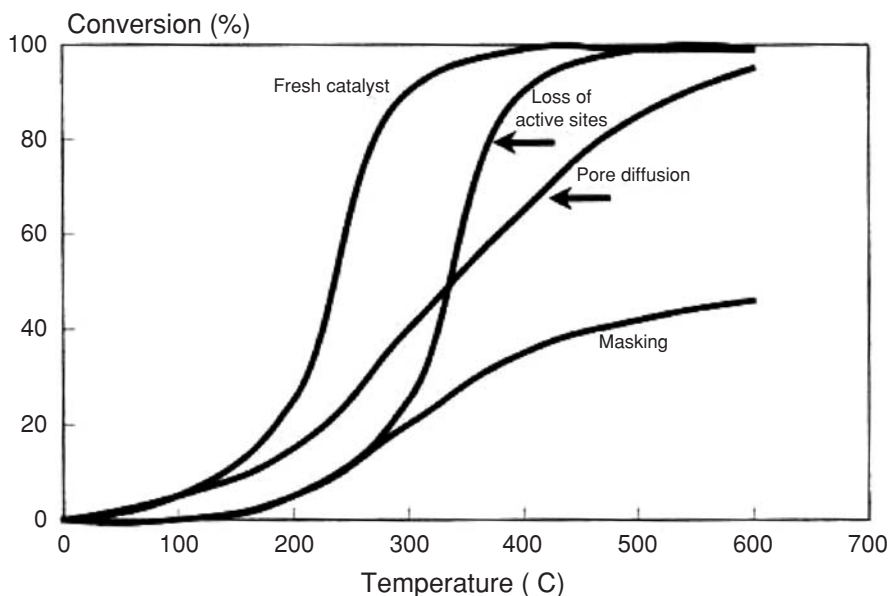


FIG. 19-19 Relative changes in conversion versus temperature behavior for various deactivation models. (Fig. 5.4 in Heck, Farrauto, and Gulati, *Catalytic Air Pollution Control: Commercial Technology*, Wiley-Interscience, 2002.)

The various mechanisms for catalyst poisoning have been discussed in Sec. 7 of the Handbook. The nature and shape of a monolith light-off curve for a facile hydrocarbon oxidation often indicate the poisoning mechanism, as shown in Fig. 19-19. The figure shows the light-off curve for a fresh catalyst. A reduction in the number of active sites (due to either poisoning or sintering of the catalytic metal) results in movement of the curve to the right. In contrast, when the pores within the catalyst become plugged with reactants or products (such as coke), the light-off curve shifts to the right and downward. In the case of deactivation due to masking, the active sites are covered with masking agents that may also plug the pores (such as in the case of silica deposition), resulting in more severe deactivation. Understanding the root cause of deactivation may allow for the design of improved catalysts, contaminant guard beds, catalyst regeneration procedures, and catalyst replacement protocols.

A good reference on monolith applications is by Heck, Farrauto, and Gulati (*Catalytic Air Pollution Control: Commercial Technology*, Wiley-Interscience, 2002).

Examples

- For the control of carbon monoxide, hydrocarbon, and nitrogen oxide emissions from automobiles, oval-shaped extruded cordierite or metal monolith catalysts are wrapped in ceramic wool and placed inside a stainless steel casing (Fig. 19-18a). The catalytic metals are Pt-Rh or Pd-Rh, or combinations. Cell sizes typically range between 400 and 600 cells per square inch. The catalysts achieve over 90 percent reduction in all three pollutants.
- Monolith catalysts are used for the control of carbon monoxide and hydrocarbon (known as volatile organic compounds or VOCs) emissions from chemical plants and cogeneration facilities. In this case, square bricks are stacked on top of one another in a wall perpendicular to the flow of exhaust gases at the appropriate temperature location within the heat recovery boiler. The size of the brick can vary from 6 in (ceramic) to 21 ft (metal). Pt and Pd catalysts are used at operating temperatures between 600 and 1200°F. Cell sizes typically range between 100 and 400 cells per square inch. Typical pressure drop requirements for monoliths are less than 2 in of water.
- *Selective catalytic reduction* (SCR) catalysts are used for controlling nitrogen oxide emissions from power plants. The reducing agent is

ammonia, and the active ingredients are $V_2O_5/WO_3/TiO_2$. Operating temperatures are 300 to 450°C. Cell sizes vary between 9 and 50 cells per square inch. The paper by Beekman and Hegedus [*Ind. Chem. Eng. Res.* **30**: 969 (1991)] is a good reaction engineering reference on SCR catalysts.

Fixed Beds A fixed-bed reactor typically is a cylindrical vessel that is uniformly packed with catalyst pellets. Nonuniform packing of catalyst may cause channeling that could lead to poor heat transfer, poor conversion, and catalyst deactivation due to hot spots. The bed is loaded by pouring and manually packing the catalyst or by sock loading. As discussed earlier, catalysts may be regular or shaped porous supports, uniformly impregnated with the catalytic ingredient or containing a thin external shell of catalyst. Catalyst pellet sizes usually are in the range of 0.1 to 1.0 cm (0.039 to 0.39 in).

Packed-bed reactors are easy to design and operate. The reactor typically contains a manhole for vessel entry and openings at the top and bottom for loading and unloading catalyst, respectively. A metal support grid is placed near the bottom, and screens are placed over the grid to support the catalyst and prevent the particles from passing through. In some cases, inert ceramic balls are placed above and below the catalyst bed to distribute the feed uniformly and to prevent the catalyst from passing through, respectively. One has to guard the bed from sudden pressure surges as they can disturb the packing and cause maldistribution and bypassing of feed.

As discussed earlier, heat management is an important issue in the design of fixed-bed reactors. A series of adiabatic fixed beds with interbed cooling (heating) may be used. For very highly exothermic (endothermic) reactions, a multitubular reactor with catalyst packed inside the tubes and cooling (heating) fluids on the shell side may be used. The tube diameter is typically greater than 8 times the diameter of the pellets (to minimize flow channeling), and the length is limited by allowable pressure drop. The heat transfer required per volume of catalyst may impose an upper limit on diameter as well. Multitubular reactors require special procedures for catalyst loading that charge the same amount of catalyst to each tube at a definite rate to ensure uniform loading, which in turn ensures uniform flow distribution from the common header. After filling, each tube is checked for pressure

drop. In addition to the high surface area for heat transfer/volume, the advantage of a multitubular fixed-bed reactor is its easy scalability. A bench-scale unit can be a full-size single tube, a pilot plant can be several dozen tubes, and a large-scale commercial reactor can have thousands of tubes. Disadvantages include high cost and a limit on maximum size (tube length and diameter, and number of tubes).

As discussed in Sec. 7, the intrinsic reaction rate and the reaction rate per unit volume of reactor are obtained based on laboratory experiments. The kinetics are incorporated into the corresponding reactor model to estimate the required volume to achieve the desired conversion for the required throughput. The acceptable pressure drop across the reactor often can determine the reactor aspect ratio. The pressure drop may be estimated by using the Ergun equation

$$\frac{\Delta P}{L} = \frac{150u_0\mu}{(\phi_p d_p)^2} \frac{(1 - \varepsilon_b)^2}{\varepsilon_b^3} + \frac{1.75\rho u_0^2}{\phi_p d_p} \left(\frac{1 - \varepsilon_b}{\varepsilon_b^3} \right) \quad (19-62)$$

where u_0 is the superficial velocity, ε_b is the bed porosity, ϕ_s is the shape factor, and d_p is the particle diameter. Correlations that provide estimates for the heat-transfer and mass transport properties are available in the literature. For example, if the dispersion model is used to simulate concentration and temperature profiles along the reactor, the axial dispersion coefficient may be estimated from Wen [in Petho and Noble (eds.), *Residence Time Distribution Theory in Chemical Engineering*, Verlag Chemie, 1982].

$$\frac{1}{\text{Pe}} = \frac{0.3}{(\text{Re})(\text{Sc})} + \frac{0.5}{3.8} \quad 0.008 \leq \text{Re} \leq 400 \quad \text{and} \quad 0.28 \leq \text{Sc} \leq 2.2 \quad (19-63)$$

where $\text{Pe} = d_p u_0 / (\varepsilon_b D_e)$, $\text{Re} = d_p \rho u_0 / \mu$, u_0 is the superficial velocity, and d_p is the particle diameter.

Mathematical Models Catalytic packed-bed reactors are used for exothermic (e.g., hydrogenations, Fischer-Tropsch synthesis, oxidations) and endothermic (e.g., steam reforming and ammonia synthesis) reactions. The two primary modes of heat management are (1) adiabatic operation usually in a single or series of packed zones, the later with interstage cooling or heating and (2) multitubular reactors with cooling (e.g., shell-and-tube heat exchange with a coolant) or heating (e.g., locating the tubes in a furnace with heat supplied by combustion of a fuel). Other more complex schemes can include heat exchange between the feed and the effluent, reverse flow operation, etc., and are discussed in the multifunctional reactors section.

The mechanism for heat transfer includes the following steps: (1) conduction in the catalyst particle; (2) convection from the particle to the gas phase; (3) conduction at contact points between particles; (4) convection between the gas and vessel wall; (5) radiation heat transfer between the particles, the gas, and the vessel wall; (6) conduction in the wall; and (7) convection to the coolant. There are a number of ways, through reactor models, that these steps are correlated to provide design and analysis estimates and criteria for preventing runaway in exothermic reactors.

The temperature profile depends on the relative rates of heat generation by reaction and heat transfer. The temperature rise or drop in a reactor affects catalyst life, product selectivity, and equilibrium conversion, and excessive heat release can lead to reaction runaway. Hence, reactor design and analysis requires good understanding of the coupling of reaction and heat transfer. Mathematical models for fixed-bed reactors can vary in the level of detail depending on the end use. For more details see Froment and Bischoff (*Chemical Reactor Analysis and Design*, Wiley, 1990) and Harriott (*Chemical Reactor Design*, Marcel Dekker, 2003).

Homogeneous one-dimensional model This is the simplest description of a packed bed, with an overall heat-transfer coefficient U . The particle and gas temperatures are identical, and only axial variation in temperature is considered, giving the following mass and energy balance equations for any species C_i :

$$\frac{d(uC_i)}{dz} = \sum_j v_{ij} r_j \quad C_i = C_{i0} \quad \text{at } z = 0$$

$$u\rho c_p \frac{dT}{dz} = \sum_j v_{ij} (-\Delta H)_{fj} - \frac{4U}{d_R} (T - T_c) \quad (19-64)$$

$$T = T_0 \quad \text{at } z = 0$$

Equation (19-64) is similar to generic PFR Eqs. (19-17) and (19-18). The overall heat-transfer coefficient U is based on the bed side heat-transfer area A_R and includes three terms: heat transfer on the bed side b , thermal conduction in the vessel wall w , and heat transfer on the coolant side c :

$$\frac{1}{U} = \frac{1}{h_b} + \frac{d_R}{k_w} \frac{A_R}{A_m} + \frac{1}{h_c} \frac{A_R}{A_c} \quad (19-65)$$

$$A_m = \log \text{mean}(A_R, A_c) = \frac{A_c - A_R}{\ln(A_c/A_R)}$$

Here, h_i are the heat-transfer coefficients in the bed side and the coolant side, k_w is the wall thermal conductivity, and A_i are the heat-transfer areas. The coolant side heat-transfer coefficient can be obtained from general heat-transfer correlations in tubes (see any heat-transfer text and the relevant sections in this Handbook). For the process-side heat-transfer coefficient, there is a large body of literature with a variety of correlations. There is no clear advantage of one correlation over another, as these depend on the particle and fluid properties, temperature range, etc.; e.g., see the correlation of Leva, *Chem. Eng.* **56**: 115 (1949):

$$\text{Nu}_R = \begin{cases} 0.813 \text{Re}_p^{0.9} e^{6d_p/d_s} & \text{for heating} \\ 3.5 \text{Re}_p^{0.7} e^{4.6d_p/d_s} & \text{for cooling} \end{cases} \quad (19-66)$$

$$\text{Re}_p = \frac{\rho u d_p}{\mu} \quad \text{Nu}_R = \frac{h_i d_R}{\lambda_f}$$

The one-dimensional homogeneous model is useful for first-order estimates and when lab (or pilot-plant) data for the same diameter tube are available. This simple model does not provide information on the effect of the tube diameter on the effective radial temperature gradients.

Fixed-bed reactors may exhibit axial dispersion. If axial dispersion is important for reactor simulation, analysis, or design, a variant of the one-dimensional homogeneous model that contains an axial dispersion term may be used. Approximate criteria to determine if mass and heat axial dispersion have to be considered are available (see, e.g., Froment and Bischoff, *Chemical Reactor Analysis and Design*, Wiley, 1990).

Homogeneous two-dimensional model This model accounts for radial variation of composition and temperature in the bed that may be present for large heats of reaction. Corresponding material and energy balances are:

$$D_{er} \left(\frac{\partial^2 C_i}{\partial r^2} + \frac{1}{r} \frac{\partial C_i}{\partial r} \right) - \frac{\partial(uC_i)}{\partial z} + \sum_j v_{ij} r_j = 0$$

$$k_{er} \left(\frac{\partial^2 T}{\partial r^2} + \frac{1}{r} \frac{\partial T}{\partial r} \right) - u\rho c_p \frac{dT}{dz} - \sum_j v_{ij} (-\Delta H)_{fj} = 0 \quad (19-67)$$

$$C_i = C_{i0} \quad T = T_0 \quad \text{at } z = 0$$

$$\frac{\partial C_i}{\partial r} = 0 \quad \frac{\partial T}{\partial r} = 0 \quad \text{at } r = 0$$

$$\frac{\partial C_i}{\partial r} = 0 \quad \frac{\partial T}{\partial r} = -\frac{h_w}{k_w} (T_R - T_w) \quad \text{at } r = R$$

The effective radial diffusivity D_{er} is normally different from the axial diffusivity. It is often safe to neglect the radial variation of species concentration due to the relatively fast radial mixing. The effective conductivity k_{er} has to be determined from heat-transfer experiments preferably with the actual bed and fluids. This coefficient can be

either a constant (averaged radially) or a function of the radial position with a higher value for the core and a lower value near the wall due to different velocity and void fraction near the wall. There are a number of correlations for k_{er} and h_w , and there is significant variability in their utility; e.g., see the correlation of De Wash and Froment, *Chem. Eng. Sci.* **27**: 567 (1972):

$$k_{er} = k_{er0} + \frac{0.0105 \text{ Re}}{1 + 46 (dp/dR)^2} \tag{19-68}$$

$$h_w = h_{w0} + 0.0481 \text{ Re} \frac{d_R}{d_p}$$

The static contribution k_{er0} incorporates heat transfer by conduction and radiation in the fluid present in the pores, conduction through particles, at the particle contact points and through stagnant fluid zones in the particles, and radiation from particle to particle. Figure 19-20 compares various literature correlations for the effective thermal conductivity and wall heat-transfer coefficient in fixed beds [Yagi and Kunii, *AIChE J.* **3**: 373(1957)].

The two-dimensional model can be used to develop an equivalent one-dimensional model with a bed-side heat-transfer coefficient defined as [see, e.g., Froment, *Chem. Eng. Sci.* **7**: 29 (1962)]

$$\frac{1}{h_b} = \frac{1}{h_w} + \frac{R}{4k_{er}} \tag{19-69}$$

The objective is to have the radially averaged temperature profile of the 2D model match the temperature profile of the 1D model.

Heterogeneous one-dimensional model The heterogeneous model allows resolution of composition and temperature differences between the catalyst particle and the fluid.

$$\frac{d(uC_i)}{dz} = k_{Ca}(C_i - C_{is})$$

$$k_{Ca}(C_i - C_{is}) = \sum_j v_{ij}r_j$$

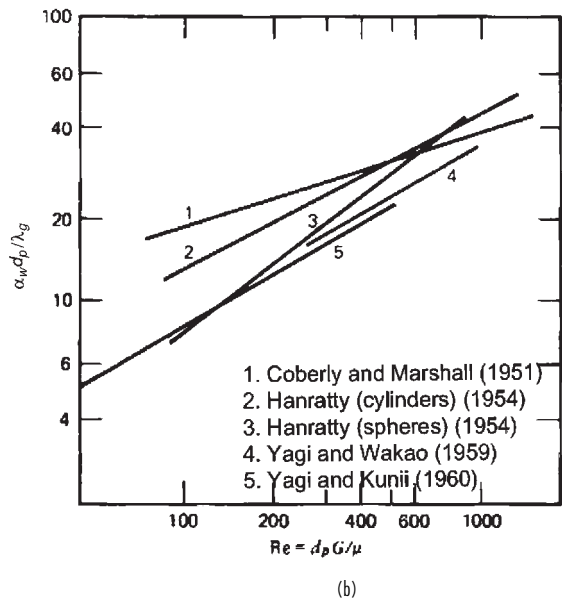
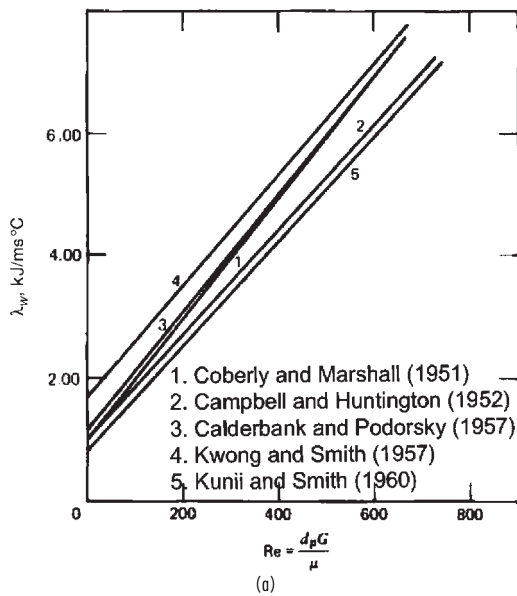


FIG. 19-20 Thermal conductivity and wall heat transfer in fixed beds. (a) Effective thermal conductivity. (b) Nusselt number for wall heat transfer. (Figs. 11.7.1-2 and 11.7.1-3 in Froment and Bischoff, *Chemical Reactor Analysis and Design*, Wiley, 1990.)

$$u\rho c_p \frac{dT}{dz} = ha(T_s - T) - \frac{4U}{d_R}(T - T_c) \tag{19-70}$$

$$ha(T_s - T) = \sum_j v_{ij}(-\Delta H)_j r_j$$

$$C_i = C_{i0} \quad T = T_0 \quad \text{at } z = 0$$

Mears developed a criterion that provides conditions for limiting interphase temperature gradients [Mears, *J. Catal.* **20**: 127 (1971) and *I&EC Proc. Des. Dev.* **10**: 541 (1971)]

$$\frac{d_p \sum_j v_{ij}(-\Delta H)_j r_j}{2hT} < 0.15 \frac{RT}{E} \tag{19-71}$$

An extension of this one-dimensional heterogeneous model is to consider intraparticle diffusion and temperature gradients, for which the lumped equations for the solid are replaced by second-order diffusion/conduction differential equations. Effectiveness factors can be used as applicable and discussed in previous parts of this section and in Sec. 7 of this Handbook (see also Froment and Bischoff, *Chemical Reactor Analysis and Design*, Wiley, 1990).

Typically the interphase temperature gradients are substantially smaller than the radial and axial temperature gradients, being on the order of 1 to 3°C, and can often be neglected.

Heterogeneous two-dimensional model Two-dimensional heterogeneous models have been developed, e.g., De Wash and Froment, *Chem. Eng. Sci.* **27**:567 (1972). Figure 19-21 compares the various models. The results indicate that the homogeneous and heterogeneous models predict similar temperature profiles; however, the heterogeneous model contains additional information on interparticle concentration and temperature gradients that may be useful in catalyst or reactor design. The 2D models predict substantially higher peak temperatures than the corresponding 1D models. The pseudohomogeneous 2D model may contain valuable information on radial temperature profiles, especially in the case of exothermic reactions. The heterogeneous 2D model also contains additional radial interparticle mass and heat-transfer information. The heterogeneous 2D model with no heat transfer through the solid shows

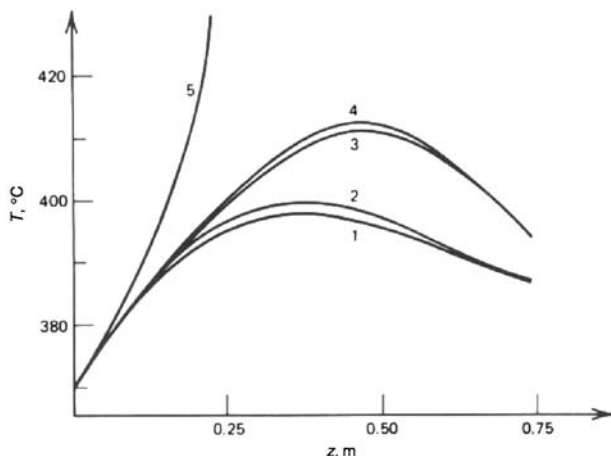


FIG. 19-21 Comparison of model predictions for radial mean temperature as a function of bed length. (1) Basic pseudohomogeneous one-dimensional model. (2) Heterogeneous model with interfacial gradients. (3) Pseudohomogeneous two-dimensional model. (4) Two-dimensional heterogeneous model with appropriate boundary conditions. (5) Two-dimensional heterogeneous model with no heat transfer through solid. (Fig. 11.10-1 in Froment and Bischoff, *Chemical Reactor Analysis and Design*, Wiley, 1990.)

a very steep temperature rise. This case illustrates the notion that a reasonably complicated model may indeed provide unrealistic results if inappropriate assumptions are made.

Examples

- Oxidation of SO_2 in large adiabatic packed-bed reactors (Fig. 19-22a). The catalyst is nominally $\frac{1}{4}$ -in Cs-promoted $\text{V}_2\text{O}_5/\text{SiO}_2$ pellets. The inlet temperature is between 350 and 450°C. The temperature increase across the bed is 50 to 100°C. The oxidation is thermodynamically limited, with lower temperatures favoring SO_3 . After each bed, the exhaust is cooled via heat exchange or injection of a cold shot. The advantage of interstage cooling is shown in Table 19-2.
- Phosgene synthesis from CO and Cl_2 in a multitubular reactor (Fig. 19-22b). The activated carbon catalyst is packed inside the tubes with water on the shell side. Reaction by-products include CCl_4 . The temperature profile in a tube (shown in the figure) is characterized by a hot spot. The position of the hot spot moves toward the exit of the reactor as the catalyst deactivates.
- Production of cumene from benzene and propylene using a phosphoric acid on quartz catalyst (Fig. 19-22c). There are four reactor beds with interbed cooling with cold feed. The reactor operates at 260°C.
- Vertical ammonia synthesizer at 300 atm with five cold shots and an internal exchanger (Fig. 19-22d). The nitrogen and hydrogen feeds are reacted over an Al_2O_3 -promoted spongy iron catalyst. The concentration of ammonia is also shown in the figure.
- Vertical methanol synthesizer at 300 atm (Fig. 19-22e). A Cr_2O_3 -ZnO catalyst is used with six cold shots totaling 10 to 20 percent of the fresh feed.
- Methanol is oxidized to formaldehyde in a thin layer of finely divided silver or a multilayer screen, with a contact time of 0.01 s at 450 to 600°C (842 to 1112°F). A shallow bed of silver catalyst is also used in the DuPont process for in situ production of methyl isocyanate by reacting monomethylformamide and oxygen at 500°C.
- The Sohio process for vapor-phase oxidation of propylene to acrylic acid uses two beds of bismuth molybdate at 20 to 30 atm (294 to 441 psi) and 290 to 400°C (554 to 752°F).
- Oxidation of ethylene to ethylene oxide also is done in two stages with supported silver catalyst, the first stage to 30 percent conversion, the second to 76 percent, with a total of 1.0-s contact time.
- Steam reforming reactors have the supported nickel catalyst packed in tubes and the endothermic heat of reaction supplied from a

furnace on the shell side. The feed is natural gas (or naphtha) and water vapor heated to over 800°C (1056°F).

- Vinyl acetate reactors that have a supported Pd/Au catalyst packed in ~ 25 -mm (0.082-ft) ID tubes and exothermic heat of reaction removed by generating steam on the shell side. The feed contains ethylene, oxygen, and acetic acid in the vapor phase at 150 to 175°C (302 to 347°F).
- Maleic anhydride is made by oxidation of benzene with air above 350°C (662°F) with V-Mo catalyst in a multitubular reactor with 2-cm tubes. The heat-transfer medium is a molten salt eutectic mixture at 375°C (707°F). Even with small tubes, the heat transfer is so limited that a peak temperature 100°C (212°F) above the shell side is developed and moves along the tubes.
- Butanol is made by the hydrogenation of crotonaldehyde in a reactor with 4000 tubes, 28-mm (0.029-ft) ID by 10.7 m (35.1 ft) long [Berty, in Leach (ed.), *Applied Industrial Catalysis*, vol. 1, Academic Press, 1983, p. 51].
- Vinyl chloride is made from ethylene and chlorine with Cu and K chlorides. The Stauffer process employs three multitubular reactors in series with 25-mm (0.082-ft) ID tubes [Naworski and Velez, in Leach (ed.), *Applied Industrial Catalysis*, vol. 1, Academic Press, 1983, p. 251].

Moving Beds In a moving-bed reactor, the catalyst, in the form of large granules, circulates by gravity and gas lift between reaction and regeneration zones (Fig. 19-23). The first successful operation was the Houdry cracker that replaced a plant with fixed beds that operated on a 10-min cycle between reaction and regeneration. Handling of large (hot) solids is difficult. The Houdry process was soon made obsolete by FCC units. The only currently publicized moving-bed process is a UOP platinum reformer (Fig. 19-23c) that regenerates a controlled quantity of catalyst on a continuous basis.

Fluidized Beds Fluidized beds are reactors in which small particles (with average size below 0.1 mm) are fluidized by the reactant gases or liquids. When the linear velocity is above the minimum required for fluidization, a dense fluidized bed is obtained. As the superficial velocity increases, the bed expands and becomes increasingly dilute. At a high enough linear velocity, the smallest particles entrain from the bed and have to be separated from the exhaust gases and recycled.

Advantages of fluidized beds are temperature uniformity, good heat transfer, and the ability to continuously remove catalyst for regeneration. Disadvantages are solids backmixing, catalyst attrition, and recovery of fines. Baffles have been used often to reduce backmixing.

Fluidized beds contain a bottom support plate over which the solids reside. The reactant gases typically are fed through a sparging system placed very near the bottom of the plate. These reactors employ a wide range of particle sizes and densities. Geldart (*Gas Fluidization Technology*, Wiley, 1986) developed a widely accepted particle classification system based on fluidization characteristics. Type A powders are employed in many refinery and chemical processes, such as catalytic cracking, acrylonitrile synthesis, and maleic anhydride synthesis. Type B powders are also utilized, e.g., in fluidized-bed combustion. The properties of different powders are summarized in the fluidized bed subsection of Sec. 17. Good distributor design and the presence of a substantial fraction of fines (mainly for processes employing group A powders) are essential for good fluidization, to eliminate maldistribution, and for good performance. Internals for heat transfer (e.g., cooling tubes) and other baffling for improved performance provide design challenges as their effect is not yet well understood (in spite of the voluminous literature).

The *particle size distribution* and the linear velocity are important in reactor design. The *minimum fluidization velocity* is the velocity at the onset of fluidization while the *terminal velocity* is the velocity above which a particle can become entrained from the bed. The nature of the particles and the linear velocity determine bed properties such as *gas holdup*, *equilibrium bubble size* (for bubbling systems), *entrainment rate* of particles from the bed, and the *flow regime transition velocities*. The height beyond which the concentration of entrained particles does not vary significantly is called the *transport disengagement height*. Knowledge of this height is required for the design and location of *cyclones* for solids containment. In addition to the velocity and the nature of the particles, the layout of the equipment can determine the *particle attrition rate*.

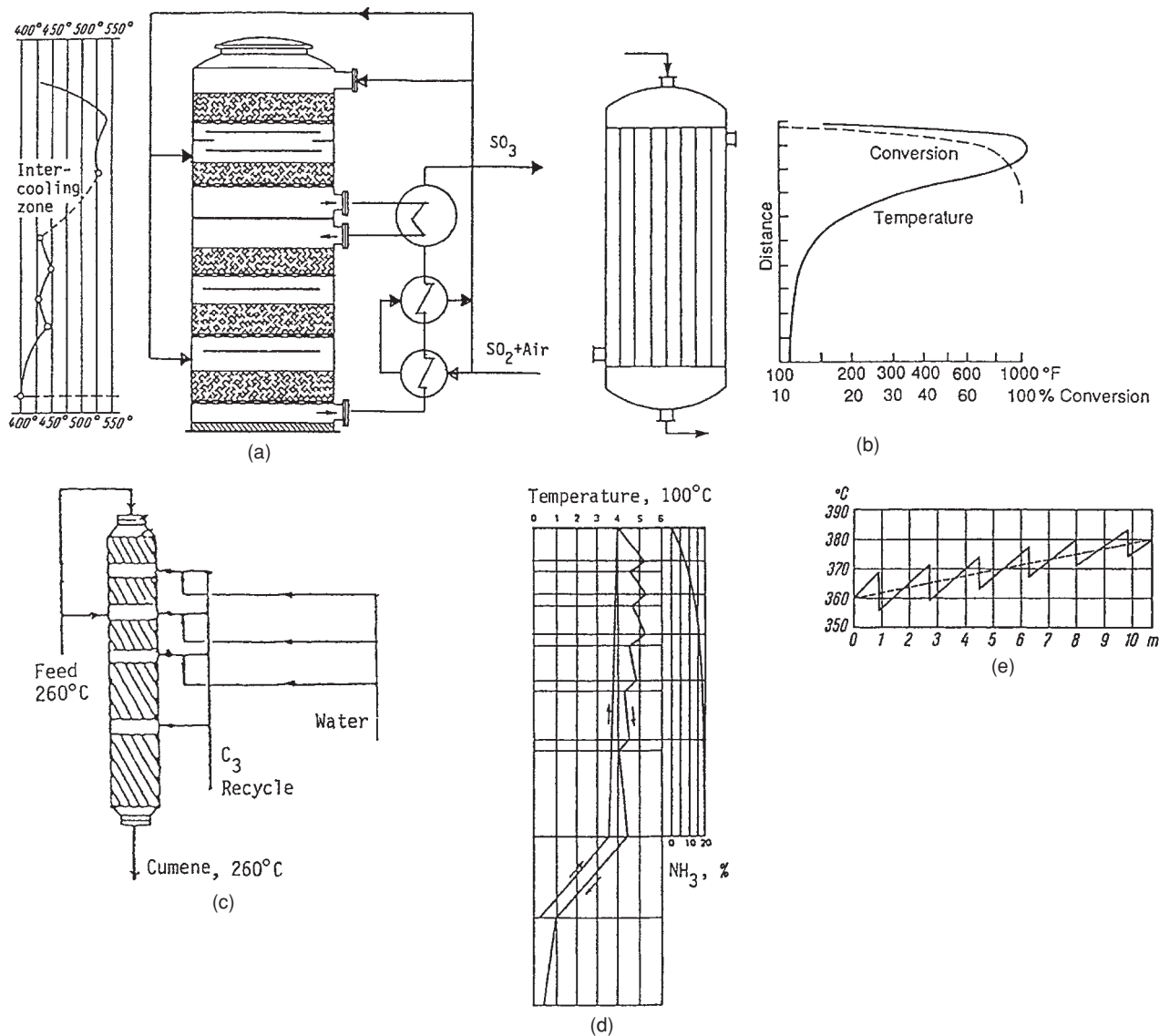


FIG. 19-22 Temperature and composition profiles. (a) Oxidation of SO₂ with intercooling and two cold shots. (b) Phosgene from CO and Cl₂, activated carbon in 2-in tubes, water-cooled. (c) Cumene from benzene and propylene, phosphoric acid on quartz with four quench zones, 260°C. (d) Vertical ammonia synthesizer at 300 atm, with five cold shots and an internal exchanger. (e) Vertical methanol synthesizer at 300 atm, Cr₂O₃-ZnO catalyst, with six cold shots totaling 10 to 20 percent of the fresh feed. To convert psi to kPa, multiply by 6.895; atm to kPa, multiply by 101.3.

The two-phase theory of fluidization has been extensively used to describe fluidization (e.g., see Kunii and Levenspiel, *Fluidization Engineering*, 2d ed., Wiley, 1990). The fluidized bed is assumed to contain a bubble and an emulsion phase. The bubble phase may be modeled by a plug flow (or dispersion) model, and the emulsion phase is assumed to be well mixed and may be modeled as a CSTR. Correlations for the size of the bubbles and the heat and mass transport from the bubbles to the emulsion phase are available in Sec. 17 of this Handbook and in textbooks on the subject. Davidson and Harrison (*Fluidization*, 2d ed., Academic Press, 1985), Geldart (*Gas Fluidization Technology*, Wiley, 1986), Kunii and Levenspiel (*Fluidization Engineering*, Wiley, 1969), and Zenz (*Fluidization and Fluid-Particle Systems*, Penn-Corp Publications, 1989) are good reference books.

Examples

- The original fluidized-bed reactor was the Winkler coal gasifier (patented 1922), followed in 1940 by the Esso cracker that has now been replaced by riser reactors with zeolite catalysts.
- Transport fluidized bed reactor is used for the Sasol Fischer-Tropsch process (Fig. 19-23a).
- Esso-type stable fluidized-bed reactor/regenerator is used for cracking petroleum oils (Fig. 19-23b).
- UOP uses a reformer with moving bed of platinum catalyst and continuous regeneration of a controlled quantity of catalyst (Fig. 19-23c).
- Acrylonitrile is made in a fixed fluidized bed by reacting propylene, ammonia, and oxygen at 400 to 510°C (752 to 950°F) over a Bi-Mo oxide catalyst. The good temperature control with embedded heat exchangers permits catalyst life of several years.

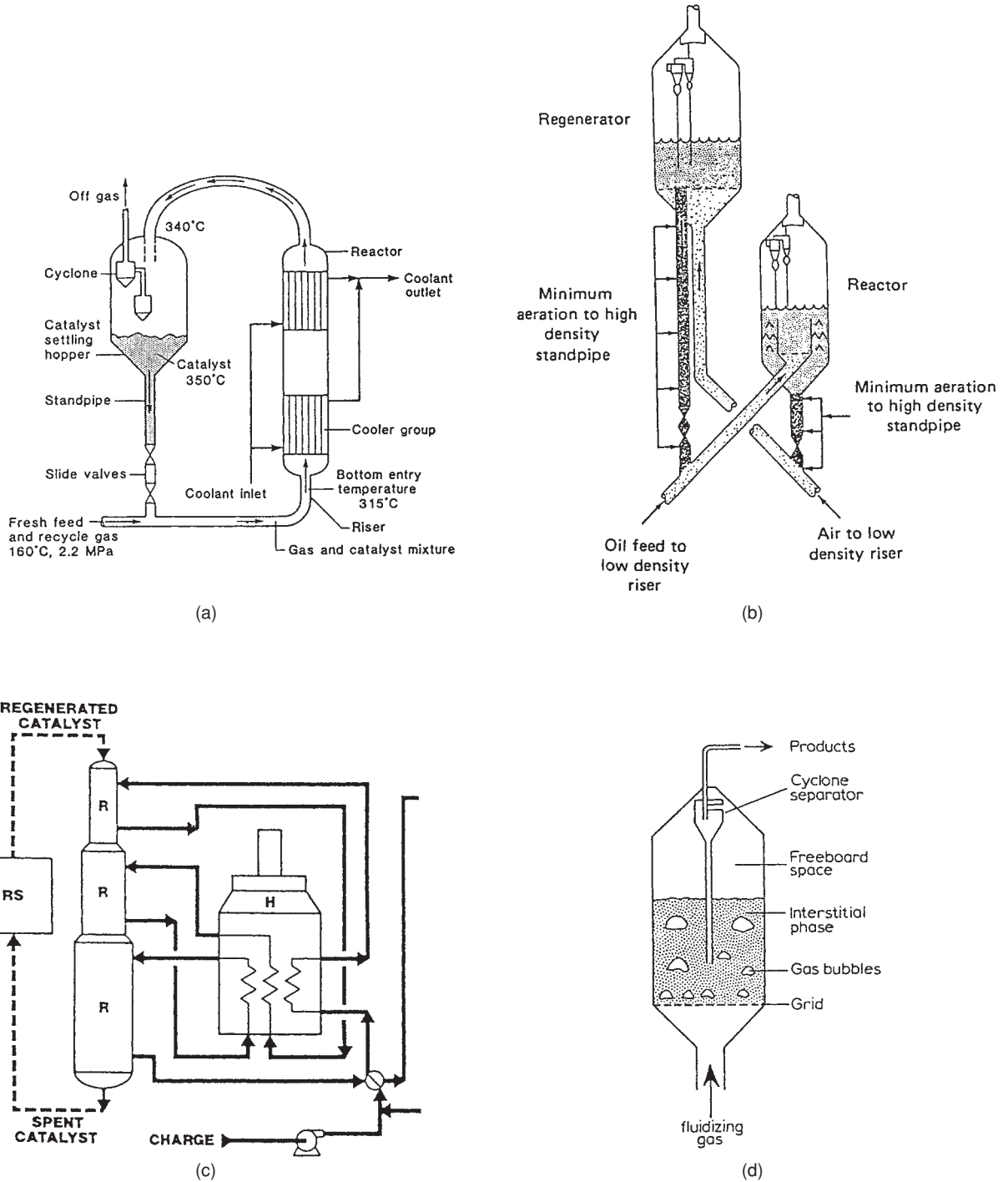


FIG. 19-23 Reactors with moving catalysts. (a) Transport fluidized type for the Sasol Fischer-Tropsch process, nonregenerating. (b) Esso type of stable fluidized-bed reactor/regenerator for cracking petroleum oils. (c) UOP reformer with moving bed of platinum catalyst and continuous regeneration of a controlled quantity of catalyst. (d) Flow distribution in a fluidized bed; the catalyst rains through the bubbles.

• Vinyl chloride is produced by chlorination of ethylene at 200 to 300°C (392 to 572°F), 2 to 10 atm (29.4 to 147 psi), with a supported cupric chloride catalyst in a fluidized bed.

Slurry Reactors Slurry reactors are akin to fluidized beds except the fluidizing medium is a liquid. In some cases (e.g., for hydrogenation), a limited amount of hydrogen may be dissolved in the liquid feed. The solid material is maintained in a fluidized state by agitation, internal or external recycle of the liquid using pipe spargers or distributor plates with perforated holes at the bottom of the reactor. Most industrial processes with slurry reactors also use a gas in reactions such as chlorination, hydrogenation, and oxidation, so the discussion will be deferred to the multiphase reactor section of slurry reactors.

Transport Reactors The superficial velocity of the gas exceeds the terminal velocity of the solid particles, and the particles are transported along with the gas. Usually, there is some “slip” between the gas and the solids—the solid velocity is slightly lower than the gas velocity. Transport reactors are typically used when the required residence time is small and the fluid reactant (or the solid reactant) can be substantially converted (consumed). They may also be used when the catalyst is substantially deactivated during its time in the reactor and has to be regenerated.

Advantages of transport reactors include low gas and solid backmixing (compared to fluidized beds) and the ability to continuously remove deactivated catalyst (and add fresh catalyst), thereby maintaining catalyst activity. The fluid and catalyst are separated downstream by using settlers, cyclones, or filters.

Transport reactors are typically cylindrical pipes. The reactants may be injected at a tee or by using injection pipes at the bottom of the reactor. The size of the pipe may be increased along the reaction path to accommodate volumetric changes that may occur during reaction. Both solid and gas phases may be modeled using a PFR model with exchange between the gas and solid phases. A core-annular concept is often used to describe transport or riser reactors, with most of the particles rising at the center and some flowing back down along the walls.

Examples

- A transport reactor is also used in the Sasol Fischer-Tropsch process. The catalyst is promoted iron. It circulates through the 1.0-m (3.28-ft) ID riser at 72,600 kg/h (160,000 lbm/h) at 340°C (644°F) and 23 atm (338 psi) and has a life of about 50 days. Figure 19-23a shows an in-line heat exchanger in the Sasol unit.
- The fluid catalytic cracking unit (FCCU) riser cracks crude oil into gasoline and distillate range products in a transport bed reactor using a zeolite-Y catalyst. The riser residence time is 4 to 10 s. The riser top temperature is between 950 and 1050°F. The ratio of catalyst to crude oil is between 4 and 8 on a weight basis. During its stay in the riser, the catalyst is deactivated by coke which is burned in the regenerator. The heat generated by burning the coke heats the catalyst and is used to vaporize the crude oil feed. A schematic of the FCCU is shown in Fig. 19-23b.

Multifunctional Reactors Reaction may be coupled with other unit operations to reduce capital and/or operating costs, increase selectivity, and improve safety. Examples are reaction and distillation and reaction with heat transfer. Concepts that combine reaction with membrane separation, extraction, and crystallization are also being explored. In each case, while possibly reducing cost, the need to accommodate both reaction and the additional operation constrains process flexibility by reducing the operating envelope.

Examples

- The Eastman process for reacting methanol with acetic acid to produce methyl acetate and water in one column. Product separation (instead of increased feed concentration) is used to drive the equilibrium to the right.
- Methyl *tert*-butyl ether (MTBE) has been produced by reactive distillation of isobutylene and methanol. The reaction is conducted in a distillation column loaded with socks containing a solid acid catalyst.
- VOC emissions from printing and chemical plants are oxidized in reverse flow reactors that couple reaction with regenerative heat transfer. The concept here is to maintain a catalyst zone in the center of a packed bed with inert heat-transfer packing on either side.

Feed is heated to the desired temperature as it travels through the hot inert bed to the catalyst zone. After the catalyst, the outlet gases lose heat to the cooler packing downstream as they leave the reactor. When the exit temperature of the gases exceeds a certain threshold temperature, the flow is reversed.

NONCATALYTIC REACTORS

These reactors may be similar to the gas-solid catalytic reactors, except for the fact that there is no catalyst involved. The gas and/or the solid may be reactants and/or products. Section 7 of this Handbook provides greater discussion on reaction types and corresponding kinetics for a range of gas-solid reactions. The oldest examples of gas-solid noncatalytic reactors are kilns. A solid is heated with hot combustion gases (that may contain a reactant) to form a desired product. Some of the equipment in use is represented in Fig. 19-24. Temperatures are usually high so the equipment is refractory-lined. The solid is in granular form, at most a few millimeters or centimeters in diameter. Historically, much of the equipment was developed for the treatment of ores and the recovery of metals. In recent years, gas-solid reactions are practiced in the electronics industry. In chemical vapor deposition (CVD), gases react to form solid films in microelectronic chips and wear protective coatings.

Rotary Kilns A rotary kiln is a long, narrow cylinder inclined 2 to 5° to the horizontal and rotated at 0.25 to 5 rpm. It is used for the decomposition of individual solids, for reactions between finely divided solids, and for reactions of solids with gases or even with liquids. The length/diameter ratio ranges from 10 to 35, depending on the reaction time needed. The solid is in granular form and may have solid fuel mixed in. The granules are scooped into the vapor space and are heated as they cascade downward. Holdup of solids is 8 to 15 percent of the cross-section. For most free-falling materials, the solids pattern approaches plug flow axially and complete mixing laterally. Rotary kilns can tolerate some softening and partial fusion of the solid. For example, CaF₂ with SO₃ is reacted in a rotary kiln to make hydrofluoric acid. The morphology of the CaF₂ solids can change considerably as they travel downward through the kiln. Approximate ranges of space velocities in rotary kilns are shown in Table 19-6.

Vertical Kilns Vertical kilns are used primarily where no fusion or softening occurs, as in the burning of limestone or dolomite, although rotary kilns may also be used for these operations. A cross-section of a continuous 50,000-kg/d (110,000-lbm/d) lime kiln is shown in Fig. 19-24c. The diameter range of these kilns is 2.4 to 4.5 m (7.9 to 14.8 ft), and height is 15 to 24 m (49 to 79 ft). Peak temperatures in lime calcination are 1200°C (2192°F), although decomposition proceeds freely at 1000°C (1832°F). Fuel supply may be coke mixed and fed with the limestone or other fuel. Space velocity of the kiln is 14 to 25 kg CaO/(m³·h) [0.87 to 1.56 lbm/(ft³·h)] or 215 to 485 kg CaO/(m³·h) [44 to 99 lbm/(ft³·h)]. Factors that influence kiln size include its vintage, the method of firing, and the lump size, which is in the range of 10 to 25 cm (3.9 to 9.8 in). A five-stage fluidized-bed calciner is sketched in Fig. 19-24d. Such a unit 4 m (13 ft) in diameter and 14 m (46 ft) high has a production of 91,000 kg CaO/d (200,000 lbm/d).

The blast furnace (Fig. 19-24f) is a vertical kiln in which fusion takes place in the lower section. This is a vertical moving-bed device; iron oxides and coal are charged at the top and flow countercurrently to combustion and reducing gases. Units of 1080 to 4500 m³ (38,000 to 159,000 ft³) may produce up to 9 × 10⁶ kg (20 × 10⁶ lbm) of molten iron per day. Figure 19-24f identifies the temperature and composition profiles. Reduction is with CO and H₂ that are made from coal, air, and water within the reactor.

In addition to rotary and vertical kilns, hearth furnaces or fluidized-bed reactors may be used. These high-temperature reactors convert minerals for easier separation from gangue or for easier recovery of metal. Fluidized beds are used for the combustion of solid fuels, and some 30 installations are listed in *Encyclopedia of Chemical Technology* (vol. 10, Wiley, 1980, p. 550). The roasting of iron sulfide in fluidized beds at 650 to 1100°C (1202 to 2012°F) is analogous. The pellets have 10-mm (0.39-in) diameter. There are numerous plants, but they are threatened with obsolescence because cheaper sources of sulfur are available for making sulfuric acid.

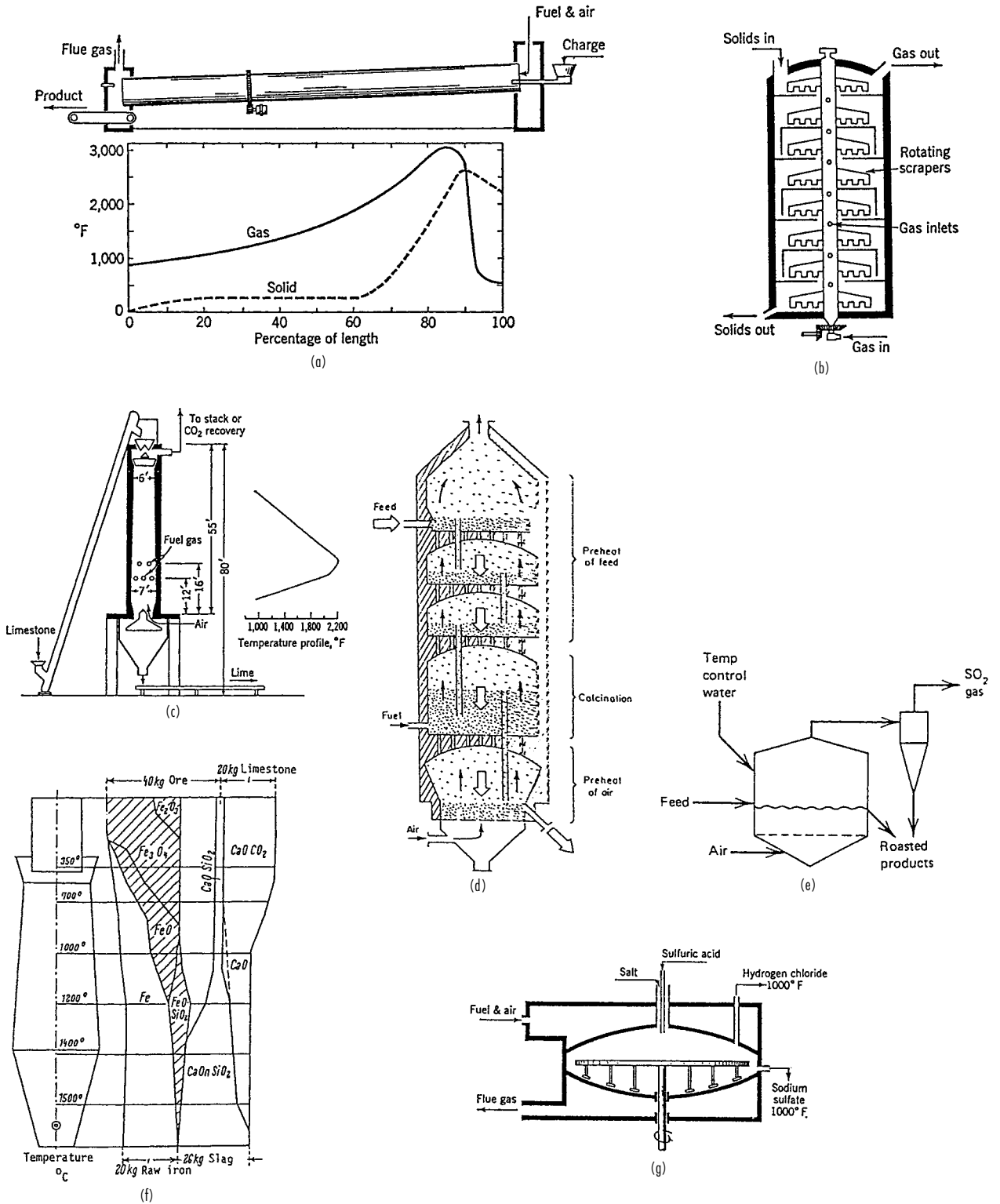


FIG. 19-24 Reactors for solids. (a) Temperature profiles in a rotary cement kiln. (b) A multiple-hearth reactor. (c) Vertical kiln for lime burning, 55 ton/d. (d) Five-stage fluidized-bed lime burner, 4 by 14 m, 100 ton/d. (e) A fluidized bed for roasting iron sulfides. (f) Conditions in a vertical moving bed (blast furnace) for reduction of iron oxides. (g) A mechanical salt cake furnace. To convert ton/d to kg/h, multiply by 907.

TABLE 19-6 Approximate Ranges of Space Velocities in Rotary Kilns

Process	Space velocity, m tons/(m ³ d)
Cement, dry process	0.4–1.1
Cement, wet process	0.4–0.8
Cement, with heat exchange	0.6–1.9
Lime burning	0.5–0.9
Dolomite burning	0.4–0.6
Pyrite roasting	0.2–0.35
Clay calcination	0.5–0.8
Magnetic roasting	1.5–2.0
Ignition of inorganic pigments	0.15–2.0
Barium sulfide preparation	0.35–0.8

There are a number of references on gas-solid noncatalytic reactions, e.g., Brown, Dollimore, and Galwey [“Reactions in the Solid State,” in Bamford and Tipper (eds.), *Comprehensive Chemical Kinetics*, vol. 22, Elsevier, 1980], Galwey (*Chemistry of Solids*, Chapman and Hall, 1967), Sohn and Wadsworth (eds.) (*Rate Processes of Extractive Metallurgy*, Plenum Press, 1979), Szekely, Evans, and Sohn (*Gas-Solid Reactions*, Academic Press, 1976), and Ullmann (*Enzyklopaedie der technischen Chemie*, “Uncatalyzed Reactions with Solids,” vol. 3, 4th ed., Verlag Chemie, 1973, pp. 395–464).

Examples

- Cement kilns are up to 6 m (17 ft) in diameter and 200 m (656 ft) long. Inclination is 3 to 4° and rotation is 1.2 to 2.0 rpm. Typical temperature profiles are shown in Fig. 19-24a. Near the flame the temperature is 1800 to 2000°C (3272 to 3632°F). The temperature of the solid reaches 1350 to 1500°C (2462 to 2732°F) which is necessary for clinker formation. In one smaller kiln, a length of 23 m (75 ft) was allowed for drying, 34 m (112 ft) for preheating, 19 m (62 ft) for calcining, and 15 m (49 ft) for clinkering. Total residence time is 40 min to 5 h, depending on the type of kiln. The time near the clinkering temperature of 1500°C (2732°F) is 10 to 20 min. Subsequent cooling is as rapid as possible. A kiln 6 m (20 ft) in diameter by 200 m (656 ft) can produce 2.7×10^9 kg/d (6×10^8 lbm/d) of cement. For production rates less than 270,000 kg/d (600,000 lbm/d), shaft kilns are used. These are vertical cylinders 2 to 3 m (6.5 to 10 ft) by 8 to 10 m (26 to 33 ft) high, fed with pellets and finely ground coal.
- Chlorination of ores ($\text{MeO} + \text{Cl}_2 + \text{C} \Rightarrow \text{MeCl}_2 + \text{CO}$, where Me is Ti, Mg, Be, U, and Zr, whose chlorides are water-soluble). For titanium, carbon is roasted with ore and chlorine is sparged through the bed ($\text{TiO}_2 + \text{C} + 2\text{Cl}_2 \Rightarrow \text{TiCl}_4 + \text{CO}_2$). The chlorine can be supplied indirectly, as in $\text{Cu}_2\text{S} + 2\text{NaCl} + \text{O}_2 \Rightarrow 2\text{CuCl} + \text{Na}_2\text{SO}_4$.
- Oxidation of sulfide ores ($\text{MeS} + 1.5\text{O}_2 \Rightarrow \text{MeO} + \text{SO}_2$, where Me is Fe, Mo, Pb, Cu, or Ni). Iron sulfide (pyrite) is burned with air for recovery of sulfur and to make the iron oxide from which the metal is more easily recovered. Sulfides of other metals also are roasted. A multiple-hearth furnace, as shown in Fig. 19-24b, is used. In some designs, the plates rotate; in others, the scraper arms rotate or oscillate and discharge the material to lower plates. Material charged at the top drops to successively lower plates while reactant and combustion

gases flow upward. A reactor with 9 trays 5 m (16 ft) in diameter and 12 m (39 ft) high can roast about 600 kg/h (1300 lbm/h) of pyrite. A major portion of the reaction is found to occur in the vapor space between trays. A unit in which most of the trays are replaced by empty space is called a *flash roaster*; its mode of operation is like that of a spray dryer. Molybdenum sulfide is roasted at the rate of 5500 kg/d (12,000 lbm/d) in a unit with 9 stages, 5-m (16-ft) diameter, at $630 \pm 15^\circ\text{C}$ ($1166 \pm 27^\circ\text{F}$) and the sulfur is reduced from 35.7 percent to 0.006 percent. A Dorr-Oliver fluidized-bed roaster is 5.5 m (18 ft) in diameter, 7.6 m (25 ft) high, with a bed height of 1.2 to 1.5 m (3.9 to 4.9 ft). It operates at 650 to 700°C (1200 to 1300°F) and has a capacity of 154,000 to 200,000 kg/d (340,000 to 440,000 lbm/d) (Kunii and Levenspiel, *Fluidization Engineering*, Butterworth, 1991). Two modes of operation can be used for a fluidized-bed unit like that shown in Fig. 19-24e. In one mode, a stable fluidized-bed level is maintained. The superficial gas velocity of 0.48 m/s (1.6 ft/s) is low. A reactor is 4.8 m (16 ft) in diameter, 1.5 m (4.9 ft) bed depth, 3 m (9.8 ft) freeboard. The capacity is 82,000 kg/d (180,000 lbm/d) pyrrhotite of 200 mesh. It operates at 875°C (1600°F) and 53 percent of the solids are entrained. In the other mode, the superficial gas velocity of 1.1 m/s (3.6 ft/s) is higher and results in 100 percent entrainment. This reactor is known as a *transfer line* or *pneumatic transport reactor*; a unit 6.6 m (22 ft) in diameter by 1.8 m (5.9 ft) can process 545,000 kg/d (1.2×10^6 lbm/d) of 200 mesh material at 780°C (1436°F).

- Sodium sulfate. A single-hearth furnace like that shown in Fig. 19-24g is used. Sodium chloride and sulfuric acid are charged continuously to the center of the pan, and the rotating scrapers gradually work the reacting mass to the periphery, where the sodium sulfate is discharged at 540°C (1000°). Pans are 3.3 to 5.5 m (11 to 18 ft) in diameter and can handle 5500 to 9000 kg/d (12,000 to 20,000 lbm/d) of salt. Rotary kilns also are used for this purpose. Such a unit 1.5 m (4.9 ft) in diameter by 6.7 m (22 ft) has a capacity of 22,000 kg/d (48,000 lbm/d) of salt cake. A pan furnace also is used, for instance, in the Leblanc soda ash process and for making sodium sulfide from sodium sulfate and coal.
- Magnetic roasting. In this process ores containing Fe_2O_3 are reduced with CO to Fe_3O_4 , which is magnetically separable from gangue. Rotary kilns are used, with temperatures of 700 to 800°C (1292 to 1472°F). Higher temperatures form FeO. The CO may be produced by incomplete combustion of a fuel. A unit for 2.3×10^6 kg/d (5×10^6 lbm/d) has a power consumption of 0.0033 to 0.0044 kWh/kg (3 to 4 kWh/ton) and a heat requirement of 180,000 to 250,000 kcal/ton (714,000 to 991,000 Btu/ton). The magnetic concentrate can be agglomerated for further treatment by pelletizing or sintering.
- Other examples include *calcination reactions* ($\text{MeCO}_3 \Rightarrow \text{MeO} + \text{CO}_2$, where Me is Ca, Mg, and Ba), *sulfating reactions* ($\text{CuS} + 2\text{O}_2 \Rightarrow \text{CuSO}_4$, of which the sulfate is water-soluble), and *reduction reactions* ($\text{MeO} + \text{H}_2 \Rightarrow \text{Me} + \text{H}_2\text{O}$, $\text{MeO} + \text{CO} \Rightarrow \text{Me} + \text{CO}_2$, where Me is Fe, W, Mo, Ge, and Zn).
- The deposition of polycrystalline silicon in microelectronic circuit fabrication ($\text{SiH}_4 \Rightarrow \text{Si} + 2\text{H}_2$) or the deposition of hard TiC films on machine tool surfaces ($\text{TiCl}_4 + \text{CH}_4 \Rightarrow \text{TiC} + 4\text{HCl}$).
- In reactive etching, a patterned film is selectively etched by reacting it with a gas such as chlorine ($\text{Si} + 2\text{Cl}_2 \Rightarrow \text{SiCl}_4$).

FLUID-FLUID REACTORS

Industrial fluid-fluid reactors may broadly be divided into gas-liquid and liquid-liquid reactors. Gas-liquid reactors typically may be used for the manufacture of pure products (such as sulfuric acid, nitric acid, nitrates, phosphates, adipic acid, and other chemicals) where all the gas and liquid react. They are also used in processes where gas-phase reactants are sparged into the reactor and the reaction takes place in the liquid phase (such as hydrogenation, halogenation, oxidation, nitration, alkylation, fermentation, oxidation of sludges, production of proteins, biochemical oxidations, and so on). Gas purification (in which relatively small amounts of impurities such as CO_2 , CO, COS, SO_2 , H_2S , NO, and

others are removed from reactants) is also an important class of gas-liquid reactions. Liquid-liquid reactors are used for synthesis of chemicals (or fuels). One of the liquids may serve as the catalyst, or the liquids may react with one another across the interface. In the latter case, the product may be soluble in one of the liquids or precipitate out as a solid.

GAS-LIQUID REACTORS

Since the reaction rate per unit reactor volume depends on the transfer of molecules from the gas to the liquid, the mass-transfer coefficient is

important. As discussed in Sec. 7, the mass-transfer coefficient in a nonreacting system depends on the physical properties of the gas and liquid and the prevailing hydrodynamics. Here D_C and D_L are diffusivities of the absorbing species in the gas and liquid phases, respectively; $p_i = f(C_i)$ or $p_i = \text{He}C_{Li}$ are the equilibrium relation at the gas-liquid interface; a = interfacial area/unit volume; and δ_C , δ_L are film thicknesses on the gas and liquid sides, respectively. The steady rates of solute transfer are

$$r = k_{cC} (p_C - p_i) = k_{lL} (C_{Li} - C_L) \tag{19-72}$$

where $k_{cC} = D_C/\delta_C$ and $k_{lL} = D_L/\delta_L$ are the mass-transfer coefficients of the individual films. Overall coefficients are defined by

$$r = K_{cC} a (p_C - p_L) = K_{lL} a (C_C - C_L) \tag{19-73}$$

Upon introducing the equilibrium relation at the interface, the relation between the various mass-transfer coefficients is

$$\frac{1}{K_{cC} a} = \frac{\text{He}}{K_{lL} a} = \frac{1}{k_{cC} a} + \frac{\text{He}}{k_{lL} a} \tag{19-74}$$

When the solubility is low, the Henry constant He is large and $k_{lL} \Rightarrow K_{lL}$; when the solubility is high, He is small and $k_{cC} \Rightarrow K_{cC}$. The reaction rate in the liquid phase determines the relative importance of the mass-transfer coefficient. For slow reactions, reaction rate in the liquid phase determines overall rate. In contrast, for fast reactions, transport of reactant from the gas to the liquid across the gas-liquid interface is rate-determining. If the reaction is fast, reaction also occurs in the film along with diffusion, thus enhancing the mass transfer. The relative role of mass transfer (across the gas-liquid interface) versus kinetics is important in gas-liquid reactor selection and design. Three modes of contacting gas with liquid are possible: (1) The gas is dispersed as bubbles in the liquid; (2) the liquid is dispersed as droplets in the gas; and (3) the liquid and gas are brought together as thin films over a packing or wall. Considerations that influence reactor selection include the magnitude and distribution of the residence times of the phases, the power requirements, the scale of the operation, the opportunity for heat transfer, and so on.

As indicated above, for purely physical absorption, the mass-transfer coefficients depend on the hydrodynamics and the physical properties of the phases. The literature contains measured values of mass-transfer coefficients and correlations (see discussion on agitated tanks and bubble columns below). Tables 19-7 and 19-8 present experimental information on apparent mass-transfer coefficients for absorption of select gases. On this basis, a tower for absorption of SO₂ with NaOH is smaller than that with pure water by a factor of roughly 0.317/7.0 = 0.045. Table 19-9 lists the main factors that are needed for

TABLE 19-7 Typical Values of $K_{cC} a$ for Absorption in Towers Packed with 1.5-in Intalox Saddles at 25% Completion of Reaction*

Absorbed gas	Absorbent	$K_{cC} a$, lb mol/(h-ft ³ ·atm)
Cl ₂	H ₂ O-NaOH	20.0
HCl	H ₂ O	16.0
NH ₃	H ₂ O	13.0
H ₂ S	H ₂ O-MEA	8.0
SO ₂	H ₂ O-NaOH	7.0
H ₂ S	H ₂ O-DEA	5.0
CO ₂	H ₂ O-KOH	3.10
CO ₂	H ₂ O-MEA	2.50
CO ₂	H ₂ O-NaOH	2.25
H ₂ S	H ₂ O	0.400
SO ₂	H ₂ O	0.317
Cl ₂	H ₂ O	0.138
CO ₂	H ₂ O	0.072
O ₂	H ₂ O	0.0072

*To convert in to cm, multiply by 2.54; lb mol/(h-ft³·atm) to kg mol/(h-m³·kPa), multiply by 0.1581.

SOURCE: From Eckert et al., *Ind. Eng. Chem.*, **59**, 41 (1967).

TABLE 19-8 Selected Absorption Coefficients for CO₂ in Various Solvents in Towers Packed with Raschig Rings*

Solvent	$K_{cC} a$, lb mol/(h-ft ³ ·atm)
Water	0.05
1-N sodium carbonate, 20% Na as bicarbonate	0.03
3-N diethanolamine, 50% converted to carbonate	0.4
2-N sodium hydroxide, 15% Na as carbonate	2.3
2-N potassium hydroxide, 15% K as carbonate	3.8
Hypothetical perfect solvent having no liquid-phase resistance and having infinite chemical reactivity	24.0

*Basis: $L = 2,500$ lb/(h-ft²); $G = 300$ lb/(h-ft²); $T = 77^\circ\text{F}$; pressure, 1.0 atm. To convert lb mol/(h-ft³·atm) to kg mol/(h-m³·kPa) multiply by 0.1581.

SOURCE: From Sherwood, Pigford, and Wilke, *Mass Transfer*, McGraw-Hill, 1975, p. 305.

mathematical representation of $K_{cC} a$ in a typical case of the absorption of CO₂ by aqueous monethanolamine. Other than Henry's law, $p = \text{He}C$, which holds for some fairly dilute solutions, there is no general simple form of equilibrium relation. A typically complex equation is that for CO₂ in contact with sodium carbonate solutions [Harte, Baker, and Purcell, *Ind. Eng. Chem.* **25**: 528 (1933)], which is

$$p_{\text{CO}_2} = \frac{137f^2 N^{1.29}}{S(1-f)(365-T)^2} \tag{19-75}$$

where f = fraction of total base present as bicarbonate
 N = normality, 0.5 to 2.0
 S = solubility of CO₂ in water at 1 atm, g-mol/L
 T = temperature, 65 to 150°F

The mass-transfer coefficient with a reactive solvent can be represented by multiplying the purely physical mass-transfer coefficient by an *enhancement factor E* that depends on a parameter called the *Hatta number* (analogous to the *Thiele* modulus in porous catalyst particles).

$$\text{Ha}^2 = \frac{\text{maximum possible reaction in film}}{\text{maximum diffusional transport through film}} \tag{19-76}$$

TABLE 19-9 Correlation of $K_{cC} a$ for Absorption of CO₂ by Aqueous Solutions of Monoethanolamine in Packed Towers*

Packing	F	Basis for calculation of F
5- to 6-mm glass rings	7.1×10^{-3}	Shneerson and Leibush data, 1-in column, atmospheric pressure
3/8-in ceramic rings	3.0×10^{-3}	Unpublished data for 4-in column, atmospheric pressure
3/4- by 2-in polyethylene Tellerettes	3.0×10^{-3}	Teller and Ford data, 8-in column, atmospheric pressure
1-in steel rings		
1-in ceramic saddles	2.1×10^{-3}	
1 1/2- and 2-in ceramic rings	$0.4\text{--}0.6 \times 10^{-3}$	Gregory and Scharmann and unpublished data for two commercial plants, pressures 30 to 300 psig

*To convert in to cm multiply by 2.54.

SOURCE: From Kohl and Riesenfeld, *Gas Purification*, Gulf, 1985.

19-40 REACTORS

For example, for the reaction $A(g) + bB(l) \rightarrow P$ with liquid reactant B in excess,

$$Ha^2 = \frac{kC_{aLi}C_{bL}\delta_L}{D_{aL}(C_{aLi} - 0)/\delta_L} = \frac{kC_{bL}\delta_L^2}{D_{aL}} = \frac{kC_{bL}D_{aL}}{k_L^2} \quad (19-77)$$

When $Ha \gg 1$, all the reaction occurs in the film and the amount of interfacial area is controlling, necessitating equipment that generates a large interfacial area. When $Ha \ll 1$, no reaction occurs in the film and the bulk volume is controlling. As guidance the following criteria may be used:

$Ha < 0.3$	Reaction needs large bulk liquid volume.
$0.3 < Ha < 3.0$	Reaction needs large interfacial area and large bulk liquid volume.
$Ha > 3.0$	Reaction needs large interfacial area.

Of the parameters making up the Hatta number, liquid diffusivity and mass-transfer coefficient data and measurement methods are well reviewed in the literature.

As discussed in Sec. 7, the factor E represents an enhancement of the rate of transfer of A caused by the reaction compared with physical absorption, i.e., K_G is replaced by EK_G . The theoretical variation of E with Hatta number for a first- and second-order reaction in a liquid film is shown in Fig. 19-25. The uppermost line on the upper right represents the pseudo first-order reaction, for which $E = Ha \coth(Ha)$. Three regions are identified with different requirements of liquid holdup ϵ and interfacial area a , and for which particular kinds of contacting equipment may be best:

Region I, $Ha > 2$. Reaction is fast and occurs mainly in the liquid film so $C_{aL} \approx 0$. The rate of reaction $r_a = k_L a E C_{aLi}$ will be large when a is large, but liquid holdup is not important. Packed towers or stirred tanks will be suitable.

Region II, $0.02 < Ha < 2$. Most of the reaction occurs in the bulk of the liquid. Both interfacial area and holdup of liquid should be high. Stirred tanks or bubble columns will be suitable.

Region III, $Ha < 0.02$. Reaction is slow and occurs in the bulk liquid. Interfacial area and liquid holdup should be high, especially the latter. Bubble columns will be suitable.

The above analysis and Fig. 19-25 provide a theoretical foundation similar to the Thiele-modulus effectiveness factor relationship for fluid-solid systems. However, there are no generalized closed-form expressions of E for the more general case of a complex reaction network, and its value has to be determined by solving the complete diffusion-reaction equations for known intrinsic mechanism and kinetics, or alternatively estimated experimentally.

Some of this theoretical thinking may be utilized in reactor analysis and design. Illustrations of gas-liquid reactors are shown in Fig. 19-26. Unfortunately, some of the parameter values required to undertake a rigorous analysis often are not available. As discussed in Sec. 7, the intrinsic rate constant k_c for a liquid-phase reaction without the complications of diffusional resistances may be estimated from properly designed laboratory experiments. Gas- and liquid-phase holdups may be estimated from correlations or measured. The interfacial area per unit reactor volume a may be estimated from correlations or measurements that utilize techniques of transmission or reflection of light, though these are limited to small diameters. The combined volumetric mass-transfer coefficient $k_L a$, can be also directly measured in reactive or nonreactive systems (see, e.g., Charpentier, *Advances in Chemical Engineering*, vol. 11, Academic Press, 1981, pp. 2-135). Mass-transfer coefficients, interfacial areas, and liquid holdup typical for various gas-liquid reactors are provided in Tables 19-10 and 19-11.

There are numerous examples of commercial gas-liquid reactions in the literature. These include common operations such as absorption of ammonia to make fertilizers and of carbon dioxide to make soda ash. Other examples are recovery of phosphine from off-gases of phosphorous plants; recovery of HF; oxidation, halogenation, and hydrogenation of various organics; hydration of olefins to alcohols; oxo reaction for higher aldehydes and alcohols; ozonolysis of oleic acid; absorption of carbon monoxide to make sodium formate; alkylation of acetic acid with isobutylene to make *tert*-butyl acetate; absorption of olefins to make various products; HCl and HBr plus higher alcohols to make alkyl halides; and so on. By far the greatest number of applications is for the removal or recovery of mostly small concentrations of acidic and other components from air, hydrocarbons, and hydrogen. Two lists of gas-liquid reactions of industrial importance have been compiled. The literature survey by Danckwerts (*Gas-Liquid*

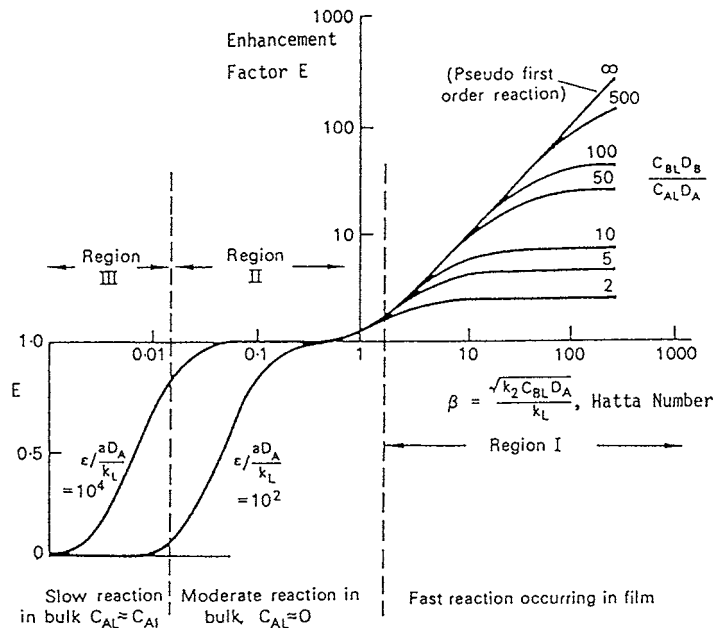


FIG. 19-25 Enhancement factor E and Hatta number of first- and second-order gas-liquid reactions. (Coulson and Richardson, *Chemical Engineering*, vol. 3, Pergamon, 1971, p. 80.)

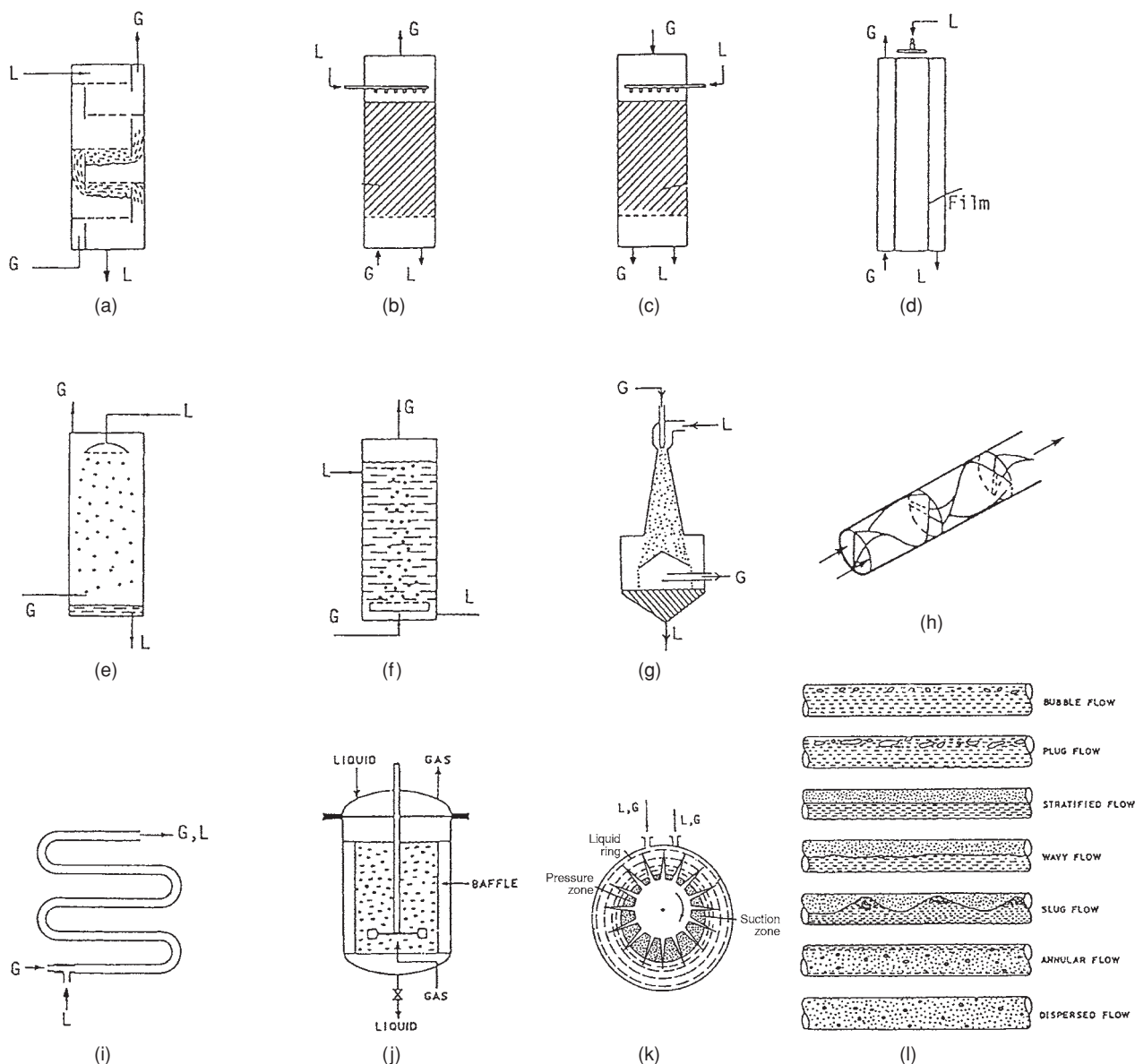


FIG. 19-26 Types of industrial gas-liquid reactors. (a) Tray tower. (b) Packed, countercurrent. (c) Packed, co-current. (d) Falling liquid film. (e) Spray tower. (f) Bubble tower. (g) Venturi mixer. (h) Static in-line mixer. (i) Tubular flow. (j) Stirred tank. (k) Centrifugal pump. (l) Two-phase flow in horizontal tubes.

Reactions, McGraw-Hill, 1970) cites 40 different systems. A supplementary list by Doraiswamy and Sharma (*Heterogeneous Reactions: Fluid-Fluid-Solid Reactions*, Wiley, 1984) cites another 50 cases and indicates the most suitable kind of reactor to be used for each. A number of devices have been in use for estimating mass-transfer coefficients, and correlations are available. This topic is reviewed in books, for example, by Danckwerts (*Gas-Liquid Reactions*, McGraw-Hill, 1970) and Charpentier [in Ginetto and Silveston (eds.), *Multiphase Chemical Reactor Theory, Design, Scaleup*, Hemisphere, 1986]. One of the issues associated with designing commercial reactors is to properly understand whether data obtained on the laboratory scale are applicable or whether larger scale data are needed to reduce the scale-up risk.

LIQUID-LIQUID REACTORS

Much of the thinking on gas-liquid reactors is also applicable to liquid-liquid reactors. The liquids are usually not miscible, and the transport of reactants can determine the specific reaction rate. Liquid-liquid reactors require dispersion of one of the liquid phases to provide sufficient interfacial area for mass transfer. This can be achieved by the use of static mixers, jets, or mechanical means such as in a CSTR.

In a stirred tank, either liquid can be made continuous by charging that liquid first, starting the agitator, and introducing the liquid to be dispersed. For other reactor types, the choice of which phase is continuous and which is dispersed will depend on the physicochemical properties of the phases and operating conditions (such as temperature,

TABLE 19-10 Mass-Transfer Coefficients, Interfacial Areas, and Liquid Holdup in Gas-Liquid Reactions

Type of reactor	ϵ_L , %	k_G , gm mol/(cm ² ·s·atm) × 10 ⁴	k_L , cm/s × 10 ²	a , cm ² /cm ³ reactor	$k_L a$, s ⁻¹ × 10 ²
Packed columns					
Countercurrent	2-25	0.03-2	0.4-2	0.1-3.5	0.04-7
Cocurrent	2-95	0.1-3	0.4-6	0.1-17	0.04-102
Plate columns					
Bubble cap	10-95	0.5-2	1-5	1-4	1-20
Sieve plates	10-95	0.5-6	1-20	1-2	1-40
Bubble columns	60-98	0.5-2	1-4	0.5-6	0.5-24
Packed bubble columns	60-98	0.5-2	1-4	0.5-3	0.5-12
Tube reactors					
Horizontal and coiled	5-95	0.5-4	1-10	0.5-7	0.5-70
Vertical	5-95	0.5-8	2-5	1-20	2-100
Spray columns	2-20	0.5-2	0.7-1.5	0.1-1	0.07-1.5
Mechanically agitated bubble reactors	20-95	—	0.3-4	1-20	0.3-80
Submerged and plunging jet	94-99	—	0.15-0.5	0.2-1.2	0.03-0.6
Hydrocyclone	70-93	—	10-30	0.2-0.5	2-15
Ejector reactor	—	—	—	1-20	—
Venturi	5-30	2-10	5-10	1.6-25	8-25

SOURCE: From Charpentier, *Advances in Chemical Engineering*, vol. 11, Academic Press, 1981, pp. 2-135.

pressure, and flow rates). Equipment suitable for reactions between liquids is represented in Fig. 19-27. Almost invariably, one of the phases is aqueous and the other organic, with reactants distributed between phases. Such reactions can be carried out in any kind of equipment that is suitable for physical extraction, including mixer-settlers and towers of various kinds: empty or packed, still or agitated, either phase dispersed, provided that adequate heat transfer can be incorporated. Mechanically agitated tanks are favored because the interfacial area can be made large, as much as 100 times that of spray towers, for instance. Power requirements for liquid-liquid mixing are about 5 hp/1000 gal. Agitator tip speed of turbine-type impellers is 4.6 to 6.1 m/s (15 to 20 ft/s). Table 19-12 provides data for common types of liquid-liquid contactors. As shown, the given range of $k_L a$ is more than 100/1 even for the same equipment. It is provided merely for guidance, and correlations need to be validated with data at some reasonable scale.

Efficiencies of several kinds of small-scale extractors are shown in Fig. 19-28. Larger-diameter equipment may have less than one-half these efficiencies. Spray columns are inefficient and are used only when other kinds of equipment may become clogged. Packed columns as liquid-liquid reactors are operated at 20 percent of flooding. Their *height equivalent to theoretical stage* (HETS) range is from 0.6 to 1.2 m (1.99 to 3.94 ft). Sieve trays minimize backmixing and provide repeated coalescence and redispersion. Mixer-settlers provide approximately one theoretical stage, but several stages can be incorporated in a single shell, although with some loss of operating flexibility. The HETS of rotating disk contactor (RDC) is 1 to 2 m (3.2 to 6.4 ft). More elaborate staged extractors bring this down to 0.35 to 1.0 m (1.1 to 3.3 ft).

When liquid-liquid contactors are used as reactors, values of their mass-transfer coefficients may be enhanced by reaction, analogously to those of gas-liquid processes. Reactions can occur in either or both phases or near the interface. Nitration of aromatics with HNO₃-H₂SO₄ occurs in the aqueous phase [Albright and Hanson (eds.), *Industrial and Laboratory Nitrations*, ACS Symposium Series 22

(1975)]. An industrial example of reaction in both phases is the oximation of cyclohexanone, a step in the manufacture of caprolactam for nylon (Rod, *Proc. 4th Int./6th European Symp. Chemical Reactions*, Heidelberg, Pergamon, 1976, p. 275). The formation of dioxane from isobutene in a hydrocarbon phase and aqueous formaldehyde occurs preponderantly in the aqueous phase where the rate equation is first-order in formaldehyde, although the specific rate is also proportional to the concentration of isobutene in the organic phase [Hellin et al., *Genie. Chim.* 91: 101 (1964)]. Doraiswamy and Sharma (*Heterogeneous Reactions*, Wiley, 1984) have compiled a list of 26 classes of reactions. The reactions include examples such as making soap with alkali, nitration of aromatics to make explosives, and alkylation of C4s with sulfuric acid to make gasoline alkylate.

REACTOR TYPES

The discussion is centered around gas-liquid reactors. If the dissolved gas content exceeds the amount needed for the reaction, the liquid may be first saturated with gas and then sent through a stirred tank or tubular reactor as a single phase. If the residence times for the liquid and gas are comparable, both gas and liquid may be pumped in and out of the reactor together. If the gas has limited solubility, it is bubbled through the reactor and the residence time for gas is much smaller. Figure 19-29 provides examples of gas-liquid reactors for specific processes.

Agitated Stirred Tanks Stirred tanks are common gas-liquid reactors. Reaction requirements dictate whether the gas and liquid are in a batch or continuous mode. For a liquid-phase reaction with a long time constant, a batch mode may be used. The reactor is filled with liquid, and gas is continuously fed into the reactor to maintain pressure. If by-product gases form, these gases may need to be purged continuously. If gas solubility is limiting, a higher-purity gas may be continuously fed (and, if required, recycled). As the liquid residence time decreases, product may be continuously removed as well. A

TABLE 19-11 Order-of-Magnitude Data of Equipment for Contacting Gases and Liquids

Device	$k_L a$, s ⁻¹	V , m ³	$k_L a V$, m ³ /s (duty)	a , m ⁻¹	ϵ_L	Liquid mixing	Gas mixing	Power per unit volume, kW/m ³
Baffled agitated tank	0.02-0.2	0.002-100	10 ⁻⁴ -20	~200	0.9	~Backmixed	Intermediate	0.5-10
Bubble column	0.05-0.01	0.002-300	10 ⁻³ -3	~20	0.95	~Plug	Plug	0.01-1
Packed tower	0.005-0.02	0.005-300	10 ⁻⁵ -6	~200	0.05	Plug	~Plug	0.01-0.2
Plate tower	0.01-0.05	0.005-300	10 ⁻⁵ -15	~150	0.15	Intermediate	~Plug	0.01-0.2
Static mixer (bubble flow)	0.1-2	Up to 10	1-20	~1000	0.5	~Plug	Plug	10-500

SOURCE: From J. C. Middleton, in Hamby, Edwards, and Nienow, *Mixing in the Process Industries*, Butterworth, 1985.

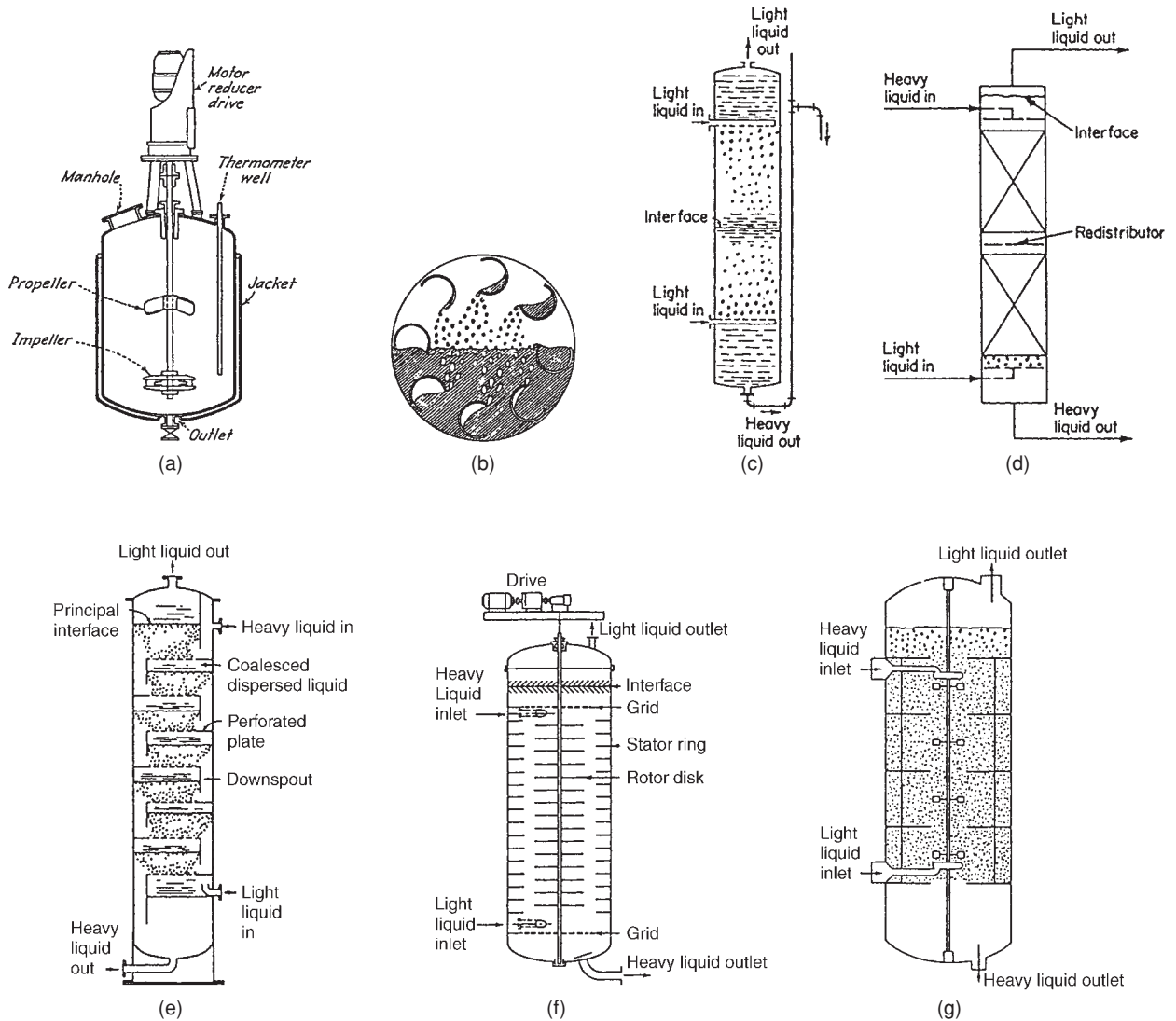


FIG. 19-27 Equipment for liquid-liquid reactions. (a) Batch stirred sulfonator. (b) Raining bucket (RTL S A, London). (c) Spray tower with both phases dispersed. (d) Two-section packed tower with light phase dispersed. (e) Sieve tray tower with light phase dispersed. (f) Rotating disk contactor (RDC) (Escher B V, Holland). (g) Oldshue-Rushton extractor (Mixing Equipment Co.).

TABLE 19-12 Continuous-Phase Mass-Transfer Coefficients and Interfacial Areas in Liquid-Liquid Contactors*

Type of equipment	Dispersed phase	Continuous phase	ϵ_D	τ_D	$k_L \times 10^3$, cm/s	a , cm ² /cm ³	$k_{La} \times 10^2$, s ⁻¹
Spray columns	P	M	0.05–0.1	Limited	0.1–1	1–10	0.1–10
Packed columns	P	P	0.05–0.1	Limited	0.3–1	1–10	0.3–10
Mechanically agitated contactors	PM	M	0.05–0.4	Can be varied over a wide range	0.3–1	1–800	0.3–800
Air-agitated liquid/liquid contactors	PM	M	0.05–0.3	Can be varied over a wide range	0.1–0.3	10–100	1.0–30
Two-phase cocurrent (horizontal) contactors	P	P	0.05–0.2	Limited	0.1–1.0	1–25	0.1–25

*P = plug flow, M = mixed flow, ϵ_D = fractional dispersed phase holdup, τ_D = residence time of the dispersed phase.

SOURCE: From Doraiswamy and Sharma, *Heterogeneous Reactions*, Wiley, 1984.

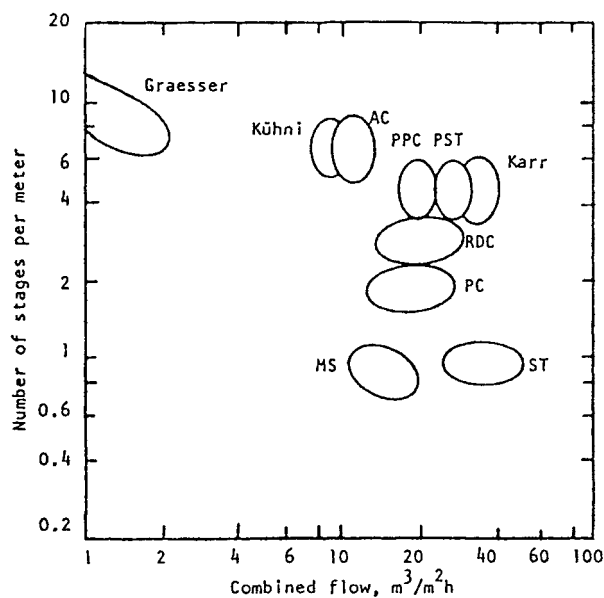


FIG. 19-28 Efficiency and capacity range of small-diameter extractors, 50- to 150-mm diameter. Acetone extracted from water with toluene as the disperse phase, $V_d/V_c = 1.5$. Code: AC = agitated cell; PPC = pulsed packed column; PST = pulsed sieve tray; RDC = rotating disk contactor; PC = packed column; MS = mixer-settler; ST = sieve tray. [Stichlmair, Chem. Ing. Tech. 52(3): 253-255 (1980).]

hybrid reactor type is the semibatch reactor. Gas and liquid are continuously fed to the reactor until the reactor is full of liquid. The reactor then operates as a batch reactor.

Agitated stirred tanks are preferred when high gas-liquid interfacial area is needed. Disadvantages include maintenance of the motor and seals, potential for contamination in biological and food applications, and higher cost.

A basic stirred tank design is shown in Fig. 19-30. Height/diameter ratio is $H/D = 1$ to 3. Heat transfer may be provided through a jacket or internal coils. Baffles prevent movement of the mass as a whole. A draft tube can enhance vertical circulation. The vapor space is about 20 percent of the total volume. A hollow shaft and impeller increase gas circulation by entraining the gas from the vapor space into the liquid. A splasher can be attached to the shaft at the liquid surface to improve entrainment of gas. A variety of impellers is in use. The pitched propeller moves the liquid axially, the flat blade moves it radially, and inclined blades move it both axially and radially. The anchor and some other designs are suited to viscous liquids. For gas dispersion, the six-bladed turbine is preferred. When the ratio of liquid height to diameter is $H/D \leq 1$, a single impeller suffices, and in the range $1 \leq H/D \leq 1.8$ two are needed.

Gases may be dispersed in liquids by spargers or nozzles. However, more intensive dispersion and redispersion are obtained by mechanical agitation. The gas is typically injected at the point of greatest turbulence near the injector tip. Agitation also provides the heat transfer and, if needed, keeps catalyst particles (in a three-phase or slurry reactor) in suspension. Power inputs of 0.6 to 2.0 kW/m³ (3.05 to 10.15 hp/1000 gal) are suitable. Bubble sizes depend on agitation as well as on the physical properties of the liquid. They tend to be greater than a minimum size regardless of power input due to coalescence. Pure liquids are of a coalescing type; solutions with electrolytes are noncoalescing. Agitated bubble size in air/water is about 0.5 mm (0.020 in), holdup fractions are about 0.10 for coalescing and 0.25 for noncoalescing liquids; however, more elaborate correlations are available and required for reactor sizing. The reactor may be modeled as two ideal reactors, one for each phase, with mass transfer between the phases. More elaborate models that utilize CFD have

also been used. For example, if the gas has limited solubility and is sparged through a liquid, the gas may be modeled as a PFR and the liquid as a CSTR. Mass-transfer coefficients vary, e.g., as the 0.7 exponent on the power input per unit volume (with the dimensions of the vessel and impeller and the superficial gas velocity as additional factors). A survey of such correlations is made by van't Riet [Ind. Eng. Chem. Proc. Des. Dev. 18: 357 (1979)]. Also, Charpentier [in Gianetto and Silveston (eds.), *Multiphase Chemical Reactors*, Hemisphere, 1986, pp. 104-151] discusses hydrodynamic parameters for stirred tank (and other) reactors, and typical values are shown in Tables 19-10 and 19-11.

Examples

- **Production of penicillin.** An agitated stirred tank is used for the large-scale aerobic fermentation of penicillin by the growth of a specific mold. Commercial vessel sizes are 40,000 to 200,000 L (1400 to 7000 ft³). The operation is semibatch in that the lactose or glucose nutrient and air are charged at controlled rates to a precharged batch of liquid nutrients and cell mass. Reaction time is 5 to 6 d. The broth is limited to 7 to 8 percent sugars, which is all the mold will tolerate. Solubility of oxygen is limited, and air must be supplied over a long period as it is used up. The air is essential to the growth. Dissolved oxygen must be kept at a high level for the organism to survive. Air also serves to agitate the mixture and to sweep out the CO₂ and any noxious by-products that are formed. Air supply is in the range of 0.5 to 1.5 volumes/(volume of liquid)(min). For organisms grown on glucose, the oxygen requirement is 0.4 g/g dry weight; on methanol it is 1.2 g/g. The pH is controlled at about 6.5 and the temperature at 24°C (75°F). The heat of reaction requires cooling water at the rate of 10 to 40 L/(1000 L holdup)(h). Vessels under about 500 L (17.6 ft³) are provided with jackets, larger ones with coils. For a 55,000-L vessel, 50 to 70 m² may be taken as average. Mechanical agitation is needed to break up the gas bubbles but must avoid rupturing the cells. The disk turbine with radial action is most suitable. It can tolerate a superficial gas velocity up to 120 m/h (394 ft/h) without flooding [whereas the propeller is limited to about 20 m/h (66 ft/h)]. When flooding occurs, the impeller is working in a gas phase and cannot assist the transfer of gas to the liquid phase. Power input by agitation and air sparger is 1 to 4 W/L [97 to 387 Btu/(ft³·h)] of liquid.

- **Refinery alkylation.** C3-C4 olefins are reacted with isobutane in the presence of concentrated acid to form higher-molecular-weight hydrocarbons that may be blended into the gasoline pool. Commercial alkylation processes are catalyzed by either sulfuric or hydrofluoric acid. For both processes, alkylation product quality and acid consumption are impacted by temperature, isobutene/olefin ratio, space velocity, and acid concentration. DuPont Stratco's contactor reactor is a horizontal pressure vessel containing an inner circulation tube, a tube bundle to remove the heat of reaction, and a mixing impeller. The hydrocarbon feed and sulfuric acid enter on the suction side of the impeller inside the circulation tube, producing an emulsion. The reaction emulsion is partially separated in a settler, and the acid emulsion is recycled to the contactor's shell side. The hydrocarbon effluent is directed to the contactor's tube bundle where flash vaporization removes the heat of reaction. Contactor arrangements are also utilized when the alkylation reaction is conducted using hydrofluoric acid.

Bubble Columns Nozzles or spargers disperse the gas. The mixing is due to rising bubbles, not mechanical agitation. Bubble action provides agitation about equivalent to that of mechanical stirrers (and similar mass- and heat-transfer coefficients) at the same power input per volume. The reaction medium may be a liquid (or slurry containing a heterogeneous catalyst). To improve the operation, redispersion of gas in liquid or an approach to plug flow may be achieved by using static mixers (such as perforated plates) at regular intervals. Because of their large volume fraction of liquid, bubble column reactors are suited to slow reactions where the rate of reaction is limiting. Major advantages are an absence of moving parts, the ability to handle solid particles without erosion or plugging, good heat transfer at the wall or coils, high interfacial area, and high mass-transfer coefficients. A disadvantage is backmixing in the liquid phase and some backmixing in the gas phase. The static head of the liquid will increase gas pressure drop, and this may be undesirable.

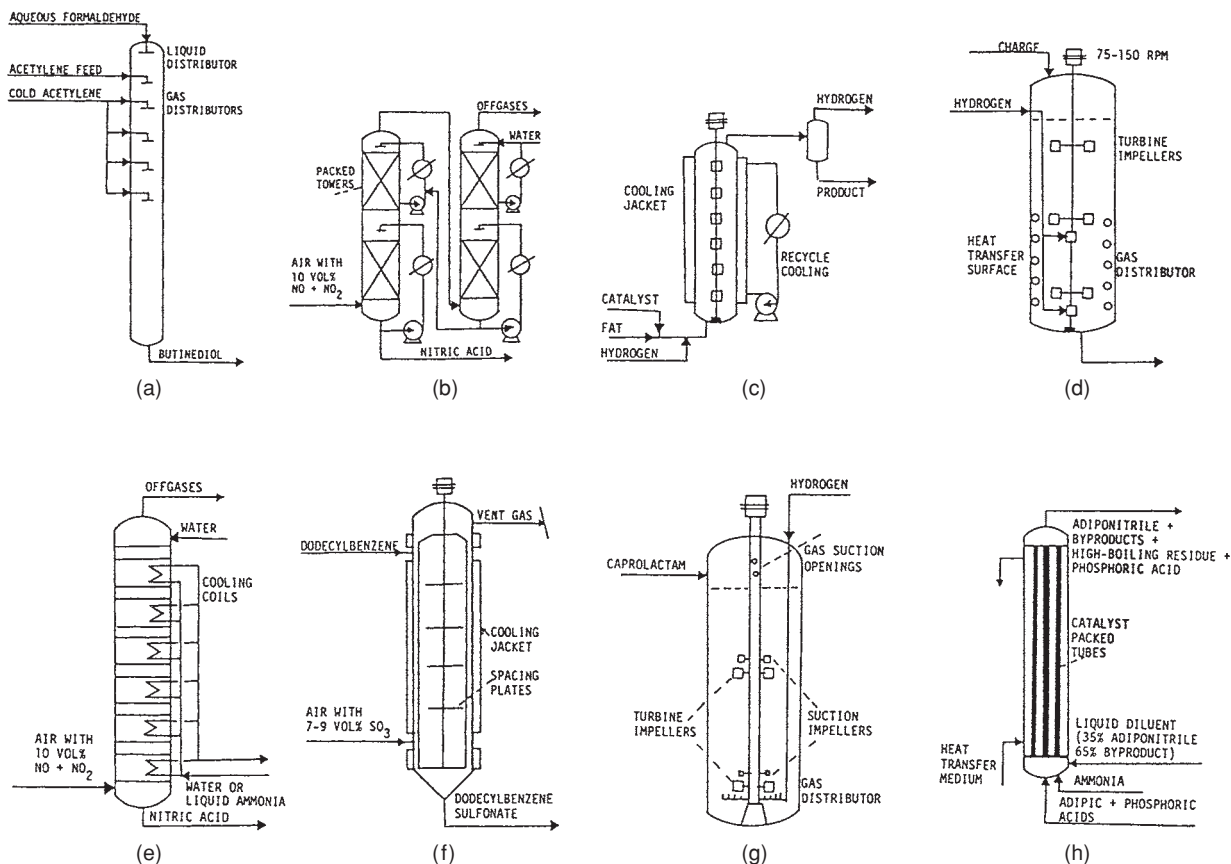


FIG. 19-29 Examples of reactors for specific gas-liquid processes. (a) Trickle reactor for synthesis of butanediol, 1.5-m diameter by 18 m high. (b) Nitrogen oxide absorption in packed columns. (c) Continuous hydrogenation of fats. (d) Stirred tank reactor for batch hydrogenation of fats. (e) Nitrogen oxide absorption in a plate column. (f) A thin-film reactor for making dodecylbenzene sulfonate with SO₃. (g) Stirred tank reactor for the hydrogenation of caprolactam. (h) Tubular reactor for making adiponitrile from adipic acid in the presence of phosphoric acid.

Generally, the bubble column height can be greater than for tray or packed towers.

From a mechanical standpoint, a bubble column reactor is a vertical cylindrical vessel with nozzles or a sparger grid at the bottom. The sparger grid is an array of parallel pipes connected to a manifold or several radial arms in a spider pattern or concentric circles, all with downward-facing holes every few inches or so. The holes are sized to give exit velocities of 100 to 300 ft/s, and the gas enters the liquid as jets that break up into bubbles after a short distance. The height/diameter ratio of the vessel is at least 1.5 and may be as large as 20. Depending on the heat-transfer requirements, coils or a jacket may be needed.

The liquid may be in batch mode or enter from the top or bottom. The simplest mathematical model may assume that the liquid is well mixed and the gas is in plug flow. Liquid backmixing may have a detrimental effect on selectivity. In the oxidation of liquid *n*-butane, for instance, the ratio of methyl ethyl ketone to acetic acid is much higher in plug flow than in backmixed reactors. Similarly, in the air oxidation of isobutane to *tert*-butyl hydroperoxide, where *tert*-butanol also is obtained, plug flow is more desirable. Backmixing in the liquid may be reduced with packing or perforated plates. Packed bubble columns operate with flooded packing, in contrast with normal packed columns that usually operate below 70 percent of the flooding point. With packing, liquid backmixing is reduced and interfacial area is increased 15 to 80 percent, but the true mass-transfer coefficient remains the same. At relatively high superficial

gas velocities [10 to 15 cm/s (0.33 to 0.49 ft/s)] and for taller columns, backmixing is reduced so the vessel performs as a CSTR battery. Radial baffles (also called disk-and-doughnut baffles) are also helpful. A rule of thumb is that the hole should be about 0.7 times the vessel diameter, and the spacing should be 0.8 times the diameter.

The literature may provide guidance on several parameters: bubble diameter and bubble rise velocity, gas holdup, interfacial area, mass-transfer coefficient k_L , axial liquid-phase and gas-phase dispersion coefficients, and heat-transfer coefficient to the wall. The key design variable is the superficial velocity of the gas that affects the gas holdup, the interfacial area, and the mass-transfer coefficient. Each of these has been described in some detail by Deckwer (*Bubble Column Reactors*, Wiley, 1992). The effect of vessel diameter on these parameters is not well understood beyond $D \geq 0.15$ to 0.3 m (0.49 to 1 ft), the range for most of the existing literature correlations. From a qualitative standpoint, increasing the superficial gas velocity increases the holdup of gas, the interfacial area, and the overall mass-transfer coefficient. The ratio of height to diameter is not very important in the range of 4 to 10. Decreasing viscosity and decreasing surface tension increase the interfacial area. Electrolyte solutions have smaller bubbles, higher gas holdup, and higher interfacial area. Sparger design is unimportant for superficial gas velocities > 5 to 10 cm/s (0.16 to 0.32 ft/s) and tall columns. Liquid entrainment considerations (discussed in the appropriate section of the Handbook) provide an upper bound on gas superficial velocity; however, gas conversion falls off at higher

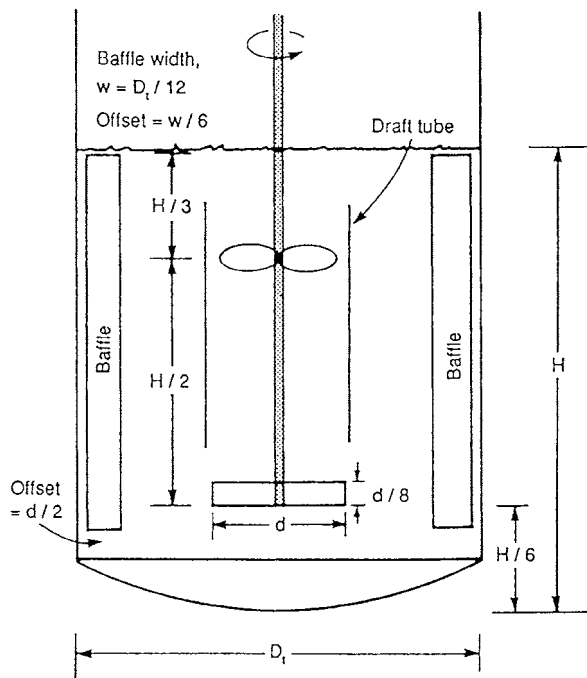


FIG. 19-30 A basic stirred tank design, not to scale, showing a lower radial impeller and an upper axial impeller housed in a draft tube. Four equally spaced baffles are standard. H = height of liquid level, D_t = tank diameter, d = impeller diameter. For radial impellers, $0.3 \leq d/D_t \leq 0.6$.

superficial velocities, so values under 10 cm/s (0.32 ft/s) are often desirable. Some examples of bubble column reactor types are illustrated in Fig. 19-31. Figure 19-31a is a conventional bubble column with no internals. Figure 19-31b is a tray bubble column. The trays are used to redistribute the gas into the liquid and to induce staging to approximate plug flow. Figure 19-31c is a packed bubble column with the packing being either an inert or a catalyst. Bubble columns are further discussed in the multiphase reactor section.

An excellent reference is Deckwer (*Bubble Column Reactors*, Wiley, 1992). Two complementary reviews of this subject are by Shah et al. [*AIChE J.* **28**: 353–379 (1982)] and Deckwer [in de Lasa (ed.), *Chemical Reactor Design and Technology*, Martinus Nijhoff, 1985, pp. 411–461]. Useful comments are made by Doraiswamy and Sharma (*Heterogeneous Reactions*, Wiley, 1984).

Examples

- A number of reactions in the production of pharmaceuticals or crop protection chemicals are conducted in bubble columns. Oxygen, chlorine, etc., may be the reactant gas.
- Hydrogenation reactions may be carried out in bubble column reactors. Often a slurry catalyst may be used which makes it a multiphase reactor.
- Aerobic fermentations are carried out in bubble columns when scale advantage is required, and the cells can be considered a third phase, making these multiphase reactors.

Tubular Reactors In a tubular or pipeline reactor, gas and liquid flow concurrently. A variety of flow patterns, ranging from a small quantity of bubbles in the liquid to small quantities of droplets in the gas, are possible, depending on the flow rate of the two streams. Figure 19-26f shows the patterns in horizontal flow; those in vertical flow are a little different.

Two-phase tubular reactors offer opportunities for temperature control, accommodate wide ranges of T and P , and approach plug flow, and the high velocities prevent settling of slurries or accumulations on the walls. Mixing of the phases may be improved by helical

in-line static mixing inserts. Idealized models use a PFR for both gas and liquid phases.

Depending on the gas and liquid residence times required, the reactor could be operated horizontally or vertically with either downflow or upflow. Weikard (in Ullmann, *Enzyklopaedie*, 4th ed., vol. 3, Verlag Chemie, 1973, p. 381) discusses possible reasons for operating an upflow concurrent flow tubular reactor for the production of adipic acid nitrile (from adipic acid and ammonia). The reactor has a liquid holdup of 20 to 30 percent and a residence time of 1.0 s for gas and 3 to 5 min for liquid.

1. The process has a large Hatta number; that is, the rate of reaction is much greater than the rate of diffusion, so a large interfacial area is desirable for carrying out the reaction.

2. With normal excess ammonia the gas/liquid ratio is about 3500 m^3/m^3 . At this high ratio there is danger of fouling the surface with tarry reaction products. The ratio is brought down to a more satisfactory value of 1000 to 1500 by recycle of some of the effluent.

3. High selectivity of the nitrile is favored by short contact time.

4. The reaction is highly endothermic so heat input must be at a high rate.

Points 2 and 4 are the main ones governing the choice of reactor type. The high gas/liquid ratio restricts the choice to types d , e , i , and k in Fig. 19-26. Due to the high rate of heat transfer needed, the choice is a falling film or tubular reactor.

A loop reactor is used for the bioconversion of methane to produce biomass used, e.g., as fish meal. This is a large-diameter pipe operated at high liquid circulation velocity with the O_2/CH_4 feed injected at several locations along the reactor. Cooling of the exothermic aerobic fermentation is accomplished by external heat exchangers. Static mixers are used to maintain gas dispersion in the liquid.

Packed, Tray, and Spray Towers Packed and tray towers have been discussed in the subsection “Mass Transfer” in Sec. 5. Typically, the gas and liquid are countercurrent to each other, with the liquid flowing downward. Each phase may be modeled using a PFR or dispersion (series of stirred tanks) model. The model is solved numerically.

Spray columns are used with slurries or when the reaction product is a solid. The coefficient k_L in spray columns is about the same as in packed columns, but the spray interfacial area is much lower. Considerable backmixing of the gas also takes place, which makes the spray volumetrically inefficient. An entrainment control device (e.g., mist eliminator) usually is needed at the outlet. In the treatment of phosphate rock with sulfuric acid, off-gases contain HF and SiF_4 . In a spray column with water, solid particles of fluorosilic acid are formed but do not harm the spray operation.

In venturi scrubbers the gas is the motive fluid. This equipment is of simple design and is able to handle slurries and large volumes of gas, but the gas pressure drop may be high. When the reaction is slow, further holdup in a spray chamber is necessary.

In liquid ejectors or aspirators, the liquid is the motive fluid, so the gas pressure drop is low. Flow of slurries in the nozzle may be erosive. Otherwise, the design is as simple as that of the venturi. Kohl and Riesenfeld (*Gas Purification*, Gulf, 1985, pp. 268–288) describe the application of liquid dispersion reactors to the absorption of fluorine gases.

Examples

- Process effluent gas emissions of CO_2 and H_2S are controlled in packed or tray towers. Aqueous solutions of monethanolamine (MEA), diethanolamine (DEA), and K_2CO_3 are the principal reactive solvents for the removal of acidic constituents from gas streams (Danckwerts and Sharma, *The Chemical Engineer*, 202, 1966, CE244). These solvents are all regenerable. Absorption proceeds at a lower temperature or higher pressure and regeneration is done in a subsequent vessel at higher temperature or lower pressure, usually with some assistance from stripping steam. The CO_2 can be recovered to make dry ice. H_2S is treated for recovery of the sulfur. Vessel diameters and allowable gas and liquid flow rates are established by the same correlations as for physical absorption. The calculation of tower heights utilizes vapor-liquid equilibrium data and enhanced mass-transfer coefficients for the

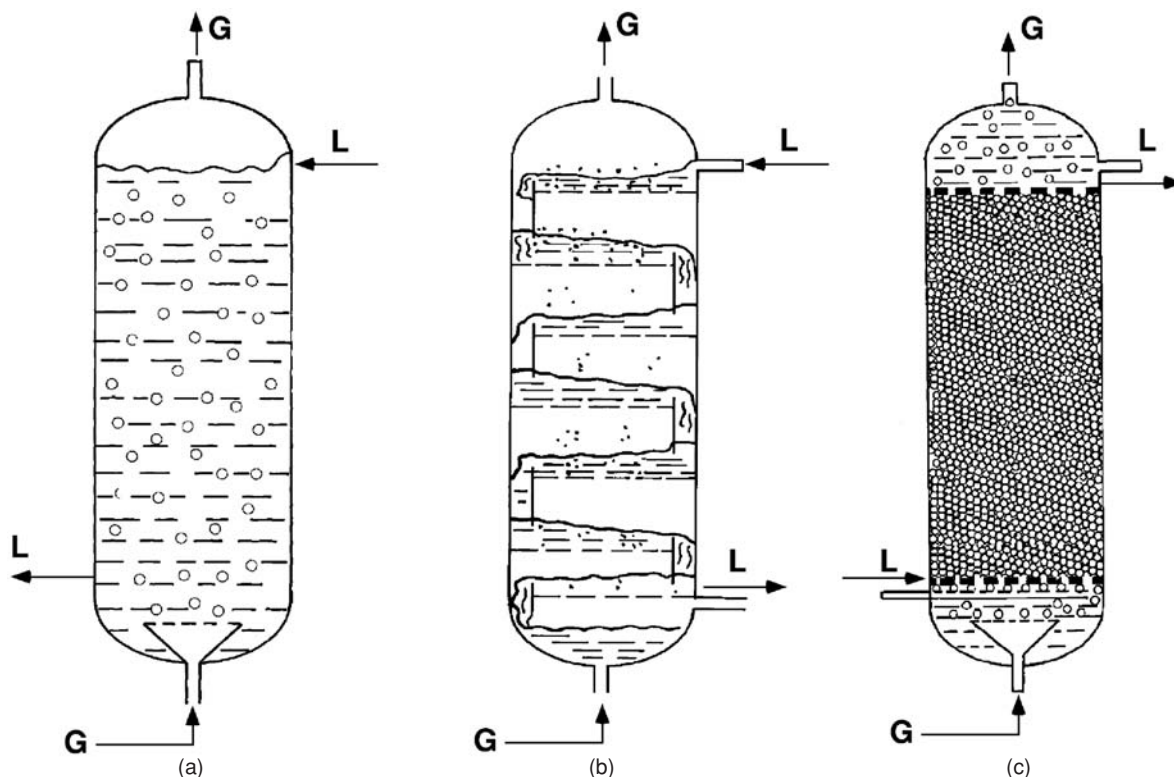


FIG. 19-31 Some examples of bubble column reactor types. (a) Conventional bubble column with no internals. (b) Tray bubble column. (c) Packed bubble column with the packing being either an inert or a catalyst. [From Mills, Ramachandran, and Chaudhari, "Multiphase Reaction Engineering for Fine Chemicals and Pharmaceuticals," *Reviews in Chemical Engineering*, 8(1-2), 1992, Figs. 2, 3, and 4.]

particular system. Such calculations are complex enough to warrant the use of the professional methods of tower design that are available from a number of service companies. Partly because of their low cost, aqueous solutions of sodium or potassium carbonate also are used for CO_2 and H_2S removal. Potassium bicarbonate has the higher solubility so the potassium salt is preferred. In view of the many competitive amine and carbonate plants that are in operation, the economics of alternative options have to be reviewed rather carefully. Additives are often used to affect equilibria and enhance absorption coefficients. Sodium arsenite is the major additive in use; however, sodium hypochlorite and small amounts of amines also are effective. *Sterically hindered amines* as promoters are claimed by Say et al. [*Chem. Eng. Prog.* **80**(10): 72-77 (1984)] to result in 50 percent more capacity than ordinary amine promoters of carbonate solutions. Kohl and Riesenfeld (*Gas Purification*, Gulf, 1985) cite operating data for carbonate plants. Pilot-plant tests are reported on 0.10- and 0.15-m (4- and 6-in) columns packed to depths of 9.14 m (30 ft) of Raschig rings by Benson et al. [*Chem. Eng. Prog.* **50**: 356 (1954)].

- SO_2 emissions from sulfuric acid plants are controlled in spray towers. Effluent gases contain less than 0.5 percent SO_2 . The SO_2 emissions have to be controlled (or recovered as elemental sulfur by, for example, the Claus process). An approach is to absorb the SO_2 in a lime (or limestone) slurry (promoted by small amounts of carboxylic acids, such as adipic acid). Flow is in parallel downward. The product calcium salt is sent to a landfill or sold as a by-product. Limestone is pulverized to 80 to 90 percent through 200 mesh. Slurry concentrations of 5 to 40 percent have been used in pilot plants.

Rotary wheel atomizers require 0.8 to 1.0 kWh/1000 L. The lateral throw of a spray wheel requires a large diameter to prevent accumulation on the wall; the ratio of length to diameter of 0.5 to 1.0 is in use in such cases. The downward throw of spray nozzles permits smaller diameters but greater depths; L/D ratios of 4 to 5 or more are used. Spray vessel diameters of 15 m (50 ft) or more are known. Liquid/gas ratios are 0.2 to 0.3 gal/MSCF. Flue gas enters at 149°C (300°F) at a velocity of 2.44 m/s (8 ft/s). Utilization of 80 percent of the solid reagent may be approached. Residence times are 10 to 12 s. At the outlet the particles are made just dry enough to keep from sticking to the wall, and the gas is within 11 to 28°C (20 to 50°F) of saturation. The fine powder is recovered with fabric filters. In one test facility, a gas with 4000 ppm SO_2 had 95 percent removal with lime and 75 percent removal with limestone.

- A study on the hydrolysis of fats with water was conducted at 230 to 260°C (446 to 500°F) and 41 to 48 atm (600 to 705 psi) in a continuous commercial spray tower. A small amount of water dissolved in the fat and reacted to form an acid and glycerine. Most of the glycerine migrated to the water phase. The tower was operated at about 18 percent of flooding, at which condition the HETS was found to be about 9 m (30 ft) compared with an expected 6 m (20 ft) for purely physical extraction [Jeffreys, Jenson, and Miles, *Trans. Inst. Chem. Eng.* **39**: 389-396 (1961)].
- There are instances where an extractive solvent is employed to force completion of a reversible homogeneous reaction by removing the reaction product. In the production of KNO_3 from KCl and HNO_3 , for instance, the HCl can be removed continuously from the aqueous phase by contact with amyl alcohol, thus forcing completion [Baniel and Blumberg, *Chim. Ind.* **4**: 27 (1957)].

SOLIDS REACTORS

Reactions of solids are typically feasible only at elevated temperatures. High temperatures are achieved by direct contact with combustion gases. Often, the product of reaction is a gas. The gas has to diffuse away from the reactant, sometimes through a solid product. Thermal and mass-transfer resistances are major factors in the performance of solids reactors. There are a number of commercial processes that utilize solid reactors. Reactor analysis and design appear to rely on empirical models that are used to fit the kinetics of solids decomposition. Most of the information on commercial reactors is proprietary.

General references on solids reactions include Brown, Dollimore, and Galwey ["Reactions in the Solid State," in Bamford and Tipper (eds.), *Comprehensive Chemical Kinetics*, vol. 22, Elsevier, 1980], Galwey (*Chemistry of Solids*, Chapman and Hall, 1967), Sohn and Wadsworth (eds.) (*Rate Processes of Extractive Metallurgy*, Plenum Press, 1979), Szekely, Evans, and Sohn (*Gas-Solid Reactions*, Academic Press, 1976), and Ullmann (ed.) (*Enzyklopaedie der technischen Chemie*, "Uncatalyzed Reactions with Solids," vol. 3, 4th ed., Verlag Chemie, 1973, pp. 395-464).

THERMAL DECOMPOSITION

Thermal decompositions may be exothermic or endothermic. Solids that decompose on heating without melting often form gaseous products. When the product is a gas, the reaction rate can be affected by diffusion so particle size can be important. Aging of solids can result in crystallization of the surface. Annealing reduces strains and slows the decomposition rate. The decomposition of some fine powders follows a first-order rate law. Otherwise, empirical rate equations are available (e.g., in Galwey, *Chemistry of Solids*, Chapman and Hall, 1967).

A few organic compounds decompose before melting. These decomposition processes are highly exothermic and may cause explosions. Decomposition kinetics may follow an autocatalytic law. The temperature range for decomposition is 100 to 200°C (212 to 392°F). The decomposition of oxalic acid (m.p. 189°C) obeyed a zero-order law at 130 to 170°C (266 to 338°F). The decomposition of malonic acid has been measured for both the solid and the supercooled liquid.

Exothermic decompositions are nearly always irreversible. When several gaseous products are formed, the reverse reaction would require that these products all combine together, which is unlikely. Commercial interest in such materials lies more in their energy storage properties than as a source of desirable products. These are often nitrogen-containing compounds such as azides, diazo compounds, and nitramines. Ammonium nitrate, an important explosive, decomposes into nitrous oxide and water. In the solid phase, decomposition begins at about 150°C (302°F) but becomes extensive only above its melting point (170°C) (338°F). The reaction is first-order, with activation energy of about 40 kcal/(g-mol) [72,000 Btu/(lb-mol)]. Traces of moisture and Cl⁻ lower the decomposition temperature. Many investigations have reported on the decomposition of azides of barium, calcium, strontium, lead, copper, and silver in the range of 100 to 200°C (212 to 392°F). Activation energies were found to be 30 to 50 kcal/(g-mol) [54,000 to 90,000 Btu/(lb-mol)] or so. Some difficulties with data reproducibility were encountered with these hazardous materials. Lead styphnate (styphnic acid contains nitrogen) monohydrate was found to detonate at 229°C (444°F). The course of decomposition could be followed at 228°C and below. Sodium azide is a propellant in most motor vehicle SRS systems (airbags). Silver oxalate decomposes smoothly and completely in the range of 100 to 160°C (212 to 320°F). Ammonium chromates and some other solids exhibit aging effects. Material that has been stored for months or years follows a different decomposition rate than a fresh material. Examples of such materials are available in the review by Brown et al. ("Reactions in the Solid State," in Bamford and Tipper, *Comprehensive Chemical Kinetics*, vol. 22, Elsevier, 1980).

Endothermic decompositions are generally reversible. Hydroxides (which give off water) and carbonates (which give off CO₂) have been the most investigated compounds. Activation energies are nearly the same as reaction enthalpies. As the reaction proceeds, the rate of reaction may be limited by diffusion of the water through the product layer.

Since a particular compound may have several hydrates, the level of dehydration will depend on the partial pressure of water vapor in the gas. For example, FeCl₂ combines with 4, 5, 7, or 12 molecules of water with melting points ranging from about 75 to 40°C (167 to 104°F). The dehydration of CuSO₄ pentahydrate at 53 to 63°C (127 to 145°F) and of the trihydrate at 70 to 86°C (158 to 187°F) obeys the Avrami-Erofeyev equation $[-\ln(1-x) = kt^n, n = 3.5, 4]$. The rate of water loss from Mg(OH)₂ at lower temperatures is sensitive to the partial pressure of water. Its decomposition above 297°C (567°F) yields appreciable amounts of hydrogen and is not reversible. Carbonates decompose at relatively high temperatures, e.g., 660 to 740°C (1220 to 1364°F) for CaCO₃. When deep beds are used, the rate of heat transfer or the rate of CO₂ removal controls the decomposition rate. Some ammonium salts decompose reversibly and release ammonia, e.g., (NH₄)₂SO₄ ⇌ NH₄HSO₄ + NH₃ at 250°C (482°F). Further heating can release SO₃ irreversibly. The decomposition of silver oxide was one of the earliest solid reactions studied. It is smoothly reversible below 200°C (392°F). The reaction is sensitive to the presence of metallic silver at the start (indicating autocatalysis) and to the presence of silver carbonate, which was accidentally present in some investigations.

SOLID-SOLID REACTIONS

In solid-solid reactions, ions or molecules in solids diffuse to the interface prior to reaction. This diffusion takes place through the normal crystal lattices of reactants and products as well as in channels and fissures of imperfect crystals. Solid diffusion is slow compared to liquids even at the elevated temperatures at which these reactions have to be conducted. Solid-solid reactions are conducted in powder metallurgy. Typical particle sizes are 0.1 to 1000 μm and pressures are 138 to 827 MPa (20,000 to 60,000 psi). Reactions of solids occur in ceramic, metallurgical, and other industries. Even though cement manufacture has been discussed in the gas-solid reactor section, solid-solid reactions take place as well. Large contact areas between solid phases are essential. These may be obtained by forming and mixing fine powders and compressing them. Reaction times are 2 to 3 h at 1200 to 1500°C (2192 to 2732°F) even with 200-mesh particles.

The literature reports several examples of laboratory solid-solid reactions. The mechanism of zinc ferrite formation (ZnO + Fe₂O₃ ⇒ ZnFe₂O₄) has been studied up to temperatures of 1200°C (2192°F). At lower temperatures, ZnO is the mobile phase that migrates and coats the Fe₂O₃ particles. Similarly, MgO is the mobile phase in the MgO + Fe₂O₃ ⇒ MgFe₂O₄ reaction. Smaller particles (< 1 μm) obey the power law $x = k \ln t$, but larger ones have a more complex behavior. In the reaction 2AgI + HgI₂ ⇒ Ag₂HgI₄, nearly equivalent amounts of the ions Ag⁺ and Hg₂²⁺ were found to migrate in opposite directions and arrive at their respective interfaces after 66 days at 65°C (149°F).

Several reactions that yield gaseous products have attracted attention because their progress is easily followed. Examples include MnO₃ + 2MoO₃ ⇒ 2MnMoO₄ + 0.5O₂ (where MoO₃ was identified as the mobile phase) and Ca₃(PO₄)₂ + 5C ⇒ 3CaO + P₂ + 5CO. For the reaction KClO₄ + 2C ⇒ KCl + CO₂, fine powders were compressed to 69 MPa (10,000 psi) and reacted at 350°C (662°F), well below the 500°C (932°F) melting point. The reaction CuCr₂O₄ + CuO ⇒ Cu₂Cr₂O₄ + 0.5O₂ eventually becomes diffusion-controlled and is described by the relationship $[1 - (1-x)^{1/3}]^2 = k \ln t$. In the reaction, CsCl + NaI ⇒ CsI + NaCl, two solid products are formed. The rate-controlling step is the diffusion of iodide ion in CsCl.

Carbothermic reactions are solid-solid reactions with carbon that apparently take place through intermediate CO and CO₂. The reduction of iron oxides has the mechanism Fe_xO_y + yCO ⇒ xFe + yCO₂, CO₂ + C ⇒ 2CO. The reduction of hematite by graphite at 907 to 1007°C in the presence of lithium oxide catalyst was correlated by the equation $1 - (1-x)^{1/3} = kt$. The reaction of solid ilmenite ore and carbon has the mechanism FeTiO₃ + CO ⇒ Fe + TiO₂ + CO₂, CO₂ + C ⇒ 2CO. A similar case is the preparation of metal carbides from metal and carbon, C + 2H₂ ⇒ CH₄, Me + CH₄ ⇒ MeC + 2H₂.

Self-Propagating High-Temperature Synthesis (SHS) Conventional methods of synthesizing materials via solid reactions involve

multiple grinding, heating, and cooling of suitable precursor compounds. Reactions need extended time periods mainly because interdiffusion in solids is slow, even at high temperatures. By contrast, in SHS, highly reactive metal particles ignite in contact with boron, carbon, nitrogen, and silica to form boride, carbide, nitride, and silicide ceramics. Since the reactions are extremely exothermic, the reaction fronts propagate rapidly through the precursor powders. Usually, the

ultimate particle size can be controlled by the particle size of the precursors. In recent years, several commercial and semicommercial facilities have been built (in Russia, the United States, Spain, and Japan) to synthesize TiC powders, nitrided ferroalloys, silicon nitride (β -phase) and titanium hydride powders, high-temperature insulators, lithium niobate, boron nitride, etc. (e.g., Weimer, *Carbide, Nitride and Boride Materials Synthesis and Processing*, Chapman & Hall, 1997).

MULTIPHASE REACTORS

Multiphase reactors include, for instance, gas-liquid-solid and gas-liquid-liquid reactions. In many important cases, reactions between gases and liquids occur in the presence of a porous solid catalyst. The reaction typically occurs at a catalytic site on the solid surface. The kinetics and transport steps include dissolution of gas into the liquid, transport of dissolved gas to the catalyst particle surface, and diffusion and reaction in the catalyst particle. Say the concentration of dissolved gas A in equilibrium with the gas-phase concentration of A is C_{aL} . Neglecting the gas-phase resistance, the series of rates involved are from the liquid side of the gas-liquid interface to the bulk liquid where the concentration is C_{aL} , and from the bulk liquid to the surface of catalyst where the concentration is C_{as} and where the reaction rate is ηwkC_{as}^m . At steady state,

$$r_a = k_{La}(C_{aL} - C_{aL}) = k_s a_s (C_{aL} - C_{as}) = \eta wk C_{as}^m \quad (19-78)$$

where w is the catalyst loading (mass of catalyst per slurry volume). For a first-order reaction, $m = 1$, the catalyst effectiveness η is independent of C_{as} , so that after elimination of C_{aL} and C_{as} the explicit solution for the observed specific rate is

$$r_{a,observed} = C_{aL} \left(\frac{1}{k_{La}} + \frac{1}{k_s a_s} + \frac{1}{\eta wk} \right)^{-1} \quad (19-79)$$

More complex chemical rate equations will require numerical solution. Ramachandran and Chaudhari (*Three-Phase Chemical Reactors*, Gordon and Breach, 1983) apply such rate equations to the sizing of plug flow, CSTR, and dispersion reactors. They list 75 reactions and identify reactor types, catalysts, temperature, and pressure for processes such as hydrogenation of fatty oils, hydrodesulfurization, Fischer-Tropsch synthesis, and miscellaneous hydrogenations and oxidations. A list of 74 gas-liquid-solid reactions with literature references has been compiled by Shah (*Gas-Liquid-Solid Reactions*, McGraw-Hill, 1979), classified into groups where the solid is a reactant, a catalyst, or an inert. Other references include de Lasa (*Chemical Reactor Design and Technology*, Martinus Nijhoff, 1986), Gianetto and Silveston (eds.) (*Multiphase Chemical Reactors*, Hemisphere, 1986), Ramachandran et al. (eds.) (*Multiphase Chemical Reactors*, vol. 2, Sijthoff & Noordhoff, 1981) and Satterfield [*Trickle Bed Reactors*, *AIChE J.* **21**: 209–228 (1975)]. Some contrasting charac-

teristics of the main kinds of three-phase reactors are summarized in Table 19-13.

BIOREACTORS

Bioreactors use live cells or enzymes to perform biochemical transformations of feedstocks to desired products. Bioreactor operation is restricted to conditions at which these biological systems can function. Most plant and animal cells live at moderate temperatures and do not tolerate extremes of pH. The vast majority of microorganisms also prefer mild conditions, but some thrive at temperatures above the boiling point of water or at pH values far from neutral. Some can endure concentrations of chemicals that most other cells find highly toxic. Commercial operations depend on having the correct organisms or enzymes and preventing death (or deactivation) or the entry of foreign organisms that could harm the process.

The pH, temperature, redox potential, and nutrient medium may favor certain organisms and discourage the growth of others. In mixed culture systems, especially those for biological waste treatment, there is an ever-shifting interplay between microbial populations and their environments that influences performance and control. Although open systems may be suitable for hardy organisms or for processes in which the conditions select the appropriate culture, many bioprocesses are closed and elaborate precautions including sterilization and cleaning are taken to prevent contamination. The optimization of the complicated biochemical activities of isolated strains, of aggregated cells, of mixed populations, and of cell-free enzymes or components presents engineering challenges. Performance of a bioprocess can suffer from changes in any of the many biochemical steps functioning in concert, and genetic controls are subject to mutation. Offspring of specialized mutants, especially bioengineered ones that yield high concentrations of product, tend to revert during propagation to less productive strains—a phenomenon called *rundown*.

Developments such as immobilized enzymes and cells have been exploited partially, and genetic manipulations through recombinant DNA techniques are leading to practical processes for molecules that could previously be found only in trace quantities in plants or animals.

Bioreactors may have either two phases (liquid-solid, e.g., in anaerobic processes) or three phases (gas-liquid-solid, e.g., aerobic processes). The solid phase typically contains cells that serve as the biocatalyst. The

TABLE 19-13 Characteristics of Gas-Liquid-Solid Reactors

Property	Trickle bed	Flooded	Stirred tank	Entrained solids	Fluidized bed
Gas holdup	0.25–0.45	Small	0.2–0.3		
Liquid holdup	0.05–0.25	High	0.7–0.8		
Solid holdup	0.5–0.7		0.01–0.10		0.5–0.7
Liquid distribution	Good only at high liquid rate		Good	Good	Good
RTD, liquid phase	Narrow	Narrower than for entrained solids reactor	Wide	Wide	Narrow
RTD, gas phase	Nearly plug flow		Backmixed	Backmixed	Narrow
Interfacial area	20–50% of geometrical	Like trickle bed reactor	100–1500 m ² /m ³	100–400 m ² /m ³	Less than for entrained solids reactor
MTC, gas/liquid	High		Intermediate		
MTC, liquid/solid	High		High		
Radial heat transfer	Slow		Fast	Fast	Fast
Pressure drop	High with small d_p		Hydrostatic head		

RTD = residence time distribution; MTC = mass-transfer coefficient.

solid can be either the free biocatalyst (bacteria, fungi, algae, etc.), also called the biotic phase (with density close to water), or an immobilized version, in which case the cells are immobilized on a solid structure (e.g., porous particles). The liquid is primarily water with dissolved feed (usually a sugar together with mineral salts and trace elements) and products (referred to as metabolites). In aerobic bioreactors, the gas phase is primarily air with the product gas containing product CO_2 produced by the organism and evaporated water. Bioreactors are mainly mechanically agitated tanks, bubble columns and air lift reactors. For low biomass concentrations (e.g., less than 60 g/L) bioreactor design is similar to that of a gas-liquid reactor. For some specialized applications, such as in some wastewater treatment processes, packed beds or slurry reactors with immobilized biocatalyst are used. Figure 19-32 shows some typical bioreactors.

While bioreactors do not differ fundamentally from other two- and three-phase reactors, as indicated above, there are more stringent requirements regarding control of temperature, pH, contamination (presence and growth of other microorganisms or phage), and toxicity (that may result from high feed and product concentrations). In aerobic processes, since O_2 is required for respiration, it must be properly distributed and managed. Whereas bacteria and yeast cells are very robust, cultivations of filamentous fungi and especially animal cell cultures and plant cell cultures are quite shear-sensitive. To maintain a robust culture of animal and plant cells, very gentle stirring either by a mechanical stirrer or by gas sparging is usually necessary. Unlike chemical catalysis, one of the (main) bioreaction products is biomass (new cells), leading to autocatalytic behavior; i.e., the rate of production of new cells per liquid volume is proportional to the cell concentration. Section 7 of this Handbook presents more details on the kinetics of bioreactions.

Bioreactors mainly operate in batch or semibatch mode, which allows better control of the key variables. However, an increasing number of bioprocesses are operated in continuous mode, typically processes for treating wastewater, but also large-scale processes such as lactic acid production, conversion of natural gas to biomass (single-cell protein production), and production of human insulin using genetically engineered yeast. Continuous operation requires good process control, especially of the sterility of the feed, but also that the biocatalyst be robust and its traits (especially for bioengineered strains) persist over many generations.

Several special terms are used to describe traditional reaction engineering concepts. Examples include *yield coefficients* for the generally fermentation environment-dependent stoichiometric coefficients, *metabolic network* for reaction network, *substrate* for feed, *metabolite* for secreted bioreaction products, *biomass* for cells, *broth* for the fermenter medium, *aeration rate* for the rate of air addition, *vvm* for volumetric airflow rate per broth volume, *OUR* for O_2 uptake rate per broth volume, and *CER* for CO_2 evolution rate per broth volume. For continuous fermentation, *dilution rate* stands for feed or effluent rate (equal at steady state), *washout* for a condition where the feed rate exceeds the cell growth rate, resulting in washout of cells from the reactor. Section 7 discusses a simple model of a CSTR reactor (called a chemostat) using empirical kinetics.

The mass conservation equations for a batch reactor are as follows:

$$\text{Cells: } V_r \frac{dC_x}{dt} = (r_g - r_d)V_r \quad (19-80)$$

$$\text{Substrate: } V_r \frac{dC_s}{dt} = Y_{xs}(-r_g)V_r - r_{sm}V_r \quad (19-81)$$

$$\text{Product: } V_r \frac{dC_p}{dt} = Y_{xp}(r_g)V_r \quad (19-82)$$

Several of the terms above have been discussed in Sec. 7: r_g and r_d are the specific rates (per broth volume) for cell growth and death, respectively; r_{sm} is the specific rate of substrate consumed for cell maintenance, and Y_{xi} are the stoichiometric yield coefficient of species i relative to biomass x . The maintenance term in Eq. (19-81) can result

also in an increased production of product p [additional term required in Eq. (19-82)] for metabolites such as lactic acid, but not for protein production. In many cases, a semibatch reactor is used, where the reactants are added with an initial cells and sugar concentration, and a certain feed profile or recipe is used—this is also called *fed batch* operation mode.

Further modeling details are available in the books by Nielsen, Villadsen, and Liden (*Bioreaction Engineering Principles*, Kluwer Academic/Plenum Press, 2003) and Fogler (*Elements of Chemical Reaction Engineering*, 3d ed., Prentice-Hall, 1999). Bioreactors and bioreaction engineering are discussed in detail by Bailey and Ollis (*Biochemical Engineering Fundamentals*, 2d ed., McGraw-Hill, 1986), Clark (*Biochemical Engineering*, Marcel Dekker, 1997), and Schugerl and Bellgardt (*Bioreaction Engineering, Modeling and Control*, Springer, 2000).

ELECTROCHEMICAL REACTORS

Electrochemical reactors are used for electrolysis (conversion of electric energy to chemicals, e.g., chlor-alkali), power generation (conversion of chemicals to electric energy, e.g., batteries or fuel cells), or for chemical separations (electrodialysis). An electrochemical cell contains at least two electronically conducting electrode phases and one ionic conducting electrolyte phase. The electrolyte phase separates the two electrode phases. The electrode phases are also connected to each other through an electronically conducting pathway, typically external of the electrochemical cell; but in the case of corrosion, the electrode phases may be localized regions on the same piece of metal, the bulk metal allowing electron flow between the regions. Thus a series electric circuit is completed beginning at one electrode through the electrolyte to the second electrode and then out of the reactor through the external circuit back into the starting electrode.

An electrochemical cell reaction involves the transfer of electrons across an electrode/electrolyte interface. There are two types of electrochemical cell reactions. In one reaction the electron transfer is from an electrode to a chemical species within the electrolyte, resulting in a reduction process, and in this case the electrode is defined as the cathode. The second electrochemical reaction involves the electron transfer from a chemical species within the electrolyte to an electrode, resulting in an oxidation process; in this case the electrode is defined as the anode. Each of these cathode (reduction) or anode (oxidation) electrochemical reactions is considered a half-cell reaction. Since an electrochemical cell requires a complete series electric circuit, the overall electrochemical cell reaction is the stoichiometric sum of the electrochemical half-cell reactions, and all electrochemical cell reactions are close-coupled to maintain the conservation of electric charge. Electrochemical cell reactions are considered heterogeneous reactions since they occur at the interface of the electrode surface and electrolyte. Sometimes the electrochemical product species is employed, in turn, as a reducing or oxidizing species, either in the bulk electrolyte or in a separate external process vessel. Subsequently, the spent reducing or oxidizing species is regenerated within the electrochemical reactor. This augmentation is known as a mediated (or indirect) electrochemical process. More details on the mechanism and kinetics of electrochemical reactions are given in Sec. 7.

An electrochemical reactor is a controlled volume containing the electrolyte and two electrodes. The electrode phases may be a solid, e.g., carbon or metal, or a liquid, e.g., mercury. The geometry of the electrodes is optimized to maximize energy efficiency and/or cell life and usually consists of parallel plates or concentric cylinders. The electrolyte may be a liquid (such as concentrated brine in the production of caustic or a molten salt in the production of aluminum) or a solid (such as a proton-conducting Nafion® membrane in fuel cells). As the electric current passes through the electrolyte, a voltage drop occurs that represents an energy loss; therefore, the gap or spacing between the electrodes is usually minimized. The electrodes may also be separated by a membrane, a diaphragm, or a separator so as to prevent the unwanted mixing of chemical species, ensure process safety, and maintain product purity and yield. One or both of the electrodes may evolve a gas (e.g., chlorine); or alternatively, one or both of the electrodes may be fed with a gas (e.g., hydrogen or oxygen) to reduce cell voltage or utilize gaseous fuels. Examples of electrochemical reactors are shown in Fig. 19-33.

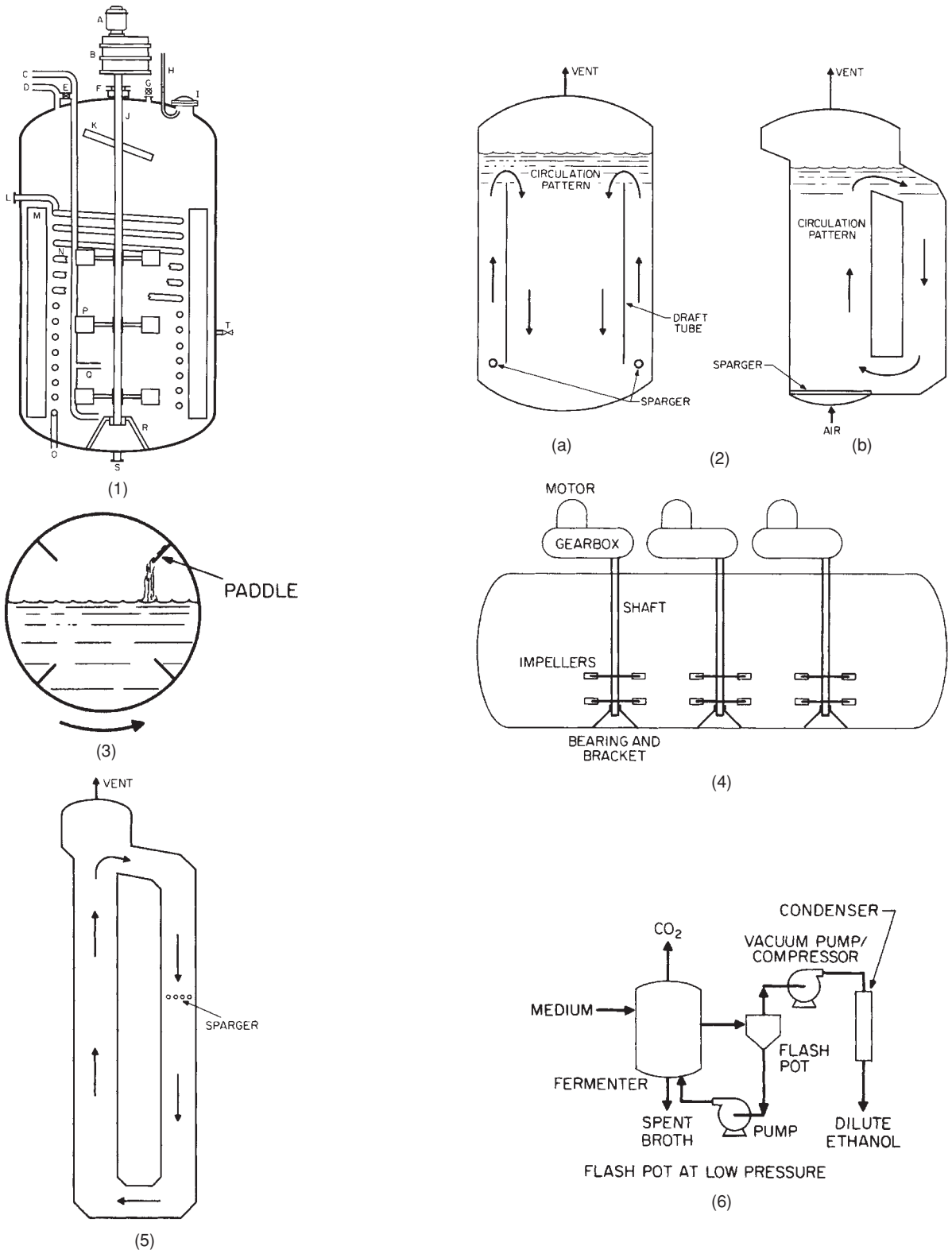


FIG. 19-32 Some examples of fermenters. (1) Conventional batch fermenter. (2) Air lift fermenters: (a) Concentric cylinder or bubble column with draft tube; (b) external recycle. (3) Rotating fermenter. (4) Horizontal fermenter. (5) Deep-shaft fermenter. (6) Flash-pot fermenter.

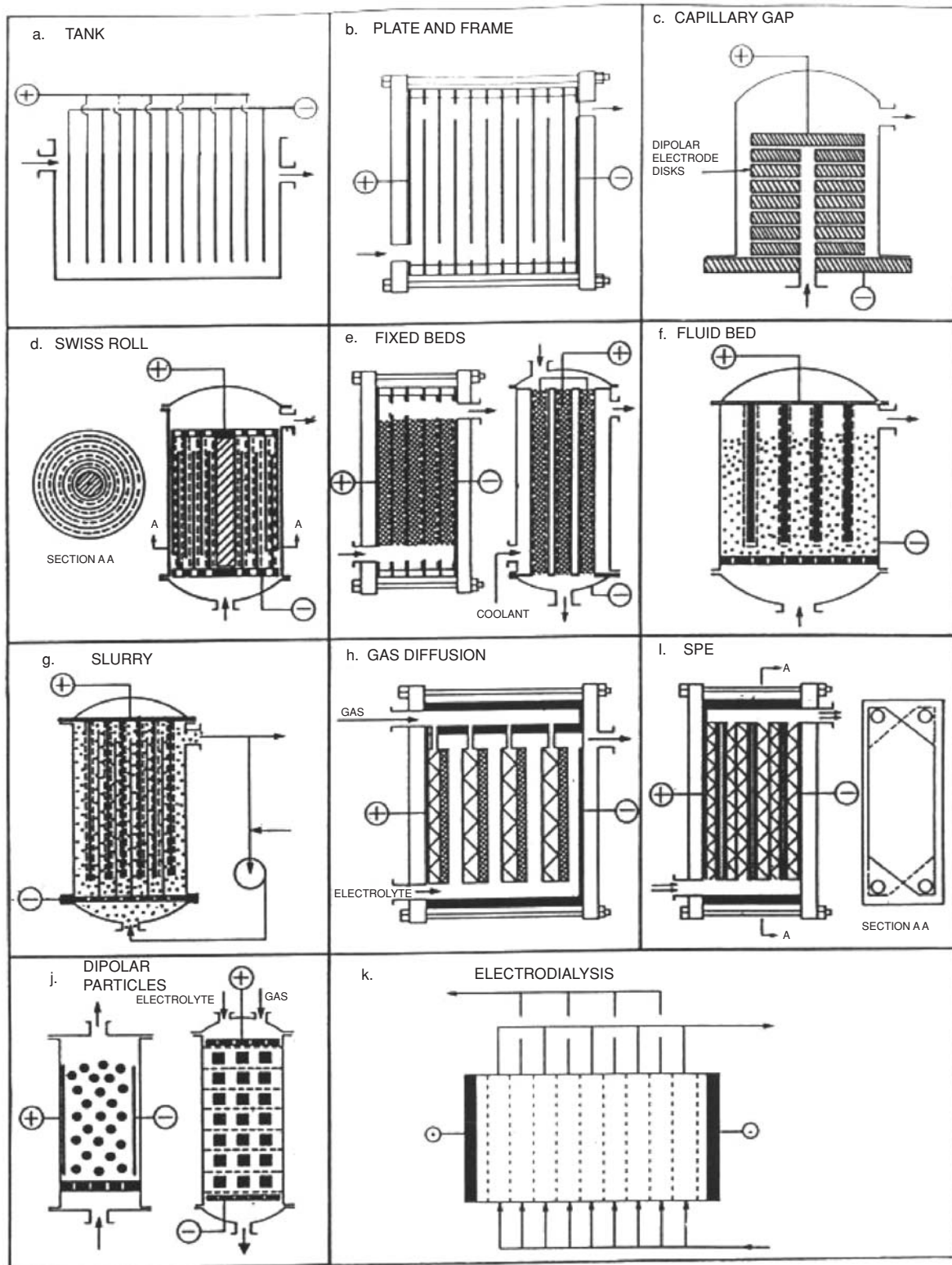


FIG. 19-33 Electrochemical reactor configurations. [From Oloman, *Electrochemical Processing for the Pulp and Paper Industry*, The Electrochemical Consultancy, 1999, p. 79, Fig. 2.10; printed in Great Britain by Alresford Press Ltd. Referring to "Tutorial Lectures in Electrochemical Engineering and Technology" (D. Chin and R. Alkire, eds.), AIChE Symposium Series 229, vol. 79, 1983; reproduced with permission.]

The size of an electrochemical reactor may be determined by evaluating the capital costs and the operating costs (on a dollar per unit mass basis) as a function of the operating current density (production rate per unit electrode area basis). Typically, the capital costs decrease with increasing current density, and the operating cost increase with current density, thus, a minimum in the total costs may be observed and serve as a basis for the sizing of the electrochemical reactor. Given an optimal current density, the electrochemical reactor design is refined to minimize voltage losses and maximize current efficiency. This is done by taking into consideration the component availability (e.g., membrane widths), the management of the excess heat removal, the minimization of pressure drops (due to liquid and gas traffic within the electrochemical reactor), and the maintenance costs (associated with reactor rebuilding). The largest, cost-effective reactor size is then replicated to meet production capacity needs. An electrochemical reactor usually has shorter operating life than the rest of the plant facility, requiring the periodic rebuilding of the reactors.

In electrochemical engineering, several terms share similar definitions to traditional reaction engineering. These include fractional conversion, yield, selectivity, space velocity, and space time yield. Several terms are unique to electrochemical reaction engineering such as *cell voltage* (the electric potential difference between the two electrodes within the electrochemical cell) and *cell overpotentials* (voltage losses within the electrochemical cell). Voltage losses include (1) *ohmic overpotential* (associated with passage of electric current in the bulk of the electrolyte phase and the bulk electrode phases and the electrical conductors between the electrochemical cell and the power supply or electrical load); (2) *activation overpotential* (associated with the limiting rates at which some steps in the electrode reactions can proceed); and (3) *concentration overpotential* (generated from the local depletion of reactants and accumulation of products at the electrode/electrolyte interface relative to the bulk electrolyte phase due to mass transport limitations). The *current density* is the current per unit surface area of the electrode. Typically, the geometric or projected area is utilized since the true electrode area is usually difficult to estimate due to surface roughness and/or porosity. It is related to the production rate of the electrolytic cell through the Faraday constant. The *current efficiency* is the ratio of the theoretical electric charge (coulombs) required for the amount of product obtained to the total amount of electric charge passed through the electrochemical cell. Many of these and other terms are discussed in Sec. 7, in Pletcher and Walsh (*Industrial Electrochemistry*, 2d ed., Chapman and Hall, 1984) and in Gritzner and Kreysa ["Nomenclature, Symbols and Definitions in Electrochemical Engineering," *Pure & Appl. Chem.* **65**: 5, 1009–1020 (1993)].

A discussion of electrochemical reactors is available in books by Prentice (*Electrochemical Engineering Principles*, Prentice-Hall, 1991), Hine (*Electrode Processes and Electrochemical Engineering*, Plenum Press, 1985), Oloman (*Electrochemical Processing for the Pulp and Paper Industry*, The Electrochemical Consultancy, 1996), and Goodridge and Scott (*Electrochemical Process Engineering: A Guide to the Design of Electrolytic Plant*, Plenum, 1995).

REACTOR TYPES

Multiphase reactors are typically mechanically agitated vessels, bubble columns, trickle bed, flooded fixed beds, gas-liquid-solid fluidized beds, and entrained solids reactors. *Agitated reactors* keep solid catalysts in suspension mechanically; the overflow may be a clear liquid or slurry, and the gas disengages from the vessel. *Bubble column reactors* keep the solids in suspension as a result of agitation caused by the sparging gas. In *trickle bed reactors* both gas and liquid phases flow down through a packed bed of catalyst. The reactor is gas continuous with liquid "trickling" as a film over the solid catalyst. In *flooded reactors*, the gas and liquid flow upward through a fixed bed. The reactor is liquid continuous. As the superficial velocity is increased, the solids first become suspended (as a dense fluidized bed) and may eventually be entrained and the effluent separated into its phases in downstream equipment. When the average residence time of solids approaches that of the liquid, the reactor becomes an *entrained solids reactor*.

Agitated Slurry Reactors The gas reactant and solid catalyst are dispersed in a continuous liquid phase by mechanical agitation using stirrers. Most issues associated with gas-liquid-solid stirred tanks are analogous to the gas-liquid systems. In addition to providing good

gas-liquid contacting, the agitation has to be sufficient to maintain the solid phase suspended. Catalytic reactions in stirred gas-liquid-solid reactors are used in a large number of applications including hydrogenations, oxidations, halogenations, and fermentations.

The benefits of using a mechanically agitated tank include nearly isothermal operation, excellent heat transfer, good mass transfer, and use of high-activity powder catalyst with minimal intraparticle diffusion limitations. The reactors may be operated in a batch, semibatch, or continuous mode; and catalyst deactivation may be managed by on-line catalyst makeup. Scale-up is relatively straightforward through geometric similarity and by providing the agitator power/volume required to produce the same volumetric mass-transfer coefficient at different scales. The hydrodynamics are decoupled from the gas flow rate. Some downsides of stirred gas-liquid-solid reactors include difficulty with catalyst/liquid product separation and lower volumetric productivity than fixed beds (due to lower catalyst loading per reactor volume). In addition, the reactor size may be limited due to high power consumption (due to horsepower limitations on agitator motor)—typically the limit is at around 50 m³. Sealing of the agitator system can also be challenging for large reactors (magnetic coupling is used for small to midrange units). These result in increased capital and operating costs.

Solid particles are in the range of 0.01 to 1.0 mm (0.0020 to 0.039 in), the minimum size limited by filterability. Small diameters are used to provide as large an interface as possible to minimize the liquid-solid mass-transfer resistance and intraparticle diffusion limitations. Solids concentrations up to 30 percent by volume may be handled; however, lower concentrations may be used as well. For example, in hydrogenation of oils with Ni catalyst, the solids content is about 0.5 percent. In the manufacture of hydroxylamine phosphate with Pd-C, the solids content is 0.05 percent.

The hydrodynamic parameters that are required for stirred tank design and analysis include phase holdups (gas, liquid, and solid); volumetric gas-liquid mass-transfer coefficient; liquid-solid mass-transfer coefficient; liquid, gas, and solid mixing; and heat-transfer coefficients. The hydrodynamics are driven primarily by the stirrer power input and the stirrer geometry/type, and not by the gas flow. Hence, additional parameters include the power input of the stirrer and the pumping flow rate of the stirrer.

The reactant gas either is sparged below the stirrer or is induced from the vapor space by a *gas-inducing* agitator which has a hollow shaft with suction orifices on the shaft and discharge orifices on the impeller. Impellers vary with applications. For low-viscosity applications, flat-bladed Rushton turbines are widely used and provide radial mixing and gas dispersion. Pitched-blade turbines may also be used to induce axial flow. Often multiple impellers are provided on one shaft, sometimes with a mix of flat blade and pitched-blade type agitators. Additional information may be obtained from the corresponding section in this Handbook and from Baldyga and Bourne (*Turbulent Mixing and Chemical Reactions*, Wiley, 1998).

As the stirrer speed is increased, different flow regimes are observed depending on the stirrer type/geometry and the nature of the gas-liquid system considered. For example, for a Rushton turbine with a low-viscosity liquid, three primary flow regimes are observed (Fig. 19-34). Regime I (Fig. 19-34a) has single bubbles that rise, and the gas is not dispersed uniformly. Regime II (Fig. 19-34b) has the gas dispersed radially as the bubbles ascend. Regime III (Fig. 19-34c) has the gas recirculated to the stirrer in an increasingly complex pattern [see, e.g., Baldi, *Hydrodynamics and Gas-Liquid Mass Transfer in Stirred Slurry Reactors*, in Gianetto and Silveston (eds.), *Multiphase Chemical Reactors*, Hemisphere, 1986].

For gas-liquid systems, the power dissipated by the stirrer at the same stirrer speed N is lower than the corresponding power input for liquid systems due to reduced drag on the impeller. The power of the gassed system P_G is related to that of the ungassed system P_0 by using the power number N_p correlation with the aeration number N_a :

$$N_p = \frac{P_G}{P_0} \quad (19-83)$$

$$N_a = \frac{Q_G}{ND_i^3} \quad (19-84)$$

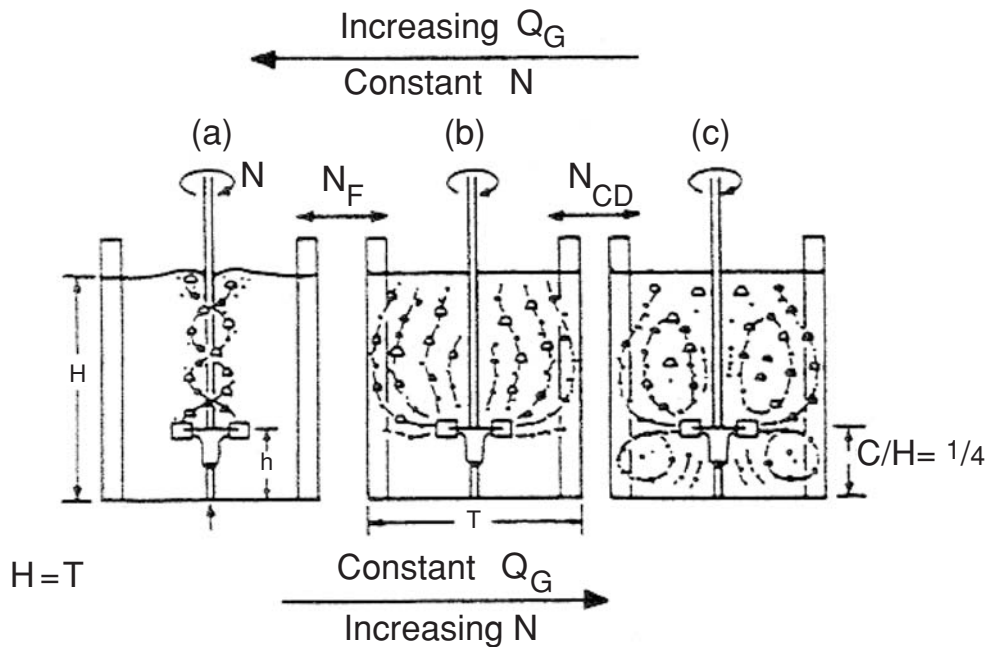


FIG. 19-34 Gas circulation as a function of stirrer speed. (From Nienow et al., 5th European Conference on Mixing, Wurzburg, 1985; published by BHRA, The Fluid Engineering Centre, Cranfield, England; Fig. 1.)

The power number is a decreasing function of the aeration rate, as shown in Fig. 19-35.

For instance, Hughmark [*Ind. Eng. Chem. Proc. Des. Dev.* **19**: 638 (1980)] developed a correlation for the power number of Rushton turbines that correlates a large database:

$$N_p = 0.1 N_a^{-0.25} \left(\frac{D_I^3}{V_L} \right)^{-0.25} \left(\frac{N^2 D_I^4}{g H_1 V_L^{2/3}} \right)^{-0.2} \quad (19-85)$$

Increasing the solids content increases the power number, as indicated, e.g., by Wiedman et al. [*Chem. Eng. Comm.* **6**: 245 (1980)].

With solids present, a minimum agitator speed is required to suspend all the solids, e.g., the correlation of Baldi et al. [*Chem. Eng. Sci.* **33**: 21 (1978)]:

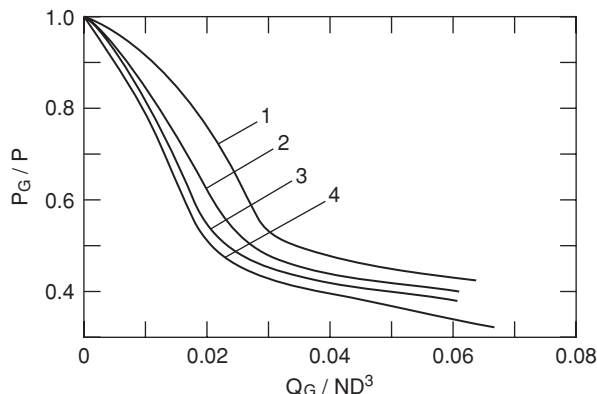


FIG. 19-35 Effect of aeration number and stirrer speed on the power number— N increases in order of $N_1 < N_2 < N_3 < N_4$. [Adapted from Baldi, "Hydrodynamics and Mass Transfer in Stirred-Slurry Reactors," in Gianetto and Silveston (eds.), *Multiphase Chemical Reactors*, Hemisphere Publishing Corp., 1986, Fig. 14.8.]

$$N_m = \frac{\beta_2 \mu_L^{0.17} [g(\rho_p - \rho_L)]^{0.42} d_p^{0.14} w^{0.125}}{\rho_L^{0.58} D_I^{0.89}} \quad (19-86)$$

where w is the catalyst loading in weight percent and parameter β_2 depends on reactor/impeller ratio, e.g., from Nienow [*Chem. Eng. J.* **9**: 153 (1975)], $\beta_2 = 2(d_R/D_I)^{1.33}$

Gas holdup and volumetric gas-liquid mass-transfer coefficients are correlated with the gassed power input/volume and with the aeration rate (actual gas superficial velocity), e.g., the correlation of van't Riet [*Ind. Eng. Chem. Proc. Des. Dev.* **18**: 357 (1979)] for the volumetric mass-transfer coefficient of coalescing and noncoalescing systems:

$$k_L a = \begin{cases} 2.6 \times 10^{-2} \left(\frac{P_G}{V_L} \right)^{0.4} u_C^{0.5} & \text{for coalescing nonviscous liquids} \\ 2.0 \times 10^{-3} \left(\frac{P_G}{V_L} \right)^{0.7} u_C^{0.2} & \text{for noncoalescing nonviscous liquids} \end{cases} \quad (19-87)$$

For the gas holdup a similar correlation was developed by Loiseau et al. [*AIChE J.* **23**: 931 (1977)]:

$$\epsilon_G = \begin{cases} 0.011 \sigma^{-0.36} \mu_L^{-0.056} \left(\frac{P'_G}{V_L} \right)^{0.27} u_C^{0.36} & \text{for nonfoaming systems} \\ 0.0051 \left(\frac{P'_G}{V_L} \right)^{0.57} u_C^{0.24} & \text{for nonfoaming system} \end{cases} \quad (19-88)$$

$$\frac{P'_G}{V_L} = \frac{P_G}{V_L} + 0.03 \frac{Q_G \rho_C u_0^2}{V_L} + \frac{Q_G \rho_C R T}{V_L M W_C} \ln \frac{P_1}{P_2}$$

The last two terms of the power/volume equation include the power/volume from the isothermal expansion of the gas through the gas distributor holes having a velocity u_0 and the power/volume to transfer the gas across the hydrostatic liquid head.

Increasing the solids loading leads to a decrease in gas holdup and gas-liquid volumetric mass-transfer coefficient at the same power/volume [e.g., Inga and Morsi, *Can. J. Chem. Eng.* **75**: 872 (1997)].

Liquid-solid mass transfer is typically not limiting due to the small particle size resulting in large particle surface area/volume of reactor, unless the concentration of the particles is very low, and/or larger particles are used. In the latter case, intraparticle mass-transfer limitations would also occur. Ramachandran and Chaudhari (*Three-Phase Catalytic Reactors*, Gordon and Breach, 1983) present several correlations for liquid-solid mass transfer, typically as a Sherwood number versus particle Reynolds and Schmidt numbers, e.g., the correlation of Levins and Glastonbury [*Trans. Inst. Chem. Engrs.* **50**: 132 (1972)]:

$$\text{Sh} = \begin{cases} 2 + 0.44\text{Re}_p^{0.5}\text{Sc}^{0.38} \\ \frac{k_s d_p}{D} \end{cases} \quad \text{Re}_p = \frac{\rho_L u_c d_p}{\mu_L} \quad \text{Sc} = \frac{\nu_L}{D} \quad (19-89)$$

Here u_c is a characteristic velocity, and the velocity terms composing it are estimated from additional correlations.

There is good heat transfer in agitated gas-liquid-solid slurry reactors; see, e.g., van't Riet and Tramper for correlations (*Basic Bioreactor Design*, Marcel Dekker, 1991).

Additional information on mechanically agitated gas-liquid-solid reactors can be obtained in van't Riet and Tramper (*Basic Bioreactor Design*, Marcel Dekker, 1991), Ramachandran and Chaudhari (*Three-Phase Catalytic Reactors*, Gordon and Breach, 1983), and Gianetto and Silveston (*Multiphase Chemical Reactors*, Hemisphere, 1986).

Examples

- Liquid benzene is chlorinated in the presence of metallic iron turnings or Raschig rings at 40 to 60°C (104 to 140°F).
- Carbon tetrachloride is made from CS₂ by bubbling chlorine into it in the presence of iron powder at 30°C (86°F).
- Substances that have been hydrogenated in slurry reactors include nitrobenzene with Pd-C, butynediol with Pd-CaCO₃, chlorobenzene with Pt-C, toluene with Raney® Ni, and acetone with Raney® Ni.
- Some oxidations in slurry reactors include cumene with metal oxides, cyclohexene with metal oxides, phenol with CuO, and *n*-propanol with Pt.
- Aerobic fermentations.

For many hydrogenations, semibatch operations often are preferred to continuous ones because of the variety of feedstocks or product specifications, or long reaction times, or small production rates. A sketch of a batch hydrogenator is shown in Fig. 19-36.

The vegetable oil hydrogenator, which is to scale, uses three impellers. The best position for inlet of gas is at a point of maximum turbulence near the impeller, or at the bottom of the draft tube. A sparger is desirable; however, an open pipe is often used. A two-speed motor is desirable to prevent overloading. Since the gassed power requirement is significantly less than ungassed, the lower speed is used when the gas supply is cut off but agitation is to continue. In tanks of 5.7 to 18.9 m³ (1500 to 5000 gal), rotation speeds are from 50 to 200 rpm and power requirements are 2 to 75 hp; both depend on superficial velocities of gas and liquid [Hicks and Gates, *Chem. Eng.*, pp. 141-148 (July 1976)]. As a rough guide, power requirements and impeller tip speeds are shown in Table 19-14.

Edible oils are mixtures of unsaturated compounds with molecular weights in the vicinity of 300. The progress of the hydrogenation reaction is expressed in terms of iodine value (IV), which is a measure of unsaturation. The IV is obtained by a standardized procedure in which the iodine adds to the unsaturated double bond in the oil. IV is the ratio of the amount of iodine absorbed per 100 g of oil.

To start a hydrogenation process, the oil and catalyst are charged, then the vessel is evacuated for safety and hydrogen is continuously added and maintained at some fixed pressure, usually in the range of 1 to 10 atm (14.7 to 147 psi). Internal circulation of hydrogen is provided by axial and radial impellers or with a hollow impeller that throws the gas out centrifugally and sucks gas in from the vapor space through the hollow shaft. Some plants have external gas circulators. Reaction times are 1 to 4 h. For edible oils, the temperature is kept at about 180°C (356°F). Since the reaction is exothermic and because space for heat-transfer coils in the vessel is limited, the process is organized to give a maximum IV drop of about 2.0/min. The rate of

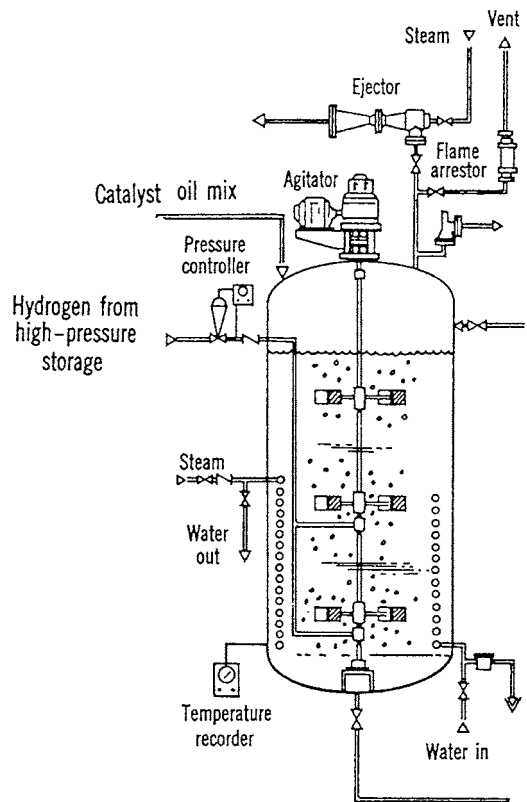


FIG. 19-36 Stirred tank hydrogenator for edible oils. (Votator Division, Chemetron Corporation.)

reaction drops off rapidly as the reaction proceeds, so a process may take several hours. The endpoint of a hydrogenation is a specified IV of the product. Hardness or refractive index also can be measured to follow reaction progress.

Saturation of the oil with hydrogen is maintained by agitation. The rate of reaction depends on agitation and catalyst concentration. Beyond a certain agitation rate, resistance to mass transfer is eliminated, and the rate becomes independent of pressure. The effect of catalyst concentration also reaches limiting values. The effects of pressure and temperature on the rate are indicated by Fig. 19-37.

A supported nickel catalyst (containing 20 to 25 weight percent Ni on a porous silica particle) is typically used. The pores allow access of the reactants to the extended pore surface, which is in the range of 200 to 600 m²/g (977 × 10³ to 2931 × 10³ ft²/lbm) of which 20 to 30 percent is catalytically active. The concentration of catalyst in the slurry can vary over a wide range but is usually under 0.1% Ni. After the reaction is complete, the catalyst can be easily separated from the product. Catalysts are subject to degradation and poisoning, particularly by sulfur compounds. Accordingly, 10 to 20 percent of the recovered catalyst is replaced by fresh catalyst before reuse. Other catalysts are applied in

TABLE 19-14 Power Requirements and Impeller Tip Speed Guidelines

Operation	hp/1000 gal ^a	Tip speed, ft/s
Homogeneous reaction	0.5-1.5	7.5-10
With heat transfer	1.5-5	10-15
Liquid-liquid mixing	5	15-20
Gas-liquid mixing	5-10	15-20

^a 1 hp/1000 gal = 0.197 kW/m³.

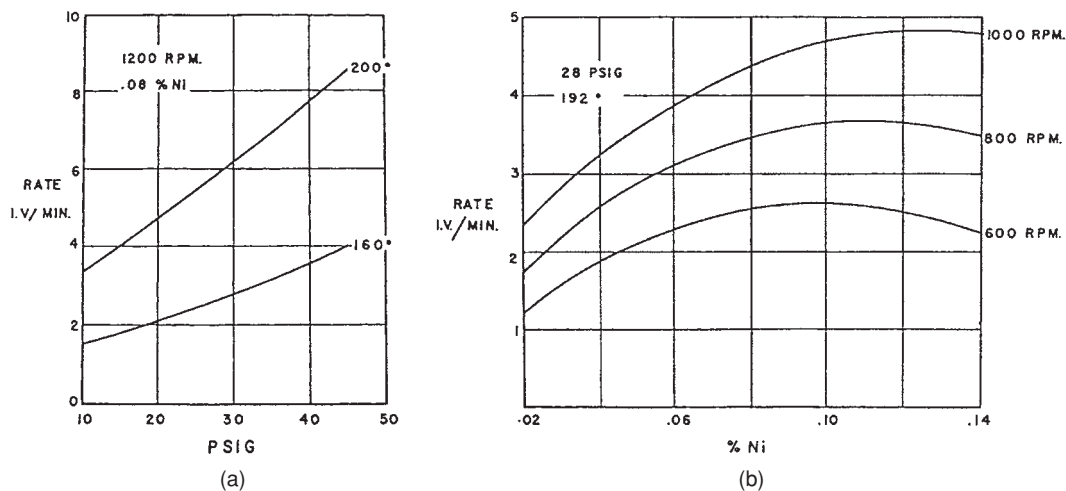


FIG. 19-37 Hydrogenation of soybean oil. (a) Effect of reaction pressure and temperature on rate. (b) Effect of catalyst concentration and stirring rate on hydrogenation. [Swern (ed.), Bailey's Industrial Oil and Fat Products, vol. 2, Wiley, 1979.]

special cases. Expensive palladium has about 100 times the activity of nickel and is effective at lower temperatures. A case study of the hydrogenation of cottonseed oil was made by Rase (*Chemical Reactor Design for Process Plants*, vol. 2, Wiley, 1977, pp. 161-178).

Slurry Bubble Column Reactors As in the case of gas-liquid slurry agitated reactors, bubble column reactors may also be used when solids are present. Most issues associated with multiphase bubble columns are analogous to the gas-liquid bubble columns. In addition, the gas flow and/or the liquid flow have to be sufficient to maintain the solid phase suspended. In the case of a bubble column fermenter, the sparged oxygen is partly used to grow biomass that serves as the catalyst in the system. Many bubble columns operate in semibatch mode with gas sparged continuously and liquid and catalyst in batch mode.

The benefits of using slurry bubble columns include nearly isothermal operation, excellent heat transfer, good mass transfer, and use of high-activity powder catalyst with minimal intraparticle diffusion limitations. The reactors may be operated in a batch, semibatch, or continuous mode and require less power input than mechanically agitated reactors. Catalyst deactivation may be managed by on-line catalyst makeup. The reactor (essentially an empty shell with a sparger grid at the bottom) is easy to design, and the capital investment can be low. Some downsides of slurry bubble column reactors include catalyst/liquid product separation difficulty and lower volumetric productivity than fixed beds (due to lower catalyst loading per reactor volume), and catalyst distribution can be skewed with higher concentration at the bottom than at the top of the reactor. Also, accounting for the effect of internals (e.g., heat exchange tubes) and of increased diameter on the hydrodynamics is not well understood. Hence gradual scale-up is often required over multiple intermediate scales before commercialization. Cold flow models can also be useful in determining hydrodynamics in the absence of reaction.

As is the case for reactors with two or more mobile phases, a variety of flow regimes exist depending primarily on the gas superficial velocity (the driver for bubble column hydrodynamics) and column diameter. A qualitative flow regime map is shown in Fig. 19-38.

In the homogeneous flow regime at low gas superficial velocity, bubbles are relatively small and rise at constant rate (about 20 to 25 cm/s). As the flow rate is increased, bubbles become larger and irregular in shape, they frequently coalesce and break up, and the transition to churn turbulent regime is obtained. In small-diameter columns, the larger bubbles may bridge the column, creating slugs—hence the slug flow regime. The large transition zones in Fig. 19-38 are indicative of the lack of accurate knowledge and of the dependence of the transition region on conditions (temperature, pressure) and physical properties of the gas and liquid.

Hydrodynamic parameters that are required for bubble column design and analysis include phase holdups (gas, liquid, and solid for

slurry bubble columns); volumetric gas-liquid mass-transfer coefficient; liquid-solid mass-transfer coefficient; liquid, gas, and solid axial and radial mixing; and heat-transfer coefficients. These parameters depend strongly on the prevailing flow regime.

Correlations for gas holdup and the volumetric gas-liquid mass-transfer coefficient can have the general form

$$\epsilon_G = \alpha u_G^\beta \quad k_{LG} = \gamma u_G^\delta \quad (19-90)$$

where u_G is the superficial gas velocity, ϵ_G is the gas holdup (fraction of gas volume), k_L is the liquid-side gas-liquid mass-transfer coefficient, and a is the interfacial area per volume of either the liquid or the expanded liquid (liquid + gas). The exponents are $\beta, \delta \sim 1$ for the homogeneous bubbly flow regime and $\beta, \delta < 1$ for heterogeneous turbulent flow regime. The correlations depend on the gas-liquid-solid system properties. Gas-liquid systems can be classified as coalescing leading to increased bubble size, and noncoalescing, leading to larger gas holdup and volumetric mass-transfer coefficients for the latter. There is a voluminous literature for these parameters, and there is substantial variability in estimated values—one should be careful to validate the parameters with data applicable to the real system considered. For instance, for gas holdup see the correlation of Yoshida

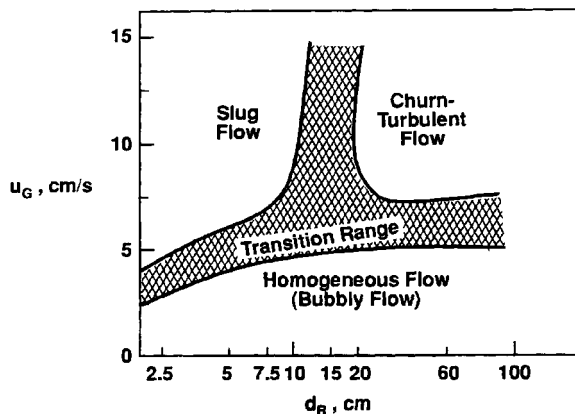


FIG. 19-38 Flow regime map for gas-liquid bubble columns. [Fig. 16 in Deckwer et al., *Ind. Eng. Chem. Process Des. Dev.* 19:699-708 (1980).]

and Akita [*AIChE J.* **11**: 9 (1965)]

$$\frac{\epsilon_C}{(1-\epsilon_C)^4} = \alpha \left(\frac{\rho_L g d_R^2}{\sigma} \right)^{1/8} \left(\frac{\rho_L^2 g d_R^3}{\mu_L^2} \right)^{1/12} \frac{u_C}{\sqrt{g d_R}}$$

$$\alpha = \begin{cases} 0.2 & \text{for pure liquids and nonelectrolytes} \\ 0.25 & \text{for salt solutions} \end{cases} \quad (19-91)$$

and for volumetric gas-liquid mass-transfer coefficient, see the correlation of Akita and Yoshida [*I&EC Proc. Des. Dev.*, **12**: 76 (1973)]:

$$k_{LA} = 0.6 \frac{D}{d_R^2} \left(\frac{\mu_L}{\rho_L D} \right)^{0.5} \left(\frac{\rho_L g d_R^2}{\sigma} \right)^{0.62} \left(\frac{\rho_L^2 g d_R^3}{\mu_L^2} \right)^{0.31} \epsilon_C^{1.1} \quad (19-92)$$

More recent correlations for gas holdup and mass transfer include the effect of pressure and bimodal bubble size distribution (small and large bubbles), in a manner analogous to the treatment of dilute and dense phases in fluidized beds [see, e.g., Letzel et al., *Chem. Eng. Sci.*, **54**: (13): 2237 (1999)].

Increasing the catalyst loading decreases the gas holdup and the volumetric gas-liquid mass transfer coefficient [see, e.g., Marett and Krishna, *Catalysis Today*, **52**: 279 (1999)].

Axial mixing in the liquid, induced by the upflow of the gas bubbles, can be substantial in commercial-scale bubble columns, especially in the churn turbulent regime. Due to typically small particle size, the axial dispersion of the solid catalyst in slurry bubble columns is expected to follow closely that of the liquid; exceptions are high-density particles. The liquid axial mixing can be represented by an *axial dispersion coefficient*, which typically has the form

$$D_{aL} = \alpha u_C^\beta d_R^\gamma \quad (19-93)$$

Based on theoretical considerations (Kolmogoroff's theory of isotropic turbulence), $\beta = 1/3$ and $\gamma = 4/3$. For example, Deckwer et al. [*Chem. Eng. Sci.* **29**: 2177 (1973)] developed the following correlation:

$$D_{aL} = 2.7 u_C^{0.3} d_R^{1.4} \quad (19-94)$$

It is expected that the strong dependence on reactor diameter only extends up to a maximum diameter beyond which there is no effect of diameter; however, there is disagreement among experts as to what that maximum diameter may be. There are a large number of correlations for liquid axial dispersion with widely different predictions, and care must be exerted to validate the predictions with data at some significant scale, even if only in a cold flow mockup.

The gas axial mixing is due to the bubble size distribution resulting in a distribution of bubble rise velocities, which varies along the column due to bubble breakup and coalescence. There are a variety of correlations in the literature, with varying results and reliability, for instance, the correlation of Mangartz and Pilhofer [*Verfahrenstechn.*, **14**: 40 (1980)].

$$D_{aG} = 5 \times 10^{-4} \left(\frac{u_C}{\epsilon_C} \right)^3 d_R^{1.5} \quad (19-95)$$

This equation is dimensional, and cm/s for u_C , cm for d_R , and cm²/s for D_{aG} should be used. The radial mixing can be represented by radial dispersion coefficients for the gas and the liquid. For instance, the liquid radial dispersion coefficient is estimated at less than one-tenth of the axial one.

Correlations for the heat-transfer coefficient have the general form

$$\text{St} = f(\text{Re Fr Pr}^2)$$

$$\text{Re Fr} = \frac{u_C^3 \rho_L}{\mu_L g} \quad \text{Pr} = \frac{c_{pL} \mu_L}{\lambda_L} \quad \text{St} = \frac{h_w}{u_C \rho_L c_{pL}} \quad (19-96)$$

For instance, see the correlation of Deckwer et al. [*Chem. Eng. Sci.* **35**(6): 1341–1346 (1980)].

$$\text{St} = 0.1(\text{Re Fr Pr}^2)^{-1/4} \quad (19-97)$$

Additional information on hydrodynamics of bubble columns and slurry bubble columns can be obtained from Deckwer (*Bubble Column Reactors*, Wiley, 1992), Nigam and Schumpe (*Three-Phase Sparged Reactors*, Gordon and Breach, 1996), Ramachandran and Chaudhari (*Three-Phase Catalytic Reactors*, Gordon and Breach, 1983), and Gianetto and Silvestro (*Multiphase Chemical Reactors*, Hemisphere, 1986). Computational fluid mechanics approaches have also been recently used to estimate mixing and mass-transfer parameters [e.g., see Gupta et al., *Chem. Eng. Sci.* **56**(3): 1117–1125 (2001)].

Examples There are a number of examples including Fischer-Tropsch synthesis in the presence of Fe or Co catalysts, methanol synthesis in the presence of Cu/Zn solid catalyst, and hydrocracking in the presence of zeolite catalyst. Fermentation reactions are conducted in bubble column reactors when there is a benefit for increased scale and for reduced cost. The oxygen is sparged from the bottom, and the liquid reactants are added in a semibatch mode. The absence of reactor internals is an advantage as it prevents contamination. Heat transfer has to be managed through a cooling jacket. If heat removal is an issue, cooling coils may be installed.

Fluidized Gas-Liquid-Solid Reactors In a gas-liquid-solid fluidized bed reactor, only the fluid mixture leaves the vessel. Gas and liquid enter at the bottom. Liquid is continuous, gas is dispersed. Particles are larger than in bubble columns, 0.2 to 1.0 mm (0.008 to 0.04 in). Bed expansion can be small. Bed temperatures are uniform within 2°C (3.6°F) in medium-size beds, and heat transfer to embedded surfaces is excellent. Catalyst may be bled off and replenished continuously, or reactivated continuously.

Figure 19-39 shows examples of gas-liquid-solid fluidized-bed reactors. Figure 19-39a illustrates a conventional gas-liquid-solid fluidized bed reactor. Figure 19-39b shows an *ebullating bed* reactor for the hydroprocessing of heavy crude oil. A stable fluidized bed is maintained by recirculation of the mixed fluid through the bed and a draft tube. Reactor temperatures may range from 350 to 600°C (662 to 1112°F) and 200 atm (2940 psi). An external pump sometimes is used instead of the built-in impeller shown. Such units were developed for the liquefaction of coal.

A biological treatment process (Dorr-Oliver Hy-Flo) employs a vertical column filled with sand on which bacterial growth takes place while waste liquid and air are charged. A large interfacial area for reaction is provided, about 33 cm²/cm³ (84 in²/in³). BOD removal of 85 to 90 percent is claimed in 15 min compared with 6 to 8 h in conventional units.

In entrained beds, the three-phase mixture flows through the vessel and is separated downstream. These reactors are used in preference to fluidized beds when catalyst particles are very fine or subject to disintegration or if the catalyst deactivates rapidly in the process.

Trickle Bed Reactors Reactant gas and liquid flow cocurrently downward through a packed bed of solid catalyst particles. The most common use of trickle bed reactors is for hydrogenation reactions. The solubility of feed hydrogen in the liquid even at the higher pressure is insufficient to provide the stoichiometric needs of the reaction, and a gas flow exceeding the need is fed into the reactor. High hydrogen partial pressures can prevent catalyst deactivation due to undesirable reactions, such as coking. Cooling (or heating) is typically done between stages either with heat transfer to a coolant outside the reactor or through direct cooling with a cold reactant gas or liquid.

Advantages of a trickle bed are ease of installation, low liquid holdup (and therefore less undesirable homogeneous reactions), minimal catalyst handling issues, low catalyst attrition, and catalyst life of 1 to 4 years. The liquid and gas flow in trickle beds approaches plug flow (leading to higher conversion than slurry reactors for the same reactor volume). Downsides of trickle beds include flow maldistribution (bypassing), sensitivity to packing uniformity and prewetting (leading to hot spots), incomplete contacting/wetting, intraparticle diffusion resistance, potential for fouling and bed plugging due to particulate matter in the feed, and high pressure drop. A significant fraction of the flow is gas that has to be compressed and recycled (i.e., increased compressor costs).

A schematic of a trickle bed reactor is shown in Fig. 19-40. The reactor is a high-pressure vessel equipped with a drain and a manhole for vessel entry. Typical vessel diameters may range from 3 to 30 ft with height from 6 to 100 ft. The liquid enters the reactor and is

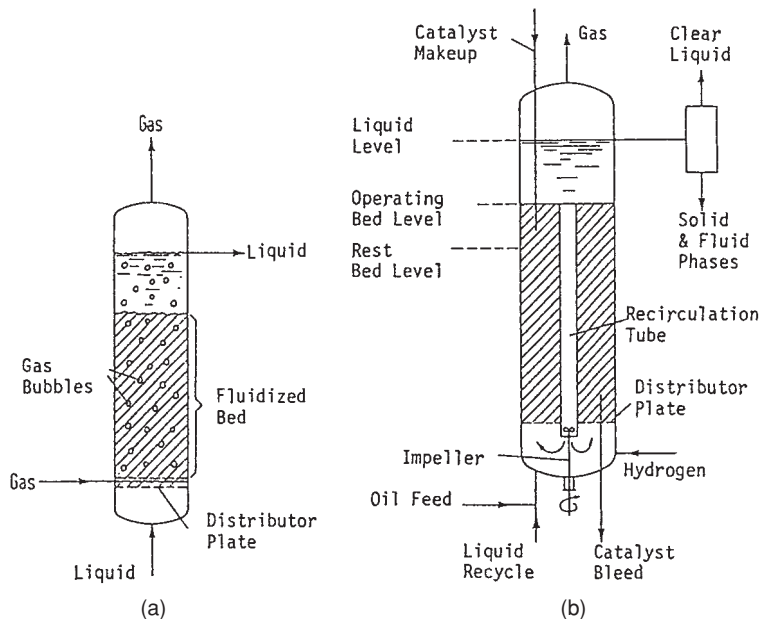


FIG. 19-39 Gas-liquid-solid reactors. (a) Three-phase fluidized-bed reactor. (b) Ebullating bed reactor for hydrotreatment of coal. (Kampiner, in Winnacker-Keuchler, *Chemische Technologie*, vol. 3, Hanser, 1972, p. 252.)

distributed across the cross-section by a distributor plate. The liquid feed flows downward due to gravity helped along by the drag of the gas at such a low rate that it is distributed over the catalyst as a thin film. The gas enters and is distributed along with the liquid. In the simplest arrangement, the liquid distributor is a perforated plate with about 10 openings/dm² (10 openings/15.5 in²), and the gas enters

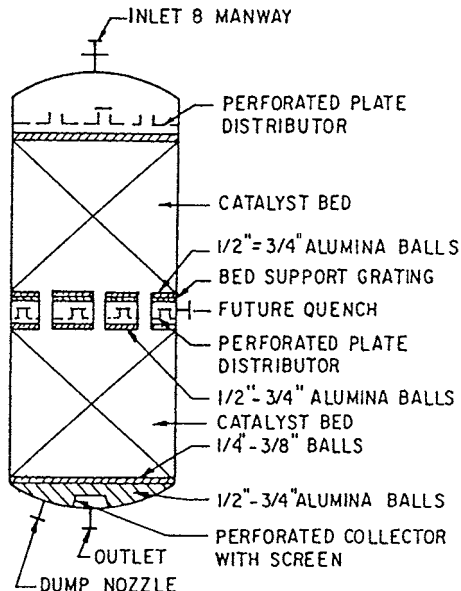


FIG. 19-40 Trickle bed reactor for hydrotreating 20,000 bbl/d of light catalytic cracker oil at 370°C and 27 atm. To convert atm to kPa, multiply by 101.3. (Baldi in Gianetto and Silvestro, *Multiphase Chemical Reactors*, Hemisphere, 1986, pp. 533-563.)

through several risers about 15 cm (5.9 in) high. More elaborate distributor caps also are used. Uniform distribution of liquid across the reactor is critical to reactor performance. The aspect ratio of the reactor can vary between 1 and 10 depending on the pressure drop that can be accommodated by the compressor. It is not uncommon to redistribute the liquid using a redistribution grid every 8 to 15 ft.

The catalyst is often loaded on screens supported by a stainless steel grid near the bottom of the reactor. Often, large inert ceramic balls are loaded at the very bottom, with slightly smaller ceramic balls above the first layer, and then the catalyst. Smaller inert ceramic balls can also be loaded above the catalyst bed and topped off with the larger balls. The layer of inert balls can be 6 in to 2 ft in depth. The balls restrict the movement of the bed and distribute the liquid across the catalyst.

As is the case when two or more mobile phases are present, cocurrent gas-liquid downflow through packed beds produces a variety of flow regimes depending on the gas and liquid flow rates and the physical properties of the gas and the liquid. In Fig. 19-41, a flow regime map for trickle beds of foaming and nonfoaming systems is presented. Here *L* and *G* are the liquid and gas fluxes (mass flow rate per total flow cross-sectional area). In the low interaction or trickle flow regime, gas is the continuous phase and the liquid is flowing as rivulets. Increasing the liquid and gas flow results in high interaction or pulse flow, with the liquid and gas alternatively bridging the bed voids. At high liquid flow and low gas flow, the liquid becomes the continuous phase and the gas is the dispersed phase, called dispersed bubble flow. Finally at high gas flow and low liquid flow, the spray flow regime exists with liquid being the dispersed phase.

The literature contains a number of references to other flow regime maps; however, there is no clear advantage of using one map versus another. Wall effects can also have a major effect on the hydrodynamics of trickle bed reactors. Most of the data reported in the literature are for small laboratory units of 2-in diameter and under.

Hydrodynamic parameters that are required for trickle bed design and analysis include *bed void fraction*, *phase holdups* (gas, liquid, and solid), *wetting efficiency* (fraction of catalyst wetted by liquid), *volumetric gas-liquid mass-transfer coefficient*, *liquid-solid mass-transfer coefficient* (for the wetted part of the catalyst particle surface), *gas-solid*

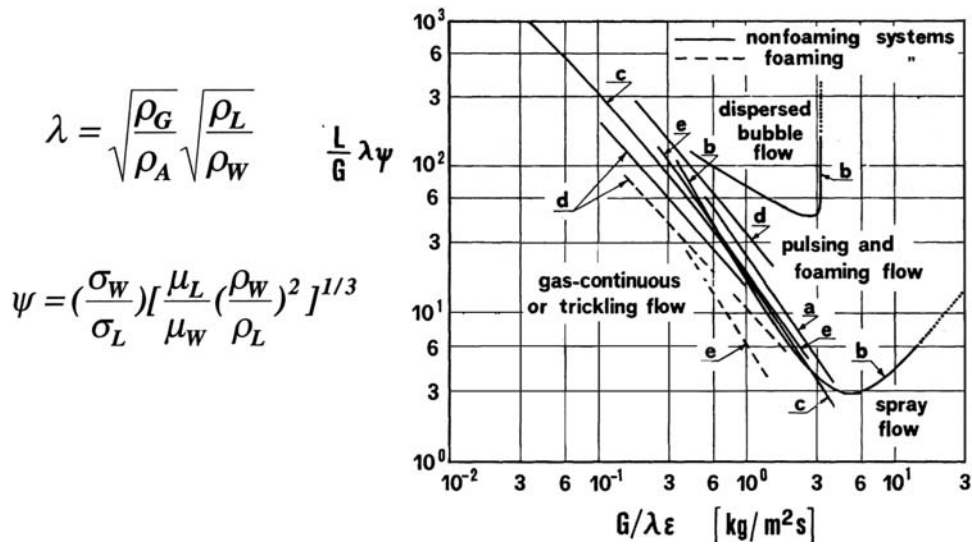


FIG. 19-41 Trickle bed flow regime map. [From Gianetto et al., *AIChE J.* 24(6):1087-1104 (1978); reproduced with permission.]

mass-transfer coefficient (for the unwetted part of the catalyst particle surface), liquid and gas axial mixing, pressure drop, and heat-transfer coefficients. These parameters vary with the flow regime (i.e., for the low and high interaction regimes).

There are a number of pressure drop correlations for two-phase flow in packed beds originating from the Lockhart-Martinelli correlation for two-phase flow in pipes. These correlate the two-phase pressure drop to the single-phase pressure drops of the gas and the liquid obtained from the Ergun equation. See, for instance, the Larkins correlation [Larkins, White, and Jeffrey, *AIChE J.* 7: 231 (1967)]

$$\ln \frac{\Delta P_{CL}}{\Delta P_L + \Delta P_C} = \frac{5.0784}{3.531 + (\ln X)^2}$$

where $X = \sqrt{\frac{\Delta P_L}{\Delta P_C}} \quad 0.05 \leq X \leq 30 \quad (19-98)$

Since some of the published pressure drop correlations can differ by an order of magnitude, it is best to verify the relationship with actual data before designing a reactor. Other approaches to two-phase pressure drop include the relative permeability method of Saez and Carbonell [*AIChE J.* 31(1): 52-62 (1985)].

The bed void volume available for flow and for gas and liquid holdup is determined by the particle size distribution and shape, the particle porosity, and the packing effectiveness. The total voidage and the total liquid holdup can be divided into external and internal terms corresponding to interparticle (bed) and intraparticle (porosity) voidage. The external liquid holdup is further subdivided into static holdup ϵ_{Ls} (holdup remaining after bed draining due to surface tension forces) and dynamic holdup ϵ_{Ld} . Additional expressions for the liquid holdup are the pore fillup F_i and the liquid saturation S_L :

$\epsilon_t = \epsilon_B + \epsilon_p(1 - \epsilon_B)$	total voidage	
$\epsilon_L = \epsilon_{Ld} + \epsilon_{Ls}$	total liquid holdup	
$\epsilon_{Ld} = \epsilon_{Ld} + \epsilon_{Ls}$	external liquid holdup	(19-99)
$\epsilon_{Ls} = F_i \epsilon_p(1 - \epsilon_B)$	internal liquid holdup	
$S_L = \frac{\epsilon_L}{\epsilon_B}$	liquid saturation	

The static holdup can be correlated with the Eotvos number N_{Eo} as it results from a balance of surface tension and gravity forces on the liquid held up in the pores in absence of flow:

$$N_{Eo} = \frac{\text{gravity force}}{\text{surface tension force}} = \frac{\rho_L g d_p^2}{\sigma_L} \quad (19-100)$$

For instance Fig. 19-42 illustrates the dependence of the static holdup on the Eotvos number for porous and nonporous packings.

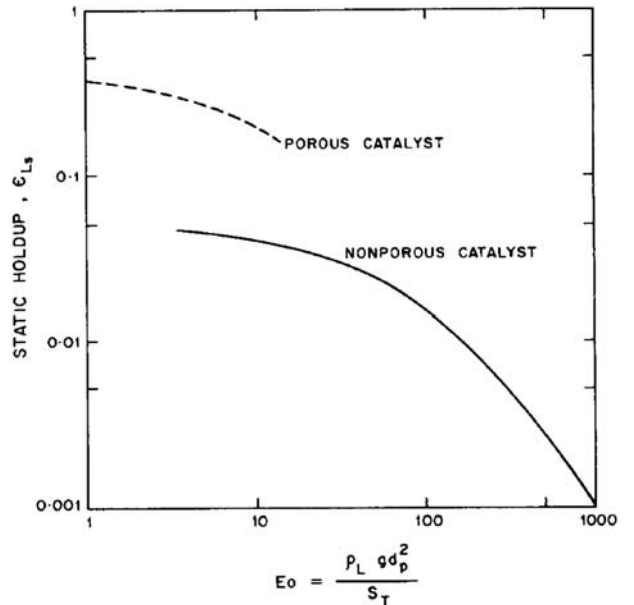


FIG. 19-42 The static liquid holdup for porous and nonporous solids. (Fig. 7.7 in Ramachandran and Chaudhari, *Three-Phase Catalytic Reactors*, Gordon and Breach, 1983.)

A variety of correlations have been developed for the total and the dynamic liquid holdup. For instance, the total liquid holdup has been correlated with the Lockhardt-Martinelli parameter X for spherical and cylindrical particles [Midou, Favier, and Charpentier, *J. Chem. Eng. Japan*, **9**: 350 (1976)]

$$\frac{\epsilon_L}{\epsilon_b} = \frac{0.66X^{0.81}}{1 + 0.66X^{0.81}} \quad (19-101)$$

Correlations for the dynamic liquid holdup have also been developed as function of various dimensionless numbers including the liquid and gas Reynolds number, and the two-phase pressure drop [see, e.g., Ramachandran and Chaudhari, *Three-Phase Catalytic Reactors*, Gordon and Breach, 1983; and Hofmann, *Hydrodynamics and Hydrodynamic Models of Fixed Bed Reactors*, in Gianetto and Silveston (eds.), *Multiphase Chemical Reactors*, Hemisphere 1986].

The various volumetric mass-transfer coefficients are defined in a manner similar to that discussed for gas-liquid and fluid-solid mass transfer in previous sections. There are a large number of correlations obtained from different gas-liquid-solid systems. For more details see Shah (*Gas-Liquid-Solid Reactor Design*, McGraw-Hill, 1979), Ramachandran and Chaudhari (*Three-Phase Catalytic Reactors*, Gordon and Breach, 1983), and Shah and Sharma [*Gas-Liquid-Solid Reactors* in Carberry and Varma (eds.), *Chemical Reaction and Reactor Engineering*, Marcel Dekker, 1987].

Axial mixing of the liquid is an important factor in the design of trickle bed reactors, and criteria were proposed to establish conditions that limit axial mixing. Mears [*Chem. Eng. Sci.* **26**: 1361 (1971)] developed a criterion that when satisfied, ensures that the conversion will be within 5 percent of that predicted by plug flow:

$$Pe = \frac{u_L L}{D} > 20n \ln \frac{1}{1-x} \quad (19-102)$$

where n is the order of the reaction with respect to the limiting reactant and x is the fractional conversion of that reactant. Correlations for axial dispersion can be found in Ramachandran and Chaudhari, *Three-Phase Catalytic Reactors*, Gordon and Breach, 1983.

Incomplete wetting can be also a critical factor in reactor design and analysis, leading usually to lower performance due to incomplete utilization of the catalyst bed. In a few select cases, the opposite may be the case, e.g., when a volatile reactant reacts faster than its liquid phase because it is not limited by the gas-liquid mass-transfer resistance and higher gas diffusivity. Correlations for the fraction of catalyst surface wetted are available, although not very reliable and strongly system-dependent (e.g., Shah, *Gas-Liquid-Solid Reactor Design*, McGraw-Hill, 1979).

Due to the complex hydrodynamics and the dependence of the hydrodynamic parameters on the flow regime, trickle beds are notoriously difficult to scale up. Laboratory units (used for kinetics and process development) and commercial units typically are operated at the same *liquid hourly space velocity* (LHSV). Since the LHSV represents the ratio of the superficial liquid velocity to the reactor length, the superficial velocity in a laboratory reactor will be lower than in a commercial reactor by the ratio of reactor lengths, which is often well over an order of magnitude. This means that heat and mass transport parameters may be considerably different in laboratory reactors operated at the target LHSV. This also shifts the flow regime from trickle flow (low interaction) in the lab and small pilot plants to the high-interaction regime in large-scale commercial reactors.

Wall effects in lab units of 50-mm (1.97-in) diameter can be important while these are negligible for commercial reactors of 1 m or more diameter. Wall effects in the lab can be reduced by using reactor/particle diameter ratios greater than 8. If that is not possible, inert fines are added in the lab to reduce wall effects. Also, in large-diameter beds, uniform liquid distribution is difficult, even with a large number of distributor nozzles, and unless the flow is redistributed, the nonuniformity can persist along the bed, leading to potential hot spots that can cause by-products and fast catalyst deactivation. In trickle beds that are not prewetted, a *hysteresis* phenomenon related to wetting

occurs, where the behavior with increasing flow of the liquid phase is not retraced with decreasing liquid flow. This can often be avoided by prewetting the reactor before start-up.

In practice, the thickness of liquid films in trickle beds has been estimated to vary between 0.01 and 0.2 mm (0.004 and 0.008 in). The dynamic liquid holdup fraction is 0.03 to 0.25, and the static fraction is 0.01 to 0.05. The high end of the static fraction includes the liquid that partially fills the pores of the catalyst. The effective gas-liquid interface is 20 to 50 percent of the geometric surface of the particles, but it can approach 100 percent at high liquid loading. This results in an increase of reaction rate as the amount of wetted surface increases (i.e., when the gas-solid reaction rate is negligible).

Examples Hydrodesulfurization of petroleum oils was the first large-scale application of trickle bed reactors commercialized in 1955. In this application, organosulfur species contained in refinery feeds are removed in the presence of hydrogen and a catalyst and released as hydrogen sulfide. Conditions depend on the quality and boiling range of the oil. The reactor pressure is optimized to increase the solubility of the hydrogen and minimize catalyst deactivation due to coking. Over the life of the catalyst, the temperature is increased to maintain a constant conversion. Temperatures are in the range of 345 to 425°C (653 to 797°F) with pressures of 34 to 102 atm (500 to 1500 psi). A large commercial reactor may have 20 to 25 m (66 to 82 ft) of total depth of catalyst, and may be up to 3-m (9.8-ft) diameter or above in several beds of 3- to 6-m (9.8- to 19.7-ft) depth. Bed depth is often limited by pressure drop, the catalyst crush strength, and the maximum adiabatic temperature increase for stable operation. The need to limit pressure drop is driven by the capital and operating costs associated with the hydrogen recycle compressor. Catalyst granules are 1.5 to 3.0 mm (0.06 to 0.12 in), sometimes a little more. Catalysts are 10 to 20 percent Co and Mo (or Ni and W) on alumina. The adiabatic temperature rise in each bed usually is limited to 30°C (86°F) by injection of cold hydrogen between beds. Since the liquid trickles over the catalyst, the wetting efficiency of the catalyst is important in determining the volumetric reaction rate. As expected, wetting efficiency increases with increasing liquid rate. Catalyst effectiveness of particles 3 to 5 mm (0.12 to 0.20 in) in diameter has been found to be about 40 to 60 percent.

Packed Bubble Columns (Cocurrent Upflow) These reactors are also called flooded-bed reactors. In contrast to trickle beds, both gas and liquid flow up cocurrently. A screen is needed at the top to retain the catalyst particles. Such a unit has been used for the hydrogenation of nitro and double-bond compounds and nitriles [Ovcinnikov et al., *Brit. Chem. Eng.* **13**: 1367 (1968)]. High gas rates can cause movement and attrition of the particles. Accordingly, such equipment is restricted to low gas flow rates, for instance, where a hydrogen atmosphere is necessary but the consumption of hydrogen is slight. The liquid is the continuous phase, and the gas, the dispersed phase. Benefits of cocurrent upflow versus trickle (cocurrent downflow) include high wetting efficiency (resulting in good liquid-solid contacting), good liquid distribution, and better heat and mass transfer. Disadvantages include higher pressure drop and liquid backmixing, the latter resulting in increased extent of undesirable homogeneous reactions.

A number of flow regime maps are available for packed bubble columns [see, e.g., Fukushima and Kusaka, *J. Chem. Eng. Japan*, **12**: 296 (1979)]. Correlations for the various hydrodynamic parameters can be found in Shah (*Gas-Liquid-Solid Reactor Design*, McGraw-Hill, 1979), Ramachandran and Chaudhari (*Three-Phase Catalytic Reactors*, Gordon and Breach, 1983), and Shah and Sharma [*Gas-Liquid-Solid Reactors* in Carberry and Varma (eds.), *Chemical Reaction and Reactor Engineering*, Marcel Dekker, 1987].

Countercurrent Flow The gas flows up countercurrent with the downflow liquid. This mode of operation is not as widely used for catalytic reactions since operation is limited by flooding at high gas velocity: at flooding conditions increasing the liquid flow does not result in increase of the liquid holdup.

For more details see Shah (*Gas-Liquid-Solid Reactor Design*, McGraw-Hill, 1979) and Hofmann [*Hydrodynamics and Hydrodynamic Models of Fixed Bed Reactors*, in Gianetto and Silveston (eds.), *Multiphase Chemical Reactors*, Hemisphere 1986].

SOME CASE STUDIES

The literature contains case studies that may be useful for analysis or design of new reactors. Several of these are listed for reference.

Rase (*Case Studies and Design Data*, vol. 2 of *Chemical Reactor Design for Process Plants*, Wiley, 1977):

- Styrene polymerization
- Cracking of ethane to ethylene
- Quench cooling in the ethylene process
- Toluene dealkylation
- Shift conversion
- Ammonia synthesis
- Sulfur dioxide oxidation
- Catalytic reforming
- Ammonia oxidation
- Phthalic anhydride production
- Steam reforming
- Vinyl chloride polymerization
- Batch hydrogenation of cottonseed oil
- Hydrodesulfurization

Rase (*Fixed Bed Reactor Design and Diagnostics*, Butterworths, 1990) has several case studies and a general computer program for reactor design:

- Methane-steam reaction
- Hydrogenation of benzene to cyclohexane
- Dehydrogenation of ethylbenzene to styrene

Tarhan (*Catalytic Reactor Design*, McGraw-Hill, 1983) has computer programs and results for these cases:

- Toluene hydrodealkylation to benzene and methane
- Phthalic anhydride by air oxidation of naphthalene
- Trickle bed reactor for hydrodesulfurization

Ramage et al. (*Advances in Chemical Engineering*, vol. 13, Academic Press, 1987, pp. 193–266):

- Mobil's kinetic reforming model Dente and Ranzi [in Albright et al. (eds.), *Pyrolysis Theory and Industrial Practice*, Academic Press, 1983, pp. 133–175]:
- Mathematical modeling of hydrocarbon pyrolysis reactions Shah and Sharma [in Carberry and Varma (eds.), *Chemical Reaction and Reaction Engineering Handbook*, Marcel Dekker, 1987, pp. 713–721]:
- Hydroxylamine phosphate manufacture in a slurry reactor

Exploration for an acceptable or optimum design for a new reactor may require consideration of several feed and product specifications, reactor types, catalysts, operating conditions, and economic evaluations. Modifications to an existing process likewise may need to consider many cases. Commercial software may be used to facilitate examination of options. A typical package can handle a number of reactions in various ideal reactors under isothermal, adiabatic, or heat-transfer conditions in one or two phases. Outputs can provide profiles of composition, pressure, and temperature as well as vessel size.

Thermodynamic software packages may be used to find equilibrium compositions at prescribed temperatures and pressures. Such calculations require knowledge of feed components and products and their thermodynamic properties and are based on Gibbs free energy minimization techniques. Examples of thermodynamic packages may be found in Smith and Missen (*Chemical Reaction Equilibrium Analysis Theory and Algorithms*, Wiley, 1982) and in Walas (*Phase Equilibria in Chemical Engineering*, Butterworths, 1985).

For some widely practiced processes, especially in the petroleum industry, computer models are available from a number of vendors or, by license, from proprietary sources. Such processes include fluid catalytic cracking, hydrotreating, hydrocracking, alkylation with HF or H₂SO₄, reforming with Pt or Pt-Re catalysts, tubular steam cracking of hydrocarbon fractions, noncatalytic pyrolysis to ethylene, and ammonia synthesis. Catalyst vendors may sometimes also provide simple process models. The reader is advised to peruse some of the process simulation packages listed for sale in the *CEP Software Directory* (e.g., AIChE, 1994) that gets periodically updated with new offerings.

SECTION 20

Alternative
Separation
Processes

PERRY'S CHEMICAL ENGINEERS' HANDBOOK

8TH EDITION



MICHAEL E. PRUDICH, HUANLIN CHEN
TINGYUE GU, RAM B. GUPTA
KEITH P. JOHNSTON, HERB LUTZ
GUANGHUI MA, ZHIGUO SU

Copyright © 2008, 1997, 1984, 1973, 1963, 1950, 1941, 1934 by The McGraw-Hill Companies, Inc. All rights reserved. Manufactured in the United States of America. Except as permitted under the United States Copyright Act of 1976, no part of this publication may be reproduced or distributed in any form or by any means, or stored in a database or retrieval system, without the prior written permission of the publisher.

0-07-154227-2

The material in this eBook also appears in the print version of this title: 0-07-151143-1.

All trademarks are trademarks of their respective owners. Rather than put a trademark symbol after every occurrence of a trademarked name, we use names in an editorial fashion only, and to the benefit of the trademark owner, with no intention of infringement of the trademark. Where such designations appear in this book, they have been printed with initial caps.

McGraw-Hill eBooks are available at special quantity discounts to use as premiums and sales promotions, or for use in corporate training programs. For more information, please contact George Hoare, Special Sales, at george_hoare@mcgraw-hill.com or (212) 904-4069.

TERMS OF USE

This is a copyrighted work and The McGraw-Hill Companies, Inc. (“McGraw-Hill”) and its licensors reserve all rights in and to the work. Use of this work is subject to these terms. Except as permitted under the Copyright Act of 1976 and the right to store and retrieve one copy of the work, you may not decompile, disassemble, reverse engineer, reproduce, modify, create derivative works based upon, transmit, distribute, disseminate, sell, publish or sublicense the work or any part of it without McGraw-Hill’s prior consent. You may use the work for your own noncommercial and personal use; any other use of the work is strictly prohibited. Your right to use the work may be terminated if you fail to comply with these terms.

THE WORK IS PROVIDED “AS IS.” McGRAW-HILL AND ITS LICENSORS MAKE NO GUARANTEES OR WARRANTIES AS TO THE ACCURACY, ADEQUACY OR COMPLETENESS OF OR RESULTS TO BE OBTAINED FROM USING THE WORK, INCLUDING ANY INFORMATION THAT CAN BE ACCESSED THROUGH THE WORK VIA HYPERLINK OR OTHERWISE, AND EXPRESSLY DISCLAIM ANY WARRANTY, EXPRESS OR IMPLIED, INCLUDING BUT NOT LIMITED TO IMPLIED WARRANTIES OF MERCHANTABILITY OR FITNESS FOR A PARTICULAR PURPOSE. McGraw-Hill and its licensors do not warrant or guarantee that the functions contained in the work will meet your requirements or that its operation will be uninterrupted or error free. Neither McGraw-Hill nor its licensors shall be liable to you or anyone else for any inaccuracy, error or omission, regardless of cause, in the work or for any damages resulting therefrom. McGraw-Hill has no responsibility for the content of any information accessed through the work. Under no circumstances shall McGraw-Hill and/or its licensors be liable for any indirect, incidental, special, punitive, consequential or similar damages that result from the use of or inability to use the work, even if any of them has been advised of the possibility of such damages. This limitation of liability shall apply to any claim or cause whatsoever whether such claim or cause arises in contract, tort or otherwise.

DOI: 10.1036/0071511431

Alternative Separation Processes*

Michael E. Prudich, Ph.D. Professor of Chemical Engineering, Ohio University; Member, American Institute of Chemical Engineers, American Chemical Society, American Society for Engineering Education (Section Editor, *Alternative Solid/Liquid Separations*)

Huanlin Chen, M.Sc. Professor of Chemical and Biochemical Engineering, Zhejiang University (Selection of *Biochemical Separation Processes—Affinity Membrane Chromatography*)

Tingyue Gu, Ph.D. Associate Professor of Chemical Engineering, Ohio University (Selection of *Biochemical Separation Processes*)

Ram B. Gupta, Ph.D. Alumni (Chair) Professor of Chemical Engineering, Department of Chemical Engineering, Auburn University; Member, American Institute of Chemical Engineers, American Chemical Society (*Supercritical Fluid Separation Processes*)

Keith P. Johnston, Ph.D., P.E. M. C. (Bud) and Mary Beth Baird Endowed Chair and Professor of Chemical Engineering, University of Texas (Austin); Member, American Institute of Chemical Engineers, American Chemical Society, University of Texas Separations Research Program (*Supercritical Fluid Separation Processes*)

Herb Lutz Consulting Engineer, Millipore Corporation; Member, American Institute of Chemical Engineers, American Chemical Society (*Membrane Separation Processes*)

Guanghui Ma, Ph.D. Professor, State Key Laboratory of Biochemical Engineering, Institute of Process Engineering, CAS, Beijing, China (Selection of *Biochemical Separation Processes—Gigaporous Chromatography Media*)

Zhiguo Su, Ph.D. Professor and Director, State Key Laboratory of Biochemical Engineering, Institute of Process Engineering, CAS, Beijing, China (Selection of *Biochemical Separation Processes—Protein Refolding, Expanded-Bed Chromatography*)

CRYSTALLIZATION FROM THE MELT

Introduction	20-3	Pertinent Variables in Zone Melting	20-6
Progressive Freezing	20-4	Applications	20-6
Component Separation by Progressive Freezing	20-4	Melt Crystallization from the Bulk	20-6
Pertinent Variables in Progressive Freezing	20-5	Investigations	20-6
Applications	20-5	Commercial Equipment and Applications	20-9
Zone Melting	20-5	Falling-Film Crystallization	20-10
Component Separation by Zone Melting	20-5	Principles of Operation	20-13
		Commercial Equipment and Applications	20-13

*The contributions of Dr. Joseph D. Henry (*Alternative Solid/Liquid Separations*), Dr. William Eykamp (*Membrane Separation Processes*), Dr. T. Alan Hatton (*Selection of Biochemical Separation Processes*), Dr. Robert Lemlich (*Adsorptive-Bubble Separation Methods*), Dr. Charles G. Moyers (*Crystallization from the Melt*), and Dr. Michael P. Thien (*Selection of Biochemical Separation Processes*), who were authors for the seventh edition, are acknowledged.

20-2 ALTERNATIVE SEPARATION PROCESSES

SUPERCRITICAL FLUID SEPARATION PROCESSES

Introduction	20-14
Physical Properties of Pure Supercritical Fluids	20-14
Thermodynamic Properties	20-14
Transport Properties	20-15
Phase Equilibria	20-15
Liquid-Fluid Equilibria	20-15
Solid-Fluid Equilibria	20-15
Polymer-Fluid Equilibria and the Glass Transition	20-15
Cosolvents and Complexing Agents	20-15
Surfactants and Colloids in Supercritical Fluids	20-15
Phase Equilibria Models	20-16
Mass Transfer	20-16
Process Concepts in Supercritical Fluid Extraction	20-16
Applications	20-16
Decaffeination of Coffee and Tea	20-16
Extraction of Flavors, Fragrances, Nutraceuticals, and Pharmaceuticals	20-16
Temperature-Controlled Residuum Oil Supercritical Extraction (ROSE)	20-16
Polymer Devolatilization, Fractionation, and Plasticization	20-16
Drying and Aerogel Formation	20-17
Cleaning	20-17
Microelectronics Processing	20-17
Precipitation/Crystallization to Produce Nano- and Microparticles	20-17
Rapid Expansion from Supercritical Solution and Particles from Gas Saturated Solutions	20-17
Reactive Separations	20-17
Crystallization by Chemical Reaction	20-18

ALTERNATIVE SOLID/LIQUID SEPARATIONS

Separation Processes Based Primarily on Action in an Electric Field	20-19
Theory of Electrical Separations	20-19
Electrophoresis	20-20
Electrofiltration	20-21
Cross-Flow-Electrofiltration	20-21
Dielectrophoresis	20-23
Surface-Based Solid-Liquid Separations Involving a Second Liquid Phase	20-28
Process Concept	20-28
Theory	20-29
Adsorptive-Bubble Separation Methods	20-29
Principle	20-29
Definitions and Classification	20-30
Adsorption	20-31
Factors Affecting Adsorption	20-31
Operation in the Simple Mode	20-32
Finding Γ	20-32
Bubble Sizes	20-32
Enriching and Stripping	20-32
Foam-Column Theory	20-32
Limiting Equations	20-33
Column Operation	20-33
Foam Drainage and Overflow	20-34
Foam Coalescence	20-34
Foam Breaking	20-34
Bubble Fractionation	20-34
Systems Separated	20-35

MEMBRANE SEPARATION PROCESSES

Topics Omitted from This Section	20-36
General Background and Definitions	20-36
Applications	20-36
Membrane Types	20-37
Component Transport	20-38
Modules and Membrane Systems	20-40

Process Configurations	20-42
Reverse Osmosis (RO) and Nanofiltration (NF)	20-45
Applications	20-45
Membranes, Modules, and Systems	20-47
Component Transport in Membranes	20-48
Pretreatment and Cleaning	20-48
Design Considerations and Economics	20-49
Ultrafiltration	20-50
Applications	20-50
Membranes, Modules, and Systems	20-51
Component Transport in Membranes	20-52
Design Considerations and Economics	20-53
Microfiltration	20-54
Process Description	20-54
Brief Examples	20-54
MF Membranes	20-54
Membrane Characterization	20-55
Process Limitations	20-56
Equipment Configuration	20-56
Representative Process Applications	20-56
Economics	20-57
Gas-Separation Membranes	20-57
Process Description	20-57
Leading Examples	20-57
Basic Principles of Operation	20-58
Selectivity and Permeability	20-59
Gas-Separation Membranes	20-60
Membrane System Design Features	20-60
Energy Requirements	20-61
Economics	20-61
Competing Technologies	20-63
Pervaporation	20-63
Process Description	20-63
Definitions	20-64
Operational Factors	20-65
Vapor Feed	20-65
Leading Examples	20-65
Pervaporation Membranes	20-65
Modules	20-66
Electrodialysis	20-66
Process Description	20-66
Leading Examples	20-66
Membranes	20-67
Membrane Efficiency	20-67
Process Description	20-67
Process Configuration	20-69
Energy Requirements	20-70
Equipment and Economics	20-71

SELECTION OF BIOCHEMICAL SEPARATION PROCESSES

General Background	20-71
Initial Product Harvest and Concentration	20-73
Cell Disruption	20-73
Protein Refolding	20-74
Clarification Using Centrifugation	20-75
Clarification Using Microfiltration	20-75
Selection of Cell-Separation Unit Operation	20-76
Initial Purification	20-76
Precipitation	20-76
Liquid-Liquid Partitioning	20-76
Adsorption	20-78
Membrane Ultrafiltration	20-78
Final Purification	20-79
Chromatography	20-79
Product Polishing and Formulation	20-83
Lyophilization and Drying	20-83
Integration of Unit Operations in Downstream Processing	20-84
Integration of Upstream and Downstream Operations	20-84

CRYSTALLIZATION FROM THE MELT

GENERAL REFERENCES: Van't Land, *Industrial Crystallization of Melts*, Taylor & Francis, New York, 2004. Mullin, *Crystallization*, 4th ed., Butterworth-Heinemann, 2001. Myerson, *Handbook of Industrial Crystallization*, 2d ed., Butterworth-Heinemann, 2001. Pfann, *Zone Melting*, 2d ed., Wiley, New York, 1966. U.S. Patents 3,621,664 and 3,796,060. Zief and Wilcox, *Fractional Solidification*, Marcel Dekker, New York, 1967.

INTRODUCTION

Purification of a chemical species by solidification from a liquid mixture can be termed either **solution** crystallization or crystallization from the **melt**. The distinction between these two operations is somewhat subtle. The term **melt crystallization** has been defined as the separation of components of a binary mixture without addition of solvent, but this definition is somewhat restrictive. In **solution crystallization** a diluent solvent is added to the mixture; the solution is then directly or indirectly cooled, and/or solvent is evaporated to effect crystallization. The solid phase is formed and maintained somewhat below its pure-component freezing-point temperature. In melt crystallization no diluent solvent is added to the reaction mixture, and the solid phase is formed by cooling of the melt. Product is frequently maintained near or above its pure-component freezing point in the refining section of the apparatus.

A large number of techniques are available for carrying out crystallization from the melt. An abbreviated list includes partial freezing and solids recovery in cooling crystallizer-centrifuge systems, partial melting (e.g., sweating), staircase freezing, normal freezing, zone melting, and column crystallization. A description of all these methods is not within the scope of this discussion. Zief and Wilcox (op. cit.) and Myerson (op. cit.) describe many of these processes. Three of the more common methods—progressive freezing from a falling film, zone melting, and melt crystallization from the bulk—are discussed here to illustrate the techniques used for practicing crystallization from the melt.

High or ultrahigh product purity is obtained with many of the melt-purification processes. Table 20-1 compares the product quality and product form that are produced from several of these operations. Zone refining can produce very pure material when operated in a batch mode; however, other melt crystallization techniques also provide high purity and become attractive if continuous high-capacity processing is desired. Comparison of the features of melt crystallization and distillation are shown on Table 20-2.

A brief discussion of solid-liquid phase equilibrium is presented prior to discussing specific crystallization methods. Figures 20-1 and 20-2 illustrate the phase diagrams for binary solid-solution and eutectic systems, respectively. In the case of binary solid-solution systems, illustrated in Fig. 20-1, the liquid and solid phases contain equilibrium quantities of both components in a manner similar to vapor-liquid phase behavior. This type of behavior causes separation difficulties since multiple stages are required. In principle, however, high purity

TABLE 20-1 Comparison of Processes Involving Crystallization from the Melt

Processes	Approximate upper melting point, °C	Materials tested	Minimum purity level obtained, ppm, weight	Product form
Progressive freezing	1500	All types	1	Ingot
Zone melting				
Batch	3500	All types	0.01	Ingot
Continuous	500	SiI ₄	100	Melt
Melt crystallization				
Continuous	300	Organic	10	Melt
Cyclic	300	Organic	10	Melt

Abbreviated from Zief and Wilcox, *Fractional Solidification*, Marcel Dekker, New York, 1967, p. 7.

TABLE 20-2 Comparison of Features of Melt Crystallization and Distillation

Distillation	Melt crystallization
Phase equilibria	
Both liquid and vapor phases are totally miscible. Conventional vapor/liquid equilibrium.	Liquid phases are totally miscible; solid phases are not. Eutectic system.
Neither phase is pure. Separation factors are moderate and decrease as purity increases.	Solid phase is pure, except at eutectic point. Partition coefficients are very high (theoretically, they can be infinite).
Ultrahigh purity is difficult to achieve.	Ultrahigh purity is easy to achieve.
No theoretical limit on recovery.	Recovery is limited by eutectic composition.
Mass-transfer kinetics	
High mass-transfer rates in both vapor and liquid phases.	Only moderate mass-transfer rate in liquid phase, zero in solid.
Close approach to equilibrium.	Slow approach to equilibrium; achieved in brief contact time. Included impurities cannot diffuse out of solid.
Adiabatic contact assures phase equilibrium.	Solid phase must be remelted and refrozen to allow phase equilibrium.
Phase separability	
Phase densities differ by a factor of 100–10,000:1.	Phase densities differ by only about 10%.
Viscosity in both phases is low.	Liquid phase viscosity moderate, solid phase rigid.
Phase separation is rapid and complete.	Phase separation is slow; surface-tension effects prevent completion.
Countercurrent contacting is quick and efficient.	Countercurrent contacting is slow and imperfect.

Wynn, *Chem. Eng. Prog.*, **88**, 55 (1992). Reprinted with permission of the American Institute of Chemical Engineers. Copyright © 1992 AIChE. All rights reserved

and yields of both components can be achieved since no eutectic is present.

If the impurity or minor component is completely or partially soluble in the solid phase of the component being purified, it is convenient to define a distribution coefficient k , defined by Eq. (20-1):

$$k = C_s / C_\ell \quad (20-1)$$

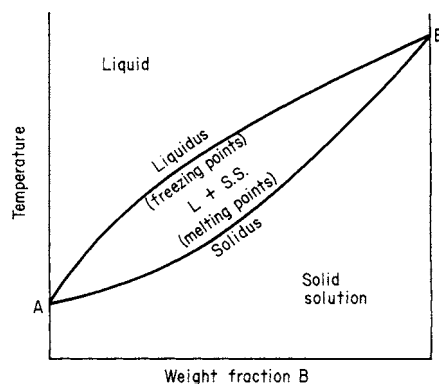


FIG. 20-1 Phase diagram for components exhibiting complete solid solution. (Zief and Wilcox, *Fractional Solidification*, vol. 1, Marcel Dekker, New York, 1967, p. 31.)

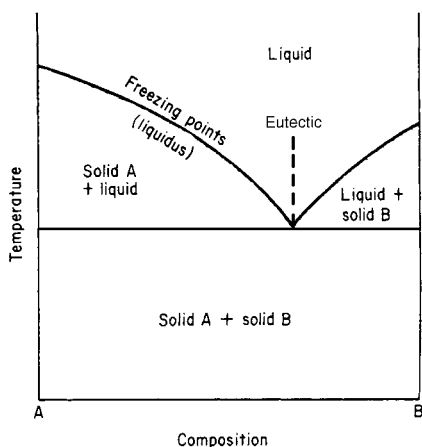


FIG. 20-2 Simple eutectic-phase diagram at constant pressure. (Zief and Wilcox, *Fractional Solidification*, vol. 1, Marcel Dekker, New York, 1967, p. 24.)

C_s is the concentration of impurity or minor component in the solid phase, and C_l is the impurity concentration in the liquid phase. The distribution coefficient generally varies with composition. The value of k is greater than 1 when the solute raises the melting point and less than 1 when the melting point is depressed. In the regions near pure A or B the liquidus and solidus lines become linear; i.e., the distribution coefficient becomes constant. This is the basis for the common assumption of constant k in many mathematical treatments of fractional solidification in which ultrapure materials are obtained.

In the case of a simple eutectic system shown in Fig. 20-2, a pure solid phase is obtained by cooling if the composition of the feed mixture is not at the eutectic composition. If liquid composition is eutectic, then separate crystals of both species will form. In practice it is difficult to attain perfect separation of one component by crystallization of a eutectic mixture. The solid phase will always contain trace amounts of impurity because of incomplete solid-liquid separation, slight solubility of the impurity in the solid phase, or volumetric inclusions. It is difficult to generalize on which of these mechanisms is the major cause of contamination because of analytical difficulties in the ultrahigh-purity range.

The distribution-coefficient concept is commonly applied to fractional solidification of eutectic systems in the ultrapure portion of the phase diagram. If the quantity of impurity entrapped in the solid phase for whatever reason is proportional to that contained in the melt, then assumption of a constant k is valid. It should be noted that the theoretical yield of a component exhibiting binary eutectic behavior is fixed by the feed composition and position of the eutectic. Also, in contrast to the case of a solid solution, only one component can be obtained in a pure form.

There are many types of phase diagrams in addition to the two cases presented here; these are summarized in detail by Zief and Wilcox (op. cit., p. 21). Solid-liquid phase equilibria must be determined experimentally for most binary and multicomponent systems. Predictive methods are based mostly on ideal phase behavior and have limited accuracy near eutectics. A predictive technique based on extracting liquid-phase activity coefficients from *vapor-liquid* equilibria that is useful for estimating nonideal binary or multicomponent *solid-liquid* phase behavior has been reported by Muir (Pap. 71f, 73d ann. meet., AIChE, Chicago, 1980).

PROGRESSIVE FREEZING

Progressive freezing, sometimes called *normal* freezing, is the slow, directional solidification of a melt. Basically, this involves slow solidification at the bottom or sides of a vessel or tube by indirect cooling. The impurity is rejected into the liquid phase by the advancing solid

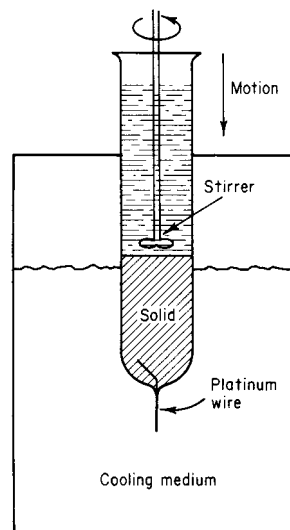


FIG. 20-3 Progressive freezing apparatus.

interface. This technique can be employed to concentrate an impurity or, by repeated solidifications and liquid rejections, to produce a very pure ingot. Figure 20-3 illustrates a progressive freezing apparatus. The solidification rate and interface position are controlled by the rate of movement of the tube and the temperature of the cooling medium. There are many variations of the apparatus; e.g., the residual-liquid portion can be agitated and the directional freezing can be carried out vertically as shown in Fig. 20-3 or horizontally (see Richman et al., in Zief and Wilcox, op. cit., p. 259). In general, there is a solute redistribution when a mixture of two or more components is directionally frozen.

Component Separation by Progressive Freezing When the distribution coefficient is less than 1, the first solid which crystallizes contains less solute than the liquid from which it was formed. As the fraction which is frozen increases, the concentration of the impurity in the remaining liquid is increased and hence the concentration of impurity in the solid phase increases (for $k < 1$). The concentration gradient is reversed for $k > 1$. Consequently, in the absence of diffusion in the solid phase a concentration gradient is established in the frozen ingot.

One extreme of progressive freezing is equilibrium freezing. In this case the freezing rate must be slow enough to permit diffusion in the solid phase to eliminate the concentration gradient. When this occurs, there is no separation if the entire tube is solidified. Separation can be achieved, however, by terminating the freezing before all the liquid has been solidified. Equilibrium freezing is rarely achieved in practice because the diffusion rates in the solid phase are usually negligible (Pfann, op. cit., p. 10).

If the bulk-liquid phase is well mixed and no diffusion occurs in the solid phase, a simple expression relating the solid-phase composition to the fraction frozen can be obtained for the case in which the distribution coefficient is independent of composition and fraction frozen [Pfann, *Trans. Am. Inst. Mech. Eng.*, **194**, 747 (1952)].

$$C_s = kC_0(1 - X)^{k-1} \quad (20-2)$$

C_0 is the solution concentration of the initial charge, and X is the fraction frozen. Figure 20-4 illustrates the solute redistribution predicted by Eq. (20-2) for various values of the distribution coefficient.

There have been many modifications of this idealized model to account for variables such as the freezing rate and the degree of mixing in the liquid phase. For example, Burton et al. [*J. Chem. Phys.*, **21**, 1987 (1953)] reasoned that the solid rejects solute faster than it can diffuse into the bulk liquid. They proposed that the effect of the

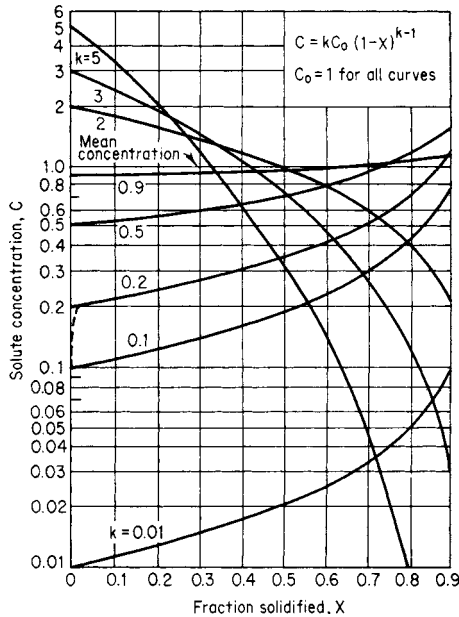


FIG. 20-4 Curves for progressive freezing, showing solute concentration C in the solid versus fraction-solidified X . (Pfann, *Zone Melting*, 2d ed., Wiley, New York, 1966, p. 12.)

freezing rate and stirring could be explained by the diffusion of solute through a stagnant film next to the solid interface. Their theory resulted in an expression for an effective distribution coefficient k_{eff} which could be used in Eq. (20-2) instead of k .

$$k_{eff} = \frac{1}{1 + (1/k - 1)e^{-f\delta/D}} \quad (20-3)$$

where f = crystal growth rate, cm/s; δ = stagnant film thickness, cm; and D = diffusivity, cm²/s. No further attempt is made here to summarize the various refinements of Eq. (20-2). Zief and Wilcox (op. cit., p. 69) have summarized several of these models.

Pertinent Variables in Progressive Freezing The dominant variables which affect solute redistribution are the degree of mixing in the liquid phase and the rate of solidification. It is important to attain sufficient mixing to facilitate diffusion of the solute away from the solid-liquid interface to the bulk liquid. The film thickness δ decreases as the level of agitation increases. Cases have been reported in which essentially no separation occurred when the liquid was not stirred. The freezing rate which is controlled largely by the lowering rate of the tube (see Fig. 20-3) has a pronounced effect on the separation achieved. The separation is diminished as the freezing rate is increased. Also fluctuations in the freezing rate caused by mechanical vibrations and variations in the temperature of the cooling medium can decrease the separation.

Applications Progressive freezing has been applied to both solid solution and eutectic systems. As Fig. 20-4 illustrates, large separation factors can be attained when the distribution coefficient is favorable. Relatively pure materials can be obtained by removing the desired portion of the ingot. Also in some cases progressive freezing provides a convenient method of concentrating the impurities; e.g., in the case of $k < 1$ the last portion of the liquid that is frozen is enriched in the distributing solute.

Progressive freezing has been applied on the commercial scale. For example, aluminum has been purified by continuous progressive freezing [Dewey, *J. Metals*, 17, 940 (1965)]. The Proabd refiner described by Molinari (Zief and Wilcox, op. cit., p. 393) is also a commercial example of progressive freezing. In this apparatus the mixture is directionally solidified on cooling tubes. Purification is achieved

because the impure fraction melts first; this process is called sweating. This technique has been applied to the purification of naphthalene and *p*-dichlorobenzene and commercial equipment is available from BEFS PROKEM, Houston, Tx.

ZONE MELTING

Zone melting also relies on the distribution of solute between the liquid and solid phases to effect a separation. In this case, however, one or more liquid zones are passed through the ingot. This extremely versatile technique, which was invented by W. G. Pfann, has been used to purify hundreds of materials. Zone melting in its simplest form is illustrated in Fig. 20-5. A molten zone can be passed through an ingot from one end to the other by either a moving heater or by slowly drawing the material to be purified through a stationary heating zone.

Progressive freezing can be viewed as a special case of zone melting. If the zone length were equal to the ingot length and if only one pass were used, the operation would become progressive freezing. In general, however, when the zone length is only a fraction of the ingot length, zone melting possesses the advantage that a portion of the ingot does not have to be discarded after each solidification. The last portion of the ingot which is frozen in progressive freezing must be discarded before a second freezing.

Component Separation by Zone Melting The degree of solute redistribution achieved by zone melting is determined by the zone length l , ingot length L , number of passes n , the degree of mixing in the liquid zone, and the distribution coefficient of the materials being purified. The distribution of solute after one pass can be obtained by material-balance considerations. This is a two-domain problem; i.e., in the major portion of the ingot of length $L - l$ zone melting occurs in the conventional sense. The trailing end of the ingot of length l undergoes progressive freezing. For the case of constant-distribution coefficient, perfect mixing in the liquid phase, and negligible diffusion in the solid phase, the solute distribution for a single pass is given by Eq. (20-4) [Pfann, *Trans. Am. Inst. Mech. Eng.*, 194, 747 (1952)].

$$C_s = C_0[1 - (1 - k)e^{-kx/l}] \quad (20-4)$$

The position of the zone x is measured from the leading edge of the ingot. The distribution for multiple passes can also be calculated from a material balance, but in this case the leading edge of the zone encounters solid corresponding to the composition at the point in question for the previous pass. The multiple-pass distribution has been numerically calculated (Pfann, *Zone Melting*, 2d ed., Wiley, New York, 1966, p. 285) for many combinations of k , L/l , and n . Typical solute-composition profiles are shown in Fig. 20-6 for various numbers of passes.

The ultimate distribution after an infinite number of passes is also shown in Fig. 20-6 and can be calculated for $x < (L - l)$ from the following equation (Pfann, op. cit., p. 42):

$$C_s = Ae^{Bx} \quad (20-5)$$

where A and B can be determined from the following relations:

$$k = B\ell/(e^{B\ell} - 1) \quad (20-6)$$

$$A = C_0BL/(e^{BL} - 1) \quad (20-7)$$

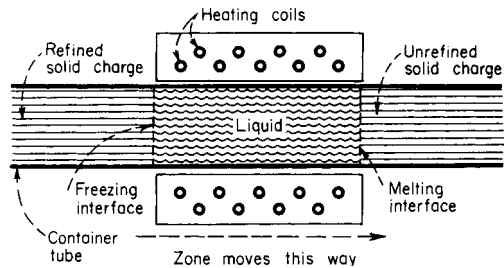


FIG. 20-5 Diagram of zone refining.

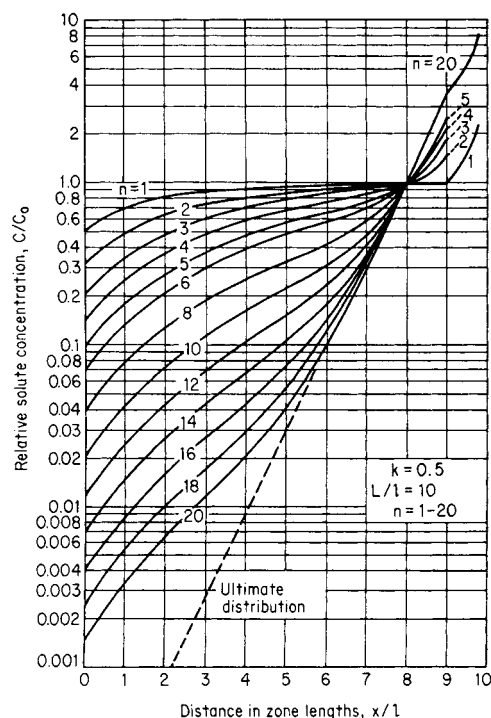


FIG. 20-6 Relative solute concentration C/C_0 (logarithmic scale) versus distance in zone lengths x/l from beginning of charge, for various numbers of passes n . L denotes charge length. (Pfann, *Zone Melting*, 2d ed., Wiley, New York, 1966, p. 290.)

The ultimate distribution represents the maximum separation that can be attained without cropping the ingot. Equation (20-5) is approximate because it does not include the effect of progressive freezing in the last zone length.

As in progressive freezing, many refinements of these models have been developed. Corrections for partial liquid mixing and a variable distribution coefficient have been summarized in detail (Zief and Wilcox, op. cit., p. 47).

Pertinent Variables in Zone Melting The dominant variables in zone melting are the number of passes, ingot-length-zone-length ratio, freezing rate, and degree of mixing in the liquid phase. Figure 20-6 illustrates the increased solute redistribution that occurs as the number of passes increases. Ingot-length-zone-length ratios of 4 to 10 are commonly used (Zief and Wilcox, op. cit., p. 624). An exception is encountered when one pass is used. In this case the zone length should be equal to the ingot length; i.e., progressive freezing provides the maximum separation when only one pass is used.

The freezing rate and degree of mixing have effects in solute redistribution similar to those discussed for progressive freezing. Zone travel rates of 1 cm/h for organic systems, 2.5 cm/h for metals, and 20 cm/h for semiconductors are common. In addition to the zone-travel rate the heating conditions affect the freezing rate. A detailed summary of heating and cooling methods for zone melting has been outlined by Zief and Wilcox (op. cit., p. 192). Direct mixing of the liquid region is more difficult for zone melting than progressive freezing. Mechanical stirring complicates the apparatus and increases the probability of contamination from an outside source. Some mixing occurs because of natural convection. Methods have been developed to stir the zone magnetically by utilizing the interaction of a current and magnetic field (Pfann, op. cit., p. 104) for cases in which the charge material is a reasonably good conductor.

Applications Zone melting has been used to purify hundreds of inorganic and organic materials. Many classes of inorganic compounds including semiconductors, intermetallic compounds, ionic salts, and

oxides have been purified by zone melting. Organic materials of many types have been zone-melted. Zief and Wilcox (op. cit., p. 624) have compiled tables which give operating conditions and references for both inorganic and organic materials with melting points ranging from -115°C to over 3000°C .

Some materials are so reactive that they cannot be zone-melted to a high degree of purity in a container. Floating-zone techniques in which the molten zone is held in place by its own surface tension have been developed by Keck et al. [*Phys. Rev.*, **89**, 1297 (1953)].

Continuous-zone-melting apparatus has been described by Pfann (op. cit., p. 171). This technique offers the advantage of a close approach to the ultimate distribution, which is usually impractical for batch operation.

Performance data have been reported by Kennedy et al. (*The Purification of Inorganic and Organic Materials*, Marcel Dekker, New York, 1969, p. 261) for continuous-zone refining of benzoic acid.

MELT CRYSTALLIZATION FROM THE BULK

Conducting crystallization inside a vertical or horizontal column with a countercurrent flow of crystals and liquid can produce a higher product purity than conventional crystallization or distillation. The working concept is to form a crystal phase from the bulk liquid, either internally or externally, and then transport the solids through a countercurrent stream of enriched reflux liquid obtained from melted product. The problem in practicing this technology is the difficulty of controlling solid-phase movement. Unlike distillation, which exploits the specific-gravity differences between liquid and vapor phases, melt crystallization involves the contacting of liquid and solid phases that have nearly identical physical properties. Phase densities are frequently very close, and gravitational settling of the solid phase may be slow and ineffective. The challenge of designing equipment to accomplish crystallization in a column has resulted in a myriad of configurations to achieve reliable solid-phase movement, high product yield and purity, and efficient heat addition and removal.

Investigations Crystallization conducted inside a column is categorized as either **end-fed** or **center-fed** depending on whether the feed location is upstream or downstream of the crystal forming section. Figure 20-7 depicts the features of an end-fed commercial column described by McKay et al. [*Chem. Eng. Prog. Symp. Ser.*, no. 25, 55, 163 (1969)] for the separation of xylenes. Crystals of *p*-xylene are formed by indirect cooling of the melt in scraped-surface heat exchangers, and the resultant slurry is introduced into the column at the top. This type of column has no mechanical internals to transport solids and instead relies upon an imposed hydraulic gradient to force the solids through the column into the melting zone. Residue liquid is removed through a filter directly above the melter. A pulse piston in the product discharge improves washing efficiency and column reliability.

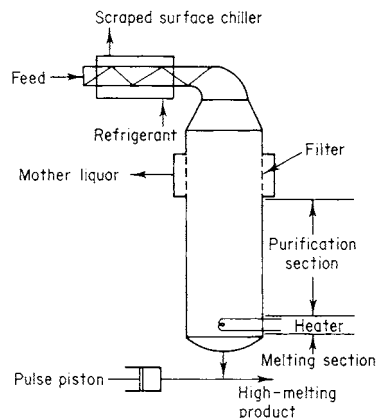


FIG. 20-7 End-fed column crystallizer. (Phillips Petroleum Co.)

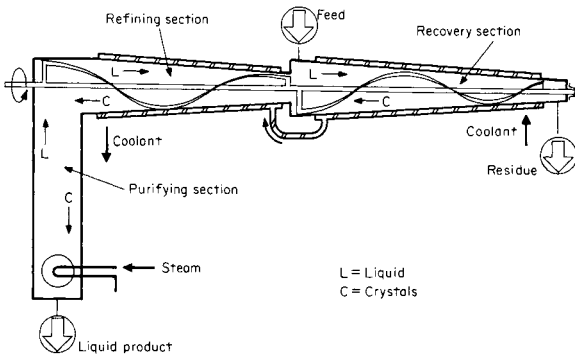


FIG. 20-8 Horizontal center-fed column crystallizer. (The C. W. Nofsinger Co.)

Figure 20-8 shows the features of a horizontal center-fed column [Brodie, *Aust. Mech. Chem. Eng. Trans.*, **37** (May 1979)] which has been commercialized for continuous purification of naphthalene and *p*-dichlorobenzene. Liquid feed enters the column between the hot purifying section and the cold freezing or recovery zone. Crystals are formed internally by indirect cooling of the melt through the walls of the refining and recovery zones. Residue liquid that has been depleted of product exits from the coldest section of the column. A spiral conveyor controls the transport of solids through the unit.

Another center-fed design that has only been used on a preparative scale is the vertical spiral conveyor column reported by Schildknecht [*Angew. Chem.*, **73**, 612 (1961)]. In this device, a version of which is shown on Fig. 20-9, the dispersed-crystal phase is formed in the freezing section and conveyed downward in a controlled manner by a rotating spiral with or without a vertical oscillation.

Differences have been observed in the performance of end- and center-fed column configurations. Consequently, discussions of center- and end-fed column crystallizers are presented separately. The design and operation of both columns are reviewed by Powers (Zief and Wilcox, *op. cit.*, p. 343). A comparison of these devices is shown on Table 20-3.

Center-Fed Column Crystallizers Two types of center-fed column crystallizers are illustrated on Figs. 20-8 and 20-9. As in a simple distillation column, these devices are composed of three distinct sections: a freezing or recovery section, where solute is frozen from the

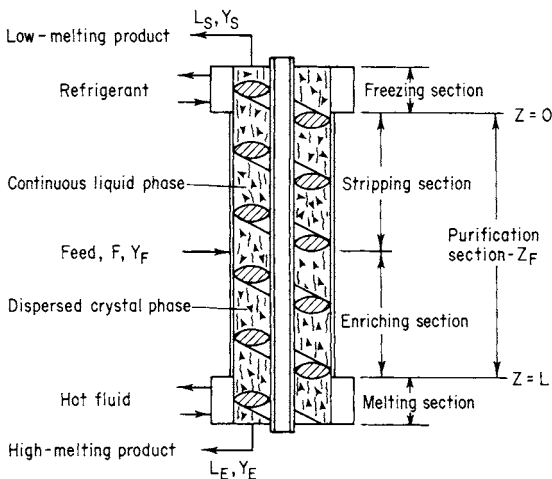


FIG. 20-9 Center-fed column crystallizer with a spiral-type conveyor.

TABLE 20-3 Comparison of Melt-Crystallizer Performance

Center-fed column	End-fed column
Solid phase is formed internally; thus, only liquid streams enter and exit the column.	Solid phase is formed in external equipment and fed as slurry into the purifier.
Internal reflux can be controlled without affecting product yield.	The maximum internal liquid reflux is fixed by the thermodynamic state of the feed relative to the product stream. Excessive reflux will diminish product yield.
Operation can be continuous or batchwise at total reflux.	Total reflux operation is not feasible.
Center-fed columns can be adapted for both eutectic and solid-solution systems.	End-fed columns are inefficient for separation of solid-solution systems.
Either low- or high-porosity-solids-phase concentrations can be formed in the purification and melting zones.	End-fed units are characterized by low-porosity-solids packing in the purification and melting zones.
Scale-up depends on the mechanical complexity of the crystal-transport system and techniques for removing heat. Vertical oscillating spiral columns are likely limited to about 0.2 m in diameter, whereas horizontal columns of several meters are possible.	Scale-up is limited by design of melter and/or crystal-washing section. Vertical or horizontal columns of several meters in diameter are possible.

impure liquor; the purification zone, where countercurrent contacting of solids and liquid occurs; and the crystal-melting and -refluxing section. Feed position separates the refining and recovery portions of the purification zone. The section between feed location and melter is referred to as the refining or enrichment section, whereas the section between feed addition and freezing is called the recovery section. The refining section may have provisions for sidewall cooling. The published literature on column crystallizers connotes stripping and refining in a reverse sense to distillation terminology, since refined product from a melt crystallizer exits at the hot section of the column rather than at the cold end as in a distillation column.

Rate processes that describe the purification mechanisms in a column crystallizer are highly complex since phase transition and heat- and mass-transfer processes occur simultaneously. Nucleation and growth of a crystalline solid phase along with crystal washing and crystal melting are occurring in various zones of the apparatus. Column hydrodynamics are also difficult to describe. Liquid- and solid-phase mixing patterns are influenced by factors such as solids-transport mechanism, column orientation, and, particularly for dilute slurries, the settling characteristics of the solids.

Most investigators have focused their attention on a differential segment of the zone between the feed injection and the crystal melter. Analysis of crystal formation and growth in the recovery section has received scant attention. Table 20-4 summarizes the scope of the literature treatment for center-fed columns for both solid-solution and eutectic forming systems.

The dominant mechanism of purification for column crystallization of solid-solution systems is recrystallization. The rate of mass transfer resulting from recrystallization is related to the concentrations of the solid phase and free liquid which are in intimate contact. A model based on height-of-transfer-unit (HTU) concepts representing the composition profile in the purification section for the high-melting component of a binary solid-solution system has been reported by Powers et al. (in Zief and Wilcox, *op. cit.*, p. 363) for total-reflux operation. Typical data for the purification of a solid-solution system, azobenzene-stilbene, are shown in Fig. 20-10. The column crystallizer was operated at total reflux. The solid line through the data was computed by Powers et al. (*op. cit.*, p. 364) by using an experimental HTU value of 3.3 cm.

TABLE 20-4 Column-Crystallizer Investigations

	Treatments	
	Theoretical	Experimental
Solid solutions		
Total reflux—steady state	1, 2, 4, 6	1, 4, 6
Total reflux—dynamic	2	
Continuous—steady state	1, 4	4, 8, 9
Continuous—dynamic		
Eutectic systems		
Total reflux—steady state	1, 3, 4, 7	1, 3, 6
Total reflux—dynamic		
Continuous—steady state	1, 5, 10, 11, 12	5, 8, 9, 10, 11, 13
Continuous—dynamic		

1. Powers, *Symposium on Zone Melting and Column Crystallization*, Karlsruhe, 1963.

2. Anikin, *Dokl. Akad. Nauk SSSR*, **151**, 1139 (1969).

3. Albertins et al., *Am. Inst. Chem. Eng. J.*, **15**, 554 (1969).

4. Gates et al., *Am. Inst. Chem. Eng. J.*, **16**, 648 (1970).

5. Henry et al., *Am. Inst. Chem. Eng. J.*, **16**, 1055 (1970).

6. Schildknecht et al., *Angew. Chem.*, **73**, 612 (1961).

7. Arkenbout et al., *Sep. Sci.*, **3**, 501 (1968).

8. Betts et al., *Appl. Chem.*, **17**, 180 (1968).

9. McKay et al., *Chem. Eng. Prog. Symp. Ser.*, no. 25, 55, 163 (1959).

10. Bolsaitis, *Chem. Eng. Sci.*, **24**, 1813 (1969).

11. Moyers et al., *Am. Inst. Chem. Eng. J.*, **20**, 1119 (1974).

12. Griffin, M.S. thesis in chemical engineering, University of Delaware, 1975.

13. Brodie, *Aust. Mech. Chem. Eng. Trans.*, **37** (1971).

Most of the analytical treatments of center-fed columns describe the purification mechanism in an adiabatic oscillating spiral column (Fig. 20-9). However, the analyses by Moyers (op. cit.) and Griffin (op. cit.) are for a nonadiabatic dense-bed column. Differential treatment of the horizontal-purifier (Fig. 20-8) performance has not been reported; however, overall material and enthalpy balances have been described by Brodie (op. cit.) and apply equally well to other designs.

A dense-bed center-fed column (Fig. 20-11) having provision for internal crystal formation and variable reflux was tested by Moyers et al. (op. cit.). In the theoretical development (ibid.) a nonadiabatic, plug-flow axial-dispersion model was employed to describe the performance of the entire column. Terms describing interphase transport of impurity between adhering and free liquid are not considered.

A comparison of the axial-dispersion coefficients obtained in oscillating-spiral and dense-bed crystallizers is given in Table 20-5. The dense-bed column approaches axial-dispersion coefficients similar to those of densely packed ice-washing columns.

The concept of minimum reflux as related to column-crystallizer operation is presented by Brodie (op. cit.) and is applicable to all types

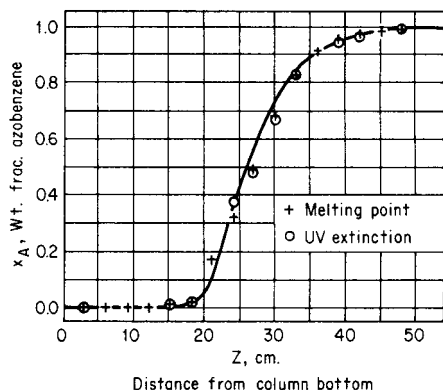


FIG. 20-10 Steady-state separation of azobenzene and stilbene in a center-fed column crystallizer with total-reflux operation. To convert centimeters to inches, multiply by 0.3937. (Zief and Wilcox, *Fractional Solidification*, vol. 1, Marcel Dekker, New York, 1967, p. 356.)

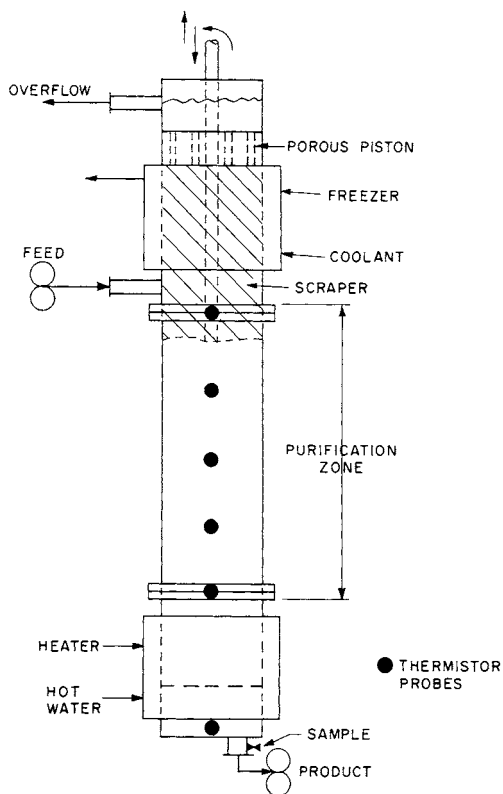


FIG. 20-11 Dense-bed center-fed column crystallizer. [Moyers et al., *Am. Inst. Chem. Eng. J.*, **20**, 1121 (1974).]

of column crystallizers, including end-fed units. In order to stabilize column operation the sensible heat of subcooled solids entering the melting zone should be balanced or exceeded by the heat of fusion of the refluxed melt. The relationship in Eq. (20-8) describes the minimum reflux requirement for proper column operation.

$$R = (T_p - T_F) C_p / \lambda \quad (20-8)$$

R = reflux ratio, g reflux/g product; T_p = product temperature, °C; T_F = saturated-feed temperature, °C; C_p = specific heat of solid crystals, cal/(g·°C); and λ = heat of fusion, cal/g.

All refluxed melt will refreeze if reflux supplied equals that computed by Eq. (20-8). When reflux supplied is greater than the minimum, jacket cooling in the refining zone or additional cooling in the

TABLE 20-5 Comparison of Axial-Dispersion Coefficients for Several Liquid-Solid Contactors

Column type	Dispersion coefficient, cm ² /s	Reference
Center-fed crystallizer (oscillating spiral)	1.6–3.5	1
Center-fed crystallizer (oscillating spiral)	1.3–1.7	2
Counter-current ice-washing column	0.025–0.17	3
Center-fed crystallizer	0.12–0.30	4

References:

1. Albertins et al., *Am. Inst. Chem. Eng. J.*, **15**, 554 (1969).

2. Gates et al., *Am. Inst. Chem. Eng. J.*, **16**, 648 (1970).

3. Ritter, Ph.D. thesis, Massachusetts Institute of Technology, 1969.

4. Moyers et al., *Am. Inst. Chem. Eng. J.*, **20**, 1119 (1974).

recovery zone is required to maintain product recovery. Since high-purity melts are fed near their pure-component freezing temperatures, little refreezing takes place unless jacket cooling is added.

To utilize a column-crystallizer design or rating model, a large number of parameters must be identified. Many of these are empirical in nature and must be determined experimentally in equipment identical to the specific device being evaluated. Hence macroscopic evaluation of systems by large-scale piloting is the rule rather than the exception. Included in this rather long list of critical parameters are factors such as impurity level trapped in the solid phase, product quality as a function of reflux ratio, degree of liquid and solids axial mixing in the equipment as a function of solids-conveyor design, size and shape of crystals produced, and ease of solids handling in the column. Heat is normally removed through metal surfaces; thus, the stability of the solution to subcooling can also be a major factor in design.

End-Fed Column Crystallizer End-fed columns were developed and successfully commercialized by the Phillips Petroleum Company in the 1950s. The sections of a typical end-fed column, often referred to as a Phillips column, are shown on Fig. 20-7. Impure liquor is removed through filters located between the product-freezing zone and the melter rather than at the end of the freezing zone, as occurs in center-fed units. The purification mechanism for end-fed units is basically the same as for center-fed devices. However, there are reflux restrictions in an end-fed column, and a high degree of solids compaction exists near the melter of an end-fed device. It has been observed that the free-liquid composition and the fraction of solids are relatively constant throughout most of the purification section but exhibit a sharp discontinuity near the melting section [McKay et al., *Ind. Eng. Chem.*, **52**, 197 (1969)]. Investigators of end-fed column behavior are listed in Table 20-6. Note that end-fed columns are adaptable only for eutectic-system purification and cannot be operated at total reflux.

Performance information for the purification of *p*-xylene indicates that nearly 100 percent of the crystals in the feed stream are removed as product. This suggests that the liquid which is refluxed from the melting section is effectively refrozen by the countercurrent stream of sub-cooled crystals. A high-melting product of 99.0 to 99.8 weight percent *p*-xylene has been obtained from a 65 weight percent *p*-xylene feed. The major impurity was *m*-xylene. Figure 20-12 illustrates the column-cross-section-area-capacity relationship for various product purities.

Column crystallizers of the end-fed type can be used for purification of many eutectic-type systems and for aqueous as well as organic systems (McKay, loc. cit.). Column crystallizers have been used for xylene isomer separation, but recently other separation technologies including more efficient melt crystallization equipment have tended to supplant the Phillips style crystallizer.

Commercial Equipment and Applications In the last two decades the practice of melt crystallization techniques for purification of certain organic materials has made significant commercial progress. The concept of refining certain products by countercurrent staging of crystallization in a column has completed the transition from laboratory and pilot equipment to large-scale industrial configurations. Chemicals which have been purified by suspension crystallization-purifier column techniques are listed on Table 20-7. The practice of crystal formation and growth from the bulk liquid (as is practiced in suspension crystallization techniques described in Sec. 18 of this handbook) and subsequent crystal melting and refluxing in a purifier

TABLE 20-6 End-Fed-Crystallizer Investigations

Eutectic systems	Treatments	
	Theoretical	Experimental
Continuous—steady state	1, 2, 4	1, 4
Batch	3	3

1. McKay et al., *Ind. Eng. Chem. Process Des. Dev.*, **6**, 16 (1967).
2. Player, *Ind. Eng. Chem. Process Des. Dev.*, **8**, 210 (1969).
3. Yagi et al., *Kagaku Kogaku*, **72**, 415 (1963).
4. Shen and Meyer, Prepr. 19F, AIChE Symp., Chicago, 1970.

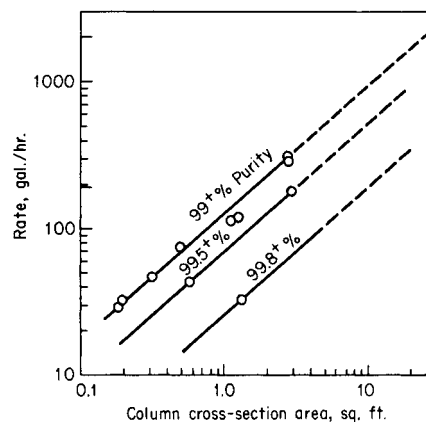


FIG. 20-12 Pulsed-column capacity versus column size for 65 percent *p*-xylene feed. To convert gallons per hour to cubic meters per hour, multiply by 0.9396; to convert square feet to square meters, multiply by 0.0929. (McKay et al., *prepr.*, 59th nat. meet. AIChE, East Columbus, Ohio.)

column has evolved into two slightly different concepts: (1) the horizontal continuous crystallization technique with vertical purifier invented by Brodie (op. cit.) and (2) the continuous multistage or stepwise system with vertical purifier developed by Tsukishima Kikai Co., Ltd. (TSK). A recent description of these processes has been published by Meyer [*Chem. Proc.*, **53**, 50 (1990)].

The horizontal continuous Brodie melt crystallizer is basically an indirectly cooled crystallizer with an internal ribbon conveyor to transport crystals countercurrent to the liquid and a vertical purifier for final refining. Figure 20-8 describes the operation of a single tube unit and Fig. 20-13 depicts a multitube unit. The multitube design has been successfully commercialized for a number of organic chemicals. The Brodie purifier configuration requires careful control of process and equipment temperature differences to eliminate internal encrustations and is limited by the inherent equipment geometry to capacities of less than 15,000 tons per year per module.

In the multistage process described on Fig. 20-14 feed enters one of several crystallizers installed in series. Crystals formed in each crystallizer are transferred to a hotter stage and the liquid collected in the clarified zone of the crystallizer is transferred to a colder stage and eventually discharged as residue. At the hot end, crystals are transferred to a vertical purifier where countercurrent washing is performed by pure, hot-product reflux. TSK refers to this multistage process as the countercurrent cooling crystallization (CCCC) process. In

TABLE 20-7 Chemicals Purified by TSK CCCC Process (The C. W. Nofsinger Co.)

Acetic acid	Isophthaloyl chloride
Acrylic acid	Isopregol
Adipic acid	Lutidine
Benzene	Maleic anhydride
Biphenyl	Naphthalene
Bisphenol-A	<i>p</i> -Nitrochloro benzene
Caprolactam	<i>p</i> -Nitrotoluene
Chloroacetic acid	Phenol
<i>p</i> -Chloro toluene	<i>b</i> -Picoline
<i>p</i> -Cresol	<i>g</i> -Picoline
Combat (proprietary)	Pyridine
Dibutyl hydroxy toluene (BHT)	Stilbene
<i>p</i> -Dichloro benzene	Terephthaloyl chloride
2,5 Dichlorophenol	Tertiary butyl phenol
Dicumyl peroxide	Toluene diisocyanate
Diene	Trioxane
Heliotropin	<i>p</i> -Xylene
Hexachloro cyclo butene	3,4 Xylidine
Hexamethylene diamine	

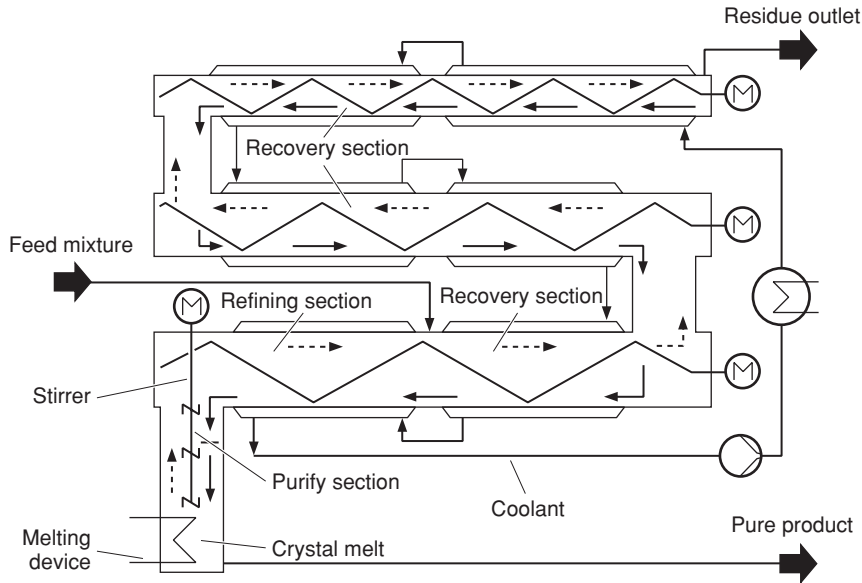


FIG. 20-13 Horizontal continuous Brodie melt crystallizer—multitube unit. (The C. W. Nofisinger Co.)

principle any suitable type of crystallizer can be used in the stages as long as the crystals formed can be separated from the crystallizer liquid and settled and melted in the purifier.

Commercial applications for both the Brodie and CCCC process are indicated on Table 20-8. Both the Brodie Purifier and the CCCC processes are available from The C. W. Nofisinger Company, PO Box 419173, Kansas City, MO 64141-0173.

FALLING-FILM CRYSTALLIZATION

Falling-film crystallization utilizes progressive freezing principles to purify melts and solutions. The technique established to practice the process is inherently cyclic. Figure 20-15 depicts the basic working concept. First a crystalline layer is formed by subcooling a liquid film on a vertical surface inside a tube. This coating is then

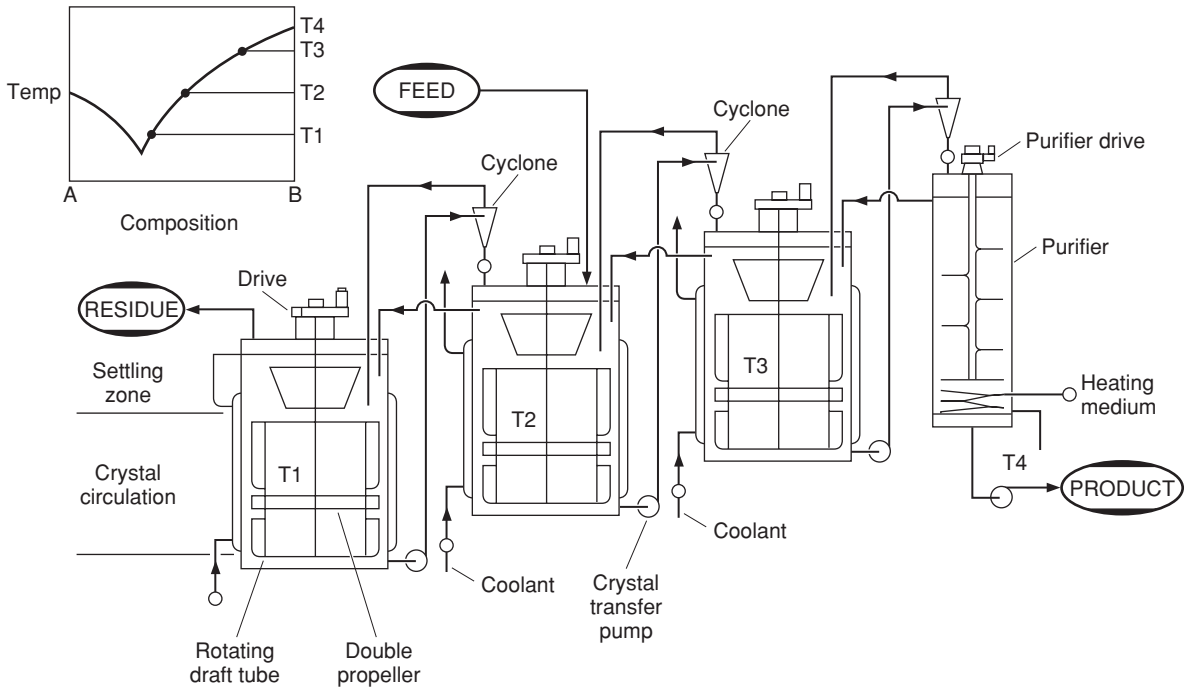


FIG. 20-14 Crystallizer—multistage process. (The C. W. Nofisinger Co.)

TABLE 20-8 Commercial TSK Crystallization Operating Plants

	Capacity MM lb/yr	Company	Date & location
Countercurrent Cooling Crystallization (CCCC) Process			
Nofsinger license			
Nofsinger design & construct			
<i>p</i> -Dichlorobenzene	Confidential	Monsanto Co.	1989—Sauget, IL
TSK license			
TSK design & construct			
Confidential ¹	Confidential	Confidential	1988—Japan
<i>p</i> -Xylene	137	MGC	1986—Mizushima, Japan
Confidential ²	Confidential	Confidential	1985—Japan
<i>p</i> -Xylene	132	MGC	1983—Mizushima, Japan
<i>p</i> -Xylene	expanded to 160		1984—Japan
<i>p</i> -Xylene	26.5	MGC	1981—Mizushima, Japan
Brodie			
TSK license			
TSK design & construct			
Naphthalene	8	SHSM	1985—China
<i>p</i> -DCB	13	Hodogaya	1981—Japan
<i>p</i> -DCB	5.5	Sumitomo	1978—Japan
UCAL license & design			
TSK hardware			
Naphthalene	16	Nippon Steel	1974—Japan
<i>p</i> -DCB	13	Hodogaya	1974—Japan
UCAL license & design			
Naphthalene	10	British Tar	1972—U.K.
<i>p</i> -DCB	3	UCAL	1969—Australia

ABBREVIATIONS:

Nofsinger	The C. W. Nofsinger Company
TSK	Tsukishima Kikai Co., Ltd.
SHSM	Shanghai Hozan Steel Mill
UCAL	Union Carbide Australia, Ltd.
MGC	Mitsubishi Gas Chemical Co., co-developer with TSK of the application for <i>p</i> -Xylene

1. Commercial scale plant started up in the spring of 1988 purifying a bulk chemical. This is the first application of the CCCC process on this bulk chemical.

2. This small unit is operating in Japan with an 800-mm crystallizer and 300-mm purifier. Because of confidentiality, we cannot disclose the company, capacity, or product.

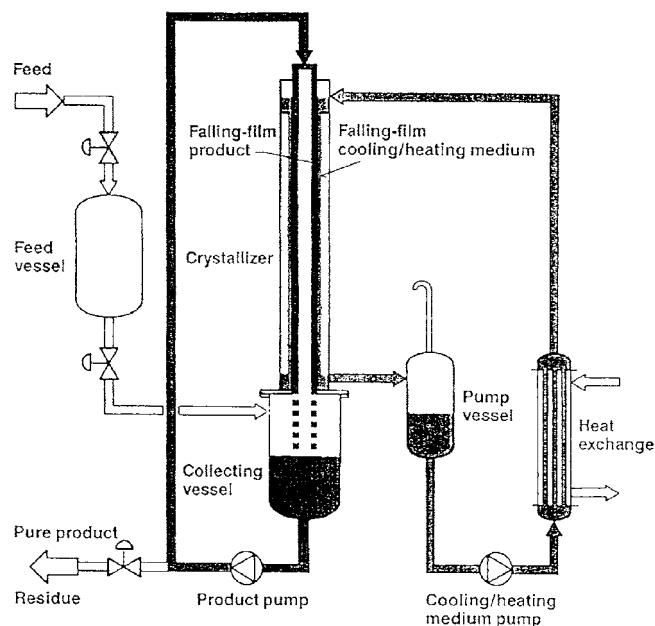


FIG. 20-15 Dynamic crystallization system. (Sulzer Chemtech.)

20-12 ALTERNATIVE SEPARATION PROCESSES

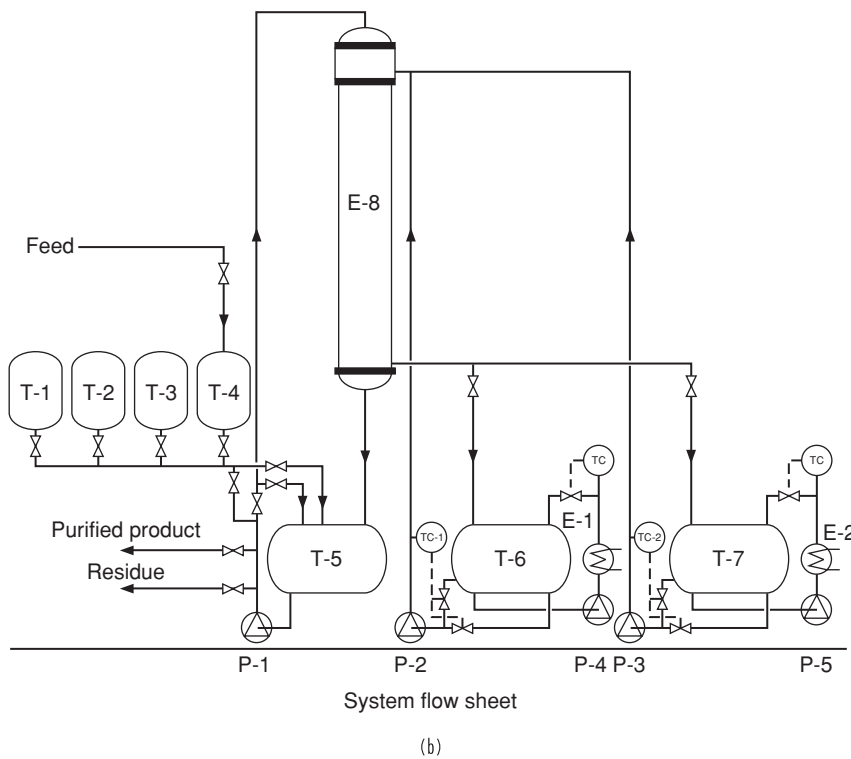
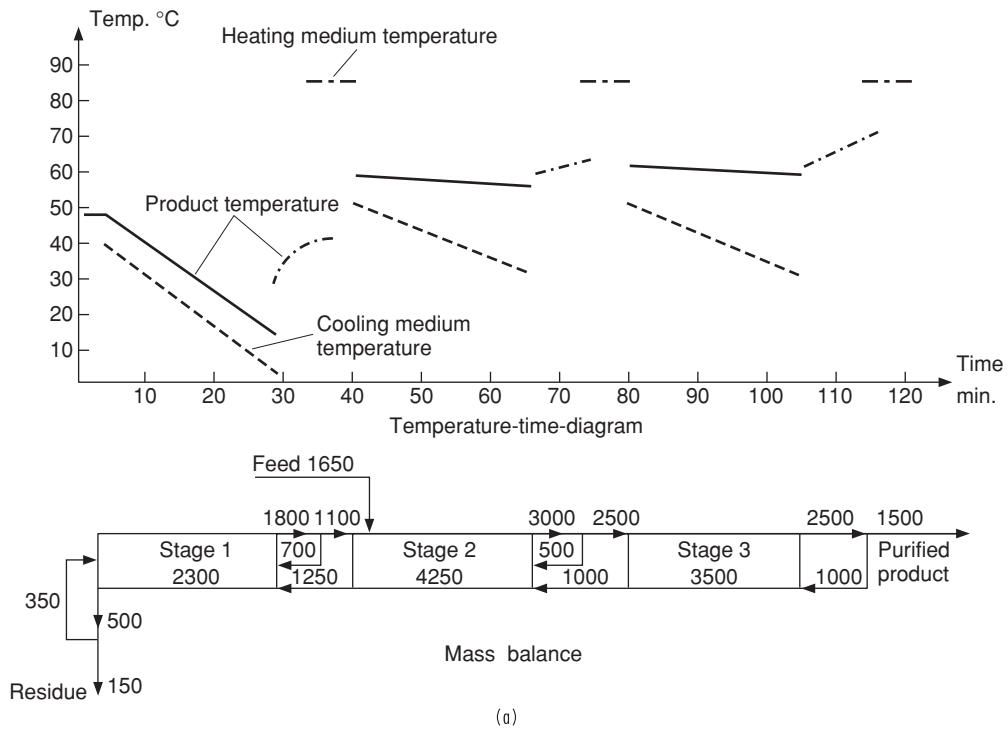


FIG. 20-16 Sulzer MWB-crystallization process. (a) Stepwise operation of the process. (b) System flow sheet. (Sulzer Chemtech.)

grown by extracting heat from a falling film of melt (or solution) through a heat transfer surface. Impure liquid is then drained from the crystal layer and the product is reclaimed by melting. Variants of this technique have been perfected and are used commercially for many types of organic materials. Both static and falling-film techniques have been described by Wynn [*Chem. Eng. Progr.*, (1992)]. Mathematical models for both static and dynamic operations have been presented by Gilbert [*AIChE J.*, **37**, 1205 (1991)].

Principles of Operation Figure 20-16 describes a typical three-stage falling-film crystallization process for purification of MCA (monochloro acetic acid). Crystallizer E-8 consists of a number of vertical tubular elements working in parallel enclosed in a shell. Normal tube length is 12 meters with a 50- to 75-millimeter tube inside diameter. Feed enters stage two of the sequential operation, is added to the kettle (T-5), and is then circulated to the top of the crystallizer and distributed as a falling film inside the tubes. Nucleation is induced at the inside walls and a crystal layer starts to grow. Temperature of the coolant is progressively lowered to compensate for reduced heat transfer and lower melt freezing point

until the thickness inside the tube is between 5 and 20 millimeters depending on the product. Kettle liquid is evacuated to the first-stage holding tank (T-3) for eventual recrystallization at a lower temperature to maximize product yield and to strip product from the final liquid residue. Semirefined product frozen to the inside of the tube during operation of stage two is first heated above its melting point and slightly melted (sweated). This semipurified melted material (sweat) is removed from the crystallizer kettle, stored in a stage tank (T-4), and then added to the next batch of fresh feed. The remaining material inside the crystallizer is then melted, mixed with product sweat from stage three, recrystallized, and sweated to upgrade the purity even further (stage 3).

Commercial Equipment and Applications The falling-film crystallization process was invented by the MWB company in Switzerland. The process is now marketed by Sulzer Chemtech. Products successfully processed in the falling-film crystallizer are listed on Table 20-9. The falling-film crystallization process is available from the Chemtech Div. of Sulzer Canada Inc., 60 Worcester Rd., Rexdale, Ontario N9W 5X2 Canada.

TABLE 20-9 Fractional Crystallization Reference List

Product	Main characteristics	Capacity, tons/year	Purity	Type of plant	Country	Client
Acrylic acid	Very low aldehyde content, no undesired polymerization in the plant	Undisclosed Undisclosed	99.95% 99.9%	Falling film Falling film	Undisclosed Undisclosed	Undisclosed Undisclosed
Benzoic acid	Pharmaceutical grade, odor- and color free	4,500	99.97%	Falling film	Italy	Chimica del Friuli
Bisphenol A	Polycarbonate grade, no solvent required	150,000	Undisclosed	Falling film	USA	General Electric
Carbonic acid		1,200	Undisclosed	Falling film	Germany	Undisclosed
Fatty acid	Separation of tallow fatty acid into saturated and unsaturated fractions	20,000	Stearic acid: Iodine no. 2 Oleic acid: Cloud pt 5°C	Falling film	Japan	Undisclosed
Fine chemicals		<1,000 <1,000 <1,000 <1,000 <1,000 <1,000	Undisclosed Undisclosed Undisclosed Undisclosed Undisclosed Undisclosed	Falling film Static Falling film Falling film Falling film Falling film	GUS Switzerland Switzerland Switzerland USA Germany Japan	Undisclosed Undisclosed Undisclosed Undisclosed Undisclosed Undisclosed Undisclosed
Hydrazine	Satellite grade	3	>99.9%	Falling film	Germany	ESA
Monochloro acetic acid (MCA)	Low DCA content	6,000	>99.2%	Falling film	USA	Undisclosed
Multipurpose	Separation or purification of two or more chemicals, alternatively	1,000 1,000	Various grades Undisclosed	Falling film Falling film	Belgium Belgium	UCB Reibelco
Naphthalene	Color free and color stable with low thionaphthene content	60,000 20,000 10,000 12,000	99.5% 99.5% 99.8% Various grades	Falling film Falling film/static Falling film/static Falling film	Germany P.R. China P.R. China The Netherlands	Rütgers-Werke Anshan Jining Cindu Chemicals
<i>p</i> -Dichlorobenzene	No solvent washing required	40,000 5,000 4,000 3,000 3,000	99.95% 99.98% 99.8% 99.95% >97%	Falling film Falling film Falling film/distillation Falling film Static	USA Japan Brazil P.R. China P.R. China	Standard Chlorine Toa Gosei Nitroclor Fuyang Shandong
<i>p</i> -Nitrochlorobenzene		18,000 10,000	99.3% 99.5%	Falling film/distillation Static	P.R. China India	Jilin Chemical Mardia
Toluene diisocyanate (TDI)	Separation of TDI 80 into TDI 100 & TDI 65	20,000	Undisclosed	Falling film	Undisclosed	Undisclosed
Trioxan		<1,000	99.97%	Falling film	Undisclosed	Undisclosed

SUPERCRITICAL FLUID SEPARATION PROCESSES

GENERAL REFERENCES: Yeo and Kiran, *J. Supercritical Fluids*, **34**, 287–308 (2005). York, Kompella, and Shekumov, *Supercritical Fluid Technology for Drug Product Development*, Marcel Dekker, New York, 2004. Shah, Hanrath, Johnston, and Korgel, *J. Physical Chemistry B*, **108**, 9574–9587 (2004). Eckert, Liotta, Bush, Brown, and Hallett, *J. Physical Chemistry B*, **108**, 18108–18118 (2004). DeSimone, *Science*, **297**, 799–803 (2002). Arai, Sako, and Takebayashi, *Supercritical Fluids: Molecular Interactions, Physical Properties, and New Applications*, Springer, New York, 2002. Kiran, Debenedetti, and Peters, *Supercritical Fluids: Fundamentals and Applications*, Kluwer Academic, Dordrecht, 2000. McHugh and Krukonic, *Supercritical Fluid Extraction Principles and Practice*, 2d ed., Butterworth, Stoneham, Mass., 1994. Brunner, *Gas Extraction: An Introduction to Fundamentals of Supercritical Fluids and the Application to Separation Processes*, Springer, New York, 1994. Gupta and Shim, *Solubility in Supercritical Carbon Dioxide*, CRC Press, Boca Raton, Fla., 2007. Gupta and Kompella, *Nanoparticle Technology for Drug Delivery*, Taylor & Francis, New York, 2006.

INTRODUCTION

Fluids above their critical temperatures and pressures, called supercritical fluids (SCFs), exhibit properties intermediate between those of gases and liquids. Consequently, each of these two boundary conditions sheds insight into the nature of these fluids. Unlike gases, SCFs possess a considerable solvent strength, and transport properties are more favorable. In regions where a SCF is highly compressible, its density and hence its solvent strength may be adjusted over a wide range with modest variations in temperature and pressure. This tunability may be used to control phase behavior, separation processes (e.g., SCF extraction), rates and selectivities of chemical reactions, and morphologies in materials processing. For SCF separation processes to be feasible, the advantages (Table 20-10) must compensate for the costs of high pressure; examples of commercial applications are listed in Table 20-11.

The two SCFs most often studied—CO₂ and water—are the two least expensive of all solvents. CO₂ is nontoxic and nonflammable and has a near-ambient critical temperature of 31.1°C. CO₂ is an environmentally friendly substitute for organic solvents including chlorocarbons and chlorofluorocarbons. Supercritical water ($T_c = 374^\circ\text{C}$) is of interest as a substitute for organic solvents to minimize waste in extraction and reaction processes. Additionally, it is used for hydrothermal oxidation of hazardous organic wastes (also called supercritical water oxidation) and hydrothermal synthesis. (See also Sec. 15 for additional discussion of supercritical fluid separation processes.)

PHYSICAL PROPERTIES OF PURE SUPERCRITICAL FLUIDS

Thermodynamic Properties The variation in solvent strength of a SCF from gaslike to liquidlike values (see Table 20-12) may be described qualitatively in terms of the density ρ , as shown in Fig. 20-17, or the solubility parameter.

Similar characteristics are observed for other density-dependent variables including enthalpy, entropy, viscosity, and diffusion coefficient. Above the critical temperature, it is possible to tune the solvent

TABLE 20-10 Advantages of Supercritical Fluid Separations

Solvent strength is adjustable to tailor selectivities and yields.
 Diffusion coefficients are higher and viscosities lower, compared with liquids.
 Low surface tension favors wetting and penetration of small pores.
 There is rapid diffusion of CO₂ through condensed phases, e.g., polymers and ionic liquids.
 Solvent recovery is fast and complete, with minimal residue in product.
 Collapse of structure due to capillary forces is prevented during solvent removal.
 Properties of CO₂ as a solvent:
 Environmentally acceptable solvent for waste minimization, nontoxic, nonflammable, inexpensive, usable at mild temperatures.
 Properties of water as a solvent:
 Nontoxic, nonflammable, inexpensive substitute for organic solvents.
 Extremely wide variation in solvent strength with temperature and pressure.

TABLE 20-11 Commercial Applications of Supercritical Fluid Separations Technology

Extraction of foods and pharmaceuticals
 Caffeine from coffee and tea
 Flavors, cholesterol, and fat from foods
 Nicotine from tobacco
 Solvents from pharmaceutical compounds and drugs from natural sources
 Extraction of volatile substances from substrates
 Drying and aerogel formation
 Cleaning fabrics, quartz rods for light guide fibers, residues in microelectronics
 Removal of monomers, oligomers, and solvent from polymers
 Fractionation
 Residuum oil supercritical extraction (ROSE) (petroleum deasphalting)
 Polymer and edible oils fractionation
 CO₂ enhanced oil recovery
 Analytical SCF extraction and chromatography
 Infusion of materials into polymers (dyes, pharmaceuticals)
 Reactive separations
 Extraction of *sec*-butanol from isobutene
 Polymerization to form Teflon
 Depolymerization, e.g., polyethylene terephthalate and cellulose hydrolysis
 Hydrothermal oxidation of organic wastes in water
 Crystallization, particle formation, and coatings
 Antisolvent crystallization, rapid expansion from supercritical fluid solution (RESS)
 Particles from gas saturated solutions
 Crystallization by reaction to form metals, semiconductors (e.g., Si), and metal oxides including nanocrystals
 Supercritical fluid deposition

TABLE 20-12 Physical Properties of a Supercritical Fluid Fall between Those of a Typical Gas and Liquid

	Liquid	Supercritical fluid	Gas
Density, g/mL	1	0.05 – 1	10 ⁻³
Viscosity, Pa·s	10 ⁻³	10 ⁻⁴ – 10 ⁻⁵	10 ⁻⁵
Diffusion coefficients, cm ² /s	10 ⁻⁵	10 ⁻³	10 ⁻¹
Surface tension, mN/m	20–50	0	0

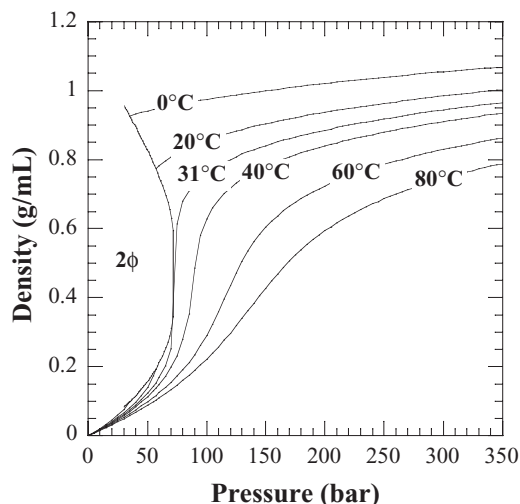


FIG. 20-17 Density versus pressure and temperature for CO₂. ($T_c = 31.1^\circ\text{C}$, $P_c = 73.8$ bar.)

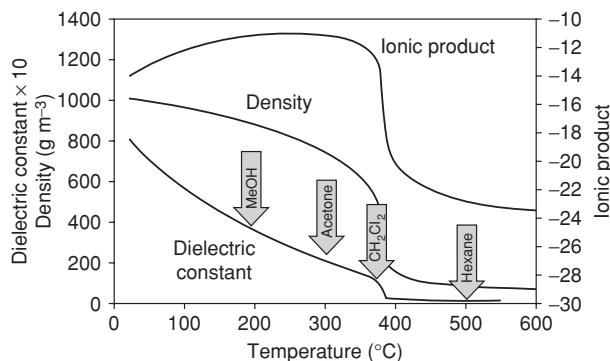


FIG. 20-18 Physical properties of water versus temperature at 240 bar. [Reprinted from Kritzer and Dinjus, "An Assessment of Supercritical Water Oxidation (SCWO): Existing Problems, Possible Solutions and New Reactor Concepts," Chem. Eng. J., vol. 83(3), pp. 207–214, copyright 2001, with permission from Elsevier.]

strength continuously over a wide range with either a small isothermal pressure change or a small isobaric temperature change. This unique ability to tune the solvent strength of a SCF may be used to extract and then recover selected products. A good indicator of the van der Waals forces contributed by a SCF is obtained by multiplying ρ by the molecular polarizability α , which is a constant for a given molecule. CO_2 's small $\alpha\rho$ and low solvent strength are more like those of a fluorocarbon than those of a hydrocarbon.

Water, a key SCF, undergoes profound changes upon heating to the critical point. It expands by a factor of 3, losing about two-thirds of the hydrogen bonds, the dielectric constant drops from 80 to 5 (Shaw et al., op. cit.), and the ionic product falls several orders of magnitude (see Fig. 20-18). At lower densities, supercritical water (SCW) behaves as a "nonaqueous" solvent, and it dissolves many organics and even gases such as O_2 . Here it does not solvate ions significantly.

Transport Properties Although the densities of SCFs can approach those of conventional liquids, transport properties are more favorable because viscosities remain lower and diffusion coefficients remain higher. Furthermore, CO_2 diffuses through condensed-liquid phases (e.g., adsorbents and polymers) faster than do typical solvents which have larger molecular sizes. For example, at 35°C the estimated pyrene diffusion coefficient in polymethylmethacrylate increases by 4 orders of magnitude when the CO_2 content is increased from 8 to 17 wt % with pressure [Cao, Johnston, and Webber, *Macromolecules*, 38(4), 1335–1340 (2005)].

PHASE EQUILIBRIA

Liquid-Fluid Equilibria Nearly all binary liquid-liquid phase diagrams can be conveniently placed in one of six classes (Prausnitz, Lichtenthaler, and de Azevedo, *Molecular Thermodynamics of Fluid Phase Equilibria*, 3d ed., Prentice-Hall, Upper Saddle River, N.J., 1998). Two-phase regions are represented by an area and three-phase regions by a line. In class I, the two components are completely miscible, and a single critical mixture curve connects their critical points. Other classes may include intersections between three phase lines and critical curves. For a ternary system, the slopes of the tie lines (distribution coefficients) and the size of the two-phase region can vary significantly with pressure as well as temperature due to the compressibility of the solvent.

Solid-Fluid Equilibria The solubility of the solid is very sensitive to pressure and temperature in compressible regions, where the solvent's density and solubility parameter are highly variable. In contrast, plots of the log of the solubility versus density at constant temperature often exhibit fairly simple linear behavior (Fig. 20-19). To understand the role of solute-solvent interactions on solubilities and selectivities, it is instructive to define an enhancement factor E as the actual solubility y_2 divided by the solubility in an ideal gas, so that $E = y_2 P_2^{\text{sat}} / P_2^{\text{sat}}$, where P_2^{sat} is the vapor pressure. The solubilities in CO_2 are governed primarily by vapor pressures, a property of the solid

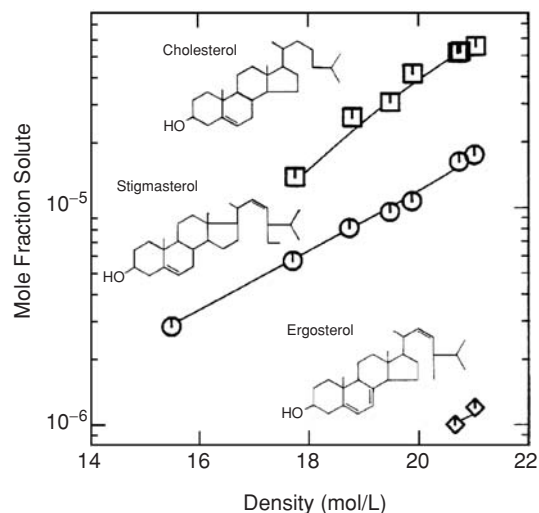


FIG. 20-19 Solubility of sterols in pure CO_2 at 35°C [Wong and Johnston, *Biotech. Prog.*, 2, 29 (1986)].

crystals, and only secondarily by solute-solvent interactions in the SCF phase. For example, for a given fluid at a particular T and P , the E 's are similar for the three sterols, each containing one hydroxyl group, even though the actual solubilities vary by many orders of magnitude (Fig. 20-19).

Polymer-Fluid Equilibria and the Glass Transition Most polymers are insoluble in CO_2 , yet CO_2 can be quite soluble in the polymer-rich phase. The solubility in CO_2 may be increased by a combination of lowering the cohesive energy density (which is proportional to the surface tension of the polymer [O'Neill et al., *Ind. Eng. Chem. Res.*, 37, 3067–79 (1998)]), branching, and the incorporation of either acetate groups in the side chain or carbonate groups in the backbone of the polymer [Sarbu, Styranec, and Beckman, *Nature*, 405, 165–168 (2000)]. Polyfluoromethacrylates are extremely soluble, and functionalized polyethers and copolymers of cyclic ethers and CO_2 have been shown to be more soluble than most other nonfluorinated polymers. The sorption of CO_2 into silicone rubber is highly dependent upon temperature and pressure, since these properties have a large effect on the density and activity of CO_2 . For glassy polymers, sorption isotherms are more complex, and hysteresis between the pressurization and depressurization steps may appear. Furthermore, CO_2 can act as a plasticizer and depress the glass transition temperature by as much as 100°C or even more, producing large changes in mechanical properties and diffusion coefficients. This phenomenon is of interest in conditioning membranes for separations and in commercial foaming of polymers to reduce VOC emissions.

Cosolvents and Complexing Agents Many nonvolatile polar substances cannot be dissolved at moderate temperatures in nonpolar fluids such as CO_2 . Cosolvents (also called entrainers) such as alcohols and acetone have been added to fluids to raise the solvent strength for organic solutes and even metals. The addition of only 2 mol % of the complexing agent tri-*n*-butyl phosphate (TBP) to CO_2 increases the solubility of hydroquinone by a factor of 250 due to Lewis acid-base interactions.

Surfactants and Colloids in Supercritical Fluids Because very few nonvolatile molecules are soluble in CO_2 , many types of hydrophilic or lipophilic species may be dispersed in the form of polymer latexes (e.g., polystyrene), microemulsions, macroemulsions, and inorganic suspensions of metals and metal oxides (Shah et al., op. cit.). The environmentally benign, nontoxic, and nonflammable fluids water and CO_2 are the two most abundant and inexpensive solvents on earth. Fluorocarbon and hydrocarbon-based surfactants have been used to form reverse micelles, water-in- CO_2

microemulsions (2- to 10-nm droplets) and macroemulsions (50-nm to 5- μm droplets) in SCFs including CO_2 . These organized molecular assemblies extend SCF technology to include nonvolatile hydrophilic solutes and ionic species such as amino acids and even proteins. Surfactant micelles or microemulsions are used commercially in dry cleaning and have been proposed for applications including polymerization, formation of inorganic and pharmaceutical particles, and removal of etch/ash residues from low- k dielectrics used in microelectronics. CO_2 -in-water macroemulsions, stabilized by surfactants with the proper hydrophilic- CO_2 -philic balance, are used in enhanced oil recovery to raise the viscosity of the flowing CO_2 phase for mobility control. Alkane ligands with various head groups have been used to stabilize inorganic nanocrystals in SCW and to stabilize Si and Ge nanocrystals in SCF hydrocarbons and CO_2 at temperatures from 350 to 500°C. Furthermore, colloids may be stabilized by electrostatic stabilization in CO_2 [Smith, Ryoo, and Johnston, *J. Phys. Chem. B.*, **109**(43), 20155 (2005)].

Phase Equilibria Models Two approaches are available for modeling the fugacity of a solute in a SCF solution. The compressed gas approach includes a fugacity coefficient which goes to unity for an ideal gas. The expanded liquid approach is given as

$$f_i^L = x_i \gamma_i(P^\circ, x_i) f_i^{\text{ol}}(P^\circ) \exp\left(\int_{P^\circ}^P \frac{\bar{v}_i}{RT} dP\right) \quad (20-9)$$

where x_i is the mole fraction, γ_i is the activity coefficient, P° and f_i° are the reference pressure and fugacity, respectively, and \bar{v}_i is the partial molar volume of component i . A variety of equations of state have been applied in each approach, ranging from simple cubic equations such as the Peng-Robinson equation of state to the more complex statistical associating fluid theory (SAFT) (Prausnitz et al., op. cit.). SAFT is successful in describing how changes in H bonding of SCF water influence thermodynamic and spectroscopic properties.

MASS TRANSFER

Experimental gas-solid mass-transfer data have been obtained for naphthalene in CO_2 to develop correlations for mass-transfer coefficients [Lim, Holder, and Shah, *Am. Chem. Soc. Symp. Ser.*, **406**, 379 (1989)]. The mass-transfer coefficient increases dramatically near the critical point, goes through a maximum, and then decreases gradually. The strong natural convection at SCF conditions leads to higher mass-transfer rates than in liquid solvents. A comprehensive mass-transfer model has been developed for SCF extraction from an aqueous phase to CO_2 in countercurrent columns [Seibert and Moosberg, *Sep. Sci. Technol.*, **23**, 2049 (1988); Brunner, op. cit.].

PROCESS CONCEPTS IN SUPERCRITICAL FLUID EXTRACTION

Figure 20-20 shows a one-stage extraction process that utilizes the adjustability of the solvent strength with pressure or temperature. The solvent flows through the extraction chamber at a relatively high pressure to extract the components of interest from the feed. The products are then recovered in the separator by depressurization, and the solvent is recompressed and recycled. The products can also be precipitated from the extract phase by raising the temperature after the extraction to lower the solvent density. Multiple extractions or multiple stages may be used with various profiles, e.g., successive increases in pressure or decreases in pressure. Solids may be processed continuously or semicontinuously by pumping slurries or by using lock hoppers. For liquid feeds, multi-stage separation may be achieved by continuous countercurrent extraction, such as in conventional liquid-liquid extraction. In SCF chromatography, selectivity may be tuned with pressure and temperature programming, with greater numbers of theoretical stages than in liquid chromatography and lower temperatures than in gas chromatography.

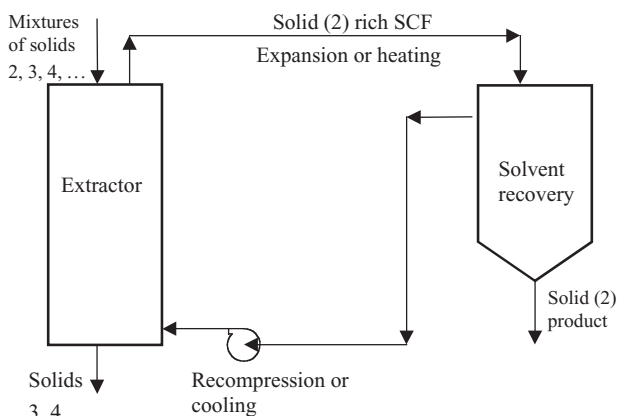


FIG. 20-20 Idealized diagram of a supercritical fluid extraction process for solids.

APPLICATIONS

Decaffeination of Coffee and Tea This application is driven by the environmental acceptability and nontoxicity of CO_2 as well as by the ability to tailor the extraction with the adjustable solvent strength. It has been practiced industrially for more than two decades. Caffeine may be extracted from green coffee beans, and the aroma is developed later by roasting. Various methods have been proposed for recovery of the caffeine, including washing with water and adsorption.

Extraction of Flavors, Fragrances, Nutraceuticals, and Pharmaceuticals Flavors and fragrances extracted by using supercritical CO_2 are significantly different from those extracted by using steam distillation or solvent extraction. The SCF extract can almost be viewed as a new product due to changes in composition associated with the greater amounts of extraction, as shown in Table 20-13. In many instances the flavor or fragrance of the extract obtained with CO_2 is closer to the natural one relative to steam distillation.

Temperature-Controlled Residuum Oil Supercritical Extraction (ROSE) The Kerr-McGee ROSE process has been used worldwide for over two decades to remove asphaltenes from oil. The extraction step uses a liquid solvent that is recovered at supercritical conditions to save energy, as shown in Fig. 20-21. The residuum is contacted with butane or pentane to precipitate the heavy asphaltene fraction. The extract is then passed through a series of heaters, where it goes from the liquid state to a lower-density SCF state. Because the entire process is carried out at conditions near the critical point, a relatively small temperature change is required to produce a fairly large density change. After the light oils have been removed, the solvent is cooled back to the liquid state and recycled.

Polymer Devolatilization, Fractionation, and Plasticization Supercritical fluids may be used to extract solvent, monomers, and oligomers from polymers, including biomaterials. After extraction the pressure is reduced to atmospheric, leaving little residue in the

TABLE 20-13 Comparison of Percent Yields of Flavors and Fragrances from Various Natural Products*

Natural substance	Steam distillation (% yield)	Supercritical CO_2 (% yield)
Ginger	1.5–3.0	4.6
Garlic	0.06–0.4	4.6
Pepper	1.0–2.6	8–18
Rosemary	0.5–1.1	7.5

* Mukhopadhyay, *Natural Extracts Using Supercritical Carbon Dioxide*, CRC Press, Boca Raton, Fla., 2000; Moyler, Extraction of flavours and fragrances with compressed CO_2 , in *Extraction of Natural Products Using Near-Critical Solvents*, King and Bott (eds.), Blackie Academic & Professional, London, 1993.

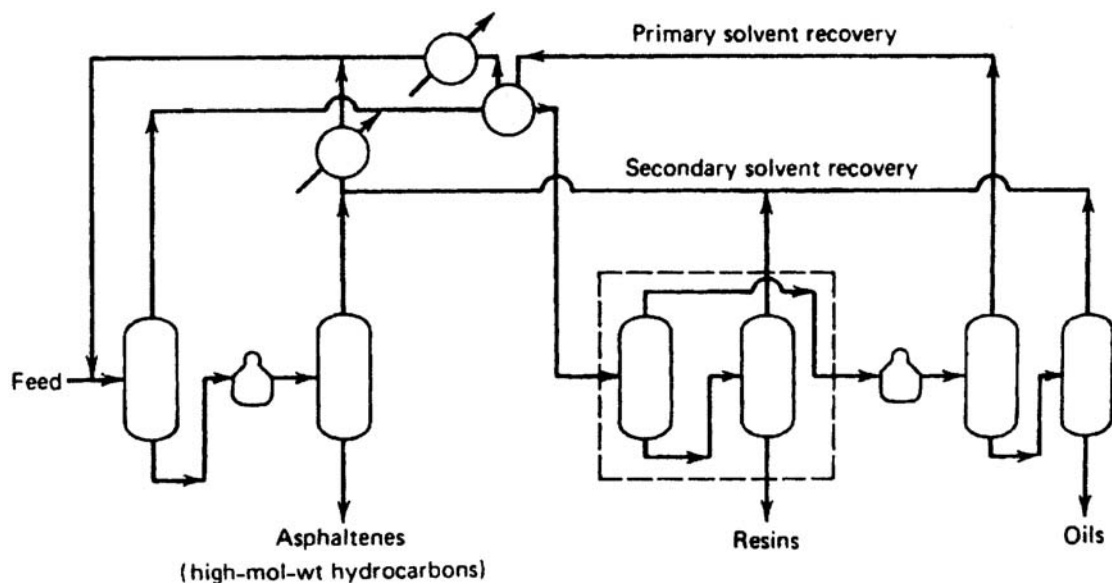


FIG. 20-21 Schematic diagram of the Kerr-McGee ROSE process.

substrate; furthermore, the extracted impurities are easily recovered from the SCF. The swelling and lowering of the glass transition temperature of the polymer by the SCF can increase mass-transfer rates markedly. This approach was used to plasticize block copolymer templates for the infusion of reaction precursors in the synthesis of porous low- k dielectrics. For homopolymers, plasticization may be used to infuse dyes, pharmaceuticals, etc., and then the SCF may be removed to trap the solute in the polymer matrix. SCFs may be used to fractionate polymers on the basis of molecular weight and/or composition with various methods for programming pressure and/or temperature (McHugh, op. cit.).

Drying and Aerogel Formation One of the oldest applications of SCF technology, developed in 1932, is SCF drying. The solvent is extracted from a porous solid with a SCF; then the fluid is depressurized. Because the fluid expands from the solid without crossing a liquid-vapor phase transition, capillary forces that would collapse the structure are not present. Using SCF drying, aerogels have been prepared with densities so low that they essentially float in air and look like a cloud of smoke. Also, the process is used in a commercial instrument to dry samples for electron microscopy without perturbing the structure.

Cleaning SCFs such as CO_2 can be used to clean and degrease quartz rods utilized to produce optical fibers, products employed in the fabrication of printed-circuit boards, oily chips from machining operations, precision bearings in military applications, and so on. Research is in progress for removing residues in etch/ash processes in microelectronics.

Microelectronics Processing SCF CO_2 is proposed as a “dry,” environmentally benign processing fluid enabling replacement of aqueous and organic solvents in microelectronics fabrication (Desimone, op. cit.). Proposed applications include drying, lithography, solvent spin coating, stripping, cleaning, metal deposition, and chemical mechanical planarization. Due to its low surface tension, tunable solvent strength, and excellent mass-transfer properties, CO_2 offers advantages in wetting of surfaces and small pores, and in removal of contaminants at moderate temperatures.

Precipitation/Crystallization to Produce Nano- and Microparticles Because fluids such as CO_2 are weak solvents for many solutes, they are often effective antisolvents in fractionation and precipitation. In general, a fluid antisolvent may be a compressed gas, a gas-expanded liquid, or a SCF. Typically a liquid solution is sprayed through a nozzle into CO_2 to precipitate a solute. As CO_2 mixes with the liquid phase, it

decreases the cohesive energy density (solvent strength) substantially, leading to precipitation of dissolved solutes (e.g., crystals of progesterone). The high diffusion rates of the organic solvent into CO_2 and vice versa can lead to rapid phase separation, and the supersaturation curve may be manipulated to vary the crystalline morphology (Yeo and Kiran, op. cit.).

Nanoparticles of controllable size can be obtained in the supercritical antisolvent-enhanced mass-transfer (SAS-EM) process, which can produce commercial quantities of pharmaceuticals (see Fig. 20-22) [Chattopadhyay and Gupta, *Ind. Engr. Chem. Res.*, **40**, 3530–3539 (2001)]. Here, the solution jet is injected onto an ultrasonic vibrating surface H inside the antisolvent chamber to aid droplet atomization. The particle size is controlled by varying the vibration intensity. For most pharmaceuticals, organic compounds, proteins, and polymers, average particle diameters range from 100 to 1000 nm; even smaller particles may be obtained for certain inorganic compounds.

Rapid Expansion from Supercritical Solution and Particles from Gas Saturated Solutions Rapid expansion from supercritical solution (RESS) of soluble materials may be used to form microparticles or microfibers. A variety of inorganic crystals have been formed naturally and synthetically in SCF water, and organic crystals have been formed in SCF CO_2 . Recently, the addition of a solid cosolvent (e.g., menthol, which can be removed later by sublimation) has overcome key limitations by greatly enhancing solubilities in CO_2 and producing smaller nanoparticles by reducing particle-particle coagulation [Thakur and Gupta, *J. Sup. Fluids*, **37**, 307–315 (2006)]. Another approach is to expand the solutions into aqueous solutions containing soluble surfactants to arrest growth due to particle collisions. RESS typically uses dilute solutions. For concentrated solutions, the process is typically referred to as particle formation from gas saturated solutions (PGSS). Here CO_2 lowers the viscosity of the melt to facilitate flow. Union Carbide developed the commercial UNICARB process to replace organic solvents with CO_2 as a diluent in coating applications to reduce volatile organic carbon emissions and form superior coatings. For aqueous solutions, the expansion of CO_2 facilitates atomization, and the resulting cooling may be used to control the freezing of the solute.

Reactive Separations Reactions may be integrated with SCF separation processes to achieve a large degree of control for producing a highly purified product. Reaction products may be recovered by

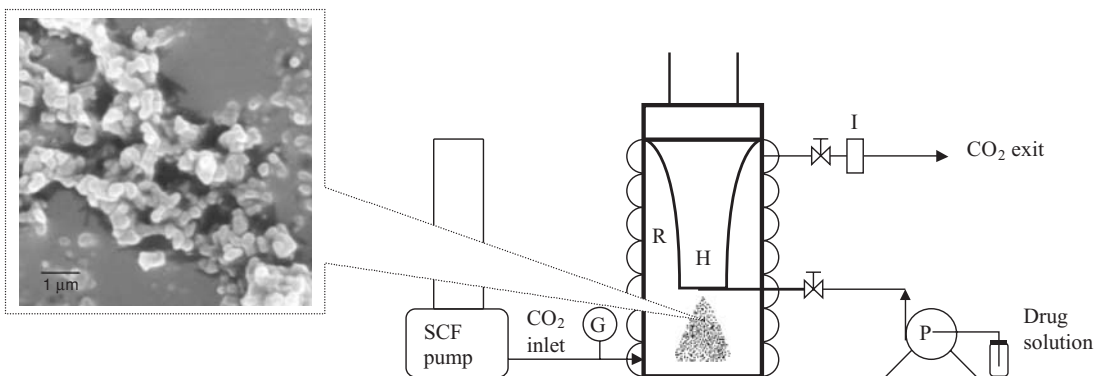


FIG. 20-22 Schematic of supercritical antisolvent with enhanced mass-transfer process to produce nanoparticles of controllable size. R, precipitation chamber; SCF pump, supply of supercritical CO₂; I, inline filter; H, ultrasonic horn; P, pump for drug solution; G, pressure gauge.

volatilization into, or precipitation from, a SCF phase. A classic example is the high-pressure production of polyethylene in SCF ethylene. The molecular weight distribution may be controlled by choosing the temperature and pressure for precipitating the polymer from the SCF phase. Over a decade ago, Idemitsu commercialized a 5000 metric ton per/year integrated reaction and separation process in SCF isobutene. The reaction of isobutene and water produces *sec*-butanol, which is extracted from water by the SCF solvent. SCF solvents have been tested for reactive extractions of liquid and gaseous fuels from heavy oils, coal, oil shale, and biomass. In some cases the solvent participates in the reaction, as in the hydrolysis of coal and heavy oils with SCW. Related applications include conversion of cellulose to glucose in water, delignification of wood with ammonia, and liquefaction of lignin in water.

Gas-expanded liquids (GXLs) are emerging solvents for environmentally benign reactive separation (Eckert et al., op. cit.). GXLs, obtained by mixing supercritical CO₂ with normal liquids, show intermediate properties between normal liquids and SCFs both in solvation power and in transport properties; and these properties are highly tunable by simple pressure variations. Applications include chemical reactions with improved transport, catalyst recycling, and product separation.

Hydrothermal oxidation (HO) [also called supercritical water oxidation (SCWO)] is a reactive process to convert aqueous wastes to water, CO₂, O₂, nitrogen, salts, and other by-products. It is an enclosed and complete water treatment process, making it more desirable to the public than incineration. Oxidation is rapid and efficient in this one-phase solution, so that wastewater containing 1 to 20 wt % organics may be oxidized rapidly in SCW with the potential for higher energy efficiency and less air pollution than in conventional incineration. Temperatures range from about 375 to 650°C and pressures from 3000 to about 5000 psia.

Crystallization by Chemical Reaction

Supercritical Fluid Deposition (SFD) Metal films may be grown from precursors that are soluble in CO₂. The SFD process yields copper films with fewer defects than those possible by using chemical vapor deposition, because increased precursor solubility removes mass-transfer limitations and low surface tension favors penetration of high-aspect-ratio features [Blackburn et al., *Science*, **294**, 141–145 (2001)].

High-Temperature Crystallization The size-tunable optical and electronic properties of semiconductor nanocrystals are attractive for a variety of optoelectronic applications. In solution-phase crystallization, precursors undergo chemical reaction to form nuclei, and particle growth is arrested with capping ligands that

passivate the surface. However, temperatures above 350°C are typically needed to crystallize the group IV elements silicon and germanium, due to the covalent network structure. Whereas liquid solvents boil away at these elevated temperatures, SCFs under pressure are capable of solvating the capping ligands to stabilize the nanocrystals (Shah et al., op. cit.). Crystalline Si and Ge nanocrystals, with an average size of 2 to 70 nm, may be synthesized in supercritical CO₂, hexane, or octanol at 400 to 550°C and 20 MPa in a simple continuous flow reactor. UV-visible absorbance and photoluminescence (PL) spectra of Ge nanocrystals of 3- to 4-nm diameter exhibit optical absorbance and PL spectra blue-shifted by approximately 1.7 eV relative to the band gap of bulk Ge, as shown in Fig. 20-23. One-dimensional silicon nanowires may be grown from relatively monodisperse gold nanocrystals stabilized with dodecanethiol ligands, as shown in Fig. 20-24. The first crystalline silicon nanowires with diameters smaller than 5 nm and lengths greater than 1 μm made by any technique were produced in SCF hexane. Hydrothermal crystallization has also been used to produce metal oxide nano- and microcrystals by rapid generation of supersaturation during hydrolysis of precursors, such as metal nitrates, during rapid heating of aqueous solutions.

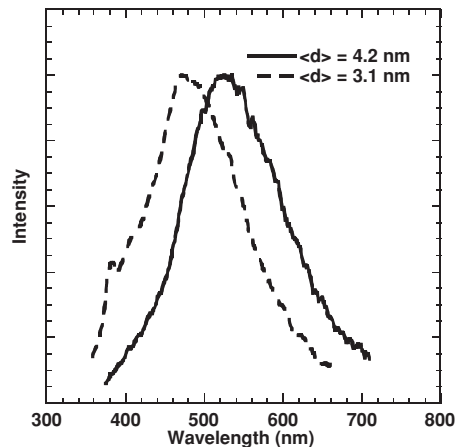


FIG. 20-23 Normalized photoluminescence spectra of 3.1-nm ($\lambda_{\text{excitation}} = 320 \text{ nm}$) and 4.2-nm ($\lambda_{\text{excitation}} = 340 \text{ nm}$) Ge nanoparticles dispersed in chloroform at 25°C with quantum yields of 6.6 and 4.6 percent, respectively. [Reprinted with permission from Lu et al., *Nano Lett.*, **4**(5), 969–974 (2004). Copyright 2004 American Chemical Society.]

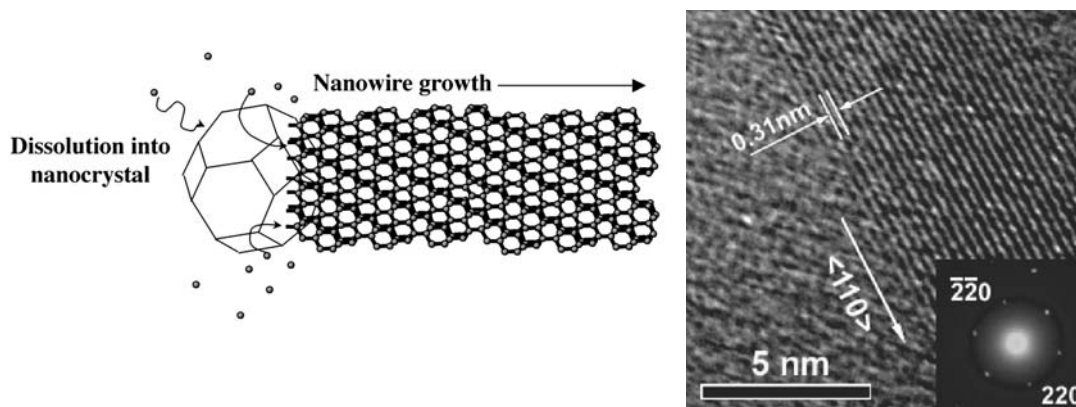


FIG. 20-24 High-resolution TEM image of Si nanowires produced at 500°C and 24.1 MPa in supercritical hexane from gold seed crystals. *Inset:* Electron diffraction pattern indexed for the <110> zone axis of Si indicates <110> growth direction. [Reprinted with permission from Lu et al., *Nano Lett.*, **3**(1), 93–99 (2003). Copyright 2003 American Chemical Society.]

ALTERNATIVE SOLID/LIQUID SEPARATIONS

SEPARATION PROCESSES BASED PRIMARILY ON ACTION IN AN ELECTRIC FIELD

Differences in mobilities of ions, molecules, or particles in an electric field can be exploited to perform useful separations. Primary emphasis is placed on electrophoresis and dielectrophoresis. Analogous separation processes involving magnetic and centrifugal force fields are widely applied in the process industry (see Secs. 18 and 19).

Theory of Electrical Separations

GENERAL REFERENCES: Newman, *Adv. Electrochem. Electrochem. Eng.*, **5**, 87 (1967); *Ind. Eng. Chem.*, **60**(4), 12 (1968). Ptasinaki and Kerkhof, *Sep. Sci. Technol.*, **27**, 995 (1992).

For electrolytic solutions, migration of charged species in an electric field constitutes an additional mechanism of mass transfer. Thus the flux of an ionic species N_i in (g-mol)/(cm²·s) in dilute solutions can be expressed as

$$N_i = -z_i u_i \mathcal{F} c_i \nabla E - D_i \nabla c_i + c_i v \quad (20-10)$$

The ionic mobility u_i is the average velocity imparted to the species under the action of a unit force (per mole). v is the stream velocity, cm/s. In the present case, the electrical force is given by the product of the electric field ∇E in V/cm and the charge $z_i \mathcal{F}$ per mole, where \mathcal{F} is the Faraday constant in C/g equivalent and z_i is the valence of the i th species. Multiplication of this force by the mobility and the concentration c_i [(g-mol)/cm³] yields the contribution of migration to the flux of the i th species.

The diffusive and convective terms in Eq. (20-10) are the same as in nonelectrolytic mass transfer. The ionic mobility u_i , (g-mol·cm²)/(J·s), can be related to the ionic-diffusion coefficient D_i , cm²/s, and the ionic conductance of the i th species λ_i , cm²/(Ω·g equivalent):

$$u_i = D_i / RT = \lambda_i / |z_i| \mathcal{F}^2 \quad (20-11)$$

where T is the absolute temperature, K; and R is the gas constant, 8.3143 J/(K·mol). Ionic conductances are tabulated in the literature (Robinson and Stokes, *Electrolyte Solutions*, Academic, New York, 1959). For practical purposes, a bulk electrolytic solution is electrically neutral.

$$\sum_i z_i c_i = 0 \quad (20-12)$$

since the forces required to effect an appreciable separation of charge are prohibitively large.

The **current density** (A/cm²) produced by movement of charged species is described by summing the terms in Eq. (20-13) for all species:

$$i = \mathcal{F} \sum_i z_i N_i = -\kappa \nabla E - \mathcal{F} \sum_i z_i D_i \nabla c_i \quad (20-13)$$

where the electrical conductivity κ in S/cm is given by

$$\kappa = \mathcal{F}^2 \sum_i z_i^2 u_i c_i \quad (20-14)$$

In solutions of uniform composition, the diffusional terms vanish and Eq. (20-13) reduces to Ohm's law.

Conservation of each species is expressed by the relation

$$\partial c_i / \partial t = -\nabla \cdot N_i \quad (20-15)$$

provided that the species is not produced or consumed in homogeneous chemical reactions. In two important cases, this conservation law reduces to the equation of convective diffusion:

$$(\partial c_i / \partial t) + \mathbf{v} \cdot \mathbf{c}_i = D \nabla^2 c_i \quad (20-16)$$

First, when a large excess of inert electrolyte is present, the electric field will be small and migration can be neglected for minor ionic components; Eq. (20-16) then applies to these minor components, where D is the ionic-diffusion coefficient. Second, Eq. (20-16) applies when the solution contains only one cationic and one anionic species. The electric field can be eliminated by means of the electroneutrality relation.

In the latter case the diffusion coefficient D of the electrolyte is given by

$$D = (z_+ u_+ D_- - z_- u_- D_+) / (z_+ u_+ - z_- u_-) \quad (20-17)$$

which represents a compromise between the diffusion coefficients of the two ions. When Eq. (20-16) applies, many solutions can be obtained by analogy with heat transfer and nonelectrolytic mass transfer.

Because the solution is electrically neutral, conservation of charge is expressed by differentiating Eq. (20-13):

$$\nabla \cdot \mathbf{i} = 0 = -\kappa \nabla^2 E - \mathcal{F} \sum_i z_i D_i \nabla^2 c_i \quad (20-18)$$

For solutions of uniform composition, Eq. (20-18) reduces to Laplace's equation for the potential:

$$\nabla^2 E = 0 \quad (20-19)$$

This equation is the starting point for determination of the current-density distributions in many electrochemical cells.

Near an interface or at solution junctions, the solution departs from electroneutrality. Charges of one sign may be preferentially adsorbed at the interface, or the interface may be charged. In either case, the charge at the interface is counterbalanced by an equal and opposite charge composed of ions in the solution. Thermal motion prevents this countercharge from lying immediately adjacent to the interface, and the result is a "diffuse-charge layer" whose thickness is on the order of 10 to 100 Å.

A tangential electric field ∇E_t acting on these charges produces a relative motion between the interface and the solution just outside the diffuse layer. In view of the thinness of the diffuse layer, a balance of the tangential viscous and electrical forces can be written

$$\mu(\partial^2 v_t / \partial y^2) + \rho_e \nabla E_t = 0 \quad (20-20)$$

where μ is the viscosity and ρ_e is the electric-charge density, C/cm³. Furthermore, the variation of potential with the normal distance satisfies Poisson's equation:

$$\partial^2 E / \partial y^2 = -(\rho_e / \epsilon) \quad (20-21)$$

with ϵ defined as the **permittivity** of the solution. [The relative dielectric constant is ϵ/ϵ_0 , where ϵ_0 is the permittivity of free space; $\epsilon_0 = 8.8542 \times 10^{-14}$ C/(V·cm).] Elimination of the electric-charge density between Eqs. (20-20) and (20-21) with two integrations, gives a relation between ∇E_t and the velocity v_0 of the bulk solution relative to the interface.

$$\mu[v_0(\infty) - v_0(0)] = \epsilon \nabla E_t [E(\infty) - E(0)] \quad (20-22)$$

$$\text{or} \quad v_0 = -(\epsilon \nabla E_t \zeta / \mu) \quad (20-23)$$

The potential difference across the mobile part of the diffuse-charge layer is frequently called the **zeta potential**, $\zeta = E(0) - E(\infty)$. Its value depends on the composition of the electrolytic solution as well as on the nature of the particle-liquid interface.

There are four related electrokinetic phenomena which are generally defined as follows: **electrophoresis**—the movement of a charged surface (i.e., suspended particle) relative to a stationary liquid induced by an applied electrical field, **sedimentation potential**—the electric field which is created when charged particles move relative to a stationary liquid, **electroosmosis**—the movement of a liquid relative to a stationary charged surface (i.e., capillary wall), and **streaming potential**—the electric field which is created when liquid is made to flow relative to a stationary charged surface. The effects summarized by Eq. (20-23) form the basis of these electrokinetic phenomena.

For many particles, the diffuse-charge layer can be characterized adequately by the value of the zeta potential. For a spherical particle of radius r_0 which is large compared with the thickness of the diffuse-charge layer, an electric field uniform at a distance from the particle will produce a tangential electric field which varies with position on the particle. Laplace's equation [Eq. (20-19)] governs the distribution of potential outside the diffuse-charge layer; also, the Navier-Stokes equation for a creeping-flow regime can be applied to the velocity distribution. On account of the thinness of the diffuse-charge layer, Eq. (20-23) can be used as a local boundary condition, accounting for the effect of this charge in leading to movement of the particle relative to the solution. The result of this computation gives the velocity of the particle as

$$v = \epsilon \zeta \nabla E / \mu \quad (20-24)$$

and it may be convenient to tabulate the mobility of the particle

$$U = v / \nabla E = \epsilon \zeta / \mu \quad (20-25)$$

rather than its zeta potential. Note that this mobility gives the velocity of the particle for unit electric field rather than for unit force on the particle. Related equations can be developed for the velocity of electroosmotic flow. The subsections presented below ("Electrophoresis," "Electrofiltration," and "Cross-Flow-Electrofiltration") represent both established and emerging commercial applications of electrokinetic phenomena.

Electrophoresis

GENERAL REFERENCE: Wankat, *Rate-Controlled Separations*, Elsevier, London, 1990.

Electrophoretic Mobility Macromolecules move at speeds measured in tenths of micrometers per second in a field (gradient) of 1 V/cm. Larger particles such as bubbles or bacteria move up to 10 times as fast because U is usually higher. To achieve useful separations, therefore, voltage gradients of 10 to 100 V/cm are required. High voltage gradients are achieved only at the expense of power dissipation within the fluid, and the resulting heat tends to cause undesirable convection currents.

Mobility is affected by the dielectric constant and viscosity of the suspending fluid, as indicated in Eq. (20-25). The ionic strength of the fluid has a strong effect on the thickness of the double layer and hence on ζ . As a rule, mobility varies inversely as the square root of ionic strength [Overbeek, *Adv. Colloid Sci.*, **3**, 97 (1950)].

Modes of Operation There is a close analogy between sedimentation of particles or macromolecules in a gravitational field and their electrophoretic movement in an electric field. Both types of separation have proved valuable not only for analysis of colloids but also for preparative work, at least in the laboratory. Electrophoresis is applicable also for separating mixtures of simple cations or anions in certain cases in which other separating methods are ineffectual.

Electrodecantation or electroconvection is one of several operations in which one mobile component (or several) is to be separated out from less mobile or immobile ones. The mixture is introduced between two vertical semipermeable membranes; for separating cations, anion membranes are used, and vice versa. When an electric field is applied, the charged component migrates to one or another of the membranes; but since it cannot penetrate the membrane, it accumulates at the surface to form a dense concentrated layer of particles which will sink toward the bottom of the apparatus. Near the top of the apparatus immobile components will be relatively pure. Murphy [*J. Electrochem. Soc.*, **97**(11), 405 (1950)] has used silver-silver chloride electrodes in place of membranes. Frilette [*J. Phys. Chem.*, **61**, 168 (1957)], using anion membranes, partially separated H⁺ and Na⁺, K⁺ and Li⁺, and K⁺ and Na⁺.

Countercurrent electrophoresis can be used to split a mixture of mobile species into two fractions by the electrical analog of elutriation. In such countercurrent electrophoresis, sometimes termed an ion still, a flow of the suspending fluid is maintained parallel to the direction of the voltage gradient. Species which do not migrate fast enough in the applied electric field will be physically swept out of the apparatus. An apparatus based mainly on this principle but using also natural convection currents has been developed (Bier, *Electrophoresis*, vol. II, Academic, New York, 1967).

Membrane electrophoresis which is based upon differences in ion mobility, has been studied by Glueckauf and Kitt [*J. Appl. Chem.*, **6**, 511 (1956)]. Partial exclusion of coions by membranes results in large differences in coion mobilities. Superposing a cation and an anion membrane gives high transference numbers (about 0.5) for both cations and anions while retaining the selectivity of mobilities. Large voltages are required, and flow rates are low.

In continuous-flow zone electrophoresis the "solute" mixture to be separated is injected continuously as a narrow source within a body of carrier fluid flowing between two electrodes. As the "solute" mixture passes through the transverse field, individual components migrate sideways to produce zones which can then be taken off separately downstream as purified fractions.

Resolution depends upon differences in mobilities of the species. Background electrolyte of low ionic strength is advantageous, not only to increase electrophoretic (solute) mobilities, but also to achieve low electrical conductivity and thereby to reduce the thermal-convection current for any given field [Finn, in Schoen (ed.), *New Chemical Engineering Separation Techniques*, Interscience, New York, 1962].

The need to limit the maximum temperature rise has resulted in two main types of apparatus, illustrated in Fig. 20-25. The first consists of multicomponent ribbon separation units—apparatus capable of separating small quantities of mixtures which may contain few or many species. In general, such units operate with high voltages, low

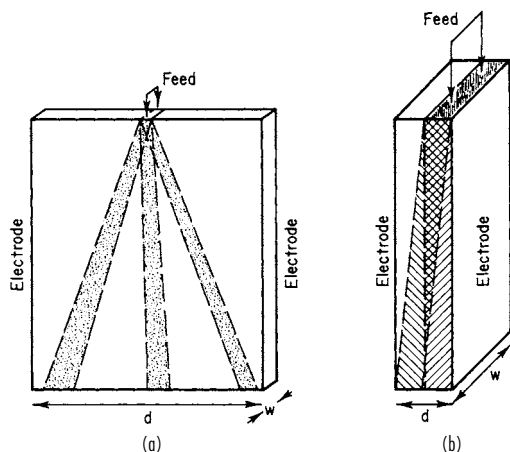


FIG. 20-25 Types of arrangement for zone electrophoresis or electrochromatography. (a) Ribbon unit, with $d > w$; cooling at side faces. (b) Block unit, with $w > d$; cooling at electrodes.

currents, a large transverse dimension, and a narrow thickness between cooling faces. Numerous units developed for analytic chemistry, generally with filter-paper curtains but sometimes with granular "anticonvectant" packing, are of this type. The second type consists of block separation units—apparatus designed to separate larger quantities of a mixture into two (or at most three) species or fractions. Such units generally use low to moderate voltages and high currents, with cooling by circulation of cold electrolyte through the electrode compartments. Scale-up can readily be accomplished by extending the thickness dimension w .

Both types of units have generally been operated in trace mode; that is, "background" or "elutant" electrolyte is fed to the unit along with the mixture to be separated. A desirable and possible means of operation for preparative applications is in bulk mode, in which one separated component follows the other without background electrolyte being present, except that other ions may be required to bracket the separated zones. Overlap regions between components should be recycled, and pure components collected as products.

For block units, the need to stabilize flow has given rise to a number of distinct techniques.

Free flow. Dobry and Finn [*Chem. Eng. Prog.*, **54**, 59 (1958)] used upward flow, stabilized by adding methyl cellulose, polyvinyl alcohol, or dextran to the background solution. Upward flow was also used in the electrode compartments, with cooling efficiency sufficient to keep the main solution within 1°C of entering temperature.

Density gradients to stabilize flow have been employed by Philpot [*Trans. Faraday Soc.*, **36**, 38 (1940)] and Mel [*J. Phys. Chem.*, **31**, 559 (1959)]. Mel's Staflo apparatus [*J. Phys. Chem.*, **31**, 559 (1959)] has liquid flow in the horizontal direction, with layers of increasing density downward produced by sucrose concentrations increasing to 7.5 percent. The solute mixture to be separated is introduced in one such layer. Operation at low electrolyte concentrations, low voltage gradients, and low flow rates presents no cooling problem.

Packed beds. A packed cylindrical electrochromatograph 9 in (23 cm) in diameter and 48 in (1.2 m) high, with operating voltages in the 25- to 100-V range, has been developed by Hybarger, Vermeulen, and coworkers [*Ind. Eng. Chem. Process Des. Dev.*, **10**, 91 (1971)]. The annular bed is separated from inner and outer electrodes by porous ceramic diaphragms. The unit is cooled by rapid circulation of cooled electrolyte between the diaphragms and the electrodes.

An interesting modification of zone electrophoresis resolves mixtures of ampholytes on the basis of **differing isoelectric points** rather than differing mobilities. Such **isoelectric spectra** develop when a pH gradient is established parallel to the electric field. Each species then migrates until it arrives at the region of pH where it possesses no net surface charge. A strong focusing effect is thereby

achieved [Kolin, in Glick (ed.), *Methods of Biochemical Analysis*, vol. VI, Interscience, New York, 1958].

Electrofiltration

GENERAL REFERENCE: P. Krishnaswamy and P. Klinkowski, "Electrokinetics and Electrofiltration," in *Advances in Solid-Liquid Separation*, H. S. Murad-dhara (ed.), Battelle Press, Columbus, OH, 1986.

Process Concept The application of a direct electric field of appropriate polarity when filtering should cause a net charged-particle migration relative to the filter medium (electrophoresis). The same direct electric field can also be used to cause a net fluid flow relative to the pores in a fixed filter cake or filter medium (electroosmosis). The exploitation of one or both of these phenomena form the basis of conventional electrofiltration.

In conventional filtration, often the object is to form a high-solids-content filter cake. At a single-filter surface, a uniform electric field can be exploited in one of two ways. The first method of exploitation occurs when the electric field is of a polarity such that the charged-particle migration occurs toward the filter medium. In this case, the application of the electric field increases the velocity of the solid particles toward the filter surface (electrosedimentation), thereby hastening the clarification of the feed suspension and, at the same time, increasing the compaction of the filter cake collected on the filter surface. In this first case, electroosmotic flow occurs in a direction away from the filter media. The magnitude of the pressure-driven fluid flow toward the filter surface far exceeds the magnitude of the electroosmotic flow away from the surface so that the electroosmotic flow results in only a minor reduction of the rate of production of filtrate. The primary benefits of the applied electric field in this case are increased compaction, and hence increased dewatering, of the filter cake and an increased rate of sedimentation or movement of the particles in bulk suspension toward the filter surface.

The second method of exploitation occurs when the electric field is of a polarity such that the charged-particle migration occurs away from the filter medium. The contribution to the net-particle velocity of the electrophoretically induced flow away from the filter medium is generally orders of magnitude less than the contribution to the net-particle velocity of the flow induced by drag due to the pressure-induced flow of the bulk liquid toward the filter media. (In conventional or cake filtration, the velocity of liquid in dead-end flow toward the filter is almost always sufficient to overcome any electrophoretic migration of particles away from the filter media so that the prevention of the formation of filter cake is not an option. This will not necessarily be the case for cross-flow electrofiltration.) The primary enhancement to filtration caused by the application of an electrical field in this manner is the increase in the filtrate flux due to electroosmotic flow through the filter cake. This electroosmotic flow is especially beneficial during the latter stages of filtration when the final filter-cake thickness has been achieved. At this stage, electroosmosis can be exploited to draw filtrate out from the pore structure of the filter cake. This type of drying of the filter cake is sometimes called **electroosmotic dewatering**.

Commercial Applications Krishnaswamy and Klinkowski, *op. cit.*, describe the Dorr-Oliver EAVF[®]. The EAVF[®] combines vacuum filtration with electrophoresis and electroosmosis and has been described as a series of parallel platelike electrode assemblies suspended in a tank containing the slurry to be separated. When using the EAVF[®], solids are collected at both electrodes, one collecting a compacted cake simply by electrophoretic attraction and the second collecting a compacted cake through vacuum filtration coupled with electroosmotic dewatering. Upon the completion of a collection cycle, the entire electrode assembly is withdrawn from the slurry bath and the cake is removed. The EAVF[®] is quoted as being best suited for the dewatering of ultrafine slurries (particle sizes typically less than $10\ \mu\text{m}$).

Cross-Flow-Electrofiltration

GENERAL REFERENCES: Henry, Lawler, and Kuo, *Am. Inst. Chem. Eng. J.*, **23**(6), 851 (1977). Kuo, Ph.D. dissertation, West Virginia University, 1978.

Process Concept The application of a direct electric field of appropriate polarity when filtering should cause a net charged-particle

migration away from the filter medium. This electrophoretic migration will prevent filter-cake formation and the subsequent reduction of filter performance. An additional benefit derived from the imposed electric field is an electroosmotic flux. The presence of this flux in the membrane and in any particulate accumulation may further enhance the filtration rate.

Cross-flow–electrofiltration (CF-EF) is the multifunctional separation process which combines the electrophoretic migration present in electrofiltration with the particle diffusion and radial-migration forces present in cross-flow filtration (CFF) (microfiltration includes cross-flow filtration as one mode of operation in “Membrane Separation Processes” which appears later in this section) in order to reduce further the formation of filter cake. Cross-flow–electrofiltration can even eliminate the formation of filter cake entirely. This process should find application in the filtration of suspensions when there are charged particles as well as a relatively low conductivity in the continuous phase. Low conductivity in the continuous phase is necessary in order to minimize the amount of electrical power necessary to sustain the electric field. Low-ionic-strength aqueous media and nonaqueous suspending media fulfill this requirement.

Cross-flow–electrofiltration has been investigated for both aqueous and nonaqueous suspending media by using both rectangular- and tubular-channel processing configurations (Fig. 20-26). Henry, Lawler, and Kuo (op. cit.), using a rectangular-channel system with a 0.6- μ -pore-size polycarbonate Nuclepore filtration membrane, investigated CF-EF for 2.5- μ m kaolin-water and 0.5- to 2- μ m oil-in-water emulsion systems. Kuo (op. cit.), using similar equipment, studied 5- μ m kaolin-water, ~100- μ m Cr₂O₃-water, and ~6- μ m Al₂O₃-methanol and/or -butanol systems. For both studies electrical fields of 0 to 60 V/cm were used for aqueous systems, and to 5000 V/cm were used for nonaqueous systems. The studies covered a wide range of processing variables in order to gain a better understanding of CF-EF fundamentals. Lee, Gidaspow, and Wasan [Ind. Eng. Chem. Fundam., 19(2), 166 (1980)] studied CF-EF by using a porous stainless-steel tube (pore size = 5 μ m) as the filtration medium. A platinum wire running down the center of the tube acted as one electrode, while the porous steel tube itself acted as the other electrode. Nonaqueous suspensions of 0.3- to 2- μ m Al₂O₃-tetralin and a coal-derived liquid diluted with xylene and tetralin were studied. By operating with applied electric fields (1000 to 10,000 V/cm) above the critical voltage, clear particle-free filtrates were produced. It should be noted that the

pore size of the stainless-steel filter medium (5 μ m) was greater than the particle size of the suspended Al₂O₃ solids (0.3 to 2 μ m). Cross-flow–electrofiltration has also been applied to biological systems. Brors, Kroner, and Deckwer [ECB6: Proc. 6th Eur. Cong. Biotech., 511 (1994)] separated malate dehydrogenase from the cellular debris of Baker’s yeast using CF-EF. A two- to fivefold increase in the specific enzyme transport rate was reported when electric field strengths of 20 to 40 V/cm were used.

Theory Cross-flow–electrofiltration can theoretically be treated as if it were cross-flow filtration with superimposed electrical effects. These electrical effects include electroosmosis in the filter medium and cake and electrophoresis of the particles in the slurry. The addition of the applied electric field can, however, result in some qualitative differences in permeate-flux-parameter dependences.

The membrane resistance for CF-EF can be defined by specifying two permeate fluxes as

$$J_{om} = \Delta P/R_{om} \quad (20-26)$$

$$J_m = \Delta P/R_m \quad (20-27)$$

where J_{om} is the flux through the membrane in the absence of an electric field and any other resistance, m/s; J_m is the same flux in the presence of an electric field; and R_{om} is the membrane resistance in the absence of an electric field, (N·s)/m². When electroosmotic effects do occur,

$$J_m = J_{om} + K_m E \quad (20-28)$$

where K_m is the electroosmotic coefficient of the membrane, m²/(V·s); and E is the applied-electric-field strength, V/m. Equations (20-26), (20-27), and (20-28) can be combined and rearranged to give Eq. (20-29), the membrane resistance in the presence of an electric field.

$$R_m = \frac{R_{om}}{1 + \left(\frac{K_m E}{J_{om}}\right)} \quad (20-29)$$

Similarly, cake resistance can be represented as

$$R_c = \frac{R_{oc}}{1 + \left(\frac{K_c E}{J_{oc}}\right)} \quad (20-30)$$

where J_{oc} is the flux through the cake in the absence of an electric field or any other resistance, R_{oc} is the cake resistance in the absence of an electric field, and K_c is the electroosmotic coefficient of the cake. The cake resistance is not a constant but is dependent upon the cake thickness, which is in turn a function of the transmembrane pressure drop and electrical-field strength.

Particulate systems require the addition of the term $\mu_e E$ in order to account for the electrophoretic migration of the particle. The constant μ_e is the electrophoretic mobility of the particle, m²/(V·s). For the case of the CF-EF, the film resistance R_f can be represented as

$$R_f = \frac{\Delta P}{k \ln \left(\frac{C_s}{C_b}\right) + U_e + \mu_e E} \quad (20-31)$$

The resistances, when incorporated into equations descriptive of cross-flow filtration, yield the general expression for the permeate flux for particulate suspensions in cross-flow–electrofiltration systems.

There are three distinct regimes of operation in CF-EF. These regimes (Fig. 20-27) are defined by the magnitude of the applied electric field with respect to the critical voltage E_c . The critical voltage is defined as the voltage at which the net particle migration velocity toward the filtration medium is zero. At the critical voltage, there is a balance between the electrical-migration and radial-migration velocities away from the filter and the velocity at which the particles are swept toward the filter by bulk flow. There is no diffusive transport at $E = E_c$ (Fig. 20-27b) because there is no gradient in the particle concentration normal to the filter surface. At field strengths below the critical voltage (Fig. 20-27a), all migration velocities occur in the same direction as in the cross-flow-filtration systems discussed earlier. At values of applied voltage above the critical voltage (Fig. 20-27c) qualitative differences

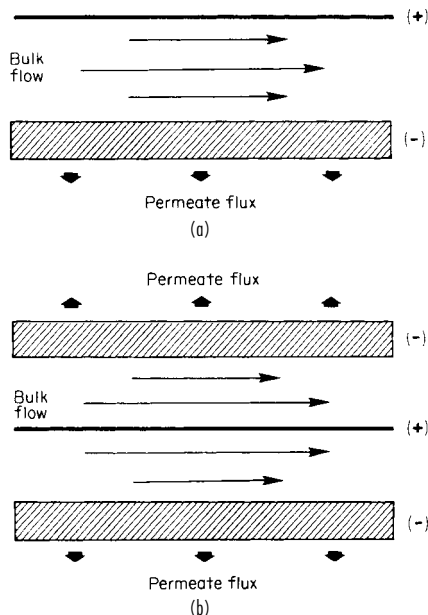


FIG. 20-26 Alternative electrode configurations for cross-flow–electrofiltration.

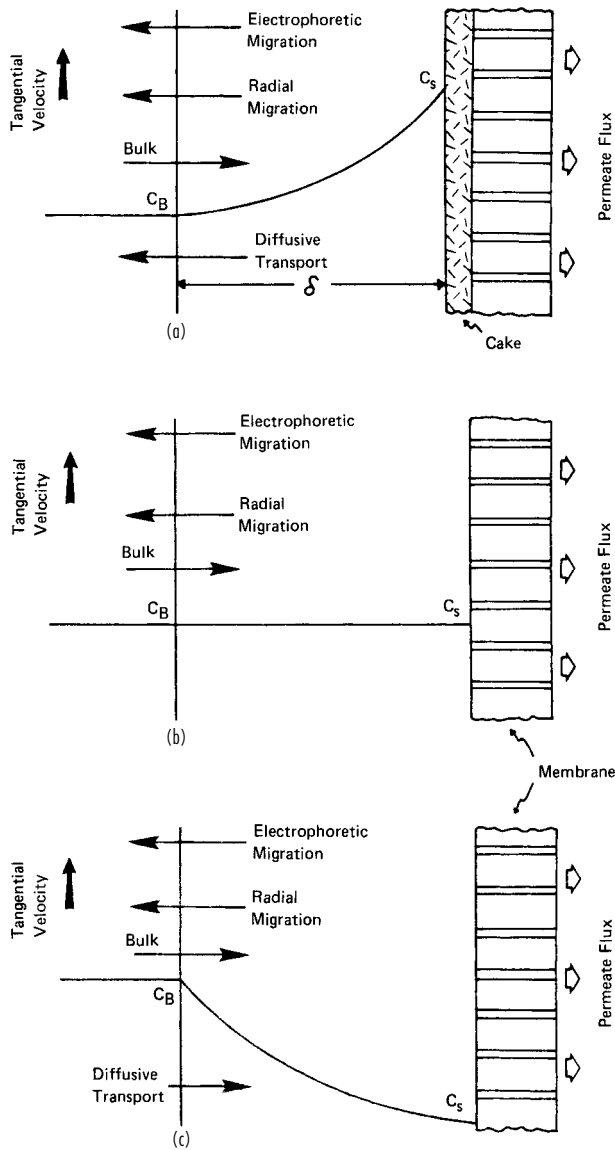


FIG. 20-27 Regimes of operation of cross-flow-electrofiltration: (a) voltage less than critical, (b) voltage equal to the critical voltage, (c) voltage greater than critical.

are observed. In this case, the electrophoretic-migration velocity away from the filter medium is greater than the velocity caused by bulk flow toward the filtration medium. Particles concentrate away from the filter medium (in actuality, a clear boundary layer has been observed). The influence of fluid shear still improves the transfer of particles down the concentration gradient, but in this case it is toward the filtration medium. When the particles are small and diffusive transport dominates radial migration, increasing the circulation velocity will decrease the permeate flux rate in this regime. When the particles are large and radial migration dominates, the increase in circulation velocity will still improve the filtration rate. These effects are illustrated qualitatively in Fig. 20-28a. The solid lines represent systems in which the particle diffusive effect dominates the radial-migration effect, while the dashed lines represent the inverse. Figure 20-28b illustrates the increase in filtration rate with increasing electric field strength. For field strengths

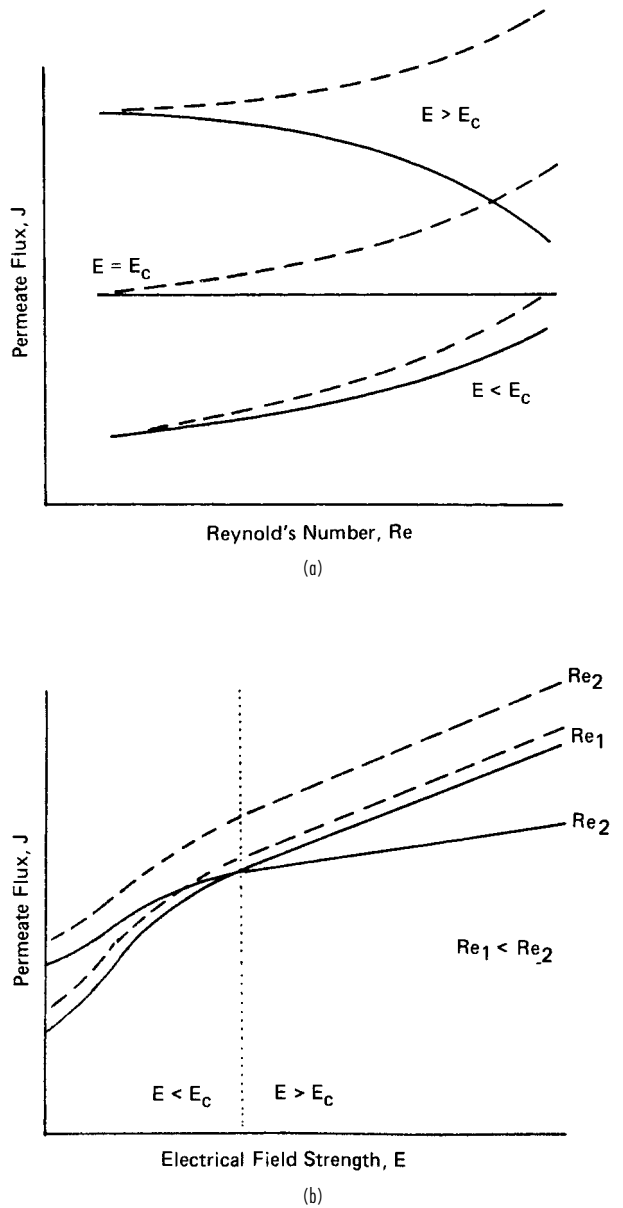


FIG. 20-28 Qualitative effects of Reynolds number and applied electric-field strength on the filtration permeate flux J . Dashed lines indicate large particles (radial migration dominates); solid lines, small particles (particle diffusion dominates).

$E > E_c$, increases in permeate flux rate are due only to electroosmosis in the filtration medium.

One potential difficulty with CF-EF is the electrodeposition of the particles at the electrode away from the filtration medium. This phenomenon, if allowed to persist, will result in performance decay of CF-EF with respect to maintenance of the electric field. Several approaches such as momentary reverses in polarity, protection of the electrode with a porous membrane or filter medium, and/or utilization of a high fluid shear rate can minimize electrodeposition.

Dielectrophoresis

GENERAL REFERENCES: Gascoyne and Vykoukal, *Electrophoresis*, **23**, 1973–1983 (2002). Pohl, in Moore (ed.), *Electrostatics and Its Applications*,

Wiley, New York, 1973, chap. 14 and chap. 15 (with Crane). Pohl, in Catsimpoalas (ed.), *Methods of Cell Separation*, vol. I, Plenum Press, New York, 1977, chap. 3. Pohl, *Dielectrophoresis: The Behavior of Matter in Nonuniform Electric Fields*, Cambridge, New York, 1978.

Introduction Dielectrophoresis (DEP) is defined as the motion of neutral, polarizable matter produced by a nonuniform electric (ac or dc) field. DEP should be distinguished from electrophoresis, which is the motion of charged particles in a uniform electric field (Fig. 20-29).

The DEP of numerous particle types has been studied, and many applications have been developed. Particles studied have included aerosols, glass, minerals, polymer molecules, living cells, and cell organelles. Applications developed include filtration, orientation, sorting or separation, characterization, and levitation and materials handling. Effects of DEP are easily exhibited, especially by large particles, and can be applied in many useful and desirable ways. DEP effects can, however, be observed on particles ranging in size even down to the molecular level in special cases. Since thermal effects tend to disrupt DEP with molecular-sized particles, they can be controlled only under special conditions such as in molecular beams.

Principle The principle of particle and cell separation, control, or characterization by the action of DEP lies in the fact that a net force can arise upon even neutral particles situated in a nonuniform electric field. The force can be thought of as arising from the imaginary two-step process of (1) induction or alignment of an electric dipole in a particle placed in an electric field followed by (2) unequal forces on the ends of that dipole. This arises from the fact that the force of an electric field upon a charge is equal to the amount of the charge and to the local field strength at that charge. Since the two (equal) charges of the (induced or oriented) dipole of the particle lie in unequal field strengths of the diverging field, a net force arises. If the particle is suspended in a fluid, then the polarizability of that medium enters, too.

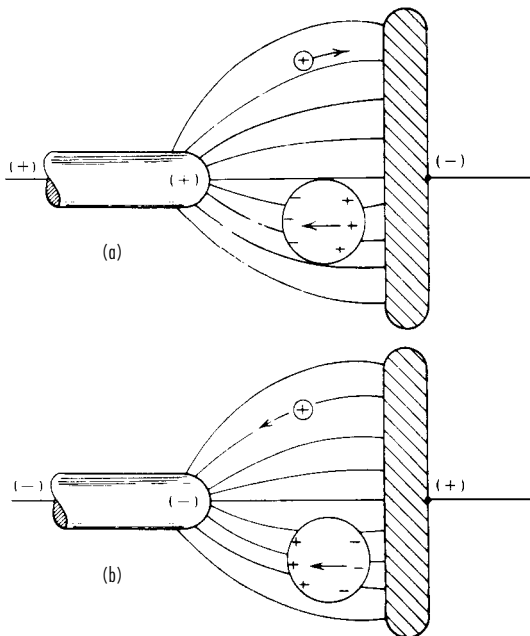


FIG. 20-29 Comparison of behaviors of neutral-charged bodies in an alternating nonuniform electric field. (a) Positively charged body moves toward negative electrode. Neutral body is polarized, then is attracted toward point where field is strongest. Since the two charge regions on the neutral body are equal in amount of charge but the force is proportional to the local field, a net force toward the region of more intense field results. (b) Positively charged body moves toward the negative electrode. Again, the neutral body is polarized, but it does not reverse direction although the field is reversed. It still moves toward the region of highest field intensity.

If, for example, the particle is more polarizable than the fluid, then the net force is such as to impel the particle to regions of greater field strength. Note that this statement implies that the effect is independent of the absolute sign of the field direction. This is found to be the case. Even rapidly alternating (ac) fields can be used to provide *unidirectional* motion of the suspended particles.

Formal Theory A small neutral particle at equilibrium in a static electric field experiences a net force due to DEP that can be written as $\mathbf{F} = (\mathbf{p} \cdot \nabla)\mathbf{E}$, where \mathbf{p} is the dipole moment vector and \mathbf{E} is the external electric field. If the particle is a simple dielectric and is isotropically, linearly, and homogeneously polarizable, then the dipole moment can be written as $\mathbf{p} = \alpha v \mathbf{E}$, where α is the (scalar) polarizability, v is the volume of the particle, and \mathbf{E} is the external field. The force can then be written as:

$$\mathbf{F} = \alpha v (\mathbf{E} \cdot \nabla)\mathbf{E} = \frac{1}{2} \alpha v \nabla |\mathbf{E}|^2 \quad (20-32)$$

This force equation can now be used to find the force in model systems such as that of an ideal dielectric sphere (relative dielectric constant K_2) in an ideal perfectly insulating dielectric fluid (relative dielectric constant K_1). The force can now be written as

$$\mathbf{F} = 2\pi a^3 \epsilon_0 K_1 \left(\frac{K_2 - K_1}{K_2 + 2K_1} \right) \nabla |\mathbf{E}|^2 \quad (20-33)$$

(ideal dielectric sphere in ideal fluid).

Heuristic Explanation As we can see from Fig. 20-30, the DEP response of *real* (as opposed to perfect insulator) particles with frequency can be rather complicated. We use a simple illustration to account for such a response. The force is proportional to the difference between the dielectric permittivities of the particle and the surrounding medium. Since a part of the polarization in real systems is thermally activated, there is a delayed response which shows as a phase lag between \mathbf{D} , the dielectric displacement, and \mathbf{E} , the electric-field intensity. To take this into account we may replace the simple (absolute) dielectric constant ϵ by the complex (absolute) dielectric constant $\hat{\epsilon} = \epsilon' - i\epsilon'' = \epsilon' - i\sigma/\omega$, where ω is the angular frequency of the applied field. For treating spherical objects, for example, the replacement

$$F \propto \frac{\epsilon_1(\epsilon_2 - \epsilon_1)}{\epsilon_2 + 2\epsilon_1} \rightarrow \text{Re} \left\{ \frac{\hat{\epsilon}_1^* (\hat{\epsilon}_2 - \hat{\epsilon}_1)}{\hat{\epsilon}_2 + 2\hat{\epsilon}_1} \right\} \quad (20-34)$$

can be made, where $\hat{\epsilon}^*$ is the complex conjugate of $\hat{\epsilon}$.

With this force expression for real dielectrics, we can now explain the complicated DEP response with the help of Fig. 20-30.

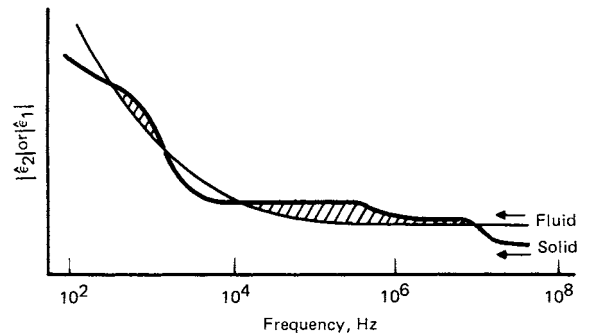


FIG. 20-30 A heuristic explanation of the dielectrophoretic-collection-rate (DCR)-frequency spectrum. The curves for the absolute values of the complex permittivities of the fluid medium and of the suspended particles are shown lying nearly, but not entirely, coincident over the frequency range of the applied electric field. When the permittivity (dielectric constant) of the particles exceeds that of the suspending medium, the collection, or "positive dielectrophoresis," occurs. In the frequency ranges in which the permittivity of the particles is less than that of the suspending medium no collection at the regions of higher field intensity occurs. Instead there is "negative dielectrophoresis," i.e., movement of the particles into regions of lower field intensity.

A particle, such as a living cell, can be imagined as having a number of different frequency-dependent polarization mechanisms contributing to the total effective polarization of the particle $|\epsilon_2|$. The heavy curve in Fig. 20-30 shows that the various mechanisms in the particle drop out stepwise as the frequency increases. The light curve in Fig. 20-30 shows the polarization for a simple homogeneous liquid that forms the surrounding medium. This curve is a smooth function which becomes constant at high frequency. As the curves cross each other (and hence $|\epsilon_2| = |\epsilon_1|$), various responses occur. The particle can thus be attracted to the strongest field region, be repelled from that region, or experience no force depending on the frequency.

Limitations It is desirable to have an estimate for the smallest particle size that can be effectively influenced by DEP. To do this, we consider the force on a particle due to DEP and also due to the osmotic pressure. This latter diffusional force will randomize the particles and tend to destroy the control by DEP. Figure 20-31 shows a plot of these two forces, calculated for practical and representative conditions, as a function of particle radius. As we can see, the smallest particles that can be effectively handled by DEP appear to be in range of 0.01 to 0.1 μm (100 to 1000 \AA).

Another limitation to be considered is the volume that the DEP force can affect. This factor can be controlled by the design of electrodes. As an example, consider electrodes of cylindrical geometry. A practical example of this would be a cylinder with a wire running down the middle to provide the two electrodes. The field in such a system is proportional to $1/r$. The DEP force is then $F_{\text{DEP}} \propto \nabla |E|^2 \propto 1/r^3$, so that any differences in particle polarization might well be masked merely by positional differences in the force. At the outer cylinder the DEP force may even be too small to affect the particles appreciably. The

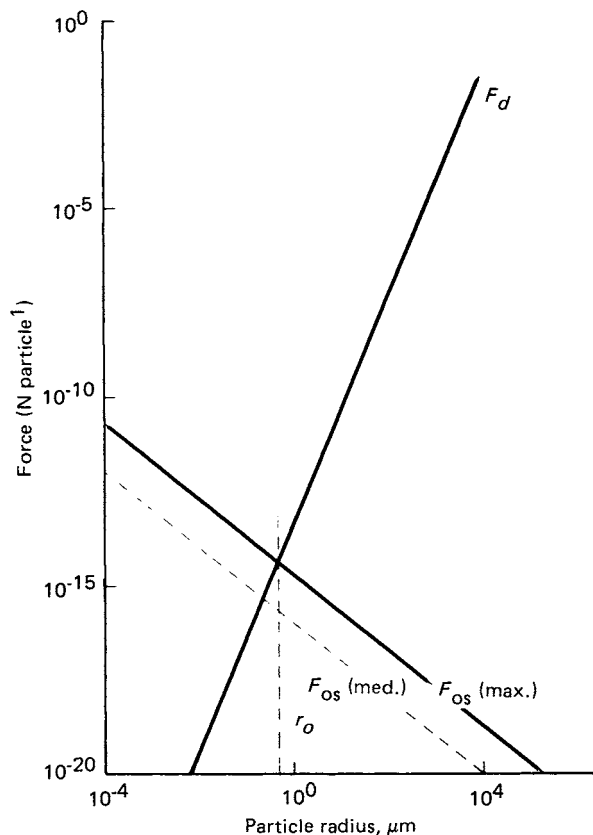


FIG. 20-31 Comparison of the dielectrophoretic (F_d) and osmotic (F_{os}) forces as functions of the particle size.

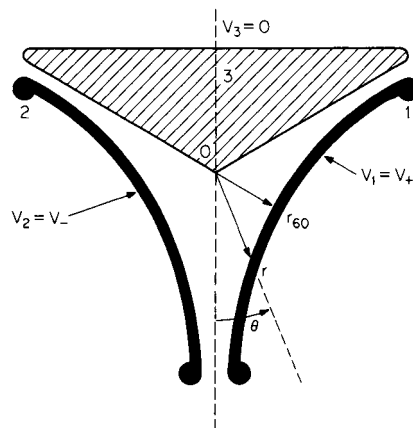


FIG. 20-32 A practical isomotive field geometry, showing r_{60} , the critical radius characterizing the isomotive electrodes. Electrode 3 is at ground potential, while electrodes 1 and 2 are at $V_1 = V_+$ and $V_2 = V_- = -V_+$, respectively. The inner faces of electrodes 1 and 2 follow $r = r_0 [\sin(3\theta/2)]^{-2.3}$, while electrode 3 forms an angle of 120° about the midline.

most desirable electrode shape is one in which the force is independent of position within the nonuniform field. This "isomotive" electrode system is shown in Fig. 20-32.

Applications of Dielectrophoresis Over the past 20 years the use of DEP has grown rapidly to a point at which it is in use for biological [Hughes, *Electrophoresis*, **23**, 2569–2582 (2002)], colloidal, and mineral materials studies and handling. The effects of nonuniform electric fields are used for handling particulate matter far more often than is usually recognized. This includes the removal of particulate matter by "electrofiltration," the sorting of mixtures, or its converse, the act of mixing, as well as the coalescence of suspensions. In addition to these effects involving the translational motions of particles, some systems apply the orientational or torsional forces available in nonuniform fields. One well-known example of the latter is the placing of "tip-up" grit on emery papers commercially. Xerography and many other imaging processes are examples of multibillion-dollar industries which depend upon DEP for their success.

A clear distinction between **electrophoresis** (field action on an object carrying excess free charges) and **dielectrophoresis** (field gradient action on neutral objects) must be borne in mind at all times.

A dielectrofilter [Lin and Benguigui, *Sep. Purif. Methods*, **10**(1), 53 (1981); Sisson et al., *Sep. Sci. Technol.*, **30**(7–9), 1421 (1995)] is a device which uses the action of an electric field to aid the filtration and removal of particulates from fluid media. A dielectrofilter can have a very obvious advantage over a mechanical filter in that it can remove particles which are much smaller than the flow channels in the filter. In contrast, the ideal mechanical filter must have all its passages smaller than the particles to be removed. The resultant flow resistance can be use-restrictive and energy-consuming unless a phenomenon such as dielectrofiltration is used.

Dielectrofiltration can (and often does) employ both electrophoresis and dielectrophoresis in its application. The precise physical process which dominates depends on a number of physical parameters of the system. Factors such as field intensity and frequency and the electrical conductivity and dielectric constants of the materials present determine this. Although these factors need constant attention for optimum operation of the dielectrofilter, this additional complication is often more than compensated for by the advantages of dielectrofiltration such as greater throughput and lesser sensitivity to viscosity problems, etc. To operate the dielectrofilter in the dominantly electrophoretic mode requires that excess free charges of one sign or the other reside on the particulate matter. The necessary charges can be those naturally present, as upon a charged sol; or they may need to be artificially implanted such as by passing the particles through a corona discharge.

Dielectrofiltration by the corona-charging, electrophoresis-dominated Cottrell technique is now widely used.

To operate the dielectrofilter (dominantly dielectrophoretic mode), on the other hand, one must avoid the presence of free charge on the particles. If the particles can become charged during the operation, a cycle of alternate charging and discharging in which the particles dash to and from the electrodes can occur. This is most likely to occur if static or very low frequency fields are used. For this reason, corona and like effects may be troublesome and need often to be minimized. To be sure, the DEP force is proportional to the field applied [actually to $\nabla(E)^2$], but fields which are too intense can produce such troublesome charge injection. A compromise for optimal operation is necessary between having $\nabla(E)^2$ so low that DEP forces are insufficient for dependable operation, on the one hand, and having E so high that troublesome discharges (e.g., coronalike) interfere with dependable operation of the dielectrofilter. In insulative media such as air or hydrocarbon liquids, for example, one might prefer to operate with fields in the range of, say, 10 to 10,000 V/cm. In more conductive media such as water, acetone, or alcohol, for example, one would usually prefer rather lower fields in the range of 0.01 to 100 V/cm. The higher field ranges cited might become unsuitable if conductive sharp asperities are present.

Another factor of importance in dielectrofiltration is the need to have the DEP effect firmly operative upon *all* portions of the fluid passing through. Oversight of this factor is a most common cause of incomplete dielectrofiltration. Good dielectrofilter design will emphasize this crucial point. To put this numerically, let us consider the essential field factor for DEP force, namely $\nabla(E_0)^2$. Near sharp points, e.g., E , the electric field varies with the radial distance r as $E \propto r^{-2}$, hence our DEP force factor will vary as $\nabla(E)^2 \propto r^{-5}$. In the neighborhood of sharp "line" sources such as at the edge of electrode plates, $E \propto r^{-1}$, hence, $\nabla(E)^2 \propto r^{-3}$. If, for instance, the distance is varied by a factor of 4 from the effective field source in these cases, the DEP force can be expected to weaken by a factor of 1024 or 64 respectively for the point source and the line source. The matter is even more keenly at issue when field-warping dielectrics (defined later) are used to effect maximal filtration. In this case the field-warping material is made to produce dipole fields as induced by the applied electric field. If we ask how the crucial factor, $\nabla(E)^2$, varies with distance away from such a dipole, we find that since the field E_d about a dipole varies approximately as r^{-3} , then $\nabla(E)^2$ can be expected to vary as r^{-7} . It then becomes critically important that the particles to be removed from the passing fluid do, indeed, pass very close to the surface of the field-warping material, or it will not be effectively handled. Clearly, it would be difficult to maintain successfully uniform dielectrofiltration treatment of fluid passing through such wildly variant regions. The problems can be minimized by ensuring that all the elements of the passing fluid go closely by such field sources in the dielectrofilter. In practice this is done by constructing the dielectrofilter from an assembly of highly comminuted electrodes or else by a set of relatively simple and widely spaced metallic electrodes between which is set an assembly of more or less finely divided solid dielectric material having a complex permittivity different from that of the fluid to be treated. The solid dielectric (fibers, spheres, chunks) serves to produce field nonuniformities or **field warpings** to which the particles to be filtered are to be attracted. In treating fluids of low dielectric constant such as air or hydrocarbon fluids, one sees field-warping materials such as sintered ceramic balls, glass-wool matting, open-mesh polyurethane foam, alumina, chunks, or BaTiO₃ particles.

An example of a practical dielectrofilter which uses both of the features described, namely, sharp electrodes *and* dielectric field-warping filler materials, is that described in Fig. 20-33 [H. J. Hall and R. F. Brown, *Lubric. Eng.*, **22**, 488 (1966)]. It is intended for use with hydraulic fluids, fuel oils, lubricating oils, transformer oils, lubricants, and various refinery streams. Performance data are cited in Fig. 20-34. It must be remarked that in the opinion of Hall and Brown the action of the dielectrofilter was "electrostatic" and due to free charge on the particles dispersed in the liquids. It is the present authors' opinion, however, that both electrophoresis and dielectrophoresis are operative here but that the dominant mechanism is that of DEP, in which neutral particles are polarized and attracted to the regions of highest field intensity.

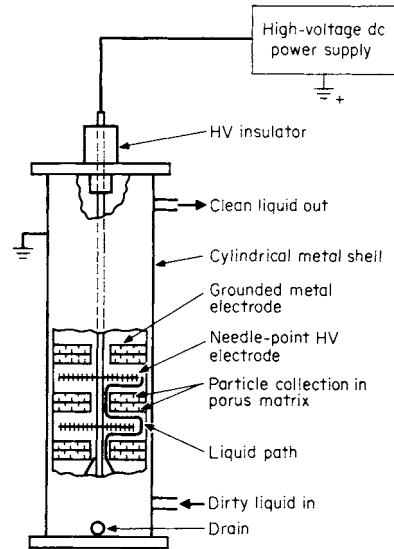


FIG. 20-33 Diagram illustrating the function of an electrostatic liquid cleaner.

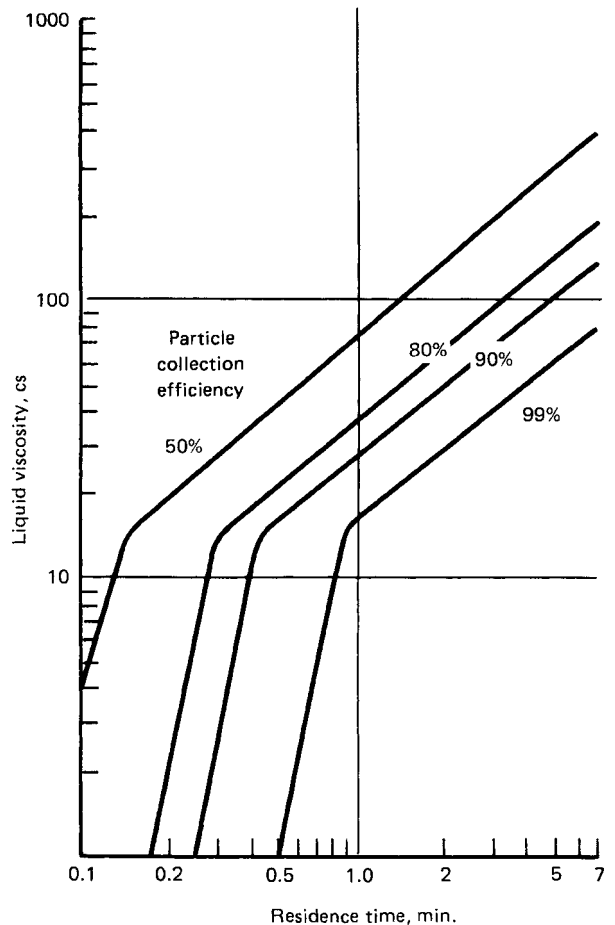


FIG. 20-34 Performance data for a typical high-efficiency electrostatic liquid cleaner.

A second commercial example of dielectric filtration is the Gulftronic® separator [G. R. Fritsche, *Oil & Gas J.*, **75**, 73 (1977)] which was commercialized in the late 1970s by Gulf Science and Technology Company. Instead of using needle-point electrodes as shown in Fig. 20-33, the Gulftronic® separator relied on the use of a bed of glass beads to produce the field nonuniformities required for dielectric filtration. Either ac or dc electric fields could be used in this separator. The Gulftronic® separator has been used primarily to remove catalyst fines from FCC decant oils and has been reported to exhibit removal efficiencies in excess of 80 percent for this fine-particle separation problem.

Another example of the commercial use of DEP is in polymer clarification [A. N. Wennerberg, U.S. Patent 2,914,453, 1959; assignor to Standard Oil Co. (Indiana)]. Here, either ac or dc potentials were used while passing suspensions to be clarified through regions with an area-to-electrode-area ratio of 10:1 or 100:1 and with fields in the order of 10 kV/cm. Field warping by the presence of various solid dielectrics was observed to enhance filtration considerably, as expected for DEP. The filtration of molten or dissolved polymers to free them of objectionable quantities of catalyst residues, for example, was more effective if a solid dielectric material such as Attapulugus clay, silica gel, fuller's earth, alumina, or bauxite was present in the region between the electrodes. The effectiveness of percolation through such absorptive solids for removing color bodies is remarkably enhanced by the presence of an applied field. A given amount of clay is reported to remove from 4 to 10 times as much color as would be removed in the absence of DEP. Similar results are reported by Lin et al. [Lin, Yaniv, and Zimmels, *Proc. XIIIth Int. Miner. Process. Congr.*, Wroclaw, Poland, 83-105 (1979)].

The instances cited were examples of the use of DEP to filter liquids. We now turn to the use of DEP to aid in dielectrofiltration of gases. Fielding et al. observe that the effectiveness of high-quality fiberglass air filters is dramatically improved by a factor of 10 or more by incorporating DEP in the operation. Extremely little current or power is required, and no detectable amounts of ozone or corona need result. The DEP force, once it has gathered the particles, continues to

act on the particles already sitting on the filter medium, thereby improving adhesion and minimizing blowoff.

The degree by which the DEP increases the effectiveness of gas filtration, or the dielectrophoretic augmentation factor (DAF), is definable. It is the ratio of the volumes of aerosol-laden gas which can be cleaned effectively by the filter with and without the voltage applied. For example, the application of 11 kV/cm gave a DAF of 30 for 1.0- μ m-diameter dioctyl phthalate particles in air, implying that the penetration of the glass filter is reduced thirtyfold by the application of a field of 1100 kV/m. Similar results were obtained by using "standard" fly ash supplied by the Air Pollution Control Office of the U.S. Environmental Protection Agency. The data obtained for several aerosols tested are shown in Table 20-14 and in Fig. 20-35. The relation $DAF = kV^2/v$ is observed to hold approximately for each aerosol. Here, the DEP augmentation factor DAF is observed to depend upon a constant K , a characteristic of the material, upon the square of the applied voltage, and upon the inverse of the volume flow rate v through the filter.

It is worth noting that in the case of the air filter described DEP serves as an augmenting rather than as an exclusive mechanism for the removal of particulate material. It is a unique feature of the dielectrophoretic gas filter that the DEP force is maximal when the particulates are at or on the fiber surface. This causes the deposits to be strongly retained by this particular filtration mechanism. It thus contrasts importantly with other types of gas filter in which the filtration mechanism no longer acts after the capture of the particle. In particular, in the case of the older electrostatic mechanisms involving only coulombic attraction, a simple charge alternation on the particle, such as caused by normal conduction, often evokes disruption of the filter operation because of particle repulsion from the contacting electrode. On the other hand, ordinary mechanical filtration depends upon the action of adventitious particle trapping or upon van der Waals forces, etc., to hold the particles. The high efficiency possible with electrofilters suggests their wider use.

TABLE 20-14 Dielectrophoretic Augmentation of Filtration of a Liquid Aerosol*

Air speed, cm/s	DAF at			
	2 kV	3.5 kV	5 kV	7 kV
0.3- μ m-diameter dioctyl phthalate aerosol				
3	8	19	95	330
6	3	13	39	120
9	3	11	28	100
15	2	6	13	42
20	2	5	9	27
28	2	4	6	14
39	2	3	4	9
50	1	2	3	6
1.0- μ m-diameter dioctyl phthalate aerosol				
3	30	110	300	1100
6	6	3	95	360
9	4	18	50	170
15	3	10	20	50
20	2	6	13	35
28	2	4	8	18
39	2	3	5	11
50	1	2	3	7
Fly-ash aerosol				
6	10	30	80	
10	8	30	80	
14	5	20	40	
20	4	10	30	70
35	3	7	10	20
45	1	2	6	
53	1	2	7	10

*Experimentally measured dielectrophoretic augmentation factor DAF as a function of air speed and applied voltage for a glass-fiber filter (HP-100, Farr Co.). Cf. Fielding, Thompson, Bogardus, and Clark, *Dielectrophoretic Filtration of Solid and Liquid Aerosol Particulates*, Prepr. 75-32.2, 68th ann. meet., Air Pollut. Control Assoc., Boston, June 1975.

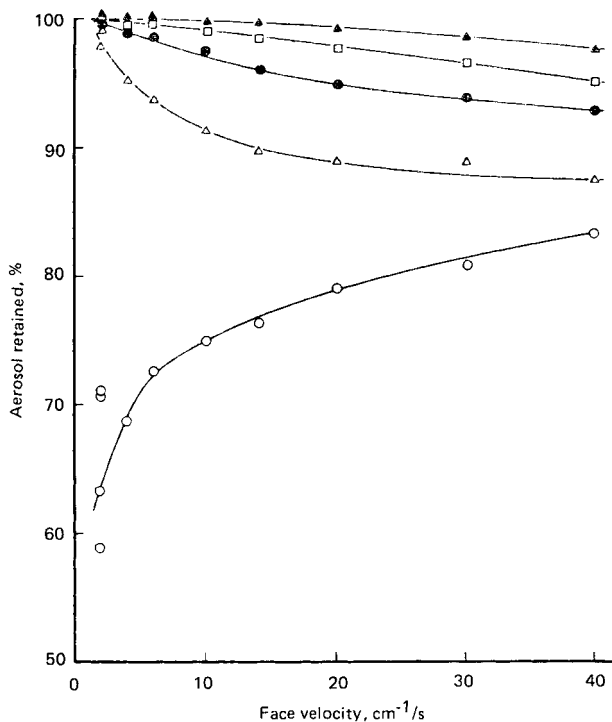


FIG. 20-35 Efficiency of an electrofilter as a function of gas flow rate at 5 different voltages. Experimental materials: 1- μ m aerosol of dioctyl phthalate; glass-fiber filter. Symbols: O, no voltage applied; Δ , 2 kV; \bullet , 3.5 kV; \square , 5 kV; \blacktriangle , 7 kV. (After Fielting et al., *Dielectrophoretic Filtration of Solid and Liquid Aerosol Particulates*, Prepr. 75-32.2, 68th ann. meet., Air Pollut. Control Assoc., Boston, June 1975.)

SURFACE-BASED SOLID-LIQUID SEPARATIONS INVOLVING A SECOND LIQUID PHASE

GENERAL REFERENCES: Fuerstenau, "Fine Particle Flotation," in Somasundaran (ed.), *Fine Particles Processing*, vol. 1, American Institute of Mining, Metallurgical, and Petroleum Engineers, New York, 1980. Henry, Prudich, and Lau, *Colloids Surf.*, **1**, 335 (1980). Henry, Prudich, and Vaidyanathan, *Sep. Purif. Methods*, **8**(2), 31 (1979). Jacques, Hovarongkura, and Henry, *Am. Inst. Chem. Eng. J.*, **25**(1), 160 (1979). Stratton-Crawley, "Oil Flotation: Two Liquid Flotation Techniques," in Somasundaran and Arbitter (eds.), *Beneficiation of Mineral Fines*, American Institute of Mining, Metallurgical, and Petroleum Engineers, New York, 1979.

Process Concept Three potential surface-based regimes of separation exist when a second, immiscible liquid phase is added to another, solids-containing liquid in order to effect the removal of solids. These regimes (Fig. 20-36) are:

1. Distribution of the solids into the bulk second liquid phase
2. Collection of the solids at the liquid-liquid interface
3. Bridging or clumping of the solids by the added fluid in order to form an agglomerate followed by settling or filtration

These separation techniques should find particular application in systems containing fine particles. The surface chemical differences involved among these separation regimes are only a matter of degree; i.e., all three regimes require the wetting of the solid by the second liquid phase. The addition of a surface-active agent is sometimes needed in order to achieve the required solids wettability. In spite of this similarity, applied processing (equipment configuration, operating conditions, etc.) can vary widely. Collection at the interface would normally be treated as a flotation process (see also "Adsorptive-Bubble Separation Methods" in Sec. 20), distribution to the bulk liquid as a liquid-liquid extraction analog, and particle bridging as a settling (sedimentation) or filtration process.

Even though surface-property-based liquid-solid-liquid separation techniques have yet to be widely used in significant industrial applications, several studies which demonstrate their effectiveness have appeared in literature.

Albertsson (*Partition of Cell Particles and Macromolecules*, 3d ed., Wiley, New York, 1986) has extensively used particle distribution to

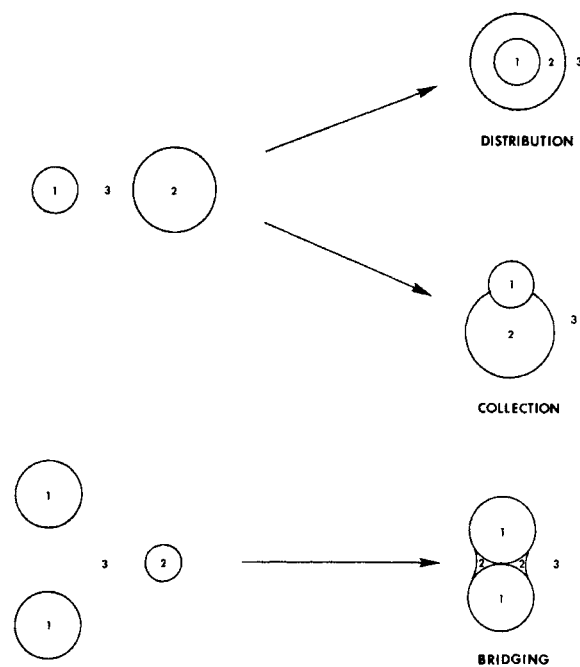


FIG. 20-36 Regimes of separation in a liquid-solid-liquid system. Phase 1 = particle; phase 2 = liquid (dispersed); phase 3 = liquid (continuous).

TABLE 20-15 Separations of Particles between Two Phases

System	Top phase	Bottom phase
Polyethylene glycol salt	Polystyrene	All others
PEG	Algae	All others
Dextran; 20,000 MW	Red cells	All others
PEG	Cellulose particles	Starch
Dextran; 200,000 MW		
Methyl cellulose		
Dextran		

fractionate mixtures of biological products. (See also Sec. 15.) In order to demonstrate the versatility of particle distribution, he has cited the example shown in Table 20-15. The feed mixture consisted of polystyrene particles, red blood cells, starch, and cellulose. Liquid-liquid particle distribution has also been studied by using mineral-matter particles (average diameter = 5.5 μm) extracted from a coal liquid as the solid in a xylene-water system [Prudich and Henry, *Am. Inst. Chem. Eng. J.*, **24**(5), 788 (1978)]. By using surface-active agents in order to enhance the water wettability of the solid particles, recoveries of better than 95 percent of the particles to the water phase were observed. All particles remained in the xylene when no surfactant was added.

Particle collection at a liquid-liquid interface is a particularly favorable separation process when applied to fine-particle systems. Advantages of this type of processing include:

- Decreased liquid-liquid interfacial tension (when compared with a gas-liquid system) results in higher liquid-liquid interfacial areas, which favor solid-particle droplet collisions.
- Liquid-solid interactions due to long-range intermolecular forces are much larger than are gas-solid interactions. This means that it is easier to collect fine particles at a liquid-liquid interface than at a gas-liquid interface.
- The increased momentum of liquid droplets (when compared with gas) should favor solid-particle collection.

Fuerstenau [Lai and Fuerstenau, *Trans. Am. Inst. Min. Metall. Pet. Eng.*, **241**, 549 (1968); Raghavan and Fuerstenau, *Am. Inst. Chem. Eng. Symp. Ser.*, **71**(150), 59 (1975)] has studied this process with respect to the removal of alumina particles (0.1 μm) and hematite particles (0.2 μm) from an aqueous solution by using isooctane. The use of isooctane as the collecting phase for the hematite particles resulted in an increase in particle recovery of about 50 percent over that measured when air was used as the collecting phase under the same conditions. The effect of the wettability of the solid particles (as measured by the three-phase contact angle) on the recovery of hematite in the water-isooctane system is shown in Fig. 20-37. This behavior is typical of particle collection. Particle collection at an oil-water interface has also been studied with respect to particle removal from a coal liquid. Particle removals averaging about 80 percent have been observed when water is used as the collecting phase (Lau, master's thesis, West Virginia University, 1979). Surfactant addition was necessary in order to control the wettability of the solids.

Particle bridging has been chiefly investigated with respect to spherical agglomeration. Spherical agglomeration involves the collecting or transferring of the fine particles from suspension in a liquid phase into spherical aggregates held together by a second liquid phase. The aggregates are then removed from the slurry by filtration or settling. Like the other liquid-solid-liquid separation techniques, the solid must be wet by the second liquid phase. The spherical agglomeration process has resulted in the development of a pilot unit called the Shell Pelletizing Separator [Zuiderweg and Van Lookeren Campagne, *Chem. Eng. (London)*, **220**, CE223 (1968)].

The ability to determine in advance which of the separation regimes is most advantageous for a given liquid-solid-liquid system would be desirable. No set of criteria with which to make this determination presently exists. Work has been done with respect to the

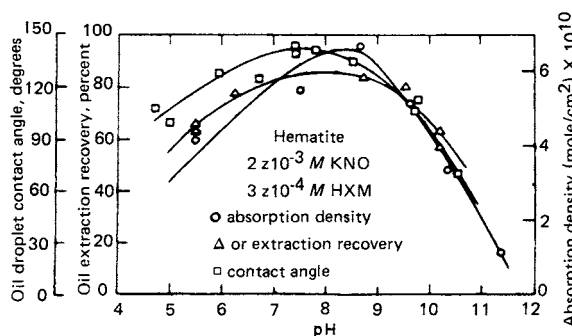


FIG. 20-37 The variation of adsorption density, oil-droplet contact angle, and oil-extraction recovery of hematite as a function of pH. To convert gram-moles per square centimeter to pound-moles per square foot, multiply by 2.048. [From Raghavan and Fuerstenau, *Am. Inst. Chem. Eng. Symp. Ser.*, **71**(150), 59 (1975).]

identification of system parameters which make these processes technically feasible. The results of these studies can be used to guide the selection of the second liquid phase as well as to suggest approximate operating conditions (dispersed-liquid droplet size, degree and type of mixing, surface-active-chemical addition, etc.).

Theory Theoretical analyses of spherical particles suspended in a planar liquid-liquid interface have appeared in literature for some time, the most commonly presented forms being those of a free energy and/or force balance made in the absence of all external body forces. These analyses are generally used to define the boundary criteria for the shift between the collection and distribution regimes, the bridging regime not being considered. This type of analysis shows that for a spherical particle possessing a three-phase contact angle between 0 and 180°, as measured through the receiving or collecting phase, collection at the interface is favored over residence in either bulk phase. These equations are summarized, using a derivation of Young's equation, as

$$\frac{\gamma_{s2} - \gamma_{s1}}{\gamma_{12}} > 1 \text{ particles wet to phase 1} \quad (20-35)$$

$$\frac{\gamma_{s2} - \gamma_{s1}}{\gamma_{12}} < -1 \text{ particles wet to phase 2} \quad (20-36)$$

$$\left| \frac{\gamma_{s2} - \gamma_{s1}}{\gamma_{12}} \right| \leq 1 \text{ particle at interface} \quad (20-37)$$

where γ_{ij} is the surface tension between phases i and j , N/m (dyn/cm); s indicates the solid phase; and subscripts 1 and 2 indicate the two liquid phases.

Several additional studies [Winitzer, *Sep. Sci.*, **8**(1), 45 (1973); *ibid.*, **8**(6), 647 (1973); Maru, Wasan, and Kintner, *Chem. Eng. Sci.*, **26**, 1615 (1971); and Rapacchiotta and Neumann, *J. Colloid Interface Sci.*, **59**(3), 555 (1977)] which include body forces such as gravitational acceleration and buoyancy have been made. A typical example of a force balance describing such a system (Fig. 20-38) is summarized in Eq. (20-38):

$$[(\gamma_{s1} - \gamma_{s2}) \cos \delta + \gamma_{12} \cos B]L = g[V_{\text{total}}\rho_s - V_1\rho_1 - V_2\rho_2] \quad (20-38)$$

where V_1 is the volume of the particle in fluid phase 1, V_2 is the volume in fluid phase 2, L is the particle circumference at the interface between the two liquid phases, ρ_i is the density of phase i , and g is the gravitational constant. The left-hand side of the equation represents the surface forces acting on the solid particle, while the right-hand side includes the gravitational and buoyancy forces. This example illustrates the fact that body forces can have a significant effect on system behavior. The solid-particle size as well as the densities of the solid and both liquid phases are introduced as important system parameters.

A study has also been performed for particle distribution for cases in which the radii of curvature of the solid and the liquid-liquid interface

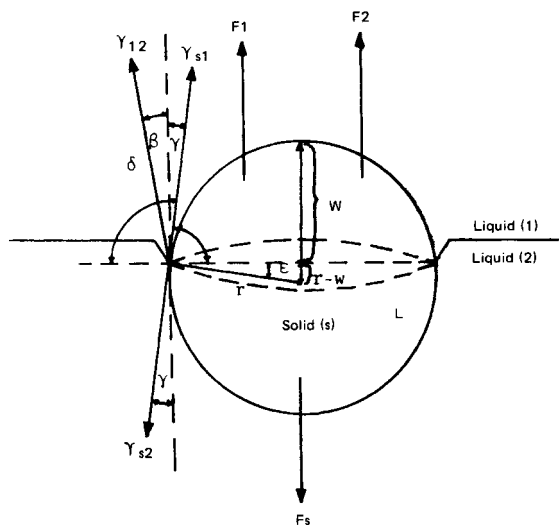


FIG. 20-38 Solid sphere suspended at the liquid-liquid interface. F_1 and F_2 are buoyancy forces; F_s is gravity. [From Winitzer, *Sep. Sci.*, **8**(1), 45 (1973).]

are of the same order of magnitude [Jacques, Hovrongkura, and Henry, *Am. Inst. Chem. Eng. J.*, **25**(1), 160 (1979)]. Differences between the final and initial surface free energies are used to analyze this system. Body forces are neglected. Results (Fig. 20-39) demonstrate that n , the ratio of the particle radius to the liquid-liquid-interface radius, is an important system parameter. Distribution of the particle from one phase to the other is favored over continued residence in the original phase when the free-energy difference is negative. For a solid particle of a given size, these results show that as the second-phase droplet size decreases, the contact angle required in order to effect distribution decreases (the required wettability of the solid by the second phase increases). The case of particle collection at a curved liquid-liquid interface has also been studied in a similar manner [Smith and Van de Ven, *Colloids Surf.*, **2**, 387 (1981)]. This study shows that collection is preferred over distribution for any n in systems without external body forces when the contact angle lies between 0 and 180°.

While thermodynamic-stability studies can be valuable in evaluating the technical feasibility of a process, they are presently inadequate in determining which separation regime will dominate a particular liquid-solid-liquid system. These analyses ignore important processing phenomena such as the mechanism of encounter of the dispersed-phase liquid with the solid particles, the strength of particle attachment, and the mixing-energy input necessary to effect the separation. No models of good predictive value which take all these variables into account have yet been offered. Until the effects of these and other system variables can be adequately understood, quantified, and combined into such a predictive model, no a priori method of performance prediction will be possible.

ADSORPTIVE-BUBBLE SEPARATION METHODS

GENERAL REFERENCES: Lemlich (ed.), *Adsorptive Bubble Separation Techniques*, Academic, New York, 1972. Carleson, "Adsorptive Bubble Separation Processes" in Scaemhorn and Harwell (eds.), *Surfactant-Based Separation Processes*, Marcel Dekker, New York, 1989.

Principle The adsorptive-bubble separation methods, or adsorbable methods for short [Lemlich, *Chem. Eng.* **73**(21), 7 (1966)], are based on the selective adsorption or attachment of material on the surfaces of gas bubbles passing through a solution or suspension. In most of the methods, the bubbles rise to form a foam or froth which carries the material off overhead. Thus the material (desirable or undesirable) is removed from the liquid, and not vice versa as in, say,

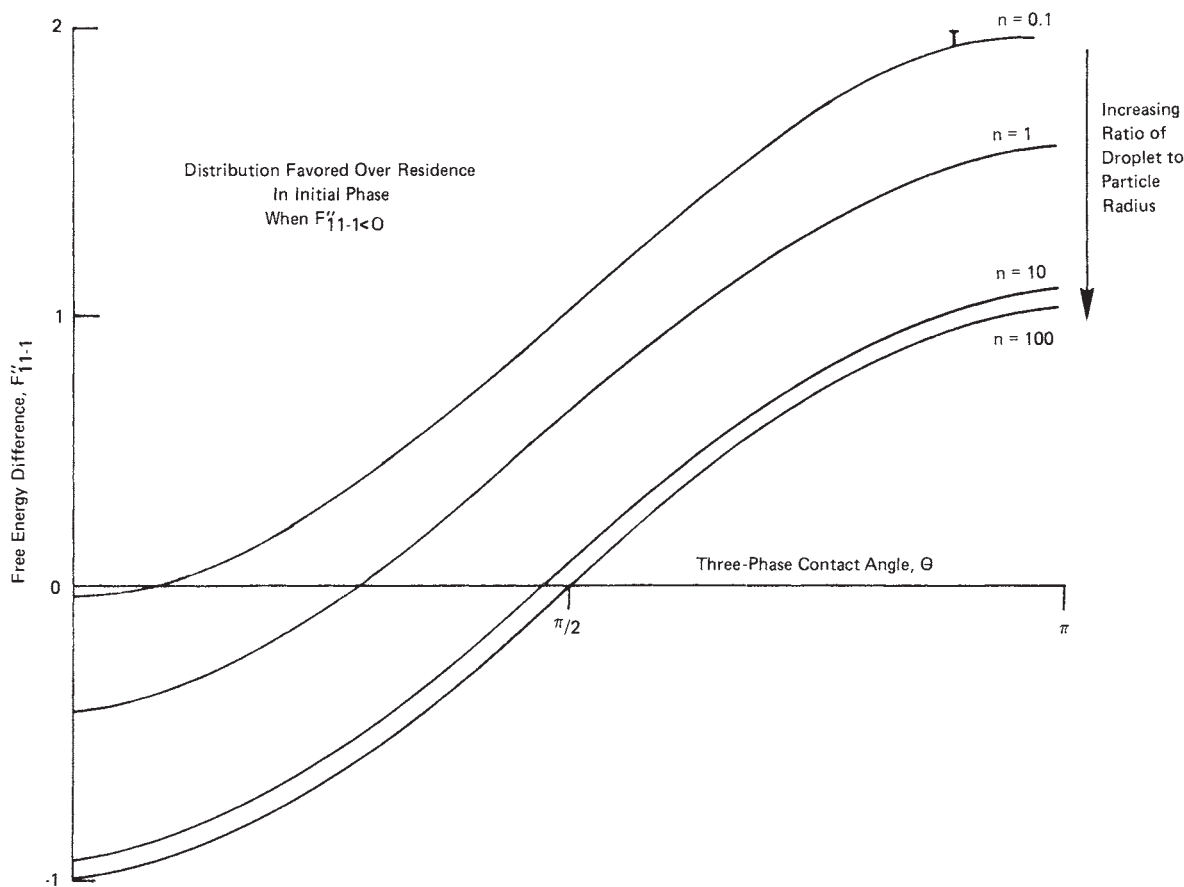


FIG. 20-39 Normalized free-energy difference between distributed (II) and nondistributed (I) states of the solid particles versus three-phase contact angle (collection at the interface is not considered). A negative free-energy difference implies that the distributed state is preferred over the nondistributed state. Note especially the significant effect of n , the ratio of the liquid droplet to solid-particle radius. [From Jacques, Hovarrongkura, and Henry, *Am. Inst. Chem. Eng. J.*, **25**(1), 160 (1979).]

filtration. Accordingly, the foaming methods appear to be particularly (although not exclusively) suited to the removal of small amounts of material from large volumes of liquid.

For any adsorbable method, if the material to be removed (termed the **colligend**) is not itself surface-active, a suitable surfactant (termed the **collector**) may be added to unite with it and attach or adsorb it to the bubble surface so that it may be removed (Sebba, *Ion Flotation*, Elsevier, New York, 1962). The union between colligend and collector may be by chelation or other complex formation. Alternatively, a charged colligend may be removed through its attraction toward a collector of opposite charge.

Definitions and Classification Figure 20-40 outlines the most widely accepted classification of the various adsorbable methods [Karger, Grieves, Lemlich, Rubin, and Sebba, *Sep. Sci.*, **2**, 401 (1967)]. It is based largely on actual usage of the terms by various workers, and so the definitions include some unavoidable inconsistencies and overlap.

Among the methods of foam separation, **foam fractionation** usually implies the removal of dissolved (or sometimes colloidal) material. The overflowing foam, after collapse, is called the *foamate*. The solid lines of Fig. 20-41 illustrate simple continuous foam fractionation. (Batch operation would be represented by omitting the feed and bottoms streams.)

On the other hand, **flotation** usually implies the removal of solid particulate material. Most important under the latter category is **ore flotation**.

Also under the category of flotation are to be found **macroflotation**, which is the removal of macroscopic particles; **microflotation** (also called **colloid flotation**), which is the removal of microscopic particles, particularly colloids or microorganisms [Dognon and Dumontet, *Comptes Rendus*, **135**, 884 (1941)]; **molecular flotation**, which is the removal of surface-inactive molecules through the use of a collector (surfactant) which yields an insoluble product; **ion flotation**, which is the removal of surface-inactive ions via a collector which yields an insoluble product, especially a removable scum [Sebba, *Nature*, **184**, 1062 (1959)]; **adsorbing colloid flotation**, which is the removal of dissolved material in piggyback fashion by adsorption on colloidal particles; and **precipitate flotation**, in which a precipitate is removed by a collector which is not the precipitating agent [Baarson and Ray, "Precipitate Flotation," in Wadsworth and Davis (eds.), *Unit Processes in Hydrometallurgy*, Gordon and Breach, New York, 1964, p. 656]. The last definition has been narrowed to precipitate flotation of the first kind, the second kind requiring no separate collector at all [Mahne and Pinfold, *J. Appl. Chem.*, **18**, 52 (1968)].

A separation can sometimes be obtained even in the absence of any foam (or any floated floc or other surrogate). In **bubble fractionation** this is achieved simply by lengthening the bubbled pool to form a vertical column [Dorman and Lemlich, *Nature*, **207**, 145 (1965)]. The ascending bubbles then deposit their adsorbed or attached material at the top of the pool as they exit. This results in a concentration gradient which can serve as a basis for separation. Bubble fractionation can operate either alone or as a booster section below a foam

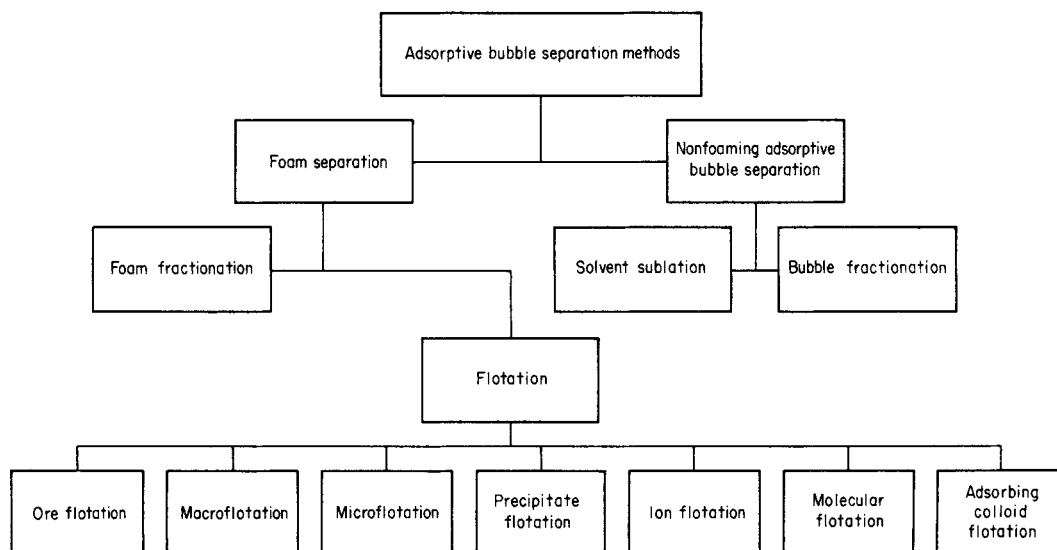


FIG. 20-40 Classification for the adsorptive-bubble separation methods.

fractionator, perhaps to raise the concentration up to the foaming threshold.

In **solvent sublation** an immiscible liquid is placed atop the main liquid to trap the material deposited by the bubbles as they exit (Sebba, *Ion Flotation*, Elsevier, New York, 1962). The upper liquid should dissolve or at least wet the material. With appropriate selectivity, the separation so achieved can sometimes be much greater than that with bubble fractionation alone.

The droplet analogs to the adsorbable methods have been termed the **adsoplet methods** (from adsorptive droplet separation methods) [Lemlich, "Adsorptive Bubble Separation Methods," *Ind. Eng. Chem.*, **60**(10), 16 (1968)]. They are omitted from Fig. 20-40, since they involve adsorption or attachment at *liquid-liquid* interfaces. Among them are **emulsion fractionation** [Eldib, "Foam and Emulsion Fractionation," in Kobe and McKetta (eds.), *Advances in Petroleum Chemistry and Refining*, vol. 7, Interscience, New York, 1963, p. 66], which is the analog of foam fractionation; and **droplet fractionation** [Lemlich, loc.

cit.; and Strain, *J. Phys. Chem.*, **57**, 638 (1953)], which is the analog of bubble fractionation. Similarly, the old beneficiation operation called bulk oil flotation (Gaudin, *Flotation*, 2d ed., McGraw-Hill, New York, 1957) is the analog of modern ore flotation. By and large, the adsoplet methods have not attracted the attention accorded to the adsorbable methods.

Of all the adsorbable methods, foam fractionation is the one for which chemical engineering theory is the most advanced. Fortunately, some of this theory also applies to other adsorbable methods.

Adsorption The separation achieved depends in part on the selectivity of adsorption at the bubble surface. At equilibrium, the adsorption of dissolved material follows the Gibbs equation (Gibbs, *Collected Works*, Longmans Green, New York, 1928).

$$d\gamma = -RT\Sigma\Gamma_i d \ln a_i \quad (20-39)$$

Γ_i is the surface excess (Davies and Rideal, *Interfacial Phenomena*, 2d ed., Academic, New York, 1963). For most purposes, it is sufficient to view Γ_i as the concentration of adsorbed component i at the surface in units of, say (g-mol)/cm². R is the gas constant, T is the absolute temperature, γ is the surface tension, and a_i is the activity of component i . The minus sign shows that material which concentrates at the surface generally lowers the surface tension, and vice versa. This can sometimes be a guide in determining preliminarily what materials can be separated.

When applied to a nonionic surfactant in pure water at concentrations below the critical micelle concentration, Eq. (20-39) simplifies into Eq. (20-40)

$$\Gamma_s = -\frac{1}{RT} \frac{d\gamma}{d \ln C_s} \quad (20-40)$$

C is the concentration in the bulk, and subscript s refers to the surfactant. Under some conditions, Eq. (20-40) may apply to an ionic surfactant as well (Lemlich, loc. cit.).

The major surfactant in the foam may usually be considered to be present at the bubble surfaces in the form of an adsorbed monolayer with a substantially constant Γ_s , often of the order of 3×10^{-10} (g-mol)/cm², for a molecular weight of several hundred. On the other hand, trace materials follow the linear-adsorption isotherm $\Gamma_i = K_i C_i$ if their concentration is low enough. For a wider range of concentration a Langmuir or other type of isotherm may be applicable (Davies and Rideal, loc. cit.).

Factors Affecting Adsorption K_i for a colligend can be adversely affected (reduced) through an insufficiency of collector. It can also be reduced through an excess of collector, which competes

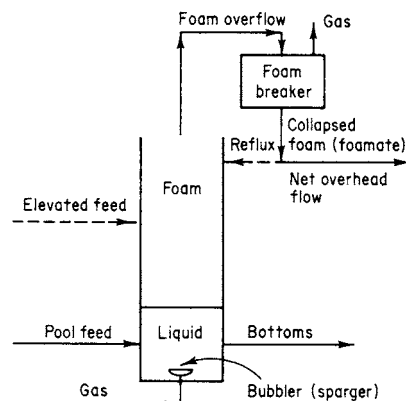


FIG. 20-41 Four alternative modes of continuous-flow operation with a foam-fractionation column: (1) The simple mode is illustrated by the solid lines. (2) Enriching operation employs the dashed reflux line. (3) In stripping operation, the elevated dashed feed line to the foam replaces the solid feed line to the pool. (4) For combined operation, reflux and elevated feed to the foam are both employed.

for the available surface against the collector-colligend complex [Schnepf, Gaden, Mirocznik, and Schonfeld, *Chem. Eng. Prog.*, **55**(5), 42 (1959)].

Excess collector can also reduce the separation by forming micelles in the bulk which adsorb some of the colligend, thus keeping it from the surface. This effect of the micelles on K_i for the colligend is given theoretically [Lemlich, "Principles of Foam Fractionation," in Perry (ed.), *Progress in Separation and Purification*, vol. 1, Interscience, New York, 1968, chap. 1] by Eq. (20-41) [Lemlich (ed.), *Adsorptive Bubble Separation Techniques*, Academic, New York, 1972] if Γ_s is constant when $C_s > C_{sc}$:

$$\frac{1}{K_2} = \frac{1}{K_1} + \frac{C_s - C_{sc}}{\Gamma_s E} \quad (20-41)$$

K_1 is K_i just below the collector's critical micelle concentration, C_{sc} . K_2 is K_i at some higher collector concentration, C_s . E is the relative effectiveness, in adsorbing colligend, of surface collector versus micellar collector. Generally, $E > 1$. Γ_s is the surface excess of collector. More about each K is available [Lemlich, "Adsorbable Methods," in Li (ed.), *Recent Developments in Separation Science*, vol. 1, CRC Press, Cleveland, 1972, pp. 113-127; Jashnani and Lemlich, *Ind. Eng. Chem. Process Des. Dev.*, **12**, 312 (1973)].

The controlling effect of various ions can be expressed in terms of thermodynamic equilibria [Karger and DeVivo, *Sep. Sci.*, **3**, 393 (1968)]. Similarities with ion exchange have been noted. The selectivity of counterionic adsorption increases with ionic charge and decreases with hydration number [Jorne and Rubin, *Sep. Sci.*, **4**, 313 (1969); and Kato and Nakamori, *J. Chem. Eng. Japan*, **9**, 378 (1976)]. By analogy with other separation processes, the relative distribution in multicomponent systems can be analyzed in terms of a selectivity coefficient $\alpha_{mn} = \Gamma_m C_n / \Gamma_n C_m$ [Rubin and Jorne, *Ind. Eng. Chem. Fundam.*, **8**, 474 (1969); *J. Colloid Interface Sci.*, **33**, 208 (1970)].

Operation in the Simple Mode If there is no concentration gradient within the liquid pool and if there is no coalescence within the rising foam, then the operation shown by the solid lines of Fig. 20-41 is truly in the simple mode, i.e., a single theoretical stage of separation. Equations (20-42) and (20-43) will then apply to the steady-flow operation.

$$C_Q = C_W + (GS\Gamma_W/Q) \quad (20-42)$$

$$C_W = C_F - (GS\Gamma_W/F) \quad (20-43)$$

C_F , C_W , and C_Q are the concentrations of the substance in question (which may be a colligend or a surfactant) in the feed stream, bottoms stream, and foamate (collapsed foam), respectively. G , F , and Q are the volumetric flow rates of gas, feed, and foamate, respectively. Γ_W is the surface excess in equilibrium with C_W . S is the surface-to-volume ratio for a bubble. For a spherical bubble, $S = 6/d$, where d is the bubble diameter. For variation in bubble sizes, d should be taken as $\sum n_i d_i^3 / \sum n_i d_i^2$, where n_i is the number of bubbles with diameter d_i in a representative region of foam.

Finding Γ Either Eq. (20-42) or Eq. (20-43) can be used to find the surface excess indirectly from experimental measurements. To assure a close approach to operation as a single theoretical stage, coalescence in the rising foam should be minimized by maintaining a proper gas rate and a low foam height [Brunner and Lemlich, *Ind. Eng. Chem. Fundam.*, **2**, 297 (1963)]. These precautions apply particularly with Eq. (20-42).

For laboratory purposes it is sometimes convenient to recycle the foamate directly to the pool in a manner analogous to an equilibrium still. This eliminates the feed and bottoms streams and makes for a more reliable approach to steady-state operation. However, this recycling may not be advisable for colligend measurements in the presence of slowly dissociating collector micelles.

To avoid spurious effects in the laboratory, it is advisable to employ a prehumidified chemically inert gas.

Bubble Sizes Subject to certain errors (de Vries, *Foam Stability*, Rubber-Stichting, Delft, 1957), foam bubble diameters can be measured photographically. Some of these errors can be minimized by taking pains to generate bubbles of fairly uniform size, say, by using a bubbler with identical orifices or by just using a bubbler with a single orifice (gas rate permitting). Otherwise, a correction for planar statistical sampling bias in

the foam should be incorporated with actual diameters [de Vries, op. cit.] or truncated diameters [Lemlich, *Chem. Eng. Commun.*, **16**, 153 (1982)]. Also, size segregation can reduce mean mural bubble diameter by roughly half the standard deviation [Cheng and Lemlich, *Ind. Eng. Chem. Fundam.*, **22**, 105 (1983)]. Bubble diameters can also be measured in the liquid pool, either photographically or indirectly via measurement of the gas flow rate and stroboscopic determination of bubble frequency [Leonard and Lemlich, *Am. Inst. Chem. Eng. J.*, **11**, 25 (1965)].

Bubble sizes at formation generally increase with surface tension and orifice diameter. Prediction of sizes in swarms from multiple orifices is difficult. In aqueous solutions of low surface tension, bubble diameters of the order of 1 mm are common. Bubbles produced by the more complicated techniques of pressure flotation or vacuum flotation are usually smaller, with diameters of the order of 0.1 mm or less.

Enriching and Stripping Unlike truly simple foam fractionation without significant changes in bubble diameter, coalescence in a foam column destroys some bubble surface and so releases adsorbed material to trickle down through the rising foam. This downflow constitutes internal reflux, which enriches the rising foam by countercurrent action. The result is a richer foamate, i.e., higher C_Q than that obtainable from the single theoretical stage of the corresponding simple mode. Significant coalescence is often present in rising foam, but the effect on bubble diameter and enrichment is frequently overlooked.

External reflux can be furnished by returning some of the externally broken foam to the top of the column. The concentrating effect of reflux, even for a substance which saturates the surface, has been verified [Lemlich and Lavi, *Science*, **134**, 191 (1961)].

Introducing the feed into the foam some distance above the pool makes for stripping operation. The resulting countercurrent flow in the foam further purifies the bottoms, i.e., lowers C_W .

Enriching, stripping, and combined operations are shown in Fig. 20-41.

Foam-Column Theory The counterflowing streams within the foam are viewed as consisting *effectively* of a descending stream of interstitial liquid (equal to zero for the simple mode) and an ascending stream of interstitial liquid plus bubble surface. (By considering this ascending surface as analogous to a vapor, the overall operation becomes analogous in a way to distillation *with entrainment*.)

An effective concentration [\bar{C}] in the ascending stream at any level in the column is defined by Eq. (20-44):

$$\bar{C} = C + (GS\Gamma/U) \quad (20-44)$$

where U is the volumetric rate of interstitial liquid upflow, C is the concentration in this ascending liquid at that level, and Γ is the surface excess in equilibrium with C . Any effect of micelles should be included.

For simplicity, U can usually be equated to Q . An effective equilibrium curve can now be plotted from Eq. (20-44) in terms of \bar{C} (or rather C°) versus C .

Operating lines can be found in the usual way from material balances. The slope of each such line is $\Delta\bar{C}/\Delta C = L/U$, where L is the downflow rate in the particular column section and C is now the concentration in the descending stream.

The number of theoretical stages can then be found in one of the usual ways. Figure 20-42 illustrates a graphical calculation for a stripper.

Alternatively, the number of transfer units (NTU) in the foam based on, say, the ascending stream can be found from Eq. (20-45):

$$NTU = \int_{C_w}^{C_Q} \frac{d\bar{C}}{C^\circ - C} \quad (20-45)$$

\bar{C}° is related to C by the effective equilibrium curve, and \bar{C}_w° is similarly related to C_w . \bar{C} is related to C by the operating line.

To illustrate this integration analytically, Eq. (20-45) becomes Eq. (20-46) for the case of a stripping column removing a colligend which is subject to the linear-equilibrium isotherm $\Gamma = KC$.

$$NTU = \frac{F}{GSK - W} \ln \frac{FW + F(GSK - W)C_F/C_W}{GSK(GSK + F - W)} \quad (20-46)$$

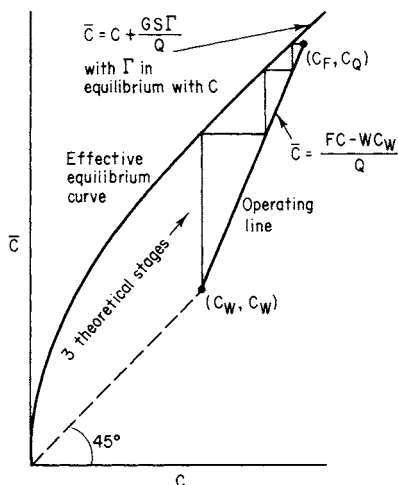


FIG. 20-42 Graphical determination of theoretical stages for a foam-fractionation stripping column.

As another illustration, Eq. (20-45) becomes Eq. (20-47) for an enriching column which is concentrating a surfactant with a constant Γ :

$$NTU = R \ln \frac{RG\Gamma(F - D)}{(R + 1)G\Gamma(F - D) - (R + 1)FD(C_D - C_F)} \quad (20-47)$$

Unless the liquid pool is purposely lengthened vertically in order to give additional separation via bubble fractionation, it is usually taken to represent one theoretical stage. A bubbler submergence of 30 cm or so is usually ample for a solute with a molecular weight that does not exceed several hundred.

In a colligend stripper, it may be necessary to add some collector to the pool as well as the feed because the collector is also stripped off.

Limiting Equations If the height of a foam-fractionation column is increased sufficiently, a concentration pinch will develop between the counterflowing interstitial streams (Brunner and Lemlich, loc. cit.). For an enricher, the separation attained will then approach the predictions of Eq. (20-48) and, interestingly enough, Eq. (20-43).

$$C_D = C_W + (GS\Gamma_W/D) \quad (20-48)$$

D is the volumetric rate at which net foamate (net overhead liquid product) is withdrawn. $D = Q/(R + 1)$. The concentration in the net foamate is C_D . In the usual case of total foam breakage (no dephlegmation), $C_D = C_Q$.

If the tall column is a stripper, the separation will approach that of Eqs. (20-49) and (20-50):

$$C_Q = C_F + (GS\Gamma_F/Q) \quad (20-49)$$

$$C_W = C_F - (GS\Gamma_F/W) \quad (20-50)$$

For a sufficiently tall combined column, the separation will approach that of Eqs. (20-51) and (20-50):

$$C_D = C_F + (GS\Gamma_F/D) \quad (20-51)$$

The formation of micelles in the foam breaker does not affect the limiting equations because of the theoretically unlimited opportunity in a sufficiently tall column for their transfer from the reflux to the ascending stream [Lemlich, "Principles of Foam Fractionation," in Perry (ed.), *Progress in Separation and Purification*, vol. 1, Interscience, New York, 1968, chap. 1].

In practice, the performance of a well-operated foam column several feet tall may actually approximate the limiting equations, provided there is little channeling in the foam and provided that reflux is either absent or is present at a low ratio.

Column Operation To assure intimate contact between the counterflowing interstitial streams, the volume fraction of liquid in the foam should be kept below about 10 percent—and the lower the better. Also, rather uniform bubble sizes are desirable. The foam bubbles will thus pack together as blunted polyhedra rather than as spheres, and the suction in the capillaries (Plateau borders) so formed will promote good liquid distribution and contact. To allow for this desirable deviation from sphericity, $S = 6.3/d$ in the equations for enriching, stripping, and combined column operation [Lemlich, *Chem. Eng.*, **75**(27), 95 (1968); **76**(6), 5 (1969)]. Diameter d still refers to the sphere.

Visible channeling or significant deviations from plug flow of the foam should be avoided, if necessary by widening the column or lowering the gas and/or liquid rates. The superficial gas velocity should probably not exceed 1 or 2 cm/s. Under proper conditions, HTU values of several cm have been reported [Hastings, Ph.D. dissertation, Michigan State University, East Lansing, 1967; and Jashnani and Lemlich, *Ind. Eng. Chem. Process Des. Dev.*, **12**, 312 (1973)]. The foam column height equals $NTU \times HTU$.

For columns that are wider than several centimeters, reflux and feed distributors should be used, particularly for wet foam [Haas and Johnson, *Am. Inst. Chem. Eng. J.*, **11**, 319 (1965)]. Liquid content within the foam can be monitored conductometrically [Chang and Lemlich, *J. Colloid Interface Sci.*, **73**, 224 (1980)]. See Fig. 20-43. Theoretically, as the limit $\mathcal{D} = K = 0$ is very closely approached, $\mathcal{D} = 3K$ [Lemlich, *J. Colloid Interface Sci.*, **64**, 107 (1978)].

Wet foam can be handled in a bubble-cap column (Wace and Banfield, *Chem. Process Eng.*, **47**(10), 70 (1966)] or in a sieve plate column [Aguayo and Lemlich, *Ind. Eng. Chem. Process Des. Dev.*, **13**, 153 (1974)]. Alternatively, individual short columns can be connected in countercurrent array [Banfield, Newson, and Alder, *Am. Inst. Chem. Eng. Symp. Ser.*, **1**, 3 (1965); Leonard and Blacyki, *Ind. Eng. Chem. Process Des. Dev.*, **17**, 358 (1978)].

A high gas rate can be used to achieve maximum throughput in the simple mode (Wace, Alder, and Banfield, AERE-R5920, U.K. Atomic Energy Authority, 1968) because channeling is not a factor in that mode. A horizontal drainage section can be used overhead [Haas and Johnson, *Ind. Eng. Chem. Fundam.*, **6**, 225 (1967)]. The highly mobile dispersion produced by a very high gas rate is not a true foam but is

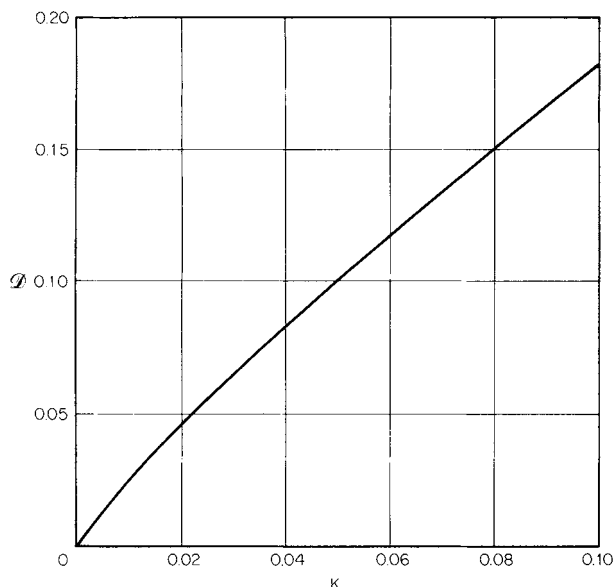


FIG. 20-43 Empirical relationship between \mathcal{D} , the volumetric fraction of liquid in common polydisperse foam, and K , the electrical conductivity of the foam divided by the electrical conductivity of the liquid. [Chang and Lemlich, *J. Colloid Interface Sci.*, **73**, 224 (1980).]

rather a so-called **gas emulsion** [Bikerman, *Ind. Eng. Chem.*, **57**(1), 56 (1965)].

A very low gas rate in a column several feet tall with internal reflux can sometimes be used to effect difficult multicomponent separations in batch operation [Lemlich, "Principles of Foam Fractionation," in Perry (ed.), *Progress in Separation and Purification*, vol. 1, Interscience, New York, 1968, chap. 1].

The same end may be achieved by continuous operation at total external reflux with a small U bend in the reflux line for foamate holdup [Rubin and Melech, *Can. J. Chem. Eng.*, **50**, 748 (1972)].

The slowly rising foam in a tall column can be employed as the sorbent for continuous chromatographic separations [Talman and Rubin, *Sep. Sci.*, **11**, 509 (1976)]. Low gas rates are also employed in short columns to produce the scumlike froth of batch-operated ion flotation, microflotation, and precipitate flotation.

Foam Drainage and Overflow The rate of foam overflow on a gas-free basis (i.e., the total volumetric foamate rate Q) can be estimated from a detailed theory for foam drainage [Leonard and Lemlich, *Am. Inst. Chem. Eng. J.*, **11**, 18 (1965)]. From the resulting relationship for overflow [Fanlo and Lemlich, *Am. Inst. Chem. Eng. Symp. Ser.*, **9**, 75, 85 (1965)], Eq. (20-52) can be employed as a convenient approximation to the theory so as to avoid trial and error over the usual range of interest for foam of low liquid content ascending in plug flow:

$$\frac{Q}{G} = 22 \left(\frac{v_g^3 \mu \mu_s^2}{g^3 \rho^3 d^8} \right)^{1/4} \quad (20-52)$$

The superficial gas velocity v_g is G/A , where A is the horizontal cross-sectional area of the empty vertical foam column. Also, g is the acceleration of gravity, ρ is the liquid density, μ is the ordinary liquid viscosity, and μ_s is the effective surface viscosity.

To account for inhomogeneity in bubble sizes, d in Eq. (20-52) should be taken as $\sqrt{\sum n_i d_i^3 / \sum n_i d_i}$ and evaluated at the top of the vertical column if coalescence is significant in the rising foam. Note that this average d for overflow differs from that employed earlier for S . Also, see "Bubble Sizes" regarding the correction for planar statistical sampling bias and the presence of size segregation at a wall.

For theoretical reasons, Q determined from Eq. (20-52) should be multiplied by the factor $(1 + 3Q/G)$ to give a final Q . However, for foam of sufficiently low liquid content this multiplication can be omitted with little error.

The effective surface viscosity is best found by experiment with the system in question, followed by back calculation through Eq. (20-52). From the precursors to Eq. (20-52), such experiments have yielded values of μ_s on the order of 10^{-4} (dyn·s)/cm for common surfactants in water at room temperature, which agrees with independent measurements [Lemlich, *Chem. Eng. Sci.*, **23**, 932 (1968); and Shih and Lemlich, *Am. Inst. Chem. Eng. J.*, **13**, 751 (1967)]. However, the expected high μ_s for aqueous solutions of such skin-forming substances as saponin and albumin was not attained, perhaps because of their non-newtonian surface behavior [Shih and Lemlich, *Ind. Eng. Chem. Fundam.*, **10**, 254 (1971); and Jashnani and Lemlich, *J. Colloid Interface Sci.*, **46**, 13 (1974)].

The drainage theory breaks down for columns with tortuous cross section, large slugs of gas, or heavy coalescence in the rising foam.

Foam Coalescence Coalescence is of two types. The first is the growth of the larger foam bubbles at the expense of the smaller bubbles due to interbubble gas diffusion, which results from the smaller bubbles having somewhat higher internal pressures (Adamson and Gast, *Physical Chemistry of Surfaces*, 6th ed., Wiley, New York, 1997). Small bubbles can even disappear entirely. In principle, the rate at which this type of coalescence proceeds can be estimated [Ranavive and Lemlich, *J. Colloid Interface Sci.*, **70**, 392 (1979)].

The second type of coalescence arises from the rupture of films between adjacent bubbles [Vrij and Overbeek, *J. Am. Chem. Soc.*, **90**, 3074 (1968)]. Its rate appears to follow first-order reaction kinetics with respect to the number of bubbles [New, *Proc. 4th Int. Congr. Surf. Active Substances*, Brussels, 1964, **2**, 1167 (1967)] and to decrease with film thickness [Steiner, Hunkeler, and Hartland, *Trans.*

Inst. Chem. Eng., **55**, 153 (1977)]. Many factors are involved [Bikerman, *Foams*, Springer-Verlag, New York, 1973; and Akers (ed.), *Foams*, Academic, New York, 1976].

Both types of coalescence can be important in the foam separations characterized by low gas flow rate, such as batchwise ion flotation producing a scum-bearing froth of comparatively long residence time. On the other hand, with the relatively higher gas flow rate of foam fractionation, the residence time may be too short for the first type to be important, and if the foam is sufficiently stable, even the second type of coalescence may be unimportant.

Unlike the case for Eq. (20-52), when coalescence is significant, it is better to find S from d evaluated at the feed level for Eqs. (20-49) to (20-51) and at the pool surface for Eqs. (20-43) and (20-48).

Foam Breaking It is usually desirable to collapse the overflowing foam. This can be accomplished by chemical means (Bikerman, op. cit.) if external reflux is not employed or by thermal means [Kishimoto, *Kolloid Z.*, **192**, 66 (1963)] if degradation of the overhead product is not a factor.

Foam can also be broken with a rotating perforated basket [Lemlich, "Principles of Foam Fractionation," in Perry (ed.), *Progress in Separation and Purification*, vol. 1, Interscience, New York, 1968, chap. 1]. If the foamate is aqueous (as it usually is), the operation can be improved by discharging onto Teflon instead of glass [Haas and Johnson, *Am. Inst. Chem. Eng. J.*, **11**, 319 (1965)]. A turbine can be used to break foam [Ng, Mueller, and Walden, *Can. J. Chem. Eng.*, **55**, 439 (1977)]. Foam which is not overly stable has been broken by running foamate onto it [Brunner and Stephan, *Ind. Eng. Chem.*, **57**(5), 40 (1965)]. Foam can also be broken by sound or ultrasound, a rotating disk, and other means [Ohkawa, Sakagawa, Sakai, Futai, and Takahara, *J. Ferment. Technol.*, **56**, 428, 532 (1978)].

If desired, dephlegmation (partial collapse of the foam to give reflux) can be accomplished by simply widening the top of the column, provided the foam is not too stable. Otherwise, one of the more positive methods of foam breaking can be employed to achieve dephlegmation.

Bubble Fractionation Figure 20-44 shows continuous bubble fractionation. This operation can be analyzed in a simplified way in terms of the adsorbed carry-up, which furthers the concentration gradient, and the dispersion in the liquid, which reduces the gradient [Lemlich, *Am. Inst. Chem. Eng. J.*, **12**, 802 (1966); **13**, 1017 (1967)].

To illustrate, consider the limiting case in which the feed stream and the two liquid takeoff streams of Fig. 20-44 are each zero, thus resulting in batch operation. At steady state the rate of adsorbed carry-up will equal the rate of downward dispersion, or $af\Gamma = \overline{D}AdC/dh$. Here a is the surface area of a bubble, f is the frequency of bubble formation, \overline{D} is the dispersion (effective diffusion) coefficient based on the column cross-sectional area A , and C is the concentration at height h within the column.

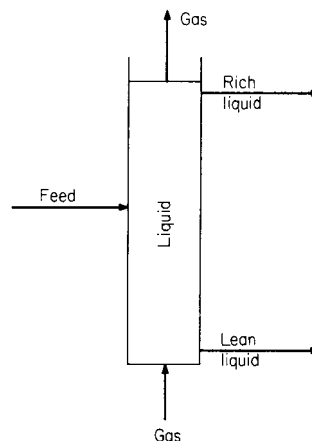


FIG. 20-44 Continuous bubble fractionation.

There are several possible alternative relationships for Γ (Lemlich, op. cit.). For simplicity, consider $\Gamma = K'C$, where K' is not necessarily the same as the equilibrium constant K . Substituting and integrating from the boundary condition of $C = C_B$ at $h = 0$ yield

$$C/C_B = \exp(Jh) \quad (20-53)$$

C_B is the concentration at the bottom of the column, and parameter $J = K'af/DA$. Combining Eq. (20-53) with a material balance against the solute in the initial charge of liquid gives

$$\frac{C}{C_i} = \frac{JH \exp(Jh)}{\exp(JH) - 1} \quad (20-54)$$

C_i is the concentration in the initial charge, and H is the total height of the column.

The foregoing approach has been extended to steady continuous flow as illustrated in Fig. 20-44 [Cannon and Lemlich, *Chem. Eng. Prog. Symp. Ser.*, **68**(124), 180 (1972); Bruin, Hudson, and Morgan, *Ind. Eng. Chem. Fundam.*, **11**, 175 (1972); and Wang, Granstrom, and Kown, *Environ. Lett.*, **3**, 251 (1972), **4**, 233 (1973), **5**, 71 (1973)]. The extension includes a rough method for estimating the optimum feed location as well as a very detailed analysis of column performance which takes into account the various local phenomena around each rising bubble (Cannon and Lemlich, op. cit.).

Uraizee and Narsimhan [*Sep. Sci. Technol.*, **30**(6), 847 (1995)] have provided a model for the continuous separation of proteins from dilute solutions. Although their work is focused on protein separation, the model should find general application to other separations.

In agreement with experiment [Shah and Lemlich, *Ind. Eng. Chem. Fundam.*, **9**, 350 (1970); and Garmendia, Perez, and Katz, *J. Chem. Educ.*, **50**, 864 (1973)], theory shows that the degree of separation that is obtained increases as the liquid column is made taller. But unfortunately it decreases as the column is made wider. In simple terms, the latter effect can be attributed to the increase in the dispersion coefficient as the column is widened.

In this last connection it is important that the column be aligned precisely vertically (Valdes-Krieg, King, and Sephton, *Am. Inst. Chem. Eng. J.*, **21**, 400 (1975)). Otherwise, the bubbles with their dragged liquid will tend to rise up one side of the column, thus causing liquid to flow down the other side, and in this way largely destroy the concentration gradient. A vertical foam-fractionation column should also be carefully aligned to be plumb.

The escaping bubbles from the top of a bubble-fractionation column can carry off an appreciable quantity of adsorbed material in an aerosol of very fine film drops [various papers, *J. Geophys. Res., Oceans Atmos.*, **77**(27), (1972)]. If the residual solute is thus appreciably depleted, C_i in Eq. (20-54) should be replaced with the average residual concentration.

This carry-off of film drops, which may also occur with breaking foam, in certain cases can partially convert water pollution into air pollution. If such is the case, it may be desirable to recirculate the gas. Such recirculation is also indicated if hydrocarbon vapors or other volatiles are incorporated in the gas stream to improve adsorptive selectivity [Maas, *Sep. Sci.*, **4**, 457 (1969)].

A small amount of collector (surfactant) or other appropriate additive in the liquid may greatly increase adsorption (Shah and Lemlich, op. cit.). Column performance can also be improved by skimming the surface of the liquid pool or, when possible, by removing adsorbed solute in even a tenuous foam overflow. Alternatively, an immiscible liquid can be floated on top. Then the concentration gradient in the tall pool of main liquid, plus the trapping action of the immiscible layer above it, will yield a combination of bubble fractionation and solvent sublation.

Systems Separated Some of the various separations reported in the literature are listed in Rubin and Gaden, "Foam Separation," in Schoen (ed.), *New Chemical Engineering Separation Techniques*, Interscience, New York, 1962, chap. 5; Lemlich, *Ind. Eng. Chem.*, **60**(10), 16 (1968); Pushkarev, Egorov, and Khrustalev, *Clarification and Deactivation of Waste Waters by Frothing Flotation*, in Russian, Atomizdat, Moscow, 1969; Kuskin and Golman, *Flotation of Ions and Molecules*, in Russian, Nedra, Moscow, 1971; Lemlich (ed.), *Adsorptive Bubble*

Separation Techniques, Academic, New York, 1972; Lemlich, "Adsorbable Methods," in Li (ed.), *Recent Developments in Separation Science*, vol. 1, CRC Press, Cleveland, 1972, chap. 5; Grieves, *Chem. Eng. J.*, **9**, 93 (1975); Valdes-Krieg King, and Sephton, *Sep. Purif. Methods*, **6**, 221 (1977); Clarke and Wilson, *Foam Flotation*, Marcel Dekker, New York, 1983; and Wilson and Clarke, "Bubble and Foam Separations in Waste Treatment," in Rousseau (ed.), *Handbook of Separation Processes*, Wiley, New York, 1987.

Of the numerous separations reported, only a few can be listed here. Except for minerals beneficiation [ore flotation], the most important industrial applications are usually in the area of pollution control.

A pilot-sized foaming unit reduced the alkyl benzene sulfonate concentration of 500,000 gal of sewage per day to nearly 1 mg/L, using a G/F of 5 and producing a Q/F of no more than 0.03 [Brunner and Stephan, *Ind. Eng. Chem.*, **57**(5), 40 (1965); and Stephan, *Civ. Eng.*, **35**(9), 46 (1965)]. A full-scale unit handling over 45,420 m³/day (12 million gal/day) performed nearly as well. The foam also carried off some other pollutants. However, with the widespread advent of biodegradable detergents, large-scale foam fractionation of municipal sewage has been discontinued.

Other plant-scale applications to pollution control include the flotation of suspended sewage particles by depressurizing so as to release dissolved air [Jenkins, Scherfig, and Eckhoff, "Applications of Adsorptive Bubble Separation Techniques to Wastewater Treatment," in Lemlich (ed.), *Adsorptive Bubble Separation Techniques*, Academic, New York, 1972, chap. 14; and Richter, *Internat. Chem. Eng.*, **16**, 614 (1976)]. Dissolved-air flotation is also employed in treating wastewater from pulp and paper mills [Coertze, *Prog. Water Technol.*, **10**, 449 (1978); and Severeid, *TAPPI* **62**(2), 61, 1979]. In addition, there is the flotation, with electrolytically released bubbles [Chambers and Cottrell, *Chem. Eng.*, **83**(16), 95 (1976)], of oily iron dust [Ellwood, *Chem. Eng.*, **75**(16), 82 (1968)] and of a variety of wastes from surface-treatment processes at the maintenance and overhaul base of an airline [Roth and Ferguson, *Desalination*, **23**, 49 (1977)].

Fats and, through the use of lignosulfonic acid, proteins can be floated from the wastewaters of slaughterhouses and other food-processing installations [Hopwood, *Inst. Chem. Eng. Symp. Ser.*, **41**, M1 (1975)]. After further treatment, the floated sludge has been fed to swine.

A report of the recovery of protein from potato-juice wastewater by foaming [Weijenberg, Mulder, Drinkenberg, and Stemerding, *Ind. Eng. Chem. Process Des. Dev.*, **17**, 209 (1978)] is reminiscent of the classical recovery of protein from potato and sugar-beet juices [Ostwald and Siehr, *Kolloid Z.*, **79**, 11 (1937)]. The isoelectric pH is often a good choice for the foam fractionation of protein (Rubin and Gaden, loc. cit.). Adding a salt to lower solubility may also help. Additional applications of foam fractionation to the separation of protein have been reported by Uraizee and Narsimhan [*Enzyme Microb. Technol.* **12**, 232 (1990)].

With the addition of appropriate additives as needed, the flotation of refinery wastewaters reduced their oil content to less than 10 mg/L in pilot-plant operation [Steiner, Bennett, Mohler, and Clere, *Chem. Eng. Prog.*, **74**(12), 39 (1978)] and full-scale operation [Simonsen, *Hydrocarb. Process. Pet. Refiner*, **41**(5), 145, 1962]. Experiments with a cationic collector to remove oils reportedly confirmed theory [Angelidon, Keskavarz, Richardson, and Jameson, *Ind. Eng. Chem. Process Des. Dev.*, **16**, 436 (1977)].

Pilot-plant [Hyde, Miller, Packham, and Richards, *J. Am. Water Works Assoc.*, **69**, 369 (1977)] and full-scale [Ward, *Water Serv.*, **81**, 499 (1977)] flotation in the preparation of potable water is described.

Overflow at the rate of 2700 m³ (713,000 gal) per day from a zinc-concentrate thickener is treated by ion flotation, precipitate flotation, and ultrafine-particle flotation [Nagahama, *Can. Min. Metall. Bull.*, **67**, 79 (1974)]. In precipitate flotation only the surface of the particles need be coated with collector. Therefore, in principle less collector is required than for the equivalent removal of ions by foam fractionation or ion flotation.

By using an anionic collector and external reflux in a combined (enriching and stripping) column of 3.8-cm (1.5-in) diameter with a feed rate of 1.63 m/h [40 gal/(h-ft²)] based on column cross section,

D/F was reduced to 0.00027 with C_w/C_F for Sr^{2+} below 0.001 [Shonfeld and Kibbey, *Nucl. Appl.*, **3**, 353 (1967)]. Reports of the adsorbable separation of 29 heavy metals, radioactive and otherwise, have been tabulated [Lemlich, "The Adsorptive Bubble Separation Techniques," in Sabadell (ed.), *Proc. Conf. Traces Heavy Met. Water*, 211–223, Princeton University, 1973, EPA 902/9-74-001, U.S. EPA, Reg. II, 1974]. Some separation of ^{15}N from ^{14}N by foam fractionation has been reported [Hitchcock, Ph.D. dissertation, University of Missouri, Rolla, 1982].

The numerous separations reported in the literature include surfactants, inorganic ions, enzymes, other proteins, other organics, biological cells, and various other particles and substances. The scale of the systems ranges from the simple Crits test for the presence of surfactants in water, which has been shown to operate by virtue of transient foam fractionation [Lemlich, *J. Colloid Interface Sci.*, **37**, 497 (1971)], to the natural adsorbable processes that occur on a grand scale in the ocean [Wallace and Duce, *Deep Sea Res.*, **25**, 827 (1978)]. For further information see the reviews cited earlier.

MEMBRANE SEPARATION PROCESSES

GENERAL REFERENCES: Cheryan, *Ultrafiltration and Microfiltration Handbook*, Technomic Publishing Company, Pa., 1988. Ho and Sirkar (eds.), *Membrane Handbook*, Van Nostrand Reinhold, New York, 1992. Baker, *Membrane Technology and Applications*, 2d ed., Wiley, 2000. Eykamp, Sec. 22: Membrane Separation Processes, in *Perry's Chemical Engineers' Handbook*, 7th ed., Perry and Green (eds.), McGraw-Hill, New York, 1997. Millipore Corporation, *Protein Concentration and Diafiltration by Tangential Flow Filtration*, Lit. No. TB032 Rev. B, 1999. Zeman and Zydney, *Microfiltration and Ultrafiltration: Principles and Applications*, Marcel Dekker, New York, 1996. A review of membrane retention mechanisms can be found in Deen, *AIChE J.*, **33**, 1409–1425 (1987).

New developments in membranes are found in journals and trade magazines (e.g., *J. Membrane Sci.*, *BioPharm International*), vendor communications (e.g., websites), patent filings, and conference presentations (e.g., annual ACS or NAMS meetings). Areas of active research include new membrane polymers and surface modification with accompanying diagnostic methods (to reduce fouling, increase flux and retention, improve consistency), new module designs (to improve flux, cleanability, ease of use, scalability, reliability), new processing skids (better components, recovery, less holdup, better mixing, disposability, software for automated processing and archiving), new processing methods (diafiltration strategies, turbulence enhancements), and new applications (e.g., protein-protein separations, plasmids).

Topics Omitted from This Section In order to concentrate on the membrane processes of widest industrial interest, several are left out.

Dialysis and Hemodialysis Historically, dialysis has found some industrial use. Today, much of that is supplanted by ultrafiltration. Donan dialysis is treated briefly under electrodialysis. Hemodialysis is a huge application for membranes, and it dominates the membrane field in area produced and in monetary value. This medical application is omitted here.

An excellent description of the engineering side of both topics is provided by Kessler and Klein [in Ho and Sirkar (eds.), op. cit., pp. 163–216]. A comprehensive treatment of diffusion appears in: Von Halle and Shachter, "Diffusional Separation Methods," in *Encyclopedia of Chemical Technology*, pp. 149–203, Wiley, 1993.

Facilitated Transport Transport by a reactive phase through a membrane is promising but problematic. Way and Noble [in Ho and Sirkar (eds.), op. cit., pp. 833–866] have a description and a complete bibliography.

Liquid Membranes Several types of liquid membranes exist: molten salt, emulsion, immobilized/supported, and hollow-fiber-contained liquid membranes. Araki and Tsukube (*Liquid Membranes: Chemical Applications*, CRC Press, 1990) and Sec. IX and Chap. 42 in Ho and Sirkar (eds.) (op. cit., pp. 724, 764–808) contain detailed information and extensive bibliographies.

Catalytic Membranes Falconer, Noble, and Sperry (Chap. 14—"Catalytic Membrane Reactors" in Noble and Stern, op. cit., p. 669–712) give a detailed review and an extensive bibliography. Additional information can be found in a work by Tsotsis et al. ["Catalytic Membrane Reactors," pp. 471–551, in Becker and Pereira (eds.), *Computer-Aided Design of Catalysts*, Dekker, 1993].

GENERAL BACKGROUND AND DEFINITIONS

Applications Membranes create a boundary between different bulk gas or liquid mixtures. Different solutes and solvents flow through membranes at different rates. This enables the use of membranes in separation processes. Membrane processes can be operated at moderate temperatures for sensitive components (e.g., food, pharmaceuticals). Membrane processes also tend to have low relative capital and energy costs. Their modular format permits reliable scale-up and operation. This unit operation has seen widespread commercial adoption since the 1960s for component enrichment, depletion, or equilibration. Estimates of annual membrane module sales in 2005 are shown in Table 20-16. Applications of membranes for diagnostic and bench-scale use are not included. Natural biological systems widely employ membranes to isolate cells, organs, and nuclei.

Common Definitions Membrane processes have been evolving since the 1960s with each application tending to generate its own terminology. Recommended nomenclature is provided along with alternatives in current use.

Fluid Stream Designations For the generalized membrane module shown in Fig. 20-45, a feed stream enters a membrane module while both a permeate and a retentate stream exit the module. The permeate (or filtrate) stream flows through the membrane and has been depleted of retained components. The term *filtrate* is commonly used for NFF operation while permeate is used for TFF operation. The retentate (or concentrate) stream flows through the module, not the membrane, and has been enriched in retained components.

TABLE 20-16 Membrane Market in 2005

Segment	\$/M/yr Size	Applications	Characteristics
Dialysis	~2,000	Medical	Mature growing 5%
Reverse osmosis	~500	Water treatment	Growing 10%
Microfiltration	~500	Water, food, pharm.	
Ultrafiltration	~400	Water, food, pharm.	Growing 10%
Gas separation	~500	Nitrogen	
Electrodialysis	~100	Water	
Pervaporation	~5	Solvent/water	Nascent
Facilitated transport	0	None	In development

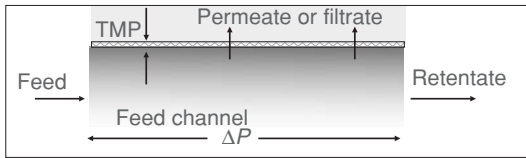


FIG. 20-45 Fluid stream schematic.

Flow Types: Normal Flow and Tangential Flow Filtration If the retentate flow in Fig. 20-45 is zero and all the feed stream flows as a velocity vector normal to the membrane surface, this type of filtration is referred to as *normal flow filtration (NFF)*, also called dead-end flow. If there is a stream that flows as a velocity vector tangent to the membrane surface, creating a velocity gradient at the membrane surface, and that exits the module as a retentate stream, this is referred to as *tangential flow filtration (TFF)*, also called crossflow filtration. A retentate stream that flows through a module without creating a surface velocity gradient is merely a bypass and not TFF.

TFF mitigates the accumulation of retained components on the membrane surface, reducing the plugging of the membrane and permitting a more steady-state operation. TFF is used in processing feeds with a high concentration of retained components.

Flow: Flux, Permeability, Conversion The productivity of a membrane module is described by its flux J = volumetric permeate flow rate/membrane area with units of volume per area per time. Relatively high flux rates imply that relatively small membrane areas are required. The permeate volume is usually greater than the feed volume for a given process. Flux is also the magnitude of the normal flow velocity with units of distance per time.

The sensitivity of productivity or flux to *transmembrane pressure (TMP)* is referred to as the permeability L = flux/transmembrane pressure. TMP refers to a module average. Pure-component permeability (e.g., water permeability) refers to membrane properties while the more industrially relevant process permeability includes fouling and polarization effects.

The efficiency of a membrane module is characterized by the recovery or conversion ratio CR = permeate flow rate/feed flow rate. Low conversion means that fluid has to be repeatedly cycled past the TFF module to generate permeate. High-efficiency NFF has $CR = 1$.

Flux Decline: Plugging, Fouling, Polarization Membranes operated in NFF mode tend to show a steady flux decline while those operated in TFF mode tend to show a more stable flux after a short initial decline. Irreversible flux decline can occur by membrane compression or retentate channel spacers blinding off the membrane. Flux decline by fouling mechanisms (molecular adsorption, precipitation on the membrane surface, entrapment within the membrane structure) are amenable to chemical cleaning between batches. Flux decline amenable to mechanical disturbance (such as TFF operation) includes the formation of a secondary structure on the membrane surface such as a static cake or a fluid region of high component concentration called a polarization layer.

Understanding polarization and controlling its effects are key to implementing a good TFF process. Solutes entrained by the permeate flow are retained by the membrane. They accumulate on the membrane surface and form a region of high concentration called the polarization boundary layer. A steady state is reached between back transport away from the membrane surface, tangential convective transport along the membrane surface, and normal convective flow toward the membrane. The back transport leading to steady-state operation gives TFF a high capacity. Plugging is commonly used to describe flux decline through fouling and caking mechanisms.

Single-Component Separation: Passage, Retention, LRV The passage of a component through a membrane (also called the sieving coefficient or transmission) is calculated as the ratio $S = c_p/c_f$, where c_p and c_f refer to the permeate concentration, and the feed concentration, respectively. These concentrations may change with position within a module. In industrial practice, it is common to measure these concentrations in the permeate stream exiting a module and the feed stream entering a module to give an observed passage or S_{obs} .

Membrane vendors and researchers may use the feed concentration at the membrane surface or c_w to calculate an intrinsic passage $S_{int} = c_p/c_w$. The intrinsic passage characterizes the membrane while the observed passage characterizes the module.

Complementary to the passage, one can also consider the *retention* of a component as $R = 1 - S$ (also called rejection). Retention can also be either an observed or an intrinsic measurement. Retention is useful in considering retained products during concentration mode operation. Other component separation characterizations include the *log reduction value* $LRV = -\log S$ which is used to characterize high-efficiency separations with permeate products (sterilization). The beta ratio $\beta = 1/S$ is sometimes used in NFF for clarification applications.

Multiple-Component Separation: Separation Factor Consistent with the characterization of different separation methods, one can define a separation factor α_{ij} (also called selectivity) for components i and j that compares their relative concentrations in the permeate stream to those in the feed stream:

$$\alpha_{ij} = \frac{c_{ip}/c_{jp}}{c_{if}/c_{jf}} = \frac{S_i}{S_j} \quad (20-55)$$

The convention is to designate the component with higher passage as component i so that $\alpha_{ij} > 1$.

Membrane Types Key membrane properties include their size rating, selectivity, permeability, mechanical robustness (to allow module fabrication and withstand operating conditions), chemical robustness (to fabrication materials, process fluids, cleaners, and sanitizers), low extractibles, low fouling characteristics, high capacity, low cost, and consistency.

Size Ratings The relative sizes of common components and the associated membrane classes capable of retaining them are shown in Fig. 20-46.

Vendors characterize their filters with ratings indicating the approximate size (or corresponding molecular weight) of components retained by the membrane. This rating should be used as a rough guide only and followed up with retention testing. Among the factors affecting retention are the application-specific retention requirements, variable component size and shapes depending on solution environment, membrane fouling and compaction, degree of module polarization, and interaction between feed components.

Composition and Structure Commercial membranes consist primarily of polymers and some ceramics. Other membrane types include sintered metal, glass, and liquid film. Polymeric membranes are formed by precipitating a 5 to 25 wt % casting solution (lacquer) into a film by solvent evaporation (air casting), liquid extraction (immersion casting), or cooling (melt casting or thermally induced phase separation). Membranes can be cast as flat sheets on a variety of supports or as fibers through a die. Ceramic membranes are formed by depositing successive layers of smaller and smaller inorganic particles on a monolith substrate, to create smaller and smaller interstices or "pores" between particles. These layers are then sintered below the melting point to create a rigid structure.

Membranes may be surface-modified to reduce fouling or improve chemical resistance. This can involve adding surface-modifying agents directly to the lacquer or modifying the cast membrane through chemical or physical treatment. Membranes can also be formed by selective etching or track-etching (radiation treatment followed by etching). Stretching is used to change pore morphology.

Liquid film membranes consist of immiscible solutions held in membrane supports by capillary forces. The chemical composition of these solutions is designed to enhance transport rates of selected components through them by solubility or coupled chemical reaction.

Membrane Morphology—Pores, Symmetric, Composite Only nucleopore and anodyne membranes have relatively uniform pores. Reverse osmosis, gas permeation, and pervaporation membranes have nonuniform angstrom-sized pores corresponding to spaces in between the rigid or dynamic membrane molecules. Solute-membrane molecular interactions are very high. Ultrafiltration membranes have nonuniform nanometer sized pores with some solute-membrane interactions. For other microfiltration membranes with nonuniform pores on the submicrometer to micrometer range, solute-membrane interactions are small.

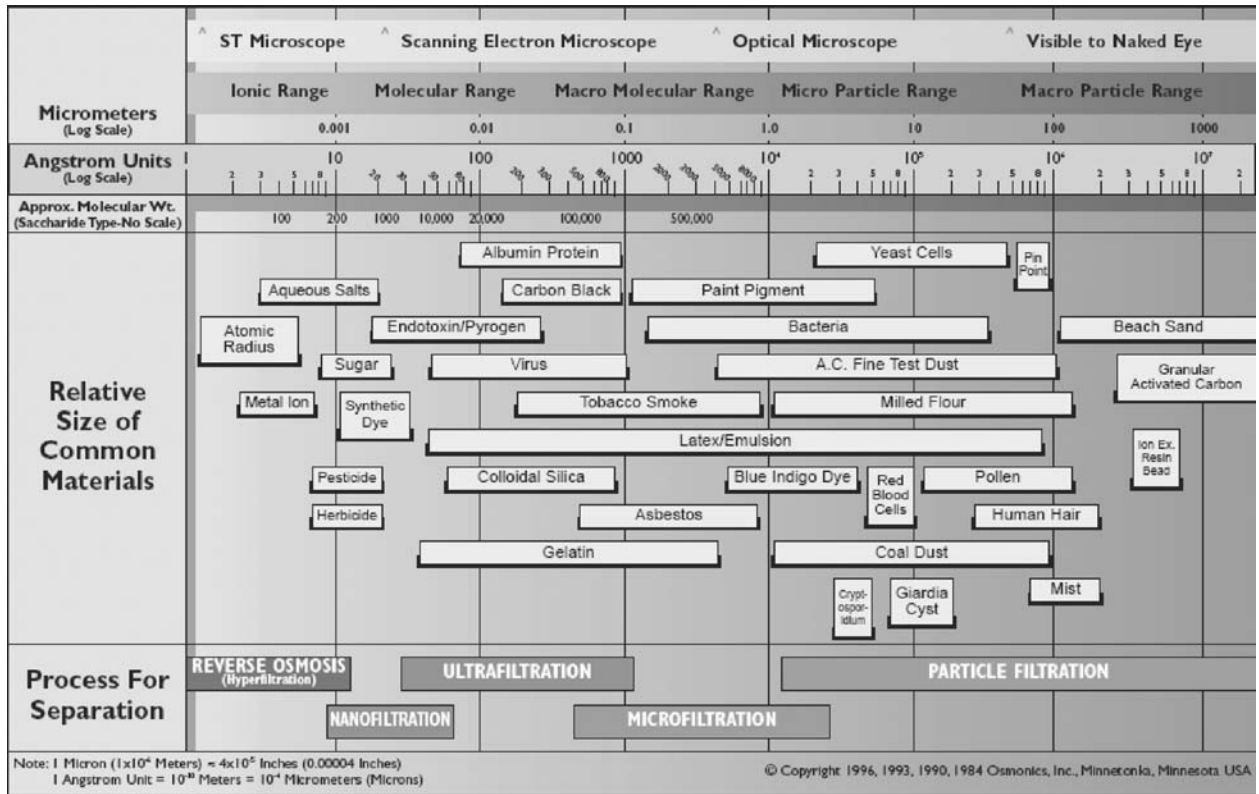


FIG. 20-46 Size spectrum. (Copyright © 1996. Reprinted by permission of Osmonics, Minnetonka, Minn.)

Membranes with a relatively uniform pore size distribution throughout the thickness of the membrane are referred to as symmetric or homogeneous membranes. Others may be formed with tight skin layers on the top or on both the top and bottom of the membrane surfaces. These are referred to as asymmetric or nonhomogeneous membranes. In addition, membranes can be cast on top of each other to form a composite membrane.

Asymmetric membranes have a “tight,” low-permeability, retentive zone that performs the desired separation and a more open, high-permeability zone that provides mechanical strength to the overall membrane. This structure is particularly critical to the economic viability of reverse-osmosis membranes. Asymmetric membranes operated in TFF mode must have the tight side facing the feed channel so that particles are retained on its surface and can be acted upon by the tangential flow. Asymmetric membranes operated in NFF mode can

be operated with the open side facing the feed flow so that retained particles can penetrate the membrane and be dispersed without blinding off the membrane surface and plugging it quickly.

Component Transport Transport through membranes can be considered as mass transfer in series: (1) transport through a polarization layer above the membrane that may include static or dynamic cake layers, (2) partitioning between the upstream polarization layer and membrane phases at the membrane surface, (3) transport through the membrane, and (4) partitioning between the membrane and downstream fluid.

Surface Polarization in TFF The simplified model of polarization shown in Fig. 20-47 is used as a basis for analyzing more complex systems. Consider a single component with no reaction in a thin, two-dimensional boundary layer near the membrane surface. Axial diffusion is negligible along the membrane surface compared to convection.

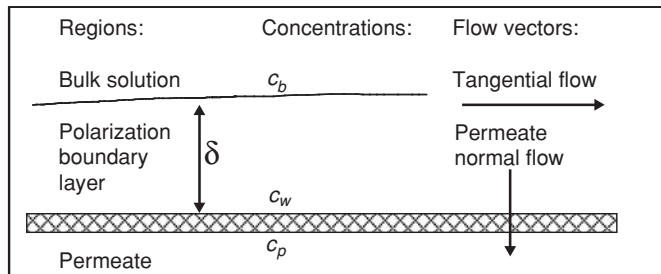


FIG. 20-47 Polarization in tangential flow filtration.

Fluid density and component brownian diffusivity D are also assumed constant. A steady-state component mass balance can be written for component concentration c :

$$u \frac{\partial c}{\partial x} + v \frac{\partial c}{\partial y} = D \frac{\partial^2 c}{\partial y^2} \quad u \text{ and } v \text{ are normal and tangential velocities} \quad (20-56)$$

Further neglecting the first term allows integration from $y = 0$ at the wall (membrane surface) into the boundary layer. At the wall, the net flux is represented by convection into the permeate

$$vc - D \frac{dc}{dy} = vc_p \quad (20-57)$$

This can be further integrated from the wall to the boundary layer thickness $y = \delta$, where the component is at the bulk concentration c_b . Substituting $J = -v$ and $k = D/\delta$, the mass-transfer coefficient yields the stagnant film model [Brian, *Desalination by Reverse Osmosis*, Merten (ed.), M.I.T. Press, Cambridge, Mass., 1966, pp. 161–292]:

$$\frac{v\delta}{D} = \ln\left(\frac{c_b - c_p}{c_w - c_p}\right) = -\frac{J}{k} \quad (20-58)$$

Although allowing for axial variations in v with a constant wall concentration c_w yields Eq. (20-59), as a more rigorous expression applicable to higher concentrations [Trettin et al., *Chem. Eng. Comm.*, **4**, 507 (1980)] the form of Eq. (20-58) is convenient in analyzing a variety of complex behavior.

$$J = 2.046k \left(\frac{c_w - c_p}{c_b - c_p}\right)^{1/3} \quad (20-59)$$

Substituting the intrinsic passage into Eq. (20-58) and rearranging yields an expression for the polarization modulus c_w/c_b :

$$\frac{c_w}{c_b} = \frac{e^{J/k}}{1 + S_{int}(e^{J/k} - 1)} \quad (20-60)$$

Figure 20-48 shows Wijmans's plot [Wijmans et al., *J. Membr. Sci.*, **109**, 135 (1996)] along with regions where different membrane processes operate (Baker, *Membrane Technology and Applications*, 2d ed., Wiley, 2004, p. 177). For RO and UF applications, $S_{int} < 1$, and $c_w > c_b$. This may cause precipitation, fouling, or product denaturation. For gas separation and pervaporation, $S_{int} > 1$ and $c_w < c_b$. MF is not shown since other transport mechanisms besides Brownian diffusion are at work.

Substituting the observed passage into Eq. (20-60) and rearranging yields Eq. (20-61). A plot of the LHS versus J data yields the mass-transfer coefficient from the slope, similar to the Wilson plot for heat transfer-coefficient determination:

$$\ln\left(1 - \frac{1}{S_{obs}}\right) = \ln\left(1 - \frac{1}{S_{int}}\right) - \frac{J}{k} \quad (20-61)$$

A generalized model of transport allowing for component interactions is provided by nonequilibrium thermodynamics where the flux of component i through the membrane J_i [gmol/(cm²·s)] is written as a first-order perturbation of the chemical potential $d\mu_i/dx$ [cal/(gmol·cm)]:

$$J_i = \sum_i L_i \frac{d\mu_i}{dx} \quad (20-62)$$

and L_i [1/(cal·cm·s)] is a component permeability. The chemical potential gradient provides the driving force for flow and may include contributions from pressure, concentration, electrical field, and temperature. A complementary description of transport is obtained by modeling each transport mechanism in some detail. See each application section for appropriate models.

Application of Eq. (20-62) to the polarization for two components. A and B requires solution of the component balances (Saksena, Ph.D. dissertation, University of Delaware, 1995):

$$u \frac{\partial c_A}{\partial x} + v \frac{\partial c_A}{\partial y} = \frac{\partial}{\partial y} \left(D_A \frac{\partial c_A}{\partial y} + D_{AB} \frac{\partial c_B}{\partial y} \right) \quad (20-63a)$$

$$u \frac{\partial c_B}{\partial x} + v \frac{\partial c_B}{\partial y} = \frac{\partial}{\partial y} \left(D_B \frac{\partial c_B}{\partial y} + D_{AB} \frac{\partial c_A}{\partial y} \right) \quad (20-63b)$$

Larger components with smaller brownian diffusivity polarize more readily. They can exclude smaller components, reducing their concentration at the membrane surface and increasing their retention by the membrane.

Solvent Transport through the Membrane The fluid flux J through a membrane is commonly modeled as an assembly of n_p parallel tubes per unit area with a uniform radius r and length l displaying Hagen-Poiseuille flow:

$$J = \frac{n_p \pi r^4 \Delta P}{8 \eta l} \quad (20-64)$$

where η is the fluid viscosity and ΔP the pressure drop. The dependence of flow on r^4 means that larger pores take most of the flow.

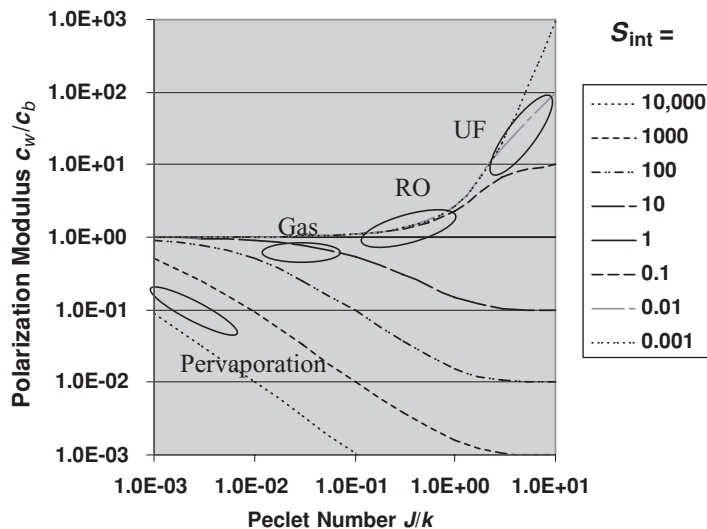


FIG. 20-48 TFF polarization.

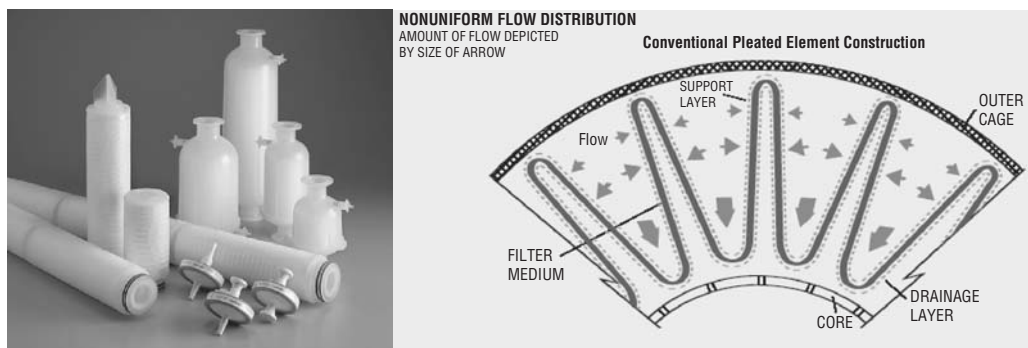


FIG. 20-49 NFF pleated cartridges and capsules. (Courtesy Millipore Corporation, Pall Corporation.)

MODULES AND MEMBRANE SYSTEMS

Membranes are packaged into modules for convenient operation. Key module properties include mechanical robustness (providing good sealing between fluid streams and membrane support), good flow distribution (low pressure drops, high TFF membrane shear, low dead volumes, and low sensitivity to feed channel plugging), cleanability, chemical robustness, low extractibles, low cost, ease of assembly, scalability, high product recovery, and high consistency. Cleanability considerations evolved from the dairy industry (3A Sanitary Standards for Crossflow Membrane Modules, USPHS No. 45-00, 1990). Modules may be integrity-tested for the absence of punctures, improper sealing, or other defects.

NFF modules (Figs. 20-49 and 20-50) include cartridges or capsules, stacked disks, and flat sheet. Pleated cartridges, the most common format, are available in a variety of sizes and are installed into multi-round stainless-steel housings. As shown in Fig. 20-49, multiple layers of materials such as support layers or membranes with different pore ratings may be pleated together. Capsules are made by sealing individual cartridges within their own plastic housing. Pleated cartridge manufacturing is shown in Fig. 20-51.

TFF module types include plate-and-frame (or cassettes), hollow fibers, tubes, monoliths, spirals, and vortex flow. Figures 20-52 and 20-53 show several common module types and the flow paths within each. Hollow fiber or tubular modules are made by potting the cast membrane fibers or tubes into end caps and enclosing the assembly in a shell. Similar to fibers or tubes, monoliths have their retentive layer coated on the inside of tubular flow channels or lumens with a high-permeability porous structure on the shell side.

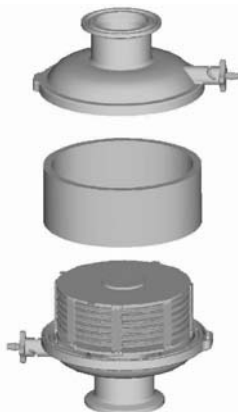


FIG. 20-50 NFF stacked disk modules. (Courtesy Millipore Corporation.)

Spiral-wound modules are made by assembling a membrane packet or leaf consisting of a permeate channel spacer sheet with two flat sheets of membranes on either side (facing outward from the permeate sheet). The sides of this packet are glued together, and the top is glued to a central core collection tube containing small holes that allow passage of permeate from the spacer channel into the collection tube. A feed-side spacer is placed on the packet, and the packet is wound around the core to create the module. The wound packet assembly is sometimes inserted into a shell. Spiral modules frequently use a multileaf construction in which several packets are glued to the central core before winding. This design reduces the pressure drop associated with a long permeate path length.

Cassettes use feed and permeate spacers with one set of precut holes for the feed/retentate and another, smaller set of holes for the permeate. The feed spacer has a raised-edge seal around the permeate hole to prevent flow, and the permeate spacer has a similar seal around the feed/retentate hole. Similar to spiral assembly, membrane packets are glued together around their edges and assembled into a stack, and the stack is glued together around the edges.

For fibers or tubular modules, the feed is generally introduced into the inside of the tubes, or lumen, while permeate is withdrawn from the shell side. This flow orientation enhances the shear at the membrane surface for TFF operation. These modules may also be run at high conversion or NFF mode with the feed introduced on the outside of the tubes or shell side. In this case, the shell side offers greater surface area.

Table 20-17 summarizes TFF module characteristics. The preferred TFF module type depends on the characteristics of each application.

In designing TFF modules, the polarization equation [Eq. (20-58)] indicates that for given fixed concentrations, increases in the mass-transfer coefficient k will increase the flux. This can be accomplished by (1) increasing the shear rate at the wall through higher tangential flow velocities and smaller channel heights, or mechanically moving the membrane by spinning or vibration; (2) altering the geometry of the feed channel to increase turbulent mixing in the normal direction by using feed channel screens or curving channels to introduce Dean or Taylor vortices; (3) introducing pulsatile flow in the feed channel or periodic bursts of gas bubbles; and (4) introducing body forces (centrifugal, gravitational, or electromagnetic) to augment transport away from the membrane and introducing large particles in the feed (e.g., $>0.5 \mu\text{m}$ PVC latex beads) that disrupt boundary layers and cause shear-induced diffusion.

Another device that finds frequent use is the stirred cell shown in Fig. 20-54. This device uses a membrane coupon at the bottom of the reservoir with a magnetic stir bar. Stirred cells use low fluid volumes and can be used in screening and R&D studies to evaluate membrane types and membrane properties. The velocity profiles have been well defined (Schlichting, *Boundary Layer Theory*, 6th ed., McGraw-Hill, New York, 1968, pp. 93–99).

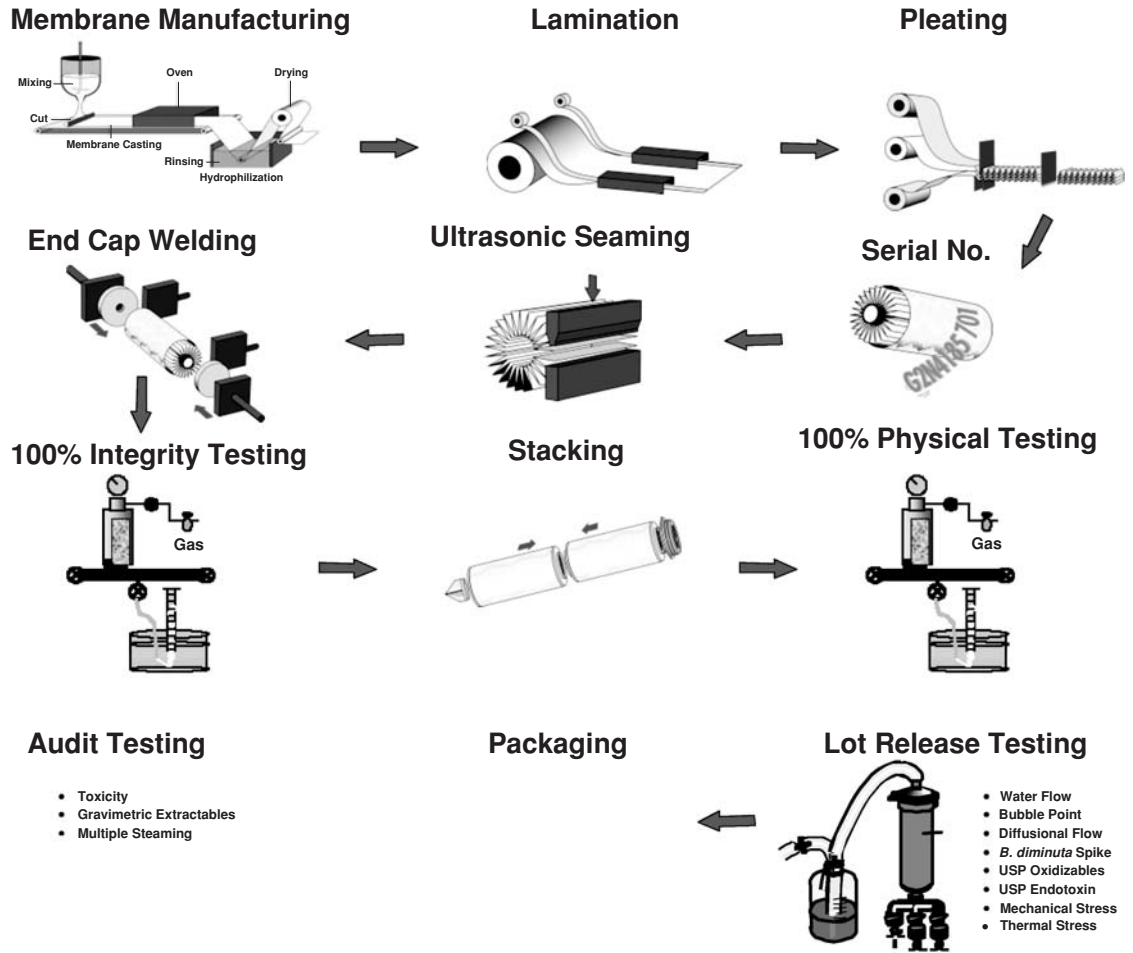


FIG. 20-51 Pleated cartridge manufacturing.

Mass-transfer coefficients for a single newtonian component in various module types and flow regimes can be correlated by Eq. (20-65) with values for the constants in Table 20-18:

$$Sh = aRe^b Sc^c (d_h/L)^e \quad (20-65)$$

where $Sh = kD/d_h$

$$Re = \frac{\rho u d_h}{\mu} \text{ (tube, slit or spacer with hydraulic diameter } d_h)$$

$$Re = \frac{\rho \omega d^2}{\mu} \text{ (stirred cell diameter } d)$$

$$Re = \frac{2\rho\omega R d}{\mu} \text{ (rotating-cylinder inner radius } R \text{ and gap diameter } d)$$

$$Sc = \frac{\mu}{\rho D}$$

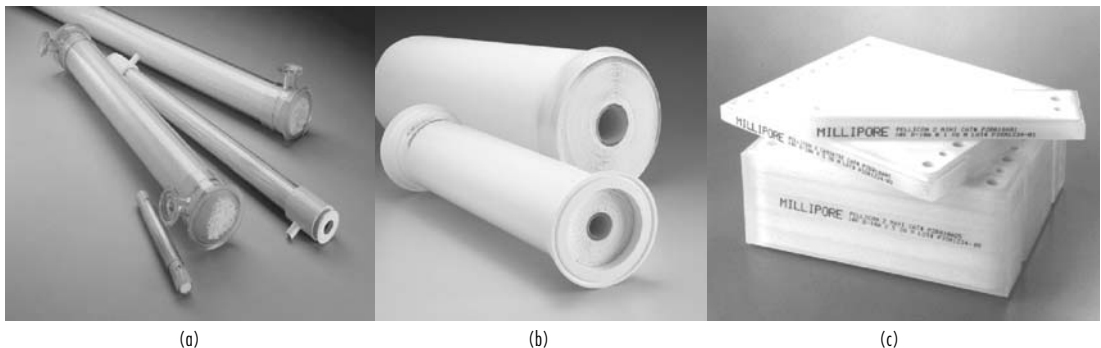


FIG. 20-52 Commercial TFF modules: (a) hollow fibers; (b) spirals; (c) cassettes. (Courtesy Millipore Corporation.)

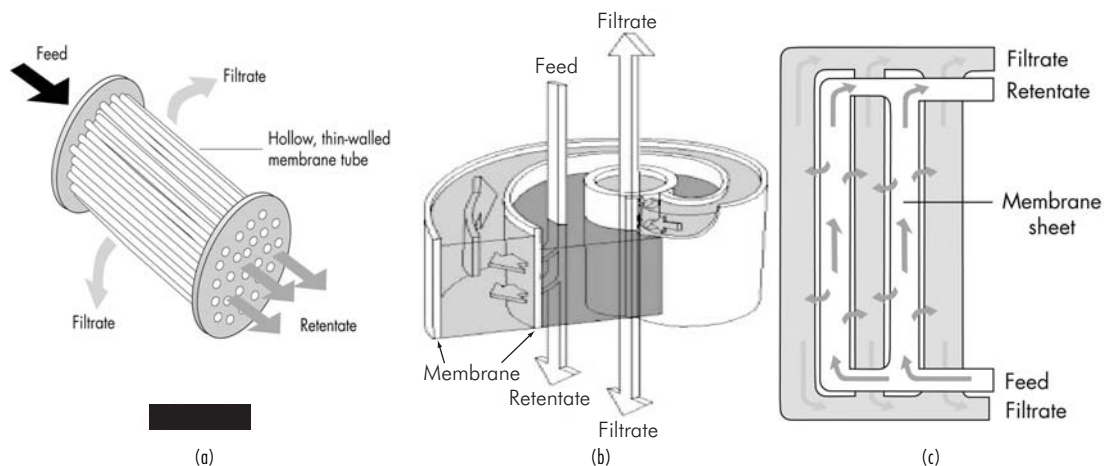


FIG. 20-53 TFF module flow paths: (a) hollow fibers; (b) spirals; (c) cassettes. (Courtesy Millipore Corporation.)

Large-Area Configurations NFF membrane systems consist primarily of large, multiround housings that contain pleated cartridges inserted into a common base plate. These cartridges share a common feed and collect a common filtrate.

TFF membrane systems generally use a common feed distributed among parallel modules with a collection of common retentate and common permeate streams. In some applications, it is also useful to plumb TFF modules with the retentate in series where the retentate flow from one module provides the feed flow to the next module. This type of configuration is equivalent to increasing the length of the retentate channel. Permeate flows may or may not be plumbed together.

Process Configurations Basic membrane process configurations shown in Fig. 20-55 include single-pass, batch, fed-batch, and continuous.

Single-Pass Operation A single-pass configuration is used for NFF system operation (no retentate). Component concentrations change along the length of the retentate channel. For dilute streams such as water, assemblies of TFF modules that run in NFF mode (retentate closed) are also used. For nondilute streams, a single pass through a module may be insufficient to generate either the desired permeate flow or a concentrated retentate.

Steady-state component and solvent mass balances can be written for single-pass operation by considering an incremental area element dA in the axial or flow direction for a feed channel, module, or membrane

assembly of constant width. For volumetric crossflow Q in the feed channel and observed solute passage S_i ,

$$\frac{d(c_i Q)}{dA} = c_i \frac{dQ}{dA} + Q \frac{dc_i}{dA} = -J c_i S_i \quad (20-66)$$

$$\frac{dQ}{dA} = -J \quad (20-67)$$

Combining these equations and integrating yield $c_i = c_{i0} X^{1-S_i}$ for a volume reduction factor $X = Q/Q_0$ and the observed component passage S_i . This allows one to determine either final concentrations from crossflow rates or the reverse. For a fully retained product ($S_i = 0$), a 10-fold volume reduction ($X = 10$) produces a 10-fold more concentrated product. However, if the product is only partially retained, the volume reduction does not proportionately increase the final concentration due to losses through the membrane.

The area required for processing $A = (Q_0 - Q)/\bar{J}$, where $Q_0 - Q$ is the permeate volumetric flow, can be estimated by using the approximation $\bar{J} \approx 0.33J_{\text{initial}} + 0.67J_{\text{final}}$ (Cheryan, *Ultrafiltration Handbook*, Technomic, Lancaster, Pa., 1986) and a suitable flux model. An appropriate model relating flux to crossflow, concentration, and pressure is then applied. Pressure profiles along the retentate channel are empirically correlated with flow for spacer-filled channels to obtain $\Delta P = \Delta P_0(Q/A)^n$.

TABLE 20-17 Commercial TFF Modules

	Spiral	Fiber	Cassette
Screens/spacers	Yes	No	Yes/no
Typical no. in series	1-2	1-2	1-2
Packing density, m ² /m ³	800	1000-6000	500
Feed flow, L/m ² /h (LMH)	700-5000	500-18,000	400
Feed pressure drop, psi/module	5-15	1-5	10-50
Channel height, mm	0.3-1	0.2-3	0.3-1
Plugging sensitivity	High	Moderate	High
Working volume, L/m ²	1	0.5	0.4
Holdup volume, L/m ²	0.03	0.03	0.02
Module cost, \$/m ²	40-200	200-900	500-1000
Ruggedness	Moderate	Low-moderate	High
Module areas, m ²	0.1-35	0.001-5	0.05-2.5
Membrane types	RO-UF	RO-UF-MF	UF-MF
Relative mass-transfer efficiency*	6	4	10
Ease of use	Moderate	High	Moderate
Scalability†	Fair	Moderate	Good

* Qualitative, based on relative fluxes.

† Cassettes keep retentate path length constant and require lower feed flow rates.



FIG. 20-54 Stirred cell TFF module. (Courtesy Millipore Corporation.)

Batch and Fed-Batch Operation Batch operation involves recycling the retentate to the feed tank to create a multipass flow of the feed through the module. The compositions in batch systems change over time. Recycling is necessary for nondilute streams to generate either the desired permeate flow or a concentrated retentate. Multipass operation increases residence times and pump passes that may degrade retentate components. For systems requiring high pressures to generate permeate flow, it is useful to run the entire system at high pressure to save energy.

An unsteady-state component mass balance, Eq. (20-68), can be written for batch operation by assuming a uniform average retentate concentration c_i within the system. Assuming a constant solvent concentration and a 100 percent passage, the solvent balance becomes Eq. (20-69).

$$\frac{d(c_i V)}{dt} = -J A c_i S_i \quad (20-68)$$

$$\frac{dV}{dt} = -J A \quad (20-69)$$

Dividing Eq. (20-68) by Eq. (20-69) and integrating yield the relationship in Table 20-19 between retentate concentration, the volume reduction factor $X = (\text{initial retentate volume})/(\text{final retentate volume})$, and the observed component passage S_i . For a fully retained product ($S_i = 0$), a 10-fold volume reduction ($X = 10$) produces a 10-fold more concentrated product. However, if the product is only partially retained, the volume reduction does not proportionately increase the

final concentration due to losses through the membrane. The component mass in the retentate is obtained as the product of the retentate concentration and retentate volume, as shown in Table 20-19.

TFF systems have a maximum volume reduction capability, typically about 40X. This arises because tanks must be large enough to hold the batch volume while allowing operation at a minimum working volume. The minimum working volume may be limited by air entrainment into the feed pump, mixing in the feed tank, or level measurement capabilities. Fed-batch operation extends the volume reduction capability to 100X and provides some flexibility in processing a variety of batch volumes in a single skid. For a fed-batch operation, the retentate is returned to a smaller tank, not the large feed tank. Feed is added to the small retentate tank as permeate is withdrawn, so the system volume remains constant. The smaller retentate tank can allow a smaller working volume without entrainment. While one could make the retentate tank a section of pipe that returns the retentate directly into the pump feed (bypass line), such a configuration can be problematic to flush, vent, and drain, leading to cleaning and product recovery issues.

Equation (20-70) is the unsteady-state component mass balance for fed-batch concentration at constant retentate volume. Integration yields the equations for concentration and yield in Table 20-19.

$$V \frac{dc_i}{dt} = J A c_F - J A c_i S_i \quad (20-70)$$

Retentate concentration over the course of the process is shown in Fig. 20-56 for a fully retentive product ($S_i = 0$). The tank ratio = $V_0/\text{retentate tank volume}$, C_0 is the feed concentration, and V_0 is the feed volume. The benefits sought from higher concentrations can lead to other problems such as reduced fluxes, larger area and pumps, possible denaturation, and extra lines that may have issues with cleaning and product recovery. This not only has caused significant commissioning and validation delays but also has led to the scrapping of a process skid as unworkable. The number of pump passes will also be higher, leading to greater potential protein degradation. Fed batch and bypass should be used only when necessary.

Diafiltration After concentration has removed permeable components from the system, a new buffer can be added to dilute the retained product back to its original volume. Repeated application of this procedure, known as batch diafiltration, is used to exchange one buffer for another and is conveniently implemented at lab scale.

An operating mode known as constant volume diafiltration involves adding a new buffer to the system while withdrawing permeate at the same rate. Figure 20-57 shows the relationship between retentate concentration and diavolumes $N = (\text{buffer volumes added})/(\text{fixed retentate volume})$ for batch and constant volume diafiltration with $S = 1$ (Cheryan, 1998). For a fully passing solute ($S = 1$) such as a buffer, the retentate concentration decays 10-fold with each 2.3 diavolumes. Partially retained solutes do not decay as quickly and require more diavolumes to reach a final concentration target. A fully retained solute ($S = 0$) maintains its retentate concentration constant at the initial value. For fully passing solutes, > 4.6 diavolumes are needed to achieve a specification of < 1 percent of the original buffer

TABLE 20-18 Mass-Transfer Correlations

Geometry	Flow	a	b	c	e	Comments
Tube	Laminar	1.62	0.33	0.33	0.33	Theoretical ¹
Slit	Laminar	1.86	0.33	0.33	0.33	Theoretical ¹
	Turbulent	0.023	0.80	0.33	—	Theoretical ²
	Turbulent	0.023	0.875	0.25	—	Theoretical ³
	—	0.664	0.50	0.33	0.50	Experimental ⁴
Spacer	—	0.664	0.50	0.33	0.50	Experimental ⁴
Stirred cell	Laminar	0.23	0.567	0.33	—	Experimental ⁵
Rotating	Laminar	0.75	0.50	0.33	0.42	Experimental ⁶

¹Leveque, *Ann. Mines*, **13**, 201 (1928).

²Gekas et al., *J. Membr. Sci.*, **30**, 153 (1987).

³Deissler in *Advances in Heat and Mass Transfer*, Harnett (ed.), McGraw-Hill, New York, 1961.

⁴DaCosta et al., *J. Membr. Sci.*, **87**, 79 (1994) with $L = \text{spacer mesh length}/2$, $d_h = 4e/[2/h + (1 - e)s]$ for spacer length channel height h , porosity e , and specific area s . See Costa for additional correction k_{dc} .

⁵Smith et al., *Chem. Eng. Prog. Symp. Ser.*, **64**, 45 (1968).

⁶Holeschovsky et al., *AIChE J.*, **37**, 1219 (1991).

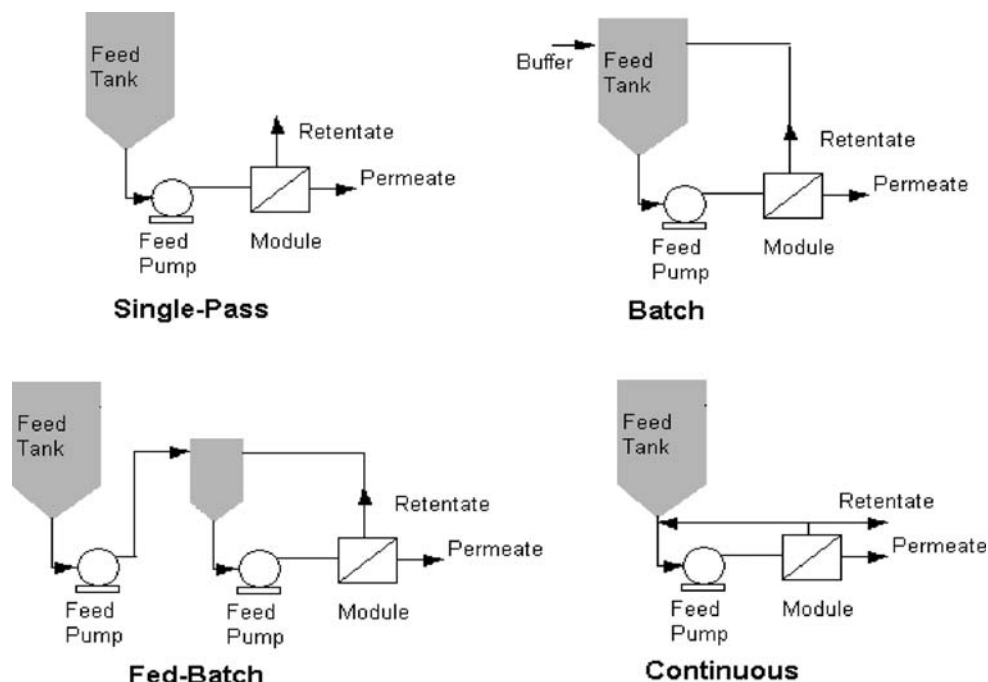


FIG. 20-55 Process configurations.

components. It is common to add an extra 1 to 2 diavolumes as a safety factor to ensure complete buffer exchange. Note that incomplete mixing (due to dead legs and liquid droplets on tank walls) becomes significant at high diavolumes ($N > 10$) and causes the curves in Fig. 20-57 to flatten out.

System sizing involves integration of Eq. (20-69) using a flux model to give Eq. (20-71), where V_p is the permeate volume and J is the average flux. Note the direct tradeoff between area and process time. Table 20-19 shows the concentration and diafiltration steps separated and processing time.

$$A = \frac{V}{Jt} \quad \text{where} \quad \frac{V_p}{Jt} = \int_0^{V_p} \frac{dV}{J} \quad (20-71)$$

The formulas for concentration and diafiltration can be combined for the entire process to derive an expression for the loss of product in the permeate. This loss is shown in Fig. 20-58 and Table 20-19 for

different levels of processing and membrane retention characteristics ($R = 1 - S$). Note that a membrane with 1 percent passage (99 percent retention) can have yield losses much higher than 1 percent because the protein is repeatedly cycled past the membrane during the entire process with losses at every pass. A high-yielding process (< 1 percent loss) requires membrane passage of < 0.1 percent (retention of > 99.9 percent).

The purification of a product p from an impurity i by an ultrafiltration process is shown in Fig. 20-59 and Eq. (20-72), where C_{i0} and C_{p0} are the initial concentrations (g/L) of the two components, Y_p is the yield of product in the retentate, and $\Psi = S_i/S_p$, the ratio of passages. High yields are obtained in purifying out small solutes (high selectivity) but are compromised in removing larger impurities with similar passages to the product.

$$\text{Purification factor PF} = \frac{c_i/c_{i0}}{c_p/c_{p0}} = \left(\frac{\text{ppm in product}}{\text{ppm in feed}} \right) = Y_p \Psi^{-1} \quad (20-72)$$

TABLE 20-19 Batch and Fed-Batch Performance Equations

	Batch concentration and diafiltration	Fed-batch concentration
Retentate concentration	$c_i = c_{i0} X^{1-S} e^{-SN}$	$c_i = \frac{c_{i0}}{S_i} [1 - (1 - S_i) e^{-S_i(X-1)}]$
Retentate mass	$M_i = M_{i0} e^{-S(N+\ln X)}$	$M_i = \frac{M_{i0}}{S_i} [1 - (1 - S_i) e^{-S_i(X-1)}]$
Sizing	$A = \frac{V_0}{t} \left(\frac{1-1/X}{J_{\text{conc}}} + \frac{NX}{J_{\text{diaf}}} \right)$	$A = \frac{V_0}{t} \left(\frac{1-1/X}{J_{\text{conc}}} \right)$
Comments	<ul style="list-style-type: none"> Simplest system and control scheme Smaller area or process time Limited to $X < 40$ 	<ul style="list-style-type: none"> Required for $40 < X < 100$ Minimize fed-batch ratio (= total V_0 / recycle tank V) to minimize area Can require larger area and time Integrate for J or use Cheryan approximation Test process performance using proposed fed-batch ratio

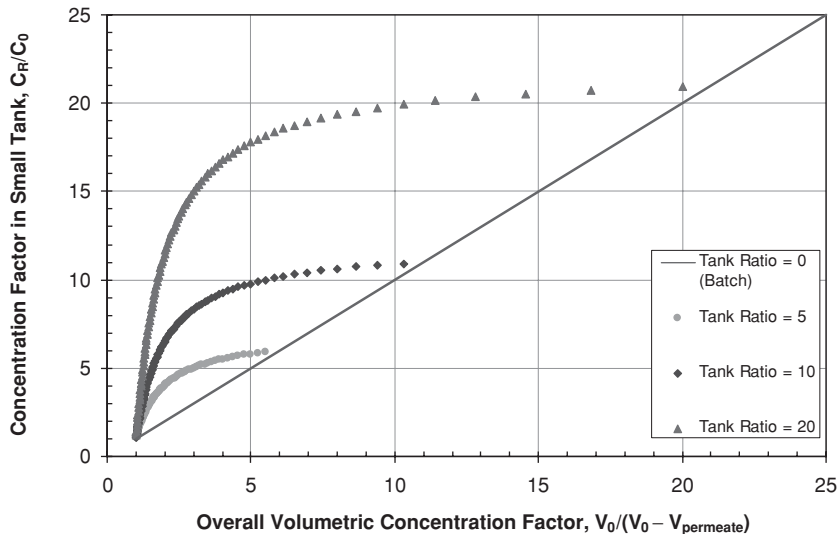


FIG. 20-56 Batch and fed-batch concentration.

Continuous Operation Continuous operation (also called feed-and-bleed) involves the partial recycle of the retentate. The residence time and number of pump passes are in between those of single-pass and batch operation, depending on the fraction of retentate recycled. Several continuous units can be plumbed with the retentate flow feeding the next consecutive system. This configuration is commonly used for large-scale membrane systems.

System Operation NFF system requirements depend on each application but should generally allow for installation, flushing, integrity testing, cleaning or sanitization, processing, recovery, and change-out.

Continued decline in performance indicates a membrane cleaning or compatibility issue. The adequacy of the cleaning step is determined by the recovery of at least 80 percent of the initial normalized water flux. Although some variability in water flux is typical, any consistent decline reflects an inadequate cleaning procedure.

Process Development/Scale-up Feasibility is evaluated by using small single-module systems. This involves selection of membrane type, operating processing conditions, processing strategies (concentration, diafiltration, etc.), cleaning procedures, performance evaluation, and sensitivity to feedstock variations. Pilot operation employs a larger skid, representative of planned commercial operation, running representative feedstock over extended periods to assess longer-term repeatable performance (product quality and retention, costs, yields, process flux, and membrane integrity).

Module change-out is based on preset number of uses, time, or when performance (retention, flux, integrity) drops below preset specifications.

Fluxes scale directly and volumes scale proportionately with the feed volume. A safety factor will be built into the scale-up design so that process times will not be the same.

REVERSE OSMOSIS (RO) AND NANOFILTRATION (NF)

RO and NF processes employ pressure driving forces of 0.3 to 10.5 MPa to drive liquid solvents (primarily water) through membranes while retaining small solutes. Reverse-osmosis (RO) membranes are commonly rated by a > 90 percent NaCl retention and retention of > 50 Da neutral organics while passing smaller liquid solvents. Nanofiltration membranes (sometimes called low-pressure RO, loose RO, or hyperfiltration) have 20 to 80 percent NaCl retention and retain > 200 to 1000 Da neutral organics. Dissolved gases have low retention. Neutral or undissociated solutes have lower retention than charged or dissociated

solutes. Although virus-retaining membranes are sometimes referred to as nanofilters, in keeping with membrane scientist classification they are described under ultrafiltration. RO membranes will remove bacteria and viruses. Lab-scale sample preparation in dilute solutions can be run as NFF in centrifuge tubes. TFF is used in large commercial processes and small home and shipboard water purification systems.

Commercial interest in RO began with the first high-flux, high-NaCl-retention Loeb-Sourirajan anisotropic cellulose acetate membrane. Practical application began with the *thin film composite (TFC)* membrane and implementation for seawater desalination at Jeddah, Saudi Arabia [Muhurji et al., *Desalination*, **76**, 75 (1975)].

Applications RO is primarily used for water purification: seawater desalination (35,000 to 50,000 mg/L salt, 5.6 to 10.5 MPa operation), brackish water treatment (5000 to 10,000 mg/L, 1.4 to 4.2 MPa operation), and *low-pressure RO (LPRO)* (500 mg/L, 0.3 to 1.4 MPa operation). A list of U.S. plants can be found at www2.hawaii.edu, and a 26 Ggal/yr desalination plant is under construction in Ashkelon, Israel. Purified water product is recovered as permeate while the concentrated retentate is discarded as waste. Drinking water specifications of total dissolved solids (TDS) ≤ 500 mg/L are published by the U.S. EPA and of ≤ 1500 mg/L by the WHO [Williams et al., chap. 24 in *Membrane Handbook*, Ho and Sirkar (eds.), Van Nostrand, New York, 1992]. Application of RO to drinking water is summarized in Eisenberg and Middlebrooks (*Reverse Osmosis Treatment of Drinking Water*, Butterworth, Boston, 1986).

RO competes well with multistage flash evaporation in desalination applications and is the current benchmark due to advantages in both capital and operating costs. It may be too costly to compete against freshwater sourced from wells and pipelines. LPRO and electro dialysis compete for brackish water treatment applications. Compact home kitchen RO runs on 0.4-MPa line pressure for < 2000-mg/L TDS feed solutions to reduce salts, odor, and trace metals such as As. These units range from \$200 to \$500 (U.S. 2005) to produce water at \$0.06 to \$0.25 per gallon. RO processes were estimated to represent 23 percent of the 3 Ggal/day of worldwide potable water production in 1986 [Wangnick, *IDA Magazine*, **1**, 53 (1986)].

Useful conversions are as follows:

Volume: $1 \text{ m}^3 = 1000 \text{ L} = 264.2 \text{ U.S. gal} = 8.11 \times 10^{-4} \text{ acre-ft} = 35.32 \text{ ft}^3$

Pressure: $1 \text{ bar} = 14.5 \text{ psi} = 0.1 \text{ MPa}$

Flow: $1 \text{ U.S. gal/min} = 1440 \text{ gal/day} = 227 \text{ L/h} = 5.47 \text{ m}^3/\text{day}$

Concentration: $1 \text{ mg/L} = 1 \text{ ppm} = 17.1 \text{ grains/gal}$

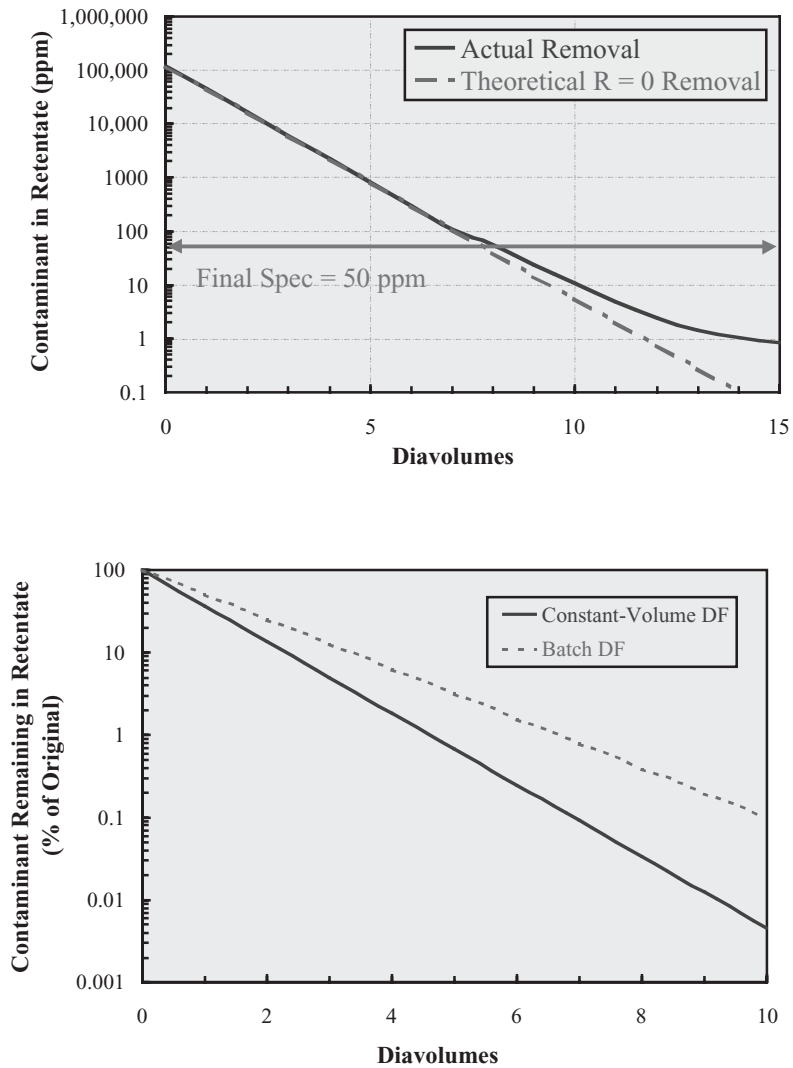


FIG. 20-57 Diafiltration performance (Cheryan, 1998).

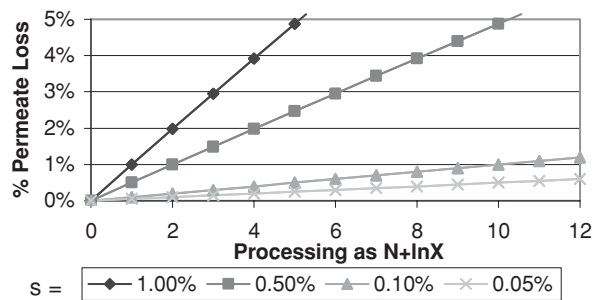


FIG. 20-58 Permeate losses.

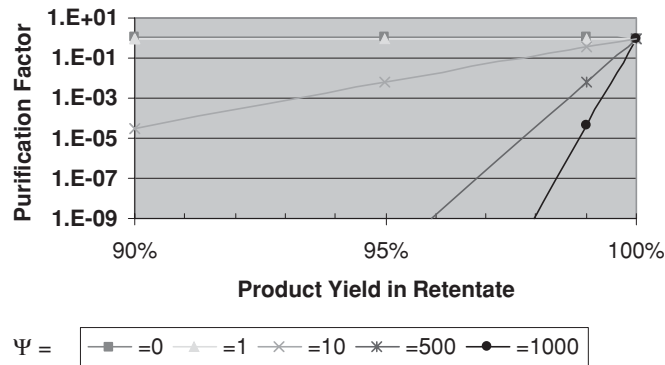


FIG. 20-59 Purification versus yield.

Process water applications include boiler water feed pretreatment before ion exchange or electrodialysis. RO is also used for ultrahigh-purity water production for use in laboratories, medical devices (kidney dialysis), microelectronic manufacturing (rinse fluids per ASTM D-19 D5127-90, 1990), and pharmaceutical manufacturing (purified water or water for injection as specified by USP).

RO applications recovering valuable product in the retentate include tomato, citrus, and apple juice dewatering, sometimes in combination with thermal evaporators at \$0.15 to \$0.18 per gallon [Short, chap. 9 in *Bioseparation Processes in Foods*, Singh and Rezvi (eds.), Marcel Dekker, New York, 1995]. Dealcoholization of wine or beer involves diafiltering alcohol through RO membranes while retaining flavor compounds in the retentate (Meier, *Wine East*, Nov./Dec., 10, 1991). LPRO is used to desalt soy sauce and dairy whey. Small-molecule drugs (e.g., penicillin) can be recovered by RO membranes.

RO can recover metals, antifreeze, paint, dyes, and oils in the retentate while generating cleaned up wastewater permeate for disposal. RO is also used to reduce the volume of waste liquids (e.g., spent sulfite liquor in paper manufacturing). Wastewater treatment application removals of 95 percent TOC, > 90 percent COD, > 98 percent PAH compounds, and pesticides > 99 percent have been seen [Williams et al., chap. 24 in *Membrane Handbook*, Sirkar and Ho (eds.), Van Nostrand, 1992].

Membranes, Modules, and Systems

Membranes RO membranes are designed for high salt retention, high permeability, mechanical robustness (to allow module fabrication and withstand operating conditions), chemical robustness (to fabrication materials, process fluids, cleaners, and sanitizers), low extractables, low fouling characteristics, high capacity, low cost, and consistency.

The predominant RO membranes used in water applications include cellulose polymers, *thin film composites (TFCs)* consisting of aromatic polyamides, and crosslinked polyetherurea. Cellulosic membranes are formed by immersion casting of 30 to 40 percent polymer lacquers on a web immersed in water. These lacquers include cellulose acetate, triacetate, and acetate-butyrate. TFCs are formed by interfacial polymerization that involves coating a microporous membrane substrate with an aqueous prepolymer solution and immersing in a water-immiscible solvent containing a reactant [Petersen, *J. Membr. Sci.*, **83**, 81 (1993)]. The Dow FilmTec FT-30 membrane developed by Cadotte uses 1-3 diaminobenzene prepolymer crosslinked with 1-3 and 1-4 benzenedicarboxylic acid chlorides. These membranes have NaCl retention and water permeability claims.

Cellulose membranes can generally tolerate a pH of 3 to 6 and 0.3 to 1.0 ppm of chlorine while TFC membranes can generally tolerate a pH of 3 to 11 and < 0.05 ppm of chlorine. Membrane tolerance is also described as the permitted cumulative ppm-hours of membrane exposure to chlorine. TFC membranes can range from 1000 to 12,000 ppm-h. Always check specific filter specifications. RO membranes

approved for food use by the FDA include aromatic polyamides, polypiperazinamide, and aryl-alkyl polyetherurea (Code of Federal Regulations, Title 21, Part 177, U.S. GPO, Washington, D.C., annually).

Nanofiltration membranes are negatively charged and reject multivalent anions at a much higher level than monovalent anions, an effect described as Donnan exclusion. Nanofiltration membranes have MgSO₄ retention and water permeability claims.

Modules RO modules are available in spiral, hollow fiber, tubular, and plate and frame formats. A comparison of characteristics is shown in Table 20-20. Spirals are used the most since they are compact, easy-to-use modules; have low feed-side pressure drops; are less prone to clogging; and are easily cleaned, mechanically robust, and economical. The standard spiral module has an 8-in diameter, is 40 in long with about 30-m² area. An anti-telescoping end cap is used to prevent the leaves from being pushed out of alignment by axial retentate flow. Hollow fibers are run with the feed on the shell side, flowing radially inward and out along the lumen. This places less mechanical stress on the fibers. Tubular modules are used with high-suspended-solids and high-viscosity fluids.

System Configurations Figure 20-60 shows common RO system configurations for permeate product recovery. For single-pass operation, the feed passes once through a membrane to generate acceptable permeate product. Double-pass operation uses permeate staging (the permeate from the first module feeds the second module) with allowance for blending to generate acceptable product. This configuration may be needed for high-concentration, hard-to-remove impurities, high product purities, and lower-retention modules. Double-pass operation has been recommended for desalination of > 38,000 mg/L [Klinko et al., *Desalination*, **54**, 3 (1985)] or modules with salt retention < 99.2 percent [Kaschemekat et al., *Desalination*, **46**, 151 (1983)]. It is also common in ultrahigh-purity water systems.

Spirals are normally packed at 5 to 7 modules per cylindrical housing and operate with staged retentates where the retentate from the first module feeds the second module. Retentate staging increases the length of the feed channel. Retentate staging of housings is used to increase the conversion ratio from around 25 to 50 percent in one housing stage to 50 to 75 percent for two housing stages and 75 to 90 percent in three housing stages. Since the feed flow is reduced by the

TABLE 20-20 RO Module Performance

	Spiral	Hollow fiber	Tubular	Plate and frame
Packing density, m ² /m ³	800	6000	70	500
Feed flow, m ³ /(m ² ·s)	0.3–0.5	0.005	1–5	0.3–0.5
Feed ΔP, psi	40–90	1.5–4.5	30–45	45–90
Plugging sensitivity	High	High	Low	Moderate
Cleanability	Fair	Poor	Excellent	Good
Relative cost	Low	Low	High	High
Chemistries available	C and TFC	C and TFC	C only	C and TFC

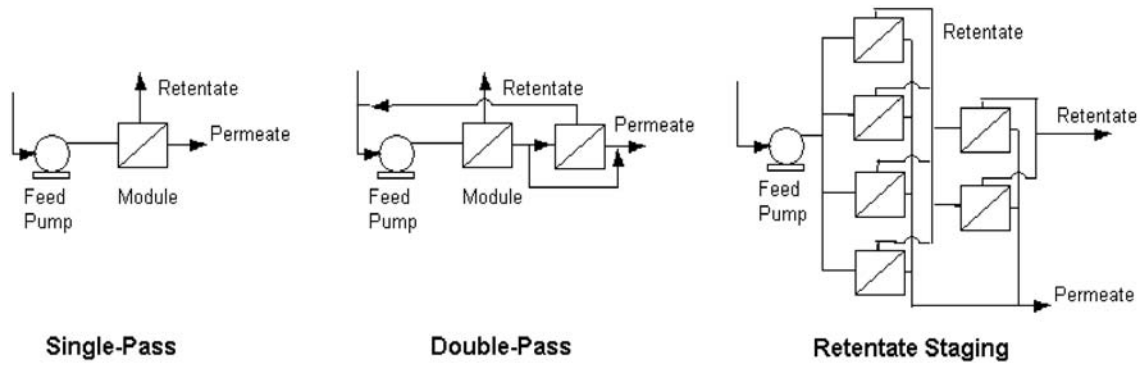


FIG. 20-60 RO system configurations.

conversion ratio after passing through the first module stage, maintaining a minimum crossflow rate requires that the second module stage have less membrane area in what has been called a “Christmas tree” design. Interstage pumping between housings may be required to maintain pressures and flows.

Retentate product recovery employs the batch, fed-batch, or continuous processing systems, and concentration or diafiltration modes of operation (see general membrane section). Beer and wine dealcoholization uses batch diafiltration.

Component Transport in Membranes RO is analyzed as a rate, not equilibrium, process. Polarization of retained salts and other low-MW components is described in the general membrane section. Solvent flux J_w and solute flux J_i through RO membranes can be described by using Eq. (20-73), the solution diffusion imperfection model [Sherwood et al., *Ind. Eng. Chem. Fund.*, **6**, 2 (1967)]. This model considers transport through the membrane in parallel with transport through a small number of nonretentive defects. Transport of solvent or solute through the membrane occurs by partitioning between the upstream polarization layer and membrane phases at the membrane surface, diffusion through the membrane, and partitioning between the membrane and downstream fluid. This process is reflected in permeabilities P_w and P_2 . Dissolution in the membrane and diffusion through it can be modeled as an activated process with an associated inverse exponential temperature dependence of the permeabilities. Transport of solvent or solute through defects occurs by convective flow. Water viscosity increases roughly 2 percent/°C near 25°C.

$$J_w = \frac{P_w}{l} (\Delta P - \Delta\pi) + \frac{P_3}{l} \Delta P \quad J_i = \frac{P_2}{l} (c_w - c_p) + \frac{P_3}{l} \Delta P c_w \quad (20-73)$$

In accordance with observed data, this model shows that water flux J_w increases linearly with applied pressure ΔP , decreases with higher salt concentration through its impact on osmotic pressure π , increases with a smaller membrane thickness l , and increases with temperature through the temperature dependence of the water permeability P_w . The model also demonstrates that the solute or salt flux J_i increases linearly with applied pressure ΔP , increases with higher salt concentration c_w , increases with a smaller membrane thickness l , and increases with temperature through the temperature dependence of the solute permeability P_2 . Polarization, as described early in this section, causes the wall concentration c_w to exceed the bulk concentration c_b .

Osmotic Pressure The osmotic pressure π of salt solutions is calculated from

$$\pi = -\frac{RT}{\bar{V}_w} \ln a_w = \frac{RTM_w}{1000\bar{V}_w} \sum_i m_i \phi_i \quad (20-74)$$

for water activity a_w , water partial molal volume \bar{V}_w , gas constant R , absolute temperature T , water molecular weight M_w , ion molality m_i , and osmotic coefficient ϕ_i for each ionic species i . Note that both Na^+

and Cl^- are counted as separate species for NaCl. For seawater at 35,000 to 50,000 mg/L (ppm) and 25°C, the osmotic pressure is in the range of 2.7 to 3.8 MPa (~11 kPa/1000 ppm).

Solute Retention Retention is determined by the relative rates of solute and solvent transport through the membrane. The impact of operation on solute retention $R_i = 1 - c_p/c_w$ can be evaluated from Eq. (20-73) by using the mass balance $J_i = c_p J_w$. Assuming high retention, $c_p \ll c_w$, and the solvent flux through defects is negligible, so the retention is calculated as

$$R_i = 1 - \frac{J_i}{J_w c_w} = 1 - \frac{P_2 + P_3 \Delta P}{P_w (\Delta P - \Delta\pi)} \quad (20-75)$$

At low pressures where $\Delta P \sim \Delta\pi$, solvent flux is low but solute flux is high (it is insensitive to pressure and occurs under a concentration gradient). This results in low solute retention. Pressures of 1 MPa over the feed osmotic pressure are needed to maintain high retention. Increasing the applied pressure ΔP increases the solvent flux, diluting the solute flux with solvent and resulting in a higher retention. Increasing the feed solute concentration lowers the solvent flux through its impact on osmotic pressure π , and decreases retention. Increasing temperature increases the solvent permeability P_w , the solute permeability P_2 , and the osmotic pressure. Solute retention tends to drop slightly at higher temperature.

Ionic solutions require charge neutrality to prevent a higher flux of species of one charge causing an associated electric current and voltage. This may limit the net salt flux through the membrane by the ion with the lowest permeability so that the sodium ion will show different retentions depending on the anion it is paired with. Charge neutrality can also enrich the permeate concentration of a salt relative to the feed to create a negative retention. For example, a feed solution containing Na^+ , Li^+ , Cl^- , and SO_4^{2-} ions would show a permeate with enriched levels of Cl^- to balance permeated Na^+ and Li^+ ions.

Nanofilters incorporate negative membrane charge for higher anion rejection. High feed salinities can passivate these charges and reduce anion retention.

Pretreatment and Cleaning Pretreatment is commonly used to extend membrane life and increase recovery. The representative pretreatment train for water purification applications in Fig. 20-61 controls feed channel clogging, mineral scaling, fouling by organic films and microorganisms, and oxidants that can degrade the membranes.

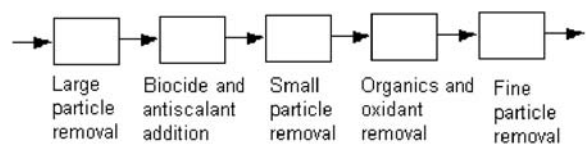


FIG. 20-61 RO pretreatment schematic.

TABLE 20-21 SDI Interpretation

SDI value	Operability
<1	Can run several years without colloidal fouling
1-3	Can run several months between cleaning
3-5	Frequent cleaning required
>5	Pretreatment required to reduce colloids

Particle Removal Solid particles can plug feed channel spacer channels and deposit as a cake layer on the membrane surface, causing increased flow resistance and lowering fluxes. Table 20-19 indicates the sensitivity of different module types to feed channel plugging. Particles may consist of organic colloids, rust flakes, precipitated iron hydroxide, algae, clay, colloidal silica, or silt. Pretreatment includes using a combination of coarse screening, hydrocyclones, flocculent addition (e.g., alum, ferric sulfate, polyelectrolytes), a sand or multimedia filtration bed with periodic backflushing, and depth filter cartridges or ultrafiltration systems.

The ability of a feed solution to plug a membrane is determined by the *silt density index* (SDI) employing a 0.45- μm PVDF microfilter at 30-psi differential pressure (ASTM Standard D-4189-82, 1987).

$$\text{SDI} = \frac{100(1 - T_i/T_f)}{15} \quad (20-76)$$

where T_i is the time it takes to filter the first 0.5 L and T_f is the time it takes to filter 0.5 L starting when 15 min of test time has elapsed. Table 20-21 is an interpretation of SDI values.

Antiscalants Precipitation of salts can form a scale on the membrane surface when solubility limits (Table 20-22) are exceeded in the retentate. This decreases flux.

Metal hydroxides (e.g., Fe, Mn, Al) can also be a problem (Rautenbach and Albrecht, *Membrane Processes*, Wiley, New York, 1989). A chemical analysis of the feed solution composition along with consideration of solubility products allows one to determine the significance of precipitation. Solubility products can be affected by temperature, pH, and ionic strength. Seasonal temperature variations must be considered. Concentrations of silica need to be < 120 mg/L in the feed.

Water hardness in milligrams per liter of total Ca^{2+} and Mg^{2+} is considered soft at 0 to 17 mg/L, moderately hard at 60 to 120 mg/L, and very hard at > 180 mg/L. The Langelier saturation index, a measure of CaCO_3 solubility, should be < 0 in the retentate to prevent precipitation (*Pure Water Handbook*, Osmonics, 1997).

Scale prevention methods include operating at low conversion and chemical pretreatment. Acid injection to convert CO_3^{2-} to CO_2 is commonly used, but cellulosic membranes require operation at pH 4 to 7 to prevent hydrolysis. Sulfuric acid is commonly used at a dosing of 0.24 mg/L while hydrochloric acid is to be avoided to minimize corrosion. Acid addition will precipitate aluminum hydroxide. Water softening upstream of the RO by using lime and sodium zeolites will precipitate calcium and magnesium hydroxides and entrap some silica. Antiscalant compounds such as sodium hexametaphosphate, EDTA, and polymers are also commonly added to encapsulate potential precipitants. Oxidant addition precipitates metal oxides for particle removal (converting soluble ferrous Fe^{2+} ions to insoluble ferric Fe^{3+} ions).

Oxidant Removal The presence of oxidizers such as chlorine or ozone can degrade polyamide RO membranes, causing a drop in salt retention. Cellulosic membranes are less sensitive to attack. Addition of 1.5 to 6 mg sodium bisulfite/ppm chlorine or contacting with activated carbon will remove oxidizers. Vacuum degassing with a hydrophobic filter module is also used.

Biocides Microorganisms can form biofilms on membrane surfaces, causing lower fluxes [Flemming in *Reverse Osmosis*, Z. Amjad (ed.), Van Nostrand, New York, 1993, p. 163]. Cellulosic membranes

TABLE 20-22 Solubility Limits at 30°C

CaCO_3	MgSO_4	CaSO_4	BaSO_4	SiO_2	SrSO_4
65 mg/L	9 mg/L	2090 mg/L	2 mg/L	120 mg/L	114 mg/L

can be consumed by bacteria, causing lower retention. Control involves pretreatment with chemicals or UV light and membrane chemical sanitization on a regular or periodic basis. Chemical sanitants include chlorine, bromine, ozone and peroxide/peracetic acid oxidants (subject to membrane limits), formaldehyde, sodium bisulfite, copper sulfate for algae and plankton control, or chloramines. The use of oxidizers will also remove dissolved hydrogen sulfide. Cellulosic membranes are commonly sanitized with 0.2 mg/L of free chlorine.

Organic Fouling Organic components can range from 1 mg/L in the open ocean to 80 to 100 mg/L in coastal waters. Components include humic and fulvic acids (800 to 50,000 kDa) from decayed vegetation, or contaminating petroleum that can adsorb to the membranes and reduce their flux. Carbon beds used for dechlorination can also remove these organics by adsorption. For wastewater purification to remove organics, high pH and ozonation improve retention and reduce flux decline (Bhattacharyya et al., *Separation of Hazardous Organics by LPRO—Phase II*, U.S. EPA, 1990).

Cleaning/Sanitization Membrane cleaning restores initial membrane flux without compromising retention to extend membrane life. Appropriate treatment depends on the nature of the foulants, membrane compatibility, and compatibility of the chemicals with the application. Cleaning generally uses acid flushing (for scalants) but may include base or enzyme flushing (for organics) and 80°C hot water flushing (for sanitization/microorganism control).

Design Considerations and Economics

Osmotic Pinch As the feed travels along the feed channels, friction losses lower the feed pressure. Solvent flux along the feed channel dewater the feed and increases solute concentration and osmotic pressure. For a recovery or conversion ratio CR, a module solute retention R , and an inlet solute concentration of c_o , the bulk concentration c_b is

$$c_b = c_o(1 - \text{CR})^{-R} \quad (20-77)$$

Both the feed pressure drop and the osmotic pressure increase lower the driving force for solvent flow $\Delta P - \Delta \pi$ along the feed channel, and the point at the end of the feed channel, having the lowest driving force, is the *osmotic pinch point*. This point has both the lowest solvent flux and the lowest solute retention. If the driving force falls below 0 along the feed channel, the solvent flux will reverse (from permeate into the feed) and subsequent membrane area will perform "negative work." Economic justification of membrane at the pinch point requires that it generate adequate flux to pay for itself. This, in turn, requires that the driving force be about 1 MPa.

Process Economics and Optimization Table 20-23 shows some representative process economics for several large 1 Mgal/day system designs [adapted from Ray, chap. 25 in *Membrane Handbook*, Ho and Sirkar (eds.), Van Nostrand, New York, 1992]. These costs are a useful guide, within ± 25 percent, but specific quotes are needed to account for site-specific differences between projects. No energy recovery technologies are included. For capacities above 50 to 100 gal/day, system costs scale almost linearly, as (gal/day capacity)^{0.85-0.95}, and can be conveniently expressed as dollars per gallon per day. Total costs are split evenly between capital and operating costs.

Energy use (pumping high flows to high pressures) represents the biggest operating cost while membrane replacement operating costs are only 10 to 15 percent. These operating costs can be represented as

$$\begin{aligned} \$E (\$/1000 \text{ gal}) &= (0.724 \text{ kWh/psig} \cdot 1000 \text{ gal}) \\ &\times (\Delta P \text{ psid}) (\$/\text{kWh}) / \text{CR} \cdot \text{Ef} \end{aligned} \quad (20-78)$$

where CR is the fractional conversion ratio (recovery), Ef is the pump efficiency, and

$$\$A (\$/1000 \text{ gal}) = (0.432) (\$/\text{m}^2) / \text{CR} \cdot J \cdot T \quad (20-79)$$

where J is the average system flux, L/(m²·h), and T is the years of membrane life.

By incorporating a flux model [Eq. (20-73)], solute concentration [Eq. (20-77)], and polarization model [Eq. (20-60)] into the area cost

TABLE 20-23 Representative RO Process Costs

Costs	Seawater	Brackish water	Softening	Notes
Operating conditions				
Inlet pressure	6.9 MPa	3.1 MPa	1.4 MPa	
Flux	25 LMH*	42 LMH	42 LMH	
Conversion	40%	60%	75%	
Total cost, \$/1000 gal	4.7	2.3	1.3	15-yr life
Capital cost	2.1	1.1	0.6	12% interest
Operating cost	2.6	1.2	0.7	15% downtime
Total capital cost, \$/(gal/day)	4.5	2.3	1.3	
Direct costs	3.7	1.9	1.1	
Equipment	3.3	1.6	0.8	
Indirect costs	0.8	0.4	0.2	
Total operating cost, \$/1000 gal	2.6	1.2	0.7	
Energy	1.6	0.4	0.2	\$0.075/kWh
Membrane replacement	0.4	0.2	0.2	3-yr life
Chemicals	0.2	0.2	0.1	2 per shift @\$14/h
Labor	0.3	0.3	0.2	
Other	0.1	0.1	0.0	

*LMH = liters per square meter per hour.

[Eq. (20-79)], the operating cost term ($\$A + \E) varies with ΔP and CR. The osmotic pinch constraint requires a minimum ΔP to overcome the average osmotic pressure and requires a maximum CR where the concentrated retentate osmotic pressure exceeds the feed pressure. Assuming that solute retention is sufficient to maintain permeate quality, there exist optimum conversion ratios and ΔP that depend on the feed (osmotic pressure), module (mass transfer, permeability, life, cost), and pump (energy cost, efficiency). Conversion ratios per module stage range from 25 to 50 percent, and typical inlet pressures are shown in Table 20-23. No provision has been made here for costs of disposing of the retentate.

One can also rearrange Eq. (20-79) to solve for ΔP in terms of area and substitute in Eq. (20-78) to express the operating costs in terms of membrane area. The energy operating cost is inverse in area, while the membrane replacement cost is linear, reflecting the existence of an optimum area. Addition of capital costs leads to total costs that scale as $b(\text{area}^{0.95}) + c(\text{area}^{-0.6})$. Module vendors provide good general recommendations and support to design and economic evaluation.

Recognizing that the high-pressure retentate contains considerable kinetic energy before it is passed through a retentate valve provides an opportunity for energy recycling. A variety of energy recovery technologies have been proposed including Pelton wheels, reverse-running pumps, hydraulic turbochargers, and pressure exchangers with pumping energy reductions of 22 to 60 percent [Darwish et al., *Desalination*, **75**, 143 (1989)]. Energy recovery technologies are most useful for high-pressure desalination but may not be worth the investment for brackish water and LPRO applications (Glueckstein et al., chap. 12 in *Synthetic Membrane Processes*, Academic Press, New York, 1984).

The capital cost of a 15 kgal/day RO skid, uninstalled with instrumentation, is about \$35,000 (U.S., 2005) and scales with gallons-per-day capacity to the 0.52 power [Ray, chap. 25 in *Membrane Handbook*, Sirkar and Ho (eds.), Van Nostrand, New York, 1992]. Approximately 25 to 30 percent of this cost is associated with membranes and housings. Operating costs are roughly \$0.30/1000 gal for energy and membrane replacement, and \$0.09/1000 gal for pretreatment, maintenance, and cleaning. High-purity water systems employing double-pass staging operate at conversions of 70 to 80 percent in the first pass and 70 to 75 percent in the second pass. Home units using line pressure run at 5 to 15 percent conversion.

System Operation For corrosive pressurized seawater, 316L stainless steel is commonly used for piping and housings although specialized alloys may be needed (Oldfield et al., *Desalination*, **55**, 261 (1985)). Sensors are used to measure inlet pH and temperature (to control scaling), pump pressure (to prevent surges and ensure sufficient driving force), pump flow (to ensure crossflow to prevent excessive polarization), permeate flow (to monitor performance), and permeate conductivity (to ensure module integrity and product

quality). Control systems are used to monitor and display sensor values, track and optimize operation over time, trigger alarms, and store the data. Provisions for module replacement and start-up are needed.

For batch processing, systems comparable to ultrafiltration are used.

Posttreatment of the permeate for potable water use can include dissolved CO₂ removal to prevent corrosion (by aeration, lime treatment), chlorination for microbial control, and oxygenation to improve taste.

ULTRAFILTRATION

Ultrafiltration processes (commonly UF or UF/DF) employ pressure driving forces of 0.2 to 1.0 MPa to drive liquid solvents (primarily water) and small solutes through membranes while retaining solutes of 10 to 1000 Å diameter (roughly 300 to 1000 kDa). Commercial operation is almost exclusively run as TFF with water treatment applications run as NFF. Virus-retaining filters are on the most open end of UF and can be run as NFF or TFF. Small-scale sample preparation in dilute solutions can be run as NFF in centrifuge tubes.

The first large commercial application of UF was paint recycling, followed by dairy whey recovery in the mid-1970s. UF applications are enabled by low-temperature and low-cost operation.

Applications Electrodeposition of cationic paint resin on automobiles (connected to the cathode) provides a uniform, defect-free coating with high corrosion resistance, but carries with it about 50 percent excess paint that must be washed off. UF is used to maintain the paint concentration in the paint bath while generating a permeate that is used for washing. The spent wash is fed back into the paint path (Zeman et al., *Microfiltration and Ultrafiltration*, Marcel Dekker, New York, 1996).

During cheese making, the coagulated milk or curd is used to make cheese while the supernatant whey is a waste product rich in salts, proteins, and lactose. Whey concentration and desalting by UF produce a retentate product that can be used as an animal feed supplement or food additive. The MMV process (Maubois et al., French Patent 2,052,121) involves concentrating the milk by UF after centrifugation to remove the cream and before coagulation to improve yields and reduce disposal costs.

UF is used in biopharmaceutical purification (proteins, viral and bacterial vaccines, nucleic acids) for initial concentration of clarified fluids or lysates (to reduce subsequent column sizes and increasing binding), to change buffer conditions (for loading on to columns), and to concentrate and change buffers (for final formulation into a storage buffer) [Lutz et al., in *Process Scale Bioseparations for the Biopharmaceutical Industry*, Shukla, et al. (eds.), CRC Press, New York, 2006]. For these applications, the drug product is recovered in the retentate. For drug products with potential viral contaminants

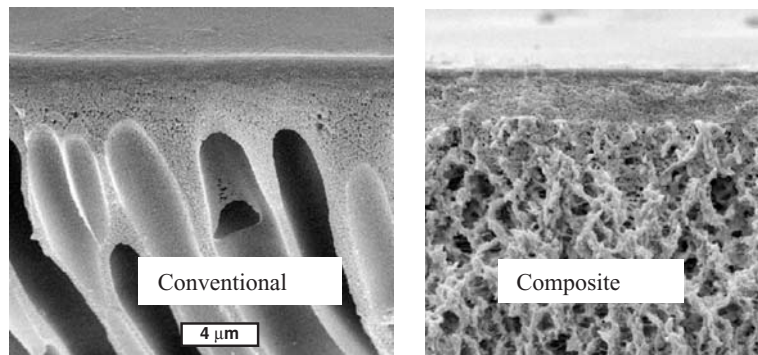


FIG. 20-62 Ultrafiltration membranes. (Courtesy Millipore Corporation.)

(sourced from mammalian cells or human and animal blood plasma), virus removal filters employed in either a TFF or NFF mode retain the viruses while the drug product is recovered in the permeate.

UF is used to clarify various fruit juices (apple, grape, pear, pineapple, cranberry, orange, lemon) which are recovered as the permeate [Blanck et al., *AIChE Symp. Ser.* **82**, 59 (1986)]. UF has also been used to remove pigments and reducing browning in wine production [Kosikowski in *Membrane Separations in Biotechnology*, McGregor (ed.), Marcel Dekker, New York, 1986].

Wastewater treatment and water purification applications employ UF in a TFF or NFF mode to produce permeate product with reduced colloids, pyrogens, and viruses. Oil droplets in wastewater are retained by UF for recycle or disposal at a significantly reduced volume.

Membranes, Modules, and Systems

Membranes UF membranes consist primarily of polymeric structures (polyethersulfone, regenerated cellulose, polysulfone, polyamide, polyacrylonitrile, or various fluoropolymers) formed by immersion casting on a web or as a composite on a MF membrane. Hydrophobic polymers are surface-modified to render them hydrophilic and thereby reduce fouling, reduce product losses, and increase flux [Cabasso in *Ultrafiltration Membranes and Applications*, Cooper (ed.), Plenum Press, New York, 1980]. Some inorganic UF membranes (alumina, glass, zirconia) are available but only find use in corrosive applications due to their high cost.

Early ultrafiltration membranes had thin surface retentive layers with an open structure underneath, as shown in Fig. 20-62. These membranes were prone to defects and showed poor retention and consistency. In part, retention by these membranes would rely on large retained components in the feed that polarize or form a cake layer that plugs defects. Composite membranes have a thin retentive layer cast on top of a microfiltration membrane in one piece. These composites demonstrate consistently high retention and can be integrity-tested by using air diffusion in water.

Table 20-24 compares properties of commonly used polyethersulfone (PES) or regenerated cellulose membranes. Membrane selection is based on experience with vendors, molecular weight rating for high

yields, chemical and mechanical robustness during product processing and clean-in-place (extractables, adsorption, swelling, shedding, class VI), process flux for sizing and costing, and the quality/consistency (ISO, cGMP) of the vendor and the membrane. Membranes are described by their normal water permeability (NWP), the ratio of their flux at 25°C to the average transmembrane pressure (TMP). Measurements taken at different temperatures can be adjusted to 25°C using a viscosity ratio correction. Process fluxes will be somewhat lower due to fouling. Membranes containing a hydrophilic surface generally have lower fouling and produce higher process fluxes.

UF membranes are assigned a nominal molecular weight limit (NMWL) corresponding roughly to their ability to retain a solute of a particular molecular weight. While tight membranes (i.e., low-molecular-weight cutoff ratings) provide high retention, they have corresponding low flow rates requiring greater membrane area to do the job. This leads to larger pumps with large holdup volumes and potential negative impact on product quality. A rule of thumb for selecting membrane NMWL is to take 0.2 to 0.3 of the MW of the solute that is to be retained by the membrane. However, the NMWL values should only be used as a very rough guide or screening method to select membranes for testing. Retention is based on hydrodynamic size, not molecular weight, so linear chain dextrans show a higher passage than globular proteins of the same molecular weight. In addition, there is no standardization of rating methods so specific retention properties vary considerably among membranes and vendors depending on the marker solute selected (e.g., protein, dextran in a particular buffer) and the level of retention selected for the marker solute (90, 95, 99 percent). Retention is affected by fouling due to adsorbed components and polarized solutes on the membrane surface. See retention below for additional discussion.

Modules and Systems UF modules include cassettes, spirals, hollow fibers, tubes, flat sheets, and inorganic monoliths. These are primarily run in TFF operation to increase flux by reducing plugging. Exceptions run in NFF operation include virus removal and water treatment applications where both cartridges and hollow fibers are used. Continuous operation provides lower-cost operation, but the biologicals process requires batch processing to meet regulatory requirements. Applications with high solids require multiple-pass operation to obtain a significant conversion ratio, but water treatment

TABLE 20-24 Ultrafiltration Membrane Properties

Material	Advantages	Disadvantages
Polyethersulfone (PES)	Resistance to temperature, Cl ₂ , pH, easy fabrication	Hydrophobic
Regenerated cellulose	Hydrophilic, low-fouling	Sensitive to temperature, pH, Cl ₂ , microbial attack, mechanical creep
Polyamide		Sensitive to Cl ₂ , microbial attack
Inorganic	Resistance to temperature, Cl ₂ , pH, high pressure, long life	Cost, brittleness, high crossflow rates

TABLE 20-25 UF Modules and Systems

Application	Paint recovery	Whey processing	Biologicals	Water treatment	Juice processing
Membrane	PES	PES	Cellulose, PES, PVDF	PES	PES, PVDF
Module	Fibers	Spirals	Cassette	Fibers	Tubes
System	Continuous	Continuous	Batch, NFF	Continuous, single-pass	Batch
Characteristics	Cost, plugging	Cost	Recovery	Cost	Plugging, cost

can achieve high conversion in one pass. The properties of these modules and system operation are described in the general section. Table 20-25 indicates where these modules are used.

Component Transport in Membranes UF is analyzed as a rate, not equilibrium, process. Pure solvent transport in UF is characterized by $J = \text{TMP}/R_{\text{membrane}}$, where TMP (transmembrane pressure) is the pressure difference across the membrane and R is the membrane resistance. Resistance R can be related to membrane properties by using Eq. (20-64) with pore size distributions following a lognormal distribution [Zydney et al., *J. Membr. Sci.*, **91**, 293 (1994)]. At ionic strengths $< 0.1 M$, charged membranes generate a streaming potential across their thickness which can lead to a 15 percent or more diminished solvent flux by counterelectroosmosis (Newman, *Electrochemical Systems*, Prentice-Hall, Englewood Cliffs, N.J., 1973). Most UF process fluids are aqueous with higher ionic strengths, but permeability measurements using low-conductivity water can encounter this effect.

Figure 20-63 shows that in the presence of retained solutes, the solvent flux flattens out at high pressures. UF has a high level of polarization where the membrane surface concentration can range up to 100 times the bulk concentration. Retained antibodies at a wall concentration of 191 g/L have an osmotic pressure Π of 30 psi (Mitra, 1978). That is, an elevated pressure of 30 psig must be applied to the protein-rich retentate side of a water-permeable membrane containing 191 g/L of antibody in order to prevent water backflow from the permeate side of the membrane containing water at 0 psig. This diminishes the driving force for flow and leads to the mechanistic-based osmotic flux model (Vilker, 1984):

$$\text{Polarization flux model } J = \frac{\text{TMP} - R \cdot \Delta\Pi(c_w)}{\mu \cdot (R_{\text{membrane}} + R_{\text{fouling}})} \quad (20-80)$$

where R is the intrinsic membrane retention and $\Delta\Pi(c_w)$ is the osmotic pressure at the wall concentration. An empirically based flux model can also be defined by omitting the osmotic term and adding a compressible polarization resistance term in the denominator (Cheryan, 1998).

Equation (20-80) requires a mass transfer coefficient k to calculate c_w and a relation between protein concentration and osmotic pressure. Pure water flux obtained from a plot of flux versus pressure is used to calculate membrane resistance (typically small). The LMH/psi slope is referred to as the NWP (normal water permeability). The membrane plus fouling resistances are determined after removing the reversible polarization layer through a buffer flush. To illustrate the components of the osmotic flux model, Fig. 20-63 shows flux versus TMP curves corresponding to just the membrane in buffer ($R_{\text{fouling}} = 0, c_w = 0$), fouled membrane in buffer ($c_w = 0$), and fouled membrane with osmotic pressure.

The region at low flux/low TMP is called the linear region and is dependent on TMP but independent of crossflow and bulk concentration. The region at high flux/high TMP is called the polarized region and is independent of TMP but dependent on crossflow and bulk concentration. This extremely counterintuitive result is the consequence of polarization. In between these two regions lies what is termed the “knee” of the flux curve. Increasing pressure beyond the knee gives diminishing returns in improving flux.

In the polarized region, the empirical gel model of Eq. (20-81) can provide a good description of the flux behavior. The gel model is based on polarization [Eq. (20-58)] with a constant wall concentration C_g and complete retention. The mass-transfer coefficient k is dependent on crossflow velocity, as shown in Table 20-18 for different geometries and flow regimes. Concentration-dependent transport (viscosity and diffusivity) will alter the velocity exponents. Operating at the knee of the flux curve, either by design or due to fouling that causes a shift in the flux curve to the right, will decrease the velocity dependence. Note that the empirical gel point concentration does not correspond to an actual gel on the membrane surface. As the feed concentration rises to within 5 to 10 percent of the gel point, the flux tends to drop off less rapidly than Eq. (20-81) would predict. The gel point is insensitive to crossflow but can increase with temperature. Cheryan summarizes gel point and velocity exponent values for a variety of solutions.

$$J = k \ln c_g/c \quad (20-81)$$

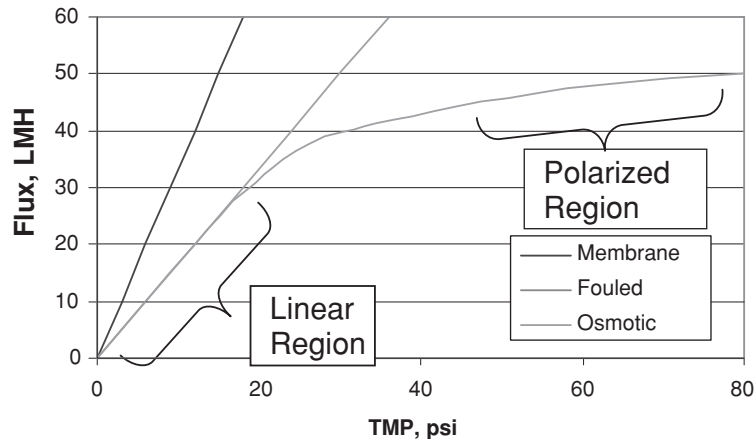


FIG. 20-63 Ultrafiltration flux behavior.

Solute Flux Solute partitioning between the upstream polarization layer and the solvent-filled membrane pores can be modeled by considering a spherical solute and a cylindrical pore. The equilibrium partition coefficient ϕ (pore/bulk concentration ratio) for steric exclusion (no long-range ionic or other interactions) can be written as

$$\text{Solute partitioning} \quad \phi = (1 - \lambda)^2 \quad (20-82)$$

where λ = solute radius/pore radius.

Solute flux within a pore can be modeled as the sum of hindered convection and hindered diffusion [Deen, *AIChE J.*, **33**, 1409 (1987)]. Diffusive transport is seen in dialysis and system start-up but is negligible for commercially practical operation. The steady-state solute convective flux in the pore is $J_s = K_c J_c = \phi K_c J_{c_w}$, where c is the radially averaged solute concentration and K_c is the convective hindrance factor (from pore wall drag, solute lag, and long-range solute pore wall and solute-solute potential interactions). For uncharged cylindrical pores $\phi K_c = \phi(2 - \phi) \exp(-0.7146\lambda^2)$ to within 2 percent [Zeman et al., in *Synthetic Membranes*, vol. 2, Turbak (ed.), *ACS Symp. Ser.*, **54**, ACS, Washington, D.C. (1981), p. 412].

A charged solute in a pore has a higher potential energy due to the distortion of its electrical field when it penetrates the pore wall into the polymer. This effect increases solute retention. The apparent size of solutes can be magnified by more than an order of magnitude by this effect. See Deen for other pore geometries and the impacts of long-range solute pore wall and solute-solute interactions. The use of electrostatic interactions to separate solutes is discussed by van Reis [*Biotechn. and Bioeng.*, **56**(1), 71 (1997)].

Solute Passage/Retention The intrinsic passage (c_p/c_w) is determined by the ratio of the solute flux to the solvent flux as $s_i = \phi K_c$. The intrinsic passage is inherent to the membrane and solute. As shown in Fig. 20-64 for a single pore, solute passage (or retention) does not follow a step change. Figure 20-65 shows passage for a membrane with a pore size distribution [Tkacik et al., *Biotechnology*, **9**, 941 (1991)].

The observed passage (c_p/c_b) varies with both the intrinsic passage and the extent of polarization, as shown in Eq. (20-83):

$$\text{Observed passage} \quad s_o = \frac{1}{1 + \left(1/s_i - 1\right) \cdot \exp(-J/k)} \quad (20-83)$$

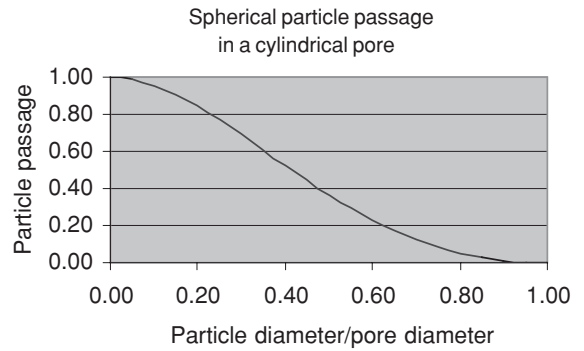


FIG. 20-64 Solute passage.

At low flux these passages are equivalent. At high fluxes the wall concentration is high due to polarization and the observed passage increases, approaching 100 percent, regardless of the intrinsic passage.

In multicomponent systems, large solutes with lower diffusivity, polarize more and exclude smaller solutes from the membrane surface, decreasing their passage. Operation at the “knee” of the flex curve reduces this effect.

Design Considerations and Economics The selection among batch, fed-batch, single-pass, or continuous operation has been described earlier in this section. Important performance considerations for UF applications involve product purity and/or concentration, product yield, and cost/sizing for a given production rate.

Batch or Fed-Batch Operation This mode of operation is typical of biologicals and juice processing where high solids and low fluxes require multiple passes, and batch operation is characteristic of the manufacturing process. Formulas in Table 20-19 can be used to calculate the required volume reduction factor X , diafiltration volumes

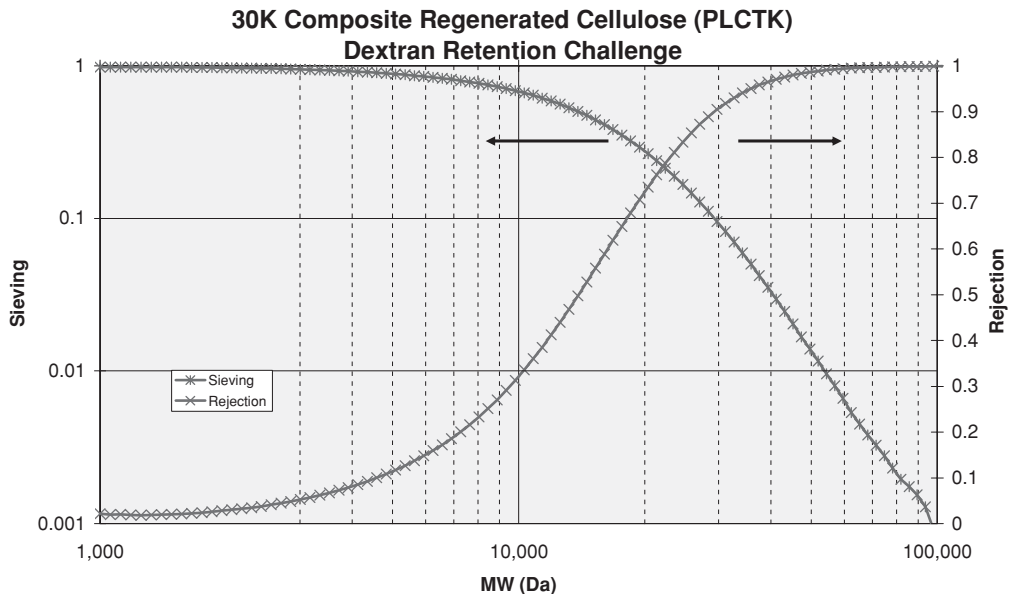


FIG. 20-65 Intrinsic membrane retention.

N , and solute passage S_i needed to produce desired retentate product with impurity concentrations c_i and retentate product yield M_i/M_{i0} . Permeate product characteristics for batch operation can be determined by mass balances using a permeate volume of $V_p = V_0(1 - 1/X + N/X)$, a mass of solute i in the permeate as $M_{i, \text{permeate}} = M_{i0}(1 - e^{-S_i(N+1/X)})$ and the permeate concentration as the ratio of the mass to volume. Fed-batch equations are obtained by using the same approach.

The system area A needed for batch or fed-batch operation can be calculated by using the formulas in Table 20-19 for production rates V_0/t based on feed volume V_0 and average fluxes during process steps. The final retentate batch volume $V_R = V_0/X$ or permeate batch volume $V_p = V_0(1 - 1/X + N/X)$ can be used to restate the production rate on other bases. Although experience can be used to estimate solute passage and process fluxes, they should be determined experimentally for each application.

Single-Pass TFF Single-pass TFF or NFF operation is typical of water treatment. Low solids allow high fluxes with high permeate product recovery and low retentate disposal costs. NFF operation is also used for virus retention in small-batch biologicals processing where low NFF fluxes (high areas) are compensated by ease of use, low residence time, and low capital costs.

Equations (20-66) and (20-67) present single-pass formulas relating retentate solute concentration, retentate crossflow, permeate flow, and membrane area. For relevant low-feed-concentration applications, polarization is minimal and the flux is mainly a function of pressure. Spiral or hollow fiber modules with low feed channel and permeate pressure drops are preferred.

Continuous Operation This mode of operation is typical of paint recovery, whey processing, and wastewater processing where high solids and low fluxes require multiple passes, and continuous operation is allowed by the manufacturing process. For a feed concentration c_F , a volumetric concentration factor X (= retentate flow/feed flow), and retention R , the outlet retentate concentration is

$$c = c_F \left[\frac{X}{X - R(X - 1)} \right] \quad (20-84)$$

In comparison to batch processing, this process operates at the final concentration with associated low fluxes. The use of multiple stages where the retentate outlet from one stage feeds the next allows successive systems to operate at different fluxes and will improve membrane productivities.

MICROFILTRATION

Process Description Microfiltration (MF) separates particles from true solutions, be they liquid or gas phase. Alone among the membrane processes, microfiltration may be accomplished without the use of a membrane. The usual materials retained by a microfiltration membrane range in size from several μm down to $0.2 \mu\text{m}$. At the low end of this spectrum, very large soluble macromolecules are retained by a microfilter. Bacteria and other microorganisms are a particularly important class of particles retained by MF membranes. Among membrane processes, dead-end filtration is uniquely common to MF, but cross-flow configurations are often used.

Brief Examples Microfiltration is the oldest and largest membrane field. It was important economically when other disciplines were struggling for acceptance, yet because of its incredible diversity and lack of large applications, it is the most difficult to categorize. Nonetheless, it has had greater membrane sales than all other membrane applications combined throughout most of its history. The early success of microfiltration was linked to an ability to separate microorganisms from water, both as a way to detect their presence, and as a means to remove them. Both of these applications remain important.

Laboratory Microfiltration membranes have countless laboratory uses, such as recovering biomass, measuring particulates in water, clarifying and sterilizing protein solutions, and so on. There are countless examples for both general chemistry and biology, especially for analytical procedures. Most of these applications are run in dead-end flow, with the membrane replacing a more conventional medium such as filter paper.

Medical MF membranes provide a convenient, reliable means to sterilize fluids without heat. Membranes are used to filter injectable fluids during manufacture. Sometimes they are inserted into the tube leading to a patient's vein.

Process Membrane microfiltration competes with conventional filtration, particularly with diatomaceous earth filtration in general-process applications. A significant advantage for membrane MF is the absence of a diatomaceous earth residue for disposal. Membranes have captured most of the final filtration of wine (displacing asbestos), are gaining market share in the filtration of gelatin and corn syrup (displacing diatomaceous earth), are employed for some of the cold pasteurization of beer, and have begun to be used in the pasteurization of milk. Wine and beer filtration operate dead-end; gelatin, corn syrup, and milk are cross-flow operations. MF is used to filter all fluid reactants in the manufacture of microcircuits to ensure the absence of particulates, with point-of-use filters particularly common.

Gas Phase Microfiltration plays an important and unique role in filtering gases and vapors. One important example is maintaining sterility in tank vents, where incoming air passes through a microfilter tight enough to retain any microorganisms, spores, or viruses. A related application is the containment of biological activity in purge gases from fermentation. An unrelated application is the filtration of gases, even highly reactive ones, in microelectronics fabrication to prevent particulates from contaminating a chip.

Downstream Processing Microfiltration plays a significant role in downstream processing of fermentation products in the pharmaceutical and bioprocessing industry. Examples are clarification of fermentation broths, sterile filtration, cell recycle in continuous fermentation, harvesting mammalian cells, cell washing, mycelia recovery, lysate recovery, enzyme purification, vaccines, and so forth.

MF Membranes Microfiltration is a mature field that has proliferated and subdivided. The scope and variety of MF membranes far exceeds that in any other field. A good overview is given by Strathmann [in Porter (ed.), op. cit., pp. 1-78]. MF membranes may be classified into those with tortuous pores or those with capillary pores. Tortuous-pore membranes are far more common, and are sponge-like structures. The pore openings in MF are much larger than those in any other membrane. Surface pores may be observed by electron microscope, but tortuous pores are much more difficult to observe directly. Membranes may be tested by bubble-point techniques. Many materials not yet useful for tighter membranes are made into excellent MF membranes. Retention is the primary attribute of an MF membrane, but important as well are permeability, chemical and temperature resistance, dirt capacity (for dead-end filters), FDA-USP approval, inherent strength, adsorption properties, wetting behavior, and service life.

Membrane-production techniques listed below are applicable primarily or only to MF membranes. In addition, the Loeb-Sourirajan process, used extensively for reverse osmosis and ultrafiltration membranes, is used for some MF membranes.

Membranes from Solids Membranes may be made from microparticles by sintering or agglomeration. The pores are formed from the interstices between the solid particles. The simplest of this class of membrane is formed by sintering metal, metal oxide, graphite, ceramic, or polymer. Silver, tungsten, stainless steel, glass, several ceramics, and other materials are made into commercial membranes. Sintered metal may be coated by TiO_2 or zirconium oxide to produce MF and UF membranes. Membranes may be made by the careful winding of microfibers or wires.

Ceramic Ceramic membranes are made generally by the sol-gel process, the successive deposition of ever smaller ceramic precursor spheres, followed by firing to form multitube monoliths. The diameter of the individual channels is commonly about 2 to 6 mm. Monoliths come in a variety of shapes and sizes. A 19-channel design is common. One manufacturer makes large monoliths with square channels.

Track-Etched Track-etched membranes (Fig. 20-66) are now made by exposing a thin polymer film to a collimated beam of radiation strong enough to break chemical bonds in the polymer chains. The film is then etched in a bath which selectively attacks the damaged polymer. The technique produces a film with photogenic pores,

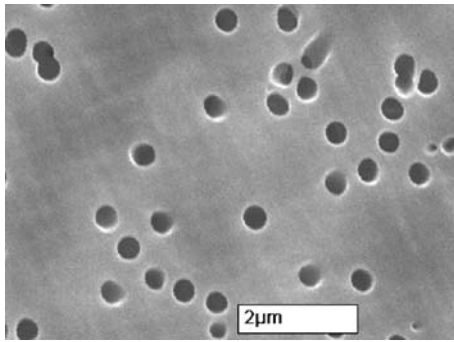


FIG. 20-66 Track-etched 0.4- μm polycarbonate membrane. (Courtesy Millipore Corporation.)

whose diameter may be varied by the intensity of the etching step. Commercially available membranes have a narrow pore size distribution and are reportedly resistant to plugging. The membranes have low flux, because it is impossible to achieve high pore density without sacrificing uniformity of diameter.

Chemical Phase Inversion Symmetrical phase-inversion membranes (Fig. 20-67) remain the most important commercial MF membranes produced. The process produces tortuous-flow membranes. It involves preparing a concentrated solution of a polymer in a solvent. The solution is spread into a thin film, then precipitated through the slow addition of a nonsolvent, usually water, sometimes from the vapor phase. The technique is impressively versatile, capable of producing fairly uniform membranes whose pore size may be varied within broad limits.

Thermal Phase Inversion Thermal phase inversion is a technique which may be used to produce large quantities of MF membrane economically. A solution of polymer in poor solvent is prepared at an elevated temperature. After being formed into its final shape, a sudden drop in solution temperature causes the polymer to precipitate. The solvent is then washed out. Membranes may be spun at high rates using this technique.

Stretched Polymers MF membranes may be made by stretching (Fig. 20-68). Semicrystalline polymers, if stretched perpendicular to the axis of crystallite orientation, may fracture in such a way as to make reproducible microchannels. Best known are Goretex[®] produced from Teflon[®], and Celgard[®] produced from polyolefin. Stretched polymers have unusually large fractions of open space, giving them very high fluxes in the microfiltration of gases, for example. Most such materials are very hydrophobic.

Membrane Characterization MF membranes are rated by flux and pore size. Microfiltration membranes are uniquely testable by

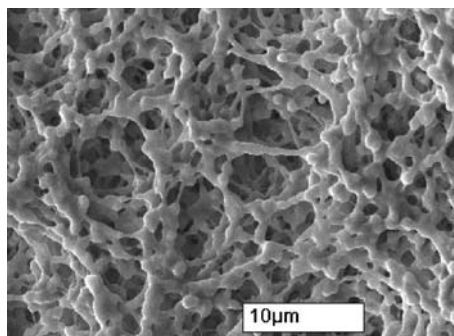


FIG. 20-67 Chemical phase inversion 0.45- μm polyvinylidene fluoride membrane. (Courtesy Millipore Corporation.)

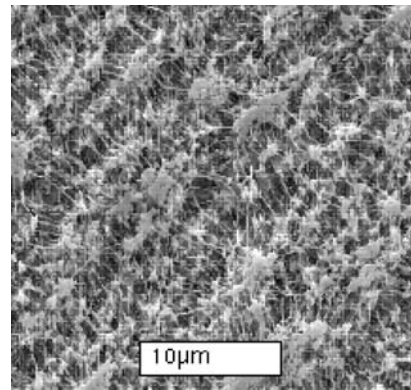


FIG. 20-68 Stretched polytetrafluoroethylene membrane. (Courtesy Millipore Corporation.)

direct examination, but since the number of pores that may be observed directly by microscope is so small, microscopic pore size determination is mainly useful for membrane research and verification of other pore-size-determining methods. Furthermore, the most critical dimension may not be observable from the surface. Few MF membranes have neat, cylindrical pores. Indirect means of measurement are generally superior. Accurate characterization of MF membranes is a continuing research topic for which interested parties should consult the current literature.

Bubble Point Large areas of microfiltration membrane can be tested and verified by a bubble test. Pores of the membrane are filled with liquid, then a gas is forced against the face of the membrane. The Young-Laplace equation, $\Delta P = (4\gamma \cos \Theta)/d$, relates the pressure required to force a bubble through a pore to its radius, and the interfacial surface tension between the penetrating gas and the liquid in the membrane pore. γ is the surface tension (N/m), d is the pore diameter (m), and P is transmembrane pressure (Pa). Θ is the liquid-solid contact angle. For a fluid wetting the membrane perfectly, $\cos \Theta = 1$.

By raising the gas pressure on a wet membrane until the first bubble appears, the largest pore may be identified, and its size computed. This is a good test to run on a membrane apparatus used to sterilize a fluid, since bacteria larger than the identified largest pore (or leak) cannot readily penetrate the assembly. Pore-size distribution may also be run by bubble point. Bubble-point testing is particularly useful in assembled microfilters, since the membrane and all seals may be verified. Periodic testing ensures that the assembly retains its integrity. Diffusional flow of gas is a complication in large MF assemblies. It results from gas dissolving in pore liquid at the high-pressure side, and desorbing at the low-pressure side. If the number of pores and the average pore length are known, the effect can be computed. Special protocols are used when this method is used for critical applications. Detail is provided in ASTM F316-86, "Standard test method for pore size characteristics of membrane filters by bubble point and mean flow pore test." The bubble-point test may also be run using two liquids. Because interfacial surface tensions of liquids can be quite low, this technique permits measurements on pores as small as 10 nm.

Charged Membranes The use of tortuous-flow membranes containing a positive electrical charge may reduce the quantity of negatively charged particles passing even when the pore size is much larger than the particle. The technique is useful for making prefilters or layered membranes that withstand much higher solids loadings before becoming plugged.

Bacteria Challenge Membranes are further tested by challenge with microorganisms of known size: their ability to retain all of the organisms is taken as proof that all pores are smaller than the organism. The best-known microorganism for pore-size determination is *Pseudomonas diminuta*, an asporogenous gram-negative rod with a mean diameter of 0.3 μm . Membranes with pore size smaller than that are used to ensure sterility in many applications. Leahy and

Sullivan [*Pharmaceutical Technology*, 2(11), 65 (1978)] provide details of this validation procedure.

Membrane thickness is a factor in microbial retention. Tortuous-pore membranes rated at 0.22 μm typically have surface openings as large as 1 μm (Fig. 20-67). Narrower restrictions are found beneath the surface. In challenge tests, *P. diminuta* organisms are found well beneath the surface of a 0.2- μm membrane, but not in the permeate.

Latex Latex particles of known size are available as standards. They are useful to challenge MF membranes.

Process Configuration As befits a field with a vast number of important applications and a history of innovation, there are countless variations on how an MF process is run.

Dead-end versus Cross-flow Conventional filtration is usually run dead-end, and is facilitated by amendments that capture the particulates being removed. Membranes have very low dirt capacity, so only applications with very low solids to be removed are run in conventional dead-end flow. A rough upper limit to solids content is about 0.5 percent; streams containing <0.1 percent are almost always processed by dead-end devices. Since dead-end membrane equipment is much less expensive than cross-flow, great ingenuity is applied to protecting the critical membrane pores by structured prefilters to remove larger particles and debris. The feed may also be pretreated. It is common practice to dispose of the spent membrane rather than clean it. The membrane may be run inverted. A review of dead-end membrane filtration is given by Davis and Grant [in Ho and Sirkar (eds.), op. cit., pp. 461–479].

Cross-flow is the usual case where cake compressibility is a problem. Cross-flow microfiltration is much the same as cross-flow ultrafiltration in principle. In practice, the devices are often different. As with UF, spiral-wound membranes provide the most economical configuration for many large-scale installations. However, capillary devices and cassettes are widely employed, especially at smaller scale. A detailed description of cross-flow microfiltration had been given by Murkes and Carlsson [*Crossflow Filtration*, Wiley, New York (1988)].

Membrane Inverted Most membranes have larger openings on one face than on the other. Common practice is to run the tightest face against the feed in order to avoid plugging of the backing by particles. The rationale is that anything that makes it past the "skin" will have relatively unimpeded passage into the backing and out with the permeate. For very low solids this convention is reversed, the rationale being that the porous backing provides a trap for particulates, rather like filter aid.

If the complete passage of soluble macromolecules is required, a highly polarized membrane is an advantage. The upside-down membrane hinders the back diffusion of macrosolutes. Countering the tendency of the retained particulates to "autofilter" soluble macrosolutes, the inhibition of back diffusion raises the polarization and thus the passage of macrosolutes such as proteins. The particulates are physically retained by the membrane. Blinding and plugging can be controlled if the membrane is backwashed frequently. This technique has been demonstrated at high solids loadings in an application where high passage of soluble material is critical, the microfiltration of beer [Wenten, Rasmussen, and Jonsson, *North Am. Membrane Soc. Sixth Annual Meeting*, Breckenridge, CO (1994)].

Liquid Backpulse Solid membranes are backwashed by forcing permeate backward through the membrane. Frequent pulsing seems to be the key.

Air Backflush A configuration unique to microfiltration feeds the process stream on the shell side of a capillary module with the permeate exiting the tube side. The device is run as an intermittent dead-end filter. Every few minutes, the permeate side is pressurized with air. First displacing the liquid permeate, a blast of air pushed backward through the membrane pushes off the layer of accumulated solids. The membrane skin contacts the process stream, and while being backwashed, the air simultaneously expands the capillary and membrane pores slightly. This momentary expansion facilitates the removal of imbedded particles.

Process Limitations The same sorts of process limitations affecting UF apply to MF. The following section will concentrate on the differences.

Concentration Polarization The equations governing cross-flow mass transfer are developed in the section describing ultrafiltration.

The velocity, viscosity, density, and channel-height values are all similar to UF, but the diffusivity of large particles (MF) is orders-of-magnitude lower than the diffusivity of macromolecules (UF). It is thus quite surprising to find the fluxes of cross-flow MF processes to be similar to, and often higher than, UF fluxes. Two primary theories for the enhanced diffusion of particles in a shear field, the inertial-lift theory and the shear-induced theory, are explained by Davis [in Ho and Sirkar (eds.), op. cit., pp. 480–505], and Belfort, Davis, and Zydney [*J. Membrane Sci.*, 96, 1–58 (1994)]. While not clear-cut, shear-induced diffusion is quite large compared to Brownian diffusion except for those cases with very small particles or very low cross-flow velocity. The enhancement of mass transfer in turbulent-flow microfiltration, a major effect, remains completely empirical.

Fouling Fouling affects MF as it affects all membrane processes. One difference is that the fouling effect caused by deposition of a foulant in the pores or on the surface of the membrane can be confounded by a rearrangement or compression of the solids cake which may form on the membrane surface. Also, the high, open space found in tortuous-pore membranes makes them slower to foul and harder to clean.

Equipment Configuration Since the early days when membrane was available only in flat-sheet form, the variety of offerings of various geometry and fabricated filter component types has grown geometrically. An entire catalog is devoted just to list the devices incorporating membranes whose area ranges from less than 1 cm^2 up to 3 m^2 . Microfiltration has grown to maturity selling these relatively small devices. Replacement rather than reuse has long been the custom in MF, and only with later growth of very large applications, such as water, sewage, and corn sweeteners, has long membrane life become an economic necessity on a large scale.

Conventional Designs Designs familiar from other unit operations are also used in microfiltration. Cartridge-filter housings may be fitted with pleated MF membrane making a high-area dead-end membrane filter. Plate-and-frame type devices are furnished with MF sheet stock, and are common in some applications. Capillary bundles with tube-side feed are used for cross-flow applications, and are occasionally used in dead-end flow. A few tubular membranes are used. Spiral-wound modules are becoming increasingly important for process applications where economics are paramount. Belt filters have been made using MF membrane.

Ceramics Ceramic microfilters for commercial applications are almost always employed as tube-side feed multitube monoliths. They are also available as flat sheet, single tubes, discs, and other forms primarily suited to lab use. They are used for a few high-temperature applications, in contact with solvents, and particularly at very high pH.

Cassettes *Cassette* is a term used to describe two different cross-flow membrane devices. The less-common design is a usually large stack of membrane separated by a spacer, with flow moving in parallel across the membrane sheets. This variant is sometimes referred to as a **flat spiral**, since there is some similarity in the way feed and permeate are handled. The more common cassette has long been popular in the pharmaceutical and biotechnical field. It too is a stack of flat-sheet membranes, but the membrane is usually connected so that the feed flows across the membrane elements in series to achieve higher conversion per pass. Their popularity stems from easy direct scale-up from laboratory to plant-scale equipment. Their limitation is that fluid management is inherently very limited and inefficient. Both types of cassette are very compact and capable of automated manufacture.

Representative Process Applications

Pharmaceutical Removal of suspended matter is a frequent application for MF. Processes may be either clarification, in which the main product is a clarified liquid, or solids recovery. Separating cells or their fragments from broth is the most common application. Clarification of the broth in preparation for product recovery is the usual objective, but the primary goal may be recovery of cells. Cross-flow microfiltration competes well with centrifugation, conventional filtration by rotary vacuum filter or filter press and decantation. MF delivers a cleaner permeate, an uncontaminated, concentrated cell product

which may be washed in the process, and generally gives high yields. There is no filter-aid disposal problem. Microfiltration has higher capital costs than the other processes, although total cost may be lower. The recovery of penicillin is an example of a process for which cross-flow microfiltration is generally accepted.

Water and Wastewater Microfiltration is beginning to be applied to large-scale potable-water treatment. Its major advantage is positive removal of cryptosporidium and giardia cysts, and its major disadvantage is cost. MF is used in a few large sewage-treatment facilities, where its primary advantage is that it permits a major reduction in the physical size of the facility.

Chemical MF is used in several applications to recover caustic values from cleaning or processing streams. An example is the caustic solution used to clean dairy evaporators, which may be cleaned for reuse by passing it through a microfilter. Significant savings in caustic purchase and disposal costs provide the incentive. Acids are also recovered and reused. Ceramic microfilters are most commonly used in these applications.

Food and Dairy Microfiltration has many applications in the food and dairy industries. An innovative dairy application uses MF membranes to remove bacteria as a nonthermal means of disinfection for milk. A special flow apparatus maintains a carefully controlled transmembrane pressure as the milk flows across the membrane. The concentrate contains the bacteria and spores, as well as any fat. The concentrate may be heat sterilized and recombined with the sterile permeate. In another milk application, some success is reported in separating fat from milk or other dairy streams by cross-flow microfiltration instead of centrifugation. Transmembrane pressure must be kept very low to prevent fat penetration into the membrane. In the food industry, MF membranes are replacing diatomaceous earth filtration in the processing of gelatin. The gelatin is passed with the permeate, but the haze producing components are retained. UF may be used downstream to concentrate the gelatin.

Flow Schemes The outline of batch, semibatch, and stages-in-series is given in the section describing ultrafiltration. Diafiltration is also described there. All these techniques are common in MF, except for stages-in-series, used rarely. MF features uses of special techniques to control transmembrane pressure in some applications. An example is one vendor's device for the microfiltration of milk. In most devices the permeate simply leaves by the nearest exit, but for this application the permeate is pumped through the device in such a way as to duplicate the pressure drop in the concentrate side, thus maintaining a constant transmembrane-pressure driving force. In spite of the low-pressure driving force, the flux is extremely high.

Limitations Some applications which seem ideal for MF, for example the clarification of apple juice, are done with UF instead. The reason is the presence of deformable solids which easily plug and blind an MF membrane. The pores of an ultrafiltration membrane are so small that this plugging does not occur, and high fluxes are maintained. UF can be used because there is no soluble macromolecule in the juice that is desired in the filtrate. There are a few other significant applications where MF seems obvious, but is not used because of deformable particle plugging.

Economics Microfiltration may be the triumph of the Lilliputians; nonetheless, there are a few large-industrial applications. Dextrose plants are very large, and as membrane filtration displaces the precoat filters now standard in the industry, very large membrane microfiltration equipment will be built.

Site Size Most MF processes require a smaller footprint than competing processes. Reduction in total-area requirements are sometimes a decisive economic advantage for MF. It may be apparent that the floor-space costs in a pharmaceutical facility are high, but municipal facilities for water and sewage treatment are often located on expensive real estate, giving MF an opportunity despite its higher costs otherwise.

Large Plants The economics of microfiltration units costing about \$10⁶ is treated under ultrafiltration. When ceramic membranes are used, the cost optimum may shift energy consumption upward to as much as 10 kWh/m³.

Disposables For smaller MF applications, short membrane life is a traditional characteristic. In these applications, costs are dominated by the disposables, and an important characteristic of equipment design is the ease, economy, and safety of membrane replacement.

Hygiene and Regulation Almost unique to MF is the influence of regulatory concerns in selection and implementation of a suitable microfilter. Since MF is heavily involved with industries regulated by the Food and Drug Administration, concerns about process stability, consistency of manufacture, virus reduction, pathogen control, and material safety loom far larger than is usually found in other membrane separations.

GAS-SEPARATION MEMBRANES

Process Description Gas-separation membranes separate gases from other gases. Some gas filters, which remove liquids or solids from gases, are microfiltration membranes. Gas membranes generally work because individual gases differ in their solubility and diffusivity through nonporous polymers. A few membranes operate by sieving, Knudsen flow, or chemical complexation.

Selective gas permeation has been known for generations, and the early use of palladium silver-alloy membranes achieved sporadic industrial use. Gas separation on a massive scale was used to separate U²³⁵ from U²³⁸ using porous (Knudsen flow) membranes. An upgrade of the membranes at Oak Ridge cost \$1.5 billion. Polymeric membranes became economically viable about 1980, introducing the modern era of gas-separation membranes. H₂ recovery was the first major application, followed quickly by acid gas separation (CO₂/CH₄) and the production of N₂ from air.

The more permeable component is called the *fast gas*, so it is the one enriched in the permeate stream. Permeability through polymers is the product of solubility and diffusivity. The diffusivity of a gas in a membrane is inversely proportional to its kinetic diameter, a value determined from zeolite cage exclusion data (see Table 20-26 after Breck, *Zeolite Molecular Sieves*, Wiley, New York, 1974, p. 636). Tables 20-27, 20-28, and 20-29 provide units conversion factors useful for calculations related to gas-separation membrane systems.

Leading Examples These applications are commercial, some on a very large scale. They illustrate the range of application for gas-separation membranes. Unless otherwise specified, all use polymeric membranes.

Hydrogen Hydrogen recovery was the first large commercial membrane gas separation. Polysulfone fiber membranes became available in 1980 at a time when H₂ needs were rising, and these novel membranes quickly came to dominate the market. Applications include recovery of H₂ from ammonia purge gas, and extraction of H₂ from petroleum cracking streams. Hydrogen once diverted to low-quality fuel use is now recovered to become ammonia, or is used to desulfurize fuel, etc. H₂ is the fast gas.

Carbon Dioxide-Methane Much of the natural gas produced in the world is coproduced with an acid gas, most commonly CO₂ and/or H₂S. While there are many successful processes for separating the gases, membrane separation is a commercially successful competitor, especially for small installations. The economics work best for feeds with very high or very low CH₄ content. Methane is a slow gas; CO₂, H₂S, and H₂O are fast gases.

Oxygen-Nitrogen Because of higher solubility, in many polymers, O₂ is faster than N₂ by a factor of 5. Water is much faster still. Since simple industrial single-stage air compressors provide sufficient pressure to drive an air-separating membrane, moderate purity N₂ (95–99.5%) may be produced in low to moderate quantities quite

TABLE 20-26 Kinetic Diameters for Important Gases

Penetrant	He	H ₂	NO	CO ₂	Ar	O ₂	N ₂	CO	CH ₄	C ₂ H ₄	Xe	C ₃ H ₈
Kinetic dia, nm	0.26	0.289	0.317	0.33	0.34	0.346	0.364	0.376	0.38	0.39	0.396	0.43

TABLE 20-27 Gas-Permeation Units

Quantity	Engineering units	Literature units	SI units
Permeation rate	Standard cubic feet/minute		kmol/s
Permeation flux	ft ³ /ft ² ·day	cm/sec (STP)	kmol/m ² ·s
Permeability	ft ³ ·ft/ft ² ·day·psi	Barrers	kmol/m·s·Pa
Permeance	ft ³ /ft ² ·day·psi	Barrers/cm	kmol/m ² ·s·Pa

economically by membrane separation. (Argon is counted as part of the nitrogen.) An O₂-enriched stream is a coproduct, but it is rarely of economic value. The membrane process to produce O₂ as a primary product has a limited market.

Helium Helium is a very fast gas, and may be recovered from natural gas through the use of membranes. More commonly, membranes are used to recover He after it has been used and become diluted.

Gas Dehydration Water is extremely permeable in polymer membranes. Dehydration of air and other gases is a growing membrane application.

Vapor Recovery Organic vapors are recovered from gas streams using highly permeable rubbery polymer membranes which are generally unsuitable for permanent gas separations because of poor selectivity. The high sorption of vapors in these materials makes them ideal for stripping and recovering vapors from gases.

Competing Processes Membranes are not the only way to make these separations, neither are they generally the dominant way. In many applications, membranes compete with cryogenic distillation and with pressure-swing adsorption; in others, physical absorption is the dominant method. The growth rate for membrane capacity is higher than that for any competitor.

Basic Principles of Operation Gas-separation literature often uses nomenclature derived from distillation, a practice that will generally be followed here. L is the molar feed rate, V is the molar permeate rate, R is the molar residue ($L - V$). Mole fractions of components i, j , in the feed-residue phase will be x_i, x_j, \dots and in the permeate phase y_i, y_j, \dots . Stage cut, Θ , is permeate volume/feed volume, or V/L .

Basic Equations In "Background and Definitions," the basic equation for gas permeation was derived with the major assumptions noted.

$$J_i \sim N_i = (\rho_i/z)(p_{i,\text{feed}} - p_{i,\text{permeate}}) \quad (20-85)$$

where ρ_i is the permeability of component i through the membrane, J_i is the flux of component i through the membrane for the *partial pressure difference* (Δp) of component i . z is the effective thickness of the membrane. By choosing units appropriately, $J = \rho \Delta p$.

A similar equation may be written for a second component, j , and any additional number of components, employing partial pressures:

$$J_j = (\rho_j/z)(p_{j,\text{feed}} - p_{j,\text{permeate}}) \quad (20-86)$$

The total pressure is the sum of the partial pressures:

$$P_{\text{feed}} = \sum (p_{\text{feed}})_{i,j,\dots} \quad (20-87)$$

$$P_{\text{permeate}} = \sum (p_{\text{permeate}})_{i,j,\dots} \quad (20-88)$$

For simplicity, consider a two-component system. The volume fraction of a component is

$$x_i = \frac{p_{\text{feed}}}{P_{\text{feed}}} \quad (20-89)$$

$$y_i = \frac{p_{\text{permeate}}}{P_{\text{permeate}}} \quad (20-90)$$

TABLE 20-28 Barrer Conversion Factors

Quantity	Multiply	By	To get
Permeability	Barrers	3.348×10^{-19}	kmol/m·s·Pa
Permeability	Barrers	4.810×10^{-8}	ft ³ (STP)/ft·psi·day
Permeance	Barrers/cm	3.348×10^{-17}	kmol/m ² ·s·Pa
Permeance	Barrers/cm	1.466×10^{-6}	ft ³ (STP)/ft ² ·psi·day

When two species are permeating through a membrane, the ratio of their fluxes can be written following Eqs. (20-85) and (20-86) as:

$$\frac{J_i}{J_j} = \frac{\frac{\rho_i}{z}(p_{i,\text{feed}} - p_{i,\text{permeate}})}{\frac{\rho_j}{z}(p_{j,\text{feed}} - p_{j,\text{permeate}})} \quad (20-91)$$

Recalling Eq. (20-55), and restating it in the nomenclature for gas membranes:

$$\alpha = \frac{y_i/y_j}{x_i/x_j} \quad (20-92)$$

Defining the pressure ratio $\Phi = P_{\text{feed}}/P_{\text{permeate}}$ and applying Eqs. (20-87) through (20-90) gives:

$$J_i = \alpha \left[\frac{x_i - (y_i/\Phi)}{x_j - (y_j/\Phi)} \right] \quad (20-93)$$

Combining these equations and rearranging, the permeate composition may be solved explicitly:

$$y_i = \left(\frac{\Phi}{2} \right) \left[x_i + \frac{1}{\Phi} + \frac{1}{\alpha - 1} - \sqrt{\left(x_i + \frac{1}{\Phi} + \frac{1}{\alpha - 1} \right)^2 - \frac{4\alpha x_i}{(\alpha - 1)\Phi}} \right] \quad (20-94)$$

Equation (20-94) gives a permeate concentration as a function of the feed concentration at a stage cut, $\Theta = 0$. To calculate permeate composition as a function of Θ , the equation may be used iteratively if the permeate is unmixed, such as would apply in a test cell. The calculation for real devices must take into account the fact that the driving force is variable due to changes on both sides of the membrane, as partial pressure is a point function, nowhere constant. Using the same caveat, permeation rates may be calculated component by component using Eq. (20-86) and permeance values. For any real device, both concentration and permeation require iterative calculations dependent on module geometry.

Driving Force Gas moves across a membrane in response to a difference in chemical potential. Partial pressure is sufficiently proportional to be used as the variable for design calculations for most gases of interest, but fugacity must be used for CO₂ and usually for H₂ at high pressure. Gas composition changes as a gas passes along a membrane. As the fast gas passes through the membrane, x_i drops. Total pressure on the upstream side of the membrane drops because of frictional losses in the device. Frictional losses on the permeate side will affect the permeate pressure. The partial pressure of a component in the permeate may thus rise rapidly. Permeation rate is a point function, dependent on the difference in partial pressures at a point on the membrane. Many variables affect point partial pressures, among them are membrane structure, module design, and permeate gas-sweep rates. Juxtaposition of feed and permeate is a function of permeator design, and a rapid decline in driving force may result when it is not expected (see "Membrane System Design Features").

TABLE 20-29 Industry-Specific Gas Measures

Industry-unit	How measured	Cubic feet per pound mole	kmol per mscf
STP, Mscf	1000 ft ³ at 32°F	359.3	1.262
Gas industry, Mscf	1000 ft ³ at 60°F	379.8	1.194
Air industry, Mnsf	1000 ft ³ at 70°F	387.1	1.172

An additional complication may arise in a few cases from the Joule-Thompson effect during expansion of a gas through a membrane changing the temperature. High-pressure CO₂ is an example.

Plasticization Gas solubility in the membrane is one of the factors governing its permeation, but the other factor, diffusivity, is not always independent of solubility. If the solubility of a gas in a polymer is too high, plasticization and swelling result, and the critical structure that controls diffusion selectivity is disrupted. These effects are particularly troublesome with condensable gases, and are most often noticed when the partial pressure of CO₂ or H₂S is high. H₂ and He do not show this effect. This problem is well known, but its manifestation is not always immediate.

Limiting Cases Equation (20-94) has two limiting cases for a binary system. First, when $\alpha \gg \phi$. In this case, selectivity is no longer very important.

$$y_i \cong x_i \frac{P_{\text{feed}}}{P_{\text{permeate}}} = x_i \Phi \quad (20-95)$$

Module design is very important for this case, as the high α may result in high permeate partial pressure. An example is the separation of H₂O from air.

Conversely, when $\Phi \gg \alpha$, pressure ratio loses its importance, and permeate composition is:

$$y_i \cong \frac{x_i \alpha}{[1 + x_i(\alpha - 1)]} \quad (20-96)$$

Module design for this case is of lesser importance.

Selectivity and Permeability

State of the Art A desirable gas membrane has high separating power (α) and high permeability to the fast gas, in addition to critical requirements discussed below. The search for an ideal membrane produced copious data on many polymers, neatly summarized by Robeson [*J. Membrane Sci.*, **62**, 165 (1991)]. Plotting log permeability versus log selectivity (α), an "upper bound" is found (see Fig. 20-69) which all the many hundreds of data points fit. The data were taken between 20 and 50°C, generally at 25 or 35°C.

The lower line in Fig. 20-69 shows the upper bound in 1980. Although no breakthrough polymers have been reported in the past

TABLE 20-30 High-Performance Polymers for O₂/N₂*

Polymer	α (O ₂ /N ₂)	ρ (O ₂)—Barrers
Poly (trimethylsilylpropyne)	2.0	4000
Tetrabromo Bis A polycarbonate	7.47	1.36
Poly (tert-butyl acetylene)	3.0	300
Vectra polyester	15.3	0.00046
Poly (triazole)	9.0	1.2
Polypyrrolone	6.5	7.9

*Polymers that are near the upper bound and their characteristics.

few years, it would be surprising if these lines remain the state of the art forever. Performance parameters for polymers used for O₂/N₂ separations are given in Table 20-30.

The upper-bound line connects discontinuous points, but polymers exist near the bound for separations of interest. Whether these will be available as membranes is a different matter. A useful membrane requires a polymer which can be fabricated into a device having an active layer around 50 nm thick. At this thickness, membrane properties may vary significantly from bulk properties, although not by a factor of 2.

The data reported are *permeabilities*, not *fluxes*. Flux is proportional to permeability/thickness. The separations designer must deal with real membranes, for which thickness is determined by factors outside the designer's control. It is vital that flux data are used in design.

Glassy polymers are significantly overrepresented in the high-selectivity region near the upper bound, and rubbery polymers are overrepresented at the high-permeability end, although the highest-permeability polymer discovered, poly(trimethylsilylpropyne) is glassy. Most of the polymers with interesting properties are noncrystalline. Current membrane-materials research is strongly focused on glassy materials and on attempts to improve diffusivity, as it seems more promising than attempts to increase solubility [Koros, *North Am. Membrane Soc. Sixth Annual Meeting*, Breckenridge, CO (1994)].

Robeson [*J. Membrane Sci.*, **62**, 165 (1991); *Polymer*, **35**, 4970 (1994)] has determined upper-bound lines for many permeant pairs in hundreds of polymers. These lines may be drawn from Eq. (20-97) and the data included in Table 20-31. These values will give ρ_i in

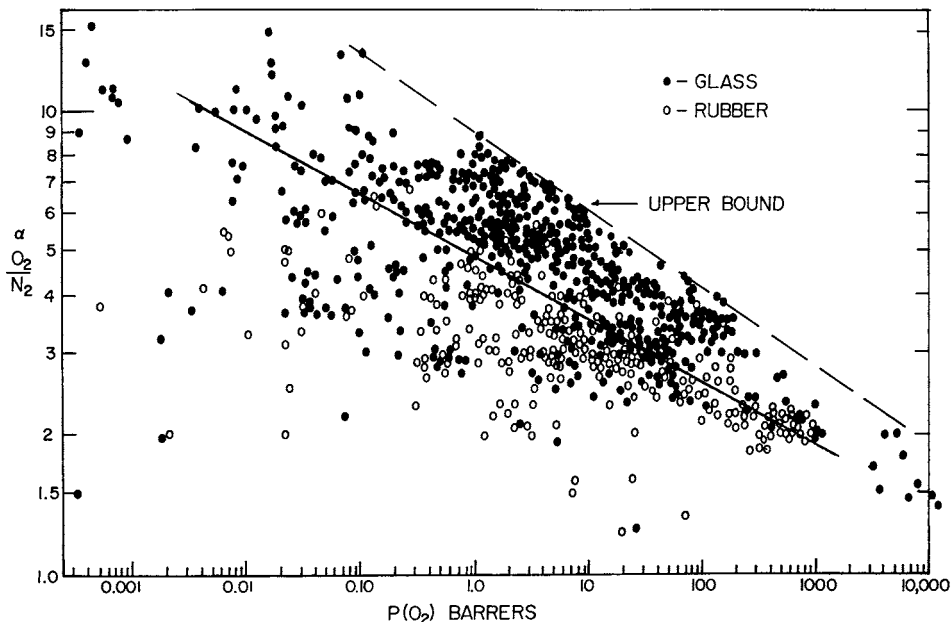


FIG. 20-69 Plot of separation factor versus permeability for many polymers, O₂/N₂. Abscissa—"Fast Gas Permeability, ρ (O₂) Barrers." Ordinate—"Selectivity, α (O₂/N₂)."

TABLE 20-31 Upper-Bound Coordinates for Gas Pairs

Gas pair	log k	m
He/N ₂	4.0969	1.0242
H ₂ /N ₂	4.7236	1.5275
He/CH ₄	3.6991	0.7857
H ₂ /CH ₄	4.2672	1.2112
O ₂ /N ₂	5.5902	5.800
He/O ₂	3.6628	1.295
H ₂ /O ₂	4.5534	2.277
CO ₂ /CH ₄	6.0309	2.6264
He/H ₂	2.9823	4.9535
He/CO ₂	2.8482	1.220
H ₂ /CO ₂	3.0792	1.9363

Barrers; α is dimensionless. Robeson [op.cit., (1991); op. cit., (1994)] lists high-performance polymers for most of these gas pairs, like Table 20-31.

$$\log p_i = \log k - m \log \alpha_{ij} \quad (20-97)$$

Temperature Effects A temperature increase in a polymer membrane permits larger segmental motions in the polymer, producing a dramatic increase in diffusivity. Countering this is a decrease in solubility. It increases the size of the gaps in the polymer matrix, decreasing diffusivity selectivity. The net result is that for a glassy polymer, permeability rises while selectivity declines. For organic permeants in rubbery polymers, this trend is often reversed.

Plasticization and Other Time Effects Most data from the literature, including those presented above are taken from experiments where one gas at a time is tested, with α calculated as a ratio of the two permeabilities. If either gas permeates because of a high-sorption coefficient rather than a high diffusivity, there may be an increase in the permeability of all gases in contact with the membrane. Thus, the α actually found in a real separation may be much lower than that calculated by the simple ratio of permeabilities. The data in the literature do not reliably include the plasticization effect. If present, it results in the sometimes slow relaxation of polymer structure giving a rise in permeability and a dramatic decline in selectivity.

Other Caveats Transport in glassy polymers is different from transport in rubbery ones. In glassy polymers, there are two sites in which sorption may occur, and the literature dealing with dual-mode sorption is voluminous. The simplest case describes behavior when the downstream pressure is zero. It is of great help in understanding the theory but of limited value in practice. There are concerns about permeation of mixtures in glassy polymers with reports of crowding out and competitive sorption. Practical devices are built and operated for many streams, and the complications are often minor. But taking data independently determined for two pure gases and dividing them to obtain α in the absence of other facts is risky.

Gas-Separation Membranes

Organic Organic polymer membranes are the basis for almost all commercial gas-separation activity. Early membranes were cellulose esters and polysulfone. These membranes have a large installed base. New installations are dominated by specialty polymers designed for the purpose, including some polyimides and halogenated polycarbonates. In addition to skinned membranes, composites are made from "designer" polymers, requiring as little as 2 g/1000 m². The rapid rise of N₂/O₂ membranes in particular is the result of stunning improvements in product uniformity and quality. A few broken fibers in a 100 m² module results in the module's being scrapped.

Caulked Membrane manufacturing defects are unavoidable, and pinholes are particularly deleterious in gas-separation membranes. A very effective remedy is to **caulk** the membrane by applying a highly permeable, very thin topcoat over the finished membrane. While the coating will have poor selectivity, it will plug up the gross leaks while impairing the fast gas permeance only slightly. Unless the as-cast membrane is almost perfect, caulking dramatically improves membrane performance.

Metallic Palladium films pass H₂ readily, especially above 300°C. α for this separation is extremely high, and H₂ produced by purification through certain Pd alloy membranes is uniquely pure. Pd alloys are used to overcome the crystalline instability of pure Pd during heating-cooling cycles. Economics limit this membrane to high-purity applications.

Advanced Materials Experimental membranes have shown remarkable separations between gas pairs such as O₂/N₂ whose kinetic diameters (see Table 20-26) are quite close. Most prominent is the carbon molecular sieve membrane, which operates by ultramicroporous molecular sieving. Preparation of large-scale permeators based on ultramicroporous membranes has proven to be a major challenge.

Catalytic A catalytic-membrane reactor is a combination heterogeneous catalyst and permselective membrane that promotes a reaction, allowing one component to permeate. Many of the reactions studied involve H₂. Membranes are metal (Pd, Ag), nonporous metal oxides, and porous structures of ceramic and glass. Falconer, Noble, and Sperry [in Noble and Stern (eds.), op. cit., pp. 669–709] review status and potential developments.

Membrane System Design Features For the rate process of permeation to occur, there must be a driving force. For gas separations, that force is partial pressure (or fugacity). Since the ratio of the component fluxes determines the separation, the partial pressure of each component at each point is important. There are three ways of driving the process: Either high partial pressure on the feed side (achieved by high total pressure), or low partial pressure on the permeate side, which may be achieved either by vacuum or by introduction of a sweep gas. Both of the permeate options have negative economic implications, and they are less commonly used.

Figure 20-70 shows three of the principal operating modes for gas membranes. A critical issue is the actual partial pressure of permeant at a point on the membrane. Flow arrangements for the permeate are very important in determining the efficiency of the separation, in rough analogy to the importance of arrangements in heat exchangers.

Spiral membranes are the usual way to form flat sheet into modules. They have the characteristic that the feed and the permeate move at

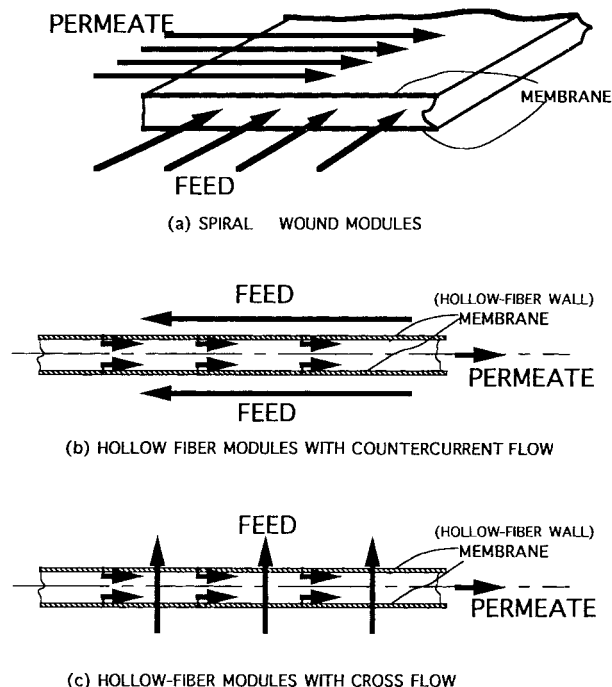


FIG. 20-70 Flow paths in gas permeators. (Courtesy Elsevier.)

right angles. Since the membrane is always cast on a porous support, point-permeate values are influenced by the substrate.

Hollow-fiber membranes may be run with shell-side or tube-side feed, cocurrent, countercurrent or in the case of shell-side feed and two end permeate collection, co- and countercurrent. Not shown is the scheme for feed inside the fiber, common practice in lower-pressure separations such as air.

The design of the membrane device will influence whether the membrane is operating near its theoretical limit. Sengupta and Sirkar [in Noble and Stern (eds.), op. cit., pp. 499–552] treat module design thoroughly (including numerical examples for most module configurations) and provide an extensive bibliography.

For a hollow-fiber device running with shell-side feed with the membrane on the outside, Giglia et al. [*Ind. Eng. Chem. Research*, **29**, 1239–1248 (1991)] analyzed the effect of membrane-backing porosity on separation efficiency. The application is production of N_2 from air, the desired result being the lowest possible O_2 content in the retentate at a given stage cut. The modules used were operated cocurrent and countercurrent. If the porous-membrane backing prevented the permeate from mixing with the gas adjacent to the membrane, a result approximating cross-flow is expected. For the particular membrane structure used, the experimental result for cocurrent flow was quite close to the calculated cocurrent value, while for countercurrent flow, the experimental data were between the values calculated for the crosscurrent model and the countercurrent model. For a membrane to be commercially useful in this application, the mass transfer on the permeate side must exceed the crosscurrent model.

Air is commonly run with tube-side feed. The permeate is run countercurrent with the separating skin in contact with the permeate. (The feed gas is in contact with the macroporous back side of the membrane.) This configuration has proven to be superior, since the permeate-side mass-transfer problem is reduced to a minimum, and the feed-side mass-transfer problem is not limiting.

Partial Pressure Pinch An example of the limitations of the partial pressure pinch is the dehumidification of air by membrane. While O_2 is the fast gas in air separation, in this application H_2O is faster still. Special dehydration membranes exhibit $\alpha = 20,000$. As gas passes down the membrane, the partial pressure of H_2O drops rapidly in the feed. Since the H_2O in the permeate is diluted only by the O_2 and N_2 permeating simultaneously, p_{H_2O} rises rapidly in the permeate. Soon there is no driving force. The commercial solution is to take some of the dry air product and introduce it into the permeate side as a countercurrent sweep gas, to dilute the permeate and lower the H_2O partial pressure. It is in effect the introduction of a leak into the membrane, but it is a controlled leak and it is introduced at the optimum position.

Fouling Industrial streams may contain condensable or reactive components which may coat, solvate, fill the free volume, or react with the membrane. Gases compressed by an oil-lubricated compressor may contain oil, or may be at the water dew point. Materials that will coat or harm the membrane must be removed before the gas is treated. Most membranes require removal of compressor oil. The extremely permeable poly(trimethylsilylpropyne) may not become a practical membrane because it loses its permeability rapidly. Part of the problem is pore collapse, but it seems extremely sensitive to contamination even by diffusion pump oil and gaskets [Robeson, op. cit., (1994)].

A foulinglike problem may occur when condensable vapors are left in the residue. Condensation may result which in the best case results in blinding of the membrane, and in the usual case, destruction of the membrane module. Dew-point considerations must be part of any gas-membrane design exercise.

Modules and Housings Modern gas membranes are packaged either as hollow-fiber bundles or as spiral-wound modules. The former uses extruded hollow fibers. Tube-side feed is preferable, but it is limited to about 1.5 MPa. Higher-pressure applications are usually fed on the shell side. A large industrial permeator contains fibers 400 μm by 200 μm i.d. in a 6-inch shell 10 feet long. Flat-sheet membrane is wound into spirals, with an 8- by 36-inch permeator containing 25 m^2 of membrane. Both types of module are similar to those illustrated in "Background and Definitions." Spiral modules are useful when feed

flows are very high and especially in vapor-permeation applications. Otherwise, fiber modules have a large and growing share of the market.

Energy Requirements The thermodynamic minimum energy requirement to separate a metric ton of N_2 from air and compress it to atmospheric pressure at 25°C is independent of separation method, 20.8 MJ or 5.8 kWh. In practice, a cryogenic distillation plant requires twice this energy, and it produces a very pure product as a matter of course. The membrane process requires somewhat more energy than distillation at low purity and much more energy at high purity. Membranes for O_2 -reduced air are economical and are a rapidly growing application, but not because of energy efficiency. Figure 20-71 may be used to estimate membrane energy requirements. From the required purity, locate the stage cut on either of the countercurrent flow curves. The compressor work required is calculated using the pressure and the term (product flow rate)/(1 - Θ). The N_2 -rich product is produced at pressure, and the O_2 -enriched permeate is vented. For example, if gas is required containing 97 percent inerts, assume the product composition would be 96 percent N_2 , 2 percent O_2 , 1 percent Ar, and 3 percent O_2 , giving a calculated molar mass of 28.2. One tonne would thus contain 35.4 kmol. For 98 percent inerts, Fig. 20-71 shows a stage cut of 67 percent when operating at 690 kPa (abs) and 25°C. Therefore, $35.5/(1 - 0.67) = 108$ kmol of air are required as feed. The adiabatic compression of 108 kmol of air from atmospheric pressure and 300 K (it would subsequently be cooled to 273 + 25 = 298 K) requires 192 kWh. Assuming 75 percent overall compressor + driver efficiency, 256 kWh are required. For comparison, a very efficient, large N_2 distillation plant would produce 99.99 percent N_2 at 690 kPa for 113 kWh/metric ton. The thermodynamic minimum to separate ($N_2 + Ar$) and deliver it at the given P and T is 72 kWh.

Economics It is ironic that a great virtue of membranes, their versatility, makes economic optimization of a membrane process very difficult. Designs can be tailored to very specific applications, but each design requires a sophisticated computer program to optimize its costs. Spillman [in Noble and Stern (eds.), op. cit., pp. 589–667] provides an overall review and numerous specific examples including circa 1989 economics.

Rules of Thumb With a few notable exceptions such as H_2 through Pd membranes, membrane separations are not favored when a component is required at high purity. Often, membranes serve these needs by providing a moderate purity product which may be inexpensively upgraded by a subsequent process. Increasing the purity of N_2 by the introduction of H_2 or CH_4 to react with unwanted O_2 is a good example. Unless permeates are recycled, high product purity is accompanied by lower product recovery.

Pressure ratio (Φ) is quite important, but transmembrane ΔP matters as well. Consider the case of a vacuum permeate ($\Phi = \infty$): The membrane area will be an inverse function of P . Φ influences separation and area, transmembrane ΔP influences area.

In a binary separation, the highest purity of integrated permeate occurs at $\Theta = 0$. Purity decreases monotonically until it reaches the feed purity at $\Theta = 1$. In a ternary system, the residue concentration of the gas with the intermediate permeability will reach a maximum at some intermediate stage cut.

Concentration polarization is a significant problem only in vapor separation. There, because the partial pressure of the penetrant is normally low and its solubility in the membrane is high, there can be depletion in the gas phase at the membrane. In other applications it is usually safe to assume bulk gas concentration right up to the membrane.

Another factor to remember is that for $\alpha = 1$, or for $\Phi = 1$, or for $(1/\Theta) = 1$ there is no separation at all. Increasing any of the quantities as defined make for a better separation, but the improvement is diminishing in all cases as the value moves higher. An example of the economic tradeoff between permeability and α is illustrated in Fig. 20-72 where the economics are clearly improved by sacrificing selectivity for flux.

Compression If compression of either feed or permeate is required, it is highly likely that compression capital and operating costs will dominate the economics of the gas-separation process. In some applications, pressure is essentially "free," such as when removing small quantities of CO_2 from natural gas. The gas is often

O₂ RETENTATE CONCENTRATION vs STAGE CUT
FLOW PATTERN COMPARISON

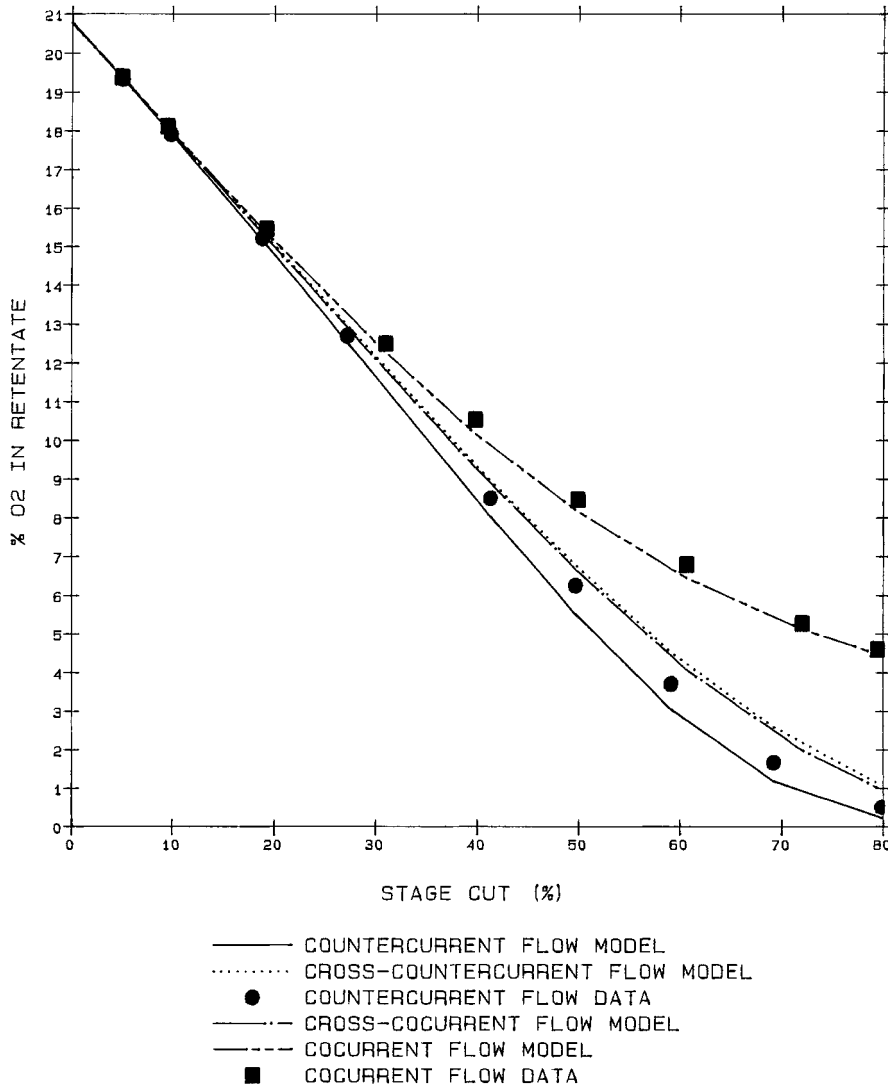


FIG. 20-71 Air fractionation by membrane. O₂ in retentate as a function of feed fraction passed through the membrane (stage cut) showing the different result with changing process paths. Process has shell-side feed at 690 kPa (abs) and 298 K. Module comprised of hollow fibers, diameter 370 μm od × 145 μm id × 1500 mm long. Membrane properties α = 5.7 (O₂/N₂), permeance for O₂ = 3.75 × 10⁻⁶ Barrer/cm. (Courtesy Innovative Membrane Systems/Praxair.)

produced at pressure, but is compressed for transmission anyway, and since the residue constitutes the product, it continues downstream at pressure. H₂ frequently enters the separation process at pressure, an advantage for membranes. Unlike CH₄, the H₂ is in the permeate, and recompression may be a significant cost. A relative area cure for CO₂/CH₄ is shown in Fig. 20-73. When the permeate is the product (H₂, CO₂) the increasing membrane area shown in Fig. 20-74 is largely the effect of more gas to pass through the membrane, since the curve is based on a constant volume of feed gas, not a constant output of H₂. The facts of life in compressor economics are in painful opposition to the desires of the membrane designer. Pressure ratios higher than six become expensive; vacuum is very expensive, and scale is important.

Because of compressor economics, staging membranes with recompression is unusual. Designers can assume that a flow sheet that mixes unlike streams or reduces pressure through a throttling valve will increase cost in most cases.

Product Losses Account must be taken of the product loss, the slow gas in the permeate (such as CH₄), or the fast gas in the residue (such as H₂). Figure 20-75 illustrates the issue for a membrane used to purify natural gas from 93 percent to pipeline quality, 98 percent. In the upper figure, the gas is run through a permeator bank operating as a single stage. For the membrane and module chosen, the permeate contains 63 percent CH₄. By dividing the same membrane area into two stages, two permeates (or more) may be produced, one of which

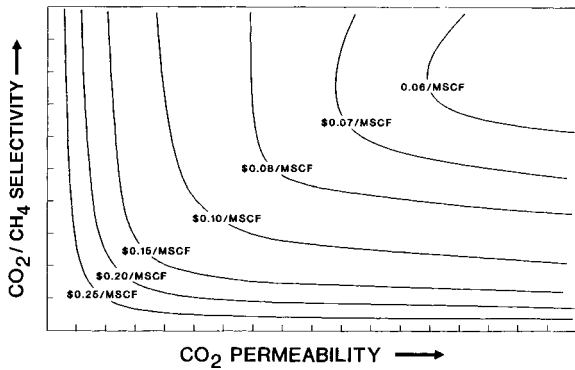


FIG. 20-72 Constant-cost lines as a function of permeability and selectivity for CO₂/CH₄. Cellulose-acetate membrane "mscf" is one thousand standard cubic feet. (Courtesy W. R. Grace.)

may have significantly higher economic value than the single mixed permeate. In fact, where CH₄ is involved, another design parameter is the local economic value of various waste streams as fuel.

Membrane Replacement Membrane replacement is a significant cost factor, but membrane life and reliability are now reasonable. Membranes are more susceptible to operating upsets than more traditional equipment, but their field-reliability record in properly engineered, properly maintained installations is good to excellent. In N₂ separations, membrane life is very long.

Competing Technologies The determination of which separation technique is best for a specific application is a dynamic function of advances in membranes and several other technologies. At this writing, very small quantities of pure components are best obtained by purchase of gas in cylinders. For N₂, membranes become competitive at moderate flow rates where purity required is <99.5 percent. At higher flow rates and higher purity, *pressure swing adsorption* (PSA) is better (see Sec. 16: "Adsorption and Ion Exchange"). At still higher volumes, delivered liquid N₂, pipeline N₂, or on-site distillation will be superior. For O₂, membranes have little economic importance. The problem is the economic cost of using vacuum on the permeate side, or the equally unattractive prospect of compressing the feed and operating at low stage cut. For H₂, membranes are dominant when the feed is at high pressure, except for high purity (excepting Pd noted above) and very large volume. Higher purity or lower feed pressure favor PSA. Very high volume favors cryogenic separation. For CH₄, membranes compete at low purity and near pipeline (98 percent)

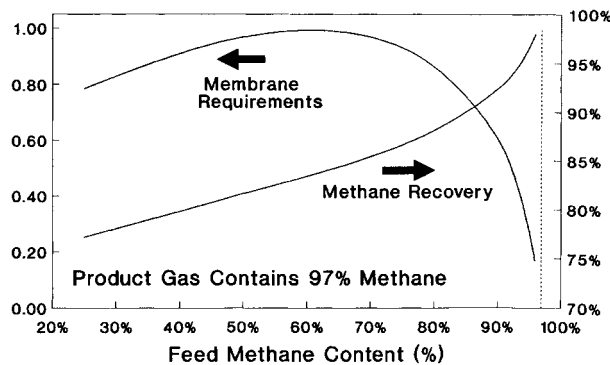


FIG. 20-73 Influence of feed purity on total membrane area when the residue gas at fixed purity is the product. Feed-gas volume is constant. CO₂/CH₄ cellulose-acetate membrane, $\alpha = 21$. (Courtesy W. R. Grace.)

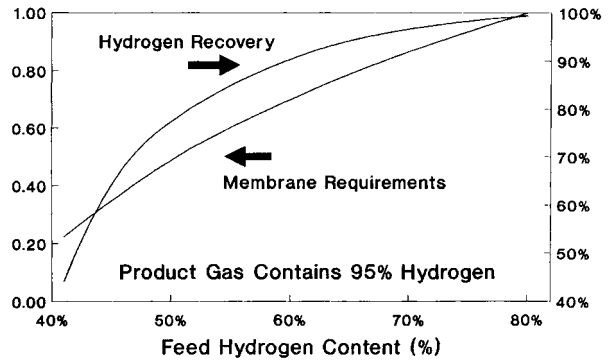


FIG. 20-74 Influence of feed purity on total membrane area when the permeate gas at fixed purity is the product. Feed-gas volume is constant. H₂/CH₄ cellulose-acetate membrane, $\alpha = 45$. (Courtesy W. R. Grace.)

purity, but distillation and absorption are very competitive at large scale and for intermediate CO₂ contamination levels.

Membranes are found as adjuncts to most conventional processes, since their use can improve overall economics in cases where membrane strength coincides with conventional process weakness.

PERVAPORATION

Process Description Pervaporation is a separation process in which a liquid mixture contacts a nonporous permselective membrane. One component is transported through the membrane preferentially. It evaporates on the downstream side of the membrane leaving as a vapor. The name is a contraction of permeation and evaporation. Permeation is induced by lowering partial pressure of the permeating component, usually by vacuum or occasionally with a sweep gas. The permeate is then condensed or recovered. Thus, three steps are necessary: Sorption of the permeating components into the membrane, diffusive transport across the nonporous membrane, then desorption into the permeate space, with a heat effect. Pervaporation membranes are chosen for high selectivity, and the permeate is often highly purified.

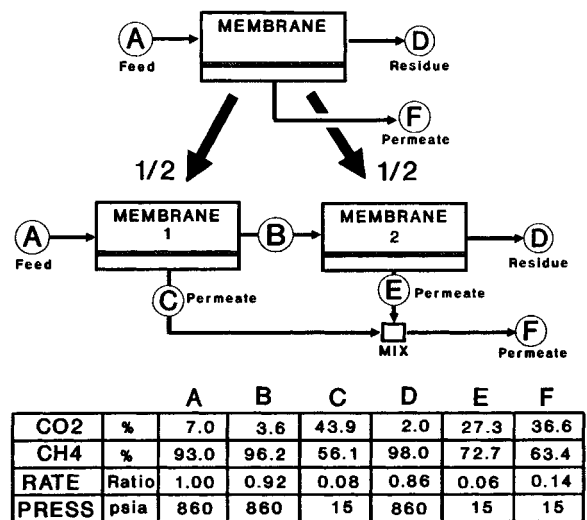


FIG. 20-75 Effect on permeate of dividing a one-stage separation into two equal stages having the same total membrane area. Compositions of A, D, and F are equal for both cases. (Courtesy W. R. Grace.)

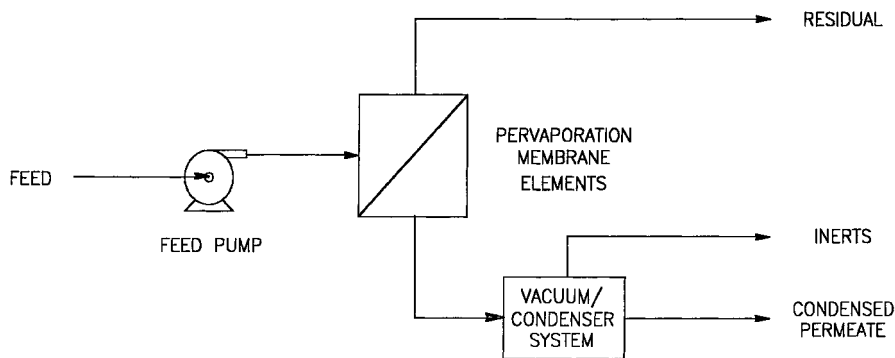


FIG. 20-76 Simplified flow schematic for a pervaporation system. Heated feed enters from left through a feed pump. Heaters in a recirculating feed loop may be required (not shown). Stripped liquid exits at the top of the pervaporation membrane. Vapor exits at the bottom to a condenser. Liquid and noncondensibles are removed under vacuum. (Courtesy Hoechst Celanese.)

In the flow schematic (Fig. 20-76), the condenser controls the vapor pressure of the permeating component. The vacuum pump, as shown, pumps both liquid and vapor phases from the condenser. Its major duty is the removal of noncondensibles. Early work in pervaporation focused on organic-organic separations. Many have been demonstrated; few if any have been commercialized. Still, there are prospects for some difficult organic separations.

An important characteristic of pervaporation that distinguishes it from distillation is that it is a rate process, not an equilibrium process. The more permeable component may be the less-volatile component. Pervaporation has its greatest utility in the resolution of azeotropes, as an adjunct to distillation. Selecting a membrane permeable to the minor component is important, since the membrane area required is roughly proportional to the mass of permeate. Thus pervaporation devices for the purification of the ethanol-water azeotrope (95 percent ethanol) are always based on a hydrophilic membrane.

Pervaporation membranes are of two general types. **Hydrophilic membranes** are used to remove water from organic solutions, often from azeotropes. **Hydrophobic membranes** are used to remove organic compounds from water. The important operating characteristics of hydrophobic and hydrophilic membranes differ. Hydrophobic membranes are usually used where the solvent concentration is about 6 percent or less—above this value, other separation methods are usually cheaper unless the flow rate is small. At low-solvent levels the usual membrane (silicone rubber) is not swollen appreciably, and movement of solvent into the membrane makes depletion of solvent in the boundary layer (concentration polarization) an important design problem. Hydrophilic pervaporation membranes operate such that the upstream portion is usually swollen with water, while the downstream face is low in water concentration because it is being depleted by vaporization. Fluxes are low enough ($<5 \text{ kg/m}^2\text{-hr}$) that boundary layer depletion (liquid side) is not limiting.

The simplifying assumptions that make Fick's law useful for other processes are not valid for pervaporation. The activity gradient across the membrane is far more important than the pressure gradient. Equation (20-98) is generally used to describe the pervaporation process:

$$J_i = -D_i C \frac{d \ln a_i}{dz} \quad (20-98)$$

where a_i is the activity coefficient of component i .

This equation is not particularly useful in practice, since it is difficult to quantify the relationship between concentration and activity. The Flory-Huggins theory does not work well with the crosslinked semicrystalline polymers that comprise an important class of pervaporation membranes. Neel (in Noble and Stern, op. cit., pp. 169–176) reviews modifications of the Stefan-Maxwell approach and other equations of state appropriate for the process.

A typical permeant-concentration profile in a pervaporation membrane is shown in Fig. 20-77. The concentration gradient at the permeate (vapor) side of the hydrophilic membrane is usually rate controlling. Therefore the downstream pressure (usually controlled by condenser temperature) is very important for flux and selectivity. Since selectivity is the ratio of fluxes of the components in the feed, as downstream pressure increases, membrane swelling at the permeate interface increases, and the concentration gradient at the permeate interface decreases. The permeate flux drops, and the more swollen membrane is less selective. A rise in permeate pressure may result in a drastic drop in membrane selectivity. This effect is diminished at low water concentrations, where membrane swelling is no longer dominant. In fact, when the water concentration drops far enough, permeate backpressure loses its significance. (See Fig. 20-78.)

For rubbery membranes (hydrophobic), the degree of swelling has less effect on selectivity. Thus the permeate pressure is less critical to the separation, but it is critical to the driving force, thus flux, since the vapor pressure of the organic will be high compared to that of water.

Definitions Following the practice presented under "Gas-Separation Membranes," distillation notation is used. Literature articles often use mass fraction instead of mole fraction, but the substitution of one to the other is easily made.

$$\beta = \frac{y_i}{x_i} \quad (20-99)$$

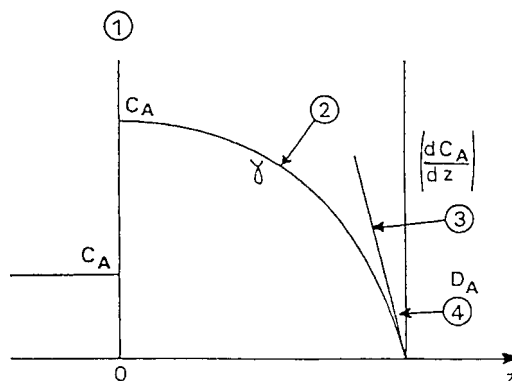


FIG. 20-77 Permeant-concentration profile in a pervaporation membrane. 1—Upstream side (swollen). 2—Convex curvature due to concentration-dependent permeant diffusivity. 3—Downstream concentration gradient. 4—Exit surface of membrane, depleted of permeant, thus unswollen. (Courtesy Elsevier.)

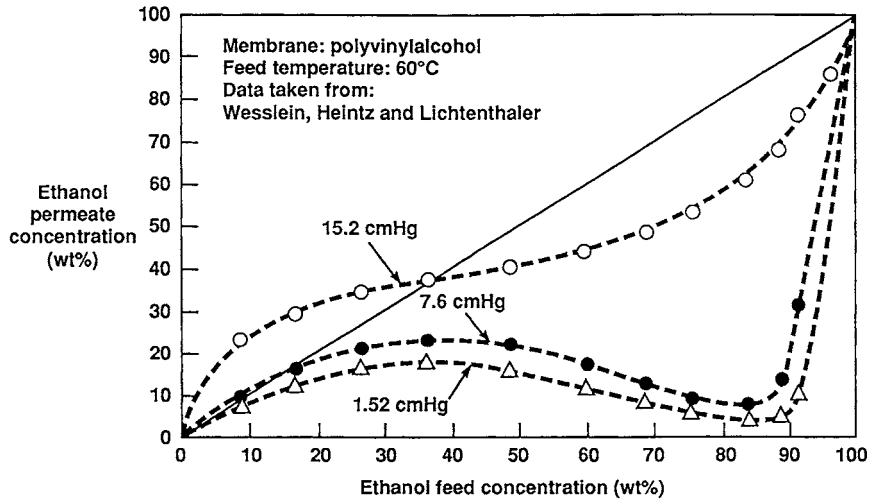


FIG. 20-78 Pervaporation schematic for ethanol-water. The illustration shows the complex behavior for a simple system at three pressures. Only the region above 90 percent is of commercial interest. (Courtesy Elsevier.)

where β is the enrichment factor. β is related to α [Eq. (20-92)], the separation factor, by

$$\beta = \frac{\alpha}{1 + (\alpha - 1)x_i} \quad \alpha = \frac{\beta(1 - x_i)}{1 - x_i\beta} \quad (20-100)$$

α is larger than β , and conveys more meaning when the membrane approaches the ideal. β is preferred in pervaporation because it is easier to use in formulations for cost, yield, and capacity. In fact, note that neither factor is constant, and that both generally change with x_i and temperature.

Operational Factors In industrial use, pervaporation is a continuous-flow single-stage process. Multistage cascade devices are unusual. Pervaporation is usually an adjunct separation, occasionally a principal one. It is used either to break an azeotrope or to concentrate a minor component. Large stand-alone uses may develop in areas where distillation is at a disadvantage, such as with closely boiling components, but these developments, have not yet been made. Notable exceptions occur when a stream is already fairly pure, such as a contaminated water source, or isopropanol from microelectronics fabrication washing containing perhaps 15 percent water.

In continuous flow, the feed will begin with concentration ($x_{i,feed}$) and be stripped until it reaches some desired ($x_{i,residue}$). If significant mass is removed from the feed, it will cool, since the general rule for liquids is that the latent heat exceeds the specific heat per °C by two orders of magnitude (more for water). So the membrane has a concentration gradient and a temperature gradient both across it and along it. Pervaporation is a complex multigradient process.

The term β is not constant for some important separations. Even worse, it can exhibit maxima that make analytic treatment difficult. Operating diagrams are often used for preliminary design rather than equations. Because of the very complex behavior in the membrane as concentrations change, all design begins with an experiment. For water removal applications, design equations often mispredict the rate constants as the water content of the feed approaches zero. The estimates tend to be lower than the experimental values, which would lead to oversize. Therefore it is necessary to obtain experimental data over the entire range of water concentrations encountered in the separation. Once the kinetic data are available, heat transfer and heat capacity are the problem. It is general practice to pilot the separation on a prototype module to measure the changes due to thermal effects. This is particularly true for water as the permeant, given its high latent heat.

For removal of an organic component from water, swelling of the organophilic membrane would result in a higher flux and lower α . At organic levels below about 10 percent, that has not been a major

problem. In most applications, boundary-layer mass-transfer limitations become limiting. Pilot data must therefore be taken with hydrodynamic similarity to the module that will be used and the actual organic permeation rate may become limited by the boundary layer. In organic-organic pervaporation, membrane swelling is a major concern.

Vapor Feed A variant on pervaporation is to use vapor, rather than liquid, as a feed. While the resulting process could be classified along with gas-separation membranes, it is customarily regarded as pervaporation.

The residue at the top of a distillation column is a vapor, so there is logic in using it as the feed to a membrane separator. Weighed against the obvious advantage are disadvantages of vapor handling (compressors cost more than pumps) and equipment size to handle the larger vapor volume. When the more volatile component permeates, heat must be added to maintain superheat. The vapor feed technique has been used in a few large installations where the advantages outweigh the disadvantages.

Leading Examples

Dehydration The growing use of isopropanol as a clean-rinse fluid in microelectronics produces significant quantities of an 85–90 percent isopropanol waste. Removing the water and trace contaminants is required before the alcohol can be reused. Pervaporation produces a 99.99 percent alcohol product in one step. It is subsequently polished to remove metals and organics. In Europe, dehydration of ethanol is the largest pervaporation application. For the very large ethanol plants typical of the United States, pervaporation is not competitive with thermally integrated distillation.

Organic from Water An area where pervaporation may become important is in flavors, fragrances, and essential oils. Here, high-value materials with unique properties are recovered from aqueous or alcohol solutions.

Pollution Control Pervaporation is used to reduce the organic loading of a waste stream, thus effecting product recovery and a reduction in waste-treatment costs. An illustration is a waste stream containing 11 percent (wt) *n*-propanol. The residue is stripped to 0.5 percent and 96 percent of the alcohol is recovered in the permeate as a 45 percent solution. This application uses a hydrophobic, rubbery membrane. The residue is sent to a conventional waste-treatment plant.

Pervaporation Membranes Pervaporation has a long history, and many materials have found use in pervaporation experiments. Cellulosic-based materials have given way to polyvinyl alcohol and blends of polyvinyl alcohol and acrylics in commercial water-removing membranes. These membranes are typically solution cast (from

water) on ultrafiltration membrane substrates. It is important to have enough crosslinking in the final polymer to avoid dissolution of the membrane in use. A very thin membrane with little penetration into the UF substrate is required. The substrate can be a problem, as it provides significant pressure drop to the vapor passing through it which, as mentioned above, has serious ramifications for flux and separation efficiency. Many new membranes are under development. Ion-exchange membranes, and polymers deposited by or polymerized by plasma, are frequently mentioned in the literature.

Modules Every module design used in other membrane operations has been tried in pervaporation. One unique requirement is for low hydraulic resistance on the permeate side, since permeate pressure is very low (0.1–1 Pa). The rule for near-vacuum operation is the bigger the channel, the better the transport. Another unique need is for heat input. The heat of evaporation comes from the liquid, and intermediate heating is usually necessary. Of course economy is always a factor. Plate-and-frame construction was the first to be used in large installations, and it continues to be quite important. Some smaller plants use spiral-wound modules, and some membranes can be made as capillary bundles. The capillary device with the feed on the inside of the tube has many advantages in principle, such as good vapor-side mass transfer and economical construction, but it is still limited by the availability of membrane in capillary form.

ELECTRODIALYSIS

GENERAL REFERENCES: This section is based on three publications by Heiner Strathmann, to which the interested reader is referred for greater detail [chap. 6, pp. 213–281, in Noble and Stern (eds.), op. cit.; sec. V, pp. 217–262, in Ho and Sirkar, op. cit.; chap. 8, pp. 8-1–8-53, Baker et al., op. cit.].

Process Description *Electrodialysis* (ED) is a membrane separation process in which ionic species are separated from water, macrosolutes, and all uncharged solutes. Ions are induced to move by an electrical potential, and separation is facilitated by ion-exchange membranes. Membranes are highly selective, passing either anions or cations and very little else. The principle of ED is shown in Fig. 20-79.

The feed solution containing ions enters a compartment whose walls are a cation-exchange and an anion-exchange membrane. If the

anion-exchange membrane is in the direction of the anode, as shown for the middle feed compartment, anions may pass through that membrane in response to an electrical potential. The cations can likewise move toward the cathode. When the ions arrive in the adjacent compartments, however, their further progress toward the electrodes is prevented by a membrane having the same electrical charge as the ion. The two feed compartments to the left and right of the central compartment are concentrate compartments. Ions entering these two compartments, either in the feed or by passing through a membrane, are retained, either by a same-charged membrane or by the EMF driving the operation. The figure shows two cells (four membranes) between anode and cathode. In an industrial application, a membrane stack can be composed of hundreds of cells, where mobile ions are alternately being depleted and concentrated.

Many related processes use charged membranes and/or EMF. Electrolytic water dissociation (water splitting), diffusion dialysis, Donnan dialysis, and electrolysis are related processes. **Electrolysis** (chlorine-caustic) is a process of enormous importance much of which is processed through very special membranes.

Leading Examples Electrodesialysis has its greatest use in removing salts from brackish water, where feed salinity is around 0.05–0.5 percent. For producing high-purity water, ED can economically reduce solute levels to extremely low levels as a hybrid process in combination with an ion-exchange bed. ED is not economical for the production of potable water from seawater. Paradoxically, it is also used for the concentration of seawater from 3.5 to 20 percent salt. The concentration of monovalent ions and selective removal of divalent ions from seawater uses special membranes. This process is unique to Japan, where by law it is used to produce essentially all of its domestic table salt. ED is very widely used for deashing whey, where the desalted product is a useful food additive, especially for baby food.

Many ED-related processes are practiced on a small scale, or in unique applications. Electrodesialysis may be said to do these things well: separate electrolytes from nonelectrolytes and concentrate electrolytes to high levels. It can do this even when the pH is very low. ED does not do well at: removing the last traces of salt (although the hybrid process, electrodeionization, is an exception), running at high pH, tolerating surfactants, or running under conditions where solubility

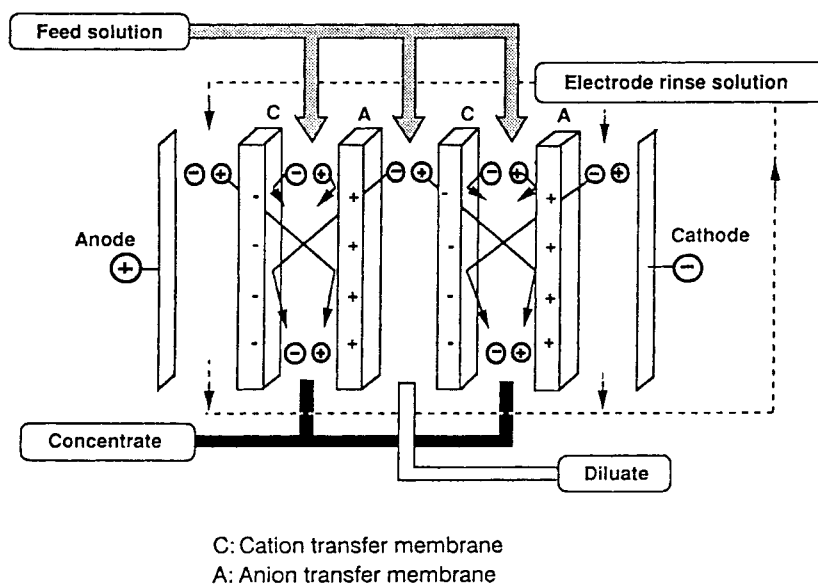


FIG. 20-79 Schematic diagram of electrodesialysis. Solution containing electrolyte is alternately depleted or concentrated in response to the electrical field. Feed rates to the concentrate and diluate cells need not be equal. In practice, there would be many cells between electrodes.

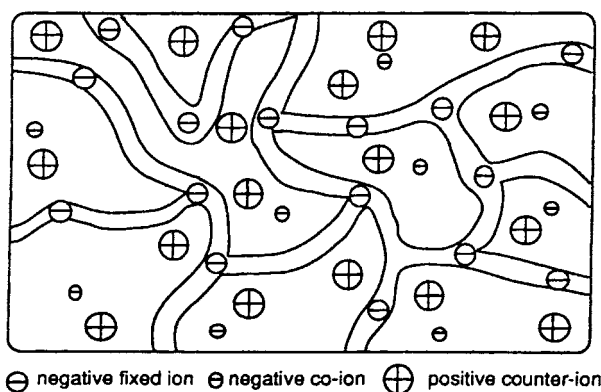


FIG. 20-80 Schematic diagram of a cation-exchange membrane showing the polymer matrix with fixed negative charges and mobile positive counterions. The density of fixed negative charges is sufficient to prevent the passage (exchange) of anions.

limits may be exceeded. Hydroxyl ion and especially hydrogen ion easily permeate both types of ED membrane. Thus, processes that generate a pH gradient across a membrane are limited in their scope.

Water splitting, a closely related process, is useful for reconstituting an acid and a base out of a salt. It is used to reclaim salts produced during neutralization.

Membranes Ion-exchange membranes are highly swollen gels containing polymers with a fixed ionic charge. In the interstices of the polymer are mobile counterions. A schematic diagram of a cation-exchange membrane is depicted in Fig. 20-80.

Figure 20-80 is a schematic diagram of a cation-exchange membrane. The parallel, curved lines represent the polymer matrix composed of an ionic, crosslinked polymer. Shown in the polymer matrix are the fixed negative charges on the polymer, usually from sulfonate groups. The spaces between the polymer matrix are the water-swollen interstices. Positive ions are mobile in this phase, but negative ions are repelled by the negative charge from the fixed charges on the polymer.

In addition to high permselectivity, the membrane must have low-electrical resistance. That means it is conductive to counterions and does not unduly restrict their passage. Physical and chemical stability are also required. Membranes must be mechanically strong and robust, they must not swell or shrink appreciably as ionic strength changes, and they must not wrinkle or deform under thermal stress. In the course of normal use, membranes may be expected to encounter the gamut of pH, so they should be stable from $0 < \text{pH} < 14$ and in the presence of oxidants.

Optimization of an ion-exchange membrane involves major trade-offs. Mechanical properties improve with crosslink density, but so does high electrical resistance. High concentration of fixed charges favors low electrical resistance and high selectivity, but it leads to high swelling, thus poor mechanical stability. Membrane developers try to combine stable polymeric backbones with stable ionic functional groups. The polymers are usually hydrophobic and insoluble. Polystyrene is the major polymer used, with polyethylene and polysulfone finding limited application.

Most commercial ion-exchange membranes are homogeneous, produced either by polymerization of functional monomers and crosslinking agents, or by chemical modification of polymers. Many heterogeneous membranes have been prepared both by melting and pressing a mixture of ion-exchange resin and nonfunctional polymer, or by dissolving or dispersing both functional and support resins in a solvent and casting into a membrane. Microheterogeneous membranes have been made by block and graft polymerization.

No membrane and no set of membrane properties has universal applicability. Manufacturers who service multiple applications have a variety of commercial membranes. One firm lists 20 different membranes having a broad spectrum of properties.

Cation-Exchange Membranes Polystyrene copolymerized with divinylbenzene, then sulfonated, is the major building block for cation-exchange membranes. These membranes have reasonable stability and versatility and are highly ionized over most of the pH range. Other chemistries mentioned in the literature include carboxylic acid membranes based on acrylic acid, PO_3^{2-} , HPO_2^- , AsO_3^{2-} , and SeO_3^- . Many specialty membranes have been produced for electro dialysis applications. A notable example is a membrane selective to monovalent cations made by placing a thin coating of positive charge on the cation-exchange membrane. Charge repulsion for polyvalent ions is much higher than that for monovalent ions, but the resistance of the membrane is also higher.

Anion-Exchange Membranes Quaternary amines are the major charged groups in anion-exchange membranes. Polystyrene-divinylbenzene polymers are common carriers for the quaternary amines. The literature mentions other positive groups based on N, P, and S. Anion-exchange membranes are problematic, for the best cations are less robust chemically than their cation exchange counterparts. Since most natural foulants are colloidal polyanions, they adhere preferentially to the anion-exchange membrane, and since the anion-exchange membrane is exposed to higher local pH there is a greater likelihood that precipitates will form there.

Membrane Efficiency The permselectivity of an ion-exchange membrane is the ratio of the transport of electric charge through the membrane by specific ions to the total transport of electrons. Membranes are not strictly semipermeable, for coions are not completely excluded, particularly at higher feed concentrations. For example, the Donnan equilibrium for a univalent salt in dilute solution is:

$$C_{\text{Co}}^M = \left(\frac{C_{\text{Co}}^F}{C_R^M} \right) \left(\frac{\gamma_{\pm}^F}{\gamma_{\pm}^M} \right)^2 \quad (20-101)$$

where C_{Co}^M is the concentration of coions (the ions having the same electrical charge as the fixed charges on the membrane); C_{Co}^F is the concentration of such coions in the ambient solution; C_R^M is the concentration of fixed charges in the gel water of the membrane; and γ_{\pm}^F and γ_{\pm}^M are, respectively, the geometric mean of the activity coefficients of the salt ions in the ambient solution and in the membrane. Equation (20-101) is applicable only when $C_{\text{Co}}^F \ll C_R^M$. Since the membrane properties are constant, coion transport rises roughly with the square of concentration.

Process Description Figure 20-81 gives a schematic view of an ED cell pair, showing the salt-concentration profile. In the solution compartment on the left, labeled "Diluate," anions are being attracted to the right by the anode. The high density of fixed cations in membrane "A" is balanced by a high mobile anion concentration within it. Cations move toward the cathode at the left, and there is a similar high mobile cation concentration in the fixed anion membrane "C" separating the depleting compartment from the concentrating compartment further left (not shown). For the anion permeable membrane "A," two boundary layers are shown. They represent depletion in the boundary layer on the left, and an excess in the boundary layer on the right, both due to the concentration polarization effects common to all membrane processes—ions must diffuse through a boundary layer whether they are entering or leaving a membrane. That step must proceed down a concentration gradient.

With every change in ion concentration, there is an electrical effect generated by an electrochemical cell. The anion membrane shown in the middle has three cells associated with it, two caused by the concentration differences in the boundary layers, and one resulting from the concentration difference across the membrane. In addition, there are ohmic resistances for each step, resulting from the E/I resistance through the solution, boundary layers, and the membrane. In solution, current is carried by ions, and their movement produces a friction effect manifested as a resistance. In practical applications, I^2R losses are more important than the power required to move ions to a compartment with a higher concentration.

Transfer of Ions Mass transfer of ions in ED is described by many electrochemical equations. The equations used in practice are empirical. If temperature, the flux of individual components, electroosmotic effects, streaming potential and other indirect effects are

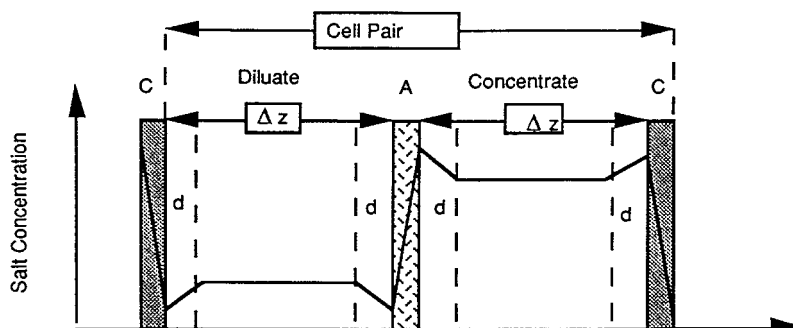


FIG. 20-81 Concentration profile of electrolyte across an operating ED cell. Ion passage through the membrane is much faster than in solution, so ions are enriched or depleted at the cell-solution interface. "d" is the concentration boundary layer. The cell gap Δz should be small. The ion concentration in the membrane proper will be much higher than shown. (Courtesy Elsevier.)

minor, an equation good to a reasonable level of approximation is:

$$J_n = C_{mn} U_{mn} \Delta\phi / \Delta x \quad (20-102)$$

where J is the component flux through the membrane $\text{kmol}/\text{m}^2\cdot\text{s}$, C_{mn} is the concentration in phase m of component n , kmol/m^3 , U_{mn} is the ion mobility of n in m , $\text{m}^2/\text{v}\cdot\text{s}$, ϕ is the electrical potential, volts, and x is distance, m.

Equation (20-102) assumes that all mass transport is caused by an electrical potential difference acting only on cations and anions. Assuming the transfer of electrical charges is due to the transfer of ions.

$$i = F \sum_n |z_n J_n| \quad (20-103)$$

where i is the current density, amperes/ m^2 , F is the Faraday constant and z is the valence. The transport number, T_n , is the ratio of the current carried by an ion to the current carried by all ions.

$$T_n = \frac{J_n z_n}{\sum_n J_n z_n} \quad (20-104)$$

The transport number is a measure of the permselectivity of a membrane. If, for example, a membrane is devoid of coions, then all current through the membrane is carried by the counterion, and the transport number = 1. The transport numbers for the membrane and the solution are different in practical ED applications.

Concentration Polarization As is shown in the flow schematic, ions are depleted on one side of the membrane and enriched on the other. The ions leaving a membrane diffuse through a boundary layer into the concentrate, so the concentration of ions will be higher at the membrane surface, while the ions entering a membrane diffuse through a boundary layer from the diluate, so the bulk concentration in the diluate must be higher than it is at the membrane. These effects occur because the transport number of counterions in the membrane is always very much higher than their transport number in the solution. Were the transport numbers the same, the boundary layer effects would vanish. This concentration polarization is similar to that experienced in reverse osmosis, except that it has both depletion and enrichment components. The equations governing concentration polarization and depolarization of a membrane are given in the section describing ultrafiltration. The depolarizing strategies used for ED are similar to those employed in other membrane processes, as they involve induced flow past the membrane.

Two basic flow schemes are used: tortuous path flow and sheet flow (Fig. 20-82). Tortuous path spacers are cut to provide a long path between inlet and outlet, providing a relatively long residence time and high velocity past the membrane. The flow channel is open. Sheet flow units have a net spacer separating the membranes. Mass transfer is enhanced either by the spacer or by higher velocity.

Enhanced depolarization requires capital equipment and energy, but it achieves savings in overall capital costs (permits the use of a smaller stack) and energy (permits lower voltage.) The designer's task is to achieve an optimum balance in these requirements. Sheet-flow units have lower capital and operating costs in general, yet both sheet-flow and tortuous-flow units remain competitive. The fact that most ED reversal units (see below) are tortuous flow, and that ED reversal is the dominant technology for water and many waste treatment applications may explain the paradox.

Limiting Current Density As the concentration in the diluate becomes ever smaller, or as the current driving the process is increased, eventually a situation arises in which the concentration of ions at the membranes surrounding the diluate compartment approaches zero. When that occurs, there are insufficient ions to carry additional current, and the cell has reached the limiting current. Forcing the voltage higher results in the dissociation of water at the membrane, giving rise to a dramatic increase in pH due to OH^- ions emerging

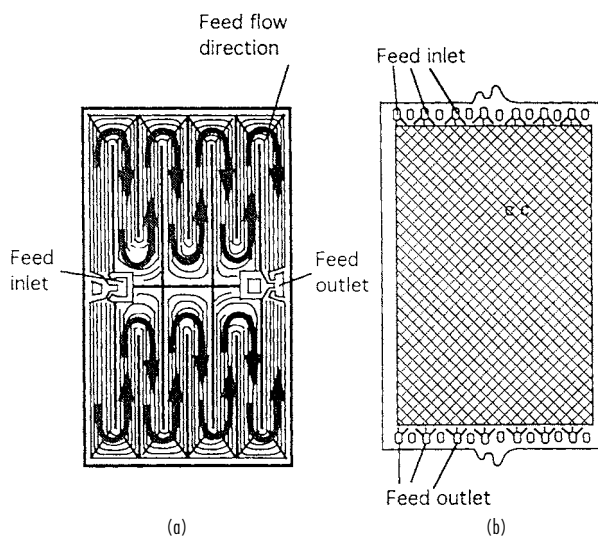


FIG. 20-82 Schematic of two ways to pass solution across an ED membrane. Tortuous flow (left) uses a special spacer to force the solution through a narrow, winding path, raising its velocity, mass transfer, and pressure drop. Sheet feed (right) passes the solution across the plate uniformly, with lower pressure drop and mass transfer. (Courtesy Elsevier.)

from the anion-exchange membrane. The high pH promotes precipitation of metal hydroxides and CaCO_3 on the membrane surface leading to flow restrictions, poor mass transfer, and subsequent membrane damage. Once a precipitate forms, its presence initiates a vicious cycle fostering the formation of more precipitates. The general expression for the limiting current density is $i_{\text{lim}} \sim (C_{\text{bulk diluate}})(\text{diluate velocity})^m$, where m is an experimental constant (often 0.6). Thus, the concentration at the membrane is limiting, and at constant current that is proportional to the bulk concentration and the mass-transfer coefficient. Flow in the compartment is laminar but mass transfer is enhanced by the spacer. A normal operating practice is to operate a stack at around 75 percent of the limiting current.

Process Configuration Figure 20-79 shows a basic cell pair. A stack is an assembly of many cell pairs, electrodes, gaskets, and manifolds needed to supply them. An exploded schematic of a portion of a sheet-flow stack is shown in Fig. 20-83.

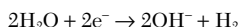
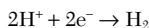
Gaskets are very important, since they not only keep the streams separated and prevent leaks from the cell, they have the manifolds to conduct feeds, both concentrate and diluate, built into them. No other practical means of feeding the stack is used in the very cramped space required by the need to keep cells thin because the diluate has very low conductivity. The manifolds are formed by aligning holes in membrane and gasket.

The membranes are supported and kept apart by feed spacers. A typical cell gap is 0.5–2 mm. The spacer also helps control solution distribution and enhances mass transfer to the membrane. Given that an industrial stack may have up to 500 cell pairs, assuring uniform flow distribution is a major design requirement.

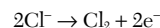
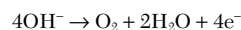
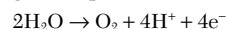
Since electro dialysis membranes are subject to fouling, it is sometimes necessary to disassemble a stack for cleaning. Ease of reassembly is a feature of ED.

Process Flow The schematic in Fig. 20-79 may imply that the feed rates to the concentrate and diluate compartments are equal. If they are, and the diluate is essentially desalted, the concentrate would leave the process with twice the salt concentration of the feed. A higher ratio is usually desired, so the flow rates of feed for concentrate and feed for diluate can be independently controlled. Since sharply differing flow rates lead to pressure imbalances within the stack, the usual procedure is to recirculate the brine stream using a feed-and-bleed technique. This is usually true for ED reversal plants. Some nonreversal plants use slow flow on the brine side avoiding the recirculating pumps. Diluate production rates are often $10\times$ brine-production rates.

Electrodes No matter how many cells are put in series, there will be electrodes. The more cells, the less the relative importance of the electrodes. The cathode reactions are relatively mild, and depending on the pH:



Anode reactions can be problematic. The anode may dissolve or be oxidized. Or, depending on the pH and the chloride concentration:



Dissolution of metal is avoided by selecting a resistant material such as Pt, Pt coated on Ti, or Pt on Nb. Base metals are sometimes used, as are graphite electrodes.

Electrode isolation is practiced to minimize chlorine production and to reduce fouling. A flush solution free of chlorides or with reduced pH is used to bathe the electrodes in some plants. Further information on electrodes may be found in a work by David ["Electrodialysis," pp. 496–499, in Porter (ed.), op. cit.].

Peripheral Components In addition to the stack, a power supply, pumps for diluate and concentrate, instrumentation, tanks for cleaning, and other peripherals are required. Safety devices are mandatory given the dangers posed by electricity, hydrogen, and chlorine.

Pretreatment Feed water is pretreated to remove gross objects that could plug the stack. Additives that inhibit the formation of scale, frequently acid, may be introduced into the feed.

Electrodialysis Reversal Two basic operating modes for ED are used in large-scale installations. **Unidirectional operation** is the mode described above in the general explanation of the process. The electrodes maintain their polarity and the ions always move in a constant direction. **ED reversal** is an intermittent process in which the polarity in the stack is reversed periodically. The interval may be from several minutes to several hours. When the polarity is reversed, the identity of compartments is also reversed, and diluate compartments become concentrate compartments and vice versa. The scheme requires instruments and valves to redirect flows appropriately after a reversal. The advantages that often justify the cost are a major reduction in membrane scaling and fouling, a reduction in feed additives required to prevent scaling, and less frequent stack-cleaning requirements.

Water Splitting A modified electro dialysis arrangement is used as a means of regenerating an acid and a base from a corresponding salt. For instance, NaCl may be used to produce NaOH and HCl. Water splitting is a viable alternative to disposal where a salt is produced by neutralization of an acid or base. Other potential applications include the recovery of organic acids from their salts and the treating of effluents from stack gas scrubbers. The new component required is a bipolar membrane, a membrane that splits water into H^+ and OH^- . At its simplest, a bipolar membrane may be prepared by laminating a cation and an anion membrane. In the absence of mobile ions, water sorbed in the membrane splits into its components when a sufficient electrical gradient is applied. The intimate contact of the two membranes minimizes the problem of the low ionic conductivity of ion-depleted water. As the water is split, replacement water readily

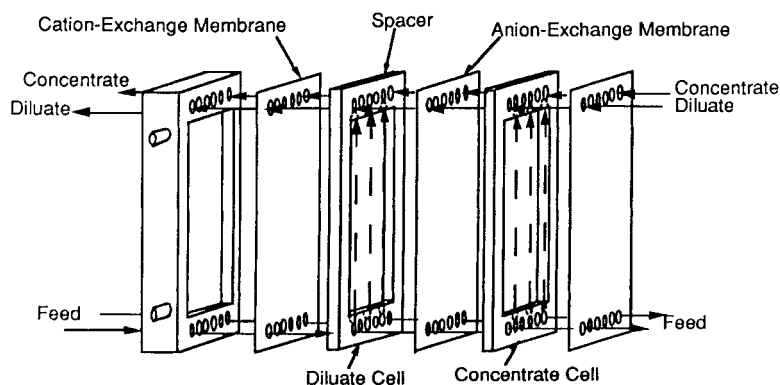


FIG. 20-83 Exploded view of a sheet-feed ED stack. Manifolds are built into the membranes and spacers as the practical way to maintain a narrow cell gap. (Courtesy Elsevier.)

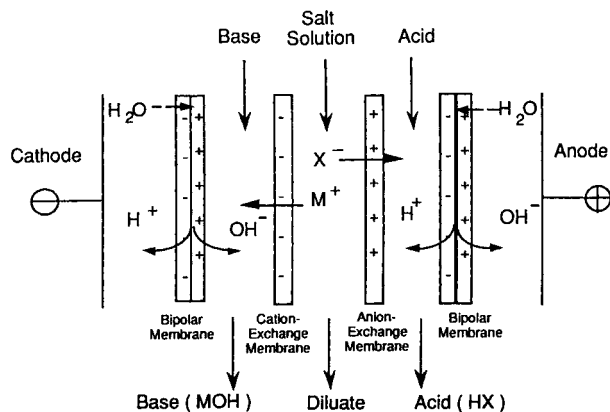


FIG. 20-84 Electrodiolysis water dissociation (water splitting) membrane inserted into an ED stack. Starting with a salt, the device generates the corresponding acid and base by supplying H^+ and OH^- from the dissociation of water in a bipolar membrane. (Courtesy Elsevier.)

diffuses from the surrounding solution. Properly configured, the process is energy efficient.

A schematic of the production of acid and base by electrodiolytic water dissociation is shown in Fig. 20-84. The bipolar membrane is inserted in the ED stack as shown. Salt is fed into the center compartment, and base and acid are produced in the adjacent compartments. The bipolar membrane is placed so that the cations are paired with OH^- ions and the anions are paired with H^+ . Neither salt ion penetrates the bipolar membrane. As is true with conventional electrodiolysis, many cells may be stacked between the anode and the cathode.

If recovery of both acid and base is unnecessary, one membrane is left out. For example, in the recovery of a weak acid from its salt, the anion-exchange membrane may be omitted. The process limitations relate to the efficiency of the membranes, and to the propensity for H^+ and OH^- to migrate through membranes of like fixed charge, limiting the attainable concentrations of acid and base to 3–5 N. The problem is at its worst for HCl and least troublesome for organic acids. Ion leakage limits the quality of the products, and the regenerated acids and bases are not of high enough quality to use in regenerating a mixed-bed ion-exchange resin.

Diffusion Dialysis The propensity of H^+ and OH^- to penetrate membranes is useful in diffusion dialysis. An anion-exchange membrane will block the passage of metal cations while passing hydrogen ions. This process uses special ion-exchange membranes, but does not employ an applied electric current.

As an example, in the aircraft industry heavy-aluminum sections are shaped as airfoils, then masked. The areas where the metal is not required to be strong are then unmasked and exposed to NaOH to etch away unneeded metal for weight reduction. Sodium aluminate is generated, a potential waste problem. Cation-exchange membranes leak OH^- by a poorly understood mechanism that is not simply the transport of OH^- with its waters of hydration. The aluminate anion is retained in the feed stream while the caustic values pass through. NaOH recovery is high, because all the Na^+ participates in the driving force. There is considerable passage of water due to the osmotic pressure difference as well. This scheme operates efficiently only because aluminum hydroxide forms highly supersaturated solutions. Hydroxide precipitation within the apparatus is reported to be a minor problem. $Al(OH)_3$ is precipitated in a downstream crystallizer, and is reported to be of high quality.

Donnan Dialysis Another nonelectrical process using ED membranes is used to exchange ions between two solutions. The common application is to use H^+ to drive a cation from a dilute compartment to a concentrated one. A schematic is shown in Fig. 20-85. In the right compartment, the pH is 0, thus the H^+ concentration is 10^7 higher

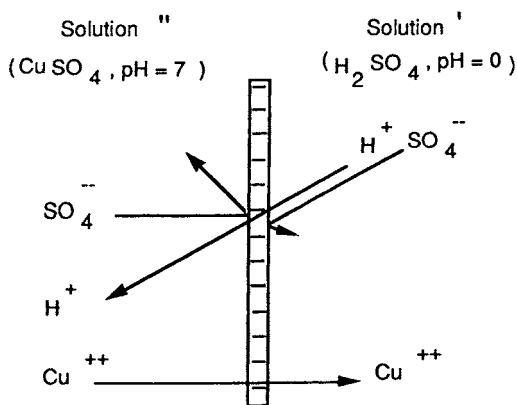


FIG. 20-85 Schematic of Donnan dialysis using a cation-exchange membrane. Cu^{2+} is “pumped” from the lower concentration on the left to a higher concentration on the right maintaining electrical neutrality accompanying the diffusion of H^+ from a low pH on the right to a higher pH on the left. The membrane’s fixed negative charges prevent mobile anions from participating in the process. (Courtesy Elsevier.)

than in the pH 7 compartment on the left. H^+ diffuses leftward, creating an electrical imbalance that can only be satisfied by a cation diffusing rightward through the cation-selective membrane. By this scheme, Cu^{2+} can be “pumped” from left to right against a significant concentration difference.

Electrodiolysis-Moderated Ion Exchange The production of ultrapure water is facilitated by incorporating a mixed-bed ion-exchange resin between the membranes of an ion-exchange stack. Already pure water is passed through the bed, while an electric current is passed through the stack. Provided the ion-exchange beads are in contact with each other and with the membranes, an electrical current can pass through the bed even though the conductivity of the very pure water is quite low. In passing, the current conducts any ions present into adjacent compartments, simultaneously and continuously regenerating the resin in situ.

Energy Requirements The thermodynamic limit on energy is the ideal energy needed to move water from a saline solution to a pure phase. The theoretical minimum energy is given by:

$$\Delta G = RT \ln (a/a_s) \quad (20-105)$$

where ΔG is the Gibbs free energy required to move one mole of water from a solution, a is the activity of pure water ($\equiv 1$), and a_s is the activity of water in the salt solution. In a solution, the activity of water is approximately equal to the molar fraction of water in the solution. So that approximate activity is

$$a_s = \frac{n_s}{n_s + v \cdot s_s} \quad \frac{1}{a_s} = 1 + \frac{v \cdot s_s}{n_s} \quad (20-106)$$

where n_s is the number of moles of water in the salt solution, v is the number of atoms in the salt molecule (2 for NaCl, 3 for $CaCl_2$) and s_s is the number of moles of salt in the salt solution. The ratio of moles of salt in the salt solution to the number of moles of water in the salt solution is a very small number for a dilute solution. This permits using the approximation $\ln(1+x) = x$, when x is of the magnitude 0.01, making this an applicable approximation for saline water. That permits rewriting Eq. (20-105) as

$$\Delta G = vRT(s_s/n_s) \quad (20-107)$$

where ΔG is still the free energy required to move one mole of water from the saline solution to the pure water compartment.

The conditions utilized in the above development of minimum energy are not sufficient to describe electrodiolysis. In addition to the desalination of water, salt is moved from a saline feed to a more concentrated compartment. That free-energy change must be added to the free energy given in Eq. (20-107), which describes the movement

of water from salt solution, the reverse of the actions in the diluate compartment (but having equal free energy). Schaffer & Mintz develop that change, and after solving the appropriate material balances, they arrive at a practical simplified equation for a monovalent ion salt, where activities may be approximated by concentrations:

$$\Delta G = RT(C_f - C_d) \left(\frac{\ln C_{fc}}{C_{fc} - 1} - \frac{\ln C_{fd}}{C_{fd} - 1} \right); C_{fc} = \frac{C_f}{C_c}; C_{fd} = \frac{C_d}{C_c} \quad (20-108)$$

where C_f is the concentration of ions in the feed, C_d is the concentration in the diluate, and C_c is the concentration in the concentrate, all in kmol/m^3 . When $C_{fc} \rightarrow 1$ and $C_{fd} \rightarrow$ infinity, the operation is one approximating the movement of salt from an initial concentration into an unlimited reservoir of concentrate, while the diluate becomes pure. This implies that the concentrate remains at a constant salt concentration. In that case, Eq. (20-108) reduces to $RT(C_f - C_d)$. As a numerical example of Eq. (20-108) consider the desalting of a feed with initial concentration 0.05 M to 0.005 M, roughly approximating the production of drinking water from a saline feed. If 10 ℓ of product are produced for every 3 ℓ of concentrate, the concentrate leaves the process at 0.2 M. The energy calculated from Eq. (20-108) is 0.067 kWh/m^3 at 25°C. If the concentrate flow is infinite, $C_c = 0.05$ M, and the energy decreases to 0.031 kWh/m^3 .

This minimum energy is that required to move ions only, and that energy will be proportional to the ionic concentration in the feed. It assumes that all resistances are zero, and that there is no polarization. In a real stack, there are several other important energy dissipaters. One is overcoming the electrical resistances in the many components. Another is the energy needed to pump solution through the stack to reduce polarization and to remove products. Either pumping or desalting energy may be dominant in a working stack.

Energy Not Transporting Ions Not all current flowing in an electro dialysis stack is the result of the transport of the intended ions. Current paths that may be insignificant, minor, or significant include electrical leakage through the brine manifolds and gaskets, and transport of co-ions through a membrane. A related indirect loss of current is water transport through a membrane either by osmosis or with solvated ions, representing a loss of product, thus requiring increased current.

Pump Energy Requirements If there is no forced convection within the cells, the polarization limits the current density to a very uneconomic level. Conversely, if the circulation rate is too high, the

energy inputs to the pumps will dominate the energy consumption of the process. Furthermore, supplying mechanical energy to the cells raises the pressure in the cells, and raises the pressure imbalance between portions of the stack, thus the requirements of the confining gear and the gaskets. Also, cell plumbing is a design problem made more difficult by high circulation rates.

A rule of thumb for a modern ED stack is that the pumping energy is roughly 0.5 kWh/m^3 , about the same as is required to remove 1700 mg/ℓ dissolved salts.

Equipment and Economics A very large electro dialysis plant would produce 500 ℓ/s of desalted water. A rather typical plant was built in 1993 to process 4700 m^3/day (54.4 ℓ/s). Capital costs for this plant, running on low-salinity brackish feed were \$1,210,000 for all the process equipment, including pumps, membranes, instrumentation, and so on. Building and site preparation cost an additional \$600,000. The building footprint is 300 m^2 . For plants above a threshold level of about 40 m^3/day , process-equipment costs usually scale at around the 0.7 power, not too different from other process equipment. On this basis, process equipment (excluding the building) for a 2000 m^3/day plant would have a 1993 predicted cost of \$665,000.

The greatest operating-cost component, and the most highly variable, is the charge to amortize the capital. Many industrial firms use capital charges in excess of 30 percent. Some municipalities assign long amortization periods and low-interest rates, reflecting their cost of capital. Including buildings and site preparation, the range of capital charges assignable to 1000 m^3 of product is \$90 to \$350.

On the basis of 1000 m^3 of product water, the operating cost elements (as shown in Table 20-32) are anticipated to be:

TABLE 20-32 Electro dialysis Operating Costs

\$ 66	Membrane-replacement cost (assuming seven-year life)
32	Plant power
16	Filters and pretreatment chemicals
11	Labor
8	Maintenance
\$133	Total

These items are highly site specific. Power cost is low because the salinity removed by the selected plant is low. The quality of the feed water, its salinity, turbidity, and concentration of problematic ionic and fouling solutes, is a major variable in pretreatment and in conversion.

SELECTION OF BIOCHEMICAL SEPARATION PROCESSES

GENERAL REFERENCES: Ahuja (ed.), *Handbook of Bioseparations*, Academic Press, London, 2000. Albertsson, *Partition of Cell Particles and Macromolecules*, 3d ed., Wiley, New York, 1986. Belter, Cussler, and Hu, *Bioseparations*, Wiley Interscience, New York, 1988. Cooney and Humphrey (eds.), *Comprehensive Biotechnology*, vol. 2, Pergamon, Oxford, 1985. Flickinger and Drew (eds.), *The Encyclopedia of Bioprocess Technology: Fermentation, Biocatalysis, and Bioseparations*, Wiley, New York, 1999. Harrison, Todd, Scott, and Petrides, *Bioseparations Science and Engineering*, Oxford University Press, Oxford, 2003. Hatti-Kaul and Mattiasson (eds.), *Isolation and Purification of Proteins*, Marcel Dekker, New York, 2003. Janson and Ryden (eds.), *Protein Purification*, VCH, New York, 1989. Ladisch, *Bioseparations Engineering: Principles, Practice, and Economics*, Wiley, New York, 2001. Scopes, *Protein Purification*, 2d ed., Springer-Verlag, New York, 1987. Stephanopoulos (ed.), *Biotechnology*, 2d ed., vol. 3, VCH, Weinheim, 1993. Subramanian (ed.), *Bioseparation and Bioprocess—A Handbook*, Wiley, New York, 1998. Zaslavsky, *Aqueous Two-Phase Partitioning—Physical Chemistry and Bioanalytical Applications*, Marcel Dekker, New York, 1995.

GENERAL BACKGROUND

The biochemical industry derives its products from two primary sources. Natural products are yielded by plants, animal tissue, and fluids, and they are obtained via fermentation from bacteria, molds, and fungi and from mammalian cells. Products can also be obtained by

recombinant methods through the insertion of foreign DNA directly into the hosting microorganism to allow overproduction of the product in this unnatural environment. The range of bioproducts is enormous, and the media in which they are produced are generally complex and ill-defined, containing many unwanted materials in addition to the desired product. The product is almost invariably at low concentration to start with. The goals of downstream processing operations include removal of these unwanted impurities, bulk-volume reduction with concomitant concentration of the desired product, and, for protein products, transfer of the protein to an environment where it will be stable and active, ready for its intended application. This always requires a multistage process consisting of multiple-unit operations. A general strategy for downstream processing of biological materials and the types of operations that may be used in the different steps is shown in Fig. 20-86 [see also Ho, in M. R. Ladisch et al. (eds.), *Protein Purification from Molecular Mechanisms to Large-Scale Processes*, ACS Symp. Ser., 427, ACS, Washington, D.C. (1990), pp. 14–34]. Low-molecular-weight products, generally secondary metabolites such as alcohols, carboxylic and amino acids, antibiotics, and vitamins, can be recovered by using many of the standard operations such as liquid-liquid partitioning, adsorption, and ion exchange, described elsewhere in this handbook. Biofuel molecules also belong

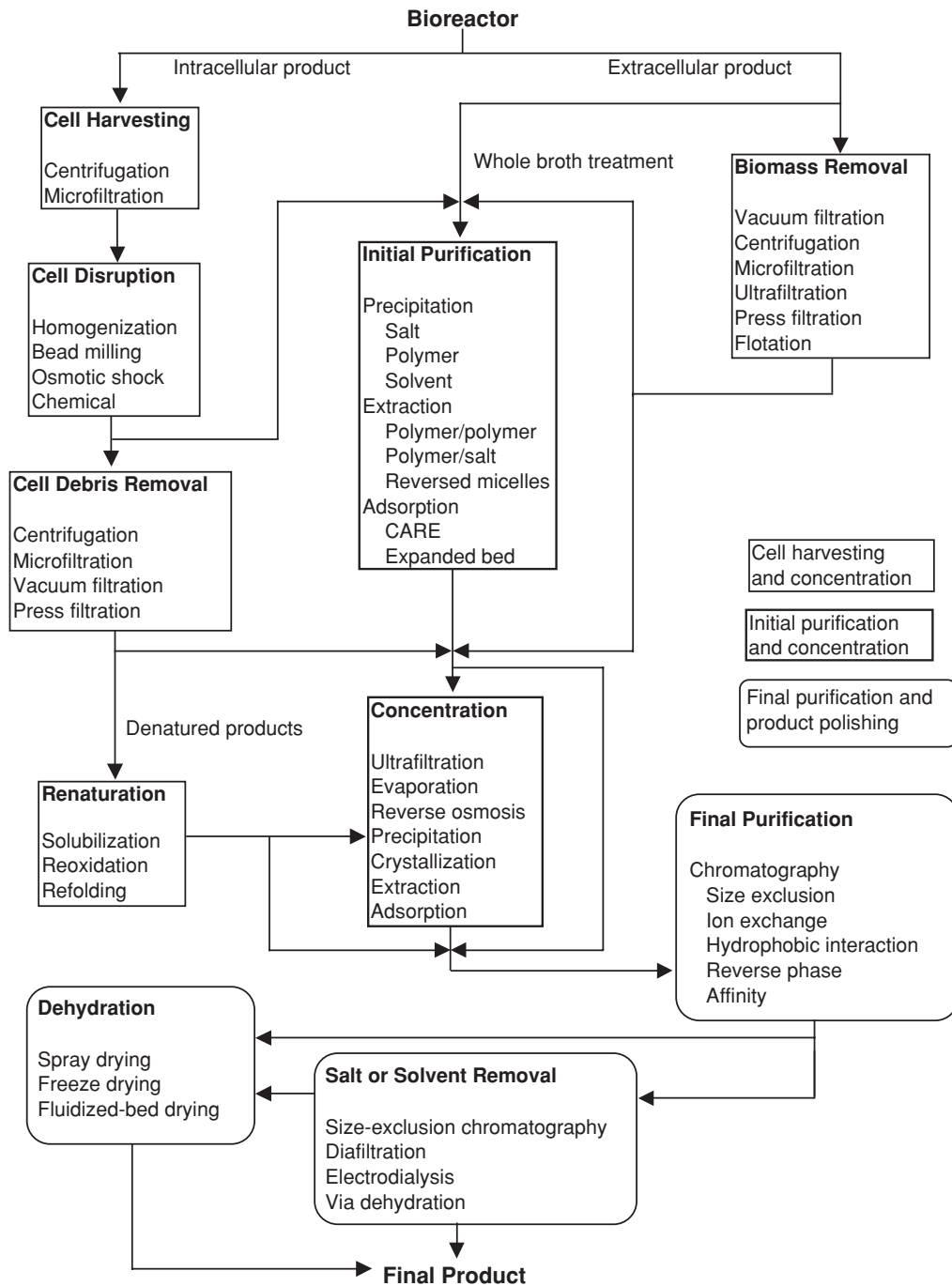


FIG. 20-86 General stages in downstream processing for protein production indicating representative types of unit operations used at each stage.

to this category. They are becoming more and more important. Less expensive and high-throughput unit operations are needed to make a biorefinery process economically feasible. Proteins require special attention, however, as they are sufficiently more complex, their function depending on the integrity of a delicate three-dimensional tertiary structure that can be disrupted if the protein is not handled correctly. For this reason, this section focuses primarily on protein separations.

Techniques used in bioseparations depend on the nature of the product (i.e., the unique properties and characteristics which provide a "handle" for the separation) and on its state (i.e., whether soluble or insoluble, intra- or extracellular, etc.). All early isolation and recovery steps remove whole cells, cellular debris, suspended solids, and colloidal particles; concentrate the product; and in many cases, achieve some degree of purification, all the while maintaining high yield. For intracellular compounds, the initial harvesting of the cells is important for their concentration prior to release of the product. Following this phase, a range of purification steps are employed to remove the remaining impurities and enhance the product purity; this purification phase, in turn, is followed by polishing steps to remove the last traces of contaminating components and process-related additions (e.g., buffer salts, detergents) and to prepare the product for storage and/or distribution. The prevention and/or avoidance of contamination is another important goal of downstream processing. Therapeutic proteins require very high purities that cannot be measured by weight percentages alone. To avoid potential harmful effects in humans, the levels of pyrogens and microbial and viral contaminants in final products must meet stringent safety and regulatory requirements.

Even for good yields of 80 to 95 percent per step, the overall yield can be poor for any process that requires a large number of steps. Thus, careful consideration must be given to optimization of the process in terms of both the unit operations themselves and their sequencing. A low-yield step should be replaced if improvement is unattainable to eliminate its impact on the overall yield. It is usually desirable to reduce the process volume early in the downstream processing, and to remove any components that can be removed fairly easily (particulates, small solutes, large aggregates, nucleic acids, etc.), so as not to overly burden the more refined separation processes downstream. Possible shear and temperature damage, and deactivation by endogenous proteases, must be considered in the selection of separation processes. Protein stability in downstream processing was discussed in depth by Hejnaes et al. [in Subramanian (ed.), vol. 2, op. cit., pp. 31–66].

INITIAL PRODUCT HARVEST AND CONCENTRATION

The initial processing steps are determined to a large extent by the location of the product species, and they generally consist of cell/broth separation and/or cell debris removal. For products retained within the biomass during production, it is first necessary to concentrate the cell suspension before homogenization or chemical treatment to release the product. Clarification to remove the suspended solids is the process goal at this stage.

Regardless of the location of the protein and its state, cell separation needs to be inexpensive, simple, and reliable, as large amounts of fermentation-broth dilute in the desired product may be handled. The objectives are to obtain a well-clarified supernatant and solids of maximum dryness, avoiding contamination by using a contained operation. Centrifugation or crossflow filtration is typically used for cell separation, and both unit operations can be run in a continuous-flow mode [Datar and Rosen, in Stephanopoulos (ed.), op. cit., pp. 369–503]. In recent years, expanded-bed adsorption has become an alternative. It combines broth clarification and adsorption separation in a single step.

Intracellular products can be present either as folded, soluble proteins or as dense masses of unfolded protein (inclusion bodies). For these products, it is first necessary to concentrate the cell suspension before effecting release of the product. Filtration can result in a suspension of cells that can be of any desired concentration up to 15 to 17 percent and that can be diafiltered into the desired buffer system. In contrast, the cell slurry that results from centrifugation will be that of

either a dry mass (requiring resuspension but substantially free of residual broth, i.e., from a tubular bowl centrifuge) or a wet slurry (containing measurable residual broth and requiring additional resuspension). During the separation, conditions that result in cell lysis (such as extremes in temperature) must be avoided. In addition, while soluble protein is generally protected from shear and external proteolysis, these proteins are still subject to thermal denaturation.

Cell Disruption Intracellular protein products are present as either soluble, folded proteins or inclusion bodies. Intracellular protein products are very common because *Escherichia coli* is a main workhorse for recombinant proteins. *E. coli* is a gram-negative bacterium that precipitates recombinant proteins in the form of inclusion bodies. Release of folded proteins must be carefully considered. Active proteins are subject to deactivation and denaturation and thus require the use of "gentle" conditions. In addition, due consideration must be given to the suspending medium; lysis buffers are often optimized to promote protein stability and protect the protein from proteolysis and deactivation. Inclusion bodies, in contrast, are protected by virtue of the protein agglomeration. More stressful conditions are typically employed for their release, which includes going to higher temperatures if necessary. For "native" proteins, gentler methods and temperature control are required.

The release of intracellular protein product is achieved through rupture of the cell walls, and release of the protein product to the surrounding medium, through either mechanical or nonmechanical means, or through chemical, physical, or enzymatic lysis [Engler, in Cooney and Humphrey (eds.), op. cit., pp. 305–324; Schutte and Kula, in Stephanopoulos (ed.), op. cit., pp. 505–526]. Mechanical methods use pressure, as in the Manton/APV-Gaulin/French Press, or the Microfluidizer, or mechanical grinding, as in ball mills, the latter being used typically for flocs and usually only for natural products. Nonmechanical means include use of desiccants or solvents, while cell lysis can also be achieved through physical means (osmotic shock, freeze/thaw cycles), chemical (detergents, chaotropes), or enzymatic (lysozyme, phages).

In a high-pressure homogenizer, a pressurized cell suspension is forced through a valve and undergoes a rapid pressure change from up to 50 MPa to the atmospheric pressure. This results in the instant rupture of cells. Product release, which generally follows first-order kinetics, occurs through impingement of the high-velocity cell suspension jet on the stationary surfaces, and possibly also by the high-shear forces generated during the acceleration of the liquid through the gap. While sufficiently high pressures can be attained using commercially available equipment to ensure good release in a single pass, the associated adiabatic temperature increases ($-1.8^{\circ}\text{C}/1000$ psig) may cause unacceptable activity losses for heat-labile proteins. Further denaturation can occur on exposure to the lysis medium. Thus, multiple passes may be preferred, with rapid chilling of the processed cell suspension between passes. The number of passes and the heat removal ability should be carefully optimized. The efficiency of the process depends on the homogenizing pressure and the choice of the valve unit, for which there are many designs available. Materials of construction are important to minimize erosion of the valve, to provide surface resistance to aggressive cleaning agents and disinfectants, and to permit steam cleaning and sanitization.

The release of inclusion bodies, in contrast, may follow a different strategy. Since inclusion bodies are typically recovered by centrifugation, it is often advantageous to send the lysate through the homogenizer with multiple passes to decrease the particle size of the cell debris. Since the inclusion bodies are much denser than the cell debris, the debris, now much reduced in size, can be easily separated from the inclusion bodies by centrifugation at low speeds. The inclusion bodies may be resuspended and centrifuged multiple times (often in the presence of low concentrations of denaturants) to clean up these aggregates. Since the inclusion bodies are already denatured, temperature control is not as important as in the case of native proteins.

Another popular method for cell disruption is to use a bead mill. In a bead mill, a cell suspension is mixed with glass or metal beads and agitated by using a rotating agitator at high speed. Bead mills have a controllable residence time compared with high-pressure homogenization.

However, they are susceptible to channeling and also fracturing of the beads. Tough cells require multiple passes to achieve a desired yield.

Chemical lysis, or solubilization of the cell wall, is typically carried out by using detergents such as Triton X-100, or the chaotropes urea, and guanidine hydrochloride. This approach does have the disadvantage that it can lead to some denaturation or degradation of the product. While favored for laboratory cell disruption, these methods are not typically used at the larger scales. Enzymatic destruction of the cell walls is also possible, and as more economical routes to the development of appropriate enzymes are developed, this approach could find industrial application. Again, the removal of these additives is an issue.

Physical methods such as osmotic shock, in which the cells are exposed to high salt concentrations to generate an osmotic pressure difference across the membrane, can lead to cell wall disruption. Similar disruption can be obtained by subjecting the cells to freeze/thaw cycles, or by pressurizing the cells with an inert gas (e.g., nitrogen) followed by a rapid depressurization. These methods are not typically used for large-scale operations.

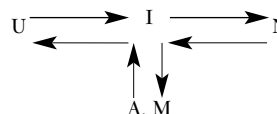
On homogenization, the lysate may drastically increase in viscosity due to DNA release. This can be ameliorated to some extent by using multiple passes to reduce the viscosity. Alternatively, precipitants or nucleic acid digesting enzymes can be used to remove these viscosity-enhancing contaminants.

For postlysis processing, careful optimization must be carried out with respect to pH and ionic strength. Often it is necessary to do a buffer exchange. Cell debris can act as an ion exchanger and bind proteins ionically, thus not allowing them to pass through a filtration device or causing them to be spun out in a centrifuge. Once optimal conditions are found, these conditions can be incorporated in the lysis buffer by either direct addition (if starting from cell paste) or diafiltration (if starting from a cell concentrate).

Protein Refolding Although protein refolding is not a bioseparation operation, it is an integral part of a downstream process for the production of an inactive (typically intracellular) protein. So far, it still remains a challenging art casting an uncertainty on the success of a process. Early in the product development stage, animal cell culture may be required to produce many bioactive candidates for initial screening of efficacy. To commercialize the product protein, it may be reexpressed in a far more economic and productive host such as *E. coli*. The commercial products of recombinant DNA technology are frequently not produced in their native, biologically active form, because the foreign hosts such as *E. coli* in which they are produced lack the appropriate apparatus for the folding of the proteins. Thus, the overproduced proteins are generally recovered as refractile or inclusion bodies, or aggregates, typically 1 to 3 μm in size, and all cysteine residues are fully reduced. It is necessary at some stage in the processing to dissolve the aggregates and then refold them to obtain the desired biologically active product [Cleland and Wang, in Stephanopoulos (ed.), op. cit., pp. 527–555].

Advantages of inclusion bodies in the production stage are their ease of separation by centrifugation following cell disruption, because of their size and density, and their provision of excellent initial-purification possibilities, as long as impurities are not copurified to any significant extent with the inclusion bodies. They also provide a high expression level and prevent endogenous proteolysis. There can be, however, significant product loss during protein refolding to the

active form. Figure 20-87 shows a typical process for refolding. The inclusion body which is released from the host cell by cell disruption is washed and then solubilized by using a denaturant such as guanidine hydrochloride (4 to 9 M), urea (7 to 8 M), sodium thiocyanate (4 to 9 M), or detergents such as Triton X-100 or sodium dodecyl sulfate. This step disrupts the hydrogen and ionic bonds to obtain fully denatured and stretched peptide chains. For proteins with disulfide bonds, addition of appropriate reducing agents (e.g., beta mercaptoethanol) is required to break all incorrectly formed intramolecular disulfide bonds. To permit proper refolding of the protein, it is necessary to remove the denaturant or detergent molecules from the surroundings of the stretched and solubilized peptides. This will initiate self-refolding of the protein molecules. For proteins with disulfide bonds, an oxidative reaction with oxygen or other oxidants is required to join two free SH groups to form an S—S covalent bond. This in vitro refolding operation is traditionally achieved by dilution with a refolding buffer. However, misfolding or aggregation is usually found in the refolding process. Analysis of in vitro refolding kinetics shows that there is at least an intermediate (I) between the unfolded protein (U) and the fully active refolded native protein (N), as illustrated below [Kuwajima and Arai, in R. H. Pain (ed.), *Mechanism of Protein Folding*, 2d ed., Oxford University Press, Oxford, 2000, pp. 138–171; Tsumoto et al., *Protein Expr. Purif.*, **28**, 1–8 (2003)].



The process to convert U to I may be fast. The process for I to N, however, may be slow and highly reversible. Some intermediate molecules may form aggregates (A) or misfolded proteins (M). Figure 20-87 is a simplified refolding pathway. In reality, the situation can be more complicated where several intermediates (I_1 , I_2 , I_3 , etc.) are present with numerous possibilities of aggregation and misfolding. For most proteins, refolding is a self-assembly process that follows a first-order kinetics. Aggregation, on the other hand, involves interactions between two or more molecules and follows the second- or higher-order kinetics. Therefore, in vitro refolding at higher protein concentrations would lead to the formation of more aggregates. Many observations have shown that a low final protein concentration, usually 10 to 100 $\mu\text{g}/\text{mL}$, is required for dilution refolding [Schlegl et al., *Chem. Engng. Sci.*, **60**, 5770–5780 (2005)]. In an industrial process, this strategy generally features large volumes of buffers, exerting an extra burden for subsequent purification steps because the concentration is low. Optimization of dilution strategy, such as the way of dilution, the speed of dilution, and the solution composition of a refolding buffer, is beneficial for an increased refolding yield.

A number of studies [Kuwajima and Arai, loc. cit.; Sadana, *Biotech. Bioeng.*, **48**, 481–489 (1995)] demonstrated that the presence of some molecules in the refolding buffer may suppress misfolding or aggregation. Molecular chaperones such as GroES and GroEL can promote correct refolding, but they are very expensive. Other molecules have been tried as artificial chaperones. The most commonly used molecules are polyethylene glycol (PEG) of various molecular weights and

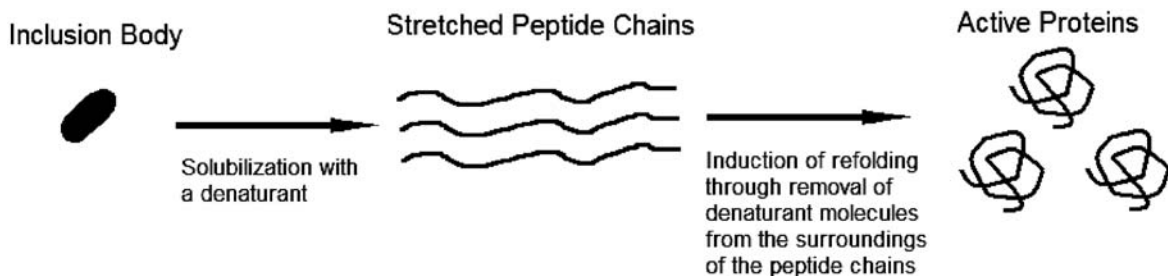


FIG. 20-87 Illustration of a refolding process for a protein from inclusion body.

concentrations, L-arginine (0.4 to 1 M), low concentrations of denaturants such as urea (1 to 2 M) and guanidine hydrochloride (0.5 to 1.5 M), and some detergents such as SDS, CTAB, and Triton X-100. The effects of these additives on protein refolding are still under investigation. A new direction of protein refolding involves the use of chromatographic techniques [Li et al., *Protein Expr. Purif.*, **33**, 1–10 (2004)]. Size exclusion, ion exchange, hydrophobic interaction, and metal chelate affinity chromatographic techniques have been studied with successful results. Chromatographic refolding explores the interaction between the protein molecule to be refolded and the packing medium in the column. It may reduce the interaction between protein molecules and increase the chance of self-assembly with the aid of the functional groups and pores in the matrix of the packing medium. An advantage for chromatographic refolding is the availability of gradient elution that creates a gradual change of the solution environment, leading to a gentle removal of the denaturant and a gradual change of favorable conditions such as pH and the artificial chaperone concentration. Simultaneous refolding and partial purification are possible with this new technique.

For extracellular products, which are invariably water-soluble, the first step is the removal of cells and cell debris using a clarification method and, in the case of typical protein products, the removal of dissolved low-molecular-weight compounds. This must be done under relatively gentle conditions to avoid undesired denaturation of the product. Again, either filtration or centrifugation can be applied. Filtration results in a cell-free supernatant with dilution associated with the diafiltration of the final cell slurry. Centrifugation, regardless of the mode, will result in a small amount of cells in the centrate, but there is no dilution of the supernatant. During the process development careful studies should be conducted to examine the effects of pH and ionic strength on the yield, as cells and cell debris may retain the product through charge interactions. If the broth or cell morphology does not allow for filtration or if dry cell mass is required, tubular-bowl centrifugation is typically utilized. Note that plant and animal cells cannot sustain the same degree of applied shear as can microbial cells, and thus crossflow filtration or classical centrifugation may not be applicable. Alternatives using low-shear equipment under gentle conditions are often employed in these situations.

For whole broths the range of densities and viscosities encountered affects the concentration factor that can be attained in the process, and can also render crossflow filtration uneconomical because of the high pumping costs, and so on. Often, the separation characteristics of the broth can be improved by broth conditioning using physicochemical or biological techniques, usually of a proprietary nature. The important characteristics of the broth are rheology and conditioning.

Clarification Using Centrifugation Centrifugation relies on the enhanced sedimentation of particles of density different from that of the surrounding medium when subjected to a centrifugal force field [Axelsson, in Cooney and Humphrey (eds.), op. cit., pp. 325–346] (see also Sec. 18, “Liquid-Solid Operations and Equipment”). Advantages of centrifugal separations are that they can be carried out continuously and have short retention times, from a fraction of a second to seconds, which limit the exposure time of sensitive biologicals to shear stresses. Yields are high, provided that temperature and other process conditions are adequately controlled. They have small space requirements, and an adjustable separation efficiency makes them a versatile unit operation. They can be completely closed to avoid contamination, and, in contrast to filtration, no chemical external aids are required that can contaminate the final product. The ability now to contain the aerosols typically generated by centrifuges adds to their operability and safety.

Sedimentation rates must be sufficiently high to permit separation, and they can be enhanced by modifying solution conditions to promote the aggregation of proteins or impurities. An increase in precipitation of the contaminating species can often be accomplished by a reduction in pH or an elevation in temperature. Flocculating agents, which include polyelectrolytes, polyvalent cations, and inorganic salts, can cause a 2000-fold increase in sedimentation rates. Some examples are polyethylene imine, EDTA, and calcium salts. Cationic bioprocessing aids (cellulosic or polymeric) reduce pyrogen, nucleic acid, and acidic protein loads which can foul chromatography columns. The removal of these additives during both centrifugation and subsequent processing must be clearly demonstrated.

There are many different types of centrifuges, classified according to the way in which the transport of the sediment is handled [Medronho, in Hatti-Kaul and Mattiasson (eds.), op. cit., pp. 131–190]. The selection of a particular centrifuge type is determined by its capacity for handling sludge; the advantages and disadvantages of various separator types are discussed by Axelsson [in Cooney and Humphrey (eds.), op. cit., pp. 325–346]. Solids-retaining centrifuges are operated in a semibatch mode, as they must be shut down periodically to remove the accumulated solids; they are primarily used when solids concentrations are low, and they have found application during the clarification and simultaneous separation of two liquids. In solids-ejecting centrifuges, the solids are removed intermittently either through radial slots or axially while the machine is running at full speed. These versatile machines can be used to handle a variety of feeds, including yeast, bacteria, mycelia, antibiotics, enzymes, and so on. Solids-discharging nozzle centrifuges have a large capacity and can accommodate up to 30 percent solids loading. Decanter centrifuges consist of a drum, partly cylindrical and partly conical, and an internal screw conveyor for transport of the solids, which are discharged at the conical end; liquids are discharged at the cylindrical end. Levels within the drum are set by means of external nozzles.

Continuous-flow units, the scroll decanter and disk-stack centrifuges, are easiest to use from an operational perspective; shutdown of the centrifuge during the processing of a batch is not expected. While the disk-stack centrifuge enjoys popularity as a process instrument within the pharmaceutical and biotechnology industries, the precise timing of solids ejection and the continuous high-speed nature of the device make for complex equipment and frequent maintenance. It is often used to harvest cells, since the solids generated are substantially wet and could lead to measurable yield losses in extracellular product systems. For intracellular product processing, the wet cell sludge is easily resuspended for use in subsequent processing.

The tubular bowl, in contrast, is a semibatch processing unit owing to the limited solids capacity of the bowl. The use of this unit requires shutdown of the centrifuge during the processing of the batch. The semibatch nature of these centrifuges can thus greatly increase processing cycle times. The introduction of disposable sheets to act as bowl liners has significantly impacted turnaround times during processing. The dry nature of the solids generated makes the tubular-bowl centrifuge well suited for extracellular protein processing, since losses to the cell sludge are minimal. In contrast, the dry, compact nature of the sludge can make the cells difficult to resuspend. This can be problematic for intracellular protein processing where cells are homogenized in easily clogged, mechanical disrupters.

Clarification Using Microfiltration Crossflow filtration (microfiltration includes crossflow filtration as one mode of operation in “Membrane Separation Processes,” which appears earlier in this section) relies on the retention of particles by a membrane. The driving force for separation is pressure across a semipermeable membrane, while a tangential flow of the feed stream parallel to the membrane surface inhibits solids settling on and within the membrane matrix [Datar and Rosen, loc. cit.].

Microfiltration is used for the removal of suspended particles, recovery of cells from fermentation broth, and clarification of homogenates containing cell debris. Particles removed by microfiltration typically average greater than 500,000 nominal molecular weight [Tutunjian, in Cooney and Humphrey (eds.), op. cit., pp. 367–381; Gobler, in Cooney and Humphrey (eds.), op. cit., pp. 351–366]. Ultrafiltration focuses on the removal of low-molecular-weight solutes and proteins of various sizes, and it operates in the less than 100,000 nominal-molecular-weight cutoff (NMWCO) range [Le and Howell, in Cooney and Humphrey (eds.), op. cit., pp. 383–409]. Both operations consist of a concentration segment (of the larger particles) followed by diafiltration of the retentate [Tutunjian, in Cooney and Humphrey (eds.), op. cit., pp. 411–437].

Generally, the effectiveness of the separation is determined not by the membrane itself, but rather by the formation of a secondary or dynamic membrane caused by interactions of the solutes and particles with the membrane. The buildup of a gel layer on the surface of an ultrafiltration membrane owing to rejection of macromolecules can provide the primary separation characteristics of the membrane. Similarly, with colloidal suspensions, pore blocking and bridging of

pore entries can modify the membrane performance, while molecules of size similar to the membrane pores can adsorb on the pore walls, thereby restricting passage of water and smaller solutes. Media containing poorly defined ingredients may contain suspended solids, colloidal particles, and gel-like materials that prevent effective microfiltration. In contrast to centrifugation, specific interactions can play a significant role in membrane separation processes.

The factors to consider in the selection of crossflow filtration include the flow configuration, tangential linear velocity, transmembrane pressure drop (driving force), separation characteristics of the membrane (permeability and pore size), size of particulates relative to the membrane pore dimensions, low protein-binding ability, and hydrodynamic conditions within the flow module. Again, since particle-particle and particle-membrane interactions are key, broth conditioning (ionic strength, pH, etc.) may be necessary to optimize performance.

Selection of Cell-Separation Unit Operation The unit operation selected for cell separations can depend on the subsequent separation steps in the train. In particular, when the operation following cell separation requires cell-free feed (e.g., chromatography), filtration is used, since centrifugation is not absolute in terms of cell separation. In addition, if cells are to be stored (i.e., they contain the desired product) because later processing is more convenient (e.g., only two-shift operation, facility competes for equipment with other products, batch is too big for single pass in equipment), it is generally better to store the cells as a frozen concentrate than a paste, since the concentrate thaws more completely, avoiding small granules of unfrozen cell solids that can foul homogenizers, columns, and filters. Here the retentate from filtration is desired, although the wet cell mass from a disc stack-type centrifuge may be used.

Centrifugation is generally necessary for complex media used to make natural products, for while the media components may be sifted prior to use, they can still contain small solids that can easily foul filters. The medium to be used should be tested on a filter first to determine the fouling potential. Some types of organisms, such as filamentous organisms, may sediment too slowly owing to their larger cross sections, and they are better treated by filtration (mycelia have the potential to easily foul tangential-flow units; vacuum-drum filtration using a filter aid, e.g., diatomaceous earth, should also be considered). Often the separation characteristics of the broth can be improved by broth conditioning using physicochemical or biological techniques, usually of a proprietary nature.

Regardless of the machine device, centrifuges are typically maintenance-intensive. Filters can be cheaper in terms of capital and maintenance costs and should be considered first unless centrifugal equipment already exists. Small facilities (< 1000 L) use filtration, since centrifugation scale-down is constrained by equipment availability. Comparative economics of the two classes of operations are discussed by Datar and Rosen (loc. cit.).

INITIAL PURIFICATION

Initial purification is the rough purification (considered by many people as isolation) to prepare a feed for subsequent high-resolution steps. In initial purification steps the goal is to obtain concentration with partial purification of the product, which is recovered as a precipitate (precipitation), a solution in a second phase (liquid-liquid partitioning), or adsorbed to solids (adsorption, chromatography).

Precipitation Precipitation of products, impurities, or contaminants can be induced by the addition of solvents, salts, or polymers to the solution; by increasing temperature; or by adjusting the solution pH (Scopes, op. cit., pp. 41–71; Ersson et al., in Janson and Ryden, op. cit., pp. 3–32). This operation is used most often in the early stages of the separation sequence, particularly following centrifugation, filtration, and/or homogenization steps. Precipitation is often carried out in two stages, the first to remove bulk impurities and the second to precipitate and concentrate the target protein. Generally, amorphous precipitates are formed, owing to occlusion of salts or solvents, or to the presence of impurities.

Salts can be used to precipitate proteins by “salting out” effects. The effectiveness of various salts is determined by the Hofmeister series, with anions being effective in the order citrate > PO₄²⁻ > SO₄²⁻

> CH₃COO⁻ > Cl⁻ > NO₃⁻, and cations according to NH₄⁺ > K⁺ > Na⁺ (Ersson et al., op. cit., p. 10; Belter et al., op. cit., pp. 221–236).

Salts should be inexpensive owing to the large quantities used in precipitation operations. Ammonium sulfate appears to be the most popular precipitant because it has an effective cation and an effective anion, high solubility, easy disposal, and low cost. Drawbacks to this approach include low selectivity, high sensitivity to operating conditions, and downstream complications associated with salt removal and disposal of the high-nitrogen-content stream. Generally, aggregates formed on precipitation with ammonium sulfate are fragile, and are easily disrupted by shear. Thus, these precipitation operations are, following addition of salt, often aged without stirring before being fed to a centrifuge by gravity feed or using low-shear pumps (e.g., diaphragm pumps).

The organic solvents most commonly used for protein precipitation are acetone and ethanol (Ersson et al., op. cit.). These solvents can cause some denaturation of the protein product. Temperatures below 0°C can be used, since the organic solvents depress the freezing point of the water. The precipitate formed is often an extremely fine powder that is difficult to centrifuge and handle. With organic solvents, in-line mixers are preferred, as they minimize solvent-concentration gradients and regions of high-solvent concentrations, which can lead to significant denaturation and local precipitation of undesired components typically left in the mother liquors. In general, precipitation with organic solvents at lower temperature increases yield and reduces denaturation. It is best carried out at ionic strengths of 0.05 to 0.2 M.

Water-soluble polymers and polyelectrolytes (e.g., polyethylene glycol, polyethylene imine polyacrylic acid) have been used successfully in protein precipitations, and there has been some success in affinity precipitations wherein appropriate ligands attached to polymers can couple with the target proteins to enhance their aggregation. Protein precipitation can also be achieved by using pH adjustment, since proteins generally exhibit their lowest solubility at their isoelectric point. Temperature variations at constant salt concentration allow for fractional precipitation of proteins.

Precipitation is typically carried out in standard cylindrical tanks with low-shear impellers. If in-line mixing of the precipitating agent is to be used, this mixing is employed just prior to the material's entering the aging tank. Owing to their typically poor filterability, precipitates are normally collected by using a centrifugal device.

Liquid-Liquid Partitioning Liquid-liquid partitioning (see also Sec. 15 on liquid-liquid extraction) involving an organic solvent is commonly known as solvent extraction or extraction. Solvent extraction is routinely used to separate small biomolecules such as antibiotics and amino acids. However, it is typically not suitable for protein fractionation with only a few exceptions because organic solvents may cause protein denaturation or degradation. A recent review of solvent extraction for bioseparations including a discussion on various parameters that can be controlled for solvent extraction was given by Gu [in Ahuja (ed.), op. cit., pp. 365–378]. As a replacement of solvent extraction, aqueous two-phase partitioning is typically used for protein purification. It uses two water-soluble polymers (and sometimes with some salts when polyelectrolytes are involved) to form two aqueous phases [Albertsson, op. cit.; Kula, in Cooney and Humphrey (eds.), op. cit., pp. 451–471]. Both phases contain water but differ in polymer (and salt) concentration(s). The high water content, typically greater than 75 percent, results in a biocompatible environment not attainable with traditional solvent extraction systems. Biomolecules such as proteins have different solubilities in the two phases, and this provides a basis for separation. Zaslavsky (op. cit., pp. 503–667) listed 163 aqueous two-phase systems including PEG-dextran-water, PEG-polyvinylmethylether-water, PEG-salt-water, polyvinylpyrrolidone-dextran-water, polyvinylalcohol-dextran-water, and Ficoll-dextran-water systems. Partitioning between the two aqueous phases is controlled by the polymer molecular weight and concentration, protein net charge and size, and hydrophobic and electrostatic interactions. Aqueous two-phase polymer systems are suitable for unclarified broths since particles tend to collect at the interface between the two phases, making their removal very efficient. They can also be used early on in the processing train for initial bulk-volume reduction and partial purification. One of the drawbacks of these systems is the subsequent need for the removal of phase-forming reagents.

Affinity partitioning is carried out by adding affinity ligands to an aqueous two-phase partitioning system. The biospecific binding of a biomolecule with the ligand moves the biomolecule to a preferred phase that enhances the partitioning of the biomolecule [Johansson and Tjerneld, in Street (ed.), *Highly Selective Separations in Biotechnology*, Blackie Academic & Professional, London, 1994, pp. 55–85]. Diamond and Hsu [in Fiechter (ed.), *Advances in Biochemical Engineering/Biotechnology*, vol. 47, Springer-Verlag, Berlin-New York, 2002, pp. 89–135] listed several dozens of biomolecules, many of which are proteins that have been separated by using affinity partitioning. Fatty acids and triazine are the two common types of affinity ligand while metallated iminodiacetic acid (IDA) derivatives of PEG such as Cu(II)IDA-PEG can be used for binding with proteins rich in surface histidines. The drawbacks of affinity partitioning include the costs of ligands and the need to couple the ligands to the polymers used in the aqueous two-phase partitioning.

Product recovery from these systems can be accomplished by changes in either temperature or system composition. Composition changes can be affected by dilution, backextraction, and micro- and ultrafiltration. As the value of the product decreases, recovery of the polymer may take on added significance. A flow diagram showing one possible configuration for the extraction and product and polymer recovery operations is shown in Fig. 20-88 [Greve and Kula, *J. Chem. Tech. Biotechnol.*, **50**, 27–42 (1991)]. The phase-forming polymer and salt are added directly to the fermentation broth. The cells or cell debris and contaminating proteins report to the salt-rich phase and are discarded. Following pH adjustment of the polymer-rich phase, more salt is added to induce formation of a new two-phase system in which the product is recovered in the salt phase, and the polymer can be recycled. In this example, disk-stack centrifuges are used to enhance the phase separation rates. Other polymer recycling options include extraction with a solvent or supercritical fluid, precipitation, or diafiltration. Electrodialysis can be used for salt recovery and recycling.

Reversed micellar solutions can also be used for the selective extraction of proteins [Kelley and Hatton, in Stephanopoulos (ed.), *op. cit.*, pp. 593–616]. In these systems, detergents soluble in an oil phase aggregate to stabilize small water droplets having dimensions similar to those of the proteins to be separated. These droplets can host hydrophilic species such as proteins in an otherwise inhospitable organic solvent, thus enabling these organic phases to be used as protein extractants. Factors affecting the solubilization effectiveness of the solvents include charge effects, such as the net charge determined

by the pH relative to the protein isoelectric point; charge distribution and asymmetry on the protein surface; and the type (anionic or cationic) of the surfactant used in the reversed micellar phase. Ionic strength and salt type affect the electrostatic interactions between the proteins and the surfactants, and affect the sizes of the reversed micelles. Attachment of affinity ligands to the surfactants has been demonstrated to lead to enhancements in extraction efficiency and selectivity [Kelley et al., *Biotech. Bioeng.*, **42**, 1199–1208 (1993)].

Product recovery from reversed micellar solutions can often be attained by simple backextraction, by contacting with an aqueous solution having salt concentration and pH that disfavors protein solubilization, but this is not always a reliable method. Addition of cosolvents such as ethyl acetate or alcohols can lead to a disruption of the micelles and expulsion of the protein species, but this may also lead to protein denaturation. These additives must be removed by distillation, e.g., to enable reconstitution of the micellar phase. Temperature increases can similarly lead to product release as a concentrated aqueous solution. Removal of the water from the reversed micelles by molecular sieves or silica gel has also been found to cause a precipitation of the protein from the organic phase.

Extraction using liquid emulsion membranes involves the use of a surface-active agent such as a surfactant to form dispersed droplets that encapsulate biomolecules. Its economic viability for large-scale applications is still weak [Patnaik, in Subramanian (ed.), *op. cit.*, vol. 1, pp. 267–303]. Another less-known method involving the use of a surfactant is the foam fractionation method that has seen limited applications. Ionic fluids have found commercial applications in chemical reactions by replacing volatile solvents. They are emerging as an environmentally friendly solvent replacement in liquid-liquid phase partitioning. Room-temperature ionic liquids are low-melting-point salts that stay as liquids at room temperature. Partition behavior in a system involving a room-temperature ionic liquid and an aqueous phase is influenced by the type of ionic liquid used as well as pH change [Visser et al., *Green Chem.*, Feb. 1–4, 2000]. An ionic fluid was also reportedly used in the mobile phase for liquid chromatography [He et al., *J. Chromatogr. A*, **1007**, 39–45 (2003)]. More research needs to be done in this area to develop this new green technology [Freemantle, *C&EN*, **83**, 33–38 (2005)].

Aqueous-detergent solutions of appropriate concentration and temperature can phase-separate to form two phases, one rich in detergents, possibly in the form of micelles, and the other depleted of the detergent [Pryde and Phillips, *Biochem. J.*, **233**, 525–533 (1986)].

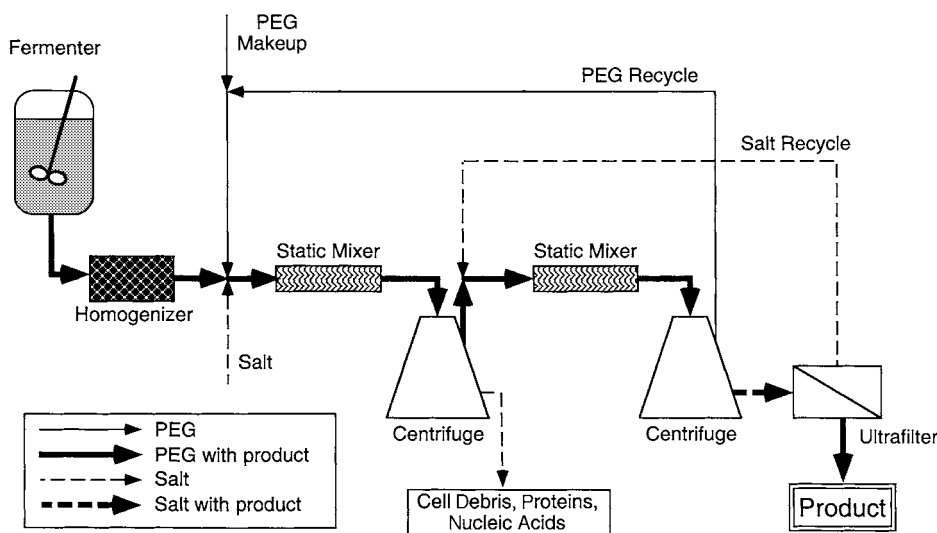


FIG. 20-88 Process scheme for protein extraction in aqueous two-phase systems for the downstream processing of intracellular proteins, incorporating PEG and salt recycling. [Reprinted from Kelly and Hatton in Stephanopoulos (ed.), *op. cit.*; adapted from Greve and Kula, *op. cit.*]

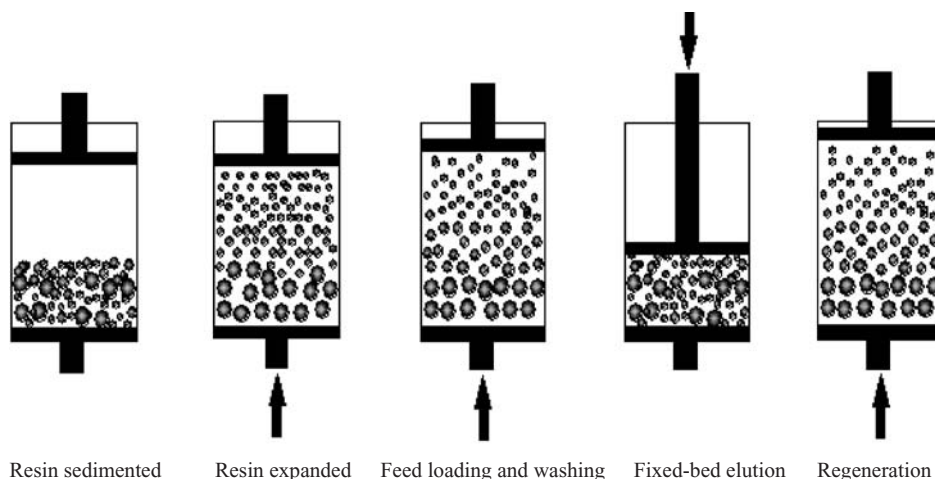


FIG. 20-89 An operation cycle in expanded-bed adsorption.

Proteins distribute between the two phases, hydrophobic (e.g., membrane) proteins reporting to the detergent-rich phase and hydrophilic proteins to the detergent-free phase. Indications are that the size-exclusion properties of these systems can also be exploited for viral separations. These systems would be handled in the same way as the aqueous two-phase systems.

On occasion, for extracellular products, cell separation can be combined with an initial volume reduction and purification step by using liquid-liquid extraction. This is particularly true for low-molecular-weight products, and it has been used effectively for antibiotic and vitamin recovery. Often scroll decanters can be used for this separation. The solids are generally kept in suspension (which requires that the solids be denser than heavy phase), while the organic phase, which must be lighter than water (cells typically sink in water), is removed. Experience shows that scrolls are good for handling the variability seen in fermentation feedstock. Podbielniak rotating-drum extraction units have been used often, but only when solids are not sticky, gummy, or flocculated, as they can get stuck in perforations of the concentric drums, but will actually give stages to the extraction in short-residence time (temperature-sensitive product). The Karr reciprocating-plate column can handle large volumes of whole-broth materials efficiently, and it is amenable to ready scale-up from small laboratory-scale systems to large plant-scale equipment.

Adsorption Adsorption (see also Sec. 16, "Adsorption and Ion Exchange") can be used for the removal of pigments and nucleic acids, e.g., or can be used for direct adsorption of the desired proteins. Stirred-batch or expanded-bed operations allow for presence of particulate matter, but fixed beds are not recommended for unclarified broths owing to fouling problems. These separations can be effected through charge, hydrophobic, or affinity interactions between the species and the adsorbent particles, as in the chromatographic steps outlined below. The adsorption processes described here are different from those traditionally ascribed to chromatography in that they do not rely on packed-bed operations.

In continuous affinity recycle extraction (CARE) operations, the adsorbent beads are added directly to the cell homogenate, and the mixture is fed to a microfiltration unit. The beads loaded with the desired solute are retained by the membrane, and the product is recovered in a second stage by changing the buffer conditions to disfavor binding.

Expanded-bed adsorption (EBA) has gained popularity in bioprocessing since its commercial introduction in the 1990s because of its ability to handle a crude feedstock that contains cells or other particulates. EBA eliminates the need for a dedicated clarification step by combining solid-liquid separation and adsorption into a single-unit operation [Hjorth et al., in Subramanian (ed.), op. cit., vol. 1, pp. 199–226; Mattiasson et al., in Ahuja (ed.), op. cit., pp. 417–451]. A

typical EBA operation cycle is illustrated in Fig. 20-89. A bed packed with an adsorption medium (or a resin), usually spherical particles of different sizes, is expanded by an upward-flow liquid stream from the bottom. An unclarified feed is introduced after a stable expansion of the bed is achieved. Particulates pass through the void spaces between the resin particles, while the soluble product molecules are adsorbed by the resin and retained in the column. After a washing step, the resin particles are left to settle in the column to form a fixed bed. The product molecules are then eluted out with a mobile phase entering from the top of the column in a way similar to that in conventional fixed-bed chromatography, to achieve a high-resolution separation. The elution can also be performed in expanded mode if needed. The regeneration step in the expanded mode flushes away residual particulates and refreshes the media for the next cycle. The difference between EBA and conventional fluidized-bed adsorption lies in the adsorption resin. In conventional fluidized-bed adsorption, the resin particles are randomly distributed in the column. In EBA, however, the resin particles are distributed vertically with large ones near the column bottom and the small ones near the top. There is no backmixing along the axial direction of the vertically standing column, thus achieving adsorption similar to that in a fixed-bed column. The resin particles have to be prepared to possess a suitable size distribution, or alternatively a distribution based on density differences if the particles sizes are uniform. An EBA column should have a length typically 3 to 4 times of the settled bed height to allow for bed expansion. An adjustable adapter at the top is needed to push the resin downward for elution in the fixed-bed mode. A proper design of the bottom frit is critical. Its holes must be smaller enough to retain the smallest resin particles but large enough to allow the particulates to enter and exit the column freely. In practical applications, plugging of the frit and nonuniform upward flow tend to be problematic, especially in columns with large diameters. To mitigate this problem, some EBA columns use an optimized inlet design and a mechanical stirrer at the bottom.

The advantages of EBA are its ability to adsorb the soluble product molecules directly from a cell suspension, a cell homogenate, or a crude biological fluid containing various particulates, thus making the "whole-broth processing" concept a reality. EBA eliminates the solid-liquid separation step (such as microfiltration and centrifugation) and enables a fast, more compact process requiring fewer steps and less time. It performs solid removal, concentration, and purification, all in a single-unit operation. By doing so, it can also minimize the risk of proteolytic breakdown of the product.

Membrane Ultrafiltration Membrane ultrafiltration is often one of the favored unit operations used for the isolation and concentration of biomolecules because they can be easily scaled up to process large feed volumes at low costs. Toward the end of an ultrafiltration operation, additional water or buffer is added to facilitate the passage of

smaller molecules. This is known as diafiltration. Diafiltration is especially helpful in the removal of small contaminating species such as unspent nutrients including salts and metabolites. Salt removal is usually necessary if the next step is ion-exchange or reverse-phase chromatography. For a protein that is not very large, two ultrafiltration steps can be used in sequence. In the first one, the protein ends up in the permeate, allowing the removal of large contaminating molecules including pyrogens and also viral particles. In the second ultrafiltration, the protein stays in the retentate. This removes small contaminating molecules and concentrates the feed up to the protein's solubility limit. Membrane materials, configurations, and design considerations were discussed earlier in this section. Proper membrane materials must be selected to avoid undesirable binding with proteins. External fouling, pore blockage, and internal fouling were discussed by Ghosh (*Protein Bioseparation Using Ultrafiltration*, Imperial College Press, London, 2003).

FINAL PURIFICATION

The final purification steps are responsible for the removal of the last traces of impurities. The volume reduction in the earlier stages of the separation train is necessary to ensure that these high-resolution operations are not overloaded. Generally, chromatography is used in these final stages. Electrophoresis can also be used, but since it is rarely found in process-scale operations, it is not addressed here. The final product preparation may require removal of solvent and drying, or lyophilization of the product.

Chromatography Liquid chromatography steps are ubiquitous in the downstream processing. It is the most widely used downstream processing operation because of its versatility, high selectivity, and efficiency, in addition to its adequate scale-up potential based on wide experience in the biochemical processing industries. As familiarity is gained with other techniques such as liquid-liquid extraction, they will begin to find greater favor in the early stages of the separation train, but are unlikely to replace chromatography in the final stages, where high purities are needed.

Chromatography is typically a fixed-bed adsorption operation, in which a column filled with chromatographic packing materials is fed with the mixture of components to be separated. Apart from size-exclusion (also known as gel-permeation or gel-filtration) chromatography, in the most commonly practiced industrial processes the solutes are adsorbed strongly to the packing materials until the bed capacity has been reached. The column may then be washed to remove impurities in the interstitial regions of the bed prior to elution of the solutes. This latter step is accomplished by using buffers or solvents which weaken the binding interaction of the proteins with the packings, permitting their recovery in the mobile phase. To minimize product loss of a high-value product, a small load far below the saturation capacity is applied to the column. A complete baseline separation can then be achieved after elution. Gradient elution uses varied modifier strength in the mobile phase to achieve better separations of more chemical species.

Types of Chromatography Practiced Separation of proteins by using chromatography can exploit a range of different physical and chemical properties of the proteins and the chromatography adsorption media [Janson and Ryden, op. cit.; Scopes, op. cit.; Egerer, in Finn and Prave (eds.), *Biotechnology Focus 1*, Hanser Publishers, Munich, 1988, pp. 95–151]. Parameters that must be considered in the selection of a chromatographic method include composition of the feed, the chemical structure and stability of the components, the electric charge at a defined pH value and the isoelectric point of the proteins, the hydrophilicity and hydrophobicity of the components, and molecular size. The different types of interactions are illustrated schematically in Fig. 20-90.

Ion-exchange chromatography relies on the coulombic attraction between the ionized functional groups of proteins and oppositely charged functional groups on the chromatographic support. It is used to separate the product from contaminating species having different charge characteristics under well-defined eluting conditions, and for concentration of the product, owing to the high-adsorptive capacity of most ion-exchange resins and the resolution attainable. Elution is carried out by using a mobile phase with competing ions or varied pH. Ion-exchange chromatography is used effectively at the front

end of a downstream processing train for early volume reduction and purification.

The differences in sizes and locations of hydrophobic pockets or patches on proteins can be exploited in *hydrophobic interaction chromatography (HIC)* and *reverse-phase chromatography (RPC)*; discrimination is based on interactions between the exposed hydrophobic residues and hydrophobic ligands which are distributed evenly throughout a hydrophilic porous matrix. As such, the binding characteristics complement those of other chromatographic methods, such as ion-exchange chromatography. In HIC, the hydrophobic interactions are relatively weak, often driven by salts in high concentration, and depend primarily on the exposed residues on or near the protein surface; preservation of the native, biologically active state of the protein is a desirable feature of HIC. HIC's popularity is on the rise in recent years because of this feature. Elution can be achieved differentially by decreasing salt concentration or increasing the concentration of polarity perturbants (e.g., ethylene glycol) in the eluent.

Reverse-phase chromatography relies on significantly stronger hydrophobic interactions than in HIC, which can result in unfolding and exposure of the interior hydrophobic residues, i.e., leads to protein denaturation and irreversible inactivation; as such, RPC depends on total hydrophobic residue content. Elution is effected by organic solvents applied under gradient conditions. RPC is the most commonly used analytical chromatographic method due to its ability to separate a vast array of chemicals with high resolutions. Denaturation of proteins does not influence the analytical outcome unless protein precipitation in the mobile phase becomes a problem.

HIC typically uses polymer-based resins with phenyl, butyl, or octyl ligands while RPC uses silica beads with straight-chain alkanes with 4, 8, or 18 carbons. Larger ligands provide stronger interactions. Polymeric beads are used in RPC when basic pH is involved because silica beads are unstable at such pH. In HIC, the mobile phase remains an aqueous salt solution, while RPC uses solvent in its mobile phase to regulate binding. Raising the temperature increases the hydrophobic interactions at the temperatures commonly encountered in biological processing.

HIC is most effective during the early stages of a purification strategy and has the advantage that sample pretreatment such as dialysis or desalting after salt precipitation is not usually required. It is also finding increased use as the last high-resolution step to replace gel filtration. It is a group separation method, and generally 50 percent or more of extraneous impurities are removed. This method is characterized by high adsorption capacity, good selectivity, and satisfactory yield of active material.

Despite the intrinsically nonspecific nature of ion-exchange and reversed-phase/hydrophobic interactions, it is often found that chromatographic techniques based on these interactions can exhibit remarkable resolution. This is attributed to the dynamics of multisite interactions being different for proteins having differing surface distributions of hydrophobic and/or ionizable groups.

Size-exclusion chromatography's (SEC's) separation mechanism is based on the sizes and shapes of proteins and impurities. The effective size of a protein is determined by its steric geometry and solvation characteristics. Smaller proteins are able to penetrate the small pores in the beads while large proteins are excluded, making the latter elute out of column more quickly. To suppress the ion-exchange side effects, a salt is typically added to the mobile phase. Ammonium carbonate or bicarbonate is used if the salt is to be removed by sublimation alone during lyophilization. In rare cases, a solvent at a low concentration is added to the mobile phase to suppress hydrophobic interactions between the protein molecules and the stationary phase. In industrial production processes, SEC columns are used to separate small molecules from proteins. It is also a choice for desalting and buffer exchange in the product polishing stage. SEC columns are typically very large because the feed loads to SEC columns are limited to 3 to 5 percent of the bed volumes. This loading capacity is far less than those with packings that have binding interactions.

Protein affinity chromatography can be used for the separation of an individual compound, or a group of structurally similar compounds from crude-reaction mixtures, fermentation broths, or cell lysates by exploiting very specific and well-defined molecular interactions

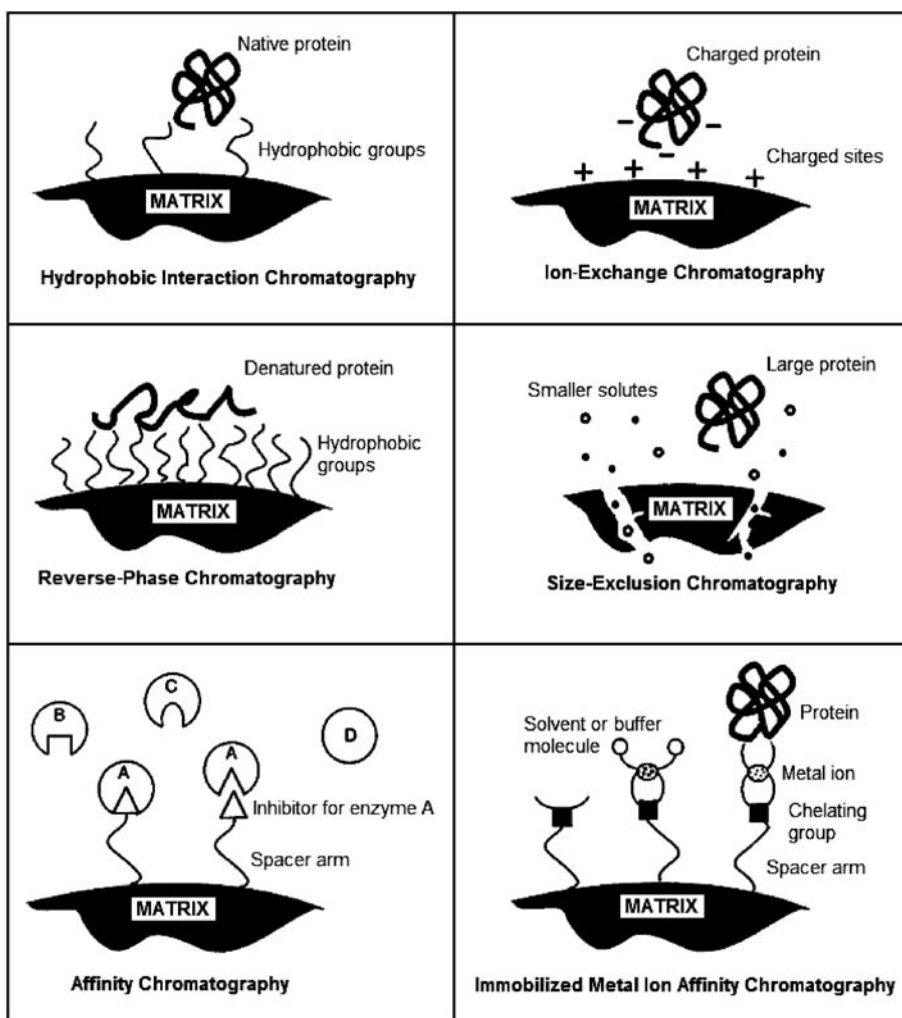


FIG. 20-90 Schematic illustration of the chromatographic methods most commonly used in downstream processing of protein products.

between the protein and affinity groups immobilized on the packing-support material. Examples of affinity interactions include antibody-antigen, hormone-receptor, enzyme-substrate/analog/inhibitor, metal ion-ligand, and dye-ligand pairs. Monoclonal antibodies are particularly effective as biospecific ligands for the purification of pharmaceutical proteins. Affinity chromatography may be used for the isolation of a pure product directly from crude fermentation mixtures in a single chromatographic step. Immunosorbents should not be subjected to crude extracts, however, as they are particularly susceptible to fouling and inactivation. Despite its high resolution and the ability to treat a very dilute feed, affinity chromatography is still costly on the process scale if protein ligands such as protein A or protein G is to be used, or a custom affinity matrix is required. Considerable research efforts are devoted to its development in part due to the increased number of protein pharmaceuticals produced at low concentrations.

After more than two decades of development, membrane chromatography has emerged as an attractive alternative to packed column chromatography. Using a porous membrane as the stationary phase in liquid chromatography has several potential advantages that include a very high flow rate through a very short and wide bed with only a modest transmembrane pressure drop. Elimination or minimization of diffusional mass-transfer resistance shifts the rate-controlling step to faster-binding kinetics, resulting in adsorptive separation of proteins

in a fraction of the time required by conventional packed columns. To achieve sufficient adsorptive separation, it is necessary to use a medium that binds strongly with target molecules when a very short flow path is involved. Thus, membrane chromatography typically uses an affinity membrane, and the combination of membrane chromatography with affinity interaction provides high selectivity and fast processing for the purification of proteins from dilute feeds. To a much less extent, ion-exchange, hydrophobic interaction, and reverse-phase membrane chromatography have also been reported [Charcosset, *J. Chem. Technol. Biotechnol.* **71**, 95–110 (1998)].

Figure 20-91 shows the interaction between proteins in the mobile phase and the affinity membrane matrix. The mechanical strength, hydrophobicity, and ligand density of the membranes can be engineered through chemical modifications to make them suitable for affinity membrane chromatography. A preferred membrane medium to be prepared for affinity membrane chromatography should provide (1) desirable physical characteristics such as pore structure and mechanical strength, allowing fast liquid flow at a small pressure loss; (2) reactive groups (such as $-\text{OH}$, $-\text{NH}_2$, $-\text{SH}$, $-\text{COOH}$) for coupling ligands or spacer arms; (3) physical and chemical stabilities to endure heat or chemical sterilization; and (4) a nondenaturing matrix to retain protein bioactivity [Zou et al., *J. Biochem. Biophys. Methods*, **49**, 199–240 (2001)]. Base membranes

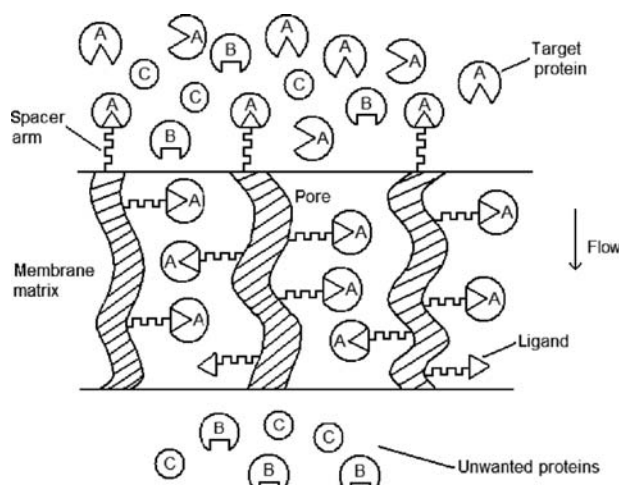


FIG. 20-91 Illustration of the interactions between proteins and membrane matrix in affinity membrane chromatography.

can be chosen from commercial membrane materials including organic, inorganic, polymeric, and composite materials. The selected membrane is first activated to create functional groups for chemical attachment of affinity ligands. If there is steric hindrance to binding between the immobilized ligand and the target molecule, a suitable spacer arm is used to bridge the activated membrane surface and the ligand. The ligand should retain its reversible binding capacity after immobilization onto the support membrane. Affinity ligands typically fall into two categories: (1) those derived from enzyme/substrate, antibody/antigen pairs that are capable of very strong and highly biospecific binding and (2) protein A and protein G, coenzyme, lectin, dyes, and metal chelates, etc., each capable of binding with a whole class of molecules. A highly specific ligand provides an unsurpassed resolution and an ability to handle a large volume of a dilute feed. However, they are typically fragile and expensive and may be unavailable off the shelf due to their narrow applications involving just one or a few molecules that can bind. Elution can also prove to be a difficult task because some biospecific bindings can be extremely tenacious. In contrast, a somewhat less specific ligand has a much wider market and thus is considerably less expensive. Various membrane cartridges have been used for affinity membrane chromatography including those with multiple layers of flat sheet membranes, hollow fibers, and spiral-wound and Chromarod membranes (Zou et al., loc. cit.).

Immobilized metal-ion affinity chromatography (IMAC) relies on the interaction of certain amino acid residues, particularly histidine, cysteine, and tryptophan, on the surface of the protein with metal ions fixed to the support by chelation with appropriate chelating compounds, invariably derivatives of iminodiacetic acid. Commonly used metal ions are Cu^{2+} , Zn^{2+} , Ni^{2+} , and Co^{2+} . Despite its relative complexity in terms of the number of factors that influence the process, IMAC is beginning to find industrial applications. The choice of chelating group, metal ion, pH, and buffer constituents will determine the adsorption and desorption characteristics. Elution can be effected by several methods, including pH gradient, competitive ligands, organic solvents, and chelating agents.

Following removal of unbound materials in the column by washing, the bound substances are recovered by changing conditions to favor desorption. A gradient or stepwise reduction in pH is often suitable. Otherwise, one can use competitive elution with a gradient of increasing concentration. IMAC eluting agents include ammonium chloride, glycine, histamine, histidine, or imidazol. Inclusion of a chelating agent such as EDTA in the eluent will allow all proteins to be eluted indiscriminately along with the metal ion.

Chromatographic Development The basic concepts of chromatographic separations are described elsewhere in this handbook. Proteins differ from small solutes in that the large number of charged and/or hydrophobic residues on the protein surface provide multiple

binding sites, which ensure stronger binding of the proteins to the adsorbents, as well as some discrimination based on the surface distribution of amino acid residues. The proteins are recovered by elution with a buffer that reduces the strength of this binding and permits the proteins to be swept out of the column with the buffer solution. In isotocratic elution, the buffer concentration is kept constant during the elution period. Since the different proteins may have significantly different adsorption isotherms, the recovery may not be complete, or it may take excessive processing time and cause excessive band spreading to recover all proteins from the column. In gradient elution operations, the composition of the mobile phase is changed during the process to decrease the binding strength of the proteins successively, the more loosely bound proteins being removed first before the eluent is strengthened to enable recovery of the more strongly adsorbed species. The change in eluent composition can be gradual and continuous, or it can be stepwise. Industrially, in large-scale columns it is difficult to maintain a continuous gradient owing to difficulties in fluid distribution, and thus stepwise changes are still used. In some adsorption modes, the protein can be recovered by the successive addition of competing compounds to displace the adsorbed proteins. In all cases, the product is eluted as a chromatographic peak, with some possible overlap between adjacent product peaks.

Displacement chromatography relies on a different mode of elution. Here a displacer that is more strongly adsorbed than any of the proteins is introduced with the mobile phase. As the displacer concentration front develops, it pushes the proteins ahead of itself. The more strongly adsorbed proteins then act as displacers for the less strongly bound proteins, and so on. This leads to the development of a displacer train in which the different molecules are eluted from the column in abutting roughly rectangular peaks in the reverse order of their binding strength with the column's stationary phase. Many displacers have been developed in the past two decades including both high- and low-molecular-weight molecules. Displacement chromatography may be practical as an earlier chromatography step in a downstream process when baseline separations are not necessary. It has been considered for some industrial processes. However, displacer reuse and possible contamination of the protein product in addition to its inherent inability to achieve a clear-cut baseline separation make the use of displacement chromatography still a challenge. So far, no FDA-approved process exists [Shukla and Cramer, in Ahuja (ed.), op. cit., pp. 379-415].

For efficient adsorption it is advisable to equilibrate both the column and the sample with the optimum buffer for binding. Prior to this, the column must be cleaned to remove tightly bound impurities by increasing the salt concentration beyond that used in the product elution stages. At the finish of cleaning operation, the column should be washed with several column volumes of the starting buffer to remove remaining adsorbed material. In desorption, it is necessary to drive the favored binding equilibrium for the adsorbed substance from the stationary to the mobile phase. Ligand-protein interactions are generally a combination of electrostatic, hydrophobic, and hydrogen bonds, and the relative importance of each of these and the degree of stability of the bound protein must be considered in selecting appropriate elution conditions; frequently compromises must be made. Gradient elution often gives good results.

Changes in pH or ionic strength are generally nonspecific in elution performance; ionic strength increases are effective when the protein binding is predominantly electrostatic, as in IEC. Polarity changes are effective when hydrophobic interactions play the primary role in protein binding. By reducing the polarity of the eluting mobile phase, this phase becomes a more thermodynamically favorable environment for the protein than adsorption to the packing support. A chaotropic salt (KSCN , KCNO , KI in range of 1 to 3 M) or denaturing agent (urea, guanidine HCl; 3 to 4 M) in the buffer can also lead to enhanced desorption. For the most hydrophobic proteins (e.g., membrane proteins) one can use detergents just below their critical micelle concentrations to solubilize the proteins and strip them from the packing surface. Specific elution requires more selective eluents. Proteins can be desorbed from ligands by competitive binding of the eluting agent (low concentration of 5 to 100 mM) either to the ligand or to the protein.

Specific eluents are most frequently used with group-specific adsorbents since selectivity is greatly increased in the elution step.

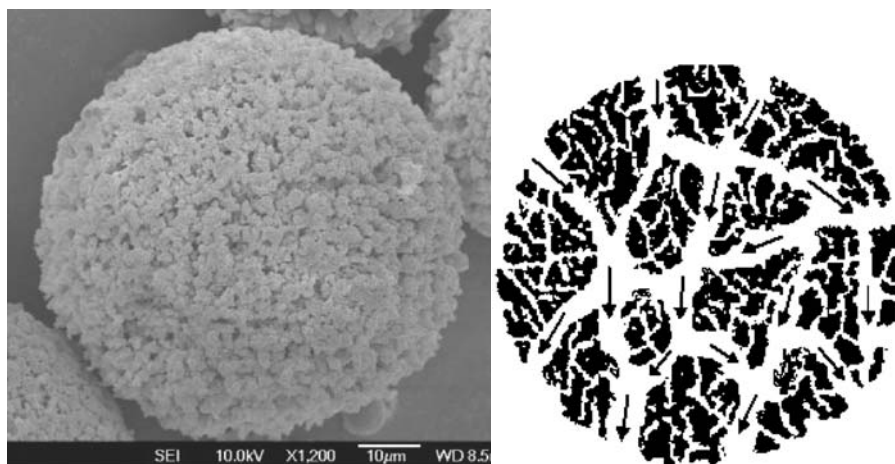


FIG. 20-92 SEM image of a poly(styrene-co-divinylbenzene) gigaporous particle synthesized from suspension polymerization and schematic of a gigaporous particle showing through-pores and diffusion pores [Gu et al., *China Particology*, 3, 349 (2005)].

The effectiveness of the elution step can be tailored by using a single eluent, pulses of different eluents, or eluent gradients. These systems are generally characterized by mild desorption conditions. If the eluting agent is bound to the protein, it can be dissociated by desalting on a gel filtration column or by diafiltration.

Column Packings The quality of the separation obtained in chromatographic separations will depend on the capacity, selectivity, and hydraulic properties of the stationary phase, which usually consists of porous beads of hydrophilic polymers filled with the solvent. The xerogels (e.g., crosslinked dextran) shrink and swell depending on solvent conditions, while aerogels have sizes independent of solution conditions. A range of materials are used for the manufacture of gel beads, classified according to whether they are inorganic, synthetic, or polysaccharides. The most widely used materials are based on neutral polysaccharides and polyacrylamide. Cellulose gels, such as crosslinked dextran, are generally used as gel filtration media, but can also be used as a matrix for ion exchangers. The primary use of these gels is for desalting and buffer exchange of protein solutions, as nowadays fractionation by gel filtration is performed largely with composite gel matrices. Agarose, a low-charge fraction of the seaweed polysaccharide agar, is a widely used packing material.

Microporous gels made by point crosslinking dextran or polyacrylamides are used for molecular-sieve separations such as size-exclusion chromatography and gel filtration, but are generally too soft at the porosities required for efficient protein chromatography. Macroporous gels are most often obtained from aggregated and physically crosslinked polymers. Examples include agarose, macroreticular polyacrylamide, silica, and synthetic polymers. These gels are good for ion-exchange and affinity chromatography as well as for other adsorption chromatography techniques. Composite gels, in which the microporous gel is introduced into the pores of macroreticular gels, combine the advantages of both types.

High matrix rigidity is offered by porous inorganic silica, which can be derivatized to enhance its compatibility with proteins, but it is unstable at alkaline pH. Hydroxyapatite particles have high selectivity for a wide range of proteins and nucleic acids.

Traditional porous media have pore sizes typically in the range of 100 to 300 Å. To reduce intraparticle diffusion for fast chromatography, column packing materials can be made either nonporous or extremely porous. Gustavsson and Larsson [in Hatti-Kaul and Mattiasson (eds), op. cit., pp. 423–454] discussed various chromatography media for fast chromatography of proteins. Nonporous particles such as the popular 5- μm modified silica beads for reverse-phase chromatography are excellent for analytical applications. However, due to their limited binding sites that exist only on the outer surface of the particles, nonporous particles are not suitable for preparative- or large-scale applications. Gigaporous media are gaining momentum in

recent years. They are particles with pore sizes above 1000 Å. Some have large enough interconnecting pores in the range of 4000 to 8000 Å that allow even convective flow inside the particles. POROS[®] perfusion chromatography media are the first commercial products in this category introduced in the 1980s. A few more products are being commercialized. POROS[®] media are synthesized in two steps. Nanosize subparticles are first synthesized and then polymerized to form 10- to 50- μm particles in a second step. In recent years, advances in suspension polymerization produced a new type of integral gigaporous media with improved physical strength. The spherical particles are formed in a single polymerization step. An oil phase (dispersed phase) consisting of a monomer (such as styrene), a crosslinking agent (such as divinylbenzene), an initiator, a diluent, and a special porogen is used. By dispersing the oil phase in a water phase containing a stabilizer, a suspension can be obtained. The suspension polymerization is carried out at an elevated temperature above the decomposition temperature of the initiator to obtain the polymer particles. The diluent and porogen in the particles form smaller diffusion pores and much larger through-pores, respectively. Figure 20-92 shows such a particle with both conventional diffusion pores and gigaporous through-pores. The through-pores allow convective flow to improve mass transfer, and the diffusion pores provide an overall large surface area required for a large binding capacity.

In the scale-up of a chromatographic column with conventional packing media, the column length scale-up is limited because of the subsequently increased column pressure. To increase the feed load, the column is typically scaled up by enlarging the column diameter after the column length reaches a certain limit. The resultant pancake-shaped column leads to a deteriorating resolution due to poor flow distribution in the column cross-section. With rigid gigaporous particles, axial direction scale-up becomes possible because the flow rate can be up to 40 times higher than that for the conventional media. This kind of scale-up is far superior because of the enhanced resolution together with increased feed capacity when the column axial length is increased. With the advances made in rigid gigaporous media, chromatography columns can potentially process large volumes of very dilute feeds when combined with strong binding kinetics such as those involved in affinity chromatography. This may have a significant impact on the overall downstream process design.

Alternative Chromatographic Columns Commercial radial-flow chromatography (RFC) columns first appeared in the mid-1980s. RFC is an alternative to the conventional axial-flow chromatography for preparative- and large-scale applications. In a RFC column, the mobile phase flows in the radial direction rather than the axial direction. Computer simulation proves that RFC is somewhat equivalent to a pancakelike axial-flow column [Gu, in Flickinger and Drew (eds),

op. cit., pp. 627–639]. Both configurations offer a short flow path and thus a low pressure drop.

Continuous chromatography can be achieved by using a simulated moving-bed (SMB) process shown in Sec. 16, in which several columns are linked with a switching device to simulate a continuous countercurrent flow process. This design maximizes productivity while minimizing eluent consumption [Nicoud, in Ahuja (ed.), op. cit., pp. 475–509]. It is suitable for a simple feed that results in only a limited fraction [Imamoglu, in Freitag (ed.), op. cit., pp. 212–231]. By switching the feed, eluant input positions and raffinate, extract output positions periodically in a series of columns to simulated countercurrent movement of the liquid phase and the solid (resin) phase, continuous chromatography is obtained through the use of multiple columns in series. A four-zone SMB consisting of four columns is capable of producing two fractions as a pair of raffinate and extract. To have two pairs (with a total of four fractions) of raffinate and extract outputs an eight-zone SMB system is needed. Another alternative design described in Sec. 16 is the so-called annual-flow column that rotates continuously in the angular direction. Despite its obvious advantage of being straightforwardly continuous, it suffers from angular dispersion and reduced bed volume. This design so far has seen very limited application since its commercial introduction in 1999 [Wolfgang and Prior, in Freitag (ed.), op. cit., pp. 233–255].

In the past decade, monolithic columns have gained popularity for analytical applications. Instead of using discrete packing particles, a whole polymer block is used as a column. Their continuous homogeneous structure provides fast mass-transfer rates and very high flow rates inside the column [Strancar et al., in Freitag (ed.), op. cit., pp. 50–85]. Thin monolithic disks with affinity binding are capable of fast chromatographic separations. They act much as affinity membrane chromatography cartridges do. To utilize long monolithic columns for process-scale separations, a breakthrough in column fabrication is needed to produce large columns suitable for commercial applications.

Sequencing of Chromatography Steps The sequence of chromatographic steps used in a protein purification train should be designed such that the more robust techniques are used first, to obtain some volume reduction (concentration effect) and to remove major impurities that might foul subsequent units; these robust units should have high chemical and physical resistance to enable efficient regeneration and cleaning, and they should be of low material cost. These steps should be followed by the more sensitive and selective operations, sequenced such that buffer changes and concentration steps between applications to chromatographic columns are avoided. Frequently, ion-exchange chromatography is used as the first step. The elution peaks from such columns can be applied directly to hydrophobic interaction chromatographic columns or to a gel filtration unit, without the need for desalting of the solution between applications. These columns can also be used as desalting operations, and the buffers used to elute the columns can be selected to permit direct application of the eluted peaks to the next chromatographic step.

Factors to be considered in making the selection of chromatography processing steps are cost, sample volume, protein concentration and sample viscosity, degree of purity of protein product, presence of nucleic acids, pyrogens, and proteolytic enzymes. Ease with which different types of adsorbents can be washed free from adsorbed contaminants and denatured proteins must also be considered.

Scale-up of Liquid Chromatography The chromatography columns in downstream processing typically are operated in the non-linear region due to a concentrated or overloaded feed. Their scale-up remains a challenging task. There are two general approaches: (1) the rule-based method using equations for column resizing [Ladisch, op. cit., pp. 299–448] and (2) the computer simulation method using rate models [Gu, *Mathematical Modeling and Scale-Up of Liquid Chromatography*, Springer-Verlag, Berlin-New York, 1995] with simulation software such as Chromulator[®] to predict column performance for a particular column setting and operating conditions.

PRODUCT POLISHING AND FORMULATION

The product from the final purification unit operation is typically in a liquid fraction containing water, a solvent, or a buffer. Based on the

requirement for the final product, they may need to be removed. A solid protein is usually far more stable with a much longer shelf life. Product formulation may also require an excipient to be added. Thus, additional unit operations are needed after the final purification step.

Lyophilization and Drying After the last high-performance purification steps it is usually necessary to prepare the finished product for special applications. For instance, final enzyme products are often required in the form of a dry powder to provide for stability and ease of handling, while pharmaceutical preparations also require high purity, stability during formulation, absence of microbial load, and extended shelf life. This product formulation step may involve drying of the final products by freeze drying, spray drying, fluidized-bed drying, or crystallization (Golker, in Stephanopoulos, op. cit., pp. 695–714). Crystallization can also serve as an economical purification step [Lee and Kim, in Hatti-Kaul and Mattiasson (ed.), op. cit., pp. 277–320] in addition to its role as a unit operation for product polishing.

Freeze drying, or lyophilization, is normally reserved for temperature-sensitive materials such as vaccines, enzymes, microorganisms, and therapeutic proteins, as it can account for a significant portion of total production cost. This process is characterized by three distinct steps, beginning with freezing of the product solution, followed by water removal by sublimation in a primary drying step, and ending with secondary drying by heating to remove residual moisture.

Freezing is carried out on cooled plates in trays or with the product distributed as small particles on a drum cooler; by dropping the product solution in liquid nitrogen or some other cooling liquid; by cospraying with liquid CO₂ or liquid nitrogen; or by freezing with circulating cold air. The properties of the freeze-dried product, such as texture and ease of rehydration, depend on the size and shape of the ice crystals formed, which in turn depend on the degree of undercooling. It is customary to cool below the lowest equilibrium eutectic temperature of the mixture, although many multicomponent mixtures do not exhibit eutectic points. Freezing should be rapid to avoid effects from local concentration gradients. Removal of water from solution by the formation of ice crystals leads to changes in salt concentration and pH, as well as enhanced concentration of the product, in the remaining solution; this in turn can enhance reaction rates, and even reaction order can change, resulting in cold denaturation of the product. If the feed contains a solvent and an acid, the solvent tends to sublimate faster than the acid, causing acidic damage to the protein. With a high initial protein concentration the freeze concentration factor and the amount of ice formed will be reduced, resulting in greater product stability. For aseptic processing, direct freezing in the freeze-drying plant ensures easier loading of the solution after filtration than if it is transferred separately from remote freezers.

In the primary drying step, heat of sublimation is supplied by contact, conduction, or radiation to the sublimation front. It is important to avoid partial melting of the ice layer. Many pharmaceutical preparations dried in ampoules are placed on heated shelves. The drying time depends on the quality of ice crystals, indicating the importance of controlling the freezing process; smaller crystals offer higher interfacial areas for heat and mass transfer, but larger crystals provide pores for diffusion of vapor away from the sublimation front.

A high percentage of water remains after the sublimation process, present as adsorbed water, water of hydration, or dissolved in the dry amorphous solid; this is difficult to remove. Usually, shelf temperature is increased to 25 to 40°C and chamber pressure is lowered as far as possible. This still does not result in complete drying, however, which can be achieved only by using even higher temperatures, at which point thermally induced product degradation can occur.

Excipients can be used to improve stability and prevent deterioration and inactivation of biomolecules through structural changes such as dissociation from multimeric states into subunits, decrease in α -helical content accompanied by an increase in β -sheet structure, or complete unfolding of helical structure. These are added prior to the freeze-drying process. Examples of these protective agents include sugars, sugar derivatives, and various amino acids, as well as polymers such as dextran, polyvinyl pyrrolidone, hydroxyethyl starch, and polyethylene glycol. Some excipients, the lyoprotectants, provide protection during freezing, drying, and storage, while others, the cryoprotectants, offer protection only during the freezing process. Spray drying can use up to 50 percent less energy than freeze-drying operations and finds applica-

tion in the production of enzymes used as industrial catalysts, as additives for washing detergents, and as the last step in the production of single-cell protein. The product is usually fed to the dryer as a solution, a suspension, or a free-flowing wet substance.

Spray drying is an adiabatic process, the energy being provided by hot gas (usually hot air) at temperatures between 120 and 400°C. Product stability is ensured by a very short drying time in the spray-drying equipment, typically in the subsecond to second range, which limits exposure to the elevated temperatures in the dryer. Protection can be offered by addition of additives (e.g., galactomannan, polyvinyl pyrrolidone, methyl cellulose, cellulose). The spray-drying process requires dispersion of the feed as small droplets to provide a large heat- and mass-transfer area. The dispersion of liquid is attained by using rotating disks, different types of nozzles, or ultrasound, and is affected by interfacial tension, density, and dynamic viscosity of the feed solution, as well as the temperature and relative velocities of the liquid and air in the mixing zone. Rotating-disk atomizers operate at 4000 to 50,000 rpm to generate the centrifugal forces needed for dispersion of the liquid phase; typical droplet sizes of 25 to 950 µm are obtained. These atomizers are especially suitable for dispersing suspensions that would tend to clog nozzles. For processing under aseptic conditions, the spray drier must be connected to a filling line that allows aseptic handling of the product.

Thickeners and binders such as acacia, agar, starch, sodium alginate, gelatin, methyl cellulose, bentonite, and silica are used to improve product stability and enhance the convenience of the administration of a liquid formulation. Surface-active agents, colors, flavors; and preservatives may also be used in the final formulation (Garcia et al., *Bioseparation Process Science*, Blackwell Science, Malden, Mass., 1999, p. 374).

INTEGRATION OF UNIT OPERATIONS IN DOWNSTREAM PROCESSING

Generally speaking, a typical downstream process consisting of four stages: removal of insolubles, isolation, purification, and polishing (Belter et al., op. cit., p. 5). Cell disruption is required for intracellular products. One or two, and sometimes more chromatography steps will serve as the center-stage unit operations. The steps before them serve the purposes of feed volume reduction and removal of the majority of impurities. The steps after them are polishing and formulation operations. Based on these general outlines, a few rules of thumb may be used (Harrison et al., op. cit., p. 322; Garcia et al., op. cit., p. 358): (1) Reduce the feed volume early in the process, (2) remove the most abundant impurities or the easy-to-remove impurities first, (3) reduce the amount of impurities as much as possible before the delicate high-resolution chromatography steps, and (4) sequence the unit operations that exploit different separation mechanisms.

The purification of proteins to be used for therapeutic purposes presents more than just the technical problems associated with the separation process. Owing to the complex nature and intricate three-dimensional structure, the routine determination of protein structure as a quality control tool, particularly in its final medium for use, is not well established. In addition, the complex nature of the human immune system allows for even minor quantities of impurities and contaminants to be biologically active. Thus, regulation of biologics production has resulted in the concept of the process defining the product since even small and inadvertent changes in the process may affect the safety and efficacy of the product. Indeed, it is generally acknowledged that even trace amounts of contaminants introduced from other processes, or contaminants resulting from improper equipment cleaning, can compromise the product. From a regulatory perspective, then, operations should be chosen for more than just efficiency. The consistency of the unit operation, particularly in the face of potentially variable feed from the culture/fermentation process, is the cornerstone of the process definition. Operations that lack robustness or are subject to significant variation should not be considered. Another aspect of process definition is the ability to quantify the operation's performance. Finally, the ease with which the equipment can

be cleaned in a verifiable manner should play a role in unit operation selection. Obviously, certain unit operations are favored over others because they are easier to validate. Process validation was covered in a book edited by Subramanian (op. cit., vol. 2, pp. 379–460).

Keep in mind that some unit operations are not as scalable as others. The evolution of a bench-scale process to production scale will see changes in the types and number of unit operations selected. To configure an effective and efficient bioseparations process, a thorough understanding of the various unit operations in downstream processing described above is a prerequisite. Different process-scale and purity requirements can necessitate changes and may result in quite different configurations for the same product. Existing process examples and past experiences help greatly. Due to regulatory restrictions, once a process is approved for a biopharmaceutical, any change in unit operations requires time-consuming and costly new regulatory approval. This means that an optimized process design is much desired before seeking approval. The involvement of biochemical engineers early in the design process is highly recommended.

INTEGRATION OF UPSTREAM AND DOWNSTREAM OPERATIONS

Upstream fermentation (or cell culture) has a direct impact on the design and optimization of its downstream process. Different media or different operating conditions in fermentation result in a different feed for the downstream process. In the development of new products, optimization of the fermentation medium for titer only often ignores the consequences of the medium properties on subsequent downstream processing steps such as filtration and chromatography. It is imperative, therefore, that there be effective communication and understanding between workers on the upstream and downstream phases of the product development if rational tradeoffs are to be made to ensure overall optimality of the process. One example is to make the conscious decision, in collaboration with those responsible for the downstream operations, of whether to produce a protein in an unfolded form or in its native folded form. The purification of the aggregated unfolded proteins is simpler than that of the native protein, but the refolding process itself to obtain the product in its final form may lack scalability or certainty in its method development.

In some instances, careful consideration of the conditions used in the fermentation process, or manipulation of the genetic makeup of the host, can simplify and even eliminate some unit operations in the downstream processing sequence [Kelley and Hatton, *Bioseparation*, 1, 303–349 (1991)]. Some of the advances made in this area are the engineering of strains of *E. coli* to allow the inducible expression of lytic enzymes capable of disrupting the wall from within for the release of intracellular protein products, the use of secretion vectors for the expression of proteins in bacterial production systems. Fusion proteins can be genetically engineered to attach an extra peptide or protein that can bind with an affinity chromatography medium [Whitmarsh and Hornby, in Street (ed.), op. cit., pp. 163–177]. This can enhance the purification of an otherwise difficult to purify protein greatly. The cell culture medium can be selected to avoid components that can hinder subsequent purification procedures. Integration of the fermentation and initial separation/purification steps in a single operation can also lead to enhanced productivity, particularly when the product can be removed as it is formed to prevent its proteolytic destruction by the proteases which are frequently the by-product of fermentation processes. The introduction of a solvent directly to the fermentation medium (e.g., phase-forming polymers), the continuous removal of products by using ultrafiltration membranes, and the use of continuous fluidized-bed operations are examples of this integration.

Process economics for biological products was discussed by Harrison et al. (op. cit., pp. 334–369) and Datar and Rosen [in Asenjo (ed.), *Separation Processes in Biotechnology*, Dekker, New York, 1990, pp. 741–793] at length, and also by Ladisch (op. cit., pp. 401–430). They provided some illustrative examples with cost analyses. Bioprocess design software can also prove helpful in the overall design process (Harrison et al., op. cit., pp. 343–369).

SECTION 21

Solid-Solid
Operations and
Processing

PERRY'S CHEMICAL ENGINEERS' HANDBOOK

8TH EDITION



BRYAN J. ENNIS, WOLFGANG WITT
RALF WEINEKÖTTER, DOUGLAS SPHAR
ERIK GOMMERAN, RICHARD H. SNOW
TERRY ALLEN, GRANTGES J. RAYMUS
JAMES D. LITSTER

Copyright © 2008, 1997, 1984, 1973, 1963, 1950, 1941, 1934 by The McGraw-Hill Companies, Inc. All rights reserved. Manufactured in the United States of America. Except as permitted under the United States Copyright Act of 1976, no part of this publication may be reproduced or distributed in any form or by any means, or stored in a database or retrieval system, without the prior written permission of the publisher.

0-07-154228-0

The material in this eBook also appears in the print version of this title: 0-07-151144-X.

All trademarks are trademarks of their respective owners. Rather than put a trademark symbol after every occurrence of a trademarked name, we use names in an editorial fashion only, and to the benefit of the trademark owner, with no intention of infringement of the trademark. Where such designations appear in this book, they have been printed with initial caps.

McGraw-Hill eBooks are available at special quantity discounts to use as premiums and sales promotions, or for use in corporate training programs. For more information, please contact George Hoare, Special Sales, at george_hoare@mcgraw-hill.com or (212) 904-4069.

TERMS OF USE

This is a copyrighted work and The McGraw-Hill Companies, Inc. (“McGraw-Hill”) and its licensors reserve all rights in and to the work. Use of this work is subject to these terms. Except as permitted under the Copyright Act of 1976 and the right to store and retrieve one copy of the work, you may not decompile, disassemble, reverse engineer, reproduce, modify, create derivative works based upon, transmit, distribute, disseminate, sell, publish or sublicense the work or any part of it without McGraw-Hill’s prior consent. You may use the work for your own noncommercial and personal use; any other use of the work is strictly prohibited. Your right to use the work may be terminated if you fail to comply with these terms.

THE WORK IS PROVIDED “AS IS.” McGRAW-HILL AND ITS LICENSORS MAKE NO GUARANTEES OR WARRANTIES AS TO THE ACCURACY, ADEQUACY OR COMPLETENESS OF OR RESULTS TO BE OBTAINED FROM USING THE WORK, INCLUDING ANY INFORMATION THAT CAN BE ACCESSED THROUGH THE WORK VIA HYPERLINK OR OTHERWISE, AND EXPRESSLY DISCLAIM ANY WARRANTY, EXPRESS OR IMPLIED, INCLUDING BUT NOT LIMITED TO IMPLIED WARRANTIES OF MERCHANTABILITY OR FITNESS FOR A PARTICULAR PURPOSE. McGraw-Hill and its licensors do not warrant or guarantee that the functions contained in the work will meet your requirements or that its operation will be uninterrupted or error free. Neither McGraw-Hill nor its licensors shall be liable to you or anyone else for any inaccuracy, error or omission, regardless of cause, in the work or for any damages resulting therefrom. McGraw-Hill has no responsibility for the content of any information accessed through the work. Under no circumstances shall McGraw-Hill and/or its licensors be liable for any indirect, incidental, special, punitive, consequential or similar damages that result from the use of or inability to use the work, even if any of them has been advised of the possibility of such damages. This limitation of liability shall apply to any claim or cause whatsoever whether such claim or cause arises in contract, tort or otherwise.

DOI: 10.1036/007151144X

Solid-Solid Operations and Processing

Bryan J. Ennis, Ph.D. *President, E&G Associates, Inc., and CEO, iPowder Systems, Inc.; Co-Founder and Member, Particle Technology Forum, American Institute of Chemical Engineers; Member, American Association of Pharmaceutical Scientists (Section Editor, Bulk Flow Characterization, Solids Handling, Size Enlargement)*

Wolfgang Witt, Dr. rer. nat. *Technical Director, Sympatec GmbH–System Partikel Technik; Member, ISO Committee TC24/SC4, DIN, VDI Gesellschaft für Verfahrenstechnik und Chemieingenieurwesen Fachausschuss “Partikelmesstechnik” (Germany) (Particle-Size Analysis)*

Ralf Weinekötter, Dr. sc. techn. *Managing Director, Gericke AG, Switzerland; Member, DECHEMA (Solids Mixing)*

Douglas Sphar, Ph.D. *Research Associate, DuPont Central Research and Development (Size Reduction)*

Erik Gommeran, Dr. sc. techn. *Research Associate, DuPont Central Research and Development (Size Reduction)*

Richard H. Snow, Ph.D. *Engineering Advisor, IIT Research Institute (retired); Fellow, American Institute of Chemical Engineers; Member, American Chemical Society, Sigma Xi (Size Reduction)*

Terry Allen, Ph.D. *Senior Research Associate (retired), DuPont Central Research and Development (Particle-Size Analysis)*

Grantges J. Raymus, M.E., M.S. *President, Raymus Associates, Inc.; Manager of Packaging Engineering (retired), Union Carbide Corporation; Registered Professional Engineer (California); Member, Institute of Packaging Professionals, ASME (Solids Handling)*

James D. Litster, Ph.D. *Professor, Department of Chemical Engineering, University of Queensland; Member, Institution of Chemical Engineers (Australia) (Size Enlargement)*

PARTICLE-SIZE ANALYSIS

Particle Size	21-8	Dispersion	21-11
Specification for Particulates	21-8	Wet Dispersion	21-12
Particle Size	21-8	Dry Dispersion	21-12
Particle-Size Distribution	21-8	Particle-Size Measurement	21-12
Model Distribution	21-9	Laser Diffraction Methods	21-12
Moments	21-9	Image Analysis Methods	21-13
Average Particle Sizes	21-9	Dynamic Light Scattering Methods	21-14
Specific Surface	21-9	Acoustic Methods	21-14
Particle Shape	21-10	Single-Particle Light Interaction Methods	21-15
Equivalent Projection Area of a Circle	21-10	Small-Angle X-Ray Scattering Method	21-15
Feret's Diameter	21-10	Focused-Beam Techniques	21-15
Sphericity, Aspect Ratio, and Convexity	21-10	Electrical Sensing Zone Methods	21-16
Fractal Logic	21-10	Gravitational Sedimentation Methods	21-16
Sampling and Sample Splitting	21-10	Sedimentation Balance Methods	21-17
		Centrifugal Sedimentation Methods	21-17

21-2 SOLID-SOLID OPERATIONS AND PROCESSING

Sieving Methods	21-18
Elutriation Methods and Classification	21-18
Differential Electrical Mobility Analysis (DMA)	21-18
Surface Area Determination	21-18
Particle-Size Analysis in the Process Environment	21-18
At-line	21-19
On-line	21-19
In-line	21-19
Verification	21-19
Reference Materials	21-19

SOLIDS HANDLING: BULK SOLIDS FLOW CHARACTERIZATION

An Introduction to Bulk Powder Behavior	21-20
Permeability and Aeration Properties	21-20
Permeability and Deaeration	21-20
Classifications of Fluidization Behavior	21-22
Classifications of Conveying Behavior	21-22
Bulk Flow Properties	21-23
Shear Cell Measurements	21-23
Yield Behavior of Powders	21-25
Powder Yield Loci	21-27
Flow Functions and Flowability Indices	21-28
Shear Cell Standards and Validation	21-29
Stresses in Cylinders	21-29
Mass Discharge Rates for Coarse Solids	21-30
Extensions to Mass Discharge Relations	21-31
Other Methods of Flow Characterization	21-31

SOLIDS MIXING

Principles of Solids Mixing	21-33
Industrial Relevance of Solids Mixing	21-33
Mixing Mechanisms: Dispersive and Convective Mixing	21-33
Segregation in Solids and Demixing	21-34
Transport Segregation	21-34
Mixture Quality: The Statistical Definition of Homogeneity	21-34
Ideal Mixtures	21-36
Measuring the Degree of Mixing	21-37
On-line Procedures	21-38
Sampling Procedures	21-38
Equipment for Mixing of Solids	21-38
Mixed Stockpiles	21-38
Bunker and Silo Mixers	21-38
Rotating Mixers or Mixers with Rotating Component	21-39
Mixing by Feeding	21-40
Designing Solids Mixing Processes	21-42
Goal and Task Formulation	21-42
The Choice: Mixing with Batch or Continuous Mixers	21-42
Batch Mixing	21-43
Feeding and Weighing Equipment for a Batch Mixing Process	21-44
Continuous Mixing	21-45

PRINCIPLES OF SIZE REDUCTION

Introduction	21-45
Industrial Uses of Grinding	21-45
Types of Grinding: Particle Fracture vs. Deagglomeration	21-45
Wet vs. Dry Grinding	21-46
Typical Grinding Circuits	21-46
Theoretical Background	21-46
Introduction	21-46
Single-Particle Fracture	21-46
Energy Required and Scale-up	21-47
Energy Laws	21-47
Fine Size Limit	21-48
Breakage Modes and Grindability	21-48
Grindability Methods	21-49
Operational Considerations	21-50
Mill Wear	21-50
Safety	21-50
Temperature Stability	21-51
Hygroscopicity	21-51
Dispersing Agents and Grinding Aids	21-51
Cryogenic Grinding	21-51
Size Reduction Combined with Other Operations	21-51
Size Reduction Combined with Size Classification	21-51
Size Classification	21-52
Other Systems Involving Size Reduction	21-52
Liberation	21-52

MODELING AND SIMULATION OF GRINDING PROCESSES

Modeling of Milling Circuits	21-52
Batch Grinding	21-53
Grinding Rate Function	21-53
Breakage Function	21-53
Solution of Batch-Mill Equations	21-53
Continuous-Mill Simulation	21-53
Residence Time Distribution	21-53
Solution for Continuous Milling	21-54
Closed-Circuit Milling	21-54
Data on Behavior of Grinding Functions	21-55
Grinding Rate Functions	21-55
Scale-Up and Control of Grinding Circuits	21-55
Scale-up Based on Energy	21-55
Parameters for Scale-up	21-55

CRUSHING AND GRINDING EQUIPMENT: DRY GRINDING—IMPACT AND ROLLER MILLS

Jaw Crushers	21-56
Design and Operation	21-56
Comparison of Crushers	21-57
Performance	21-57
Gyratory Crushers	21-57
Design and Operation	21-57
Performance	21-58
Control of Crushers	21-58
Impact Breakers	21-58
Hammer Crusher	21-58
Cage Mills	21-59
Prebreakers	21-59
Hammer Mills	21-59
Operation	21-59
Roll Crushers	21-60
Roll Press	21-60
Roll Ring-Roller Mills	21-60
Raymond Ring-Roller Mill	21-60
Pan Crushers	21-61
Design and Operation	21-61
Performance	21-61

CRUSHING AND GRINDING EQUIPMENT: FLUID-ENERGY OR JET MILLS

Design	21-61
Types	21-61
Spiral Jet Mill	21-61
Opposed Jet Mill	21-61
Other Jet Mill Designs	21-62

CRUSHING AND GRINDING EQUIPMENT: WET/DRY GRINDING—MEDIA MILLS

Overview	21-62
Media Selection	21-62
Tumbling Mills	21-63
Design	21-63
Multicompartmented Mills	21-63
Operation	21-64
Material and Ball Charges	21-64
Dry vs. Wet Grinding	21-64
Dry Ball Milling	21-64
Wet Ball Milling	21-64
Mill Efficiencies	21-65
Capacity and Power Consumption	21-65
Stirred Media Mills	21-65
Design	21-65
Attritors	21-65
Vertical Mills	21-65
Horizontal Media Mills	21-65
Annular Gap Mills	21-66
Manufacturers	21-66
Performance of Bead Mills	21-66
Residence Time Distribution	21-66
Vibratory Mills	21-66
Performance	21-67
Residence Time Distribution	21-67

Hicom Mill 21-67
 Planetary Ball Mills 21-67
 Disk Attrition Mills 21-67
 Dispersers and Emulsifiers 21-68
 Media Mills and Roll Mills 21-68
 Dispersion and Colloid Mills 21-68
 Pressure Homogenizers 21-68
 Microfluidizer 21-68

CRUSHING AND GRINDING PRACTICE

Cereals and Other Vegetable Products 21-68
 Flour and Feed Meal 21-68
 Soybeans, Soybean Cake, and Other Pressed Cakes 21-68
 Starch and Other Flours 21-69
 Ores and Minerals 21-69
 Metalliferous Ores 21-69
 Types of Milling Circuits 21-69
 Nonmetallic Minerals 21-69
 Clays and Kaolins 21-69
 Talc and Soapstone 21-70
 Carbonates and Sulfates 21-70
 Silica and Feldspar 21-70
 Asbestos and Mica 21-70
 Refractories 21-70
 Crushed Stone and Aggregate 21-70
 Fertilizers and Phosphates 21-70
 Fertilizers 21-70
 Phosphates 21-70
 Cement, Lime, and Gypsum 21-71
 Portland Cement 21-71
 Dry-Process Cement 21-71
 Wet-Process Cement 21-71
 Finish-Grinding of Cement Clinker 21-71
 Lime 21-71
 Gypsum 21-71
 Coal, Coke, and Other Carbon Products 21-71
 Bituminous Coal 21-71
 Anthracite 21-71
 Coke 21-72
 Other Carbon Products 21-72
 Chemicals, Pigments, and Soaps 21-72
 Colors and Pigments 21-72
 Chemicals 21-72
 Soaps 21-72
 Polymers 21-72
 Gums and Resins 21-72
 Rubber 21-72
 Molding Powders 21-72
 Powder Coatings 21-72
 Processing Waste 21-72
 Pharmaceutical Materials 21-73
 Biological Materials—Cell Disruption 21-73

PRINCIPLES OF SIZE ENLARGEMENT

Scope and Applications 21-73
 Mechanics of Size-Enlargement Processes 21-74
 Granulation Rate Processes 21-74
 Compaction Microlevel Processes 21-76
 Process vs. Formulation Design 21-77
 Key Historical Investigations 21-80
 Product Characterization 21-80
 Size and Shape 21-80
 Porosity and Density 21-81
 Strength of Agglomerates 21-81
 Strength Testing Methods 21-81
 Flow Property Tests 21-82
 Redispersion Tests 21-82
 Permeability 21-82
 Physiochemical Assessments 21-82

AGGLOMERATION RATE PROCESSES AND MECHANICS

Wetting 21-82
 Mechanics of the Wetting Rate Process 21-83
 Methods of Measurement 21-83
 Examples of the Impact of Wetting 21-86
 Regimes of Nucleation and Wetting 21-86
 Growth and Consolidation 21-89

Granule Deformability 21-89
 Types of Granule Growth 21-90
 Deformability and Interparticle Forces 21-92
 Deformability and Wet Mass Rheology 21-93
 Low Agitation Intensity—Low Deformability Growth 21-95
 High Agitation Intensity Growth 21-96
 Determination of St^* 21-98
 Granule Consolidation and Densification 21-99
 Breakage and Attrition 21-100
 Fracture Properties 21-101
 Fracture Measurements 21-101
 Mechanisms of Attrition and Breakage 21-102
 Powder Compaction 21-103
 Powder Feeding 21-104
 Compact Density 21-105
 Compact Strength 21-105
 Compaction Pressure 21-105
 Stress Transmission 21-106
 Hiestand Tableting Indices 21-107
 Compaction Cycles 21-107
 Controlling Powder Compaction 21-108
 Paste Extrusion 21-108
 Compaction in a Channel 21-108
 Drag-Induced Flow in Straight Channels 21-108
 Paste Rheology 21-108

CONTROL AND DESIGN OF GRANULATION PROCESSES

Engineering Approaches to Design 21-110
 Scales of Analysis 21-110
 Scale: Granule Size and Primary Feed Particles 21-111
 Scale: Granule Volume Element 21-112
 Scale: Granulator Vessel 21-113
 Controlling Processing in Practice 21-113
 Controlling Wetting in Practice 21-113
 Controlling Growth and Consolidation in Practice 21-117
 Controlling Breakage in Practice 21-117

SIZE ENLARGEMENT EQUIPMENT AND PRACTICE

Tumbling Granulators 21-118
 Disc Granulators 21-118
 Drum Granulators 21-119
 Controlling Granulation Rate Processes 21-120
 Moisture Control in Tumbling Granulation 21-121
 Granulator-Driers for Layering and Coating 21-122
 Relative Merits of Disc vs. Drum Granulators 21-122
 Scale-up and Operation 21-123
 Mixer Granulators 21-123
 Low-Speed Mixers 21-123
 High-Speed Mixers 21-123
 Powder Flow Patterns and Scaling of Mixing 21-125
 Controlling Granulation Rate Processes 21-126
 Scale-up and Operation 21-128
 Fluidized-Bed and Related Granulators 21-130
 Hydrodynamics 21-130
 Mass and Energy Balances 21-130
 Controlling Granulation Rate Processes 21-130
 Scale-up and Operation 21-133
 Draft Tube Designs and Spouted Beds 21-133
 Centrifugal Granulators 21-134
 Centrifugal Designs 21-134
 Particle Motion and Scale-up 21-134
 Granulation Rate Processes 21-135
 Spray Processes 21-135
 Spray Drying 21-135
 Prilling 21-135
 Flash Drying 21-136
 Pressure Compaction Processes 21-136
 Piston and Molding Presses 21-137
 Tableting Presses 21-137
 Roll Presses 21-137
 Pellet Mills 21-139
 Screw and Other Paste Extruders 21-139
 Thermal Processes 21-142
 Sintering and Heat Hardening 21-142
 Drying and Solidification 21-143

21-4 SOLID-SOLID OPERATIONS AND PROCESSING

MODELING AND SIMULATION OF GRANULATION PROCESSES

The Population Balance	21-143
Modeling Individual Growth Mechanisms	21-144
Nucleation	21-144
Layering	21-144
Coalescence	21-144

Attrition	21-145
Solution of the Population Balance	21-146
Effects of Mixing	21-146
Analytical Solutions	21-146
Numerical Solutions	21-146
Simulation of Granulation Circuits with Recycle	21-147

Nomenclature and Units for Particle-Size Analysis

Symbol	Definition	SI units	U.S. customary units	Symbol	Definition	SI units	U.S. customary units
A	Empirically determined constant	—	—	$q^z(z)$	Logarithmic normal distribution	—	—
a	Distance from the scatterer to the detector	m	ft	q_r^z	Logarithmic density distribution of dimension r	—	—
a_s	Specific surface per mass unit	m ² /g	ft ² /s	$q_0(x)$	Number density distribution	1/m	1/in
B	Empirically determined constant	—	—	$q_l(x)$	Length density distribution	1/m	1/in
C	Empirically determined constant	—	—	$q_s(x)$	Area density distribution	1/m	1/in
C	BET number	—	—	$q_{3s}(x)$	Volume or mass density distribution	1/m	1/in
C_{PF}	Area concentration	1/cm ²	1/in ²	$\bar{q}_{3s,i}$	Volume density distribution of class i	1/m	1/in
D	Translational diffusion coefficient	m ² /s	ft ² /s	$\bar{q}_{3s,i}^z$	Logarithmic volume density distribution of class i	1/m	1/in
D_m	Concentration undersize	—	—	r, r_i	Measurement radius	m	in
e	Elementary charge	C	C	s	Dimensionless standard deviation	—	—
f_i	Frequency i	Hz	Hz	s, s_i	Surface radius of a centrifuge	m	in
g	Acceleration due to gravity	m/s ²	ft/s ²	S_V	Volume specific surface	m ² /m ³	—
I_0	Illuminating intensity	W/m ²	fc	$S_1(\theta), S_2(\theta)$	Dimensionless, complex functions describing the change and amplitude in the perpendicular and the parallel polarized light	—	—
i	Index of size class	—	—	T	Absolute temperature	K	K
I	Measured sound intensity	W/m ²	W/ft ²	t	Time	s	s
I	Measured sound intensity	W/m ²	W/ft ²	u	Settling velocity of particles	m/s	ft/s
I_0	Illuminating intensity	W/m ²	fc	v_1, v_2	Particle velocities	m/s	ft/s
I_θ	Primary sound intensity	W/m ²	W/ft ²	W	Weight undersize	g	lb
$I(\theta)$	Total scattered intensity	W/m ²	W/ft ²	x_{EQPC}	Particle size of the equivalent projection area of a circle	m	in
K	Related extinction cross section	—	—	\bar{x}_F	Average Feret diameter	m	in
Kn	Knudsen number	—	—	$x_{F,max}$	Maximum Feret diameter	m	in
$k_c \rightarrow k_B$	Wave number	—	—	$x_{F,max,90}$	Feret diameter measured 90° to the maximum Feret diameter	m	in
k_1, k_2	Incident illumination vectors	1/m	1/ft	$x_{F,min}$	Minimum Feret diameter	m	in
L	Loschmidt number	1/mol	1/mol	x_i	Size of class i	m	in
l	Mean path of gas molecules	m	ft	$\bar{x}_{k,0}$	Arithmetic average particle size for a number distribution	m	in ²
$M_{k,r}$	k th moment of dimension r	—	—	$\bar{x}_{k,r}$	Average particle size	m	in
m	Refractive index	—	—	x_{min}	Minimum particle size	m	in
n	Real part of the refractive index	—	—	x_s	Stokes diameter	m	in
n	Number of classes	—	—	$\bar{x}_{1,r}$	Weighted average particle size	m	in
n_a	Amount of absorbed gas	mol/g	mol/lb	$\bar{x}_{1,2}$	Sauter diameter	m	in
n_m	Monolayer capacity	mol/g	mol/lb	$x_{50,r}$	Mean size of dimension r	m	in
P	Settled weight	g	lb	z	Integration variable	m	in
p	Number of elementary charges	—	—	$Z(x)$	Electrical mobility of particle size x	C	C
p	Pressure	Pa	psi			Pa·s·m	Pa·s·m
p_0	Starting pressure	Pa	psi				
$Q_0(x)$	Cumulative number distribution	—	—				
$Q_1(x)$	Cumulative length distribution	—	—				
$Q_2(x)$	Cumulative area distribution	—	—				
$Q_3(x)$	Cumulative volume or mass distribution	—	—				
$Q_{3,i}$	Cumulative volume distribution till class i	—	—				
q	Modulus of the scattering vector	1/m	1/ft				
\bar{q}	Scattering vector	1/m	1/ft				

Greek Symbols

Δl	Thickness of the suspension layer	m	in	ρ_f	Density of the liquid	g/cm ³	lb/in ³
$\Delta Q_{3,i}$	Normalized volume fraction in size class i	—	—	ρ_s	Density of the particle	g/cm ³	lb/in ³
Δx_i	Width of size class i	m	in	θ	Scattering angle	rad	deg
ϵ	Extension of a particle ensemble in the direction of a camera	m	in	σ	Dimensionless wave number	—	—
Γ	Decay rate	1/s	1/s	ω	Radial velocity of an agglomerate	rad/s	rad/s
η	Hydrodynamic viscosity of the dispersing liquid	Pa·s	Poise	ω	Radial velocity of a centrifuge	rad/s	rad/s
κ	Imaginary part of refractive index	—	—	ψ_s	Sphericity	—	—
				ψ_A	Aspect ratio	—	—
				ψ_C	Convexity	—	—

Nomenclature and Units for Solids Mixing

Symbol	Definition	Units	Symbol	Definition	Units
d	Mixer diameter	m	t_f, t_m, t_e, t_i	Filling, mixing, discharging, and idle time	s
D	Axial coefficient of dispersion	m^2/s	$\#^{\circ}$	Mixing time	—
E_{Mix}	Mixing energy	W	T_p	Feed fluctuation period	s
g	Gravitational acceleration	m^2/s	v	Axial velocity	m/s
H	Height of fluidized bed	m	VRR	Variance reduction ratio	—
L	Mixer length	m	$W\{ \}$	Probability	—
m_p, m_q	Average particle weight of two components p and q in mixture	kg	x	Concentration of tracer component	—
M	Coefficient of mixing	m^2/s	x_i	Concentration in i sample	—
M	Mass of a sample	kg	Greek Symbols		
M	Mass of a batch	kg	μ	Mean concentration	—
n	Random sampling scope	—	ρ	Density of solids	kg/m^3
n	Rotational frequency	Hz	ρ_{bulk}	Bulk density	kg/m^3
Ne	Newton number	—	ρ_s	Density of solids	kg/m^3
N_g	Number of samples in basic whole	—	σ_p, σ_q	Standard deviation of particle weight for two ingredients in mix	kg
p	Tracer component concentration in basic whole	—	σ^2	Variance	—
p_g	Proportional mass volume of coarse ingredient	—	σ_z^2	Variance of a random mix	—
P	Power	W	$\Phi(\chi^2)$	Cumulative function of	—
q	$1-p$	—	χ^2	Chi square distribution	—
r	Mixer radius	m	χ^2_l, χ^2_u	Chi square distribution variables. In a two-sided confidence interval, l stands for lower and u for upper limit.	—
RSD	Relative standard deviation	—	ω	Angular velocity	1/s
S	Empirical standard deviation	—			
S^2	Random sample variance	—			
t, t'	Time	s			
t_e	Mean residence times	s			

21-6 SOLID-SOLID OPERATIONS AND PROCESSING

Nomenclature and Units for Size Enlargement and Practice

Symbol	Definition	SI units	U.S. customary units	Symbol	Definition	SI units	U.S. customary units
A	Parameter in Eq. (21-108)			k	Coalescence rate constant	1/s	1/s
A	Apparent area of indenter contact	cm ²	in ²	K	Agglomerate deformability		
A	Attrition rate	cm ³ /s	in ³ /s	K_c	Fracture toughness	MPa·m ^{1/2}	MPa·m ^{1/2}
A_i	Spouted-bed inlet orifice area	cm ²	in ²	l	Wear displacement of indenter	cm	in
B	Nucleation rate	cm ³ /s	in ³ /s	L	Roll loading	dyn	lbf
B_f	Fragmentation rate	g/s	lb/s	$(\Delta L/L)_c$	Critical agglomerate deformation strain		
B_f	Wear rate	g/s	lb/s	N_t	Granules per unit volume	1/cm ³	1/ft ³
c	Crack length	cm	in	n	Feed droplet size	cm	in
δ_c	Effective increase in crack length due to process zone	cm	in	$n(v,t)$	Number frequency size distribution by size volume	1/cm ⁶	1/ft ⁶
c	Unloaded shear strength of powder	kg/cm ²	psf	N_c	Critical drum or disc speed	rev/s	rev/s
d	Harmonic average granule diameter	cm	in	P	Applied load	dyn	lbf
d	Primary particle diameter	cm	in	P	Pressure in powder	kg/cm ²	psf
d	Impeller diameter	cm	in	Q	Maximum compressive force	kg/cm ²	psf
d	Roll press pocket depth	cm	in	\dot{Q}	Granulator flow rate	cm ³ /s	ft ³ /s
d_i	Indenter diameter	cm	in	r_p	Process zone radius	cm	in
d_p	Average feed particle size	cm	in	\bar{R}	Capillary radius	cm	in
D	Die diameter	cm	in	S	Volumetric spray rate	cm ³ /s	ft ³ /s
D	Disc or drum diameter	cm	in	St	Stokes number, Eq. (21-48)		
D	Roll diameter	cm	in	St°	Critical Stokes number representing energy required for rebound		
D_c	Critical limit of granule size	cm	in	St_0	Stokes number based on initial nuclei diameter		
e_r	Coefficient of restitution			t	Time	s	s
E	Strain energy stored in particle	J	J	u, v	Granule volumes	cm ³	in ³
E°	Reduced elastic modulus	kg/cm ²	psf	u_0	Relative granule collisional velocity	cm/s	in/s
f_c	Unconfined yield stress of powder	kg/cm ²	psf	U	Fluidization gas velocity	cm/s	ft/s
g	Acceleration due to gravity	cm/s ²	ft/s ²	U_{mf}	Minimum fluidization gas velocity	cm/s	ft/s
G_c	Critical strain energy release rate	J/m ²	ft ² /m ²	U_i	Spouted-bed inlet gas velocity	cm/s	ft/s
F	Indentation force	dyn	lbf	V	Volumetric wear rate	cm ³ /s	in ³ /s
F	Roll separating force	dyn	lbf	V_R	Mixer swept volume ratio of impeller	cm ³ /s	ft ³ /s
G	Layering rate	cm ³ /s	in ³ /s	V	Volume of granulator	cm ³	ft ³
h	Height of liquid capillary rise	cm	in	w	Weight fraction liquid		
h	Roll press gap distance	cm	in	w°	Granule volume	cm ³	in ³
h	Binder liquid layer thickness	cm	in	W	Critical average granule volume	cm ³	in ³
h_b	Fluid-bed height	cm	in	x	Roll width	cm	in
h_a	Height of surface asperities	cm	in	y	Granule or particle size	cm	in
h_c	Maximum height of liquid capillary rise	cm	in	Y	Liquid loading		
H	Individual bond strength	dyn	lbf		Calibration factor		
H	Hardness of agglomerate or compact	kg/cm ²	psf				

Greek Symbols

Symbol	Definition	SI units	U.S. customary units	Symbol	Definition	SI units	U.S. customary units
$\beta(u, v)$	Coalescence rate constant for collisions between granules of volumes u and v	1/s	1/s	$\Delta\rho$	Relative fluid density with respect to displaced gas or liquid	g/cm ³	
ε	Porosity of packed powder			ρ	Apparent agglomerate or granule density	g/cm ³	lb/ft ³
ε_b	Interagglomerate bed voidage			ρ_a	Apparent agglomerate or granule density	g/cm ³	lb/ft ³
ε_g	Intraagglomerate granule porosity			ρ_b	Bulk density	g/cm ³	lb/ft ³
κ	Compressibility of powder			ρ_g	Apparent agglomerate or granule density	g/cm ³	lb/ft ³
ϕ	Disc angle to horizontal	deg	deg	ρ_l	Liquid density	g/cm ³	lb/ft ³
ϕ	Internal angle of friction	deg	deg	ρ_s	True skeletal solids density	g/cm ³	lb/ft ³
ϕ_c	Effective angle of friction	deg	deg	σ_0	Applied axial stress	kg/cm ²	psf
ϕ_w	Wall angle of friction	deg	deg	σ_c	Resulting axial stress in powder	kg/cm ²	psf
ϕ_w	Roll friction angle	deg	deg	σ	Powder normal stress during shear	kg/cm ²	psf
$\phi(\eta)$	Relative size distribution			σ_c	Powder compaction normal stress	kg/cm ²	psf
γ^{lc}	Liquid-vapor interfacial energy	dyn/cm	dyn/cm	σ_f	Fracture stress under three-point bend loading	kg/cm ²	psf
γ^{sl}	Solid-liquid interfacial energy	dyn/cm	dyn/cm	σ_T	Granule tensile strength	kg/cm ²	psf
γ^{sv}	Solid-vapor interfacial energy	dyn/cm	dyn/cm	σ_y	Granule yield strength	kg/cm ²	psf
μ	Binder or fluid viscosity	poise		τ	Powder shear stress	kg/cm ²	psf
μ	Coefficient of internal friction			θ	Contact angle	deg	deg
ω	Impeller rotational speed	rad/s	rad/s	ζ	Parameter in Eq. (21-108)		
				η	Parameter in Eq. (21-108)		

Nomenclature and Units for Size Reduction and Size Enlargement

Symbol	Definition	SI units	U.S. customary units	Symbol	Definition	SI units	U.S. customary units
A	Coefficient in double Schumann equation			q_f	Fine-fraction mass flow rate	g/s	lb/s
a	Constant			q_o	Feed mass flow rate	g/s	lb/s
$a_{k,k}$	Coefficient in mill equations			q_p	Mass flow rate of classifier product	g/s	lb/s
$a_{k,n}$	Coefficient in mill equations			q_R	Mass flow rate of classifier tailings	g/s	lb/s
\mathbf{B}	Matrix of breakage function			q_R	Recycle mass flow rate to a mill	g/s	lb/s
$\Delta B_{k,n}$	Breakage function			R	Recycle		
b	Constant			R	Reid solution		
C	Constant			r	Dimensionless parameter in size-distribution equations		
C_s	Impact-crushing resistance	kWh/cm	ft-lb/in	S	Rate function	S^{-1}	S^{-1}
D	Diffusivity	m^2/s	ft^2/s	\bar{S}	Corrected rate function	S^{-1}	S^{-1}
D	Mill diameter	m	ft	\mathbf{S}'	Matrix of rate function	Mg/kWh	ton/(hp-h)
D_b	Ball or rod diameter	cm	in	$S_G(X)$	Grindability function	S^{-1}	S^{-1}
D_{mill}	Diameter of mill	m	ft	S_u	Grinding-rate function		
d	Differential			s	Parameter in size-distribution equations		
d	Distance between rolls of crusher	cm	in	s	Peripheral speed of rolls	cm/min	in/min
E	Work done in size reduction	kWh	hp-h	t	Time	s	s
E	Energy input to mill	kW	hp	u	Settling velocity of particles	cm/s	ft/s
E_i	Bond work index	kWh/Mg	hp-h/ton	\mathbf{W}	Vector of differential size distribution of a stream		
E_i	Work index of mill feed			w_k	Weight fraction retained on each screen		
E_2	Net power input to laboratory mill	kW	hp	w_u	Weight fraction of upper-size particles		
erf	Normal probability function			w_r	Material holdup in mill	g	lb
F	As subscript, referring to feed stream			X	Particle size or sieve size	cm	in
F	Bonding force	kg/kg	lb/lb	X'	Parameter in size-distribution equations	cm	in
g	Acceleration due to gravity	cm/s^2	ft/s^2	ΔX_i	Particle-size interval	cm	in
\mathbf{I}	Unit matrix in mill equations			X_i	Midpoint of particle-size interval ΔX_i	cm	in
i	Tensile strength of agglomerates	kg/cm ²	lb/in ²	X_0	Constant, for classifier design		
K	Constant			X_f	Feed-particle size	cm	in
k	Parameter in size-distribution equations	cm	in	X_m	Mean size of increment in size-distribution equations	cm	in
k	As subscript, referring to size of particles in mill and classifier parameters			X_p	Product-particle size	cm	in
L	As subscript, referring to discharge from a mill or classifier			X_p	Size of coarser feed to mill	cm	in
L	Length of rolls	cm	in	X_{25}	Particle size corresponding to 25 percent classifier-selectivity value	cm	in
L	Inside length of tumbling mill	m	ft	X_{50}	Particle size corresponding to 50 percent classifier-selectivity value	cm	in
\mathbf{M}	Mill matrix in mill equations			X_{75}	Particle size corresponding to 75 percent classifier-selectivity value	cm	in
m	Dimensionless parameter in size-distribution equations			ΔX_k	Difference between opening of successive screens	cm	in
N	Mean-coordination number			x	Weight fraction of liquid		
N_c	Critical speed of mill	r/min	r/min	Y	Cumulative fraction by weight undersize in size-distribution equations		
ΔN	Incremental number of particles in size-distribution equation			Y	Cumulative fraction by weight undersize or oversize in classifier equations		
n	Dimensionless parameter in size-distribution equations			ΔY	Fraction of particles between two sieve sizes		
n	Constant, general			ΔY	Incremental weight of particles in size-distribution equations	g	lb
n_r	Percent critical speed of mill			ΔY_{ci}	Cumulative size-distribution intervals of coarse fractions	cm	in
O	As subscript, referring to inlet stream			ΔY_{fi}	Cumulative size-distribution intervals of fine fractions	cm	in
P	As subscript, referring to product stream			\mathbf{Z}	Matrix of exponentials		
P_k	Fraction of particles coarser than a given sieve opening						
p	Number of short-time intervals in mill equations						
Q	Capacity of roll crusher	cm^3/min	ft^3/min				
q	Total mass throughput of a mill	g/s	lb/s				
q_c	Coarse-fraction mass flow rate	g/s	lb/s				
q_F	Mass flow rate of fresh material to mill	g/s	lb/s				

Greek Symbols

β	Sharpness index of a classifier			ρ_l	Density of liquid	g/cm^3	lb/in^3
δ	Angle of contact	rad	0	ρ_s	Density of solid	g/cm^3	lb/in^3
ε	Volume fraction of void space			Σ	Summation		
Z	Residence time in the mill	s	s	σ	Standard deviation		
η_c	Size-selectivity parameter			σ	Surface tension	N/cm	dyn/cm
μ	Viscosity of fluid	$N \cdot S/m^2$	P	υ	Volumetric abundance ratio of gangue to mineral		
ρ_f	Density of fluid	g/cm^3	lb/in^3				

PARTICLE-SIZE ANALYSIS

GENERAL REFERENCES: Allen, *Particle Size Measurement*, 4th ed., Chapman and Hall, 1990. Bart and Sun, Particle Size Analysis Review, *Anal. Chem.*, **57**, 151R (1985). Miller and Lines, *Critical Reviews in Analytical Chemistry*, **20**(2), 75–116 (1988). Herdan, *Small Particles Statistics*, Butterworths, London. Orr and DalleValle, *Fine Particle Measurement*, 2d ed., Macmillan, New York, 1960. Kaye, *Direct Characterization of Fine Particles*, Wiley, New York, 1981. Van de Hulst, *Light Scattering by Small Particles*, Wiley, New York, 1957. K. Leschonski, Representation and Evaluation of Particle Size Analysis Data, *Part. Part. Syst. Charact.*, **1**, 89–95 (1984). Terence Allen, *Particle Size Measurement*, 5th ed., Vol. 1, Springer, 1996. Karl Sommer, *Sampling of Powders and Bulk Materials*, Springer, 1986. M. Alderliesten, Mean Particle Diameters, Part I: Evaluation of Definition Systems, *Part. Part. Syst. Charact.*, **7**, 233–241 (1990); Part II: Standardization of Nomenclature, *Part. Part. Syst. Charact.*, **8**, 237–241 (1991); Part III: An Empirical Evaluation of Integration and Summation Methods for Estimating Mean Particle Diameters from Histogram Data, *Part. Part. Syst. Charact.*, **19**, 373–386 (2002); Part IV: Empirical Selection of the Proper Type of Mean Particle Diameter Describing a Product or Material Property, *Part. Part. Syst. Charact.*, **21**, 179–196 (2004); Part V: Theoretical Derivation of the Proper Type of Mean Particle Diameter Describing a Product or Process Property, *Part. Part. Syst. Charact.*, **22**, 233–245 (2005). ISO 9276, Representation of Results of Particle Size Analysis. H. C. van de Hulst, Light Scattering by Small Particles, Structure of Matter Series, Dover, 1981. Craig F. Bohren and Donald R. Huffman, Absorption and Scattering of Light by Small Particles, Wiley-Interscience, new edition. Bruce J. Berne and Robert Pecora, Dynamic Light Scattering: With Applications to Chemistry, Biology, and Physics, unabridged edition, Dover, 2000. J. R. Allegra and S. A. Hawley, Attenuation of Sound in Suspensions and Emulsions: Theory and Experiment, *J. Acoust. Soc. America* **51**, 1545–1564 (1972).

PARTICLE SIZE

Specification for Particulates The behavior of dispersed matter is generally described by a large number of parameters, e.g., the powder's bulk density, flowability, and degree of aggregation or agglomeration. Each parameter might be important for a specific application. In solids processes such as comminution, classification, agglomeration, mixing, crystallization, or polymerization, or in related material handling steps, particle size plays an important role. Often it is the dominant quality factor for the suitability of a specific product in the desired application.

Particle Size As particles are extended three-dimensional objects, only a perfect spherical particle allows for a simple definition of the particle size x , as the diameter of the sphere. In practice, spherical particles are very rare. So usually **equivalent diameters** are used, representing the diameter of a sphere that behaves as the real (nonspherical) particle in a specific sizing experiment. Unfortunately, the measured size now depends on the method used for sizing. So one can only expect identical results for the particle size if either the particles are spherical or similar sizing methods are employed that measure the same equivalent diameter.

In most applications more than one particle is observed. As each individual may have its own particle size, methods for data reduction have been introduced. These include the particle-size distribution, a variety of model distributions, and moments (or averages) of the distribution. One should also note that these methods can be extended to other particle attributes. Examples include pore size, porosity, surface area, color, and electrostatic charge distributions, to name but a few.

Particle-Size Distribution A particle-size distribution (PSD) can be displayed as a table or a diagram. In the simplest case, one can divide the range of measured particle sizes into size intervals and sort the particles into the corresponding size class, as displayed in Table 21-1 (shown for the case of volume fractions).

Typically the fractions $\Delta Q_{r,i}$ in the different size classes i are summed and normalized to 100 percent, resulting in the **cumulative distribution** $Q(x)$, also known as the percentage undersize. For a

TABLE 21-1 Tabular Presentation of Particle-Size Data

1	2	3	4	5	6	7
i	x_i μm	$\Delta Q_{3,i}$	Δx_i μm	$\bar{q}_{3,i} = \Delta Q_{3,i} / \Delta x_i$ $1/\mu\text{m}$	$Q_{3,i}$	$\bar{q}_{3,i}^*$
0	0.063				0.0000	
1	0.090	0.0010	0.027	0.0370	0.0010	0.0028
2	0.125	0.0009	0.035	0.0257	0.0019	0.0027
3	0.180	0.0016	0.055	0.0291	0.0035	0.0044
4	0.250	0.0025	0.070	0.0357	0.0060	0.0076
5	0.355	0.0050	0.105	0.0476	0.0110	0.0143
6	0.500	0.0110	0.145	0.0759	0.0220	0.0321
7	0.710	0.0180	0.210	0.0857	0.0400	0.0513
8	1.000	0.0370	0.290	0.1276	0.0770	0.1080
9	1.400	0.0610	0.400	0.1525	0.1380	0.1813
10	2.000	0.1020	0.600	0.1700	0.2400	0.2860
11	2.800	0.1600	0.800	0.2000	0.4000	0.4755
12	4.000	0.2100	1.200	0.1750	0.6100	0.5888
13	5.600	0.2400	1.600	0.1500	0.8500	0.7133
14	8.000	0.1250	2.400	0.0521	0.9750	0.3505
15	11.20	0.0240	3.200	0.0075	0.9990	0.0713
16	16.000	0.0010	4.800	0.0002	1.0000	0.0028

given particle size x , the Q value represents the percentage of the particles finer than x .

If the quantity measure is “number,” $Q_n(x)$ is called a **cumulative number distribution**. If it is length, area, volume, or mass, then the corresponding length [$Q_l(x)$], area [$Q_s(x)$], volume, or mass distributions are formed [$Q_v(x)$]; mass and volume are related by the specific density ρ . The index r in this notation represents the quantity measure (ISO 9276, *Representation of Results—Part 1 Graphical Representation*). The choice of the quantity measured is of decisive importance for the appearance of the PSD, which changes significantly when the dimension r is changed. As, e.g., one 100- μm particle has the same volume as 1000 10- μm particles or $10^6/1\text{-}\mu\text{m}$ particles, a number distribution is always dominated by and biased to the fine fractions of the sample while a volume distribution is dominated by and biased to the coarse.

The normalization of the fraction $\Delta Q_{r,i}$ to the size of the corresponding interval leads to the **distribution density** $\bar{q}_{r,i}$, or

$$\bar{q}_{r,i} = \frac{\Delta Q_{r,i}}{\Delta x_i} \quad \text{and} \quad \sum_{i=1}^n \Delta Q_{r,i} = \sum_{i=1}^n \bar{q}_{r,i} \Delta x_i = 1 = 100\% \quad (21-1)$$

If $Q_r(x)$ is differentiable, the distribution density function $q_r(x)$ can be calculated as the first derivative of $Q_r(x)$, or

$$q_r(x) = \frac{dQ_r(x)}{dx} \quad \text{or} \quad Q_r(x_i) = \int_{x_{\text{min}}}^{x_i} q_r(x) dx \quad (21-2)$$

It is helpful in the graphical representation to identify the distribution type, as shown for the cumulative volume distribution $Q_3(x)$ and volume distribution density $q_3(x)$ in Fig. 21-1. If $q_r(x)$ displays one maximum only, the distribution is called a **monomodal size distribution**. If the sample is composed of two or more different-size regimes, $q_r(x)$ shows two or more maxima and is called a **bimodal** or **multimodal size distribution**.

PSDs are often plotted on a logarithmic abscissa (Fig. 21-2). While the $Q_r(x)$ values remain the same, care has to be taken for the transformation of the distribution density $q_r(x)$, as the corresponding areas under the distribution density curve must remain constant (in particular

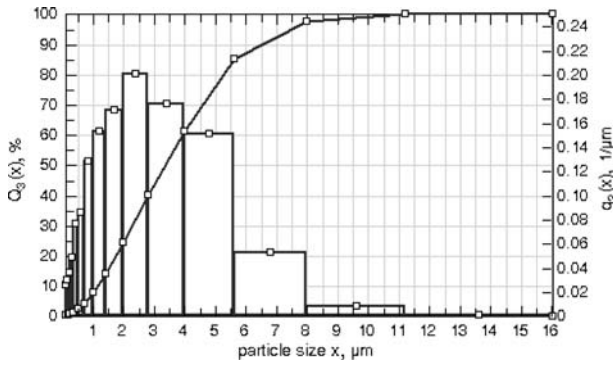


FIG. 21-1 Histogram $\bar{q}_3(x)$ and $Q_3(x)$ plotted with linear abscissa.

the total area remains 1, or 100 percent) independent of the transformation of the abscissa. So the transformation has to be performed by

$$\bar{q}_r^*(\ln x_{i-1}, \ln x_i) = \frac{\Delta Q_{r,i}}{\ln(x_i/x_{i-1})} \quad (21-3)$$

This equation also holds if the natural logarithm is replaced by the logarithm to base 10.

Example 1: From Table 21-1 one can calculate, e.g.,

$$\begin{aligned} \bar{q}_{3,11} &= \frac{\Delta Q_{3,11}}{\Delta x_{11}} = \frac{0.16}{0.8 \mu\text{m}} = 0.2 \mu\text{m}^{-1} \\ \bar{q}_{3,11}^* &= \bar{q}_3^*(\ln x_{10}, \ln x_{11}) = \frac{\Delta Q_{3,11}}{\ln(x_{11}/x_{10})} = \frac{0.16}{\ln(2.8 \mu\text{m}/2.0 \mu\text{m})} \\ &= \frac{0.16}{\ln 1.4} = 0.4755 \end{aligned}$$

Model Distribution While a PSD with n intervals is represented by $2n + 1$ numbers, further data reduction can be performed by fitting the size distribution to a specific mathematical model. The logarithmic normal distribution or the logarithmic normal probability function is one common model distribution used for the distribution density, and it is given by

$$q_r^*(z) = \frac{1}{\sqrt{2\pi}} e^{-0.5z^2} \quad \text{with} \quad z = \frac{1}{s} \ln \left[\frac{x}{x_{50,r}} \right] \quad (21-4)$$

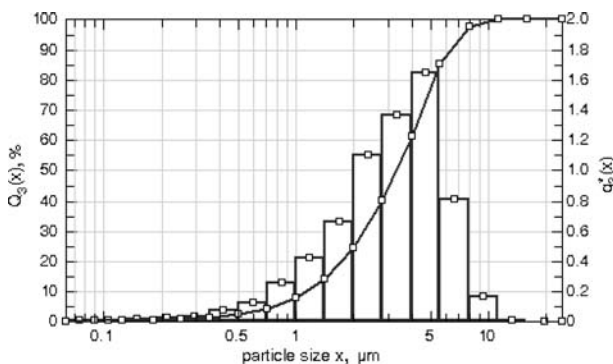


FIG. 21-2 Histogram $\bar{q}_3(x)$ and $Q_3(x)$ plotted with a logarithmic abscissa.

The PSD can then be expressed by two parameters, namely, the mean size $x_{50,r}$ and, e.g., by the dimensionless standard deviation s (ISO 9276, Part 5: *Methods of Calculations Relating to Particle Size Analysis Using Logarithmic Normal Probability Distribution*). The data reduction can be performed by plotting $Q_r(x)$ on logarithmic probability graph paper or using the fitting methods described in upcoming ISO 9276-3, *Adjustment of an Experimental Curve to a Reference Model*. This method is mainly used for the analysis of powders obtained by grinding and crushing and has the advantage that the transformation between PSDs of different dimensions is simple. The transformation is also log-normal with the same slope s .

Other model distributions used are the **normal distribution** (Laplace-Gauss), for powders obtained by precipitation, condensation, or natural products (e.g., pollens); the **Gates-Gaudin-Schulmann distribution** (bilogarithmic), for analysis of the extreme values of fine particle distributions (Schulmann, *Am. Inst. Min. Metall. Pet. Eng.*, Tech. Paper 1189 Min. Tech., 1940); or the **Rosin-Rammler-Sperling-Bennet distribution** for the analysis of the extreme values of coarse particle distributions, e.g., in monitoring grinding operations [Rosin and Rammler, *J. Inst. Fuel.* **7**, 29–36 (1933); Bennett, *ibid.*, **10**, 22–29 (1936)].

Moments Moments represent a PSD by a single value. With the help of moments, the average particle sizes, volume specific surfaces, and other mean values of the PSD can be calculated. The general definition of a moment is given by (ISO 9276, Part 2: *Calculation of Average Particle Sizes/Diameters and Moments from Particle Size Distributions*)

$$M_{k,r} = \int_{x_{\min}}^{x_{\max}} x^k q_r(x) dx \quad (21-5)$$

where $M_{k,r}$ is the k th moment of a $q_r(x)$ distribution density and k is the power of x .

Average Particle Sizes A PSD has many average particle sizes. The general equation is given by

$$\bar{x}_{k,r} = \sqrt[k]{M_{k,r}} \quad (21-6)$$

Two typically employed average particle sizes are the **arithmetic average particle size** $\bar{x}_{k,0} = M_{k,0}$ [e.g., for a number distribution ($r = 0$) obtained by counting methods], and the **weighted average particle size** $\bar{x}_{1,r} = \bar{M}_{1,r}$ [e.g., for a volume distribution ($r = 3$) obtained by sieve analysis], where $\bar{x}_{1,r}$ represents the center of gravity on the abscissa of the $q_r(x)$ distribution.

Specific Surface The **specific surface area** can be calculated from size distribution data. For spherical particles this can simply be calculated by using moments. The volume specific surface is given by

$$S_V = \frac{6}{\bar{x}_{1,2}} \quad \text{or} \quad S_V = \frac{6}{M_{1,2}} = \frac{M_{2,0}}{M_{3,0}} = 6 \cdot M_{-1,3} \quad (21-7)$$

where $\bar{x}_{1,2}$ is the weighted average diameter of the area distribution, also known as **Sauter mean diameter**. It represents a particle having the same ratio of surface area to volume as the distribution, and it is also referred to as a **surface-volume average diameter**. The Sauter mean is an important average diameter used in solids handling and other processing applications where aspects of two-phase flow become important, as it appropriately weights the contributions of the fine fractions to surface area. For nonspherical particles, a shape factor has to be considered.

Example 2: The Sauter mean diameter and the volume weighted particle size and distribution given in Table 21-1 can be calculated by using FDIS-ISO 9276-2, *Representation of Results of Particle Size Analysis—Part 2: Calculation of Average Particle Sizes/Diameters and Moments from Particle Size Distributions* via Table 21-2.

The Sauter mean diameter is

$$\bar{x}_{1,2} = M_{1,2} = \frac{M_{3,0}}{M_{2,0}} = \frac{1}{M_{-1,3}} \quad \text{with} \quad M_{-1,3} = \sum_{i=1}^n \Delta Q_{3,i} \frac{\ln(x_i/x_{i-1})}{x_i - x_{i-1}}$$

TABLE 21-2 Table for Calculation of Sauter Mean Diameter and Volume Weighted Particle Size

<i>I</i>	$x_i, \mu\text{m}$	$\Delta Q_{3,i}$	$\ln(x_i/x_{i-1})$	$\ln(x_i/x_{i-1}) / (x_i - x_{i-1})$	$\Delta Q_{3,i}^s$	$\Delta Q_{3,i}^s / (x_i + x_{i-1}), \mu\text{m}$
0	0.0630					
1	0.0900	0.0010	0.3567	13.2102	0.013210	0.000153
2	0.1250	0.0009	0.3285	9.3858	0.008447	0.000194
3	0.1800	0.0016	0.3646	6.6299	0.010608	0.000488
4	0.2500	0.0025	0.3285	4.6929	0.011732	0.001075
5	0.3550	0.0050	0.3507	3.3396	0.016698	0.003025
6	0.5000	0.0110	0.3425	2.3620	0.025982	0.009405
7	0.7100	0.0180	0.3507	1.6698	0.030056	0.021780
8	1.0000	0.0370	0.3425	1.1810	0.043697	0.063270
9	1.4000	0.0610	0.3365	0.8412	0.051312	0.146400
10	2.0000	0.1020	0.3567	0.5945	0.060635	0.346800
11	2.8000	0.1600	0.3365	0.4206	0.067294	0.768000
12	4.0000	0.2100	0.3567	0.2972	0.062418	1.428000
13	5.6000	0.2400	0.3365	0.2103	0.050471	2.304000
14	8.0000	0.1250	0.3567	0.1486	0.018577	1.700000
15	11.2000	0.0240	0.3365	0.1051	0.002524	0.460800
16	16.0000	0.0010	0.3567	0.0743	0.000074	0.027200
					$\Sigma 0.473736$	7.280590

which yields

$$\bar{x}_{1,2} = \frac{1}{0.473736} = 2.110882$$

The volume weighted average particle size is

$$\bar{x}_{1,3} = M_{1,3} = \frac{1}{2} \sum_{i=1}^n \Delta Q_{3,i} (x_i + x_{i-1})$$

which yields

$$\bar{x}_{1,3} = \frac{1}{2} \cdot 7.280590 = 3.640295$$

PARTICLE SHAPE

For many applications not only the particle size but also the shape are of importance; e.g., toner powders should be spherical while polishing powders should have sharp edges. Traditionally in microscopic methods of size analysis, direct measurements are made on enlarged images of the particles by using a calibrated scale. While such measurements are always encouraged to gather a direct sense of the particle shape and size, care should be taken in terms of drawing general conclusions from limited particle images. Furthermore, with the strong progress in computing power, instruments have become available that acquire the projected area of many particles in short times, with a significant reduction in data manipulation times. Although a standardization of shape parameters is still in preparation (upcoming ISO 9276, *Part 6: Descriptive and Qualitative Representation of Particle Shape and Morphology*), there is wide agreement on the following parameters.

Equivalent Projection Area of a Circle Equivalent projection area of a circle (Fig. 21-3) is widely used for the evaluation of particle sizes from the projection area *A* of a nonspherical particle.

$$x_{EQPC} = 2\sqrt{A/\pi} \tag{21-8}$$

Feret's Diameter Feret's diameter is determined from the projected area of the particles by using a slide gauge. In general it is defined as the distance between two parallel tangents of the particle at an arbitrary angle. In practice, the **minimum** $x_{F,min}$ and **maximum** **Feret** diameters $x_{F,max}$, the **mean Feret diameter** \bar{x}_F , and the Feret diameters obtained at 90° to the direction of the minimum and maximum Feret diameters $x_{F,max,90}$ are used. The minimum Feret diameter is often used as the diameter equivalent to a sieve analysis.

Other diameters used in the literature include **Martin's diameter** or the edges of an **enclosing rectangle**. Martin's diameter is a line, parallel to a fixed direction, which divides the particle profile into two equal areas.

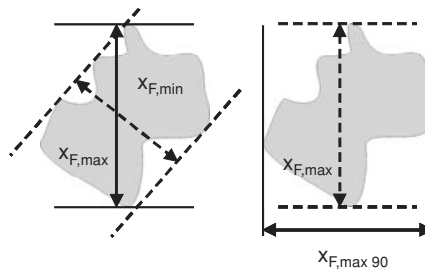


FIG. 21-3 Definition of Feret diameters.

These diameters offer an extension over volume equivalent diameters to account for shape deviations from spherical. As with any other quality measure of size, many particles must be measured to determine distributions of these particle-size diameters.

Sphericity, Aspect Ratio, and Convexity Parameters describing the shape of the particles include the following:

The **sphericity** ψ_s ($0 < \psi_s \leq 1$) is defined by the ratio of the perimeter of a circle with diameter x_{EQPC} to the perimeter of the corresponding projection area *A*. And $\psi_s = 1$ represents a sphere.

The **aspect ratio** ψ_A ($0 < \psi_A \leq 1$) is defined by the ratio of the minimum to the maximum Feret diameter $\psi_A = x_{Feret,min}/x_{Feret,max}$. It gives an indication of the **elongation** of the particle. Some literature also used $1/\psi_A$ as the definition of sphericity.

The **convexity** ψ_C ($0 < \psi_C \leq 1$) is defined by the ratio of the projection area *A* to the convex hull area *A* + *B* of the particle, as displayed in Fig. 21-4.

In **Fourier techniques** the shape characteristic is transformed to a signature waveform, Beddow and coworkers (Beddow, *Particulate Science and Technology*, Chemical Publishing, New York, 1980) take the particle centroid as a reference point. A vector is then rotated about this centroid with the tip of the vector touching the periphery. A plot of the magnitude of the vector versus its angular position is a wave-type function. This waveform is then subjected to Fourier analysis. The lower-frequency harmonics constituting the complex wave correspond to the gross external morphology, whereas the higher frequencies correspond to the texture of the fine particle.

Fractal Logic This was introduced into fine particles science by Kaye and coworkers (Kaye, op. cit., 1981), who show that the noneuclidean logic of Mandelbrot can be applied to describe the ruggedness of a particle profile. A combination of fractal dimension and geometric shape factors such as the aspect ratio can be used to describe a population of fine particles of various shapes, and these can be related to the functional properties of the particle.

SAMPLING AND SAMPLE SPLITTING

As most of the sizing methods are limited to small sample sizes, an important prerequisite to accurate particle-size analysis is proper powder sampling and sample splitting (upcoming ISO 14488, *Particulate Materials—Sampling and Sample Splitting for the Determination of Particulate Properties*).

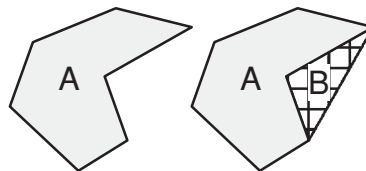


FIG. 21-4 Definition of the convex hull area *A* + *B* for the projection area *A* of a particle.

When determining particle size (or any other particle attribute such as chemical composition or surface area), it is important to recognize that the error associated in making such a measurement can be described by its variance, or

$$\sigma_{\text{observed}}^2 = \sigma_{\text{actual}}^2 + \sigma_{\text{measurement}}^2 \quad (21-9)$$

$$\sigma_{\text{measurement}}^2 = \sigma_{\text{sampling}}^2 + \sigma_{\text{analysis}}^2 \quad (21-10)$$

That is, the *observed* variance in the particle-size measurement is due to both the actual physical variance in size as well as the variance in the measurement. More importantly, the variance in measurement has two contributing factors: variance due to sampling, which would include systematic errors in the taking, splitting, and preparation of the sample; and variance due to the actual sample analysis, which would include not only the physical measurement at hand, but also how the sample is *presented* to the measuring zone, which can be greatly affected by instrument design and sample dispersion (discussed below). Successful characterization of the sample (in this discussion, taken to be measurement of particle size) requires that the errors in measurement be much less than actual physical variations in the sample itself, especially if knowledge of sample deviations is important. In this regard, great negligence is unfortunately often exhibited in sampling efforts. Furthermore, measured deviations in particle size or other properties are often incorrectly attributed to and reflect upon the measuring device, where in fact they are caused by inattention to proper sampling and sample splitting. Worse still, such deviations caused by poor sampling may be taken as true sample deviations, causing undue and frequent process corrections.

Powders may be classified as nonsegregating (cohesive) or segregating (free-flowing). Representative samples can be more easily taken from **cohesive powders**, provided that they have been properly mixed. For wet samples a sticky paste should be created and mixed from which the partial sample is taken.

In the case of **free-flowing powders**, four key rules should be followed, although some apply or can be equally employed for cohesive materials as well. These rules are especially important for in-line and on-line sampling, discussed below. As extended from Allen, *Powder Sampling and Particle Size Determination* (Elsevier, 2003):

1. The particles should be analyzed while in motion. Transfer points are often convenient and relevant for this. Sampling a stagnant bed of segregating material by, e.g., thieves disrupts the state of the mixture and may be biased to coarse or fines.

2. The whole stream of powder should be taken in many short time intervals in preference to part of the stream being taken over the whole time, i.e., a complete slice of the particle stream. Furthermore, any mechanical collection point should not be allowed to overflow, since this will make the sample bias toward fines, and coarse material rolls off formed heaps.

3. The entire sample should be analyzed, splitting down to a smaller sample if necessary. In many cases, segregation of the sample will not affect the measurement, provided the entire sample is analyzed. There are, however, exceptions in that certain techniques may only analyze one surface of the final sample. In the case of chemical analysis, an example would be near infrared spectroscopy operated in reflectance mode as opposed to transmission. Such a technique may still be prone to segregation during the final analysis. (See the subsection "Material Handling: Impact of Segregation on Measurements.")

4. A minimum sample size exists for a given size distribution, generally determined by the sample containing a minimum number of coarse particles representative of the customer application. While many applications involving fine pharmaceuticals may only require milligrams to establish a representative sample, other cases such as detergents and coffee might require kilograms. Details are given in the upcoming standard ISO/DIS14488, *Particulate Materials—Sampling and Sample Splitting for the Determination of Particulate Properties*.

In this regard, one should keep in mind that the sample size may also reflect variation in the degree of mixing in the bed, as opposed to true size differences. (See also the subsection "Solids Mixing: Measuring the Degree of Mixing.") In fact, larger samples in this case help minimize the impact of segregation on measurements.

TABLE 21-3 Reliability of Selected Sampling Method

Method	Estimated maximum sampling error, %
Cone and quartering	22.7
Scoop sampling	17.1
Table sampling	7.0
Chute splitting	3.4
Spinning riffling	0.42

The estimated maximum sampling error on a 60:40 blend of free-flowing sand using different sampling techniques is given in Table 21-3.

The **spinning riffler** (Fig. 21-5) generates the most representative samples. In this device a ring of containers rotates under the powder feed. If the powder flows a long time with respect to the period of rotation, each container will be made up of many small fractions from all parts of the bulk. Many different configurations are commercially available. Devices with small numbers of containers (say, 8) can be cascaded *n* times to get higher splitting ratios 1:8ⁿ. This usually creates smaller sampling errors than does using splitters with more containers. A splitter simply divides the sample into two halves, generally pouring the sample into a set of intermeshed chutes. Figure 21-6 illustrates commercial rifflers and splitters.

For reference materials sampling errors of less than 0.1 percent are achievable (S. Röhle and W. Witt, Standards in Laser Diffraction, PARTEC, 5th European Symposium Particle Characterization, Nürnberg, 1992, pp. 625–642).

DISPERSION

Many sizing methods are sensitive to the agglomeration state of the sample. In some cases, this includes primary particles, possibly with some percentage of such particles held together as weak agglomerates by interparticle cohesive forces. In other cases, strong aggregates of

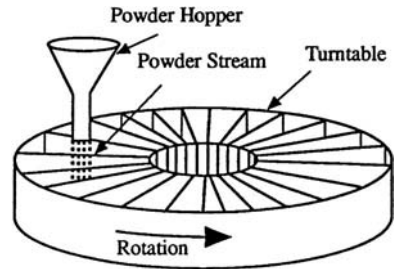


FIG. 21-5 Spinning riffler sampling device.



FIG. 21-6 Examples of commercial splitting devices. Spinning riffler and standard splitters. (Courtesy of Retsch Corporation.)

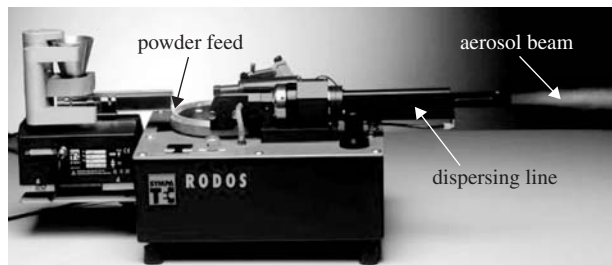


FIG. 21-7 Dry disperser RODOS with vibratory feeder VIBRI creating a fully dispersed aerosol beam from dry powder. (Courtesy of Sympatec GmbH.)

the primary particles may also exist. Generally, the size of either the primary particles or the aggregates is the matter of greatest interest. In some cases, however, it may also be desirable to determine the level of agglomerates in a sample, requiring that the intensity of dispersion be controlled and variable. Often the agglomerates have to be dispersed smoothly without comminution of aggregates or primary particles. This can be done either in gas (dry) or in liquid (wet) by using a suitable dispersion device which is stand-alone or integrated in the particle-sizing instrument. If possible, dry particles should be measured in gas and wet particles in suspension.

Wet Dispersion Wet dispersion separates agglomerates down to the primary particles by a suitable liquid. Dispersing agents and optional cavitation forces induced by ultrasound are often used. Care must be taken that the particles not be soluble in the liquid, or that they not flocculate. Microscopy and zeta potential measurements may be of utility in specifying the proper dispersing agents and conditions for dispersion.

Dry Dispersion Dry dispersion uses mechanical forces for the dispersion. While a simple fall-shaft with impact plates may be sufficient for the dispersion of coarse particles, say, $>300\ \mu\text{m}$, much higher forces have to be applied to fine particles.

In Fig. 21-7 the agglomerates are sucked in by the vacuum generated through expansion of compressed gas applied at an injector. They arrive at low speed in the dispersing line, where they are strongly accelerated. This creates three effects for the dispersion, as displayed in Fig. 21-8.

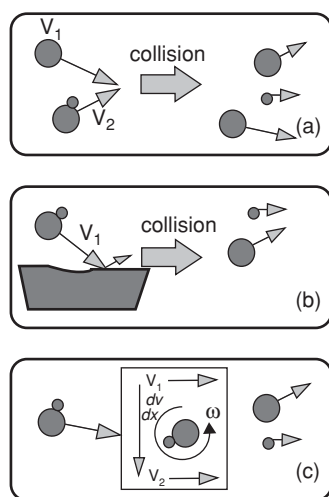


FIG. 21-8 Interactions combined for dry dispersion of agglomerates. (a) Particle-to-particle collisions. (b) Particle-to-wall collisions. (c) Centrifugal forces due to strong velocity gradients.

With suitable parameter settings agglomerates can be smoothly dispersed down to $0.1\ \mu\text{m}$ [K. Leschonski, S. Röhle, and U. Menzel, *Entwicklung und Einsatz einer trockenen Dosier-Dispergiereinheit zur Messung von Partikelgrößenverteilungen in Gas-Feststoff-Freistrahl aus Laser-Beugungsspektren; Part. Charact.*, **1**, 161–166 (1984)] without comminution of the primary particles.

PARTICLE-SIZE MEASUREMENT

There are many techniques available to measure the particle-size distribution of powders or droplets. The wide size range, from nanometers to millimeters, of particulate products, however, cannot be analyzed by using only a single measurement principle.

Added to this are the usual constraints of capital costs versus running costs, speed of operation, degree of skill required, and, most important, the end-use requirement.

If the particle-size distribution of a powder composed of hard, smooth spheres is measured by any of the techniques, the measured values should be identical. However, many different size distributions can be defined for any powder made up of nonspherical particles. For example, if a rod-shaped particle is placed on a sieve, then its diameter, not its length, determines the size of aperture through which it will pass. If, however, the particle is allowed to settle in a viscous fluid, then the calculated diameter of a sphere of the same substance that would have the same falling speed in the same fluid (i.e., the Stokes diameter) is taken as the appropriate size parameter of the particle. Since the Stokes diameter for the rod-shaped particle will obviously differ from the rod diameter, this difference represents added information concerning particle shape. The ratio of the diameters measured by two different techniques is called the **shape factor**.

While historically mainly methods using mechanical, aerodynamic, or hydrodynamic properties for discrimination and particle sizing have been used, today methods based on the interaction of the particles with electromagnetic waves (mainly light), ultrasound, or electric fields dominate.

Laser Diffraction Methods Over the past 30 years **laser diffraction** has developed into a leading principle for particle-size analysis of all kinds of aerosols, suspensions, emulsions, and sprays in laboratory and process environments.

The scattering of unpolarized laser light by a single spherical particle can be mathematically described by

$$I(\theta) = \frac{I_0}{2k^2a^2} \{ [S_1(\theta)]^2 + [S_2(\theta)]^2 \} \quad (21-11)$$

where $I(\theta)$ is the total scattered intensity as function of angle θ with respect to the forward direction; I_0 is the illuminating intensity; k is the wave number $2\pi/\lambda$; a is the distance from the scatterer to the detector; and $S_1(\theta)$ and $S_2(\theta)$ are dimensionless, complex functions describing the change and amplitude in the perpendicular and parallel polarized light. Different algorithms have been developed to calculate $I(\theta)$. The **Lorenz-Mie theory** is based on the assumption of spherical, isotropic, and homogenous particles and that all particles can be described by a common complex refractive index $m = n - i\kappa$. Index m has to be precisely known for the evaluation, which is difficult in practice, especially for the imaginary part κ , and inapplicable for mixtures with components having different refractive indices.

The **Fraunhofer theory** considers only scattering at the contour of the particle and the near forward direction. No preknowledge of the refractive index is required, and $I(\theta)$ simplifies to

$$I(\theta) = \frac{I_0}{2k^2a^2} \alpha^4 \left[\frac{J_1(\alpha \sin \theta)}{\alpha \sin \theta} \right]^2 \quad (21-12)$$

with J_1 as the Bessel function of first kind and the dimensionless size parameter $\alpha = \pi r/\lambda$. This theory does not predict polarization or account for light transmission through the particle.

For a single spherical particle, the diffraction pattern shows a typical ring structure. The distance r_0 of the first minimum to the center depends on the particle size, as shown in Fig. 21-9a. In the

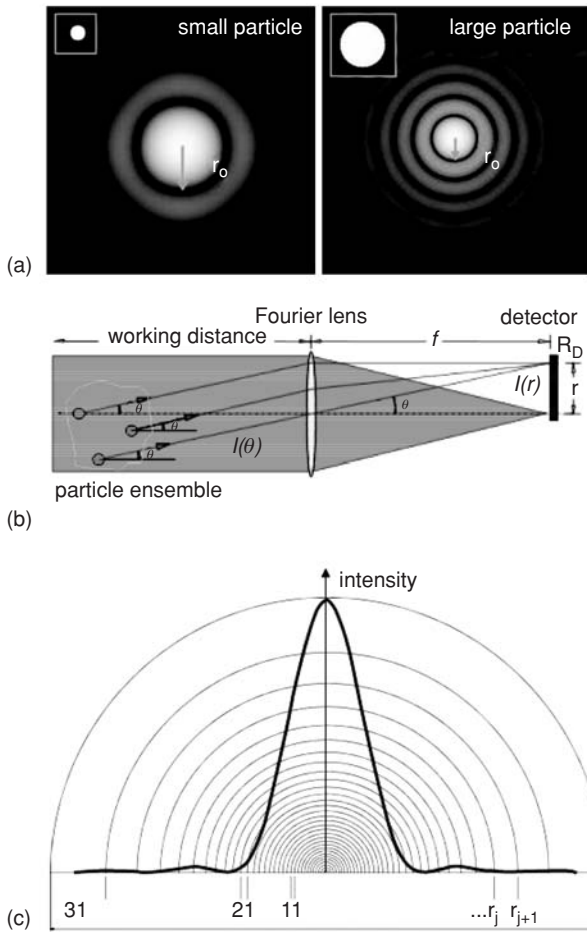


FIG. 21-9 (a) Diffraction patterns of laser light in forward direction for two different particle sizes. (b) The angular distribution $I(\theta)$ is converted by a Fourier lens to a spatial distribution $I(r)$ at the location of the photodetector. (c) Intensity distribution of a small particle detected by a semicircular photodetector.

particle-sizing instrument, the acquisition of the intensity distribution of the diffracted light is usually performed with the help of a multielement photodetector.

Diffraction patterns of static nonspherical particles are displayed in Fig. 21-10. As all diffraction patterns are symmetric to 180° , semicircular detector elements integrate over 180° and make the detected intensity independent of the orientation of the particle.

Simultaneous diffraction on more than one particle results in a superposition of the diffraction patterns of the individual particles, provided that particles are moving and diffraction between the particles is averaged out. This simplifies the evaluation, providing a parameter-free and model-independent mathematical algorithm for the inversion process (M. Heuer and K. Leschonski, Results Obtained with a New Instrument for the Measurement of Particle Size Distributions from Diffraction Patterns, *Part. Syst. Charact.* **2**, 7–13, 1985).

Today the method is standardized (ISO 13320-1, 1999, *Particle Size Analysis—Laser Diffraction Methods—Part 1: General Principles*), and many companies offer instruments, usually with the choice of Fraunhofer and/or Mie theory for the evaluation of the PSD. The size ranges of the instruments have been expanded by combining low-angle laser light scattering with 90° or back scattering, the use of different wavelengths, polarization ratio, and white light scattering, etc.

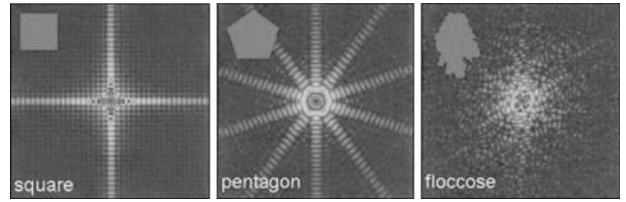


FIG. 21-10 Calculated diffraction patterns of laser light in forward direction for nonspherical particles: square, pentagon, and floccose. All diffraction patterns show a symmetry to 180° .

It is now ranging from below $0.1 \mu\text{m}$ to about 1 cm . Laser diffraction is currently the fastest method for particle sizing at highest reproducibility. In combination with dry dispersion it can handle large amounts of sample, which makes this method well suited for process applications.

Instruments of this type are available, e.g., from Malvern Ltd. (Mastersizer), Sympatec GmbH (HELOS, MYTOS), Horiba (LA, LS series), Beckmann Coulter (LS 13320), or Micromeritics (Saturn).

Image Analysis Methods The extreme progress in image capturing and exceptional increase of the computational power within the last few years have revolutionized microscopic methods and made image analysis methods very popular for the characterization of particles, especially since, in addition to size, relevant shape information becomes available by the method. Currently, mainly instruments creating a 2D image of the 3D particles are used. Two methods have to be distinguished.

Static image analysis is characterized by nonmoving particles, e.g., on a microscope slide (Fig. 21-11). The depth of sharpness is well defined, resulting in a high resolution for small particles. The method is well established and standardized (ISO 13322-1:2004, *Particle Size Analysis—Image Analysis Methods, Part 1: Static Image Analysis Methods*), but can handle only small amounts of data. The particles are oriented by the base; overlapping particles have to be separated by time-consuming software algorithms, and the tiny sample size creates a massive sampling problem, resulting in very low statistical relevance of the data. Commercial systems reduce these effects by using large or even stepping microscopic slides and the deposition of the particles via a dispersing chamber. As all microscopic techniques can be used, the size range is only defined by the microscope used.

Dynamic image analysis images a flow of moving particles. This allows for a larger sample size. The particles show arbitrary orientation, and the number of overlapping particles is reduced. Several companies offer systems which operate in either reflection or transmission, with wet dispersion or free fall, with matrix or line-scan cameras. The free-fall systems are limited to well flowing bulk materials. Systems with wet dispersion only allow for smallest samples sizes and slow particles. As visible light is used for imaging, the size range is

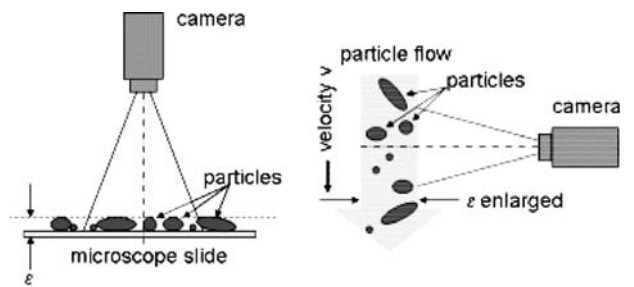


FIG. 21-11 Setup of static (left) and dynamic (right) image analysis for particle characterization.

limited to about 1 μm at the fine end. This type of instruments has been standardized (ISO/FDIS 13322-2:2006, *Particle Size Analysis—Image Analysis Methods, Part 2: Dynamic Methods*).

Common to all available instruments are small particle numbers, which result in poor statistics. Thus recent developments have yielded a combination of powerful dry and wet dispersion with high-speed image capturing. Particle numbers up to 10^7 can now be acquired in a few minutes. Size and shape analysis is available at low statistical errors [W. Witt, U. Köhler, and J. List, *Direct Imaging of Very Fast Particles Opens the Application of the Powerful (Dry) Dispersion for Size and Shape Characterization*, PARTEC 2004, Nürnberg].

Dynamic Light Scattering Methods Dynamic light scattering (DLS) is now used on a routine basis for the analysis of particle sizes in the submicrometer range. It provides an estimation of the average size and its distribution within a measuring time of a few minutes.

Submicrometer particles suspended in a liquid are in constant **brownian motion** as a result of the impacts from the molecules of the suspending fluid, as suggested by W. Ramsay in 1876 and confirmed by A. Einstein and M. Smoluchowski in 1905/06.

In the Stokes-Einstein theory of brownian motion, the particle motion at very low concentrations depends on the viscosity of the suspending liquid, the temperature, and the size of the particle. If viscosity and temperature are known, the particle size can be evaluated from a measurement of the particle motion. At low concentrations, this is the **hydrodynamic diameter**.

DLS probes this motion optically. The particles are illuminated by a coherent light source, typically a laser, creating a diffraction pattern, showing in Fig. 21-12 as a fine structure from the diffraction between the particles, i.e., its near-order. As the particles are moving from impacts of the thermal movement of the molecules of the medium, the particle positions change with the time, t .

The change of the position of the particles affects the phases and thus the fine structure of the diffraction pattern. So the intensity in a certain point of the diffraction pattern fluctuates with time. The fluctuations can be analyzed in the time domain by a correlation function analysis or in the frequency domain by frequency analysis. Both methods are linked by Fourier transformation.

The measured decay rates Γ are related to the translational diffusion coefficients D of spherical particles by

$$\Gamma = Dq^2 \quad \text{with} \quad q = \frac{4\pi}{\lambda_0} \sin \frac{\theta}{2} \quad \text{and} \quad D = \frac{k_B T}{2\pi\eta x} \quad (21-13)$$

where q is the modulus of the scattering vector, k_B is the Boltzmann constant, T is the absolute temperature, and η is the hydrodynamic viscosity of the dispersing liquid. The particle size x is then calculated by the Stokes-Einstein equation from D at fixed temperature T and η known.

DLS covers a broad range of diluted and concentrated suspension. As the theory is only valid for light being scattered once, any contribution of multiple scattered light leads to erroneous PCS results and misinterpretations. So different measures have been taken to minimize the influence of multiple scattering.

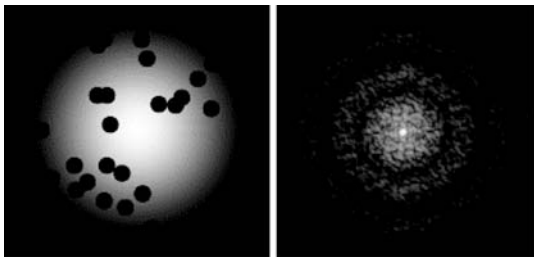


FIG. 21-12 Particles illuminated by a gaussian-shaped laser beam and its corresponding diffraction pattern show a fine structure.

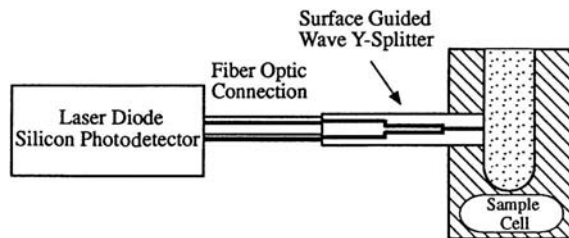


FIG. 21-13 Diagram of Leeds and Northrup Ultrafine Particle Size Analyzer (UPA), using fiber optics in a backscatter setup.

The well-established **photon correlation spectroscopy** (PCS) uses highly diluted suspensions to avoid multiple scattering. The low concentration of particles makes this method sensitive to impurities in the liquid. So usually very pure liquids and a clean-room environment have to be used for the preparation and operation (ISO 13321:1996, *Particle Size Analysis—Photon Correlation Spectroscopy*).

Another technique (Fig. 21-13) utilizes an optical system which minimizes the optical path into and out of the sample, including the use of backscatter optics, a moving cell assembly, or setups with the maximum incident beam intensity located at the interface of the suspension to the optical window (Trainer, Freud, and Weiss, *Pittsburg Conference, Analytical and Applied Spectroscopy, Symp. Particle Size Analysis*, March 1990; upcoming ISO 22412, *Particle Size Analysis—Dynamic Light Scattering*).

Photon cross-correlation spectroscopy (PCCS) uses a novel three-dimensional cross-correlation technique which completely suppresses the multiple scattered fractions in a special scattering geometry. In this setup two lasers A and B are focused to the same sample volume, creating two sets of scattering patterns, as shown in Fig. 21-14. Two intensities are measured at different positions but with identical scattering vectors.

$$\vec{q} = \vec{k}_A - \vec{k}_1 = \vec{k}_B - \vec{k}_2 \quad (21-14)$$

Subsequent cross-correlation of these two signals eliminates any contribution of multiple scattering. So highly concentrated, opaque suspensions can be measured as long as scattered light is observed. High count rates result in short measuring times. High particle concentrations reduce the sensitivity of this method to impurities, so standard liquids and laboratory environments can be used, which simplifies the application [W. Witt, L. Aberle, and H. Geers, *Measurement of Particle Size and Stability of Nanoparticles in Opaque Suspensions and Emulsions with Photon Cross Correlation Spectroscopy*, *Particulate Systems Analysis*, Harrogate (UK), 2003].

Acoustic Methods **Ultrasonic attenuation spectroscopy** is a method well suited to measuring the PSD of colloids, dispersions, slurries, and emulsions (Fig. 21-15). The basic concept is to measure the frequency-dependent attenuation or velocity of the ultrasound as it passes through the sample. The attenuation includes

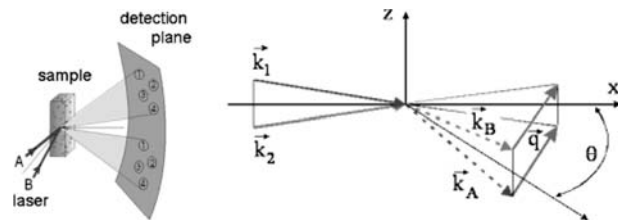


FIG. 21-14 Scattering geometry of a PCCS setup. The sample volume is illuminated by two incident beams. Identical scattering vectors \vec{q} and the scattering volumes are used in combination with cross-correlation to eliminate multiple scattering.

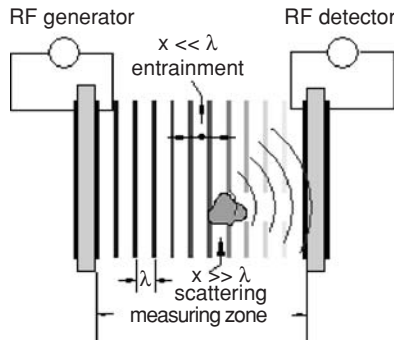


FIG. 21-15 Setup of an ultrasonic attenuation system for particle-size analysis.

contributions from the scattering or absorption of the particles in the measuring zone and depends on the size distribution and the concentration of the dispersed material. (ISO 20998:2006, *Particle Characterization by Acoustic Methods, Part 1: Ultrasonic Attenuation Spectroscopy*).

In a typical setup (see Fig. 21-15) an electric high-frequency generator is connected to a piezoelectric ultrasonic transducer. The generated ultrasonic waves are coupled into the suspension and interact with the suspended particles. After passing the measuring zone, the ultrasonic plane waves are received by an ultrasonic detector and converted to an electric signal, which is amplified and measured. The attenuation of the ultrasonic waves is calculated from the ratio of the signal amplitudes on the generator and detector sides.

PSD and concentration can be calculated from the attenuation spectrum by using either complicated theoretical calculations requiring a large number of parameters or an empirical approach employing a reference method for calibration. Following U. Riebel (Die Grundlagen der Partikelgrößenanalyse mittels Ultraschallspektrometrie, PhD-Thesis, University of Karlsruhe), the ultrasonic extinction of a suspension of monodisperse particles with diameter x can be described by Lambert-Beer's law. The extinction $-\ln(I/I_0)$ at a given frequency f is linearly dependent on the thickness of the suspension layer Δl , the projection area concentration C_{PF} , and the related extinction cross section K . In a polydisperse system the extinctions of single particles overlay:

$$-\ln\left(\frac{I}{I_0}\right) \cong \Delta l \cdot C_{PF} \cdot \sum_j K(f_i, x_j) \cdot q_2(x_j) \Delta x \quad (21-15)$$

When the extinction is measured at different frequencies f_i , this equation becomes a linear equation system, which can be solved for C_{PF} and $q_2(x)$. The key for the calculation of the particle-size distribution is the knowledge of the related extinction cross section K as a function of the dimensionless size parameter $\sigma = 2\pi x/\lambda$. For spherical particles K can be evaluated directly from the acoustic scattering theory. A more general approach is an empirical method using measurements on reference instruments as input.

This disadvantage is compensated by the ability to measure a wide size range from below 10 μm to above 3 mm and the fact that PSDs can be measured at very high concentrations (0.5 to >50 percent of volume) without dilution. This eliminates the risk of affecting the dispersion state and makes this method ideal for in-line monitoring of, e.g., crystallizers (A. Pankewitz and H. Geers, LABO, "In-line Crystal Size Distribution Analysis in Industrial Crystallization Processes by Ultrasonic Extinction," May 2000).

Current instruments use different techniques for the attenuation measurement: with *static* or *variable* width of the measuring zone, measurement in *transmission* or *reflection*, with *continuous* or *swept* frequency generation, with *frequency burst* or *single-pulse* excitation.

For process environment, probes are commercially available with a frequency range of 100 kHz to 200 MHz and a dynamic range of

>150 dB, covering 1 to 70 percent of volume concentration, 0 to 120°C, 0 to 40 bar, pH 1 to 14, and hazardous areas as an option.

Vendors of this technology include Sympatec GmbH (OPUS), Malvern Instruments Ltd. (Ultrazizer), Dispersion Technology Inc. (DT series), and Colloidal Dynamics Pty Ltd. (AcoustoSizer).

Single-Particle Light Interaction Methods Individual particles have been measured with light for many years. The measurement of the particle size is established by (1) the determination of the *scattered light* of the particle, (2) the measurement of the amount of *light extinction* caused by the particle presence, (3) the measurement of the *residence time* during motion through a defined distance, or (4) *particle velocity*.

Many commercial instruments are available, which vary in optical design, light source type, and means, and how the particles are presented to the light.

Instruments using **light scattering** cover a size range of particles of 50 nm to about 10 μm (liquid-borne) or 20 μm (gas-borne), while instruments using **light extinction** mainly address liquid-borne particles from 1 μm to the millimeter size range. The size range capability of any single instrument is typically 50 : 1. International standards are currently under development (ISO 13323-1:2000, *Determination of Particle Size Distribution—Single-Particle Light Interaction Methods, Part 1: Light Interaction Considerations*; ISO/DIS 21501-2, *Determination of Particle Size Distribution—Single Particle Light-Interaction Methods, Part 2: Light-Scattering Liquid-Borne Particle Counter*; ISO/DIS 21501-3, *Part 3: Light-Extinction Liquid-Borne Particle Counter*; ISO/DIS 21501-4, *Part 4: Light-Scattering Airborne Particle Counter for Clean Spaces*).

Instruments using the **residence time**, such as the aerodynamic particle sizers, or the **particle velocity**, as used by the phase Doppler particle analyzers, measure the particle size primarily based on the aerodynamic diameter.

Small-Angle X-Ray Scattering Method Small angle X-ray scattering can be used in a size range of about 1 to 300 nm. Its advantage is that the scattering mainly results from the differences in the electron density between the particles and their surrounding. As internal crystallites of external agglomerates are not visible, the measured size always represents the size of the primary particles and the requirement for dispersion is strongly reduced [Z. Jinyuan, L. Chulan, and C. Yan, Stability of the Dividing Distribution Function Method for Particle Size Distribution Analysis in Small Angle X-Ray Scattering, *J. Iron & Steel Res. Inst.*, 3(1), (1996); ISO/TS 13762:2001, *Particle Size Analysis—Small Angle X-ray Scattering Method*].

Focused-Beam Techniques These techniques are based on a focused light beam, typically a laser, with the focal point spinning on a circle parallel to the surface of a glass window. When the focal point passes a particle, the reflected and/or scattered light of the particle is detected. The focal point moves along the particle on circular segments, as displayed in Fig. 21-16. Sophisticated threshold algorithms are used to determine the start point and endpoint of the chord, i.e., the edges of the particle. The chord length is calculated from the time interval and the track speed of the focal point. Focused-beam techniques measure a chord length distribution, which corresponds to the size and shape information of the particles typically in a complicated way (J. Worlische, T. Hocker, and M. Mazzoti, Restoration of PSD from Chord Length Distribution Data Using the Method of Projections onto Convex Sets, *Part. Part. Syst. Char.*, 22, 81 ff.). So often the chord length distribution is directly used as the fingerprint information of the size, shape, and population status.

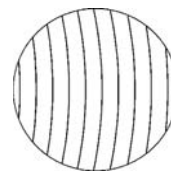


FIG. 21-16 Different chords measured on a constantly moving single spherical particle by focused-beam techniques.



FIG. 21-17 Multisizer™ 3 COULTER COUNTER® from Beckman Coulter, Inc., uses the electrical sensing zone method.

Instruments of this type are commercially available as robust finger probes with small probe diameters. They are used in on-line and preferably in in-line applications, monitoring the chord length distribution of suspensions and emulsions. Special flow conditions are used to reduce the sampling errors. Versions with fixed focal distance [Focused Beam Reflectance Measurement (FBRM®)] and variable focal distance (3D ORM technology) are available. The latter improves this technique for high concentrations and widens the dynamic range, as the focal point moves horizontally and vertically with respect to the surface of the window. For instruments refer, e.g., to Mettler-Toledo International Inc. (Lasentec FBRM probes) and Messtechnik Schwartz GmbH (PAT).

Electrical Sensing Zone Methods In the electric sensing zone method (Fig. 21-17), a well-diluted and -dispersed suspension in an electrolyte is caused to flow through a small aperture [Kubitschek, *Research*, **13**, 129 (1960)]. The changes in the resistivity between two electrodes on either side of the aperture, as the particles pass through, are related to the volumes of the particles. The pulses are fed to a pulse-height analyzer where they are counted and scaled. The method is limited by the resolution of the pulse-height analyzer of about 16,000:1 (corresponding to a volume diameter range of about 25:1) and the need to suspend the particles in an electrolyte (ISO 13319:2000, *Determination of Particle Size Distributions—Electrical Sensing Zone Method*).

Gravitational Sedimentation Methods In gravitational sedimentation methods, the particle size is determined from the settling velocity and the undersize fraction by changes of concentration in a settling suspension. The equation relating particle size to settling velocity is known as **Stokes' law** (ISO 13317, *Part 1: General Principles and Guidelines*):

$$x_{st} = \sqrt{\frac{18\eta u}{(\rho_s - \rho_l)g}} \quad (21-16)$$

where x_{st} is the Stokes diameter, η is viscosity, u is the particle settling velocity under gravity, ρ_s is the particle density, ρ_l is the liquid density, and g is the gravitational acceleration.

The **Stokes diameter** is defined as the diameter of a sphere having the same density and the same velocity as the particle settling in a liquid of the same density and viscosity under laminar flow conditions. Corrections for the deviation from Stokes' law may be necessary at the coarse end of the size range. Sedimentation methods are limited to sizes above 1 μm due to the onset of thermal diffusion (brownian motion) at smaller sizes.

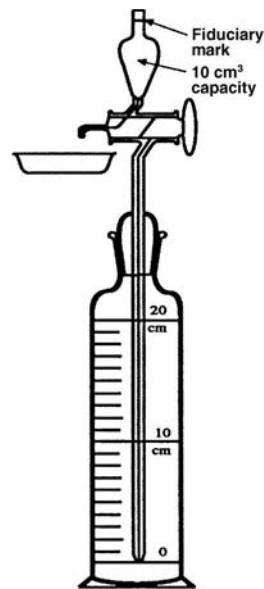


FIG. 21-18 Equipment used in the pipette method of size analysis.

An experimental problem is to obtain adequate dispersion of the particles prior to a sedimentation analysis. For powders that are difficult to disperse, the addition of dispersing agents is necessary, along with ultrasonic probing. It is essential to examine a sample of the dispersion under a microscope to ensure that the sample is fully dispersed. (See "Wet Dispersion.")

Equations to calculate size distributions from sedimentation data are based on the assumption that the particles sink freely in the suspension. To ensure that particle-particle interaction can be neglected, a volume concentration below 0.2 percent is recommended.

There are various procedures available to determine the changing solid concentration of a sedimenting suspension:

In the **pipette method**, concentration changes are monitored by extracting samples from a sedimenting suspension at known depths and predetermined times. The method is best known as Andreasen modification [Andreasen, *Kolloid-Z.*, **39**, 253 (1929)], shown in Fig. 21-18. Two 10-mL samples are withdrawn from a fully dispersed, agitated suspension at zero time to corroborate the 100 percent concentration given by the known weight of powder and volume of liquid making up the suspension. The suspension is then allowed to settle in a temperature-controlled environment, and 10-mL samples are taken at time intervals in geometric 2:1 time progression starting at 1 min (that is, 1, 2, 4, 8, 16, 32, 64 min). The amount of powder in the extracted samples is determined by drying, cooling in a desiccator, and weighing. Stokes diameters are determined from the predetermined times and the depth, with corrections for the changes in depth due to the extractions. The cumulative mass undersize distribution comprises a plot of the normalized concentration versus the Stokes diameter. A reproducibility of ± 2 percent is possible by using this apparatus. The technique is versatile in that it is possible to analyze most powders dispersible in liquids; its disadvantages are that it is a labor-intensive procedure, and a high level of skill is needed (ISO 13317, *Part 2: Fixed Pipette Method*).

The **hydrometer method** is simpler in that the density of the suspension, which is related to the concentration, is read directly from the stem of the hydrometer while the depth is determined by the distance of the hydrometer bulb from the surface (ASTM Spec. Pub. 234, 1959). The method has a low resolution but is widely used in soil science studies.

In **gravitational photo sedimentation methods**, the change of the concentration with time and depth of sedimentation is monitored



FIG. 21-19 The Sedigraph III 5120 Particle Size Analysis System determines particle size from velocity measurements by applying Stokes' law under the known conditions of liquid density and viscosity and particle density. Settling velocity is determined at each relative mass measurement from knowledge of the distance the X-ray beam is from the top of the sample cell and the time at which the mass measurement was taken. It uses a narrow, horizontally collimated beam of X-rays to measure directly the relative mass concentration of particles in the liquid medium.

by using a light point or line beam. These methods give a continuous record of changing optical density with time and depth and have the added advantage that the beam can be scanned to the surface to reduce the measurement time. A correction needs to be applied to compensate for a deviation from the laws of geometric optics (due to diffraction effects the particles cut off more light than geometric optics predicts). The normalized measurement is a $Q_2(x)$ distribution (coming ISO 1337, *Part 4: Photo Gravitational Method*).

In **gravitational X-ray sedimentation methods**, the change of the concentration with time and depth of sedimentation is monitored by using an X-ray beam. These methods give a continuous record of changing X-ray density with time and depth and have the added advantage that the beam can be scanned to the surface to reduce the measurement time. The methods are limited to materials having a high atomic mass (i.e., X-ray-opaque material) and give a $Q_3(x)$ distribution directly (ISO 13317, *Part 3: X-ray Gravitational Technique*). See Fig. 21-19.

Sedimentation Balance Methods In sedimentation balances the weight of sediment is measured as it accumulates on a balance pan suspended in an initial homogeneous suspension. The technique is slow due to the time required for the smallest particle to settle out over a given height. The relationship between settled weight P , weight undersize W , and time t is given by

$$P = W - \frac{dP}{d \ln t} \quad (21-17)$$

Centrifugal Sedimentation Methods These methods extend sedimentation methods well into the submicrometer size range. Alterations of the particle concentration may be determined space- and time-resolved during centrifugation (T. Detloff and D. Lerche, "Determination of Particle Size Distributions Based on Space and Time Resolved Extinction Profiles in Centrifugal Field," Proceedings of Fifth World Congress on Particle Technology, Session Particle

Measurement, Orlando, Fla., April 23–27, 2006). Sizes are calculated from a modified version of the Stokes equation:

$$x_{st} = \sqrt{\frac{18\eta u}{(\rho_s - \rho_f)\omega^2}} \quad (21-18)$$

where ω is the radial velocity of the centrifuge. The concentration calculations are complicated due to radial dilution effects (i.e., particles do not travel in parallel paths as in gravitational sedimentation but move away from each other as they settle radially outward). Particle velocities are given by

$$u = \frac{\ln(r/s)}{t} \quad (21-19)$$

where both the measurement radius r and the surface radius s can be varying. The former varies if the system is a scanning system, and the latter if the surface falls due to the extraction of samples.

Concentration undersize D_m is determined by

$$D_m = \int_{x_{min}}^x \exp(-2ktz^2) q_3(x) dz \quad (21-20)$$

with

$$k = \frac{\rho_s - \rho_f}{18\eta} \omega^2 \quad (21-21)$$

where $q_3(x) = dQ_3(x)/dx$ is the volume or mass density distribution and z is the integration variable.

The solution of the integral for measuring the concentration at constant position over time is only approximately possible. A common way uses Kamack's equation [Kamack, *Br. J. Appl. Phys.*, **5**, 1962–1968 (1972)] as recommend by ISO 13318 (*Part 1: Determination of Particle Size by Centrifugal Liquid Sedimentation Methods*).

An analytical solution is provided by measuring the concentration to at least one time at different sedimentation heights:

$$Q_3(x) = \int_1^{D_s} \left(\frac{r_1}{s}\right)^2 dD_m \quad (21-22)$$

where r_1 is the measurement position and s the surface radius; $Q_3(x)$ is the cumulative mass or volume concentration, and $(r_1/s)^2$ is the radial dilution correction factor.

The **disc centrifuge**, developed by Slater and Cohen and modified by Allen and Svarovsky [Allen and Svarovsky, *Dechema Monogram*, Nuremberg, Nos. 1589–1625, pp. 279–292 (1975)], is essentially a centrifugal pipette device. Size distributions are measured from the solids concentration of a series of samples withdrawn through a central drainage pillar at various time intervals.

In the **centrifugal disc photodensitometer**, concentration changes are monitored by a light point or line beam. In one high-resolution mode of operation, the suspension under test is injected into clear liquid in the spinning disc through an entry port, and a layer of suspension is formed over the free surface of liquid (the line start technique). The analysis can be carried out using a homogeneous suspension. Very low concentrations are used, but the light-scattering properties of small particles make it difficult to interpret the measured data.

Several **centrifugal cuvette photocentrifuges** are commercially available. These instruments use the same theory as the photocentrifuges but are limited in operation to the homogeneous mode of operation (ISO 13318:2001, *Determination of Particle Size Distribution by Centrifugal Liquid Sedimentation Methods—Part 1: General Principles and Guidelines; Part 2: Photocentrifuge Method*).

The **X-ray disc centrifuge** is a centrifuge version of the gravitational instrument and extends the measuring technique well into the submicrometer size range (ISO 13318-3:2004, *Part 3: Centrifugal X-ray Method*).

Sieving Methods Sieving is probably the most frequently used and abused method of analysis because the equipment, analytical procedure, and basic concepts are deceptively simple. In sieving, the particles are presented to equal-size apertures that constitute a series of go-no go gauges. Sieve analysis implies three major difficulties: (1) with woven-wire sieves, the weaving process produces three-dimensional apertures with considerable tolerances, particularly for fine-woven mesh; (2) the mesh is easily damaged in use; (3) the particles must be efficiently presented to the sieve apertures to prevent blinding.

Sieves are often referred to their mesh size, which is a number of wires per linear unit. Electroformed sieves with square or round apertures and tolerances of $\pm 2 \mu\text{m}$ are also available (ISO 3310, *Test Sieves—Technical Requirements and Testing*, 2000/2004; Part 1: *Test Sieves of Metal Wire Cloth*; 1999; Part 2: *Test Sieves of Perforated Metal Plate*; 1990; Part 3: *Test Sieves of Electroformed Sheets*).

For coarse separation, dry sieving is used, but other procedures are necessary for finer and more cohesive powders. The most aggressive agitation is performed with Pascal Inclyno and Tyler Ro-tap sieves, which combine gyratory and jolting movement, although a simple vibratory agitation may be suitable in many cases. With Air-Jet sieves, a rotating jet below the sieving surface cleans the apertures and helps the passage of fines through the apertures. The sonic sifter combines two actions, a vertical oscillating column of air and a repetitive mechanical pulse. Wet sieving is frequently used with cohesive powders.

Elutriation Methods and Classification In gravity elutriation the particles are classified in a column by a rising fluid flow. In centrifugal elutriation the fluid moves inward against the centrifugal force. A cyclone is a centrifugal elutriator, although it is not usually so regarded. The cyclosizer is a series of inverted cyclones with added apex chambers through which water flows. Suspension is fed into the largest cyclone, and particles are separated into different size ranges.

Differential Electrical Mobility Analysis (DMA) Differential electrical mobility analysis uses an electric field for the classification and analysis of charged aerosol particles ranging from about 1 nm to about 1 μm in a gas phase. It mainly consists of four parts: (1) A *pre-separator* limits the upper size to a known cutoff size. (2) A *particle charge conditioner* charges the aerosol particles to a known electric charge (a function of particle size). A bipolar diffusion particle charger is commonly used. The gas is ionized either by radiation from a radioactive source (e.g., ^{85}Kr), or by ions emitted from a corona electrode. Gas ions of either polarity diffuse to the aerosol particles until charge equilibrium is reached. (3) A *differential electrical mobility spectrometer* (DEMS) discriminates particles with different electrical mobility by particle migration perpendicular to a laminar sheath flow. The voltage between the inner cylinder and the outer cylinder (GND) is varied to adjust the discrimination level. (4) An *aerosol particle detector* uses, e.g., a continuous-flow condensation particle counter (CPC) or an aerosol electrometer (AE).

A typical setup of the DEMS is shown in Fig. 21-20. It shows the flow rates of the sheath flow F_1 , the polydisperse aerosol sample F_2 , the monodisperse (classified) aerosol exiting the DEMS F_3 , and the excess air F_4 .

The electrical mobility Z depends on the particle size x and the number of elementary charges e :

$$Z(x) = \frac{p \cdot e}{3\pi\eta x} [1 + \text{Kn}(A + B e^{C/\text{Kn}})] \quad (21-23)$$

with the number of elementary charges p , the Knudsen number Kn of $2l/x$, the mean path l of the gas molecule, η the dynamic fluid viscosity, and numeric constants A , B , C determined empirically.

Commercial instruments are available for a variety of applications in aerosol instrumentation, production of materials from aerosols, contamination control, etc. (ISO/CD 15900 2006, *Determination of Particles Size Distribution—Differential Electrical Mobility Analysis for Aerosol Particles*).

Surface Area Determination The surface-to-volume ratio is an important powder property since it governs the rate at which a powder interacts with its surroundings, e.g., in chemical reactions. The surface area may be determined from size-distribution data or measured directly by flow through a powder bed or the adsorption of gas molecules on the powder surface. Other methods such as gas diffusion, dye adsorption from solution, and heats of adsorption have also been used. The most commonly used methods are as follows:

In **mercury porosimetry**, the pores are filled with mercury under pressure (ISO 15901-1:2005, *Pore Size Distribution and Porosity of Solid Materials—Evaluation by Mercury Porosimetry and Gas Adsorption—Part 1: Mercury Porosimetry*). This method is suitable for many materials with pores in the diameter range of about 3 nm to 400 μm (especially within 0.1 to 100 μm).

In **gas adsorption** for micro-, meso- and macropores, the pores are characterized by adsorbing gas, such as nitrogen at liquid-nitrogen temperature. This method is used for pores in the ranges of approximately <2 nm (*micropores*), 2 to 50 nm (*mesopores*), and >50 nm (*macropores*) (ISO/FDIS 15901-2, *Pore Size Distribution and Porosity of Solid Materials—Evaluation by Mercury Porosimetry and Gas Adsorption, Part 2: Analysis of Meso-pores and Macro-pores by Gas Adsorption*; ISO/FDIS 15901-3, *Part 3: Analysis of Micro-pores by Gas Adsorption*). An isotherm is generated of the amount of gas adsorbed versus gas pressure, and the amount of gas required to form a monolayer is determined.

Many theories of gas adsorption have been advanced. For mesopores the measurements are usually interpreted by using the BET theory [Brunauer, Emmet, and Teller, *J. Am. Chem. Soc.*, **60**, 309 (1938)]. Here the amount of adsorbed n_a is plotted against the relative pressure p/p_0 . The monolayer capacity n_m is calculated by the BET equation:

$$\frac{p/p_0}{n_a(1 - p/p_0)} = \frac{1}{n_m C} + \frac{C - 1}{n_m C} \cdot \frac{p}{p_0} \quad (21-24)$$

The specific surface per unit mass of the sample is then calculated by assessing a value a_m for the average area occupied by each molecule in the complete monolayer (say, $a_m = 0.162 \text{ nm}^2$ for N_2 at 77 K) and the Loschmidt number L :

$$a_s = n_m \cdot a_m \cdot L \quad (21-25)$$

PARTICLE-SIZE ANALYSIS IN THE PROCESS ENVIRONMENT

The growing trend toward automation in industry has resulted in the development of particle-sizing equipment suitable for continuous

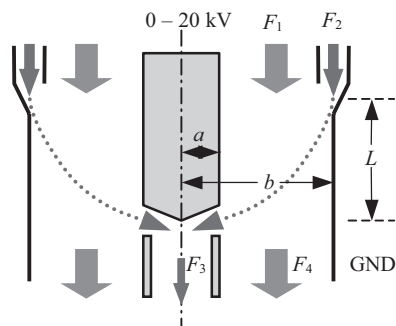


FIG. 21-20 Schematic of a differential electrical mobility analyzer.

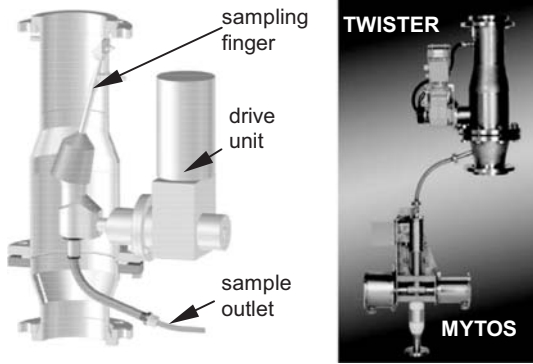


FIG. 21-21 A typical on-line application with a representative sampler (TWISTER) in a pipe of 150-mm, which scans the cross section on a spiral line, and dry disperser with particle-sizing instrument (MYTOS) based on laser diffraction. (Courtesy of Sympatec GmbH.)

work under process conditions—even in hazardous areas (Fig. 21-21). The acquisition of particle-size information in real time is a prerequisite for feedback control of the process.

Today the field of particle sizing in process environment is subdivided into three branches of applications.

At-line At-line is the fully automated analysis in a laboratory. The sample is still taken manually or by stand-alone devices. The sample is transported to the laboratory, e.g., by pneumatic delivery. Several hundred samples can be measured per day, allowing for precise quality control of slow processes. At-line laser diffraction is widely used for quality control in the cement industry. See Fig. 21-22.

On-line On-line places the measuring device in the process environment close to, but not in, the production line. The fully automated system includes the sampling, but the sample is transported to the measuring device. Mainly laser diffraction, ultrasonic extinction, and dynamic light scattering are used. See Fig. 21-23.

In-line In-line implements sampling, sample preparation, and measurement directly in the process, keeping the sample inside the production line. This is the preferred domain of laser diffraction

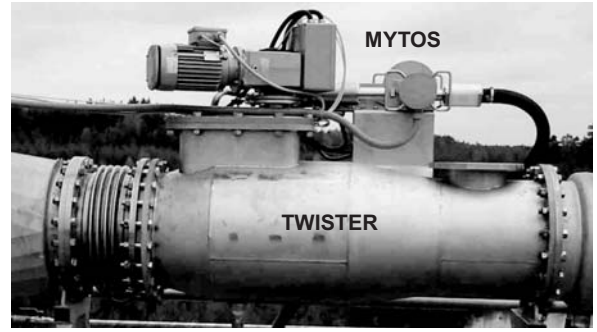


FIG. 21-23 Typical on-line outdoor application with a representative sampler TWISTER 440, which scans the cross section on a spiral line in a pipe of 440-mm, and a hookup dry disperser with laser diffraction particle sizer MYTOS. (Courtesy of Sympatec GmbH.)

(mainly dry), image analysis, focused-beam techniques, and ultrasonic extinction devices (wet). See Fig. 21-24.

VERIFICATION

The use of **reference materials** is recommended to verify the correct function of the particle-sizing equipment. A simple electrical, mechanical, or optical test is generally not sufficient, as all functions of the measuring process, such as dosing, transportation, and dispersion, are only tested with sample material applied to the instrument.

Reference Materials Many vendors supply certified standard reference materials which address either a single instrument or a group of instruments. As these materials are expensive, it is often advisable to perform only the primary tests with these materials and perform secondary tests with a stable and well-split material supplied by the user. For best relevance, the size range and distribution type of this material should be similar to those of the desired application. It is essential that the total operational procedure be adequately described in full detail (S. Röhlele and W. Witt, Standards in Laser Diffraction, 5th European Symposium Particle Char., Nuremberg, March 24–26, 1992).

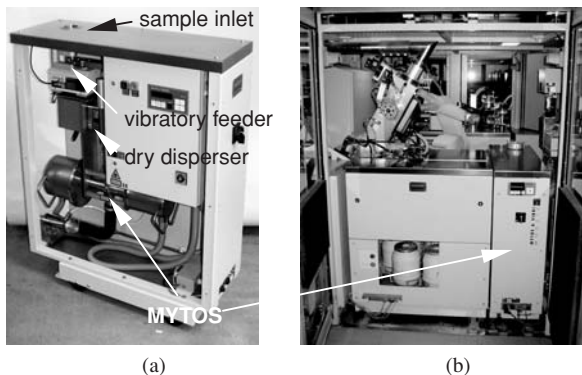


FIG. 21-22 (a) At-line particle sizing MYTOS module (courtesy of Sympatec GmbH) based on laser diffraction, with integrated dosing and dry dispersion stage. (b) Module integrated into a Polysius Polab® AMT for lab automation in the cement industry.

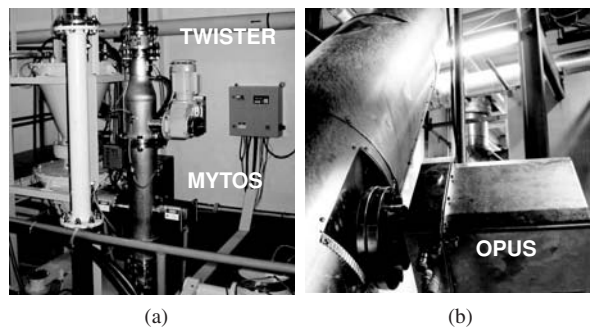


FIG. 21-24 (a) Typical in-line laser diffraction system with a representative sampler (TWISTER and MYTOS), all integrated in a pipe of 100-mm. (b) In-line application of an ultrasonic extinction (OPUS) probe monitoring a crystallization process in a large vessel. (Both by courtesy of Sympatec GmbH.)

SOLIDS HANDLING: BULK SOLIDS FLOW CHARACTERIZATION

GENERAL REFERENCES: Nedderman, *Statics and Kinematics of Granular Materials*, Cambridge University Press, 1992. Wood, *Soil Behavior and Critical State Soil Mechanics*, Cambridge University Press, 1990. J. F. Carr and D. M. Walker, *Powder Technology*, **1**, 369 (1967). Thompson, Storage of Particulate Solids, in *Handbook of Powder Science and Technology*, Fayed and Otten (eds.), Van Nostrand Reinhold, 1984. Brown and Richards, *Principles of Powder Mechanics*, Pergamon Press, 1970. Schofield and Wroth, *Critical State Soil Mechanics*, McGraw-Hill, 1968. M. J. Hvorslev, On the Physical Properties of Disturbed Cohesive Soils, *Ingeniorvidenskabelige Skrifter A*, no. 45, 1937. Janssen, *Zeits. D. Vereins Deutsch Ing.*, **39**(35), 1045 (1895). Jenike, Storage and Flow of Bulk Solids, *Bull. 123*, Utah Eng. Expt. Stn., 1964. O. Reynolds, On the Dilatancy of Media Composed of Rigid Particles in Contact: With Experimental Illustrations, *Phil. Mag.*, Series 5, **20**, 269 (1885). K. H. Roscoe, A. N. Schofield, and C. P. Wroth, On the Yielding of Soils, *Geotechnique*, **8**, 22 (1958). Dhodapkar et al., Fluid-Solid Transport in Ducts, in *Multiphase Flow Handbook*, Crowe (ed.), Taylor and Francis, 2006. Sanchez et al., *Powder Technology*, **138**, 93 (2003). Geldart, *Powder Technology*, **7**, 285 (1973). Kaye, *Powder Technology*, **1**, 11 (1967).

AN INTRODUCTION TO BULK POWDER BEHAVIOR

Bulk solids flow affects nearly all solids processing operations through material handling problems and mechanical behavior. Measurements of powder flow properties date back to Reynolds (loc. cit. 1885), Gibbs, Prandtl, Coulomb, and Mohr. However, the term **flowability** is rarely defined in an engineering sense. This often leads to a number of misleading analogies being made with fluid behavior. Unique features with regard to powder behavior are as follows:

1. Powders can withstand stress without flowing, in contrast to most liquids. The strength or **yield stress** of this powder is a function of previous compaction, and is not unique, but depends on stress application. Powders fail only under applied shear stress, and not isotropic load, although they do compress. For a given applied horizontal load, failure can occur by either raising or lowering the normal stress, and two possible values of failure shear stress are obtained (**active versus passive failure**).

2. When failure does occur, the flow is **frictional** in nature and often is a weak function of strain rate, depending instead on **shear strain**. Prior to failure, the powder behaves as an elastic solid. In this sense, bulk powders do *not* have a viscosity in the bulk state.

3. Powders do not readily transmit stress. In the case of columns, normal stress or weight of the bulk solid is held by wall friction. In addition, normal stress is not isotropic, with radial stress being only a fraction of normal stress. In fact, the end result is that stress in silos scales with diameter rather than bed height, a most obvious manifestation of this being the narrow aspect ratio of a corn silo.

4. A powder will not necessarily maintain a shear stress-imposed strain rate gradient in the fluid sense. Due to force instabilities, it will search for a characteristic slip plane, with one mass of powder flowing against the next, an example being rat-hole discharge from a silo.

5. Bulk solids are also capable of two-phase flow, with large gas interactions in silo mass discharge, fluidization, pneumatic conveying, and rapid compression and mixing. Under fluidized conditions, the bulk solid may now obtain traditional fluid behavior, e.g., pressure scaling with bed height. But there are other cases where fluidlike rheology is misinterpreted, and is actually due to time-dependent compression of interstitial fluid. After characteristic time scales related to permeability, stresses are transmitted to the solid skeleton. It may not be of utility to combine the rheology of the solid and interstitial fluids, but rather to treat them as separate, as is often done in soil mechanics.

PERMEABILITY AND AERATION PROPERTIES

Permeability and Deaeration Various states of fluidization and pneumatic conveying exist for bulk solid. Fluidization and aeration behavior may be characterized by a fluidization test rig, as illustrated in Fig. 21-25. A loosely poured powder is supported by a porous or perforated distributor plate. The quality and uniformity of this plate are critical to the design. Various methods of filling have been explored to include vibration and vacuum filling of related **permeameters**

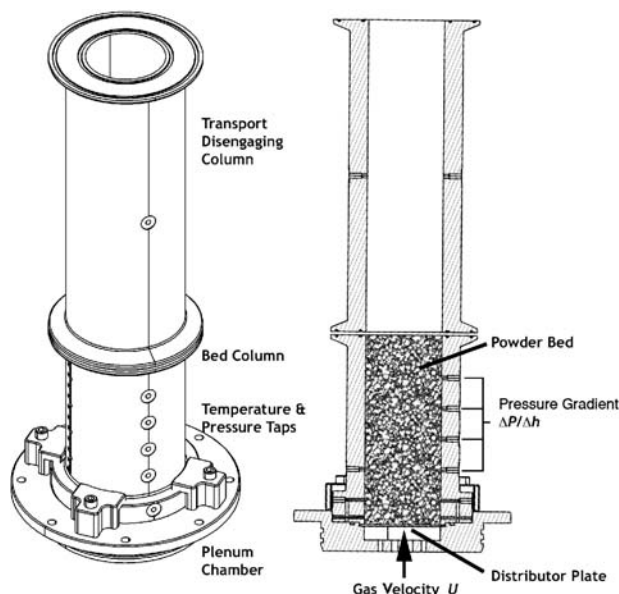


FIG. 21-25 iFluid™ fluidization permeameter, illustrating powder bed supported by distributor plate fluidized at a gas velocity U , with associated pressure taps for multiple pressure gradient measurements dP/dh . (Courtesy iPowder Systems, E&G Associates, Inc.)

[Kaye, *Powder Technology*, **1**, 11 (1967); Juhasz, *Powder Technology*, **42**, 123 (1985)]. Two key types of measurements may be performed. In the first, air or gas is introduced through the distributor, and the pressure drop across the bed is measured as a function of flow rate or superficial gas velocity (Fig. 21-26). In the second, the gas flow is stopped to an aerated bed, and the pressure drop or bed height is measured as a function of time, as the bed collapses and deaerates (Fig. 21-27).

For the first **fluidization measurement**, pressure drop will increase with gas velocity while powder remains in a **fixed-bed** state until it reaches a maximum plateau, after which the pressure drop equals the weight of the bed, provided the bed becomes uniformly fluidized. Bed expansion will also occur. The point of transition is referred to as the **minimum fluidization velocity** U_{mf} . Various states of a **fluidized bed** occur. For fine materials of limited cohesion, the bed will initially undergo **homogeneous fluidization** (also referred to as particulate fluidization), where bed expansion occurs without the formation of bubbles, and with further increases in gas velocity, it will transition to a bubbling bed, or **heterogeneous fluidization** (also referred to as bubbling or aggregative fluidization). Coarse materials do not expect the initial state of homogeneous fluidization, and $U_{mb} = U_{mf}$. The point at which bubbles form in the bed is referred to as the **minimum bubbling velocity** U_{mb} . The various stages of fluidization are described in detail in Sec. 17. In addition, for fine, cohesive powders, channeling may occur instead of uniform fluidization, resulting in lower, more erratic pressure drops. Various states of fluidization are indicated in Fig. 21-26. Lastly, mixing, bed expansion, heat and mass transport, and forces acting in fluidized beds scale with **excess gas velocity**, or $U - U_{mf}$.

Prior to reaching minimum bubbling, a homogeneous fluidized powder will undergo a peak in pressure prior to settling down to its plateau. This peak represents a measure of **aerated cohesion**, and it ranges from 10 percent for fine, low-cohesion powders capable of homogeneous fluidization, to 50 percent for fine, extremely cohesive material, which generally undergoes channeling when fluidized.

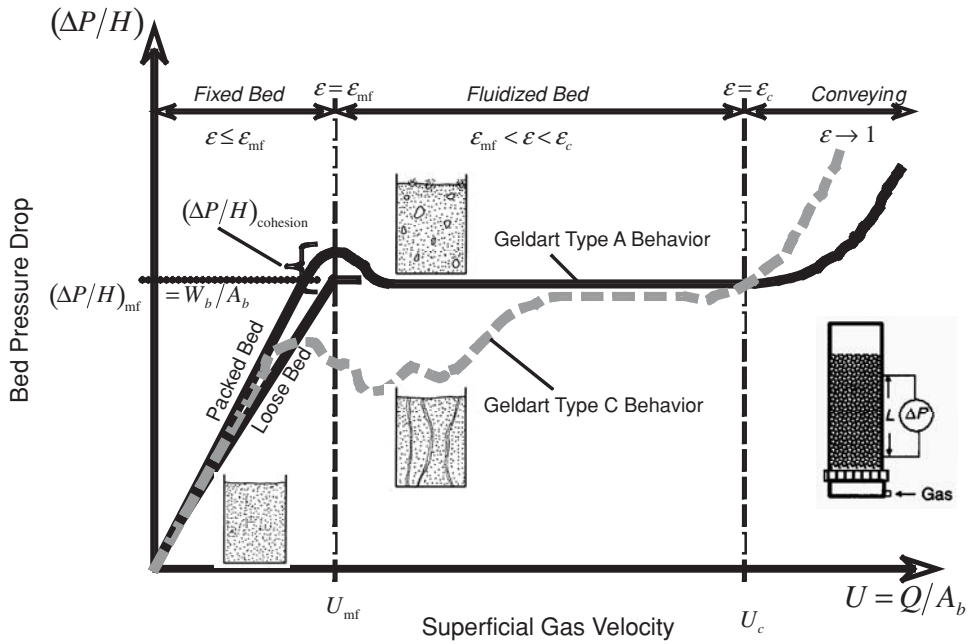


FIG. 21-26 Fluidization measurement of permeability and fluidization behavior. Bed pressure drop $\Delta P/H$ for fixed and fluidized beds as a function of gas velocity U . (After Rumpf, Particle Technology, Kluwer Academic, 1990.)

The pressure drop across the initial fixed bed (or final previously aerated bed) is a measure of **permeability** k_p as defined by Darcy (1856), given by

$$U = \frac{Q}{A_b} = k_p \frac{\Delta P/H_b}{\mu_g} \quad (21-26)$$

otherwise known as **Darcy's law**, which is strictly only valid for low Reynolds number. Comparing to the **Kozeny-Carman relation** [Kozeny (1927); Carman (1937)], permeability may be predicted from particle size (surface-volume average) and packing voidage:

$$k_{p0} = \frac{d_p^2 \epsilon^3}{C_{p1}(1 - \epsilon)^2} \quad (21-27)$$

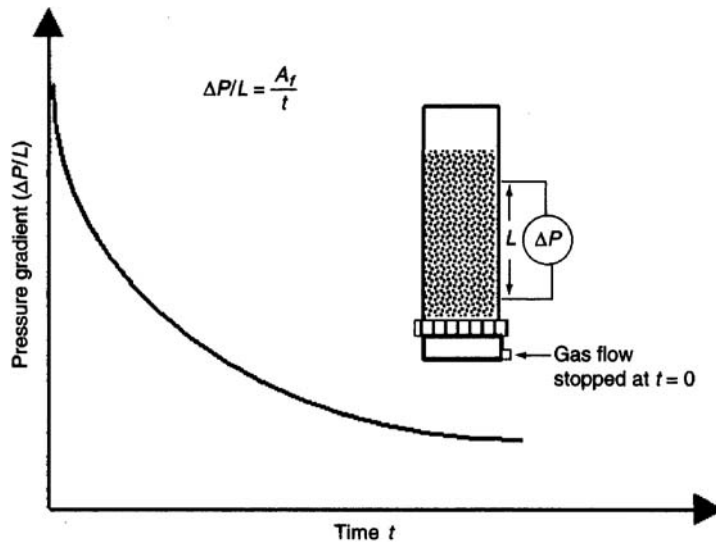


FIG. 21-27 Deaeration measurement of deaeration time and constant. Bed pressure drop $(\Delta P/H)$ decay following fluidization as a function of time. [Dhodapkar et al., Fluid-Solid Transport in Ducts, in Multiphase Flow Handbook, Crowe (ed.), Taylor & Francis, 2006, with permission.]

21-22 SOLID-SOLID OPERATIONS AND PROCESSING

which is valid for low Reynolds number and loose packing. C_{p1} equals 180 from the Kozeny-Carman relation and 150 from the Ergun relation. For a wider range of gas velocities, **Ergun's relation** should be utilized instead, where the pressure drop is given by

$$\frac{dP}{dh} = \frac{\mu_g U}{k_{p0}} (1 + 1.75 \text{Re}_p) \quad \text{where} \quad \text{Re}_p = \frac{\rho_g U d_p}{\mu_g (1 - \epsilon)} \quad (21-28)$$

which can be rewritten to give

$$\frac{1}{p_f} = \frac{\mu_g}{k_p} = \frac{dP/dh}{U} = E_1 + E_2 U \quad (21-29)$$

where E_1 and E_2 may be determined from plotting the slope in the fixed-bed region divided by velocity [or $(dP/dh)/U$] versus gas velocity. Theoretically, these constants are given by

$$E_1 = \frac{\mu_g}{k_{p0}} = \frac{C_{p1} \mu_g (1 - \epsilon)^2}{d_p^3 \epsilon^3} \quad \text{and} \quad E_2 = \frac{C_{p2} \rho_g (1 - \epsilon)}{d_p \epsilon^3} \quad (21-30)$$

where $C_{p1} = 150$ and $C_{p2} = 1.75$ based on Ergun's relation. The standard value of permeability is then related to the intercept E_1 , but a velocity dependence can be determined as well for high velocity related to conveying. And p_f is another common definition of permeability, or **permeability factor**, which incorporates gas viscosity.

As with bulk density, permeability is a function of packing voidage and its uniformity, and in practice, it is best measured. It can vary substantially with previous compaction of the sample. An example is the change in bulk density—and therefore interstitial voidage—that occurs with a material as it moves through a hopper. By applying a load to the upper surface of the bed, permeability may be also determined as a function of solids consolidation pressure (see "Bulk Flow Properties"). Permeability is a decreasing function of applied solids pressure, and bulk density is often written in log form, or

$$k_p = k_{p0} \left(\frac{\rho_{bo}}{\rho_b} \right)^m \quad (21-31)$$

From the second **deaeration measurement**, pressure drop is measured as a decaying function of time, given by one of the forms (Fig. 21-27)

$$\frac{\Delta P}{dh} = ae^{-t/t_d} \quad \text{or} \quad \frac{\Delta P}{dh} = \frac{A_d}{t} \quad (21-32)$$

where t_d and A_d are a characteristic **deaeration time** and **deaeration factor**, respectively. Large deaeration time or factor implies that the powder retains air for long times. Also an additional deaeration factor has been defined to account for particle density, or

$$X_d = \frac{A_d \rho_s}{(\Delta P/H)_{mf}} \quad (21-33)$$

Permeability and deaeration control both fluidization and pneumatic conveying. In addition, they impact the gas volume and pressure requirement for **air-augmented flow** in hoppers and feeders. Materials of low permeability have lower mass discharge rates from hopper openings (see "Mass Discharge Rates") and limit the rate of production in roll pressing, extrusion, and tableting, requiring vacuum to speed deaeration ("Compaction Processes"). Lastly permeability impacts wetting phenomena and the rate of drop uptake in granulation ("Wetting and Nucleation").

Classifications of Fluidization Behavior Geldart [*Powder Technology*, **7**, 285 (1973)] and later Dixon [*Pneumatic Conveying, Plastics Conveying and Bulk Storage*, Butters (ed.), Applied Science Publishers, 1981] developed a classification of fluidization/aeration behavior from studies of fluidized beds and slugging in vertical tubes,

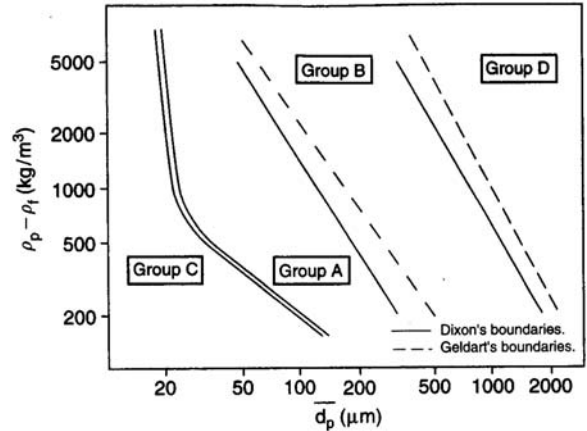


FIG. 21-28 Geldart's classification of aeration behavior with Dixon and Geldart boundaries. (From Mason, Ph.D. thesis, Thames Polytechnic, London, 1991, with permission.)

respectively (Fig. 21-28). The classification is based on particle size (surface-volume average for wide size distributions) and relative particle density. Particle size controls interparticle cohesive forces, whereas density controls the driving force to be overcome by drag. A summary of aeration behavior is provided in Table 21-4, where from **Geldart's classification** powders are broken down into group A (aeratable) for fine materials of low cohesion, which can exhibit homogeneous fluidization; group B (bubbling) for coarser material, which immediately bubbles upon fluidization; group C (cohesive), which typically channels and retains air for long periods; and group D (spoutable), which is coarse material of high permeability with no air retention capability.

Classifications of Conveying Behavior Aeration behavior also impacts mode and ease of pneumatic conveying [Dhodapkar et al., Fluid-Solid Transport in Ducts, in *Multiphase Flow Handbook*, Crowe (ed.), Taylor & Francis, 2006]. Figure 21-29 illustrates the impact of decreasing conveying velocity on flow pattern. At high gas flow, ideal dilute, homogeneous solids flow may occur (1). As gas velocity is reduced past some characteristic velocity, the solids can no longer be uniformly suspended and increasing amounts of solid will form on the bottom of the pipe, forming a moving stand of solids (2,3). With further decrease of gas velocity and deposited solids, moving dunes (4,5) and later slugs (6,7,8) will form which completely fill the pipe. Finally, ripple flow (9) and pipe pluggage (10) will occur. **Dilute-phase conveying** encompassed patterns 1 to 3, where **dense-phase conveying** includes the remainder of 4 to 10. Dhodapkar et al. (loc. cit.) further classified conveying patterns according to particle size. Fine materials (plastic powder, fly ash, cement, fine coal, carbon fines) may be transported in all patterns, with a smooth, predictable transition between regimes. At intermediate gas velocities, two-phase strand flow (2,3) is observed followed by dune flow at lower velocities (4–8), where the solid flow can appear as turbulent or fast-moving bed, wave, or fluidized-bed modes. Conveying might also be achieved in patterns 9 and 10 for materials that readily aerate and retain air, in which case they are conveyed as a fluidized plug. Coarse materials (pellets, grains, beans, large granules), however, form slugs when conveyed at low velocities, which form on a regular, periodic basis. The transition from dilute- to dense-phase conveying for coarse material is unstable and occurs under dune flow. Some coarse materials with substantial fines exhibit fine conveying modes.

Figure 21-30 provides classifications of conveying ability, where permeability and deaeration factor are plotted against pressure drop at minimum fluidization for a variety of materials [Mainwaring and Reed, *Bulk Solids Handling*, **7**, 415 (1987)]. Lines of constant minimum fluidization $U_{mf} = 0.05$ m/s and deaeration factor $X_d = 0.001$ m³ · s/kg are shown. From Fig. 21-30a, materials which lie above the line of high permeability can be conveyed in plug or slug form as they do

TABLE 21-4 Characteristics of Geldart (1973) or Dixon (1981) Classification

Properties	Group A	Group B	Group C	Group D
Material	Fine/medium powder Fly ash, pulverized coal, plastic powders, alumina, granular sugar, pharma excipients	Course powder Sand, salt, granules, mineral powders, glass beads	Cohesive fine powder Cement, corn starch, tit anium dioxide, carbon-black powder, many pharma actives	Granular Plastic pellets, wheat, large glass beads, tablets, coarse sand, seeds
Fluidization characteristics	Good air retention, small bubble size, considerable bed expansion	Poor air retention, low bed expansion, large bubble, asymmetric slugging at higher velocity or small beds	Cohesive and difficult to fluidize, tends to channel, retains gas for extended period once aerated, adhesion to walls and surfaces	Highly permeable, negligible expansion and no air retention, large bubbles, spouts, or axisymmetric slugs can form
Conveying characteristics	Can be conveyed in fluidized- or moving-bed mode, easy to convey, does not form slugs naturally	Unlikely to convey in conventional dense phase, unsteady and unpredictable plug formation, large pipe vibrations	Difficult but possible to convey in dense phase, forms impermeable plugs that break up, requires special conveying	Natural slugging ability and high permeability aid in slug or plug flow conveying; operationally easiest to dense phase convey
Pressure drop at U_{mf} : $(\Delta P/H)_{mf}$ [mbar/m]	<50	>80	50–130	5–150
Permeability factor $(k_p/\mu_g) = [m^2/(bar \cdot s)]$	0.1	0.01–0.1 to 1	0.1 to 1	>1
Deaeration	Collapses slowly, air retention	Collapses rapidly	Collapses slowly, long air retention	Collapses very rapidly

Adapted from Dhodapkar et al., Fluid-Solid Transport in Ducts, in *Multiphase Flow Handbook*, Crowe (ed.), Taylor & Francis, 2006; and Sanchez et al., *Powder Technology*, 138, 93 (2003).

not readily retain air, whereas those below the line of low permeability can be conveyed by moving-bed flow, as they more readily retain air, or by dilute-phase flow. Similarly from Fig. 21-30b, materials which lie below the line with small deaeration constant (or time) can be conveyed in plug or slug form, whereas those above the line with large deaeration constant (or time) can be conveyed by moving-bed flow or dilute-phase flow, as they retain air. Jones and Miller [*Powder Handling and Processing*, 2, 117 (1990)] combined deaeration behavior and permeability in a single classification, as shown in Fig. 21-31. Group 1 includes Geldart type A powders of low permeability and

large deaeration time which conveyed as moving-bed flow, whereas at the other extreme, group 3 includes Geldart type D materials with high permeability and short deaeration time conveyed as plug-type flow. Dilute- and dense-phase conveying is possible for group 2 or typically type B powder with (1) intermediate permeability and deaeration time, (2) small deaeration time and permeability, or (3) large deaeration time and permeability. Type C material exhibits all three forms of conveying. Sanchez et al. [*Powder Technology*, 138, 93 (2003)] and Dhodapkar et al. (loc. cit.) provide current summaries of these classifications.

BULK FLOW PROPERTIES

Shear Cell Measurements The yield or flow behavior of bulk solids may be measured by **shear cells**. Figure 21-32 illustrates these principles for the case of a direct rotary split cell. For **flow measurements**, powder is contained within two sets of rings. **Normal stress** is applied to the powder bed through a horizontal roughened or patterned lid. The upper ring containing approximately one-half of the powder is sheared with respect to the lower ring, forming a **shear plane** or lens between the two halves of powder. This is accomplished by rotating the lower half of the powder mounted to a motorized base, which in turn attempts to rotate the upper half of powder through rotational shear stress transmitted through the shear plane. The upper half of powder is instead held fixed by the upper lid, which transmits this shear stress through an air bearing to a force transducer. Through this geometry, the **shear stress** between the two halves of powder, measured as a torque by the force transducer, is measured versus time or displacement as a function of applied normal stress. In addition, any corresponding changes in powder density are measured by changes in vertical displacement for a linear voltage displacement transducer.

For **wall friction measurements**, a wall coupon is inserted between the rings, and powder in the upper ring alone is sheared against a coupon of interest. Wall friction and adhesion, both static and dynamic, may be assessed against different materials of construction or surface finish.

Shear cell testing of powders has its basis in the more comprehensive field of **soil mechanics** (Schofield and Wroth, *Critical State Soil Mechanics*, McGraw-Hill, 1968), which may be further considered a subset of **solid mechanics** (Nadia, *Theory of Flow and Fracture of Solids*, vols. 1 and 2, McGraw-Hill, 1950). The most comprehensive testing of the shear and flow properties of soils is accomplished in

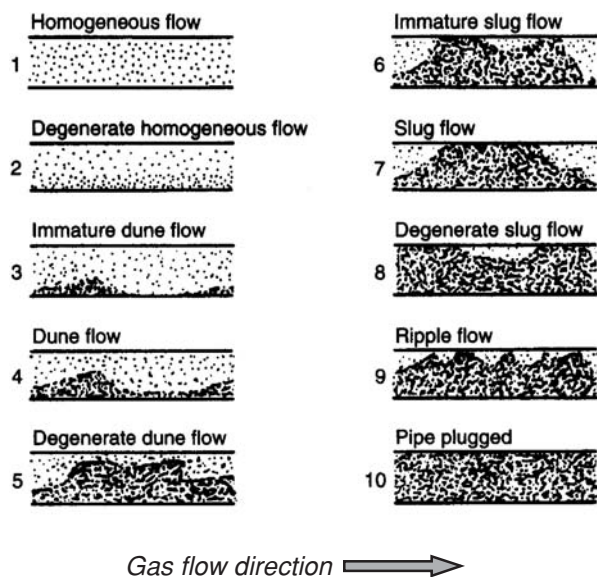


FIG. 21-29 Pattern of solids flow in pneumatic conveying. [From Wen, U.S. Dept. of Interior, Bureau of Mines, PA, IC 8314 (1959) with permission.]

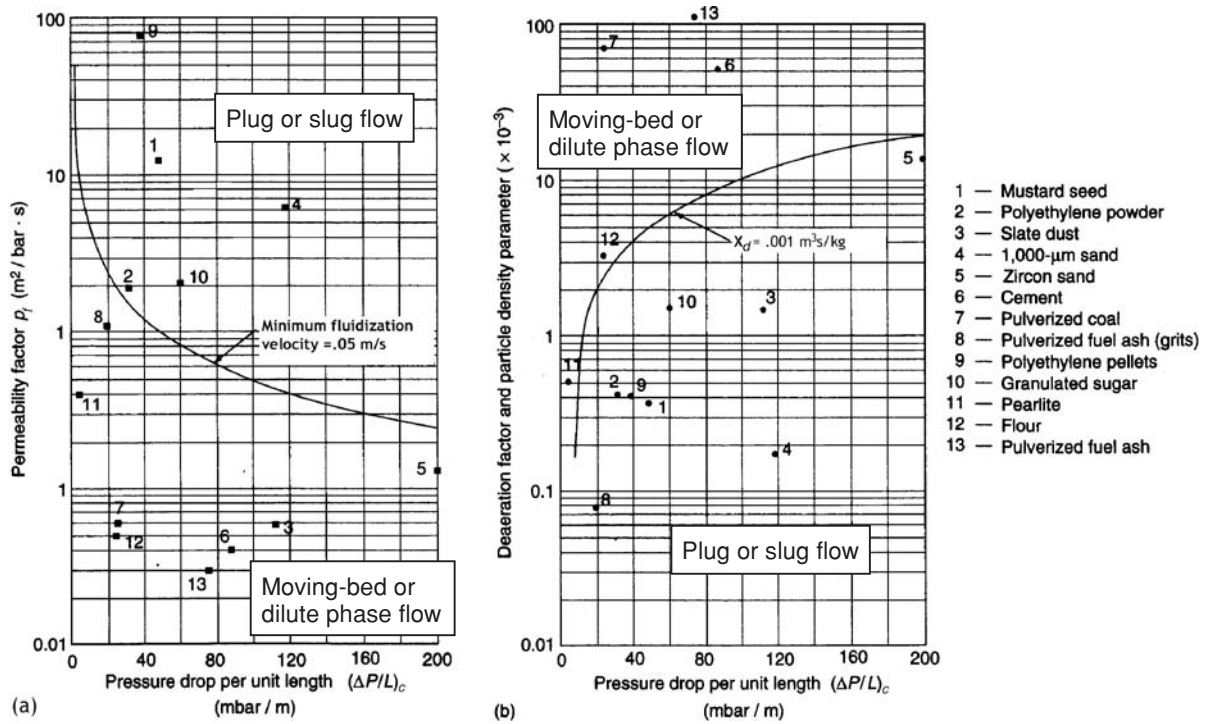


FIG. 21-30 Classification of pneumatic conveying based on (a) permeability factor and (b) deaeration factor. [From Mainwaring and Reed, Bulk Solids Handling, 7, 415 (1987) with permission.]

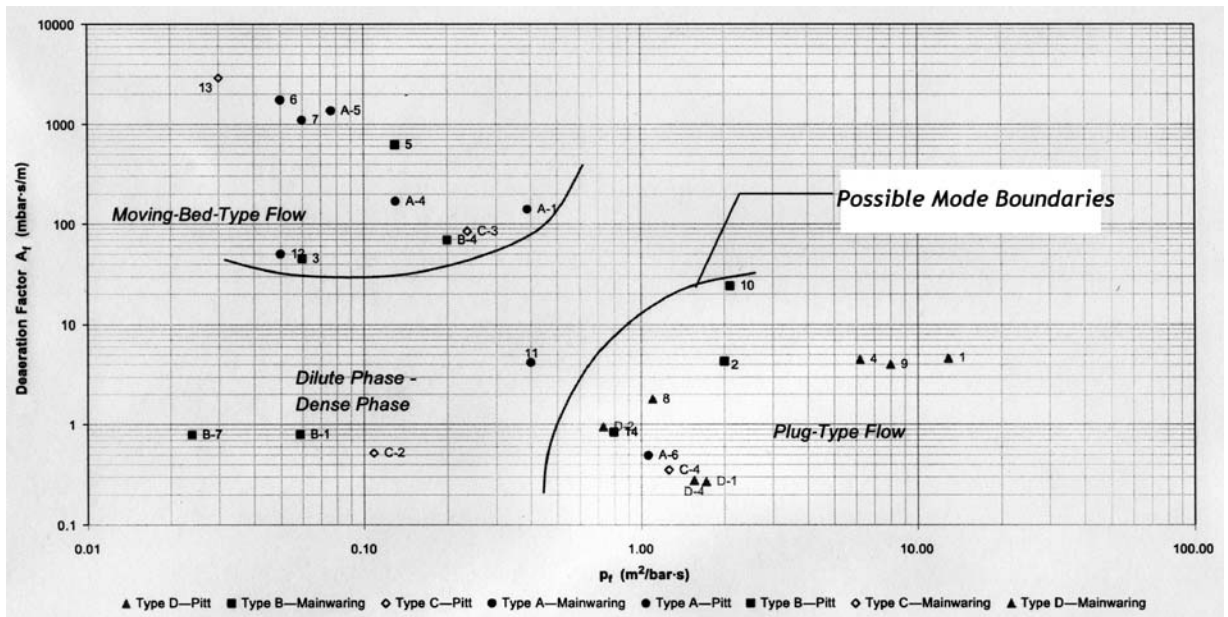


FIG. 21-31 Classification of pneumatic conveying based on combined permeability and deaeration factors, based on Jones and Miller. [Sanchez et al., Powder Technology, 138, 93 (2003), with permission.]

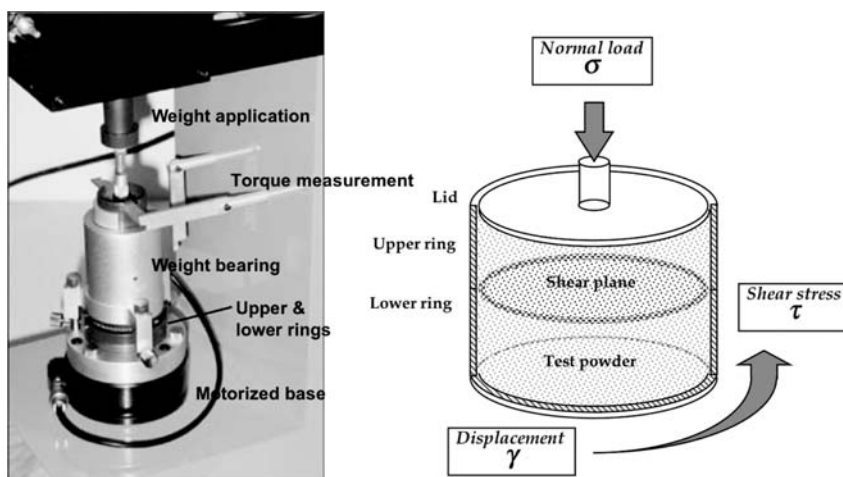


FIG. 21-32 iShear™ rotary, full annulus split cell, illustrating normal load weight application, rotational base, and shear stress/torque measurement. Vertical displacement of lid is monitored by displacement transducer. (Courtesy E&G Associates, Inc.)

triaxial shear cells (Fig. 21-33). There are two such types of triaxial shear cells. In the traditional cylindrical triaxial cell, the axial and radial pressures acting on the sample contained within a rubber membrane are directly controlled through applied axial force and radial hydraulic oil pressure. Deviatoric stress, i.e., shear stress due to difference in axial and radial pressure, is applied to the sample until failure. In a true triaxial cell, all three principal stresses may be varied; whereas only the major and minor principal stresses are controlled in the traditional cylindrical triaxial cell. Lastly, shear displacements are measured through a variety of strain gauges, and both the drained and undrained tests are possible. Such tests refer to simultaneous measurement of pressure of any interstitial fluid or gas. Interstitial fluid can have pronounced effects on mitigating powder friction and changing flow properties. While triaxial cells are not typically employed for powder characterization in industrial processing, they do provide the most comprehensive information as well as a knowledge base of application in such results for bulk solids flow, including detailed simulations of multiphase flow of such systems. Their disadvantage is their difficulty of use and time required to perform measurements. Future advances in employing these designs are likely.

Direct shear cells were introduced due to drastically reduced testing times, although the exact nature of stresses in the failure zone is not as precisely defined as with triaxial cells. Direct cells have undergone substantial automation in the last two decades. All have as a common feature that only the applied axial force or axial stress is controlled (Fig. 21-33). The shear stress required to accomplish failure is measured as a function of the applied axial stress, where translational or rotational motion is employed. Both **cup** and **split cell** designs are available. Rotational cells include both full **annulus** and **ring cells**. For a properly designed direct shear cell, failure occurs within a specific region, in which both the plane of failure and the acting stresses may be clearly defined. In addition, direct shear cells may be validated against an independent vendor standard, or the BCR116 limestone powder (see "Shear Cell Standards and Validation"). Rotary split cell designs have two possible advantages: (1) Unlimited displacement of the sample is possible, allowing ease of sample conditioning and repeated sample shear on a single sample. (2) The shear plane is induced in a defined region between the two cell halves, allowing unconfined expansion in the shear plane (Fig. 21-32).

Yield Behavior of Powders The yield behavior of a powder depends on the existing **state of consolidation** within the powder bed when it is caused to flow or yield under a given state of stress, defined by the acting normal and shear stresses. The consolidation state controls the current bed voidage or **porosity**. Figure 21-34 illustrates a times series of shears occurring for the BCR116 limestone standard for a rotary shear cell. For each shear step, torque is applied

to the sample by cell rotation until sample failure; the cell is then reversed until the shear force acting on the sample is removed. Two stages of a typical experiment may be noted. The first is a **consolidation stage** wherein repeated shears take place on the sample until the shear stress τ reaches a steady state, defined by either the maximum value or the steady value occurring after an initial peak. This occurs with a constant normal consolidation stress $\sigma = \sigma_c$ acting on the sample. During this step, the sample reaches a characteristic or **critical density** or **critical porosity** ϵ_c related to the consolidation normal stress. A set of shear steps is then performed during a **shear stage** with progressively smaller normal loads. In all cases, each shear step is preceded by a shear at the original consolidation normal stress.

Three characteristic displacement profiles may be observed during shear for shear stress and density (Fig. 21-35), which are unique to the state of consolidation:

1. **Critically consolidated.** If a powder is sheared sufficiently, it will obtain a constant density or critical porosity ϵ_c for this consolidation normal stress σ_c . This is defined as the critical state of the powder, discussed below. If a powder in such a state is sheared, initially the material will deform elastically, with shear forces increasing linearly with displacement or strain. Beyond a certain shear stress, the material will fail or flow, after which the shear stress will remain approximately constant as the bulk powder deforms plastically. Depending on the type of material, a small peak may be displayed originating from differences between static and dynamic density. Little change in density is observed during shear, as the powder has already reached the desired density for the given applied normal consolidation stress σ_c .

2. **Overconsolidated.** If the same sample is sheared, but at a lower normal stress of $\sigma < \sigma_c$, the shear stress will increase elastically to a peak and then fail, with this peak being less than that observed for the critically consolidated state, as the applied normal stress is lower. After the failure peak, the shear stress will decrease as the powder expands due to **dilation** and density decreases, eventually leveling off to a lower shear stress and lower density. Overconsolidated shears are observed during the shear stage of a shear cell experiment.

3. **Underconsolidated.** If the same sample is sheared, but at a higher normal stress of $\sigma > \sigma_c$, the shear stress will progressively increase to some value, while the material simultaneously densifies. Such underconsolidated responses are observed in the consolidation stage of an experiment.

In practice, following the filling of a cell, the powder is in an underconsolidated state. A set of shear steps is performed under a chosen consolidation stress in the consolidation stage to increase its density and bring it into a critical state. A set of shears is then performed at small normal stresses in the shear stage to determine the strength of

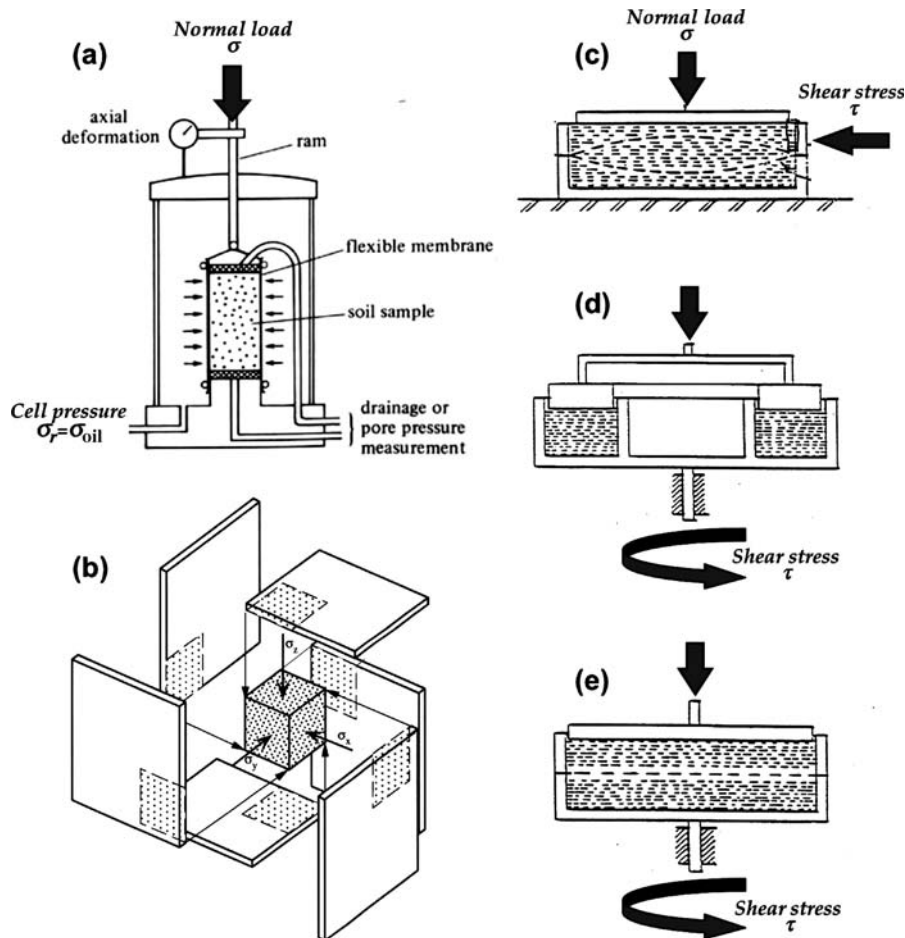


FIG. 21-33 Examples of powder shear cells. **Triaxial cells:** (a) Traditional triaxial cell; (b) true triaxial. **Direct shear cells:** (c) Translational split, Collin (1846), Jenike™ (1964), Carr and Walker (1967), Schulze™ (2000); (d) rotational annulus, Carr and Walker (1967), Schulze™ (2000); (e) rotational split, Peschl and Colijn (1976), iShear™ (2003). (From Measuring Powder Flowability and Its Applications, E-G Associates, 2006, with permission.)

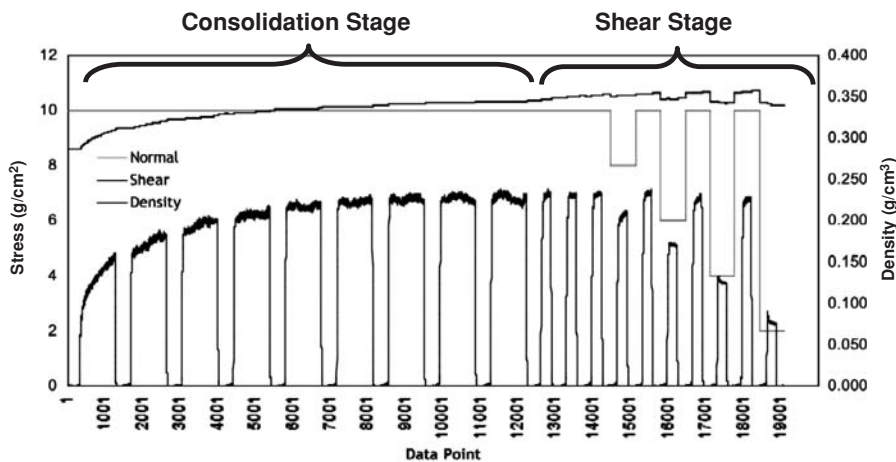


FIG. 21-34 Time-series shearing profile for the BCR116 limestone validation powder, in an iShear rotary split cell. (From Measuring Powder Flowability and Its Applications, E-G Associates, 2006, with permission.)

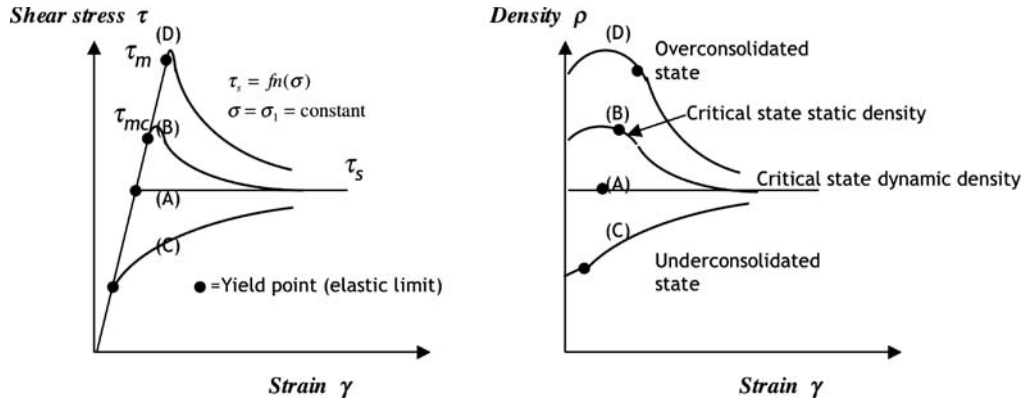


FIG. 21-35 Examples of yield behavior. (From Measuring Powder Flowability and Its Applications, E&G Associates, 2006, with permission.)

the powder as a function of normal load, in the overconsolidated or overcompacted state, each time reconsolidating the powder before performing the next shear step.

Powder Yield Loci For a given shear step, as the applied shear stress is increased, the powder will reach a maximum sustainable shear stress τ , at which point it yields or flows. The functional relationship between this limit of shear stress τ and applied normal load σ is referred to as a **yield locus**, i.e., a locus of yield stresses that may result in powder failure beyond its elastic limit. This functional relationship can be quite complex for powders, as illustrated in both principal stress space and shear versus normal stress in Fig. 21-36. See Nadia (loc. cit.), Stanley-Wood (loc. cit.), and Nedderman (loc. cit.) for details. Only the most basic features for **isotropic hardening** of the yield surface are mentioned here.

1. There exists a **critical state line**, also referred to as the **effective yield locus**. The effective yield locus represents the relationship between shear stress and applied normal stress for powders always in a critically consolidated state. That is, the powder is not over- or undercompacted but rather has obtained a steady-state density. This density increases along the line with increases in normal stress, and bed porosity decreases.

2. A given yield locus generally has an envelope shape; the initial density for all points forming this locus prior to shear is constant. That is, the locus represents a set of points all beginning at the porosity; this critical state porosity is determined by the intersection with the effective yield locus.

3. Points to the left of the effective yield locus are in a state of overconsolidation, and they dilate upon shear. If sheared long enough, the density and shear stress will continue to drop until reaching the effective yield locus. Points to the right are underconsolidated and compact with shear.

4. For negative normal stresses, a state of tension exists in the sample along the yield locus. This area is generally not measured by direct shear cells, but can be measured by triaxial shear and tensile split cells.

5. Multiple yield loci exist. As a powder is progressively compacted along the effective yield locus, it gains strength as density rises, reaching progressively higher yield loci. Yield loci of progressively larger envelope size have higher critical density and lower critical voidage, as shown in Fig. 21-36. Therefore, the shear strength of a powder τ is a function of the current normal stress σ , as well as its consolidation history or stress σ_c , which determined the starting density prior to shear.

Currently in industrial practice, we are most concerned with the overcompacted state of the powder, and applications of the undercompacted and tensile data are less common, although they are finding applications in compaction processes of size enlargement (see "Powder Compaction").

Although the yield locus in the overcompacted state may possess significant curvature, especially for fine materials, a common **Mohr-Coulomb** linear approximation to the yield locus as shown in Fig. 21-37 is given by

$$\tau = c + \mu\sigma = c + \sigma \tan \phi \tag{21-34}$$

Here, μ is the **coefficient of internal friction**, ϕ is the **internal angle of friction**, and c is the shear strength of the powder in the absence of any applied normal load. Overcompacted powders dilate when sheared, and the ability of powders to change volume with shear results in the powder's shear strength τ being a strong function of previous compaction. There are therefore a series of yield loci (YL), as illustrated in Fig. 21-37, for increasing previous consolidation stress. The individual yield loci terminate at a critical state line or effective yield locus (EYL) defined early, which typically passes through the stress-strain origin, or

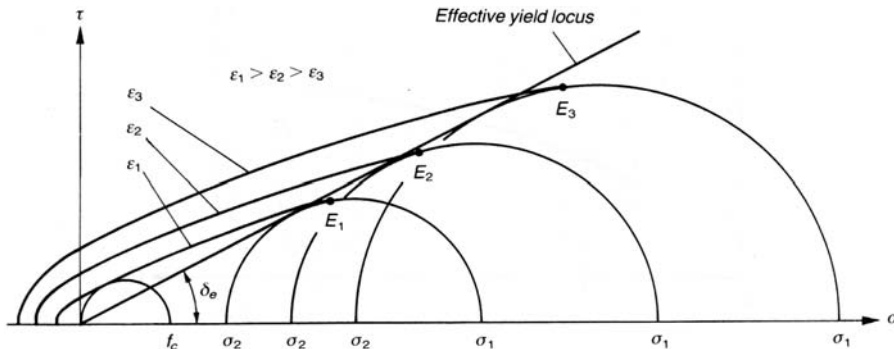


FIG. 21-36 Family of yield loci for a typical powder. (Rumpf, loc. cit., with permission.)

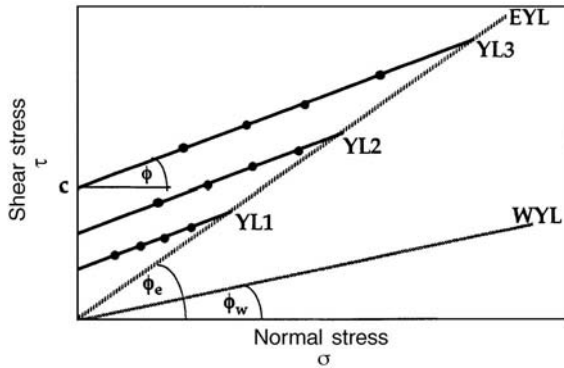


FIG. 21-37 The yield loci of a powder, reflecting the increased shear stress required for flow as a function of applied normal load. YL1 through YL3 represent yield loci for increasing previous compaction stress. EYL and WYL are the effective and wall yield loci, respectively.

$$\tau = \mu_e \sigma = \sigma \tan \phi_e \tag{21-35}$$

where μ_e is the **effective coefficient of powder friction** and ϕ_e is the **effective angle of powder friction** of the powder. In practice, there may be a small cohesion offset in the effective yield locus, in which case the effective angle is determined from a line intercepting an origin and touching the effective yield locus. In this case, the effective angle of friction is an asymptotic function of normal stress.

When sheared powders also experience friction along a wall, this relationship is described by the **wall yield locus**, or

$$\tau = \mu_w \sigma = \sigma \tan \phi_w \tag{21-36}$$

where μ_w is the **effective coefficient of wall friction** and ϕ_w is the **effective angle of wall friction**, respectively. In practice, there is a small **wall adhesion** offset, making the effective angle of wall friction an asymptotic function of normal stress, as with effective powder friction.

Lastly, both static (incipient powder failure) and dynamic (continued-flow) yield loci may be measured, giving both static and dynamic values of wall and powder friction angles as well as wall adhesion.

Flow Functions and Flowability Indices Consider a powder compacted in a mold at a **compaction pressure** σ_1 . When it is removed from the mold, we may measure the powder's strength, or **unconfined uniaxial compressive yield stress** f_c (Fig. 21-38). The unconfined yield and compaction stresses are determined directly from Mohr circle constructions to yield loci measurements (Fig. 21-36). This strength increases with increasing previous compaction, with this relationship referred to as the powder's **flow function** FF.

The flow function is the paramount characterization of powder strength and **powder flowability**. Common examples are illustrated in Fig. 21-38. Typically the flow function curves toward the normal stress axis with increasing load (A). An upward shift in the flow function indicates an overall gain of strength (B). If one were comparing the flowability of two lots of material, this would indicate a decrease in flowability. In other words, greater stresses would be required in processing for lot B than for lot A (e.g., hoppers, feeders, mixers) to overcome the strength of the powder and to induce flow of the mass. An upward shift also occurs with **time consolidation**, where a specified time of consolidation is allowed prior to each shear step of the yield locus. The resulting flow function is a **time flow function**, and it indicates the effect of prolonged storage on flow. Flow functions often cross (C vs. A), indicating lot C is more flowable at low pressure than lot A, but less flowable at high pressure. An upward curvature of the flow function is indicative of powder or granule degradation (C), with large gains of strength as breakdown of the material occurs, raising powder density and interparticle contacts.

Under the linear Mohr-Coloumb approximation, if parallel yield loci are assumed with constant angle of internal friction, and with zero intercept of the effective yield locus, the flow function is a straight line through the origin D, given by

$$f_c = f_{co} + A\sigma_1 = \left[\frac{2}{\cos \phi} \left(\frac{1 + \sin \phi}{1 + \sin \phi_e} \right) (\sin \phi_e - \sin \phi) \right] \sigma_1 \quad \text{where } f_{co} = 0 \tag{21-37}$$

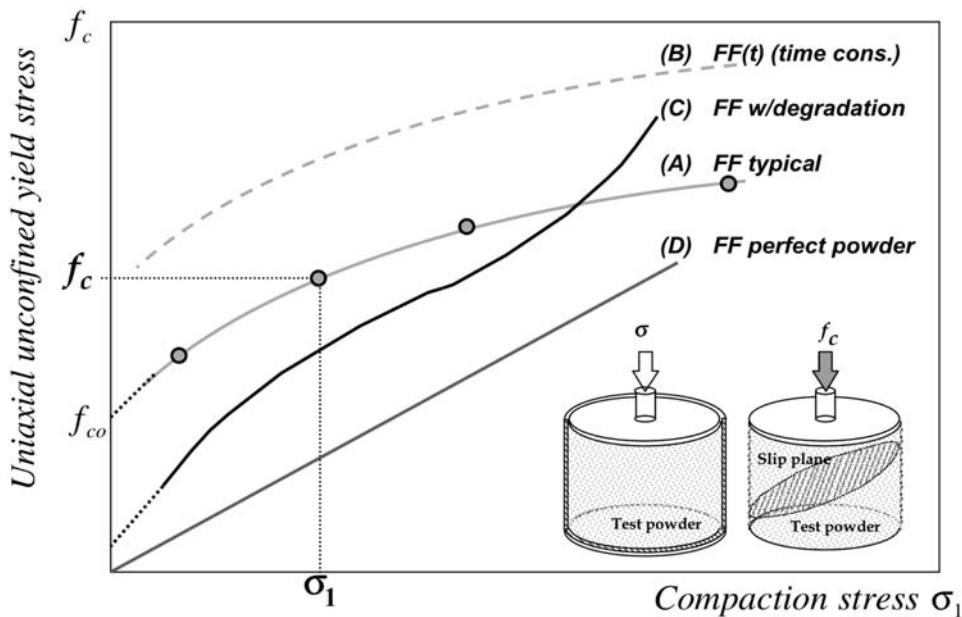


FIG. 21-38 Common flow functions of powder. (From Measuring Powder Flowability and Its Applications, E&G Associates, 2006, with permission.)

Other workers assume a linear form with a nonzero intercept f_c . This implies a minimum powder strength in the absence of gravity or any other applied consolidation stresses. As described above, the flow function is often curved, likely due to the angles of friction being a function of applied stress, and various fitting relations are extrapolated to zero to determine f_c . While this is a typical practice, it has questionable basis as the flow function may have pronounced curvature at low stress.

The flow function and powder strength have a large impact on minimum discharge opening sizes of hoppers to prevent arching and rat holing, mass discharge rates, mixing and segregation, and compact strength.

One may compare the flowability of powders at similar pressures by comparing their unconfined yield stress f_c at a single normal stress, or one point off a flow function. In this case one should clearly state the pressure of comparison. **Flow indices** have been defined to aid such one-point comparisons, given by the ratio of normal stress to strength, or

$$Rel_p = \frac{\sigma_1 - \sigma_3}{f_c} \quad \text{or} \quad Rel_j = \frac{\sigma_1}{f_c} \quad (21-38)$$

The first is due to Peschl (Peschl and Colijn, New Rotational Shear Testing Technique, Bulk Solids Handling and Processing Conference, Chicago, May 1976). For powders in the absence of caking it has a minimum value of 1 for a perfectly plastic, cohesive powder. The second definition is due to Jenike (Jenike, Storage and Flow of Bulk Solids, *Bull. 123*, Utah Eng Expt. Stn., 1964). The reciprocal of these **relative flow indices** represents a normalized yield strength of the powder, normalized by maximum consolidation shear in the case of Peschl and consolidation stress in the case of Jenike. Flowability increases with decreasing powder strength, or increasing flow index. Table 21-5 provides typical ranges of behavior for varying flow index. For powders of varying bulk density, **absolute flow indices** should be used, or

$$Abs_{p \text{ or } j} = Rel_{p \text{ or } j} \times (\rho_b/\rho_{H_2O}) \quad (21-39)$$

Therefore, for powders of equal powder strength, flowability increases with increasing bulk density for gravity-driven flow.

Shear Cell Standards and Validation While shear cells vary in design, and may in some cases provide differing values of powder strength, the testing does have an engineering basis in geotechnical engineering, and engineering properties are measured, i.e., yield stresses of a powder versus consolidation. As opposed to other phenomenological, or *instrument-specific*, characterizations of powder flowability, shear cells generally provide a common reliable ranking of flowability, and such data are directly used in design, as discussed below. (See also “Solids Handling: Storage, Feeding, and Weighing.”) Rotary split cells (ASTM D6682-01), translation Jenike cells (ASTM D6128-97), and rotary annular ring cells (ASTM D6682-01) all have ASTM test methods. In addition, units may be validated against an independent, international powder standard, namely, the BCR-116 limestone validation powder for shear cell testing (Commission of the European Communities: Community Bureau of Reference). Table 21-6 provides an excerpt of shear values expected for the standard, and Fig. 21-39 provides a yield loci comparison between differing cell designs and a comparison to the standard values.

Stresses in Cylinders Bulk solids do not uniformly transmit stress. Consider the forces acting on a differential slice of material in,

TABLE 21-5 Typical Ranges of Flowability for Varying Flow Index, Modified after Peschl

Flow index	Level of cohesion	Example
Rel _p : < 1	Bonding, solid	Caked material, time consolidated
= 1	Plastic material	Wet mass
1-2	Extremely cohesive	Magstearate, starch (nongravity)
2-4	Very cohesive	Coarse organics
4-10	Cohesive	Granules inorganics
10-15	Slightly cohesive	Hard silica, sand
15-25	Cohesionless	If fine, floodable

From Measuring Powder Flowability and Its Applications, E&C Associates, 2006, with permission.

TABLE 21-6 BCR-116 Limestone Validation Powder for Shear Cell Testing

COMMISSION OF THE EUROPEAN COMMUNITIES CERTIFIED REFERENCE MATERIAL CERTIFICATE OF MEASUREMENT CRM 116 LIMESTONE POWDER FOR JENIKER SHEAR TESTING			
CONSOLIDATION NORMAL STRESS kPa	SHEAR NORMAL STRESS kPa	MEAN SHEAR STRESS kPa	UNCERTAINTY kPa
3.0	3.0	2.14	± 0.31
3.0	2.0	1.75	± 0.19
3.0	1.75	1.64	± 0.17
3.0	1.5	1.54	± 0.14
3.0	1.25	1.41	± 0.13
3.0	1.0	1.27	± 0.10

say, a cylindrical bin (Fig. 21-40). Prior to failure or within the elastic limit, the axial stresses σ_z and radial stresses σ_r , under the assumption they are principal stresses, are related by

$$\sigma_r = \frac{\nu}{1 - \nu} \sigma_z \quad (21-40)$$

where ν is the Poisson ratio. Under active incipient failure, the axial and radial stresses are related by a lateral stress coefficient K_a given by

$$K_a = \frac{\sigma_r}{\sigma_z} = \frac{1 - \sin \phi_w}{1 + \sin \phi_w} \quad (\text{active}) \quad (21-41)$$

In the case of wall friction, the axial and radial stresses differ somewhat from the true principal stresses, and the stress coefficient becomes

$$K_a = \frac{\sigma_r}{\sigma_z} = \frac{1 - \sin \phi_w \cos(\omega - \phi_w)}{1 + \sin \phi_w \cos(\omega - \phi_w)} \quad \text{where} \quad \sin \omega = \frac{\sin \phi_w}{\sin \phi_c} \quad (21-42)$$

This may be contrasted to, e.g., the isotropic pressure developed in a fluid under pressure, with only nonnewtonian fluids able to develop and sustain a nonisotropic distribution of normal stress. In addition, the radial normal stress acting at the wall develops a wall shear stress that opposes gravity and helps support the weight of the powder. As originally developed by Janssen [*Zeits. D. Vereins Deutsch Ing.*, **39**(35), 1045 (1895)], from a balance of forces on a differential slice, the axial stress σ_z as a function of depth z is given by

$$\sigma_z = \frac{\rho_b g D}{4\mu_w K_a} (1 - e^{-(4\mu_w K_a/D)z}) \quad (21-43)$$

where D is the diameter of the column. Several comments may be made of industrial practicality:

1. Pressure initially scales with height as one would expect for a fluid, which may be verified by expanding Eq. (21-35) for small z . Or $\sigma_z \approx \rho_b g z$.

2. For sufficient depth (at least one diameter), the pressure reaches a maximum value given by $\sigma_z = \rho_b g D / (4\mu_w K_a)$. Note that this pressure scales with cylinder diameter, and not height. This is a critical property to keep in mind in processing; that diameter often controls pressure in a powder rather than depth. A commonplace example would be comparing the tall aspect ratio of a corn silo to that of a liquid storage vessel. The maximum pressure in the base of such a silo is controlled by diameter, which is kept small.

3. The exact transition to constant pressure occurs at roughly $2z_c$, where $z_c = D / (4\mu_w K_a)$.

Stress transmission in powders controls flow out of hoppers, feeders, filling of tubes, and compaction problems such as tableting and roll pressing. (See “Powder Compaction.”)

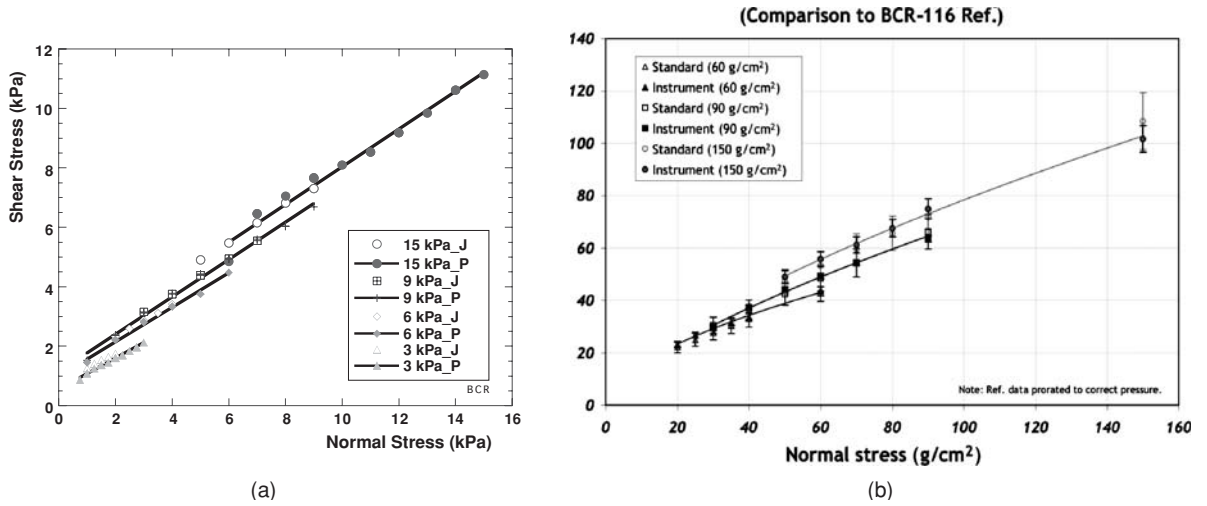


FIG. 21-39 Shear cell BCR-116 limestone validation yield loci. (a) Comparison of Jenike translational to Peschl rotary shear cell data (*DuPont, 1994, used with permission*). (b) Typical validation set performed on an iShear™ rotary shear cell as compared to BCR standard (2005). (*Courtesy E&G Associates, Inc.*)

Mass Discharge Rates for Coarse Solids The mass discharge rate from a flat-bottom bin with a circular opening of diameter B has been shown experimentally to be independent of bin diameter D and bed fill height H , for $H > 2B$. Dimensional analysis then indicates that the mass discharge rate W must be of the form $W = C\rho\sqrt{g}B^{3/2}$, where C is a constant function of powder friction. Such a form was verified by Beverloo [Beverloo et al., *Chem. Eng. Sci.*, **15**, 260 (1961)] and Hagen (1856), leading to the **Beverloo equation** of mass discharge, or

$$W_o = C\rho_b\sqrt{g(B - kd_p)^{2.5}} \approx 0.52\rho_bA\sqrt{2gB} \quad \text{for } B \gg d_p \quad (21-44)$$

Here, ρ_b is loose poured bulk density, $C \sim 0.58$ and is nearly independent of friction, $k = 1.5$ for spherical particles and is somewhat larger for angular powders, d_p is particle size, and A is the area of the opening. The correction term of particle size represents an excluded annulus effective lowering the opening diameter. See Nedderman (*Statics and Kinematics of Granular Materials*, Cambridge University Press, 1992) and Brown and Richards (*Principles of Powder Mechanics*, Pergamon Press, 1970) for reviews.

The Beverloo relation for solids discharge may be contrasted with the mass flow rate of an inviscid fluid from an opening of area A , or

$$W = 0.64\rho_bA\sqrt{2gH} \quad (21-45)$$

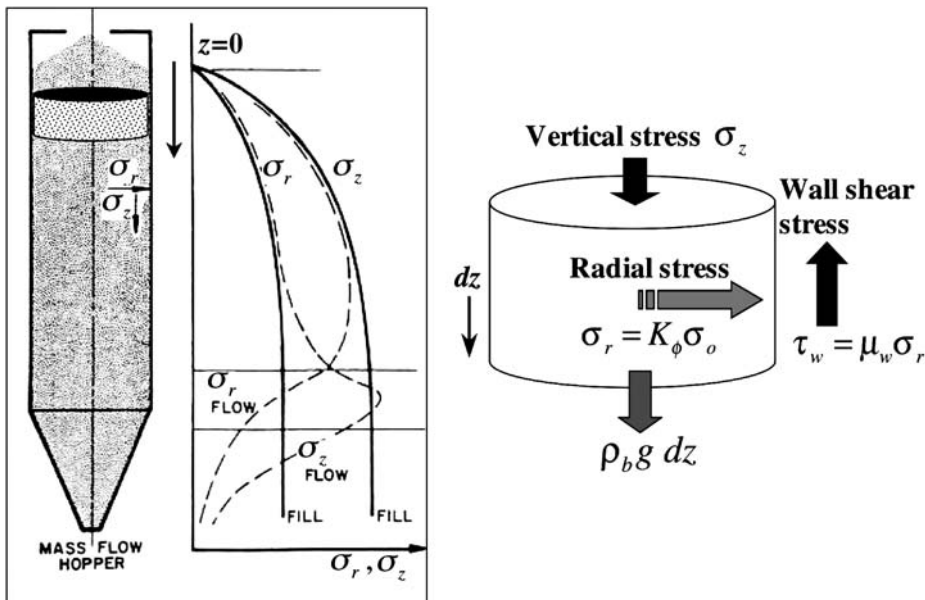


FIG. 21-40 Stresses in a vertical cylinder. [*From Measuring Powder Flowability and Its Applications, E&G Associates, 2006, with permission.*]

where ρ_f is fluid density. Note that mass flow rate scales with height, which controls fluid pressure, compared to mass discharge rates, which scale with orifice diameter.

For coarse materials of typical friction, discharge rates predicted by the Beverloo relation are within 5 percent for experimental values for discharge from flat-bottom bins or from hoppers emptying by **funnel flow**, and are most reliable for material of low powder cohesion, in the range of $400 \mu\text{m} < d_p < B/6$. However, for fine materials less than $100 \mu\text{m}$ or materials large enough to give mechanical interlocking, the Beverloo relation can substantially overpredict discharge.

Equation (21-45) may be generalized for noncircular openings by replacing diameter by hydraulic diameter, given by 4 times the opening area divided by the perimeter. The excluded annulus effect can be incorporated by subtracting kd_p from all dimensions. For slot opening of length $L \gg B$ with B as slot width, discharge rates have been predicted to within 1 percent for coarse materials (Myers and Sellers, Final Year Project, Department of Chemical Engineering, University of Cambridge, UK, 1977) by

$$W_o = \frac{4\sqrt{2}C}{\pi} \rho_b \sqrt{g(L - kd_p)} (B - kd_p)^{2.5} \quad (21-46)$$

Through solutions of radial stress fields acting at the opening, the discharge rate for smooth, wedge-shaped hoppers emptying by **mass flow** is given by the **hourglass theory** of discharge [Savage, *Br. J. Mech. Sci.*, **16**, 1885 (1967); Sullivan, Ph.D. thesis, California Institute of Technology, 1972; Davidson and Nedderman, *Trans. Inst. Chem. Eng.*, **51**, 29 (1973)]:

$$W = \frac{W_o}{\sin^{1/2} \alpha} \quad \text{where} \quad C(K_p) = \frac{\pi}{4} \sqrt{\frac{1 + K_p}{2(2K_p - 3)}} \quad (21-47)$$

where α is the vertical hopper half-angle, $C = fn(K_p)$, and K_p is the passive Rankine stress coefficient given by

$$K_p = \frac{1 + \sin \phi_e}{1 - \sin \phi_e} \quad (21-48)$$

Here C is a decreasing function of powder friction, ranging from 0.64 to 0.47 for values of ϕ_e ranging from 30° to 50° . Equation (21-46) generally overpredicts wedge hopper rates by a factor of 2, primarily due to neglect of wall friction. The impact of wall friction may be incorporated through the work of Kaza and Jackson [*Powder Technology*, **39**, 915 (1984)] by replacing K_p with a modified coefficient κ given by

$$\kappa = K_p + \frac{(\omega + \phi_w) \sin \phi_e}{\alpha(1 - \sin \phi_e)} \quad (21-49)$$

From Eqs. (21-46) to (21-48), the mass flow discharge rate from wedge hopper increases with increasing orifice diameter $B^{2.5}$, increasing bulk density, decreasing powder friction and wall friction, and decreasing vertical hopper half-angle, and is independent of bed height.

Extensions to Mass Discharge Relations Johanson (*Trans. Soc. Min. Eng.*, March 1965) extended the Beverloo relations to include the effect of powder cohesion, with mass discharge rate given by

$$W_{sc} = 1.354 W_o \sqrt{\frac{1}{2m \tan \alpha} \left(1 - \frac{f_c}{\sigma_{ia}}\right)} \quad (21-50)$$

Here W_{sc} is the steady-state discharge rate for a cohesive powder for unconfined uniaxial compressive strength f_c , and $m = 1$ or 2 for a slot hopper or a conical hopper, respectively. σ_{ia} is the major consolidation stress acting at the hopper opening. Note that the discharge rate increases with increasing stress at the opening and decreasing powder strength, and that the major stress σ_{ia} must exceed the powder's strength f_c for flow to occur. In addition, Johanson determined an initial dynamic mass discharge rate given by

$$W_{dc} = W_{sc} \left(1 - 1.39 \frac{T}{t}\right) \quad \text{where} \quad T = \frac{W_{sc}}{2\rho_f g A} \left(\frac{1}{1 - f_c/\sigma_{ia}}\right) \quad (21-51)$$

where T is the period required to achieve steady-state state flow, which increases with the increases in the required steady discharge rate and increasing powder cohesion f_c .

It is also especially critical to note that an **applied surface pressure** to the top of the powder bed will *not* increase the flow rate. In fact, it is more likely to decrease the flow rate by increasing powder cohesive strength f_c . Similarly, **vibration** will increase flow rate only if the powder is in motion, primarily by lowering wall friction. If discharge is halted, vibration can lower or stop the discharge rate by compacting and raising powder strength.

Stresses in powders are an increasing function of diameter [cf. Eq. (21-43)]. Therefore, as a powder moves toward the opening, the stress acting upon it decreases and the powder undergoes a decrease in bulk density. The displaced solids volume due to the corresponding increase in powder voidage must be matched by an inflow of gas. For coarse solids governed by the Beverloo relation, this inflow of gas occurs with little air pressure change with negligible effect on mass discharge. However, for fine powders of low permeability defined above, large gas pressure gradients will be created at the opening, which opposes solids discharge. There is therefore a decrease in mass discharge with decreasing powder **permeability**, or decreasing particle size of the bulk solid. Verghese (Ph.D. thesis, University of Cambridge, UK, 1991) proposed an initial relation of the form

$$W = W_o \left(1 - \frac{\lambda}{\rho_b g d_p^2}\right)^{1/2} \frac{\lambda}{\rho_b g} \approx 1.48 \times 10^{-8} \text{ m}^3 \quad (21-52)$$

The decrease in mass discharge rate from the Beverloo relation for decreasing particle size is illustrated in Fig. 21-41. For fine enough materials, bubbling and fluidization actually halt flow from the orifice, after which a gain in bulk density will again initialize flow. This may be witnessed with fine sands discharging from hourglasses. A similar relation based on venting required predicted from the Carman-Kozeny equation gives a fine powder mass discharge rate of

$$W \approx \frac{2\pi(B/\sin \alpha)^3 \rho_b^2 d_p^2 g (1 - \cos \alpha) \epsilon^3}{180 \mu_g (1 - \epsilon)^3} \quad (21-53)$$

where μ_g is gas viscosity and ϵ is the bed voidage.

Gas venting may be used to increase discharge rate, either through venting in the hopper wall or through imposed pressure gradients. The involved pressure drops or required air volumes may be calculated from standard pressure drop correlations, based on, e.g., Darcy's law or the Ergun equation. For air-augmented flow, discharge rates are given by

$$W = W_o \left[1 + \left(\frac{2\kappa - 3}{2\kappa - 1}\right) \frac{\Delta P}{\rho g r_o}\right]^{1/2} \quad \text{for } Re_o < 10 \quad (21-54)$$

$$W = W_o \left[1 + \left(\frac{2\kappa - 3}{2\kappa - 1}\right) \frac{3 \Delta P}{\rho g r_o}\right]^{1/2} \quad \text{for } Re_o \text{ large} \quad (21-55)$$

$$W = W_o \left[1 + \left(\frac{150 + 5.25 Re_o}{150 + 1.75 Re_o}\right) \left(\frac{2\kappa - 3}{2\kappa - 1}\right) \left(\frac{\Delta P}{\rho g r_o}\right)\right]^{1/2} \quad \text{for intermediate } Re_o \quad (21-56)$$

where r_o is the radial distance from the hopper apex, $\Delta P/r_o$ is the pressure drop imposed across the orifice, and Re_o is the gas Reynolds number acting at the orifice (see Nedderman, *Statics and Kinematics of Granular Materials*, Cambridge University Press, 1992).

Other Methods of Flow Characterization A variety of other test methods to characterize flowability of powders have been proposed, which include density ratios, flow from funnels and orifices, angles of repose and sliding, simplified indicizer flow testing, and

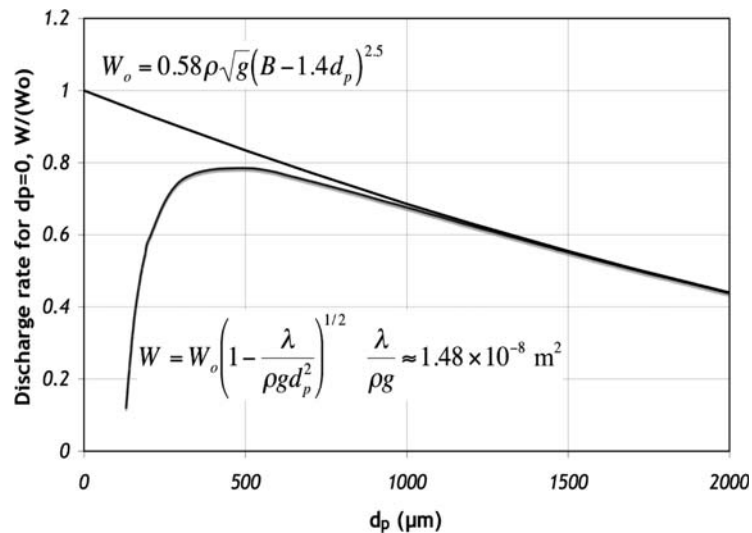


FIG. 21-41 The impact of decreasing particle size and bulk permeability on mass discharge rate.

tumbling avalanche methods. These methods should be used with caution, as (1) they are often a strong function of the test method and instrument itself, (2) engineering properties useful for either scale-up or a priori design are not measured, (3) they are only a crude characterization of flowability, and often suffer from lack of reproducibility, (4) they lack a fundamental basis of use, and (5) they suffer from the absence of validation powders and methods. The first two points are particularly crucial, the end result of which is that the ranking of powders determined by the apparatus cannot be truly linked to process performance, as the states of stress in the process may differ from the apparatus, and further, the ranking of powders may very well change with scale-up. In contrast, shear cells and permeability properties may be used directly for design, with no need for arbitrary scales of behavior, and the effect of changing stress state with scale-up can be predicted. Having said this, many of these methods have found favor due to the misleading ease of use. In some defined cases they may be useful for quality control, but should not be viewed as a replacement for more rigorous flow testing offered by shear cell and permeability testing.

Various **angles of repose** may be measured, referring to the horizontal angle formed along a powder surface. These include the angle of a heap, the angle of drain for material remaining in a flat-bottom bin, the angle of sliding occurring when a dish of powder is inclined, rolling angles in cylinders, and dynamic and static discharge angles onto vibrating feed chutes (Thompson, *Storage of Particulate Solids*, in *Handbook of Powder Science and Technology*, Fayed and Otten (eds.), Van Nostrand Reinhold Co., 1984). From Eq. (21-37) describing the impact of the angles of friction—as measured by shear cell—on cohesive strength, the angle of repose may be demonstrated to lack a true connection to flowability. For cohesive powders, there will be large differences between the internal and effective angles of friction, and the unconfined strength increases with an increase in the difference in sine of the angles. When one is measuring the angle of repose in this case, wide variations in the angle of the heap will be observed, and it likely varies between the angles of friction, making the measurement of little utility in a practical, measurement sense. However, when the difference in the angles of friction approaches zero, the angle of repose will be equal to both the internal and effective angle of friction. But at that point, the cohesive strength of the powder is zero [Eq. (21-37)], regardless of the angle of repose.

In is likely the above has formed the basis for the use of rotating **avalanche testers**, where the size and frequency of avalanches formed on the sliding, rotating bed are analyzed as a deviation of the time between avalanches, as well as strange attractor diagrams. This

approach is more consistent with the *variation* in the angle of repose being related to powder strength [Eq. (21-37)].

The typical density ratios are the **Carr** and **Hausner ratios**, given by

$$FI_{\text{Carr}}[\%] = 100 \frac{\rho_{b(\text{tapped})} - \rho_{b(\text{loose})}}{\rho_{b(\text{tapped})}} \quad \text{and} \quad FI_H[-] = \frac{\rho_{b(\text{tapped})}}{\rho_{b(\text{loose})}} \quad (21-57)$$

where $\rho_{b(\text{tapped})}$ is the equilibrium packed bulk density achieved under tapping. It could equally be replaced with a bulk density achieved under a given pressure. The Carr index is a measure of **compressibility**, or the gain in bulk density under stress, and is directly related to gain in powder strength. Large gains in density are connected to differences in the state of packing in the over- and critically consolidated state defined above (see “Yield Behavior of Powders”), which in turn results in differences between the internal and effective angles of friction, leading to a gain in unconfined yield strength [Eq. (21-37)]. However, the results are a function of the method and may not be discriminating for free-flowing materials. Lastly, changes in density are only one of many contributions to unconfined yield stress and powder flowability. Hence, Carr and Hausner indices may incorrectly rank flowability across ranges of material class that vary widely in particle mechanical and surface properties.

Two methods of **hopper flow characterization** are used. The first is the Flowdex™ tester, which consists of a cup with interchangeable bottoms of varying orifice size. The cup is filled from a funnel, and the covering lid then drops from the opening. The minimum orifice in millimeters required for flow to occur is determined as a ranking of flowability. This minimum orifice is analogous to the minimum orifice diameter determined from shear cell data for hopper design. Alternatively, the mass discharge rate out of the cup or from a funnel may be determined. Various methods of vibration both before and after initiation of flow may be utilized. Mass discharge rates, as expected, rank with the correlations described above. The disadvantage of this characterization method is that it is a direct function of hopper/cup geometry and wall friction, and has a low state of stress that may differ from the actual process. If a process hopper differs in vertical half-angle, wall friction, opening size, solids pressure, filling method, or a range of other process parameters, the ranking of powder behavior in practice may differ from the lab characterization, since scalable engineering properties are not measured.

The last set of tests includes **solid indicizers** pioneered by Johanson. These include the Flow Rate and Hang-Up Indicizers™ [cf. Bell et al., Practical Evaluation of the Johanson Hang-Up Indicizer, *Bulks Solids Handling*, 14(1), 117 (Jan. 1994)]. They represent simplified versions of permeability and shear cell tests. Assumptions are made with regard to typical pressures and wall frictions, and based on these, a

flow ranking is created. Their degree of success in an application will largely rest on the validity of the property assumptions. For defined conditions, they can give similar ranking to shear cell and permeability tests. The choice of use is less warranted than in the past due to the progress in automating shear cell and permeability tests, which has simplified their ease of use.

SOLIDS MIXING

GENERAL REFERENCES: Fan, Chen, and Lai, Recent Developments in Solids Mixing, *Powder Technology*, 61, 255–287 (1990); N. Harnby, M. F. Edwards, A. W. Nienow (eds.), *Mixing in the Process Industries*, 2d ed., Butterworth-Heinemann, 1992; B. Kaye, *Powder Mixing*, 1997; Ralf Weinekötter and Herman Gericke, *Mixing of Solids, Particle Technology Series*, Brian Scarlett (ed.), Kluwer Academic Publishers, Dordrecht 2000.

PRINCIPLES OF SOLIDS MIXING

Industrial Relevance of Solids Mixing The mixing of powders, particles, flakes, and granules has gained substantial economic importance in a broad range of industries, including, e.g., the mixing of human and animal foodstuff, pharmaceutical products, detergents, chemicals, and plastics. As in most cases the mixing process adds significant value to the product, the process can be regarded as a key unit operation to the overall process stream.

By far the most important use of mixing is the production of a homogeneous blend of several ingredients which neutralizes variations in concentration. But if the volume of material consists of one ingredient or compound exhibiting fluctuating properties caused by an upstream production process, or inherent to the raw material itself, the term *homogenization* is used for the neutralization of these fluctuations. By mixing, a new product or intermediate is created for which the quality and price are very often dependent upon the efficiency of the mixing process. This efficiency is determined both by the materials to be mixed, e.g., particle size and particle-size distribution, density, and surface roughness, and by the process and equipment used for performing the mixing. The design and operation of the mixing unit itself have a strong influence on the quality produced, but upstream material handling process steps such as feeding, sifting, weighing, and transport determine also both the quality and the capacity of the mixing process. Downstream processing may also destroy the product quality due to segregation (demixing). Continuous mixing is one solution which limits segregation by avoiding storage equipment.

The technical process of mixing is performed by a multitude of equipment available on the market. However, mixing processes are not always designed with the appropriate care. This causes a significant financial loss, which arises in two ways:

1. *The quality of the mix is poor:* In cases where the mixing produces the end product, this will be noticed immediately at the product's quality inspection. Frequently, however, mixing is only one in a series of further processing stages. In this case, the effects of unsatisfactory blending are less apparent, and might possibly be overlooked to the detriment of final product quality.

2. *The homogeneity is satisfactory but the effort employed is too great (overmixing):* Overmixing in batch blending is induced by an overlong mixing time or too long a residence time in the case of continuous blending. This leads to increased strain on the mixture, which can have an adverse effect on the quality of sensitive products. Furthermore, larger or more numerous pieces of equipment must be used than would be necessary in the case of an optimally configured mixing process.

Mixing Mechanisms: Dispersive and Convective Mixing The mixing process can be observed in diagrammatic form as an over-

lap of **dispersion** and **convection** (Fig. 21-42). Movement of the particulate materials is a prerequisite of both mechanisms. **Dispersion** is understood to mean the completely random change of place of the individual particles. The frequency with which the particles of *ingredient A* change place with those of another is related to the number of particles of the other ingredients in the *direct vicinity* of the particles of *ingredient A*. Dispersion is therefore a local effect (**micromixing**) taking place in the case of premix systems where a number of particles of different ingredients are in proximity, leading to a fine mix localized to very small areas. If the ingredients are spatially separated at the beginning of the process, long times will be required to mix them through dispersion alone, since there is a very low number of *assorted neighbors*. Dispersion corresponds to diffusion in liquid mixtures. However, in contrast to diffusion, mixing in the case of dispersion is not caused by any concentration gradient. The particles have to be in motion to get dispersed. **Convection** causes a movement of large groups of particles relative to each other (**macromixing**). The whole volume of material is continuously divided up and then mixed again after the portions have changed places (Fig. 21-42). This forced convection can be achieved by rotating elements. The dimension of the groups, which are composed of just one unmixed ingredient, is continuously reduced splitting action of the rotating paddles. Convection increases the number of *assorted neighbors* and thereby promotes the exchange processes of dispersive mixing. A material mass is divided up

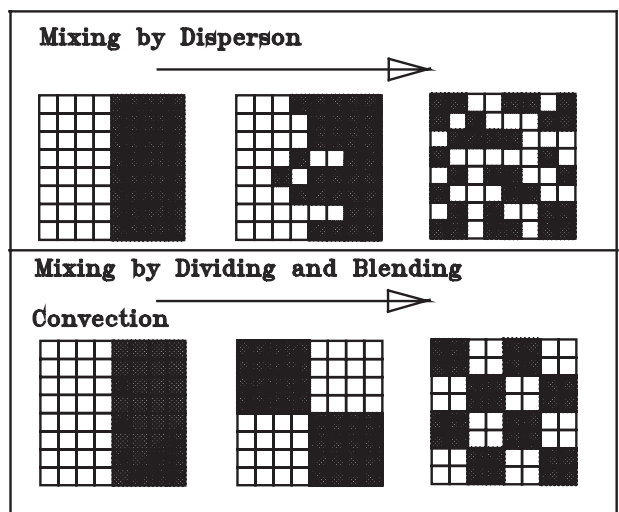


FIG. 21-42 The mixing process can be observed in diagrammatic form as an overlap of *dispersion* and *convection*. Mixture consists of two components A and B; A is symbolized by the white block and B by the hatched block. Dispersion results in a random arrangement of the particles; convection results in a regular pattern.

or convectively mixed through the rearrangement of a solid's layers by rotating devices in the mixer or by the fall of a stream of material in a static gravity mixer, as discussed below.

Segregation in Solids and Demixing If the ingredients in a solids mixture possess a selective, individual motional behavior, the mixture's quality can be reduced as a result of segregation. As yet only a partial understanding of such behavior exists, with particle movement behavior being influenced by particle properties such as size, shape, density, surface roughness, forces of attraction, and friction. In addition, industrial mixers each possess their own specific flow conditions. Particle size is, however, the dominant influence in segregation (J. C. Williams, *Mixing, Theory and Practice*, vol. 3, V. W. Uhl and J. B. Gray, (eds.), Academic Press, Orlando, Fla., 1986). Since there is a divergence of particle sizes in even a single ingredient, nearly all industrial powders can be considered as solid mixtures of particles of different size, and segregation is one of the characteristic problems of solids processing which must be overcome for successful processing. If mixtures are unsuitably stored or transported, they will separate according to particle size and thus segregate. Figure 21-43 illustrates typical mechanisms of segregation.

Agglomeration segregation arises through the preferential self-agglomeration of one component in a two-ingredient mixture (Fig. 21-43a). Agglomerates form when there are strong interparticle forces, and for these forces to have an effect, the particles must

be brought into close contact. In the case of agglomerates, the particles stick to one another as a result, e.g., of liquid bridges formed in solids, if a small quantity of moisture or other fluid is present. Electrostatic and van der Waals forces likewise induce cohesion of agglomerates. Van der Waals forces, reciprocal induced and dipolar, operate particularly upon finer grains smaller than $30\ \mu\text{m}$ and bind them together. High-speed impellers or knives are utilized in the mixing chamber to create shear forces during mixing to break up these agglomerates. Agglomeration can, however, have a positive effect on mixing. If a solids mix contains a very fine ingredient with particles in the submicrometer range (e.g., pigments), these fine particles coat the coarser ones. An **ordered mixture** occurs, which is stabilized by the van der Waals forces and is thereby protected from segregation.

Flotation segregation can occur if a solids mix is *vibrated*, where the coarser particles *float up* against the gravity force and collect near the top surface, as illustrated in Fig. 21-43b for the case of a large particle in a mix of finer material. During vibration, smaller particles flow into the vacant space created underneath the large particle, preventing the large particle from reclaiming its original position. If the large particle has a higher density than the fines, it will compact the fines, further reducing their mobility and the ability of the large particle to sink. Solely because of the blocking effect of the larger particle's geometry there is little probability that this effect will run in reverse and that a bigger particle will take over the place left by a smaller one which has been lifted up. The large particle in this case would also have to displace several smaller ones. As a result the probability is higher that coarse particles will climb upward with vibration.

Percolation segregation is by far the most important segregational effect, which occurs when finer particles trickle down through the gaps between the larger ones (Fig. 21-43c). These gaps act as a sieve. If a solids mixture is moved, gaps briefly open up between the grains, allowing finer particles to selectively pass through the particle bed. Granted a single layer has a low degree of separation, but a bed of powder consists of many layers and interconnecting grades of particles which taken together can produce a significant division between fine and coarse grains (see Fig. 21-43), resulting in widespread segregation. Furthermore, percolation occurs even where there is but a small difference in the size of the particles (250- and $300\text{-}\mu\text{m}$ particles) [J. C. Williams, *Fuel Soc. J.*, University of Sheffield, **14**, 29 (1963)]. The most significant economical example is the poured heap appearing when filling and discharging bunkers or silos. A mobile layer with a high-speed gradient forms on the surface of such a cone, which, like a sieve, bars larger particles from passing into the cone's core. Large grains on the cone's mantle obviously slide or roll downward. But large, poorly mixed areas occur even inside the cone. Thus filling a silo or emptying it from a central discharge point is particularly critical. Remixing of such segregated heaps can be achieved through **mass flow** discharge; i.e., the silo's contents move downward in blocks, slipping at the walls, rather than emptying from the central core (**funnel flow**).

Transport Segregation This encompasses several effects which share the common factor of a gas contributing to the segregation processes. Trajectory and fluidized segregation can be defined, first, as occurring in cyclones or conveying into a silo where the particles are following the individual trajectories and, second, in fluidization. During fluidization particles are exposed to drag and gravity forces, which may lead to a segregation.

Williams (see above) gives an overview of the literature on the subject and suggests the following measures to counter segregation: The addition of a small quantity of water forms water bridges between the particles, reducing their mobility and thus stabilizing the condition of the mixture. Because of the cohesive behavior of particles smaller than $30\ \mu\text{m}$ ($\rho_s = 2$ to $3\ \text{kg/L}$) the tendency to segregate decreases below this grain size. Inclined planes down which the particles can roll should be avoided. In general, having ingredients of a uniform grain size is an advantage in blending.

Mixture Quality: The Statistical Definition of Homogeneity To judge the efficiency of a solids blender or of a mixing process in general, the status of mixing has to be quantified; thus a *degree of*

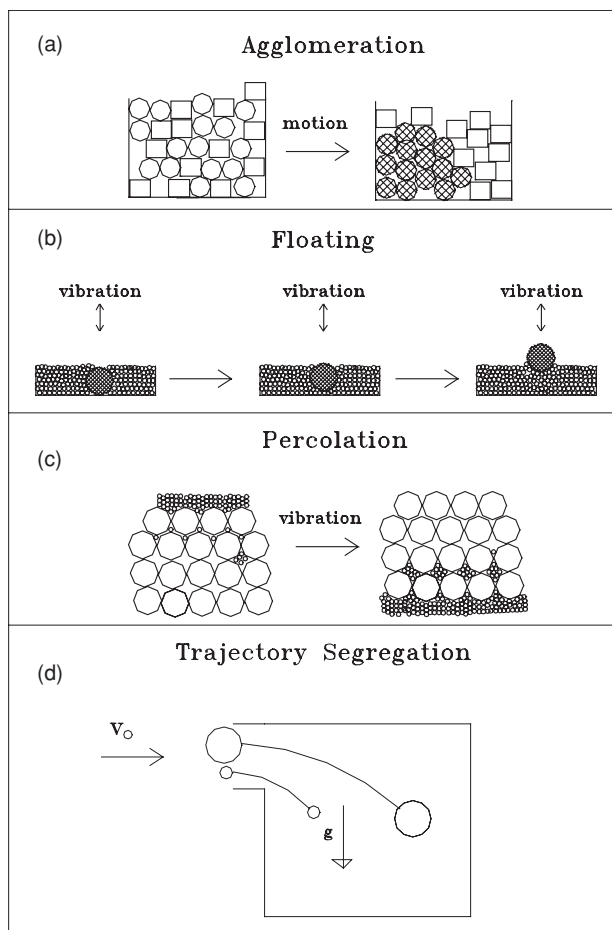


FIG. 21-43 Four mechanisms of segregation, following Williams.

mixing has to be defined. Here one has to specify what *property* characterizes a mixture, examples being composition, particle size, and temperature. The end goal of a mixing process is the uniformity of this property throughout the volume of material in the mixer. There are circumstances in which a good mix requires uniformity of several properties, e.g., particle size and composition. The mixture's condition is traditionally checked by taking a number of samples, after which these samples are examined for uniformity of the property of interest. The quantity of material sampled, or **sample size**, and the location of these samples are essential elements in evaluating a solids mixture.

Sample size thus represents the resolution by which a mixture can be judged. The smaller the size of the sample, the more closely the condition of the mixture will be scrutinized (Fig. 21-44). Dankwerts terms this the **scale of scrutiny** [P. V. Dankwerts, *The Definition and Measurement of Some Characteristics of Mixtures, Appl. Sci. Res.*, 279ff (1952)]. Specifying the size of the sample is therefore an essential step in analyzing a mixture's quality, since it quantifies the mixing task from the outset. The size of the sample can only be meaningfully specified in connection with the mixture's further application. In pharmaceutical production, active ingredients must be equally distributed; e.g., within the individual tablets in a production batch, the sample size for testing the condition of a mixture is one tablet. In less critical industries the sample size can be in tons. The traditional and general procedure is to take *identically sized* samples of the mixture from various points at *random* and to analyze them in an off-line analysis. Multielement mixtures can also be described as twin ingredient mixes when a particularly important ingredient, e.g., the active agent in pharmaceutical products, is viewed as a tracer element and all the other constituents are combined into one common ingredient. This is a simplification of the statistical description of solids mixtures. When two-element mixtures are being examined, it is sufficient to trace the concentration path of just one ingredient, the tracer. There will be a complementary concentration of the other ingredients. The description is completely analogous when the property or characteristic feature in which we are interested is not the concentration but is, e.g., moisture, temperature, or the particle's shape. If the tracer's concentration in the mixture is p and that of the other ingredients is q , we have the following relationship: $p + q = 1$. If you take samples of a specified size from the mixture and analyze them for their content of the tracer, the concentration of tracer x_i in the samples will fluctuate randomly around that tracer's concentration p in the whole mixture (the "base whole"). Therefore a mixture's quality can only be

described by using statistical means. The smaller the fluctuations in the samples' concentration x_i around the mixture's concentration p , the better its quality. This can be quantified by the statistical **variance** of sample concentration σ^2 , which consequently is frequently defined as the **degree of mixing**.

There are many more definitions of mix quality in literature on the subject, but in most instances these relate to an initial or final variance and are frequently too complicated for industrial application (K. Sommer, *Mixing of Solids*, in *Ullmann's Encyclopaedia of Industrial Chemistry*, vol. B4, Chap. 27, VCH Publishers Inc., 1992). The theoretical variance for finite sample numbers is calculated as follows:

$$\sigma^2 = \frac{1}{N_g} \sum_{i=1}^{N_g} (x_i - p)^2 \tag{21-58}$$

The relative standard deviation (RSD) is used as well for judging mixture quality. It is defined by

$$\text{RSD} = \sqrt{\sigma^2} / p \tag{21-59}$$

The variance is obtained by dividing up the whole mix, the base whole, into N_g samples of the same size and determining the concentration x_i in each sample. Figure 21-44 illustrates that smaller samples will cause a larger variance or degree of mixing.

If one analyzes not the whole mix but a number n of randomly distributed samples across the base whole, one determines instead the **sample variance** S^2 . If this procedure is repeated several times, a new value for the sample variance will be produced on each occasion, resulting in a statistical distribution of the sample variance. Thus each S^2 represents an estimated value for the unknown variance σ^2 . In many cases the concentration p is likewise unknown, and the random sample variance is then defined by using the **arithmetical average** μ of the sample's concentration x_i .

$$S^2 = \frac{1}{n-1} \sum_{i=1}^n (x_i - \mu)^2 \quad \mu = \frac{1}{n} \sum_{i=1}^n x_i \tag{21-60}$$

Random sample variance data are of little utility without knowing how accurately they describe the unknown, true variance σ^2 . The variance is therefore best stated as a desired **confidence interval** for σ^2 . The confidence interval used in mixing is mostly a unilateral one, derived by the χ^2 distribution. Interest is focused on the upper confidence limit, which, with a given degree of probability, will not be exceeded by the variance [Eq. (21-61)] [J. Raasch and K. Sommer, *The Application of Statistical Test Procedures in the Field of Mixing Technology*, in German, *Chemical Engineering*, 62(1), 17-22 (1990)], which is given by

$$W\left(\sigma^2 < (n-1) \frac{S^2}{\chi^2_1}\right) = 1 - \Phi(\chi^2_1) \tag{21-61}$$

Figure 21-45 illustrates how the size of the confidence interval normalized with the sample variance decreases as the number of random samples n increases. The confidence interval depicts the accuracy of the analysis. The smaller the interval, the more exactly the mix quality can be estimated from the measured sample variance. If there are few samples, the mix quality's confidence interval is very large. An evaluation of the mix quality with a high degree of accuracy (a small confidence interval) requires that a large number of samples be taken and analyzed, which can be expensive and can require great effort. Accuracy and cost of analysis must therefore be balanced for the process at hand.

Example 3: Calculating Mixture Quality Three tons of a sand (80 percent by weight) and cement (20 percent by weight) mix has been produced. The quality of this mix has to be checked. Thirty samples at 2 kg of the material mixture have been taken at random, and the sand content in these samples established.

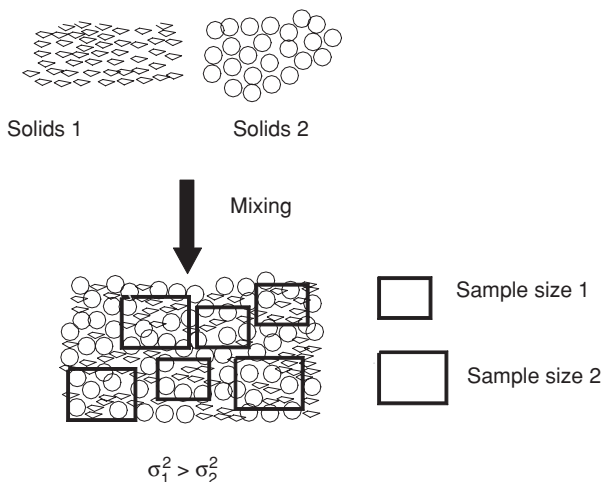


FIG. 21-44 The influence of the size of the sample on the numerical value of the degree of mixing.

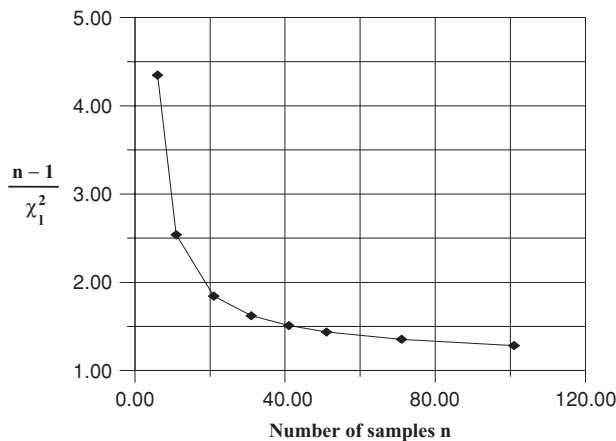


FIG. 21-45 The size of the unilateral confidence interval (95 percent) as a function of the number n of samples taken, measured in multiples of S^2 [cf. Eq. (21-62)]. Example: If 31 samples are taken, the upper limit of the variance's confidence interval assumes a value of 1.6 times that of the experimental sample variance S^2 .

The mass fraction of the sand x_i ($\text{kg}_{\text{sand}}/\text{kg}_{\text{mix}}$) in the samples comes to

3 samples @ 0.75; 7 @ 0.77; 5 @ 0.79; 6 @ 0.81; 7 @ 0.83; 2 @ 0.85

The degree of mixing defined as the variance of the mass fraction of sand in the mix needs to be determined. It has to be compared with the variance for a fully segregated system and the ideal variance of a random mix. First, the random sample variance S^2 [Eq. (21-60)] is calculated, and with it an upper limit for the true variance σ^2 can then be laid down. The sand's average concentration μ in the whole 3-ton mix is estimated by using the random sample average μ :

$$\mu = \frac{1}{n} \sum_{i=1}^n x_i = \frac{1}{30} \sum_{i=1}^{30} x_i = 0.797$$

$$S^2 = \frac{1}{n-1} \sum_{i=1}^n (x_i - \mu)^2 = \frac{1}{29} \sum_{i=1}^{30} (x_i - 0.797)^2$$

$$= \frac{1}{29} (3 \cdot 0.047^2 + 7 \cdot 0.027^2 + 5 \cdot 0.007^2 + 6 \cdot 0.013^2 + 7 \cdot 0.033^2 + 2 \cdot 0.053^2)$$

$$= 9.04 \times 10^{-4}$$

Ninety-five percent is set as the probability W determining the size of the confidence interval for the variance σ^2 . An upper limit (unilateral confidence interval) is then calculated for variance σ^2 :

$$W \left[\sigma^2 < (n-1) \frac{S^2}{\chi^2_1} \right] = 0.95 = 1 - \Phi(\chi^2_1) \Rightarrow \Phi(\chi^2_1) = 0.05$$

From the table of the χ^2 distribution summation function (in statistical teaching books) $\Phi(\chi^2_1; n-1)$ the value 17.7 is derived for 29 degrees of freedom. Figure 21-45 allows a fast judgment of these values without consulting statistical tables. Values for $(n-1)/\chi^2_1$ are shown for different number of samples n .

$$\sigma^2 < (n-1) \frac{S^2}{\chi^2_1} = 29 \cdot \frac{9.04 \times 10^{-4}}{17.7} = 14.8 \times 10^{-4} \quad (21-62)$$

It can therefore be conclusively stated with a probability of 95 percent that the mix quality σ^2 is better (equals less) than 14.8×10^{-4} .

Ideal Mixtures A perfect mixture exists when the concentration at any randomly selected point in the mix in a sample of any size is the same as that of the overall concentration. The variance of a perfect mixture has a value of 0. This is only possible with gases and liq-

uids which can be mixed molecularly and where sample volumes of the mixture are many times larger than its ingredients, i.e., molecules. In the case of solids mixtures, particle size must be considered in comparison to both sample size and sensor area. Thus σ^2 depends on the size of the sample (Fig. 21-46). There are two limiting conditions of maximum homogeneity which are the equivalent of a minimum variance: an **ordered** and a **random mixture**.

Ordered Mixtures The components align themselves according to a defined pattern. Whether this ever happens in practice is debatable. There exists the notion that because of interparticle processes of attraction, this mix condition can be achieved. The interparticle forces find themselves in an interplay with those of gravity and other dispersive forces, which would prevent this type of ordered mix in the case of coarser particles. Interparticle forces predominate in the case of finer particles, i.e., cohesive powders. Ordered agglomerates or layered particles can arise. Sometimes not only the mix condition but also the mixing of powders in which these forces of attraction are significant is termed **ordered mixing** [H. Egermann and N. A. Orr, Comments on the paper "Recent Developments in Solids Mixing" by L. T. Fan et al., *Powder Technology*, **68**, 195–196 (1991)]. However, Egermann [L. T. Fan, Y. Chen, and F. S. Lai, Recent Developments in Solids Mixing, *Powder Technology* **61**, 255–287 (1990)] points to the fact that one should only use ordered mixing to describe the condition and not the mixing of fine particles using powerful interparticle forces.

Random Mixtures A random mixture also represents an ideal condition. It is defined as follows: A uniform random mix occurs when the probability of coming across an ingredient of the mix in any subsection of the area being examined is equal to that of any other point in time for all subsections of the same size, provided

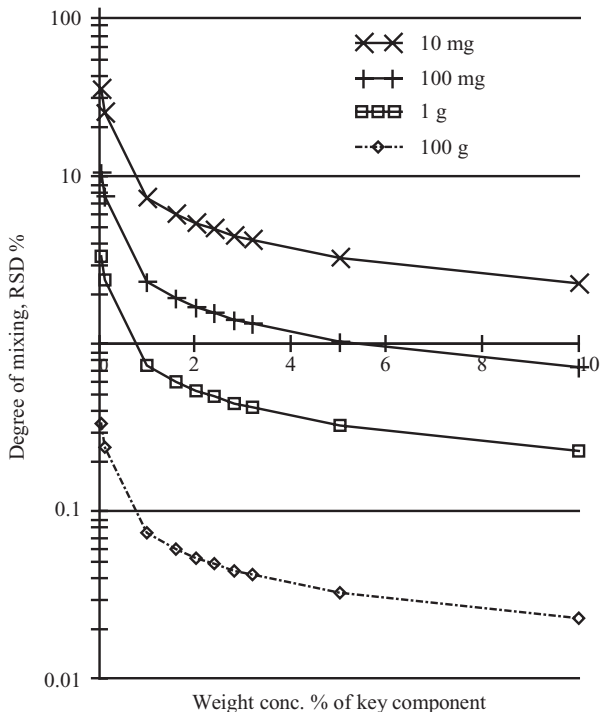


FIG. 21-46 Degree of mixing expressed as $RSD = \sqrt{\sigma^2}/P$ for a random mixture calculated following Sommer. The two components have the same particle-size distribution, $dp_{50} = 50 \mu\text{m}$, $d_{\text{max}} = 130 \mu\text{m}$, $m = 0.7$ (exponent of the power density distribution of the particle size) parameter: sample size ranging from 10 mg to 100 g (R. Weinekötter, Degree of Mixing and Precision for Continuous Mixing Processes, Proceedings Partec, Nuremberg, 2007).

that the condition exists that the particles can move freely. The variance of a random mixture is calculated as follows for a two-ingredient blend in which the particles are of the same size [P. M. C. Lacey, *The Mixing of Solid Particles, Trans. Instn. Chem. Engrs.*, **21**, 53-59 (1943)]:

$$\sigma^2 = \frac{p \cdot q}{n_p} \tag{21-63}$$

where p is the concentration of one of the ingredients in the mix, q is the other ($q = 1 - p$), and n_p is number of particles in the sample. Note that the variance of the random mix grows if the sample size decreases. The variance for a **completely segregated system** is given by

$$\sigma_{\text{segregated}}^2 = p \cdot q \tag{21-64}$$

Equation (21-63) is a highly simplified model, for no actual mixture consists of particles of the same size. It is likewise a practical disadvantage that the number of particles in the sample has to be known in order to calculate variance, rather than the usually specified sample volume. Stange calculated the variance of a random mix in which the ingredients possess a distribution of particle sizes. His approach is based on the fact that an ingredient possessing a distribution in particle size by necessity also has a distribution in particle mass. He made an allowance for the average mass m_p and m_q of the particles in each component and the particle mass's standard deviation σ_p and σ_q [K. Stange, *Die Mischgüte einer Zufallmischung als Grundlage zur Beurteilung von Mischversuchen* (The mix quality of a random mix as the basis for evaluating mixing trials), *Chem. Eng.*, **26**(6), 331-337 (1954)]. He designated the **variability** c as the quotient of the standard deviation and average particle mass, or

$$c_p = \frac{\sigma_p}{m_p} \quad c_q = \frac{\sigma_q}{m_q} \tag{21-65}$$

Variability is a measure for the width of the particle-size distribution. The higher the value of c , the broader the particle-size distribution.

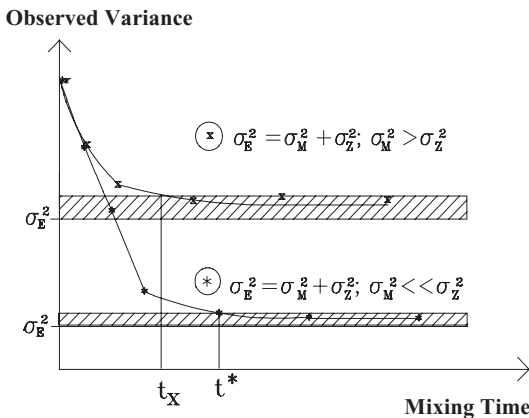


FIG. 21-47 Illustration of the influence of the measurement's accuracy on the variance as a function of the mixing time [following K. Sommer, *How to Compare the Mixing Properties of Solids Mixers* (in German), *Prep. Technol.* no. 5, 266-269 (1982)]. A set of samples have been taken at different mixing times for computing the sample variance. Special attention has to be paid whether the experimental sample variance monitors the errors of the analysis procedure (x) or detects really the mixing process (*). Confidence intervals for the final status σ_E^2 are shown as hatched sections.

The size of the sample is now specified in practice by its mass M and no longer by the number of particles n_p , as shown in Eq. (21-63). The variance in random mixture for the case of two-component mixes can be given by

$$\sigma^2 = \frac{pq}{M} [pm_q(1 + c_q^2) + qm_p(1 + c_p^2)] \tag{21-66}$$

Equation (21-66) estimates the variance of a random mixture, even if the components have different particle-size distributions. If the components have a small size (i.e., small mean particle mass) or a narrow particle-size distribution, that is, c_q and c_p are low, the random mix's variance falls. Sommer has presented mathematical models for calculating the variance of random mixtures for particulate systems with a particle-size distribution (Karl Sommer, *Sampling of Powders and Bulk Materials*, Springer-Verlag, Berlin, 1986, p. 164). This model has been used for deriving Fig. 21-46.

Measuring the Degree of Mixing The mixing process uniformly distributes one or more properties within a quantity of material. These can be physically recordable properties such as size, shape, moisture, temperature, or color. Frequently, however, it is the mixing of **chemically** differing components which forms the subject under examination. Off-line and on-line procedures are used for this examination (compare to subsection "Particle-Size Analysis"). Off-line procedure: A specified portion is (randomly or systematically) taken from the volume of material. These samples are often too large for a subsequent analysis and must then be split. Many analytical processes, e.g., the chemical analysis of solids using infrared spectroscopy, require the samples to be prepared beforehand. At all these stages there exists the danger that the mix status within the samples will be changed. As a consequence, when examining a mixing process whose efficiency can be characterized by the variance expression $\sigma_{\text{process}}^2$, all off- and on-line procedures give this variance only indirectly:

$$\sigma_{\text{observed}}^2 = \sigma_{\text{process}}^2 + \sigma_{\text{measurement}}^2 \tag{21-67}$$

The observed variance $\sigma_{\text{observed}}^2$ also contains the variance $\sigma_{\text{measurement}}^2$ resulting from the test procedure and which arises out of errors in the systematic or random taking, splitting, and preparation of the samples and from the actual analysis. A lot of attention is often paid to the accuracy of an analyzer when it is being bought. However, the preceding steps of sampling and preparation also have to fulfil exacting requirements so that the following can apply:

$$\sigma_{\text{process}}^2 \gg \sigma_{\text{measurement}}^2 \Rightarrow \sigma_{\text{process}}^2 = \sigma_{\text{observed}}^2 \tag{21-68}$$

Figure 21-47 illustrates the impact of precision of the determination of mixing time for batch mixers. It is not yet possible to theoretically forecast mixing times for solids, and therefore these have to be ascertained by experiments. The traditional method of determining mixing times is once again sampling followed by off-line analysis. The mixer is loaded and started. After the mixer has been loaded with the ingredients in accordance with a defined procedure, it is run and samples are taken from it at set time intervals. To do this the mixer usually has to be halted. The concentration of the tracer in the samples is established, and the random sample variance S^2 ascertained. This random sample variance serves as an estimated value for the variance σ_p^2 , which defines the mixture's condition. All analyses are burdened by errors, and this is expressed in a variance σ_m^2 derived from the sampling itself and from the analysis procedure. Initially there is a sharp fall in the random sample variance, and it runs asymptotically toward a final value of σ_E^2 as the mixing time increases. This stationary end value σ_E^2 is set by the variance of the mix in the stationary condition σ_Z^2 , for which the minimum would be the variance of an ideal random mix, and the variance σ_M^2 caused by errors in the analyzing process. The **mixing time** denotes that period in which the experimental random sample variance S^2 falls within the confidence interval of the stationary final condition σ_E^2 . Two cases can be considered. In the first case with large measurement errors, σ_E^2 is determined by the analyzing process itself since for sufficient mixing time the mixing process's fluctuations in

its stationary condition are much smaller than those arising out of the analysis or $\sigma_p^2 \ll \sigma_M^2$. In this case, the mixing process can only be tracked at its commencement, where $\sigma_p^2 > \sigma_M^2$. The “mixing time” t_x obtained under these conditions does not characterize the process. In the second case where the measurement errors are small, or $\sigma_p^2 \gg \sigma_M^2$, the analyzing process is sufficiently accurate for the mixing process to be followed through to its stationary condition. This allows an accurate determination of the true mixing time t^* . The “mixing time” t_x obtained on the basis of an unsatisfactory analysis is always deceptively shorter than the true time t^* .

On-line Procedures Advances in sensor technology and data processing are enabling an increased number of procedures to be completely monitored using **on-line procedures**. The great leap forward from off-line to on-line procedures lies in the fact that the whole process of preparing and analyzing samples has been automated. As a result of this automation, the amount of collectible test data has risen considerably, thereby enabling a more comprehensive statistical analysis and, in ideal cases, even regulation of the process. On-line procedures in most cases must be precisely matched to the process, and the expense in terms of equipment and investment is disparately higher. The accuracy of laboratory analyses in the case of off-line procedures cannot be produced by using on-line processes. There are as yet few on-line procedures for chemically analyzing solids. Near-infrared spectrometers fitted with fiber-optic sensors are used solely in the field of foodstuffs and for identifying raw materials in the pharmaceuticals industry and have also been applied to mixtures [Phil Williams and Karl Norris (eds.), *Near-Infrared Technology in the Agricultural and Food Industries*, American Association of Cereal Chemists, St. Paul, Minn., 1987; R. Weinekötter, R. Davies, and J. C. Steichen, Determination of the Degree of Mixing and the Degree of Dispersion in Concentrated Suspensions, Proceedings of the Second World Congress, Particle Technology, pp. 239–247, September 19–22, 1990, Kyoto, Japan]. For pharmaceutical mixes the NIR method has been proposed for the control of mixing efficiency (A. Niemöller, Conformity Test for Evaluation of Near Infrared Data, Proc. Int. Meeting on Pharmaceutics, Biopharmaceutics and Pharmaceutical Technology, Nuremberg, March 15–18, 2004). This method records the specific adsorption of groups of chemicals on a particle’s surface. If these spectrometers are based on modern diode array technology, a spectrum covering the whole wave range is obtained in a fraction of a second.

Sampling Procedures The purpose of taking samples is to record the properties of the whole volume of material from a small, analyzed portion of it. This is difficult to achieve with solids since industrial mixes in particular always present a distribution of grain sizes, shape, or density and can also separate out when samples are being taken, on account of the ingredients’ specific motional behavior (see the subsection “Sampling”).

EQUIPMENT FOR MIXING OF SOLIDS

A wide variety of equipment is commercially available to suit a multiplicity of mixing tasks. In this overview mixers and devices for mixing solids are divided into four groups: (1) mixed stockpiles, (2) bunker mixers, (3) rotating mixers or mixers with rotating tools, and (4) direct mixing of feeding streams.

Mixed Stockpiles Many bulk goods that are often stored in very large stockpiles do not possess uniform material properties within these stockpiles. In the case of raw materials, this may be caused by natural variations in deposits; or in the case of primary material, by variations between different production batches. In the iron and steel industry, e.g., there are fluctuations in the ore and carbon content of the finished material. If these stockpiles are emptied in the “first-in, first-out” principle, material with a variance in properties will find its way into the subsequent process and reduce its efficiency. To provide a uniform finished material, a mix is obtained by following a defined scheme for building up and emptying large stockpiles (Fig. 21-48). Such mixing processes are also called *homogenization*. As in any mixing process, the volume of material is homogenized by moving portions of it relative to each other. A long

stockpile is built up by a movable conveyor belt or other corresponding device traveling *lengthwise*. During loading the belt continuously travels up and down the whole length. In the strata thereby created is stored a temporal record of the material’s delivery. If the material is now systematically removed *crosswise* to these layers, each portion removed from the stockpile (Fig. 21-48) will contain material from all the strata and therefore from the times it was supplied. Since such bins are built up over days or weeks, mixed stockpiles reduce the degree of long-term fluctuations in the material’s properties.

Bunker and Silo Mixers Bunker and silo mixers (Fig. 21-49) are sealed vessels, the biggest of which may likewise serve to homogenize large quantities of solids. They are operated batchwise, continuously or with partial recirculation of the mixture. Their sealed construction also enables material to be conditioned, e.g., humidified, granulated, dried, or rendered inert, as well as mixed. In gravity mixers, granular material is simultaneously drawn off by a system of tubes at various heights and radial locations, brought together, and mixed. Other types of construction use a central takeoff tube into which the solids travel through openings arranged at various heights up this pipe. If the quality of the mix does not meet requirements, the withdrawn material is fed back into the bunker (Eichler and Dau, Geometry and Mixing of Gravity Discharge Silo Mixers, The First European Congress on Chemical Engineering, Florence, Italy, 1997, *Proceedings*, 2, 971–974). In this fashion the bunker’s entire contents are recirculated several times and thus homogenized. The material drawn off in most cases is carried to the top of the bunker by air pressure (using an external circulation system).

Gravity mixers are designed for free-flowing powders and are offered in sizes ranging between 5 and 200 m³. The specific energy consumption, i.e., the energy input per product mass, is very low at under 1 to 3 kWh/t. Silo screw mixers are silos with a special funnel mixer at their outlet and are grouped with the gravity mixers. A concentric double cone gives a different residence time period for the material in the inner and outer cones, inducing remixing. Such mixers are available for quantities of material between 3 and 100 m³. In the case of granulate mixers, material from various areas of the vessel is brought together in its lower section and then carried upward by air pressure in a central pipe (using an internal circulating system) where the solids are separated from the gas and at the same time distributed on the surface. Design sizes reach up to 600 m³, and the specific energy input, like that of gravity mixers, is low. The rotating screw of a **conical screw mixer** transports the material upward from the bottom. This screw is at the same time driven along the wall of the vessel by a swiveling arm. This type of mixer also processes both pastes and cohesive powders. The solids at the container wall are continuously replaced by the action of the screw so that the mix can be indirectly heated or cooled through the container’s outer wall. It is also used for granulation and drying. Mixers of this design are offered in capacities of between 25 L and 60 m³. In **blast air** or **air jet mixers**, air is blown in through jets arranged around the circumference of a mixing head placed in the bottom of the vessel. The specific air consumption is 10 to 30 N·m³/t, and the largest mixers have a capacity of 100 m³. If a fluid flowing through a bed of particles against the force of gravity reaches a critical speed (minimum fluidization velocity), the particles become suspended or fluidized by the fluid (see Sec. 17, “Gas-Solid Operations and Equipment”).

Through increased particle mobility, **fluidized beds** possess excellent mix properties for solids in both a vertical and radial axis. In **circulating fluidized beds** often used in reaction processes, this is combined with elevated heat transfer and material circulation as a result of the high relative velocities of the gas and solids. Lower fluidizing speeds to limit air consumption are generally used if the fluidized bed serves only the purpose of mixing. Furthermore, differing volumes of air are fed to the air-permeable segments installed in the container’s floor which serve to distribute air. The largest fluidized bed mixers as used in cement making reach a capacity of 10⁴ m³. The material must be fluidizable, i.e., free-flowing (with a particle size greater than 50 μm), and dry. The specific



FIG. 21-48 Recovery of the fine homogenized coal by system Chevron (Central Coking Plant, Saar GmbH, Germany); width of the bridge scraper is 57.5 m; capacity is 1200 t/h. (Courtesy of PWH-Krupp Engineering.)

power input lies between 1 and 2 kWh/t, but air consumption rises sharply in the case of particle sizes above 500 μm . **Fluidized-bed granulators** utilize the mixing properties of fluidization for granulation, atomized fluid distribution, and drying (see "Size Enlargement Equipment: Fluidized-Bed Granulators").

Rotating Mixers or Mixers with Rotating Component

Figure 21-50 shows four categories of mixers where the mix is agitated by rotating the whole unit or where movement in the mix is produced by rotating components built into the apparatus. These mixers are classified according to their Froude number (Fr):

$$Fr = \frac{r\omega^2}{g} = \frac{m^2 4\pi^2}{g} \quad (21-69)$$

Here r denotes the mixer's radius or that of the mixer's agitators, g the gravitational acceleration, and ω the angular velocity. The Froude number therefore represents a dimensionless rotating frequency. The Froude number is the relationship between centrifugal and gravitational acceleration. No material properties are accounted for in the Froude number: Subject to this limitation, a distinction is drawn in Fig. 21-50 between $Fr < 1$, $Fr > 1$, and $Fr \gg 1$. **Free-fall mixers** are only suitable for free-flowing solids. Familiar examples of free-fall units are drum mixers and V-blenders. However, as the solids are generally free-flowing, demixing and segregation may also occur, leading to complete separation of the ingredients. Since drums are also used in related processes such as rotary tubular kilns or granulating drums for solids, these processes may also be prone to size segregation. In some cases, this may even be intentional, such as

with rotating disc granulators common in iron ore processing. Despite these risks of segregation, mixers without built-in agitators are particularly widely used in the pharmaceuticals and foodstuffs industries since they can be cleaned very thoroughly. **Asymmetrically moved mixers** in which, e.g., a cylinder is tilted obliquely to the main axis, turning over the mix, also belong in the free-fall category, e.g., being fertilizer drum granulation processes. Mixing is done gently. Because of the material's distance from the central axis, high torques have to be applied by the drive motor, and these moments have to be supported by the mixer's bearings and bed. Units with a capacity of 5000 L are offered. There are also mixers with operating range $Fr < 1$ where the work of moving the mix is undertaken by rotating agitators. The particles of solids are displaced relative to one another by agitators inside the mixer. This design is suitable for both cohesive, moist products and those which are free-flowing. Examples of **displacement mixers** are ribbon blenders or paddle mixers. Because of their low rpm the load on the machine is slight, but the mixing process is relatively slow. The specific energy input is low and lies under 5 kW/m^3 .

Ploughshear and centrifugal mixers operate in a range with $Fr > 1$. The consequence is that, at least in the vicinity of the outer edge of the agitator, the centrifugal forces exceed that of gravity and the particles are spun off. Thus instead of a pushing motion there is a flying one. This accelerates the mixing process both radially and axially. If the ingredients still need to be disagglomerated, high-speed cutters are brought into the mixing space to disagglomerate the mix by impact. At very high Froude number ranges ($Fr > 7$) there is a sharp increase in the shear forces acting on the mix. The impact load is large and sufficient to heat the product as a result of

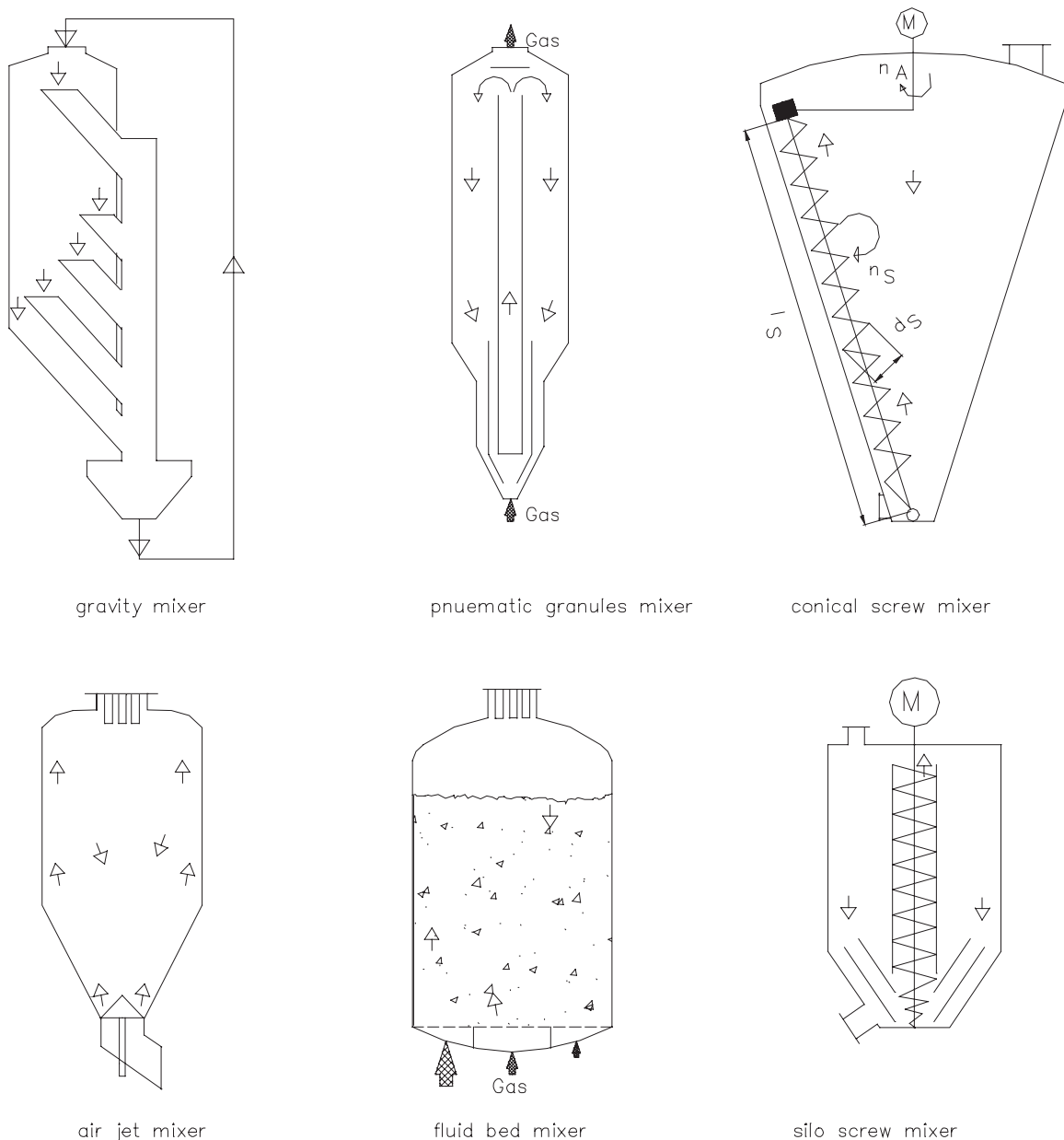


FIG. 21-49 Classification of bunker or silo mixers following Müller [W. Müller, Methoden und derzeitiger Kenntnisstand für Auslegungen beim Mischen von Feststoffen [Methods and the current state of the art in solids mixing configurations], *Chem. Eng.*, **53**, 831-844 (1981)].

dissipated energy. The heat is caused by friction between the mixer's tools and the solids as well as by friction among the solids' particles. As well as simple mixing, here the mixer's task is often disagglomeration, agglomeration, moistening, and sintering. Such mixers are especially used for producing plastics and in the pharmaceutical industry for granulation.

Mixing by Feeding Direct mixing of feed streams represents a continuous mixing process (Fig. 21-51). The solids are blended by metering in each ingredient and bringing these streams of solids together locally. There is no axial mixing (transverse or back mixing), or as such it is very low, with the result that the quality of the meter-

ing determines the mix's homogeneity. Metered feeder units should therefore ideally be used, preferably operated **gravimetrically** with appropriate feedback control of weight loss. According to the requirements of the case in question, mixing is also required obliquely to the direction of travel. If the ingredients are brought together in a perpendicular fall, this is achieved by their merging together. If this oblique mixing is not sufficient, **static mixers** can be used for free-flowing powders or granules where, e.g., the stream of solids is repeatedly divided up and brought back together by baffles as it drops down a tube. The energy input into the mixer is very low, but such systems need sufficient height to achieve mix quality.

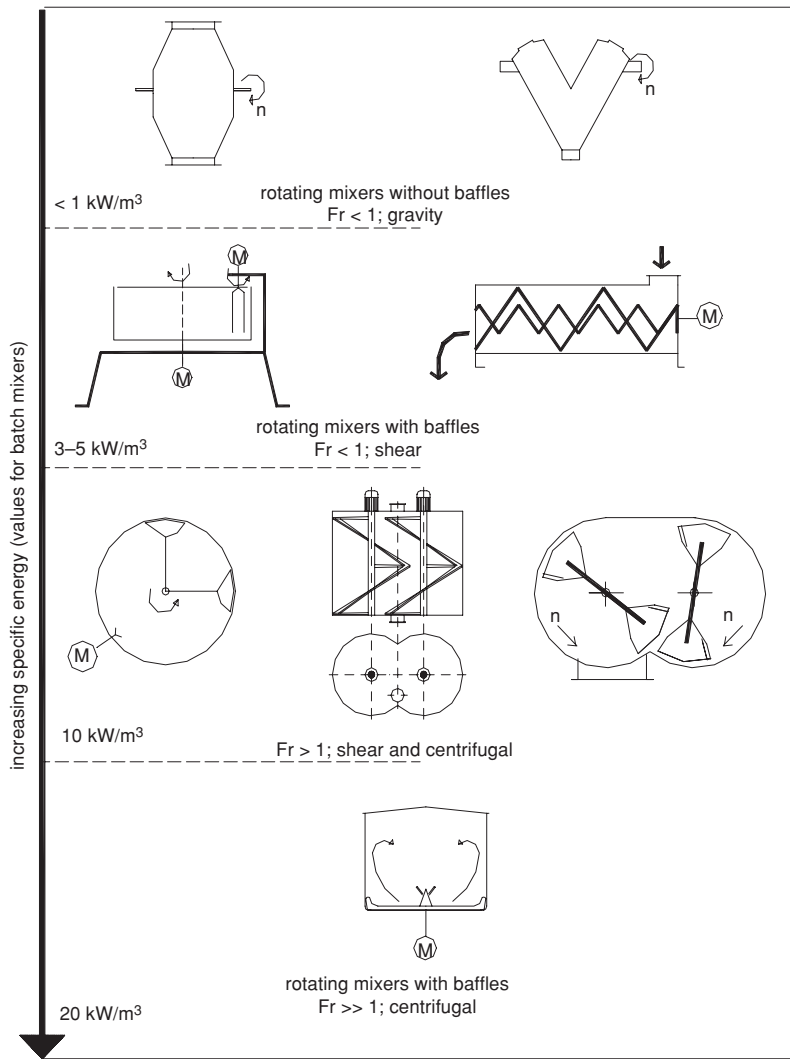


FIG. 21-50 Classification of mixers—movement of material by rotating agitators or revolving containers. [W. Müller, Methoden und derzeitiger Kenntnisstand für Auslegungen beim Mischen von Feststoffen [Methods and the current state of the art in solids mixing configurations], *Chem. Eng.*, **53**, 831-844 (1981)].

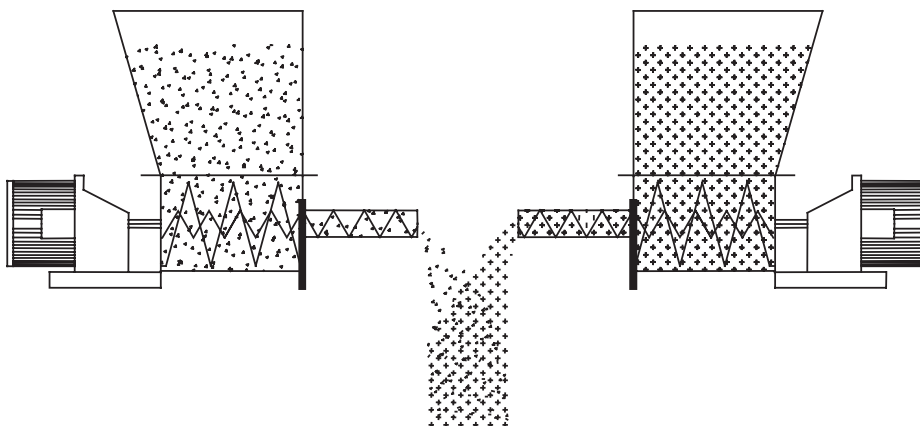


FIG. 21-51 Direct mixing of feeder streams.

21-42 SOLID-SOLID OPERATIONS AND PROCESSING

It was shown that the efficiency for radial mixing depends on the gas phase as well (O. Eichstädt, Continuous Mixing of Fine Particles within Fluid Dynamic Vertical Tube Mixers, Dissertation, in German, ETH-Zurich, 1997). At best they operate with low volume concentration and for particles between 20 and 200 μm . Static mixers have been used for very abrasive free-flow materials such as silicon carbide. Since any rotating equipment is avoided inside static mixers, abrasion is limited. As will be shown below, mixture quality is dependent on feed consistency and residence time within the static mixer. Since the latter is very short in static mixers (seconds or fractions of a second), short-time feeding precision has to be very high to achieve high-quality mix.

DESIGNING SOLIDS MIXING PROCESSES

Goal and Task Formulation An essential prerequisite for the efficient design of a mixing process is a clear, exact, and comprehensive formulation of the task and objective. Applying Table 21-7a as a checklist guarantees a systematic formulation of the *mixing task* along with the major *formative conditions*. Priority *objectives* covering the economic requirements, quality targets, and operating conditions have to be met when one is engineering a mixing system. Besides a definition of the stipulated quality of the mix and an average production throughput (minimum or maximum), the *quality target* can include additional physical (moisture, grain size, temperature) and chemical properties required of the mixed product. Furthermore, the general principles of quality assurance frequently demand production documentation. This means that material batches must be coded, mixture recipes recorded, and the flow of materials in and out balanced out against their inventories and consumption. Clearly *formative economic conditions* such as investment, maintenance requirements, and utilization of existing space often determine the actual technical features of a design when it is put into practice. Specifications arising from the mixing system's operation are grouped under *formative operating conditions*. These set the requirements on

- Staff numbers and training
- Process monitoring, process management system design, and the degree of automation
- Operating, cleaning, and maintenance
- Safety, dust, explosion, and emission protection and the alarm system

Sometimes raw material costs exceed the processing cost by far; or manufacturing contributes a negligible part of the overall cost; e.g., the marketing and R&D determine the manufacturing cost of a newly patented pharmaceutical product.

The Choice: Mixing with Batch or Continuous Mixers Mixing processes can be designed as a batch or a continuous process.

TABLE 21-7a Checklist for Formulating a Mixing Task

<i>Mix recipes (mixture composition)</i>	
<ul style="list-style-type: none"> • Number and designation of the recipes • The preparation's composition (the ingredients' percentages and margins of accuracy to be observed, particularly in the case of low-dosage ingredients) • The percentage of each recipe as part of the total production output • The frequency with which the recipe is changed and any desired sequence • Cleaning operations when a recipe is changed [dry, wet, cleaning in place (CIP)] • Sampling and analyses 	
<i>Ingredients</i>	
<ul style="list-style-type: none"> • Designation • Origin, supplier, packaging • Bulk density, solids density • Grain size (grain size distribution) and shape • Flow properties, gradient • Abrasiveness • Moistness (damp, hygroscopic, dry) • Temperature, sensitivity to thermal stress • Sensitivity to mechanical stress (crushing, abrasion, fracture) 	
<i>Product (mixture)</i>	
<ul style="list-style-type: none"> • Mix quality • Bulk density • Fluidizability (air take-up during mixing) • Tendency to segregation • The mix's flow properties • Agglomeration, disagglomeration required 	
<i>The mixer performance</i>	
<ul style="list-style-type: none"> • Mix performance: production volume per unit of production (average, minimum, maximum) • For batch mixers: Batch mix size (final volume after mixing); start-up filling level; the filled mixer's idle time • For continuous mixers: The production volume with an unchanged recipe; feed/mix output tolerance range 	
<i>Integrating the mixers into the system</i>	
<ul style="list-style-type: none"> • Material flow diagram (average, maximum, and minimum figures) • The ingredients' inflow and outflow • Spatial requirements, height, layout • The mixture's usage • Storing, feeding, and weighing devices • The type of process inspection, process control, storage, and data exchange • Safety requirements 	
<i>Mixer design</i>	
<ul style="list-style-type: none"> • Raw material, surfaces, and the inflow and outflow configuration • Heating, cooling, inertizing, pressurization, vacuum • The addition of liquid into the mixer • Disagglomeration • Current, steam, and water connections, adjuncts, types of protection, protection against explosion 	
<i>Formative economic conditions</i>	
<ul style="list-style-type: none"> • Investment costs • Maintenance, running, and staff costs • Profitability 	

TABLE 21-7b Comparison of Discontinuous and Continuous Mixing Processes

Implementation data	Discontinuous	Continuous
The number of ingredients	As many as wanted	2–10; any more ingredients are usually combined in a premix
Frequency with which the recipe is changed	Several times per hour	A recipe must remain unchanged for several hours
Cleaning frequency or idle time	Several times a day	Once a day or less
Production output, throughput	Any rate	More than 100 kg/h. Exception: feeding laboratory extrusions
Risk of separation	Present, therefore there must be short transportation paths, few intermediate silos	Low risk when the material is taken directly to the next processing stage or directly drawn off
Spatial requirement	Large amount of space and intermediate silos required for machines with a throughput greater than 5000 kg/h	Low spatial requirement even for machines with a high throughput
Requirements placed on the equipment	Simple feeding but high demands on the mixer	Accurate continuous feeding (feeding scales necessary) but low demands on the mixer
Safety	Steps have to be taken in the case of materials with a risk of explosion	The small quantities of material present during processing have a low potential risk, which simplifies safety design
Automation	Variable degree of automation	Contained in the processing



FIG. 21-52 Classical automated batch mixing installation. The components are stored in small silos shown at the top of picture. The materials are extracted from these hoppers in a downstream weighing hopper according to the recipe. Once all components are fed into this weighing hopper, a valve is opened and the exact batch falls into the downstream batch mixer.

Table 21-7*b* gives a detailed comparison of discontinuous and continuous mixing processes, to help guide the selection of a mixing method.

Batch Mixing Batch or discontinuous mixing is characterized by the fact that the mixer is filled with the ingredients, and after a certain **mixing time** the mixture is discharged. The feeding (or filling), mixing, and discharging operations are performed *one after the other*. Batch processing presents advantages for small quantities of material because of its lower investment costs and greater flexibility. Batch mixers are used even when very large volumes of material are being homogenized since continuous mixers are limited by their lower volume. However, in the batch mixer's very flexibility lies the danger that it is not being optimally utilized. For example, overmixing can occur, whereby the product could be damaged and the process's effectiveness suffers.

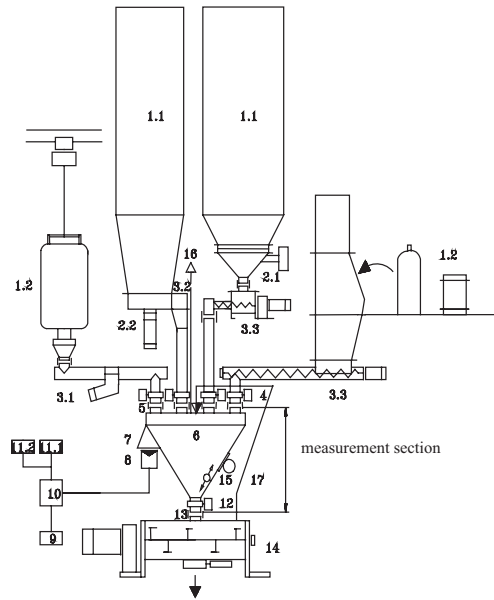


FIG. 21-53 Weighing hopper with additive weighing for feeding a batch mixer. 1.1 Storage silos; 1.2 big bag, bag, drum; 2.1–2.2 dischargers; 3.1–3.3 feeder units; 4 cutoff; 5 flexible connections; 6 weighing hopper; 7 support for gravity force; 8 gravity-operated sensor (load cell); 9 set point; 10 weighing analysis and regulation; 11.1 measured value indicator or output; 11.2 recorder (printer); 12 cutoff; 13 flexible connection; 14 mixer; 15 discharger; 16 dust extraction and weighing hopper ventilation; 17 mixer ventilation.

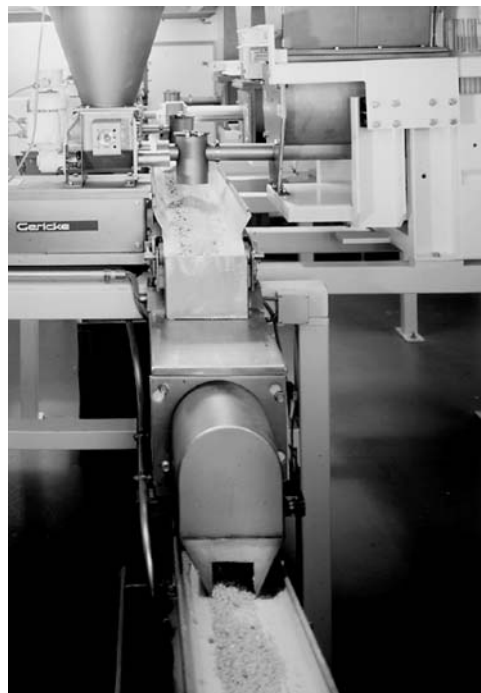


FIG. 21-54 Continuous mixing for the production of Muesli: Continuous gravimetric solids feeder (loss-in-weight feeding) supplies the components (raisins, flakes, etc.) at constant rate onto a belt, which delivers the components to the continuous mixer (bottom of the picture). The continuous mixer discharges onto a second belt.

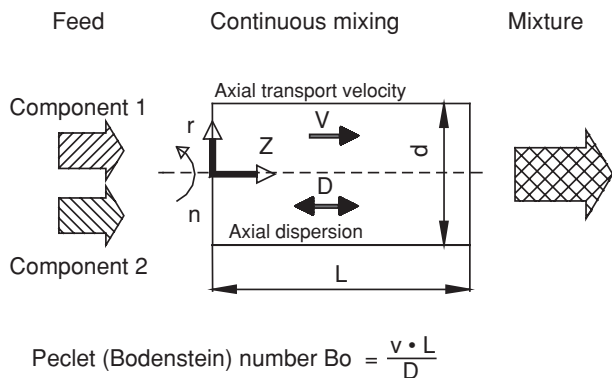


FIG. 21-55 The continuous mixing of two ingredients: Axial mixing or dispersion shows up as well as residence time distribution of the product inside the mixer.

Feeding and Weighing Equipment for a Batch Mixing Process The number of mix cycles multiplied by the usable mixer capacity gives the set mixture output per hour. The mix cycle consists of the filling, mixing, discharge, and idle times (Fig. 21-52). To this is added in special cases the time taken for sampling and analysis and that for associated processes such as disagglomeration and granulation. The capacity (throughput rate) of a batch mixing process having a mixture charge with a mass M is shown in Eq. (21-70):

$$\dot{m} = \frac{M}{t_f + t_m + t_d + t_i} \quad \frac{\text{kg}}{\text{s}} \quad (21-70)$$

The mixing time t_m depends on the selected mixer design and size, the filling time t_f on the system's configuration, while the discharge time t_d depends on both the mixer's design and the system's layout. The choice of feed and weighing devices is determined by the number of ingredients, their mass and proportions, the throughput volume, the stocking and mode of delivery, the spatial circumstances, degree of automation, etc. In the simplest case the ingredients are manually weighed into the mixer. In some cases, *sandwiching* of specific ingredients may be desirable, i.e., staged delivery of multiple layers of key ingredients between other excipients. Where there are higher

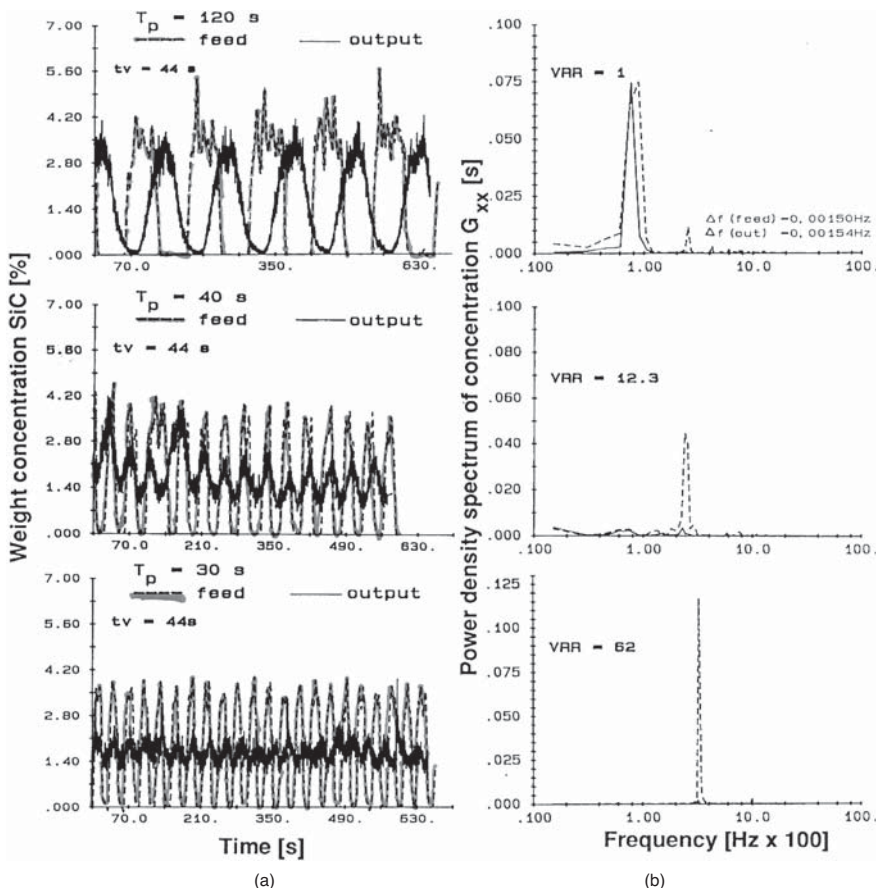


FIG. 21-56 Dampening of feed fluctuation in a continuous mixer—variance reduction ratio (VRR). The efficiency of continuous mixing processes is described by the variance reduction ratio. The variances in concentration of inlet and outlet are compared. Tracer-feed oscillating with different periods T_p , main component feed at constant rate (20 g/s), mean residence time in the continuous mixer $t_v = 44$ s. (a) Variation in time of SiC concentration: dotted line at the entrance of the continuous mixer, bold line at the outlet of the continuous mixer. (b) Power density spectrum of SiC concentration. High variance reduction ratios are achieved if the period of the tracer feed is small compared to the mean residence time in the mixer.

requirements in respect of accuracy, safety, and recording, a hopper scale represents a simple device for weighing and releasing the components into the mixing equipment (Fig. 21-53).

Continuous Mixing In a **continuous mixing** process (compare Figs. 21-52 and 21-54) the ingredients are continuously fed into the mixer, then mixed and prepared for the next processing stage. The operations of feeding, mixing, and discharging follow each other locally but occur simultaneously. In continuous mixing, the weighing and filling of a batch mixer are replaced by the ingredients' controlled continuous addition. The blending time in a continuous mixer is in fact the material's **residence time**, which is determined by the feed rate to the mixer. Losses of product during start-up or shutdown added to this lower degree of flexibility come as further disadvantages of the continuous process. Yet it possesses considerable advances over batch processing both in financial terms and in respect of process control: Even high-throughput continuous mixers are compact. A smaller-volume scale provides short mixing paths and ease of mixing. When integrated into a continuous production system, a continuous mixing process saves on reservoirs or silos and automating the course of the process is simplified. In the case of dangerous products or base materials, there is less potential risk with a continuous process since only a small quantity of material accumulates in the mixer. Segregation can be limited in a continuous mixer by its smaller required scale. A continuous mixer, which on account of its compact construction can be positioned before the next station in the processing chain, guarantees that a mix of a higher quality will in fact be made available to that next stage of the process, with smaller material handling distances.

The continuous mixer has principally two tasks (Fig. 21-55): The ingredients, which in an extreme case arrive in the mixer side by side, have to be **radially mixed** (*r*). In this case *radial* means lateral to the direction of the material's conveyance into the mixer. If in addition there are large feed rate fluctuations or the ingredients are themselves unho-

mogenized, the mixer must also minimize any differences in concentration in an axial direction (*z*), i.e., in the direction of the material's conveyance, or the mixture must be **axially mixed** as well. If a mixer only has to perform its task radially, it can have a very compact structure, since slim-line mixers with a high rpm very quickly equalize concentrations radially over short mixing paths. Feed fluctuations (Fig. 21-56) are damped by the residence time distribution of the material inside the mixer [R. Weinekötter and L. Reh, *Continuous Mixing of Fine Particles, Part. Part. Syst. Charact.*, **12**, 46–53 (1995)]. The residence time distribution describes the degree of axial dispersion occurring in the mixer. The Peclet (=Bodenstein) number *Bo* (Fig. 21-55) characterizes the ratio of axial transport velocity and axial dispersion coefficient *D*. The capability to reduce incoming fluctuations (thus variance) inside continuous mixers depends on the ratio of period of entrance fluctuation to the mean residence time as well as the residence time distribution. Besides the number of ingredients in the mix, a decisive feature in selecting the process is the individual component's flow volumes. Since the feed's constancy can only be maintained with a limited degree of accuracy at continuous feeding rates below 300 g/h, ingredients with low flow volumes necessitate a premixing operation. There is an increasing trend toward continuous mixing installations. Widely used are continuous processes in the plastics industry, detergents, and foodstuffs. Although less common, **pharmaceutical processes utilizing continuous mixing are growing in appeal** due to the small volume of the apparatus. The U.S. Food and Drug Administration, e.g., has promoted a **Process Analytical Technology (PAT) Initiative** with the objective of facilitating continuous processing to improve efficiency and manage variability (<http://www.fda.gov/cder/ops/Pat.htm>; Henry Berthiaux et al., *Continuous Mixing of Pharmaceutical Powder Mixtures*, 5th World Congress on Particle Technology, 2006; Marcos Lusa and Fernando Muzzio, *The Effect of Shear Mixing on the Blending of Cohesive Lubricants and Drugs*, *Pharmaceutical Technol.*, Dec. 2005).

PRINCIPLES OF SIZE REDUCTION

GENERAL REFERENCES: Annual reviews of size reduction, *Ind. Eng. Chem.*, October or November issues, by Work from 1934 to 1965, by Work and Snow in 1966 and 1967, and by Snow in 1968, 1969, and 1970; and in *Powder Technol.*, **5**, 351 (1972), and **7** (1973); Snow and Luckie, **10**, 129 (1973), **13**, 33 (1976), **23**(1), 31 (1979). *Chemical Engineering Catalog*, Reinhold, New York, annually. Cremer-Davies, *Chemical Engineering Practice*, vol. 3: *Solid Systems*, Butterworth, London, and Academic, New York, 1957. *Crushing and Grinding: A Bibliography*, Chemical Publishing, New York, 1960. European Symposia on Size Reduction: 1st, Frankfurt, 1962, publ. 1962, Rumpf (ed.), *Verlag Chemie*, Düsseldorf; 2d, Amsterdam, 1966, publ. 1967, Rumpf and Pietsch (eds.), *DECHEMA-Monogr.*, **57**; 3d, Cannes, 1971, publ. 1972, Rumpf and Schönert (eds.), *DECHEMA-Monogr.*, **69**. Gaudin, *Principles of Mineral Dressing*, McGraw-Hill, New York, 1939. International Mineral Processing Congresses: *Recent Developments in Mineral Dressing*, London, 1952, publ. 1953, Institution of Mining and Metallurgy; *Progress in Mineral Dressing*, Stockholm, 1957, publ. London, 1960, Institution of Mining and Metallurgy; 6th, Cannes, 1962, publ. 1965, Roberts (ed.), Pergamon, New York; 7th, New York, 1964, publ. 1965, Arbitter (ed.), vol. 1: *Technical Papers*, vol. 2: *Milling Methods in the Americas*, Gordon and Breach, New York; 8th, Leningrad, 1968; 9th, Prague, 1970; 10th, London, 1973; 11th, Cagliari, 1975; 12th, São Paulo, 1977. Lowrison, *Crushing and Grinding*, CRC Press, Cleveland, Ohio, 1974. *Pit and Quarry Handbook*, Pit & Quarry Publishing, Chicago, 1968. Richards and Locke, *Text Book of Ore Dressing*, 3d ed., McGraw-Hill, New York, 1940. Rose and Sullivan, *Ball, Tube and Rod Mills*, Chemical Publishing, New York, 1958. Snow, *Bibliography of Size Reduction*, vols. 1 to 9 (an update of the previous bibliography to 1973, including abstracts and index). U.S. Bur. Mines Rep. SO122069, available IIT Research Institute, Chicago, Ill. 60616. Stern, Guide to Crushing and Grinding Practice, *Chem. Eng.*, **69**(25), 129 (1962). Taggart, *Elements of Ore Dressing*, McGraw-Hill, New York, 1951. Since a large part of the literature is in German, availability of English translations is important. Translation numbers cited in this section refer to translations available through the National Translation Center, Library of Congress, Washington, D.C. Also, volumes of selected papers in English translation are available from the Institute for Mechanical Processing Technology, Karlsruhe Technical University, Karlsruhe, Germany.

INTRODUCTION

Industrial Uses of Grinding Grinding operations are critical to many industries, including mining cement manufacture, food processing, agricultural processes, and many chemical industries. Nearly every solid material undergoes size reduction at some point in its processing cycle. Grinding equipment is used both to reduce the size of a solid material by fracture and to intimately mix materials, *usually a solid and a liquid (dispersion)*.

Some of the common reasons for size reduction are to liberate a desired component for subsequent separation, as in separating ores from gangue; to prepare the material for subsequent chemical reaction, i.e., by enlarging the specific surface as in cement manufacture; to meet a size requirement for the quality of the end product, as in fillers or pigments for paints, plastics, agricultural chemicals, etc.; and to prepare wastes for recycling.

Types of Grinding: Particle Fracture vs. Deagglomeration There are two primary types of size reduction that occur in grinding equipment: deagglomeration and particle fracture. In deagglomeration, an aggregate of smaller particles (often with a fractal structure) is size-reduced by breaking clusters of particles off the main aggregate without breaking any of the "primary particles" that form the aggregates. In particle fracture, individual particles are broken rather than simply separating individual particles. Most operations involving particles larger than 10 μm (including materials thought of as rocks and stones) usually involve at least some particle fracture, whereas finer grinding is often mostly deagglomeration. At similar particle scales, deagglomeration requires much less energy than particle fracture. For example, fracture of materials down to a size of 0.1 μm is extremely difficult, whereas deagglomeration of materials in this size range is commonly practiced

in several industries, including the automotive paint industry and several electronics industries.

Wet vs. Dry Grinding Grinding can occur either wet or dry. Some devices, such as ball mills, can be fed either slurries or dry feeds. In practice, it is found that finer size can be achieved by wet grinding than by dry grinding. In wet grinding by media mills, product sizes of $0.5\ \mu\text{m}$ are attainable with suitable surfactants, and deagglomeration can occur down to much smaller sizes. In dry grinding, the size in ball mills is generally limited by ball coating (Bond and Agthe, *Min. Technol.*, AIME Tech. Publ. 1160, 1940) to about $15\ \mu\text{m}$. In dry grinding with hammer mills or ring-roller mills, the limiting size is about 10 to $20\ \mu\text{m}$. Jet mills are generally limited to a mean product size of $10\ \mu\text{m}$. However, dense particles can be ground to 2 to $3\ \mu\text{m}$ because of the greater ratio of inertia to aerodynamic drag. Dry processes can sometimes deagglomerate particles down to about $1\ \mu\text{m}$.

Typical Grinding Circuits There are as many different configurations for grinding processes as there are industries that use grinding equipment; however, many processes use the circuit shown in Fig. 21-57a. In this circuit a process stream enters a mill where the particle size is reduced; then, upon exiting the mill, the stream goes to some sort of classification device. There a stream containing the oversized particles is recycled back to the mill, and the product of desired size exits the circuit. Some grinding operations are simply one-pass without any recycler or classifier. For very fine grinding or dispersion (under $1\ \mu\text{m}$), classifiers are largely unavailable, so processes are either single-pass or recirculated through the mill and tested off-line until a desired particle size is obtained.

The fineness to which a material is ground has a marked effect on its production rate. Figure 21-57b shows an example of how the capacity decreases while the specific energy and cost increase as the product is ground finer. Concern about the rising cost of energy has led to publication of a report on this issue [National Materials Advisory Board, *Comminution and Energy Consumption*, Publ. NMAB-364, National Academy Press, Washington, 1981; available from National Technical Information Service, Springfield, Va. 22151]. This has shown that U.S. industries use approximately 32 billion kWh of electrical energy per annum in size-reduction operations. More than one-half of this energy is consumed in the crushing and grinding of minerals, one-quarter in the production of cement, one-eighth in coal, and one-eighth in agricultural products.

THEORETICAL BACKGROUND

Introduction The theoretical background for size reduction is often introduced with particle breakage (or, equivalently, droplet

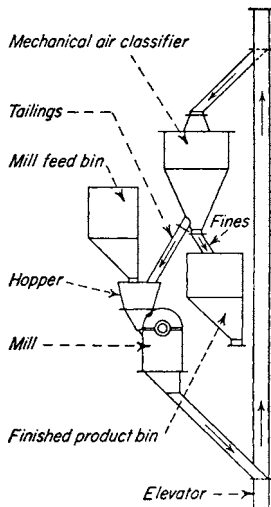


FIG. 21-57a Hammer mill in closed circuit with an air classifier.

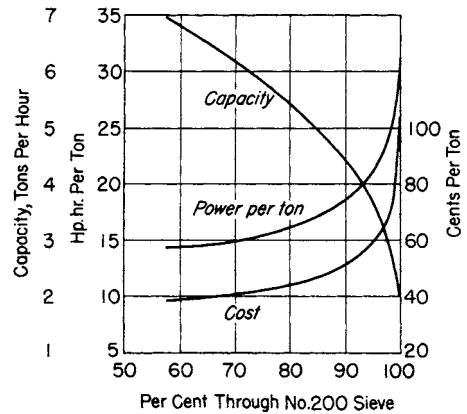


FIG. 21-57b Variation in capacity, power, and cost of grinding relative to fineness of product.

breakup for liquid-liquid system and bubble breakup for gas-liquid systems). It is relatively easy to write down force balances around a particle (or droplet) and make some predictions about how particles might break. Of particular interest in size reduction processes are predictions about the size distribution of particles after breakage and the force/energy required to break particles of a given size, shape, and material.

It has, however, proved difficult to relate theories of particle fracture to properties of interest to the grinding practitioner. This is so, in part, because single particle testing machines, although they do exist, are expensive and time-consuming to use. To get any useful information, many particles must be tested, and it is unclear that these tests reflect the kind of forces encountered in a given piece of grinding equipment. Even if representative fracture data can be obtained, this information needs to be combined with information on the force distribution and particle mechanics inside a particular grinding device to be useful for scale-up or predicting the effectiveness of a device. Most of this information (force distribution and particle motion inside devices) has not been studied in detail from either a theoretical or an empirical point of view, although this is beginning to change with the advent of more powerful computers combined with advances in numerical methods for fluid mechanics and discrete element models.

The practitioner is therefore limited to scale-up and scale-down from testing results of geometrically similar equipment (see "Energy Required and Scale-up," below) and using models which treat the devices as empirical "black boxes" while using a variety of population balance and grind rate theories to keep track of the particle distributions as they go into and out of the mills (see "Modeling of Milling Circuits," below).

Single-Particle Fracture The key issue in all breakage processes is the creation of a stress field inside the particle that is intense enough to cause breakage. The state of stress and the breakage reaction are affected by many parameters that can be grouped into both particle properties and loading conditions, as shown in Fig. 21-58.

The reaction of a particle to the state of stress is influenced by the material properties, the state of stress itself, and the presence of microcracks and flaws. Size reduction will start and continue as long as energy is available for the creation of new surface. The stresses provide the required energy and forces necessary for the crack growth on the inside and on the surface of the particle. However, a considerable part of the energy supplied during grinding will be wasted by processes other than particle breakage, such as the production of sound and heat, as well as plastic deformation.

The breakage theory of spheres is a reasonable approximation of what may occur in the size reduction of particles, as most size-reduction processes involve roughly spherical particles. An equation for the force required to crush a single particle that is spherical near the contact regions is given by the equation of Hertz (Timoshenko and Goodier, *Theory of*

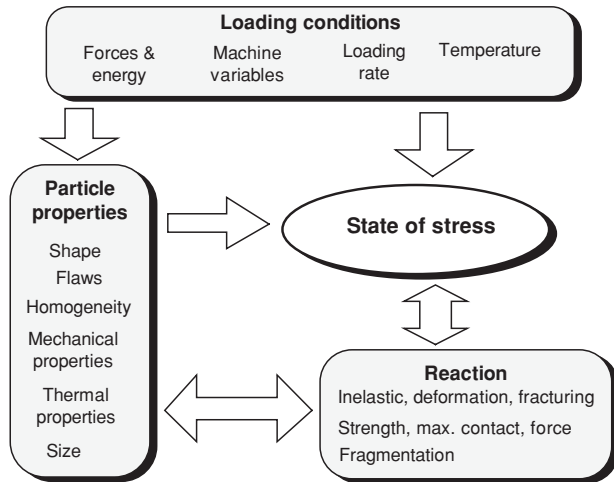


FIG. 21-58 Factors affecting the breakage of a particle. (After Heiskanen, 1995.)

Elasticity, 2d ed., McGraw-Hill, New York, 1951). In an experimental and theoretical study of glass spheres, Frank and Lawn [*Proc. R. Soc. (London)*, A299(1458), 291 (1967)] observed the repeated formation of ring cracks as increasing load was applied, causing the circle of contact to widen. Eventually a load is reached at which the ring crack deepens to form a cone crack, and at a sufficient load this propagates across the sphere to cause breakage into fragments. The authors' photographs show how the size of flaws that happen to be encountered at the edge of the circle of contact can result in a distribution of breakage strengths. Thus the mean value of breakage strength depends partly on intrinsic strength and partly on the extent of flaws present. Most industrial solids contain irregularities such as microscopic cracks and weaknesses caused by dislocations, nonstoichiometric composition, solid solutions, gas- and liquid-filled voids, or grain boundaries.

Inglis showed that these irregularities play a predominant role in particle breakage as the local stresses σ_i generated at the tips of the crack, as shown in Fig. 21-59, were much higher than the gross applied stress σ_N . The effect is expressed by stress concentration factor k

$$k = \frac{\sigma_i}{\sigma_N} = \frac{l}{r} \tag{21-71}$$

which is a function of the crack length l and the tip radius r .

Griffith found that tensile stresses always occur in the vicinity of crack tips, even when the applied gross stresses are compressive. He also showed that the largest tensile stresses are produced at cracks having a 30° angle to the compressive stress. Thus cracks play a key

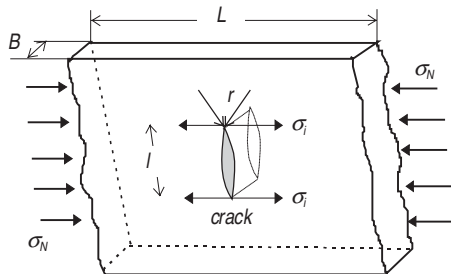


FIG. 21-59 A microcrack in an infinitely large plate.

role in propagation, and their effects greatly overshadow the theoretically calculated values for breakage of spheres or other ideal particles.

ENERGY REQUIRED AND SCALE-UP

Energy Laws Fracture mechanics expresses failure of materials in terms of both stress intensity and fracture toughness, in terms of energy to failure. Due to the difficulty of calculating the stresses on particles in grinding devices, many theoreticians have relied on energy-based theories to connect the performance of grinding devices to the material properties of the material being ground. In these cases, the energy required to break an ensemble of particles can be estimated without making detailed assumptions about the exact stress state of the particles, but rather by calculating the energy required to create fresh surface area with a variety of assumptions.

A variety of energy laws have been proposed. These laws are encompassed in a general differential equation (Walker et al., *Principles of Chemical Engineering*, 3d ed., McGraw-Hill, New York, 1937):

$$dE = -C dX/X^n \tag{21-72}$$

where E is the work done, X is the particle size, and C and n are constants.

For $n = 1$ the solution is Kick's law (Kick, *Das Gasetz der proportionalen Widerstande und seine Anwendung*, Leipzig, 1885). The law can be written

$$E = C \log (X_F/X_P) \tag{21-73}$$

where X_F is the feed-particle size, X_P is the product size, and X_F/X_P is the reduction ratio. For $n > 1$ the solution is

$$E = \left(\frac{C}{n-1} \right) \left(\frac{1}{X_P^{n-1}} - \frac{1}{X_F^{n-1}} \right) \tag{21-74}$$

For $n = 2$ this becomes *Rittinger's law*, which states that the energy is proportional to the new surface produced (Rittinger, *Lehrbuch der Aufbereitungskunde*, Ernst and Korn, Berlin, 1867).

The *Bond law* corresponds to the case in which $n = 1.5$ [Bond, *Trans. Am. Inst. Min. Metall. Pet. Eng.*, **193**, 484 (1952)]:

$$E = 100E_i \left(\frac{1}{\sqrt{X_P}} - \frac{1}{\sqrt{X_F}} \right) \tag{21-75}$$

where E_i is the **Bond work index**, or work required to reduce a unit weight from a theoretical infinite size to 80 percent passing 100 μm . Extensive data on the work index have made this law useful for rough mill sizing especially for ball mills. Summary data are given in Table 21-8. The work index may be found experimentally from laboratory crushing and grinding tests or from commercial mill operations. Some rules of thumb for extrapolating the work index to conditions different from those measured are that for dry grinding the index must be increased by a factor of 1.34 over that measured in wet grinding; for open-circuit operations another factor of 1.34 is required over that measured in closed circuit; if the product size X_P is extrapolated below 70 μm , an additional correction factor is $(10.3 + X_P)/1.145X_P$. Also for a jaw or gyratory crusher, the work index may be estimated from

$$E_i = 2.59C_s/\rho_s \tag{21-76}$$

where C_s = impact crushing resistance, (ft-lb)/in of thickness required to break; ρ_s = specific gravity, and E_i is expressed in kWh/ton.

The relation of energy expenditure to the size distribution produced has been thoroughly examined [Arbiter and Bhrany, *Trans. Am. Inst. Min. Metall. Pet. Eng.*, **217**, 245-252 (1966); Harris, *Inst. Min. Metall. Trans.*, **75**(3), C37 (1966); Holmes, *Trans. Inst. Chem. Eng. (London)*, **35**, 125-141 (1957); and Kelleher, *Br. Chem. Eng.*, **4**, 467-477 (1959); **5**, 773-783 (1960)].

The energy laws have not proved very successful in practice, most likely because only a very small amount of energy used in milling

TABLE 21-8 Average Work Indices for Various Materials*

Material	No. of tests	Specific gravity	Work index†	Material	No. of tests	Specific gravity	Work index†
All materials tested	2088	—	13.81	Taconite	66	3.52	14.87
Andesite	6	2.84	22.13	Kyanite	4	3.23	18.87
Barite	11	4.28	6.24	Lead ore	22	3.44	11.40
Basalt	10	2.89	20.41	Lead-zinc ore	27	3.37	11.35
Bauxite	11	2.38	9.45	Limestone	119	2.69	11.61
Cement clinker	60	3.09	13.49	Limestone for cement	62	2.68	10.18
Cement raw material	87	2.67	10.57	Manganese ore	15	3.74	12.46
Chrome ore	4	4.06	9.60	Magnesite, dead burned	1	5.22	16.80
Clay	9	2.23	7.10	Mica	2	2.89	134.50
Clay, calcined	7	2.32	1.43	Molybdenum	6	2.70	12.97
Coal	10	1.63	11.37	Nickel ore	11	3.32	11.88
Coke	12	1.51	20.70	Oil shale	9	1.76	18.10
Coke, fluid petroleum	2	1.63	38.60	Phosphate fertilizer	3	2.65	13.03
Coke, petroleum	2	1.78	73.80	Phosphate rock	27	2.66	10.13
Copper ore	308	3.02	13.13	Potash ore	8	2.37	8.88
Coral	5	2.70	10.16	Potash salt	3	2.18	8.23
Diorite	6	2.78	19.40	Pumice	4	1.96	11.93
Dolomite	18	2.82	11.31	Pyrite ore	4	3.48	8.90
Emery	4	3.48	58.18	Pyrrhotite ore	3	4.04	9.57
Feldspar	8	2.59	11.67	Quartzite	16	2.71	12.18
Ferrosilicon	18	6.75	8.87	Quartz	17	2.64	12.77
Ferromanganese	10	5.91	7.77	Rutile ore	5	2.84	12.12
Ferrosilicon	15	4.91	12.83	Sandstone	8	2.68	11.53
Flint	5	2.65	26.16	Shale	13	2.58	16.40
Fluorspar	8	2.98	9.76	Silica	7	2.71	13.53
Gabbro	4	2.83	18.45	Silica sand	17	2.65	16.46
Galena	7	5.39	10.19	Silicon carbide	7	2.73	26.17
Garnet	3	3.30	12.37	Silver ore	6	2.72	17.30
Glass	5	2.58	3.08	Sinter	9	3.00	8.77
Gneiss	3	2.71	20.13	Slag	12	2.93	15.76
Gold ore	209	2.86	14.83	Slag, iron blast furnace	6	2.39	12.16
Granite	74	2.68	14.39	Slate	5	2.48	13.83
Graphite	6	1.75	45.03	Sodium silicate	3	2.10	13.00
Gravel	42	2.70	25.17	Spodumene ore	7	2.75	13.70
Gypsum rock	5	2.69	8.16	Syenite	3	2.73	14.90
Ilmenite	7	4.27	13.11	Tile	3	2.59	15.53
Iron ore	8	3.96	15.44	Tin ore	9	3.94	10.81
Hematite	79	3.76	12.68	Titanium ore	16	4.23	11.88
Hematite—specular	74	3.29	15.40	Trap rock	49	2.86	21.10
Oolitic	6	3.32	11.33	Uranium ore	20	2.70	17.93
Limanite	2	2.53	8.45	Zinc ore	10	3.68	12.42
Magnetite	83	3.88	10.21				

*Allis-Chalmers Corporation.

†Caution should be used in applying the average work index values listed here to specific installations since individual variations between materials in any classification may be quite large.

devices is actually used for breakage. A great deal of energy input into a mill is used to create noise and heat as well as simply move the material around the device. Although few systematic studies have been done, less (often, much less) than 5 percent of the energy input into a typical grinding device actually goes into breaking the material. The majority of the remaining energy is eventually converted to frictional heat, most of which heats up the product and the mill.

Mill efficiency can be judged in terms of energy input into the device as compared to the particle size achieved for a given material. It is rare that one grinding device will be more than twice as energy-efficient as another device in order to achieve the same particle size for the same material, and there are usually other tradeoffs for the more energy-efficient device. In particular, more energy-efficient devices have a tendency to have large, heavy mechanical components that cause great damage to equipment when moved, swung, etc. These, however, tend to be much more costly for the same capacity and harder to maintain than smaller, high-speed devices. For example, for many materials, roll mills are more energy-efficient than hammer mills, but they are also significantly more costly and have higher maintenance costs.

Fine Size Limit (See also “Single-Particle Fracture” above.) It has long been thought that a limiting size is attainable, and, in fact, it is almost a logical necessity that grinding cannot continue down to the molecular level. Nonetheless, recent results suggest that stirred

media mills are capable of grinding many materials down to particle sizes near 100 nm, finer than many predicted limits [see, e.g., S. Mende et al., *Powder Tech.*, **132**, 64–73 (2003) or F. Stenger et al., *Chem. Eng. Sci.*, **60**, 4557–4565 (2005)]. The requirements to achieve these sizes are high-energy input per unit volume, very fine media, a slurry formulated with dispersants designed to prevent deagglomeration of the very fine particles, and a great deal of energy and time. With improved technology and technique, finer grinds than ever before are being achieved, at least on the laboratory scale. The energy requirements of these processes are such that it is unlikely that many will be cost-effective. From a practical point of view, if particles much under 1 μm are desired, it is much better to synthesize them close to this size than to grind them down.

Breakage Modes and Grindability Different materials have a greater or lesser ease of grinding, or grindability. In general, soft, brittle materials are easier to grind than hard or ductile materials. Also, different types of grinding equipment apply forces in different ways, and this makes them more suited to particular classes of materials. Figure 21-60 lists the modes of particle loading as they occur in industrial mills. This loading can take place either by slow compression between two planes or by impact against a target. In these cases the force is normal to the plane. If the applied normal forces are too weak to affect the whole of the particle and are restricted to a partial volume at the surface of the particle, the mode is attrition. An alternative way

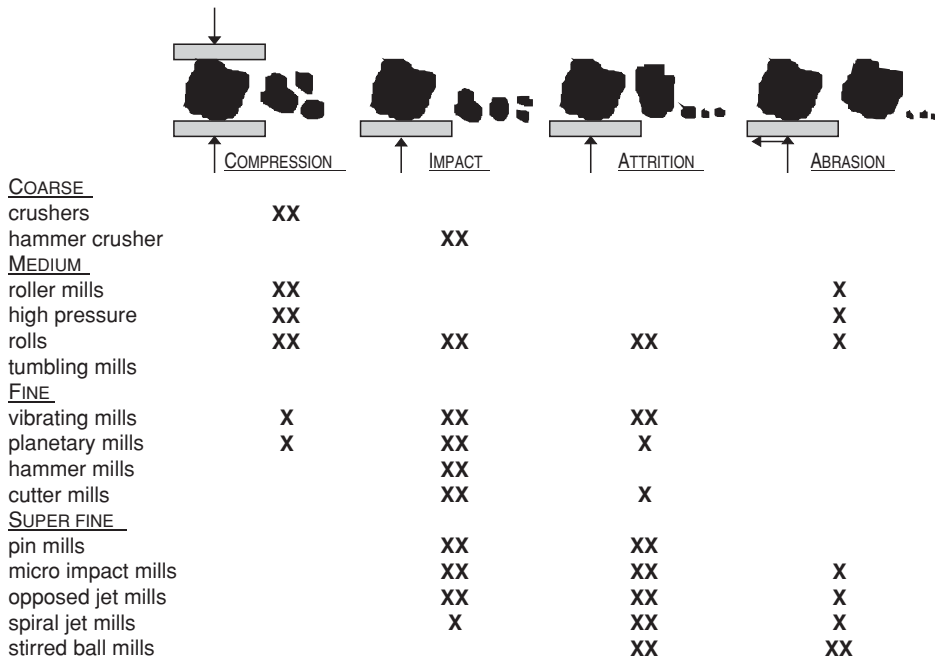


FIG. 21-60 Breakage modes in industrial mills. (Heiskanen, 1995.)

of particle loading is by applying a shear force by moving the loading planes horizontally. The table indicates that compression and impact are used more for coarse grinding, while attrition and abrasion are more common in fine and superfine grinding.

Hard materials (especially Mohs hardness 7 and above) are usually ground by devices designed for abrasion/attrition modes. For example, roll mills would rarely, if ever, be used for grinding of quartz, but media mills of various sorts have been successfully used to grind industrial diamonds. This is so primarily because both compression and high-energy impact modes have substantial contact between the mill and the very hard particles, which causes substantial wear of the device. Many attrition and abrasion devices, on the other hand, are designed so that a large component of grinding occurs by impact of particles on one another, rather than impact with the device. Wear still occurs, but its less dramatic than with other devices.

Ductile materials are an especially difficult problem for most grinding devices. Almost all grinding devices are designed for brittle materials and have some difficulties with ductile materials. However, devices with compression or abrasion modes tend to have the greatest difficulty with these kinds of materials. Mills with a compression mode will tend to flatten and flake these materials. Flaking can also occur in mills with a tangential abrasion mode, but smearing of the material across the surface of the mill is also common. In both cases, particle agglomeration can occur, as opposed to size reduction. Impact and attrition devices tend to do somewhat better with these materials, since their high-speed motion tends to cause more brittle fracture.

Conversely, mills with impact and attrition modes often do poorly with heat-sensitive materials where the materials become ductile as they heat up. Impact and attrition mills cause significant heating at the point of impact, and it is not uncommon for heat-sensitive materials (e.g., plastics) to stick to the device rather than being ground. In the worst cases, cryogenic grinding can be necessary for highly ductile or heat-sensitive materials.

Grindability Methods Laboratory experiments on single particles have been used to correlate grindability. In the past it has usually

been assumed that the total energy applied could be related to the grindability whether the energy is applied in a single blow or by repeated dropping of a weight on the sample [Gross and Zimmerly, *Trans. Am. Inst. Min. Metall. Pet. Eng.*, **87**, 27, 35 (1930)]. In fact, the results depend on the way in which the force is applied (Axelson, Ph.D. thesis, University of Minnesota, 1949). In spite of this, the results of large mill tests can often be correlated within 25 to 50 percent by a simple test, such as the number of drops of a particular weight needed to reduce a given amount of feed to below a certain mesh size. Two methods having particular application for coal are known as the ball-mill and Hardgrove methods. In the ball-mill method, the relative amounts of energy necessary to pulverize different coals are determined by placing a weighed sample of coal in a ball mill of a specified size and counting the number of revolutions required to grind the sample so that 80 percent of it will pass through a No. 200 sieve. The grindability index in percent is equal to 50,000 divided by the average of the number of revolutions required by two tests (ASTM designation D-408).

In the Hardgrove method, a prepared sample receives a definite amount of grinding energy in a miniature ball-ring pulverizer. The unknown sample is compared with a coal chosen as having 100 grindability. The Hardgrove grindability index = $13 + 6.93W$, where W is the weight of material passing the No. 200 sieve (see ASTM designation D-409).

Chandler [*Bull. Br. Coal Util. Res. Assoc.*, **29**(10), 333; (11), 371 (1965)] finds no good correlation of grindability measured on 11 coals with roll crushing and attrition, and so these methods should be used with caution. The Bond grindability method is described in the subsection "Capacity and Power Consumption." Manufacturers of various types of mills maintain laboratories in which grindability tests are made to determine the suitability of their machines. When grindability comparisons are made on small equipment of the manufacturers' own class, there is a basis for scale-up to commercial equipment. This is better than relying on a grindability index obtained in a ball mill to estimate the size and capacity of different types such as hammer or jet mills.

OPERATIONAL CONSIDERATIONS

Mill Wear Wear of mill components costs nearly as much as the energy required for comminution—hundreds of millions of dollars a year. The finer stages of comminution result in the greatest wear, because the grinding effort is greatest, as measured by the energy input per unit of feed. Parameters that affect wear fall under three categories: (1) the ore, including hardness, presence of corrosive minerals, and particle size; (2) the mill, including composition, microstructure, and mechanical properties of the material of construction, size of mill, and mill speed; and (3) the environment, including water chemistry and pH, oxygen potential, slurry solids content, and temperature [Moore et al., *Int. J. Mineral Processing*, **22**, 313–343 (1988)]. An abrasion index in terms of kilowatt-hour input per pound of metal lost furnishes a useful indication. In *wet grinding*, a synergy between mechanical wear and corrosion results in higher metal loss than with either mechanism alone [Iwasaki, *Int. J. Mineral Processing*, **22**, 345–360 (1988)]. This is due to removal of protective oxide films by abrasion, and by increased corrosion of stressed metal around gouge marks (Moore, loc. cit.). Wear rate is higher at lower solids content, since ball coating at high solids protects the balls from wear. This indicates that the mechanism is different from dry grinding. The rate of wear without corrosion can be measured with an inert atmosphere such as nitrogen in the mill. Insertion of marked balls into a ball mill best measures the wear rate at conditions in industrial mills, so long as there is not a galvanic effect due to a different composition of the balls. The mill must be cleared of dissimilar balls before a new composition is tested.

Sulfide ores promote corrosion due to galvanic coupling by a chemical reaction with oxygen present. Increasing the pH generally reduces corrosion. The use of harder materials enhances wear resistance, but this conflicts with achieving adequate ductility to avoid catastrophic brittle failure, so these two effects must be balanced. Wear-resistant materials can be divided into three groups: (1) abrasion-resistant steels, (2) alloyed cast irons, and (3) nonmetallics [see Durman, *Int. J. Mineral Processing*, **22**, 381–399 (1988) for a detailed discussion of these].

Cast irons of various sorts are often used for structural parts of large mills such as large ball mills and jaw crushers, while product contact parts such as ball-mill liners and cone crusher mantels are made from a variety of steels.

In many milling applications, mill manufacturers offer a choice of steels for product-contact surfaces (such as mill liner), usually at least one low-alloy “carbon” steel, and higher-alloy stainless steels. The exact alloys vary significantly with mill type. Stainless steels are used in applications where corrosion may occur (many wet grinding operations, but also high-alkali or high-acid minerals), but are more expensive and have lower wear resistance.

Nonmetallic materials include natural rubber, polyurethane, and ceramics. Rubber, due to its high resilience, is extremely wear-resistant in low-impact abrasion. It is inert to corrosive wear in mill liners, pipe linings, and screens. It is susceptible to cutting abrasion, so that wear increases in the presence of heavy particles, which penetrate, rather than rebound from, the wear surface. Rubber can also swell and soften in solvents. Advantages are its low density, leading to energy savings, ease of installation, and soundproofing qualities. Polyurethane has similar resilient characteristics. Its fluidity at the formation stage makes it suitable for the production of the wearing surface of screens, diaphragms, grates, classifiers, and pump and flotation impellers. The low heat tolerance of elastomers limits their use in dry processing where heat may build up.

Ceramics fill a niche in comminution where metal contamination cannot be tolerated such as pigments, cement, electronic materials, and pharmaceuticals (where any sort of contamination must be minimized). Use of ceramics has greatly increased in recent years, in part due to finer grinding requirements (and therefore higher energy and higher wear) for many industries and in part due to an increased production of electronic materials and pharmaceuticals. Also, the technology to produce mill parts from very hard ceramics such as tungsten carbide and yttria-stabilized zirconia have advanced, making larger parts available (although these are often expensive). Ceramic tiles

have been used for lining roller mills and chutes and cyclones, where there is a minimum of impact.

Safety The explosion hazard of nonmetallic materials such as sulfur, starch, wood flour, cereal dust, dextrin, coal, pitch, hard rubber, and plastics is often not appreciated [Hartmann and Nagy, U.S. Bur. Mines Rep. Invest., **3751** (1944)]. Explosions and fires may be initiated by discharges of static electricity, sparks from flames, hot surfaces, and spontaneous combustion. Metal powders also present a hazard because of their **flammability**. Their combustion is favored during grinding operations in which ball, hammer, or ring-roller mills are employed and during which a high grinding temperature may be reached. Many finely divided metal powders in suspension in air are potential **explosion hazards**, and causes for ignition of such dust clouds are numerous [Hartmann and Greenwald, *Min. Metall.*, **26**, 331 (1945)]. Concentration of the dust in air and its particle size are important factors that determine explosibility. Below a lower limit of concentration, no explosion can result because the heat of combustion is insufficient to propagate it. Above a maximum limiting concentration, an explosion cannot be produced because insufficient oxygen is available. The finer the particles, the more easily is ignition accomplished and the more rapid is the rate of combustion. This is illustrated in Fig. 21-61.

Isolation of the mills, use of nonsparking materials of construction, and magnetic separators to remove foreign magnetic material from the feed are useful **precautions** [Hartman, Nagy, and Brown, U.S. Bur. Mines Rep. Invest., **3722** (1943)]. Stainless steel has less sparking tendency than ordinary steel or forgings. Reduction of the oxygen content of air present in grinding systems is a means for preventing dust explosions in equipment [Brown, *U.S. Dep. Agri. Tech. Bull.* **74** (1928)]. Maintenance of oxygen content below 12 percent should be safe for most materials, but 8 percent is recommended for sulfur grinding. The use of **inert gas** has particular adaptation to pulverizers equipped with air classification; flue gas can be used for this purpose, and it is mixed with the air normally present in a system (see subsection “Chemicals and Soaps” for sulfur grinding). Despite the protection afforded by the use of inert gas, equipment should be provided with explosion vents, and structures should be designed with venting in mind [Brown and Hanson, *Chem. Metall. Eng.*, **40**, 116 (1933)].

Hard rubber presents a fire hazard when reduced on steam-heated rolls (see subsection “Organic Polymers”). Its dust is explosive [Twiss

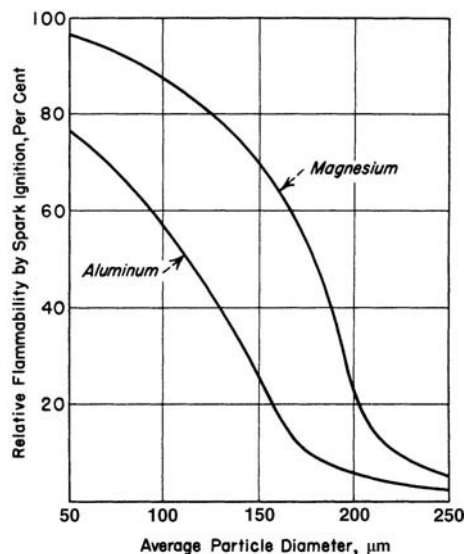


FIG. 21-61 Effect of fineness on the flammability of metal powders. (Hartmann, Nagy, and Brown, U.S. Bur. Mines Rep. Invest. 3722, 1943.)

and McGowan, *India Rubber J.*, **107**, 292 (1944)]. The annual publication *National Fire Codes for the Prevention of Dust Explosions* is available from the National Fire Protection Association, Quincy, Massachusetts, and should be of interest to those handling hazardous powders.

Temperature Stability Many materials are temperature-sensitive and can tolerate temperatures only slightly above room temperature, including many food products, polymers, and pharmaceuticals. This is a particular problem in grinding operations, as grinding inevitably adds heat to the ground material. The two major problems are that either the material will simply be damaged or denatured in some way, such as food products, or the material may melt or soften in the mill, usually causing significant operational problems.

Ways to deal with heat-sensitive materials include choosing a less energy-intensive mill, or running a mill at below optimum energy input. Some mills run naturally cooler than others. For example, jet mills can run cool because they need high gas flow for operation, and this has a significant cooling effect despite their high-energy intensity. Variable-speed drives are commonly used in stirred media mills to control the energy input to heat-sensitive slurries as energy input (and therefore temperature) is a strong function of stirrer speed.

Adding more cooling capability is often effective, but it can be expensive. Compositions containing fats and waxes are pulverized and blended readily if refrigerated air is introduced into their grinding systems (U.S. Patents 1,739,761 and 2,098,798; see also subsection "Organic Polymers" and Hixon, loc. cit., for flow sheets).

Hygroscopicity Some materials, such as salt, are very hygroscopic; they pick up water from air and deposit on mill surfaces, forming a hard cake. Mills with air classification units may be equipped so that the circulating air can be conditioned by mixing with hot or cold air, gases introduced into the mill, or dehumidification to prepare the air for the grinding of hygroscopic materials. Flow sheets including air dryers are also described by Hixon.

Dispersing Agents and Grinding Aids Grinding aids are helpful under some conditions. For example, surfactants make it possible to ball-mill magnesium in kerosene to 0.5- μm size [Fochtman, Bitten, and Katz, *Ind. Eng. Chem. Prod. Res. Dev.*, **2**, 212–216 (1963)]. Without surfactants the size attainable was 3 μm ; the rate of grinding was very slow at sizes below this. Also, the water in wet grinding may be considered to act as an additive.

Chemical agents that increase the rate of grinding are an attractive prospect since their cost is low. However, despite a voluminous literature on the subject, there is no accepted scientific method to choose such aids; there is not even agreement on the mechanisms by which they work. The subject has been reviewed [Fuerstenau, *KONA Powder and Particle*, **13**, 5–17 (1995)]. In wet grinding there are several theories, which have been reviewed [Somasundaran and Lin, *Ind. Eng. Chem. Process Des. Dev.*, **11**(3), 321 (1972); Snow, annual reviews, op. cit., 1970–1974; see also Rose, *Ball and Tube Milling*, Constable, London, 1958, pp. 245–249]. Additives can alter the rate of wet ball milling by changing the slurry viscosity or by altering the location of particles with respect to the balls. These effects are discussed under "Tumbling Mills." In conclusion, there is still no theoretical way to select the most effective additive. Empirical investigation, guided by the principles discussed earlier, is the only recourse. There are a number of commercially available grinding aids that may be tried. Also, a kit of 450 surfactants that can be used for systematic trials (Model SU-450, Chem Service Inc., West Chester, Pa. 19380) is available. Numerous experimental studies lead to the conclusion that dry grinding is limited by ball coating and that additives function by reducing the tendency to coat (Bond and Agthe, op. cit.). Most materials coat if they are ground finely enough, and softer materials coat at larger sizes than do hard materials. The presence of more than a few percent of soft gypsum promotes ball coating in cement-clinker grinding. The presence of a considerable amount of coarse particles above 35 mesh inhibits coating. Balls coat more readily as they become scratched. Small amounts of moisture may increase or decrease ball coating. Dry materials also coat. Materials used as grinding aids include solids such as graphite, oleoresinous liquid materials, volatile solids, and vapors. The complex effects of vapors have been extensively studied [Goette and Ziegler, *Z. Ver. Dtsch. Ing.*,

98, 373–376 (1956); and Locher and von Seebach, *Ind. Eng. Chem. Process Des. Dev.*, **11**(2), 190 (1972)], but water is the only vapor used in practice. The most effective additive for dry grinding is fumed silica that has been treated with methyl silazane [Tulis, *J. Hazard. Mater.*, **4**, 3 (1980)].

Cryogenic Grinding Cryogenic grinding is increasingly becoming a standard option for grinding of rubbers and plastics (especially powder coatings, but also some thermoplastics), as well as heat-sensitive materials such as some pharmaceuticals and chemicals. Many manufacturers of fine-grinding equipment have equipment options for cryogrinding, especially manufacturers of hammer mills and other rotary impact mills.

Cryogrinding adds to operating expenses due to the cost and recovery of liquid nitrogen, but capital cost is a more significant drawback to these systems. Modified mills, special feeders, as well as enhanced air handling and recovery systems are required and these tend to add significant cost to cryogenic systems. Partly for this reason, there is a healthy toll industry for cryogrinding where specialty equipment can be installed and used for a variety of applications to cover its cost. Many manufacturers of liquid nitrogen have information on cryogrinding applications on their Web sites.

SIZE REDUCTION COMBINED WITH OTHER OPERATIONS

Size Reduction Combined with Size Classification Grinding systems are batch or continuous in operation (Fig. 21-62). Most large-scale operations are continuous; batch ball or pebble mills are used only when small quantities are to be processed. Batch operation involves a high labor cost for charging and discharging the mill. Continuous operation is accomplished in open or closed circuit, as illustrated in Figs. 21-62 and 21-57a. **Operating economy** is the object of closed-circuit grinding with size classifiers. The idea is to remove the material from the mill before all of it is ground, separate the fine product in a classifier, and return the coarse for regrinding with the new feed to the mill. A mill with the fines removed in this way performs much more efficiently. Coarse material returned to a mill by a classifier is known as the **circulating load**; its rate may be from 1 to 10 times the production rate. The ability of the mill to transport material may limit the recycle rate; tube mills for use in such circuits may be designed with a smaller length-to-diameter ratio and hence a larger hydraulic gradient for greater flow or with compartments separated by diaphragms with lifters.

Internal size classification plays an essential role in the functioning of machines for dry grinding in the fine-size range; particles are retained in the grinding zone until they are as small as required in the finished product; then they are allowed to discharge. By closed-circuit operation the product size distribution is narrower and will have a larger proportion of particles of the desired size. On the other hand, making a *product size within narrow limits* (such as between 20 and 40 μm) is often requested but usually is not possible regardless of the grinding circuit used. The reason is that particle breakage is a random process, both as to the probability of breakage of particles and as to the sizes of fragments produced from each breakage event. The narrowest size distribution ideally attainable is one that has a slope of 1.0 when plotted on Gates-Gaudin-Schumann coordinates [$Y = (X/k)^m$]. This can be demonstrated by examining the Gaudin-Meloy size distribution [$Y = 1 - (1 - XX^r)^n$]. This is the distribution produced in a mill when particles are cut into pieces of random size, with r cuts per event. The case in which r is large corresponds to a breakage event producing many fines. The case

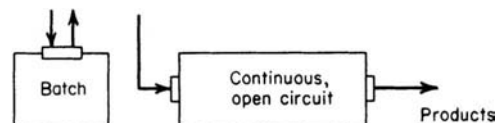


FIG. 21-62 Batch and continuous grinding systems.

in which r is 1 corresponds to an ideal case such as a knife cutter, in which each particle is cut once per event and the fragments are removed immediately by the classifier. The Meloy distribution with $r = 1$ reduces to the Schumann distribution with a slope of 1.0. Therefore, no practical grinding operation can have a slope greater than 1.0. Slopes typically range from 0.5 to 0.7. The specified product may still be made, but the finer fraction may have to be disposed of in some way. Within these limits, the size distribution of the classifier product depends both on the recycle ratio and on the sharpness of cut of the classifier used.

Size Classification The most common objective is **size classification**. Often only a particular range of product sizes is wanted for a given application. Since the particle breakage process always yields a spectrum of sizes, the product size cannot be directly controlled; however, mill operation can sometimes be varied to produce fewer fines at the expense of producing more coarse particles. By recycling the classified coarse fraction and regrinding it, production of the wanted size range is optimized. Such an arrangement of classifier and mill is called a **mill circuit** and is dealt with further below. More complex systems may include several unit operations such as mixing (Sec. 18), drying (Sec. 12), and agglomerating (see "Size Enlargement," in this section). Inlet and outlet silencers are helpful to reduce noise from high-speed mills. Chillers, air coolers, and explosion proofing may be added to meet requirements. Weighing and packaging facilities complete the system. Batch ball mills with low ball charges can be used in dry mixing or standardizing of dyes, pigments, colors, and insecticides to incorporate wetting agents and inert extenders. Disk mills, hammer mills, and other high-speed disintegration equipment are useful for final intensive blending of insecticide compositions, earth colors, cosmetic powders, and a variety of other finely divided materials that tend to agglomerate in ribbon and conical blenders. Liquid sprays or gases may be injected into the mill or airstream, for mixing with the material being pulverized to effect chemical reaction or surface treatment.

Other Systems Involving Size Reduction Industrial applications usually involve a number of processing steps combined with size reduction [Hixon, *Chem. Eng. Progress*, **87**, 36–44 (May 1991)].

Drying The **drying** of materials while they are being pulverized or disintegrated is known variously as *flash* or *dispersion* drying; a generic term is *pneumatic conveying* drying.

Beneficiation Ball and pebble mills, batch or continuous, offer considerable opportunity for combining a number of **processing steps** that include grinding [Underwood, *Ind. Eng. Chem.*, **30**, 905 (1938)]. Mills followed by air classifiers can serve to **separate components of mixtures** because of differences in specific gravity and the component that is pulverized readily. Grinding followed by *froth flotation* has become the beneficiation method most widely used for metallic ores and for nonmetallic minerals such as feldspar. Magnetic separation is the chief means used for upgrading taconite iron ore (see subsection "Ores and Minerals"). Magnetic separators frequently are employed to remove tramp magnetic solids from the feed to high-speed hammer and disk mills.

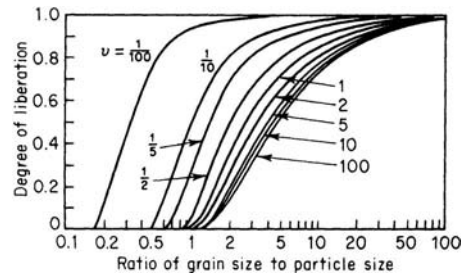


FIG. 21-63 Fraction of mineral B that is liberated as a function of volumetric abundance ratio v of gangue to mineral B (1/grade), and ratio of grain size to particle size of broken fragments (1/fineness). [Wiegel and Li, *Trans. Soc. Min. Eng.-Am. Inst. Min. Metall. Pet. Eng.*, **238**, 179 (1967).]

Liberation Most ores are heterogeneous, and the objective of grinding is to release the valuable mineral component so that it can be separated. Calculations based on a random-breakage model assuming no preferential breakage [Wiegel and Li, *Trans. Am. Inst. Min. Metall. Pet. Eng.*, **238**, 179–191 (1967)] agreed, at least in general trends, with plant data on the efficiency of release of mineral grains. Figure 21-63 shows that the desired mineral B can be liberated by coarse grinding when the grade is high so that mineral A becomes a small fraction and mineral B a large fraction of the total volume; mineral B can be liberated only by fine grinding below the grain size, when the grade is low so that there is a small proportion of grains of B . Similar curves, somewhat displaced in size, resulted from a more detailed integral geometry analysis by Barbery [*Minerals Engg.*, **5**(2), 123–141 (1992)]. There is at present no way to measure grain size on-line and thus to control liberation. A review of liberation modeling is given by Mehta et al. [*Powder Technol.*, **58**(3), 195–209 (1989)]. Many authors have assumed that breakage occurs preferentially along grain boundaries, but there is scant evidence for this. On the contrary, Gorski [*Bull. Acad. Pol. Sci. Ser. Sci. Tech.*, **20**(12), 929 (1972); CA 79, 20828k], from analysis of microscope sections, finds an intercrystalline character of comminution of dolomite regardless of the type of crusher used. The liberation of a valuable constituent does not necessarily translate directly into recovery in downstream processes. For example, flotation tends to be more efficient in intermediate sizes than at coarse or fine sizes [McIvor and Finch, *Minerals Engg.*, **4**(1), 9–23 (1991)]. For coarser sizes, failure to liberate may be the limitation; finer sizes that are liberated may still be carried through by the water flow. A conclusion is that overgrinding should be avoided by judicious use of size classifiers with recycle grinding.

MODELING AND SIMULATION OF GRINDING PROCESSES

MODELING OF MILLING CIRCUITS

Grinding processes have not benefited as much as some other types of processes from the great increase in computing power and modeling sophistication in the 1990s. Complete simulations of most grinding processes that would be useful to practicing engineers involve breakage mechanics and gas-phase or liquid-phase particle motion coupled in a complex way that is not yet practical to study. However, with the continuing increase of computing power, it is unlikely that this state will continue much longer. Fluid mechanics modeling is well advanced, and the main limitation to modeling many devices is having

enough computer power to keep track of a large number of particles as they move and are size-reduced. Traditionally, particle breakage is modeled by using variations of population balance methodology described below, but more recent models have tended to use discrete elements models which track the particles individually. The latter requires greater computing power, but may provide a more realistic way of accounting for particle dynamics in a device.

Computer simulation, based on population-balance models [Bass, *Z. Angew. Math. Phys.*, **5**(4), 283 (1954)], traces the breakage of each size of particle as a function of grinding time. Furthermore, the simulation models separate the breakage process into two aspects: a

breakage rate and a mean fragment-size distribution. These are both functions of the size of particle being broken. They usually are not derived from knowledge of the physics of fracture but are empirical functions fitted to milling data. The following formulation is given in terms of a discrete representation of size distribution; there are comparable equations in integro-differential form.

BATCH GRINDING

Grinding Rate Function Let w_k = the weight fraction of material retained on each screen of a nest of n screens; w_k is related to P_k , the fraction coarser than size X_k , by

$$w_k = (\partial P_k / \partial X_k) \Delta X_k \tag{21-77a}$$

where ΔX_k is the difference between the openings of screens k and $k + 1$. The **grinding-rate function** S_u is the rate at which the material of upper size u is selected for breakage in an increment of time, relative to the amount of that size present:

$$dw_u/dt = -S_u w_u \tag{21-77b}$$

Breakage Function The **breakage function** $\Delta B_{k,u}$ gives the size distribution of product breakage of size u into all smaller sizes k . Since some fragments from size u are large enough to remain in the range of size u , the term $\Delta B_{u,u}$ is not zero, and

$$\sum_{k=n}^u \Delta B_{k,u} = 1 \tag{21-78}$$

The differential equation of batch grinding is deduced from a balance on the material in the size range k . The rate of accumulation of material of size k equals the rate of production from all larger sizes minus the rate of breakage of material of size k :

$$\frac{dw_k}{dt} = \sum_{u=1}^k [w_u S_u(t) \Delta B_{k,u}] - S_k(t) w_k \tag{21-79}$$

In general, S_u is a function of all the milling variables. Also $\Delta B_{k,u}$ is a function of breakage conditions. If it is assumed that these functions are constant, then relatively simple solutions of the grinding equation are possible, including an analytical solution [Reid, *Chem. Eng. Sci.*, **20**(11), 953-963 (1965)] and matrix solutions [Broadbent and Callcott, *J. Inst. Fuel*, **29**, 524-539 (1956); **30**, 18-25 (1967); and Meloy and Bergstrom, *7th Int. Min. Proc. Congr. Tech. Pap.*, 1964, pp. 19-31].

Solution of Batch-Mill Equations In general, the grinding equation can be solved by numerical methods, e.g., the Euler technique (Austin and Gardner, *1st European Symposium on Size Reduction*, 1962) or the Runge-Kutta technique. The matrix method is a particularly convenient formulation of the Euler technique. Reid's **analytical solution** is useful for calculating the product as a function of time t for a constant feed composition. It is

$$w_{L,k} = \sum_{n=1}^k a_{k,n} \exp(-\bar{S}_n \Delta t) \tag{21-80}$$

where the subscript L refers to the discharge of the mill, 0 to the entrance, and $\bar{S}_n = 1$ "corrected" rate function defined by $\bar{S}_n = (1 - \Delta B_{n,n})$ and B is then normalized with $\Delta B_{n,n} = 0$. The coefficients are

$$a_{k,k} = w_{0k} - \sum_{n=1}^{k-1} a_{k,n} \tag{21-81a}$$

and

$$a_{k,n} = \sum_{u=n}^{k-1} \frac{S_u \Delta B_{k,u} a_{n,u}}{\bar{S}_k - \bar{S}_n} \tag{21-81b}$$

The coefficients are evaluated in order since they depend on the coefficients already obtained for larger sizes.

The basic idea behind the **Euler method** is to set the change in w per increment of time as

$$\Delta w_k = (dw_k/dt) \Delta t \tag{21-82}$$

where the derivative is evaluated from Eq. (21-79). Equation (21-82) is applied repeatedly for a succession of small time intervals until the desired duration of milling is reached. In the matrix method a modified rate function is defined $S'_k = S_k \Delta t$ as the amount of grinding that occurs in some small time Δt . The result is

$$\mathbf{w}_L = (\mathbf{I} + \mathbf{S}'\mathbf{B} - \mathbf{S}')\mathbf{w}_F = \mathbf{M}\mathbf{w}_F \tag{21-83}$$

where the quantities \mathbf{w} are vectors, \mathbf{S}' and \mathbf{B} are the matrices of rate and breakage functions, and \mathbf{I} is the unit matrix. This follows because the result obtained by multiplying these matrices is just the sum of products obtained from the Euler method. Equation (21-83) has a physical meaning. The unit matrix times \mathbf{w}_F is simply the amount of feed that is not broken. $\mathbf{S}'\mathbf{B}\mathbf{w}_F$ is the amount of feed that is selected and broken into the vector of products; $\mathbf{S}'\mathbf{w}_F$ is the amount of material that is broken out of its size range and hence must be subtracted from this element of the product. The entire term in parentheses can be considered as a mill matrix \mathbf{M} . Thus the milling operation transforms the feed vector to the product vector. Meloy and Bergstrom (op. cit.) pointed out that when Eq. (21-83) is applied over a series of p short-time intervals, the result is

$$\mathbf{w}_L = \mathbf{M}^p \mathbf{w}_F \tag{21-83a}$$

Matrix multiplication happens to be cumulative in this special case. It is easy to raise a matrix to a power on a computer since three multiplications give the eighth power, etc. Therefore the matrix formulation is well adapted to computer use.

CONTINUOUS-MILL SIMULATION

Residence Time Distribution Batch-grinding experiments are the simplest type of experiments to produce data on grinding coefficients. But scale-up from batch to continuous mills must take into account the **residence-time distribution** in a continuous mill. This distribution is apparent if a tracer experiment is carried out. For this purpose, background ore is fed continuously, and a pulse of tagged feed is introduced at time t_0 . This tagged material appears in the effluent distributed over a period of time, as shown by a typical curve in Fig. 21-64. Because of this distribution some portions are exposed to grinding for longer times than others. Levenspiel (*Chemical Reaction Engineering*, Wiley, New York, 1962) shows several types of residence time distribution that can be observed. Data on large mills indicate that a curve like that of Fig. 21-64 is typical (Keienberg et al., *3d European Symposium on Size Reduction*, op. cit., 1972, p. 629). This curve

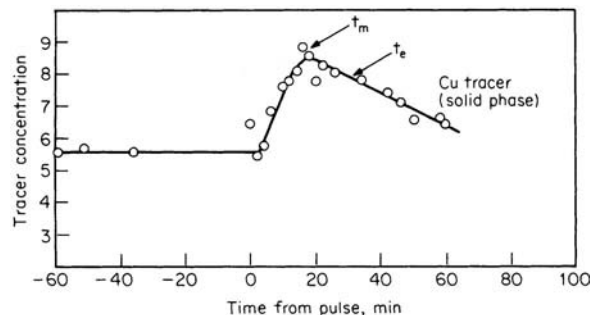


FIG. 21-64 Ore transit through a ball mill. Feed rate is 500 lb/h. (Courtesy Phelps Dodge Corporation.)

can be accurately expressed as a series of arbitrary functions (Merz and Molerus, *3d European Symposium on Size Reduction*, op. cit., 1972, p. 607). A good fit is more easily obtained if we choose a function that has the right shape since then only the first two moments are needed. The log-normal probability curve fits most available mill data, as was demonstrated by Mori [*Chem. Eng. (Japan)*, 2(2), 173 (1964)]. Two examples are shown in Fig. 21-65. The log-normal plot fails only when the mill acts nearly as a perfect mixer. To measure a residence time distribution, a pulse of tagged feed is inserted into a continuous mill and the effluent is sampled on a schedule. If it is a dry mill, a soluble tracer such as salt or dye may be used and the samples analyzed conductimetrically or colorimetrically. If it is a wet mill, the tracer must be a solid of similar density to the ore. Materials such as copper concentrate, chrome brick, or barites have been used as tracers and analyzed by X-ray fluorescence. To plot results in log-normal coordinates, the concentration data must first be normalized from the form of Fig. 21-64 to the form of cumulative percent discharged, as in Fig. 21-65. For this, one must either know the total amount of pulse feed or determine it by a simple numerical integration using a computer. The data are then plotted as in Fig. 21-65, and the coefficients in the log-normal formula of Mori can be read directly from the graph. Here $t_e = t_{50}$ is the time when 50 percent of the pulse has emerged. The standard deviation σ is the time between t_{16} and t_{50} or between t_{50} and t_{84} . Knowing t_e and σ , one can reconstruct the straight line in log-normal coordinates. One can also calculate the vessel dispersion number Dt_e/L^2 , which is a measure of the sharpness of the pulse (Levenspiel, *Chemical Reactor Omnibook*, Oregon State University Bookstores Inc., 1979, p. 100.6). This number has erroneously been called by some the Peclet number. Here D is the particle diffusivity. A few available data are summarized (Snow, *International Conference on Particle Technology*, IIT Research Institute, Chicago, 1973, p. 28) for wet mills. Other experiments are presented for dry mills [Hogg et al., *Trans. Am. Inst. Min. Metall. Pet. Eng.*, 258, 194 (1975)]. The most important variables affecting the vessel dispersion number are L /diameter of the mill, ball size, mill speed, scale expressed either as diameter or as throughput, degree of ball filling, and degree of material filling.

Solution for Continuous Milling In the method of Mori (op. cit.), the residence time distribution is broken up into a number of

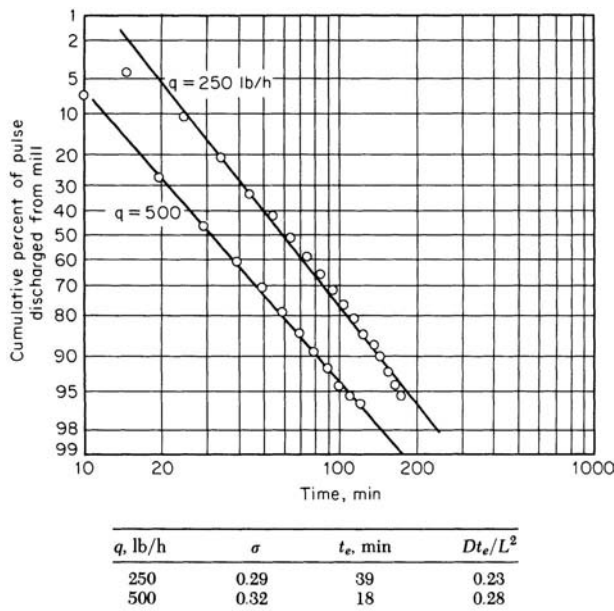


FIG. 21-65 Log-normal plot of residence-time distribution in Phelps Dodge mill.

segments, and the batch-grinding equation is applied to each of them. The resulting size distribution at the mill discharge is

$$w(L) = w(t) \Delta\phi \tag{21-84}$$

where $w(t)$ is a matrix of solutions of the batch equation for the series of times t , with corresponding segments of the cumulative residence time curve. Using the Reid solution, Eq. (21-80), this becomes

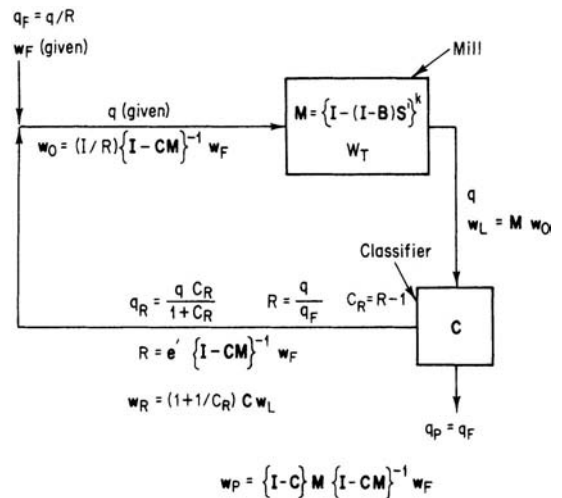
$$w(L) = RZ \Delta\phi \tag{21-85}$$

since the Reid solution [Eq. (21-80)] can be separated into a matrix Z of exponentials $\exp(-St)$ and another factor R involving only particle sizes. Austin, Klimpel, and Luckie (*Process Engineering of Size Reduction: Ball Milling*, Society of Mining Engineers of AIME, 1984) incorporated into this form a tanks-in-series model for the residence time distribution.

CLOSED-CIRCUIT MILLING

In closed-circuit milling, the tailings from a classifier are mixed with fresh feed and recycled to the mill. Calculations can be based on a material balance and an explicit solution such as Eq. (21-83a). Material balances for the normal circuit arrangement (Fig. 21-66) give

$$q = q_F + q_R \tag{21-86}$$



Nomenclature

- C_R = circulating load, $R - 1$
 - C = classifier selectivity matrix, which has classifier selectivity-function values η on diagonal zeros elsewhere
 - I = identity matrix, which has ones on diagonal, zeros elsewhere
 - M = mill matrix, which transforms mill-feed-size distribution into mill-product-size distribution
 - q = flow rate of a material stream
 - R = recycle ratio q/q_F
 - w = vector of differential size distribution of a material stream
 - w_T = holdup, total mass of material in mill
- Subscripts:
 0 = inlet to mill
 F = feed stream
 L = mill-discharge stream
 P = product stream
 R = recycle stream, classifier tailings

FIG. 21-66 Normal closed-circuit continuous grinding system with stream flows and composition matrices, obtained by solving material-balance equations. [Callcott, *Trans. Inst. Min. Metall.*, 76(1), C1-11 (1967).]

where q = total mill throughput, q_F = rate of feed of new material, and q_R = recycle rate. A material balance on each size gives

$$w_{0,k} = \frac{q_F w_{F,k} + \frac{q_R}{R} \eta_k w_{L,k}}{q} \quad (21-87)$$

where $w_{0,k}$ = fraction of size k in the mixed feed streams, R = recycle ratio, and η_k = classifier selectivity for size k . With these conditions, a calculation of the transient behavior of the mill can be performed by using any method of solving the milling equation and iterating over intervals of time τ = residence time in the mill. This information is important for evaluating mill circuit control stability and strategies. If the throughput q is controlled to be a constant, as is often the case, then τ is constant, and a closed-form matrix solution can be found for the steady state [Callcott, *Trans. Inst. Min. Metall.*, **76**(1), C1-11 (1967)]. The resulting flow rates and composition vectors are given in Fig. 21-66. Callcott (loc. cit.) gives equations for the reverse-circuit case, in which the feed is classified before it enters the mill. These results can be used to investigate the effects of changes in feed composition on the product. Separate calculations can be made to find the effects of classifier selectivity, mill throughput or recycle, and grindability (rate function) to determine optimum mill-classifier combinations [Lynch, Whiten, and Draper, *Trans. Inst. Min. Metall.*, **76**, C169, 179 (1967)]. Equations such as these form the basis for computer codes that are available for modeling mill circuits (Austin, Klimpel, and Luckie, loc. cit.).

DATA ON BEHAVIOR OF GRINDING FUNCTIONS

Several breakage functions were early suggested [Gardner and Austin, *1st European Symposium on Size Reduction*, op. cit., 1962, p. 217; Broadbent and Calcott, *J. Inst. Fuel*, **29**, 524 (1956); 528 (1956); 18 (1957); **30**, 21 (1957)]. The simple Gates-Gaudin-Schumann equation has been most widely used to fit ball-mill data. For example, this form was assumed by Herbst and Fuerstenau [*Trans. Am. Inst. Min. Metall. Pet. Eng.*, **241**(4), 538 (1968)] and Kelsall et al. [*Powder Technol.*, **1**(5), 291 (1968); **2**(3), 162 (1968); **3**(3), 170 (1970)]. More recently it has been observed that when the Schumann equation is used, the amount of coarse fragments cannot be made to agree with the mill-product distribution regardless of the choice of rate function. This observation points to the need for a breakage function that has more coarse fragments, such as the function used by Reid and Stewart (Chemica meeting, 1970) and Stewart and Restarick [*Proc. Australas. Inst. Min. Metall.*, **239**, 81 (1971)] and shown in Fig. 21-67. This graph can be fitted by a double Schumann equation

$$B(X) = A \left(\frac{X}{X_0} \right)^s + (1-A) \left(\frac{X}{X_0} \right)^r \quad (21-88)$$

where A is a coefficient less than 1.

In the investigations mentioned earlier, the breakage function was assumed to be normalizable; i.e., the shape was independent of X_0 . Austin and Luckie [*Powder Technol.*, **5**(5), 267 (1972)] allowed the coefficient A to vary with the size of particle breaking when grinding soft feeds.

Grinding Rate Functions These were determined by tracer experiments in laboratory mills by Kelsall et al. (op. cit.) and in similar work by Szanthy and Fuhrmann [*Aufbereit. Tech.*, **9**(5), 222 (1968)]. These curves can be fitted by the following equation:

$$\frac{S}{S_{\max}} = \left(\frac{X}{X_{\max}} \right)^\alpha \exp \left(- \frac{X}{X_{\max}} \right) \quad (21-89)$$

That a maximum must exist should be apparent from the observation of Coghill and Devaney (U.S. Bur. Mines Tech. Pap., 1937, p. 581) that there is an optimum ball size for each feed size. The position of this maximum depends on the ball size. In fact, the feed size for

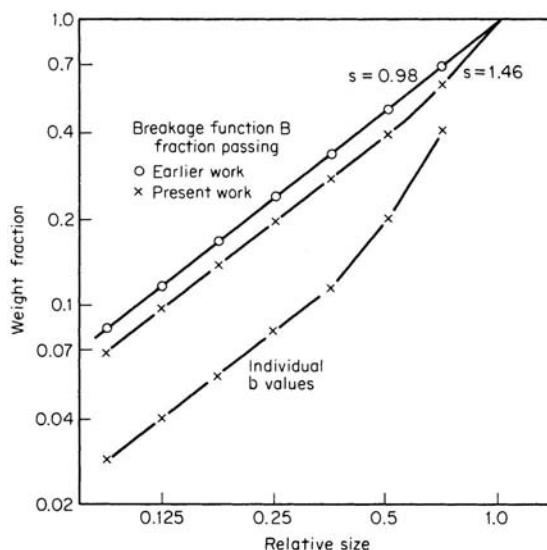


FIG. 21-67 Experimental breakage functions. (Reid and Stewart, *Chemical meeting*, 1970.)

which S is a maximum can be estimated by inverting the formula for optimum ball size given by Coghill and Devaney under "Tumbling Mills."

SCALE-UP AND CONTROL OF GRINDING CIRCUITS

Scale-up Based on Energy Since large mills are usually sized on the basis of power draft (see subsection "Energy Laws"), it is appropriate to scale up or convert from batch to continuous data by

$$S(X)_{\text{cont}} = S(X)_{\text{batch}} \frac{(W_T/KW)_{\text{batch}}}{(W_T/KW)_{\text{cont}}} \quad (21-90)$$

Usually W_T is not known for continuous mills, but it can be determined from $W_T = t_e Q$, where t_e is determined by a tracer measurement. Equation (21-90) will be valid if the holdup W_T is geometrically similar in the two mills or if operating conditions are in the range in which total production is independent of holdup. Studies of the kinetics of milling [Patat and Mempel, *Chem. Ing. Tech.*, **37**(9), 933; (11), 1146; (12), 1259 (1965)] indicate that there is a range of holdup in which this is true. More generally, Austin, Luckie, and Klimpel (loc. cit.) developed empirical relations to predict S as holdup varies. In particular, they observe a slowing of grinding rate when mill filling exceeds ball void volume due to cushioning.

Parameters for Scale-up Before simulation equations can be used, the parameter matrices **S** and **B** must be back-calculated from experimental data, which turns out to be difficult. One reason is that **S** and **B** occur as a product, so they are to some extent indeterminate; errors in one tend to be compensated by the other. Also, the number of parameters is larger than the number of data values from a single size-distribution measurement; but this is overcome by using data from grinding tests at a series of grinding times. This should be done anyway, since the empirical parameters should be determined to be valid over the experimental range of grinding times.

It may be easier to fit the parameters by forcing them to follow specified functional forms. In earliest attempts it was assumed that the forms should be normalizable (have the same shape whatever the size being broken). With complex ores containing minerals of different friability, the grinding functions **S** and **B** exhibit complex behavior

near the grain size (Choi et al., *Particulate and Multiphase Processes Conference Proceedings*, **1**, 903–916). Grinding function **B** is not normalizable with respect to feed size, and **S** does not follow a simple power law.

There are also experimental problems: When a feed-size distribution is ground for a short time, there is not enough change in the size distribution in the mill to distinguish between particles being broken into and out of intermediate sizes, unless individual feed-size ranges are tagged. Feeding narrow-size fractions alone solves the problem, but changes the milling environment; the presence of fines affects the grinding of coarser sizes. Gupta et al. [*Powder Technol.*, **28**(1), 97–106 (1981)] ground narrow fractions separately, but subtracted out the effect of the first 3 min of grinding, after which the behavior had become steady. Another experimental difficulty arises from the recycle of fines in a closed circuit, which soon “contaminates” the size distribution in the mill; it is better to conduct experiments in open circuit, or in batch mills on a laboratory scale.

There are few data demonstrating scale-up of the grinding-rate functions **S** and **B** from pilot- to industrial-scale mills. Weller et al. [*Int. J. Mineral Processing*, **22**, 119–147 (1988)] ground chalcocopyrite ore in pilot and plant mills and compared predicted parameters with laboratory data of Kelsall [*Electrical Engg. Trans.*, Institution of

Engineers Australia, **EE5**(1), 155–169 (1969)] and Austin, Klimpel, and Luckie (*Process Engineering of Size Reduction, Ball Milling*, Society of Mining Engineers, New York, 1984) for quartz. Grinding function **S** has a maximum for a particle size that depends on ball size, which can be expressed as $X_s/X_t = (d_s/d_t)^{2.4}$, where s = scaled-up mill, t = test mill, d = ball size, and X = particle size of maximum rate. Changing ball size also changes the rates according to $S_s/S_t = (d_s/d_t)^{0.55}$. These relations shift one rate curve onto another and allow scale-up to a different ball size. Mill diameter also affects rate by a factor $(D_s/D_t)^{0.5}$. Lynch (*Mineral Crushing and Grinding Circuits, Their Simulation Optimization Design and Control*, Elsevier Scientific Publishing Co., Amsterdam, 1977) and Austin, Klimpel, and Luckie (loc. cit.) developed scale-up factors for ball load, mill filling, and mill speed. In addition, slurry solids content is known to affect the rate, through its effect on slurry rheology. Austin, Klimpel, and Luckie (loc. cit.) present more complete simulation examples and compare them with experimental data to study scale-up and optimization of open and closed circuits, including classifiers such as hydrocyclones and screen bends. Differences in the classifier will affect the rates in a closed circuit. For these reasons scale-up is likely to be uncertain unless conditions in the large mill are as close as possible to those in the test mill.

CRUSHING AND GRINDING EQUIPMENT: DRY GRINDING—IMPACT AND ROLLER MILLS

JAW CRUSHERS

Design and Operation These crushers may be divided into two main groups, the *Blake* (Fig. 21-68), with a movable jaw pivoted at the top, giving greatest movement to the smallest lumps; and the *overhead eccentric*, which is also hinged at the top, but through an *eccentric-driven* shaft which imparts an elliptical motion to the jaw. Both types have a removable crushing plate, usually corrugated, fixed in a vertical position at the front end of a hollow rectangular frame. A similar plate is attached to the swinging movable jaw. The Blake jaw is moved through a knuckle action by the rising and falling of a second lever (pitman) car-

ried by an eccentric shaft. The vertical movement is communicated horizontally to the jaw by double-toggle plates. Because the jaw is pivoted at the top, the throw is greatest at the discharge, preventing choking.

The *overhead eccentric jaw crusher* falls into the second type. These are single-toggle machines. The lower end of the jaw is pulled back against the toggle by a tension rod and spring. The choice between the two types of jaw crushers is generally dictated by the feed characteristics, tonnage, and product requirements (Pryon, *Mineral Processing*, Mining Publications, London, 1960; Wills, *Mineral Processing Technology*, Pergamon, Oxford, 1979). Greater wear caused by the elliptical motion of the overhead eccentric and direct transmittal of

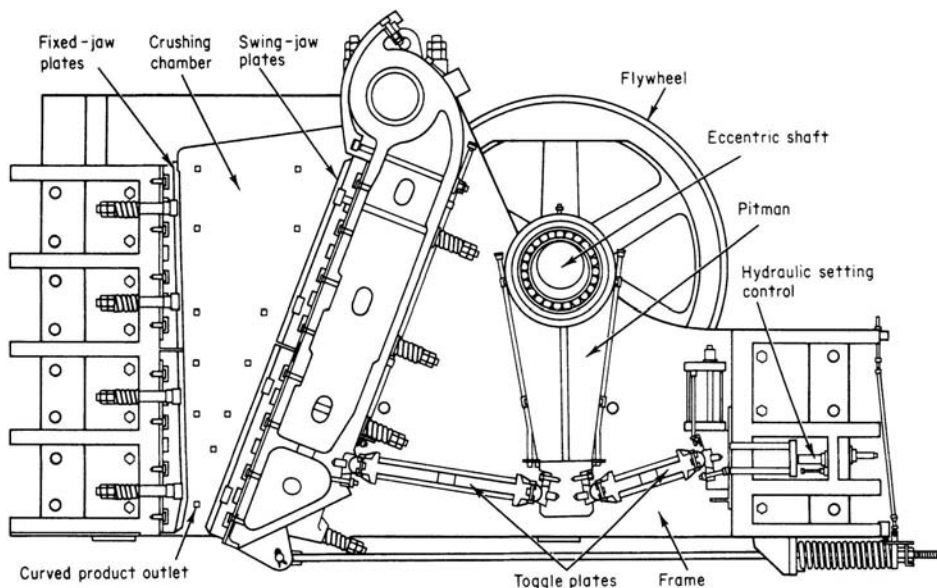


FIG. 21-68 Blake jaw crusher. (Allis Mineral Systems Grinding Div., Svedala Industries, Inc.)

shocks to the bearing limit use of this type to readily breakable material. Overhead eccentric crushers are generally preferred for crushing rocks with a hardness equal to or lower than that of limestone. Operating costs of the overhead eccentric are higher for the crushing of hard rocks, but its large reduction ratio is useful for simplified low-tonnage circuits with fewer grinding steps. The double-toggle type of crushers cost about 50 percent more than the similar overhead-eccentric type of crushers.

Comparison of Crushers The jaw crusher can accommodate the same size rocks as a gyratory, with lower capacity and also lower capital and maintenance costs, but similar installation costs. Therefore they are preferred when the crusher gape is more important than the throughput. Relining the gyratory requires greater effort than for the jaw, and also more space above and below the crusher.

Performance Jaw crushers are applied to the primary crushing of hard materials and are usually followed by other types of crushers. In smaller sizes they are used as single-stage machines. Typical capabilities and specifications are shown in Table 21-9a.

GYRATORY CRUSHERS

The development of improved supports and drive mechanisms has allowed gyratory crushers to take over most large hard-ore and

mineral-crushing applications. The largest expense of these units is in relining them. Operation is intermittent; so power demand is high, but the total power cost is not great.

Design and Operation The gyratory crusher consists of a cone-shaped pestle oscillating within a larger cone-shaped mortar or bowl. The angles of the cones are such that the width of the passage decreases toward the bottom of the working faces. The pestle consists of a mantle which is free to turn on its spindle. The spindle is oscillated from an eccentric bearing below. Differential motion causing attrition can occur only when pieces are caught simultaneously at the top and bottom of the passage owing to different radii at these points. The circular geometry of the crusher gives a favorably small **nip angle** in the horizontal direction. The nip angle in the vertical direction is less favorable and limits feed acceptance. The vertical nip angle is determined by the shape of the mantle and bowl liner; it is similar to that of a jaw crusher.

Primary crushers have a steep cone angle and a small reduction ratio. **Secondary** crushers have a wider cone angle; this allows the finer product to be spread over a larger passage area and also spreads the wear over a wider area. Wear occurs to the greatest extent in the lower, fine-crushing zone. These features are further extended in cone crushers; therefore secondary gyratories are much less popular than secondary cone crushers, but they can be used as primaries when

TABLE 21-9a Performance of Nordberg C Series Eccentric Jaw Crushers

	C95	C105	C 0	C100	C 05	C110	C125	C10	C15	C10	C200
Feed opening width mm (in)	930 (37)	1060 (42)	800 (32)	1000 (40)	1375 (54)	1100 (44)	1250 (49)	1400 (55)	1400 (55)	1600 (63)	2000 (79)
Feed opening depth mm (in)	580 (23)	700 (28)	510 (20)	760 (30)	760 (30)	850 (34)	950 (37)	1070 (42)	1100 (43)	1200 (47)	1500 (59)
Power kW (HP)	90 (125)	110 (150)	75 (100)	110 (150)	160 (200)	160 (200)	160 (200)	200 (250)	200 (300)	250 (350)	400 (500)
Speed (rpm)	330	300	350	260	260	230	220	220	220	220	200
Product size mm (in)											
Closed side setting mm (in)	tph (Stph)	tph (Stph)	tph (Stph)	tph (Stph)	tph (Stph)	tph (Stph)	tph (Stph)	tph (Stph)	tph (Stph)	tph (Stph)	tph (Stph)
0-30	20		*								
0-1 1/8	3/4		*								
0-35	25	*	*	*							
0-1 3/8	1	*	*	*							
0-45	30	*	*	*							
0-1 3/4	1 1/8	*	*	*							
0-60	40	*	*	55 - 75	*	*	*				
0-2 3/8	1 5/8	*	*	60 - 80	*	*	*				
0-75	50	*	*	65 - 95	*	*	*				
0-3	2	*	*	75 - 100	*	*	*				
0-90	60	105 - 135	*	80 - 110	*	*	*				
0-3 1/2	2 3/8	115 - 150	*	90 - 120	*	*	*				
0-105	70	125 - 155	135 - 175	95 - 135	125 - 175	210 - 270	160 - 220				
0-4 1/8	2 3/4	135 - 170	150 - 190	110 - 145	140 - 190	230 - 295	175 - 240				
0-120	80	140 - 180	155 - 195	110 - 150	145 - 200	240 - 300	175 - 245	*			
0-4 3/4	3 1/8	155 - 200	170 - 215	120 - 165	160 - 215	260 - 330	195 - 270	*			
0-135	90	160 - 200	175 - 225	125 - 175	160 - 220	260 - 330	190 - 275	*	*	*	
0-5 3/8	3 1/2	175 - 220	195 - 245	140 - 190	175 - 240	285 - 360	215 - 300	*	*	*	
0-150	100	175 - 225	195 - 245	140 - 190	180 - 250	285 - 365	215 - 295	245 - 335	*	*	*
0-6	4	195 - 250	210 - 270	150 - 210	200 - 275	315 - 400	235 - 325	270 - 370	*	*	*
0-185	125	220 - 280	245 - 315	175 - 245	220 - 310	345 - 435	260 - 360	295 - 405	325 - 445	335 - 465	*
0-7	5	240 - 310	270 - 345	195 - 270	245 - 340	375 - 480	285 - 395	325 - 445	355 - 490	370 - 510	*
0-225	150	265 - 335	295 - 375	210 - 290	265 - 365	405 - 515	310 - 430	345 - 475	380 - 530	395 - 545	430 - 610
0-9	6	290 - 370	325 - 410	230 - 320	290 - 400	445 - 565	340 - 470	380 - 525	420 - 580	435 - 600	475 - 670
0-260	175	310 - 390	345 - 435	245 - 335	310 - 430	465 - 595	350 - 490	395 - 545	435 - 605	455 - 625	495 - 695
0-10	7	340 - 430	380 - 480	270 - 370	340 - 470	515 - 650	390 - 540	435 - 600	480 - 665	500 - 690	545 - 765
0-300	200		390 - 500		355 - 490	530 - 670	405 - 555	445 - 615	495 - 685	510 - 710	560 - 790
0-12	8		430 - 550		390 - 535	580 - 740	445 - 610	490 - 675	545 - 750	565 - 780	615 - 870
0-340	225							495 - 685	550 - 760	570 - 790	625 - 880
0-13	9							545 - 750	605 - 835	630 - 870	685 - 965
0-375	250							545 - 755	610 - 840	630 - 870	685 - 965
0-15	10							600 - 830	670 - 925	695 - 960	755 - 1060
0-410	275								690 - 950	745 - 1055	940 - 1321
0-16	11								760 - 1045	820 - 1160	1030 - 1451
0-450	300									815 - 1145	1015 - 1431
0-18	12									895 - 1260	1120 - 1571

*Smaller closed side settings can be often used depending on application and production requirements. (From Metso Minerals brochure.)

quarrying produces suitable feed sizes. The three general types of gyratory crusher are the **suspended-spindle**, **supported-spindle**, and **fixed-spindle** types. Primary gyratories are designated by the size of feed opening, and secondary or reduction crushers by the diameter of the head in feet and inches. There is a close opening and a wide opening as the mantle gyrates with respect to the concave ring at the outlet end. The close opening is known as the close setting or the closed-side setting, while the wide opening is known as the wide-side or open-side setting. Specifications usually are based on closed settings. The setting is adjustable by raising or lowering the mantle.

The length of the crushing stroke greatly affects the capacity and the screen analysis of the crushed product. A very short stroke will give a very evenly crushed product but will not give the greatest capacity. A very long stroke will give the greatest capacity, but the product will contain a wider product-size distribution.

Performance Crushing occurs through the full cycle in a gyratory crusher, and this produces a higher crushing capacity than a similar-sized jaw crusher, which crushes only in the shutting half of the cycle. Gyratory crushers also tend to be easier to operate. They operate most efficiently when they are fully charged, with the main shaft fully buried in charge. Power consumption for gyratory crushers is also lower than that of jaw crushers. These are preferred over jaw crushers when capacities of 800 Mg/h (900 tons/h) or higher are required.

Gyratories make a product with open-side settings of 5 to 10 in at discharge rates from 600 to 6000 tons/h, depending on size. Most manufacturers offer a throw from 1/4 to 2 in. The throughput and power draw depend on the throw and the hardness of the ore, and on the amount of undersized material in the feed. Removal of undersized material (which can amount to one-third of the feed) by a stationary grizzly can reduce power draw. See Table 21-9b.

Gyratory crushers that feature wide-cone angles are called **cone crushers**. These are suitable for secondary crushing, because crushing of fines requires more work and causes more wear; the cone shape provides greater working area than primary or jaw crushers for grinding of the finer product. Crusher performance is harmed by sticky material in the feed, more than 10 percent fines in the feed smaller than the crusher setting, excessive feed moisture, feed-size segregation, uneven distribution of feed around the circumference, uneven feed control, insufficient capacity of conveyors and closed-circuit screens, extremely hard or tough feed material, and operation at less than recommended

speed. Rod mills are sometimes substituted for crushing of tough ore, since they provide more easily replaceable metal for wear.

Control of Crushers The objective of crusher control is usually to maximize crusher throughput at some specified product size, without overloading the crusher. Usually only three variables can be adjusted: feed rate, crusher opening, and feed size in the case of a secondary crusher. Four modes of control for a crusher are:

1. Setting overload control, where the gape setting is fixed except that it opens when overload occurs. A hardness change during high throughput can cause a power overload on the crusher, which control should protect against.
2. Constant power setting control, which maximizes throughput.
3. Pressure control, which provides settings that give maximum crusher force, and hence also throughput.
4. Feeding-rate control, for smooth operation. Setting control influences mainly product size and quality, while feed control determines capacity. Flow must also be synchronized with the feed requirements of downstream processes such as ball mills, and improved crusher efficiency can reduce the load on the more costly downstream grinding.

IMPACT BREAKERS

Impact breakers include heavy-duty hammer crushers, rotor impact breakers, and cage mills. They are generally coarse breakers which reduce the size of materials down to about 1 mm. Fine hammer mills are described in a following subsection. Not all rocks shatter well by impact. Impact breaking is best suited for the reduction of relatively nonabrasive and low-silica-content materials such as limestone, dolomite, anhydrite, shale, and cement rock, the most popular application being on limestone. Most of these devices, such as the hammer crusher shown in Fig. 21-69, have top-fed rotors (of various types) and open bottoms through which product discharge occurs. Some hammer crushers have screens or grates.

Hammer Crusher Pivoted hammers are mounted on a horizontal shaft, and crushing takes place by impact between the hammers and breaker plates. Heavy-duty hammer crushers are frequently used in the quarrying industry, for processing municipal solid waste, and to scrap automobiles.

The rotor of these machines is a cylinder to which is affixed a tough steel bar. Breakage can occur against this bar or on rebound from the

TABLE 21-9b Performance of Nordberg Superior MK-II Gyratory Crusher [in mtph (stph)]*

				Open Side Settings of Discharge Opening — Millimeters (Inches)										
Size	Feed Opening mm (in.)	Pinion RPM	Max. KW (HP)	125mm (5.0")	140mm (5 1/2")	150mm (6")	165mm (6 1/2")	175mm (7")	190mm (7 1/2")	200mm (8")	215mm (8 1/2")	230mm (9")	240mm (9 1/2")	250mm (10")
42-65	1065 (42)	600	375 (500)		1635 (1800)	1880 (2075)	2100 (2315)	2320 (2557)						
50-65	1270 (50)	600	375 (500)			2245 (2475)	2625 (2895)	2760 (3040)						
54-75	1370 (54)	600	450 (600)			2555 (2820)	2855 (3145)	3025 (3335)	3215 (3545)	3385 (3735)				
62-75	1575 (62)	600	450 (600)			2575 (2840)	3080 (3395)	3280 (3615)	3660 (4035)	3720 (4205)				
60-89	1525 (60)	600	600 (800)				4100 (4520)	4360 (4805)	4805 (5295)	5005 (5520)	5280 (5820)	5550 (6115)		
60-110	1525 (60)	514	1000 (1400)					5575 (6150)	5845 (6440)	6080 (6705)	6550 (7220)	6910 (7620)	7235 (7975)	7605 (8385)

*From Metso Minerals brochure.

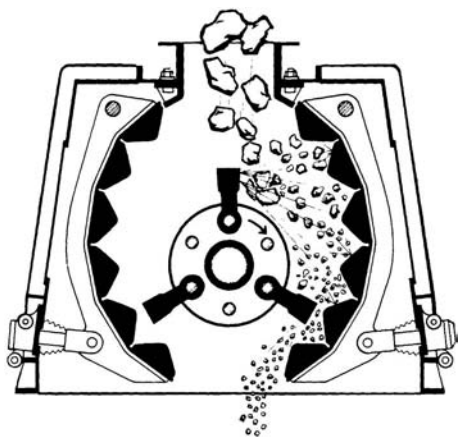


FIG. 21-69 Reversible impactor. (Pennsylvania Crusher Corp.)

walls of the device. Free impact breaking is the principle of the rotor breaker, and it does not rely on pinch crushing or attrition grinding between rotor hammers and breaker plates. The result is a high reduction ratio and elimination of secondary and tertiary crushing stages. By adding a screen on a portable mounting, a complete, compact mobile crushing plant of high capacity and efficiency is provided for use in any location.

The ring granulator features a rotor assembly with loose crushing rings, held outwardly by centrifugal force, which chop the feed. It is suitable for highly friable materials which may give excessive fines in an impact mill. For example, bituminous coal is ground to a product below 2 cm ($\frac{3}{4}$ in). They have also been successfully used to grind abrasive quartz to sand size, due to the ease of replacement of the ring impact elements.

Cage Mills In a cage mill, cages of one, two, three, four, six, and eight rows, with bars of special alloy steel, revolving in opposite directions produce a powerful impact action that pulverizes many materials. Cage mills are used for many materials, including quarry rock, phosphate rock, and fertilizer and for disintegrating clays, colors, press cake, and bones. The advantage of multiple-row cages is the achievement of a greater reduction ratio in a single pass, and these devices can produce products significantly finer than other impactors in many cases, as fine as 325 mesh. These features and the low cost of the mills make them suitable for medium-scale operations where complicated circuits cannot be justified.

Prebreakers Aside from the normal problems of grinding, there are special procedures and equipment for breaking large masses of feed to smaller sizes for further grinding. There is the breaking or shredding of bales, as with rubber, cotton, or hay, in which the compacted mass does not readily come apart. There also is often caking in bags of plastic or hygroscopic materials which were originally fine. Although crushers are sometimes used, the desired size-reduction ratio often is not obtainable. Furthermore, a lower capital investment may result through choosing a less rugged device which progressively attacks the large mass to remove only small amounts at a time. Typically, these devices are toothed rotating shafts in casings.

HAMMER MILLS

Operation Hammer mills for fine pulverizing and disintegration are operated at high speeds. The rotor shaft may be vertical or horizontal, generally the latter. The shaft carries hammers, sometimes called beaters. The hammers may be T-shaped elements, stirrups, bars, or rings fixed or pivoted to the shaft or to disks fixed to the shaft. The grinding action results from **impact** and **attrition** between lumps or particles of the material being ground, the housing, and the grinding elements. A cylindrical screen or grating usually encloses all or part of the rotor. The fineness of product can be regulated by changing rotor speed, feed rate, or clearance between hammers and

grinding plates, as well as by changing the number and type of hammers used and the size of discharge openings.

The **screen** or **grating discharge** for a hammer mill serves as an internal classifier, but its limited area does not permit effective usage when small apertures are required. A larger external screen may then be required. The feed must be nonabrasive with a hardness of 1.5 or less. Hammer mills can reduce many materials so that substantially all the product passes a 200-mesh screen.

One of the subtleties of operating a hammer mill is that, in general, screen openings should be sized to be much larger than the desired product size. The screen serves to retain very large particles in the mill, but particles that pass through the screen are usually many times smaller than the screen opening. Thus, changing the screen opening size may strongly affect the coarse end of a product-size distribution, but will have limited effect on the median particle size and very little effect at all on the fines. These are more strongly affected by the speed, number, and type of hammers, and, most of all, the speed of the hammers. Screens with very fine openings (500 μ m and less) can be used in smaller laboratory mills to produce very fine product, but tend not to be rugged enough for large-scale use. Particle-size distribution in hammer mill products tends to be very broad, and in cases where relatively narrow product-size distribution is desired, some sort of grinding circuit with an external classifier is almost always needed.

There are a large number of hammer mill manufacturers. The basic designs are very similar, although there are subtle differences in performance and sturdiness that can lead to varying performance. For example, some machines have lower maximum rotation speeds than others. Less rugged and powerful machines might be fully adequate for vegetable materials (e.g., wood), but not suitable for fine mineral grinding. Occasionally, vendors are particularly experienced in a limited set of products and have designs which are especially suited for these. For relatively common materials, it is usually better to use vendors with practical experience in these materials.

Pin Mills In contrast to peripheral hammers of the rigid or swing types, there is a class of high-speed mills having pin breakers in the grinding circuit. These may be on a rotor with stator pins between circular rows of pins on the rotor disk, or they may be on rotors operating in opposite directions, thereby securing an increased differential of speed. There are machines with both vertical and horizontal shafts. In the devices with horizontal shafts, feed is through the top of the mill similar to hammer mills. In devices with vertical shafts, feed is along the shaft, and centrifugal force helps impact the outer ring of pins.

Unlike hammer mills, pin mills do not have screens. Pin mills have a higher energy input per pass than hammer mills and can generally grind softer materials to a finer particle size than hammer mills, while hammer mills perform better on hard or coarse materials. Because they do not have retaining screens, residence time in pin mills is shorter than in hammer mills, and pin mills are therefore more suitable for heat-sensitive materials or cryogrinding.

Universal Mills Several manufacturers are now making "universal mills," which are essentially hammer mill-style devices with fairly narrow chambers that can be fitted with either a variety of hammer mill type of hammers and screens (although usually only fixed hammers) or set up as a pin mill. These are useful where frequent product changes are made and it is necessary to be able to rapidly change the grind characteristics of the devices, such as small lot manufacturing or grinding research.

Hammer Mills with Internal Air Classifiers A few mills are designed with internal classifiers. These are generally capable of reducing products to particle sizes below 45 μ m, down to about 10 μ m, depending on the material. A good example of this type of mill is the Hosokawa Mikro-ACM mill, which is a pin mill fitted with an air classifier. There are also devices more like hammermills, such as the Raymond vertical mill, which do not grind quite as fine as the pin mill-based machine but can handle slightly more abrasive materials.

The **Mikro-ACM pulverizer** is a pin mill with the feed being carried through the rotating pins and recycled through an attached vane classifier. The classifier rotor is separately driven through a speed control which may be adjusted independently of the pin-rotor speed. Oversize particles are carried downward by the internal circulating airstream and are returned to the pin rotor for further reduction. The

constant flow of air through the ACM maintains a reasonable low temperature, which makes it ideal for handling heat-sensitive materials, and it is commonly used in the powder coating and pharmaceutical industries for fine grinding.

ROLL CRUSHERS

Once popular for coarse crushing in the minerals industry, these devices long ago lost favor to gyratory and jaw crushers because of their poorer wear characteristics with hard rocks. Roll crushers are still commonly used for grinding of agricultural products such as grains, and for both primary and secondary crushing of coal and other friable rocks such as oil shale and phosphate. The roll surface is smooth, corrugated, or toothed, depending on the application. *Smooth rolls* tend to wear ring-shaped corrugations that interfere with particle nipping, although some designs provide a mechanism to move one roll from side to side to spread the wear. *Corrugated rolls* give a better bite to the feed, but wear is still a problem. *Toothed rolls* are still practical for rocks of not too high silica content, since the teeth can be regularly resurfaced with hard steel by electric arc welding. Toothed rolls are frequently used for crushing coal and chemicals. For further details, see Edition 6 of this handbook.

The **capacity** of roll crushers is calculated from the ribbon theory, according to the formula

$$Q = dLs/2.96 \quad (21-91)$$

where Q = capacity, cm^3/min ; d = distance between rolls, cm ; L = length of rolls, cm ; and s = peripheral speed, cm/min . The denominator becomes 1728 in engineering units for Q in cubic feet per minute, d and L in inches, and s in inches per minute. This gives the theoretical capacity and is based on the rolls discharging a continuous, solid uniform ribbon of material. The actual capacity of the crusher depends on roll diameter, feed irregularities, and hardness and varies between 25 and 75 percent of theoretical capacity.

ROLL PRESS

One of the newer comminution devices, the **roll press**, has achieved significant commercial success, especially in the cement industry. It is used for fine crushing, replacing the function of a coarse ball mill or of tertiary crushers. Unlike ordinary roll crushers, which crush individual particles, the roll press is choke-fed and acts on a thick stream or ribbon of feed. Particles are crushed mostly against other particles, so wear is very low. A roll press can handle a hard rock such as quartz. Energy efficiency is also greater than in ball mills.

The product is in the form of agglomerated slabs. These are broken up in either a ball mill or an impact or hammer mill running at a speed too slow to break individual particles. Some materials may even deagglomerate from the handling that occurs in conveyors. A large proportion of fines is produced, but a fraction of coarse material survives. This makes recycle necessary.

From experiments to grind cement clinker to $-80 \mu\text{m}$, as compression is increased from 100 to 300 MPa, the required recycle ratio decreases from 4 to 2.8. The energy required per ton of throughput increases from 2.5 to 3.5 kWh/ton. These data are for a 200-mm-diameter pilot-roll press. Status of 150 installations in the cement industry is reviewed [Strasser et al., *Rock Products*, **92**(5), 60-72 (1989)]. In cement clinker milling, wear is usually from 0.1 to 0.8 g/ton, and for cement raw materials it is between 0.2 and 1.2 g/ton, whereas it may be 20- to 40-in ball mills.

The size of the largest feed particles should not exceed $0.04 \times$ roll diameter D according to Schoenert (loc. cit.). However, it has been found [Wuestner et al., *Zement-Kalk-Gips*, **41**(7), 345-353 (1987); English edition, 207-212] that particles as large as 3 to 4 times the roll gap may be fed to an industrial press.

Machines with up to 2500-kW installed power and 1000-ton/h (900-ton/h) capacity have been installed. The largest presses can supply feed for four or five ball mills. Operating experience (Wuestner et al., loc. cit.) has shown that roll diameters of about 1 m are preferred, as a compromise between production rate and stress on the equipment.

The press must be operated choke-fed, with a substantial depth of feed in the hopper; otherwise it will act as an ordinary roll crusher.

ROLL RING-ROLLER MILLS

Roll ring-roller mills (Fig. 21-70) are equipped with rollers that operate against grinding rings. Pressure may be applied with heavy springs or by centrifugal force of the rollers against the ring. Either the ring or the rollers may be stationary. The grinding ring may be in a vertical or horizontal position. Ring-roller mills also are referred to as ring roll mills or roller mills or medium-speed mills. The ball-and-ring and bowl mills are types of ring-roller mill. Ring-roller mills are more energy-efficient than ball mills or hammer mills. The energy to grind coal to 80 percent passing 200 mesh was determined (Luckie and Austin, *Coal Grinding Technology—A Manual for Process Engineers*) as ball mill, 13 hp/ton; hammer mill, 22 hp/ton; roller mill, 9 hp/ton.

Raymond Ring-Roller Mill The Raymond ring-roller mill (Fig. 21-70) is a typical example of a ring-roller mill. The base of the mill carries the grinding ring, rigidly fixed in the base and lying in the horizontal plane. Underneath the grinding ring are tangential air ports through which the air enters the grinding chamber. A vertical shaft driven from below carries the roller journals. Centrifugal force urges the pivoted rollers against the ring. The raw material from the feeder drops between the rolls and ring and is crushed. Both centrifugal air motion and plows move the coarse feed to the nips. The air entrains fines and conveys them up from the grinding zone, providing some classification at this point. An air classifier is also mounted above the grinding zone to return oversize particles. The method of classification used with Raymond mills depends on the fineness desired. If a medium-fine product is required (up to 85 or 90 percent through a No. 100 sieve), a single-cone air classifier is used.

This consists of a housing surrounding the grinding elements with an outlet on top through which the finished product is discharged. This is known as the low-side mill. For a finer product and when frequent changes in fineness are required, the whizzer-type classifier is

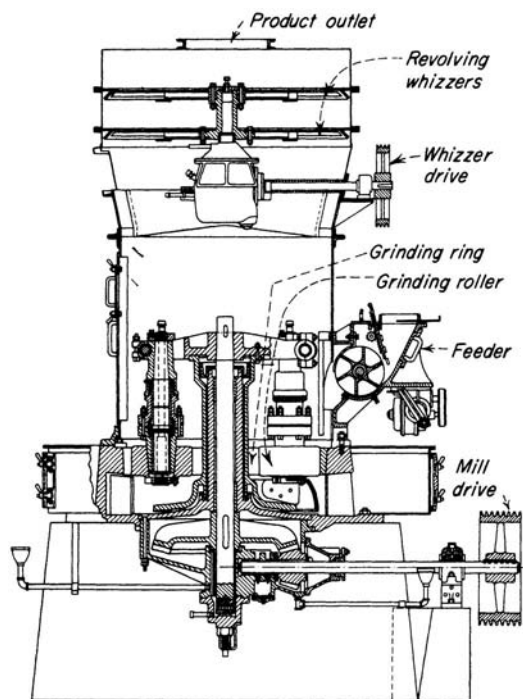


FIG. 21-70 Raymond high-side mill with an internal whizzer classifier. (ABB Raymond Div., Combustion Engineering Inc.)

used. This type of mill is known as the *high-side mill*. The Raymond ring-roll mill with internal air classification is used for the large-capacity fine grinding of most of the softer nonmetallic minerals. Materials with a Mohs-scale hardness up to and including 5 are handled economically on these units. Typical natural materials handled include barites, bauxite, clay, gypsum, magnesite, phosphate rock, iron oxide pigments, sulfur, talc, graphite, and a host of similar materials. Many of the manufactured pigments and a variety of chemicals are pulverized to high fineness on such units. Included are such materials as calcium phosphates, sodium phosphates, organic insecticides, powdered cornstarch, and many similar materials. When properly operated under suction, these mills are entirely dust-free and automatic.

PAN CRUSHERS

Design and Operation The pan crusher consists of one or more grinding wheels or mullers revolving in a pan; the pan may remain stationary and the mullers be driven, or the pan may be driven while the

mullers revolve by friction. The mullers are made of tough alloys such as Ni-Hard. Iron scrapers or plows at a proper angle feed the material under the mullers.

Performance The dry pan is useful for crushing medium-hard and soft materials such as clays, shales, cinders, and soft minerals such as barites. Materials fed should normally be 7.5 cm (3 in) or smaller, and a product able to pass No. 4 to No. 16 sieves can be delivered, depending on the hardness of the material. High reduction ratios with low power and maintenance are features of pan crushers. Production rates can range from 1 to 54 Mg/h (1 to 60 tons/h) according to pan size and hardness of material as well as fineness of feed and product.

The **wet pan** is used for developing plasticity or molding qualities in ceramic feed materials. The abrasive and kneading actions of the mullers blend finer particles with the coarser particles as they are crushed [Greaves-Walker, *Am. Refract. Inst. Tech. Bull.* 64 (1937)], and this is necessary so that a high packing density can be achieved to result in strength.

CRUSHING AND GRINDING EQUIPMENT: FLUID-ENERGY OR JET MILLS

DESIGN

Jet milling, also called fluid-energy grinding, is an increasingly used process in the chemical industry for processing brittle, heat-sensitive materials into very fine powders with a narrow size distribution. For more than 90 years jet mills have been built and applied successfully on a semilarge scale in the chemical industry. A number of famous designs are extensively described in a number of patents and publications.

Most such mills are variations on one of the fundamental configurations depicted in Fig. 21-71. The designs differ from each other by the arrangement of the nozzles and the classification section. In the following paragraphs the jet mill types are briefly discussed.

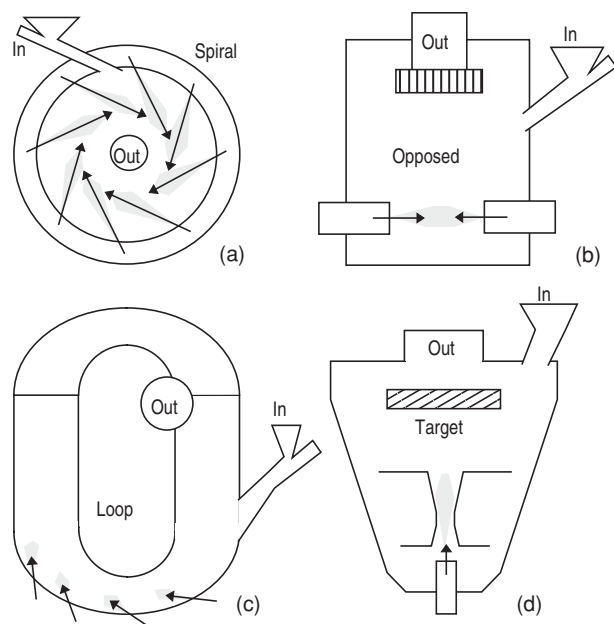


FIG. 21-71 Schematic representation of basic jet mill designs: (a) spiral; (b) opposed; (c) loop; (d) target.

The key feature of jet mills is the conversion of high pressure to kinetic energy. The operating fluid enters the grinding chamber through nozzles placed in the wall. The feed particles brought into the mill through a separate inlet are entrained by expanding jets and accelerated to velocities as high as the velocity of sound. In fact three collision geometries can be distinguished:

Interparticle collisions in a free jet

Collisions between particles accelerated by opposed jets

Impact of particles on a target

The turbulent nature of the jets causes particles to have differences in velocities and directions. Particle breakage in jet mills is mainly a result of interparticle collisions: wall collisions are generally thought to be of minor importance only, except in mill type D (Fig. 21-71). Fluid-energy-driven mills are a class of impact mills with a considerable degree of attrition due to eccentric and gliding interparticle impacts. The grinding mechanism via mutual collisions means that jet mills operate with virtually no product contact. In other words, the contamination grade is low.

The classification of product leaving the mill depends on a balance between centrifugal forces and drag forces in the flow field around the mill outlet. Mill types A and C create a free vortex at the outlet, while jet mill D makes use of gravity. Type B has an integrated rotor. The final product quality is largely determined by the success of classification.

TYPES

Spiral Jet Mill The original design of the spiral jet mill, also called a pancake mill, is shown in Fig. 21-71. This design was first described by Andrews in 1936 and patented under the name Micronizer. A number of nozzles are placed in the outer wall of the mill through which the grinding medium, a gas or steam, enters the mill.

A spiral jet mill combines both grinding and classification by the same jets. The vortex causes coarse particles of the mill contents to be transferred to the outer zone, as fines can leave through the central outlet. The solid feed is brought into the mill by an air pusher. The outlet is placed in the center of the mill chamber. The working principle of this mill was extensively investigated by Rumpf.

Spiral jet mills are notable for their robust design and compactness. Their direct air operation avoids the need for separate drive units. Another significant argument for the use of jet mills is the lower risk for dust explosions.

Opposed Jet Mill Opposed jet mills are fluid-energy-driven mills that contain two or more jets aligned toward each other (see Fig. 21-71b). Different versions are on the market, based on a design patented by Willoughby (1917). In this type of jet mill, opposed gas

streams entrain the mill holdup. At the intersection of the jets the coarse particles hit one another. The grinding air carries the particles upward in a kind of fluidized bed to the classification zone.

Adjustment of the rotor speed allows a direct control of the particle size of the end product. The feed is entered by a rotary valve. Drawbacks are the higher cost of investment and maintenance. These types of mills are described by Vogel and Nied.

Other Jet Mill Designs Figure 21-71d shows one of the earliest jet mill designs (around 1880), but it is still in use today. In this mill a jet loaded with particles is impacting on an anvil. Consequently the impact

efficiency is high for relatively large particles. Very fine grinding becomes difficult as small particles are decelerated in the stagnant zone in front of the target. Fines are dragged out in an airstream by a fan, as coarse material is recirculated to the jet entry. Points of improvement have included better classification and abrasive-resistant target material. This device is suitable to incorporate as a pregrinder.

The loop mill (Fig. 21-71c), also called Torus mill, was designed by Kidwell and Stephanoff (1940). The grinding fluid is brought into the grinding section. The fines leave the mill through the classification section.

CRUSHING AND GRINDING EQUIPMENT: WET/DRY GRINDING—MEDIA MILLS

OVERVIEW

Another class of grinding mills is media mills. These are mills which grind materials primarily through the action of mechanically agitated balls made out of metals (mostly steel) or various ceramics. Different mills use different methods of agitation. Some are more commonly used for dry grinding, others for wet grinding, and still others can be used in both modes. Types of media mills include tumbling mills, stirred media mills, and vibratory mills.

MEDIA SELECTION

A key to the performance of media mills is the selection of an appropriate grinding medium. Jorg Schwedes and his students have developed correlations which are effective in determining optimal media size for stirred media mills [Kwade et al., *Powder Technol.*, **86** (1996); and Becker et al., *Int. J. Miner. Process.*, **61** (2001)]. Although these correlations were developed for stirred media mills, the principles developed apply to all media mills.

In this methodology, energy input is broken up into stress intensity (SI) and stress frequency (SF), defined as:

$$SI = (\rho_m - \rho) D_m^3 V_t^2$$

$$SF = \omega (D_m/D)^2 t$$

where ρ is slurry density, ρ_m is media density, D_m is media diameter, ω is the rotational speed of a rotating mill, D is the rotor diameter of a rotating mill, and V_t is the tip speed of a rotating mill.

Stress intensity is related to the kinetic energy of media beads, and stress frequency is related to the frequency of collisions.

When stress intensity is plotted versus media particle size achieved at constant grinding energy (such as Fig. 21-72) for limestone, it can be seen that a large number of experimental data can be collapsed onto a single curve. There is a relatively narrow range of stress intensity which gives the smallest particle size, and larger or smaller stress intensities give increasingly larger particle sizes at the same energy input.

This can be explained in physical terms in the following way. For each material, there is a critical stress intensity. If the stress intensity applied during grinding is less than the critical stress intensity, then very little grinding occurs. If the applied stress intensity is much greater than the critical stress intensity, then unnecessary energy is being used in bead collisions, and a greater grinding rate could be obtained by using smaller beads that would collide more frequently. This has a very practical implication for choosing the size and, to some extent, the density of grinding beads. At a constant stirring rate (or tumbling rate or vibration rate), a small range of media sizes give an optimal grinding rate for a given material in a given mill. In practice, most mills are operated using media slightly larger than the optimal size, as changes in feed and media quality can shift the value of the

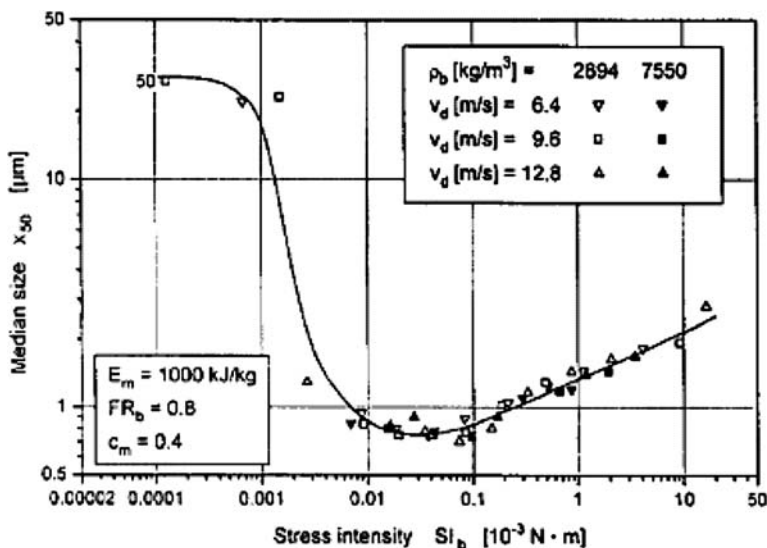


FIG. 21-72 Influence of stress intensity on the size of limestone for a specific energy input of 1000 kJ/kg. [From A. Kwade et al., *Powder Technol.* **86** (1996).]

critical stress intensity over the lifetime of an industrial process, and the falloff in grinding rate when one is below the critical stress intensity is quite dramatic.

Another important factor when choosing media mills is media and mill wear. Most media mills have fairly rapid rates of media wear, and it is not uncommon to have to replace media monthly or at least add partial loads of media weekly. Media wear will reduce the grind rate of a mill and can cause significant product contamination. Very hard media materials often have low wear rates, but can cause very rapid mill wear. Media with a good balance of properties tend to be specialty ceramics. Commonly used ceramics include glass, specialty sand, alumina, zirconia (although this is higher in mill wear), zirconia-silica composites, and yttria- or Ceria-stabilized zirconia. Yttria-stabilized zirconia is particularly wear resistant but is very expensive. Steel is often used as a medium and has a very good combination of low cost, good wear life, and gentle mill wear if a product can handle slight discoloration and iron content from the medium.

TUMBLING MILLS

Ball, pebble, rod, tube, and compartment mills have a cylindrical or conical shell, rotating on a horizontal axis, and are charged with a grinding medium such as balls of steel, flint, or porcelain or with steel rods. The **ball mill** differs from the tube mill by being short in length; its length, as a rule, is not far from its diameter (Fig. 21-73). Feed to ball mills can be as large as 2.5 to 4 cm (1 to 1½ in) for very fragile materials, although the top size is generally 1 cm (½ in). Most ball mills operate with a reduction ratio of 20:1 to 200:1. The largest balls are typically 13 cm (5 in) in diameter. The tube mill is generally long in comparison with its diameter, uses smaller balls, and produces a finer product. The compartment mill consists of a cylinder divided into two or more sections by perforated partitions; preliminary grinding takes place at one end and finish grinding at the charge end. These mills have a length-to-diameter ratio in excess of 2 and operate with a reduction ratio of up to 600:1.

Rod mills deliver a more uniform granular product than other revolving mills while minimizing the percentage of fines, which are sometimes detrimental. The **pebble mill** is a tube mill with flint or ceramic pebbles as the grinding medium and may be lined with

ceramic or other nonmetallic liners. The **rock-pebble mill** is an autogenous mill in which the medium consists of larger lumps scalped from a preceding step in the grinding flow sheet.

Design The conventional type of **batch mill** consists of a cylindrical steel shell with flat steel-flanged heads. Mill length is equal to or less than the diameter [Coghill, De Vaney, and O'Meara, *Trans. Am. Inst. Min. Metall. Pet. Eng.*, **112**, 79 (1934)]. The discharge opening is often opposite the loading manhole and for wet grinding usually is fitted with a valve. One or more vents are provided to release any pressure developed in the mill, to introduce inert gas, or to supply pressure to assist discharge of the mill. In dry grinding, the material is discharged into a hood through a grate over the manhole while the mill rotates. Jackets can be provided for heating and cooling.

Material is fed and discharged through hollow trunnions at opposite ends of **continuous mills**. A grate or diaphragm just inside the discharge end may be employed to regulate the slurry level in wet grinding and thus control retention time. In the case of **air-swept mills**, provision is made for blowing air in at one end and removing the ground material in air suspension at the same end or the other end. Ball mills usually have **liners** which are replaceable when they wear. Both all-rubber liners and rubber liners with metal lifter bars are currently used in large ball mills [McTavish, *Mining Engg.*, **42**, 1249–1251 (Nov. 1990)]. Lifters must be at least as high as the ball radius, to key the ball charge and ensure that the balls fall into the toe area of the mill [Powell, *Int. J. Mineral Process.*, **31**, 163–193 (1991)]. Special operating problems occur with smooth-lined mills owing to erratic slip of the charge against the wall. At low speeds the charge may **surge** from side to side without actually tumbling; at higher speeds tumbling with **oscillation** occurs. The use of lifters prevents this [Rose, *Proc. Inst. Mech. Eng. (London)*, **170**(23), 773–780 (1956)].

Pebble mills are frequently lined with nonmetallic materials when iron contamination would harm a product such as a white pigment or cement. Belgian silex (silica) and porcelain block are popular linings. Silica linings and ball media have proved to wear better than other nonmetallic materials. Smaller mills, up to about 50-gal capacity, are made in one piece of ceramic with a cover.

Multicompartmented Mills Multicompartmented mills feature grinding of coarse feed to finished product in a single operation, wet or dry. The primary grinding compartment carries large grinding balls

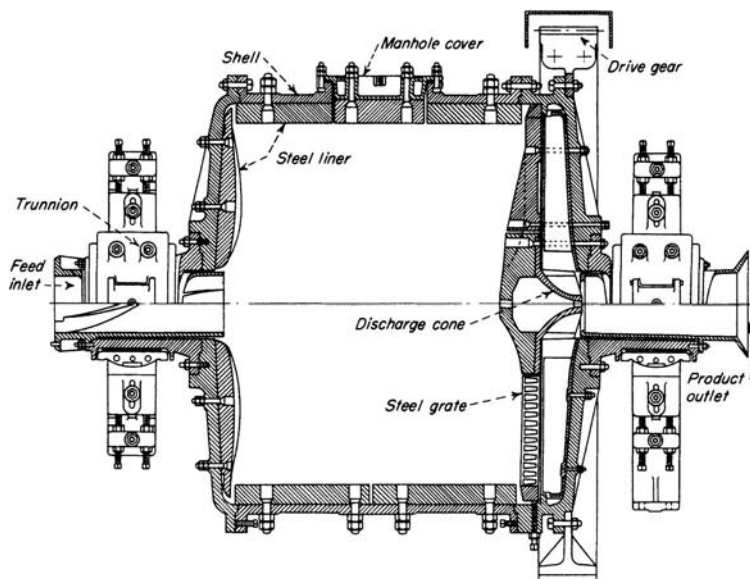


FIG. 21-73 Marcy grate-type continuous ball mill. (Allis Mineral Systems, Svedala Inc.)

or rods; one or more secondary compartments carry smaller media for finer grinding.

Operation Cascading and cataracting are the terms applied to the motion of grinding media. The former applies to the rolling of balls or pebbles from top to bottom of the heap, and the latter refers to the throwing of the balls through the air to the toe of the heap. The criterion by which the ball action in mills of various sizes may be compared is the concept of **critical speed**. It is the theoretical speed at which the centrifugal force on a ball in contact with the mill shell at the height of its path equals the force on it due to gravity:

$$N_c = 42.3/\sqrt{D} \quad (21-92)$$

where N_c is the critical speed, r/min, and D is diameter of the mill, m (ft), for a ball diameter that is small with respect to the mill diameter. The numerator becomes 76.6 when D is expressed in feet. **Actual mill speeds** range from 65 to 80 percent of critical. It might be generalized that 65 to 70 percent is required for fine wet grinding in viscous suspension and 70 to 75 percent for fine wet grinding in low-viscosity suspension and for dry grinding of large particles up to 1-cm (½-in) size. Unbaffled mills can run at 105 percent of critical to compensate for slip. The chief factors determining the size of **grinding balls** are fineness of the material being ground and maintenance cost for the ball charge. A coarse feed requires a larger ball than a fine feed. The need for a calculated ball-size feed distribution is open to question; however, methods have been proposed for calculating a rationed ball charge [Bond, *Trans. Am. Inst. Min. Metall. Pet. Eng.*, **153**, 373 (1943)]. The recommended optimum size of makeup rods and balls is [Bond, *Min. Eng.*, **10**, 592–595 (1958)]

$$D_b = \sqrt{\frac{X_p E_i}{K n_r}} \sqrt{\frac{\rho_s}{\sqrt{D}}} \quad (21-93)$$

where D_b = rod or ball diameter, cm (in); D = mill diameter, m (ft); E_i is the work index of the feed; n_r is speed, percent of critical; ρ_s is feed specific gravity; and K is a constant = 214 for rods and 143 for balls. The constant K becomes 300 for rods and 200 for balls when D_b and D are expressed in inches and feet, respectively. This formula gives reasonable results for production-sized mills but not for laboratory mills. The ratio between the recommended ball and rod sizes is 1.23.

Material and Ball Charges The load of a grinding medium can be expressed in terms of the percentage of the volume of the mill that it occupies; i.e., a bulk volume of balls half filling a mill is a 50 percent ball charge. The void space in a static bulk volume of balls is approximately 41 percent. The amount of material in a mill can be expressed conveniently as the ratio of its volume to that of the voids in the ball load. This is known as the **material-to-void ratio**. If the solid material and its suspending medium (water, air, etc.) just fill the ball voids, the M/V ratio is 1, for example. Grinding-media loads vary from 20 to 50 percent in practice, and M/V ratios are usually near 1.

The material charge of continuous mills, called the **holdup**, cannot be set directly. It is indirectly determined by operating conditions. There is a maximum throughput rate that depends on the shape of the mill, the flow characteristics of the feed, the speed of the mill, and the type of feed and discharge arrangement. Above this rate the holdup increases unstably. The holdup of material in a continuous mill determines the mean residence time, and thus the extent of grinding. Gupta et al. [*Int. J. Mineral Process.*, **8**, 345–358 (Oct. 1981)] analyzed published experimental data on a 40·40-cm grate discharge laboratory mill, and determined that holdup was represented by $H_w = (4.020 - 0.176WI) F_w + (0.040 + 0.01237WI) S_w - (4.970 + 0.395WI)$, where WI is Bond work index based on 100 percent passing a 200-mesh sieve, F_w is the solids feed rate, kg/min, and S_w is weight percent of solids in the feed. This represents experimental data for limestone, feldspar, sulfide ore, and quartz. The influence of WI is believed to be due to its effect on the amount of fines present in the mill. Parameters that did not affect H_w are specific gravity of feed material and feed size over the narrow range studied. Sufficient data were not available to develop a correlation for overflow mills, but the data indicated a linear variation of H_w with F as well. The mean resi-

dence time τ (defined as H_w/F) is the most important parameter since it determines the time over which particles are exposed to grinding. Measurements of the water (as opposed to the ore) of several industrial mills (Weller, *Automation in Mining Mineral and Metal Processing*, 3d IFAC Symposium, 303–309, 1980) showed that the maximum mill filling was about 40 percent, and the maximum flow velocity through the mill was 40 m/h. Swaroop et al. [*Powder Technol.*, **28**, 253–260 (Mar.–Apr. 1981)] found that the material holdup is higher and the vessel dispersion number $D\tau/L^2$ (see subsection “Continuous-Mill Simulation”) is lower in the rod mill than in the ball mill under identical dimensionless conditions. This indicates that the known narrow-product-size distribution from rod mills is partly due to less mixing in the rod mill, in addition to different breakage kinetics.

The holdup in grate-discharge mills depends on the grate openings. Kraft et al. [*Zement-Kalk-Gips Int.*, **42**(7), 353–359 (1989); English edition, 237–239] measured the effect of various hole designs in wet milling. They found that slots tangential to the circumference gave higher throughput and therefore lower holdup in the mill. Total hole area had little effect until the feed rate was raised to a critical value (30 m/h in a mill with 0.26-m diameter and 0.6 m long); above this rate the larger area led to lower holdup. The open area is normally specified between 3 and 15 percent, depending on the number of grinding chambers and other conditions. The slots should be 1.5 to 16 mm wide, tapered toward the discharge side by a factor of 1.5 to 2 to prevent blockage by particles.

Dry vs. Wet Grinding The choice between wet and dry grinding is generally dictated by the end use of the product. If the presence of liquid with the finished product is not objectionable or the feed is moist or wet, wet grinding generally is preferable to dry grinding, but power consumption, liner wear, and capital costs determine the choice. Other factors that influence the choice are the performance of subsequent dry or wet classification steps, the cost of drying, and the capability of subsequent processing steps for handling a wet product. The net production in wet grinding in the Bond grindability test varies from 145 to 200 percent of that in dry grinding depending on mesh [Maxson, Cadena, and Bond, *Trans. Am. Inst. Min. Metall. Pet. Eng.*, **112**, 130–145, 161 (1934)]. Ball mills have a large field of application for wet grinding in closed circuit with size classifiers, which also perform advantageously wet.

Dry Ball Milling In fine dry grinding, surface forces come into action, causing cushioning and ball coating, resulting in a less efficient use of energy. Grinding media and liner-wear consumption per ton of ground product are lower for a dry-grinding system. However, power consumption for dry grinding is about 30 percent larger than for wet grinding. Dry grinding requires the use of dust-collecting equipment.

Wet Ball Milling See Fig. 21-74. The **rheological properties** of the slurry affect the grinding behavior in ball mills. Rheology depends on solids content, particle size, and mineral chemical properties [Kawatra and Eisele, *Int. J. Mineral Process.*, **22**, 251–259 (1988)]. Above 50 vol. % solids, a mineral slurry may become pseudoplastic, i.e., it exhibits a yield value (Austin, Klimpel, and Luckie, *Process Engineering of Size Reduction: Ball Milling*, AIME, 1984). Above the yield value the grinding rate decreases, and this is believed to be due to adhesion of grinding media to the mill wall, causing centrifuging [Tangsatitkulchai and Austin, *Powder Technol.*, **59**(4), 285–293 (1989)]. Maximum power draw and fines production is achieved when the solids content is just below that which produces the critical yield. The solids concentration in a pebble-mill slurry should be high enough to give a slurry viscosity of at least 0.2 Pa·s (200 cP) for best grinding efficiency [Creyke and Webb, *Trans. Br. Ceram. Soc.*, **40**, 55 (1941)], but this may have been required to key the charge to the walls of the smooth mill used.

Since viscosity increases with amount of fines present, mill performance can often be improved by closed-circuit operation to remove fines. Chemicals such as surfactants allow the solids content to be increased without increasing the yield value of the pseudoplastic slurry, allowing a higher throughput. They may cause foaming problems downstream, however. Increasing temperature lowers the viscosity of water, which controls the viscosity of the slurry under high-shear conditions such as those encountered in the cyclone, but does not

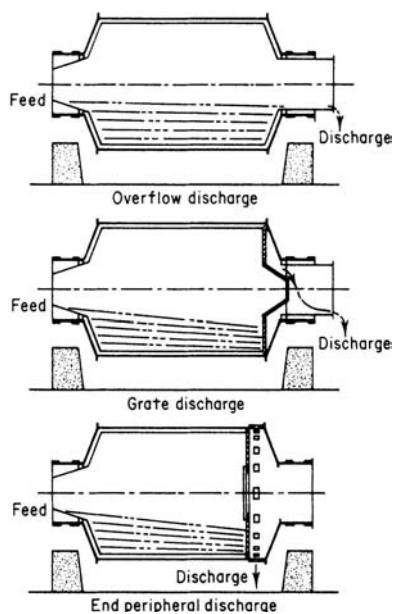


FIG. 21-74 Continuous ball-mill discharge arrangements for wet grinding.

greatly affect chemical forces. Slurry viscosity can be most directly controlled by controlling solids content.

MILL EFFICIENCIES

In summary, controlling factors for cylindrical mills are as follows:

1. Mill speed affects capacity, as well as liner and ball wear, in direct proportion up to 65 to 75 percent of critical speed.
2. Ball charge equal to 35 to 50 percent of the mill volume gives the maximum capacity.
3. Minimum-size balls capable of grinding the feed give maximum efficiency.
4. Bar-type lifters are essential for smooth operation.
5. Material filling equal to ball-void volume is optimum.
6. Higher-circulating loads tend to increase production and decrease the amount of unwanted fine material.
7. Low-level or grate discharge with recycle from a classifier increases grinding capacity over the center or overflow discharge; but liner, grate, and media wear is higher.
8. Ratio of solids to liquids in the mill must be considered on the basis of slurry rheology.

Capacity and Power Consumption One of the methods of mill sizing is based on the observation that the amount of grinding depends on the amount of energy expended, if one assumes comparable good practice of operation in each case. The energy applied to a ball mill is primarily determined by the size of mill and load of balls. Theoretical considerations show the net power to drive a ball mill to be proportional to $D^{2.5}$, but this exponent may be used without modification in comparing two mills only when operating conditions are identical [Gow, et al., *Trans. Am. Inst. Min. Metall. Pet. Eng.*, **112**, 24 (1934)]. The net power (the gross power draw of the mill minus the power to turn an empty mill) to drive a ball mill was found to be

$$E = [(1.64L - 1)K + 1][(1.64D)^{2.5}E_2] \quad (21-94)$$

where L is the inside length of the mill, m (ft); D is the mean inside diameter of the mill, m (ft); E_2 is the net power used by a 0.6- by 0.6-m (2- by 2-ft) laboratory mill under similar operating condi-

tions; and K is 0.9 for mills less than 1.5 m (5 ft) long and 0.85 for mills over 1.5 m long. This formula may be used to scale up pilot milling experiments in which the diameter and length of the mill are changed, but the size of balls and the ball loading as a fraction of mill volume are unchanged. More accurate computer models are now available.

Morrell [*Trans. Instn. Min. Metall.*, Sect. C, **101**, 25–32 (1992)] established equations to predict power draft based on a model of the shape of the rotating ball mass. Photographic observations from laboratory and plant-sized mills, including autogenous, semiautogenous, and ball mills, showed that the shape of the material charge could roughly be represented by angles that gave the position of the toe and shoulder of the charge. The power is determined by the angular speed and the torque to lift the balls. The resulting equations show that power increases rapidly with mill filling up to 35 percent, then varies little between 35 and 50 percent. Also, net power is related to mill diameter to an exponent less than 2.5. This agrees with Bond [*Brit. Chem. Engr.*, 378–385 (1960)] who stated from plant experience that power increases with diameter to the 2.3 exponent or more for larger mills. Power input increases faster than volume, which varies with diameter squared. The equations can be used to estimate holdup for control of autogenous mills.

STIRRED MEDIA MILLS

Stirred media mills have a wide range of applications. They are often found in minerals processing grinding circuits for grinding in the size range of 5 to 50 μm , and they are the only mill capable of reliably grinding materials to submicrometer sizes. They are very commonly used for grinding and dispersion of dyes, clays, and pigments and are also used for biological cell disruption.

Stirred media mills are also the dominant process equipment used for dispersing fine powders into liquid, e.g., pigment dispersions, and have largely displaced ball mills in these applications. In these applications, they are capable of dispersing powders down to particle sizes below 100 nm effectively and reliably.

Stirred media mills are used almost exclusively for wet grinding. In general, the higher the tip speed of the rotor, the lower the viscosity that can be tolerated by the mill. At high viscosity, very little bead motion occurs. Similarly, mills with lower tip speeds can tolerate the use of larger, heavier media, since gravity will cause additional motion in this case.

Design In stirred mills, a central paddle wheel or disc ed armature stirs the media at speeds from 100 to 3000 r/min (for some lab units). Stirrer tip speeds vary from 2 m/s for some attritors to 18 m/s for some high-energy mills.

Attritors In the *Attritor* (Union Process Inc.) a single vertical armature rotates several long radial arms. The rotation speeds are much slower than with other stirred media mills, and the grinding behavior in these mills tends to be more like that in tumbling mills than in other stirred media mills. They can be used for higher-viscosity applications. These are available in batch, continuous, and circulation types.

Vertical Mills Vertical mills are, generally speaking, older designs whose chief advantage is that they are inexpensive. They are vertical chambers of various shapes with a central agitator shaft. The media are stirred by discs or pegs mounted on the shaft. Some mills are open at the top, while others are closed at the top. Most mills have a screen at the top to retain media in the mill.

The big drawback to vertical mills is that they have a limited flow rate range due to the need to have a flow rate high enough to help fluidize the media and low enough to avoid carrying media out of the top of the mill. The higher the viscosity of the slurry in the mill, the more difficult it is to find the optimal flow rate range. Slurries that change viscosity greatly during grinding, such as some high solid slurries, can be particularly challenging to grind in vertical mills.

Horizontal Media Mills Horizontal media mills are the most common style of mill and are manufactured by a large number of companies. Figure 21-75 illustrates the Drais continuous stirred media mill. The mill has a horizontal chamber with a central shaft. The media are stirred by discs or pegs mounted on the shaft. The

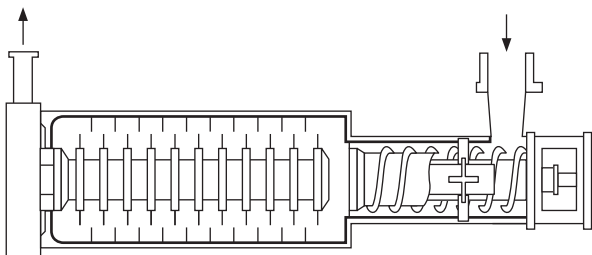


FIG. 21-75 Drais wet-grinding and dispersing system (U.S. patent 3,957,210) Draiserwerke GmbH. [Stehr, International J. Mineral Processing, **22**(1-4), 431-444 (1988).]

advantage of horizontal machines is the elimination of gravity segregation of the feed. The feed slurry is pumped in at one end and discharged at the other where the media are retained by a screen or an array of closely spaced, flat discs. Most are useful for slurries up to about 50 Pa·s (50,000 cP). Also note that slurries with very low viscosities (under 1 Pa·s) can sometimes cause severe mill wear problems. Several manufacturers have mill designs where either the screen rotates or the mill outlet is designed in such a way as to use centrifugal force to keep media off the screen. These mills can use media as fine as 0.2 mm. They also have the highest flow rate capabilities. Hydrodynamically shaped screen cartridges can sometimes accommodate media as fine as 0.2 mm.

Agitator discs are available in several forms: smooth, perforated, eccentric, and pinned. The effect of disc design has received limited study, but pinned discs are usually reserved for highly viscous materials. Cooling water is circulated through a jacket and sometimes through the central shaft. The working speed of disc tips ranges from 5 to 18 m/s regardless of mill size. A series of mills may be used with decreasing media size and increasing rotary speed to achieve desired fine particle size.

Annular Gap Mills Some mills are designed with a large interior rotor that has a narrow gap between the rotor and the inner chamber wall. These annular gap mills generally have higher energy input per unit volume than do the other designs. Media wear tends to be correspondingly higher as well. Despite this, these mills can be recommended for heat-sensitive slurries, because the annular design of the mills allows for a very large heat-transfer surface.

Manufacturers There are many manufacturers of stirred media mills worldwide. Major manufacturers of stirred media mills include Netzsch, Buhler, Drais (now part of Buhler), Premier (now part of SPX), Union Process, and MorehouseCowles. Many of these manufacturers have devices specifically adapted for specific industries. For example, Buhler has some mills specifically designed to handle higher-viscosity inks, and Premier has a mill designed specifically for milling/flaking of metal powders.

PERFORMANCE OF BEAD MILLS

Variables affecting the milling process are listed below:

- Agitator speed
- Feed rate
- Size of beads
- Bead charge, percent of mill volume
- Feed concentration
- Density of beads
- Temperature
- Design of blades
- Shape of mill chamber
- Residence time

The availability of more powerful, continuous machines has extended the possible applications to both lower and higher size ranges, from 5- to 200- μ m product size, and to a feed size as large as 5 mm. The energy density may be 50 times larger than that in tumbling-ball mills, so that a smaller mill is required (Fig. 21-76). Mills range in size from

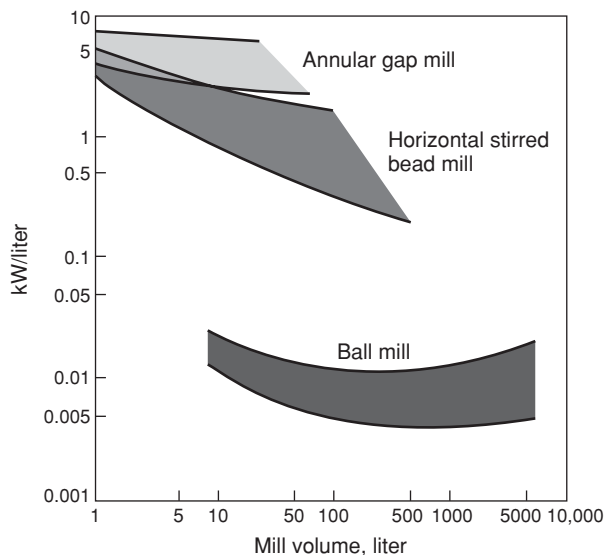


FIG. 21-76 Specific power of bead and ball mills [Kolb, Ceramic Forum International, **70**(5), 212-216 (1993)].

1 to 1000 L, with installed power up to 320 kW. Specific power ranges from 10 to 200 or even 2000 kWh/t, with feed rates usually less than 1 t. For stirred media mills, an optimum media size is about 20 times greater than the material to be ground. It is possible to relate Reynolds number to mill power draw in the same way that this is done for rotating mixers (see Fig. 21-77).

In vertical disc-stirred mills, the media should be in a fluidized condition (White, *Media Milling*, Premier Mill Co., 1991). Particles can pack in the bottom if there is not enough stirring action or feed flow; or in the top if flow is too high. These conditions are usually detected by experiment. A study of bead milling [Gao and Forssberg, *Int. J. Mineral Process.*, **32**(1-2), 45-59 (1993)] was done in a continuous Drais mill of 6-L capacity having seven 120·10-mm horizontal discs. Twenty-seven tests were done with variables at three levels. Dolomite was fed with 2 m²/g surface area in a slurry ranging from 65 to 75 percent solids by weight, or 39.5 to 51.3 percent by volume. Surface area produced was found to increase linearly with grinding time or specific-energy consumption. The variables studied strongly affected the milling rate; two extremes differed by a factor of 10. An optimum bead density for this feed material was 3.7. Evidently the discs of the chosen design could not effectively stir the denser beads. Higher slurry concentration above 70 wt % solids reduced the surface production per unit energy. The power input increased more than proportionally to speed.

Residence Time Distribution Commercially available bead mills have a diameter-to-length ratio ranging from 1:2.5 to 1:3.5. The ratio is expected to affect the *residence time distribution* (RTD). A wide distribution results in overgrinding some feed and undergrinding others. Data from Kula and Schuette [*Biotechnol. Progress*, **3**(1), 31-42 (1987)] show that in a Netzsch LME20 mill, RTD extends from 0.2 to 2.5 times the nominal time, indicating extensive stirring. (See "Biological Materials—Cell Disruption.") The RTD is even more important when the objective is to reduce the top size of the product as Stadler et al. [*Chemie-Ingenieur-Technik*, **62**(11), 907-915 (1990)] showed, because much of the feed received less than one-half the nominal residence time. A narrow RTD could be achieved by rapidly flowing material through the mill for as many as 10 passes.

VIBRATORY MILLS

The dominant form of industrial vibratory mill is the type with two horizontal tubes, called the **horizontal tube mill**. These tubes are mounted on springs and given a circular vibration by rotation of a

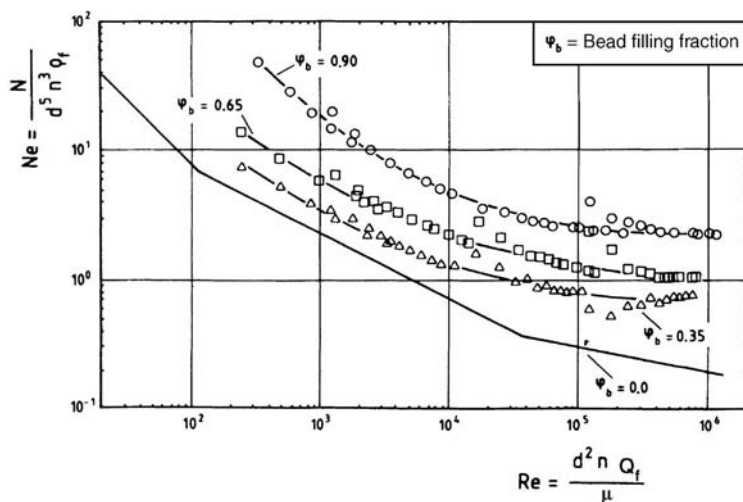


FIG. 20-77 Newton number as a function of Reynolds number for a horizontal stirred bead mill, with fluid alone and with various filling fractions of 1-mm glass beads [Weit and Schvedes, *Chemical Engineering and Technology*, **10**(6), 398–404 (1987)]. (N = power input, W; d = stirrer disk diameter, n = stirring speed, 1/s; μ = liquid viscosity, Pa·s; Q_f = feed rate, m^3/s .)

counterweight. Many feed flow arrangements are possible, adapting to various applications. Variations include polymer lining to prevent iron contamination, blending of several components, and milling under inert gas and at high and low temperatures.

The vertical vibratory mill has good wear values and a low-noise output. It has an unfavorable residence time distribution, since in continuous operation it behaves as a well-stirred vessel. Tube mills are better for continuous operation. The mill volume of the vertical mill cannot be arbitrarily scaled up because the static load of the upper media, especially with steel beads, prevents thorough energy introduction into the lower layers. Larger throughputs can therefore only be obtained by using more mill troughs, as in tube mills. The primary applications of vibratory mills are in fine milling of medium to hard minerals primarily in dry form, producing particle sizes of 1 μm and finer. Throughputs are typically 10 to 20 t/h. Grinding increases with residence time, active mill volume, energy density and vibration frequency, and media filling and feed charge.

The amount of energy that can be applied limits the tube size to 600 mm, although one design reaches 1000 mm. Larger vibratory amplitudes are more favorable for comminution than higher frequency. The development of larger vibratory mills is unlikely in the near future because of excitation problems. This has led to the use of mills with as many as six grinding tubes.

Performance The grinding-media diameter should preferably be 10 times that of the feed and should not exceed 100 times the feed diameter. To obtain improved efficiency when reducing size by several orders of magnitude, several stages should be used with different media diameters. As fine grinding proceeds, rheological factors alter the charge ratio, and power requirements may increase. Size availability varies, ranging from 1.3 cm ($\frac{1}{2}$ in) down to 325 mesh (44 μm).

Advantages of vibratory mills are (1) simple construction and low capital cost, (2) very fine product size attainable with large reduction ratio in a single pass, (3) good adaptation to many uses, (4) small space and weight requirements, and (5) ease and low cost of maintenance. Disadvantages are (1) limited mill size and throughput, (2) vibration of the support and foundation, and (3) high-noise output, especially when run dry. The vibratory-tube mill is also suited to wet milling. In fine wet milling, this narrow residence time distribution lends itself to a simple open circuit with a small throughput. But for tasks of grinding to colloid-size range, the stirred media mill has the advantage.

Residence Time Distribution Hoeffel [Freiberger, *Forschungshefte A*, **750**, 119 pp. (1988)] carried out the first investigations of

residence time distribution and grinding on vibratory mills, and derived differential equations describing the motion. In vibratory horizontal tube mills, the mean axial transport velocity increases with increasing vibrational velocity, defined as the product $r_s\Omega$, where r_s = amplitude and Ω = frequency. Apparently the media act as a filter for the feed particles and are opened by vibrations. Nevertheless, good uniformity of transport is obtained, indicated by *vessel dispersion numbers* $D\tau/L^2$ (see “Simulation of Milling Circuits” above) in the range 0.06 to 0.08 measured in limestone grinding under conditions where both throughput and vibrational acceleration are optimum.

HICOM MILL

The Hicom mill is technically a vertical vibratory mill, but its design allows much higher energy input than do typical vibratory mills. The Hicom mill uses an irregular “nutating” motion to shake the mills, which allows much higher than normal g forces. Consequently, smaller media can be used and much higher grinding rates can be achieved. Hicom mill dry grinding performance tends to be competitive with jet mills, a substantial improvement over other vibratory mills. The Hicom mill is primarily used for dry grinding although it can also be used for wet grinding.

PLANETARY BALL MILLS

In planetary ball mills, several ball mill chambers are mounted on a frame in a circular pattern. The balls are all rotated in one direction (clockwise or counterclockwise), and the frame is rotated in the opposite direction, generating substantial centrifugal forces (10 to 50 g , depending on the device).

Planetary ball mills are difficult to make at large scale due to mechanical limitations. The largest mills commercially available have volumes in the range of 5 gal. Larger mills have been made, but they have tended to have very significant maintenance difficulties.

DISK ATTRITION MILLS

The disk or attrition mill is a modern counterpart of the early buhrstone mill. Stones are replaced by steel disks mounting interchangeable metal or abrasive grinding plates rotating at higher speeds, thus permitting a much broader range of application. They have a place in the grinding of tough organic materials, such as wood pulp and corn

grits. Grinding takes place between the plates, which may operate in a vertical or a horizontal plane. One or both disks may be rotated; if both, then in opposite directions. The assembly, comprising a shaft, disk, and grinding plate, is called a **runner**. Feed material enters a chute near the axis, passes between the grinding plates, and is discharged at the periphery of the disks. The grinding plates are bolted to the disks; the distance between them is adjustable.

DISPERSERS AND EMULSIFIERS

Media Mills and Roll Mills Both media mills and roll mills are commonly used for powder dispersion, especially in the paint and ink industries. Media mills used for these operations are essentially the same as described above, although finer media are used than are common in particle-grinding operations (down to 0.2 mm). Often, some sort of high-speed mixer is needed to disperse the powder into a liquid before trying to disperse powder in the media mill. Otherwise, large clumps of powder in the slurry can clog the mill.

Paint-grinding roller mills (Fig. 21-78) consist of two to five smooth rollers operating at differential speeds. A paste is fed between the first two rollers (low-speed) and is discharged from the final roller (high-speed) by a scraping blade. The paste passes from the surface of one roller to that of the next because of the differential speed, which also applies shear stress to the film of material passing between the rollers. Roll mills are sometimes heated so that higher-viscosity pastes can be ground and, in some cases, so that solvent can be removed.

Both of these mills can achieve very small particle-size dispersion (below 100 nm, if the primary particle size of the powder is small enough). However, formulation with surfactants is absolutely necessary to achieve fine particle dispersions. Otherwise, the particles will simply reaggregate after leaving the shear field of the machine.

Dispersion and Colloid Mills Colloid mills have a variety of designs, but all have a rotating surface, usually a cone or a disc, with another surface near the rotor that forms a uniform gap (e.g., two discs parallel to each other). The liquid to be emulsified is pumped between the gaps. Sometimes, the design allows some pumping action between the rotor and the stator, and some machines of this type resemble centrifugal pumps in design. Colloid mills are relatively easy to clean and can handle materials with viscosity. For this reason, they are very common in the food and cosmetic industries for emulsifying pastes, creams, and lotions.

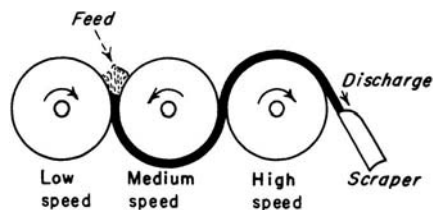


FIG. 21-78 Roller mill for paint grinding.

Pressure Homogenizers These are the wet grinding equivalents to jet mills, but they are used almost exclusively for emulsion and disagglomeration. There are several different styles of these, but all operate by generating pressures between 1000 and 50,000 psi using high-pressure pumps, with all the pressure drop occurring in a very small volume, such as flowing through an expansion valve. Some devices also have liquid jets which impinge on each other, similar to certain kinds of jet mills.

A **high-pressure valve homogenizer** such as the Gaulin and Rannie (APV Gaulin Group) forces the suspension through a narrow orifice. The equipment has two parts: a high-pressure piston pump and a homogenizer valve [Kula and Schuette, *Biotechnol. Progress*, **3**(1), 31–42 (1987)]. The pump in production machines may have up to six pistons. The valve opens at a preset or adjustable value, and the suspension is released at high velocity (300 m/s) and impinges on an impact ring. The flow changes direction twice by 90°, resulting in turbulence. There is also a two-stage valve, but it has been shown that it is better to expend all the pressure across a single stage. The temperature of the suspension increases about 2.5°C per 10-MPa pressure drop. Therefore intermediate cooling is required for multiple passes. Submicrometer-size emulsions can be achieved with jet homogenizers.

Microfluidizer The microfluidizer operates much the same as the valve homogenizers, but has a proprietary interaction chamber rather than an expansion valve. While valve homogenizers often have difficulties with particle slurries due to wear and clogging of the homogenizing valves, microfluidizers are much more robust and are often used in pharmaceutical processing. Interaction chambers for these applications must be made of specialized materials and can be expensive. Slurry particle sizes similar in size to those in media mill operations can be achieved with the microfluidizer.

CRUSHING AND GRINDING PRACTICE

CEREALS AND OTHER VEGETABLE PRODUCTS

Hammer mills or roll mills are used for a wide variety of vegetable products, from fine flour products to pulping for ethanol fermentation. Choice of mill usually depends on the exact nature of the feed and the desired product. For example, although usually cheaper to install and easier to operate, hammer mills cannot handle moist feeds as easily as roll mills, and roll mills tend to produce products with narrower size distributions.

Flour and Feed Meal The roller mill is the traditional machine for grinding wheat and rye into high-grade flour. A typical mill used for this purpose is fitted with two pairs of rolls, capable of making two separate reductions. After each reduction, the product is taken to a bolting machine or classifier to separate the fine flour; the coarse product is returned for further reduction. Feed is supplied at the top where a vibratory shaker spreads it out in a thin stream across the full width of the rolls. Rolls are made with various types of corrugation. Two standard types are generally used: the dull and the sharp. The former is mainly used on wheat and rye, and the latter on corn and feed. Under ordinary conditions, a sharp roll is used against a sharp roll for very tough wheat. A sharp, fast roll is used against a dull, slow roll for mod-

erately tough wheat; a dull, fast roll against a sharp, slow roll for slightly brittle wheat; and a dull roll against a dull roll for very brittle wheat. The speed ratio usually is 2½:1 for corrugated rolls and 1¼:1 for smooth rolls. By examining the marks made on the grain fragments, it has been concluded (Scott, *Flour Milling Processes*, Chapman & Hall, London, 1951) that the differential action of the rolls actually can open up the berry and strip the endosperm from the hulls.

High-speed hammer or pin mills result in some *selective grinding*. Such mills combined with air classification can produce fractions with controlled protein content. Flour with different protein content is needed for the baking of breads and cakes; these types of flour were formerly available only by selection of the type of wheat, which is limited by growing conditions prevailing in particular locations [Wichser, *Milling*, **3**(5), 123–125 (1958)].

Soybeans, Soybean Cake, and Other Pressed Cakes After granulation on rolls, the granules are generally treated in presses or solvent-extracted to remove the oil. The product from the presses goes to attrition mills or flour rolls and then to bolters, depending upon whether the finished product is to be a feed meal or a flour. The method used for grinding pressed cakes depends upon the nature of the cake, its purity, its residual oil, and its moisture content. If the whole cake is to be

pulverized without removal of fibrous particles, it may be ground in a hammer mill with or without air classification. A 15-kW (20-hp) hammer mill with an air classifier, grinding pressed cake, had a capacity of 136 kg/h (300 lb/h), 90 percent through a No. 200 sieve; a 15-kW (20-hp) screen hammer mill grinding to 0.16-cm (1/16-in) screen produced 453 kg/h (1000 lb/h). In many cases the hammer mill is used merely as a preliminary disintegrator, followed by an attrition mill. A finer product may be obtained in a hammer mill in a closed circuit with an external screen or classifier. High-speed hammer mills are extensively used for the grinding of soy flour.

Starch and Other Flours Grinding of starch is not particularly difficult, but precautions must be taken against explosions; starches must not come in contact with hot surfaces, sparks, or flame when suspended in air. See "Operational Considerations: Safety" for safety precautions. When a product of medium fineness is required, a hammer mill of the screen type is employed. Potato, tapioca, banana, and similar flours are handled in this manner. For finer products a high-speed impact mill such as the Entoleter pin mill is used in closed circuit with bolting cloth, an internal air classifier, or vibrating screens.

ORES AND MINERALS

Metalliferous Ores The most extensive grinding operations are done in the ore-processing and cement industries, which frequently require size reduction from rocks down to powder in the range of 100 μm and sometimes below 325 mesh (45 μm). Grinding is one of the major problems in milling practice and one of the main items of expense. These industries commonly use complicated grinding circuits, and manufacturers, operators, and engineers find it necessary to compare grinding practices in one plant with that in another, attempting to evaluate circuits and practices (Arbiter, *Milling in the Americas*, 7th International Mineral Processing Congress, Gordon and Breach, New York, 1964). Direct-shipping ores are high in metal assay, and require only preliminary crushing before being fed to a blast furnace or smelter. As these high-grade ores have been depleted, it has become necessary to concentrate ores of lower mineral value.

Autogenous milling, where media are replaced with large rocks of the same material as the product, is becoming increasing popular in the minerals industry. In many cases, however, semiautogenous milling (SAM), where a small load of steel balls is added in addition to the product "media," is preferred over autogenous grinding. The advantage of autogenous mills is reduction of ball wear costs, but power costs are at least 25 percent greater because irregular-shaped media are less effective than balls.

Autogenous milling of iron and copper ores has been widely accepted. When successful, this method results in economies due to elimination of media wear. Probably another reason for efficiency is the use of higher circulating loads and better classification. These improvements resulted from the need to use larger-diameter mills to obtain grinding with rock media that have a lower density than do steel balls. The major difficulty lies in arranging the crushing circuits and the actual mining so as to ensure a steady supply of large ore lumps to serve as grinding media. With rocks that are too friable this cannot be achieved.

With other ores there has been a problem of buildup of intermediate-sized particles, but this has been solved either by using semiautogenous grinding or by sending the scalped intermediate-sized particles through a cone crusher.

Types of Milling Circuits A typical grinding circuit with three stages of gyratory crushers, followed by a wet rod mill followed by a ball mill, is shown in Fig. 21-79. This combination has high-power efficiency and low steel consumption, but higher investment cost because rod mills are limited in length to 20 ft by potential tangling of the rods. Other variations of this grinding circuit include [Allis Chalmers, *Engg. & Mining J.*, 181(6), 69-171 (1980)] similar crusher equipment followed by one or two stages of large ball mills (depending on product size required), or one stage of a gyratory crusher followed by large-diameter semiautogenous ball mills followed by a second stage of autogenous or ball mills.

Circuits with larger ball mills have higher energy and media wear costs. A fourth circuit using the roll press has been widely accepted in the cement industry (see "Roll Press" and "Cement, Lime, and

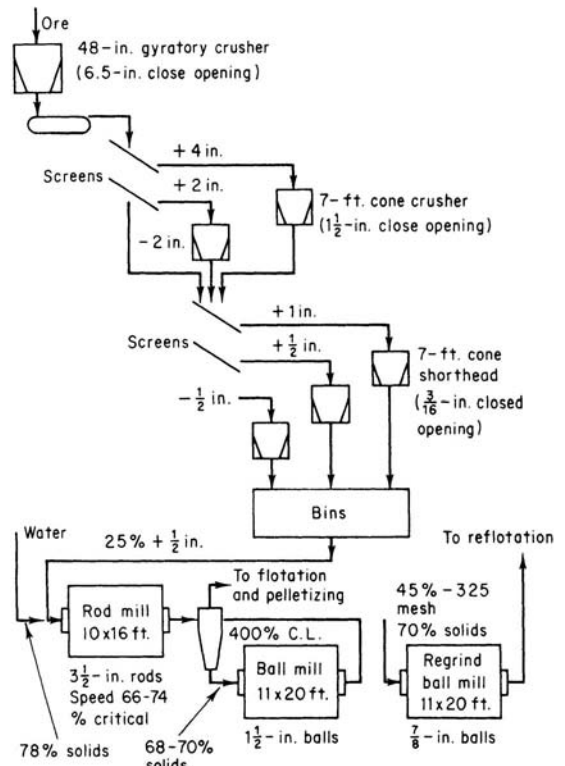


FIG. 21-79 Ball- and rod-mill circuit. Simplified flow sheet of the Cleveland-Cliffs Iron Co. Republic mine iron-ore concentrator. To convert inches to centimeters, multiply by 2.54; to convert feet to centimeters, multiply by 30.5. (Johnson and Bjorne, *Milling in the Americas*, Gordon and Breach, New York, 1964.)

Gypsum") and could be used in other mineral plants. It could replace the last stage of crushers and the first stage of ball or rod mills, at substantially reduced power and wear. For the grinding of softer copper ore, the rod mill might be eliminated, with both coarse-crushing and ball-milling ranges extended to fill the gap. Larger stirred media mills are increasingly available and are sometimes used in the final grinding stages for fine products.

Nonmetallic Minerals Many nonmetallic minerals require much finer sizes than ore grinding, sometimes down below 5 μm. In general, dry-grinding circuits with ball, roller, or hammer mills with a closed-circuit classifier are used for products above about 20 μm. For products less than 20 μm, either jet mills or wet milling is used. Either option adds significantly to the cost, jet mills because of significantly increased energy costs, and in wet milling because of additional drying and classification steps.

Clays and Kaolins Because of the declining quality of available clay deposits, beneficiation is becoming more required [Uhlig, *Ceram. Forum Int.*, 67(7-8), 299-304 (1990)], English and German text]. Beneficiation normally begins with a size-reduction step, not to break particles but to dislodge adhering clay from coarser impurities.

In **dry processes** this is done with low-energy impact mills. Mined clay with 22 percent moisture is broken up into pieces of less than 5 cm (2 in) in a rotary impact mill without a screen, and is fed to a rotary gas-fired kiln for drying. The moisture content is then 8 to 10 percent, and this material is fed to a mill, such as a Raymond ring-roll mill with an internal whizzer classifier. Hot gases introduced to the mill complete the drying while the material is being pulverized to the required fineness. After grinding, the clay is agglomerated to a flowable powder with water mist in a balling drum.

In the **wet process**, the clay is masticated in a pug mill to break up lumps and is then dispersed with a dispersing aid and water to make a 40 percent solids slurry of low viscosity. A high-speed agitator such as a Cowles dissolver is used for this purpose. Sands are settled out, and then the clay is classified into two size fractions in either a hydrosettler or a continuous Sharples or Bird centrifuge. The fine fraction, with sizes of less than 1 μm , is used as a pigment and for paper coating, while the coarser fraction is used as a paper filler. A process for upgrading kaolin by grinding in a stirred bead mill has been reported [Stanczyk and Feld, *U.S. Bur. Mines Rep. Invest.*, **6327** and **6694** (1965)]. By this means the clay particles are delaminated, and the resulting platelets give a much improved surface on coated paper.

Talc and Soapstone Generally these are easily pulverized. Certain fibrous and foliated talcs may offer greater resistance to reduction to impalpable powder, but these are no longer produced because of their asbestos content. Talc milling is largely a grinding operation accompanied by air separation. Most of the industrial talcs are dry-ground. Dryers are commonly employed to predry ahead of the milling operation because the wet material reduces mill capacity by as much as 30 percent. Conventionally, in talc milling, rock taken from the mines is crushed in primary and then in secondary crushers to at least 1.25 cm ($\frac{1}{2}$ in) and frequently as fine as 0.16 cm ($\frac{1}{16}$ in). Ring-roll mills with internal air separation are widely used for the large-capacity fine grinding of the softer talcs. High-speed hammer mills with internal air separation have also had outstanding success on some of the softer high-purity talcs for very fine fineness. Talcs of extreme fineness and high surface area are used for various purposes in the paint, paper, plastics, and rubber industries.

Carbonates and Sulfates Carbonates include limestone, calcite, marble, marls, chalk, dolomite, and magnesite; the most important sulfates are barite, celestite, anhydrite, and gypsum. These are used as fillers in paint, paper, and rubber. (Gypsum and anhydrite are discussed below as part of the cement, lime, and gypsum industries.)

Silica and Feldspar These very hard minerals can be ground in ball/pebble mills with silex linings and flint balls. A feldspar mill is described in *U.S. Bur. Mines Cir.* **6488** (1931). It uses pebble mills with a Gayco air classifier. They can also be processed in ring-roller mills as the rings are easily replaced as they wear. Feldspar is also ground in continuous-tube mills with classification. Feldspar for the ceramic and chemical industries is ground finer than for the glass industry.

Asbestos and Mica Asbestos is no longer mined in the United States because of the severe health hazard. See previous editions of this handbook for process descriptions.

The micas, as a class, are difficult to grind to a fine powder; one exception is disintegrated schist, in which the mica occurs in minute flakes. For dry grinding, hammer mills equipped with an air transport system are generally used. Maintenance is often high. It has been established that the method of milling has a definite effect on the particle characteristics of the final product. Dry grinding of mica is customary for the coarser sizes down to 100 mesh. Micronized mica, produced by high-pressure steam jets, is considered to consist of highly delaminated particles.

Refractories Refractory bricks are made from fireclay, alumina, magnesite, chrome, forsterite, and silica ores. These materials are crushed and ground, wetted, pressed into shape, and fired. To obtain the maximum brick density, furnishes of several sizes are prepared and mixed. Thus a magnesia brick may be made from 40 percent coarse, 40 percent middling, and 20 percent fines. Preliminary crushing is done in jaw crushers or gyratories, intermediate crushing in pan mills or ring rolls, and fine grinding in open-circuit ball mills. Since refractory plants must make a variety of products in the same equipment, pan mills and ring rolls are preferred over ball mills because the former are more easily cleaned.

Sixty percent of refractory magnesite is made synthetically from Michigan brines. When calcined, this material is one of the hardest refractories to grind. Gyratory crushers, jaw crushers, pan mills, and ball mills are used. Alumina produced by the Bayer process is precipitated and then calcined [Krawczyk, *Ceram. Forum Int.*, **67**(7-8), 342-348 (1990)]. Aggregates are typically 20 to 70 μm and have to be reduced. The standard product is typically made in continuous dry

ball or vibratory mills to give a product d_{50} size of 3 to 7 μm , 98 percent finer than 45 μm . The mills are lined with wear-resistant alumina blocks, and balls or cylinders are used with an alumina content of 80 to 92 percent. The products containing up to 96 percent Al_2O_3 are used for bricks, kiln furniture, grinding balls and liners, high-voltage insulators, catalyst carriers, etc.

Ultrafine grinding is carried out batchwise in vibratory or ball mills, either dry or wet. The purpose of batch operation is to avoid the residence time distribution which would pass less-ground material through a continuous mill. The energy input is 20 to 30 times greater than that for standard grinding, with inputs of 1300 to 1600 kWh/ton compared to 40 to 60. Jet milling is also used, followed by air classification, which can reduce the top size below 8 μm . Among new mill developments, annular-gap bead mills and stirred bead mills are being used. These have a high cost, but result in a steep particle-size distribution when used in multipass mode [Kolb, *Ceram. Forum Int.*, **70**(5), 212-216 (1993)]. Costs for fine grinding typically exceed the cost of raw materials. Products are used for high-performance ceramics. Silicon carbide grains were reduced from 100 to 200 mesh to 80 percent below 1 μm in a version of stirred bead mill, using 20- to 30-mesh silicon carbide as media [Hoyer, *Rep. Investigations U.S. Bur. Mines*, **9097**, 9 pp. (1987)].

Crushed Stone and Aggregate In-pit crushing is increasingly being used to reduce the rock to a size that can be handled by a conveyor system. In quarries with a long, steep haul, conveyors may be more economic than trucks. The primary crusher is located near the quarry face, where it can be supplied by shovels, front-end loaders, or trucks. The crusher may be fully mobile or semimobile. It can be of any type listed below. The choices depend on individual quarry economics and are described by Faulkner [*Quarry Management and Products*, **7**(6), 159-168 (1980)]. Primary crushers used are jaw, gyratory, impact, and toothed roll crushers. Impact mills are limited to limestone and softer stone. With rocks containing more than 5 percent quartz, maintenance of hammers may become prohibitive. Gyratory and cone crushers dominate the field for secondary crushing of hard and tough stone. Rod mills have been employed to manufacture stone sand when natural sands are not available. Crushed stone for road building must be relatively strong and inert and must meet specifications regarding size distribution and shape. Both size and shape are determined by the crushing operation. The purpose of these specifications is to produce a mixture where the fines fill the voids in the coarser fractions, thus to increase load-bearing capacity. (See "Refractories" above.) Sometimes a product that does not meet these requirements must be adjusted by adding a specially crushed fraction. No crushing device available will give any arbitrary size distribution, and so crushing with a small reduction ratio and recycle of oversize is practiced when necessary.

FERTILIZERS AND PHOSPHATES

Fertilizers Many of the materials used in the fertilizer industry are pulverized, such as those serving as sources for calcium, phosphorus, potassium, and nitrogen. The most commonly used for their lime content are limestone, oyster shells, marls, lime, and, to a small extent, gypsum. Limestone is generally ground in hammer mills, ring-roller mills, and ball mills. Fineness required varies greatly from a No. 10 sieve to 75 percent through a No. 100 sieve.

Phosphates Phosphate rock is generally ground for one of two major purposes: for direct application to the soil or for acidulation with mineral acids in the manufacture of fertilizers. Because of larger capacities and fewer operating-personnel requirements, plant installations involving production rates over 900 Mg/h (100 tons/h) have used ball-mill grinding systems. Ring-roll mills are used in smaller applications. Rock for direct use as fertilizer is usually ground to various specifications, ranging from 40 percent minus 200 mesh to 70 percent minus 200 mesh. For manufacture of normal and concentrated superphosphates, the fineness of grind ranges from 65 percent minus 200 mesh to 85 percent minus 200 mesh.

Inorganic salts often do not require fine pulverizing, but they frequently become lumpy. In such cases, they are passed through a double-stage mill or some type of hammer mill.

Basic slag is often used as a source of phosphorus. Its grinding resistance depends largely upon the way in which it has been cooled; slowly cooled slag generally is more easily pulverized. The most common method for grinding basic slag is in a ball mill, followed by a tube mill or a compartment mill. Both systems may be in closed circuit with an air classifier. A 2.1- by 1.5-m (7- by 5-ft) mill, requiring 94 kW (125 hp), operating with a 4.2-m (14-ft) 22.5-kW (30-hp) classifier, gave a capacity of 4.5 Mg/h (5 tons/h) from the classifier, 95 percent through a No. 200 sieve. Mill product was 68 percent through a No. 200 sieve, and circulating load 100 percent.

CEMENT, LIME, AND GYPSUM

Portland Cement Portland cement manufacture requires grinding on a very large scale and entails a large use of electric power. Raw materials consist of sources of lime, alumina, and silica and range widely in properties, from crystalline limestone with silica inclusions to wet clay. Therefore a variety of crushers are needed to handle these materials. Typically a crushability test is conducted by measuring the product size from a laboratory impact mill on core samples [Schaefter and Gallus, *Zement- Kalk-Gips*, 41(10), 486-492 (1988); English ed., 277-280]. Abrasiveness is measured by the weight loss of the hammers. The presence of 5 to 10 percent silica can result in an abrasive rock, but only if the silica grain size exceeds 50 μm . Silica inclusions can also occur in soft rocks. The presence of sticky clay will usually result in handling problems, but other rocks can be handled even if moisture reaches 20 percent. If the rock is abrasive, the first stage of crushing may use gyratory or jaw crushers, otherwise a rotor-impact mill. Their reduction ratio is only 1:12 to 1:18, so they often must be followed by a hammer mill, or they can feed a roll press. Rotor crushers have become the dominant primary crusher for cement plants because of the characteristics. All these types of crushers may be installed in movable crusher plants. In the grinding of raw materials, two processes are used: the dry process in which the materials are dried to less than 1 percent moisture and then ground to a fine powder, and the wet process in which the grinding takes place with addition of water to the mills to produce a slurry.

Dry-Process Cement After crushing, the feed may be ground from a size of 5 to 6 cm (2 to 2½ in) to a powder of 75 to 90 percent passing a 200-mesh sieve in one or several stages. The first stage, reducing the material size to approximately 20 mesh, may be done in vertical, roller, ball-race, or ball mills. The last named rotate from 15 to 18 r/min and are charged with grinding balls 5 to 13 cm (2 to 5 in) in diameter. The second stage is done in tube mills charged with grinding balls of 2 to 5 cm (¾ to 2 in). Frequently ball and tube mills are combined into a single machine consisting of two or three compartments, separated by perforated steel diaphragms and charged with grinding media of different sizes. Rod mills are hardly ever used in cement plants. The compartments of a tube mill may be combined in various circuit arrangements with classifiers, as shown in Fig. 21-80. A dry-process plant has been described by Bergstrom [*Rock Prod.*, 59-62 (August 1968)].

Wet-Process Cement Ball, tube, and compartment mills of essentially the same construction as for the dry process are used for grinding. A water or clay slip is added at the feed end of the initial grinder, together with the roughly proportioned amounts of limestone and other components. In modern installations wet grinding is sometimes accomplished in ball mills alone, operating with excess water in

closed circuit with classifiers and hydroseparators. The circuits of Fig. 21-80 may also be used as a closed-circuit wet-grinding system incorporating a liquid solid cyclone as the classifier. A wet-process plant making cement from shale and limestone has been described by Bergstrom [*Rock Prod.*, 64-71 (June 1967)]. There are separate facilities for grinding each type of stone. The ball mill operates in closed circuit with a battery of Dutch State Mines screens. Material passing the screens is 85 percent minus 200 mesh.

Finish-Grinding of Cement Clinker Typically the hot clinker is first cooled and then ground in a compartment mill in a closed circuit with an air classifier. To crush the clinkers, balls as large as 5 in may be needed in the first compartment. A roll press added before the ball mill can reduce clinkers to a fine size and thus reduce the load on the ball mills. The main reason for adding a roll press has been to increase capacity of the plant and to lower cost. Installation of roll presses in several cement plants is described (31st IEEE Cement Industry Technical Conference, 1989). Considerable modification of the installation was required because of the characteristics of the press. A roll press is a constant-throughput machine, and the feed rate cannot easily be reduced to match the rate accepted by the ball mill that follows it. Several mills attempted to control the rate by increasing the recycle of coarse rejects from the air classifier, but the addition of such fine material was found to increase the pulling capacity of the rolls, e.g., from 180 to 250 t/h. With the resulting high recycle ratio of 5:1, the roll operation became unstable, and power peaks occurred. Deaeration of fines occurs in the nip, and this also interferes with feeding fines to the rolls. In some plants these problems were overcome by recirculating slabs of product directly from the roll discharge. In other cases the rolls were equipped with variable-speed drives to allow more versatile operation when producing several different grades/finenesses of cement. The roll press was found to be 2.5 times as efficient as the ball mill, in terms of new surface per unit energy. Tests showed that the slab from pressing of clinker at 120 bar and 20 percent recycle contained 97 percent finer than 2.8 mm, and 39 percent finer than 48 μm . Current operation is at 160 bar. The wear was small; after 4000 h of operation and 1.5 million tons of throughput, the wear rate was less than 0.1 g/ton, or 0.215 g/ton of finished cement. There is some wear of the working parts of the press, requiring occasional maintenance. The press is controlled by four control loops. The main control adjusts the gates that control slab recycle. Since this adjustment is sensitive, the level in the feed bin is controlled by adjusting the clinker-feed rate to ensure choke-feed conditions. Hydraulic pressure is also controlled. Separator reject rate is fixed. The investment cost was only \$42,000 per ton of increased capacity. Energy savings is 15 kWh/ton. This together with off-peak power rates results in energy cost savings of \$500,000/yr.

Lime Lime used for agricultural purposes generally is ground in hammer mills. It includes burned, hydrated, and raw limestone. When a fine product is desired, as in the building trade and for chemical manufacture, ring-roller mills, ball mills, and certain types of hammer mills are used.

Gypsum When gypsum is calcined in rotary kilns, it is first crushed and screened. After calcining it is pulverized. Tube mills are usually used. These impart plasticity and workability. Occasionally such calcined gypsum is passed through ring-roller mills ahead of the tube mills.

COAL, COKE, AND OTHER CARBON PRODUCTS

Bituminous Coal The grinding characteristics of bituminous coal are affected by impurities it contains, such as inherent ash, slate, gravel, sand, and sulfur balls. The grindability of coal is determined by grinding it in a standard laboratory mill and comparing the results with those obtained under identical conditions on a coal selected as a standard. This standard coal is a low-volatile coal from Jerome Mines, Upper Kintanning bed, Somerset County, Pennsylvania, and is assumed to have a grindability of 100. Thus a coal with a grindability of 125 could be pulverized more easily than the standard, while a coal with a grindability of 70 would be more difficult to grind. (Grindability and grindability methods are discussed under "Energy Required and Scale-up.")

Anthracite Anthracite is harder to reduce than bituminous coal. It is pulverized for foundry-facing mixtures in ball mills or hammer mills

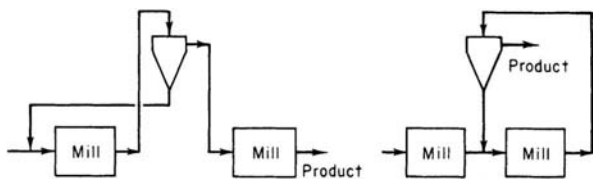


FIG. 21-80 Two cement-milling circuits. [For others, see Tonry, Pit Quarry (February-March 1959).]

followed by air classifiers. A 3- by 1.65-m (10-ft by 66-in) Hardinge mill in closed circuit with an air classifier, grinding 4 mesh anthracite with 3.5 percent moisture, produced 10.8 Mg/h (12 tons/h), 82 percent through No. 200 sieve. The power required for the mill was 278 kW (370 hp); for auxiliaries, 52.5 kW (70 hp); speed of mill, 19 r/min; ball load, 25.7 Mg (28.5 tons). Anthracite for use in the manufacture of electrodes is calcined, and the degree of calcination determines the grinding characteristics. Calcined anthracite is generally ground in ball and tube mills or ring-roller mills equipped with air classification.

Coke The grinding characteristics of coke vary widely. By-product coke is hard and abrasive, while certain foundry and retort coke is extremely hard to grind. For certain purposes it may be necessary to produce a uniform granule with minimum fines. This is best accomplished in rod or ball mills in closed circuit with screens. Petroleum coke is generally pulverized for the manufacture of electrodes; ring-roller mills with air classification and tube mills are generally used.

Other Carbon Products **Pitch** may be pulverized as a fuel or for other commercial purposes; in the former case the unit system of burning is generally employed, and the same equipment is used as described for coal. Grinding characteristics vary with the melting point, which may be anywhere from 50 to 175°C.

Natural graphite may be divided into three grades in respect to grinding characteristics: flake, crystalline, and amorphous. Flake is generally the most difficult to reduce to fine powder, and the crystalline variety is the most abrasive. Graphite is ground in ball mills, tube mills, ring-roller mills, and jet mills with or without air classification. Beneficiation by flotation is an essential part of most current procedures. Artificial graphite has been ground in ball mills in a closed circuit with air classifiers. For lubricants the graphite is ground wet in a paste in which water is eventually replaced by oil. The colloid mill is used for production of graphite paint.

Mineral black, a type of shale sometimes erroneously called *rotten stone*, contains a large amount of carbon and is used as a filler for paints and other chemical operations. It is pulverized and classified with the same equipment as shale, limestone, and barite.

Bone black is sometimes ground very fine for paint, ink, or chemical uses. A tube mill often is used, the mill discharging to a fan, which blows the material to a series of cyclone collectors in tandem.

Decolorizing carbons of vegetable origin should not be ground too fine. Standard fineness varies from 100 percent through No. 30 sieve to 100 percent through No. 50, with 50 to 70 percent on No. 200 sieve as the upper limit. Ball mills, hammer mills, and rolls, followed by screens, are used. When the material is used for filtering, a product of uniform size must be used.

Charcoal usually is ground in hammer mills with screen or air classification. For absorption of gases it is usually crushed and graded to about No. 16 sieve size. Care should be taken to prevent it from igniting during grinding.

Gilsonite sometimes is used in place of asphalt or pitch. It is easily pulverized and is generally reduced on hammer mills with air classification.

CHEMICALS, PIGMENTS, AND SOAPS

Colors and Pigments **Dry colors** and **dyestuffs** generally are pulverized in hammer mills. The jar mill or a large pebble mill is often used for small lots. There is a special problem with some dyes, which are coarsely crystalline. These are ground to the desired fineness with hammer or jet mills using air classification to limit the size. Synthetic pigments (mineral or organic) are usually fine agglomerates produced from aqueous crystallization processes. They are often lightly ground in media mills prior to drying. Dried pigments can be ground in hammer or jet mills to disintegrate aggregation that occurs during grinding.

Dispersion of pigments into liquids is done predominantly by stirred media mills in the ink and paint industries. Roll mills are sometimes used for very fine dispersion or for very viscous materials such as some inks. Some grades of pigments disperse readily, or go into products with less stringent particle-size requirements, such as house-paints, and these require only high-speed dispersing mixers or colloid mills. Very difficult to disperse pigments, such as carbon black, are usually processed with a combination of these two processes, where a

high-speed disperser is used to premix the carbon black into the paint vehicle prior to processing in a media mill.

White pigments are basic commodities processed in large quantities. Titanium dioxide is the most important. The problem of cleaning the mill between batches does not exist as with different colors. These pigments are finish-ground to sell as dry pigments using mills with air classification. For the denser, low-oil-absorption grades, roller and pebble mills are employed. For looser, fluffier products, hammer and jet mills are used. Often a combination of the two mill actions is used to set the finished quality.

Chemicals Fine powder organic chemicals (herbicides are one example) can be processed similar to fine pigments: media mills for wet slurries of crystals, followed by drying and hammer mills or jet mill for dry material.

Sulfur The ring-roller mill can be used for the fine grinding of sulfur. Inert gases are supplied instead of hot air (see "Properties of Solids: Safety" for use of inert gas).

Soaps Soaps in a finely divided form may be classified as soap powder, powdered soap, and chips or flakes. The term *soap powder* is applied to a granular product, No. 12 to No. 16 sieve size with a certain amount of fines, which is produced in hammer mills with perforated or slotted screens. The oleates and erucates are best pulverized by multicage mills; laurates and palmitates, in cage mills and also in hammer mills if particularly fine division is not required. Stearates may generally be pulverized in multicage mills, screen mills, and air classification hammer mills.

POLYMERS

The grinding characteristics of various resins, gums, waxes, hard rubbers, and molding powders depend greatly upon their softening temperatures. When a finely divided product is required, it is often necessary to use a water-jacketed mill or a pulverizer with an air classifier in which cooled air is introduced into the system. Hammer and cage mills are used for this purpose. Some low-softening-temperature resins can be ground by mixing with 15 to 50 percent by weight of dry ice before grinding. Refrigerated air sometimes is introduced into the hammer mill to prevent softening and agglomeration [Dorris, *Chem. Metall. Eng.*, 51, 114 (July 1944)].

Gums and Resins Most **gums and resins**, natural or artificial, when used in the paint, varnish, or plastic industries, are not ground very fine, and hammer or cage mills will produce a suitable product. Roll crushers will often give a sufficiently fine product. Ring mills are sometimes used.

Rubber **Hard rubber** is one of the few combustible materials which is generally ground on heavy steam-heated rollers. The raw material passes to a series of rolls in closed circuit with screens and air classifiers. Farrel-Birmingham rolls are used extensively for this work. There is a differential in the roll diameters. The motor should be separated from the grinder by a firewall.

Molding Powders Specifications for **molding powders** vary widely, from a No. 8 to a No. 60 sieve product; generally the coarser products are No. 12, 14, or 20 sieve material. Specifications usually prescribe a minimum of fines (below No. 100 and No. 200 sieve). Molding powders are produced with hammer mills, either of the screen type or equipped with air classifiers. The following materials may be ground at ordinary temperatures if only the regular commercial fineness is required: amber, arabac, tragacanth, rosin, olibanum, gum benzoin, myrrh, guaiacum, and montan wax. If a finer product is required, hammer mills or attrition mills in closed circuit, with screens or air classifiers, are used.

Powder Coatings Powder coatings are quite fine, often 40 µm or less, and tend to be heat-sensitive. Also, to give a good finish, large particles, which have a detrimental effect on gloss, must be minimized. These are typically ground in air classifying mills or jet mills.

PROCESSING WASTE

In flow sheets for processing *municipal solid waste* (MSW), the objective is to separate the waste into useful materials, such as scrap metals, plastics, and *refuse-derived fuels* (RDFs). Usually size reduction is the

first step, followed by separations with screens or air classifiers, which attempt to recover concentrated fractions [Savage and Diaz, *Proc. ASME National Waste Processing Conference*, Denver, Colo., 361–373 (1986)]. Many installed circuits proved to be ineffective or not cost-effective, however. Begnaud and Noyon [*Biocycle*, **30**(3), 40–41 (1989)] concluded from a study of French operations that milling could not grind selectively enough to separate different materials. Size reduction uses either hammer mills or blade cutters (shredders). Hammer mills are likely to break glass into finer sizes, making it hard to separate. Better results may be obtained in a flow sheet where size reduction follows separation (Savage, Seminar on the Application of U.S. Water and Air Pollution Control Technology to Korea, Korea, May 1989). Wear is also a major cost, and wear rates are shown in Fig. 21-81. The maximum capacity of commercially available hammer mills is about 100 tons/h.

PHARMACEUTICAL MATERIALS

Specialized modification of fine grinding equipment for pharmaceutical grinding has become increasingly common. Most grinding is accomplished using a variety of air classifying mills and jet mills. Wet grinding with homogenizers and bead mills is becoming more common. Equipment for grinding pharmaceuticals must be readily cleaned to very high standards; many materials are very poisonous, and many materials are quite heat-sensitive. To meet cleanliness requirements, mills are often fitted with extra seals, stainless-steel parts of high-quality finish, and other expensive modifications. Modified mills can cost 5 times what a standard mill of the same type would cost.

BIOLOGICAL MATERIALS—CELL DISRUPTION

Mechanical disruption is the most practical first step in the release and isolation of proteins and enzymes from microorganisms on a commercial scale. The size-reduction method must be gently tuned to the strength of the organisms to minimize formation of fine fragments that interfere with subsequent clarification by centrifugation or filtration. Typically, fragments as fine as 0.3 μm are produced. High-speed stirred-bead mills and high-pressure homogenizers have been applied for cell disruption [Kula and Schuette, *Biotechnol. Progress*, **3**(1), 31–42 (1987)]. There are two limiting cases in the operation of bead mills for disruption of bacterial cells. When the energy imparted by

collision of beads is insufficient to break all cells, the rate of breakage is proportional to the specific energy imparted [Bunge et al., *Chem. Engg. Sci.*, **47**(1), 225–232 (1992)]. On the other hand, when the energy is high due to higher speed above 8 m/s, larger beads above 1 mm, and low concentrations of 10 percent, each bead impact has more than enough energy to break any cells that are captured, which causes problems during subsequent separations. The strength of cell walls differs among bacteria, yeasts, and molds. The strength also varies with the species and the growth conditions, and must be determined experimentally. Beads of 0.5 mm are typically used for yeast and bacteria. Recommended bead charge is 85 percent for 0.5-mm beads and 80 percent for 1-mm beads [Schuette et al., *Enzyme Microbial Technol.*, **5**, 143 (1983)]. Residence time distribution is important in continuous mills.

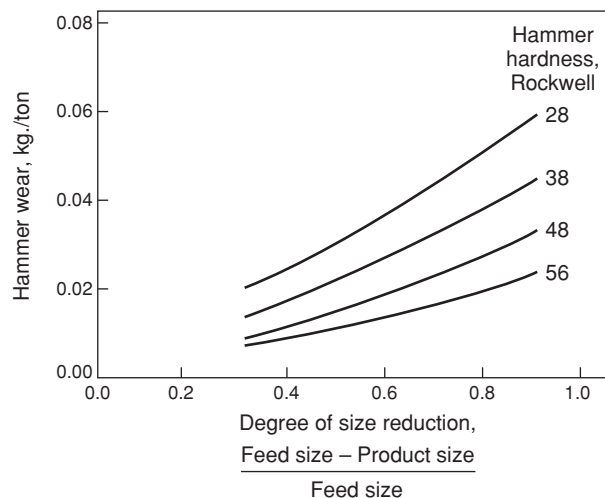


FIG. 21-81 Hammer wear as a consequence of shredding municipal solid waste. (Savage and Diaz, *Proceedings ASME National Waste Processing Conference*, Denver, CO, pp 361–373, 1986.)

PRINCIPLES OF SIZE ENLARGEMENT

GENERAL REFERENCES: Benbow and Bridgwater, *Paste Flow and Extrusion*, Oxford University Press, 1993. Ennis, *Design and Optimization of Granulation and Compaction Processes for Enhanced Product Performance*, E&G Associates, Nashville, Tenn., 2006. Ennis, On the Mechanics of Granulation, Ph.D. thesis 1990, The City College of the City University of New York, University Microfilms International, 1991. Ennis, *Powder Technology*, June 1996. Kapur, *Adv. Chem. Eng.*, **10**, 55 (1978). Kristensen, *Acta Pharm. Suec.*, **25**, 187 (1988). Lütster and Ennis, *The Science and Engineering of Granulation Processes*, Kluwer Academic Publishers, 2005. Masters, *Spray Drying Handbook*, Wiley, 1979. Masters, *Spray Drying in Practice*, SprayDryConsult International, 2002. Parikh (ed.), *Handbook of Pharmaceutical Granulation Technology*, 2d ed., Taylor & Francis, 2005. Pietsch, *Size Enlargement by Agglomeration*, Wiley, Chichester, 1992. Randolph and Larson, *Theory of Particulate Processes*, Academic Press, San Diego, 1988. Stanley-Wood (ed.), *Enlargement and Compaction of Particulate Solids*, Butterworth & Co. Ltd., 1983. Ball et al., *Agglomeration of Iron Ores*, Heinemann, London, 1973. Capes, *Particle Size Enlargement*, Elsevier, New York, 1980. King, "Tablets, Capsules and Pills," in *Remington's Pharmaceutical Sciences*, Mack Pub. Co., Easton, Pa., 1970. Knepper (ed.), *Agglomeration*, Interscience, New York, 1962. Mead (ed.), *Encyclopedia of Chemical Process Equipment*, Reinhold, New York, 1964. Pietsch, *Roll Pressing*, Heyden, London, 1976. Sastry (ed.), *Agglomeration 77*, AIME, New York, 1977. Sauchelli (ed.), *Chemistry and Technology of Fertilizers*, Reinhold, New York, 1960. Sherrington and Oliver, *Granulation*, Heyden, London, 1981.

SCOPE AND APPLICATIONS

Size enlargement is any process whereby small particles are agglomerated, compacted, or otherwise brought together into larger, relatively permanent masses in which the original particles can still be distinguished. Size enlargement processes are employed by a wide range of industries, including pharmaceutical and food processing, consumer products, fertilizer and detergent production, and the mineral processing industries. The term encompasses a variety of unit operations or processing techniques dedicated to particle agglomeration. **Agglomeration** is the formation of aggregates through the sticking together of feed and/or recycle material. These processes can be loosely broken down into agitation and compression methods. Although terminology is industry-specific, agglomeration by agitation will be referred to as **granulation**. As depicted in Fig. 21-82, a particulate feed is introduced to a process vessel and is agglomerated, either batchwise or continuously, to form a granulated product. **Agitative agglomeration** processes or granulation include fluid-bed, pan (or disc), drum, and mixer granulators as well as many hybrid designs. Such processes are also used as coating operations for controlled release, taste masking, and cases where solid cores may act as a

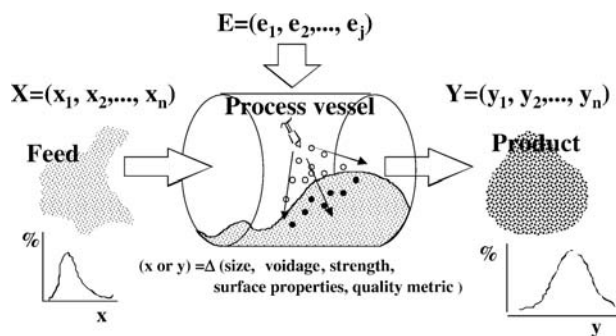


FIG. 21-82 The unit operation of agitative agglomeration, or granulation. (Reprinted from *Design and Optimization of Granulation and Compaction Processes for Enhanced Product Performance*, Ennis, 2006, with permission of E&G Associates. All rights reserved.)

carrier for a drug coating. The feed typically consists of a mixture of solid ingredients, referred to as a **formulation**, which include, an active or key ingredient, binders, diluents, disintegrants, flow aids, surfactants, wetting agents, lubricants, fillers, or end-use aids (e.g. sintering aids, colors or dyes, taste modifiers). The active ingredient is often referred to as the **technical** or **API** (active product ingredient), and it is the end-use ingredient of value, such as a drug substance, fertilizer, pesticide, or a key detergent agent. Agglomeration can be induced in several ways. A solvent or slurry can be atomized onto the bed of particles that coats either the particle or granule surfaces promoting agglomeration, or the spray drops can form small nuclei in the case of a powder feed that subsequently can agglomerate. The solvent or slurry may contain a binder, or a solid binder may be present as one component of the feed. Alternatively, the solvent may induce dissolution and recrystallization in the case of soluble particles. Slurries often contain the same particulate matter as the dry feed, and granules may be formed, either completely or partially, as the droplets solidify in flight prior to reaching the particle bed. **Spray-drying** is an extreme case where no further, intended agglomeration takes place after granule formation. Agglomeration may also be induced by heat, which either leads to controlled **sintering** of the particle bed or induces sintering or partial melting of a binder component of the feed, e.g., a polymer. Product forms generally include agglomerated or layered granules, coated carrier cores, or spray-dried product consisting of agglomerated solidified drops.

An alternative approach to size enlargement is by **compressive agglomeration** or **compaction** processes, where the mixture of particulate matter is fed to a compression device which promotes agglomeration due to pressure as depicted in Fig. 21-83. Either continuous sheets or strands of solid material are produced or some solid form such as a **briquette** or **tablet**. Either continuous sheets or strands may break down in subsequent handling to form a *granulated* material, or the material may be further processing through a variety of chopping or forced screening methods. Heat or cooling may be applied, in addition to induced frictional heating and particle deformation, and reaction may be induced such as with sintering processes. Carrier fluids may be present, either added or induced by melting, in which case the product is **wet-extruded**. Compaction processes range from confined compression devices such as tableting, briquetting machines, and ram extrusion to unconfined devices such as roll presses and extrusion and a variety of pellet mills. Capsule, vial, and blister pack filling operations could also be considered low-pressure compaction processes.

At the level of a manufacturing plant, the size-enlargement process involves several peripheral, unit operations such as milling, blending, drying or cooling, and classification, referred to generically as an **agglomeration circuit** (Fig. 21-84). In addition, more than one agglomeration step may be present, as in the case of pharmaceutical or detergent processes. In the case of pharmaceutical granulation,

granulated material formed by an agitative process is generally an intermediate product form, which is then followed by the compressive process of tableting. Upstream of this circuit might also involve spray-drying or crystallization of an active ingredient, or multiple granulation steps may be employed, as is the case with detergent and mineral processing, respectively.

In troubleshooting process upsets or product quality deviations, it is important to consider the high degree of interaction between the unit operations, which is much higher in the case of solids processing operations. Tableting failures might often be the result of granule properties originating in the upstream granulation step, or further still, due to production deviations of ingredients by spray-drying or crystallization, or blending and grinding steps.

Numerous benefits result from size-enlargement processes, as will be appreciated from Table 21-10. A wide variety of size-enlargement methods are available; a classification of these is given in Table 21-11 with key process attributes as well as typical subsequent processing. A primary purpose of wet granulation in the case of pharmaceutical processing is to create free-flowing, nonsegregating blends of ingredients of controlled strength, which may be reproducibly metered in subsequent tableting or for vial- or capsule-filling operations. The wet granulation process must generally achieve desired granule properties within some prescribed range. These attributes clearly depend on the application at hand. However, common to most processes is a specific granule size distribution and granule voidage. Size distribution affects flow and segregation properties as well as compaction behavior. Granule voidage controls strength, and impacts capsule and tablet dissolution behavior, as well as compaction behavior and tablet hardness. Control of granule size and voidage is discussed in detail. The approach taken here relies heavily on attempting to understand interactions at a particle level, and scaling this understanding to bulk effects. Developing an understanding of these microlevel processes of agglomeration allows a rational approach to the design, scale-up, and control of agglomeration processes. Although the approach is difficult, qualitative trends are uncovered along the way that aid in formulation development and process optimization, and that emphasize powder characterization as an integral part of product development and process design work.

MECHANICS OF SIZE-ENLARGEMENT PROCESSES

Granulation Rate Processes Granulation is controlled by four key **rate processes**, as outlined by Ennis [On the Mechanics of Granulation, Ph.D. thesis, The City College of the City University of New York, University Microfilms International No. 1416, 1990, printed 1991; *Design and Optimization of Granulation and Compaction Processes for Enhanced Product Performance*, E&G Associates, 2006; Theory of Granulation: An Engineering Perspective, in Parikh (ed.), *Handbook of Pharmaceutical Granulation Technology*, 2d ed., Taylor & Francis, 2005]. These include (1) wetting and nucleation,

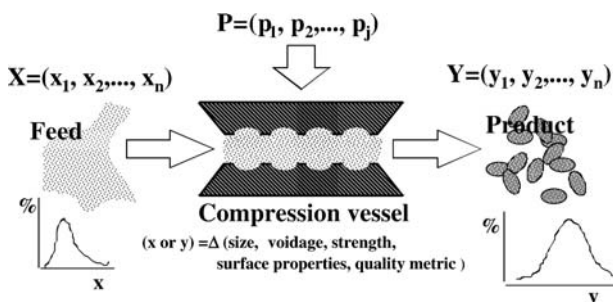


FIG. 21-83 The unit operation of compressive agglomeration, or compaction. (Reprinted from *Design and Optimization of Granulation and Compaction Processes for Enhanced Product Performance*, Ennis, 2006, with permission of E&G Associates. All rights reserved.)

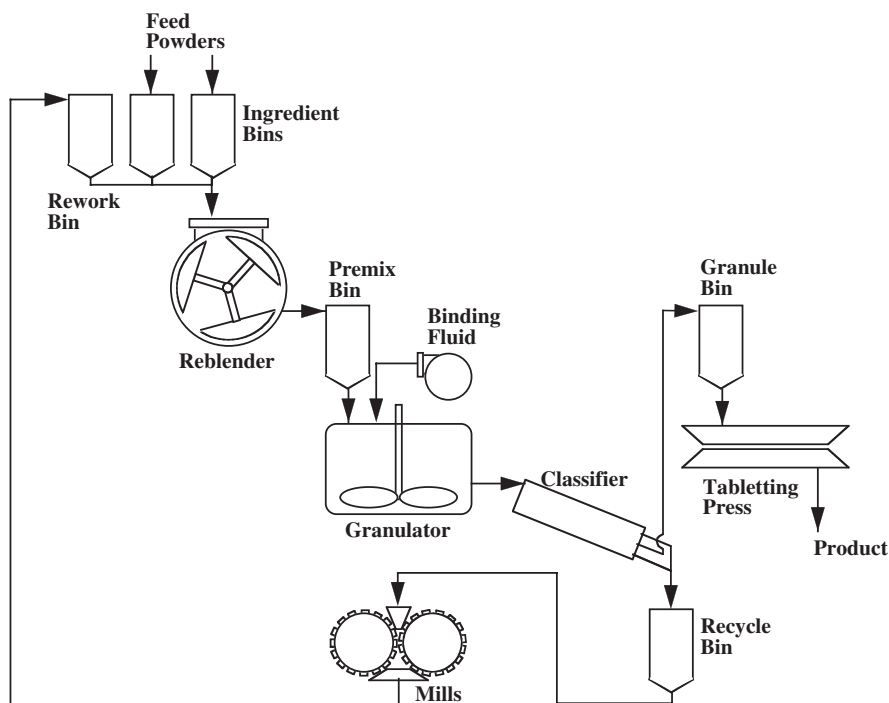


FIG. 21-84 A typical agglomeration circuit utilized in the processing of pharmaceutical or agricultural chemicals involving both granulation and compaction techniques. (Reprinted from *Design and Optimization of Granulation and Compaction Processes for Enhanced Product Performance*, Ennis, 2006, with permission of E&G Associates. All rights reserved.)

(2) coalescence or growth, (3) consolidation and densification, and (4) breakage or attrition (Fig. 21-85). Initial **wetting** of the feed powder and existing granules by the binding fluid is strongly influenced by spray rate or fluid distribution as well as feed formulation properties, in comparison with mechanical mixing. Wetting promotes **nucleation** of fine powders, or **coating** in the case of feed particle size in excess of drop size. Often wetting agents such as surfactants are carefully chosen to enhance poorly wetting feeds. In the **coales-**

cence or **growth** stage, partially wetted primary particles and larger nuclei coalesce to form granules composed of several particles. The term **nucleation** is typically applied to the initial coalescence of primary particles in the immediate vicinity of the larger wetting drop, whereas the more general term of **coalescence** refers to the successful collision of two granules to form a new, larger granule. In addition, the term **layering** is applied to the coalescence or layering of granules by primary feed powder. Nucleation is promoted from some initial distribution of moisture, such as a drop distribution or from the homogenization of a fluid feed to the bed, as with high-shear mixing, or by any maldistribution fluid such as dripping nozzles or flaking of caked wall material. The nucleation process is strongly linked with the wetting stage. As granules grow, they are consolidated by compaction forces due to bed agitation. This **consolidation** or densification stage strongly influences internal granule voidage or granule porosity, and therefore end-use properties such as granule strength, hardness, or dissolution. Formed granules may be particularly susceptible to **attrition** if they are inherently weak or if flaws develop during drying.

These mechanisms can occur simultaneously in all granulation operations, ranging from spray-drying to fluidized beds to high-shear mixers. However, certain mechanisms may dominate in a particular process. For example, fluidized-bed granulators are strongly influenced by the wetting process, whereas mechanical redispersion of binding fluid by impellers and particularly high-intensity choppers diminish the wetting contributions to granule size in high-shear mixing. On the other hand, granule consolidation is far more pronounced in high-shear mixing than fluidized-bed granulation. These simultaneous rate processes taken as a whole—and sometimes competing against one another—determine the final granule size distribution and granule structure and voidage resulting from a process, and therefore the final end-use or product quality attributes of the granulated product.

TABLE 21-10 Objectives of Size Enlargement

Production of useful structural forms, as in pressing of intricate shapes in powder metallurgy.
Provision of a defined quantity to facilitate dispensing and metering, as in agricultural chemical granules or pharmaceutical tablets.
Elimination of dust-handling hazards or losses, as in briquetting of waste fines.
Improved product appearance, or product renewal.
Reduced caking and lump formation, as in granulation of fertilizer.
Improved flow properties, generally defined as enhanced flow rates with improved flow rate uniformity, as in granulation of pharmaceuticals for tableting or ceramics for pressing.
Increased bulk density for storage and tableting feeds.
Creation of nonsegregating blends of powder ingredients with ideally uniform distribution of key ingredients, as in sintering of fines for steel or agricultural chemical or pharmaceutical granules.
Control of solubility, as in instant food products.
Control of porosity and surface-to-volume ratio, as with catalyst supports.
Improvement of heat-transfer characteristics, as in ores or glass for furnace feed.
Remove of particles from liquid, as with polymer additives, which induce clay flocculation.

Reprinted from *Design and Optimization of Granulation and Compaction Processes for Enhanced Product Performance*, Ennis, 2006, with permission of E&G Associates. All rights reserved.

TABLE 21-11 Size Enlargement Methods and Application

Method	Product size (mm)	Granule density	Scale of operation	Additional comments and processing	Typical applications
Tumbling granulators Drums Discs	0.2–20	Moderate	0.5–800 tons/h	Very spherical granules Fluid-bed or rotary kiln drying	Fertilizers, iron and other ores, agricultural chemicals
Mixer-granulators Continuous high-shear (e.g., Shugi mixer) Batch high-shear (e.g., vertical mixer)	0.1–0.5 0.1–2	Low Moderate to high	Up to 50 tons/h Up to 500-kg batch	Handles cohesive materials, both batch and continuous, as well as viscous binders and nonwetable powders Fluid-bed, tray, or vacuum/ microwave on-pot drying	Chemicals, detergents, clays, carbon black Pharmaceuticals, ceramics, clays
Fluidized granulators Fluidized beds Spouted beds Wurster coaters	0.1–1	Low (agglomerated) Moderate (layered)	100–900 kg batch 50 tons/h continuous	Flexible, relatively easy to scale, difficult for nonwetable powders and viscous binders, good for coating applications Same vessel drying, air handling requirements	Continuous: fertilizers, inorganic salts, food, detergents Batch: pharmaceuticals, agricultural chemicals, nuclear wastes
Centrifugal granulators	0.3–3	Moderate to high	Up to 200-kg batch	Powder layering and coating applications. Fluid-bed or same-pot drying	Pharmaceuticals, agricultural chemicals
Spray methods Spray drying Prilling	0.05–0.2 0.7–2	Low Moderate		Morphology of spray-dried powders can vary widely. Same vessel drying	Instant foods, dyes, detergents, ceramics, pharmaceuticals Urea, ammonium nitrate
Pressure compaction Extrusion Roll press Tablet press Molding press Pellet mill	>0.5 >1 10	High to very high	Up to 5 tons/h Up to 50 tons/h Up to 1 ton/h	Very narrow size distributions, very sensitive to powder flow and mechanical properties Often subsequent milling and blending operations	Pharmaceuticals, catalysts, inor- ganic chemicals, organic chemi- cals, plastic preforms, metal parts, ceramics, clays, minerals, animal feeds
Thermal processes Sintering	2–50	High to very high	Up to 100 tons/h	Strongest bonding	Ferrous and nonferrous ores, cement clinker, minerals, ceramics
Liquid systems Immiscible wetting in mixers Sol-gel processes Pellet flocculation	<0.3	Low	Up to 10 tons/h	Wet processing based on flocculation properties of particulate feed, subsequent drying	Coal fines, soot, and oil removal from water Metal dicarbide, silica hydrogels Waste sludges and slurries

Reprinted from *Design and Optimization of Granulation and Compaction Processes for Enhanced Product Performance*, Ennis, 2006, with permission of E&G Associates. All rights reserved.

Compaction Microlevel Processes Compaction is a forming process controlled by mechanical properties of the feed in relationship to applied stresses and strains. Microlevel processes are controlled by particle properties such as friction, hardness, size, shape, surface energy, and elastic modulus (Fig. 21-86). The performance of compaction techniques is controlled by the ability of the particulate phase to uniformly **transmit stress**, and the relationship between applied stress and the compaction and strength characteristics of the final compacted particulate phase.

Key steps in any compaction process include (1) powder filling or feeding, (2) stress application and removal, and (3) compact ejection in the case of confined compression techniques. Powder filling and compact weight variability are strongly influenced by bulk density and powder flowability (cf. subsection “Solids Handling”), as well as any contributing segregation tendencies of the feed. The steps of **stress application** and **removal** consist of several competing mechanisms, as depicted in Fig. 21-86. Powders do not transmit stress uniformly. Wall friction impedes the applied load, causing a drop in stress as one moves away from the point of the applied load, e.g., a punch face in tableting or roll surface in roll pressing. Therefore, the applied load and resulting density are not uniform throughout the compact, and powder frictional properties control the **stress transmission** and distribution in the com-

compact [cf. subsection “Bulk Powder Characterization” in Brown and Richards, *Principles of Powder Mechanics*, Pergamon Press Ltd., Oxford, 1970; Stanley-Wood (ed.), *Enlargement and Compaction of Particulate Solids*, Butterworth & Co. Ltd., 1983]. For a local level of applied stress, particles deform at their point contacts, including plastic deformation for forces in excess of the particle surface **hardness**. This allows intimate contact at surface point contacts, allowing cohesion/adhesion to develop between particles, and therefore interfacial bonding, which is a function of their **interfacial surface energy**. During the short time scale of the applied load, any entrapped air must escape, which is a function of feed **permeability**, and a portion of the elastic strain energy is converted to permanent plastic deformation. Upon stress removal, the compact expands due to remaining elastic recovery of the matrix, which is a function of **elastic modulus**, as well as any expansion of remaining entrapped air. This can result in loss of particle bonding and flaw development, and this is exacerbated for cases of wide distributions in compact stress due to poor stress transmission. The final step of stress removal involves **compact ejection**, where any remaining radial elastic stresses are removed. If recovery is substantial, it can lead to capping or delamination of the compact.

These microlevel processes of compaction control the final flaw and density distribution throughout the compact, whether it is a roll

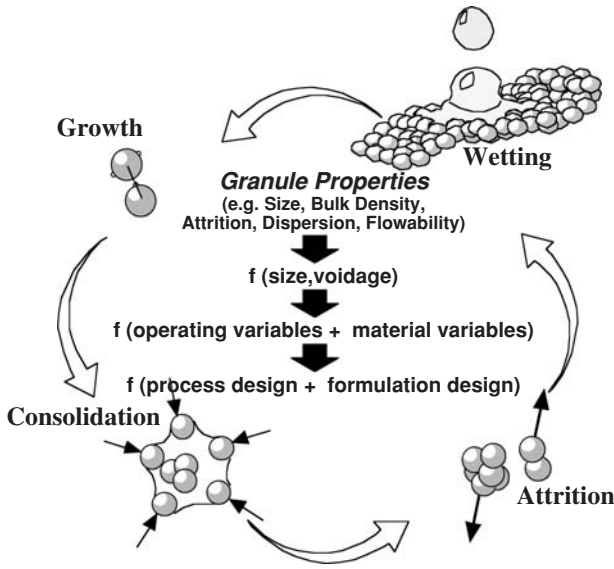


FIG. 21-85 The rate processes of agitative agglomeration, or granulation, which include powder wetting, granule growth, granule consolidation, and granule attrition. These processes combined control granule size and porosity, and they may be influenced by formulation or process design changes. (Reprinted from Design and Optimization of Granulation and Compaction Processes for Enhanced Product Performance, Ennis, 2006, with permission of E&G Associates. All rights reserved.)

pressed, extruded, or tableted product, and as such, control compact strength, hardness, and dissolution behavior.

Process vs. Formulation Design The end-use properties of granulated material are primarily controlled by granule size and inter-

nal granule **voidage** or **porosity**. Internal granule voidage ϵ_g and bed voidage ϵ_b , or voidage between granules, are related by

$$\rho_b = \rho_g(1 - \epsilon_b) = \rho_s(1 - \epsilon_b)(1 - \epsilon_g) \quad (21-95)$$

where ρ_b , ρ_g , and ρ_s are bulk, granule (or apparent), and skeletal primary particle density, respectively. Here, granule voidage and granule porosity are used interchangeably. Granule structure may also influence properties. Similar linkages exist in the case of compaction processes where hardness, voidage, and distribution of compact voidage are critical. To achieve a desired product quality as defined by metrics of end-use properties, granule size and voidage or compact properties may be manipulated by changes in either process operating variables or product material variables (Figs. 21-85 and 21-86), as initially outlined by Ennis (loc. cit., 2005, 2006). The first approach is the realm of traditional **process engineering**, whereas the second is **product engineering**. Both approaches are critical and must be integrated to achieve a desired endpoint in product quality. **Operating variables** are defined by the chosen granulation technique and peripheral processing equipment, as illustrated for a fluidized-bed and mixer-granulator in Fig. 21-87. In addition, the choice of agglomeration technique dictates the **mixing pattern** of the vessel. **Material variables** include parameters such as binder viscosity, surface tension, feed particle size distribution, powder friction, wall friction and lubrication, hardness, elastic modulus, and the adhesive properties of the solidified binder. Material variables are specified by the choice of ingredients, or **product formulation**. Both operating and material variables together define the granulation kinetic mechanisms and rate constants of wetting, growth, consolidation, and attrition, or the compaction processes for compressive techniques. Overcoming a given size-enlargement problem often requires changes in both processing conditions and product formulation.

The importance of granule voidage or density to final product quality is illustrated in Figs. 21-88 to 21-90 for a variety of formulations. Here, bulk density is observed to decrease, granule attrition to increase, and dissolution rate to increase with an increase in granule voidage. Bulk density is clearly a function of both granule size distribution, which controls bed voidage or porosity between granules, and

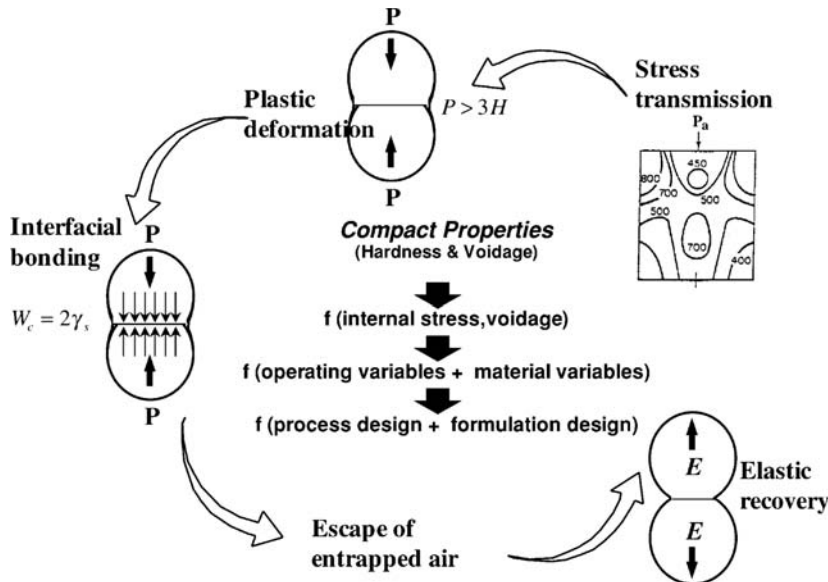
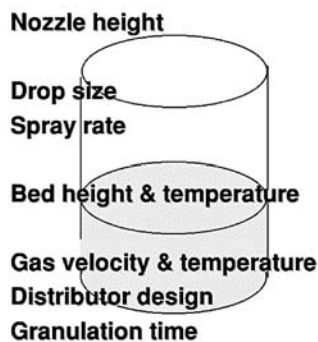


FIG. 21-86 The microlevel processes of compressive agglomeration, or compaction. These processes combined control compact strength, hardness, and porosity, and they may be influenced by formulation or process design changes. (Reprinted from Design and Optimization of Granulation and Compaction Processes for Enhanced Product Performance, Ennis, 2006, with permission of E&G Associates. All rights reserved.)

Batch Fluid-Bed Granulator



Batch High-Shear Granulator

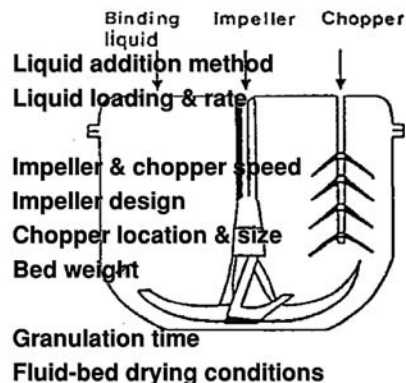


FIG. 21-87 Typical operating variable for granulation processes. (Reprinted from Design and Optimization of Granulation and Compaction Processes for Enhanced Product Performance, Ennis, 2006, with permission of E&G Associates. All rights reserved.)

the voidage within the granule itself. The data of Fig. 21-88 are normalized with respect to its zero-intercept, or its effective bulk density at zero granule voidage. The granule attrition results of Fig. 21-89 are based on a CIPAC test method, which is effectively the percentage of fines passing a fine mesh size following attrition in a tumbling apparatus. Granules weaken with increased voidage. The dissolution results of Fig. 21-90 measure the length required for granule dissolution in a long tube, or disintegration length also based on CIPAC test method. Increased granule voidage results in increased dissolution rate and shorter disintegration length. All industries have their own specific quality and in-process evaluation tests. However, what they have in common are the important contributing effects of granule size and granule voidage.

An example of the importance of distinguishing the effects of process and formulation changes can be illustrated with the help of Figs. 21-89 and 21-90. Let us assume the particular formulation and current process conditions produce a granulated material with a given attrition resistance and dissolution behavior (indicated as *current product*). If one desires instead to reach a given *target*, either formulation or process variables may be changed. Changes to the process, or operating variables, generally readily alter granule voidage. Examples to decrease voidage might include increased bed height, increased processing time, or increased peak bed moisture. However, only a range of such changes in voidage, and therefore attrition resistance and dissolution, are possible. The various curves in Figs. 21-89 and 21-90 are due to changes in formulation properties. Therefore, it may

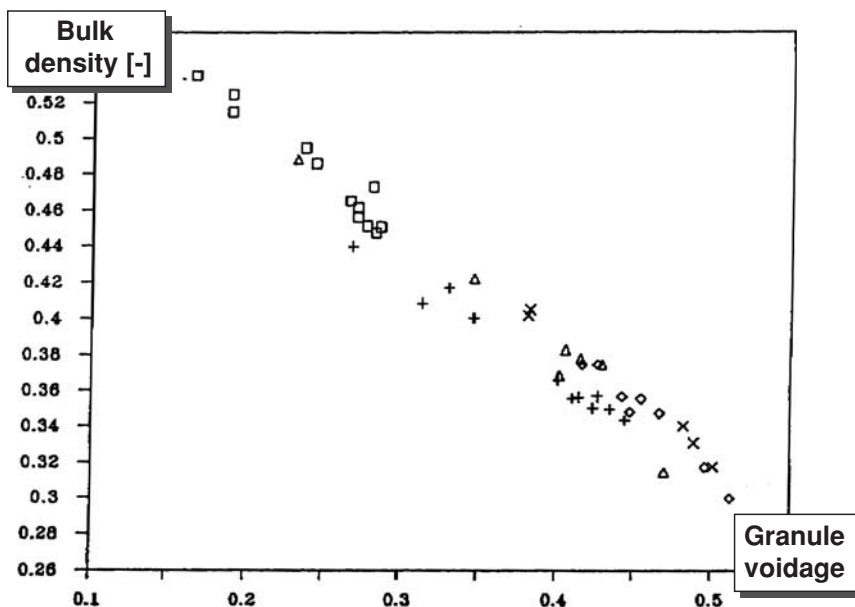


FIG. 21-88 Impact of granule voidage on bulk density. Normalized bulk density as a function of granule voidage. (After Maroglou, reprinted from Design and Optimization of Granulation and Compaction Processes for Enhanced Product Performance, Ennis, 2006, with permission of E&G Associates. All rights reserved.)

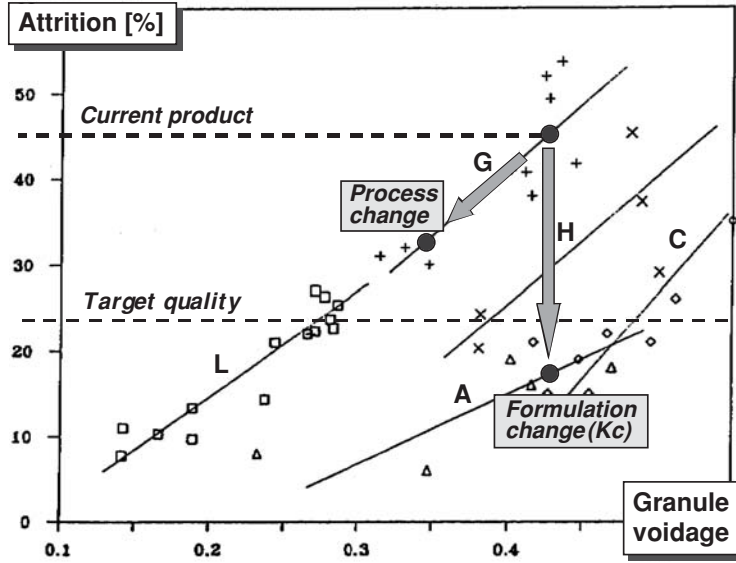


FIG. 21-89 Impact of granule voidage on strength and attrition. Illustration of process changes vs. formulation changes. (After Maroglou, reprinted from Design and Optimization of Granulation and Compaction Processes for Enhanced Product Performance, Emis, 2006, with permission of E&G Associates. All rights reserved.)

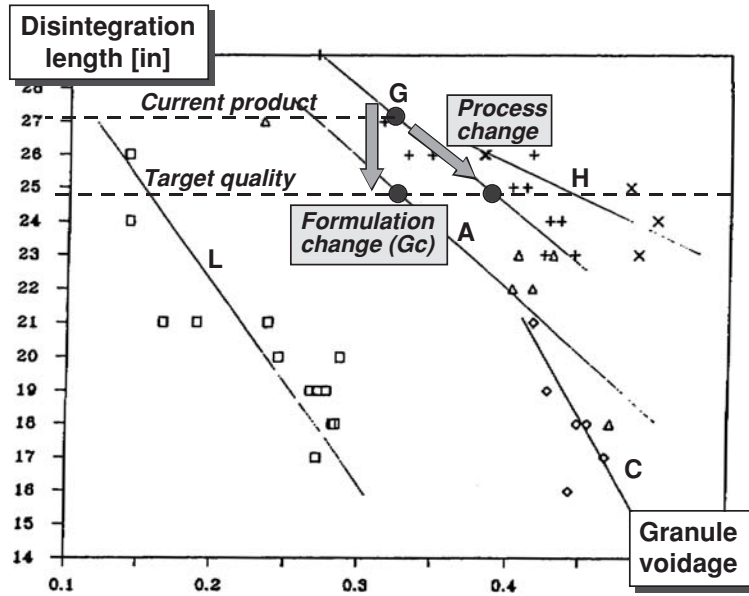


FIG. 21-90 Impact of granule voidage on dissolution. (After Maroglou, reprinted from Design and Optimization of Granulation and Compaction Processes for Enhanced Product Performance, Emis, 2006, with permission of E&G Associates. All rights reserved.)

not be possible to reach a target change in dissolution without changes in formulation, or material variables. Examples of a key material variable affecting voidage would include feed primary particle size, inherent formulation bond strength, and binder solution viscosity, as discussed in detail in the following subsections. This critical interaction between and manipulation of operating and material variables is crucial for successful formulation development, and requires substantial collaboration between processing and formulation groups and a clear knowledge of the effect of scale-up on this interaction.

Key Historical Investigations A range of historical investigations have been undertaken involving the impact of operating variables on granulation behavior [cf. Ennis, loc. cit., 1991, 2006; Ennis, *Powder Technol.*, **88**, 203 (1996); Litster and Ennis, *The Science and Engineering of Granulation Processes*, Kluwer Academic Publishers, 2005; Parikh (ed.), *Handbook of Pharmaceutical Granulation Technology*, 2d ed., Taylor & Francis, 2005; Turton et al., *Fluidized Bed Coating and Granulation*, Noyes Publications, 1999, p. 331; Pietsch, *Size Enlargement by Agglomeration*, Wiley, Chichester, 1992]. Typical variables have included the effects of bed hydrodynamics and agitation intensity, pan angle and speed, fluid-bed excess gas velocity, mixer impeller and chopper speeds, drum rotation speed, spray method, drop size, nozzle location, and binder and solvent feed rates. While such studies are important, their general application and utility to studies beyond the cited formulations and process conditions can be severely limited. Often the state of mixing, moisture distribution and rates, and material properties such as formulation size distribution, powder frictional properties, and solution viscosity are insufficiently defined. As such, these results should be used judiciously and with care. Often even the directions of the impact of operating variables on granule properties are altered by formulation changes.

Two key pieces of historical investigation require mention. The first involves growth and breakage mechanisms that control the evolution of the granule size distribution [Sastry and Fuerstenau, *Agglomeration '77*, Sastry (ed.), AIME, New York, 1977, p. 381], as illustrated in Fig. 21-91. These include the nucleation of existing fine powder to form initial primary granules, the coalescence of existing granules, and the layering of raw material onto previously formed nuclei or granules. Granules may be simultaneously compacted by consolidation and reduced

in size by breakage. There are strong interactions between these rate processes. In addition, these mechanisms in various forms have been incorporated into population balances modeling to predict granule size in the work of Sastry (loc. cit.) and Kapur [*Adv. Chem. Eng.*, **10**, 55 (1978); *Chem. Eng. Sci.*, **26**, 1093 (1971); *Ind. Eng. Chem. Eng. (Proc. Des. & Dev.)*, **5**, 5 (1966); *Chem. Eng. Sci.*, **27**, 1863 (1972)]. See subsection "Modeling and Simulation of Grinding Processes" for details. Given the progress made in connecting rate constants to formulation properties, the utility of population balance modeling has increased substantially.

The second important area of contribution involves the work of Rumpf [*The Strength of Granules and Agglomerates*, Knepper (ed.), *Agglomeration*, Interscience, New York, 1962, pp. 379–414; and *Particle Adhesion*, Sastry (ed.), *Agglomeration '77*, AIME, New York, 1977, pp. 97–129], which studied the impact of interparticle force H on granule static tensile strength, or

$$\sigma_T = \frac{9}{8} \left(\frac{1 - \epsilon_g}{\epsilon_g} \right) \frac{H}{a^2} = A \left(\frac{1 - \epsilon_g}{\epsilon_g} \right) \frac{\gamma \cos \theta}{a} \quad (21-96)$$

with $A = 9/4$ for pendular state
 $A = 6$ for capillary state

Forces of a variety of forms were studied, including viscous, semisolid, solid, electrostatic, and van der Waals forces. Of particular importance was the contribution of pore filling force between primary particles of size a arising from surface tension γ with a contact angle θ . This force summed over the granule area results in a granule static tensile strength σ_T , which is a function of pore saturation S as experimentally plotted (Fig. 21-92, with $U = 0$). The states of pore filling have been defined as pendular (single bridges), funicular (partial complete filling and single bridges), capillary (nearly complete filling $S \sim 80$ to 100 percent), followed by drop formation and loss of static strength. This approach is extended in subsequent subsections to include viscous forces and dynamic strength behavior ($U \neq 0$).

The approach taken here follows that of Rumpf and Kapur, namely, relating granule and particle level interactions to bulk behavior through the development of the rate processes of wetting and nucleation, granule growth and consolidation, and granule breakage and attrition.

PRODUCT CHARACTERIZATION

Powders are agglomerated to modify physical or physicochemical properties. Effective measurement of **agglomerate properties** is vital. However, many tests are industry-specific and take the form of empirical indices based on standardized protocols. Such tests as described below are useful for quality control, if used with care. However, since they often reflect an end use rather than a specific defined agglomerate property, they often are of little developmental utility for recommending process or formulation changes. Significant improvements have been made in the ability to measure real agglomerate properties. Key agglomerate properties are **size**, **porosity**, and **strength** and their associated distributions because these properties directly affect end-use attributes of the product, such as attrition resistance, flowability, bulk solid permeability, wettability and dispersibility, appearance, or the active agent release rate.

Size and Shape Agglomerate **mean size** and **size distribution** are both important properties. (See "Particle-Size Analysis"). For granular materials, sieve analysis is the most common sizing technique. Care is needed in sizing wet granules. Handling during sampling and sieving can cause changes in the size distribution through coalescence or breakage. Sieves are also easily blinded. Snap freezing the granules with liquid nitrogen prior to sizing overcomes these problems [Hall, *Chem. Eng. Sci.*, **41**, 187 (1986)]. **On-line** or **in-line measurement** of granules as large as 9 mm is now available by laser diffraction techniques, making improved granulation control schemes possible (Ogunnaike et al., *I.E.C. Fund.*, 1996). Modern methods of rapid imaging also provide a variety of shape assessments (see "Particle-Size Analysis").

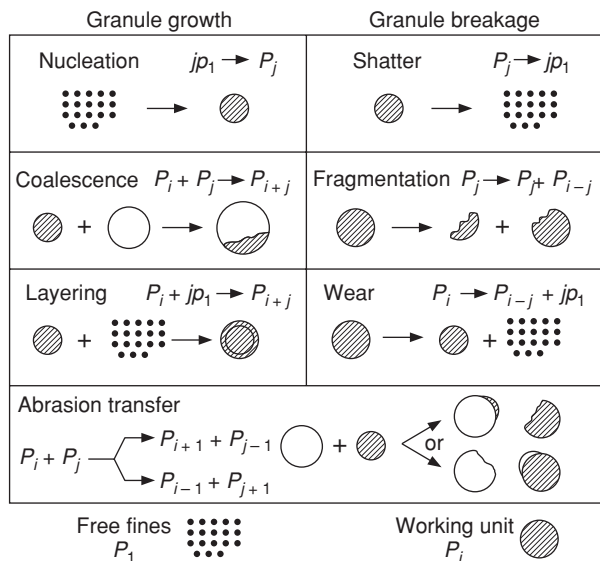


FIG. 21-91 Growth and breakage mechanisms in granulation processes. [After Sastry and Fuerstenau, *Agglomeration '77*, Sastry (ed.), AIME, New York, 1977, p. 381.]

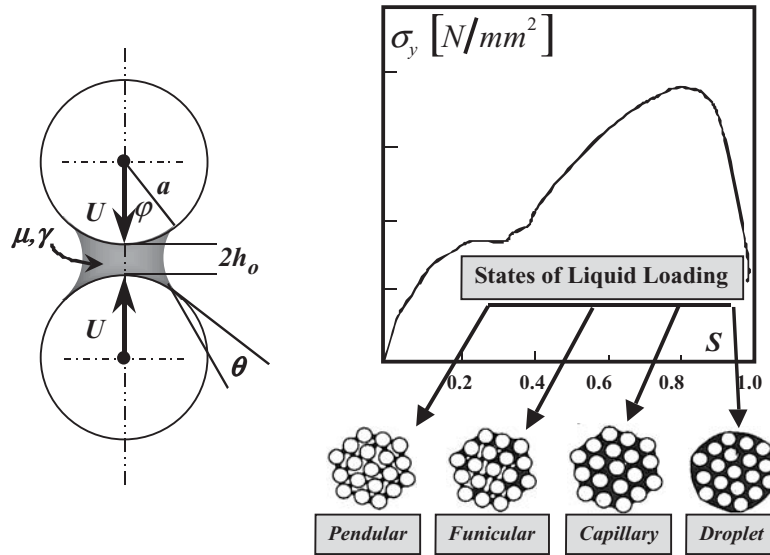


FIG. 21-92 Static yield strength of wet agglomerates versus pore saturation (collisional velocity $U = 0$). Here a is the size of a primary particle within the granule, and S is pore saturation resulting from the filling angle ϕ . [After Rumpf (*loc. cit.*), reprinted from Design and Optimization of Granulation and Compaction Processes for Enhanced Product Performance, Ennis, 2006, with permission of E&G Associates. All rights reserved. Also, Newitt and Conway-Jones, Trans. Inst. Chem. Engineers (London), **36**, 422 (1958)].

Porosity and Density There are three important densities of granular or agglomerated materials: **bulk density** ρ_b (related to the volume occupied by the bulk solid), the apparent or **agglomerate density** ρ_a (related to the volume occupied by the agglomerate including internal porosity), and the true or **skeletal solids density** ρ_s . These densities are related to one another and the interagglomerate **voidage** ϵ_b and the intraagglomerate **porosity** ϵ_g [Eq. (21-96)].

Bulk density is easily measured from the volume occupied by the bulk solid and is a strong function of sample preparation. True density is measured by standard techniques using liquid or gas pycnometry. Apparent (agglomerate) density is difficult to measure directly. Hinkley et al. [*Int. J. Min. Proc.*, **41**, 53–69 (1994)] describe a method for measuring the apparent density of wet granules by kerosene displacement. Agglomerate density may also be inferred from direct measurement of true density and porosity by using Eq. (21-96).

Agglomerate porosity can be measured by gas adsorption or mercury porosimetry. However, any breakage or compression of the granules under high pressure during porosimetry will invalidate the results. Often raw curves must be carefully analyzed to correct for penetration between granules and possible deformation. Some progress has also been made in the use of tomography to evaluate pore structure and distribution from X-ray images (Farber et al., *Powder Technol.*, **132**, 57 (2003)).

Strength of Agglomerates Agglomerate bonding mechanisms may be divided into five major groups [Rumpf, in Knepper (ed.), *Agglomeration*, op. cit., p. 379]. More than one mechanism may apply during a given size-enlargement operation. (In addition, see Krupp [*Adv. Colloid. Int. Sci.*, **1**, 111 (1967)] for a review of adhesion mechanisms.)

Solid bridges can form between particles by the sintering of ores, the crystallization of dissolved substances during drying as in the granulation of fertilizers, and the hardening of bonding agents such as glue and resins.

Mobile liquid binding produces cohesion through interfacial forces and capillary suction. Three states can be distinguished in an assembly of particles held together by a mobile liquid (Fig. 21-92).

Small amounts of liquid are held as discrete lens-shaped rings at the points of contact of the particles; this is the **pendular state**. As the liquid content increases, the rings coalesce and there is a continuous network of liquid interspersed with air; this is the **funicular state**. When all the pore spaces in the agglomerate are completely filled, the **capillary state** has been reached. When a mobile liquid bridge fails, it constricts and divides without fully exploiting the adhesion and cohesive forces in the bridge in the absence of viscous effects. Binder viscosity markedly increases the strength of the pendular bridge due to dynamic lubrication forces, and aids the transmission of adhesion. For many systems, viscous forces outweigh interfacial capillary effects, as demonstrated by Ennis et al. [*Chem. Eng. Sci.*, **45**, 3071 (1990)].

In the limit of high viscosity, **immobile liquid bridges** formed from materials such as asphalt or pitch fail by tearing apart the weakest bond. Then adhesion and/or cohesion forces are fully exploited, and binding ability is much larger.

Intermolecular and electrostatic forces bond very fine particles without the presence of material bridges. Such bonding is responsible for the tendency of particles less than about 1 mm in diameter to form agglomerates spontaneously under agitation. With larger particles, however, these short-range forces are insufficient to counterbalance the weight of the particle, and adhesion does not occur without applied pressure. High compaction pressures act to plastically flatten interparticle contacts and substantially enhance short-range forces.

Mechanical interlocking of particles may occur during the agitation or compression of, for example, fibrous particles, but it is probably only a minor contributor to agglomerate strength in most cases.

Equation (21-96) gives the tensile strength of an agglomerate of equal-sized spherical particles for an interparticle bonding force H (Rumpf, *loc. cit.*, p. 379). Figure 21-93 indicates values of tensile strength to be expected in various size-enlargement processes for a variety of binding mechanisms. In particular, note that viscous mechanisms of binding (e.g., adhesives) can exceed capillary effects in determining agglomerate strength.

Strength Testing Methods Compressed agglomerates often fail in **tension** along their diameter. This is the basis of the commonly

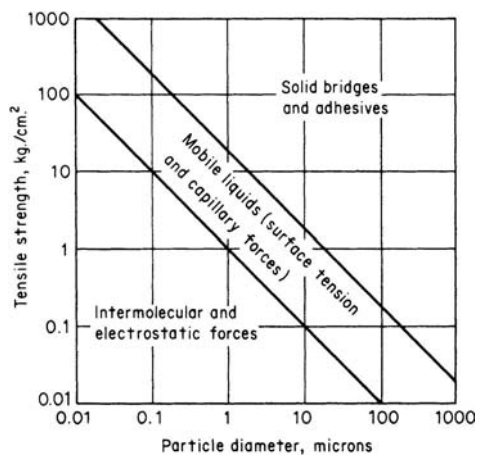


FIG. 21-93 Theoretical tensile strength of agglomerates. [Adapted from Rumpf, "Strength of Granules and Agglomerates," in Knepper (ed.), *Agglomeration*, Wiley, New York, 1962.]

used measurement of **crushing strength** of an agglomerate as a method to assess tensile strength. However, the brittle failure of a granule depends on the flaw distribution as well as the inherent tensile strength of bonds as given by the Griffith crack theory (Lawn, *Fracture of Brittle Solids*, 2d ed., Cambridge University Press, 1975). Therefore, it is more appropriate to characterize granule strength by **fracture toughness** K_{IC} [Kendall, *Nature*, **272**, 710 (1978); see also subsections "Theoretical Background" and "Breakage and Attrition"].

Several strength-related indices are measured in different industries which give some measure of resistance to attrition. These tests do not measure strength or toughness directly, but rather the size distribution of fragments after handling the agglomerates in a defined way. The handling could be repeated drops, tumbling in a drum, fluidizing, circulating in a pneumatic conveying loop, etc. These indices should only be used for quality control if the test procedure simulates the actual handling of the agglomerates during processing and transportation.

Flow Property Tests **Flowability** of the product granules can be characterized by **unconfined yield stress** and **angle of friction** by shear cell tests as used generally for bulk solids (see subsection "Powder Compaction"). **Caking** refers to deterioration in the flow properties of the granules due to chemical reaction or hydroscopic effects. Caking tests as used for fertilizer granules consist of two parts [Bookey and Raistrick, in Sauchelli (ed.), *Chemistry and*

Technology of Fertilizers, p. 454 year]. A cake of the granules is first formed in a compression chamber under controlled conditions of humidity, temperature, etc. The crushing strength of the cake is then measured to determine the degree of caking.

The propensity to cake may also be assessed by caking and thermal **dilatometry**, which assess compaction of powder and thermal softening under a variety of loading, temperature, and humidity conditions [Ennis et al., *Chem. Engg. Progress* (2007)].

Redispersion Tests Agglomerated products are often **redispersed** in a fluid by a customer. Examples include the dispersion of fertilizer granules in spray-tank solutions or of tablets within the gastrointestinal tract of the human body. The mechanisms comprising this redispersion process of product **wetting**, agglomerate **disintegration**, and final **dispersion** are related to interfacial properties (for details, see subsection "Wetting"). There are a wide range of industry-specific empirical indices dealing with redispersion assessment.

Disintegration height tests consist of measuring the length required for complete agglomerate disintegration in a long, narrow tube. Small fragments may still remain after initial agglomerate disintegration. The residual of material which remains undispersed is measured by a related test, or **long-tube sedimentation test**. The residual undispersed material is reported by the level in the bottom tip of the tube. A variation of this test is the **wet screen test**, which measures the residual remaining on a fine mesh screen (e.g., 350 mesh) following pouring the beaker solution through the screen.

Tablet-disintegration tests consist of cyclical immersion in a suitable dissolving fluid of pharmaceutical tablets contained in a basket. Acceptable tablets disintegrate completely by the end of the specified test period (*United States Pharmacopeia*, 17th rev., Mack Pub. Co., Easton, Pa., 1965, p. 919).

Permeability **Bulk solid permeability** is important in the iron and steel industry where gas-solid reactions occur in the sinter plant and blast furnace. It also strongly influences compaction processes, where entrapped gas can impede compaction, and solids-handling equipment, where restricted gas flow can impede product flowability. The permeability of a granular bed is inferred from measured pressure drop under controlled gas-flow conditions.

Physicochemical Assessments A variety of methods remain to assess both the chemical and physical nature of granulated and compacted product. Some of these include nitrogen adsorption measurements of surface area; adsorption isotherm measures of humidity and gas interactions; surface chemical assessment by inverse gas chromatography and near infrared and Rauman spectroscopy; X-ray powder diffraction measurements of polymorphism; and measurements of electrostatic charge. [See Parikh (ed.), *Handbook of Pharmaceutical Granulation Technology*, 2d ed., Taylor & Francis, 2005; Stanley-Wood (ed.), *Enlargement and Compaction of Particulate Solids*, Butterworth & Co. Ltd., 1983.]

AGGLOMERATION RATE PROCESSES AND MECHANICS

GENERAL REFERENCES: Adetayo et al., *Powder Technol.*, **82**, 37 (1995). Benbow and Bridgwater, *Paste Flow and Extrusion*, Oxford University Press, 1993. Brown and Richards, *Principles of Powder Mechanics*, Pergamon Press, 1970. Ennis, *Design and Optimization of Granulation and Compaction Processes for Enhanced Product Performance*, E&G Associates, Nashville, Tenn., 2006. Ennis, On the Mechanics of Granulation, Ph.D. thesis, 1990, The City College of the City University of New York, University Microfilms International, 1991. Ennis et al., *Powder Technol.*, **65**, 257 (1991). Ennis and Sunshine, *Tribology Int.*, **26**, 319 (1993). Ennis, *Powder Technol.*, June 1996. Holm et al. Parts V and VI, *Powder Technol.*, **43**, 213–233 (1985). Kristensen, *Acta Pharm. Suec.*, **25**, 187 (1988). Lawn, *Fracture of Brittle Solids*, 2d ed., Cambridge University Press, 1975. Litster and Ennis, *The Science and Engineering of Granulation Processes*, Kluwer Academic Publishers, 2005. Owens and Wendt, *J. Appl. Polym. Sci.*, **13**, 1741 (1969). Parfitt (ed.), *Dispersion of Powders in Liquids*, Elsevier Applied Science Publishers Ltd., 1986. Parikh (ed.), *Handbook of Pharmaceutical Granulation Technology*, 2d ed., Taylor & Francis, 2005. Stanley-Wood (ed.), *Enlargement and Compaction of Particulate Solids*, Butterworth & Co. Ltd., 1983.

WETTING

The initial distribution of binding fluid can have a pronounced influence on the size distribution of seed granules or **nuclei** that are formed from fine powder. Both the final **extent** of and **rate** at which the fluid wets the particulate phase are important. Poor wetting results in drop coalescence and fewer, larger nuclei with ungranulated powder and overwettered masses, leading to broad nuclei distributions. Granulation can retain a memory, with nuclei size distribution impacting final granule size distribution. Therefore, initial wetting can be critical to uniform nuclei formation and often a narrow, uniform product. Wide nuclei distributions can lead to wide granule-size distributions. When the size of a particulate feed material is larger than drop size, wetting dynamics controls the distribution of **coating** material, which has a strong influence on the later stages of growth. Wetting phenomena also influence redistribution of individual ingredients

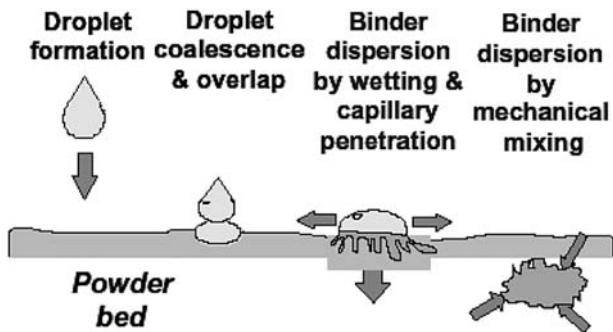


FIG. 21-94 Stages of wetting for fine powder compared to drop size.

within a granule, drying processes, and redispersion of granules in a fluid phase. Other granule properties such as voidage, strength, and attrition resistance may be influenced as well. **Preferential wetting** of certain formulation ingredients can cause component segregation with granule size. Extensive reviews of wetting research are available [Parfitt (ed.), *Dispersion of Powders in Liquids*, Elsevier Applied Science Publishers Ltd., 1986; Hapgood, *Nucleation and Binder Dispersion in Wet Granulation*, Ph.D. thesis, University of Queensland, 2000].

Mechanics of the Wetting Rate Process As outlined previously, wetting is the first stage in wet granulation involving liquid binder distribution to the feed powder. There are two extremes: (1) Liquid drop size is large compared to unit or primary particle size of the feed, and (2) particle size is large compared to the drop size. For the first case as depicted in Fig. 21-94 for fine feeds compared to drop size, the wetting process consists of several steps. First, droplets are formed related to spray distribution, or spray flux defined as the wetting area of the bed per unit time. Important operating variables include nozzle position, spray area, spray rate, and drop size. Second, droplets impact and coalesce on the powder bed surface if mixing or wet-in time is slow. Third, droplets spread and penetrate into the moving powder bed to form loose nuclei, again coalescing if wet-in is slow. In the case of high-shear processes, shear forces break down overwet clumps, also producing nuclei. For the second case of small drop size compared to the primary particle size, the liquid will coat the particles as depicted in Fig. 21-95. Coating is produced by collisions between the drop and the particle followed by spreading of the liquid over the particle surface. If the particle is porous, then liquid will also suck into the pores by capillary action. The wetting dynamics control the distribution of coating material, which has a strong influence on the later stages of growth as well as coating quality.

Methods of Measurement Methods of characterizing the rate process of wetting include four approaches, as illustrated in Table 21-12. The first considers the ability of a drop to spread across the powder. This approach involves the measurement of a **contact angle** of a drop on a powder compact. The contact angle is a measure of the affinity of the fluid for the solid as given by the Young-Dupré equation, or

$$\gamma^{sv} - \gamma^{sl} = \gamma^{lv} \cos \theta \tag{21-97}$$

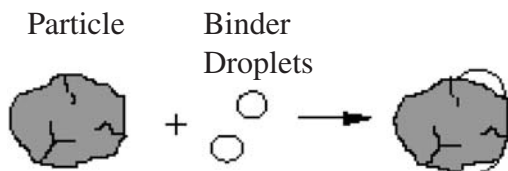


FIG. 21-95 Stages of wetting for coarse powder compared to drop size.

where γ^{sv} , γ^{sl} , and γ^{lv} are the solid-vapor, solid-liquid, and liquid-vapor interfacial energies, respectively, and θ is the contact angle measured through the liquid, as illustrated in Fig. 21-96. When the solid-vapor interfacial energy exceeds the solid-liquid energy, the fluid wets the solid with a contact angle less than 90° . In the limit of $\gamma^{sv} - \gamma^{sl} \geq \gamma^{lv}$, the contact angle equals 0° and the fluid **spreads** on the solid. The extent of wetting is controlled by the group $\gamma^{lv} \cos \theta$, which is referred to as the **adhesion tension**. Sessile drop studies of contact angle can be performed on powder compacts in the same way as on planar surfaces. As illustrated in Fig. 21-97, methods involve (1) direct measurement of the contact angle from the tangent to the air-binder interface, (2) solution of the Laplace-Young equation involving the contact angle as a boundary condition, or (3) indirect calculations of the contact angle from measurements of, e.g., drop height. Either the compact can be saturated with the fluid for static measurements, or dynamic measurements may be made through a computer imaging goniometer (Pan et al., *Dynamic Properties of Interfaces and Association Structure*, American Oil Chemists' Society Press, 1995).

For granulation processes, the dynamics of wetting are often crucial, requiring that powders be compared on the basis of a short time scale, **dynamic contact angle**. Important factors are the physical nature of the powder surface (particle size, pore size, porosity, environment, roughness, pretreatment). Powders which are **formulated** for granulation often are composed of a combination of ingredients. The dynamic wetting process is therefore influenced by the rates of ingredient dissolution and surfactant adsorption and desorption kinetics (Pan et al., loc. cit.).

The second approach to characterize wetting considers the ability of the fluid to penetrate a powder bed, as illustrated in Fig. 21-98. It involves the measurement of the extent and rate of fluid rise by capillary suction into a column of powder, better known as the **Washburn test**. Considering the powder to consist of capillaries of radius R , the equilibrium height of rise h_e is determined by equating capillary and gravimetric pressures, or

$$h_e = \frac{2\gamma^{lv} \cos \theta}{\Delta\rho gR} \tag{21-98a}$$

where $\Delta\rho$ is the fluid density with respect to air, g is gravity, and $\gamma^{lv} \cos \theta$ is the adhesion tension as before. In addition to the equilibrium height of rise, the dynamics of penetration can be equally important. By ignoring gravity and equating viscous losses with the capillary pressure, the rate dh/dt and dynamic height of rise h are given by

$$\frac{dh}{dt} = \frac{R\gamma^{lv} \cos \theta}{4\mu h} \quad \text{or} \quad h = \sqrt{\left(\frac{R\gamma^{lv} \cos \theta}{2\mu}\right)t} \tag{21-98b}$$

where t is time and μ is binder fluid viscosity [Parfitt (ed.), *Dispersion of Powders in Liquids*, Elsevier Applied Science Publishers Ltd., 1986, p. 10]. The grouping of terms in parentheses involves the material properties which control the dynamics of fluid penetration, namely, average pore radius, or **tortuosity** R (related to particle size and void distribution of the powder), adhesion tension, and binder viscosity.

The contact angle or adhesion tension of a binder solution with respect to a powder can be determined from the slope of the penetration profile. Washburn tests can also be used to investigate the

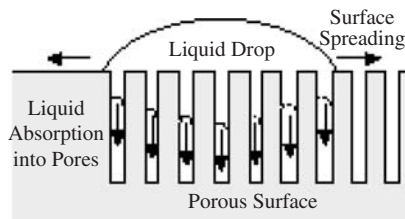
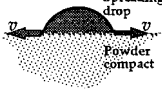
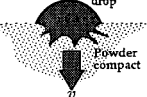
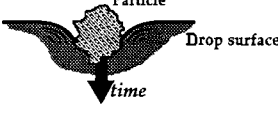
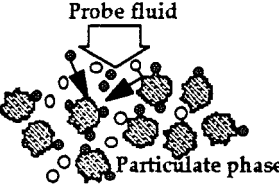


TABLE 21-12 Methods of Characterizing Wetting Dynamics of Particulate Systems

Mechanism of wetting	Characterization method
Spreading of drops on powder surface 	Contact angle goniometer Contact angle Drop height or volume Spreading velocity References: Kossen and Heertjes, <i>Chem. Eng. Sci.</i> , 20 , 593 (1965). Pan et al., <i>Dynamic Properties of Interfaces and Association Structure</i> , American Oil Chemists' Society Press, 1995.
Penetration of drops into powder bed 	Washburn test Rate of penetration by height or volume Bartell cell Capillary pressure difference References: Parfitt (ed.), <i>Dispersion of Powders in Liquids</i> , Elsevier Applied Science Publishers Ltd., 1986. Washburn, <i>Phys. Rev.</i> , 17 , 273 (1921). Bartell and Osterhof, <i>Ind. Eng. Chem.</i> , 19 , 1277 (1927).
Penetration of particles into fluid 	Flotation tests Penetration time Sediment height Critical solid surface energy distribution References: R. Ayala, Ph.D. thesis, Chemical Engineering, Carnegie Mellon University, 1985. Fuerstaneau et al., <i>Colloids and Surfaces</i> , 60 , 127 (1991). Vargha-Butler et al., in <i>Interfacial Phenomena in Coal Technology</i> , Botsaris & Glazman (eds.), Chap. 2, 1989.
Chemical probing of powder 	Inverse gas chromatography Preferential adsorption with probe gases Electrokinetics Zeta potential and charge Surfactant adsorption Preferential adsorption with probe surfactants References: Lloyd et al. (eds.), <i>ACS Symposium Series 391</i> , ACS, Washington, 1989. Aveyard and Haydon, <i>An Introduction to the Principles of Surface Chemistry</i> , Cambridge University Press, 1973. Shaw, <i>Introduction to Colloid and Surface Chemistry</i> , Butterworths & Co. Ltd., 1983.

Reprinted from *Design and Optimization of Granulation and Compaction Processes for Enhanced Product Performance*, Ennis, 2006, with permission of E & G Associates. All rights reserved.

influence of powder preparation on penetration rates. The **Bartell cell** is related to the Washburn test, except that here adhesion tension is determined by a variable gas pressure which opposes penetration [Bartell and Osterhof, *Ind. Eng. Chem.*, **19**, 1277 (1927)].

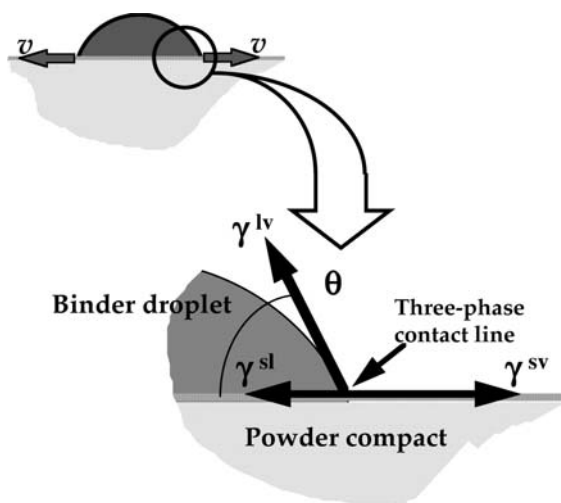


FIG. 21-96 Contact angle on a powder surface, where γ^{lv} , γ^{sl} , and γ^{sv} are the solid-vapor, solid-liquid, and liquid-vapor interfacial energies, and θ is the contact angle measured through the liquid.

The contact angle of a binder-particle system is not itself a primary thermodynamic quantity, but rather is a reflection of individual interfacial energies [Eq. 21-97], which are a function of the molecular interactions of each phase with respect to one another. An interfacial energy may be broken down into its **dispersion** and **polar** components. These components reflect the chemical character of the interface, with the polar component due to hydrogen bonding and other polar interactions and the dispersion component due to van der Waals interactions. These components may be determined by the wetting tests described here, where a variety of solvents are chosen as the wetting fluids to probe specific molecular interactions as described by Zisman [Contact Angle, Wettability, and Adhesion, *Advances in Chemistry Series*, ACS, **43**, 1 (1964)]. These components of interfacial energy are strongly influenced by trace impurities, which often arise in crystallization of the active ingredient, or other forms of processing such as grinding, and they may be modified by judicious selection of **surfactants** (R. Ayala, Ph.D. thesis, Chemical Engineering, Carnegie Mellon University, 1985). Charges may also exist at interfaces. In the case of solid-fluid interfaces, these may be characterized by **electrokinetic** studies (Shaw, *Introduction to Colloid & Surface Chemistry*, Butterworths & Co. Ltd., 1983).

The total solid-fluid interfacial energy (i.e., both dispersion and polar components) is also referred to as the **critical solid surface energy** of the particulate phase. It is equal to the surface tension of a fluid which just wets the solid with zero contact angle. This property of the particle feed may be determined by a third approach to characterize wetting, involving the penetration of particles into a series of fluids of varying surface tension [R. Ayala, Ph.D. thesis, Chemical Engineering, Carnegie Mellon University, 1985; Fuerstaneau et al., *Colloids & Surfaces*, **60**, 127 (1991)]. The critical surface energy may also be determined from the variation of sediment height with the surface tension of the solvent [Vargha-Butler et al., *Colloids & Surfaces*,

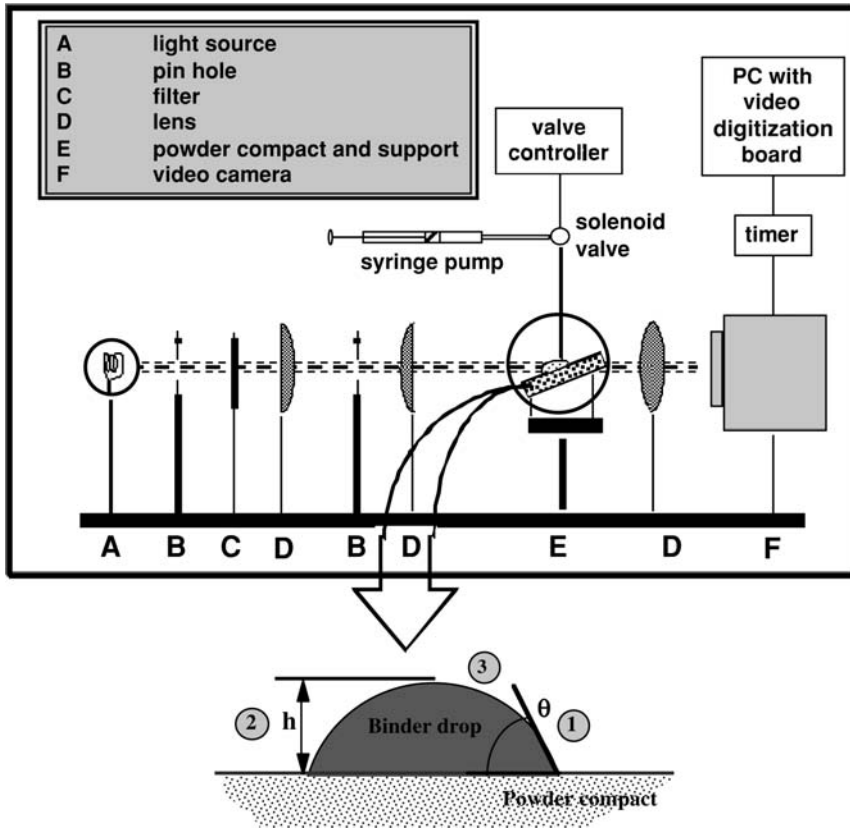


FIG. 21-97 Characterizing wetting by dynamic contact angle goniometry. (Reprinted from Design and Optimization of Granulation and Compaction Processes for Enhanced Product Performance, Ennis, 2006, with permission of E&G Associates. All rights reserved.)

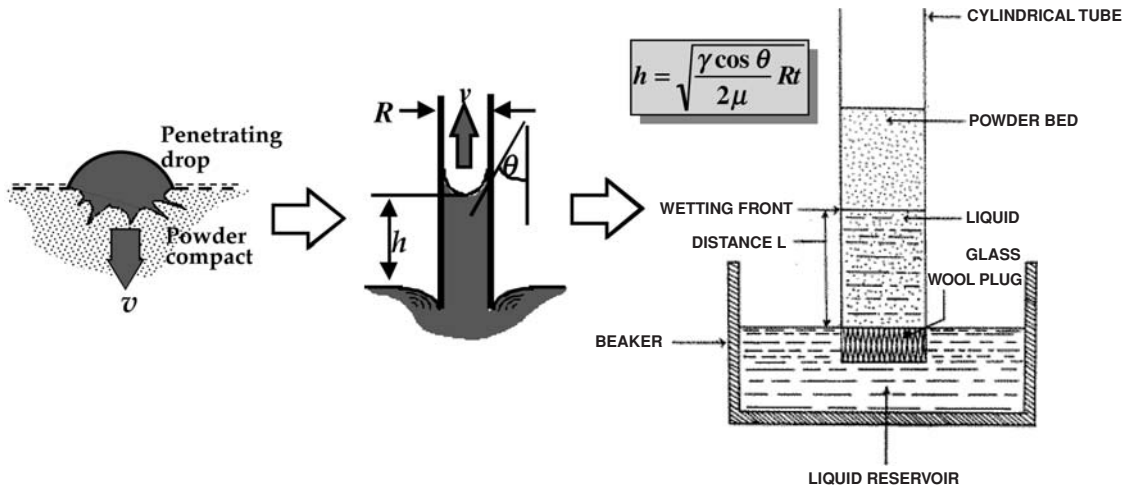


FIG. 21-98 Characterizing wetting by Washburn test and capillary rise. (Reprinted from Design and Optimization of Granulation and Compaction Processes for Enhanced Product Performance, Ennis, 2006, with permission of E&G Associates. All rights reserved.)

24, 315 (1987)]. Distributions in surface energy and its components often exist in practice, and these may be determined by the wetting measurements described here.

The last approach to characterizing wetting involves chemical probing of properties which control surface energy. As an example, **inverse gas chromatography** (IGC) uses the same principles and equipment as standard gas chromatography. In IGC, however, the mobile phase is comprised of probe gas molecules that move through a column packed with the powder of interest, which is the stationary phase. Surface energies of the powder are determined from the adsorption kinetics of both alkane and various polar probes. A distinct advantage of IGC over other methods is reproducible measurements of physical chemical surface properties, which control adhesion tension.

Examples of the Impact of Wetting Wetting dynamics have a pronounced influence on the initial nuclei distribution formed from fine powder. The influence of powder contact angle on the average size of nuclei formed in fluid-bed granulation is illustrated in Fig. 21-99, where the contact angle of the powder with respect to water was varied by changing the weight ratios of the ingredients of lactose and salicylic acid, which are hydrophilic and hydrophobic, respectively (Aulton and Banks, *Proceedings of Powder Technology in Pharmacy Conference*, Powder Advisory Centre, Basel, Switzerland, 1979). Note that granule size in this study is actually *nuclei* size, since little growth has taken place in the process. Nuclei size is seen to improve with contact angle. In addition, the x coordinate would more appropriately be replaced with adhesion tension. Aulton et al. [*J. Pharm. Pharmacol.*, **29**, 59P (1977)] also demonstrated the influence of surfactant concentration on shifting nuclei size due to changes in adhesion tension.

Figure 21-100a illustrates an example of dynamic wetting, where a drop is imaged as it wets in to a formulation tablet. The time scale of wetting is 2 s, with nearly complete wet-in occurring in 1 s. This particular formulation was granulated on a continuous pan system in excess of 2 tons/h. Figure 21-100b compares differences in lots of the formulation. Note that a second lot, referred to as problem technical, experiences significantly degraded granule strength and reduction in production rates. This is associated with nearly twice the initial con-

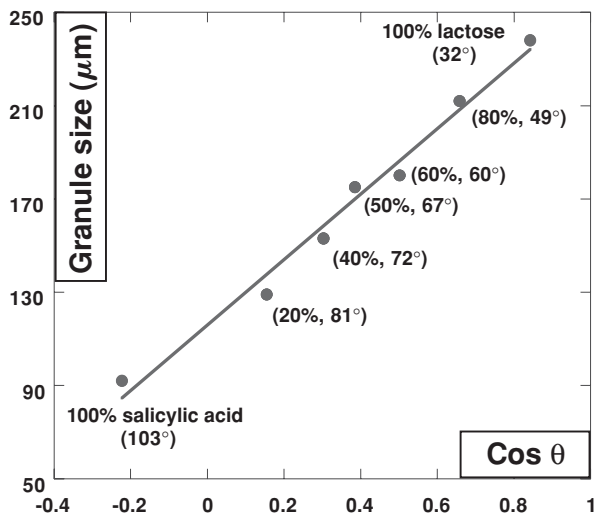


FIG. 21-99 The influence of contact angle on nuclei size formed in fluid-bed granulation of lactose/salicylic acid mixtures. Formulations ranged from hydrophobic (100% salicylic acid) to hydrophilic (100% lactose). Powder contact angle θ determined by goniometry and percent lactose of each formulation are given in parentheses. (Aulton and Banks, *Proceedings of Powder Technology in Pharmacy Conference*, Powder Advisory Centre, Basel, Switzerland, 1979.)

tact angle (120°) and slower-spreading velocity when compared with the good technical. Poor wetting in practice can translate to reduced production rates to compensate for increased time for drops to work into the powder bed surface. Weaker granules are also often observed, since poor wetting leads to repulsive bonding and high granule voidage. Note that differences in the lots are only observed over the first $\frac{1}{4}$ to $\frac{1}{2}$ s, illustrating the importance of comparing dynamic behavior of formulations, after which time surfactant adsorption/desorption reduces contact angle.

As an example of Washburn approaches, the effect of fluid penetration rate and the extent of penetration on granule-size distribution for drum granulation was shown by Gluba et al. [*Powder Hand. & Proc.*, **2**, 323 (1990)]. Increasing penetration rate, as reflected by Eq. (21-98b), increased granule size, and decreased asymmetry of the granule-size distribution as shown in Fig. 21-101.

Regimes of Nucleation and Wetting Two key features control this wetting and nucleation process. One is the time required for a drop to wet into the moving powder bed, in comparison to some circulation time of the process. As discussed previously, this wet-in time is strongly influenced by formulation properties [e.g., Eq. (21-98b)]. The second is the actual spray rate or spray flux, in comparison to solids flux moving through the spray zones. Spray flux is strongly influenced by manufacturing and process design.

One can envision that drop penetration time and spray flux define **regimes of nucleation** and wetting. If the wet-in is rapid and spray fluxes are low, individual drops will form discrete nuclei somewhat larger than the drop size, defining a **droplet-controlled regime**. At the other extreme, if drop penetration is slow and spray flux is large, drop coalescence and pooling of binder material will occur throughout the powder bed, which must be broken down by mechanical dispersion. In this **mechanical dispersion regime** of nucleation, shear forces control the breakdown of wetting clumps, independent of drop distribution.

Following between these two extreme regimes, drop overlap and coalescence occur to varying extent, defining an **intermediate regime** of nucleation, being a function of penetration time and spray flux. To better define wetting, particularly in the sense of process engineering and scale-up, we consider drop penetration or wet-in time and spray flux in greater detail.

Beginning with penetration time, Eq. (21-98b) defines key formulation properties controlling capillary rise in powder beds. From considering a distribution of macro- and micropores in the moving powder bed as shown in Fig. 21-102, Hapgood (loc. cit.) determined a total drop penetration time t_p of

$$t_p = 1.35 \frac{V_d^{2/3}}{\epsilon_{\text{eff}}^2} \left(\frac{\mu}{R_{\text{eff}} \gamma \cos \theta} \right) \quad (21-99)$$

As shown previously, drop wet-in time decreases with increasing pore radius R_{eff} , decreasing binder viscosity and increasing adhesion tension. In addition, drop penetration time decreases with decreasing drop size V_d and increasing bed porosity ϵ_{eff} . Effective pore radius R_{eff} is related to the surface-volume average particle size d_{32} , particle shape, and effective porosity of packing ϵ_{eff} by

$$R_{\text{eff}} = \frac{\phi d_{32}}{3} \left(\frac{\epsilon_{\text{eff}}}{1 - \epsilon_{\text{eff}}} \right) \quad (21-100)$$

To remain within a droplet-controlled regime of nucleation, the penetration time given by Eq. (21-99) should be much less than some characteristic circulation time t_c of the granulator in question. Circulation time is a function of mixing and bed weight, and it can change with scale-up.

In the case of spray flux, Fig. 21-103 illustrates an idealized powder bed of width B moving past a flat spray of spray rate dV/dt at a solids velocity of w . For a given spray rate, the number of drops is determined by drop volume, which in turn defines the drop area a per unit time that will be covered by the spray, giving a spray flux of

$$\frac{da}{dt} = \frac{dV/dt}{V_d} \left(\frac{\pi d_d^2}{4} \right) = \frac{3}{2} \frac{dV/dt}{d_d} \quad (21-101)$$

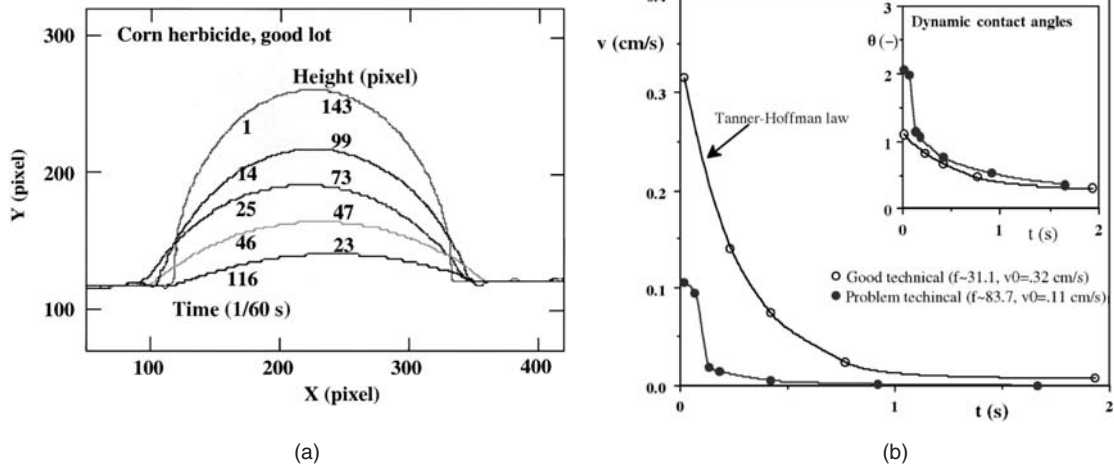


FIG. 21-100 Dynamic imaging of wetting, and its impact on continuous pan granulation. (a) Dynamic images of a drop wetting into a formulation with good active ingredient. (b) Comparison of surface spreading velocity and dynamic contact angle versus time for good and bad active ingredients or technical. (Reprinted from Design and Optimization of Granulation and Compaction Processes for Enhanced Product Performance, Ennis, 2006, with permission of E&G Associates. All rights reserved.)

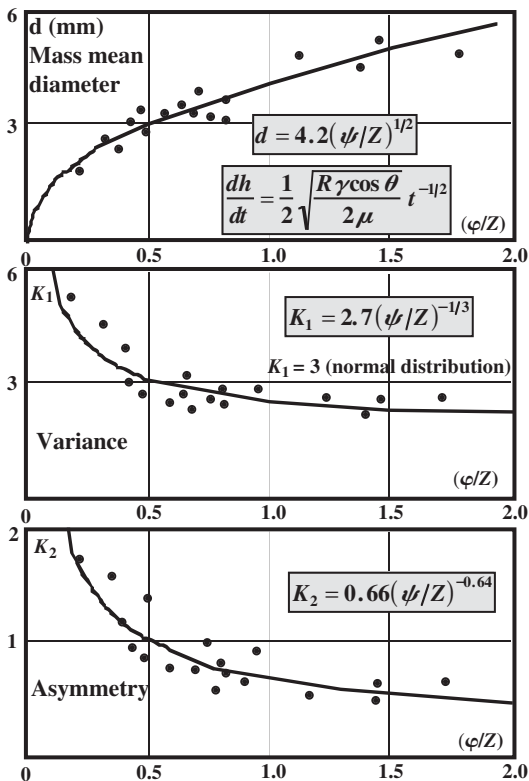


FIG. 21-101 Influence of capillary penetration on drum granule size. Increasing penetration rate increases granule size and decreases asymmetry of the granule-size distribution. [After Gluba et al., Powder Hand. & Proc., 2, 323 (1990).]

As droplets contact the powder bed at a certain rate, the powder moves past the spray zone at its own velocity, or at solids flux given for this simple example by

$$\frac{dA}{dt} = Bw \tag{21-102}$$

The ratio of the droplet spray flux to the solids flux defines a dimensionless spray flux given by

$$\psi_a = \frac{da/dt}{dA/dt} = \frac{3}{2} \frac{dV/dt}{d_s(dA/dt)} \tag{21-103}$$

The dimensionless spray flux is the ratio of the rate at which wetted area is covered by droplets to the area of flux of powder through the spray zone, and it is a measure of the density of drops falling on the powder surface. As with drop penetration time, it plays a role in defining the regimes of nucleation as illustrated in Fig. 21-104. For small spray flux ($\psi_a \ll 1$), drops will not overlap on contact and will form separate discrete nuclei for fast penetration time. For large spray flux ($\psi_a \approx 1$), however, significant drop overlap occurs, forming nuclei much larger than drop size, and, in the limit, independent of drop size.

For the case of random drop deposition as described by a Poisson distribution, Hapgood (loc. cit.) showed the fraction of surface

$$R_{\text{eff}} = \frac{\varphi d_{32}}{3} \frac{\epsilon_{\text{eff}}}{1 - \epsilon_{\text{eff}}} \quad \epsilon_{\text{eff}} = \epsilon_{\text{tap}} (1 - \epsilon + \epsilon_{\text{tap}})$$

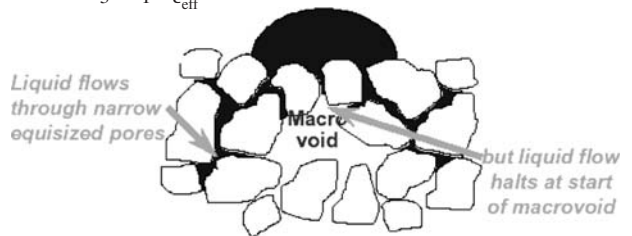


FIG. 21-102 Drop penetration in a moving powder bed. [After Hapgood (loc. cit.).]

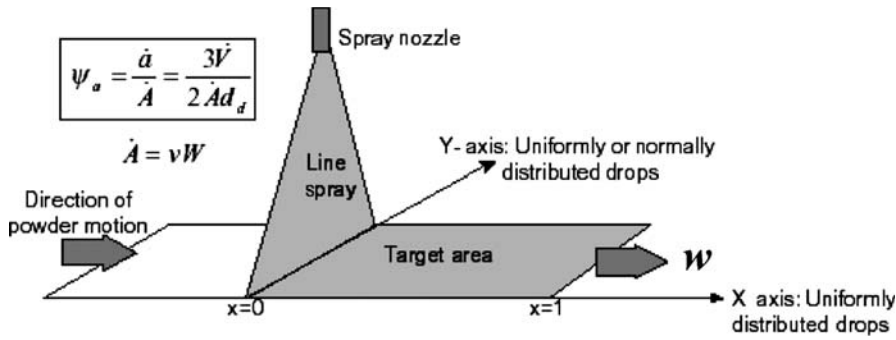


FIG. 21-103 Idealized flat spray zone in a spinning riffle granulator. [After Hapgood (loc. cit.).]

covered by spray was given by

$$f_{\text{single}} = 1 - \exp(-\psi_a) \quad (21-104)$$

In addition, the fraction of single drops forming individual nuclei (assuming rapid drop penetration) versus the number of agglomerates formed was given by

$$f_{\text{single}} = \exp(-4\psi_a) \quad (21-105)$$

$$f_{\text{agglom}} = 1 - \exp(-4\psi_a) \quad (21-106)$$

Examples of the above as applied to nucleation are depicted in Fig. 21-105. Here, nuclei distributions were studied as a function of drop size and spray flux. Lactose was sprayed with a flat spray in a spinning riffle granulator, mimicking the geometry of Fig. 21-103. For a small spray flux of $\psi_a = 0.22$, a clear relationship is seen between nuclei size and spray distribution, with nuclei formed somewhat larger than drop size. However, as the speed of the riffler is slowed (i.e., solids velocity and solids flux are decreased, and spray flux increased), the nuclei distribution widens with the formation of agglomerates.

The spray flux captures the impact of equipment operating variables on nucleation, and as such is very useful for scale-up if nucleation rates and nuclei sizes are to be maintained constant. The overall impact of dimensionless spray flux on nucleation and agglomerate formation is illustrated in Fig. 21-106, with agglomerates increasing with increased spray flux as clearly governed by Eq. (21-106) for the case of rapid drop penetration.

Regimes of nucleation may be defined (Fig. 21-107) with the help of dimensionless drop penetration time τ_p and spray flux ψ_a , or

$$\tau_p = \frac{t_p}{t_c} = \frac{\text{penetration time}}{\text{circulation time}} \quad \text{and} \quad \psi_a = \frac{da/dt}{dA/dt} \quad (21-107)$$

$$= \frac{\text{spray flux}}{\text{solids flux}}$$

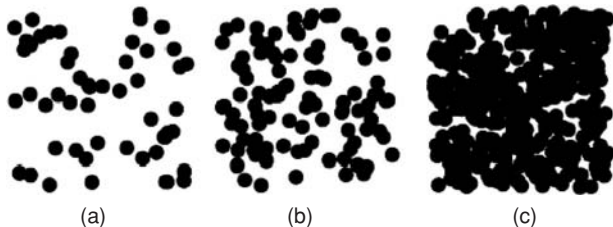


FIG. 21-104 Monte Carlo simulations of drop coverage: (a) 50 discs, $\psi_a = 0.29$, $f_{\text{covered}} = 0.26$; (b) 100 discs, $\psi_a = 0.59$, $f_{\text{covered}} = 0.45$; (c) 400 discs, $\psi_a = 2.4$, $f_{\text{covered}} = 0.91$. Image, 500 × 500 pixels; disc radius, 20 pixels. [After Hapgood (loc. cit.).]

A droplet-controlled nucleation regime occurs when there is both low spray flux (relatively few drops overlap) and fast droplet penetration—drops wet into the bed completely before bed mixing allows further drop contact. Nuclei will be formed of the order of drop size. A mechanical dispersion regime occurs at the other extreme of high spray flux, giving large drop overlap and coalescence, and large drop penetration times, promoted by poor wet-in rates and slow circulation

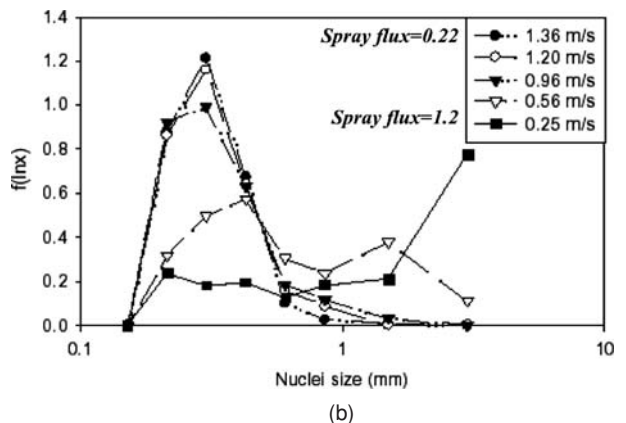
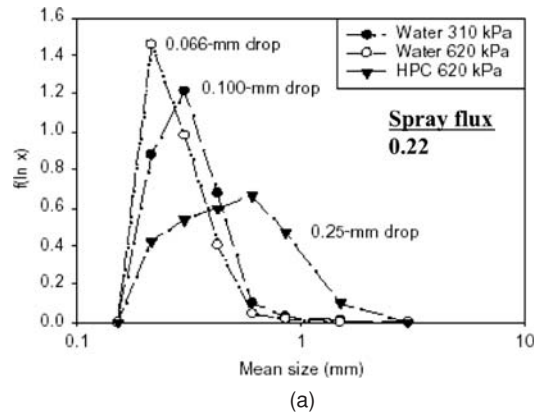


FIG. 21-105 Effect of (a) spray drop distribution (b) (low spray flux—water and HPC) and (b) powder velocity (variable spray flux—water) on nuclei size distribution. Lactose feed powder in spinning granulator. (Litster and Emnis, loc. cit.)

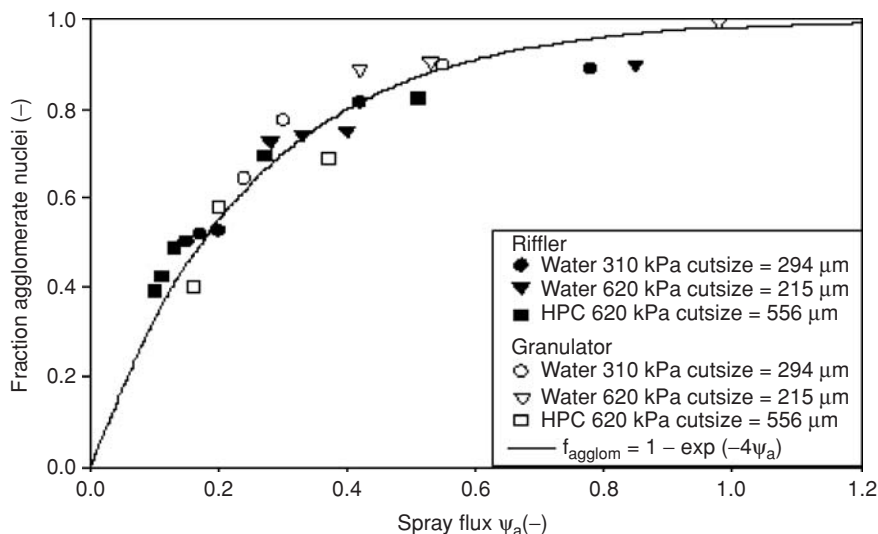


FIG. 21-106 Agglomerate formation vs. spray flux. Lactose powder with water and HPLC solutions. [After Hapgood (loc. cit.).]

times and poor mixing. In the regime, nucleation and binder dispersion occurs by mechanical agitation. Viscous, poorly wetting binders are slow to flow through pores in the powder bed in the case of poor penetration time. Drop coalescence on the powder surface occurs (also known as *pooling*), creating very broad nuclei size distributions. The binder solution delivery method (drop size, nozzle height) typically has minimal effect on the nuclei size distribution, although interfacial properties may affect nuclei and final granule strength. An intermediate regime exists for moderate drop penetration times and moderate spray flux, with the resulting nuclei regime narrowing with decreases in both.

There are several implications with regard to the nucleation regime map of Fig. 21-107 with regard to troubleshooting of wetting and nucleation problems. If drop penetration times are large, making adjustments to spray may not be sufficient to narrower granule size distributions if remaining in the mechanical regime. Significant changes to wetting and nucleation occur only if changes take the system across a regime boundary. This can occur in an undesirable way if processes are not scaled with due attention to remaining in the drop-controlled regime.

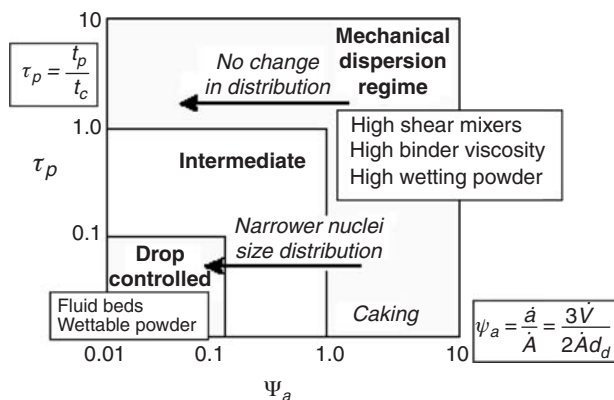


FIG. 21-107 A possible regime map of nucleation, relating spray flux, solids mixing (solids flux and circulation time), and formulation properties.

GROWTH AND CONSOLIDATION

The evolution of the granule-size distribution of a particulate feed in a granulation process is controlled by several mechanisms, as illustrated in Figs. 21-85 and 21-91. These include the **nucleation** of fine powder to form initial primary granules, the **coalescence** of existing granules, and the **layering** of raw material onto previously formed nuclei or granules. The breakdown of wet clumps into a stable nuclei distribution can also be included among coalescence mechanisms. As granules grow by coalescence, they are simultaneously compacted by **consolidation** mechanisms, which reduce internal granule voidage or porosity. Lastly, granules may be reduced in size by **breakage**. Dominant mechanisms of growth and consolidation are dictated by the relationship between critical particle properties and operating variables as well as by mixing, size distribution, and the choice of processing.

There are strong interactions between the growth and consolidation mechanisms, as illustrated for the case of drum granulation of fine feed (Fig. 21-108). Granule size progresses through three stages of growth, including rapid, exponential growth in the initial **nucleation** stage, followed by linear growth in the **transition** stage, and finishing with very slow growth in a final **balling** stage. Simultaneously with growth, granule porosity or voidage decreases with time as the granules are compacted. Granule growth and consolidation are intimately connected; increases in granule size are shown here to be associated with a decrease in granule porosity. This is a dominant theme in wet granulation.

As originally outlined in Ennis (loc. cit., 1991), these growth patterns are common throughout fluidized-bed, drum, pan, and high-shear mixer processes for a variety of formulations. Specific mechanisms of growth may dominate for a process—sometimes to the exclusion of others. However, what all processes have in common is that the prevailing mechanisms are dictated by a balance of critical particle level properties, which control formulation deformability, and operating variables, which control the local level of shear, or bed agitation intensity.

Granule Deformability In order for two colliding granules to coalesce rather than break up, the **collisional kinetic energy** must first be dissipated to prevent rebound, as illustrated in Fig. 21-109. In addition, the strength of the bond must resist any subsequent breakup forces in the process. The ability of the granules to deform during processing may be referred to as the formulation's **deformability**, and

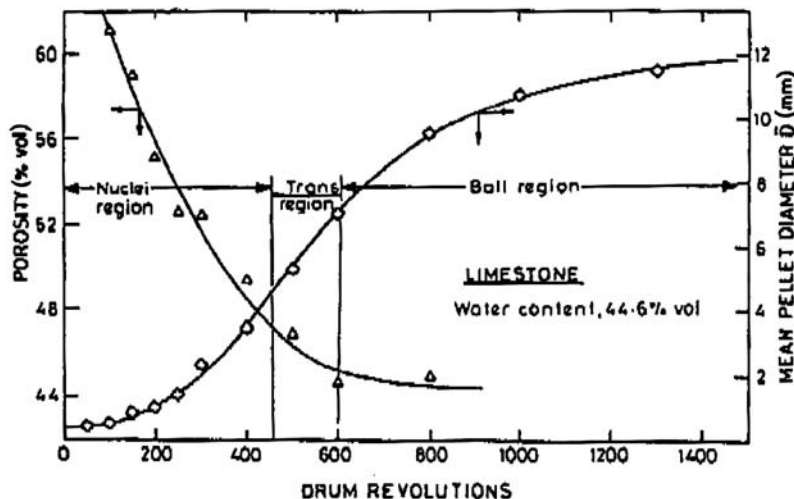


FIG. 21-108 Granule porosity and mean (pellet) size. Typical regimes of granule growth and consolidation. [After Kapur, *Adv. Chem. Eng.*, **10**, 55 (1978); *Chem. Eng. Sci.*, **26**, 1093 (1971).]

deformability has a large effect on growth rate. Increases in deformability increase the bonding or contact area, thereby dissipating and resisting breakup forces. From a balance of binding and separating forces and torque acting within the area of granule contact, Ouchiyama and Tanaka [*I&EC Proc. Des. & Dev.*, **21**, 29 (1982)] derived a **critical limit of size** above which coalescence becomes impossible, or a maximum growth limit given by

$$D_c = (AQ^{3/2}K^{3/2}\sigma_T)^{1/4 - (3/2)\eta} \quad (21-108)$$

where K is deformability, a proportionality constant relating the maximum compressive force Q to the deformed contact area; A is a constant with units of L^3/F , which relates granule volume to impact compression force; and σ_T is the **tensile strength** of the granule bond [see Eq. (21-98)]. Granules are compacted as they collide. This expels pore fluid to the granule surface, thereby increasing local liquid satu-

ration in the contact area of colliding granules. This surface fluid (1) increases the tensile strength of the liquid bond σ_T and (2) increases surface plasticity and deformability K .

Here D_c represents the largest granule that may be grown in a granulation process, and it is a harmonic *average* granule size. Therefore, it is possible for the collision of two large granules to be unsuccessful, their average being beyond this critical size, whereas the collision of a large granule and a small granule leads to successful coalescence. The growth limit D_c is seen to increase with increased formulation deformability K (which will be shown to be a strong function of moisture and primary particle-size distribution), increased compressive forces Q (which are related to local shear levels in the process), and increased tensile forces σ_T (which are related to interparticle forces). The parameters ζ and η depend on the deformation mechanism within the contact area. For plastic deformation, $\zeta = 1$, $\eta = 0$, and $K \propto 1/H$, where H is hardness. For elastic, hertzian deformation, $\zeta = 2/3$, $\eta = 2/3$, and $K \propto (1/E^*)^{2/3}$, where E^* is the reduced elastic modulus. Granule deformation is generally dominated by **inelastic** behavior of the contacts during collision, with such deformation treated by the area of inelastic **contact mechanics** (Johnson, *Contact Mechanics*, Cambridge University Press, 1985).

Types of Granule Growth The importance of deformability to the growth process depends on **bed agitation intensity**. If little deformation takes place during granule collisions, the system is referred to as a **low-deformability** or **low-agitation-intensity** process. This generally includes fluid-bed, drum, and pan granulators. Growth is largely controlled by the extent of any surface fluid layer and surface deformability, with surface fluid playing a large role in dissipating collisional kinetic energy. Growth generally occurs at a faster time scale than overall granule deformation and consolidation. This is depicted in Fig. 21-110, where smaller granules can still be distinguished as part of a larger granule structure, or a popcorn-type appearance, as often occurs in fluid-bed granulation. Note that such a structure may not be observed if layering and nucleation alone dominate with little coalescence of large granules; in addition, the surface structure may be compacted and smoother over time due to the longer time-scale process of consolidation. In this case, granule coalescence and consolidation have less interaction than they do with high-deformability systems, making low deformability–low agitation systems easier to scale and model.

For high-shear rates or bed agitation intensity, large granule deformation occurs during granule collisions, and granule growth and consolidation occur on the same time scale. Such a system is referred to

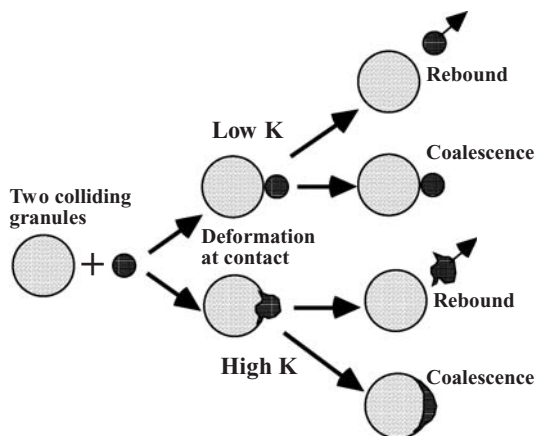


FIG. 21-109 Mechanisms of granule coalescence for low- and high-deformability systems. Rebound occurs for average granule sizes greater than the critical granule size D_c . K = deformability. (Reprinted from Design and Optimization of Granulation and Compaction Processes for Enhanced Product Performance, Ennis, 2006, with permission of E&C Associates. All rights reserved.)

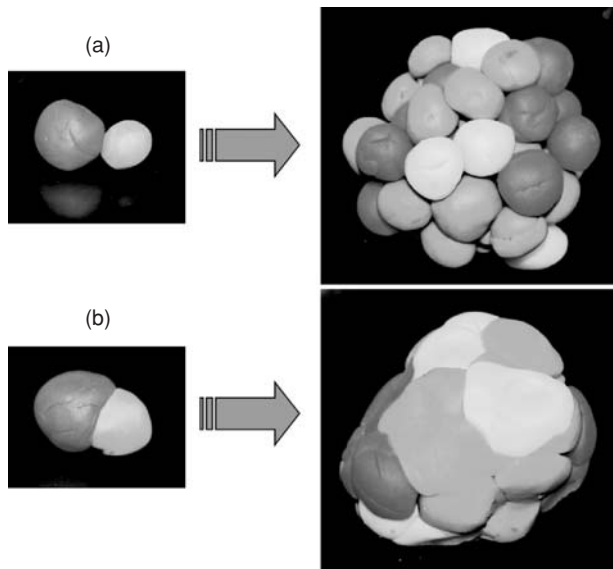


FIG. 21-110 Granule structures resulting from (a) low- and (b) high-deformability systems, typical for fluid-bed and high-shear mixer-granulators, respectively. (Reprinted from Design and Optimization of Granulation and Compaction Processes for Enhanced Product Performance, Ennis, 2006, with permission of E&G Associates. All rights reserved.)

as a **deformable** or **high-agitation-intensity** process, and this generally includes continuous pin and plow shear-type mixers, as well as batch high-shear pharmaceutical mixers. In these cases, substantial collisional kinetic energy is dissipated with deformation of the wet mass composing the granule. Rather than a *sticking-together* process

as often occurs in the low-deformability process of fluid beds, granules are *smashed* or *kneaded* together as with a high-shear mixer, and smaller granules are not distinguishable with the granule structure, as depicted in Fig. 21-110. High-agitation, highly deformable processes generally produce denser granules than low-deformability, low-agitation-intensity ones. In addition, the combined and competing effects of granule coalescence and consolidation make high-agitation processes difficult to model and scale. Both coalescence and consolidation initially increase with both increases in shear level and deformability, while at the same time as granules densify, they become less deformable, which works to lower coalescence in the later stages of growth.

Bed agitation intensity is controlled by mechanical variables of the process such as fluid-bed excess gas velocity or mixer impeller and chopper speed. Agitation intensity controls the relative collisional and shear velocities of granules within the process and therefore growth, breakage, consolidation, and final product density. Figure 21-111 summarizes typical characteristic velocities, agitation intensities and compaction pressures, and product relative densities achieved for a variety of size-enlargement processes.

Lastly, note that the process or formulation itself *cannot* uniquely define whether it falls into a low- or high-agitation-intensity process. As discussed more fully below, it is a function of *both* the level of shear and the formulation deformability. A very stiff formulation with low deformability may behave as a low-deformability system in a high-shear mixer; or a very pliable formulation may act as a high deformable system in a fluid-bed granulator.

Granule deformability and limiting size D_c are a strong function of moisture, as illustrated in Fig. 21-112. Deformability K is related to both the **yield strength** of the material σ_y , i.e., the ability of the material to resist stresses, and the ability of the surface to be strained without degradation or rupture of the granule, with this maximum allowable **critical deformation strain** denoted by $(\Delta L/L)_c$. Figure 21-113 illustrates the low-shear-rate stress-strain behavior of agglomerates during compression as a function of liquid saturation, with strain denoted by $\Delta L/L$. In general, high deformability K requires low yield strength σ_y and high critical strain $(\Delta L/L)_c$. Increasing moisture

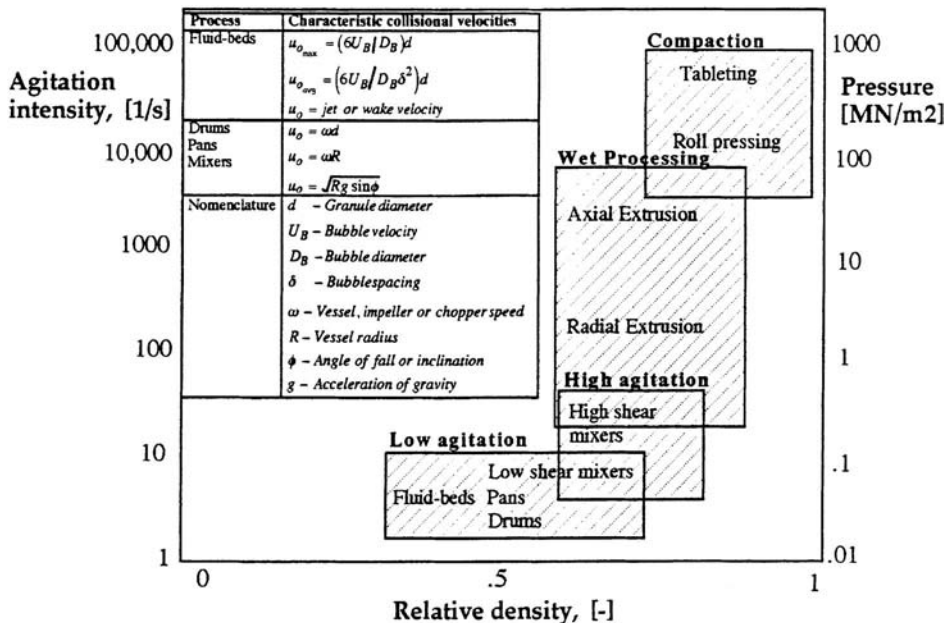


FIG. 21-111 Classification of agglomeration processes by agitation intensity and compaction pressure. (Reprinted from Design and Optimization of Granulation and Compaction Processes for Enhanced Product Performance, Ennis, 2006, with permission of E&G Associates. All rights reserved.)

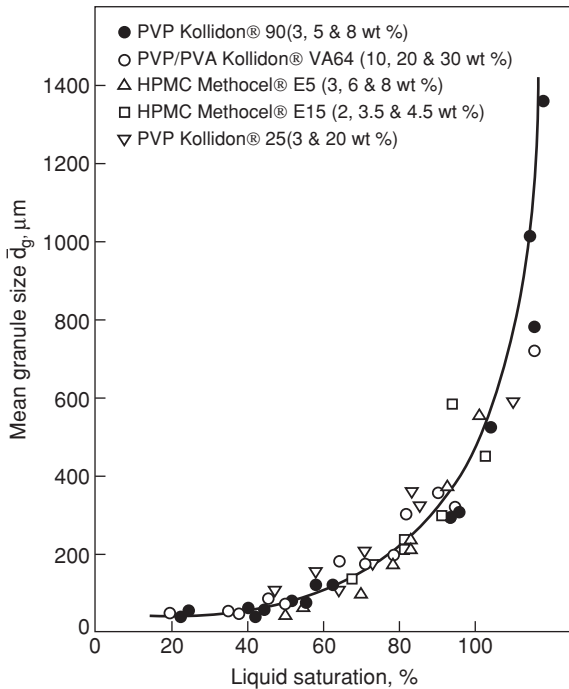


FIG. 21-112 Effect of granule saturation on mean granule diameter, indicating the marked increase in granule deformability with increased moisture. Mean granule diameter is a measure of the critical limit of size D_c . Granulation of calcium hydrogen phosphate with aqueous binder solutions in a Fielder PMAT 25 VC, high-shear mixer. [Ritala et al., Drug Dev. & Ind. Pharm., **14**(8), 1041 (1988).]

increases deformability by lowering interparticle frictional resistance, leading to an increase in mean granule size (Fig. 21-112). Saturation S is defined here as the volumetric percent of pore volume filled with moisture, with this pore volume controlled by granule porosity or voidage.

Deformability and Interparticle Forces In most cases, granule deformability increases with increasing moisture, decreasing binder viscosity, decreasing surface tension, decreasing interparticle friction, and increasing average primary particle size, as well as increasing bed agitation intensity. Interstitial fluid leads to pendular bridges between the primary particles composing a granule, giving rise to capillary and viscous interparticle forces. In addition, frictional forces develop as primary particles come into contact. Interparticle forces and their impact on deformability warrant further attention. Figure 21-114 illustrates two particles of radius a separated by a gap distance $2h_o$ (or in contact) approaching each other at a velocity U , bound by a pendular bridge of viscosity μ , density ρ , and surface tension γ . The two particles may represent two primary particles within the granule, in which case we are concerned about the contribution of interparticle forces to granule strength and deformability. Or they may represent two colliding granules, in which case we are concerned with the ability of the pendular bridge to dissipate granule kinetic energy and resist breakup forces in the granulation process. The pendular bridge consists of the binding fluid in the process, which includes the added solvent and any solubilized components. In some cases, it may also be desirable to include very fine solid components within the definition of the binding fluid and, therefore, consider instead a suspension viscosity and surface tension. These material parameters vary on a local level throughout the process and are time-dependent and a function of drying conditions.

For the case of a static liquid bridge of contact angle θ , surface tension induces an attractive capillary force F_{cap} between the two particles

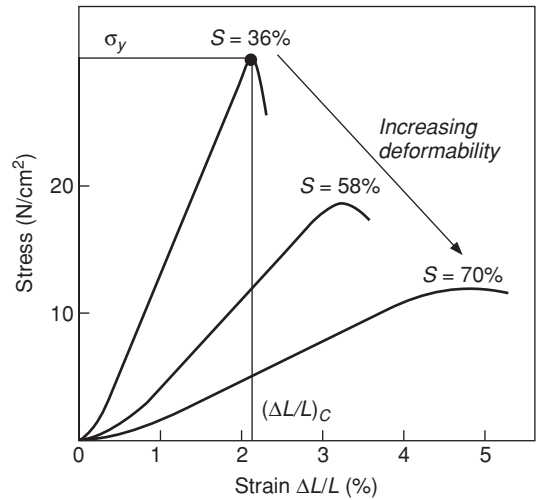


FIG. 21-113 The influence of sample saturation S on granule deformability. Deformation strain $(\Delta L/L)$ is measured as a function of applied stress, with the peak stress and strain denoted by tensile strength σ_y and critical strain $(\Delta L/L)_c$ of the material. Dicalcium phosphate with 15 wt % binding solution of PVP/PVA Kollidon® VA64, 50% compact porosity. [Holm et al., Powder Technol., **43**, 213 (1985), with kind permission from Elsevier Science SA, Lausanne, Switzerland.]

due to a three-phase contact line force and a pressure deficiency arising from interfacial curvature H_o and filling angle ϕ , given by

$$F_{cap} = \pi\gamma a (2 \cos \theta - 2H_o) \sin^2 \phi \quad (21-109)$$

The impact of this static pendular bridge force on static granule strength has been studied extensively, as illustrated in Fig. 21-92 (Ennis, loc. cit., 1991; Rumpf, loc. cit.; Kapur, loc. cit.). It is important to recognize that in most processes, however, the particles are moving relative to one another and, therefore, the bridge liquid is in motion. This gives rise to viscous lubrication forces F_{vis} that can contribute significantly to the total bridge strength, given by

$$F_{vis} = 3\pi\mu Ua/\epsilon \quad (21-110)$$

This viscous force increases with increasing binder viscosity μ and collision velocity U , and decreasing dimensionless gap distance $\epsilon = 2h_o/a$ [Ennis, loc. cit., 1991; Ennis et al., *Chem. Eng. Sci.*, **45** (10), 3071 (1990); Mazzone et al., *J. Colloid Interface Sci.*, **113**, 544 (1986)]. Written in dimensionless form, total dynamic bridge strength for newtonian fluids for particles in close contact is given by

$$F^* = \frac{1}{\pi\gamma a} (F_{cap} + F_{vis}) = F_o + 3Ca/\epsilon$$

where $F_o = (2 \cos \theta - 2H_o) \sin^2 \phi \quad (21-111)$

$$Ca = \mu U/\gamma$$

where Ca is a capillary number representing the ratio of viscous-to-capillary forces and is proportional to velocity. Dynamic bridge force consists of an initial constant, static bridge strength for small Ca (or near zero velocity) and then increases linearly with Ca (or velocity). This is confirmed experimentally as illustrated in Fig. 21-115 for the case of two spheres approaching axially. Extensions of the theory have also been conducted for nonnewtonian fluids, shearing motions, particle roughness, wettability, and time-dependent drying binders (Ennis, loc. cit., 1991).

For small velocities, small binder viscosity, and large gap distances, the strength of the bridge will approximate a static pendular bridge, or

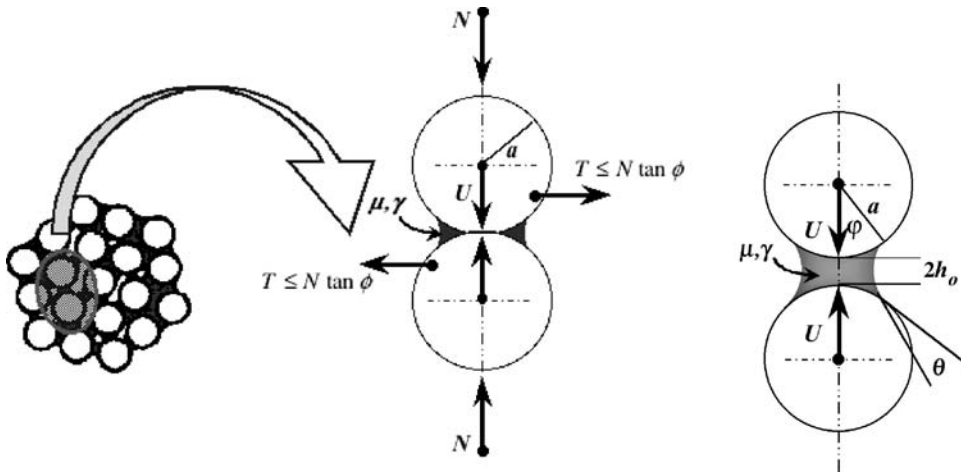


FIG. 21-114 Interparticle forces and granule deformability. Interparticle forces include capillary forces, viscous lubrication forces, and frictional forces. (Reprinted from Design and Optimization of Granulation and Compaction Processes for Enhanced Product Performance, Ennis, 2006, with permission of E&G Associates. All rights reserved.)

F_{cap} , which is proportional to and increases with increases in surface tension. This force is equivalent to the static pendular force H previously given in Eq. (21-96) as studied by Rumpf (loc. cit.). On the other hand, for large binder viscosities and velocities, or small gap distances, the bridge strength will approximately be equal to F_{vis} , which is proportional to and increases with increases in binder viscosity and velocity. This viscous force is singular in the gap distance and increases dramatically for small separation of the particles. It is important to note that as granules are consolidated, resulting in decreases in effective interparticle gap distance, and binders dry, resulting in large increases in binder viscosity, the dynamic bridge strength can exceed the static strength by orders of magnitude.

The important contributions of binder viscosity and friction to granule deformability are illustrated by fractions of energy dissipated during computer simulations of granule collisions, as depicted in Fig. 21-116.

Of the energy, 60 percent is dissipated through viscous losses, with the majority of the remainder through interparticle friction. Very little loss is due to capillary forces. Therefore, modern approaches to granule coalescence rest in understanding the impact of granule deformability on growth, rather than the original framework put for regarding pendular and funicular forces due to interparticle liquid bridges alone.

Deformability and Wet Mass Rheology The static yield stress of wet compacts has previously been reported in Fig. 21-113. However, the dependence of interparticle forces on shear rate clearly impacts **wet mass rheology** and therefore deformability. Figure 21-117 illustrates the dynamic stress-strain response of compacts, demonstrating that the peak flow or yield stress increases proportionally with compression velocity [Iveson et al., *Powder Technol.*, **127**, 149 (2002)]. Peak flow stress of wet unsaturated compacts (initially pendular state) can be seen to also increase with Ca as follows (Fig. 21-118):

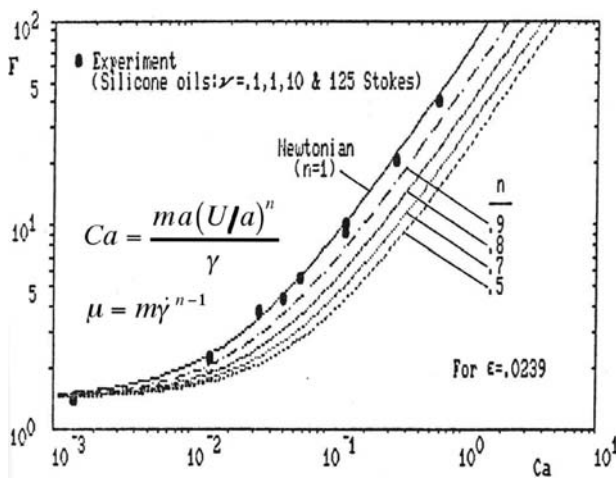


FIG. 21-115 Maximum strength of a liquid bridge between two axial moving particles as a function of Ca for newtonian and shear thinning fluids. (After Ennis, *On the Mechanics of Granulation*, Ph.D. thesis, 1990, The City College of the City University of New York, University Microfilms International, 1991, with permission.)

$$\frac{\sigma_y^{Peak}}{\gamma a} = \sigma_o + A \overline{Ca}^B \quad \text{where} \quad \sigma_o = 5.0 - 5.3$$

$$A = 280 - 320 \quad B = 0.58 - 0.64$$

$$\overline{Ca} = \mu \dot{\epsilon} a / \gamma \quad (21-112)$$

There are several important issues worth noting with regard to these results. First is the similarity between the strength of the assembly or compact [Eq. (21-112)] and the strength of the individual dynamic pendular bridge given by Eq. (21-111); both curves are similar in shape with a capillary number dependency. As with the pendular bridge, two regions may be defined. In region 1 for a bulk capillary number of $Ca < 10^{-4}$, the strength or yield stress of the compact depends on the static pendular bridge, and therefore on surface tension, particle size, and liquid loading. In region 2 for $Ca > 10^{-4}$, the strength depends on the viscous contribution to bridge strength, and therefore on binder viscosity and strain rate, in addition to particle size.

Second is that the results of Figs. 21-117 and 21-118 do not clearly depict the role of saturation and compact porosity. Decreases in compact porosity generally increase compact strength through increases in interparticle friction, whereas increases in saturation lower strength (e.g., Figs. 21-112 and 21-113 and Holm et al. [Parts V and VI, *Powder Technol.*, **43**, 213-233 (1985)]). Hence, the curve of Fig. 21-118 should be expected to shift with these variables, particularly since the viscous force for axial approach is singular in the interparticle gap distance [Eq. 21-111)].

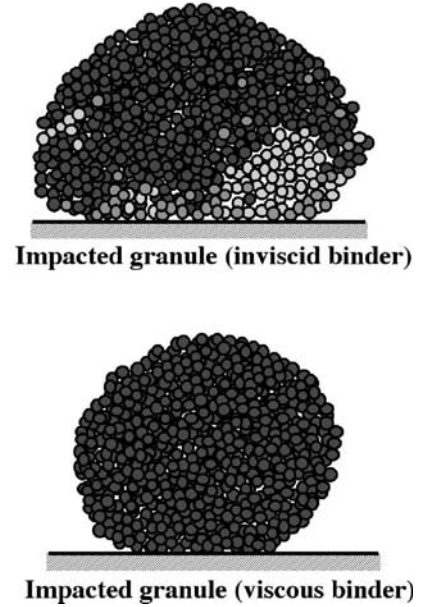
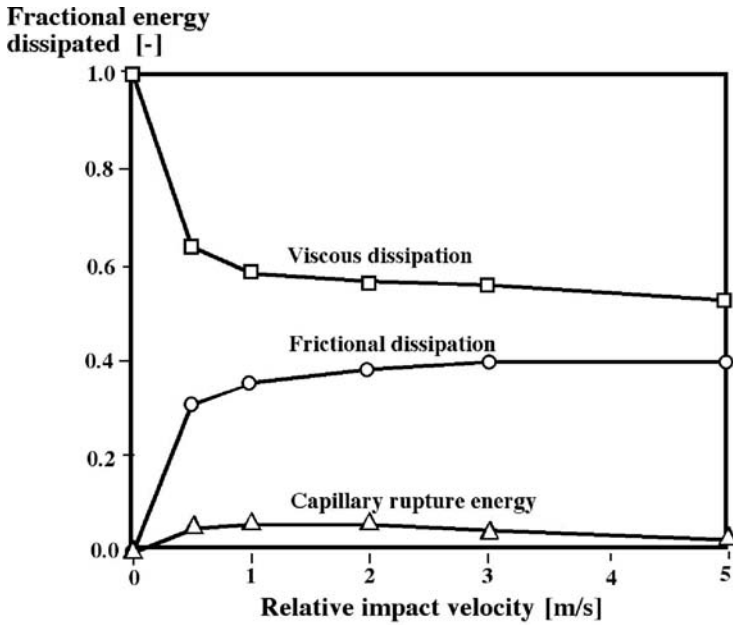


FIG. 21-116 Distribution of energy dissipation during agglomerate collisions, with granular simulations of wall impact for 128- μ s duration for inviscid and viscous binder agglomerates. [After Adams, Thornton, and Lian, *Agglomeration and Size Enlargement*, Proc. 1st Int. Particle Technology Forum, vol.1, Denver, Colo., AIChE, New York, 1994, pp. 155-286, with permission.]

Last is that the mechanism of compact failure also depends on strain rate. Figure 21-118 illustrates schematically the crack behavior observed in compacts as a function of capillary number. At low Ca , compacts fail by brittle fracture with macroscopic crack propagation, whereas at high Ca , compacts fail by plastic flow, which is more desirable to promote growth.

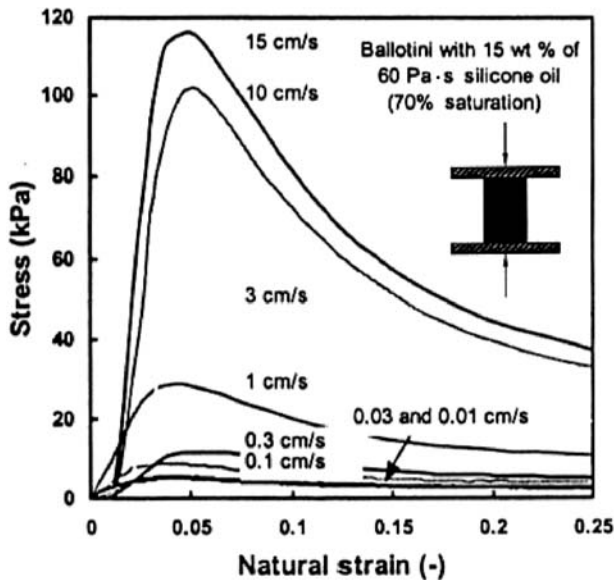


FIG. 21-117 Typical compact stress response for fast compression vs. crosshead compression velocity for glass ballotini ($d_{32} = 35 \mu\text{m}$) and compact diameter 20 mm, length 25 mm. [After Iveson et al., *Powder Technol.*, **127**, 149 (2002), with permission.]

Within the context of granulation, small yield stresses at low Ca may result in unsuccessful growth when these stresses are compared with large breakup forces. With increased yield stress come stronger granules but also decreased deformability. Therefore, high strength might imply a low-deformability growth mechanism for low-shear processes such as a fluid-bed. On the other hand, it might imply smaller growth rates for high-shear processes, which are able to overcome this yield stress and bring about kneading action and plastic flow in the process. Therefore, it is important to bear in mind that increased liquid saturation may initially lower yield stress, allowing greater plastic deformation during granule collisions. However, as granules grow and consolidate and decrease in voidage, they also strengthen and rise in yield stress, becoming less deformable with

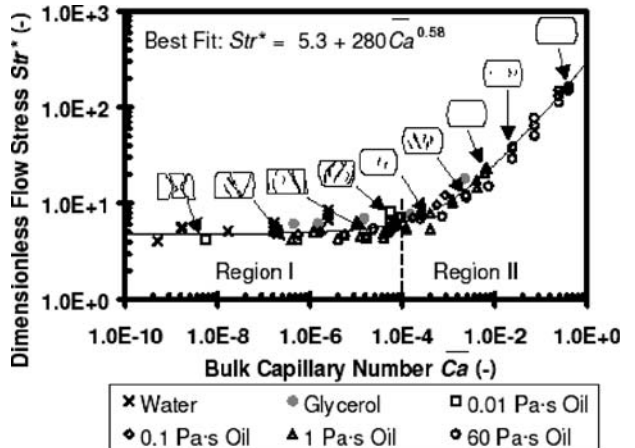


FIG. 21-118 Dimensionless peak flow stress of Fig. 21-154 vs. bulk capillary number, for various binder solutions. [After Iveson et al., *Powder Technol.*, **127**, 149 (2002), with permission.]

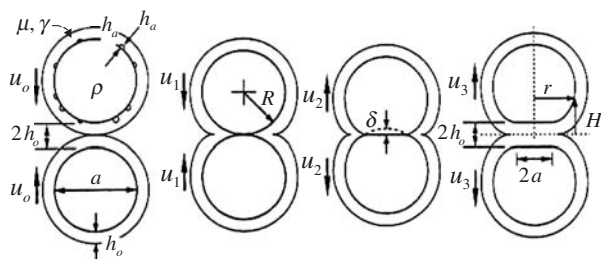


FIG. 21-119 Collisions between surface wet granules, beginning with approach and ending with separation [Liu et al., *AIChE J.*, **46**(3), 529 (2000)]. Note that no deformation takes place in the original Stokes model [Ennis et al., *Powder Technol.*, **65**, 257 (1991)].

time and withstanding shear forces in the granulator. Hence, the desired granule strength and deformability is linked in a complex way to granulator shear forces and consolidation behavior, and is the subject of current investigations.

Low Agitation Intensity—Low Deformability Growth For low-agitation processes or for formulations which allow little granule deformation during granule collisions, consolidation of the granules occurs at a much slower rate than growth, and granule deformation can be ignored to a first approximation. The growth process can be modeled by the collision of two nearly stiff granules, each coated by a liquid layer of thickness h (Fig. 21-119). For the case of zero plastic deformation and neglecting capillary contributions to bridge strength, the probability of successful coalescence is governed by a dimensionless energy of collision, or **viscous Stokes number** St_v , given by

$$St_v = \frac{4\rho u_o d}{9\mu} \quad (21-113)$$

where u_o is the relative collisional velocity of the granules, ρ is granule density, d is the harmonic average of granule diameter, and μ is the solution-phase binder viscosity. The Stokes number represents the ratio of **initial collisional kinetic energy** to the **energy dissipated by viscous lubrication** forces, and it is one measure of normalized bed agitation energy. Successful growth by coalescence or layering requires that

$$St_v < St^* \quad \text{where} \quad St^* = \left(1 + \frac{1}{e_r}\right) \ln\left(\frac{h}{h_a}\right) \quad (21-114)$$

where St^* is a **critical Stokes number** representing the energy required for rebound. The binder layer thickness h is related to liquid loading, e_r is the coefficient of restitution of the granules, and h_a is a measure of surface roughness or asperities. The critical condition given by Eq. (21-114) controls the growth of low-deformability systems where viscous forces dominate (large Ca) (Fig. 21-109) [Ennis et al., *Powder Technol.*, **65**, 257 (1991)]. This criterion has also been extended to capillary coalescence (Ennis, loc. cit., 1991) and for the case of plastic deformation [Liu et al., *AIChE J.*, **46**(3), 529 (2000)].

Both the **binder solution viscosity** μ and the granule density are largely properties of the feed. Binder viscosity is a function of local temperature, collisional strain rate (for nonnewtonian binders), and binder concentration, which is dictated by drying rate and local mass transfer and bed moisture. Viscosity can be manipulated in formulation through judicious selection of binding and surfactant agents and measured by standard rheological techniques (Bird et al., *Dynamics of Polymeric Liquids*, vol.1, Wiley, 1977). The **collisional velocity** is a function of process design and operating variables, and is related to bed agitation intensity and mixing. Possible choices of u_o are summarized in Fig. 21-111, and discussed further below. Note that u_o is an **interparticle collisional velocity**, which is not necessarily the local average granular flow velocity.

Three regimes of granule growth may be identified for low-agitation-intensity, low-deformability processes [Ennis et al., *Powder Technol.*, **65**, 257 (1991)], as depicted for fluid-bed granulation in Fig. 21-120. For small granules or high binder viscosity lying within a **noninertial regime** of granulation, all values of St_v will lie below the critical value St^* and therefore all granule collisions result in successful coalescence and growth *provided* binder is present. Growth rate is independent of granule kinetic energy, particle size, and binder viscosity (provided other rate processes are constant). *Distribution of binding fluid* and *degree of mixing* then control growth, and this is strongly coupled with the rate process of wetting. (See subsection “Wetting”.) As shown in Fig. 21-120, both binders have the same initial growth rate for similar spray rates, independent of binder viscosity. Increases in bed moisture (e.g., spray rate, drop rate) and increases in granule collisions in the presence of binder will increase the overall rate of growth. Bear in mind, however, that there is a 100 percent success of these collisions, since dissipation of energy far exceeds collisional kinetic energy.

As granules grow in size, their collisional momentum increases, leading to localized regions in the process where St_v exceeds the critical value St^* . In this **inertial regime** of granulation, the granule size, binder viscosity, and collision velocity determine the proportion of the bed in which granule rebound or unsuccessful coalescence is possible. Increases in binder viscosity and decreases in agitation intensity increase the **extent of granule growth**, i.e., the largest granule that may be grown [for example, D_c of Eq. (21-108)]. This is confirmed in Fig. 21-120 with the CMC binder continuing to grow, whereas the PVP system with lower viscosity slows in growth. However, note that binder distribution and mixing, and not binder viscosity, control the rate of growth. For example, increasing binder viscosity will not affect growth rate, or initial granule size, but it will result in an increased growth limit. For deformable systems, the opposite will hold true.

When the spatial average of St_v exceeds St^* , growth is balanced by granule disruption or breakup, leading to the **coating regime** of granulation. Growth continues by coating of granules by binding fluid alone. The PVP system with lower viscosity is seen to reach its growth limit and therefore coating regime in Fig. 21-120.

Transitions between granulation regimes depend on bed hydrodynamics. As demonstrated by Fig. 21-120, granulation of an initially fine powder may exhibit characteristics of all three granulation regimes as time progresses, since St_v increases with increasing granule size. Implications and additional examples regarding the regime analysis are highlighted by Ennis [loc. cit., 2006; *Powder Technol.*, **88**, 203 (1996)]. In particular, increases in fluid-bed excess gas velocity exhibit a similar but opposite effect on growth rate to binder viscosity; namely, it is observed to not affect growth rate in the initial inertial regime of growth, but instead lowers the growth limit in the inertial regime.

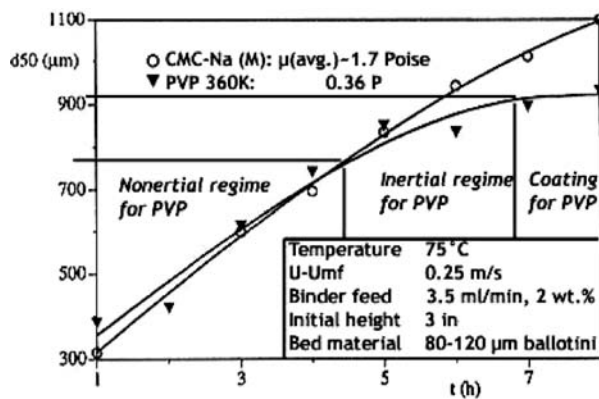


FIG. 21-120 Median granule diameter for fluid-bed granulation of ballottini with binders of different viscosity indicating regimes of growth [Ennis et al., *Powder Technol.*, **65**, 257 (1991)].

Example 4: Extent of Noninertial Growth Growth by coalescence in granulation processes may be modeled by the population balance. (See "Modeling and Simulation of Granulation Processes" subsection.) It is necessary to determine both the mechanism and kernels—or rate constants—which describe growth. For fine powders within the noninertial regime of growth, all collisions result in successful coalescence provided binder is present. Coalescence occurs via a random, size-independent kernel, which is only a function of liquid loading y , since all collisions are successful in the presence of binder, or

$$\beta(u, v) = k = k^* f(y) \tag{21-115}$$

The dependence of growth on liquid loading $f(y)$ strongly depends on wetting properties, spray distribution, and mixing. For random growth and in the presence of sufficient binding fluid, it may be rigorously proved that the average granule size increases exponentially with time, or

$$d = d_0 e^{kt} \tag{21-116}$$

This exponential increase in size with time is confirmed experimentally in Fig. 21-121a, where increases in liquid loading $f(y)$ increase growth rate. (Note granule saturation S is connected to liquid loading y and porosity.) Based on the regime analysis above, growth will continue in a process while the conditions of Eq. (21-114) are met; i.e., dissipation exceeds collisional kinetic energy, or put another way, granules do not have sufficient momentum based on their current size to exceed the energy dissipated during the collision. Examples of these growth limits are seen in the drum granulation work of Kapur (loc. cit.) in Fig. 21-121a, as well as fluid beds (Fig. 21-120) and mixers (Fig. 21-122). It may be shown that the **maximum extent** of granulation $(kt)_{\max}$ occurring within the noninertial regime is given by

$$(kt)_{\max} = \ln\left(\frac{d_{\max}}{d_0}\right) = 6 \ln (St^*/St_0) f(y) \propto \ln \frac{\mu}{\rho u_c d_0} \tag{21-117}$$

where St_0 is the Stokes number based on initial nuclei diameter d_0 [Adetayo et al., *Powder Technol.*, **82**, 37 (1995)]. Extent $(kt)_{\max}$ is taken as the logarithm of the growth limit in the first random stage of growth, or d_{\max} . The growth limits d_{\max} of Fig. 21-121a are replotted as extents in Fig. 21-121b. Here, $(kt)_{\max}$ is observed to depend linearly on liquid loading y . Therefore, the maximum granule size depends exponentially on liquid loading, as observed experimentally (Fig. 21-112).

From Eq. (21-117), it is possible to scale or normalize a variety of drum granulation data to a common drum speed and binder viscosity. Maximum granule size d_{\max} and extent $(kt)_{\max}$ depend linearly and logarithmically, respectively, on binder viscosity and the inverse of agitation velocity. This is illustrated based on the data of Fig. 21-121b, where the slope of each formulation line depends linearly on binder viscosity. Figure 21-121c provides the normalization of extent $(kt)_{\max}$ for the drum granulation of limestone and fertilizers, correcting for differences in binder viscosity, granule density, and drum rotation speed, with the data collapsing onto a common line.

High Agitation Intensity Growth For high-agitation processes involving **high-shear mixing** or for readily deformable formulations, granule deformability, plastic deformation, and granule consolidation can no longer be neglected as they occur at the same rate as granule growth. Typical growth profiles for high-shear mixers are illustrated in Fig. 21-122. Two stages of growth are evident, which reveal the possible effects of binder viscosity and impeller speed, as shown for data replotted vs. impeller speed in Fig. 21-123. The **initial, nonequilibrium stage** of growth is controlled by granule deformability and is of greatest practical significance in manufacturing for high-shear mixers for deformable formulations. Increases in St due to lower viscosity or higher impeller speed increase the rate of growth, as shown in Fig. 21-122, since the system becomes more deformable and easier to **knead** into larger granule structures. These effects are contrary to what is predicted

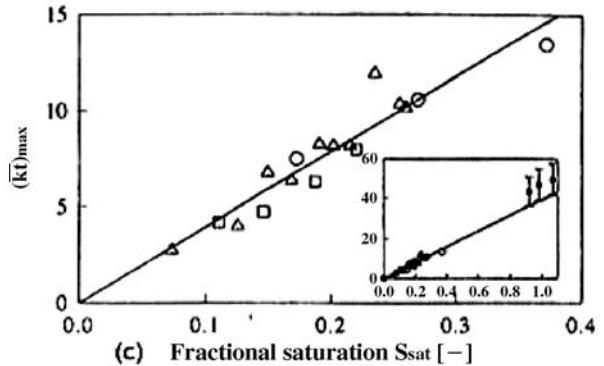
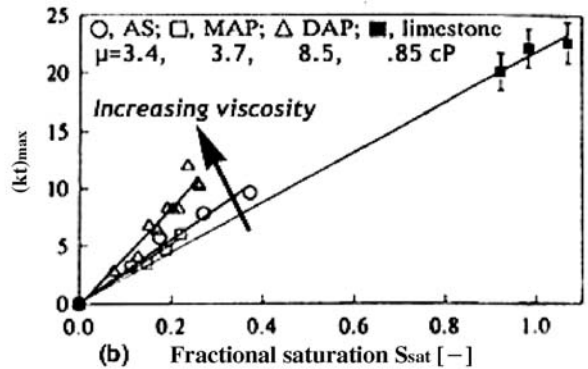
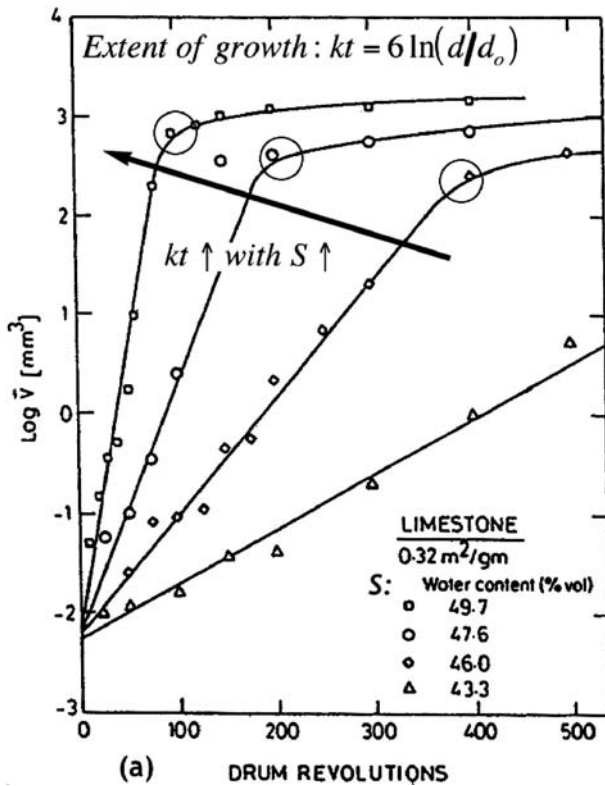


FIG. 21-121 (a) Exponential growth in drum granulation reaching a growth limit d_{\max} or maximum extent of growth $(kt)_{\max}$, which are functions of moisture saturation (Kapur, loc. cit.). (b) Maximum extent of noninertial growth $(kt)_{\max}$ as a linear function of saturation of the powder feed and binder viscosity. (c) Maximum extent normalized for differences in binder viscosity, drum speed, and granule density by Stokes number. [Adetayo et al., *Powder Technol.*, **82**, 37 (1995).]

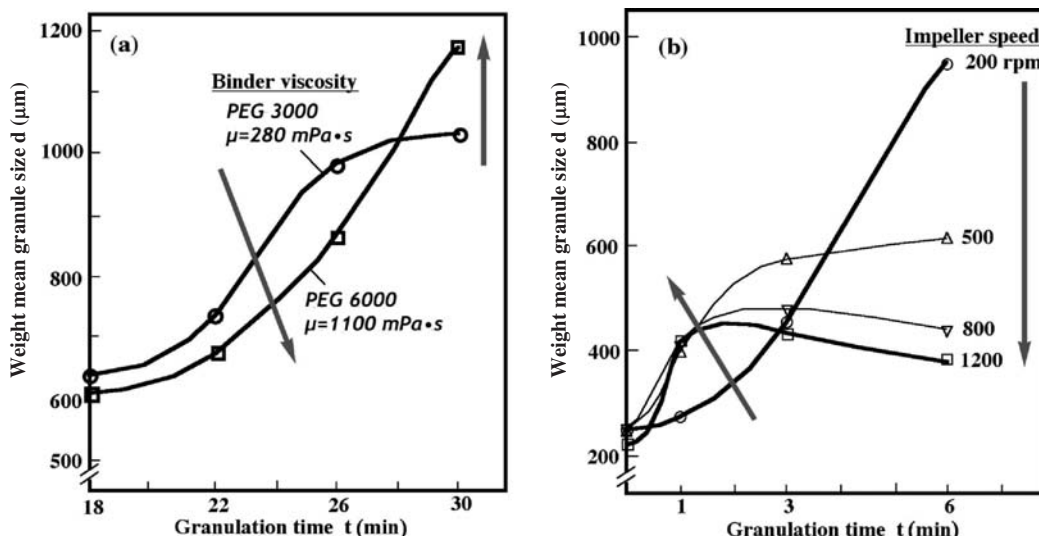


FIG. 21-122 Granule diameter as a function of time for high-shear mixer granulation, illustrating the influence of deformability on growth behavior. Directions of increasing viscosity and impeller speed are indicated by arrows. (a) A 10-L vertical high-shear melt granulation of lactose with liquid loading of 15 wt % binder and impeller speed of 1400 rpm for two different viscosity grades of polyethylene glycol binders. [Schaefer et al., *Drug Dev. & Ind. Pharm.*, **16**(8), 1249 (1990), with permission.] (b) A 10-L vertical high-shear mixer granulation of dicalcium phosphate with 15 wt % binder solution of PVP/PVA Kollidon® VA64, liquid loading of 16.8 wt %, and chopper speed of 1000 rpm for varying impeller speed. [Schaefer et al., *Pharm. Ind.*, **52**(9), 1147 (1990), with permission.]

from the Stokes analysis based on rigid, low deformable granules [Eq. (21-114)], where high viscosity and low velocity increase the growth limit. In this nonequilibrium deformable stage, high viscosity and low velocity give less growth due to less kneading action.

Growth continues until disruptive and growth forces are balanced in the process, similar to a coating stage of growth. This last **equilibrium stage** of growth represents a balance between dissipation and

collisional kinetic energy, and so increases in St_t decrease the final granule size, as expected from the Stokes analysis [Eq. (21-114)]. Note that the equilibrium granule diameter decreases with the inverse square root of the impeller speed, as it should based on $St = St^*$, with $u_o = d \cdot (du/dx) = \omega d$.

The Stokes analysis is used to determine the effect of operating variables and binder viscosity on *equilibrium* growth, where disruptive and growth forces are balanced. In the early stages of growth for high-shear mixers, the Stokes analysis in its present form is inapplicable. Freshly formed, uncompacted granules are easily deformed, and as growth proceeds and consolidation of granules occur, they will surface-harden and become more resistant to deformation. This increases the importance of the elasticity of the granule assembly. Therefore, in later stages of growth, older granules approach the ideal Stokes model of rigid collisions. For these reasons, the Stokes approach has had reasonable success in providing an overall framework with which to compare a wide variety of granulating materials (Ennis, *Powder Technol.*, 1996). In addition, the Stokes number controls in part the degree of deformation occurring during a collision since it represents the importance of collision kinetic energy in relation to viscous dissipation, although the exact dependence of deformation on St is presently unknown.

The Stokes coalescence criteria of Eq. (21-114) must be generalized to account for substantial plastic deformation to treat the initial nonequilibrium stages of growth in high-agitation systems such as high-shear mixers. In this case, granule growth and deformation are controlled by a generalization of St_t , or a deformation Stokes number St_{def} , as originally defined by Tardos et al. [Tardos and Khan, AIChE Annual Meeting, Miami, 1995; Tardos et al., *Powder Technol.*, **94**, 245 (1997)]:

$$St_{\text{def}} = \frac{\rho u_o^2}{\sigma_y} (\text{impact}) \quad \text{or} \quad \frac{\rho (du/dx)^2 d^2}{\sigma_y} (\text{shear}) \quad (21-118)$$

Viscosity has been replaced by a generalized form of plastic deformation controlled by the yield stress σ_y , which may be determined by compression experiments (e.g., Fig. 21-117). As shown previously, yield stress is related to deformability of the wet mass and is a function of shear rate, binder viscosity, and surface tension (captured by a bulk

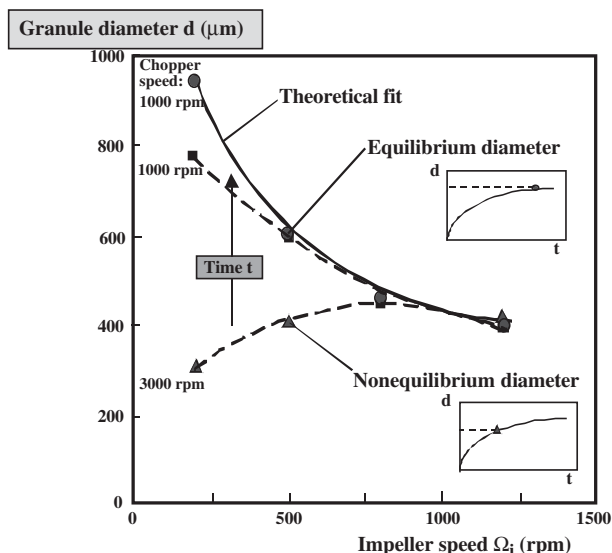


FIG. 21-123 Granule diameter as a function of impeller speed for both initial nonequilibrium and final equilibrium growth limits for high-shear mixer granulation, data from Fig. 21-124. [Ennis, *Powder Technol.*, **88**, 203 (1996), with permission.]

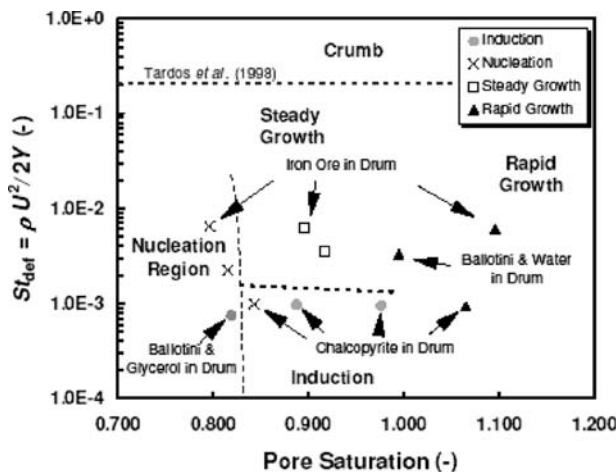


FIG. 21-124 Regime map of growth mechanisms, based on moisture level and deformability of formulations [Iveson et al., *Powder Technol.*, **117**, 83 (2001)].

capillary number), as well as primary particle size, friction, saturation, and voidage as previously presented [cf. Eq. (21-112)].

Critical conditions required for granule coalescence may be defined in terms of the viscous and deformation Stokes numbers, or St_v and St_{def} , respectively. These represent a complex generalization of the critical Stokes number given by Eq. (21-114) and are discussed in detail elsewhere [Litster and Ennis, *The Science and Engineering of Granulation Processes*, Kluwer Academic, 2004; Iveson et al., *Powder Technol.*, **88**, 15 (1996)].

An overall view of the impact of deformability of growth behavior may be gained from Fig. 21-124, where types of granule growth are plotted vs. deformability in a regime map, and yield stress has been measured by compression experiments [Iveson et al., *Powder Technol.*, **117**, 83 (2001)]. Growth mechanism depends on the competing effects of high shear promoting growth by deformation, on the one hand, and the breakup of granules giving a growth limit, on the otherhand. For high velocities that exceed the dissipation energy [Eq. (21-114)] or significantly exceed the dynamic strength of the granule, growth is not possible by deformation due to high shear or high St_{def} , and the material remains in a crumb state. For low pore saturation and lower St_{def} , growth is possible by initial wetting and nucleation, with surrounding powder remaining ungranulated and the formed nuclei surviving breakup forces. At intermediate levels of moisture, growth occurs at a steady rate for moderate deformability, where larger granules grow preferentially or by crushing and layering [Newitt and Conway Jones, loc. cit.; Capes and Danckwerts, *Trans. Inst. Chem. Eng.*, **43**, T116 (1965); Linkson et al., *Trans. Inst. Chem. Eng.*, **51**, 251 (1973)]. Linear or power law behavior as observed is shown by Kapur (loc. cit.), where for preferential growth

$$d^m - d_o^m = m(kt) \quad (21-119)$$

For nondeformable systems, random exponential growth is expected for sufficient saturation (Fig. 21-121). However, for lower levels of saturation, a delay with little or no growth may be observed. This delay, or induction time, is related to the time required to work moisture to the surface to promote growth, and in some cases, the growth can be rapid and unstable, which also occurs in all cases of high moisture. Pore saturation may be calculated by

$$S = \frac{w\rho_s(1 - \epsilon_g)}{\rho\epsilon_g} \quad (21-120)$$

where w is the liquid-solid mass ratio. The current regime map, while providing a starting point, requires considerable development.

Overall growth depends on the mechanics of local growth, as well as the overall mixing pattern and local/overall moisture distribution. Levels of shear are poorly understood in high-shear processes. In addition, growth by both deformation and the rigid growth model is possible. Lastly, deformability is intimately linked to both voidage and moisture. They are not a constant for a formation, but depend on time and the growth process itself through the interplay of growth and consolidation.

Determination of St^* The extent of growth is controlled by some **limit of granule size**, reflected either by the critical Stokes number St^* or by the critical limit of granule size D_c . There are three possible methods to determine this critical limit. The first involves measuring the critical rotation speed for the survival of a series of liquid binder drops during drum granulation (Ennis, On the Mechanics of Granulation, Ph.D. thesis, 1990, The City College of the City University of New York, University Microfilms International, 1991). A second refined version involves measuring the survival of granules in a couette-fluidized shear device (Tardos and Khan, loc. cit.; Tardos et al., loc. cit.). Both the onset of granule deformation and complete granule rupture are determined from the dependence of granule shape and the number of surviving granules, respectively, on shear rate (Fig. 21-125). The critical shear rate describing complete granule rupture defines St^* , whereas the onset of deformation and the beginning of granule breakdown define an additional critical value $St_{def} = St^*$. The third approach is to measure the deviation in the growth rate curve from random exponential growth (Adetayo and Ennis, *AIChE J.*, 1996). The deviation from random growth indicates a value of w^* , or the **critical granule diameter** at which noninertial growth ends (Fig. 21-126). This value is related to D_c . (See the "Modeling and Simulation" subsection for further discussion.) The last approach is through the direct measurement of the yield stress through compression experiments.

Example 5: High-Shear Mixer Growth An important case study for high-deformability growth was conducted by Holm et al. [Parts V and VI, *Powder Technol.*, **43**, 213 (1985)] for high-shear mixer granulation. Lactose, dicalcium phosphate, and dicalcium phosphate/starch mixtures (15 and 45 percent starch) were granulated in a Fielder PMAT 25 VG laboratory-scale mixer. Granule size, porosity, power level, temperature rise, and fines disappearance were monitored during liquid addition and wet massing phases. Impeller and chopper speeds were kept constant at 250 and 3500 rpm, respectively, with 7.0 to 7.5 kg of starting material. Liquid flow rates and amount of binder added were varied according to the formulation. Figure 21-127 illustrates typical power profiles during granulation, whereas Fig. 21-128 illustrates the resulting granule size and voidage (or porosity). Note that wet massing time (as opposed to total process time) is defined as the amount of time following the end of liquid addition, and the beginning of massing time is indicated in Fig. 21-127.

Clear connections may be drawn between granule growth, consolidation, power consumption, and granule deformability (Figs. 21-127 and 21-128). For the case of lactose, there is no further rise in power following the end of water addition (beginning of wet massing), and this corresponds to no further changes in granule size and porosity. In contrast, dicalcium phosphate continues to grow through the wet massing stage, with corresponding continual increases in granule size and porosity. Lastly, the starch formulations are noted to have power increase for approximately 2 min into the wet massing stage, corresponding to 2 min of growth; however, growth ceased when power consumption leveled off. Therefore, power clearly tracks growth and consolidation behavior.

Further results connecting power and growth to compact deformability are provided in Holm (Holm et al., loc. cit.). The deformability of lactose compacts, as a function of saturation and porosity, is shown to increase with moisture in a stable fashion. In other words, the lactose formulation is readily deformable, and growth begins immediately with water addition. This steady growth is consistent with values observed in drum granulation. Growth rates and power rise do not lag behind spray addition, and growth ceases with the end of spraying. Dicalcium phosphate compacts, on the other hand, remain undeformable until a critical moisture is reached, after which they become extremely deformable and plastic. This unstable behavior is reflected by an inductive lag in growth and power after the end of spray addition (consistent with data for drum granulation), ending by unstable growth and bowl sticking as moisture is finally worked to the surface.

In closing, a comment should be made with regard to using power for control and scale-up. While it is true the power is reflective of the growth process, it is a dependent variable in many respects. Different lots of a set formulation, e.g., may have different yield properties and deformability, and a different dependence on moisture. This may be due to minute particle property changes

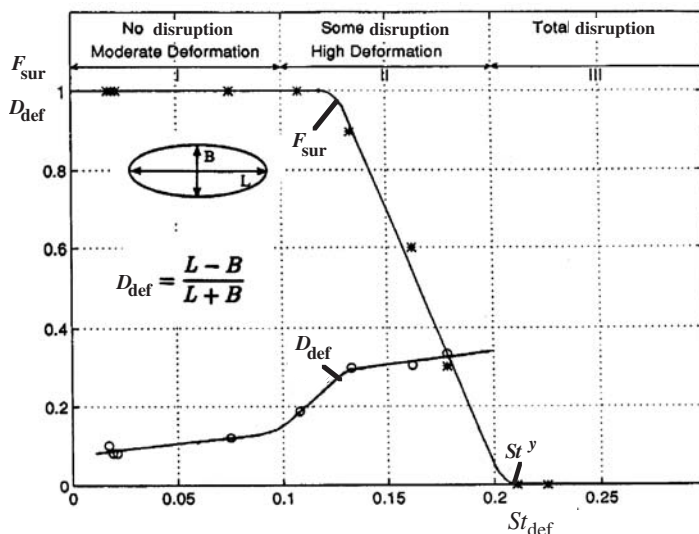


FIG. 21-125 Determination of the onset of granule deformation and complete granule breakdown with the fluidized-couette constant-shear device. St_{def} is a deformation yield, F_{sur} is the fraction of surviving granules, and D_{def} is the average degree of granule deformation; $St_{def} = St^y$ and $F_{sur} = 0$ complete granule breakdown. [Tardos and Khan, *AIChE Annual Meeting*, 1995; Tardos et al., *Powder Technol.*, **94**, 245 (1997).]

controlling the rate processes. Therefore, there is not a unique relationship between power and growth. However, power measurements might be useful to indicate a shift in formation properties. Lastly, **specific power** should be used for scale-up, where power is normalized by the *active* portion of the powder bed, which could change over wet massing time. The impact of scale-up on mixing and distribution of power in a wet mass, however, is only partly understood at this point.

Granule Consolidation and Densification Consolidation or densification of granules determines **granule porosity** and hence **granule density**. Granules may consolidate over extended times and achieve high densities if there is no simultaneous drying to stop the consolidation process. The extent and rate of consolidation are determined by the balance between the collision energy and the granule resistance to deformation, as described by the Stokes numbers previously defined.

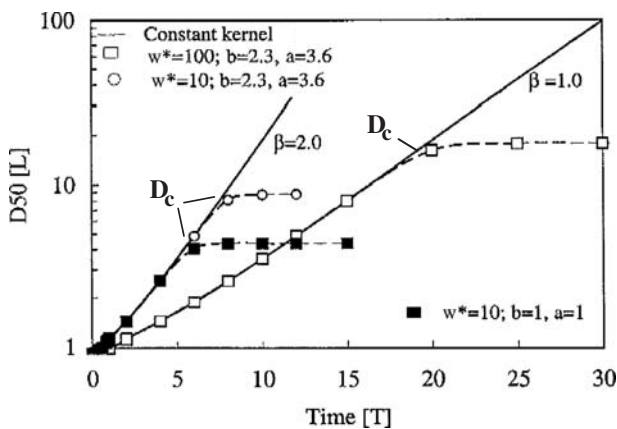


FIG. 21-126 Determination of critical granule diameter, or growth limit, from the evolution of the granule-size distribution (Adetayo and Ennis, *AIChE J.*, 1996).

The voidage ϵ_g may be shown to depend on time as follows:

$$\frac{\epsilon_g - \epsilon_{min}}{\epsilon_o - \epsilon_{min}} = \exp(-\beta t) \quad \text{where} \quad \beta = f_n(S, St, St_{def}) \quad (21-121)$$

Here S is granule saturation related to liquid loading; ϵ_o and ϵ_{min} are the beginning and final (minimum) granule porosity, respectively [Iveson et al., *Powder Technol.*, **88**, 15 (1996)]. The consolidation process and final granule voidage control the granule strength, dissolution behavior, and attrition resistance (cf. Figs. 21-88 to 21-90), in addition to controlling the growth process through its impact on deformability. Granule voidage also impacts bulk density, mass flow rates for feeding, and possible subsequent compact properties such as hardness or compact uniformity.

The effects of binder viscosity and liquid content are complex and interrelated. For low-viscosity binders, consolidation *increases* with

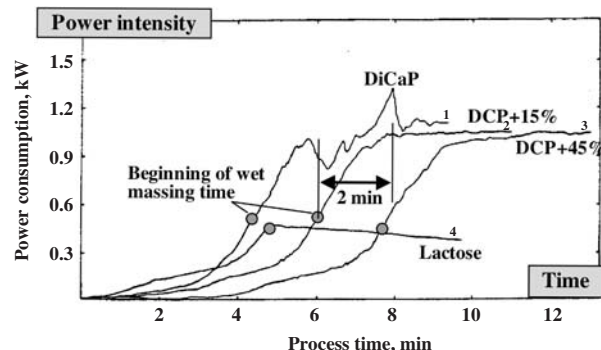


FIG. 21-127 Power consumption for lactose, dicalcium phosphate, and dicalcium phosphate/starch mixtures (15 and 45 percent starch) granulated in a Fielder PMAT 25 VG. Impeller speed is 250 rpm, chopper speed 3000 rpm. [Holm et al., Parts V and VI, *Powder Technol.*, **43**, 213 (1985); Kristensen et al., *Acta Pharm. Sci.*, **25**, 187 (1988).]

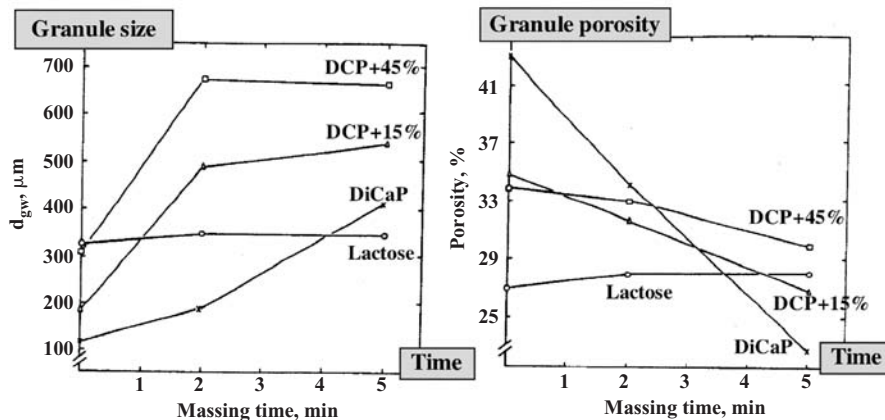


FIG. 21-128 Granule size and porosity vs. wet massing time for lactose, dicalcium phosphate, and dicalcium phosphate/starch mixtures (15 and 45 percent starch) granulated in a Fielder PMAT 25 VG. Impeller speed is 250 rpm, chopper speed 3000 rpm. [Holm et al., *Parts V and VI, Powder Technol.*, **43**, 213 (1985); Kristensen et al., *Acta Pharm. Sci.*, **25**, 187 (1988).]

liquid content, as shown in Fig. 21-129. This is the predominant effect for the majority of granulation systems, with liquid content related to peak bed moisture on average. Increased drop size and spray flux are also known to increase consolidation. Drying affects peak bed moisture and consolidation as well by varying both moisture level and binder viscosity; generally increased drying slows the consolidation process. For very viscous binders, consolidation *decreases* with increasing liquid content (Fig. 21-130). As a second important effect, decreasing feed particle size decreases the rate of consolidation due to the high specific surface area and low permeability of fine powders, thereby decreasing granule voidage. Lastly, increasing agitation intensity and process residence time increases the degree of consolidation by increasing the energy of collision and compaction time. The exact combined effect of formulation properties is determined by the balance between viscous dissipation and particle frictional losses, and therefore the rate is expected to depend on the viscous and deformation Stokes numbers.

BREAKAGE AND ATTRITION

Dry granule strength impacts three key areas of processing. These include the physical attrition or breakage of granules during the granulation and drying processes, the breakage of granules in subsequent material handling steps such as conveying or feeding, and lastly the deformation and breakdown of granules in compaction processes such as tableting. (Note that breakage also includes breakdown of wet granules or overmassed wet cake in granulation, which is outside the scope of this subsection.) Modern approaches to granule strength rely on **fracture mechanics** (Lawn, *Fracture of Brittle Solids*, 2d ed., Cambridge University Press, 1975). In this context, a granule is viewed as a nonuniform **physical composite** possessing certain macroscopic mechanical properties, such as a generally anisotropic **yield stress**, as well as an inherent **flaw distribution**. Hard materials may fail in tension, with the breaking strength being much less than the inherent tensile strength of bonds because of the existence of flaws. Flaws act to

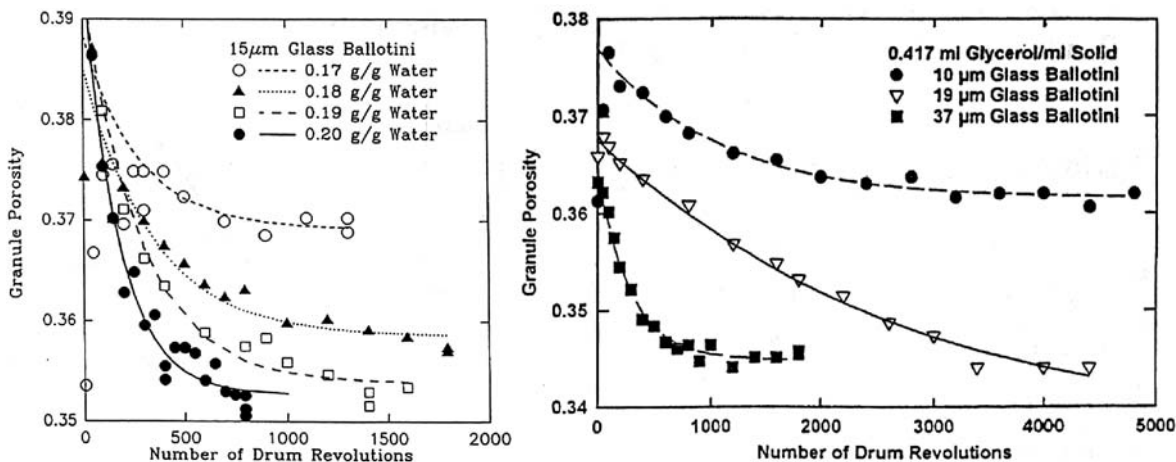


FIG. 21-129 Effect of binder liquid content and primary feed particle size on granule porosity for the drum granulation of glass ballotini. Decreasing granule porosity corresponds to increasing extent of granule consolidation. [Iveson et al., *Powder Technol.*, **88**, 15 (1996).]

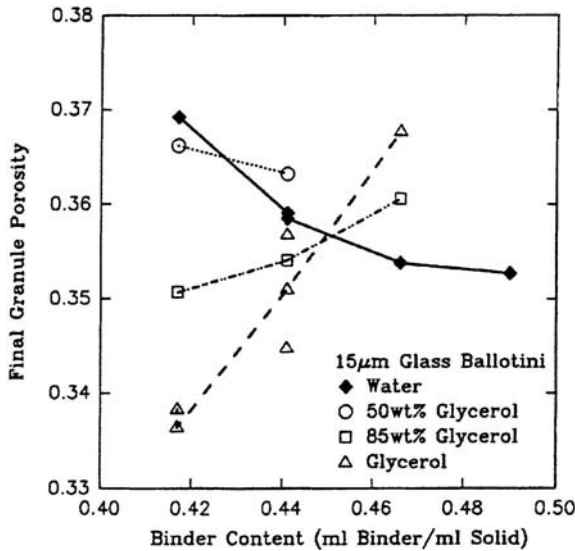


FIG. 21-130 Effect of binder viscosity and liquid content on final granule porosity for the drum granulation of 15-µm glass ballotini. Decreasing granule porosity corresponds to increasing extent of granule consolidation. (Iveson et al., Powder Technol., 1996.)

concentrate stress, as depicted in Fig. 21-131 for commercial Metamucil tablets. Here, razor scores or notches have been added to the tablets, which were subsequently broken under three-point bend loading described below. In all cases, the tablets break at the razor score—which acts as a sharp flaw to concentrate stress—rather than at the tableted original indentation notch.

Bulk breakage tests of granule strength measure both the inherent bond strength of the granule and its flaw distribution [Ennis, loc. cit., 1991; Ennis and Sunshine, Tribology Int., 26, 319 (1993)]. Figure 21-89 previously illustrated granule attrition results for a variety of formulations. Attrition clearly increases with increasing voidage; note that this voidage is a function of granule consolidation discussed previously. Different formulations fall on different curves, due to inherently differing interparticle bond strengths. It is often important to separate the impact of bond strength vs. voidage on attrition and granule strength. Processing influences flaw distribution and granule voidage, whereas inherent bond strength is controlled by formulation properties.

The mechanism of granule breakage (Fig. 21-91) is a strong function of the materials properties of the granule itself as well as the type of loading imposed by the test conditions [Bemros and Bridgewater, Powder Technol., 49, 97 (1987)]. Ranking of product breakage

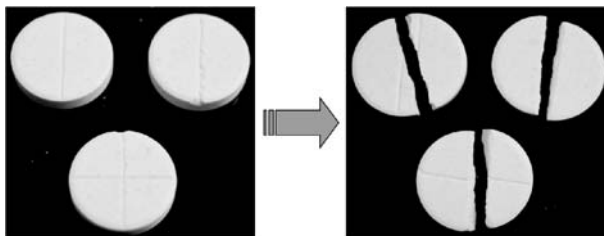


FIG. 21-131 Breakage of Metamucil tablets under three-point loading with razor scoring. (Reprinted from Design and Optimization of Granulation and Compaction Processes for Enhanced Product Performance, Ennis, 2006, with permission of E-L-G Associates. All rights reserved.)

resistance by ad hoc tests may be test-specific, and in the worst case differs from actual process conditions. Instead, material properties should be measured by standardized mechanical property tests which minimize the effect of flaws and loading conditions under well-defined geometries of internal stress, as described below.

Fracture Properties Fracture toughness K_c defines the stress distribution in the body (Fig. 21-132) just before fracture and is given by

$$K_c = Y_{cf} \sigma_f \sqrt{\pi c} \quad (21-122)$$

where σ_f is the applied fracture stress, c is the length of the crack in the body, and Y_{cf} is a calibration factor introduced to account for different body geometries (Lawn, loc. cit.). The elastic stress is increased dramatically as the crack tip is approached. In practice, however, the elastic stress cannot exceed the yield stress of the material, implying a region of local yielding at the crack tip.

To nevertheless apply the simple framework of linear elastic fracture mechanics, Irwin [J. Applied Mech., 24, 361 (1957)] proposed that this process zone size r_p be treated as an effective increase in crack length δ_c . Fracture toughness is then given by

$$K_c = Y_{cf} \sigma_f \sqrt{\pi(c + \delta_c)} \quad \text{with} \quad \delta_c \sim r_p \quad (21-123)$$

The process zone is a measure of the yield stress or plasticity of the material in comparison to its brittleness. Yielding within the process zone may take place either plastically or by diffuse microcracking, depending on the brittleness of the material. For plastic yielding, r_p is also referred to as the plastic zone size.

The critical strain energy release rate G_c is the energy equivalent to fracture toughness, first proposed by Griffith [Phil. Trans. Royal Soc., A221, 163 (1920)]. With an elastic modulus of E , toughness and release rate are related by

$$G_c = K_c^2/E \quad (21-124)$$

Fracture Measurements To ascertain fracture properties in any reproducible fashion, very specific test geometries must be used since it is necessary to know the stress distribution at predefined, induced cracks of known length. Three traditional methods are (1) the three-point bend test, (2) indentation fracture testing, and (3) hertzian contact compression between two spheres of the material (see “Fracture” under “Size Reduction”). Figure 21-133 illustrates a typical geometry and force response for the case of a three-point bend test. By breaking a series of dried formulation bars under three-point bend loading of varying crack length, the fracture toughness is determined from the variance of fracture stress on crack length, as given by Eq. (21-123). Here, δ_c is initially taken as zero and determined in addition to toughness (Ennis and Sunshine, loc. cit.).

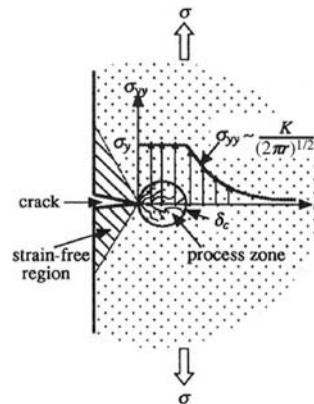


FIG. 21-132 Fracture of a brittle material by crack propagation. [Ennis and Sunshine, Tribology Int., 26, 319 (1993), with permission.]

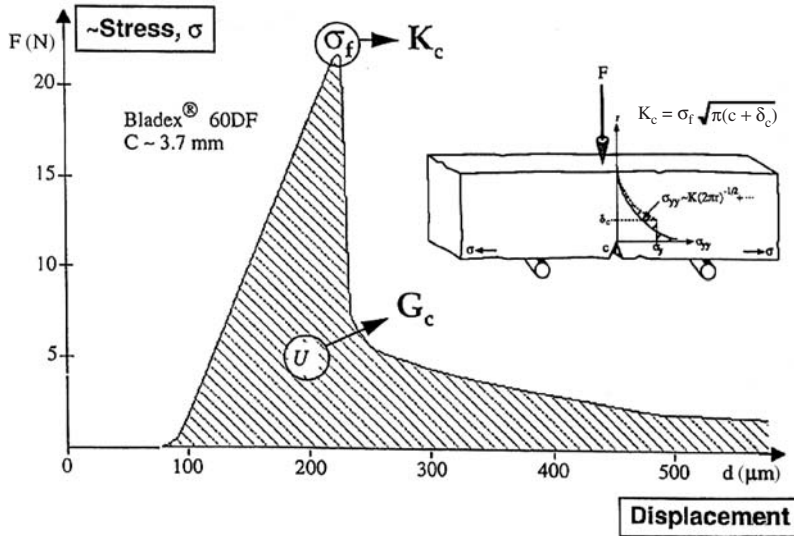


FIG. 21-133 Typical force-displacement curve for three-point bend semistable failure. [Ennis and Sunshine, Tribology Int., 26, 319 (1993), with permission.]

In the case of indentation fracture (Fig. 21-134), one determines the **hardness** H from the area of the residual plastic impression and the fracture toughness from the lengths of cracks propagating from the indent as a function of indentation load F (Johnson and Ennis, *Proc. First International Particle Technology Forum*, vol. 2, AICHe, Denver, 1994, p. 178). Hardness is a measure of the yield strength of the material. Toughness and hardness in the case of indentation are given by

$$K_c = \beta \sqrt{\frac{E}{H}} \frac{F}{c^{3/2}} \quad \text{and} \quad H \sim \frac{F}{A} \quad (21-125)$$

Table 21-13 compares typical fracture properties of agglomerated materials. Fracture toughness K_c is seen to range from 0.01 to 0.06 $\text{Mpa}\cdot\text{m}^{1/2}$, less than that typical for polymers and ceramics, presumably due to the high agglomerate voidage. Critical strain energy release rates G_c from 1 to 200 J/m^2 , are typical for ceramics but less than that for polymers. Process zone sizes δ_c are seen to be large and of the order of 0.1 to 1 mm, values typical for polymers. Ceramics, however typically have process zone sizes less than 1 μm . Critical displacements

required for fracture may be estimated by the ratio G_c/E , which is an indication of the **brittleness** of the material. This value was of the order of 10^{-7} to 10^{-8} mm for polymer-glass agglomerates, similar to polymers, and of the order of 10^{-9} mm for herbicide bars, similar to ceramics. In summary, granulated materials behave similar to brittle ceramics which have small critical displacements and yield strains but also similar to ductile polymers which have large process or plastic zone sizes.

Mechanisms of Attrition and Breakage The process zone plays a large role in determining the mechanism of granule breakage (Fig. 21-91). (Ennis and Sunshine, loc. cit.). Agglomerates with process zones small in comparison to granule size break by a brittle fracture mechanism into smaller fragments, or **fragmentation or fracture**. However, for agglomerates with process zones of the order of their size, there is insufficient volume of agglomerate to concentrate enough elastic energy to propagate gross fracture during a collision. The mechanism of breakage for these materials is one of **wear, erosion, or attrition** brought about by diffuse microcracking. In the limit of very weak bonds, agglomerates may also **shatter** into small fragments or primary particles.

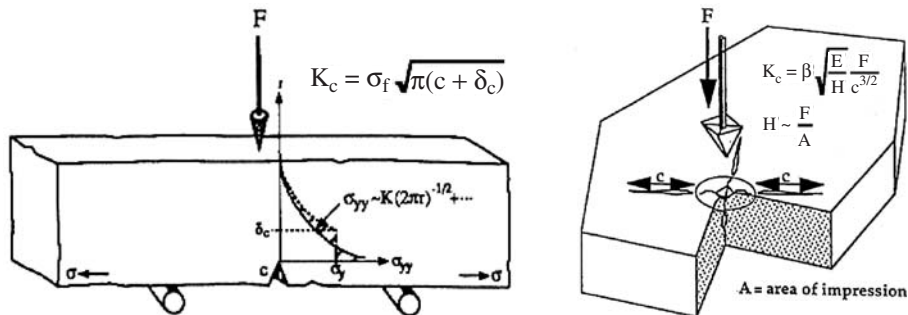


FIG. 21-134 Three-point bend and indentation testing for fracture properties. (Reprinted from Design and Optimization of Granulation and Compaction Processes for Enhanced Product Performance, Ennis, 2006, with permission of E-G Associates. All rights reserved.)

TABLE 21-13 Fracture Properties of Agglomerated Materials

Material	Id	K_c (MPa·m ^{1/2})	G_c (J/m ²)	δ_c (μ m)	E (MPa)	G_c/E (m)
Bladex 60 ^o	B60	0.070	3.0	340	567	5.29e-09
Bladex 90 ^o	B90	0.014	0.96	82.7	191	5.00e-09
Glean ^o	G	0.035	2.9	787	261	1.10e-08
Glean ^o Aged [†]	GA	0.045	3.2	3510	465	6.98e-09
CMC-Na (M) [†]	CMC	0.157	117.0	641	266	4.39e-07
Klucel GF [†]	KGF	0.106	59.6	703	441	1.35e-07
PVP 360K [†]	PVP	0.585	199.0	1450	1201	1.66e-07
CMC 2% 1kN [†]	C2/1	0.097	16.8	1360	410	4.10e-08
CMC 2% 5kN [†]	C2/5	0.087	21.1	1260	399	5.28e-08
CMC 5% 1kN [†]	C5/1	0.068	15.9	231	317	5.02e-08

^oDupont corn herbicides.

[†]50-μm glass beads with polymer binder.

Ennis and Sunshine, *Tribology Int.*, **26**, 319 (1993).

Each mechanism of breakage implies a different functional dependence of breakage rate on material properties. Granules generally have been found to have a large process zone (Table 21-13), which suggests granule wear as a dominant mechanism or breakage or attrition. For the case of **abrasive wear** of ceramics due to surface scratching by loaded indentors, Evans & Wilshaw [*Acta Metallurgica*, **24**, 939 (1976)] determined a volumetric wear rate V of

$$V = \frac{d_i^{1/2}}{A^{1/4} K_c^{3/4} H^{1/2}} P^{5/4} l \quad (21-126)$$

where d_i is indenter diameter, P is applied load, l is wear displacement of the indenter, and A is apparent area of contact of the indenter with the surface. Therefore, wear rate depends inversely on fracture toughness. For the case of fragmentation, Yuregir et al. [*Chem. Eng. Sci.*, **42**, 843 (1987)] have shown that the fragmentation rate of organic and inorganic crystals is given by

$$V \sim \frac{H}{K_c^2} \rho u^2 a \quad (21-127)$$

where a is crystal length, ρ is crystal density, and u is impact velocity. Note that hardness plays an opposite role for fragmentation than for wear, since it acts to concentrate stress for fracture. Fragmentation rate is a stronger function of toughness as well.

Drawing on analogies with this work, the breakage rates by wear B_w and fragmentation B_f for the case of fluid-bed granulation and drying

processes should be of the forms

$$B_w = \frac{d_0^{1/2}}{K_c^{3/4} H^{1/2}} h_b^{5/4} (U - U_{mf}) \quad (21-128)$$

$$B_f \sim \frac{H}{K_c^2} \rho (U - U_{mf})^2 a \quad (21-129)$$

where d is granule diameter, d_0 is primary particle diameter, $U - U_{mf}$ is fluid-bed excess gas velocity, and h_b is bed height. Figure 21-135 illustrates the dependence of erosion rate on material properties for bars and fluid-bed granules undergoing a wear mechanism of breakage, as governed by Eqs. (21-126 and 21-128).

POWDER COMPACTION

Compressive or **compaction** techniques of agglomeration encompass a variety of unit operations with varying degrees of confinement (Fig. 21-136), ranging from completely confined as in the case of tableting to unconfined as in the case of roll pressing. Regardless of the unit of operation, the ability of powders to freely flow, easily compact, forming permanent interparticle bonding, and maintain strength during stress unloading determines the success of compaction. As opposed to the kinetic rate processes of granulation, compaction is a forming process consisting of a variety of microlevel powder processes (Fig. 21-86) strongly influenced by mechanical properties of the feed. These key areas are now discussed.

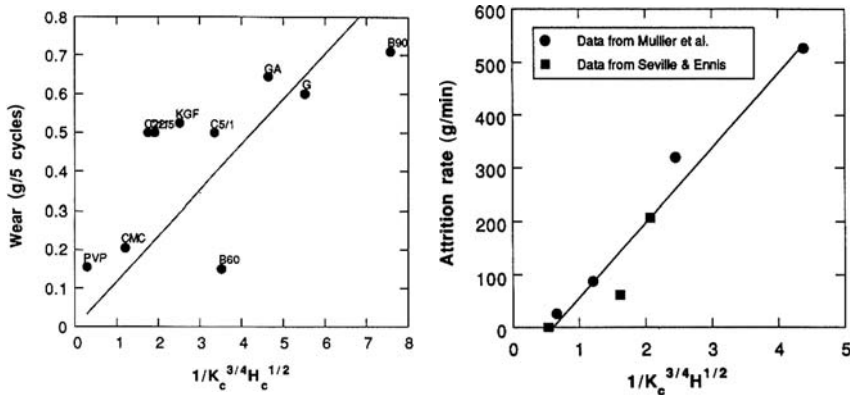


FIG. 21-135 Bar wear rate and fluid-bed erosion rate as a function of granule material properties. K_c is fracture toughness and H is hardness as measured by three-point bend tests. [Ennis and Sunshine, *Tribology Int.*, **26**, 319 (1993), with permission.]

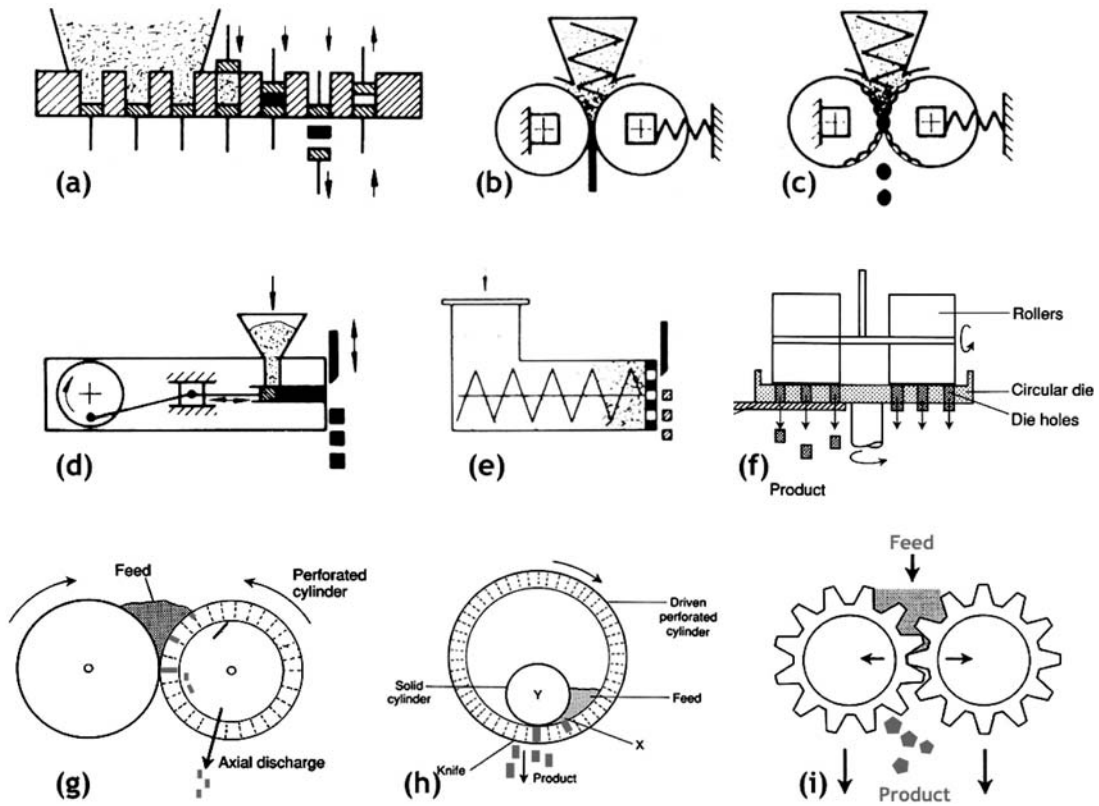


FIG. 21-136 Examples of compressive agglomeration, or compaction, processes. Dry compaction: (a) tableting, (b) roll pressing, (c) briquetting, (d) ram extrusion. Paste extrusion: (e) screw extrusion, (f) table pelletizing, (g) double-roll pelletizing, (h) concentric-roll pelletizing, and (i) tooth extrusion. (After Pietsch, *Size Enlargement by Agglomeration*, Wiley, Chichester, 1992; and Benbow and Bridgwater, *Paste Flow and Extrusion*, Oxford University Press, New York, 1993.)

Powder Feeding Bulk density control of feed materials and reproducible powder feeding are crucial to the smooth operation of compaction techniques. **Flowability data** developed from bulk shear cell and permeability measurements are invaluable in designing machine hoppers for device filling.

As an example, mass flow rates W_s out of openings of diameter B for coarse materials may be estimated by

$$W_s = 0.785\rho_b(B - 1.4d_p)^{2.5} \sqrt{\frac{g}{2m \tan \alpha} \left(1 - \frac{ff}{\text{Rel}}\right)} \quad (21-130)$$

Here, ff is the **flow factor** determining the stress at the opening which is a function of wall and powder friction, Rel is a **relative flow index** giving the ratio of opening stress to the powder's **cohesive strength**, α is the hopper angle, d_p is particle diameter, and $m = 1$ or 2 for slot or conical hoppers, respectively (cf. "Solids Handling"). The relative flow index is indirectly proportional to powder strength. Increasing powder strength lowers feed rate both here and in a general sense. Examples would include hopper discharge, flow into dies, or screw feeding of roll presses. Powder strength generally increases with decreasing particle size, increasing size distribution, decreasing particle hardness, increasing surface energy and increasing shape factor.

Lubricants or glidants are also added in small amounts to improve flow properties. **Glidants** such as fumed silica are often added to lower powder strength. Also note that in contrast, **lubricants** such as magnesium stearate may actually increase powder strength and adversely lower the flow rate. The primary purpose of

lubricants is to modify die friction as discussed below, rather than alter powder flow rates.

Equally important to powder strength and bulk density of the feed is bulk **gas permeability**. Permeability controls the gas pressure developed within the bulk powder during feeding. Lower powder permeability means greater time is required for gas depressurization after movement of the powder, e.g., filling of a roll press gap or tablet die. Permeability is given by the dependence of gas pressure drop in a powder bed on gas velocity. In addition, as powders discharge from feed hoppers, they undergo expansion during movement, requiring in turn that gas flow into the powder. This concurrent flow of gas impedes the powder discharge, with mass discharge rate as given by, e.g., Eq. (21-130) decreasing with decreasing gas permeability. Permeability decreases with decreasing particle size.

Production rate of compaction processes, and the associated quality issues of pushing production limits, is intimately linking to flow properties and permeability. Poor flow properties associated with large cohesive strength will lower filling of dies and presses. In addition to impeding feed rate, low-permeability powders entrap gas, which later becomes pressurized in compaction, leading to compact flaws during stress removal and compact ejection. Low-permeability powders therefore require larger dwell times to allow escape of entrapped gas, if such gas is not removed prior to filling. Feeding problems are most acute for direct **powder filling** of compression devices, as opposed to **granular feeds**. Although industry- and process-specific, gravimetric feeding is preferred, in which variations in flow rate are used in feedback control to modify screw rate, which helps compensate for variations in feed bulk density and cohesive strength. In addition,

complex-force feeding and vacuum-assisted systems have been developed to aid filling and ensure uniform bulk density; such designs aid immensely in compensating for low feed permeability.

Compact Density Compact strength depends on the number and strength of interparticle bonds [Eq. (21-96)] created during consolidation, and both generally increase with increasing compact density. Compact density is in turn a function of the maximum pressure achieved during compaction. The mechanisms of compaction have been discussed by Cooper and Eaton [J. Am. Ceramic Soc., 45, 97 (1962)] in terms of two largely independent probabilistic processes. The first is the filling of large holes with particles from the original size distribution. The second is the filling of holes smaller than the original particles by plastic flow or fragmentation. Additional possible mechanisms include the low-pressure elimination of arches and cavities created during die filling due to wall effects, and the final high-pressure consolidation of the particle phase itself. As these mechanisms manifest themselves over different pressure ranges, four stages of compression are generally observed in the compressibility diagram when density is measured over a wide pressure range (Fig. 21-137). The slope of the intermediate- and high-pressure regions is defined as $1/\kappa$, where κ is the compressibility of the powder. The density at an arbitrary pressure σ is given by a compaction equation of the form

$$\rho = \rho_o \left[\frac{\sigma}{\sigma_o} \right]^{1/\kappa} \tag{21-131}$$

where ρ_o is the density at an arbitrary pressure or stress σ_o . Table 21-14 gives a summary of common compaction relations. For a complete review of compaction equations, see Kawakita and Lüdde [Powder Technol., 4, 61 (1970/71)] and Hersey et al. [Proc. First International Conf. of Compaction & Consolidation of Particulate Matter, Brighton, 165 (1972)].

Compact Strength Both particle size and bond strength control final compact strength for a given compact density or voidage [Eq. (21-96), Fig. 21-93]. Krupp [Adv. Colloidal Interface Sci., 1, 111 (1967)] has shown the adhesive force between two compressed particles varies inversely with hardness, and is proportional to the initial compressive force and surface energy of the particles. Although surface energy and elastic deformation play a role, increasing plastic deformation at particle contacts with decreasing hardness is likely the major mechanism contributing to large permanent bond formation and successful compaction in practice. Figure 21-138 illustrates the strength of mineral compacts of varying hardness and size cut. To obtain significant strength, Benbow (Enlargement and Compaction of Particulate Solids, Stanley-Wood (ed.), Butterworths, 1983, p. 169) found that a critical yield pressure must be exceeded which was independent of size but found to increase linearly with particle hardness. Strength also increases linearly with compaction pressure, with the slope inversely related to particle size. Similar results were obtained by others for ferrous powder, sucrose, sodium chloride, and coal [Hardman and Lilly, Proc. Royal Soc. A., 333, 183 (1973)]. Particle hardness and elasticity may be characterized directly by nanoindentation [Johnson and Ennis,

TABLE 21-14 Common Compaction Relations*

Equation	Authors
$\ln \frac{\rho_t - \rho_c}{\rho_t - \rho_c} = KP_A$	Athy, Shapiro, Heckel, Konopicky, Seelig
$\ln \frac{\rho_c}{\rho_t} \left(\frac{\rho_c - \rho_i}{\rho_t - \rho_c} \right) = KP_A$	Ballhausen
$\ln \frac{\rho_t}{\rho_t} \left(\frac{\rho_t - \rho_i}{\rho_t - \rho_c} \right) = KP_A$	Spencer
$\ln \frac{\rho_c}{\rho_t} = KP_A^a$	Nishihara, Nutting
$\ln \frac{\rho_t - \rho_c}{\rho_t} + K \left(\frac{\rho_c}{\rho_t - \rho_c} \right)^{1/3} = aP_A$	Murray
$\ln \frac{\rho_t}{\rho_c} \left(\frac{\rho_c - \rho_i}{\rho_t - \rho_i} \right) = \ln Ka - (b + c)P_A$	Cooper and Eaton
$\frac{\rho_t}{\rho_c} = 1 - KP_A^a$	Umeya
$\rho_c = KP_A^a$	Jaky
$\rho_c = K(1 - P_A)^a$	Jenike
$\rho_c - \rho_i = KP_A^{1/3}$	Smith
$\rho_c - \rho_i = KP_A^2$	Shaler
$\frac{\rho_c - \rho_i}{\rho_c} = \frac{K \times aP_A}{1 + aP_A}$	Kawakita
$\frac{\rho_t}{\rho_c} \left(\frac{\rho_c - \rho_i}{\rho_t - \rho_i} \right) = \frac{KP_A}{1 + KP_A}$	Aketa
$\frac{1}{\rho_c} = K - a \ln P_A$	Walker, Bal'shin, Williams, Higuchi, Terzaghi
$\rho_c = K + a \ln P_A$	Gurnham
$\frac{1}{\rho_c} = K - a \ln P_A$	Jones
$\frac{1}{\rho_c} = K - a \ln (P_A - b)$	Mogami
$\frac{\rho_c - \rho_i}{\rho_c} = KP_A \rho_i + a \left(\frac{P_A}{P_A + b} \right)$	Tanimoto
$\frac{\rho_c - \rho_i}{\rho_c} = \ln (KP_A + b)$	Rieschel

* ρ_o , density of powder; ρ_i , initial apparent density of powder; ρ_c , density of powder applied pressure P_A ; K , a , b and c are constants.

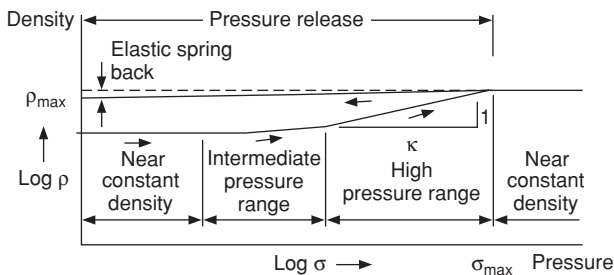


FIG. 21-137 Compressibility diagram of a typical powder illustrating four stages of compaction.

Proc. First International Particle Technology Forum, vol. 2, AIChE, Denver, 1994, p. 178), whereas surface energy can be characterized by inverse gas chromatography and other adsorption techniques. Particle yield pressures and elastic moduli of the powder feeds can also be determined by uniaxial compaction experiments which monitor deformation and pressure throughout the compaction cycles. In addition, rate effects are investigated, as plastic and elastic properties can be rate-dependent for some materials.

Compaction Pressure The minimum compaction pressure is the pressure that induces significant plastic deformation or yielding of the feed particles or granules; i.e., particle/granule strength must be exceeded, such that this pressure exceeds any unloading forces inducing compact failure. Plastic deformation is necessary to produce some measure of final compact strength. While brittle fragmentation may also help increase compact density and points of interparticle bonding as well, in the end some degree of plastic deformation and

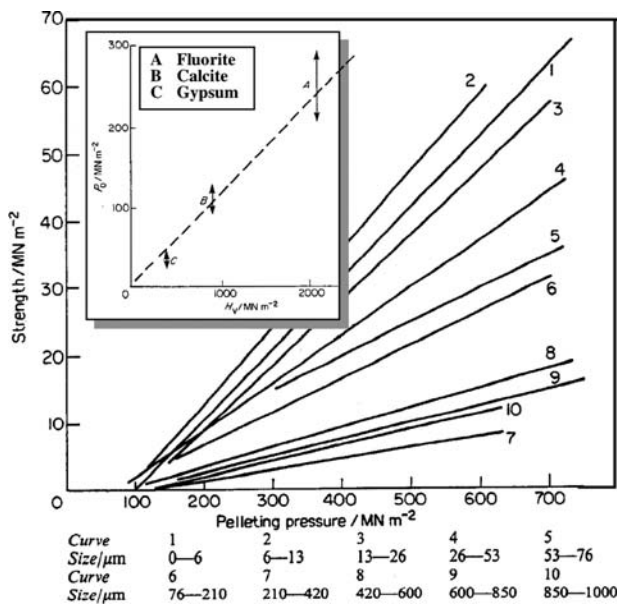


FIG. 21-138 Effect of pelleting pressure on axial crushing strength of compacted calcite particles of different sizes, demonstrating existence of a critical yield pressure. Inset shows the effect of hardness of critical yield pressure. [Benbow, Enlargement and Compaction of Particulate Solids, Stanley-Wood (ed.), Butterworths, 1983, p. 169.]

interlocking is required to achieve some minimum compact strength. Lastly, keep in mind that low powder permeability and entrapped gas may act to later destroy permanent bonding. At the other extreme, compaction pressure is limited since as pressure is raised (e.g., roll load or tableting pressure), elastic effects also increase. During pressure unloading, elastic recovery and gas expansion can induce flaw formation by destroying bonding that was originally created by plastic deformation and adhesion. Therefore, most materials have an allowable compaction pressure range. This range may be narrowed further by other product quality attributes, e.g., desired conveying strength, storage, or redispersion properties. Compacts can be

produced through an automated die compaction simulator, and then the compacts are tested for quality attributes. Such simulators measure all relevant die forces, allowing a connection between powder properties and compaction behavior and product quality. This approach helps identify specific shortcomings in feed properties that require reformulation or improvement. Various quality tests may be employed including compact hardness testing, uniaxial compaction of compacts, shear testing, conveying tests, dust tests, and wetting and dissolution tests.

The development of **flaws** and the loss of interparticle bonding during decompression substantially weaken compacts (see "Breakage and Attrition" subsection). **Delamination** during load removal involves the fracture of the compact into layers, and it is induced by strain recovery in excess of the elastic limit of the material, which cannot be accommodated by plastic flow. Delamination also occurs during compact ejection, where the part of the compact which is clear of the die elastically recovers in the radial direction while the lower part remains confined. This differential strain sets up shear stresses, causing fracture along the top of the compact referred to as **capping**.

Stress Transmission After determination of the necessary compaction pressure range, the compactor must be designed to achieve this desired pressure within the compact geometry for a given loading and dwell time. In this regard, it is key to realize that powders do not uniformly transmit stress with fluids (see "Bulk Powder Characterization Methods: Powder Mechanics"). As pressure is applied to a powder in a die or roll press, various zones in the compact are subjected to **differing intensities of pressure** and shear. Typical pressure and density distributions for uniaxial die compaction are shown in Fig. 21-139. High- and low-density annuli are apparent along the die corners, with a dense axial core in the lower part of the compact and a low-density core just below the moving upper punch. These density variations are due to the formation of a dense conical wedge acting along the top punch (A) with a resultant force directed toward the center of the compact (B). The wedge is densified to the greatest extent by the shearing forces developed by the axial motion of the upper punch along the stationary wall whereas the corners along the bottom stationary die are densified the least (C). The lower axial core (B) is densified by the wedge, whereas the upper low-density region (D) is shielded by the wedge from the full axial compressive force. These variations in pressure lead to local variations in compact density and strength as well as differential zones of expansion upon compact unloading, which in turn can lead to flaws in the compact.

From another point of view, the relationships between compaction pressure and compact strength and density discussed [Table 21-14, Eq. (21-96), Fig. 21-93) and the controlling compaction mechanisms

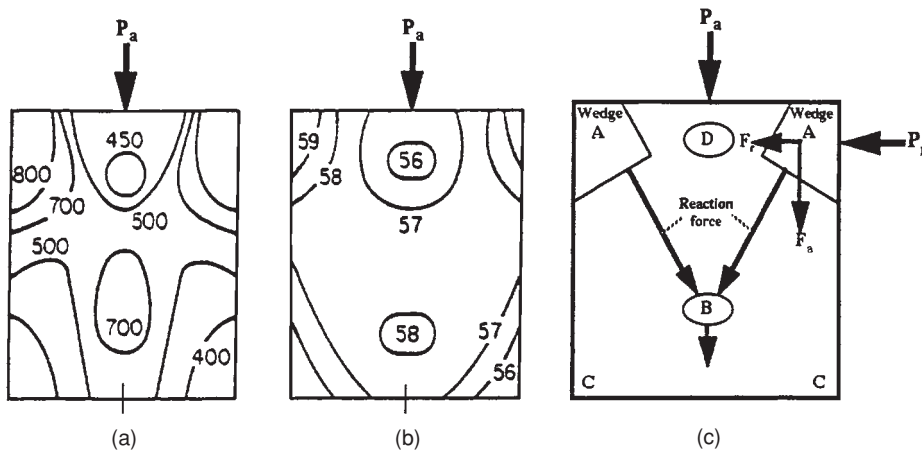


FIG. 21-139 Reaction in compacts of magnesium carbonate when pressed ($P_a = 671 \text{ kg/cm}^2$). (a) Stress contour levels in kilograms per square centimeter. (b) Density contours in percent solids. (c) Reaction force developed at wedge responsible for stress and density patterns. [Train, Trans. Inst. Chem. Eng. (London), 35, 258 (1957).]

are in reality *local relationships* restricted to a small region of the tablet for the given localized pressure. These local volume regions taken together form a compact. The *uniformity of pressure* across these regions is absolutely critical to successful compaction. Applied compaction pressure in fact must be sufficient to induce deformation and bonding in the regions of lowest pressure and weakest resultant strength. If there are wide variations in local pressure, this will by necessity result in high compaction in other regions with associated large elastic recovery during unloading, possibly inducing compact failure. If compact pressure is uniform, less applied average compaction pressure will be required overall, minimizing flaw development and compact ejection forces.

Compaction stress decreases exponentially with axial distance from the applied pressure [Strijbos et al., *Powder Technol.*, **18**, 187, 209 (1977)] due to **frictional properties** of the powder and die wall. As originally demonstrated by Janseen [Zeits. D. Vereins Deutsch Ing., **39**(35), 1045 (1895)], the axial stress experienced within a cylindrical die due to an applied axial load σ_o may be estimated by

$$\sigma_z = \sigma_o e^{-(4\mu_w K_\phi/D)z} \tag{21-132}$$

where D is die diameter, z is axial distance from the applied load, K_ϕ is a lateral stress transmission coefficient (**Janseen coefficient**), and μ_w is the **wall friction coefficient** (see “Bulk Characterization Methods: Powder Mechanics”). The explanation for this drop in compaction pressure may be demonstrated in Fig. 21-140. The given applied load σ_o results in a radial pressure σ_r acting at the wall given by

$$\sigma_r = K_\phi \sigma_o \quad \text{with} \quad K_\phi = (1 - \sin \phi_w)/(1 + \sin \phi_w) \tag{21-133}$$

Radial pressure is therefore controlled by the **effective angle of powder friction** ϕ_w . Typical values range from 40 to 60°, with *increases* in powder friction leading to a decrease in radial pressure for a given loading. Further, note the contrast with typical fluids that develop an isotropic pressure under load. The radial pressure σ_r in turn produces a wall shear stress τ_w which acts to oppose the applied load σ_o , given by:

$$\tau_w = \mu_w \sigma_r \quad \text{with} \quad \mu_w = \tan \phi_w \tag{21-134}$$

and ϕ_w is the **effective angle of wall friction**. Decreasing wall friction lowers the wall shear stress acting to decrease the compaction pressure, for a given radial wall pressure.

The ratio σ_r/σ_o may be taken as a measure of stress uniformity. In practice, it increases toward unity with decreasing aspect ratio of the compact, decreasing diameter, increasing powder friction, and, most important, decreasing wall friction, as controlled by the addition of lubricants. Low stress transmission results in not only poor compact uniformity, but also large residual radial stresses after stress unloading, giving rise to flaws and delamination as well as large die ejection forces.

Equation (21-132) provides only an approximate relation for determining stress distribution during compaction. With modern finite element codes based on soils and plasticity models of powder behavior

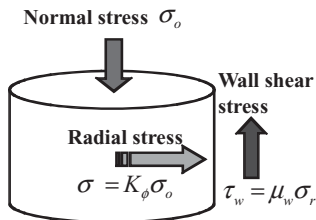


FIG. 21-140 Stresses developed in a column of powder with applied load as a function of powder frictional properties, neglecting gravity. [After Janseen, Zeits. D. Vereins Deutsch Ing., **39**(35), 1045 (1895)].

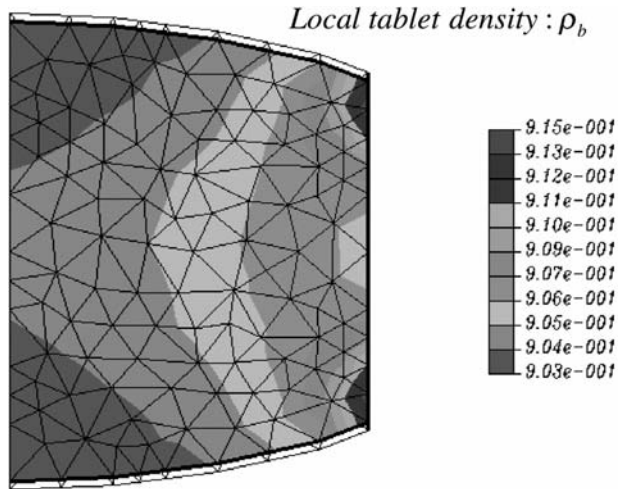


FIG. 21-141 Density developed in one-half of a tablet during compression, based on plasticity and compaction models. (Lewis et al., *Casting and Powder Compaction Group, Department of Mechanical Engineering, University of Wales Swansea*, <http://www.swan.ac.uk/nfa/>, with permission.)

using the above frictional properties, compact density and stress may be determined for any geometry, as illustrated in Fig. 21-141.

Hiestand Tableting Indices Likelihood of failure during decompression depends on the ability of the material to relieve elastic stress by plastic deformation without undergoing brittle fracture, and this is time-dependent. Those which relieve stress rapidly are less likely to cap or delaminate. Hiestand and Smith [*Powder Technol.*, **38**, 145 (1984)] developed three pharmaceutical **tableting indices**, which are applicable for general characterization of powder compactability. The **strain index** (SI) is a measure of the elastic recovery following plastic deformation, the **bonding index** (BI) is a measure of plastic deformation at contacts and bond survival, and the **brittle fracture index** (BFI) is a measure of compact brittleness.

Compaction Cycles Insight into compaction performance is gained from direct analysis of pressure/density data over the cycle of axial compact compression and decompression. Figure 21-142 illustrates typical **Heckel profiles** for plastic and brittle deforming materials which are determined from density measurements of *unloading* compacts. The slope of the curves gives an indication of the yield pressure of the particles. The contribution of fragmentation and rearrangement to densification is indicated by the low-pressure deviation from linearity. In addition, elastic recovery contributes to the degree of hysteresis which occurs in the *at-pressure* density curve during compression followed by decompression [Doelker, *Powder*

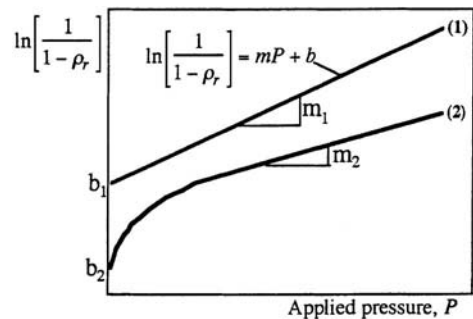


FIG. 21-142 Heckel profiles of the unloaded relative compact density for (1) a material densifying by pure plastic deformation and (2) a material densifying with contributions from brittle fragmentation and particle rearrangement.

Technology and Pharmaceutical Processes, Chulia et al. (eds.), Elsevier, 1994, p. 403].

Controlling Powder Compaction Compaction properties of powders are generally improved by improving flow properties. In particular, stress transmission improves with either lowering the wall friction angle or increasing the angle of friction of the powder. **Internal lubricants** may be mixed with the feed material to be compacted. They aid stress transmission by reducing the wall friction, but may also weaken bonding properties and the unconfined yield stress of the powder as well as lower powder friction, which acts to lower stress transmission. **External lubricants** are applied to the die surface, to impact wall friction alone.

Binders improve the strength of compacts through increased plastic deformation or chemical bonding. They may be classified as **matrix type**, **film type**, and **chemical**. Komarek [*Chem. Eng.*, 74(25), 154 (1967)] provides a classification of binders and lubricants used in the tableting of various materials. See also Parikh (ed.), *Handbook of Pharmaceutical Granulation Technology*, 2d ed., Taylor & Francis, 2005, and Stanley-Wood (ed.), *Enlargement and Compaction of Particulate Solids*, Butterworth & Co. Ltd., 1983.

Particle properties such as size, shape, elastic/plastic properties, and surface properties are equally important. Generally decreased particle or granule hardness, increased surface energy, and raising particle size improve flow properties. Increasing particle size, which raises powder permeability, and applied vacuum and forces loading (e.g., screw or ram designs) help aid powder deaeration. Improved deaeration, powder flowability, and improved stress transmission generally improve all compaction processes, eliminate delamination and flaw formation, and improve production rates.

PASTE EXTRUSION

As in dry compaction processes, size-enlargement processes involving **paste extrusion** are also dominated by powder friction, including, e.g., both radial and axial extrusion in addition to some pressing operations. To illustrate the impact of frictional properties, we consider here an example of axial extrusion, as illustrated in Fig. 21-143 for a single screw extruder. Three key regions may be identified in this case: (1) a metering, mixing, and kneading zone; (2) a solids conveying zone where material is compacted and transported, largely in a plug flow fashion; and (3) the die plate extrusion region. In the conveying region, pressure increases as one moves down the barrel to reach some **maximum backpressure**, which is a function of screw speed, barrel and flight friction, and rheological properties of the paste. In other words, the extruder acts as a pump that can develop a certain total pumping or backpressure. In addition, the plug velocity, and hence throughput, is also a function of friction and rheological properties of the paste. The relationship between this maximum pressure and throughput is referred to as an **extruder characteristic**. The second region is the extrusion process through the die. Given the backpressure developed in the first conveying region, and again the paste rheology and friction, the paste will extrude at a certain rate through the die holes. The relationship between die plate pressure drop and throughput is referred to as a **die plate characteristic**. Therefore, the two regions are coupled through the operating backpressure of the extruder.

Compaction in a Channel Consider a powder being compacted in a channel of wetted perimeter C and cross-sectional area A , as shown in Fig. 21-144. The pressure which develops at the end of the

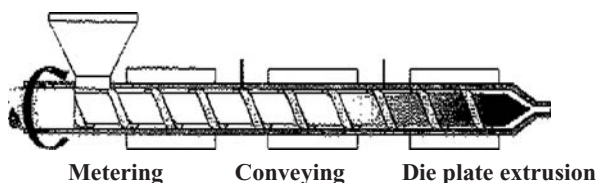


FIG. 21-143 Typical single-screw extruder, identifying key regions.

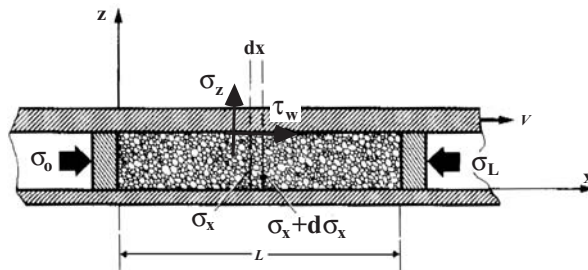


FIG. 21-144 Powder compaction in a channel, and associated force balance.

channel σ_L of width W and length $x = L$ will be given by

$$\sigma_L = \sigma_0 e^{\pm(\mu K_0 C/A)L} = \sigma_0 e^{\pm\mu K_0 [L(2W+2H)/(WH)]} \quad \text{for } v = \pm \text{value} \quad (21-135)$$

where σ_0 is the applied feed pressure and K_0 and μ_w are the stress transmission and wall friction coefficients defined above. Note in comparison Eq. (21-132), where in contrast the sign of the exponential coefficient here depends on the direction of velocity v in Fig. 21-144. For positive velocity, the movement of the walls forward acts to increase the applied feed pressure, with the degree of pressurization increases with increasing wall friction coefficient and aspect ratio (CL/A), as well as increasing K_0 or decreasing powder friction [Eq. (21-133)]. This degree of pressurization is a key source in the driving pressure of extrusion.

Drag-Induced Flow in Straight Channels Consider now a rectangular channel sliding over an infinite plate (Fig. 21-145). The channel represents the unwound flight of a screw of width W and depth H ; and the plate, a barrel moving at a linear velocity V at an angle θ to the down channel direction x . The solids plug formed within the channel moves forward in the down channel direction x at a velocity u due to the friction of the moving upper plate, which conveys it forward as the screw moves backward. The vectorial difference between the plate velocity V and the plug velocity u gives the relative velocity at which the plate slides over the moving plug, or V^* . This produces a frictional wall stress τ_w acting at this top plate (or barrel) on the plug in the same direction as V^* . The angle difference between the plate velocity V and shear stress τ_w is referred to as the solids conveying angle, which is easily shown to be given by

$$\tan \Theta = \frac{u \sin \theta}{V - u \cos \theta} \quad (21-136)$$

The solids conveying angle Θ is zero for stationary solids ($u = 0$) and increases with increasing flow rate or throughput (increasing u). Neglecting the impact of cross-channel modification in friction, a force balance on the plug allows us to determine a relation akin to Eq. (21-135) for compaction in a channel, or

$$\sigma_L = \sigma_0 e^{+(C_b \mu_b \cos(\Theta+\theta) - C_s \mu_s) K_f L/A} = \sigma_0 e^{+(W \mu_b \cos(\Theta+\theta) - (W+2H) \mu_s) K_f L/WH} \quad (21-137)$$

where μ_b and μ_s are the barrel and screw flight friction, respectively. As conveying angle Θ increases, $\cos(\Theta + \theta)$ decreases, and therefore the overall pressure rise in the extruder *decreases*. Since conveying angle increases with increasing throughput [Eq. (21-136)], an inverse relationship exists between throughput and pressure rise. This suggests the following potential implications with regard to extruder operation: (1) Increasing pressure rise *decreases* conveying throughput for constant frictional coefficients, (2) increasing barrel friction or lowering flight friction increases pressure for constant throughput, and (3) increasing barrel friction or lowering flight friction increases throughput for constant pressure rise. Barrel friction acts to increase extruder pressurization, whereas flight friction works against this pressurization. Note also that the exact operating pressure must be determined in conjunction with die face pressure drop.

Paste Rheology Paste frictional and rheological properties control the flow rate through the final extrusion die face or basket. One

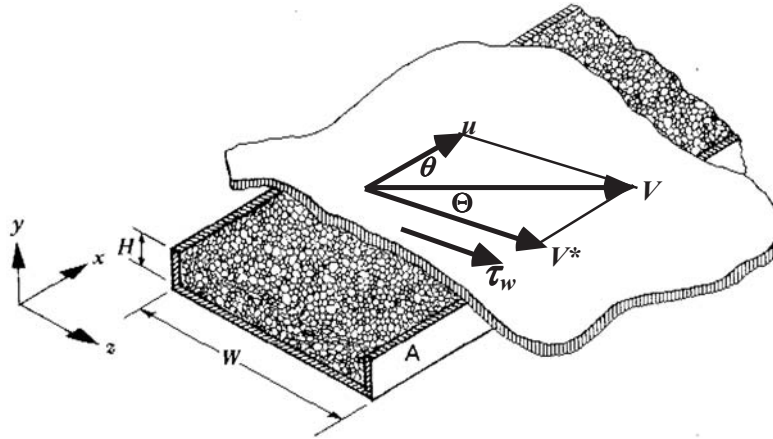


FIG. 21-145 The unwound screw channel, illustrating the barrel moving at a velocity V and at an angle θ with respect to the down channel direction x . The barrel slides over the solids at a relative velocity V^* , resulting in a frictional shear stress along the wall of τ_w and a solids conveying angle of Θ .

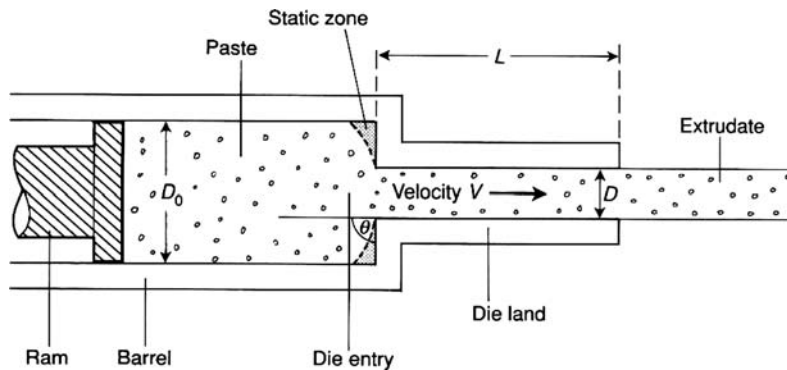


FIG. 21-146 Paste extrusion through a cylindrical die land with square entry. Note that the pressure drop consists of both an orifice pressure drop due to changing area (yielding within the paste) and a die land pressure drop (yielding along the wall). (Benbow and Bridgwater, *Paste Flow and Extrusion*, Oxford University Press, New York, 1993.)

approach to paste rheology is that of **capillary rheometry**, where parameters are determined for the paste as a function of die geometry and velocity, which can be used to determine die pressure drop for the production geometry, or the die characteristic. Figure 21-146 illustrates a typical die geometry, for which the pressure drop is typically modeled by a relationship of the form

$$P_e = P_o + P_f = (\sigma_o + \alpha V^b) \ln A_o/A_1 + (\tau_o + \alpha' V^{b'}) \frac{4L}{D} \quad (21-138)$$

As proposed in the work of Benbow and Bridgwater (*Paste Flow and Extrusion*, Oxford University Press, New York, 1993), the first term P_o represents an orifice pressure in a converging section, required to overcome internal yield stresses within the material as the cross-sectional area is reduced from A_o to A_1 . The second term P_f represents frictional stresses that must be overcome to extrude through the die

land of aspect ratio L/D and constant diameter D . Through capillary rheometry experiments of varying die geometry and throughput, the various constants of Eq. (21-138) are estimated from measured pressure drops. These parameters are then used to calculate the die characteristic for the extruder at hand, namely, the die pressure drop vs. rate.

Although relatively unexplored, an alternative approach is to determine frictional yield properties by high-pressure shear and triaxial cells, and to incorporate these properties into soils or plasticity models for finite element simulations of flow within the extruder body, as has been done for compaction (cf. Fig. 21-141).

With increasing pressure, the conveying throughput provided by the screw will be less, whereas the possible throughput through the die face will be more. The intersection of the extruder and die characteristics determines the critical output of the extruder. (See "Screw and Other Paste Extruders" subsection for details.)

CONTROL AND DESIGN OF GRANULATION PROCESSES

ENGINEERING APPROACHES TO DESIGN

Advances in the understanding of granulation phenomena rest heavily in engineering process design. A change in granule size or voidage is akin to a change in chemical species, and so analogies exist between growth kinetics and chemical kinetics and the unit operations of size enlargement and chemical reaction (Fig. 21-147), where several scales of analysis must be considered for successful process design.

Scales of Analysis Consider the molecular or primary particle/single granule interactions occurring within a small volume element of material *A* within a mixing process, as shown in Fig. 21-148. On this molecular or **granule scale of scrutiny**, the designs of chemical reactors and of granulation processes differ conceptually in that the former deals with **chemical transformations** whereas the latter deals primarily with **physical transformations** controlled by **mechanical processing**. Here, the rate processes of granulation are controlled by a set of key physicochemical interactions defined in the following sections. These mechanisms or rate processes compete to control granule growth on a **granule volume scale of scrutiny**, as shown for the small volume element of material *A* of Fig. 21-148. Within this small volume of material, one is concerned with the rate at which one or more chemical species is converted to a product in the case of chemical kinetic. This is generally dictated by a reaction rate or **kinetic constant**, which is in turn a local function of temperature, pressure, and the concentration of

feed species, as was established from previous physicochemical considerations. These local variables are in turn a function of overall heat, mass, and momentum transfer of the vessel controlled by mixing and heating/cooling. The chemical conversion occurring within this local volume element may be integrated over the entire vessel to determine the chemical yield or extent of conversion for the reactor vessel; the impact of mixing and heat transfer is generally considered in this step at the **process volume scale of scrutiny**. In the case of a granulation process, an identical mechanistic approach exists for design, where chemical kinetics is replaced by **granulation kinetics**. The performance of a *granulator* may be described by the **extent of granulation** of a species. Let (x_1, x_2, \dots, x_n) represent a list of attributes such as average granule size, porosity, strength, and any other generic quality metric and associated variances. Alternatively, (x_1, x_2, \dots, x_n) might represent the concentrations or numbers of certain granule size or density classes, just as in the case of chemical reactors. The proper design of a chemical reactor or a *granulator* then relies on understanding and controlling the evolution (both *time* and *spatial*) of the feed vector *X* to the desired product vector *Y*. Inevitably, the reactor or granulator is contained within a larger plant-scale process chain, or **manufacturing circuit**, with overall plant performance being dictated by the interaction between individual unit operations. At the **plant scale of scrutiny**, understanding interactions between unit operations can be critical to plant performance and product quality. These interactions are far more

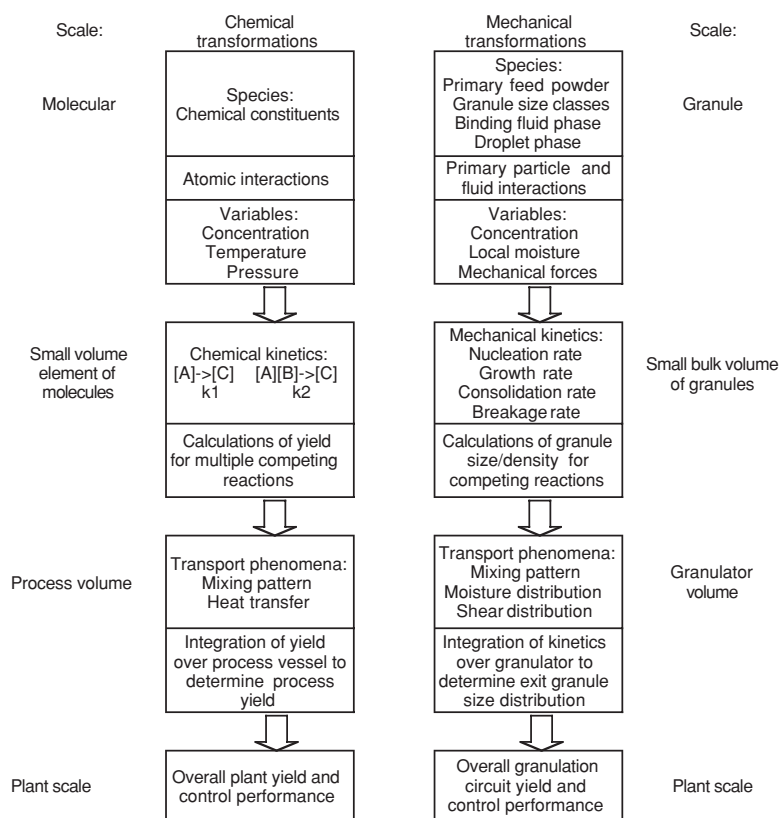


FIG. 21-147 Changes in state as applied to granulator and reactor kinetics and design. [Emis, *Theory of Granulation: An Engineering Approach*, in *Handbook of Pharmaceutical Granulation Technology*, 2d ed., Parikh (ed.), Taylor & Francis, 2005. With permission.]

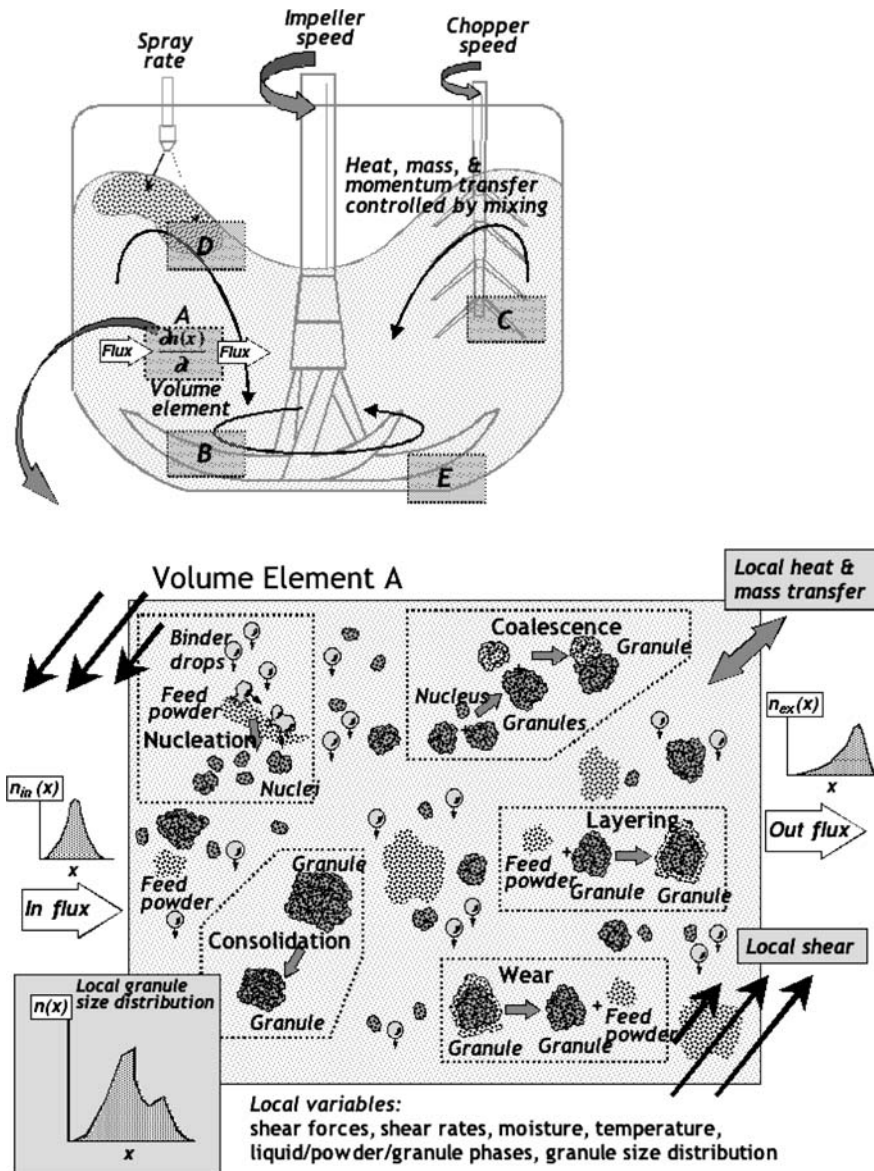


FIG. 21-148 Granulation within a local volume element, as a subvolume of a process granulator volume, which controls local size distribution. [Ennis, *Theory of Granulation: An Engineering Approach*, in Handbook of Pharmaceutical Granulation Technology, 2d ed., Parikh (ed.), Taylor & Francis, 2005. With permission.]

substantial with solids processing than with liquid-gas processing. Ignoring these interactions often leads processing personnel to misdiagnose sources of poor plant performance. We consider each of these scales in greater detail below.

There are several important points worth noting with regard to this approach. First, the design of chemical reactors is well developed and an integral part of traditional chemical engineering education. (See, e.g., Levenspiel, *Chemical Reaction Engineering*, 2d ed., Wiley, New York, 1972.) In contrast, only the most rudimentary elements of reaction kinetics have been applied to granulator design. Second, an appreciation of this engineering approach is absolutely vital to properly scale up granulation processes for difficult formulations. Lastly, this perspective provides a logical framework with which to approach and unravel

complex processing problems, often involving several competing phenomena. Significant progress had been made with this approach in crystallization (Randolph and Larson, *Theory of Particulate Processes*, Academic Press, 1988) and grinding (Prasher, *Crushing and Grinding Process Handbook*, Wiley, 1987). Many complexities arise when applying the results of the previous subsections detailing granulation mechanisms to granulation processing. The purpose of this subsection is to summarize approaches to controlling these rate processes by placing them within the context of actual granulation systems and granulator design. See also "Modeling and Simulation of Granulation Processes."

Scale: Granule Size and Primary Feed Particles When considering a scale of scrutiny of the order of granules, we ask what controls the rate processes. This step links formulation or material

variables to the process operating variables, and successful granulator design hinges on this understanding. Two key local variables of the volume element A include the *local bed moisture* and the local level of shear (both *shear rate* and *shear forces*). These variables play an analogous role of species concentration and temperature in controlling kinetics in chemical reaction. In the case of chemical reaction, increased temperature or concentration of a feed species generally increases the reaction rate. For the case of granulation considered here, increases in shear rate and moisture result in increased granule/powder collisions in the presence of binding fluid, resulting in an increased frequency of successful growth events and increases in granule growth rate. Increases in shear forces also increase the granule consolidation rate and aid growth for deformable formulations. In the limit of very high shear (e.g., due to choppers), they promote wet and dry granule breakage, or limit the growth rate. Lastly, in the case of simultaneous drying, bed and gas-phase moisture and temperature control heat and mass transfer and the resulting drying kinetics, which can be important in fluid-bed granulation and temperature-induced drying in high-shear mixing.

Scale: Granule Volume Element A small bulk volume element A of granules (Fig. 21-148) has a particular granule size distribution, which is controlled by the local granulation rate processes shown pictorially in Fig. 21-149. In the wetting and nucleation rate process, droplets interact with fine powder to form initial nuclei, either directly or through mechanical breakdown of pooled overwetted regions. It is generally useful to consider the initial **powder phase** and **drop phases** as independent feed phases to the **granule phase**. In addition, the granule phase can be broken down into separate **species**, each species corresponding to a particular granule mesh size cut. Nucleation therefore results in a loss of powder and drop phases and the **birth** of granules. Granules and initial nuclei collide within this volume element with one another and with the surrounding powder phase, resulting in both granule growth and consolidation due to compaction forces. Granule growth by coalescence also results in the discrete birth of granules to a new granule size class or species, as well as loss or **death** of granules from the originating size classes. On the other hand, granule growth by layering and granule consolidation result in a slow differential increase and decrease in granule size, respectively. Granule breakage by fracture and attrition (or wear) act in a similar but opposite fashion to granule coalescence and layering,

and increase the powder phase and species of smaller granules. Lastly, this volume element of granules interacts with surrounding bed material, as granulated, powder, and drop phases flow to and from surrounding volume elements. The rate processes of granulation and the mass exchange with surrounding elements combine to control the local granule size distribution and growth rate within this small volume element.

As illustrated in Fig. 21-149, conducting an inventory of all granules entering and leaving a given size class $n(x)$ leads to a microlevel population balance over the volume element A, which governs the **local** average growth rate, given by

$$\frac{\partial n_a}{\partial t} + \frac{\partial}{\partial x_i} (n_a u_i) = G_a = B_a - D_a \quad (21-139)$$

where $n(x,t)$ is the instantaneous granule size distribution, which varies with time and position; G , B , and D are growth, birth, and death rates due to granule coalescence and granule fracture. The second term on the left side reflects contributions to the distribution from layering and wear as well as exchanges of granules with surrounding volume elements. Nucleation rate would be considered a boundary condition of Eq. (21-139), providing a source of initial granules or nuclei.

Solutions to this population balance are described in greater detail in the subsection "Modeling and Simulation of Grinding Processes." Analytical solutions are only possible in the simplest of cases. Although actual processes would require specific examination, some general comments are warranted. Beginning with nucleation, in the case of fast drop penetration into fine powders and for small spray flux, new granules will be formed of the order of the drop size distribution, and will contribute to those particular size cuts or granule species. If spray is stopped at low moisture levels, one might obtain a bimodal distribution of nuclei size superimposed on the original feed distribution. Very little growth may occur for these low moisture levels. This should not be confused with induction-type growth, which is a result of low overall formulation deformability. In fact, the moisture level of the nuclei themselves will be found to be high and nearly saturated. Moisture, however, is locked up within these nuclei, surrounded by large amounts of fine powder. Therefore, it is important not to confuse granule moisture, local moisture, and the overall

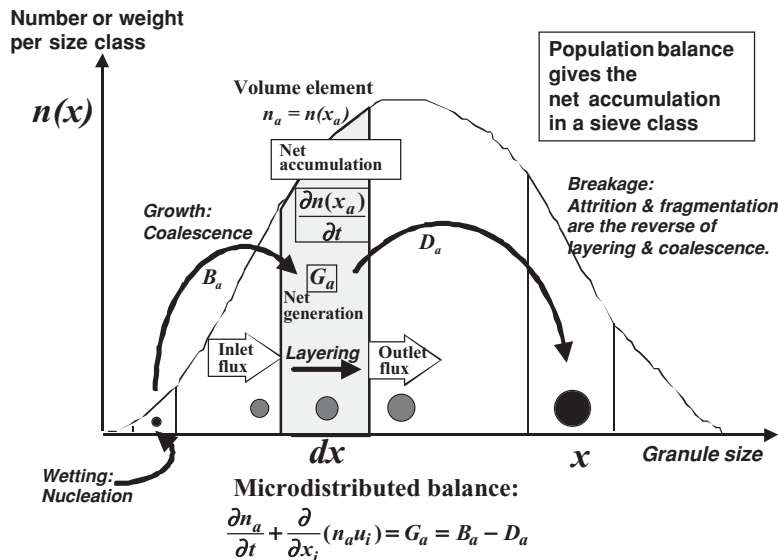


FIG. 21-149 The population balance over a sieve class, over specific granule size class. (Reprinted from Design and Optimization of Granulation and Compaction Processes for Enhanced Product Performance, Ennis, 2006, with permission of E&G Associates. All rights reserved.)

average peak bed moisture of the process; they are very much not the same and are influenced by proper vessel design and operation. As moisture levels increase and the concentration of the *ungranulated* powder phase decreases, the portion of the granule phase increases. As granules begin to interact more fully due to decreased surrounding powder and greater chances to achieve wet granule interaction, granule coalescence begins to occur. This in turn results in a decrease in granule number, and a rapid, often exponential, increase in granule size as previously demonstrated. Coalescence generally leads to an initial widening of the granule-size distribution until the **granule growth limit** is reached. As larger granules begin to exceed this growth limit, they can no longer coalesce with granules of similar size. Their growth rate drops substantially as they can continue to grow only by coalescence with fine granules or by layering with any remaining fine powder. At this point, the granule-size distribution generally narrows with time. Note that this is a *local* description of growth, whereas the overall growth rate of the process depends greatly on mixing, described next, as controlled by process design.

Scale: Granulator Vessel The local variables of moisture and shear level vary with volume element, or position in the granulator, which leads to the kinetics of nucleation, growth, consolidation, and breakage being dependent on position in the vessel, leading to a scale of scrutiny of the vessel size. As shown in Fig. 21-147, moisture levels and drop phase concentration and nucleation will be high at position *D*. Significant growth will occur at position *B* due to increased shear forces and granule deformation, as well as increased contacting. Significant breakage can occur at position *C* in the vicinity of choppers. Each of these positions or volume elements will have its own specific granule-size distribution.

Solids mixing impacts overall granulation in several ways, with mixing details given in subsection "Solids Mixing." (See also Weinekötter and Gericke, *Mixing of Solids*, Kluwer Academic, 2000.) First, it controls the local shear. Local shear rates and forces are a function of shear stress transfer through the powder bed, which is in turn a function of mixer design and bed bulk density, granule size distribution, and frictional properties. Local shear rates determine granule collisional velocities. This first area is possibly one of the least understood areas of powder processing, and it requires additional research to establish the connection between operating variables and local shear rates and forces. It is also a very important scale-up consideration. Second, solids mixing controls the interchange of moisture, powder phase, and droplet phases among the local volume elements. Third, it controls the interchange of the granulated phase.

Within the context of reaction kinetics (Levenspiel, loc.cit.), one considers extremes of mixing between well-mixed continuous and plug flow continuous or well-mixed batch processes. The impact of mixing on reaction kinetics is well understood, and similar implications exist for granulation growth kinetics. In particular, well-mixed continuous processes would be expected to provide the widest granule size distribution (deep continuous fluidized beds are an example), whereas plug flow or well-mixed batch processes should result in narrower distributions. *All else being equal*, plug flow continuous and batch well-mixed processes should produce identical size distributions. An example might include comparing a continuous shallow to a batch fluid-bed granulator. In addition, it is possible to narrow the distribution further by purposely segregating the bed by granule size, or staging the addition of ingredients, although this is a less explored area of granulator design. Pan granulation is a specific process promoting segregation by granule size. Since large granules interact less with smaller granule size classes, layering can be promoted at the expense of coalescence, thereby narrowing the granule-size distribution. Lastly, it should be possible to predict effects of dispersion, backmixing, and dead/stagnant zones on granule-size distribution, based on previous chemical kinetic studies.

Equation (21-139) reflects the evolution of granule size distribution for a particular volume element. When integrating this equation over the entire vessel, one is able to predict the granule-size distribution vs. time and position within the granulator. Lastly, it is important to understand the complexities of scaling rate processes on a local level to overall growth rate of the granulator. If such considerations are not

taken into account, misleading conclusions with regard to granulation behavior may be drawn. Wide distributions in moisture and shear level, as well as granule size, and how this interacts with scale-up must be kept in mind when applying the detailed description of rate processes discussed in the previous subsections.

CONTROLLING PROCESSING IN PRACTICE

Tables 21-15 and 21-16 summarize formulation and operating variables and their impact on granulation. From a processing perspective, we begin with the uniformity of the process in terms of solids mixing. Approaching a uniform state of mixing as previously described will ensure equal moisture and shear levels and therefore uniform granulation kinetics throughout the bed; however, poor mixing will lead to differences in local kinetics. If not accounted for in design, these local differences will lead to a wider distribution in granule-size distribution and properties than is necessary, and often in unpredictable fashions—particularly with scale-up.

Increasing fluid-bed excess gas velocity ($U - U_{mf}$) will increase solids flux and decrease circulation time. This can potentially narrow nuclei distribution for intermediate drop penetration times. Growth rates will be minimally affected due to increased contacting; however, the growth limit will decrease. There will be some increase in granule consolidation, and potentially a large increase in attrition. Lastly, initial drying kinetics will increase. Impeller speed in mixers will play a similar role in increasing solids flux. However, initial growth rates and granule consolidation are likely to increase substantially with an increase in impeller speed. The growth limit will decrease, partly controlled by chopper speed.

Fluidized beds can be one of the most uniform processes in terms of mixing and temperature. Powder frictional forces are overcome as drag forces of the fluidizing gas support bed weight, and gas bubbles promote rapid and intensive mixing. In the case of mixers, impeller speed in comparison to bed mass promotes mixing, with choppers eliminating any gross maldistribution of moisture and overgrowth.

With regard to bed weight, forces in fluid beds and therefore consolidation and granule density generally scale with bed height. As a gross rule of thumb, ideally the power input per unit mass should be maintained with mixer scale-up. However, cohesive powders can be ineffective in transmitting stress, meaning that only a portion of the bed may be activated with shear at large scale, whereas the entire bowl may be in motion at a laboratory scale. Therefore, mixing may not be as uniform in mixers as it is in fluidized beds. Equipment design also plays a large role, including air distributor and impeller/chopper design for fluid beds and mixers, respectively.

Increasing bed moisture and residence time increases overall growth and consolidation. However, it also increases the chances of bed defluidization or overmassing/bowl buildup in fluid beds and mixers, respectively. Increasing bed temperature normally acts to lower bed moisture due to drying. This acts to raise effective binder viscosity and lower granule consolidation and density, as well as initial growth rates for the case of high-shear mixers. This effect of temperature and drying generally offsets the inverse relationship between viscosity and temperature.

Spray distribution generally has a large effect in fluid beds, but in many cases, a small effect in mixers. In fact, fluid-bed granulation is only practical for wettable powders with short drop penetration time, since otherwise defluidization of the bed would be promoted to local pooling of fluid. Mechanical dispersion counteracts this in mixers. There may be a benefit, however, to slowing the spray rate in mixers for formulation with inductive growth behavior, as this will minimize the lag between spray and growth, as discussed previously.

In summary, for the case of fluid-bed granulation, growth rate is largely controlled by spray rate and distribution and consolidation rate by bed height and peak bed moisture. For the case of mixers, growth and consolidation are controlled by impeller and chopper speed. From a formulation perspective, we now turn to each rate process.

Controlling Wetting in Practice Table 21-17 summarizes typical changes in material and operating variables which improve wetting uniformity. Also listed are appropriate routes to achieve these changes

TABLE 21-15 Impact of Key Operating Variables in Fluid-Bed and Mixer Granulation

Effect of changing key process variables	Fluidized beds (including coating and drying)	High-shear mixers
Increasing solids mixing, solids flux, and bed agitation	Increasing excess gas velocity: Improves bed uniformity Increases solids flux Decreases solids circulation time Potentially improves nucleation Has no effect on noninertial growth rate Lowers growth limit Shows some increase in granule consolidation Increases granule attrition Increases initial drying kinetics Distributor design: Impacts attrition and defluidization	Increasing impeller/chopper speed: Improves bed uniformity Increases solids flux Decreases solids circulation time Potentially improves nucleation Increases growth rate Lowers growth limit Increases granule consolidation Increases granule attrition Impeller/chopper design: Improvements needed to improve shear transmission for cohesive powders
Increasing bed weight	Increasing bed height: Increases granule consolidation, density, and strength	Increasing bed weight: Generally lowers power per unit mass in most mixers, lowering growth rate Also increases nonuniformity of cohesive powders, and lowers solids flux and increases circulation time
Increasing bed moisture (Note: Increasing bed temperature normally acts to lower bed moisture due to drying.) Increasing residence time	Increases rates of nucleation, growth, and consolidation, giving larger, denser granules with generally a wider distribution. Distribution can narrow if growth limit is reached. Increases chances of defluidization	Increases rates of nucleation, growth, and consolidation giving larger, denser granules with generally a wider distribution Distribution can narrow if growth limit is reached. Increases chances of over massing and bowl buildup
Increasing spray distribution: Lowers liquid feed or spray rate Lowers drop size Increases number of nozzles Increases air pressure (two-fluid nozzles) Increases solids mixing (above)	Largely affected Wettable powders and short penetration times generally required For fast penetration: Decreases growth rate Decreases spread of size distribution Decreases granule density and strength For slow penetration: Poor process choice Defluidization likely	Less affected Poorly wetting powders and longer penetration time possible For fast penetration: Decreases growth rate Decreases spread of size distribution Decreases granule density and strength For slow penetration: Mechanical dispersion of fluid Little effect on distribution; however, slowing rate of addition minimizes lag in growth rate
Increasing feed particle size (can be controlled by milling)	Requires increase in excess gas velocity Has minimal effect on growth rate Increases in granule consolidation and density	Increases growth rate Increases granule consolidation and density

Ennis, *Theory of Granulation: An Engineering Approach*, in Handbook of Pharmaceutical Granulation Technology, 2d ed., Parikh (ed.), Taylor & Francis, 2005. With permission.

in a given variable through changes in either the formulation or processing. Improved wetting uniformity generally implies a tighter granule size distribution and improved product quality. Equations (21-99), (21-103), and (21-107) provide basic trends of the impact of material variables on wetting dynamics and extent, as described by the dimensionless spray flux and drop penetration time.

Since drying occurs simultaneously with wetting, the effect of drying can substantially modify the expected impact of a given process variable, and this should not be overlooked. In addition, simultaneously drying often implies that the *dynamics* of wetting are far more important than the *extent*.

Adhesion tension should be maximized to increase the rate and extent of both binder spreading and binder penetration. Maximizing adhesion tension is achieved by minimizing contact angle and maximizing surface tension of the binding solution. These two aspects work against each other as surfactant is added to a binding fluid, and in general, there is an optimum surfactant concentration for the formulation. Surfactant type influences adsorption and desorption kinetics at the three-phase contact line. Inappropriate surfactants can lead to

Marangoni interfacial stresses which slow the dynamics of wetting. Additional variables which influence adhesion tension include (1) impurity profile and particle habit/morphology typically controlled in the particle formation stage such as crystallization, (2) temperature of granulation, and (3) technique of grinding, which is an additional source of impurity as well.

Decreases in binder viscosity enhance the rate of both binder spreading and binder penetration. The prime control over the viscosity of the binding solution is through binder concentration. Therefore, liquid loading and drying conditions strongly influence binder viscosity. For processes *without simultaneous drying*, binder viscosity generally decreases with increasing temperature. For processes *with simultaneous drying*, however, the dominant observed effect is that lowering temperature lowers binder viscosity and enhances wetting due to decreased rates of drying and increased liquid loading.

Changes in particle-size distribution affect the pore distribution of the powder. Large pores between particles enhance the *rate* of binder penetration, whereas they decrease the final *extent*. In addition, the particle size distribution affects the ability of the particles to pack

TABLE 21-16 Summary of Governing Groups for Granulation and Compaction

Rate process and governing groups	Key formulation properties governing group increases with:	Key process parameters governing group increases with:
Wetting and nucleation Spray flux ψ_s (small flux desirable)	Decreasing binder viscosity, per its effect on atomization	Increasing spray volume or rate Decreasing number on nozzles Decreasing solids flux Decreasing solids velocity, e.g., impeller or drum speed, fluidization velocity Decreasing spray area Decreasing spray time Decrease bed circulation time Increasing drop size
Drop penetration time τ_p (small time desirable)	Decreasing adhesion tension Increasing binder viscosity Decreasing effective powder pore size	
Growth and consolidation Viscous and deformation Stokes numbers St_v and St_{def} Granule saturation S Bulk capillary number Ca	Decreasing formulation yield stress Decreasing binder viscosity Increasing granule density Increasing granule size Increasing primary particle size or granule voidage Increasing binder viscosity Increasing particle friction Decreasing surface tension	Increase bed moisture or saturation Increasing granule collision velocity (Table 21-41) Increasing impeller and chopper speeds, drum speed, fluidization velocity Increasing bed height or scale Increasing granule collision velocity
Breakage Viscous and deformation Stokes numbers St_v and St_{def} for wet breakage Some relationship between toughness, hardness, and energy (yet undefined)	As above for growth and consolidation Decreasing fracture toughness Mechanism-dependent, hardness Increasing granule density Increasing granule voidage	As above for growth and consolidation Increasing granule collision velocity Increasing bed turnover and erosion displacement
Solids mixing Froude number Fr Some measure of frictional shear to inertia (yet undefined)	Increasing granule density Increasing interparticle friction Decreasing granule density	Increasing impeller diameter or vessel scale Increasing impeller speed Increasing collision velocity
Compaction Stress transmission ratio (high desirable) (low desirable) Relative deaeration time (low desirable) Relative permanent adhesion	Decreasing wall friction Increasing powder friction Decreasing bulk permeability Decreasing particle hardness Increasing surface energy (See also Hiestand indices)	Decreasing gap and die aspect ratio Increasing production rate Increasing compaction pressure

Reprinted from Design and Optimization of Granulation and Compaction Processes for Enhanced Product Performance, Ennis, 2006, with permission of E&G Associates. All rights reserved.

TABLE 21-17 Controlling Wetting in Granulation Processes

Typical changes in material or operating variables that improve wetting uniformity	Appropriate routes to alter variable through formulation changes	Appropriate routes to alter variable through process changes
Increase adhesion tension. Maximize surface tension. Minimize contact angle.	Alter surfactant concentration or type to maximize adhesion tension and minimize Marangoni effects. Precoat powder with wettable monolayers, e.g., coatings or steam.	Control impurity levels in particle formation. Alter crystal habit in particle formation. Minimize surface roughness in milling.
Decrease binder viscosity.	Lower binder concentration. Change binder. Decrease any diluents and polymers that act as thickeners.	Raise temperature for processes without simultaneous drying. Lower temperature for processes with simultaneous drying since binder concentration will decrease due to increased liquid loading.
Increase pore size to increase rate of fluid penetration. Decrease pore size to increase extent of fluid penetration.	Modify particle-size distribution of feed ingredients.	Alter milling, classification or formation conditions of feed if appropriate to modify particle size distribution.
Improve spray distribution (related to dimensionless spray flux, given by ratio of spray to solid fluxes).	Improve atomization by lowering binder fluid viscosity.	Increase wetted area of the bed per unit mass per unit time by increasing the number of spray nozzles, lowering spray rate; increase air pressure or flow rate of two fluid nozzles.
Increase solids mixing (related to dimensionless spray flux).	Improve powder flowability of feed.	Increase agitation intensity (e.g., impeller speed, fluidization gas velocity, or rotation speed).
Minimize moisture buildup and losses.	Avoid formulations that exhibit adhesive characteristics with respect to process walls.	Maintain spray nozzles to avoid caking and nozzle drip. Avoid spray entrainment in process airstreams and spraying process walls.

Reprinted from Design and Optimization of Granulation and Compaction Processes for Enhanced Product Performance, Ennis, 2006, with permission of E&G Associates. All rights reserved.

21-116 SOLID-SOLID OPERATIONS AND PROCESSING

TABLE 21-18 Controlling Growth and Consolidation in Granulation Processes

Typical changes in material or operating variables that maximize growth and consolidation	Appropriate routes to alter variable through formulation changes	Appropriate routes to alter variable through process changes
Rate of growth (low deformability): Increase rate of nuclei formation. Increase collision frequency. Increase residence time.	Improve wetting properties. (See "Wetting" subsection.) Increase binder distribution.	Increase spray rate and number of drops. Increase mixer impeller or drum rotation speed or fluid-bed gas velocity. Increase batch time or lower feed rate.
Rate of growth (high deformability): Decrease binder viscosity. Increase agitation intensity. Increase particle density. Increase rate of nuclei formation, collision frequency, and residence time, as above for low-deformability systems.	Decrease binder concentration or change binder. Decrease any diluents and polymers that act as thickeners.	Decrease operating temperature for systems with simultaneous drying. Otherwise increase temperature. Increase mixer impeller or drum rotation speed or fluid-bed gas velocity.
Extent of growth: Increase binder viscosity. Decrease agitation intensity. Decrease particle density. Increase liquid loading.	Increase binder concentration, change binder, or add diluents and polymers as thickeners.	Increase operating temperature for systems with simultaneous drying. Otherwise decrease temperature. Decrease mixer impeller or drum rotation speed or fluid-bed gas velocity. Extent observed to increase linearly with moisture.
Rate of consolidation: Decrease binder viscosity. Increase agitation intensity. Increase particle density. Increase particle size.	As above for high-deformability systems. Particle size and friction strongly interact with binder viscosity to control consolidation. Feed particle size may be increased and fine tail of distribution removed.	As above for high-deformability systems. In addition, increase compaction forces by increasing bed weight, or altering mixer impeller or fluid-bed distributor plate design. Size is controlled in milling and particle formation.

Reprinted from Design and Optimization of Granulation and Compaction Processes for Enhanced Product Performance, Ennis, 2006, with permission of E&G Associates. All rights reserved.

TABLE 21-19 Controlling Breakage in Granulation Processes

Typical changes in material or operating variables which minimize breakage	Appropriate routes to alter variable through formulation changes	Appropriate routes to alter variable through process changes
Increase fracture toughness. Maximize overall bond strength. Minimize agglomerate voidage.	Increase binder concentration or change binder. Bond strength is strongly influenced by formulation and compatibility of binder with primary particles.	Decrease binder viscosity to increase agglomerate consolidation by altering process temperatures (usually decrease for systems with simultaneous drying). Increase bed agitation intensity (e.g., increase impeller speed, increase bed height) to increase agglomerate consolidation. Increase granulation residence time to increase agglomerate consolidation, but minimize drying time.
Increase hardness to reduce wear: Minimize binder plasticity. Minimize agglomerate voidage.	Increase binder concentration or change voidage. binder. Binder plasticity is strongly influenced by binder type.	See above effects which decrease agglomerate voidage.
Decrease hardness to reduce fragmentation: Maximize binder plasticity. Maximize agglomerate voidage.	Change binder. Binder plasticity is strongly influenced by binder type. Apply coating to alter surface hardness.	Reverse the above effects to increase agglomerate voidage.
Decrease load to reduce wear.	Lower formulation density.	Decrease bed agitation and compaction forces (e.g., mixer impeller speed, fluid-bed height, bed weight, fluid-bed excess gas velocity). Decrease contacting by lowering mixing and collision frequency (e.g., mixer impeller speed, excess fluid-bed gas velocity, drum rotation speed).
Decrease contact displacement to reduce wear.		
Decrease impact velocity to reduce fragmentation.	Lower formulation density.	Decrease bed agitation intensity (e.g., mixer impeller speed, fluid-bed excess gas velocity, drum rotation speed). Also it is strongly influenced by distributor plate design in fluid beds, or impeller and chopper design in mixers.

Reprinted from Design and Optimization of Granulation and Compaction Processes for Enhanced Product Performance, Ennis, 2006, with permission of E&G Associates. All rights reserved.

within the drop as well as the final degree of saturation [Waldie, *Chem. Eng. Sci.*, **46**, 2781 (1991)].

The drop distribution and spray rate of binder fluid have a major influence on wetting. Generally, finer drops will enhance wetting as well as the distribution of binding fluid. The more important question, however, involves how large may the drops be or how high a spray rate is possible. The answer depends on the wetting propensity of the feed. If the liquid loading for a given spray rate exceeds the ability of the fluid to penetrate and spread on the powder, maldistribution in binding fluid will develop in the bed. This maldistribution increases with increasing spray rate, increasing drop size, and decreasing spray area (due to, e.g., bringing the nozzle closer to the bed or switching to fewer nozzles). The maldistribution will lead to large granules on one hand and fine ungranulated powder on the other. In general, the width of the granule-size distribution will increase, and generally the average size will decrease. Improved spray distribution can be aided by increases in agitation intensity (e.g., mixer impeller or chopper speed, drum rotation rate, or fluidization gas velocity) and by minimizing moisture losses due to spray entrainment, dripping nozzles, or powder caking on process walls.

Controlling Growth and Consolidation in Practice Table 21-18 summarizes typical changes in material and operating variables which maximize granule growth and consolidation. Also listed are appropriate routes to achieve these changes in a given variable through changes in either the formulation or processing. Growth and consolidation of granules are strongly influenced by rigid (especially fluid-beds) and deformability (especially mixers) Stokes numbers. Increasing St increases energy with respect to dissipation during deformation of granules. Therefore, the rate of growth for deformable

systems (e.g., deformable formulation or high-shear mixing) and the rate of consolidation of granules generally increase with increasing St . St may be increased by decreasing binder viscosity or increasing agitation intensity. Changes in binder viscosity may be accomplished by formulation changes (e.g., the type or concentration of binder) or by operating temperature changes. In addition, simultaneous drying strongly influences the effective binder concentration and viscosity. The *maximum* extent of growth increases with decreasing St and increased liquid loading. Increasing particle size also increases the rate of consolidation, and this can be modified by upstream milling or crystallization conditions.

Controlling Breakage in Practice Table 21-19 summarizes typical changes in material and operating variables necessary to minimize breakage. Also listed are appropriate routes to achieve these changes in a given variable through changes in either the formulation or processing. Both fracture toughness and hardness are strongly influenced by the compatibility of the binder with the primary particles, as well as the elastic and plastic properties of the binder. In addition, hardness and toughness increase with decreasing voidage and are influenced by previous consolidation of the granules. While the direct effect of increasing gas velocity and bed height is to increase breakage of dried granules, increases in these variables may also act to increase consolidation of wet granules, lower voidage, and therefore lower the final breakage rate. Granule structure also influences breakage rate; e.g., a layered structure is less prone to breakage than a raspberry-shaped agglomerate. However, it may be impossible to compensate for extremely low toughness by changes in structure. Measurements of fracture properties help define expected breakage rates for a product and aid product development of formulations.

SIZE ENLARGEMENT EQUIPMENT AND PRACTICE

GENERAL REFERENCES: Ball et al., *Agglomeration of Iron Ores*, Heinemann, London, 1973. Benbow and Bridgwater, *Paste Flow and Extrusion*, Oxford University Press, New York, 1993. Ennis, *Design and Optimization of Granulation and Compaction Processes for Enhanced Product Performance*, E&G Associates, Nashville, Tenn., 2006. Kristensen, *Acta Pharm. Suec.*, **25**, 187 (1988). Lister and Ennis, *The Science and Engineering of Granulation Processes*, Kluwer Academic Publishers, 2005. Parikh (ed.), *Handbook of Pharmaceutical Granulation Technology*, 2d ed., Taylor & Francis, 2005. Masters, *Spray Drying in Practice*, SprayDryConsult International ApS, 2002. Master, *Spray Drying Handbook*, 5th ed., Longman Scientific Technical, 1991. Pietsch, *Size Enlargement by Agglomeration*, Wiley, Chichester, 1992. Pietsch, *Roll Pressing*, Heyden, London, 1976. Stanley-Wood, *Enlargement and Compaction of Particulate Solids*, Butterworth & Co. Ltd., 1983.

Particle-size enlargement equipment can be classified into several groups, with typical objectives summarized in Table 21-10 and advantages and applications summarized in Table 21-11. See "Scope and Applications." Comparisons of bed agitation intensity, compaction pressures, and product bulk density for select agglomeration processes are highlighted in Fig. 21-111. Terminology is industry-specific. In the following discussion, particle-size enlargement in tumbling, mixer, and fluidized-bed granulators is referred to as **granulation**. Granulation processes vary from low to medium levels of applied shear and stress, producing granules of low to medium density. The presence of liquid binder is essential for granule growth and green strength. Granulation includes pelletization or balling as used in the iron ore industry, but does not include the breakdown of compacts by screening as used in some tableting industries. The term *pelleting* or *pelletization* is used for extrusion processes only. **Spray processes** include slurry atomization operations such as prilling and spray drying. **Pressure compaction processes** include dry compaction techniques such as roll pressing and tableting and wet techniques such as radial and axial extrusion. Compaction processes rely on pressure to

increase agglomerate density and give sufficient compact strength, either with or without liquid binder, with a resulting high compact density.

In fluidized-bed granulators, the bed of solids is supported and mixed by fluidization gas, generally with simultaneously drying. With small bed agitation intensities and high binder viscosities due to drying, **fluidized-bed granulators** can produce one of the lowest-density granules of all processes, with the exception of spray drying. Fluidized and spouted fluidized beds are also used for coating or layering applications from solution or melt feeds, which can produce spherical, densely layered granules. At the other extreme of granulation processes are **high-shear mixer-granulators**, where mechanical blades and choppers induce binder distribution and growth, producing dense, sometimes irregular granules. Fluidized beds are generally a low-agitation, low-deformability process where spray distribution is critical, whereas mixer-granulators lie at the other end of bed agitation as a high-agitation, high-deformability process dominated by shear forces and formulation deformability. (See "Growth and Consolidation," Figs. 21-110 and 21-111.) **Tumbling granulators** such as rotating discs and drums produce spherical granules of low to medium density, and lie between fluidized bed and mixer in terms of bed agitation intensity and granule density. They have the highest throughput of all granulation processes, often with high recycle ratios. Preferential segregation in, e.g., disc granulators can produce very tight size distributions of uniform spherical granules. Mixer and fluid-bed granules operate as both continuous and batch-processed, dependent on the specific industry. See "Growth and Consolidation" and "Controlling Wetting in Practice" subsections for a discussion of granulation mechanisms and controlling properties.

Extrusion processes can operate wet or dry to produce narrowly sized, dense agglomerates or pellets. Wet extrusion is also often followed by spherization techniques to round the product. Extrusion

operates on the principle of forcing powder in a plastic state through a die, perforated plate, or screen. Material undergoes substantial shear in the equipment, and operation and product attributes are strongly influenced by the frictional interaction between the powder and wall. For wet extrusion, the rheology of the wet mass or paste is also important. In compaction processes, material is directly consolidated between two opposing surfaces, with varying degrees of powder confinement. These processes exert the highest applied force of any size enlargement device to give the highest density product. Successful operation depends on good transmission of the applied force through the powder, escape of any entrapped gases, and development of strong interparticle bonds. Both extrusion and compaction processes are very sensitive to powder flow and mechanical properties of the feed. See "Powder Compaction" and "Powder Extrusion" for a discussion of feed property impact on equipment performance.

The choice of size enlargement equipment for a product at hand is subject to a variety of constraints, some of which are listed in Table 21-20. Ideally, the choice of equipment should be made on the basis of the desired final product attributes, making allowances for any special processing requirements (e.g., heat, moisture sensitivity, polymorphism). In practice, however, the dominant driver behind technology selection for a company relies heavily on historical process experience. Unfortunately, this can lead to long-term challenges if a new product is envisioned which differs significantly in formulation feed and final product attributes. Mixers do not generally produce porous, low-density granules, can be difficult to scale over large volume changes, and can produce significant frictional heating. On the other hand, fluid beds cannot process hydrophobic formulations or produce dense granules, with layering for slurry sprays being an exception, but are easier to scale up in practice and are robust to feed property changes. Compaction of fine powder (direct compression) and extrusion processes are sensitive to frictional properties and cannot tolerate large upstream variations in size distribution of a formulation. In many cases tradeoffs must be made. For example, a desire to eliminate solvent and dust handling in fluid-bed processing must be balanced by the fact that this process produces porous granules that might be highly desirable for their fast dissolution behavior. Lastly, in choosing and designing a granulation process, one must consider both product and process engineering, as discussed above ("Process vs. Formulation Design"). The range of possible product attributes is set during feed powder formulation, or **product engineering**, and control within this range is specific to the operating variables chosen during **process engineering**. The degree of interaction of these endeavors governs the success of the size-enlargement process as well as any scale-up efforts. We now discuss the myriad equipment choices avail-

TABLE 21-20 Considerations for Choice of Size-Enlargement Process

Final product attributes, in particular agglomerate size, size distribution, voidage, strength, and dissolution behavior
Form of the active ingredient (dry powder, melt, slurry, or solution), and its amount and nature (hydrophobic, hydrophilic, moisture or heat sensitivity, polymorphic changes)
Need for moisture-sensitive (dry processing) formulations or heat-sensitive formulations
Robustness of a process to handle a wide range of formulations, as opposed to a dedicated product line
Air and solvent handling requirements as well as degree of unit containment due to dust or solvent hazards
Desired scale of operation, and type (batch vs. continuous). Ease of process scale-up and scale-down, as well as range of granule property control at one scale
Multiple unit operations in one vessel (e.g., granulation, drying, coating in a fluidized bed)
Process monitoring capabilities and ease of integration into process control schemes
Maintenance and utility requirements; ease of cleaning to prevent product cross-contamination
Integration of size enlargement equipment into existing process plant
Existing company and supporting vendor experience with specific granulation equipment

able. Related granulation and compaction mechanisms have been discussed previously within the context of formulation and product engineering (see "Agglomeration Rate Processes and Mechanics.")

TUMBLING GRANULATORS

In **tumbling granulators**, particles are set in motion by the tumbling action caused by the balance between gravity and centrifugal forces. The most common types of tumbling granulators are **drum** and inclined **disc granulators**. Their use is widespread including the iron ore industry (where the process is sometimes called **balling** or **wet pelletization**), fertilizer manufacturer, and agricultural chemicals.

Tumbling granulators generally produce granules in the size range of 1 to 20 mm and are not suitable for making granules smaller than 250 μm . Granule density generally falls between that of fluidized-bed and mixer granulators (Fig. 21-111), and it is difficult to produce highly porous agglomerates in tumbling granulators. Tumbling equipment is also suitable for coating large particles, but it is difficult to coat small particles, as growth by **coalescence** of the seed particles is hard to control.

Drum and disc granulators generally operate in **continuous feed** mode. A key advantage to these systems is the ability to run at large scale. Drums with diameters up to 4 m and throughputs up to 100 tons/h are widely used in the mineral industry.

Disc Granulators Figure 21-150 shows the elements of a **disc granulator**. It is also referred to as a **pelletizer** in the iron ore industry or a **pan granulator** in the agricultural chemical industry. The equipment consists of a rotating tilted disc or pan with a rim. Solids and fluid agents are continuously added to the disc. A coating of the feed material builds up on the disc, and the thickness of this layer is controlled by scrapers or a plow, which oscillate mechanically. The surface of the pan may also be lined with expanded metal or an abrasive coating to promote proper lifting and cascading of the particulate bed, although this is generally unnecessary for fine materials. Solids are typically introduced to the disc by either volumetric or gravimetric feeders, preferable at the bottom edge of the rotating granular bed. Gravimetric feeding generally improves granulation performance due to smaller fluctuations in feed rates. Such fluctuations act to disrupt rolling action in the disc and can lead to maldistributions in moisture and local buildup on the disc surface. Wetting fluids that promote growth are generally applied by a series of single-fluid spray nozzles distributed across the face of the bed. Solids feed and spray nozzle locations have a pronounced effect on granulation performance and granule structure.

Variations of the simple disc shape include (1) an outer reroll ring which allows granules to be simultaneously coated or densified without further growth, (2) multisteped sidewalls, and (3) a pan in the form of a truncated cone (Capes, *Particle Size Enlargement*, Elsevier, 1980). Discs in the form of deep pans running close to horizontal with internal blades and choppers are also available, as a hybrid disc-mixer system.

The required disc rotation speed is given in terms of the **critical speed**, i.e., the speed at which a single particle is held stationary on the rim of the disc due to centripetal forces. The critical speed N_c is given by

$$N_c = \sqrt{\frac{g \sin \delta}{2\pi^2 D}} \quad (21-140)$$

where g is the gravitational acceleration, δ is the angle of the disc to the horizontal, and D is the disc diameter. The typical operating range for discs is 50 to 75 percent of critical speed, with angles δ of 45 to 55°. This range ensures a good tumbling action. If the speed is too low, sliding will occur. If the speed is too high, particles are thrown off the disc or openings develop in the bed, allowing spray *blow-through* and uneven buildup on the disc bottom. Proper speed is influenced by flow properties of the feed materials, bed moisture, and pan angle, in addition to granulation performance.

Discs range in size from laboratory units of 30 cm in diameter up to production units of 10 m in diameter with throughputs ranging from 1000 lb/h up to 100 tons/h in the iron ore industry. Figure 21-151

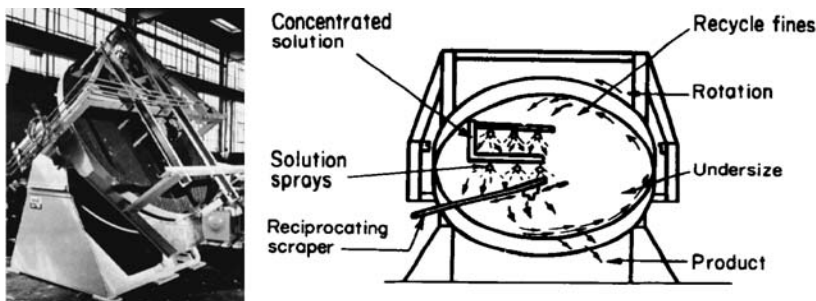


FIG. 21-150 A typical disc granulator [Capes, Particle Size Enlargement, Elsevier, 1980].

shows throughput capacities for discs of varying diameters for different applications and formulation feed densities. When scaling up from laboratory or pilot tests, it is usual to keep the same disc angle and fraction of critical speed. Power consumption and throughput are approximately proportional to the square of disc diameters, and disc height is typically 10 to 20 percent of diameter. It should be emphasized that these relationships are best used as a guide and in combination with actual experimental data on the system in question to indicate the approximate effect of scale-up.

A key feature of disc operation is the inherent **size classification** (Fig. 21-152). Centripetal forces throw small granules and ungranulated feed high on the disc, whereas large granules remain in the **eye** and exit as product. In addition, the granular bed generally sits on a bed of ungranulated powder and freshly formed nuclei. **Size segregation** leads to exit of only product granules from the eye at the rim of the disc. This classification effect substantially narrows exit granule-size distribution, as compared to drum granulators, and discs typically operate with little or no pellet recycle. Due to this segregation, positioning of the feed and spray nozzles is key in controlling the balance of granulation rate processes and resultant granule structure. Disc granulators produce the narrowest first-pass granule size distribution

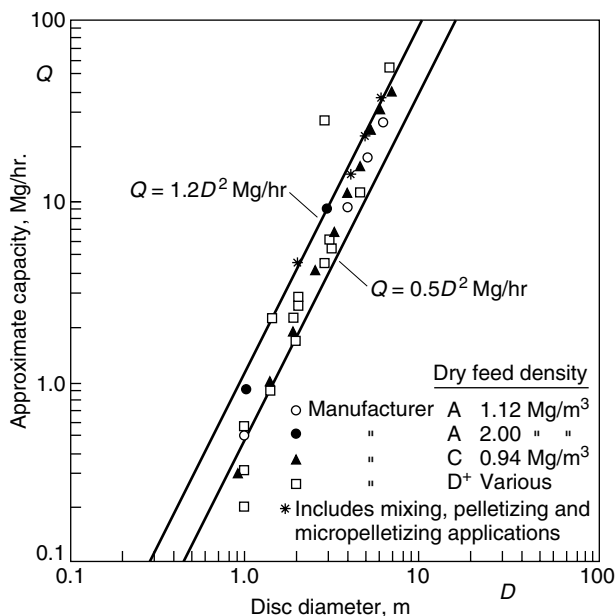


FIG. 21-151 Capacity of inclined disc granulators of varying diameter and formulation feed densities. [Capes, Particle Size Enlargement, Elsevier, 1980.]

of all granulation systems, second only to compaction processes of wet extrusion or fluid-bed coating systems.

Total holdup and granule residence time distribution vary with changes in operating parameters, which affect granule motion on the disc. Total holdup (mean residence time) increases with decreasing pan angle, increasing speed, and increasing moisture content. The residence time distribution for a disc lies between the mixing extremes of plug flow and completely mixed, and can have a marked effect on granule-size distribution and structure (e.g., layered vs. agglomerated). Increasing the disc angle narrows the residence time distribution and promotes layered growth. Several mixing models for disc granulators have been proposed. One- to two-minute residence times are common.

Drum Granulators Granulation drums are common in the metallurgical and fertilizer industries and are primarily used for very large throughput applications (see Table 21-21). In contrast to discs, there is no output size classification and high recycle rates of off-size product are common. As a first approximation, granules can be considered to flow through the drum in plug flow, although back mixing to some extent is common.

As illustrated in Fig. 21-153, a granulation drum consists of an inclined cylinder, which may be either open-ended or fitted with annular retaining rings. Either feeds may be premoistened by mixers to form granule nuclei, or liquid may be sprayed onto the tumbling bed via nozzles or distributor pipe systems. Drums are usually tilted longitudinally a few degrees from the horizontal (0 to 10°) to assist flow of granules through the drum. The critical speed for the drum is calculated from Eq. (21-140) with $\delta = 80$ to 90° . To achieve a cascading, tumbling motion of the load, drums operate at lower fractions of critical speed than discs, typically 30 to 50 percent of N_c . If drum speed is too low, intermittent sliding of the bed will occur with poor tumbling motion; if too high, material will be pinned to the drum wall, increasing the likelihood of bed cataracting and spray blow-through. Scrapers of various designs are often employed to control buildup of the drum wall. Holdup in the drum is between 10 and 20 percent of the drum volume. Drum length

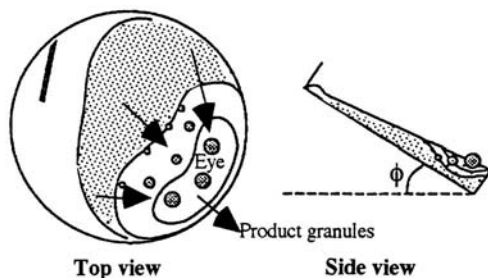


FIG. 21-152 Granule segregation on a disc granulator, illustrating a size classified granular bed sitting on ungranulated feed powder.

TABLE 21-21 Characteristics of Large-Scale Granulation Drums

Diameter (ft)	Length (ft)	Power (hp)	Speed (rpm)	Approximate capacity (tons/h)*
Fertilizer granulation				
5	10	15	10-17	7.5
6	12	25	9-16	10
7	14	30	9-15	20
8	14	60	20-14	25
8	16	75	20-14	40
10	20	150	7-12	50
Iron ore balling				
9	31	60	12-14	54
10	31	60	12-14	65
12	33	75	10	98

*Capacity excludes recycle. Actual drum throughput may be much higher.
 NOTE: To convert feet to centimeters, multiply by 30.48; to convert tons per hour to megagrams per hour, multiply by 0.907; and to convert horsepower to kilowatts, multiply by 0.746.
 From Capes, *Particle Size Enlargement*, Elsevier, 1980.

ranges from 2 to 5 times diameter, and power and capacity scale with drum volume. Holdup and mean residence time are controlled by drum length, with difficult systems requiring longer residence times than those that agglomerate readily. One- to two-minute residence times are common.

Variations of the basic cylindrical shape are the multicone drum, which contains a series of compartments formed by annular baffles [Stirling, in Knepper (ed.), *Agglomeration*, Interscience, New York, 1962], falling curtain and fluidized drum granulators (having an internal distributor running the length of the drum), the Sacket star granulator, and deep disc granulators with internal screens and recycle.

Drum granulation plants often have significant **recycle** of under-size, and sometimes crushed oversize, granules. Recycle ratios between 2:1 and 5:1 are common in iron ore balling and fertilizer **granulation circuits**. This large recycle stream has a major effect on circuit operation, stability, and control. A surge of material in the recycle stream affects both the moisture content and the size distribution in the drum. Surging and limit cycle behavior are common. There are several possible reasons for this, including:

1. A shift in controlling mechanism from coalescence to layering when the ratio of recycled pellets to new feed changes [Sastry and Fuerstenau, *Trans. Soc. Mining Eng., AIME*, **258**, 335-340 (1975)]

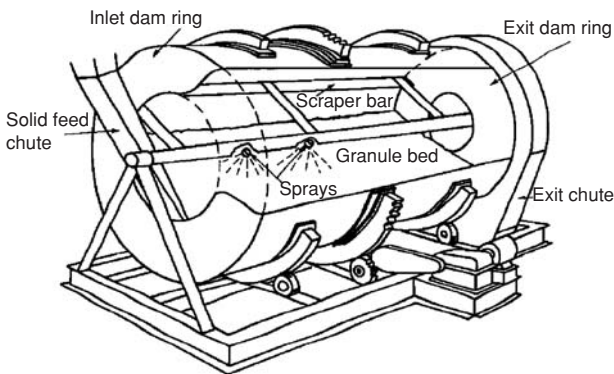


FIG. 21-153 A rolling drum granulator [Capes, *Particle Size Enlargement*, Elsevier, 1980].

2. Significant changes in the moisture content in the drum due to recycle fluctuations (recycle of dry granules in fertilizer granulation) [Zhang et al., *Control of Particulate Processes IV* (1995)] In many cases, plants simply live with these problems. However, use of modern model-based control schemes in conjunction with improved methods for on-line moisture and particle-size analysis can help overcome these effects [Ennis (ed.), *Powder Technol.*, **82** (1995); Zhang et al., *Control of Particulate Processes IV* (1995)].

Controlling Granulation Rate Processes Granulation rate processes have been discussed in detail above (see "Agglomeration Rate Processes and Mechanics" subsection). Nucleation, coalescence, consolidation, and layering are all important processes in tumbling granulation, which could be considered a low- to medium-agitation-intensity process. See also Tables 21-15 to 21-19.

Nucleation, or the formation of seed granules, is critically controlled by spray distribution and interfacial properties of the particulate feed. **Nuclei** are generated from liquid spray drops, scraper bars, or initial coalescence of feed particles. Bed agitation intensity is low to moderate and has only a secondary effect in breaking up/down large nuclei or overwet regions. Therefore, tumbling systems should be maintained in a droplet-controlled regime of nucleation. Spray flux ψ_n should be maintained at less than 0.2, where the solids flux may be estimated from the width of the spray zone and the drum peripheral speed DN [see Eqs. (21-102) and (21-103)]. Fast drop penetration times are most suitable, with low binder viscosities, wetting powder, and larger feed. Fine powders are also possible with layered growth or high recycle. Poor wetting inhibits capacity, particularly in disc granulation. Poor wetting limits production rate to prevent overwet masses. In addition, nucleation determines the initial granule-size distribution and is therefore critical in low-agitation-intensity processes. Wetting and nucleation can be enhanced by increasing temperature and feed particle size, by decreasing binder viscosity, or by improved spray distribution, e.g., by multiple nozzles.

Granule coalescence or growth in tumbling granulators can be complex for a number of reasons:

1. Granules remain wet and can deform and consolidate. The behavior of a granule is therefore a function of its history.
2. Different granulation behavior is observed for broad and narrow feed-size distributions.
3. There is often complex competition between growth mechanisms. As a general rule, growth is linked to consolidation. For a batch process beginning with fine feed, random exponential growth initially occurs followed by a transition to a slower preferential balling stage of growth [Eqs. (21-116) and (21-119)]. This is tied to a similar decrease in granule voidage through the consolidation process.

For less deformable systems, an induction time may be observed, with time required to work moisture to the surface. Such systems are often unstable. For highly deformable and weak formulations, initial linear, preferential growth may be observed with large granules crushing weaker small granules, which are then layered onto the surviving large granules, referred to as crushing and layering.

The granule-size distribution generally narrows with residence time for broad feed-size distribution, whereas fine feeds widen until reaching the critical limiting size of the formulation, after which they will narrow. This limiting size of growth depends linearly on binder viscosity and inversely on agitation velocity and granule density, or

$$d_{max} \propto \frac{\mu}{\rho u_o} \tag{21-141}$$

Table 21-22 gives possible choices for the collision velocity. Figure 21-121 demonstrates that successful scaling of these effects has been achieved in practice.

Note that many of the above observations are based on batch experiments, whereas in most drum granulation systems, very high recycle ratios are present. This recycle material is often composed of well-formed granules, and so the above observations may be masked.

Growth rate is very sensitive to liquid content for narrow initial-size distributions, with increases in liquid content for fine powders leading to an approximate exponential increase in granule size. For low-viscosity liquids, granulation occurs when very close to the saturation of the

TABLE 21-22 Possible Choices of Impact Velocity u_0 or u_c for Stokes Numbers

Granulation process	Collision velocity (maxima)	Shear velocity (averages)
Tumbling (pans and drums)	ND (N is drum/disk speed) (D is drum/disk diameter)	Nd (N is drum/disk speed)
Mixers	$N_i D_i$ (D_i is impeller diameter) $N_c D_c$ (D_c is chopper diameter)	$N_i d$ (i is impeller) $N_c d$ (c is chopper)
Fluidized beds	$(6U_B/D_B)d$ (U_B, D_B is bubble velocity & diameter) U_j (U_j is distributor jet velocity)	$N_i \delta$ (δ is impeller wall gap) $(6U_B/\delta D_B)d$ (δ is bubble gap)

Reprinted from Design and Optimization of Granulation and Compaction Processes for Enhanced Product Performance, Ennis, 2006, with permission of E&G Associates.

granule. This leads to the following equation to estimate moisture requirements (Capes, *Particle Size Enlargement*, Elsevier, 1980):

$$w = \frac{\epsilon \rho_l}{\epsilon \rho_l + (1 - \epsilon) \rho_s}$$

$$w = \frac{1}{1 + 1.85(\rho_s/\rho_l)} \quad d_p < 30 \mu\text{m} \quad (21-142)$$

$$w = \frac{1}{1 + 2.17(\rho_s/\rho_l)} \quad d_p > 30 \mu\text{m}$$

where w is the weight fraction of the liquid, ϵ is the porosity of the close-packed material, ρ_s is true particle density, ρ_l is liquid density, and d_p is the average size of the feed material. Equation (21-142) is suitable for preliminary mass balance requirements for liquid binders with similar properties to water. If possible, however, the liquid requirements should be measured in a balling test on the material in question, since unusual packing and wetting effects, particle internal porosity and solubility, air inclusions, etc., may cause error. Approximate moisture requirements for balling several systems are given in Table 21-23. In addition, for materials containing soluble constituents, such as fertilizer formulations, the total solution phase ratio controls growth, and not simply the amount of binding fluid used.

When fines are recycled as in iron ore sinter feed or fertilizer drum granulation, fines are rapidly granulated and removed from the distribution up to some critical size, which is a function of both moisture content and binder viscosity. Changing the initial-size distribution changes the granule porosity and hence moisture requirements [Adetayo et al., *Chem. Eng. Sci.*, **48**, 3951 (1993)]. Since recycle rates in drum systems are high, differences in size distribution between feed and recycle streams are one source of the limit cycle behavior observed in practice.

Growth by **layering** is important for the addition of fine powder feed to recycled, well-formed granules in drum granulation circuits and for disc granulators. In each case, layering will compete with **nuclei formation** and coalescence as growth mechanisms. Layered growth leads to a smaller number of larger, denser granules with a narrower size distribution than growth by coalescence. Layering is favored by a high ratio of pellets to new feed, low moisture, and positioning powder feed to fall onto tumbling granules.

Mechanisms of growth in disc granulation may be altered by spray location, as illustrated in Fig. 21-154. Spraying toward the eye and granule region promotes agglomerated growth with wide size distribution and low bulk density, whereas spraying feed powder promotes denser, layered growth with narrow size distribution and high bulk density, largely due to the fact that the formed granules have a larger effective residence time. Similar implications would apply in drum granulation as well, and staged moisture addition or dry feed addition is yet relatively unexplored.

Consolidation of the granules in tumbling granulators directly determines granule density and porosity. Since there is typically no in

situ drying to stop the consolidation process, granules consolidate over extended times. Consolidation rates are controlled by Eq. (21-121) (cf. "Granule Consolidation and Densification" subsection.) The maximum collision velocity u_c increases with both drum or disc speed as well as size, with $u_c = ND/2$. Increasing bed moisture and size and speed and angle of drums and discs will increase the rate of consolidation. Increasing residence time through lower feed rates will increase the extent of consolidation. With disc granulators, residence time can be increased by increasing bed depth (controlled by bottom inserts), raising disc speed, or lowering disc angle. With drum granulators, residence time can be influenced by internal baffling.

Moisture Control in Tumbling Granulation Maldistributions in moisture often occur in granulation systems. There are two key sources. One is caused by local variations in spray rate, poor wetting, and fluctuations in solids feed rate. The other is due to induction-like growth (cf. Fig. 21-128), where time is required to work moisture to the surface of granules, and when such moisture is finally available, it is often too much for stable growth to occur. In addition, for such instable formulations, operators may inherently overspray the process, or during scale-up, greater consolidation of granules occurs, again providing excess moisture.

Additives have been explored particularly in the minerals industry to damp out moisture maldistribution. Figure 21-155 illustrates the

TABLE 21-23 Moisture Requirements for Granulating Various Materials

Raw material	Approximate size of raw material, less than indicated mesh	Moisture content of balled product, wt % H ₂ O
Precipitated calcium carbonate	200	29.5–32.1
Hydrated lime	325	25.7–26.6
Pulverized coal	48	20.8–22.1
Calcined ammonium metavanadate	200	20.9–21.8
Lead-zinc concentrate	20	6.9–7.2
Iron pyrite calcine	100	12.2–12.8
Specular hematite concentrate	150	8.0–10.0
Taconite concentrate	150	8.7–10.1
Magnetic concentrate	325	9.8–10.2
Direct-shipping open-pit iron ores	10	10.3–10.9
Underground iron ore	¼ in.	10.4–10.7
Basic oxygen converter fume	1 μ	9.2–9.6
Raw cement meal	150	13.0–13.9
Fly ash	150	24.9–25.8
Fly ash-sewage sludge composite	150	25.7–27.1
Fly ash-clay slurry composite	150	22.4–24.9
Coal-limestone composite	100	21.3–22.8
Coal-iron ore composite	48	12.8–13.9
Iron ore-limestone composite	100	9.7–10.9
Coal-iron ore-limestone composite	14	13.3–14.8

Dravo Corp.

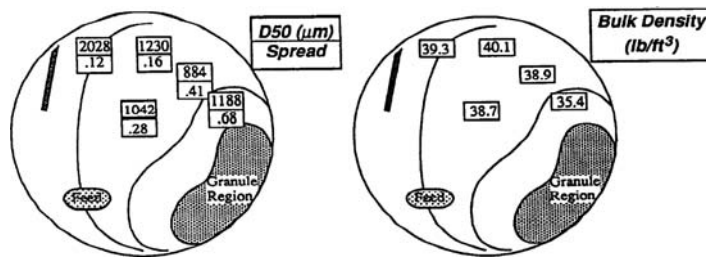


FIG. 21-154 Impact of single nozzle location on granule-size distribution and bulk density for disc granulation, 3-ft diameter, 200 lb/h. (Reprinted from Design and Optimization of Granulation and Compaction Processes for Enhanced Product Performance, Ennis, 2006, with permission of E&G Associates. All rights reserved.)

decrease in drum growth rate for taconite ores that occurs with increasing amounts of bentonite clay [Kapur et al., *Chem. Eng. Sci.*, **28**, 1535 (1973)]. However, what merits particular mention is that the decrease in balling rate is disproportionate with the level of moisture, as illustrated in Fig. 21-156. In other words, high moisture levels are more affected by bentonite level. As illustrated for a bentonite level of 0.23 wt %, a moisture level of 46 vol % behaves or is converted to an equivalent balling rate of 43 vol % at zero bentonite, whereas a moisture level of 44 percent is converted to an equivalent rate of 42.5 percent. In other words, a 2 percent deviation of moisture is converted to a 0.5 percent deviation in moisture in the presence of the bentonite, which as a result narrows the wide variations in balling rate that might otherwise be possible due to moisture maldistribution. In addition, the overall balling rate is slowed, making the granulation process more controllable. Although unexplored, similar effects would be expected in fluid-bed and mixer granulation.

Granulator-Dryers for Layering and Coating Some designs of tumbling granulators also act as driers specifically to encourage layered growth or coating and discourage coalescence or agglomeration, e.g., the fluidized drum granulator [Anon, *Nitrogen*, **196**, 3-6 (1992)]. These systems have drum internals designed to produce a falling curtain of granules past an atomized feed solution or slurry. Layered granules are dried by a stream of warm air before circulating through the coating zone again. Applications are in fertilizer and industrial chemicals manufacture. Analysis of these systems is similar to that of fluidized-bed granulator-dryers.

In the pharmaceutical industry, pan granulators are still widely used for coating application. Pans are only suitable for coating relatively

large granules or tablets. For smaller particles, the probability of coalescence is too high.

Relative Merits of Disc vs. Drum Granulators The principal difference between disc and drum granulators is the classifying action of the disc, resulting in disc granulators having narrower exit granule-size distributions than do drums. This can alleviate the need for product screening and recycle for disc granulators in some industries. For industries with tight granule-size specifications, however, recycle rates are rarely more than 1:2 compared to drum recycle rates often as high as 5:1. The classified mixing action of the disc affects product bulk density, growth mechanisms, and granule structure as well. Generally, drum granulators produce denser granules than disks. Control of growth mechanisms on discs is complex, since regions of growth overlap and mechanisms compete. Both layered and partially agglomerated structures are therefore possible in disc granulators (Fig. 21-154). Other advantages claimed for the disc granulator include low equipment cost, sensitivity to operating controls, and easy observation of the granulation/classification action, all of which lend versatility in agglomerating many different materials. Dusty materials and chemical reactions such as the ammonization of fertilizer are handled less readily in the disc granulator than in the drum.

Advantages claimed for the drum granulator over the disc are greater capacity, longer retention time for materials difficult to agglomerate or of poor flow properties, and less sensitivity to upsets in the system due to the damping effect of a large recirculated load.

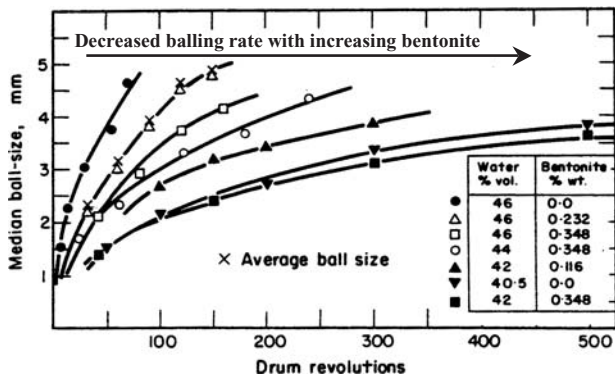


FIG. 21-155 Median ball size vs. drum revolutions for the granulation of taconite ore for varying moisture and bentonite clay levels. [Kapur et al., *Chem. Eng. Sci.*, **28**, 1535 (1973).]

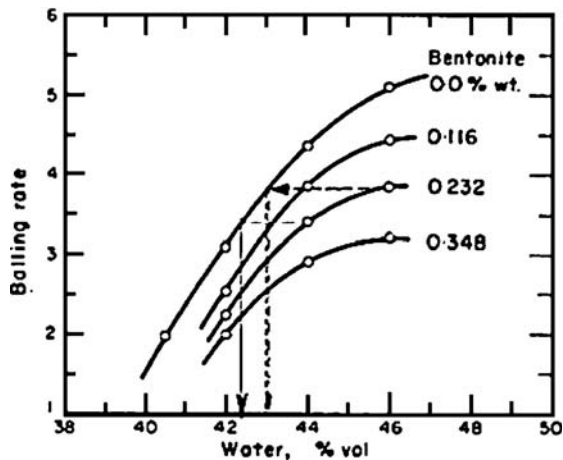


FIG. 21-156 Balling rate for drum granulation of taconite ore as a function of moisture and bentonite clay levels. [Kapur et al., *Chem. Eng. Sci.*, **28**, 1535 (1973).]

TABLE 21-24 Dimensions and Scale-up Rules for Tumbling Granulators

Inclined disc	Drum
Throughput or capacity: $Q \propto D^3$ (area)	$Q \propto LD^2$ (10–20% of volume)
Power consumption: $P \propto D^2$ (area)	$P \propto LD^2$ (volume)
Speed: 50–75% of N_c	30–50% of N_c
Angle: 40–70° from vertical (45–55° most common)	0–10° from horizontal
Height or Length: 20% of D (10–30% of D range)	2–5 times D

Disadvantages are high recycle rates that can promote limit cycle behavior or degradation of properties of the product.

Scale-up and Operation Typical dimensions and scale-up rules for discs and drums are summarized in Table 21-24. Table 21-16 summarizes key groups governing scale-up. For drum granulators, powder consumption and capacity scale with volume, allowing greater throughput than is possible with discs, where capacity scales with area. Although powder properties are not strictly taken into account, similar mixing patterns may be maintained to a first approximation with scale-up by maintaining constant Froude number. In this case, the peripheral speed and velocity of the drum scale with diameter as

$$Fr = \frac{DN^2}{g} = \text{const} \Rightarrow N \propto D^{-0.5} \quad \text{and} \quad u_c = \frac{ND}{2} \propto D^{0.5} \quad (21-143)$$

As a first approximation to scale-up, it is desirable to maintain similar spray flux, which controls nucleation, and similar Stokes numbers, which control growth (see “Mechanics of Size Enlargement Processes”). Both depend for tumbling granulators on the peripheral velocity. In the case of wetting and nucleation, powder or solids flux past the nozzle will scale with the peripheral speed, or with $D^{0.5}$. On the other hand, spray rate will scale with volume to maintain similar moisture (for geometric similarity D^3), which requires a larger spray area to maintain the same dimensionless spray flux [Eq. (21-103)]. This is most easily achieved by increasing the number of nozzles, which can be estimated for constant flux to be given by

$$\psi_a = \frac{\text{spray flux}}{\text{solid flux}} \propto \frac{D^3}{nBu_c} \propto \frac{D^{2.5}}{nB} = \text{const} \leq 0.2$$

or $n \propto \frac{D^{2.5}}{B}$ (21-144)

where n is the number of nozzles and B is the spray width. In practice, fewer nozzles than predicted by Eq. (21-144) will likely be required due to greater consolidation forces or residence time with scale-up.

The impact of scale on growth and consolidation depends upon the choice of collisional velocity (Table 21-22). Granule consolidation and density likely increase with the maximum peripheral speed, or scale-up by $D^{0.5}$. For growth, on the basis of a critical viscous Stokes number with a shear assumption for collisional velocity, or $u_c = Nd$, the maximum growth limit scales with

$$d_{\max} \propto \frac{\mu}{\rho u_c} \propto \sqrt{\frac{\mu}{\rho N}} \propto \sqrt{\frac{\mu D^{0.5}}{\rho}} \quad (21-145)$$

when constant Froude number is maintained.

Other key operational issues are to employ gravimetric feeding preferred to volumetric to control moisture and upsets in flow patterns.

Fluctuations in mass feed rate may also be matched by changes in spray rates through load cell measurements of flow and feedforward control. Dripping nozzles should be prevented through pressure monitoring as well as wetting of process walls. On-line measurements of moisture by near-infrared and of granule size (up to 9 mm) are possible by laser diffraction and imaging.

MIXER GRANULATORS

Mixer granulators contain an agitator to mix particles and liquid and cause granulation. In fact, mixing any wet solid will cause some granulation, even if unintentionally. Mixer granulators have a wide range of applications including ceramics, pharmaceuticals, agrichemicals, and detergents (Table 21-11), and they have the following advantages:

- They can process plastic, sticky materials and can spread viscous binders. That is, they can operate in the mechanical dispersion regime of wetting and the deformable regime of growth (see “Granulation Rate Processes”).
- They are less sensitive to operating conditions than tumbling and fluid-bed granulators, although associated with this is less understanding of control and scale-up of granulation mechanisms.
- High-intensity mixers are the only type of granulator that can produce small (<2 mm) high-density granules.

Power and maintenance costs are higher than for tumbling granulators. Outside of high-intensity continuous systems (e.g., the Schugi in-line mixer), mixers are not feasible for very large throughput applications if substantial growth is required. Granules produced in mixer granulators may not be as spherical as those produced in tumbling granulators, and are generally denser due to higher agitation intensity (see Fig. 21-111). Control of the amount of liquid phase and the intensity and duration of mixing determine agglomerate size and density. Due to greater compaction and kneading action, generally less liquid is required in mixers than in tumbling and fluid-bed granulation. As opposed to tumbling and fluidized-bed granulators, an extremely wide range of mixer granulator equipment is available. The equipment can be divided somewhat arbitrarily into low- and high-shear mixers, although there is considerable overlap in shear rates, and actual growth mechanisms also depend on wet mass rheology in addition to shear rates.

Low-Speed Mixers Low-speed mixers include (1) ribbon or paddle blenders, (2) planetary mixers, (3) orbiting screw mixers, (4) sigma blade mixers, and (5) double-cone or V blenders, operating with rotation rates or impeller speeds less than 100 rpm. (See Fig. 21-157 and subsection “Solids Mixing”.) **Pug mills** and **paddle mills** as well as ribbon blenders are used for both batch and continuous applications. These devices have horizontal troughs in which rotate central shafts with attached mixing blades of bar, rod, paddle, and other designs. The vessel may be of single- or double-trough design. The rotating blades throw material forward and to the center to achieve a kneading, mixing action. Characteristics of a range of pug mills available for fertilizer granulation are given in Table 21-25. These mills have largely been replaced by tumbling granulators in metallurgical and fertilizer applications, but they are still used as a premixing step for blending very different raw materials, e.g., filter cake with dry powder.

Batch planetary mixers are used extensively in the pharmaceutical industry for powder granulation. A typical batch size of 100 to 200 kg has a power input of 10 to 20 kW. Mixing times in these granulators are quite long (20 to 40 min), and many have been replaced with batch high-shear mixers.

High-Speed Mixers High-speed mixers include continuous shaft mixers and batch high-speed mixers. **Continuous shaft mixers** have blades or pins rotating at high speed on a central shaft. Both horizontal and vertical shaft designs are available (Figs. 21-158 and 21-159). Examples include the vertical **Schugi™ mixer** and the horizontal **pin or peg mixers**. These mixers operate at high speed (200 to 3500 rpm) to produce granules of 0.5 to 1.5 mm with a residence time of a few seconds, during which intimate mixing of a sprayed liquid binder and fine cohesive feed powder is achieved. However, little time is available for substantial product growth or densification, and the granulated product is generally fine, irregular, and fluffy with low bulk density. Schugi™ and pin mixer capacities may range up to 200 tons/h with

TABLE 21-25 Characteristics of Pug Mixers for Fertilizer Granulation*

Model	Material bulk density, lb/ft ³	Approximate capacity, tons/h	Size (width × length), ft	Plate thickness, in	Shaft diameter, in	Speed, r/min	Drive, hp
A	25	8	2 × 8	¼	3	56	15
	50	15	2 × 8	¼	3	56	20
	75	22	2 × 8	¼	3	56	25
B	100	30	2 × 8	¼	3	56	30
	25	30	4 × 8	¾	4	56	30
	50	60	4 × 8	¾	4	56	50
C	75	90	4 × 8	¾	4	56	75
	100	120	4 × 8	¾	5	56	100
	25	30	4 × 12	¾	5	56	50
	50	60	4 × 12	¾	5	56	100
	75	90	4 × 12	¾	6	56	150
	100	120	4 × 12	¾	6	56	200
	125	180	4 × 12	¾	7	56	300

*Fecco International, Inc. To convert pounds per cubic foot to kilograms per cubic meter, multiply by 16; to convert tons per hour to megagrams per hour, multiply by 0.907; to convert feet to centimeters, multiply by 30.5; to convert inches to centimeters, multiply by 2.54; and to convert horsepower to kilowatts, multiply by 0.746.

power requirements up to 200 kW. Typical plant capacities of pug mixers are 10 to 20 tons/h (Capes, *Particle Size Enlargement*, 1980). Examples of applications include detergents, agricultural chemicals, foodstuffs, clays, ceramics, and carbon black.

Batch high-shear mixer granulators are used extensively in the pharmaceutical industry, where they are valued for their robustness to processing a range of powders as well as their ease of enclosure. Plow-shaped mixers rotate on a horizontal shaft at 60 to 800 rpm, with impeller tip speeds of the order of 10 ms⁻¹. Most designs incorporate an off-center high-speed cutter or chopper rotating at much higher speed (500 to 3500 rpm), which breaks down overwetting powder mass and limits the maximum granule size. Scale ranges from 10 to 1200 L, with granulation

times on the order of 5 to 10 min, which includes both wet massing and granulation stages operating at low and high impeller speed, respectively. Several designs with both vertical and horizontal shafts are available (Figs. 21-160). [Schaefer, *Acta. Pharm. Sci.*, **25**, 205 (1988)].

Variations in equipment, impeller, and chopper geometry result in very wide variations in shear rate and powder flow patterns among manufacturers (Fig 21-161). Therefore, great caution should be exercised in transferring formulations and empirical knowledge between mixer designs. For example, the effect of chopper on granule attributes has been observed to be small for Fielder™ and Diosna™ vertical bottom-driven mixer designs, provided the chopper is on (Litster et al., loc. cit., 2002), whereas chopper effects are large in the

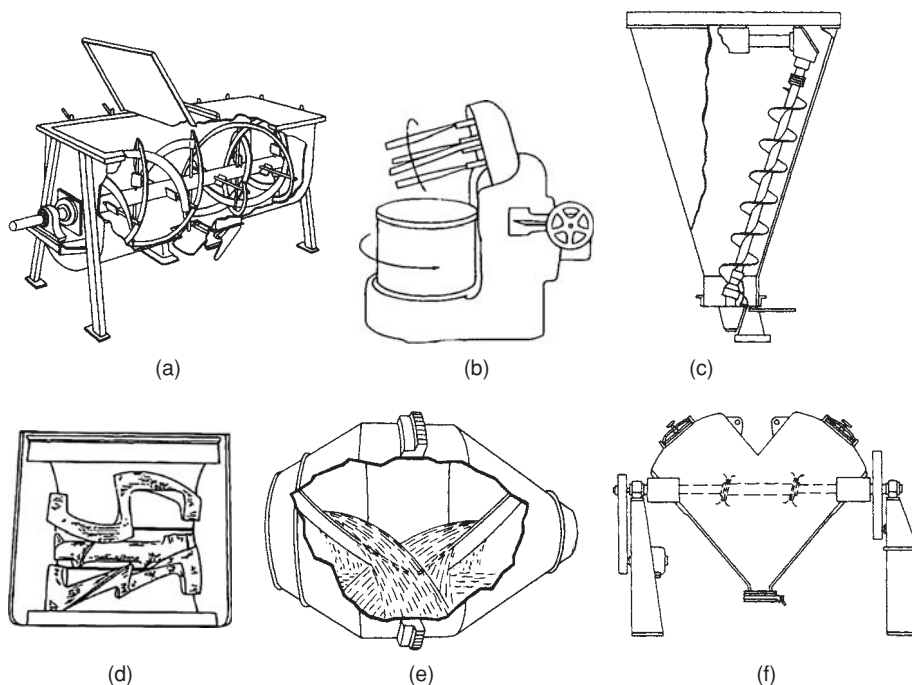


FIG. 21-157 Examples of low-shear mixers used in granulation. (a) Ribbon blender; (b) planetary mixer; (c) orbiting screw mixer; (d) sigma blender; (e) double-cone blender with baffles; (f) v blender with breaker bar. (See also "Solids Mixing.") [(b) and (d), Chirkot and Propst, in Parikh (ed.), *Handbook of Pharmaceutical Granulation Technology*, 2d ed., Taylor & Francis, 2005.]



FIG. 21-158 The Schugi Flexomix® vertical high-shear continuous granulator. (Courtesy Bepex Corp.)

Lödige™ horizontal plough shear design where tools push material into relatively large chopper zones (Iveson et al., loc. cit., 2000), or in Gral™ top-driven designs, which possess much larger choppers.

The Eirich mixer granulator is a unique design commonly employed in ceramics and clay industries (Fig. 21-161d). Here both impeller blades and the chopper rotate on eccentrically mounted vertical shafts, while in addition the cylindrical bowl rotates. This provides a hybrid of mixer and tumbling granulation, and generally more spherical granules are produced than those achieved in other batch mixer processes.

Powder Flow Patterns and Scaling of Mixing Powder flow properties have a significant impact on high-shear mixing, particularly

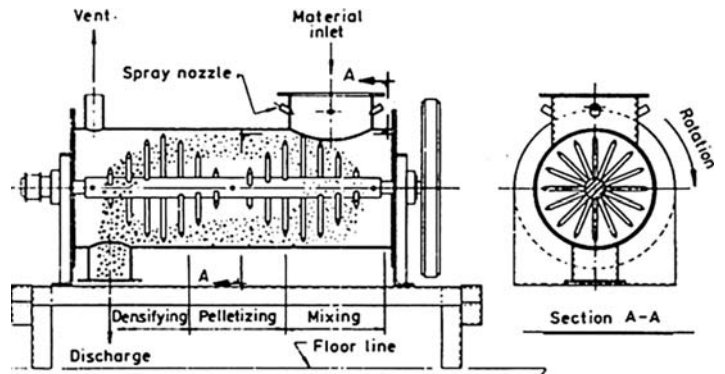
in the presence of cohesive powders and moisture. Frictional properties play a key role as in bulk solids flow (cf. “Bulk Flow Properties” subsection), as well as particle inertia and two-phase interactions with interstitial gas. As yet, the rheological behavior of rapid powder flow under shear is only partly understood in an engineering design sense. However, as with bulk solids flow, powder beds under shear do not readily transmit shear stress, and often develop shear zones in which large shear velocities exist between more relatively stagnant masses of powder. Put another way, traditional scaling approaches based on liquid mixing should be used with great caution. This greatly impacts scale-up since the entire mass of the powder bed is not activated, with only a portion of the bed being sheared and mixed, and this activated portion generally varies over the life of the granulation. In some cases, small shear zones between blades and vessel walls could dominate growth. Furthermore, such powder mixing is very sensitive to equipment geometry, varying widely among manufacturers.

Key visual studies and mixing studies have been undertaken to attempt to understand equipment interactions [Litster et al., *Powder Technol.*, **124**, 272 (2002); Ramaker et al., *Int. J. Pharm.*, **166**, 89 (1998); Knight et al., *Chem. Eng. Sci.*, **56**, 4457 (2001); Forest et al., *Proc. World Congress of Chem. Eng.*, Melbourne, 2001]. In the case of horizontal plough shears, large masses were found to cycle around the shaft undergoing little internal shear, with high shear occurring between the masses and at the wall. In the case of vertical batch mixers, two regimes were observed as illustrated in Figs. 21-162 and 21-163. At low impeller speed, the blade slips along the bottom surface of the powder, with powder being displaced upward momentarily in a **bumping flow** regime. Little turnover of the bed occurs, with rotational motion or **powder surface velocity** increasing with increasing impeller speed. At high impeller speed, material is forced upward along the walls tumbling downward along the bed surface toward the central impeller axis in a **roping flow** regime. There is significant rotational motion of the bed with good turnover, with the entire bed being activated. In the case of Fielder™ mixer design, the powder surface velocity was observed to remain approximately constant (Litster et al., loc. cit.) indicating that slip and substantial shear may still be occurring between the impeller blade and solid mass. In addition, note that the surface velocity of the powder is typically no more than 10 percent of the impeller tip speed (Fig. 21-163).

The transition between regimes occurs at a critical velocity N_c , or critical Froude number $Fr_c = DN_c^2/g$, representing a shift in the balance between gravity and powder rotational inertia. Fr_c is expected to be an increasing function of dimensionless bed height and a decreasing function of powder cohesion, although this has yet to be confirmed. Generally it should decrease with increasing bed moisture due to sprayed binder fluid, potentially giving a shift between regimes occurring during the granulation. Furthermore, Knight et al. (loc. cit.) found the mixer torque measurements scaled with



(a)



(b)

FIG. 21-159 Examples of horizontal high-shear mixers. (a) CB 75 horizontal pin mixer (Courtesy Lödige GmbH). (b) Peg granulator [Capes, Size Enlargement, 1985].

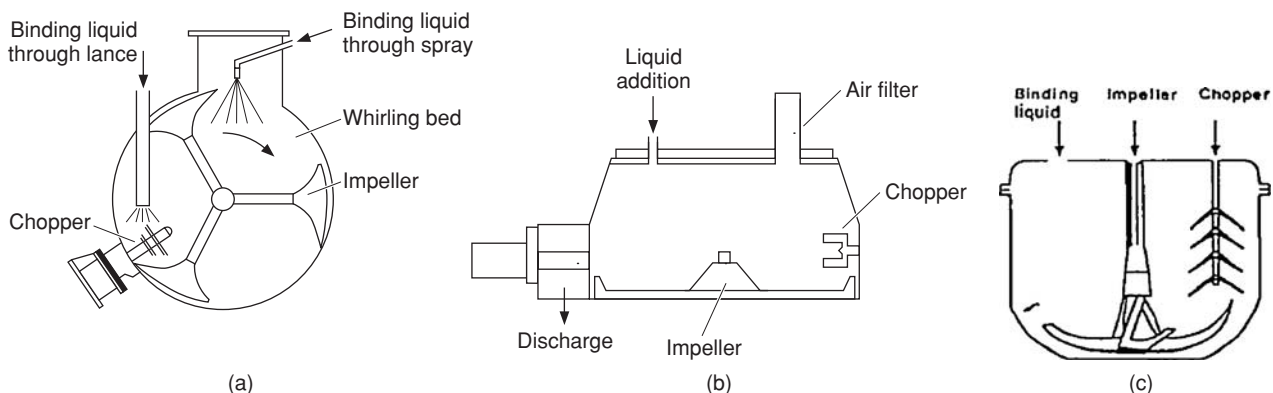


FIG. 21-160 High-shear mixer granulators for pharmaceutical granule preparation for subsequent tableting. (a) Horizontal plough shear, (b) vertical bottom-driven shear, and (c) vertical top-driven shear.

Froude number, potentially providing a scale-up rule for mixer granulation.

Controlling Granulation Rate Processes Despite their robustness with respect to processing a wide variation in formulation types, mixers present the greatest challenge for predicting granule properties of all granulation techniques. All rate processes often play a role, and they are often intertwined (see “Agglomeration Rate Processes and Mechanics”). Granule deformation is important due to the high-shear forces existing in mixers as compared with tumbling and fluid-bed granulators. As deformability is linked to granule saturation and voidage, consolidation and growth are highly coupled. High-speed choppers also bring about significant granule breakage, both wet and dry, often providing a limit on granule growth. Furthermore, a very wide range of shear rates and impact velocities exist throughout the bed, which vary over the life of the granulation, are strongly impacted by powder flow properties, and are equipment-specific (see “Powder Flow Patterns and Scaling of Mixing”). To further complicate matters, geometric similarity is often not preserved for commercial equipment and dominates rate processes by shift with scale-up. It is not surprising there are wide opinions about control of such processes and their method of scale-up.

Some key questions to be addressed as part of formulation, processing, and scale-up efforts include these:

1. Is the formulation wettable with fast drop penetration time? Is there possible preferential wetting of active vs. excipients? Is little growth required, applying only a nucleation stage of granulation?
2. If substantial growth is required, what is the deformability of the formulation? Does it readily grow, or is the formulation stiffer, requiring an induction time to work moisture to the surface? How much moisture is required, and how does it impact deformability?
3. What is the relative volume occupied by the chopper? If large growth is desired, does the formulation reach its maximum limit of granule size during latter stages of growth?
4. What granule density is required, and what is its impact on downstream processing such as tableting and final product quality? Is additional processing required to densify wet granules, e.g., by second-stage mixing or fluid-bed drying?
5. Is dry granule attrition occurring in the process, or is the product prone to dust formation?

These questions are now addressed within the context of rate processes. See also Tables 21-15 to 21-19.

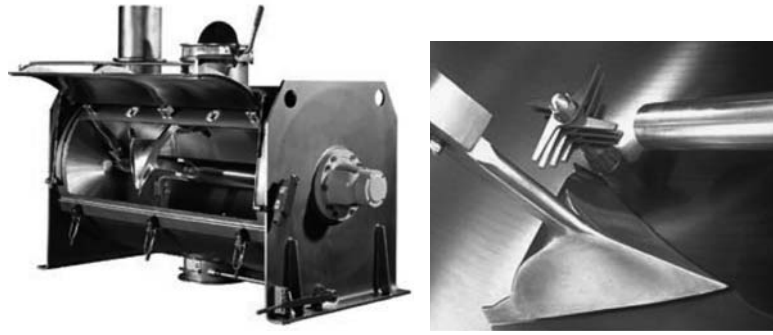
If little growth is desired, granulation may be halted early in growth, or limited to **nucleation**. If the formulation is wettable by the binding fluid, this is best achieved in the **drop-controlled** regime of nucleation, which requires fast drop penetration and low spray flux [Eq. (21-107)], Fig. 21-107). Small drop penetration time t_p is possible for low binder viscosity, high adhesion tension, coarse feed powders, and

fine drops for a given bed circulation time [Eq. 21-99]. Small dimensionless spray flux $\psi_a < 0.2$ occurs for low spray rate for a given area and high solids flux past the spray zone, which is influenced by the number of nozzles and surface solids velocity. Drop-controlled growth gives the tightest nuclei distribution, as illustrated in Fig. 21-164 for commercial mixers. For large spray rates, pumping of binding solution, viscous binders, unwettable powder, or poor powder mixing, nucleation will occur by **mechanical dispersion** of the fluid and breakdown of overwet masses by impellers and choppers, resulting in wider nuclei size distributions.

Large solids fluxes may be necessary for drop-controlled nucleation, implying operating the mixer in the roping regime of mixing for vertical mixers in excess of a critical velocity or Froude number Fr_c (see “Powder Flow Patterns and Scaling of Mixing”). However, it is quite possible that this might also set off simultaneous bumping. In practice, binding fluid is often added at low impeller speed (bumping flow), followed by wet massing at high speed (roping fluid). This interaction between initial nucleation, subsequent growth, and powder mixing is product-specific and illustrates the source of current disagreement behind the method of binder addition. For a readily growing formulation, operating in roping flow during binder addition will readily initiate growth, whereas operating in bumping flow may lead to wider nuclei distributions.

In most mixers, granule grows by a **high-agitation, high-deformability** mechanism, where deformability cannot be ignored (see “Growth and Consolidation” and Figs. 21-109 and 21-110). An example of such growth in mixers is detailed above (see Example 5 High-Shear Mixer Growth.) **Granule growth** and **granule consolidation** are initially controlled by the deformability of the wet mass. This **deformability** is a strong function of saturation [Eq. (21-120), Figs. 21-112 and 21-113] as well as shear level as represented by the deformation Stokes number St_{def} [Eq. (21-118)]. Saturations of 80 to 100 percent are generally required to initiate growth, although this is formulation-dependent. Ideally plastic deformation of the wet mass is desired without crumbling. Overall deformability increases with increasing primary particle size, decreasing binder viscosity, and increasing granule voidage, implying fresh granules are more deformable and capable of growth than older, compacted granules.

Initial growth in mixing is associated with compaction and decreases in granule porosity (Fig. 21-128). Granule size should increase with increasing St_{def} , implying increasing impeller speed, granule density, and bed moisture and decreasing solution viscosity and wet mass deformability. In this stage, granule-size distribution is expected to increase in proportion to granule size in a **self-preserving** fashion (Adetayo and Ennis, loc. cit., 1996). However, the material may reach a **limiting granule size**, in which case the distribution will then narrow. This limit is strongly dependent on chopper and impeller speed and mixer design. In the later stages of growth, granules



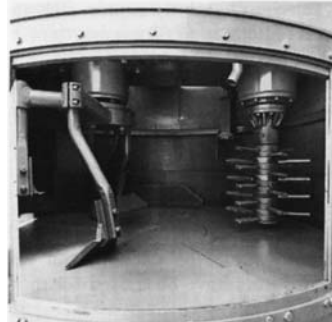
(a)



(b)



(c)



(d)

FIG. 21-161 Commercial examples of available high-shear granulators. (a) Horizontal plough shear; FKM 1200 with plough shovel tools, chopper, and liquid addition lance. (Courtesy Loedige Corp.) (b) Vertical top-driven shear; GMX top-driven mixer with mixing impeller blade. (Courtesy Vector Corp.) (c) Vertical bottom-driven shear; Glatt VG bottom-driven mixer with mixing impeller and chopper blade. (Courtesy Glatt GmbH.) (d) Eccentric vertical shear mixer; Eirich vertical mixer with rotation bowl and eccentric rotating blade and chopper. (Courtesy Eirich GmbH.)

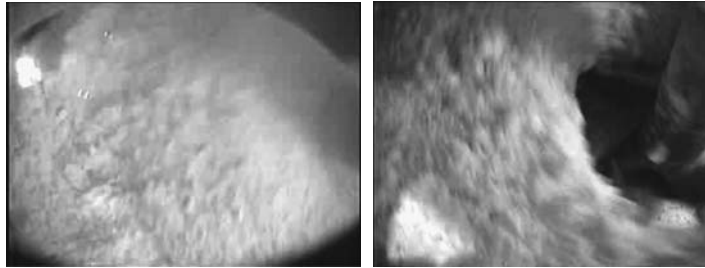


FIG. 21-162 Examples of bumping and roping flow in commercial batch high-shear mixers. *Left:* Bumping flow at low impeller speed during spray cycles. *Right:* Roping flow at high impeller speed in wet massing. GMX top-driven mixer. (Courtesy Vector Corporation.)

may become less deformable, switching to a nondeformable method of growth as with tumbling granulation. Here, the limit of growth will increase with increasing binder viscosity and decrease with increasing impeller speed [cf. Eq. (21-145) and Figs. 21-121 and 21-122].

Scale-up and Operation As discussed above, scale-up of high-shear mixers is difficult due to complex powder flow patterns, wide variations in shear rates among mixers, and competition among granulation rate processes. Ideally, the following should be preserved with scale-up.

1. Geometric similarity, including dimensionless powder bed height
2. Dimensionless spray flux and drop penetration time
3. Collisional shear velocities in terms of viscous and deformation Stokes numbers
4. Constant maximum collisional velocities controlling breakage

In practice, it may not be possible to meet all these objectives, and only limited understanding exists with regard to the best choice of shear rates in scaling. Table 21-16 summarizes key governing groups governing scale-up.

For many commercial mixers, since geometric similarity is often not preserved—even within a given manufacturer—Kristensen recommends constant relative swept volume ratio \dot{V} as a scale-up parameter as a starting point, defined as

$$\dot{V}_R = \frac{\dot{V}_{imp}}{V_{tot}} \quad (21-146)$$

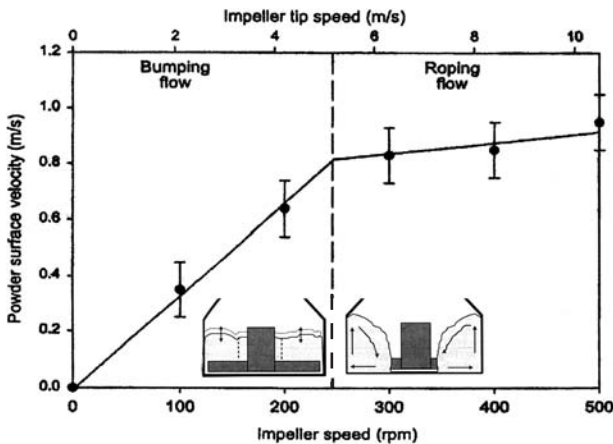


FIG. 21-163 Powder surface velocities as a function of impeller tip speed. Dry lactose in a 25-L Fielder™. (Litster and Ennis, *The Science and Engineering of Granulation Processes*, Kluwer, 2004.)

where \dot{V}_{imp} is the volume rate swept by the impeller and V_{tot} is the total volume of the granulator. For constant geometric similarity (where impeller diameter would scale with bed diameter), maintaining constant relative swept volume is equivalent to maintaining constant tip speed, or

$$u_o = ND = \text{const} \quad \text{or} \quad N \propto 1/D \quad (21-147)$$

where N and D are impeller speed and diameter, respectively. Depending on mixer design, relative swept volume may decrease significantly with scale when similarity is not preserved (Schaefer, loc. cit.), requiring increases in impeller speed over Eq. (21-147) with scale-up to compensate. Alternatively, dimensionless bed height might be reduced to maintain a constant swept mass rate. In reality, maintaining a constant percentage of swept mass rate is required, but this is complicated by complex powder flow patterns and cannot be easily achieved in practice with many impeller designs. In general, scale-up leads to poorer liquid distribution, higher-porosity granules, and wider granule-size distributions. Required granulation time may increase with scale although this depends on the importance of consolidation kinetics, as discussed above.

To improve upon maintaining swept volume as a scale-up criterion, one must also consider the impact of scale-up on wetting, nucleation, growth, and granule consolidation. To maintain bed moisture with scale-up requires that the sprayed binding fluid increase with the bed volumetric scaling ratio β , or

$$V_2 = \dot{V}_2 \Delta t_2 = \beta V_1 = \beta \dot{V}_1 \Delta t_1 \quad \text{where} \quad \beta = V_2^B / V_1^B \quad (21-148)$$

where V^B is the bed volume. This requires that either the spray time Δt_s or the spray rate \dot{V} be increased. To maintain constant wetting in the case of drop-controlled nucleation, spray flux and penetration time must be maintained constant [Eqs. (21-103) and (21-107)]. If drop size is maintained, a constant spray flux constrains the number of nozzles n required upon scale-up, or

$$\Psi_a = \frac{3}{2} \frac{\dot{V}}{d_n w B} = \text{const} \Rightarrow \Psi_{a2} = \frac{\beta \dot{V}_{s1} (n_1 \Delta t_1 / n_2 \Delta t_2)}{w_2 B_2} = \Psi_{a1} \quad (21-149)$$

Therefore to maintain constant spray flux with increasing scale, one may increase the number of nozzles, spray time, spray width, or solids velocity through the spray zone. Spray width would be altered by nozzle height on nozzle design, whereas solids velocity is related to impeller speed. In bumping flow, solids velocity most likely increases with tip speed for horizontal mixers, whereas in roping flow it is constant. A decision about which regime of mixing is desired must be reached. If roping flow is chosen, $Fr > Fr_c$ (see “Powder Flow Patterns and Scaling of Mixing”) maintains this regime of mixing with scale-up.

Equation (21-149) assumes a very fast drop penetration time, and that spray zones do not interact, or multiple passes do not cause drop overlap on previous nuclei. To compensate for this, smaller fluxes may

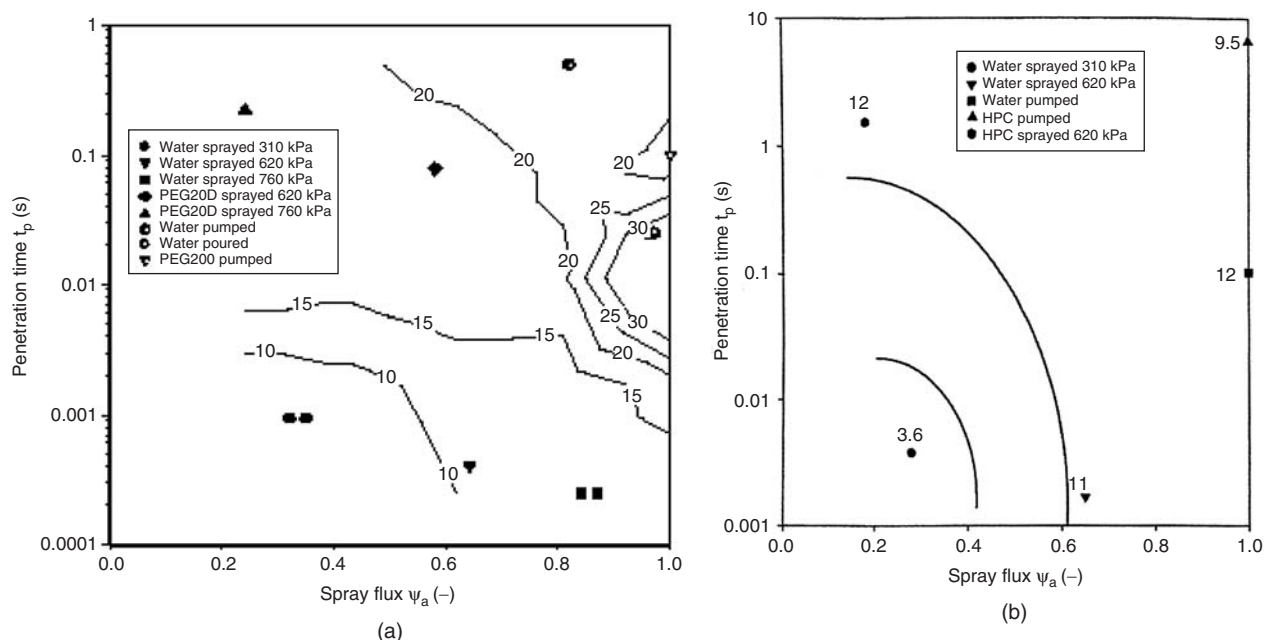


FIG. 21-164 Nucleation regime maps for high-shear batch mixing of lactose. Standard deviations in granule-size distribution are indicated by contour and directly. (a) 6L Hobart for 10 s [Hapgood, *loc. cit.*, 2000]. (b) 25L Fielder, 15% liquid content [Hapgood *et al.*, *AIChE J.*, **49**, 350, (2003)].

be desirable with scale-up. Furthermore, greater compaction forces at large scale may require less moisture, or an effectively smaller β , requiring further adjustment in spray parameters.

For nonwettable powders or viscous binders, nucleation will occur through mechanical distribution of the fluid, and spray nozzles are likely unwarranted. Instead fluid should be added upstream and in the vicinity of chopper locations, where choppers will break down over-wetted nonuniform masses. Little is known at present about such scaling, although maintaining constant chopper swept volume with scale-up is desirable.

For deformable growth and consolidation where a limit of growth is not achieved, a constant deformation Stokes number St_{def} [Eq. (21-118)] should be maintained with scale-up. Depending upon the choice of impact velocity u_o (Table 21-22) and assuming a constant profile of developing yield stress Y , this leads to different scaling criteria as follows:

$$\text{Constant tip speed: } u_o = ND \Rightarrow N \propto 1/D \quad (21-150a)$$

$$\text{Constant granular shear: } u_o = Nd \Rightarrow N = \text{const} \quad (21-150b)$$

$$\text{Constant Froude number: } Fr = DN^2/g \Rightarrow N \propto 1/\sqrt{D} \quad (21-150c)$$

The last criterion of maintaining constant Froude number will lead to an increase in deformation Stokes number if the tip speed controls growth, or a decrease if a granular shear velocity is a more appropriate choice. A conservative recommendation is to scale with constant Fr for deformable growth systems far from a limit of growth. Note that if scaling is performed on the basis of constant tip speed, Froude number will decrease with scale-up, and could alter mixing regimes from roping to bumping flow (see “Bulk Flow Properties”). Lastly, any changes in speed could alter bulk capillary number and dynamic yield stress Y [Eq. (21-112), Fig. 21-118].

For systems approaching a limiting granule growth with less deformation, constant viscous Stokes number should be maintained. This does not alter the scaling criteria based on the deformation Stokes

number [Eq. (21-118)]. Depending on the most appropriate measure of impact velocity, the limit of growth is given by

$$\text{Constant tip speed: } u_o = ND \Rightarrow d_{max} \propto \mu/\rho ND \quad (21-151a)$$

$$\text{Constant granular shear: } u_o = Nd \Rightarrow d_{max} \propto \sqrt{\mu/\rho N} \quad (21-151b)$$

If constant Froude number scaling is chosen, these limits become:

$$d_{max} \propto \begin{cases} \mu/\rho\sqrt{D} & \text{tip speed} \\ \sqrt{\mu D^{0.5}/\rho} & \text{granular shear} \end{cases} \quad (21-152)$$

It is also possible to stage the growth process, allowing for changes in both impeller and chopper speed. Three stages to consider would be nucleation, initial deformable growth, and final equilibrium growth. For example, one might choose constant-Froude-number scaling for nucleation and initial deformable growth, followed by a decrease in impeller speed to constant tip speed in the later stages of growth.

Staged growth is also possible by staging granulation processes as performed in detergent manufacture (Fig. 21-165), consisting of a nucleation stage at high shear and short residence time in a pin mixer followed by a growth and consolidation stage at moderate shear and long residence time in a plough shear mixer. Feed and exit granule distributions are given in Fig. 21-166.

Power dissipation can lead to temperature increases of up to 40°C in the mass. Note that evaporation of liquid as a result of this increase needs to be accounted for in determining liquid requirements for granulation.

Impeller shaft **power intensity** (kW/kg) has been used both as a rheological tool to characterize formulation deformability and as a control technique to judge granulation endpoint, primarily due to its relationship to granule deformation [see Kristensen *et al.*, *Acta. Pharm. Sci.*, **25**, 187 (1988), and Holm *et al.*, *Powder Technol.*, **43**, 225 (1985)]. Swept volume ratio is a preliminary estimate of expected

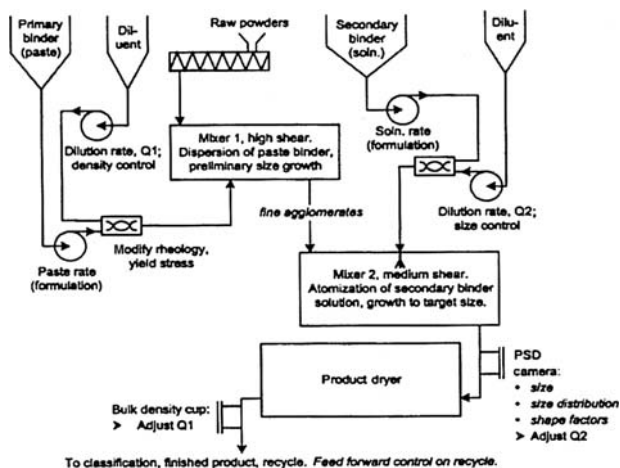


FIG. 21-165 Two-stage continuous granulation process, consisting of high-shear nucleation (pin mixer) and moderate shear growth and consolidation (plough shear). [Mort et al., Powder Technol., 117, 173 (2003).]

power intensity. There are two key issues associated with this approach: (1) The portion of the bed mass activated may only be local to the impeller, and this percentage of the bed changes with impeller speed, life of the granulation, and scale-up. (2) The relationship between deformability, growth, and power will vary from lot to lot if there are variations in physical properties of the formulation such as surface chemistry or size distribution. There have been attempts to account for these variations through the use of specific work [Sirois and Craig, *Pharm Dev. Technol.*, 5, 365 (2000)].

FLUIDIZED-BED AND RELATED GRANULATORS

In fluidized granulators (**fluidized beds** and **spouted beds**), particles are set in motion by air rather than by mechanical agitation. Applications include fertilizers, industrial chemicals, agricultural chemicals, pharmaceutical granulation, and a range of coating processes. Fluidized granulators produce either high-porosity granules due to the agglomeration of powder feeds or high-strength, layered granules due to coating of seed particles or granules by liquid feeds.

Figure 21-167 shows a typical production-size **batch** fluid-bed granulator. The air handling unit dehumidifies and heats the inlet air. Heated fluidization air enters the processing zone through a distributor, which also supports the particle bed. Liquid binder is sprayed through an air atomizing nozzle located above, in, or below the bed. Bag filters or cyclones are needed to remove dust from the exit air. Other fluidization gases such as nitrogen are also used in place of or in combination with air to avoid potential explosion hazards due to fine powders. **Continuous** fluid-bed granulators are used in the fertilizer, food, and detergent industries. For fertilizer applications, near-size granules are recycled to control the granule-size distribution. Dust is not recycled directly, but is first remelted or slurried in the liquid feed.

Advantages of fluidized beds over other granulation systems include high volumetric intensity, simultaneous drying and granulation, high heat- and mass-transfer rates, and robustness with respect to operating variables on product quality. Disadvantages include high operating costs with respect to air handling and dust containment and the potential of defluidization due to uncontrolled growth, making them unsuitable generally for very viscous fluid binders or unwettable powders. [See Parikh (ed.) *Handbook of Pharmaceutical Granulation Technology*, 2d ed., 2005) for additional details.]

Hydrodynamics The hydrodynamics of fluidized beds is covered in detail in Sec. 17. Only aspects specifically related to particle-size enlargement are discussed here. Granular products from

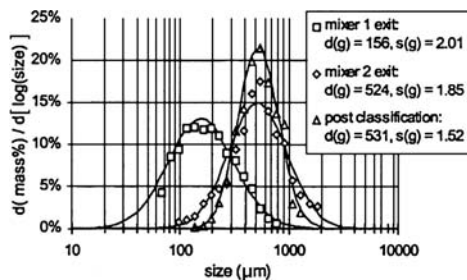


FIG. 21-166 Two-stage continuous granulation process, consisting of high-shear nucleation (pin mixer) and moderate shear growth and consolidation (plough shear). Exit granule size distributions are determined by in-line imaging. [Mort et al., Powder Technol., 117, 173 (2003).]

fluidized beds are generally **group B** or **group D** particles under Geldart's powder classification. However, for batch granulation, the bed may initially consist of a **group A** powder. For granulation, fluidized beds typically operate in the range $1.5U_{mf} < U < 5U_{mf}$, where U_{mf} is the minimum fluidization velocity and U is the operating superficial gas velocity. For batch granulation, the gas velocity may need to be increased significantly during operation to maintain the velocity in this range as the bed particle size increases.

For groups B and D particles, nearly all the excess gas velocity $U - U_{mf}$ flows as bubbles through the bed. The flow of bubbles controls particle mixing, attrition, and elutriation. Therefore, elutriation and attrition rates are proportional to excess gas velocity. Readers should refer to Sec. 17 for important information and correlations on Geldart's powder classification, minimum fluidization velocity, bubble growth and bed expansion, and elutriation.

In summary however, it is important that mixing, bed turnover, solids flux, bed expansion, shear within the dense phase of the bed, and heat and mass transfer control drying scale with fluid-bed excess gas velocity $U - U_{mf}$.

Mass and Energy Balances Due to the good mixing and heat-transfer properties of fluidized beds, the exit gas temperature is assumed to be the same as the bed temperature, when operating with proper fluidization. Fluidized-bed granulators also act simultaneously as dryers and therefore are subject to the same **mass and energy balance limits** as dryers, namely:

1. Solvent concentration of the atomized binding fluid in the **exit air** cannot exceed the saturation value for the solvent in the fluidizing gas at the bed temperature.

2. The supplied energy in the **inlet air** must be sufficient to evaporate the solvent and maintain the bed at the desired temperature. Both these limits restrict the maximum rate of liquid feed or binder addition for given inlet gas velocity and temperature. The liquid feed rate, however, is generally further restricted to avoid excess coalescence or **quenching**, as defined by low spray flux ψ_n .

Controlling Granulation Rate Processes Table 21-26 summarizes the typical effect of feed properties (material variables) and operating variables on fluidized-bed granulation. (See also Fig. 21-168.) Due to the range of mechanisms operating simultaneously, the combined effect of these variables can be complex. Understanding individual rate processes allows at least semiquantitative analysis to be used in design and operation. See also Tables 21-15 to 21-19 on controlling the individual granulation rate processes of wetting, coalescence and consolidation, and breakage, respectively.

Nucleation in fluidized-bed granulation by necessity occurs within a **drop-controlled** regime, which requires fast drop penetration and low spray flux [Eq. (21-107), Figure. 21-107]. Spray flux ψ_n should be no more than 0.2, and quite possibly much lower. Increasing wettability has been shown to increase nuclei size, presumably due to more stable operation (Fig. 21-99). Figure 21-168 illustrates the impact of increasing spray flux and fluid-bed gas velocity on size distribution. Decreasing dimensional spray flux (which is inverse to

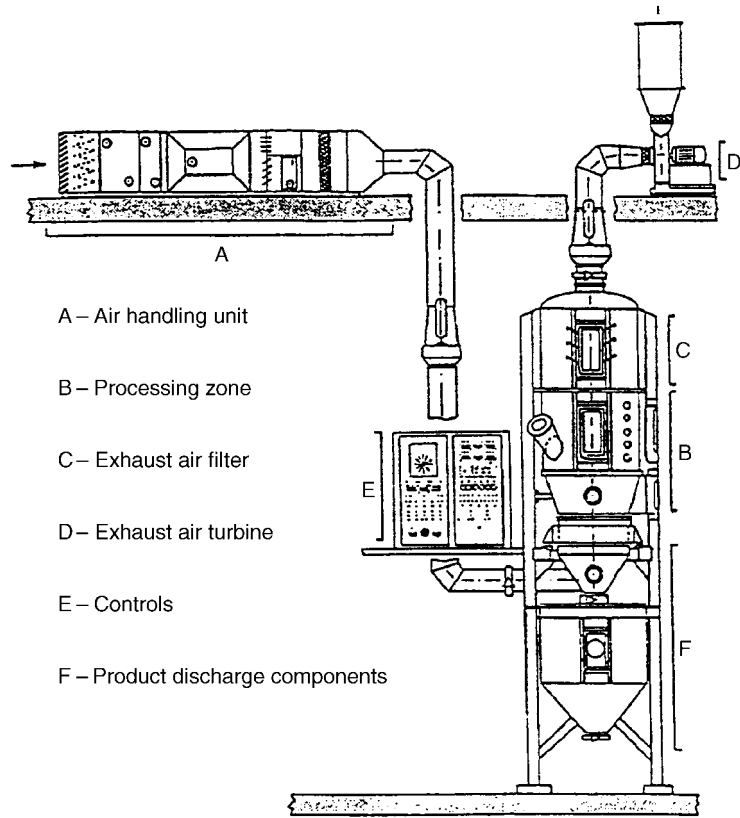


FIG. 21-167 Fluid-bed granulator for batch processing of powder feeds [Ghebre-Sellasie (ed.), *Pharmaceutical Pelletization Technology*, Marcel Dekker, 1989].

TABLE 21-26 Effect of Variables on Fluidized-Bed Granulation

Operating or material variable	Effect of increasing variable
Liquid feed or spray rate	Increases size and spread of granule size distribution Increases granule density and strength Increases chance of defluidization due to quenching
Liquid droplet size (decreases with increasing atomization air or nozzle atomization ratio NAR)	Increases size and spread of granule size distribution
Gas velocity	Increases attrition and elutriation rates (major effect) Decreases coalescence for inertial growth Has no effect on coalescence for noninertial growth, unless altering bed moisture through drying Increases granule consolidation and density
Bed height	Increases granule density and strength
Bed temperature	Decreases granule density and strength
Binder viscosity	Increases coalescence for inertial growth Has no effect on coalescence for noninertial growth Decreases granule density
Particle or granule size	Decreases chance of coalescence Increases required gas velocity to maintain fluidization

Reprinted from *Design and Optimization of Granulation and Compaction Processes for Enhanced Product Performance*, Ennis, 2006, with permission of E&G Associates. All rights reserved.

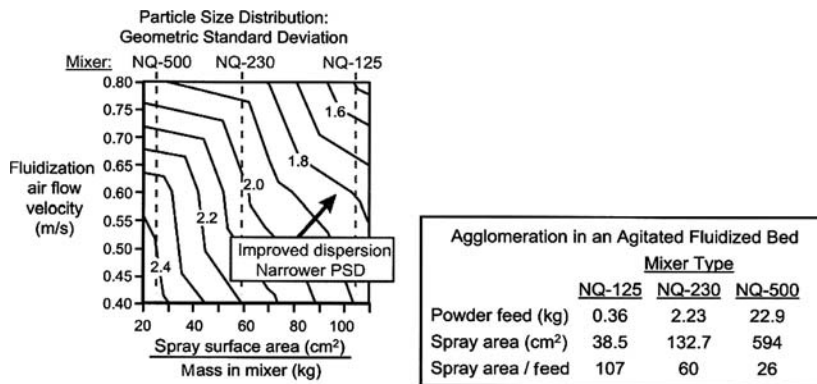


FIG. 21-168 Geometric standard deviation of granule size distribution in an agitated fluid-bed granulator as a function of spray flux, as controlled by fluidization velocity and spray surface area. (Mort et al., 1998; Tardos et al., 1997.)

spray area) leads to a narrower granule-size distribution, as well as increasing fluidization velocity, which increases solids flux through the nozzle zone. In general, bed turnover rate and solids flux increase with increasing $U - U_{mf}$. Dimensionless spray flux ψ_a decreases with decreasing nozzle spray flux and increasing solids flux. In addition, drop penetration time increases with finer drops or increasing atomization ratio.

Air atomizing nozzles are commonly used to control the droplet size distribution independently of the liquid feed rate (Fig. 21-169), as controlled by the nozzle atomization ratio (NAR), given by the volumetric ratio of air-to-liquid flow. **Defluidization** may occur due to large drops and growth. At the other extreme, fine drops with large air volumes may be entrained into the freeboard of the fluid bed, coating bags, vessel wall, leading to caked material, or promoting nozzle dripping.

The formation of large, wet agglomerates that dry slowly is called **wet quenching**, and it is brought about by too high a spray flux and poor drop penetration time. Large, wet agglomerates defluidize, causing channeling, and poor mixing and ultimately leading to shutdown. Sources of wet quenching include high liquid spray rates,

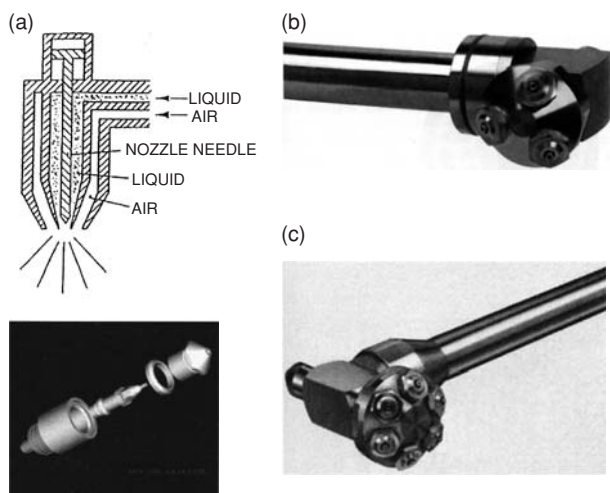


FIG. 21-169 Examples of atomization nozzles. (a) Schematic of single-port nozzle (courtesy Niro Pharma Systems). (b) Three-port nozzle (courtesy Vector Corporation). (c) Six-port nozzle (courtesy Glatt Group). [After Parikh (ed.), Handbook of Pharmaceutical Granulation Technology, 2d ed., 2005.]

large spray droplets, dripping nozzles, or insufficient mixing due to low excess gas velocity $U - U_{mf}$. It is also linked to the drying capacity of the gas, which should be considered during scale-up. **Dry quenching** (uncontrolled coalescence) is the formation and defluidization of large, stable dry agglomerates, which also may ultimately lead to shutdown and can be related again to high spray flux and/or rapid granule coalescence, particularly in the last stages of growth where the bed is dominated by granules with little available fine powder.

Competing mechanisms of growth include **layering**, which results in dense, strong granules with a very tight size distribution, and **coalescence**, which results in raspberry-like agglomerates of higher voidage. Growth rates range from 10 to 100 $\mu\text{m}/\text{h}$ to 100 to 1000 $\mu\text{m}/\text{h}$ for growth by layering and coalescence, respectively. Layering is generally more prevalent in coating processes or continuous processes with seeded recycle. In terms of coalescence, fluid-bed granulation follows a nondeformable growth model and generally remains within a noninertial regime of growth. Here, growth rate is *not* a function of gas velocity or binder viscosity (Fig. 21-120), and the distribution of spray and the design of the spray zone dominate successful operation. The *final* maximum growth limit, however, does vary in proportion to binder solution viscosity and inversely with gas velocity, as controlled by relative collision velocities within the bed. Possible choices of collision velocity include the relative shear occurring within the dense phase and entrance velocities existing at the distributor. In terms of consolidation, bed height is also critical in terms of compaction forces discussed below. From two-phase fluidization theory (see Dalton et al., 1973, and Sec. 17), the relative shear collisional velocity u_c occurring in the dense phase between bubbles is controlled by bubble velocity U_B and diameter D_B , or

$$u_c = \left(\frac{6U_B}{D_B} \right) d \quad \text{max} \quad \text{and} \quad u_c = \left(\frac{6U_B}{8D_B} \right) d \quad \text{(average)} \quad (21-153)$$

where

$$U_B = 0.71 \sqrt{gD_B} + (U - U_{mf})$$

$$\text{and} \quad D_B = 0.54(U - U_{mf})^{0.4} H^{0.8} / g^{0.2} \quad (21-154)$$

In most cases it may be shown that this collisional velocity is a weakly increasing function of excess gas velocity and bed height. As a general rule, increasing excess velocity $U - U_{mf}$ decreases overall growth for a number of reasons. It limits the maximum diameter as predicted by Stokes criteria [Eqs. (21-117) and (21-118)]; it lowers spray flux, giving less drop overlap and finer nuclei, but with a tighter distribution; and it increases drying rate during the spray cycle.

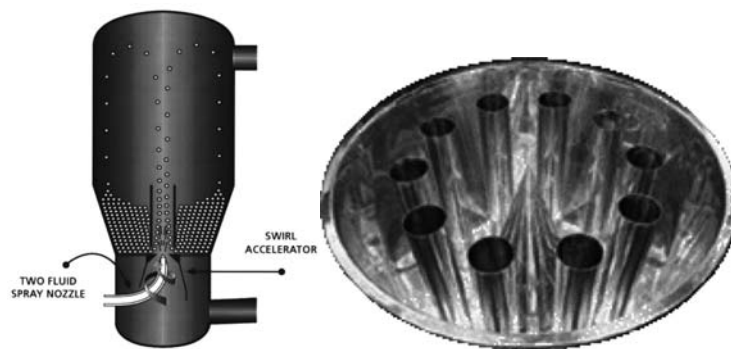


FIG. 21-170 Niro™ Precision Granulation process. Agglomeration in bottom-spray draft tube fluid-bed granulation. Scale-up is accomplished by replicating draft tube geometry. (Courtesy Niro Pharma Systems.)

Granule **consolidation**, which controls granule voidage, and hence indirectly granule **breakage**, generally increases with increasing peak bed moisture, increasing bed height, increasing gas velocity, decreasing primary particle size, increasing spray flux and drop size, and decreasing bed temperature. Increasing bed temperature and gas velocity increases the drying rate, thereby lowering bed moisture, leading to more porous, weaker granules. Increased bed turnover rate, and greater distributor velocities with increasing $U - U_{mf}$ can increase attrition and lower average growth. Note that high collisional velocities and bed height can also promote nonuniform granule density, or shell formation, which can impact redispersion and attrition behavior.

Scale-up and Operation Spray nozzles suffer from caking on the outside and clogging on the inside. When the nozzle is below the bed surface, fast capture of the liquid drops by bed particles, as well as scouring of the nozzle by particles, prevents caking. Blockages inside the nozzle are also common, particularly for slurries. The nozzle design should be as simple as possible, and provision for in situ cleaning or easy removal is essential.

Early detection of quenching is important. The initial stages of defluidization are detected by monitoring the bed temperature just above the distributor. A sudden increase (dry quenching) or decrease (wet quenching) indicates the onset of bed defluidization. Wet quenching is avoided by reducing the liquid feed rate and improving the nozzle operation. In situ jet grinding is sometimes used to limit the maximum stable size of dry agglomerates.

Control is accomplished by monitoring bed temperature as well as granule size and density of samples. Temperature may be controlled by adjusting the liquid feed rate or inlet air temperature. For batch granulation, the fluidizing air velocity should be increased during the batch to maintain constant $U - U_{mf}$, accomplished most easily by staged changes. **Bed pressure fluctuations** can be used to monitor the quality of fluidization and to indicate when gas velocity increases are required. In addition, intermittent sampling systems may be employed with **on-line size analyzers** to monitor granule size.

Scale-up of fluid-bed granulators relies heavily on pilot-scale tests. The pilot plant fluid bed should be at least 0.3 m in diameter so that bubbling rather than slugging fluidization behavior occurs. Key in scale-up is the increase in agitation intensity with increasing bed height. In particular, granule density and attrition resistance increase linearly with operating bed height, whereas the rate of granule dispersion decreases.

There are a variety of approaches to scale-up. One is to maintain constant bed height, resulting in similar compaction forces. In this case, peak bed moisture should be maintained to produce similar rates of granule consolidation and growth. In addition, nucleation rate may be kept constant by maintaining spray flux ψ_w . This is accomplished by increasing the number of nozzles in proportion to scale to maintain spray per unit area, and by maintaining constant solids flux through the

spray zone by maintaining constant excess gas velocity $U - U_{mf}$. In essence, this approach simply replicates the bed to achieve scale-up and the basis of cross-sectional area. A recent batch commercial example is the Niro™ Precision Granulation process illustrated in Fig. 21-170. This approach is also directly applicable to continuous processes.

In many batch processes, however, fluid-bed height increases with scale, complicating scale-up. Competing changes in spray flux, drying rate which controls peak bed moisture, and compaction forces scaling with bed height must be balanced. If peak bed moisture is maintained, denser granules will likely result. This may be compensated by increasing gas velocity or raising bed temperature to lower bed moisture with scale-up. The dependence of granule voidage on bed height and moisture must be explored at small scale to determine how much compensation is required. To maintain constant hydrodynamics, Horio et al. (*Proc. Fluidization V*, New York, Engineering Foundation, 1986, p. 151) suggested that excess velocity be increased as

$$(U - U_{mf})_2 = \sqrt{m}(U - U_{mf})_1 \quad (21-155)$$

$$m = (H_2/H_1) \quad (dU_{p_{gas}}/U_{p_{gas}}) > 30$$

where geometric similarity of the bed is maintained. The spray rate should be adjusted on the basis of the modified drying rate and desired peak bed moisture desired at scale-up. The number of nozzles can then be determined by maintaining similar spray flux.

Draft Tube Designs and Spouted Beds A **draft tube** is often employed to regulate particle circulation patterns. The most common design is the **Wurster** draft tube fluid bed employed extensively in the pharmaceutical industry, usually for coating and layered growth applications. The **Wurster coater** uses a bottom positioned spray, but other variations are available (Table 21-27).

The **spouted-bed granulator** consists of a central high-velocity **spout** surrounded by a **moving bed annular region**. All air enters

TABLE 21-27 Sizes and Capacities of Wurster Coaters*

Bed diameter, in	Batch size, kg
7	3-5
9	7-10
12	12-20
18	35-55
24	95-125
32	200-275
46	400-575

*Ghebre-Sellase (ed.), *Pharmaceutical Pelletization Technology*. Marcel Dekker, 1989.

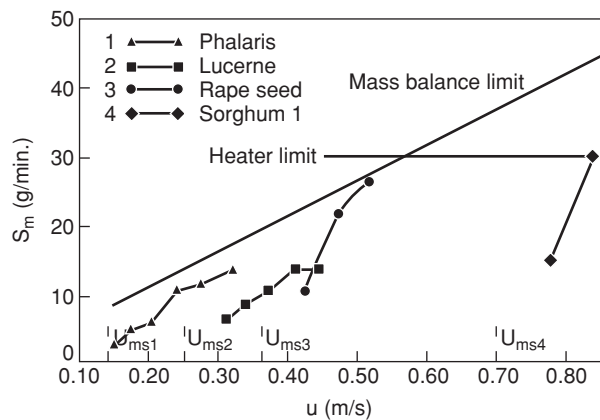


FIG. 21-171 Effect of gas velocity on maximum liquid rate for a spouted-bed seed coater. [Liu and Litster, *Powder Technol.*, **74**, 259 (1993). With permission from Elsevier Science SA, Lausanne, Switzerland.]

through the orifice at the base of the spout. Particles entrained in the spout are carried to the bed surface and rain down on the annulus as a fountain. Bottom-sprayed designs are the most common. Due to the very high gas velocity in the spout, granules grow by layering only. Therefore, spouted beds are good for coating applications. However, attrition rates are also high, so the technique is not suited to weak granules. Spouted beds are well suited to group D particles and are more tolerant of nonspherical particles than a fluid bed. Particle circulation is better controlled than in a fluidized bed, unless a draft tube design is employed. Spouted beds are difficult to scale past two meters in diameter.

The liquid spray rate to a spouted bed may be limited by agglomerate formation in the spray zone causing spout collapse [Liu and Litster, *Powder Tech.*, **74**, 259 (1993)]. The maximum liquid spray rate increases with increasing gas velocity, increasing bed temperature, and decreasing binder viscosity (see Fig. 21-171). The maximum

liquid flow rate is typically between 20 and 90 percent of that required to saturate the exit air, depending on operating conditions. Elutriation of fines from spouted-bed granulators is due mostly to the attrition of newly layered material, rather than spray drying. The elutriation rate is proportional to the kinetic energy in the inlet air [see Eq. (21-158)].

CENTRIFUGAL GRANULATORS

In the pharmaceutical industry, a range of centrifugal granulator designs are used. In each of these, a horizontal disc rotates at high speed causing the feed to form a rotating **rope** at the walls of the vessel (see Fig. 21-172). There is usually an allowance for drying air to enter around the edge of the spinning disc. Applications of such granulators include spherulization of extruded pellets, dry-powder layering of granules or sugar spheres, and coating of pellets or granules by liquid feeds.

Centrifugal Designs Centrifugal granulators tend to give denser granules or powder layers than fluidized beds and more spherical granules than mixer granulators. Operating costs are reasonable but capital cost is generally high compared to other options. Several types are available including the **CF granulator** (Fig. 21-172) and **rotary fluidized-bed** designs, which allow high gas volumes and therefore significant drying rates (Table 21-28). CF granulator capacities range from 3 to 80 kg with rotor diameters of 0.36 to 1.3 m and rotor speeds of 45 to 360 rpm [Ghebre-Selassie (ed.), *Pharmaceutical Pelletization Technology*, Marcel Dekker, 1989].

Particle Motion and Scale-up Very little fundamental information is published on centrifugal granulators. Qualitatively, good operation relies on maintaining a smoothly rotating **stable rope** of tumbling particles. Operating variables which affect the particle motion are disc speed, peripheral air velocity, and the presence of baffles.

For a given design, good rope formation is only possible for a small range of disc speeds. If the speed is too low, a rope does not form. If the speed is too high, very high attrition rates can occur. Scale-up on the basis of either **constant peripheral speed** ($DN = \text{const.}$), or **constant Froude number** ($DN^2 = \text{const.}$) is possible. Increasing peripheral air velocity and baffles helps to increase the rate of rope turnover. In designs with tangential powder or liquid feed tubes, additional baffles are usually not necessary. The motion of particles in the equipment is also a function of the frictional properties of the feed, so the optimum operating conditions are feed specific.

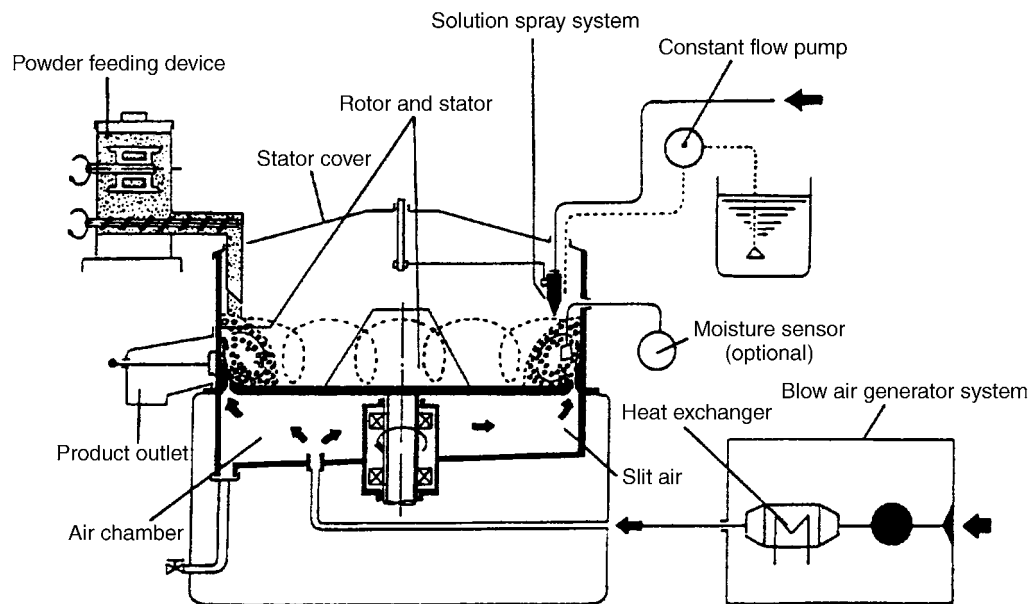


FIG. 21-172 Schematic of a CF granulator. (Ghebre-Selassie, 1989.)

TABLE 21-28 Specifications of Glatt Rotary Fluid-Bed Granulators*

Parameter	15	60	200	500
Volume, L	45	220	670	1560
Fan				
Power, kW	11	22	37	55
Capacity, m ³ /h	1500	4500	8000	12000
Heating capacity, kW	37	107	212	370
Diameter, m	1.7	2.5	3.45	4.0

*Glatt Company, in Ghebre-Selassie (ed.), *Pharmaceutical Pelletization Technology*, Marcel Dekker, 1989.

Granulation Rate Processes Possible granulation processes occurring in centrifugal granulators are extrudate breakage, consolidation, rounding (spheronization), coalescence, powder layering and coating, and attrition. Very little information is available about these processes as they occur in centrifugal granulators; however, similar principles from tumbling and fluid-bed granulators will apply.

SPRAY PROCESSES

Spray processes include **spray dryers**, **prilling towers**, **spouted and fluid beds**, and **flash dryers**. Feed solids in a fluid state (solution, gel, paste, emulsion, slurry, or melt) are dispersed in a gas and converted to granular solid products by heat and/or mass transfer. In spray processes, the size distribution of the particulate product is largely set by the drop size distribution; i.e., **nucleation** is the dominant granulation process, or more precisely **particle formation**. Exceptions are where fines are recycled to coalesce with new spray droplets and where spray-dried powders are rewet in a second tower to encourage agglomeration. For spray drying, a large amount of solvent must be evaporated whereas prilling is a spray-cooling process. Fluidized or spouted bed may be used to capture nucleated fines as hybrid granulator designs, e.g., **fluid-bed spray dryers**.

Product diameter is small and bulk density is low in most cases, except prilling. Feed liquids must be pumpable and capable of atomization or dispersion. Attrition is usually high, requiring fines recycle or recovery. Given the importance of the droplet size distribution, nozzle design and an understanding of the fluid mechanics of drop formation are critical. In addition, heat- and mass-transfer rates during drying can strongly affect the particle morphology, of which a wide range of characteristics are possible.

Spray Drying Detailed descriptions of spray dispersion dryers, together with application, design, and cost information, are given in Sec. 12. Product quality is determined by a number of properties such as particle form, size, flavor, color, and heat stability. Particle size and size distribution, of course, are of greatest interest from the point of view of size enlargement.

Figures 21-173 and 21-174 illustrate typical process and the stages of spray atomization, spray-air contacting and evaporation, and final product collection. A range of particle structures may be obtained, depending on the tower temperature in comparison to the boiling point and rheological properties of the feed (Fig. 21-175). Particle sizes ranging from 3 to 200 μm are possible with two-fluid atomizers producing the finest material, followed by rotary wheel and pressure nozzles.

In general, particle size is a function of atomizer operating conditions and of the solids content, liquid viscosity, liquid density, and feed rate. Coarser, more granular products can be made by increasing viscosity (through greater solids content, lower temperature, etc.), by increasing feed rate, and by the presence of binders to produce greater agglomeration of semidry droplets. Less-intense atomization and spray-air contact also increase particle size, as does a lower exit temperature, which yields a moister (and hence a more coherent) product. This latter type of spray-drying agglomeration system has been described by Masters and Stoltze [*Food Eng.*, 64 (February 1973)] for the production of instant skim-milk powders in which the completion of drying and cooling takes place in vibrating conveyors (see Sec. 17) downstream of the spray dryer.

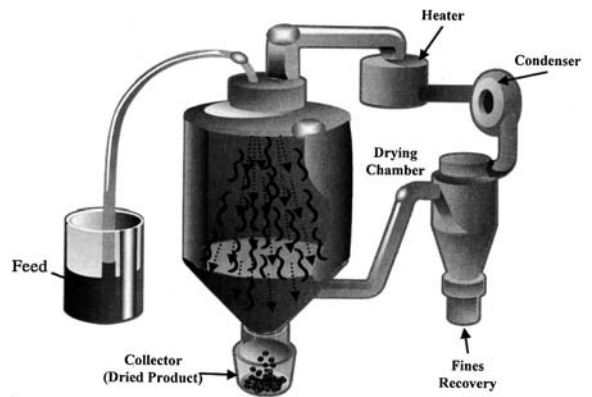


FIG. 21-173 Schematic of a typical spray-drying process. [Çelik and Wendel, in Parikh (ed.), *Handbook of Pharmaceutical Granulation Technology*, 2d ed., Taylor & Francis, 2005. With permission.]

Prilling The prilling process is similar to spray drying and consists of spraying droplets of liquid into the top of a tower and allowing these to fall against a countercurrent stream of air. During their fall the droplets are solidified into approximately spherical particles or prills which are up to about 3 mm in diameter, or larger than those formed in spray drying. The process also differs from spray drying since the

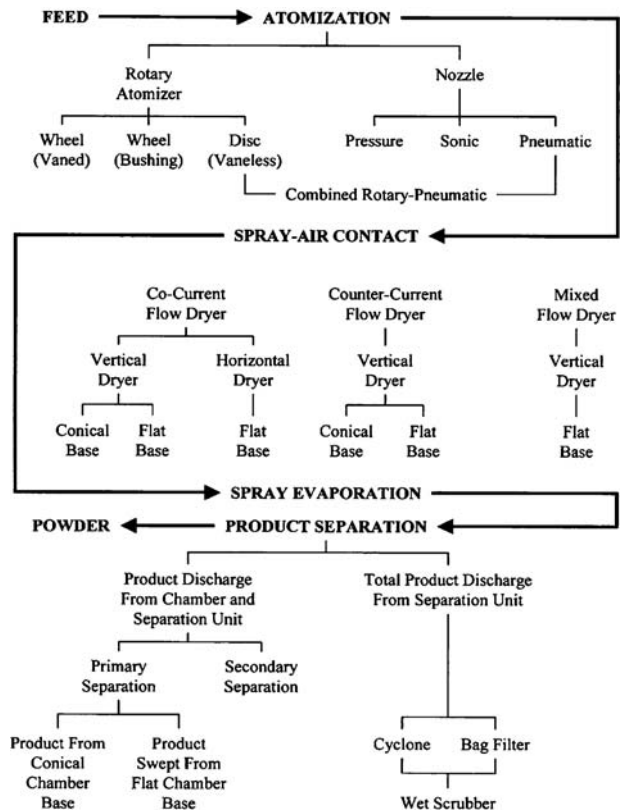


FIG. 21-174 Typical stages of a spray-drying process: atomization, spray-air contact/evaporation, and product collection. (Masters, *Spray Drying Handbook*, 5th ed., Longman Scientific Technical, 1991. With permission.)

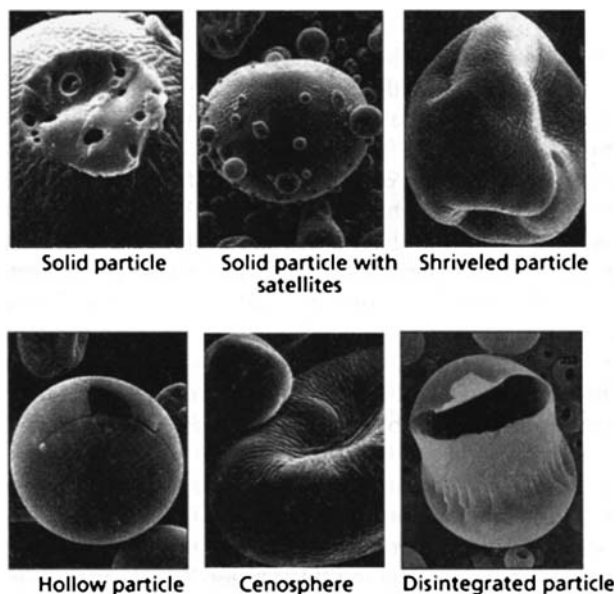


FIG. 21-175 Types of spray-dried particles, depending on drying conditions and feed boiling point. (Courtesy Niro Pharma Systems.)

droplets are formed from a melt which solidifies primarily by cooling with little, if any, contribution from drying. Traditionally, ammonium nitrate, urea, and other materials of low viscosity and melting point and high surface tension have been treated in this way. Improvements in the process now allow viscous and high-melting-point materials and slurries containing undissolved solids to be treated as well.

The design of a prilling unit first must take into account the properties of the material and its sprayability before the tower design can proceed. By using data on the melting point, viscosity, surface tension, etc., of the material, together with laboratory-scale spraying tests, it is possible to specify optimum temperature, pressure, and orifice size for the required prill size and quality. Tower sizing basically consists of specifying the cross-sectional area and the height of fall. The former is determined primarily by the number of spray nozzles necessary for the desired production rate. Tower height must be sufficient to accomplish solidification and is dependent on the heat-transfer characteristics of the prills and the operating conditions (e.g., air temperature). Because of relatively large prill size, narrow but very tall towers are used to ensure that the prills are sufficiently solid when they reach

the bottom. Table 21-29 describes the principal characteristics of a typical prilling tower.

Theoretical calculations are possible to determine tower height with reasonable accuracy. Simple parallel streamline flow of both droplets and air is a reasonable assumption in the case of prilling towers compared with the more complex rotational flows produced in spray dryers. For velocity of fall, see, for example, Becker [*Can. J. Chem.*, **37**, 85 (1959)]. For heat transfer, see, e.g., Kramers [*Physica*, **12**, 61 (1946)]. Specific design procedures for prilling towers are available in the *Proceedings of the Fertilizer Society (England)*; see Berg and Hallie, no. 59, 1960; and Carter and Roberts, no. 110, 1969.

Recent developments in nozzle design have led to drastic reductions in the required height of prilling towers. However, such nozzle designs are largely proprietary, and little information is openly available.

Flash Drying Special designs of pneumatic conveyor dryers, described in Sec. 12, can handle filter and centrifuge cakes and other sticky or pasty feeds to yield granular size-enlarged products. The dry product is recycled and mixed with fresh, cohesive feed, followed by disintegration and dispersion of the mixed feed in the drying air stream.

PRESSURE COMPACTION PROCESSES

The success of **compressive agglomeration** or **pressure compaction** processes depends on the effective utilization and transmission of the applied external force and on the ability of the material to form and maintain permanent interparticle bonds during **pressure compaction** (or **consolidation**) and **decompression**. Both of these aspects are controlled in turn by the geometry of the confined space, the nature of the applied loads, and the physical properties of the particulate material and of the confining walls.

Pressure compaction is carried out in two classes of equipment (Fig. 21-136). These are **dry confined-pressure devices** (molding, piston, tableting, briquetting, and roll presses), in which material is directly consolidated in closed molds or between two opposing surfaces, where the degree of confinement varies with design; and **paste extrusion devices** (pellet mills, screw extruders, table and cylinder pelletizers), in which material undergoes considerable shear and mixing as it is consolidated while being pressed through a die. See Table 21-11 for examples of use. Product densities and pressures are substantially higher than with agitative agglomeration techniques, as shown in Fig. 21-111. For detailed equipment discussion, see also Pietsch (*Size Enlargement by Agglomeration*, Wiley, Chichester, 1992) and Benbow and Bridgwater (*Paste Flow and Extrusion*, Oxford University Press, New York, 1993).

Powder hardness, friction, particle size, and permeability have a considerable impact on process performance and developed compaction pressures. As a general rule, the success of **dry compaction** improves with the following (Table 21-16):

TABLE 21-29 Some Characteristics of a Typical Prilling Operations*

Tower size		
Prill tube height, ft	130	
Rectangular cross section, ft	11 by 21.4	
Cooling air		
Rate, lb/h	360,000	
Inlet temperature	Ambient	
Temperature rise, °F	15	
Melt		
Type	Urea	Ammonium nitrate
Rate, lb/h	35,200 (190 lb H ₂ O)	43,720 (90 lb H ₂ O)
Inlet temperature, °F	275	365
Prills		
Outlet temperature, °F	120	225
Size, mm	Approximately 1 to 3	

*HPD Incorporated. To convert feet to centimeters, multiply by 30.5; to convert pounds per hour to kilograms per hour, multiply 0.4535; °C = (°F - 32) × 5/9.

1. **Increased stress transmission**, improving uniformity of pressure throughout the compact. For the case of die-type compaction, transmission increases with decreasing wall or die friction, increasing powder friction, decreasing aspect ratio, and decreasing compact size. Increased stress transmission improves the uniformity of compact density, and decreases residual radial stresses after compact unloading, which in turn lowers the likelihood of capping and delamination and lowers ejection forces.

2. **Decreased deaeration time** of the powder feed. If large deaeration is required, it becomes more likely that air will be entrapped within the die or feed zone, which not only can lower the powder feed rate, but also can result in gas pressurization during compact formation, which can create flaws and delamination during unloading. Relative deaeration time improves with decreasing production rate, increased bulk powder permeability, increased vacuum and forced feeding, and any upstream efforts to densify the product, one example being granulation.

3. **Increased permanent bonding**. Generally this increases with applied force (given good stress transmission), decreasing particle hardness, increased elastic modulus, and decreasing particle size. See also Hiestand tableting indices under "Powder Compaction" subsection.

4. **Increase powder flowability**. Powder feed rates improve with decreasing powder cohesive strength, increasing flow gaps, and increasing bulk permeability. See "Solids Handling: Bulk Solids Flow Characterization."

A range of compaction processes are discussed below, and these rules of thumb generally extend to all such processes in one form or another. See "Powder Compaction" for detailed discussion.

Piston and Molding Presses Piston or molding presses are used to create uniform and sometimes intricate compacts, especially in powder metallurgy and plastics forming. Equipment comprises a mechanically or hydraulically operated press and, attached to the platens of the press, a two-part mold consisting of top (male) and bottom (female) portions. The action of pressure and heat on the particulate charge causes it to flow and take the shape of the cavity of the mold. Compacts of metal powders are then sintered to develop metallic properties, whereas compacts of plastics are essentially finished products on discharge from the molding machine.

Tableting Presses Tableting presses are employed in applications having strict specifications for weight, thickness, hardness, density, and appearance in the agglomerated product. They produce simpler shapes at higher production rates than do molding presses. A single-punch press is one that will take one station of tools consisting of an upper punch, a lower punch, and a die. A rotary press employs a rotating round die table with multiple stations of punches and dies. Older rotary machines are single-sided; that is, there is one fill station and one compression station to produce one tablet per station at every revolution of the rotary head. Modern high-speed rotary presses are double-sided; that is, there are two feed and compression stations to produce two tablets per station at every revolution of the rotary head. Some characteristics of tableting presses are shown in Table 21-30.

For successful tableting, a material must have suitable flow properties to allow it to be fed to the tableting machine. Wet or dry granulation is used to improve the flow properties of materials. In the case of **wet granulation**, agitative granulation techniques such as fluidized beds or mixer granulators as discussed above are often employed.

TABLE 21-30 Characteristics of Tableting Presses*

	Single-punch	Rotary
Tablets per minute	8-140	72-6000
Tablet diameter, in.	1/8-4	3/4-2 1/2
Pressure, tons	1 1/2-100	4-100
Horsepower	1/4-15	1 1/2-50

*Browning, *Chem. Eng.*, **74**(25), 147 (1967).

NOTE: To convert inches to centimeters, multiply by 2.54; to convert tons to megagrams, multiply by 0.907; and to convert horsepower to kilowatts, multiply by 0.746.

In **dry granulation**, the blended dry ingredients are first densified in a heavy-duty rotary tableting press which produces "slugs" 1.9 to 2.5 cm (3/4 to 1 in) in diameter. These are subsequently crushed into particles of the size required for tableting. Predensification can also be accomplished by using a rotary compactor-granulator system. A third technique, direct compaction, uses sophisticated devices to feed the blended dry ingredients to a high-speed rotary press.

Figure 21-176 illustrates the stations of a typical rotary tablet press of die filling, weight adjustment, compaction, punch unloading, tablet ejection, and tablet knockoff. See "Powder Compaction" for detailed discussion of the impact of powder properties on die filling, compaction, and ejection forces. As discussed above, these stages of compaction improve with increased stress transmission (controlled by lubrication and die geometry), decreased deaeration time (increasing powder permeability and decreasing production rate), increased plastic, permanent deformation, and increased powder flowability (decreasing powder cohesion, increasing flow index, and increased die diameter and clearances).

Excellent accounts of tableting in the pharmaceutical industry have been given by Kibbe [*Chem. Eng. Prog.*, **62**(8), 112 (1966)], Carstensen (*Handbook of Powder Science & Technology*, Fayed & Otten (eds.), Van Nostrand Reinhold Inc., 1983, p. 252), Stanley-Wood (ed.) (loc. cit.), and Doelker (loc. cit.).

Figure 21-177 illustrates typical **defects** that occur in tableting as well as other compaction processes. Lamination or more specifically **delamination** occurs during compact ejection where the compact or tablet breaks into several layers perpendicular to its compression axis. **Capping** is a specific case where a conical endpiece dislodges from the surface of the compact. **Weak equators** are similar to delamination, where failure occurs at the midline of the compact. A key cause of these flaws is poor stress transmission resulting in large radial stresses and wall shear stresses, and it can be improved through lowering wall friction with lubrication or changing the compact aspect ratio. Such flaws occur during compact ejection but also within the compact itself, and they may be hidden, thereby weakening overall compact strength. Note that delamination can often be prevented in split dies, where the residual radial stress is relieved radially rather than by axial ejection. Sticking to punch surfaces or **die fouling** may also contribute to capping and delamination, and it can be assessed through wall friction and adhesion measurements. **Localized cracks** form in complex geometries during both compression and unloading, again due to nonuniform compression related to stress transmission. Small amounts of very hard or elastic material differing from the overall powder bed matrix can cause irregular **spontaneous fracture** of the compact, and it is often caused by recycle material, nonuniform feed, or entrapped air due to high production rate and low feed permeability. **Flashing and skirting** leading to a ring of weak material around edges are due to worn punches.

Roll Presses Roll presses compact raw material as it is carried into the gap between two rolls rotating at equal speeds (Fig. 21-178). The size and shape of the agglomerates are determined by the geometry of the roll surfaces. Pockets or indentations in the roll surfaces form briquettes the shape of eggs, pillows, teardrops, or similar forms from a few grams up to 2 kg (5 lb) or more in weight. Smooth or corrugated rolls produce a solid sheet, which can be granulated or broken down into the desired particle size on conventional grinding equipment.

Roll presses can produce large quantities of materials at low cost, but the product is less uniform than that from molding or tableting presses. The introduction of the proper quantity of material into each of the rapidly rotating pockets in the rolls is the most difficult problem in the briquetting operation. Various types of feeders have helped to overcome much of this difficulty.

The impacting rolls can be either solid or divided into segments. Segmented rolls are preferred for hot briquetting, as the thermal expansion of the equipment can be controlled more easily.

Roll presses provide a **mechanical advantage** in amplifying the feed pressure P_0 to some maximum value P_m . This maximum pressure P_m and the roll compaction time control compact density. Generally speaking, as compaction time decreases (e.g., by increasing roll speed), the minimum necessary pressure for quality compacts increases. There may be an upper limit of pressure as well for friable materials or elastic materials prone to delamination.

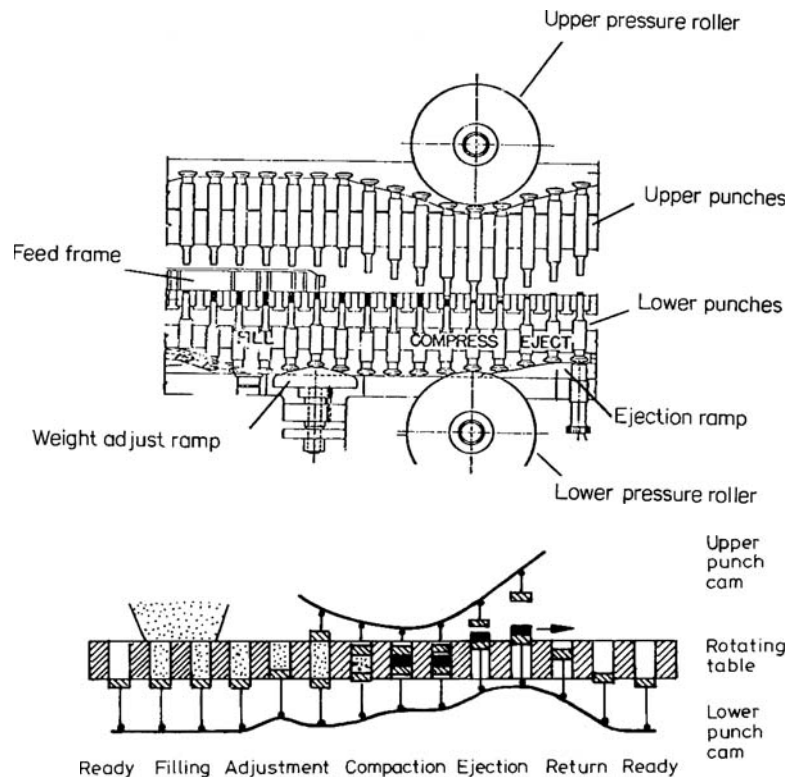


FIG. 21-176 Typical multistation rotary tableting press, indicating stages of tableting for one station. (Pietsch, *Size Enlargement by Agglomeration*, Wiley, Chichester, 1992.)

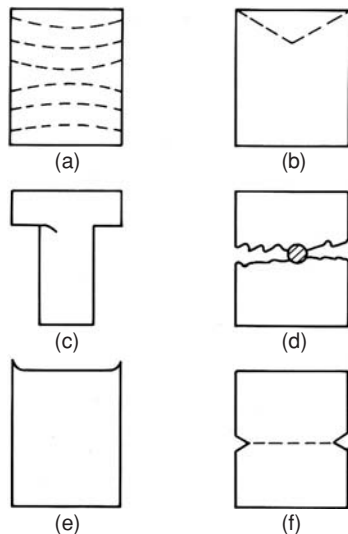


FIG. 21-177 Common defects occurring during tableting and compaction: (a) lamination, (b) capping, (c) localized cracks, (d) spontaneous cracking, (e) flashing or skirting, and (f) weak equator. (Benbow and Bridgwater, *Paste Flow and Extrusion*, Oxford University Press, New York, 1993.)

Pressure amplification occurs in two regions of the press (Fig. 21-178). Above the **angle of nip**, sliding occurs between the material and roll surface as material is forced into the rolls, with intermediate pressure ranging from 1 to 10 psi. Energy is dissipated primarily through overcoming particle friction and cohesion. Below the angle of nip, no slip occurs as the powder is compressed into a compact and pressure may increase up to several thousand psi. Both of these intermediate and high-pressure regions of densification are indicated in the compressibility diagram of Fig. 21-137.

The overall performance of the press and its mechanical advantage (P_m/P_0) depend on the mechanical and frictional properties of the powder. (See "Powder Compaction" subsections.) For design procedures, see Johanson [*Proc. Inst. Briquet. Agglom. Bien. Conf.*, **9**, 17 (1965).] Nip angle α generally increases with decreasing compressibility κ , or with increasing roll friction angle ϕ_w and effective angle of friction ϕ_e . Powders compress easily and have high-friction grip high in the rolls. The mechanical advantage pressure ratio (P_m/P_0) increases and the time of compaction decreases with decreasing nip angle since the pressure is focused over a smaller roll area. In addition, the mechanical advantage generally increases with increasing compressibility and roll friction.

The most important factor that must be determined in a given application is the pressing force required for the production of acceptable compacts. Roll loadings (i.e., roll separating force divided by roll width) in commercial installations vary from 4.4 MN/m to more than 440 MN/m (1000 lb/in to more than 100,000 lb/in). Roll sizes up to 91 cm (36 in) in diameter by 61 cm (24 in) wide are in use.

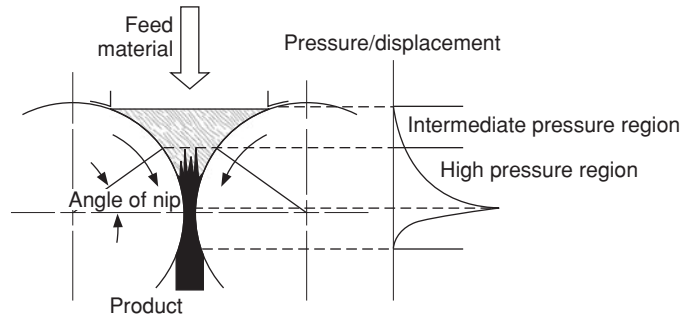


FIG. 21-178 Regions of compression in roll presses. Slippage and particle rearrangement occur above the angle of nip, and powder compaction at high pressure occurs in the nonslip region below the angle of nip.

The roll loading L is related to the maximum developed pressure and roll diameter by

$$L = \frac{F}{W} = \frac{1}{2} f P_m D \propto P_m D^{1/2} (h + d)^{1/2} \quad (21-156)$$

where F is the **roll-separating force**, D and W are the roll diameter and width, f is a **roll-force factor** dependent on compressibility κ and gap thickness as given in Fig. 21-179, h is the gap thickness, and $d/2$ is the pocket depth for briquette rolls. (Pietsch, *Size Enlargement by Agglomeration*, Wiley, Chichester, 1992.) The maximum pressure P_m is established on the basis of required compact density and quality, and it is a strong function of roll gap distance and powder properties as discussed above, particularly compressibility. Small variations in feed properties can have a pronounced effect on maximum pressure P_m and press performance. Roll presses are scaled on the basis of constant maximum pressure. The required roll loading increases approximately with the square root of increasing roll diameter or gap width.

The appropriate roll force then scales as follows:

$$F_2 = F_1 \sqrt{\frac{D_2}{D_1}} \sqrt{\frac{(h+d)_2}{(h+d)_1}} \left(\frac{W_2}{W_1} \right) \quad (21-157)$$

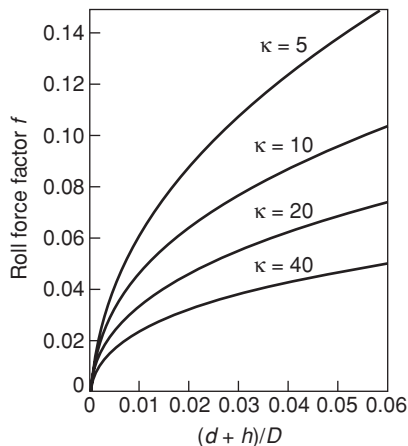


FIG. 21-179 Roll force factor as a function of compressibility κ and dimensionless gap distance $(d + h)/D$. [Pietsch (ed.), *Roll Pressing*, Powder Advisory Centre, London, 1987.]

It may be difficult to achieve geometric scaling of gap distance in practice. In addition, the impact of entrapped air and deaeration must be considered as part of scale-up, and this is not accounted for in the scale work of Johanson (loc. cit.).

The allowable roll width is inversely related to the required pressing force because of mechanical design considerations. The throughput of a roll press at constant roll speed decreases as pressing force increases since the allowable roll width is less. Machines with capacities up to 45 Mg/h (50 tons/h) are available. Some average figures for the pressing force and energy necessary to compress a number of materials on roll-type briquette machines are given in Table 21-31. Typical capacities are given in Table 21-32.

During compression in the slip region, escaping air may induce fluidization or erratic pulsating of the feed. This effect, which is controlled by the permeability of the powder, limits the allowable roll speed of the press, and may also induce compact delamination. Increases in roll speed or decreases in permeability require larger feed pressures.

Recent advances in roll press design focus heavily on achieving rapid deaeration of the feed, screw design (double or single), screw loading, and vacuum considerations to remove entrapped air. Fluctuations in screw feed pressure have been shown to correlate with frequency of turns, which brings about density variations in the sheets exiting the rolls. See Miller [in Parikh (ed.), *Handbook of Pharmaceutical Granulation Technology*, 2d ed., 2005] for a review.

Pellet Mills Pellet mills operate on the principle shown in Fig. 21-180. Moist, plastic feed is pushed through holes in dies of various shapes. The friction of the material in the die holes supplies the resistance necessary for compaction. Adjustable knives shear the rodlike extrudates into pellets of the desired length. Although several designs are in use, the most commonly used pellet mills operate by applying power to the die and rotating it around a freely turning roller with fixed horizontal or vertical axis. Concentric cylinder, double-roll cylinder, and table roll are commonly available designs (Fig. 21-136).

Pellet quality and capacity vary with properties of the feed such as moisture, lubricating characteristics, particle size, and abrasiveness, as well as die characteristics and speed. A readily pelleted material will yield about 122 kg/kWh [200 lb/(hp·h)] by using a die with 0.6-cm (1/4-in) holes. Some characteristics of pellet mills are given in Table 21-33.

Wet mass rheology heavily impacts performance through controlling both developed pressures and extrusion through the die, as in the case of paste extrusion (see "Paste Extrusion" and "Screw and Other Paste Extruders" subsections). In addition, the developed pressure in the roller nips behaves in a similar fashion to roll presses (see "Roll Presses" subsection).

Screw and Other Paste Extruders Screw extruders employ a screw to force material in a plastic state continuously through a die. If the die hole is round, a compact in the form of a rod is formed, whereas if the hole is a thin slit, a film or sheet is formed.

21-140 SOLID-SOLID OPERATIONS AND PROCESSING

TABLE 21-31 Pressure and Energy Requirements to Briquette Various Materials*

Pressure range, lb/in ³	Approximate energy required, kWh/ton	Type of material being briquetted or compacted		
		Without binder	With binder	Hot
Low 500–20,000	2–4	Mixed fertilizers, phosphate ores, shales, urea	Coal, charcoal, coke, lignite, animal feed, candy	Phosphate ores, urea
Medium 20,000–50,000	4–8	Acrylic resins, plastics, PVC, ammonium chloride, DMT, copper compounds, lead	Ferroalloys, fluorspar, nickel	Iron, potash, glass-making mixtures
High 50,000–80,000	8–16	Aluminum, copper, zinc, vanadium, calcined dolomite, lime, magnesia, magnesium carbonates, sodium chloride, sodium and potassium compounds	Flue dust, natural and reduced iron ores	Flue dust, iron oxide, natural and reduced iron ores, scrap metals
Very high >80,000	>16	Metal powders, titanium	—	Metal chips

*Courtesy Bepex Corporation. To convert pounds per square inch to newtons per square meter, multiply by 6895; to convert kilowatthours per ton to kilowatthours per megagram, multiply by 1.1.

TABLE 21-32 Some Typical Capacities (tons/h) for a Range of Roll Presses*

Roll diameter, in	10	16	12	10.3	13	20.5	28	36
Maximum roll-face width, in	3.25	6	4	6	8	13.5	27	10
Roll-separating force, tons	25	50	40	50	75	150	300	360
Carbon								
Coal, coke		2	1		3	6	25	
Charcoal			8			13		
Activated					3	7		
Metal and ores								
Alumina					5	10	28	
Aluminum				2	4	8	20	
Brass, copper	0.5			1.5	3	6	16	
Steel-mill waste					5	10		
Iron				3	6	15	40	
Nickel powder					2.5	5.0		
Nickel ore						20	40	
Stainless steel				2	5	10		
Steel								25
Bauxite		1.5				10	20	
Ferrometals						10		
Chemicals								
Copper sulfate	0.5	1.5		1	3	6	15	
Potassium hydroxide				1	4	8		
Soda ash	0.5				3	6	15	
Urea	0.25					10		
DMT	0.25				2	6		
Minerals								
Potash						20	80	
Salt				2	5	9		
Lime					4	8	15	
Calcium sulfate							13	40
Fluorspar						5	10	28
Magnesium oxide						1.5	5	
Asbestos						1.5	3	
Cement						5		
Glass batch						5	12	

*Courtesy Bepex Corporation. To convert inches to centimeters, multiply by 2.54; to convert tons to megagrams, multiply by 0.907; and to convert tons per hour to megagrams per hour, multiply by 0.907.

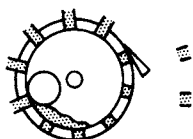


FIG. 21-180 Operating principle of a pellet mill.

TABLE 21-33 Characteristics of Pellet Mills

Horsepower range	10–250
Capacity, lb/(hp-h)	75–300
Die characteristics	
Size	Up to 26 in inside diameter × approximately 8 in wide
Speed range	75–500 r/min
Hole-size range	1/16–1/4 in inside diameter
Rollers	As many as three rolls; up to 10-in diameter

NOTE: To convert horsepower to kilowatts, multiply by 0.746; to convert pounds per horsepower-hour to kilograms per kilowatthour, multiply by 0.6; and to convert inches to centimeters, multiply by 2.54.

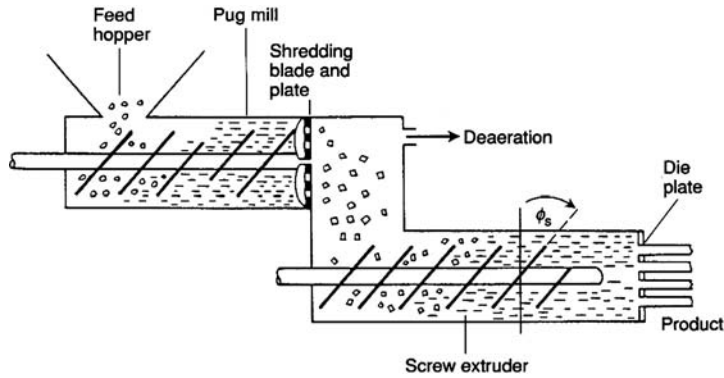


FIG. 21-181 Screw extruder with upstream pug mill, shredding plate, and deaeration stage. (Benbow and Bridgwater, *Paste Flow and Extrusion*, Oxford University Press, 1993, with permission.)

Basic types of extruders include both screw extruders such as axial endplate, radial screen, and basket designs, as well as pelletization equipment described above, such as rotary cylinder or gear and ram or piston extruders (Fig. 21-136). See Newton [*Powder Technology and Pharm. Processes*, Chulia et al. (eds.), Elsevier, 1994, p. 391], Pietsch (*Size Enlargement by Agglomeration*, Wiley, 1992), and Benbow and Bridgwater (*Paste Flow and Extrusion*, Oxford University Press, 1993).

Figure 21-181 illustrates a typical extruder layout, with upstream pug mill, shredding plate, and deaeration stage. Premixing and extrusion through a pug mill help achieve initial densification prior to final screw extrusion. As with all compaction processes, deaeration must be accounted for, which often occurs under vacuum. A wider variety of single- and twin-screw designs are available, which vary in screw and barrel geometry, the degrees of intermeshing, and rotation direction (Fig. 21-182).

Both wet and dry extrusion techniques are available, and both are strongly influenced by the frictional properties of the particulate phase and wall. In the case of wet extrusion, rheological properties

of the liquid phase are equally important. See Pietsch (*Size Enlargement by Agglomeration*, Wiley, Chichester, 1992, p. 346), and Benbow et al. [*Chem. Eng. Sci.*, **422**, 2151 (1987)] for a review of design procedures for dry and wet extrusion, respectively. Die face throughput increases with increasing pressure developed at the die, whereas the developed pressure from the screw decreases with increasing throughput. These relationships are referred to as the **die and screw characteristics** of the extruder, respectively, as illustrated in Fig. 21-183 (see "Screw and Other Paste Extruders" subsection), and in addition to rheology and wall friction, they are influenced by wear of dies, screws, and barrels over equipment life, which modify wall friction properties and die entrance effects. The intersection of these characteristics determines the **operating point**, or throughput, of the extruder.

The formation of **defects** and **phase separation** is an important consideration in paste extrusion. Typical defects include lamination or **delamination** (occurring with joining of adjacent past streams) and **surface fracture**, often referred to as shark-skin formation. Surface fracture generally increases with decreasing paste liquid

Single screw	Twin screw (tangential)	Twin screw (intermeshing)
Decreasing pitch	Co-rotating	Co-rotating self-cleaning
Increasing core	Counter-rotating	Partly self-cleaning
Threaded barrel		Counter-rotating cylindrical
Conical barrel		Counter-rotating conical
Alternating pin-type screw		

FIG. 21-182 Available screw extruder systems, illustrated barrel and screw type, as well as rotation. (After Benbow and Bridgwater, *Paste Flow and Extrusion*, Oxford University Press, 1993. Courtesy Werner and Pfliederer.)

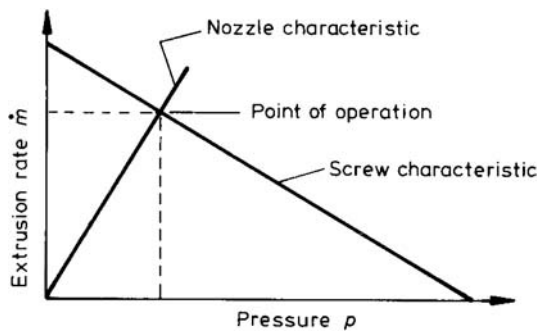


FIG. 21-183 Determination of extruder capacity or throughput based on the intersection of screw and nozzle (die face) characteristics. (From Pietsch, Size Enlargement by Agglomeration, Wiley, 1992.)

content (Fig. 21-184), increasing extrusion die velocity, and decreasing die length. Phase separation can lead to extruder or die failure, with rapid rise in pressures associated with the fluid phase separating from the powder matrix. The chance of phase separation increases with increased operating pressure, increased bulk powder permeability (or increasing particle size), and decreasing liquid viscosity. See Benbow and Bridgwater (loc. cit.) for detailed discussions of these effects.

A common use of screw extruders is in the forming and compounding of plastics. Table 21-34 shows typical outputs that can be expected per horsepower for various plastics and the characteristics of several popular extruder sizes.

Deairing pugmill extruders, which combine mixing, densification, and extrusion in one operation, are available for agglomerating clays, catalysts, fertilizers, etc. Table 21-35 gives data on screw extruders for the production of catalyst pellets.

THERMAL PROCESSES

Bonding and agglomeration by temperature elevation or reduction are applied either in conjunction with other size-enlargement processes or as a separate process. Agglomeration occurs through one or more of the following mechanisms:

1. Drying of a concentrated slurry or wet mass of fines
2. Fusion
3. High-temperature chemical reaction
4. Solidification and/or crystallization of a melt or concentrated slurry during cooling

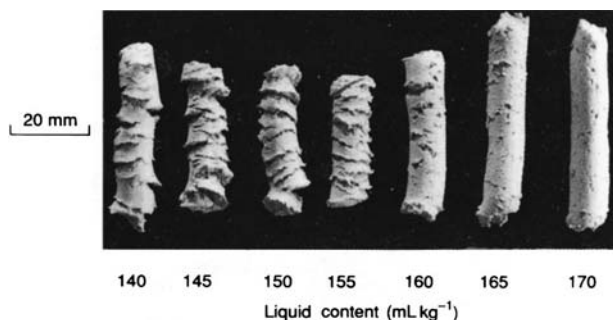


FIG. 21-184 Effect of liquid content of surface fracture. α -alumina and 5 wt % Celacol in water, with die ($D = 9.5$ mm, $L = 3.14$ mm) at a velocity $V = 1.2$ mm/s. (Benbow and Bridgwater, Paste Flow and Extrusion, Oxford University Press, 1993, with permission.)

TABLE 21-34 Characteristics of Plastics Extruders*

Efficiencies		lb/(hp-h)	
Rigid PVC		7-10	
Plasticized PVC		10-13	
Impact polystyrene		8-12	
ABS polymers		5-9	
Low-density polyethylene		7-10	
High-density polyethylene		4-8	
Polypropylene		5-10	
Nylon		8-12	

Relation of size, power, and output			
hp	Diameter		Output, lb/h, low-density polyethylene
	in	mm	
15	2	45	Up to 125
25	2½	60	Up to 250
50	3½	90	Up to 450
100	4½	120	Up to 800

*The Encyclopedia of Plastics Equipment, Simonds (ed.), Reinhold, New York, 1964.

NOTE: To convert inches to centimeters, multiply by 2.54; to convert horsepower to kilowatts, multiply by 0.746; to convert pounds per hour to kilograms per hour, multiply by 0.4535; and to convert pounds per horsepower-hour to kilograms per kilowatt-hour, multiply by 0.6.

Sintering and Heat Hardening In powder metallurgy compacts are sintered with or without the addition of binders. In ore processing the agglomerated mixture is either sintered or indurated. Sintering refers to a process in which fuel is mixed with the ore and burned on a grate. The product is a porous cake. Induration, or heat hardening, is accomplished by combustion of gases passed through the bed. The aim is to harden the pellets without fusing them together, as is done in the sintering process.

Ceramic bond formation and grain growth by diffusion are the two prominent reactions for bonding at the high temperature (1100 to 1370°C, or 2000 to 2500°F, for iron ore) employed. The minimum temperature required for sintering may be measured by modern dilatometry techniques, as well as by differential scanning calorimetry. See Compo et al. [Powder Tech., 51(1), 87 (1987); Particle Characterization, 1, 171 (1984)] for reviews.

In addition to agglomeration, other useful processes may occur during sintering and heat hardening. For example, carbonates and sulfates, may be decomposed, or sulfur may be eliminated. Although the major application is in ore beneficiation, other applications, such as the preparation of lightweight aggregate from fly ash and the formation of clinker from cement raw meal, are also possible. Nonferrous sinter is produced from oxides and sulfides of manganese, zinc, lead, and nickel. An excellent account of the many possible applications is given by Ban et al. [Knepper (ed.), Agglomeration, op. cit., p. 511] and Ball et al. (Agglomeration of Iron Ores, 1973). The highest tonnage use at present is in the beneficiation of iron ore.

TABLE 21-35 Characteristics of Pelletizing Screw Extruders for Catalysts*

Screw diameter, in	Drive hp	Typical capacity, lb/h
2.25		60
4	7.5-15	200-600
6	Up to 60	600-1500
8	75-100	Up to 2000

*Courtesy The Bonnot Co. To convert inches to centimeters, multiply by 2.54; to convert horsepower to kilowatts, multiply by 0.746; and to convert pounds per hour to kilograms per hour, multiply by 0.4535.

NOTE:

1. Typical feeds are high alumina, kaolin carriers, molecular sieves, and gels.
2. Water-cooled worm and barrel, variable-speed drive.
3. Die orifices as small as 1/16 in.
4. Vacuum-deairing option available.

The machine most commonly used for sintering iron ores is a traveling grate, which is a modification of the Dwight-Lloyd continuous sintering machine formerly used only in the lead and zinc industries. Modern sintering machines may be 4 m (13 ft) wide by 60 m (200 ft) long and have capacities of 7200 Mg/day (8000 tons/day).

The productive capacity of a sintering strand is related directly to the rate at which the burning zone moves downward through the bed. This rate, which is of the order of 2.5 cm/min (1 in/min), is controlled by the air rate through the bed, with the air functioning as the heat-transfer medium.

Heat hardening of green iron-ore pellets is accomplished in a vertical shaft furnace, a traveling-grate machine, or a grate-plus-kiln combination (see Ball et al., op. cit.).

Drying and Solidification Granular free-flowing solid products are often an important result of the drying of concentrated slurries and pastes and the cooling of melts. Size enlargement of originally finely divided solids results. Pressure agglomeration including extrusion, pelleting, and briquetting is used to preform wet material into forms suitable for drying in through-circulation and other types of dryers. Details are given in Sec. 12 in the account of solids-drying equipment.

Rotating-drum-type and belt-type heat-transfer equipment forms granular products directly from fluid pastes and melts without intermediate preforms. These processes are described in Sec. 5 as examples of indirect heat transfer to and from the solid phase. When solidification results from melt freezing, the operation is known as *flaking*. If evaporation occurs, solidification is by drying.

MODELING AND SIMULATION OF GRANULATION PROCESSES

For granulation processes, granule size distribution is an important if not the most important property. The evolution of the granule size distribution within the process can be followed using population balance modeling techniques. This approach is also used for other size-change processes including crushing and grinding. (See section "Principles of Size Reduction.") The use of the **population balance (PB)** is outlined briefly below. For more in-depth analysis see Randolph and Larson (*Theory of Particulate Processes*, 2d ed., Academic Press, 1991), Ennis and Litster (*The Science and Engineering of Granulation Processes*, Chapman-Hall, 1997), and Sastry and Loftus [*Proc. 5th Int. Symp. Agglom.*, IChemE, 623 (1989)]. See also Cameron and Wang for a recent review of modeling and control [in Parikh (ed.), *Handbook of Pharmaceutical Granulation Technology*, 2d ed., Taylor & Francis, 2005].

- The key uses of PB modeling of granulation processes are
- Critical evaluation of data to determine controlling granulation mechanisms
 - In design, to predict the mean size and size distribution of product granules

- Sensitivity analysis: to analyze quantitatively the effect of changes to operating conditions and feed variables on product quality
- Circuit simulation, optimization, and process control

The use of PB modeling by practitioners has been limited for two reasons. First, in many cases the kinetic parameters for the models have been difficult to predict and are very sensitive to operating conditions. Second, the PB equations are complex and difficult to solve. However, recent advances in understanding of granulation micromechanics, as well as better numerical solution techniques and faster computers, means that the use of PB models by practitioners should expand.

THE POPULATION BALANCE

The PB is a statement of continuity for particulate systems. It includes a **kinetic expression** for each mechanism which changes a particle property. Consider a section of a granulator as illustrated in Fig. 21-185. The PB follows the change in the granule size distribution as granules are born, die, grow, and enter or leave the control

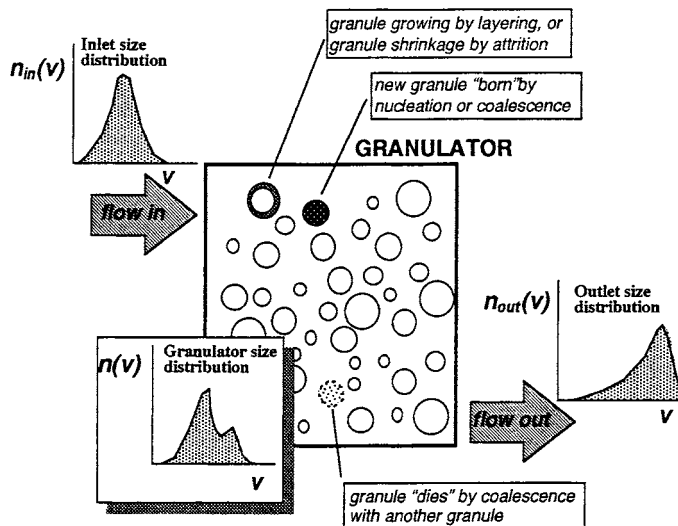


FIG. 21-185 Changes to the granule size distribution due to granulation-rate processes as particles move through the granulator. (Reprinted from Design and Optimization of Granulation and Compaction Processes for Enhanced Product Performance, Ennis, 2006, with permission of E&G Associates. All rights reserved.)

volume. As discussed in detail previously (“Agglomeration Rate Processes and Mechanics”), the granulation mechanisms which cause these changes are nucleation, layering, coalescence, and attrition (Fig. 21-91 and Table 21-36). The number of particles-per-unit volume of granulator between size volume v and $v + dv$ is $n(v) dv$, where $n(v)$ is the **number frequency size distribution** by size volume, having dimensions of number per unit granulator and volume per unit size volume. For constant granulator volume, the macroscopic PB for the granulator in terms of $n(v)$ is:

$$\frac{\partial n(v,t)}{\partial t} = \frac{Q_{in}}{V} n_{in}(v) - \frac{Q_{ex}}{V} n_{ex}(v) - \frac{\partial(G^\circ - A^\circ)n(v,t)}{\partial v} + B_{nuc}(v) + \frac{1}{2N_t} \int_0^v \beta(u,v-u,t)n(u,t)n(v-u,t) du - \frac{1}{N_t} \int_0^\infty \beta(u,v,t)n(u,t)n(v,t) du \quad (21-158)$$

where V is the volume of the granulator; Q_{in} and Q_{ex} are the inlet and exit flow rates from the granulator; $G(v)$, $A(v)$, and $B_{nuc}(v)$ are the layering, attrition, and nucleation rates, respectively; $B(u,v,t)$ is the coalescence kernel and N_t is the total number of granules-per-unit volume of granulator. The left-hand side of Eq. (21-158) is the accumulation of particles of a given size volume. The terms on the right-hand side are in turn: the bulk flow into and out of the control volume, the convective flux along the size axis due to layering and attrition, the birth of new particles due to nucleation, and birth and death of granules due to coalescence. Equation (21-158) is written in terms of granule volume v , but could also be written in terms of granule size x or could also be expanded to follow changes in other granule properties, e.g., changes in granule density or porosity due to consolidation.

MODELING INDIVIDUAL GROWTH MECHANISMS

The **granule size distribution (GSD)** is a strong function of the balance between different mechanisms for size change shown in Table 21-33—layering, attrition, nucleation, and coalescence. For example, Fig. 21-186 shows the difference in the GSD for a doubling in mean granule size due to (1) layering only, or (2) coalescence only for batch, plug-flow, and well-mixed granulators. Table 21-36 describes how four key rate mechanisms effect the GSD.

Nucleation Nucleation increases both the mass and number of the granules. For the case where new granules are produced by liquid

feed, which dries or solidifies, the nucleation rate is given by the new feed, droplet size n_s , and the volumetric spray rate S :

$$B(v)_{nuc} = S n_s(v) \quad (21-159)$$

In processes where new powder feed has a much smaller particle size than the smallest granular product, the feed powder can be considered as a **continuous phase** that can nucleate to form new granules [Sastry & Fuerstenau, *Powder Technol.*, **7**, 97 (1975)]. The size of the nuclei is then related to nucleation mechanism. In the case of nucleation by spray, the size of the nuclei is of the order of the droplet size and proportional to $\cos\theta$, where θ is binder fluid-particle contact angle (see Fig. 21-99).

Layering Layering increases granule size and mass by the progressive coating of new material onto existing granules, but it does not alter the number of granules in the system. As with nucleation, the new feed may be in liquid form (where there is simultaneous drying or cooling) or may be present as a fine powder. Where the feed is a powder, the process is sometimes called **pseudolayering** or **snowballing**. It is often reasonable to assume a linear-growth rate $G(x)$ which is independent of granule size. For batch and plug-flow granulators, this causes the initial feed distribution to shift forward in time with the shape of the GSD remaining unaltered and governed by a traveling-wave equation (Table 21-37). As an example, Fig. 21-187 illustrates size-independent growth of limestone pellets by snowballing in a batch drum. Size-independent linear growth rate implies that the volumetric growth rate $G^\circ(v)$ is proportional to projected granule surface area, or $G^\circ(v) \propto v^{2/3} \propto x^2$. This assumption is true only if all granules receive the same exposure to new feed. Any form of segregation will invalidate this assumption [Liu and Litster, *Powder Technol.*, **74**, 259 (1993)]. The growth rate $G^\circ(v)$ by layering only can be calculated directly from the mass balance:

$$\dot{V}_{feed} = (1 - \epsilon) \int_0^\infty G^\circ(v)n(v)dv \quad (21-160)$$

where \dot{V}_{feed} is the volumetric flow rate of new feed and ϵ is the granule porosity.

Coalescence Coalescence is the most difficult mechanism to model. It is easiest to write the population balance [Eq. (21-158)] in terms of number distribution by volume $n(v)$ because granule volume is conserved in a coalescence event. The key parameter is the **coalescence kernel** or rate constant $\beta(u,v)$. The kernel dictates the overall rate of coalescence, as well as the effect of granule size on coalescence rate. The **order** of the kernel has a major effect on the shape and evolution of the granule size distribution. [See Adetayo & Ennis, *AIChE J.* 1997.] Several empirical kernels have been proposed and used (Table 21-38).

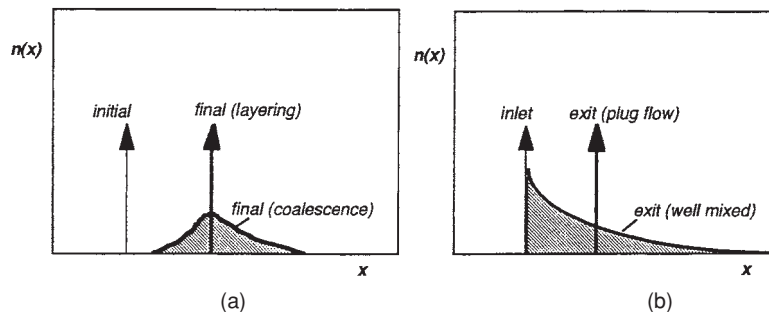
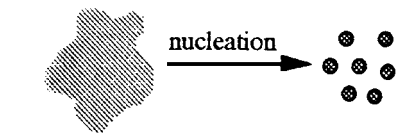
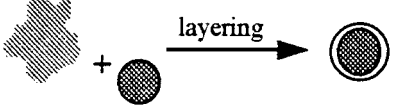
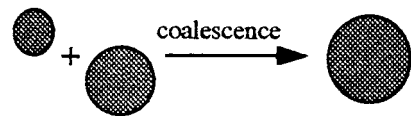
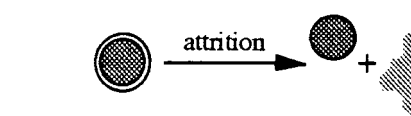


FIG. 21-186 The effect of growth mechanism and mixing on product granule size distribution for (a) batch growth by layering or coalescence, and (b) layered growth in well-mixed or plug-flow granulators. (Reprinted from Design and Optimization of Granulation and Compaction Processes for Enhanced Product Performance, Ennis, 2006, with permission of E&G Associates. All rights reserved.)

TABLE 21-36 Impact of Granulation Mechanisms on Size Distribution

Mechanism	Changes number of granules?	Changes mass of granules?	Discrete or differential?
	yes	yes	discrete
	no	yes	differential
	yes	no	discrete
	no	yes	differential

Reprinted from Design and Optimization of Granulation and Compaction Processes for Enhanced Product Performance, Ennis, 2006, with permission of E&G Associates. All rights reserved.

All the kernels are empirical, or semiempirical and must be fitted to plant or laboratory data. The kernel proposed by Adetayo and Ennis is consistent with the granulation regime analysis described above (see section on growth) and is therefore recommended:

$$\beta(u,v) = \begin{cases} k, w < w^* \\ 0, w > w^* \end{cases} \quad w = \frac{(uv)^a}{(u+v)^b} \quad (21-161)$$

where w^* is the **critical average granule volume** in a collision corresponding to $St = St^*$, and it is related to the critical cutoff diameter defined above. For fine powders in the noninertial regime (see section "Growth and Consolidation") where $St \ll St^*$, this kernel collapses to the simple **random** or size-independent kernel $\beta = k$ for

which the mean granule size increases exponentially with time. Where deformation is unimportant, coalescence occurs only in the noninertial regime and stops abruptly when $St_v = St^*$. Based on the granulation regime analysis, the effects of feed characteristics and operating variables on granulation extent has been predicted [Adetayo et al., *Powder Tech.*, **82**, 47-59 (1995)].

Modeling growth where deformation is significant is more difficult. It can be assumed that a critical cutoff size exists w^* , which determines which combination of granule sizes are capable of coalescence, based on their inertia. When the harmonic average of sizes of two colliding granules w is less than this critical cutoff size w^* , coalescence is successful, or

$$w = \frac{(uv)^b}{(u+v)^a} = w^* = \frac{\pi}{6} \left(\frac{16\mu}{\rho u_0} St^* \right)^3 \quad (21-162)$$

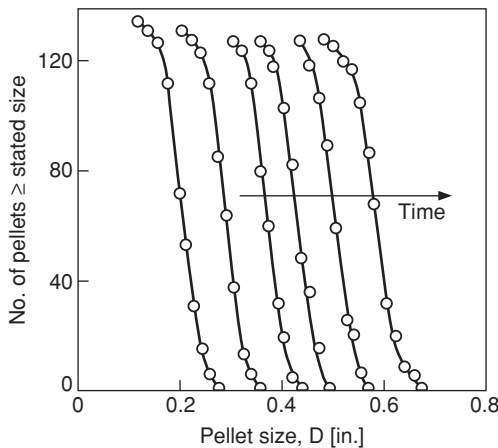


FIG. 21-187 Batch drum growth of limestone pellets by layering with a size-independent linear growth rate [Capes, Chem. Eng., **45**, CE78 (1967).]

where a and b are model parameters expected to vary with granule deformability, and u and v are granule volumes. To be dimensionally consistent, $2b - a = 1$. w^* and w involving the parameters a and b represent a generalization of the Stokes analysis for nondeforming systems, for which case $a = b = 1$. For deformable systems, the kernel is then represented by Eq. (21-161). Figure 21-188 illustrates the evolution of the granule size distribution as predicted by this cutoff-based kernel that accounts for deformability. The cutoff kernel is seen to clearly track the experimental average granule size over the life of the granulation, illustrating that multiple kernels are not necessary to describe the various stages of granule growth, including the initial stage of random noninertial coalescence and the final stage of nonrandom preferential inertial growth by balling or crushing and layering (see Fig. 21-91).

Attrition The wearing away of granule surface material by attrition is the direct opposite of layering. It is an important mechanism when drying occurs simultaneously with granulation and granule velocities are high, e.g., fluidized beds and spouted beds. In a fluid bed [Ennis and Sunshine, *Tribology Int.*, **26**, 319 (1993)], attrition rate is proportional to excess gas velocity $U - U_{mf}$ and approximately inversely proportional to granule-fracture toughness K_c , or $A \propto (U - U_{mf})/K_c$. For

TABLE 21-37 Some Analytical Solutions to the Population Balance*

Mixing state	Mechanisms operating	Initial or inlet size distribution	Final or exit size distribution
Batch	Layering only: $G(x) = \text{constant}$	Any initial size distribution, $n_0(x)$	$n(x) = n_0(x - \Delta x)$ where $\Delta x = Ct$
Continuous & well-mixed	Layering only: $G(x) = \text{constant}$	$n_{in}(x) = N_{in} \delta(x - x_{in})$	$n(x) = \frac{N_0 G}{\tau} \exp\left(-\frac{\tau(x - x_m)}{G}\right)$
Batch	Coalescence only, size independent: $\beta(u, v) = \beta_0$	$n_0(v) = N_0 \delta(v - v_0)$	$n(v) = \frac{N_0}{\bar{v}} \exp\left(-\frac{v}{\bar{v}}\right)$ where $\bar{v} = v_0 \exp\left(\frac{\beta_0 t}{6}\right)$
Batch	Coalescence only, size independent: $\beta(u, v) = \beta_0$	$n_0(v) = \frac{N_0}{v_0} \exp\left(-\frac{v}{v_0}\right)$	$n(v) = \frac{4 N_0}{v_0(N_0 \beta_0 t + 2)^2} \exp\left[\frac{-2v/v_0}{N_0 \beta_0 t + 2}\right]$

*Randolph and Larson, *Theory of Particulate Processes*, 2d ed., Academic Press, New York (1988); Gelbart and Seinfeld, *J. Computational Physics*, **28**, 357 (1978).

spouted beds, most attrition occurs in the spout and the attrition rate may be expressed as

$$A \propto \frac{A_i U_i^3}{K} \quad (21-163)$$

where A_i and U_i are the inlet orifice area and gas velocity, respectively. Attrition rate also increases with increasing slurry feed rate [Liu and Lister, *Powder Tech.*, **74**, 259 (1993)]. Granule breakage by fragmentation

is also possible, with its rate being described by an **on function**, which plays a similar role as the coalescence kernel does for growth. (See "Principles of Size Reduction" and "Breakage Modes and Grindability" sections for additional details.)

SOLUTION OF THE POPULATION BALANCE

Effects of Mixing As with chemical reactors, the **degree of mixing** within the granulator has an important effect on the final granule size distribution because of its influence on the **residence time distribution**. Figure 21-186 shows the difference in exit size distribution for a plug-flow and well-mixed granulator for growth by layering only. In general, the exit size distribution is broadened and the extent of growth (for constant rate constants) is diminished for an increased degree of mixing in the granulator. With layering and attrition rates playing the role of generalized velocities, coalescence, and fragmentation rates, the role of reaction rate constants, methodologies of traditional reaction engineering may be employed to design granulation systems or optimize the granule size distribution. [For the related example of crystallization, see Randolph and Larson (*Theory of Particulate Processes*, 2d ed., Academic Press, 1991).] Table 21-39 lists some mixing models that have been used for several types of granulators.

Analytical Solutions Solution of the population balance is not trivial. Analytical solutions are available for only a limited number of special cases, of which some examples of practical importance are summarized in Table 21-37. For other analytical solutions, see general references on population balances given above.

In general, analytical solutions are only available for specific initial or inlet size distributions. However, for batch granulation where the only growth mechanism is coalescence, at long times the size distribution may become **self-preserving**. The size distribution is self-preserving if the normalized size distributions $\phi = \phi(\eta)$ at long times are independent of mean size \bar{v} , or

$$\phi = \phi(\eta) \quad \text{only where} \quad \eta = v/\bar{v}$$

$$\bar{v} = \int_0^\infty v \cdot n(v, t) dv \quad (21-164)$$

Analytical solutions for self-preserving growth do exist for some coalescence kernels and such behavior is sometimes seen in practice (Fig. 21-189). Roughly speaking, self-preserving growth implies that the width of the size distribution increases in proportion to mean granule size, i.e., the width is uniquely related to the mean of the distribution.

Numerical Solutions For many practical applications, numerical solutions to the population balance are necessary. Several numerical solution techniques have been proposed. It is usual to break the

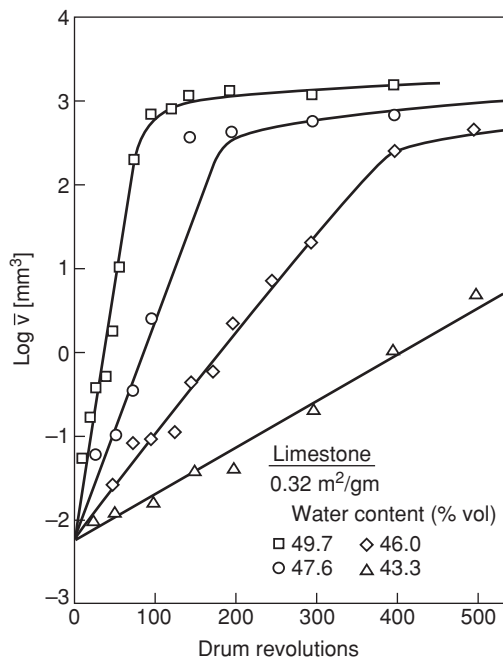


FIG. 21-188 Batch drum growth of limestone by coalescence. Note granule size increases exponentially with time in the first stage of noninertial growth. Experimental data of Kapur [Adv. Chem. Eng., **10**, 56 (1978)] compared with single deformable granulation kernel [Eqs. (21-161), and (21-162)]. [Adetayo & Ennis, AIChE]. (In press.) Reproduced with permission of the American Institute of Chemical Engineers. Copyright AIChE. All rights reserved.

TABLE 21-38 Coalescence Kernels for Granulation

Kernel	Reference and comments
$\beta = \beta_0$	Kapur & Fuerstenau [<i>I & EC Proc. Des. & Dev.</i> , 8(1), 56 (1969)], size-independent kernel.
$\beta = \beta_0 \frac{(u+v)^a}{(uv)^b}$	Kapur [<i>Chem. Eng. Sci.</i> , 27, 1863 (1972)], preferential coalescence of limestone.
$\beta = \beta_0 \frac{(u^{2/3} + v^{2/3})}{1/u + 1/v}$	Sastry [<i>Int. J. Min. Proc.</i> , 2, 187 (1975)], preferential balling of iron ore and limestone.
$\beta(u,v) = \begin{cases} k, & w < w^* \\ 0, & w > w^* \end{cases} \quad w = \frac{(uv)^a}{(u+v)^b}$	Adetayo & Ennis [<i>AIChE J.</i> , (1997)], based on granulation regime analysis.

TABLE 21-39 Mixing Models for Continuous Granulators

Granulator	Mixing model	Reference
Fluid bed	Well-mixed	See Sec. 17
Spouted bed	Well-mixed	Liu and Litster, <i>Powder Tech.</i> , 74, 259 (1993)
	Two-zone model	Litster et al. [<i>Proc. 6th Int. Symp. Agglom., Soc. Powder Tech., Japan</i> , 123 (1993)].
Drum	Plug-flow	Adetayo et al., <i>Powder Tech.</i> , 82, 47-59 (1995)
Disc	Two well-mixed tanks in series with classified exit	Sastry & Loftus [<i>Proc. 5th Int. Symp. Agglom.</i> , IChemE, 623 (1989)]
	Well-mixed tank and plug-flow in series with fines bypass	Ennis, Personal communication (1986)

size range into discrete intervals and then solve the resulting series of ordinary differential equations. A geometric discretization reduces the number of size intervals (and equations) that are required. Litster et al. [*AIChE J.*, (1995)] give a general discretized PB for nucleation,

growth, and coalescence with a geometric discretization of $v_j = 2^{1/q} v_{j-1}$ where q is an integer. Accuracy is increased (at the expense of computational time) by increasing the value of q . Their discretized PB is recommended for general use.

SIMULATION OF GRANULATION CIRCUITS WITH RECYCLE

When granulation circuits include recycle streams, both steady-state and dynamic responses can be important. Computer simulation packages are now widely used to design and optimize many process flow sheets, e.g., comminution circuits, but simulation of granulation circuits is much less common. Commercial packages do not contain library models for granulators. Some researchers have developed simulations and used these for optimization and control studies [Sastry, *Proc. 3d Int. Symp. Agglom.* (1981); Adetayo et al., *Computers Chem. Eng.*, 19, 383 (1995); Zhang et al., *Control of Part. Processes IV* (1995)]. For these simulations, dynamic population-balance models have been used for the granulator. Standard literature models are used for auxiliary equipment such as screens, dryers, and crushers. These simulations are valuable tools for optimization studies and development of control strategies in granulation circuits, and may be employed to investigate the effects of transient upsets in operating variables, particularly moisture level and recycle ratio, on circuit performance.

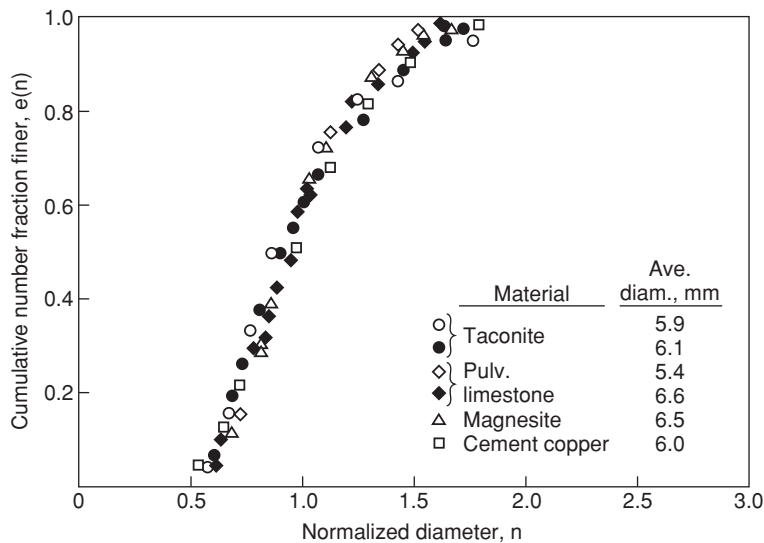


FIG. 21-189 Self-preserving size distributions for batch coalescence in drum granulation. [Sastry, *Int. J. Min. Proc.*, 2, 187 (1975).] With kind permission of Elsevier Science -NL, 1055 KV Amsterdam, the Netherlands.

SECTION 22

Waste
Management

PERRY'S CHEMICAL ENGINEERS' HANDBOOK

8TH EDITION



LOUIS THEODORE, KENNETH N. WEISS
JOHN D. MCKENNA, F. LEE SMITH
ROBERT R. SHARP, JOSEPH J. SANTOLERI
THOMAS F. MCGOWAN

Copyright © 2008, 1997, 1984, 1973, 1963, 1950, 1941, 1934 by The McGraw-Hill Companies, Inc. All rights reserved. Manufactured in the United States of America. Except as permitted under the United States Copyright Act of 1976, no part of this publication may be reproduced or distributed in any form or by any means, or stored in a database or retrieval system, without the prior written permission of the publisher.

0-07-154229-9

The material in this eBook also appears in the print version of this title: 0-07-151145-8.

All trademarks are trademarks of their respective owners. Rather than put a trademark symbol after every occurrence of a trademarked name, we use names in an editorial fashion only, and to the benefit of the trademark owner, with no intention of infringement of the trademark. Where such designations appear in this book, they have been printed with initial caps.

McGraw-Hill eBooks are available at special quantity discounts to use as premiums and sales promotions, or for use in corporate training programs. For more information, please contact George Hoare, Special Sales, at george_hoare@mcgraw-hill.com or (212) 904-4069.

TERMS OF USE

This is a copyrighted work and The McGraw-Hill Companies, Inc. (“McGraw-Hill”) and its licensors reserve all rights in and to the work. Use of this work is subject to these terms. Except as permitted under the Copyright Act of 1976 and the right to store and retrieve one copy of the work, you may not decompile, disassemble, reverse engineer, reproduce, modify, create derivative works based upon, transmit, distribute, disseminate, sell, publish or sublicense the work or any part of it without McGraw-Hill’s prior consent. You may use the work for your own noncommercial and personal use; any other use of the work is strictly prohibited. Your right to use the work may be terminated if you fail to comply with these terms.

THE WORK IS PROVIDED “AS IS.” McGRAW-HILL AND ITS LICENSORS MAKE NO GUARANTEES OR WARRANTIES AS TO THE ACCURACY, ADEQUACY OR COMPLETENESS OF OR RESULTS TO BE OBTAINED FROM USING THE WORK, INCLUDING ANY INFORMATION THAT CAN BE ACCESSED THROUGH THE WORK VIA HYPERLINK OR OTHERWISE, AND EXPRESSLY DISCLAIM ANY WARRANTY, EXPRESS OR IMPLIED, INCLUDING BUT NOT LIMITED TO IMPLIED WARRANTIES OF MERCHANTABILITY OR FITNESS FOR A PARTICULAR PURPOSE. McGraw-Hill and its licensors do not warrant or guarantee that the functions contained in the work will meet your requirements or that its operation will be uninterrupted or error free. Neither McGraw-Hill nor its licensors shall be liable to you or anyone else for any inaccuracy, error or omission, regardless of cause, in the work or for any damages resulting therefrom. McGraw-Hill has no responsibility for the content of any information accessed through the work. Under no circumstances shall McGraw-Hill and/or its licensors be liable for any indirect, incidental, special, punitive, consequential or similar damages that result from the use of or inability to use the work, even if any of them has been advised of the possibility of such damages. This limitation of liability shall apply to any claim or cause whatsoever whether such claim or cause arises in contract, tort or otherwise.

DOI: 10.1036/0071511458

Waste Management*

Louis Theodore, Eng.Sc.D. Professor of Chemical Engineering, Manhattan College; Member, Air and Waste Management Association (Section Editor, Pollution Prevention)

Kenneth N. Weiss, P.E., Diplomate AAEE Partner and North American Director of Compliance Assurance, ERM; Member, Air and Waste Management Association (Introduction to Waste Management and Regulatory Overview)

John D. McKenna, Ph.D. President and Chairman, ETS International, Inc.; Member, American Institute of Chemical Engineers, Air and Waste Management Association (Air-Pollution Management of Stationary Sources)

(Francis) Lee Smith, Ph.D., M.Eng. Principal, Wilcrest Consulting Associates, Houston, Texas; Member, American Institute of Chemical Engineers, Society of American Value Engineers, Water Environment Federation, Air and Waste Management Association (Biological APC Technologies, Estimating Henry's Law Constants)

Robert R. Sharp, Ph.D., P.E. Professor of Environmental Engineering, Manhattan College; Environmental Consultant; Member, American Water Works Association; Water Environment Federation Section Director (Wastewater Management)

Joseph J. Santoleri, P.E. Senior Consultant, RMT Inc. & Santoleri Associates; Member, American Institute of Chemical Engineers, American Society of Mechanical Engineers (Research Committee on Industrial and Municipal Waste), Air and Waste Management Association (Solid Waste Management)

Thomas F. McGowan, P.E. President, TMTS Associates; Member, American Institute of Chemical Engineers, American Society of Mechanical Engineers, Air and Waste Management Association (Solid Waste Management)

INTRODUCTION TO WASTE MANAGEMENT AND REGULATORY OVERVIEW

Multimedia Approach to Environmental Regulations in the United States	22-4	Clean Air Act of 1990	22-9
Plant Strategies	22-5	Regulatory Direction	22-12
Corporate Strategic Planning	22-5	United States Water Quality Legislation and Regulations	22-12
United States Air Quality Legislation and Regulations	22-6	Federal Water Pollution Control Act	22-12
Clean Air Act of 1970	22-6	Source-Based Effluent Limitations	22-14
Prevention of Significant Deterioration (PSD)	22-6	Clean Water Act of 1977	22-15
Nonattainment (NA)	22-8	Control of Toxic Pollutants	22-15
Controlled-Trading Program	22-9	1987 CWA Amendments	22-15
		Biological Criteria	22-15
		Metal Bioavailability and Toxicity	22-16
		Total Maximum Daily Load (TMDL)	22-16
		Water Quality Trading	22-16
		Bioterrorism Act of 2003	22-17

*The contributions of Dr. Anthony J. Buonicore to material from the seventh edition of this handbook are acknowledged.

22-2 WASTE MANAGEMENT

Cooling Water Intake Regulation	22-17
Water Reuse	22-17
Regulatory Direction	22-17
United States Solid Waste Legislation and Regulations	22-17
Rivers and Harbors Act, 1899	22-17
Solid Waste Disposal Act, 1965	22-17
National Environmental Policy Act, 1969	22-17
Resource Recovery Act, 1970	22-17
Resource Conservation and Recovery Act, 1976	22-17
Toxic Substances Control Act, 1976	22-18
Regulatory Direction	22-18

POLLUTION PREVENTION

Introduction	22-19
Pollution-Prevention Hierarchy	22-20
Multimedia Analysis and Life-Cycle Analysis	22-21
Multimedia Analysis	22-21
Life-Cycle Analysis	22-21
Pollution-Prevention Assessment Procedures	22-22
Planning and Organization	22-22
Assessment Phase	22-22
Feasibility Analysis	22-22
Implementation	22-23
Sources of Information	22-23
Industry Programs	22-23
Assessment Phase: Material Balance Calculations	22-23
Barriers and Incentives to Pollution Prevention	22-24
Barriers to Pollution Prevention ("The Dirty Dozen")	22-24
Pollution-Prevention Incentives ("A Baker's Dozen")	22-24
Economic Considerations Associated with Pollution-Prevention Programs	22-25
Pollution Prevention at the Domestic and Office Levels	22-26
Ethical Considerations	22-27
Future Trends	22-27

AIR-POLLUTION MANAGEMENT OF STATIONARY SOURCES

Introduction	22-28
Gaseous Pollutants	22-28
Particulate Pollutants	22-29
Estimating Emissions from Sources	22-31
Effects of Air Pollutants	22-31
A Source-Control-Problem Strategy	22-35
Strategy	22-35
Factors in Control-Equipment Selection	22-36
Dispersion From Stacks	22-37
Preliminary Design Considerations	22-37
Design Calculations	22-39
Miscellaneous Effects	22-40
Control of Gaseous Emissions	22-41
Absorption	22-41
Adsorption	22-42
Combustion	22-44
Condensation	22-47
Biological APC Technologies	22-48
Membrane Filtration	22-51
Source Control of Particulate Emissions	22-53
Emissions Measurement	22-54
Introduction	22-54
Sampling Methodology	22-55

INDUSTRIAL WASTEWATER MANAGEMENT

Introduction	22-58
United States Legislation, Regulations, and Government Agencies	22-58
Federal Legislation	22-58
Environmental Protection Agency	22-60
State Water-Pollution-Control Offices	22-60
Wastewater Characteristics	22-60
Priority Pollutants	22-60
Organics	22-60
Inorganics	22-62
pH and Alkalinity	22-62

Temperature	22-62
Dissolved Oxygen	22-62
Solids	22-62
Nutrients and Eutrophication	22-62
Whole Effluent Toxicity (WET)	22-63
Oil and Grease	22-63
Wastewater Treatment	22-63
Pretreatment	22-63
Equalization	22-63
Neutralization	22-63
Grease and Oil Removal	22-64
Toxic Substances	22-64
Primary Treatment	22-64
Screens	22-64
Grit Chambers	22-64
Gravity Sedimentation	22-64
Chemical Precipitation	22-65
Secondary Treatment	22-65
Design of Biological Treatment Systems	22-66
Reactor Concepts	22-67
Determination of Kinetic and Stoichiometric Pseudo Constants	22-68
Activated Sludge	22-69
Lagoons	22-72
Fixed-Film Reactor Systems	22-74
Trickling Filters	22-74
Rotating Biological Contactors (RBCs)	22-74
Packed-Bed Fixed-Film Systems	22-74
Biological Fluidized Beds	22-75
Physical-Chemical Treatment	22-76
Adsorption	22-76
Ion Exchange	22-77
Stripping	22-77
Chemical Oxidation	22-77
Advanced Oxidation Processes	22-77
Membrane Processes	22-78
Membrane Bioreactors (MBRs)	22-78
Industrial Reuse	22-78
Sludge Processing	22-78
Objectives	22-78
Concentration: Thickening and Flotation	22-79
Stabilization (Anaerobic Digestion, Aerobic Digestion, High Lime Treatment)	22-79
Sludge Disposal	22-80
Incineration	22-80
Sanitary Landfills	22-80
Beneficial Reuse of Biosolids	22-80

MANAGEMENT OF SOLID WASTES

Introduction	22-81
Functional Elements	22-81
United States Legislation, Regulations, and Government Agencies	22-82
Generation of Solid Wastes	22-82
Types of Solid Waste	22-82
Hazardous Wastes	22-83
Sources of Industrial Wastes	22-84
Properties of Solid Wastes	22-84
Quantities of Solid Wastes	22-86
On-Site Handling, Storage, and Processing	22-88
On-Site Handling	22-89
On-Site Storage	22-89
On-Site Processing of Solid Wastes	22-90
Processing and Resource Recovery	22-90
Processing Techniques for Solid Waste	22-90
Processing of Hazardous Waste	22-91
Materials-Recovery Systems	22-92
Recovery of Biological Conversion Products	22-92
Thermal Processes	22-92
Concentration of WTE Incinerators	22-96
Regulations Applicable to Municipal Waste Combustors	22-96
Ultimate Disposal	22-98
Landfilling of Solid Waste	22-98
Planning	22-106

List of Abbreviations

Abbreviation	Definition	Abbreviation	Definition
3P	Pollution prevention pays	LCC	Life cycle costing
ABS	Alkyl benzene sulfonate	LOX	Liquid oxygen
ACC	Annualized capital costs	MACT	Maximum achievable control technology
BACT	Best available control technology	MSDA	Material safety data sheets
BAT	Best available technology	MSW	Municipal solid waste
BCOD	Biodegradable chemical oxygen demand	MWC	Municipal waste combustors
BCT	Best conventional technology	MWI	Medical waste incinerators
BOD	Biochemical oxygen demand	NBOD	Nitrogenous biochemical oxygen demand
BSRT	Biomass solids retention time	NIMBY	Not in my back yard
BTEX	Benzene, toluene, xylene	NPDES	National pollutant discharge elimination system
CAA	Clean Air Act	NSPS	New source performance standards
CAAA	Clean Air Act Amendments	PCB	Polychlorinated biphenyl
CCP	Comprehensive costing procedures	PIES	Pollution prevention information exchange systems
CFR	Code of federal regulations	PM	Particulate matter
CKD	Cement kiln dust	POTW	Publicly owned treatment work
COD	Chemical oxygen demand	PPIC	Pollution prevention information clearinghouse
CPI	Chemical process industries	PSD	Prevention of significant deterioration
CRF	Capital recovery factor	RCRA	Resource Conservation and Recovery Act
CTDMPLUS	Complex terrain dispersion model plus algorithms for unstable situations	RDF	Refuse-derived fuel
CWRT	Center for Waste Reduction Technologies	SARA	Superfund Amendments and Reauthorization Act
DCF	Direct installation cost factor	SCR	Selective catalytic reduction
DO	Dissolved oxygen	SCS	Stationary-container systems
DRE	Destruction and removal efficiency	SE	Strength of the treated waste
EBCT	Empty bed contact time	SMART	Save money and reduce toxics
EMAS	Eco-management and audit scheme	SO	Strength of the untreated waste
EMS	Environmental management system	SS	Suspended solids
EPA	Environmental Protection Agency	TCC	Total capital cost
FML	Flexible membrane liner	TCP	Traditional costing procedures
GAX	Granular activated carbon	TGNMO	Total gas nonmethane organics
HAPS	Hazardous air pollutants	TOC	Total organic carbon
HAZWOPER	Hazardous waste operators	TSA	Total systems approach
HCS	Hauled-container systems	TSCA	Toxic Substances Control Act
HRT	Reactor hydraulic retention time	TSD	Treatment, storage, and disposal
HSWA	Hazardous and Solid Waste Act	UASB	Upflow anaerobic sludge blanket
I-TEF	International toxic equivalency factor	VOC	Volatile organic compound
ICF	Indirect installation cost factor	VOST	Volatile organic sampling train
ISO	International Organization for Standardization	VSS	Volatile suspended solids
LCA	Life cycle assessment	WRAP	Waste reduction always pays
		WTE	Waste-to-energy (systems)

GENERAL REFERENCES

1. United States EPA, *Pollution Prevention Fact Sheet*, Washington, DC, March 1991.
2. Keoleian, G., and D. Menerey, "Sustainable Development by Design: Review of Life Cycle Design and Related Approaches," *Air & Waste*, **44**, May 1994.
3. Theodore, L. Personal notes.
4. Dupont, R., L. Theodore, and K. Ganesan, *Pollution Prevention: The Waste Management Approach for the 21st Century*, Lewis Publishers, 2000.
5. World Wildlife Fund, *Getting at the Source*, 1991, p. 7.
6. United States EPA, *1987 National Biennial RCRA Hazardous Waste Report—Executive Summary*, Washington, DC, GPO, 1991, p. 10.
7. ASTM, Philadelphia, PA.
8. Theodore, L., and R. Allen, *Pollution Prevention: An ETS Theodore Tutorial*, Roanoke, VA, ETS International, Inc., 1993.
9. United States EPA, *The EPA Manual for Waste Minimization Opportunity Assessments*, Cincinnati, OH, August 1988.
10. Santoleri, J., J. Reynolds, and L. Theodore, *Introduction to Hazardous Waste Incineration*, 2d ed., Wiley, 2000.
11. ICF Technology Incorporated, *New York State Waste Reduction Guidance Manual*, Alexandria, VA, 1989.
12. Details available from L. Theodore.
13. Neveril, R. B., *Capital and Operating Costs of Selected Air Pollution Control Systems*, EPA Report 450/5-80-002, Gard, Inc., Niles, IL, December 1978.
14. Vatauvuk, W. M., and R. B. Neveril, "Factors for Estimating Capital and Operating Costs," *Chemical Engineering*, November 3, 1980, pp. 157–162.
15. Vogel, G. A., and E. J. Martin, "Hazardous Waste Incineration," *Chemical Engineering*, September 5, 1983, pp. 143–146 (part 1).
16. Vogel, G. A., and E. J. Martin, "Hazardous Waste Incineration," *Chemical Engineering*, October 17, 1983, pp. 75–78 (part 2).
17. Vogel, G. A., and E. J. Martin, "Estimating Capital Costs of Facility Components," *Chemical Engineering*, November 28, 1983, pp. 87–90.
18. Ulrich, G. D., *A Guide to Chemical Engineering Process Design and Economics*, Wiley-Interscience, New York, 1984.
19. California Department of Health Services, *Economic Implications of Waste Reduction, Recycling, Treatment, and Disposal of Hazardous Wastes: The Fourth Biennial Report*, California, 1988, p. 110.
20. Wilcox, J., and L. Theodore, *Engineering and Environmental Ethics*, Wiley, 1998.
21. Varga, A., *On Being Human*, Paulist Press, New York, 1978.
22. Theodore, L., "Dissolve the USEPA . . . Now," *Environmental Manager* (AWMA publication), vol. 1, November 1995.
23. Theodore, L., and R. Kunz, *Nanotechnology: Environmental Implications and Solutions*, Wiley, 2005.
24. Yang, Y., and E. R. Allen, "Biofiltration Control of Hydrogen Sulfide. 2. Kinetics, Biofilter Performance, and Maintenance," *JAWA*, vol. 44, p. 1315.
25. Mycock, J., and J. McKenna, *Handbook of Air Pollution Control and Technology*, ETS, Inc., chap. 21.
26. Ottengraf, S. P. P., "Biological Systems for Waste Gas Elimination," 1987.
27. Hubert, F. L., "Consider Membrane Pervaporation," *Chemical Engineering Progress*, July 1992, p. 46.
28. Caruana, Claudia M., "Membranes Vie for Pollution Cleanup Role," *Chemical Engineering Progress*, October 1993, p. 11.
29. Winston, W. S., and Kamalesh K. Sirkar, *Membrane Handbook*, Van Nostrand Reinhold, NY, 1992, p. 78.
30. Tabak et al., "Biodegradability Studies with Organic Priority Pollutant Compounds," USEPA, MERL, Cincinnati, Ohio, April 1980.
31. Levin, M. A., and M. A. Gealt, *Biotreatment of Industrial and Hazardous Waste*, McGraw-Hill Inc., 1993.
32. Sutton, P. M., and P. N. Mishra, "Biological Fluidized Beds for Water and Wastewater Treatment: A State-of-the-Art Review," WPCF Conference, October 1990.
33. Envirex equipment bulletin FB. 200-R2 and private communication, Waukesha, WI, 1994.
34. Donovan, E. J., Jr., "Evaluation of Three Anaerobic Biological Systems Using Paper Mill Foul Condensate," HydroQual, Inc., EPA, IERL contract 68-03-3074.
35. Mueller, J. A., K. Subburama, and E. J. Donovan, *Proc. 39th Ind. Waste Conf.*, 599, Ann Arbor, 1984.
36. ASME Research Committee on Industrial and Municipal Waste—Keeping Society's Options Open—MWCs, A Case Study on Environmental Regulation.
37. *Chartwell Information*, EBI, Inc., San Diego, June 2004.
38. Wilson, D. G. (ed.), *Handbook of Solid Waste Management*, Van Nostrand Reinhold, New York, 1997.
39. *Wastes: Engineering Principles and Management Issues*, McGraw-Hill, New York, 1977.
40. Montenay Montgomery LP, 2001.

INTRODUCTION TO WASTE MANAGEMENT AND REGULATORY OVERVIEW

In this section, a number of references are made to laws and procedures that have been formulated in the United States with respect to waste management. An engineer handling waste-management problems in another country would well be advised to know the specific laws and regulations of that country. Nevertheless, the treatment given here is believed to be useful as a general guide.

MULTIMEDIA APPROACH TO ENVIRONMENTAL REGULATIONS IN THE UNITED STATES

Among the most complex problems to be faced by industry during the 1990s is the proper control and use of the natural environment. In the 1970s the engineering profession became acutely aware of its responsibility to society, particularly for the protection of public health and welfare. The decade saw the formation and rapid growth of the U.S. Environmental Protection Agency (EPA) and the passage of federal and state laws governing virtually every aspect of the environment. The end of the decade, however, brought a realization that only the more simplistic problems had been addressed. A limited number of

large sources had removed substantial percentages of a few readily definable air pollutants from their emissions. The incremental costs to improve the removal percentages would be significant and would involve increasing numbers of smaller sources, and the health hazards of a host of additional toxic pollutants remained to be quantified and control techniques developed.

Moreover, in the 1970s, air, water, and waste were treated as separate problem areas to be governed by their own statutes and regulations. Toward the latter part of the decade, however, it became obvious that environmental problems were closely interwoven and should be treated in concert. The traditional type of regulation—command and control—had severely restricted compliance options.

The 1980s began with EPA efforts redirected to take advantage of the case-specific knowledge, technical expertise, and imagination of those being regulated. Providing plant engineers with an incentive to find more efficient ways of abating pollution would greatly stimulate innovation in control technology. This is a principal objective, for example, of EPA's "controlled trading" air pollution program, established in the Offsets Policy Interpretative Ruling issued by the EPA in 1976, with statutory foundation given by the Clean Air Act Amendments of 1977. The Clean Air Act Amendments of

1990 expanded the program even more to the control of sulfur oxides under Title IV. In effect, a commodities market on “clean air” was developed.

The rapidly expanding body of federal regulation presents an awesome challenge to traditional practices of corporate decision-making, management, and long-range planning. Those responsible for new plants must take stock of the emerging requirements and construct a fresh approach.

The full impact of the Clean Air Act Amendments of 1990, the Clean Water Act, the Safe Drinking Water Act, the Resource Conservation and Recovery Act, the Comprehensive Environmental Responsibility, Compensation and Liability (Superfund) Act, and the Toxic Substances Control Act is still not generally appreciated. The combination of all these requirements, sometimes imposing conflicting demands or establishing differing time schedules, makes the task of obtaining all regulatory approvals extremely complex.

One of the dominant impacts of environmental regulations is that the lead time required for the planning and construction of new plants is substantially increased. When new plants generate major environmental complexities, the implications can be profound. Of course, the exact extent of additions to lead time will vary widely from one case to another, depending on which permit requirements apply and on what difficulties are encountered. For major expansions in any field of heavy industry, however, the delay resulting from federal requirements could conceivably add 2 to 3 years to total lead time. Moreover, there is always the possibility that regulatory approval will be denied. So, contingency plans for fulfilling production needs must be developed.

The 1990s saw the emergence of environmental management systems (EMSs) across the globe including the ISO 14001 environmental management system and the European Union’s Eco-Management and Audit Scheme (EMAS). Any EMS is a continual cycle of planning, implementing, reviewing, and improving the processes and actions that an organization undertakes to meet its business and environmental goals. EMSs are built on the “Plan, Do, Check, Act” model (Fig. 22-1) that leads to continual improvement. Planning includes identifying environmental aspects and establishing goals (plan); implementing includes training and operational controls (do); checking includes monitoring and corrective action (check); and reviewing includes progress review and acting to make needed changes to the EMS (act). Organizations that have implemented an EMS often require all their suppliers to become EMS-certified as environmental programs become part of everyday business.

Any company planning a major expansion must concentrate on environmental factors from the outset. Since many environmental approvals require a public hearing, the views of local elected officials and the community at large are extremely important. To an unprecedented degree, the political acceptability of a project can now be crucial.

PLANT STRATEGIES

At the plant level, a number of things can be done to minimize the impact of environmental quality requirements. These include:

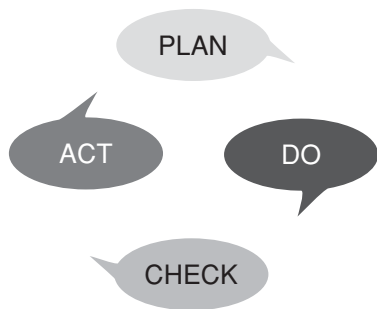


FIG. 22-1 “Plan, Do, Check, Act” model.

1. Maintaining an accurate source-emission inventory
2. Continually evaluating process operations to identify potential modifications that might reduce or eliminate environmental impacts
3. Ensuring that good housekeeping and strong preventive-maintenance programs exist and are followed
4. Investigating available and emerging pollution-control technologies
5. Keeping well informed of the regulations and the directions in which they are moving
6. Working closely with the appropriate regulatory agencies and maintaining open communications to discuss the effects that new regulations may have
7. Keeping the public informed through a good public-relations program
8. Implementing an EMS

It is unrealistic to expect that at any point in the foreseeable future Congress will reverse direction, reduce the effect of regulatory controls, or reestablish the preexisting legal situation in which private companies are free to construct major industrial facilities with little or no restraint by federal regulation.

CORPORATE STRATEGIC PLANNING

Contingency planning represents an essential component of sound environmental planning for a new plant. The environmental uncertainties surrounding a large capital project should be specified and related to other contingencies (such as marketing, competitive reactions, politics, foreign trade, etc.) and mapped out in the overall corporate strategy.

Environmental factors should also be incorporated into a company’s technical or research and development program. Since the planning horizons for new projects may now extend to 5 to 10 years, R&D programs can be designed for specific projects. These may include new process modifications or end-of-pipe control technologies.

Another clear need is to integrate environmental factors into financial planning for major projects. It must be recognized that strategic environmental planning is as important to the long-range goal of the corporation as is financial planning. Trade-off decisions regarding financing may have to change as the project goes through successive stages of environmental planning and permit negotiations. For example, requirements for the use of more expensive pollution control technology may significantly increase total project costs; or a change from end-of-pipe to process modification technology may preclude the use of industrial revenue bond financing under Internal Revenue Service (IRS) rules. Regulatory delays can affect assumptions as to both the rate of expenditure and inflation factors. Investment, production, environmental, and legal factors are all interrelated and can have a major impact on corporate cash flow.

Most companies must learn to deal more creatively with local officials and public opinion. The social responsibility of companies can become an extremely important issue. Companies should apply thoughtfulness and skill to the timing and conduct of public hearings. Management must recognize that local officials have views and constituencies that go beyond attracting new jobs.

From all these factors, it is clear that the approval and construction of major new industrial plants or expansions is a far more complicated operation than it has been in the past, even the recent past. Stringent environmental restrictions are likely to preclude construction of certain facilities at locations where they otherwise might have been built. In other cases, acquisition of required approvals may generate a heated technical and political debate that can drag out the regulatory process for several years.

In many instances, new requirements may be imposed while a company is seeking approval for a proposed new plant. Thus, companies intending to expand their basic production facilities should anticipate their needs far in advance, begin preparation to meet the regulatory challenge they will eventually confront, and select sites with careful consideration of environmental attributes. It is the objective of this section to assist the engineer in meeting this environmental regulatory challenge.

UNITED STATES AIR QUALITY LEGISLATION AND REGULATIONS

Although considerable federal legislation dealing with air pollution has been enacted since the 1950s, the basic statutory framework now in effect was established by the Clean Air Act of 1970; amended in 1974 to deal with energy-related issues; amended in 1977, when a number of amendments containing particularly important provisions associated with the approval of new industrial plants were adopted; and amended in 1990 to address toxic air pollutants and ozone nonattainment areas.

Clean Air Act of 1970 The Clean Air Act of 1970 was founded on the concept of attaining National Ambient Air Quality Standards (NAAQS). Data were accumulated and analyzed to establish the quality of the air, identify sources of pollution, determine how pollutants disperse and interact in the ambient air, and define reductions and controls necessary to achieve air-quality objectives.

EPA promulgated the basic set of current ambient air-quality standards in April 1971. The specific regulated pollutants were particulates, sulfur dioxide, photochemical oxidants, hydrocarbons, carbon monoxide, and nitrogen oxides. In 1978, lead was added. Table 22-1 enumerates the present standards.

To provide basic geographic units for the air-pollution control program, the United States was divided into 247 air quality control regions (AQCRs). By a standard rollback approach, the total quantity of pollution in a region was estimated, the quantity of pollution that could be tolerated without exceeding standards was then calculated, and the degree of reduction called for was determined. States were required by EPA to develop state implementation plans (SIPs) to achieve compliance.

The act also directed EPA to set new source performance standards (NSPS) for specific industrial categories. New plants were required to use the best system of emission reduction available. EPA gradually issued these standards, which now cover a number of basic industrial categories (as listed in Table 22-2). The 1977 amendments to the Clean Air Act directed EPA to accelerate the NSPS program and included a regulatory program to prevent significant deterioration in those areas of the country where the NAAQS were being attained.

Finally, Sec. 112 of the Clean Air Act required that EPA promulgate National Emission Standards for Hazardous Air Pollutants

(NESHAPs). Between 1970 and 1989, standards were promulgated for asbestos, beryllium, mercury, vinyl chloride, benzene, arsenic, radionuclides, and coke-oven emissions.

Prevention of Significant Deterioration (PSD) Of all the federal laws placing environmental controls on industry (and, in particular, on new plants), perhaps the most confusing and restrictive are the limits imposed for the prevention of significant deterioration (PSD) of air quality. These limits apply to areas of the country that are already cleaner than required by ambient air-quality standards. This regulatory framework evolved from judicial and administrative action under the 1970 Clean Air Act and subsequently was given full statutory foundation by the 1977 Clean Air Act Amendments.

EPA established an area classification scheme to be applied in all such regions. The basic idea was to allow a moderate amount of industrial development but not enough to degrade air quality to a point at which it barely complied with standards. In addition, states were to designate certain areas where pristine air quality was especially desirable. All air-quality areas were categorized as Class I, Class II, or Class III. Class I areas were pristine areas subject to the tightest control. Permanently designated Class I areas included international parks, national wilderness areas, memorial parks exceeding 5000 acres, and national parks exceeding 6000 acres. Although the nature of these areas is such that industrial projects would not be located within them, their Class I status could affect projects in neighboring areas where meteorological conditions might result in the transport of emissions into them. Class II areas were areas of moderate industrial growth. Class III areas were areas of major industrialization. Under EPA regulations promulgated in December 1974, all areas were initially categorized as Class II. States were authorized to reclassify specified areas as Class I or Class III.

The EPA regulations also established another critical concept known as the *increment*. This was the numerical definition of the amount of additional pollution that may be allowed through the combined effects of all new growth in a particular locality (see Table 22-3). To assure that the increments would not be used up hastily, EPA specified that each major new plant must install best available control technology (BACT) to limit emissions. BACT is determined based on a case-by-case engineering analysis and is more stringent than NSPS.

To implement these controls, EPA requires that every new source undergo preconstruction review. The regulations prohibited a company

TABLE 22-1 National Ambient Air Quality Standards

Pollutant	Primary stds.	Averaging times	Secondary stds.
Carbon monoxide	9 ppm (10 mg/m ³) 35 ppm (40 mg/m ³)	8-h ^e 1-h ^e	None None
Lead	1.5 µg/m ³	Quarterly average	Same as primary
Nitrogen dioxide	0.053 ppm (100 µg/m ³)	Annual (arithmetic mean)	Same as primary
Particulate matter (PM ₁₀)	50 µg/m ³	Annual ^b (arithmetic mean)	Same as primary
Particulate matter (PM _{2.5})	150 µg/m ³	24-h ^c	Same as primary
	15.0 µg/m ³	Annual ^c (arithmetic mean)	
Ozone	65 µg/m ³	24-h ^d	Same as primary
	0.08 ppm	8-h ^e	
Sulfur oxides	0.12 ppm	1-h ^f	Same as primary
	0.03 ppm	Annual (arithmetic mean)	—
	0.14 ppm	24-h ^e 3-h ^e	—
	—		0.5 ppm (1300 µg/m ³)

^aNot to be exceeded more than once per year.

^bTo attain this standard, the expected annual arithmetic mean PM₁₀ concentration at each monitor within an area must not exceed 50 µg/m³.

^cTo attain this standard, the 3-year average of the annual arithmetic mean PM_{2.5} concentrations from single or multiple community-oriented monitors must not exceed 15.0 µg/m³.

^dTo attain this standard, the 3-year average of the 98th percentile of 24-h concentrations at each population-oriented monitor within an area must not exceed 65 µg/m³.

^eTo attain this standard, the 3-year average of the fourth-highest daily maximum 8-h average ozone concentrations measured at each monitor within an area over each year must not exceed 0.08 ppm.

^f(1) The standard is attained when the expected number of days per calendar year with maximum hourly average concentrations above 0.12 ppm is ≤ 1.

(2) The 1-h NAAQS will no longer apply to an area 1 year after the effective date of the designation of that area for the 8-h ozone NAAQS. The effective designation date for most areas is June 15, 2004. [40 CFR 50.9; see Federal Register of April 30, 2004 (69 FR 23996)].

TABLE 22-2 New Source Performance Standards (NSPS) from 40 CFR Part 60 as of June 2004

40 CFR 60	NSPS
Subpart C	Emission Guidelines and Compliance Times (Reserved)
Subpart Ca	
Subpart Cb	Emissions Guidelines and Compliance Times for Large Municipal Waste Combustors That Are Constructed On or Before September 20, 1994
Subpart Cc	Emission Guidelines and Compliance Times for Municipal Solid Waste Landfills
Subpart Cd	Emission Guidelines and Compliance Times for Sulfuric Acid Production Units
Subpart Ce	Emission Guidelines and Compliance Times for Hospital/Medical/Infectious Waste Incinerators
Subpart D	Standards of Performance for Fossil-Fuel-Fired Steam Generators for Which Construction is Commenced After August 17, 1971
Subpart Da	Standards of Performance for Electric Utility Steam Generating Units for Which Construction Is Commenced After September 18, 1978
Subpart Db	Standards of Performance for Industrial-Commercial-Institutional Steam Generating Units
Subpart Dc	Standards of Performance for Small Industrial-Commercial-Institutional Steam Generating Units
Subpart E	Standards of Performance for Incinerators
Subpart Ea	Standards of Performance for Municipal Waste Combustors for which Construction is Commenced after December 20, 1989 and on or before September 20, 1994
Subpart Eb	Standards of Performance for Large Municipal Waste Combustors for Which Construction is Commenced after September 20, 1994 or for which Modification of Reconstruction is Commenced after June 19, 1996
Subpart Ec	Standards of Performance for Hospital/Medical/Infectious Waste Incinerators for which Construction Is Commenced after June 20, 1996
Subpart F	Standards of Performance for Portland Cement Plants
Subpart G	Standards of Performance for Nitric Acid Plants
Subpart H	Standards of Performance for Sulfuric Acid Plants
Subpart I	Standards of Performance for Hot Mix Asphalt Facilities
Subpart J	Standards of Performance for Petroleum Refineries
Subpart K	Standards of Performance for Storage Vessels for Petroleum Liquids Constructed After June 11, 1973 and Prior to May 19, 1978
Subpart Ka	Standards of Performance for Storage Vessels for Petroleum Liquids for Which Construction, Reconstruction, or Modification Commenced After May 18, 1978, and Prior to July 23, 1984
Subpart Kb	Standards of Performance for Volatile Organic Liquid Storage Vessels (Including Petroleum Liquid Storage Vessels) for Which Construction, Reconstruction, or Modification Commenced after July 23, 1984
Subpart L	Standards of Performance for Secondary Lead Smelters
Subpart M	Standards of Performance for Secondary Brass and Bronze Production Plants
Subpart N	Standards of Performance for Primary Emissions from Basic Oxygen Process Furnaces for Which Construction Is Commenced After June 11, 1973
Subpart Na	Standards of Performance for Secondary Emissions From Basic Oxygen Process Steelmaking Facilities for Which Construction Is Commenced After January 20, 1983
Subpart O	Standards of Performance for Sewage Treatment Plants
Subpart P	Standards of Performance for Primary Copper Smelters
Subpart Q	Standards of Performance for Primary Zinc Smelters
Subpart R	Standards of Performance for Primary Lead Smelters
Subpart S	Standards of Performance for Primary Aluminum Reduction Plants
Subpart T	Standards of Performance for the Phosphate Fertilizer Industry: Wet-Process Phosphoric Acid Plants
Subpart U	Standards of Performance for the Phosphate Fertilizer Industry: Superphosphoric Acid Plants
Subpart V	Standards of Performance for the Phosphate Fertilizer Industry: Diammonium Phosphate Plants
Subpart W	Standards of Performance for the Phosphate Fertilizer Industry: Triple Superphosphate Plants
Subpart X	Standards of Performance for the Phosphate Fertilizer Industry: Granular Triple Superphosphate Storage Facilities
Subpart Y	Standards of Performance for Coal Preparation Plants
Subpart Z	Standards of Performance for Ferroalloy Production Facilities
Subpart AA	Standards of Performance for Steel Plants: Electric Arc Furnaces Constructed After October 21, 1974, and On or Before August 17, 1983
Subpart AAa	Standards of Performance for Steel Plants: Electric Arc Furnaces and Argon-Oxygen Decarburization Vessels Constructed After August 17, 1983
Subpart BB	Standards of Performance for Kraft Pulp Mills
Subpart CC	Standards of Performance for Glass Manufacturing Plants
Subpart DD	Standards of Performance for Grain Elevators
Subpart EE	Standards of Performance for Surface Coating of Metal Furniture
Subpart FF	(Reserved)
Subpart GG	Standards of Performance for Stationary Gas Turbines
Subpart HH	Standards of Performance for Lime Manufacturing Plants
Subpart KK	Standards of Performance for Lead-Acid Battery Manufacturing Plants
Subpart LL	Standards of Performance for Metallic Mineral Processing Plants
Subpart MM	Standards of Performance for Automobile and Light Duty Truck Surface Coating Operations
Subpart NN	Standards of Performance for Phosphate Rock Plants
Subpart PP	Standards of Performance for Ammonium Sulfate Manufacture
Subpart QQ	Standards of Performance for the Graphic Arts Industry: Publication Rotogravure Printing
Subpart RR	Standards of Performance for Pressure Sensitive Tape and Label Surface Coating Operations
Subpart SS	Standards of Performance for Industrial Surface Coating: Large Appliances
Subpart TT	Standards of Performance for Metal Coil Surface Coating
Subpart UU	Standards of Performance for Asphalt Processing and Asphalt Roofing Manufacture
Subpart VV	Standards of Performance for Equipment Leaks of VOC in the Synthetic Organic Chemicals Manufacturing Industry
Subpart WW	Standards of Performance for the Beverage Can Surface Coating Industry
Subpart XX	Standards of Performance for Bulk Gasoline Terminals
Subpart AAA	Standards of Performance for New Residential Wood Heaters

TABLE 22-2 New Source Performance Standards (NSPS) from 40 CFR Part 60 as of June 2004 (Concluded)

40 CFR 60	NSPS
Subpart BBB	Standards of Performance for the Rubber Tire Manufacturing Industry (Reserved)
Subpart CCC	Standards of Performance for Volatile Organic Compound (VOC) Emissions from the Polymer Manufacturing Industry
Subpart DDD	(Reserved)
Subpart EEE	Standards of Performance for Flexible Vinyl and Urethane Coating and Printing
Subpart FFF	Standards of Performance for Equipment Leaks of VOC in Petroleum Refineries
Subpart GGG	Standards of Performance for Synthetic Fiber Production Facilities
Subpart HHH	Standards of Performance for Volatile Organic Compound Emissions From the Synthetic Organic Chemical Manufacturing Industry (SOCMI) Air Oxidation Unit Processes
Subpart III	Standards of Performance for Petroleum Dry Cleaners
Subpart JJJ	Standards of Performance for Equipment Leaks of VOC From Onshore Natural Gas Processing Plants
Subpart KKK	Standards of Performance for Onshore Natural Gas Processing; SO(2) Emissions (Reserved)
Subpart LLL	Standards of Performance for Volatile Organic Compound Emissions from Synthetic Organic Chemical Manufacturing Industry Distillation Operations
Subpart MMM	Standards of Performance for Nonmetallic Mineral Processing Plants
Subpart NNN	Standards of Performance for Wool Fiberglass Insulation Manufacturing Plants
Subpart OOO	Standards of Performance for VOC Emissions From Petroleum Refinery Wastewater Systems
Subpart PPP	Standards of Performance for Volatile Organic Compound Emissions From Synthetic Organic Chemical Manufacturing Industry (SOCMI) Reactor Processes
Subpart QQQ	Standards of Performance for Magnetic Tape Coating Facilities
Subpart RRR	Standards of Performance for Industrial Surface Coating; Coating of Plastic Parts for Business Machines
Subpart SSS	Standards of Performance for Calciners and Dryers in Mineral Industries
Subpart TTT	Standards of Performance for Polymeric Coating of Supporting Substrates Facilities
Subpart UUU	Standards of Performance for Municipal Solid Waste Landfills
Subpart VVV	Standards of Performance for Small Municipal Waste Combustion Units for Which Construction Is Commenced After August 30, 1999 or for Which Modification or Reconstruction Is Commenced After June 6, 2001
Subpart WWW	Emission Guidelines and Compliance Times for Small Municipal Waste Combustion Units Constructed On or Before August 30, 1999
Subpart AAAA	Standards of Performance for Commercial and Industrial Solid Waste Incineration Units for Which Construction Is Commenced After November 30, 1999 or for Which Modification or Reconstruction Is Commenced on or After June 1, 2001
Subpart BBBB	Emissions Guidelines and Compliance Times for Commercial and Industrial Solid Waste Incineration Units that Commenced Construction On or Before November 30, 1999

from commencing construction on a new source until the review had been completed and provided that, as part of the review procedure, public notice should be given and an opportunity provided for a public hearing on any disputed questions.

Sources Subject to Prevention of Significant Deterioration (PSD) Sources subject to PSD regulations (40 CFR, Sec. 52.21) are major stationary sources and major modifications located in attainment areas and unclassified areas. A major stationary source was defined as any source listed in Table 22-4 with the potential to emit 100 tons per year or more of any pollutant regulated under the Clean Air Act (CAA) or any other source with the potential to emit 250 tons per year or more of any CAA pollutant. The "potential to emit" is defined as the maximum capacity to emit the pollutant under applicable emission standards and permit conditions (after application of any air pollution control equipment) excluding secondary emissions. A "major modification" is defined as any physical or operational change of a major stationary source producing a "significant net emissions increase" of any CAA pollutant (see Table 22-5).

Ambient monitoring is required of all CAA pollutants with emissions greater than or equal to Table 22-5 values for which there are

NAAQS. Continuous monitoring is also required for other CAA pollutants for which the EPA or the state determines that monitoring is necessary. The EPA or the state may exempt any CAA pollutant from these monitoring requirements if the maximum air-quality impact of the emissions increase is less than the values in Table 22-6 or if present concentrations of the pollutant in the area that the new source would affect are less than the Table 22-6 values. The EPA or the state may accept representative existing monitoring data collected within 3 years of the permit application to satisfy monitoring requirements.

EPA regulations provide exemption from BACT and ambient air-impact analysis if the modification that would increase emissions is accompanied by other changes within the plant that would net a zero increase in total emissions. This exemption is referred to as the "no net increase" exemption.

A full PSD review would include a case-by-case determination of the controls required by BACT, an ambient air-impact analysis to determine whether the source might violate applicable increments or air-quality standards; an assessment of the effect on visibility, soils, and vegetation; submission of monitoring data; and full public review.

Nonattainment (NA) Those areas of the United States failing to attain compliance with ambient air-quality standards are considered nonattainment areas. New plants could be constructed in nonattainment areas only if stringent conditions are met. Emissions have to be controlled to the greatest degree possible, and more than equivalent offsetting emission reductions have to be obtained from other sources to assure progress toward achievement of the ambient air-quality standards. Specifically, (1) the new source must be equipped with pollution controls to assure lowest achievable emission rate (LAER), which in no case can be less stringent than any applicable NSPS; (2) all existing sources owned by an applicant in the same region must be in compliance with applicable state implementation plan requirements or be under an approved schedule or

TABLE 22-3 PSD Air Quality Increments ($\mu\text{g}/\text{m}^3$)

	Class I area	Class II area	Class III area
Sulfur dioxide			
Annual	2	20	40
24-h	5	91	182
3-h	25	512	700
PM ₁₀			
Annual	4	17	34
24-h	8	30	60
Nitrogen dioxide			
Annual	2.5	25	50

TABLE 22-4 Sources Subject to PSD Regulation If Their Potential to Emit Equals or Exceeds 100 Tons per Year

Fossil-fuel-fired steam electric plants of more than 250 million Btu/h heat input
Coal-cleaning plants (with thermal dryers)
Kraft-pulp mills
Portland-cement plants
Primary zinc smelters
Iron and steel mill plants
Primary aluminum-ore-reduction plants
Primary copper smelters
Municipal incinerators capable of charging more than 250 tons of refuse per day
Hydrofluoric, sulfuric, and nitric acid plants
Petroleum refineries
Lime plants
Phosphate-rock-processing plants
Coke-oven batteries
Sulfur-recovery plants
Carbon-black plants (furnace process)
Primary lead smelters
Fuel-conversion plants
Sintering plants
Secondary metal-production plants
Chemical-process plants
Fossil-fuel boilers (or combinations thereof) totaling more than 250 million Btu/h heat input
Petroleum-storage and -transfer units with total storage capacity exceeding 300,000 bbl
Taconite-ore-processing plants
Glass-fiber-processing plants
Charcoal-production plants

an enforcement order to achieve such compliance; (3) the applicant must have sufficient offsets to more than make up for the emissions to be generated by the new source (after application of LAER); and (4) the emission offsets must provide “a positive net air quality benefit in the affected area.”

LAER was deliberately a technology-forcing standard of control. The statute stated that LAER must reflect (1) the most stringent emission limitation contained in the implementation plan of any state for such category of sources unless the applicant can demonstrate that such a limitation is not achievable, or (2) the most stringent limitation achievable in practice within the industrial category, whichever is more stringent. In no event could LAER be less stringent than any applicable NSPS. While the statutory language defining BACT directed that “energy, environmental, and economic impacts and other costs” be taken into account, the comparable provision on LAER provided no instruction that economics be considered.

TABLE 22-5 Significant Net Emissions Increase

Pollutant	Tons/yr
PM ₁₀	15
SO ₂	40
NO _x	40
VOC	40
CO	100
Lead	0.6
PM	25
Fluorides	3
Sulfuric acid mist	7
Hydrogen sulfide	10
Total reduced sulfur	10
Municipal waste combustor	
Acid gases	40
Metals	15
Organics	3.5 × 10 ⁻⁶
CFCs (11, 12, 113, 114 & 115)	Any increase
Halons (1211, 1301, 2402)	Any increase
Any emissions increase resulting in a >1 μ/m ³ 24-h impact in a Class I area	

TABLE 22-6 Concentration Impacts below Which Ambient Monitoring May Not Be Required

	μg/m ³	Average time
CO	575	8-h maximum
NO ₂	14	Annual
PM ₁₀	10	24-h maximum
SO ₂	13	24-h maximum
Lead	0.1	3-month
Fluorides	0.25	24-h maximum
Total reduced sulfur	10	1-h maximum
H ₂ S	0.2	1-h maximum
Reduced-sulfur compounds	10	1-h maximum

For existing sources emitting pollutants for which the area is nonattainment, reasonable available control technology (RACT) would be required. EPA defines RACT by industrial category.

Minor Source Preconstruction Permits Commonly after the application of air pollution controls the emissions associated with new facilities or modifications of existing facilities will be less than the emissions thresholds necessary to trigger PSD or nonattainment new source review. In such instances, a minor source preconstruction permit is required from the state permitting authority and new source performance standards (NSPS) apply.

Controlled-Trading Program The legislation enacted under the Clean Air Act Amendments of 1977 provided the foundation for EPA’s controlled-trading program, the essential elements of which include:

- No-net-increase provisions of PSD
- Offsets policy (under nonattainment)
- Banking and brokerage (under nonattainment)

While these different policies vary broadly in form, their objective is essentially the same: to substitute flexible economic-incentive systems for the current rigid, technology-based regulations that specify exactly how companies must comply. These market mechanisms have made regulating easier for EPA and less burdensome and costly for industry.

PSD No-Net-Increase Provisions Under the PSD program, the affected source is the entire plant. This source definition allows a company to determine the most cost-effective means to control pollution any time a plant is modified. Emission increases associated with a new process or production line may be compensated for by emission increases at other parts of the plant. As long as the entire site net emissions increase is maintained below the levels identified in Table 22-5, a PSD review is not required.

Offsets Policy Offsets were EPA’s first application of the concept that one source could meet its environmental protection obligations by getting another source to assume additional control actions. In nonattainment areas, pollution from a proposed new source, even one that controls its emissions to the lowest possible level, would aggravate existing violations of ambient air-quality standards and trigger the statutory prohibition. The offsets policy provided these new sources with an alternative. The source could proceed with construction plans, provided that:

1. The source would control emissions to the lowest achievable level.
2. Other sources owned by the applicant were in compliance or on an approved compliance schedule.

3. Existing sources were persuaded to reduce emissions by an amount at least equal to the pollution that the new source would add.

Banking and Brokerage Policy EPA’s banking policy is aimed at providing companies with incentives to find more offsets. Under the original offset policy, a firm shutting down or modifying a facility could apply the reduction in emissions to new construction elsewhere in the region only if the changes were made simultaneously. However, with banking a company can “deposit” the reduction for later use or sale. Such a policy will clearly establish that clean air (or the right to use it) has direct economic value.

Clean Air Act of 1990 In November 1990, Congress adopted the Clean Air Act Amendments of 1990, providing substantial

TABLE 22-7 Ozone Nonattainment Area Classifications and Associated Requirements

Nonattainment area classification	One-hour ozone concentration design value, ppm	Attainment date	Major source threshold level, tons VOCs/yr	Offset ratio for new/modified sources
Marginal	0.121–0.138	Nov. 15, 1993	100	1.1 to 1
Moderate	0.138–0.160	Nov. 15, 1996	100	1.15 to 1
Serious	0.160–0.180	Nov. 15, 1999	50	1.2 to 1
Severe	0.180–0.190	Nov. 15, 2005	25	1.3 to 1
	0.190–0.280	Nov. 15, 2007	25	1.3 to 1
Extreme	0.280 and up	Nov. 15, 2010	10	1.5 to 1

changes to many aspects of the existing CAAA. The concepts of NAAQS, NSPS, and PSD remain virtually unchanged. However, significant changes have occurred in several areas that directly affect industrial facilities and electric utilities and air-pollution control at these facilities. These include changes and additions in the following major areas:

- Title I Nonattainment areas
- Title III Hazardous air pollutants
- Title IV Acid deposition control
- Title V Operating permits
- Title VI Stratospheric ozone protection

Title I: Nonattainment Areas The existing regulations for nonattainment areas were made more stringent in several areas. The CAAA of 1990 requires the development of comprehensive emission inventory-tracking for all nonattainment areas and establishes a classification scheme that defined nonattainment areas into levels of severity. For example, ozone nonattainment areas were designated as marginal, moderate, serious, severe (two levels), and extreme, with compliance deadlines of 3, 6, 9, 15–17, and 20 years, respectively, with each classification having more stringent requirements regarding strategies for compliance (see Table 22-7). Volatile organic compound (VOC) emissions reductions of 15 percent were required in moderate areas by 1996 and 3 percent a year thereafter for severe or extreme areas until compliance was achieved. In addition, the definition of a major source of ozone precursors (previously 100 tons per year of NO_x, CO, or VOC emissions) was redefined to as little as 10 tons per year in the extreme classification, with increased offset requirements of 1.5 to 1 for new and modified sources. In 2004, EPA adopted a new 8-h ozone ambient air quality standard. Ultimately the 8-h standard will replace the 1-h standard although both standards apply during a several year transition period. The new standard adopted the same regulatory approach as previously existed for the 1-h standard. New extended deadlines for compliance are being adopted based on the same marginal to extreme area approach previously described with the new deadlines identified in Table 22-8. These requirements place major constraints on affected industries in these nonattainment areas. A similar approach is being taken in PM₁₀ and CO nonattainment areas.

Title III: Hazardous Air Pollutants The Title III provisions on hazardous air pollutants (HAPs) represent a major departure from the previous approach of developing NESHAPs. While only eight HAPs were designated in the 20 years since enactment of the CAAA of 1970, the new CAAA of 1990 designated 189 pollutants as HAPs requiring regulation. The state allows EPA to list additional HAPs or to delist any HAP. As of 2004 there were 188 HAPs identified in Table 22-9. Major sources are defined as any source (new or existing) that emits (after control) 10 tons a year or more of any regulated HAP or 25 tons a year or more of any combination of HAPs. A major source of HAPs must comply with emissions standards known as MACT standards that EPA has been adopting since 1992. Table 22-10 provides a list of MACT standards as of 2004 that affect all named existing and new major HAP sources. If a proposed new source is not of a type identified in Table 22-10, then the new source must undergo a case-by-case MACT evaluation to identify the appropriate level of control which is generally the most stringent achieved in practice.

For existing sources, MACT is defined as a stringency equivalent to the average of the best 12 percent of the sources in the category. For

new sources, MACT is defined as the best controlled system. New sources are required to meet MACT immediately, while existing sources have three years from the date of promulgation of the appropriate MACT standard.

Title IV: Acid Deposition Control The Acid Deposition Control Program is designed to reduce emissions of SO₂ in the United States by 10 million tons per year, resulting in a net yearly emission of 8.9 million tons by the year 2000. Phase I of the program requires 111 existing uncontrolled coal-fired power plants (≥ 100 MW) to reduce emissions to 2.5 pounds of SO₂ per 10⁶ Btu by 1995 (1997 if scrubbers are used to reduce emissions by at least 90 percent). The reduction is to be accomplished by issuing all affected units emission “allowances” equivalent to what their annual average SO₂ emissions would have been in the years 1985–1987 based on 2.5 pounds SO₂ per 10⁶ Btu coal. The regulations represent a significant departure from previous regulations where specified SO₂ removal efficiencies were mandated; rather, the utilities will be allowed the flexibility of choosing which strategies will be used (e.g., coal washing, low-sulfur coal, flue gas desulfurization, etc.) and which units will be controlled, as long as the overall “allowances” are not exceeded. Any excess reduction in SO₂ by a utility will create “banked” emissions that can be sold or used at another unit.

Phase II of Title IV limits the majority of plants ≥ 20 MW and all plants ≥ 75 MW to maximum emissions of 1.2 pounds of SO₂ per 10⁶ Btu after the year 2000. In general, new plants would have to acquire banked emission allowances in order to be built. Emission allowances will be traded through a combination of sell/purchase with other utilities, EPA auctions and direct sales.

Control of NO_x under the CAAA of 1990 will be accomplished through the issuance of a revised NSPS in 1994, with the objective of reducing emissions by 2 million tons a year from 1980 emission levels. The technology being considered is the use of low-NO_x burners (LNBs). The new emission standards will not apply to cyclone and wet bottom boilers, unless alternative technologies are found, as these cannot be retrofitted with existing LNB technologies.

Title V: Operating Permits Title V of the 1990 Clean Air Act Amendments established a new operating permit program to be administered by state agencies in accordance with federal guidelines. The program basically requires a source to obtain a permit that covers

TABLE 22-8 The 8-h Ozone NAAQS Classifications and Attainment Dates*

Area classification ¹	8-h ozone concentration, ppm	Attainment date ¹
Marginal	0.081–0.092	2007
Moderate	0.092–0.107	2010
Serious	0.107–0.120	2013
Severe-15	0.120–0.127	2019
Severe-17	0.127–0.187	2021
Extreme	0.187 and up	2024

*Areas newly designated as nonattainment under the 8-h standard which were never previously nonattainment must comply with the standard within 5 years of being designated nonattainment or generally in 2009.

¹These classifications and attainment dates apply to areas previously designated nonattainment under the 1-h ozone NAAQS.

TABLE 22-9 Regulated Hazardous Air Pollutants (HAPs) from 40 CFR Part 63 as of June 2004

CAS no.	HAP	CAS no.	HAP
75070	Acetaldehyde	108101	Methyl isobutyl ketone (Hexene)
60355	Acetamide	624839	Methyl isocyanate
75058	Acetonitrile	80626	Methyl methacrylate
98862	Acetophenone	1634044	Methyl tert butyl ether
53963	Acetylaminofluorene	101144	4,4-Methyiene bis(2-chloroaniline)
107028	Acrolein	75092	Methylene chloride (Dichloromethane)
79061	Acrylamide	101688	Methylene diphenyl diisocyanate (MDI)
79107	Acrylic acid	101779	4,4-Methylenedianiline
107131	Acrylonitrile	91203	Naphthalene
107051	Allyl chloride	98953	Nitrobenzene
92671	4-Aminobiphenyl	92933	4-Nitrobiphenyl
62533	Aniline	100027	4-Nitrophenol
90040	o-Anisidine	79469	2-Nitropropane
1332214	Asbestos	684935	N-Nitroso-N-methylurea
71432	Benzene (including benzene from gasoline)	62759	N-Nitrosodimethylamine
92875	Benzidine	59892	N-Nitrosomorpholine
98077	Benzotrichloride	56382	Parathion
100447	Benzyl chloride	82688	Pentachloronitrobenzene (Quintobenzene)
92524	Biphenyl	87865	Pentachlorophenol
117817	Bis(2-ethylhexyl)phthalate (DEHP)	108952	Phenol
54288	Bis(chloromethyl)ether	106503	p-Phenylenediamine
75252	Bromoform	75445	Phosgene
106990	1,3-Butadiene	7803512	Phosphine
156627	Calcium cyanamide	7723140	Phosphorus
133062	Captan	85449	Phthalic anhydride
63252	Carbaryl	1336363	Polychlorinated biphenyls (Aroclors)
75150	Carbon disulfide	1120714	1,3-Propane sultone
56235	Carbon tetrachloride	57578	beta-Propiolactone
463581	Carbonyl sulfide	123386	Propionaldehyde
120809	Catechol	114261	Propoxur (Baygon)
133904	Chloramben	78875	Propylene dichloride (1,2-Dichloropropane)
57749	Chlordane	542756	1,3-Dichloropropene
7782505	Chlorine	62737	Dichlorvos
79118	Chloroacetic acid	111422	Diethanolamine
532274	2-Chloroacetophenone	121697	N,N-Diethyl aniline (N,N-Dimethylaniline)
108907	Chlorobenzene	64675	Diethyl sulfate
510156	Chlorobenzilate	119904	3,3-Dimethoxybenzidine
67663	Chloroform	60117	Dimethyl aminoazobenzene
107302	Chloromethyl methyl ether	119937	3,3'-Dimethyl benzidine
126998	Chloroprene	79447	Dimethyl carbamoyl chloride
1319773	Cresols/Cresylic acid (isomers and mixture)	68122	Dimethyl formamide
95487	o-Cresol	57147	1,1-Dimethyl hydrazine
108394	m-Cresol	131113	Dimethyl phthalate
106445	p-Cresol	77781	Dimethyl sulfate
98828	Cumene	534521	4,6-Dinitro-o-cresol, and salts
94757	2,4-D, salts and esters	51285	2,4-Dinitrophenol
3547044	DDE	121142	2,4-Dinitrotoluene
334883	Diazomethane	123911	1,4-Dioxane (1,4-Diethyleneoxide)
132649	Dibenzofurans	122667	1,2-Diphenylhydrazine
96128	1,2-Dibromo-3-chloropropane	106898	Epichlorohydrin (1-Chloro-2,3-epoxypropane)
84742	Dibutylphthalate	106887	1,2-Epoxybutane
106467	1,4-Dichlorobenzene(p)	140885	Ethyl acrylate
91941	3,3-Dichlorobenzidene	100414	Ethyl benzene
111444	Dichloroethyl ether (Bis (2-chloroethyl)ether)	51796	Ethyl carbamate (Urethane)
76448	Heptachlor	75003	Ethyl chloride (Chloroethane)
118741	Hexachlorobenzene	106934	Ethylene dibromide (Dibromoethane)
87683	Hexachlorobutadiene	107062	Ethylene dichloride (1,2-Dichloroethane)
77474	Hexachlorocyclopentadiene	107211	Ethylene glycol
67721	Hexachloroethane	151564	Ethylene imine (Aziridine)
822060	Hexamethylene-1,6-diisocyanate	75218	Ethylene oxide
680319	Hexamethylphosphoramide	96457	Ethylene thiourea
110543	Hexane	75343	Ethylidene dichloride (1,1-Dichloroethane)
302012	Hydrazine	50000	Formaldehyde
7647010	Hydrochloric acid	75569	Propylene oxide
7664393	Hydrogen fluoride (Hydrofluoric acid)	75558	1,2-Propylenimine (2-Methyl aziridine)
123319	Hydroquinone	91225	Quinoline
78591	Isophorone	106514	Quinone
58899	Lindane (all isomers)	100425	Styrene
108316	Maleic anhydride	96093	Styrene oxide
67561	Methanol	1746016	2,3,7,8-Tetrachlorodibenzo-p-dioxin
72435	Methoxychlor	79345	1,1,2,2-Tetrachloroethane
74839	Methyl bromide (Bromomethane)	127184	Tetrachloroethylene (Perchloroethylene)
74873	Methyl chloride (Chloromethane)	7550450	Titanium tetrachloride
71556	Methyl chloroform (1,1,1-Trichloroethane)	108883	Toluene
78933	Methyl ethyl ketone (2-Butanone)	95807	2,4-Toluene diamine
60344	Methyl hydrazine	584849	2,4-Toluene diisocyanate
74884	Methyl iodide (Iodomethane)	95534	o-Toluidine

TABLE 22-9 Regulated Hazardous Air Pollutants (HAPs) from 40 CFR Part 63 as of June 2004 (Concluded)

CAS no.	HAP	CAS no.	HAP
8001352	Toxaphene (chlorinated camphene)	—	Antimony compounds
120821	1,2,4-Trichlorobenzene	—	Arsenic compounds (inorganic including arsine)
79005	1,1,2-Trichloroethane	—	Beryllium compounds
79016	Trichloroethylene	—	Cadmium compounds
95954	2,4,5-Trichlorophenol	—	Chromium compounds
88062	2,4,6-Trichlorophenol	—	Cobalt compounds
121448	Triethylamine	—	Coke oven emissions
1582098	Trifluralin	—	Cyanide compounds ¹
540841	2,2,4-Trimethylpentane	—	Glycol ethers ²
108054	Vinyl acetate	—	Lead compounds
593602	Vinyl bromide	—	Manganese compounds
75014	Vinyl chloride	—	Mercury compounds
75354	Vinylidene chloride (1,1-Dichloroethylene)	—	Fine mineral fibers ³
1330207	Xylenes (isomers and mixture)	—	Nickel compounds
95476	o-Xylenes	—	Polycyclic organic matter ⁴
108383	m-Xylenes	—	Radionuclides (including radon) ⁵
106423	p-Xylenes	—	Selenium compounds

NOTE: For all listings above which contain the word "compounds" and for glycol ethers, the following applies: Unless otherwise specified, these listings are defined as including any unique chemical substance that contains the named chemical (i.e., antimony, arsenic, etc.) as part of that chemical's infrastructure.

¹XCN where X = H' or any other group where a formal dissociation may occur, for example, KCN or Ca (CN)₂.

²Includes mono- and di-ethers of ethylene glycol, diethylene glycol, and triethylene glycol R-(OCH₂CH₂)_n-OR' where n = 1, 2, or 3; R = alkyl or aryl groups; R' = R, H, or groups which, when removed, yield glycol ethers with the structure R-(OCH₂CH)n-OH. Polymers are excluded from the glycol category.

³Includes mineral fiber emissions from facilities manufacturing or processing glass, rock, or slag fibers (or other mineral derived fibers) of average diameter 1 micrometer or less.

⁴Includes organic compounds with more than one benzene ring, and which have a boiling point greater than or equal to 100°C.

⁵A type of atom which spontaneously undergoes radioactive decay.

each and every requirement applicable to the source under the Clean Air Act. A major impact of the Title V program is that sources are required to implement measures to demonstrate routinely that they are operating in compliance with permit terms. This represents a dramatic shift from previous practices where, to bring an enforcement action, regulatory authorities were required to demonstrate that a source was in noncompliance.

Initially, all "major" sources of air pollution are required to obtain an operating permit. However, any state permitting authority may extend the applicability of the operating permit to minor sources as well. Once a source is subject to the permit program as a major source for any one pollutant, emissions of every regulated air pollutant must be addressed in the permit application.

The operating permit must outline specifically how and when a source will be allowed to operate over the five-year term of the permit. The permit the state develops from an application becomes the principal mechanism for enforcement of all air-quality regulations. As such, it is critically important to submit an application that allows maximum operating flexibility.

Sources must also include in their permit applications monitoring protocols sufficient to document compliance with each permit term and condition.

The Title V operating permit requires the submission of at least five types of reports:

1. The initial compliance report
2. The annual compliance certification
3. Monitoring reports submitted at least every six months
4. Progress reports for sources not in compliance when the application is submitted
5. Prompt reports on any deviations from the permit terms

Permit fees are a mandatory element of the Title V program. In most cases, fees are assessed for emissions on a dollars-per-ton-emitted basis.

Title VI: Stratospheric Ozone Protection Title VI of the 1990 Clean Air Act Amendments established a program to implement the provisions of the Montreal Protocol, a worldwide agreement to reduce the use and emission of ozone-depleting substances. EPA's regulations adopted in response to Title VI outline a series of requirements for facilities that use equipment containing ODS compounds. Facilities must be certain that they handle and manage ODS compounds as prescribed in the rules. Only certified technicians and staff may maintain

affected equipment, and detailed records must be maintained. Table 22-11 identifies common ODS compounds.

Regulatory Direction The current direction of regulations and air-pollution control efforts is clearly toward significantly reducing the emissions to the environment of a broad range of compounds, including:

1. Volatile organic compounds and other ozone precursors (CO and NO_x)
2. Hazardous air pollutants, including carcinogenic organic emissions and heavy metal emissions
3. Acid rain precursors, including SO_x and NO_x

In addition, the PM_{2.5} NAAQS will continue to place emphasis on quantifying and reducing particulate emissions in the less than 2.5 μm particle-size range. Particle size-specific emission factors have been developed for many sources, and size-specific emission standards have been developed in a number of states. These standards are addressing concerns related to nitrates and suitable condensates in the atmosphere.

Although it is not possible to predict the future, it is possible to prepare for it and influence it. It is highly recommended that maximum flexibility be designed into new air-pollution control systems to allow for increasingly more stringent emission standards for both particulates and gases. Further, it is everyone's responsibility to provide a thorough review of existing and proposed new processes and to make every attempt to identify economical process modifications and/or material substitutions that reduce or, in some cases, eliminate both the emissions to the environment and the overdependency on retrofitted or new end-of-pipe control systems.

UNITED STATES WATER QUALITY LEGISLATION AND REGULATIONS

Federal Water Pollution Control Act In 1948, the original Federal Water Pollution Control Act (FWPCA) was passed. This act and its various amendments are often referred to as the Clean Water Act (CWA). It provided loans for treatment plant construction and temporary authority for federal control of interstate water pollution. The enforcement powers were so heavily dependent on the states as to make the act almost unworkable. In 1956, several amendments to the FWPCA were passed that made federal enforcement procedures less cumbersome. The provision for state consent was removed by amendments passed in 1961, which also extended federal authority to include navigable waters in the United States.

TABLE 22-10 Maximum Achievable Control Technology (MACT) Standards from 40 CFR Part 63 as of June 2004

40 CFR 63	MACT Standard	40 CFR 63	MACT Standard
Subpart F	National Emission Standards for Organic Hazardous Air Pollutants from the Synthetic Organic Chemical Manufacturing Industry	Subpart RR	National Emission Standards for Individual Drain Systems
Subpart G	National Emission Standards for Organic Hazardous Air Pollutants From Synthetic Organic Chemical Manufacturing Industry Process Vents, Storage Vessels, Transfer Operations, and Wastewater	Subpart SS	National Emission Standards for Closed Vent Systems, Control Devices, Recovery Devices and Routing to a Fuel Gas System or a Process
Subpart H	National Emission Standards for Organic Hazardous Air Pollutants for Equipment Leaks	Subpart TT	National Emission Standards for Equipment Leaks—Control Level 1
Subpart I	National Emission Standards for Organic Hazardous Air Pollutants for Certain Processes Subject to the Negotiated Regulation for Equipment Leaks	Subpart UU	National Emission Standards for Equipment Leaks—Control Level 2 Standards
Subpart J	National Emission Standards for Organic Hazardous Air Pollutants for Polyvinyl Chloride and Copolymers Production	Subpart VV	National Emission Standards for Oil-Water Separators and Organic-Water Separators
Subpart K	(Reserved)	Subpart WW	National Emission Standards for Storage Vessels (Tanks)—Control Level 2
Subpart L	National Emission Standards for Coke Oven Batteries	Subpart XX	National Emission Standards for Ethylene Manufacturing Process Units: Heat Exchange Systems and Waste Operations
Subpart M	National Perchloroethylene Air Emission Standards for Dry Cleaning Facilities	Subpart YY	National Emission Standards for Hazardous Air Pollutants for Source Categories: Generic Maximum Achievable Control Technology Standards
Subpart N	National Emission Standards for Chromium Emissions from Hard and Decorative Chromium Electroplating and Chromium Anodizing Tanks	Subpart CCC	National Emission Standards for Hazardous Air Pollutants for Steel Pickling—HCI Process Facilities and Hydrochloric Acid Regeneration Plants
Subpart O	Ethylene Oxide Emissions Standards for Sterilization Facilities	Subpart DDD	National Emission Standards for Hazardous Air Pollutants for Mineral Wool Production
Subpart Q	National Emission Standards for Hazardous Air Pollutants for Industrial Process Cooling Towers	Subpart EEE	National Emission Standards for Hazardous Air Pollutants From Hazardous Waste Combustors
Subpart R	National Emission Standards for Gasoline Distribution Facilities (Bulk Gasoline Terminals and Pipeline Breakout Stations)	Subpart GGG	National Emission Standards for Pharmaceuticals Production
Subpart S	National Emission Standards for Hazardous Air Pollutants from the Pulp and Paper Industry	Subpart HHH	National Emission Standards for Hazardous Air Pollutants From Natural Gas Transmission and Storage Facilities
Subpart T	National Emission Standards for Halogenated Solvent Cleaning	Subpart III	National Emission Standards for Hazardous Air Pollutants for Flexible Polyurethane Foam Production
Subpart U	National Emission Standards for Hazardous Air Pollutant Emissions: Group I Polymers and Resins	Subpart JJJ	National Emission Standards for Hazardous Air Pollutant Emissions: Group IV Polymers and Resins
Subpart W	National Emission Standards for Hazardous Air Pollutants for Epoxy Resins Production and Non-Nylon Polyamides Production	Subpart LLL	National Emission Standards for Hazardous Air Pollutants From the Portland Cement Manufacturing Industry
Subpart X	National Emission Standards for Hazardous Air Pollutants From Secondary Lead Smelting	Subpart MMM	National Emission Standards for Hazardous Air Pollutants for Pesticide Active Ingredient Production
Subpart Y	National Emission Standards for Marine Tank Vessel Tank Loading Operations	Subpart NNN	National Emission Standards for Hazardous Air Pollutants for Wool Fiberglass Manufacturing
Subpart AA	National Emission Standards for Hazardous Air Pollutants From Phosphoric Acid Manufacturing Plants	Subpart OOO	National Emission Standards for Hazardous Air Pollutant Emissions: Manufacture of Amino/Phenolic Resins
Subpart BB	National Emission Standards for Hazardous Air Pollutants From Phosphate Fertilizers Production Plants	Subpart PPP	National Emission Standards for Hazardous Air Pollutant Emissions for Polyether Polyols Production
Subpart CC	National Emission Standards for Hazardous Air Pollutants From Petroleum Refineries	Subpart QQQ	National Emission Standards for Hazardous Air Pollutants for Primary Copper Smelting
Subpart DD	National Emission Standards for Hazardous Air Pollutants from Off-Site Waste and Recovery Operations	Subpart RRR	National Emission Standards for Hazardous Air Pollutants for Secondary Aluminum Production
Subpart EE	National Emission Standards for Magnetic Tape Manufacturing Operations	Subpart TTT	National Emission Standards for Hazardous Air Pollutants for Primary Lead Smelting
Subpart GG	National Emission Standards for Aerospace Manufacturing and Rework Facilities	Subpart UUU	National Emission Standards for Hazardous Air Pollutants for Petroleum Refineries: Catalytic Cracking Units, Catalytic Reforming Units, and Sulfur Recovery Units
Subpart HH	National Emission Standards for Hazardous Air Pollutants From Oil and Natural Gas Production Facilities	Subpart VVV	National Emission Standards for Hazardous Air Pollutants: Publicly Owned Treatment Works
Subpart II	National Emission Standards for Shipbuilding and Ship Repair (Surface Coating)	Subpart XXX	National Emission Standards for Hazardous Air Pollutants for Ferroalloys Production: Ferromanganese and Silicomanganese
Subpart JJ	National Emission Standards for Wood Furniture Manufacturing Operations	Subpart AAAA	National Emission Standards for Hazardous Air Pollutants: Municipal Solid Waste Landfills
Subpart KK	National Emission Standards for the Printing and Publishing Industry	Subpart CCCC	National Emission Standards for Hazardous Air Pollutants: Manufacturing of Nutritional Yeast
Subpart LL	National Emission Standards for Hazardous Air Pollutants for Primary Aluminum Reduction Plants	Subpart EEEE	National Emission Standards for Hazardous Air Pollutants: Organic Liquids Distribution (Non-Gasoline)
Subpart MM	National Emission Standards for Hazardous Air Pollutants for Chemical Recovery Combustion Source at Kraft, Soda, Sulfite, and Stand-Alone Semichemical Pulp Mills	Subpart FFFF	National Emission Standards for Hazardous Air Pollutants: Miscellaneous Organic Chemical Manufacturing
Subpart OO	National Emission Standards for Tanks—Level 1	Subpart GGGG	National Emission Standards for Hazardous Air Pollutants: Solvent Extraction for Vegetable Oil Production
Subpart PP	National Emission Standards for Containers		
Subpart QQ	National Emission Standards for Surface Impoundments		

22-14 WASTE MANAGEMENT

TABLE 22-10 Maximum Achievable Control Technology (MACT) Standards from 40 CFR Part 63 as of June 2004 (Concluded)

40 CFR 63	MACT Standard	40 CFR 63	MACT Standard
Subpart HHHH	National Emission Standards for Hazardous Air Pollutants for Wet-Formed Fiberglass Mat Production	Subpart CCCCC	National Emission Standards for Hazardous Air Pollutants for Coke Ovens: Pushing, Quenching, and Battery Stacks
Subpart JJJJ	National Emission Standards for Hazardous Air Pollutants: Paper and Other Web Coating	Subpart FFFFF	National Emission Standards for Hazardous Air Pollutants for Integrated Iron and Steel Manufacturing Facilities
Subpart KKKK	National Emission Standards for Hazardous Air Pollutants: Surface Coating of Metal Cans	Subpart GGGGG	National Emission Standards for Hazardous Air Pollutants: Site Remediation
Subpart MMMM	National Emission Standards for Hazardous Air Pollutants for Surface Coating of Miscellaneous	Subpart HHHHH	National Emission Standards for Hazardous Air Pollutants: Miscellaneous Coating Manufacturing
Subpart NNNN	National Emission Standards for Hazardous Air Pollutants: Surface Coating of Large Appliances	Subpart IIIII	National Emission Standards for Hazardous Air Pollutants: Mercury Emissions from Mercury Cell Chlor-Alkali Plants
Subpart OOOO	National Emission Standards for Hazardous Air Pollutants: Printing, Coating, and Dyeing of Fabrics and Other Textiles	Subpart JJJJJ	National Emission Standards for Hazardous Air Pollutants for Brick and Structural Clay Products Manufacturing
Subpart QQQQ	National Emission Standards for Hazardous Air Pollutants: Surface Coating of Wood Building Products	Subpart KKKKK	National Emission Standards for Hazardous Air Pollutants for Clay Ceramics Manufacturing
Subpart RRRR	National Emission Standards for Hazardous Air Pollutants: Surface Coating of Metal Furniture	Subpart LLLLL	National Emission Standards for Hazardous Air Pollutants: Asphalt Processing and Asphalt Roofing Manufacturing
Subpart SSSS	National Emission Standards for Hazardous Air Pollutants: Surface Coating of Metal Coil	Subpart MMMM	National Emission Standards for Hazardous Air Pollutants: Flexible Polyurethane Foam Fabrication Operations
Subpart TTTT	National Emission Standards for Hazardous Air Pollutants for Leather Finishing Operations	Subpart NNNNN	National Emission Standards for Hazardous Air Pollutants: Hydrochloric Acid Production
Subpart UUUU	National Emission Standards for Hazardous Air Pollutants for Cellulose Products Manufacturing	Subpart PPPPP	National Emission Standards for Hazardous Air Pollutants for Engine Test Cells/Stands
Subpart VVVV	National Emission Standards for Hazardous Air Pollutants for Boat Manufacturing	Subpart QQQQQ	National Emission Standards for Hazardous Air Pollutants for Friction Materials Manufacturing Facilities
Subpart WWWW	National Emission Standards for Hazardous Air Pollutants: Reinforced Plastic Composites Production	Subpart RRRRR	National Emission Standards for Hazardous Air Pollutants: Taconite Iron Ore Processing
Subpart XXXX	National Emission Standards for Hazardous Air Pollutants: Rubber Tire Manufacturing	Subpart SSSSS	National Emission Standards for Hazardous Air Pollutants for Refractory Products Manufacturing
Subpart YYYYY	National Emission Standards for Hazardous Air Pollutants for Stationary Combustion Turbines	Subpart TTTTT	National Emission Standards for Hazardous Air Pollutants for Primary Magnesium Refining
Subpart AAAAA	National Emission Standards for Hazardous Air Pollutants for Lime Manufacturing Plants		
Subpart BBBBB	National Emission Standards for Hazardous Air Pollutants for Semiconductor Manufacturing		

In 1965 the Water Quality Act established a new trend in water pollution control. It provided that the states set water quality standards in accordance with federal guidelines. If the states failed to do so, the federal government, subject to a review hearing, would set the standards. In 1966, the Clean Water Restoration Act transferred the Federal Water Pollution Control Administration from the Department of Health, Education, and Welfare to the Department of the Interior. It also gave the Interior Department the responsibility for the Oil Pollution Act.

After the creation of EPA in 1970, the EPA was given the responsibility previously held by the Department of the Interior with respect to water pollution control. In subsequent amendments to the FWPCA in 1973, 1974, 1975, 1976, and 1977, additional federal programs were established. The goals of these programs were to make waterways of the United States fishable and swimmable by 1983 and to achieve zero discharge of pollutants by 1985. The National Pollutant Discharge Elimination System (NPDES) was established as the basic regulatory mechanism for water pollution control. Under this program, the states

were given the authority to issue permits to “point-source” dischargers provided the dischargers gave assurance that the following standards would be met:

1. Source-specific effluent limitations [including new source performance standards (NSPS)]
 2. Toxic pollutant regulations (for specific substances regardless of source)
 3. Regulations applicable to oil and hazardous substance liability
- To achieve that stated water quality goal of fishable and swimmable waters by 1983, each state was required by EPA to adopt water quality standards that met or exceeded the federal water quality criteria. After each state submitted its own water quality standards, which were subsequently approved by EPA, the federal criteria were removed from the Code of Federal Regulations. The state water quality standards are used as the basis for establishing both point-source-based effluent limitations and toxic pollutant limitations used in issuing NPDES permits to point-source discharges.

Source-Based Effluent Limitations Under the FWPCA, EPA was responsible for establishing point-source effluent limitations for municipal dischargers, industrial dischargers, industrial users of municipal treatment works, and effluent limitations for toxic substances (applicable to all dischargers).

Standards promulgated or proposed by EPA under 40 CFR, Parts 402 through 699, prescribe effluent limitation guidelines for existing sources, standards of performance for new sources, and pretreatment standards for new and existing sources. Effluent limitations and new source performance standards apply to discharges made directly into receiving bodies of water. The new standards require best-available technology (BAT) and are to be used by the states when issuing NPDES permits for all sources 18 months after EPA makes them final. Pretreatment standards apply to waste streams from industrial sources that are sent to publicly owned treatment works (POTW) for final treatment. These regulations are meant to

TABLE 22-11 Common ODS Compounds

Class I-CFCs	Class II-HCFCs
CFC-11	HCFC-22
CFC-12	HCFC-123
CFC-13	HCFC-124
CFC-111	HCFC-141
CFC-112	HCFC-142
CFC-113	
CFC-114	
CFC-115	
Halons	Others
Halon-1211	Carbon tetrachloride
Halon-1301	Methyl chloroform
Halon-1202	Methyl bromide

protect the POTW from any materials that would either harm the treatment facility or pass through untreated. They are to be enforced primarily by the local POTW. These standards are applicable to particular classes of point sources and pertain to discharges into navigable waters without regard to the quality of the receiving water. Standards are specific for numerous subcategories under each point-source category.

Limitations based upon application of the best practicable control technology currently available (BPT) apply to existing point sources and should have been achieved by July 1, 1977. Limitations based upon application of the BATEA (best-available technology economically achievable) that will result in reasonable further progress toward elimination of discharges had to be achieved by July 1, 1984.

Clean Water Act of 1977 The 1977 Clean Water Act directed EPA to review all BAT guidelines for conventional pollutants in those industries not already covered.

On August 23, 1978 (43 FR 37570), the EPA proposed a new approach to the control of conventional pollutants by effluent guideline limitations. The new guidelines were known as best conventional (pollutants control) technology (BCT). These guidelines replaced the existing BAT limitations, which were determined to be unreasonable for certain categories of pollutants.

To determine if BCT limitations would be necessary, the cost-effectiveness of conventional pollutant reduction to BAT levels beyond BPT levels had to be determined and compared to the cost of removal of this same amount of pollutant by a publicly owned treatment works of similar capacity. If it was equally cost-effective for the industry to achieve the reduction required for meeting the BAT limitations as the POTW, then the BCT limit was made equal to the BAT level. When this test was applied, the BAT limitations set for certain categories were found to be unreasonable. In these subcategories EPA proposed to remove the BAT limitations and revert to the BPT limitations until BCT control levels could be formulated.

Control of Toxic Pollutants Since the early 1980s, EPA's water quality standards guidance placed increasing importance on toxic pollutant control. The agency urged states to adopt criteria into their standards for priority toxic pollutants, particularly those for which EPA had published criteria guidance. EPA also provided guidance to help and support state adoption of toxic pollutant standards with the *Water Quality Standards Handbook* (1983) and the *Technical Support Document for Water Quality Toxics Control* (1985 and 1991).

Despite EPA's urging and guidance, state response was disappointing. A few states adopted large numbers of numeric toxic pollutant criteria, primarily for the protection of aquatic life. Most other states adopted few or no water quality criteria for priority toxic pollutants. Some relied on "free from toxicity" criteria and "action levels" for toxic pollutants or occasionally calculated site-specific criteria. Few states addressed the protection of human health by adopting numeric human health criteria.

State development of case-by-case effluent limits using procedures that did not rely on the statewide adoption of numeric criteria for the priority toxic pollutants frustrated Congress. Congress perceived that states were failing to aggressively address toxics and that EPA was not using its oversight role to push the states to move more quickly and comprehensively. Many in Congress believed that these delays undermined the effectiveness of the act's framework.

1987 CWA Amendments In 1987, Congress, unwilling to tolerate further delays, added Section 303(c)(2)(B) to the CWA. The section provided that whenever a state reviews water quality standards or revises or adopts new standards, the state has to adopt criteria for all toxic pollutants listed pursuant to Section 307(a)(1) of the act for which criteria have been published under Section 304(a), discharge or presence of which in the affected waters could reasonably be expected to interfere with those designated uses adopted by the state, as necessary to support such designated uses. Such criteria had to be specific numerical criteria for such toxic pollutants. When numerical criteria are not available, wherever a state reviews water quality standards, or revises or adopts new standards, the state has to adopt criteria based on biological monitoring or assessment methods consistent with information published pursuant to Section 304(a)(8).

Nothing in this section was to be construed to limit or delay the use of effluent limitations or other permit conditions based on or involving biological monitoring or assessment methods or previously adopted numerical criteria.

In response to this new congressional mandate, EPA redoubled its efforts to promote and assist state adoption of numerical water quality standards for priority toxic pollutants. EPA's efforts included the development and issuance of guidance to the states on acceptable implementation procedures. EPA attempted to provide the maximum flexibility in its options that complied not only with the express statutory language but also with the ultimate congressional objective: prompt adoption of numeric toxic pollutant criteria. The agency believed that flexibility was important so that each state could comply with Section 303(c)(2)(B) within its resource constraints. EPA distributed final guidance on December 12, 1988. This guidance was similar to earlier drafts available for review by the states. The availability of the guidance was published in the Federal Register on January 5, 1989 (54 FR 346).

The structure of Section 303(c) is to require states to review their water quality standards at least once each 3-year period. Section 303(c)(2)(B) instructs states to include reviews for toxics criteria whenever they initiate a triennial review. EPA initially looked at February 4, 1990, the 3-year anniversary of the 1987 CWA amendments, as a convenient point to index state compliance. The April 17, 1990, Federal Register Notice (55 FR 14350) used this index point for the preliminary assessment of state compliance. However, some states were very nearly completing their state administrative processes for ongoing reviews when the 1987 amendments were enacted and could not legally amend those proceedings to address additional toxics criteria. Therefore, in the interest of fairness, and to provide such states a full 13-year review period, EPA's FY 1990 Agency Operating Guidance provided that states should complete adoption of the numeric criteria to meet Section 303(c)(2)(B) by September 30, 1990.

Section 303(c) does not provide penalties for states that do not complete timely water quality standard reviews. In no previous case had an EPA Administrator found that state failure to complete a review within 3 years jeopardized the public health or welfare to such an extent that promulgation of federal standards pursuant to Section 303(c)(4)(8) was justified. However, the pre-1987 CWA never mandated state adoption of priority toxic pollutants or other specific criteria. EPA relied on its water quality standards regulation (40 CFR 131.11) and its criteria and program guidance to the states on appropriate parametric coverage in state water quality standards, including toxic pollutants. With congressional concern exhibited in the legislative history for the 1987 Amendments regarding undue delays by states and EPA, and because states have been explicitly required to adopt numeric criteria for appropriate priority toxic pollutants since 1983, the agency is proceeding to promulgate federal standards pursuant to Section 303(c)(4)(B) of the CWA and 40 CFR 131.22(b).

States have made substantial recent progress in the adoption, and EPA approval, of toxic pollutant water quality standards. Furthermore, virtually all states have at least proposed new toxics criteria for priority toxic pollutants since Section 303(c)(2)(B) was added to the CWA in February 1987. Unfortunately, not all such state proposals address, in a comprehensive manner, the requirements of Section 303(c)(2)(B). For example, some states have proposed to adopt criteria to protect aquatic life, but not human health; other states have proposed human health criteria that do not address major exposure pathways (such as the combination of both fish consumption and drinking water). In addition, in some cases final adoption of proposed state toxics criteria that would be approved by EPA has been substantially delayed due to controversial and difficult issues associated with the toxic pollutant criteria adoption process.

Biological Criteria While the overall mandate of the Clean Water Act may now be more clearly stated and understood, the tools needed are still under development, and their full application is being worked out. The direction is toward a more comprehensive approach to water quality protection, which might be more appropriately termed *water resource protection* to encompass the living resources and their habitat along with the water itself.

In 1991, EPA directed states to adopt biological criteria into their water quality standards by September 30, 1993. To assist the states, EPA issued its "Policy on the Use of Biological Assessments and Criteria in the Water-Quality Program," which sets forth the key policy directions governing the shift to the use of biological criteria:

- "Biological surveys shall be fully integrated with toxicity and chemical-specific assessment methods in state water-quality programs."
- "Biological surveys should be used together with whole-effluent and ambient toxicity testing, and chemical-specific analyses to assess attainment/nonattainment of designated aquatic life uses in state water-quality standards."
- "If any one of the three assessment methods demonstrate that water-quality standards are not attained, it is EPA's policy that appropriate action should be taken to achieve attainment, including use of regulatory authority" (the independent applicability policy).
- "States should designate aquatic life uses that appropriately address biological integrity and adopt biological criteria necessary to protect those uses."

These policy statements are founded on the existing language and authorities in Clean Water Act Sections 303(c)(2)(A) and (B). EPA defined biological criteria as "numerical values or narrative expressions used to describe the expected structure and function of the aquatic community."

Most states currently conduct biological surveys. These consist of the collection and analysis of resident aquatic community data and a subsequent determination of the aquatic community's structure and function. A limiting factor in the number of surveys conducted is simply the funding to support field sampling. Most states also take their survey data through the next level of analysis, which is a biological assessment, in which the biological condition of the water body is evaluated. A state needs to conduct a biological assessment to justify designated waters as having uses less than the Clean Water Act goal of "fishable/swimmable" [Sec. 101(a)(2)].

Implementing biological criteria requires that the state establish what the expected condition of a biological community should be. This expected condition (or reference condition) is based on measurements at either unimpacted sites or sites that are minimally impacted by human activities. A key element of developing and adopting biological criteria is to develop a set of metrics (biological measurements) and indices (summations of those metrics) that are sensitive to reflecting the community changes that occur as a result of human perturbation. Metrics may include measures of species richness, percentages of species of a particular feeding type, and measures of species abundance and condition. The development of metrics and indices has been a major technical advance that effectively brought the field to the point of implementing biological integrity measures.

Aside from the need for additional monitoring and data as a basis for biological criteria, the largest impediment is currently related to the question of how or whether biological criteria should be translated directly to NPDES permit requirements. A strict reading of the NPDES regulations leads some individuals to conclude that every water quality standard potentially affected by a discharge must have a specific effluent limit. In the case of biological criteria, the direct translation isn't always possible. The preferred approach is to use biological criteria as a primary means to identify impaired waters that will then need additional study. Appropriate discharge controls can then be applied.

The other area of contention in adopting biocriteria is the EPA policy of *independent applicability*. This policy recognizes that chemical-specific criteria, toxicity testing (WET tests), and biological criteria each have unique as well as overlapping attributes, limitations, and program applications. No single approach is superior to another; rather, the approaches are complementary. When any one of these approaches indicates that water quality is impaired, appropriate regulatory action is needed. Critics of this approach most frequently cite biological criteria as the superior, or determining, measure and would use it to override an exceedance of chemical-specific criteria.

EPA and many states are now moving toward a watershed or basin management approach to water management. This is a holistic approach that looks at the multiple stresses and activities that affect a basin and evaluates these effects in the context of the survival of ecological systems. Biological criteria are recognized by states as a necessary

tool for detecting impacts to important aquatic resources that would otherwise be missed, particularly those caused by non-point-source activities, and for defining the desired endpoint of environmental restoration activities.

To assist states, EPA has issued programmatic guidance (*Biological Criteria: National Program Guidance for Surface Waters*, April 1990; *Procedures for Initiating Narrative Biological Criteria*, October 1992). In addition, EPA will be issuing over the next couple of years technical guidance specific to developing biological criteria for streams and small rivers, lakes and reservoirs, estuaries, and wetlands.

Metal Bioavailability and Toxicity Another area of policy and regulatory change that bears directly on questions of biological integrity is the application of toxic metal water quality criteria. EPA is in the midst of reconsidering its approach to implementing toxic metals criteria. This was prompted in part by the difficulty that some dischargers are having in meeting the state ambient water quality criteria for metals, which generally are expressed as total recoverable metals (a measurement that includes the metal dissolved in water plus metal that becomes dissolved when the sample is treated with acid). At issue is whether the criteria can be expressed in a form that more accurately addresses the toxicity of the metal to aquatic life, thereby providing the desired level of aquatic life protection, while allowing greater leeway in the total amount of metal discharged. This is a technically complex issue that will require long-term research even if short-term solutions are implemented.

The bioavailability, and hence the toxicity, of metal depends on the physical and chemical form of the metal, which in turn depends on the chemical characteristics of the surrounding water. The dissolved form of the metal is generally viewed as more bioavailable and therefore more toxic than the particulate form. Particulate matter and dissolved organic matter can bind the metal, making it less bioavailable. What is not well known or documented is the various chemical transformations that occur both within the effluent stream and when the effluent reaches and mixes with the receiving water. Metal that is not bioavailable in the effluent may become bioavailable under ambient chemical conditions.

The NPDES regulations (40 CFR 122.45) require effluent limits to be expressed as total recoverable metal. This requirement makes sense as a means to monitor and regulate both the total metal loading and the effectiveness of wastewater treatment that involves chemical precipitation of the metal.

From the perspective of ecological integrity called for in the Clean Water Act, any adjustment to the implementation of toxic metals criteria needs to be integrated with both sediment criteria and biological criteria to provide ecosystem protection envisioned by the act.

Total Maximum Daily Load (TMDL) Under Section 303(d) of the 1972 Clean Water Act, states, territories, and authorized tribes were required to develop a list of impaired waters. The impaired waters do not meet water quality standards that states, territories, and authorized tribes have set for them, even after point sources of pollution have installed the minimum required levels of pollution control technology. The law requires that these jurisdictions establish priority rankings for waters on the lists and develop TMDLs for these waters.

This part of the Clean Water Act was relatively neglected until 1996. A Federal Advisory Committee was convened and produced in 1998 a report and subsequent proposed changes for implementation of the TMDL program and associated changes in the National Pollutant Discharge Elimination System for point sources. A number of court orders were also motivating factors in the implementation and proposed changes to the rule.

The TMDL specifies the amount of a particular pollutant that may be present in a water body, allocates allowable pollutant loads among sources, and provides the basis for attaining or maintaining water quality standards.

The TMDL regulations were issued as draft in 1999 and finally published on July 13, 2000.

Water Quality Trading Within the approach to TMDL rules and subsequent management policy, the emphasis on *Pollutant trading* or *water quality trading* has evolved. Trading allows sources with responsibility for discharge reductions the flexibility to determine where reduction will occur. Within the trading approach, the economic advantages are emphasized. This is driven by the TMDL or more

stringent water quality-based requirement in an NPDES permit and the potential fact that discharge sources have significantly different costs to control the pollutant of concern.

In January 2003, EPA published the *Water Quality Trading Policy*. The policy outlines the trading objectives, requirements, and elements of a trading program. While barriers exist to the implementation of an effective water quality trading program, the cost of discharge quality compliance would warrant consideration of the approach.

Bioterrorism Act of 2003 While not directly related to water quality regulations, the security and vulnerability of community drinking water systems were addressed in the Public Health Security and Bioterrorism Preparedness and Response Act of 2002 (Bioterrorism Act). The vulnerability assessments were intended to examine a facility's ability to defend against adversarial actions that might substantially disrupt the ability of a water system to provide a safe and reliable supply of drinking water.

For community drinking water systems serving more than 3300 persons, it was required to conduct a vulnerability assessment (VA), certify and submit a copy of the VA to the EPA Administrator, prepare or revise an emergency response plan based on the results of the VA, and within 6 months certify to the EPA Administrator that an emergency response plan has been completed or updated. The VA requirement was to be completed by all facilities in June 2004.

Cooling Water Intake Regulation The EPA established requirements for facilities with cooling water intake structure to implement best-available technologies to minimize adverse environmental impacts. Under Section 316(b) of the CWA, the protection of aquatic organisms from being killed or injured by impingement or entrainment was established. The rule was divided into three phases. Phase I was published in December 2001 and addressed new facilities. Phase II was published in July 2004. The Phase II rule addressed existing electric generating plants that withdraw greater than 50 million gallons per day and use at least 25 percent of their withdrawn water for cooling purposes only. Phase III was prepublished in November 2004. The Phase III rule addresses other electric generating facilities and industrial sectors that withdraw water. It is anticipated that Phase III will be published within 1 to 2 years.

The rule provides that the facility may choose one of five compliance alternatives for establishing best available technology for minimizing adverse environmental impact at the site. Under current NPDES program regulations, the 316(b) requirements would occur when an existing NPDES permit was reissued or when an existing permit was modified or revoked and reissued.

Water Reuse With increasing water sustainability and scarcity issues in the United States, the U.S. Environmental Protection Agency (EPA) and the U.S. Agency for International Development (USAID) are revising portions of the 1992 EPA *Guidelines for Water Reuse* to reflect significant technical advancements and institutional developments since 1992. The guidelines will also address new areas, including national reclaimed water use trends, endocrine disrupters, and approaches to integrated water resources management.

Across the world, reclaimed water is becoming a critical water source, and reuse strategies are recognized in many U.S. states as an integral part of water resources management. The original guidelines, published in 1980, gave many state agencies direction in establishing reuse permits and helped to foster state water reuse regulations. The revised guidelines will include an updated inventory of state reuse regulations.

Regulatory Direction EPA and states are directed by the Clean Water Act to develop programs to meet the act's stated objective: "to restore and maintain the chemical, physical, and biological integrity of the Nation's waters" [Section 101 (a)]. Efforts to date have emphasized "clean water" quite literally, by focusing on the chemical makeup of discharges and their compliance with chemical water quality standards established for surface water bodies. These programs have successfully addressed many water pollution problems, but they are not sufficient to identify and address all of them. A continuing large gap in the current regulatory scheme is the absence of a direct measure of the condition of the biological resources that we are intending to protect (the biological integrity of the water body). Without such a measure it will be difficult to determine whether our water management

approaches are successful in meeting the intent of the act. Taken together, chemical, physical, and biological integrity is equivalent to the *ecological integrity* of a water body. It is highly likely the future will see the interpretation of biological integrity and ecological integrity, and the management of ecological systems, assume a much more prominent role in water quality management.

To ensure technically sound decision making, EPA should review its water quality criteria at a minimum of every 10 years. EPA's water quality criteria consist of information regarding the concentrations of chemicals or levels of parameters in water that protect aquatic life and human health, and act as regulatory thresholds for determination of impaired waters. Many of EPA's current water quality criteria are outdated, and have not been developed using consistent methodologies.

To the extent that EPA does pursue changes or additions to the current water quality standards program, it is critical that such modifications not be simply added onto existing requirements as independent new program elements. In pursuing any modifications EPA should carefully examine opportunities for coordinating and streamlining requirements within the context of the overall water quality standards program to maximize efficiency in the face of substantial resource constraints.

UNITED STATES SOLID WASTE LEGISLATION AND REGULATIONS

Much of the current activity in the field of solid waste management, especially with respect to hazardous wastes and resources recovery, is a direct consequence of recent legislation. Therefore, it is important to review the principal legislation that has affected the entire field of solid-waste management.

What follows is a brief review of existing legislation that affects the management of solid wastes. The actual legislation must be consulted for specific detail. Implementation of the legislation is accomplished through regulations adopted by federal, state, and local agencies. Because these regulations are revised continuously, they must be monitored continuously, especially when design and construction work is to be undertaken.

Rivers and Harbors Act, 1899 Passed in 1899, the Rivers and Harbors Act directed the U.S. Army Corps of Engineers to regulate the dumping of debris in navigable waters and adjacent lands.

Solid Waste Disposal Act, 1965 Modern solid-waste legislation dates from 1965, when the Solid Waste Disposal Act, Title II of Public Law 88-272, was enacted by Congress. The principal intent of this act was to promote the demonstration, construction, and application of solid waste management and resource-recovery systems that preserve and enhance the quality of air, water, and land resources.

National Environmental Policy Act, 1969 The National Environmental Policy Act (NEPA) of 1969 was the first federal act that required coordination of federal projects and their impacts with the nation's resources. The act specified the creation of the Council on Environmental Quality in the Executive Office of the President. This body has the authority to force every federal agency to submit to the council an environmental impact statement on every activity or project which it may sponsor or over which it has jurisdiction.

Resource Recovery Act, 1970 The Solid Waste Disposal Act of 1965 was amended by Public Law 95-512, the Resources Recovery Act of 1970. This act directed that the emphasis of the national solid-waste-management program should be shifted from disposal as its primary objective to that of recycling and reuse of recoverable materials in solid wastes or the conversion of wastes to energy.

Resource Conservation and Recovery Act, 1976 RCRA is the primary statute governing the regulation of solid and hazardous waste. It completely replaced the Solid Waste Disposal Act of 1965 and supplemented the Resource Recovery Act of 1970; RCRA itself was substantially amended by the Hazardous and Solid Waste Amendments of 1984 (HSWA). The principal objectives of RCRA as amended are to:

- Promote the protection of human health and the environment from potential adverse effects of improper solid and hazardous waste management
- Conserve material and energy resources through waste recycling and recovery

- Reduce or eliminate the generation of hazardous waste as expeditiously as possible

To achieve these objectives, RCRA authorized EPA to regulate the generation, treatment, storage, transportation, and disposal of hazardous wastes. The structure of the national hazardous waste regulatory program envisioned by Congress is laid out in Subtitle C of RCRA (Sections 3001 through 3019), which authorized EPA to:

- Promulgate standards governing hazardous waste generation and management
 - Promulgate standards for permitting hazardous waste treatment, storage, and disposal facilities
 - Inspect hazardous waste management facilities
 - Enforce RCRA standards
 - Authorize states to manage the RCRA Subtitle C program, in whole or in part, within their respective borders, subject to EPA oversight
- Federal RCRA hazardous waste regulations are set forth in 40 CFR Parts 260 through 279. The core of the RCRA regulations establishes the “cradle to grave” hazardous waste regulatory program through seven major sets of regulations:
- Identification and listing of regulated hazardous wastes (Part 261)
 - Standards for generators of hazardous waste (Part 262)
 - Standards for transporters of hazardous waste (Part 263)
 - Standards for owners/operators of hazardous waste treatment, storage, and disposal facilities (Parts 264, 265, and 267)
 - Standards for the management of specific hazardous wastes and specific types of hazardous waste management facilities (Part 266)
 - Land disposal restriction standards (Part 268)
 - Requirements for the issuance of permits to hazardous waste facilities (Part 270)
 - Approved state hazardous waste management programs (Part 272)
 - Standards for unusual waste management (Part 273)
 - Standards for management of used oil (Part 279)
 - Standards and procedures for authorizing state hazardous waste programs to be operated in lieu of the federal program (Part 271)

EPA, under Section 3006 of RCRA, may authorize a state to administer and enforce a state hazardous waste program in lieu of the federal Subtitle C program. To receive authorization, a state program must:

- Be equivalent to the federal Subtitle C program
- Be consistent with, and no less stringent than, the federal program and other authorized state programs
- Provide adequate enforcement of compliance with Subtitle C requirements

Toxic Substances Control Act, 1976 The two major goals of the Toxic Substances Control Act (TSCA), passed by Congress in 1976, are (1) the acquisition of sufficient information to identify and evaluate potential hazards from chemical substances and (2) the regulation of the manufacture, processing, distribution, use, and disposal of any substance that presents an unreasonable risk of injury to health of the environment.

Under TSCA, the EPA has issued a ban on the manufacture, processing, and distribution of products containing PCBs. Exporting of PCBs has also been banned. TSCA also required that PCB mixtures containing more than 50 ppm PCBs must be disposed of in an acceptable incinerator or chemical waste landfill. All PCB containers or products containing PCBs had to be clearly marked and records maintained by the operator of each facility handling at least 45 kilograms of PCBs. These records include PCBs in use in transformers and capacitors, PCBs in transformers and capacitors removed from service, PCBs stored for disposal, and a report on the ultimate disposal of the PCBs. Additionally, PCB transformers, must be registered, and records must be kept of hydraulic systems, natural gas pipeline systems, voltage regulators, electromagnetic switches, and ballasts.

TSCA also placed restrictions on the use of chlorofluorocarbons, asbestos, and fully halogenated chlorofluoroalkanes such as aerosol propellants.

Regulatory Direction There is no doubt that pollution prevention continues to be the regulatory direction. The development of new and more efficient processes and waste minimization technologies will be essential to support this effort.

An area certain to receive regulatory attention in the future is nanotechnology. The applications and implications of nanotechnology not only are changing lives every day, but also are moving so fast that many

have not yet grasped their tremendous impact (Theodore, L., and R. Kunz, *Nanotechnology: Environmental Implications and Solutions*, Wiley, Hoboken, N.J., 2002). It is clear that nanotechnology will revolutionize the way industry operates, creating chemical processes and products that are more efficient and less expensive. A primary obstacle to achieving this goal will be the need to control, reduce, and ultimately eliminate the environmental and related problems associated with nanotechnology, or dilemmas that may develop through its misuse.

Completely new legislation and regulatory rulemaking may be necessary for environmental control of nanotechnology. However, in the meantime, one may speculate on how the existing regulatory framework might be applied to the nanotechnology area as this emerging field develops over the next several years.

Commercial applications of nanotechnology are likely to be regulated under the Toxic Substances Control Act (TSCA), which authorized EPA to review and establish limits on the manufacture, processing, distribution, use, and/or disposal of new materials the EPA determines to pose “an unreasonable risk of injury to human health or the environment.” The term *chemicals* is defined broadly by TSCA. Unless qualifying for an exemption under the law [R&D (a statutory exemption requiring no further approval by EPA), low-volume production, low environmental releases along with low volume, or plans for limited test marketing], a prospective manufacturer is subject to the full-blown premanufacture notice (PMN) procedure. This requires submittal of said notice, along with toxicity and other data to EPA at least 90 days before commencing production of the chemical substance. (Theodore, L., and R. Kunz, *Nanotechnology: Environmental Implications and Solutions*, Wiley, Hoboken, N.J., 2002).

Approval then involves recordkeeping, reporting, and other requirements under the statute. Requirements will differ, depending on whether EPA determines that a particular application constitutes a “significant new use” or a “new chemical substance.” EPA can impose limits on production, including an outright ban when it is deemed necessary for adequate protection against “an unreasonable risk of injury to health or the environment.” EPA may revisit a chemical’s status under TSCA and change the degree or type of regulation when new health and environmental data warrant. EPA is expected to be issuing several new TSCA test rules in 2004 [Bergeson, L. L., “Expect a Busy Year at EPA,” *Chem. Processing* 17 (April 14, 2004)]. If the experience with genetically engineered organisms is any indication, there will be a push for EPA to update regulations in the future to reflect changes, advances, and trends in nanotechnology [Bergeson, L. L., “Genetically Engineered Organisms Face Changing Regulations,” *Chem. Processing* (March 2004)].

Workplace exposure to chemical substances and the potential for pulmonary toxicity are subject to regulation by the Occupational Safety and Health Administration under the Occupational Safety and Health Act (OSHA), including the requirement that potential hazards be disclosed on material safety data sheets (MSDS). (An interesting question arises as to whether carbon nanotubes, chemically carbon but with different properties because of their small size and structure, are indeed to be considered the same as or different from carbon black for MSDS purposes.) Both government and private agencies can be expected to develop the requisite threshold limit values (TLVs) for workplace exposure. Also, EPA may once again utilize TSCA to assert its own jurisdiction, appropriate or not, to minimize exposure in the workplace.

Wastes from a commercial-scale nanotechnology facility would be treated under the Resource Conservation and Recovery Act (RCRA), provided that they meet the criteria for RCRA waste. RCRA requirements could be triggered by a listed manufacturing process or the act’s specified hazardous waste characteristics. The type and extent of regulation would depend on how much hazardous waste is generated and whether the wastes generated are treated, stored, or disposed of on-site.

Finally, opponents of nanotechnology, especially, may be able to use the National Environmental Policy Act (NEPA) to impede nanotechnology research funded by the U.S. government. A “major Federal action significantly affecting the quality of the human environment” is subject to the environmental impact provision under NEPA. (Various states also have environmental impact assessment requirements that could delay or put a stop to construction of nanotechnology facilities.) Time will tell.

POLLUTION PREVENTION

This subsection is drawn in part from “Pollution Prevention Overview,” prepared by B. Wainwright and L. Theodore, copyright 1993.

FURTHER READING: American Society of Testing and Materials, *Standard Guide for Industrial Source Reduction*, draft copy dated June 16, 1992. American Society of Testing and Materials, *Pollution Prevention, Reuse, Recycling and Environmental Efficiency*, June, 1992. California Department of Health Services, *Economic Implications of Waste Reduction, Recycling, Treatment, and Disposal of Hazardous Wastes: The Fourth Biennial Report*, California, 1988. Citizen’s Clearinghouse for Hazardous Waste, *Reduction of Hazardous Waste: The Only Serious Management Option*, Falls Church, CCHW, 1986. Congress of the United States. Office of Technology Assessment, *Serious Reduction of Hazardous Waste: For Pollution Prevention and Industrial Efficiency*, Washington, D.C., GPO, 1986. Dupont, R., L. Theodore, and K. Ganesan, *Pollution Prevention: The Waste Management Option for the 21st Century*, Lewis Publishers, 2000. Friedlander, S., “Pollution Prevention—Implications for Engineering Design, Research, and Education,” *Environment*, May 1989, p. 10. Theodore, L., and R. Kunz, *Nanotechnology: Environmental Implications and Solutions*, Wiley, 2005. Theodore, L. and R. Allen, *Pollution Prevention: An ETS Theodore Tutorial*, Roanoke, VA, ETS International, Inc., 1994. Theodore, L., *A Citizen’s Guide to Pollution Prevention*, East Williston, NY, 1993. United States EPA, *Facility Pollution Prevention Guide*. (EPA/600/R-92/088), Washington, D.C., May 1992. United States EPA, “Pollution Prevention Fact Sheets,” Washington, D.C., GPO, 1991. United States EPA, *1987 National Biennial RCRA Hazardous Waste Report—Executive Summary*, Washington, D.C., GPO, 1991. United States EPA, Office of Pollution Prevention, *Report on the U.S. Environmental Protection Agency’s Pollution Prevention Program*, Washington, D.C., GPO, 1991. Wilcox, J., and L. Theodore, *Engineering and Environmental Ethics*, Wiley, 1998. World Wildlife Fund, *Getting at the Source—Executive Summary*, 1991.

INTRODUCTION

The amount of waste generated in the United States has reached staggering proportions; according to the United States Environmental Protection Agency (EPA), 250 million tons of solid waste alone are generated annually. Although both the Resource Conservation and Recovery Act (RCRA) and the Hazardous and Solid Waste Act (HSWA) encourage businesses to minimize the wastes they generate, the majority of the environmental protection efforts are still centered around treatment and pollution clean-up.

The passage of the Pollution Prevention Act of 1990 has redirected industry’s approach to environmental management; pollution prevention has now become the environmental option of the 21st century. Whereas typical waste-management strategies concentrate on “end-of-pipe” pollution control, pollution prevention attempts to handle waste at the source (i.e., source reduction). As waste handling and disposal costs increase, the application of pollution prevention measures is becoming more attractive than ever before. Industry is currently exploring the advantages of multimedia waste reduction and developing agendas to *strengthen* environmental design while *lessening* production costs.

There are profound opportunities for both industry and the individual to prevent the generation of waste; indeed, pollution prevention is today primarily stimulated by economics, legislation, liability concerns, and the enhanced environmental benefit of managing waste at the source. The Pollution Prevention Act of 1990 established pollution prevention as a national policy, declaring that “waste should be prevented or reduced at the source wherever feasible, while pollution that cannot be prevented should be recycled in an environmentally safe manner” (Ref. 1). The EPA’s policy establishes the following hierarchy of waste management:

1. Source reduction
2. Recycling/reuse
3. Treatment
4. Ultimate disposal

The hierarchy’s categories are prioritized so as to promote the examination of each individual alternative prior to the investigation of subsequent options (i.e., the most preferable alternative should be thoroughly evaluated before consideration is given to a less accepted option). Practices that decrease, avoid, or eliminate the generation of

waste are considered source reduction and can include the implementation of procedures as simple and economical as good house-keeping. Recycling is the use, reuse, or reclamation of wastes and/or materials that may involve the incorporation of waste recovery techniques (e.g., distillation, filtration). Recycling can be performed at the facility (i.e., on-site) or at an off-site reclamation facility. Treatment involves the destruction or detoxification of wastes into nontoxic or less toxic materials by chemical, biological, or physical methods, or any combination of these control methods. Disposal has been included in the hierarchy because it is recognized that residual wastes will exist; the EPA’s so-called “ultimate disposal” options include land-filling, land farming, ocean dumping, and deep-well injection. However, the term *ultimate disposal* is a misnomer, but is included here because of its earlier adaptation by the EPA.

Table 22-12 provides a rough timetable demonstrating the United States’ approach to waste management. Note how waste management has begun to shift from pollution *control*-driven activities to pollution *prevention* activities.

The application of waste-management practices in the United States has recently moved toward securing a new pollution prevention ethic. The performance of pollution prevention assessments and their subsequent implementation will encourage increased activity into methods that will further aid in the reduction of hazardous wastes. One of the most important and propitious consequences of the pollution-prevention movement will be the development of life-cycle design and standardized life-cycle cost-accounting procedures. These two consequences are briefly discussed in the two paragraphs that follow. Additional information is provided in a later subsection.

The key element of life-cycle design is Life-Cycle Assessment (LCA). LCA is generally envisioned as a process to evaluate the environmental burdens associated with the cradle-to-grave life cycle of a product, process, or activity. A product’s life cycle can be roughly described in terms of the following stages:

1. Raw material
2. Bulk material processing
3. Production
4. Manufacturing and assembly
5. Use and service
6. Retirement
7. Disposal

Maintaining an objective process while spanning this life cycle can be difficult given the varying perspective of groups affected by different parts of that cycle. LCA typically does not include any direct or indirect monetary costs or impacts to individual companies or consumers.

Another fundamental goal of life-cycle design is to promote sustainable development at the global, regional, and local levels. There is significant evidence that suggests that current patterns of human and industrial activity on a global scale are not following a sustainable path. Changes to achieve a more sustainable system will require that environmental issues be more effectively addressed in the future. Principles for achieving sustainable development should include (Ref. 2):

TABLE 22-12 Waste Management Timetable

Prior to 1945	No control
1945–1960	Little control
1960–1970	Some control
1970–1975	Greater control (EPA is founded)
1975–1980	More sophisticated control
1980–1985	Beginning of waste-reduction management
1985–1990	Waste-reduction management
1990–1995	Formal pollution prevention programs (Pollution Prevention Act)
1995–2000	Widespread acceptance of pollution prevention
After 2000	The sky’s the limit

1. *Sustainable resource use (conserving resources, minimizing depletion of nonrenewable resources, using sustainable practices for managing renewable resources).* There can be no product development or economic activity of any kind without available resources. Except for solar energy, the supply of resources is finite. Efficient designs conserve resources while also reducing impacts caused by material extraction and related activities. Depletion of nonrenewable resources and overuse of otherwise renewable resources limits their availability to future generations.

2. *Maintenance of ecosystem structure and function.* This is a principal element of sustainability. Because it is difficult to imagine how human health can be maintained in a degraded, unhealthy natural world, the issue of ecosystem health should be a more fundamental concern. Sustainability requires that the health of all diverse species as well as their interrelated ecological functions be maintained. As only one species in a complex web of ecological interactions, humans cannot separate their success from that of the total system.

3. *Environmental justice.* The issue of environmental justice has come to mean different things to different people. Theodore (Ref. 3) has indicated that the subject of environmental justice contains four key elements that are interrelated: environmental racism, environmental health, environmental equity, and environmental politics. (Unlike many environmentalists, Theodore has contended that only the last issue, politics, is a factor in environmental justice.) A major challenge in sustainable development is achieving both intergenerational and intersocietal environmental justice. Overconsuming resources and polluting the planet in such a way that it enjoins future generations from access to reasonable comforts irresponsibly transfer problems to the future in exchange for short-term gains. Beyond this intergenerational conflict, enormous inequities in the distribution of resources continue to exist between developed and less developed countries. Inequities also occur within national boundaries.

Life cycle is a perspective that can consider the true costs of product production and/or services provided and utilized by analyzing the price associated with potential environmental degradation and energy consumption, as well as more customary costs like capital expenditure and operating expenses. A host of economic and economic-related terms have appeared in the literature. Some of these include total cost assessment, life-cycle costing, and full-cost accounting. Unfortunately, these terms have come to mean different things to different people at different times. In an attempt to remove this ambiguity, the following three economic terms are defined below.

1. *Traditional costing procedure (TCP).* This accounting procedure *only* takes into account capital and operating (including environmental) costs.

2. *Comprehensive costing procedure (CCP).* The economic procedure includes not only the traditional capital and operating costs but also peripheral costs such as liability, regulatory related expenses, borrowing power, and social considerations.

3. *Life-cycle costing (LCC).* This type of analysis requires that all the traditional costs of project or product system, from raw-material acquisition to end-result product disposal, be considered.

The TCP approach is relatively simple and can be easily applied to studies involving comparisons of different equipment, different processes, or even parts of processes. CCP has now emerged as the most realistic approach that can be employed in economic project analyses. It is the recommended procedure for pollution-prevention studies. The LCC approach is usually applied to the life-cycle analysis (LCA) of a product or service. It has found occasional application in project analysis.

The remainder of this subsection on pollution prevention will be concerned with providing the reader with the necessary background to understand the meaning of pollution prevention and its useful implementation. Assessment procedures and the economic benefits derived from managing pollution at the source are discussed along with methods of cost accounting for pollution prevention. Additionally, regulatory and nonregulatory methods to promote pollution prevention and overcome barriers are examined, and ethical considerations are presented. By eliminating waste at the source, all can participate in the protection of the environment by reducing the amount of waste mate-

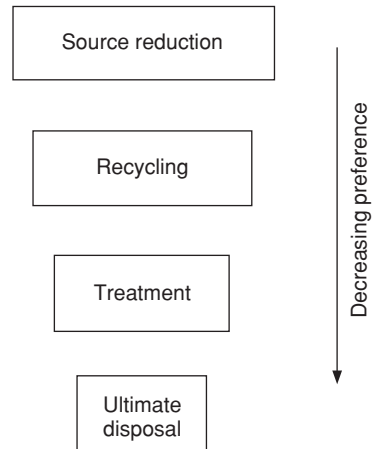


FIG. 22-2 Pollution prevention hierarchy.

rial that would otherwise need to be treated or ultimately disposed; accordingly, attention is also given to pollution prevention in both the domestic and business office environments.

POLLUTION-PREVENTION HIERARCHY

As discussed in the Introduction, the hierarchy set forth by the EPA in the Pollution Prevention Act establishes an order to which waste-management activities should be employed to reduce the quantity of waste generated. The preferred method is source reduction, as indicated in Fig. 22-2. This approach actually precedes traditional waste management by addressing the source of the problem prior to its occurrence.

Although the EPA's policy does not consider recycling or treatment as actual pollution prevention methods per se, these methods present an opportunity to reduce the amount of waste that might otherwise be discharged into the environment. Clearly, the definition of pollution prevention and its synonyms (e.g., waste minimization) must be understood to fully appreciate and apply these techniques.

Waste minimization generally considers all of the methods in the EPA hierarchy (except for disposal) appropriate to reduce the volume or quantity of waste requiring disposal (e.g., source reduction). The definition of *source reduction* as applied in the Pollution Prevention Act, however, is "any practice that reduces the amount of any hazardous substance, pollutant, or contaminant entering any waste stream or otherwise released into the environment . . . prior to recycling, treatment or disposal" (Ref. 1). Source reduction reduces the amount of waste generated; it is therefore considered true pollution prevention and has the highest priority in the EPA hierarchy.

Recycling (or reuse) refers to the use (or reuse) of materials that would otherwise be disposed of or treated as a waste product. A good example is a rechargeable battery. Wastes that cannot be directly reused may often be recovered on-site through methods such as distillation. When on-site recovery or reuse is not feasible due to quality specifications or the inability to perform recovery on-site, off-site recovery at a permitted commercial recovery facility is often a possibility. Such management techniques are considered secondary to source reduction and should only be used when pollution cannot be prevented.

The treatment of waste is the third element of the hierarchy and should be utilized only in the absence of feasible source reduction or recycling opportunities. Waste treatment involves the use of chemical, biological, or physical processes to reduce or eliminate waste material. The incineration of wastes is included in this category and is considered "preferable to other treatment methods (i.e., chemical, biological, and physical) because incineration can permanently destroy the

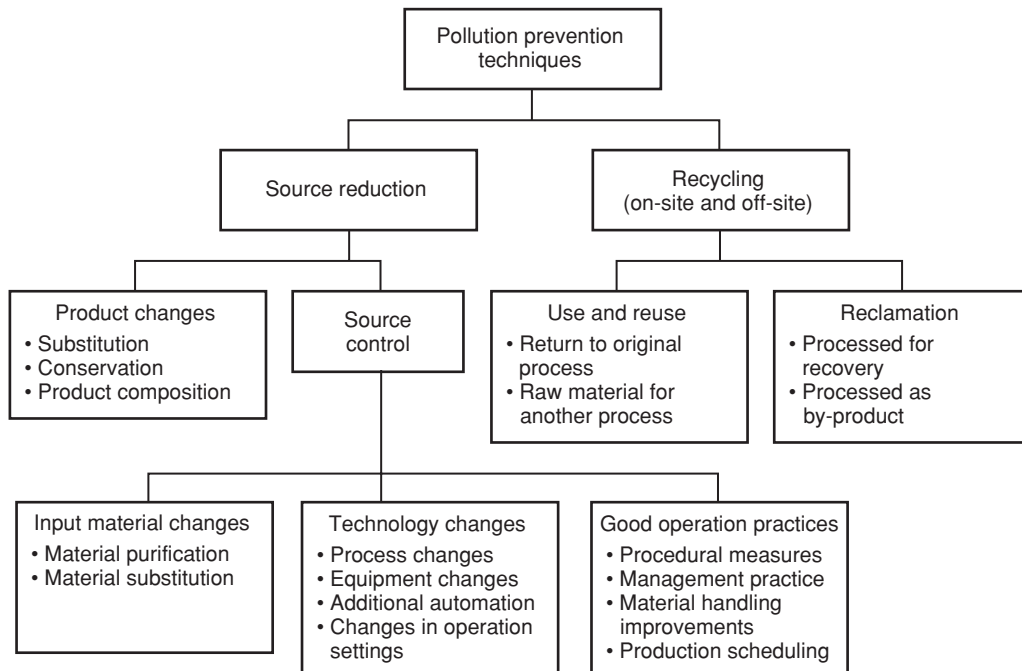


FIG. 22-3 Pollution prevention techniques.

hazardous components in waste materials” (Ref. 4). It can also be employed to reduce the volume of waste to be treated.

Several of these pollution-prevention elements are used by industry in combination to achieve the greatest waste reduction. Residual wastes that cannot be prevented or otherwise managed are then disposed of only as a last resort.

Figure 22-3 provides a more detailed schematic representation of the two preferred pollution prevention techniques (i.e., source reduction and recycling).

MULTIMEDIA ANALYSIS AND LIFE-CYCLE ANALYSIS

Multimedia Analysis In order to properly design and then implement a pollution prevention program, sources of all wastes must be fully understood and evaluated. A multimedia analysis involves a multifaceted approach. It must not only consider one waste stream but all potentially contaminated media (e.g., air, water, land). Past waste-management practices have been concerned primarily with treatment. All too often, such methods solve one waste problem by transferring a contaminant from one medium to another (e.g., air stripping); such waste shifting is *not* pollution prevention or waste reduction.

Pollution prevention techniques must be evaluated through a thorough consideration of all media, hence the term multimedia. This approach is a clear departure from previous pollution treatment or control techniques where it was acceptable to transfer a pollutant from one source to another in order to solve a waste problem. Such strategies merely provide short-term solutions to an ever increasing problem. As an example, air pollution control equipment prevents or reduces the discharge of waste into the air but at the same time can produce a solid (hazardous) waste problem.

Life-Cycle Analysis The aforementioned multimedia approach to evaluating a product’s waste stream(s) aims to ensure that the treatment of one waste stream does not result in the generation or increase in an additional waste output. Clearly, impacts resulting during the production of a product or service must be evaluated over its entire

history or life cycle. This life-cycle analysis or total systems approach (Ref. 3) is crucial to identifying opportunities for improvement. As described earlier, this type of evaluation identifies “energy use, material inputs, and wastes generated during a product’s life: from extraction and processing of raw materials to manufacture and transport of a product to the marketplace and finally to use and dispose of the product” (Ref. 5).

During a forum convened by the World Wildlife Fund and the Conservation Foundation in May 1990, various steering committees recommended that a three-part life-cycle model be adopted. This model consists of the following:

1. An inventory of materials and energy used, and environmental releases from all stages in the life of a product or process
2. An analysis of potential environmental effects related to energy use and material resources and environmental releases
3. An analysis of the changes needed to bring about environmental improvements for the product or process under evaluation

Traditional cost analysis often fails to include factors relevant to future damage claims resulting from litigation, the depletion of natural resources, the effects of energy use, and the like. As such, waste-management options such as treatment and disposal may appear preferential if an overall life-cycle cost analysis is not performed. It is evident that environmental costs from cradle to grave have to be evaluated together with more conventional production costs to accurately ascertain genuine production costs. In the future, a total systems approach will most likely involve a more careful evaluation of pollution, energy, and safety issues. For example, if one was to compare the benefits of coal versus oil as a fuel source for an electric power plant, the use of coal might be considered economically favorable. In addition to the cost issues, however, one must be concerned with the environmental effects of coal mining (e.g., transportation and storage prior to use as a fuel). Society often has a tendency to overlook the fact that there are serious health and safety matters (e.g., miner exposure) that must be considered along with the effects of fugitive emissions. When these effects are weighed alongside standard economic factors, the full cost benefits of coal

usage may be eclipsed by environmental costs. Thus, many of the economic benefits associated with pollution prevention are often unrecognized due to inappropriate cost-accounting methods. For this reason, economic considerations are briefly detailed later.

POLLUTION-PREVENTION ASSESSMENT PROCEDURES

The first step in establishing a pollution prevention program is the obtaining of management commitment. This is necessary given the inherent need for project structure and control. Management will determine the amount of funding allotted for the program as well as specific program goals. The data collected during the actual evaluation is then used to develop options for reducing the types and amounts of waste generated. Figure 22-4 depicts a systematic approach that can be used during the procedure. After a particular waste stream or area of concern is identified, feasibility studies are performed involving both economic and technical considerations. Finally, preferred alternatives are implemented. The four phases of the assessment (i.e., planning and organization, assessment, feasibility, and implementation) are introduced in the following subsections. Sources of additional information as well as information on industrial programs are also provided.

Planning and Organization The purpose of this phase is to obtain management commitment, define and develop program goals, and assemble a project team. Proper planning and organization are crucial to the successful performance of the pollution-prevention assessment. Both managers and facility staff play important roles in the assessment procedure by providing the necessary commitment and familiarity with the facility, its processes, and current waste-management operations. It is the benefits of the program, including economic advantages, liability

reduction, regulatory compliance, and improved public image that often leads to management support.

Once management has made a commitment to the program and goals have been set, a program task force is established. The selection of a team leader will be dependent upon many factors including the ability to effectively interface with both the assessment team and management staff.

The task force must be capable of identifying pollution reduction alternatives as well as be cognizant of inherent obstacles to the process. Barriers frequently arise from the anxiety associated with the belief that the program will negatively affect product quality or result in production losses. According to an EPA survey, 30 percent of industry comments responded that they were concerned that product quality would decline if waste minimization techniques were implemented (Ref. 6). As such, the assessment team, and the team leader in particular, must be ready to react to these and other concerns (Ref. 2).

Assessment Phase The assessment phase aims to collect data needed to identify and analyze pollution-prevention opportunities. Assessment of the facility's waste-reduction needs includes the examination of (hazardous) waste streams, process operations, and the identification of techniques that often promise the reduction of waste generation. Information is often derived from observations made during a facility walk-through, interviews with employees (e.g., operators, line workers), and review of site or regulatory records. One professional organization suggests the following sources of information be reviewed, as available (Ref. 7):

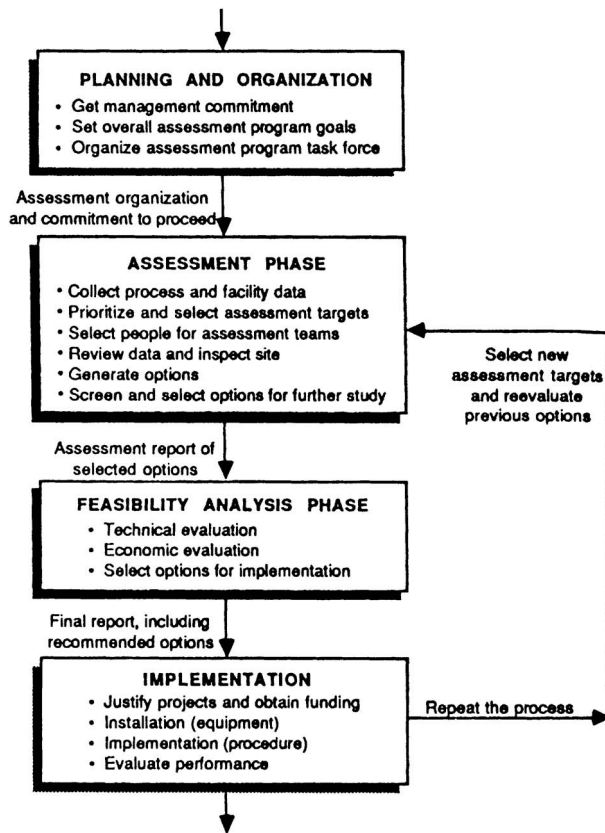
1. Product design criteria
2. Process flow diagrams for all solid waste, wastewater, and air emissions sources
3. Site maps showing the location of all pertinent units (e.g., pollution-control devices, points of discharge)
4. Environmental documentation, including: Material Safety Data Sheets (MSDS), military specification data, permits (e.g., NPDES, POTW, RCRA), SARA Title III reports, waste manifests, and any pending permits or application information
5. Economic data, including: cost of raw materials; cost of air, wastewater, and (hazardous) waste treatment; waste management operating and maintenance costs; and waste disposal costs
6. Managerial information: environmental policies and procedures; prioritization of waste-management concerns; automated or computerized waste-management systems; inventory and distribution procedures; maintenance scheduling practices; planned modifications or revisions to existing operations that would impact waste-generation activities; and the basis of source reduction decisions and policies

The use of process flow diagrams and material balances are worthwhile methods to quantify losses or emissions and provide essential data to estimate the size and cost of additional equipment, other data to evaluate economic performance, and a baseline for tracking the progress of minimization efforts (Ref. 3). Material balances should be applied to individual waste streams or processes and then utilized to construct an overall balance for the facility. Details on these calculations are available in the literature (Ref. 8). In addition, an introduction to this subject is provided in the next section.

The data collected is then used to prioritize waste streams and operations for assessment. Each waste stream is assigned a priority based on corporate pollution-prevention goals and objectives. Once waste origins are identified and ranked, potential methods to reduce the waste stream are evaluated. The identification of alternatives is generally based on discussions with the facility staff; review of technical literature; and contacts with suppliers, trade organizations, and regulatory agencies.

Alternatives identified during this phase of the assessment are evaluated using screening procedures so as to reduce the number of alternatives requiring further exploration during the feasibility analysis phase. Some criteria used during this screening procedure include: cost-effectiveness; implementation time; economic, compliance, safety and liability concerns; waste-reduction potential; and whether the technology is proven (Refs. 4, 8). Options that meet established criteria are then examined further during the feasibility analysis.

Feasibility Analysis The selection procedure is performed by an evaluation of technical and economic considerations. The technical



Pollution prevention assessment procedure.

FIG. 22-4 Pollution prevention assessment procedure.

evaluation determines whether a given option will work as planned. Some typical considerations follow:

1. Safety concerns
2. Product quality impacts or production delays during implementation
3. Labor and/or training requirements
4. Creation of new environmental concerns
5. Waste reduction potential
6. Utility and budget requirements
7. Space and compatibility concerns

If an option proves to be technically ineffective or inappropriate, it is deleted from the list of potential alternatives. Either following or concurrent with the technical evaluation, an economic study is performed, weighing standard measures of profitability such as payback period, investment returns, and net present value. Many of these costs (or, more appropriately, cost savings) may be substantial yet are difficult to quantify. (Refer to *Economic Considerations Associated with Pollution Prevention*.)

Implementation The findings of the overall assessment are used to demonstrate the technical and economic worthiness of program implementation. Once appropriate funding is obtained, the program is implemented not unlike any other project requiring new procedures or equipment. When preferred waste-pollution-prevention techniques are identified, they are implemented and should become part of the facility's day-to-day management and operation. Subsequent to the program's execution, its performance should be evaluated in order to demonstrate effectiveness, generate data to further refine and augment waste-reduction procedures, and maintain management support.

It should be noted that waste reduction, energy conservation, and safety issues are interrelated and often complementary to each other. For example, the reduction in the amount of energy a facility consumes usually results in reduced emissions associated with the generation of power. Energy expenditures associated with the treatment and transport of waste are similarly reduced when the amount of waste generated is lessened; at the same time, worker safety is elevated due to reduced exposure to hazardous materials. However, this is not always the case. Addition of air-pollution control systems at power plants decreases net power output due to the power consumed by the equipment. This in turn requires more fuel to be combusted for the same power exported to the grid. This additional fuel increases pollution from coal mining, transport, ash disposal, and the like. In extreme cases, very high recovery efficiencies for some pollutants can raise, not lower, overall total emissions. Seventy percent removal might produce a 2 percent loss in power output; 90 percent recovery could lead to a 3 percent loss; 95 percent, a 5 percent loss; 99 percent, a 10 percent loss, and so on. The point to be made is that pollution control is generally not a "free lunch."

Sources of Information The successful development and implementation of any pollution prevention program is not only dependent on a thorough understanding of the facility's operations but also requires an intimate knowledge of current opportunities and advances in the field. In fact, 32 percent of industry respondents to an earlier EPA survey identified the lack of technical information as a major factor delaying or preventing the implementation of a waste-minimization program (Ref. 6). One of EPA's positive contributions has been the development of a national Pollution Prevention Information Clearinghouse (PPIC) and the Pollution Prevention Information Exchange System (PIES) to facilitate the exchange of information needed to promote pollution prevention through efficient information transfer (Ref. 2).

PPIC is operated by the EPA's Office of Research and Development and the Office of Pollution Prevention. The clearinghouse is comprised of four elements:

1. Repository, including a hard copy reference library and collection center and an on-line information retrieval and ordering system.
2. PIES, a computerized conduit to databases and document ordering, accessible via modem and personal computer: (703) 506-1025.
3. PPIC uses the RCRA/Superfund and Small Business Ombudsman Hotlines as well as a PPIC technical assistance line to answer pollution-prevention questions, access information in the PPIC, and

assist in document ordering and searches. To access PPIC by telephone, call:

- RCRA/Superfund Hotline, (800) 242-9346
- Small Business Ombudsman Hotline, (800) 368-5888
- PPIC Technical Assistance, (703) 821-4800

4. PPIC compiles and disseminates information packets and bulletins, and initiates networking efforts with other national and international organizations.

Additionally, the EPA publishes a newsletter entitled *Pollution Prevention News* that contains information including EPA news, technologies, program updates, and case studies. The EPA's Risk Reduction Engineering Laboratory and the Center for Environmental Research Information has published several guidance documents, developed in cooperation with the California Department of Health Services. The manuals supplement generic waste reduction information presented in the EPA's *Waste Minimization Opportunity Assessment Manual* (Ref. 9).

Pollution prevention or waste minimization programs have been established at the State level and as such are good sources of information. Both Federal and State agencies are working with universities and research centers and may also provide assistance. For example, the American Institute of Chemical Engineers has established the Center for Waste Reduction Technologies (CWRT), a program based on targeted research, technology transfer, and enhanced education.

Industry Programs A significant pollution-prevention resource may very well be found with the "competition." Several large companies have established well-known programs that have successfully incorporated pollution-prevention practices into their manufacturing processes. These include, but are not limited to: 3M—Pollution Prevention Pays (3P); Dow Chemical—Waste Reduction Always Pays (WRAP); Chevron—Save Money and Reduce Toxics (SMART); and, the General Dynamics Zero Discharge Program.

Smaller companies can benefit by the assistance offered by these larger corporations. It is clear that access to information is of major importance when implementing efficient pollution-prevention programs. By adopting such programs, industry is affirming pollution prevention's application as a good business practice and not simply a "noble" effort.

ASSESSMENT PHASE: MATERIAL BALANCE CALCULATIONS

(The reader is directed to Refs. 4 and 10 for further information.)

One of the key elements of the assessment phase of a pollution prevention program involves mass balance equations. These calculations are often referred to as material balances; the calculations are performed via the conservation law for mass. The details of this often-used law are described below.

The conservation law for mass can be applied to any process or system. The general form of the law follows:

$$\text{mass in} - \text{mass out} + \text{mass generated} = \text{mass accumulated}$$

This equation can be applied to the total mass involved in a process or to a particular species, on either a mole or mass basis. The conservation law for mass can be applied to steady-state or unsteady-state processes and to batch or continuous systems. A steady-state system is one in which there is no change in conditions (e.g., temperature, pressure) or rates of flow with time at any given point in the system; the accumulation term then becomes zero. If there is no chemical reaction, the generation term is zero. All other processes are classified as unsteady state.

To isolate a system for study, the system is separated from the surroundings by a boundary or envelope that may either be real (e.g., a reactor vessel) or imaginary. Mass crossing the boundary and entering the system is part of the mass-in term. The equation may be used for any compound whose quantity does not change by chemical reaction or for any chemical element, regardless of whether it has participated in a chemical reaction. Furthermore, it may be written for one piece of equipment, several pieces of equipment, or around an entire process (i.e., a total material balance).

The conservation of mass law finds a major application during the performance of pollution-prevention assessments. As described earlier,

a pollution-prevention assessment is a systematic, planned procedure with the objective of identifying methods to reduce or eliminate waste. The assessment process should characterize the selected waste streams and processes (Ref. 11)—a necessary ingredient if a material balance is to be performed. Some of the data required for the material balance calculation may be collected during the first review of site-specific data; however, in some instances, the information may not be collected until an actual site walk-through is performed.

Simplified mass balances should be developed for each of the important waste-generating operations to identify sources and gain a better understanding of the origins of each waste stream. Since a mass balance is essentially a check to make sure that what goes into a process (i.e., the total mass of all raw materials) is what leaves the process (i.e., the total mass of the products and by-products), the material balance should be made individually for all components that enter and leave the process. When chemical reactions take place in a system, there may be an advantage to performing “elemental balances” for specific chemical elements in a system. Material balances can assist in determining concentrations of waste constituents where analytical test data are limited. They are particularly useful when there are points in the production process where it is difficult or uneconomical to collect analytical data.

Mass-balance calculations are particularly useful for quantifying fugitive emissions such as evaporative losses. Waste stream data and mass balances will enable one to track flow and characteristics of the waste streams over time. Since in most cases the accumulation equals zero (steady-state operation), it can then be assumed that any buildup is actually leaving the process through fugitive emissions or other means. This will be useful in identifying trends in waste/pollutant generation and will also be critical in the task of measuring the performance of implemented pollution prevention options. The result of these activities is a catalog of waste streams that provides a description of each waste, including quantities, frequency of discharge, composition, and other important information useful for material balance. Of course, some assumptions or educated estimates will be needed when it is impossible to obtain specific information.

By performing a material balance in conjunction with a pollution prevention assessment, the amount of waste generated becomes known. The success of the pollution prevention program can therefore be measured by using this information on baseline generation rates (i.e., that rate at which waste is generated without pollution prevention considerations) (Ref. 12).

BARRIERS AND INCENTIVES TO POLLUTION PREVENTION

As discussed previously, industry is beginning to realize that there are profound benefits associated with pollution prevention, including cost effectiveness, reduced liability, enhanced public image, and regulatory compliance. Nevertheless, there are barriers or disincentives identified with pollution prevention. This section will briefly outline both barriers and incentives that may need to be confronted or considered during the evaluation of a pollution prevention program.

Barriers to Pollution Prevention (“The Dirty Dozen”)

There are numerous reasons why more businesses are not reducing the wastes they generate. The following “dirty dozen” are common disincentives:

1. *Technical limitations.* Given the complexity of present manufacturing processes, waste streams exist that cannot be reduced with current technology. The need for continued research and development is evident.

2. *Lack of information.* In some instances, the information needed to make a pollution-prevention decision may be confidential or is difficult to obtain. In addition, many decision makers are simply unaware of the potential opportunities available regarding information to aid in the implementation of a pollution-prevention program.

3. *Consumer preference obstacles.* Consumer preference strongly affects the manner in which a product is produced, packaged, and marketed. If the implementation of a pollution-prevention program results in an increase in the cost of a product or decreased convenience or availability, consumers might be reluctant to use it.

4. *Concern over product quality decline.* The use of a less hazardous material in a product’s manufacturing process may result in decreased life, durability, or competitiveness.

5. *Economic concerns.* Many companies are unaware of the economic advantages associated with pollution prevention. Legitimate concerns may include decreased profit margins or the lack of funds required for the initial capital investment.

6. *Resistance to change.* The unwillingness of many businesses to change is rooted in their reluctance to try technologies that may be unproven or based on a combination of the barriers discussed in this section.

7. *Regulatory barriers.* Existing regulations that have created incentives for the control and containment of wastes are at the same time discouraging the exploration of pollution-prevention alternatives. Moreover, since regulatory enforcement is often intermittent, current legislation can weaken waste-reduction incentives.

8. *Lack of markets.* The implementation of pollution-prevention processes and the production of environmentally friendly products will be of no avail if markets do not exist for such goods. As an example, the recycling of newspaper in the United States has resulted in an overabundance of waste paper without markets prepared to take advantage of this raw material.

9. *Management apathy.* Many managers capable of making decisions to begin pollution-prevention activities do not realize the potential benefits of pollution prevention.

10. *Institutional barriers.* In an organization without a strong infrastructure to support pollution-prevention plans, waste-reduction programs will be difficult to implement. Similarly, if there is no mechanism in place to hold individuals accountable for their actions, the successful implementation of a pollution-prevention program will be limited.

11. *Lack of awareness of pollution prevention advantages.* As mentioned in reason no. 5, decision makers may merely be uninformed of the benefits associated with pollution reduction.

12. *Concern over the dissemination of confidential product information.* If a pollution-prevention assessment reveals confidential data pertinent to a company’s product, fear may exist that the organization will lose a competitive edge with other businesses in the industry.

Pollution-Prevention Incentives (“A Baker’s Dozen”) Various means exist to encourage pollution prevention through regulatory measures, economic incentives, and technical assistance programs. Since the benefits of pollution prevention can surpass prevention barriers, a “baker’s dozen” incentives is presented below:

1. *Economic benefits.* The most obvious economic benefits associated with pollution prevention are the savings that result from the elimination of waste storage, treatment, handling, transport, and disposal. Additionally, less tangible economic benefits are realized in terms of decreased liability, regulatory compliance costs (e.g., permits), legal and insurance costs, and improved process efficiency. Pollution prevention almost always pays for itself, particularly when the time required to comply with regulatory standards is considered. Several of these economic benefits are discussed separately below.

2. *Regulatory compliance.* Quite simply, when wastes are not generated, compliance issues are not a concern. Waste-management costs associated with record keeping, reporting, and laboratory analysis are reduced or eliminated. Pollution prevention’s proactive approach to waste management will better prepare industry for future regulation of many hazardous substances and wastes that are currently unregulated. Regulations have, and will continue to be, a moving target.

3. *Liability reduction.* Facilities are responsible for their wastes from “cradle-to-grave.” By eliminating or reducing waste generation, future liabilities can also be decreased. Additionally, the need for expensive pollution liability insurance requirements may be abated.

4. *Enhanced public image.* Consumers are interested in purchasing goods that are safer for the environment, and this demand, depending on how they respond, can mean success or failure for many companies. Businesses should therefore be sensitive to consumer demands and use pollution-prevention efforts to their utmost advantage by producing goods that are environmentally friendly.

5. *Federal and state grants.* Federal and state grant programs have been developed to strengthen pollution-prevention programs initiated by states and private entities. The EPA's "Pollution Prevention by and for Small Business" grant program awards grants to small businesses to assist their development and demonstration of new pollution-prevention technologies.

6. *Market incentives.* Public demand for environmentally preferred products has generated a market for recycled goods and related products; products can be designed with these environmental characteristics in mind, offering a competitive advantage. In addition, many private and public agencies are beginning to stimulate the market for recycled goods by writing contracts and specifications that call for the use of recycled materials.

7. *Reduced waste-treatment costs.* As discussed in reason no. 5 of the dirty dozen, the increasing costs of traditional end-of-pipe waste-management practices are avoided or reduced through the implementation of pollution-prevention programs.

8. *Potential tax incentives.* In an effort to promote pollution prevention, taxes may eventually need to be levied to encourage waste generators to consider reduction programs. Conversely, tax breaks could be developed for corporations that utilize pollution-prevention methods to foster pollution prevention.

9. *Decreased worker exposure.* By reducing or eliminating chemical exposures, businesses benefit by lessening the potential for chronic workplace exposure and serious accidents and emergencies. The burden of medical monitoring programs, personal exposure monitoring, and potential damage claims are also reduced.

10. *Decreased energy consumption.* As mentioned previously, methods of energy conservation are often interrelated and complementary to each other. Energy expenditures associated with the treatment and transport of waste are usually but not always reduced when the amount of waste generated is lessened, while at the same time the pollution associated with energy consumed by these activities is abated.

11. *Increased operating efficiencies.* A potential beneficial side effect of pollution-prevention activities is a concurrent increase in operating efficiency. Through a pollution-prevention assessment, the assessment team can identify sources of waste that result in (hazardous) waste generation and loss in process performance. The implementation of a reduction program will often rectify such problems through modernization, innovation, and the implementation of good operating practices.

12. *Competitive advantages.* By taking advantage of the many benefits associated with pollution prevention, businesses can gain a competitive edge.

13. *Reduced negative environmental impacts.* Through an evaluation of pollution-prevention alternatives, which consider a total systems approach, consideration is given to the negative impact of environmental damage to natural resources and species that occur during raw-material procurement and waste disposal. The performance of pollution-prevention endeavors will therefore result in enhanced environmental protection.

ECONOMIC CONSIDERATIONS ASSOCIATED WITH POLLUTION-PREVENTION PROGRAMS

The purpose of this subsection is to outline the basic elements of a pollution-prevention cost-accounting system that incorporates both traditional and less tangible economic variables. The intent is not to present a detailed discussion of economic analysis but to help identify the more important elements that must be considered to properly quantify pollution-prevention options.

The greatest driving force behind any pollution-prevention plan is the promise of economic opportunities and cost savings over the long term. Pollution prevention is now recognized as one of the lowest-cost options for waste/pollutant management. Hence, an understanding of the economics involved in pollution prevention programs/options is quite important in making decisions at both the engineering and management levels. Every engineer should be able to execute an economic evaluation of a proposed project. If the project cannot be justified economically after *all* factors—and these will be discussed in

TABLE 22-13 Economic Analysis Timetable

Prior to 1945	Capital costs only
1945–1960	Capital and some operating costs
1960–1970	Capital and operating costs
1970–1975	Capital, operating, and some environmental control costs
1975–1980	Capital, operating, and environmental control costs
1980–1985	Capital, operating, and more sophisticated environmental control costs
1985–1990	Capital, operating, and environmental controls, and some life-cycle analysis (Total Systems Approach)
1990–1995	Capital, operating, and environmental control costs and life-cycle analysis (Total Systems Approach)
1995–2000	Widespread acceptance of Total Systems Approach
After 2000	To be detailed at a later date

more detail below—have been taken into account, it should obviously not be pursued. The earlier such a project is identified, the fewer resources will be wasted.

Before the true cost or profit of a pollution-prevention program can be evaluated, the factors contributing to the economics must be recognized. There are two traditional contributing factors (capital costs and operating costs), but there are also other important costs and benefits associated with pollution prevention that need to be quantified if a meaningful economic analysis is going to be performed. Table 22-13 demonstrates the evolution of various cost-accounting methods. Although Tables 22-12 (see Introduction) and 22-13 are not directly related, the reader is left with the option of comparing some of the similarities between the two.

The Total Systems Approach (TSA) referenced in Table 22-13 aims to quantify not only the economic aspects of pollution prevention but also the social costs associated with the production of a product or service from cradle to grave (i.e., life cycle). The TSA attempts to quantify less tangible benefits such as the reduced risk derived from not using a hazardous substance. The future is certain to see more emphasis placed on the TSA approach in any pollution-prevention program. As described earlier, a utility considering the option of converting from a gas-fired boiler to coal-firing is usually not concerned with the environmental effects and implications associated with such activities as mining, transporting, and storing the coal prior to its usage as an energy feedstock. Pollution-prevention approaches since the mid-to-late 1990s have become more aware of this need.

The economic evaluation referred to above is usually carried out using standard measures of profitability. Each company and organization has its own economic criteria for selecting projects for implementation. (For example, a project can be judged on its payback period. For some companies, if the payback period is more than 3 years, it is a dead issue.) In performing an economic evaluation, various costs and savings must be considered. As noted earlier, the economic analysis presented in this subsection represents a preliminary, rather than a detailed, analysis. For smaller facilities with only a few (and perhaps simple) processes, the entire pollution-prevention assessment procedure will tend to be much less formal. In this situation, several obvious pollution-prevention options such as the installation of flow controls and good operating practices may be implemented with little or no economic evaluation. In these instances, no complicated analyses are necessary to demonstrate the advantages of adopting the selected pollution-prevention option. A proper perspective must also be maintained between the magnitude of savings that a potential option may offer and the amount of manpower required to do the technical and economic feasibility analyses. A short description of the various aforementioned economic factors—including capital and operating costs and other considerations—follows.

Once identified, the costs and/or savings are placed into their appropriate categories and quantified for subsequent analysis. Equipment cost is a function of many variables, one of the most significant of which is capacity. Other important variables include operating temperature and/or pressure conditions, and degree of equipment sophistication. Preliminary estimates are often made using simple cost-capacity relationships that are valid when the other variables are confined to a narrow range of values.

The usual technique for determining the capital costs (i.e., total capital costs, which include equipment design, purchase, and installation) for the facility is based on the factored method of establishing direct and indirect installation costs as a function of the known equipment costs. This is basically a modified Lang method, whereby cost factors are applied to known equipment costs (Refs. 13 and 14). The first step is to obtain from vendors the purchase prices of the primary and auxiliary equipment. The total base price, designated by X , which should include instrumentation, control, taxes, freight costs, and so on, serves as the basis for estimating the direct and indirect installation costs. These costs are obtained by multiplying X by the cost factors, which are available in the literature (see Refs. 13–19).

The second step is to estimate the direct installation costs by summing all the cost factors involved in the direct installation costs, which include piping, insulation, foundation and supports, and so on. The sum of these factors is designated as the DCF (direct installation cost factor). The direct installation costs are then the product of the DCF and X . The third step consists of estimating the indirect installation cost. Here all the cost factors for the indirect installation costs (engineering and supervision, startup, construction fees, and so on) are added; the sum is designated by ICF (indirect installation cost factor). The indirect installation costs are then the product of ICF and X . Once the direct and indirect installation costs have been calculated, the total capital cost (TCC) may be evaluated as follows:

$$TCC = X + (DCF)(X) + (ICF)(X)$$

This can then be converted to annualized capital costs (ACC) with the use of the capital recovery factor (CRF). The CRF can be calculated from the following equation:

$$CRF = \frac{(i)(1+i)^n}{(1+i)^n - 1}$$

where n = projected lifetime of the project, years
 i = annual interest rate, expressed as a fraction

The annualized capital cost (ACC) is the product of the CRF and TCC and represents the total annualized installed equipment cost distributed over the lifetime of the project. The ACC reflects the cost associated with the initial capital outlay over the depreciable life of the system. Although investment and operating costs can be accounted for in other ways such as present-worth analysis, the capital recovery method is often preferred because of its simplicity and versatility. This is especially true when comparing somewhat similar systems having different depreciable lives. In such decisions, there are usually other considerations besides economic, but if all other factors are equal, the alternative with the lowest total annualized cost should be the most viable.

Operating costs can vary from site to site since these costs reflect local conditions (e.g., staffing practices, labor, utility costs). Operating costs, like capital costs, may be separated into two categories: direct and indirect costs. Direct costs are those that cover material and labor and are directly involved in operating the facility. These include labor, materials, maintenance and maintenance supplies, replacement parts, wastes, disposal fees, utilities, and laboratory costs. However, the major direct operating costs are usually those associated with labor and materials. Indirect costs are those operating costs associated with, but not directly involved in, operating the facility; costs such as overhead (e.g., building/land leasing and office supplies), administrative fees, property taxes, and insurance fees fall into this category.

The main problem with the traditional type of economic analysis is that it is difficult—nay, in some cases impossible—to quantify some of the not-so-obvious economic merits of a pollution-prevention program. Several considerations have just recently surfaced as factors that need to be taken into account in any meaningful economic analysis of a pollution-prevention effort. What follows is a summary listing of these considerations, most which have been detailed earlier.

1. Decreased long-term liabilities
2. Regulatory compliance
3. Regulatory recordkeeping
4. Dealings with the EPA

5. Dealings with state and local regulatory bodies
6. Elimination or reduction of fines and penalties
7. Potential tax benefits
8. Customer relations
9. Stockholder support (corporate image)
10. Improved public image
11. Reduced technical support
12. Potential insurance costs and claims
13. Effect on borrowing power
14. Improved mental and physical well-being of employees
15. Reduced health-maintenance costs
16. Employee morale
17. Other process benefits
18. Improved worker safety
19. Avoidance of rising costs of waste treatment and/or disposal
20. Reduced training costs
21. Reduced emergency response planning

Many proposed pollution-prevention programs have been squelched in their early stages because a comprehensive economic analysis was not performed. Until the effects described above are included, the true merits of a pollution-prevention program may be clouded by incorrect and/or incomplete economic accounting. Can something be done by industry to remedy this problem? One approach is to use a modified version of the standard Delphi panel. In order to estimate these other economic benefits of pollution prevention, several knowledgeable individuals within and perhaps outside the organization are asked to independently provide estimates, with explanatory details, on these economic benefits. Each individual in the panel is then allowed to independently review all responses. The cycle is then repeated until the group's responses approach convergence.

Finally, pollution-prevention measures can provide a company with the opportunity of looking their neighbors in the eye and truthfully saying that all that can reasonably be done to prevent pollution is being done. In effect, the company is doing right by the environment. Is there an economic advantage to this? It is not only a difficult question to answer quantitatively but also a difficult one to answer qualitatively. Industry is left to ponder the answer to this question.

POLLUTION PREVENTION AT THE DOMESTIC AND OFFICE LEVELS

Concurrent with the United States' growth as an international economic superpower during the years following World War II, a new paradigm was established whereby society became accustomed to the convenience and ease with which goods could be discarded after a relatively short useful life. Individuals have come to expect these everyday comforts with what may be considered an unconscious ignorance towards the ultimate effect of the throwaway lifestyle. In fact, many, while fearful of environmental degradation, are not aware of the ill effect these actions have on the world as a whole. Many individuals who abide by the "not in my back yard" (NIMBY) mind-set also feel pollution prevention does not have to occur "in my house."

The past three decades have seen an increased social awareness of the impact of modern-day lifestyles on the environment. Public environmental concerns include issues such as waste disposal; hazardous-material regulations; depletion of natural resources; and air, water, and land pollution. Nevertheless, roughly one-half of the total quantity of waste generated each year can be attributed to domestic sources!

More recently, concern about the environment has begun to stimulate environmentally correct behavior. After all, the choices made today affect the environment of tomorrow. Simple decisions can be made at work and at home that conserve natural resources and lessen the burden placed on a waste-management system. By eliminating waste at the source, society is participating in the protection of the environment by reducing the amount of waste that would otherwise need to be treated or ultimately disposed.

There are numerous areas of environmental concern that can be directly influenced by the consumer's actions. The first issue, which is described above, is that of waste generation. Second, energy conservation has significantly affected Americans and has resulted in cost-saving

measures that have directly reduced pollution. As mentioned previously, energy conservation is directly related to pollution prevention since a reduction in energy use usually corresponds to less energy production and, consequently, less pollution output. A third area of concern is that of accident and emergency planning. Relatively recent accidents like Chernobyl and Bhopal have increased public awareness and helped stimulate regulatory policies concerned with emergency planning. Specifically, Title III of the Superfund Amendments and Reauthorization Act (SARA) of 1986 established the Emergency Planning and Community Right-to-Know Act, which has forever changed the concept of environmental management. This law attempts to avert potential emergencies through careful planning and the development of contingency plans. Planning for emergency situations can help protect human health and the environment (Ref. 3).

Based on the above three areas of potential concern, a plethora of waste reduction activities can be performed at home or in an office environment. One can easily note the similarities between these activities and those pollution-prevention activities performed in industry. The following few examples are identified by category according to this notation (Ref. 3):

- Waste reduction
- ★ Accidents, health, and safety
- Energy conservation

At home

- Purchase products with the least amount of packaging
- Borrow items used infrequently
- ★ Handle materials to avoid spills (and slips, trips)
- ★ Keep hazardous materials out-of-reach of children
- Use energy-efficient lighting (e.g., fluorescent)
- Install water-flow restriction devices on sink faucets and showerheads

At the office

- Pass on verbal memos when written correspondence isn't required
- Reuse paper before recycling it
- ★ Know building evacuation procedures
- ★ Adhere to company medical policies (e.g., annual physicals)
- Don't waste utilities simply because you are not paying for them
- Take public transportation to the office

The use of pollution-prevention principles on the home front clearly does not involve the use of high-technology equipment or major lifestyle changes; success is only dependent upon active and willing public participation. All can help to make a difference.

Before pollution prevention becomes a fully accepted way of life, considerable effort still needs to be expended to change the way one looks at waste management. A desire to use "green" products and services will be of no avail in a market where these goods are not available. Participation in pollution-prevention programs will increase through continued education, community efforts, and lobbying for change. Market incentives can be created and strengthened by tax policies, price preferences, and packaging regulations created at the federal, state, and local levels. Individuals should take part by communicating with industry and expressing their concerns. For example, citizens should feel free to write letters to decision makers at both business organizations and government institutions regarding specific products or legislation. Letters can be positive, demonstrating personal endorsement of a green product, or disapproving, expressing discontent and reluctance to use a particular product because of its negative environmental effect (Ref. 3).

By starting now, society will learn through experience to better manage its waste while providing a safer and cleaner environment for future generations.

ETHICAL CONSIDERATIONS

Given the evolutionary nature of pollution prevention, it is evident that as technology changes and continued progress is achieved, society's

opinion of both what is possible and desirable will also change. Government officials, scientists, and engineers will face new challenges to fulfill society's needs while concurrently meeting the requirements of changing environmental regulations. It is now apparent that attention should also be given to ethical considerations and their application to pollution prevention policy. How one makes decisions on the basis of ethical beliefs is clearly a personal issue but one that should be addressed. In order to examine this issue, the meaning of ethics must be known, although the intent here is not to provide a detailed discussion regarding the philosophy of ethics or morality.

Ethics can simply be defined as the analysis of the rightness and wrongness of an act or actions. According to Dr. Andrew Varga, director of the Philosophical Resources Program at Fordham University, in order to discern the morality of an act, it is customary to look at the act on the basis of four separate elements: its object, motive, circumstances, and consequences (Ref. 21). Rooted in this analysis is the belief that if one part of the act is bad, then the overall act itself cannot be considered good. Of course, there are instances where the good effects outweigh the bad, and therefore there may be a reason to permit the evil. The application of this principle is not cut and dry and requires decisions to be made on a case-by-case basis. Each must make well-judged decisions rooted in an understanding of the interaction between technology and the environment. After all, the decisions made today will have an impact not only on this generation but on many generations to come. If one chooses today not to implement a waste-reduction program in order to meet a short-term goal of increased productivity, this might be considered a good decision since it benefits the company and its employees. However, should a major release occur that results in the contamination of a local sole-source of drinking water, what is the good?

As an additional example, toxicological studies have indicated that test animals exposed to small quantities of toxic chemicals had better health than control groups that were not exposed. A theory has been developed that says that a low-level exposure to the toxic chemical results in a challenge to the animal to maintain homeostasis; this challenge increases the animal's vigor and, correspondingly, its health. However, larger doses seem to cause an inability to adjust, resulting in negative health effects. Based on this theory, some individuals would believe that absolute pollution reduction might not be necessary.

FUTURE TRENDS

The reader should keep an open mind when dealing with the types of issues discussed above and facing challenges perhaps not yet imagined. Clearly, there is no simple solution or answer to many of the questions. The EPA is currently *attempting* to develop a partnership with government, industry, and educators to produce and distribute pollution-prevention educational materials. Given EPA's past history and performance, there are understandable doubts as to whether this program will succeed (Ref. 22).

Finally, no discussion on pollution prevention would be complete without reference to the activities of the 50-year-old International Organization for Standardization (ISO) and the general subject of nanotechnology (Ref. 23). Both are briefly described below.

ISO created Technical Committee 207 (TC 207) to develop new standards for environmental management systems (EMS). The ramifications, especially to the chemical industry, which has become heavily involved in the continued development and application of these standards, will be great. TC 207's activities are being scrutinized closely. The new environmental management set of standards is entitled ISO 14000. With this new standard in place, it is expected that customers will require their product suppliers to be certified by ISO 14000. In addition, some service suppliers who have an impact on the environment are expected to obtain an ISO 14000 certification. Certification will imply to the customer that, when the product or service was prepared, the environment was not significantly damaged in the process. This will effectively require that the life-cycle design mentality discussed earlier be applied to all processes. Implementing the life-cycle design framework will require significant organizational and operational changes in business. To effectively promote the goals of

sustainable development, life-cycle designs will have to successfully address cost, performance, and cultural and legal factors.

Nanotechnology is concerned with the world of invisible miniscule particles that are dominated by forces of physics and chemistry that cannot be applied at the macro or human-scale level. These particles have come to be defined by some as nanomaterials, and these materials possess unusual properties not present in traditional and/or ordinary materials. The new technology allows the engineering of matter by systems and/or processes that effectively deal with atoms. Interestingly, the classic laws of science are different at the nanoscale. Nanoparticles possess large surface areas and essentially no inner mass; i.e., their surface-to-mass ratio is extremely high. This new "science" is based on the knowledge that particles in the nanometer range, and nanostructures or nanomachines that are developed from these nanoparticles, possess special properties and exhibit unique behavior; and can significantly impact physical, chemical, electrical, biological, mechanical, etc., functional qualities. These new characteristics can be harnessed and exploited by applied scientists to engineer "Industrial Revolution II" processes. Present-day and future applications include chemical products, e.g., parts, plastics, specialty metals, powders; computer chips and computer systems; pollution prevention areas that can include energy conservation, environmental control, and health/safety issues, plus addressing crime and terrorism concerns. In effect, the sky's the limit regarding efforts in this area. As far as the environment is concerned, this new technology can terminate pollution as it is known today. By ingeniously controlling the building

of small and large products via a process of precise controlled building, there is no waste since environmental engineering is built in by design. However, activists have begun to organize against the science, calling for a moratorium on nanotechnology products until the social (health) and environmental risks are better understood. At the time of the preparation of this manuscript, justifiably (in the opinion of the author) no nanoregulations had been put into place. One of the main obstacles to achieving this goal will be to control, reduce, and ultimately eliminate environmental and related problems, or problems that may develop through the misuse or use of nanotechnology.

The impact of all of the above on both the industry and the consumer will be significant. All have heard the expression "I've met the enemy . . . and we're it." After all, it is the consumer who can and will ultimately have the final say. Once the consumer refuses to buy and/or accept products and/or services that damage the environment, that industry is either out of business or must change its operations to environmentally acceptable alternatives. With the new standards, customers (in addition to other organizations) of certified organizations will be assured that the products or services they purchase have been produced in accordance with universally accepted standards of environmental management. Organizational claims, which today can be misleading or erroneous, will, under the standards, be backed up by comprehensive and detailed environmental management systems that must withstand the scrutiny of intense audits.

Can all of the above be achieved in the near future? If it can, then society need only key its environmental efforts on educating the consumer.

AIR-POLLUTION MANAGEMENT OF STATIONARY SOURCES

FURTHER READING: Billings and Wilder, *Fabric Filter Handbook*, U.S. EPA, NTIS Publ. PB 200-648 (vol. 1), PB 200-649 (vol. 2), PB 200-651 (vol. 3), and PB 200-650 (vol. 4), 1970. Buonicore, "Air Pollution Control," *Chem. Eng.*, **87**(13), 81 (June 30, 1980). Buonicore and Theodore, *Industrial Control Equipment for Gaseous Pollutants*, vols. I and II, CRC Press, Boca Raton, Florida, 1975. Calvert, *Scrubber Handbook*, U.S. EPA, NTIS Publ. PB 213-016 (vol. 1) and PB 213-017 (vol. 2), 1972. Danielson, *Air Pollution Engineering Manual*, EPA Publ. AP-40, 1973. Davis, *Air Filtration*, Academic, New York, 1973. Kleet and Galeski, *Flare Systems Study*, EPA-600/2-76-079 (NTIS), 1976. Lund, *Industrial Pollution Control Handbook*, McGraw-Hill, New York, 1971. Oglesby and Nichols, *Manual of Electrostatic Precipitator Technology*, U.S. EPA, NTIS Publ. PB 196-380 (vol. 1), PB 196-381 (vol. 2), PB 196-370 (vol. 3), and PB 198-150 (vol. 4), 1970. *Package Sorption System Study*, EPA-R2-73-202 (NTIS), 1973. Rolke et al., *Afterburner Systems Study*, U.S. EPA, NTIS Publ. PB 212-500, 1972. Slade, *Meteorology and Atomic Energy*, AEC (TID-24190), Oak Ridge, Tennessee, 1969. Stern, *Air Pollution*, Academic, New York, 1974. Strauss, *Industrial Gas Cleaning*, Pergamon, New York, 1966. Buonicore and Theodore, *Industrial Control Equipment for Gaseous Pollutants*, vol. 1, 2d ed., CRC Press, Boca Raton, Florida, 1992. Theodore and Buonicore, *Air Pollution Control Equipment: Selection, Design, Operation, and Maintenance*, Prentice Hall, Englewood Cliffs, New Jersey, 1982. Treybal, *Mass Transfer Operations*, 3d ed., McGraw-Hill, New York, 1980. Turner, *Workbook of Atmospheric Dispersion Estimates*, U.S. EPA Publ. AP-26, 1970. White, *Industrial Electrostatic Precipitation*, Addison-Wesley, Reading, Massachusetts, 1963. McKenna, Mycock, and Theodore, *Handbook of Air Pollution Control Engineering and Technology*, CRC Press, Boca Raton, Florida, 1995. Theodore and Allen, *Air Pollution Control Equipment*, ETSI Prof. Training Inst., Roanoke, VA, 1993. *Air Pollution Engineering Manual*, 2d ed., Wiley, New York, 2000. *Guideline on Air Quality Models (CAQM)*, rev. ed., EPA-450/2-78-027R, July 1986. *Compilation of Air Pollution Emission Factors (AP-42)*, 4th ed., U.S. EPA, Research Triangle Park, North Carolina, September, 1985. McKenna and Turner, *Fabric Filter—Baghouses I—Theory, Design, and Selection*, ETSI Prof. Training Inst., Roanoke, Virginia, 1993. Greiner, *Fabric Filter—Baghouses II—Operation, Maintenance, and Troubleshooting*, ETS Prof. Training Inst., Roanoke, Virginia, 1993. Yang, Yonghua, and Allen, "Biofiltration Control of Hydrogen Sulfide. 2. Kinetics Biofilter Performance and Maintenance," *JAWA*, **44**, p. 1315.

INTRODUCTION

Air pollutants may be classified into two broad categories: (1) natural and (2) human-made. Natural sources of air pollutants include:

- Windblown dust
- Volcanic ash and gases

- Ozone from lightning and the ozone layer
- Esters and terpenes from vegetation
- Smoke, gases, and fly ash from forest fires
- Pollens and other aeroallergens
- Gases and odors from biologic activities
- Natural radioactivity

Such sources constitute background pollution and that portion of the pollution problem over which control activities can have little, if any, effect.

Human-made sources cover a wide spectrum of chemical and physical activities and are the major contributors to urban air pollution. Air pollutants in the United States pour out from over 10 million vehicles, the refuse of approximately 300 million people, the generation of billions of kilowatts of electricity, and the production of innumerable products demanded by everyday living. Hundreds of millions of tons of air pollutants are generated annually in the United States alone. The six pollutants identified in the Clean Air Act are shown in Table 22-14. Annual emission statistics for these six pollutants are considered major indicators of the U.S. air quality. During the 1970 to 2003 period, the total emissions of the six pollutants declined by 51 percent, while at the same time the gross domestic product increased by 176 percent, the population by 39 percent, and energy consumption by 45 percent. Total emissions in the United States are summarized by source category for the year 1998 in Table 22-15.

Air pollutants may also be classified as to the origin and state of matter:

1. Origin
 - a. Primary. Emitted to the atmosphere from a process
 - b. Secondary. Formed in the atmosphere as a result of a chemical reaction
 2. State of matter
 - a. Gaseous. True gases such as sulfur dioxide, nitrogen oxide, ozone, carbon monoxide, etc.; vapors such as gasoline, paint solvent, dry cleaning agents, etc.
 - b. Particulate. Finely divided solids or liquids; solids such as dust, fumes, and smokes; and liquids such as droplets, mists, fogs, and aerosols
- Gaseous Pollutants** Gaseous pollutants may be classified as inorganic or organic. Inorganic pollutants consist of:
1. *Sulfur gases.* Sulfur dioxide, sulfur trioxide, hydrogen sulfide
 2. *Oxides of carbon.* Carbon monoxide, carbon dioxide

TABLE 22-14 Six Principal Pollutants' Annual Emission Statistics, Millions of Tons per Year

	1970	1975	1980	1985 ^a	1990	1995	2000 ^a	2002	2003 ^b
Carbon monoxide (CO)	197.3	184.0	177.8	169.6	143.6	120.0	102.4	96.4	93.7
Nitrogen oxides (NO _x) ^c	26.9	26.4	27.1	25.8	25.1	24.7	22.3	20.8	20.5
Particulate matter (PM) ^d									
PM ₁₀	12.2 ^e	7.0	6.2	3.6	3.2	3.1	2.3	2.4	2.3
PM _{2.5} ^e	NA	NA	NA	NA	2.3	2.2	1.8	1.8	1.8
Sulfur dioxide (SO ₂)	31.2	28.0	25.9	23.3	23.1	18.6	16.3	15.3	15.8
Volatile organic compounds (VOC)	33.7	30.2	30.1	26.9	23.1	21.6	16.9	15.8	15.4
Lead ^f	0.221	0.16	0.074	0.022	0.005	0.004	0.003	0.003	0.003
Totals ^g	301.5	275.8	267.2	249.2	218.1	188.0	160.2	150.2	147.7

NOTES:

- ^a In 1985 and 1996 EPA refined its methods for estimating emissions. Between 1970 and 1975, EPA revised its methods for estimating particulate matter emissions.
- ^b The estimates for 2003 are preliminary.
- ^c NO_x estimates prior to 1990 include emissions from fires. Fires would represent a small percentage of the NO_x emissions.
- ^d PM estimates do not include condensable PM, or the majority of PM_{2.5} that is formed in the atmosphere from "precursor" gases such as SO₂ and NO_x.
- ^e EPA has not estimated PM_{2.5} emissions prior to 1990.
- ^f The 1999 estimate for lead is used to represent 2000 and 2003 because lead estimates do not exist for these years.
- ^g PM_{2.5} emissions are not added when calculating the total because they are included in the PM₁₀ estimate.

SOURCE: EPA 2003 Emissions Report (www.epa.gov/air/urbanair/6poll.html).

3. *Nitrogen gases.* Nitrous oxide, nitric oxide, nitrogen dioxide, other nitrous oxides

4. *Halogens, halides.* Hydrogen fluoride, hydrogen chloride, chlorine, fluorine, silicon tetrafluoride

5. *Photochemical products.* Ozone, oxidants

6. *Cyanides.* Hydrogen cyanide

7. *Ammonium compounds.* Ammonia

8. *Chlorofluorocarbons.* 1,1,1-trichloro-2,2,2-trifluoroethane; trichlorofluoromethane, dichlorodifluoromethane; chlorodifluoromethane; 1,2-dichloro-1,1,2,2-tetrafluoroethane; chloropentafluoroethane

Organic pollutants consist of:

1. Hydrocarbons

- a. Paraffins. Methane, ethane, octane
- b. Acetylene
- c. Olefins. Ethylene, butadiene
- d. Aromatics. Benzene, toluene, benzopyrene, xylene, styrene

2. Aliphatic oxygenated compounds

- a. Aldehydes. Formaldehyde
- b. Ketones. Acetone, methylethylketone
- c. Organic acids
- d. Alcohols. Methanol, ethanol, isopropanol
- e. Organic halides. Cyanogen chloride bromobenzyl cyanide
- f. Organic sulfides. Dimethyl sulfide
- g. Organic hydroperoxides. Peroxyacetyl nitrite or nitrate (PAN)

The most common gaseous pollutants and their major sources and significance are presented in Table 22-16.

Particulate Pollutants Particulates may be defined as solid or liquid matter whose effective diameter is larger than a molecule but smaller than approximately 100 μm. Particulates dispersed in a gaseous medium are collectively termed an *aerosol*. The terms *smoke*, *fog*, *haze*, and *dust* are commonly used to describe particular types of aerosols, depending on the size, shape, and characteristic behavior of the dispersed particles. Aerosols are rather difficult to classify on a scientific basis in terms of their fundamental properties such as settling rate under the influence of external forces, optical activity, ability to absorb an electrical charge, particle size and structure, surface-to-volume ratio, reaction activity, physiological action, and so on. In general, particle size and settling rate have been the most characteristic properties for many purposes. On the other hand, particles on the order of 1 μm or less settle so slowly that, for all practical purposes, they are regarded as permanent suspensions. Despite possible advantages of scientific classification schemes, the use of popular descriptive terms such as smoke, dust, and mist, which are essentially based on the mode of formation, appears to be a satisfactory and convenient method of classification. In addition, this approach is so well established and understood that it undoubtedly would be difficult to change.

Dust is typically formed by the pulverization or mechanical disintegration of solid matter into particles of smaller size by processes such as grinding, crushing, and drilling. Particle sizes of dust range from a lower limit of about 1 mm up to about 100 or 200 μm and larger. Dust particles are usually irregular in shape, and particle size refers to some average dimension for any given particle. Common examples include

TABLE 22-15 1998 National Point and Area Emissions by Source Category and Pollutant, 1000 Short Tons

Source category	CO			NO _x			VOC			SO ₂		
	Point	Area	Total	Point	Area	Total	Point	Area	Total	Point	Area	Total
Fuel comb. elec. util.	413	4	417	6,095	8	6,103	54	0	54	13,217	0	13,217
Fuel comb. industrial	908	206	1,114	2,142	827	2,969	144	17	161	2,075	820	2,895
Fuel comb. other	83	3,760	3,843	142	975	1,117	12	666	678	191	418	609
Chemical & allied product mfg.	1,129	0	1,129	152	0	152	312	84	396	299	0	299
Metals processing	1,494	1	1,495	88	0	88	75	0	76	444	0	444
Petroleum & related industries	365	3	368	122	16	138	223	273	496	344	0	345
Other industrial processes	629	3	632	402	6	408	388	62	450	366	3	370
Solvent utilization	2	0	2	2	0	2	639	4,640	5,278	1	0	1
Storage & transport	80	0	80	7	0	7	298	1,025	1,324	3	0	3
Waste disposal & recycling	31	1,123	1,154	38	59	97	27	406	433	19	24	42
Highway vehicles	0	50,386	50,386	0	7,765	7,765	0	5,325	5,325	0	326	326
Off-highway	0	19,914	19,914	0	5,280	5,280	0	2,461	2,461	0	1,084	1,084
Natural sources	0	0	0	0	0	0	0	14	14	0	0	0
Miscellaneous	0	8,920	8,920	1	327	328	2	770	772	0	12	12
Total	5,134	84,319	89,454	9,190	15,264	24,454	2,174	15,743	17,917	16,960	2,688	19,647

SOURCE: National Air Pollution Trends: 1900-1998, EPA 454/R-00-002, March 2000 (www.epa.gov/ttn/chieftrends/index.html).

22-30 WASTE MANAGEMENT

TABLE 22-16 Typical Gaseous Pollutants and Their Principal Sources and Significance

Air pollutants	From manufacturing sources such as these	In typical industries	Cause these damaging effects
Alcohols	Used as a solvent in coatings	Surface coatings, printing	Sensory and respiratory irritation
Aldehydes	Results from thermal decomposition of fats, oil, or glycerol; used in some glues and binders	Food processing, light process, wood furniture, chip board	An irritating odor, suffocating, pungent, choking; not immediately dangerous to life; can become intolerable in a very short time
Ammonia	Used in refrigeration, chemical processes such as dye making, explosives, lacquer, fertilizer	Textiles, chemicals	Corrosive to copper, brass, aluminum, and zinc; high concentration producing chemical burns on wet skin
Aromatics	Used as a solvent in coatings	Surface coatings, printing	Irritation of mucous membranes, narcotic effects; some are carcinogens
Arsine	Any soldering, pickling, etching, or plating process involving metals or acids containing arsenic	Chemical processing, smelting	Breakdown of red cells in blood
Carbon dioxide	Fuel combustion; calcining	Industrial boilers, cement and lime production	Greenhouse gas
Carbon monoxide	Fuming of metallic oxides, gas-operated fork trucks	Primary metals; steel and aluminum	Reduction in oxygen-carrying capacity of blood
Chlorine	Manufactured by electrolysis, bleaching cotton and flour; by-product of organic chemicals	Textiles, chemicals	Attacks entire respiratory tract and mucous membrane of eye
Chlorofluorocarbons	Used in refrigeration and production of porous foams; degreasing agent	Refrigeration, plastic foam production, metal fabricating	Attacks stratospheric ozone layer; greenhouse gas
Hydrochloric acid	Combustion of coal or wastes containing chlorinated plastics	Coal-fired boilers, incinerators	Irritant to eyes and respiratory system
Hydrogen cyanide	From metal plating, blast furnaces, dyestuff works	Metal fabricating, primary metals, textiles	Capable of affecting nerve cells
Hydrogen fluoride	Catalyst in some petroleum refining, etching glass, silicate extraction; by-product in electrolytic production of aluminum	Petroleum, primary metals, aluminum	Strong irritant and corrosive action on all body tissue; damage to citrus plants, effect on teeth and bones of cattle from eating plants
Hydrogen sulfide	Refinery gases, crude oil, sulfur recovery, various chemical industries using sulfur compounds	Petroleum and chemicals; Kraft pulping process	Foul odor of rotten eggs; irritating to eyes and respiratory tract; darkening exterior paint
Ketones	Used as a solvent in coatings	Surface coatings, printing	Sensory and respiratory irritation
Lead	Incineration, smelting and casting, transportation	Copper and lead smelting, MSWs	Neurological impairments; kidney, liver, and heart damage.
Nitrogen oxides	High-temperature combustion: metal cleaning, fertilizer, explosives, nitric acid; carbon-arc combustion; manufacture of H ₂ SO ₄	Metal fabrication, heavy chemicals	Irritating gas affecting lungs; vegetation damage
Odors	Slaughtering and rendering animals, tanning animal hides, canning, smoking meats, roasting coffee, brewing beer, processing toiletries	Food processing, allied industries	Objectionable odors
Ozone	Reaction product of VOC and nitrogen oxides	Not produced directly	Irritant to eyes and respiratory system
Phosgenes	Thermal decomposition of chlorinated hydrocarbons, degreasing, manufacture of dyestuffs, pharmaceuticals, organic chemicals	Metal fabrication, heavy chemicals	Damage capable of leading to pulmonary edema, often delayed
Sulfur dioxide	Fuel combustion (coal, oil), smelting and casting, manufacture of paper by sulfite process	Primary metals (ferrous and nonferrous); pulp and paper	Sensory and respiratory irritation, vegetation damage, corrosion, possible adverse effect on health

fly ash, rock dusts, and ordinary flour. *Smoke* implies a certain degree of optical density and is typically derived from the burning of organic materials such as wood, coal, and tobacco. Smoke particles are very fine, ranging in size from less than 0.01 μm up to 1 μm . They are usually spherical in shape if of liquid or tarry composition and irregular in shape if of solid composition. Owing to their very fine particle size, smokes can remain in suspension for long periods of time and exhibit lively brownian motion.

Fumes are typically formed by processes such as sublimation, condensation, or combustion, generally at relatively high temperatures. They range in particle size from less than 0.1 μm to 1 μm . Similar to smokes, they settle very slowly and exhibit strong brownian motion.

Mists or fogs are typically formed either by the condensation of water or other vapors on suitable nuclei, giving a suspension of small liquid droplets, or by the atomization of liquids. Particle sizes of natural fogs and mists lie between 2 and 200 μm . Droplets larger than 200 μm are more properly classified as drizzle or rain. Many of the important properties of aerosols that depend on particle size are presented in Sec. 17, Fig. 17-34.

When a liquid or solid substance is emitted to the air as particulate matter, its properties and effects may be changed. As a substance is broken up into smaller and smaller particles, more of its surface area is exposed to the air. Under these circumstances, the substance, whatever its chemical composition, tends to combine physically or chemically

with other particles or gases in the atmosphere. The resulting combinations are frequently unpredictable. Very small aerosol particles (from 0.001 to 0.1 μm) can act as condensation nuclei to facilitate the condensation of water vapor, thus promoting the formation of fog and ground mist. Particles less than 2 or 3 μm in size (about half by weight of the particles suspended in urban air) can penetrate the mucous membrane and attract and convey harmful chemicals such as sulfur dioxide. In order to address the special concerns related to the effects of very fine, inhalable particulates, EPA now has ambient standards in place for both PM_{10} and $\text{PM}_{2.5}$.

By virtue of the increased surface area of the small aerosol particles and as a result of the adsorption of gas molecules or other such properties that are able to facilitate chemical reactions, aerosols tend to exhibit greatly enhanced surface activity. Many substances that oxidize slowly in their massive state will oxidize extremely fast or possibly even explode when dispersed as fine particles in the air. Dust explosions, for example, are often caused by the unstable burning or oxidation of combustible particles, brought about by their relatively large specific surfaces. Adsorption and catalytic phenomena can also be extremely important in analyzing and understanding the problems of particulate pollution. The conversion of sulfur dioxide to corrosive sulfuric acid assisted by the catalytic action of iron oxide particles, for example, demonstrates the catalytic nature of certain types of particles in the atmosphere. Finally, aerosols can absorb radiant energy and rapidly conduct heat to the surrounding gases of the atmosphere. These are gases that ordinarily would be incapable of absorbing radiant energy by themselves. As a result, the air in contact with the aerosols can become much warmer.

Estimating Emissions from Sources Knowledge of the types and rates of emissions is fundamental to evaluation of any air pollution problem. A comprehensive material balance on the process can often assist in this assessment. Estimates of the rates at which pollutants are discharged from various processes can also be obtained by utilizing published emission factors. See *Compilation of Air Pollution Emission Factors (AP-42)*, 4th ed., U.S. EPA, Research Triangle Park, North Carolina, September, 1985, with all succeeding supplements and the EPA Technology Transfer Network's CHIEF. The emission factor is a statistical average of the rate at which pollutants are emitted from the burning or processing of a given quantity of material or on the basis of some other meaningful parameter. Emission factors are affected by the techniques employed in the processing, handling, or burning operations, by the quality of the material used, and by the efficiency of the air-pollution control. Since the combination of these factors tends to be unique to a source, emission factors appropriate for one source may not be satisfactory for another source. Hence, care and good judgment must be exercised in identifying appropriate emission factors. If appropriate emission factors cannot be found or if air-pollution control equipment is to be designed, specific source sampling should be conducted. The major industrial sources of pollutants, the air contaminants emitted, and typical control techniques are summarized in Table 22-17.

Effects of Air Pollutants

Materials The damage that air pollutants can do to some materials is well known: ozone in photochemical smog cracks rubber, weakens fabrics, and fades dyes; hydrogen sulfide tarnishes silver; smoke dirties laundry; acid aerosols ruin nylon hose. Among the most important effects are discoloration, corrosion, the soiling of goods, and impairment of visibility.

1. **Discoloration.** Many air pollutants accumulate on and discolor buildings. Not only does sooty material blacken buildings, but it can accumulate and become encrusted. This can hide lines and decorations and thereby disfigure structures and reduce their aesthetic appeal. Another common effect is the discoloration of paint by certain acid gases. A good example is the blackening of white paint with a lead base by hydrogen sulfide.

2. **Corrosion.** A more serious effect and one of great economic importance is the corrosive action of acid gases on building materials. Such acids can cause stone surfaces to blister and peel; mortar can be reduced to powder. Metals are also damaged by the corrosive action of some pollutants. Another common effect is the deterioration of tires

and other rubber goods. Cracking and apparent "drying" occur when these goods are exposed to ozone and other oxidants.

3. **Soiling of goods.** Clothes, real estate, automobiles, and household goods can easily be soiled by air contaminants, and the more frequent cleaning thus required can become expensive. Also, more frequent cleaning often leads to a shorter life span for materials and to the need to purchase goods more often.

4. **Impairment of visibility.** The impairment of atmospheric visibility (i.e., decreased visual range through a polluted atmosphere) is caused by the scattering of sunlight by particles suspended in the air. It is not a result of sunlight being obscured by materials in the air. Since light scattering, and not obscuration, is the main cause of the reduction in visibility, reduced visibility due to the presence of air pollutants occurs primarily on bright days. On cloudy days or at night there may be no noticeable effect, although the same particulate concentration may exist at these times as on sunny days. Reduction in visibility creates several problems. The most significant are the adverse effects on aircraft, highway, and harbor operations. Reduced visibility can reduce quality of life and also cause adverse aesthetic impressions that can seriously affect tourism and restrict the growth and development of any area. Extreme conditions such as dust storms or sandstorms can actually cause physical damage by themselves.

Vegetation Vegetation is more sensitive than animals to many air contaminants, and methods have been developed that use plant response to measure and identify contaminants. The effects of air pollution on vegetation can appear as death, stunted growth, reduced crop yield, and degradation of color. It is interesting to note that in some cases of color damage such as the silvering of leafy vegetables by oxidants, the plant may still be used as food without any danger to the consumer; however, the consumer usually will not buy such vegetables on aesthetic grounds, so the grower still sustains a loss. Among the pollutants that can harm plants are sulfur dioxide, hydrogen fluoride, and ethylene. Plant damage caused by constituents of photochemical smog has been studied extensively. Damage has been attributed to ozone and peroxyacetyl nitrites, higher aldehydes, and products of the reaction of ozone with olefins. However, none of the cases precisely duplicates all features of the damage observed in the field, and the question remains open to some debate and further study.

Animals Considerable work continues to be performed on the effects of pollutants on animals, including, for a few species, experiments involving mixed pollutants and mixed gas-aerosol systems. In general, such work has shown that mixed pollutants may act in several different ways. They may produce an effect that is additive, amounting to the sum of the effects of each contaminant acting alone; they may produce an effect that is greater than the simply additive (synergistic) or less than the simply additive (antagonistic); or they may produce an effect that differs in some other way from the simply additive.

The mechanism by which an animal can become poisoned in many instances is completely different from that by which humans are affected. As in humans, inhalation is an important route of entry in acute air-pollution exposures such as the Meuse Valley and Donora incidents (see the paragraph on **humans** below). However, probably the most common exposure for herbivorous animals grazing within a zone of pollution will be the ingestion of feed contaminated by air pollutants. In this case, inhalation is of secondary importance.

Air pollutants that present a hazard to livestock, therefore, are those that are taken up by vegetation or deposited on the plants. Only a few pollutants have been observed to cause harm to animals. These include arsenic, fluorides, lead, mercury, and molybdenum.

Humans There seems to be little question that, during many of the more serious episodes, air pollution can have a significant effect on health, especially upon the young, elderly, or people already in ill health. Hundreds of excess deaths have been attributed to incidents in London in 1952, 1956, 1957, and 1962; in Donora, Pennsylvania, in 1948; in New York City in 1953, 1963, and 1966; and Bhopal, India in 1989. Many of the people affected were in failing health, and they were generally suffering from lung conditions. In addition, hundreds of thousands of persons have suffered from serious discomfort and inconvenience, including eye irritation and chest pains, during these and other such incidents. Such acute problems are actually the lesser of the health problems. There is considerable evidence of a chronic threat to

22-32 WASTE MANAGEMENT
TABLE 22-17 Control Techniques Applicable to Unit Processes at Important Emission Sources

Industry	Process of operation	Air contaminants emitted	Control techniques
Aluminum reduction plants	Materials handling: Buckets and belt Conveyor or pneumatic conveyor	Particulates (dust)	Exhaust systems and baghouse
	Anode and cathode electrode preparation: Cathode (baking) Anode (grinding and blending)	Hydrocarbon emissions from binder Particulates (dust) Particulates (dust), CO, SO ₂ , hydrocarbons, and fluorides	Exhaust systems and mechanical collectors High-efficiency cyclone, electrostatic precipitators, scrubbers, catalytic combustion or incinerators, flares, baghouse
	Baking Pot charging	Particulates (dust), CO, HF, SO ₂ , CF ₄ , and hydrocarbons	High-efficiency cyclone, baghouse, spray towers, floating-bed scrubber, electrostatic precipitators, chemisorption, wet electrostatic precipitators
	Metal casting	Cl ₂ , HCl, CO, and particulates (dust)	Exhaust systems and scrubbers
Asphalt plants	Materials handling, storage and classifiers: elevators, chutes, vibrating screens Drying: rotary oil- or gas-fired	Particulates (dust) Particulates, SO ₂ , NO _x , VOC, CO, and smoke	Wetting; exhaust systems with a scrubber or baghouse Proper combustion controls, fuel-oil preheating where required; local exhaust system, cyclone and a scrubber or baghouse
	Truck traffic	Dust	Paving, wetting down truck routes
Cement plants	Quarrying: primary crusher, secondary crusher, conveying, storage	Particulates (dust)	Wetting; exhaust systems with fabric filters
	Dry processes: materials handling, air separator (hot-air furnace)	Particulates (dust)	Local exhaust system with mechanical collectors and baghouse
	Grinding Pneumatic, conveying and storage	Particulates (dust) Particulates (dust)	Local exhaust system with cyclones and baghouse
	Wet process: materials handling, grinding, storage Kiln operations: rotary kiln	Wet materials, no dust Particulates (dust), CO, SO ₂ , NO _x , hydrocarbons, aldehydes, ketones Particulates (dust)	Electrostatic precipitators, acoustic horns and baghouses, scrubber
	Clinker cooling: materials handling	Particulates (dust)	Local exhaust system and electrostatic precipitators or fabric filters
	Grinding and packing, air separator, grinding, pneumatic conveying, materials handling, packaging	Particulates (dust)	Local exhaust system and fabric filters
Coal-preparation plants	Materials handling: conveyors, elevators, chutes	Particulates (dust)	Local exhaust system and cyclones
	Sizing: crushing, screening, classifying Dedusting	Particulates (dust) Particulates (dust)	Local exhaust system and cyclones Local exhaust system, cyclone precleaners, and baghouse
	Storing coal in piles Refuse piles	Blowing particulates (dust) H ₂ S, particulates, and smoke from burning storage piles	Wetting, plastic-spray covering Digging out fire, pumping water onto fire area, blanketing with incombustible material
	Coal drying: rotary, screen, suspension, fluid-bed, cascade	Dust, smoke, particulates, sulfur oxides, H ₂ S	Exhaust systems with cyclones and fabric filters
Coke plants	By-product-ovens charging	Smoke, particulates (dust)	Pipe-line charging, careful charging techniques, portable hooding and scrubber or baghouses
	Pushing	Smoke, particulates (dust), SO ₂	Minimizing green-coke pushing, scrubbers and baghouses
	Quenching	Smoke, particulates (dust and mists), phenols, and ammonia	Baffles and spray tower
	By-product processing	CO, H ₂ S, methane, ammonia, H ₂ , phenols, hydrogen cyanide, N ₂ , benzene, xylene, etc.	Electrostatic precipitator, scrubber, flaring
	Material storage (coal and coke)	Particulates (dust)	Wetting, plastic spray, fire-prevention techniques
Electric utilities (industrial and commercial facilities)	Coal-fired boilers	Particulates SO _x , NO _x	Baghouses Precipitators, SCR, and SNCR Acid gas scrubbers
Fertilizer industry (chemical)	Phosphate fertilizers: crushing, grinding, and calcining Hydrolysis of P ₂ O ₅ Acidulation and curing Granulation Ammoniation	Particulates (dust) PH ₃ , P ₂ O ₃ PO ₄ mist HF, SiF ₄ Particulates (dust)(product recovery) NH ₃ , NH ₄ Cl, SiF ₄ , HF	Exhaust system, scrubber, cyclone, baghouse Scrubbers, flare Scrubbers Exhaust system, scrubber, or baghouse Cyclone, electrostatic precipitator, baghouse, high-energy scrubber

TABLE 22-17 Control Techniques Applicable to Unit Processes at Important Emission Sources (Continued)

Industry	Process of operation	Air contaminants emitted	Control techniques
Fertilizer industry (chemical)	Nitric acid acidulation Superphosphate storage and shipping Ammonium nitrate reactor Prilling tower	NO _x , gaseous fluoride compounds Particulates (dust) NH ₃ , NO _x NH ₄ , NO ₃	Scrubber, addition of urea Exhaust system, cyclone or baghouse Scrubber Proper operation control, scrubbers
Foundries: Iron	Melting (cupola): Charging Melting Pouring Bottom drop	Smoke and particulates Smoke and particulates, fume Oil, mist, CO Smoke and particulates	Closed top with exhaust system, CO afterburner, gas-cooling device and scrubbers, baghouse or electrostatic precipitator, wetting to extinguish fire
Brass and bronze	Melting: Charging Melting Pouring	Smoke particulates, oil mist Zinc oxide fume, particulates, smoke Zinc oxide fume, lead oxide fume	Low-zinc-content red brass: use of good combustion controls and slag cover; high-zinc-content brass: use of good combustion controls, local exhaust system, and baghouse or scrubber
Aluminum	Melting: charging, melting, pouring	Smoke and particulates	Charging clean material (no paint or grease); proper operation required; no air-pollution-control equipment if no fluxes are used and degassing is not required; dirty charge requiring exhaust system with scrubbers and baghouses
Zinc	Melting: Charging Melting Pouring Sand-handling shakeout Magnetic pulley, conveyors, and elevators, rotary cooler, screening, crusher-mixer Coke-making ovens	Smoke and particulates Zinc oxide fume Oil mist and hydrocarbons from diecasting machines Particulates (dust), smoke, organic vapors Particulates (dust) Organic acids, aldehydes, smoke, hydrocarbons	Exhaust system with cyclone and baghouse, charging clean material (no paint or grease) Careful skimming of dross Use of low-smoking die-casting lubricants Exhaust system, cyclone, and baghouse Use of binders that will allow ovens to operate at less than 204°C (400°F) or exhaust systems and afterburners
Galvanizing operations	Hot-dip-galvanizing-tank kettle: dipping material into the molten zinc; dusting flux onto the surface of the molten zinc	Fumes, particulates (liquid), vapors: NH ₄ Cl, ZnO, ZnCl ₂ , Zn, NH ₃ , oil, and carbon	Close-fitting hoods with high in-draft velocities (in some cases, the hood may not be able to be close to the kettle, so the in-draft velocity must be very high), baghouses, electrostatic precipitators
Kraft pulp mills	Digesters: batch and continuous Multiple-effect evaporators Recovery furnace Weak and strong black-liquor oxidation Smelt tanks Lime kiln	Mercaptans, methanol (odors) H ₂ S, other odors H ₂ S, mercaptans, organic sulfides, and disulfides H ₂ S Particulates (mist or dust) Particulates (dust), H ₂ S	Condensers and use of lime kiln, boiler, or furnaces as afterburners Caustic scrubbing and thermal oxidation of noncondensables Proper combustion controls for fluctuating load and unrestricted primary and secondary air flow to furnace and dry-bottom electrostatic precipitator; noncontact evaporator Packed tower and cyclone Demisters, venturi, packed tower, or impingement-type scrubbers Venturi scrubbers
Municipal and industrial incinerators	Single-chamber incinerators Multiple-chamber incinerators (retort, inline): Flue-fed Wood waste Municipal incinerators (50 tons and up per day):	Particulates, smoke, volatiles, CO, SO _x , ammonia, organic acids, aldehydes, NO _x , dioxins, hydrocarbons, odors, HCl, furans Particulates, smoke, and combustion contaminants Particulates, smoke, and combustion contaminants Particulates, smoke, and combustion contaminants Particulates, smoke, volatiles, CO, ammonia, organic acids, aldehydes, NO _x , furans, hydrocarbons, SO _x ,	Afterburner, combustion controls Operating at rated capacity, using auxiliary fuel as specified, and good maintenance, including timely cleanout of ash Use of charging gates and automatic controls for draft; afterburner Continuous-feed systems; operation at design load and excess air; cyclones Preparation of materials, including weighing, grinding, shredding; control of tipping area, furnace design with

22-34 WASTE MANAGEMENT
TABLE 22-17 Control Techniques Applicable to Unit Processes at Important Emission Sources (Continued)

Industry	Process of operation	Air contaminants emitted	Control techniques
Municipal and industrial incinerators	Municipal incinerators (50 tons and up per day):	hydrogen chloride, dioxins and odors	proper automatic controls; proper start-up techniques; maintenance of design operating temperatures; use of electrostatic precipitators, scrubbers, and baghouses; proper ash cleanout Proper charging, acid gas scrubber, baghouse Modified fuel feed, auxiliary fuel and dryer systems, cyclones, scrubbers
	Pathological incinerators	Odors, hydrocarbons, HCl, dioxins, furans	
	Industrial waste	Particulates, smoke, and combustion contaminants	
Nonferrous smelters, primary: Copper	Roasting	SO ₂ , particulates, fume	Exhaust system, settling chambers, cyclones or scrubbers and electrostatic precipitators for dust and fumes and sulfuric acid plant for SO ₂ Exhaust system, settling chambers, cyclones or scrubbers and electrostatic precipitators for dust and fumes and sulfuric acid plant for SO ₂ Exhaust system, settling chambers, cyclones or scrubbers and electrostatic precipitators for dust and fumes and sulfuric acid plant for SO ₂
	Reverberatory furnace	Smoke, particulates, metal oxide fumes, SO ₂	
	Converters: charging, slag skim, pouring, air or oxygen blow	Smoke, fume, SO ₂	
Lead	Sintering	SO ₂ , particulates, smoke	Exhaust system, cyclones and baghouse or precipitators for dust and fumes, sulfuric acid plant for SO ₂ Exhaust system, settling chambers, afterburner and cooling device, cyclone, and baghouse Exhaust system, settling chambers, cyclone and cooling device, baghouse Local exhaust system, cooling device, baghouse or precipitator
	Blast furnace	SO ₂ , CO, particulates, lead oxide, zinc oxide	
	Dross reverberatory furnace	SO ₂ , particulates, fume	
	Refining kettles	SO ₂ , particulates	
Cadmium	Roasters, slag, fuming furnaces, deleading kilns	Particulates	Local exhaust system, baghouse or precipitator
Zinc	Roasting	Particulates (dust) and SO ₂	Exhaust system, humidifier, cyclone, scrubber, electrostatic precipitator, and acid plant Exhaust system, humidifier, electrostatic precipitator, and acid plant Exhaust system, baghouse, scrubber or acid plant
	Sintering	Particulates (dust) and SO ₂	
	Calcining	Zinc oxide fume, particulates, SO ₂ , CO	
	Retorts: electric arc		
Nonferrous smelters, secondary	Blast furnaces and cupolas-recovery of metal from scrap and slag	Dust, fumes, particulates, oil vapor, smoke, CO	Exhaust systems, cooling devices, CO burners and baghouses or precipitators Exhaust systems, and baghouses or precipitators, or venturi scrubbers Precleaning metal and exhaust systems with afterburner and baghouse Scrubbers and afterburners
	Reverberatory furnaces	Dust, fumes, particulates, smoke, gaseous fluxing materials	
	Sweat furnaces	Smoke, particulates, fumes	
	Wire reclamation and autobody burning	Smoke, particulates	
Paint and varnish manufacturing	Resin manufacturing: closed reaction vessel	Acrolein, other aldehydes and fatty acids (odors), phthalic anhydride (sublimed)	Exhaust systems with scrubbers and fume burners Exhaust system with scrubbers and fume burners; close-fitting hoods required for open kettles Exhaust system with fume burners
	Varnish: cooking-open or closed vessels	Ketones, fatty acids, formic acids, acetic acid, glycerine, acrolein, other aldehydes, phenols and terpenes; from tall oils, hydrogen sulfide, alkyl sulfide, butyl mercaptan, and thiofen (odors)	
	Solvent thinning	Olefins, branched-chain aromatics and ketones (odors), solvents	
Rendering plants	Feedstock storage and housekeeping	Odors	Quick processing, washdown of all concrete surfaces, paving of dirt roads, proper sewer maintenance, enclosure, packed towers Exhaust system, condenser, scrubber, or incinerator Exhaust system and scrubber
	Cookers and percolators	SO ₂ , mercaptans, ammonia, odors	
	Grinding	Particulates (dust)	
Roofing plants (asphalt saturators)	Felt or paper saturators: spray section, asphalt tank, wet looper	Asphalt vapors and particulates (liquid)	Exhaust system with high inlet velocity at hoods (3658 m/s [>200 ft/min]) with either scrubbers, baghouses, or two-stage low-voltage electrostatic precipitators

TABLE 22-17 Control Techniques Applicable to Unit Processes at Important Emission Sources (Concluded)

Industry	Process of operation	Air contaminants emitted	Control techniques
Roofing plants (asphalt saturators)	Crushed rock or other minerals handling	Particulates (dust)	Local exhaust system, cyclone or multiple cyclones
Steel mills	Blast furnaces: charging, pouring	CO, fumes, smoke, particulates (dust)	Good maintenance, seal leaks; use of higher ratio of pelletized or sintered ore; CO burned in waste-heat boilers, stoves, or coke ovens; cyclone, scrubber, and baghouse
	Electric steel furnaces: charging, pouring, oxygen blow	Fumes, smoke, particulates (dust), CO	Segregating dirty scrap; proper hooding, baghouses or electrostatic precipitator
	Open-hearth furnaces: oxygen blow, pouring	Fumes, smoke, SO _x , particulates (dust), CO, NO _x	Proper hooding, settling chambers, waste-heat boiler, baghouse, electrostatic precipitator, and wet scrubber
	Basic oxygen furnaces: oxygen blowing	Fumes, smoke, CO, particulates (dust)	Proper hooding (capturing of emissions and dilute CO), scrubbers, or electrostatic precipitator
	Raw material storage Pelletizing Sintering	Particulates (dust) Particulates (dust) Smoke, particulates (dust), SO ₂ , NO _x	Wetting or application of plastic spray Proper hooding, cyclone, baghouse Proper hooding, cyclones, wet scrubbers, baghouse, or precipitator

human health from air pollution. This evidence ranges from the rapid rise of emphysema as a major health problem, through identification of carcinogenic compounds in smog, to statistical evidence that people exposed to polluted atmospheres over extended periods of time suffer from a number of ailments and a reduction in their life span. There may even be a significant indirect exposure to air pollution. As noted above, air pollutants may be deposited onto vegetation or into bodies of water, where they enter the food chain. The impact of such indirect exposures is still under review.

A large body of evidence is available to indicate that atmospheric pollution in varying degrees does affect health adversely. [Amdur, Melvin, and Drinker, "Effect of Inhalation of Sulfur Dioxide by Man," *Lancet*, **2**, 758 (1953); Barton, Corn, Gee, Vassallo, and Thomas, "Response of Healthy Men to Inhaled Low Concentrations of Gas-Aerosol Mixtures," *Arch. Environ. Health*, **18**, 681 (1969); Bates, Bell, Burnham, Hazucha, and Mantha, "Problems in Studies of Human Exposure to Air Pollutants," *Can. Med. Assoc. J.*, **103**, 833 (1970); Ciocco and Thompson, "A Follow-Up of Donora Ten Years After: Methodology and Findings," *Am. J. Public Health*, **51**, 155 (1961); Daly, "Air Pollution and Causes of Death," *Br. J. Soc. Med.*, **13**, 14 (1959); Jaffe, "The Biological Effect of Photochemical Air Pollutants on Man and Animals," *Am. J. Public Health*, New York, **57**, 1269 (1967); New York Academy of Medicine, Committee on Public Health, "Air Pollution and Health," *Bull. N.Y. Acad. Med.*, **42**, 588 (1966); Pemberton and Goldberg, "Air Pollution and Bronchitis," *Br. Med. J.*, London, **2**, 567 (1954); Snell and Luchsinger, "Effect of Sulfur Dioxide on Expiratory Flowrates and Total Respiratory Resistance in Normal Human Subjects," *Arch. Environ. Health*, Chicago, **18**, 693 (1969); Speizer and Frank, "A Comparison of Changes in Pulmonary Flow Resistance in Healthy Volunteers Acutely Exposed to SO₂ by Mouth and by Nose," *J. Ind. Med.*, **23** 75 (1966); Stocks, "Cancer and Bronchitis Mortality in Relation to Atmospheric Deposit and Smoke," *Br. Med. J. London*, **1**, 74 (1959); Toyama, "Air Pollution and Its Health Effects in Japan," *Arch. Environ. Health*, Chicago, **8**, 153 (1963); U.K. Ministry of Health, "Mortality and Morbidity During London Fog of December 1952," Report on Public Health and Medical Subjects No. 95, London, 1954; U.S. Public Health Service, "Air Pollution in Donora, Pa.: Preliminary Report," Public Health Bull. 306.] It contributes to excesses of death, increased morbidity, and earlier onset of chronic respiratory diseases. There is evidence of a relationship between the intensity of the pollution and the severity of attributable health effects and a consistency of the relationship between these environmental stresses and diseases of the target organs. Air pollutants can both initiate and aggravate a variety of respiratory diseases including asthma. In fact, the clinical presentation of asthma may be considered an air pollution host-defense disorder brought on by specific airborne irritants: pollens, infectious agents, and gaseous and particulate chemicals. The bronchopulmonary response to these foreign irritants is bronchospasm and hypersecretion; the airways are intermittently and reversibly obstructed.

Air-pollutant effects on neural and sensory functions in humans vary widely. Odorous pollutants cause only minor annoyance; yet, if persistent, they can lead to irritation, emotional upset, anorexia, and mental depression. Carbon monoxide can cause death secondary to the depression of the respiratory centers of the central nervous system. Short of death, repeated and prolonged exposure to carbon monoxide can alter sensory protection, temporal perception, and higher mental functions. Lipid-soluble aerosols can enter the body and be absorbed in the lipids of the central nervous system. Once there, their effects may persist long after the initial contact has been removed. Examples of agents of long-term chronic effects are organic phosphate pesticides and aerosols carrying the metals lead, mercury, and cadmium.

The acute toxicological effects of most air contaminants are reasonably well understood, but the effects of exposure to heterogenous mixtures of gases and particulates at very low concentrations are only beginning to be comprehended. Two general approaches can be used to study the effects of air contaminants on humans: epidemiology, which attempts to associate the effect in large populations with the cause, and laboratory research, which begins with the cause and attempts to determine the effects. Ideally, the two methods should complement each other.

EPA recognizes that scientific studies show a link between inhalable PM (alone and in combination with other pollutants in the air) and a series of health effects. While both coarse and fine particles accumulated in the respiratory system and are associated with numerous adverse health effects, fine particles have been more clearly tied to the most serious health effects. Fine particles have been associated with decreased lung functions, disease, and even premature death. The elderly and children are notable in the sensitive groups that appear to be at greatest risk (JAWMA Special Issues, July and August 2000; PM2000, *Particulate Matter and Health—The Scientific Basis for Regulatory Decision Making*).

Epidemiology, the more costly of the two, requires great care in planning and often suffers from incomplete data and lack of controls. One great advantage, however, is that moral barriers do not limit its application to humans as they do with some kinds of laboratory research. The method is therefore highly useful and has produced considerable information. Laboratory research is less costly than epidemiology, and its results can be checked against controls and verified by experimental repetition.

A SOURCE-CONTROL-PROBLEM STRATEGY

Strategy Control technology is self-defeating if it creates undesirable side effects in meeting objectives. Air pollution control must be considered in terms of regulatory requirements, total technological systems (equipment and processes), and ecological consequences,

such as the problems of treatment and disposal of collected pollutants. It should be noted that the 1990 Clean Air Act Amendments (CAAA) have impacted on the control approach in a significant manner. In particular, the CAAA have placed an increased emphasis on control technology by requiring Best Available Control Technology (BACT) on new major sources and modifications, and by requiring Maximum Achievable Control Technology (MACT) on new and *existing* major sources of Hazardous Air Pollutants (HAPs).

The control strategy for environmental-impact assessment often focuses on five alternatives whose purpose would be the reduction and/or elimination of pollutant emissions:

1. Elimination of the operation entirely or in part
2. Modification of the operation
3. Relocation of the operation
4. Application of appropriate control technology
5. Combinations thereof

In light of the relatively high costs often associated with pollution-control systems, engineers are directing considerable effort toward process modification to eliminate as much of the pollution problem as possible at the source. This includes evaluating alternative manufacturing and production techniques, substituting raw materials, and improving process-control methods. Unfortunately, if there is no alternative, the application of the correct pollution-control equipment is essential. The equipment must be designed to comply with regulatory emission limitations on a continual basis, interruptions being subject to severe penalty depending upon the circumstances. The requirement for design performance on a continual basis places very heavy emphasis on operation and maintenance practices. The escalating costs of energy, labor, and materials can make operation and maintenance considerations even more important than the original capital cost.

Factors in Control-Equipment Selection In order to solve an air-pollution problem, the problem must be defined in detail. A number of factors must be considered prior to selecting a particular piece of air-pollution-control equipment. In general, these factors can be grouped into three categories: environmental, engineering, and economic.

Environmental Factors These include (1) equipment location, (2) available space, (3) ambient conditions, (4) availability of adequate utilities (i.e., power, water, etc.) and ancillary-system facilities (i.e., waste treatment and disposal, etc.), (5) maximum allowable emission (air pollution codes), (6) aesthetic considerations (i.e., visible steam or water-vapor plume, etc.), (7) contributions of the air-pollution-control system to wastewater and land pollution, and (8) contribution of the air-pollution-control system to plant noise levels.

Engineering Factors These include:

1. Contaminant characteristics (e.g., physical and chemical properties, concentration, particulate shape and size distribution [in the case of particulates], chemical reactivity, corrosivity, abrasiveness, and toxicity)
2. Gas-stream characteristics (e.g., volume flow rate, temperature, pressure, humidity, composition, viscosity, density, reactivity, combustibility, corrosivity, and toxicity)
3. Design and performance characteristics of the particular control system (i.e., size and weight, fractional efficiency curves [in the case of particulates]), mass-transfer and/or contaminant-destruction capability (in the case of gases or vapors), pressure drop, reliability, turndown capability, power requirements, utility requirements, temperature limitations, maintenance requirements, operating cycles (including startup and shutdown) and flexibility toward complying with more stringent air-pollution codes.

Economic Factors These include capital cost (equipment, installation, engineering, etc.), operating cost (utilities, maintenance, etc.), emissions fees, and life-cycle cost over the expected equipment lifetime.

Comparing Control-Equipment Alternatives The final choice in equipment selection is usually dictated by the equipment capable of achieving compliance with regulatory codes at the lowest uniform annual cost (amortized capital investment plus operation and maintenance costs). To compare specific control-equipment alternatives, knowledge of the particular application and site is essential. A preliminary screening, however, may be performed by reviewing the advantages and disadvantages of each type of air-pollution-control equipment. General advantages and disadvantages of the most popular types of air-pollution

TABLE 22-18 Advantages and Disadvantages of Cyclone Collectors

Advantages

1. Low cost of construction
2. Relatively simple equipment with few maintenance problems
3. Relatively low operating pressure drops (for degree of particulate removal obtained) in the range of approximately 2- to 6-in water column
4. Temperature and pressure limitations imposed only by the materials of construction used
5. Collected material recovered dry for subsequent processing or disposal
6. Relatively small space requirements

Disadvantages

1. Relatively low overall particulate collection efficiencies, especially on particulates below 10 μm in size
2. Inability to handle tacky materials

equipment for gases and particulates are presented in Tables 22-18 through 22-30. Other activities that must be accomplished before final compliance is achieved are presented in Table 22-31.

In addition to using annualized cost comparisons in evaluating an air-pollution-control (APC) equipment installation, the impact of the 1990 Clean Air Act Amendments (CAAA) and resulting regulations also must be included in the evaluation. The CAAA prescribes specific pollution-control requirements for particular industries and locations. As an example, the CAAA requires that any major stationary source or major modification plan that is subject to Prevention of Significant Deterioration (PSD) requirements must undergo a Best Available Control Technology (BACT) analysis. The BACT analysis is done on a case-by-case basis. The process involves evaluating the possible types of air-pollution-control equipment that could be used for technology and energy and in terms of the environment and economy. The analysis uses a top-down approach that lists all available control technologies in descending order of effectiveness. The most stringent technology is chosen unless it can be demonstrated that, due to technical, energy, environmental, or economic considerations, this type of APC technology is not feasible.

The 1990 CAAA introduced a new level of control for hazardous (toxic) air pollutants (HAPs). As a result, EPA has identified 188 HAPs for regulation. Rather than rely upon ambient air quality standards to set acceptable exposures to HAPs, the CAAA requires that EPA promulgate through the end of the decade Maximum Achievable Control Technology (MACT) standards for controlling HAPs emitted from specified industries. These standards are based on the level of control established by the best performing 12 percent of industries in each of the categories identified by EPA.

TABLE 22-19 Advantages and Disadvantages of Wet Scrubbers

Advantages

1. No secondary dust sources
2. Relatively small space requirements
3. Ability to collect gases as well as particulates (especially "sticky" ones)
4. Ability to handle high-temperature, high-humidity gas streams
5. Capital cost low (if wastewater treatment system not required)
6. For some processes, gas stream already at high pressures (so pressure-drop considerations may not be significant)
7. Ability to achieve high collection efficiencies on fine particulates (however, at the expense of pressure drop)
8. Ability to handle gas streams containing flammable or explosive materials

Disadvantages

1. Possible creation of water-disposal problem
2. Product collected wet
3. Corrosion problems more severe than with dry systems
4. Steam plume opacity and/or droplet entrainment possibly objectionable
5. Pressure-drop and horsepower requirements possibly high
6. Solids buildup at the wet-dry interface possibly a problem
7. Relatively high maintenance costs
8. Must be protected from freezing
9. Low exit gas temperature reduces exhaust plume dispersion
10. Moist exhaust gas precludes use of most additional controls

TABLE 22-20 Advantages and Disadvantages of Dry Scrubbers*Advantages*

1. No wet sludge to dispose of
2. Relatively small space requirements
3. Ability to collect acid gases at high efficiencies
4. Ability to handle high-temperature gas streams
5. Dry exhaust allows addition of fabric filter to control particulate

Disadvantages

1. Acid gas control efficiency not as high as with wet scrubber
2. No particulate collection—dry scrubber generates particulate
3. Corrosion problems more severe than with dry systems
4. Solids buildup at the wet-dry interface possibly a problem
5. Relatively high maintenance costs
6. Must be protected from freezing
7. Low exit gas temperature reduces exhaust plume dispersion

DISPERSION FROM STACKS

Stacks discharging to the atmosphere have long been the most common industrial method of disposing of waste gases. The concentrations to which humans, plants, animals, and structures are exposed at ground level can be reduced significantly by emitting the waste gases from a process at great heights. Although tall stacks may be effective in lowering the ground-level concentration of pollutants, they do not in themselves reduce the amount of pollutants released into the atmosphere. However, in certain situations, their use can be the most practical and economical way of dealing with an air-pollution problem.

Preliminary Design Considerations To determine the acceptability of a stack as a means of disposing of waste gases, the acceptable ground-level concentration (GLC) of the pollutant or pollutants must be determined. The topography of the area must also be considered so that the stack can be properly located with respect to buildings and hills that might introduce a factor of air turbulence into the operation of the stack. Awareness of the meteorological conditions prevalent in the area, such as the prevailing winds, humidity, and rainfall, is also essential. Finally, an accurate knowledge of the constituents of the waste gas and their physical and chemical properties is paramount.

TABLE 22-21 Advantages and Disadvantages of Electrostatic Precipitators*Advantages*

1. Extremely high particulate (coarse and fine) collection efficiencies attainable (at a relatively low expenditure of energy)
2. Collected material recovered dry for subsequent processing or disposal
3. Low pressure drop
4. Designed for continuous operation with minimum maintenance requirements
5. Relatively low operating costs
6. Capable of operation under high pressure (to 150 lb/in²) or vacuum conditions
7. Capable of operation at high temperatures [to 704°C(1300°F)]
8. Relatively large gas flow rates capable of effective handling

Disadvantages

1. High capital cost
2. Very sensitive to fluctuations in gas-stream conditions (in particular, flows, temperature, particulate and gas composition, and particulate loadings)
3. Certain particulates difficult to collect owing to extremely high- or low-resistivity characteristics
4. Relatively large space requirements required for installation
5. Explosion hazard when treating combustible gases and/or collecting combustible particulates
6. Special precautions required to safeguard personnel from the high voltage
7. Ozone produced by the negatively charged discharge electrode during gas ionization
8. Relatively sophisticated maintenance personnel required
9. Gas ionization may cause dissociation of gas stream constituents and result in creation of toxic byproducts
10. Sticky particulates may be difficult to remove from plates
11. Not effective in capturing some contaminants that exist as vapors at high temperatures (e.g., heavy metals, dioxins)

TABLE 22-22 Advantages and Disadvantages of Fabric-Filter Systems*Advantages*

1. Extremely high collection efficiency on both coarse and fine (sub-micrometer) particles
2. Relatively insensitive to gas-stream fluctuation; efficiency and pressure drop relatively unaffected by large changes in inlet dust loadings for continuously cleaned filters
3. Filter outlet air capable of being recirculated within the plant in many cases (for energy conservation)
4. Collected material recovered dry for subsequent processing or disposal
5. No problems with liquid-waste disposal, water pollution, or liquid freezing
6. Corrosion and rusting of components usually not problems
7. No hazard of high voltage, simplifying maintenance and repair and permitting collection of flammable dusts
8. Use of selected fibrous or granular filter aids (precoating), permitting the high-efficiency collection of submicrometer smokes and gaseous contaminants
9. Filter collectors available in a large number of configurations, resulting in a range of dimensions and inlet and outlet flange locations to suit installation requirements
10. Relatively simple operation

Disadvantages

1. Temperatures much in excess of 288°C (550°F) requiring special refractory mineral or metallic fabrics that are still in the developmental stage and can be very expensive
2. Certain dusts possibly requiring fabric treatments to reduce dust seeping or, in other cases, assist in the removal of the collected dust
3. Concentrations of some dusts in the collector (~50 g/m³) forming a possible fire or explosion hazard if a spark or flame is admitted by accident; possibility of fabrics burning if readily oxidizable dust is being collected
4. Relatively high maintenance requirements (bag replacement, etc.)
5. Fabric life possibly shortened at elevated temperatures and in the presence of acid or alkaline particulate or gas constituents
6. Hygroscopic materials, condensation of moisture, or tarry adhesive components possibly causing crusty caking or plugging of the fabric or requiring special additives
7. Replacement of fabric, possibly requiring respiratory protection for maintenance personnel
8. Medium pressure-drop requirements, typically in the range 4- to 10-in water column

Wind Direction and Speed Wind direction is measured at the height at which the pollutant is released, and the mean direction will indicate the direction of travel of the pollutants. In meteorology, it is conventional to consider the wind direction as the direction from which the wind blows; therefore, a northwest wind will move pollutants to the southeast of the source.

The effect of wind speed is twofold: (1) Wind speed will determine the travel time from a source to a given receptor; and (2) wind speed will affect dilution in the downwind direction. Generally, the concentration of air pollutants downwind from a source is inversely proportional to wind speed.

Wind speed has velocity components in all directions so that there are vertical motions as well as horizontal ones. These random motions of widely different scales and periods are essentially responsible for the movement and diffusion of pollutants about the mean downwind path. These motions can be considered atmospheric turbulence. If the scale of a turbulent motion (i.e., the size of an eddy) is larger than the size of the pollutant plume in its vicinity, the eddy will move that portion of the plume. If an eddy is smaller than the plume, its effect will be to diffuse or spread out the plume. This diffusion caused by eddy motion is widely variable in the atmosphere, but even when the effect of this diffusion is least, it is in the vicinity of three orders of magnitude greater than diffusion by molecular action alone.

Mechanical turbulence is the induced-eddy structure of the atmosphere due to the roughness of the surface over which the air is passing. Therefore, the existence of trees, shrubs, buildings, and terrain features will cause mechanical turbulence. The height and spacing of the elements causing the roughness will affect the turbulence. In general, the higher the roughness elements, the greater the mechanical turbulence. In addition, mechanical turbulence increases as wind speed increases.

TABLE 22-23 Advantages and Disadvantages of Absorption Systems (Packed and Plate Columns)*Advantages*

1. Relatively low pressure drop
2. Standardization in fiberglass-reinforced plastic (FRP) construction permitting operation in highly corrosive atmospheres
3. Capable of achieving relatively high mass-transfer efficiencies
4. Increasing the height and/or type of packing or number of plates capable of improving mass transfer without purchasing a new piece of equipment
5. Relatively low capital cost
6. Relatively small space requirements
7. Ability to collect particulates as well as gases
8. Collected substances may be recovered by distillation

Disadvantages

1. Possibility of creating water (or liquid) disposal problem
2. Product collected wet
3. Particulates deposition possibly causing plugging of the bed or plates
4. When FRP construction is used, sensitive to temperature
5. Relatively high maintenance costs
6. Must be protected from freezing

Thermal turbulence is turbulence induced by the stability of the atmosphere. When the Earth's surface is heated by the sun's radiation, the lower layer of the atmosphere tends to rise and thermal turbulence becomes greater, especially under conditions of light wind. On clear nights with wind, heat is radiated from the Earth's surface, resulting in the cooling of the ground and the air adjacent to it. This results in extreme stability of the atmosphere near the Earth's surface. Under these conditions, turbulence is at a minimum. Attempts to relate different measures of turbulence of the wind (or stability of the atmosphere) to atmospheric diffusion have been made for some time. The measurement of atmospheric stability by temperature-difference measurements on a tower is frequently utilized as an indirect measure of turbulence, particularly when climatological estimates of turbulence are desired.

Lapse Rate and Atmospheric Stability Apart from mechanical interference with the steady flow of air caused by buildings and other obstacles, the most important factor that influences the degree of turbulence and hence the speed of diffusion in the lower air is the variation of temperature with height above the ground, referred to as the "lapse rate." The dry-adiabatic lapse rate (DALR) is the temperature change for a rising parcel of dry air. The dry-adiabatic lapse rate can be approximated as -1°C per 100 m, or $dT/dz = -10^{-2}^{\circ}\text{C}/\text{m}$ or $-5.4^{\circ}\text{F}/1000$ ft. If the rising air contains water vapor, the cooling due to adiabatic expansion will result in the relative humidity being increased, and saturation may be reached. Further ascent would then lead to condensation of water vapor, and the latent heat thus released would reduce the rate of cooling of the rising air. The buoyancy force on a warm-air parcel is caused by the difference between its density and that of the surrounding air. The perfect-gas law shows that, at a fixed pressure (altitude), the temperature and density of an air parcel are inversely related; temperature is normally used to determine buoyancy because it is easier to measure than density. If the temperature gradient (lapse rate) of the atmosphere is the same as the adiabatic lapse rate, a parcel of air displaced from its original position will expand or contract in such a manner that its density and temperature remain the same as its surroundings. In this case there will be no buoyancy forces on the displaced parcel, and the atmosphere is termed "neutrally stable."

TABLE 22-24 Comparison of Plate and Packed Columns*Packed column*

1. Lower pressure drop
2. Simpler and cheaper to construct
3. Preferable for liquids with high-foaming tendencies

Plate column

1. Less susceptible to plugging
2. Less weight
3. Less of a problem with channeling
4. Temperature surge resulting in less damage

TABLE 22-25 Advantages and Disadvantages of Adsorption Systems*Advantages*

1. Possibility of product recovery
2. Excellent control and response to process changes
3. No chemical-disposal problem when pollutant (product) recovered and returned to process
4. Capability of systems for fully automatic, unattended operation
5. Capability to remove gaseous or vapor contaminants from process streams to extremely low levels

Disadvantages

1. Product recovery possibly requiring an exotic, expensive distillation (or extraction) scheme
2. Adsorbent progressively deteriorating in capacity as the number of cycles increases
3. Adsorbent regeneration requiring a steam or vacuum source
4. Relatively high capital cost
5. Prefiltering of gas stream possibly required to remove any particulate capable of plugging the adsorbent bed
6. Cooling of gas stream possibly required to get to the usual range of operation (less than 49°C [120°F])
7. Relatively high steam requirements to desorb high-molecular-weight hydrocarbons
8. Spent adsorbent may be considered a hazardous waste
9. Some contaminants may undergo a violent exothermic reaction with the adsorbent

If the atmospheric temperature decreases faster with increasing altitude than the adiabatic lapse rate (superadiabatic), a parcel of air displaced upward will have a higher temperature than the surrounding air. Its density will be lower, giving it a net upward buoyancy force. The opposite situation exists if the parcel of air is displaced downward, and the parcel experiences a downward buoyancy force. Once a parcel of air has started moving up or down, it will continue to do so, causing unstable atmospheric conditions. If the temperature decreases more slowly with increasing altitude than the adiabatic lapse rate, a displaced parcel of air experiences a net restoring force. The buoyancy forces then cause stable atmospheric conditions (see Fig. 22-5).

Strongly stable lapse rates are commonly referred to as *inversions*. The strong stability inhibits mixing across the inversion layer. Normally these conditions of strong stability extend for only several hundred meters vertically. The vertical extent of the inversion is referred to as the *inversion depth*. Two distinct types are observed: the ground-level inversion, caused by radiative cooling of the ground at night, and inversions aloft, occurring between 500 and several thousand meters above the ground (see Fig. 22-6). Some of the more common lapse-rate profiles with the corresponding effect on stackplumes are presented in Fig. 22-7.

From the viewpoint of air pollution, both stable surface layers and low-level inversions are undesirable because they minimize the rate of dilution of contaminants in the atmosphere. Even though the surface layer may be unstable, a low-level inversion will act as a barrier to vertical mixing, and contaminants will accumulate in the surface layer

TABLE 22-26 Advantages and Disadvantages of Combustion Systems*Advantages*

1. Simplicity of operation
2. Capability of steam generation or heat recovery in other forms
3. Capability for virtually complete destruction of organic contaminants

Disadvantages

1. Relatively high operating costs (particularly associated with fuel requirements)
2. Potential for flashback and subsequent explosion hazard
3. Catalyst poisoning (in the case of catalytic incineration)
4. Incomplete combustion, possibly creating potentially worse pollution problems
5. Even complete combustion may produce SO_2 , NO_x , and CO_2
6. High temperature components and exhaust may be hazardous to maintenance personnel and birds
7. High maintenance requirements—especially if operation is cyclic

TABLE 22-27 Advantages and Disadvantages of Condensers

Advantages

1. Pure product recovery (in the case of indirect-contact condensers)
2. Water used as the coolant in an indirect-contact condenser (i.e., shell-and-tube heat exchanger), not in contact with contaminated gas stream, and is reusable after cooling
3. May be used to produce vacuum to remove contaminants from process

Disadvantages

1. Relatively low removal efficiency for gaseous contaminants (at concentrations typical of pollution-control applications)
2. Coolant requirements possibly extremely expensive
3. Direct-contact condenser may produce water discharge problems

below the inversion. Stable atmospheric conditions tend to be more frequent and longest in persistence in the autumn, but inversions and stable lapse rates are prevalent at all seasons of the year.

Design Calculations For a given stack height, the calculational sequence begins by first estimating the effective height of the emission, employing an applicable plume-rise equation. The maximum GLC may then be determined by using an appropriate atmospheric-diffusion equation. A simple comparison of the calculated GLC for the particular pollutant with the maximum GLC permitted by the local air-pollution codes dictates whether the stack is operating satisfactorily. Conversely, with knowledge of the maximum acceptable GLC standards, a stack that will satisfy these standards can be properly designed.

Effective Height of an Emission The effective height of an emission rarely corresponds to the physical height of the stack. If the plume is caught in the turbulent wake of the stack or of buildings in the vicinity of the stack, the effluent will be mixed rapidly downward toward the ground. If the plume is emitted free of these turbulent zones, a number of source emission characteristics and meteorological factors influence the rise of the plume. The source emission characteristics include the gas flow rate and the temperature of the effluent at the top of the stack and the diameter of the stack opening. The meteorological factors influencing plume rise include wind speed, air temperature, shear of the wind speed with height, and atmospheric stability. No theory on plume rise presently takes into account all of these variables. Most of the equations that have been formulated for computing the effective height of an emission are semi-empirical. When considering any of these plume-rise equations, it is important to evaluate each in terms of the assumptions made and the circumstances existing at the time that the particular correlation was formulated. The formulas generally are not applicable to tall stacks (above 305 m [1000 ft] effective height).

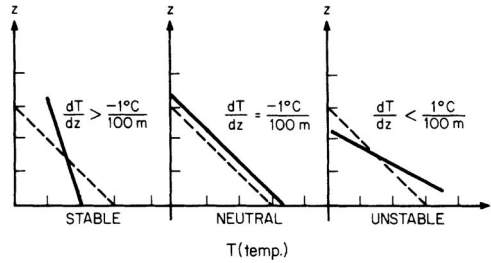


FIG. 22-5 Stability criteria with measured lapse rate.

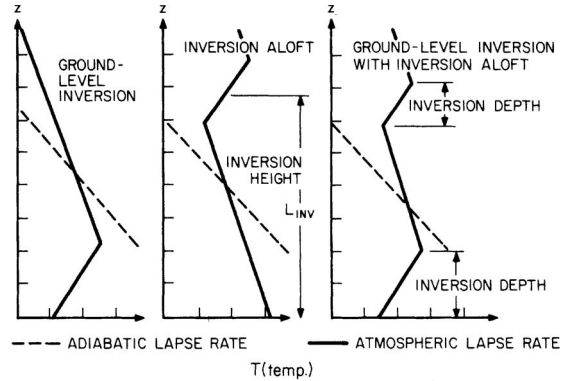


FIG. 22-6 Characteristic lapse rates under inversion conditions.

The effective stack height (equivalent to the effective height of the emission) is the sum of the actual stack height, the plume rise due to the exhaust velocity (momentum) of the issuing gases, and the buoyancy rise, which is a function of the temperature of the gases being emitted and the atmospheric conditions.

Some of the more common plume-rise equations have been summarized by Buonicore and Theodore (*Industrial Control Equipment for Gaseous Pollutants*, vol. 2, CRC Press, Boca Raton, Florida, 1975) and include:

Temperature gradient	Observation	Description
		Strong lapse—looping (unstable) This is usually a fair-weather daytime condition, since strong solar heating of the ground is required. Looping is not favored by cloudiness, snow cover, or strong winds.
		Weak lapse—coning (slightly unstable or neutral) This is usually favored by cloudy and windy conditions and may occur day or night. In dry climates it may occur infrequently, and in cloudy climates it may be the most frequent type observed.
		Inversion—fanning (stable) This is principally a nighttime condition. It is favored by light winds, clear skies, and snow cover. The condition may persist in some climates for several days at a time during winter, especially in the higher latitudes.
		Inversion below, lapse aloft—lofting (transition from unstable to stable) This condition occurs during transition from lapse to inversion and should be observed most frequently near sunset; it may be very transitory or persist for several hours. The shaded zone of strong effluent concentration is caused by trapping by the inversion of effluent carried into the stable layer by turbulent eddies that penetrate the layer for a short distance.
		Lapse below, inversion aloft—fumigation (transition from stable to unstable) This occurs when the nocturnal inversion is dissipated by heat from the morning sun. The lapse layer usually starts at the ground and works its way upward (less rapidly in winter than in summer). Fumigation may also occur in sea-breeze circulations during late morning or early afternoon. The shaded zone of strong concentration is that portion of the plume which has not yet been mixed downward.

FIG. 22-7 Lapse-rate characteristics of atmospheric-diffusion transport of stack emissions.

TABLE 22-28 Advantages and Disadvantages of Biofiltration*Advantages*

1. Uses natural biological processes and materials
2. Relatively simple and economical
3. High destruction efficiencies for oxygen-rich, low-contaminant concentration gas streams
4. Waste products are CO₂ and water

Disadvantages

1. Raw gas must not be lethal to microorganisms
2. Gas stream must be maintained at proper temperature and humidity
3. Heavy particulate loadings can damage pore structure of filter bed

- ASME, *Recommended Guide for the Prediction of the Dispersion of Airborne Effluents*, ASME, New York, 1968.
 - Bosanquet-Carey-Halton, *Proc. Inst. Mech. Eng. (London)*, **162**, 355 (1950).
 - Briggs, *Plume Rise*, AEC Critical Review ser., U.S. Atomic Energy Commission, Div. Tech. Inf.
 - Brummage et al., *The Calculation of Atmospheric Dispersion from a Stack*, CONCAWE, The Hague, 1966.
 - Carson and Moses, *J. Air Pollut. Control Assoc.*, **18**, 454 (1968) and **19**, 862 (1969).
 - Csnaday, *Int. J. Air Water Pollut.*, **4**, 47 (1961).
 - Davison-Bryant, *Trans. Conf. Ind. Wastes*, 14th Ann. Meet. Ind. Hyg. Found. Am., **39**, 1949.
 - Holland, *Workbook of Atmospheric Dispersion Estimates*, U.S. EPA Publ. AP-26, 1970.
 - Lucas, Moore, and Spurr, *Int. J. Air Water Pollut.*, **7**, 473 (1963).
 - Montgomery et al., *J. Air Pollut. Control Assoc.*, **22**(10), 779, TVA (1972).
 - Stone and Clarke, *British Experience with Tall Stacks for Air Pollution Control on Large Fossil-Fueled Power Plants*, American Power Conference, Chicago, 1967.
 - Stumke, *Staub*, **23**, 549 (1963).
- See also:
- Briggs, G. A., *Plume Rise Predications: Lectures on Air Pollution and Environmental Impact Analyses*, Workshop Proceedings, American Meteorological Society, Boston, Massachusetts, 1975, pp. 59–111.
 - Randerson, Darryl (ed.), *Plume Rise and Buoyancy Effects, Atmospheric Science and Power Production*, DOE Report DOE/TIC-27601, 1981.

Maximum Ground-Level Concentrations The effective height of an emission having been determined, the next step is to study its path downward by using the appropriate atmospheric-dispersion formula. Some of the more popular atmospheric-dispersion calculational procedures have been summarized by Buonicore and Theodore (op. cit.) and include:

- Bosanquet-Pearson model [Pasquill, *Meteorol. Mag.*, **90**, 33, 1063 (1961), and Gifford, *Nucl. Saf.*, **2**, 4, 47 (1961).]
 - Sutton model [Q.J.R. *Meteorol. Soc.*, **73**, 257 (1947).]
 - TVA Model [Carpenter et al., *J. Air Pollut. Control Assoc.*, **21**(8), (1971), and Montgomery et al., *J. Air Pollut. Control Assoc.*, **23**(5), 388 (1973).]
- See also:
- Bornstein et al., *Simulation of Urban Barrier Effects on Polluted Urban Boundary Layers Using the Three-Dimensional URBMET/IVM Model with Urban Topography*, Air Pollution Proceedings, 1993.

TABLE 22-29 Advantages and Disadvantages of Membrane Filtration*Advantages*

1. Low energy utilization
2. Modular design
3. Low capital costs
4. Low maintenance
5. Superior separation ability

Disadvantages

1. Potential particulate fouling problems if not properly designed

TABLE 22-30 Advantages and Disadvantages of Selective Catalytic Reduction of Nitrogen Oxides*Advantages*

1. Capable of 90% NO_x removal
2. Uses readily available urea reagent
3. Exhaust products are N₂ and water

Disadvantages

1. Spent catalyst may be considered hazardous waste
2. Gas stream must be maintained at proper temperature and humidity
3. Heavy particulate loadings can damage pore structure of filter bed

- EPA, *Guidance on the Application of Refined Dispersion Models for Air Toxins Releases*, EPA-450/4-91-007.
- Zannetti, Paolo, *Air Pollution Modeling: Theories, Computational Methods, and Available Software*, Van Nostrand, Reinhold, New York, 1990.
- Zannetti, Paolo, *Numerical Simulation Modeling of Air Pollution: An Overview*, Ecological Physical Chemistry, 2d International Workshop, May 1992.

Miscellaneous Effects

Evaporative Cooling When effluent gases are washed to absorb certain constituents prior to emission, the gases are cooled and become saturated with water vapor. Upon release of the gases, further cooling due to contact with cold surfaces of ductwork or stack is likely. This cooling causes water droplets to condense in the gas stream. Upon release of the gases from the stack, the water droplets evaporate, withdrawing the latent heat of vaporization from the air and cooling the plume. The resulting negative buoyancy reduces the effective stack height. The result may be a plume (with a greater density than that of the ambient atmosphere) that will fall to the ground. If any pollutant remains after scrubbing, its full effect will be felt on the ground in the vicinity of the stack.

Aerodynamic Downwash Should the stack exit velocity be too low as compared with the speed of the crosswind, some of the effluent can be pulled downward by the low pressure on the lee side of the stack. This phenomenon, known as “stack-tip downwash,” can be minimized by keeping the exit velocity greater than the mean wind speed (i.e., typically twice the mean wind speed). Another way to minimize stack-tip downwash is to fit the top of the stack with a flat disc that extends for at least one stack diameter outward from the stack.

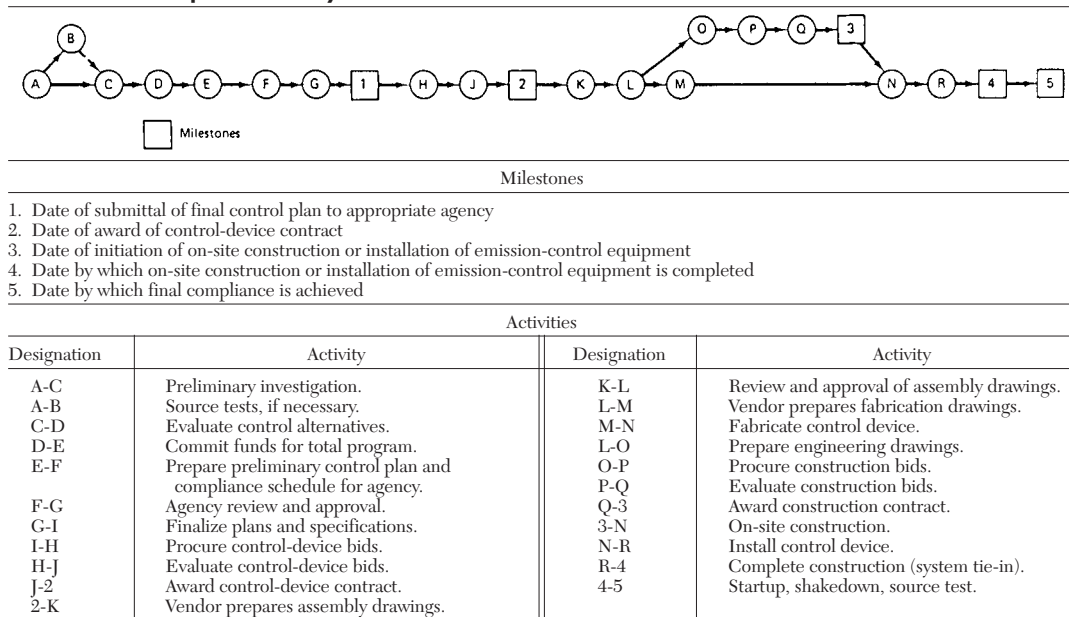
If it becomes necessary to increase the stack-gas exit velocity to avoid downwash, it may be necessary to remodel the stack exit. A venturi-nozzle design has been found to be the most effective. This design also keeps pressure losses to a minimum.

Building Downwash A review must be conducted for each stack to determine if building downwash effects need to be considered. Atmospheric flow is disrupted by aerodynamic forces in the immediate vicinity of structures or terrain obstacles. The disrupted flow near either building structures or terrain obstacles can both enhance the vertical dispersion of emissions from the source and reduce the effective height of the emissions from the source, resulting in an increase in the maximum GLC.

EPA Air Dispersion Models EPA addresses modeling techniques in the “Guideline on Air Quality Models” [Appendix W (July 2003) of 40 CFR Part 51]. The guideline provides a common basis for estimating the air quality concentrations of criteria pollutants used in assessing control strategies and developing emission limits. The continuing development of new air quality models in response to regulatory requirements and the expanded requirements for models to cover ever more complex problems have emphasized the need for periodic review and update of guidance on these techniques. Information on the current status of modeling guidance can always be obtained from EPA’s regional offices.

The guideline recommends air quality modeling techniques that should be applied to State Implementation Plan (SIP) revisions for existing sources and to new source reviews (NSRs), including prevention of significant deterioration (PSD). In addition the guideline serves to identify, for all interested parties, those techniques and databases that EPA considers acceptable. Dispersion models, while uniquely filling

TABLE 22-31 Compliance Activity and Schedule Chart



one program need, have become a primary analytical tool in most air quality assessments. Air quality measurements can be used in a complementary manner to dispersion models, with due regard for the strengths and weaknesses of both analysis techniques. The diversity of the nation's topography and climate, and variations in source configurations and operating characteristics dictate against a strict modeling "cookbook." There is no one model capable of properly addressing all conceivable situations even within a broad category such as point sources.

The guideline provides a consistent basis for selection of the most accurate models and databases for use in air quality assessments. There are two levels of sophistication of models. The first level consists of relatively simple estimation techniques that generally use pre-set, worst-case meteorological conditions to provide conservative estimates of the air quality impact of a specific source, or source category. These are called screening techniques or screening models. The purpose of such techniques is to eliminate the need for more detailed modeling for those sources that clearly will not cause or contribute to ambient concentrations in excess of either the National Ambient Air Quality Standards (NAAQS) or the allowable PSD concentration increments. The second level consists of those analytical techniques that provide more detailed treatment of physical and chemical atmospheric processes, require more detailed and precise input data, and provide more specialized concentration estimates. Most of the screening and refined models discussed in the guideline, codes, associated documentation, and other useful information are available for download from EPA's Support Center for Regulatory Air Modeling (SCRAM) Internet web site at <http://www.epa.gov/scram001>.

CONTROL OF GASEOUS EMISSIONS

There are four chemical-engineering unit operations commonly used for the control of gaseous emissions:

1. *Absorption.* See Sec. 4, "Thermodynamics"; and Sec. 18, "Liquid Gas Systems." For plate columns, see Sec. 18, "Gas-Liquid Contacting: Plate Columns." For packed columns, see Sec. 18, "Gas-Liquid Contacting: Packed Columns."
2. *Adsorption.* See Sec. 16, "Adsorption and Ion Exchange."
3. *Combustion.* See Sec. 9, "Heat Generation" and "Fired Process Equipment." For incinerators, see material under these subsections.
4. *Condensation.* See Sec. 10, "Heat Transmission"; Sec. 11, "Heat-Transfer Equipment"; and Sec. 12, "Evaporative Cooling." For direct-

contact condensers, See Sec. 11, "Evaporator Accessories"; and Sec. 12, "Evaporative Cooling." For indirect-contact condensers, see Sec. 10, "Heat Transfer with Change of Phase" and "Thermal Design of Heat-Transfer Equipment"; and Sec. 11, "Shell and Tube Heat Exchangers" and "Other Heat Exchangers for Liquids and Gases."

These operations, which are routine chemical engineering operations, have been treated extensively in other sections of this handbook.

There are three additional chemical engineering unit operations that are increasing in use in recent years. They are:

1. *Biofiltration*
2. *Membrane filtration*
3. *Selective catalytic reduction*

and are discussed further in this section.

Absorption The engineering design of gas absorption equipment must be based on a sound application of the principles of diffusion, equilibrium, and mass transfer as developed in Secs. 5 and 14 of the handbook. The main requirement in equipment design is to bring the gas into intimate contact with the liquid; that is, to provide a large interfacial area and a high intensity of interface renewal and to minimize resistance and maximize driving force. This contacting of the phases can be achieved in many different types of equipment, the most important being packed and plate columns. The final choice between them rests with the various criteria that must be met. For example, if the pressure drop through the column is large enough that compression costs become significant, a packed column may be preferable to a plate-type column because of the lower pressure drop.

In most processes involving the absorption of a gaseous pollutant from an effluent gas stream, the gas stream is the processed fluid; hence, its inlet condition (flow rate, composition, and temperature) are usually known. The temperature and composition of the inlet liquid and the composition of the outlet gas are usually specified. The main objectives in the design of an absorption column, then, are the determination of the solvent flow rate and the calculation of the principal dimensions of the equipment (column diameter and height to accomplish the operation). These objectives can be obtained by evaluating, for a selected solvent at a given flow rate, the number of theoretical separation units (stage or plates) and converting them into practical units, column heights or number of actual plates by means of existing correlations.

The general design procedure consists of a number of steps to be taken into consideration. These include:

1. Solvent selection
2. Equilibrium-data evaluation
3. Estimation of operating data (usually consisting of a mass and energy in which the energy balance decides whether the absorption balance can be considered isothermal or adiabatic)
4. Column selection (should the column selection not be obvious or specified, calculations must be carried out for the different types of columns and the final based on economic considerations)
5. Calculation of column diameter (for packed columns, this is usually based on flooding conditions, and, for plate columns, on the optimum gas velocity or the liquid-handling capacity of the plate)
6. Estimation of column height or number of plates (for packed columns, column height is obtained by multiplying the number of transfer units, obtained from a knowledge of equilibrium and operating data, by the height of a transfer unit; for plate columns, the number of theoretical plates determined from the plot of equilibrium and operating lines is divided by the estimated overall plate efficiency to give the number of actual plates, which in turn allows the column height to be estimated from the plate spacing)
7. Determination of pressure drop through the column (for packed columns, correlations dependent of packing type, column-operating data, and physical properties of the constituents involved are available to estimate the pressure drop through the packing; for plate columns, the pressure drop per plate is obtained and multiplied by the number of plates)

Solvent Selection The choice of a particular solvent is most important. Frequently, water is used, as it is very inexpensive and plentiful, but the following properties must also be considered:

1. *Gas solubility.* A high gas solubility is desired, since this increases the absorption rate and minimizes the quantity of solvent necessary. Generally, solvents of a chemical nature similar to that of the solute to be absorbed will provide good solubility.
2. *Volatility.* A low solvent vapor pressure is desired, since the gas leaving the absorption unit is ordinarily saturated with the solvent, and much may thereby be lost.
3. *Corrosiveness.*
4. *Cost.*
5. *Viscosity.* Low viscosity is preferred for reasons of rapid absorption rates, improved flooding characteristics, lower pressure drops, and good heat-transfer characteristics.
6. *Chemical stability.* The solvent should be chemically stable and, if possible, nonflammable.
7. *Toxicity.*
8. *Low freezing point.* If possible, a low freezing point is favored, since any solidification of the solvent in the column makes the column inoperable.

Equipment The principal types of gas-absorption equipment may be classified as follows:

1. Packed columns (continuous operation)
2. Plate columns (staged operations)
3. Miscellaneous

Of the three categories, the packed column is by far the most commonly used for the absorption of gaseous pollutants. Miscellaneous gas-absorption equipment could include acid gas scrubbers that are commonly classified as either "wet" or "dry." In wet scrubber systems, the absorption tower uses a lime-based sorbent liquor that reacts with the acid gases to form a wet/solid by-product. Dry scrubbers can be grouped into three categories: (1) spray dryers; (2) circulating spray dryers; and (3) dry injection. Each of these systems yields a dry product that can be captured with a fabric filter baghouse downstream and thus avoids costly wastewater treatment systems. The baghouse is highly efficient in capturing the particulate emissions, and a portion of the overall acid gas removal has been found to occur within the baghouse. Additional information may be found by referring to the appropriate sections in this *handbook* and the many excellent texts available, such as McCabe and Smith, *Unit Operations of Chemical Engineering*, 3d ed., McGraw-Hill, New York, 1976; Sherwood and Pigford, *Absorption and Extraction*, 2d ed., McGraw-Hill, New York, 1952; Smith, *Design of Equilibrium Stage Processes*, McGraw-Hill, New York, 1963; Treybal, *Mass Transfer Operations*, 3d ed., McGraw-Hill, New York, 1980; McKenna, Mycock, and Theodore, *Handbook of Air Pollution Control Engineering and Technology*, CRC Press, Boca

Raton, Florida, 1995; Theodore and Allen, *Air Pollution Control Equipment*, ETSI Prof. Training Inst., Roanoke, Virginia, 1993.

Adsorption The design of gas-adsorption equipment is in many ways analogous to the design of gas-absorption equipment, with a solid adsorbent replacing the liquid solvent (see Secs. 16 and 19). Similarity is evident in the material- and energy-balance equations as well as in the methods employed to determine the column height. The final choice, as one would expect, rests with the overall process economics.

Selection of Adsorbent Industrial adsorbents are usually capable of adsorbing both organic and inorganic gases and vapors. However, their preferential adsorption characteristics and other physical properties make each of them more or less specific for a particular application. General experience has shown that, for the adsorption of vapors of an organic nature, activated carbon has superior properties, having hydrocarbon-selective properties and high adsorption capacity for such materials. Inorganic adsorbents, such as activated alumina or silica gel, can also be used to adsorb organic materials, but difficulties can arise during regeneration. Activated alumina, silica gel, and molecular sieves will also preferentially adsorb any water vapor with the organic contaminant. At times this may be a considerable drawback in the application of these adsorbents for organic-contaminant removal.

The normal method of regeneration of adsorbents is by use of steam, inert gas (i.e., nitrogen), or other gas streams, and in the majority of cases this can cause at least slight decomposition of the organic compound on the adsorbent. Two difficulties arise: (1) incomplete recovery of the adsorbate, although this may be unimportant; and (2) progressive deterioration in capacity of the adsorbent as the number of cycles increases owing to blocking of the pores from carbon formed by hydrocarbon decomposition. With activated carbon, a steaming process is used, and the difficulties of regeneration are thereby overcome. This is not feasible with silica gel or activated alumina because of the risk of breakdown of these materials when in contact with liquid water.

In some cases, none of the adsorbents has sufficient retaining capacity for a particular contaminant. In these applications, a large-surface-area adsorbent can be impregnated with an inorganic compound or, in rare cases, with a high-molecular-weight organic compound that can react chemically with the particular contaminant. For example, iodine-impregnated carbons are used for removal of mercury vapor and bromine-impregnated carbons for ethylene or propylene removal. The action of these impregnants is either catalytic conversion or reaction to a nonobjectionable compound or to a more easily adsorbed compound. For this case, general adsorption theory no longer applies to the overall effects of the process. For example, mercury removal by an iodine-impregnated carbon proceeds faster at a higher temperature, and a better overall efficiency can be obtained than in a low-temperature system.

Since adsorption takes place at the interphase boundary, the adsorption surface area becomes an important consideration. Generally, the higher the adsorption surface area, the greater its adsorption capacity. However, the surface area has to be "available" in a particular pore size within the adsorbent. At low partial pressure (or concentration) a surface area in the smallest pores in which the adsorbate can enter is the most efficient. At higher pressures the larger pores become more important; at very high concentrations, capillary condensation will take place within the pores, and the total micropore volume becomes the limiting factor.

The action of molecular sieves is slightly different from that of other adsorbents in that selectivity is determined more by the pore-size limitations of the particular sieve. In selecting molecular sieves, it is important that the contaminant to be removed be smaller than the available pore size. Hence, it is important that the particular adsorbent not only have an affinity for the contaminant in question but also have sufficient surface area available for adsorption.

Design Data The adsorbent having been selected, the next step is to calculate the quantity of adsorbent required and eventually consider other factors such as the temperature rise of the gas stream due to adsorption and the useful life of the adsorbent under operating conditions. The sizing and overall design of the adsorption system depend on the properties and characteristics of both the feed gas to be treated and the adsorbent. The following information should be known or available for design purposes:

1. Gas stream
 - a. Adsorbate concentration.
 - b. Temperature.
 - c. Temperature rise during adsorption.
 - d. Pressure.
 - e. Flow rate.
 - f. Presence of adsorbent contaminant material.
2. Adsorbent
 - a. Adsorption capacity as used on stream.
 - b. Temperature rise during adsorption.
 - c. Isothermal or adiabatic operation.
 - d. Life, if presence of contaminant material is unavoidable.
 - e. Possibility of catalytic effects causing an adverse chemical reaction in the gas stream or the formation of solid polymerizates on the adsorbent bed, with consequent deterioration.
 - f. Bulk density.
 - g. Particle size, usually reported as a mean equivalent particle diameter. The dimensions and shape of particles affect both the pressure drops through the adsorbent bed and the diffusion rate into the particles. All things being equal, adsorbent beds consisting of smaller particles, although causing a higher pressure drop, will be more efficient.
 - h. Pore data, which are important because they may permit elimination from consideration of adsorbents whose pore diameter will not admit the desired adsorbate molecule.
 - i. Hardness, which indicates the care that must be taken in handling adsorbents to prevent the formation of undesirable fines.
 - j. Regeneration information.

The design techniques used include both stagewise and continuous-contacting methods and can be applied to batch, continuous, and semicontinuous operations.

Adsorption Phenomena The adsorption process involves three necessary steps. The fluid must first come in contact with the adsorbent, at which time the adsorbate is preferentially or selectively adsorbed on the adsorbent. Next the fluid must be separated from the adsorbent-adsorbate, and, finally, the adsorbent must be regenerated by removing the adsorbate or by discarding used adsorbent and replacing it with fresh material. Regeneration is performed in a variety of ways, depending on the nature of the adsorbate. Gases or vapors are usually desorbed by either raising the temperature (thermal cycle) or reducing the pressure (pressure cycle). The more popular thermal cycle is accomplished by passing hot gas through the adsorption bed in the direction opposite to the flow during the adsorption cycle. This ensures that the gas passing through the unit during the adsorption cycle always meets the most active adsorbent last and that the adsorbate concentration in the adsorbent at the outlet end of the unit is always maintained at a minimum.

In the first step, in which the molecules of the fluid come in contact with the adsorbent, an equilibrium is established between the adsorbed fluid and the fluid remaining in the fluid phase. Figures 22-8 through 22-10 show several experimental equilibrium adsorption isotherms for a number of components adsorbed on various adsorbents. Consider Fig. 22-8, in which the concentration of adsorbed gas on the solid is plotted against the equilibrium partial pressure p^0 of the vapor or gas at constant temperature. At 40°C, for example, pure propane vapor at a pressure of 550 mm Hg is in equilibrium with an adsorbate concentration at point P of 0.04 lb adsorbed propane per pound of silica gel. Increasing the pressure of the propane will cause more propane to be adsorbed, while decreasing the pressure of the system at P will cause propane to be desorbed from the carbon.

The adsorptive capacity of activated carbon for some common solvent vapors is shown in Table 22-32.

Adsorption-Control Equipment If a gas stream must be treated for a short period, usually only one adsorption unit is necessary, provided, of course, that a sufficient time interval is available between adsorption cycles to permit regeneration. However, this is usually not the case. Since an uninterrupted flow of treated gas is often required, it is necessary to employ one or more units capable of operating in this fashion. The units are designed to handle gas flows without interruption and are characterized by their mode of contact, either staged or continuous. By far the most common type of adsorption system used to remove an objectionable pollutant from a gas stream consists of a

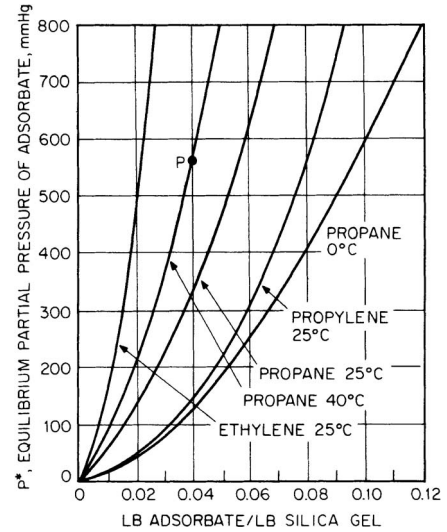


FIG. 22-8 Equilibrium partial pressures for certain organics on silica gel.

number of fixed-bed units operating in such a sequence that the gas flow remains uninterrupted. A two- or three-bed system is usually employed, with one or two beds bypassed for regeneration while one is adsorbing. A typical two-bed system is shown in Fig. 22-11a, while a typical three-bed system is shown in Fig. 22-11b. The type of system best suited for a particular job is determined from several factors, including the amount and rate of material being adsorbed, the time between cycles, the time required for regeneration, and the cooling time, if required.

Typical of continuous-contact operation for gaseous-pollutant adsorption is the use of a fluidized bed. During steady-state staged-contact operation, the gas flows up through a series of successive fluidized-bed stages, permitting maximum gas-solid contact on each stage. A typical arrangement of this type is shown in Fig. 22-12 for multistage countercurrent adsorption with regeneration. In the upper part of the tower, the particles are contacted countercurrently

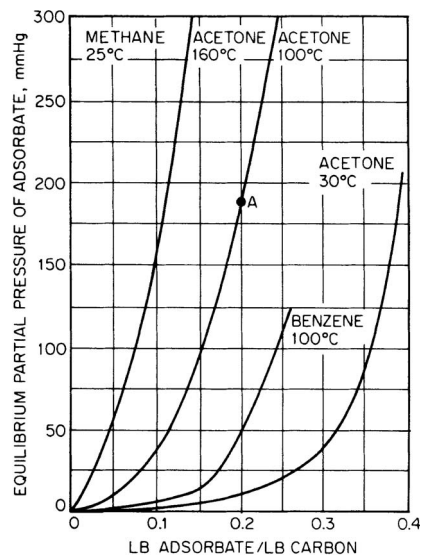


FIG. 22-9 Equilibrium partial pressures for certain organics on carbon.

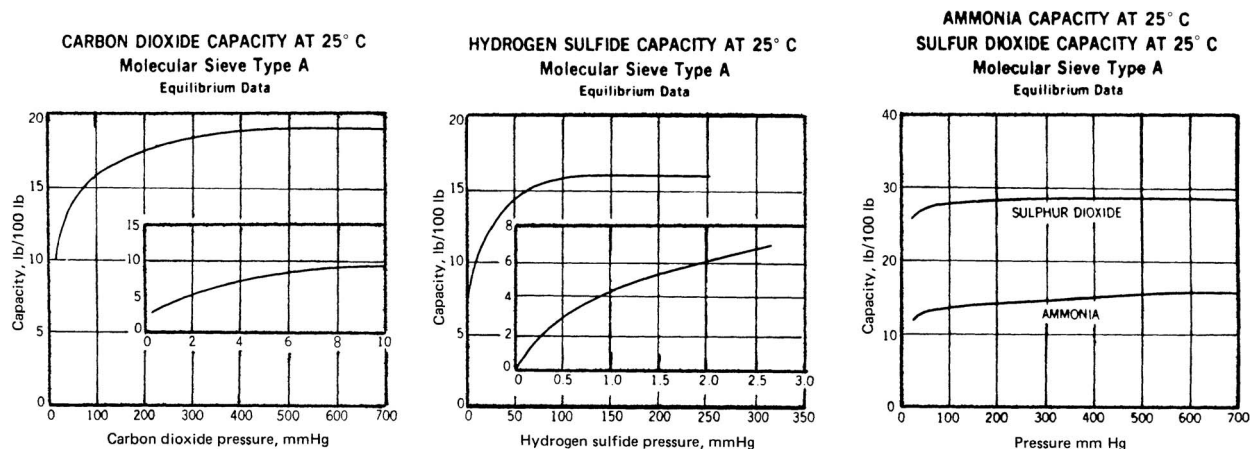


FIG. 22-10 Equilibrium partial pressures for certain gases on molecular sieves. (A. J. Buonicore and L. Theodore, *Industrial Control Equipment for Gaseous Pollutants*, vol. I, CRC Press, Boca Raton, Fla., 1975.)

on perforated trays in relatively shallow beds with the gas stream containing the pollutant, the adsorbent solids moving from tray to tray through downspouts. In the lower part of the tower, the adsorbent is regenerated by similar contact with hot gas, which desorbs and carries off the pollutant. The regenerated adsorbent is then recirculated by an airlift to the top of the tower.

Although the continuous-countercurrent type of operation has found limited application in the removal of gaseous pollutants from process streams (for example, the removal of carbon dioxide and sulfur compounds such as hydrogen sulfide and carbonyl sulfide), by far the most common type of operation presently in use is the fixed-bed adsorber. The relatively high cost of continuously transporting solid particles as required in steady-state operations makes fixed-bed adsorption an attractive, economical alternative. If intermittent or batch operation is practical, a simple one-bed system, cycling alternately between the adsorption and regeneration phases, will suffice.

Additional information may be found by referring to the appropriate sections of this *handbook*. A comprehensive treatment of adsorber design principles is given in Buonicore and Theodore, *Industrial Control Equipment for Gaseous Pollutants*, vol. 1, 2d ed., CRC press, Boca Raton, Florida, 1992.

Combustion Many organic compounds released from manufacturing operations can be converted to innocuous carbon dioxide and water by rapid oxidation (chemical reaction): combustion. However, combustion of gases containing halides may require the addition of acid gas treatment to the combustor exhaust.

Three rapid oxidation methods are typically used to destroy combustible contaminants: (1) flares (direct-flame-combustion), (2) thermal combustors, and (3) catalytic combustors. The thermal and flare methods are characterized by the presence of a flame during combus-

tion. The combustion process is also commonly referred to as "after-burning" or "incineration."

To achieve complete combustion (i.e., the combination of the combustible elements and compounds of a fuel with all the oxygen that they can utilize), sufficient space, time, and turbulence and a temperature high enough to ignite the constituents must be provided.

The three T's of combustion—time, temperature, and turbulence—govern the speed and completeness of the combustion reaction. For complete combustion, the oxygen must come into intimate contact with the combustible molecule at sufficient temperature and for a sufficient length of time for the reaction to be completed. Incomplete reactions may result in the generation of aldehydes, organic acids, carbon, and carbon monoxide.

Combustion-Control Equipment Combustion-control equipment can be divided into three types: (1) flares, (2) thermal incinerators, (3) catalytic incinerators.

Flares In many industrial operations and particularly in chemical plants and petroleum refineries, large volumes of combustible waste gases are produced. These gases result from undetected leaks in the operating equipment, from upset conditions in the normal operation of a plant in which gases must be vented to avoid dangerously high pressures in operating equipment, from plant startups, and from emergency shutdowns. Large quantities of gases may also result from off-specification product or from excess product that cannot be sold. Flows are typically intermittent, with flow rates during major upsets of up to several million cubic feet per hour.

The preferred control method for excess gases and vapors is to recover them in a blowdown recovery system. However, large quantities of gas, especially those during upset and emergency conditions, are difficult to contain and reprocess. In the past all waste gases were vented directly to the atmosphere. However, widespread venting caused safety and environmental problems, and, in practice, it is now customary to collect such gases in a closed flare system and to burn them as they are discharged.

Although flares can be used to dispose of excess waste gases, such systems can present additional safety problems. These include the explosion potential, thermal-radiation hazards from the flame, and the problem of toxic asphyxiation during flameout. Aside from these safety aspects, there are several other problems associated with flaring that must be dealt with during the design and operation of a flare system. These problems include the formation of smoke, the luminosity of the flame, noise during flame, and the possible emission of by-product air pollutants during flaring.

The heat content of the waste stream to be disposed is another important consideration. The heat content of the waste gas falls into two classes. The gases can either support their own combustion or not. In general, a waste gas with a heating value greater than 7443 kJ/m³

TABLE 22-32 Adsorptive Capacity of Common Solvents on Activated Carbons*

Solvent	Carbon bed weight, %†
Acetone	8
Heptane	6
Isopropyl alcohol	8
Methylene chloride	10
Perchloroethylene	20
Stoddard solvent	2-7
1,1,1-Trichloroethane	12
Trichloroethylene	15
Trichlorotrifluoroethane	8
VM&P naphtha	7

* Assuming steam desorption at 5 to 10 psig.

† For example, 8 lb of acetone adsorbed on 100 lb of activated carbon.

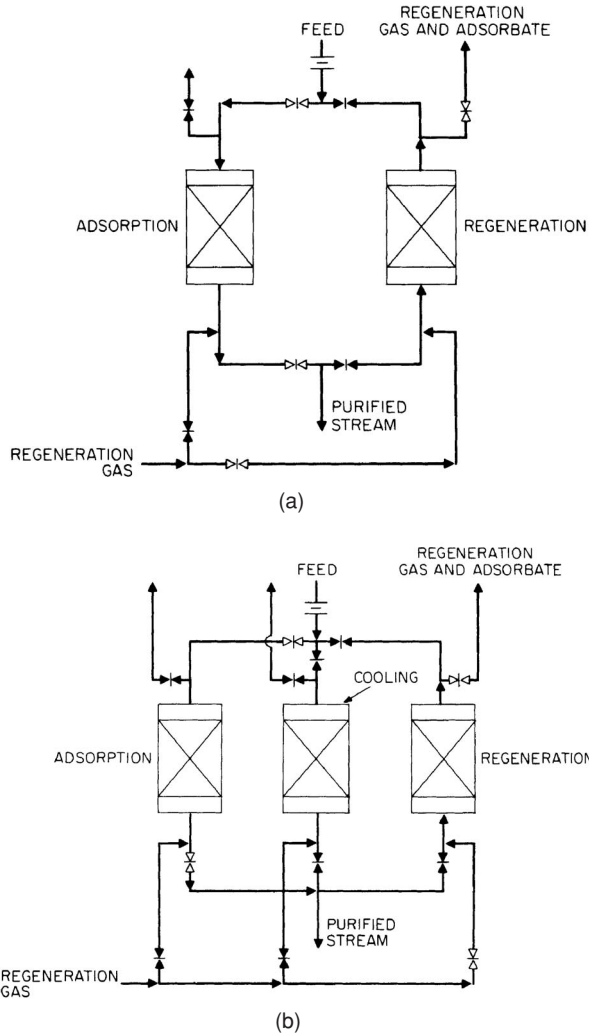


FIG. 22-11 (a) Typical two-bed adsorption system. (b) Typical three-bed adsorption system.

(200 Btu/ft³) can be flared successfully. The heating value is based on the lower heating value of the waste gas at the flare. Below 7443 kJ/m³, enriching the waste gas by injecting another gas with a higher heating value may be necessary. The addition of such a rich gas is called "endothermic flaring." Gases with a heating value as low as 2233 kJ/m³ (60 Btu/ft³) have been flared but at a significant fuel demand. It is usually not feasible to flare a gas with a heating value below 3721 kJ/m³ (100 Btu/ft³). If the flow of low-Btu gas is continuous, thermal or catalytic incineration can be used to dispose of the gas. For intermittent flows, however, endothermic flaring may be the only possibility.

Although most flares are used to dispose of intermittent waste gases, some continuous flares are in use, but generally only for relatively small volumes of gases. The heating value of large-volume continuous-flow waste gases is usually too valuable to lose in a flare. Vapor recovery or the use of the vapor as a fuel in a process heater is preferred over flaring. Since auxiliary fuel must be added to the gas in order to flare, large continuous flows of a low-heating-value gas are usually more efficient to burn in a thermal incinerator than in the flame of a flare.

Flares are mostly used for the disposal of hydrocarbons. Waste gases composed of natural gas, propane, ethylene, propylene, butadi-

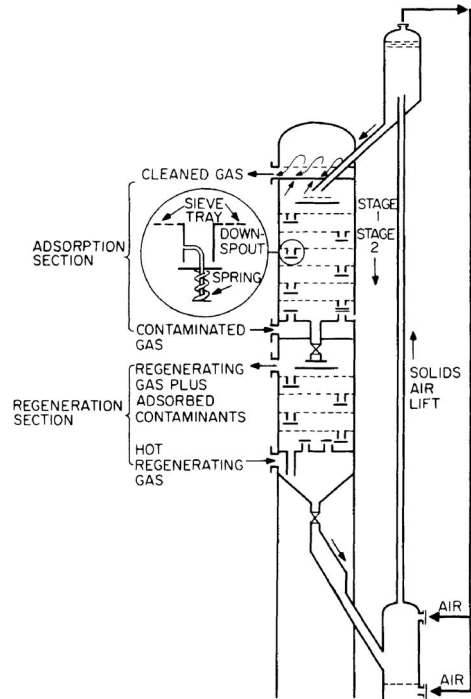


FIG. 22-12 Multistage countercurrent adsorption with regeneration.

ene, and butane probably constitute over 95 percent of the material flared. Flares have been used successfully to control malodorous gases such as mercaptans and amines, but care must be taken when flaring these gases. Unless the flare is very efficient and gives good combustion, obnoxious fumes can escape unburned and cause a nuisance.

Flaring of hydrogen sulfide should be avoided because of its toxicity and low odor threshold. In addition, burning relatively small amounts of hydrogen sulfide can create enough sulfur dioxide to cause crop damage or a local nuisance. For gases whose combustion products may cause problems, such as those containing hydrogen sulfide or chlorinated hydrocarbons, flaring is not recommended.

Thermal Incinerators Thermal incinerators or afterburners can be used over a fairly wide but low range of organic vapor concentration. The concentration of the organics in air must be substantially below the lower flammable level (lower explosive limit). As a rule, a factor of four is employed for safety precautions. Reactions are conducted at elevated temperatures to ensure high chemical-reaction rates for the organics. To achieve this temperature, it is necessary to preheat the feed stream using auxiliary energy. Along with the contaminant-laden gas stream, air and fuel are continuously delivered to the incinerator (see Fig. 22-13). The fuel and contaminants are combusted with air in a firing unit (burner). The burner may utilize the air in the process-waste stream as the combustion air for the auxiliary fuel, or it may use a separate source of outside air. The products of combustion and the unreacted feed stream are intensely mixed and enter the reaction zone of the unit. The pollutants in the process-gas stream are then reacted at the elevated temperature. Thermal incinerators generally require operating temperatures in the range of 650 to 980°C (1200 to 1800°F) for combustion of most organic pollutants (see Table 22-33). A residence time of 0.2 to 1.0 is often recommended, but this factor is dictated primarily by complex kinetic considerations. The kinetics of hydrocarbon (HC) combustion in the presence of excess oxygen can be simplified into the following first-order rate equation:

$$\frac{d(\text{HCl})}{dt} = -k[\text{HCl}] \quad (22-1)$$

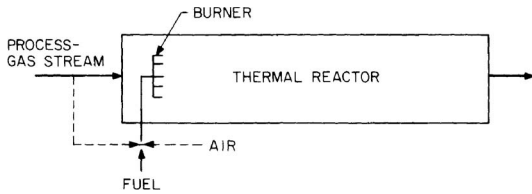


FIG. 22-13 Thermal-combustion device.

where k = pseudo-first-order rate constant (s^{-1}). If the initial concentration is $C_{A,0}$, the solution of Eq. (22-1) is:

$$\ln\left(\frac{C_A}{C_{A,0}}\right) = -kt \quad (22-2)$$

Equation (22-2) is frequently used for a kinetic modeling of a burner using mole fractions in the range of 0.15 and 0.001 for oxygen and HC, respectively. The rate constant is generally of the following Arrhenius form:

$$k = Ae^{-E/RT} \quad (22-3)$$

where: A = pre-exponential factor, s^{-1} (see Table 2, *Air Pollution Engineering Manual*, Van Nostrand Reinhold, New York, 1992, p. 62)
 E = activation energy, cal/gmol (see Table 2, *Air Pollution Engineering Manual*, Van Nostrand Reinhold, New York, 1992, p. 62)
 R = universal gas constant, 1.987 cal/gmol °K
 T = absolute temperature, °K

The referenced table for A and E is a summary of first-order HC combustion reactions.

The end combustion products are continuously emitted at the outlet of the reactor. The average gas velocity can range from as low as 3 m/s (10 ft/s) to as high as 15 m/s (50 ft/s). These high velocities are required to prevent settling of particulates (if present) and to minimize the dangers of flashback and fire hazards. Space velocity calculations are given in the "Incinerator Design and Performance Equation" section.

The fuel is usually natural gas. The energy liberated by reaction may be directly recovered in the process or indirectly recovered by suitable external heat exchange (see Fig. 22-14).

Because of the high operating temperatures, the unit must be constructed of metals capable of withstanding this condition. Combustion

TABLE 22-33 Thermal Afterburners: Conditions Required for Satisfactory Performance in Various Abatement Applications

Abatement category	Afterburner residence time, s	Temperature, °F
Hydrocarbon emissions: 90 + % destruction of HC	0.3-0.5	1100-1250°
Hydrocarbons + CO: 90 + % destruction of HC + CO	0.3-0.5	1250-1500
Odor		
50-90% destruction	0.3-0.5	1000-1200
90-99% destruction	0.3-0.5	1100-1300
99 + % destruction	0.3-0.5	1200-1500
Smokes and plumes		
White smoke (liquid mist)		
Plume abatement	0.3-0.5	800-1000†
90 + % destruction of HC + CO	0.3-0.5	1250-1500
Black smoke (soot and combustible particulates)	0.7-1.0	1400-2000

°Temperatures of 1400 to 1500°F (760 to 816°C) may be required if the hydrocarbon has a significant content of any of the following: methane, cellulose, and substituted aromatics (e.g., toluene and xylenes).

†Operation for plume abatement only is not recommended, since this merely converts a visible hydrocarbon emission into an invisible one and frequently creates a new odor problem because of partial oxidation in the afterburner.

devices are usually constructed with an outer steel shell that is lined with refractory material. Refractory-wall thickness is usually in the 0.05- to 0.23-m (2- to 9-in) range, depending upon temperature considerations.

Some of the advantages of the thermal incinerators are:

1. Removal of organic gases
2. Removal of submicrometer organic particles
3. Simplicity of construction
4. Small space requirements

Some of the disadvantages are:

1. High operating costs
2. Fire hazards
3. Flashback possibilities

Catalytic Incinerators Catalytic incinerators are an alternative to thermal incinerators. For simple reactions, the effect of the presence of a catalyst is to (1) increase the rate of the reaction, (2) permit the reaction to occur at a lower temperature, and (3) reduce the reactor volume.

In a typical catalytic incinerator for the combustion of organic vapors, the gas stream is delivered to the reactor continuously by a fan at a velocity in the range of 3 to 15 m/s (10 to 30 ft/s), but at a lower temperature, usually in the range of 350 to 425°C (650 to 800°F), than the thermal unit. (Design and performance equations used for calculating space velocities are given in the next section). The gases, which may or may not be preheated, pass through the catalyst bed, where the combustion reaction occurs. The combustion products, which again are made up of water vapor, carbon dioxide, inerts and unreacted vapors, are continuously discharged from the outlet at a higher temperature. Energy savings can again be effected by heat recovery from the exit stream.

Metals in the platinum family are recognized for their ability to promote combustion at low temperatures. Other catalysts include various oxides of copper, chromium, vanadium, nickel, and cobalt. These catalysts are subject to poisoning, particularly from halogens, halogen and sulfur compounds, zinc, arsenic, lead, mercury, and particulates. It is therefore important that catalyst surfaces be clean and active to ensure optimum performance.

Catalysts may be porous pellets, usually cylindrical or spherical in shape, ranging from 0.16 to 1.27 cm (1/16 to 1/2 in) in diameter. Small sizes are recommended, but the pressure drop through the reactor increases. Among other shapes are honeycombs, ribbons, and wire mesh. Since catalysis is a surface phenomenon, a physical property of these particles is that the internal pore surface is nearly infinitely greater than the outside surface.

The following sequence of steps is involved in the catalytic conversion of reactants to products:

1. Transfer of reactants to and products from the outer catalyst surface
2. Diffusion of reactants and products within the pores of the catalyst
3. Activated adsorption of reactants and the desorption of the products on the active centers of the catalyst

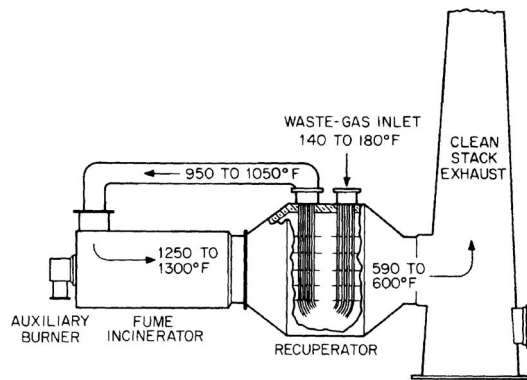


FIG. 22-14 Thermal combustion with energy (heat) recovery.

4. Reaction or reactions on active centers on the catalyst surface
 At the same time, energy effects arising from chemical reaction can result in the following:

1. Heat transfer to or from active centers to the catalyst-particle surface
2. Heat transfer to and from reactants and products within the catalyst particle
3. Heat transfer to and from moving streams in the reactor
4. Heat transfer from one catalyst particle to another within the reactor
5. Heat transfer to or from the walls of the reactor

Some of the advantages of catalytic incinerators are:

1. Lower fuel requirements as compared with thermal incinerators
2. Lower operating temperatures
3. Minimum insulation requirements
4. Reduced fire hazards
5. Reduced flashback problems

The disadvantages include:

1. Higher initial cost than thermal incinerators
2. Catalyst poisoning
3. Necessity of first removing large particulates
4. Catalyst-regeneration problems
5. Catalyst disposal

Incinerator Design and Performance Equations The key incinerator design and performance calculations are the required fuel usage and physical dimensions of the unit. The following is a general calculation procedure to use in solving for these two parameters, assuming that the process gas stream flow, inlet temperature, combustion temperature, and required residence time are known. The combustion temperature and residence time for thermal incinerators can be estimated using Table 22-33 and Eqs. (22-1) through (22-3).

1. The heat load needed to heat the inlet process gas stream to the incinerator operating temperature is:

$$Q = \Delta H \tag{22-4}$$

2. Correct the heat load for radiant heat losses, *RL*:

$$Q = (1 + RL) (\Delta H); \text{RL} = \text{fractional basis} \tag{22-5}$$

3. Assuming that natural gas is used to fire the burner with a known heating value of *HV_C*, calculate the available heat at the operating temperature. A shortcut method usually used for most engineering purposes is:

$$HA_T = (HV_C) \left(\frac{HA_T}{HV_C} \right)_{\text{ref}} \tag{22-6}$$

where the subscript "ref" refers to a reference fuel. For natural gas with a reference *HV_C* of 1059 Btu/scf, the heat from the combustion using no excess air would be given by:

$$(HA_T)_{\text{ref}} = -0.237(t) + 981; T = F \tag{22-7}$$

4. The amount of natural gas needed as fuel (*NG*) is given by:

$$NG = \frac{Q}{HA}; \text{consistent units} \tag{22-8}$$

5. The resulting volumetric flow rate is the sum of the combustion of the natural gas *q* and the process gas stream *p* at the operating temperature:

$$q_T = q_p + q_c \tag{22-9}$$

A good estimate for *q_c* is:

$$q_c = (11.5)(NG) \tag{22-10}$$

6. The diameter of the combustion device is given by:

$$S = \frac{q_T}{v_t} \tag{22-11}$$

where *v_t* is defined as the velocity of the gas stream at the incinerator operating temperature.

Condensation Frequently in air-pollution-control practice, it becomes necessary to treat an effluent stream consisting of a con-

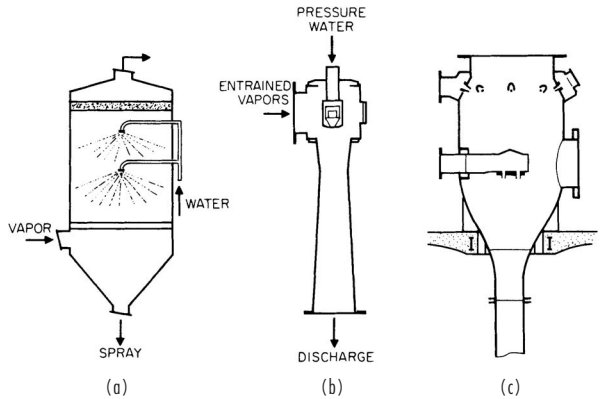


FIG. 22-15 Typical direct-contact condensers. (a) Spray chamber. (b) Jet. (c) Barometric.

densable pollutant vapor and a noncondensable gas. One control method to remove such pollutants from process-gas streams that is often overlooked is condensation. Condensers can be used to collect condensable emissions discharged to the atmosphere, particularly when the vapor concentration is high. This is usually accomplished by lowering the temperature of the gaseous stream, although an increase in pressure will produce the same result. The former approach is usually employed by industry, since pressure changes (even small ones) on large volumetric gas-flow rates are often economically prohibitive.

Condensation Equipment There are two basic types of condensers used for control: contact and surface. In contact condensers, the gaseous stream is brought into direct contact with a cooling medium so that the vapors condense and mix with the coolant (see Fig. 22-15). The more widely used system, however, is the surface condenser (or heat exchanger), in which the vapor and the cooling medium are separated by a wall (see Fig. 22-16). Since high removal efficiencies cannot be obtained with low-condensable vapor concentrations, condensers are typically used for pretreatment prior to some other more efficient control device such as an incinerator, absorber, or adsorber.

Contact Condensers Spray condensers, jet condensers, and barometric condensers all utilize water or some other liquid in direct contact with the vapor to be condensed. The temperature approach between the liquid and the vapor is very small, so the efficiency of the condenser is high, but large volumes of the liquid are necessary. If the vapor is soluble in the liquid, the system is essentially an absorptive one. If the vapor is not soluble, the system is a true condenser, in which case the temperature of the vapor must be below the dew point. Direct-contact condensers are seldom used for the removal of organic solvent vapors because the condensate will contain an organic-water mixture that must be separated or treated before disposal. They are, however, the most effective method of removing heat from hot gas streams when the recovery of organics is not a consideration.

In a direct-contact condenser, a stream of water or other cooling liquid is brought into direct contact with the vapor to be condensed. The liquid stream leaving the chamber contains the original cooling liquid plus the condensed substances. The gaseous stream leaving the

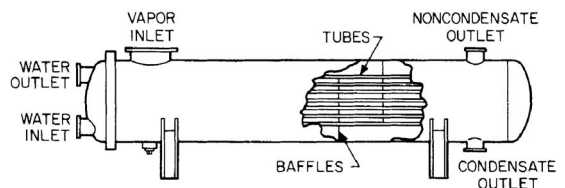


FIG. 22-16 Typical surface condenser (shell-and-tube).

chamber contains the noncondensable gases and such condensable vapor as did not condense; it is reasonable to assume that the vapors in the exit gas stream are saturated. It is then the temperature of the exit gas stream that determines the collection efficiency of the condenser.

The advantages of contact condensers are that (1) they can be used to produce a vacuum, thereby creating a draft to remove odorous vapors and also reduce boiling points in cookers and vats; (2) they usually are simpler and less expensive than the surface type; and (3) they usually have considerable odor-removing capacity because of the greater condensate dilution (13 lb of 60°F water is required to condense 1 lb of steam at 212°F and cool the condensate to 140°F). The principal disadvantage is the large water requirement. Depending on the nature of the condensate, odor in the wastewater can be offset by using treatment chemicals.

Direct-contact condensers involve the simultaneous transfer of heat and mass. Design procedures available for absorption, humidification, cooling towers, and the like may be applied with some modifications.

Surface Condensers Surface condensers (indirect-contact condensers) are used extensively in the chemical-process industry. They are employed in the air-pollution-equipment industry for recovery, control, and/or removal of trace impurities or contaminants. In the surface type, coolant does not contact the vapor condensate. There are various types of surface condensers including the shell-and-tube, fin-fan, finned-hairpin, finned-tube-section, and tubular. The use of surface condensers has several advantages. Salable condensate can be recovered. If water is used for coolant, it can be reused, or the condenser may be air-cooled when water is not available. Also, surface condensers require less water and produce 10 to 20 times less condensate. Their disadvantage is that they are usually more expensive and require more maintenance than the contact type.

Biological APC Technologies

GENERAL REFERENCES

BIOFILTRATION: Ottengraph, S. S. P., "Exhaust Gas Purification," in *Biotechnology*, vol. 8, Rehn, H. J., and G. Reed, eds., VCH Verlagsgesellschaft, Weinheim, Germany, 1986; Ottengraph, S. S. P., "Biological Elimination of Volatile Xenobiotic Compounds in Biofilters," *Bioprocess Eng.*, 1986, **1**: 61–69; Smith, F. L., et al., "Development and Demonstration of an Explicit Lumped Parameter Biofilter Model and Design Equation Incorporating Monod Kinetics," *J. Air & Waste Manage. Assoc.*, 2002, **52**(2): 208–219; Margulis, L., *Microcosmos*, Summit Books, New York, 1986.

HENRY'S LAW CONSTANTS: Subsection "Solubilities" in Sec. 2 of this handbook; DIPPR 911; ENVIRON, EPCON International, Houston; "Environmental Simulation Program": OLI Systems, Inc., Morris Plains, N. J. (www.olisystems.com); Mackay, D., et al., "A Critical Review of Henry's Law Constants for Chemicals of Environmental Interest," *J. Phys. Chem. Ref. Data*, 1981, **10**(4): 1175–1199; Tse, G., et al., "Infinite Dilution Activity Coefficients and Henry's Law Coefficients of Some Priority Water Pollutants Determined by Relative Gas Chromatographic Method," *Environ. Sci. Technol.*, 1992, **26**: 2017–2022; Smith, F. L., and A. H. Harvey, "Avoid Common Pitfalls When Using Henry's Law," *Chem. Eng. Prog.* **103**(9), 2007.

PHASE-EQUILIBRIUM DATA: Shaw, D. G., and A. Maczynski (eds.), IUPAC Solubility Data Series, Vol. 81: "Hydrocarbons in Water and Seawater—Revised and Updated," published in 12 parts in *J. Phys. Chem. Ref. Data*, 2005 and 2006; Gmehling, J., et al., "Vapor-Liquid Equilibrium Data Collection: Aqueous-Organic Systems," *DECHEMA Chemistry Data Series*, Vol. I, Part 1-1d, Schön & Wetzel GmbH, Frankfurt/Main, Germany, 1988.

Bioscrubbers, biotrickling filters, and biofilters are biological APC technologies which use enzymatic catalytic oxidation to completely break down (metabolize) biodegradable air pollutants to H₂O, CO₂, and salts. These pollutants, present in the airstream as vapors, can be either organic or inorganic (H₂S, NH₃, CO, etc.). The oxidation catalysts (enzymes) are produced and maintained within moist, living, active biomass, which operates near ambient temperature and pressure. In practice, these biological APC processes represent a subclass of gas adsorption processes, in which pollutant mass transfer from the gas phase to the liquid phase is enhanced by a fast chemical reaction in the liquid phase, which contains the biomass. Unlike incineration, biodegradation of compounds containing sulfur, nitrogen, and halogens produces benign by-products, biomass, and inorganic ions (SO₄²⁻, NO₃⁻, Cl⁻, etc.), which require little or no subsequent treatment prior

to their release into the environment. Biological processes can be particularly desirable because they neither transfer the identified pollutants into another phase (as with carbon adsorption, condensation, etc.) nor produce additional, collateral air pollution from fuel combustion [as does incineration (SO₂, NO_x, CO, CO₂, particulates, etc.)].

Biomass: The Community of Microorganisms* The microorganisms which make up the biomass in these devices are similar to those found in soil and in biological wastewater treatment plants: bacteria, often with smaller populations of fungi, ciliates, and other protists. Bacteria are extremely diverse in their biochemical degradation abilities. They all lack cellular nuclei. Individually, a bacterium has limited metabolic capabilities, because a single bacterium has limited quantities of DNA. However, individual bacteria can modify their DNA by exchange and transfer with other bacteria present. Nevertheless, this limited DNA restricts the ability of one kind of bacterium to produce all the different enzymes needed to completely break down all available substrates. Consequently, at steady state, differing bacteria live together in mixed consortia (communities) such that, taken together, these consortia can produce all the enzymes needed to completely break down the available substrates to CO₂, H₂O, salts, etc.

In bioscrubbers, biotrickling filters, and biofilters, the principal microbial populations metabolize the primary substrates, the biodegradable air pollutants. The secondary and generally smaller microbial populations assist the process of total breakdown by consuming bacterial metabolic intermediates from the primary substrates as well as other waste products produced by the other bacteria. In biotrickling filters and biofilters, the biomass exists within the airstream as a fixed biofilm, a thin layer of microbes growing on an inert attachment surface. An important advantage of an attached biofilm is that the microbes tend to become distributed along chemical gradients by depth within the biofilm. Often, the most rapidly growing microbes are concentrated near the outer surface, where both oxygen and the primary substrate are most abundant, and the slower-growing, secondary microbes are concentrated near the attachment surface. This configuration protects the secondary microbes with an outer layer of expendable microbes. It also provides a nearly infinite mean cell residence time for the often slow-growing but essential secondary microbes, needed for complete breakdown of the pollutants. These bacterial populations are consumed by still other predatory microbial populations, which decompose them, recycling their substances to the consortia. Acting together, these microbial populations finish the complete breakdown of the primary substrates.

Biofiltration: Theoretical Considerations

Maximum biofilter inlet pollutant concentration For an aerobic fixed-film device, the local total flux for all pollutants into the biofilm must not exceed the local flux of oxygen into the biofilm, on a stoichiometric basis. Therefore, the maximum acceptable total pollutant concentration is fixed, at the biofilter inlet, by the low maximum oxygen solubility in the biofilm, at the biofilm interface. This oxygen concentration is about 8 mg/L (8 ppm) for air at ambient conditions. If the total pollutant concentration exceeds this maximum limit, aerobic biological conditions cannot be maintained throughout the biofilter, a condition which can result in biofilter failure.

For a single pollutant biofilter application, using the stoichiometric coefficients v for complete pollutant oxidation, diffusivities D , and molecular weights (MW), the maximum acceptable inlet biofilm interface pollutant POL concentration S_{POL} can be estimated from the maximum available biofilm interface oxygen concentration S_{O_2} :

$$S_{POL} = \left[\frac{v_{POL}}{v_{O_2}} \right] \left[\frac{D_{O_2}}{D_{POL}} \right] \left[\frac{MW_{POL}}{MW_{O_2}} \right] S_{O_2} \quad (22-12)$$

Pollutant solubility At these very low biofilm interface concentrations, biodegradable pollutant solubility in water can be described by using Henry's law:

$$p_i = H_i C_i \quad (22-13)$$

where p is the partial pressure of the solute i in the gas phase; C is the concentration of the solute in the aqueous liquid phase; and H is the

*The contributions to this subsection by Prof. Lynn Margulis, University of Massachusetts, Amherst, are gratefully appreciated.

proportionality constant, generally referred to as the Henry's law constant. (Henry's law constants are not true constants but rather functions of temperature.) Experimental data are needed to estimate H , however, because pollutant-water mixtures are highly nonideal. The best reference for these solubilities is corroborated data from a computerized data bank that specializes in environmental aqueous systems. Such data banks are especially helpful for calculating solubilities for uncommon pollutants of environmental interest, as well as for compounds that dissociate in water, i.e., are acidic or basic.

Estimating Henry's law constants Henry's law constants can be estimated from extensive data published for solute-water LLE (liquid-liquid equilibria):

$$H_i = \frac{(1 - x_{\text{water}})P_i^{\text{sat}}}{x_i} \quad (22-14)$$

where x_{water} is the equilibrium mole fraction of water in the organic phase (often negligible), P_i^{sat} is the vapor pressure of the organic solute, and x_i is the equilibrium mole fraction of the solute in the water phase.

Extensive, reviewed tabulated pollutant data also exist (see subsection "Solubilities" in Sec. 2 of this handbook). Any single tabulated Henry's law constant H is published with its measurement temperature, typically 20 or 25°C. The constant H for a subcritical pollutant (i.e., toluene) is proportional to its pure component vapor pressure P^{sat} , and therefore H is an exponential function of temperature T . Using Henry's and Raoult's laws, a pollutant's constant H for a given ambient design temperature can be estimated by using its tabulated value and its vapor pressure, by extrapolating $\leq 25^\circ\text{C}$ over the ambient temperature range ($4^\circ\text{C} < T < 50^\circ\text{C}$), from T_1 to T_2 :

$$H_2 = \frac{\gamma_2 P_2^{\text{sat}}}{\gamma_1 P_1^{\text{sat}}} H_1 \cong \frac{P_2^{\text{sat}}}{P_1^{\text{sat}}} H_1 \quad (22-15a)$$

For a more soluble (or completely miscible) pollutant (i.e., ethanol), a Henry's law constant can be similarly estimated by using its tabulated infinite dilution activity coefficient γ_{∞} , measured at T_1 , by extrapolation using P_2^{sat} , from T_1 to T_2 :

$$H_2 = \gamma_{\infty 2} P_2^{\text{sat}} \cong \gamma_{\infty 1} P_2^{\text{sat}} \quad (22-15b)$$

Such estimations for H_2 are single-point extrapolations of nonlinear functions, and therefore should be used with caution. In both cases estimation error is introduced due to the nonlinear temperature dependence of the activity coefficient.

Biofilter kinetics and design model These biological systems are complex, so that normal simplifying assumptions are approximate at best: biomass homogeneity, independent and uniform multisubstrate kinetics, etc. Nevertheless, for understanding the basics of these bioabsorbers, it is helpful to consider them in terms of a single substrate system, with uniform classic kinetics and mass transfer, and no liquid layer external to the fixed biofilm. Chemical and environmental engineers use different expressions to describe the kinetics of substrate (pollutant) utilization—the shifting order form and the Monod (or Michaelis-Menten) form:

$$\frac{d(S_f)}{dt} = \frac{k_1 S_f}{1 + k_2 S_f} = \frac{k X_f S_f}{K_s + S_f} \quad (22-16)$$

where the variables are rate-limiting substrate concentration S_f , first-order reaction rate coefficient $k^1 = k_1$, zero-order rate coefficient $k^0 = k_1/k_2$, maximum utilization rate coefficient for the rate-limiting substrate k , density of the active substrate degraders X_f , and Monod half-velocity coefficient K_s .

Biofilters are chemically enhanced absorbers, and therefore mass transfer limited (see "Absorption with Chemical Reaction" in Sec. 14). The magnitudes for the Hatta [= Damkohler II = (Thiele modulus)²] numbers are quite low, perhaps below 5. Nevertheless, for design simplicity, mass-transfer limitation is generally assumed to be in the liquid phase (the biofilm). For a single-component biofilter, the simplified biofilter model and design equation is

$$\tau = \frac{H}{k_L a_f} \ln \left| \frac{S_{g(\text{IN})}}{S_{g(\text{OUT})}} \right| \quad (22-17)$$

where the variables are the empty-bed residence time τ , a dimensionless variable H , liquid-phase local mass-transfer coefficient k_L , and air-liquid phase effective specific surface a_f . (The units used for the dimensionless H must be the same as those used for S_g [Eq. (22-17)].) If the mass-transfer coefficient were for an ideal, single-component, fast first-order reaction system, for a biofilm having no external liquid layer of any significant thickness (i.e., not more than a moist surface), and all other variables are assumed to have constant magnitudes, then

$$k_L = \sqrt{k^1 D_f} = \sqrt{\frac{k X_f D_f}{K_s}} \quad (22-18a)$$

where D_f is the pollutant diffusion coefficient within the biofilm and k_L has a single magnitude, a function of temperature. For a single component following Monod reaction kinetics, k_L is defined as

$$k_L = \sqrt{\frac{2k X_f D_f}{S_i^2} \left(S_i - S_{\text{min}} - K_s \ln \frac{K_s + S_i}{K_s + S_{\text{min}}} \right)} \quad (22-18b)$$

where S_i and S_{min} are the pollutant biofilm concentrations, at the biofilm interface (maximum) and at the biofilm attachment surface (minimum), respectively. All other variables are assumed to have constant magnitudes throughout the biofilter. (For a "deep biofilm," S_{min} is assumed to approach the limit of zero.) Therefore, k_L is a function of the local pollutant concentration as well as a function of temperature. Note that Eq. (22-18b) predicts a lower value for k_L than does Eq. (22-18a), until the pollutant concentration approaches the limit of zero, where they are equal.

General Process Description For any APC design it is difficult to accurately characterize variations of temperature, flow rate, and composition for the polluted source stream, especially during the engineering design of the upstream process source. For biological APC design is added the state of the art, the imperfect scientific understanding of the behavior of biomass under long-term steady-state operation, but more importantly as the biomass and media respond to stream variations, especially significant step change variations. This APC field remains a technical art. The magnitude of $k_L a_f$ cannot be calculated with confidence for any media formulation from first principles, especially for multiple pollutants. Consequently, and especially for multiple components, responsible vendors can be expected to recommend field pilot testing for unfamiliar applications, as an appropriate expense for achieving a minimum annualized system cost design. What follows is written to assist chemical engineers to effectively discuss their project needs with responsible vendors of biological APC technologies, and to comprehend what they receive from such vendors.

Most natural, and most artificial, organic compounds can be biodegraded. However, only some biodegradable compounds are candidates for economical biological APC, which typically means a residence time measured in minutes [Eq. (22-17)]. Although $k_L a_f$ is important, its practical range of magnitudes is modest, and candidate suitability for treatment is principally determined by its solubility, coupled with the ratio of the design inlet and outlet concentrations. Note, for instance, that economical designs are achievable for pollutants with low concentrations and low solubility (flavors and fragrances) or for high concentrations and high solubility (ethanol, butyric acid). In practice, compounds such as ethanol, acetone, formaldehyde, acetic acid, and diethylether are good candidates; BTEX, pinenes, and similarly soluble compounds are acceptable candidates; and largely nonpolar hydrocarbons such as alkanes (and highly halogenated compounds in general) are poor candidates. The most expensive media typically can offer the highest values for $k_L a_f$ and are generally justified through reduction of the required EBRT (reduced media volume) needed for a specific application.

An ID fan, which minimizes leakage of polluted air, is normally used to maintain airflow through the process and to overcome the total system pressure drop, typically measured in centimeters of water. The optimum design temperature is determined by the trade-off between solubility, which decreases with temperature, and biological kinetics, which increases. Another optimization factor is how much heating or cooling is necessary for the inlet stream. Operation is

generally controlled to within a narrow range of a couple of degrees. The selected design temperature may range from perhaps 20 to 45°C, commonly 30 to 35°C. Particulates or aerosols, including organic liquid droplets, should be removed (perhaps > 15 µm). The inlet stream is usually prehumidified to 95 to nearly 100 percent relative humidity. Finally, temperature, particulate, and humidity control is often managed in a single step.

Biofilters Biofilters fall into two categories: soil bed biofilter (open bed) and artificial media biofilters (confined media).

Soil bed biofilters consist of an air distribution system of perforated piping buried under a layer of soil media, typically exposed outdoors. The treated air is emitted directly to atmosphere (Fig. 22-17). The soil media used can consist of a blend of natural soil components and other materials. This is a fixed-film bioreactor, with the biofilm attached to other inert soil materials. Soil media are biologically self-sustaining, hydrophilic, and self-buffering and often last for decades of use. Over a hundred are in operation. Although most soil beds are employed for odor control, any otherwise suitable candidate pollutant should be treatable in a soil bed. Soil bed operating temperature is maintained by inlet air temperature control, and soil biofilters are practical for any climate, including very cold conditions (i.e., Calgary, Alberta, Canada).

Artificial media biofilters employ a biologically active medium housed in a containment vessel (Fig. 22-18). The support media can consist of natural and synthetic materials, including compost, peat, bark, wood chips, etc., and polymer foam, activated carbon, rubber tire waste, ceramic pellets, etc., respectively. The media are typically blended, wetted, and biologically seeded (inoculated) before installation. Inert materials, such as polystyrene beads, may be blended with the media to prevent compaction and pressure drop increase and to maintain biofilm specific surface. Media moisture content can be a critical operating parameter. Secondary humidification is often employed, via water spraying, which can be accurately controlled by weigh cell measurement of the total media bed mass. Media replacement may be required 1 to 2 times per decade. Depending on the media and the pollutants, nutrients and/or pH buffers may be applied with the water spray. Some biofilters are maintained wet enough to drip, to purge soluble waste salts. Generally, artificial media biofilters can be designed for higher loadings than can soil bed biofilters. Upflow and downflow designs are practical.

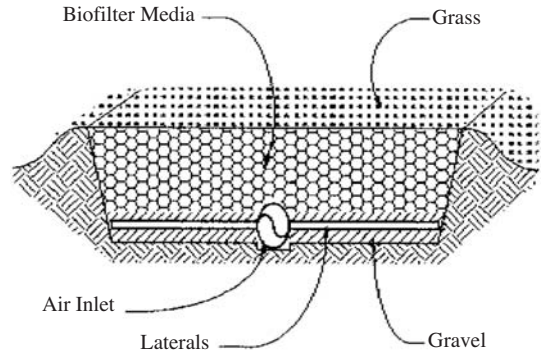


FIG. 22-17 Pretreated contaminated air flows into an inlet manifold, lateral piping, and into a continuous layer of gravel or crushed stone, providing even air distribution across the bottom of the media. Air is biofiltered, flowing upward through the biofilter media, exiting to atmosphere through the media surface or a grass cover. (Courtesy of Bohn Biofilter, www.bohnbiofilter.com.)

Bioscrubbers Bioscrubbers combine physical absorption with biological degradation, using two separate unit operations. The pollutants are absorbed into water within the scrubber. This water is then directed to an external biological reactor, where the pollutants are degraded. The treated liquid is recycled to the bioscrubber. One configuration employs water and a fixed-film bioreactor, while a second configuration employs MLSS and a slurry reactor. In both cases, separating absorption from reaction permits scrubbing pollutant concentrations far above those which a fixed-film system would survive (due to O₂ limitation). Scrubbing can be designed to attenuate substantial and rapid composition change in the inlet, assisting the performance of a downstream biotreatment step. The scrubber can be multistaged (packed column, Fig. 22-18) or single-staged (a venturi scrubber or spray chamber, Fig. 22-19). Scrubbers with horizontal airflow are also available. Nutrients, pH buffers, and makeup water are added, and biomass and waste salts are purged, as needed. Bioscrubbing is commonly combined with

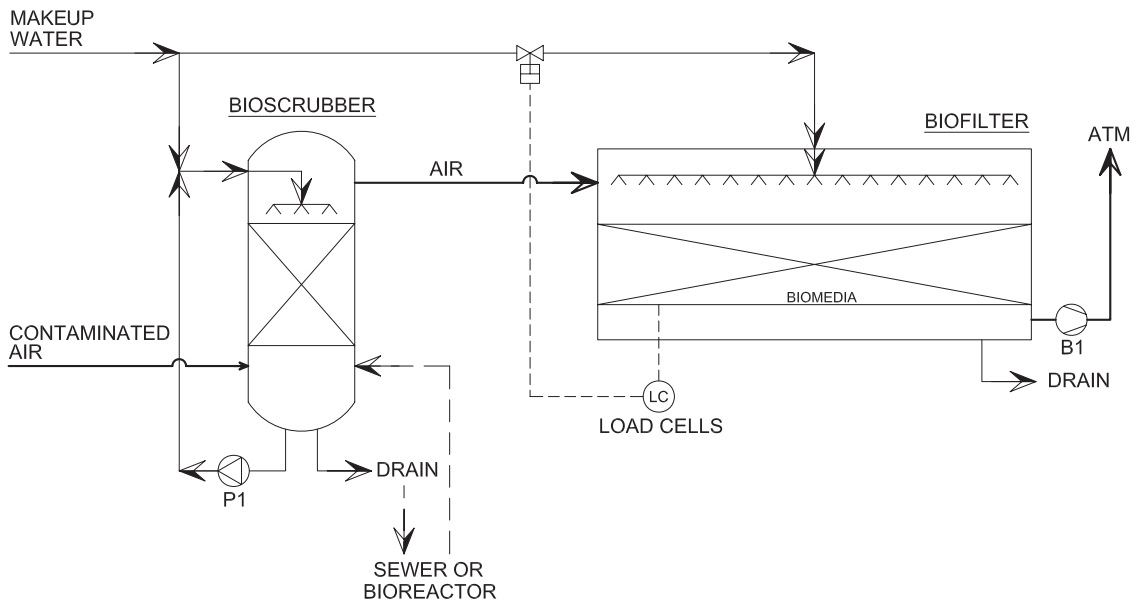


FIG. 22-18 Contaminated air is pretreated (shown: a countercurrent bioscrubber), before passing into the biofilter. Air is biofiltered, flowing downward through the media. Biomedium moisture content is accurately controlled via load-cell control of water sprays on media surface. (Courtesy of Waterleau Biofilter-Bioton, Bel-Air, www.waterleau.com.)

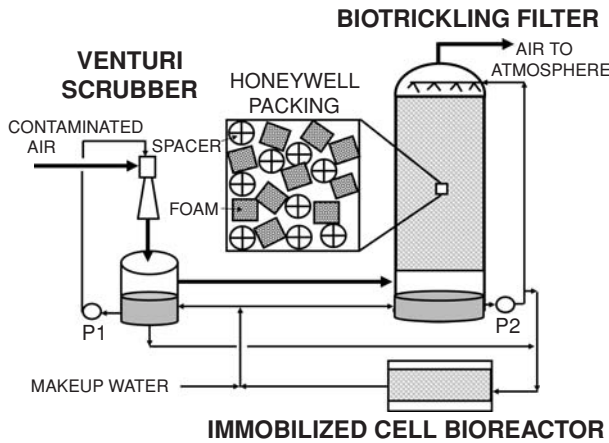


FIG. 22-19 Contaminated air is pretreated (shown: a Venturi scrubber), before passing into the biotrickling filter. Air is biofiltered, flowing downward through the media. (Courtesy of Honeywell PAI—Biological Air Treatment System, www.honeywellpai.com.)

temperature, particulate, and humidity control as feed pretreatment to biotrickling filters and biofilters. A combined multipollutant plot of $\log H = f(1/T)$ is a helpful design aid in the selection of the optimum stream composition for the scrubber effluent stream.

Biotrickling Filters Biotrickling filters are a hybrid of bioscrubbers and biofilters. A fixed biofilm (often a deep biofilm) is employed, typically attached to a synthetic medium containing blocks of polymer foam, lava rock, sintered ceramics, etc. (Fig. 22-19). Water permeability is preferred for the biofilm support media. Inert materials, such as Pall rings or other distillation-type packing materials, may be blended with the media to prevent compaction and pressure drop increase and to maintain biofilm specific surface. Water is recirculated through the filter. Although the water layer forms a resistance to pollutant mass transfer into the fixed biofilm, the water stream also absorbs pollutants which can be removed from the filter for separate biological treatment, as described above for bioscrubbers. As for a bioscrubber, this hybrid can respond more effectively to rapid changes in the feed, and can survive

higher inlet concentrations, than can a biofilter. This feature, in turn, can assist the performance of a downstream biotreatment step. Nutrients, pH buffers and makeup water are added, and biomass and waste salts are purged, as needed. Upflow, downflow, and horizontal airflow designs are practical.

Use of Activated Carbon Activated carbon (AC) can be used to enhance these processes in at least three ways. Positioned in front of the process, AC can provide pollutant concentration capacitance, reducing concentration peak magnitudes and rapid rate of variation and providing minimum concentrations during periods of no or low source pollutant flow. Positioned behind the process, AC can increase the overall process elimination efficiency, as well as scavenging nonbiologically degradable compounds (i.e., poly-halogenated organics). Mixed with the media, AC is reported to combine these two functions, enhancing biological removal and protecting the system during periods of high pollutant inlet variation. Note that AC positioned in front can present a fire hazard for certain pollutants, such as acetone. AC positioned in back is exposed to very high humidity, which restricts adsorption capacity.

Relative Biofiltration Treatment Costs The true final annualized cost for treating a polluted airstream with any specific APC technology is complex and will be affected by many factors, including project-specific factors. Nevertheless, Fig. 22-20 can provide helpful guidance to the relationships between the probable final costs for treating a polluted airstream using different APC technologies.

Membrane Filtration Membrane systems have been used for several decades to separate colloidal and molecular slurries by the chemical process industries (CPI). Membrane filtration was not viewed as a commercially viable pollution control technology until recently. This conventional wisdom was due to fouling problems exhibited when handling process streams with high solid content. This changed with the advent of membranes composed of high-flux cellulose acetate. In Europe and Asia, membrane filtration systems have been used for several years, primarily for ethanol dewatering for synthetic fuel plants. Membrane systems were selected in these cases for their (1) low energy utilization; (2) modular design; (3) low capital costs; (4) low maintenance; and (5) superior separations. In the United States, as EPA regulations become increasingly stringent, a renewed interest in advanced membrane filtration systems has occurred. In this case, the driving factors are the membrane system's ability to operate in a pollution-free, closed-loop manner with minimum wastewater output. Low capital and maintenance costs also result from the small amount of moving parts within the membrane systems.

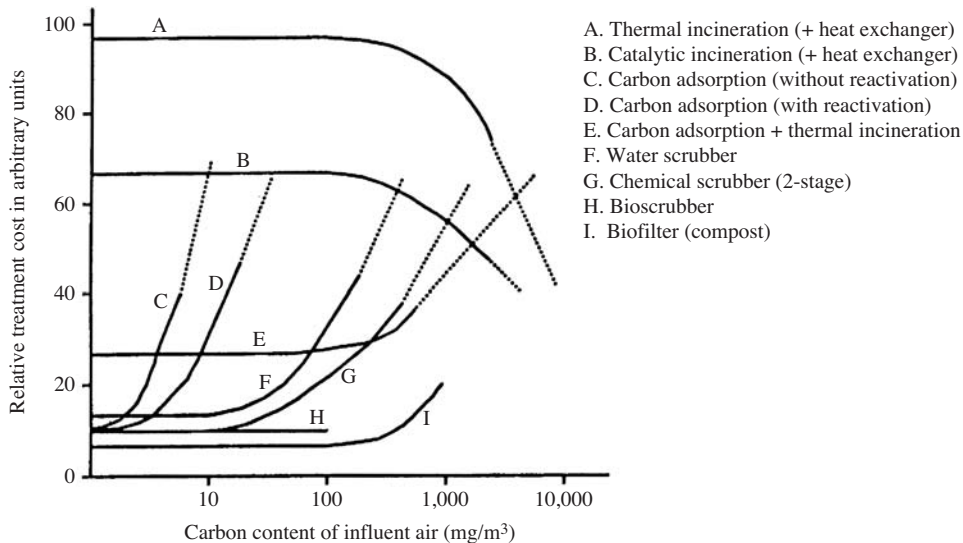


FIG. 22-20 Relative (and approximate) treatment costs for removing VOCs from air (Kosky and Neff, 1988). Assumption: 40,000 m³/h at 1982 price level. (Note: Current costs for chemical scrubbing can be 2 or more times greater than for biofiltration.)

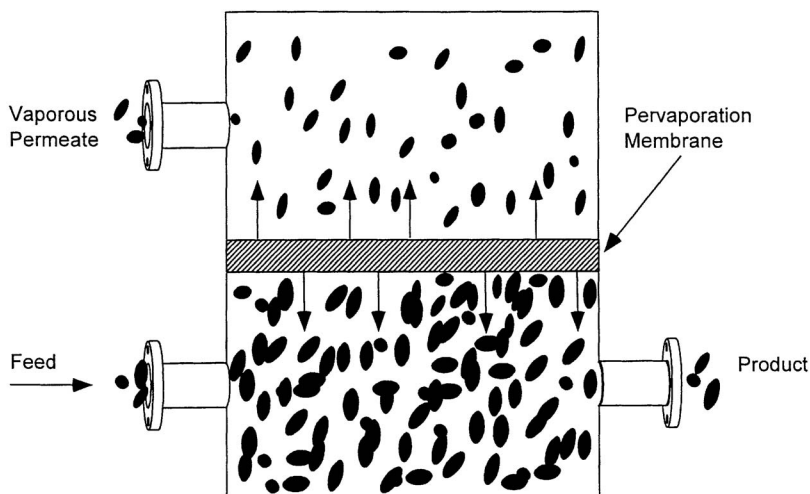


FIG. 22-21 Pervaporation of gas from liquid feed across membrane to vaporous permeate. (SOURCE: Redrawn from Ref. 24.)

Process Descriptions Selectively permeable membranes have an increasingly wide range of uses and configurations as the need for more advanced pollution control systems are required. There are four major types of membrane systems: (1) pervaporation; (2) reverse osmosis (RO); (3) gas absorption; and (4) gas adsorption. Only membrane pervaporation is currently commercialized.

Membrane Pervaporation Since 1987, membrane pervaporation has become widely accepted in the CPI as an effective means of separation and recovery of liquid-phase process streams. It is most commonly used to dehydrate liquid hydrocarbons to yield a high-purity ethanol, isopropanol, and ethylene glycol product. The method basically consists of a selectively-permeable membrane layer separating a liquid feed stream and a gas phase permeate stream as shown in Fig. 22-21. The permeation rate and selectivity is governed by the physicochemical composition of the membrane. Pervaporation differs from reverse osmosis systems in that the permeate rate is not a function of osmotic pressure, since the permeate is maintained at saturation pressure (Ref. 24).

Three general process groups are commonly used when describing pervaporation: (1) water removal from organics; (2) organic removal from water (solvent recovery); and (3) organic/organic separation. Organic/organic separations are very uncommon and therefore will not be discussed further.

Ethanol Dehydration The membrane-pervaporation process for dehydrating ethanol was first developed by GFT in West Germany in the mid 1970s, with the first commercial units being installed in Brazil and the Philippines. At both sites, the pervaporation unit was coupled to a continuous sugarcane fermentation process that produced ethanol at concentrations up to 96 percent after vacuum pervaporation. The key advantages of the GFT process are (1) no additive chemicals are required; (2) the process is skid-mounted (low capital costs and small footprint); (3) and there is a low energy demand. The low energy requirement is achieved because only a small fraction of the water is actually vaporized and that the required permeation driving force is provided by only a small vacuum pump. The basic ethanol dehydration process schematic is shown in Fig. 22-22. A key advantage of all pervaporation processes is that vapor-liquid equilibria and possible resulting azeotropic effects are irrelevant (see Fig. 22-23 and Ref. 24).

Solvent Recovery The largest current industrial use of pervaporation is the treatment of mixed organic process streams that have become contaminated with small (10 percent) quantities of water. Pervaporation becomes very attractive when dehydrating streams down to less than 1 percent water. The advantages result from the small operating costs relative to distillation and adsorption. Also, dis-

tillation is often impossible, since azeotropes commonly form in multicomponent organic/water mixtures.

Pervaporation occurs in three basic steps:

1. Preferential sorption of chemical species
2. Diffusion of chemical species through the membrane
3. Desorption of chemical species from the membrane

Steps 1 and 2 are controlled by the specific polymer chemistry and its designed interaction with the liquid phase. The last step, consisting of evaporation of the chemical species, is considered to be a fast, nonselective process. Step 2 is the rate-limiting step. The development by the membrane manufacturers of highly selective, highly permeable composite membranes that resist fouling from solids has subsequently been the key to commercialization of pervaporation systems. The membrane composition and structure are designed in layers, with each layer fulfilling a specific requirement. Using membrane dehydration as an example, a membrane filter would be composed of a support layer of nonwoven porous polyester below a layer of polyacrylonitrile (PAN) or polysulfone ultrafiltration membrane and a layer of 0.1- μm -thick crosslinked polyacrylate, polyvinyl alcohol (PVA). Other separations membranes generally use the same two sublayers. The top layer is interchanged according to the selectivity desired.

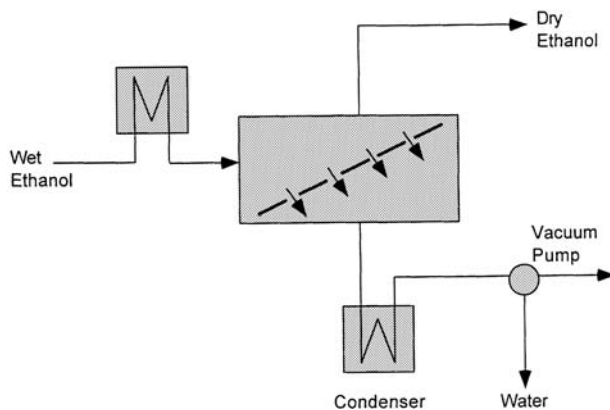


FIG. 22-22 Ethanol dehydration using pervaporation membrane. (SOURCE: Redrawn from Ref. 24.)

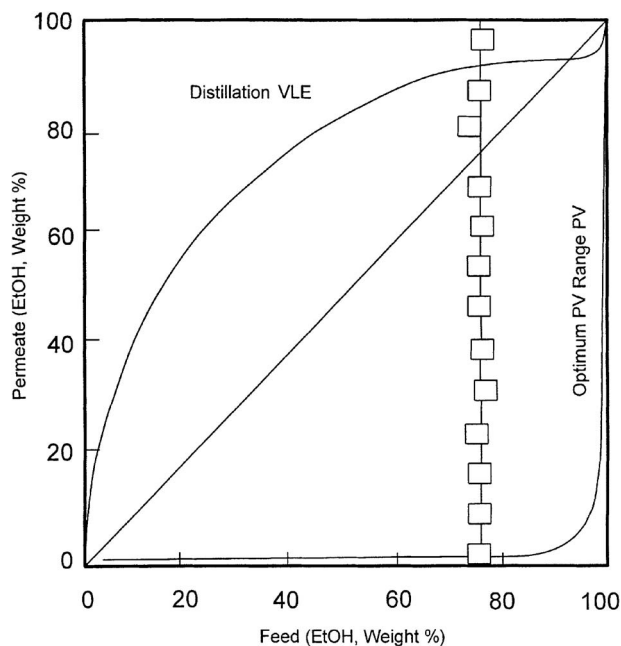


FIG. 22-23 Comparison of two types of pervaporation membranes to distillation of ethanol-water mixtures. (SOURCE: Redrawn from Ref. 24.)

Emerging Membrane Control Technologies The recent improvements in membrane technology have spawned several potentially commercial membrane filtration uses.

Reverse Osmosis (RO) Membranes A type of membrane system for treating oily wastewater is currently undergoing commercialization by Bend Research, Inc. The system uses a tube-side feed module that yields high fluxes while being able to handle high-solids-content waste streams (Ref. 25). Another type of reverse osmosis technique is being designed to yield ultrapurified HF recovered from spent etching solutions. It is estimated that 20,000 tons of spent solution is annually generated in the United States and that using membrane RO could save 1 million bbl/yr of oil.

In Situ Filter Membranes In situ membranes are being fitted into incinerator flue-gas stacks in an attempt to reduce hydrocarbon emissions. Two types of commercially available gas separation membranes are being studied: (1) flat cellulose acetate sheets; and (2) hollow-tube fiber modules made of polyamides.

Vibratory Shear-Enhanced Membranes The vibratory shear-enhancing process (VSEP) is just starting commercialization by Logic International, Emeryville, CA. It employs the use of intense sinusoidal shear waves to ensure that the membrane surfaces remain active and clean of solid matter. The application of this technology would be in the purification of wastewater (Ref. 2).

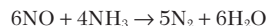
Vapor Permeation Vapor permeation is similar to vapor pervaporation except that the feed stream for permeation is a gas. The future commercial viability of this process is based upon energy and capital costs savings derived from the feed already being in the vapor-phase, as in fractional distillation, so no additional heat input would be required. Its foreseen application areas would be the organics recovery from solvent-laden vapors and pollution treatment. One commercial unit was installed in Germany in 1989 (Ref. 26).

Selective Catalytic Reduction of Nitrogen Oxides The traditional approach to reducing ambient ozone concentrations has been to reduce VOC emissions, an ozone precursor. In many areas, it has now been recognized that elimination of persistent exceedances of the National Ambient Air Quality Standard for ozone may require more

attention to reductions in the other ingredients in ozone formation, nitrogen oxides (NO_x). In such areas, ozone concentrations are controlled by NO_x rather than VOC emissions.

Selective catalytic reduction (SCR) has been used to control NO_x emissions from utility boilers in Europe and Japan for over a decade. Applications of SCR to control process NO_x emissions in the chemical industry are becoming increasingly common. A typical SCR system is shown in Fig. 22-24.

NO_x -laden fumes are preheated by effluent from the catalyst vessel in the feed/effluent heat exchanger and then heated by a gas- or oil-fired heater to over 600°F. A controlled quantity of ammonia is injected into the gas stream before it is passed through a metal oxide, zeolite, or promoted zeolite catalyst bed. The NO_x is reduced to nitrogen and water in the presence of ammonia in accordance with the following exothermic reactions:



NO_x analyzers at the preheater inlet and catalyst vessel outlet monitor NO_x concentrations and control the ammonia feed rate. The effluent gives up much of its heat to the incoming gas in the feed/effluent exchanger. The vent gas is discharged at about 350°F.

SOURCE CONTROL OF PARTICULATE EMISSIONS

There are four conventional types of equipment used for the control of particulate emissions:

1. Mechanical collectors
2. Wet scrubbers
3. Electrostatic precipitators
4. Fabric filters

Each is discussed in Sec. 17 of this handbook under "Gas-Solids Separations." The effectiveness of conventional air-pollution-control equipment for particulate removal is compared in Fig. 22-25. These fractional efficiency curves indicate that the equipment is least efficient in removing particulates in the 0.1- to 1.0- μm range. For wet scrubbers and fabric filters, the very small particulates (0.1 μm) can be efficiently removed by brownian diffusion. The smaller the particulates, the more intense their brownian motion and the easier their collection by diffusion forces. Larger particulates (>1 μm) are collected principally by impaction, and removal efficiency increases with particulate size. The minimum in the fractional efficiency curve for scrubbers and filters occurs in the transition range between removal by brownian diffusion and removal by impaction.

A somewhat similar situation exists for electrostatic precipitators. Particulates larger than about 1 μm have high mobilities because they are highly charged. Those smaller than a few tenths of a micrometer can achieve moderate mobilities with even a small charge because of aerodynamic slip. A minimum in collection efficiency usually occurs in the transition range between 0.1 and 1.0 μm . The situation is further complicated because not all particulates smaller than about 0.1 μm acquire charges in an ion field. Hence, the efficiency of removal of very small particulates decreases after reaching a maximum in the submicrometer range.

The selection of the optimum type of particulate collection device (i.e., ESP or fabric filter baghouse) is often not obvious without conducting a site-specific economic evaluation. This situation has been brought about by both the recent reductions in the allowable emissions levels and advancements with fabric filter and ESP technologies. Such technoeconomic evaluations can result in application and even site-specific differences in the final optimum choice (see *Precip Newsletter*, 220, June, 1994 and *Fabric Filter Newsletter*, 223, June, 1994).

Improvements in existing control technology for fine particulates and the development of advanced techniques are top-priority research goals. Conventional control devices have certain limitations. Precipitators, for example, are limited by the magnitude of charge on

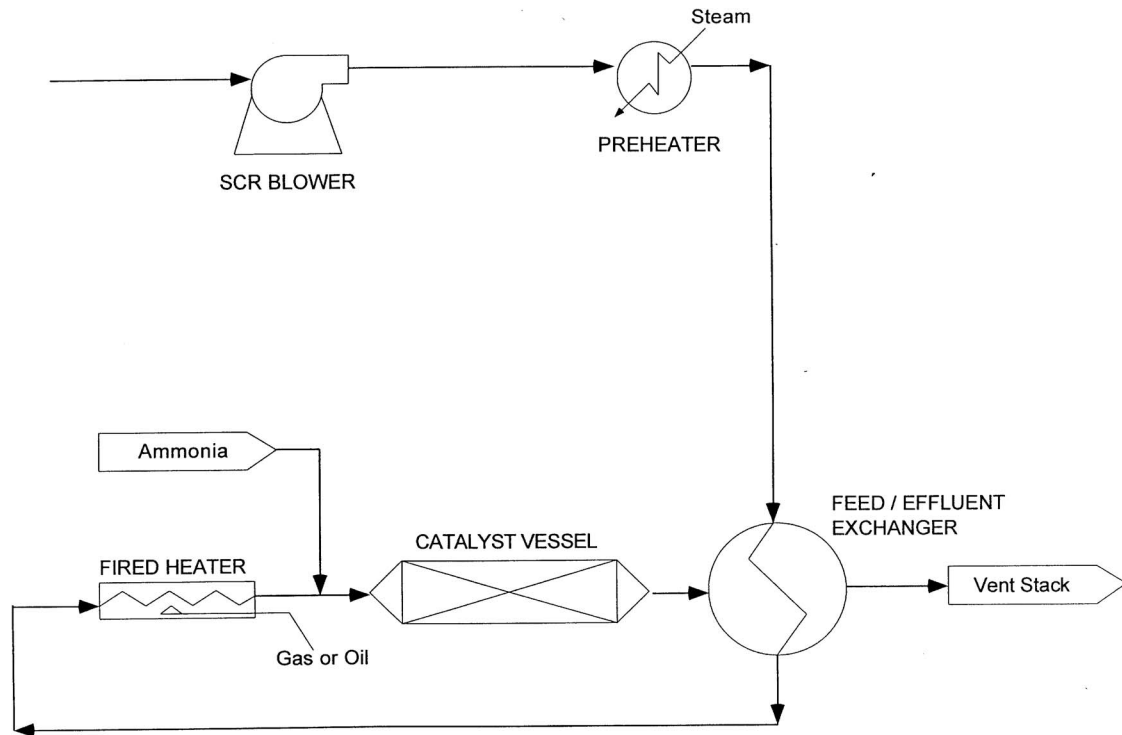


FIG. 22-24 Selective catalytic reduction of nitrogen oxides.

the particulate, the electric field, and dust reentrainment. Also, the resistivity of the particulate material may adversely affect both charge and electric field. Advances are needed to overcome resistivity and extend the performance of precipitators not limited by resistivity (see Buonicore and Theodore, "Control Technology for Fine Particulate Emissions," DOE Rep. ANL/ECT-5, Argonne National Laboratory, Argonne, Illinois, October 1978). Recent design developments with the potential to improve precipitator performance include pulse energization, electron beam ionization, wide plate spacing, and precharged units [Balakrishnan et al., "Emerging Technologies for Air Pollution Control," *Pollut. Eng.*, **11**, 28-32 (Nov. 1979); "Pulse Energization," *Environ. Sci. Technol.* **13**(9), 1044 (1974); and Midkaff, "Change in Precipitator Design Expected to Help Plants Meet Clean Air Laws," *Power*, **126**(10), 79 (1979)]; Robert A. Mastropietro, "Impact of ESP Performance on $PM_{2.5}$," European Particulate Control Users Group Meeting, Pisa, Italy, Nov. 7, 2000.

Fabric filters are limited by physical size and bag-life considerations. Some sacrifices in efficiency might be tolerated if higher air-cloth ratios could be achieved without reducing bag life (improved pulse-jet systems). Improvements in fabric filtration may also be possible by enhancing electrostatic effects that may contribute to rapid formation of a filter cake after cleaning. J.C. Mycock, J. Turner, and J. Farmer, "Baghouse Filtration Products Verification Testing, How It Benefits the Boiler Baghouse Operator," Council of Industrial Boiler Owners Conference, May 6, 2002; C. Jean Bustard et al. "Long Term Evaluation of Activated Carbon Injection for Mercury Control Upstream of a Cohnpac Fabric Filter," Air Quality IV, Arlington, Va., Sept. 22, 2003.

Scrubber technology is limited by scaling and fouling, overall reliability, and energy consumption. The use of supplementary forces acting on particulates to cause them to grow or otherwise be more easily collected at lower pressure drops is being closely investigated. The development of electrostatic and flux-force-condensation scrubbers is a step in this direction.

The electrostatic effect can be incorporated into wet scrubbing by charging the particulates and/or the scrubbing-liquor droplets. Electrostatic scrubbers may be capable of achieving the same efficiency for fine-particulate removal as is achieved by high-energy scrubbers, but at substantially lower power input. The major drawbacks are increased maintenance of electrical equipment and higher capital cost.

Flux-force-condensation scrubbers combine the effects of flux force (diffusiophoresis and thermophoresis) and water-vapor condensation. These scrubbers contact hot, humid gas with subcooled liquid, and/or they inject steam into saturated gas, and they have demonstrated that a number of these novel devices can remove fine particulates (see Fig. 22-26). Although limited in terms of commercialization, these systems may find application in many industries.

EMISSIONS MEASUREMENT

Introduction An accurate quantitative analysis of the discharge of pollutants from a process must be determined prior to the design and/or selection of control equipment. If the unit is properly engineered by utilizing the emission data as input to the control device and the code requirements as maximum-effluent limitations, most pollutants can be successfully controlled.

Sampling is the keystone of source analysis. Sampling methods and tools vary in their complexity according to the specific task; therefore, a degree of both technical knowledge and common sense is needed to design a sampling function. Sampling is done to measure quantities or concentrations of pollutants in effluent gas streams, to measure the efficiency of a pollution-abatement device, to guide the designer of pollution-control equipment and facilities, and/or to appraise contamination from a process or a source. A complete measurement requires a determination of the concentration and contaminant characteristics as well as the associated gas flow. Most statutory limitations require mass rates of emissions; both concentration and volumetric-flow-rate data are therefore required.

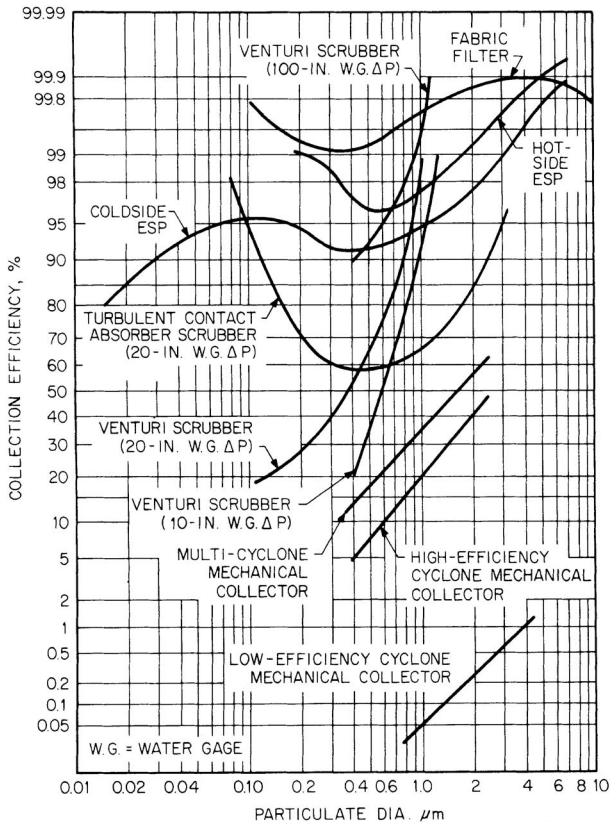


FIG. 22-25 Fractional efficiency curves for conventional air-pollution-control devices. [Chem. Eng., 87(13), 83 (June 30, 1980).]

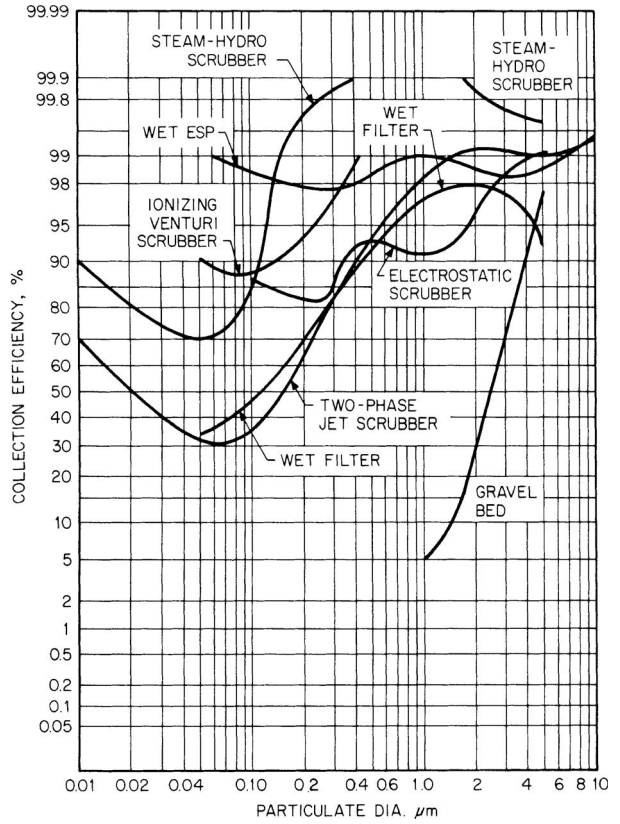


FIG. 22-26 Fractional efficiency curves for novel air-pollution-control devices. [Chem. Eng., 87(13), 85 (June 30, 1980).]

The selection of a sampling site and the number of sampling points required are based on attempts to get representative samples. To accomplish this, the sampling site should be at least eight stack or duct diameters downstream and two diameters upstream from any flow disturbance, such as a bend, expansion, contraction, valve, fitting, or visible flame.

Once the sampling location has been decided on, the flue cross section is laid out in a number of equal areas, the center of each being the point where the measurement is to be taken. For rectangular stacks, the cross section is divided into equal areas of the same shape, and the traverse points are located at the center of each equal area, as shown in Fig. 22-27. The ratio of length to width of each elemental area should be selected. For circular stacks, the cross section is divided into equal annular areas, and the traverse points are located at the centroid of each area. The location of the traverse points as a percentage of diameter from the inside wall to the traverse point for circular-stack sampling is given in Table 22-34. The number of traverse points necessary on each of two perpendiculars for a particular stack may be estimated from Fig. 22-28.

Once these traverse points have been determined, velocity measurements are made to determine gas flow. The stack-gas velocity is usually determined by means of a pitot tube and differential-pressure gauge. When velocities are very low (less than 3 m/s [10 ft/s]) and when great accuracy is not required, an anemometer may be used. For gases moving in small pipes at relatively high velocities or pressures, orifice-disk meters or venturi meters may be used. These are valuable as continuous or permanent measuring devices.

Once a flow profile has been established, sampling strategy can be considered. Since sampling collection can be simplified and greatly

reduced depending on flow characteristics, it is best to complete the flow-profile measurement before sampling or measuring pollutant concentrations.

Sampling Methodology The following subsections review the methods specified for sampling commonly regulated pollutants as well as sampling for more exotic volatile and semivolatile organic compounds. In all sampling procedures, the main concern is to obtain a representative sample; the U.S. EPA has published

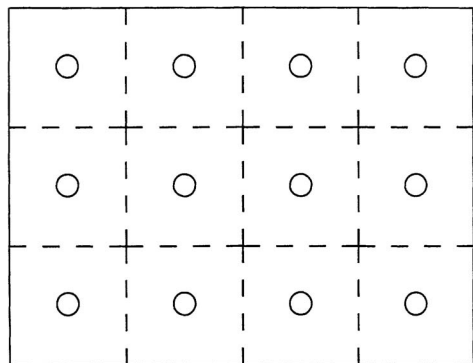


FIG. 22-27 Example showing rectangular stack cross section divided into 12 equal areas, with a traverse point at centroid of each area.

TABLE 22-34 Location of Traverse Points in Circular Stacks

(Percent of stack diameter from inside wall to traverse point)

Traverse point number on a diameter	Number of traverse points on a diameter										
	2	4	6	8	10	12	14	18	20	22	24
1	14.6	6.7	4.4	3.2	2.6	2.1	1.8	1.4	1.3	1.1	1.1
2	85.4	25.0	14.6	10.5	8.2	6.7	5.7	4.4	3.9	3.5	3.2
3		75.0	29.6	19.4	14.6	11.8	9.9	7.5	6.7	6.0	5.5
4		93.3	70.4	32.3	22.6	17.7	14.6	10.9	9.7	8.7	7.9
5			85.4	67.7	34.2	25.0	20.1	14.6	12.9	11.6	10.5
6			95.6	80.6	65.8	35.6	26.9	18.8	16.5	14.6	13.2
7				89.5	77.4	64.4	36.6	23.6	20.4	18.0	16.1
8				96.8	85.4	75.0	63.4	29.6	25.0	21.8	19.4
9					91.8	82.3	73.1	38.2	30.6	26.2	23.0
10					97.4	88.2	79.9	61.8	38.8	31.5	27.2
11						93.3	85.4	70.4	61.2	39.3	32.3
12						97.9	90.1	76.4	69.4	60.7	39.8
13							94.3	81.2	75.0	68.5	60.2
14							98.2	85.4	79.6	73.8	67.7
15								89.1	83.5	78.5	72.8
16								92.5	87.1	82.0	77.0
17								95.6	90.3	85.4	80.8
18								98.6	93.3	88.4	83.9
19									96.1	91.3	86.8
20									96.7	94.0	89.5
21										96.5	92.1
22										98.9	94.5
23											96.8
24											96.9

reference sampling methods for measuring emissions of specific pollutants so that uniform procedures can be applied in testing to obtain a representative sample. Table 22-35 provides a list of some of the most commonly employed test methods. A complete listing of all EPA test methods can be found by going online to the USEPA Technology Transfer Network Emission Measurement Center at www.epa.gov/ttn/emc/promgate.html. These are the CFR Promulgated test methods published in the Federal Register and are the federal government's official legal versions. The test methods reviewed in the following subsections address measuring the emissions of the following pollutants: particulate matter, sulfur dioxide, nitrogen oxides, carbon monoxide, fluorides, hydrogen chloride, total gaseous organics, multiple metals, volatile organic compounds, and semivolatile organic compounds.

Each sampling method requires the use of complex sampling equipment that must be calibrated and operated in accordance with specified reference methods. Additionally, the process or source that is being tested must be operated in a specific manner, usually at rated capacity, under normal procedures.

Velocity and Volumetric Flow Rate The U.S. EPA has published Method 2 as a reference method for determining stack-gas velocity and volumetric flow rate. At several designated sampling points, which represent equal portions of the stack volume (areas in the stack), the velocity and temperature are measured with instrumentation shown in Fig. 22-29.

Measurements to determine volumetric flow rate usually require approximately 30 min. Since sampling rates depend on stack-gas velocity, a preliminary velocity check is usually made prior to testing for pollutants to aid in selecting the proper equipment and in determining the approximate sampling rate for the test.

The volumetric flow rate determined by this method is usually within ± 10 percent of the true volumetric flow rate.

Sources of Methods and Information For the person trying to obtain current information or to enter into the field of source measurements, several particularly helpful information sources are available. The U.S. EPA methods fall in two groups—those used by EPA's Office of Air Quality Planning and Standards (OAQPS) and those used by EPA's Office of Solid Waste (OSW).

The Emission Measurement Technical Information Center (EMTIC) at Research Triangle Park, N.C., is supported by EPA's Office of Air Quality Planning and Standards. Perhaps the most efficient of several available forms of assistance is the EMTIC Bulletin Board System (BBS). Test methods are included along with announcements, utility programs, miscellaneous documents, and other information. The EMTIC/BBS may be reached through TTN 2000 on the Internet at <http://www.epa.gov/ttn>. An EMTIC representative can be reached by telephone at 919-541-0200. EMTIC sponsors workshops and training courses jointly with EPA's Air Pollution Training Institute. Training videotapes, a newsletter, and other mailings are also available from EMTIC.

An excellent source for information concerning OSW's SW-846 Methods is the Methods Information Communication Exchange (MICE). MICE can be reached on the Internet at mice@lan828.ehsg.saic.com. A telephone call to the MICE line, at 703-821-4690, will put the information seeker in touch with an automated information service or with a live representative. Although the function of MICE is to provide information, they will usually send copies of up to three methods. They will not provide copies of the entire SW-846 Methods Manual. The SW-846 Methods Manual may be obtained on CD-ROM or hard copy from National Technical Information Service (NTIS). The NTIS order number for the CD-ROM which includes the third edition and updates 1-3 is PB97-501928INQ. NTIS has a web site at <http://www.ntis.gov> and may also be reached by telephone at 703-487-4650. SW-846 may also be obtained from the Government Printing Office (GPO). Ordering information for GPO is *Test Methods for Evaluating Solid Waste, Physical/Chemical Methods, SW-846 Manual*, 3d ed., Document No. 955-001-000001. Available from Superintendent of Documents, U.S. Government Printing Office, Washington, D.C., November 1986.

The full document is available from the U.S. Government Printing Office, telephone 202-783-3238. GPO also has a web site at <http://www.access.gpo.gov>.

For more information or copies of the California Environmental Protection Agency, Air Resources Board Methods (a.k.a. CARB Methods), contact <http://www.arb.ca.gov/testmeth/testmeth.htm> or telephone the Engineering and Laboratory Branch at 916-263-1630.

EPA reports may be ordered from NTIS at the web site or telephone number given above.

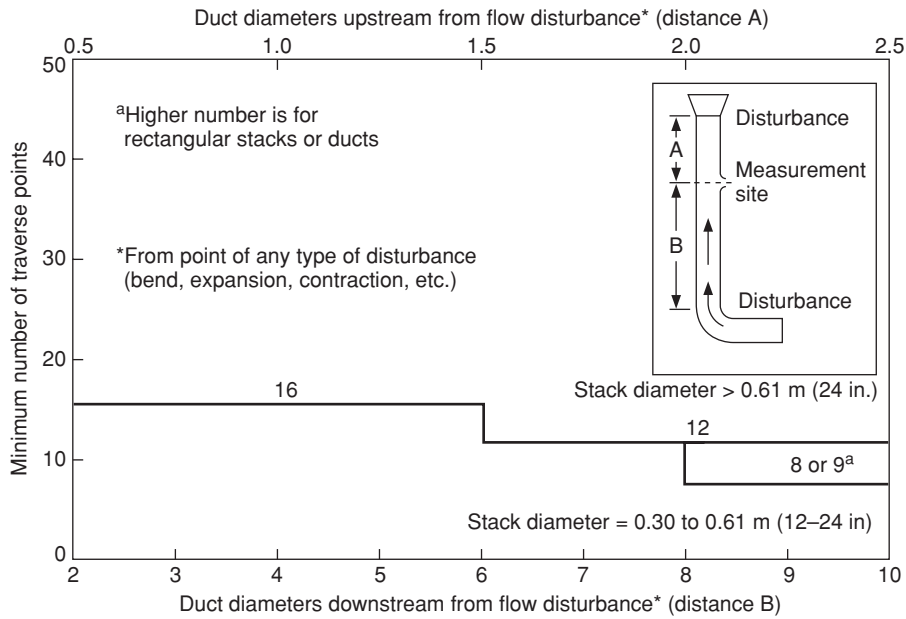
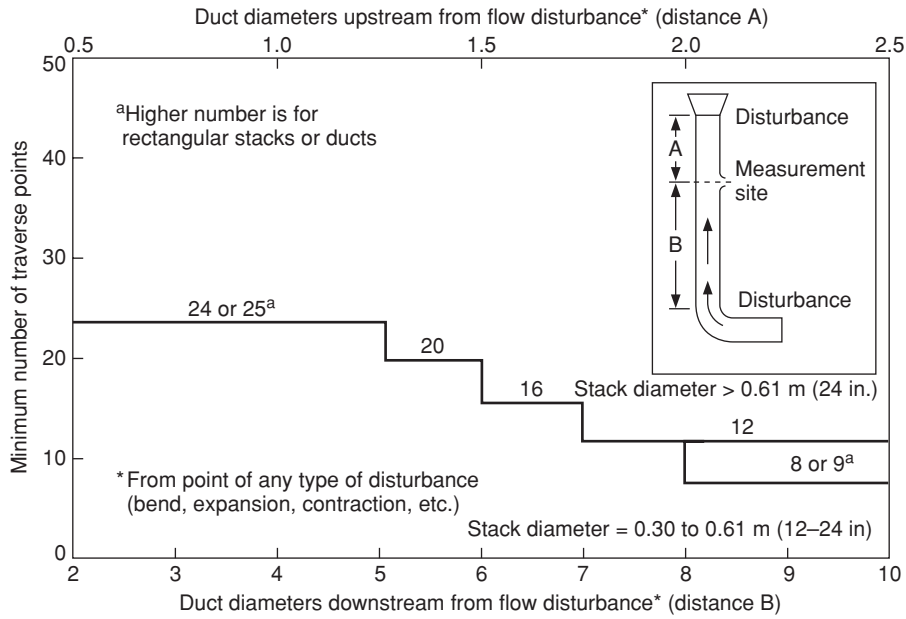


FIG. 22-28 Minimum number of traverse points for (a) particulate traverse and (b) velocity (nonparticulate) traverse.

TABLE 22-35 Selected EPA Test Methods

Commonly Used in Stationary Source Compliance Tests

Method	Test parameter(s)
Office of Air Quality Planning and Standards (OAQPS)	
Methods 1-4	Test location, volumetric flow, gas composition, moisture content
Method 5	Particulate matter
Method 6	Sulfur dioxide
Method 7	Nitrogen oxides
Method 9	Opacity
Method 10	Carbon monoxide
Method 13	Total fluoride
Method 23	Dioxins and furans
Method 25	VOCs
Method 26	Halogens, halides
Method 29	Metals
Method 201	Particulate PM ₁₀
Method 202	Condensible particulate matter
Office of Solid Waste (OSW)	
Method 0010	Modified Method 5, semivolatile organics
Method 0030	Volatile organics

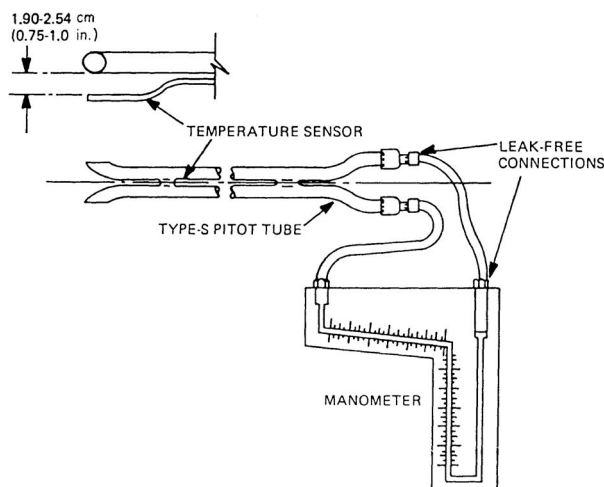


FIG. 22-29 Velocity-measurement system.

INDUSTRIAL WASTEWATER MANAGEMENT

FURTHER READING: Eckenfelder, W. W., *Industrial Water Pollution Control*, 2d ed., McGraw-Hill, 1989. Metcalf & Eddy, Inc., *Wastewater Engineering, Treatment, Disposal and Reuse*, 3d ed., McGraw-Hill, 1990. Nemerow, N. L. and A. Dasgupta, *Industrial and Hazardous Waste Treatment*, Van Nostrand Reinhold, New York, 1991.

INTRODUCTION

All industrial operations produce some wastewaters which must be returned to the environment. Wastewaters can be classified as (1) domestic wastewaters, (2) process wastewaters, and (3) cooling wastewaters. Domestic wastewaters are produced by plant workers, shower facilities, and cafeterias. Process wastewaters result from spills, leaks, product washing, and noncooling processes. Cooling wastewaters are the result of various cooling processes and can be once-pass systems or multiple-recycle cooling systems. Once-pass cooling systems employ large volumes of cooling waters that are used once and returned to the environment. Multiple-recycle cooling systems have various types of cooling towers to return excess heat to the environment and require periodic blowdown to prevent excess buildup of salts.

Domestic wastewaters are generally handled by the normal sanitary-sewerage system to prevent the spread of pathogenic microorganisms which might cause disease. Normally, process wastewaters do not pose the potential for pathogenic microorganisms, but they do pose potential damage to the environment through either direct or indirect chemical reactions. Some process wastes are readily biodegraded and create an immediate oxygen demand. Other process wastes are toxic and represent a direct health hazard to biological life in the environment. Cooling wastewaters are the least dangerous, but they can contain process wastewaters as a result of leaks in the cooling systems. Recycle cooling systems tend to concentrate both inorganic and organic contaminants to a point at which damage can be created.

Recently, concern for subtle aspects of environmental damage has started to take precedence over damage referred to above. It has been realized that the presence of substances in water at concentrations far below those that will produce overt toxicity or excessive reduction of dissolved oxygen levels can have a major impact by altering the predomination of organisms in the aquatic ecosystem. This is beginning to have an effect on water-quality standards and, consequently, allow-

able discharges. Unfortunately, the extent of knowledge is not sufficient upon which to base definitive standards for these subtle effects. Emerging chemicals of concern include pharmaceutically active agents, endocrine disrupters, and low concentrations of heavy metals and metalloids. Over the next decade, it is anticipated that accumulation of knowledge will make it possible to delineate defensible standards. Another recent concern is that of contaminated storm water from industrial sites. Federal guidelines to control this wastewater are presently being developed. Most concern is for product spills on plant property but outside the production facility and from rain contact with spoil piles.

UNITED STATES LEGISLATION, REGULATIONS, AND GOVERNMENT AGENCIES

Federal Legislation Public Law 92-500 promulgated in 1972 created the primary framework for management of water pollution in the United States. This act has been amended many times since 1972. Major amendments occurred in 1977 (Public Laws 95-217 and 95-576), 1981 (Public Laws 97-117 and 97-164), and 1987 (Public Law 100-4). This law and its various amendments are referred to as the Clean Water Act. The Clean Water Act addresses a large number of issues of water pollution management. A general review of these issues has been presented in an earlier chapter in this handbook. Primary with respect to control of industrial wastewater is the National Pollutant Discharge Elimination System (NPDES), originally established by PL 92-500. Any municipality or industry that discharges wastewater to the navigable waters of the United States must obtain a discharge permit under the regulations set forth by the NPDES. Under this system, there are three classes of pollutants (conventional pollutants, priority pollutants, and nonconventional/nonpriority pollutants). Conventional pollutants are substances such as biochemical oxygen demand (BOD), suspended solids (SS), pH, oil and grease, and coliforms. Priority pollutants are a list of 129 substances originally set forth in a consent decree between the Environmental Protection Agency and several environmental organizations. This list was incorporated into the 1977 amendments. Most of the substances on this list are organics, but it does include most of the heavy metals. These substances are generally considered to be toxic. However, the toxicity is not absolute; it depends on the concentration. In addition, many of

the organics on the list are under appropriate conditions biodegradable. In reality, substances for inclusion on the priority pollutant list were chosen on the basis of a risk assessment rather than only a hazard assessment. The third class of pollutants could include any pollutant not in the first two categories. Examples of substances that are presently regulated in the third category are nitrogen, phosphorous, sodium, and chlorine residual. The overall goals of the Clean Water Act are to restore and maintain water quality in the navigable waters of the United States. The initial standard was to ensure that these waters would be clean enough for recreation (swimmable) and ecologically secure (fishable). Initially this was to be achieved by curtailment of the discharge of pollutants. Eventually the regulatory system was essentially to phase out discharge of any pollutant into water. Obviously, if no discharge of pollutants occurs, the waters will be maintained in close to a pristine condition. However, the early reduction of pollutant discharge to zero was realized as impractical. Thus, at present, the NPDES has prescribed the limits on discharges as a function of the type of pollutant, the type of industry discharging, and the desired water quality. The specific requirements for each individual discharger are established in the NPDES permit issued to the discharger. These permits are reviewed every five years and are subject to change at the time of review.

A major tactic that was adopted in the Clean Water Act was to establish uniform technology standards, by class of pollutant and specific industry type, which applied nationwide to all dischargers. Thus, a kraft mill in Oregon would have to meet essentially the same discharge standards as a kraft mill in New York. In establishing these standards, the EPA took into account the state of the art of waste treatment in each particular industry as well as cost and ecological effectiveness. These discharge standards have been published in the *Federal Register* for more than thirty industrial categories and several hundred subcategories (the Commerce Department Industrial Classification System was used to establish these categories) in the *Federal Register*. These have been promulgated over an extensive period of time. The reader is advised to consult the index to this document to ascertain regulations that apply to a particular industry. Table 22-36 presents the major industrial categories.

TABLE 22-36 Industry Categories

1. Adhesives and sealants
2. Aluminum forming
3. Asbestos manufacturing
4. Auto and other laundries
5. Battery manufacturing
6. Coal mining
7. Coil coating
8. Copper forming
9. Electric and electronic components
10. Electroplating
11. Explosives manufacturing
12. Ferroalloys
13. Foundries
14. Gum and wood chemicals
15. Inorganic chemicals manufacturing
16. Iron and steel manufacturing
17. Leather tanning and finishing
18. Mechanical products manufacturing
19. Nonferrous metals manufacturing
20. Ore mining
21. Organic chemicals manufacturing
22. Pesticides
23. Petroleum refining
24. Pharmaceutical preparations
25. Photographic equipment and supplies
26. Plastic and synthetic materials manufacturing
27. Plastic processing
28. Porcelain enamelling
29. Printing and publishing
30. Pulp and paperboard mills
31. Soap and detergent manufacturing
32. Steam electric power plants
33. Textile mills
34. Timber products processing

As indicated above, not only are the discharge standards organized on an industry-by-industry basis, but they are different depending upon which of the three classes of pollutants is being regulated. The standards for conventional pollutants are referred to as best conventional technology (BCT). The standards for priority pollutants are referred to as best available technology (BAT), as are those for non-conventional, nonpriority pollutants. These standards envision that the technology will not be limited to treatment but may include revision in the industrial processing and/or reuse of effluents (pollution prevention). They are usually presented as mass of pollutant discharged per unit of product produced.

In some situations it is anticipated that application of BCT and BAT may not be sufficient to ensure that water-quality standards are achieved in a stream segment. Studies have indicated that approximately 10 percent of the stream segments in the United States will have their water-quality standards violated, even if all the dischargers to that stream segment meet BCT and BAT regulations. These segments are referred to as water quality limited segments. The NPDES permit for those who discharge into water quality limited segments must provide for pollutant removal in excess of that required by BCT and BAT so that water-quality standards (which are jointly established by each state and EPA) are achieved. The stream segments in which water-quality standards will be met by application of BCT and BAT are referred to as "effluent quality limited segments."

For industrial discharges that enter municipal sewers and thus eventually municipal treatment plants, NPDES regulations are nominally the same as for industries that discharge directly to navigable waters; i.e., they must meet BCT and BAT standards. These are referred to as "categorical industrial pretreatment standards." However if it can be demonstrated that the municipal treatment plant can remove a pollutant in the industrial waste, a "removal credit" can be assigned to the permit, thus lowering the requirement on the industrial discharger. The monetary charge to the industry by the municipality for this service is negotiable but must be within parameters established by EPA for industrial user charges if the municipality received a federal grant for construction of the treatment plant. A removal credit cannot be assigned if removal of the industrial pollutant results in difficulty in ultimate disposal of sludge from the municipal plant. In addition, an industry cannot discharge any substance that can result in physical damage to the municipal sewer and/or interfere with any aspect of treatment plant performance even if the substance is not covered by BCT or BAT regulations.

The EPA has established a National Pretreatment Program to address the growing impacts industrial effluents have on publicly owned treatment works (POTWs). These impacts include biological toxicity and inhibition causing biological upsets that can reduce plant efficiency; accumulation of heavy metals in primary and secondary sludge that may impact beneficial reuse applications; increase in whole effluent toxicity (WET) which can impact plant discharge permit requirements; and increasing organic and solid loadings on plants that are reaching their design capacity. The EPA has established two sets of rules that are the basis of the National Pretreatment Program, the categorical pretreatment standards and prohibited discharge standards. The categorical pretreatment standards are industry- or technology-based limitations on pollutant discharges to POTWs promulgated by USEPA in accordance with Section 307 of the Clean Water Act. These standards apply to specific process wastewaters of particular industrial categories (see 40 CFR 403.6 and 40 CFR Parts 405 to 471). The prohibited discharge standards forbid certain chemicals and discharges by any sewer system. These specific discharges are described in full in the *Federal Register* and include 126 specific chemicals. The program requires all POTWs with a flow greater than 5 mgd or those receiving significant industrial flow to establish an industrial pretreatment program. States and individual municipalities can develop their own pretreatment programs to address system-specific industrial wastewater impacts. Currently, over 1500 municipalities have established their own pretreatment programs that either meet or exceed the EPA pretreatment standards. Along with setting standards for pretreatment, the EPA identifies best-available technologies to economically control industrial effluents. In addition to industrial discharges, the EPA has initiated a program to better control

stormwater discharges associated with industrial activity. This program is part of the national NPDES Phase I Stormwater Program.

Environmental Protection Agency President Nixon created the EPA in 1970 to coordinate all environmental pollution-control activities at the federal level. The EPA was placed directly under the Office of the President so that it could be more responsive to the political process. In the succeeding decade, the EPA produced a series of federal regulations increasing federal control over all wastewater-pollution-control activities. In January 1981, President Reagan reversed the trend of greater federal regulation and began to decrease the role of the federal EPA. However, during the 1980s, an equilibrium was achieved between those who wish less regulation and those who wish more. In general, industry and the EPA reached agreement on the optimum level of regulation.

State Water-Pollution-Control Offices Every state has its own water-pollution-control office. Some states have reorganized along the lines of the federal EPA with state EPA offices, while others have kept their water-pollution-control offices within state health departments. Prior to 1965, each state controlled its own water-pollution-control programs. Conflicts between states and uneven enforcement of state regulations resulted in the federal government's assuming the leadership role. Unfortunately, conflicts between states shifted to being conflicts between the states and the federal EPA. By 1980, the state water-pollution-control offices were primarily concerned with handling most of the detailed permit and paperwork for the EPA and in furnishing technical assistance to industries at the local level. In general, most of the details of regulation are carried out by state water-pollution-control agencies with oversight by EPA.

WASTEWATER CHARACTERISTICS

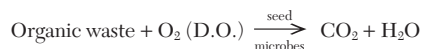
Wastewater characteristics vary widely from industry to industry. Obviously, the specific characteristics will affect the treatment techniques chosen for use in meeting discharge requirements. Some general characteristics that should be considered in planning are given in Table 22-37. Because of the large number of pollutant substances, wastewater characteristics are not usually considered on a substance-by-substance basis. Rather, substances of similar pollution effects are grouped together into classes of pollutants or characteristics as indicated below.

Priority Pollutants Recently, greatest concern has been for this class of substances for the reasons given previously. These materials are treated on an individual-substance basis for regulatory control. Thus, each industry could receive a discharge permit that lists an acceptable level for each priority pollutant. Table 22-38 presents a list of these substances; most are organic, but some inorganics are included. All are considered toxic, but, as indicated previously, there is wide variation in their toxicity. Most of the organics are biologically degradable despite their toxicity (Refs. 30 and 31). USEPA has collected data on the occurrence of these substances in various industrial

wastes and their treatability. A recent trend has been to avoid their use in industrial processing.

Organics The organic composition of industrial wastes varies widely, primarily due to the different raw materials used by each specific industry. These organics include proteins, carbohydrates, fats and oils, petrochemicals, solvents, pharmaceutical, small and large molecules, solids and liquids. Another complication is that a typical industry produces many diverse wastestreams. Good practice is to conduct a material balance throughout an entire production facility. This survey should include a flow diagram, location and sizes of piping, tanks and flow volumes, as well as an analysis of each stream. Results of an industrial waste survey for an industry are given in Table 22-39. Noteworthy is the range in waste sources, including organic soap, toilet articles, ABS (alkyl benzene sulfonate), and the relatively clean but hot condenser water that makes up half the plant flow, while the strongest wastes—spent caustic and fly ash—have the lowest flows. See Tables 22-39 and 22-40 for information on the average characteristics of wastes from specific industries.

An important measure of the waste organic strength is the 5-day biochemical oxygen demand (BOD₅). As this test measures the demand for oxygen in the water environment caused by organics released by industry and municipalities, it has been the primary parameter in determining the strength and effects of a pollutant. This test determines the oxygen demand of a waste exposed to biological organisms (controlled seed) for an incubation period of five days. Usually this demand is caused by degradation of organics according to the following simplified equation, but reduced inorganics in some industries may also cause demand (i.e., Fe²⁺, S²⁻, and SO₃²⁻).



This wet lab test measures the decrease in dissolved oxygen (D.O.) concentration in 5 days, which is then related to the sample strength. If the test is extended over 20 days, the BOD₂₀ (ultimate BOD) is obtained and corresponds more closely to the Chemical Oxygen Demand (COD) test. The COD test uses strong chemical oxidizing agents with catalysts and heat to oxidize the wastewater and obtain a value that is almost always larger than the 5- and 20-day BOD values. Some organic compounds (like pyridene, a ring structure containing nitrogen) resists chemical oxidation giving a low COD. A major advantage of the COD test is the completion time of less than 3 hours, versus 5 days for the BOD₅ test. Unfortunately, state and federal regulations generally require BOD₅ values, but approximate correlations can be made to allow computation of BOD from COD. A more rapid measure of the organic content of a waste is the instrumental test for total organic carbon (TOC), which takes a few minutes and may be correlated to both COD and BOD for specific wastes. Unfortunately, BOD₅ results are subject to wide statistical variations and require close scrutiny and experience. For municipal wastewaters, BOD₅ is about 67 percent of the ultimate BOD and 40–45 percent of the COD, indicating a large amount of nonbiodegradable COD and the continuing need to run BOD as well as COD and TOC. An example of BOD, COD, and TOC relationships for chemical industry wastewater is given in Table 22-40. The concentrations of the wastewaters vary by two orders of magnitude, and the BOD/COD, COD/TOC, and BOD/TOC ratios vary less than twofold. The table indicates that correlation/codification is possible, but care and continual scrutiny must be exercised.

Another technique for organics measurement that overcomes the long period required for the BOD test is the use of continuous respirometry. Here the waste (full-strength rather than diluted as in the standard BOD test) is contacted with biomass in an apparatus that continuously measures the dissolved oxygen consumption. This test determines the ultimate BOD in a few hours if a high level of biomass is used. The test can also yield information on toxicity, the need to develop an acclimated biomass, and required rates of oxygen supply.

In general, low-molecular-weight water-soluble organics are biodegraded readily. As organic complexity increases, solubility and biodegradability decrease. Soluble organics are metabolized more easily than insoluble organics. Complex carbohydrates, proteins, and

TABLE 22-37 Wastewater Characteristics

Property	Characteristic	Example	Size or concentration
Solubility	Soluble	Sugar	>100 gm/L
	Insoluble	PCB	<1 mg/L
Stability, biological	Degradable	Sugar	
	Refractory	DDT, metals	
Solids	Dissolved	NaCl	<10 ⁻⁹ m
	Colloidal	Carbon	>10 ⁻⁶ –<10 ⁻⁹ m
	Suspended	Bacterium	>10 ⁻⁶ m
Organic	Carbon	Alcohol	
Inorganic	Inorganic	Cu ²⁺	
	Acidic	HNO ₃	
	Neutral	Salt (NaCl)	1–12
	Basic	NaOH	
Temperature	High–low	Cooling	>5°
		Heat exchange	>30°
Toxicity	Biological effect	Heavy metals	Varies
Nutrients	Priority compounds		
		N	NH ₃
		P	PO ₄ ³⁻

TABLE 22-38 List of Priority Chemicals*

Compound name	Compound name	Compound name
1. Acenaphthene†	37. 1,2-Diphenylhydrazine†	83. Indeno (1,2,3-cd) pyrene (2,3- <i>o</i> -phenylene)pyrene)
2. Acrolein†	38. Ethylbenzene†	84. Pyrene
3. Acrylonitrile†	39. Fluoranthene†	85. Tetrachloroethylene†
4. Benzene†		86. Toluene†
5. Benzidine†		87. Trichloroethylene†
6. Carbon tetrachloride† (tetrachloromethane)	Haloethers† (other than those listed elsewhere)	88. Vinyl chloride† (chloroethylene)
Chlorinated benzenes (other than dichlorobenzenes)	40. 4-Chlorophenyl phenyl ether	Pesticides and metabolites
7. Chlorobenzene	41. 4-Bromophenyl phenyl ether	89. Aldrin†
8. 1,2,4-Trichlorobenzene	42. Bis(2-chloroisopropyl) ether	90. Dieldrin†
9. Hexachlorobenzene	43. Bis(2-chloroethoxy) methane	91. Chlordane† (technical mixture and metabolites)
Chlorinated ethanes† (including 1,2-dichloroethane, 1,1,1-trichloroethane, and hexachloroethane)	Halomethanes† (other than those listed elsewhere)	DDT and metabolites†
10. 1,2-Dichloroethane	44. Methylene chloride (dichloromethane)	92. 4,4'-DDT
11. 1,1,1-Trichloroethane	45. Methyl chloride (chloromethane)	93. 4,4'-DDE (<i>p,p'</i> -DDX)
12. Hexachloroethane	46. Methyl bromide (bromomethane)	94. 4,4'-DDD (<i>p,p'</i> -TDE)
13. 1,1-Dichloroethane	47. Bromoform (tribromomethane)	Endosulfan and metabolites†
14. 1,1,2-Trichloroethane	48. Dichlorobromomethane	95. α -Endosulfan-alpha
15. 1,1,2,2-Tetrachloroethane	49. Trichlorofluoromethane	96. β -Endosulfan-beta
16. Chloroethane (ethyl chloride)	50. Dichlorodifluoromethane	97. Endosulfan sulfate
Chloroalkyl ethers† (chloromethyl, chloroethyl, and mixed ethers)	51. Chlorodibromomethane	Endrin and metabolites†
17. Bis(chloromethyl) ether	52. Hexachlorobutadiene†	98. Endrin
18. Bis(2-chloroethyl) ether	53. Hexachlorocyclopentadiene†	99. Endrin aldehyde
19. 2-Chloroethyl vinyl ether (mixed)	54. Isophorone†	Heptachlor and metabolites†
Chlorinated naphthalene†	55. Naphthalene†	100. Heptachlor
20. 2-Chloronaphthalene	56. Nitrobenzene†	101. Heptachlor epoxide
Chlorinated phenols† (other than those listed elsewhere; includes trichlorophenols and chlorinated cresols)	Nitrophenols† (including 2,4-dinitrophenol and dinitrocresol)	Hexachlorocyclohexane (all isomers)†
21. 2,4,6-Trichlorophenol	57. 2-Nitrophenol	102. α -BHC-alpha
22. <i>para</i> -Chloro- <i>meta</i> -cresol	58. 4-Nitrophenol	103. β -BHC-beta
23. Chloroform (trichloromethane)†	59. 2,4-Dinitrophenol†	104. γ -BHC (lindane)-gamma
24. 2-Chlorophenol†	60. 4,6-Dinitro- <i>o</i> -cresol	105. δ -BHC-delta
Dichlorobenzenes†	Nitrosamines†	Polychlorinated biphenyls (PCB)†
25. 1,2-Dichlorobenzene	61. <i>N</i> -Nitrosodimethylamine	106. PCB-1242 (Arochlor 1242)
26. 1,3-Dichlorobenzene	62. <i>N</i> -Nitrosodiphenylamine	107. PCB-1254 (Arochlor 1254)
27. 1,4-Dichlorobenzene	63. <i>N</i> -Nitrosodi- <i>n</i> -propylamine	108. PCB-1221 (Arochlor 1221)
Dichlorobenzidine†	64. Pentachlorophenol†	109. PCB-1232 (Arochlor 1232)
28. 3,3'-Dichlorobenzidine	65. Phenol†	110. PCB-1248 (Arochlor 1248)
Dichloroethylenes† (1,1-dichloroethylene and 1,2-dichloroethylene)	Phthalate esters†	111. PCB-1260 (Arochlor 1260)
29. 1,1-Dichloroethylene	66. Bis(2-ethylhexyl) phthalate	112. PCB-1016 (Arochlor 1016)
30. 1,2- <i>trans</i> -Dichloroethylene	67. Butyl benzyl phthalate	113. Toxaphene†
31. 2,4-Dichlorophenol†	68. Di- <i>n</i> -butyl phthalate	114. antimony (total)
Dichloropropane and dichloropropene†	69. Di- <i>n</i> -octyl phthalate	115. arsenic (total)
32. 1,2-Dichloropropane	70. Diethyl phthalate	116. asbestos (fibrous)
33. 1,2-Dichloropropylene (1,2-dichloropropene)	71. Dimethyl phthalate	117. beryllium (total)
34. 2,4-Dimethylphenol†	Polynuclear aromatic hydrocarbons (PAH)†	118. cadmium (total)
Dinitrotoluene†	72. Benzo(a)anthracene (1,2-benzanthracene)	119. chromium (total)
35. 2,4-Dinitrotoluene	73. Benzo(a)pyrene (3,4-benzopyrene)	120. copper (total)
36. 2,6-Dinitrotoluene	74. 3,4-Benzofluoranthene	121. cyanide (total)
	75. Benzo(k)fluoranthene (11,12-benzofluoranthene)	122. lead (total)
	76. Chrysene	123. mercury (total)
	77. Acenaphthylene	124. nickel (total)
	78. Anthracene	125. selenium (total)
	79. Benzo(ghi)perylene (1,12-benzoperylene)	126. silver (total)
	80. Fluorene	127. thallium (total)
	81. Phenanthrene	128. zinc (total)
	82. Dibenzo(a,h)anthracene (1,2,5,6-dibenzanthracene)	129. 2,3,7,8-Tetrachlorodibenzo- <i>p</i> -dioxin (TCDD)

*Adapted from Eckenfelder, W. W. Jr., *Industrial Water Pollution Control*, 2d ed., McGraw-Hill, New York, 1989.

†Specific compounds and chemical classes as listed in the consent degree.

TABLE 22-39 Industrial Waste Components of a Soap, Detergents, and Toilet Articles Plant

Waste source	Sampling station	COD, mg/L	BOD, mg/L	SS, mg/L	ABS, mg/L	Flow, gal/min
Liquid soap	D	1,100	565	195	28	300
Toilet articles	E	2,680	1,540	810	69	50
Soap production	R	29	16	39	2	30
ABS production	S	1,440	380	309	600	110
Powerhouse	P	66	10	50	0	550
Condenser	C	59	21	24	0	1100
Spent caustic	B	30,000	10,000	563	5	2
Tank bottoms	A	120,000	150,000	426	20	1.5
Fly ash	F			6750		10
Main sewer		450	260	120	37	2150

NOTE: gal/min = 3.78×10^{-3} m³/min.

SOURCE: Eckenfelder, W. W., *Industrial Water Pollution Control*, 2d ed., McGraw-Hill, New York, 1989.

fats and oils must be hydrolyzed to simple sugars, aminos, and other organic acids prior to metabolism. Petrochemicals, pulp and paper, slaughterhouse, brewery, and numerous other industrial wastes containing complex organics have been satisfactorily treated biologically, but proper testing and evaluation is necessary.

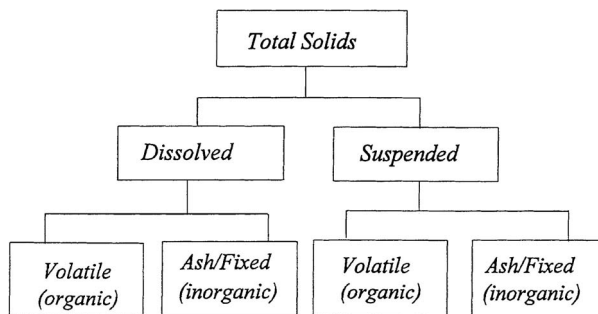
Inorganics The inorganics in most industrial wastes are the direct result of inorganic compounds in the carriage water. Soft-water sources will have lower inorganics than hard-water or saltwater sources. However, some industrial wastewaters can contain significant quantities of inorganics which result from chemical additions during plant operation. Many food processing wastewaters are high in sodium. While domestic wastewaters have a balance in organics and inorganics, many process wastewaters from industry are deficient in specific inorganic compounds. Biodegradation of organic compounds requires adequate nitrogen, phosphorus, iron, and trace salts. Ammonium salts or nitrate salts can provide the nitrogen, while phosphates supply the phosphorus. Either ferrous or ferric salts or even normal steel corrosion can supply the needed iron. Other trace elements needed for biodegradation are potassium, calcium, magnesium, cobalt, molybdenum, chloride, and sulfur. Carriage water or demineralizer wastewaters or corrosion products can supply the needed trace elements for good metabolism. Occasionally, it is necessary to add specific trace elements or nutrient elements.

pH and Alkalinity Wastewaters should have pH values between 6 and 9 for minimum impact on the environment. Wastewaters with pH values less than 6 will tend to be corrosive as a result of the excess hydrogen ions. On the other hand, raising the pH above 9 will cause some of the metal ions to precipitate as carbonates or as hydroxides at higher pH levels. Alkalinity is important in keeping pH values at the right levels. Bicarbonate alkalinity is the primary buffer in wastewaters. It is important to have adequate alkalinity to neutralize the acid waste components as well as those formed by partial metabolism of organics. Many neutral organics such as carbohydrates, aldehydes, ketones, and alcohols are biodegraded through organic acids which must be neutralized by the available alkalinity. If alkalinity is inadequate, sodium carbonate is a better form to add than lime. Lime tends to be hard to control accurately and results in high pH levels and pre-

TABLE 22-40 BOD, COD, and TOC Relationships

Type of waste	BOD ₅ , mg/L	COD, mg/L	TOC, mg/L	BOD ₅ /COD	COD/TOC	BOD ₅ /TOC
Chemical	700	1,400	450	0.50	3.12	1.55
Chemical	850	1,900	580	0.45	3.28	1.47
Chemical	8,000	17,500	5,800	0.46	3.02	1.38
Chemical	9,700	15,000	5,500	0.65	2.72	1.76
Chemical	24,000	41,300	9,500	0.58	4.35	2.53
Chemical	60,700	78,000	26,000	0.78	3.00	2.34
Chemical	62,000	143,000	48,140	0.43	2.96	1.28

Adapted from Eckenfelder, W.W. and D.L. Ford, *Water Pollution Control*, Pemberton Press, Austin and New York, 1970.

**FIG. 22-30** Solids identification. Abbreviations: TS, total solids; SS, suspended solid; D, dissolved; V, volatile.

cipitation of the calcium which forms part of the alkalinity. In a few instances, sodium bicarbonate may be the best source of alkalinity.

Temperature Most industrial wastes tend to be on the warm side. For the most part, temperature is not a critical issue below 37°C if wastewaters are to receive biological treatment. It is possible to operate thermophilic biological wastewater-treatment systems up to 65°C with acclimated microbes. Low-temperature operations in northern climates can result in very low winter temperatures and slow reaction rates for both biological treatment systems and chemical treatment systems. Increased viscosity of wastewaters at low temperatures makes solid separation more difficult. Efforts are generally made to keep operating temperatures between 10 and 30°C if possible.

Dissolved Oxygen Oxygen is a critical environmental resource in receiving streams and lakes. Aquatic life requires reasonable dissolved-oxygen (DO) levels. EPA has set minimum stream DO levels at 5 mg/L during summer operations, when the rate of biological metabolism is a maximum. It is important that wastewaters have maximum DO levels when they are discharged and have a minimum of oxygen-demanding components so that DO remains above 5 mg/L. DO is a poorly soluble gas in water, having a solubility around 9.1 mg/L at 20°C and 101.3-kPa (1-atm) air pressure. As the temperature increases and the pressure decreases with higher elevations above sea level, the solubility of oxygen decreases. Thus, DO is a minimum when BOD rates are a maximum. Lowering the temperature yields higher levels of DO saturation, but the biological metabolism rate decreases. Warm-wastewater discharges tend to aggravate the DO situation in receiving waters.

Solids Total solids is the residue remaining from a wastewater dried at 103–105°C. It includes the fractions shown in Fig. 22-30. The first separation is the portion that passes through a 2- μ m filter (dissolved) and those solids captured on the filter (suspended). Combustion at 500°C further separates the solids into volatile and ash (fixed) solids. Although ash and volatile solids do not distinguish inorganic from organic solids exactly, due to loss of inorganics on combustion, the volatile fraction is often used as an approximate representation of the organics present. Another type of solids, settleable solids, refers to solids that settle in an Imhoff cone in one hour. Industrial wastes vary substantially in these types of solids and require individual wastewater treatment process analysis. An example of possible variation is given in Table 22-41.

Nutrients and Eutrophication Nitrogen and phosphorus cause significant problems in the environment and require special attention in industrial wastes. Nitrogen, phosphorus, or both may cause aquatic

TABLE 22-41 Solids Variation in Industrial Wastewater

Type of solids	Plating	Pulp and paper
Total	High	High
Dissolved	High	High
Suspended	Low	High
Organic	Low	High
Inorganic	High	High

TABLE 22-42 Nutrient Forms

Parameter	Example
Organic N	protein
Ammonia	NH ₃
Ammonium	NH ₄ ⁺
Nitrite	NO ₂ ⁻
Nitrate	NO ₃ ⁻
Organic P	malathion
Ortho-P	PO ₄ ³⁻
Poly-P	(PO ₄ ³⁻) _x

biological productivity to increase, resulting in low dissolved oxygen and eutrophication of lakes, rivers, estuaries, and marine waters. Table 22-42 gives the primary nutrient forms causing problems, while the following equation shows the biological oxidation or oxygen-consuming potential of the most common nitrogen forms.

When organics containing reduced nitrogen are degraded, they usually produce ammonium, which is in equilibrium with ammonia. As the pK for NH₃ ↔ NH₄⁺ is 9.3, the ammonium ion is the primary form present in virtually all biological treatment systems, as they operate at pH < 8.5 and usually in the pH range of 6.5–7.5. In aerobic reactions, ammonium is oxidized by nitrifying bacteria (nitrosomonas) to nitrite and each mg of NH₄⁺—N oxidized will require 3.43 mg D.O. Further oxidation of nitrite by nitrobacter yields nitrate and uses an additional 1.14 mg of D.O. for a total D.O. consumption of 4.57 mg. Thus, organic and ammonium nitrogen can exert significant biochemical oxygen demand in the water environment. This nitrogen demand is referred to as nitrogenous or NBOD, whereas organic BOD is CBOD (carbonaceous). In treatment of wastewaters with organics and ammonium, the total oxygen demand (TOD) may have to be satisfied in accordance with the approximate formula:

$$\text{TOD} \cong 1.5 \text{ BOD}_5 + 4.5 (\text{TKN})$$

where TKN (total Kjeldahl nitrogen) = Organic N + NH₄⁺—N.

Phosphorus is not oxidized or reduced biologically, but ortho-P may be formed from organic and poly-P. Ortho-P may be removed by chemical precipitation or biologically with sludges and will be covered in a later section.

While many industrial wastes are so low in nitrogen and phosphorus that these must be added if biologically based treatment is to be used, others contain very high levels of these nutrients. For example, paint-production wastes are high in nitrogen, and detergent production wastes are high in phosphorus. Treatment for removal of these nutrients is required in areas where eutrophication is a problem.

Whole Effluent Toxicity (WET) Whole effluent toxicity testing is an important part of the EPA's approach to protecting receiving waters from toxic effluents. The EPA has established 17 analytical methods for testing acute and chronic toxicity of point sources (municipal and industrial wastewater effluents) and their impact on surface water environments. WET is a term used to describe the toxic effects imposed on a species or population of aquatic organisms caused by exposure to an effluent. WET is determined analytically by exposing sensitive indigenous organisms to effluents using WET test protocols established by the EPA. WET tests report on the general acute and chronic toxicity of all constituents in a complex effluent and do not represent the toxicity of specific chemicals. To this end, the WET test results could represent the combined toxic effect of heavy metals, un-ionized ammonia, and other toxic constituents in an effluent. The EPA and state regulators have been using WET as an analytical tool for controlling industrial discharges and developing and enforcing industrial pretreatment programs.

Oil and Grease These substances are found in many industrial wastes (i.e., meat packing, petrochemical, and soap production). They tend to float on the water surface, blocking oxygen transfer, interfering with recreation, and producing an aesthetically poor appearance in the water. Measurement is by a solvent extraction procedure. Many somewhat different substances will register as oil and grease in this test. Often oil and grease interfere with other treatment operations, so they must be removed as part of the initial stages of treatment.

WASTEWATER TREATMENT

As indicated above, industrial wastewater contains a vast array of pollutants in soluble, colloidal, and particulate forms, both inorganic and organic. In addition, the required effluent standards are also diverse, varying with the industrial and pollutant class. Consequently, there can be no standard design for industrial water-pollution control. Rather, each site requires a customized design to achieve optimum performance. However, each of the many proven processes for industrial waste treatment is able to remove more than one type of pollutant and is in general applicable to more than one industry. In the sections that follow, waste-treatment processes are discussed more from the broad-based generalized perspective than with narrow specificity. Generally, a combination of several processes is utilized to achieve the degree of treatment required at the least cost.

Much of the experience and data from wastewater treatment has been gained from municipal treatment plants. Industrial liquid wastes are similar to wastewater but differ in significant ways. Thus, typical design parameters and standards developed for municipal wastewater operations must not be blindly utilized for industrial wastewater. It is best to run laboratory and small pilot tests with the specific industrial wastewater as part of the design process. It is most important to understand the temporal variations in industrial wastewater strength, flow, and waste components and their effect on the performance of various treatment processes. Industry personnel in an effort to reduce cost often neglect laboratory and pilot studies and depend on waste characteristics from similar plants. This strategy often results in failure, delay, and increased costs. Careful studies on the actual waste at a plant site cannot be overemphasized.

PRETREATMENT

Many industrial-wastewater streams should be pretreated prior to discharge to municipal sewerage systems or even to a central industrial sewerage system. Many POTWs have pretreatment programs that follow the EPA program by regulating specific industries and specific chemical constituents. Product substitution, process alteration, or pretreatment should be considered to address wastewater streams that may fall under the local or federal pretreatment program. Pretreatment may include single- or multiple-unit processes aimed at reducing the overall toxicity and adverse impact of the waste stream on the total treatment system.

Equalization Equalization is one of the most important pretreatment devices. The batch discharge of concentrated wastes is best suited for equalization. It may be important to equalize wastewater flows, wastewater concentrations, or both. Periodic wastewater discharges tend to overload treatment units. Flow equalization tends to level out the hydraulic loads on treatment units. It may or may not level out concentration variations, depending upon the extent of mixing within the equalization basin. Mechanical mixing may be adequate if the wastes are purely chemical in their reactivity. Biodegradable wastes normally require aeration mixing so that the microbes are kept aerobic and nuisance odors are prevented. Diffused aeration systems offer better mixing under variable load conditions than mechanical surface aeration equipment. Mixing and oxygen transfer are both important with biodegradable wastewaters. Operation on regular cycles determines the size of the equalization basin. There is no advantage in making the equalization basin any larger than necessary to level out wastewater variations. Industrial operation on a 5-day, 40-h week will normally make a 2-day equalization basin as large as needed for continuous operation of the wastewater-treatment system under uniform conditions.

Neutralization Acidic or basic wastewaters must be neutralized prior to discharge. If an industry produces both acidic and basic wastes, these wastes may be mixed together at the proper rates to obtain neutral pH levels. Equalization basins can be used as neutralization basins. When separate chemical neutralization is required, sodium hydroxide is the easiest base material to handle in a liquid form and can be used at various concentrations for in-line neutralization with a minimum of equipment. Yet, lime remains the most widely used base for acid neutralization. Limestone is used when reaction

rates are slow and considerable time is available for reaction. Sulfuric acid is the primary acid used to neutralize high-pH wastewaters unless calcium sulfate might be precipitated as a result of the neutralization reaction. Hydrochloric acid can be used for neutralization of basic wastes if sulfuric acid is not acceptable. For very weak basic wastewaters carbon dioxide can be adequate for neutralization.

Grease and Oil Removal Grease and oils tend to form insoluble layers with water as a result of their hydrophobic characteristics. These hydrophobic materials can be easily separated from the water phase by gravity and simple skimming, provided they are not too well mixed with the water prior to separation. If the oils and greases form emulsions with water as a result of turbulent mixing, the emulsions are difficult to break. Separation of oil and grease should be carried out near the point of their mixing with water. In a few instances, air bubbles can be added to the oil and grease mixtures to separate the hydrophobic materials from the water phase by flotation. Chemicals have also been added to help break the emulsions. American Petroleum Institute (API) separators have been used extensively by the petroleum industry to remove oils from wastewaters. The food industries use grease traps to collect the grease prior to its discharge. Unfortunately, grease traps are designed for regular cleaning of the trapped grease. Too often they are allowed to fill up and discharge the excess grease into the sewer or are flushed with hot water and steam to fluidize the grease for easy discharge to the sewer. A grease trap should be designed for a specific volume of grease to be collected over specific time periods. Care should be taken to design the trap so that the grease can easily be removed and properly handled. Neglected or poorly designed grease traps are worse than no grease traps at all.

Toxic Substances Recent federal legislation has made it illegal for industries to discharge toxic materials in wastewaters. Each industry is responsible for determining if any of its wastewater components are toxic to the environment and to remove them prior to the wastewater discharge. The EPA has identified a number of priority pollutants which must be removed and kept under proper control from their origin to their point of ultimate disposal. Major emphasis has recently been placed on heavy metals and on complex organics that have been implicated in possible cancer production. Pretreatment is essential to reduce heavy metals below toxic levels and to prevent discharge of any toxic organics. Many industries will be required to pretreat waste streams under the local or federal pretreatment program. In the past, these pretreatment programs have focused on heavy metals and toxic organics. More recently they have begun to concentrate on whole effluent toxicity, with future emphasis likely to be on low concentrations of heavy metals and metalloids, pharmaceutical agents, endocrine disrupters, and other emerging pollutants of concern.

PRIMARY TREATMENT

Wastewater treatment is directed toward removal of pollutants with the least effort. Suspended solids are removed by either physical or chemical separation techniques and handled as concentrated solids.

Screens Fine screens such as hydroscreens are used to remove moderate-size particles that are not easily compressed under fluid flow. Fine screens are normally used when the quantities of screened particles are large enough to justify the additional units. Mechanically cleaned fine screens have been used for separating large particles. A few industries have used large bar screens to catch large solids that could clog or damage pumps or equipment following the screens.

Grit Chambers Industries with sand or hard, inert particles in their wastewaters have found aerated grit chambers useful for the rapid separation of these inert particles. Aerated grit chambers are relatively small, with total volume based on 3-min retention at maximum flow. Diffused air is normally used to create the mixing pattern shown in Fig. 22-31, with the heavy, inert particles removed by centrifugal action and friction against the tank walls. The air flow rate is adjusted for the specific particles to be removed. Floatable solids are removed in the aerated grit chamber. It is important to provide for regular removal of floatable solids from the surface of the grit chamber; otherwise, nuisance conditions will be created. The settled grit is normally removed with a continuous screw and buried in a landfill.

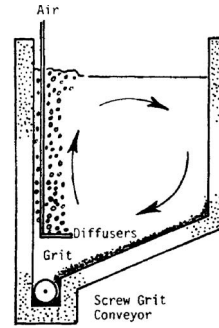


FIG. 22-31 Schematic diagram of an aerated grit chamber.

Gravity Sedimentation Slowly settling particles are removed with gravity sedimentation tanks. For the most part, these tanks are designed on the basis of retention time, surface overflow rate, and minimum depth. A sedimentation tank can be rectangular or circular. The important factor affecting its removal efficiency is the hydraulic flow pattern through the tank. The energy contained in the incoming-wastewater flow must be dissipated before the solids can settle. The wastewater flow must be distributed properly through the sedimentation volume for maximum settling efficiency. After the solids have settled, the settled effluent should be collected without creating serious hydraulic currents that could adversely affect the sedimentation process. Effluent weirs are placed at the end of rectangular sedimentation tanks and around the periphery of circular sedimentation tanks to ensure uniform flow out of the tanks. Once the solids have settled, they must be removed from the sedimentation-tank floor by scraping and hydraulic flow. Conventional sedimentation tanks have sludge hoppers to collect the concentrated sludge and to prevent removal of excess volumes of water with the settled solids. Cross-sectional diagrams of conventional sedimentation tanks are shown in Figs. 22-32 and 22-33.

Design criteria for gravity sedimentation tanks normally provide for 2-h retention based on average flow, with longer retention periods used for light solids or inert solids that do not change during their retention in the tank. Care should be taken that sedimentation time is not too long; otherwise, the solids will compact too densely and affect

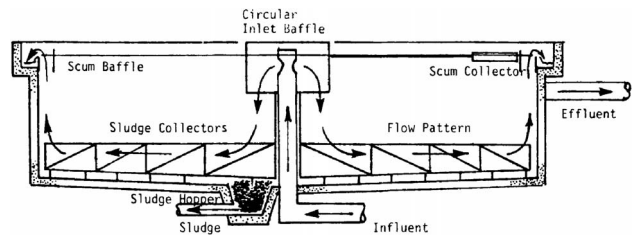


FIG. 22-32 Schematic diagram of a circular sedimentation tank.

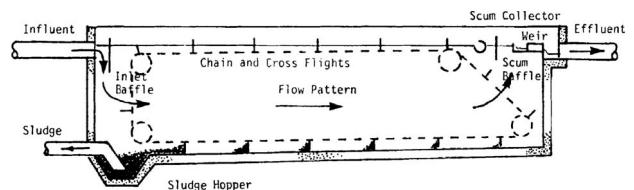


FIG. 22-33 Schematic diagram of a rectangular sedimentation tank.

solids collection and removal. Organic solids generally will not compact to more than 5 to 10 percent. Inorganic solids will compact up to 20 or 30 percent. Centrifugal sludge pumps can handle solids up to 5 or 6 percent, while positive-displacement sludge pumps can handle solids up to 10 percent. With solids above 10 percent the sludge tends to lose fluid properties and must be handled as a semi-solid rather than a fluid. Circular sedimentation tanks have steel truss boxes with angled sludge scrapers on the lower side. As the sludge scrapers rotate, the solids are pushed toward the sludge hopper for removal on a continuous or semicontinuous basis. The rectangular sedimentation tanks employ chain-and-flight sludge collectors or rail-mounted sludge collectors. When floating solids can occur in primary sedimentation tanks, surface skimmers are mounted on the sludge scrapers so that the surface solids are removed at regular intervals.

The surface overflow rate (SOR) for primary sedimentation is normally held close to 40.74 m³/(m²·day) [1000 gal/(ft²·day)] for average flow rates, depending upon the solids characteristics. Lowering the SOR below 40.74 m³/(m²·day) does not produce improved effluent quality in proportion to the reduction in SOR. Generally, the minimum depth of sedimentation tanks is 3.0 m (10 ft), with circular sedimentation tanks having a minimum diameter of 6.0 m (20 ft) and rectangular sedimentation tanks having length-to-width ratios of 5:1. Chain-and-flight limitations generally keep the width of rectangular sedimentation tanks to increments of 6.0 m (20 ft) or less. While hydraulic overflow rates have been limited on the effluent weirs, operating experience has indicated that the recommended limit of 186 m³/(m·day) [15,000 gal/(ft·day)] is lower than necessary for good operation. A circular sedimentation tank with a single-edge weir provides adequate weir length and is easier to adjust than one with a double-sided weir. More problems appear to be created from improper adjustment of the effluent weirs than from improper length.

Chemical Precipitation Lightweight suspended solids and colloidal solids can be removed by chemical precipitation and gravity sedimentation. In effect, the chemical precipitate is used to agglomerate the tiny particles into large particles that settle rapidly in normal sedimentation tanks. Aluminum sulfate, ferric chloride, ferrous sulfate, lime, and polyelectrolytes have been used as coagulants. The choice of coagulant depends upon the chemical characteristics of the particles being removed, the pH of the wastewaters, and the cost and availability of the precipitants. While the precipitation reaction results in removal of the suspended solids, it increases the amount of sludge to be handled. The chemical sludge must be considered along with the characteristics of the original suspended solids in evaluating sludge-processing systems.

Normally, chemical precipitation requires a rapid mixing system and a flocculation system ahead of the sedimentation tank. With a rectangular sedimentation tank, the rapid-mixer and flocculation units are added ahead of the tank. With a circular sedimentation tank the rapid-mixer and flocculation units are built into the tank. Schematic diagrams of chemical treatment systems are shown in Figs. 22-34 and 22-35. Rapid mixers are designed to provide 30-s retention at average flow with sufficient turbulence to mix the chemicals with the incoming wastewaters. The flocculation units are designed for slow mixing at 20-min retention. These units are designed to cause the particles to collide and increase in size without excessive shearing. Care must be taken to move the flocculated mixture from the flocculation unit to the sedimentation unit without disrupting the large floc particles.

The parameter used to design rapid mix and flocculation systems is the root mean square velocity gradient *G*, which is defined by equation

$$G = \left(\frac{P}{VU} \right)^{1/2} \left(\frac{1}{s} \right)$$

where *P* = power input to the water (ft·lb/s)
V = mixer or flocculator volume (ft³)
U = absolute viscosity of water (lb·s/ft²)

Optimum mixing usually requires a *G* value of greater than 1000 inverse seconds. Optimum flocculation occurs when *G* is in the range 10–100 inverse seconds.

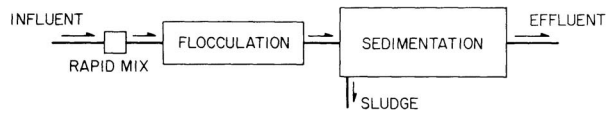


FIG. 22-34 Schematic diagram of a chemical precipitation system for rectangular sedimentation tanks.

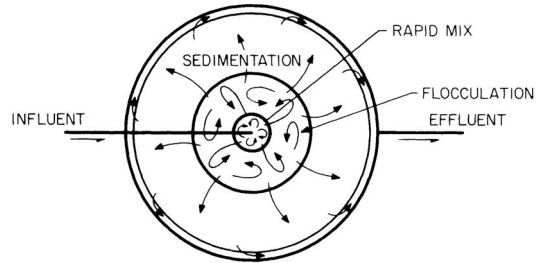
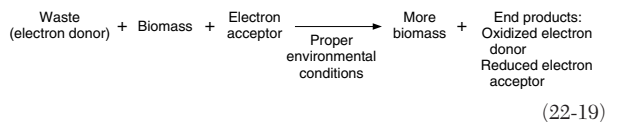


FIG. 22-35 Schematic diagram of a chemical precipitation system for circular sedimentation tanks.

Chemical precipitation can remove 95 percent of the suspended solids, up to 50 percent of the soluble organics and the bulk of the heavy metals in a wastewater. Removal of soluble organics is a function of the coagulant chemical, with iron salts yielding best results and lime the poorest. Metal removal is primarily a function of pH and the ionic state of the metal. Guidance is available from solubility product data.

SECONDARY TREATMENT

Secondary treatment utilizes processes in which microorganisms, primarily bacteria, stabilize waste components. The mixture of microorganisms is usually referred to as biomass. A portion of the waste is oxidized, releasing energy, the remainder is utilized as building blocks of protoplasm. The energy released by biomass metabolism is utilized to produce the new units of protoplasm. Thus, the incentive for the biomass to stabilize waste is that it provides the energy and basic chemical components required for reproduction. The process of biological waste conversion is illustrated by Eq. (22-19).



As this equation indicates, the waste generally serves as an electron donor, necessitating that an electron acceptor be supplied. A variety of substances can be utilized as electron acceptors, including molecular oxygen, carbon dioxide, oxidized forms of nitrogen, sulfur, and organic substances. The characteristics of the end products of the reaction are determined by the electron acceptor. Table 22-43 is a list of typical end products as a function of the electron acceptor. In general, the end products of this reaction are at a much lower energy level than the waste components, thus resulting in the release of energy referred to above. Although this process is usually utilized for the stabilization of organic substances, it can also be utilized for oxidation of inorganics. For example, biomass-mediated oxidation of iron, nitrogen, and sulfur is known to occur in nature and in anthropogenic processes.

Equation (22-19) describes the biomass-mediated reaction and indicates that proper environmental conditions are required for the reaction to take place. These conditions are required by the biomass, not the electron donor or acceptor. The environmental conditions include pH, temperature, nutrients, ionic balance, and so on. In general, biomass can function over a wide pH range generally from 5 to 9. However,

TABLE 22-43 Electron Acceptors and End Products for Biological Reactions

Electron acceptors	End product
Molecular oxygen	Water, CO ₂ , oxidized nitrogen
Oxidized nitrogen	N ₂ , N ₂ O, NO, CO ₂ , H ₂ O
Oxidized sulfur	H ₂ S, S, CO ₂ , H ₂ O
CO ₂ , acetic acid, formic acid	CH ₄ , CO ₂ , H ₂
Complex organics	H ₂ , simple organics, CO ₂ , H ₂ O

some microbes require a much narrower pH range; i.e., effective methane fermentation requires a pH in the range of 6.5–7.5. It is just as important to maintain a relatively constant pH in the process as it is to stay within the range given above. Microorganisms can function effectively at the extremes of their pH range provided they are given the opportunity to acclimate to these conditions. Continual changes in pH are detrimental, even if the organisms are on the average near the middle of their effective pH range. A similar situation prevails for temperature. Most organisms can function well over a broad range of temperature but do not adjust well to frequent fluctuations of even a few degrees. There are three major temperature ranges in which microorganisms function. The psychrophilic range (5 to 20°C), the mesophilic range (20 to 45°C), and the thermophilic range (45 to 70°C). In general the microbes that function in one of these temperature ranges cannot function efficiently in the other ranges. As it is generally uneconomical to adjust the temperature of a waste, most processes are operated in the mesophilic range. If the normal temperature of the waste is above or below the mesophilic range, the process will be operated in the psychrophilic or thermophilic range as appropriate. However, occasionally the temperature of the waste is altered to improve performance. For example, some anaerobic treatment processes are operated under thermophilic conditions, even though the waste must be heated to achieve this temperature range. This is carried out in order to speed up the degradation of complex organics and/or to achieve kill of mesophilic pathogens. It should be noted that any time the biological operation of a process moves away from its optimum or most effective range, be it pH, temperature, nutrients, or what have you, the rate of biological processing is reduced.

All microorganisms require varying amounts of a large number of nutrients. These are required because they are necessary components of bacterial protoplasm. The nutrients can be divided into three groups: macro, minor, and micro. The macronutrients are those that comprise most of the biomass. These are given by the commonly accepted formula for biomass (C₆₀H₈₇O₂₃N₁₂P). The carbon, hydrogen, and oxygen are normally supplied by the waste and water, but the nitrogen and phosphorous must often be added to industrial wastes to ensure that a sufficient amount is present. A good rule is that the mass of nitrogen should be at least 5 percent of the BOD, and the mass of phosphorous should be at least 20 percent of the mass of nitrogen. One of the major operational expenses is the purchase of nitrogen and phosphorous for addition to biologically based treatment processes. The quantities of nitrogen and phosphorous referred to above as required are actually in excess of the minimum amounts needed. The actual amount required depends upon the quantity of excess biomass wasted from the system and the amount of N and P available in the waste. This will be expanded upon later in this section. The minor nutrients include the typical inorganic components of water. These are given in Table 22-44. The range of concentrations required in the wastewater for the minor nutrients is 1–100 mg/L. The micronutrients include the substances that we normally refer to as trace metals and vitamins. It is interesting to note that the trace metals include virtually all of the toxic heavy metals. This reinforces the statement made above that toxicity is a function of concentration and not an absolute parameter. Whether or not the substances referred to as vitamins will be required depends upon the type of microorganisms required to stabilize the waste materials. Many microorganisms have the ability to make their own vitamins from the waste components; thus, a supplement is not needed. However, occasionally the addition of an external source of vitamins is essential to the success of a biologically based waste-treatment sys-

TABLE 22-44 Minor and Micro Nutrients Required for Biologically Mediated Reactors

Minor 1–100 mg/L
Sodium, potassium, calcium, magnesium, iron, chloride, sulfate
Micro 1–100 µg/L
Copper, cobalt, nickel, manganese, boron, vanadium, zinc, lead, molybdenum, various organic vitamins, various amino acids

tem. In general, the trace nutrients must be present in a waste at a level of a few micrograms per liter.

One aspect of the basic equation describing biological treatment of waste that has not been referred to previously is that biomass appears on both sides of the equation. As was indicated above, the only reason that microorganisms function in waste-treatment systems is because it enables them to reproduce. Thus, the quantity of biomass in a waste-treatment system is higher after the treatment process than before it. This is favorable in that there is a continual production of the organisms required to stabilize the waste. Thus, one of the major reactants is, in effect, available free of charge. However, there is an unfavorable side in that unless some organisms are wasted from the system, an excess level will build up, and the process could choke on organisms. The wasted organisms are referred to as sludge. A major cost component of all biologically based processes is the need to provide for the ultimate disposal of this sludge.

Biologically based treatment processes probably account for the majority of the treatment systems used for industrial waste management because of their low cost and because most substances are amenable to biological breakdown. However, some substances are difficult to degrade biologically. Unfortunately, it is not possible at present to predict a priori the biodegradability of a specific organic compound; rather, we must depend upon experience and testing. The collective experience of the field has been put into compendia by EPA in a variety of documents. However, these data are primarily qualitative. There have been some attempts to develop a system of prediction of biodegradability based on a number of compound parameters such as solubility, presence or absence of certain functional groups, compound polarity, and so on. Unfortunately, none of these systems has advanced to the point where reliable quantitative predictions are possible. Another complication is that some organics that are easily biodegradable at low concentration exert a toxic effect at high concentration. Thus, literature data can be confusing. Phenol is a typical compound that shows ease of biodegradation when the concentration is below 500 mg/L but poor biodegradation at higher concentrations. Another factor affecting both biodegradation and toxicity is whether or not a substance is in solution. In general, if a substance is not in solution, it is not available to affect the biomass. Thus, the presence of a waste in substances that can precipitate, complex, or absorb other waste components can have a significant effect on reports of biodegradability and/or toxicity. A quantitative estimate of toxicity can be obtained in terms of the change in kinetic parameters of a system. These kinetic parameters are discussed below.

Design of Biological Treatment Systems In the past, the design of biologically based waste-treatment systems has been derived from rules of thumb. During the past two decades, however, a more fundamental system has been developed and is presently widely used to design such systems. This system is based upon a fundamental understanding of the kinetics and stoichiometry of biological reactions. The system is codified in terms of equations in which four pseudo constants appear. These pseudo constants are k_m , the maximum substrate utilization rate (1/time); K_s , the half maximal velocity concentration (mg/L); Y , the yield coefficient; and b , the endogenous respiration rate (1/time). These are referred to as pseudo constants because, in the mathematical manipulation of the equations in which they appear, they are treated as constants. However, the value of each is a function of the nature of the microbes, the pH, the temperature, and the components of the waste. It is important to remember that if any of these change, the value of the pseudo

constants may change as well. The kinetics of biological reactions are described by Eq. (22-20).

$$\frac{dS}{dt} = \frac{k_m SX}{K_s + S} \tag{22-20}$$

where t = time (days)
 S = waste concentration (mg/L)
 X = biomass concentration (mg/L)
 k_m = (mg/L substrate ÷ mg/L biomass) – time

The accumulation or growth of biosolids is given by Eq. (22-21).

$$\frac{dX}{dt} = Y \frac{dS}{dt} - bX \tag{22-21}$$

where X = biomass level (mg/L).

The equations that have been developed for design using these pseudo constants are based on steady-state mass balances of the biomass and the waste components around both the reactor of the system and the device used to separate and recycle microorganisms. Thus, the equations that can be derived will be dependent upon the characteristics of the reactor and the separator. It is impossible here to present equations for all the different types of systems. As an illustration, the equations for a common system (a complete mix – stirred tank reactor with recycle) are presented below.

$$S_e = \frac{K_s [1 + \text{BSRT}(b)]}{\text{BSRT}(YK_m - b) - 1} \tag{22-22}$$

$$X = \frac{(\text{BSRT})(Y)(S_o - S_e)}{\text{HRT}[1 + (b)\text{BSRT}]} \tag{22-23}$$

where S_o = influent waste concentration (mg/L)
 S_e = treated waste concentration (mg/L)
 HRT = reactor hydraulic retention time

Note that these equations predict some unexpected results. The strength of the untreated waste (S_o) has no effect on the strength of the treated waste (S_e). Neither does the size of the reactor (HRT). Rather, a parameter referred to as the biomass solids retention time (BSRT) is the key parameter determining the system performance. This is illustrated in Fig. 22-36. As the BSRT increases, the concentration of untreated waste in the effluent decreases irrespective of the reactor size or the waste strength. However, the reactor size and waste strength have a significant effect on the level of biomass (X) that is maintained in the system at steady state. Since the development of an excess level of biomass in the system can lead to system upset, it is important to take cognizance of the waste strength and the reactor size. But treatment performance with respect to removal of the waste components is again a function only of BSRT and the value of the

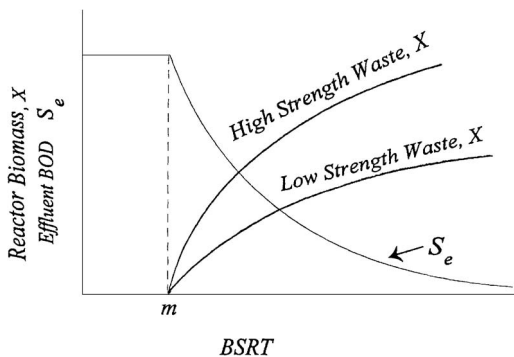


FIG. 22-36 Effect of BSRT on biological treatment process performance. m = minimum BSRT.

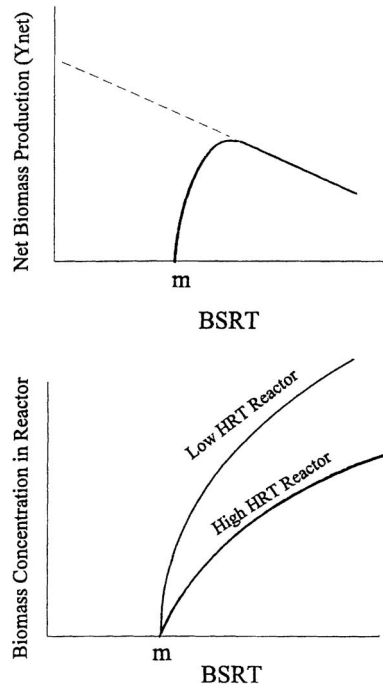


FIG. 22-37 Biomass production.

pseudo constants referred to above. The BSRT also has an effect on the level of biomass in the system and the quantity of excess biomass produced (Fig. 22-37). The latter will determine the quantity of waste sludge which must be dealt with as well as the N and P requirement. The N and P in the biomass removed from the system each day must be replaced. From the formula given previously for biomass, N is 12 percent and P is 2.3 percent by weight in biomass grown under ideal conditions (see Fig. 22-37). Also, note that m , the minimum BSRT, is the minimum time required for the microorganisms to double in mass. Below this minimum, washout occurs and substrate removal approaches zero.

Although identical results are not obtained for other reactor configurations, the design equations yield similar patterns. The dominant parameters in determining system performance are again the BSRT and the pseudo constants. The latter are not under the control of the design engineer as they are functions of the waste and the microorganisms that developed in the system. The BSRT is the major design parameter under the control of the design engineer. This parameter has been defined as the ratio of the biomass in the reactor to the biomass produced from the waste each day. At steady state, the level of biomass in the system is constant; thus, the biomass produced must equal the biomass wasted. The minimum BSRT that can be utilized is that which will produce the degree of treatment required. Generally, this minimum value is less than the range of BSRT used in design and operation. This provides not only a safety factor, but, in addition, it is necessary in order to foster the growth of certain favorable groups of microorganisms in the system. Generally, BSRT values in the range of 3–15 days are utilized in most systems, although BSRT values of less than 1 day for high rate systems are usually adequate to ensure greater than 95 percent destruction of waste components in all but anaerobic systems. For the latter, a minimum BSRT of 8 days is needed for 95 percent destruction. BSRT is controlled by the concentration of biomass (X) in the system and the quantity wasted each day; thus, the treatment plant operator can alter BSRT by altering the rate of biomass wasting.

Reactor Concepts A large number of reactor concepts seem to be used in biologically based treatment systems. However, this diversity

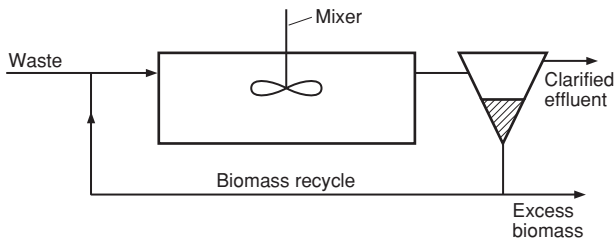


FIG. 22-38 Diagram of a suspended growth system.

is more apparent than real. In reality, there are only two major reactor types that are used. One is referred to as a suspended growth reactor, the other is referred to as a fixed film reactor. In the former, the waste and the microorganisms move through the reactor, with the microorganisms constantly suspended in the flow. After exiting the reactor, the suspension flows through a separator, which separates the organisms from the liquid. Some of the organisms are wasted as sludge, while the remainder are returned to the reactor. The supernatant is discharged either to the environment or to other treatment units (Fig. 22-38). The functioning of the separator is very important, as poor performance of the separator will result in high solids in the effluent and reduction of organisms in the recycle and eventually also in the reactor. As indicated above, the level of the BSRT used in design of suspended growth systems is set to produce a biomass of the proper level in the system; i.e., a level at which waste degradation is rapid but not so high that excess loading on the separator will occur. BSRT also influences the ability of biomass to self flocculate and thus be removed in the separator (usually a clarifier).

In the fixed-film reactor, the organisms grow on an inert surface that is maintained in the reactor. The inert surface can be granular material, proprietary plastic packing, rotating discs, wood slats, mass-transfer packing, or even a sponge-type material. The reactor can be flooded or have a mixed gas-liquid space (Fig. 22-39). The biomass level on the packing is controlled by hydraulic scour produced as the waste liquid flows through the reactor. There is no need of a separator to ensure that the biomass level in the reactor is maintained. The specific surface area of the packing is the design parameter used to ensure an adequate level of biomass. However, a separator is usually supplied to capture biomass washed from the packing surface by the flow of the waste, thus providing a clarified effluent. As with the suspended growth system, if this biomass escapes the system, it will result

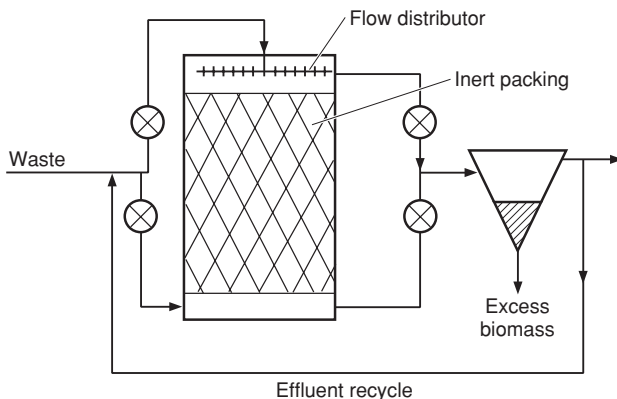


FIG. 22-39 Diagram of a fixed-film system.

in a return to the environment of organic laden material, thus negating the effectiveness of the waste treatment. As indicated above, biomass level in a fixed film reactor is maintained by a balance between the rate of growth on the packing (which is a function of the strength of the waste, the yield coefficient and the BSRT), and the rate of hydraulic flushing by the waste flow. Recycle of treated wastewater is used to control the degree of hydraulic flushing. Thus, typical design parameters for fixed film reactors include both an organic loading and a hydraulic loading. Details on the typical levels for these will be given in a later section.

The reactor concepts described above can be utilized with any of the electron acceptor systems previously discussed, although some reactor types perform better with specific electron acceptors. For example, suspended growth systems are generally superior to fixed film systems when molecular oxygen is the electron acceptor because it is easier to supply oxygen to suspended growth systems.

On the other hand, fixed-film systems that use nitrate as the electron acceptor can be superior to activated sludge systems since nitrogen bubbles produced won't affect sludge settling and oxygen diffusion limitations are not an issue. Different reactor types are better suited for different strengths and types of wastewater. Weak wastewaters are generally easier to treat with fixed-film systems since the appropriate amount of biomass is inherently maintained in the system. Very strong wastes are typically better treated using anaerobic systems to eliminate oxygen limitation and significantly reduce waste sludge production. In addition, the yield coefficient \bar{Y} is much lower for anaerobic systems, reducing sludge production and excessive biomass accumulation. Different types and combinations of activated and fixed-film reactor types can be utilized to perform tertiary treatment on wastewaters and to reclaim hazardous waste streams that are contaminated with recalcitrant chemicals such as PCBs, halogenated aliphatics, and PAHs. Table 22-45 summarizes some of the advantages and disadvantages of various combinations of reactor type, electron acceptor, and waste strength.

Determination of Kinetic and Stoichiometric Pseudo Constants As indicated above, these parameters are most important for predicting the performance of biologically based treatment systems. It would be ideal if tabulations of these were available for various industrial wastes as a function of pH temperature and nutrient levels. Unfortunately, little reliable data has been codified. Only certain trends have been established, and these are primarily the result of studies on municipal wastewater. For example, the yield coefficient \bar{Y} has been shown to be much higher for systems that are aerobic (molecular oxygen as the electron acceptor) than for anaerobic systems (sulfate or carbon dioxide as the electron acceptors). Systems where oxidized nitrogen is the electron acceptor (termed *anoxic*) exhibit yield values intermediate between aerobic and

TABLE 22-45 Favorable (F) and Unfavorable (U) Combinations of Electron Acceptor, Waste Strength, and Reactor Type

Suspended growth reactor		
Electron acceptor	Waste strength	Condition
Aerobic	Low–modest	F
Aerobic	High	U
Anoxic	Low–modest	F
Anoxic	High	U
Anaerobic	Low–modest	U
Anaerobic	High	F
Fixed film reactor		
Electron acceptor	Waste strength	Condition
Aerobic	Low	F
Aerobic	Modest–high	U
Anoxic	Low–modest	F
Anoxic	High	U
Anaerobic	Low–modest	F
Anaerobic	High	F

anaerobic systems. The endogenous respiration rate is higher for aerobic and anoxic systems than anaerobic systems. However, no trends have been established for values of the maximum specific growth rate or the half maximal velocity concentration. Thus, the values applicable to a specific waste must be determined from laboratory studies.

The laboratory studies utilized small-scale (1–5-L) reactors. These are satisfactory because the reaction rates observed are independent of reactor size. Several reactors are operated in parallel on the waste, each at a different BSRT. When steady state is reached after several weeks, data on the biomass level (X) in the system and the untreated waste level in the effluent (usually in terms of BOD or COD) are collected. These data can be plotted for equation forms that will yield linear plots on rectangular coordinates. From the intercepts and the slope of the lines, it is possible to determine values of the four pseudo constants. Table 22-46 presents some available data from the literature on these pseudo constants. Figure 22-40 illustrates the procedure for their determination from the laboratory studies discussed previously.

Activated Sludge This treatment process is the most widely used aerobic suspended growth reactor system. It will consistently produce a high-quality effluent (BOD₅ and SS of 20–30 mg/L). Operational costs are higher than for other secondary treatment processes primarily because of the need to supply molecular oxygen using energy-intensive mechanical aerator- or sparger-type equipment. Removal of soluble organics, colloidal, particulates, and inorganics are achieved in this system through a combination of biological metabolism, adsorption, and entrapment in the biological floc. Indeed, many pollutants that are not biologically degradable are removed during activated sludge treatment by adsorption or entrapment by the floc. For example, most heavy metals form hydroxide or carbonate precipitates under the pH conditions maintained in activated sludge, and most organics are easily adsorbed to the surface of the biological floc. A qualitative guide to the latter is provided by the octanol-water partition coefficient of a compound.

All activated sludge systems include a suspended growth reactor in which the wastewater, recycled sludge, and molecular oxygen are mixed. The latter must be dissolved in the water; thus the need for an energy-intensive pure oxygen or air supply system. Usually, air is the source of the molecular oxygen rather than pure oxygen. Energy for mixing of the reactor contents is supplied by the aeration equipment. All systems include a separator and pump station for sludge recycle and sludge wasting. The separator is usually a sedimentation tank that is designed to function as both a clarifier and a thickener. Many modifications of the activated sludge process have been developed over the years and are described below. Most of these involve differences in the way the reactor is compartmentalized with respect to introduction of waste, recycle, and/or oxygen supply.

Modifications The modifications of activated sludge systems offer considerable choice in processes. Some of the most popular modifications of the activated sludge process are illustrated in Fig. 22-41. Conventional activated sludge uses a long narrow reactor with air supplied along the length of the reactor. The recycle sludge and waste are introduced at the head end of the reactor producing a zone of high waste to biomass concentration and high oxygen demand.

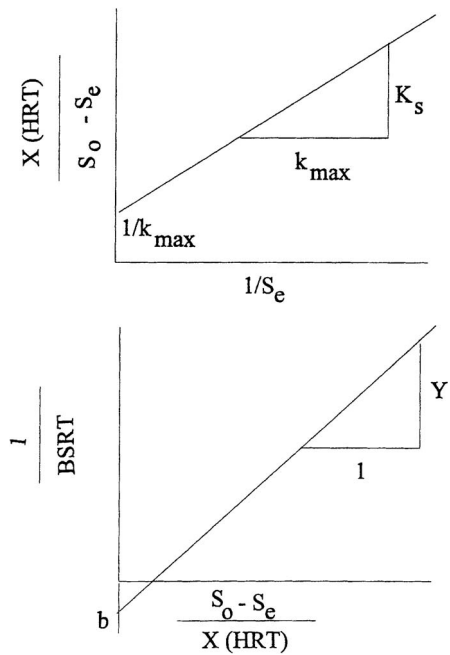


FIG. 22-40 Determination of pseudo-kinetic constants.

This modification is used for relatively dilute wastes such as municipal wastewater. Step aeration systems distribute the waste along the length of the aerator, thus reducing the oxygen demand at the head end of the reactor and spreading the oxygen demand more uniformly over the whole reactor. In the complete mix system, the waste and sludge recycle are uniformly distributed over the whole reactor, resulting in the waste load and oxygen demand being uniform in the entire reactor. Complete-mixing activated sludge is the most popular system for industrial wastes because of its ability to absorb shock loads better than other modifications. Contact stabilization is a modification of activated sludge that is best suited to wastewaters having high suspended solids and low soluble organics. Contact stabilization employs a short-term mixing tank to adsorb the suspended solids and metabolize the soluble organics, a sedimentation tank for solids separation, and a reaeration tank for stabilization of the suspended organics. Extended-aeration systems are actually long-term-aeration, completely mixed activated-sludge systems. They employ 24- to 48-h aeration periods and high mixed-liquor suspended solids to provide complete stabilization of the organics and aerobic digestion of the activated sludge in the same aeration tank. The oxidation ditch is a popular form of the extended-aeration system employing mechanical aeration. Pure-oxygen systems are designed to treat strong industrial

TABLE 22-46 Typical of Values for Pseudo Constants

Biomass type	Substrate	k_{max} mg substrate mg biomass-day	Y , mg biomass mg substrate	K_s , mg substrate liter	b , 1 day	Remarks
Mixed culture	Sewage (COD)	5–10	0.5	50	0.05	Aerobic 20°C
Mixed culture	Glucose (COD)	7.5	0.6	10	0.07–.1	Aerobic 20°C
Mixed culture	Skim milk (COD)	5	—	100	0.05	Aerobic 20°C
Mixed culture	Soybean waste (COD)	12	—	355	0.144	Aerobic 20°C
Methane bacteria	Acetic acid (COD)	8.7	.04	165	0.035	35°C
Anaerobic mixed	Propanoic acid (COD)	7.7	.04	60	0.035	35°C
Anaerobic mixed	Sewage sludge (COD)	6.7	.04	1,800	0.03	35°C
Anoxic	NO ₃ as N	0.375	0.8	0.1	0.04	Methanol feed
Aerobic	NH ₄ ⁺ as N	5	0.2	1.4	.05	20°C

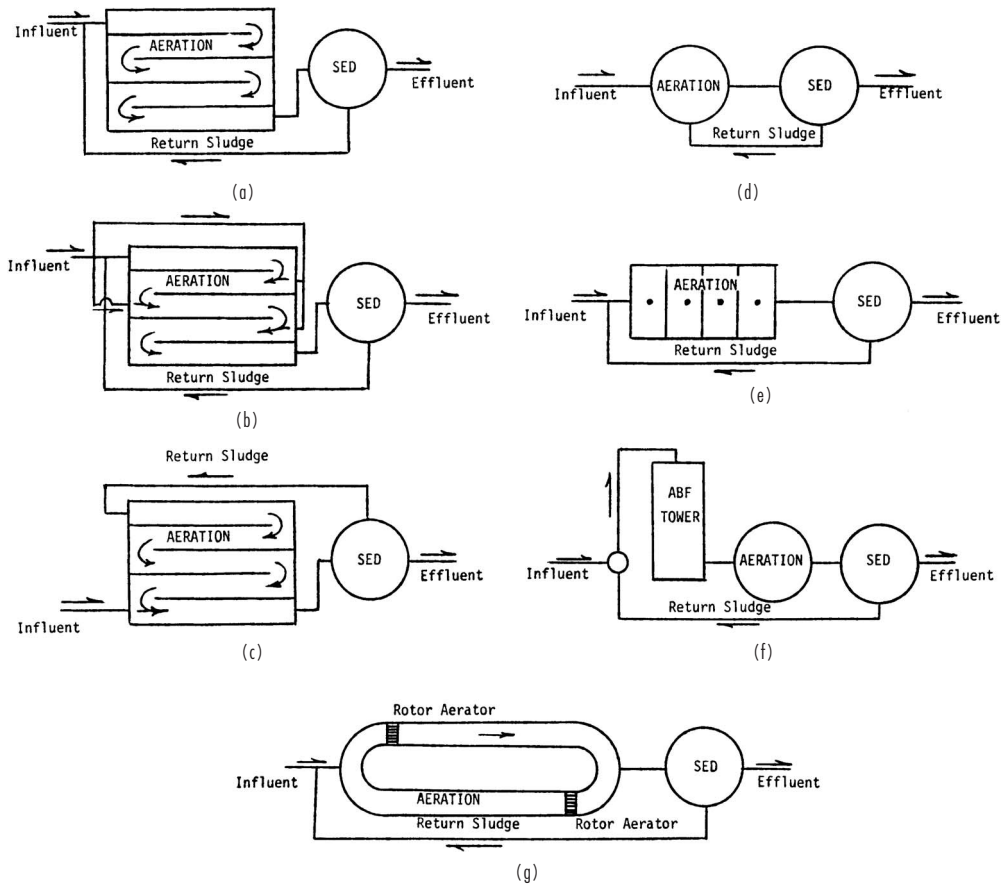


FIG. 22-41 Schematic diagrams of various modifications of the activated-sludge process. (a) Conventional activated sludge. (b) Step aeration. (c) Contact stabilization. (d) Complete mixing. (e) Pure oxygen. (f) Activated biofiltration (ABF). (g) Oxidation ditch.

wastes in a series of completely mixed units having relatively short contact periods. One of the latest modifications of activated sludge employs powdered activated carbon to adsorb complex organics and assist in solids separation. Another modification employs a redwood-medium trickling filter ahead of a short-term aeration tank with mixed liquor recycled over the redwood-medium tower to provide heavy microbial growth on the redwood as well as in the aeration tank.

As indicated previously, success with the activated sludge process requires that the biomass have good self-flocculating properties. Significant research effort has been expended to determine the conditions that favor the development of good settling biomass cultures. These have indicated that nutritional deficiency, levels of dissolved oxygen between 0 to 0.5 mg/L, and pH values below 6.0 will favor the predomination of filamentous biomass. Filamentous organisms settle and compact poorly and thus are difficult to separate from liquid. By avoiding the above conditions, and with the application of selector technology, the predomination of filaments in the biomass can be eliminated. A selector is often a short contact (15–30 min) reactor set ahead of the main activated sludge reactor. All of the recycle sludge and all of the waste are routed to the selector. In the selector, either a high rate of aeration (aerobic selector) is used to keep the dissolved oxygen above 2 mg/L, or no aeration occurs (anaerobic selector) so that the dissolved oxygen is zero. Because filamentous organisms are microaerophilic, they cannot predominate when the dissolved oxygen level is zero or high. The anaerobic selector

not only selects in favor of nonfilamentous biomass but also fosters luxury uptake of phosphorous and is used in systems where phosphorous removal is desired.

Aeration Systems These systems control the design of aeration tanks. Aeration equipment has two major functions: mixing and oxygen transfer. Diffused-aeration equipment employs either a fixed-speed positive-displacement blower or a high-speed turbine blower for readily adjustable air volumes. Air diffusers can be located along one side of the aeration tank or spread over the entire bottom of the tank. They can be either fine-bubble or coarse-bubble diffusers. Fine-bubble diffusers are more efficient in oxygen transfer but require more extensive air-cleaning equipment to prevent them from clogging as a result of dirty air. Mechanical-surface-aeration equipment is more efficient than diffused-aeration equipment but is not as flexible. Economics has dictated the use of large-power aerators, but tank configuration has tended to favor the use of greater numbers of lower-power aerators. Oxidation ditches use horizontal rotor-type aerators. Mixing is a critical problem with mechanical-surface aerators since they are a point-source pump of limited capacity. Experience has indicated that bearings are a serious problem with mechanical-aeration equipment. Wave action generated within the aeration tank tends to produce lateral stresses on the bearings and has resulted in failures and increased maintenance costs. Slow-speed mechanical-surface-aeration units present fewer problems than the high-speed mechanical-surface-aeration units. Deep tanks, greater than 3.0 m (10 ft), require draft tubes to ensure proper hydraulic flow through the aeration tank.

Short-circuiting is one of the major problems associated with mechanical aeration equipment. Combined mechanical- and diffused-aeration systems have enjoyed some popularity for industrial-waste systems that treat variable organic loads. The mechanical mixers provide the fluid mixing with the diffused aeration varied for different oxygen-transfer rates.

Diffused-aeration systems transfer from 20 to 40 mg/(L O₂·h). Combined mechanical- and diffused-aeration systems can transfer up to 65 mg/(L O₂·h), while mechanical-surface aerators can provide up to 90 mg/(L O₂·h). Pure-oxygen systems can provide the highest oxygen-transfer rate, up to 150 mg/(L O₂·h). Aeration equipment must provide sufficient oxygen to meet the peak oxygen demand; otherwise, the system will fail to provide proper treatment. For this reason, the peak oxygen demand and the rate of transfer for the desired equipment determine the size of the aeration tank in terms of retention time. Economics dictates a balance between the size of the aeration tank and the size of the aeration equipment. As the cost of power increases, economics will favor constructing a larger aeration tank and smaller aerators. It is equally important to examine the hydraulic flow pattern around each aerator to ensure maximum efficiency of oxygen transfer. Improper spacing of aeration equipment can waste energy.

There is no standard aeration-tank shape or size. Aeration tanks can be round, square, or rectangular. Shallow aeration tanks are more difficult to mix than deeper tanks. Yet aeration-tank depths have ranged from 0.6 m (2 ft) to 18 m (60 ft). The oxidation-ditch systems tend to be shallow, while some high-rate diffused-aeration systems have used very deep tanks to provide more efficient oxygen transfer.

Regardless of the aeration equipment employed, oxygen-transfer rates must provide from 0.6 to 1.4 kg of oxygen/kg BOD₅ (0.6 to 1.4 lb oxygen/lb BOD₅) stabilized in the aeration tank for carbonaceous-oxygen demand. Nitrogen oxidation can increase oxygen demand at the rate of 4.3 kg (4.3 lb) of oxygen/kg (lb) of ammonia nitrogen oxidized. At low oxygen-transfer rates more excess activated sludge must be removed from the system than at high oxygen-transfer rates. Here again the economics of sludge handling must be balanced against the cost of oxygen transfer. The quantity of waste activated sludge will depend upon wastewater characteristics. The inert suspended solids entering the treatment system must be removed with the excess activated sludge. The soluble organics are stabilized by converting a portion of the organics into suspended solids, producing from 0.3 to 0.8 kg (0.3 to 0.8 lb) of volatile suspended solids/kg (lb) of BOD₅ stabilized. Biodegradable suspended solids in the wastewaters will result in destruction of the original suspended solids and their conversion to a new form. Depending upon the chemical characteristics of the biodegradable suspended solids, the conversion factor will range from 0.7 to 1.2 kg (0.7 to 1.2 lb) of microbial solids produced/kg (lb) of suspended solids destroyed. If the suspended solids produced by metabolism are not wasted from the system, they will eventually be discharged in the effluent. While considerable efforts have been directed toward developing activated-sludge systems which totally consume the excess solids, no such system has proved to be practical. The concept of total oxidation of excess sludge is fundamentally unsound and should be recognized as such.

A definitive determination of the waste sludge production and the oxygen requirement can be obtained using the pseudo constants referred to previously. The ultimate BOD in the waste will be accounted for by the sum of the oxidation and sludge synthesis [Eq. (22-24)].

Thus:

$$\text{Waste BOD}_u = \text{oxygen required} + \text{BOD}_u \text{ of sludge produced} \quad (22-24)$$

where: BOD_u of sludge = $(Y_{\text{net}})(1.42)(\text{Waste BOD}_u)$

$$Y_{\text{net}} = \frac{Y}{1 + b(\text{BSRT})}$$

1.42 = Factor converting biomass to oxygen units; i.e.,
 $\text{BOD}_u \approx \text{COD}$

Sedimentation Tanks These tanks are an integral part of any activated-sludge system. It is essential to separate the suspended solids from the treated liquid if a high-quality effluent is to be produced. Circular sedimentation tanks with various types of hydraulic sludge collectors have become the standard secondary sedimentation system. Square tanks have been used with common-wall construction for compact design with multiple tanks. Most secondary sedimentation tanks use center-feed inlets and peripheral-weir outlets. Recently, efforts have been made to employ peripheral inlets with submerged-orifice flow controllers and either center-weir outlets or peripheral-weir outlets adjacent to the peripheral-inlet channel.

Aside from flow control, basic design considerations have centered on surface overflow rates, retention time, and weir overflow rate. Surface overflow rates have been slowly reduced from 33 m³/(m²·day) [800 gal/(ft²·day)] to 24 m³/(m²·day) to 16 m³/(m²·day) [600 gal/(ft²·day) to 400 gal/(ft²·day)] and even to 12 m³/(m²·day) [300 gal/(ft²·day)] in some instances, based on average raw-waste flows. Operational results have not demonstrated that lower surface overflow rates improve effluent quality, making 33 m³/(m²·day) [800 gal/(ft²·day)] the design choice in most systems. Retention time has been found to be an important design factor, averaging 2 h on the basis of raw-waste flows. Longer retention periods tend to produce rising sludge problems, while shorter retention periods do not provide for good solids separation with high-return sludge flow rates. Effluent-weir overflow rates have been limited to 186 m³/(m·day) [15,000 gal/(ft·day)] with a tendency to reduce the rate to 124 m³/(m·day) [10,000 gal/(ft·day)]. Lower effluent-weir overflow rates are obtained by using dual-sided effluent weirs cantilevered from the periphery of the tank. Unfortunately, proper adjustment of dual-side effluent weirs has created more hydraulic problems than the weir overflow rate. Field data have shown that effluent quality is not really affected by weir overflow rates up to 990 m³/(m·day) [80,000 gal/(ft·day)] or even 1240 m³/(m·day) [100,000 gal/(ft·day)] in a properly designed sedimentation tank. A single peripheral weir, being easy to adjust and keep clean, appears to be optimal for secondary sedimentation tanks from an operational point of view.

Depth tends to be determined from the retention time and the surface overflow rate. As surface overflow rates were reduced, the depth of sedimentation tanks was reduced to keep retention time from being excessive. It was recognized that depth was a valid design parameter and was more critical in some systems than retention time. As mixed-liquor suspended-solids (MLSS) concentrations increase, the depth should also be increased. Minimum sedimentation-tank depths for variable operations should be 3.0 m (10 ft) with depths to 4.5 m (15 ft) if 3000 mg/L MLSS concentrations are to be maintained under variable hydraulic conditions. With MLSS concentrations above 4000 mg/L, the depth of the sedimentation tank should be increased to 6.0 m (20 ft). The key is to keep a definite freeboard over the settled-sludge blanket so that variable hydraulic flows do not lift the solids over the effluent weir.

Scum baffles around the periphery of the sedimentation tank and radial scum collectors are standard equipment to ensure that rising solids or other scum materials are removed as quickly as they form. Hydraulic sludge-collection tubes have replaced the center sludge well, but they have caused a new set of operational problems. These tubes were designed to remove the settled sludge at a faster rate than conventional sludge scrapers. To obtain good hydraulic distribution in the sludge-collection tubes, it was necessary to increase the rate of return sludge flow and decrease the concentration of return sludge. The higher total inflow to the sedimentation tank created increased forces that lifted the settled-solids blanket at the wall, causing loss of excessive suspended solids and lower effluent quality. Operating data tend to favor conventional secondary sedimentation tanks over hydraulic sludge-collection systems. Return-sludge rates normally range from 25 to 50 percent for MLSS concentrations up to 3300 mg/L. Most return-sludge pumps are centrifugal pumps with capacities up to 100 percent raw-waste flow.

Gravity settling can concentrate activated sludge to 10,000 mg/L, but hydraulic sludge-collecting tubes tend to operate best below 8,000 mg/L. The excess activated sludge can be wasted either from the

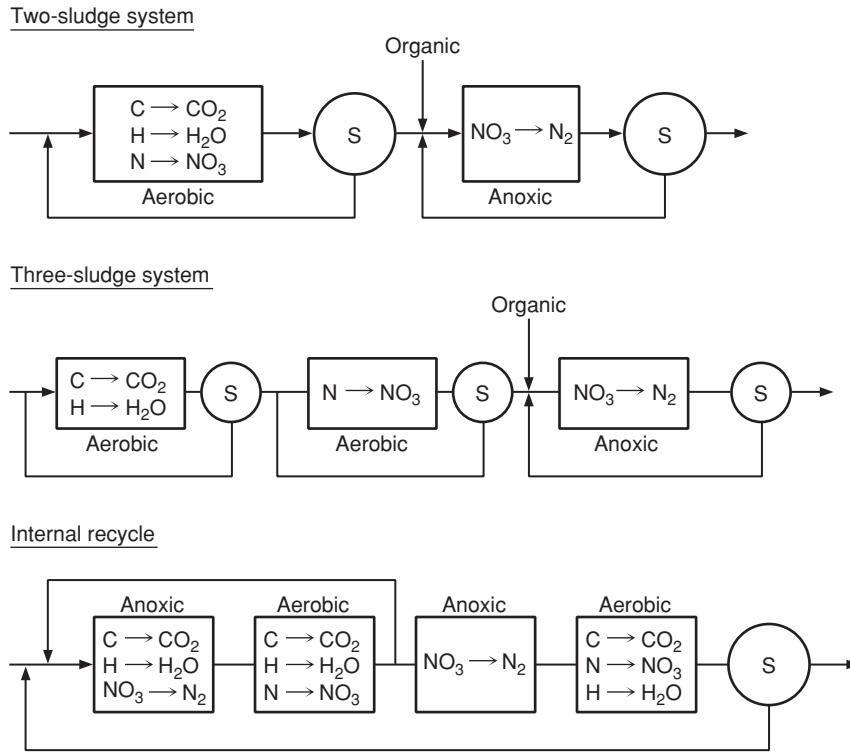


FIG. 22-42 Nitrogen removal systems.

return sludge or from a separate waste-sludge hopper near the center of the tank. The low solids concentrations result in large volumes of waste activated sludge in comparison with primary sludge. Unfortunately, the physical characteristics of waste activated sludge prevent significant concentration without the expenditure of considerable energy. Gravity thickening can produce 2 percent solids, while air flotation can produce 4 percent solids concentration. Centrifuges are able to concentrate activated sludge from 10 to 15 percent solids, but the capture is limited. Vacuum filters can equal the performance of centrifuges if the sludge is chemically conditioned. Filter presses and belt-press filters can produce cakes with 15 to 25 percent solids. It is very important that the excess activated sludge formed in the aeration tanks be wasted on a regular basis; otherwise, effluent quality will deteriorate. Care should be taken to ensure that sludge-thickening systems do not control activated-sludge operations. Alternative sludge-handling provisions should be available during maintenance on sludge-thickening equipment. At no time should final sedimentation tanks be used for the storage of sludge beyond that required by daily operational variations.

Anaerobic/Anoxic Activated Sludge The activated sludge concept (i.e., suspended growth reactor) can be used for anaerobic or anoxic systems in which no oxygen or air is added to the reactor. An anoxic activated sludge is used for systems in which removal of nitrate is a goal or where nitrate is used as the electron acceptor. These systems (denitrification) will be successful if the nitrate is reduced to low levels in the reactor so that nitrate reduction to nitrogen gas does not take place in the clarifier-thickener. Nitrogen gas production in the clarifier will result in escape of biological solids with the effluent as nitrogen bubbles floating sludge to the clarifier surface. For nitrogen reduction, a source of organics (electron donor) is required. Any inexpensive carbohydrate can be effectively used for nitrate removal. Many systems utilize methanol as the donor because it is rapidly

metabolized; others use the organics in sewage in order to reduce chemical costs. Nitrate reduction is invariably used as part of a system in which organics and nitrogen removal are goals. In such systems, the nitrogen in the waste is first oxidized to nitrate and then reduced to nitrogen gas. Figure 22-42 presents some flow sheets for such systems. Table 22-47 presents some design parameters for nitrate-reduction-activated sludge systems. Anaerobic activated sludge has been used for strong industrial wastes high in degradable organic solids. In these systems, a high rate of gasification takes place in the sludge separator so that a highly clarified effluent is usually not obtained. A vacuum degasifier is incorporated in such systems to reduce solids loss. Such systems have been used primarily with meat packing wastes that are warm, high in BOD and yield a high level of bicarbonate buffer as a result of ammonia release from protein breakdown. All of these conditions favor anaerobic processing. The use of this process scheme provides a high BSRT (15–30 days), usually required for anaerobic treatment, at a low HRT (1–2 days).

Lagoons Lagoons are low-cost, easy-to-operate wastewater-treatment systems capable of producing satisfactory effluents. Nominally, a lagoon is a suspended-growth no-recycle reactor with a variable degree of mixing. In lagoons in which mechanical or diffused aeration is used, mixing may be sufficient to approach complete mixing

TABLE 22-47 Design Parameter for Nitrogen Removal

System	BSRT, d	HRT, h	X, mg/L	pH
Carbon removal†	2–5	1–3	1000–2000	6.5–8.0
Nitrification†	10–20	0.5–3	1000–2000	7.4–8.6
Denitrification†	1–5	0.2–2	1000–2000	6.5–7.0
Internal recycle*	10–40	8–20	2000–4000	6.5–8.0

*Total for all reactors

†Separate reactors

(i.e., solids maintained in suspension). In other types of lagoons, most solids settle and remain on the lagoon bottom, but some mixing is achieved as a result of gas production from bacterial metabolism and wind action. Lagoons are categorized as aerobic, facultative, or anaerobic on the basis of degree of aeration. Aerobic lagoons primarily depend on mechanical or diffused air supply. Significant oxygen supply is also realized through natural surface aeration. A facultative lagoon is dependent primarily on natural surface aeration and oxygen generated by algal cells. These two lagoon types are relatively shallow to encourage surface aeration and provide for maximum algal activity. The third type of lagoon is maintained under anaerobic conditions to foster methane fermentation. This system is often covered with floating polystyrene panels to block surface aeration and help prevent a drop in temperature. Anaerobic lagoons are several meters deeper than the other two types. Lagoon flow schemes can be complex, employing lagoons in series and recycle from downstream to upstream lagoons. The major effect of recycle is to maintain control of the solids. If solids escape the lagoon system, a poor effluent is produced. Periodically controlled solids removal must take place or solids will escape.

Lagoons are, in effect, inexpensive reactors. They are shallow basins either cut below grade or formed by dikes built above grade or a combination of a cut and dike. The bottom must be lined with an impermeable barrier and the sides protected from wind erosion. These systems are best used where large areas of inexpensive land are available.

Facultative Lagoons These lagoons have been designed to use both aerobic and anaerobic reactions. Normally, facultative lagoons consist of two or more cells in series. The settleable solids tend to settle out in the first cell and undergo anaerobic metabolism with the production of organic acids and methane gas, which bubbles out to the atmosphere. Algae at the surface of the lagoon utilize sunlight for their energy in converting carbon dioxide, water, and ammonium ions into algal protoplasm with the release of oxygen as a waste product. Aerobic bacteria utilize the oxygen released by the algae to stabilize the soluble and colloidal organics. Thus, the bacteria and algae form a symbiotic relationship as shown in Fig. 22-43. The interesting aspect of facultative lagoons is that the organic matter in the incoming wastewaters is not stabilized but rather is converted to microbial protoplasm, which has a slower rate of oxygen demand. In fact, in some facultative lagoons inorganic compounds in the wastewaters are converted to organic compounds with a total increase in organics within the lagoon system.

Facultative lagoons are designed on the basis of organic load in relationship to the potential sunlight availability. In the northern part of the United States facultative lagoons are designed on the basis of 2.2 g/(m²·day) [20 lb BOD₅/(acre·day)]. In the middle part of the United States the organic load can be increased to 3.4 to 4.5 g/(m²·day) [30 to 40 lb BOD₅/(acre·day)], while in the southern part the organic load can be increased to 6.7 g/(m²·day) [60 lb BOD₅/(acre·day)]. The depth of lagoons is normally maintained between 1.0 and 1.7 m (3 and 5 ft). A depth less than 1.0 m (3 ft) encourages the growth of aquatic

weeds and permits mosquito breeding. In dry areas the maximum depth may be increased above 1.7 m (5 ft) depending upon evaporation. Most facultative lagoons depend upon natural wind action for mixing and should not be placed in screened areas where wind action is blocked.

Effluent quality from facultative lagoons is related primarily to the suspended solids created by living and dead microbes. The long retention period in the lagoons allows the microbes to die off, leaving a small particle that settles slowly. The release of nutrients from the dead microbes permits the algae to survive by recycling the nutrients. Thus, the algae determine the ultimate effluent quality. Use of series ponds with well-designed transfer structures between ponds permits maximum retention of algae within the ponds and the best-quality effluent. Normally the soluble BOD₅ is under 5 or 10 mg/L with a total effluent BOD₅ under 30 mg/L. The effluent suspended solids will vary widely during the different seasons of the year, being a maximum of 70 to 100 mg/L in the summer months and a minimum of 10 to 20 mg/L in the winter months. If suspended-solids removal is essential, chemical precipitation is the best method available at the present time. Slow sand filters and rock filters have been studied for suspended-solids removal; they work well as long as the effluent suspended solids are relatively low, 40 to 70 mg/L.

Aerated Lagoons These lagoons originated from efforts to control overloaded facultative lagoons. Since the lagoons were deficient in oxygen, additional oxygen was supplied by either mechanical surface aerators or diffused aerators. Mechanical surface aerators were quickly accepted as the primary aerators because they could be quickly added to existing ponds and moved to strategic locations. Unfortunately, the high-speed, floating surface aeration units were not efficient, and large numbers were required for existing lagoons. The problem was simply one of poor mixing in a very shallow lagoon.

Eventually, diffused aeration equipment was added to relatively deep lagoons [3.0 to 6.0 m (10 to 20 ft)]. Mixing became the most significant parameter for good oxygen transfer in aerated lagoons. From an economical point of view, it was found that a completely mixed aerated lagoon with 24-h retention provided the best balance between mixing and oxygen transfer. As the organic load increased, the fluid-retention time also increased. Short-term aeration permitted metabolism of the soluble organics by the bacteria, but time did not permit metabolism of the suspended solids. The suspended solids were combined with the microbial solids produced from metabolism and discharged from the aerated lagoon to a solids-separation pond. Data from the short-term aerated lagoon indicated that 50 percent BOD₅ stabilization occurred, with conversion of the soluble organics to microbial cells. The problem was separation and stabilization of the microbial cells. Short-term sedimentation ponds permitted separation of the solids without significant algae growths but required cleaning at frequent intervals to keep them from filling with solids and flowing into the effluent. Long-term lagoons permitted solids separation and stabilization but also permitted algae to grow and affect effluent quality.

Aerated lagoons were simply dispersed microbial reactors which permitted conversion of the organic components in the wastewaters to microbial solids without stabilization. The residual organics in solution were very low, less than 5 mg/L BOD₅. By adding oxygen and improving mixing, the microbial metabolism reaction was speeded up, but the stabilization of the microbial solids has remained a problem to be solved.

Anaerobic Lagoons These lagoons were developed when a major fraction of the organic contaminants consisted of suspended solids that could be removed easily by gravity sedimentation. The anaerobic lagoons are relatively deep [8.0 to 6.0 m (10 to 20 ft)], with a short fluid-retention time (3 to 5 days) and a high BOD₅ loading rate, up to 3.2 kg/(m³·day) [200 lb/(1000 ft³·day)]. Microbial metabolism in the settled-solids layer produces methane and carbon dioxide, which quickly rise to the surface, carrying some of the suspended solids. A scum layer that retards oxygen transfer and release of obnoxious gases is quickly produced in anaerobic lagoons. Mixing with a grinder pump can provide a better environment for metabolism of the suspended solids. The key for anaerobic lagoons is adequate buffer to keep the

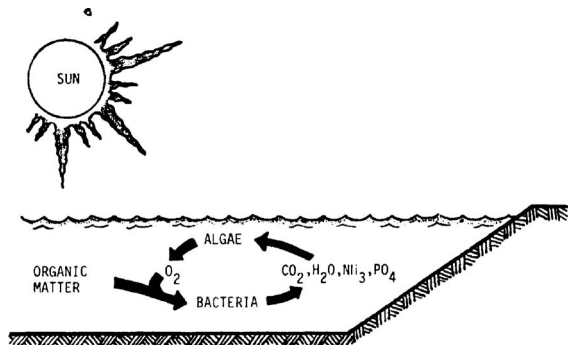


FIG. 22-43 Schematic diagram of oxidation-pond operations.

pH between 6.5 and 8.0. Protein wastes have proved to be the best pollutants to be treated by anaerobic lagoons, with the ammonium ions reacting with carbon dioxide and water to form ammonium bicarbonate as the primary buffer. High-carbohydrate wastes are poor in anaerobic lagoons since they produce organic acids without adequate buffer, making it difficult to maintain a suitable pH for good microbial growth.

Anaerobic lagoons do not produce a high-quality effluent but are able to reduce the BOD load by 80 to 90 percent with a minimum of effort. Since anaerobic lagoons work best on strong organic wastes, their effluent must be treated by either aerated lagoons or facultative lagoons. An anaerobic lagoon is simply the first stage in the treatment of strong organic wastewaters.

Fixed-Film Reactor Systems A major advantage of fixed film systems is that a flocculent-type biomass is not necessary as the biomass remains in the reactor attached to inert packing. Biomass does periodically slough off or break away from the packing, usually in large chunks that can be easily removed in a clarifier. On the other hand, the time of contact between the biomass and the waste is much shorter than in suspended growth systems, making it difficult to achieve the same degree of treatment especially in aerobic systems. Aerobic, anoxic, and anaerobic fixed film systems are utilized for waste treatment.

Aerobic systems including trickling filters and rotating biological contactors (RBC) are operated in a nonflooded mode to ensure adequate oxygen supply. Other aerobic, anoxic, and anaerobic systems employ flooded reactors. The most common systems are packed beds (anaerobic trickling filter) and fluidized or expanded bed systems.

Trickling Filters For years trickling filters were the mainstay of biological wastewater treatment systems because of their simplicity of design and operation. Trickling filters were displaced as the primary biological treatment system by activated sludge because of better effluent quality. Trickling filters are simply fixed-medium biological reactors with the wastewaters being spread over the surface of a solid medium where the microbes are growing. The microbes remove the organics from the wastewaters flowing over the fixed medium. Oxygen from the air permits aerobic reactions to occur at the surface of the microbial layer, but anaerobic metabolism occurs at the bottom of the microbial layer where oxygen does not penetrate.

Originally, the medium in trickling filters was rock, but rock has largely been replaced by plastic, which provides greater void space per unit of surface area and occupies less volume within the filter. A plastic medium permitted trickling filters to be increased from a medium depth of 1.8 m (6 ft) to one of 4.2 m (14 ft) and even 6.0 m (20 ft). The wastewaters are normally applied by a rotary distributor or a fixed-spray nozzle. The spraying or discharging of wastewaters above the trickling-filter medium permits better distribution over the medium and oxygen transfer before reaching the medium. The effluent from the trickling-filter medium is captured in a clay-tile underdrain system or in a tank below the plastic medium. It is important that the bottom of the trickling filter be open for air to move quickly through the filter and bring adequate oxygen for the microbial reactions.

If a high-quality effluent is required, trickling filters must be operated at a low hydraulic-loading rate and a low organic-loading rate. Low-rate trickling filters are operated at hydraulic loadings of 2.2×10^{-5} to 4.3×10^{-5} $\text{m}^3/(\text{m}^2\cdot\text{s})$ [2 million to 4 million gal/(acre·day)]. High-rate trickling filters are designed for 10.8×10^{-5} to 40.3×10^{-5} $\text{m}^3/(\text{m}^2\cdot\text{s})$ [10 million to 40 million gal/(acre·day)] hydraulic loadings and organic loadings up to 1.4 kg/($\text{m}^3\cdot\text{day}$) [90 lb BOD₅/(1000 ft³·day)]. Plastic-medium trickling filters have been designed to operate up to 108×10^{-5} $\text{m}^3/(\text{m}^2\cdot\text{s})$ [100 million gal/(acre·day)] or even higher, with organic loadings up to 4.8 kg/($\text{m}^3\cdot\text{day}$) [300 lb BOD₅/(1000 ft³·day)]. Low-rate trickling filters will produce better than 90 percent BOD₅ and suspended-solids reductions, while high-rate trickling filters will produce from 65 to 75 percent BOD₅ reduction. Plastic-medium trickling filters will produce from 59 to 85 percent BOD₅ reduction depending upon the organic-loading rate. It is important to recognize that concentrated industrial wastes will require considerable hydraulic recirculation around the trickling filter to obtain the proper hydraulic-loading rate without excessive organic loads. With high recirculation rates the organic load is distributed over the entire volume of the trickling filter for maximum organic removal.

The short fluid-retention time within the trickling filter is the primary reason for the low treatment efficiency.

Rotating Biological Contactors (RBCs) The newest form of trickling filter is the rotating biological contactor with a series of circular plastic disks, 3.0 to 3.6 m (10 to 12 ft) in diameter, immersed to approximately 40 percent diameter in a shaped contact tank. The RBC disks rotate at 2 to 5 r/min. As the disks travel through the wastewaters, a small layer adheres to them. As the disks travel into the air, the microbes on the disk surface oxidize the organics. Thus, only a small amount of energy is required to supply the required oxygen for wastewater treatment. As the microbes build up on the plastic disks, the shearing velocity that is created by the movement of the disks through the water causes the excess microbes to be removed from the disks and discharged to the final sedimentation tank.

Rotating biological contactors have been very popular in treating industrial wastes because of their relatively small size and their low energy requirements. Unfortunately, there have occurred a number of problems which should be recognized prior to using RBCs. Strong industrial wastes tend to create excessive microbial growths which are not easily sheared off and which create high oxygen-demand rates with the production of hydrogen sulfide and other obnoxious odors. The heavy microbial growths have damaged some of the disks and caused some shaft failures. The disks are currently being covered with plastic shells to prevent nuisance odors from occurring. Air must be forced through the covered RBC systems and be chemically treated before being discharged back into the environment. Recirculation of wastewater flow around the RBC units can distribute the load over all the units and reduce the heavy initial microbial growths. RBC units also work best under uniform organic loads, requiring surge tanks for many industrial wastes. The net result has been for the cost of RBC units to approach that of other treatment units in terms of organic matter stabilized.

RBCs should be designed on both a hydraulic-loading rate and an organic-loading rate. Normally, hydraulic-loading rates of up to 0.16 $\text{m}^3/(\text{m}^2\cdot\text{day})$ [4 gal/(ft²·day)] of surface area are used with organic loading rates up to 44 kg/($\text{m}^2\cdot\text{day}$) [9 lb BOD₅/(ft²·day)]. Treatment efficiency is primarily a function of the fluid-retention time and the organic-loading rate. At low organic-loading rates the RBC units will produce nitrification in the same way as low-rate trickling filters.

Packed-Bed Fixed-Film Systems These systems were originally termed anaerobic trickling filters because the first systems were submerged columns filled with stones run under anaerobic conditions. A wide variety of packed media is now used ranging in size from granules 40 mesh to 7.5-cm (3-in) stones. Many systems use open structure plastic packing similar to that used in aerobic trickling filters.

The systems using granular media packing are used for anoxic denitrification. They are usually downflow, thus serving the dual function of filtration and denitrification. Contact times are short (EBCT < 15 min), but excellent removal is achieved due to the high level of biomass retained in the reactor. Pacing the methanol dose to the varying feed nitrate concentration is crucial. Frequent, short-duration backwash (usually several times per day) is required or the nitrogen bubbles formed will bind the system, causing poor results. Extended backwash every two to three days is required or the system will clog on the biomass growth. Thus, several units in parallel or a large holding tank are needed to compensate for the down time during backwash. Backwash does not remove all the biomass; a thin film remains coating the packing. Thus, denitrification begins immediately when the flow is restored.

The systems using the larger packing are used in the treatment of relatively strong, low-suspended-solids industrial waste. These systems are closed columns usually run in an upflow mode with a gas space at the top. These are operated under anaerobic conditions with waste conversion to methane and carbon dioxide as the goal. Effluent recycle is often used to help maintain the pH in the inlet zone in the correct range 6.5–7.5 for the methane bacteria. Some wastes require the addition of alkaline material to prevent a pH drop. Sodium bicarbonate is often recommended for pH control because it is easier to handle than lime or sodium hydroxide, and because an overdose of bicarbonate will only raise the pH modestly. An overdose of lime or sodium hydroxide can easily raise the pH above 8.0. Table 22-48 gives

TABLE 22-48 Anaerobic Process Performance on Industrial Wastewater UASB, Submerged Filter (SF), FBR

Process	Wastewater	Reactor size, MG	COD, g/l	OVL, kg/m ³ d	%CODr	HRT-d	°C
SF	Rum slops	3.5	80-105	15	71	7.8	35
SF	Modified guar	0.27	9.1	7.5	60	1.0	37
SF	Chemical	1.5	14	11	90	0.7	H
SF	Milk	0.2	3	7.5	60	0.5	32
SF	PMFC	10 ⁻⁵	13.7	23	72	0.6	36
UASB	Potato	0.58	2.5	3	85	0.7	35
UASB	Sugar beet	0.21	3	16	88	—	—
UASB	Brewery	1.16	1.6-2.2S	4.4	83	0.4	30
UASB	Brewery	1.16	2.0-2.4S	8.7	78	0.2	30
UASB	PMFC	10 ⁻⁵	13.7	4-5	87	2.9	36
FBR	PMFC	10 ⁻⁵	13.7	35-48	88	0.4	36
FBR	Soft drink	0.04	3.0	6-7	75	0.5	35
FBR	Chemical	0.04	35	14	95	2.5	35

OVL = organic volumetric load (COD); S = settled effluent; H = heated; PMFC = paper mill foul condensate (5,6).
NOTE: MG = 3785 m³.

some performance data with systems treating industrial wastes. HRTs of 1 to 2 days are used, as the buildup of growth on the packing ensures a BSRT of 20-50 days. It should be possible to lower the HRT further, but in practice this has not been successful because biomass starts to escape from the system or plugging occurs. Some escape is due to high gasification rates, and some is due to the fact that anaerobic sludge attaches less tenaciously to packing than aerobic or anoxic sludge. These systems can handle wastes with moderate solids levels. Periodically, solids must be removed from the reactor to prevent plugging of the packing or loss of solids in the effluent.

Biological Fluidized Beds This high-rate process has been used successfully for aerobic, anoxic, and anaerobic treatment of municipal and industrial wastewaters. Numerous small- and large-scale applications for hazardous waste, contaminated groundwater, nontoxic industrial waste and municipal wastewater have been reported (Refs. 32 and 33). The basic element of the process is a bed of solid carrier particles, such as sand or granular activated carbon, placed in a reactor through which wastewater is passed upflow with sufficient velocity to impart motion or fluidize the carrier. An active growth of biological organisms grow as firmly attached mass surrounding each of the carrier particles. As the wastewater contaminants pass by the biologically covered carrier, they are removed from the wastewater through biological and adsorptive mechanisms. Figure 22-44 is a schematic of the process.

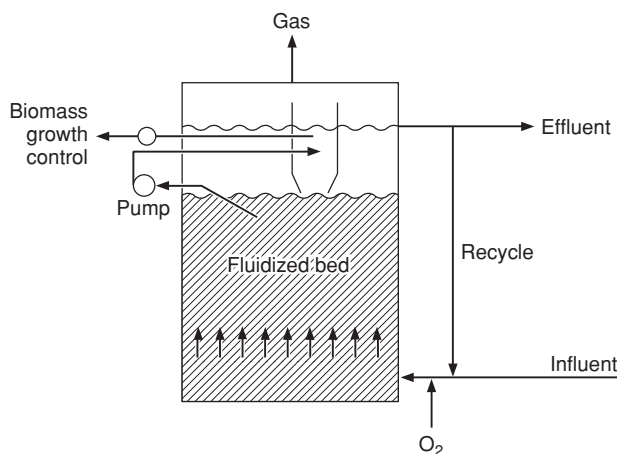


FIG. 22-44 Schematic of fluidized bed process.

The influent wastewater enters the reactor through a pipe manifold and is introduced downflow through nozzles that distribute the flow uniformly at the base of the reactor. Reversing direction at the bottom, the flow fluidizes the carrier when the fluid drag overcomes the buoyant weight of the carrier and its attached biomass layer. During startup (before much biomass has accumulated), the flow velocity required to achieve fluidization is higher than after the biomass attaches. Recycle of treated effluent is adjusted to achieve the desired degree of fluidization. As biomass accumulates, the particles of coated biomass will separate to a greater extent at constant flow velocity. Thus, as the system ages and more biomass accumulates, the extent of bed expansion increases (the volume of voids increases). This phenomenon is advantageous because it prevents clogging of the bed with biomass. Consequently, higher levels of biomass attachment are possible than in other types of fixed film systems. However, eventually, the degree of bed expansion may become excessive. Reduction of recycle will reduce expansion but may not be feasible because recycle has several purposes (i.e., supply of nutrients, alkalinity, and dilution of waste strength). Control of the expanded bed surface level is automatically accomplished using a sensor that activates a biomass growth control system at a prescribed level and maintains the bed at the proper depth. A pump removes a portion of the attached biomass, separates the biomass and inert carrier by abrasion, and pumps the mixture into a separator. Here the heavy carrier settles back into the fluidized bed and the abraded biomass, which is less dense, is removed from the system by gravity or a second pump. Other growth control designs are also used. Effluent is withdrawn from the supernatant layer above the fluidized bed. The reactor is usually not covered unless it is operating under anaerobic conditions and methane, odorous gases, or other safety precautions are mandated.

When aerobic treatment is to be provided to high concentrations of organics, pure oxygen or hydrogen peroxide may be injected into the wastewater prior to entering the reactor. Liquid oxygen (LOX) or pressure swing absorption (PSA) systems have been used to supply oxygen. Air may be used at low D.O. demands.

In full-scale applications, this process has been found to operate at significantly higher volumetric loading rates for wastewater treatment than other processes. The primary reasons for the very high rates of contaminant removal is the high biologically active surface area available (approximately 1000 ft²/ft³ of reactor) and the high concentration of reactor biological solids (8,000-40,000 mg/L) that can be maintained (Table 22-49). Because of these atypical high values, designs usually indicate a 200-500 percent reduction in reactor volume when compared to other fixed film and suspended growth treatment processes. In Table 22-50, is a list of full-scale commercial applications of the process operated at high wastewater concentrations including aerobic oxidation of organics, anoxic denitrification and anaerobic treatment systems.

TABLE 22-49 Process Comparisons

Biological process	MLVSS, mg/L	Surface area, ft ² /ft ³
Activated sludge	1500–3000	—
Pure oxygen activated sludge	2000–5000	—
Suspended growth nitrification	1000–2000	—
Suspended growth denitrification	1500–3000	—
Fluidized bed-CBOD removal	12,000–20,000	800–1200
Fluidized bed-nitrification	8,000–12,000	800–1200
Fluidized bed-denitrification	25,000–40,000	800–1200
Trickling filter-CBOD removal	—	12–50
RBC-CBOD removal	—	30–40

Of special note is the enhancement to the process when granular activated carbon (GAC) is used as the carrier. Because GAC has adsorptive properties, organic compounds present in potable waters and wastewater at low concentrations, often less than ten mg/L, are removed by adsorption and subsequently consumed by the biological organisms that grow in the fluidized bed. The BTEX compounds, methylene chloride, chlorobenzene, plastics industry toxic effluent, and many others are removed in this manner. BTEX contamination of groundwater from leaking gasoline storage tanks is a major problem, and sixteen full-scale fluidized bed process applications have been made. Contaminated groundwater is pumped to the ground surface for treatment using the fluidized bed in the aerobic mode. Often the level of BTEX is 1–10 mg/L and about 99 percent is removed in less than ten minutes detention time. Installations in operation range in size from 30 to 3000 gpm. The smaller installations are often skid-mounted and may be moved from location to location at a given site. A major advantage of this process over stripping towers and vacuum systems for treating volatile organics (VOCs) is the elimination of effluent gas treatment.

Pilot-plant studies and full-scale plants have shown successful treatment of wastewaters with 5000 to 50,000 mg/L COD from dairy, brewery, other food preparation wastes; paper pulp wastes; deicing fluids; and other hazardous and nonhazardous materials. Design criteria for biological fluidized-bed systems are included in Table 22-51.

A third type of reactor system is the upflow anaerobic sludge blanket (UASB) reactor system. The UASB is a continuous-flow system that maintains a dense flocculated biomass that is granular. The wastewater passes through this dense sludge blanket to achieve desired treatment efficiency. The UASB, anaerobic filter, and fluidized-bed systems have all been applied successfully to treat a variety of industrial waste streams. Table 22-44 summarizes some of the applications of these treatment technologies.

Design criteria for satisfactory biological fluidized bed treatment systems include the major parameters given in Table 22-51.

TABLE 22-50 Full-Scale Commercial Applications of Fluidized Bed Process

Application	Type	Reactor volume, m ³
CBOD—paint—General Motors	Aerobic	108
C.NBOD—sanitary and automotive—GM	Aerobic	165
Chemical—Grindsted Products Denmark	Aerobic	730
Nitrification—fish hatchery—Idaho	Aerobic	820
BTEX, groundwater—Ohio	Aerobic	250
Chemical, Toxicity reduction—Texas	Aerobic	225
Denitrification, Nuclear Fuel, DOE, Fernald, OH	Anoxic	53
CBOD, Denitrification—municipal, Nevada	Anoxic	1450
Petrochemical—Reliance Ind. India	Anaerobic	850
Soft drink, Delaware	Anaerobic	166
Brewery—El Aguila, Spain	Anaerobic	1570

TABLE 22-51 Typical Design Parameters for Fluidized Beds

Waste	Mode	Influent concentration, mg/L	Volumetric load, lb/ft ³ -d	Hydraulic detention time, hr	Volatile solids (biosolids), g/L
Organic COD	Aerobic	<2000	0.1–0.6	0.5–2.5	12–20
Organic COD	Aerobic	<10	0.02–0.1	0.1–0.5	4–8
NH ₃ -N	Aerobic	<25	0.05–0.3	0.1–0.5	7–14
NO ₃ -N	Anoxic	<5,000	0.4–2	0.1–2.4	20–40
Organic COD	Anaerobic	>4000	0.5–4	2–24	20–40

NOTE: lb/ft³-d = 16 kg/m³-d.

PHYSICAL-CHEMICAL TREATMENT

Processes and/or unit operations that fall under this classification include adsorption, ion exchange, stripping, chemical oxidation, and membrane separations. All of these are more expensive than biological treatment but are used for removal of pollutants that are not easily removed by biomass. Often these are utilized in series with biological treatment; but sometimes they are used as stand-alone processes.

Adsorption This is the most widely used of the physical-chemical treatment processes. It is used primarily for the removal of soluble organics with activated carbon serving as the adsorbent. Most liquid-phase-activated carbon adsorption reactions follow a Freundlich Isotherm [Eq. (22-25)].

$$y = kc^{1/n} \quad (22-25)$$

where: y = adsorbent capacity, mass pollutant/mass carbon
 c = concentration of pollutant in waste, mass/volume
 k and n = empirical constants

EPA has compiled significant data on values of k and n for environmentally significant pollutants with typical activated carbons. Assuming equilibrium is reached, the isotherm provides the dose of carbon required for treatment. In a concurrent contacting process, the capacity is set by the required effluent concentration. In a countercurrent process, the capacity of the carbon is set by the untreated waste pollutant concentration. Thus countercurrent contacting is preferred.

Activated carbon is available in powdered form (200–400 mesh) and granular form (10–40 mesh). The latter is more expensive but is easier to regenerate and easier to utilize in a countercurrent contactor. Powdered carbon is applied in well-mixed slurry-type contactors for detention times of several hours after which separation from the flow occurs by sedimentation. Often coagulation, flocculation, and filtration are required in addition to sedimentation. As it is difficult to regenerate, powdered carbon is usually discarded after use. Granular carbon is used in column contactors with EBCT of 30 minutes to 1 hour. Often several contactors are used in series, providing for full countercurrent contact. A single contactor will provide only partial countercurrent contact. When a contactor is exhausted, the carbon is regenerated either by a thermal method or by passing a solvent through the contactor. For waste-treatment applications where a large number of pollutants must be removed but the quantity of each pollutant is small, thermal regeneration is favored. In situations where a single pollutant in large quantity is removed by the carbon, solvent extraction regeneration can be used, especially where the pollutant can be recovered from the solvent and reused. Thermal regeneration is a complex operation. It requires removal of the carbon from the contactor, drainage of free water, transport to a furnace, heating under controlled conditions of temperature, oxygen, time, water vapor partial pressure, quenching, transport back to the reactor, and reloading of the column. Five to ten percent of the carbon is lost in this regeneration process due to burning and attrition during each regeneration cycle. Multiple hearth, rotary kiln, and fluidized bed furnaces have all been successfully used for carbon regeneration.

Pretreatment prior to carbon adsorption is usually for removal of suspended solids. Often this process is used as tertiary treatment after

primary and biological treatment. In either situation, the carbon columns must be designed to provide for backwash. Some solids will escape pretreatment, and biological growth will occur on the carbon, even with extensive pretreatment. Originally carbon treatment was viewed only as applicable for removal of toxic organics or those that are difficult to degrade biologically. Present practice applies carbon adsorption as a procedure for removal of all types of organics. It is realized that some biological activity will occur in virtually any activated carbon unit, so the design must be adjusted accordingly.

Ion Exchange This process has been employed for many years for treatment of industrial water supplies but not for wastes. However, some new ion-exchange materials have recently been developed that can be used for removal of specific pollutants. These new resins are primarily useful for selective removal of heavy metals, even though the target metals are present at low concentration in a wastewater containing many other inorganics. An ion-exchange process is usually operated with the waste being run downflow through a series of columns containing the appropriate ion-exchange resins. EBCT contact times of 30 min to 1 hour are used. Pretreatment for suspended solids and organics removal is practiced as well as pH adjustment.

The capacity of an ion-exchange resin is a function of the type and concentration of regenerant. Because ion-exchange resins are so selective for the target compound, a significant excess of the regenerant must be used. Up to a point, the more regenerant, the greater the capacity of the resin. Unfortunately, this results in waste of most of the regenerant. In fact, the bulk of the operational cost for this process is for regenerant purchase and its disposal; thus, regeneration must be optimized. Regenerants used (selection depends on the ion exchange resin) include sodium chloride, sodium carbonate, sulfuric acid, sodium hydroxide, and ammonia. Table 22-52 gives information on some of the new highly selective resins. These resins may provide the only practical method for reduction of heavy metals to the very low levels required by recent EPA regulations.

Stripping Air stripping is applied for the removal of volatile substances from water. Henry's law is the key relationship for use in design of stripping systems. The minimum gas-to-liquid ratio required for stripping is given by:

$$\frac{G}{L} = \frac{S_{in} - X_{out}}{(H)X_{out}}$$

for a concurrent process and

$$\frac{G}{L} = \frac{X_{in} - X_{out}}{(H)X_{in}}$$

for a countercurrent process where:

- G = airflow rate, mass/time
- L = waste flow rate, volume/time
- X = concentration of pollutant in waste, mass/volume
- H = Henry's constant for the pollutant in water, volume/mass

Higher ratios of gas to liquid flow are required than those computed above because mass-transfer limitations must be overcome. Stripping

can occur by sparging air into a tank containing the waste. Indeed, stripping of organics from activated sludge tanks is of concern because of the possibility that the public will be exposed to airborne pollutants including odors. A much more efficient stripping procedure is to use counterflow or crossflow contact towers. Procedures for design of these and mass-transfer characteristics of various packings are available elsewhere in this handbook.

Stripping has been successfully and economically employed for removal of halogenated organics from water and wastes with dispersion of the effluent gas to the atmosphere. However, recent EPA regulations have curtailed this practice. Now removal of these toxic organics from the gas stream is also required. Systems employing activated carbon (prepared for use with gas streams) are employed as well as systems to oxidize the organics in the gas stream. However, the cost of cleaning up the gas stream often exceeds the cost of stripping these organics from the water.

Chemical Oxidation This process has not been widely utilized because of its high cost. Only where the concentration of the target compound is very low will the quantity of oxidant required be low enough to justify treatment by chemical oxidation. The efficiency of this process is also low, as many side reactions can occur that will consume the oxidant. In addition, complete oxidation of organics to carbon dioxide and water often will not occur unless a significant overdose is used. However, renewed interest has recently occurred for two reasons.

1. It has been found that partial oxidation is satisfactory as a pretreatment to biological or carbon adsorption treatment. Partial oxidation often seems to make recalcitrant organics easier to degrade biologically and easier to adsorb.

2. A combination of ozone oxidation with simultaneous exposure to ultraviolet light seems to produce a self-renewing chain reaction that can significantly reduce the dose of ozone needed to accomplish oxidation.

Oxidants commonly used include ozone, permanganate, chlorine, chlorine dioxide, and ferrate, often in combination with catalysts. Standard-type mixed reactors are used with contact times of several minutes to an hour.

Advanced Oxidation Processes Advanced oxidation processes (AOPs) utilize the extremely strong oxidizing power of hydroxyl radicals to oxidize recalcitrant organic compounds to the mineral end products of CO₂, H₂O, HCL, etc. The hydroxyl radicals are produced on-site using a combination of traditional oxidation processes such as ozone/hydrogen peroxide, ultraviolet radiation/ozone, ultraviolet radiation/hydrogen peroxide, Fenton's reagent (ferrous iron and hydrogen peroxide) with ultraviolet radiation, and titanium dioxide/ultraviolet radiation (catalytic oxidation). The hydroxyl radical is a powerful nonselective oxidant, which can effectively and rapidly oxidize most organic compounds. As shown in Table 22-53, the hydroxyl radical has greater oxidizing power than do traditional oxidizing reagents. AOPs can be used to remove overall organic content (COD) or to destroy specific compounds. Table 22-53 shows the relative oxidation power of a select number of oxidizing species compared to chlorine. AOPs are most economical for treating industrial and hazardous waste streams that have a low level of recalcitrant contamination (<50 ppm). AOPs are emerging as an efficient and cost-effective treatment technology for specific industrial wastewaters and are likely to have broader applications as the various technologies are proved in the field.

TABLE 22-52 Selective Ion-Exchange Resins

Application	Exchanger type	Composition	Regenerant
Softening	Cation	Polystyrene matrix Sulfonic acid functional groups	NaCl
Heavy metals	Cation	Polystyrene matrix Chelating functional groups	Mineral acids
Chromate	Anion	Polystyrene matrix Tertiary or quaternary ammonium functional groups	Sodium carbonate or alkaline NaCl
Nitrate	Anion	Polystyrene matrix Tributyl ammonium functional group	NaCl

TABLE 22-53 Relative Oxidation Power of Select Oxidizing Reagents

Oxidizing species	Relative oxidation power
Chlorine	1.0
Hypochlorous acid	1.1
Permanganate	1.24
Hydrogen peroxide	1.31
Ozone	1.52
Atomic oxygen	1.78
Hydroxyl radical	2.05
Titanium dioxide	2.35

Membrane Processes These processes use a selectively permeable membrane to separate pollutants from water. Most of the membranes are formulated from complex organics that polymerize during membrane preparation. This allows the membrane to be tailored to discriminate by molecular size or by degree of hydrogen bonding potential. Ultrafiltration membranes discriminate by molecular size or weight, while reverse osmosis membranes discriminate by hydrogen-bonding characteristics. The permeability of these membranes is low: from 0.38–3.8 m/day (10–100 gal/d/ft²). The apparatus in which they are used must provide a high surface area per unit volume.

Membrane Bioreactors (MBRs) Membrane bioreactors are a technology that combines biological degradation of waste products with membrane filtration (Fig. 22-45). Typically, MBRs are operated as activated sludge systems with high biomass concentrations (10,000 to 15,000 mg/L MLSS) and long solids retention times (30 to 60 days). The membranes act as a solid-liquid separation to replace secondary clarifiers and granular media polishing filters. With the development of more economical, durable, and efficient membrane components, MBR systems have become feasible options for aerobic treatment of municipal wastewaters, and potentially for anaerobic treatment of industrial (i.e. low- to medium-strength) wastewaters. Two different process configurations for MBRs (sidestream or submerged modules) are used within wastewater treatment. The sidestream process is operated with high velocities and high transmembrane pressures (up to 5 bar). This results in high energy consumption and excessive shear forces within the reactor. The process with submerged modules was especially designed for biological wastewater treatment. The modules are submerged in the aerobic activated sludge zone where flow across the membrane surface is attained by aeration and mixing, resulting in a low flux rate with low transmembrane and vacuum pressures. Submerged membranes typically last longer (8+ years) and require less frequent cleaning and maintenance. With recent advances in membrane materials and process technology, MBRs have become more reliable, durable, and affordable. MBRs can be utilized for any level of treatment, but are most cost-effective when high-quality effluent is required.

The submerged MBR system is a small-footprint, single-process unit that can achieve a high-quality standard with low solids production. The membrane systems typically utilize either micro- or ultramembranes configured as hollow fibers, flat sheets, or tubes depending upon the manufacturer. Experience over the past decade has proved MBRs to be reliable and cost-effective for high-quality effluent applications, and relatively easy to maintain and operate. The key parameters for MBR

design and operation are flux rate, transmembrane pressure, fouling rate, and membrane cleaning schedule. MBRs have many possible applications in industrial and advanced municipal wastewater treatment and are becoming the preferred technology for wastewater reuse applications.

Industrial Reuse Many industries that use large volumes of freshwater are turning toward industrial reuse to minimize costs associated with attaining freshwater and disposing of wastewater. The need to minimize water consumption is a function of economics, water shortages caused by drought and overdevelopment, increasingly stringent regulations, and environmental awareness. Industrial reuse water is wastewater that is produced on-site that does not contain sewage and has been adequately treated for use in some part of the industrial operation. Reuse has become more economically feasible as a result of new treatment technologies (MBRs, AOPs, etc.) and rising costs of freshwater and wastewater disposal.

There are many industrial sources and uses of industrial reuse water. Common industrial processes that require large quantities of water, such as evaporative cooling towers and power stations, can be supplied using reclaimed wastewater. Other industrial applications for reuse water include boilers; stack scrubbing; washing of vehicles, buildings, and mechanical parts; and process water. The key to effective industrial reuse is to match the proper treatment processes (chemical, physical, biological) to achieve the desired quality of reuse water. Zero discharge industrial systems have recently been implemented in the United States and appear to be a growing trend, sustaining water resources and promoting smart industrial development. Some common industries that have implemented water reuse include the paper pulp industry, the pharmaceutical industry, chemical manufacturers, power plants, and refineries.

SLUDGE PROCESSING

Objectives Sludges consist primarily of the solids removed from liquid wastes during their processing. Thus, sludges could contain a wide variety of pollutants and residuals from the application of treatment chemicals; i.e., large organic solids, colloidal organic solids, metal sulfides, heavy-metal hydroxides and carbonates, heavy-metal organic complexes, calcium and magnesium hydroxides, calcium carbonate, precipitated soaps and detergents, and biomass and precipitated phosphates. As sludge even after extensive concentration and dewatering is still greater than 50 percent by weight water, it can also contain soluble pollutants such as ammonia, priority pollutants, and nonbiologically degradable COD.

The general treatment or management of sludge involves stabilization of biodegradable organics, concentration and dewatering, and ultimate disposal of the stabilized and dewatered residue. A large number of individual unit processes and unit operations are used in a sludge-management scheme. Those most frequently used are discussed below. Occasionally, only one of these is needed, but usually several are used in a series arrangement.

Because of the wide variability in sludge characteristics and the variation in acceptability of treated sludges for ultimate disposal (this is a function of the location and characteristics of the ultimate disposal site), it is impossible to prescribe any particular sludge-management plan. In the sections below, general performance of individual sludge-treatment processes and operations is presented.

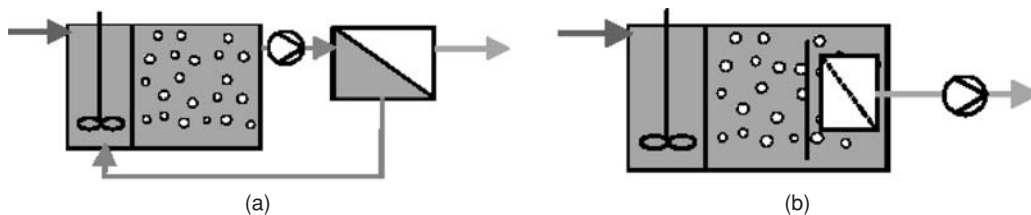


FIG. 22-45 Membrane bioreactor configurations for wastewater treatment. (a) With sidestream module; (b) with submerged module.

Concentration: Thickening and Flotation Generated sludges are often dilute (1–2 percent solids by weight). In order to reduce the volumetric loading on other processes, the first step in sludge processing is often concentration. The most popular process is gravity thickening which is carried out in treatment units similar to circular clarifiers. Organic sludges from primary treatment can usually be concentrated to 5–8 percent solids. Sludges from secondary treatment can be thickened to 2 percent solids. The potential concentration with completely inorganic sludges is higher (greater than 10 percent solids) except for sludges high in metal hydroxides. Polymers are often used to speed up thickening and increase concentration. Thickening is enhanced by long retention of the solids in the thickening apparatus. However, when biodegradable organics are present, solids retention time must be at a level that will not foster biological activity, lest odors, gas generation, and solids hydrolysis occur. Loading rates on thickeners range from 50–122 kg/m²/d (10–25 lb/ft²/d) for primary sludge to 12–45 kg/m²/d (2.5–9 lb/ft²/d). Solids detention time is 0.5 days in summer to several days in winter.

Flotation Air flotation has proved to be successful in concentrating secondary sludges to about 4 percent solids. The incoming solids are normally saturated with air at 275 to 350 kPa (40 to 50 psig) prior to being released in the flotation tank. As the air comes out of solution, the fine bubbles are trapped under the suspended solids and carry them to the surface of the tank. The air bubbles compact the solids as a floating mass. Normally, the air-to-solids ratio is about 0.01–0.05 L/g (0.16–0.8 ft³/lb). The thickened solids are scraped off the surface, while the effluent is drawn off the middle of the tank and returned to the treatment system. In large flotation tanks with high flows the effluent rather than the incoming solids is pressurized and recycled to the influent. The size of the flotation tanks is determined primarily by the solids-loading rate, directly or indirectly. A solids loading of 25 to 97 kg/(m²·day) [5 to 20 lb/(ft²·day)] has been found to be adequate. On a flow basis this translates into 0.14 to 2.7 L/(m²·day) [0.2 to 4 gal/(ft²·min)] surface area.

As with thickening, air flotation is enhanced by the addition of polymers. Flotation has been successfully used with wholly inorganic metal hydroxide sludges. Polymers and surfactants are used as additives. Engineering details on air flotation equipment has been developed by and is available from various equipment manufacturing companies. Liquid removed during thickening and flotation is usually returned to the head end of the plant.

Stabilization (Anaerobic Digestion, Aerobic Digestion, High Lime Treatment) Sludges high in organics can be stabilized by subjecting them to biological treatment. The most popular system is anaerobic digestion.

Anaerobic Digestion Anaerobic digesters are large covered tanks with detention times of 30 days, based on the volume of sludge added daily. Digesters are usually heated with an external heat exchanger to 35–37°C to speed the rate of reaction. Mixing is essential to provide good contact between the microbes and the incoming organic solids. Gas mixing and mechanical mixers have been used to provide mixing in the anaerobic digester. Following digestion, the sludge enters a holding tank, which is basically a solids-separation unit and is not normally equipped for either heating or mixing. The supernatant is recycled back to the treatment plant, while the settled sludge is allowed to concentrate to 3–6 percent solids before being further processed.

Anaerobic digestion results in the conversion of the biodegradable organics to methane, carbon dioxide, and microbial cells. Because of the energy in the methane, the production of microbial mass is quite low, less than 0.1 kg/kg (0.1 lb volatile suspended solids (VSS)/lb) BCOD metabolized except for carbohydrate wastes. The production of methane is 0.35 m³/kg (5.6 ft³/lb) BCOD destroyed. Digester gases range from 50 to 80 percent methane and 20 to 50 percent carbon dioxide, depending on the chemical characteristics of the waste organics being digested. The methane is often used on site for heat and power generation.

There are three major groups of bacteria that function in anaerobic digestion. The first group hydrolyzes large soluble and nonsoluble organic compounds such as proteins, fats and oils (grease), and carbohydrates, producing smaller water-soluble compounds. These are

then degraded by acid-forming bacteria, producing simple volatile organic acids (primarily acetic acid) and hydrogen. The last group (the methane bacteria) split acetic acid to methane and carbon dioxide and produce methane from carbon dioxide and hydrogen. Good operation requires the destruction of the volatile acids as quickly as they are produced. If this does not occur, the volatile acids will build up and depress the pH, which will eventually inhibit the methane bacteria. To prevent this from occurring, feed of organics to the digester should be as uniform as possible.

If continuous addition of solids is not possible, additions should be made at as short intervals as possible. Alkalinity levels are normally maintained at about 3000 to 5000 mg/L to keep the pH in the range 6.5–7.5 as a buffer against variable organic-acid production with varying organic loads. Proteins will produce an adequate buffer, but carbohydrates will require the addition of alkalinity to provide a sufficient buffer. Sodium bicarbonate should be used to supply the buffer.

An anaerobic digester is a no-recycle complete mix reactor. Thus, its performance is independent of organic loading but is controlled by hydraulic retention time (HRT). Based on kinetic theory and values of the pseudo constants for methane bacteria, a minimum HRT of 3 to 4 days is required. To provide a safety factor and compensate for load variation as indicated earlier, HRT is kept in the range 10 to 30 days. Thickening of feed sludge is used to reduce the tank volume required to achieve the long HRT values. When the sludge is high in protein, the alkalinity can increase to greater than 5000 mg/L, and the pH will rise past 7.5. This can result in free ammonia toxicity. To avoid this situation, the pH should be reduced below 7.5 with hydrochloric acid. Use of nitric or sulfuric acid will result in significant operational problems.

Aerobic Digestion Waste activated sludge can be treated more easily in aerobic treatment systems than in anaerobic systems. The sludge has already been partially aerobically digested in the aeration tank. For the most part, only about 25 to 35 percent of the waste activated sludge can be digested. An additional aeration period of 15 to 20 days should be adequate to reduce the residual biodegradable mass to a satisfactory level for dewatering and return to the environment. One of the problems in aerobic digestion is the inability to concentrate the solids to levels greater than 2 percent. A second problem is nitrification. The high protein concentration in the biodegradable solids results in the release of ammonia, which can be oxidized during the long retention period in the aerobic digester. Limiting oxygen supply to the aerobic digester appears to be the best method to handle nitrification and the resulting low pH.

A new concept is to use an on/off air supply cycle. During aeration, nitrates are produced. When the air is shut off, nitrates are reduced to nitrogen gas. This prevents acid buildup and removes nitrogen from the sludge. High power cost for aerobic digestion restricts the applicability of this process.

High Lime Treatment Uses doses of lime sufficient to raise the pH of sludge to 12 or above. As long as the pH is maintained at this level, biological breakdown will not occur. In this sense, the sludge is stable. However, any reduction of pH as a result of contact with CO₂ in the air will allow biological breakdown to begin. Thus, this technique should only be used as temporary treatment until further processing can occur. It is not permanent stabilization as is provided by anaerobic or aerobic digestion.

Sludge Dewatering Dewatering is different from concentration in that the latter still leaves a substance with the properties of a liquid. The former produces a product which is essentially a friable solid. When the water content of sludge is reduced to <70–80 percent, it forms a porous solid called sludge cake. There is no free water in the cake, as the water is chemically combined with the solids or tightly adsorbed on the internal pores. The operations below which are used to dewater sludge can be applied at any stage of the sludge management process, but often they follow concentration and/or biological stabilization. Chemical conditioning is almost always used to aid dewatering.

Lime, alum, and various ferric salts have been used to condition sludge prior to dewatering. Lime reacts to form calcium carbonate crystals, which act as a solid matrix to hold the sludge particles apart and allow the water to escape during dewatering. Alum and iron salts

help displace some of the bound water from hydrophilic organics and form part of the inorganic matrix. Chemical conditioning increases the mass of sludge to be ultimately handled from 10 to 25 percent, depending upon the characteristics of the individual sludge. Chemical conditioning can also help remove some of the fine particles by incorporating them into insoluble chemical precipitates. The water (supernatant) removed from the sludge during dewatering is often high in suspended solids and organics. Addition of polymers prior to, during, or after dewatering will often reduce the level of pollutants in the supernatant.

Centrifugation Both basket and solid-bowl centrifuges have been used to concentrate waste sludges. Field data have shown that it is possible to obtain 10 to 20 percent solids with waste activated sludge, 15 to 30 percent solids with a mixture of primary and waste activated sludge, and up to 30 to 35 percent solids with primary sludge alone. Centrifuges result in 85 to 90 percent solids capture with good operation. The problem is that the centrate contains the fine solids not easily removed. The centrate is normally returned to the treatment process, where it may or may not be removed. Economics do not favor centrifuges unless the sludge cake produced is at least 25 to 30 percent solids. For the most part, centrifuges are designed by equipment manufacturers from field experience. With varying sludge characteristics centrifuge characteristics will also vary widely.

Vacuum Filtration Vacuum filtration has been the most common method employed in dewatering sludges. Vacuum filters consist of a rotary drum covered with a cloth-filter medium. Various plastic fibers as well as wool have been used for the filter cloth. The filter operates by drawing a vacuum as the drum rotates into chemically conditioned sludge. The vacuum holds a thin layer of sludge, which is dewatered as the drum rotates through the air after leaving the vat. When the drum rotates the cloth to the opposite side of the apparatus, air-pressure jets replace the vacuum, causing the sludge cake to separate from the cloth medium as the cloth moves away from the drum. The cloth travels over a series of rollers, with the sludge being separated by a knife edge and dropping onto a conveyor belt by gravity. The dewatered sludge is moved on the conveyor belt to the next concentration point, while the filter cloth is spray-washed and returned to the drum prior to entering the sludge vat. Vacuum filters yield the poorest results on waste activated sludge and the best results on primary sludge. Waste activated sludge will concentrate to between 12 and 18 percent solids at a rate of 4.9 to 9.8 kg dry cake/(m²-h) [1 to 2 lb/(ft²-h)]. Primary sludge can be dewatered to 25 to 30 percent solids at a rate of 49 kg dry cake/(m²-h) [10 lb/(ft²-h)].

Pressure Filtration Pressure filtration has been used increasingly since the early 1970s because of its ability to produce a drier sludge cake. The pressure filters consist of a series of plates and frames separated by a cloth medium. Sludge is forced into the filter under pressure, while the filtrate is drawn off. When maximum pressure is reached, the influent-sludge flow is stopped and the pressure filter is allowed to discharge the residual filtrate prior to opening the filter and allowing the filter cake to drop by gravity to a conveyor belt below the filter press. The pressure filter operates at a pressure between 689 and 1380 kPa (100 and 200 psig) and takes 1.5 to 4 h for the pressure cycle. Normally, 20 to 30 min is required to remove the filter cake. The sludge cakes will vary from 20 to 25 percent for waste activated sludge to 50 percent for primary sludge. Chemical conditioning is necessary to obtain good dewatering of the sludges.

Belt-Press Filters The newest filter for handling waste activated sludge is the belt-press filter. The belt press utilizes a continuous cloth-filter belt. Waste activated sludge is spread over the filter medium, and water is removed initially by gravity. The open belt with the sludge moves into contact with a second moving belt, which squeezes the sludge layer between rollers with ever-increasing pressure. The sludge cake is removed at the end of the filter press by a knife blade, with the sludge dropping by gravity to a conveyor belt. Belt-press filters can produce sludge with 20–30 percent solids.

Sand Beds Sand filter beds can be used to dewater either anaerobically or aerobically digested sludges. They work best on relatively small treatment systems located in relatively dry areas. The sand bed consists of coarse gravel graded to fine sand in a series of layers to a depth of 0.45 to 0.6 m (1.5 to 2 ft). The digested sludge is placed over the entire filter

surface to a depth of 0.3 m (12 in) and allowed to sit until dry. Free water will drain through the sand bed to an open pipe underdrain system and be removed from the filter. Air drying will slowly remove the remaining water. The sludge must be cleaned from the bed by hand prior to adding a second layer of sludge. The sludge layer will drop from an initial thickness of 3 m (12 in) to about 0.006 m (1/4 in). An open sand bed can generally handle 49 to 122 kg dry solids/(m²-year) [10 to 25 lb/(ft²-year)]. Covered sand beds have been used in wet climates as well as in cold climates, but economics does not favor their use.

SLUDGE DISPOSAL

Incineration Incineration has been used to reduce the volume of sludge after dewatering. The organic fractions in sludges lend themselves to incineration if the sludge does not have an excessive water content. Multiple-hearth and fluid-bed incinerators have been extensively used for sludge combustion.

A multiple-hearth incinerator consists of several hearths in a vertical cylindrical furnace. The dewatered sludge is added to the top hearth and is slowly pushed through the incinerator, dropping by gravity to the next lower layer until it finally reaches the bottom layer. The top layer is used for drying the sludge with the hot gases from the lower layers. As the temperature of the furnace increases, the organics begin to degrade and undergo combustion. Air is used to add the necessary oxygen and to control the temperature during combustion. It is very important to keep temperatures above 600°C to ensure complete oxidation of the volatile organics. One of the problems with the multiple-hearth incinerator is volatilization of odorous organics during the drying phase before the temperature reaches combustion levels. Even afterburners on the exhaust-gas line may not be adequate for complete oxidation. Air-pollution-control devices are required on all incinerators to remove fly ash and corrosive gases. The ash from the incinerator must be cooled, collected, and conveyed back to the environment, normally to a sanitary landfill for burial. The residual ash will weigh from 10 to 30 percent of the original dry weight of the sludge. Supplemental fuels are needed to start the incinerator and to ensure adequate temperatures with sludges containing excessive moisture, such as activated sludge. Heat recovery from wastes is being given more consideration. It is possible to combine the sludges with other wastes to provide a better fuel for the incinerator.

A fluid-bed incinerator uses hot sand as a heat reservoir for dewatering the sludge and combusting the organics. The turbulence created by the incoming air and the sand suspension requires the effluent gases to be treated in a wet scrubber prior to final discharge. The ash is removed from the scrubber water by a cyclone separator. The scrubber water is normally returned to the treatment process and diluted with the total plant effluent. The ash is normally buried.

Sanitary Landfills Dewatered sludge, either raw or digested, is often buried in a sanitary landfill to minimize the environmental impact. Increased concern over sanitary landfills has made it more difficult simply to bury dewatered sludge. Sanitary landfills must be made secure from leachate and be monitored regularly to ensure that no environmental damage occurs. The moisture content of most sludges makes them a problem at sanitary landfills designed for solid wastes, requiring separate burial even at the same landfill.

Beneficial Reuse of Biosolids Biosolids are biological treatment sludges that are stabilized by using a variety of methods including alkaline stabilization, anaerobic digestion, aerobic digestion, composting, or heat drying and pelletization. The disposal of biosolids has typically been done through incineration and landfilling. With the severe decline in the number of landfills and the difficulty with incineration meeting stringent Clean Air Act standards, biosolids are increasingly being land-applied as a beneficial reuse. The specific type of land application is a function of the quality of biosolids being applied. Beneficial reuse of biosolids is regulated by the EPA (Part 503 Rules), which has established guidelines and specific criteria for reuse application. The EPA biosolids rules regulate chemical contaminants in the biosolids (metals), pathogen and pathogen indicator content, sludge stabilization methodology, land application site access and setback distances, vector attraction reduction methods, and the crop type and harvesting schedule.

EPA Class A or Class B biosolids can be land-applied. Land application serves two purposes: (1) to provide an inexpensive fertilizer and soil conditioner and (2) to continue treatment of the sludge through exposure to sunlight, plant uptake of metals, and desiccation of pathogens. The benefits of biosolids land application include addition

of nutrients (micro and macro) to soil, replacing agricultural dependency on chemical fertilizer; improving soil texture and increasing biological activity to promote root growth; slowly releasing nutrients to reduce off-site transport of nutrients; and lower cost than landfilling or incineration.

MANAGEMENT OF SOLID WASTES

INTRODUCTION

Solid wastes are all the wastes arising from human and animal activities that are normally solid and that are discarded as useless or unwanted. The term as used in this subsection is all-inclusive, and it encompasses the heterogeneous mass of throwaways. The three R's should be applied to solid wastes: reuse, recycle, and reduce. When these techniques have been implemented, management of the remaining residual solid waste can be addressed.

Functional Elements The activities associated with the management of solid wastes from the point of generation to final disposal have been grouped into the functional elements identified in Fig. 22-46. By considering each fundamental element separately, it is possible to (1) identify the fundamental element and (2) develop, when possible,

quantifiable relationships for the purpose of making engineering comparisons, analyses, and evaluations.

Waste Reduction Processes can be redesigned to reduce the amount of waste generated. For example, transfer lines between processes can be blown clear pneumatically to drive liquid into the batch mix tank.

Waste Generation Waste generation encompasses those activities in which materials are identified as no longer being of value and are either thrown away or gathered together for disposal. From the standpoint of economics, the best place to sort waste materials for recovery is at the source of generation.

Reuse Waste may be diverted to reuse. For example, containers may be cleaned and reused, or the waste from one process may become the feedstock for another.

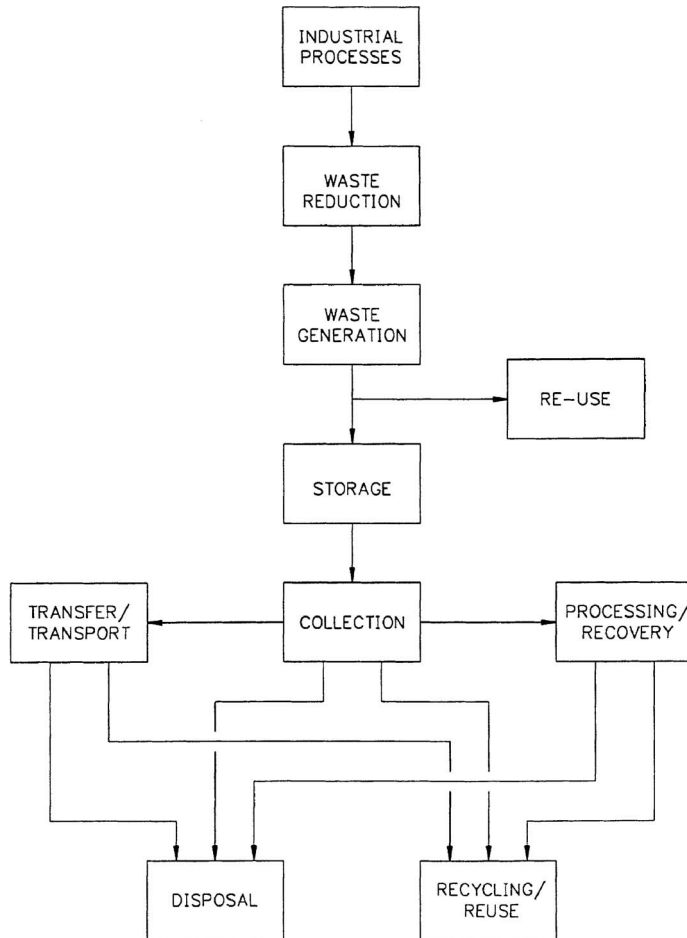


FIG. 22-46 Functional elements in a solid-waste management system. (Updated from G. Tchobanoglous, H. Theisen, and R. Eliassen, *Solid Wastes: Engineering and Management Issues*, McGraw-Hill, New York, 1977.)

On-Site Handling, Storage, and Processing The functional element encompasses those activities associated with the handling, storage, and processing of solid wastes at or near the point of generation. On-site storage is of primary importance because of the aesthetic considerations, public health, public safety, and economics involved.

Collection The functional element of collection includes the gathering of solid wastes and the hauling of wastes after collection to the location where the collection vehicle is emptied. As shown in Fig. 22-46, this location may be a transfer station, a processing station, or a landfill disposal site.

Transfer and Transport The functional element of transfer and transport involves two steps: (1) the transfer of wastes from the smaller collection containers to the larger transport equipment and (2) the subsequent transport of the wastes, usually over long distances, to the disposal site.

Processing and Recovery The functional element of processing and recovery includes all the techniques, equipment, and facilities used both to improve the efficiency of the other functional elements and to recover usable materials, conversion products, or energy from solid wastes. Materials that can be recycled are exported to facilities equipped to do so. Residues go to disposal.

Disposal The final functional element in the solid waste management system is disposal. Disposal is the ultimate fate of all solid wastes, whether they are wastes collected and transported directly to a landfill site, semisolid wastes (sludge) from industrial treatment plants and air-pollution-control devices, incinerator residue, compost, or other substances from various solid waste processing plants that are of no further use.

Solid-Waste-Management Systems Practical aspects associated with solid-waste-management systems not covered in the presentation include financing, operations, equipment management, personnel, reporting, cost accounting and budgeting, contract administration ordinances and guidelines, and public communications.

UNITED STATES LEGISLATION, REGULATIONS, AND GOVERNMENT AGENCIES

Much of the current activity in the field of solid-waste management, especially with respect to hazardous wastes and resources recovery, is a direct consequence of legislation. It is imperative to have a working knowledge of waste regulations, including RCRA and MACT (for EPA hazardous waste); TSCA (Toxic Substances Control Act) for PCBs and toxic waste; Solid Waste Disposal Act; the Clean Air Act; and PSD (prevention of significant deterioration) regulations. The Clean Air Act has far-reaching implications for any waste-related operation (e.g., incineration or landfill) that emits particulates or gaseous emissions. Primary elements of the act are Title I, dealing with fugitive emissions monitoring; Title III, with reduction of organic hazardous air pollutants; and Title V, with operating permits. The 1990 amendments have added a significant permitting burden for industrial plants and require additional controls for HAPs (hazardous air pollutants). In addition, state and local regulations apply to waste operations. The process of initiating major technology improvements in poor air quality areas, proving performance, and then spreading that technology elsewhere steadily ratcheted the emission limitations for new plants down to ever-lower levels.

Particulate emissions are an example of the ratcheting process. In the 1960s, burning 1 ton of MSW emitted about 30 lb of smoke. In 1971, the NSPS for incinerators reduced PM emissions to approximately 1.9 lb of PM per ton of MSW burned, a 94 percent reduction. In the 1980s, the focus changed to minimizing sulfur dioxide and PM. New plant PM levels have been below 0.2 lb/ton of MSW burned since the late 1980s—a 99 percent reduction from 30 lb in about two decades. Incremental improvements came from technology meeting the more stringent emission criteria. Each incremental improvement also used much more resources—energy, money and human talent—than the previous step.

Dioxin and furan emissions are another example of the ratcheting process. When first measured in the 1970s, concentrations were 1000

times greater than those routinely found 10 years later in state-of-the-art plants. The technology to control sulfur dioxide and hydrogen chloride emissions also reduced dioxin and furan emissions. Multipathway health risk assessments routinely show negligible risk from this level of dioxin and furan emissions. Even so, the 1995 Emissions Guidelines call for these low-emitting systems to demonstrate dioxin emissions another 50 times lower. This reduction is the anticipated by-product of using activated carbon to reduce mercury emissions, as it will also adsorb dioxins and furans.

The Maximum Achievable Control Technology (MACT) emission limitations required by the 1990 Clean Air Act Amendments (CAAA) show the ultimate effect of the ratcheting process. After a little more than two decades of ratcheting, MWCs have become a comparatively minor source of combustion-related air pollution. Other artificial and natural sources such as automobiles, trucks, power plants, fireplaces, wood stoves, metal production furnaces, industrial manufacturing processes, volcanoes, forest fires, and backyard trash burning are now the major known sources of combustion-related pollutants.

Regulations have been adopted by federal, state, and local agencies to implement the legislation. Before any design and construction work is undertaken, these regulations must be reviewed and care taken to factor in the nearly continuous regulatory revisions, as noted above.

GENERATION OF SOLID WASTES

Solid wastes, as noted previously, include all solid or semisolid materials that are no longer considered of sufficient value to be retained in a given setting. The types and sources of solid wastes, the physical and chemical composition of solid wastes, and typical solid-waste generation rates are considered in this subsection.

Types of Solid Waste The term *solid wastes* is all-inclusive and encompasses all sources, types of classifications, compositions, and properties. As a basis for subsequent discussions, it will be helpful to define the various types of solid wastes that are generated. It is important to note that the definitions of solid-waste terms and the classifications vary greatly in practice and in the literature. Consequently, the use of published data requires considerable care, judgment, and common sense. The following definitions are intended to serve as a guide.

1. *Food wastes.* Food wastes are the animal, fruit, or vegetable residues (also called *garbage*) resulting from the handling, preparation, cooking, and eating of foods. The most important characteristic of these wastes is that they are putrescible and will decompose rapidly, especially in warm weather.

2. *Rubbish.* Rubbish consists of combustible and noncombustible solid wastes, excluding food wastes or other putrescible materials. Typically, combustible rubbish consists of materials such as paper, cardboard, plastics, textiles, rubber, leather, wood, furniture, and garden trimmings. Noncombustible rubbish consists of items such as glass, crockery, tin cans, aluminum cans, ferrous and other nonferrous metals, dirt, and construction wastes.

3. *Ashes and residues.* These are the materials remaining from the burning of wood, coal, coke, and other combustible wastes. Residues from power plants normally are composed of fine powdery materials, cinders, clinkers, and small amounts of burned and partially burned materials. Fly ash from coal boilers and CKD (cement kiln dust) are frequently sold for stabilization of waste, waste bulking operations, and incorporation into building products such as gypsum from sulfur dioxide scrubbing.

4. *Construction and demolition wastes.* C&D wastes that come from razed buildings and other structures are classified as demolition wastes. Wastes from the construction, remodeling, and repair of commercial and industrial buildings and other similar structures are classified as construction wastes. These wastes may include dirt, stones, concrete, bricks, plaster, lumber, shingles, and plumbing, heating, and electrical parts.

5. *Special wastes.* Wastes such as street sweepings, roadside litter, catch-basin debris, dead animals, and abandoned vehicles are classified as special wastes.

6. *Treatment plant wastes.* The solid and semisolid wastes from water, wastewater, and industrial waste-treatment facilities are included in this classification.

TABLE 22-54 Sources and Types of Industrial Wastes*

Code	SIC group classification	Waste-generating processes	Expected specific wastes
19	Ordnance and accessories	Manufacturing, assembling	Metals, plastic, rubber, paper, wood, cloth, chemical residues
20	Food and kindred products	Processing, packaging, shipping	Meats, fats, oils, bones, offal, vegetables, fruits, nuts and shells, cereals
22	Textile mill products	Weaving, processing, dyeing, shipping	Cloth and filter residues
23	Apparel and other finished products	Cutting, sewing, sizing, pressing	Cloth, fibers, metals, plastics, rubber
24	Lumber and wood products	Sawmills, millwork plants, wooden containers, miscellaneous wood products, manufacturing	Scrap wood, shavings, sawdust; in some instances, metals, plastics, fibers, glues, sealers, paints, solvents
25a	Furniture, wood	Manufacture of household and office furniture, partitions, office and store fixtures, mattresses	Those listed under Code 24, in addition, cloth and padding residues
25b	Furniture, metal	Manufacture of household and office furniture, lockers, springs, frames	Metals, plastics, resins, glass, wood, rubber, adhesives, cloth paper
26	Paper and allied products	Paper manufacture, conversion of paper and paperboard, manufacture of paperboard boxes and containers	Paper and filter residues, chemicals, paper coatings and filters, inks, glues, fasteners
27	Printing and publishing	Newspaper publishing, printing, lithography, engraving, bookbinding	Paper, newsprint, cardboard, metals, chemicals, cloth, inks, glues
28	Chemicals and related products	Manufacture and preparation of inorganic chemicals (ranging from drugs and soaps to paints and varnishes and explosives)	Organic and inorganic chemicals, metals, plastics, rubber, glass, oils, paints, solvents, pigments
29	Petroleum refining and related industries	Manufacture of paving and roofing materials	Asphalt and tars, felts, paper, cloth, fiber
30	Rubber and miscellaneous plastic products	Manufacture of fabricated rubber and plastic products	Scrap rubber and plastics, lampblack, curing compounds, dyes
31	Leather and leather products	Leather tanning and finishing, manufacture of leather belting and packaging	Scrap leather, thread, dyes, oils, processing and curing compounds
32	Stone, clay, and glass products	Manufacture of flat glass, fabrication or forming of glass; manufacture of concrete, gypsum, and plaster products; forming and processing of stone products, abrasives, asbestos, and miscellaneous non-mineral products	Glass, cement, clay, ceramics, gypsum, asbestos, stone, paper, abrasives
33	Primary metal industries	Melting, casting, forging, drawing, rolling, forming, extruding operations	Ferrous and non-ferrous metals scrap, slag, sand, cores, patterns, bonding agents
34	Fabricated metal products	Manufacture of metal cans, hand tools, general hardware, non-electrical heating apparatus, plumbing fixtures, fabricated structural products, wire, farm machinery and equipment, coating and engraving of metal	Metals, ceramics, sand, slag, scale, coatings, solvents, lubricants, pickling liquors
35	Machinery (except electrical)	Manufacture of equipment for construction, elevators, moving stairways, conveyors, industrial trucks, trailers, stackers, machine tools, etc.	Slag, sand, cores, metal scrap, wood, plastics, resins, rubber, cloth, paints, solvents, petroleum products
36	Electrical	Manufacture of electrical equipment, appliances and communication apparatus, machining, drawing, forming, welding, stamping, winding, painting, plating, baking, firing operations	Metal scrap, carbon, glass, exotic metals, rubber, plastics, resins, fibers, cloth residues, PCBs
37	Transportation equipment	Manufacture of motor vehicles, truck and bus bodies, motor-vehicle parts and accessories, aircraft and parts, ship and boat building, repairing motorcycles and bicycles and parts, etc.	Metal scrap, glass, fiber, wood, rubber, plastics, cloth, paints, solvents, petroleum products
38	Professional scientific controlling instruments	Manufacture of engineering, laboratory and research instruments and associated equipment	Metals, plastics, resins, glass, wood, rubber, fibers, abrasives
39	Miscellaneous manufacturing	Manufacture of jewelry, silverware, plate ware, toys, amusements, sporting and athletic goods, costume novelties, buttons, brooms, brushes, signs, advertising displays	Metals, glass, plastics, resin, leather, rubber, composition, bone, cloth, straw, adhesives, paints, solvents

*From C. L. Mantell (ed.), *Solid Wastes: Origin, Collection, Processing, and Disposal*, Wiley-Interscience, New York, 1975. PCBs added to item 36.

7. *Agricultural wastes.* Wastes and residues resulting from diverse agricultural activities, such as the planting and harvesting of row, field, and tree and vine crops, the production of milk, the production of animals for slaughter, and the operation of feedlots are collectively called agricultural wastes.

Hazardous Wastes The US EPA has defined hazardous waste in RCRA regulations, CFR Parts 260 and 261. A waste may be hazardous if it exhibits one or more of the following characteristics: (1) ignitability, (2) corrosivity, (3) reactivity, and (4) toxicity. A detailed definition of these terms was first published in the Federal Register on May 19, 1980, pp. 22, 121–122. A waste may be hazardous if listed in Appendix VIII.

In the past, hazardous wastes were often grouped into the following categories: (1) radioactive substances, (2) chemicals, (3) biological wastes, (4) flammable wastes, and (5) explosives. The chemical category included wastes that were corrosive, reactive, and toxic. The

principal sources of hazardous biological wastes are hospitals and biological research facilities.

All hazardous waste combustors (HWCs), including hazardous waste incinerators (HWIs), cement kilns (CKs), and lightweight aggregate kilns (LWAKs), are subject to the MACT standards regardless of size or major source status. HWCs are required to be in compliance with the standards by September 30, 2003, and are required to demonstrate compliance by March 30, 2004, through a Comprehensive Performance Test (CPT). The rule allows for a 1-year extension of the compliance date for facilities that need to install pollution control equipment to meet standards.

The HWC MACT standards regulate emissions of the following pollutants:

- Dioxins and furans (D/F)
- Mercury (Hg)

- Total chlorine (HCl/Cl₂)
- Semivolatile metals (SVMs)—lead and cadmium
- Low-volatility metals (LVMs)—arsenic, beryllium, and chromium
- Particulate matter (PM)
- Carbon monoxide (CO)
- Hydrocarbons (HC)

The HWC MACT standards require continuous monitoring of both emissions and operating parameters to demonstrate compliance at all times. Continuous emissions monitoring is required for CO or HC. In the future, facilities will also be required to use continuous emission monitors for PM. In addition, cement kilns may be required to use an opacity monitor.

The Federal Register (vol. 69, no. 76, April 20, 2004) issued Proposed Rules for Existing and New Sources of HWCs. This included not only the HWIs, CKs, and LWAKs, but also for the first time the solid-fuel-fired boilers, liquid-fuel-fired boilers, and hydrochloric acid production furnaces. The boilers and HCl furnaces had been covered by the Boilers and Industrial Furnaces standards issued as Boiler and Industrial Furnace Act (BIF) in 1991. When MACT was enacted for HWCs on September 30, 1999, the BIFs were not included. The proposed standards were listed in Tables 1 and 2 of the FR of April 20, 2004.

Sources of Industrial Wastes Knowledge of the sources and types of solid wastes, along with data on the composition and rates of generation, is basic to the design and operation of the functional elements associated with the management of solid wastes.

Conventional Wastes Sources and types of industrial solid wastes generated by Standard Industrial Classification (SIC) group classification are reported in Table 22-54. The expected specific wastes in the table are most readily identifiable.

Hazardous Waste Hazardous wastes are generated in limited amounts throughout most industrial activities. In terms of generation, concern is with the identification of amounts and types of hazardous wastes developed at each source, with emphasis on those sources where significant waste quantities are generated.

The USEPA released "National Biennial RCRA Hazardous Waste Report" based on 2001 data. The three-volume report, which represents comprehensive data on the generation and management of hazardous waste in the United States during 2001, includes the National Analysis, the State Detail Analysis, and the List of Reported RCRA Sites. The report noted a decrease to 40.8 million

tons compared to 206 million tons of hazardous waste generated in 1991. The number of large-quantity generators decreased to 19,024 from 23,426 in 1991. The number of waste treatment, storage, and disposal (TSD) facilities decreased to 2479 from 3862 in 1991.

The majority—56.1 percent—of the hazardous wastes generated during 2001 were managed in aqueous waste treatment units. Land disposal accounted for another 4.6 percent of the total, divided as follows: 2.1 million tons sent to landfills and 65,000 tons managed by land farming. Resource recovery operations managed 3.7 percent of the 46 million tons, with solvent-recovery units managing 3.6 million tons; fuel-blending units, 1.4 million tons; metals recovery, 1.46 million tons; and other methods such as acid regeneration and waste oil recovery accounting for 9.8 million tons. Thermal treatment systems burned 6.3 percent of the hazardous wastes generated in 2001: 1.65 million tons was incinerated, and 1.7 million tons was used as fuel in boilers and industrial furnaces.

The generation of hazardous wastes by spillage must also be considered. The quantities of hazardous wastes that are involved in spillage usually are not known. After a spill, the wastes requiring collection and disposal are often significantly greater than the amount of spilled wastes, especially when an adsorbing material, such as straw, sand, and "oil-dry," is used to soak up liquid hazardous wastes. Similarly, the volume and mass of contaminated soil requiring excavation are far greater than the waste volume involved in a spill. Both the adsorbing material and the liquid are classified as hazardous waste.

Properties of Solid Wastes Information on the properties of solid wastes is important in evaluating alternative equipment needs, systems, and management programs and plans.

Physical Composition Information and data on the physical composition of solid wastes including (1) identification of the individual components that make up industrial and municipal solid wastes, (2) density of solid wastes, and (3) moisture content are presented below.

1. *Individual components.* Components that typically make up most industrial and municipal solid wastes and their relative distribution are reported in Table 22-55. Although any number of components could be selected, those listed in the table have been chosen because they are readily identifiable, are consistent with component categories reported in the literature, and are adequate for the characterization of solid wastes for most applications.

2. *Density.* Typical densities for various wastes as found in containers are reported by source in Table 22-56. Because the densities of

TABLE 22-55 Typical Data on Distribution of Industrial Wastes Generated by Major Industries and Municipalities*

SIC code	SIC group classification	Percent by mass									
		Food wastes [†]	Paper	Wood	Leather	Rubber	Plastics	Metals	Glass	Textiles	Miscellaneous
20	Food and kindred products	15–20	50–60	5–10	0–2	0–2	0–5	5–10	4–10	0–2	5–15
22	Textile mill products	0–2	40–50	0–2	0–2	0–2	3–10	0–2	0–2	20–40	0–5
23	Apparel and other finished products	0–2	40–60	0–2	0–2	0–2	0–2	0–2	0–2	30–50	0–5
24	Lumber and wood products	0–2	10–20	60–80	0–2	0–2	0–2	0–2	0–2	0–2	5–10
25a	Furniture, wood	0–2	20–30	30–50	0–2	0–2	0–2	0–2	0–2	0–5	0–5
25b	Furniture, metal	0–2	20–40	10–20	0–2	0–2	0–2	20–40	0–2	0–5	0–10
26	Paper and allied products	0–2	40–60	10–15	0–2	0–2	0–2	5–15	0–2	0–2	10–20
27	Printing and publishing	0–2	60–90	5–10	0–2	0–2	0–2	0–2	0–2	0–2	0–5
28	Chemicals and related products	0–2	40–60	2–10	0–2	0–2	5–15	5–10	0–5	0–2	15–25
29	Petroleum refining and related industries	0–2	60–80	5–15	0–2	0–2	10–20	2–10	0–12	0–2	2–10
30	Rubber and miscellaneous plastic products	0–2	40–60	2–10	0–2	5–20	10–20	0–2	0–2	0–2	0–5
31	Leather and leather products	0–2	5–10	5–10	40–60	0–2	0–2	10–20	0–2	0–2	0–5
32	Stone, clay, and glass products	0–2	20–40	2–10	0–2	0–2	0–2	5–10	10–20	0–2	30–50
33	Primary metal industries	0–2	30–50	5–15	0–2	0–2	2–10	2–10	0–5	0–2	20–40
34	Fabricated metal products	0–2	30–50	5–15	0–2	0–2	0–2	15–30	0–2	0–2	5–15
35	Machinery (except electrical)	0–2	30–50	5–15	0–2	0–2	1–5	15–30	0–2	0–2	0–5
36	Electrical	0–2	60–80	5–15	0–2	0–2	2–5	2–5	0–2	0–2	0–5
37	Transportation equipment	0–2	40–60	5–15	0–2	0–2	2–5	0–2	0–2	0–2	15–30
38	Professional scientific controlling instruments	0–2	30–50	2–10	0–2	0–2	5–10	5–15	0–2	0–2	0–5
39	Miscellaneous manufacturing	0–2	40–60	10–20	0–2	0–2	5–15	2–10	0–2	0–2	5–15
Municipal	Municipal	10–20	40–60	1–4	0–2	0–2	2–10	3–15	4–16	0–4	5–30

*Adapted in part from D. G. Wilson (ed.), *Handbook of Solid Waste Management*, Van Nostrand Reinhold, New York, 1977.

†With the exception of food and kindred products, food wastes are from company cafeterias, canteens, etc.

TABLE 22-56 Typical Density and Moisture-Content Data for Domestic, Commercial, and Industrial Solid Waste

Item	Density, kg/m ³		Moisture content, % by mass	
	Range	Typical	Range	Typical
Residential (uncompacted)				
Food wastes (mixed)	130–480	290	50–80	70
Paper	40–130	85	4–10	6
Cardboard	40–80	50	4–8	6
Plastics	40–130	65	1–4	2
Textiles	40–100	65	6–15	10
Rubber	100–200	130	1–4	2
Leather	100–260	160	8–12	10
Garden trimmings	60–225	100	30–80	60
Wood	130–320	240	15–40	20
Glass	160–480	195	1–4	2
Tin cans	50–160	90	2–4	3
Nonferrous metals	65–240	160	2–4	2
Ferrous metals	130–1150	320	2–4	2
Dirt, ashes, etc.	320–1000	480	6–12	8
Ashes	650–830	745	6–12	6
Rubbish (mixed)	90–180	130	5–20	15
Residential (compacted)				
In compactor truck	180–450	300	15–40	20
In landfill (normally compacted)	360–500	450	15–40	30°
In landfill (well-compacted)	590–740	600	15–40	30°
Commercial				
Food wastes (wet)	475–950	535	50–85	75
Appliances	150–200	180	0–5	
Wooden crates	110–160	110	10–30	20
Tree trimmings	100–180	150	20–80	50
Rubbish (combustible)	50–180	120	5–25	15
Rubbish (noncombustible)	180–360	300	5–15	10
Rubbish (mixed)	140–180	160	5–20	12
Construction; demolition; remediation				
Mixed demolition (noncombustible)	1000–1600	1420	2–10	4
Mixed demolition (combustible)	300–400	360	4–15	8
Mixed construction (combustible)	180–360	260	4–15	8
Broken concrete	1200–1800	1540	0–5	—
Contaminated soil	1200–1900	1600	5–25	10
Industrial wastes				
Chemical sludges (wet)	800–1100	1000	75–99	80
Fly ash	700–900	800	2–10	4
Leather scraps	100–250	160	6–15	10
Metal scraps (heavy)	1500–2000	1780	0–5	
Metal scraps (light)	500–900	740	0–5	
Metal scraps (mixed)	700–1500	900	0–5	
Oils, tars, asphalt	800–1000	950	0–5	2
Sawdust	100–350	290	10–40	15
Textile wastes	100–220	180	6–15	10
Wood (mixed)	400–675	500	10–40	20
Agricultural wastes				
Agricultural (mixed)	400–750	560	48–80	50
Fruit wastes (mixed)	250–750	360	60–90	75
Manure (wet)	900–1050	1000	75–96	94
Vegetable wastes (mixed)	200–700	360	50–80	65

°Depends on degree of surface water infiltration.

solid waste vary markedly with geographic location, season of the year, and length of time in storage, great care should be used in selecting typical values.

3. *Moisture content.* The moisture content of solid wastes usually is expressed as the mass of moisture per unit mass of wet or dry material. In the wet-mass method of measurement, the moisture in a sample is expressed as a percentage of the wet mass of the material; in the dry-mass method, it is expressed as a percentage of the dry mass of the material. In equation form, the wet-mass moisture content is expressed as

$$\text{Moisture content (\%)} = \left\{ a - \frac{b}{a} \right\} \times 100 \quad (22-26)$$

where *a* = initial mass of sample as delivered and *b* = mass of sample after drying. Typical data on the moisture content for the solid-waste

components are given in Table 22-56. For most industrial solid wastes, the moisture content will vary from 10 to 25 percent.

4. *Particle size.* The material handling properties of solid wastes are dependent upon particle size. This applies as well to feed preparation and air pollution control which are affected by solid-waste particle size and cohesiveness. For wastes such as bulk soils, the amount of fines (from clay and silt) is critical for system design. Cohesiveness, which varies with moisture content, is important for bin and conveyor design.

Chemical Composition Information on the chemical composition of solid wastes is important in evaluating alternative processing and recovery options. If solid wastes are to be used as fuel, the six most important properties to be known are

1. Proximate analysis
- a. Moisture (loss at 105°C for 1 h)

TABLE 22-57 Typical Proximate-Analysis and Energy-Content Data for Components in Domestic, Commercial, and Industrial Solid Waste*

Component	Proximate analysis, % by mass				Energy content, kJ/kg		
	Moisture	Volatile matter	Fixed carbon	Non-combustible	As collected	Dry	Moisture- and ash-free
Food and food products							
Fats	2.0	95.3	2.5	0.2	37,530	38,296	38,374
Food wastes (mixed)	70.0	21.4	3.6	5.0	4,175	13,917	16,700
Fruit wastes	78.7	16.6	4.0	0.7	3,970	18,638	19,271
Meat wastes	38.8	56.4	1.8	3.1	17,730	28,970	30,516
Paper products							
Cardboard	5.2	77.5	12.3	5.0	16,380	17,278	18,240
Magazines	4.1	66.4	7.0	22.5	12,220	12,742	16,648
Newsprint	6.0	81.1	11.5	1.4	18,550	19,734	20,032
Paper (mixed)	10.2	75.9	8.4	5.4	15,815	17,611	18,738
Waxed cartons	3.4	90.9	4.5	1.2	26,345	27,272	27,615
Plastics							
Plastics (mixed)	0.2	95.8	2.0	2.0	32,000	32,064	32,720
Polyethylene	0.2	98.5	<0.1	1.2	43,465	43,552	44,082
Polystyrene	0.2	98.7	0.7	0.5	38,190	38,266	38,216
Polyurethane	0.2	87.1	8.3	4.4	26,060	26,112	27,316
Polyvinyl chloride	0.2	86.9	10.8	2.1	22,690	22,735	23,224
Wood, trees, etc.							
Garden trimmings	60.0	30	9.5	0.5	6,050	15,125	15,316
Green wood	50.0	42.3	7.3	0.4	4,885	9,770	9,848
Hardwood	12.0	75.1	12.4	0.5	17,100	19,432	19,542
Wood (mixed)	20.0	67.9	11.3	0.8	15,444	19,344	19,500
Leather, rubber, textiles, etc.							
Leather (mixed)	10	68.5	12.5	9.0	18,515	20,572	22,858
Rubber (mixed)	1.2	83.9	4.9	9.9	25,330	25,638	28,493
Textiles (mixed)	10	66.0	17.5	6.5	17,445	19,383	20,892
Glass, metals, etc.							
Glass and mineral	2	—	—	96–99+	196†	200	200
Metal, tin cans	5	—	—	94–99+	1,425†	1,500	1,500
Metals, ferrous	2	—	—	96–99+	—	—	—
Metals, nonferrous	2	—	—	94–99+	—	—	—
Miscellaneous							
Office sweepings	3.2	20.5	6.3	70	8,535	8,817	31,847
Multiple wastes	20 (15–40)	53 (30–60)	7 (5–15)	20 (9–30)	10,470	13,090	17,450
Industrial wastes	15 (10–30)	58 (30–60)	7 (5–15)	20 (10–30)	11,630	13,682	17,892

*Adapted in part from D. G. Wilson (ed.), *Handbook of Solid Waste Management*, Van Nostrand Reinhold, New York, 1977, and G. Tchobanoglous, H. Theisen, and R. Eliassen, *Solid Wastes: Engineering Principles and Management Issues*, McGraw-Hill, New York, 1977.
 †Energy content is from coatings, labels, and attached materials.

- b. Volatile matter (additional loss on heating to 950°C)
- c. Ash (residue after burning)
- d. Fixed carbon (remainder)
- 2. Fusion point of ash
- 3. Ultimate analysis, percent of C (carbon), H (hydrogen), O (oxygen), N (nitrogen), S (sulfur), and ash
- 4. Heating value
- 5. Organic chlorine
- 6. Organic sulfur

Typical proximate-analysis data for the combustible components of industrial and municipal solid wastes are presented in Table 22-57.

Typical data on the inert residue and energy values for solid wastes may be converted to a dry basis by using Eq. (22.27):

$$\frac{\text{kJ}}{\text{kg (dry basis)}} = \frac{\text{kJ}}{\text{kg (as discarded)}} \left(\frac{100}{100 - \% \text{ moisture}} \right) \quad (22-27)$$

The corresponding equation on an ash-free basis is

$$\frac{\text{kJ}}{\text{kg (ash-free dry basis)}} = \frac{\text{kJ}}{\text{kg (as discarded)}} \times \left(\frac{100}{100 - \% \text{ ash} - \% \text{ moisture}} \right) \quad (22-28)$$

Representative data on the ultimate analysis of typical industrial and municipal-waste components are presented in Table 22-58. If energy values are not available, approximate values can be determined by using Eq. (22-29), known as the modified Dulong formula, and the data in Table 22-58.

$$\text{kJ/kg} = 337C + 1428 \left(H - \frac{1}{8} O \right) + 95S \quad (22-29)$$

where C = carbon, percent
 H = hydrogen, percent
 O = oxygen, percent
 S = sulfur, percent

Quantities of Solid Wastes Representative data on the quantities of solid wastes and factors affecting the generation rates are considered briefly in the following paragraphs.

Typical Generation Rates Typical unit waste generation rates from selected industrial sources are reported in Table 22-59. Because waste generation practices are changing so rapidly, the presentation of “typical” waste generation data may not be reliable.

Factors That Affect Generation Rates Factors that influence the quantity of industrial wastes generated include (1) the extent of salvage and recycle operations, (2) company attitudes, and (3) legislation

TABLE 22-58 Typical Ultimate-Analysis Data for Components in Domestic, Commercial, and Industrial Solid Waste*

Components	Percent by mass (dry basis)					
	Carbon	Hydrogen	Oxygen	Nitrogen	Sulfur	Ash
Foods and food products						
Fats	73.0	11.5	14.8	0.4	0.1	0.2
Food wastes (mixed)	48.0	6.4	37.6	2.6	0.4	5.0
Fruit wastes	48.5	6.2	39.5	1.4	0.2	4.2
Meat wastes	59.6	9.4	24.7	1.2	0.2	4.9
Paper products	45.4	6.1	42.1	0.3	0.1	6.0
Cardboard	43.0	5.9	44.8	0.3	0.2	5.0
Magazines	32.9	5.0	38.6	0.1	0.1	23.3
Newsprint	49.1	6.1	43.0	< 0.1	0.2	23.3
Paper (mixed)	43.4	5.8	44.3	0.3	0.2	6.0
Waxed cartons	59.2	9.3	30.1	0.1	.1	1.2
Plastics						
Plastics (mixed)	60.0	7.2	22.8	—	—	10.0
Polyethylene	85.2	14.2	—	< 0.1	< 0.1	0.4
Polystyrene	87.1	8.4	4.0	0.2	—	0.3
Polyurethane†	63.3	6.3	17.6	6.0	< 0.1	4.3
Polyvinyl chloride‡	45.2	5.6	1.6	0.1	0.1	2.0
Wood, trees, etc.						
Garden trimmings	46.0	6.0	38.0	3.4	0.3	6.3
Green timber	50.1	6.4	42.3	0.1	0.1	1.0
Hardwood	49.6	6.1	43.2	0.1	< 0.1	0.9
Wood (mixed)	49.5	6.0	42.7	0.2	< 0.1	1.5
Wood chips (mixed)	48.1	5.8	45.5	0.1	< 0.1	0.4
Glass, metals, etc.						
Glass and mineral	0.5	0.1	0.4	< 0.1	—	98.9
Metals (mixed)	4.5	0.6	4.3	< 0.1	—	90.5
Leather, rubber, textiles						
Leather (mixed)	60.0	8.0	11.6	10.0	0.4	10.0
Rubber (mixed)	69.7	8.7	—	—	1.6	20.0
Textiles (mixed)	48.0	6.4	40.0	2.2	0.2	3.2
Miscellaneous						
Office sweepings	24.3	3.0	4.0	0.5	0.2	68.0
Oils, paints	66.9	9.6	5.2	2.0	—	16.3
Refuse-derived fuel (RAF)	44.7	6.2	38.4	0.7	< 0.1	9.9

*Adapted in part from D. G. Wilson (ed.), *Handbook of Solid Waste Management*, Van Nostrand Reinhold, New York, 1977, and G. Tehobanoulous, H. Theissen, and R. Eliassen, *Solid Wastes Engineering Principles and Management Issues*, McGraw-Hill, New York, 1977.

†Organic content is from coatings, labels and other attached materials.

‡Remainder is chlorine.

and regulations. The existence of salvage and recycling operations within an industry definitely affects the quantities of wastes collected. Whether such operations affect the quantities generated is another matter. The subsection "Pollution Prevention" by Louis Theodore points out actions taken by industrial plants as a result of the 1990 Pollution Prevention Act. Significant reductions in the quantities of solid wastes generated will occur when and if companies are willing to change—of their own volition—to conserve natural resources, to handle waste at its source rather than use "end-of-pipe" pollution control, and to reduce the economic burdens associated with the management of solid wastes. Perhaps the most important factor affecting the generation of certain types of waste is the existence of local, state, and federal regulations concerning the use and disposal of specific material. In general, the more regulated the waste, the higher the cost for treatment and disposal and the greater the incentive to reduce generation of the waste.

In 2001, U.S. residents, businesses, and institutions produced more than 229 million tons of MSW, which is approximately 4.4 lb of

waste per person per day, up from 2.7 lb per person per day in 1960. Several waste management practices, such as source reduction, recycling, and composting, prevent or divert materials from the waste stream. Source reduction involves altering the design, manufacture, or use of products and materials to reduce the amount and toxicity of what gets thrown away. A portion of each material category was recycled or composted in 2001. The highest rates of recovery were achieved with yard trimmings, paper products, and metal products. About 57 percent (5.8 million tons) of yard trimmings were recovered for composting in 2001. This represents a 4-fold increase from 1990. About 45 percent (36.7 million tons) of paper and paperboard was recovered for recycling in 2001. Recycling these organic materials alone diverted nearly 23 percent of MSW from landfills and combustion facilities. In addition, about 6.3 million tons, or about 35 percent, of metals were recovered for recycling. See Figs. 22-47 and 22-48.

EPA has ranked the most environmentally sound strategies for MSW. Source reduction (including reuse) is the most preferred

TABLE 22-59 Unit Solid-Waste Generation Rates for Selected Industrial Sources

Source	Unit	Range
Canned and frozen foods	Metric tons/metric tons of raw product	0.04–0.06
Printing and publishing	Metric tons/metric tons of raw paper	0.08–0.10
Automotive	Metric tons/vehicle produced	0.6–0.8
Petroleum refining	Metric tons/(employee day)	0.04–0.05
Rubber	Metric tons/metric tons of raw rubber	0.01–0.3

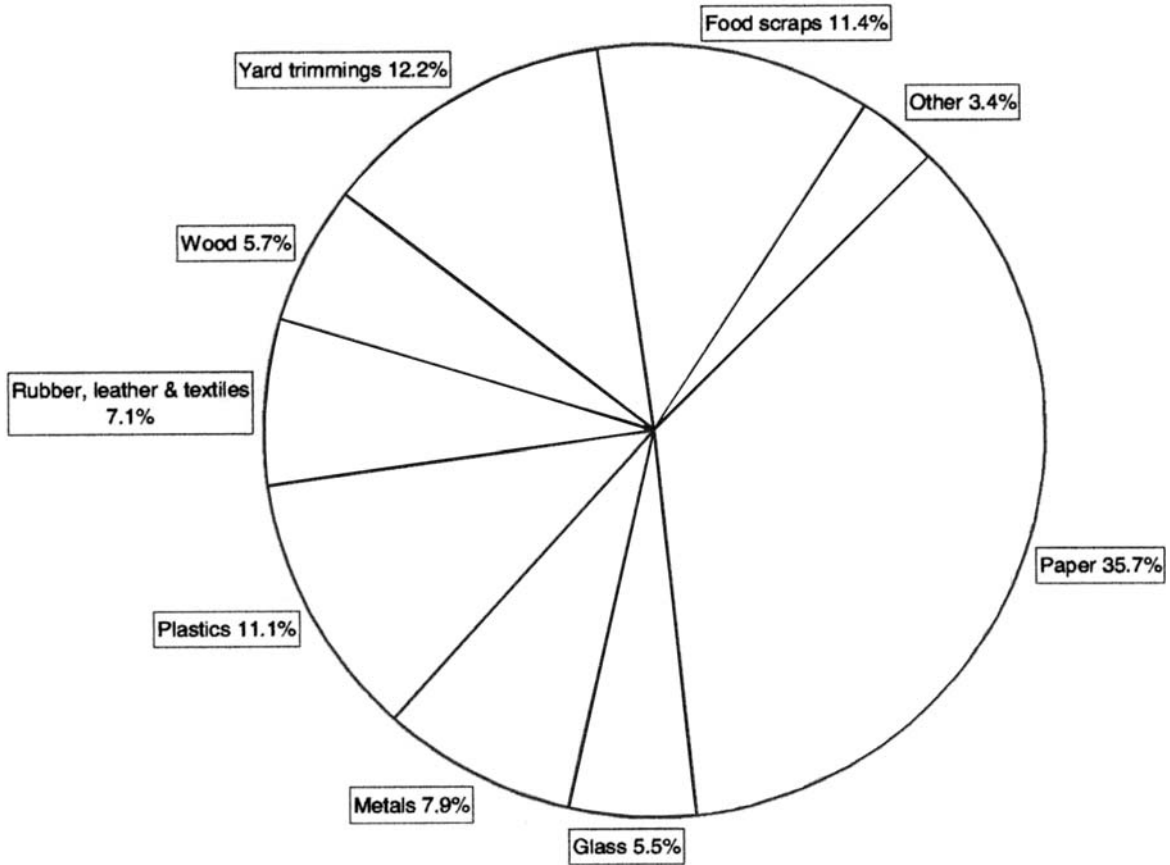


FIG. 22-47 2001 total MSW generation—229 million tons.

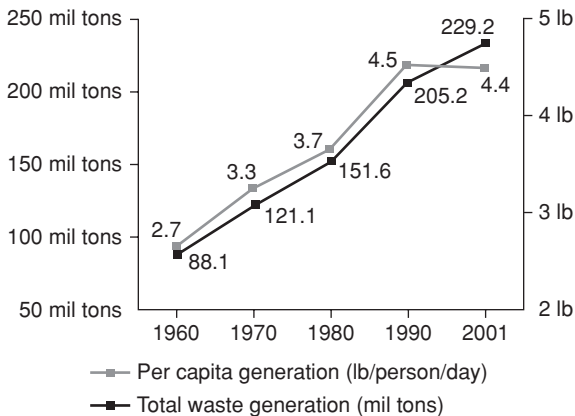


FIG. 22-48 Trends in MSW generation, 1960–2001.

method, followed by recycling and composting, and, lastly, disposal in MWCs and landfills. Currently, in the United States, 30 percent is recovered and recycled or composted, 15 percent is burned at combustion facilities (MWCs and WTEs), and the remaining 56 percent is disposed of in landfills. See Fig. 22-49.

Source reduction can be a successful method of reducing waste generation. Practices such as grass recycling, backyard composting, two-sided copying of paper, and transport packaging reduction by industry have yielded substantial benefits through source reduction. Source reduction has many environmental benefits. It prevents emissions of many greenhouse gases, reduces pollutants, saves energy, conserves resources, and reduces the need for new landfills and MWCs. Table 22-60 shows the total source reduction between 1992 and 2000 in millions of tons. Note the rapid rise in the first 4 years from 0.6 million to 31.0 million tons. From 1996 to 2000, a period of 4 years, a reduction of 77 percent has continued. The materials that made up these reductions are noted in Table 22-61.

Recycling, including composting, diverted 68 million tons of material away from landfills and MWCs in 2001, up from 34 million tons in 1990. See Fig. 22-50.

ON-SITE HANDLING, STORAGE, AND PROCESSING

The handling, storage, and processing of solid wastes at the source before they are collected are the second element of the six functional elements in the solid-waste-management system.

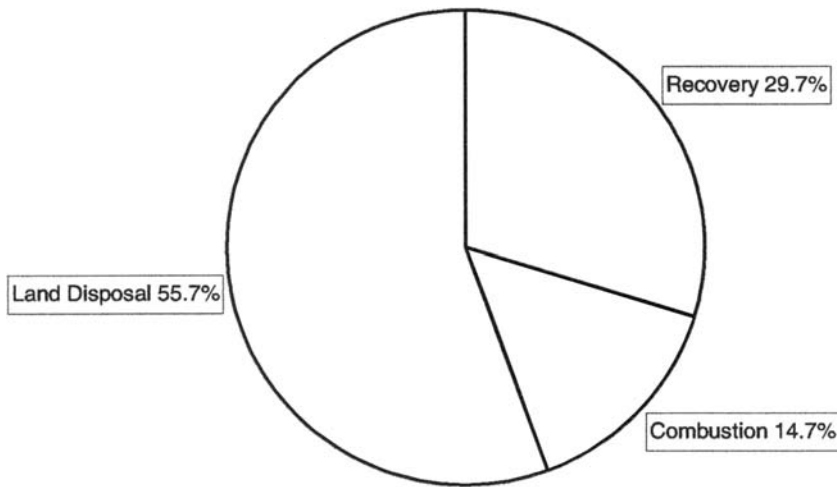


FIG. 22-49 Management of MSW in the United States, 2001.

On-Site Handling On-site handling refers to the activities associated with the handling of solid wastes until they are placed in the containers used for storage before collection. Depending on the type of collection service, handling may also be required to move loaded containers to the collection point and to return the empty containers to the point where they are stored between collections.

Conventional Solid Wastes In most office, commercial, and industrial buildings, solid wastes that accumulate in individual offices or work locations usually are collected in relatively large containers mounted on casters. Once filled, these containers are removed by means of the service elevator, if there is one, and emptied into (1) large storage containers, (2) compactors used in conjunction with the storage containers, (3) stationary compactors that can compress the material into bales or into specially designed containers, or (4) other processing equipment.

Hazardous Wastes When hazardous wastes are generated, special containers are usually provided, and trained personnel (OSHA

1910.120 required such workers to have HAZWOPER training) are responsible for the handling of these wastes. Hazardous wastes include solids, sludges, and liquids; hence, container requirements vary with the form of waste.

On-Site Storage Factors that must be considered in the on-site storage of solid wastes include (1) the type of container to be used, (2) the container location, (3) public health and aesthetics, (4) the collection methods to be used, and (5) future transport method.

Containers To a large extent, the types and capacities of the containers used depend on the characteristics of the solid wastes to be collected, the collection frequency, and the space available for the placement of containers.

1. *Containers for conventional wastes.* The types and capacities of containers now commonly used for on-site storage of solid wastes are summarized in Table 22-62. The small containers are used in individual offices and workstations. The medium-size and large containers are used at locations where large volumes are generated.

2. *Containers for hazardous wastes.* On-site storage practices are a function of the types and amounts of hazardous wastes generated and the time period over which waste generation occurs. Usually, when large quantities are generated, special facilities are used that have sufficient capacity to hold wastes accumulated over a period of

TABLE 22-60 Source Reduction of Municipal Solid Waste since 1990

Year	Million tons of source reduced
1992	0.6
1994	8.0
1995	21.4
1996	31.0
1997	31.8
1998	37.3
1999	42.8
2000	55.1

TABLE 22-61 Source Reduction by Major Material Categories, 2000

Waste stream	Million tons of source reduced
Durable goods (e.g., appliances, furniture)	5.4
Nondurable goods (e.g., newspapers, clothing)	9.3
Containers and packaging (e.g., bottles, boxes)	15.5
Other MSW (e.g., yard trimmings, food scraps)	25.0
Total source reduction (1990 baseline)	55.1

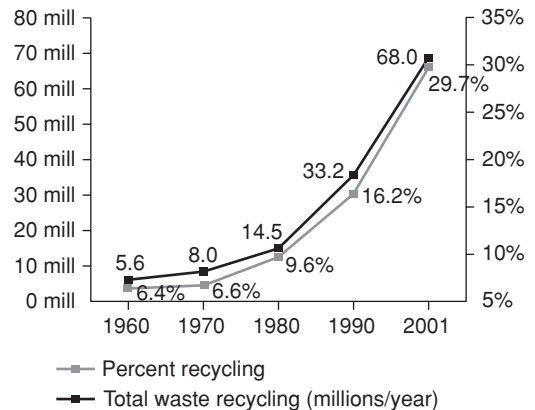


FIG. 22-50 Waste recycling rates, 1960–2001.

TABLE 22-62 Data on the Types and Sizes of Containers Used for On-Site Storage of Solid Wastes

Container type	Capacity			Dimensions*	
	Unit	Range	Typical	Unit	Typical
Small-capacity					
Plastic or metal (office type)	L	16–40	28	mm	(180 × 300)B × (260 × 380)T × 380H
Plastic or galvanized metal	L	75–150	120	mm	510D × 660H
Barrel, plastic, aluminum, or fiber barrel	L	20–250	120	mm	510D × 660H
Disposable paper bags (standard, leak-resistant, and leakproof)	L	75–210	120	mm	380W × 380d × 1100H
Disposal plastic bag	L	20–200	170	mm	460W × 380d × 1000H
Medium-capacity					
Side or top loading	m ³	0.75–9	3	mm	1830W × 1070d × 1650H
Bulk bags	m ³	0.3–2	1	mm	1000W × 1000d × 1000H
Large-capacity					
Open top, rolloff (also called debris bags)	m ³	9–38	27	mm	2440W × 1830H × 6100L
Used with stationary compactor	m ³	15–30	23	mm	2440W × 1830H × 5490L
Equipped with self-contained compaction mechanism	m ³	15–30	23	mm	2440W × 2440H × 6710L
Trailer-mounted					
Open top	m ³	15–38	27	mm	2440W × 3660H × 6100L
Enclosed, equipped with self-contained compaction mechanism	m ³	15–30	27	mm	2440W × 3660H × 7320L

*B = bottom, T = top, D = diameter, H = height, W = width, L = length, and d = depth.

several days. When only small amounts of hazardous wastes are generated on an intermittent basis, they may be containerized, and limited quantities may be stored for periods covering months or years. General information on the storage containers used for hazardous wastes and the conditions of their use is presented in Table 22-63.

Container Location The location of containers at existing commercial and industrial facilities depends on both the location of available space and service-access conditions. In newer facilities, specific service areas have been included for this purpose. Often, because the containers are not owned by the commercial or industrial activity, the locations and types of containers to be used for on-site storage must be worked out jointly between the industry and the public or private collection agency.

On-Site Processing of Solid Wastes On-site processing methods are used to (1) recover usable materials from solid wastes, (2) reduce the volume, or (3) alter the physical form. The most common on-site processing operations as applied to large commercial and industrial sources include manual sorting, compaction, and incineration. These and other processing operations are considered in the portion of this subsection dealing with processing and resource recovery. Factors that should be considered in the selection of on-site processing equipment are summarized in Table 22-64.

PROCESSING AND RESOURCE RECOVERY

The purpose of this subsection is to introduce the reader to the techniques and methods used to recover materials, conversion products,

and energy from solid wastes. Topics to be considered include (1) processing techniques for solid waste, (2) processing techniques for hazardous wastes, (3) materials-recovery systems, (4) recovery of biological conversion products, (5) thermal processes, and (6) waste-to-energy systems.

Because so many of the techniques, especially those associated with the recovery of materials and energy and the processing of solid hazardous wastes, are in a state of flux with respect to application and design criteria, the objective here is only to introduce them to the reader. If these techniques are to be considered in the development of waste-management systems, current engineering design and performance data must be obtained from consultants, operating records, field tests, equipment manufacturers, and available literature.

Processing Techniques for Solid Waste Processing techniques used in solid-waste-management systems (1) improve the efficiency of the systems, (2) recover resources (usable materials), and (3) prepare materials for recovery of conversion products and energy. The more important techniques used for processing solid wastes are summarized below:

- **Manual component separation.** The manual separation of solid-waste components can be accomplished at the source where solid wastes are generated, at a transfer station, at a centralized processing station, or at the disposal site. Manual sorting at the source of generation is the most positive way to achieve the recovery and reuse of materials. The number and types of components salvaged or sorted (e.g., cardboard and high-quality paper, metals, and wood) depend on the location, the opportunities for recycling, and the resale market.

TABLE 22-63 Typical Data on Containers Used for Storage and Transport of Hazardous Waste

Waste category	Container		Auxiliary equipment and conditions of use
	Type	Capacity	
Radioactive substances	Lead encased in concrete	Varies with waste	Isolated storage buildings; high-capacity hoists and lighting equipment; special container markings
Corrosive, reactive, and toxic chemicals	Lined metal drums	210 L	
	Metal drums	210 L	Washing facilities for empty containers, special blending precautions to prevent hazardous reactions; incompatible wastes stored separately
Liquids and sludges	Plastic drums	210 L, up to 500 L	
	Lined metal drums	210 L	
	Lined and unlined storage tanks	Up to 20 m ³	Drums, hand-trucks, pallets, forklifts
Biological wastes	Drums	142–3400 L	
	Trucks	11–30 m ³	Transfer piping, hoses, pumps
Flammable wastes	Vacuum tankers	11–15 m ³	
	Explosives	Sealed plastic bags	120 L
Lined boxes, lined metal drums		57 L	
Explosives	Metal drums	210 L	Fume ventilation, temperature control
	Storage tanks	Up to 20 m ³	
	Shock-absorbing containers	Varies	Temperature control; special container markings

TABLE 22-64 Factors That Should Be Considered in Evaluating On-Site Processing Equipment

Factor	Evaluation
Capabilities	What will the device or mechanism do? Will its use be an improvement over conventional practices?
Reliability	Will the equipment perform its designated functions with little attention beyond preventive maintenance? Has the effectiveness of the equipment been demonstrated in use over a reasonable period of time or merely predicted?
Service	Will servicing capabilities beyond those of the local building maintenance staff be required occasionally? Are properly trained service personnel available through the equipment manufacturer or the local distributor?
Safety of operation	Is the proposed equipment reasonably foolproof so that it may be operated by tenants or building personnel with limited mechanical knowledge or abilities? Does it have adequate safeguards to discourage careless use?
Ease of operation	Is the equipment easy to operate by a tenant or building personnel? Unless functions and actual operations of equipment can be carried out easily, they may be ignored or bypassed by paid personnel and most often by "paying" tenants.
Efficiency	Does the equipment perform efficiently and with a minimum of attention? Under most conditions, equipment that completes an operational cycle each time that it is used should be selected.
Environmental effects	Does the equipment pollute or contaminate the environment? When possible, equipment should reduce environmental pollution presently associated with conventional functions.
Health hazards	Does the device, mechanism, or equipment create or amplify health hazards?
Aesthetics	Do the equipment and its arrangement offend the senses? Every effort should be made to reduce or eliminate offending sights, odors, and noises.
Economics	What are the economics involved? Both first and annual costs must be considered. Future operation and maintenance costs must be assessed carefully. All factors being equal, equipment produced by well-established companies, having a proven history of satisfactory operations should be given appropriate consideration.
Flexibility	Will the equipment or its placement allow future changes to the process to handle wastes with differing characteristics?

*From G. Tchobanoglous, H. Theissen, and R. Eliassen, *Solid Wastes: Engineering Principles and Management Issues*, McGraw-Hill, New York, 1977.

There has been an evolution in the solid-waste industry to combine manual and automatic separation techniques to reduce overall costs and produce a cleaner product, especially for recyclable materials. Component separation is the heart of recycling, and it is required to raise the concentration of the material to the point that it is worth reclaiming, and reduce the amount of tramp materials to meet specifications. Recycling occurs on a major scale, and for MSW, it accounted for 30 percent of the waste stream in 2001.

- **Storage and transfer.** When solid wastes are to be processed for material recovery, storage and transfer facilities should be considered an essential part of the processing operation. Important factors in the design of such facilities include (1) the size of the material before and after processing, (2) the density of the material, (3) the angle of repose before and after processing, (4) the abrasive characteristics of the materials, and (5) the moisture content.
- **Mechanical volume reduction.** Mechanical volume reduction is perhaps the most important factor in the development and opera-

tion of solid-waste-management systems. Vehicles equipped with compaction mechanisms are used for the collection of most industrial solid wastes. To increase the useful life of landfills, wastes are compacted there also via mobile compaction equipment. Paper for recycling is baled for shipping to processing centers. When compacting industrial solid wastes, it has been found that the final density (typically about 1100 kg/m³) is essentially the same regardless of the starting density and applied pressure. This fact is important in evaluating manufacturer's claims.

- **Chemical volume reduction.** Incineration has been the method commonly used to reduce the volume of wastes chemically. One of the most attractive features of the incineration process is that it can be used to reduce the original volume of combustible solid wastes by 80 to 90 percent. The technology of incineration has advanced with many mass burn facilities now having two or more combustors with capacities of 1000 tons/day of refuse per unit. However, regulations limiting low volatile and semivolatile metals, acid gases, free chlorine and hydrogen chloride, unburned hydrocarbons, polychlorinated dioxin and furan (PCDD/PCDF) emissions have resulted in higher costs and operating complexity.
- **Mechanical size alteration.** The objective of size reduction is to obtain a final product that is reasonably uniform and considerably reduced in size in comparison to its original form. It is important to note that size reduction does not necessarily imply volume reduction. In some situations, the total volume of the material after size reduction may be greater than the original volume. Shredding is most often used for size reduction. Two-stage (coarse, fine) low-speed shredders and a single-stage shredder with screen and recycle of oversize are the most common systems. The gain in ease of materials handling must be weighed against the substantial operating costs for shredding equipment. A substantial market for the technology lies in shredding tires to produce fuel for cement kilns and utility boilers. With finer shredding, the product can be used to make thick resilient mats for play areas or for inclusion in asphalt pavement.
- **Mechanical component separation.** Component separation is a necessary operation in the recovery of resources from solid wastes and in instances when energy and conversion products are to be recovered from process wastes.
- **Magnetic and electromechanical separation.** Magnetic separation of ferrous materials is a well-established technique. More recently, a variety of electromechanical techniques have been developed for the removal of several nonferrous materials.
- **Drying and dewatering.** In many solid-waste energy-recovery and incineration systems, the shredded light fraction is predried to decrease weight. Although energy requirements for drying wastes vary with the application, the required energy input can be established by using a value of about 4300 kJ/kg of water evaporated. Drying can frequently increase waste throughput in many treatment systems. For incinerators, it produces more stable combustion and better ash quality.
- **Bulking of liquid wastes.** Liquid wastes are prohibited from landfills. Wastes with free liquids are mixed with a bulking agent such as dry sawdust, cement kiln dust, or fly ash.

Processing of Hazardous Waste As with conventional solid wastes, the processing of hazardous wastes is undertaken for three purposes: (1) to recover useful materials, (2) to reduce the amount of wastes that must be disposed in landfills, and (3) to prepare the wastes for ultimate disposal.

Processing Techniques The processing of hazardous wastes on a batch basis can be accomplished by physical, chemical, thermal, and biological means. The various individual processes in each category are reported in Table 22-65. Clearly, the number of possible treatment-process combinations is staggering. In practice, the physical, chemical, and thermal treatment operations and processes are the ones most commonly used.

Identification of Waste Constituents In any processing (and disposal) scheme, the key item is knowledge of the characteristics of the waste being handled. Without this information, effective processing or treatment is impossible. For this reason, the characteristics of the wastes must be known before they are accepted and hauled to a

TABLE 22-65 Biological and Thermal Processes Used for Recovery of Conversion Products from Solid Waste

Process	Conversion product	Preprocessing required	Comments
Biological Composting	Humuslike material	Shredding, air separation	Lack of markets a primary shortcoming; technically proved in full-scale application
Anaerobic digestion	Methane gas	Shredding, air separation	Technology on laboratory scale only
Biological conversion to protein	Protein, alcohol	Shredding, air separation	Technology on pilot scale only
Biological fermentation	Glucose, furfural	Shredding, air separation	Used in conjunction with the hydrolytic process
Thermal Incineration with heat recovery	Energy in the form of steam	None	Markets for steam required; proved in numerous full-scale applications; air-quality regulations possibly prohibiting use
Thermal desorption	Clean soil used for fill or reclaimed raw materials such as deoiled metal turnings	Sizing, blending, dilution	In routine use for Superfund organic contaminated soil
Supplementary fuel firing in boilers	Energy in the form of steam	Shredding, air separation, magnetic separation	If at least capital investment desired, existing air-quality regulations possibly prohibiting use
Gasification	Energy in the form of low-energy gas	Shredding, air separation, magnetic separation	Gasification also capable of being used for codisposal for industrial sludges
Pyrolysis	Energy in the form of gas or oil and char	Shredding, magnetic separation	Technology proved only in pilot applications but full-scale use has rarely succeeded due to high operating costs and lack of materials for gas, oil, and char only.
Hydrolysis	Glucose, furfural	Shredding, air separation	Technology on pilot scale only
Chemical conversion	Oil, gas, cellulose acetate	Shredding, air separation	Technology on pilot scale only

treatment or disposal site. In most states, proper identification of the constituents of the waste is the responsibility of the waste generator.

Materials-Recovery Systems Paper, rubber, plastics, textiles, glass, metals, and organic and inorganic materials are the principal recoverable materials contained in industrial solid wastes.

Once a decision has been made to recover materials and/or energy, process flow sheets must be developed for the removal of the desired components, subject to predetermined materials specifications. A typical flow sheet for the recovery of specific components and the preparation of combustible materials for use as a fuel source is presented in Fig. 22-51. The light combustible materials are often identified as refuse-derived fuel (RDF).

The design and layout of the physical facilities that make up the processing-plant flow sheet are an important aspect in the implementation and successful operation of such systems. Important factors that must be considered in the design and layout of such systems include (1) process performance efficiency, (2) reliability and flexibility, (3) ease and economy of operation, (4) aesthetics, and (5) environmental controls.

Recovery of Biological Conversion Products Biological conversion products that can be derived from wastes include alcohols and a variety of other intermediate organic compounds. The principal processes that have been used are reported in Table 22-68. Composting and anaerobic digestion, the two most highly developed processes, are considered further. The recovery of gas from landfills is discussed in the portion of this subsection dealing with ultimate disposal.

Composting If the organic materials, excluding plastics, rubber, and leather, are separated from municipal solid wastes and subjected to bacterial decomposition, the end product remaining after dissimilatory and assimilatory bacterial activity is called *compost* or *humus*. The entire process involving both separation and bacterial conversion of the organic solid wastes is known as *composting*. Decomposition of the organic solid wastes may be accomplished either aerobically or anaerobically, depending on the availability of oxygen.

Most composting operations involve three basic steps—(1) preparation of solid wastes, (2) decomposition of the solid wastes, and (3) size reduction—and moisture and nutrient addition are part of the preparation step. Several techniques have been developed to accomplish the decomposition step. Once the solid wastes have been con-

verted to a humus, they are ready for the third step of product preparation and marketing. This step may include fine grinding, blending with various additives, granulation, bagging, storage, shipping, and, in some cases, direct marketing. The principal design considerations associated with the biological decomposition of prepared solid wastes are presented in Table 22-66.

Anaerobic Digestion Anaerobic digestion or anaerobic fermentation, as it is often called, is the process used for the production of methane from solid wastes. In most processes in which methane is to be produced from solid wastes by anaerobic digestion, three basic steps are involved. The first step involves preparation of the organic fraction of the solid wastes for anaerobic digestion and usually includes receiving, sorting, separation, and size reduction. The second step involves the addition of moisture and nutrients, blending, pH adjustment to about 6.7, heating of the slurry to between 327 and 333 K (130 and 140°F), and anaerobic digestion in a reactor with continuous flow, in which the contents are well mixed for a time varying from 8 to 15 days. The third step involves capture, storage, and, if necessary, separation of the gas components evolved during the digestion process. The fourth step is the disposal of the digested sludge, an additional task that must be accomplished. Some important design considerations are reported in Table 22-67. Because of the variability of the results reported in the literature, it is recommended that pilot-plant studies be conducted if the digestion process is to be used for the conversion of solid wastes.

Thermal Processes Conversion products that can be derived from solid wastes include heat, gases, a variety of oils, and various related organic compounds. The principal thermal processes that have been used for the recovery of usable conversion products from solid wastes are reported in Table 22-65.

Incineration with Heat Recovery Heat contained in the gases produced from the incineration of solid wastes can be recovered as steam. The low-level heat remaining in the gases after heat recovery can also be used to preheat the combustion air, boiler makeup water, or solid-waste fuel.

1. *In existing incinerators.* With existing incinerators, waste-heat boilers can be installed to extract heat from the combustion gases without introducing excess amounts of air or moisture. Typically,

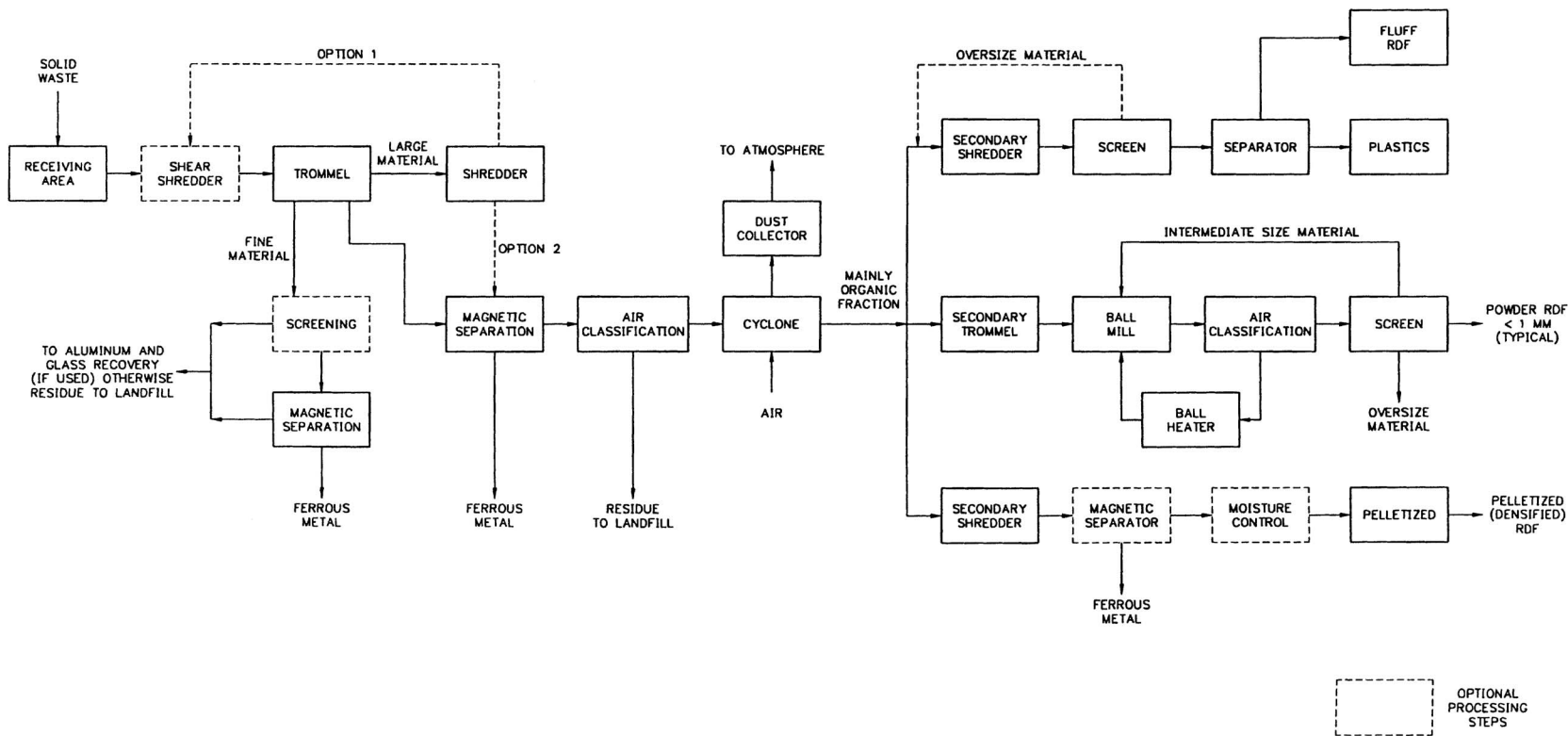


FIG. 22-51 Typical flow sheet for the recovery of materials and production of refuse-derived fuels (RDF). [Adapted in part from D. C. Wilson (ed.), Waste Management: Planning, Evaluation, Technologies, Oxford University Press, Oxford, 1981.]

TABLE 22-66 Important Design Considerations for Anaerobic Composting Processes*

Item	Comment
Particle size	For optimum results the size of solid waste should be between 25 and 75 mm (1 and 3 in).
Seeding and mixing	Composting time can be reduced by seeding with partially decomposed solid wastes to the extent of about 1 to 5 percent by weight. Sewage sludge can also be added to prepared solid wastes. When sludge is added, the final moisture content is the controlling variable.
Mixing or turning	To prevent drying, caking, and air channeling, material in the process of being composted should be mixed or turned on a regular schedule or as required. Frequency of mixing or turning will depend on the type of composting operation.
Air requirements	Air with at least 50 percent of the initial oxygen concentration remaining should reach all parts of the composting material for optimum results, especially in mechanical systems.
Total oxygen requirements	The theoretical quantity of oxygen required can be estimated.
Moisture content	Moisture content should be in the range between 50 and 60 percent during the composting process. The optimum value appears to be about 55 percent.
Temperature	For best results, temperature should be maintained between 322 and 327 K (130 and 140°F) for the first few days and between 327 and 333 K (130 and 140°F) for the remainder of the active composting period. If temperature goes beyond 339 K (150°F), biological activity is reduced significantly.
Carbon-nitrogen ratio	Initial carbon-nitrogen ratios (by mass) between 35 and 50 are optimum for aerobic composting. At lower ratios ammonia is given off. Biological activity is also impeded at lower ratios. At higher ratios nitrogen may be a limiting nutrient.
pH	To minimize the loss of nitrogen in the form of ammonia gas, pH should not rise above about 8.5.
Control of pathogens	If the process is properly conducted, it is possible to kill all the pathogens, weeds, and seeds during the composting process. To do this, the temperature must be maintained between 333 and 334 K (140 and 160°F) for 24 h.

*Adapted from G. Tchobanoglous, H. Theisen, and R. Eliassen, *Solid Wastes: Engineering Principles and Management Issues*, McGraw-Hill, New York, 1977.

incinerator gases will be cooled from a range of 1250 to 1375 K (1800 to 2000°F) to a range of 500 to 800 K (600 to 1000°F) before being discharged to the air-pollution-control system. Apart from the production of steam, the use of a boiler system is beneficial in reducing the volume of gas to be processed in the air-pollution-control equipment. The compounds in the waste stream will generate products of combustion and ash that may create serious corrosion and fouling problems in waste-heat boilers (WHBs). WHBs also tend to generate dioxins and furans when particulates, combined with free chlorine and other dioxin/furan precursors, attach to the tubes at proper reformation temperatures and time to cause the reformation of D/Fs.

2. *In water-wall incinerators.* The internal walls of the combustion chamber are lined with boiler tubes that are arranged vertically and welded together in continuous sections. When water walls are employed in place of refractory materials, they are not only useful for the recovery of steam but also extremely effective in controlling furnace temperature without introducing excess air; however, they are subject to corrosion by the hydrochloric acid produced from the burning of some plastic compounds and the molten ash containing salts (chlorides and sulfates) that attach to the tubes.

Combustion Combustion of industrial and municipal waste is an attractive waste management option because it reduces the volume of waste by 70 to 90 percent. In the face of shrinking landfill availability, municipal waste combustion capacity in the United States has grown at a rate significantly faster than the growth rate for municipal refuse generation.

Types of Combustors The three main classes of facilities used to combust municipal refuse are mass-burn, modular, and RDF-fired facilities. Mass-burn combustors are field-erected and generally range in size

from 50 to over 1000 tons/day of refuse feed per unit (Fig. 22-52). Modular combustors burn waste with little more preprocessing than do the mass-burn units. These range in size from 5 to 100 tons/day. Total U.S. MSW waste-to-energy plants had a design capacity of 98,719 tons/day per a 2004 survey. There were 72 plants in 2004. In addition to traditional WTE contained in the first two classes, the third major class of municipal waste combustor burns RDF. The types of waste-to-energy boilers used to combust RDF can include suspension, stoker, and fluidized-bed designs. RDF fuels can also be fired directly in large industrial and utility boilers that are now used for the production of power with pulverized or stoker coal, oil, and gas. Although the process is not well established with coal, it appears that about 15 to 20 percent of the heat input can be from RDF. With oil as the fuel, about 10 percent of the heat input can be from RDF. Depending on the degree of processing, suspension, spreader-stoker, and double-vortex firing systems have been used. RDF includes source-separated material, such as whole tires and chipped tires fired in cement kilns and boilers, and wood waste. Combustion of this material was estimated to be 2.4 million tons in 2001.

The system shown in Fig. 22-52 is a schematic of the Montenegro Montgomery LP located in Plymouth Township, Montgomery County, Pa. The facility specifications are as follows:

Waste throughput:	1200 tons/day (2 × 600)
Technology:	L&C Steimmuller, GmbH
Steam output:	324,000 lb/h (2 × 162,000)
Steam quality:	650 psig/750°F
Boiler mfr.:	L&C Steimmuller, GmbH
Extraction turbine:	36 MW gross
Turbine mfr.:	General Electric
Generator:	General Electric

TABLE 22-67 Important Design Considerations for Anaerobic Digestion*

Item	Comment
Size of material shredded	Wastes to be digested should be shredded to a size that will not interfere with the efficient functioning of pumping and mixing operations.
Mixing equipment	To achieve optimum results and to avoid scum buildup, mechanical mixing is recommended.
Percentage of solid wastes mixed with sludge	Although amounts of waste varying from 50 to 90+ percent have been used, 60 percent appears to be a reasonable compromise.
Hydraulic and mean cell residence time, $\Theta_h = \Theta_c$	Washout time is in the range of 3 to 4 days. Use 8 to 15 days for design of base design on results of pilot-plant studies.
Loading rate	0.6 to 1.6 kg/(m ³ ·day) [0.04 to 0.10 lb/(ft ³ ·day)]. It is not well defined at present. Significantly higher rates have been reported.
Temperature	Between 327 and 333 K (130 and 140°F)
Destruction of volatile solid wastes	Varies from about 60 to 80 percent; 70 percent can be used for estimating purposes.
Total solids destroyed	Varies from 40 to 60 percent, depending on amount of inert material present originally.
Gas production	0.5 to 0.75 m ³ /kg (8 to 12 ft ³ /lb) of volatile solids destroyed (CH ₄ = 60 percent; CO ₂ = 40 percent)

*From G. Tchobanoglous, H. Theisen, and R. Eliassen, *Solid Wastes: Engineering Principles and Management Issues*, McGraw-Hill, New York, 1977.

NOTE: Actual removal rates for volatile solids may be less, depending on the amount of material diverted to the scum layer.



FIG. 22-52 1200-tons/day MSW plant of Montenay Montgomery.

Dry scrubber:	Research-Cottrell (slaked lime)
Baghouse:	Research-Cottrell (reverse air)
CEMs:	Environmental elements
DeNO _x :	Fuel tech
Mercury removal:	Sorbaline
Material recovery:	Ferrous metals

The construction of the facility began on May 23, 1989, and went into full operation on February 17, 1992, on an interim basis upon completion of the performance tests. The facility achieved full acceptance on May 23, 1994, and began a 20-year service agreement with the Eastern District of Montgomery County. The plant serves 24 municipalities in the Eastern District with a population of 425,000. The processing capacity is 1200 tons/day; 377,000 tons/yr with an electrical capacity of 36 MW. The electricity produced is sold to Philadelphia Electric Company (PECO).

See Fig. 22-53, which is typical of most waste-to-energy (WTE) plants burning MSW. Trucks deliver MSW to the scale house of the facility, where the truck is weighed and identified. At (2), the trucks unload waste into a storage pit in an enclosed tipping hall. The truck fumes and waste odors are drawn into the furnaces by large fans to provide combustion air and to prevent escape of odors. The waste is inspected in the storage pit (3), prior to feeding the waste into the fur-

nace by large overhead cranes. Waste is burned at high temperatures (over 2000°F) in the furnaces (4). The waste moves through the furnaces through drying, combustion, and final burnout stages over a 60-min period.

The heat of combustion generates steam in the boiler (5). The steam is used in making electricity in a steam turbine/generator set. After providing the in-plant electrical needs, excess energy is sold to the local electric utility and/or utilized by nearby process steam industries. After the combustion of the waste, ferrous metals are removed from the remaining residue by screening and magnetic separation (6). These ferrous metals are then recycled. The remaining residue can be beneficially reused or recycled, further reducing reliance on landfilling.

State-of-the-art pollution control equipment (7) removes particulates, acid gases, and other air emissions following the waste combustion process. Clean Air Act and other environmental standards are achieved through a combination of equipment such as spray dryers, baghouses, and carbon injection systems. Exhaust gases are drawn into an induced-draft fan which maintains a negative pressure throughout the entire system from waste feeding through the pollution controls. This prevents fugitive emissions from the process. These gases are then pushed into the exhaust stack and into the atmosphere. Stack gas sampling is conducted on platforms in the vertical stack section.

Gasification The gasification process involves the partial combustion of a carbonaceous or hydrocarbon fuel to generate a combustible fuel gas rich in carbon monoxide and hydrogen. A gasifier is similar to an incinerator operating under reducing conditions. Heat to sustain the process is derived from exothermic reactions, while the combustible components of the low-energy gas are primarily generated by endothermic reactions. The reaction kinetics of the gasification process are quite complex and still the subject of considerable debate.

When a gasifier is at atmospheric pressure with air as the partial oxidant, the end products of the gasification process are a low-energy gas typically containing (by volume) 10 percent CO₂, 20 percent CO, 15 percent H₂, and 2 percent CH₄, with the balance being N₂ and a carbon-rich ash. Because of the diluting effect of the nitrogen in the input air, the low-energy gas has an energy content in the range of the 5.2 to 6.0 MJ/m³ (140 to 160 Btu/ft³). Dual-bed gasifiers produce a gas with double this heating value. When pure oxygen is used as the oxidant, a medium-energy gas with an energy content in the range of 12.9 to 13.8 MJ/m³ (345 to 370 Btu/ft³) is produced. Gasifiers were in widespread use on coal and wood until natural gas displaced them in the 1930s through the 1950s. Some large coal gasifiers are in use today in the United States and worldwide. While the process can work on solid waste, incinerators (which gasify and burn in one chamber) are favored over gasifiers.

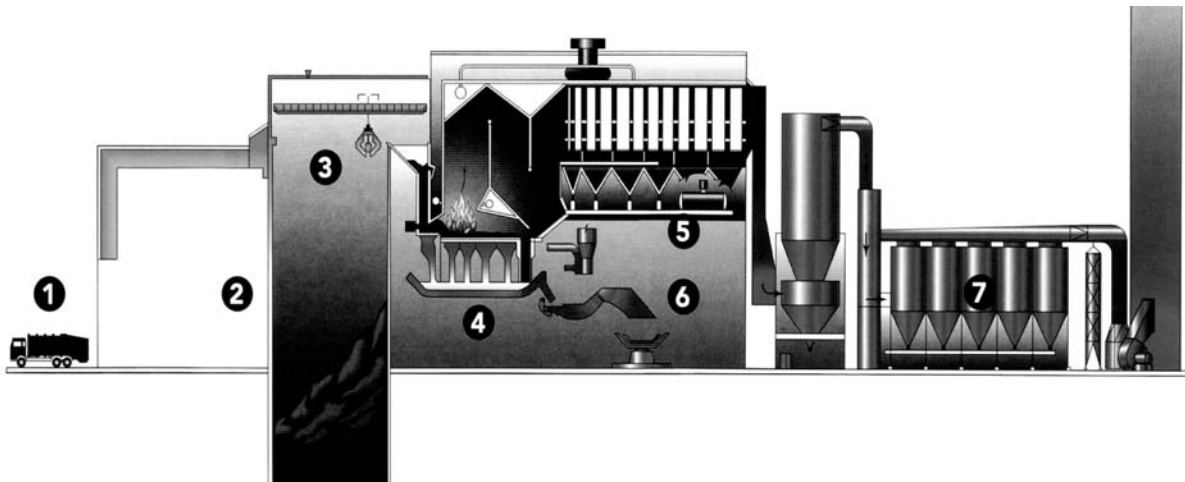


FIG. 22-53 1200-tons/day MSW plant schematic.

Pyrolysis Of the main alternative chemical conversion processes that have been investigated, pyrolysis has received the most attention. Pyrolysis has been tested in countless pilot plants, and many full-scale demonstration systems have operated. Few attained any long-term commercial use. Major issues were lack of market for the unstable and acidic pyrolytic oils and the char and high operating costs.

Depending on the type of reactor used, the physical form of solid wastes to be pyrolyzed can vary from unshredded raw wastes to the finely ground portion of the wastes remaining after two stages of shredding and air classification. Upon heating in an oxygen-free atmosphere, most organic substances can be split via thermal cracking and condensation reactions into gaseous, liquid, and solid fractions. *Pyrolysis* is the term used to describe the process while the term *destructive distillation* is also often used. In contrast to the combustion process, which is highly exothermic, the pyrolytic process involves both highly endothermic and exothermic reactions. For this reason, the term *destructive distillation* is often used as an alternative for *pyrolysis*.

The characteristics of the three major component fractions resulting from the pyrolysis are (1) a gas stream containing primarily hydrogen, methane, carbon monoxide, reduced sulfur compounds, carbon disulfide, and various other gases, depending on the organic characteristics of the material being pyrolyzed; (2) a fraction that consists of a tar and/or oil stream that is liquid at room temperature and has been found to contain hundreds of chemicals such as acetic acid, acetone, methanol, and phenols; and (3) a char consisting of almost pure carbon plus any inert material that may have entered the process. It has been found that distribution of the product fractions varies with the temperature at which the pyrolysis is carried out. Under conditions of maximum gasification, the energy content of pyrolytic oils has been estimated to be about 23.2 MJ/kg (10,000 Btu/lb).

Waste-to-Energy Systems The preceding subsection ended at the production of steam. WTE systems take over at this point, using high-pressure/high-temperature steam to drive turbines and produce shaft horsepower for prime movers at industrial plants or to generate electricity.

This fuel may be solid or gas or oil or fuels from a gasifier or pyrolysis system.

Typical flow sheets for alternative energy-recovery systems are shown in Fig. 22-54. Perhaps the most common flow sheet for the production of electric energy involves the use of a steam turbine-generator combination. As shown, when solid wastes are used as the basic fuel source, four operating modes are possible. A flow sheet using a gas turbine-generator combination is shown in Fig. 22-54. The low-energy gas is compressed under high pressure so that it can be used more effectively in the gas turbine. Use of low- or medium-Btu gas for gas turbines has been attempted, and success requires good design and operation of gas cleaning equipment prior to introduction into the combustor of the gas turbine.

Efficiency Factors Representative efficiency data for boilers, pyrolytic reactors, gas turbines, steam turbine-generator combinations, electric generators, and related plant use and loss factors are given in Table 22-68. In any installation in which energy is being produced, allowance must be made for the power needs of that station or process and for unaccounted-for process-heat losses. Typically, the auxiliary power allowance varies from 4 to 8 percent of the power produced. Process-heat losses usually will vary from 2 to 8 percent. In general, steam pressures of 600 psig and temperatures of 650°F are considered minimum for economical power generation. Industrial plants may choose a cogeneration topping cycle, with steam exhaust from the turbine at the plant's process steam pressure, typically in the 125 to 250 psig range. For commercial WTE plants, condensing turbines are the norm.

Determination of Energy Output and Efficiency for Energy-Recovery Systems An analysis of the amount of energy produced from a solid-waste energy conversion system using an incinerator boiler system turbine electric generator combination with a capacity of 1000 t/day of waste is presented in Table 22-69. If it is assumed that 10 percent of the power generated is used for the front-end processing system (typical values vary from 8 to 14 percent), then the net power for export is 24,604 kW and the overall efficiency is 17.4 percent.

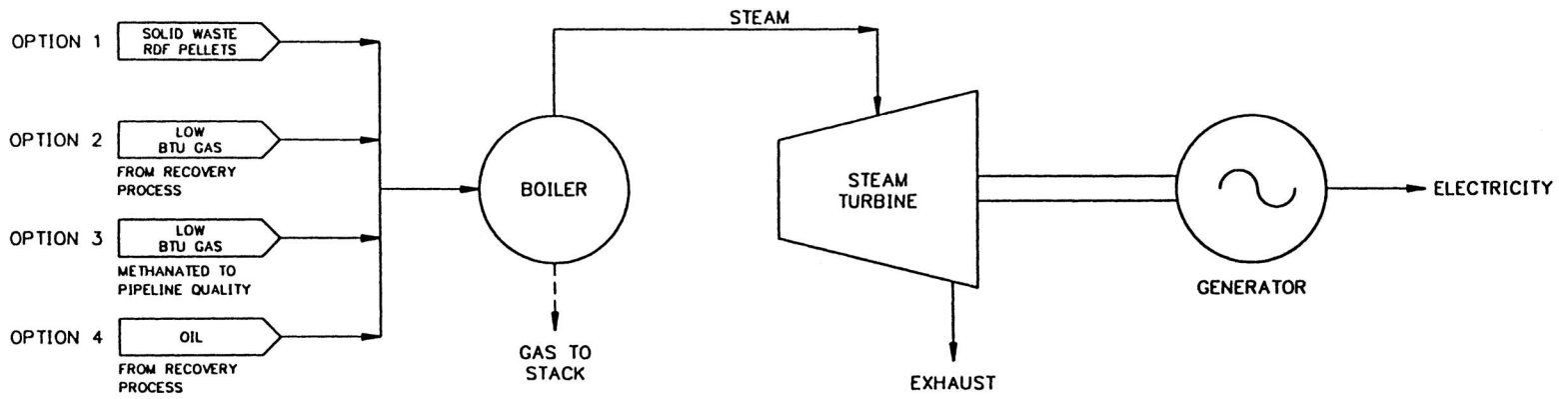
Concentration of WTE Incinerators The total number of municipal waste incinerator facilities as listed in the *Solid Waste Digest*, vol. 14, no. 6, June 2004 (a publication of Chartwell Information, EBI, Inc., of San Diego, Calif.), is 72. This is an increase of 10 facilities since September 1994 (a 10-year period). See Table 22-70. The wastes burned in these facilities total 8.96 percent of total municipal wastes managed in landfills, incinerators, and transfer stations. This amounts to 98,719 tons/day of combusted municipal waste. This also is an increase of 10,248 tons over the 88,471 tons in September 1994, an average of 1000 tons/yr.

One notes that the heavily populated areas of the country also have the highest number of WTE facilities as well as the highest intake of municipal waste into incinerators. This is also due to the lack of low-cost land and open space for landfills compared to the midwest and western states. The amount of waste combusted in the northeastern states is 25.6 percent of the total generated compared to 8.96 percent of all municipal wastes combusted nationwide. The WTE cost per ton averages \$62 in the northeastern states compared to \$59 for the nation. Incinerator costs are similar to landfill costs in the northeastern states. However, landfill costs are far lower than WTE tipping fees across the nation. For example, in states such as Idaho (landfill costs, \$18.80/ton) and Texas (landfill costs \$21.03/ton), WTE incinerator plants cannot compete at this time. However, it is interesting to note that the landfill costs have doubled in 10 years while WTE tipping fees have dropped about 10 percent. The stricter regulations applied to landfills have caused this increase in landfill tipping fees. The NIMBY (Not In My Back Yard) syndrome concerning incineration systems has also hurt the siting and permitting of many of these facilities. Figure 22-55 shows the range of costs for all solid-waste management in June 2004. The national index was \$39.49/ton in 2004, up from \$37.93/ton in 1994. This is an average increase of only 0.1 percent per year, which is well below the inflation rate for this 10-year period.

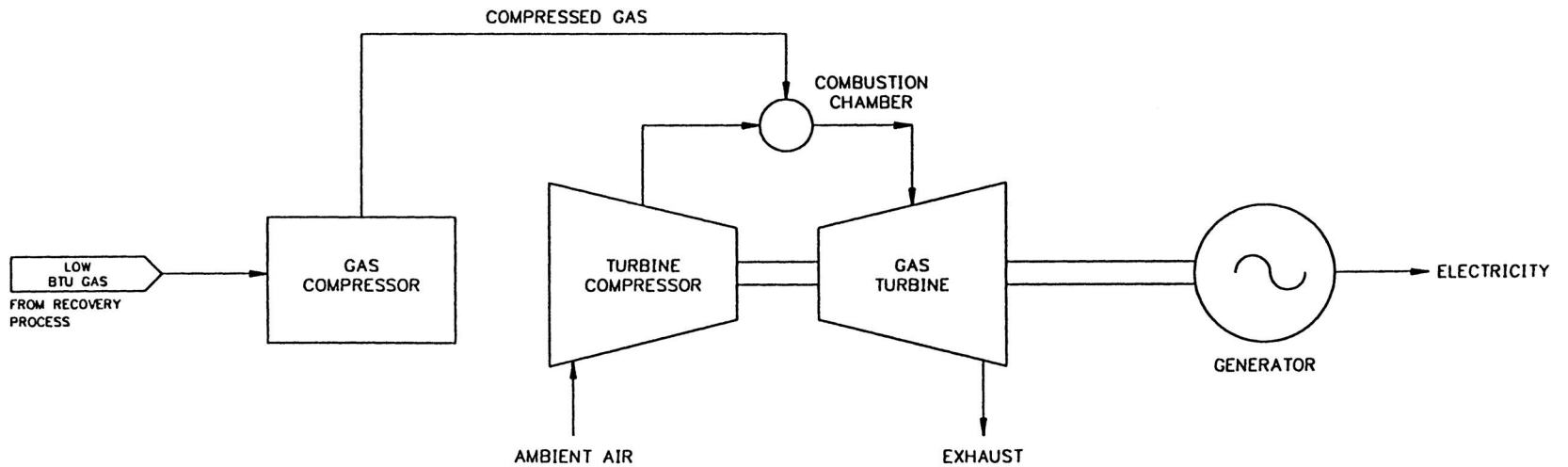
REGULATIONS APPLICABLE TO MUNICIPAL WASTE COMBUSTORS

New Source Performance Standards (NSPS) were promulgated under Sections 111(b) and 129 of the CAA Amendments of 1990. The NSPS applies to new municipal solid-waste combustors (MWCs) with capacity to combust more than 250 tons/day of municipal solid waste that commenced construction after September 20, 1994. The proposed standards and guidelines were published in the Federal Register on September 20, 1994. They are listed in Title 40, Protection of the Environment, Chapter 1, Part 60 Standards of Performance for New Stationary Sources (<http://a257.g.akamaitech.net/7/25/23422/14mar20010800/edocket.access.gpo.gov/cfr2001>). Section 129 of the CAA of 1990 applies to a range of solid-waste incinerators including MWCs, medical waste incinerators (MWIs), and industrial waste incinerators. On June 28, 2004, the Federal Register (vol. 69, no. 123) established that Section 129(a)(5) of the CAA requires EPA to review, and if necessary revise, those standards every 5 years. This rulemaking addresses those requirements and is the first 5-year review of the MACT standards. Implementation of these MACT standards has been highly effective and has reduced dioxin/furan emissions by more than 99 percent since 1990. Similar reductions have occurred for other CAA Section 129 pollutants. Incinerators for hazardous solid and liquid wastes are covered under RCRA and MACT regulations (40 CFR Parts 260 through 272) and TSCA, Toxic Substances Control Act, 1976 (40 CFR Parts 700 through 766).

Regulated Pollutants The NSPS regulates MWC emissions and nitrogen oxides (NO_x) emissions from individual MWC units larger than 250 tons/day capacity. MWC emissions are subcategorized as MWC metal emissions, MWC organic emissions, and MWC acid gas emissions. The NSPS establishes emission limits for organic emissions (measured as dioxins and furans), MWC metal emissions (measured as particulate matter PM, opacity, cadmium, lead, and mercury), and MWC acid gas emissions as sulfur dioxide SO₂ and hydrogen chloride HCl, as well as NO_x emission limits.



OPTIONS WITH STEAM-TURBINE-GENERATOR COMBINATION



OPTIONS WITH GAS-COMPRESSOR-GAS-TURBINE-GENERATOR COMBINATION

FIG. 22-54 Flow sheet—alternative energy recovery systems.

TABLE 22-68 Typical Thermal Efficiency and Plant Use and Loss Factors for Individual Components and Processes Used for Recovery of Energy from Solid Wastes

Component	Efficiency ^a		Comments
	Range	Typical	
Incinerator-boiler	40–68	63	Mass-fired
Boiler			
Solid fuel	60–75	72	Processed solid wastes (RDF)
Low-btu gas	60–80	75	Necessity to modify burners
Oil-fired	65–85	80	Oils produced from solid wastes possibly required to be blended to reduce corrosiveness
Gasifier	60–70	70	
Pyrolysis reactor	65–75	70	
Turbines			
Combustion gas			
Simple cycle	8–12	10	
Regenerative	20–26	24	Including necessary appurtenances
Expansion gas	30–50	40	
Steam turbine-generator system			
Less than 10 MW	24–40	29 ^{††}	
10 MW	28–32	31.6 ^{††}	Including condenser, heaters, and all other necessary appurtenances but not boiler
Electric generator			
Less than 10 MW	88–92	90	
Over 10 MW	94–98	96	

^aTheoretical value for mechanical equivalent of heat = 3600 kJ/kWh.

[†]Efficiency varies with exhaust pressure. Typical value given is based on an exhaust pressure in the range of 50 to 100 mmHg.

^{††}Heat rate = 11,395 kJ/kWh = (3600 kJ/kWh)/0.316.

MWCs Organic Emissions The NSPS limits organic emissions to a total dioxin plus furan emission mass limit of 13 ng/scfm (at 7 percent O₂ dry volume). This level is approximately equivalent to a toxic equivalent (TEQ) of 2.0 ng/dscm, using the 1990 international toxic equivalent factor (I-TEF) approach.

MWCs Metal Emissions The NSPS includes a PM emission limit of 0.015 grain per dry standard cubic feet (gr/dscf) at 7 percent oxygen dry/volume and an opacity limit of 10 percent (6-min average). Cadmium is limited to 0.020 ng/dnm³ and lead to 0.3 ng/dnm³, all at 7 percent O₂ dry volume.

MWCs Acid Gas Emissions The NSPS requires a 95 percent reduction of HCl emissions and an 80 percent reduction of SO₂ emissions for new MWCs or an emission limit of 25 ppmv for HCl and 30 ppmv for SO₂ (at 7 percent O₂ dry volume).

Nitrogen Oxides Emissions The NSPS limits NO_x emission to 150 ppmv (at 7 percent O₂ dry volume).

MWC Air-Pollution-Control Systems MWCs generate flue gas that contains particulates, acid gases, and trace amounts of organic and volatile metals. Particulates have traditionally been removed by use of cyclone separators, baghouses, and electrostatic precipitators. Acid gases require neutralization and removal from the gas stream. This can be accomplished by adding reagents or chemicals to the gas stream and removing products of the chemical reaction when these materials are mixed together. Two major types of APCs are employed for PM, metals and acid gas removal:

- Dry systems, where the gas stream is humidified and chemicals (lime, sodium hydroxide, or carbonate and activated carbon) are added to the system
- Wet systems, where large quantities of water-containing chemicals

(lime, sodium hydroxide or carbonates, activated carbon) wash the gas stream

MWC facilities are required to meet some of the toughest environmental air emissions standards in the country. Complying with these standards makes modern waste combustors among the cleanest producers of electricity—and may even provide a means of improving a community's overall air quality.

ULTIMATE DISPOSAL

Disposal on or in the earth's mantle is, at present, the only viable method for the long-term handling of (1) solid wastes that are collected and are of no further use, (2) the residual matter remaining after solid wastes have been processed, and (3) the residual matter remaining after the recovery of conversion products and/or energy has been accomplished. The three land disposal methods used most commonly are (1) landfilling, (2) landfarming, and (3) deep-well injection. Although incineration is being used more often as a disposal method, it is, in reality, a processing method. Recently, the concept of using muds in the ocean floor as a waste storage location also has received some attention.

Landfilling of Solid Waste Landfilling involves the controlled disposal of solid wastes on or in the upper layer of the earth's mantle. Important aspects in the implementation of sanitary landfills include (1) site selection, (2) landfilling methods and operations, (3) occurrence of gases and leachate in landfills, (4) movement and control of landfill gases and leachate, and (5) landfill design. Landfilling is a large-scale operation. The number of landfills decreased substantially over the period from 1988 to 2001. There were nearly 8000 in 1988,

TABLE 22-69 Energy Output and Efficiency for 1000 t/day of Waste Steam Boiler Turbine-Generator Energy-Recovery Plant Using Unprocessed Industrial Solid Wastes with Energy Content of 12,000 kJ/kg

Item	Value
Energy available in solid wastes, million kJ/h [(1000 t/day × 1000 kg/t × 12,000 kJ/kg) / (24 h/day × 10 ⁶ kJ/million kJ)]	500
Steam energy available, million kJ/h (500 million kJ/h × 0.7)	350
Electric power generation, kW (350 million kJ/h)/(11,395 kJ/kWh)	30,715
Station-service allowance, kW [30,715 (0.06)]	-1,843
Unaccounted heat losses, kW [30,715 (0.05)]	1,536
Net electric power for export, kW	27,336
Overall efficiency, percent [(27,336 kW)/((500,000,000 kJ/h)/(3600 kJ/kWh))](100)	19.7

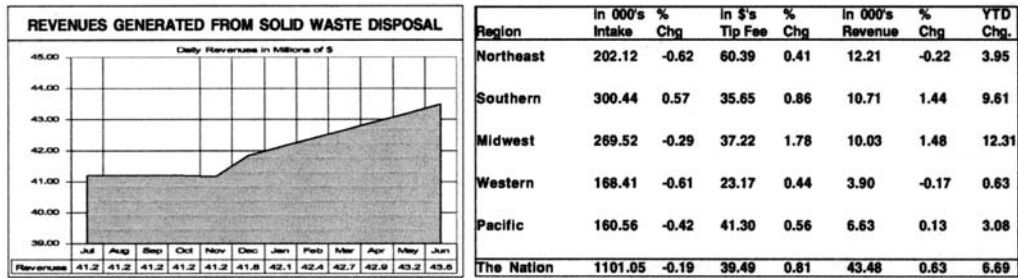
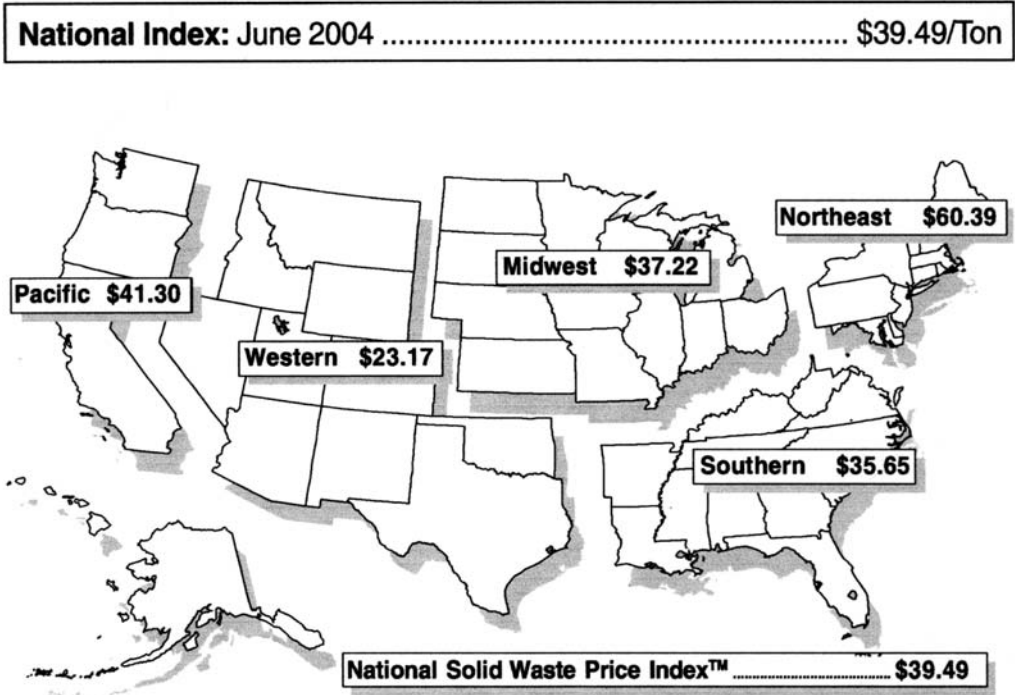


FIG. 22-55 Solid-waste management costs, June 2004.

down to 1858 landfills in service nationwide in 2001 accepting approximately 160 million tons of waste. The number of landfills is decreasing, and the capacity of remaining landfills is rising, as new landfills are larger. New landfills are more sophisticated than older ones and are therefore more costly to design and operate. Over the long term, the tonnage of MSW landfilled in 1990 was 140.1 million tons, but decreased to 122.4 million tons in 1995. The tonnage increased to 131.8 million tons in 1999, then declined to 127.6 in 2001. The tonnage landfilled results from an interaction among generation, recycling, and combustion, which do not necessarily rise and fall at the same time. Figure 22-56 shows the decrease of landfills that has occurred over the 13-year period from 1988 to 2001.

The landfilling of hazardous waste is considered separately.

Site Selection Factors that must be considered in evaluating potential solid-waste-disposal sites are summarized in Table 22-71. Final selection of a disposal site usually is based on the results of a preliminary site survey, results of engineering design and cost studies, and an environmental impact assessment.

Landfilling Methods and Operations To use the available area at a landfill site effectively, a plan of operation for the placement of solid wastes must be prepared. Various operational methods have been developed primarily on the basis of field experience. The principal methods used for landfilling dry areas may be classified as (1) area and (2) depression.

1. *Area method.* The area method is used when the terrain is unsuitable for the excavation of trenches in which to place the solid wastes. The filling operation usually is started by building an earthen levee against which wastes are placed in thin layers and then compacted (see Fig. 22-57). Each layer is compacted as the filling progresses until the thickness of the compacted wastes reaches a height varying from 2 to 3 m (6 to 10 ft). At that time, and at the end of each day's operation, a 150- to 300-mm (6- to 12-in) layer of cover material is placed over the completed fill. The cover material must be hauled in by truck or earthmoving equipment from adjacent land or from borrow-pit areas. In some newer landfill operations, the daily cover material is omitted, and reusable geotextile covers, similar to very

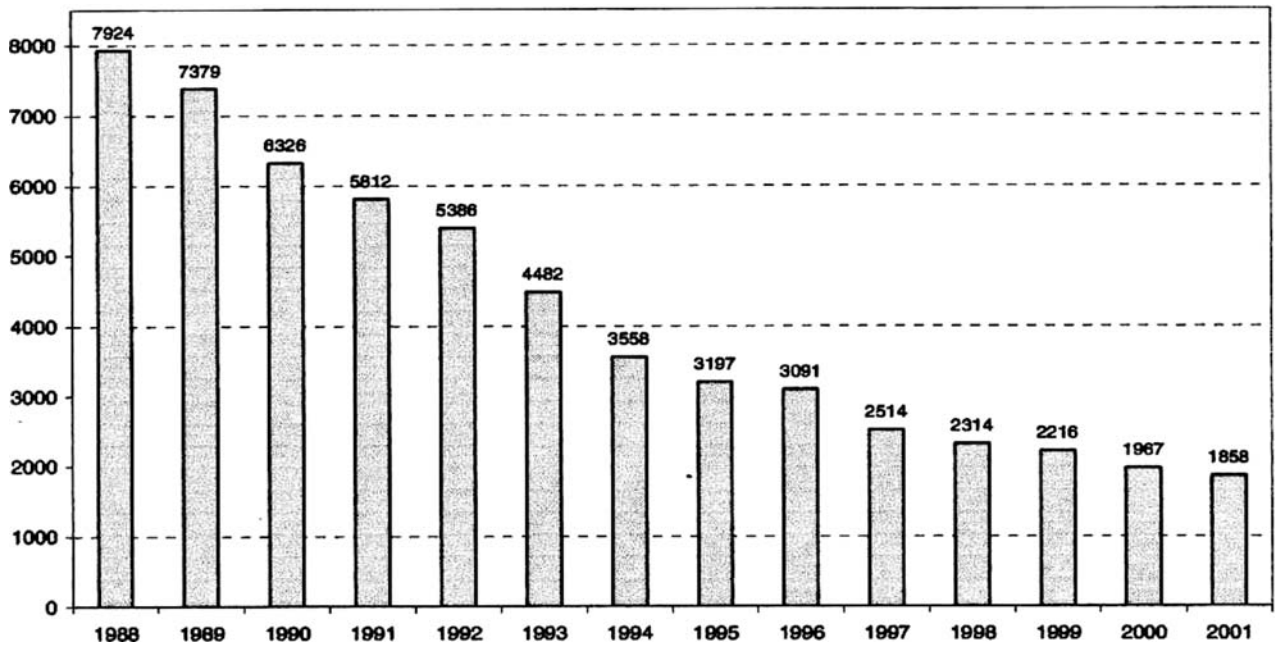


FIG. 22-56 Number of landfills, 1988–2001.

large tarps, are used. A completed lift including the cover material is called a *cell* (see Fig. 22-58). Successive lifts are placed on top of one another until the final grade called for in the ultimate development plan is reached. A final layer of cover material is used when the fill reaches the final design height.

2. *Depression method.* At locations where natural or artificial depressions exist, it is often possible to use them effectively for landfilling operations. Canyons, ravines, dry borrow pits, and quarries have been used for this purpose. The techniques to place and compact solid wastes in depression landfills vary with the geometry of the site,

the characteristics of the cover material, the hydrology and geology of the site, and access of the site. In a canyon site, filling starts at the head end of the canyon (see Fig. 22-59) and ends at the mouth. The practice prevents the accumulation of water behind the landfill. Wastes usually are deposited on the canyon floor and from there are pushed up against the canyon face at a slope of about 2 : 1. In this way, a high degree of compaction can be achieved.

3. *Landfills in wet areas.* Because of the problems associated with contamination of local groundwater, the development of odors, and structural stability, landfills must be avoided in wetlands. If wet

TABLE 22-71 Important Factors in Preliminary Selection of Landfill Sites

Factor	Remarks
Available land area	In selecting potential land disposal sites, it is important to ensure that sufficient land area is available. Sufficient area to operate for at least 1 year at a given site is needed to minimize costs.
Impact of processing and resource recovery	It is important to project the extent of resource-recovery processing activities that are likely to occur in the future and determine their impact on the quantity and condition of the residual materials to be disposed of.
Haul distance	Although minimum haul distances are desirable, other factors must also be considered. These include collection-route location, types of wastes to be hauled, local traffic patterns, and characteristics of the routes to and from the disposal site (condition of the routes, traffic patterns, and access conditions).
Soil conditions and topography	Because it is necessary to provide material for each day's landfill and a final layer of cover after the filling has been completed, data on the amounts and characteristics of the soils in the area must be obtained. Local topography will affect the type of landfill operation to be used, equipment requirements, and the extent of work necessary to make the site usable.
Climatological conditions	Local weather conditions must also be considered in the evaluation of potential sites. Under winter conditions where freezing is severe, landfill cover material must be available in stockpiles when excavation is impractical. Wind and wind patterns must also be considered carefully. To avoid blowing or flying papers, windbreaks must be established.
Surface-water hydrology	The local surface-water hydrology of the area is important in establishing the existing natural drainage and runoff characteristics that must be considered.
Geologic and hydrogeologic conditions	Geologic and hydrogeologic conditions are perhaps the most important factors in establishing the environmental suitability of the area for a landfill site. Data on these factors are required to assess the pollution potential of the proposed site and to establish what must be done to the site to control the movement of leachate or gases from the landfill.
Local environmental conditions	The proximity of both residential and industrial developments is extremely important. Great care must be taken in their operation if they are to be environmentally sound with respect to noise, odor, dust, flying paper, and vector control.
Ultimate uses	Because the ultimate use affects the design and operation of the landfill, this issue must be resolved before the layout and design of the landfill are started.

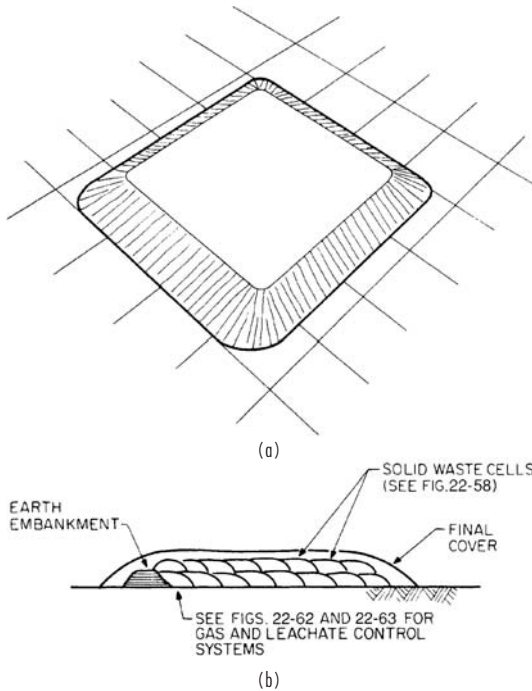


FIG. 22-57 Area method for landfilling solid wastes. (a) Pictorial view of completed landfill. (b) Section through landfill.

areas such as ponds, pits, or quarries must be used as landfill sites, special provisions must be made to contain or eliminate the movement of leachate and gases from completed cells. Usually this is accomplished by first draining the site and then lining the bottom with a clay liner or other appropriate sealants. If a clay liner is used, it is important to continue operation of the drainage facility until the site is filled to avoid the creation of uplift pressures that could cause the liner to rupture from heaving.

Occurrence of Gases and Leachate in Landfills The following biological, physical, and chemical events occur when solid wastes are placed in a sanitary landfill: (1) biological decay of organic materials, either aerobically or anaerobically, with the evolution of gases and liquids; (2) chemical oxidation of waste materials; (3) escape of gases from the fill; (4) movement of liquids caused by differential heads; (5) dissolving and leaching of organic and inorganic materials by water and leachate moving through the fill; (6) movement of dissolved material by concentration gradients and osmosis; and (7) uneven settlement caused by consolidation of material into voids.

With respect to item 1, bacterial decomposition initially occurs under aerobic conditions because a certain amount of air is trapped within the landfill. However, the oxygen in the trapped air is exhausted within days, and long-term decomposition occurs under anaerobic conditions.

1. **Gases in landfills.** Gases found in landfills include air, ammonia, carbon dioxide, carbon monoxide, hydrogen, hydrogen sulfide, methane, nitrogen, and oxygen. Data on the molecular weight and density of these gases are presented in Sec. 2. Carbon dioxide and methane are the principal gases produced from the anaerobic decomposition of the organic solid-waste components.

The anaerobic conversion of organic compounds is thought to occur in three steps. The first involves the enzyme-mediated transformation (hydrolysis) of higher-weight molecular compounds into compounds suitable for use as a source of energy and cell carbon; the second is associated with the bacterial conversion of the compounds resulting

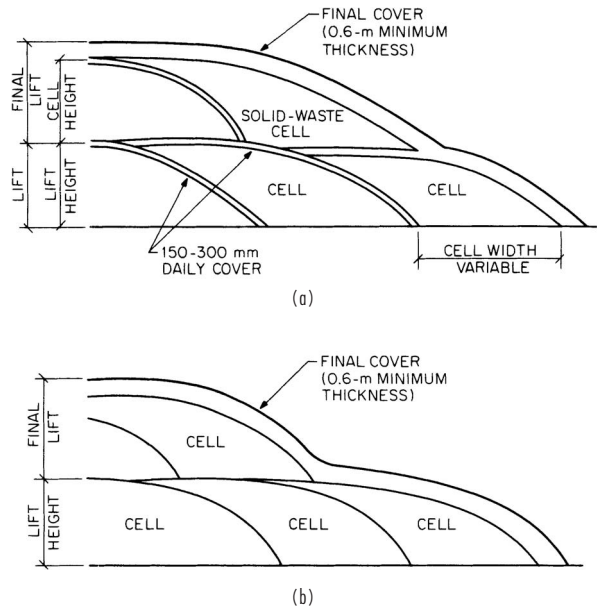


FIG. 22-58 Typical section through a landfill. (a) With daily or intermediate cover. (b) Without daily or intermediate cover.

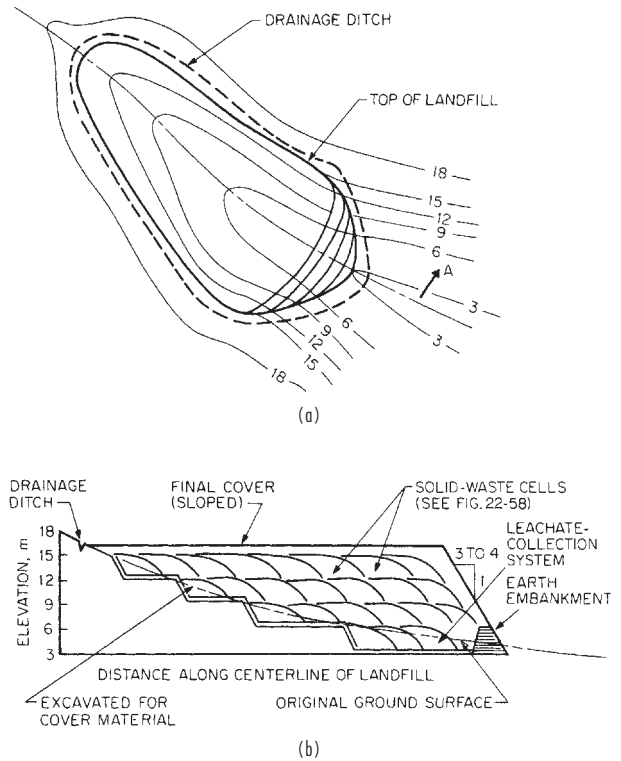
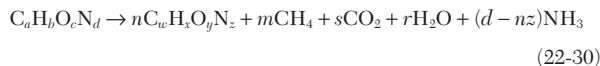


FIG. 22-59 Depression method for landfilling solid wastes. (a) Plan view: canyon-site landfill. (b) Section through landfill.

from the first step into identifiable lower-molecular-weight intermediate compounds; and the third step involves the bacterial conversion of the intermediate compounds into simpler end products, such as carbon dioxide (CO₂) and methane (CH₄). The overall anaerobic conversion of organic industrial wastes can be represented with the following equation:



where $s = a - nw = m$ and $r = c - ny - 2s$. The terms $C_aH_bO_cN_d$ and $C_wH_xO_yN_z$ are used to represent on a molar basis the composition of the material present at the start of the process.

The rate of decomposition in unmanaged landfills, as measured by gas production, reaches a peak within the first 2 years and then slowly tapers off, continuing in many cases for periods of up to 25 years or more. The total volume of the gases released during anaerobic decomposition can be estimated in a number of ways. If all the organic constituents in the wastes (with the exception of plastics, rubber, and leather) are represented with a generalized formula of the form $C_aH_bO_cN_d$, the total volume of gas can be estimated by using Eq. (22-30) with the assumption of completed conversion to carbon dioxide and methane.

2. *Leachate in landfills.* Leachate may be defined as liquid that has percolated through solid waste and has extracted dissolved or suspended materials from it. In most landfills, the liquid portion of the leachate is composed of the liquid produced from the decomposition of the wastes and liquid that has entered the landfill from external sources, such as surface drainage, rainfall, groundwater, and water from underground springs. Representative data on chemical characteristics of leachate are reported in Table 22-72.

Gas and Leachate Movement and Control Under ideal conditions, the gases generated from a landfill should be either vented to the atmosphere or, in larger landfills, collected for the production of energy. Landfills with >2.5 million cubic meters of waste or >50 Mg/yr NMOC (nonmethane organic compounds) emissions may require landfill-gas collection and flare systems, per EPA support WWW, CFR 60 Regulations. The leachate should be either contained within the landfill or removed for treatment.

1. *Gas movement.* In most cases, over 90 percent of the gas volume produced from the decomposition of solid wastes consists of methane and carbon dioxide. Although most of the methane escapes to the atmosphere, both methane and carbon dioxide have been found in concentrations of up to 40 percent at lateral distances of up to 120 m (400 ft) from the edges of landfills. Methane can accumulate below buildings or in other enclosed spaces or close to a sanitary landfill. With proper venting at the landfill source, methane should not pose a problem.

Because carbon dioxide is about 1.5 times as dense as air and 2.8 times as dense as methane, it tends to move toward the bottom of the landfill. As a result, the concentration of carbon dioxide in the lower portions of landfill may be high for years. Ultimately, because of its density, carbon dioxide will also move downward through the underlying formation until it reaches the groundwater. Because carbon dioxide is readily soluble in water, it usually lowers the pH, which in turn can increase the hardness and mineral content of the groundwater through the solubilization of calcium and magnesium carbonates.

Currently, MSW landfills are estimated to release approximately 14,300 tons/yr of NMOC. Methane and carbon dioxide contribute to the greenhouse effect, and the release of VOCs cause air quality issues such as smog and ozone formation. In the gas of a MSW landfill, VOCs comprise about 39 percent of NMOC.

2. *Control of gas movement.* The lateral movement of gases produced in a landfill can be controlled by installing vents made of materials that are more permeable than the surrounding soil. Typically, as shown in Fig. 22-60a, gas vents are constructed of gravel. The spacing of cell vents depends on the width of the waste cell but usually varies from 18 to 60 m (60 to 200 ft). The thickness of the gravel layer should be such that it will remain continuous even though there may be dif-

ferential settling; 300 to 450 mm (12 to 18 in) thick is recommended. Barrier vents (see Fig. 22-60b) also can be used to control the lateral movements of gases. Well vents are often used in conjunction with lateral surface vents buried below grade in a gravel trench (see Fig. 22-60c). Details of a gas vent are shown in Fig 22-61. Control of the downward movement of gases can be accomplished by installing perforated pipes in the gravel layer at the bottom of the landfill. If the gases cannot be vented laterally, it may be necessary to install gas wells and vent the gas to atmosphere. This is considered a passive venting system. See Fig. 22-62. The movement of landfill gases through adjacent soil formation can be controlled by constructing barriers of materials that are more impermeable than soil. See Fig. 22-63a. Some of the landfill sealants that are available for this use are identified in Table 22-73. Of these, the use of compacted clays is the most common. The thickness will vary depending on the type of clay and the degree of control required; thicknesses ranging from 0.015 to 1.25 m (6 to 48 in) have been used. Covers of landfills are also typically multilayered and may include foundation layer, clay layer, membrane, drainage layer (synthetic or natural), root zone layer, or soil.

3. *Control of gas movement by recovery.* The movement of gases in landfills can also be controlled by installing gas-recovery wells in completed landfills (see Fig. 22-63b). This is considered an active venting system. Clay and other lines are used when landfill gas is to be

TABLE 22-72 Typical Leachate Quality of Municipal Waste

S1 number	Parameter	Overall range (mg/L except as indicated)
1	TDS	584-55,000
2	Specific conductance	480-72,500 μ mho/cm
3	Total suspended solids	2-140,900
4	BOD	ND-195,000
5	COD	6.6-99,000
6	TOC	ND-40,000
7	pH	3.7-8.9 units
8	Total alkalinity	ND-15,050
9	Hardness	0.1-225,000
10	Chloride	2-11,375
11	Calcium	3.0-2,500
12	Sodium	12-6,010
13	Total Kjeldahl nitrogen	2-3,320
14	Iron	ND-4,000
15	Potassium	ND-3,200
16	Magnesium	4.0-780
17	Ammonia-nitrogen	ND-1,200
18	Sulfate	ND-1,850
19	Aluminum	ND-85
20	Zinc	ND-731
21	Manganese	ND-400
22	Total phosphorus	ND-234
23	Boron	0.87-13
24	Barium	ND-12.5
25	Nickel	ND-7.5
26	Nitrate-nitrogen	ND-250
27	Lead	ND-14.2
28	Chromium	ND-5.6
29	Antimony	ND-3.19
30	Copper	ND-9.0
31	Thallium	ND-0.78
32	Cyanide	ND-6
33	Arsenic	ND-70.2
34	Molybdenum	0.07-1.43
35	Tin	ND-0.16
36	Nitrite-nitrogen	ND-1.46
37	Selenium	ND-1.85
38	Cadmium	ND-0.4
39	Silver	ND-1.96
40	Beryllium	ND-0.36
41	Mercury	ND-3.0
42	Turbidity	40-500 Jackson units

From McGinley, P. M., and P. Kmet, *Formation Characteristics, Treatment, and Disposal of Leachate from Municipal Solid Waste Landfills*, Bureau of Solid Waste Management, Wisconsin Department of Natural Resources, Madison, 1984.

22-104 WASTE MANAGEMENT

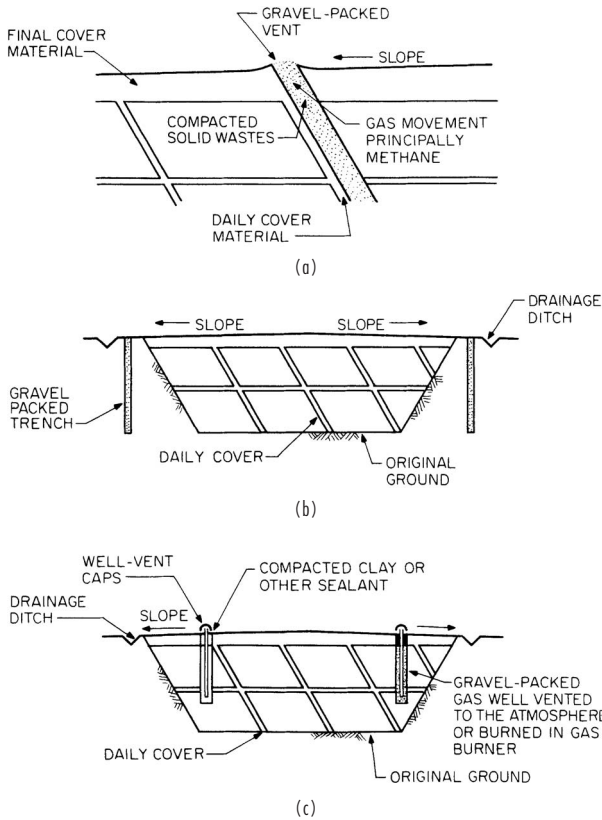


FIG. 22-60 Vents used to control the lateral movement of gases in landfills. (a) Cell. (b) Barrier. (c) Well. (From G. Tchobanoglous, H. Theisen, and R. Eliassen, *Solid Wastes: Engineering Principles and Management Issues*, McGraw-Hill, New York, 1977.)

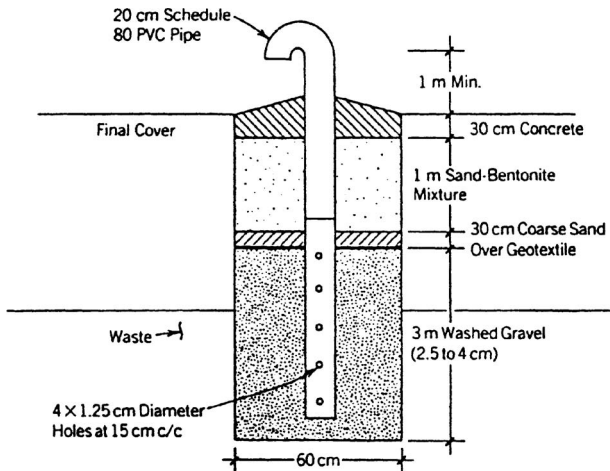


FIG. 22-61 Typical detail of an isolated gas vent. (From Bagchi, A., *Design, Construction, and Monitoring of Sanitary Landfill*, Wiley, 1990.)

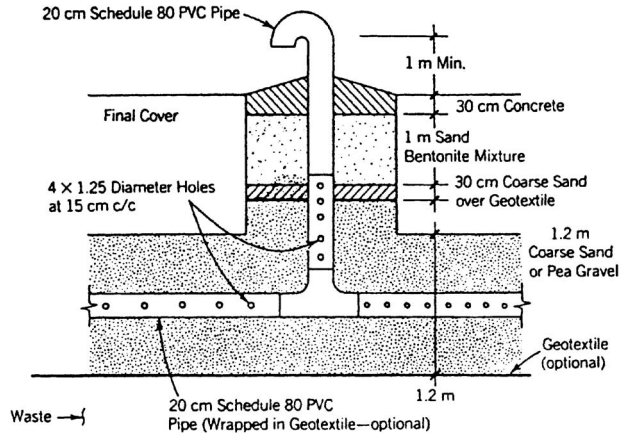


FIG. 22-62 Typical detail of a passive gas venting system with a header pipe. (From Bagchi, A., *Design, Construction, and Monitoring of Sanitary Landfill*, Wiley, 1990.)

recovered. In some gas-recovery systems, leachate is collected and recycled to the top of the landfill and reinjected through perforated lines located in drainage trenches. Typically, the rate of gas production is greater in leachate-recirculation systems.

Gas recovery systems have been installed in some large municipal landfills, with the gas flared used to run spark-ignition diesel engines to generate power for sale to the grid or the gas is cleaned up and piped to nearby users. The economics of such operations must be reviewed for each site. The end use of gas will affect the overall economics. The

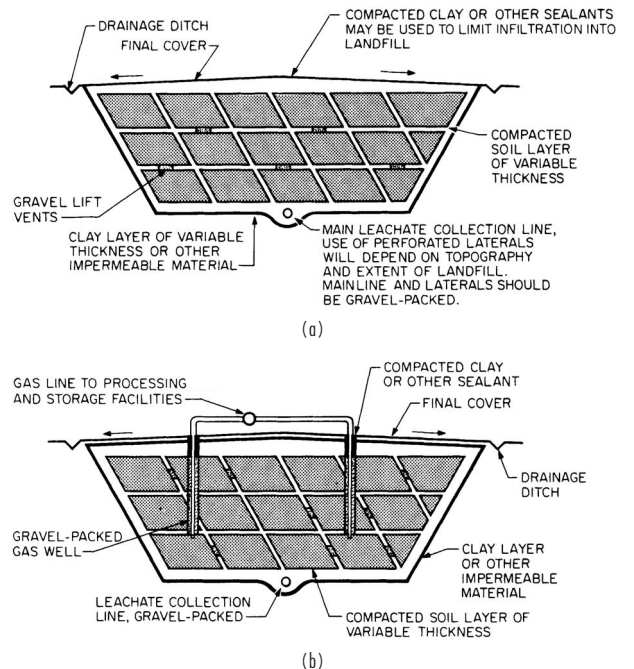


FIG. 22-63 Use of an impermeable liner to control the movement of gases and leachate in landfills. (a) Without gas recovery. (b) With gas recovery. (From G. Tchobanoglous, H. Theisen, and R. Eliassen, *Solid Wastes: Engineering Principles and Management Issues*, McGraw-Hill, New York, 1977.)

TABLE 22-73 Landfill Sealants for the Control of Gas and Leachate Movement

Classification	Sealant	
	Representative types	
Compacted soil Compacted clay	Bentonites, illites, kaolinites	
Inorganic chemicals Synthetic chemicals Synthetic membrane liners	Sodium carbonate, silicate, or pyrophosphate Polymers, rubber, latex Polyvinyl chloride, butyl rubber, Hypalon, polyethylene, nylon-reinforced liners	
Asphalt	Modified asphalt, asphalt-covered polypropylene fabric, asphalt concrete	
Others	Gumite concrete, soil, cement, plastic soil cement	

*From G. Tchobanoglous, H. Theisen, and R. Eliassen, *Solid Wastes: Engineering Principles and Management Issues*, McGraw-Hill, New York, 1977.

cost of gas cleanup and processing equipment will limit the recovery of landfill gases, especially from small landfills.

4. *Leachate movement.* Under normal conditions, leachate is found in the bottom of landfills. From there it moves through the underlying strata, although some lateral movement may also occur, depending on the characteristics of the surrounding material. The rate of seepage of leachate from the bottom of a landfill can be estimated by Darcy's law by assuming that the material below the landfill to the top of the water table is saturated and that a small layer of leachate exists at the bottom of the fill. Under these conditions, the leachate discharge rate per unit area is equal to the value of the coefficient of permeability *K*, expressed in meters per day. The computed value represents the maximum amount of seepage that would be expected, and this value should be used for design purposes. Under normal conditions, the actual rate would be less than this value because the soil column below the landfill would not be saturated. Models have been developed to aid in the estimation of leachate quantity. Bagchi has covered details of these models in the *Design, Construction, and Monitoring of Sanitary Landfill*.

5. *Control of leachate movement.* As leachate percolates through the underlying strata, many of the chemical and biological constituents originally contained in it will be removed by the filtering and adsorptive action of the material composing the strata. In general, the extent of this action depends on the characteristics of the soil, especially the clay content. Because of the potential risk involved in allowing leachate to percolate to the groundwater, best practice calls for its elimination or containment. Ultimately, it will be necessary to collect and treat the leachate.

The use of clay has been the favored method of reducing or eliminating the percolation of leachate (see Fig. 22-63 and Table 22-73). Membrane liners are used most often today but require care so that they will not be damaged during the filling operations. Equally important in controlling the movement of leachate is the elimination of surface-water infiltration, which is the major contributor to the total volume of leachate. With the use of an impermeable clay layer, membrane liners, an appropriate surface slope (1 to 2 percent), and adequate drainage, surface infiltration can be controlled effectively.

TABLE 22-74 Short- and Long-Term Actions for Effective Industrial Solid-Waste Management*

Actions	Remarks
Short-term	
1. Inventory wastes.	Document all types, quantities, and sources of wastes (both nonhazardous and hazardous wastes).
2. Inventory inactive sites.	All inactive sites where wastes have been disposed of in the past should be inventoried. Data should be gathered on buried wastes, including types, quantity, and sources. A groundwater-monitoring program should be developed.
3. Characterize wastes.	In addition to general information on the characteristics of the wastes, all hazardous wastes should be individually characterized.
4. Assign responsibilities.	Assign responsibilities and authority at plant and headquarters for the storage, collection, treatment, and disposal of all types of hazardous wastes.
5. Track the movement of wastes.	Develop a logging system for hazardous wastes containing the date, waste description, source, volume shipped or hauled, name of hauler, and destination. Follow through to be sure that wastes reach their destination.
6. Develop emergency procedures.	Develop procedures for dealing with emergency situations involving the storage, collection, treatment, and disposal of hazardous wastes.
7. Obtain permits.	Start obtaining the necessary waste-disposal permits as soon as possible.
Long-term	
1. Remove all accumulated wastes.	Develop a systematic program for removing all accumulated wastes stored on the plant site.
2. Separate wastes.	Institute a long-term program to separate wastes at the source of production.
3. Reduce wastes.	A systematic program should be undertaken to examine all sources of waste production and to develop alternative operations and processes to reduce waste generation.
4. Improve facilities.	Upgrade facilities to meet RCRA requirements. A data-collection program should be instituted to obtain any needed data.
5. Review all waste-management agreements.	Develop detailed contracts with outside waste-management firms. Define clearly the duties and responsibilities of plant personnel and waste-collection personnel.
6. Review and develop disposals-tie options.	Develop long-term projections for landfill requirements and initiate a program to secure the needed sites.
7. Secure appropriate engineering and consulting services.	Make sure that your engineering departments are involved early in the process.
8. Monitor legislative programs.	Retain outside consultants for specific tasks. Develop a program for monitoring new regulations and for inputting to appropriate federal, state, and local agencies on the modification and development of new regulations.

*Adapted in part from R. Sobel, "How Industry Can Prepare for RCRA," *Chem. Eng.*, 86(1), 82 (Jan. 29, 1979).

22-106 WASTE MANAGEMENT

6. *Settlement and structural characteristics of landfills.* The settlement of landfills depends on the initial compaction, characteristics of wastes, degree of decomposition, and effects of consolidation when the leachate and gases are formed in the landfill. The height of the completed fill will also influence the initial compaction and degree of consolidation.

PLANNING

Because of the ever-growing number of federal regulations governing the disposal of nonhazardous and hazardous solid wastes, it is prudent to develop both short-term and long-term action programs to deal with all aspects of solid-waste management. Important short- and long-term actions are identified in Table 22-74.

SECTION **23**

Process Safety

PERRY'S CHEMICAL ENGINEERS' HANDBOOK

8TH EDITION



DANIEL A. CROWL, LAURENCE G. BRITTON
WALTER L. FRANK, STANLEY GROSSEL
DENNIS HENDERSHOT, W. G. HIGH
ROBERT W. JOHNSON, TREVOR A. KLETZ
JOSEPH C. LEUNG, DAVID A. MOORE
ROBERT ORMSBY, RICHARD W. PRUGH
JACK E. OWENS, RICHARD SIWEK
THOMAS O. SPICER III, ANGELA SUMMERS
RONALD WILLEY, JOHN L. WOODWARD

Copyright © 2008, 1997, 1984, 1973, 1963, 1950, 1941, 1934 by The McGraw-Hill Companies, Inc. All rights reserved. Manufactured in the United States of America. Except as permitted under the United States Copyright Act of 1976, no part of this publication may be reproduced or distributed in any form or by any means, or stored in a database or retrieval system, without the prior written permission of the publisher.

0-07-154230-2

The material in this eBook also appears in the print version of this title: 0-07-154205-1.

All trademarks are trademarks of their respective owners. Rather than put a trademark symbol after every occurrence of a trademarked name, we use names in an editorial fashion only, and to the benefit of the trademark owner, with no intention of infringement of the trademark. Where such designations appear in this book, they have been printed with initial caps.

McGraw-Hill eBooks are available at special quantity discounts to use as premiums and sales promotions, or for use in corporate training programs. For more information, please contact George Hoare, Special Sales, at george_hoare@mcgraw-hill.com or (212) 904-4069.

TERMS OF USE

This is a copyrighted work and The McGraw-Hill Companies, Inc. (“McGraw-Hill”) and its licensors reserve all rights in and to the work. Use of this work is subject to these terms. Except as permitted under the Copyright Act of 1976 and the right to store and retrieve one copy of the work, you may not decompile, disassemble, reverse engineer, reproduce, modify, create derivative works based upon, transmit, distribute, disseminate, sell, publish or sublicense the work or any part of it without McGraw-Hill’s prior consent. You may use the work for your own noncommercial and personal use; any other use of the work is strictly prohibited. Your right to use the work may be terminated if you fail to comply with these terms.

THE WORK IS PROVIDED “AS IS.” McGRAW-HILL AND ITS LICENSORS MAKE NO GUARANTEES OR WARRANTIES AS TO THE ACCURACY, ADEQUACY OR COMPLETENESS OF OR RESULTS TO BE OBTAINED FROM USING THE WORK, INCLUDING ANY INFORMATION THAT CAN BE ACCESSED THROUGH THE WORK VIA HYPERLINK OR OTHERWISE, AND EXPRESSLY DISCLAIM ANY WARRANTY, EXPRESS OR IMPLIED, INCLUDING BUT NOT LIMITED TO IMPLIED WARRANTIES OF MERCHANTABILITY OR FITNESS FOR A PARTICULAR PURPOSE. McGraw-Hill and its licensors do not warrant or guarantee that the functions contained in the work will meet your requirements or that its operation will be uninterrupted or error free. Neither McGraw-Hill nor its licensors shall be liable to you or anyone else for any inaccuracy, error or omission, regardless of cause, in the work or for any damages resulting therefrom. McGraw-Hill has no responsibility for the content of any information accessed through the work. Under no circumstances shall McGraw-Hill and/or its licensors be liable for any indirect, incidental, special, punitive, consequential or similar damages that result from the use of or inability to use the work, even if any of them has been advised of the possibility of such damages. This limitation of liability shall apply to any claim or cause whatsoever whether such claim or cause arises in contract, tort or otherwise.

DOI: 10.1036/0071542051

Process Safety

Daniel A. Crowl, Ph.D. *Professor of Chemical Engineering, Michigan Technological University; Fellow, American Institute of Chemical Engineers (Section Editor, Process Safety Introduction, Combustion and Flammability Hazards, Gas Explosions, Vapor Cloud Explosions, Boiling-Liquid Expanding-Vapor Explosions)*

Laurence G. Britton, Ph.D. *Process Safety Consultant; Consulting Scientist, Neolytica, Inc.; Fellow, American Institute of Chemical Engineers; Fellow, Energy Institute; Member, Institute of Physics (U.K.) (Flame Arresters)*

Walter L. Frank, P.E., B.S.Ch.E. *Senior Consultant, ABS Consulting; Fellow, American Institute of Chemical Engineers (Hazards of Vacuum, Hazards of Inerts)*

Stanley Grossel, M.S.Ch.E. *President, Process Safety & Design; Fellow, American Institute of Chemical Engineers (Emergency Relief Device Effluent Collection and Handling, Flame Arresters)*

Dennis Hendershot, M.S.Ch.E. *Principal Process Safety Specialist, Chilworth Technology, Inc.; Fellow, American Institute of Chemical Engineers (Hazard Analysis)*

W. G. High, C.Eng., B.Sc., F.I.Mech.E. *Consultant, Burgoyne Consultants (Estimation of Damage Effects)*

Robert W. Johnson, M.S.Ch.E. *President, Unwin Company; Member, American Institute of Chemical Engineers (Reactivity, Storage and Handling of Hazardous Materials)*

Trevor A. Kletz, D.Sc. *Visiting Professor, Department of Chemical Engineering, Loughborough University (U.K.); Adjunct Professor, Department of Chemical Engineering, Texas A&M University; Fellow, American Institute of Chemical Engineers; Fellow, Royal Academy of Engineering (U.K.); Fellow, Institution of Chemical Engineers (U.K.); Fellow, Royal Society of Chemistry (U.K.) (Inherently Safer and More User-Friendly Design, Incident Investigation and Human Error, Institutional Memory, Key Procedures)*

Joseph C. Leung, Ph.D. *President, Leung Inc.; Member, American Institute of Chemical Engineers (Pressure Relief Systems)*

David A. Moore, MBA, B.Sc. *President, AcuTech Consulting Group; Registered Professional Engineer (FPE, PA); Certified Safety Professional (CSP); ASSE, ASIS, NFPA (Security)*

Robert Ormsby, M.S.Ch.E. *Process Safety Consultant; Fellow, American Institute of Chemical Engineers (Risk Analysis)*

Jack E. Owens, B.E.E. *Electrostatics Consultant, E. I. Dupont de Nemours and Co.; Member, Institute of Electrical and Electronics Engineers; Member, Electrostatics Society of America (Static Electricity)*

Richard W. Prugh, M.S.P.E., C.S.P. *Senior Process Safety Specialist, Chilworth Technology, Inc.; Fellow, American Institute of Chemical Engineers; Member, National Fire Protection Association (Toxicity)*

23-2 PROCESS SAFETY

Carl A. Schiappa, B.S.Ch.E. *Retired, The Dow Chemical Company (Project Review and Audit Processes)*

Richard Siwek, M.S. *Managing Director, President, FireEx Consultant Ltd.; Member, European Committee for Standardization (CEN/TC305); Member, Association of German Engineers (VDI 2263,3673); Member, International Section for Machine Safety (ISSA) (Dust Explosions, Preventive Explosion Protection, Explosion Protection through Design Measures)*

Thomas O. Spicer III, Ph.D., P.E. *Professor and Head, Ralph E. Martin Department of Chemical Engineering, University of Arkansas; Member, American Institute of Chemical Engineers (Atmospheric Dispersion)*

Angela Summers, Ph.D., P.E. *President, SIS-TECH; Adjunct Professor, Department of Environmental Management, University of Houston—Clear Lake; Senior Member, Instrumentation, Systems and Automation Society; Member, American Institute of Chemical Engineers (Safety Instrumented Systems)*

Ronald Willey, Ph.D., P.E. *Professor, Department of Chemical Engineering, Northeastern University; Fellow, American Institute of Chemical Engineers (Case Histories)*

John L. Woodward, Ph.D. *Senior Principal Consultant, Baker Engineering and Risk Consultants, Inc.; Fellow, American Institute of Chemical Engineers (Discharge Rates from Punctured Lines and Vessels)*

PROCESS SAFETY INTRODUCTION

CASE HISTORIES

Introduction	23-5
Hydrocarbon Fires and Explosions	23-5
Dust Explosions	23-5
Reactive Chemicals	23-5
Materials of Construction	23-6
Toxicology	23-6
Nitrogen Asphyxiation	23-6

HAZARDOUS MATERIALS AND CONDITIONS

Flammability	23-6
Introduction	23-6
The Fire Triangle	23-7
Definition of Terms	23-7
Combustion and Flammability Hazards	23-8
Explosions	23-11
Vapor Cloud Explosions	23-13
Boiling-Liquid Expanding-Vapor Explosions	23-13
Dust Explosions	23-15
Static Electricity	23-22
Chemical Reactivity	23-24
Introduction	23-25
Life-Cycle Considerations	23-25
Designing Processes for Control of Intended Chemical Reactions	23-26
Designing Facilities for Avoidance of Unintended Reactions	23-27
Designing Mitigation Systems to Handle Uncontrolled Reactions	23-29
Reactive Hazard Reviews and Process Hazard Analyses	23-30
Reactivity Testing	23-30
Sources of Reactivity Data	23-30
Toxicity	23-30
Introduction	23-30
Inhalation Toxicity: The Haber Equation	23-31
Dosage Equation	23-31
Probit Equation	23-31
Ingestion Toxicity	23-32
Skin-Contact Toxicity	23-32
Compilation of Data	23-32
Safeguards against Toxicity Hazards	23-34
Conclusion	23-34
Other Hazards	23-34
Hazards of Vacuum	23-34
Hazards of Inerts	23-36

INHERENTLY SAFER DESIGN AND OTHER PRINCIPLES

Inherently Safer and More User-Friendly Design	23-38
Introduction	23-38
Intensification or Minimization	23-38
Substitution	23-38
Attenuation or Moderation	23-38
Limitation of Effects of Failures	23-38
Simplification	23-38
Knock-on Effects	23-38
Making Incorrect Assembly Impossible	23-39
Making Status Clear	23-39
Tolerance	23-39
Low Leak Rate	23-39
Ease of Control	23-39
Software	23-39
Actions Needed for the Design of Inherently Safer and User-Friendly Plants	23-39
Incident Investigation and Human Error	23-39
Institutional Memory	23-40

PROCESS SAFETY ANALYSIS

Hazard Analysis	23-41
Introduction	23-41
Definitions of Terms	23-41
Process Hazard Analysis Regulations	23-42
Hazard Identification and Analysis Tools	23-42
Hazard Ranking Methods	23-45
Logic Model Methods	23-47
Risk Analysis	23-47
Introduction	23-48
Frequency Estimation	23-49
Consequence Estimation	23-51
Risk Estimation	23-52
Risk Criteria	23-53
Risk Decision Making	23-53
Discharge Rates from Punctured Lines and Vessels	23-54
Overview	23-55
Types of Discharge	23-55
Energy Balance Method for Orifice Discharge	23-55
Momentum Balance in Dimensionless Variables	23-56
Analytical Solutions for Orifice and Pipe Flow	23-57
Orifice Discharge for Gas Flow	23-57
Blowdown of Gas Discharge through Orifice	23-57
Pipe and Orifice Flow for Subcooled Liquids	23-57
Numerical Solution for Orifice Flow	23-57

Omega Method Model for Compressible Flows 23-58
 Homogeneous Equilibrium Omega Method for Orifice
 and Horizontal Pipe Flow 23-58
 HEM for Inclined Pipe Discharge 23-59
 Nonequilibrium Extension of Omega Method 23-61
 Differences between Subcooled and Saturated
 Discharge for Horizontal Pipes 23-61
 Accuracy of Discharge Rate Predictions 23-61
 Atmospheric Dispersion 23-61
 Introduction 23-62
 Parameters Affecting Atmospheric Dispersion 23-62
 Atmospheric Dispersion Models 23-64
 Estimation of Damage Effects 23-66
 Inert, Ideal Gas-Filled Vessels 23-67
 Blast Characteristics 23-67
 Fragment Formation 23-67
 Initial Fragment Velocity 23-68
 Vessel Filled with Reactive Gas Mixtures 23-68
 Vessels Completely Filled with an Inert
 High-Pressure Liquid 23-68
 Distance Traveled by Fragments 23-68
 Fragment Striking Velocity 23-69
 Damage Potential of Fragments 23-69
 Local Failure 23-69
 Overall Response 23-69
 Response to Blast Waves 23-69
 Project Review and Audit Processes 23-71
 Introduction 23-71
 Project Review Process 23-71
 Audit Process 23-73

SAFETY EQUIPMENT, PROCESS DESIGN, AND OPERATION

Pressure Relief Systems 23-74
 Introduction 23-74
 Relief System Terminology 23-74
 Codes, Standards, and Guidelines 23-75
 Relief Design Scenarios 23-75
 Pressure Relief Devices 23-76
 Sizing of Pressure Relief Systems 23-77
 Emergency Relief Device Effluent Collection and Handling 23-80
 Introduction 23-80

Types of Equipment 23-80
 Equipment Selection Criteria and Guidelines 23-86
 Sizing and Design of Equipment 23-88
 Flame Arresters 23-92
 General Considerations 23-92
 Deflagration Arresters 23-94
 Detonation and Other In-Line Arresters 23-95
 Arrestor Testing and Standards 23-96
 Special Arrestor Types and Alternatives 23-96
 Storage and Handling of Hazardous Materials 23-97
 Introduction 23-98
 Established Practices 23-98
 Basic Design Strategies 23-98
 Site Selection, Layout, and Spacing 23-99
 Storage 23-99
 Design of Tanks, Piping, and Pumps 23-100
 Loss-of-Containment Causes 23-102
 Maintaining the Mechanical Integrity of the Primary
 Containment System 23-102
 Release Detection and Mitigation 23-102
 Safety Instrumented Systems 23-102
 Glossary 23-102
 Introduction 23-103
 Hazard and Risk Analysis 23-103
 Design Basis 23-103
 Engineering, Installation, Commissioning,
 and Validation (EICV) 23-104
 Operating Basis 23-104
 Security 23-104
 Definition of Terms 23-104
 Introduction 23-105
 Threats of Concern 23-106
 Security Vulnerability Assessment 23-106
 SVA Methodologies 23-106
 Defining the Risk to Be Managed 23-107
 Security Strategies 23-108
 Countermeasures and Security Risk Management
 Concepts 23-108
 Security Management System 23-109
 Key Procedures 23-109
 Preparation of Equipment for Maintenance 23-109
 Inspection and Testing of Protective Equipment 23-110
 Key Performance Indicators 23-110

PROCESS SAFETY INTRODUCTION

GENERAL REFERENCES: AIChE/CCPS, *Guidelines for Chemical Process Quantitative Risk Analysis*, 2d ed., American Institute of Chemical Engineers, New York, 2000. AIChE/CCPS, *Guidelines for Hazards Evaluation Procedures*, 2d ed., American Institute of Chemical Engineers, New York, 1992. Crowl and Louver, *Chemical Process Safety: Fundamentals with Applications*, 2d ed., Prentice-Hall, Englewood Cliffs, N.J., 2002. Mannan, *Lees' Loss Prevention in the Process Industries*, 3d ed., Elsevier, Amsterdam.

Process safety differs from the traditional approach to accident prevention in several ways (Mannan, *Lees' Loss Prevention in the Process Industries*, 3d ed., Elsevier, 2005, p. 1/9):

- There is greater concern with accidents that arise out of the technology.
- There is greater emphasis on foreseeing hazards and taking action before accidents occur.
- There is greater emphasis on a systematic rather than a trial-and-error approach, particularly on systematic methods of identifying hazards and of estimating the probability that they will occur and their consequences.
- There is concern with accidents that cause damage to plant and loss of profit but do not injure anyone, as well as those that do cause injury.
- Traditional practices and standards are looked at more critically.

The term *loss prevention* can be applied in any industry but is widely used in the process industries where it usually means the same as *process safety*.

Chemical plants, and other industrial facilities, may contain large quantities of hazardous materials. The materials may be hazardous due to toxicity, reactivity, flammability, or explosivity. A chemical plant may also contain large amounts of energy—the energy either is required to process the materials or is contained in the materials themselves. An *accident* occurs when control of this material or energy is lost. An *accident* is defined as an unplanned event leading to undesired consequences. The consequences might include injury to people, damage to the environment, or loss of inventory and production, or damage to equipment.

A *hazard* is defined as a chemical or physical condition that has the potential for causing damage to people, property, or the environment (AIChE/CCPS, *Guidelines for Chemical Process Quantitative Risk Analysis*, 2d ed., American Institute of Chemical Engineers, New York, 2000, p. 6). Hazards exist in a chemical plant due to the nature of the materials processed or due to the physical conditions under which the materials are processed, i.e., high pressure or temperature. These hazards are present most of the time. An initiating event is required to begin the accident process. Once initiated, the accident follows a sequence of steps, called the event sequence, that results in an incident outcome. The consequences of the accident are the resulting effects of the incident. For instance, a rupture in a pipeline due to corrosion (initiating event) results in leakage of a flammable liquid from the process. The liquid evaporates and mixes with air to form a flammable cloud, which finds an ignition source (event sequence), resulting in a fire (incident outcome). The consequences of the accident are considerable fire damage and loss of production.

Risk is defined as a measure of human injury, environmental damage, or economic loss in terms of both the incident likelihood (probability) and the magnitude of the loss or injury (consequence) (AIChE/CCPS, *Guidelines for Chemical Process Quantitative Risk Analysis*, 2d ed., American Institute of Chemical Engineers, New York, 2000, pp. 5–6). It is important that both likelihood and consequence be included in risk. For instance, seat belt use is based on a reduction in the consequences of an accident. However, many people argue against seat belts based on probabilities, which is an incorrect application of the risk concept.

A good safety program identifies and removes existing hazards. An outstanding safety program prevents the existence of safety hazards in the

first place. An outstanding safety program is achieved by company commitment, visibility, and management support. This is usually achieved by a corporatewide safety policy. This safety policy usually includes the following items: (1) the company is very serious about safety, (2) safety cannot be prioritized and is a part of everyone's job function, (3) everyone is responsible for safety, including management.

To ensure that the safety program is working, most companies have a safety policy follow-through. This includes monthly safety meetings, performance reviews, and safety audits. The monthly safety meetings include a discussion of any accidents (and resolution of prevention means), training on specific issues, inspection of facilities, and delegation of work. Performance reviews within the company for all employees must have a visible safety performance component.

Safety audits are a very important means of ensuring that the safety program is operating as intended. Audits are usually done yearly by an audit team. The audit team is comprised of corporate and site safety people and other experts, as needed, including industrial hygiene, toxicology, and/or process safety experts. The audit team activities include (1) reviewing records (including accident reports, training, monthly meetings), (2) inspecting random facilities to see if they are in compliance, (3) interviewing the employees to determine how they participate in the safety program, (4) making recommendations on

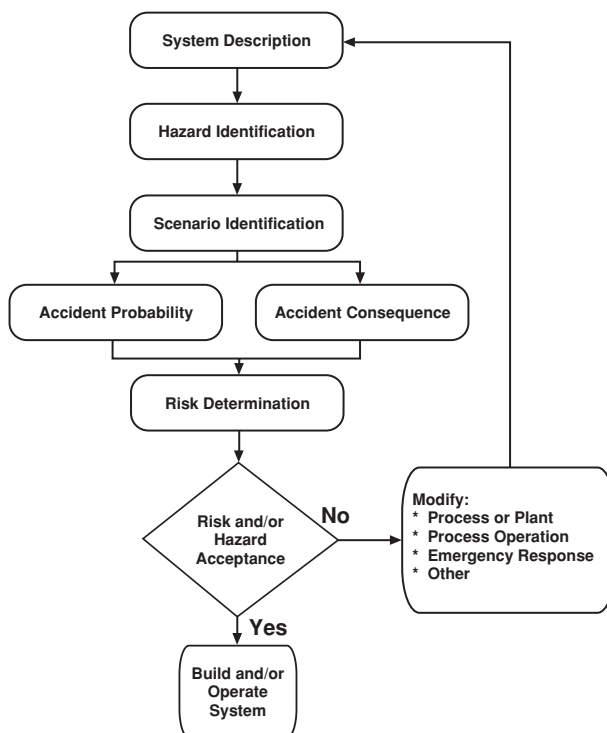


FIG. 23-1 The hazard identification and risk assessment procedure. [Guidelines for Hazards Evaluation Procedures, *Center for Chemical Process Safety (CCPS) of the American Institute of Chemical Engineers (AIChE)*; copyright 1985 AIChE and reproduced with permission.]

how the program can be improved, and (5) rating the performance of the unit. The audit results are reported to upper management with the expectation that the designated unit will implement improvements in short order. Many companies perform a combined audit, which may include environmental and quality issues.

Figure 23-1 shows the hazards identification and risk assessment procedure. The procedure begins with a complete description of the process. This includes detailed PFD and P&I diagrams, complete specifications on all equipment, maintenance records, operating procedures, and so forth. A hazard identification procedure is then selected (see Hazard Analysis subsection) to identify the hazards and their nature. This is followed by identification of all potential event sequences and potential incidents (scenarios) that can result in loss of control of energy or material. Next is an evaluation of both the consequences and the probability. The consequences are estimated by using source models (to describe the

release of material and energy) coupled with a consequence model to describe the incident outcome. The consequence models include dispersion, fire, and explosion modeling. The results of the consequence models are used to estimate the impacts on people, environment, and property. The accident probability is estimated by using fault trees or generic databases for the initial event sequences. Event trees may be used to account for mitigation and postrelease incidents. Finally, the risk is estimated by combining the potential consequence for each event with the event frequency and summing over all events.

Once the risk is determined, a decision must be made on risk acceptance. This can be done by comparison to a relative or absolute standard. If the risk is acceptable, then the decision is made to build and/or operate the process. If the risk is not acceptable, then something must be changed. This could include the process design, the operation, or maintenance, or additional layers of protection might be added.

CASE HISTORIES

GENERAL REFERENCES: *One Hundred Largest Losses: A Thirty Year Review of Property Damage Losses in the Hydrocarbon Chemical Industry*, 20th ed. (M&M Protection, Consultants, Chicago); Mannan, S., ed., *Lees' Loss Prevention in the Process Industries*, Elsevier, 2005; Kletz, T. A., *Learning from Accidents*, Gulf Professional Publishing, 2001; Kletz, T. A., *What Went Wrong? Case Histories of Process Plant Disasters*, Editions Technip, 1998; and Sanders, R. E., *Chemical Process Safety: Learning from Case Histories*, Editions Technip, 1999.

INTRODUCTION

Engineers must give significant thought to the consequences of their decisions and indecisions. A wise step during conceptual and design phases is to review previous negative experiences of others and within your own organization. Periodically review the status of recent chemical accidents. The U.S. Chemical Safety and Hazards Investigation Board web site, www.csb.gov, offers details on many investigations related to chemical industry accidents within the United States. Look for similarities and dissimilarities to your current practice, and carefully make appropriate changes and improvements to avoid repeating similar accidents.

HYDROCARBON FIRES AND EXPLOSIONS

The explosion and fires at the Texaco Refinery, Milford Haven, Wales, 24 July 1994. Reference: Health and Safety Executive (HSE); HSE Books, Her Majesty's Stationary Office, Norwich, England, 1997.

On July 24, 1994, an explosion followed by a number of fires occurred at 13:23 at the Texaco refinery in Milford Haven, Wales, England. Prior to this explosion, around 9 a.m., a severe coastal electrical storm caused plant disturbances that affected the vacuum distillation, alkylation, butamer, and FCC units. The explosion occurred due to a combination of failures in management, equipment, and control systems. Given its calculated TNT equivalent of at least 4 tons, significant portions of the refinery were damaged. That no fatalities occurred is attributed partially to the accident occurring on a Sunday, as well as the fortuitous location of those who were near the explosion.

As the plant attempted adjustments to the upsets caused by the electrical storm, liquid was continuously pumped into a process vessel with a closed outlet valve. The control system indicated that this valve was open. As the unit overfilled, the only means of exit was a relief system designed for vapor. When the liquid reached the relief system, its momentum was high enough to rip apart the ductwork and cause a massive release of hydrocarbons into the environment. Minutes prior to the explosion, operating personnel were responding to 275 alarms of which 80 percent had high priority. An ignition source was found 110 m away. Recommendations from the accident investigation included

the necessity of operating personnel having knowledge about simple volumetric and mass balances; that control systems be configured to provide an overview of the condition of the process; that safety critical alarms be distinguishable from other alarms; and that liquid knockout drums exist for relief systems designed for vapor.

DUST EXPLOSIONS

West Pharmaceutical Services Plant in Kinston, North Carolina, 29 January 2003, and CTA Acoustics Manufacturing Plant in Corbin, Kentucky, 20 February 2003. Reference: U.S. Chemical Safety Board (CSB); www.csb.gov/index.cfm?folder=completed_investigations&page=info&INV_ID=34 and [ID=35](http://www.csb.gov/index.cfm?folder=completed_investigations&page=info&INV_ID=35)

On January 29, 2003, the West Pharmaceutical explosion killed six workers and injured dozens more. The CSB determined that fine polyethylene dust particles, released during the production of rubber products, had accumulated above the tiles of a false ceiling, creating an explosion hazard at the plant. A similar incident occurred a few weeks later, at the CTA Acoustics manufacturing plant in Corbin, Kentucky, fatally injuring seven workers and injuring more than 30 others. This facility produced fiberglass insulation for the automotive industry. CSB investigators found that the explosion was fueled by resin dust accumulated in a production area, likely ignited by flames from a malfunctioning oven. The resin involved was a phenolic binder used in producing fiberglass mats.

CSB investigators determined that both disasters resulted from accumulations of combustible dust. Workers and workplaces need to be protected from this insidious hazard. The lesson learned here is the importance of housekeeping. Some companies will allow only $\frac{1}{32}$ in of dust to accumulate before cleaning. Suspended ceilings must be suspected as areas that can accumulate dust. Often the first explosion may be minor, but the dust dislodged can be explosive enough to level the building on the second ignition.

REACTIVE CHEMICALS

Explosion, Morton International, Inc., Paterson, New Jersey, 8 April 1998. Reference: CSB; www.csb.gov/completed_investigations/docs/MortonInvestigationReport.pdf

On April 8, 1998, at 20:18, an explosion and fire occurred during the production of Automate Yellow 96 Dye at Morton International, Inc. Yellow 96 dye was produced by mixing and reacting two chemicals, *ortho*-nitrochlorobenzene (*o*-NCB) and 2-ethylhexylamine (2-EHA). The explosion and fire were the consequence of a runaway reaction, which overpressurized a 2000-gal capacity chemical reactor vessel and released flammable material that ignited. Nine employees were injured, including two seriously, and potentially hazardous materials were released into

23-6 PROCESS SAFETY

the community. The CSB investigation team determined that the reaction accelerated beyond the heat removal capability of the kettle. The resulting high temperature led to a secondary runaway reaction (decomposition of *o*-NCB). The initial runaway reaction was most likely caused by a combination of the following factors: (1) The reaction was started at a temperature higher than normal, (2) the steam used to initiate the reaction was left on for too long, and (3) the use of cooling water to control the reaction rate was not initiated soon enough. The Paterson facility was not aware of the decomposition reaction. A similar incident occurred with a process using *o*-NCB in Sauget, Illinois, in 1974 (Vincent, G. C., *Loss Prev.* 1971, 5: 46–52).

MATERIALS OF CONSTRUCTION

Ruptured chlorine hose. Reference: CSB; www.csb.gov/safety_publications/docs/ChlorineHoseSafetyAdvisory.pdf

On August 14, 2002, a 1-in chlorine transfer hose (CTH) used in a rail-car offloading operation at DPC Enterprises in Festus, Missouri, catastrophically ruptured and initiated a sequence of events that led to the release of 48,000 lb of chlorine into neighboring areas. The material of construction of the ruptured hose was incorrect. The distributor fabricated bulk CTH with Schedule 80 Monel 400 end fittings and a high-density polyethylene spiral guard. Three hoses were shipped directly to the Festus facility from the distributor; two were put into service on June 15, 2002. The hose involved in the incident failed after 59 days in service.

Most plastics react chemically with chlorine because of their hydrocarbon structural makeup. This reactivity is avoided with some plastics in which fluorine atoms have been substituted into the hydrocarbon molecule. The Chlorine Institute recommends that hoses constructed with such an inner lining “have a structural layer braid of polyvinylidene fluoride (PVDF) monofilament material or a structural braid of Hastelloy C-276.” An underlying lesson here is material compatibility. Material compatibility tables exist that engineers can consult, including in other sections within this volume.

TOXICOLOGY

Vessel explosion, D. D. Williamson & Co., Inc., Louisville, Kentucky, 11 April 2003. Reference: CSB; www.csb.gov/completed_investigations/docs/CSB_DDWilliamsonReport.pdf

On April 11, 2003, at approximately 2:10 a.m., a 2200-gal stainless steel spray dryer feed tank at the D. D. Williamson & Co., Inc. (DDW), plant in Louisville, Kentucky, exploded. One operator was killed. The other four men working at the plant at the time of the incident were not injured. The incident was most likely initiated by overheating by a 130-psi steam supply. The feed tank was manually

controlled for temperature and pressure. The tank had a maximum working pressure of 40 psi. A concrete block wall to the east separated the feed tank from a 12,000-gal aqua ammonia storage tank (29.4% ammonia). After the explosion, the feed tank's shell split open in a vertical line. It was propelled through the wall and struck the ammonia storage tank, located 15 ft to the west. The ammonia storage tank was knocked off its foundation approximately 10 ft, and piping was ripped loose. This resulted in a 26,000-lb aqua ammonia leak. Metro Louisville Health Department obtained maximum ammonia readings of 50 parts per million (ppm) at the fence line and 35 ppm on a nearby street. No injuries were reported in the area of the ammonia release.

A number of management decisions factor into this case. There was no program to evaluate necessary layers of protection on the spray dryer feed tanks. Likewise, there was no recognition of the need to provide process control and alarm instrumentation on the two feed tanks. Reliance on a single local temperature indicator that must be read by operators is insufficient. On the morning of the incident, the operators were unaware that the system had exceeded normal operating conditions. The feed tanks were installed for use in the spray dryer process without a review of their design versus system requirements. Safety valves on the spray dryer feed tanks had been removed to transport the tanks to Louisville and were never reinstalled. Inadequate hazard analysis systems didn't identify feed tank hazards. The ASME Code, Section VIII (2001 ASME Boiler and Pressure Vessel Code: Design and Fabrication of Pressure Vessels, American Society of Mechanical Engineers, 2001), requires that all vessels having an internal operating pressure exceeding 15 psi be provided with pressure relief devices. Finally, equipment layout should always be considered in the design stage. Methods such as the Dow Fire and Explosion Index (AIChE, 1994) can assist in determining the optimum spacing between critical units.

NITROGEN ASPHYXIATION

Union Carbide Corporation, Hahnville, Louisiana, 27 March 1998. Reference: CSB; [www.csb.gov/completed_investigations/docs/Final Union Carbide Report.pdf](http://www.csb.gov/completed_investigations/docs/Final%20Union%20Carbide%20Report.pdf) and [SB-Nitrogen-6-11-03.pdf](http://www.csb.gov/completed_investigations/docs/SB-Nitrogen-6-11-03.pdf)

On March 27, 1998, at approximately 12:15 p.m., two workers at Union Carbide Corporation's Taft/Star Manufacturing Plant in Hahnville, Louisiana, were overcome by nitrogen gas while performing a black light inspection at an open end of a 48-in-wide horizontal pipe. One Union Carbide employee was killed, and an independent contractor was seriously injured due to nitrogen asphyxiation. Nitrogen was being injected into a nearby reactor to prevent contamination of a catalyst by oxygen and related materials. The nitrogen also flowed through some of the piping systems connected to the reactors. No warning sign was posted on the pipe opening identifying it as a confined space. Nor was there a warning that the pipe contained potentially hazardous nitrogen.

HAZARDOUS MATERIALS AND CONDITIONS

FLAMMABILITY

Nomenclature

K_C	deflagration index for gases (bar·m/s)
K_{St}	deflagration index for dusts (bar·m/s)
LFL	lower flammability limit (vol % fuel in air)
LOC	limiting oxygen concentration
n	number of combustible species
P	pressure
T	temperature (°C)
t	time (s)
UFL	upper flammability limit (vol. % fuel in air)
V	vessel volume (m ³)
y_i	mole fraction of component i on a combustible basis
z	stoichiometric coefficient for oxygen
ΔH_c	net heat of combustion (kcal/mol)

GENERAL REFERENCES: Crowl and Louvar, *Chemical Process Safety: Fundamentals with Applications*, 2d ed., Prentice-Hall, Upper Saddle River, N.J., 2002, Chaps. 6 and 7. Crowl, *Understanding Explosions*, American Institute of Chemical Engineers, New York, 2003. Eckhoff, *Dust Explosions in the Process Industries*, 2d ed., Butterworth-Heinemann, now Elsevier, Amsterdam, 1997. Kinney and Graham, *Explosive Shocks in Air*, 2d ed., Springer-Verlag, New York, 1985. Lewis and von Elbe, *Combustion, Flames and Explosions of Gases*, 3d ed., Academic Press, New York, 1987. Mannan, *Lees' Loss Prevention in the Process Industries*, 3d ed., Elsevier, Amsterdam, 2005, Chap. 16: Fire, Chap. 17: Explosion.

Introduction Fire and explosions in chemical plants and refineries are rare, but when they do occur, they are very dramatic.

Accident statistics have shown that fires and explosions represent 97 percent of the largest accidents in the chemical industry (J. Coco, ed., *Large Property Damage Losses in the Hydrocarbon-Chemical Industry: A Thirty Year Review*, J. H. Marsh and McLennan, New York, 1997).

Prevention of fires and explosions requires

1. An understanding of the fundamentals of fires and explosions
2. Proper experimental characterization of flammable and explosive materials

3. Proper application of these concepts in the plant environment
The technology does exist to handle and process flammable and explosive materials safely, and to mitigate the effects of an explosion. The challenges to this problem are as follows:

1. Combustion behavior varies widely and is dependent on a wide range of parameters.
2. There is an incomplete fundamental understanding of fires and explosions. Predictive methods are still under development.
3. Fire and explosion properties are not fundamentally based and are an artifact of a particular experimental apparatus and procedure.
4. High-quality data from a standardized apparatus that produces consistent results are lacking.
5. The application of these concepts in a plant environment is difficult.

The Fire Triangle The fire triangle is shown in Fig. 23-2. It shows that a fire will result if fuel, oxidant, and an ignition source are present. In reality, the fuel and oxidant must be within certain concentration ranges, and the ignition source must be robust enough to initiate the fire. The fire triangle applies to gases, liquids, and solids. Liquids are volatilized and solids decompose prior to combustion in the vapor phase. For dusts arising from solid materials, the particle size, distribution, and suspension in the gas are also important parameters in the combustion—these are sometimes included in the fire triangle.

The usual oxidizer in the fire triangle is oxygen in the air. However, gases such as fluorine and chlorine; liquids such as peroxides and chlorates; and solids such as ammonium nitrate and some metals can serve the role of an oxidizer. Exothermic decomposition, without oxygen, is also possible, e.g., with ethylene oxide or acetylene.

Ignition arises from a wide variety of sources, including static electricity, hot surfaces, sparks, open flames, and electric circuits. Ignition sources are elusive and difficult to eliminate entirely, although efforts should always be made to reduce them.

If any one side of the fire triangle is removed, a fire will not result. In the past, the most common method for fire control was elimination of ignition sources. However, experience has shown that this is not robust enough. Current fire control prevention methods continue with elimination of ignition sources, while focusing efforts more strongly on preventing flammable mixtures.

Definition of Terms The following are terms necessary to characterize fires and explosions (Crowl and Louvar, *Chemical Process Safety: Fundamentals with Applications*, 2d ed. Prentice-Hall, Upper Saddle River, N.J., 2002, pp. 227–229).

Autoignition temperature (AIT) This is a fixed temperature above which adequate energy is available in the environment to provide an ignition source.

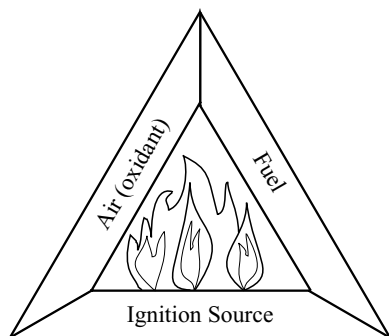


FIG. 23-2 The fire triangle showing the requirement for combustion of gases and vapors. [D. A. Crowl, *Understanding Explosions*, Center for Chemical Process Safety (CCPS) of the American Institute of Chemical Engineers (AIChE); copyright 2003 AIChE and reproduced with permission.]

Boiling-liquid expanding-vapor explosion (BLEVE) A BLEVE occurs if a vessel that contains a liquid at a temperature above its atmospheric pressure boiling point ruptures. The subsequent BLEVE is the explosive vaporization of a large fraction of the vessel contents, possibly followed by combustion or explosion of the vaporized cloud if it is combustible. This type of explosion occurs when an external fire heats the contents of a tank of volatile material. As the tank contents heat, the vapor pressure of the liquid within the tank increases, and the tank's structural integrity is reduced because of the heating. If the tank ruptures, the hot liquid volatilizes explosively.

Combustion or fire Combustion or fire is a chemical reaction in which a substance combines with an oxidant and releases energy. Part of the energy released is used to sustain the reaction.

Confined explosion This explosion occurs within a vessel or a building.

Deflagration In this explosion the reaction front moves at a speed less than the speed of sound in the unreacted medium.

Detonation In this explosion the reaction front moves at a speed greater than the speed of sound in the unreacted medium.

Dust explosion This explosion results from the rapid combustion of fine solid particles. Many solid materials (including common metals such as iron and aluminum) become flammable when reduced to a fine powder and suspended in air.

Explosion An explosion is a rapid expansion of gases resulting in a rapidly moving pressure or shock wave. The expansion can be mechanical (by means of a sudden rupture of a pressurized vessel), or it can be the result of a rapid chemical reaction. Explosion damage is caused by the pressure or shock wave.

Fire point The fire point is the lowest temperature at which a vapor above a liquid will continue to burn once ignited; the fire point temperature is higher than the flash point.

Flammability limits Vapor-air mixtures will ignite and burn only over a well-specified range of compositions. The mixture will not burn when the composition is lower than the lower flammable limit (LFL); the mixture is too lean for combustion. The mixture is also not combustible when the composition is too rich, i.e., that is, when it is above the upper flammable limit (UFL). A mixture is flammable only when the composition is between the LFL and the UFL. Commonly used units are volume percent of fuel (percentage of fuel plus air).

Lower explosion limit (LEL) and upper explosion limit (UEL) are used interchangeably with LFL and UFL.

Flash point (FP) The flash point of a liquid is the lowest temperature at which it gives off enough vapor to form an ignitable mixture with air. At the flash point, the vapor will burn but only briefly; inadequate vapor is produced to maintain combustion. The flash point generally increases with increasing pressure.

There are several different experimental methods used to determine flash points. Each method produces a somewhat different value. The two most commonly used methods are open cup and closed cup, depending on the physical configuration of the experimental equipment. The open-cup flash point is a few degrees higher than the closed-cup flash point.

Ignition Ignition of a flammable mixture may be caused by a flammable mixture coming in contact with a source of ignition with sufficient energy or by the gas reaching a temperature high enough to cause the gas to autoignite.

Mechanical explosion A mechanical explosion results from the sudden failure of a vessel containing high-pressure, nonreactive gas.

Minimum ignition energy This is the minimum energy input required to initiate combustion.

Overpressure The pressure over ambient that results from an explosion.

Shock wave This is an abrupt pressure wave moving through a gas. A shock wave in open air is followed by a strong wind; the combined shock wave and wind is called a blast wave. The pressure increase in the shock wave is so rapid that the process is mostly adiabatic.

Unconfined explosion Unconfined explosions occur in the open. This type of explosion is usually the result of a flammable gas spill. The gas is dispersed and mixed with air until it comes in contact with an ignition source. Unconfined explosions are rarer than confined explosions because the explosive material is frequently diluted below the LFL by

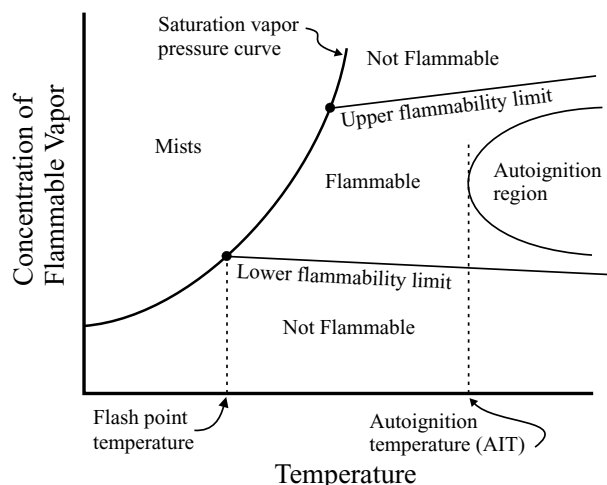


FIG. 23-3 The relationship between the various flammability properties. (D. A. Crowl and J. F. Louvar, *Chemical Process Safety: Fundamentals with Applications*, 2d ed., © 2002. Adapted by permission of Pearson Education, Inc., Upper Saddle River, N.J.)

wind dispersion. These explosions are destructive because large quantities of gas and large areas are frequently involved.

Figure 23-3 is a plot of concentration versus temperature and shows how several of these definitions are related. The exponential curve in Fig. 23-3 represents the saturation vapor pressure curve for the liquid material. Typically, the UFL increases and the LFL decreases with temperature. The LFL theoretically intersects the saturation vapor pressure curve at the flash point, although experimental data are not always consistent. The autoignition temperature is actually the lowest temperature of an autoignition region. The behavior of the autoignition region and the flammability limits at higher temperatures are not well understood.

The flash point and flammability limits are not fundamental properties but are defined only by the specific experimental apparatus and procedure used.

Section 2 provides flammability data for a number of compounds.

Combustion and Flammability Hazards

Vapor Mixtures Frequently, flammability data are required for vapor mixtures. The flammability limits for the mixture are estimated by using LeChatelier's rule [LeChatelier, "Estimation of Firedamp by Flammability Limits," *Ann. Mines* (1891), ser. 8, 19: 388–395, with translation in *Process Safety Progress*, 23(3): 172].

$$LFL_{\text{mix}} = \frac{1}{\sum_{i=1}^n y_i / LFL_i} \quad (23-1)$$

where LFL_i = lower flammability limit for component i (in volume %)
 y_i = mole fraction of component i on a combustible basis
 n = number of combustible species

An identical equation can be written for the UFL.

Note that Eq. (23-1) is only applied to the combustible species, and the mole fraction is computed using only the combustible species.

LeChatelier's rule is empirically derived and is not universally applicable. Mashuga and Crowl [Mashuga and Crowl, "Derivation of LeChatelier's Mixing Rule for Flammable Limits," *Process Safety Progress*, 19(2): 112–118 (2000)] determined that the following assumptions are present in LeChatelier's rule:

1. The product heat capacities are constant.
2. The number of moles of gas is constant.

3. The combustion kinetics of the pure species is independent of and unchanged by the presence of other combustible species.

4. The adiabatic temperature rise at the flammability limit is the same for all species.

These assumptions were found to be reasonably valid at the LFL and less so at the UFL.

Liquid Mixtures Flash point temperatures for mixtures of liquids can be estimated if only one component is flammable and the flash point temperature of the flammable component is known. In this case the flash point temperature is estimated by determining the temperature at which the vapor pressure of the flammable component in the mixture is equal to the pure component vapor pressure at its flash point. Estimation of flash point temperatures for mixtures of several flammable components can be done by a similar procedure, but it is recommended that the flash point temperature be measured experimentally.

Flammability Limit Dependence on Temperature In general, as the temperature increases, the flammability range widens, i.e., the LFL decreases and the UFL increases. Zabetakis et al. (Zabetakis, Lambiris, and Scott, "Flame Temperatures of Limit Mixtures," *7th Symposium on Combustion*, Butterworths, London, 1959) derived the following empirical equations, which are approximate for many hydrocarbons:

$$LFT_T = LFL_{25} - \frac{0.75}{\Delta H_c} (T - 25) \quad (23-2)$$

$$UFL_T = UFL_{25} + \frac{0.75}{\Delta H_c} (T - 25)$$

where ΔH_c is the net heat of combustion (kcal/mol) and T is the temperature ($^{\circ}\text{C}$).

Flammability Limit Dependence on Pressure Pressure has little effect on the LFL except at very low pressures (<50 mmHg absolute) where flames do not propagate.

The UFL increases as the pressure is increased. A very approximate equation for the change in UFL with pressure is available for some hydrocarbon gases (Zabetakis, "Fire and Explosion Hazards at Temperature and Pressure Extremes," *AIChE Inst. Chem. Engr. Symp.*, ser. 2, pp. 99-104, 1965):

$$UFL_P = UFL + 20.6 (\log P + 1) \quad (23-3)$$

where P is the pressure (megapascals absolute) and UFL is the upper flammability limit (vol % fuel in air at 1 atm).

Estimating Flammability Limits There are a number of very approximate methods available to estimate flammability limits. However, for critical safety values, experimental determination as close as possible to actual process conditions is always recommended.

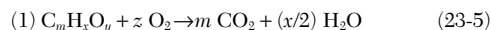
Jones [Jones, "Inflammation Limits and Their Practical Application in Hazardous Industrial Operations," *Chem. Rev.*, 22(1): 1–26 (1938)] found that for many hydrocarbon vapors the LFL and UFL can be estimated from the stoichiometric concentration of fuel:

$$LFL = 0.55C_{\text{st}} \quad (23-4)$$

$$UFL = 3.50C_{\text{st}}$$

where C_{st} is the stoichiometric fuel concentration (vol % fuel in air).

For a stoichiometric combustion equation of the form



it follows that

$$z = m + \frac{x}{4} - \frac{y}{2} \quad (23-6)$$

and furthermore that

$$C_{\text{st}} = \frac{100}{1 + z/0.21} \quad (23-7)$$

TABLE 23-1 Limiting Oxygen Concentrations (Volume Percent Oxygen Concentrations above Which Combustion Can Occur)

Gas or vapor	N ₂ / Air	CO ₂ / Air
Methane	12	14.5
Ethane	11	13.5
Propane	11.5	14.5
<i>n</i> -Butane	12	14.5
Isobutane	12	15
<i>n</i> -Pentane	12	14.5
Isopentane	12	14.5
<i>n</i> -Hexane	12	14.5
<i>n</i> -Heptane	11.5	14.5
Ethylene	10	11.5
Propylene	11.5	14
1-Butene	11.5	14
Isobutylene	12	15
Butadiene	10.5	13
3-Methyl-1-butene	11.5	14
Benzene	11.4	14
Toluene	9.5	—
Styrene	9.0	—
Cyclopropane	11.5	14
Gasoline		
(73/100)	12	15
(100/130)	12	15
(115/145)	12	14.5
Kerosene	10 (150°C)	13 (150°C)
JP-1 fuel	10.5 (150°C)	14 (150°C)
Natural gas	12	14.5
Acetone	11.5	14
<i>t</i> -Butanol	NA	16.5 (150°C)
Carbon disulfide	5	7.5
Carbon monoxide	5.5	5.5
Ethanol	10.5	13
Ethyl ether	10.5	13
Hydrogen	5	5.2
Hydrogen sulfide	7.5	11.5
Isobutyl formate	12.5	15
Methanol	10	12
Methyl acetate	11	13.5

Data from NFPA 68, *Venting of Deflagrations* (Quincy, Mass.: National Fire Protection Association, 1994).

Equation (23-7) can be used with (23-4) to estimate the LFL and UFL.

Suzuki [Suzuki, "Empirical Relationship between Lower Flammability Limits and Standard Enthalpies of Combustion of Organic Compounds," *Fire and Materials*, 18: 333–336 (1994); Suzuki and Koide, "Correlation between Upper Flammability Limits and Thermochemical Properties of Organic Compounds," *Fire and Materials*, 18: pp. 393–397 (1994)] provides more detailed correlations for the UFL and LFL in terms of the heat of combustion.

Flammability limits can also be estimated by using calculated adiabatic flame temperatures and a chemical equilibrium program [Mashuga and Crowl, "Flammability Zone Prediction Using Calculated Adiabatic Flame Temperatures," *Process Safety Progress*, 18 (3) (1999)].

Limiting Oxygen Concentration (LOC) Below the limiting oxygen concentration it is not possible to support combustion, independent of the fuel concentration. The LOC is expressed in units of volume percent of oxygen. The LOC is dependent on the pressure and temperature, and on the inert gas. Table 23-1 lists a number of LOCs, and it shows that the LOC changes if carbon dioxide is the inert gas instead of nitrogen.

The LOC can be estimated for many hydrocarbons from

$$\text{LOC} = z \text{ LFL} \quad (23-8)$$

where z is the stoichiometric coefficient for oxygen [see Eq. (23-5)] and LFL is the lower flammability limit.

Flammability Diagram Figure 23-4 shows a typical flammability diagram. Point A shows how the scales are oriented—at any point on

the diagram the concentrations must add up to 100 percent. At point A we have 60% fuel, 20% oxygen, and 20% nitrogen. The air line represents all possible combinations of fuel and air—it intersects the nitrogen axis at 79% nitrogen which is the composition of air. The stoichiometric line represents all stoichiometric combinations of fuel and oxygen. If the combustion reaction is written according to Eq. (23-5), then the intersection of the stoichiometric line with the oxygen axis is given by

$$100 \left(\frac{z}{1+z} \right) \quad (23-9)$$

The LFL and UFL are drawn on the air line from the fuel axis values.

The flammability zone for most hydrocarbon vapors is shown as drawn in Fig. 23-4. Any concentration within the flammability zone is defined as flammable.

The LOC is the oxygen concentration at the very nose of the flammability zone. It is found from a line drawn from the nose of the flammability zone to the oxygen axis.

Crowl (*Understanding Explosions*, American Institute of Chemical Engineers, New York, 2003, App. A) derived a number of rules for using flammability diagrams:

1. If two gas mixtures R and S are combined, the resulting mixture composition lies on a line connecting points R and S on the flammability diagram. The location of the final mixture on the straight line depends on the relative moles in the mixtures combined: If mixture S has more moles, the final mixture point will lie closer to point S . This is identical to the lever rule used for phase diagrams.

2. If a mixture R is continuously diluted with mixture S , the mixture composition follows along the straight line between points R and S on the flammability diagram. As the dilution continues, the mixture composition moves closer and closer to point S . Eventually, at infinite dilution the mixture composition is at point S .

3. For systems having composition points that fall on a straight line passing through an apex corresponding to one pure component, the other two components are present in a fixed ratio along the entire line length.

Figure 23-5 shows how nitrogen can be used to avoid the flammable zone during the vessel preparation for maintenance. In this case nitrogen is pumped into the vessel until a concentration is reached at point S . Then air can be pumped in, arriving at point R . Figure 23-6 shows the reverse procedure. Now nitrogen is added until point S is reached, then fuel is pumped in until point R is reached. In both cases the flammable zone is avoided.

A complete flammability diagram requires hundreds of tests in a combustion sphere [Mashuga and Crowl, "Application of the Flammability Diagram for the Evaluation of Fire and Explosion Hazards of Flammable Vapors," *Proc. Safety Prog.*, 17 (3): 176–183 (1998)]. However, an approximate diagram can be drawn by using the LFL, UFL, LOC, and flammability limits in pure oxygen. The following procedure is used:

1. Draw the flammability limits in air as points on the air line, using the fuel axis values.

2. Draw the flammability limits in pure oxygen as points on the oxygen scale, using the fuel axis values. Table 23-2 provides a number of values for the flammability limits in pure oxygen. These are drawn on the oxygen axis using the fuel axis concentrations.

3. Use Eq. (23-9) to draw a point on the oxygen axis, and then draw the stoichiometric line from this point to the 100 percent nitrogen apex.

4. Locate the LOC on the oxygen axis. Draw a line parallel to the fuel axis until it intersects the stoichiometric line. Draw a point at the intersection.

5. Connect the points to estimate the flammability zone.

In reality, not all the data are available, so a reduced form of the above procedure is used to draw a partial diagram (Crowl, *Understanding Explosions*, American Institute of Chemical Engineers, New York, 2003, p. 27).

Ignition Sources and Energy Table 23-3 provides a list of the ignition sources for major fires. As seen in Table 23-3, ignition sources are very common and cannot be used as the only method of fire prevention.

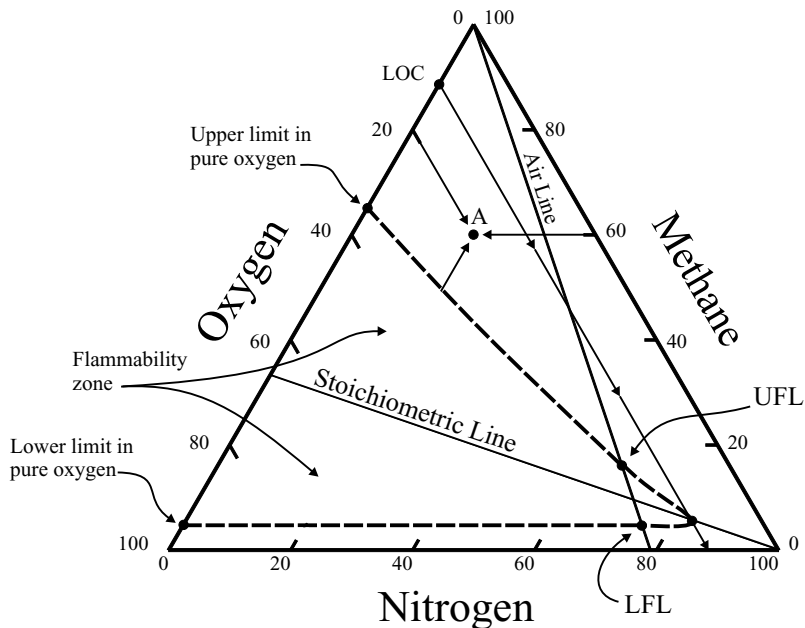


FIG. 23-4 Flammability diagram for methane at an initial temperature and pressure of 25°C and 1 atm. [C. V. Mashuga and D. A. Crowl, "Application of the Flammability Diagram for Evaluation of Fire and Explosion Hazards of Flammable Vapors," *Process Safety Progress*, vol. 17, no. 3; copyright 1998 American Institute of Chemical Engineers (AIChE) and reproduced with permission.]

The minimum ignition energy (MIE) is the minimum energy input required to initiate combustion. All flammable materials (including dusts) have an MIE. The MIE depends on the species, concentration, pressure, and temperature. A few MIEs are provided in Table 23-4. In general, experimental data indicate that

1. The MIE increases with increasing pressure.
2. The MIE for dusts is, in general, at energy levels somewhat higher than that of combustible gases.

3. An increase in nitrogen concentration increases the MIE.
- Most hydrocarbon vapors have an MIE of about 0.25 mJ. This is very low—a static spark that you can feel is greater than about 20 mJ. Dusts typically have MIEs of about 10 mJ. In both the vapor and dust cases, wide variability in the values is expected.

Aerosols and Mists The flammability behavior of vapors is affected by the presence of liquid droplets in the form of aerosols or mists. Aerosols are liquid droplets or solid particles of size small

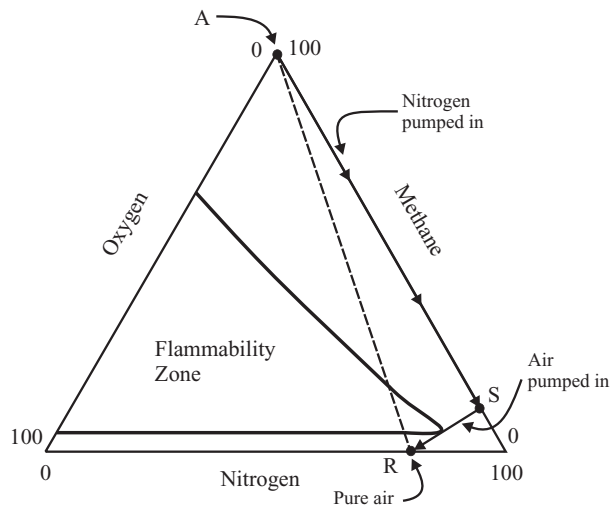


FIG. 23-5 A procedure for avoiding the flammability zone for taking a vessel out of service. [D. A. Crowl, *Understanding Explosions*, Center for Chemical Process Safety (CCPS) of the American Institute of Chemical Engineers (AIChE); copyright 2003 AIChE and reproduced with permission.]

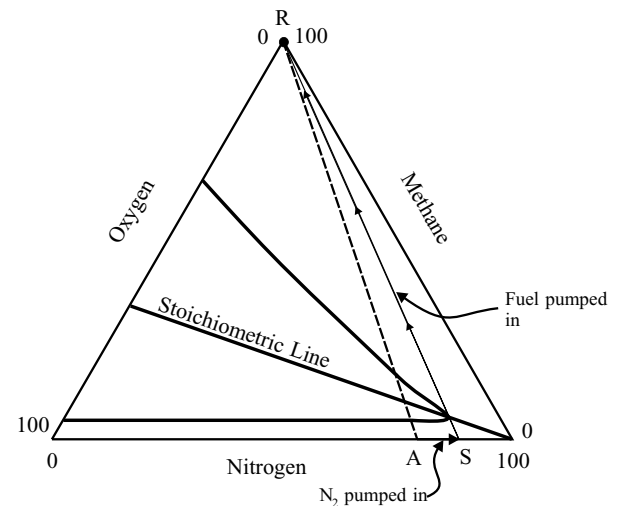


FIG. 23-6 A procedure for avoiding the flammability zone for placing a vessel into service. [D. A. Crowl, *Understanding Explosions*, Center for Chemical Process Safety (CCPS) of the American Institute of Chemical Engineers (AIChE); copyright 2003 AIChE and reproduced with permission.]

TABLE 23-2 Flammability Limits in Pure Oxygen

Compound	Formula	Limits of flammability in pure oxygen	
		Lower	Upper
Hydrogen	H ₂	4.0	94
Carbon monoxide*	CO	15.5	94
Ammonia	NH ₃	15.0	79
Methane	CH ₄	5.1	61
Ethane	C ₂ H ₆	3.0	66
Ethylene	C ₂ H ₄	3.0	80
Propylene	C ₃ H ₆	2.1	53
Cyclopropane	C ₃ H ₆	2.5	60
Diethyl ether	C ₄ H ₁₀ O	2.0	82
Divinyl ether	C ₄ H ₆ O	1.8	85

*The limits are insensitive to p_{H_2O} above a few millimeters of mercury.

Data from B. Lewis and G. von Elbe, *Combustion, Flames and Explosions of Gases* (New York: Harcourt Brace Jovanovich, 1987).

enough to remain suspended in air for prolonged periods. Mists are suspended liquid droplets produced by condensation of vapor into liquid or by the breaking up of liquid into a dispersed state by splashing, spraying, or atomizing.

For liquid droplets with diameters less than 0.01 mm, the LFL is virtually the same as the substance in vapor form. For mechanically formed mists with drop diameters between 0.001 and 0.2 mm, the LFL decreases as the drop diameter increases. In experiments with larger drop diameters the LFL was less than one-tenth of the vapor LFL. Thus, suspended droplets have a profound effect on flammability.

Explosions

Introduction Gas explosions depend on a large number of parameters, including temperature, pressure, gas composition, ignition source, geometry of surroundings, turbulence in the gas, mixing, time before ignition, and so forth. Thus, gas explosions are difficult to characterize and predict.

An explosion occurs when energy is released into the gas phase in a very short time, typically milliseconds or less. If the energy is released into the gas phase, the energy causes the gases to expand very rapidly, forcing back the surrounding gas and initiating a pressure wave that moves rapidly outward from the blast origin. The pressure wave contains energy which causes damage to the surroundings. A prediction of the damage effects from an explosion requires a clear understanding of how this pressure wave behaves.

TABLE 23-3 Ignition Sources of Major Fires*

Electrical (wiring of motors)	23%
Smoking	18
Friction (bearings or broken parts)	10
Overheated materials (abnormally high temperatures)	8
Hot surfaces (heat from boilers, lamps, etc.)	7
Burner flames (improper use of torches, etc.)	7
Combustion sparks (sparks and embers)	5
Spontaneous ignition (rubbish, etc.)	4
Cutting and welding (sparks, arcs, heat, etc.)	4
Exposure (fires jumping into new areas)	3
Incendiarism (fires maliciously set)	3
Mechanical sparks (grinders, crushers, etc.)	2
Molten substances (hot spills)	2
Chemical action (processes not in control)	1
Static sparks (release of accumulated energy)	1
Lightning (where lightning rods are not used)	1
Miscellaneous	1

**Accident Prevention Manual for Industrial Operations* (Chicago: National Safety Council, 1974).

TABLE 23-4 Minimum Ignition Energy (MIE) for Selected Gases

Chemical	Minimum ignition energy, mJ
Acetylene	0.020
Benzene	0.225
1,3-Butadiene	0.125
<i>n</i> -Butane	0.260
Cyclohexane	0.223
Cyclopropane	0.180
Ethane	0.240
Ethene	0.124
Ethylacetate	0.480
Ethylene oxide	0.062
<i>n</i> -Heptane	0.240
Hexane	0.248
Hydrogen	0.018
Methane	0.280
Methanol	0.140
Methyl acetylene	0.120
Methyl ethyl ketone	0.280
<i>n</i> -Pentane	0.220
2-Pentane	0.180
Propane	0.250

Data from I. Glassman, *Combustion*, 3d ed. (New York: Academic Press, 1996).

Detonation and Deflagration The difference between a detonation and deflagration depends on how fast the pressure wave moves out from the blast origin. If the pressure wave moves at a speed less than the speed of sound in the ambient gas, then a deflagration results. If the pressure wave moves at a speed greater than the speed of sound in the ambient gas, then a detonation results.

For ideal gases, the speed of sound is a function of temperature and molecular weight only. For air at 20°C the speed of sound is 344 m/s (1129 ft/s).

For a detonation, the reaction front moves faster than the speed of sound, pushing the pressure wave or shock front immediately ahead of it. For a deflagration, the reaction front moves at a speed less than the speed of sound, resulting in a pressure wave that moves at the speed of sound, moving away from the reaction front. A noticeable difference is found in the resulting pressure-time or pressure-distance plots.

The difference in behavior between a detonation and deflagration results in a significant difference in the damage. For a detonation, the damage is usually localized. However, for a deflagration, the damage is more widespread.

For high explosives, such as TNT, detonations are the normal result. However, for flammable vapors, deflagrations are more common.

Confined Explosions A confined explosion occurs in a building or process. Empirical studies on deflagrations (Tang and Baker, "A New Set of Blast Curves from Vapor Cloud Explosions," 33d Loss Prevention Symposium, AIChE, 1999; Mercx, van Wees, and Opschoor, "Current Research at TNO on Vapour Cloud Explosion Modeling," *Plant/Operations Progress*, October 1993) have shown that the behavior of the explosion is highly dependent on the degree of confinement. Confinement may be due to process equipment, buildings, storage vessels, and anything else that impedes the expansion of the reaction front.

These studies have found that increased confinement leads to flame acceleration and increased damage. The flame acceleration is caused by increased turbulence which stretches and tears the flame front, resulting in a larger flame front surface and an increased combustion rate. The turbulence is caused by two phenomena. First, the unburned gases are pushed and accelerated by the combustion products behind the reaction front. Second, turbulence is caused by the interaction of the gases with obstacles. The increased combustion rate results in additional turbulence and additional acceleration, providing a feedback mechanism for even more turbulence.

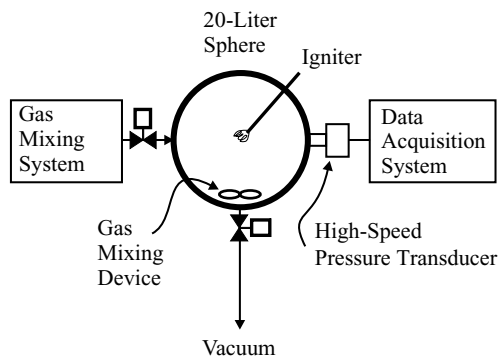


FIG. 23-7 An apparatus for collecting explosion data for gases and vapors. [D. A. Crowl, *Understanding Explosions*, Center for Chemical Process Safety (CCPS) of the American Institute of Chemical Engineers (AIChE); copyright 2003 AIChE and reproduced with permission.]

Characterizing Explosive Behavior for Vapors and Dusts

Figure 23-7 is a schematic of a device used to characterize explosive vapors. This vessel is typically 3 to 20 L. It includes a gas handling and mixing system (not shown), an igniter to initiate the combustion, and a high-speed pressure transducer capable of measuring the pressure changes at the millisecond level.

The igniter can be of several types, including a fuse wire, spark, or chemical ignition system. A typical energy for ignition is 10 J, although gases can be ignited at much lower levels.

The gas is metered into the chamber to provide a mixture of a known composition. At a specified time the igniter is activated, and data are collected from the pressure transducer.

A typical pressure time plot is shown in Fig. 23-8. After ignition, the pressure increases rapidly, reaches a peak, and then diminishes as the reaction products are consumed and the gases are quenched and cooled by the vessel wall.

The experiment is repeated over a range of concentrations. A plot of the maximum pressure versus fuel concentration is used to determine the flammability limits, as shown in Fig. 23-9. A pressure increase of 7 percent over initial ambient pressure is used to define

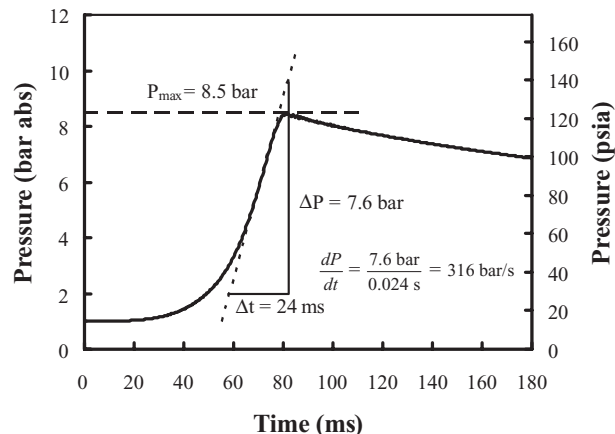


FIG. 23-8 Typical pressure versus time data obtained from gas explosion apparatus shown in Fig. 23-9. [Daniel A. Crowl and Joseph F. Louvar, *Chemical Process Safety: Fundamentals with Applications*, 2d ed., © 2002. Adapted by permission of Pearson Education, Inc., Upper Saddle River, N.J.]

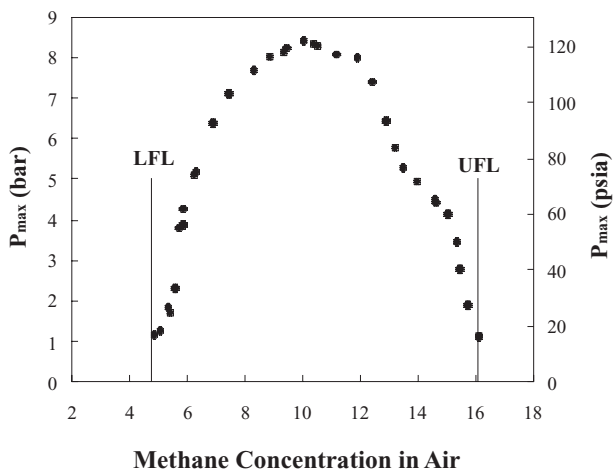


FIG. 23-9 Maximum pressure as a function of volume percent concentration for methane in air in a 20-L test sphere. The initial temperature and pressure are 25°C and 1 atm. The stoichiometric concentration is 9.51% methane. [C. V. Mashuga and D. A. Crowl, "Application of the Flammability Diagram for Evaluation of Fire and Explosion Hazards of Flammable Vapors," *Process Safety Progress*, vol. 17, no. 3; copyright 1998 American Institute of Chemical Engineers (AIChE) and reproduced with permission.]

the flammability limits (ASTM E918, *Standard Procedure for Determining Flammability Limits at Elevated Temperature and Pressure*, American Society for Testing and Materials, Philadelphia, 1992).

Figure 23-10 shows a device used to characterize the combustion of dusts. In this case, the dusts are initially contained in a small carrier external to the vessel, and the dust is blown in just prior to ignition. A typical pressure-time curve for the dust apparatus is shown in Fig. 23-11. The vessel is initially at a pressure less than atmospheric, but the pressure increases to atmospheric after the dust sample is blown in. After the dust is blown in, a delay time occurs in order for the dust to become quiescent but still suspended in the gas. The results are highly dependent on the delay time.

Two parameters are used to characterize the combustion for both the vapor and dust cases. The first is the maximum pressure during the combustion process, and the second is the maximum rate of

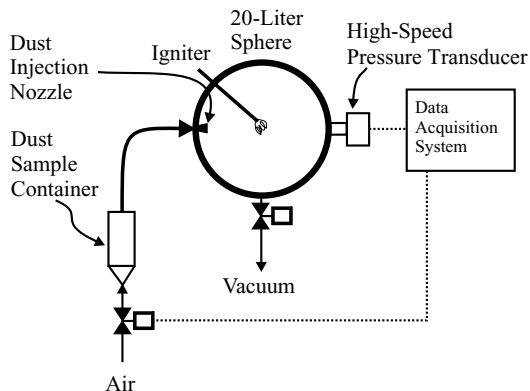


FIG. 23-10 An apparatus for collecting explosion data for dusts. [D. A. Crowl, *Understanding Explosions*, Center for Chemical Process Safety (CCPS) of the American Institute of Chemical Engineers (AIChE); copyright 2003 AIChE and reproduced with permission.]

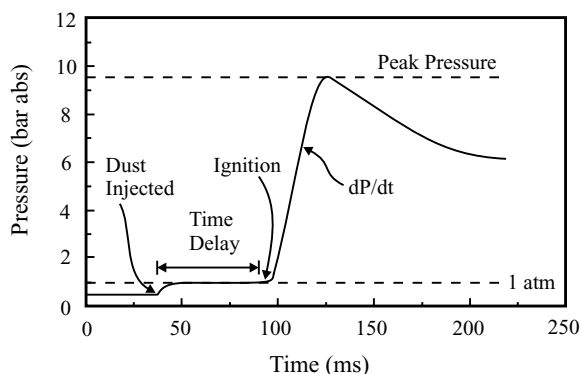


FIG. 23-11 Pressure data from dust explosion device. (Daniel A. Crowl and Joseph F. Louvar, *Chemical Process Safety: Fundamentals with Applications*, 2d ed., © 2002. Adapted by permission of Pearson Education, Inc., Upper Saddle River, N.J.)

pressure increase. Empirical studies have shown that a deflagration index can be computed from the maximum rate of pressure increase:

$$K_G \text{ or } K_{St} = \left(\frac{dP}{dt} \right)_{\max} V^{1/3} \quad (23-10)$$

where K_G = deflagration index for gases (bar·m/s)

K_{St} = deflagration index for dusts (bar·m/s)

P = pressure (bar)

t = time (s)

V = is the vessel volume (m^3)

The higher the value of the deflagration index, the more robust the combustion. Table 23-5 contains combustion data for gases while Table 23-6 contains combustion data for dusts.

Vapor Cloud Explosions A vapor cloud explosion (VCE) occurs when a large quantity of flammable material is released, is mixed with enough air to form a flammable mixture, and is ignited. Damage from a VCE is due mostly to the overpressure, but significant damage to equipment and personnel may occur due to thermal radiation from the resulting fireball.

A VCE requires several conditions to occur (*Estimating the Flammable Mass of a Vapor Cloud*, American Institute of Chemical Engineers, New York, 1999):

1. The released material must be flammable.
2. A cloud of sufficient size must form prior to ignition.
3. The released material must mix with an adequate quantity of air to produce a sufficient mass in the flammable range.
4. The speed of the flame propagation must accelerate as the vapor cloud burns. This acceleration can be due to turbulence, as discussed in the section on confined explosions. Without this acceleration, only a flash fire will result.

Most VCEs involving flammable liquids or gases result only in a deflagration—detonations are unlikely. As the confinement of the vapor cloud increases, due to congestion from process equipment, the flame accelerates and higher overpressures are achieved. The higher overpressures may approach the severity of a detonation.

Four methods are available to estimate the damage from a VCE: TNT equivalency, TNO Multi-Energy method, Baker-Strehlow-Tang method, and computational fluid dynamics. The TNT equivalency method is discussed in the Estimation of Damage Effects section. The other methods are discussed elsewhere (*Guidelines for Evaluating the Characteristics of Vapor Cloud Explosions, Flash Fires and BLEVES*, American Institute of Chemical Engineers, New York, 1994; *Guidelines for Chemical Process Quantitative Risk Analysis*, 2d ed., American Institute of Chemical Engineers, 2000).

Boiling-Liquid Expanding-Vapor Explosions A boiling-liquid expanding-vapor explosion, commonly called a BLEVE (pronounced ble-vee), occurs when a vessel containing a liquid stored at a temperature above its normal boiling point fails catastrophically. After failure, a fraction of the liquid flashes almost instantaneously into vapor. Damage may be caused, in part, by the rapid expansion of the vapor and fragments from the failing vessel. The liquid may be water.

TABLE 23-5 Maximum Pressures and Deflagration Indices for a Number of Gases and Vapors

Chemical	Maximum pressure P_{\max} , barg			Deflagration index K_G , bar·m/s		
	NFPA 68 1997	Bartknecht 1993	Senecal 1998	NFPA 68 1997	Bartknecht 1993	Senecal 1998
Acetylene	10.6			109		
Ammonia	5.4			10		
Butane	8.0	8.0		92	92	
Carbon disulfide	6.4			105		
Diethyl ether	8.1			115		
Ethane	7.8	7.8	7.4	106	106	78
Ethyl alcohol	7.0			78		
Ethyl benzene	6.6	7.4		94	96	
Ethylene			8.0			171
Hydrogen	6.9	6.8	6.5	659	550	638
Hydrogen sulfide	7.4			45		
Isobutane			7.4			67
Methane	7.05	7.1	6.7	64	55	46
Methyl alcohol		7.5	7.2		75	94
Methylene chloride	5.0			5		
Pentane	7.65	7.8		104	104	
Propane	7.9	7.9	7.2	96	100	76
Toluene		7.8			94	

Data selected from:

NFPA 68: *Venting of Deflagrations* (Quincy, Mass.: National Fire Protection Association, 1997).

W. Bartknecht, *Explosionsschutz: Grundlagen und Anwendung* (New York: Springer-Verlag, 1993).

J. A. Senecal and P. A. Beaulieu, "K_G: Data and Analysis," *31st Loss Prevention Symposium* (New York: American Institute of Chemical Engineers, 1997).

TABLE 23-6 Combustion Data for Dust Clouds*

Dust	Median particle size, μm	Minimum explosive dust conc., g/m^3	P_{max} , barg	K_{St} , bar·m/s	Minimum ignition energy, mJ
<i>Cotton, Wood, Peat</i>					
Cotton	44	100	7.2	24	—
Cellulose	51	60	9.3	66	250
Wood dust	33	—	—	—	100
Wood dust	80	—	—	—	7
Paper dust	<10	—	5.7	18	—
<i>Feed, Food</i>					
Dextrose	80	60	4.3	18	—
Fructose	200	125	6.4	27	180
Fructose	400	—	—	—	>4000
Wheat grain dust	80	60	9.3	112	—
Milk powder	165	60	8.1	90	75
Rice flour	—	60	7.4	57	>100
Wheat flour	50	—	—	—	540
Milk sugar	10	60	8.3	75	14
<i>Coal, Coal Products</i>					
Activated carbon	18	60	8.8	44	—
Bituminous coal	<10	—	9.0	55	—
<i>Plastics, Resins, Rubber</i>					
Polyacrylamide	10	250	5.9	12	—
Polyester	<10	—	10.1	194	—
Polyethylene	72	—	7.5	67	—
Polyethylene	280	—	6.2	20	—
Polypropylene	25	30	8.4	101	—
Polypropylene	162	200	7.7	38	—
Polystyrene (copolymer)	155	30	8.4	110	—
Polystyrene (hard foam)	760	—	8.4	23	—
Polyurethane	3	<30	7.8	156	—
<i>Intermediate Products, Auxiliary Materials</i>					
Adipinic acid	<10	60	8.0	97	—
Naphthalene	95	15	8.5	178	<1
Salicylic acid	—	30	—	—	—
<i>Other Technical, Chemical Products</i>					
Organic dyestuff (blue)	<10	—	9.0	73	—
Organic dyestuff (red)	<10	50	11.2	249	—
Organic dyestuff (red)	52	60	9.8	237	—
<i>Metals, Alloys</i>					
Aluminum powder	<10	60	11.2	515	—
Aluminum powder	22	30	11.5	110	—
Bronze powder	18	750	4.1	31	—
Iron (from dry filter)	12	500	5.2	50	—
Magnesium	28	30	17.5	508	—
Magnesium	240	500	7.0	12	—
Silicon	<10	125	10.2	126	54
Zinc (dust from collector)	<10	250	6.7	125	—
<i>Other Inorganic Products</i>					
Graphite (99.5% C)	7	<30	5.9	71	—
Sulfur	20	30	6.8	151	—
Toner	<10	60	8.9	196	4

St Classes for Dusts

Deflagration index K_{St} , bar·m/s	St class
0	St-0
1–200	St-1
200–300	St-2
>300	St-3

*Data selected from R. K. Eckoff, *Dust Explosions in the Process Industries* (Oxford, England: Butterworth-Heinemann, 1997).

The most damaging BLEVE occurs when a vessel contains a flammable liquid stored at a temperature above its normal boiling point. The vessel walls below the liquid level are maintained at a low temperature due to the rapid heat transfer to the liquid. However, the vessel walls exposed to the fire above the liquid level will heat rapidly due to the much lower heat transfer to the vapor. The vessel wall temperature

will increase to a point where the strength of the vessel wall is significantly reduced. The vessel wall will fail catastrophically, resulting in the flashing of a large quantity of flammable liquid into vapor. Since a fire is already present, the resulting vapor cloud will ignite almost immediately. Overpressures from the vessel failure may result, but most of the damage is caused by radiation from the resulting large fireball.

Dust Explosions

Nomenclature

A	Area of a vent opening, m^2
A_w	Effective vent area, m^2
A_k	Geometric vent area, m^2
$(dP/dt)_{\max}$	Maximum rate of pressure rise, $\text{bar}\cdot\text{s}^{-1}$
K_{\max}	Maximum explosion constant, $\text{m}\cdot\text{bar}\cdot\text{s}^{-1}$
K_{\min}	Minimum explosion constant, $\text{m}\cdot\text{bar}\cdot\text{s}^{-1}$
ℓ	Length of a pipe, m
L_D	Length of vent duct, m
L_{DS}	Maximum length of vent duct, m
L_F	Flame length, m
P_a	Activation overpressure, bar
P_{ext}	Maximum external peak of overpressure, bar
P_{\max}	Maximum explosion overpressure, bar
P_{red}	Reduced explosion overpressure, bar
$P_{\text{red,max}}$	Maximum reduced explosion overpressure, bar
P_{stat}	Static activation overpressure, bar
R	Distance to vent area, m
T_{\max}	Maximum permissible surface temperature, $^{\circ}\text{C}$
V	Vessel volume, m^3
v_c	Relative circumferential speed, $\text{m}\cdot\text{s}^{-1}$
W_F	Width of flame, m
α	Angle between the horizontal and vertical axes of vent area, deg

GENERAL REFERENCES: Bartknecht, *Dust Explosions*, Springer, New York, 1989. Bartknecht, *Explosionsschutz* (Explosion Protection), Springer, Berlin, 1993. Crowl and Louvar, *Chemical Process Safety*, Prentice-Hall, New Jersey, 1990. "Dust Explosions," 28th Annual Loss Prevention Symposium, Atlanta, 1994. Eckhoff, *Dust Explosions in the Process Industries*, 2d ed., Butterworth-Heinemann, London, 1997. Health, Safety and Loss Prevention in the Oil, Chemical and Process Industries, Butterworth/Heinemann, Singapore, 1993. NFPA 69, *Standard on Explosion Prevention Systems*, Quincy, Mass., 1997. Hattwig and Steen, eds., *Handbook of Explosion Prevention and Protection*, Wiley-Vch Verlag GmbH & Co. KGaA, Weinheim, 2004. VDI-Report 1601, *Safe Handling of Combustible Dust*, VDI-Verlag GmbH, Düsseldorf, 2001. VDI-Guideline 2263, *Dust Fires and Dust Explosions*, Beuth Verlag, Berlin, 1992. European Standard EN 1127-1, *Explosives atmospheres: Explosion prevention and protection*, Pt. 1: *Basic Concepts and Methodology*, 1997.

Definition of Dust Explosion A dust explosion is the rapid combustion of a dust cloud. In a confined or nearly confined space, the explosion is characterized by relatively rapid development of pressure with flame propagation and the evolution of large quantities of heat and reaction products. The required oxygen for this combustion is mostly supplied by the combustion air. The condition necessary for a dust explosion is a simultaneous presence of a dust cloud of proper concentration in air that will support combustion and a suitable ignition source.

Explosions are either deflagrations or detonations. The difference depends on the speed of the shock wave emanating from the explosion. If the pressure wave moves at a speed less than or equal to the speed of sound in the unreacted medium, it is a deflagration; if it moves faster than the speed of sound, the explosion is a detonation.

The term *dust* is used if the maximum particle size of the solids mixture is below 500 μm .

In the following, dusts are called combustible in the airborne state only if they require oxygen from the air for exothermic reaction.

Glossary

Activation overpressure P_a That pressure threshold, above the pressure at ignition of the reactants, at which a firing signal is applied to the suppressor(s).

Cubic law The correlation of the vessel volume with the maximum rate of pressure rise. $V^{1/3} \cdot (dP/dt)_{\max} = \text{constant} = K_{\max}$.

Dust explosions class, St Dusts are classified in accordance with the K_{\max} values.

Explosion Propagation of a flame in a premixture of combustible gases, suspended dust(s), combustible vapor(s), mist(s), or mixtures thereof, in a gaseous oxidant such as air, in a closed or substantially closed vessel.

Explosion pressure resistant (EPR) Design of a construction following the calculation and construction directions for pressure vessels.

Explosion pressure-shock resistant (EPSR) Design of a construction allowing greater utilization of the material strength than the EPR design.

Maximum reduced explosion overpressure $P_{\text{red,max}}$ The maximum pressure generated by an explosion of a dust-air mixture in a vented or suppressed vessel under systematically varied dust concentrations.

Minimum ignition energy (MIE) Lowest electrical energy stored in a capacitor which, upon discharge, is just sufficient to effect ignition of the most ignitable atmosphere under specified test conditions.

Minimum ignition temperature of a dust cloud (MIT_C) The lowest temperature of a hot surface on which the most ignitable mixture of the dust with air is ignited under specified test conditions.

Minimum ignition temperature of a dust layer (MIT_L) The lowest temperature of a hot surface on which a dust layer is ignited under specified test conditions.

Static activation overpressure P_{stat} Pressure at which the retaining element breaks or releases such that the venting element is able to open when the rate of pressure rise is ≤ 0.1 bar/min .

Vent area A Area of an opening for explosion venting.

Venting efficiency EF Ratio of the effective vent area A_w to the geometric vent area A_k .

Venting element That part of vent area device that covers the vent area and opens under explosion conditions.

Vessel length-to-diameter ratio (L/D) The ratio of the longest linear dimension L (length, height) of a round vessel to its geometric or equivalent diameter D .

Prevention and Protection Concept against Dust Explosions

Explosion protection encompasses the measures implemented against explosion hazards in the handling of combustible substances and the assessment of the effectiveness of protective measures for the avoidance or dependable reduction of these hazards. The explosion protection concept is valid for all mixtures of combustible substances and distinguishes between

1. Measures that prevent or restrict formation of a hazardous explosive atmosphere
2. Measures that prevent the ignition of a hazardous, explosive atmosphere
3. Constructional measures that limit the effects of an explosion to a harmless level

From a safety standpoint, priority must be given to the measures in item 1. Item 2 cannot be used as a sole protective measure for flammable gas or solvent vapors in industrial practice with sufficient reliability, but can be applied as the sole protective measure when only combustible dusts are present if the minimum ignition energy of the dusts is high (≥ 10 mJ) and the operating area concerned can easily be monitored.

If the measures under items 1 and 2, which are also known as preventive measures, cannot be used with sufficient reliability, the constructional measures must be applied.

In practice, in most cases it is sufficient to determine and judge systematically the explosion risk with a sequence of specific questions, shown in Fig. 23-12.

During the evaluation it is assumed that ignition of an existing combustible atmosphere is always possible. The assessment is thus independent of the question of whether ignition sources are present.

Preventive Explosion Protection The principle of preventive explosion protection comprises the reliable exclusion of one of the requirements necessary for the development of an explosion. An explosion can thus be excluded with certainty by

- Avoiding the development of explosive mixtures
- Replacing the atmospheric oxygen by *inert gas*, working in a vacuum, or using *inert dust*
- Preventing the occurrence of effective ignition sources

Avoidance or Reduction of Explosive Combustible Fuel-Air Mixtures

Flammable gas or vapor-air mixtures This can be achieved if the flammable substance can be replaced by a nonflammable substance or the concentration of flammable substance can be kept so low that the gas or vapor-air mixture is too lean for an explosion.

The development of a hazardous atmosphere can also be prevented by ventilation measures. A distinction is made here between *natural* ventilation, which is usually sufficient only in the open air, and *artificial*

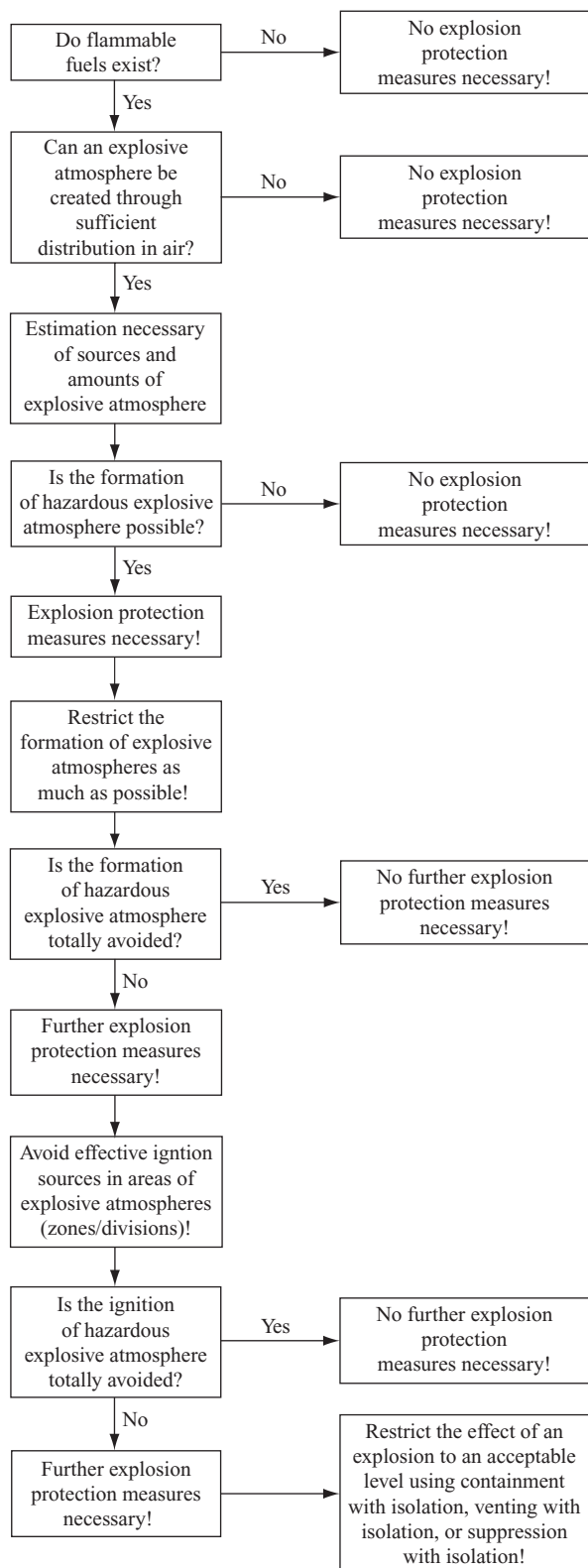


FIG. 23-12 Evaluation flowchart for preventing and/or limiting explosions.

ventilation (IEC 60079-10, "Electrical Apparatus for Explosive Atmospheres. Part 10: Classification of Hazardous Areas"). *Artificial* ventilation permits the use of greater amounts of air and the selective circulation of air in areas surrounding the equipment. Its use and the calculation of the minimum volume flow rate for the supply and exhaust air are subject to certain requirements.

The use of *gas alarm devices* in connection with, e.g., ventilation measures is also possible. The factors influencing the decision regarding setting of the required gas detectors include the relative density of the flammable gases and vapors. With gases and vapors that are heavier than air, the sensors and the waste air openings should be installed near the floor, with those that are lighter than air near the ceiling.

Combustible dust-air mixtures These mixtures can be avoided or restricted if the combustible dust can be replaced by a noncombustible dust or the dust concentration can be kept so low that an explosive dust-air mixture is never actually formed.

The explosibility limits do not have the same meaning as with flammable gases and flammable vapors, owing to the interaction between dust layers and suspended dust. This protective measure can, e.g., be used when dust deposits are avoided in operating areas or in the airstream of clean air lines after filter installation, where in normal operation the lower explosion limit (LEL) is not reached. However, dust deposits must be anticipated with time. When these dust deposits are whirled up in the air, an explosion hazard can arise. Such a hazard can be avoided by regular cleaning. The dust can be extracted directly at its point of origin by suitable ventilation measures.

Avoidance of Explosions through Inerting The introduction of inert gas in the area to be protected against explosions lowers the oxygen volume content below the limiting oxygen concentration (LOC) so that ignition of the mixture can no longer take place. This process is called *inerting* (CEN/TR 15281, "Guidance on Inerting for the Prevention of Explosions").

One has to be aware of the danger of asphyxiation from gases in inerted equipment. This is also important for surrounding areas in case of major leaks.

Inerting is not a protective measure to avoid exothermic decomposition. For the avoidance of (smoldering) fires, oxygen concentrations lower than the LOC must usually be adhered to and must be determined from case to case. In addition to the nitrogen normally used, all nonflammable gases which do not support combustion or react with the combustible dust can be considered for use as the inert gas. The inerting effect generally decreases in the following order: carbon dioxide → water vapor → flue gas → nitrogen → noble gases. In special cases, liquid nitrogen or dry ice is used.

The LOC depends upon the combustible material and the type of inert gas used. It decreases with increased temperature and pressure. A distinction has to be made between the determined LOC value and the concentration which results by subtracting a safety margin.

The maximum allowable oxygen concentration (MAOC), which is, in general, 2 vol % below the LOC, has to include the following considerations: Fluctuation in oxygen concentrations due to process and breakdown conditions per time and location, as well as the requirement for protective measures or emergency measures to become effective. In addition, a concentration level for an alarm has to be set below the MAOC.

Explosive dusts can also be changed into mixtures which are no longer explosive by the addition of inert dusts (e.g., rock salt, sodium sulfate). In general, inert dust additions of more than 50 wt % are necessary here. It is also possible to replace flammable solvents and cleaning agents by nonflammable halogenated hydrocarbons or water, or flammable pressure transmission fluids by halocarbon oils.

Avoidance of Effective Ignition Sources Explosions can be prevented if ignition sources capable of igniting combustible material-air mixtures can successfully be avoided. A distinction is made between trivial ignition sources (e.g., welding, smoking, cutting) and mechanically generated spark, mechanically generated hot surfaces, lumps of smoldering material, and static electricity. Trivial ignition sources can also reliably be excluded by organizational measures such as the systematic employment of permits. This measure should always be employed, even when constructional measures are applied, unless the explosive atmosphere is avoided with certainty.

TABLE 23-7 Zone Classification versus Minimum Extent of Preventive Measures against Danger of Ignition

Explosion hazard zone	Avoid ignition sources which can occur:
20/0	During normal operation, during frequent malfunction, and during rare malfunction
21/1	During normal operation and during frequent malfunction
22/2	During normal operation

Hazardous places are classified in terms of zones (divisions) on the basis of the frequency and duration of the occurrence of an explosive atmosphere (IEC 60079-10:200X, "Classification of Hazardous Areas"; European Standard EN 50281-3:200X, "Classification of Areas Where Combustible Dusts Are or May Be Present").

Fundamentally all 13 kinds of ignition sources mentioned and also described in detail in EN 1127-1 must be considered. In EN 1127-1, the descriptions refer to both the ignition mechanisms of the different kinds of ignition source and the necessary scope of protection (material- and zone-dependent). The ignition sources should be classified according to the likelihood of their occurrence in the following manner:

1. Sources of ignition which can occur *continuously or frequently*
2. Sources of ignition which can occur in *rare* situations
3. Sources of ignition which can occur in *very rare* situations

In terms of the equipment, protective systems, and components used, this classification must be considered equivalent to

1. Sources of ignition which can occur during *normal operation*
2. Sources of ignition which can occur solely as a result of *malfunctions*

3. Sources of ignition which can occur solely as a result of *rare malfunctions*

Ignition sources at devices, protective systems, and components must be avoided, depending on zones (Table 23-7); i.e., the zone determines the minimum extent of preventive measures against danger of ignition.

Flammable gas or vapor-air mixtures Due to their low minimum ignition energies (<1 mJ), avoidance of effective ignition sources in flammable gas or vapor-air mixtures is in principle possible only in exceptional cases. For *hot surfaces* a maximum permissible surface temperature T_{\max} must be specified, with the help of the minimum ignition temperature (MIT) of flammable gases, vapors, or liquids, so that the temperature of all surfaces is not exceeded (Table 23-8).

Combustible dust-air mixtures For every installation a check has to be made to determine which ignition source may become effective and whether it can be prevented with a sufficient degree of safety. With more sensitive products and complex installations, it becomes more and more difficult to exclude ignition sources with ample safety.

With dusts the avoidance of effective ignition sources depends on the ignition sensitivity, i.e., on the temperature-related minimum ignition energy (MIE). Because a low MIE means that both the number of effective ignition sources rises and the probability of the release of an ignition of a dust-air mixture rises. Safe handling of particularly or extremely ignition-sensitive dusts requires in general increased use of preventive measures in comparison to normally ignitable sensitive dusts.

It is therefore usual to combine the evaluation of the ignition sensitivity (MIE) of the dusts with the type and extent of protective measures in accordance with Table 23-9.

TABLE 23-8 Measures against Ignition of Flammable Gas, Vapors, and Liquids by Hot Surfaces

Zone	Protection by limiting the hot surface temperature (EN 1127-1)
0	$T_{\max} \leq 0.8 \text{ MIT}$
1	$T_{\max} \leq 0.8 \text{ MIT}$
2	$T_{\max} \leq \text{MIT}$

TABLE 23-9 Ignition Sensitivity of Dusts as a Function of Protective Measures

Ignition sensitivity of dusts	Protective measures
Normally sensitive (MIE ≥ 10 mJ)	Avoidance of effective ignition sources.
Easily sensitive (3 mJ \leq MIE < 10 mJ)	Expert decision or Avoidance of effective ignition sources and additional protective measures.
Extremely sensitive (MIE < 3 mJ)	Avoidance of effective ignition sources and additional protective measures.

Protective measures: Inerting or constructional explosion protection (e.g., containment).

For hot surfaces a maximum permissible surface temperature T_{\max} must be specified, with the help of the minimum ignition temperature of a dust cloud MIT_C and the minimum ignition temperature of a dust layer MIT_L (usually 5-mm dust layer = glow temperature), so that the temperature of all surfaces is not exceeded. Independent of the zone the T_{\max} for dust clouds is $\frac{2}{3} \text{MIT}_C$ and for dust layers $\text{MIT}_L - 75 \text{ K}$.

Mechanically generated sparks and resultant *hot surfaces* together are regarded as one of the more important causes of ignition in industrial practice. The hot surfaces show considerably better incendiarity in comparison with the short-lived, mechanically generated sparks. Neither ignition source appears in industrial practice from the normal metallic materials of construction rubbing against each other or against stone if the relative circumferential speeds v_c are less than or equal to 1 m/s and the power requirement is no more than 4 kW (Table 23-10). This is not valid for cerium-iron, titanium, and zirconium.

Regarding *electrostatic ignition sources*, see the subsection "Static Electricity," later. In addition, see CENELEC CLC/TR 50404, "Electrostatics—Code of Practice for the Avoidance of Hazards due to Static Electricity," June 2003.

Explosion Protection through Design Measures Design measures which restrict the effects of an explosion to a safe level are always necessary when the goal of avoiding explosions cannot be achieved—or at least not with sufficient reliability—through the use of preventive explosion protection. This ensures that people are not injured and further that the protected equipment is usually ready for operation a short time after an explosion. In applying design measures, the possibility of an explosion is not prevented. Therefore, all exposed equipment has to be built to be explosion-pressure-resistant in order to withstand the anticipated explosion pressure. The anticipated explosion pressure may be the maximum explosion overpressure or the maximum reduced explosion overpressure. In addition, *any propagation of an explosion to other parts or process areas has to be prevented*. Depending on the anticipated explosion pressure, a distinction is made between the following explosion-pressure-resistant designs:

- Those capable of withstanding the maximum explosion overpressure
- Those capable of withstanding an explosion overpressure reduced by explosion suppression or explosion venting

The strength of the protected vessels or apparatus may be either explosion-pressure-resistant or explosion pressure shock-resistant.

Containment Containment is understood to mean the possibility of designing vessels and equipment for the full *maximum explosion overpressure*, which is generally from $P_{\max} = 7$ to 10 bar. The explosion-resistant vessel can then be designed as explosion-pressure-resistant or

TABLE 23-10 Influence of Relative Circumferential Speed v_c on Danger of Ignition for Combustible Dusts

$*v_c \leq 1$ m/s	There is no danger of ignition.
$v_c > 1$ –10 m/s	Every case has to be judged separately, considering the product and material-specific characteristics.
$v_c > 10$ m/s	In every case there is danger of ignition.

* In addition, low power requirements $W \leq 4 \text{ kW}$.

TABLE 23-11 Explosion Venting System Design Parameters

Explosion hazard definition	Venting system definition
Volume of vessel (free volume)	Type of venting device
Shape of vessel (cubic or elongated vessel)	Detection method for triggering a shutdown
Length-to-diameter ratio of vessel	Static activation overpressure P_{stat} of venting device
Strength of vessel	Venting capability of venting device
Type of dust cloud distribution (ISO method/pneumatic-loading method)	Location of venting device on the vessel
Dust explosibility characteristics:	Position of equipment to be protected in the building
maximum explosion overpressure P_{max}	Length and shape of relief pipe if existent
maximum explosion constant K_{max}	Recoil force during venting
toxicity of the product	Duration of recoil force
Maximum flame length	Total transferred impulse
Pressure outside the vent areas	

explosion pressure shock-resistant. This protective measure is generally employed when small vessel volumes need to be protected, such as small filter units, fluidized-bed dryers, cyclones, rotary vales, or mill housings.

One has to consider that all connected devices must also withstand the maximum explosion overpressure. The NFPA 69 Standard, *Explosion Prevention System*, 1997; European Standard prEN 14460, *Explosion Resistant Equipment*, 2005; and Kirby and Siwek, "Preventing Failures of Equipment Subject to Explosions," *Chemical Engineering*, June 23, 1986, provide excellent guidance on the practice of containment.

Explosion venting The concept of explosion venting encompasses all measures used to open the originally closed vessels and equipment either briefly or permanently in a nonhazardous direction following an explosion. *Explosion venting is inadmissible when the escape of toxic or corrosive, irritating, carcinogenic, harmful-to-fruit, or genetically damaging substances* is anticipated. In contrast to containment, explosions in a vented vessel are characterized by the maximum reduced explosion overpressure $P_{red,max}$ instead of the maximum explosion overpressure P_{max} and by the maximum reduced rate of pressure rise $(dP/dt)_{red,max}$ instead of the maximum rate of pressure rise $(dP/dt)_{max}$.

By this method in general, the expected inherent maximum explosion overpressure on the order of $P_{max} = 7$ to 10 bar will be reduced to a value of $P_{red,max} < 2$ bar. In this case, the static activation overpressure of the venting device is $P_{stat} \leq 0.1$ bar. The resulting $P_{red,max}$ may not exceed the design pressure of the equipment. The explosion as such is not prevented; only the dangerous consequences are limited. However, subsequent fires must be expected.

Among other things, one prerequisite to calculate the pressure relief openings needed on the apparatus is knowledge about the explosion threat definition and venting system hardware definition. The various factors are summarized in Table 23-11.

The inertia, the opening behavior of a bursting disk or of the movable cover of an explosion device, and its arrangement (horizontal, vertical) can affect the venting efficiency and may result in a higher maximum reduced explosion overpressure inside the protected vessel (Fig. 23-13). This venting efficiency is mainly dependent upon the specific mass of the venting device.

If the specific mass of a venting device is $< 0.5 \text{ kg/m}^2$, then it has a venting efficiency of $EF = 1$ and is called inertia-free and does not impede the venting process" (European Standard prEN 14797-2006, "Explosion Venting Devices"). For such explosion venting devices EF testing is therefore not required. Explosion venting devices with venting elements with a specific mass $> 0.5 \text{ kg/m}^2$ can influence the venting process by their opening and release behavior. Experiments have shown that explosion venting devices with a specific mass $> 0.5 \text{ kg/m}^2$ and $\leq 10 \text{ kg/m}^2$ can be considered as inertia-free, which means having a venting efficiency $EF = 1$ provided that

$$\frac{A}{V} < 0.07 \quad (23-11)$$

The equations are only valid for

- Vessel volumes of $0.1 \text{ m}^3 \leq V \leq 10,000 \text{ m}^3$
- Static activation overpressure of venting device $P_{stat} \leq 0.1$ bar

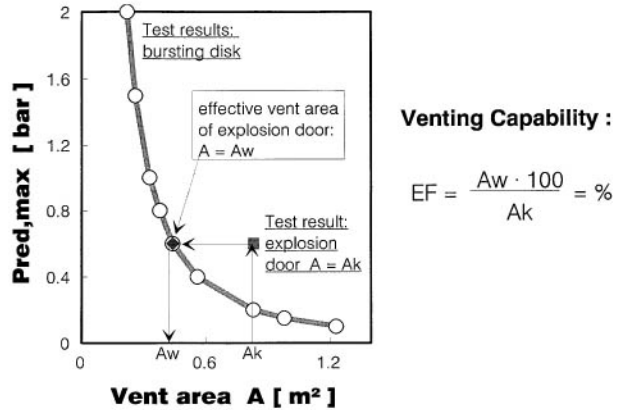


FIG. 23-13 Definition of the venting capability EF of an explosion door in comparison with a plastic foil rupture disk.

- Vessel strength ($= P_{red,max}$) of $0.1 \text{ bar} < P \leq 2 \text{ bar}$
- $P_{red,max} > P_{stat}$

For all other conditions EF has to be determined by tests (Fig. 23-13). EF and therefore the effective vent area A_w of a non-inertia-free explosion device are smaller than the venting efficiency of an inertia-free vent device (specific mass $< 0.5 \text{ kg/m}^2$) with the same vent area. Therefore, such devices need testing to determine the mechanical strength before actual use, and the EF or the pressure rise, respectively, has to be chosen relative to the $P_{red,max}$ of the rupture disk of the same area.

When explosion doors that close the vent area after the explosion are in use, the cooling of the hot gases of combustion may create a vacuum in the vessel, resulting in its deformation. To prevent this from happening, vacuum breakers have to be provided.

Sizing of vent areas The empirical equation (23-12) can be used to calculate the required vent area for flammable gas or solvent vapor explosions. The equation is valid for flammable gas-air mixtures which have been ignited in a quiescent state (nonturbulent) with an ignition source of $E = 10 \text{ J}$.

$$A = [(0.1265 \log K_{max} - 0.0567) P_{red,max}^{-0.5817} + 0.1754 P_{red,max}^{-0.5722} (P_{stat} - 0.1)] \times V^{2/3} + \frac{[AK_{max}(L/D - 2)^2]}{750} \quad (23-12)$$

The equation is valid for

- Vessel volumes $0.1 \text{ m}^3 \leq V \leq 1000 \text{ m}^3$
- Vessel length-to-diameter ratio $1 \leq L/D \leq 5$
- Static activation overpressure of rupture disk $0.1 \text{ bar} \leq P_{stat} \leq 0.5 \text{ bar}$
- Maximum reduced explosion overpressure $0.1 \text{ bar} \leq P_{red,max} \leq 2 \text{ bar}$
- $P_{red,max} > P_{stat} + 0.05 \text{ bar}$

- Maximum explosion constant $50 \text{ bar}\cdot\text{m/s} \leq K_{\text{max}} \leq 550 \text{ bar}\cdot\text{m/s}$
- Gas-air mixtures ignited at zero turbulence
- Venting efficiency $EF = 1$

If it is necessary to locate equipment with explosion vents inside buildings, vent ducts should be used to direct vented material from the equipment to the outdoors. Vent ducts will significantly increase the pressure development in the equipment during venting. They require at least the same cross section as the vent area and the same design pressure as the protected equipment.

The use of vent ducts results in an increase in $P_{\text{red,max}}$. The maximum reduced explosion overpressure $P'_{\text{red,max}}$ caused by the downstream vent duct can be calculated with Eqs. (23-13) and (23-14).

Length of vent duct = $0 \text{ m} < L_D \leq 3 \text{ m}$:

$$P'_{\text{red,max}} = 1.24P_{\text{red,max}}^{0.8614} \quad (23-13)$$

Length of vent duct = $3 \text{ m} < L_D \leq 6 \text{ m}$:

$$P'_{\text{red,max}} = 2.48P_{\text{red,max}}^{0.5165} \quad (23-14)$$

where $P'_{\text{red,max}}$ = maximum explosion overpressure with vent duct, bar, and $P_{\text{red,max}}$ = maximum explosion overpressure without vent duct, bar.

The following empirical equations, Eqs. (23-15) to (23-17), allow the calculation of the size of a vent area A for combustible dust-air-mixture explosions.

For $P_{\text{red,max}} < 1.5 \text{ bar}$

$$A = B \left(1 + C \log \frac{L}{D} \right) \text{ m}^2 \quad (23-15)$$

For $P_{\text{red,max}} \geq 1.5 \text{ bar}$

$$A = B \text{ m}^2$$

with

$$B = [3.264 \cdot 10^{-5} \cdot P_{\text{max}} K_{\text{max}} P_{\text{red,max}}^{-0.569} + 0.27(P_{\text{stat}} - 0.1)P_{\text{red,max}}^{-0.5}] V^{0.753} \quad (23-16)$$

$$C = -4.305 \log P_{\text{red,max}} + 0.758 \quad (23-17)$$

The equations are valid for

- Vessel volumes $0.1 \text{ m}^3 \leq V \leq 10,000 \text{ m}^3$
- Static activation overpressure of venting device $0.1 \text{ bar} \leq P_{\text{stat}} \leq 1 \text{ bar}$
- Maximum reduced explosion overpressure $0.1 \text{ bar} < P_{\text{red,max}} \leq 2 \text{ bar}$
- $P_{\text{red,max}} > P_{\text{stat}}$
- Maximum explosion overpressure $5 \text{ bar} \leq P_{\text{max}} \leq 10 \text{ bar}$ for a maximum explosion constant $10 \text{ bar}\cdot\text{m/s} \leq K_{\text{max}} \leq 300 \text{ bar}\cdot\text{m/s}$
- Maximum explosion overpressure $5 \text{ bar} \leq P_{\text{max}} \leq 12 \text{ bar}$ for a maximum explosion constant $300 \text{ bar}\cdot\text{m/s} \leq K_{\text{max}} \leq 800 \text{ bar}\cdot\text{m/s}$
- Length-to-diameter ratio of the vessel $L/D \leq 20$
- L/D limited in that the maximum vent area shall not be greater than the cross-sectional area of the equipment
- Venting efficiency $EF = 1$

The required area for pressure venting increases with increased length (height) to diameter ratio of the vessel, in comparison with the area requirement for $L/D = 1$ vessel. For low $P_{\text{red,max}}$, the required effective vent area will be markedly influenced by the ratio L/D . Such influence diminishes with increasing reduced explosion overpressure and ceases at $P_{\text{red,max}} = 1.5 \text{ bar}$ as per experimental results. However, with $P_{\text{red,max}} \geq 1.5 \text{ bar}$, no influence of the L/D ratio of the vessel can be noticed.

The influence of the vent duct upon the pressure increase is most pronounced when the flame propagation from the secondary explosion in the vent duct reaches the velocity of sound. This is valid for vent ducts of

$$L_D = L_{DS} = 4.564P_{\text{red,max}}^{-0.37} \text{ m} \quad (23-18)$$

Vent ducts with a length of $L_D > L_{DS}$ have no additional effect upon the pressure increase. Therefore, L_{DS} will be the maximum vent duct length that has to be considered. *The above-mentioned equation (23-18) is not valid for metal dusts.*

Independent of the location of the vent duct, the maximum reduced explosion overpressure $P'_{\text{red,max}}$ caused by the downstream vent duct can be calculated for vessels having an L/D ratio of 1 with Eq. (23-19).

Vessel ratio $L/D = 1$ (longitudinal und transversal):

$$P'_{\text{red,max}} = P_{\text{red,max}} [1 + 17.3L_D(AV^{-0.753})^{1.6}] \quad (23-19)$$

where $P'_{\text{red,max}}$ = maximum explosion overpressure with vent duct, bar

$P_{\text{red,max}}$ = maximum explosion overpressure without vent duct, bar

A = vent area, m^2 , without vent duct

V = volume of protected vessel, m^3

L_D = length of vent duct, m

The equation is valid for

- Vessel volumes $0.1 \text{ m}^3 \leq V \leq 10,000 \text{ m}^3$
- Static activation overpressure of the venting device $0.1 \text{ bar} \leq P_{\text{stat}} \leq 1 \text{ bar}$
- Maximum reduced explosion overpressure $0.1 \text{ bar} < P_{\text{red,max}} \leq 2 \text{ bar}$, with $P_{\text{red,max}} > P_{\text{stat}}$
- Maximum explosion overpressure $5 \text{ bar} \leq P_{\text{max}} \leq 12 \text{ bar}$ and a maximum explosion constant $10 \text{ m}\cdot\text{bar/s} \leq K_{\text{max}} \leq 800 \text{ m}\cdot\text{bar/s}$
- Vessel $L/D = 1$
- Vent duct length $L_D \leq L_{DS}$

Experimental studies have proved that the influence of vent duct with longitudinal arrangement—located on the roof—decreases markedly with increased vessel length-to-diameter ratio. The increase of the maximum explosion overpressure is at its maximum if vessel ratio $L/D = 1$.

Hazard due to flame and pressure in the surroundings The maximum outside range of a flame L_F originating from a vessel increases with increased volume of the vented vessel.

Pressure and blast effects external to a vent arise from pressures generated by the vented explosion inside the plant and the explosion area outside the vent.

Explosion suppression During a suppression of an explosion, not products, residues from combustion, residues from gases, or flames can escape from the protected vessel, because an explosion suppression system reduces the effects of these explosions to a harmless level, by restricting the action of the flames during the initial phase of the explosion. This prevents the installation in question from being destroyed and people standing in the area of the installation from being injured. A further benefit of explosion suppression systems is that they can be deployed for combustible products with toxic properties and can be used irrespective of the equipment location.

An explosion can generally be considered suppressed if the expected maximum explosion pressure P_{max} at the optimum concentration of the combustible product (7 to 10 bar)—assuming the explosion suppression system has an activation overpressure P_a of 0.1 bar—is reduced to a maximum reduced explosion overpressure $P_{\text{red,max}} \leq 1 \text{ bar}$. This means that a vessel safeguarded in this way needs to be designed so that it is secured against explosions of up to 1 bar (equivalent to $P_{\text{red,max}}$). The activation overpressure P_a is that pressure at which an explosion suppression system will be activated.

To initiate an explosion suppression system, a detector is used to sense either an overpressure generated by, or a flame of, an incipient explosion. It is important to locate the detector in a position that ensures sufficient time for the suppression system to sense and activate the devices to extinguish the explosion.

Optical detectors shall be used in more open configurations where pressure buildup due to the incipient explosion is limited. Optical detectors shall not be used where high dust concentrations limit the reliability of the suppression system. Both uv and ir detectors are available for optical detection. The use of daylight-sensitive sensors shall be avoided to avoid spurious activation. The sensor shall be mounted such that the angle of vision allows it to cover all the protected hazard area. The performance of an optical detector will also be affected by any obstacles within its vision, and this shall be overcome by the introduction of more detectors. Optical detectors shall be fitted with air shields to keep the optical lens clean.

TABLE 23-12 Suppression System Design Parameters

Explosion hazard definition	Suppression system hardware definition
Volume of vessel (free volume V)	Type of explosion suppressant and its suppression efficiency
Shape of vessel (area and aspect ratio)	Type of HRD suppressors: number and free volume of HRD suppressors and the outlet diameter and valve opening time
Type of dust cloud distribution (ISO method/pneumatic-loading method)	Suppressant charge and propelling agent pressure
Dust explosibility characteristics:	Fittings: elbow and/or stub pipe and type of nozzle
Maximum explosion overpressure P_{max}	Type of explosion detector(s): dynamic or threshold pressure, UV or IR radiation, effective system activation overpressure P_a
Maximum explosion constant K_{max}	Hardware deployment: location of HRD suppressor(s) on vessel
Minimum ignition temperature MIT	

Pressure detection shall be used for closed enclosure applications. Threshold detectors provide an electric signal when a preset overpressure is exceeded. Dynamic detectors provide an electric signal to the control and indicating equipment (CIE). Typically they have both rate-of-rise and pressure threshold triggering points that can be configured specifically to the application conditions. Although this type of detector minimizes spurious activation of the isolation system (due to pressure fluctuations other than explosion pressure rise), care shall be taken to set up such detectors to meet appropriate detection response criteria for the particular application and protected enclosure geometry.

The suppressants deployed in suppression systems are water and dry and liquid chemicals. Apart from the effectiveness of the suppressant used, the compatibility of the suppressant with the process shall be considered. A suppressant is regarded as being very effective when an increase of the activation pressure P_a of the explosion suppression system leads to a small increase in the maximum reduced explosion overpressure $P_{red,max}$. The application of a suppressant is dependent upon how effective it is at suppressing an explosion. Testing shall be used to determine the effectiveness and performance of the suppressant, thus quantifying the applicability of the suppressant. The following parameters shall be considered when selecting a suppressant:

- Any adverse reaction with the process products
- The toxicity levels of the suppressant relating to occupational exposure limits

- The temperature stability of the suppressant

In addition, the following properties shall be taken into account where necessary:

- Will the suppressant have to be food-compatible?
- Will the suppressant cause the onset of corrosion?
- Is the suppressant environmentally friendly?
- Can the suppressant be easily removed from the process?

Suppression system design parameters fall into the two categories of explosion hazard definition and suppression system hardware definition. The various influences are summarized in Table 23-12.

Comparison of explosion protection design measures In Table 23-13, comparison is made of the explosion protection design measures of containment, explosion venting and explosion suppression. In addition all three design measures are in combination with explosion isolation. Regarding the effectiveness of the different explosion design measures, all three techniques are equal if the design of these measures is performed properly and the design measures are inspected by a competent person at least once a year or more often depending on the process and/or environmental conditions.

Explosion Isolation For all equipment systems protected by design safety measures it is also necessary to prevent the propagation of an explosion from these protected vessels into operating areas or equipment connected via interconnecting pipeline. Such an approach is referred to as *explosion isolation*.

To prevent an explosion occurring in, e.g., a constructional protected installation from spreading through a pipeline ($\ell > 6$ m) to part of the installation fitted with preventive explosion protection, explosion isolation measures (see Fig. 23-14) must be implemented. As explosions are generally propagated by *flames* and not by pressure waves, it is especially important to detect, extinguish, or block this flame front at an early stage, i.e., to isolate or disengage the explosion. If there is no explosion isolation, then the flame issuing from the equipment, e.g., from the equipment protected through design (equipment part 1), through the connecting pipeline comes into contact with a highly turbulent recompressed mixture in the equipment with preventive protection (equipment part 2). The mixture will ignite in an instant and explode; a large increase in the rate of combustion reaction and, naturally, in the reduced explosion overpressure is the result. The equipment in question may be destroyed.

The isolation can be done with very different systems, which have in common that they become effective only by an explosion.

Since the action of the isolation systems requires the physical effects of an explosion, in the selection of a suitable system consideration must be given to process engineering and machine boundary

TABLE 23-13 Comparison of Explosion Protection Design Measures

	Containment with isolation	Explosion venting with isolation	Explosion suppression with isolation
Pressure resistance P	7–10 bar	Without relief pipe, up to 2 bar With relief pipe, up to 4 bar	St 1 up to 0.5 bar St 2+3 up to 1.0 bar
Location	Independent	Dependent	Independent
Limits of application	Products which decompose spontaneously	Toxic products and products which decompose spontaneously	Products which decompose spontaneously, metal dust hazard
Environmentally friendly	Yes	No (flame, pressure, and product)	Yes
Loss of material ^o	++++	++++	++
Maintenance requirements [†]	+++	+++	++++

^oThe loss of material by using containment and explosion venting is always much greater than that by using explosion suppression.

[†]To ensure the reliability of explosion protection devices, regular servicing and maintenance are required. The nature and time intervals of these activities depend on technical specifications and on the plant situation. Normally, after commissioning of the plant, inspections are carried out in comparatively short intervals, e.g., every month. Positive experience may subsequently provide for longer service intervals (every three months). It is recommended to contract service and maintenance to reliable, specialized companies.

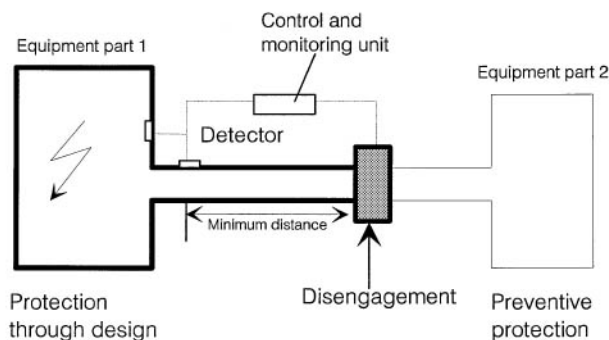


FIG. 23-14 Principle of the constructional measure explosion isolation.

conditions, particularly since the function and operability of these systems are not generally unrestricted.

Dust-carrying pipelines are different from gas-carrying pipelines— isolation devices can only be used which do not lose their function by the presence of the dust.

Today it is usual to divide the assigned isolation system in accordance with its mode of operation in *passive* isolation systems and *active* isolation systems. The passive isolation systems work without additional control units; i.e., the function (release) is determined by the physical effects of the explosion. Active isolation systems, however, are dependent on additional control and/or release mechanisms, without which they are nonfunctioning. Table 23-14 summarizes the different isolation systems.

Proper installation is dependent on the existing explosion protection measures and on the corresponding isolation system to be used. This guarantees operability. In addition the application and installation remarks of the manufacturer as well as the limits of application in accordance with the Type-Examination Certificate are to be obeyed in every detail. In Table 23-15 the most frequently used isolation systems for explosion protection measures are summarized.

An optical flame sensor installed at the beginning of the pipeline is the most suitable device for such an isolation system, since the propagating flame from the explosion has to be detected and extinguished. Pressure detectors alone are, in principle, not suited to the case on hand because there is no distinct separation between the pressure and flame fronts for explosion in pipelines. Optical ir sensors that have a relatively low sensitivity to daylight are normally chosen and have proved themselves amply in industrial practice. Therefore, daylight into the pipe in the vicinity of the sensor must be avoided. It is necessary to flush the optical lens with gas (e.g., nitrogen, air) to keep it dust-free.

TABLE 23-14 Different Isolation Devices

Type of isolation	Suitable for:
Rotary air lock (active)	Dusts
Extinguishing barrier (active)	Gas, dusts, and hybrid mixtures
Explosion protection valve (passive or active)	Gas, dusts, and hybrid mixtures
Explosion diverter (passive)	Gas, dusts, and hybrid mixtures
Double slide valve (active)	Gas, dusts, and hybrid mixtures
Product layer as a barrier (active)	Dusts and solvent humid products
Screw conveyer (passive)	Dusts and solvent humid products
Extinguishing barrier or explosion protection valve in combination with explosion diverter (active)	Gas, dusts, and hybrid mixtures
Flame arresters	Gas (see subsection "Flame Arresters," later)

TABLE 23-15 Most Frequently Used Isolation Systems as Related to the Installed Construction Explosion Protection Measure

Isolation system	Containment	Explosion venting	Explosion suppression
Double slide valve system	✓	✓	✓
Explosion diverter	✓	✓	✓
Explosion protection valve system	✓	✓	✓
Extinguishing barrier	—	✓	✓
Extinguishing barrier in combination with explosion diverter	—	✓	✓
Explosion protection valve in combination with explosion diverter	✓	✓	✓
Product layer as a barrier	—	✓	✓
Screw conveyer	✓	✓	✓
Rotary valve	✓	✓	✓

In difficult situations, it is recommended to install both types of sensors—pressure detector in the vessel and flame detector in the pipe—and they must be switched in an OR-logic to activate the isolation device (see Fig. 23-14).

The pressure detector in the vessel provides the earliest detection of an explosion in the interconnected vessel, whereas the flame detector in the pipeline provides assured detection, even for lazy flames, as they propagate down the pipeline toward the extinguishing barrier.

For the explosion protection valves always two installation distances are to be indicated, namely, the *minimum* and *maximum* installation distances. The *minimum installation distance* ensures that the given isolation system can react in time to prevent an explosion propagation beyond the installation place. The *maximum installation distance* ensures that a detonation in the piping cannot be formed up to the isolation system and/or that excessive pressure loads are avoided at the isolation system.

With extinguishing barriers the minimum and the maximum installation distances and the *extinguishing distance* must be considered after the extinguishing barrier. This *extinguishing distance* is specified as the minimum length after the extinguishing barrier to guarantee proper function of that extinguishing barrier. Only after this extinguishing distance may the piping connect to other equipment.

The minimum installation distance between the detector which activates the isolation system and the isolation system itself depends essentially on

- Type of detectors (pressure/flame)
- Volume of the vessel to be protected
- Maximum explosion overpressure P_{max} or maximum reduced explosion overpressure $P_{red,max}$ in the protected vessel
- Diameter of the pipeline
- Reaction time of the isolation system
- Maximum explosion overpressure P_{max} of the fuel
- Maximum explosion constant K_{max} of the fuel
- Minimum explosion constant K_{min} of the fuel (typically $\frac{1}{3} K_{max}$, but minimum 50 m-bar/s)
- Forward air velocity in the pipeline
- Minimum ignition temperature of a dust cloud (only for extinguishing barriers)
- Type of suppressant (only for extinguishing barriers)

Finally, it must be pointed out that all explosion protection devices or systems used in practice may be used only when their pressure rating, flameproof, and functional testing have been proved by competent bodies and their test results including the limits of application are documented in a type test certificate.

Static Electricity

Nomenclature

C	Capacitance
C/kg	Unit of charge density
C/m ²	Unit surface charge density
F	Farad
J	Unit of energy (joules)
K _r	Relative dielectric constant, dimensionless
kV/m	Unit of electric field intensity
m	Meter
MIE	Minimum ignition energy, mJ
mJ	Millijoule
Ω ²	Resistivity value, ohms per square, usually used for fabrics and films
pS	Unit of conductivity (picosiemens)
pS/m	Unit of electrical conductivity of liquid
RH	Relative humidity, %
S	Siemen, formerly mho
T	Time, s
V	Electric potential, V
V/m	Unit of electrical field intensity

GENERAL REFERENCES: Gibson and Lloyd, "Incendivity of Discharges from Electrostatically Charged Plastics," *Brit. J. of Appl. Phys.* **16**, pp. 1619–1631, 1965. *Plant/Operations Progress* **7**, No. 1, Jan. 1988. Entire issue devoted to papers on static electricity, presented at AIChE meeting, Minneapolis, Minn., August 1987. "Protection Against Ignitions Arising Out of Static, Lightning and Stray Currents," American Petroleum Institute Recommended Practice 2003, 1998. M. Glor, "Electrostatic Ignition Hazards Associated with Flammable Substances in the Form of Gases, Vapors, Mists, and Dusts," *Inst. Phys. Conf. Ser. No. 163*, London, pp. 199–206, 1999. National Fire Protection Association, "Recommended Practice on Static Electricity," NFPA 77, Quincy, Mass., 2007. National Fire Protection Association, "Standard for the Manufacture of Organic Coatings," NFPA 35, 2005. "Safety of Machinery; Guidance and Recommendations for the Avoidance of Hazards due to Static Electricity," Cenelec Report RO 44-001, European Committee for Electrotechnical Standardization, Brussels, 1999.

Introduction Spark ignition hazards must be considered whenever static charges may accumulate in an environment that contains a flammable gas, liquid, or dust. The need for electrical bonding and grounding of conductive process equipment in hazardous (classified) locations is widely recognized. Less well understood are the ignition hazards associated with static charges on poorly conductive, flammable liquids, solids, and powders. Static charges, generated on these materials by normal handling and processing, cannot be conducted to ground quickly, and may cause hazardous charge accumulations. The electric fields associated with these charges may stress the surrounding air sufficiently to cause breakdown by some type of electrical discharge.

Electrical discharges from poorly conductive materials take several forms, each differing in its ability to ignite flammable mixtures. It is not possible to calculate the incendivity of most of these discharges, because of their varying time and spatial distributions. Several engineering rules of thumb for estimating the relative hazard of these discharges are discussed below.

An analysis of static ignition hazard should start with data on the ignition sensitivity of the particular flammable material at its most flammable concentration in air, i.e., its MIE. This is especially important for dusts. It is prudent to determine this value on fines of the specific dust of interest, rather than to rely on published data. *Hybrid mixtures*, i.e., mixtures of dust and vapor for which vapor concentrations may be below their lower flammable limit, can be ignited by smaller discharge energies than might be expected.

The key to safe operation is to provide an adequate means of charge dissipation from charged materials to ground. This requires mobility of charges in or on the charged material *plus* electrical continuity from the material to ground.

Definitions

Bonding A method of providing electrical continuity between two or more conductive objects to prevent electrical sparking between them.

Charge relaxation time The time required for a charge in a liquid or on a solid material to dissipate to 36.8 percent of its initial value when the material is grounded.

Electrical discharge A current flow that occurs when the electrical field strength exceeds the dielectric breakdown value of a medium such as air.

Flammable mixture A mixture of a gas, vapor, mist, or dust in air which is within its flammable range.

Grounding A special form of bonding in which a conductive object is connected to (earth) ground.

Incendive discharge Any electrical discharge that has sufficient energy to ignite a specified flammable mixture.

Minimum ignition energy The smallest amount of spark energy that has been found capable of igniting a specified flammable mixture in a standard test.

Static-dissipative (antistatic) material One with an electrical resistivity that is low enough to make it incapable of accumulating hazardous concentrations of static charges when grounded.

Electrostatic Charging The primary cause of electrostatic charging is contact electrification, which takes place when two different materials are brought into contact and separated. Other causes include induction charging, the formation of sprays, and impingement of charged mist or particles on an ungrounded conductor.

Contact electrification involves the contact and separation of solid-solid, solid-liquid, or liquid-liquid surfaces. Pure gases do not cause charging unless they carry droplets or dust particles.

Efforts to quantify the magnitude and polarity of contact charging have had limited success, because minute variations in the types and concentration of contaminants exert a large influence on charge separation. Even like solid-solid surfaces can produce significant charge separation. The charge density on separated surfaces is usually very nonuniform. Each surface may contain both + and – charges, with more of one polarity than of the other. After separation, the charges dissipate slowly or rapidly, depending upon the electrical resistivity of the material and the presence of a path to ground.

Contact electrification at liquid-liquid and liquid-solid surfaces is attributed to the adsorption of ions of one polarity by one surface. Ions of opposite polarity form a diffuse layer near the interface. If the diffuse layer is carried along by moving liquid, or in a pipeline, the flowing charges (called a *streaming current*) may create a sparking hazard downstream. One protective measure is to keep the charged liquid in a closed, grounded system (a *relaxation chamber*) long enough to allow for safe dissipation of the charges.

The magnitude of the streaming current in any given situation is not readily calculated. Equations, derived experimentally, for some liquids (Bustin and Dukek, *Electrostatic Hazards in the Petroleum Industry*, Research Studies Press, Letchworth, England, 1983) show that flow velocity and filters have the greatest influence on pipeline charging. Streaming currents can usually be limited to safe levels by limiting velocities to less than 1 m/s.

Charge induction takes place when a conducting object is exposed to electric fields from other objects. Examples include the induction charging of a human body by charged clothing, the charging of a conductive liquid in a charged plastic container, and the charging of the conductive coating on one-side-metallized film by static charges on the uncoated surface.

Although charge induction can take place whether or not the conductive object is grounded, a sparking hazard is present only if the conductor is not grounded. This phenomenon can convert a relatively innocuous charge buildup on a nonconductor to a serious sparking hazard by raising the potential of the conductor aboveground (Owens, "Spark Ignition Hazards Caused by Charge Induction," *Plant/Operations Progress* **7**, no. 1, pp. 37–39, 1988).

Droplets, formed by **spray nozzles**, tend to be highly charged, even if the conductivity of the liquid is high. Because there is no path to ground from the droplets, their charges can accumulate on an ungrounded conductor to cause sparking. If flammable vapor is present, as in some tank cleaning operations, it is essential that the spray nozzle and the tank be bonded or separately grounded. Other precautions include the use of a nonflammable cleaning solvent or the use of an inert gas.

Although charged **mists** are unable to cause ignition of flammable vapor by self-generated sparking, it is important that the mist not impinge on an ungrounded conductor.

Charge Dissipation It is an experimental fact that charged objects exert a force on other charged objects. This behavior is explained by the presence of an *electric field*, i.e., electric lines of force, each of which emanates from a + charge and terminates on a - charge. The *magnitude* of the field is defined as the force on a unit test charge, placed at the point of interest. The *direction* of the field is the direction of the force on a + test charge placed at that point.

Static charge generation causes an ignition hazard only if the accumulated charges create an electric field that is sufficient to produce an electrical discharge in a flammable atmosphere. In most processes, this means that the electric field intensity at some location must reach the dielectric breakdown strength of air (nominally 3×10^6 V/m). The objective of static control measures is to ensure that electric field intensities cannot reach this value.

Bonding and grounding are the primary means of dissipating charges from **conductive objects**. Bonding clamps should be of the single-point type, which bites through oxide or enamel coatings to make contact with the bare metal. Owing to the sturdy construction of bonding clamps and cables, their initial resistance is less than 1Ω . It is good practice to visually inspect the condition of bonding cables and clamps during each use, and to measure the resistance of temporary bonding cables at least annually, to confirm that it is less than, say, 25Ω .

Charge-dissipative materials allow static charges to dissipate without causing hazardous accumulations. Charge dissipation normally takes place by conduction along the material to ground. The charge-dissipating behavior of such materials is measured at a controlled temperature and relative humidity, in terms of Ω^2 (ohms per square) of *electrical surface resistivity*. The maximum safe resistivity depends, in part, upon the rate of charge generation, but is typically in the range of 10^8 to $10^{11} \Omega^2$ for fabrics and films [ASTM Standard Test Method D257-99 (2005), "DC Resistance or Conductance of Insulating Materials"].

An alternate test for charge-dissipating performance is the *charge decay* test, in which the time of charge decay is measured after a potential of 5 kV has been applied to the specimen (Federal Test Method Standard 101C, Method 4046.1). For many purposes, a charge decay time of 0.5 s to 500 V, measured at the RH in end use, indicates acceptable performance.

The electrical surface resistivity and the charge decay time of most materials vary substantially with RH. It is important that test specimens be conditioned and tested at the lowest RH expected during use. Items that are acceptable at 50 percent RH may not be safe at 20 percent RH.

Some fabrics contain a small percentage of conductive or antistatic fibers or staple, which limit charge accumulation by *air ionization*. These static-dissipative fabrics do not depend upon electrical conduction of static charges, and may not pass the resistivity or the charge decay test. Their performance is not humidity-dependent. Antistatic performance is determined by measuring the charge transferred in electrical discharges from the charged fabric, and by the ability of these discharges to ignite flammable mixtures having a known MIE.

The rate of dissipation of charges in **liquid**, assuming that its conductivity and dielectric properties are constant, can be expressed as

$$T = 8.85K_r/C \quad (23-20)$$

where T = time required for charge density to dissipate to 36.8% of its initial value, s

K_r = relative dielectric constant of liquid, dimensionless

C = electrical conductivity of liquid, pS/m

Flammable liquids are considered particularly static-prone if their electrical conductivity is within the range of 0.1 to 10 pS/m. If no particulates or immiscible liquids are present, these liquids are considered safe when their conductivity has been raised to 50 pS/m or higher. Blending operations or other two-phase mixing may cause such a high rate of charging that a conductivity of at least 1000 pS/m is needed for safe charge dissipation (British Standard 5958, part 1, "Control of Undesirable Static Electricity," para. 8, 1991).

Electrostatic Discharges An electrostatic discharge takes place when a gas- or a vapor-air mixture is stressed electrically to its break-

down value. Depending upon the specific circumstances, the breakdown usually appears as one of four types of discharges, which vary greatly in origin, appearance, duration, and incendivity.

Spark discharges are most common between solid conductors, although one electrode may be a conductive liquid or the human body. They appear as a narrow, luminous channel and carry a large peak current for a few microseconds or less. Sparks are the only form of discharge for which a maximum energy can be calculated, by using the expression

$$J = 0.5CV^2 \quad (23-21)$$

where J = total energy dissipated, J

C = capacitance of charged system, F

V = initial potential difference between electrodes, V

Incident investigations often require that estimates be made of the possible spark energy from an ungrounded conductor. If the discharge path contains significant resistance, some of the stored energy is dissipated in the resistance, thereby lowering the energy in the spark gap.

A **corona** is generated when a highly nonuniform electric field of sufficient strength terminates on a conductor that has a small radius of curvature, i.e., a point, wire, or knife edge. The luminous (breakdown) region is confined to a small volume near the corona electrode. Because of their small peak currents and long duration, corona discharges do not have sufficient energy to ignite most flammable materials found in industry, i.e., materials having an MIE greater than 0.2 mJ. For this reason, nonpowered devices that employ corona discharges for static neutralization can be used safely in most hazardous (classified) locations. Corona discharges *can* ignite hydrogen-air and oxygen-enriched gas mixtures.

Brush discharges take place between conductors and charged nonconductors, where the radius of curvature of the conductor is too large for corona generation. The name refers to the brushlike appearance of the discharge, which spreads from the conductor to discrete areas on the nonconductor. The brush discharge may have a hot "stem" near the conductor, which may cause ignition by raising the temperature of the flammable mixture to its *autoignition* value.

Brush discharges from - charged nonconductors have been found more incendive than those from + charged nonconductors. Brush discharges may ignite flammable mixtures that have an MIE of less than 4 mJ. This limitation arises because charges from a small area on the nonconductor are able to participate in the discharge. Most dust-air mixtures cannot be ignited by brush discharges, because their MIE exceeds 4 mJ.

Surface charge densities cannot exceed the theoretical value of 2.7×10^{-5} C/m² set by air breakdown, and are normally less than 1.5×10^{-5} C/m².

Propagating brush discharges are much less common than brush discharges. They may occur when a nonconductive film or plastic layer acquires a double layer of charges, i.e., + charges on one surface and - charges on the opposite surface. With the electric fields within the film, surface charge densities can be large, because they are not limited by air breakdown.

The double layer can be formed by contact (triboelectric) charging on one surface of the nonconductor while the opposite surface is in contact with a conductor, e.g., a nonconductive coating on a metal chute or a plastic-lined, metal pipe for powders. A less frequent cause is contact charging of one surface of a nonconductor while air ions collect on the opposite surface.

Investigations by Glor ("Discharges and Hazards Associated with the Handling of Powders," *Electrostatics* 1987, Inst. Phys. Conf. Ser. no. 85, pp. 207-216, 1987) and others conclude that propagating brush discharges require surface charge densities above 2.7×10^{-4} C/m². In addition, the dielectric breakdown voltage of the insulating layer must exceed 4 kV for a thickness of 10 μ m, or 8 kV for a thickness of 200 μ m.

If a conductor approaches the charged surface, the electric field will produce air ionization at the surface, which creates a semiconductive layer, thereby allowing charges from a large area to participate

in a single discharge. Because these discharges can have energies of 1 J or more, they are very hazardous in a flammable environment. They may also cause severe shocks to operators who reach into a nonconductive container that is receiving charged powder, pellets, or fibers.

Causes of Hazardous Discharges with Liquids Self-generated discharges in vapor-air mixtures can be ignited by static discharges from highly charged liquids. Such liquids are said to "carry their own match." Typical causes of such charging for poorly conductive (<50 pS/m) liquids include

1. High-velocity flow
2. Free-fall/splashing
3. Filtering
4. Spraying
5. Agitation with air
6. Blending with powder
7. Settling of an immiscible component, e.g., water in gasoline
8. Liquid sampling from pressurized lines, using ungrounded or nonconductive containers

Conductive liquids in nonconductive containers may cause sparking if the outside of the container is charged by rubbing.

External causes of incendive static discharges include

1. Sparks from ungrounded conductors or persons
2. Brush discharges from flexible intermediate bulk containers (FIBCs), plastic bags, stretch wrap, or other plastic film
3. Propagating brush discharges from metal-backed, plastic film or linings

Powders Contact charging of powders occurs whenever particles move relative to one another or to a third surface. Significant charging is most often generated by pneumatic transfer. Maximum charge densities (C/kg) on airborne powders increase as particle size decreases, because of larger surface/mass ratios. Dry fines can be expected to charge more highly than those containing moisture. While suspended in air, charged powder poses an ignition risk only if nonconductive piping is used in the conveying lines, or if conductive piping is not bonded. The collected powder may accumulate so much charge per unit volume that the associated electric fields cause breakdown of the surrounding air in the form of a corona or a brush discharge. For receiving containers larger than about 1 m³, bulking or cone discharges may be present. These discharges typically have energies of less than 10 mJ, but the value is sometimes higher. The ignition hazard from bulking discharges can be minimized by, e.g., using a rotary valve or bag filter to prebulk small volumes of charged powder prior to its collection in a large receiver.

Personnel and Clothing Sparks from ungrounded persons pose a serious ignition hazard in flammable gas-air, vapor-air, and some dust-air mixtures, because the body is a conductor and can store energies as high as 40 mJ. Induction of static charges on a person's ungrounded body by charged clothing is a common cause of personnel electrification. Even at the *threshold of shock sensation*, the stored energy is about 1 mJ.

It is essential that persons be grounded in hazardous (classified) locations. For most chemical operations, the resistance from skin to ground should not exceed 100 M Ω . A lower allowable resistance may be specified for locations where the presence of primary explosives, hydrogen-air mixtures, oxygen-enriched mixtures, or certain solid-state devices requires faster charge dissipation.

The combination of conductive flooring and conductive (ESD) footwear is the preferred method of grounding. Untreated concrete flooring with conductive footwear is usually adequate, but the resistance to ground should be measured. Where this method is impractical, personnel-grounding devices are available.

In most chemical plants, grounded persons can wear any type of clothing safely. For the unusually sensitive environments noted above, charge-dissipative or conductive clothing should be worn, and personnel should be grounded. Removal of outer garments in a flammable location can cause hazardous discharges and should be avoided. Although most gloves used in the chemical industry show a resistance of less than 100 M Ω from the wearer's palm to a handheld electrode, this value should be verified.

CHEMICAL REACTIVITY

GENERAL REFERENCES: ASTM E 1231, "Practice for Calculation of Hazard Potential Figures-of-Merit for Thermally Unstable Materials," ASTM International, West Conshohocken, Penn. ASTM E 1445, "Standard Terminology Relating to Hazardous Potential of Chemicals," ASTM International. ASTM E 2012, "Standard Guide for the Preparation of a Binary Chemical Compatibility Chart," ASTM International. Bartknecht, *Explosions: Course, Prevention, Protection*, Springer-Verlag, Berlin, 1981. Barton and Rogers, eds., *Chemical Reaction Hazards: A Guide to Safety*, 2d ed., Gulf Publishing Co., Houston, Tex., 1997. Beever, "Hazards in Drying Thermally Unstable Powders," *Inst. Chem. Engr., Hazards X*, Symp. Ser. 115, 1989. Beever, "Scaling Rules for Prediction of Thermal Runaway," *Intl. Symp. on Runaway Reactions*, CCPS-AIChE, Cambridge, Mass., 1989. Bollinger et al., *Inherently Safer Chemical Processes: A Life Cycle Approach*, CCPS-AIChE, New York, 1996. Bowes, "A General Approach to the Prediction and Control of Potential Runaway Reaction," *Inst. Chem. Engr., Symp. Ser. 68*, 1981. Bowes, *Self-heating: Evaluating and Controlling the Hazards*, Elsevier, 1984. *Bretherick's Reactive Chemical Hazards Database*, Version 3.0, Butterworth-Heinemann, Oxford, 1999. Brogli, et al., "Assessment of Reaction Hazards by Means of a Bench Scale Calorimeter," *Inst. Chem. Engr., Symp. Ser. 68*, 1981. Brogli, Gygax, and Myer, "Differential Scanning Calorimetry—A Powerful Screening Method for the Estimation of the Hazards Inherent in Industrial Chemical Reactions," *Therm. Analy.*, 6th Symp., vol. 1, 549, 1980. Center for Chemical Process Safety (CCPS), *Guidelines for Chemical Reactivity Evaluation and Application to Process Design*, CCPS-AIChE, New York, 1995. CCPS, *Guidelines for Safe Storage and Handling of Reactive Materials*, CCPS-AIChE, New York, 1995. CCPS, *Guidelines for Process Safety in Batch Reaction Systems*, CCPS-AIChE, New York, 1999. CCPS, Safety Alert, "Reactive Material Hazards: What You Need To Know," CCPS-AIChE, New York, 2001. Coates, "The ARC™ in Chemical Hazard Evaluation," *Thermochim. Acta* 85: 369–372, 1984. Davies, *Organic Peroxides*, Butterworths, London, 1961. ESCIS, *Thermal Process Safety: Data, Assessment Criteria, Measures*, Safety Series, Booklet 8, Expert Commission for Safety in the Swiss Chemical Industry, Basel, Switzerland, April 1993. Fenlon, "Calorimetric Methods Used in the Assessment of Thermally Unstable or Reactive Chemicals," *Intl. Symp. for the Prevention of Major Chemical Accidents*, AIChE, 1987. Fisher et al., "Emergency Relief System Design Using DIERS Technology: The Design Institute for Emergency Relief Systems (DIERS) Project Manual," AIChE, New York, 1992. Frank and Kamenetskii, *Diffusion and Heat Transfer in Chemical Kinetics*, Plenum Press, 1969. Frurip et al., "A Review of Chemical Compatibility Issues," *AIChE Loss Prevention Symp.*, Houston, Tex., 1997. Grever, "Direct Assessment and Scaling of Runaway Reaction and Decomposition Behavior Using Oven and DEWAR Tests," *Inst. Chem. Engr., Symp. Ser.*, 68, 1981. Grever, "Use of DEWAR Calorimetry," *Proc. Runaway Chem. React. Haz. Symp.*, IBC, Amsterdam, November 1986. Grever, *Thermal Hazards of Chemical Reactions*, Elsevier Science, London, 1994. Halk, "SEDEX Versatile Instrument for Investigating Thermal Stability," *Inst. Chem. Engr., Symp. Ser.*, 68, 1981. Hazard Investigation, "Improving Reactive Hazard Management," Report no. 2001-01-H, U.S. Chemical Safety and Hazard Investigation Board, Washington, October 2002. Hender-shot, "A Checklist for Inherently Safer Chemical Reaction Process Design and Operation," *Intl. Symp. on Risk, Reliability and Security*, CCPS-AIChE, New York, October 2002. HSE, *Designing and Operating Safe Chemical Reaction Processes*, U.K. Health and Safety Executive, 2000. "How to Prevent Runaway Reactions, Case Study: Phenol-Formaldehyde Reaction Hazards," EPA 550-F99-004, U.S. Environmental Protection Agency, Washington, August 1999. Hub, "Adiabatic Calorimetry and SIKAREX Technique," *Inst. Chem. Engr., Symp. Ser.*, 68, 1981. Hub, "Experiences with the TSC 500 and RADEX Calorimeter," *Proc. Runaway Chem. React. Haz. Symp.*, IBC, Amsterdam, November 1986. Hub, "Heat Balance Calorimetry and Automation of Testing Procedures," *Proc. Runaway Chem. React. Haz. Symp.*, IBC, Amsterdam, November 1986. *International Conference/Workshop on Modeling and Mitigating the Consequences of Accidental Releases of Hazardous Materials*, CCPS-AIChE, New York, 1991. *International Conference on Hazard Identification and Risk Analysis, Human Factors and Human Reliability in Process Safety*, CCPS-AIChE, New York, 1992. *International Conference on Managing Chemical Reactivity Hazards and High Energy Release Events*, CCPS-AIChE, New York, 2003. *International Symp. on Runaway Reactions and Pressure Relief Design*, DIERS-AIChE, New York, 1995. Johnson et al., *Essential Practices for Managing Chemical Reactivity Hazards*, CCPS-AIChE, New York, 2003. Johnson and Lodal, "Screen Your Facilities for Chemical Reactivity Hazards," *Chem. Eng. Prog.* 99(8): 50–58, 2003. Johnson and Unwin, "Addressing Chemical Reactivity Hazards in Process Hazard Analysis," *Proc. Intl. Conf. and Workshop on Managing Chemical Reactivity Hazards and High Energy Release Events*, CCPS-AIChE, New York, 2003. Kohlbrand, "Reactive Chemical Screening for Pilot Plant Safety," *Chem. Eng. Prog.* 81(4): 52, 1985. Kohlbrand, "The Relationship Between Theory and Testing in the Evaluation of Reactive Chemical Hazards," *Intl. Symp. for the Prevention of Major Chemical Accidents*, AIChE, New York, 1987. Leggett, "Chemical Reaction Hazard Identification and Evaluation: Taking the First Steps," *AIChE Loss Prevention Symp.*, New Orleans, March 2002.

Lewis, *Sax's Dangerous Properties of Industrial Materials*, 11th ed., Wiley, New York, 2004. Mannan, *Lees' Loss Prevention in the Process Industries*, 3d ed., Elsevier, Amsterdam, 2005. Manufacturing Chemists Association (now American Chemistry Council), *Selected Case Histories*, Washington, 1951–1973. Mosley et al., "Screen Reactive Chemical Hazards Early in Process Development," *Chem. Eng. Prog.* 96(11): 51–65, 2000. NFPA 430, "Code for the Storage of Liquid and Solid Oxidizers," National Fire Protection Association, Quincy, Mass. NFPA 432, "Code for the Storage of Organic Peroxide Formulations," National Fire Protection Association, Quincy, Mass. NFPA 49, "Hazardous Chemicals Data," and NFPA 491, "Hazardous Chemical Reactions," in *Fire Protection Guide to Hazardous Materials*, 13th ed., National Fire Protection Association, Quincy, Mass., 1997. NFPA 704, "Standard System for the Identification of the Hazards of Materials for Emergency Response," National Fire Protection Association, Quincy, Mass., 2001. NOAA, Chemical Reactivity Worksheet, Version 1.5, U.S. National Oceanic and Atmospheric Administration, *response, restoration. noaa.gov/chemaids/react.html*, 2002. Pohanish and Green, *Wiley Guide to Chemical Incompatibilities*, 2d ed., Wiley, New York, 2003. *Second Intl. Symp. on Runaway Reactions, Pressure Relief Design and Effluent Handling*, DIERS-AIChE, New York, 1998. Stull, *Fundamentals of Fire and Explosion*, AIChE, New York, 1976. Stull, "Linking Thermodynamics and Kinetics to Predict Real Chemical Hazards," *Loss Prevention* 7, p. 67, AIChE, 1976. Thomas, "Self Heating and Thermal Ignition—A Guide to Its Theory and Application," ASTM STP 502, pp. 56–82, ASTM International, 1972. Townsend, "Accelerating Rate Calorimetry," *Inst. Chem. Eng., Symp. Ser.* 68, 1981. Townsend and Kohlbrand, "Use of ARC™ to Study Thermally Unstable Chemicals and Runaway Reactions," *Proc. Runaway Chem. React. Haz. Symp.*, IBC, Amsterdam, November 1986. Townsend and Tou, "Thermal Hazard Evaluation by an Accelerating Rate Calorimeter," *Thermochem. Acta* 73: 1–30 and references therein, 1980. Urben, ed., *Bretherick's Handbook of Reactive Chemical Hazards*, 6th ed., Butterworth-Heinemann, Oxford, 1999. Yoshida et al., *Safety of Reactive Chemicals and Pyrotechnics*, Elsevier Science, London, 1995.

Introduction *Chemical reactivity* is the tendency of substances to undergo chemical change. A *chemical reactivity hazard* is a situation with the potential for an uncontrolled chemical reaction that can result directly or indirectly in serious harm to people, property, or the environment. A chemical reaction can get out of control whenever the reaction environment is not able to safely absorb the energy and products released by the reaction. The possibility of such situations should be anticipated not only in the reaction step of chemical processes but also in storage, mixing, physical processing, purification, waste treatment, environmental control systems, and any other areas where reactive materials are handled or reactive interactions are possible.

The main business of most chemical companies is to manufacture products by means of controlled chemical reactions. The reactivity that makes chemicals useful can also make them hazardous. Chemical reactions are usually carried out without mishap, but sometimes they get out of control because of problems such as the wrong or contaminated raw material being used, changed operating conditions, unanticipated time delays, failed equipment, incompatible materials of construction, or loss of temperature control. Such mishaps can be worse if the chemistry under both normal and abnormal conditions is not fully understood. Therefore, it is essential that chemical process designers and operators understand the nature of the reactive materials and chemistry involved and what it takes to control intended reactions and avoid unintended reactions throughout the entire life cycle of a process facility.

Life-Cycle Considerations

Considering Chemical Reactivity during Process Development Decisions made at the early development stages of a process facility, including conceptual and research phases, will in large part determine the nature and magnitude of the chemical reactivity hazards that will need to be contained and controlled throughout the entire life cycle of the facility. For this reason, chemical reactivity hazards should be considered from the outset of process development, including creative thinking regarding feasible alternatives to the use of reactive materials or the employment of highly energetic reactive systems. What may seem reasonable to the research chemist—handling materials in very small quantities—will have vast implications to the design and ongoing operation of a full-scale facility that must safely control the intended chemical reactions and avoid unintended reactions throughout the entire facility lifetime.

Mosley et al. describe a chemistry hazard and operability (CHA-ZOP) analysis approach, similar to a HAZOP study but applied at the early development stages of a new process.

Many companies designate a particular person or position as the "owner" of the process chemistry; this responsibility is likely to change as the life cycle progresses from development to design, construction, and operation. Data on the hazardous properties of the chemical reactions to be employed and the materials to be handled should begin to be assembled into a formal documentation package. Screening tests (described later in this section) may also need to be performed early in the development process to identify consequences of abnormal reactions and of deviations such as exceeding the normal reaction temperature. This documentation package will then form part of the information base upon which safeguards can be developed to control chemical reactivity hazards.

Considering Inherently Safer Approaches Specific to Reactivity Hazards The basic concepts of inherently safer plants, and the general strategies for making a facility inherently safer, are detailed in the later subsection on Inherently Safer and More User-Friendly Design. Strategies that focus on chemical reactivity hazards, and steps to conduct a review of these strategies, are highlighted in that section.

Instead of choosing to receive and store a highly reactive raw material, it may be possible to use a less hazardous material that is one step farther along in the formulation or synthesis chain. Alternatively, a decision may be made to generate the material on demand and eliminate all or most storage and handling of the material. Many reactive materials can be handled in dilute solutions, dissolved in less hazardous solvents, or otherwise handled under inherently safer conditions. (For some reactive materials such as benzoyl peroxide, handling as a dilute paste or solution is essential to the safe handling of the material.)

Inherently safer facilities with respect to chemical reactivity hazards must focus on the magnitude of stored chemical energy, the kinetics of how fast the energy could be released, and the possible reaction products that may themselves have hazardous properties such as toxicity or flammability.

With respect to kinetics, a slower reaction might be considered at first glance to be the inherently safer option as compared to a rapid reaction. This may indeed be the case, if the energy and products of the slower reaction can always be dissipated safely without causing harm or loss. However, this is often not the case, for two important reasons. First, regardless of the speed of the reaction, the same potential chemical energy is still thermodynamically present if only the kinetics is changed, and may be available under abnormal conditions such as an external fire or the introduction of a catalytic contaminant. Second, a slower reaction may allow unreacted material to accumulate. Hence faster reactions are generally more desirable, as discussed in the general reaction considerations below.

Finally, with respect to reaction products, a chemical reaction that does not generate hazardous reaction products or by-products is inherently safer than one that does. Thought must be given not only to hazardous reaction products, however. The generation of any kind of noncondensable gases can cause a vessel rupture due to internal overpressurization, if not adequately vented or relieved.

The following is a typical agenda for an inherent safety review at the concept or development stage of a new facility involving reactivity hazards (Johnson et al. 2003):

1. Review what is known of the chemical reactivity hazards (as well as other hazards) that will need to be contained and controlled in the proposed process. This existing level of knowledge might come from past experience, suppliers, literature reviews, incident reports, etc.
2. Based on the level of knowledge of chemical reactivity hazards, determine if additional screening of reactivity hazards is necessary. Having reactive functional groups might indicate the need to perform literature searches, access databases, or run differential scanning calorimetry.
3. Discuss possible process alternatives and their relative hazards, including discussions on such topics as alternative solvents and possible incompatibilities to avoid.
4. Brainstorm and discuss possible ways to reduce the hazards.
5. Obtain consensus on significant unknowns that will need to be addressed.

6. Document the review, including attendees, scope, approach, and decisions.

7. Assign follow-up items, with responsibilities, goal completion dates, and a closure mechanism such as reconvening after a designated number of weeks.

Scale-up Considerations A key consideration when scaling up a reactive process, such as from a pilot plant to a full-scale facility, is to ensure adequate heat removal for normal or abnormal exothermic reactions. Heat generation is proportional to *volume* (mass) in a reactive system, whereas heat removal is only proportional to *area* (surface area) at best. Even though the reaction temperature can be easily controlled in the laboratory, this does not mean that it can be adequately controlled in a plant-scale reactor. Increasing the size of a reactor, or of another process or storage vessel where, e.g., polymerization or slow degradation can occur, without adequately considering heat transfer can have disastrous effects. The careful design of the agitation or recirculation system is likewise important when scaling up, and the combined effects on the design of the emergency relief system must be taken into account.

Scale-up can also have a significant effect on the basic process control system and safety systems in a reactive process. In particular, a larger process will likely require more temperature sensors at different locations in the process to be able to rapidly detect the onset of out-of-control situations. Consideration should be given to the impact of higher-temperature gradients in plant-scale equipment compared to a laboratory or pilot plant reactor (Hendershot 2002).

Designing Processes for Control of Intended Chemical Reactions

General Considerations The following should be taken into account whenever designing or operating a chemical process that involves intended chemical reactions (Hendershot 2002). CCPS (1999) also details many key issues and process safety practices to consider that are oriented toward the design and operation of batch reaction systems.

- Know the heat of reaction for the intended and other potential chemical reactions.
- Calculate the maximum adiabatic temperature for the reaction mixture.
- Determine the stability of all individual components of the reaction mixture at the maximum adiabatic reaction temperature. This might be done through literature searching, supplier contacts, or experimentation.
- Understand the stability of the reaction mixture at the maximum adiabatic reaction temperature. Are there any chemical reactions, other than the intended reaction, that can occur at the maximum adiabatic reaction temperature? Consider possible decomposition reactions, particularly those which generate gaseous products.
- Determine the heat addition and heat removal capabilities of the reactor. Don't forget to consider the reactor agitator as a source of energy—about 2550 Btu/(h·hp).
- Identify potential reaction contaminants. In particular, consider possible contaminants, which are ubiquitous in a plant environment, such as air, water, rust, oil, and grease. Think about possible catalytic effects of trace metal ions such as sodium, calcium, and others commonly present in process water.
- Consider the impact of possible deviations from intended reactant charges and operating conditions. For example, is a double charge of one of the reactants a possible deviation, and, if so, what is the impact?
- Identify all heat sources connected to the reaction vessel and determine their maximum temperature.
- Determine the minimum temperature to which the reactor cooling sources could cool the reaction mixture.
- Understand the rate of all chemical reactions. Thermal hazard calorimetry testing can provide useful kinetic data.
- Consider possible vapor-phase reactions. These might include combustion reactions, other vapor-phase reactions such as the reaction of organic vapors with a chlorine atmosphere, and vapor-phase decomposition of materials such as ethylene oxide or organic peroxide.

- Understand the hazards of the products of both intended and unintended reactions.
- Rapid reactions are desirable. In general, you want chemical reactions to occur immediately when the reactants come into contact.
- Avoid batch processes in which all the potential chemical energy is present in the system at the start of the reaction step.
- Avoid using control of reaction mixture temperature as a means for limiting the reaction rate.
- Avoid feeding a material to a reactor at a higher temperature than the boiling point of the reactor contents. This can cause rapid boiling of the reactor contents and vapor generation.

Exothermic Reactions and “Runaway Reactions” The term *runaway reaction* is often improperly used to refer to any uncontrolled chemical reaction. As properly used, it refers to loss of control of a kinetically limited, exothermic reaction that proceeds at a stable, controlled rate under normal conditions and that includes adequate removal of the heat of reaction (Fig. 23-15). When the situation changes such that the heat of reaction is not adequately removed, the excess heat increases the temperature of the reaction mass, which in turn increases the reaction rate and thus the rate of heat release as an exponential function of reaction temperature. If not limited by some means such as (1) the limiting reactant being exhausted, (2) a solvent removing the heat of reaction by boiling off, or (3) quenching or inhibiting the reaction, this “bootstrap” situation can result in an exponential temperature rise that can reach as high as hundreds of degrees Celsius per minute. The resulting temperature increase, generation of gaseous reaction products, and/or boiloff of evaporated liquid can easily exceed a pressure and/or thermal limit of the containment system, if not adequately relieved. The elevated temperatures may also initiate a secondary or side reaction that is even more rapid or energetic.

This runaway situation can be understood by comparing Fig. 23-15 with Fig. 23-16, which has two new lines added, for two possible upset conditions in a process with a cooling coil or other heat exchanger being used to absorb the heat of an exothermic reaction. The temperature of the cooling medium might increase (shift from line 1 to line 2), or the heat-transfer coefficient might decrease, such as by heat exchanger fouling (shift from line 1 to line 3). When one of these shifts gets past point T_{NR} (temperature of no return), the heat removal line no longer crosses the heat generation line, and stable operation is no longer possible. The heat of reaction causes the system temperature to increase, which further increases the rate of heat generation, which further increases the system temperature, etc.

Many possible abnormal situations can initiate a runaway reaction. These include

- Loss of flow of cooling medium to/from the reactor
- An increase in the temperature of the cooling medium

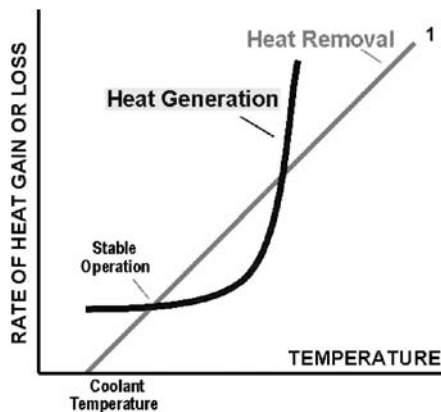


FIG. 23-15 For stable operation, all heat generated by an exothermic reaction is transferred to the surroundings, by whatever means (conduction, evaporation, etc.).

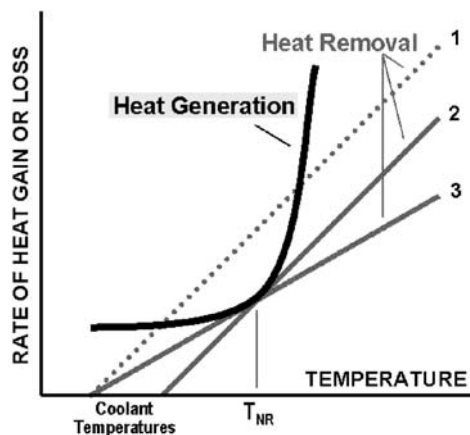


FIG. 23-16 For an exothermic reaction system with heat removal, e.g., to a vessel jacket and cooling coil, the limit of stable operation is reached as the reaction temperature increases to T_{NR} (temperature of no return), beyond which the rate of heat generation, which increases exponentially with increasing temperature, exceeds the capability of the system to remove the heat of reaction (see text).

- A general increase in the temperature of the storage or process configuration, such as due to an extreme ambient condition or loss of refrigeration
- Abnormal heat addition to the reactive material or mixture, such as by an external fire or the injection of steam to a vessel jacket or directly into the material or mixture
- Intentional heating of a vessel containing thermally sensitive material, due to lack of recognition of the runaway hazard or other reason
- Gradual fouling of the heat exchange surfaces to the point that maximum coolant flow is no longer sufficient to remove the heat of reaction
- Loss of agitation or circulation of the reactant mass or other reduction in the heat-transfer coefficient or contact with the heat exchange surface
- Insulation of the system, resulting in less heat dissipation
- Addition of a contaminant or excess catalyst which would increase the reaction rate
- Excess or too rapid addition of a limiting reactant
- Blockage of a vapor line or other means of increasing the system pressure
- Loss of a moderating diluent or solvent
- Inadequate inhibitor concentration in a storage container, or inadequate mixing of the inhibitor (including due to freezing of the material)
- Transfer of the reactive material or mixture to a location not capable of removing the heat of reaction

As can be seen from the above list, runaway reactions do not occur by a single mechanism. They can take place not only in reactors but also in raw material and product storage containers and vessels, purification systems, and anywhere else exothermic reactive systems and self-reacting materials (as described below) are involved.

Historical perspective An analysis of thermal runaways in the United Kingdom (Barton and Nolan, "Incidents in the Chemical Industry due to Thermal Runaway Chemical Reactions," *Hazards X: Process Safety in Fine and Specialty Chemical Plants*, IChem 115: 3–18) indicated that such incidents occur because of the following general causes:

- Inadequate understanding of the process chemistry and thermochemistry
- Inadequate design for heat removal
- Inadequate control systems and safety systems
- Inadequate operational procedures, including training

Semibatch reactions The inherently safer way to operate exothermic reaction processes is to determine a temperature at which the reaction occurs very rapidly (Hendershot 2002). The reactor can be

operated at this temperature, while feeding at least one of the reactants gradually to limit the potential energy contained in the reactor. This type of gradual addition process is often called *semibatch*. A physical limit to the possible rate of addition of the limiting reactant is desirable—e.g., a metering pump, flow limited by using a small feed line, or a restriction orifice. Ideally, the limiting reactant should react immediately, or very quickly, when it is charged. The reactant feed can be stopped if necessary, if there is any kind of a failure (e.g., loss of cooling, power failure, loss of agitation), and the reactor will contain little or no potential chemical energy from unreacted material. Some means to confirm actual reaction of the limiting reagent is also desirable. A direct measurement is best, but indirect methods such as monitoring of the demand for cooling from an exothermic batch reactor can also be effective.

Design of Emergency Relief and Effluent Treatment Systems Containment systems are only rarely designed with sufficient pressure and temperature rating to fully contain a runaway reaction. For this reason, overpressure protection is of obvious critical importance as a last line of defense against loss events that can result from runaway reactions. The latter sections in this chapter on Pressure Relief Systems and on Emergency Relief Device Effluent Collection and Handling address design basis selection, relief calculations, and effluent treatment system configurations for reactive system overpressure protection.

Endothermic Reactions An endothermic reaction process is generally easier to bring to a safe state if an out-of-control situation is detected. Discontinuing the heat input is usually the primary line of defense to stop the operation. In this regard, the endothermic reaction is inherently safer than an exothermic reaction.

The following should especially be taken into account:

- The final product of an endothermic chemical reaction has a greater energy content than the starting materials. For this reason, materials with net positive heats of formation are often termed *endothermic compounds*. (Most explosives, e.g., are endothermic compounds.) This energy content can potentially be released in an uncontrolled manner if sufficient energy is again added to the material, such as by heating it to a decomposition temperature.
- Likewise, if control is lost of an endothermic reaction process, such as by a heating control valve opening too far or by a steam leak directly into the reaction mass, a degradation reaction or other secondary or side reaction may be initiated that can be exothermic and can lead to a thermal runaway.
- Some endothermic compounds can gradually degrade, decompose, become more concentrated, or become sensitized over time.

Designing Facilities for Avoidance of Unintended Reactions

General Considerations The following general design and operational considerations for avoiding unintended chemical reactions are summarized from a CCPS Safety Alert (2001):

- Train all personnel to be aware of reactivity hazards and incompatibilities and to know maximum storage temperatures and quantities.
- Design storage and handling equipment with all compatible materials of construction.
- Avoid heating coils, space heaters, and all other heat sources for thermally sensitive materials.
- Avoid confinement when possible; otherwise, provide adequate emergency relief protection.
- Avoid the possibility of pumping a liquid reactive material against a closed or plugged line.
- Locate storage areas away from operating areas in secured and monitored locations.
- Monitor material and building temperatures where feasible with high-temperature alarms.
- Clearly label and identify all reactive materials and what must be avoided (e.g., heat, water).
- Positively segregate and separate incompatible materials, using dedicated equipment if possible.
- Use dedicated fittings and connections to avoid unloading a material to the wrong tank.
- Rotate inventories for materials that can degrade or react over time.

- Pay close attention to housekeeping and fire prevention around storage/handling areas.

Identifying Potential Reactions The U.S. Chemical Safety and Hazard Investigation Board's Hazard Investigation "Improving Reactive Hazard Management" (2002) highlighted the importance of identifying chemical reactivity hazards as a result of an examination of 167 previous reactive incidents. CCPS has published a preliminary screening methodology for identifying where reactive hazards are likely to exist (Johnson et al., 2003). The flowchart for the preliminary screening methodology is shown later in the Hazard Analysis subsection.

The following paragraphs break down the types of reactive materials and reactive interactions that an engineer may need to address in the design of a chemical process or other facility such as a warehouse where reactive materials are handled (Johnson and Lodal, 2003; Johnson et al., 2003). These can be considered to be in three larger categories:

- Self-reactive substances (polymerizing, decomposing, rearranging)
- Substances that are reactive with ubiquitous substances such as air (spontaneously combustible/pyrophoric, peroxide-forming), water (water-reactive), or ordinary combustibles (oxidizers)
- Incompatible materials

Polymerizing, Decomposing, and Rearranging Substances Most of these substances are stable under normal conditions or with an added inhibitor, but can energetically self-react with the input of thermal, mechanical, or other form of energy sufficient to overcome its activation energy barrier (see Sec. 4, Reaction Kinetics, Reactor Design, and Thermodynamics). The rate of self-reaction can vary from imperceptibly slow to violently explosive, and is likely to accelerate if the reaction is exothermic or self-catalytic.

The tendency of a material such as acrylic acid or styrene to *polymerize* is usually recognized, and the material safety data sheet should be checked and the supplier can be contacted as to whether hazardous polymerization might be expected. A less energetic means of self-reaction is by molecular *rearrangement* such as by isomerizing, tautomerizing, disproportionating, or condensing.

The *decomposition* of some materials into smaller, more stable molecules can be initiated by mechanical shock alone, and they are known as *shock-sensitive*. Many commercially important chemicals are *thermally sensitive* and decompose with the addition of heat. For storage situations, the critical temperature at which the thermal energy is sufficient to start an uncontrolled reaction in a particular storage configuration for a specified time is known as the *self-accelerating decomposition temperature* (SADT), as described in NFPA 49.

Decomposing materials are sometimes referred to as *unstable*, and generally they have a positive heat of formation such that energy will be released when the decomposition reaction occurs. Self-reactive materials can often be recognized by the presence of certain chemical structures that tend to confer reactivity. These include

- Carbon-carbon double bonds not in benzene rings (e.g., ethylene, styrene)
- Carbon-carbon triple bonds (e.g., acetylene)
- Nitrogen-containing compounds (NO₂ groups, adjacent N atoms, etc.)
- Oxygen-oxygen bonds (peroxides, hydroperoxides, ozonides)
- Ring compounds with only three or four atoms (e.g., ethylene oxide)
- Metal- and halogen-containing complexes (metal fulminates, halites, halates, etc.).

A more complete list is given by CCPS (1995), and specific compounds can be investigated in resources such as Urben (1999).

General considerations for avoiding unintended reactions with self-reacting substances include knowing the mechanisms and boundaries of what will initiate a self-reaction, maintaining diluents or inhibitors to extend the boundaries where feasible and avoiding the mechanisms (such as shock and overtemperature) that would initiate the self-reaction, and having reliable controls and last-resort safety systems in place to detect and deal with an incipient out-of-control condition.

Specific design considerations for a few substances including acrylic acid, styrene, organic peroxides, ethylene oxide, and 1,3-butadiene are given in CCPS (1995) on the basis of an industry-practice survey. Detailed information for other substances is distributed by industry

user groups. These include methacrylic acid and methacrylate esters (www.mpaua.org) and ethylene oxide (www.ethyleneoxide.com).

Spontaneously Combustible and Pyrophoric Substances *Spontaneously combustible* substances will readily react with the oxygen in the atmosphere, igniting and burning even without an ignition source. Ignition may be immediate, or may result from a self-heating process that may take minutes or hours (hence, some spontaneously combustible substances are known as *self-heating* materials).

Pyrophoric materials ignite spontaneously on short exposure to air under ordinary ambient conditions. Some materials that are considered pyrophoric require a minimum relative humidity in the atmosphere for spontaneous ignition to occur. The potential of pyrophoric materials to exhibit this behavior is usually well known due to the extreme care required for their safe handling.

Pyrophoric and other spontaneously combustible substances will generally be identified as such on their product literature, material safety data sheets (MSDSs), or International Chemical Safety Cards (ICSCs). If transported, these substances should be identified as DOT/UN Hazard Class 4.2 materials for shipping purposes and labeled as spontaneously combustible. For pyrophoric substances, the NFPA 704 diamond for container or vessel labeling has a red (top) quadrant with a rating of 4, indicating the highest severity of flammability hazard (NFPA 704, 2001). Note that pyrophoric materials often exhibit one or more other reactivity hazards as well, such as water reactivity.

A scenario that has resulted in many fires and explosions in petroleum refineries involves iron sulfide. An impure, pyrophoric sulfide is formed when streams containing hydrogen sulfide or other volatile sulfur compounds are processed in ferrous equipment. Oxidation of moist iron sulfide is highly exothermic. Opening sulfide-containing equipment without adequate purging can result in rapid self-heating and ignition of the iron sulfide, which can then ignite other residual flammable gases or liquids in the equipment.

Many scenarios involving spontaneous combustion involve a combination of materials exposed to sufficient air, often in an insulating situation that prevents heat from a slow oxidation reaction from dissipating, which results in a self-heating situation.

Lists of pyrophoric materials that include less common chemicals, including metals, can be found in volume 2 of *Bretherick's Handbook of Reactive Chemical Hazards* (Urben, 1999). Other spontaneously combustible substances are tabulated by their proper shipping names and UN/NA numbers in the U.S. Dept. of Transportation regulation 49 CFR 172.101.

Possible causes of uncontrolled reactions associated with pyrophoric and other spontaneously combustible materials are listed in Johnson et al. (2003).

Peroxide Formers *Peroxide formers* will react with the oxygen in the atmosphere to form unstable peroxides, which in turn might explosively decompose if concentrated. Peroxide formation, or peroxidation, usually happens slowly over time, when a peroxide-forming liquid is stored with limited access to air.

Substances that are peroxide formers will often have an inhibitor or stabilizer added to prevent peroxidation. They are often not easily identifiable as peroxide formers by using MSDSs or ICSCs. Rather, they are frequently identified by another characteristic, such as flammability, for storage and shipping purposes. Examples of peroxide formers include 1,3-butadiene, 1,1-dichloroethylene, isopropyl ether, and alkali metals. Johnson et al. (2003) tabulate other chemical structures susceptible to peroxide formation.

The total exclusion of air from vessels and equipment containing peroxide formers, and the establishment and observing of strict shelf life limitations, are basic strategies for managing peroxide-forming hazards.

Water-Reactive Substances *Water-reactive substances* will chemically react with water, particularly at normal ambient conditions. For fire protection purposes, a material is considered water-reactive if a gas or at least 30 cal/g (126 kJ/kg) of heat is generated when it is mixed with water (NFPA 704, 2001), using a two-drop mixing calorimeter.

Water reactivity can be hazardous by one or more of several mechanisms. The heat of reaction can cause thermal burns, ignite combustible materials, or initiate other chemical reactions. Flammable,

corrosive or toxic gases are often formed as reaction products. The violence of some reactions may disperse hazardous materials. Even slow reactions can generate sufficient heat and off-gases to overpressurize and rupture a closed container.

Substances that are water-reactive will nearly always be identified as such on their MSDSs or ICSCs. They may be identified as DOT/UN Hazard Class 4.3 materials for shipping purposes and labeled as dangerous when wet. However, some water-reactive materials are classified otherwise. Acetic anhydride is designated Class 8; it may also be identified as a combustible liquid.

The total exclusion of water from vessels and equipment containing water-reactive substances, and the maintenance of the primary containment integrity over time, are the obvious design and operational considerations when handling water-reactive substances. Drying of equipment prior to start-up and careful design of provisions for cleaning and purging of equipment are also essential.

Oxidizers and Organic Peroxides An oxidizer is any material that readily yields oxygen or other oxidizing gas, or that readily reacts to promote or initiate combustion of combustible materials (NFPA 430, 2000). Thus, most oxidizers can be thought of as being reactive with ordinary combustible liquids or solids, which are commonly used as process, packaging, general use, or structural materials. They can also react with many other reducing substances.

Oxidizers will nearly always be identified as such on their MSDSs or ICSCs. They may be identified as DOT/UN Hazard Class 5.1 materials for shipping purposes and labeled as oxidizers. However, some oxidizers are classified otherwise.

Volume 2 of *Bretherick's Handbook of Reactive Chemical Hazards* (Urban, 1999) lists many structures and individual chemical compounds having oxidizing properties. NFPA 432 can be consulted for typical organic peroxide formulations. Note, however, that some organic peroxide formulations burn with even less intensity than ordinary combustibles and present no chemical reactivity hazard.

NFPA 430 contains safety provisions for the storage of liquid and solid oxidizers. NFPA 432 contains safety provisions for the storage of organic peroxide formulations.

Incompatible Materials In this context, *incompatible* refers to two materials not able to contact each other without undesired consequences. ASTM E 2012 gives a method for preparing a binary compatibility chart for identifying incompatibilities. The NOAA Chemical Reactivity Worksheet uses a group compatibility method to predict the results of mixing any binary combination of the 6080 chemicals in the CAMEO database, including many common mixtures and solutions. Materials to be considered include not only raw materials and products but also by-products, waste products, cleaning solutions, normal and possible abnormal materials of construction, possible contaminants and degradation products, material that could be left in the process from a previous batch or cleanout, and materials in interconnected piping, heat-transfer systems, waste collection systems, or collocated storage.

The essence of the ASTM E 2012 approach is to determine incompatibility scenarios that could foreseeably occur by examining all possible binary combinations. It may be necessary to review a process by using a systematic method such as a process hazard analysis (PHA) to identify all incompatibility scenarios that have a significant likelihood of occurrence and severity of consequences. The same review can then be used to evaluate whether adequate safeguards exist or whether further risk reduction is warranted.

Where the consequences of combining two or more materials under given conditions of temperature, confinement, etc., are unknown and cannot be predicted with certainty, testing may need to be performed to screen for potential incompatibilities. Two common test methods used for this purpose are differential scanning calorimetry and mixing cell calorimetry (described later in this section).

Design considerations to avoid contact of incompatible materials include total exclusion of an incompatible substance from the facility; quality control and sampling of incoming materials; approval procedures for bringing new chemicals and materials of construction on-site; dedicated fittings and unloading spots; vessel, piping, and container labeling; dedicated or segregated storage; segregated diking, drainage, and vent systems; quality control of raw materials and of

materials of construction (both initial construction and ongoing maintenance and modifications); sealless pumps, double tube sheets, and other means of excluding seal fluid, heat-transfer fluid, and other utility substances; positive isolation of interconnections by physical disconnects, blinding, or double block and bleed valves; avoidance of manifolds with flexible connections; and use of compatible purge gases, cleaning solutions, heat-transfer fluids, insulation, fire-extinguishing and suppression agents whenever possible; and removal of unused materials from the site. These design considerations will always need to be accompanied by procedure training, hazard awareness, and operating discipline for them to be effective on an ongoing basis.

Designing Mitigation Systems to Handle Uncontrolled Reactions (From CCPS, *Guidelines for Safe Storage and Handling of Reactive Materials*, 1995, Chap. 5.) Last-resort safety systems are intended to be used in many reactive chemical storage and handling operations as last-ditch efforts to avert a loss event such as an explosion or a hazardous material release, if the operation exceeds safe operating limits and it is not possible to regain control by using the operation's normal control mechanisms.

Inhibitor Injection Inhibitor injection systems are primarily used with polymerizing materials such as vinyl acetate. If the material begins to self-react in an uncontrolled manner, then injection of a polymerization inhibitor can interfere with the reaction before sufficient pressure and temperature have built up to cause a release from the storage/handling containment. The type of inhibitor needed will depend on the nature of the polymerization reaction; e.g., a free-radical scavenger may be used as an inhibitor for a material that reacts by free-radical polymerization. The inhibitor is often the same inhibitor used for normal storage stability requirements, but injected in a much larger quantity. If a different inhibitor is used that is designed to quickly kill the reaction, it is generally called a *short-stop* system.

Inhibitor injection systems need to be carefully designed and maintained to provide a highly reliable last-resort safety system. Since the inhibitor injection system is on standby and may not be used for months, attention must be paid to how the system components can be functionally and effectively tested on a periodic basis, such as once a month, without excessive disruption of normal operations. CCPS' *Guidelines for Engineering Design for Process Safety* (CCPS-AIChE, New York, 1993, pp. 273–275) discusses testing of continuous-process safety systems. This functional testing is important not only for the checking of adequate inhibitor supply and properly functioning delivery system, but also as the means of detecting an out-of-control situation and actuating the inhibitor injection system. Such systems, as well as other last-resort safety systems, are likely to be considered *safety instrumented systems* (SISs); and they should be selected, designed, and maintained accordingly (see the later section on SISs).

Quench Systems Quench systems are used for essentially all types of reactive chemicals. A quench system involves the addition of flooding quantities of water or other quenching medium to the reactive material; the quenching medium might be a subcooled material such as liquid nitrogen or dry ice in special applications.

The means by which a quench system works depends on the nature of the reactive material; e.g., for water-reactive materials, a quench system will destroy the material in a last-resort situation and generally form less-hazardous products, and will at the same time absorb some of the heat of reaction. Most quench systems are designed to both cool down and dilute a material that may be reacting uncontrollably; the quenching medium may also actually interfere with the chemical reaction or deactivate a catalyst.

Dump Systems For an inhibitor injection or quench system, the inhibitor or quenching medium is transferred from an external supply to the reactive material; in a dump system, the reactive material is transferred from the storage/handling facility to a safer location that is the same size or, more commonly, larger than the normal capacity of the facility. This allows depressurizing and deinventory of the reacting mass from the facility in an out-of-control situation, such as an incipient runaway reaction.

Depressuring Systems A last-resort depressurizing system can be added to a reactive system to vent off excessive pressure buildup in a tank vessel in a controlled manner before reaching the relief valve or

rupture disk set pressure. Such a depressurizing system typically consists of a remotely actuated vent valve connected to the vapor space of the vessel, with the venting discharge directed to a scrubber or other treatment system of adequate capacity. The system can be designed to be actuated either manually, by a control room or field operator, or by detection of high pressure and/or high temperature in the vessel.

Reactive Hazard Reviews and Process Hazard Analyses Reactive hazards should be evaluated using reviews on all new processes and on all existing processes on a periodic basis. Reviews should include

1. Review of process chemistry, including reactions, side reactions, heat of reaction, potential pressure buildup, and characteristics of intermediate streams
2. Review of reactive chemicals test data for evidence of flammability characteristics, exotherms, shock sensitivity, and other evidence of instability
3. Review of planned operation of process, especially the possibility of upsets, modes of failure, unexpected delays, redundancy of equipment and instrumentation, critical instruments and controls, and worst-credible-case scenarios

These reviews can be either in addition to or combined with periodic process hazard analyses (PHAs) by using methods such as what-if analysis and HAZOP studies. The latter should consciously focus on identifying scenarios in which intended reactions could get out of control and unintended reactions could be initiated. One means of accomplishing this as part of a HAZOP study has been to include *chemical reaction* as one of the parameters to be investigated for each study node. Johnson and Unwin (2003) describe other PHA-related approaches for studying chemical reactivity hazards.

Worst-Case Thinking At every point in the operation, the process designer should conceive of the worst possible combination of circumstances that could realistically exist, such as loss of cooling water, power failure, wrong combination or amount of reactants, wrong valve position, plugged lines, instrument failure, loss of compressed air, air leakage, loss of agitation, deadheaded pumps, and raw material impurities. An engineering evaluation should then be made of the worst-case consequences, with the goal that the plant will be safe even if the worst case occurs. The previous discussion of calculating the maximum adiabatic temperature rise, then considering what might happen if it is realized, is an example of this type of analysis. A hazard and operability (HAZOP) study could be used to help identify abnormal situations and worst-case consequences.

Reactivity Testing Many of the data needed for the design of facilities with reactivity hazards involve the determination of thermal stability and of

1. The temperature at which an exothermic reaction starts
2. The rate of reaction as a function of temperature
3. Heat generated per unit mass of material

In many cases, data on the increase of pressure during a reaction are also required, especially for vent sizing, and on the composition of the product gases.

The term *onset temperature* T_{onset} is used in two contexts:

1. In a testing context, it refers to the first detection of exothermic activity on the thermogram. The differential scanning calorimeter (DSC) has a scan rate of 10°C/min, whereas the accelerating rate calorimeter (ARC[®]) has a sensitivity of 0.02°C/min. Consequently, the temperature at which thermal activity is detected by the DSC can be as much as 50°C different from ARC data.

2. The second context is the process reactor. There is a potential for a runaway if the net heat gain of the system exceeds its total heat loss capability. A self-heating rate of 3°C/day is not unusual for a monomer storage tank in the early stages of a runaway. This corresponds to 0.00208°C/min, which is 10 percent of the ARC's detection limit.

Sources of Reactivity Data Several important sources of reactivity data are described in the following paragraphs.

Calculations Potential energy that can be released by a chemical system can often be predicted by thermodynamic calculations. If there is little energy, the reaction still may be hazardous if gaseous products are produced. Kinetic data are usually not available in this way. Thermodynamic calculations should be backed up by actual tests.

Differential Scanning Calorimetry Sample and inert reference materials are heated in such a way that the temperatures are always equal. Onset-of-reaction temperatures reported by the DSC are higher than the true onset temperatures, so the test is mainly a screening test.

Differential Thermal Analysis (DTA) A sample and inert reference material are heated at a controlled rate in a single heating block. This test is basically qualitative and can be used for identifying exothermic reactions. Like the DSC, it is also a screening test. Reported temperatures are not reliable enough to be able to make quantitative conclusions. If an exothermic reaction is observed, it is advisable to conduct tests in the ARC.

Mixing Cell Calorimetry (MCC) The MCC provides information regarding the instantaneous temperature rise resulting from the mixing of two compounds. Together, DSC and MCC provide a reliable overview of the thermal events that may occur in a process.

Accelerating Rate Calorimetry (ARC) This equipment determines the self-heating rate of a chemical under near-adiabatic conditions. It usually gives a conservative estimate of the conditions for, and consequences of, a runaway reaction. Pressure and rate data from the ARC may sometimes be used for pressure vessel emergency relief design. Activation energy, heat of reaction, and approximate reaction order can usually be determined. For multiphase reactions, agitation can be provided. Nonstirred ARC runs may give answers that do not adequately duplicate plant results when there are reactants that may settle out or that require mixing for the reaction to be carried out (DeHaven and Dietsche, "Catalyst Explosion: A Case History," *Plant/Oper. Prog.*, April 1990).

Vent Sizing Package (VSP2™) The VSP is an extension of ARC technology. The VSP2 is a bench-scale apparatus for characterizing runaway chemical reactions. It makes possible the sizing of pressure relief systems with less engineering expertise than is required with the ARC or other methods.

Advanced Reactive System Screening Tool (ARSST™) The ARSST measures sample temperature and pressure within a sample containment vessel. The ARSST determines the potential for runaway reactions and measures the rate of temperature and pressure rise (for gassy reactions) to allow determinations of the energy and gas release rates. This information can be combined with simplified methods to assess reactor safety system relief vent requirements.

Shock Sensitivity Shock-sensitive materials react exothermically when subjected to a pressure pulse. Materials that do not show an exotherm on a DSC or DTA are presumed not to be shock-sensitive. Testing methods include

- **Drop weight test** A weight is dropped on a sample in a metal cup. The test measures the susceptibility of a chemical to decompose explosively when subjected to impact. This test should be applied to any materials known or suspected to contain unstable atomic groupings.
- **Confinement cap test** Detonatability of a material is determined by using a blasting cap.
- **Adiabatic compression test** High pressure is applied rapidly to a liquid in a U-shaped metal tube. Bubbles of hot compressed gas are driven into the liquid and may cause explosive decomposition of the liquid. This test is intended to simulate water hammer and sloshing effects in transportation, such as humping of railway tank cars. It is very severe and gives worst-case results.

Obtaining test data for designing a facility with significant reactivity hazards requires familiarity with a range of test equipment and a significant amount of experience in the interpretation of test results.

TOXICITY

Introduction Many natural and artificial substances are toxic to humans (and animals). Liquids and solids can be ingested, or exposure can be through the skin, eyes, or other external passages to the body. Where these substances are gaseous or volatile, toxic effects can result from inhalation. As a result of accidents and tests, it has been discovered that some of these substances are more toxic than others. Quantification of the degree of hazard has become important in devising appropriate measures for containing these substances.

Several chemical companies have established toxicology laboratories to develop quantitative information concerning the toxicity of raw materials, products, by-products, and waste materials. They include Dow, Du Pont, Eastman Kodak, and Union Carbide (Fawcett and Wood, *Safety and Accident Prevention in Chemical Operations*, 2d ed., pp. 262 and 281, 1982). Also, the Chemical Industry Institute of Toxicology was established in 1975 to provide toxicological hazards services, and The Netherlands Organization of Applied Scientific Research [TNO] has performed similar toxicological research in the Netherlands (The Institution of Chemical Engineers, *Chlorine Toxicity Monograph*, p. 34, 1989).

The present "Process Safety Management" standard of the Occupational Safety and Health Act requires "toxicity information" and "a qualitative evaluation of a range of the possible safety and health effects of failure of controls on employees in the workplace" [U.S. Department of Labor, *Occupational Safety and Health Standards*, 29 CFR 1910.119(d)(1)(i), (e)(3)(vii), and (f)(1)(iii)(A), 1992]. Similarly, the "Risk Management Programs for Chemical Accidental Release Prevention" standard of the Environmental Protection Agency's Clean Air Act Amendments [U.S. Environmental Protection Agency, *Risk Management Programs for Chemical Accidental Release Prevention*, 40 CFR 68.15(b)(3), 15(c), 24(c)(7), and 26(b)(1), 1993] requires toxicity information, a qualitative evaluation of a range of the possible safety and health effects of failure of controls on public health and the environment, and analysis of the off-site consequences of the worst-case release scenario and the other more likely significant accidental release scenarios.

To perform safety and health evaluations, quantitative knowledge of the effects of exposure to toxic materials would be needed. Some of the available data for inhalation toxicity (quantitative), skin-absorption toxicity (qualitative), and ingestion (quantitative) of hazardous materials are presented in Table I (American Industrial Hygiene Association, *Emergency Response Planning Guidelines and Workplace Environmental Exposure Level*, No. AEAH05-559, 2005; National Institute for Occupational Safety and Health, *Pocket Guide to Chemical Hazards*, 1994; American Conference of Governmental Industrial Hygienists, *Threshold Limit Values for Chemical Substances and Physical Agents*, 2001; National Institute for Occupational Safety and Health, *Registry of Toxic Effects of Chemical Substances*, 1983). To facilitate use of these data, several types of graphical and "probit" equation methods are available (Griffiths, "The Use of Probit Expressions in the Assessment of Acute Population Impact of Toxic Releases," *Journal of Loss Prevention in the Process Industries*, 4: 49, January 1991; Prugh, "Quantitative Evaluation of Inhalation-Toxicity Hazards," 29th Annual Loss Prevention Symposium, 1995).

The scope of this section is limited to dangerous and life-threatening exposures of the public to toxic materials (primarily gases and vapors) and non-life-threatening exposures of employees to toxic materials. Data concerning life-threatening concentrations and doses of many toxic gases, vapors, and liquids are available (National Institute for Occupational Safety and Health, *Registry of Toxic Effects of Chemical Substances*, 1983).

Inhalation Toxicity: The Haber Equation In 1924, Fritz Haber reported on his analysis of the results of animal inhalation tests on chemical warfare agents. He discovered that the product of gas or vapor concentration and duration of exposure was nearly constant for a given physiological effect. This relationship has been termed the *Haber law* (Haber, *Fünf Vorträge aus den Jahren 1920-1923*, Springer-Verlag, 1924; Fleming et al., *Modern Occupational Medicine*, p. 78, 1960):

$$Ct = K = D \quad (23-22)$$

When the concentration C is expressed in parts per million (ppm) and the duration of exposure t is expressed in minutes, the values of the constant K and the dose D are in units of ppm-minutes.

It is now recognized that Haber's law does not apply for long exposures to low concentrations. Apparently, there are metabolic processes in the human body (and in animals) that can (for many toxic materials) result in biotransformation or detoxification, elimination, or excretion of toxic materials, or can repair damaged cells or tissues (Elkins, *The Chemistry of Industrial Toxicology*, 2d ed., p. 242, 1959; U.S. Federal

Emergency Management Agency, *Handbook of Chemical Hazard Analysis Procedures*, p. 6-7, 1989). It is likely that the absorption process functions in proportion to the square root of the duration of exposure (Perry, *Chemical Engineers' Handbook*, 4th ed., p. 14-13 and Figs. 14-7, 14-9, and 14-21, 1963).

Dosage Equation The Haber law apparently applies to short exposures (less than 30 min) (The Institution of Chemical Engineers, *Chlorine Toxicity Monograph*, Table 5, Rat Group Codes U, N, E, X, and Z, and Mouse Group Codes N and R, 1989), but does not apply for long exposures to toxic vapors and gases. Eisenberg and others (Eisenberg et al., *Vulnerability Model—A Simulation System for Assessing Damage Resulting from Marine Spills*, U.S. Coast Guard Report CG-D-136-75, pp. 77, 83-89, and 257-267, 1975); also, 3d International Symposium on Loss Prevention in the Process Industries, p. 15/1158, and Proceedings, p. 190, 1980) attempted to modify the dose equation to fit the data over a useful range of interest, between 5 min and 2 h (Lees, *Loss Prevention in the Process Industries*, pp. 206-209, 527, 594, 599, 651-653, and 661, 1980). They found that the following equation could be used:

$$C^n t = K \quad (23-23)$$

Eisenberg found that a value of 2.75 for n was appropriate for the chlorine and ammonia data which were available.

In the 20 years since Eisenberg's report, many inhalation toxicity tests have been conducted, and many of the earlier data have been reexamined, with the result that values for n ranging from 0.6 to 4.9 have been applied to the above dose equation. It appears (Griffiths, "The Use of Probit Expressions in the Assessment of Acute Population Impact of Toxic Releases," *Journal of Loss Prevention in the Process Industries*, 4, p. 49, 1991) that the value of n may be related to the degree of breathing rate stimulation (high value of n) or repression (low values of n), and the value of n apparently increases with increasing exposure times (decreasing slope of ordinate C versus abscissa t). A value of 1.0 is frequently used by investigators if there are few data.

Probit Equation The probit equation has been used in an attempt to quantitatively correlate hazardous material concentration, duration of exposure, and probability of effect/injury, for several types of exposures. The objective of such use is to transform the typical sigmoidal (S-shaped) relationship between cause and effect to a straight-line relationship (Mannan, *Lees' Loss Prevention in the Process Industries*, 3d ed., p. 9/68, 2005).

Probit equations have the following form (Mannan, *Lees' Loss Prevention in the Process Industries*, 3d ed., Table 9.29, 2005):

$$Y = k_1 + k_2 \ln V \quad (23-24)$$

where Y = probit value

V = value of "intensity of causative factor which harms the vulnerable resource"

k_1 = constant that is intercept of Y versus V line (where value of V is 1.0 and $\ln V$ is 0).

k_2 = constant that is slope of Y versus $\ln V$ line.

The following table can be used to convert from probit values to probability percentages (Mannan, *Lees' Loss Prevention in the Process Industries*, 3d ed., Table 9.29, 2005):

Percentage	Probit value P
0.001 (1 in 10 ⁵)	0.73
0.01 (1 in 10 ⁴)	1.28
0.1 (1 in 10 ³)	1.90
1 [1%] (1 in 100)	2.67
3 [3%] (3 in 100)	3.12
10 [10%] (1 of 10)	3.72
30 [30%] (3 of 10)	4.48
50 [50%] (5 of 10)	5.00

23-32 PROCESS SAFETY

For the inhalation hazards of toxic vapors and gases, the function V has the form

$$V = C^n t \quad (23-25)$$

where C = concentration by volume, ppm
 t = duration of exposure, min
 n = exponent that expresses difference between dosage and dose

The term *dosage* typically refers to an environmental hazard and is the product of the concentration of toxic gas or vapor at a particular point and the duration of the hazardous environment at that point. Thus, the *dosage* can be expressed as an average concentration multiplied by an average duration, or

$$D = Ct \quad \text{ppm} \cdot \text{min} \quad (23-26)$$

Dose typically refers to the amount of toxic material actually retained and is sometimes referred to as the *toxic load*. Thus, the dose can be expressed as the product of a concentration term and a duration-of-exposure term, by either of the following relationships:

$$TL = V = C^n t \quad \text{ppm}^n \cdot \text{min} \quad (23-27)$$

$$TL = V = Ct^{1/n} \quad \text{ppm} \cdot \text{min}^{1/n} \quad (23-28)$$

Ingestion Toxicity Data are available for the *acute* (single-dose) ingestion/oral toxicity of many toxic materials (National Institute for Occupational Safety and Health, *Registry of Toxic Effects of Chemical Substances*, 1983; Lewis, *Sax's Dangerous Properties of Industrial Materials*, 9th ed., 1996). However, very few data are available for prolonged ingestion or periodic doses of toxic materials. It is likely that metabolic processes would operate to increase the total *burden* required for toxic effects for such chronic exposures, except for some materials (such as mercury and lead) which apparently can accumulate in the body.

The primary route for ingestion of toxic materials (especially dusts, mists, and vapors) is by the swallowing of mucus and saliva that has absorbed these materials during breathing. Cilia in the nose and esophagus (windpipe) sweep foreign materials that have been embedded or absorbed by these fluids toward the pharynx, where the contaminated fluid is swallowed (Guyton, *Textbook of Medical Physiology*, 3d ed., pp. 555, 556, 880, and 894, 1966).

Skin-Contact Toxicity Data for acute (short-term) exposures of the skin to corrosive and toxic liquids, solids, and gases are extremely limited, particularly where the consequences are severe or fatal injury, and the available data may not be useful, from an engineering standpoint. For example, the skin toxicity of hydrogen peroxide to rats is stated as 4060 mg/kg, but the skin area and duration of exposure are not stated. Thus, it is not possible (with the available data) to estimate the relationship among percent of body surface exposed to a corrosive material, the concentration of the corrosive material, the duration of exposure (before removal of the corrosive material), and the severity of the effect.

Somewhat in contrast, there are considerable data concerning the relatively long-term effects of exposure to toxic materials, where there are irritation, tumorigenic, reproductive, or mutation consequences (National Institute for Occupational Safety and Health, *Registry of Toxic Effects of Chemical Substances*, 1983). In the

absence of better skin-contact data, it might be appropriate to use parenteral or subcutaneous injection data for a worst-case exposure (e.g., through a cut in the skin). However, use of intravenous or intraperitoneal data might overstate the skin exposure toxicity of a material.

The U.S. Department of Transportation and others have developed guidance for the corrosivity of chemical substances (U.S. Department of Transportation, *Shippers—General Requirements for Shipments and Packagings*, 49 CFR 173.136, *Definitions*, and 49 CFR 173.137, *Assignment of Packing Group*, 1998); American Society for Testing and Materials, *Practice for Laboratory Immersion Corrosion Testing of Metals*, G-31, 2002; Organization for Economic Cooperation and Development, *Guideline for Testing of Chemicals—Acute Dermal Irritation/Corrosion*, no. 404, 1992). The following definitions apply for Class 8 corrosive materials:

Packing Group 1—Great Danger: Full thickness destruction of human skin (exposure time, 3 min or less; observation time, 60 min).

Packing Group 2—Medium Danger: Full thickness destruction of human skin (exposure time, 3 to 60 min; observation time, 14 days).

Packing Group 3—Minor Danger: Full thickness destruction of human skin (exposure time, 1 to 4 h; observation time, 14 days).

Examples of assignments to packing groups are shown in the table at the bottom of the page.

Another effect of skin-contact toxicity is dermatitis. This can be caused by "physical" agents, such as detergents and solvents that remove the natural oils from the skin and thereby render the skin susceptible to materials that ordinarily do not affect the skin (National Safety Council, *Fundamentals of Industrial Hygiene*, 3d ed., p. 23, 1988). Dermatitis also can be caused by desiccants and water-reactive chemicals that remove moisture from the skin, generating heat and causing burns. Other causes are oxidizers; protein precipitants; allergic or anaphylactic proteins; friction, pressure, and trauma; thermal and electromagnetic radiation; biological agents; and plant poisons. Dermatitis can be prevented or controlled by containment of skin-contact hazards and use of tools to avoid contact (engineering controls) or by the wearing of protective clothing, including gloves and eye and face protection, and good personal hygiene, including hand and face washing (administrative controls) (National Safety Council, *Fundamentals of Industrial Hygiene*, 3d ed., pp. 106, 108, 467, 469, and 471, 1988).

Compilation of Data Table 23-16 presents inhalation toxicity data for the following criteria:

The emergency response planning guidelines (ERPG) concentrations for the following types of effects, for 1-h exposures (American Industrial Hygiene Association, *Emergency Response Planning Guidelines and Workplace Environmental Exposure Level*, no. AEAH05-559, 2005):

- ERPG-1 Mild, transient health effects, without objectionable odor
- ERPG-2 No irreversible or action-impairing effects
- ERPG-3 No life-threatening effects

The immediately dangerous to life and health (IDLH) concentrations (National Institute for Occupational Safety and Health, *Pocket Guide to Chemical Hazards*, 1994), for 30-min exposures.

Values for workplace environmental exposure levels (WEELs) for many materials not listed in Table 23-16 can be obtained from the American Industrial Hygiene Association, at www.aiha.org.

The threshold limit values (TLVs) or time-weighted averages (TWAs) for 8-h exposures of workers (American Conference of Governmental Industrial Hygienists, *Threshold Limit Values for Chemical Substances and Physical Agents*, 2001).

Group	Acids	Alcohols	Oxides	Hydroxides	Halogens	Anhydrides
1	Hydrofluoric acid; selenic acid	Alkyl phenols			Fluorine; chlorine; bromine	
2	Hydrochloric acid; acetic acid; nitric acid	Pentol	Phosphorus pentoxide	Potassium hydroxide; sodium hydroxide		Acetic anhydride
3	Phosphoric acid		Calcium oxide	Ammonium hydroxide		Propionic anhydride

TABLE 23-16 ERPG Values and Other Toxicity Values for Toxic Materials

For materials that are listed in the USEPA 40 CFR 68.130 list and in the NJTCPA Group A and B lists (as of January 1, 2005; refer to current issues for changes).

Definitions:

ERPG-1 The maximum airborne concentration below which it is believed nearly all individuals could be exposed for up to 1 h without experiencing other than mild, transient adverse health effects or without perceiving a clearly defined objectionable odor.

ERPG-2 The maximum airborne concentration below which it is believed nearly all individuals could be exposed for up to 1 h without experiencing or developing irreversible or other serious health effects or symptoms that could impair an individual's ability to take protective action.

ERPG-3 The maximum airborne concentration below which it is believed nearly all individuals could be exposed for up to 1 h without experiencing or developing life-threatening health effects.

IDLH Immediately dangerous to life and health, for 1-h exposures. Where no IDLH data are available, the 50% lethal concentration is shown, as LC50: ppm/time.

WEEL-8 Workplace environmental exposure level, for 8-h time-weighted average (TWA).

WEEL-C Workplace environmental exposure level, as a ceiling (not to be exceeded) value.

TLV-TWA Threshold limit value, time-weighted average for 8-h exposures, with ceiling concentrations shown as C, and with skin absorption hazard as S. The OSHA permissible exposure limit (PEL) is the lower of the TWA or the ceiling limit.

Oral LD50 data are recorded where they are available (— indicates a toxicity listing but no oral toxicity data). Where the material is a gas at normal temperatures and pressure (25°C and 1 atm), the atmospheric-pressure boiling point is given.

Material	CAS no.	ERPG-1	ERPG-2	ERPG-3	IDLH	WEEL-8	WEEL-C	TLV-TWA	Oral, mg/kg
Acetaldehyde	75-07-0	10 ppm	200 ppm	1000 ppm	Ca (2000 ppm)	—	—	0.25 ppm C	1930
Acrolein	107-02-8	0.1 ppm	0.5 ppm	3 ppm	2 ppm	—	—	0.1 ppm C	7
Acrylonitrile	107-13-1	10 ppm	35 ppm	75 ppm	LC50: 576/4 h	—	—	2 ppm	27
Ammonia	7664-41-7	25 ppm	150 ppm	750 ppm	300 ppm	—	—	25 ppm	350
Arsine	7784-42-1	—	0.5 ppm	1.5 ppm	Ca (3 ppm)	—	—	0.05 ppm	-62.5°C
Boron trifluoride	7637-07-2	2 mg/m ³	30 mg/m ³	100 mg/m ³	25 ppm	—	—	1 ppm C	-99.8°C
Bromine	7726-95-6	0.1 ppm	0.5 ppm	5 ppm	3 ppm	—	—	0.1 ppm	14
Carbon disulfide	75-15-0	1 ppm	50 ppm	500 ppm	500 ppm	—	—	10 ppm	2125
Carbon monoxide	630-08-0	200 ppm	350 ppm	500 ppm	1200 ppm	—	—	25 ppm	-191.5°C
Chlorine	7782-50-5	1 ppm	3 ppm	20 ppm	10 ppm	—	—	0.5 ppm	-34.1°C
Chlorine dioxide	10049-04-4	—	0.5 ppm	3 ppm	5 ppm	—	—	0.1 ppm	10.9°C
Chloroform	67-66-3	—	50 ppm	5000 ppm	Ca (500 ppm)	—	—	10 ppm	36
Chloropicrin	76-06-2	0.1 ppm	0.3 ppm	1.5 ppm	2 ppm	—	—	0.1 ppm	250
Chloroprene	126-99-8	—	—	—	Ca (300 ppm)	—	—	10 ppm	260
Dichlorosilane	4109-96-0	—	—	—	LC50: 215/	—	—	—	—
Diethylamine	109-89-7	—	—	—	200 ppm	—	—	5 ppm	540
Dimethylamine	124-40-3	0.6 ppm	100 ppm	350 ppm	500 ppm	—	—	5 ppm	240
Dimethylhydrazine	57-14-7	—	—	—	Ca (15 ppm)	—	—	0.01 ppm	122
Epichlorohydrin	106-89-8	2 ppm	20 ppm	100 ppm	Ca (75 ppm)	—	—	0.5 ppm	90
Ethylamine	75-04-7	—	—	—	600 ppm	—	—	5 ppm	400
Ethylenediamine	107-15-3	—	—	—	1000 ppm	—	—	10 ppm	470
Ethyleneimine	151-56-4	—	—	—	Ca (100 ppm)	—	—	0.5 ppm	15
Ethylene oxide	75-21-8	NA	50 ppm	500 ppm	Ca (800 ppm)	—	—	1 ppm	72
Ethylmercaptan	75-08-1	—	—	—	500 ppm	—	—	0.5 ppm	1960
Fluorine	7782-41-4	0.5 ppm	5 ppm	20 ppm	25 ppm	—	—	1 ppm	-188.3°C
Formaldehyde	50-00-0	1 ppm	10 ppm	25 ppm	Ca (20 ppm)	—	—	0.3 ppm C	42
Furan	110-00-9	—	—	—	LC50: 43/1 h	Minimize	—	—	—
Hydrazine	302-01-2	0.5 ppm	5 ppm	30 ppm	Ca (50 ppm)	—	—	0.01 ppm	49
Hydrogen bromide	10035-10-6	—	—	—	30 ppm	—	—	3 ppm C	-66.7°C
Hydrogen chloride	7647-01-0	3 ppm	20 ppm	150 ppm	50 ppm	—	—	5 ppm C	-85.0°C
Hydrogen cyanide	74-90-8	NA	10 ppm	25 ppm	50 ppm	—	—	4.7 ppm C	2
Hydrogen fluoride	7664-39-3	2 ppm	20 ppm	50 ppm	30 ppm	—	—	3 ppm C	-19.5°C
Hydrogen selenide	7783-07-5	NA	0.2 ppm	2 ppm	1 ppm	—	—	0.05 ppm	-41°C
Hydrogen sulfide	7783-06-4	0.1 ppm	30 ppm	100 ppm	100 ppm	—	—	10 ppm	-60°C
Iron pentacarbonyl	13463-40-6	—	—	—	LC50: 870/10 min	—	—	0.1 ppm	12
Isopropylamine	75-31-0	—	—	—	750 ppm	—	—	5 ppm	820
Ketene	143-50-0	—	—	—	5 ppm	—	—	0.5 ppm	1300
Methacrylonitrile	126-98-7	—	—	—	LC50: 36/4 h	—	—	1 ppm	15
Methylamine	74-89-5	10 ppm	100 ppm	500 ppm	100 ppm	—	—	5 ppm	-6.3°C
Methyl bromide	74-83-9	NA	50 ppm	200 ppm	Ca (250 ppm)	—	—	1 ppm	214
Methyl chloride	74-87-3	NA	400 ppm	1000 ppm	Ca (2000 ppm)	—	—	50 ppm	-24°C
Methylhydrazine	60-34-4	—	—	—	Ca (20 ppm)	—	—	0.01 ppm	22
Methyl iodide	74-88-4	25 ppm	50 ppm	125 ppm	Ca (100 ppm)	—	—	2 ppm	150
Methyl isocyanate	624-83-9	0.025 ppm	0.25 ppm	1.5 ppm	3 ppm	—	—	0.02 ppm	69
Methyl mercaptan	74-93-1	0.005 ppm	25 ppm	100 ppm	150 ppm	—	—	0.5 ppm	6.0°C
Methyl chlorosilane	75-79-6	0.5 ppm	3 ppm	15 ppm	LC50: 29/2 h	1 ppm	1 ppm	—	1000
Methylvinylketone	78-94-4	—	—	—	LC50: 2.4/4 h	—	—	0.2 ppm	31
Nickel carbonyl	13463-39-3	—	—	—	Ca (2 ppm)	—	—	0.05 ppm	43°C
Nitric acid (white fuming)	7697-37-2	1 ppm	6 ppm	78 ppm	25 ppm	—	—	2 ppm	430
Nitric oxide	10102-43-9	—	—	—	LC50: 315/15 min	—	—	25 ppm	-151.8°C
Nitrogen dioxide	10102-44-0	1 ppm	15 ppm	30 ppm	20 ppm	—	—	3 ppm	20.8°C
Oleum	8014-95-7	2 mg/m ³	10 mg/m ³	30 mg/m ³	LC50: 347/1 h	—	—	—	—
Ozone	10028-15-6	—	—	—	5 ppm	—	—	0.05 ppm	-112°C
Perchloryl fluoride	7616-94-6	—	—	—	100 ppm	—	—	3 ppm	-47°C
Phosgene	75-44-5	NA	0.2 ppm	1 ppm	2 ppm	—	—	0.1 ppm	7.6°C
Phosphine	7803-51-2	NA	0.5 ppm	5 ppm	50 ppm	—	—	0.3 ppm	-87°C
Phosphorus oxychloride	10025-87-3	—	—	—	LC50: 48/4 h	—	—	0.1 ppm	380
Phosphorus trichloride	7719-12-2	0.5 ppm	3 ppm	15 ppm	25 ppm	—	—	0.2 ppm	550
Propylene oxide	75-56-9	50 ppm	250 ppm	750 ppm	Ca (400 ppm)	—	—	2 ppm	380
Stibine	7803-52-3	ID	0.5 ppm	1.5 ppm	5 ppm	—	—	0.1 ppm	-18°C

TABLE 23-16 ERPG Values and Other Toxicity Values for Toxic Materials (Concluded)

Material	CAS no.	ERPG-1	ERPG-2	ERPG-3	IDLH	WEEL-8	WEEL-C	TLV-TWA	Oral, mg/kg
Sulfur dioxide	7446-09-5	0.3 ppm	3 ppm	15 ppm	100 ppm	—	—	2 ppm	-10°C
Sulfuric acid	7664-93-9	2 mg/m ³	10 mg/m ³	30 mg/m ³	15 mg/m ³	—	—	0.25 ppm	2140
Sulfur trioxide	7446-11-9	2 mg/m ³	10 mg/m ³	30 mg/m ³	LC50: >9/6 h	—	—	—	—
Tetranitromethane	509-14-8	—	—	—	4 ppm	—	—	0.005 ppm	130
Thionyl chloride	7719-09-7	0.2 ppm	2 ppm	10 ppm	LC50: 500/1 h	—	—	1 ppm	—
Titanium tetrachloride	7550-45-0	5 mg/m ³	20 mg/m ³	100 mg/m ³	LC50: 13/2 h	0.5 mg/m ³	—	—	—
Toluene di-isocyanate	584-84-9	0.01 ppm	0.15 ppm	0.6 ppm	Ca (2.5 ppm)	—	—	0.005 ppm	5800
Trimethylamine	75-50-3	—	—	—	LC50: 3500/4 h	1 ppm	—	5 ppm	2.9°C
Vinyl acetate	108-05-4	5 ppm	75 ppm	500 ppm	LC50: 1550/4 h	—	—	10 ppm	1613
Vinyl trichlorosilane	75-94-5	—	—	—	LC50: 500/4 h	1 ppm	1 ppm	—	1.280

The 50 percent lethal doses of ingested toxic materials that could cause fatal injury (National Institute for Occupational Safety and Health, *Registry of Toxic Effects of Chemical Substances*, 1983).

Where data for the above categories could not be found in the available literature, but the material was listed in the USEPA or NJTCPA standards, the LC50 value (op. cit.) was entered in the IDLH column.

Additional data concerning relatively long-term exposures of the public to toxic chemicals are presented in Table 23-17.

Safeguards against Toxicity Hazards Certainly the best protection against toxicity hazards is complete containment of hazardous materials within processing equipment.

Where complete containment is impractical, exhaust ventilation (preferably to a scrubber) can limit or eliminate exposure to toxic materials. The exhaust ventilation rate (velocity or volumetric rate) may be calculable for volatile liquids from spill size and vapor pressure (U.S. Environmental Protection Agency, *Risk Management Program Guidance for Offsite Consequence Analysis*, Appendix D, Equation D-1, 1999), but tests to determine concentrations in air usually would be needed for dusty processes and fugitive releases of gases.

If containment and exhaust ventilation are not considered adequate, cartridge respirators or self-contained breathing apparatus can provide protection against inhalation (and, in some cases, ingestion) of toxic materials. In 1994, the Occupational Safety and Health Standards were amended to require that "the employer shall assess the workplace to determine if hazards are present, or are likely to be present, which necessitate the use of personal protective equipment (PPE). If such hazards are present, or likely to be present, the employer shall select, and have each affected employee use, the types of PPE that will protect the affected employee from the hazards identified in the hazard assessment" [U.S. Department of Labor, *Occupational Safety and Health Standards*, 29 CFR 1910.132(d), 1999]. This hazard assessment would aid in determining the type of breathing protection that is appropriate for the toxicity hazard. Guidelines for appropriate use of breathing protection are given in this Standard (U.S. Department of Labor, *Occupational Safety and Health Standards*, 29 CFR 1910.134 and Appendices A, B, and C to 1910.134, and Appendix B to Subpart I, 1999). OSHA has not yet provided official Assigned Protection Factors, in Table I of this Standard, but manufacturers do provide these factors. As examples, a full-face cartridge respirator typically has a protection factor of 50 × PEL, and a self-contained breathing apparatus typically has a protection factor of 10,000 × PEL.

Conclusion Toxicity data are available for many thousands of solid, liquid, and gaseous chemicals and other materials. The data for inhalation toxicity provide guidance for concentration and duration limits, for protection of the public, chemical plant employees, and emergency response personnel. Similar data for ingestion and skin contact with toxic materials are not as readily available. Investigation into toxic effects is continuing, so that toxic materials can be handled safely.

OTHER HAZARDS

Hazards of Vacuum

Introduction Storage tanks and many other equipment items often have a relatively low resistance to the damage that can be caused

by internal vacuum. The low vacuum rating for such equipment and the amount of damage that can result are often surprising and potentially costly lessons learned by plant engineers and operators.

Equipment Limitations A robust internal pressure rating for a piece of equipment is no guarantee that it will withstand an appreciable vacuum. Industry loss experience includes failures of vessels with design pressure ratings in excess of 25 psig (Sanders, "Victims of Vacuum," *Proceedings of the 27th Annual Loss Prevention Symposium*, AIChE, 1993). Low-pressure storage tanks are particularly fragile. For example, an atmospheric fixed-roof storage tank may only withstand a vacuum of 2.5 mbar (0.036 psi or 1 in water) (British Petroleum, *Hazards of Trapped Pressure and Vacuum*, 2003).

Jacketed vessels can be particularly vulnerable to internal vacuum, since the operating pressure of the heat-transfer medium in the jacket adds to the differential pressure that would otherwise exist between the atmosphere and the vessel interior.

While many pressure vessels may withstand a significant vacuum, design calculations are required to confirm this. Unless specifically rated for vacuum service, equipment should be assumed to be subject to damage by vacuum. When equipment is procured, consideration should be given to including the vacuum rating in the pressure vessel calculations and code stamp. In many instances, the additional cost of doing so will be an insignificant fraction of the total procurement cost for the vessel (see Protective Measures for Equipment).

Consequences of Vacuum Damage Vessels, tank trucks, or railcars can be dimpled by partial collapse or, more significantly, crushed like used drink cans. Fortunately, equipment damaged by underpressurization does not fail explosively, as might occur with overpressurized equipment. Nevertheless, loss of containment of equipment contents is a real risk, due to damage to the vessel or to the piping connected to the vessel. Significant releases of toxic, flammable, or otherwise hazardous materials can result, with severe consequences.

Alternatively, vacuum within equipment could lead to ingress of air into inerted or fuel-rich systems, posing a fire or explosion hazard within the equipment.

The potential for "knock-on" effects resulting from equipment damage should be considered.

Common Causes of Equipment Underpressurization Equipment can be exposed to excessive vacuum due to an unanticipated mechanism creating a vacuum and/or the failure or inadequate design of protective systems provided to mitigate the hazard.

A common scenario involves the pumping, draining, or siphoning of liquid from a tank that has no, or an inadequate, venting capacity and thus cannot allow the entry of air at a rate sufficient to backfill behind the dropping liquid level.

Similarly, vacuums can be created when a blower, fan, compressor, or jet ejector removes gases from equipment. The magnitude of the vacuum attainable will be governed by the performance characteristics of the device. Other mechanisms for generating a vacuum, which have been demonstrated by industry experience, include the following.

- **Condensation of vapors or cooling of hot gases.** For example, steam is commonly used to clean vessels and, less frequently, to create an inert atmosphere inside of equipment. Steam condensing inside a closed vessel can create a significant vacuum, and vessels (e.g., railcars) have collapsed when all vessel inlets were

TABLE 23-17 Emergency and Continuous Exposure Guidance Levels for Selected Airborne Contaminants

Committee on Toxicology National Research Council

Vol.	Material (concentrations in ppm, except for mg/m ³)	Emergency exposure limits		Continuous exposure limit
		60-min	24-h	90-day
1	Acetone	8,500	1,000	200
1	Acrolein	0.05	0.01	0.01
4	Aluminum oxide	15*	N/L	N/L
IV	Ammonia	10	N/L	N/L
1	Arsine	1.0	0.1	0.01
3	Bromotrifluoromethane	25,000	N/L	100
1	Carbon disulfide	200	100	50
VI	Carbon monoxide	25	N/L	N/L
4	Carbon monoxide	400	50	20
VIII	Chlorine	0.5	N/L	N/L
2	Chlorine	3	0.5	0.1
2	Chlorine trifluoride	1	N/L	N/L
1	Chloroform	100	30	1
2	Dichlorodifluoromethane	10,000	1,000	100
2	Dichlorofluoromethane	100	3	1
2	Dichlorotetrafluoroethane	10,000	1,000	100
V	Dimethyl hydrazine	15	N/L	N/L
5	Dimethyl hydrazine	0.24	0.01	N/L
2	Ethanolamine	50	3	0.5
4	Ethylene glycol	40	20	4
1	Fluorine	15	10	7.5
V	Hydrazine	5	N/L	N/L
5	Hydrazine	0.12	0.005	N/L
II	Hydrogen chloride	2	N/L	N/L
III	Hydrogen fluoride	4	N/L	N/L
4	Hydrogen sulfide	N/L	10	1
2	Isopropyl alcohol	400	200	1
1	Mercury vapor	N/L	0.2*	0.01*
1	Methane	N/L	5,000	5,000
4	Methanol	200	10	N/L
V	Methyl hydrazine	15	N/L	N/L
5	Methyl hydrazine	0.24	0.01	N/L
4	Nitrogen dioxide	1	0.04	N/L
1	Nitrogen oxides	2	N/L	N/L
4	Nitrous oxide	10,000	N/L	N/L
1	Ozone	1	0.1	0.02
2	Phosgene	0.2	0.02	0.01
1	Sulfuric acid	5*	2*	1*
2	Trichlorofluoromethane	1,500	500	100
2	Trichlorotrifluoroethane	1,500	500	100
2	Sodium hydroxide	2*	N/L	N/L
2	Sulfur dioxide	10	5	1
2	Vinylidene chloride	N/L	10	0.15
2	Xylene	200	100	50

N/L = not listed; no guidance is given.

*Concentration in milligrams per cubic meter.

closed immediately after steam cleaning. The rapid addition of cool liquid to a vessel containing a hot, volatile liquid can markedly reduce the vapor pressure of the liquid. The sudden cooling of a storage tank by a thunderstorm can create a vacuum when gases in the vessel head space cool and/or vapors of volatile liquids condense. The American Petroleum Institute (API, *Venting Atmospheric and Low-Pressure Storage Tanks*, Standard 2000, Washington, 1998) provides guidance for in-breathing requirements as a function of tank capacity to protect against this latter scenario.

- *Absorption of a gas in a liquid.* Vessels have collapsed when ammonia vapor from the head space dissolved in water within the vessel (Lees, *Loss Prevention in the Process Industries*, 2d ed., Butterworths, London, 1996). A similar potential should be considered for HCl and water.
- *Chemical reactions that remove gases from the head space.* The corrosion of the interior of a steel vessel, especially if the vessel is newly fabricated or has been chemically cleaned, can consume and

remove a significant quantity of the oxygen from the vessel atmosphere. Other chemical reactions (e.g., ammonia reacting with hydrogen chloride to form ammonium chloride) can reduce the amount of gas or vapor in the vessel.

Prudent design requires that equipment be protected from credible underpressurization scenarios. Equipment damage can result when such protections are omitted, improperly sized, incorrectly designed or installed, or inadequately maintained. Common failures include the following.

- *Failure to consider appropriate challenges when determining the required relief capacity* (e.g., maximum rates of liquid withdrawal or cooling of vessel contents). Credible contingencies (e.g., thunderstorm cooling a vessel during steam-out) should be considered.
 - *Inadequate capacity, or failure, of vessel blanketing systems.* Inert gas supplies are often piped to vessels to maintain a reduced-oxygen atmosphere during liquid withdrawal. Coincident high demand for inert elsewhere, closure of a valve, or depletion of the supply could result in the failure to prevent a vacuum. A common means of initially inerting a vessel is to fill the vessel with liquid, then drain the liquid while allowing the blanketing system to backfill the head space with inert gas. Unless the blanketing system is sized to accommodate the drainage rate (which may exceed the normal process demand), there is a risk of collapsing the vessel.
 - *Operating errors.* Many vessel collapses have resulted from closing or failing to open a valve in a vent line. For this reason, valves in vacuum relief lines should be avoided, and they may be prohibited by some design codes.
 - *Maintenance errors.* One common error is the failure to remove an isolation blind in a vent line when returning a vessel to service. Even a thin sheet of plastic placed over an open nozzle may be sufficient to allow a vessel-damaging vacuum to be produced (BP, *Hazards of Trapped Pressure and Vacuum*, 2003).
 - *Inappropriate modifications.* In one incident, a hose was connected to a vent line that was provided for both pressure and vacuum protection. The hose was submerged into a drum of liquid in an attempt to scrub vapors emitted from the vent. Only a few inches of submergence were required to ensure that the vent was effectively blocked the next time a vacuum was pulled on the vessel (Lees, *Loss Prevention in the Process Industries*, 2d ed., Butterworths, London, 1996).
 - *Failure of vacuum control loop.* Control failures can either initiate events (e.g., increase the speed of an exhaustor) or disable protections (e.g., reduce the rate of supply of inert gas to a vessel).
 - *Plugging of vent lines or devices.* Process materials can migrate into and occlude vent systems when they polymerize, crystallize, condense, or solidify. Monomers requiring an inhibitor to prevent polymerization can evaporate from a tank and then condense in the vent line, free of the inhibitor. Waxes and other high-melting-point materials can solidify upon cooling in the vent system, dusts can accumulate, and water vapor can condense to form liquid seals in low points of vent lines or freeze in the winter. Such scenarios are a particular problem in cases where flame arrestors, screens, and other devices introduce small apertures in the vent flow path. Plugging of vent lines by animal or insect nests is not uncommon.
 - *Inadequate or incorrect maintenance.* Mechanical devices such as vacuum breakers and flame arrestors require routine maintenance attention to ensure that they provide their intended protective function. Incorrect maintenance (e.g., changing the vacuum breaker set pressure) could defeat the intended protection.
- Lees (*Loss Prevention in the Process Industries*, 2d ed., Butterworths, London, 1996), BP (*Hazards of Trapped Pressure and Vacuum*, 2003), and Kletz (*What Went Wrong?—Case Histories of Process Plant Disaster*, Gulf Publishing Company, 1989) include additional case histories providing valuable lessons about how equipment failures and human errors can combine to inflict vacuum damage.
- Protective Measures for Equipment** If equipment is subject to experiencing a vacuum, the inherently safer alternative would be to design the equipment to withstand a full vacuum. While this may not be

economically feasible for large storage tanks, the incremental cost for smaller vessels may not be prohibitive, particularly when traded off against the capital and continued operating and maintenance costs of some alternatives (e.g., protective instrumentation systems). The incremental fabrication cost of providing a suitable vacuum rating can be less than 10 percent for vessels of up to 3000-gal nominal capacity and having a 15-psig pressure rating (Wintner, "Check the Vacuum Rating of Your Tanks," *Chemical Engineering*, pp. 157–159, February 1991).

Careful process hazards analysis may show that a particular vessel need not be designed to withstand a full vacuum (e.g., if the maximum attainable vacuum is limited to the performance characteristics of an exhauster). Whatever the vacuum rating, rated vessels must be periodically inspected to ensure that internal or external corrosion has not diminished the vessel strength.

Reliable protections against excessive vacuum should be provided whenever equipment cannot withstand the vacuums that can credibly be achieved. In some low-risk situations, protections may consist of administrative controls implemented by adequately trained personnel. Where the risk of damage is higher or where design standards or codes require, engineered protections should be implemented.

Where process, safety, and environmental considerations permit, vacuum protection may be provided by properly sized ever-open vents. Alternatively, active protective devices and systems are required. Vacuum breaker valves designed to open and admit air at a predetermined vacuum in the vessel are commonly used on storage tanks, but may not be suitable for some applications involving flammable liquids. Inert gas blanketing systems may be used if adequate capacity and reliability can be ensured. Where the source of the vacuum can be deenergized or isolated, suitably reliable safety instrumented systems (e.g., interlocks) can be provided.

API (*Venting Atmospheric and Low-Pressure Storage Tanks*, Standard 2000, Washington, 1998) provides guidance for vacuum protection of low-pressure storage tanks. Where vacuum relief devices are provided, they should communicate directly with the vapor space in the vessel and should be installed so that they cannot be sealed off by the liquid contents in the vessel. Valves should be avoided in the inlets or outlets of vacuum relief devices unless the valves are reliably car-sealed or locked open, or excess relief capacity is provided (e.g., via multiple-way valves).

Hazards of Inerts

Introduction The use of inert gases to displace oxygen from equipment atmospheres in order to prevent combustion and, perhaps, consequent explosions has been described in the subsection "Flammability." Other applications for inerting exist, including preventing (1) corrosion or other deterioration of out-of-service equipment, (2) degradation of oxygen-sensitive products, or (3) exothermic reactions with air- or water-reactive materials. While the risk of personnel asphyxiation in an oxygen-deficient environment is the most frequently recognized concern, other hazards such as toxicity, temperature and pressure extremes, and chemical incompatibilities also need to be considered.

Sources of Inerts The most commonly used inert gases are N₂ and CO₂, but other gases and vapors such as argon (Ar), helium (He), steam, and exhaust gases from combustion devices are also used. The choice of the most appropriate inert for a given application must be based upon factors such as cost, availability, reliability of supply, effectiveness, and compatibility with process streams (Cumliff, "Avoiding Explosions by Means of Inerting Systems," IChemE Symposium Series no. 148, 2001; Grossel and Zalosh, *Guidelines for Safe Handling of Powders and Bulk Solids*, CCPS-AIChE, 2004).

Traditionally, inerts have been obtained from sources such as high-pressure gas cylinders or tube trailers or through evaporation of cryogenic liquids from bulk tanks. Other sources of inerts include (NFPA 69, *Standard on Explosion Prevention Systems*, National Fire Protection Association, 2002; FM Global, Loss Prevention Data Sheet 7-59, *Inerting and Purging of Tanks, Process Vessels, and Equipment*, 2000)

- On-site cryogenic air separation plants
- Gas generators burning or catalytically oxidizing a hydrocarbon to produce an oxygen-deficient product gas
- Nitrogen produced by the air oxidation of ammonia

- Nitrogen produced by removal of oxygen from air using pressure swing adsorption (PSA) or membrane separation units

Inert gas streams generated on site should be carefully monitored to ensure detection of an excessively high O₂ concentration in the product gas in the event of equipment failure or operational upset (e.g., due to a too high air-to-fuel ratio in a combustion generator or the failure of a membrane in a membrane separator). Consideration should be given to monitoring other indicators of problems in the inert generator (e.g., monitoring for low differential pressure across the membrane as an indication of the failure of a membrane separator).

Asphyxiation and Toxicity Hazards An asphyxiant is a chemical (either a gas or a vapor) that can cause death or unconsciousness by suffocation (BP, *Hazards of Nitrogen and Catalyst Handling*, 2003). A simple asphyxiant is a chemical, such as N₂, He, or Ar, whose effects are caused by the displacement of O₂ in air, reducing the O₂ concentration below its normal value of approximately 21 vol %. The physiological effects of oxygen concentration reduction by simple asphyxiants are illustrated in Table 23-18 (BP, *Hazards of Nitrogen and Catalyst Handling*, 2003).

The physiological processes leading to death from hypoxia (i.e., insufficient supply of oxygen to the body tissues) are described by Air Products (Air Products, *Dangers of Oxygen-Deficient Atmospheres*, Safetygram 17, 1998). At very low oxygen concentrations, loss of consciousness occurs within about 10 s of the first breath, followed by death within 2 to 4 min. A person exposed to an oxygen-deficient environment may not recognize the warning signs and may not be able to reason or take protective action before unconsciousness occurs. Victims removed from an O₂-deficient atmosphere require resuscitation through the administration of O₂ to prevent death [U.S. Chemical Safety and Hazard Investigation Board (CSB), *Hazards of Nitrogen Asphyxiation*, Safety Bulletin no. 2003-10-B, 2003].

Physical exertion increases oxygen demand and may result in oxygen deficiency symptoms at higher oxygen concentrations (CGA, *Oxygen-Deficient Atmospheres*, Publication SB-2, 2001), and individuals in poor health may be less tolerant of reduced oxygen concentrations. The guidance in Table 23-18 assumes a sea-level location and should be applied cautiously for facilities at significant altitudes; however, OSHA's Respiratory Protection Standard accepts 19.5 vol % as a safe O₂ concentration up to an altitude of 8000 ft (OSHA, 29 CFR 1910.134, Respiratory Protection Standard, 1998).

In its safety bulletin on the hazards of nitrogen asphyxiation, CSB identified 80 nitrogen asphyxiation deaths and 50 injuries occurring in 85 incidents between 1992 and 2002 (CSB, *Hazards of Nitrogen Asphyxiation*, Safety Bulletin no. 2003-10-B, 2003).

A chemical asphyxiant works by interfering with the body's ability to absorb or transport O₂ to the tissues. A relevant example of a chemical asphyxiant is CO, which can be present in inert gas streams produced

TABLE 23-18 Physiological Effects of Reduced O₂ Atmospheres

O ₂ (vol %)	Effects
23.5	Maximum "safe level" (23 vol % is often the high-level alarm of most O ₂ detectors)
21	Typical O ₂ concentration in air
19.5	Minimum "safe level" (19 vol % is often the low-level alarm of most O ₂ detectors)
15–19	First sign of hypoxia. Decreased ability to work strenuously. May induce early symptoms in persons with coronary, pulmonary, or circulatory problems.
12–14	Respiration increases with exertion; pulse up; impaired muscular coordination, perception, and judgment
10–12	Respiration further increases in rate and depth, poor judgment, lips blue
8–10	Mental failure, fainting, unconsciousness, ashen face, blueness of lips, nausea, vomiting, inability to move freely
6–8	6 min, 50% probability of death; 8 min, 100% probability of death
4–6	Coma in 40 s, convulsions, respiration ceases, death

TABLE 23-19 Physiological Effects of Exposure to CO₂

CO ₂ (vol %)	Effects
1	Slight increase in breathing rate.
2	Breathing rate increases to 50% above normal. Prolonged exposure can cause headache and tiredness.
3	Breathing increases to the normal rate and becomes labored. Weak narcotic effect. Impaired hearing, headache, increase in blood pressure and pulse rate.
4-5	Breathing increases to approximately four times the normal rate, symptoms of intoxication become evident, and slight choking may be felt.
5-10	Characteristic sharp odor noticeable. Very labored breathing, headache, visual impairment, and ringing in the ears. Judgment may be impaired, followed within minutes by loss of consciousness.
50-100	Unconsciousness occurs more rapidly above 10 vol % level. Prolonged exposure to high concentrations may eventually result in death from asphyxiation.

by combustion. Exposure to CO concentrations of approximately 1000 and 13,000 ppm can cause, respectively, loss of consciousness after 1 h and unconsciousness and danger of death after 1 to 3 min (Meidl, *Explosive and Toxic Hazardous Materials*, Table 28, p. 293, Glencoe Press, 1970).

Note that CO₂ acts as neither a simple asphyxiant (like N₂) nor a chemical asphyxiant (like CO). The normal concentration of CO₂ in air is approximately 300 ppm (0.03 vol %). Table 23-19 (Air Products, *Carbon Dioxide*, Safetygram 18, 1998) illustrates that exposure to air diluted by 5 vol % CO₂ (yielding an oxygen concentration of 21 × 0.95, or approximately 20 vol %) prompts physiological effects that are more severe than those inferred from Table 23-18 for dilution by the same amount of nitrogen.

Injuries and fatalities from asphyxiation are often associated with personnel entry into inerted equipment or enclosures. Guidance on safe procedures for confined space access are provided by OSHA (OSHA, 29 CFR 1910.146, *Confined Space Entry Standard*, 2000), the American National Standards Institute (ANSI, Z117.1, *Safety Requirements for Confined Spaces*, 2003), Hodson (Hodson, "Safe Entry into Confined Spaces," *Handbook of Chemical Health and Safety*, American Chemical Society, 2001), and BP (BP, *Hazards of Nitrogen and Catalyst Handling*, 2003). OSHA has established 19.5 vol % as the minimum safe oxygen concentration for confined space entry without supplemental oxygen supply (see Table 23-18). Note that OSHA imposes a safe upper limit on O₂ concentration of 23.5 vol % to protect against the enhanced flammability hazards associated with O₂-enriched atmospheres.

Physical Hazards A variety of physical hazards are presented by the various inerts in common usage.

High temperature The high-temperature off-gases from combustion-based sources of inerts typically must be quenched before use. Water scrubbing, in addition to reducing the temperature, can remove soot and sulfur compounds (which could react with moisture to form corrosive acids) present in the off-gas. The humidity of the resultant gas stream may make it unsuitable for inerting applications where moisture cannot be tolerated.

Use of steam as an inert requires that equipment be maintained at an elevated temperature to limit condensation that would lower the inert concentration. FM Global (FM Global, Loss Prevention Data Sheet 7-59, *Inerting and Purging of Tanks, Process Vessels, and Equipment*, 2000) recommends a minimum temperature of 160°F. The Compressed Gas Association (CGA, *Safe Handling of Compressed Gases in Containers*, Publication P-1, 2000) cautions against the use of steam in (1) systems where brittle materials (such as cast iron) may be stressed by thermal expansion, (2) systems with close clearances where high temperatures may cause permanent warping or maladjustment, and (3) systems where pipe coatings or plastic materials may be damaged by high temperatures. Protection for personnel to prevent thermal burns from equipment may be required.

In addition, some equipment or equipment supports may not have the strength to support a significant load of condensate, and provisions must be made for removal of condensate from the inerted equipment.

Low temperature The atmospheric boiling points for N₂, CO₂, He, and Ar are -196, -79, -269, and -186°C, respectively. The potential for cryogenic burns must be addressed in operating and maintenance procedures and in specifying personal protective equipment requirements.

Cryogenic temperatures can cause embrittlement of some materials of construction (e.g., carbon steel) and must be considered in the design of inert gas delivery systems. Controls should be provided to ensure that operational upsets do not allow the migration of cryogenic liquids to piping or equipment not designed to withstand such low temperatures.

The potential for the condensation and fractional distillation of air on the outside of equipment containing cryogenic liquids with boiling points less than that of O₂ must be considered. For example, because N₂ boils at a lower temperature than O₂ (-196 versus -183°C), air can condense on the outside of liquid N₂-bearing piping. The liquid that drops off of the piping will be enriched in O₂ and can pose an enhanced fire or explosion risk in the vicinity of the equipment.

High pressure Cryogenic liquids produce large volumes of gas upon evaporation (for example, 1 volume of liquid N₂ produces 694 volumes of gas at 20°C) (Air Products, *Safe Handling of Cryogenic Liquids*, Safetygram 16, 1999). Containers such as transport and storage vessels must be provided with overpressure relief to address this hazard. An additional concern is the hydrostatic pressure that can be produced if cryogenic liquids are trapped in a liquid-full system. Absent a vapor space to allow liquid expansion, extremely high pressures can be produced; accordingly, pressure relief devices must be installed in sections of equipment where cryogenic liquids might become trapped between closed valves.

Given the large liquid-to-gas expansion ratio, consideration should be given to limiting the quantity of cryogenic liquid stored inside tight enclosures or buildings that could become pressurized. The asphyxiation hazard associated with inert gases was addressed previously.

Portable containers of high-pressure inert gases can operate at pressures of thousands of pounds per square inch. Suitable precautions are required to protect containers and associated regulators and piping from damage. Refer to CGA (CGA, *Safe Handling of Compressed Gases in Containers*, Publication P-1, 2000; CGA, *Precautions for Connecting Compressed Gas Containers to Systems*, Publication SB-10, 2003) and Air Products (Air Products, *Handling, Storage, and Use of Compressed Gas Cylinders*, Safetygram 10, 2000) for guidance.

Air Products (Air Products, *Product Migration of Liquefied Compressed Gases in Manifolder Systems*, Safetygram 38, 2003) provides precautionary guidance with respect to manifolding of liquid-containing cylinders. A temperature difference of only a few degrees between cylinders can cause gas from the warmer cylinder to migrate through the manifold to the cooler cylinder, where it could condense and potentially fill the cylinder. A liquid-filled cylinder could rupture if it was subsequently valved closed.

Static electricity The use of high-pressure CO₂ for inerting poses a concern for potential static electricity hazards. CO₂ converts directly to a solid if the liquid is depressurized below 61 psig (Air Products, *Carbon Dioxide*, Safetygram 18, 1998). Consequently, discharge of liquid CO₂ produces CO₂ "snow" that, when moving at a high velocity, can generate static electric charge. Incendive sparks (5 to 15 mJ at 10 to 20 kV) have been reported (Urban, *Bretherick's Handbook of Reactive Chemical Hazards*, 6th ed., Butterworth-Heinemann Ltd., 1999).

Chemical Incompatibility Hazards While N₂ and CO₂ may act as inerts with respect to many combustion reactions, they are far from being chemically inert. Only the noble gases (e.g., Ar and He) can, for practical purposes, be regarded as true inerts. Frank (Frank, "Inerting for Explosion Prevention," *Proceedings of the 38th Annual Loss Prevention Symposium*, AIChE, 2004) lists a number of incompatibilities for N₂, CO₂, and CO (which can be present in gas streams from combustion-based inert gas generators). Notable incompatibilities for N₂ are lithium metal and titanium metal (which is reported to burn in N₂). CO₂ is incompatible with many metals (e.g., aluminum and the alkali metals), bases, and amines, and it forms carbonic acid in water,

which can corrode some materials. CO is a strong reducing agent and is incompatible with oxidizers, potassium, sodium, some aluminum compounds, and certain metal oxides. Trace metals and residual organic compounds may contaminate gas streams from combustion-based inert gas generators, posing a variety of potential incompatibility and product quality concerns.

Certain polymerization inhibitors added to stabilize monomers require a small concentration of dissolved O₂ to be effective (NFPA

69, *Standard on Explosion Prevention Systems*, National Fire Protection Association, 2002). For example, methyl acrylate and ethyl acrylate are commonly stabilized with hydroquinone monomethyl ether. Industry guidance recommends a minimum concentration of 5 vol % O₂ in the atmosphere above the acrylate to prevent polymerization (Intercompany Committee for the Safety and Handling of Acrylic Monomers, *Acrylate Esters, A Summary of Safety and Handling*, 3d ed., 2002).

INHERENTLY SAFER DESIGN AND OTHER PRINCIPLES

INHERENTLY SAFER AND MORE USER-FRIENDLY DESIGN

Introduction For many years the usual procedure in plant design was to identify the hazards, by one of the systematic techniques described later or by waiting until an accident occurred, and then add protective equipment to control them or to protect people from their consequences. This protective equipment is often complex and expensive and requires regular testing and maintenance. It often interferes with the smooth operation of the plant and is sometimes bypassed. Gradually the industry came to realize that, whenever possible, we should design user-friendly plants that can withstand human error and equipment failure without serious effects on safety (and output and efficiency). When we handle flammable, explosive, toxic, or corrosive materials, we can tolerate only very low failure rates, of people and equipment, rates which it may be impossible or impracticable to achieve consistently for long periods.

The most effective way of designing user-friendly plants is to avoid, when possible, large inventories of hazardous materials in process or storage. "What you don't have, can't leak." This sounds obvious, but until the explosion at Flixborough in 1974, little systematic thought was given to ways of reducing inventories. The industry simply designed a plant and accepted whatever inventory the design required, confident it could be kept under control. Flixborough weakened that confidence, and 10 years later Bhopal almost destroyed it. Plants in which we avoid a hazard, by reducing inventories or avoiding hazardous reactions, are usually called inherently safer.

The principle ways of designing inherently safer plants, and other ways of making plants user-friendly, are summarized below, with examples (Kletz, *Process Plants: A Handbook for Inherently Safer Design*, Taylor & Francis, 1998).

Intensification or Minimization One approach is to use so little hazardous material that it does not matter if it all leaks out. For example, at Bhopal methyl isocyanate (MIC), the material that leaked and killed over 2000 people, was an intermediate that was convenient but not essential to store. Within a few years many companies had reduced their stocks of MIC and other hazardous intermediates.

Intensification is the preferred route to inherently safer design as the plants, being smaller, are also cheaper (Bell, *Loss Prevention in the Process Industries*, Institution of Chemical Engineers Symposium Series no. 34, 1971 p. 50).

Substitution If intensification is not possible, then an alternative is to use a safer material in place of a hazardous one. Thus it is possible to replace flammable solvents, refrigerants, and heat-transfer media by nonflammable or less flammable (high-boiling) ones, hazardous products by safer ones, processes that use hazardous raw materials or intermediates by processes that do not. As an example of the latter, the product manufactured at Bhopal (carbaryl) was made from three raw materials. Methyl isocyanate is formed as an intermediate. It is possible to react the same raw materials in a different order so that a different and less hazardous intermediate is formed.

Attenuation or Moderation Another alternative to intensification is attenuation, or using a hazardous material under the least hazardous conditions. Thus large quantities of liquefied chlorine, ammonia, and petroleum gas can be stored as refrigerated liquids at atmospheric pressure instead of under pressure at ambient tempera-

ture. (Leaks from the refrigeration equipment should also be considered, so there is probably no net gain in refrigerating quantities less than a few hundred tons.) Dyestuffs that form explosive dusts can be handled as slurries.

Limitation of Effects of Failures Effects of failures can be limited by equipment design or change in reaction conditions, rather than by adding protective equipment. For example:

- Heating media such as steam or hot oil should not be hotter than the temperature at which the materials being heated are liable to ignite spontaneously or react uncontrollably.
- Spiral-wound gaskets are safer than fiber gaskets because if the bolts work loose or are not tightened correctly, the leak rate is much lower.
- Tubular reactors are safer than pot reactors as the inventory is usually lower and a leak can be stopped by closing a valve.
- Vapor-phase reactors are safer than liquid-phase ones as the mass flow rate through a hole of a given size is much less. (This is also an example of attenuation.)
- A small, deep diked area around a storage tank is safer than a large shallow one as the evaporation rate is lower and the area of any fire is smaller.
- Changing the order of operations, reducing the temperature, or changing another parameter can prevent many runaway reactions.
- Reduce the frequency of hazardous operations such as sampling or maintenance. We should consider the optimum balance between reliability and maintenance.

Simplification Simpler plants are friendlier than complex ones as they provide fewer opportunities for error and less equipment which can go wrong. Some of the reasons for complication in plant design are

- The need to control hazards. If we can intensify or carry out one of the other actions already discussed, we need less added protective equipment and plants will therefore be simpler.
- A desire for flexibility. Multistream plants with numerous crossovers and valves, so that any item can be used on any stream, have numerous leakage points, and errors in valve settings are easily made.
- Lavish provision of installed spares with the accompanying isolation and changeover valves.
- Continued adherence to traditional rules or practices that are no longer necessary.
- Design procedures that result in a failure to identify hazards until late in design. By this time it is impossible to avoid the hazard, and all we can do is to add complex equipment to control it.

Knock-on Effects Plants should be designed so that those incidents that do occur do not produce knock-on or domino effects. This can be done, e.g., by

- Providing firebreaks, about 15 m wide, between sections, similar to firebreaks in a forest, to restrict the spread of fire.
- Locating equipment that is liable to leak out-of-doors so that leaks of flammable gases and vapors are dispersed by natural ventilation. Indoors a few tens of kilograms are sufficient for an explosion that can destroy the building. Outdoors a few tons are necessary for serious damage. A roof over a piece of equipment, such as a compressor, is acceptable, but walls should be avoided. If leaks of toxic gases are liable to occur, it may be safer to locate the plant indoors, unless leaks will disperse before they reach members of the public or employees on other units.

- Constructing storage tanks so that the roof-wall weld will fail before the base-wall weld, thus preventing spillage of the contents. In general, in designing equipment we should consider the way in which it is most likely to fail and, when possible, locate or design the equipment so as to minimize the consequences.

Making Incorrect Assembly Impossible Plants should be designed so that incorrect assembly is difficult or impossible. For example, compressor valves should be designed so that inlet and exit valves cannot be interchanged; hose connections of different types or sizes should be used for compressed air and nitrogen.

Making Status Clear It should be possible to see at a glance if equipment has been assembled or installed incorrectly or whether it is in the open or shut position. For example:

- Check valves should be marked so that installation the wrong way round is obvious. It should not be necessary to look for a faint arrow hardly visible beneath the dirt.
- Gate valves with rising spindles are friendlier than valves with non-rising spindles, as it is easy to see whether they are open or shut. Ball valves and cocks are friendly if the handles cannot be replaced in the wrong position.
- Figure 8 plates are friendlier than slip plates (blinds) as their position is apparent at a glance. If slip plates are used, their projecting tags should be readily visible, even when the line is insulated. In addition, spectacle plates are easier to fit than slip plates, if the piping is rigid, and are always available on the job. It is not necessary to search for one, as with slip plates.

Tolerance Whenever possible, equipment should tolerate poor installation or operation without failure. Expansion loops in pipework are more tolerant of poor installation than are expansion joints (bellows). Fixed pipes, or articulated arms, if flexibility is necessary, are friendlier than hoses. For most applications, metal is friendlier than glass or plastic.

Bolted joints are friendlier than quick-release couplings. The former are usually dismantled by a fitter after issue of a permit-to-work. One worker prepares the equipment and another opens it up; the issue of the permit provides an opportunity to check that the correct precautions have been taken. In addition, if the joints are unbolted correctly, any trapped pressure is immediately apparent and the joint can be remade or the pressure allowed to blow off. In contrast, many accidents have occurred because operators opened up equipment that was under pressure, without independent consideration of the hazards, using quick-release couplings. There are, however, designs of quick-release coupling which give the operator a second chance.

Low Leak Rate If friendly equipment does leak, it does so at a low rate which is easy to stop or control. Examples already mentioned are spiral-wound gaskets, tubular reactors, and vapor-phase reactors.

Ease of Control Processes with a flat response to change are obviously friendlier than those with a steep response. Processes in which a rise of temperature decreases the rate of reaction are friendlier than those with a positive temperature coefficient, but this is a difficult ideal to achieve in the chemical industry. However, there are a few examples of processes in which a rise in temperature reduces the rate of reaction. For example, in the manufacture of peroxides, water is removed by a dehydrating agent. If magnesium sulfate is used as the agent, a rise in temperature causes release of water by the agent, diluting the reactants and stopping the reaction (Gerrison and van't Land, *I&EC Process Design*, 24, 1985, p. 893).

Software In some programmable electronic systems (PESs), errors are much easier to detect and correct than in others. Accidentally pressing the wrong key should never produce serious consequences. If we press the delete key on our computers, sometimes we are asked if we really want to do so; but stocks and currency have been accidentally sold or bought because someone pressed the wrong key. If we use the term *software* in the wider sense to cover all procedures, as distinct from hardware or equipment, some software is much friendlier than others. For example, if many types of gaskets or nuts and bolts are stocked, sooner or later the wrong type will be installed. It is better, and cheaper in the long run, to keep the number of types stocked to a minimum even though more expensive types than are strictly necessary are used for some applications.

Actions Needed for the Design of Inherently Safer and User-Friendly Plants

1. Designers need to be made aware that there is scope for improving the friendliness of the plants they design.

2. To achieve many of the changes suggested above, it is necessary to carry out much more critical examination and systematic consideration of alternatives during the early stages of design than has been customary in most companies. Two studies are suggested, one at the conceptual or business analysis stage when the process is being chosen and another at the flow sheet stage. For the latter the usual hazard and operability study (HAZOP) questions may be suitable but with one difference. In a normal HAZOP study on a line diagram, if we are discussing "more of temperature," say, we assume that it is undesirable and look for ways of preventing it. In a HAZOP of a flow sheet, we should ask if "more of temperature" would be better. For the conceptual study, different questions are needed.

Many companies will say that they do consider alternatives during the early stages of plant design. However, what is lacking in many companies is a formal, systematic structured procedure of the HAZOP type.

When a new plant is needed, it is usually wanted as soon as possible, and so there is no time to consider and develop inherently safer designs (or other innovations). When we are designing a new plant, we are conscious of all the improvements we could have made if we had had more time. These possible improvements should be noted and work on their feasibility started, ready for the plant after next. Unless we do so, we will never innovate and will ultimately lose to those who do.

3. To achieve the more detailed improvements suggested above, it may be necessary to add a few questions to those asked during a normal HAZOP. For example, what types of valve, gasket, blind, etc. will be used?

INCIDENT INVESTIGATION AND HUMAN ERROR

Although most companies investigate accidents (and many investigate dangerous incidents in which no one was injured), these investigations are often superficial and we fail to learn all the lessons for which we have paid the high price of an accident. The collection of evidence is usually adequate, but often only superficial conclusions are drawn from it. Identifying the causes of an accident is like peeling an onion. The outer layers deal with the immediate technical causes and triggering events while the inner layers deal with ways of avoiding the hazard and with the underlying weaknesses in the management system (Kletz, *Learning from Accidents*, 3d ed., Gulf Professional, 2001).

Dealing with the immediate technical causes of a leak, e.g., will prevent another leak for the same reason. If we can use so little of the hazardous material that leaks do not matter, or a safer material instead, as discussed above, we prevent all significant leaks of this hazardous material. If we can improve the management system or improve our designs, we may be able to prevent many more accidents.

Other points to watch when you are drawing conclusions from the facts are as follows:

1. Avoid the temptation to list causes we can do little or nothing about. For example, a source of ignition should not be listed as the primary cause of a fire or explosion as leaks of flammable gases are liable to ignite even though we remove known sources of ignition. The cause is whatever led to the formation of a flammable mixture of gas or vapor and air. (Removal of known sources of ignition should, however, be included in the recommendations.)

Similarly, human error should not be listed as a cause. See item 7 below.

2. Do not produce a long list of recommendations without any indication of the relative contributions they will make to the reduction of risk or without any comparison of costs and benefits. Resources are not unlimited, and the more we spend on reducing one hazard, the less there is left to spend on reducing others.

3. A named person should be made responsible for carrying out each agreed recommendation, and a completion date agreed with him or her. The report should be brought forward at this time; otherwise, nothing will happen except a repeat of the accident.

4. Avoid the temptation to overreact after an accident and install an excessive amount of protective equipment or complex procedures that

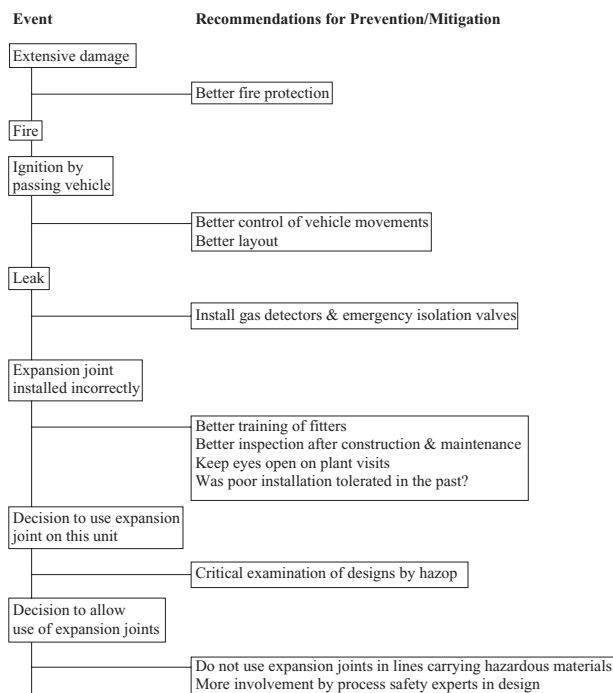


FIG. 23-17 An example of the many ways by which an accident could have been prevented.

are unlikely to be followed after a few years have elapsed. Sometimes an accident occurs because the protective equipment available was not used, but nevertheless the report recommends installation of more protective equipment; or an accident occurs because complex procedures were not followed, and the report recommends extra procedures. It would be better to find out why the original equipment was not used or the original procedures were not followed.

5. Remember that few, if any, accidents have a single cause. In most cases many people had an opportunity to prevent it, from the chemist who developed the process to the operator who closed the wrong valve. Figure 23-17 shows by example the opportunities that were available to prevent a fire or minimize the consequences of an apparently simple incident: an expansion joint (bellows) was incorrectly installed in a pipeline so that it was distorted. After some months it leaked, and a passing vehicle ignited the escaping vapor. Damage was extensive as the surrounding equipment had not been fire-protected to save on costs.

The fitter who installed the expansion joint incorrectly could have prevented the fire. So could the person who was responsible for her or his training and supervision; so could the designers if they had not specified an expansion joint, had carried out a HAZOP, or had consulted experts; so could the author of the company's design standards, and those responsible for the training of designers; those responsible for inspection of workmanship, and anyone who kept his or her eyes open when walking round the plant.

6. When you are reading an accident report, look for the things that are not said. For example, a gland leak on a liquefied flammable gas pump caught fire and caused considerable damage. The report drew attention to the congested layout, the amount of redundant equipment in the area, the fact that a gearbox casing had been made of aluminum, which melted, and several other unsatisfactory features. It did not stress that there had been a number of gland leaks on this pump over the years, that reliable glands are available for liquefied gases at

ambient temperatures, and therefore there was no need to have tolerated a leaky pump on this duty.

7. At one time most accidents were said to be due to human error, and in a sense they all are. If someone, designer, manager, operator, or maintenance worker had done something differently, the accident would not have occurred. However, the term *human error* is not very helpful as different types of error require quite different actions to prevent their happening again. The following classification of errors is recommended as it helps us see the type of action needed to prevent a repeat (Kletz, *An Engineer's View of Human Error*, 3d ed., Institution of Chemical Engineers, United Kingdom, and Taylor and Francis, 2001).

a. Some errors, called mistakes, are due to poor training or instructions—someone did not know what to do. It is a management responsibility to provide good training and instructions and avoid instructions that are designed to protect the writer rather than help the reader. However many instructions we write, problems will arise that are not covered, and so people, particularly operators, should be trained in flexibility, i.e., the ability to diagnose and handle unforeseen situations. If the instructions are hard to follow, can the job be simplified?

b. Some accidents, called violations or noncompliance, occur because someone knew what to do but made a decision not to do it. We should, if possible, simplify the job (if the correct method is difficult, an incorrect one will be used); explain the reasons for the instructions; carry out checks from time to time to see that instructions are being followed; and not turn a blind eye if they are not. While some violations make the job easier, many are made by people who think they have found a better way of doing the job. If instructions are incorrect, a violation can prevent an accident.

The methods of behavioral science can be used to reduce violations. Specially trained members of the workforce keep their eyes open and tactfully draw the attention of fellow workers to violations such as failures to wear protective clothing. These techniques can reduce the incidence of everyday accidents, but they have little or no influence on process safety.

c. Some accidents—mismatches—occur because the job is beyond the physical or mental ability of the person asked to do it, sometimes beyond anyone's ability. We should improve the plant design or method of working.

d. The fourth category is the commonest, a momentary slip or lapse of attention. This happens to everyone from time to time and cannot be prevented by telling people to be more careful, telling them to keep their minds on the job, or better training. In fact, slips and lapses of attention occur only when we are well trained. We put ourselves on autopilot and carry out the task without continually monitoring our progress, though we may check it from time to time. These errors are more likely to occur when we are distracted or stressed. To avoid slips and lapses of attention, all we can do is to change the plant design or method of working so as to remove opportunities for error (or minimize the consequences or provide opportunities for recovery). We should, whenever possible, design user-friendly plants (see above) that can withstand errors (and equipment failures) without suffering serious effects on safety (and output and efficiency). It is more effective to change the behavior of equipment than to try to change the behavior of people.

When an accident report says that an accident was due to human error, the writer usually means an error by an operator or other front line worker. But designers and managers also make errors, not slips or lapses of attention as they usually have time to check their work, as well as mistakes or, less often, violations.

INSTITUTIONAL MEMORY

Most accidents occur not because we do not know how to prevent them but because we do not use the information that is available. The recommendations made after an accident are forgotten when the people involved have left the plant; the procedures they introduced are allowed to lapse, the equipment they installed is no longer used, and the accident happens again. The following actions can prevent or reduce this loss of information.

- Include a note on the reason why in every instruction, code, and standard as well as accounts of accidents that would not have occurred if the instruction, code, or standard had been followed.
- Describe old accidents as well as recent ones in safety bulletins and newsletters, and discuss them at safety meetings.
- Follow up at regular intervals (e.g., during audits) to see that the recommendations made after accidents are being followed, in design as well as operations.
- Make sure that recommendations for changes in design are acceptable to the design organization.
- Remember that the first step down the road to an accident is taken when someone turns a blind eye to a missing blind (or other feature).
- On each unit keep a memory book, a folder of reports on past accidents, which is compulsory reading for new recruits and which others dip into from time to time. It should include relevant reports from other companies but should not include cuts and bruises.
- Never remove equipment before you know why it was installed. Never abandon a procedure before you know why it was adopted.
- When people are moving to other jobs in the company or leaving it, make sure that the remaining employees at all levels have adequate knowledge and experience.
- Include important accidents of the past in the training of undergraduates and company employees. The training should start with accounts of accidents that demonstrate the need for codes, standards, or instructions. Ask audience members to say what *they think* should be done to prevent similar accidents from happening again. More will be remembered after a discussion than after a lecture, and audience members are more likely to be convinced when they have worked out for themselves the actions that should be taken (Kletz, *Lessons from Disaster—How Organizations Have No Memory and Accidents Recur*, Institution of Chemical Engineers, Rugby, United Kingdom, 1993, Chap. 10). Suitable accidents for discussion can be found in books of accident case histories, but local accidents have the greatest impact.
- There are many databases of accidents as well as books of case histories, but they have been little used. We need better retrieval systems so that we can find, more easily than at present, details of past accidents, in our own and other companies, and the recommendations made afterward.

PROCESS SAFETY ANALYSIS

HAZARD ANALYSIS

GENERAL REFERENCES: Alaimo, *Handbook of Chemical Health and Safety*, Oxford University Press, New York, 2001; *Chemical Exposure Index*, 2d ed., AIChE, New York, 1994; Council of the European Union, Directive 96/82/EC, *Prevention of Major Accidents*, December 9, 1996; CPQRA, *Guidelines for Chemical Process Quantitative Risk Analysis*, 2d ed., CCPS-AIChE, New York, 2000; Crawley, Preston, and Tyler, *HAZOP: Guide to Best Practice*, IChemE, Rugby, Warwickshire, U.K., 2002; Crowl and Louvar, *Chemical Process Safety: Fundamentals with Applications*, 2d ed., Prentice-Hall, Englewood Cliffs, N.J., 2002; Dowell, "Managing the PHA Team," *Process Safety Progress* **13**, no. 1, January 1994; *Dow Fire and Explosion Index*, AIChE, New York, January 1994; Harris, *Patty's Industrial Hygiene*, 5th ed., Wiley, New York, 2000; *Guidelines for Design Solutions for Process Equipment Failures*, AIChE, New York, 1997; *HEP Guidelines for Hazard Evaluation Procedures*, 2d ed., AIChE, New York, 1992; Johnson, Rudy, and Unwin, *Essential Practices for Managing Chemical Reactivity Hazards*, AIChE, New York, 2003; Knowlton, *Hazard and Operability Studies*, Chemetics International Co., Ltd., Vancouver, British Columbia, February 1989; *LOPA Layer of Protection Analysis*, AIChE, New York, 2001; Maman, *Lees' Loss Prevention in the Process Industries*, Butterworth-Heinemann, London, 2005; Mosley, Ness, and Hendershot, "Screen Reactive Chemical Hazards Early in Process Development," *Chemical Engineering Progress*, 96(1), pp. 51-65; NOAA, *Chemical Reactivity Worksheet*, Version 1.6, U.S. National Oceanic and Atmospheric Administration, 2004 (<http://response.restoration.noaa.gov/chemaids/react.html>); Skelton, *Process Safety Analysis: An Introduction*, Gulf Publishing, Houston, Tex., 1997; *SVA Guidelines for Analyzing and Managing the Security Vulnerabilities of Fixed Chemical Sites*, AIChE, New York, 2003; Tweeddale, *Managing Risk and Reliability of Process Plants*, Gulf Professional, Houston, Tex., 2003; USEPA, "Risk Management Programs for Chemical Accidental Release Prevention Requirements," 40 CFR 68; U.S. OSHA, "Process Safety Management of Highly Hazardous Chemicals, Explosives and Blasting Agents," 29 CFR 1910.119; Wells, *Hazard Identification and Risk Assessment*, IChemE, Rugby, Warwickshire, U.K., 1996.

Introduction The meaning of *hazard* is often confused with *risk*. *Hazard* is defined as the inherent potential of a material or activity to harm people, property, or the environment. Hazard does not have a probability component.

There are differences in terminology on the meaning of *risk* in the published literature that can lead to confusion. *Risk* has been defined in various ways (CPQRA, 2000, pp. 5, 6). In this edition of the handbook, *risk* is defined as "a measure of human injury, environmental damage, or economic loss in terms of both the incident likelihood and magnitude of the injury, damage, or loss." *Risk* implies a probability of something occurring.

Definitions of Terms Following are some definitions that are useful in understanding the components of hazards and risk.

Accident A specific combination of events or circumstances that leads to an undesirable consequence.

Acute hazard The potential for injury or damage to occur as a result of a short-duration exposure to the effects of an accident.

Cause-consequence A procedure using diagrams to illustrate the causes and consequences of a particular scenario. They are not widely used because, even for simple systems, displaying all causes and outcomes leads to very complex diagrams.

Chemical Exposure Index (CEI) A method of rating the relative potential of acute health hazard to people from possible chemical release incidents, developed by Dow Chemical Company.

Chronic hazard The potential for injury or damage to occur as a result of prolonged exposure to an undesirable condition.

Consequence The direct, undesirable result of an accident, usually measured in health and safety effects, environmental impacts, loss of property, or business costs.

Consequence analysis Once hazards and specific incident scenarios through which those hazards might impact people, the environment, or property have been identified, methods exist for analyzing their consequences (size of vapor cloud, blast damage radius, overpressure expected, etc.). This is independent of frequency or probability.

Domino effect An incident which starts in one piece of equipment and affects other nearby items, such as vessels containing hazardous materials, by thermal blast or fragment impact. This can lead to escalation of consequences or frequency of occurrence. This is also known as a *knock-on effect*.

Event An occurrence involving equipment performance or human action or an occurrence external to the system that causes system upset. An event is associated with an incident, either as a cause or a contributing cause of the incident, or as a response to an initiating event.

Event tree A graphical logic model that identifies and potentially quantifies possible outcomes following an initiating event.

Failure mode and effect analysis (FMEA) A hazard identification technique in which all known failure modes of components or features of a system are considered in turn and undesired outcomes are noted. It is often used in combination with hazard and operability (HAZOP) studies or fault tree analysis.

Fault tree A graphical logic model for representing the combinations of various system states which lead to a particular outcome, known as the *top event*.

Fire and Explosion Index (F&EI) A hazard index developed by Dow Chemical Company used to rank fire and explosion hazards in a chemical process.

Hazard An inherent physical or chemical characteristic that has the potential for causing harm to people, the environment, or property.

HAZOP (HAZard and OPerability study) A formal hazard identification and evaluation procedure based on the application of guide words to identify possible deviations from the intended operation of the process.

Incident The loss of containment of material or energy, e.g., a leak of a flammable and toxic gas.

Interaction matrix A two-dimensional matrix listing all components of interest on the *x* and *y* axes and recording the consequences of mixing of these components for each combination of the components. It is useful for identifying chemical reaction hazards and incompatibilities.

Layer-of-protection analysis (LOPA) A method, based on event tree analysis, of evaluating the effectiveness of independent protection layers in reducing the likelihood or severity of an undesired event.

Process hazard analysis (PHA) Any of a number of techniques for understanding and managing the risk of a chemical process or plant. Examples of PHA techniques include HAZOP, checklists, what-if methods, fault tree analysis, event tree analysis, and others.

Process Hazard Analysis Regulations In the United States, the OSHA rule for Process Safety Management (PSM) of Highly Toxic Hazardous Chemicals, 29 CFR 1910.119, part (e), requires an initial PHA and an update every 5 years for processes that handle listed chemicals or contain over 10,000 lb (4356 kg) of flammable material. The PHA must be done by a team, must include employees such as operators and mechanics, and must have at least one person skilled in the methodology employed. Suggested methodologies from Process Safety Management are listed in Table 23-20. The PHA must consider hazards listed in the PSM Rule, part (e), including information from previous incidents with potential for catastrophic consequences, engineering and administrative controls and consequences of their failure, facility siting, and human factors. Consequences of failure of controls must be considered. The key to good PHA documentation is to do it right away while the information is fresh. Periodic follow-up of the PHA study is needed by management and safety professionals to confirm that all recommendations have been addressed. The PHA must be reviewed as part of the management of change procedures when the facility is modified in any way. (Dowell, 1994, pp. 30–34.)

As required by the Clean Air Act Amendments of 1990, the USEPA mandates a Risk Management Program (RMP) for listed substances (40 CFR 68). RMP requires (1) a hazard assessment that details the potential effects of an accidental release, an accident history of the last 5 years, and an evaluation of worst-case and alternative accidental releases; (2) a prevention program that includes safety precautions and maintenance, monitoring, and employee training measures; and (3) an emergency response program that spells out emergency health care, employee training measures, and procedures for informing the public and response agencies, should an accident occur.

Most countries also have regulations analogous to the U.S. regulations. For example, the European Union issued the “Seveso II” Directive in 1996 (replacing the original 1982 directive) which requires all member states to implement regulations for the control of major accident hazards. Also, in addition to the U.S. government requirements,

many state and local governments have implemented regulations requiring process hazard analysis and risk management.

Hazard Identification and Analysis Tools The hazard and risk assessment tools used vary with the stage of the project from the early design stage to plant operations. Many techniques are available. In the following discussion, they will be categorized as hazard identification and analysis tools, hazard ranking methods, and logic model methods. Reviews done early in projects often result in easier, more effective changes.

Safety, Health, Environmental, and Loss Prevention Reviews Most chemical companies have specific internal protocols defining these reviews, which may have different names or descriptions in different organizations. In most organizations, these reviews are conducted at various stages in the process life cycle, from initial process conceptualization, through laboratory development, scale-up, plant design, start-up, operation, modification, and shutdown. The scope and focus of the review will be different at different stages in development, with reviews early in process development focusing on major hazards and strategies for managing the risks. As the process and plant become clearly defined, the reviews will focus more on details of the design and operation. The purpose of the reviews is to have an independent (from the development, design, or operation team) evaluation of the process and layout from safety, industrial hygiene, environmental, and loss prevention points of view. It is often desirable to combine these reviews to improve the efficiency of the use of time for the reviewers (*HEP* Chaps. 4.1, 4.4, 6.1, 6.4, 13).

Checklists Checklists are simple means of applying experience to designs or situations to ensure that the features appearing in the list are not overlooked. Checklists tend to be general and may not be appropriate to a specific situation. They may not handle adequately the novel design or unusual process. (*HEP*, Chaps. 4.2, 6.2, 16, 20). The CCPS *Design Solutions for Process Equipment Failures* (1997) provides a useful set of checklists for common chemical processing equipment.

What-if At each process step, what-if questions are formulated and answered to evaluate the effects of component failures or procedural errors. This technique relies on the experience level of the questioner. What-if methods are often used in conjunction with checklists (*HEP* Chaps. 4.5, 4.6, 6.5, 6.6, 12, 20).

Failure Mode and Effect Analysis (FMEA) This is a systematic study of the causes of failures and their effects. All causes or modes of failure are considered for each element of a system, and then all possible outcomes or effects are recorded (*HEP* Chaps. 4.8, 6.8, 19).

Reactive Chemistry Reviews The process chemistry is reviewed for evidence of exotherms, shock sensitivity, and other instability, with emphasis on possible exothermic reactions. The purpose of this review is to prevent unexpected and uncontrolled chemical reactions. Reviewers should be knowledgeable people in the field of reactive chemicals and include people from loss prevention, manufacturing, and research. The CCPS *Essential Practices for Managing Chemical Reactivity Hazards* provides a useful protocol for identifying chemical reactivity hazards (Johnson et al., 2003). A series of questions about the chemical handling operations and the materials are used to determine if there are possible reactivity hazards. Figure 23-18 summarizes the CCPS protocol for identifying reaction hazards.

Interaction Matrix (Compatibility Chart) An interaction matrix is a tool for identifying and understanding potential hazards, including reaction hazards, from combinations of materials (*HEP*, 1992, Chaps. 3.3, 11.3). The most common representation is a two-dimensional matrix, listing all components of interest (including, e.g., chemicals; materials of construction; potential contaminants; environmental contaminants such as air, rust, or water; utilities). The consequences of mixing the materials for each row-column intersection are identified. Figure 23-19 is an example of an interaction matrix. Johnson et al. (2003) describe the use of the interaction matrix, and Mosley et al. (2000) provide a specific example. The U.S. National Oceanic and Atmospheric Administration (NOAA) has developed a computer tool, the *Chemical Reactivity Worksheet*, which can generate an interaction matrix for materials in the program's database (NOAA, 2004).

Industrial Hygiene Reviews These reviews evaluate the potential of a process to cause harm to the health of people. The review

TABLE 23-20 Process Hazard Analysis Methods Listed in the OSHA Process Safety Management Rule

- What-if
- Checklist
- What-if/checklist
- Hazard and operability study (HAZOP)
- Failure mode and effect analysis (FMEA)
- Fault tree analysis (FTA)
- An appropriate equivalent methodology

SOURCE: Dowell, 1994, pp. 30–34.

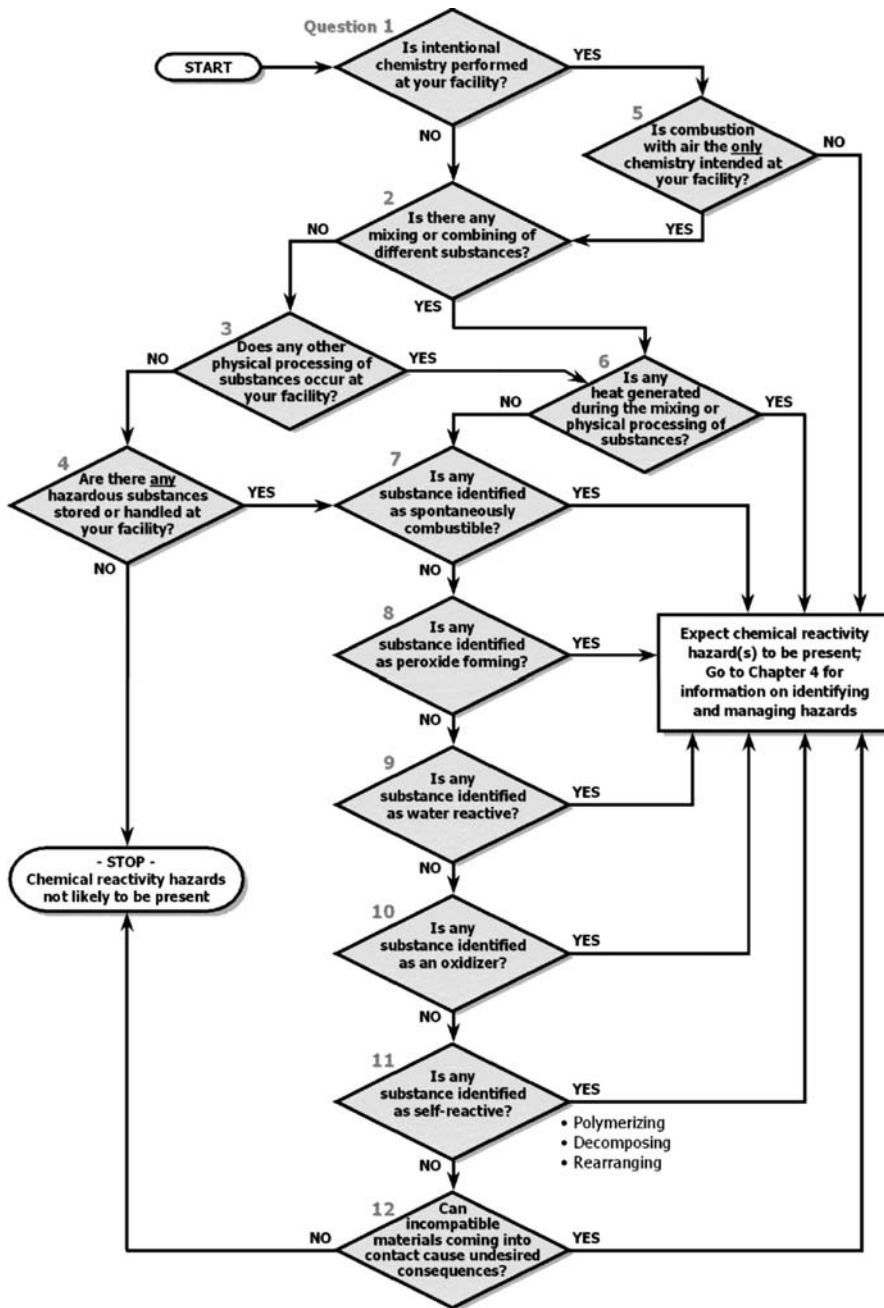


FIG. 23-18 CCPS preliminary screening for chemical reactivity hazards. [From Johnson et al. (2003); copyright AIChE; reproduced with permission.]

normally deals with chronic effects of exposure to chemicals and other harmful agents (e.g., noise, heat, repetitive motion) in the workplace. Chapter 44 of *Patty's Industrial Hygiene* reviews industrial hygiene survey procedures.

Facilities Reviews There are many kinds of facilities reviews that are useful in detecting and preventing process safety problems. They include prestart-up reviews (before the plant operates), new-plant reviews (the plant has started, but is still new), reviews of exist-

ing plants (safety, technology, and operations audits and reviews), management reviews, critical instrument reviews, and hazardous materials transportation reviews.

HAZOP (HEP, 1992, Chaps. 4.7, 6.7, 14, 18; Knowlton, 1989; Lees, 2005; CPQRA, 2000, pp. 583–587). HAZOP is a formal hazard identification and evaluation procedure designed to identify hazards to people, process plants, and the environment. The techniques aim to stimulate, in a systematic way, the imagination of designers and people

SUBSTANCE							
1	Hydrochloric Acid (35%)				1		
2	Sulfuric Acid (90%)	R ¹			2		
3	Acetic Acid	? ⁸	R ²		3		
4	Ethanol	NR ³	R ⁴	NR ¹⁵	4		
5	Ethylenediamine	R ⁵	R ⁶	R ⁷	NR ¹²	5	
6	Water	R ⁹	R ¹⁰	NR ¹¹	NR ¹³	R ¹⁴	6

Legend:

R	Reactive under the stated scenario - incompatible
NR	Non-Reactive under the stated scenario - compatible
?	unknown – assume incompatible until further information is obtained

Footnotes/Information Sources:

- 1 Unlikely to be compatible – USCG chart NVC 4-75 indicates a hazard with non-oxidizing acids plus sulfuric acid. Heat of mixing may be significant.
- 2 Unlikely to be compatible – the P-168 chart indicates that gas and heat are formed; USCG chart NVC 4-75 indicates a hazard when combining sulfuric and organic acids.
- 3 Primary alcohols do not react with aq. HCl at ambient temperature.
- 4 Heat of solution followed by reaction to form ethyl hydrogen sulfate.
- 5 Lab experiment 980001 (50/50 mix) resulted in a significant heat of neutralization.
- 6 Lab experiment 980002 (50/50 mix by volume) resulted in a XXX C adiabatic temperature rise.
- 7 Organic acids and amines are generally incompatible due to acid/base neutralization heat.
- 8 The P-168 and USCG charts indicate no hazard; most likely compatible, but lab testing should be performed.
- 9 Heat of mixing may be a concern in some circumstances. The maximum adiabatic temperature rise is XX C (see XYZ Encyclopedia of Chemical Technology).
- 10 Heat of mixing may be a concern in some circumstances. The maximum adiabatic temperature rise is XX C (see XYZ Encyclopedia of Chemical Technology). Violent reaction with splattering if water is added to the acid.
- 11 Lab experiment 98005 showed that mixing acetic acid and water is endothermic at room temperature.
- 12 Lab experiments 98003 and 98008 indicate that the materials do not generate heat or gases when mixed nor when heated to 100 C. Although the USCG chart NVC 4-75 indicates that some alcohols and amines are incompatible, ethylene diamine has been found to be compatible with many alcohols; see Appendix of USCG Guide.
- 13 Plant experience has shown materials to be compatible.
- 14 Mildly exothermic hydrate formation.
- 15 Very slow, nearly thermoneutral, equilibrium-limited esterification at ambient temperature.

FIG. 23-19 Hypothetical compatibility chart. (Copyright ASTM International. Reprinted with permission.)

who operate plants or equipment to identify potential hazards. HAZOP studies assume that a hazard or operating problem can arise when there is a deviation from the design or operating intention. Actions to correct identified hazard or operational scenarios can then be taken before a real incident occurs. The primary goal in performing a HAZOP study is to identify, not analyze or quantify, the hazards in a process. The end product of a HAZOP is a list of concerns and recommendations for prevention of problems, not an analysis of the occurrence, frequency, overall effects, and the definite solution. A HAZOP study is most cost-effective when done during plant design—it is easier and cheaper to change a design than to modify an existing plant. However, HAZOP is a valuable process hazard analysis tool at any stage in the life cycle of a plant.

These studies make use of the combined experience and training of a group of knowledgeable people in a structured setting. Some key HAZOP terms are as follows.

Intention How the part or process is expected to operate.

Guide words Simple words used to qualify the intention in order to guide and stimulate creative thinking and so discover deviations. Table 23-21 describes commonly used guide words.

Deviations Departures from the intention discovered by systematic application of guide words.

Causes Reasons that deviations might occur.

Consequences Results of deviations if they occur.

Safeguards Prevention, mitigation, and control features which already exist in the plant, or which are already incorporated in a new design.

Actions Prevention, mitigation, and control features which do not currently exist and are recommended by the HAZOP team. Actions may also include recommendations for additional study if the HAZOP team does not have sufficient information, or time to understand a concern sufficiently to make a specific recommendation.

TABLE 23-21 Some HAZOP Guide Words Used in Conjunction with Process Parameters

Guide word	Meanings	Comments
No, Not, None	Complete negation of design intentions	No part of intention is achieved and nothing else occurs
More	Quantitative increases	Quantities and relevant physical properties such as flow rates, heat, pressure
Less	Quantitative decreases of any relevant physical parameters	Same as above
As well as	Qualitative increase	All design and operating intentions are achieved as well as some additional activity
Part of	A qualitative decrease	Some parts of the intention are achieved, others are not
Reverse	Logical opposite of intention	Activities such as reverse flow or chemical reaction, or poison instead of antidote
Other than	Complete substitution	No part of intention is achieved; something quite different happens

SOURCE: Knowlton, 1989.

The HAZOP study is not complete until response to actions has been documented. Initial HAZOP planning should establish the management follow-up procedure that will be used.

The guide words are used in conjunction with the process intentions to generate possible deviations from the intended operation (see Table 23-21). Some examples of deviations that might be generated in the course of a HAZOP study include

- No flow
- Reverse flow
- Less flow
- Increased temperature
- Decreased temperature
- Composition change
- Sampling
- Corrosion/erosion

The HAZOP team then determines the specific causes of each deviation; e.g., no flow of a particular material in a specified pipe might include causes such as a manual valve improperly closed, pump stops, pipe plugged with solids, etc. The HAZOP team then determines the consequences of the deviation for each cause and qualitatively decides the magnitude of hazard. The team identifies any existing safeguards in the plant or design and qualitatively judges whether they are adequate. If the team determines that additional safeguards are required, it may recommend specific actions. The team may determine that the issue requires greater study than can be accommodated in the time frame of a HAZOP meeting and recommend more extensive evaluation to determine if further action is needed, and what that action should be.

Many HAZOP studies incorporate a qualitative evaluation of risk to assist the team in evaluating the adequacy of existing safeguards, and the need for additional safeguards. This involves constructing a risk matrix, such as the one shown in Fig. 23-20. The team determines, based on its knowledge of the plant, experience, and engineering judgment, which of the several consequence and likelihood categories in the risk matrix best describe the particular deviation-cause-consequence sequence under consideration. Scenarios with high consequence and high frequency represent a large risk, those with low likelihood and consequence are of low risk. An organization can use the matrix to establish guidelines for which of the boxes in the risk matrix require action.

HAZOP studies may be made on batch as well as continuous processes. For a continuous process, the working document is usually a set of flow sheets or piping and instrument diagrams (P&IDs). Batch processes have another dimension: time. Time is usually not significant with a continuous process that is operating smoothly, although start-up and shutdown must also be considered, when the continuous process will resemble a batch process. For batch processes, the working documents consist not only of the flow sheets or P&IDs but also

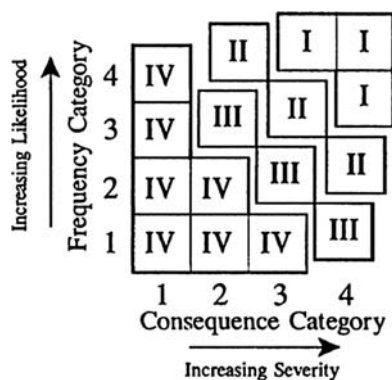


FIG. 23-20 Example of PHA qualitative risk matrix.

TABLE 23-22 HAZOP Guide Words Associated with Time

Guide word	Meaning
No time	Step(s) missed
More time	Step does not occur when it should
Less time	Step occurs before previous step is finished
Wrong time	Flow or other activity occurs when it should not

SOURCE: Knowlton, 1989.

the operating procedures. One method to incorporate this fourth dimension is to use guide words associated with time, such as those described in Table 23-22.

HAZOP studies involve team members, at least some of whom have had experience in the plant design to be studied. These team members apply their expertise to achieve the aims of HAZOP. There are four overall aims to which any HAZOP study should be addressed:

1. Identify as many deviations as possible from the way the design is expected to work, their causes, and problems associated with these deviations.
2. Decide whether action is required, and identify ways in which the problem can be solved.
3. Identify cases in which a decision cannot be made immediately, and decide what information or action is required.
4. Ensure that required actions are followed through.

The team leader is a key to the success of a HAZOP study and should have adequate training for the job. Proper planning is important to success. The leader is actually a facilitator (a discussion leader and one who keeps the meetings on track) whose facilitating skills are just as important as technical knowledge. The leader outlines the boundaries of the study and ensures that the design intention is clearly understood. The leader applies guide words and encourages the team to discuss causes, consequences, and possible remedial actions for each deviation. Prolonged discussions of how a problem may be solved should be avoided. Ideally, the team leader should be accompanied by a scribe or recorder, freeing the leader for full-time facilitating. The scribe should take notes in detail for full recording of as much of the meeting as is necessary to capture the intent of actions and recommendations.

Many companies offer computer tools to help facilitate and document HAZOP studies.

Team size is important. Having fewer than three contributing members, excluding the secretary and leader, will probably reduce team effectiveness. A team size of five to eight, including the leader and scribe, is probably optimum. The time required for HAZOP studies is significant. It has been estimated that each line or node (a node is usually a line or an item of equipment) may require in the range of 30 min for an experienced team, although the time may vary widely depending on the complexity of the system. It should be recognized that the time required for HAZOP studies may not really be additional time for the project as a whole, particularly if started early enough in the design, and may actually save time on the project. It also should make possible smoother start-ups and make the process or plant safer and easier to operate, which will more than pay back the cost of the HAZOP study during the life of the plant.

Hazard Ranking Methods Hazard ranking methods (HEP, 1992, Chaps. 4.3, 6.3) allow the analyst to compare the hazards of several processes, plants, or activities. They can be used to compare alternative chemical process routes, plant designs, plant siting options, or other design choices. Hazard ranking methods can also be useful for prioritizing facilities for additional risk management studies. They generally produce a numerical score for the process being evaluated. The scores generally do not have units and are only meaningful relative to each other in the context of the hazard index being used. Some of the more commonly used hazard ranking methods are briefly discussed.

NFPA Standard System for Identification of Health, Flammability, Reactivity, and Related Hazards (NFPA 704, 2001) This printed material is not the complete and official position of the National Fire Protection Association on the referenced subject, which is represented only by the standard in its entirety.

TABLE 23-23 NFPA 704 System for Identification of Hazards

Degree of hazard	Health hazard color code: blue	Flammability hazard color code: red	Instability hazard color code: yellow
4	Materials that, under emergency conditions, can be lethal	Materials that will rapidly or completely vaporize at atmospheric pressure and normal ambient temperature or that are readily dispersed in air and will burn readily.	Materials that in themselves are readily capable of detonation or explosive decomposition or explosive reaction at normal temperatures and pressures.
3	Materials that, under emergency conditions, can cause serious or permanent injury	Liquids and solids that can be ignited under almost all ambient temperature conditions. Materials in this degree produce hazardous atmospheres with air under almost all ambient temperatures or, though unaffected by ambient temperatures, are readily ignited under almost all conditions.	Materials that in themselves are capable of detonation or explosive decomposition or explosive reaction, but that require a strong initiating source or that must be heated under confinement before initiation.
2	Materials that, under emergency conditions, can cause temporary incapacitation or residual injury	Materials that must be moderately heated or exposed to relatively high ambient temperatures before ignition can occur. Materials in this degree would not, under normal conditions, form hazardous atmospheres with air, but under high ambient temperatures or under moderate heating could release vapor in sufficient quantities to produce hazardous atmospheres with air.	Materials that readily undergo violent chemical change at elevated temperatures and pressures.
1	Materials that, under emergency conditions, can cause significant irritation	Materials that must be preheated before ignition can occur. Materials in this degree require considerable preheating, under all ambient temperature conditions, before ignition and combustion can occur.	Materials that in themselves are normally stable, but that can become unstable at elevated temperatures and pressures.
0	Materials that, under emergency conditions, would offer no hazard beyond that of ordinary combustible materials	Materials that will not burn under typical fire conditions, including intrinsically noncombustible materials such as concrete, stone, and sand.	Materials that in themselves are normally stable, even under fire conditions.

SOURCE: Reprinted with permission from NFPA 704, *Standard System for the Identification of the Fire Hazards of Materials*, National Fire Protection Association, Quincy, Mass., 2001. This printed material is not the complete and official position of the National Fire Protection Association on the referenced subject, which is represented only by the standard in its entirety.

This is a brief summary of NFPA 704 which addresses hazards that may be caused by short-term exposure to a material during handling under conditions of fire, spill, or similar emergencies. This standard provides a simple, easily recognized and understood system of markings. The objective is to provide on-the-spot identification of hazardous materials. The markings provide a general idea of the hazards of a material and the severity of these hazards as they relate to handling, fire protection, exposure, and control. This standard is not applicable to transportation or to use by the general public. It is also not applicable to chronic exposure. For a full description of this standard, refer to NFPA 704.

The system identifies the hazards of a material in four principal categories: health, flammability, reactivity, and unusual hazards such as reactivity with water. The degree of severity of health, flammability, and reactivity is indicated by a numerical rating that ranges from 0 (no hazard) to 4 (severe hazard). Table 23-23 describes the characteristics associated with the various ratings; for a detailed description of the degree of severity ratings, see NFPA 704. The information is presented in a square-on-point (diamond) field of numerical ratings, e.g., as shown in Figs. 23-21 through 23-23. Information is presented as follows:

- Health rating in blue at nine o'clock
- Flammability rating in red at twelve o'clock
- Reactivity hazard rating in yellow at three o'clock
- Unusual hazards at six o'clock

Materials that demonstrate unusual reactivity with water are identified as W, and materials that possess oxidizing properties shall be identified by the letters OX. Other special hazard symbols may be used to identify radioactive hazards, corrosive hazards, substances that are toxic to fish, and so on. The use of this system provides a standard method of identifying the relative degree of hazard that is contained in various tanks, vessels, and pipelines.

Fire and Explosion Index (F&EI) (*Dow Fire and Explosion Index Hazard Classification Guide*, 1994; Mannan, 2005, pp. 8/13–8/22.)

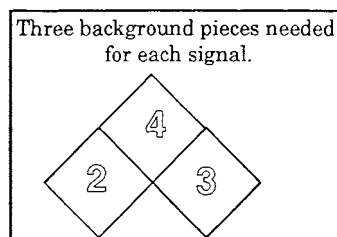


FIG. 23-21 NFPA 704 hazard ratings for use where specified color background is used with numerals of contrasting colors. (NFPA 704, 2001.)

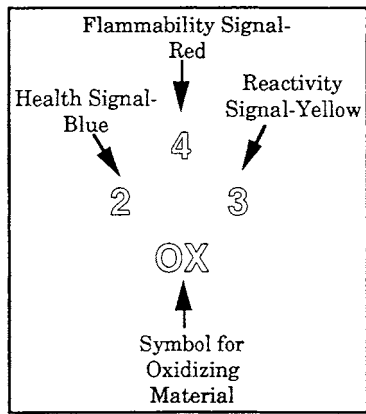


FIG. 23-22 For use where white background is used. (NFPA 704, 2001.)

The F&EI is used to rate the potential of hazard from fires and explosions. Its purpose is to quantify damage from an incident. It identifies equipment that could contribute to an incident and ways to mitigate possible incidents. It is a way to communicate to management the quantitative hazard potential. The F&EI measures realistic maximum loss potential under adverse operating conditions. It is based on quantifiable data. It is designed for flammable, combustible, and reactive materials that are stored, handled, or processed. It does not address frequency (risk) except indirectly, nor does it address specific hazards to people except indirectly. The goals of the F&EI are to raise awareness of loss potential and identify ways to reduce potential severity and potential dollar loss in a cost-effective manner. The index number has significance as a comparison and in calculations to estimate the *maximum probable property damage* (MPPD). It also provides a method for measuring the effect of outage (plant being shut down) on the business. It is easy for users to get credible results with a small amount of training.

Chemical Exposure Index (CEI) (*Chemical Exposure Index*, 1994; Mannan, 2005, pp. 8/22–8/26.) The CEI provides a method of rating the relative potential of acute health hazard to people from possible chemical release incidents. It may be used for prioritizing initial process hazard analysis and establishing the degree of further analysis needed. The CEI also may be used as part of the site review process. The system provides a method of ranking one risk relative to another. It is not intended to define a particular containment system as safe or unsafe, but provides a way of comparing toxic hazards. It deals with acute, not chronic, releases. Flammability and explosion hazards are not included in this index. To develop a CEI, information needs include

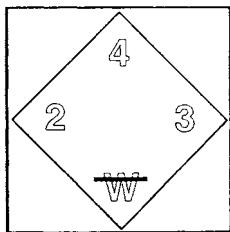


FIG. 23-23 For use where white background is used or for signs or placards. (NFPA 704, 2001.)

- An accurate plot plan of the plant and surrounding area
- A simplified process flow sheet showing containment vessels, major piping, and quantity of chemicals
- Physical, chemical, and toxicological properties of the chemicals
- Process variables such as pressures, temperatures, and quantities of materials

Substance Hazard Index The Substance Hazard Index (SHI) was developed for use by U.S. OSHA for ranking material hazards during the development of the OSHA Process Safety Management regulations. SHI is defined as “the equilibrium vapor concentration (EVC) of a material at 20°C divided by an acute toxicity concentration.” SHI is a measure of the ability of a released material to be transported through the air and impact people. The EVC is defined as the vapor pressure of the material at 20°C $\times 10^6/760$. Different organizations using the SHI may use different toxicity measures, for example, ERPG-3, IDLH, or AEGL.

Consequence-Based Ranking Systems Release consequence modeling can be used to rank potential chemical hazards. For example, the USEPA’s RMP regulations require consequence modeling for a predefined worst-case scenario—release of the entire contents of the largest container of a material in 10 min. EPA provides lookup tables and software (RMPComp) to assist in estimating the hazard distances for materials covered by the RMP regulations.

Logic Model Methods The following tools are most commonly used in quantitative risk analysis, but can also be useful qualitatively to understand the combinations of events which can cause an accident. The logic models can also be useful in understanding how protective systems impact various potential accident scenarios. These methods will be thoroughly discussed in the “Risk Analysis” subsection. Also, hazard identification and evaluation tools discussed in this section are valuable precursors to a quantitative risk analysis (QRA). Generally a QRA quantifies the risk of hazard scenarios which have been identified by using tools such as those discussed above.

- Fault tree analysis
- Event tree analysis
- Cause-consequence diagram
- Layer-of-protection analysis (LOPA)

RISK ANALYSIS

GENERAL REFERENCES: *Guidelines for Chemical Process Quantitative Risk Analysis*, 2d ed., CCPS-AIChE, New York, 2000. Arendt, “Management of Quantitative Risk Assessment in the Chemical Process Industry,” *Plant Operations Progress*, vol. 9, no. 4, AIChE, New York, October 1990. CMA, “A Manager’s Guide to Quantitative Risk Assessment,” Chemical Manufacturers’ Association, December 1989. EFCE, “Risk Analysis in the Process Industries,” European Federation of Chemical Engineering, Publication Series no. 45, 1985. Lees, *Loss Prevention in the Process Industries* 2d ed., Butterworths, Boston, 1996. World Bank, *Manual of Industrial Hazard Assessment Techniques*, Office of Environmental and Scientific Affairs, World Bank, Washington, D.C., 1985. *Guidelines for Chemical Transportation Risk Analysis*, CCPS-AIChE, New York, 1995.

FREQUENCY ESTIMATION REFERENCES: *Guidelines for Process Equipment Reliability Data*, CCPS-AIChE, New York, 1989. Billington and Allan, *Reliability Evaluation of Engineering Systems: Concepts and Techniques*, Plenum Press, New York, 1983. Fussell, Powers, and Bennetts, “Fault Trees: A State of the Art Discussion,” *IEEE Transactions on Reliability*, 1974. Roberts, N. H. et al., *Fault Tree Handbook*, NUREG-0492, Washington, D.C. Swain and Guttmann, *Handbook of Human Reliability Analysis with Emphasis on Nuclear Power Plant Applications*, NUREG/CR-1278, USNRC, Washington, D.C., 1983.

CONSEQUENCE ESTIMATION REFERENCES: *Guidelines for Use of Vapor Cloud Dispersion Models*, CCPS-AIChE, New York, 1987. TNO, *Methods for the Calculation of the Physical Effects of the Escape of Dangerous Materials: Liquids and Gases* (“The Yellow Book”), Apeldoorn, The Netherlands, 1979. *Understanding Explosions*, CCPS-AIChE, New York, 2003. *Guidelines for Evaluating the Characteristics of Vapor Cloud Explosions*, CCPS-AIChE, New York, 1994. *Guidelines for Use of Vapor Cloud Dispersion Models*, 2d ed., CCPS-AIChE, New York, 1996. *Guidelines for Consequence Analysis of Chemical Releases*, CCPS-AIChE, New York, 1999. Technical Report no. 55, *Techniques for Assessing Industrial Hazards*, World Bank, Washington, 1988.

RISK ESTIMATION REFERENCES: Health and Safety Executive, *Canvey—An Investigation of Potential Hazards from the Operations in the Canvey*

Island/Thurrock Area, HMSO, London, 1978. Rasmussen, *Reactor Safety Study: An Assessment of Accident Risk in U.S. Commercial Nuclear Power Plants*, WASH-1400 NUREG 75/014, Washington, D.C., 1975. Rijnmond Public Authority, *A Risk Analysis of 6 Potentially Hazardous Industrial Objects in the Rijnmond Area—A Pilot Study*, D. Reidel, Boston, 1982. Considine, *The Assessment of Individual and Societal Risks*, SRD Report R-310, Safety and Reliability Directorate, UKAEA, Warrington, 1984. Baybutt, "Uncertainty in Risk Analysis," Conference on Mathematics in Major Accident Risk Assessment, University of Oxford, U.K., 1986.

RISK CRITERIA AND RISK DECISION MAKING: Ale, "The Implementation of an External Safety Policy in the Netherlands," *Intl. Conference on Hazard Identification and Risk Analysis, Human Factors and Reliability in Process Safety*, AIChE, New York, pp. 173–183, 1992; Gibson, "Hazard Analysis and Risk Criteria," *Chemical Engineering Progress*, Nov. 1980, pp. 46–50; Gibson, "The Use of Risk Criteria in the Chemical Industry," *Trans. of IChemE 71*, Pt. B, pp. 117–123, 1993; Health and Safety Executive, *Reducing Risks Protecting People, HSE's Decision Making Process*, HSE Books, London, 2001; Helmers and Schaller, "Calculated Process Risks and Health Management," *Plant Operations Progress*, 1, no. 3, pp. 190–194, 1982; Renshaw, "A Major Accident Prevention Program," *Plant Operations Progress*, 9, no. 3, pp. 194–197, 1990; Pikaar and Seaman, *A Review of Risk Control*, Zoetermeer, Ministerie VROM, Netherlands, 1995; *Tools for Making Acute Risk Decisions with Chemical Process Safety Implications*, CCPS-AIChE, New York, 1995; Hamm and Schwartz, "Issues and Strategies in Risk Decision Making," *Intl. Process Safety Management Conference and Workshop*, San Francisco, AIChE, New York, pp. 351–371, 1993.

Introduction The previous sections dealt with techniques for qualitative hazard analysis only. This section addresses the quantitative methodologies available to analyze and estimate risk, which is a function of both the consequences of an incident and its frequency. The application of these methodologies in most instances is not trivial. A significant allocation of resources is necessary. Therefore, a selection process or risk prioritization process is advised before considering a risk analysis study.

Important definitions are as follows.

Accepted risk The risk is considered tolerable for a given activity by those responsible for managing or regulating the operation of a hazardous facility. The term *acceptable risk* has often been used, but this inevitably raises the question, "Acceptable to whom?" Tweeddale (*Managing Risk and Reliability of Process Plants*, Gulf Professional, Houston, Tex, 2003, p. 70) suggests that *accepted risk* is a better term because it makes it clear that the risk has been accepted by those responsible for the decisions on how to build, operate, and regulate the facility.

Event sequence A specific, unplanned sequence of events composed of initiating events and intermediate events that may lead to an incident.

Frequency The rate at which observed or predicted events occur.

Incident outcome The physical outcome of an incident; e.g., a leak of a flammable and toxic gas could result in a jet fire, a vapor cloud explosion, a vapor cloud fire, or a toxic cloud.

Probability The likelihood of the occurrence of events, the values of which range from 0 to 1.

Probability analysis Way to evaluate the likelihood of an event occurring. By using failure rate data for equipment, piping, instruments, and fault tree techniques, the frequency (number of events per unit time) can be quantitatively estimated.

Probit model A mathematical model of dosage and response in which the dependent variable (response) is a probit number that is related through a statistical function directly to a probability.

Quantitative risk assessment (QRA) The systematic development of numerical estimates of the expected frequency and consequence of potential accidents associated with a facility or an operation. Using consequence and probability analyses and other factors such as population density and expected weather conditions, QRA estimates the fatality rate for a given set of events.

Risk A measure of economic loss or human injury in terms of both incident likelihood (frequency) and the magnitude of the loss or injury (consequence).

Risk analysis The development of an estimate of risk based on engineering evaluation and mathematical techniques for combining

estimates of incident consequences and frequencies. Incidents in the context of the discussion in this chapter are acute events which involve loss of containment of material or energy.

Risk assessment The process by which results of a risk analysis are used to make decisions, either through a relative ranking of risk reduction strategies or through comparison with risk targets. The terms *risk analysis* and *risk assessment* are often used interchangeably in the literature.

A typical hazard identification process, such as a hazard and operability (HAZOP) study, is sometimes used as a starting point for selection of potential major risks for risk analysis. Other selection or screening processes can also be applied. However major risks are chosen, a HAZOP study is a good starting point to develop information for the risk analysis study. A major risk may qualify for risk analysis if the magnitude of the incident is potentially quite large (high potential consequence) or if the frequency of a severe event is judged to be high (high potential frequency) or both. A flowchart which describes a possible process for risk analysis is shown in Fig. 23-24.

The components of a risk analysis involve the estimation of the frequency of an event, an estimation of the consequences, and the selection and generation of the estimate of risk itself.

A risk analysis can have a variety of potential goals:

1. To screen or bracket a number of risks in order to prioritize them for possible future study
2. To estimate risk to employees
3. To estimate risk to the public
4. To estimate financial risk
5. To evaluate a range of risk reduction measures
6. To meet legal or regulatory requirements
7. To assist in emergency planning

The scope of a study required to satisfy these goals will be dependent upon the extent of the risk, the depth of the study required, and the level of resources available (mathematical models and tools and skilled people to perform the study and any internal or external constraints).

A risk analysis can be applied to fixed facilities or transportation movements, although much of the attention today still centers on the former. In a fixed-facility risk analysis, QRA can aid risk management decisions with respect to

1. Chemical processes
2. Process equipment
3. Operating procedures
4. Chemical inventories
5. Storage conditions

In a transportation risk analysis (TRA), the risk parameters are more extensive, but more restrictive in some ways. Examples of risk parameters that could be considered are

1. Alternate modes of transport
2. Routes
3. Travel restrictions
4. Shipment size
5. Shipping conditions (e.g., pressure, temperature)
6. Container design
7. Unit size (e.g., bulk versus drums)

The objective of a risk analysis is to reduce the level of risk wherever practical. Much of the benefit of a risk analysis comes from the discipline which it imposes and the detailed understanding of the major contributors of the risk that follows. There is general agreement that if risks can be identified and analyzed, then measures for risk reduction can be effectively selected.

The expertise required in carrying out a risk analysis is substantial. Although various software programs are available to calculate the frequency of events or their consequences, or even risk estimates, engineering judgment and experience are still very much needed to produce meaningful results. And although professional courses are available in this subject area, there is a significant learning curve required not only for engineers to become practiced risk analysts, but also for management to be able to understand and interpret the results. For these reasons, it may be useful to utilize a consultant organization in this field.

The analysis of a risk—that is, its estimation—leads to the assessment of that risk and the decision-making processes of selecting the

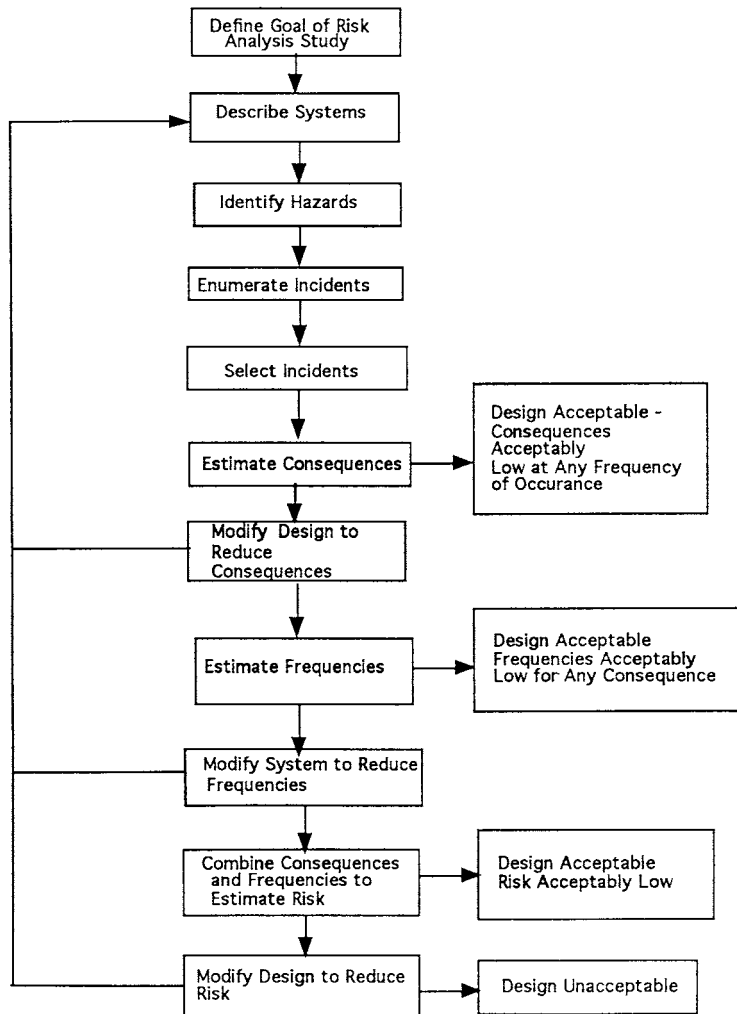


FIG. 23-24 One version of a risk analysis process. (CCPS-AIChE, 1989, p. 13, by permission.)

appropriate level of risk reduction. In most studies this is an iterative process of risk analysis and risk assessment until the risk is reduced to some specified level. The question of how safe is safe enough has to be addressed either implicitly or explicitly in the decision-making process. This subject is discussed in greater detail later on in this section.

Frequency Estimation There are two primary sources for estimates of incident frequencies. These are historical records and the application of fault tree analysis and related techniques, and they are not necessarily applied independently. Specific historical data can sometimes be usefully applied as a check on frequency estimates of various subevents of a fault tree, for example.

The use of historical data provides the most straightforward approach to the generation of incident frequency estimates but is subject to the applicability and the adequacy of the records. Care should be exercised in extracting data from long periods of the historical record over which design or operating standards or measurement criteria may have changed.

An estimate of the total population from which the incident information has been obtained is important and may be difficult to obtain.

Fault tree analysis and other related event frequency estimation techniques, such as event tree analysis, play a crucial role in the risk analysis process. Fault trees are logic diagrams that depict how components and systems can fail. The undesired event becomes the top event and subsequent subevents, and eventually basic causes, are then developed and connected through logic gates. The fault tree is completed when all basic causes, including equipment failures and human errors, form the base of the tree. There are general rules for construction, which have been developed by practitioners, but no specific rules for events or gates to use. The construction of a fault tree is still more of an art than a science. Although a number of attempts have been made to automate the construction of fault trees from process flow diagrams or piping instrumentation diagrams, these attempts have been largely unsuccessful [P. K. Andow, "Difficulties in Fault Tree Synthesis for Process Plant," *IEEE Transactions on Reliability* R-29(1): 2, 1980].

Once the fault tree is constructed, quantitative failure rate and probability data must be obtained for all basic causes. A number of equipment failure rate databases are available for general use. However, specific equipment failure rate data is generally lacking and,

23-50 PROCESS SAFETY

therefore, data estimation and reduction techniques must be applied to generic databases to help compensate for this shortcoming. Accuracy and applicability of data will always be a concern, but useful results from quantifying fault trees can generally be obtained by experienced practitioners.

Human error probabilities can also be estimated using methodologies and techniques originally developed in the nuclear industry. A number of different models are available (Swain, "Comparative Evaluation of Methods for Human Reliability Analysis," GRS Project RS 688, 1988). This estimation process should be done with great care, as many factors can affect the reliability of the estimates. Methodologies using expert opinion to obtain failure rate and probability estimates have also been used where there is sparse or inappropriate data.

In some instances, plant-specific information relating to frequencies of subevents (e.g., a release from a relief device) can be compared against results derived from the quantitative fault tree analysis, starting with basic component failure rate data.

An example of a fault tree logic diagram using AND and OR gate logic is shown in Fig. 23-25.

The logical structure of a fault tree can be described in terms of boolean algebraic equations. Some specific prerequisites to the application of this methodology are as follows.

- Equipment states are binary (working or failed).
- Transition from one state to another is instantaneous.
- Component failures are statistically independent.
- The failure rate and repair rate are consistent for each equipment item.
- After repair, the component is returned to the working state.

Minimal cut set analysis is a mathematical technique for developing and providing probability estimates for the combinations of basic component failures and/or human error probabilities, which are necessary and sufficient to result in the occurrence of the top event.

A number of software programs are available to perform these calculations, given the basic failure data and fault tree logic diagram (AIChE-CCPS, 2000). Other less well known approaches to quantifying fault tree event frequencies are being practiced, which result in gate-by-gate calculations using discrete-state, continuous-time, Markov models (Doelp et al., "Quantitative Fault Tree Analysis, Gate-by-Gate Method," *Plant Operations Progress* 4(3): 227-238, 1984).

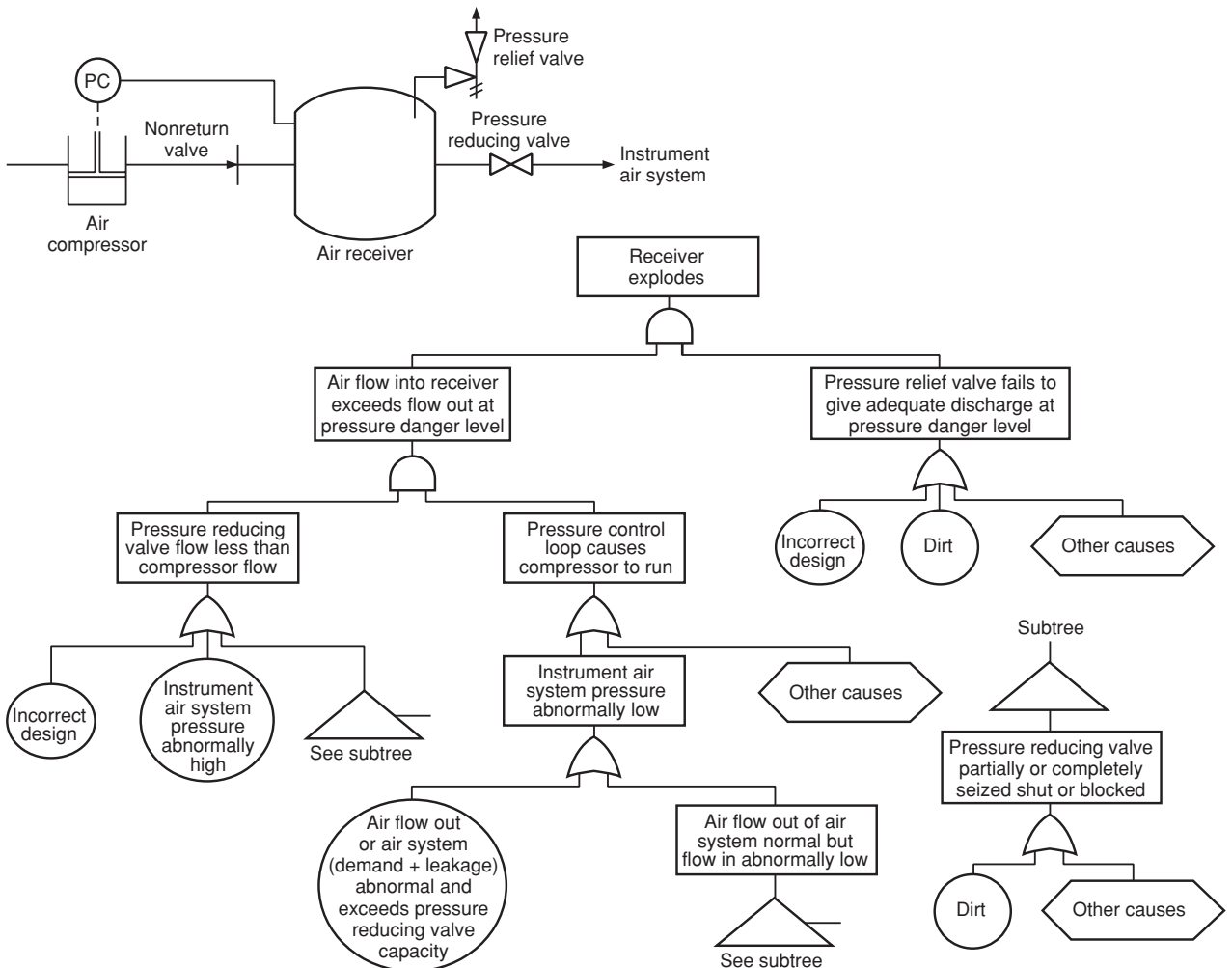


FIG. 23-25 Process drawing and fault tree for explosion of an air receiver. (From Lees, 1980, pp. 200, 201, by permission.)

Identification and quantitative estimation of common-cause failures are general problems in fault tree analysis. Boolean approaches are generally better suited to mathematically handle common-cause failures. The basic assumption is that failures are completely independent events, but in reality dependencies will exist and these are categorized as common cause failures (CCFs). Both qualitative and quantitative techniques can be applied to identify and assess CCFs. An excellent overview of CCF is available (AIChE-CCPS, 2000).

Event tree analysis is another useful frequency estimation technique used in risk analysis. It is a bottom-up logic diagram, which starts with an identifiable event. Branches are then generated, which lead to specific chronologically based outcomes with defined probabilities. Event tree analysis can provide a logic bridge from the top event, such as a flammable release into specific incident outcomes (e.g., no ignition, flash fire, or vapor cloud explosion). Probabilities for each limb in the event tree diagram are assigned and, when multiplied by the starting frequency, produce frequencies at each node point for all the various incident outcome states. The probabilities for all of the limbs at any given level of the event tree must sum to 1.0. Event trees are generally very helpful toward the generation of a final risk estimate. Figure 23-26 shows an event tree for a release of LPG (AIChE-CCPS, 2000).

Layers-of-protection analysis (LOPA) is a semiquantitative methodology for analyzing and assessing risk. It is typically applied after a qualitative hazards analysis has been completed, which provides the LOPA team with a listing of hazard scenarios with associated safeguards for consideration. LOPA uses simplified methods to characterize the process risk based on the frequency of occurrence and consequence severity of potential hazard scenarios. The process risk is compared to the owner/operator risk criteria. When the process risk exceeds the risk criteria, protection layers are identified that reduce the process risk to the risk criteria.

The protection layers are safeguards that are designed and managed to achieve seven core attributes: independence, functionality, integrity, reliability, auditability, access security, and management of change. Protection layers may include inherently safer design, control, supervisory, prevention, mitigation, limitation, barriers, and emergency response systems, depending on the owner/operator's risk management strategy.

In general, risk reduction is accomplished by implementing one or more protective layers, which reduce the frequency and/or consequence of the hazard scenario. LOPA provides specific criteria and restrictions for the evaluation of protection layers, eliminating the subjectivity of qualitative methods at substantially less cost than fully quantitative techniques. LOPA is a rational, defensible methodology that allows a rapid, cost-effective means for identifying the protection layers that lower the frequency and/or the consequence of specific hazard scenarios.

Consequence Estimation Given that an incident (release of material or energy) has been defined, the consequences can be estimated. The general logic diagram in Fig. 23-27 illustrates these calculations for the release of a volatile hazardous substance.

For any specific incident there will be an infinite number of incident outcome cases that can be considered. There is also a wide degree of consequence models which can be applied. It is important, therefore, to understand the objective of the study to limit the number of incident outcome cases to those which satisfy that objective. An example of variables which can be considered is as follows.

- Quality, magnitude, and duration of the release
- Dispersion parameters (wind speed, wind direction, weather stability)
- Ignition probability, ignition sources/location, ignition strength (flammable releases)
- Energy levels contributing to explosive effects (flammable releases)
- Impact of release on people, property, or environment (thermal radiation, projectiles, shock-wave overpressure, toxic dosage)

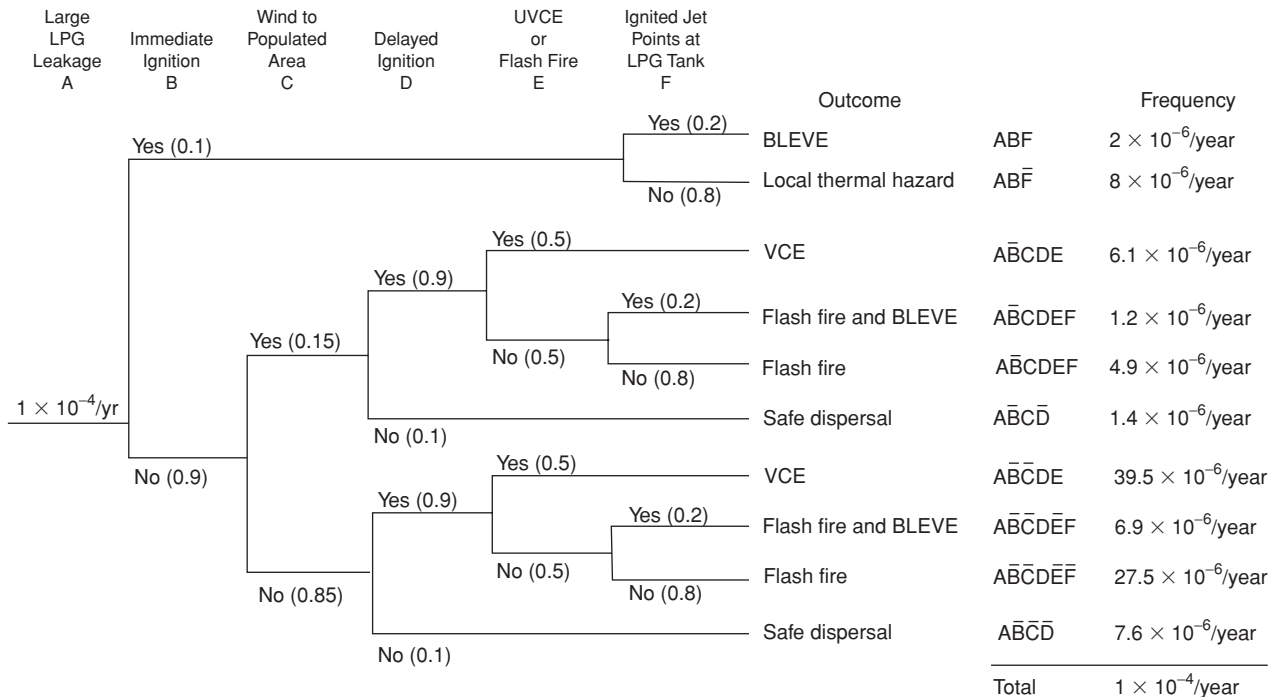


FIG. 23-26 Sample event tree for a release of LPG. (AIChE-CCPS, 2000, p. 329.)

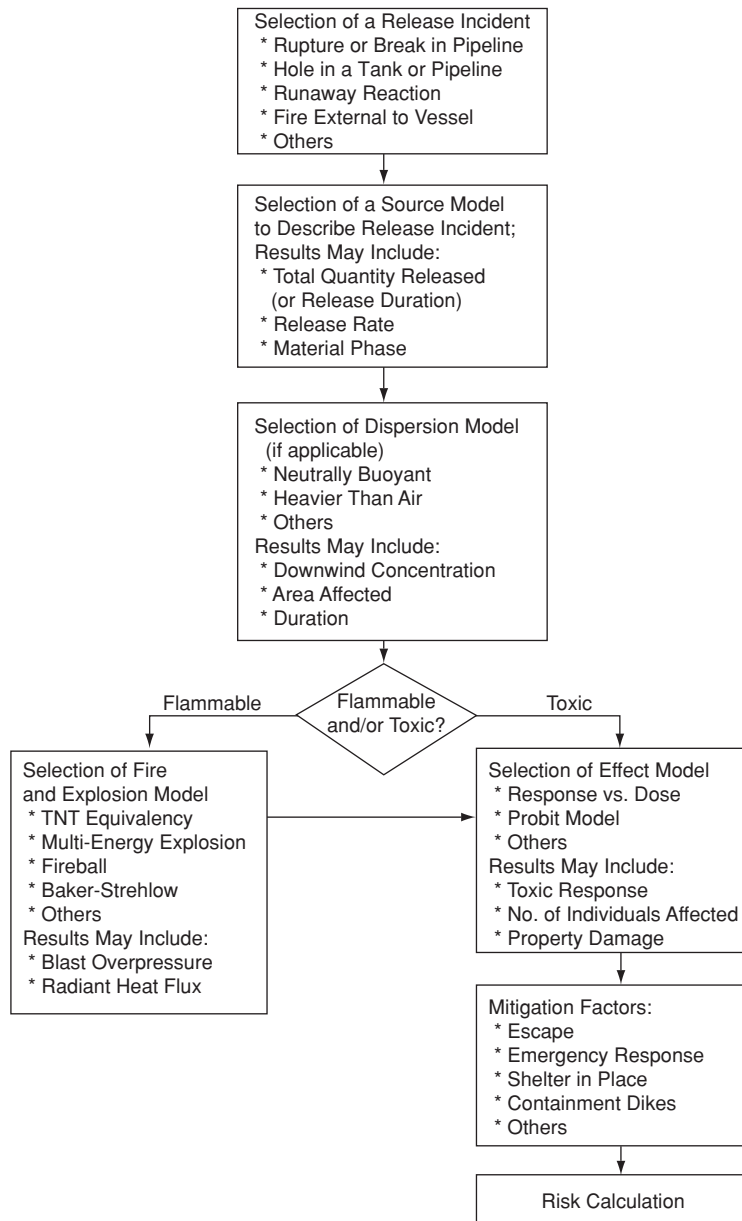


FIG. 23-27 Overall logic diagram for consequence analysis of volatile hazardous substances. (CCPS-AIChE, 1989, p. 60.)

- Mitigation effects (safe havens, evacuation, daytime/nighttime populations)

Probit models have been found generally useful to describe the effects of incident outcome cases on people or property for more complex risk analyses. At the other end of the scale, the estimation of a distance within which the population would be exposed to a concentration of ERPG-2 or higher may be sufficient to describe the impact of a simple risk analysis.

Portions or all of the more complex calculation processes, using specific consequence models, have been incorporated into a few com-

mercially available software packages (AIChE-CCPS, 2000). These programs should be used by risk analysts with extensive engineering experience, as significant judgment will still be required.

The output of these calculation processes is one or more pairs of an incident or incident outcome case frequency and its effect (consequence or impact).

Risk Estimation There are a number of risk measures which can be estimated. The specific risk measures chosen are generally related to the study objective and depth of study, and any preferences or requirements established by the decision makers. Generally, risk

measures can be broken down into three categories: risk indices, individual risk measures, and societal risk measures.

Risk indices are usually single-number estimates, which may be used to compare one risk with another or used in an absolute sense compared to a specific target. For risks to employees the *fatal accident rate* (FAR) is a commonly applied measure. The FAR is a single-number index, which is the expected number of fatalities from a specific event based on 10⁵ exposure hours. For workers in a chemical plant the FAR would be calculated for a specific event as

$$FAR = \frac{10^5}{8760} EP\tau \quad (23-29)$$

where FAR = expected number of fatalities from a specific event based on 10⁵ exposure hours

E = frequency of event, yr⁻¹

P = probability of being killed by event at a specific location

τ = fraction of time spent at specific location

However, the worker in a chemical plant could be exposed to other potential events that might result in a fatality. In this case the overall FAR for the worker would be

$$FAR = \frac{10^5}{8760} \sum_i E_i \sum_j P_{ij} \tau_j \quad (23-30)$$

Each subscript *i* is a specific event and each subscript *j* is a specific location.

References are available which provide FAR estimates for various occupations, modes of transportation, and other activities (Kletz, "The Risk Equations—What Risk Should We Run?," *New Scientist*, May 12, pp. 320-325, 1977).

Figure 23-28 is an example of an individual risk contour plot, which shows the expected frequency of an event causing a specified level of harm at a specified location, regardless of whether anyone is present at that location to suffer that level of harm.

The total individual risk at each point is equal to the sum of the individual risks at that point from all incident outcome cases.

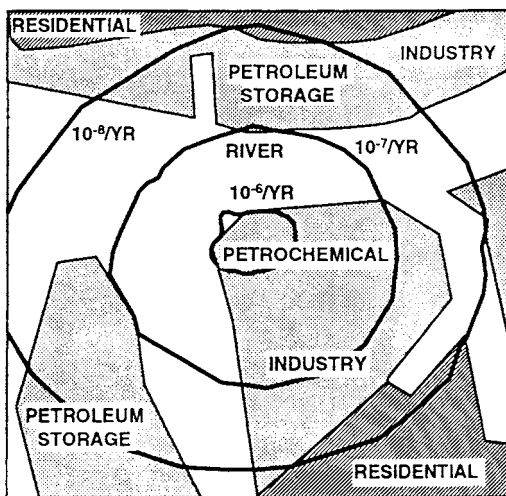


FIG. 23-28 Example of an individual risk contour plot. (CCPS-AIChE, 1989, p. 269.)

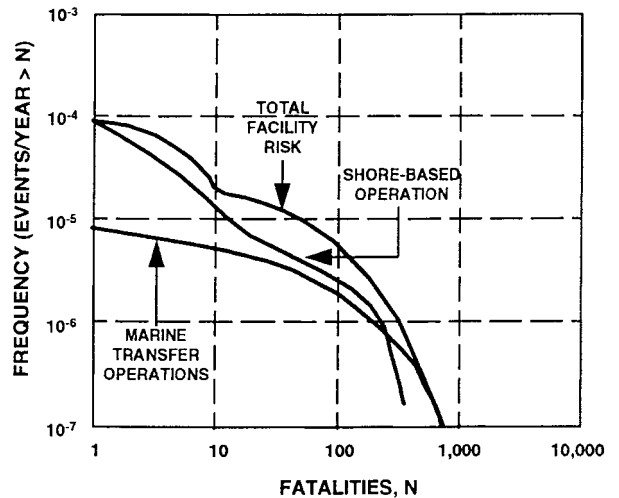


FIG. 23-29 Example of a societal risk F-N curve. (AIChE-CCPS, 1989, p. 4.4.)

$$IR_{x,y} = \sum_{i=1}^n IR_{x,y,i} \quad (23-31)$$

where IR_{x,y} = total individual risk of fatality at geographical location x,y

IR_{x,y,i} = individual risk of fatality at geographical location x,y from incident outcome case *i*

n = total number of incident outcome cases

A common form of societal risk measure is an F-N curve, which is normally presented as a cumulative distribution plot of frequency *F* versus number of fatalities *N*. An example of this type of measure is shown in Fig. 23-29.

Any individual point on the curve is obtained by summing the frequencies of all events resulting in that number of fatalities or greater. The slope of the curve and the maximum number of fatalities are two key indicators of the degree of risk.

Risk Criteria Once a risk estimate is prepared, alternatives to reduce the risk can be determined; but one always faces the challenge of how low a risk level is low enough. Different countries in the world have established numerical criteria [ALE (1992) and HSE (2001)] primarily as a tool to address the Seveso regulations. In addition, over the years various chemical companies have established numerical targets [Gibson (1980), Helmers (1982), and Renshaw (1990)]. A good survey paper on the use of risk guidelines by both governments and operating companies is provided by Pikaar and Seaman (1995).

Risk Decision Making Risk criteria represent the first step in risk decision making. Efforts must be made to reduce the risk at least to a "tolerable" risk level, which may be dictated by a government or an operating company. Once the tolerable level is reached, then additional risk reductions should still be evaluated. A number of criteria also provide guidance on a level of risk that requires no further risk reduction. In between these two levels is a range of risk where risk reduction options need to be evaluated. How far to continue reducing risk below the tolerable level is up to the individual company and is a function of costs and benefits (degree of risk reduction). At some point additional risk reductions have little benefit. Hamm and Schwartz (1993) summarize some strategies for consideration, and CCPS-AIChE (1995) provides an introduction to a number of decision analysis tools which could be applied.

DISCHARGE RATES FROM PUNCTURED LINES AND VESSELS

Nomenclature

a	Coefficient in nonequilibrium compressibility factor, Eq. (23-74)
A	Cross-sectional area perpendicular to flow, m^2
C_D	Discharge coefficient
C_{DG}	Discharge coefficient for gas flow
C_{DL}	Discharge coefficient for liquid flow
C_p	Heat capacity at constant pressure, $J/(kg \cdot K)$
C_v	Heat capacity at constant volume, $J/(kg \cdot K)$
D	Pipe diameter, m
D_T	Tank diameter, m
f	Fanning friction factor
F_l	Pipe inclination factor defined by Eq. (23-43)
g	Gravitational acceleration, m^2
G	Mass flux, $kg/(m^2 \cdot s)$
H	Specific enthalpy, J/kg
H_{GL}	Heat of vaporization ($H_G - H_L$) at saturation, J/kg
K	Slip velocity ratio, u_G/u_L
K_e	Number of velocity heads for fittings, expansions, contractions, and bends
L	Length of pipe, m
N	$4fL/D + K_e$, pipe resistance or nonequilibrium compressibility factor
P	Pressure, $Pa = N/m^2$
Q	Heat-transfer rate, W/kg
R	Gas constant, $J/(kgmol \cdot K)$
S	Specific entropy, $J/(kg \cdot K)$
t	Time, s
T	Temperature, K
u	Velocity, m/s
v	Specific volume, m^3/kg
v_{GL}	Specific volume difference, $v_G - v_L$, m^3/kg
w	Mass discharge rate, kg/s
x	Vapor quality, kg vapor/ kg mixture or mole fraction of liquid components
y	Mole fraction of vapor components
\bar{X}_m	Lockhart Martinelli parameter
z	Vertical distance, m

Greek

α	Volume fraction vapor, m^3 vapor/ m^3 mixture
ϵ	Dimensionless specific volume, v/v_0
γ	Heat capacity ratio, C_p/C_v

Greek

η	Pressure ratio, P/P_0
ϕ	Two-phase multiplier, pressure drop for two-phase flow divided by pressure drop for single-phase flow
μ	Single- or two-phase viscosity, $Pa \cdot s$
θ	Overall inclination angle of pipe to horizontal from source to break, deg
ρ	Density, kg/m^3
ω	Slope of dimensionless specific volume to reciprocal dimensionless pressure, defined by Eqs. (23-61a) and (23-61b)

Subscripts

a	Ambient
b	Backpressure
bub	Bubble point, pressure and saturation temperature when first vapor bubbles appear
c	η_{ch}/η_s , ratio of choked pressure to saturation pressure
ch	Choked
C	Condensable components (the contaminant)
d	Discharge
dew	Dew point, pressure and saturation temperature when first (or last) liquid occurs
diff	Differential form
e	Equivalent, for two-phase specific volume with slip
g, G	Gas or vapor
H	Homogeneous flow (slip velocity ratio of unity)
int	Integral form
I	Inert or padding gas component
L	Liquid
max	Maximum
N	Nonequilibrium
ori	Orifice
p	Pipe flow
s	Saturation (or bubble point)
sol	Solids
S	Constant specific entropy
v	Vapor pressure
0	Initial stagnation conditions
1	Point at which backpressure from pipe is felt after entrance from tank
2	Plane at vena contracta or at pipe puncture
\circ	Dimensionless

GENERAL REFERENCES: Bragg, "Effect of Compressibility on the Discharge Coefficient of Orifices and Convergent Nozzles," *J. Mech. Eng. Sci.*, **2**: 35-44, 1960. Chermisinoff and Gupta, eds., *Handbook of Fluids in Motion*, Ann Arbor Science, Ann Arbor, Mich., 1983. Chisholm, *Two-Phase Flow in Pipelines and Heat Exchangers*, George Godwin, New York, in association with the Institution of Chemical Engineers, 1983. Daubert and Danner, "Physical and Thermodynamic Properties of Pure Chemicals, Data Compilation," DIPPR (Design Inst. of Phys. Props. Res.) AIChE, New York, 1989. Diener and Schmidt, "Sizing of Throttling Device for Gas/Liquid Two-Phase Flow, Part 1: Safety Valves, Part 2: Control Valves, Orifices, and Nozzles," *J. Hazardous Mat.* **23**(4): 335-344, December 2004; **24**(1): 29-37, March 2005. Ely and Huber, "NIST Thermophysical Properties of Hydrocarbon Mixtures Database (STRAPP Program)," Version 1.0 Users' Guide, U.S. Dept. of Commerce, National Institute of Standards and Technology (NIST), Gaithersburg, Md., Feb. 1990. Fisher et al., *Emergency Relief System Design Using DIERS Technology*, AIChE, New York, 1992. Graham, "The Flow of Air-Water Mixtures Through Nozzles," National Engineering Laboratories (NEL) Report no. 308, East Kilbride, Glasgow, 1967. Jobson, "On the Flow of Compressible Fluids Through Orifices," *Proc. Instn. Mech. Engrs.* **169**(37): 767-776, 1955. "The Two-Phase Critical Flow of One-Component Mixtures in Nozzles, Orifices, and Short Tubes," *ASME J. Heat Transfer*, **93**(5): 179-187, 1976. Lee and Sommerfeld, "Maximum Leakage Times Through Puncture Holes for Process Vessels of Various Shapes," *J. Hazardous Mat.* **38**(1) 27-40, July 1994. Lee and Sommerfeld, "Safe Drainage or Leakage Considerations and Geometry in the Design of Process Vessels," *Trans. IChemE* **72**, part B: 88-89, May 1994. Leung, "A Generalized Correlation for One-Component Homogeneous Equilibrium Flashing Choked Flow," *AIChE J.* **32**(10): 1743-1746, 1986. Leung, "Similarity Between Flashing and Non-flashing Two-Phase Flow," *AIChE J.* **36**(5): 797, 1990. Leung, "Size Safety Relief Valves for Flashing Liquids," *Chem. Eng. Prog.* **88**(2): 70-75, February 1992. Leung, "Two-Phase Flow Discharge in Nozzles and Pipes—A Unified

Approach," *J. Loss Prevention Process Ind.* **3**(27): 27-32, January 1990. Leung and Ciolek, "Flashing Flow Discharge of Initially Subcooled Liquid in Pipes," *ASME Trans. J. Fluids Eng.* **116**(3), September 1994. Leung and Epstein, "Flashing Two-Phase Flow Including the Effects of Noncondensable Gases," *ASME Trans. J. Heat Transfer* **113**(1): 269, February 1991. Leung and Epstein, "A Generalized Correlation for Two-Phase Non-flashing Homogeneous Choked Flow," *ASME J. Heat Transfer* **112**(2), May 1990. Leung and Grolmes, "The Discharge of Two-Phase Flashing Flow in a Horizontal Duct," *AIChE J.* **33**(3): 524-527, 1987; also errata, **34**(6): 1030, 1988. Levenspiel, "The Discharge of Gases from a Reservoir Through a Pipe," *AIChE J.* **23**(3): 402-403, 1977. Lockhart and Martinelli, "Proposed Correlation of Data for Isothermal Two-Phase, Two-Component Flow in Pipes," *Chem. Eng. Prog.* **45**(1): 39-48, January 1949. Simpson, Rooney, and Grattan, "Two-Phase Flow Through Gate Valves and Orifice Plates," Int. Conf. on the Physical Modeling of Multi-phase Flow, Coventry, U.K., April 19-20, 1983. Sozzi and Sutherland, "Critical Flow of Saturated and Subcooled Water at High Pressure," General Electric Co. Report no. NEDO-13418, July 1975; also *ASME Symp. on Non-equilibrium Two-Phase Flows*, 1975. Tangren, Dodge, and Siefert, "Compressibility Effects in Two-Phase Flow," *J. Applied Phys.* **20**: 637-645, 1949. Uchida and Narai, "Discharge of Saturated Water Through Pipes and Orifices," *Proc. 3d Intl. Heat Transfer Conf.*, ASME, Chicago, **5**: 1-12, 1966. Van den Akker, Snoey, and Spoelstra, "Discharges of Pressurized Liquefied Gases Through Apertures and Pipes," *I. Chem. E. Symposium Ser.* (London) **80**: E23-35, 1983. Watson, Vaughan, and McFarlane, "Two-Phase Pressure Drop with a Sharp-Edged Orifice," National Engineering Laboratories (NEL) Report no. 290, East Kilbride, Glasgow, 1967. Woodward, "Discharge Rates Through Holes in Process Vessels and Piping," in Fthenakis, ed., *Prevention and Control of Accidental Releases of Hazardous Gases*, Van Nostrand Reinhold, New York, 1993, pp. 94-159. Woodward and Mudan, "Liquid and Gas Discharge Rates Through Holes in Process Vessels," *J. Loss Prevention*: **4**(3): 161-165, 1991.

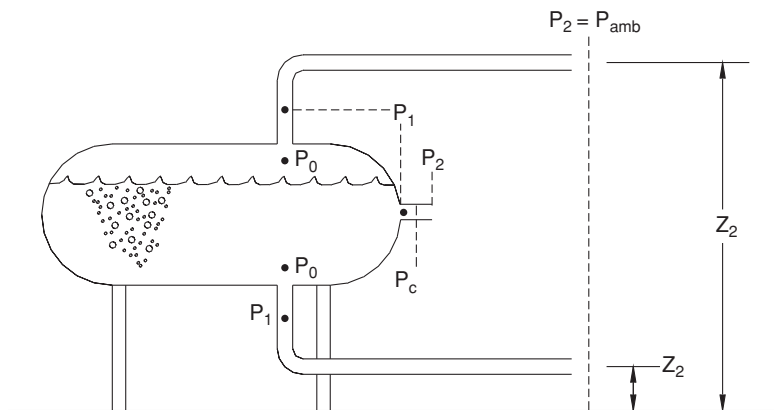


FIG. 23-30 Types of accidental discharge and pressure evaluation points.

Overview Modeling the consequences of accidental releases of hazardous materials begins with the calculation of discharge rates. In the most general case, the discharged material is made up of a volatile flashing liquid and vapor along with noncondensable gases and solid particles. Most of the model development is given in terms of two-phase, vapor + liquid flow, but it can be readily extended to three phases with vapor, liquid, plus suspended solids flow. The solids contribute primarily to the density and heat capacity of the mixture, contributing energy to the flashing and to the subsequent dispersion.

Types of Discharge Hazardous accidental releases can occur from vessels, pipelines, reactors, and distillation columns. The more common accidental events are breaks in a vessel or its associated piping. Figure 23-30 illustrates this. For a vessel, the piping attachments can be from a dip leg or from the bottom or top of the vessel. A puncture in the vapor space of the vessel or a break in a top-attachment pipe, initially at least, discharges vapor plus the padding gas used to maintain vessel pressure. This padding gas can be air for an atmospheric vessel. The discharged vapor can cool upon expansion and condense liquids when the pressure in the jet drops to the dew point pressure P_{dew} .

A puncture in the liquid space of the vessel or a break in the bottom-attachment or dip-leg pipe, initially, at least, discharges liquid plus any solids present without any noncondensable components. The liquid can begin to flash when the pressure drops to the bubble point pressure P_{bub} . If the liquid is extremely volatile, it could totally evaporate when the pressure drops below the dew point, producing vapor plus solids. The initial mass vapor fraction x_0 is zero as is the initial volume fraction α_0 .

For a puncture, break, or pressure relief valve (PRV) opening from a reactor or distillation column, there may be no clear-cut level distinguishing the liquid and vapor phases. That is, the system is initially mixed. In this case, noncondensable gases, condensable vapors, and liquid plus solids are initially discharged. The value of α_0 is nonzero and less than unity, reflecting the contributions of the gases and vapors.

For a blow-down calculation, the conditions change. With a tank vapor space release, as the pressure decreases, the liquid could reach its bubble point and begin to flash. Vapor bubbles in the liquid generate a liquid swell, so a frothy, two-phase interface rises and could drive out all the vapor (along with noncondensables) and begin two-phase flashing flow of liquid without noncondensables. Thus, the discharge calculation would also change from a vapor discharge to a two-phase flashing liquid discharge.

The energy and momentum balance equations are drawn across planes at points 0, 1, and 2, as illustrated for a general case in Fig. 23-31.

Energy Balance Method for Orifice Discharge Solutions can be found for the discharge rate by solving the energy balance and/or the momentum balance. The energy balance solution is quite simple and general, but is sensitive to inaccuracies in physical properties correlations. The equations below apply to orifice flow. A separate momentum balances solution is applied to pipe flow to find the pressure losses. The balances are written across an orifice from a plane 0 inside the tank at stagnant conditions (i.e., far enough away from the orifice that the velocity inside the tank is negligible) to a plane at the backpressure P_b at point 2.

$$H_0 = H_2 + \frac{1}{2} (G^2 v_c^2)_2 + Q \tag{23-32}$$

Rarely, if ever, is the heat-transfer term Q nonnegligible.

Perform an isentropic expansion. That is, as the pressure decreases from P_0 to the backpressure P_b (usually ambient pressure P_a), select intermediate values of pressure P_1 . At each P_1 find the temperature that keeps S constant T_{S1} . Solve for the vapor fraction x , using the entropy balance between planes 0 and 1:

$$S_0 = xS_{c1} + (1 - x - x_{sol})S_{L1} + x_{sol}S_{sol} \tag{23-33}$$

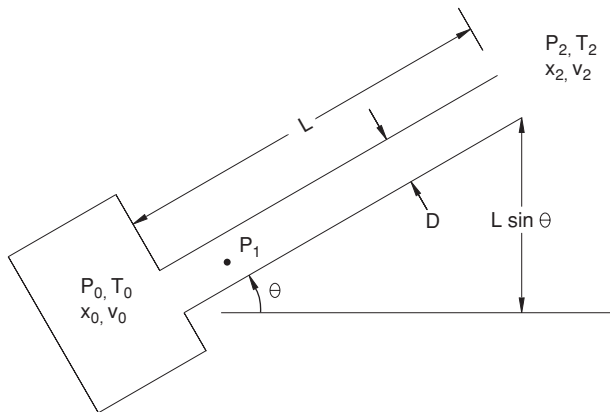


FIG. 23-31 Configuration modeled for pipe flow with elevation change.

23-56 PROCESS SAFETY

Since the mass fraction of solids is constant, the vapor flash fraction is

$$x = \frac{S_0 - [(1 - x_{\text{sol}})S_{L1} - x_{\text{sol}}S_{\text{sol}}]_{T_{s1}}}{(S_{C1} - S_{L1})_{T_{s1}}} \quad (23-34)$$

Find the enthalpy H_2 at T_{s1} from physical property correlations. Velocity is found solving Eq. (23-32) for homogeneous flow (with $Q = 0$):

$$Gv_c = u = \sqrt{2(H_0 - H_2)} \quad (23-35)$$

Find the density ρ from an equation of state at P_1, T_{s1} for the phase densities ρ_G and ρ_L , and the reciprocal of the homogeneous specific volume v_H . Calculate the mass flux from

$$G = u\rho = \frac{u}{v} \quad (23-36)$$

Search with values of P_1 until G is maximized. The choke pressure, P_{ch} is the value of P_1 that produces a maximum value of mass flux G_{max} . The discharge rate w is given from the mass flux, a discharge coefficient C_D , and the orifice cross-sectional area A as

$$w = C_D A G_{\text{max}} \quad (23-37)$$

This approach is illustrated for two-phase flashing flow with a multicomponent mixture (mole fractions 0.477 allyl alcohol, 0.3404 allyl chloride, 0.1826 dodecane). Figure 23-32 plots the flash curve showing that as pressure decreases, flashing begins at the bubble point of 7.22 bar(a) (104.7 psia) and increases to 30.8 mass %. At the same time, temperature follows the saturation curve down. Figure 23-33 plots the two-phase density, the velocity, and the product of these, the mass flux G . In the plot G is a maximum at 8586 kg/(m²·s) at the choke pressure just below the bubble point. This is so because the two-phase density drops quickly as flashing occurs at reduced pressures, while the velocity increases more slowly. With a discharge coefficient of 0.61 and a 2-in orifice (area of 0.002027 m²) the discharge rate w is 10.6 kg/s.

Momentum Balance in Dimensionless Variables For pipe flow, it is necessary to solve the momentum balance. The momentum balance is simplified by using the following dimensionless variables:

$$\text{Pressure ratio: } \eta = \frac{P}{P_0}$$

$$\text{Mass flux ratio: } G_* = \frac{G}{\sqrt{P_0 \rho_0}} \quad (23-38)$$

$$\text{Specific volume ratio: } \varepsilon = \frac{v}{v_0}$$

The discharge relationships are derived by solving the differential momentum balance over a tank plus pipe:

$$v dP + G^2 v dv + \left(4f \frac{dz}{D} + K_v\right) \frac{1}{2} G^2 v_L^2 \phi_L^2 + g \sin \theta dz = 0 \quad (23-39)$$

The terms represent, respectively, the effect of pressure gradient, acceleration, line friction, and potential energy (static head). The effect of fittings, bends, entrance effects, etc., is included in the term K_v correlated as a number of effective “velocity heads.” The inclination angle θ is the angle to the horizontal from the elevation of the pipe connection to the vessel to the discharge point. The term ϕ_L^2 is the two-phase multiplier that corrects the liquid-phase friction pressure loss to a two-phase pressure loss. Equation (23-39) is written in units of pressure/density.

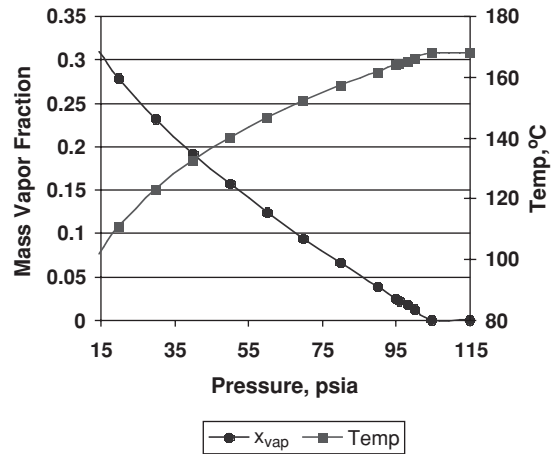


FIG. 23-32 Example flash curve for multicomponent material.

In dimensionless variables, the momentum balance is

$$\varepsilon d\eta + G_*^2 \varepsilon d\varepsilon + N \frac{1}{2} G_*^2 \varepsilon^2 \phi_L^2 + \frac{g \sin \theta dz}{P_0 v_0} = 0 \quad (23-40)$$

where N collects the friction loss terms in terms of the number of velocity heads, or

$$N = 4f_L \frac{dz}{D} + K_v \quad (23-41)$$

The two-phase flow multiplier ϕ_L^2 is discussed in a later section.

The momentum balance for homogeneous flow can be factored to a form that enables integration as

$$-N = \frac{G_{*p}^2 \varepsilon d\varepsilon + \varepsilon d\eta}{\frac{1}{2} G_{*p}^2 \varepsilon^2 + F_L} \quad (23-42)$$

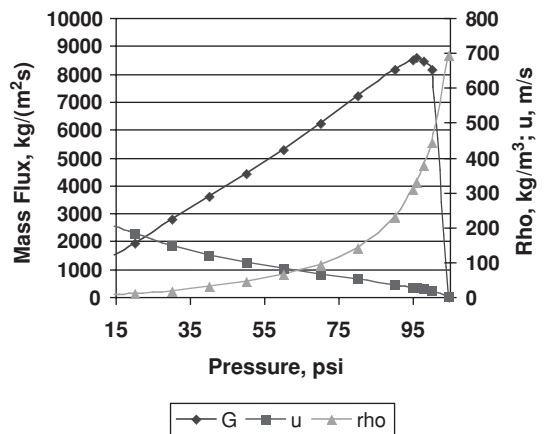


FIG. 23-33 Example of using the energy balance to find the orifice discharge flux.

by defining a pipe inclination factor F_I as

$$F_I = \frac{gD \sin \theta}{4f_{L0} P_0 v_0} \quad (23-43)$$

where F_I is positive for upflow, negative for downflow, and zero for horizontal flow.

Analytical Solutions for Orifice and Pipe Flow Equation (23-42) can be solved analytically for pipe breaks and tank punctures for the following cases:

- Subcooled liquid flow
 - Adiabatic expansion of ideal gases
 - Flashing liquid flow without noncondensable gases ($\alpha_0 = 0$)
 - Subcooled liquid mixed with noncondensable gases ($\alpha_0 > 0$) (frozen flow)
 - Flashing liquid mixed with noncondensable gases (hybrid flow)
- The solutions for all except hybrid flow follow.

Orifice Discharge for Gas Flow The analytic solution for discharge through an orifice of an ideal gas is derived by invoking the equation of state for adiabatic expansion of an ideal gas:

$$\frac{P}{P_0} = \left(\frac{\rho}{\rho_0} \right)^\gamma = \left(\frac{T}{T_0} \right)^{\gamma/(\gamma-1)} \quad (23-44)$$

where

$$\gamma = \frac{C_p}{C_v} \quad (23-45)$$

The solution is

$$G_{sg}^2 = \frac{2\gamma}{\gamma-1} \eta_2^{2\gamma} (1 - \eta_2^{(\gamma-1)/\gamma}) \quad (23-46)$$

This solution applies for both subsonic and choked flow. If the flow is choked, the exit pressure ratio η_2 is replaced by the choked pressure ratio η_{ch} , given by

$$\eta_{ch} = \left(\frac{2}{\gamma+1} \right)^{\gamma/(\gamma-1)} \quad (23-47)$$

Equation (23-47) must be evaluated to test for choked flow in any event. When η_{ch} from Eq. (23-47) is substituted into Eq. (23-46), the general solution reduces to the choked flow solution:

$$G_{sg}^2 = \gamma \left(\frac{2}{\gamma+1} \right)^{(\gamma+1)/(\gamma-1)} \quad (23-48)$$

The discharge rate is found by using Eqs. (23-37) and (23-38).

Blowdown of Gas Discharge through Orifice An analytic solution is available for blowdown (time-dependent discharge) of an ideal gas from a tank. The time-varying mass of gas in the tank m_T is the product of the tank volume V_T and the density ρ :

$$m_T(t) = V_T \rho(t) \quad (23-49)$$

Differentiating, solving for dt , and integrating gives

$$t = -V_T \int_{P_0}^P \frac{dP}{w} \quad (23-50)$$

where w is the time-varying discharge rate. Typically, all but a small fraction of the mass in a tank is discharged at sonic flow, so a sonic

flow solution is most useful. Transforming P and ρ to temperature T , using Eq. (23-44) allows Eq. (23-50) to be integrated to give a solution in terms of the initial discharge rate w_0 and the initial tank mass m_{T0} :

$$w(t) = w_0 [F(t)]^{(\gamma+1)/(\gamma-1)} \quad (23-51)$$

where

$$F(t) = (1 + At)^{-1} \quad (23-52a)$$

$$A = \frac{w_0 (\gamma + 1)}{2m_{T0}} \quad (23-52b)$$

Pipe and Orifice Flow for Subcooled Liquids Since liquids are essentially incompressible, ε is constant at ε_0 , and $d\varepsilon$ is zero in Eq. (23-42). Recognizing that η_0 and ε_0 are unity, we see that integration gives

$$-N \left(\frac{1}{2} G_{sp}^2 \varepsilon_0^2 + F_I \right) = \varepsilon_0 \int_{\eta_1}^{\eta_2} d\eta = \eta_2 - \eta_0$$

or

$$G_{sp}^2 = 2 \left(\frac{1 - \eta_2}{N} - F_I \right) \quad (23-53)$$

The solution for orifice flow is a special case with N equal to unity (entrance losses only) and F_I equal to zero, giving

$$G_{sori} = \sqrt{2(1 - \eta_2)} \quad (23-54)$$

Numerical Solution for Orifice Flow With orifice flow, the last two terms of the momentum balance (line resistance and potential energy change) are negligible. The momentum balance, Eq. (23-40), reduces to

$$G^2 \varepsilon d\varepsilon = -\varepsilon d\eta \quad (23-55)$$

This equation can be treated in differential form and in integral form. In differential form it becomes

$$G_{diff} = - \left(\frac{d\varepsilon}{d\eta} \right)^{-1/2} \quad \text{or} \quad G_{diff} = - \left(\frac{d\eta}{d\varepsilon} \right)^{-1/2} \quad (23-56)$$

For the integral form, express Eq. (23-55) as

$$\frac{1}{2} G^2 d\varepsilon^2 = -\varepsilon d\eta$$

to obtain

$$G \cdot d\varepsilon = (-2\varepsilon d\eta)^{1/2} \quad (23-57)$$

In general, the limits of integration are from ε_0 , η_0 to an arbitrary final point ε , η (recognizing that $\varepsilon_s = \varepsilon_0 = 1$). However, this method works better, using an indefinite integration of $d\varepsilon$:

$$G_{int} = \frac{1}{\varepsilon} \left(2 \int_{\eta}^{\eta_0} \varepsilon d\eta \right)^{1/2} \quad (23-58)$$

or in dimensional form

$$G_{int} = \frac{1}{v} \left(2 \int_p^{p_0} v dp \right)^{1/2} \quad (23-59)$$

Equations (23-56) and (23-59) are readily evaluated at intermediate pressure points P_1 in the range $P_a < P_1 < P_0$, giving two curves for G . The two curves cross at the choke point, which is also the point of maximum mass flux, as illustrated in Fig. 23-34 for a mixture of isobutane (90.898 mol %) and ethylene (9.102 mol %) initially at 33.0 bara and 357.4 K. The mass flux G found by evaluating Eq. (23-59) is labeled G_{int} in the figure, and the value of G found by evaluating Eq. (23-56) is labeled G_{diff} . The G_{int} curve has a maximum value of 20,637 kg/(m²·s) at the choke pressure of 20.64 bara.

The disadvantage of this solution is that it is sensitive to inaccuracies in the physical properties correlations used to evaluate the flash fraction and specific volumes. Figure 23-34 is found by using DIPPR properties (Daubert and Danner, 1989). The mass flux found does not agree well with that found by using the energy balance method that gives 24,330 kg/(m²·s). In addition, the rightmost branch of the G_{diff} curve is anomalously low and crosses the G_{int} curve spuriously to the right of the maximum flux. By using more accurate physical properties developed by the STRAPP program of NIST (Ely and Huber, 1990), the maximum value of G_{int} agrees with that found by the energy balance method and the right-hand branch of the G_{diff} curve does not fall low and cause this confusion. For this reason the method is not recommended for general use, but provides good confirmations when used with accurate physical properties correlations.

Omega Method Model for Compressible Flows The factored momentum balance, Eq. (23-42), can be analytically integrated after first relating the dimensionless specific volume ϵ to the dimensionless pressure ratio η . A method to do this, designated the *omega method*, was suggested by Leung (1986):

$$\epsilon = \begin{cases} \omega \left(\frac{\eta_s}{\eta} - 1 \right) + 1 & \text{if } \frac{\eta_s}{\eta} > 1 \\ 1.0 & \text{if } \frac{\eta_s}{\eta} \leq 1 \end{cases} \quad (23-60)$$

Equation (23-60) represents a linear relationship between the two- or three-phase specific volume and reciprocal pressure (v versus P^{-1} or ϵ

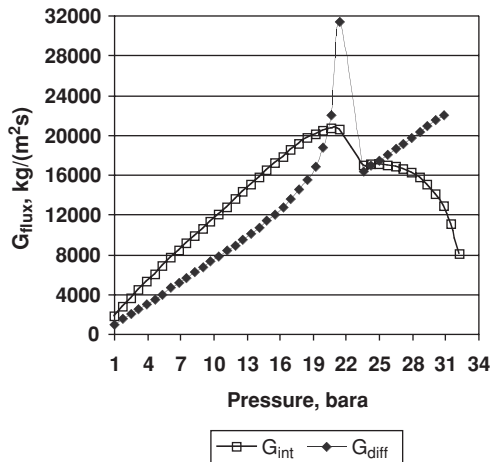


FIG. 23-34 Numerical solution of the momentum balance for orifice flow using Eqs. (23-56) and (23-59).

versus η^{-1}) beginning at the bubble point P_s , where η is η_s . For single components, ω is found by using the Clapeyron equation to give

$$\omega = \frac{C_p T_0 P_s}{v_{L0}} \left[\frac{v_{GL0}(P_s)}{H_{GL0}(P_s)} \right]^2 \quad (23-61a)$$

Alternately, use the slope of the ϵ versus η^{-1} curve between the bubble point and a second, lower pressure at ϵ_2, η_2 to evaluate ω , or

$$\omega = \frac{\epsilon_2 - 1}{\eta_s/\eta_2} - 1 \quad (23-61b)$$

This is a more convenient formula for multicomponent mixtures.

This value of ω can be called the saturation value or ω_s , since it applies only with flashing liquids (i.e., in the flashing region for pressures less than the bubble point, as seen in Fig. 23-32). A generalization defines omega to apply also with noncondensable gases by using $\alpha_0 = x_{v0} v_{v0} / v_0$

$$\omega = \alpha_0 + (1 - \alpha_0)\omega_s \quad (23-61c)$$

Homogeneous Equilibrium Omega Method for Orifice and Horizontal Pipe Flow The homogeneous equilibrium model (HEM) solution is obtained by substituting Eq. (23-60) for ϵ and integrating the momentum balance. The solution is given first for horizontal flow, with the flow inclination factor $F_I = 0$. Orifice flow is a special case in which only the orifice solution is needed. For pipe flow, two solutions are needed, the orifice flow solution giving G_{ori} and the pipe flow solution giving G_p . Plane 1 in Fig. 23-31 is at the pressure ratio η_1 where the pipe pressure balance begins and the inlet orifice pressure loss ends. The final pipe solution finds η_1 so that

$$G_{ori} = G_p \quad (23-62)$$

The integration for both solutions must be conducted over the subcooled region and the flashing region. The complicating factor is that the bubble point pressure ratio η_s could fall either in the orifice flow integration span ($\eta_s > \eta_1$), giving flashing in the orifice (case 1), or in the pipe integration span ($\eta_s < \eta_1$), giving flashing in the pipe (case 2). These two options are illustrated in Fig. 23-35.

Again, over the subcooled region from η_0 to η_s , $d\epsilon$ is zero and ϵ is constant at unity, ϵ_0 . The solutions for the two cases are as follows:

Case 1: *Flashing in Orifice, Two-Phase Flashing Flow in Pipe*

$$G_{ori}^2 = \frac{2[(1 - \eta_s) + [\omega \eta_s \ln(\eta_s/\eta_{ch}) - (\omega - 1)(\eta_s - \eta_{ch})]]}{\epsilon_{ch}^2} \quad (23-63)$$

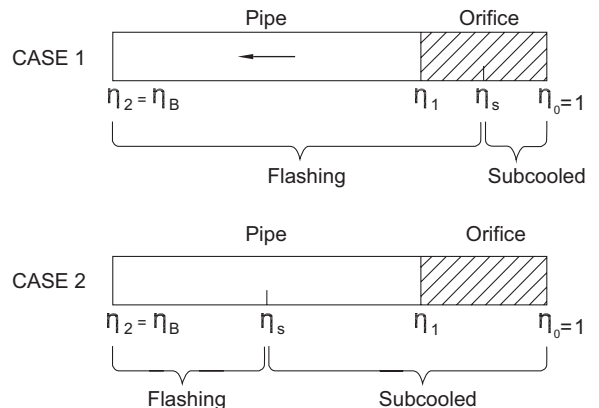


FIG. 23-35 Options for integration range of HEM omega method.

$$G_{sp}^2 = 2 \left\{ \frac{\eta_1 - \eta_2 + \frac{\omega \eta_s}{(1-\omega)^2} \ln \frac{\eta_2 \epsilon_2}{\eta_1 \epsilon_1}}{N + 2 \ln \left(\frac{\epsilon_2}{\epsilon_1} \right)} \right\} \quad (23-64)$$

Case 2: Subcooled Liquid in Orifice, Flashing in Pipe

$$G_{ori}^2 = 2(\eta_0 - \eta_1) \quad (23-65)$$

$$G_{sp}^2 = 2 \left[\frac{\eta_1 - \eta_s + \frac{\eta_s - \eta_2}{1-\omega} + \frac{\eta_s - \eta_2}{1-\omega} + \frac{\omega \eta_s}{(1-\omega)^2} \ln \left(\frac{\eta_2 \epsilon_2}{\eta_s \epsilon_s} \right)}{N + 2 \ln \left(\frac{\epsilon_2}{\epsilon_s} \right)} \right] \quad (23-66)$$

The choke point is found by the usual maximization relationship:

$$\left(\frac{dG_s}{d\eta_2} \right)_{\eta_2=\eta_b} = 0 \quad (23-67)$$

This gives an implicit equation in the choked pressure ratio η_c (short-hand for η_{ch}/η_s):

If $\omega \leq 2$:

$$\eta_c^2 + \omega(\omega - 2)(1 - \eta_c)^2 + 2\omega^2 \ln \eta_c + 2\omega^2(1 - \eta_c) = 0 \quad (23-68a)$$

An explicit equation provides an adequate approximate solution for larger values of ω :

For $\omega \geq 2$:

$$\eta_c = 0.55 + 0.217 \ln \omega - 0.046 (\ln \omega)^2 + 0.004 (\ln \omega)^3 \quad (23-68b)$$

For orifice flow, the definition of choked flow in terms of the back-pressure ratio η_b is

- Choked compressible: $\eta_b \leq \eta_{ch}$ set $\eta = \eta_{ch}$
- Subsonic compressible: $\eta_b > \eta_{ch}$ set $\eta = \eta_b$
- Subcooled liquid: always subsonic

The omega method HEM solution for orifice flow is plotted in Fig. 23-36. The solution for flashing liquids without noncondensables is to the right of $\omega = 1$, and the solution for frozen flow with subcooled liquids plus noncondensables is to the left. The omega method HEM solution for horizontal pipe flow is plotted in Fig. 23-37 as the ratio of pipe mass flux to orifice mass flux.

HEM for Inclined Pipe, Discharge If a pipe leak occurs at an elevation above or below the pump or source tank the elevation change can be idealized between the starting and ending points as shown in Fig. 23-38. That is, elevation changes can be treated as an inclined pipe with a non-zero inclination factor F_I . This is an approximation to the actual piping isometrics, but is often an adequate approximation.

The HEM solution in this case is implicit in G_{sp} :

Case 1: Flashing in Orifice, Two-Phase Flashing Flow in Pipe:

Use Eq. (23-63) for G_{ori} :

$$N + \ln \left\{ \frac{X(\eta_2)}{X(\eta_1)} \left[\frac{\eta_1}{\eta_2} \right]^2 \right\} = \frac{1-\omega}{c} (\eta_1 - \eta_2) + \frac{b(1-\omega) - c\omega \eta_s}{2c^2} \ln \frac{X(\eta_2)}{X(\eta_1)} + \frac{bc\omega \eta_s - (1-\omega)(b^2 - 2ac)}{2c^2} [I_0(\eta_2) - I_0(\eta_1)] \quad (26-69)$$

Case 2: Subcooled Liquid in Orifice, Flashing in Pipe: Use Eq. (23-65) for G_{ori} :

$$N + \ln \left\{ \frac{X(\eta_2)}{X(\eta_s)} \left[\frac{\eta_s}{\eta_2} \right]^2 \right\} = \frac{\eta_1 - \eta_s}{\frac{1}{2}G_s^2 + F_I} + \frac{1-\omega}{c} (\eta_s - \eta_2) + \frac{b(1-\omega) - c\omega \eta_s}{2c^2} \ln \frac{X(\eta_2)}{X(\eta_s)} + \frac{bc\omega \eta_s - (1-\omega)(b^2 - 2ac)}{2c^2} [I_0(\eta_2) - I_0(\eta_s)] \quad (23-70)$$

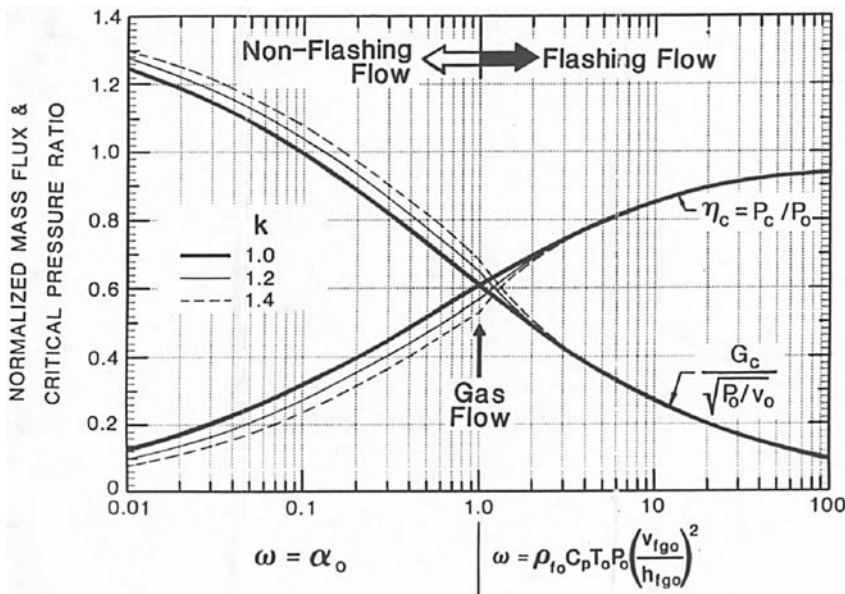


FIG. 23-36 Omega method solution for orifice flow of flashing liquids and for noncondensable gas plus subcooled liquids.

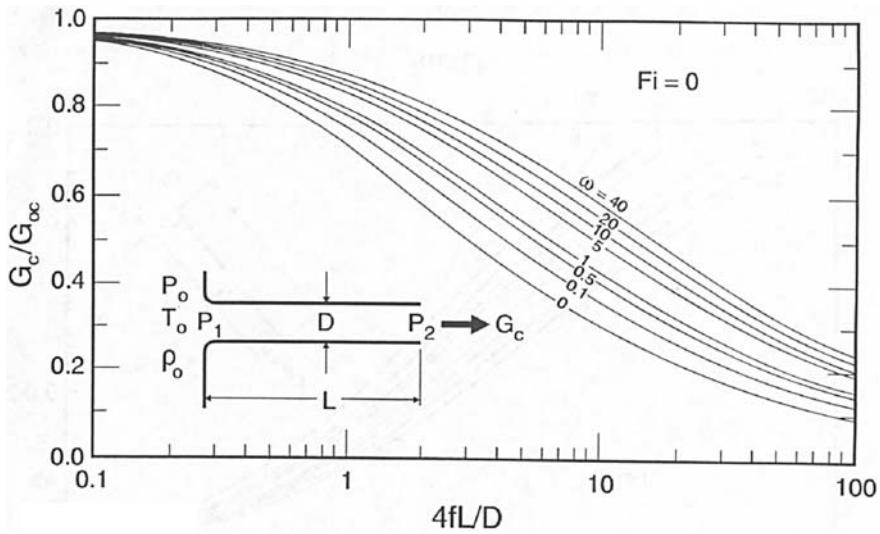


FIG. 23-37 Omega method solution for flashing liquid horizontal pipe flow.

where

$$a = \frac{1}{2} G^2 \omega^2 \eta_s^2 \quad (23-71a)$$

$$b = \frac{1}{2} G^2 2\omega (1 - \omega) \eta_s \quad (23-71b)$$

$$c = \frac{1}{2} G^2 (1 - \omega)^2 + F_I \quad (23-71c)$$

$$q = 4ac - b^2 \quad (23-71d)$$

$$X(\eta) = a + b\eta + c\eta^2 \quad (23-72)$$

$$I_0(\eta) = \int \frac{d\eta}{X(\eta)}$$

If $q > 0, F_I > 0$, upflow:

$$I_0(\eta) = \frac{2}{\sqrt{q}} \tan^{-1} \frac{2c\eta + b}{\sqrt{q}} \quad (23-73a)$$

If $q < 0, F_I < 0$, downflow:

$$I_0(\eta) = \ln \frac{2c\eta + b - \sqrt{-q}}{2c\eta + b + \sqrt{-q}} \quad (23-73b)$$

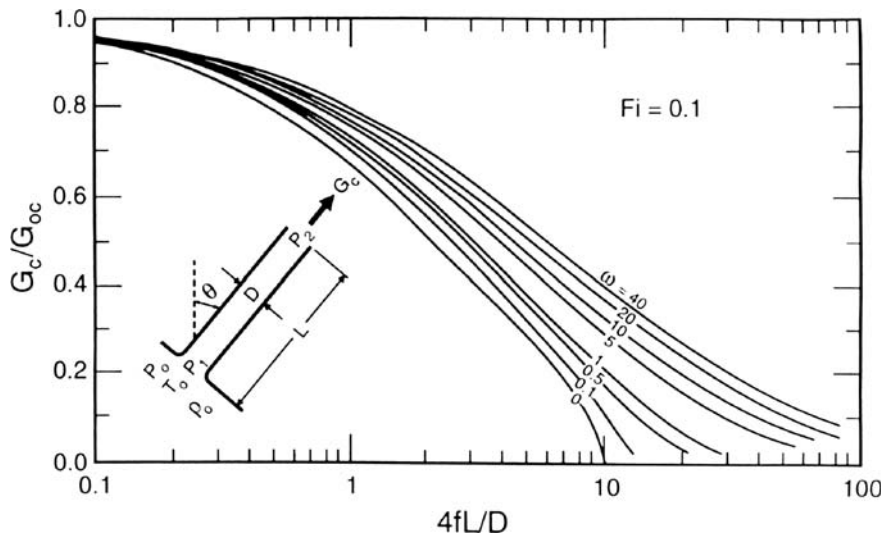


FIG. 23-38 Omega method HEM solution for inclined pipe flow at $F_I = 0.1$.

If $q = 0, F_1 = 0$, horizontal flow:

$$I_0(\eta) = \frac{-1}{(1 - \omega)\epsilon\eta} \quad (23-73c)$$

The omega method HEM solution for inclined pipe flow is illustrated in Fig. 23-38.

Nonequilibrium Extension of Omega Method The omega method HEM tends to produce discharge rates that are low, particularly for short pipes. To correct this deficiency, Diener and Schmidt proposed a modification they term the *nonequilibrium compressibility factor N*, defined by

$$N = \left[x_0 + C_{PL0} T_0 P_0 \left(\frac{v_{GL0}}{H_{GL0}^2} \right) \ln \left[\frac{1}{\eta_c} \right] \right]^a \quad (23-74)$$

with

$$a = \begin{cases} 0.6 & \text{for orifices, control valves, short nozzles} \\ 0.4 & \text{for pressure relief valves, high - lift control valves} \\ 0 & \text{for long nozzles, office with large area ratio} \end{cases}$$

The choked pressure ratio η_c is found by using Eqs. (23-68a) and (23-68b). The nonequilibrium factor N is used to modify ω :

$$\omega = \alpha_0 + \omega_s N \quad (23-75)$$

Differences between Subcooled and Saturated Discharge for Horizontal Pipes Data by Uchaida and Narai (1966) in Figs. 23-39 and 23-40 illustrate the substantial differences between subcooled and saturated-liquid discharge rates. Discharge rates decrease with increasing pipe length in both cases, but the drop in discharge rate is much more pronounced with saturated liquids. This is so, because the flashed vapor effectively chokes the flow and decreases the two-phase density.

Accuracy of Discharge Rate Predictions Model verification is difficult because agreement with data varies substantially from one set of experimental data to another. The accuracy of the HEM and the NEM correction is illustrated in Fig. 23-41 and compared with data for saturated water by Uchaida and Narai (1966). The NEM correction using the power coefficient a of 0.6 decreases omega and increases the predicted discharge rates so that good predictions are obtained for pipe lengths greater than 0.5 m.

The accuracy of the energy balance method for discharge of flashing liquids through orifices and horizontal pipes is illustrated in Figs. 23-42 and 23-43. The ratio of predicted to observed mass flux is plotted for saturated water data by Uchaida and Narai and by Sozzi and

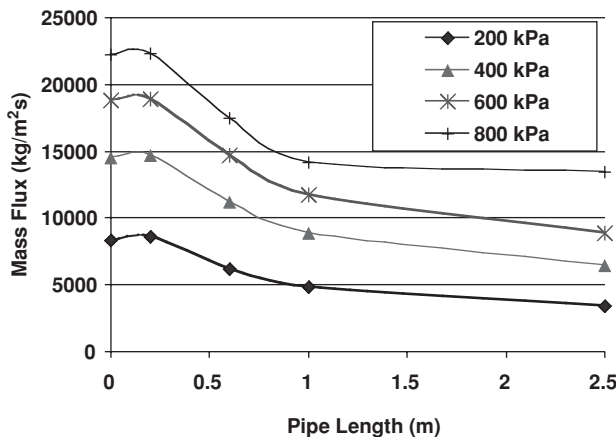


FIG. 23-39 Subcooled water data by Uchaida and Narai.

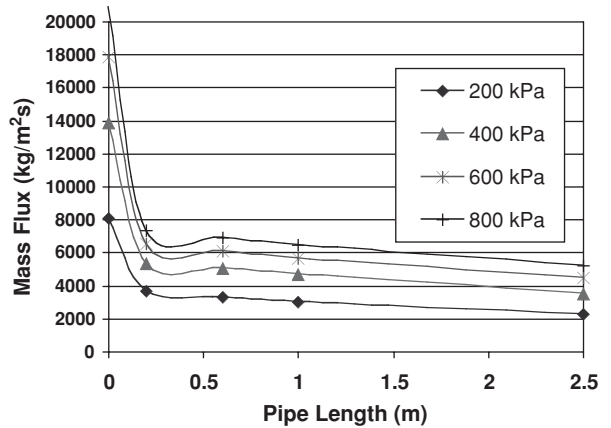


FIG. 23-40 Saturated water data by Uchaida and Narai.

Sutherland (1975). Orifice flow rates are underpredicted by about the same factor with the energy balance method and with the NEM. Discharge predictions for short (0.2-m) pipes are overpredicted by the energy balance method. In this region, the assumption of homogeneous equilibrium is not justified. A model that takes slip velocity into account may improve predictions for short pipes.

ATMOSPHERIC DISPERSION

Nomenclature

$\langle C \rangle_{t_1}$	(Ensemble) time-averaged concentration for averaging time t_1 , mass per volume
d_0	Displacement height, length
E	Airborne contaminant mass rate in a plume, mass per time
E_t	Total airborne contaminant mass in a puff, mass
g	Acceleration due to gravity, length squared per time
k	Von Karman's constant (typically 0.4)
L	Monin-Obukhov length, length
p	Index reflecting decrease in time-averaged concentration with averaging time
t_d	Along wind (x direction) dispersion time scale, time
t_h	Time scale for contaminant to pose a particular hazard, time
t_s	Source time scale, length of time for contaminant to become airborne, time
t_t	Time scale for a contaminant cloud to reach hazard endpoint distance x_h , time
u	(Characteristic) wind speed at elevation z , length per time
u_r	Wind speed at reference height z_r , length per time
u_*	Friction velocity, length per time
x_e	Virtual source distance upwind of real source, length
x	(Downwind) distance in wind direction, length
x_h	Hazard endpoint distance, length
z_0	Surface roughness, length
z_r	Reference height, length

Greek symbols

α	Monin-Obukhov length coefficient
ϵ	Height of ground covering, length
ρ	Air-contaminant mixture density at concentration C , mixture mass per mixture volume
ρ_a	Ambient air density, mass per volume
$\sigma_x, \sigma_y, \sigma_z$	Dispersion coefficients in x, y, z directions, length
σ_θ	Wind direction standard deviation, angle

Subscripts

x	Along wind direction
y	Lateral direction
z	Vertical direction

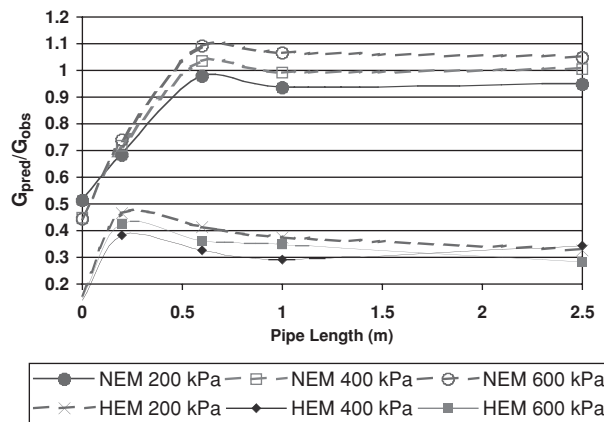


FIG. 23-41 Accuracy of Omega method HEM and NEM correction compared with saturated water data by Uchaida and Narai.

GENERAL REFERENCES: Britter and McQuaid, *Workbook on the Dispersion of Dense Gases*, Health and Safety Executive Report 17/1988, Sheffield, U.K., 1988. Mannan, *Lees' Loss Prevention in the Process Industries*, 3d ed., Chap. 15, Elsevier Butterworth-Heinemann, Oxford, U.K., 2005. Panofsky and Dutton, *Atmospheric Turbulence*, Wiley, New York, 1984. Pasquill and Smith, *Atmospheric Diffusion*, 3d ed., Ellis Horwood Limited, Chichester, U.K., 1983. Seinfeld, *Atmospheric Chemistry and Physics of Air Pollution*, Chaps. 12–15, Wiley, New York, 1986. Turner, *Workbook of Atmospheric Dispersion Estimates*, U.S. Department of Health, Education, and Welfare, 1970.

Introduction Atmospheric dispersion models predict the dilution of an airborne contaminant after its release (and depressurization) to the atmosphere. The discussion in this section focuses on episodic releases representing acute biological, toxic, or flammable hazards. Physical and mathematical dispersion models discussed here are typically used for (1) forensic purposes (in comparison with actual events such as experiments, field trials, or accidents); (2) regulatory purposes, such as estimating the consequences of releases of toxic or flammable materials for siting requirements; or (3) planning purposes. Release consequences may be used to estimate the risk to a facility and workforce or the surrounding population. All such estimates can be used to identify appropriate emergency response or mitigation measures and the priority with which such measures should be considered.

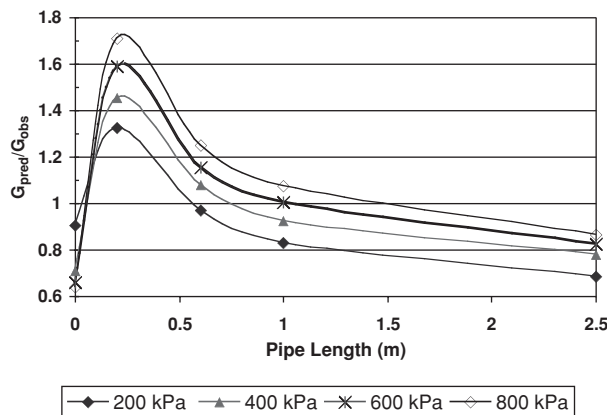


FIG. 23-42 Accuracy of energy balance method compared with saturated water data by Uchaida and Narai.

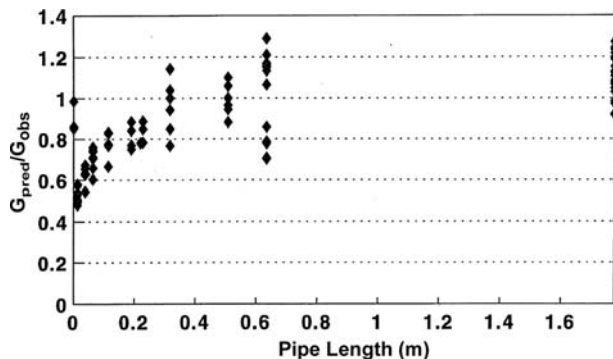


FIG. 23-43 Accuracy of energy balance method for flashing liquid discharge through orifices and horizontal pipes.

Parameters Affecting Atmospheric Dispersion The parameters important to atmospheric dispersion can be divided roughly into three categories: contaminant source; atmospheric and terrain properties; and contaminant interaction with the atmosphere.

Contaminant Source The contaminant source includes such factors as the following:

1. *Rate or total amount of contaminant that becomes airborne.*

For a continuous contaminant release, the contaminant concentration at a fixed downwind distance is roughly proportional to the rate at which the contaminant becomes airborne. Likewise, the contaminant concentration at a fixed downwind distance is roughly proportional to the amount of contaminant released if the release is instantaneous. However, materials released from containment may not immediately become airborne. For example, a liquid below its boiling point stored at atmospheric pressure will form a liquid pool when released. The rate at which the contaminant becomes airborne will depend on the heat-transfer rate to the liquid pool and the mass-transfer rate from the liquid pool to air. However, the same liquid stored at a higher pressure may form an aerosol so that the liquid phase is airborne. If the aerosol droplet size formed in the release is too large to remain suspended, the liquid phase will fall to the ground (rainout), and the resulting liquid pool evaporation will again be dictated by heat- and mass-transfer considerations.

2. *Release momentum.* For jet releases, the amount of air entrained in an unobstructed jet is proportional to the jet velocity. Depending on the orientation of the jet relative to nearby obstructions, the momentum of a jet can be dissipated without significant air entrainment. The degree of initial air entrainment can be an important determinant of the hazard extent, particularly for flammable hazards. It would be (possibly overly) conservative to assume the source momentum is dissipated without air dilution. Explosive releases are high-momentum, instantaneous releases. For explosive releases, a rough first approximation is to assume the mass of contaminant in the explosion is mixed with 10 times that mass of air.

3. *Release buoyancy.* Contaminant release buoyancy is determined by the initial contaminant temperature and molecular weight, and whether there is a suspended liquid phase as in an aerosol. Lighter-than-air contaminants will rise and be more readily dispersed. Denser-than-air contaminants will tend to stay near ground level, and the atmospheric dispersion of such materials can be importantly determined by buoyancy effects. The degree of importance is typically quantified by a Richardson number (proportional to the density difference with air and the quantity or rate of contaminant release and inversely proportional to the square of the wind speed); the higher the Richardson number, the more important the effect of buoyancy on the atmospheric dispersion (see Denser-than-Air Dispersion Models — Britter-McQuaid below). Denser-than-air contaminants can actually displace the atmospheric flow field. In contrast, contaminants which do not perturb the atmospheric flow field and can be thought of as simply following the airflow are termed *passive* contaminants.

4. *Other source conditions.* The source height and the source area are also important source characteristics. The greatest impact is typically associated with ground-level sources, so elevated sources are not considered in the model discussion below.

Atmospheric and Terrain Parameters In addition to terrain parameters, basic atmospheric parameters are listed below. There can be many other meteorological effects which can be important in some circumstances (e.g., inversion layers) and are beyond the scope of this introduction.

1. *Wind direction.* Wind direction is the most important determinant of the location of hazard zones with notable exceptions involving high-momentum releases or releases where buoyancy is important (particularly for denser-than-air contaminants involving terrain effects such as valleys and slopes especially under low-wind-speed conditions). Near ground level, lateral wind direction variability is much larger than vertical variability (typical of flat-plate boundary layers) and measured with the standard deviation σ_θ which is a function of atmospheric stability.

2. *Atmospheric stability.* Atmospheric stability is often characterized by Pasquill stability class (ranging from A through F). Atmospheric stability classes are broad classifications which are used to characterize the continuum of atmospheric turbulence available to the (mixing) dispersion process. Neutral atmospheric stability (class D) occurs most often and indicates that the vertical momentum flux is not influenced by the vertical heat flux in the lowest atmospheric layers. Unstable atmospheric conditions (instability increasing from classes C through A) indicate the atmospheric vertical heat flux is enhancing the vertical mixing of the atmosphere, such as when ground surface heating due to insolation (incident solar radiation) enhances vertical atmospheric mixing (turbulence). Stable atmospheric conditions (stability increasing from classes E through F) indicate the atmospheric vertical heat flux is suppressing the vertical mixing of the atmosphere, such as when ground surface cooling at night suppresses vertical mixing (turbulence). All atmospheric dispersion models rely in some way on measured atmospheric parameters, and these parameters are quite frequently correlated on the basis of Pasquill stability class. Consequently, atmospheric dispersion model results should be viewed as only representative of the atmospheric conditions present in a real or hypothetical release. Atmospheric stability class is an important determinant of concentration at a fixed downwind distance in dispersion models. For passive contaminants, concentration at a fixed downwind distance can be roughly an order of magnitude higher for F stability in comparison to D stability. Table 23-24 illustrates the relationship between atmospheric stability class and other meteorological conditions. Determination of Pasquill stability class should be made with detailed measurements such as discussed by Golder ("Relations among Stability Parameters in the Surface Layer," *Boundary Layer Meteorol.*, 3, pp. 47-58, 1972).

3. *General terrain characteristics.* General terrain characteristics are used to describe features with length scales much smaller than the depth of the contaminant cloud or the height of the characteristic wind speed. General terrain characteristics influencing the shape of the vertical wind speed profile are parameterized with the surface roughness and displacement height. The surface roughness z_0 is roughly proportional to the height of the ground covering ϵ (and $z_0 \sim 0.05\epsilon$ to 0.15ϵ) and can be used to infer the amount of vertical turbulence (mixing) in the atmospheric flow (higher obstacles enhance vertical turbulence above the obstacle height). However, obstacles can also displace the atmospheric flow; the displacement height is the height at which the (average) ambient wind speed is negligible. If the displacement height is negligible (flow blockage is not important), contaminant concentration at a fixed downwind distance decreases with increased surface roughness (an order-of-magnitude increase in surface roughness decreases the concentration by roughly a factor of 3).

4. *Wind speed.* Because wind speed varies with height above the ground, the reference wind speed u_r must be specified at a particular height z_r (typically 10 m provided local flow obstructions are not important at this height). For a continuous contaminant release, the contaminant concentration at a fixed downwind distance is roughly inversely proportional to the wind speed. As indicated above, denser-than-air effects are less important at higher wind speeds. The wind speed profile is affected by atmospheric stability, surface roughness z_0 , and displacement height d_0 (the height below which the wind speed is negligible). The vertical profile of the wind speed is logarithmic

$$u = \frac{u_*}{k} \left[\ln \left(\frac{z + d_0}{z_0} \right) + \alpha \left(\frac{z}{L} \right) \right] \quad (23-76)$$

for neutral and stable conditions when $z \gg z_0$ and d_0 ; k is von Karman's constant (typically 0.4), u_* is the friction velocity (u_*^2 characterizes the atmospheric vertical mixing rate), L is the Monin-Obukhov length (a measure of stability class), and α is the Monin-Obukhov length coefficient ($\alpha = 5.2$ for stable conditions). For D stability, $L = \infty$ so $z/L = 0$, and the second term in brackets is zero. Since Eq. (23-76) must also hold for u_r and z_r , u_r is proportional to u_* (all other things being equal), so reduction of the wind speed by a factor of 2 reduces the vertical atmospheric mixing by a factor of 4.

5. *Flow obstructions.* In contrast to general terrain characteristics, flow obstructions have length scales much larger than the depth or width of the contaminant cloud or the height of the characteristic wind speed. Flow obstructions can increase or decrease contaminant concentration depending on location. Flow obstructions increase concentration by delaying the dispersal of the contaminant cloud; e.g., inside a dike, concentration is higher, but downwind of the dike, concentrations can be smaller; and the downwind side of flow obstructions can temporarily trap higher concentrations. Obstructions also distort the wind speed profile given above.

Contaminant Interaction with the Atmosphere Contaminant interaction with the atmosphere is important for several reasons:

1. There are chemical reactions between the released contaminant and ambient air or surfaces. If the released contaminant reacts, any reacted material can no longer be considered airborne (although the reaction products may also be hazardous), and so chemical reactions effectively reduce the rate or amount of airborne contaminant. Some reactions can be characterized as dry or wet deposition.

2. Phase changes are typically associated with the evaporation of any suspended liquid phase in an aerosol release. As air is mixed with an aerosol, equilibrium constraints cause additional evaporation of the liquid phase which reduces the temperature of the liquid phase (and the vapor phase if thermal equilibrium is maintained).

3. Ground-to-contaminant cloud heat transfer acts to warm the contaminant cloud if the cloud temperature is lower than ambient. Ground-to-cloud heat transfer can be important for cold clouds at ground level because the buoyancy of the contaminant cloud can be significantly reduced for cold clouds with contaminant molecular weight less than that of air. At higher wind speeds, heat transfer is by forced convection, and even though such conditions produce higher heat-transfer coefficients than do low-wind-speed conditions, heat

TABLE 23-24 Typical Atmospheric Stability Classes in Terms of Wind Speed, Insolation, and State of the Sky

Surface wind speed m/s	Insolation			Night	
	Strong	Moderate	Slight	Thinly overcast or ≥4/8 low cloud	≤3/8 cloud
<2	A	A-B	B	—	—
2-3	A-B	B	C	E	F
3-5	B	B-C	C	D	E
5-6	C	C-D	D	D	D
>6	C	D	D	D	D

For A-B, take the average of values for A and B, etc. Pasquill and Smith relate insolation to conditions in England. Seinfeld (*Atmospheric Chemistry and Physics of Air Pollution*, Wiley, New York, 1986) classifies insolation greater than 700 W/m² as strong, less than 350 W/m² as slight, and between these limits as moderate. Night refers to the period from 1 h before sunset to 1 h after dawn. The neutral class D should be used, regardless of wind speed, for overcast conditions during day or night and for all sky conditions during the hour preceding or following the night period.

SOURCE: Pasquill and Smith, *Atmospheric Diffusion*, 3d ed., Ellis Horwood Limited, Chichester, U.K., 1983.

transfer is typically more important at low-wind-speed conditions because of two effects: (1) At low wind speeds, the amount of air entrainment is reduced so that the heat-transfer driving force is larger, and (2) at low wind speeds, the contact time between the contaminant cloud and the ground is longer.

Atmospheric Dispersion Models Atmospheric dispersion models generally fall into the categories discussed below. Regardless of the modeling approach, models should be verified that the appropriate physical phenomena are being modeled and validated by comparison with relevant data (at field and laboratory scale). The choice of modeling techniques may be influenced by the expected distance to the level of concern.

1. *Physical or wind tunnel models* Wind tunnel models have long been used to study the atmospheric flow around structures such as buildings and bridges to predict pressure loading and local velocities. Wind tunnel measurement of contaminant concentrations for release scenarios can be used to estimate hazard zones. However, wind tunnel models are generally considered to be incapable of simultaneously scaling mechanical turbulence and thermally induced turbulence (verification issue). Wind tunnel experiments can be very useful when considering validation of mathematical models. Wind tunnel models typically do not account for the lateral variation in wind direction.

2. *Empirical models* Empirical models rely on the correlation of atmospheric dispersion data for characteristic release types. Two examples of empirically based models are the Pasquill-Gifford model (for passive contaminants) and the Britter-McQuaid model (for denser-than-air contaminants) both of which are described below. Empirical models can be useful for the validation of other mathematical models but are limited to the characteristic release scenarios considered in the correlation. Selected empirical models are discussed in greater detail below because they can provide a reasonable first approximation of the hazard extent for many release scenarios and can be used as screening tools to indicate which release scenarios are most important to consider.

3. *First principle mathematical models* These models solve the basic conservation equations for mass and momentum in their form as partial differential equations (PDEs) along with some method of turbulence closure and appropriate initial and boundary conditions. Such models have become more common with the steady increase in computing power and sophistication of numerical algorithms. However, there are many potential problems that must be addressed. In the verification process, the PDEs being solved must adequately represent the physics of the dispersion process especially for processes such as ground-to-cloud heat transfer, phase changes for condensed phases, and chemical reactions. Also, turbulence closure methods (and associated boundary and initial conditions) must be appropriate for the dis-

person processes present, especially for denser-than-air contaminants. Regardless of the algorithm for solving the PDEs, any solution must demonstrate resolution independence (i.e., the numerical solution must be independent of grid spacing or time step). Finally, models should be validated against relevant information for the scenario considered. Despite decreased computational costs, such models still require a significant investment for investigating a release scenario.

4. *Simplified mathematical models* These models typically begin with the basic conservation equations of the first principle models but make simplifying assumptions (typically related to similarity theory) to reduce the problem to the solution of (simultaneous) ordinary differential equations. In the verification process, such models must also address the relevant physical phenomenon as well as be validated for the application being considered. Such models are typically easily solved on a computer with typically less user interaction than required for the solution of PDEs. Simplified mathematical models may also be used as screening tools to identify the most important release scenarios; however, other modeling approaches should be considered only if they address and have been validated for the important aspects of the scenario under consideration.

All mathematical models predict (ensemble) time-averaged cloud behavior for a particular set of release conditions. To illustrate in very broad terms, consider a set of trials (field experiments) with continuous contaminant releases (as plumes) that are conducted under identical atmospheric conditions. Suppose that you could measure the concentration on the plume centerline at a given downwind distance with a reasonably fast concentration sensor. Owing to the turbulent nature of the atmosphere and dispersion process, the measured concentration on the plume centerline at a given downwind location observed in each trial would not be identical. If these measurements are averaged during the period for which the contaminant is present, the average of measurements will not change after a sufficient number of trials; this is an ensemble average. This ensemble average reflects the instantaneous (ensemble average) concentration provided the averaging time of the sensor is sufficiently fast. If one considers the difference between any one measured data set and this ensemble average, the measurements will show peak concentrations higher than the average (mean). Peak-to-mean concentration values depend on many factors, but for many purposes, a peak-to-mean concentration ratio of 2 can be assumed. For this hypothetical example, the concentrations were assumed to be measured on the plume centerline. However, the plume centerline of a passive contaminant does not remain at the same ground location due to variation in the wind direction related to large-scale atmospheric turbulence, as illustrated in Fig. 23-44 for a ground-level release on flat, unobstructed terrain. This effect is termed *plume meander*. (Note that denser-than-air contaminant plumes would exhibit less of this effect because such plumes may actually displace the

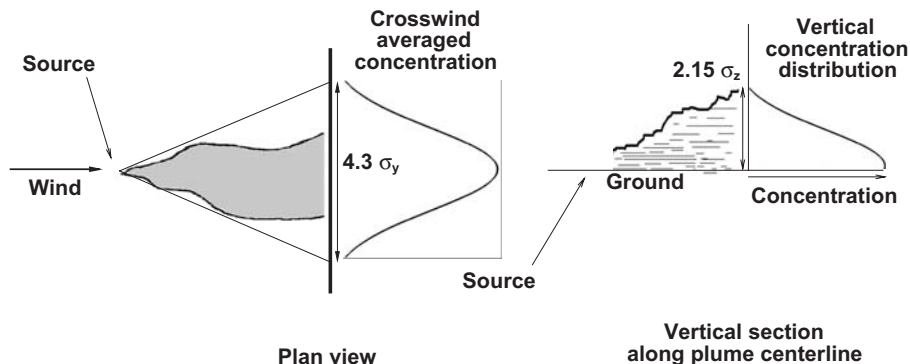


FIG. 23-44 Schematic representation of time-averaged distribution and spread for a continuous plume. σ_y and σ_z are the statistical measures of crosswind and vertical dimensions; $4.3\sigma_y$ is the width corresponding to a concentration 0.1 of the central value when the distribution is of gaussian form (a corresponding cloud height is $2.15\sigma_z$). (Redrawn from Pasquill and Smith, *Atmospheric Diffusion*, 3d ed., Ellis Horwood Limited, Chichester, U.K., 1983).

atmospheric flow field.) For a fixed ground location, the concentration sensor will be at various locations in the plume (effectively moving in and out of the plume). For a constant average wind direction, concentrations at a fixed ground location will again approach an (ensemble) average over a sufficiently long averaging time (10-min averaging time has proved to be standard). In this case, concentrations are (ensemble-averaged) 10-min concentrations. (Other properties of the concentration distribution are considered in the literature.) For the effect of plume meander, the relationship between concentrations for various averaging times for ground-level plumes can be approximated as

$$\frac{\langle C \rangle_2}{\langle C \rangle_1} = \left(\frac{t_1}{t_2} \right)^p \tag{23-77}$$

where $\langle C \rangle_1$ and $\langle C \rangle_2$ are (ensemble) time-averaged concentrations with averaging times t_1 and t_2 and p is an index typically taken to be around 0.2 for passive plumes. In addition to other more sophisticated approaches, some dispersion models adjust the dispersion coefficients to account for the effect of plume meander. Equation (23-77) shows that concentration decreases as averaging time increases. Based on comparison between passive puff and (10-min) plume coefficients, the averaging time associated with puff coefficients is about 20 s, which is the smallest value that should properly be used in Eq. (23-77). There is no correction to puff coefficients or concentrations associated with plume meander. Note that this is only a rough illustration of the processes present which are discussed in much greater detail in the literature.

Basic Scenario Time Scales There are several competing time scales that are important:

1. The source time scale t_s describes the length of time for the contaminant to become airborne; the source time scale is also limited by the inventory of contaminant.

2. The hazard endpoint time scale t_h describes the length of time required for the contaminant to pose a hazard. There are many different time scales associated with various toxicity levels (e.g., TLV-C ceiling limit values are never to be exceeded, TLV-STEL values are not to be exceeded in a 15-min period, etc.). Time scales associated with flammability hazards reflect the maximum local concentration (and also typically including peak-to-mean concentration ratios) and for reasons discussed above are considered representative of dispersion model averaging times of around 20 s.

3. The travel time t_t is the time required for a contaminant cloud to reach the endpoint distance x_e . As a first approximation, $t_t = x_e/(u_r/2)$ for ground-level clouds; for elevated releases, $t_t = x_e/u$ where u is the characteristic wind speed.

The source time scale t_s must be greater than the travel time t_t for a steady-state plume to be possible. Other time scale restrictions are considered for the models discussed here.

Scenario Development and Simulation The typical procedure for assessing the consequences of an airborne contaminant release is as follows:

1. Identify release scenarios by which containment can be lost along with the hazards of that scenario. Hazards may differ depending on the physical state of the released contaminant and the circumstances of the scenario. Hazards arise from the properties of the released material such as biological agents, toxic materials, or flammable materials; flammable or reactive materials may pose an explosion hazard depending on their reactivity and the degree to which the air-contaminant mixture is confined. Scenarios include a description of the applicable atmospheric conditions (which may be dictated by regulatory requirements).

2. Develop an appropriate source model to define the source description (see previous subsection) for each scenario.

3. Use an appropriate atmospheric dispersion model to assess the consequences or risk of each scenario. For screening purposes, atmospheric dispersion models which are less costly may be used to identify the most important scenarios; examples are discussed in the following subsection. More expensive modeling procedures can be applied to the most important scenarios provided such procedures are more appropriate and accurate. Screening methods may also be useful in considering the validity of more complicated models.

4. Determine if the resulting consequences or risk to people and property is acceptable. For unacceptable scenarios, mitigation measures should be applied such as discussed by Prugh and Johnson (*Guidelines for Vapor Release Mitigation*, AIChE, New York, 1988), and amended scenarios should be reassessed. If mitigation measures cannot sufficiently reduce the consequences or risk, the appropriate business and ethical decision would be to discontinue such operations.

Passive Contaminant (Pasquill-Gifford) Dispersion Models The gaussian dispersion model is based on the assumption of a passive contaminant release (i.e., the released contaminant does not change the atmospheric flow field). Based on the theoretical model of a passive contaminant, the spatial distribution would have a gaussian distribution with characteristic length scales. Using extensive observations of (steady-state) plumes, the Pasquill-Gifford dispersion model correlates characteristic vertical and lateral length scales (or dispersion coefficients σ_z and σ_y , respectively) with atmospheric stability class; other correlations have also been proposed for the plume dispersion coefficients taking other effects into account such as the effect of surface roughness z_0 . Less extensive observations of instantaneously released puffs have been used to characterize the length scales of puffs (with the additional length scale σ_x to characterize the along wind direction); σ_x is often assumed to be approximated by σ_y in puff models. Although the Pasquill-Gifford approach provides for the prediction of the concentration distribution, the discussion below is limited to the maximum predicted concentration since this is most important for hazard assessment purposes.

Pasquill-Gifford plume model At a given downwind distance x , the maximum (average) concentration for a (continuous) passive plume from a point source is

$$\langle C \rangle_1 = \frac{E}{\pi \sigma_y \sigma_z u} \tag{23-78}$$

where E is the mass rate at which the contaminant becomes airborne and u is the characteristic wind speed (typically taken to be u_r). Pasquill-Gifford plume dispersion coefficients as a function of downwind distance and atmospheric stability are available from many sources (Seinfeld, *Atmospheric Chemistry and Physics of Air Pollution*, Wiley, New York, 1986; Mannan, *Less' Loss Prevention in the Process Industries*, 3d ed., Chap. 15, Elsevier Butterworth-Heinemann, Oxford, U.K., 2005; Griffiths, "Errors in the Use of the Briggs Parameterization for Atmospheric Dispersion Coefficients," *Atmospheric Environment*, vol. 28, no. 17, pp. 2861–2865, 1994). Passive dispersion coefficients are typically not provided for distances less than 100 m or greater than a few kilometers because predicted concentrations outside this range must be viewed with some caution (e.g., meteorological conditions may not persist over such large time scales, and at such long distances, large-scale meteorological and terrain features may dictate plume behavior in ways not accounted for by this simple approach).

Note that the predicted values of σ_y and σ_z are sensitive to the *specification* of atmospheric stability. Between D and F stability classes, σ_y for D stability is roughly three times greater than for F stability, and σ_z is roughly two times greater. Since $\langle C \rangle_1$ is inversely proportional to $\sigma_y \sigma_z$, the predicted $\langle C \rangle_1$ for F stability is roughly six times greater than for D stability.

Pasquill-Gifford puff model At a given downwind distance x , the maximum (average) concentration for a (instantaneous) passive puff from a point source is

$$\langle C \rangle = \frac{2E_t}{(2\pi)^{3/2} \sigma_x \sigma_y \sigma_z} \tag{23-79}$$

where E_t is the total contaminant mass that becomes airborne. Pasquill-Gifford puff dispersion coefficients as function of downwind distance and atmospheric stability are available from many sources (e.g., Mannan, *Less' Loss Prevention in the Process Industries*, 3d ed., Chap. 15, Elsevier Butterworth-Heinemann, Oxford, U.K., 2005). As indicated above, σ_x is often assumed to be approximated by σ_y in puff models. As for passive plumes, note that passive puff dispersion coefficients are not provided for distances of less than 100 m (where

near source effects will be important), and predicting concentrations for distances longer than a few kilometers must be viewed with some caution for the same reasons cited above.

Note that the predicted values of σ_y and σ_z are sensitive to the specification of atmospheric stability for puffs as well. Between D and F stability classes, σ_y for D stability is roughly three times greater than for F stability, and σ_z is roughly 10 times greater. Since $\langle C \rangle$ is inversely proportional to $\sigma_y^2 \sigma_z$, the predicted $\langle C \rangle$ for F stability is roughly 40 times greater than for D stability.

Virtual sources As indicated above, the gaussian model was formulated for an idealized point source, and such an approach may be unnecessarily conservative (predict an unrealistically large concentration) for a real release. There are formulations for area sources, but such models are more cumbersome than the point source models above. For point source models, methods using a virtual source have been proposed in the past which essentially use the maximum concentration of the real source to determine the location of an equivalent upwind point source that would give the same maximum concentration at the real source. Such an approach will tend to overcompensate and unrealistically reduce the predicted concentration because a real source has lateral and along-wind extent (not a maximum concentration at a point). Consequently, the modeled concentration can be assumed to be bounded above, using the point source formulas in Eq. (23-78) or (23-79), and bounded below by concentrations predicted by using a virtual source approach.

Assuming the source concentration C_s is known, the virtual distance is found by using the known source concentration to find the virtual source distance. For a plume, solve Eq. (23-78) for the product $\sigma_y \sigma_z$, then determine the virtual source distance x_v by iterative solution (or trial and error) using E and C_s . For a puff, solve Eq. (23-79) for the product $\sigma_x \sigma_y \sigma_z$ (or $\sigma_y^2 \sigma_z$); then determine the virtual source distance x_v by iterative solution (or trial and error) using E_i and C_s . The dispersion coefficients at distance x_v will now represent a distance from the real source of $x_v - x_e$.

Passive puff or plume In addition to the restriction on plumes discussed above, there is an along-wind dispersion time scale given by $t_d = 2\sigma_x/u$, where σ_x is evaluated at the endpoint distance x_e . The release can usually be considered a plume if $t_s > 2.5 t_d$, where t_s is the source time scale defined above, and the release can be considered a puff if $t_d > t_s$. For $t_d \leq t_s \leq 2.5 t_d$, neither puff nor plume models are entirely appropriate; the predicted concentration is considered the largest of the puff and plume predictions.

Denser-than-Air Contaminant (Britter-McQuaid) Dispersion Models Britter and McQuaid (*Workbook on the Dispersion of Dense Gases*, Health and Safety Executive Report 17/1988, Sheffield, U.K., 1988) proposed a correlation for estimating the dispersion of denser-than-air contaminants from area sources for plume and puff releases. Their objective was to produce correlations which predicted the distance to a given concentration level within a factor of 2. Their analysis identified the dominant independent variables as (1) density of released contaminant after depressurization to atmospheric pressure ρ_s ; (2) volumetric rate E/ρ_s (or total volume E_t/ρ_s) of contaminant released; (3) characteristic wind speed u , (typically taken to be at 10-m elevation z_e); and (4) characteristic source dimension D_s . Based at least in part on the fact that presently available field test data for denser-than-air contaminants do not clearly indicate the importance of these parameters, Britter and McQuaid considered some independent variables to be of lesser importance, and these parameters were not considered in the correlation, including surface roughness, atmospheric stability, and exact source dimensions. (Many models for denser-than-air behavior indicate these parameters to be important.) Other effects were not included in the analysis including dilution due to source momentum and condensation of ambient humidity; such effects may be of crucial importance for contaminants that have a molecular weight less than that of air including, e.g., liquefied natural gas (LNG), ammonia, and hydrogen fluoride.

Britter and McQuaid provide correlations for denser-than-air (continuous) plumes and (instantaneous) puffs released at ambient temperature. Since many materials of practical interest are released below ambient temperature, Britter and McQuaid provide guidance as to how to predict the limiting cases for such releases.

Britter and McQuaid report that the averaging time t_1 for the plume correlation is 10 min, and Eq. (23-77) should be used with $p = 0.12$ for other averaging times (and limited to averaging times no shorter than about 20 s as for releases).

Denser-than-air puff or plume Britter and McQuaid use the ratio of the source duration to the travel time to distinguish between plumes and puffs with a slightly different definition of travel time: $t_t = x_e/(0.4u_e)$. The release can be considered a plume if $t_s > t_t$, where t_s is the source time scale defined above, and the release can be considered a puff if $t_s < t_t/4$. For $t_t/4 \leq t_s \leq t_t$, neither puff nor plume models are entirely appropriate; the predicted concentration is considered the largest of the puff and plume predictions.

Recommended Procedure for Screening Estimates The recommended procedure for making concentration estimates at a specified downwind distance with the simplified models discussed here is as follows:

1. For a given release scenario, estimate the state of the released contaminant after it has depressurized and become airborne (including any initial dilution). The initial mole fraction of hazardous components will be applied to the final reported concentrations and hazardous endpoint concentrations throughout the process. If source momentum is important (as in a jet release or for plume rise), other models are available that can address these considerations. Disregarding the dilution due to source momentum will likely result in higher concentrations downwind, but not always.
2. Consider the important time scales involved, and decide whether a puff or plume model is indicated. If this choice is unclear, assume a plume release.
3. Determine whether denser-than-air behavior is important.
4. When denser-than-air effects are important, use the Britter-McQuaid (plume or puff) models. Otherwise, assume the release is passive and use the Pasquill-Gifford (plume or puff) models. Adjust values for the virtual source correction(s) as appropriate.
5. Adjust values for the averaging time correction for plume predictions with Eq. (23-77). Note that the index p for use in the averaging time correction depends on the model used. If the hazard time scale t_h is different from the model averaging time scale (10 min for plumes), then the predicted concentration should be adjusted to t_h but only if $t_s \geq t_h$; if $t_s < t_h$, then adjust the predicted concentration to t_s .
6. For plume predictions, confirm that plume behavior applies by consideration of appropriate time scales. If plume behavior is not justified, revise the calculations with the puff model and recheck the dispersion time scale. Report the appropriate concentration or distance.

ESTIMATION OF DAMAGE EFFECTS

Nomenclature

A	Projected area of fragment, breach area, or fragment cross-sectional area
a_a	Sound velocity in atmosphere
a_e	Sound velocity in high-pressure gas prior to vessel failure
B	Batch energy availability
d	Fragment diameter
E	Explosion energy available to generate blast and fragment kinetic energy, etc.
E_p	Critical perforation energy ($1/2 MV_f^2$)
E_y	Young's modulus of elasticity
F	Dimensionless initial fragment acceleration
F	$P_e AR/Ma_e = P_e R/ma_e$ for vessel completely shattered into many small fragments
g	Acceleration due to gravity
h	Vessel wall thickness
k	Ratio of vessel outside diameter to internal diameter
L	Length of cylindrical vessel
M	Fragment mass
m	Mass per unit area of vessel shell
N	Length of cylindrical vessel forming rocketing tub fragment
N/m ²	Unit of pressure in SI system, N/m ² ; also called pascal (Pa). One psi = 6.89476 × 10 ³ Pa or 6.89476 kPa.
P	Liquid pressure
P_a	Atmospheric pressure

Nomenclature (Concluded)

P_b	Dynamic vessel burst pressure
P_e	Pressure at expanding gas contact surface
P_e	Pressure at vessel failure
P_{inc}	Incident (side-on) blast pressure
P_r	Normally reflected (face-on) blast pressure
R	Vessel radius
r	Fragment radius = $(A/\pi)^{0.5}$
R_g	Range of fragment
t	Steel target thickness
U	$U_f + U_m$
u	Ultimate tensile strength of target steel
U_f	Fluid compression energy
U_m	Elastic strain energy in vessel walls
V	Volume of gas
V_f	Fragment velocity
V_L	Liquid volume
W	Equivalent mass of TNT
w	Unsupported span of steel target
X	Distance from wall of vessel to target
Greek letters	
β_r	Fluid compressibility
γ	Ratio of specific heats of gas C_p/C_v
Φ_0	Standard steady-state availability
ν	Poisson's ratio of vessel steel
Subscripts	
0	Reference state
1	Initial state
a	Environmental state
1→ a	Denotes the path from state 1 to the environmental ambient state a

GENERAL REFERENCES: Baker, Cox et al., "Explosion Hazards and Evaluation," *Fundamental Studies in Engineering* 5, Elsevier Science Publishing, New York, 1983. Kinney and Graham, *Explosive Shocks in Air*, 2d ed., Springer-Verlag, New York, 1985. Petes, *Annals, New York Academy of Sciences* 1968, vol. 152, pp. 283-316. Holden, *Assessment of Missile Hazards: Review of Incident Experience Relevant to Major Hazard Plant*, UKAEA SRD/HSE/R477, November 1988. Lees, *Loss Prevention in the Process Industries*, Butterworths, London, 1996. Leslie and Birk, "State of the Art Review of Pressurized Liquefied Gas Container Failure Modes and Associated Projectile Hazards," *Journal of Hazardous Materials* 28, 1991, pp. 329-365. ASCE *Structural Analysis and Design of Nuclear Plant Facilities Manual and Reports on Engineering Practice* no. 58, 1980. Pritchard and Roberts, "Blast Effects from Vapour Cloud Explosions: A Decade of Progress," *Safety Science*, vol. 16 (3,4) 1993, pp. 527-548. "Explosions in the Process Industries," Major Haz. Monograph Series, I. Chem. E. (U.K.), 1994.

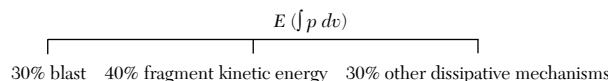
The availability of energy from an explosion can be approximately calculated in most cases but the method used depends upon the nature of the explosion.

Inert, Ideal Gas-Filled Vessels The energy available for external work following the rapid disintegration of the vessel is calculated by assuming that the gas within the vessel expands adiabatically to atmospheric pressure.

$$E = \frac{P_e V}{(\gamma - 1)} \left\{ \left[1 - \left(\frac{P_a}{P_e} \right)^{(\gamma - 1)/\gamma} \right] + (\gamma - 1) \left(\frac{P_a}{P_e} \right) \left[1 - \left(\frac{P_a}{P_e} \right)^{-1/\gamma} \right] \right\} \quad (23-80)$$

In the case of thick-walled HP vessels, the strain energy in the vessel shell can contribute to the available energy, but for vessels below about 20 MN/m² (200 barg) it is negligible and can be ignored. If a Mollier chart for the gas is available, the adiabatic energy can be measured directly. This is the preferred method, but in many cases the relevant chart is not available.

The available energy is dissipated in several ways, e.g., the strain energy to failure, plastic strain energy in the fragments, kinetic energy of the fragments, blast wave generation, kinetic energy of vessel contents, heat energy in vessel contents, etc. For damage estimation purposes, the energy distribution can be simplified to:



Blast Characteristics Accurate calculation of the magnitude of the blast wave from an exploding pressure vessel is not possible, but it may be estimated from several approximate methods that are available.

One method of estimating the blast wave parameters is to use the TNT equivalent method, which assumes that the damage potential of the blast wave from a fragmenting pressure vessel can be approximated by the blast from an equivalent mass of trinitrotoluene (TNT). The method is not valid for the region within a few vessel diameters from the vessel. However, a rough approximation can be made outside this region by calculating an equivalent mass of TNT and utilizing its well-known blast properties. The term *equivalent mass* means the mass of TNT which would produce a similar damage pattern to that of the blast from the ruptured vessel. The energy of detonation of TNT is 4.5 MJ/kg (1.5 × 10⁶ ft-lb/lb), so the TNT equivalent mass W is given by $W = 0.3E/4.5$ kg. Standard TNT data (Dept. of the Army, Navy, and Air Force, "Structures to resist the effects of accidental explosions," TM5-1300, NAVFAC P-397, AFM 88-22, U.S. Gov. Printing Office, vol. 2, November 1990, Figs. 2-7 and 2-15; or Kingery and Pannill, Memorandum Report No. 1518, Ballistic Research Laboratories, Aberdeen Proving Ground, U.S., April 1964) can then be used to determine the blast parameters of interest (Fig. 23-45). This method has limitations in the far field where the peak incident overpressure is less than 4 kN/m² (0.5 psi). In this region, local terrain and weather effects become significant.

The blast parameters also depend upon the physical location of the vessel. If the vessel is located close to or on the ground, then *surface-burst* data should be used. In other circumstances where the vessel is high in the air, either *free-air* or *air-burst* blast data may be used. These data are best presented in the form of *height-of-burst* curves (Petes, "Blast and Fragmentation Characteristics," *Ann. of New York Acad. of Sciences*, vol. 152, art. 1, fig. 3, 1968, p. 287). For incident blast pressures of 3 × 10³ N/m² (3 bar) or less, using surface-burst data may overestimate the blast pressure by about 33 percent. Generally, pressure vessel ruptures rarely cause ground craters, so no allowance for cratering should be made.

Fragment Formation The way in which a vessel breaks up into several fragments as a consequence of an explosion or metal failure is

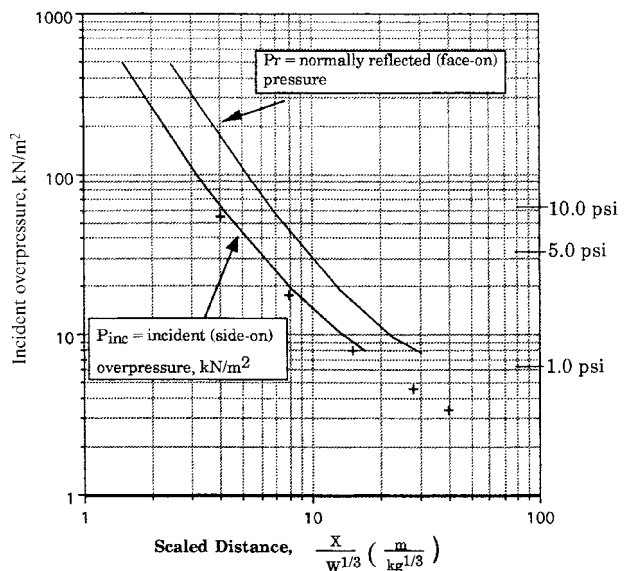


FIG. 23-45 Incident overpressure vs. scaled distance, surface burst. (The "+" points are from Kingery and Pannill, Memorandum Report No. 1518 BRL. Adapted from Department of Army, Navy, and Air Force TM5-1300, NAVFAC P-397, AFM 88-22.)

impossible to predict. Consequently, in most cases it is necessary to assume several failure geometries and to assess the effect of each. The number of fragments formed is strongly dependent upon the nature of the explosion and the vessel design. For high-speed explosions—e.g., detonations or condensed phase explosions—the vessel frequently shatters into many fragments, but for slower-speed explosions—e.g., deflagrations and BLEVEs—generally fewer than ten fragments are formed, and frequently less than five.

Initial Fragment Velocity (V_f) The process of energy transfer from the expanding gas to the vessel fragments is not efficient and seldom exceeds 40 percent of the available energy. According to Baum ("The Velocity of Missiles Generated by the Disintegration of Gas Pressurized Vessels and Pipes," *Journal of Press. Vessel Technology*, Trans. ASME, vol. 106, November 1984, pp. 362–368), there is an upper limit to the fragment velocity, which is taken to be the velocity of the contact surface between the expanding high-pressure gas and the surrounding atmospheric air. This is referred to as the *zero-mass* fragment velocity and, for most industrial low- to medium-pressure vessels, is less than about 1.3 Mach. It is calculated using ideal gas, one-dimensional shock tube theory and is given by the equation for the shock tube contact surface velocity (Wright, *Shock Tubes*, Methuen & Co., London, 1961).

$$\frac{V_f}{a_0} = -\frac{2}{(\gamma-1)} \left[\left(\frac{P_c}{P_e} \right)^{(\gamma-1)/2\gamma} - 1 \right] \quad (23-81)$$

where P_c is determined from the relationship:

$$\frac{a_c(1-\mu_a) \left(\frac{P_c}{P_a} - 1 \right)}{a_c \left[(1+\mu_a) \left(\frac{P_c}{P_a} + \mu_a \right) \right]^{1/2}} = \frac{2}{(\gamma-1)} \left[1 - \left(\frac{P_a}{P_e} \cdot \frac{P_c}{P_a} \right)^{(\gamma-1)/2\gamma} \right] \quad (23-82)$$

and
$$\mu_a = \frac{\gamma_a - 1}{\gamma_a + 1} \quad (23-83)$$

where P_c = pressure at expanding gas contact surface
 a_a = sound velocity at ambient conditions
 a_c = sound velocity in gas prior to vessel failure

The value of a_c may be approximated using physical property data for the specific gas at the temperature and pressure at the start of the expansion. Equation (23-82) must be solved using a trial-and-error method. Most fragments never achieve the zero-mass velocity and their velocity can be assessed using the correlations of Baum ("Disruptive Failure of Pressure Vessels: Preliminary Design Guidelines for Fragments Velocity and the Extent of the Hazard Zone," *J. Pressure Vessel Technology*, Trans. ASME, vol. 110, May 1988, pp. 168–176; Baum, "Rupture of a Gas-Pressurized Cylindrical Pressure Vessel. The Velocity of Rocketing Fragments," *J. Loss Prev. Process Ind.*, vol. 4, January 1991, pp. 73–86; Baum, "Velocity of a Single Small Missile Ejected from a Vessel Containing High Pressure Gas," *J. Loss Prev. Process Ind.*, vol. 6, no. 4, 1993, pp. 251–264).

Baum provides correlations for several vessel failure modes.

Vessel Filled with Reactive Gas Mixtures Most cases of damage arise not from the vessel failing at its normal operating pressure but because of an unexpected exothermic reaction occurring within the vessel. This usually is a decomposition, polymerization, deflagration, runaway reaction, or oxidation reaction. In assessing the damage potential of such incidents, the peak explosion or reaction pressure can often be calculated, and if this peak pressure P_e is then inserted into Eq. (23-80), the available energy can be assessed and the blast and fragment hazard determined. Where the expected peak explosion pressure P_e is greatly in excess of the vessel dynamic burst pressure, it is sufficient to increase the burst pressure to allow for the increase in vessel pressure during the period necessary for both the vessel to rupture and the fragments to be removed from the path of the expanding vessel contents. Where the gas pressure in the vessel is rising

rapidly, the gas may reach a much higher pressure than the estimated dynamic burst pressure of the vessel. This effect is similar to the accumulation on a relief valve. It is, therefore, conservative to assume that the gas reaches the pressure calculated on the assumption of complete reaction. The reaction is assumed to go to completion before the containing vessel fails. However, there are reactions where it is simpler to calculate the energy availability using thermodynamic methods. The maximum energy released in an explosion can be assessed from the change in the Helmholtz free energy ($-\Delta H = -\Delta E + T\Delta S$), but if the required data is not available, it may be necessary to use the Gibbs free energy ($\Delta F = \Delta H - T\Delta S$), which—especially in the case of reactions with little or no molal change, e.g., hydrocarbon/air oxidation—is similar to the Helmholtz energy. It may sometimes be more convenient to calculate the batch energy availability [$B = \phi_0 + \Delta\phi_{1 \rightarrow a} + \Delta(PV)_{1 \rightarrow a} - P_a\Delta V_{1 \rightarrow a}$] (Crowl, "Calculating the Energy of Explosion Using Thermodynamic Availability," *J. Loss Prev. Process Ind.*, **5**, no. 2, 1992, p. 109), which for an ideal gas becomes

$$B_1 = f_0 + f_{1 \rightarrow a} + nRT_1 \left[\left(\frac{P_a}{P_1} \right) - 1 \right] \quad (23-84)$$

The energy partition between blast wave energy and fragment kinetic energy is as described in paragraph 1.

Vessels Completely Filled with an Inert High-Pressure Liquid* A typical example is the pressure testing of vessels with water. The energy available to cause damage is the sum of the liquid compression energy and the strain energy in the vessel shell. The sudden release of this energy on vessel failure generally creates flying fragments but rarely any significant blast effects.

The fluid compression energy up to about 150 MN/m² (22,000 psig) can be estimated from $U_f = \frac{1}{2}\beta_f P^2 V_L$, where β_f is the liquid bulk compressibility, P is the liquid pressure, and V_L is the liquid volume. At higher pressure, this simple equation becomes too conservative and more complex methods of calculating the fluid compression energy are required. The elastic strain energy for cylindrical vessels, ignoring end closures, can be estimated from:

$$U_m = -\frac{P^2 V_L}{2E(k^2 - 1)} [3(1 - 2\nu) + 2k^2(1 + \nu)] \quad (23-85)$$

where P = pressure of liquid
 V_L = volume of liquid
 E_y = Young's modulus of elasticity
 ν = Poisson's ratio

Energy available $U = U_f + U_m$.

Only a small fraction of U is available to provide kinetic energy to the fragments. There are few data available, but in five incidents analyzed by High (unpublished data), no fraction was greater than 0.15. The fragment initial velocity can be assessed from $0.15 U = \frac{1}{2} M V_f^2$.

Distance Traveled by Fragments There is no method available to estimate the distance traveled by an irregularly shaped, possibly tumbling, subsonic fragment projected at an unknown angle. A conservative approach is to assume that all the fragments are projected at an angle of 45° to the horizontal and to ignore the aerodynamic effects of drag and/or lift. The range R_g is then given by $R_g = V_f^2/g$, where g = gravitational acceleration.

This is too conservative to provide anything more than an upper bound. Some limited guidance is given by Scilly and Crowther ("Methodology for Predicting Domino Effects from Pressure Vessel Fragmentation," *Proc. Hazards Ident. and Risk Anal., Human Factors and Human Reliability in Process Safety*, Orlando, Fla., 15 Jan 1992, p. 5, sponsored by AIChE and HSE), where the range, for vessels with walls less than 20 mm (0.79 in), is $2.8 P_b$, with the range in meters and P_b as the vessel burst pressure in bars. Other sources are Baker (*Explosion Hazards and Evaluation*, Elsevier, 1983, p. 492) and Chemical

*An excellent review of the necessary precautions to be taken is given by Saville, "Pressure Test Safety," HSE Contract Research Report 168/1998, HMSO, U.K., 1998.

Propulsion Information Agency (*Hazards of Chemical Rockets and Propellants Handbook*, vol. 1, NTIS, Virginia, May 1972, pp. 2-56, 2-60).

Fragment Striking Velocity It is generally impossible to assess the fragment velocity, trajectory, angle of incidence, and fragment attitude at the moment of striking a target; consequently, the conservative view is taken that the fragment strikes the target at right angles, in the attitude to give the greatest penetration, with a velocity equal to the initial velocity.

Damage Potential of Fragments In designing protection for fragment impact, there are two failure modes to be considered: local response and overall response. Local response includes penetration/perforation in the region of the impact. Overall response includes the bending and shear stresses in the total target element; i.e., will the whole target element fail regardless of whether the element is penetrated or perforated?

Local Failure The penetration or perforation of most industrial targets cannot be assessed using theoretical analysis methods, and recourse is made to using one of the many empirical equations. In using the equations, it is essential that the parameters of the empirical equation embrace the conditions of the actual fragment.

The penetrability of a fragment depends on its *kinetic energy density* (KED), given by

$$KED = \frac{1}{2} \frac{MV_f^2}{A} \tag{23-86}$$

where *A* is the fragment cross-sectional area. The KED is a useful comparative measure of a fragment's penetrability when comparing like with like. Several equations are given in the following sections.

Ballistics Research Laboratory (BRL) Equation for Steel Targets

$$E_p = 1.4 \times 10^9 (dt)^{1.5} \tag{23-87}$$

where *d* is the fragment diameter, *t* is the steel target plate thickness, and *E_p* is the critical perforation energy in SI units (kg, m, m/s, J), when applied to fragments between 1 kg and 19.8 kg, impacting targets 1 mm to 25 mm (1 in) thick plate with velocities from 10 m/s to 100 m/s. Neilson (*Procedures for the Design of Impact Protection of Off-shore Risers and ESVs*, U.K. AEA [ed.], 1990) found a large scatter in the results, but most were within ±30 percent.

Stanford Research Institute (SRI) Equation for Steel Targets

$$E = \frac{dut^2}{10.3} \left(42.7 + \frac{w}{t} \right) \tag{23-88}$$

where *w* is the unsupported span of the target plate (m) and *u* the ultimate tensile strength of the target steel (N/m²). The parameters for this equation are given by Brown ("Energy Release Protection for Pressurized Systems," part II, "Review of Studies into Impact/Terminal Ballistics," *Applied Mechanics Review*, vol. 39, no. 2, 1986, pp. 177-201) as 0.05 ≤ *d* ≤ 0.25m, 414 ≤ *u* ≤ 482 MN/m² for a fragment mass between 4.5 and 50 kg.

Overall Response The transition from local to overall response is difficult to define. High-velocity impact implies that the boundary conditions of the target have little influence on the local response (excluding reflected shock waves). If the fragment is small relative to the target, local response will dominate, but fragments that are of the same order of size as the target will produce an overall response. It is often necessary to consider both overall and local response. Low values of KED are associated with overall response. Design methods for dynamically applied loads are given by Newark ("An Engineering Approach to Blast Resistant Design," ASCE New York, 1953), Baker (see General References), or ASCE (*Manual and Reports on Engineering Practice*, no. 58, 1980).

Response to Blast Waves The effect of blast waves upon equipment and people is difficult to assess because there is no single blast wave parameter which can fully describe the damage potential of the blast. Some targets respond more strongly to the peak incident overpressure and others to the impulse ($\int p dt$) of the blast. The blast parameters are usually based on the conservative assumption that the

TABLE 23-25 Damage Effects

Incident, psi	Pressure, kPa	Damage effects
10	70	Damage to most refineries would be severe, although some pumps, compressors, and heat exchangers could be salvaged. All conventional brick buildings would be totally destroyed. Rail wagons (rail cars) overturned. Storage tanks ruptured. Fatalities certain.
5.0	34	Brick buildings severely damaged, 75% external wall collapse. Fired heaters badly damaged. Storage tanks leak from base. Threshold for eardrum damage to people. Domino or knock-on radius. Pipe bridges may move.
2.0	14	Doors and windows removed. Some frame distortion to steel frame buildings and cladding removed. Some electrical/instrument cables broken.*
1.0	7	Lethal glass fragments. Limit for public housing, schools, etc.
0.3	2	About 50% domestic glass broken.

*1% probability electrical cables broken at 2.0 psi inc. 99% probability electrical cables broken at 3.6 psi inc.

blast strikes the target normal to its surface, so that normal reflection parameters are used.

The pressure exerted by the blast wave on the target depends upon the orientation of the target. If the target surface faces the blast, then the target will experience the reflected or face-on blast pressure *P_r*, but if the target surface is side-on to the blast, then the target will experience the incident or side-on blast pressure *P_{inc}*. The reflected blast pressure is never less than double the incident pressure and can, for ideal gases, be as high as eight times the incident pressure. For most industrial targets where the incident pressure is less than about 17 kN/m² (25 psi), the reflected pressure is not more than 2.5 times the incident pressure.

Response of Equipment The response of equipment to blast is usually a combination of two effects: one is the displacement of the equipment as a single entity and the other is the failure of the equipment itself. The displacement of the equipment is an important consideration for small, unsecured items—e.g., empty drums, gas cylinders, empty containers. Most damage results from the failure in part or totally of the equipment or containing structure itself.

The blast parameters are usually based on the conservative assumption that the blast strikes the target normal to its surface, so that normal reflection parameters may be used.

The response of a target is a function of the ratio of the blast wave duration and the natural period of vibration of the target (*T/T_n*). Neither of these parameters can be closely defined.

Calculating the specific response of a specific target can generally be done only approximately. Accuracy is not justified when the blast properties are not well defined. A guide to the damage potential of condensed phase explosive blast is given in Table 23-25 (Scilly and High, "The Blast Effect of Explosions," *Loss Prevention and Safety Promotion in the Process Industries*, European Fed. of Chem. Eng., 337 Event, France, September 1986, table 2). Nuclear data is available (Table 23-26) (Walker, "Estimating Production and Repair Effort in Blast-damaged Petroleum Refineries," *Stanford Research Inst.*, July 1969, fig. 5, p. 45), which is based upon long positive-duration blast (±6 s). This suggests that the Walker data will be conservative for the much shorter duration blast from accidental industrial explosions.

A blast incident overpressure of 35 kN/m² (5 psi) is often used to define the region beyond which the damage caused will be minor and not lead to significant involvement of plant and equipment beyond the 35 kN/m² boundary.

Response of People The greatest hazard to people from blast is generally from the deceleration mechanism after people have been blown off their feet and they become missiles. This occurs at an incident overpressure of about 27 kN/m² (4.0 psi) for long positive-duration

TABLE 23-26 Blast Overpressure Effects on Vulnerable Refinery Parts

Equipment	Overpressure (psi)																										
	0.5	1.0	1.5	2.0	2.5	3.0	3.5	4.0	4.5	5.0	5.5	6.0	6.5	7.0	7.5	8.0	8.5	9.0	9.5	10.0	12.0	14.0	16.0	18.0	20.0	>20.0	
Control house: steel roof	a	c	d				h																				
Control house: concrete roof	a	e p	d				n													e							
Cooling tower	b		f				o																				
Tank: cone roof		d				k							u														
Instrument cubicle			a			i m						t															
Fired heater				g	i					t																	
Reactor: chemical				a			i						p						t								
Filter				h				i												v		t					
Regenerator						i				i p					t												
Tank: floating roof						k							u													d	
Reactor: cracking							i							i												t	
Pipe supports							p					s o															
Utilities: gas meter									q																		
Utilities: electric transformer								h							l						t						
Electric motor										h									l								v
Blower										q											t						
Fractionation column											r				t												
Pressure vessel: horizontal												p i								t							
Utilities: gas regulator												i									m q						
Extraction column																					v	t					
Steam turbine															l							m	s				v
Heat exchanger															i												
Tank: sphere																i										t	
Pressure vessel: vertical																						i	t				
Pump																						i					v

CODE:

- | | | | | | |
|---|-------------------------------------------|---|-------------------------------|---|---------------------------------|
| a | Windows and gauges break. | h | Debris-missile damage occurs. | p | Frame deforms. |
| b | Louvers fall at 0.3–0.5 psi. | i | Unit moves and pipes break. | q | Case is damaged. |
| c | Switchgear is damaged from roof collapse. | j | Bracing fails. | r | Frame cracks. |
| d | Roof collapses. | k | Unit uplifts (half-filled). | s | Piping breaks. |
| e | Instruments are damaged. | l | Power lines are severed. | t | Unit overturns or is destroyed. |
| f | Inner parts are damaged. | m | Controls are damaged. | u | Unit uplifts (0.9 filled). |
| g | Brick cracks. | n | Block walls fail. | v | Unit moves on foundation. |
| | | o | Frame collapses. | | |

SOURCE: F. E. Walker, "Estimating Production and Repair Effort in Blast Damaged Petroleum Refineries," SRI, July 1969.

nuclear weapon blasts. People have more blast resistance than most equipment and can survive incident overpressures of 180 kN/m² (27 psi) (Bowen, Fletcher, and Richmond, DASA-2113, Washington, D.C., October 1968), even for long-duration blasts.

PROJECT REVIEW AND AUDIT PROCESSES

GENERAL REFERENCES: Center for Chemical Process Safety (CCPS), *Guidelines for Hazard Evaluation Procedures, Second Edition with Worked Examples*, AIChE, September 1992. CCPS, *Guidelines for Technical Management of Chemical Process Safety*, AIChE, 1989. CCPS, *Guidelines for Auditing Process Safety Management Systems*, AIChE, 1993.

Introduction Review and audit processes are used in the chemical process industry to evaluate, examine, and verify the design of process equipment, operating procedures, and management systems. These processes assure compliance with company standards and guidelines as well as government regulations. Reviews and audits can encompass the areas of process and personnel safety, environmental and industrial hygiene protection, quality assurance, maintenance procedures, and so on.

A review is a critical examination or evaluation of any operation, procedure, condition, event, or equipment item. Reviews can take many forms and be identified as project reviews, design reviews, safety reviews, pre-start-up reviews, and so on. The following discussion of the review process will deal with project reviews associated with capital projects and focus on the area of process safety.

An audit is a formal, methodical examination and verification of an operation, procedure, condition, event, or series of transactions. The verification element of an audit makes it distinctive from a review. A project review will *recommend* design, procedural, maintenance, and management practices to minimize hazards and reduce risk while meeting company standards and government regulations. An audit will *verify* that the design, the procedures, and the management systems are actually in place, and are being maintained and used as intended. In fact, it is not uncommon for an audit to be done on a review process, to verify that the elements of the review process are being followed.

Project Review Process The scope of capital projects can be large, involving the construction of new plants with new technologies and products, or small, involving minor changes to existing facilities. In either case, project safety reviews can be used to evaluate and examine the process design, operating procedures, and process control scheme for process hazards, conformance to company standards and guidelines, and compliance with government regulations. Some objectives of the review process (CCPS, 1992, p. 53) are: (1) identify equipment or process changes that could introduce hazards, (2) eval-

uate the design basis of control and safety systems, (3) evaluate operating procedures for necessary revisions, (4) evaluate the application of new technology and any subsequent hazards, (5) review the adequacy of maintenance and safety inspections, and (6) evaluate the consequences of process deviations and determine if they are acceptable (CCPS, 1989, p. 46).

The project review process should be integrated with the development of the project from the conceptual stage to the start-up stage (CCPS, 1989, p. 46). Figure 23-46 depicts the various stages of a capital project. The size and complexity of a project will determine if the project progresses through all these stages and, in the same manner, determine the number and type of reviews that are needed. The earlier in a project that a review can be used to identify required changes, the less costly the change will be to implement.

As the project progresses, more information is available; therefore, the review technique used can be different at each stage of the project. The use of various hazard evaluation techniques, such as checklist analyses, relative rankings, what-if analyses, and hazard and operability studies, is documented in *Guidelines for Hazard Evaluation Procedures: Second Edition with Worked Examples* (CCPS, 1992). The need to use more quantitative techniques for hazard evaluation may be identified during these reviews, and become an action item for the project team.

The project review process involves multiple steps that should be defined in management guidelines (CCPS, 1993, pp. 57-61). The steps include: (1) review policy, (2) review scheduling, (3) review technique, (4) review team representation, (5) review documentation, (6) review follow-up, (7) review follow-up verification, and (8) review procedures change management. These steps define how a review, whether it be a safety review, environmental review, pre-start-up review, or whatever, is conducted and how closure of review action items is achieved.

Review Policy The review policy should establish when project safety reviews should be done. All capital projects, large or small, should have one or more safety reviews during the course of the project. The number and types of review should be stated in a management policy. Any reasons for exceptions to the policy should be documented as well. The policy should address not only projects internal to a company, but also any joint ventures or turnkey projects by outside firms.

Review Scheduling A review scheduling procedure should be established that documents who is responsible for initiating the review and when the review(s) should occur during the project. The scheduling needs to balance availability of process information, review technique used, and the impact of potential review action items on project costs (i.e., early enough to minimize the cost of any potential changes

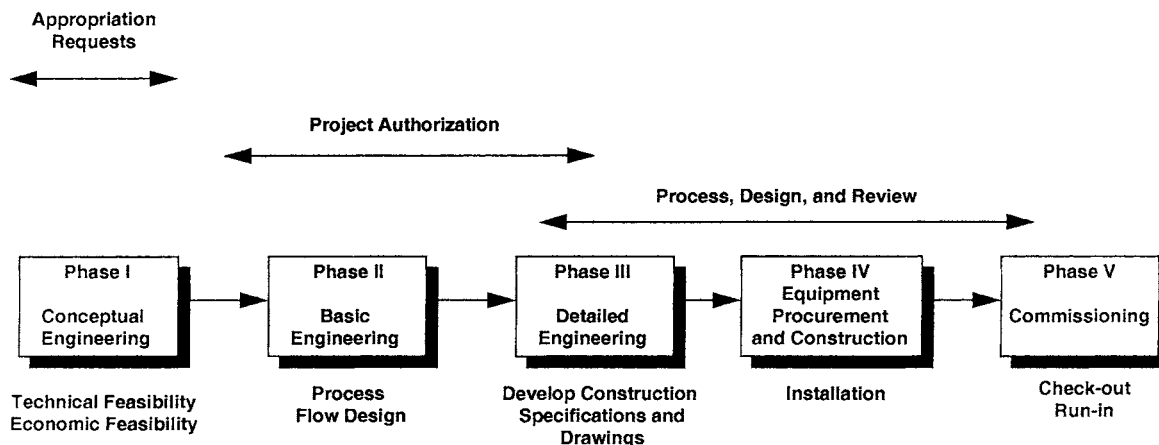


FIG. 23-46 The phases of a capital project. (CCPS, 1989, by permission of AIChE.)

to the process). The actual amount of time needed for the review should also be stated in the procedure. On the basis of the number of project reviews required and the estimated time needed for each review, the project cost estimate should include the cost for project reviews as part of the total cost for the project.

Review Team The project review should be conducted by a functionally diverse team. The team should consist of a team leader to organize and lead the team review, a scribe or secretary to record and issue a review summary with action items, and functional experts in fields relevant to the project such as safety, environmental, and industrial hygiene (CCPS, 1993, p. 58). The team leader should be experienced in the use of the selected review technique with leadership skills and no direct involvement with the project under review. The review procedure should address the minimum requirements for team leaders and team members. Some typical requirements could be years of experience, educational background, and training in the review technique. Responsibilities should be clearly defined for initiating the review, assigning the review team, recording the team findings, and monitoring follow-up of team recommendations.

Review Techniques The review techniques used at the various stages of a project should be selected based on the amount of process information and detail available. Figure 23-47 depicts some typical review techniques at the various stages of a capital project. A detailed description, including the type and amount of process information required, for each review technique can be found in *Guidelines for Hazard Evaluation Procedures: Second Edition with Worked Examples* (CCPS, 1992). The process information required for the review should be defined and documented in the review guidelines. Up-to-date and accurate process information is essential to conducting a successful review.

Review Documentation The project review team leader has the ultimate responsibility for documenting the results of the project

review. This responsibility may be delegated to a team scribe or secretary to record the review minutes and issue a summary report with listed action items. The action items could address exceptions to company or industry standards and government regulations, review team recommendations based on experience and knowledge, and further issues for study that could not be resolved during the review session.

The summary report should have a standard format and could contain a short project scope summary, a listing of review team members by function, a listing of project team members present, a meeting agenda or checklist of topics reviewed by the team, and a list of concerns and action items for project team follow-up. The distribution list for the summary report should be established and include the review team, project team, and any personnel outside the project team who have follow-up responsibilities for any of the action items. Also, include on the distribution list any appropriate management personnel, whether they be project team supervisors, manufacturing managers, or engineering managers. The documentation for the review should be archived in a process plant file with the appropriate records retention time (e.g., the life of the plant).

Review Follow-up An important element (maybe the most important) of the review process is the follow-up to action items. The project review will result in a list of potential concerns and action items, but, without follow-up, the issues will never be resolved and implemented. A person(s) should be assigned to each action item, preferably at the time of the project review. The person(s) assigned should have a combination of knowledge, resources, and authority to do a proper job in following up on the action items (CCPS, 1993, p. 59). The total action item list should not be assigned to one person, since it may overwhelm one individual. Depending on the number of action items generated, prioritizing the action item list may be helpful and a responsibility the review team can assume.

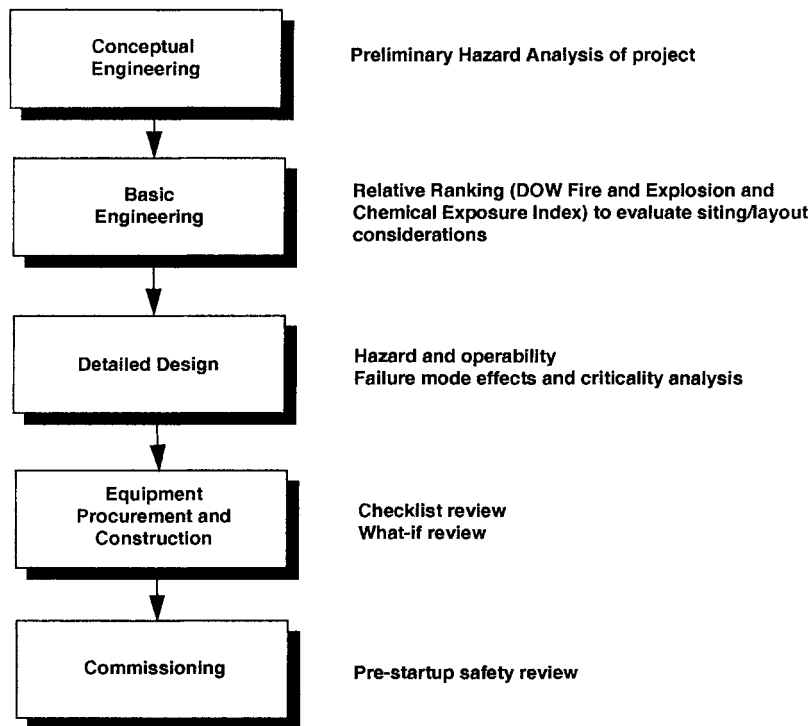


FIG. 23-47 Hazard evaluation at various project stages. (CCPS, 1993, by permission of AIChE.)

Progress on the action items should be documented in periodic progress reports to the review team leader or others assigned that functional responsibility. If no one is assigned the responsibility of tracking this progress, completion of the action list will probably be relegated to a lower priority and not be done.

Changes made to the process as a result of the project review may require a similar review before implementation, especially if the change is significant.

Review Follow-up Verification Responsibility should be assigned to verify that any process changes were actually made in the field. This verification can be done by a review team as part of a process pre-start-up review. It could also be part of the project team management responsibility or assigned to a particular functional (i.e., safety and loss prevention) representative. The closure of the review process is complete once implementation is verified.

On rare occasions, the resolution of project review concerns or action items is a point of contention between review team and project team members. In such a case, a management structure must be in place to arbitrate such disputes.

Review Procedure Change Management The project review process can require changes in policy and procedures at certain times. Therefore, the procedures should provide a management-of-change mechanism for suggesting changes and assign a person responsible for initiating and implementing any necessary changes.

Audit Process Audits in the chemical process industry can be focused on process safety, process safety management, environmental, and health areas. The discussion in this section will focus on the process safety and process safety management area, but it should be recognized that the process can be applied to the other areas as well. "Process safety audits are intended to provide management with increased assurance that operating facilities and process units have

been designed, constructed, operated, and maintained such that the safety and health of employees, customers, communities, and the environment are being properly protected" (CCPS, 1989, p. 133). Process safety management system audits "provide increased assurance that operating units have appropriate systems in place to manage process risk" (CCPS, 1989, p. 130).

The key steps in the audit process are outlined according to pre-audit activities, audit activities, and postaudit activities in Fig. 23-48. These activities are described in detail in *Guidelines for Auditing Process Safety Management Systems* (CCSP, 1993) and will be only briefly discussed in this section.

Preaudit Process Prior to the actual on-site audit, some preliminary activities should take place. These activities include selecting the facilities to be audited, scheduling the audit, selecting the audit team, and planning the audit. The selection criteria may be random, based on potential hazards of the facilities or the value of the facilities from a business standpoint. Audit scheduling must account for the availability of key facility personnel and audit team members, operational mode of the facility (i.e., it should be in normal operation), and the lead time required to obtain background information that may require advance visits to the facility and preaudit interviews. The audit team members should possess the technical training and experience to understand the facilities being audited. They should be knowledgeable in the auditing process and in the appropriate regulations and standards that will apply to the facilities. They should also be impartial and objective about audit findings. The audit plan should define the audit scope (what parts of the facility will be covered, what topics, who will do it, etc.), develop an audit protocol that is a step-by-step guide to how the audit is performed, identify any priority topics for coverage, and develop an employee interview schedule.

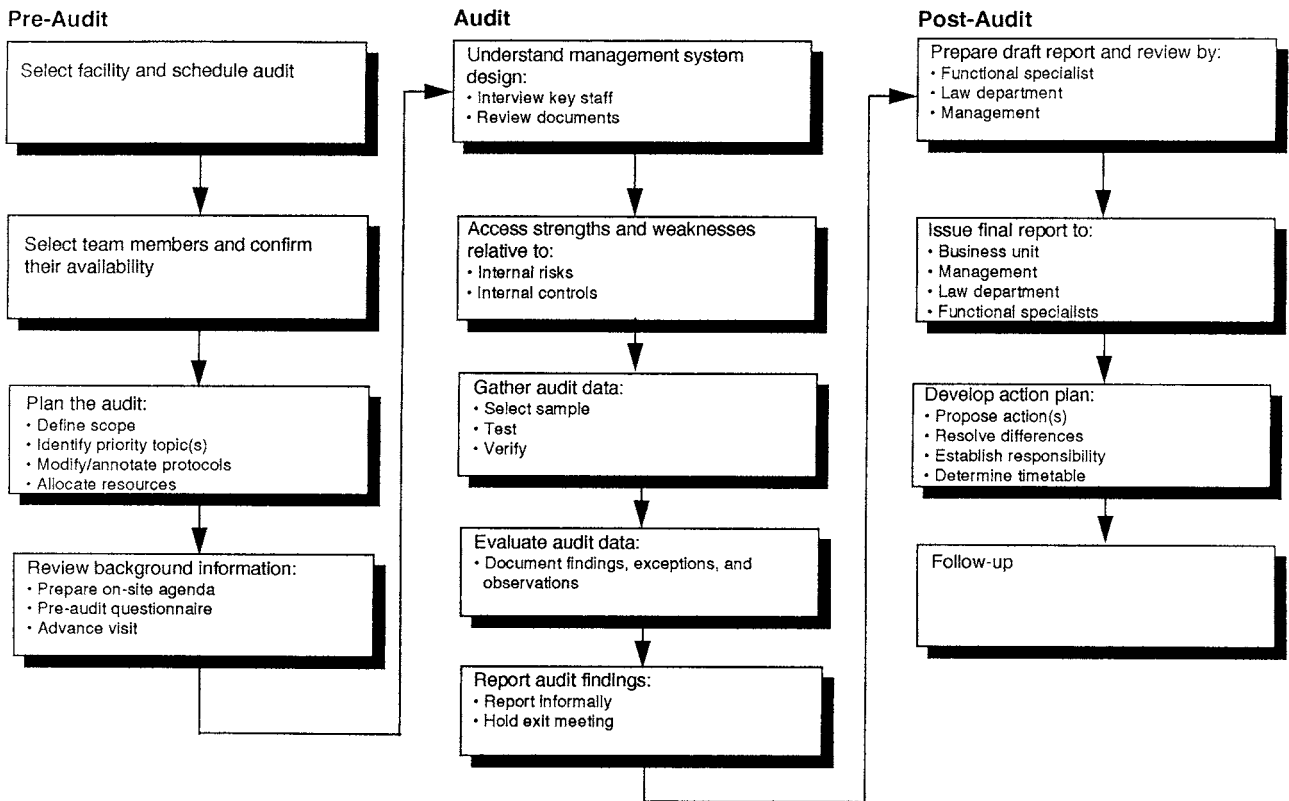


FIG. 23-48 Typical steps in the process safety management audit process. (CCSP, 1993, by permission of AIChE.)

On-Site Audit Process An opening meeting with key facility personnel is held at which the audit team covers the objectives and approach for the audit, and the facility personnel provide an overview of the site operations including site safety rules and a site tour. The on-site audit process should then follow five basic steps that include: (1) understanding management systems, (2) evaluating management systems, (3) gathering audit information, (4) evaluating audit information, and (5) reporting audit findings (CCSP, 1993, p. 17).

An understanding of the management systems in place to control and direct the process safety of the facility can be obtained from reading engineering and administrative standards, guidelines, and procedures that should be available in the background information supplied prior to the on-site audit. Informal procedures and guidelines used by the facility may only be discovered in interviews with staff management and operations management. This understanding of the formal and informal management systems is a critical step in the audit process.

The next process step evaluates the process safety management systems to determine if they are adequate to achieve the desired results, and if they are used as intended. This evaluation is highly subjective on the auditor's part. This step sets the stage for the rest of the audit, guiding the auditor's information gathering and focusing attention on critical areas.

Gathering audit data can be accomplished through observations, documents, and interviews. The data obtained is used to verify and validate that the process safety management systems are implemented and functioning as designed. Data gathering can be aided by the use of audit samples, where a representative number of items are audited to draw a conclusion, and by using self-evaluation questionnaires.

The audit data can now be evaluated, resulting in audit findings (i.e., conclusions both positive and negative). The audit team should confirm that sufficient data has been collected to support each finding. Additional data may need to be gathered if the team decides a preliminary finding needs to be strengthened. The conclusions drawn from the data evaluation should be a team consensus.

The reporting step of the on-site audit should be planned to avoid any surprises to facility personnel. Reporting sessions should be held at the end of each audit day to inform facility personnel of the findings, clear up any misunderstandings of the data, and help redirect

the audit team, if necessary. The on-site audit should end with a well-planned exit or closeout meeting between the audit team and facility personnel. All the findings of the audit team should be presented at this meeting. This verbal report is the opportunity for clarification of any ambiguities and determination of the final disposition of the findings (written audit report, for local attention only, etc.).

Postaudit Process The postaudit process consists of preparation of a draft report, preparation of a final report, development of action plans, and follow-up. A draft report of the audit findings should be prepared shortly after the completion of the on-site audit. The draft report usually undergoes review and comment by facility personnel involved with the audit, experienced auditors not involved with the subject audit, functional specialists, and attorneys. The review of the draft report is done to assure that a clear, concise, and accurate report is issued, and not to modify or change the findings. Once this review procedure is completed, a final report can be issued and distributed based on a distribution list provided by the facility personnel. The final audit report should be issued in a timely manner and meet the time requirement specified in the audit plan.

An action plan should be developed by the appropriate personnel of the audited facility to address any deficiencies stated in the audit report. Action plans should state what is to be done, who is responsible for getting it done, and when it is to be completed. Rationale for not taking any action for any of the stated deficiencies should also be documented. The action plan is an important step in closing the audit process.

It would not be unusual for some action plans to take a long time to complete. When extended implementation time is necessary, a follow-up mechanism should be used to document progress and show that an effort is being made to resolve the issues. Periodic (i.e., quarterly, semiannually) progress reports should be used as a follow-up method to ensure implementation. Future audits of the facility should include confirmation of the implementation of previous audit action plans.

The final audit report, action plans, progress reports, and any closure report should be retained by the facility based on the facility record retention policy. Typically, these items will be retained until future audit documentation replaces them. In some cases, audit records are retained for the life of the plant.

SAFETY EQUIPMENT, PROCESS DESIGN, AND OPERATION

PRESSURE RELIEF SYSTEMS

GENERAL REFERENCES: Center for Chemical Process Safety (CCPS), *Guidelines for Pressure Relief and Effluent Handling Systems*, American Institute of Chemical Engineers, New York, 1998. DIERS Project Manual, *Emergency Relief System Design Using DIERS Technology*, American Institute of Chemical Engineers, New York, 1992. Leung, "Simplified Vent Sizing Equations for Emergency Relief Requirements in Reactors and Storage Vessels," *AIChE J.* 32(10), pp. 1622-1634 (1986a). Leung, "A Generalized Correlation for One-Component Homogeneous Equilibrium Flashing Choked Flow," *AIChE J.* 32(10), pp. 1743-1746 (1986b). Leung, "Easily Size Relief Devices and Piping for Two-Phase Flow," *Chem. Eng. Prog.* 92(12), pp. 28-50 (1996). See more references under Code, Standards, and Guidelines subsection.

Introduction All process designs should attempt to arrive at an inherently safe facility. Incorporating safety features that are intrinsic (built-in) rather than extrinsic (added-on) to the basic design, together with the use of high-integrity equipment and piping, provides the first lines of defense against the dramatic, often catastrophic effects of an overpressure and subsequent rupture. In recent years, many companies have incorporated the principles of depressurizing or instrumental shutdown of key equipment as a means to control a release and avoid the actuation of pressure relief devices. This minimizes the probability of failure of the device, because, once used, the device may no longer be dependable. Since maintenance of relief devices can be sporadic, this redundancy provides yet another layer of safety. However, regardless of the number of lines of defense and depressur-

izing systems in place, overpressure protection must still be provided. Emergency pressure relief systems are intended to provide the last line of protection and thus must be designed for high reliability, even though they will have to function infrequently.

Self-actuated pressure relief systems must be designed to limit the pressure rise that can occur as a result of overcompressing, overfilling, or overheating either an inert or a chemically reactive medium in a closed system. Pressure generation is usually the result of either expansion of a single-phase medium (by material addition and/or heating) or a shift of the phase equilibrium in a multiphase medium (as a result of composition and/or temperature changes, particularly in the case of a reactive system). These mechanisms of pressure generation differ from what is commonly referred to as explosion venting. Events such as dust explosions and flammable vapor deflagrations propagate nonuniformly from a point of initiation, generating pressure or shock waves. Such venting problems are not included in these discussions.

Relief System Terminology Refer to API-RP520 Part I for complete terminology.

Accumulation The rise of pressure above the MAWP of the protected system, usually expressed as a percentage of the gauge MAWP. Maximum allowable accumulations are established by applicable codes for emergency operating and fire contingencies.

Backpressure The pressure existing at the outlet of a relief device. The value under no-flow conditions is superimposed backpressure. The value under flowing conditions consists of both

superimposed backpressure and built-up pressure due to piping pressure drop.

Blowdown The reduction in flowing pressure below the set point required for a PRV to close.

Design pressure The design pressure used to determine the minimum thickness of a vessel component and possibly used in place of MAWP where the latter has not been established. It is equal to or less than the MAWP. It is the pressure specified on the equipment purchase order.

Maximum allowable working pressure (MAWP) The maximum allowed pressure at the top of the vessel in its normal operating position at the operating temperature specified for that pressure.

Overpressure A pressure increase above the set point during relief flow, usually expressed as a percentage of the differential set pressure.

Pressure relief valve (PRV) A pressure relief device designed to open and relieve excess pressure and to reclose after normal conditions have been restored. *PRV* is a generic term applied to *relief valve* (set up for liquid flow), *safety valve* (set up for gas or vapor flow), and *safety relief valve* (set up for either liquid or compressible flow).

Relieving pressure Set pressure plus the overpressure.

Rupture disk A non-reclosing pressure relief device actuated by static differential pressure and designed to function by the bursting of a pressure-containing disk.

Set pressure The inlet gauge pressure at which a PRV will start to open (or a rupture disk will burst) under service conditions of temperature and backpressure.

Codes, Standards, and Guidelines Industry practice is to conform to the applicable regulations, codes, and recommended practices. In many cases, these will provide different guidelines. A suggested approach would be to review all applicable codes, standards, and recommended practices prior to choosing a design basis. The Design Institute for Emergency Relief Systems (DIERS) was established by AIChE to address sizing aspects of relief system for two-phase, vapor-liquid flashing flow regimes. The DIERS Project Manual (*Emergency Relief System Design Using DIERS Technology*, 1982) and the CCPS Guidelines (*Guidelines for Pressure Relief and Effluent Handling Systems*, 1998) are the generally accepted industry standard for two-phase relief venting.

NFPA 30 and API Standard 2000 provide guidance for design of overpressure protection involving storage tanks that operate at or near atmospheric pressure. In particular, NFPA 30 focuses on flammability issues, while API 2000 addresses both pressure and vacuum requirements. The ASME code (Sections I and VIII) and API RP 520 are the primary references for pressure relief device sizing requirements.

Designers of emergency pressure relief systems should be familiar with the following list of regulations, codes of practice, and industry standards and guidelines in the United States.

API RP 520. *Sizing, Selection, and Installation of Pressure-Relieving Devices in Refineries*. Part I, *Sizing and Selection*, 7th ed., January 2000, and Part II, *Installation*, 4th ed., December 1994. American Petroleum Institute, Washington.

API RP 521, 1997. *Guide for Pressure-Relieving and Depressuring Systems*, 4th ed. American Petroleum Institute, Washington.

API STD 526, 1995. *Flanged Steel Pressure Relief Valves*, 4th ed. American Petroleum Institute, Washington.

API STD 2000, 1998. *Venting Atmospheric and Low-Pressure Storage Tanks, Nonrefrigerated and Refrigerated*, 5th ed. American Petroleum Institute, Washington.

API RP 2001, 1984. *Fire Protection in Refineries*. American Petroleum Institute, Washington.

ASME, 2001. *Boiler and Pressure Vessel Code*, Section I, *Power Boilers*, and Section VIII, *Pressure Vessels*. American Society of Mechanical Engineers, New York.

ASME, 1988. *Performance Test Code PTC-25, Safety and Relief Valves*. American Society of Mechanical Engineers, New York.

CCPS, 1993. *Engineering Design for Process Safety*. American Institute of Chemical Engineers, New York.

CCPS, 1998. *Guidelines for Pressure Relief and Effluent Handling Systems*, American Institute of Chemical Engineers, New York.

DIERS, 1992. *Emergency Relief System Design Using DIERS Technology*, DIERS Project Manual. American Institute of Chemical Engineers, New York.

National Board of Boiler and Pressure Vessel Inspectors, 2004. *Pressure Relieving Device Certifications (Red Book NB-18)*. National Board of Boiler and Pressure Vessel Inspectors, Columbus, Ohio.

NFPA 30, 2000. *Flammable and Combustible Liquids Code*. National Fire Protection Association, Quincy, Mass.

OSHA 1910.106, 2005. *Flammable and Combustible Liquids, Regulations (Standards—29 CFR)*. U.S. Dept. of Labor, Occupational Safety and Health Administration, Washington.

Relief Design Scenarios The most difficult part of designing an adequate emergency pressure relief system lies in determining the emergency events (credible design scenarios) for which to design. The difficulty arises primarily because the identification of credible design scenarios usually involves highly subjective judgments, which are often influenced by economic situations. Unfortunately, there exists no universally accepted list of credible design scenarios. Relief systems must be designed for the credible chain of events that results in the most severe venting requirements (worst credible scenario). Credibility is judged primarily by the number and the time frame of causative failures required to generate the postulated emergency. Only totally independent equipment or human failures should be considered when judging credibility. A failure resulting from another failure is an effect, rather than an independent causative factor. A suggested guideline for assessing credibility as a function of the number and time frames of independent causative events is as follows:

- Any single failure is *credible*.
- Two or more simultaneous failures are *not credible*.
- Two events in sequence are *credible*.
- Three or more events in sequence are *not credible*.

The first step in scenario selection is to identify all the credible emergencies by using the preceding guidelines (or a similar set). This is perhaps best accomplished by identifying all the possible sources of pressure and vacuum. Table 23-27 lists a number of commonly existing pressure and vacuum sources.

Fire The main consequence of fire exposure is heat input causing thermal expansion, vaporization, or thermally induced runaway reaction and decomposition resulting in a pressure rise. An additional result of fire exposure is the possibility of overheating the wall of the equipment in the vapor space where the wall is not cooled by the liquid. In this case, the vessel wall may fail due to the high temperature, even though the relief system is operating. Hence API RP-521 recommends vapor depressurizing facilities for high-pressure services (greater than 17 bar or 250 psig). Guidelines for estimating the heat input from a fire are found in API Recommended Practices, NFPA 30 (for bulk storage tanks), OSHA 1910.106, and corporate engineering standards. In determining the heat input from fire exposure, NFPA allows credit for application of water spray to a vessel; API allows no such credit.

Pressure vessels (including heat exchangers and air coolers) in a plant handling flammable fluids are subject to potential exposure to external fire. A vessel or group of vessels which could be exposed to a

TABLE 23-27 Common Sources of Pressure and Vacuum

Heat Related
• Fire
• Out-of-control heaters and coolers
• Ambient temperature changes
• Runaway chemical reactions
Equipment and Systems
• Pumps and compressors
• Heaters and coolers
• Vaporizers and condensers
• Vent manifold interconnections
• Utility headers (steam, air, water, etc.)
Physical Changes
• Gas absorption (e.g., HCl in water)
• Thermal expansion
• Vapor condensation

pool fire must be protected by pressure relief device(s). Additional protection to reduce the device relief load can be provided by insulation, water spray, drainage, or remote-controlled depressurizing devices. Plant layout should consider spacing requirements, such as those set forth by NFPA, API, Industrial Risk Insurers, or Factory Mutual, and must include accessibility for firefighting personnel and equipment. Several pieces of equipment located adjacent to each other that cannot be isolated by shutoff valves can be protected by a common relief device, providing the interconnecting piping is large enough to handle the required relief load and the relief set pressure is no higher than the minimum MAWP of these pieces of equipment.

Operational Failures A number of scenarios of various operational failures may result in the generation of overpressure conditions:

- **Blocked outlet** Operation or maintenance errors (especially following a plant turnaround) can block the outlet of a liquid or vapor stream from a piece of process equipment, resulting in an overpressure condition.
- **Opening a manual valve** Manual valves which are normally closed to isolate two or more pieces of equipment or process streams can be inadvertently opened, causing the release of a high-pressure stream or resulting in vacuum conditions.
- **Cooling water failure** The loss of cooling water is one of the more commonly encountered causes of overpressurization. Different scenarios should be considered for this event, depending on whether the failure affects a single piece of equipment (or process unit) or is plantwide.
- **Power failure** The loss of power will shut down all motor-driven rotating equipment, including pumps, compressors, air coolers, and vessel agitators.
- **Instrument air failure** The consequences of the loss of instrument air should be evaluated in conjunction with the failure mode of the control valve actuators. It should not be assumed that the correct air failure response will occur on these control valves, as some valves may stick in their last operating position.
- **Thermal expansion** Equipment and pipelines that are liquid-full under normal operating conditions are subject to hydraulic expansion if the temperature increases. Common sources of heat that can result in high pressures due to thermal expansion include solar radiation, steam or other heated tracing, heating coils, and heat transfer from other pieces of equipment.
- **Vacuum** Vacuum conditions in process equipment can develop due to a wide variety of situations, including instrument malfunction, draining or removing liquid with venting, shutting off purge steam without pressurizing with noncondensable vapors, extreme cold ambient temperatures resulting in subatmospheric vapor pressures, and water addition to vessels that have been steam-purged. If vacuum conditions can develop, then either the equipment must be designed for vacuum conditions or a vacuum relief system must be installed.

Equipment Failure Most equipment failures that can lead to overpressure situations involve the rupture or break of internal tubes inside heat exchangers and other vessels and the failure of valves and regulators. Heat exchangers and other vessels should be protected with a relief system of sufficient capacity to avoid overpressure in case of internal failure. API RP 521 presents guidance in determining these requirements, including criteria for deciding when a full tube rupture is likely. In cases involving the failure of control valves and regulators, it is important to evaluate both the fail-open and fail-closed positions.

Runaway Reactions Runaway temperature and pressure in process vessels can occur as a result of many factors, including loss of cooling, feed or quench failure, excessive feed rates or temperatures, contaminants, catalyst problems, and agitation failure. Of major concern is the high rate of energy release in runaway reactions and/or formation of gaseous products, which generally cause a rapid pressure rise in the equipment. To properly assess these effects, the reaction kinetics must be either known or obtained experimentally (see "Reactivity Testing" in the earlier "Chemical Reactivity" subsection for a description of adiabatic calorimeters for runaway reactions). In general, a lower relief set pressure (much below the equipment MAWP) is desirable for these runaway reaction systems in order to relieve the

TABLE 23-28 Summary of Device Characteristics

	Reclosing devices		Nonreclosing devices
	Relief valves	Disk-valve combinations	Rupture disks
Fluid above normal boiling point	+	+	-
Toxic fluids	+	+	-
Corrosive fluids	-	+	+
Cost	-	-	+
Minimum pipe size	-	-	+
Testing and maintenance	-	-	+
Won't fatigue and fail low	+	+	-
Opens quickly and fully	-	-	+

NOTE: + indicates advantageous
- indicates disadvantageous

system at a lower reaction rate, since most reactions are Arrhenius in behavior.

Pressure Relief Devices The most common method of overpressure protection is through the use of safety relief valves and/or rupture disks which discharge into a containment vessel, a disposal system, or directly to the atmosphere. Table 23-28 summarizes some of the device characteristics and the advantages.

Safety Relief Valves (SRVs) Conventional safety relief valves are used in systems where built-up backpressures typically do not exceed 10 percent of the set pressure. The spring setting of the valve is reduced by the amount of superimposed backpressure expected. Higher built-up backpressures can result in a complete loss of continuous valve relief capacity. The designer must examine the effects of other relieving devices connected to a common header on the performance of each valve. Some mechanical considerations of conventional relief valves are presented in the ASME code; however, the manufacturer should be consulted for specific details.

Balanced safety relief valves may be used in systems where built-up and/or superimposed backpressure is high or variable. In general, the capacity of a balanced valve is not significantly affected by backpressures below 30 percent of the set pressure. Most manufacturers recommend keeping the backpressure on balanced valves below 45 to 50 percent of the set pressure. Consult API-526 and valve manufacturers for the maximum outlet pressure limit for bellows-type SRVs.

For both conventional and balanced SRVs, the inlet pressure loss, including the mounting nozzle entrance loss, rupture disk flow resistance, and inlet pipe friction, is recommended to stay below 3 percent of the differential set pressure, or else valve instability may occur, resulting in degraded relief capacity.

Pilot-Operated Relief Valves In a pilot-operated relief valve, the main valve is combined with and controlled by a smaller, self-actuating pressure relief valve. The pilot is a spring-loaded valve that senses the process pressure and opens the main valve by lowering the pressure on the top of an unbalanced piston, diaphragm, or bellows of the main valve. Once the process pressure is lowered to the blowdown pressure, the pilot closes the main valve by permitting the pressure in the top of the main valve to increase. Pilot-operated relief valves are commonly used in clean, low-pressure services and in services where a large relieving area at high set pressures is required. The set pressure of this type of valve can be close to the operating pressure. Pilot-operated valves are frequently chosen when operating pressures are within 5 percent of set pressures and a close tolerance valve is required.

Rupture Disks A rupture disk is a non-reclosing device designed to function by the bursting of a pressure-retaining disk. This assembly consists of a thin, circular membrane usually made of metal, plastic, or graphite that is firmly clamped in a disk holder. When the process reaches the bursting pressure of the disk, the disk ruptures and releases the pressure. Rupture disks can be installed alone or in combination with other types of devices. Once blown, rupture disks do not reseal; thus, the entire contents of the upstream process equipment will be vented. Rupture disks of nonfragmented type are commonly used in series (upstream) with a safety relief valve to prevent corrosive

fluids from contacting the metal parts of the valve. In addition, this combination is a reclosing system.

The burst tolerances of rupture disks are typically about ± 5 percent for set pressures above 2.76 barg (40 psig). Consult API-520-I (Section 2.3.6.1) on the proper selection and burst setting of the rupture disks.

Pressure Vacuum Relief Valves For applications involving atmospheric and low-pressure storage tanks, pressure-vacuum relief valves (PVRVs) are used to provide pressure relief. Such devices are not included in the scope of ASME Section VIII and thus are not Code-certified; hence they are used mostly in non-Coded vessels (<1.03-barg or 15-psig design). These units combine both a pressure and a vacuum relief valve into a single assembly that mounts on a nozzle on top of the tank and are usually sized to handle the normal in-breathing and out-breathing requirements.

Sizing of Pressure Relief Systems A critical point in design is to determine whether the relief system must be sized for single-phase or two-phase relief flow. Two-phase flow frequently occurs during a runaway, but it can also occur in nonreactive systems such as vessels with gas spargers, vessels experiencing high heat input rates, or systems containing known foaming agents such as latex. The *drift flux* methodology (Zuber and Findlay, "Average Volumetric Concentration in Two-Phase Flow Systems," *Trans. ASME J. Heat Transfer*, pp. 453-468, November 1965; Wallis, *One-Dimensional Two-Phase Flow*, McGraw-Hill, New York, 1969) has been extended and applied to both the volumetric heating case (uniform vapor generation throughout the liquid) and wall heating case (vaporization occurring only at vessel wall) in the DIERS (Design Institute for Emergency Relief Systems) study (DIERS, 1992). The DIERS methodology is important as a means of addressing situations, such as two-phase flow, not covered adequately by current ASME and API methods. The recent CCPS Guidelines (CCPS, 1998) is the best source of updated information on these methods. For a top-vented vessel, the important mechanism for the liquid carryover resulting in two-phase relief is *boilover*. The vessel hydrodynamic model based on drift flux formulation is used to estimate the quality (i.e., vapor mass fraction) entering the vent system. The churn-turbulent regime vessel model is generally reserved for nonfoaming and nonviscous liquids. This regime would yield the highest degree of vapor-liquid disengagement. The bubbly regime vessel model is generally applied to foamy liquids and viscous systems. The bubbly regime would yield only limited disengagement in the vessel. Finally, a conservative but often realistic case for runaway reactive systems is the homogeneous (or uniform froth) vessel model. This model assumes no vapor-liquid disengagement inside the vessel, an idealized assumption, but it leads to much simpler sizing equations.

Required Relief Rate The required relief rate is the vent rate W (kg) required to remove the volume being generated within the protected equipment when the equipment is at its highest allowed pressure:

$$W_{\text{req}} = \frac{\text{net volume generation rate}}{\text{specific volume of vent stream}} \quad (23-89)$$

For steady-state design scenarios, the required vent rate, once determined, provides the capacity information needed to properly size the relief device and associated piping. For situations that are transient (e.g., two-phase venting of a runaway reactor), the required vent rate would require the simultaneous solution of the applicable material and energy balances on the equipment together with the in-vessel hydrodynamic model. Special cases yielding simplified solutions are given below. For clarity, nonreactive systems and reactive systems are presented separately.

Nonreactive Systems

Consider constant flow into protected equipment (blocked outlet). For the steady-state design scenario with a constant flow of fluid W_{in} (kg/s) from a pressure source that is above the maximum allowed pressure in the protected equipment, volume is being generated within the equipment at a rate of $W_{\text{in}}/\rho_{\text{in}}$, where ρ_{in} (kg/m³) is the incoming fluid density evaluated at the maximum allowed pressure. Denoting ρ_{out} (kg/m³) as the vent stream fluid density, Eq. (23-89)

then yields the required vent rate:

$$W_{\text{req}} = \frac{W_{\text{in}}}{\rho_{\text{in}}} \rho_{\text{out}} \quad (23-90)$$

Consider constant heat input into protected equipment. If the addition of heat to the equipment does not cause the fluid to boil, then the volume generation rate is the thermal expansion rate of the fluid:

$$W_{\text{req}} = \frac{q\beta}{C_p} \quad (23-91)$$

where q is the heat input rate (J/s), β is the coefficient of volumetric expansion at constant pressure ($^{\circ}\text{C}^{-1}$), and C_p is the constant-pressure specific heat [J/(kg $\cdot^{\circ}\text{C}$)].

The properties are evaluated at maximum allowed pressure conditions. For liquids, β can typically be evaluated from the specific volume change over a 5 $^{\circ}\text{C}$ temperature increment. For ideal gases, Eq. (23-91) becomes

$$W_{\text{req}} = \frac{q}{C_p T} \quad (23-92)$$

where T is the absolute temperature (K).

If the fluid is at its boiling point, then volume is generated through the phase change that occurs upon vaporization. For *nonfoamy fluids*, vents sized for all-vapor relief are adequate, even if some initial two-phase venting is predicted. The required vent rate based on the volumetric rate balance criterion of Eq. (23-89) is given for a single-component fluid as (Leung, 1986a)

$$W_{\text{req}} = \frac{q}{h_{fg}} \left(\frac{v_{fg}}{v_g} \right) \quad (23-93)$$

where h_{fg} is the latent heat of vaporization (J/kg), v_g is the vapor specific volume (m³/kg), v_{fg} is the specific volume increase upon vaporization = $v_g - v_f$ (m³/kg), and v_f is the liquid specific volume (m³/kg).

Near the critical region, the property ratio h_{fg}/v_{fg} can be replaced by $T(dP/dT)_{\text{sat}}$ via the Clapeyron relation since both h_{fg} and v_{fg} are approaching zero. Here $(dP/dT)_{\text{sat}}$ is the slope of the vapor-pressure curve and has units of Pa/K. For multicomponent fluids, Eq. (23-93) is evaluated for each major component (> 10% wt), and the largest single-component venting requirement is used. Refer to CCPS Guidelines (1998) for more complex schemes.

For *foamy fluids*, the homogeneous vessel model with volumetric heating assumption is used (Leung, 1986a):

$$W(T_p - T_s) = \frac{q}{C_p} \left(\ln \frac{m_0 q v_{fg}}{W V h_{fg}} - 1 \right) + \frac{W V h_{fg}}{m_0 C_p v_{fg}} \quad (23-94)$$

where W is the vent rate (kg/s), T_p is the temperature at peak pressure ($^{\circ}\text{C}$), T_s is the temperature at set pressure ($^{\circ}\text{C}$), m_0 is the initial mass in system (kg), V is the equipment (vessel) volume (m³), q is the heat input rate (J/s), and C_p is the constant-pressure liquid specific heat [J/(kg $\cdot^{\circ}\text{C}$)].

Note that Eq. (23-94) is implicit in W ; a trial-and-error solution method is required. This equation is applicable for single-component or pseudo-one-component systems. For the latter, h_{fg} is defined to be the enthalpy (heat) required to vaporize a unit mass of liquid at equilibrium vapor composition.

Analytical equations have been presented for both the bubbly regime and churn-turbulent regime; see Leung (Leung, "Overpressure During Emergency Relief Venting in Bubbly and Churn-Turbulent Flow," *AIChE J.* 33(6), pp. 952-958, 1987) and Dalessandro (Dalessandro, "Emergency Venting Requirements for Tempered Systems Considering Partial Vapor-Liquid Separation with Disengagement Parameters Greater than Unity, Part I: Model Development, Part II: Application," *Process Safety Prog.* 23, pp. 1-15 and 86-98, 2004).

Reactive Systems Exothermic runaway (uncontrolled chemical) reactions add considerable complexity. Note that external heating (such as a fire) on a vessel containing unstable compounds would fall into this category. The added complications are due to the following:

1. Reaction rate varies exponentially with temperature.
2. Exothermic heat release rates are time-varying.
3. Volatile or noncondensable gas can be generated (in decomposition).
4. Composition change causes shift in boiling point curve.
5. Viscosity increases due to polymerization.

In dealing with such complexity, DIERS has developed a special bench-scale apparatus commercialized by Fauske & Associates, LLC, as the Vent Sizing Package 2 (VSP2™). The design and operation are described in several references [Fauske and Leung, "New Experimental Technique for Characterizing Runaway Chemical Reactions," *Chem. Eng. Prog.*, **80**(8), pp. 39–46, 1985; Leung, Fauske, and Fisher, "Thermal Runaway Reactions in a Low Thermal Inertia Apparatus," *Thermochimica Acta*, **104**, pp. 13–29, 1986; DIERS, 1992; CCPS, 1998]. This adiabatic calorimeter has been extensively used to obtain the above key information for pressure relief design. Upset scenarios such as external heating, overcharge of reactants, or loss of cooling can be directly simulated in this apparatus. Two special-case solutions are given here.

For boiling liquid reactive systems, an analytical method yielding closed-form integral equations for homogeneous vessel two-phase relief has been used for some time (Leung, 1986a). Simplifying assumptions are that (1) the vent rate is taken as constant with time, (2) average values of heat release rate per unit mass and physical properties can be used, (3) there is constant or decreasing system volatility, and (4) a pseudo-one-component approach is taken. The required vent rate is

$$W_{req} = \frac{m_0 C_p (dT/dt)_{av}}{[(V/m_0)/(h_{fg}/v_{fg})]^{1/2} + (C_p \Delta T)^{1/2}} \quad (23-95)$$

where $\Delta T = T_p - T_s$ is the "overtemperature" (°C) corresponding to the overpressure ΔP selected, and $(dT/dt)_{av}$ is the average temperature rise rate (°C/s).

The average dT/dt is typically an arithmetic average between the value at set pressure and the value at peak allowed pressure. The properties C_p , h_{fg} , v_{fg} either can be evaluated at the set conditions or can be taken as the average values between the set condition and the peak allowed pressure condition. Alternatively, the term h_{fg}/v_{fg} in Eq. (23-95) can be replaced by $T(dp/dT)_{sat}$ via the Clapeyron relation. This holds reasonably well for a multicomponent system of near constant volatility. Such an application permits direct use of the experimental pressure-temperature data obtained from a closed-system runaway VSP2 test. This form of Eq. (23-95) has been used to demonstrate the advantageous reduction in both vent rate and vent area with allowable overpressure (Leung, 1986a).

For partial disengagement venting models (in bubbly and churn-turbulent regimes), refer to publications by Leung (1987) and Dalessandro (2004).

The special case of **gas generating reactive systems** is for a decomposition reaction with negligible gas solubility in the liquid and no significant latent heat effects. Such a reaction will proceed to the maximum rate whether vented or not. The main purpose of venting is to limit the pressure rise in these "gassy" systems. The maximum gas generation rate is usually obtained from the pressure rise rate data in the DIERS-type apparatus. At the peak allowed pressure P_m , the volumetric gas generation rate for the protected equipment is given by

$$Q_{g,max} = \frac{m_0}{m_t} \frac{V_t}{P_m} \left(\frac{dP}{dt} \right)_{max} \quad (23-96)$$

where m_0 is the mass in protected equipment (kg), m_t is the sample mass in test apparatus (kg), V_t is the volume occupied by gas in test apparatus (m^3), P_m is the peak allowed pressure in equipment (Pa, psia), and $(dP/dt)_{max}$ is the maximum pressure rise rate measured in test apparatus (Pa/s, psi/s). Note that consistent pressure units can be used for P_m and dP/dt here. The required vent rate based on the volumetric rate balance criterion of Eq. (23-89) is given by

$$W_{req}^0 = \frac{Q_{g,max}}{V/m_0} \quad (23-97)$$

However, this vent rate assumes homogeneous vessel venting at the peak allowed pressure with no prior loss of mass. A less conservative design would consider the mass loss during the overpressure venting interval [Leung, "Venting of Runaway Reactions with Gas Generation," *AIChE J.*, **38**(5), pp. 723–732, 1992].

Relief System Flow Capacity This subsection establishes the relation between relief system configuration and flow capacity in order to determine the size required for a given vent rate. The mass flow rate W through a given relief system geometry, in general, requires a trial-and-error approach when the system configuration contains more than a single diameter. The generalized approach is to assume a flow rate W —this is usually governed by the limiting area such as the orifice or nozzle in a pressure relief valve (PRV) or the rupture disk (RD)—and calculate the resulting pressure profiles down the system until the final discharge pressure matches the specified value. If choked flow is encountered at any area enlargement location in the vent system, then the pressure just after the choking location is determined by calculating back up the larger pipe from a downstream point of specified pressure.

The treatment of vent flow calculations in most typical relief system configurations involves two classes of computational models: flow through nozzles and frictional flow in pipes.

The flow path in well-formed nozzles [ideal (**frictionless**) flow] follows smoothly along the nozzle contour without flow separation. The effects of small imperfections and small frictional losses are accounted for by correcting the ideal nozzle flow by an empirically determined coefficient of discharge K_d . This applies to PRV geometry. The acceleration of a fluid initially at rest to flowing conditions in an ideal nozzle is given by

$$-\frac{G^2 v}{2} = \int_{P_0}^{P_1} v \, dP \quad (23-98)$$

where P_0 is the stagnation pressure of the fluid, P_1 is the static pressure at the minimum flow area called the *throat*, G is the mass flux [$\text{kg}/(\text{m}^2 \cdot \text{s})$], and v is the fluid specific volume (m^3/kg). If the fluid is compressible, the flow will increase to a maximum value as the downstream pressure is reduced, and any further decrease in the downstream pressure will not affect the flow. This maximum flow condition is referred to as the *critical* (or *choked*) condition. The flow and pressure at this condition are related by

$$G_c = \sqrt{\frac{-1}{(dv/dP)_s}} \quad (23-99)$$

The subscript s denotes an isentropic path for ideal nozzle flow. For ideal gas with $Pv^k = \text{constant}$, substitution of this isentropic expansion law into Eq. (23-98) yields the following critical pressure ratio P_c/P_0 and critical flow rate G_c :

$$\frac{P_c}{P_0} = \left(\frac{2}{k+1} \right)^{k/(k-1)} \quad (23-100)$$

$$G_c = \left[k \left(\frac{2}{k+1} \right)^{(k+1)/(k-1)} \right]^{1/2} \sqrt{\frac{P_0}{v_0}} \quad (23-101)$$

where k is the isentropic expansion exponent for ideal gas ($k = C_p/C_v$), P_c is the choking pressure at throat (Pa), P_0 is the stagnation inlet pressure (Pa), and v_0 is the ideal gas specific volume at P_0 (m^3/kg).

Thus for a PRV system, the following relief rate formula (for choked flow) is given in SI units (kg/s , m^2 , N/m^2 , K) in API-520-I (2000):

$$W = K_d K_b A P_0 \left(\frac{M_{ic}}{RT_0 Z} \right)^{1/2} \left[k \left(\frac{2}{k+1} \right)^{(k+1)/(k-1)} \right]^{1/2} \quad (23-102)$$

where K_d is the discharge coefficient of PRV nozzle (orifice), K_b is the capacity correction factor due to backpressure (consult API-520-1), A is the PRV orifice area (m^2), M_w is the molecular weight, R is the gas constant, T_0 is the absolute temperature at inlet (K), and Z is the compressibility. For nonideal gas at near thermodynamic critical or supercritical region, special treatments other than simply applying the Z factor as in Eq. (23-102) are necessary [see Leung and Epstein, "A Generalized Critical Flow Model for Non-ideal Gases," *AICHE J.* 34(9), pp. 1568–1572, 1988; and CCPS, 1998].

The treatment for two-phase relief is more involved due to the presence of slip and thermodynamic nonequilibrium between the two phases. However, for flow capacity evaluation, the traditional homogeneous (no slip) equilibrium model (HEM) is recommended (DIERS, 1992; CCPS, 1998). For a two-phase flashing system (both single-component and multicomponent), the P - v relation can be obtained from adiabatic flash calculations—strictly speaking under constant-entropy, but constant-enthalpy flash computations are adequate for use in numerical integration of Eq. (23-98). A particularly useful simplification is the *omega* method by Leung (1986b; see the earlier subsection "Discharge Rates from Punctured Lines and Vessels" for more discussion), where a P - v relation for a two-phase fluid expansion is written as

$$\frac{v}{v_0} = \omega \left(\frac{P_0}{P} - 1 \right) + 1 \quad (23-103)$$

For a single-component or a pseudo-one-component fluid, the dimensionless parameter ω is evaluated at the inlet conditions (subscript 0) from (Leung, 1996)

$$\omega = \alpha_0 \left(1 - 2 \frac{P_0 v_{f0}}{h_{f0}} \right) + \frac{C_{p0} T_0 P_0}{v_0} \left(\frac{v_{f0}}{h_{f0}} \right)^2 \quad (23-104)$$

For multicomponent systems with boiling range greater than 80°C, a single adiabatic flash calculation to 80 to 90 percent of the inlet pressure P_0 yields the two-phase specific volume v_1 at pressure P_1 , and ω is calculated from (Nazario and Leung, "Sizing Pressure Relief Valves in Flashing and Two-Phase Service: An Alternative Procedure," *J. Loss Prev. Process Ind.* 5(5), pp. 263–269, 1992)

$$\omega = \frac{v_1/v_0 - 1}{P_0/P - 1} \quad (23-105)$$

For the case of a noncondensable gas and a nonflashing liquid (a nonflashing two-phase fluid), ω is simply defined by (Leung, 1996)

$$\omega = \frac{\alpha_0}{\Gamma} \quad (23-106)$$

where the two-phase isentropic expansion exponent for a thermal equilibrium process is given by

$$\Gamma = \frac{x C_{pg} + (1-x) C_{pf}}{x C_{vg} + (1-x) C_{vf}} \quad (23-107)$$

Note that for most cases of interest, Γ is close to unity since the flowing gas mass fraction $x \ll 1$. For the case of frozen flow (i.e., no heat transfer between the two phases), Γ would be replaced by k (or C_{pg}/C_{vg}) in Eq. (23-106). However, the difference between the two limiting cases is small (< 10 percent) in terms of the flow capacity [Leung and Epstein, "A Generalized Correlation for Two-Phase Nonflashing Homogeneous Choked Flow," *Trans. ASME J. Heat Transfer* 112 (May), pp. 528–530, 1990].

With the P - v relation given by Eq. (23-103), Eq. (23-98) can be integrated to give a generalized equation for flow through an ideal nozzle

$$\frac{G}{\sqrt{P_0 v_0}} = \frac{[-2[\omega \ln(P/P_0)] + (\omega - 1)(1 - P/P_0)]^{0.5}}{\omega(P_0/P - 1) + 1} \quad (23-108)$$

The maximum (critical) or choked flow condition occurs at the critical pressure ratio P_c/P_0 from solving (Leung, 1986a)

$$\left(\frac{P_c}{P_0} \right)^2 + (\omega^2 - 2\omega) \left(1 - \frac{P_c}{P_0} \right)^2 + 2\omega^2 \ln \frac{P_c}{P_0} + 2\omega^2 \left(1 - \frac{P_c}{P_0} \right) = 0 \quad (23-109)$$

The critical mass flux G_c is given by the dimensionless form

$$\frac{G_c}{\sqrt{P_0 v_0}} = \frac{P_c/P_0}{\sqrt{\omega}} \quad (23-110)$$

If $P_c > P_b$, the backpressure, the flow is choked, and Eq. (23-110) yields the critical mass flux. Otherwise, $P_c < P_b$, flow is not choked, and P is equated to P_b in Eq. (23-108) to obtain the unchoked mass flux.

A relief rate formula for two-phase flow similar to Eq. (23-102) for gas can be written as

$$W = K_d K_b A G \quad (23-111)$$

For the boiling-liquid system, ω is calculated from Eq. (23-104) or Eq. (23-105), while for a gas-generating system, ω is evaluated from Eq. (23-106).

For **pipe flow**, HEM requires solution of the equations of conservation of mass, energy, and momentum. The momentum equation is in differential form, which requires partitioning the pipe into segments and carrying out numerical integration. For constant-diameter pipe, these conservation equations are as follows:

Mass:

$$G = \text{constant} \quad (23-112)$$

Energy:

$$h_0 = h + \frac{G^2 v^2}{2} \quad (23-113)$$

Momentum:

$$v dP + G^2 \left(v dv + \frac{4fv^2 dL}{2D} \right) + g \cos \theta dL = 0 \quad (23-114)$$

where h_0 is enthalpy at stagnation (J/kg), h is enthalpy (J/kg), v is fluid specific volume, f is Fanning friction factor, L is flow length (m), g is acceleration due to gravity, and θ is angle of inclination from vertical.

Equation (23-114), the momentum equation, can be solved more conveniently by rewriting it and solving it numerically

$$\Delta L = - \frac{\bar{v} \Delta P + G^2 v \Delta v}{(2f/D) G^2 v^2 + g \cos \theta} \quad (23-115)$$

where \bar{v} is the average specific volume in the pressure increment ΔP and Δv is the incremental specific volume over ΔP .

In the numerical integration of Eq. (23-115) for a given pipe length L , the following steps are suggested (note that detailed thermodynamic properties are required also):

1. Either G is known or guessed.
2. Increments of pressure are taken from the initial to the final pressure.
3. Both \bar{v} and Δv are obtained for each increment for a constant stagnation enthalpy process satisfying Eq. (23-113).
4. For each ΔP taken, ΔL is computed from Eq. (23-115).
5. Total length of pipe L is $\Sigma \Delta L$.
6. If ΔL is negative, then ΔP is too large.
7. A critical flow condition corresponds to $\Delta L = 0$, and the final pressure corresponds to choked pressure.
8. If $\Sigma \Delta L > L$, then G was guessed too small, and steps 1 through 7 are repeated with a larger G . If $\Sigma \Delta L < L$, then G was guessed too large; steps 1 through 7 are repeated with a smaller G .
9. A converged solution is obtained when $\Sigma \Delta L = L$ to within a given tolerance.

The above calculations can be simplified somewhat by ignoring the kinetic energy term in the energy equation, Eq. (23-113), and simply basing calculations on an isenthalpic flash. Thus a P - v relation can be obtained from such flash calculations prior to performing the above iteration steps. In the special case of turbulent pipe flow horizontal discharge ($\cos \theta = 0$), Eq. (23-114) can be integrated based on the omega P - v relation to yield [Leung and Grolmes, "The Discharge of Two-Phase Flashing Flow in a Horizontal Duct," *AICHE J.* 33(3), pp. 524–527, 1987; also errata, 34(6), p. 1030, 1988]

$$4f \frac{L}{D} = \frac{2}{G^2} \left[\frac{\eta_1 - \eta_2}{1 - \omega} + \frac{\omega}{(1 - \omega)^2} \ln \frac{(1 - \omega)\eta_2 + \omega}{(1 - \omega)\eta_1 + \omega} \right] - 2 \ln \left[\frac{(1 - \omega)\eta_2 + \omega}{(1 - \omega)\eta_1 + \omega} \left(\frac{\eta_1}{\eta_2} \right) \right] \quad (23-116)$$

where $\eta_1 \equiv P_1/P_0$, $\eta_2 \equiv P_2/P_0$, $G^* \equiv G/\sqrt{P_0/v_0}$, P_1 is the absolute static pressure at the inlet of the pipe (N/m^2), P_2 is the absolute static pressure at the outlet of the pipe (N/m^2), and P_0 is the reference pressure typically associated with the stagnation pressure in the upstream equipment. The choking criterion at pipe exit takes the form

$$G_c^* = \frac{\eta_{2c}}{\sqrt{\omega}} \quad (23-117)$$

where subscript c denotes choking. The integrated momentum equation, Eq. (23-116), yields the pressure drop $P_1 - P_2$ in the pipe implicitly as a function of ω , $4fL/D$, and G . For the case of a pipe discharge from a vessel, the inlet acceleration pressure drop $P_0 - P_1$ is given by Eq. (23-108) above with P/P_0 being P_1/P_0 or η_1 . Essentially the inlet pipe section is treated as an ideal nozzle, and any irreversible loss due to sharp entrance effect is included in the overall $4fL/D$ term. Likewise, the velocity head loss associated with bends (elbows) is to be included in the $4fL/D$ term as well. For high-velocity, two-phase discharge, an average f value of 0.005 has been used in most applications (Wallis, 1969).

Choked pipe exit: $\eta_{2c} > \eta_b$ or $P_{2c} > P_b$. Equations (23-109), (23-116), and (23-117) are used to solve for G_c^* , η_{1c} , and η_{2c} (likewise, for G_c , P_1 , and P_2) for a given $4fL/D$ and ω value.

Unchoked pipe exit: $\eta_{2c} < \eta_b$ or $P_{2c} < P_b$. Equation (23-116) does not apply. With $\eta_2 = \eta_b$ (or $P_2 = P_b$) for an unchoked exit, only Eqs. (23-108) and (23-116) are needed to solve for G^* and η_1 (likewise, for G and P_1). Under most situations, it suffices to set $\eta_1 = 1$ and to solve for G^* readily by rearranging Eq. (23-116).

This method has been extended to inclined pipe discharge [Leung and Epstein, "The Discharge of Two-Phase Flashing Flow from an Inclined Duct," *Trans. ASME J. Heat Transfer* 112 (May), pp. 524–528, 1990], which together with some useful design charts is presented in the earlier subsection "Discharge Rates from Punctured Lines and Vessels."

EMERGENCY RELIEF DEVICE EFFLUENT COLLECTION AND HANDLING

GENERAL REFERENCES: API RP 521, *Guide for Pressure Relieving and Depressurizing Systems*, 5th ed., American Petroleum Institute, Washington, 2007. API STD 537, *Flare Details for General Refinery and Petrochemical Service*, American Petroleum Institute, Washington, September 2003. AIChE-CCPS, *Guidelines for Pressure Relief and Effluent Handling Systems*, AIChE, New York, 1998. DIERS, *Emergency Relief System Design Using DIERS Technology*, AIChE, New York, 1992. Fthenakis, *Prevention and Control of Accidental Releases of Hazardous Cases*, Van Nostrand-Reinhold, New York, 1993. Grossel and Crowl, *Handbook of Highly Toxic Materials Handling and Management*, Marcel Dekker, New York, 1995. Grossel, *Journal of Loss Prevention in the Process Industries* 3(1): 112–124, 1990. Grossel, *Plant/Operations Progress* 5(3): 129–135, 1986. Keiter, *Plant/Operations Progress* 11(3): 157–163, 1992. McIntosh and Nolan, *Journal of Loss Prevention in the Process Industries* 14(1): 17–26, 2001. McIntosh and Nolan, *Journal of Loss Prevention in the Process Industries* 14(1): 27–42, 2001. Schmidt and Giesbrecht, *Process Safety Progress* 20(1): 6–16, 2001.

Introduction In determining the disposal of an effluent vent stream from an emergency relief device (safety valve or rupture disk), a number of factors must be considered, such as

1. Is the stream single-phase (gas or vapor) or multiphase (vapor-liquid or vapor-liquid-solid)?
2. Is the stream flammable or prone to deflagration?
3. Is the stream toxic?
4. Is the stream corrosive to equipment or personnel?

Some vent streams, such as light hydrocarbons, can be discharged directly to the atmosphere even though they are flammable and explosive. This can be done because the high-velocity discharge entrains sufficient air to lower the hydrocarbon concentration below the lower explosive limit (API RP 521, 2007). Toxic vapors must be sent to a flare or scrubber to render them harmless. Multiphase streams, such as those discharged as a result of a runaway reaction, e.g., must first be routed to separation or containment equipment before final discharge to a flare, a scrubber, or a quench pool tank.

This discussion is organized into three major areas: types of equipment, criteria employed in the selection of equipment, and sizing and design of the equipment.

Types of Equipment Equipment for handling emergency relief discharge streams can be divided into two classes:

1. Vapor/gas/solid-liquid separators
2. Final vapor/gas control or destruction equipment

The two most commonly used types of vapor/gas-liquid separators are

- Gravity separators—horizontal and vertical (also called blowdown drums, knockout drums, or catch tanks)
 - Emergency cyclone separators
- The most commonly used types of final vapor/gas control or destruction equipment are
- Quench pools/catch tanks and quench towers
 - Emergency flare systems
 - Emergency scrubbers (absorbers)

Gravity Separators Three types of gravity separators are commonly used in the chemical process industries (CPI): horizontal blowdown drum/catch tank, vertical blowdown drum/catch tank, and multi-reactor knockout drum/catch tank.

Horizontal blowdown drum/catch tank This type of drum, shown in Fig. 23-49, combines both the vapor-liquid separation and holdup functions in one vessel. Horizontal drums are commonly used where space is plentiful. The two-phase mixture usually enters at one end, and the vapor exits at the other end. To overcome reentrainment of liquid droplets, due to high inlet velocities, various devices and piping arrangements are used to provide a more uniform distribution of vapor-liquid mixtures into the separator, as shown in Fig. 23-50. For two-phase streams with very high vapor flow rates, inlets may be provided at each end, with the vapor outlet at the center of the drum, thus minimizing vapor velocities at the inlet and aiding vapor-liquid separation.

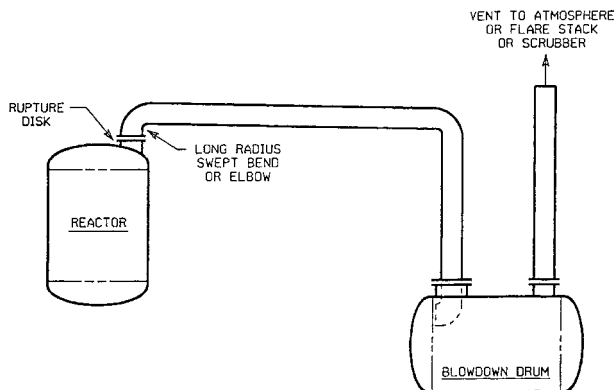


FIG. 23-49 Horizontal blowdown drum/catch tank.

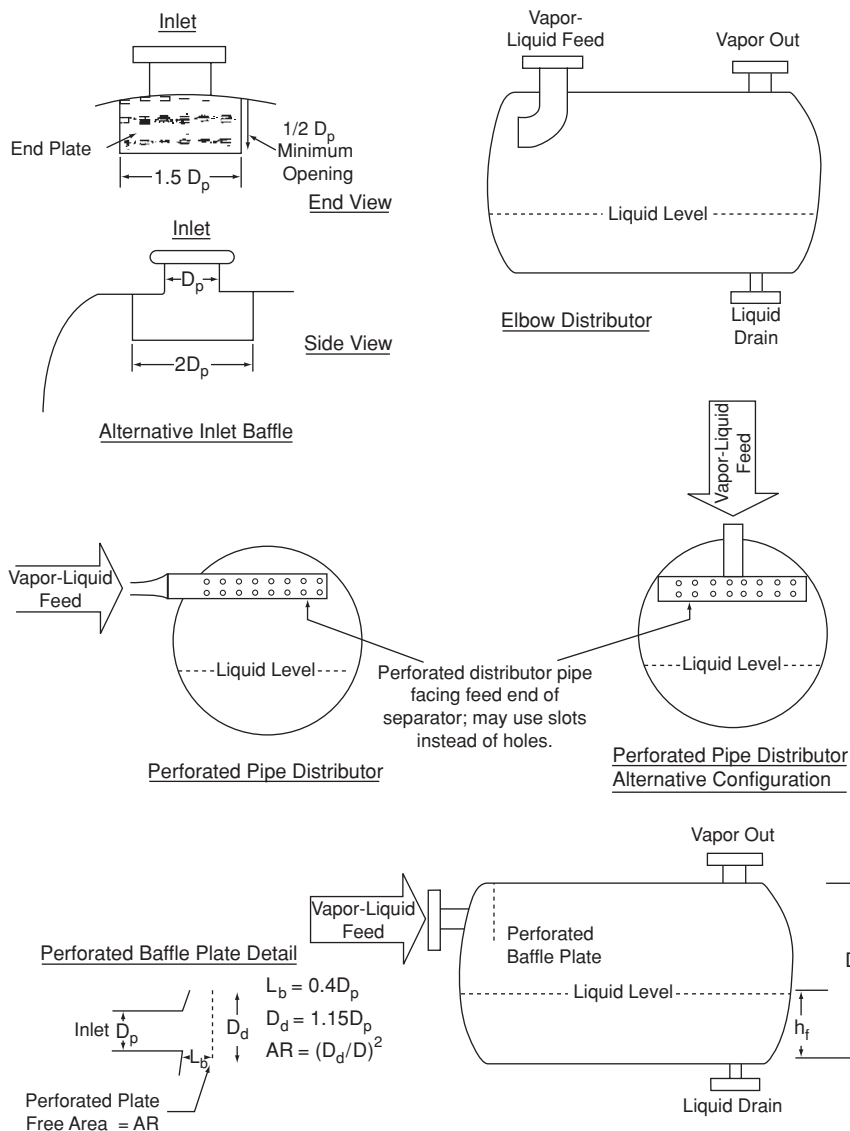


FIG. 23-50 Feed distributor devices for horizontal blowdown drums/catch tanks. (Guidelines for Pressure Relief and Effluent Handling Systems, *Center for Chemical Process Safety (CCPS) of the American Institute of Chemical Engineers (AIChE)*; copyright 1988 AIChE and reproduced with permission.)

Vertical blowdown drum/catch tank This type of drum, shown in Fig. 23-51, performs the same function and operates on similar principles as horizontal separators. These separators are usually used where horizontal space is limited. The two-phase mixture enters the vessel via a nozzle on the vertical shell and is distributed by an inlet baffle chamber.

Multireactor knockout drum/catch tank This interesting system is sometimes used as the containment vessel for a series of closely spaced reactors (Speechly et al., "Principles of Total Containment System Design," presented at I.Chem.E. North West Branch Meeting, 1979).

Emergency Cyclone Separators Two types of emergency cyclone separators are commonly used, those with a separate catch tank and those with a catch tank integral with the cyclone section.

Cyclone separator with separate catch tank This type of blowdown system, shown in Figs. 23-52 and 23-53, is frequently used in chemical plants where plot plan space is limited. The cyclone performs the vapor-liquid separation, while the catch tank accumulates the liquid from the cyclone. This arrangement allows location of the cyclone knockout drum close to the reactor so that the length of the relief device discharge line can be minimized. The cyclone has internals, vital to its proper operation, which are discussed in the following subsections.

Cyclone separator with integral catch tank This type of containment system, depicted in Fig. 23-54, is similar to the aforementioned type, except that the knockout drum and catch tank are combined in one vessel shell. This design is used when the vapor rate is quite high so that the knockout drum diameter is large.

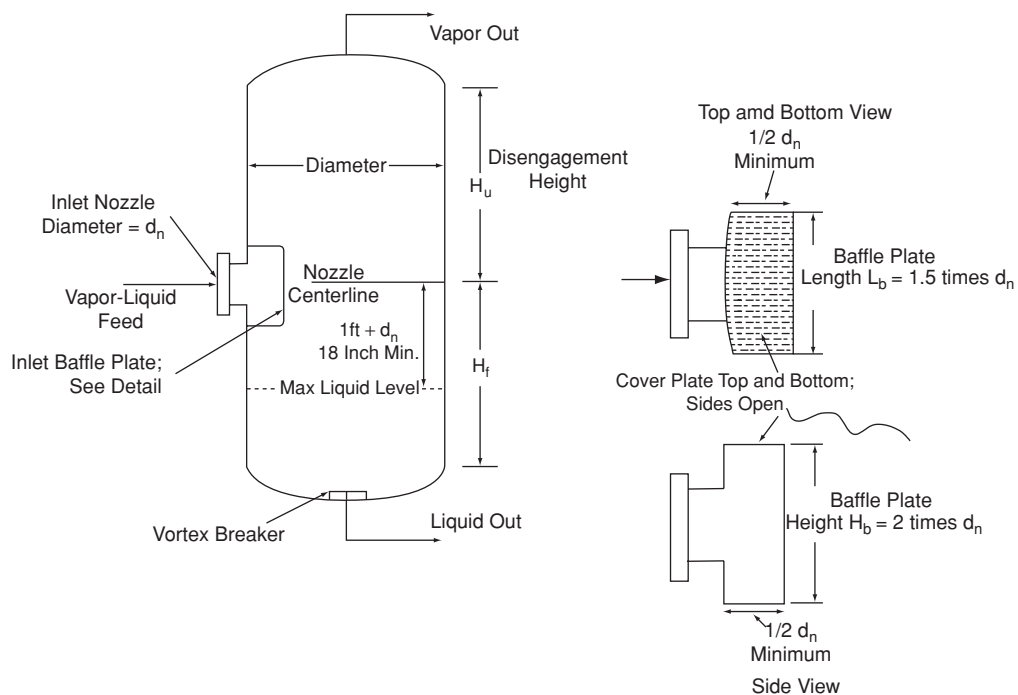


FIG. 23-51 Vertical blowdown drum/catch tank. (Guidelines for Pressure Relief and Effluent Handling Systems, *Center for Chemical Process Safety (CCPS) of the American Institute of Chemical Engineers (AIChE)*; copyright 1988 AIChE and reproduced with permission.).

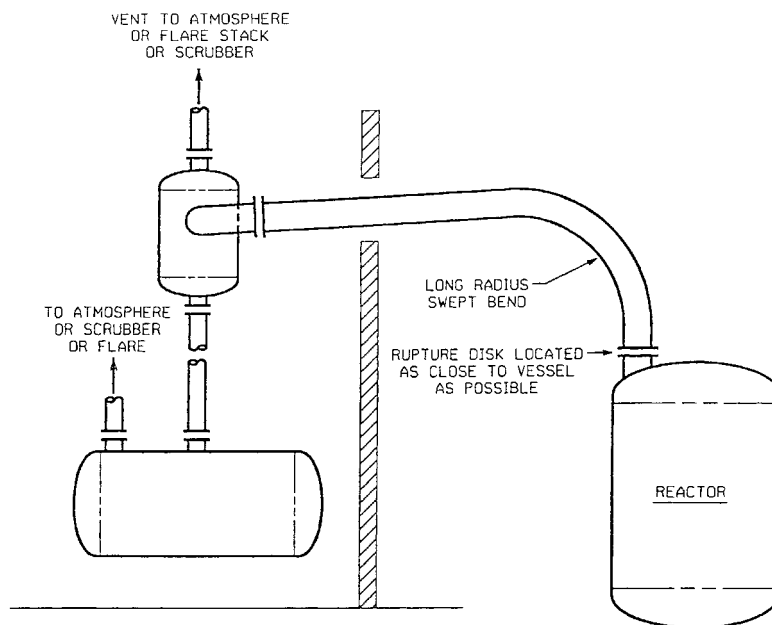


FIG. 23-52 Cyclone separator with separate liquid catch tank.

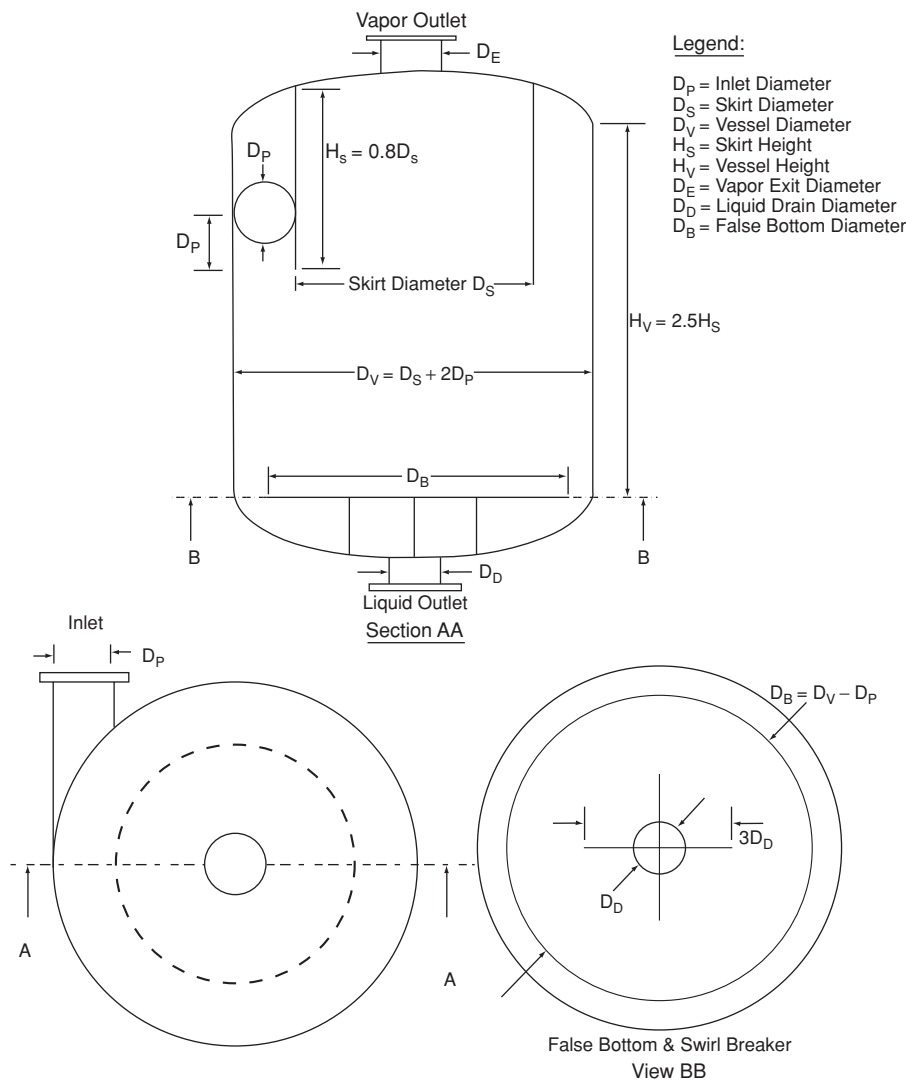


FIG. 23-53 Cyclone separator design details. (Guidelines for Pressure Relief and Effluent Handling Systems, *Center for Chemical Process Safety (CCPS) of the American Institute of Chemical Engineers (AIChE)*; copyright 1988 AIChE and reproduced with permission.)

Quench Pools/Catch Tanks and Quench Towers Two types of quench systems are commonly used: the quench pool/catch tank (also called passive scrubber) and quench tower.

Quench pool/catch tank This type of system, as shown in Fig. 23-55, is used to condense, cool, react with, and/or collect a mixture of liquid and vapors discharging from a relief device by passing them through a pool of liquid in a vessel. Feed vapor and liquid (if present) are sparged into the pool of cool liquid, where the vapors are condensed and the liquid is cooled. If the feed materials are miscible with the pool liquid, they mix with and are diluted by the pool liquid; if not, the condensate, feed liquid, and pool liquid separate into layers after the emergency relief event is over. The condensed vapors, feed liquid, and quench liquid are contained in the vessel until they are sent to final disposal.

Quench pools can be used for the neutralization or killing of reactive materials. A chemical reaction can be quenched by the cooling

effect in the pool, by the dilution effect if the reaction mass is miscible with the pool liquid, or by a killing or neutralizing agent added to the quench liquid. For example, discharge of chlorine or acid mixtures can be neutralized by adding sodium hydroxide to the quench liquid. However, systems involving slow to moderate reaction rates usually require more than one contacting stage, and a quench pool (equal to one stage only) may not be adequate to completely neutralize or kill the reactant in the entering relief device effluent stream. In this case, a multiple-stage emergency scrubber will be needed.

Depending on the relief stream components (with or without non-condensable gases) and quenching efficiency, this arrangement often obviates the need for a subsequent scrubber and/or flare stack. The design of the quencher arm is critical to efficient condensation and avoidance of water hammer. Figure 23-55 is the more conventional passive type quench pool used in the chemical and nuclear industry.

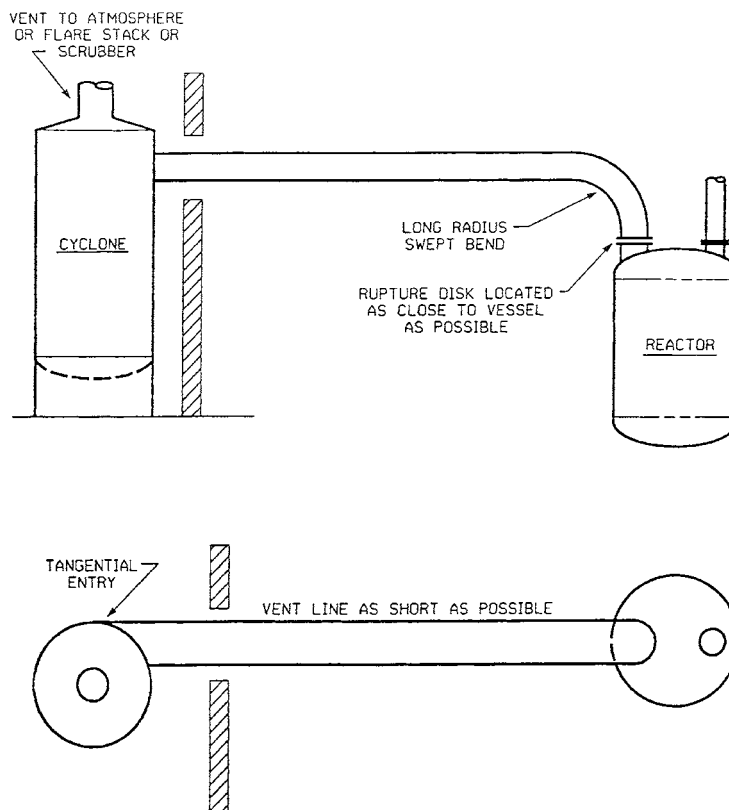


FIG. 23-54 Cyclone separator with integral catch tank.

Quench tower The type shown in Fig. 23-56, with a superimposed baffle plate section, is often used when complete condensation of the incoming vapors is not required. The exiting vapors are usually cooled to 150 to 200°F in the baffle plate section. This type is often used in petroleum refineries.

Emergency Flare Systems Single-phase effluent streams (gases or vapors) from pressure relief devices are often sent directly to emergency flares. The vapor/gas streams from gas-liquid separators are also often sent to emergency flares. Emergency flares are similar in design to normal process flares (continuous flaring), but they are only used to handle emergency releases (intermittent operation).

Flares can be grouped into two major categories, i.e., vertical and horizontal.

Vertical flares These are single-burner combusters generally oriented to fire upward. The discharge point is in an elevated position relative to the surrounding grade and/or nearby equipment. Three types of support methods are used for vertical flares:

- **Self-supported.** A mechanically and structurally designed riser supports the flame burner.
- **Guyed.** An elevated flare with the riser is supported by cables. Cables are attached to the flare riser at one or more elevations to limit the deflection of the structure. The cables (guy-wires) are typically positioned in a triangular plan to provide strong support.
- **Derrick supported.** Support is provided by a steel trussed structure that supports one or more flare risers.

The main components of an elevated flare system are the flare burner with or without smoke suppression capability, pilot(s), pilot igniter(s), support structure, and piping. A number of optional features are available, such as pilot flame detectors; air seals (buoyancy or

velocity type); knockout drum; flame/detonation arrester; liquid seal; smoke suppression control system; blower(s); flow, composition, heat content, or video monitoring; ladders (caged or with safety-climbing system) and platforms; davit for tip removal; aircraft warning lights and painting; radiation heat shields; and rain shields. Detailed information about these components can be found in API STD 537.

Smokeless flaring is required by law in the United States (40 CFR 60.18, Chap. 1) for normal process flares (continuous flaring). However, smokeless flaring is not required by the EPA for emergency flaring, but local conditions and regulations may require smokeless flaring.

Air seals (also called purge reduction or gas seals) are often recommended to prevent air from entering the stack, which could possibly cause flashbacks and explosions. More information about air seals can be found in API RP 521 (2007) and the AIChE-CCPS book *Guidelines for Pressure Relief and Effluent Handling Systems*.

Horizontal flares A horizontal flare can be either an enclosed ground flare or an open field ground flare (also called a matrix flare).

Enclosed ground flares are most commonly used as a supplement to an elevated flare on the same relief system. The primary reason for an enclosed ground flare is to reduce the visual impact of flared gas combustion on a nearby community. They are often used when it is desirable that all or part of a flare load be disposed of in a way that causes the minimum of disturbance to the immediate locality. They offer many advantages in comparison to elevated flares; there is no smoke, no visible flame, no odor, no objectionable noise, and no thermal radiation (heat shield) problems. Enclosed ground flares are typically used for normal process flow (continuous) flaring, but with recent technical advances they are now also used for emergency flaring (AIChE-CCPS, 1998).

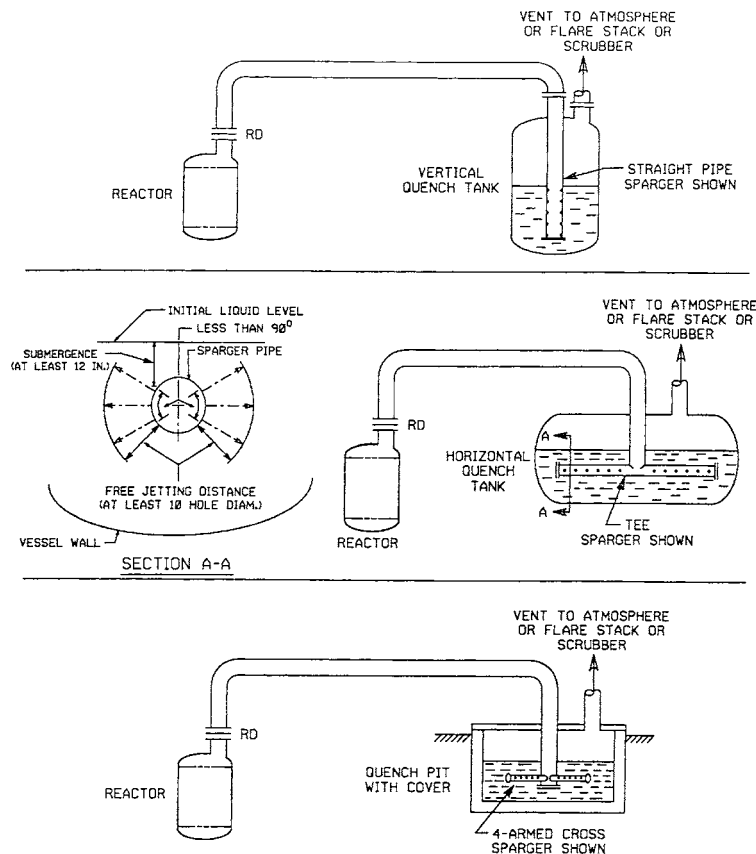


FIG. 23-55 Quench tank/catch tank.

Enclosed ground flares burn the effluent gas in multiple specially designed multitip burners placed as near to the ground as practicable to ensure good operation. The resulting flames are hidden from sight by a surrounding wall or chamber. The top of the chamber is open to the atmosphere, and allowance is made in the bottom of the chamber to permit ingress of air for combustion. Overall heights can vary according to the needs of the specific location. In some locations, a low profile of perhaps 10 m may be mandated, while in others an elevated discharge may be needed to ensure a satisfactory downwind trajectory for the flue gases. It is common for the chamber to be surrounded by a wind fence to modify the effect of crosswinds on the combustion process and to prevent unauthorized access.

An enclosed ground flare system has a number of key components: combustion chamber, burners, piping system, wind fence, and operational and safety controls. More details about enclosed ground flare system components are given in API STD 537.

Enclosed ground flares can be used to burn toxic gases, but since any noncombusted release would be near the ground, special safety dispersion systems and more stringent monitoring and control instrumentation are usually provided in this application.

There is a practical economical limit to the size of enclosed ground flares. If the maximum effluent relief rate exceeds 100 tons/h, the feasibility of an enclosed ground flare becomes questionable, and at 500 tons/h, it is impractical (AIChE-CCPS, 1998).

Open field ground flares (also called **matrix flares**) are sometimes used in lieu of elevated flares, most commonly, although not exclusively, in remote locations with relatively low population density.

A primary reason for use of an open field ground (matrix) flare is to reduce the visual impact of flared gas combustion in the manner of an enclosed ground flare. The open field ground (matrix) flare, however, has a significantly larger capacity than could be practically handled in a furnacelike structure, and the visual shielding is provided by tall fencing located some distance away from the burners themselves so that the fence encloses a small "field."

An open field (matrix) ground flare consists of a number of staged multiburners mounted on a series of horizontal pipes, arranged in manifolds, in a large field or pit. Smokeless or nonsmokeless flaring can be provided. The main structural and physical design issues are concerned with protecting the piping and manifolds inside the flare field from the effects of high radiant heat loads, while still permitting normal thermal expansions. More information about ground flare components is given in API STD 537.

Emergency Scrubbers (Absorbers) Emergency relief effluent streams are often sent to scrubbers (also called absorbers, columns, or towers) for final disposal by absorption of the gas into a solvent. Some gases or vapors can be removed by physical absorption. Other gases or vapors can be removed by chemical absorption (reaction of the vent gas/vapor into a liquid that reacts with it).

A typical emergency scrubber system consists of a scrubbing column (often filled with packing), recirculating liquid pumps, solvent cooler, and in some cases (where the entering effluent gas/vapor is at a low pressure) exhaust blowers (see Fig. 23-57). Redundant equipment and instrumentation is usually provided to ensure reliable scrubber operation at all times.

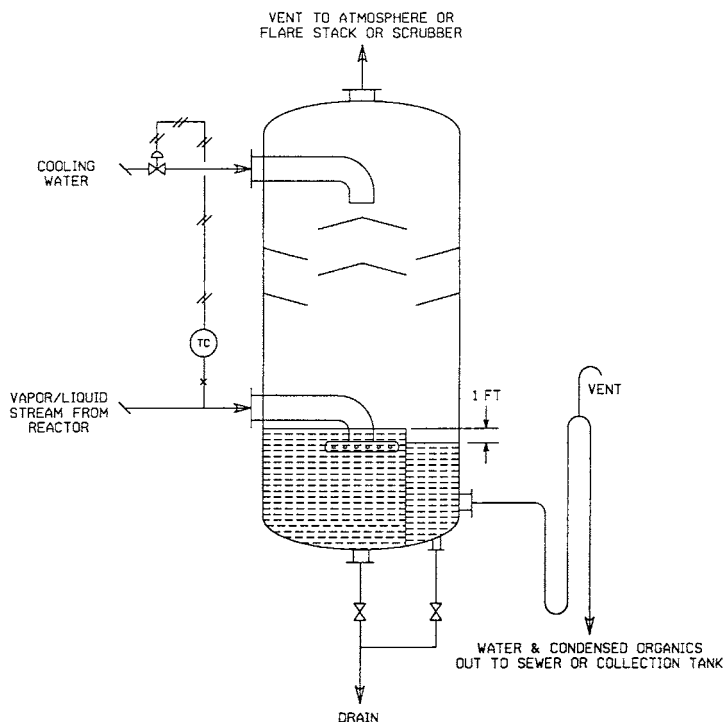


FIG. 23-56 Quench tank with direct-contact baffle tray section.

Equipment Selection Criteria and Guidelines A number of factors should be considered to determine when to select which type of vapor/gas/solid-liquid separator (blowdown drum or cyclone separator) to handle a multiphase stream from a relief device, and which final control or destruction equipment (emergency flare, emergency scrubber, or quench pool/catch tank) should be selected. These factors include the plot plan space available, the operating limitations of each type, and the physicochemical properties of the stream.

The selection of vapor/gas/solid-liquid separators and final control and destruction equipment can be helped by considering the advantages and disadvantages of each, as given below.

Gravity Separators (Horizontal and Vertical Drums/Catch Tanks)

Advantages:

- History of good performance.
 - Passive.
 - Excellent turndown up to the maximum design flow; lower vapor flow improves separation effectiveness.
 - Low pressure drop.
 - Can handle high liquid loading and provide large holdup of liquid.
 - Can be combined with secondary vapor-liquid separator such as vane impingement type.
 - Can handle high-viscosity liquids.
 - Moderate cost.
- Disadvantages:
- May be large.
 - Cannot economically remove low-density (e.g., light hydrocarbon) droplets smaller than about 150 μm .
 - Cannot handle stable foams.
 - Reacting liquids may continue to react in separator.

Cyclones

Advantages:

- Can remove over 99 percent above 20- μm droplet diameter in high liquid-loading situations.

- Some designs able to handle foamy liquids under some conditions.
 - Passive.
 - May be able to handle streams containing solids or with fouling tendencies.
 - Relatively low capital cost.
- Disadvantages:
- Performance not as well defined for emergency services as normal process cyclones.
 - Little data on handling foamy or high-viscosity mixtures.
 - May require higher pressure drop than gravity separators.

Quench Pool Tanks/Catch Tanks

Advantages:

- Passive, but must have system to verify proper liquid level, and composition if pool liquid is used as a neutralizing or kill liquid.
 - Can handle two-phase, foamy, and high-viscosity liquids.
 - Can handle high-flow-rate discharges.
 - Can handle high liquid loading with special sparger design.
 - Can contain reaction-stopping or -neutralizing chemicals and antifoam agents.
 - Complete containment possible at low levels of noncondensables.
 - Can use variety of quench liquids.
- Disadvantages:
- Pilot-plant demonstration or scale-up test possibly needed.
 - Requires sufficient discharge pressure to provide adequate pressure drop (at least 10 psig) across sparger and to overcome static head of liquid in pool.
 - Sparger piping to be supported to control vibration and the suddenly applied load from the relief discharge.
 - Some proven sparger designs are proprietary.
 - May not be suitable for systems with slow to moderate reaction rates when used as an absorber.
 - If vented, entrainment and vapor may be carried out of the vessel.

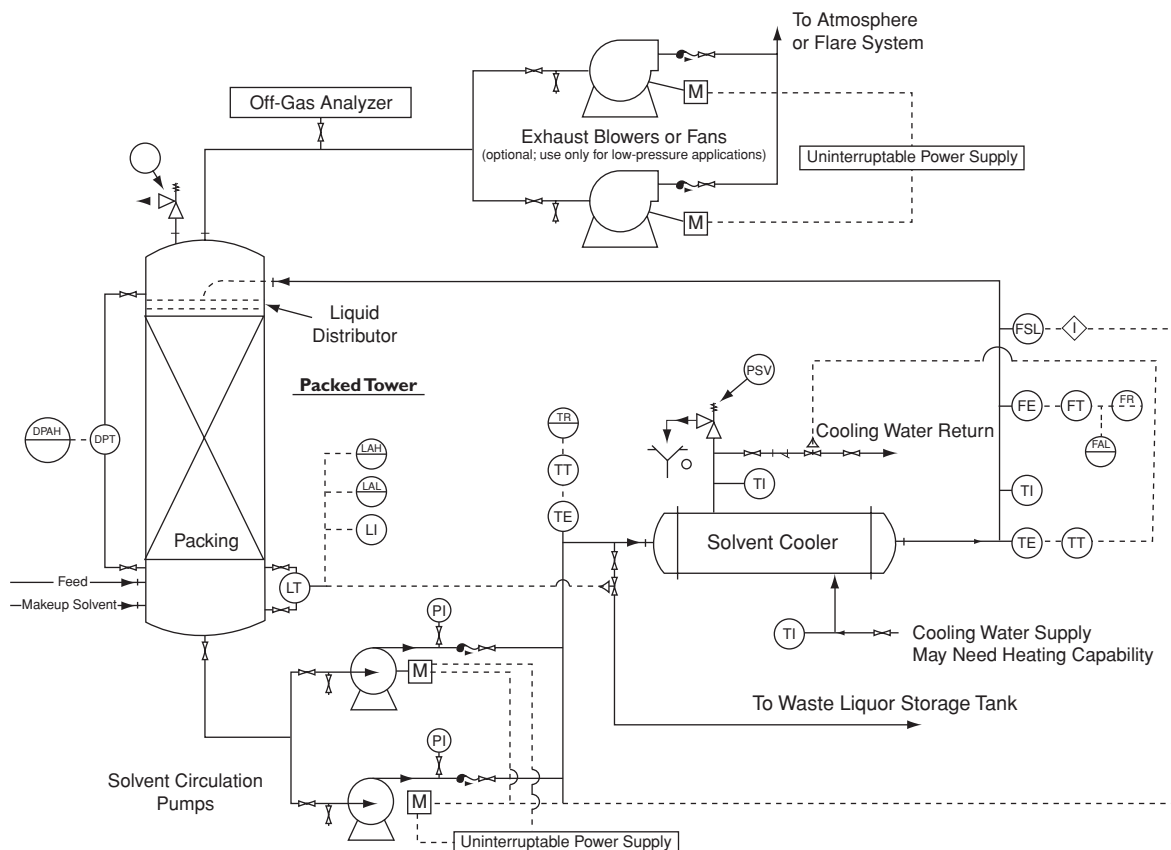


FIG. 23-57 Schematic of an emergency scrubber (absorber) system. (Guidelines for Pressure Relief and Effluent Handling Systems, *Center for Chemical Process Safety (CCPS) of the American Institute of Chemical Engineers (AIChE)*; copyright 1988 AIChE and reproduced with permission.)

- Noncondensables in the feed will lower recovery efficiency, and need to be vented.
- May require large pool to handle lower-boiling materials.

Emergency Flares

Advantages:

- Can destroy over 98 percent of combustibles.
- Experimental tests not required for most chemicals.
- Commercially proven technology.
- Very reliable—onstream over 99 percent.
- Good turndown ratio.
- Smokeless operation not needed for emergency flares (only required for continuous flares).
- No generation of appreciable liquid waste as would be the case for a quench pool or an emergency scrubber, but knockout drum required upstream of the flare to remove liquids and any condensate.
- May be used as final step after other control equipment, e.g., emergency scrubber or quench pool.

Disadvantages:

- May not be suitable for some corrosive chemicals (e.g., most chlorine-containing compounds).
- May be subject to flameout.
- Required minimum heating value of 300 Btu/SCF for nonassisted flares, or 200 Btu/SCF for assisted flares.
- Not passive; require continuous pilot fuel, electricity, oxygen analyzers for collection headers, and instrumentation.

- Require backup systems to monitor flame and provide pilot burning.
- Care needed not to feed foams or liquids into the flare stack.
- Because of maintenance of flare tip on elevated flares (and even some open ground and enclosed ground flares), crane or helicopter required possibly for access. Connection often needed for backup flare system, i.e., portable trailer flare or other temporary flare.

- Elevated flares with excessive light, noise, or odors a possible public nuisance in some situations and locales.

Emergency Scrubbers

Advantages:

- Sound basis for technology.
- High turndown ratio at constant scrubbing liquid flow rate.
- Countercurrent operation that can attain high absorption (removal) efficiency and low outlet concentration of solute.
- Can handle two-phase mixtures.
- May be able to handle unstable foams (to be confirmed by testing).
- Some types of scrubbers that can handle fouling streams, and baffle trays that can handle fouling and solids-containing streams.
- Can be used for neutralization of reactive materials.
- Generally used only for gas/vapor feed, but can handle liquid by use of a separator section in the bottom of the tower.

Disadvantages:

- Possible need for spent solvent to be treated or disposed of after the emergency release.

- Not passive. Utilities and process control instrumentation must be available at all times, and must have a sufficient and reliable supply of fresh solvent for the expected duration of the emergency.
- May need large diameter to avoid flooding.
- Possible restriction of tray towers to nonfouling materials that are free of suspended solids.
- May need continuous flow of scrubbing solvent for the scrubber to be effective at the start of the effluent flow.
- *Guidelines for Pressure Relief and Effluent Handling Systems* (AIChE-CCPS, 1998) contains more information about selection criteria and factors that affect them.

Sizing and Design of Equipment This subsection presents sizing methods and design criteria for the design of vapor/gas/solid-liquid separators for normal vapor-liquid systems (low-viscosity and nonfoamy or unstable foams). They are not applicable usually to high-viscosity (newtonian and nonnewtonian) liquids and/or systems that exhibit surface-active foaming behavior, as insufficient information is available at present relating to the separation efficiency for these types of equipment. Design information is also presented for quench pool tanks which usually can handle high-viscosity liquids as well as stable foams, and for final vapor/gas control or destruction equipment.

Vapor-Liquid Gravity Separator Design Fundamentals The critical factors in the performance of a horizontal separator are the vapor residence time and the settling rate of the liquid droplets. However, two other factors enter into the design—the vapor velocity must be limited to avoid liquid entrainment, and there must be sufficient freeboard within the vessel to allow for a feed distributor. For vertical separators, the design is based on a vapor velocity that must be less than the settling velocity of the smallest droplet that is to be collected, with due allowance for turbulence and maldistribution of the feed. The vapor residence time is a function of the vapor flow rate (mass), vapor density, and volume of vapor space in the separator, based on the following:

- The vapor flow rate (mass) is the sum of the vapor feed to the separator and any vapor generated by flashing of the liquid as the feed enters the separator.
- The vapor density depends on the compositions of the vapor fed and the vapor generated, and the pressure and temperature within the separator. The pressure in the separator is essentially the sum of the pressure drop from the outlet of the separator to the ultimate disposal point of the effluent and the pressure at the downstream discharge location (e.g., the atmosphere).
- The vapor volume is the total volume of the separator minus the volume of the liquid collected; and the volume of liquid is the volume collected (separated) from the feed minus the volume of liquid flashed when the static pressure decreases as the flow rate declines. The maximum volume of liquid collected is also a function of pressure—a greater volume is collected at higher pressure, and time.

Horizontal Blowdown Drum/Catch Tank (See Fig. 23-49.) The two main criteria used in sizing horizontal blowdown drums or catch tanks are as follows:

1. The diameter must be sufficient to provide good vapor-liquid separation.
2. The total volume must be sufficient to hold the estimated amount of liquid carryover from the reactor or process vessel. For a foamy discharge, the holding volume should be greater than the reactor or process vessel volume (to be discussed below).

The recommended method is from *Guidelines for Pressure Relief and Effluent Handling Systems* (AIChE-CCPS, 1998). It is an improvement over the method presented in the 7th edition of this Handbook. The procedure involves calculating a terminal velocity for a selected droplet size, then providing enough residence time in the vapor space to allow the droplets to fall from the top of the vessel to the level of liquid collected. Also, the vapor velocity in the separator must not exceed the value above which liquid may be entrained from the liquid surface in the separator. The tank is treated as a simple horizontal cylinder, neglecting the volume of liquid in the heads.

Other approaches for sizing a horizontal separator (blowdown drum) are given in *Guidelines for Pressure Relief and Effluent Handling Systems* (AIChE-CCPS, 1998) and API RP 521 (2007).

Vertical Blowdown Drum/Catch Tank (See Fig. 23-51.) Some of the basic equations used for sizing horizontal separators can be applied to vertical separators; however, the superficial vapor velocity for vertical separators is based on the total vessel cross-sectional area, and the vapor velocity must be less than the terminal settling velocity for the droplet size selected as the basis of design.

The recommended design procedure is also from *Guidelines for Pressure Relief and Effluent Handling Systems* (AIChE-CCPS, 1998). As with a horizontal separator, the assumed value of K is expected to be suitable for most vertical separators in emergency relief services. However, if it is necessary to remove droplets smaller than 300 to 600 μm , then lower values of K should be used.

Multireactor Knockout Drum/Catch Tank The area needed for vapor disengaging is calculated by the equations given earlier in the section on horizontal blowdown drums. The diameter and length (or height) are determined by considering a number of factors:

1. The length should be sufficient to extend beyond the locations of the reactors discharging into the vessel so as to simplify discharge pipe runs (for a horizontal vessel).
2. The height should not greatly exceed the height of the building (for vertical vessels).
3. The diameter should be sufficient to allow attenuation of the shock wave leaving the deflector plate.
4. The diameter should be sufficient to allow installation of the pipes and deflector plates in such a way as not to interfere directly with one another (particularly important for vertical vessels).
5. The cost of pressure vessels increases as the diameter increases.
6. An upper limit to the diameter is set by the need to transport complete cylindrical sections from the manufacturer to the site.
7. The volume of liquid in the reactor or reactors (assuming more than one vents at the same time) must be determined.

Mechanical Design Considerations The paper by Speechly et al. ("Principles of Total Containment System Design," presented at I. Chem. E. Northwestern Branch Meeting, 1979) discusses a number of pertinent design features:

1. Each vent device discharge pipe is extended into the vessel, and its end is fitted with a deflector device. This disperses the jet stream of solids (catalyst) and liquids discharged and dissipates this force, which should otherwise be exerted on the vessel wall immediately opposite.
2. The deflector device (baffle plate) must be carefully designed as described by Woods (*Proc. Inst. Mech. Engrs.* 180, Part 3J: 245–259, 1965–1966).
3. Isolate the catch tank from both reaction loads and forces generated by thermal expansion of the pipes; the pipes can be designed to enter the vessel through a sliding gland. Depending on layout, vessels that tend to have shorter, stiffer pipes between the building and the vessel may also require flexible bellows to be incorporated in the pipes.
4. There are usually several reactors linked to a single catch tank. To ensure that rupture of a disk on one reactor does not affect the others, each reactor is fitted with a double-rupture disk assembly. The use of double-rupture disks in this application requires installation of a leak detection device in the space between the two disks.

Gravity Separator Safety Considerations and Features A pressure relief device may be required on vapor-liquid gravity separators, based on the following assumptions:

- External fire exposure, if the vapor outlet is inadequately sized for fire relief.
- The vessel outlets could be closed.
- A chemical reaction could continue in the knockout drum/catch tank.

The pressure relief device should be evaluated and sized in accordance with the latest industry standards (i.e., DIERS, API, NFPA). An open passage (nozzle or line) from the separator to the atmosphere may be considered as the pressure relief device provided that it meets the relieving capacity requirements of the ASME Boiler and Pressure Vessel Code (BPVC).

Freeze protection is not normally provided in separators intended solely for emergency release service; however, occasionally, coils or a

jacket are used to keep high-viscosity liquids flowable, or to boil off volatile components. If internal coils or a heating jacket is used, it should be recognized that the source of heat might initiate a chemical reaction or increase its rate. Internal heating coils should be

- Designed for complete drainage.
- Provided with block valves to shut off the source of heat.
- Designed with a generous corrosion allowance.
- Braced to withstand impingement by the relief effluent stream.

Also the calculated liquid level in the separator should be corrected for the volume of the internal coils, and a heel of solvent might be retained in the separator to prevent freezing or to dissolve any components that can solidify or freeze.

Gravity Separator Vessel Design and Instrumentation Some of or all the following features might be appropriate in selected situations [also see API RP 521(2007)]:

- Liquid level indicator.
- High and low level alarms.
- Temperature indicator (with high-temperature alarm if deemed necessary).
- Pressure gauge.
- Pressure relief device.
- Manhole(s) for tank entry and cleaning.
- Pump for transferring the accumulated liquid to subsequent rework, recovery, or disposal.
- Antivortex baffle above the liquid outlet to the pump.
- Bracing of wall stiffeners to allow for possible "jet force" impingement on the vessel wall, and for intermittent buffeting and vibration if two-phase slug flow can occur.

For separators that normally operate at about atmospheric pressure, consider designing the vessel for 50 or 75 psig minimum MAWP to avoid vessel damage by an internal deflagration. For higher normal operating pressures, the design basis should be adjusted accordingly, consistent with the ASME BPVC, NFPA 68, and NFPA 69.

It should be realized that the separator may not be used for long periods, and the process control instrumentation and auxiliaries must receive regular inspection, testing, and maintenance.

Emergency Cyclone Separators Sizing of cyclone separators to handle unsteady-state discharge from emergency pressure relief devices is somewhat different from normal steady-state service (process cyclones). Emergency cyclones are designed usually for higher inlet velocity and pressure drop. Inlet velocity and cyclone pressure drop are limited only by the allowable backpressure on the pressure relief device. Emergency cyclone separator designs may allow some entrained mist or small droplets to leave the cyclone. This can be acceptable if the consequences of the release of the droplets are not significant.

Emergency cyclones often handle flashing vapor-liquid mixtures, and more vapor may be generated from flashing liquid because of the pressure drop in the cyclone; thus the mass flow rate of vapor leaving the cyclone is often greater than that entering. The cyclone size is determined by the outlet vapor volumetric flow rate. Since the discharge flow rate and ratio of vapor to liquid often vary, the cyclone design calculations should be made for conditions occurring at various times during the overpressure event.

Cyclone separator with separate catch tank (See Figs. 23-52 and 23-53.) The sizing of a cyclone knockout drum for emergency relief systems is somewhat different from that of a cyclone separator for normal process service for the following reasons:

1. In normal process service, the superficial vapor velocity at the inlet of tangential-entry vapor-liquid separators is limited to about 120 to 150 ft/s. Higher velocities may lead to
 - a. Excessive pressure drop in the separator and in the inlet piping.
 - b. Generation of fine mist in the inlet piping, which escapes collection in the separator.
2. Inlet velocity restrictions do not apply in the design of separators for emergency relief systems because
 - a. Pressure drop is usually not a penalty.
 - b. Escape of fine mist can usually be tolerated.

Sizing procedure The cyclone is sized by choosing a superficial F factor for the skirt in the range of 8.0 to 5.0 in USCS units (10 to 6 in

SI units). The higher value may be used for waterlike liquids; the lower value for liquids such as molasses. If design F factors exceed the range of 5 to 8, the liquid draining down the skirt is entrained and escapes with the vapor. These F factors were determined in small-scale lab experiments using water and a high-polymer solution as the test liquids. The high-polymer solution had a viscosity that was molasseslike, probably in the range of 1500 cP. There were no liquids of intermediate viscosity used in the tests.

The F factors of 5.0 and 8.0 are conservative in the opinion of the researcher who performed the experiments (private communication from E. I. duPont de Nemours Co., Inc., to the DIERS Project).

The sizing procedure is presented in *Guidelines for Pressure Relief and Effluent Handling Systems* (AIChE-CCPS, 1998). Figure 23-53 shows the dimensions of a cyclone separator designed in accordance with this procedure. If liquid is continuously drained from the cyclone to a separate accumulator, a vortex breaker and false bottom should be used (Fig. 23-53, view BB).

If the liquid contents of the vented vessel are to be retained in the separator for subsequent disposition, the holdup capacity may be increased by increasing the height of the vessel to increase the total volume by an amount equal to the vented liquid volume.

If the pressure drop is too high, it may be necessary to increase the inlet line size for a distance of about 3 to 5 diameters upstream of the cyclone.

A sizing method similar to the one recommended above is proposed by Schmid and Giesbrecht (2001), based on experimental work done at BASF in Germany.

Cyclone separator with integral catch tank (See Fig. 23-54.) The diameter of the knockout drum is calculated by the criteria given in the preceding subsection and Fig. 23-53. Since the liquid is also to be retained in the vessel, extend the shell height below the normal bottom tangent line to increase the total volume by an amount equal to the volume of the liquid carried over.

Quench Tank (See Figs. 23-55 and 23-56.) There is very little information in the open technical literature on the design of quench tanks in the chemical industry. Most of the information available deals with the design of quench tanks (also called suppression pools) for condensation of steam or steam-water mixtures from nuclear reactor safety valves. Information and criteria from quench tanks in the nuclear industry often can be used for the design of quench tanks in the chemical industry. *Guidelines for Pressure Relief and Effluent Handling Systems* (AIChE-CCPS, 1998) provides more information for chemical industry quench tank design. The following subsections summarize some of this information. Pertinent criteria for quench tank sizing and design are presented below:

Operating pressure There are three modes of operation of a quench tank: atmospheric pressure operation, nonvented operation, and controlled venting operation. Atmospheric operation is usually feasible when the effluent being emitted has a bubble point well above the maximum ambient temperature. A very small quantity of vapor escapes with the air that is displaced as the tank fills with the emergency discharge (typically about 0.2 percent of the reactor contents). Depending on the toxic or flammable properties of the vapor, the vent from the quench tank can be routed to the atmosphere or must be sent to a scrubber or flare.

In nonvented operation, no material is vented to the atmosphere, and this design is used when complete containment of the discharge is required. It is also used when the discharge mixture bubble point is close to or below the maximum ambient temperature and the concentration of noncondensable gas in the feed stream is very low. The tank design pressure is relatively high since the initial air in the tank is compressed by the rising liquid level, adding to the vapor pressure. The designer must take into consideration that the quench tank backpressure must be limited so as not to adversely affect the reactor relief system.

In controlled venting operation, the quench tank pressure is maintained at a desired level by a pressure controller/control valve system or pressure relief valve. This mode of operation is used when the discharge mixture bubble point is close to or below the maximum ambient temperature and it is desired to limit the maximum quench tank pressure.

Quench liquid selection The choice of the appropriate quench liquid depends on a number of factors. Water is usually the first quench liquid to consider. If water is selected as the quench liquid, the tank should be located indoors, if possible, to avoid freezing problems if the facility is in a cold climate. If the tank has to be located outdoors in a cold climate, the addition of antifreeze is preferable to heat-tracing the tank, since overheating of the tank can result from tracing, thus reducing its effectiveness.

If other quench liquids are required, the liquid should have as many of the following properties as possible: compatibility with the discharge effluent, low vapor pressure, high specific heat, low viscosity, low flammability, low freezing point, high thermal conductivity, immiscibility with the discharge effluent, low cost, and ready availability.

Quench liquid quantity A good discussion of the factors determining the quantity of quench liquid required is presented by CCPS (AIChE-CCPS, 1998).

When water is used as the quench medium and the effluent stream is a hydrocarbon or organic, separate liquid phases are often formed. In this case, heat transfer is the predominating mechanism during the quench. To achieve effective heat transfer, there must be a sufficient difference between the quench liquid temperature and the bubble point of the incoming effluent stream. The minimum temperature difference occurs at the end of the discharge, when the quench pool temperature is highest. A rule of thumb, from industry practice, is to allow a 10 to 20°C (18 to 36°F) ΔT . For atmospheric tank operation, the final quench liquid temperature is then set 10 to 20°C (18 to 36°F) below the normal boiling point of the final quench pool mixture. For nonvented or controlled venting operation, the final boiling point is elevated, permitting a greater design temperature rise and the use of less quench liquid. Therefore, the quench pool final temperature must be set 10 to 20°C (18 to 36°F) lower than the saturated temperature of the discharge effluent at the design maximum quench tank pressure.

The minimum capacity of quench liquid can be estimated by a heat balance, given the final quench pool temperature, using an equation given by AIChE-CCPS (1998). An equation is also presented there that includes the heat of reaction. In some cases, an experiment is necessary to confirm that the reaction indeed stops in the quench pool. An equation is also presented for the heat balance needed to calculate the minimum amount of quench liquid when the feed contains noncondensable gases.

It is good practice to provide 10 to 20 percent more quench liquid than the minimum amount calculated.

Quench tank volume The total volume of the quench tank should be equal to the sum of the following volumes:

- Quench liquid required
- Liquid entering in the multiphase effluent stream
- Liquid condensed from vapors in entering effluent stream
- Freeboard for noncondensables (a minimum of 10 percent is recommended)

Quench tank geometry Quench tanks can have any of the following three types of geometry:

- Horizontal cylindrical vessel
- Vertical cylindrical vessel
- Concrete pit (usually rectangular)

Usually, the geometry is determined by space limitations. Both horizontal and vertical cylindrical vessels are designed as pressure vessels and for pressures up to 50 to 75 psig. An L/D ratio of 2 to 3 results in an economic design.

Sparger design The effluent stream should be discharged into the quench liquid by means of a sparger, which breaks it up into small jets to provide good heat and mass transfer. The sparger design must also incorporate the following capabilities:

- Maximize momentum-induced recirculation in the quench pool.
- Provide adequate flow area (cross section for pressure relief without imposing high backpressure).
- Minimize shock due to vapor bubble collapse.
- Minimize unbalanced momentum forces.

Figure 23-55 shows conventional quench tank sparger arrangements. As can be seen in this figure, the sparger can be of the following types:

- Vertical straight-pipe sparger
- Tee sparger
- Four-armed cross-sparger

Alternative sparger designs are shown in AIChE-CCPS (1998).

The following design criteria are recommended:

1. The flow area of the manifold and/or distributor piping should be at least 2 times the total area of the sparger holes. This generally ensures that flow through the sparger holes will be uniform.
2. The number of holes should provide at least 0.2 hole per square foot (2.2 holes per square meter) of pool cross-sectional area, distributed evenly over the cross section of the pool.
3. Holes should be uniformly spaced in the distributor pipe—adjacent holes should be spaced at least 2 to 3 hole diameters apart, center to center.
4. Holes should discharge from the bottom or bottom half of the distributor pipe so that they can serve also as drains for liquid. Separate drain holes may be needed for the manifold pipe and in each distributor pipe.
5. Holes should be as small as possible consistent with consideration of possible plugging or fouling when handling liquids that contain polymers or suspended solids. For effluent streams consisting of only liquid and vapor, hole diameters ranging from 1/8 to 1/2 in (3 to 13 mm) are typical. Larger hole diameters (up to 2 in) may be required if the blowdown stream contains solids (polymers and/or catalyst). Smaller holes tend to minimize vibration and water hammer.
6. Sonic hole velocity is desirable in smaller holes and is essential in 1/2- to 2-in holes. A minimum sparger pressure drop of 10 psi should be used.
7. The quencher arm should be anchored to prevent pipe whip. It should also extend to the length (for horizontal vessels) or the height (for vertical vessels) of the vessel to evenly distribute the vapors in the pool.

When quenching effluents discharged by safety valves, it is preferable to use a straight, vertical sparger with holes in the end cap as well as in the pipe sidewalls. This is recommended to minimize the possibility of liquid hammer, which can occur more readily in horizontal spargers. The liquid hammer usually occurs for the following reasons: As the relief valve opens for the first time, the pressure spike is cushioned by the air trapped in the vent line. This air is blown out. If the valve recloses, the line may cool, causing slugs of condensate to accumulate. When the valve reopens, the slugs will accelerate to very high velocities and impact any elbows and end caps of the sparger. In severe cases, the sparger-arm end caps can be knocked off. The preceding recommendation avoids turns, and the holes in the end cap provide some relief from the pressure spike.

Many aspects of quench pool design (vessel, spargers, mechanical design loads, etc.) and operation are covered in *Guidelines for Pressure Relief and Effluent Handling Systems* (AIChE-CCPS, 1998), and it should be consulted when a quench pool has to be designed.

Mass-Transfer Contact Section Where there is a strong possibility that not all the incoming vapors will be condensed in the pool (the feed stream contains a large amount of noncondensable gases), a direct-contact mass-transfer section is superimposed on the quench tank. This can be a baffle tray section (as shown in Fig. 23-56) or a packed column section.

The design of direct-contact mass-transfer columns is discussed in detail by Scheiman [*Petro Chemical Engr.* 37(3): 29–33, 1965; *ibid.* 37(4): 75, 78–79] and Fair (*Chem. Eng.*, June 12, 1972).

Emergency Flare Systems A discussion of design criteria, principles, and practices for a number of flare system components is presented below.

Flare tip diameter The flare tip diameter is sized on a velocity basis, but the pressure drop must also be checked. Flare tip velocities can be chosen on the basis of EPA requirements or API recommendations. EPA recommendations are given in the AIChE-CCPS book (1998). API RP 521 states that tips may be based on velocities of 0.5 Mach number or higher, if pressure drop, noise, and other factors permit.

Flare height and thermal radiation The height of an elevated flare is based on the minimum distance from the flare flame to an object whose exposure to thermal radiation must be limited. Industrial flares are normally designed so that personnel in the vicinity are not exposed to a heat intensity greater than 1500 to 2000 Btu/(h·ft²) when flaring at the maximum design rates.

An equation by Hajek and Ludwig (*Petro/Chem. Eng.* pp. C31–38, June 1960; pp. C44–51, July 1960) may be used to determine the distance required between a flare flame and a point of exposure where thermal radiation must be limited. [See API RP 521 (2007).]

A flame under the influence of wind will tilt in the direction that the wind is blowing and will change the location of the flame center. API RP 521 (2007) presents two methods for estimating the required flare height when the flame is tilted.

Other methods for estimating the required flare height are presented in *Guidelines for Pressure Relief and Effluent Handling Systems* (AIChE-CCPS, 1998).

Purge gas requirements Purging is used to prevent the formation of explosive mixtures in flare systems by preventing the admission of air into the system through leaks, backflow of air at the flare tip at very low flows, and back diffusion of air into the flare tip. Combustible gases such as methane or natural gas, or inert gases such as nitrogen or carbon dioxide, are frequently used for purging flare systems. API RP 521 (section 7.3.3.3) presents equations for calculating the purge rate as a function of the stack diameter, the desired oxygen level, and the type of purge gas.

Air (purge reduction) seals Air seals (also called purge reduction or gas seals) are often installed near the top of flare stacks. Others are located near the base of the flare. They are used to prevent air from entering the stack and are often recommended to prevent flashbacks and explosions. They also greatly reduce the amount of purge gas required. There are two basic types of air seals primarily used: diffusion (sometimes called molecular or labyrinth seals) and velocity types.

The diffusion seal consists of a baffled concentric cylinder arrangement, which uses the difference in molecular weight of the flare gas and ambient air to prevent air from entering the stack. Diffusion seals, combined with the purge gas flow rate, are intended to form a secondary line of defense against the entry of air into the flare stack. In a vertical flare stack, gravity exerts a driving force to increase the diffusion of air into the stack. Diffusion seals create an inverted flow field to reverse the gravitational effect and reduce air entry. Use of lighter-than-air purge gas (e.g., methane or natural gas)

creates a pocket of light gas at the top of the air entry path. Use of diffusion seal and lighter-than-air purge gas allows a much lower purge gas rate. Installation of a diffusion seal at the top of the flare, and immediately below the burner tip, reduces the purge gas required to 1/50 of the volume required if the diffusion seal is not used (Niemeyer and Livingston, *Chem. Eng. Prog.*, pp. 39–44, December 1993).

Velocity seals are more recent developments in air seal design. They use conical baffles to redirect and focus the purge gas flow field just below the flare tip to sweep air from the flare stack. Some velocity seal designs can reduce the purge gas flow rate requirement to about 1/10 of the rate needed without the seal. Also, some velocity seal designs reportedly require only about 25 to 33 percent of the purge gas used in diffusion seals (AIChE-CCPS, 1998). More details about air (purge reduction) seals may be found in API RP 521 (2007).

Liquid seal drums Emergency vent streams are usually passed through a liquid seal, commonly water, before going to the flare stack. The liquid seal drum is usually located downstream of the knockout drum, and some vendors' designs include them in the base of the flare stack. A liquid seal drum is used to maintain a positive pressure in the vent header system and upstream system. It also reduces the possibility of flame flashbacks, caused when air is inadvertently introduced into the flare system and the flame front pulls down into the stack; it also acts as a mechanical damper on any explosive shock wave in the flare stack. Figure 23-58 is a schematic of a typical flare stack liquid seal drum, designed per API RP 521 criteria.

A properly designed and operated liquid seal drum should allow gas to pass through the seal with minimum surging in gas flow and/or upstream gas pressure. The design of the liquid seal internals and the design of the vessel can have a significant impact on the ability of the seal to meet the performance objective. For example, a common design for the end of a dipleg pipe uses V notches cut into the end of the pipe wall. This design is less effective than the proprietary designs developed by vendors of liquid seal drums. These proprietary designs, which use alternative design guidelines, may offer

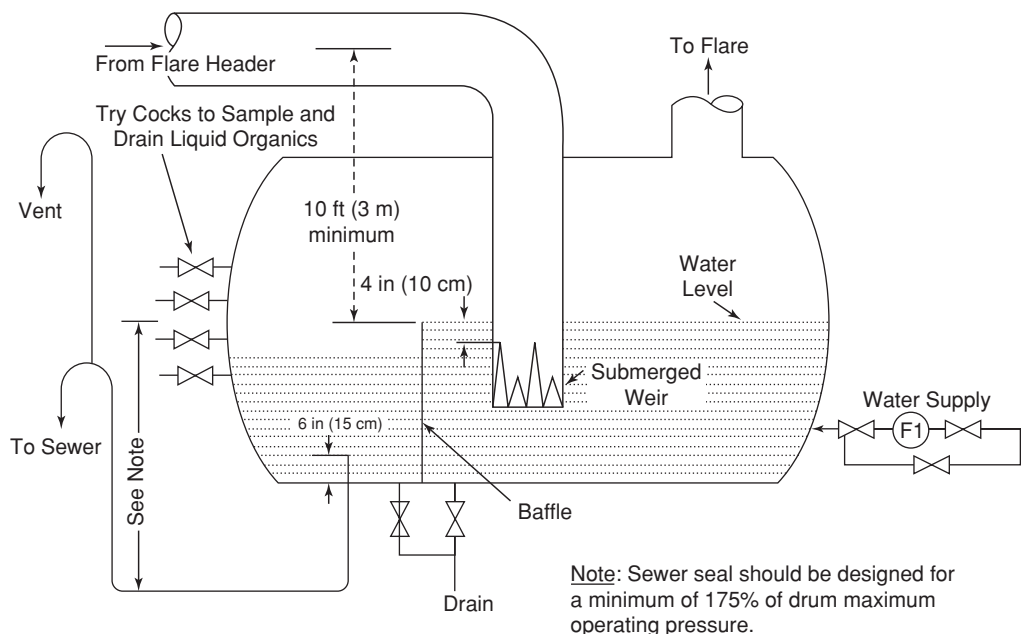


FIG. 23-58 Schematic for typical flare stack seal drum. (Adapted from API RP 521.) (Guidelines for Pressure Relief and Effluent Handling Systems, Center for Chemical Process Safety (CCPS) of the American Institute of Chemical Engineers (AIChE); copyright 1988 AIChE and reproduced with permission.).

economic or operational advantages. Details about several types of proprietary designs for liquid seal drums are presented by Grosseil (*Deflagration and Detonation Flame Arresters*, AIChE-CCPS, New York, 2002).

More detailed discussions of flare systems and their components are presented in API RP 521 (2007), API STD 537 (2003), and AIChE-CCPS (1998).

Emergency Scrubbers (Absorbers) Emergency relief discharges are often passed through scrubbers (also called absorbers, or absorption columns or towers) for removal of flammable, corrosive, or toxic chemicals. The removal mechanism in some scrubbers involves physical absorption in a solvent, whereas in others chemical absorption (reactive scrubbing) is required.

Unlike quench pools for treatment of emergency relief effluent, scrubbers are not passive. For reliable performance, all critical components, including instruments, must be working correctly. There must be a reliable and sufficient supply of solvent and utilities (cooling water, electricity, etc.), with all process variables maintained under design conditions at all times. This includes proper liquid levels, liquid concentrations, flow rates, and reliable operation of ancillary equipment (e.g., pumps, blowers, etc.). General practice is to provide redundancy in pumps and blowers and utilities to ensure reliable scrubber operation (see Fig. 23-57). In the preferred mode of operation for hazardous materials, especially toxic gases, the scrubber is in a standby mode, with solvent flow maintained at all times. An alternate mode is to have the scrubber shut down (solvent not circulating) and then started up after detecting a release from the pressure relieving system. The consequences of the delay in starting the scrubber up after it has been shut down must be considered before accepting this mode of operation.

A discussion of emergency scrubber design and operating criteria and practices is given in *Guidelines for Pressure Relief and Effluent Handling Systems* (AIChE-CCPS, 1998).

FLAME ARRESTERS

GENERAL REFERENCES: [1] Howard, W. B., Precautions in Selection, Installation and Use of Flame Arresters, *Chem. Eng. Prog.*, April 1992. [2] Piotrowski, T., Specification of Flame Arresting Devices for Manifolded Low Pressure Storage Tanks, *Plant/Operations Progress*, vol. 10, no. 2, April 1991. [3] Roussakis and Lapp, A Comprehensive Test Method for In-Line Flame Arresters, *Plant/Operations Progress*, vol. 10, no. 2, April 1991. [4] Deflagration and Detonation Flame Arresters, Chapter 13, *Guidelines for Engineering Design for Process Safety*, Center for Chemical Process Safety, American Institute of Chemical Engineers, 1993. [5] Ibid. Chapter 15, Effluent Disposal Systems. [6] Howard, W. B., Flame Arresters and Flashback Preventers, *Plant/Operations Progress*, vol. 1, no. 4, 1982. [7] Thibault, P., Britton, L., and Zhang, F., Deflagration and Detonation of Ethylene Oxide Vapor in Pipelines, *Process Safety Progress*, vol. 19, no. 3, 2000. [8] Grosseil, S. S., *Deflagration and Detonation Flame Arresters*, AIChE-CCPS Concept Book, 2002. [9] Britton, L. G., Using Maximum Experimental Safe Gap to Select Flame Arresters, *Process Safety Progress*, vol. 19, no. 3, 2000. [10] Britton, L. G., Using Heats of Oxidation to Evaluate Flammability Hazards, *Process Safety Progress*, vol. 21, no. 1, 2002. [11] Davies, M., and Heidermann, T., Investigation of Common Application Failures Proven by Life Field Testing of Endurance Burning Tested End-of-Line Flame Arresters, American Institute of Chemical Engineers, 37th Loss Prevention Symposium, 2003. [12] Brandes, E., and Redeker, T., Maximum Experimental Safe Gap of Binary and Ternary Mixtures, Fourth International Symposium on Hazards, Prevention and Mitigation of Industrial Explosions, IV ISHPMIE October 2002, pp. 207–213. [13] Förster, H., and Kersten, C., Investigation of Deflagrations and Detonations in Pipes and Flame Arresters by High Speed Framing, 4th International Symposium on Hazards, Prevention and Mitigation of Industrial Explosions (ISHPMIE), Bourges, France, October 21–25, 2002. [14] Lunn, G. A., The Maximum Experimental Safe Gap: The Effect of Oxygen Enrichment and the Influence of Reaction Kinetics, *Journal of Hazardous Materials*, 8 (1984), pp. 261–270, Elsevier Science Publisher B.V. Amsterdam. [15] European Standard EN 12874, *Flame Arrester Performance Requirements, Test Methods and Limits of Use*, European Committee for Standardization, Brussels, 2001.

General Considerations In 2002, the Center for Chemical Process Safety (CCPS) of the American Institute of Chemical Engineers (AIChE) published a Concept Book on this topic [8]. The book was intended to expand and update the coverage given in [4], providing extensive information on the history, technology, practice, and regulatory aspects of deflagration and detonation flame arresters.

Flame arresters are passive devices designed to prevent propagation of gas flames through pipelines. Typical applications are to prevent flames entering a system from outside (such as via a tank vent) or propagating within a system (such as from one tank to another). Flame arrestment is achieved by a permeable barrier, usually a metallic matrix containing narrow channels, which removes heat and free radicals from the flame fast enough to both quench it within the matrix and prevent reignition of the hot gas on the protected side of the arrester. These metallic matrices are known as *elements*. Some preliminary considerations for arrester selection and placement are as follows:

1. Identify the at-risk equipment and the potential ignition sources in the piping system to determine where arresters should be placed and what general type (deflagration or detonation, unidirectional or bidirectional) is needed.

2. Determine the worst-case gas mixture combustion characteristics, system pressure, and permissible pressure drop across the arrester, to help select the most appropriate element design. Not only does element design impact pressure drop, but also the rate of blockage due to particle impact, liquid condensation, and chemical reaction (such as monomer polymerization) can make some designs impractical even if in-service and out-of-service arresters are provided in parallel.

3. The possibility of a stationary flame residing on the arrester element surface should be evaluated, and the need for additional safeguards, should such an event occur, should be evaluated (see the subsection Endurance Burn)

4. Consider any material of construction limitations due to reactive or corrosive stream components, plus the impact of elevated temperature and pressure during flame events.

5. Consider upset conditions that could exceed the test conditions at which the arrester was certified. These include the gas composition with regard to concentration of sensitive constituents such as ethylene or hydrogen, maximum system pressure during an emergency shutdown, plus the maximum temperature and oxygen concentration. Under certain upset conditions such as a high-pressure excursion and/or elevated oxygen concentration [14], there may be no flame arrester available for the task.

6. Consider the type and location of the arrester with respect to ease of maintenance, particularly for large in-line arresters.

These questions address the type of arrester needed, the appropriate location, and the best design with respect to flow resistance, maintainability, and cost. It should be recognized that while flame arrester effectiveness is high, it is not 100 percent. To maximize effectiveness, attention should be given to proper selection, application, and maintenance of the device. Since arresters may fail on demand, it is good engineering practice to conduct layers of protection analysis to determine what additional mitigation may be required (Förster, H., *Flame Arresters—The New Standard and Its Consequences*, *Proceedings of the International ESGM Symposium, Part 2: Industrial Explosion Protection*, Nürnberg, Germany, March 27–29, 2001). For marine vapor control systems in the United States, flame arrester applications are regulated by the U.S. Coast Guard. For other applications, alternative test protocols and procedures have been developed by different agencies. Some arresters, such as hydraulic arresters and in-line types used to stop decomposition flames, have specialized applications for which general design and testing information is scarce. Where flame arresters are impractical, alternative strategies such as fast-acting valves, vapor suppression, and flammable mixture control should be considered. Dynamic systems such as fast-acting valves and suppression should be tested and certified as suitable for the required task.

Combustion: Deflagrations and Detonations A deflagration is a combustion wave propagating at less than the speed of sound as measured in the unburned gas immediately ahead of the flame front. Flame speed relative to the unburned gas is typically 10 to 100 m/s although owing to expansion of hot gas behind the flame, several hundred meters per second may be achieved relative to the pipe wall. The combustion wave propagates via a process of heat transfer and species diffusion across the flame front, and there is no coupling in time or space with the weak shock front generated ahead of it. Deflagrations typically generate maximum pressures in the range of 8 to 12 times the initial pressure. The pressure peak coincides with the flame front

although a marked pressure rise precedes it; thus the unburned gas is compressed as the deflagration proceeds, depending on the flame speed and vent paths available. The precompression of gas ahead of the flame front (also known as *cascading* or *pressure piling*) establishes the gas conditions in the arrester when the flame enters it, and hence affects both the arrestment process and the maximum pressure generated in the arrester body. A severe deflagration arrestment test involves placing a restricting orifice behind the arrester, which increases the degree of precompression. This is known as *restricted-end* deflagration testing. As discussed later, the *maximum experimental safe gap* (MESG) of the gas mixture may underestimate its tendency to defeat the arrester under such conditions. This is so because the current MESG test method minimizes precompression effects and hence the likelihood of autoignition on the "protected side" of the arrester. It is most important to consider the influences of pressure, temperature, and oxygen concentration on the safe gap. In addition the safe gap of mixtures is influenced by the chemical interaction of the different gases [12, 14].

As the deflagration flame travels through piping, its speed increases due to flow-induced turbulence and compressive heating of the unburned gas ahead of the flame front. Turbulence is especially enhanced by flow obstructions such as valves, elbows, and tees. Once the flame speed has attained the order of 100 m/s, a *deflagration-to-detonation transition* (DDT) can occur, provided that the gas composition is within the detonable limits, which lie inside the flammable limits. The travel distance for this to occur is referred to as the *run-up* distance for detonation. This distance varies with the gas mixture sensitivity and increases with pipe diameter. It is often difficult to estimate the run-up distance at which a DDT may occur in a piping system, and when to specify either a deflagration or a detonation flame arrester. However, some indication of this can be obtained from [13]. If the actual plant piping installation is different from that of the experimental configurations, then it is recommended that tests be conducted simulating the actual plant piping configurations to establish the DDT run-up length. The European Standard EN12 874 [15] limits the use of in-line deflagration arresters to $L/D = 50$ for group D and C applications and $L/D = 30$ for group B. Tabulated run-up distances are generally for straight pipe runs, and DDT can occur for much smaller distances in pipe systems containing flow obstructions. At the instant of transition, a transient state of *overdriven detonation* is achieved and persists for a distance of a few pipe diameters. Overdriven detonations propagate at speeds greater than the speed of sound (as measured in the burned gas immediately behind the flame front), and side-on pressure ratios (at the pipe wall) in the range of 50 to 100 have been measured. The peak pressure is variable depending on the amount of precompression during deflagration. A severe test for detonation-type flame arresters is to arrange for the arrester to encounter a series of overdriven detonations.

After the abnormally high velocities and pressures associated with DDT have decayed, a state of stable detonation is attained. A detonation is a combustion-driven shock wave propagating at the speed of sound as measured in the burned gas immediately behind the flame front. Since the speed of sound in this hot gas is much larger than that in the unburned gas or the ambient air, and the flame front speed is augmented by the burned gas velocity, stable detonations propagate at supersonic velocities relative to an external fixed point. A typical velocity for a stoichiometric gas mixture is 1800 m/s. The wave is sustained by chemical energy released by shock compression and ignition of the unreacted gas. The flame front is coupled in space and time with the shock front with no significant pressure rise ahead of the shock front. The high velocities and pressures associated with detonations require special element design to quench the high-velocity flames plus superior arrester construction to withstand the associated impulse loading. Since this entails narrower and/or longer element channels plus bracing of the element facing, both inherent pressure drop and the possibility of fouling of detonation arresters should be considered.

The problem of flame arrestment, of either deflagrations or detonations, depends on the properties of the gas mixture involved plus the initial temperature, pressure, and oxygen concentration. Gas mixture combustion properties cannot be quantified for direct use in

flame arrester selection, and only general characteristics can be assigned. For this reason flame arrester performance must be demonstrated by realistic testing. Such testing has demonstrated that arresters capable of stopping even overdriven detonations may fail under restricted end deflagration test conditions. It is important to understand the significance of the test conditions addressed and their possible limitations. It is recommended that users request a detailed test report from the flame arrester manufacturer and only an approved arrester tested to a recognized test standard be installed.

Combustion: Gas Characteristics and Sensitivity Combustion thermodynamic calculations allow determination of peak deflagration and detonation pressures, plus stable detonation velocity. The peak pressure calculation may be used to determine combustion product venting requirements although a conservative volume increase of 9:1 may be used for essentially closed systems. Other relevant gas characteristics are entirely experimental. The sensitivity to detonation depends on the detonable range and fundamental burning velocity, although no specific correlations or measures of sensitivity exist based on fundamental properties. National Electrical Code (NEC) groups are commonly used to rank gases for the purposes of flame arrester selection. By this method, group A gases (acetylene) are considered most sensitive to detonation (and most difficult to arrest) while group D gases (such as saturated hydrocarbons) are considered least sensitive and easiest to arrest. As formerly applied, successful testing of an arrester using one gas in a NEC Electrical Group was assumed to mean that the arrester would be suitable for all other gases in that group. As presently applied in various codes, a representative test gas from each group (such as hydrogen in group B, ethylene in group C, or propane in group D) is typically used for arrester certification, and its ability to arrest a different gas or gas mixture is deduced by comparing the respective maximum experimental safe gaps. The arrester is assumed to be suitable for any single gas or mixture having an MESG greater than or equal to that of the representative test gas. Although the arrester may be directly tested using the gas or gas mixture of interest, this is rarely carried out owing to cost. The MESG comparison procedure is currently applied to both deflagration and detonation arresters. Specific testing protocols are specified by the codes used. Since MESGs provide an independent ranking for arrester selection, reference to NEC groups is not essential. Nevertheless, arresters continue to be described in terms of the NEC group of the representative test gas used for certification. For example, an arrester might be described as a "group C (ethylene)" type. A detailed discussion of the use of MESGs is given in [9].

It is cautioned that there have been no systematic studies proving that arrester performance can be directly correlated with MESG, especially if the MESG for a mixture is estimated by using the Le Chatelier rule. An alternative way for calculating the MESG and safe gap of mixtures is given in [12]. Furthermore, major revisions to the MESG test method have caused many "historic" MESG values to increase significantly; the current test method minimizes compression of the unburned gas mixture and may therefore underestimate the likelihood of arrester failure via autoignition.

Corrosion Consideration should be given to possible corrosion of both the element material and the arrester housing, since corrosion may weaken the structure, increase the pressure drop, and decrease the effectiveness of the element. While the housing might be designed to have a corrosion allowance, corrosion of the element must be avoided by proper material specification. Common materials of construction include aluminum, carbon steel, ductile iron and 316 stainless steel housings, and aluminum or 316 stainless steel elements. While special materials such as Hastelloy might be used for situations such as high HCl concentrations, it may be more cost-effective to use a hydraulic arrester made of carbon steel and lined with a suitable polymeric lining in such applications. Also, at least one flame arrester manufacturer can provide flame arresters with PTFE (Teflon) arresting elements and lined housings up to a nominal size of 4 in for very corrosive service [8].

Directionality To select an arrester for any service, the potential sources of ignition must be established in relation to the pipe system and the equipment to be protected. The pipe connecting an arrester with an identified ignition source is the *unprotected side* of the arrester.

The pipe connecting the arrester with at-risk equipment is the *protected side*. If the arrester will encounter a flame arriving only from one direction, a *unidirectional* arrester can be used. If a flame may arrive from either direction a *bidirectional* arrester is needed. The latter either are symmetrically constructed or are certified by testing. Back-to-back use of unidirectional arresters will not usually be cost-effective unless testing reveals a specific advantage such as increased allowable operating pressure during restricted end deflagration testing.

Endurance Burn Under certain conditions a successfully arrested flame may stabilize on the unprotected side of an arrester element. Should this condition not be corrected, the flame will eventually penetrate the arrester as the channels become hot. An endurance burn time can be determined by testing, which specifies that the arrester has withstood a stabilized flame without penetration for a given period. The test should address either the actual or the worst-case geometry since heat transfer to the element will depend on whether the flame stabilizes on the top, bottom, or horizontal face. In general the endurance burn time identified by test should not be regarded as an accurate measure of the time available to take remedial action, since test conditions will not necessarily approximate the worst possible practical case. Temperature sensors may be incorporated at the arrester to indicate a stabilized flame condition and either alarm or initiate appropriate action, such as valve closure. It is very important to install an endurance burning flame arrester in the same way as tested to avoid malfunction [11].

Installation End-of-line arresters should be protected by using appropriate weather hoods or cowls. In-line arresters (notably detonation arresters and in-line deflagration arresters) must be designed to withstand the highest line pressure that might be seen, including upset conditions. The design should be verified by hydrostatic and pneumatic pressure tests. The piping system should be designed with adequate supports and should allow routine access to the arrester for inspection and maintenance.

Maintenance It is important to provide for arrester maintenance by both selection of the most suitable arrester type and judicious location. Inspection and maintenance should be performed on a regular basis depending on experience with the particular arrester in the service involved. It should also be carried out after successful function of the arrester. Some in-line designs allow removal, inspection, and cleaning of the element without the need to expand the line. Unit designs featuring multiple elements in parallel can reduce downtime by extending the period between cleaning. For systems that cannot be shut down during maintenance, parallel arresters incorporating a three-way valve may be used. Detonation arrester elements are especially prone to damage during dismantling, cleaning, and reassembly. Maintenance must be carefully done, avoiding sharp objects that could disable the delicate channels in the element. Spare elements should be available to reduce downtime and provisions made for storing, transporting, and cleaning the elements without damage.

Monitoring The differential pressure across the arrester element can be monitored to determine the possible need for cleaning. The pressure taps must not create a flame path around the arrester. It can be important to provide temperature sensors such as thermocouples at the arrester to detect flame arrival and stabilization. Since arrester function may involve damage to the arrester, the event of successful function (flame arrival) may be used to initiate inspection of the element for damage. If the piping is such that flame stabilization on the element is a realistic concern, action must be taken immediately upon indication of such stabilization (see also Endurance Burn). Such action may involve valve closure to shut off gas flow or inert gas purging.

Operating Temperature and Pressure Arresters are certified subject to maximum operating temperatures and absolute pressures normally seen at the arrester location. Arrester placement in relation to heat sources such as incinerators must be selected so that the allowable temperature is not exceeded, with due consideration for the detonation potential as run-up distance is increased. Flame arrester manufacturers can provide recommended distances from heat sources, such as open flames, to avoid thermal damage to a flame arrester element. If heat tracing is used to prevent condensation of liquids, the same temperature constraint applies. In the case of in-line arresters, there may

be certain upset conditions that produce unusually large system pressures outside the stipulated operating range of the arrester. Since the maximum operating pressure for a detonation arrester may be in the range of 16 to 26 psia, depending on the gas sensitivity and arrester design, it may be impossible to find a suitable arrester to operate during such an upset. The situation may be exacerbated by pressure drop across the device caused by high flow and/or fouling.

Pressure Drop Flow resistance depends on flame arrester channel arrangement and on a time-dependent fouling factor due to corrosion, or accumulation of liquids, particles or polymers, depending on the system involved. Monomer condensation is a difficult problem since inhibitors will usually be removed during monomer evaporation and catalysis might occur over particulates trapped in the element. Pressure drop can be a critical factor in operability, and cleaning may represent a large hidden cost. Sizing for pressure drop must be based on worst-credible-case operating conditions rather than normal operating conditions.

Fouling may be mitigated in a number of ways. First, the least sensitive element design can be selected, and in the case of end-of-line arresters, weather hoods or cowls can be used to protect against water or ice accumulation. Second, a fouling factor (20 percent or greater) might be estimated and an element with a greater tested flow capacity selected to reduce the pressure drop. This should be further increased if liquid condensation might occur. It is important that certified flow curves for the arrester be used rather than calculated curves since the latter can be highly optimistic. Condensation and polymerization may be mitigated by geometry (minimizing liquid accumulation in contact with the element) and provision for drainage. Alternatively, the arrester may be insulated and possibly heat-traced. Drains should not provide flame paths around the arrester or leak in either direction when closed. If heat tracing is used, the temperature must be limited to the certified operating range of the arrester.

In addition to using an arrester element with greater flow capacity, it is common to use two arresters in parallel where frequent cleaning is required, with one arrester in standby. A three-way valve can be used to allow uninterrupted operation during changeover. Where elements have an intrinsically high pressure drop, such as sintered metal elements used in acetylene service, multiple parallel elements can be used.

Deflagration Arresters The two types of deflagration arrester normally encountered are the *end-of-line arrester* (Figs. 23-59 and 23-60) and the *tank vent deflagration arrester*, which is mounted close to the end of the line going direct to the atmosphere. Neither type of arrester is designed to stop in-line deflagrations or detonations. If mounted sufficiently far from the atmospheric outlet of a piping system, which constitutes the unprotected side of the arrester, the flame can accelerate sufficiently to cause these arresters to fail. Failure can occur at high flame speeds even without a run-up to detonation.

If atmospheric tanks are equipped with flame arresters on the vents, fouling or blockage by extraneous material can inhibit gas flow to the degree that the tank can be damaged by underpressure. API standards allow the use of pressure vacuum (P/V) valves without flame arresters for free-venting tanks on the basis that the high vapor velocity in the narrow gap between pressure pallet (platter) and valve body will prevent flashback. However, it is important to ensure the pallet is not missing or stuck open since this will remove the protection. Absence of the pallet was a listed factor in the 1991 Coode Island fire (State Coroner Victoria, Case No. 2755/91, Inquest into Fire at Coode Island on August 21 and 22, 1991, Finding). Whether or not flame arresters are used, proper inspection and maintenance of these vent systems is required.

End-of-line arresters are mounted at the outlet of a pipe system and go directly to the atmosphere, so there is no potential for significant flame acceleration in the pipe. **Tank vent deflagration arresters** are strictly limited by the approval agency, but for group D gases they are typically mounted no more than 20 ft from the end of a straight pipe that vents directly to the atmosphere. The allowed distance must be established by proper testing with the appropriate gas mixture and the pipe diameter involved. Turbulence-promoting irregularities in the flow (bends, tees, elbows, valves, etc.) cannot be used unless testing has addressed the exact geometry. It is essential that run-up to detonation not occur in the

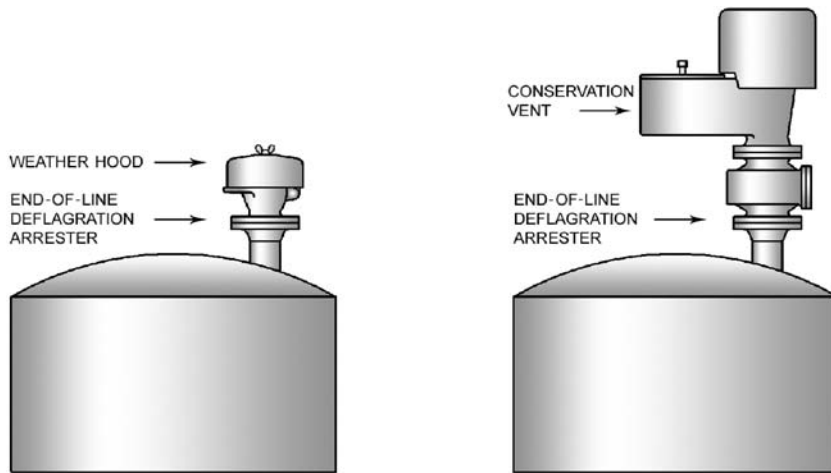


FIG. 23-59 Typical end-of-line deflagration arrester installations. (Courtesy of PROTEGO®.)

available piping system, and run-up distance can be less than 2 ft for some fast-burning gases such as hydrogen in air (group B). Thus the NEC grouping of the gas mixture must be considered. More importantly, it must be emphasized that even if run-up to detonation does not occur, a deflagration arrester can fail if the flame speed is great enough. Thus the run-up distance is not an adequate criterion for acceptable location, and this limitation can be determined only by realistic testing. A number of explosions have occurred due to misapplication of end-of-line or tank vent deflagration arresters where detonation arresters or in-line deflagration arresters should have been used. The latter are described in the next subsection.

Detonation and Other In-Line Arresters If the point of ignition is remote from the arrester location, the arrester is an in-line type such as might be situated in a vapor collection system connecting several tanks. Due to the possibility of DDT, most in-line arresters are designed to stop both deflagrations and detonations (including overdriven detonations) of the specified gas mixture. These are known as **detonation arresters**. Figure 23-61 shows a typical design. Detonation arresters may be further delineated into those types that will arrest only stable detonations and those that will arrest both stable and unstable detonations (i.e., overdriven detonations or DDT events).

In some cases, in-line arresters need to stop deflagrations only. However, in such cases it must be demonstrated that detonations

cannot occur in the actual pipework system; unless the gas mixture is intrinsically not capable of detonation, this requires full-scale testing using the exact pipe geometry to be used in practice, which must not be changed after installation. In certain exceptional cases, an in-line deflagration arrester may be mounted without regard to run-up distance. This can be done only where the system is known to be incapable of detonation. Examples are the decomposition flames of ethylene and ethylene oxide, which are briefly discussed under Special Arrester Types and Alternatives.

Detonation arresters are typically used in conjunction with other measures to decrease the risk of flame propagation. For example, in vapor control systems the vapor is often enriched, diluted, or inerted, with appropriate instrumentation and control [5]. In cases where ignition sources are present or predictable (such as most vapor destruct systems), the detonation arrester is used as a last-resort method anticipating possible failure of vapor composition control. Where vent collection systems have several vapor/oxidant sources, stream compositions can be highly variable and this can be additionally complicated when upset conditions are considered. It is often cost-effective to perform hazard analyses such as HAZOP or fault

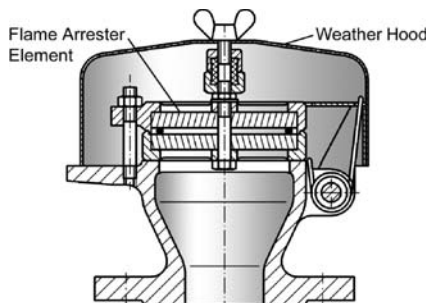


FIG. 23-60 Typical end-of-line deflagration arrester design. (Courtesy of PROTEGO®.)

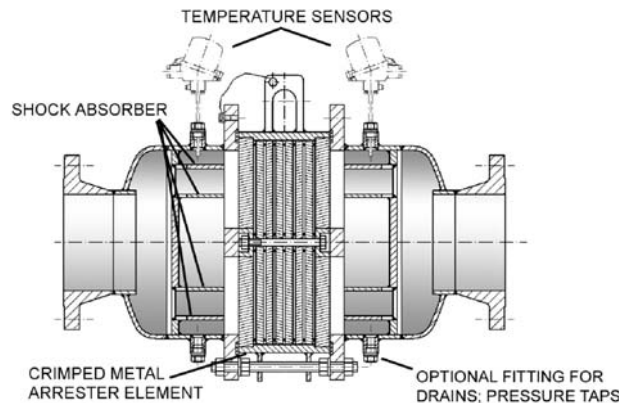


FIG. 23-61 Typical detonation arrester design (crimped ribbon type). (Courtesy of PROTEGO®.)

tree analysis to determine whether such vent streams can enter the flammable region and, if so, what composition corresponds to the worst credible case. Such an analysis is also suitable to assess alternatives to arresters.

Effect of Pipe Diameter Changes Arrester performance can be impaired by local changes in pipe diameter. It was shown that a minimum distance of 120 pipe diameters should be allowed between the arrester and any increase in pipe diameter; otherwise, a marked reduction in maximum allowable operating pressure would occur. This impairment was observed during detonation testing but was most pronounced during restricted-end deflagration testing (Lapp and Vickers, *Int. Data Exchange Symp. on Flame Arresters and Arrestment Technology*, Banff, Alberta, October 1992). As a rule, arresters should be mounted in piping either equal to or smaller than the nominal size of the arrester.

Venting of Combustion Products As gas deflagrates or detonates in the piping system, there is a volume expansion of the products and an associated pressure increase. In some instances where the pipe system volume involved is relatively large, a significant overpressure might be developed in the vapor spaces of connected tanks, especially when vapor space is minimal due to high liquid level. It can be assumed that all the gas on the unprotected side of the arrester is converted to equilibrium products; the pressure is relieved via gas expansion into the entire system volume and to the atmosphere via any vent paths present. If heat losses are neglected by the assumption of high flame speeds or detonation, and atmospheric venting paths are neglected, a conservative approach is that storage vessels be designed with a capacity to handle 9 times the pipe volume on the unprotected side of the arrester. With regard to the high pressures associated with detonations, it has been shown (Lapp, Independent Liquid Terminal Association Conference, Houston, June 23, 1992) that detonation arresters attenuate the peak detonation pressure by up to 96 percent depending on the arrester design, and therefore protect from much of the pressure pulse. To further reduce the pressure pulse, relief devices may be provided at the arrester.

Arrester Testing and Standards Regulatory and approval agencies and insurers impose *acceptance testing* requirements, sometimes as part of certification standards. The user may also request testing to demonstrate specific performance needs just as the manufacturer can help develop standards. These interrelationships have resulted in several new and updated performance test procedures. *Listing* of an arrester by a testing laboratory refers only to performance under a defined set of test conditions. The flame arrester user should develop specific application requirements based on the service involved and the safety and risk criteria adopted.

As discussed in [8], a variety of test procedures and use guidelines have been developed. General considerations are given in Chapter 9.3 of National Fire Protection Association Standard 69. The Federal Register, 33 CFR, Part 154, contains the USCG requirements for detonation arresters in marine vapor control systems. Other U.S. procedures are given in ASTM F 1273-91, UL 525, FM Procedure Classes 6061 and 7371, plus API Publications 2028 and 2210. For U.S. mining applications, the Mine Safety and Health Administration (MSHA) provides regulation and guidance; e.g., in CFR Title 30, Part 36. The International Maritime Organization (IMO) Standard MSC/Circ. 677 (1994) provides testing procedures for end-of-line deflagration and in-line detonation arresters for use on tanker ships. In Canada, CSA-Z343 is followed while in Europe the CEN Standard EN 12874 [15] has replaced previous European National Standards such as BS 7244.

Deflagration Arrester Testing For end-of-line, tank vent, and in-line deflagration flame arresters, approval agencies may require manufacturers to provide users with data for flow capacity at operating pressures, proof of success during an endurance burn or continuous flame test, evidence of flashback test results (for end-of-line arresters) or explosion test results (for in-line or tank vent arrester applications), hydraulic pressure test results, and results of a corrosion test.

Endurance burn testing generally implies that the ignited gas mixture and flow rate are adjusted to give the worst-case heating (based on temperature observations on the protected side of the element surface), that the burn continues for a specified duration, and flame penetration does not occur. Continuous flame testing implies a gas

mixture and flow rate are established at specified conditions and burn on the flame arrester for a specified duration. The endurance burn test is usually a more severe test than the continuous burn. In both cases the flame arrester attachment configuration and any connecting piping or valves should be installed in the same configuration used for testing. General reference [11] gives additional information.

Flashback tests incorporate a flame arrester on top of a tank with a large plastic bag surrounding the flame arrester. A specific gas mixture (e.g., propane, ethylene, or hydrogen at the most sensitive composition in air) flows through and fills the tank and the bag. Deflagration flames initiated in the bag (three at different bag locations) must not pass through the flame arrester into the protected vessel. On the unprotected side, piping and attachments such as valves are included as intended for installation; a series of tests, perhaps 10, is conducted.

Whatever the application, a user should be aware that not all test procedures are the same, or of the same severity, or use the same rating designations. Therefore, it is important to review the test procedure and determine whether the procedure used is applicable to the intended installation and potential hazard the flame arrester is meant to prevent.

Detonation Arrester Testing Requirements are described by various agencies in the documents listed above (UL 525, etc). For installations governed by the USCG in Appendix A of 33 CFR, Part 154 (Marine Vapor Control Systems), the USCG test procedures must be followed. These are similar but not identical to those of other agencies listed. The European Union mandates arrester testing by an approved testing laboratory according to the EN 12874 Standard. Reference [8] discusses differences between the requirements of disparate agencies.

Detonation arresters are extensively tested for proof of performance against deflagrations, detonations, and endurance burns. In the United States, arrester manufacturers frequently test detonation arresters according to the USCG protocol; other test standards might alternatively or additionally be met. Under this protocol, the test gas must be selected to have either the same or a lower MESH than the gas in question. Typical MESH benchmark gases are stoichiometric mixtures of propane, hexane, or gasoline in air to represent group D gases having an MESH equal to or greater than 0.9 mm, and ethylene in air to represent group C gases with an MESH no less than 0.65 mm. Commercially available arresters are typically certified for use with one or another of these benchmark gas types. An ethylene-type arrester is selected, should the gas in question have an MESH of less than 0.9 mm but not less than 0.65 mm. Five low and five high overpressure deflagration tests are required with and without a flow restriction on the protected side. Of these 20 tests, the restricted-end condition is usually the most severe and often limits the maximum initial pressure at which the arrester will be suitable. Five detonation tests and five overdriven detonation tests are also required, which may involve additional run-up piping and turbulence promoters to achieve DDT at the arrester. If these tests are successful, an endurance burn test is required. This test does not use propane for group D gases but hexane or gasoline, owing to their lower autoignition temperatures. For group C tests, ethylene can be used for all test stages.

Care must be taken when applying the MESH method [4, 9, 12]. The user has the option to request additional tests to address such concerns and may wish to test actual stream compositions rather than simulate them on the basis of MESH values.

Special Arrester Types and Alternatives

Hydraulic (Liquid Seal) Flame Arresters Hydraulic (liquid seal) flame arresters are most commonly used in large-pipe-diameter systems where fixed-element flame arresters are either cost-prohibitive or otherwise impractical (e.g., very corrosive gas or where the gas contains solid particles that would quickly plug a conventional arrester element). These arresters contain a liquid, usually water-based, to provide a flame barrier. Figure 23-62 shows one design. Realistic tests are needed to ensure performance, as described in EN 12874 [15]. Note that hydraulic flame arresters may fail at high flow rates, producing a sufficiently high concentration of gas bubbles to allow transmission of flame. This is distinct from the more obvious failure mode caused by failure to maintain adequate liquid level.

Alternatives to Arresters Alternatives to the use of flame arresters include fast-acting isolation valves, vapor suppression systems,

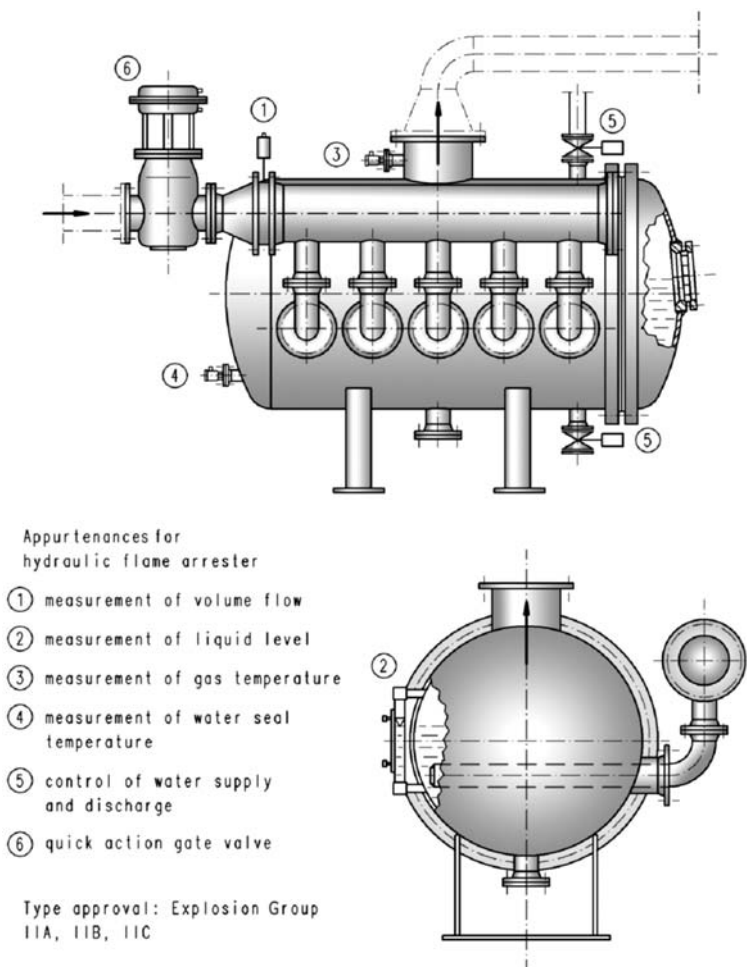


FIG. 23-62 Tested and approved hydraulic (liquid seal) flame arrester. (Courtesy of PROTEGO®.)

velocity-type devices in which gas velocity is designed to exceed flashback velocity, and control of the flammable mixture (NFPA 69 Standard, "Explosion Prevention Systems"). The latter alternative frequently involves reduction of oxygen concentration to less than the limiting oxygen concentration (LOC) of the gas stream.

STORAGE AND HANDLING OF HAZARDOUS MATERIALS

GENERAL REFERENCES: API-620, *Design and Construction of Large, Welded, Low-Pressure Storage Tanks*, American Petroleum Institute, Washington. AP-40, *Air Pollution Engineering Manual*, 2d ed., U.S. Environmental Protection Agency, Office of Air Quality Planning and Standards, 1973. AP-42, *Compilation of Emission Factors for Stationary Sources*, 5th ed., U.S. Environmental Protection Agency, Office of Transportation and Air Quality, 1995. *API Standards*, American Petroleum Institute, Washington ASME, *Process Piping: The Complete Guide to ASME B31.3*, 2d ed., American Society of Mechanical Engineers, New York, 2004. ASME, *ASME Boiler and Pressure Vessel Code; ASME Code for Pressure Piping; ASME General and Safety Standards; ASME Performance Test Codes*, American Society of Mechanical Engineers, New York. *Chemical Exposure Index*, 2d ed., AIChE, New York, 1994. *Code of Federal Regulations*, Protection of Environment, Title 40, Parts 53 to 80, Office of the Federal Register, Washington. CGA, *Handbook of Compressed Gases*, 4th ed., Compressed Gas Association, Chantilly, Va., 1999. CCPS, *Guidelines for Chemical Process Quantitative Risk Analysis*, 2d ed., CCPS-AIChE, New York, 2000. CCPS, *Guidelines for Engineering Design for Process Safety*. CCPS, *Guidelines*

for Facility Siting and Layout, CCPS-AIChE, New York, 2003. CCPS, *Guidelines for Process Safety in Batch Reaction Systems*, CCPS-AIChE, New York, 1999. CCPS, *Guidelines for Safe Storage and Handling of High Toxic Hazard Materials*, CCPS-AIChE, New York, 1988. CCPS, *Guidelines for Safe Storage and Handling of Reactive Materials*, CCPS-AIChE, New York, 1995. CCPS, *Guidelines for Mechanical Integrity Systems*, Wiley, New York, 2006. Englund, "Opportunities in the Design of Inherently Safer Chemical Plants," in J. Wei et al., eds., *Advances in Chemical Engineering*, vol. 15, Academic Press, 1990. Englund, "Design and Operate Plants for Inherent Safety," *Chem. Eng. Prog.*, pts. 1 and 2, March and May 1991. Englund, Mallory, and Grinwis, "Preventing Backflow," *Chem. Eng. Prog.*, February 1992. Englund and Grinwis, "Redundancy in Control Systems," *Chem. Eng. Prog.*, October 1992. Fisher et al., "Emergency Relief System Design Using DIERS Technology: The Design Institute for Emergency Relief Systems (DIERS) Project Manual," AIChE, New York, 1992. Grossel and Crowl, *Handbook of Highly Toxic Materials Handling and Management*, Marcel Dekker, New York, 1995. Hendershot, "Alternatives for Reducing the Risks of Hazardous Material Storage Facilities," *Environ. Prog.*, 7, August 1988, pp. 180ff. Kletz, *An Engineer's View of Human Error*, Institution of Chemical Engineers, VCH Publishers, New York, 1991. Kletz, "Friendly Plants," *Chem. Eng. Prog.*, July 1989, pp. 18-26. Kletz, *Plant Design for Safety: A User Friendly Approach*, Hemisphere Publishing, London, 1991. Kohan, *Pressure Vessel Systems: A User's Guide to Safe Operations and Maintenance*, McGraw-Hill, New York, 1987. Mannan, *Lees' Loss Prevention in the Process Industries*, 3d ed., Elsevier, Amsterdam, 2005. Prokop, "The Ashland Tank Collapse," *Hydrocarbon Processing*, May 1988. Russell and Hart, "Underground Storage Tanks, Potential for Economic Disaster," *Chemical Engineering*, March 16, 1987, pp. 61-69. Ventsorb for Industrial Air Purification,

Bulletin 23-56c, Calgon Carbon Corporation, Pittsburgh, Pa., 1986. White and Barkley, "The Design of Pressure Swing Adsorption Systems," *Chem. Eng. Prog.*, January 1989.

Introduction The inherent nature of most chemicals handled in the chemical process industries is that they each have physical, chemical, and toxicological hazards to a greater or lesser degree. This requires that these hazards be contained and controlled throughout the entire life cycle of the facility, to avoid loss, injury, and environmental damage. The provisions that will be necessary to contain and control the hazards will vary significantly depending on the chemicals and process conditions required.

Established Practices Codes, standards, regulatory requirements, industry guidelines, recommended practices, and supplier specifications have all developed over the years to embody the collective experience of industry and its stakeholders in the safe handling of specific materials. These should be the engineer's first resource in seeking to design a new facility.

The ASME Boiler and Pressure Vessel Code, Section VIII, is the standard resource for the design, fabrication, installation, and testing of storage tanks and process vessels rated as pressure vessels (i.e., above 15-psig design). ASME B31.3 is a basic resource for process piping systems.

Examples of established practices and other resources—some of which pertain to the safe storage and handling of specific hazardous chemicals, classes of chemicals, or facilities—include those listed in Table 23-29 from the publications of two U.S. organizations, the NFPA and the Compressed Gas Association (CGA). Other organizations that may have pertinent standards include the International Standards Organization (ISO), the American National Standards Institute (ANSI), ASTM International (Conshohocken, Pa; www.astm.org), and other well-established national standards such as British Standards and Deutsches Institut für Normung e.V. (DIN) standards. Local codes and regulations should be checked for applicability, and the latest version should always be used when employing established practices.

Basic Design Strategies The storage and handling of hazardous materials involve risks that can be reduced to very low levels by good planning, design, and management practices. Facilities that handle hazardous materials typically represent a variety of risks, ranging from small leaks, which require prompt attention, to large releases, which are extremely rare in well-managed facilities but which have the potential for widespread impact (CCPS, 1988). It is essential that good techniques be developed for identifying significant hazards and mitigating them where necessary. Hazards can be identified and evaluated by using approaches discussed in the section on hazard and risk analysis.

Loss of containment due to mechanical failure or improper operation is a major cause of chemical process incidents. The design of storage and piping systems should be based on minimizing the likelihood of loss of containment, with the accompanying release of hazardous materials, and on limiting the amount of the release. An effective emergency response program that can reduce the impacts of a release should be available.

Thus, the basic design strategy for storing and handling hazardous materials can be summarized as follows, with reference to other parts of this section in parentheses:

1. Understand the hazardous properties of the materials to be stored and handled (Flammability, Reactivity, Toxicity, Other Hazards), as well as the physical hazards associated with the expected process design.

2. Reduce or eliminate the underlying hazards as much as is feasible (Inherently Safer and More User-Friendly Design).

3. Evaluate the potential consequences associated with major and minor loss-of-containment events and other possible emergency situations involving the hazardous materials and energies; and take this information into account in the process of site selection and facility layout and the evaluation of the adequacy of personnel, public, and environmental protection (Source Models, Atmospheric Dispersion, Estimation of Damage Effects).

4. Design and build a robust and well-protected primary containment system following codes, standards, regulations, and other established practices (Security).

TABLE 23-29 Examples of Established Practices Related to Storage and Handling of Hazardous Materials

Designation	Title
National Fire Protection Association (Quincy, Mass.; www.nfpa.org)	
NFPA 30	Flammable and Combustible Liquids Code
NFPA 30B	Code for the Manufacture and Storage of Aerosol Products
NFPA 36	Standard for Solvent Extraction Plants
NFPA 45	Standard on Fire Protection for Laboratories Using Chemicals
NFPA 53	Recommended Practice on Materials, Equipment and Systems Used in Oxygen-Enriched Atmospheres
NFPA 55	Standard for the Storage, Use, and Handling of Compressed Gases and Cryogenic Fluids in Portable and Stationary Containers, Cylinders, and Tanks
NFPA 58	Liquefied Petroleum Gas Code
NFPA 59A	Standard for the Production, Storage, and Handling of Liquefied Natural Gas (LNG)
NFPA 68	Guide for Venting of Deflagrations
NFPA 69	Standard on Explosion Prevention System
NFPA 318	Standard for the Protection of Semiconductor Fabrication Facilities
NFPA 326	Standard for the Safeguarding of Tanks and Containers for Entry, Cleaning, or Repair
NFPA 329	Recommended Practice for Handling Releases of Flammable and Combustible Liquids and Gases
NFPA 400	Hazardous Chemical Code
NFPA 430	Code for the Storage of Liquid and Solid Oxidizers
NFPA 432	Code for the Storage of Organic Peroxide Formulations
NFPA 434	Code for the Storage of Pesticides
NFPA 484	Standard for Combustible Metals, Metal Powders, and Metal Dusts
NFPA 490	Code for the Storage of Ammonium Nitrate
NFPA 495	Explosive Materials Code
NFPA 497	Recommended Practice for the Classification of Flammable Liquids, Gases, or Vapors and of Hazardous (Classified) Locations for Electrical Installations in Chemical Process Areas
NFPA 499	Recommended Practice for the Classification of Combustible Dusts and of Hazardous (Classified) Locations for Electrical Installations in Chemical Process Areas
NFPA 654	Standard for the Prevention of Fire and Dust Explosions from the Manufacturing, Processing, and Handling of Combustible Particulate Solids
NFPA 655	Standard for Prevention of Sulfur Fires and Explosions
NFPA 704	Standard System for the Identification of the Hazards of Materials for Emergency Response
Compressed Gas Association (Chantilly, Va.; www.cganet.com)	
CGA G-1	Acetylene
CGA G-2	Anhydrous Ammonia
CGA G-3	Sulfur Dioxide
CGA G-4	Oxygen
CGA G-5	Hydrogen
CGA G-6	Carbon Dioxide
CGA G-8.1	Standard for Nitrous Oxide Systems at Consumer Sites
CGA G-12	Hydrogen Sulfide
CGA G-14	Code of Practice for Nitrogen Trifluoride (EIGA Doc. 92/03)
CGA P-1	Safe Handling of Compressed Gases in Containers
CGA P-8	Safe Practices Guide for Cryogenic Air Separation Plants
CGA P-9	The Inert Gases: Argon, Nitrogen, and Helium
CGA P-12	Safe Handling of Cryogenic Liquids
CGA P-16	Recommended Procedures for Nitrogen Purging of Tank Cars
CGA P-32	Safe Storage and Handling of Silane and Silane Mixtures
CGA P-34	Safe Handling of Ozone-Containing Mixtures Including the Installation and Operation of Ozone-Generating Equipment
CGA S-1.1	Pressure Relief Device Standards—Part 1—Cylinders for Compressed Gases
CGA S-1.2	Pressure Relief Device Standards—Part 2—Cargo and Portable Tanks for Compressed Gases
CGA S-1.3	Pressure Relief Device Standards—Part 3—Stationary Storage Containers for Compressed Gases

NOTE: Always check the latest edition when using established practices.

5. Design and implement a reliable and fault-tolerant basic process control system to ensure the design limitations of the primary containment system are not exceeded.

6. Include provisions for detecting abnormal process conditions and bringing the process to a safe state before an emergency situation occurs (Safety Instrumented Systems).

7. Design, install, and maintain reliable and effective emergency relief systems, as well as mitigation systems such as secondary containment, deluge, and suppression systems, to reduce the severity of consequences in the event an emergency situation does occur (Pressure Relief Systems; Emergency Relief Device Effluent Collection and Handling).

8. Evaluate the risks associated with the process and its safety systems taken as a whole, including consideration of people, property, business, and the environment, that could be affected by loss events; and determine whether the risks have been adequately reduced (Hazard Analysis, Risk Analysis, Source Models, Atmospheric Dispersion, Estimation of Damage Effects).

9. Take human factors into account in the design and implementation of the control system and the facility procedures (Human Error, Key Procedures).

10. Ensure staffing, training, inspections, tests, maintenance, and management of change are all adequate to maintain the integrity of the system throughout the facility lifetime (Key Procedures, Audit Process).

Designers and operating companies will address these items in different ways, according to their established procedures. The steps that are addressed elsewhere in this section are not repeated here.

Site Selection, Layout, and Spacing Facility siting decisions that will have critical, far-reaching implications are made very early in a new facility's life cycle, or in the early planning stages of a site expansion project. The degree of public and regulatory involvement in this decision-making process, as well as the extent of prescriptive requirements and established practices in this area, varies considerably among countries, regions, and companies. Insurance carriers are also generally involved in the process, particularly with regard to fire protection considerations.

From the perspective of process safety, key considerations with respect to site selection, layout, and spacing can be summarized as

- Where on-site personnel (including contractors and visitors), critical equipment, the surrounding public, and sensitive environmental receptors are located with respect to hazardous materials and processes
- Whether the design and construction of control rooms and other occupied structures, as well as detection, warning, and emergency response provisions, will provide adequate protection in the event of a major fire, explosion, or toxic release event

Recommended distances for spacing of buildings and equipment for fire protection were issued as IRI IM.2.5.2, *Plant Layout and Spacing for Oil and Chemical Plants* (Industrial Risk Insurers, Hartford, Conn). These are referenced in "Typical Spacing Tables" included as Appendix A of the CCPS *Guidelines for Facility Siting and Layout* (2003). Other resources pertaining to siting and layout include

- *Dow's Fire & Explosion Index Hazard Classification Guide*, 7th ed. (AIChE, New York, 1994), which gives an empirical radius of exposure and damage factor based on the quantity and characteristics of the material being stored and handled
- API RP 752, "Management of Hazards Associated With Location of Process Plant Buildings," 2d ed. (American Petroleum Institute, Washington, 2003), which gives a risk-based approach to evaluating protection afforded by occupied structures

Storage

Storage Facilities Dating back to at least 1974, when a vapor cloud explosion in Flixborough, U.K., claimed 28 lives and destroyed an entire chemical plant (Mannan, 2005), a major emphasis in the safe storage and handling of hazardous materials has been to reduce hazardous material inventories. Inventory reduction can be accomplished not only by using fewer and smaller storage tanks and vessels but also by eliminating any nonessential intermediate storage vessels and

batch process weigh tanks and generating hazardous materials on demand when feasible. Note, however, that reduction of inventory may require more frequent and smaller shipments and improved management.

There may be more chances for errors in connecting and reconnecting with small shipments. Quantitative risk analysis of storage facilities has revealed solutions that may run counter to intuition. [Schaller, *Plant/Oper. Prog.* 9(1), 1990]. For example, reducing inventories in tanks of hazardous materials does little to reduce risk in situations where most of the exposure arises from the number and extent of valves, nozzles, and lines connecting the tank. Removing tanks from service altogether, on the other hand, generally helps. A large pressure vessel may offer greater safety than several small pressure vessels of the same aggregate capacity because there are fewer associated nozzles and lines. Also, a large pressure vessel is inherently more robust, or it can economically be made more robust by deliberate overdesign than can a number of small vessels of the same design pressure. On the other hand, if the larger vessel has larger connecting lines, the relative risk may be greater if release rates through the larger lines increase the risk more than the inherently greater strength of the vessel reduces it. In transporting hazardous materials, maintaining tank car integrity in a derailment is often the most important line of defense in transportation of hazardous materials.

Safer Storage Conditions The hazards associated with storage facilities can often be reduced significantly by changing storage conditions. The primary objective is to reduce the driving force available to transport the hazardous material into the atmosphere in case of a leak (Hendershot, 1988). Some methods to accomplish this follow.

Dilution Dilution of a low-boiling hazardous material reduces the hazard in two ways:

1. The vapor pressure is reduced. This has a significant effect on the rate of release of material boiling at less than ambient temperature. It may be possible to store an aqueous solution at atmospheric pressure, such as aqueous ammonium hydroxide instead of anhydrous ammonia.
2. In the event of a spill, the atmospheric concentration of the hazardous material will be reduced, resulting in a smaller hazard downwind of the spill.

Refrigeration Loss of containment of a liquefied gas under pressure and at atmospheric temperature causes immediate flashing of a large proportion of the gas. This is followed by slower evaporation of the residue. The hazard from a gas under pressure is normally much less in terms of the amount of material stored, but the physical energy released if a confined explosion occurs at high pressure is large.

Refrigerated storage of hazardous materials that are stored at or below their atmospheric boiling points mitigates the consequences of containment loss in three ways:

1. The rate of release, in the event of loss of containment, will be reduced because of the lower vapor pressure in the event of a leak.
2. Material stored at a reduced temperature has little or no superheat, and there will be little flash in case of a leak. Vaporization will be mainly determined by liquid evaporation from the surface of the spilled liquid, which depends on weather conditions.
3. The amount of material released to the atmosphere will be further reduced because liquid entrainment from the two-phase flashing jet resulting from a leak will be reduced or eliminated.

Refrigerated storage is most effective in mitigating storage facility risk if the material is refrigerated when received.

The economics of storage of liquefied gases are such that it is usually attractive to use pressure storage for small quantities, pressure or semirefrigerated storage for medium to large quantities, and fully refrigerated storage for very large quantities. Quantitative guidelines can be found in Mannan (2005).

It is generally considered that there is a greater hazard in storing large quantities of liquefied gas under pressure than at low temperatures and low pressures. The trend is toward replacing pressure storage by refrigerated low-pressure storage for large inventories. However, it is necessary to consider the risk of the entire system, including the refrigeration system, and not just the storage vessel. The consequences of failure of the refrigeration system must be considered. Each case should be carefully evaluated on its own merits.

Preventing Leaks and Spills from Accumulating under Tanks or Equipment Around storage and process equipment, it is a good idea to design dikes that will not allow toxic and flammable materials to accumulate around the bottom of tanks or equipment in case of a spill. If liquid is spilled and ignites inside a dike where there are storage tanks or process equipment, the fire may be continuously supplied with fuel and the consequences can be severe. It is usually much better to direct possible spills and leaks to an area away from the tank or equipment and provide a firewall to shield the equipment from most of the flames if a fire occurs. Figure 23-63 shows a diking design for directing leaks and spills to an area away from tanks and equipment.

The surface area of a spill should be minimized for hazardous materials that have a significant vapor pressure at ambient conditions, such as acrylonitrile or chlorine. This will make it easier and more practical to collect vapor from a spill or to suppress vapor release with foam or by other means. This may require a deeper nondrained dike area than normal or some other design that will minimize surface area, in order to contain the required volume. It is usually not desirable to cover a diked area to restrict loss of vapor if the spill consists of a flammable or combustible material.

Minimal Use of Underground Tanks The U.S. Environmental Protection Agency's (EPA) Office of Underground Storage Tanks defines underground tanks as those with 10 percent or more of their volume, including piping, underground. An aboveground tank that does not have more than 10 percent of its volume (including piping) underground is excluded from the underground tank regulations. Note, however, that a 5000-gal tank sitting wholly atop the ground but having 1400 ft of 3-in buried pipe or 350 ft of 6-in buried pipe is considered an underground storage tank.

At one time, burying tanks was recommended because it minimized the need for a fire protection system, dikes, and distance separation. At many companies, this is no longer considered good practice. Mounding, or burying tanks above grade, has most of the same problems as burying tanks below ground and is usually not recommended.

Problems with buried tanks include

- Difficulty in monitoring interior and exterior corrosion (shell thickness)
- Difficulty in detecting leaks
- Difficulty of repairing a tank if the surrounding earth is saturated with chemicals from a leak
- Potential contamination of groundwater due to leakage

Government regulations concerning buried tanks have become stricter. This is so because of the large number of leaking tanks that

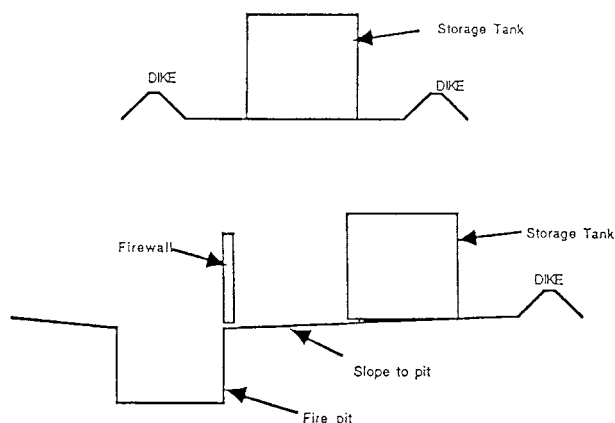


FIG. 23-63 Methods of diking for flammable liquids: (a) traditional diking method allows leaks to accumulate around the tank. In case of fire, the tank will be exposed to flames that can be supplied by fuel from the tank and will be hard to control. (b) In the more desirable method, leaks are directed away from the tank. In case of fire, the tank will be shielded from most flames and fire will be easier to fight. (From Englund, in *Advances in Chemical Engineering*, vol. 15, Academic Press, San Diego, 1990, pp. 73-135, by permission.)

have been identified as causing adverse environmental and human health problems.

Design of Tanks, Piping, and Pumps Six basic tank designs are used for the storage of organic liquids: (1) fixed-roof, (2) external floating-roof, (3) internal floating-roof, (4) variable vapor space, (5) low-pressure, and (6) high-pressure tanks. The first four tank designs listed are not generally considered suitable for highly toxic hazardous materials.

Low-Pressure Tanks (up to 15 psig) Low-pressure storage tanks for highly hazardous toxic materials should meet, as a minimum, the American Petroleum Institute (API) 620 Standard, "Recommended Rules for the Design and Construction of Large Welded, Low-Pressure Storage Tanks" (*API Standards*). This standard covers above-ground tanks designed for all pressures less than or equal to 15 psig and metal temperatures less than or equal to 250°F (121°C). There are no specific requirements in API 620 for highly hazardous toxic materials.

API 650, "Welded Steel Tanks for Oil Storage" (*API Standards*), has limited applicability to storage of highly hazardous toxic materials because it prohibits refrigerated service and limits pressures to 2.5 psig and only if designed for certain conditions. Most API 650 tanks have a working pressure approaching atmospheric pressure, and hence their pressure-relieving devices must generally vent directly to the atmosphere. Its safety factors and welding controls are less stringent than required by API 620.

Horizontal and vertical cylindrical tanks are used to store highly toxic liquids and other hazardous materials at atmospheric pressure. Horizontal, vertical, and spherical tanks are used for refrigerated liquefied gases that are stored at atmospheric pressure. The design pressure of tanks for atmospheric pressure and low-pressure storage at ambient temperature should not be less than 100 percent of the vapor pressure of the material at the maximum design temperature. The maximum design metal temperature to be used takes into consideration the maximum temperature of material entering the tank; the maximum ambient temperature, including solar radiation effects; and the maximum temperature attainable by expected or reasonably foreseeable abnormal chemical reactions.

Since discharges of vapors from highly hazardous materials cannot simply be released to the atmosphere, the use of a weak seam roof is not normally acceptable. It is best that tanks in low-pressure hazardous service be designed and stamped for 15 psig to provide maximum safety, and pressure relief systems must be provided to vent relieved overpressure to equipment that can collect, contain, and treat the effluent.

The minimum design temperature should be the lowest temperature to which the tank will be subjected, taking into consideration the minimum temperature of material entering the tank, the minimum temperature to which the material may be autorefriegerated by rapid evaporation of low-boiling liquids or mechanically refrigerated, the minimum ambient temperature of the area where the tank is located, and any possible temperature reduction by endothermic physical processes or chemical reactions involving the stored material. API 620 provides for installations in areas where the lowest recorded 1-day mean temperature is 50°F (10°C).

While either rupture disks or relief valves are allowed on storage tanks by Code, rupture disks by themselves should not be used on tanks for the storage of toxic or other highly hazardous materials since they do not close after opening and may lead to continuing release of hazardous material to the atmosphere.

The API 620 Code requires a combined pneumatic hydrotest at 125 percent of design tank loading. In tanks designed for low-density liquid, the upper portion is not fully tested. For highly hazardous materials, consideration should be given for hydrotesting at the maximum specified design liquid level. It may be required that the lower shell thickness be increased to withstand a full head of water and that the foundation be designed such that it can support a tank full of water or the density of the liquid, if it is greater than water. Testing in this manner not only tests the containment capability of the tank, but also provides an overload test for the tank and the foundation similar to the overload test for pressure vessels. API 620 also requires radiography.

Proper preparation of the subgrade and grade is extremely important for tanks that are to rest directly on grade. Precautions should be taken to prevent ground freezing under refrigerated tanks, as this can

cause the ground to heave and damage the foundation or the tank. Designing for free air circulation under the tank is a method for passive protection from ground freezing.

Steels lose their ductility at low temperatures and can become subject to brittle failure. There are specific requirements for metals to be used for refrigerated storage tanks in API 620, Appendices Q and R.

Corrosive chemicals and external exposure can cause tank failure. Materials of construction should be chosen so that they are compatible with the chemicals and exposure involved. Welding reduces the corrosion resistance of many alloys, leading to localized attack at the heat-affected zones. This may be prevented by the use of the proper alloys and weld materials, in some cases combined with annealing heat treatment.

External corrosion can occur under insulation, especially if the weather barrier is not maintained or if the tank is operating at conditions at which condensation is likely. This form of attack is hidden and may be unnoticed for a long time. Inspection holes and plugs should be installed in the insulation to monitor possible corrosion under the insulation.

Pressure Vessels (above 15 psig) The design of vessels above 15 psig falls within the scope of the American Society of Mechanical Engineers (ASME) Boiler and Pressure Vessel Code, Section VIII, "Pressure Vessels, Division I," and should be designated as lethal service if required. *Lethal service* means containing substances that are "poisonous gases or liquids of such a nature that a very small amount of the gas or vapor of the liquid mixed or unmixed with air is dangerous to life when inhaled. This class includes substances which are stored under pressure or may generate a pressure if stored in a closed vessel." This is similar to, but not exactly the same as, the same definition as that for "Category M" fluid service of the ASME Pressure Piping Code (see below). Pressure vessels for the storage of highly hazardous materials should be designed in accordance with requirements of the ASME code even if the vessels could be exempted because of high pressure or size. The code requires that the corrosion allowance be adequate to compensate for the more or less uniform corrosion expected to take place during the life of the vessel and not weaken the vessel below design strength.

Venting and Drainage Low-pressure storage tanks are particularly susceptible to damage if good venting practices are not followed. A vent that does not function properly at all times may cause damage to the tank from pressure that is too high or too low. Vapors should go to a collection system, if necessary, to contain toxic and hazardous vents.

Piping Piping systems for toxic fluids fall within Chapter VIII of the ASME Pressure Piping Code, "Piping for Category M Fluid Service." Category M fluid service is defined as "fluid service in which the potential for personnel exposure is judged to be significant and in which a single exposure to a small quantity of a toxic fluid, caused by leakage, can produce serious irreversible harm to persons on breathing or bodily contact, even when prompt restorative measures are taken."

Piping systems should meet the requirements for both Category M fluid service and for "severe cyclic conditions." Piping systems should be subjected to a flexibility analysis, and if they are found to be too rigid, flexibility should be added. Severe vibration pulsations should be eliminated. Expansion bellows, flexible connections, and glass equipment should be avoided. Pipelines should be designed with the minimum number of joints, fittings, and valves. Joints should be flanged or butt-welded. Threaded joints should not be used.

Instrumentation (CCPS, 1986.) Instrument systems are an essential part of the safe design and operation of systems for storing and handling hazardous materials. They are key elements of systems to eliminate the threat of conditions that could result in loss of containment. They are also used for early detection of releases so that mitigating action can be taken before these releases result in serious effects on people in the plant or in the public sector, or on the environment.

Pumps and Gaskets The most common maintenance problem with centrifugal pumps is with the seals. Mechanical seal problems account for most of the pump repairs in a chemical plant, with bearing failures a distant second. The absence of an external motor (on canned pumps) and a seal is appealing to those experienced with mechanical seal pumps.

Sealless pumps are very popular and are widely used in the chemical industry. Sealless pumps are manufactured in two basic types: canned-motor and magnetic-drive. Magnetic-drive pumps have thicker "cans," which hold in the process fluid, and the clearances between the internal rotor and can are greater compared to canned-motor pumps. This permits greater bearing wear before the rotor starts wearing through the can. Many magnetic-drive pump designs now have incorporated a safety clearance, which uses a rub ring or a wear ring to support the rotating member in the event of excessive bearing wear or failure. This design feature prevents the rotating member (outer magnet holder or internal rotating shaft assembly) from accidentally rupturing the can, as well as providing a temporary bearing surface until the problem bearings can be replaced. Because most magnetic-drive pumps use permanent magnets for both the internal and external rotors, there is less heat to the pumped fluid than with canned-motor pumps. Some canned-motor pumps have fully pressure-rated outer shells, which enclose the canned motor; others do not. With magnetic-drive pumps, containment of leakage through the can to the outer shell can be a problem. Even though the shell may be thick and capable of holding high pressures, there is often an elastomeric lip seal on the outer magnetic rotor shaft with little pressure containment capability.

Canned-motor pumps typically have a clearance between the rotor and the containment shell or can, which separates the fluid from the stator, of only 0.008 to 0.010 in (0.20 to 0.25 mm). The can has to be thin to allow magnetic flux to flow to the rotor. It is typically 0.010 to 0.015 in (0.25 to 0.38 mm) thick and made of Hastelloy. The rotor can wear through the can very rapidly if the rotor bearing wears enough to cause the rotor to move slightly and begin to rub against the can. The can may rupture, causing uncontrollable loss of the fluid being pumped.

It should not be assumed that just because there is no seal, sealless pumps are always safer than pumps with seals, even with the advanced technology now available in sealless pumps. Use sealless pumps with considerable caution when handling hazardous or flammable liquids.

Sealless pumps rely on the process fluid to lubricate the bearings. If the wear rate of the bearings in the fluid being handled is not known, the bearings can wear unexpectedly, causing rupture of the can.

Running a sealless pump dry can cause complete failure. If there is cavitation in the pump, hydraulic balancing in the pump no longer functions and excessive wear can occur, leading to failure of the can. *The most common problem with sealless pumps is bearing failure, which occurs either by flashing the fluid in the magnet area because of a drop in flow below minimum flow or by flashing in the impeller eye as it leaves the magnet area.* It is estimated that 9 out of 10 conventional canned-motor pump failures are the result of dry running. Canned pumps are available which, their manufacturer claims, can be operated dry for as long as 48 h.

It is especially important to avoid deadheading a sealless pump. Deadheaded sealless pumps can cause overheating. The bearings may be damaged, and the pump may be overpressurized. The pump and piping systems should be designed to avoid dead spots when pumping monomers. Monomers in dead spots may polymerize and plug the pump. There are minimum flow requirements for sealless pumps. It is recommended that a recirculation system be used to provide internal pump flow whenever the pump operates. Inlet line filters are recommended, but care must be taken not to cause excessive pressure drop on the suction side. Typical inlet filters use sieve openings of 0.0059 in (0.149 mm).

A mistreated sealless pump can rupture with potentially serious results. The can can fail if valves on both sides of the pump are closed and the fluid in the pump expands, either due to heating up from a cold condition or if the pump is started up. If the pump is run dry, the bearings can be ruined. The pump can heat up and be damaged if there is insufficient flow to take away heat from the windings. Sealless pumps, especially canned-motor pumps, produce a significant amount of heat, since nearly all the electric energy lost in the system is absorbed by the fluid being pumped. *If this heat cannot be properly dissipated, the fluid will heat up with possibly severe consequences.* Considerable care must be used when installing a sealless pump to be sure that improper operations cannot occur.

The instrumentation recommended for sealless pumps may seem somewhat excessive. However, sealless pumps are expensive, and they

can be made to last for a long time, compared to conventional centrifugal pumps where seals may need to be changed frequently. Most failures of sealless pumps are caused by running them dry and damaging the bearings. Close monitoring of temperature is necessary in sealless pumps. Three temperature sensors (resistance temperature devices, or RTDs) are recommended: (1) in the internal fluid circulation loop, (2) in the magnet, or shroud, area, and (3) in the pump case area.

It is very important that sealless pumps be flooded with liquid before starting, to avoid damage to bearings from imbalance or overheating. Entrained gases in the suction can cause immediate imbalance problems and lead to internal bearing damage. Some type of liquid sensor is recommended. Sealless pumps must not be operated deadheaded (pump liquid full with inlet and/or outlet valves closed). Properly installed and maintained, sealless pumps, both canned-motor and magnetic-drive, offer an economical and safe way to minimize hazards and leaks of hazardous liquids.

Loss-of-Containment Causes The list in Table 23-30 indicates four basic ways in which containment can be lost. These cause categories can be used both as a checklist of considerations during the design process and as a starting point for evaluating the adequacy of safeguards as part of a process hazard and risk analysis.

Maintaining the Mechanical Integrity of the Primary Containment System The second main category in the above list pertains to containment failure under design operating conditions due to imperfections in the equipment. This group of causes is the main focus of a facility's mechanical integrity (MI) program. The MI program should also detect other imperfections such as previous periods

TABLE 23-30 Summary of Loss-of-Containment Causes in the Chemical Industry

I. Containment lost via an "open-end" route to atmosphere
A. Due to genuine process relief or dumping requirements
B. Due to maloperation of equipment in service; e.g., spurious relief valve operation
C. Due to operator error; e.g., drain or vent valve left open, misrouting of materials, tank overfilled, unit opened up under pressure
II. Containment failure under design operating conditions due to imperfections in the equipment
A. Imperfections arising prior to commissioning and not detected before start-up
B. Imperfections due to equipment deterioration in service and not detected before the effect becomes significant
C. Imperfections arising from routine maintenance or minor modifications not carried out correctly, e.g., poor workmanship, wrong materials
III. Containment failure under design operating conditions due to external causes
A. Impact damage, such as by cranes, road vehicles, excavators, machinery associated with the process
B. Damage by confined explosions due to accumulation and ignition of flammable mixtures arising from small process leaks, e.g., flammable gas buildup in analyzer houses, in enclosed drains, around submerged tanks
C. Settlement of structural supports due to geologic or climatic factors or failure of structural supports due to corrosion, etc.
D. Damage to tank trucks, railcars, containers, etc., during transport of materials on- or off-site
E. Fire exposure
F. Blast effects from a nearby explosion (unconfined vapor cloud explosion, bursting vessel, etc.), such as blast overpressure, projectiles, structural damage
G. Natural events (acts of God) such as windstorms, earthquakes, floods, lightning
IV. Containment failure due to deviations in plant conditions beyond design limits
A. Overpressurizing of equipment
B. Underpressurizing of non-vacuum-rated equipment
C. High metal temperature (causing loss of strength)
D. Low metal temperature (causing cold embrittlement and overstressing)
E. Wrong process materials or abnormal impurities (causing accelerated corrosion, chemical attack of seals or gaskets, stress corrosion cracking, embrittlement, etc.)

SOURCE: Summarized from Appendix A of Prugh and Johnson, *Guidelines for Vapor Release Mitigation*, CCPS-AIChE, New York, 1988.

of operating outside design limits, or improper process materials or impurities that cause accelerated corrosion, chemical attack of seals or gaskets, stress corrosion cracking, embrittlement, etc. MI programs include quality assurance of the initial construction and of maintenance materials; routine preventive maintenance activities; regular inspections and nondestructive testing (NDT) of vessels, tanks, and piping to detect corrosion, pitting, erosion, cracking, creep, etc.; functional testing of standby equipment including alarms, safety instrumented systems, and emergency relief systems; and correcting problems that are identified while inspecting, testing, or maintaining the equipment and instrumentation. CCPS (2006) provides guidance on developing and implementing a mechanical integrity program.

Release Detection and Mitigation Mitigation means reducing the severity of consequences of an emergency situation such as a major release, fire, and/or explosion. The choice of mitigation strategies will depend on the nature of the hazardous materials and energies that can be released and the degree to which risk reduction is needed to ensure people, property, and the environment are adequately protected. The latter will be affected by the proximity of populations and sensitive environments surrounding the facility. An unstaffed remote natural gas facility will obviously not warrant the same mitigation measures as a facility using large quantities of high-toxic-hazard materials with other industry or residences nearby.

- To be effective, a mitigation strategy will need to be capable of
- Detecting either an incipient or an actual emergency situation
 - Deciding on and initiating the proper course of action to mitigate the situation
 - Reducing the severity of consequences at the source, in transit, and/or at the receptor locations
 - Preventing domino effects that could have even more severe consequences

Each of these steps might be performed either by direct action of operations or emergency response personnel or by automatic systems. An example of the latter might be an array of toxic or flammable gas detectors that might trip an emergency shutdown system that closes remotely actuated block valves and vents off the process pressure to a flare if two adjacent sensors read above a predetermined vapor concentration.

Mitigation measures can also be *passive* safeguards, meaning that they require no human intervention and no engineered sensing and actuation system to work. Examples of passive mitigation measures are secondary containment systems, blast-resistant and fire-resistant structures, insulated or low-heat-capacity spill surfaces to reduce the rate of evaporation, and an increased distance between the hazardous materials and energies and the sensitive receptors.

SAFETY INSTRUMENTED SYSTEMS

REFERENCES: *Guidelines for Safe and Reliable Instrumented Protective Systems*, American Institute of Chemical Engineers, New York, 2007; ISA TR84.00.04, *Guidelines for the Implementation of ANSI/ISA 84.00.01-2004 (IEC 61511)*, Instrumentation, Systems, and Automation Society, N.C., 2005; ANSI/ISA 84.00.01-2004, *Functional Safety: Safety Instrumented Systems for the Process Industry Sector*, Instrumentation, Systems, and Automation Society, N.C., 2004; IEC 61511, *Functional Safety: Safety Instrumented Systems for the Process Industry Sector*, International Electrotechnical Commission, Geneva, Switzerland, 2003.

GENERAL REFERENCES: *Guidelines for Hazard Evaluation Procedures, Second Edition with Worked Examples*, American Institute of Chemical Engineers, New York, 1992; *Layer of Protection Analysis: A Simplified Risk Assessment Approach*, American Institute of Chemical Engineers, New York, 2001; ISA TR84.00.02, *Safety Instrumented Functions (SIF)—Safety Integrity Level (SIL) Evaluation Techniques*, Instrumentation, Systems, and Automation Society, N.C., 2002.

Glossary

Basic process control system (BPCS) System that responds to input signals from the process, its associated equipment, other programmable systems, and/or an operator and generates output signals,

causing the process and its associated equipment to operate in the desired manner. The BPCS is commonly referred to as the *control system*.

Compensating measures Planned means for managing process risk during periods of process operation with known faults or problems that increase risk.

Control layer Protection layer that is used to maintain the process within the normal operating limits, such as standard operating procedures, basic process control system, and process alarms.

Core attribute Fundamental underlying property of a protection layer. The core attributes are independence, functionality, integrity, reliability, auditability, management of change, and access security.

Independent protection layer An IPL is a device, system, or action that is capable of preventing a hazard scenario from proceeding to the undesired consequence regardless of the initiating cause occurrence (or its consequences) or the failure of any other protection layer.

Safety instrumented function (SIF) A safety function allocated to the safety instrumented system with a safety integrity level necessary to achieve the desired risk reduction for an identified process hazard.

Safety instrumented system (SIS) Any combination of separate and independent devices (sensors, logic solvers, final elements, and support systems) designed and managed to achieve a specified safety integrity level. An SIS may implement one or more safety instrumented functions.

Safety integrity level (SIL) Discrete level (one out of a possible four SIL categories) used to specify the probability that a safety instrumented function will perform its required function under all operational states within a specified time.

Introduction The chemical processing industry relies on many types of instrumented systems, e.g., the basic process control systems (BPCSs) and safety instrumented system (SIS). The BPCS controls the process on a continuous basis to maintain it within prescribed control limits. Operators supervise the process and, when necessary, take action on the process through the BPCS or other independent operator interface. The SIS detects the existence of unacceptable process conditions and takes action on the process to bring it to a safe state. In the past, these systems have also been called emergency shutdown systems, safety interlock systems, and safety critical systems.

In 1993, the Center for Chemical Process Safety (CCPS) published *Guidelines for Safe Automation of Chemical Processes* (referred to henceforth as *Safe Automation*). *Safe Automation* provides guidelines for the application of automation systems used to control and shut down chemical and petrochemical processes. The popularity of one of the hazard and risk analysis methods presented in *Safe Automation* led to the publication of the 2001 Concept Series book from CCPS, *Layer of Protection Analysis: A Simplified Risk Assessment Approach*. This method builds upon traditional process hazards analysis techniques. It uses a semiquantitative approach to define the required performance for each identified protective system.

The Instrumentation, Systems, and Automation Society (ISA) published the Standard ANSI/ISA 84.01-1996, documenting the good engineering practice for the design, operation, maintenance, and testing of SIS. The standard established a numerical benchmark for the SIS performance known as the safety integrity level (SIL) and provided requirements on how to design and manage the SIS to achieve the target SIL.

Safe Automation and ANSI/ISA 84.01-1996 served as significant technical references for the first international standard, IEC 61511, issued by the International Electrotechnical Commission (IEC). In the United States, IEC 61511 was accepted by ISA as ISA 84.00.01-2004, replacing the 1996 standard. In 2004, the European Committee for Electrotechnical Standardization (CENELEC) and the American National Standards Institute (ANSI) recognized IEC 61511 as a consensus standard for the process industry. IEC 61511 covers the complete process safety management life cycle. With its adoption, this standard serves as the primary driving force behind the work processes followed to achieve and maintain safe operation using safety instrumented systems.

It is important that personnel understand how to achieve safe operation, but not at the exclusion of other important considerations, such as reliability, operability, and maintainability. The chemical industry has also found significant benefit to plant productivity and operability when SIS work processes are used to design and manage other instrumented protective systems (IPS), such as those mitigating potential economic and business losses. The CCPS book (2007) *Guidelines for Safe and Reliable Instrumented Protective Systems* discusses the activities and quality control measures necessary to achieve safe and reliable operation throughout the IPS lifecycle.

Hazard and Risk Analysis Consideration should be given to identifying process hazards as early as possible in the process equipment design, so that measures can be taken to reduce or eliminate the hazards. Inherently safer design strategies, such as minimize, substitute, moderate, and simplify, should be implemented.

When it is no longer practical to reduce the risk further by process design modification, protection layers are used to mitigate the remaining process risk. IPLs must meet the necessary rigor associated with seven core attributes: independence, functionality, integrity, reliability, auditability, access security, and management of change. There are two critical activities to be completed during the risk assessment phase. First, the safety functions (i.e., those functions that detect and respond to process hazards) are identified by using an accepted hazard and risk analysis (H&RA) methodology. Second, each safety function is allocated to a protection layer that is designed and managed to achieve the required risk reduction.

An H&RA involves a review of the process design and its control, operation, and maintenance practices. The review is conducted by a multidisciplinary team with expertise in the design and operation of the process unit. The team uses a systematic screening process to determine how deviations from normal operation lead to process hazards. The H&RA identifies areas where the process risk is too high, requiring the implementation of safety functions. The team's objective is to reduce the risk to below the owner/operator's risk criteria.

Process risk is defined by the frequency of the occurrence and the potential consequence severity of the process hazard. To define the frequency, the initiating causes (e.g., single causes or multiple causes and conditions) are identified for each process hazard, and their frequency of occurrence is estimated. The consequence severity is the logical conclusion to the propagation of the process hazard if no protection layers are implemented as barriers to the event.

The gap between the process risk and the owner/operator's risk criteria establishes the requirements for risk reduction. The risk gap can be managed by a single safety function or by multiple functions allocated to protection layers. The team defines the risk reduction that must be provided by each safety function and allocates the safety function to a protection layer that is designed and managed to achieve the allocated risk reduction.

When the safety function is allocated to the SIS, it is a safety instrumented function (SIF). The risk reduction allocated to the SIF defines its target safety integrity level (SIL). This target is related to the SIF probability of failure on demand (PFD), e.g., SIL 1 (PFD range: 0.01 to 0.1), SIL 2 (PFD range: 0.001 to 0.01), SIL 3 (PFD range: 0.0001 to 0.001), and SIL 4 (PFD range: 0.00001 to 0.0001).

The identification of safety functions continues until the process risk associated with the hazard is reduced to meet the risk criteria. When there is insufficient risk reduction provided by the current or planned design, the team makes recommendations for process design changes (e.g., inherently safer design), improvement to existing functions, or the design and implementation of new functions. These recommendations are generally prioritized based on the magnitude of the gap between the mitigated process risk (i.e., risk considering the presence of existing functions) and the risk criteria.

Design Basis In the design phase, the project team works together to create an SIS design basis that achieves the risk reduction strategy established in the risk reduction phase. This strategy relies, in part, on the implementation of SIFs to address identified process risk. The SIF uses dedicated devices, including process sensors that detect the process hazard, a logic solver that decides what to do, and final elements that take action on the process. Often, a single logic solver

implements multiple SIFs, so the potential for common-cause failures between SIFs should be considered during design.

The SIS is normally designed to fail-safe on loss of power and takes action only when the process demands that it do so. These demands often occur when safe operating limits are exceeded due to BPCS failures. Therefore, the SIS is designed and managed to be independent of the BPCS in terms of its hardware and software and its user interfaces, such as operator, maintenance, and engineering interfaces.

Systematic errors can occur anywhere in the design and implementation process or during the operational life of an SIS device. These errors put the SIS on the path to failure in spite of the design elements incorporated to achieve robust hardware and software systems. Systematic errors are minimized using work processes that address potential human errors in the SIS design and management (e.g., programming errors or hardware specification errors).

Random hardware failure can occur throughout the device life as components age in the environmental conditions of the process unit. These failures can cause a device to fail dangerously; i.e., it cannot perform as required. These failures are estimated by examining the dangerous failure modes of each device and their frequency of occurrence. The resulting failure rate is used to estimate the PFD of the SIS considering its specific devices, redundancy, diagnostics, common-cause failure potential, and proof test interval. The PFD is then compared to the target SIL assigned during the risk assessment phase to determine whether the design is adequate.

The design basis includes the process requirements specification and the safety requirements specification. The process requirements specification is typically developed by process engineering, with input from operations personnel. The process requirements are provided to the instrumentation, electrical, or controls systems personnel to develop the safety requirements specification with input from operations and maintenance personnel.

Process Requirements Specification Process engineering uses the H&RA findings, process design information, and operations input to

- Define safe state, including safety and nonsafety actions.
- Define reliability requirements necessary to achieve desired process unit uptime performance.
- Define operability requirements for modes of operation, such as start-up, reduced rates, maintenance modes, and shutdown.
- Identify windows of opportunity for SIS testing.
- Define process-related parameters.
- Define human-related parameters.

Guidance can be found in the CCPS book (2007) *Guidelines for Safe and Reliable Instrumented Protective Systems* related to the development of the process requirements specification.

Safety Requirements Specification The instrumentation and electrical (I&E) requirements are developed to meet the intent of any H&RA findings and the process requirements. The design documentation should establish a clear connection between each process hazard and the design of its SIFs. I&E personnel should meet with the process engineering representative responsible for the process requirements to ensure that the intent is understood.

I&E design focuses on achieving the target SIL through careful selection of the devices (e.g., user approved for safety), use of redundancy, on-line diagnostics, and frequent proof testing. The ISA technical report TR84.00.04 gives extensive guidance on design requirements for the hardware and software systems used to implement the SIS. Application-specific standards by organizations such as American Society of Mechanical Engineers (ASME), American Petroleum Institute (API), and the National Fire Protection Association (NFPA) may provide additional requirements and guidance.

There is often quite a bit of give and take between the process requirements and I&E requirements in the early stages of the project. For example, the ideal process measurement may not be practical in the existing installation. At all times, it should be recognized that the goal of the design is to prevent the process hazard from propagating to an incident.

Engineering, Installation, Commissioning, and Validation (EICV) This phase involves the physical realization of the design basis, which is developed in response to process risk identified in an H&RA study. The bulk of the work in this phase is not a process

engineering effort. Detailed engineering, installation, and commissioning is generally an I&E function. However, this is where the assumptions and requirements developed by the process engineer are put into practice and validated.

Validation of the SIS functionality is performed as part of a site acceptance test (SAT). Validation involves a full functional test that demonstrates the SIS actually works in the real-world installation. It proves the SIS devices execute the logic according to the specification and ensures that the SIS and its devices interact as intended with other systems, such as the BPCS and operator interface. From a systematic error standpoint, the SAT also provides an opportunity for a first-pass validation of the procedures developed for the operating basis (see next subsection).

Pre-start-up Safety Review (PSSR) approval of the SIS establishes the point where the SIS design and construction is considered complete. All documentation should be formally updated to as-built status, incorporating any modifications made since the last formal drawing or document revision. Once the PSSR has approved the SIS for process unit start-up, formal management of change procedures should be followed to address proposed modification to the SIS or its associated documentation. Any deviation from the approved design basis should be reviewed and approved by appropriate parties prior to change implementation.

Operating Basis As the SIS engineering design nears completion, the resources and skills of plant operations should be considered. At some point, the SIS is turned over to operations and maintenance personnel, who must be trained on the new SIS and on their responsibilities. Consequently, thought should be given to the content and depth of the information that must be communicated to various personnel. This is especially important as the responsibility for the SIS transitions from the project team to operations and maintenance control.

The process engineer is responsible for defining the content of SIS operating procedures, which should cover SIS specific information (e.g., set points, SIS actions, and the hazard that is being prevented with SIS), the correct use of bypasses and resets, the operator response to SIS alarms and trips, when to execute a manual shutdown, and provisions for operation with detected faults (e.g., compensating measures). These procedures, along with analogous ones developed by maintenance and reliability engineering for maintenance activities, make up the backbone of the operating basis.

Since a device can fail at any time during its life, periodic proof tests are performed to demonstrate the functionality of the SIS. Proof tests are covered by operation and maintenance procedures that ensure that the test is done correctly, consistently, and safely and that the device is returned to a fully operational state after test. Each test serves as an opportunity for personnel to see the SIS in action and to validate the procedures associated with its operation.

Proof testing is required for all SISs. It is used to demonstrate that the devices are operating as specified and are maintained in "as good as new" condition. Failures found during testing indicate gaps in the mechanical integrity program, necessitating root-cause investigation and corrective action.

SECURITY

Definition of Terms (American Petroleum Institute/National Petroleum Refiner's Association, *Security Vulnerability Assessment Methodology for the Petroleum Industry*, 2004.)

Adversary Any individual, group, organization, or government that conducts activities, or has the intention and capability to conduct activities detrimental to critical assets. An adversary could include intelligence services of host nations, or third-party nations, political and terrorist groups, criminals, rogue employees, and private interests. Adversaries can include site insiders, site outsiders, or the two acting in collusion.

Alert levels A progressive, qualitative measure of the likelihood of terrorist actions, from negligible to imminent, based on government or company intelligence information. Different security measures may be implemented at each alert level based on the level of threat to the facility.

Asset Any person, environment, facility, material, information, business reputation, or activity that has a positive value to an owner. The asset may have value to an adversary, as well as an owner, although

the nature and magnitude of those values may differ. Assets in the SVA include the community and the environment surrounding the site.

Asset category Assets may be categorized in many ways. Among these are by people, hazardous materials (used or produced), information, environment, equipment, facilities, activities and operations, and company reputation.

Countermeasures An action taken or a physical capability provided whose principal purpose is to reduce or eliminate one or more vulnerabilities. The countermeasure may also affect the threat(s) (intent and/or capability) as well as the asset's value. The cost of a countermeasure may be monetary, but may also include nonmonetary costs such as reduced operational effectiveness, adverse publicity, unfavorable working conditions, and political consequences.

Cyber security Protection of critical information systems including hardware, software, infrastructure, and data from loss, corruption, theft, or damage.

Delay A countermeasures strategy that is intended to provide various barriers to slow the progress of an adversary in penetrating a site, to prevent an attack or theft, or in leaving a restricted area to assist in apprehension and prevention of theft.

Detection A countermeasures strategy that is intended to identify an adversary attempting to commit a security event or other criminal activity in order to provide real-time observation as well as postincident analysis of the activities and identity of the adversary.

Deterrence A countermeasures strategy that is intended to prevent or discourage the occurrence of a breach of security by means of fear or doubt. Physical security systems such as warning signs, lights, uniformed guards, cameras, and bars are examples of countermeasures that provide deterrence.

Hazard A situation with the potential for harm.

Intelligence Information to characterize specific or general threats including the motivation, capabilities, and activities of adversaries.

Intent A course of action that an adversary intends to follow.

Likelihood of adversary success (LAS) The potential for causing a catastrophic event by defeating the countermeasures. LAS is an estimate that the security countermeasures will thwart or withstand the attempted attack, or if the attack will circumvent or exceed the existing security measures. This measure represents a surrogate for the conditional probability of success of the event.

Physical security Security systems and architectural features that are intended to improve protection. Examples include fencing, doors, gates, walls, turnstiles, locks, motion detectors, vehicle barriers, and hardened glass.

Response The act of reacting to detected or actual criminal activity either immediately following detection or after the incident.

Risk The potential for damage to or loss of an asset. Risk, in the context of process security, is the potential for a catastrophic outcome to be realized. Examples of the catastrophic outcomes that are typically of interest include an intentional release of hazardous materials to the atmosphere, or the theft of hazardous materials that could later be used as weapons, or the contamination of hazardous materials that may later harm the public, or the economic costs of the damage or disruption of a process.

Risk assessment Risk (R) assessment is the process of determining the likelihood of an adversary (T) successfully exploiting vulnerability (V) and the resulting degree of consequences (C) on an asset. A risk assessment provides the basis for rank-ordering risks and thus establishing priorities for the application of countermeasures.

Security layers of protection Also known as concentric "rings of protection," a concept of providing multiple independent and overlapping layers of protection in depth. For security purposes, this may include various layers of protection such as countersurveillance, counterintelligence, physical security, and cyber security.

Security vulnerability assessment (SVA) The process of determining the likelihood of an adversary successfully exploiting vulnerability, and the resulting degree of damage or impact. SVAs are not quantitative risk analyses, but are performed qualitatively using the best judgment of security and safety professionals. The determination of risk (qualitatively) is the desired outcome of the SVA, so that it provides the basis for rank ordering of the security-related risks and thus establishing priorities for the application of countermeasures.

Target attractiveness An estimate of the value of a target to an adversary based on the factors shown below. Experience has shown that, particularly for terrorist attacks, certain targets better accomplish the objectives of the adversaries than do others. Since the SVA is a risk-based analytical approach, consideration must be given to these factors in defining the threat and in determining the need for any enhanced countermeasures.

- Potential for mass casualties and fatalities
- Extensive property damage
- Proximity to national assets or landmarks
- Possible disruption or damage to critical infrastructure
- Disruption of the national, regional, or local economy
- Ease of access to target
- Media attention or possible interest of the media
- Company reputation and brand exposure

Threat Any indication, circumstance, or event with the potential to cause the loss of, or damage to, an asset. Threat can also be defined as the intention and capability of an adversary to undertake actions that would be detrimental to critical assets.

Threat categories Adversaries may be categorized as occurring from three general areas:

- Insiders
- Outsiders
- Insiders working in collusion with outsiders

Vulnerability Any weakness that can be exploited by an adversary to gain access to an asset. Vulnerabilities can include, but are not limited to, building characteristics; equipment properties; personnel behavior; locations of people, equipment, and buildings; or operational and personnel practices.

Introduction Prior to September 11, 2001, known as 9/11, chemical process safety activities primarily focused on accidental release risks and excluded most considerations of intentional releases. Security was provided mostly for lesser threats than such extreme acts of violence, and terrorism was generally not provided for except in high-security areas of the world. Exceptions to this included general concerns for sabotage. This was due to a perception that these risks were managed adequately, and that the threat of a terrorist attack, particularly on U.S. chemical manufacturing facilities or transportation system, was remote.

Following 9/11 it became apparent that the threat of intentional harm to infrastructure, especially where hazardous materials were manufactured, stored, processed, or transported, had to be considered a credible concern. Security for the chemical industry took on increased emphasis as a result, and such organizations as the American Institute of Chemical Engineers recognized the paradigm shift and published guidelines on analyzing these threats.^o The concerns of international terrorism have spread to many countries around the world, and addressing this concern is now a permanent part of the requirements of the chemical engineering profession. Chemical engineers now must include *chemical process security* as a critical element of the management of a process facility.

Chemical process security management has as its objectives

1. To minimize the risk of harm to the public or employees from intentional acts against a process facility
2. To protect the assets (including employees) of the process facility to maintain the ongoing integrity of the operation and to preserve the value of the investment

Process security and process safety have many parallels and use many common programs and systems for achieving their ends. Process security management requires a systems approach to develop a comprehensive security program, which shares many common elements with process safety management.

Chemical process security includes, but goes beyond, traditional *physical security*. Physical security includes such considerations as guards, barriers, surveillance equipment, and other physical system considerations. Physical security is an element of chemical process security, but physical security alone is not always adequate to address the new challenges of security against extreme acts of violence, such as terrorism.

^oGuidelines for Managing and Analyzing the Security Vulnerabilities of Fixed Chemical Sites, American Institute of Chemical Engineers, August 2002.

Effective chemical process security must also consider integration of broader process elements including technology, chemical usage and quantities, procedures, administrative controls, training, and cyber interface with those traditional physical security elements.

The chemical engineer has an opportunity to influence these considerations in all stages of a process life cycle, including concept, engineering, construction, commissioning, operations, modification, and decommissioning. Security issues that are recognized in the concept and design phases of a project may allow for cost-effective considerations that can eliminate or greatly minimize security risks. For example, if a buffer zone can be provided between the public areas and a plant fence, and then again between a plant fence and critical process equipment, those two zones can effectively provide such benefits as

- *Detection zone(s)*, given they are free of obstacles and have sufficient depth to allow for adversaries to be detected while attempting unlawful entry
- *Standoff zone(s)*, given they have sufficient depth to keep adversaries from using explosives or standoff weapons effectively from the perimeter
- *Delay zone(s)* allowing intervening force the time to respond or time for operators to take evasive action before an adversary reaches a target following detection

A chemical engineer may have a choice of inherent safety variables, such as quantity stored or process temperatures and pressures, or process safety measures such as emergency isolation valves or containment systems, all of which may greatly reduce the vulnerabilities or the consequences of intentional loss. These are in addition to traditional security measures, which may include physical security, background checks, administrative controls, access controls, or other protective measures. For a more complete discussion of the options, refer to the AIChE Center for Chemical Process Safety *Guidelines for Analyzing and Managing the Security Vulnerabilities of Fixed Chemical Sites*⁶ and other references.¹

Threats of Concern Terrorist acts can be the most problematic to defend against since they may be more extreme or malevolent than other crimes focused on monetary gains or outcomes with less malicious intent. Plus terrorists may use military tactics not often provided for in base chemical facility design. Chemical facility security must be considered in context with local and national homeland security and law enforcement activities, as well as with emergency response capabilities. There is a practical limit to the ability of a chemical site to prevent or mitigate a terrorist act. Above a certain level of threat, the facility needs to rely on law enforcement and military services to provide physical security against extreme acts of intentional harm. The security posture must be risk-based, and so extremely robust security measures are not always applicable or necessary.

The acts of concern for terrorism can be generally defined as involving the four motives shown in Table 23-31.

Other adversaries that must be considered as applicable include those capable and interested in perpetrating a full spectrum of security acts. These may include outside parties or insiders or a combination of the two working in collusion.

The threats that are applicable and the adversaries that may be culpable are characterized to understand their capabilities, intent, and therefore potential targets and tactics. The targets and acts of interest to various adversaries will vary with the group. For example, a terrorist may be interested in destroying a process through violent means, such as by the use of an explosive device. An activist may be interested only in a nonviolent protest or in causing some limited physical damage, but not in harming the environment or the public in the process. The various

⁶*Guidelines for Managing and Analyzing the Security Vulnerabilities of Fixed Chemical Sites*, American Institute of Chemical Engineers, August 2002.

¹*Counterterrorism and Contingency Planning Guide*, special publication from Security Management Magazine and American Society for Industrial Security, 2001; Dalton, D., *Security Management: Business Strategies for Success*, Butterworth-Heinemann Publishing, Newton, Mass., 1995; Walsh, Timothy J., and Richard J. Healy, eds., *Protection of Assets Manual*, Merritt Co., Santa Monica, Calif. (four-volume loose-leaf reference manual, updated monthly).

TABLE 23-31 Security Issues of Concern with Example Applications to Terrorism

Security motives of concern ^a	Example terrorist means and objectives
Intentional loss of containment	By causing a release of chemicals to the atmosphere and potential toxic release, fire, or explosion to harm the public, workers, or the environment, or to destroy the facility
Theft of chemicals	For their eventual reuse as primary or secondary improvised weapons against a third party
Contamination or spoilage of a process	To cause immediate or delayed harm to people or the environment, or to cause severe economic injury
Degradation of the asset	By causing mechanical damage or physical or cyber disruption, for purposes of causing severe direct or indirect economic damages

^aAdapted from *Guidelines for Managing and Analyzing the Security Vulnerabilities of Fixed Chemical Sites*, American Institute of Chemical Engineers, August 2002.

adversaries and strategies of interest form the basis of the vulnerability assessment, which is the foundation of a chemical process security management system specific to address the anticipated threats.

Overall Objectives of Terrorism Terrorists attempt to cause change to accomplish their goals by creating fear and uncertainty in the population they are targeting through the use of violent acts. The underlying goals include fundamentalist objectives, such as purity of religion or idealistic goals, but they may include power struggles, such as trying to overthrow a government, or reparations, such as revenge for past actions. The reason for a chemical plant being targeted may be that it serves an adversary of the terrorist (economic or military significance) or that it can be weaponized to cause third-party harm (health and safety consequences from intentional release of hazardous materials).

Security Vulnerability Assessment A security vulnerability assessment is intended to identify security vulnerabilities from a wide range of threats ranging from vandalism to terrorism. With the recognition of threats, consequences, and vulnerabilities, the risk of security events can be evaluated, and a security management system can be organized that will effectively mitigate those risks.

SVA Methodologies There are several SVA techniques and methods available to the industry, all of which share common elements. The following is a list of some available SVA methodologies published by various governments, private, and trade and professional organizations. Some are merely chapters or sections of documents that address security or risk assessment/risk management in broader terms. Some are SVA or VA publications by themselves. Some of these "methods" are complete, systematic analytical techniques, and others are mere checklists.

- American Institute of Chemical Engineers Center for Chemical Process Safety: *Guidelines for Analyzing and Managing the Security Vulnerabilities of Fixed Chemical Sites*, 2002.
- American Petroleum Institute/National Petroleum Refiner's Association, *Security Vulnerability Assessment Methodology for the Petroleum Industry*, 2003.
- National Institute of Justice, *Chemical Facility Vulnerability Assessment Methodology*, July 2002 (Sandia VAM).
- Synthetic Organic Chemical Manufacturers Association, Inc. (SOCMA), *Manual on Chemical Site Security Vulnerability Analysis Methodology and Model*, 2002.

One approach to conducting an SVA is shown in Fig. 23-64. This methodology was published by the American Institute of Chemical Engineers, Center for Chemical Process Safety, in 2002. The CCPS SVA is founded on a risk-based approach to managing chemical facility security. To begin the process, companies may perform an enterprise-level screening methodology to sort out significant risks among multiple sites and to determine priorities for analysis and implementation of any recommended changes. The screening, if performed, would result in a prioritized list of sites and forms the foundation of the choice of specific SVAs required. The book covers how to integrate chemical security

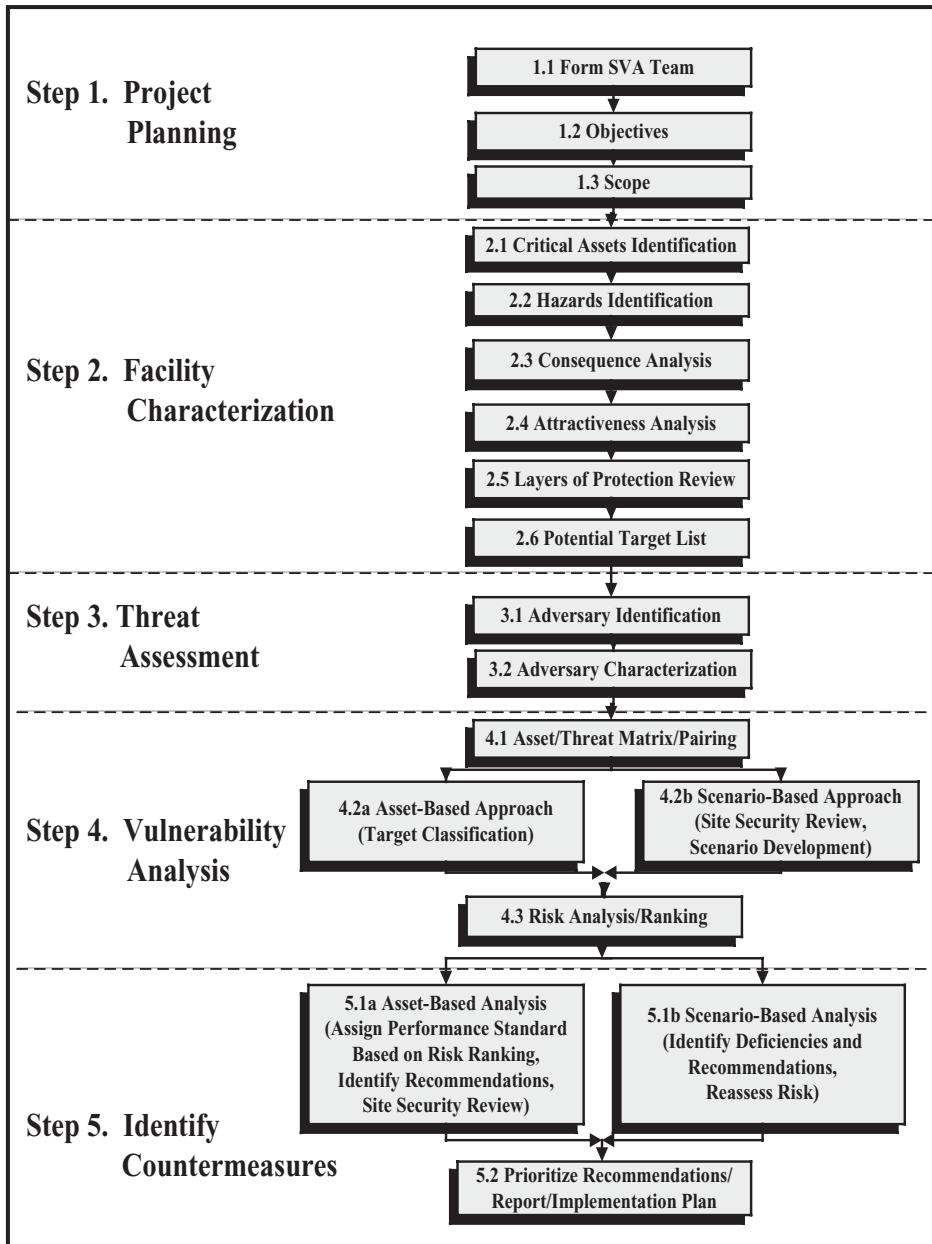


FIG. 23-64 CCPS SVA process.

management and process safety management strategies into a comprehensive process safety and security strategy. Security risk reduction opportunities during the process life cycle are explained, as well as various process risk management strategies (including inherent safety) that are applicable.

In the appendices, the book contains a set of tools including an enterprise-level screening tool, reference information available to conduct the CCPS SVA, and a workbook with worksheets for conducting the CCPS SVA, examples of enhanced security measures, and checklists for assessing security measures at a site.

Defining the Risk to Be Managed For the purposes of an SVA, the definition of risk is shown in Fig. 23-65. The risk that is being

analyzed for the SVA is defined as an expression of the likelihood that a defined threat will target and successfully attack a specific security vulnerability of a particular target or combination of targets to cause a given set of consequences. This is contrasted with the usual accidental risk definitions. The risk variables are defined as shown in Table 23-32.

A challenge for security vulnerability analysis is that the accurate prediction of the frequency and location of terrorist acts is not considered credible. As such, the analyst has a choice of assuming a frequency of a certain attack or assuming the attack frequency is 1, thereby focusing solely on the conditional likelihood of success of the adversary who attempts an attack. While the latter approach provides a baseline for making decisions about vulnerability, it does not fully

<p>Intentional release risk is a function of</p> <ul style="list-style-type: none"> • Consequences of a successful attack against an asset • Likelihood of a successful attack against an asset 	<p>Accidental release risk is a function of</p> <ul style="list-style-type: none"> • Consequences of an accidental event • Likelihood of the occurrence of the event
<p>Likelihood is a function of</p> <ul style="list-style-type: none"> • The attractiveness to the adversary of the asset • The degree of threat posed by the adversary • The degree of vulnerability of the asset 	<p>Likelihood is a function of</p> <ul style="list-style-type: none"> • The probability of an event cascading from initiating event to the consequences of interest and the frequency of the events over a given period

FIG. 23-65 Intentional release vs. accidental release.

answer the question of cost/benefit of any countermeasures. Certain crimes other than terrorism may be more predictable or frequent, allowing for statistical analysis to help frame the risks and justify countermeasure expenditures. Due to this limitation, the factor of attractiveness is considered along with consequences, threat, and vulnerability, to determine the priorities for and design of security measures for the industry.

Security Strategies A basic premise is that not all security risks can be completely prevented. Appropriate strategies for managing security can vary widely depending on the circumstances including the type of facility and the threats facing the facility. As a result, it is difficult to prescribe security measures that apply to all facilities in all industries. Instead, it is suggested to use the SVA as a means of identifying, analyzing, and reducing vulnerabilities. The specific situations must be evaluated individually by local management using best judgment of applicable practices. Appropriate security risk management decisions must be made commensurate with the risks. This flexible approach recognizes that there isn't a uniform approach to security in the chemical process industry, and that resources are best applied to mitigate high-risk situations primarily.

Security strategies for the process industries are generally based on the application of four key concepts against each threat: deterrence, detection, delay, and response.*

**Managing and Analyzing the Security Vulnerabilities of Fixed Chemical Sites*, AIChE, August 2002.

A complete security design includes these four concepts in layers of protection or a defense in depth arrangement. The most critical assets should be placed in the center of conceptual concentric levels of increasingly more stringent security measures. In the concept of rings of protection, the spatial relationship between the location of the target asset and the location of the physical countermeasures is important.

In the case of malicious acts, the layers or rings of protection must be particularly robust because the adversaries are intentionally attempting to breach the protective features and can be counted on to use whatever means are available to be successful. This could include explosions or other initiating events that result in widespread common-cause failures. Some particularly motivated adversaries might commit suicide while attempting to breach the security layers of protection.

Countermeasures and Security Risk Management Concepts Countermeasures are actions taken to reduce or eliminate one or more vulnerabilities. Countermeasures include hardware, technical systems, software, interdictive response, procedures, and administrative controls.

Security risk reduction at a site can include the following strategies:

- Physical security
- Cyber security
- Crisis management and emergency response plans
- Policies and procedures
- Information security
- Intelligence
- Inherent safety

TABLE 23-32 SVA Risk Variables

Consequences	Potential Impact of the Event
Likelihood	Likelihood is a function of the chance of being targeted for attack, and the conditional chance of mounting a successful attack (both planning and executing), given the threat and existing security measures. This is a function of three variables below.
Threat	Threat, is a function of the adversary's existence, intent, motivation, capabilities, and known patterns of potential adversaries. Different adversaries may pose different threats to various assets within a given facility.
Vulnerability	This is weakness that can be exploited by an adversary to gain access and damage or steal an asset or disrupt a critical function. This is a variable that indicates the likelihood of a successful attack, given the intent to attack an asset.
Target attractiveness	Target attractiveness is a surrogate measure for likelihood of attack. This factor is a composite estimate of the perceived value of a target to the adversary and the adversary's degree of interest in attacking the target.

SOURCE: *Managing and Analyzing the Security Vulnerabilities of Fixed Chemical Sites*, AIChE, August 2002.

TABLE 23-33 American Chemistry Council's Responsible Care® Security Code Process Security Management System*

1.	Leadership commitment
2.	Analysis of threats, vulnerabilities, and consequences
3.	Implementation of security measures
4.	Information and cyber security
5.	Documentation
6.	Training, drills, and guidance
7.	Communications, dialogue, and information exchange
8.	Response to security threats
9.	Response to security incidents
10.	Audits
11.	Third-party verification
12.	Management of change
13.	Continuous improvement

*Site Security Guidelines for the U.S. Chemical Industry, American Chemistry Council, October 2001.

Security Management System A comprehensive process security management system must include management program elements that integrate and work in concert with other management systems to control security risks. The 13 management practices shown in Table 23-33 are an example of a management system developed by the American Chemistry Council.

The purpose of a security management system is to ensure the ongoing, integrated, and systematic application of security principles and programs to protect personnel and assets in a dynamic security environment to ensure the continuity of the operation and supporting or dependent infrastructure. Traditional industrial facility security management tended to focus on protection of persons and property from crime (e.g., theft of property, workplace violence) and crime prevention, response, and investigation. While that is still an element of facility security, a management system allows incorporation of broader security concerns relating to intentional attack on fixed assets, such as by terrorists. To develop and implement a security management system not only provides a more thorough, dynamic, risk-based, and proactive approach, but also allows security management to be integrated into a facility's overall EH&S management systems.

The American Chemistry Council's Responsible Care® Security Code is designed to encourage continuous improvement in security performance by using a risk-based approach to identify, assess, and address vulnerabilities; prevent or mitigate incidents; enhance training and response capabilities; and maintain and improve relationships with key stakeholders. As a condition of membership in the council, each member company must implement the Security Code for facilities, transportation and value chain, and cyber security.

KEY PROCEDURES

Safety by design should always be our aim but is often impossible or too expensive, and then we have to rely on procedures. Key features of all procedures are as follows:

- They should be as simple as possible and described in simple language, so as to help the reader rather than protect the writer.
- They should be explained to and discussed with those who will have to carry them out, not just sent to them through the post.
- Regular checks and audits should be made to confirm that they are being carried out correctly.

Many accidents have occurred because the three procedures discussed below were unsatisfactory or were not followed.

Preparation of Equipment for Maintenance The essential feature of this procedure is a permit-to-work system: The operating team members prepare the equipment and write down on the permit the work to be done, the preparation carried out, the remaining hazards, and the precautions necessary. The permit is then accepted by the person or group who will carry out the work and is returned when the work is complete. The permit system will not make maintenance 100 percent safe, but it reduces the chance that hazards will be overlooked, lists ways of controlling them, and informs those doing the job what precautions they should take. The

system should cover such matters as who is authorized to issue and accept permits-to-work, the training they should receive (not forgetting deputies), and the period of time for which permits are valid. It should also cover the following:

Isolation of the Equipment under Maintenance Poor or missing isolation has been the cause of many serious accidents. Do not rely on valves except for quick jobs; use blinds or disconnection and blanking unless the job is so quick that blinding (or disconnection) would take as long and be as hazardous as the main job. Valves used for isolation (including isolation while fitting blinds or disconnecting) should be locked shut (e.g., by a padlock and chain). Blinds should be made to the same standard (pressure rating and material of construction) as the plant. Plants should be designed so that blinds can be inserted without difficulty; i.e., there should be sufficient flexibility in the pipework, or a slip-ring or figure 8 plate should be used. Electricity should be isolated by locking off or removal of fuses. Do not leave the fuses lying around for anyone to replace. Always try out electrical equipment after defusing to check that the correct fuses have been withdrawn.

Identification of the Equipment Many accidents have occurred because maintenance workers opened up the wrong equipment. Equipment that is under repair should be numbered or labeled unambiguously. Temporary labels should be used if there are no permanent ones. Pointing out the correct equipment is not sufficient. "The pump you repaired last week is leaking again" is a recipe for an accident.

Freeing from Hazardous Materials Equipment that is to be repaired should be freed as far as possible from hazardous materials. Gases can be removed by sweeping out with nitrogen (if the gases are flammable) or air; water-soluble liquids, by washing with water; and oils, by steaming. Some materials such as heavy oils and materials that polymerize are very difficult or impossible to remove completely. Tests should be carried out to make sure that the concentration of any hazardous material remaining is below an agreed level. Machinery should be in the lowest energy state. Thus the forks of fork lift trucks should be lowered, and springs should not be compressed or extended. For some machinery the lowest energy state is less obvious. Do not work under heavy suspended loads.

Special Jobs Certain jobs, such as entry to vessels and other confined spaces, hot work, and responsibilities of contractors, raise special problems.

Handover Permits should be handed over (and returned when the job is complete) person to person. They should not be left on the table for people to sign when they come in.

Change of Intent If there is a change in the work to be done, the permit should be returned and a new one issued (Crowl and Grossel, eds., *Handbook of Toxic Materials Handling and Management*, Marcel Dekker, 1994, Chap. 12).

Control of Modifications to Plants, Processes, and Organization Many accidents have occurred when such modifications had unforeseen and unsafe side effects (Sanders, *Chemical Process Safety Learning from Case Histories*, 3d ed., Gulf Professional, 2005). No such modifications should therefore be made until they have been authorized by a professionally qualified person who has made a systematic attempt to identify and assess the consequences of the proposal, by hazard and operability study or a similar technique. When the modification is complete, the person who authorized it should inspect it to make sure that the design intention has been followed and that it "looks right." What does not look right is usually wrong and should at least be checked.

- Unauthorized modifications are particularly liable to occur
- During start-ups, as changes may be necessary to get the plant on-line.
 - During maintenance, as the maintenance workers may be tempted to improve the plant as well as repair it. They may suggest modifications, but should put the plant back as it was unless a change has been authorized.
 - When the modification is cheap and no financial authorization is necessary. Many seemingly trivial modifications have had tragic results.
 - When the modification is temporary. Twenty-eight people were killed by the temporary modification at Flixborough, one of the

most famous of all time (Mannan, *Lees' Loss Prevention in the Process Industries*, 3d ed., Elsevier, Amsterdam, 2005, Appendix A1; Kletz, *Learning from Accidents*, 3d ed., Gulf Professional, Boston, 2001, Chap.8).

- When one modification leads to another, and then another (Kletz, *Plant/Operations Progress*, vol. 5, 1986, p. 136).
- When organizations are changed often, especially when staffing is reduced. Such changes should be studied as thoroughly as changes to equipment or processes.

Inspection and Testing of Protective Equipment All protective equipment should be scheduled for regular inspection and for testing if failure is latent (hidden); e.g., we do not know if an interlock, trip, alarm, or relief valve is in working order unless we test it. The frequency of testing or inspection depends on the failure rate and the length of time considered tolerable if it fails. Relief valves fail about once per 100 years on average, and testing every 1 or 2 years is usually adequate. Protective systems based on instruments, such as trips and alarms, fail more often, about once every couple of years on average; so more frequent testing is necessary, about once per month. Pressure systems (vessels and pipework) on noncorrosive duties can go for many years between inspections, but on some duties they may have to be inspected annually or even more often.

All protective equipment should be designed so that it can be tested or inspected, and access should be provided. Audits should include a check that the tests are carried out and the results acted on.

The supervisor, manager, or engineer responsible should be reminded when a test or inspection is due, and senior managers should be informed if it has not been carried out by the due date. Test and inspection schedules should include guidance on the methods to be used and the features that should be inspected. For example, if the time of response is critical, it should be checked.

Test results should be displayed for all to see, e.g., on a board in the control room.

Tests should be like real life. For example, a high-temperature trip failed to work despite regular testing. It was removed from its case before testing so the test did not disclose that the pointer rubbed against the case. This prevented it from indicating a high temperature.

Operators sometimes regard tests and inspections as a nuisance, interfering with the smooth operation of the plant. Operator training should emphasize that protective equipment is there for their protection and they should "own" it.

Key Performance Indicators Preparation for maintenance, the control of modifications, and the testing of protective equipment are examples of key performance indicators; i.e., taken together, they indicate the quality of the plant's and company's process safety. If they are below standard, the plant is at risk. The usual measure of safety, the lost-time accident (LTA) rate, does not measure process safety. Many companies that had a low LTA rate and assumed that their process safety was therefore under control have experienced serious fires and explosions.

SECTION **24**

Energy Resources,
Conversion,
and Utilization

PERRY'S CHEMICAL ENGINEERS' HANDBOOK

8TH EDITION



WALTER F. PODOLSKI, DAVID K. SCHMALZER
VINCENT CONRAD, DOUGLAS E. LOWENHAUPT
RICHARD A. WINSHEL, EDGAR B. KLUNDER
HOWARD G. MCILVRIED III, MASSOOD RAMEZAN
GARY J. STIEGEL, RAMESHWAR D. SRIVASTAVA
JOHN WINSLOW, PETER J. LOFTUS
CHARLES E. BENSON, JOHN M. WHEELDON
MICHAEL KRUMPELT, F. LEE SMITH

Copyright © 2008, 1997, 1984, 1973, 1963, 1950, 1941, 1934 by The McGraw-Hill Companies, Inc. All rights reserved. Manufactured in the United States of America. Except as permitted under the United States Copyright Act of 1976, no part of this publication may be reproduced or distributed in any form or by any means, or stored in a database or retrieval system, without the prior written permission of the publisher.

0-07-154231-0

The material in this eBook also appears in the print version of this title: 0-07-154206-X.

All trademarks are trademarks of their respective owners. Rather than put a trademark symbol after every occurrence of a trademarked name, we use names in an editorial fashion only, and to the benefit of the trademark owner, with no intention of infringement of the trademark. Where such designations appear in this book, they have been printed with initial caps.

McGraw-Hill eBooks are available at special quantity discounts to use as premiums and sales promotions, or for use in corporate training programs. For more information, please contact George Hoare, Special Sales, at george_hoare@mcgraw-hill.com or (212) 904-4069.

TERMS OF USE

This is a copyrighted work and The McGraw-Hill Companies, Inc. (“McGraw-Hill”) and its licensors reserve all rights in and to the work. Use of this work is subject to these terms. Except as permitted under the Copyright Act of 1976 and the right to store and retrieve one copy of the work, you may not decompile, disassemble, reverse engineer, reproduce, modify, create derivative works based upon, transmit, distribute, disseminate, sell, publish or sublicense the work or any part of it without McGraw-Hill’s prior consent. You may use the work for your own noncommercial and personal use; any other use of the work is strictly prohibited. Your right to use the work may be terminated if you fail to comply with these terms.

THE WORK IS PROVIDED “AS IS.” MCGRAW-HILL AND ITS LICENSORS MAKE NO GUARANTEES OR WARRANTIES AS TO THE ACCURACY, ADEQUACY OR COMPLETENESS OF OR RESULTS TO BE OBTAINED FROM USING THE WORK, INCLUDING ANY INFORMATION THAT CAN BE ACCESSED THROUGH THE WORK VIA HYPERLINK OR OTHERWISE, AND EXPRESSLY DISCLAIM ANY WARRANTY, EXPRESS OR IMPLIED, INCLUDING BUT NOT LIMITED TO IMPLIED WARRANTIES OF MERCHANTABILITY OR FITNESS FOR A PARTICULAR PURPOSE. McGraw-Hill and its licensors do not warrant or guarantee that the functions contained in the work will meet your requirements or that its operation will be uninterrupted or error free. Neither McGraw-Hill nor its licensors shall be liable to you or anyone else for any inaccuracy, error or omission, regardless of cause, in the work or for any damages resulting therefrom. McGraw-Hill has no responsibility for the content of any information accessed through the work. Under no circumstances shall McGraw-Hill and/or its licensors be liable for any indirect, incidental, special, punitive, consequential or similar damages that result from the use of or inability to use the work, even if any of them has been advised of the possibility of such damages. This limitation of liability shall apply to any claim or cause whatsoever whether such claim or cause arises in contract, tort or otherwise.

DOI: 10.1036/007154206X

Energy Resources, Conversion, and Utilization*

Walter F. Podolski, Ph.D. *Chemical Engineer, Electrochemical Technology Program, Argonne National Laboratory; Member, American Institute of Chemical Engineers (Section Editor)*

David K. Schmalzer, Ph.D., P.E. *Fossil Energy Program Manager, Argonne National Laboratory; Member, American Chemical Society, American Institute of Chemical Engineers (Fuels, Liquid Petroleum Fuels, Gaseous Fuels)*

Vincent Conrad, Ph.D. *Group Leader, Technical Services Development, CONSOL Energy Inc.; Member, Spectroscopy Society of Pittsburgh, Society for Analytical Chemistry of Pittsburgh, Society for Applied Spectroscopy. (Solid Fuels)*

Douglas E. Lowenhaupt, M.S. *Group Leader, Coke Laboratory, CONSOL Energy Inc.; Member, American Society for Testing and Materials, Iron and Steel Making Society, International Committee for Coal Petrology (Solid Fuels)*

Richard A. Winschel, B.S. *Director, Research Services, CONSOL Energy Inc.; Member, American Chemical Society, Technical Committee of the Coal Utilization Research Council (Solid Fuels)*

Edgar B. Klunder, Ph.D. *Project Manager, National Energy Technology Laboratory, U.S. Department of Energy (Coal Conversion)*

Howard G. McIlvried III, Ph.D. *Consulting Engineer, Science Applications International Corporation, National Energy Technology Laboratory (Coal Conversion)*

Massood Ramezan, Ph.D., P.E. *Program Manager, Science Applications International Corporation, National Energy Technology Laboratory (Coal Conversion)*

Gary J. Stiegel, P.E., M.S. *Technology Manager, National Energy Technology Laboratory, U.S. Department of Energy (Coal Conversion)*

Rameshwar D. Srivastava, Ph.D. *Principal Engineer, Science Applications International Corporation, National Energy Technology Laboratory (Coal Conversion)*

John Winslow, M.S. *Technology Manager, National Energy Technology Laboratory, U.S. Department of Energy (Coal Conversion)*

Peter J. Loftus, D.Phil. *Principal, ENVIRON International Corp.; Member, American Society of Mechanical Engineers (Heat Generation, Thermal Energy Conversion and Utilization, Energy Recovery)*

*The contributions of the late Dr. Shelby A. Miller and Dr. John D. Bacha to the seventh edition are gratefully acknowledged.

24-2 ENERGY RESOURCES, CONVERSION, AND UTILIZATION

Charles E. Benson, M.Eng. *Principal, ENVIRON International Corp.; Treasurer, American Flame Research Committee; Member, Combustion Institute (Heat Generation, Thermal Energy Conversion and Utilization, Energy Recovery)*

John M. Wheeldon, Ph.D. *Electric Power Research Institute (Fluidized-Bed Combustion)*

Michael Krumpelt, Ph.D. *Manager, Fuel Cell Technology, Argonne National Laboratory; Member, American Institute of Chemical Engineers, American Chemical Society, Electrochemical Society (Electrochemical Energy Conversion)*

(Francis) Lee Smith, Ph.D., M.Eng. *Principal, Wilcrest Consulting Associates, Houston, Texas; Member, American Institute of Chemical Engineers, Society of American Value Engineers, Water Environment Federation, Air and Waste Management Association (Energy Recovery, Economizers, Turbine Inlet Cooling)*

INTRODUCTION

FUELS

Resources and Reserves	24-4
Solid Fuels	24-4
Coal	24-4
Coke	24-6
Other Solid Fuels	24-7
Liquid Fuels	24-7
Liquid Petroleum Fuels	24-7
Nonpetroleum Liquid Fuels	24-10
Gaseous Fuels	24-10
Natural Gas	24-10
Liquefied Petroleum Gas	24-12
Other Gaseous Fuels	24-12
Fuel and Energy Costs	24-12
Coal Conversion	24-12
Coal Gasification	24-12
Coal Liquefaction	24-16

HEAT GENERATION

Combustion Background	24-21
Basic Principles	24-21
Pollutant Formation and Control in Flames	24-23
Combustion of Solid Fuels	24-25
Suspension Firing	24-25
Fuel-Bed Firing	24-28
Comparison of Suspension and Fuel-Bed Firing	24-29
Fluidized-Bed Combustion	24-29
Combustion of Liquid Fuels	24-31
Atomizers	24-31
Combustion of Gaseous Fuels	24-32
Gas Burners	24-33

THERMAL ENERGY CONVERSION AND UTILIZATION

Boilers	24-35
Boiler Design Issues	24-36

Utility Steam Generators	24-37
Industrial Boilers	24-37
Fluidized-Bed Boilers	24-39
Process Heating Equipment	24-41
Direct-Fired Equipment	24-41
Indirect-Fired Equipment (Fired Heaters)	24-41
Industrial Furnaces	24-42
Source of Heat	24-42
Function and Process Cycle	24-42
Furnace Atmosphere and Mode of Heating	24-43
Cogeneration	24-44
Typical Systems	24-45

ELECTROCHEMICAL ENERGY CONVERSION

Fuel Cells	24-45
Background	24-45
Fuel Cell Efficiency	24-46
Design Principles	24-46
Types of Fuel Cells	24-47

ENERGY RECOVERY

Economizers	24-51
Acid Dew Point	24-52
Water Dew Point	24-52
Boiler Thermal Efficiency	24-52
Conventional Economizers	24-52
Condensing Economizers	24-52
Regenerators	24-54
Checkerbrick Regenerators	24-54
Ljungstrom Heaters	24-55
Regenerative Burners	24-55
Miscellaneous Systems	24-56
Recuperators	24-56
Turbine Inlet (Air) Cooling	24-56
Evaporative Technologies	24-56
Refrigeration Technologies	24-56
Thermal Energy Storage (TES)	24-57
Summary	24-57

Nomenclature and Units

Symbol	Definition	SI units	U.S. Customary System units	Acronym	Definition
A	Area specific resistance	Ω/m^2	Ω/ft^2	AFBC	atmospheric fluidized bed combustion
c	Heat capacity	$\text{J}/(\text{kg}\cdot\text{K})$	$\text{Btu}/(\text{lb}\cdot^\circ\text{F})$	AFC	alkaline fuel cell
E	Activation energy	J/mol	$\text{Btu}/\text{lb mol}$	AGC-21	Advanced Gas Conversion Process
E	Electrical potential	V	V	BGL	British Gas and Lurgi process
f	Fugacity	kPa	psia	COE	cost of electricity
F	Faraday constant	C/mol	$\text{C}/\text{lb mol}$	COED	Char Oil Energy Development Process
ΔG	Free energy of reaction	J/mol	$\text{Btu}/\text{lb mol}$	DOE	U.S. Department of Energy
ΔH	Heat of reaction	J/mol	$\text{Btu}/\text{lb mol}$	EDS	Exxon Donor Solvent Process
i	Current density	A/m^2	A/ft^2	FBC	fluidized bed combustion
k	Rate constant	$\text{g}/(\text{h}\cdot\text{cm}^3)$	$\text{lb}/(\text{h}\cdot\text{ft}^3)$	HAO	hydrogenated anthracene oil
K	Latent heat of vaporization	kJ/kg	Btu/lb	HPO	hydrogenated phenanthrene oil
P	Pressure	kPa	psia	HRI	Hydrocarbon Research, Inc.
Q	Heating value	kJ/kg	Btu/lb	HTI	Hydrocarbon Technologies, Inc.
R	Gas constant	$\text{J}/\text{mol}\cdot\text{K}$	$\text{Btu}/\text{lb mol}\cdot^\circ\text{R}$	IGCC	integrated gasification combined-cycle
s	Relative density	Dimensionless	Dimensionless	KRW	Kellogg-Rust-Westinghouse process
T	Temperature	K	$^\circ\text{F}$	MCFC	molten carbonate fuel cell
U	Fuel utilization	percent	percent	MTG	methanol-to-gasoline process
V	Molar gas volume	m^3/mol	$\text{ft}^3/\text{lb mol}$	OTFT	once-through Fischer-Tropsch process
Z	Compressibility factor	Dimensionless	Dimensionless	PAFC	phosphoric acid fuel cell
Greek Symbol					
ϵ	Energy conversion efficiency	Percent	Percent	PC	pulverized coal
Acronyms and Unit Prefixes					
Symbol	Name	Value			
E	Exa	10^{18}		PEFC	polymer electrolyte fuel cell
G	Giga	10^9		PFBC	pressurized fluidized bed combustion
K	Kilo	10^3		Quad	10^{15} Btu
M	Mega	10^6		SASOL	South African operation of synthetic fuels plants
P	Peta	10^{15}		SMDS	Shell Middle Distillate Synthesis Process
T	Tera	10^{12}		SNG	synthetic natural gas
Z	Zetta	10^{21}		SOFC	solid oxide fuel cell
				SRC	solvent-refined coal

INTRODUCTION

GENERAL REFERENCES: Loftness, *Energy Handbook*, 2d ed., Van Nostrand Reinhold, New York, 1984. Energy Information Administration, *Emissions of Greenhouse Gases in the United States 2003*, U.S. Dept. of Energy, DOE/EIA-0573 (2004). Howes and Fainberg (eds.), *The Energy Source Book*, American Institute of Physics, New York, 1991. Johansson, Kelly, Reddy, and Williams (eds.), Burnham (exec. ed.), *Renewable Energy—Sources for Fuels and Electricity*, Island Press, Washington, 1993. Turner, *Energy Management Handbook* 5th ed., The Fairmont Press, Lilburn, Ga., 2004. *National Energy Policy*, National Energy Policy Development Group, Washington, May 2001.

Energy is usually defined as the capacity to do work. Nature provides us with numerous sources of energy, some difficult to utilize efficiently (e.g., solar radiation and wind energy), others more concentrated or energy dense and therefore easier to utilize (e.g., fossil fuels). Energy sources can be classified also as *renewable* (solar and nonsolar) and *nonrenewable*. Renewable energy resources are derived in a number of ways: gravitational forces of the sun and moon, which create the tides; the rotation of the earth combined with solar energy, which generates the currents in the ocean and the winds; the decay of radioactive minerals and the interior heat of the earth, which provide geothermal energy; photosynthetic production of organic matter; and the direct heat of the sun. These energy sources are called renewable because they are either continuously replenished or, for all practical purposes, are inexhaustible.

Nonrenewable energy sources include the fossil fuels (natural gas, petroleum, shale oil, coal, and peat) as well as uranium. Fossil fuels are both energy dense and widespread, and much of the world's industrial, utility, and transportation sectors rely on the energy contained in them. Concerns over global warming notwithstanding, fossil fuels will remain the dominant fuel form for the foreseeable future. This is so for two reasons: (1) the development and deployment of new technologies able to utilize renewable energy sources such as solar, wind, and biomass are uneconomic at present, in most part owing to the diffuse or intermittent nature of the sources; and (2) concerns persist over storage and/or disposal of spent nuclear fuel and nuclear proliferation.

Fossil fuels, therefore, remain the focus of this section; their principal use is in the generation of heat and electricity in the industrial, utility, and commercial sectors, and in the generation of shaft power in transportation. The material in this section deals primarily with the conversion of the chemical energy contained in fossil fuels to heat and electricity. Material from *Perry's Chemical Engineers' Handbook*, 7th ed., Sec. 27, has been updated and condensed. Recent improvements in materials and manufacturing methods have brought fuel cells closer to being economic for stationary and transportation power generation, but additional advances are required for broad adoption.

FUELS

RESOURCES AND RESERVES

Proven worldwide energy resources are large. The largest remaining known reserves of crude oil, used mainly for producing transportation fuels, are located in the Middle East, along the equator, and in the former Soviet Union. U.S. proven oil reserves currently account for only about 3 percent of the world's total. Large reserves of natural gas exist in the former Soviet Union and the Middle East. Coal is the most abundant fuel on earth and the primary fuel for electricity in the United States, which has the largest proven reserves. Annual world consumption of energy is still currently less than 1 percent of combined world reserves of fossil fuels. The resources and reserves of the principal fossil fuels in the United States—coal, petroleum, and natural gas—follow.

Fuel	ZJ*		
	Proven reserves	Discovered conventionally reservoiried	Total estimated resource
Coal	6.48	12.5	96.2
Petroleum	0.16	0.5	1.2
Natural gas	0.21	0.4	1.6

*ZJ = 10²¹ J. (To convert to 10¹⁸ Btu, multiply by 0.948.)

The energy content of fossil fuels in commonly measured quantities is as follows.

	Energy content	
Bituminous and anthracite coal	30.2 MJ/kg	26 × 10 ⁶ Btu/US ton
Lignite and subbituminous coal	23.2 MJ/kg	20 × 10 ⁶ Btu/US ton
Crude oil	38.5 MJ/L	5.8 × 10 ⁶ Btu/bbl
Natural-gas liquids	25.2 MJ/L	3.8 × 10 ⁶ Btu/bbl
Natural gas	38.4 MJ/m ³	1032 Btu/ft ³

1 bbl = 42 US gal = 159 L = 0.159 m³

SOLID FUELS

Coal

GENERAL REFERENCES: Lowry (ed.), *Chemistry of Coal Utilization*, Wiley, New York, 1945; suppl. vol., 1963; 2d suppl. vol., Elliott (ed.), 1981. Van Krevelen, *Coal*, Elsevier, Amsterdam, 1961. *Annual Book of ASTM Standards*, sec. 5, ASTM International, West Conshohocken, Pa., 2004. *Methods of Analyzing and Testing Coal and Coke*, U.S. Bureau of Mines Bulletin, 638, 1967.

Origin Coal originated from the arrested decay of the remains of trees, bushes, ferns, mosses, vines, and other forms of plant life, which flourished in huge swamps and bogs many millions of years ago during prolonged periods of humid, tropical climate and abundant rainfall. The precursor of coal was peat, which was formed by bacterial and chemical action on the plant debris. Subsequent actions of heat, pressure, and other physical phenomena metamorphosed the peat to the various ranks of coal as we know them today. Because of the various degrees of the metamorphic changes during this process, coal is not a uniform substance; no two coals are ever the same in every respect.

Classification Coals are classified by rank, i.e., according to the degree of metamorphism in the series from lignite to anthracite. Table 24-1 shows the classification system described in ASTM D 388-99 (2004) (ASTM International, op. cit.). The heating value on the moist *mineral-matter-free* (mmf) basis, and the fixed carbon, on the dry mmf basis, are the bases of this system. The lower-rank coals are classified according to the heating value, kJ/kg (Btu/lb), on a moist mmf basis. The agglomerating character is used to differentiate between adjacent groups. Coals are considered agglomerating if the coke button remaining from the test for volatile matter will support a specified weight or if the button swells or has a porous cell structure.

The Parr formulas, Eqs. (24-1) to (24-3), are used for classifying coals according to rank. The Parr formulas are employed in litigation cases.

$$F' = \frac{100(F - 0.15S)}{100 - (M + 1.08A + 0.55S)} \quad (24-1)$$

TABLE 24-1 Classification of Coals by Rank*

Class/group	Fixed carbon limits (dry, mineral-matter-free basis), %		Volatile matter limits (dry, mineral-matter-free basis), %		Gross calorific value limits (moist, mineral-matter-free basis)†				Agglomerating character
	Equal or greater than	Less than	Greater than	Equal or less than	MJ/kg		Btu/lb		
					Equal or greater than	Less than	Equal or greater than	Less than	
Anthracitic:									
Meta-anthracite	98	—	—	2	—	—	—	—	Nonagglomerating
Anthracite	92	98	2	8	—	—	—	—	
Semianthracite‡	86	92	8	14	—	—	—	—	
Bituminous:									
Low-volatile bituminous coal	78	86	14	22	—	—	—	—	Commonly agglomerating¶
Medium-volatile bituminous coal	69	78	22	31	—	—	—	—	
High-volatile A bituminous coal	—	69	31	—	32.6§	—	14,000§	—	
High-volatile B bituminous coal	—	—	—	—	30.2§	32.6	13,000§	14,000	
High-volatile C bituminous coal	—	—	—	—	26.7	30.2	11,500	13,000	
					24.4	26.7	10,500	11,500	Agglomerating
Subbituminous:									
Subbituminous A coal	—	—	—	—	24.4	26.7	10,500	11,500	Nonagglomerating
Subbituminous B coal	—	—	—	—	22.1	24.4	9,500	10,500	
Subbituminous C coal	—	—	—	—	19.3	22.1	8,300	9,500	
Lignitic:									
Lignite A	—	—	—	—	14.7	19.3	6,300	8,300	
Lignite B	—	—	—	—	—	14.7	—	6,300	

Adapted, with permission, from D388-99, Standard Classification of Coals by Rank; copyright ASTM International, 100 Barr Harbor Drive, West Conshohocken, PA 19428.

*This classification does not apply to certain coals, as discussed in source.

†Moist refers to coal containing its natural inherent moisture but not including visible water on the surface of the coal.

‡If agglomerating, classify in low-volatile group of the bituminous class.

§Coals having 69 percent or more fixed carbon on the dry, mineral-matter-free basis shall be classified according to fixed carbon, regardless of gross calorific value.

¶It is recognized that there may be nonagglomerating varieties in these groups of the bituminous class and that there are notable exceptions in the high-volatile C bituminous group.

$$V' = 100 - F' \quad (24-2)$$

$$Q' = \frac{100(Q - 50S)}{100 - (M + 1.08A + 0.55S)} \quad (24-3)$$

where M , F , A , and S are weight percentages, on a moist basis, of moisture, fixed carbon, ash, and sulfur, respectively; Q and Q' are calorific values (Btu/lb), on a moist non-mmf basis and a moist mmf basis, respectively. (Btu/lb = 2326 J/kg)

Composition and Heating Value Coal analyses are reported on several bases, and it is customary to select the basis best suited to the application. The **as-received** basis represents the weight percentage of each constituent in the sample as received in the laboratory. The sample itself may be coal as fired, as mined, or as prepared for a particular use. The **moisture-free** (dry) basis is a useful basis because performance calculations can be easily corrected for the actual moisture content at the point of use. The **dry, ash-free** basis is frequently used to approximate the rank and source of a coal. For example, the heating value of coal from a given deposit is remarkably constant when calculated on this basis.

The composition of the coal is reported in two different ways: the proximate analysis and the ultimate analysis, both expressed in weight percent. The **proximate analysis** [ASTM D 3172-89 (2002), ASTM International, op. cit.] is the determination by prescribed methods of moisture, volatile matter, fixed carbon, and ash. The moisture in coal consists of inherent moisture, also called equilibrium moisture, and surface moisture. Free moisture is that moisture lost when coal is air-dried under standard low-temperature conditions. The **volatile matter** is the portion of coal which, when the coal is heated in the absence of air under prescribed conditions, is liberated as gases and vapors. Volatile matter does not exist by itself in coal, except for a little absorbed methane, but results from thermal decomposition of the coal substance. **Fixed carbon**, the residue left after the volatile matter is driven off, is calculated by subtracting from 100 the percentages of moisture, volatile matter, and ash of the proximate analysis. In addition to carbon, it may contain several tenths of a percent of hydrogen and oxygen, 0.4 to 1.0 percent nitrogen, and about half of the sulfur that was in the coal. **Ash** is the inorganic residue that remains after the coal has been burned under specified conditions, and it is composed largely of compounds of silicon, aluminum, iron, and calcium, and minor amounts of compounds of magnesium, sodium, potassium, phosphorus, sulfur, and titanium. Ash may vary considerably from the original mineral matter, which is largely kaolinite, illite, montmorillonite, quartz, pyrites, and calcite. The **ultimate analysis** [ASTM D 3176-89 (2002), ASTM International, op. cit.] is the determination by prescribed methods of the ash, carbon, hydrogen, nitrogen, sulfur, and (by difference) oxygen. Other, minor constituent elements are also sometimes determined, most notably chlorine.

The **heating value**, or **calorific value**, expressed as kJ/kg (Btu/lb), is the heat produced at constant volume by the complete combustion of a unit quantity of coal in an oxygen-bomb calorimeter under specified conditions (ASTM D 5865-04, ASTM International, op. cit.). The result includes the latent heat of vaporization of the water in the combustion products and is called the gross heating or **high heating value** (HHV) Q_h . And Q_l in Btu/lb ($\times 2.326 = \text{kJ/kg}$) on a dry basis can be approximated by a formula developed by the Institute of Gas Technology:

$$Q_h = 146.58C + 568.78H + 29.4S - 6.58A - 51.53(O + N) \quad (24-4)$$

where C , H , S , A , O , and N are the weight percentages on a dry basis of carbon, hydrogen, sulfur, ash, oxygen, and nitrogen, respectively. The heating value when the water is not condensed is called the **low heating value** (LHV) Q_l and is obtained from

$$Q_l = Q_h - K \cdot W \quad (24-5)$$

where W = weight of water in the combustion products/weight of fuel burned. The factor K is the latent heat of vaporization at the partial pressure of the vapor in the gas, which, at 20°C, is 2395 kJ/kg (1030 Btu/lb) of water. Thus,

$$Q_l = Q_h - \%H \cdot 214 \quad \text{kJ/kg} \quad (24-6)$$

$$Q_l = Q_h - \%H \cdot 92.04 \quad \text{Btu/lb} \quad (24-7)$$

where $\%H$ = weight percent hydrogen in the coal and all values are on an as-determined (including moisture) basis.

Sulfur Efforts to abate atmospheric pollution have drawn considerable attention to the sulfur content of coal, since the combustion of coal results in the discharge to the atmosphere of sulfur oxides. Sulfur occurs in coal in three major forms: as organic sulfur (20 to 80 percent of the sulfur), which is a part of the coal substance; as pyrite (FeS_2); and as sulfate (<5 percent of the sulfur in unoxidized coals). Organic sulfur is chemically bound to the coal substance, and severe treatment is necessary to break the chemical bonds to remove the sulfur. There is no existing economical method that will remove organic sulfur. Pyritic sulfur can be partially removed by using standard coal-washing equipment. The degree of pyrite removal depends on the size of the coal and the size and distribution of the pyrite particles.

The sulfur content of U.S. coals varies widely, ranging from a low of 0.2 percent to as much as 7 percent by weight, on a dry basis. The estimated remaining (as of 1997) recoverable U.S. coal reserves of all ranks, by sulfur content and major producing region, are shown in Table 24-2. The values in the table are in units of 10^9 metric tonnes (Pg) as reported in *U.S. Coal Reserves: 1997 Update*, DOE/EIA-0529(97). Extensive data on sulfur and sulfur reduction potential, including washability, in U.S. coals are given in *Sulfur and Ash Reduction Potential and Selected Chemical and Physical Properties of United States Coal* (U.S. Dept. of Energy, DOE/PETC, TR-90/7, 1990; TR-91/1 and TR-91/2, 1991).

Mercury Impending regulations limiting the emission of mercury from coal-fired furnaces have created great interest in knowing the concentration of mercury in various coals, determining the fate of mercury during combustion, and developing methods to control mercury emissions to the atmosphere. Most commercially produced U.S. coals have mercury contents of about 0.05 to 0.2 mg/kg, dry basis, although numerous individual coals fall outside that range. Depending on the specific coal properties, furnace conditions, and type and configuration of pollution control devices with which the furnace is equipped, less than 10 percent or more than 90 percent of the coal mercury will be emitted to the atmosphere with the flue gas. The chemical form of the vaporized mercury in the flue gas, whether elemental or ionic, is important, because ionic mercury is easier to capture with available technology than is elemental mercury. The chemical form is apparently influenced by the chlorine content of the coal: coals with higher chlorine contents (0.05 percent and higher) tend to produce mainly ionic mercury in their flue gases, and thus the mercury emissions from these coals are more easily controlled.

Coal-Ash Characteristics and Composition When coal is to be burned, used in steel making, or gasified, it is often important to know the ash fusibility, or the temperatures at which formed pyramids of ash attain certain defined stages of fusing in either a mildly reducing or an oxidizing atmosphere; these temperatures are known as the initial deformation, softening, hemispherical, and fluid temperatures. The procedure for determining the fusibility of coal ash is prescribed by ASTM D 1857-04 (ASTM International, op. cit.). The ash fusibility temperatures are most often used as indicators of the tendency of the ash to form sintered or fused masses, which can impede gas flow through a grate and impair heat flow through furnace heat-transfer surfaces, or as indicators of the flowability of ash in slag-tap and cyclone furnaces. However, because ash fusibility is not an infallible index of ash behavior in practice, care is needed in using fusibility data for designing and operating purposes. There is an excellent discussion on this subject in *Steam: Its Generation and Use* (40th ed., Babcock & Wilcox Co., New York, 1992).

TABLE 24-2 Estimate of Recoverable U.S. Coal Reserves by Sulfur Ranges and Regions (Pg)

	Low sulfur*	Medium sulfur*	High sulfur*	Total
Appalachia	10.6	18.4	21.1	50.2
Interior	0.7	9.1	52.6	62.4
West	79.6	49.5	8.0	137.1
U.S. total	90.9	77.0	81.7	249.6

*Sulfur content ranges defined in units of kg S/kJ (lb S/MBtu) as follows: low sulfur, < 0.29 (< 0.60); medium sulfur, 0.29 to 0.80 (0.61 to 1.67); high sulfur, > 0.80 (> 1.67).

The composition of coal ash varies widely. Calculated as oxides, the composition (percent by weight) varies as follows:

SiO ₂	20–60
Al ₂ O ₃	10–35
Fe ₂ O ₃	5–35
CaO	1–20
MgO	0.3–4
TiO ₂	0.5–2.5
P ₂ O ₅	0.01–1
Na ₂ O and K ₂ O	1–4
SO ₃	0.1–12

Knowledge of the composition of coal ash is useful for estimating and predicting the fouling and corrosion of heat-exchange surfaces in pulverized-coal-fired furnaces and in coke making. Multiple correlations for ash composition and ash fusibility are discussed in *Coal Conversion Systems Technical Data Book* (part IA, U.S. Dept. of Energy, 1984). The slag viscosity-temperature relationship provided in that reference for completely melted slag is

$$\text{Log viscosity} = \frac{10^7 M}{(T - 150)^2 + C} \quad (24-8)$$

where viscosity is in poise ($\times 0.1 = \text{Pa}\cdot\text{s}$), $M = 0.00835(\text{SiO}_2) + 0.00601(\text{Al}_2\text{O}_3) - 0.109$, $C = 0.0415(\text{SiO}_2) + 0.0192(\text{Al}_2\text{O}_3) + 0.0276$ (equivalent Fe_2O_3) + $0.0160(\text{CaO}) - 3.92$, and $T = \text{temperature, K}$.

The oxides in parentheses are the weight percentages of these oxides when $\text{SiO}_2 + \text{Al}_2\text{O}_3 + \text{Fe}_2\text{O}_3 + \text{CaO} + \text{MgO}$ are normalized to 100 percent.

Physical Properties The *free-swelling index* (FSI) measures the tendency of a coal to swell when burned or gasified in fixed or fluidized beds. Coals with a high FSI (greater than 4) can usually be expected to cause difficulties in such beds. Details of the test are given by the ASTM D 720–91 (2004) (American Society for Testing and Materials, op. cit.) and U.S. Bureau of Mines Report of Investigations 3989.

The *Hardgrove grindability index* (HGI) indicates the ease (or difficulty) of grinding coal and is complexly related to physical properties such as hardness, fracture, and tensile strength. The Hardgrove machine is usually employed (ASTM D 409-02, American Society for Testing and Materials, op. cit.). It determines the relative grindability or ease of pulverizing coal in comparison with a standard coal, chosen as 100 grindability. The FSI and HGI of some U.S. coals are given in Bureau of Mines Information Circular 8025 for FSI and HGI data for 2812 and 2339 samples, respectively.

The *bulk density* of broken coal varies according to the specific gravity, size distribution, and moisture content of the coal and the amount of settling when the coal is piled. Following are some useful approximations of the bulk density of various ranks of coal.

	kg/m ³	lb/ft ³
Anthracite	800–930	50–58
Bituminous	670–910	42–57
Lignite	640–860	40–54

Size stability refers to the ability of coal to withstand breakage during handling and shipping. It is determined by dropping a sample of coal onto a steel plate in a specified manner and comparing the size distribution before and after the test, as in ASTM D 440-86 (2002) (ASTM International, op. cit.). A complementary property, *friability*, is the tendency of coal to break during repeated handling, and it is determined by the standard tumbler test, as in ASTM D 441-86 (2002) (ASTM International, op. cit.).

Spier's *Technical Data on Fuels* gives the *specific heat* of dry, ash-free coal as follows.

	kJ/(kg·K)	Btu/(lb·°F)
Anthracite	0.92–0.96	0.22–0.23
Bituminous	1.0–1.1	0.24–0.25

The relationships between specific heat and water content and between specific heat and ash content are linear. Given the specific heat on a dry, ash-free basis, it can be corrected to an as-received

basis. The specific heat and enthalpy of coal to 1366 K (2000°F) are given in *Coal Conversion Systems Technical Data Book* (part IA, U.S. Dept. of Energy, 1984).

The *mean specific heat* of coal ash and slag, which is used for calculating heat balances on furnaces, gasifiers, and other coal-consuming systems, follows.

Temperature range		Mean specific heat	
K	°F	kJ/(kg·K)	Btu/(lb·°F)
273–311	32–100	0.89	0.21
273–1090	32–1500	0.94	0.22
273–1310	32–1900	0.97	0.23
273–1370	32–2000	0.98	0.24
273–1640	32–2500	1.1	0.27

Coke Coke is the solid, cellular, infusible material remaining after the carbonization of coal, pitch, petroleum residues, and certain other carbonaceous materials. The varieties of coke generally are identified by prefixing a word to indicate the source, if other than coal, (e.g., *petroleum coke*), the process by which a coke is manufactured (e.g., vertical slot oven coke), or the end use (e.g., blast furnace coke). The carbonization of coal into coke involves a complex set of physical and chemical changes. Some of the physical changes are softening, devolatilization, swelling, and resolidification. Some of the accompanying chemical changes are cracking, depolymerization, polymerization, and condensation. More detailed theoretical information is given in the general references listed in the beginning of the section on coal.

High-Temperature Coke (1173 to 1423 K or 1652 to 2102°F.) Essentially all coal-derived coke produced in the United States is high-temperature coke for metallurgical applications; its production comprises nearly 5 percent of the total bituminous coal consumed in the United States. About 90 percent of this type of coke is made in slot-type by-product recovery ovens, and the rest is made in heat recovery ovens. Blast furnaces use about 90 percent of the production, the rest going mainly to foundries and gas plants. The ranges of chemical and physical properties of metallurgical coke used in the United States are given in Table 24-3. Blast furnaces use about 90 percent of the production, the rest going mainly to foundries and gas plants.

The typical by-product yields per U.S. ton (909 kg) of dry coal from high-temperature carbonization in ovens with inner-wall temperatures from 1273 to 1423 K (1832 to 2102°F) are: coke, 653 kg (1437 lb); gas, 154 kg (11,200 ft³); tar, 44 kg (10 gal); water, 38 kg (10 gal); light oil, 11 kg (3.3 gal); and ammonia, 2.2 kg (4.8 lb).

Foundry Coke This coke must meet specifications not required of blast furnace coke. The volatile matter should not exceed 1.0 percent, the sulfur should not exceed 0.7 percent, the ash should not exceed 8.0 percent, and the size should exceed 100 mm (4 in).

Low- and Medium-Temperature Coke (773 to 1023 K or 932 to 1382°F.) Cokes of this type are no longer produced in the United States to a significant extent. However, there is some interest in low-temperature carbonization as a source of both hydrocarbon liquids and gases to supplement petroleum and natural-gas resources.

Pitch Coke and Petroleum Coke Pitch coke is made from coal-tar pitch, and petroleum coke is made from petroleum residues from petroleum refining. Pitch coke has about 1.0 percent volatile matter, 1.0 percent ash, and less than 0.5 percent sulfur on the as-received basis. There are two kinds of petroleum coke: delayed coke and fluid coke. Delayed coke is produced by heating a gas oil or heavier feedstock to

TABLE 24-3 Chemical and Physical Properties of Metallurgical Cokes Used in the United States

Property	Range of values
Volatile matter	0.5–1.0%, dry basis
Ash content	8–12%, dry basis
Sulfur content	0.6–1.0%, dry basis
Stability factor	55–65
Hardness factor	60–68
Strength after reaction	55–65
Apparent specific gravity (water = 1.0)	0.8–0.99

TABLE 24-4 Waste Fuel Analysis

Type of waste	Heating value, Btu/lb	Percentage composition by weight					Density, lb/ft ³
		Volatiles	Moisture	Ash	Sulfur	Dry combustible	
Paper	7,572	84.6	10.2	6.0	0.20		
Wood	8,613	84.9	20.0	1.0	0.05		
Rags	7,652	93.6	10.0	2.5	0.13		
Garbage	8,484	53.3	72.0	16.0	0.52		
Coated fabric: rubber	10,996	81.2	1.04	21.2	0.79	78.80	23.9
Coated felt: vinyl	11,054	80.87	1.50	11.39	0.80	88.61	10.7
Coated fabric: vinyl	8,899	81.06	1.48	6.33	0.02	93.67	10.1
Polyethylene film	19,161	99.02	0.15	1.49	0	98.51	5.7
Foam: scrap	12,283	75.73	9.72	25.30	1.41	74.70	9.1
Tape: resin-covered glass	7,907	15.08	0.51	56.73	0.02	43.27	9.5
Fabric: nylon	13,202	100.00	1.72	0.13	0	99.87	6.4
Vinyl scrap	11,428	75.06	0.56	4.56	0.02	95.44	23.4

SOURCE: From Heschels, *MECAR Conference on Waste Disposal*, New York, 1968; and *Refuse Collection Practice*, 3d ed., American Public Works Association, Chicago, 1966.

To convert British thermal units per pound to joules per kilogram, multiply by 2326; to convert pounds per cubic foot to kilograms per cubic meter, multiply by 16.02.

755 to 811 K (900 to 1000°F) and spraying it into a large vertical cylinder where cracking and polymerization reactions occur. Fluid coke is made in a fluidized-bed reactor where preheated feed is sprayed onto a fluidized bed of coke particles. Coke product is continuously withdrawn by size classifiers in the solids loop of the reactor system. Petroleum coke contains many of the impurities from its feedstock; thus, the sulfur content is usually high, and appreciable quantities of vanadium may be present. Ranges of composition and properties are as follows:

Composition and properties	Delayed coke	Fluid coke
Volatile matter, wt %	8–18	3.7–7.0
Ash, wt %	0.05–1.6	0.1–2.8
Sulfur, wt %	—	1.5–10.0
Grindability index	40–60	20–30
True density, g/cm ³	1.28–1.42	1.5–1.6

Most petroleum coke is used for fuel, but some premium delayed coke known as “needle coke” is used to make anodes for the aluminum industry. That coke is first calcined to less than 0.5 percent volatiles at 1300 to 1400°C before it is used to make anodes.

Other Solid Fuels

Coal Char Coal char is, generically, the nonagglomerated, nonfusible residue from the thermal treatment of coal; however, it is more specifically the solid residue from low- or medium-temperature carbonization processes. Char is used as a fuel or a carbon source. Chars have compositions intermediate between those of coal and coke: the volatile matter, sulfur content, and heating values of the chars are lower, and the ash content is higher, than those of the original coal.

Peat Peat is partially decomposed plant matter that has accumulated in a water-saturated environment. It is the precursor of coal but is not classified as coal. Peat is used extensively as a fuel primarily in Ireland and the former Soviet Union, but in the United States, its main use is in horticulture and agriculture. Although analyses of peat vary widely, a typical high-grade peat has 90 percent water, 3 percent fixed carbon, 5 percent volatile matter, 1.5 percent ash, and 0.10 percent sulfur. The moisture-free heating value is approximately 20.9 MJ/kg (9000 Btu/lb).

Wood Typical higher heating values are 20 MJ/kg (8600 Btu/lb) for oven-dried hardwood and 20.9 MJ/kg for oven-dried softwood. These values are accurate enough for most engineering purposes. U.S. Department of Agriculture Handbook 72 (revised 1974) gives the specific gravity of the important softwoods and hardwoods, useful if heating value on a volume basis is needed.

Charcoal Charcoal is the residue from the destructive distillation of wood. It absorbs moisture readily, often containing as much as 10 to 15 percent water. In addition, it usually contains about 2 to 3 percent ash and 0.5 to 1.0 percent hydrogen. The heating value of charcoal is about 27.9 to 30.2 MJ/kg (12,000 to 13,000 Btu/lb).

Solid Wastes and Biomass The generation of large quantities of solid wastes is a significant feature of affluent societies. In the United

States in 2001 the rate was about 2 kg (4.4 lb) per capita per day, or nearly 208 Tg (229 M short tons) per year. Table 24-4 shows that the composition of miscellaneous refuse is fairly uniform, but size and moisture variations cause major difficulties in efficient, economical disposal. The fuel value of municipal solid wastes is usually sufficient to enable self-supporting combustion, leaving only the incombustible residue and reducing by 90 percent the volume of waste consigned to landfill. The heat released by the combustion of waste can be recovered and utilized, although this is not always economically feasible.

Wood, wood scraps, bark, and wood product plant waste streams are major elements of biomass, industrial, and municipal solid waste fuels. In 1991, about 1.7 EJ (1.6×10^{15} Btu [quads]) of energy were obtained from wood and wood wastes, representing about 60 percent of the total biomass-derived energy in the United States. *Bagasse* is the solid residue remaining after sugarcane has been crushed by pressure rolls. It usually contains from 40 to 50 percent water. The dry bagasse has a heating value of 18.6 to 20.9 MJ/kg (8000 to 9000 Btu/lb). Tire-derived fuel (TDF), which is produced by shredding and processing waste tires and which has a heating value of 30.2 to 37.2 MJ/kg (13,000 to 16,000 Btu/lb), is an important fuel for use in cement kilns and as a supplement to coal in steam raising.

LIQUID FUELS

Liquid Petroleum Fuels The discussion here focuses on burner fuels rather than transportation fuels. There is overlap, particularly for fuels in the distillate or “gas oil” range. Other factors such as the Tier II gasoline specifications, the ultralow-sulfur diesel specifications, and the gradual reduction in crude quality impact refining and blending practices for burner fuels. The principal liquid fuels are made by fractional distillation of crude petroleum (a mixture of hydrocarbons and hydrocarbon derivatives ranging from methane to heavy bitumen). As many as one-quarter to one-half of the molecules in crude may contain sulfur atoms, and some contain nitrogen, oxygen, vanadium, nickel, or arsenic. Desulfurization, hydrogenation, cracking (to lower molecular weight), and other refining processes may be performed on selected fractions before they are blended and marketed as fuels. Viscosity, gravity, and boiling ranges are given in Table 24-5.

Specifications The American Society for Testing and Materials has developed specifications (*Annual Book of ASTM Standards*, Conshohocken, Pa., updated annually) that are widely used to classify fuels. Table 24-5 shows fuels covered by ASTM D 396, Standard Specification for Fuel Oils. D 396 omits kerosenes (low-sulfur, clean-burning No. 1 fuels for lamps and freestanding flueless domestic heaters), which are covered separately by ASTM D 3699.

In drawing contracts and making acceptance tests, refer to the pertinent ASTM standards. *ASTM Standards* contain specifications (classifications) and test methods for burner fuels (D 396), motor and aviation gasolines (D 4814-03 and D 910-03), diesel fuels (D 975-03), and aviation and gas-turbine fuels (D 1655-03 and D 2880-03).

24-8 ENERGY RESOURCES, CONVERSION, AND UTILIZATION

TABLE 24-5 Detailed Requirements for Fuel Oils^a

Property	ASTM Test Method ^b	No. 1 Low Sulfur ^c	No. 1 ^c	No. 2 Low Sulfur ^c	No. 2 ^c	Grade No. 4 (Light) ^e	No. 4	No. 5 (Light)	No. 5 (Heavy)	No. 6
Flash point, °C, min	D 93—Proc. A D 93—Proc. B	38 —	38 —	38 —	38 —	38 —	— 55	— 55	— 55	— 60
Water and sediment, % vol, max	D 2709 D 95 + D 473 D 86	0.05 —	0.05 —	0.05 —	0.05 —	— (0.50) ^d	— (0.50) ^d	— (1.00) ^d	— (1.00) ^d	— (2.00) ^d
Distillation temperature, °C										
10% volume recovered, max		215	215	—	—	—	—	—	—	—
90% volume recovered, min		—	—	282	282	—	—	—	—	—
90% volume recovered, max		288	288	338	338	—	—	—	—	—
Kinematic viscosity at 40°C, mm ² /s	D 445									
min		1.3	1.3	1.9	1.9	1.9	>5.5	—	—	—
max		2.1	2.1	3.4	3.4	5.5	24.0 ^e	—	—	—
Kinematic viscosity at 100°C, mm ² /s	D 445									
min		—	—	—	—	—	—	5.0	9.0	15.0
max		—	—	—	—	—	—	8.9 ^e	14.9 ^e	50.0 ^e
Ramsbottom carbon residue on 10% distillation residue, % mass, max	D 524	0.15	0.15	0.35	0.35	—	—	—	—	—
Ash, % mass, max	D 482	—	—	—	—	0.05	0.10	0.15	0.15	—
Sulfur, % mass max ^f	D 129 D 2622	— 0.05	— 0.50	— 0.05	— 0.50	—	—	—	—	—
Copper strip corrosion rating, max, 3 h at 50°C	D 130	No. 3	No. 3	No. 3	No. 3	—	—	—	—	—
Density at 15°C, kg/m ³	D 1298									
min		—	—	—	—	>876 ^e	—	—	—	—
max		850	850	876	876	—	—	—	—	—
Pour point, °C, max ^h	D 97	-18	-18	-6	-6	-6	-6	—	—	ⁱ

Adapted, with permission, from D396-06, Standard Specification for Fuel Oils; copyright ASTM International, 100 Barr Harbor Drive, West Conshohocken, PA 19428.

^a It is the intent of these classifications that failure to meet any requirement of a given grade does not automatically place an oil in the next lower grade unless in fact it meets all requirements of the lower grade. However, to meet special operating conditions, modifications of individual limiting requirements may be agreed upon among the purchaser, seller, and manufacturer.

^b The test methods indicated are the approved referee methods. Other acceptable methods are indicated in Sections 2 and 5.1 of ASTM D 396.

^c Under U.S. regulations, Grades No. 1, No. 1 Low Sulfur, No. 2, No. 2 Low Sulfur, and No. 4 (Light) are required by 40 CFR Part 80 to contain a sufficient amount of the dye Solvent Red 164 so its presence is visually apparent. At or beyond terminal storage tanks, they are required by 26 CFR Part 48 to contain the dye Solvent Red 164 at a concentration spectrally equivalent to 3.9 lb per thousand barrels of the solid dye standard Solvent Red 26.

^d The amount of water by distillation by Test Method D 95 plus the sediment by extraction by Test method D 473 shall not exceed the value shown in the table. For Grade No. 6 fuel oil, the amount of sediment by extraction shall not exceed 0.50 mass percent, and a deduction in quantity shall be made for all water and sediment in excess of 1.0 mass percent.

^e Where low sulfur fuel oil is required, fuel oil falling in the viscosity range of a lower numbered grade down to and including No. 4 can be supplied by agreement between the purchaser and supplier. The viscosity range of the initial shipment shall be identified, and advance notice shall be required when changing from one viscosity range to another. This notice shall be in sufficient time to permit the user to make the necessary adjustments.

^f Other sulfur limits may apply in selected areas in the United States and in other countries.

^g This limit ensures a minimum heating value and also prevents misrepresentation and misapplication of this product as Grade No. 2.

^h Lower or higher pour points can be specified whenever required by conditions of storage or use. When a pour point less than -18°C is specified, the minimum viscosity at 40°C for Grade No. 2 shall be 1.7 mm²/s and the minimum 90% recovered temperature shall be waived.

ⁱ Where low sulfur fuel oil is required, Grade No. 6 fuel oil will be classified as Low Pour (+15°C max) or High Pour (no max). Low Pour fuel oil should be used unless tanks and lines are heated.

ASTM D 4057-95 contains procedures for sampling bulk oil in tanks, barges, etc.

Fuel specifications from different sources may differ in test limits on sulfur, density, etc., but the same general categories are recognized worldwide: kerosene-type vaporizing fuel, distillate (or gas oil) for atomizing burners, and more viscous blends and residuals for commerce and heavy industry.

Foreign specifications are generally available from the American National Standards Institute, New York; United States federal specifications, at Naval Publications and Forms, Philadelphia. The International Association for Stability, Handling and Use of Liquid Fuels maintains a web site, www.iash.net, with extensive references to fuel standards.

Equipment manufacturers and large-volume users often write fuel specifications to suit particular equipment, operating conditions, and economics. Nonstandard test procedures and restrictive test limits should be avoided; they reduce the availability of fuel and increase its cost.

Bunker-fuel specifications for merchant vessels were described by ASTM D 2069, Standard Specification for Marine Fuels, which was withdrawn in 2003. Specifications under ASTM D-396 or foreign specifications may be substituted as appropriate.

Chemical and Physical Properties Petroleum fuels contain paraffins, isoparaffins, naphthenes, and aromatics, plus organic sulfur, oxygen, and nitrogen compounds that were not removed by refining. Olefins are absent or negligible except when created by severe refining. Vacuum-tower distillate with a final boiling point equivalent to 730 to 840 K (850 to 1050°F) at atmospheric pressure may contain from 0.1 to

0.5 ppm vanadium and nickel, but these metal-bearing compounds do not distill into No. 1 and 2 fuel oils.

Black, viscous residuum directly from the still at 410 K (390°F) or higher serves as fuel in nearby furnaces or may be cooled and blended to make commercial fuels. Diluted with 5 to 20 percent distillate, the blend is No. 6 fuel oil. With 20 to 50 percent distillate, it becomes No. 4 and No. 5 fuel oils for commercial use, as in schools and apartment houses. Distillate-residual blends also serve as diesel fuel in large stationary and marine engines. However, distillates with inadequate solvent power will precipitate asphaltene and other high-molecular-weight colloids from *visbroken* (severely heated) residuals. A blotter test, ASTM D 4740-02, will detect sludge in pilot blends. Tests employing centrifuges, filtration (D 4870-99), and microscopic examination have also been used.

No. 6 fuel oil contains from 10 to 500 ppm vanadium and nickel in complex organic molecules, principally porphyrins. These cannot be removed economically, except incidentally during severe hydrodesulfurization (Amero, Silver, and Yanik, *Hydrodesulfurized Residual Oils as Gas Turbine Fuels*, ASME Pap. 75-WA/GT-8). Salt, sand, rust, and dirt may also be present, giving No. 6 a typical ash content of 0.01 to 0.5 percent by weight.

Ultimate analyses of some typical fuels are shown in Table 24-6.

The hydrogen content of petroleum fuels can be calculated from density with the following formula, with an accuracy of about 1 percent for petroleum liquids that contain no sulfur, water, or ash:

$$H = 26 - 15s \quad (24-9)$$

TABLE 24-6 Typical Ultimate Analyses of Petroleum Fuels

Composition, %	No. 1 fuel oil (41.5° API)	No. 2 fuel oil (33° API)	No. 4 fuel oil (23.2° API)	Low sulfur, No. 6 F.O. (12.6° API)	High sulfur, No. 6 (15.5° API)
Carbon	86.4	87.3	86.47	87.26	84.67
Hydrogen	13.6	12.6	11.65	10.49	11.02
Oxygen	0.01	0.04	0.27	0.64	0.38
Nitrogen	0.003	0.006	0.24	0.28	0.18
Sulfur	0.09	0.22	1.35	0.84	3.97
Ash	<0.01	<0.01	0.02	0.04	0.02
C/H Ratio	6.35	6.93	7.42	8.31	7.62

NOTE: The C/H ratio is a weight ratio.

where H = percent hydrogen and s = relative density at 15°C (with respect to water), also referred to as specific gravity.

Relative density is usually determined at ambient temperature with specialized hydrometers. In the United States these hydrometers commonly are graduated in an arbitrary scale termed *degrees API*. This scale relates inversely to relative density s (at 60°F) as follows (see also the abscissa scale of Fig. 24-1):

$$\text{Degrees API} = \frac{141.5}{s} - 131.5 \quad (24-10)$$

For practical engineering purposes, relative density at 15°C (288 K), widely used in countries outside the United States, is considered equivalent to specific gravity at 60°F (288.6 K). With the adoption of

SI units, the American Petroleum Institute favors absolute density at 288 K instead of degrees API.

The hydrogen content, heat of combustion, specific heat, and thermal conductivity data herein were abstracted from Bureau of Standards Miscellaneous Publication 97, *Thermal Properties of Petroleum Products*. These data are widely used, although other correlations have appeared, notably that by Linden and Othmer (*Chem. Eng.* 54[4, 5], April and May, 1947).

Heat of combustion can be estimated within 1 percent from the relative density of the fuel by using Fig. 24-1. Corrections for water and sediment must be applied for residual fuels, but they are insignificant for clean distillates.

Pour point ranges from 213 K (−80°F) for some kerosene-type jet fuels to 319 K (115°F) for waxy No. 6 fuel oils. Cloud point (which is not measured on opaque fuels) is typically 3 to 8 K higher than pour point unless the pour has been depressed by additives. Typical petroleum fuels are practically newtonian liquids between the cloud point and the boiling point and at pressures below 6.9 MPa (1000 psia).

Fuel systems for No. 1 (kerosene) and No. 2 fuel oil (diesel, home heating oil) are not heated. Systems for No. 6 fuel oil are usually designed to preheat the fuel to 300 to 320 K (90 to 120°F) to reduce viscosity for handling and to 350 to 370 K (165 to 200°F) to reduce viscosity further for proper atomization. No. 5 fuel oil may also be heated, but preheating is usually not required for No. 4. (See Table 24-5.) Steam or electric heating is employed as dictated by economics, climatic conditions, length of storage time, and frequency of use. Pressure relief arrangements are recommended on sections of heated pipelines when fuel could be inadvertently trapped between valves.

The kinematic viscosity of a typical No. 6 fuel oil declines from 5000 mm²/s (0.054 ft²/s) at 298 K (77°F) to about 700 mm²/s (0.0075 ft²/s) and 50 mm²/s (0.000538 ft²/s) on heating to 323 K (122°F) and 373 K (212°F), respectively. Viscosity of 1000 mm²/s or less is required for manageable pumping. Proper boiler atomization requires a viscosity between 15 and 65 mm²/s.

Thermal expansion of petroleum fuels can be estimated as volume change per unit volume per degree. ASTM-IP Petroleum Measurement Tables (ASTM D 1250 IP 200) are used for volume corrections in commercial transactions.

Heat capacity (specific heat) of petroleum liquids between 0 and 205°C (32 and 400°F), having a relative density of 0.75 to 0.96 at 15°C (60°F), can be calculated within 2 to 4 percent of the experimental values from the following equations:

$$c = \frac{1.685 + (0.039 \times ^\circ\text{C})}{\sqrt{s}} \quad (24-11)$$

$$c' = \frac{0.388 + (0.00045 \times ^\circ\text{F})}{\sqrt{s}} \quad (24-12)$$

where c is heat capacity, kJ/(kg·°C) or kJ/(kg·K), and c' is heat capacity, Btu/(lb·°F). Heat capacity varies with temperature, and the arithmetic average of the values at the initial and final temperatures can be used for calculations relating to the heating or cooling of oil.

The thermal conductivity of liquid petroleum products is given in Fig. 24-2. Thermal conductivities for asphalt and paraffin wax in their solid states are 0.17 and 0.23 W/(m·K), respectively, for temperatures above 273 K (32°F) (1.2 and 1.6 Btu/[h·ft²][°F/in]).

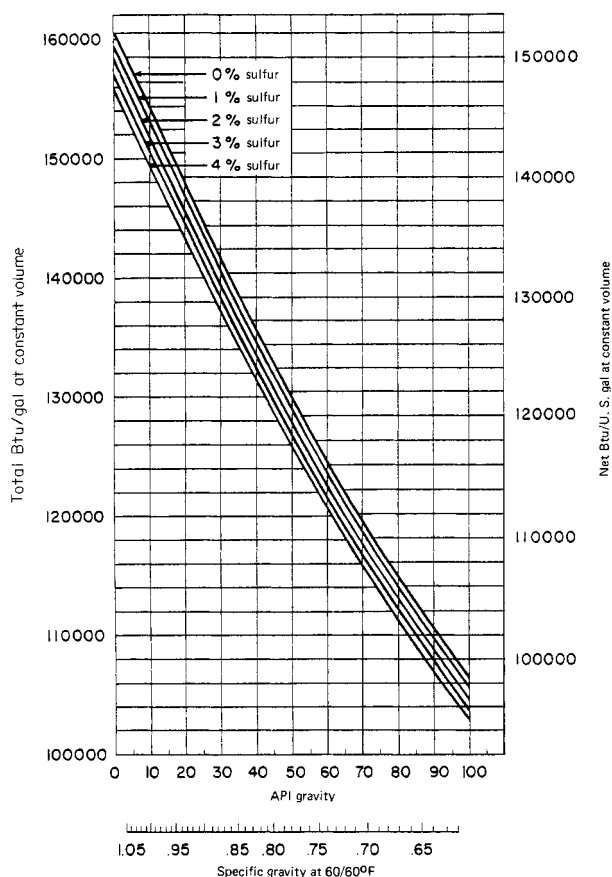


FIG. 24-1 Heat of combustion of petroleum fuels. To convert Btu/U.S. gal to kJ/m³, multiply by 278.7.

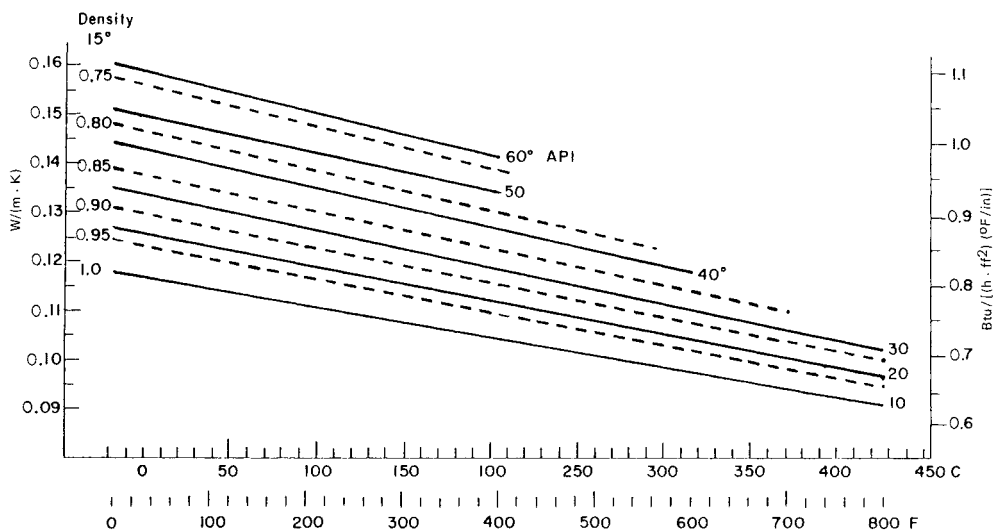


FIG. 24-2 Thermal conductivity of petroleum liquids. The solid lines refer to density expressed as degrees API; the broken lines refer to relative density at 288 K (15°C). ($K = [^{\circ}F + 459.7]/1.8$)

Commercial Considerations Fuels are sold in gallons and in multiples of the 42-gal barrel (0.159 m³) in the United States, while a weight basis is used in other parts of the world. Transactions exceeding about 20 to 40 m³ (5000 to 10,000 U.S. gal) usually involve volume corrections to 288 K (60°F) for accounting purposes. Fuel passes through an air eliminator and mechanical meter when loaded into or dispensed from trucks. Larger transfers such as pipeline, barge, or tanker movements are measured by fuel depth and strapping tables (calibration tables) in tanks and vessels, but positive-displacement meters that are proved (calibrated) frequently are gaining acceptance. After an appropriate settling period, water in the tank bottom is measured with a plumb bob or stick smeared with water-detecting paste.

Receipts of tank-car quantities or larger are usually checked for gravity, appearance, and flash point to confirm product identification and absence of contamination.

Safety Considerations Design and location of storage tanks, vents, piping, and connections are specified by state fire marshals, underwriters' codes, and local ordinances. In NFPA 30, *Flammable and Combustible Liquids Code, 2003* (published by the National Fire Protection Association, Quincy, Ma.), liquid petroleum fuels are placed in Class I through Class III B based on their flash point, boiling point, and vapor pressure.

NFPA 30 details the design features and safe placement of handling equipment for flammable and combustible liquids.

Crude oils with flash points below 311 K (100°F) have been used in place of No. 6 fuel oil. Different pumps may be required because of low fuel viscosity.

Nonpetroleum Liquid Fuels

Tar Sands Canadian tar sands either are strip-mined and extracted with hot water or employ steam-assisted gravity drainage (SAGD) for in situ recovery of heavy oil (bitumen). The bitumen is processed into naphtha, kerosine, and gasoline fractions (which are hydrotreated), in addition to gas (which is recovered). Current production of syncrude from Canadian tar sands is about 113,000 T/d (790,000 B/d) with expected increases to about 190,000 T/d (1.7 MB/d) by 2010.

Oil Shale Oil shale is nonporous rock containing organic kerogen. Raw shale oil is extracted from mined rock by pyrolysis in a surface retort, or in situ by partial combustion after breaking up the rock with explosives. Pyrolysis cracks the kerogen, yielding raw shale oil high in nitrogen, oxygen, and sulfur. **Shale oil** has been hydrotreated

and refined in demonstration tests into relatively conventional fuels. Refining in petroleum facilities is possible with significant pretreatment or by incorporating upgrading units into the refinery.

Coal-Derived Fuels Liquid fuels derived from coal range from highly aromatic coal tars to liquids resembling petroleum. Raw liquids from different hydrogenation processes show variations that reflect the degree of hydrogenation achieved. Also, the raw liquids can be further hydrogenated to refined products. Properties and cost depend on the degree of hydrogenation and the boiling range of the fraction selected. A proper balance between fuel upgrading and equipment modification is essential for the most economical use of coal liquids in boilers, industrial furnaces, diesels, and stationary gas turbines.

Coal-tar fuels are high-boiling fractions of crude tar from pyrolysis in coke ovens and coal retorts. Grades range from free-flowing liquids to pulverizable pitch. Low in sulfur and ash, they contain hydrocarbons, phenols, and heterocyclic nitrogen and oxygen compounds. Being more aromatic than petroleum fuels, they burn with a more luminous flame. From 288 to 477 K (60 to 400°F) properties include:

Heat capacity	1.47–1.67 kJ/(kg·K) (0.35–0.40 Btu/[lb·°F])
Thermal conductivity	0.14–0.15 W/(m·K) (0.080–0.085 Btu/[h·ft·°F])
Heat of vaporization	349 kJ/kg (150 Btu/lb)
Heat of fusion	Nil

Table 24-7 shows representative data for liquid fuels from tar sands, oil shale, and coal.

GASEOUS FUELS

RESERVE AND PRODUCTION INFORMATION: DOE/EIA-0216(2003), November 2004; U.S. Crude Oil, Natural Gas, and Natural Gas Liquids Reserves: 2003 Annual Report, Table 2, Table 8, Table 12; *Annual Energy Review 2003*, DOE/EIA-0364, September 2004; *Natural Gas Annual 2003*, DOE/EIA-0131(03), December 2004, Table 9.

Natural Gas Natural gas is a combustible gas that occurs in porous rock of the earth's crust and is often found with accumulations of crude oil or coal. Natural gas termed *dry* has less than 0.013 dm³/m³ (0.1 gal/1000 ft³) of gasoline. Above this amount, it is termed *wet*.

Proven reserves of conventionally reservoired natural gas in the United States total about 5.35 Tm³ (189 Tft³). An additional 0.53 Tm³ (18.7 Tft³) of proven reserves are in coal bed methane deposits. Production in 2003 was about 0.54 Tm³ (19.1 Tft³), over 75 percent

TABLE 24-7 Characteristics of Typical Nonpetroleum Fuels

	Conventional coal-tar fuels from retorting ^a		Typical coal-derived fuels with different levels of hydrogenation ^b				Synthetic crude oils, by hydrogenation		
	CTF 50	CTF 400	Minimal		Mild	Mild ^c	Severe	Oil shale	Tar sands ^d
Distillation range, °C			175–280	280–500	160–415	175–400	125–495		
Density, kg/m ³ , 15°C	1.018	1.234	0.974	1.072	0.964	0.9607	0.914	0.817	0.864
lb U.S. gal, 60°F	8.5	10.3	8.1	8.9	8.0	8.0	7.6	6.8	7.2
Viscosity, mm ² /s	2–9	9–18	3.1–3.4	50–90	3.6	—	2.18		
	At 38°C	At 121°C	At 38°C	At 38°C	At 38°C	—	At 38°C		
Ultimate analysis, %									
Carbon	87.4	90.1	86.0	89.1	87.8	89.6	89.0	86.1	87.1
Hydrogen	7.9	5.4	9.1	7.5	9.7	10.1	11.1	13.84	12.69
Oxygen	3.6	2.4	3.6–4.3	1.4–1.8	2.4	0.3	0.5	0.12	0.04
Nitrogen	0.9	1.4	0.9–1.1	1.2–1.4	0.6	0.04	0.09	0.01	0.07
Sulfur	0.2	0.7	<0.2	0.4–0.5	0.07	0.004	0.04	0.02	0.10
Ash ^e	Trace	0.15	<0.001	^f					
C/H ratio, weight	11.0	16.5	9.4	11.9	9.1	8.9	8.0	6.2	6.9
Gross calorific value, MJ/kg	38.4–40.7	36.8–37.9							
Btu/lb	16,500–17,500	15,800–16,300							

^aCTF 50 and 400 indicate approximate preheat temperature, °F, for atomization of fuel in burners (terminology used in British Standard B.S. 1469).

^bProperties depend on distillation range, as shown, and to a lesser extent on coal source.

^cUsing recycle-solvent process.

^dTar sands, although a form of petroleum, are included in this table for comparison.

^eInorganic mineral constituents of coal tar fuel:

5 to 50 ppm: Ca, Fe, Pb, Zn (Na, in tar treated with soda ash)

0.05 to 5 ppm: Al, Bi, Cu, Mg, Mn, K, Si, Na, Sn

Less than 0.05 ppm: As, B, Cr, Ge, Ti, V, Mo

Not detected: Sb, Ba, Be, Cd, Co, Ni, Sr, W, Zr

^fInherent ash is “trace” or “<0.1%,” although entrainment in distillation has given values as high as 0.03 to 0.1%.

from nonassociated gas wells. Conventional proven reserves have declined about 0.03 Tm³ (0.9 Tft³) per year from 1977 through 2003. Net gas imports in 2003 were 0.09 Tm³ (3.3 Tft³), about 15 percent of consumption. Imports as LNG were 0.4 Tft³, about 2 percent of gas consumption.

Natural gas consists of hydrocarbons with a very low boiling point.

Methane is the main constituent, with a boiling point of 119 K (–245°F). Ethane, with a boiling point of 184 K (–128°F) may be present in amounts up to 10 percent; propane, with a boiling point of 231 K (–44°F), up to 3 percent. Butane, pentane, hexane, heptane, and octane may also be present. Physical properties of these hydrocarbons are given in Sec. 2.

Although there is no single composition that may be called “typical” natural gas, Table 24-8 shows the range of compositions in large cities in the United States.

TABLE 24-8 Analysis of Natural Gas*

	Range†	
	Low	High
Composition, vol %		
Methane	86.3	95.2
Ethane	2.5	8.1
Propane	0.6	2.8
Butanes	0.13	0.66
Pentanes	0	0.44
Hexanes plus	0	0.09
CO ₂	0	1.1
N ₂	0.31	2.47
He	0.01	0.06
Heating value		
MJ/m ³ (Btu/ft ³)	38.15(1024)	40.72(1093)
Specific gravity	0.586	0.641
Ref.: Air at 288 K (60°F)		

*Adapted from *Gas Engineers Handbook*, American Gas Association, Industrial Press, New York, 1965.

†Ranges are the high and low values of annual averages reported by 13 utilities (1954 data).

Commodity natural gas is substantially free of sulfur compounds; the terms *sweet* and *sour* are used to denote the absence or presence of H₂S. Some wells, however, deliver gas containing levels of hydrogen sulfide and other sulfur compounds (e.g., thiophenes, mercaptans, and organic sulfides) that must be removed before transfer to commercial pipelines. Pipeline-company contracts typically specify maximum allowable limits of impurities; H₂S and total sulfur compounds seldom exceed 0.023 and 0.46 g/m³ (1.0 and 20.0 gr/100 std ft³), respectively. The majority of pipeline companies responding to a 1994 survey limited H₂S to less than 0.007 g/m³ (0.3 gr/100 std ft³), but a slightly smaller number continued specifying 0.023 g/m³, in accord with an American Gas Association 1971 recommendation.

Supercompressibility of Natural Gas All gases deviate from the simple gas laws to a varying extent. This deviation is called *supercompressibility* and must be taken into account in gas measurement, particularly at high line pressure. For example, since natural gas is more compressible under high pressure at ordinary temperatures than is called for by Boyle’s law, gas purchased at an elevated pressure gives a greater volume when the pressure is reduced than it would if the gas were ideal.

The supercompressibility factor may be expressed as

$$Z = (RT/PV)^{1/2} \tag{24-13}$$

where *Z* = supercompressibility factor; *R* = universal gas constant, 8.314 kPa·m³/(kmol·K); *T* = gas temperature, K; *P* = gas pressure, kPa; *V* = molar gas volume, m³/kmol.

For determining supercompressibility factors of natural gas mixtures, see *Manual for the Determination of Supercompressibility Factors for Natural Gas*, American Gas Association, New York, 1963; and A.G.A Gas Measurement Committee Report No. 3, 1969.

Liquefied Natural Gas The advantages of storing and shipping natural gas in liquefied form (LNG) derive from the fact that 0.035 m³ (1 ft³) of liquid methane at 111 K (–260°F) equals about 18 m³ (630 ft³) of gaseous methane. One cubic meter (264 U.S. gal) weighs 412 kg (910 lb) at 109 K (–263°F). The heating value is about 24 GJ/m³ (86,000 Btu/U.S. gal). The heat of vaporization of LNG at 0.1 MPa is 232 MJ/m³ of liquid. On a product gas basis, the heat required is about 0.3 kJ/m³ (10 Btu/std ft³) of gas produced.

LNG is actively traded in international commerce. In 2003 LNG was about 13 percent of gas imports to the United States but only 2 percent of gas consumption. The Energy Information Administration (EIA) projects (Annual Energy Outlook 2004) that gas imports will grow to 5.5 Tft³ in 2010 and to 7.2 Tft³ in 2025, with nearly all the increased volume being LNG.

Specialized ships are used to transport LNG. Receiving terminals have storage tankage and reevaporization facilities. Several new terminals have been proposed, but none has advanced to construction at this writing.

Liquefied Petroleum Gas The term *liquefied petroleum gas* (LPG) is applied to certain specific hydrocarbons which can be liquefied under moderate pressure at normal temperatures but are gaseous under normal atmospheric conditions. The chief constituents of LPG are propane, propylene, butane, butylene, and isobutane. LPG produced in the separation of heavier hydrocarbons from natural gas is mainly of the paraffinic (saturated) series. LPG derived from oil-refinery gas may contain varying low amounts of olefinic (unsaturated) hydrocarbons.

LPG is widely used for domestic service, supplied either in tanks or by pipelines. It is also used to augment natural gas deliveries on peak days and by some industries as a standby fuel.

Other Gaseous Fuels

Hydrogen Hydrogen is used extensively in the production of ammonia and chemicals, in the refining of petroleum, in the hydrogenation of fats and oils, and as an oven reducing atmosphere. It is also used as a fuel in industrial cutting and welding operations. There are no resources of uncombined hydrogen as there are of the other fuels. It is made industrially by the steam reforming of natural gas; as the by-product of industrial operations such as the thermal cracking of hydrocarbons; and, to a small extent, by the electrolysis of water.

Hydrogen is seen as the ultimate nonpolluting form of energy; when electrochemically combined with oxygen in fuel cells, only water, heat, and electricity are produced. Means for transforming the world's fossil energy economy into a hydrogen economy are being considered as a long-term option. Hydrogen can be stored in gaseous, liquid, or solid forms; however, currently available technologies are not suited to meet mass energy market needs. Technologies for economically producing, storing, and utilizing hydrogen are being researched in the United States, Europe, and Japan.

Acetylene Acetylene is used primarily in operations requiring high flame temperature, such as welding and metal cutting. To transport acetylene, it is dissolved in acetone under pressure and drawn into small containers filled with porous material.

Miscellaneous Fuels A variety of gases have very minor market shares. These include reformed gas, oil gases, producer gas, blue water gas, carbureted water gas, coal gas, and blast-furnace gas. The heating values of these gases range from 3.4 to 41 MJ/m³ (90 to 1100 Btu/ft³). They are produced by pyrolysis, the water gas reaction, or as by-products of pig-iron production.

Hydrogen sulfide in manufactured gases may range from approximately 2.30 g/m³ (100 gr/100 ft³) in blue and carbureted water gas to several hundred grains in coal- and coke-oven gases. Another important sulfur impurity is carbon disulfide, which may be present in amounts varying from 0.007 to 0.07 percent by volume. Smaller amounts of carbon oxysulfide, mercaptans, and thiophene may be found. However, most of the impurities are removed during the purification process and either do not exist in the finished product or are present in only trace amounts.

FUEL AND ENERGY COSTS

Fuel costs vary widely both geographically and temporally. Oil and gas markets have been highly volatile in recent years while steam coal markets have not. Much combustion equipment is designed for a specific fuel, limiting the potential for fuel switching to take advantage of price trends. The costs given in Table 24-9 are U.S. averages not necessarily applicable to a specific location; they do provide fuel cost trends.

TABLE 24-9 Time-Price Relationships for Fossil Fuels

Year	Bituminous coal, \$/Mg (\$/U.S. ton)	Wellhead natural gas, \$/1000 m ³ (\$/1000 scf)	Crude oil, domestic first purchase price, \$/m ³ (\$/bbl)
1975	21.81 (19.79)	15.54 (0.44)	48.24 (7.67)
1985	33.93 (30.78)	88.64 (2.51)	151.52 (24.09)
1995	28.17 (25.56)	54.74 (1.55)	91.96 (14.62)
2000	26.51 (24.05)	129.96 (3.68)	168.06 (26.72)
2003	29.29 (26.57)	175.87 (4.98)	173.35 (27.56)

SOURCE: *Annual Energy Review 2003*, DOE/EIA-0384, September 2004, Tables 7.8, 6.7, and 5.18, respectively.

COAL CONVERSION

Coal is the most abundant fossil fuel, and it will be available long after petroleum and natural gas are scarce. However, because liquids and gases are more desirable than solid fuels, technologies have been, and continue to be, developed to economically convert coal into liquid and gaseous fuels.

Bodley, Vyas, and Talwalker (*Clean Fuels from Coal Symposium II*, Institute of Gas Technology, Chicago, 1975) presented the chart in Fig. 24-3, which shows very simply the different routes from coal to clean gases and liquids.

Coal Gasification

GENERAL REFERENCES: *Fuel Gasification Symp.*, 152d American Chemical Society Mtg., Sept. 1966. *Chemistry of Coal Utilization*, suppl. vol., Lowry (ed.), Wiley, New York, 1963; and 2d suppl. vol., Elliot (ed.), 1981. *Coal Gasification Guidebook: Status, Applications, and Technologies*, Electric Power Research Institute, EPRI TR-102034, Palo Alto, Calif., 1993. *Riegel's Handbook of Industrial Chemistry*, 10th ed., Kent (ed.), Chap. 17, 2003. *Gasification* by Higman and van der Burgt, Elsevier, 2003. "The Case for Gasification" by Stiegel and Ramezan, EM, Dec. 2004, pp. 27-33.

Background The advantages of gaseous fuels have resulted in an increased demand for gas and led to the invention of advanced processes for coal gasification. Converting coal to combustible gas has been practiced commercially since the early 19th century. Chapter 17 of *Riegel's Handbook of Industrial Chemistry*, 10th ed., provides a good summary of the early history of coal gasification. Coal-derived gas was distributed in urban areas of the United States for residential and commercial uses until its displacement by lower-cost natural gas, starting in the 1940s. At about that time, development of oxygen-based gasification processes was initiated. An early elevated-pressure gasification process, developed by Lurgi Kohle u Mineralöltechnik GmbH, is still in use. The compositions of gases produced by this and a number of more recent gasification processes are listed in Table 24-10.

Theoretical Considerations The chemistry of coal gasification can be approximated by assuming coal is only carbon and considering the most important reactions involved (see Table 24-11). Reaction (24-14), the combustion of carbon with oxygen, which can be assumed to go to completion, is highly exothermic and supplies most of the thermal energy for the other gasification reactions. The oxygen used in the gasifier may come from direct feeding of air or may be high-purity oxygen from an air separation unit. Endothermic reactions (24-16) and (24-17), which represent the conversion of carbon to combustible gases, are driven by the heat energy supplied by reaction (24-14).

Hydrogen and carbon monoxide produced by the gasification reaction react with each other and with carbon. The hydrogenation of carbon to produce methane, reaction (24-15), is exothermic and contributes heat energy. Similarly, methanation of CO, reaction (24-19), can also contribute heat energy. These reactions are affected by the water-gas-shift reaction (24-18), the equilibrium of which controls the extent of reactions (24-16) and (24-17).

Several authors have shown [cf. Gumz, *Gas Producers and Blast Furnaces*, Wiley, New York, 1950; Elliott and von Fredersdorff, *Chemistry of Coal Utilization*, 2d suppl. vol., Lowry (ed.), Wiley, New

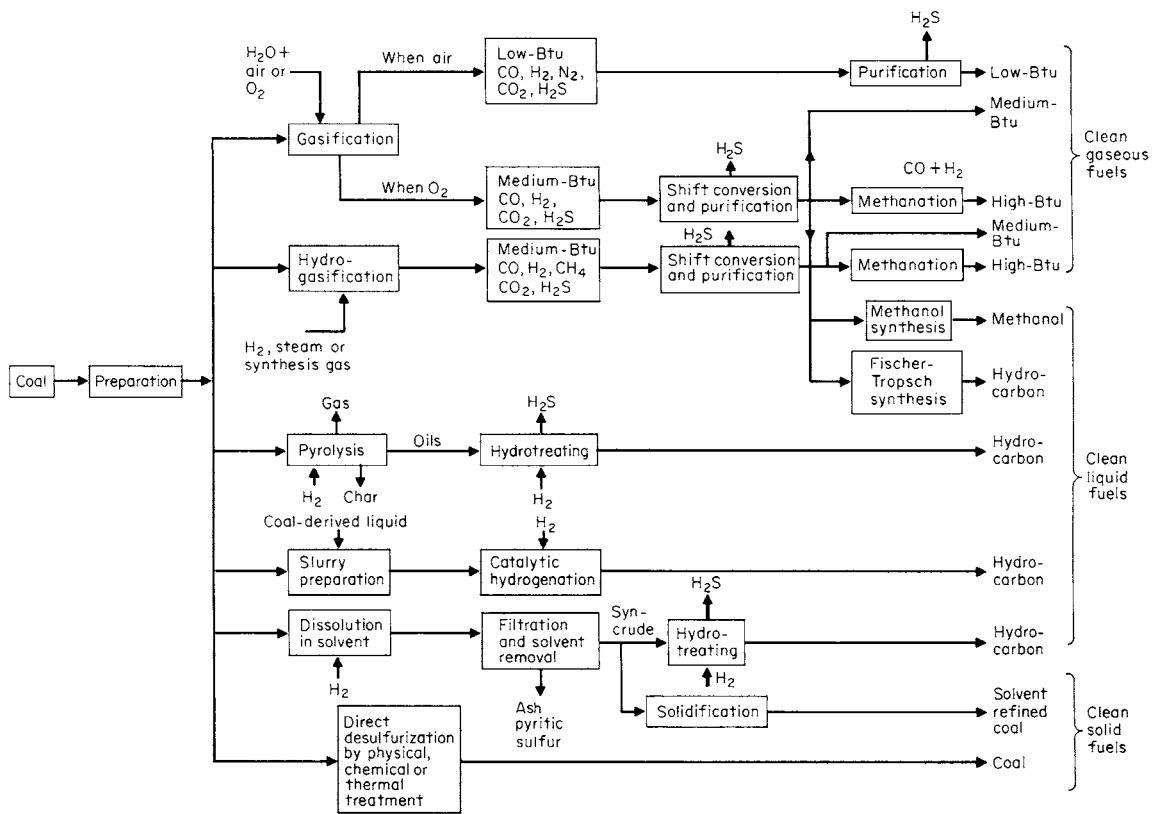


FIG. 24-3 The production of clean fuels from coal. (Based on W. Bodle, K. Vyas, and A. Talwalker; Clean Fuels from Coal Symposium II, Institute of Gas Technology, Chicago, 1975.)

York, 1963] that there are three fundamental gasification reactions: the Boudouard reaction (24-17), the heterogeneous water-gas-shift reaction (24-18), and the hydrogasification reaction (24-15). The equilibrium constants for these reactions are sufficient to calculate equi-

librium for all the reactions listed. Unfortunately, it is not possible to calculate accurate gas composition by using reactions (24-14) to (24-19). One reason is that not all reactions may be in equilibrium. Another reason is that other reactions are taking place. Since gasifica-

TABLE 24-10 Coal-Derived Gas Compositions

Gasifier technology	Sasol/Lurgi ^o	Texaco/GE Energy [†]	BGL [‡]	E-Gas/ConocoPhillips	Shell/Uhde [§]
Type of bed	Moving	Entrained	Moving	Entrained	Entrained
Coal feed form	Dry coal	Coal slurry	Dry coal	Coal slurry	Dry coal
Coal type	Illinois No. 6	Illinois No. 6	Illinois No. 6	Illinois No. 6	Illinois No. 5
Oxidant	Oxygen	Oxygen	Oxygen	Oxygen	Oxygen
Pressure, MPa (psia)	0.101 (14.7)	4.22 (612)	2.82 (409)	2.86 (415)	2.46 (357)
Ash form	Slag	Slag	Slag	Slag	Slag
Composition, vol %					
H ₂	52.2	30.3	26.4	33.5	26.7
CO	29.5	39.6	45.8	44.9	63.1
CO ₂	5.6	10.8	2.9	16.0	1.5
CH ₄	4.4	0.1	3.8	1.8	0.03
Other hydrocarbons	0.3	—	0.2	—	—
H ₂ S	0.9	1.0	1.0	1.0	1.3
COS	0.04	0.02	0.1	0.1	0.1
N ₂ + Ar	1.5	1.6	3.3	2.5	5.2
H ₂ O	5.1	16.5	16.3	—	2.0
NH ₃ + HCN	0.5	0.1	0.2	0.2	0.02
HCl	—	0.02	0.03	0.03	0.03
H ₂ S : COS	20 : 1	42 : 1	11 : 1	10 : 1	9 : 1

^oRath, "Status of Gasification Demonstration Plants," Proc. 2d Annu. Fuel Cells Contract Review Mtg., DOE/METC-9090/6112, p. 91.

[†]Coal Gasification Guidebook: Status, Applications, and Technologies, Electric Power Research Institute, EPRI TR-102034, 1993, p. 5-28.

[‡]Ibid., p. 5-58.

[§]Ibid., p. 5-48.

TABLE 24-11 Chemical Reactions in Coal Gasification

Reaction	Reaction heat, kJ/(kg·mol)	Process	Number
Solid-gas reactions			
$C + O_2 \rightarrow CO_2$	+393,790	Combustion	(24-14)
$C + 2H_2 \rightarrow CH_4$	+74,900	Hydrogasification	(24-15)
$C + H_2O \rightarrow CO + H_2$	-175,440	Steam-carbon	(24-16)
$C + CO_2 \rightarrow 2CO$	-172,580	Boudouard	(24-17)
Gas-phase reaction			
$CO + H_2O \rightarrow H_2 + CO_2$	+2,853	Water-gas shift	(24-18)
$CO + 3H_2 \rightarrow CH_4 + H_2O$	+250,340	Methanation	(24-19)
Pyrolysis and hydroxyprolysis			
CH_x	$\left(1 - \frac{x}{4}\right)C + \left(\frac{x}{4}\right)CH_4$	Pyrolysis	(24-20)
$CH_x + m H_2$	$\left[1 - \left(\frac{x+2m}{4}\right)\right]C + \left(\frac{x+2m}{4}\right)CH_4$	Hydroxyprolysis	(24-21)

tion of coal always involves elevated temperatures, thermal decomposition (pyrolysis) takes place as coal enters the gasification zone of the reactor. Reaction (24-20) treats coal as a hydrocarbon and postulates its thermal disintegration to produce carbon (coke) and methane. Reaction (24-21) illustrates the stoichiometry of hydrogasifying part of the carbon to produce methane.

These reactions can be used to estimate the effect of changes in operating parameters on gas composition. As temperature increases, endothermic reactions are favored over exothermic reactions. Methane production will decrease, and CO production will be favored as reactions are shifted in the direction in which heat absorption takes place. An increase in pressure favors reactions in which the number of moles of products is less than the number of moles of reactants. At higher pressure, production of CO_2 and CH_4 will be favored.

It is generally believed that oxygen reacts completely in a very short distance from the point at which it is mixed or comes in contact with coal or char. The heat evolved acts to pyrolyze the coal, and the char formed then reacts with carbon dioxide, steam, and other gases formed by combustion and pyrolysis. The assumption made in Table 24-11 that the solid reactant is carbon is probably close to correct, but the type of char formed affects the kinetics of gas-solid reactions. The overall reaction is probably rate-controlled below 1273 K (1832°F). Above this temperature, pore diffusion has an overriding effect, and at very high temperatures surface-film diffusion probably controls. For many gasification processes, the reactivity of the char is quite important and can depend on feed coal characteristics, the method of heating, the rate of heating, and particle-gas dynamics.

The importance of these concepts can be illustrated by the extent to which the pyrolysis reactions contribute to gas production. In a moving-bed gasifier, the particle is heated through several distinct thermal zones. In the initial heat-up zone, coal carbonization or devolatilization dominates. In the successively hotter zones, char devolatilization, char gasification, and fixed carbon combustion are the dominant processes. About 17 percent of total gas production occurs during coal devolatilization, and about 23 percent is produced during char devolatilization. The balance is produced during char gasification and combustion.

Gasifier Types and Characteristics The three main types of gasifier reactors, moving bed, fluidized bed, and entrained bed, as shown in Fig. 24-4, are all in commercial use. The moving bed is sometimes referred to as a "fixed" bed, because the coal bed is kept at a constant height. These gasifiers can differ in many ways: size, type of coal fed, feed and product flow rates, residence time, and reaction temperature. Gas compositions from the gasifiers discussed below are listed in Table 24-10.

Moving bed Depending on the temperature at the base of the coal bed, the ash can either be dry or in the form of molten slag. If excess steam is added, the temperature can be kept below the ash fusion point, in which case the coal bed rests on a rotating grate which allows the dry ash to fall through for removal. To reduce steam usage, a slagging bottom gasifier was developed by British Gas and Lurgi (BGL) in which the ash is allowed to melt and drain off through a slag tap. This gasifier has over twice the capacity per unit of cross-section

area of the dry-bottom gasifier. The BGL technology is offered commercially by Allied Syngas and Advantica.

Fluidized bed The problem of coal agglomeration is eliminated by a fluidized-bed gasifier developed by GTI. The U-Gas gasification process uses an agglomerating-ash fluidized-bed gasifier in which crushed limestone can be injected with the coal for sulfur capture. Char and ash that exit the gasifier with the product gas are recycled to the hot agglomerating and jetting zone, where temperatures are high enough to pyrolyze fresh coal introduced at that point, gasify the char, and soften the ash particles. The ash particles stick together and fall to the base of the gasifier, where they are cooled and removed. The agglomerating fluid-bed gasifier can be blown by either air or oxygen. Pressurized operation has several advantages: slightly higher methane formation, resulting in higher heating value of the gas; increased heat from the methanation reactions, which reduces the amount of oxygen needed; reduced heat losses through the wall and, consequently, improved efficiency; and higher capacity.

Entrained bed The primary example of an oxygen-blown, dry-feed, entrained-flow gasifier is the Shell gasifier. An advantage of Shell coal gasification technology is its ability to process a range of coals, with a wide variety of coals (from brown coal to anthracite) having been successfully tested. As with other entrained-flow gasifiers, disadvantages of the Shell process include a high oxygen requirement and a high waste heat recovery duty. However, the ability to feed dry coal reduces the oxygen requirement below that of single-stage entrained-flow gasifiers that use slurry feed and makes the Shell gasifier somewhat more efficient. The penalty for this small efficiency improvement is a more complex coal-feeding system. Uhde and Shell are marketing this technology.

Two slurry-fed, entrained-flow gasifiers are the Texaco gasifier (now owned by GE) and the E-Gas gasifier (now owned by ConocoPhillips). The Texaco gasifier is similar to the Shell gasifier, except that the coal is fed as a slurry. Reactor exit gas is cooled either by direct water injection or by a radiative cooler directly below the reactor. The E-Gas gasifier differs from other systems in that it uses a two-stage reactor. The bulk of the feed slurry and all the oxygen are sent to the first (horizontal) stage, where the coal is gasified. Hot gas flows into the second (vertical) stage, where the remainder of the coal slurry is injected. Hot fuel gas is cooled in a fire-tube boiler fuel gas cooler.

Gasification-Based Liquid Fuels and Chemicals Liquid fuels and chemicals from gasification-based synthesis gas are described in the coal liquefaction section following this section. While the downstream areas of power system and indirect liquefaction plants will differ markedly, the gasification sections will be quite similar and are described in this section.

Gasification-Based Power Systems An important driving force for coal gasification process development is the environmental superiority of gasification-based power generation systems, generally referred to as integrated gasification combined-cycle (IGCC) power production (Fig. 24-5). Coal is crushed prior to being fed to a reactor, where it is gasified through contact with steam and air or oxygen. Partial oxidation produces the high-temperature [1033 to 2255 K

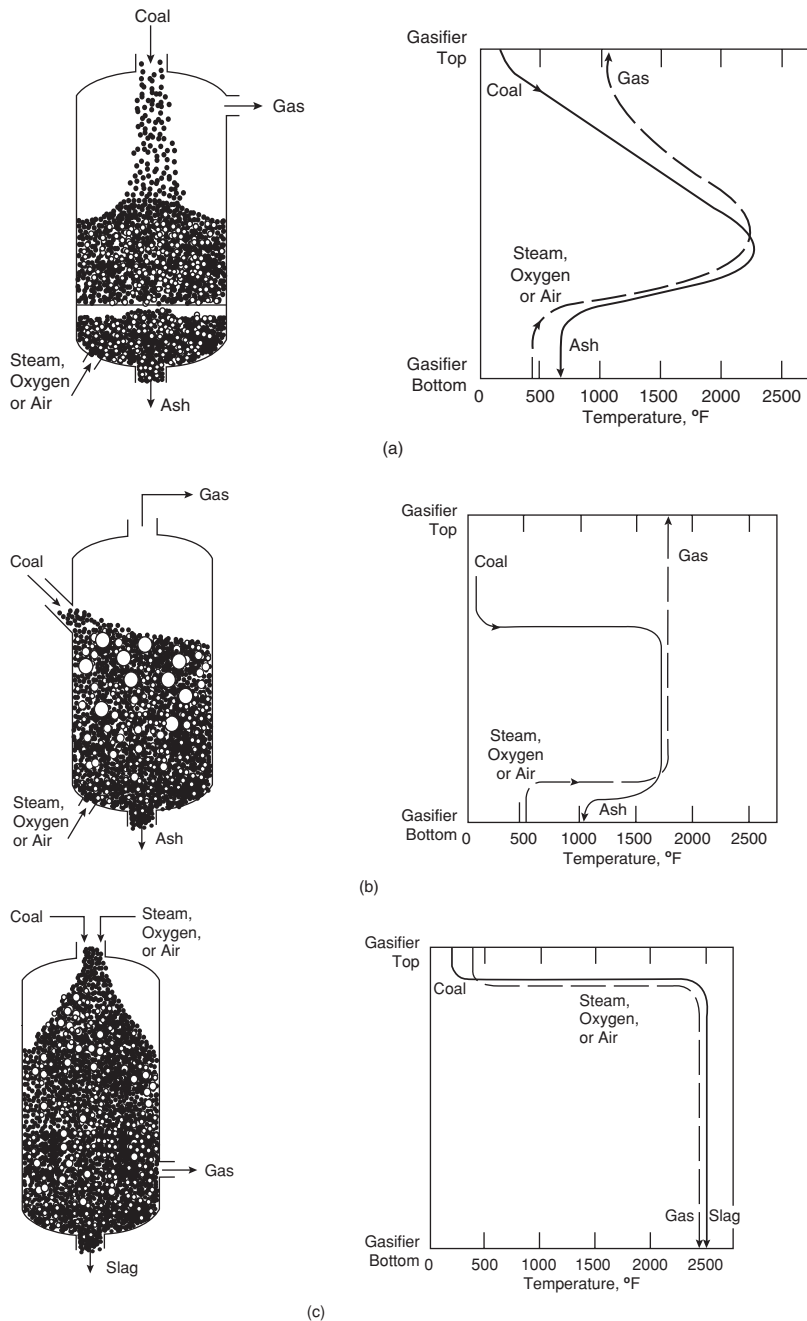


FIG. 24-4 Gasifier types and temperature profiles: (a) fixed bed (dry ash); (b) fluidized bed; (c) entrained flow. (This figure was published in N. Holt and S. Alpert, "Integrated Gasification Combined-Cycle Power," vol. 7, pp. 897–905, in *Encyclopedia of Physical Science and Technology*, 3d ed. Copyright Elsevier, 2002.)

(1400 to 3600°F), depending on the type of gasifier] reducing environment necessary for gasification. The product fuel gas passes through heat recovery and cleanup, where particulates (dust) and sulfur are removed. After cleanup, the fuel gas, composed primarily of hydrogen and carbon oxides, is burned with compressed air and expanded through a gas turbine to generate electricity. Heat is recovered from the turbine's hot exhaust gas to produce steam (at subcritical conditions), which is expanded in a steam turbine for additional electric power generation.

All three basic gasifier types could be incorporated into IGCC plant designs, although to date only entrained-flow gasifiers have actually been deployed. With each gasifier type, the oxidant can be air or oxygen, and the coal can be fed dry or in a slurry. The composition of the fuel gas, as well as its pressure and temperature, is determined by the design of the gasifier and the gas cleanup system.

There are several features of IGCC power systems that contribute to their improved thermal efficiency and environmental superiority compared to a conventional pulverized-coal fired power plant. First, the

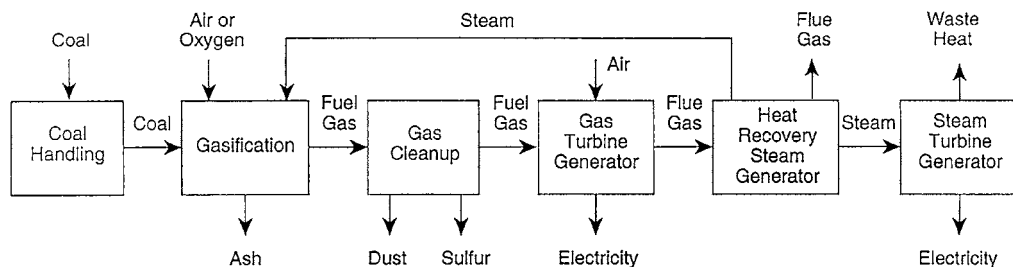


FIG. 24-5 Integrated gasification combined-cycle block diagram.

mass flow rate of gas from a gasifier is about one-fourth that from a combustor, because the gasifier is oxygen-blown and operates substoichiometrically, while the combustor is air-blown and operates with excess air. Because of the elevated operating pressure and the lack of nitrogen dilution, the volumetric gas flow to the sulfur removal system is actually only 0.5 percent to 1 percent of the volumetric flow to the flue gas desulfurization unit; this lowers the capital cost of the gas cleanup system.

Furthermore, the sulfur in coal-derived fuel gas is mainly present as hydrogen sulfide, which is much more easily recovered than the sulfur dioxide in flue gas. Not only can hydrogen sulfide be easily converted to elemental sulfur, a more valuable by-product than the calcium sulfate produced when lime is used to remove sulfur dioxide from flue gas, but also neither lime nor limestone is required. Nitrogen in the coal is largely converted to nitrogen gas or ammonia, which is easily removed by water washing, thus reducing nitrogen oxide emissions when the fuel gas is burned. Carbon dioxide can also be scrubbed from the fuel gas, and if even further reductions in carbon emissions are required, the carbon monoxide in the fuel gas can be converted to hydrogen and carbon dioxide before CO_2 removal. Finally, it has been estimated that the cost of mercury removal from an IGCC system would be only about one-tenth the cost for a conventional power plant.

Another advantage is that the IGCC system generates electricity by both combustion (Brayton cycle) and steam (Rankine cycle) turbines. The inclusion of the Brayton topping cycle improves efficiency compared to a conventional power plant's Rankine cycle-only generating system. Typically, about two-thirds of the power generated comes from the Brayton cycle and one-third from the Rankine cycle.

Current Status There have been substantial advancements in the development of gasification-based power systems during the last two decades. Programs are in place in the United States to support demonstration projects and for conducting research to improve efficiency, cost effectiveness, and environmental performance of IGCC power generation. Two areas of research that are likely to produce significant improvements in coal gasification technology are air separation (oxygen production) and fuel gas cleanup (removal of sulfur, mercury, particulates, and other pollutants).

Gasification technology is being widely used throughout the world. A study conducted in 2004 indicated that there were 156 gasification projects worldwide. Total capacity of the projects in operation was 45,000 MW (thermal) with another 25,000 MW (thermal) in various stages of development. As discussed later, in addition to producing fuel gas for power production, synthesis gas production by gasification is the first step in the indirect liquefaction of coal. Furthermore, gasification of carbonaceous, hydrogen-containing fuels is an effective method of thermal hydrogen production and is considered to be a key technology in the transition to a hydrogen economy. Therefore, the possibility exists for the coproduction of electric power and liquid fuels while sequestering carbon dioxide. Such an option could allow a gasifier in an IGCC system to operate at full capacity at all times, producing fuel gas at times of peak power demand and a mix of fuel gas and synthesis gas at other times.

In 2005, there were four coal-based IGCC power plants in operation in the world: Tampa Electric in Polk County, Florida, based on a Texaco (now GE) gasifier; Wabash repowering project in Indiana, based on E-Gas (now ConocoPhillips E-Gas); and Buggenum in The Netherlands and Puertollano in Spain, both based on Shell gasifiers (N.A.H. Holt, "IGCC Technology—Status, Opportunities, and Issues," *EM*, Dec. 2004, pp. 18–26).

Cost of Gasification-Based Power Systems Comparing power options is complicated by the many different parameters that must be considered in making a cost determination: coal cost; coal properties, including sulfur and moisture contents; ambient temperature; degree of process integration; gas turbine model; and gas cleanup method. These, and many other factors, have a significant impact on cost.

While comparison of absolute costs among different power systems is difficult, the costs of the component units are usually within given ranges. For an oxygen-blown IGCC power system, the breakdown of the capital cost for the four component units is: air separation plant, 10 to 15 percent; gasifier including gas cleanup, 30 to 40 percent; combined-cycle power unit, 40 to 45 percent; and balance of plant, 5 to 10 percent. The breakdown of the cost of electricity is: capital charge, 52 to 56 percent; operating and maintenance, 14 to 17 percent; and fuel, 28 to 32 percent.

One of the main challenges to the development and deployment of IGCC power plants has been that the capital cost was significantly higher than that of a natural-gas-fired generating unit, thereby negating the fuel cost savings. However, if natural gas prices remain substantially above \$4.75/GJ (\$5.00/10⁶ Btu), that should no longer be the case. Moreover, capital costs of IGCC power plants are likely to decline considerably as more of these facilities are built, standard designs are developed, and economies of scale are realized.

Coal Liquefaction

GENERAL REFERENCES: *Riegel's Handbook of Industrial Chemistry*, 10th ed., Kent (ed.), Ch. 17 Coal Technology, Kluwer Academic/Plenum Publishers, New York, 2003. *Chemistry of Coal Utilization*, suppl. vol., Lowry (ed.), Wiley, New York, 1963, and 2d suppl. vol., Elliott (ed.), 1981. Wu and Storch, *Hydrogenation of Coal and Tar*, U.S. Bur. Mines Bull. 633, 1968. Srivastava, McIlvried, Gray, Tomlinson, and Klunder, *American Chemical Society Fuel Chemistry Division Preprints*, Chicago, 1995. Dry, *The Fischer-Tropsch Synthesis, Catalysis Science and Technology*, vol. 1, Springer-Verlag, New York, 1981. Anderson, *The Fischer-Tropsch Synthesis*, Academic Press, New York, 1984. Sheldon, *Chemicals from Synthesis Gas*, D. Reidel Publishing Co., Dordrecht, Netherlands, 1983. Rao, Stiegel, Cinquegrane, and Srivastava, "Iron-Based Catalyst for Slurry-Phase Fischer-Tropsch Process: Technology Review," *Fuel Processing Technology*, **30**, 83–151 (1992). Wender, "Reactions of Synthesis Gas," *Fuel Processing Technology*, **48**, 189–297 (1996).

Background Coal liquefaction denotes the process of converting solid coal to a liquid fuel. The primary objective of any coal liquefaction process is to increase the hydrogen-to-carbon molar ratio. For a typical bituminous coal, this ratio is about 0.8, while for light petroleum it is about 1.8. A secondary objective is to remove sulfur, nitrogen, oxygen, and ash so as to produce a nearly pure hydrocarbon. There are several ways to accomplish liquefaction: (1) pyrolysis, (2) direct hydrogenation of the coal at elevated temperature and pressure, (3) hydrogenation of coal slurried in a solvent, and (4) gasification of coal to produce synthesis gas (a mixture of hydrogen and carbon monoxide, also referred to as syngas) followed by the use of Fischer-Tropsch (F-T) chemistry to produce liquid products. The first three of these approaches are generally referred to as direct liquefaction, in that the coal is directly converted to a liquid. The fourth approach is termed indirect liquefaction, because the coal is first converted to an intermediate product.

Pyrolysis In pyrolysis, coal is heated in the absence of oxygen to drive off volatile components, leaving behind a solid residue enriched in carbon and known as char or coke. Most coal pyrolysis operations are for the purpose of producing metallurgical coke, with the liquids

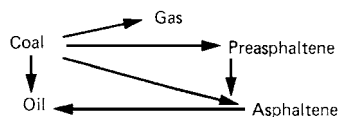
produced being considered only as a by-product. However, some small-scale work has been done to maximize liquids production by heating the coal at carefully controlled conditions of temperature vs. time, usually in several stages. Although capable of producing a significant liquid yield, this approach has two major drawbacks. First, the liquids produced are of low quality and require significant upgrading to convert them to salable products. Second, a large fraction of the original heating value of the coal remains in the char, which must be profitably marketed to make the pyrolysis process economically feasible. Two processes that reached a high state of development were the COED process developed by FMC Corporation, which used a series of fluidized beds operating at successively higher temperatures, and the TOSCOAL process, which used a horizontal rotating kiln.

Direct Hydrogenation In direct hydrogenation, pulverized coal is contacted with hydrogen at carefully controlled conditions of temperature and pressure. The hydrogen reacts with the coal, converting it to gaseous and liquid products. In some cases the coal is impregnated with a catalyst before being introduced into the reactor. Again, small-scale experiments have been successfully conducted. However, the major difficulty with this approach is scale-up to commercial size. Significant technical problems exist in feeding a large volume of powdered coal (powdered coal is necessary to provide a large surface area for reaction) into a reactor at high pressure, heating it to the desired temperature, and then quenching the products.

Direct Liquefaction of Coal Figure 24-6 presents a simplified process flow diagram of a typical direct coal liquefaction plant using coal slurry hydrogenation. Coal is ground and slurried with a process-derived solvent, mixed with a hydrogen-rich gas stream, preheated, and sent to a one- or two-stage liquefaction reactor system. In the reactor(s), the organic fraction of the coal dissolves in the solvent, and the dissolved fragments react with hydrogen to form liquid and gaseous products. Sulfur in the coal is converted to hydrogen sulfide,

nitrogen is converted to ammonia, and oxygen is converted to water. The reactor products go to vapor/liquid separation. The gas is cleaned and, after removal of a purge stream to prevent buildup of inerts, mixed with fresh hydrogen and recycled. The liquid is sent to fractionation for recovery of distillates. Heavy gas-oil is recycled as process solvent, and vacuum bottoms are gasified for hydrogen production. Ash from the gasifier is sent to disposal. Heavy direct liquefaction products contain polynuclear aromatics and are potentially carcinogenic. However, this problem can be avoided by recycling to extinction all material boiling above the desired product endpoint.

Direct Liquefaction Kinetics Hydrogenation of coal in a slurry is a complex process, the mechanism of which is not fully understood. It is generally believed that coal first decomposes in the solvent to form free radicals which are then stabilized by extraction of hydrogen from hydroaromatic solvent molecules, such as tetralin. If the solvent does not possess sufficient hydrogen transfer capability, the free radicals can recombine (undergo retrograde reactions) to form heavy, nonliquid molecules. A greatly simplified model of the liquefaction process is shown below.



Many factors affect the rate and extent of coal liquefaction, including temperature, hydrogen partial pressure, residence time, coal type and analysis, solvent properties, solvent-to-coal ratio, ash composition, and the presence or absence of a catalyst. Many kinetic expressions have appeared in the literature, but since they are generally specific to a particular process, they will not be listed here. In general, liquefaction is

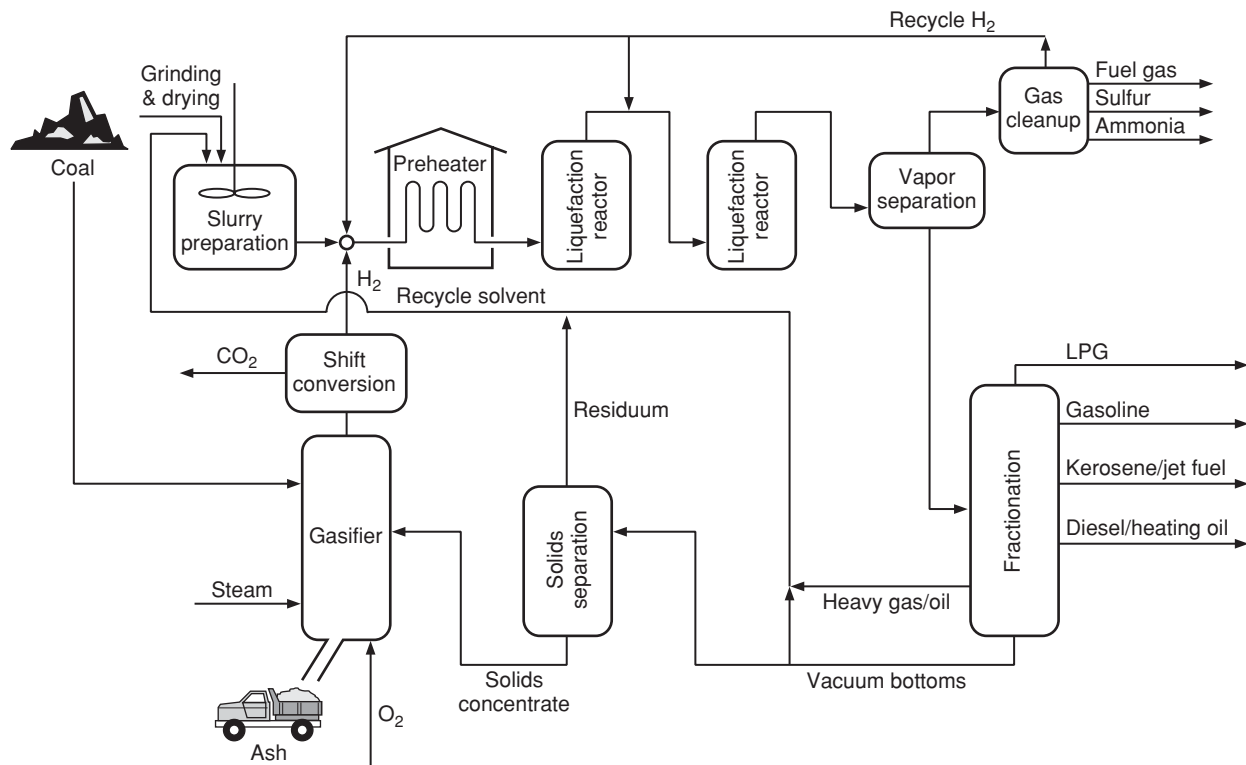


FIG. 24-6 Direct liquefaction of coal.

promoted by increasing the temperature, hydrogen partial pressure, and residence time. However, if the temperature is too high, gas yield is increased and coking can occur. Solvent-to-coal ratio is important. If the ratio is too low, there will be insufficient hydrogen transfer activity; on the other hand, if the ratio is high, a larger reactor will be necessary to provide the required residence time. Typical operating conditions are:

Temperature	670–730 K (750–850°F)
Pressure	10.3–20.7 MPa (1500–3000 psia)
Residence time	0.5 h
Solvent-to-coal ratio	1.5–2 kg/kg (1.5–2 lb/lb)

For the most highly developed processes, maf coal conversion can be as high as 90 to 95 % with a C₄+ distillate yield of 60 to 75 wt % and a hydrogen consumption of 5 to 7 wt %. When an external catalyst is used, it is typically some combination of cobalt, nickel, and molybdenum on a solid acid support, such as silica alumina. In slurry hydrogenation processes, catalyst life is typically fairly short because of the large number of potential catalyst poisons present in the system.

Several variations of the slurry hydrogenation process, depicted in Fig. 24-6 and discussed below, were tested at pilot-plant scale. Table 24-12 presents typical operating conditions and yields for these processes.

The *SRC-I process*, developed by the Pittsburg & Midway Coal Mining Co. in the early 1960s, was not really a liquefaction process; rather, it was designed to produce a solid fuel for utility applications. Only enough liquid was produced to keep the process in solvent balance. The bottoms product was subjected to filtration or solvent extraction to remove ash and then solidified to produce a low-ash, low-sulfur substitute for coal. However, the value of the product was not high enough to make this process economically viable.

The *SRC-II process*, developed by Gulf Oil Corp., was an improved version of the SRC-I process, designed to produce more valuable liquid products, rather than a solid. The major difference between SRC-II and the typical process described above was the recycle of a portion of the fractionator bottoms to the slurry feed tank. This increased the ash content of the reactor feed. This ash, particularly the iron pyrites in the ash, acted as a catalyst and improved product yield and quality.

The *Exxon Donor Solvent (EDS) Process*, developed by the Exxon Research and Engineering Co., differed from the typical process in that, before being recycled, the solvent was hydrogenated in a fixed-bed reactor using a hydrotreating catalyst, such as cobalt or nickel molybdate. Exxon found that use of this hydrogen donor solvent with carefully controlled properties improved process performance. Exxon developed a solvent index, based on solvent properties, which correlated with solvent effectiveness.

The *H-Coal Process*, based on H-Oil technology, was developed by Hydrocarbon Research, Inc. (HRI). The heart of the process was a three-phase, ebullated-bed reactor in which catalyst pellets were fluidized by the upward flow of slurry and gas through the reactor. The reactor contained an internal tube for recirculating the reaction mixture to the bottom of the catalyst bed. Catalyst activity in the reactor was maintained by the withdrawal of small quantities of spent catalyst and the addition of fresh catalyst. The addition of a catalyst to the reactor is the main feature which distinguishes the H-Coal Process from the typical process.

Two-stage liquefaction is an advanced process concept that provides higher yields of better quality products by carrying out the coal solution and the hydrogenation/hydrocracking steps in separate reactors whose conditions are optimized for the reaction that is occurring. Either or both reactors may be catalytic. Slurry catalysts have been tested, in addition to the more conventional supported catalysts, as a means of simplifying reactor design and removing process constraints. The U.S. Department of Energy and its private sector collaborators, Hydrocarbon Technologies, Inc., and others, have advanced the development of the two-stage direct liquefaction process to commercialization status during the last two decades. Coal-derived product quality has been improved dramatically (less than 50 ppm nitrogen content, for example) through the addition of in-line fixed-bed hydrotreating of the product stream.

In *coal-oil coprocessing*, coal is slurried in petroleum residuum rather than in recycle solvent, and both the coal and petroleum components are converted to high-quality fuels in the slurry reactor. This variation offers the potential for significant cost reduction by eliminating or

TABLE 24-12 Direct Liquefaction Process Conditions and Product Yields

Developer Process	Gulf ^a SRC-I	Gulf SRC-II	Exxon EDS	HRI H-Coal	SCS, ^b EPRI, Amoco Two-stage	HTI Two-stage
Coal type	Kentucky 9 & 14	Illinois No. 6	Illinois No. 6	Illinois No. 6	Illinois No. 6	Illinois No. 6
Operating conditions						
Nominal reactor residence time, h	0.5	0.97	0.67			
Coal space velocity per stage, kg/(h·m ³) (lb/(h·ft ³))				530 (33.1)	825 ^c (51.7)	310 (19.4)
Temperature, K (°F)	724 (842)	730 (855)	722 (840)	726 (847)	700 (800)	692 (787)
Total pressure, MPa (psia)	10.3 (1500)	13.4 (1950)	10.3 (1500)			19.2 (2790)
H ₂ partial pressure, MPa (psia)	9.7 (1410)	12.6 (1830)		12.6 (1827)	18.3 (2660)	
Catalyst type	Coal minerals	Coal minerals	Coal minerals	Supported catalyst (Co/Mo)	AKZO-AO-60 (Ni/Mo)	AKZO-AO-60 (Ni/Mo)
Catalyst replacement rate, kg/kg (lb/US ton) mf coal					1.5 × 10 ⁻³ (3.0)	2.3 × 10 ⁻³ (4.5)
Product yields, wt % maf coal						
H ₂	-2.4	-5.0	-4.3	-5.9	-6.0	-7.2
H ₂ O	—	—	12.2 ^d	8.3	9.7	9.8
H ₂ S, CO _x , NH ₃	—	9.6	4.2 ^e	5.0	5.2	5.2
C ₁ -C ₃	3.7 ^f	13.9 ^f	7.3	11.3	6.5	5.6
C ₄ + distillate	13.5 ^g	46.8 ^g	38.8	53.1	65.6	73.3
Bottoms ^h	68.4	30.7	41.8	28.2	19.0	13.3
Unreacted coal ⁱ	5.4	4.6	—	6.4	7.0	5.0
Distillate end point, K (°F)	727 (850)	727 (850)	911 (1180)	797 (975)	797 (975)	524 (975)

^aIn partnership with Pittsburg & Midway Coal Mining Co.

^bSouthern Company Services, Inc., prime contractor for Wilsonville Facility.

^cCoal space velocity is based on settled catalyst volume.

^dCO_x is included.

^eCO_x is excluded.

^fC₄ is included.

^gC₄ is excluded.

^hUnreacted coal is included.

ⁱ"Unreacted coal" is actually insoluble organic matter remaining after reaction.

reducing recycle streams. More importantly, fresh hydrogen requirements are reduced, because the petroleum feedstock has a higher initial hydrogen content than coal. As a result, plant capital investment is reduced substantially. Other carbonaceous materials, such as municipal waste, plastics, cellulose, and used motor oils, might also serve as cofeedstocks with coal in this technology.

Commercial Operations The world's only commercial-scale direct coal liquefaction plant, located in the Inner Mongolia Autonomous Region of China, was dedicated in 2004. The plant is scheduled to begin production in 2007. The first train of the first phase of the Shenhua Direct Coal Liquefaction Plant will liquefy 2,100,000 Mg/a (2,315,000 ton/yr) of coal from the Shangwan Mine in the Shenhua coal field of Inner Mongolia. The plant will use a combination of technologies developed in the United States, Japan, and Germany with modifications and enhancements developed in China. The first train will use a two-stage reactor system and include an in-line hydrotreater and produce 591,900 Mg/a (652,460 ton/yr) of diesel; 174,500 Mg/a (192,350 ton/yr) of naphtha; 70,500 Mg/a (77,710 ton/yr) of LPG; and 8300 Mg/a (9150 ton/yr) of ammonia. When completed, the plant will include 10 trains producing approximately 10,000,000 Mg/a (11,000,000 ton/yr) of oil products.

Unlike the processes described above, *indirect liquefaction* is not limited to coal but may be performed using any carbonaceous feed, such as natural gas, petroleum residues, petroleum coke, coal, and biomass. Figure 24-7 presents a simplified process flow diagram for a typical indirect liquefaction process using coal as the feedstock. The syngas is produced in a gasifier (see the description of coal gasifiers earlier in this section), which partially combusts the coal or other feed at high temperature [1500 to 1750 K (2200 to 2700°F)] and moderate pressure [2 to 4 MPa (300 to 600 psia)] with a mixture of oxygen (or air) and steam. In addition to H₂ and CO, the raw synthesis gas contains other constituents, such as CO₂, H₂S, NH₃, N₂, H₂O, and CH₄, as well as particulates and, with some gasifiers, tars.

The syngas leaving the gasifier is cooled and passed through particulate removal equipment. Following this, depending on the requirements of the syngas conversion process, it may be necessary to adjust the H₂/CO ratio. Modern high-efficiency gasifiers typically produce syngas with a H₂/CO molar ratio between 0.45 and 0.7, which is lower than the stoichiometric ratio of about 2 for F-T synthesis or methanol production. Some F-T catalysts, particularly iron catalysts, possess water-gas shift conversion activity and permit operation with a low H₂/CO ratio [see reaction (24-25)]. Others, such as cobalt catalysts, possess little shift activity and require adjustment of the H₂/CO ratio before the syngas enters the synthesis reactor.

After shift conversion (if required), acid gases (CO₂ and H₂S) are scrubbed from the synthesis gas. A guard chamber is sometimes used to remove the last traces of H₂S, since F-T catalysts are generally very sensitive to sulfur poisoning. The cleaned gas is sent to the synthesis reactor, where it is converted at moderate temperature and pressure, typically 498 to 613 K (435 to 645°F) and 1.5 to 6.1 MPa (220 to 880 psia). Products, whose composition depends on operating conditions, the catalyst employed, and the reactor design, include saturated hydrocarbons (mainly straight chain paraffins from methane through *n*-C₃₀ and higher), oxygenates (methanol, higher alcohols, ethers), and olefins.

Fischer-Tropsch Synthesis The best-known technology for producing hydrocarbons from synthesis gas is the Fischer-Tropsch synthesis. This technology was first demonstrated in Germany in 1902 by Sabatier and Senderens when they hydrogenated carbon monoxide (CO) to methane, using a nickel catalyst. In 1926 Fischer and Tropsch were awarded a patent for the discovery of a catalytic technique to convert synthesis gas to liquid hydrocarbons similar to petroleum.

The basic reactions in the Fischer-Tropsch synthesis are:

Paraffins formation:

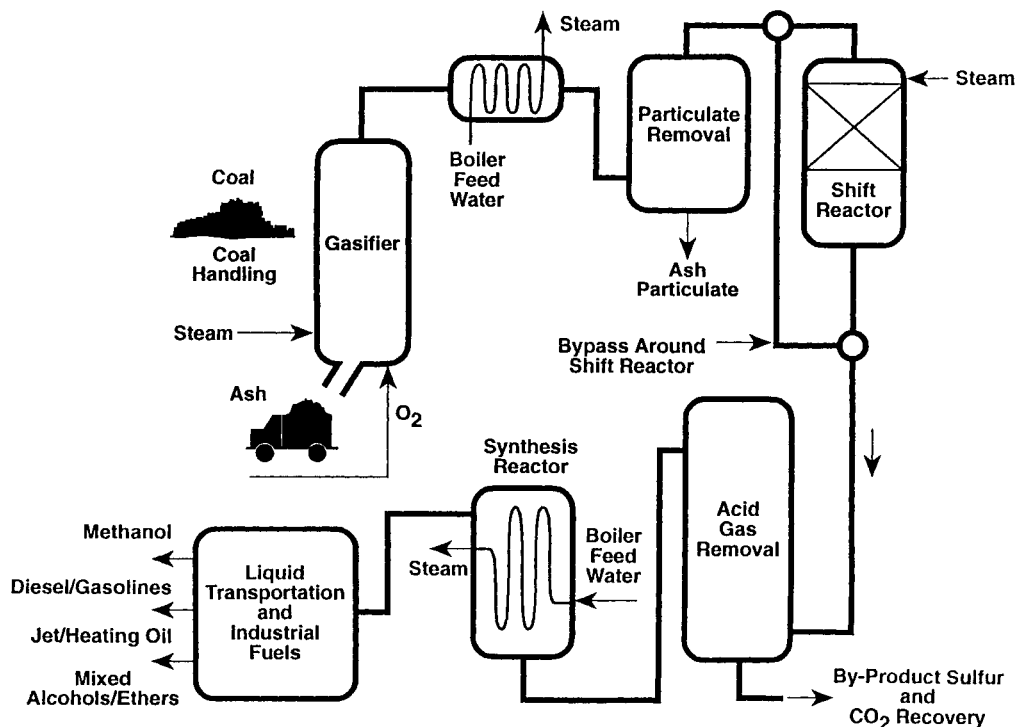
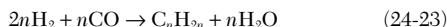


FIG. 24-7 Indirect liquefaction of coal.

Olefins formation:



Alcohols formation:

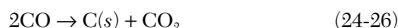


Other reactions may also occur during the Fischer-Tropsch synthesis, depending on the catalyst employed and the conditions used:

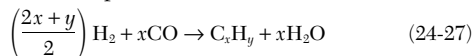
Water-gas shift:



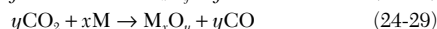
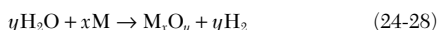
Boudouard disproportionation:



Surface carbonaceous deposition:



Catalyst oxidation-reduction:



Bulk carbide formation:



where M represents a catalytic metal atom.

The production of hydrocarbons using traditional F-T catalysts is governed by chain growth (polymerization) kinetics. The theoretical equation describing the distribution of hydrocarbon products, commonly referred to as the Anderson-Schulz-Flory (ASF) equation, is

$$\log \frac{W_n}{n} = n \log \alpha + \log \frac{(1-\alpha)^2}{\alpha} \quad (24-31)$$

where W_n is the weight fraction of products with carbon number n , and α is the chain growth probability, i.e., the probability that a carbon chain on the catalyst surface will grow by adding another carbon atom rather than desorb from the catalyst surface and terminate. In deriving Eq. (24-31), α is assumed to be independent of chain length. However, α is dependent on temperature, pressure, H_2/CO ratio, and catalyst composition. As α increases, the average carbon number of the product also increases. When α equals 0, methane is the only product formed. As α approaches 1, the product becomes predominantly wax. In practice, α is not really independent of chain length. Methane production, particularly with cobalt catalysts, is typically higher than predicted; and C_2 yield is often lower. Some investigators have found a significant deviation from the ASF distribution for higher-carbon-number products and have proposed a dual alpha mechanism to explain their results.

Figure 24-8 provides a graphical representation of Eq. 24-32 showing the weight fraction of various products as a function of α . This figure shows that there is a particular α that will maximize the yield of any desired product, such as gasoline or diesel fuel. Based on the ASF equation, the weight fraction of material between carbon numbers m and n inclusive is given by

$$W_{mn} = m\alpha^{m-1} - (m-1)\alpha^m - (n+1)\alpha^n + n\alpha^{n+1} \quad (24-32)$$

The α to maximize the yield of the carbon number range from m to n is given by

$$\alpha_{\text{opt}} = \left(\frac{m^2 - m}{n^2 + n}\right)^{1/(n-m+1)} \quad (24-33)$$

Additional gasoline and diesel fuel can be produced through further refining, such as hydrocracking or catalytic cracking of the wax product or polymerization of light olefins.

F-T Catalysts The patent literature is replete with recipes for the production of F-T catalysts, with most formulations being based on iron, cobalt, or ruthenium, typically with the addition of some promoter(s). Nickel is sometimes listed as a F-T catalyst, but nickel has too much hydrogenation activity and produces mainly methane. In practice, because of the cost of ruthenium, commercial plants use either cobalt-based or iron-based catalysts. Cobalt is usually deposited on a refractory oxide support, such as alumina, silica, titania, or zirconia. Iron is typically not supported and may be prepared by precipitation.

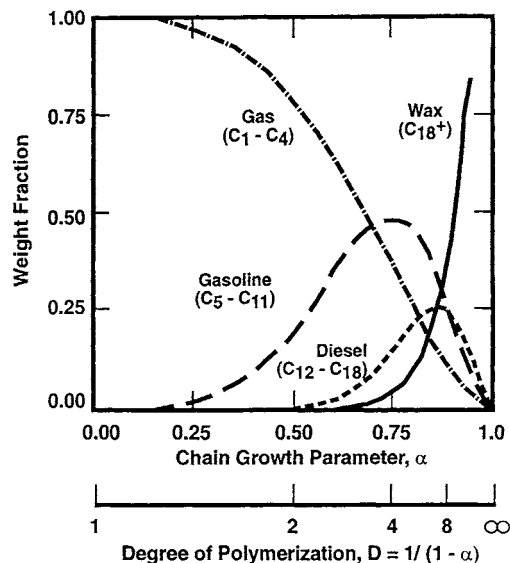
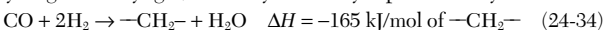


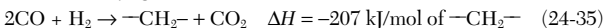
FIG. 24-8 Product yield in Fischer-Tropsch synthesis.

Of the large number of promoters listed in patents, rhenium or one of the noble metals may be used to promote cobalt, and iron is often promoted with potassium.

Reactor Design The F-T reaction is highly exothermic and, for hydrogen-rich syngas, can be symbolically represented by



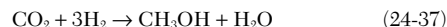
For CO-rich syngas, the overall reaction is



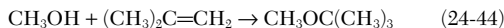
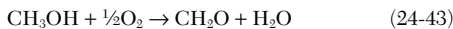
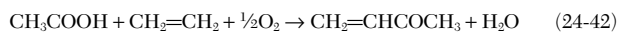
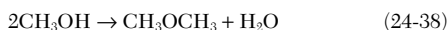
Because of the high heat release, adequate heat removal from the reactor is critical. High temperatures result in high yields of methane as well as coking and sintering of the catalyst. Three types of reactors (tubular fixed bed, fluidized bed, and slurry) provide good temperature control, and all three types are being used for synthesis gas conversion. The first plants used tubular or plate-type fixed-bed reactors. Later, SASOL, in South Africa, used fluidized-bed reactors, and most recently, slurry reactors have come into use. Fluid bed reactors are limited to the production of products that are volatile at reactor operating conditions. Nonvolatile products accumulate on the catalyst and destroy its fluidizing properties.

F-T reactor operations can be classified into two categories: high-temperature, 613 K (645°F), or low-temperature, 494-544 K (430 to 520°F). The Synthol reactor developed by SASOL is typical of high-temperature operation. Using an iron-based catalyst, this reactor produces a very good gasoline having high olefinicity and a low boiling range. The olefin fraction can readily be oligomerized to produce diesel fuel. Low-temperature operation, typical of fixed-bed reactors, produces a much more paraffinic and straight-chain product. The chain growth parameter can be tailored to give the desired product selectivity. The primary diesel fraction, as well as the diesel-range product from hydrocracking of the wax, is an excellent diesel fuel.

Chemicals from Syngas A wide range of products can be produced from syngas. These include such chemicals as methanol, ethanol, isobutanol, dimethyl ether, dimethyl carbonate, and many other chemicals. Typical methanol-producing reactions are

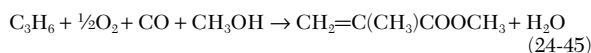


Once methanol is produced, it can be converted to an extensive range of materials. The following reactions illustrate some of the chemicals of major importance that can be made from methanol. Among these are dimethyl ether, acetic acid, methyl acetate, acetic anhydride, vinyl acetate, formaldehyde, and methyl tertiarybutyl ether (MTBE).



Reaction (24-38) can occur in parallel with the methanol-producing reactions, thereby overcoming the equilibrium limitation on methanol formation. Higher alcohols can also be formed, as illustrated by reaction (24-24), which can generate either linear or branched alcohols, depending on the catalyst used and the operating conditions. The production of methyl acetate, reaction (24-40), from synthesis gas is currently being practiced commercially. Following methanol synthesis, one-half of the methanol is reacted with carbon monoxide to form acetic acid, which is reacted with the rest of the methanol to form methyl acetate.

Methyl acrylate and methyl methacrylate, which are critical to the production of polyesters, plastics, latexes, and synthetic lubricants, can also be produced. For example, methyl methacrylate can be produced from propylene and methanol:



Commercial Operations The only commercial indirect coal liquefaction plants for the production of transportation fuels are operated by SASOL in South Africa. Construction of the original plant was begun in 1950, and operations began in 1955. This plant employed both fixed-bed (Arge) and entrained-bed (Synthol) reactors. The fixed-bed reactors have been converted to natural gas, and the Synthol reactors have been replaced by advanced fixed-fluidized bed reactors. Two additional plants that employ dry-ash Lurgi Mark IV coal gasifiers and entrained-bed (Synthol) reactors for synthesis gas conversion were constructed with start-ups in 1980 and 1983. In addition to producing a significant fraction of South Africa's transportation fuel requirements, these plants produce more than 120 other products from coal.

SASOL and others, including Exxon, Statoil, Air Products and Chemicals, Inc., and the U.S. Department of Energy, have engaged in the development of slurry bubble column reactors for F-T and oxygenate synthesis. SASOL commissioned a 5-m-diameter slurry reactor in 1993, which doubled the wax capacity of the SASOL I facility. The development work on slurry reactors shows that they have several advantages over competing reactor designs: (1) excellent heat-transfer capability resulting in nearly isothermal reactor operations, (2) high catalyst and reactor productivity, (3) ease of catalyst addition and withdrawal, (4) simple construction, and (5) ability to process hydrogenlean synthesis gas successfully. Because of the small particle size of the catalyst used in slurry reactors, effective separation of catalyst from the products can be difficult but is crucial to successful operation.

The United States has two commercial facilities that convert coal to fuels or chemicals via a syngas intermediate. The Great Plains Synfuels

Plant, located in Beulah, N. Dak., and operated by Dakota Gasification Company (DGC), produces synthetic natural gas (SNG) from North Dakota lignite. Fourteen Lurgi dry-ash gasifiers in the plant convert approximately 15,400 Mg/d (17,000 U.S. ton/day) of lignite into syngas which is methanated to about $4.7 \times 10^6 \text{ N}\cdot\text{m}^3$ ($166 \times 10^6 \text{ std ft}^3$) of pipeline-quality gas. Aromatic naphtha and tar oil are also produced in the gasification section. The plant operates at 120 percent of its original design capacity. In addition to SNG, a wide assortment of other products are produced and sold (anhydrous ammonia, ammonium sulfate, phenol, cresylic acid, naphtha, krypton and xenon gases, liquid nitrogen, and carbon dioxide).

Eastman Chemical Company has operated a coal-to-methanol plant in Kingsport, Tenn., since 1983. Two Texaco gasifiers (one is a backup) process 34 Mg/h (37 U.S. ton/h) of coal to synthesis gas. Using ICI methanol technology, the synthesis gas is converted to methanol, which is an intermediate in the production of methyl acetate and acetic acid. The plant produces about 225,000 Mg/a (250,000 U.S. ton/yr) of acetic anhydride. As part of the DOE Clean Coal Technology Program, Air Products and Chemicals, Inc., and Eastman Chemical Company constructed and operated a 9.8 Mg/h (260 U.S. ton/d) slurry-phase reactor for the conversion of synthesis gas to methanol.

Despite the success of SASOL, most of the commercial interest in Fischer-Tropsch synthesis technology is based on natural gas, as this represents a way to bring remote gas deposits to market using conventional tankers. In 1985, Mobil commercialized its Methanol-to-Gasoline (MTG) technology in New Zealand, natural gas being the feedstock. This fixed-bed process converted synthesis gas to 4000 Mg/d (4400 U.S. ton/day) of methanol; the methanol could then be converted to 2290 m³/d (14,400 bbl/d) of gasoline. Owing to economic factors, the plant was used primarily for the production of methanol; it has been shut down due to an insufficient gas supply.

Shell Gas B.V. constructed a 1987 m³/d (12,500 bbl/d) F-T plant in Malaysia that started operations in 1994. The Shell Middle Distillate Synthesis (SMDS) process uses natural gas as the feedstock to fixed-bed reactors containing cobalt-based catalyst. The heavy hydrocarbons from the F-T reactors are converted to distillate fuels by hydrocracking and hydroisomerization. The quality of the products is very high, the diesel fuel having a cetane number in excess of 75 with no sulfur.

The largest F-T facility based on natural gas is the Moss gas plant located in Mossel Bay, South Africa. Natural gas is converted to synthesis gas in a two-stage reformer and subsequently converted to hydrocarbons by SASOL's Synthol technology. The plant, commissioned in 1992, has a capacity of 7155 m³/d (45,000 bbl/d).

In addition to these commercial facilities, several companies have smaller-scale demonstration facilities, generally with capacities of a few hundred barrels per day of liquid products. For example, Exxon Research and Engineering Company developed a process for converting natural gas to high-quality refinery feedstock, the AGC-21 Advanced Gas Conversion Process. The technology involves three highly integrated process steps: fluid-bed synthesis gas generation; slurry-phase Fischer-Tropsch synthesis; and mild fixed-bed hydroisomerization. The process was demonstrated in the early 1990s with a slurry-phase reactor having a diameter of 1.2 m (4 ft) and a capacity of about 32 m³/d (200 bbl/d).

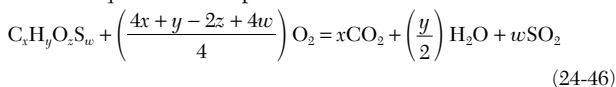
HEAT GENERATION

GENERAL REFERENCES: Stultz and Kitto (eds.), *Steam: Its Generation and Use*, 40th ed., Babcock and Wilcox, Barberton, Ohio, 1992. *North American Combustion Handbook*, 3d ed., vols. I and II, North American Manufacturing Company, Cleveland, Ohio, 1996. Singer (ed.), *Combustion: Fossil Power Systems*, 4th ed., Combustion Engineering, Inc., Windsor, Conn., 1991. Cuenca and Anthony (eds.), *Pressurized Fluidized Bed Combustion*, Blackie Academic & Professional, London, 1995. Basu and Fraser, *Circulating Fluidized Bed Boilers: Design and Operations*, Butterworth and Heinemann, Boston, 1991. *Proceedings of International FBC Conference(s)*, ASME, New York, 1991, 1993, 1995. *Application of FBC for Power Generation*, Electric Power Research Institute, EPRI PR-101816, Palo Alto, Calif., 1993. Boyen, *Thermal Energy Recovery*, 2d ed., Wiley, New York, 1980.

COMBUSTION BACKGROUND

Basic Principles

Theoretical Oxygen and Air for Combustion The amount of oxidant (oxygen or air) just sufficient to burn the carbon, hydrogen, and sulfur in a fuel to carbon dioxide, water vapor, and sulfur dioxide is the *theoretical* or *stoichiometric oxygen or air* requirement. The chemical equation for complete combustion of a fuel is



$x, y, z,$ and w being the number of atoms of carbon, hydrogen, oxygen, and sulfur, respectively, in the fuel. For example, 1 mol of methane (CH_4) requires 2 mol of oxygen for complete combustion to 1 mol of carbon dioxide and 2 mol of water. If air is the oxidant, each mol of oxygen is accompanied by 3.76 mol of nitrogen.

The volume of theoretical oxygen (at 0.101 MPa and 298 K) needed to burn any fuel can be calculated from the ultimate analysis of the fuel as follows:

$$24.45 \left(\frac{C}{12} + \frac{H}{4} - \frac{O}{32} + \frac{S}{32} \right) = m^3 \text{O}_2/\text{kg fuel} \quad (24-47)$$

where $C, H, O,$ and S are the decimal weights of these elements in 1 kg of fuel. (To convert to ft^3 per lb of fuel, multiply by 16.02.) The mass of oxygen (in kg) required can be obtained by multiplying the volume by 1.31. The volume of theoretical air can be obtained by using a coefficient of 116.4 in Eq. (24-47) in place of 24.45.

Figure 24-9 gives the theoretical air requirements for a variety of combustible materials on the basis of fuel higher heating value (HHV). If only the fuel lower heating value is known, the HHV can be calculated from Eq. (24-5). If the ultimate analysis is known, Eq. (24-4) can be used to determine HHV.

Excess Air for Combustion More than the theoretical amount of air is necessary in practice to achieve complete combustion. This excess air is expressed as a percentage of the theoretical air amount. The *equivalence ratio* is defined as the ratio of the actual fuel-air ratio to the stoichiometric fuel-air ratio. Equivalence ratio values less than 1.0 correspond to fuel-lean mixtures. Conversely, values greater than 1.0 correspond to fuel-rich mixtures.

Products of Combustion For lean mixtures, the *products of combustion* (POC) of a sulfur-free fuel consist of carbon dioxide, water vapor, nitrogen, oxygen, and possible small amounts of carbon monoxide and unburned hydrocarbon species. Figure 24-10 shows the effect of fuel-air ratio on the flue gas composition resulting from the combustion of natural gas. In the case of solid and liquid fuels, the POC may also include solid residues containing ash and unburned carbon particles.

Equilibrium combustion product compositions and properties may be readily calculated using thermochemical computer codes which minimize the Gibbs free energy and use thermodynamic databases containing polynomial curve-fits of physical properties. Two widely used versions are those developed at NASA Lewis (Gordon and McBride, NASA SP-273, 1971) and at Stanford University (Reynolds, STANJAN Chemical Equilibrium Solver, Stanford University, 1987).

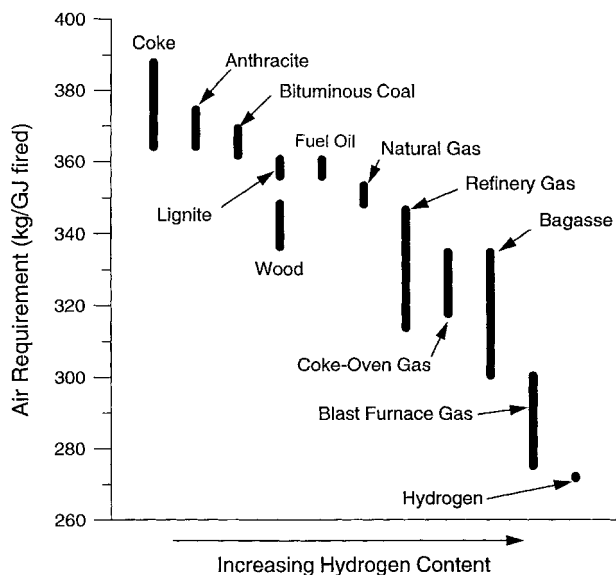


FIG. 24-9 Combustion air requirements for various fuels at zero excess air. To convert from kg air/GJ fired to lb air/10⁶ Btu fired, multiply by 2.090.

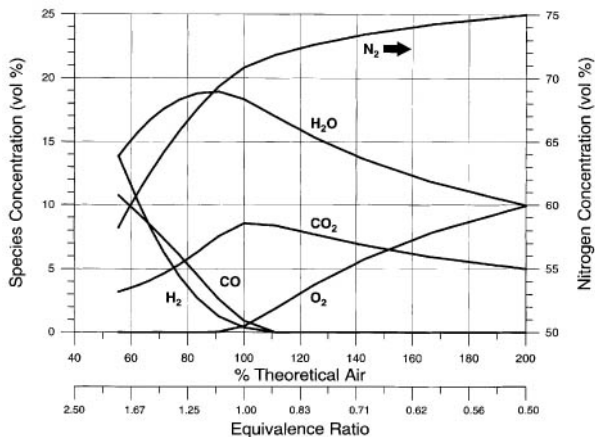


FIG. 24-10 Effect of fuel-air ratio on flue-gas composition for a typical U.S. natural gas containing 93.9% CH_4 , 3.2% C_2H_6 , 0.7% C_3H_8 , 0.4% C_4H_{10} , 1.5% N_2 and 1.1% CO_2 by volume.

Flame Temperature The heat released by the chemical reaction of fuel and oxidant heats the POC. Heat is transferred from the POC, primarily by radiation and convection, to the surroundings, and the resulting temperature in the reaction zone is the flame temperature. If there is no heat transfer to the surroundings, the flame temperature equals the theoretical, or adiabatic, flame temperature.

Figure 24-11 shows the *available heat* in the products of combustion for various common fuels. The available heat is the total heat

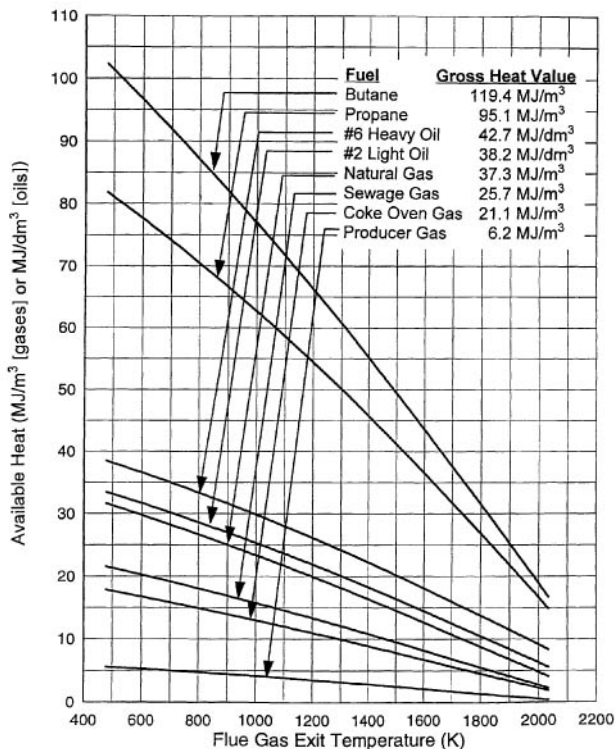


FIG. 24-11 Available heats for some typical fuels. The fuels are identified by their gross (or higher) heating values. All available heat figures are based upon complete combustion and fuel and air initial temperature of 288 K (60°F). To convert from MJ/Nm^3 to Btu/ft^3 , multiply by 26.84. To convert from MJ/dm^3 to Btu/gal , multiply by 3585.

TABLE 24-13 Combustion Characteristics of Various Fuels*

Fuel	Minimum ignition temp., K/°F	Calculated flame temperature, † K/°F		Flammability limits, % fuel gas by volume in air		Maximum flame velocity, m/s and ft/s		% theoretical air for max. flame velocity
		in air	in O ₂	lower	upper	in air	in O ₂	
Acetylene, C ₂ H ₂	578/581	2905/4770	3383/5630	2.5	81.0	2.67/8.75	—	83
Blast furnace gas	—	1727/2650	—	35.0	73.5	—	—	—
Butane, commercial	753/896	2246/3583	—	1.86	8.41	0.87/2.85	—	—
Butane, n-C ₄ H ₁₀	678/761	2246/3583	—	1.86	8.41	0.40/1.3	—	97
Carbon monoxide, CO	882/1128	2223/3542	—	12.5	74.2	0.52/1.7	—	55
Carbureted water gas	—	2311/3700	3061/5050	6.4	37.7	0.66/2.15	—	90
Coke oven gas	—	2261/3610	—	4.4	34.0	0.70/2.30	—	90
Ethane, C ₂ H ₄	745/882	2222/3540	—	3.0	12.5	0.48/1.56	—	98
Gasoline	553/536	—	—	1.4	7.6	—	—	—
Hydrogen, H ₂	845/1062	2318/4010	3247/5385	4.0	74.2	2.83/9.3	—	57
Hydrogen sulfide, H ₂ S	565/558	—	—	4.3	45.5	—	—	—
Mapp gas, (allene) C ₃ H ₄	728/850	—	3200/5301	3.4	10.8	—	4.69/15.4	—
Methane, CH ₄	905/1170	2191/3484	—	5.0	15.0	0.45/1.48	4.50/14.76	90
Methanol, CH ₃ OH	658/725	2177/3460	—	6.7	36.0	—	0.49/1.6	—
Natural gas	—	2214/3525	2916/4790	4.3	15.0	0.30/1.00	4.63/15.2	100
Producer gas	—	1927/3010	—	17.0	73.7	0.26/0.85	—	90
Propane, C ₃ H ₈	739/871	2240/3573	3105/5130	2.1	10.1	0.46/1.52	3.72/12.2	94
Propane, commercial	773/932	2240/3573	—	2.37	9.50	0.85/2.78	—	—
Propylene, C ₃ H ₆	—	—	3166/5240	—	—	—	—	—
Town gas (brown coal)	643/700	2318/3710	—	4.8	31.0	—	—	—

*For combustion with air at standard temperature and pressure. These flame temperatures are calculated for 100 percent theoretical air, disassociation considered. Data from *Gas Engineers Handbook*, Industrial Press, New York, 1965.

†Flame temperatures are theoretical—calculated for stoichiometric ratio, dissociation considered.

released during combustion minus the flue-gas heat loss (including the heat of vaporization of any water formed in the POC).

Flammability Limits There are both upper (or rich) and lower (or lean) limits of flammability of fuel-air or fuel-oxygen mixtures. Outside these limits, a self-sustaining flame cannot form. Flammability limits for common fuels are listed in Table 24-13.

Flame Speed Flame speed is defined as the velocity, relative to the unburned gas, at which an adiabatic flame propagates normal to itself through a homogeneous gas mixture. It is related to the combustion reaction rate and is important in determining burner flashback and blow-off limits. In a premixed burner, the flame can *flash back* through the flameholder and ignite the mixture upstream of the burner head if the mixture velocity at the flameholder is lower than the flame speed. Conversely, if the mixture velocity is significantly higher than the flame speed, the flame may not stay attached to the flameholder and is said to *blow off*. Flame speed is strongly dependent on fuel/air ratio, passing from nearly zero at the lean limit of flammability through a maximum and back to near zero at the rich limit of flammability. Maximum flame speeds for common fuels are provided in Table 24-13.

Pollutant Formation and Control in Flames Key combustion-generated air pollutants include nitrogen oxides (NO_x), sulfur oxides (principally SO₂), particulate matter, carbon monoxide, and unburned hydrocarbons.

Nitrogen Oxides Three reaction paths, each having unique characteristics (see Fig. 24-12), are responsible for the formation of NO_x during combustion processes: (1) *thermal* NO_x, which is formed by the combination of atmospheric nitrogen and oxygen at high temperatures; (2) *fuel* NO_x, which is formed from the oxidation of fuel-bound nitrogen; and (3) *prompt* NO_x, which is formed by the reaction of fuel-derived hydrocarbon fragments with atmospheric nitrogen. (NO_x is used to refer to NO + NO₂. NO is the primary form in combustion products [typically 95 percent of total NO_x]. NO is subsequently oxidized to NO₂ in the atmosphere.)

Thermal NO_x The formation of thermal NO_x is described by the Zeldovich mechanism:



The first of these reactions is the rate-limiting step. Assuming that O and O₂ are in partial equilibrium, the NO formation rate can be expressed as follows:

$$\frac{d[\text{NO}]}{dt} = A[\text{N}_2][\text{O}_2]^{1/2} \exp\left(\frac{-E}{RT}\right) \quad (24-51)$$

As indicated, the rate of NO formation increases exponentially with temperature, and, of course, oxygen and nitrogen must be available for thermal NO_x to form. Thus, thermal NO_x formation is rapid in high-temperature lean zones of flames.

Fuel NO_x Fuel-bound nitrogen (FBN) is the major source of NO_x emissions from combustion of nitrogen-bearing fuels such as heavy oils, coal, and coke. Under the reducing conditions surrounding the burning droplet or particle, the FBN is converted to fixed nitrogen species such as HCN and NH₃. These, in turn, are readily oxidized to form NO if they reach the lean zone of the flame. Between 20 and 80 percent of the bound nitrogen is typically converted to NO_x, depending on the design of the combustion equipment. With prolonged exposure (order of 100 ms) to high temperature and reducing conditions, however, these fixed nitrogen species may be converted to molecular nitrogen, thus avoiding the NO formation path.

Prompt NO_x Hydrocarbon fragments (such as C, CH, CH₂) may react with atmospheric nitrogen under fuel-rich conditions to yield fixed nitrogen species such as NH, HCN, H₂CN, and CN. These, in turn, can be oxidized to NO in the lean zone of the flame. In most flames, especially those from nitrogen-containing fuels, the prompt mechanism is responsible for only a small fraction of the total NO_x. Its control is important only when attempting to reach the lowest possible emissions.

NO_x emission control It is preferable to minimize NO_x formation through control of the mixing, combustion, and heat-transfer processes rather than through postcombustion techniques such as selective catalytic reduction. Four techniques for doing so, illustrated in Fig. 24-13, are air staging, fuel staging, flue-gas recirculation, and lean premixing.

Air staging Staging the introduction of combustion air can control NO_x emissions from all fuel types. The combustion air stream is split to create a fuel-rich primary zone and a fuel-lean secondary zone. The rich primary zone converts fuel-bound nitrogen to molecular nitrogen and suppresses thermal NO_x. Heat is removed prior to addition of the secondary combustion air. The resulting lower flame temperatures (below 1810 K [2800°F]) under lean conditions reduce the rate of formation of thermal NO_x. This technique has been widely applied to furnaces and boilers and it is the preferred approach for burning liquid and solid fuels. Staged-air burners are typically capable of reducing NO_x emissions by 30 to 60 percent, relative to uncontrolled levels. Air staging can also be accomplished by use of overfire air systems in boilers.

Fuel staging Staging the introduction of fuel is an effective approach for controlling NO_x emissions when burning gaseous fuels. The first combustion stage is very lean, resulting in low thermal and prompt NO_x. Heat is removed prior to injection of the secondary fuel. The secondary fuel entrains flue gas prior to reacting, further reducing flame temperatures. In addition, NO_x reduction through reburning

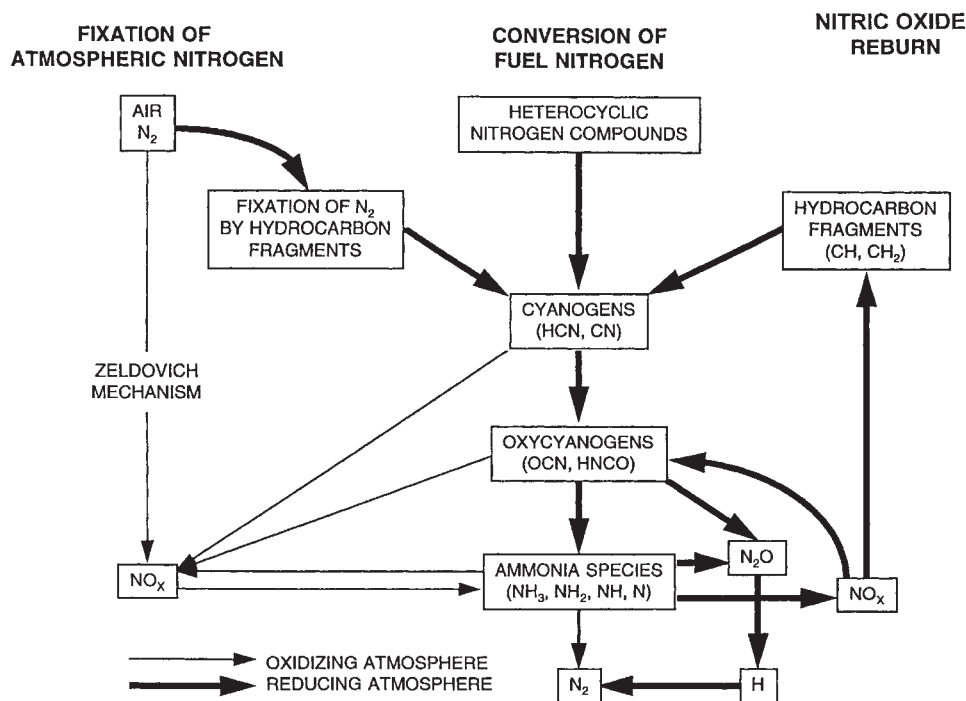


FIG. 24-12 Nitrogen oxide formation pathways in combustion.

reactions may occur in the staged jets. This technique is the favored approach for refinery- and chemical plant-fired heaters utilizing gaseous fuels. Staged-fuel burners are typically capable of reducing NO_x emissions by 40 to 70 percent, relative to uncontrolled levels.

Flue gas recirculation Flue gas recirculation, alone or in combination with other modifications, can significantly reduce thermal NO_x. Recirculated flue gas is a diluent that reduces flame temperatures. External and internal recirculation paths have been applied: internal recirculation can be accomplished by jet entrainment using either combustion air or fuel jet energy; external recirculation requires a fan or a jet pump (driven by the combustion air). When combined with staged-air or staged-fuel methods, NO_x emissions from gas-fired burners can be reduced by 50 to 90 percent. In some applications, external flue-gas recirculation can decrease thermal efficiency. Condensation in the recirculation loop can cause operating problems and increase maintenance requirements.

Lean premixing Very low NO_x emissions can be achieved by pre-mixing gaseous fuels (or vaporized liquid fuels) with air and reacting at high excess air. The uniform and very lean conditions in such systems favor very low thermal and prompt NO_x. However, achieving such low emissions requires operating near the lean stability limit. This is an attractive NO_x control approach for gas turbines, where operation at high excess air does not incur an efficiency penalty. In this application, NO_x emissions have been reduced by 75 to 95 percent.

Sulfur Oxides Sulfur occurs in fuels as inorganic minerals (primarily pyrite, FeS₂), organic structures, sulfate salts, and elemental sulfur. Sulfur contents range from parts per million in pipeline natural gas, to a few tenths of a percent in diesel and light fuel oils, to 0.5 to 5 percent in heavy fuel oils and coals. Sulfur compounds are pyrolyzed during the volatilization phase of oil and coal combustion and react in the gas phase to form predominantly SO₂ and some SO₃. Conversion of fuel sulfur to these oxides is generally high (85 to 90 percent) and is relatively independent of combustion conditions. From 1 to 4 percent of the SO₂ is further oxidized to SO₃, which is highly reactive and extremely hygroscopic. It combines with water to form sulfuric acid

aerosol, which can increase the visibility of stack plumes. It also elevates the dew point of water so that, to avoid back-end condensation and resulting corrosion, the flue-gas discharge temperature must be raised to about 420 K (300°F), reducing heat recovery and thermal efficiency. This reaction is enhanced by the presence of fine particles, which serve as condensation nuclei. Some coals may contain ash with substantial alkali content. In combustion of these fuels, the alkali may react to form condensed phase compounds (such as sulfates), thereby reducing the amount of sulfur emitted as oxides. Reductions in SO₂ emissions may be achieved either by removing sulfur from the fuel before and/or during combustion, or by postcombustion flue-gas desulfurization (wet scrubbing using limestone slurry, for example).

Particulates Combustion-related particulate emissions may consist of one or more of the following types, depending on the fuel.

Mineral matter derived from ash constituents of liquid and solid fuels can vaporize and condense as sub-micron-size aerosols. Larger mineral matter fragments are formed from mineral inclusions which melt and resolidify downstream.

Sulfate particles formed in the gas phase can condense. In addition, sulfate can become bound to metals and can be adsorbed on unburned carbon particles.

Unburned carbon includes unburned char, coke, cenospheres, and soot.

Particles of char are produced as a normal intermediate product in the combustion of solid fuels. Following initial particle heating and devolatilization, the remaining solid particle is termed *char*. Char oxidation requires considerably longer periods (ranging from 30 ms to over 1 s, depending on particle size and temperature) than the other phases of solid fuel combustion. The fraction of char remaining after the combustion zone depends on the combustion conditions as well as the char reactivity.

Cenospheres are formed during heavy oil combustion. In the early stages of combustion, the oil particle is rapidly heated and evolves volatile species, which react in the gas phase. Toward the end of the volatile-loss phase, the generation of gas declines rapidly and the

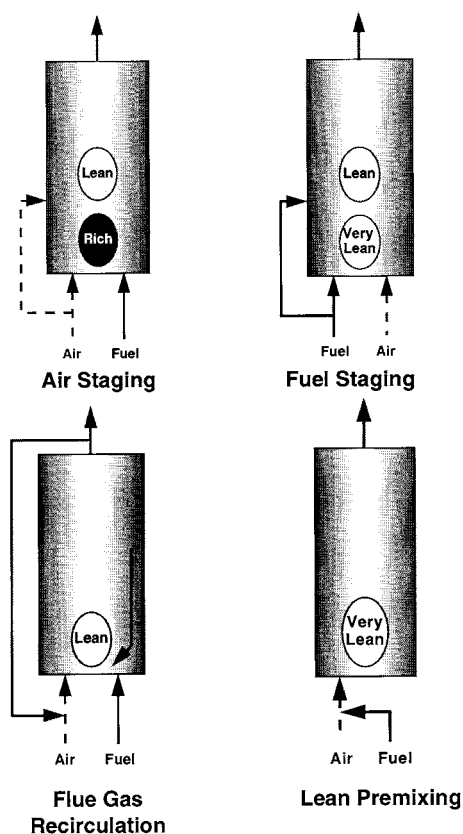


FIG. 24-13 Combustion modifications for NO_x control.

droplet (at this point, a highly viscous mass) solidifies into a porous coke particle known as a *cenosphere*. This is called *initial coke*. For the heaviest oils, the initial coke particle diameter may be 20 percent larger than the initial droplet diameter. For lighter residual oils, it may be only one third of the original droplet diameter. After a short interval, the initial coke undergoes contraction to form *final coke*. Final coke diameter is ~80 percent of the initial droplet diameter for the heaviest oils. At this time the temperature of the particle is approximately 1070 to 1270 K (1470 to 1830°F). Following coke formation, the coke particles burn out in the lean zone, but the heterogeneous oxidation proceeds slowly. Final unburned carbon levels depend on a balance between the amount of coke formed and the fraction burned out. Coke formation tends to correlate with fuel properties such as asphaltene content, C:H ratio, or Conradson Carbon Residue. Coke burnout depends on combustion conditions and coke reactivity. Coke reactivity is influenced by the presence of combustion catalysts (e.g., vanadium) in the cenospheres.

Formation of *soot* is a gas-phase phenomenon that occurs in hot, fuel-rich zones. Soot occurs as fine particles (0.02 to 0.2 μm), often agglomerated into filaments or chains which can be several millimeters long. Factors that increase soot formation rates include high C:H ratio, high temperature, very rich conditions, and long residence times at these conditions. Pyrolysis of fuel molecules leads to soot precursors such as acetylene and higher analogs and various polyaromatic hydrocarbons. These condense to form very small (< 2 nm) particles. The bulk of solid-phase material is generated by *surface growth*—attachment of gas-phase species to the surface of the particles and their incorporation into the particulate phase. Another growth mechanism is *coagulation*, in which particles collide and coalesce. Soot particle formation and growth

is typically followed by soot oxidation to form CO and CO_2 . Eventual soot emission from a flame depends on the relative balance between the soot-formation and oxidation reactions.

Carbon Monoxide Carbon monoxide is a key intermediate in the oxidation of all hydrocarbons. In a well-adjusted combustion system, essentially all the CO is oxidized to CO_2 and final emission of CO is very low indeed (a few parts per million). However, in systems which have low temperature zones (for example, where a flame impinges on a wall or a furnace load) or which are in poor adjustment (for example, an individual burner fuel-air ratio out of balance in a multiburner installation or a misdirected fuel jet which allows fuel to bypass the main flame), CO emissions can be significant. The primary method of CO control is good combustion system design and practice.

Unburned Hydrocarbons Various unburned hydrocarbon species may be emitted from hydrocarbon flames. In general, there are two classes of unburned hydrocarbons: (1) small molecules that are the intermediate products of combustion (for example, formaldehyde) and (2) larger molecules that are formed by pyro-synthesis in hot, fuel-rich zones within flames, e.g., benzene, toluene, xylene, and various polycyclic aromatic hydrocarbons (PAHs). Many of these species are listed as Hazardous Air Pollutants (HAPs) in Title III of the Clean Air Act Amendment of 1990 and are therefore of particular concern. In a well-adjusted combustion system, emission of HAPs is extremely low (typically, parts per trillion to parts per billion). However, emission of certain HAPs may be of concern in poorly designed or maladjusted systems.

COMBUSTION OF SOLID FUELS

There are three basic modes of burning solid fuels, each identified with a furnace design specific for that mode: in suspension, in a bed at rest* on a grate (fuel-bed firing), or in a fluidized bed. Although many variations of these generic modes and furnace designs have been devised, the fundamental characteristics of equipment and procedure remain intact. They will be described briefly.

Suspension Firing Suspension firing of pulverized coal (PC) is commoner than fuel-bed or fluidized-bed firing of coarse coal in the United States. This mode of firing affords higher steam-generation capacity, is independent of the caking characteristics of the coal, and responds quickly to load changes. Pulverized coal firing accounts for approximately 55 percent of the power generated by electric utilities in the United States. It is rarely used on boilers of less than 45.4 Mg/h (100,000 lb/h) steam capacity because its economic advantage decreases with size.

A simplified model of PC combustion includes the following sequence of events: (1) on entering the furnace, a PC particle is heated rapidly, driving off the volatile components and leaving a char particle; (2) the volatile components burn independently of the coal particle; and (3) on completion of volatiles combustion, the remaining char particle burns. While this simple sequence may be generally correct, PC combustion is an extremely complex process involving many interrelated physical and chemical processes.

Devolatilization The volatiles produced during rapid heating of coal can include H_2 , CH_4 , CO, CO_2 , and C_2 - C_4 hydrocarbons, as well as tars, other organic compounds, and reduced sulfur and nitrogen species. The yield of these various fractions is a function of both heating rate and final particle temperature. The resulting char particle may be larger in diameter than the parent coal particle, owing to swelling produced by volatiles ejection. The particle density also decreases.

Char oxidation dominates the time required for complete burnout of a coal particle. The heterogeneous reactions responsible for char oxidation are much slower than the devolatilization process and gas-phase reaction of the volatiles. Char burnout may require from 30 ms to over 1 s, depending on combustion conditions (oxygen level, temperature), and char particle size and reactivity. Char reactivity depends on parent coal type. The rate-limiting step in char burnout can be chemical reaction or gaseous diffusion. At low temperatures or for very large particles, chemical reaction is the rate-limiting step. At

*The burning fuel bed may be moved slowly through the furnace by the vibrating action of the grate or by being carried on a traveling grate.

higher temperatures boundary-layer diffusion of reactants and products is the rate-limiting step.

Pulverized-Coal Furnaces In designing and sizing PC furnaces, particular attention must be given to the following fuel-ash properties:

- Ash fusion temperatures, including the spread between initial deformation temperature and fluid temperature
- Ratio of basic (calcium, sodium, potassium) to acidic (iron, silicon, aluminum) ash constituents, and specifically iron-to-calcium ratio
- Ash content
- Ash friability

These characteristics influence furnace plan area, furnace volume, and burning zone size required to maintain steam production capacity for a given fuel grade or quality.

Coal properties influence pulverizer capacity and the sizing of the air heater and other heat-recovery sections of a steam generator. Furnace size and heat-release rates are designed to control slagging characteristics. Consequently, heat-release rates in terms of the ratio of net heat input to plan area range from 4.4 MW/m² (1.4×10^6 Btu/[h·ft²]) for severely slagging coals to 6.6 MW/m² (2.1×10^6 Btu/[h·ft²]) for low-slugging fuels.

The various burner and furnace configurations for PC firing are shown schematically in Fig. 24-14. The U-shaped flame, designated as *fantail vertical firing* (Fig. 24-14a), was developed initially for pulverized coal before the advent of water-cooled furnace walls. Because a large percentage of the total combustion air is withheld from the fuel stream until it projects well down into the furnace, this type of firing is well suited for solid fuels that are difficult to ignite, such as those with less than 15 percent volatile matter. Although this configuration is no longer used in central-station power plants, it may find favor again if low-volatile chars from coal-conversion processes are used for steam generation or process heating.

Modern central stations use the other burner-furnace configurations shown in Fig. 24-14, in which the coal and air are mixed rapidly in and close to the burner. The primary air, used to transport the pulverized coal to the burner, comprises 10 to 20 percent of the total combustion air. The secondary air comprises the remainder of the total air and mixes in or near the burner with the primary air and coal. The velocity of the mixture leaving the burner must be high enough to prevent flashback in the primary air-coal piping. In practice, this velocity is maintained at about 31 m/s (100 ft/s).

In *tangential firing* (Fig. 24-14b), the burners are arranged in vertical banks at each corner of a square (or nearly square) furnace and directed toward an imaginary circle in the center of the furnace. This results in the formation of a large vortex with its axis on the vertical centerline. The burners consist of an arrangement of slots one above the other, admitting, through alternate slots, primary air-fuel mixture and secondary air. It is possible to tilt the burners upward or downward, the maximum inclination to the horizontal being 30°, enabling the operator to selectively utilize in-furnace heat-absorbing surfaces, especially the superheater.

The circular burner shown in Fig. 24-15 is widely used in horizontally fired furnaces and is capable of firing coal, oil, or gas in capacities as high as 174 GJ/h (1.65×10^8 Btu/h). In such burners the air is often swirled to create a zone of reverse flow immediately downstream of the burner centerline, which provides for combustion stability.

Low-NO_x burners are designed to delay and control the mixing of coal and air in the main combustion zone. A typical low-NO_x air-staged burner is illustrated in Fig. 24-16. This combustion approach can reduce NO_x emissions from coal burning by 40 to 50 percent. Because of the reduced flame temperature and delayed mixing in a low-NO_x burner, unburned carbon emissions may increase in some applications and for some coals. *Overfire air* is another technique for

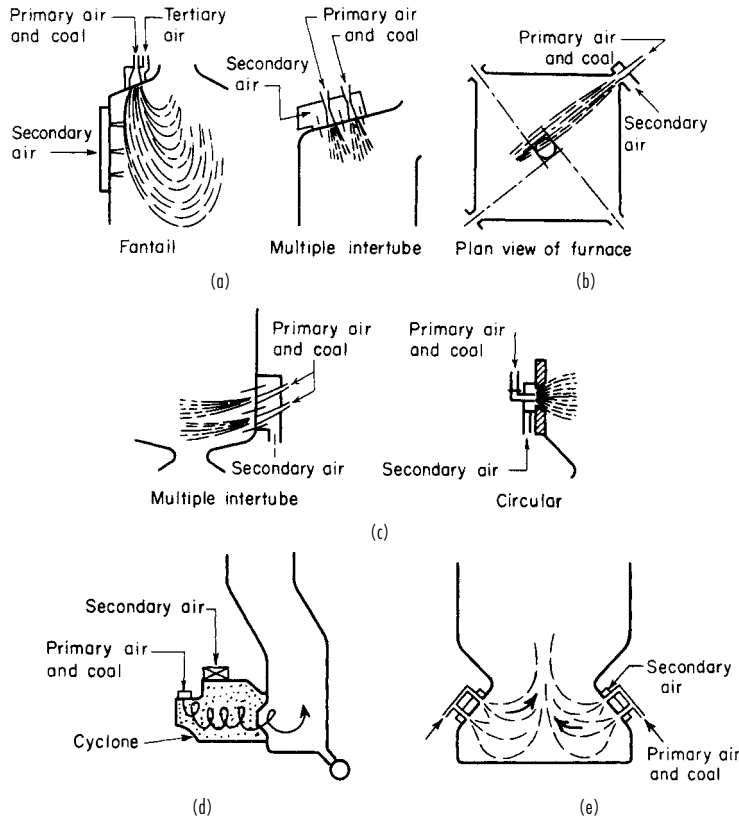


FIG. 24-14 Burner and furnace configurations for pulverized-coal firing: (a) vertical firing; (b) tangential firing; (c) horizontal firing; (d) cyclone firing; (e) opposed-inclined firing.

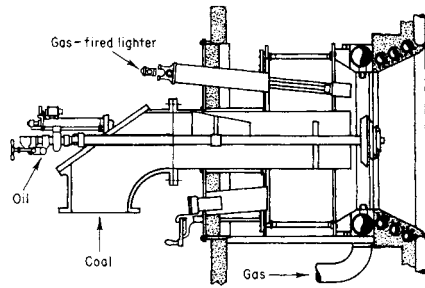


FIG. 24-15 Circular burner for pulverized coal, oil, or gas. (From Marks' Standard Handbook for Mechanical Engineers, 8th ed., McGraw-Hill, New York, 1978.)

staging the combustion air to control NO_x emissions when burning coal in suspension-firing systems. Overfire air ports are installed above the top level of burners on wall- and tangential-fired boilers. Use of overfire air can reduce NO_x emissions by 20 to 30 percent. *Reburn* is a NO_x control strategy that involves diverting a portion of the fuel from the burners to a second combustion zone (reburn zone) above the main burners. Completion air is added above the reburn zone to complete fuel burnout. The reburn fuel can be natural gas, oil, or pulverized coal, though natural gas is used in most applications. In this approach, the stoichiometry in the reburn zone is controlled to be slightly rich (equivalence ratio of ~1.15), under which conditions a portion (50 to 60 percent) of the NO_x is converted to molecular nitrogen.

Pulverizers The pulverizer is the heart of any solid-fuel suspension-firing system. Air is used to dry the coal, transport it through the pulverizer, classify it, and transport it to the burner, where the transport air provides part of the air for combustion. The pulverizers themselves are classified according to whether they are under positive or negative pressure and whether they operate at slow, medium, or high speed.

Pulverization occurs by impact, attrition, or crushing. The capacity of a pulverizer depends on the grindability of the coal and the fineness desired, as shown by Fig. 24-17. Capacity can also be seriously reduced by excessive moisture in the coal, but it can be restored by

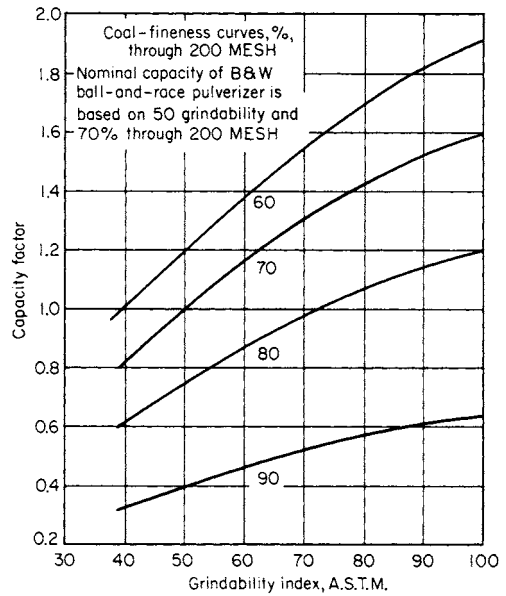


FIG. 24-17 Variation of pulverizer capacity with the grindability of the coal and the fineness to which the coal is ground. (Babcock & Wilcox Co.)

increasing the temperature of the primary air. Figure 24-18 indicates the temperatures needed. For PC boilers, the coal size usually is 65 to 80 percent through a 200-mesh screen, which is equivalent to 74 μm.

Cyclone Furnaces In *cyclone firing* (Fig. 24-14d) the coal is not pulverized but is crushed to 4-mesh (4.76-mm) size and admitted tangentially with primary air to a horizontal cylindrical chamber, called a *cyclone furnace*, which is connected peripherally to a boiler furnace. Secondary air also is admitted, so that almost all of the coal burns within the chamber. The combustion gas then flows into the boiler furnace. In the cyclone furnace, finer coal particles burn in suspension and the

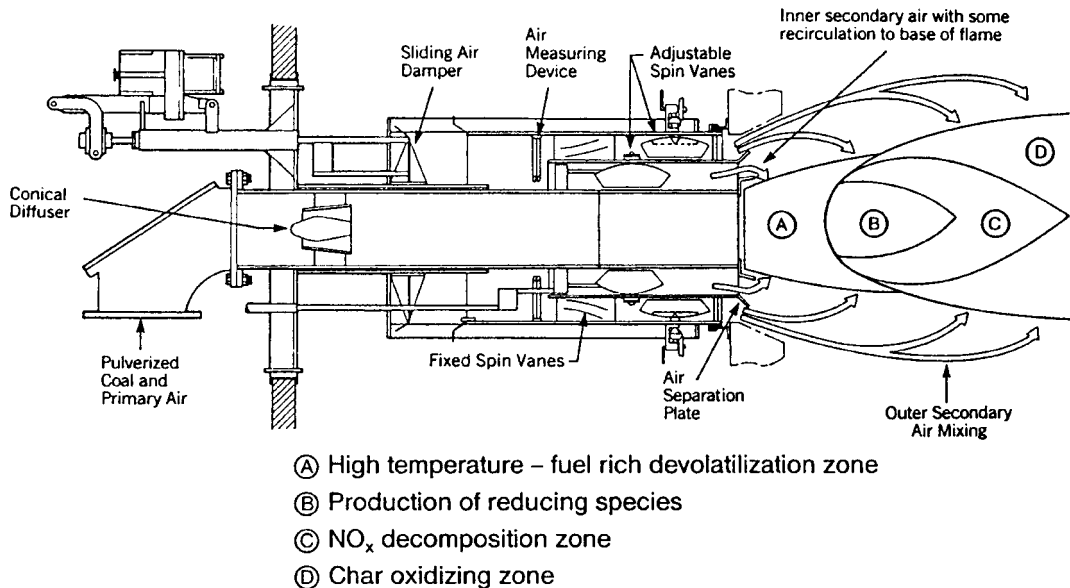


FIG. 24-16 Low-NO_x pulverized coal burner. (Babcock & Wilcox Co.)

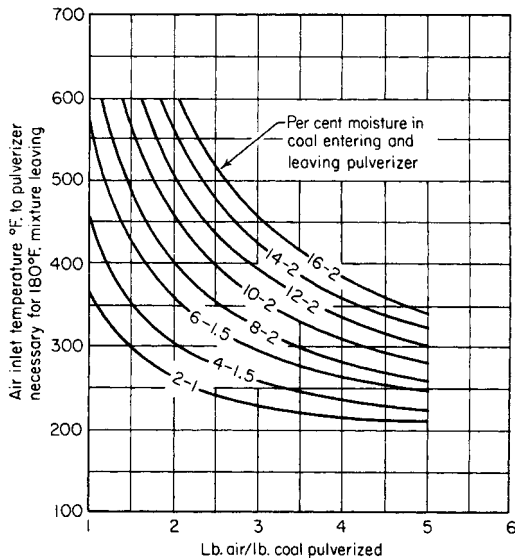


FIG. 24-18 Effect of moisture in coal on pulverizer capacity. Sufficient drying can be accomplished to restore capacity if air temperatures are high enough. [K = (°F + 459.7)/1.8] (Combustion Engineer, *Combustion Engineering Inc.*, New York, 1966.)

coarser ones are thrown centrifugally to the chamber wall, where most of them are captured in a sticky wall coating of molten slag. The secondary air, admitted tangentially along the top of the cyclone furnace, sweeps the slag-captured particles and completes their combustion. A typical firing rate is about 18.6 GJ/(h·m³) (500,000 Btu/[h·ft³]). The slag drains continuously into the boiler furnace and thence into a quenching tank. Figure 24-19 shows a cyclone furnace schematically.

Fuel-Bed Firing Fuel-bed firing is accomplished with mechanical stokers, which are designed to achieve continuous or intermittent fuel feed, fuel ignition, proper distribution of the combustion air, free release of the gaseous combustion products, and continuous or intermittent disposal of the unburned residue. These aims are met with two classes of stokers, distinguished by the direction of fuel feed to the bed: underfeed and overfeed. Overfeed stokers are represented by two types, distinguished by the relative directions of fuel and air flow (and also by the manner of fuel feed): crossfeed, also termed mass-burning, and spreader. The principles of these three methods of fuel-bed firing are illustrated schematically in Fig. 24-20.

Underfeed Firing Both fuel and air have the same relative direction in the underfeed stoker, which is built in single-retort and multiple-retort designs. In the *single-retort*, side-dump stoker, a ram pushes coal into the retort toward the end of the stoker and upward toward the tuyere blocks, where air is admitted to the bed. This type of stoker will handle most bituminous coals and anthracite, preferably in the size range 19 to 50 mm (¾ to 2 in) and no more than 50 percent through a 6-mm (¼-in) screen. Overfire air or steam jets are frequently used in the bridgeway at the end of the stoker to promote turbulence.

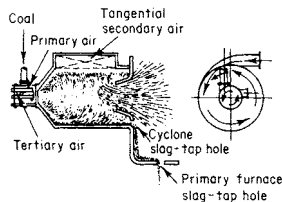


FIG. 24-19 Cyclone furnace. (From Marks' Standard Handbook for Mechanical Engineers, 9th ed., McGraw-Hill, New York, 1987.)

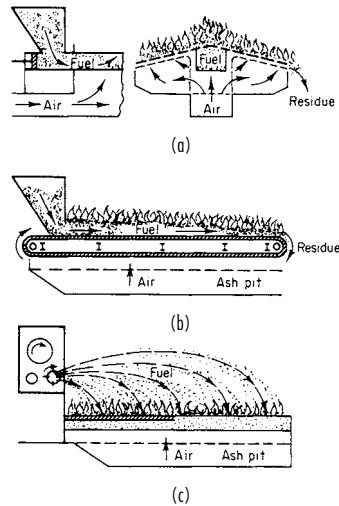


FIG. 24-20 Basic types of mechanical stokers: (a) underfeed; (b) crossfeed; (c) overfeed (spreader stoker).

In the *multiple-retort stoker*, rams feed coal to the top of sloping grates between banks of tuyeres. Auxiliary small sloping rams perform the same function as the pusher rods in the single retort. Air is admitted along the top of the banks of tuyeres, and on the largest units the tuyeres themselves are given a slight reciprocating action to agitate the bed further. This type of stoker operates best with caking coals having a relatively high ash-softening temperature. Coal sizing is up to 50 mm (2 in) with 30 to 50 percent through a 6-mm (¼-in) screen.

Overfeed Firing: Crossfeed (Mass-Burning) Stokers Crossfeed stokers are also termed mass-burning stokers because the fuel is dumped by gravity from a hopper onto one end of a moving grate, which carries it into the furnace and down its length. Because of this feature, crossfeed stokers are commonly called *traveling-grate* stokers. The grate may be either of two designs: *bar grate* or *chain grate*. Alternatively, the burning fuel bed may be conveyed by a vibratory motion of the stoker (*vibrating-grate*).

The fuel flows at right angles to the air flow. Only a small amount of air is fed at the front of the stoker, to keep the fuel mixture rich, but as the coal moves toward the middle of the furnace, the amount of air is increased, and most of the coal is burned by the time it gets halfway down the length of the grate. Fuel-bed depth varies from 100 to 200 mm (4 to 8 in), depending on the fuel, which can be coke breeze, anthracite, or any noncaking bituminous coal.

Overfeed Firing: Spreader Stokers Spreader stokers burn coal (or other fuel) by propelling it into the furnace. A portion of the coal burns in suspension (the percentage depending on the coal fineness), while the rest burns on a grate. In most units, coal is pushed off a plate under the storage hopper onto revolving paddles (either overthrow or underthrow) which distribute the coal on the grate (Fig. 24-20c). The angle and speed of the paddles control coal distribution. The largest coal particles travel the farthest, while the smallest ones become partially consumed during their trajectory and fall on the forward half of the grate. The grate may be stationary or traveling. The fuel and air flow in opposite directions.

Some spreaders use air to transport the coal to the furnace and distribute it, while others use mechanical means to transport the coal to a series of pneumatic jets.

The performance of spreader stokers is affected by changes in coal sizing. The equipment can distribute a wide range of fuel sizes, but it distributes each particle on the basis of size and weight. Normal size specifications call for 19-mm (¾-in) nut and slack with not more than 30 percent less than 6.4 mm (¼ in).

Typically, approximately 30 to 50 percent of the coal is burned in suspension. If excessive fines are present, more coal particles will be

carried out of the furnace and burned in suspension, and very little ash will be available to provide a protective cover for the grate surface. On the other hand, if sufficient fines are not present, not all the fuel will be burned on the grate, resulting in derating of the unit and excessive dumping of live coals to the ash hopper.

Excess air is usually 30 to 40 percent for stationary and dumping grates, while traveling grates are operated with from 22 to 30 percent excess air. Preheated air can be supplied for all types of grates but the temperature is usually limited to 395 to 422 K (250 to 300°F) to prevent excessive slagging of the fuel bed.

Overfire air nozzles are located in the front wall underneath the spreaders and in the rear wall from 0.3 to 0.9 m (1 to 3 ft) above the grate level. These nozzles use air directly from a fan or inspirate air with steam to provide turbulence above the grate for most effective mixing of fuel and air. They supply about 15 percent of the total combustion air.

Comparison of Suspension and Fuel-Bed Firing A major factor to consider when comparing a stoker-fired boiler with a PC boiler is the reduction in efficiency due to carbon loss. The carbon content of the ash passing out of a spreader stoker furnace varies from 30 to 50 percent. Overall efficiency of the stoker can be increased by reburning the ash: it is returned to the stoker grate by gravity or a pneumatic feed system. A continuous-ash-discharge spreader-stoker-fired unit will typically have a carbon loss of 4 to 8 percent, depending on the amount of ash reinjection. A properly designed PC boiler, on the other hand, can maintain an efficiency loss due to unburned carbon of less than 0.4 percent.

A difference between these firing methods may also be manifested in the initial fuel cost. For efficient operation of a spreader-stoker-fired boiler, the coal must consist of a proper mixture of coarse and fine particles. Normally, double-screened coal is purchased because less expensive run-of-mine coal does not provide the optimum balance of coarse and fine material.

An advantage of a stoker-fired furnace is its easy adaptability to firing almost any unsized solid fuels. Bark, bagasse, or refuse can normally be fired on a stoker to supplement the coal with a minimum amount of additional equipment. Thus, such supplementary waste fuels may be able to contribute a higher percentage of the total heat input in a stoker-fired furnace than in a PC furnace without expensive equipment modifications.

Fluidized-Bed Combustion The principles of gas-solid fluidization and their application to the chemical process industry are treated in Sec. 17. Their general application to combustion is reviewed briefly here, and their more specific application to fluidized-bed boilers is discussed later in this section.

In fluidized-bed combustion (FBC), fuel is burned in a bed of particles supported in an agitated state by an upward flow of air introduced via an air distributor. The bed particles may be sand or ash derived from the fuel, or spent sorbent (limestone or dolomite) if in-bed sulfur capture is included in the design. The fluidizing action promotes good solids mixing and gas-solids contacting that allow high combustion efficiency to be achieved at temperatures significantly lower than those of a pulverized coal (PC) furnace (typically 1116 K [1550°F] compared to over 1589 K [2400°F]). These lower temperatures also result in reduced slagging and fouling problems and significantly lower NO_x formation. This latter benefit, in conjunction with in-bed sulfur capture capability, constitutes one of the great advantages of fluidized-bed combustion: in situ pollution control. Having this control built into the furnace reduces the extent of back-end clean up required for a given emissions standard.

There are two types of FBC unit being sold commercially, *bubbling* and *circulating*, both operating at atmospheric pressure. Typical superficial fluidizing velocities are as follows.

Bubbling FBC 1.5 to 2.7 m/s (5 to 9 ft/s)

Circulating FBC 3.7 to 7.3 m/s (12 to 24 ft/s)

Pressurized FBC (PFBC) designs, bubbling and circulating, have been under development since the 1970s, but all work has now been curtailed. Work on an advanced PFBC design, incorporating partial coal gasification and char combustion, has also been curtailed. Several commercial bubbling PFBC units were built in the 1990s, covering the range 80 to 340 MWe. However, no new PFBC plants have been

announced since 1996, and consequently the technology is dropped from this edition of the Handbook.

Bubbling Beds A large proportion of the noncombustible feedstock—sand, ash, or sorbent-derived material—remains in the combustor forming the bed. Bed depth is maintained by draining off excess material. Most of the gas in excess of that required for minimum fluidization appears as bubbles (voids), and these carry particles upward in their wake, resulting in the rapid vertical mixing of the bed material that promotes even temperatures and good gas-solids contacting.

Early bubbling FBC units were designed to burn coal, and the heat released was removed by heat transfer to in-bed tubes and/or to the water-wall tubes used to enclose the furnace. These surfaces experienced high rates of metal loss through the combined effects of erosion and abrasion. Protective measures such as plasma-sprayed coatings and metal fins to disrupt the solids flow pattern were used. These were effective for only short periods before requiring replacement, and so maintenance requirements were high.

The two largest bubbling-bed FBC units built, 160 and 350 MWe, entered into service in the late 1980s burning bituminous coal. However, for coal applications, the overall performance of circulating fluidized-bed units has proved superior, and bubbling-bed designs of this size are no longer marketed. The bubbling technology is now mainly used for burning high-moisture biomass fuels for which in-bed heat-transfer surfaces are not required. These units are usually designed for generating capacities below 120 MWe, and typical fuels include wood wastes, paper mill and sewage sludges, and peat.

The boilers are of water-wall construction with the walls in the bed region lined with refractory to protect against erosion and abrasion damage. The heat released in the bed is removed from the flue gas by the exposed water walls and by convection pass tubing set in the gas path after the boiler. The coal boilers included multiclones to collect elutriated carbon and recycle it back to the boiler to increase combustion efficiency. However, because biomass is more reactive, recycle is not required.

To accommodate the wide variations in fuel moisture content while maintaining close bed temperature control, two control strategies are used.

- Operate the bed substoichiometrically so that bed temperature varies with the fluidizing air (primary combustion air). There is an equal and opposite change in the air fed above the bed (secondary combustion air) to complete the combustion process, the total air remaining constant. As the fuel moisture increases, the primary airflow rate increases, increasing the fluidizing velocity and releasing more heat in the bed to evaporate the additional water and keep the bed temperature constant. The bed operates less substoichiometrically, and in-bed combustion efficiency increases. At the same time the secondary air is reduced, and as there is less above-bed combustion, the upper furnace temperature falls. The control action is reversed when the fuel moisture content decreases. The split of primary to secondary airflow ranges from above 80:20 for high-moisture fuels to below 50:50 for low-moisture fuels.
- The above strategy results in variations in fluidizing velocity that might produce poor fluidization at some operating conditions with a resulting reduction in combustion efficiency. To maintain fluidizing velocity constant, recirculated flue gas is mixed with the primary combustion air to lower its oxygen content while keeping the combined fluidization gas flow rate constant. Air may be fed above the bed to complete combustion, but this is controlled independently of the air passing to the bed. As the fuel moisture increases, less flue gas is recirculated, the oxygen content of the primary combustion air and in-bed combustion both increase, and secondary air decreases. The control action is reversed when the fuel moisture content decreases.

Circulating Beds These fluidized beds operate at higher velocities, and virtually all the solids are elutriated from the furnace. The majority of the elutriated solids, still at combustion temperature, are captured by reverse-flow cyclone(s) and recirculated to the foot of the combustor. The foot of the combustor is a potentially very erosive region, as it contains large particles not elutriated from the bed, and they are being fluidized at high velocity. Consequently, the lower reaches of the combustor do not contain heat-transfer tubes and the water walls are protected with refractory. Some combustors have

experienced damage at the interface between the water walls and the refractory, and measures similar to those employed in bubbling beds have been used to protect the tubes in this region.

The circulating-bed design is the leading FBC technology and is the only design currently offered at sizes above 120 MWe. Units as large as 320 MWe have been built incorporating subcritical steam conditions with reheat and supercritical designs of up to 600 MWe are available. The fuels used in these designs are coals or opportunity fuels such as petroleum coke, although one 240-MWe unit is designed to operate solely on biomass. Circulating FBC boilers as small as 25 MWe have been built to fire either coal or biomass. However, as the size gets smaller, the circulating FBC becomes less competitive for biomass firing, and as indicated earlier, the bubbling FBC design is favored for this application.

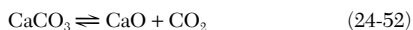
The heat released in the furnace is removed from the flue gas by the exposed upper water-wall tubes. As the units increase in size, more heat-transfer surface is required than is provided by the walls. Surface can be added by wrapping horizontal tubing over the walls of the upper furnace, or by added wing walls, sections of water wall extending short distances into the furnace enclosure. In some designs, tubes are extended across the upper furnace where, although the fluidizing velocity is still high, the erosion potential is low because the solids are finer and their concentration is lower. In some designs, heat is removed from the recirculated solids by passing them through a bubbling-bed heat exchanger before returning them to the furnace. The potential for erosion or abrasion of the tubes in this bed is low as the recirculating solids are mostly less than 500 μm and are well fluidized at velocities of only around 0.6 m/s [2 ft/s].

The combustion air is introduced at two levels, 60 to 70 percent being introduced through the distributor and 30 to 40 percent above the bed. This staged entry results in the lower reaches operating substoichiometrically, which helps to reduce NO_x emissions but tends to reduce the fluidizing velocity at the base of the combustor. To compensate for this and to increase solids mixing by increasing the local gas velocity, the portion of the combustor below the secondary air entry points is tapered.

Fuel Flexibility An advantage of FBC designs is fuel flexibility: a single unit can burn a wider range of fuels than a PC furnace, thus offering owners an improved bargaining position to negotiate lower fuel prices. Among the fuels fired are bituminous and subbituminous coals, anthracite culm, lignite, petroleum coke, refuse-derived fuel, biomass, industrial and sewage sludges, and shredded tires. But fuel flexibility can be achieved only if the unit is designed for the range of fuels intended to be burned. For example, to maintain the same firing rate, a feed system designed for a certain fuel must be capable of feeding a lower calorific fuel at a higher rate. Similarly, to maintain the same degree of sulfur capture, feeders must be capable of delivering sorbent over a range of rates matching the sulfur contents of the fuels likely to be fed. This increase in operating flexibility increases the capital cost, offsetting at least partially the economic benefits of reduced fuel pricing.

Sulfur Emissions Sulfur present in a fuel is released as SO_2 , a known contributor to acid rain deposition. By adding limestone or dolomite to a fluidized bed, much of this can be captured as calcium sulfate, a dry nonhazardous solid. As limestone usually contains over 40 percent calcium, compared to only 20 percent in dolomite, it is the preferred sorbent, resulting in lower transportation costs for the raw mineral and the resulting ash product. Moreover, the high magnesium content of the dolomite makes the ash unsuitable for some building applications and so reduces its potential for utilization. Whatever sorbent is selected, for economic reasons it is usually from a source local to the FBC plant. If more than one sorbent is available, plant trials are needed to determine the one most suitable, as results from laboratory-scale reactivity assessments are unreliable.

At atmospheric pressure, calcium carbonate almost completely calcines to free lime, and it is this that captures the sulfur dioxide. As the free lime is not completely sulfated, the resulting sorbent ash is very alkaline, consisting primarily of CaSO_4 and CaO , with small amounts of CaCO_3 .



The sulfation reaction has an optimum at a mean bed temperature of around 1116 K (1550°F). Units are usually designed to operate at this

temperature, but changes in operating conditions to achieve power output and accommodate changes in fuel composition often result in the plant operating at above or below the optimum temperature. To compensate for the ensuing reduction in sulfur capture, more sorbent is fed to the bed.

Emissions standards are becoming increasingly more stringent, and environmental permits for recent CFB projects have required sulfur capture efficiencies greater than 98 percent. Achieving this with only in-bed sulfur capture requires Ca/S molar ratios as high as 3 (3 mol of calcium in the sorbent for each mole of sulfur in the coal). For a 3 percent sulfur coal and a sorbent with 38 percent calcium, the sorbent-to-coal weight ratio is 0.3. To reduce the sorbent demand for the same sulfur capture efficiency, a back-end dry scrubber is used to remove additional SO_2 from the flue gas. This has been demonstrated to lower the Ca/S molar ratio to 1.9, a sorbent-to-coal weight ratio of 0.19. For a coal with 12 percent ash, this 37 percent reduction in sorbent feed rate reduces the amount of ash sent to disposal by 17 percent. This reduction in solids handling requirements improves process economics primarily by lowering the operating costs of the plant. The capital cost remains roughly the same, the cost of the dry scrubber being mainly offset by the reduction in solids handling equipment.

The sorbent used in the dry scrubber can be either lime or reactivated ash captured by the baghouse. The baghouse ash contains unreacted sorbent particles with a surface coating of calcium sulfate that prevents SO_2 reaching the CaO at their core. Hydrating these solids causes the material to swell and crack, thus exposing the unreacted CaO , which when recycled back to the boiler is available to react with additional SO_2 . As lime is more expensive than limestone, using the baghouse ash is the preferred approach. It also eliminates the need to provide separate handling facilities for lime.

Nitrogen Oxide Emissions FBC units achieve excellent combustion and sulfur emission performance at relatively modest combustion temperatures in the range of 1060 to 1172 K [1450 to 1650°F]. At these temperatures no atmospheric nitrogen is converted to NO_x . The prime variables influencing NO_x formation are excess air, mean bed temperature, nitrogen content of the fuel, and Ca/S molar ratio. With respect to the latter, high sorbent feed rates increase the free lime content, and this catalyzes NO_2 formation. Typical NO_x emissions, consisting of around 90 percent NO and 10 percent NO_2 , are in the range 86 to 129 mg/MJ [0.2 to 0.3 lb/MBtu]. These values have been reduced to as low as 21 mg/MJ [0.05 lb/MBtu] by injecting ammonia into the boiler freeboard to promote selective noncatalytic reduction (SNCR) reactions. This is a less costly approach than the selective catalytic reduction (SCR) units required for PC plants.

Because the operating temperature is lower, FBC units release more N_2O than do PC units. Nitrous oxide is a greenhouse gas that absorbs 270 times more heat per molecule than carbon dioxide and as such is likely to come under increased scrutiny in the future. The emissions at full load from coal-fired units are around 65 mg/MJ [0.15 lb/MBtu], but these increase as load is reduced and furnace temperature falls. Measurements from biomass-fired FBCs have not been made. Combustion processes do not contribute greatly to current U.S. N_2O emissions; agriculture and motor vehicles account for 86 percent of the total.

Particulate Emissions To meet environmental regulations, FBC boilers use a back-end particulate collector, such as a baghouse or an electrostatic precipitator (ESP). Compared to PC units, because of its sulfur sorbent content, the ash from a circulating CFB has higher resistivity and is finer because the flue gas path contains cyclones. Both factors result in a reduction in ESP collection efficiency, although lowering the gas velocity and providing additional collection fields can compensate for this albeit at increased capital cost. Bubbling FBC designs fired on biomass do not normally feed sulfur sorbents and do not include dust collectors in the flue gas path. For these applications suitably designed ESPs are often included. In general, however, baghouses are the preferred particulate collection devices.

FBC ash is irregular, whereas PC ash, because it melts at the elevated operating temperatures, is spherical. This difference in shape influences baghouse design in three ways: (1) FBC ash does not flow from the collection hoppers as readily and special attention has to be given to their design; (2) FBC ash forms a stronger cake, requiring more frequent and more robust cleaning mechanisms, e.g., shake-deflate and

pulse-jet technologies; and (3) this more robust action in conjunction with the more abrasive, irregular particles result in filter bags being more prone to failure in FBC systems. Careful selection of bag materials (synthetic felts generally perform best) and good installation and maintenance practices minimize the latter problem.

Mercury Emissions The U.S. Environmental Protection Agency (EPA) has proposed new rules that require power plants to reduce their mercury emissions by 70 percent by 2018. Tests on operating fluidized beds show that inherent mercury capture from the flue gas for bituminous coals is over 90 percent, but for lignites capture is closer to 50 percent. The reasons for this difference are not fully understood but could be explained by the higher reactivity of lignite resulting in lower unburned carbon carryover. Carbon is known to adsorb elemental and ionic mercury, and a low carbon content will result in reduced mercury capture. The combustion efficiency for less reactive bituminous coal is lower, resulting in more carbon carryover and possibly accounting for the higher mercury capture. Recent tests have shown that halide-impregnated activated carbons injected into flue gas streams can capture over 90 percent of the mercury present. So the low inherent mercury capture associated with lignite can be compensated for by activated carbon injection ahead of the dust collection device used.

COMBUSTION OF LIQUID FUELS

Oil is typically burned as a suspension of droplets generated by atomizing the fuel. As the droplets pass from the atomizer into the flame zone, they are heated both by radiation from the flame and by convection from the hot gases that surround them, and the lighter fuel components vaporize. The vapors mix with surrounding air and ignite. Depending on the fuel type, the fuel droplet may be completely vaporized or it may be partially vaporized, leaving a residual char or coke particle.

Fuel oils can contain a significant amount of sulfur: in the case of high-sulfur No. 6, it may be as much as 4 percent (Table 24-6). SO_2 is the principal product of sulfur combustion with stoichiometric or leaner fuel-air mixtures, but with the excess air customarily used for satisfactory combustion, SO_3 can form and then condense as sulfuric acid at temperatures higher than the normally expected dew point. Thus air preheaters and other heat recovery equipment in the flue-gas stream can be endangered. Figure 24-21 shows the maximum safe upper limits for dew points in the stacks of furnaces burning sulfur-containing oil and emitting unscrubbed flue gas.

Atomizers Atomization is the process of breaking up a continuous liquid phase into discrete droplets. Figure 24-22 shows the idealized process by which the surface area of a liquid sheet is increased until it forms droplets. Atomizers may be classified into two broad groups (see Fig. 24-23), pressure atomizers, in which fuel oil is injected at high pressure, and twin-fluid atomizers, in which fuel oil is injected at moderate pressure and a compressible fluid

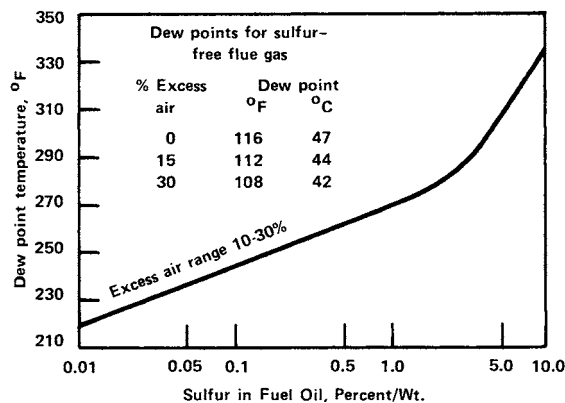


FIG. 24-21 Maximum flue-gas dew point versus percent of sulfur in typical oil fuels. ($K = [^{\circ}\text{F} + 459.7]/1.8$)

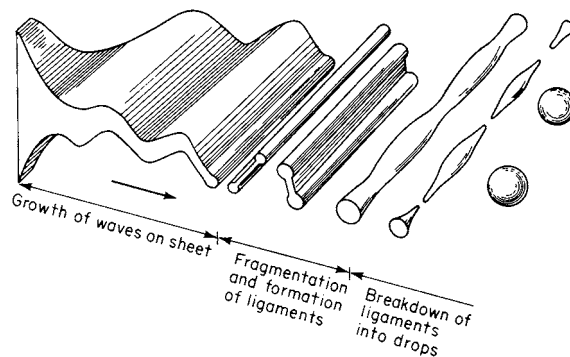


FIG. 24-22 Idealized process of drop formation by breakup of a liquid sheet. (After Dombrowski and Johns, *Chem. Eng. Sci.* 18:203, 1963.)

(steam or air) assists in the atomization process. Low oil viscosity (less than $15 \text{ mm}^2/\text{s}$) is required for effective atomization (i.e., small droplet size). Light oils, such as No. 2 fuel oil, may be atomized at ambient temperature. However, heavy oils must be heated to produce the desired viscosity. Required preheats vary from approximately 373 K (212°F) for No. 6 oil to 623 K (480°F) for vacuum bottoms.

Pressure Atomizers The commonest type of pressure atomizer is the swirl-type (Fig. 24-24). Entering a small cup through tangential orifices, the oil swirls at high velocity. The outlet forms a dam around the open end of the cup, and the oil spills over the dam in the form of a thin conical sheet, which subsequently breaks up into thin filaments and then droplets. Depending on the fuel viscosity, operating pressures range from 0.69 to 6.9 MPa (100 to 1000 psia) and the attainable

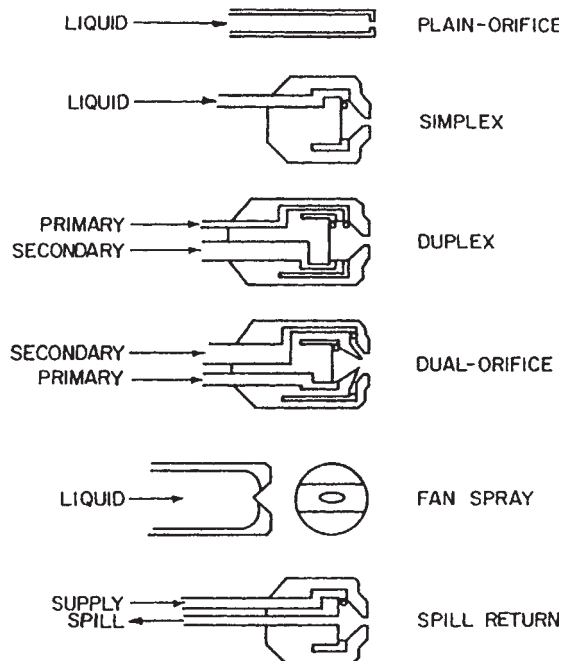


FIG. 24-23a Common types of atomizers: pressure atomizers. (From Lefebvre, *Atomization and Sprays*, Hemisphere, New York, 1989. Reproduced with permission. All rights reserved.)

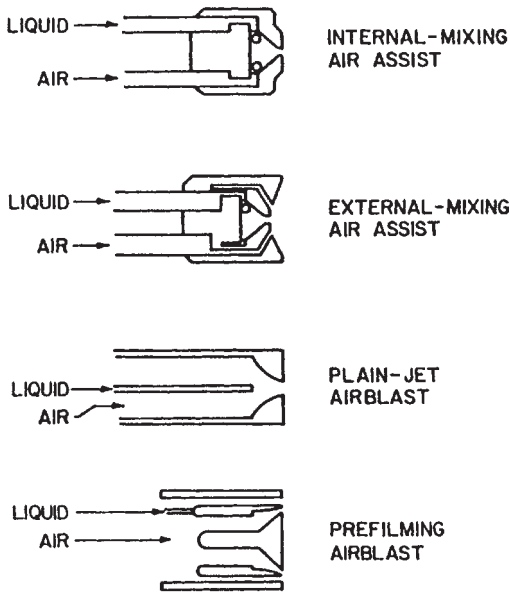


FIG. 24-23b Common types of atomizers: twin-fluid atomizers. (From Lefebvre, *Atomization and Sprays*, Hemisphere, New York, 1989. Reproduced with permission. All rights reserved.)

turndown ratio is approximately 4:1. Pressure atomization is most effective for lighter fuel oils.

Twin-Fluid Atomizers In a twin-fluid atomizer, the fuel stream is exposed to a stream of air or steam flowing at high velocity. In the internal-mixing configuration (Fig. 24-25), the liquid and gas mix inside the nozzle before discharging through the outlet orifice. In the external-mixing nozzle, the oil stream is impacted by the high-velocity gas stream outside the nozzle. The internal type requires lower flows of secondary fluid. In industrial combustion systems, steam is the preferred atomizing medium for these nozzles. In gas turbines, compressed air is more readily available. Maximum oil pressure is about 0.69 MPa (100 psia), with the steam or air pressure being maintained about 0.14 to 0.28 MPa (20 to 40 psia) in excess of the oil pressure. The mass flow of atomizing fluid varies from 5 to 30 percent of the fuel flow rate, and represents only a modest energy consumption. Turndown performance is better than for pressure atomizers and may be as high as 20:1.

A well-designed atomizer will generate a cloud of droplets with a mean size of about 30 to 40 μm and a top size of about 100 μm for light oils such as No. 2 fuel oil. Mean and top sizes are somewhat larger than this for heavier fuel oils.

Oil Burners The structure of an oil flame is shown in Fig. 24-26, and Fig. 24-27 illustrates a conventional circular oil burner for use in boilers. A combination of stabilization techniques is used, typically including swirl. It is important to match the droplet trajectories to the combustion aerodynamics of a given burner to ensure stable ignition and good turndown performance.

Many oil burners are designed as combination gas/oil burners. An example of a modern low- NO_x oil/gas forced-draft burner is shown in Fig. 24-28. This is an air-staged design, with the air divided into primary, secondary, and tertiary streams. An air-staged natural draft process heater oil/gas burner is illustrated in Fig. 24-29.

Emissions of unburned carbon (primarily coke cenospheres) may be reduced by (1) achieving smaller average fuel droplet size (e.g., by heating the fuel to lower its viscosity or by optimizing the atomizer geometry), (2) increasing the combustion air preheat temperature, or (3) firing oils with high vanadium content (vanadium appears to catalyze the burnout of coke).

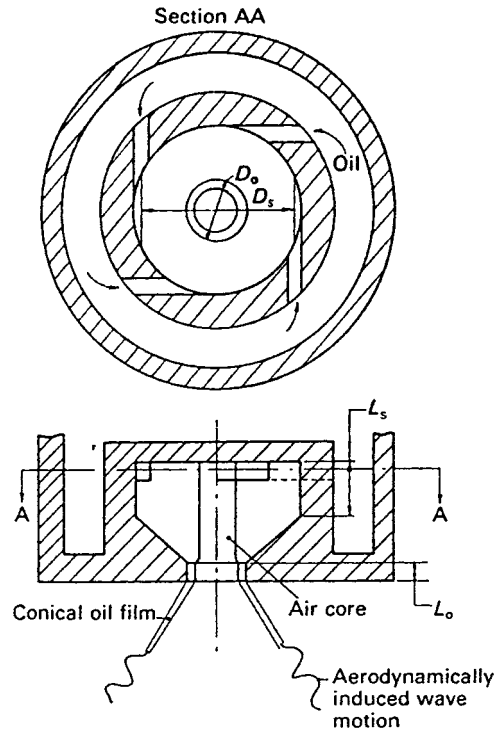


FIG. 24-24 Swirl pressure-jet atomizer. (From Lefebvre, *Atomization and Sprays*, Hemisphere, New York, 1989. Reproduced with permission. All rights reserved.)

COMBUSTION OF GASEOUS FUELS

Combustion of gas takes place in two ways, depending upon when gas and air are mixed. When gas and air are mixed before ignition, as in a Bunsen burner, burning proceeds by hydroxylation. The hydrocarbons and oxygen form hydroxylated compounds that become aldehydes; the addition of heat and additional oxygen breaks down the aldehydes to H_2 , CO , CO_2 , and H_2O . Inasmuch as carbon is converted to aldehydes in the initial stages of mixing, no soot can be developed even if the flame is quenched.

Cracking occurs when oxygen is added to hydrocarbons after they have been heated, decomposing the hydrocarbons into carbon and hydrogen, which, when combined with sufficient oxygen, form CO_2 and H_2O . Soot and carbon black are formed if insufficient oxygen is present or if the combustion process is arrested before completion.

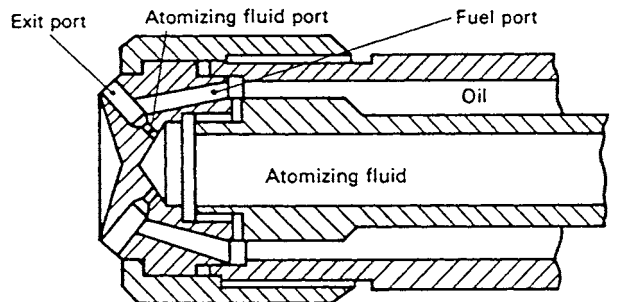


FIG. 24-25 Y-jet twin-fluid atomizer. (From Lefebvre, *Atomization and Sprays*, Hemisphere, New York, 1989. Reproduced with permission. All rights reserved.)

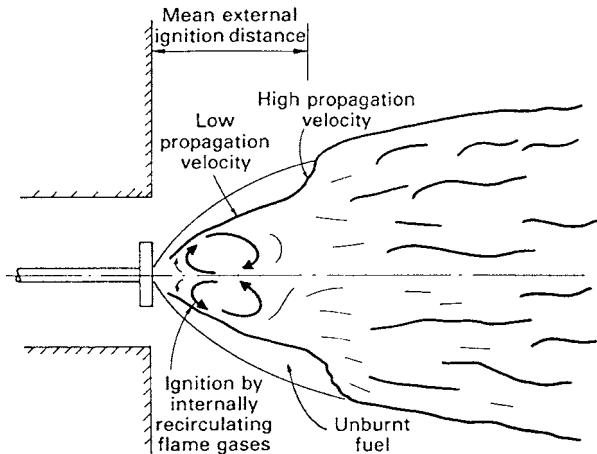


FIG. 24-26 Structure of typical oil flame. (From *Lawn, Principles of Combustion Engineering for Boilers*, Academic Press, London, 1987. Reprinted with permission.)

Gas Burners Gas burners may be classified as premixed or non-premixed. Many types of flame stabilizer are employed in gas burners. Bluff body, swirl, and combinations thereof are the predominant stabilization mechanisms.

Fully Premixed Burners A fully premixed burner includes a section for completely mixing the fuel and air upstream of the burner.

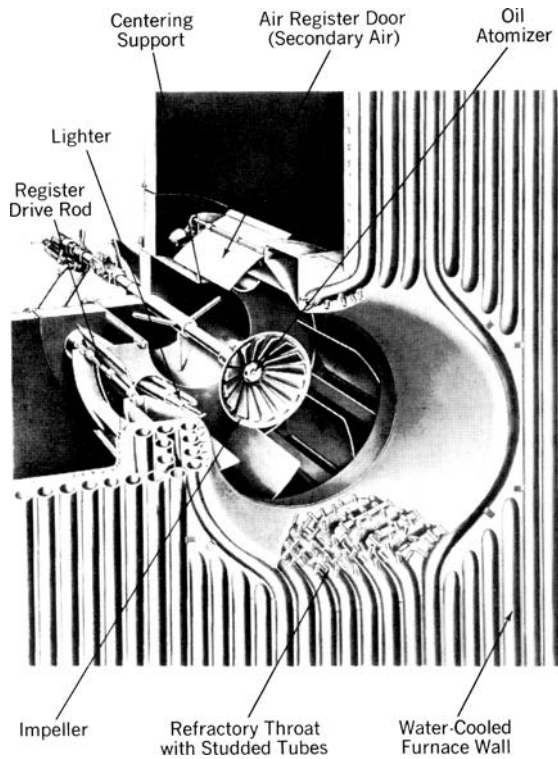


FIG. 24-27 Circular register burner with water-cooled throat for oil firing. (Babcock & Wilcox Co.)

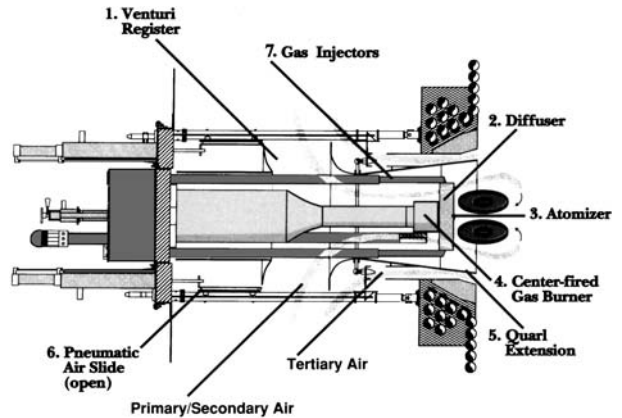


FIG. 24-28 Low-NO_x combination oil/gas forced-draft boiler burner. (Todd Combustion, Inc.)

The burner proper consists essentially of a flame holder. The porting that admits the mixture to the combustion chamber is designed to produce a fairly high velocity through a large number of orifices to avoid the possibility of the flame flashing back through the flame holder and igniting the mixture upstream of the burner.

Surface combustion devices are designed for fully premixing the gaseous fuel and air and burning it on a porous radiant surface. The close coupling of the combustion process with the burner surface results in low flame temperatures and, consequently, low NO_x formation. Surface materials can include ceramic fibers, reticulated ceramics, and metal alloy mats. This approach allows the burner shape to be customized to match the heat transfer profile with the application.

Partially Premixed Burners These burners have a premixing section in which a mixture that is flammable but overall fuel-rich is generated. Secondary combustion air is then supplied around the flame holder. The fuel gas may be used to aspirate the combustion air or vice versa, the former being the commoner. Examples of both are provided in Figs. 24-30 and 24-31.

Nozzle-Mix Burners The most widely used industrial gas burners are of the nozzle-mix type. The air and fuel gas are separated until they are rapidly mixed and reacted after leaving the ports. These burners allow a wide range of fuel-air ratios, a wide variety of flame shapes, and multifuel firing capabilities. They can be used to generate special atmospheres by firing at very rich conditions (50 percent excess fuel) or very lean conditions (1000 percent excess air). By changing nozzle shape and degree of swirl, the flame profile and mixing rates can be varied widely, from a rapid-mixing short flame ($L/D = 1$), to a conventional flame ($L/D = 5$ to 10), to a slow-mixing long flame ($L/D = 20$ to 50).

Staged Burners As was pointed out earlier under "Pollutant Formation and Control in Flames," the proper staging of fuel or air in the combustion process is one technique for minimizing NO_x emissions. Gas burners that achieve such staging are available.

Air-staged burners Low-NO_x air-staged burners for firing gas (or oil) are shown in Fig. 24-28. A high-performance, low-NO_x burner for high-temperature furnaces is shown in Fig. 24-32. In this design, both air-staging and external flue-gas recirculation are used to achieve extremely low levels of NO_x emissions (approximately 90 percent lower than conventional burners). The flue gas is recirculated by a jet-pump driven by the primary combustion air.

Fuel-staged burners Use of fuel-staged burners is the preferred combustion approach for NO_x control because gaseous fuels typically contain little or no fixed nitrogen. Figure 24-33 illustrates a fuel-staged natural draft refinery process heater burner. The fuel is split into primary (30 to 40 percent) and secondary (60 to 70 percent) streams. Furnace gas may be internally recirculated by the primary gas jets for additional NO_x control. NO_x reductions of 80 to 90 percent have been achieved by staging fuel combustion.

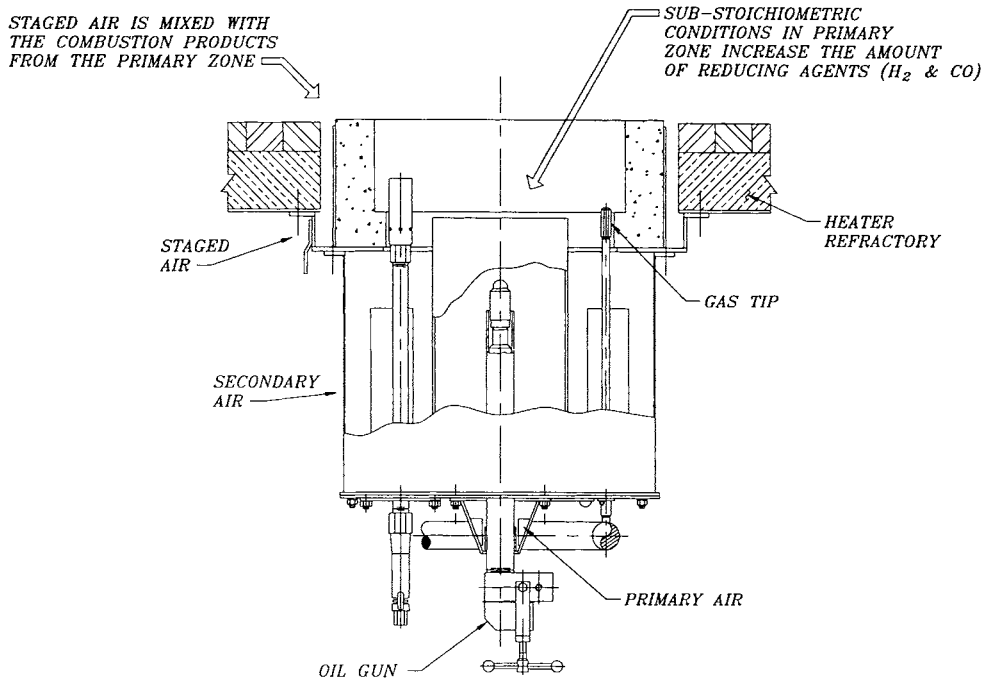


FIG. 24-29 Air-staged natural-draft combination oil/gas burner. (Callidus Technologies, Inc.)

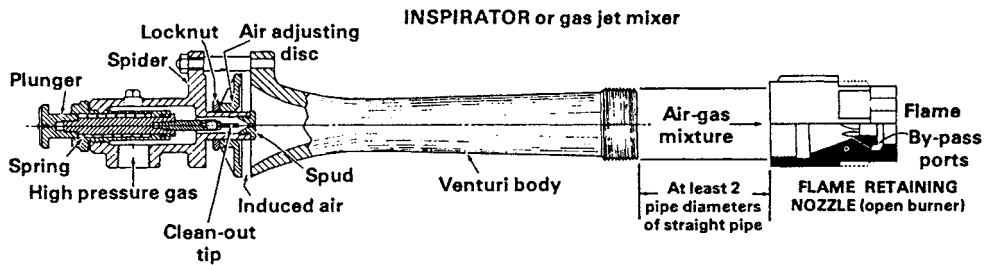


FIG. 24-30 Inspirator (gas-jet) mixer feeding a large port premix nozzle of the flame retention type. High-velocity gas emerging from the spud entrains and mixes with air induced in proportion to the gas flow. The mixture velocity is reduced and pressure is recovered in the venturi section. (From North American Combustion Handbook, 3d ed., North American Manufacturing Company, Cleveland, 1996.)

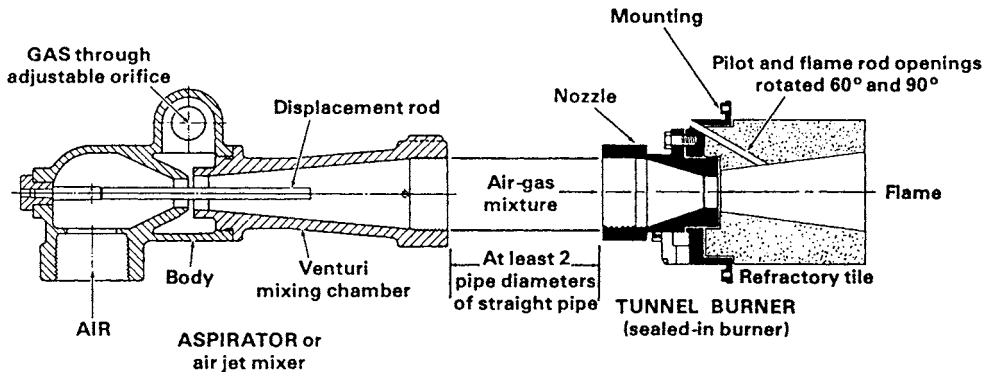


FIG. 24-31 Aspirator (air-jet) mixer feeding a sealed-in large port premix tunnel burner. Blower air enters at lower left. Gas from an atmospheric regulator is pulled into the air stream from the annular space around the venturi throat in proportion to the air flow. (From North American Combustion Handbook, 3d ed., North American Manufacturing Company, Cleveland, 1996.)

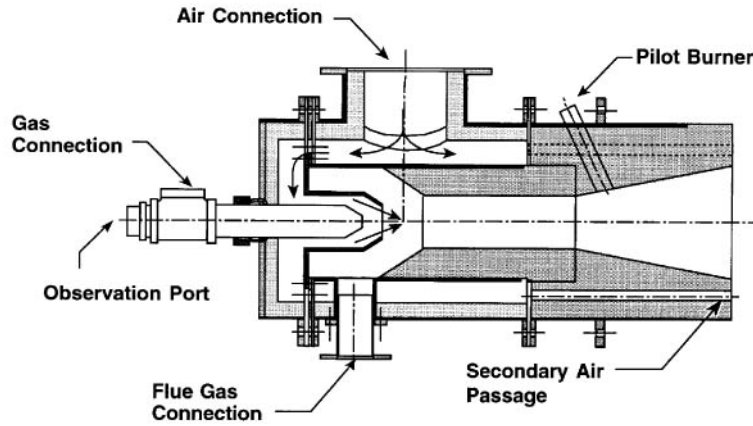


FIG. 24-32 Low- NO_x burner with air-staging and flue-gas recirculation for use in high-temperature furnaces. (Hauck Manufacturing Company. Developed and patented by the Gas Research Institute.)

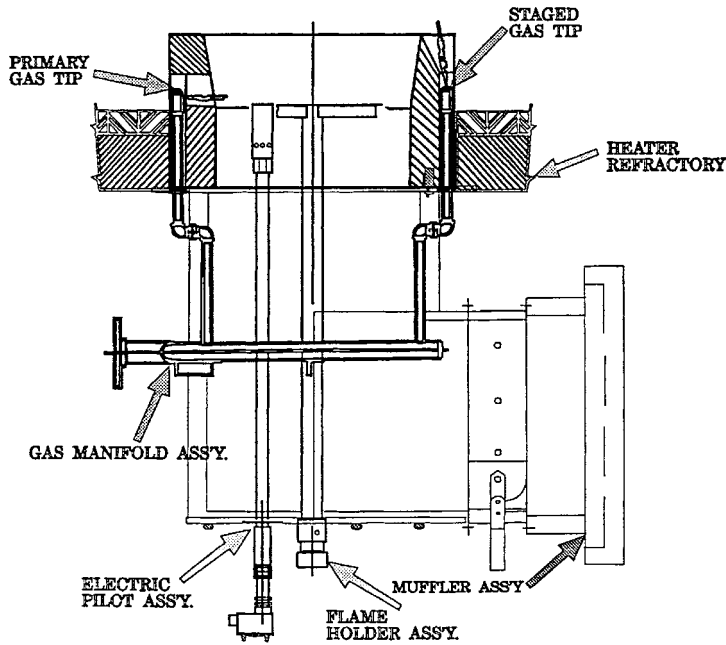


FIG. 24-33 Low- NO_x fuel-staged burner for a natural draft refinery process heater. (Callidus Technologies, Inc.)

THERMAL ENERGY CONVERSION AND UTILIZATION

BOILERS

Steam generators are designed to produce steam for process requirements, for process needs along with electric power generation, or solely for electric power generation. In each case, the goal is the most efficient and reliable boiler design for the least cost. Many factors influence the selection of the type of steam generator and its design, and some of these will be treated later in discussions of industrial and utility boilers.

Figure 24-34 shows the chief operating characteristics of a range of boilers, from small-scale heating systems to large-scale utility boilers.

In the industrial market, boilers have been designed to burn a wide range of fuels and operate at pressures up to 12.4 MPa (1800 psia) and steaming rates extending to 455,000 kg/h (1,000,000 lb/h). High-capacity shop-assembled boilers (package boilers) range in capacity from 4545 kg/h (10,000 lb/h) to about 270,000 kg/h (600,000 lb/h).

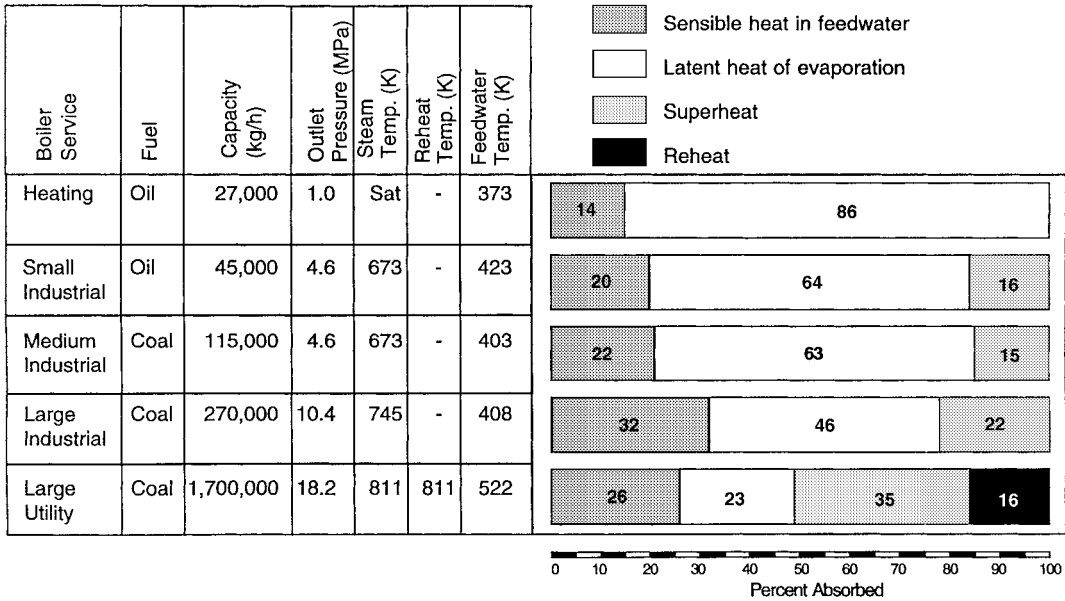


FIG. 24-34 Heat absorption distribution for various types of boilers. (Adapted from Singer, Combustion—Fossil Power, 4th ed., Combustion Engineering, Inc., Windsor, Conn., 1991.)

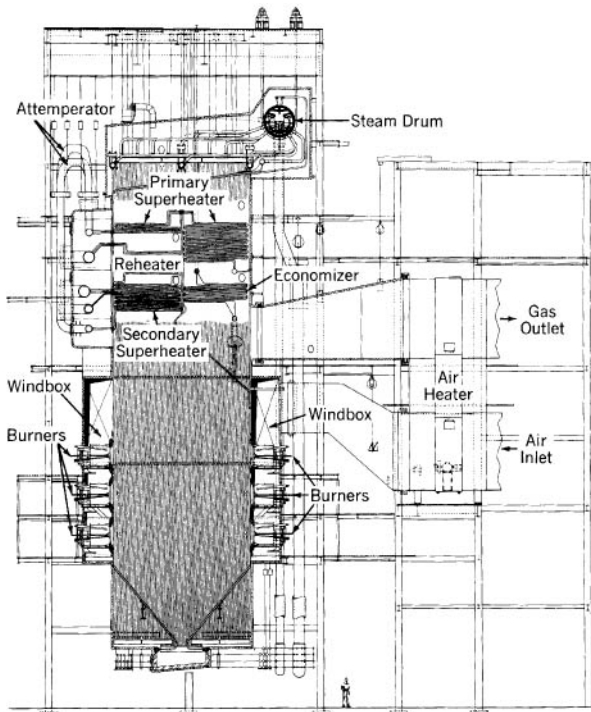


FIG. 24-35 Shop-assembled radiant boiler for natural gas or oil. (Babcock & Wilcox Co.)

These units are designed for operation at pressures up to 11.4 MPa (1650 psia) and 783 K (950°F). Figure 24-35 shows a gas- or liquid-fuel-fired unit. While most shop-assembled boilers are gas- or oil-fired, designs are available to burn pulverized coal. A field-erected coal-fired industrial boiler is shown in Fig. 24-36.

Boilers designed for service in electric power utility systems operate at both subcritical-pressure (pressures below 22.1 MPa [3205 psia]) and supercritical-pressure steam conditions. Subcritical-pressure boilers range in design pressures up to about 18.6 MPa (2700 psia) and in steaming capacities up to about 2955 Mg/h (6,500,000 lb/h). Supercritical-pressure boilers have been designed to operate at pressures up to 34.5 MPa (5000 psia). The 24.1 MPa (3500 psia) cycle has been firmly established in the utility industry, and boilers with steaming capacities up to 4227 Mg/h (9,300,000 lb/h) and superheat and reheat temperatures of 814 K (1005°F) are in service. The furnace of a large coal-fired steam generator absorbs half of the heat released, so that the gas temperature leaving the furnace is about 1376 K (2000°F).

Boiler Design Issues Boiler design involves the interaction of many variables: water-steam circulation, fuel characteristics, firing systems and heat input, and heat transfer. The furnace enclosure is one of the most critical components of a steam generator and must be conservatively designed to assure high boiler availability. The furnace configuration and its size are determined by combustion requirements, fuel characteristics, emission standards for gaseous effluents and particulate matter, and the need to provide a uniform gas flow and temperature entering the convection zone to minimize ash deposits and excessive superheater metal temperatures. Discussion of some of these factors follows.

Circulation and Heat Transfer Circulation, as applied to a steam generator, is the movement of water or steam or a mixture of both through the heated tubes. The circulation objective is to absorb heat from the tube metal at a rate that assures sufficient cooling of the furnace-wall tubes during all operating conditions, with an adequate margin of reserve for transient upsets. Adequate circulation prevents excessive metal temperatures or temperature differentials that would cause failures due to overstressing, overheating, or corrosion.

The rate of heat transfer from the tubes to the fluid depends primarily on turbulence and the magnitude of the heat flux itself. Turbulence is a

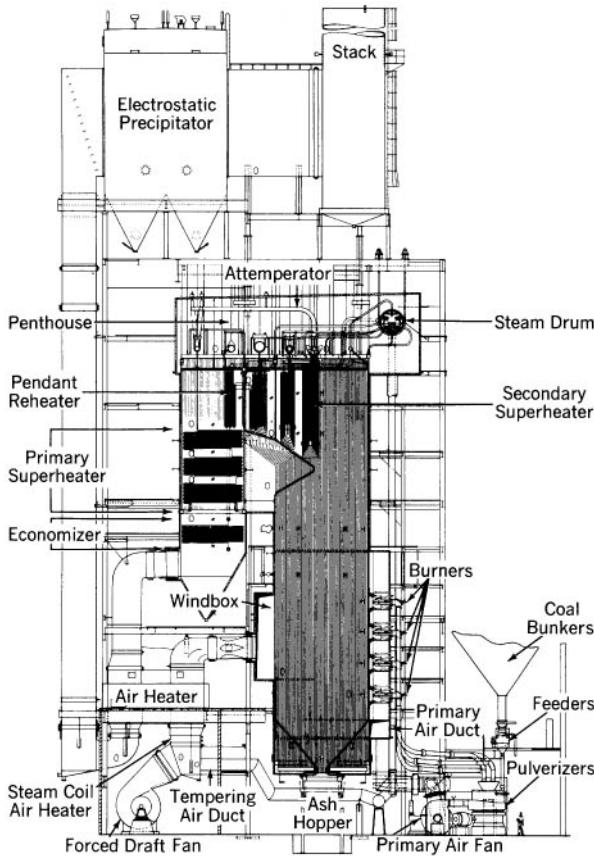


FIG. 24-36 Field-erected radiant boiler for pulverized coal. (Babcock & Wilcox Co.)

function of mass velocity of the fluid and tube roughness. Turbulence has been achieved by designing for high mass velocities, which ensure that nucleate boiling takes place at the inside surface of the tube. If sufficient turbulence is not provided, *departure from nucleate boiling* (DNB) occurs. DNB is the production of a film of steam on the tube surface that impedes heat transfer and results in tube overheating and possible failure.

Satisfactory performance is obtained with tubes having helical ribs on the inside surface, which generate a swirling flow. The resulting centrifugal action forces the water droplets toward the inner tube surface and prevents the formation of a steam film. The internally rifled tube maintains nucleate boiling at much higher steam temperature and pressure and with much lower mass velocities than those needed in smooth tubes. In modern practice, the most important criterion in drum boilers is the prevention of conditions that lead to DNB.

Utility Steam Generators

Steam-Generator Circulation System Circulation systems for utility application are generally classified as natural circulation and forced or pump-assisted circulation in drum-type boilers, and as once-through flow in subcritical- and supercritical-pressure boilers.

Natural circulation in a boiler circulation loop depends only on the difference between the mean density of the fluid (water) in the downcomers and the mean density of the fluid (steam-water mixture) in the heated furnace walls. The actual circulating head is the difference between the total gravity head in the downcomer and the integrated gravity heads in the upcoming legs of the loop containing the heated tubes. The circulating head must balance the

sum of the losses due to friction, shock, and acceleration throughout the loop.

In a once-through system, the feedwater entering the unit absorbs heat until it is completely converted to steam. The total mass flow through the waterwall tubes equals the feedwater flow and, during normal operation, the total steam flow. As only steam leaves the boiler, there is no need for a steam drum.

Fuel Characteristics Fuel choice has a major impact on boiler design and sizing. Because of the heat transfer resistance offered by ash deposits in the furnace chamber in a coal-fired boiler, the mean absorbed heat flux is lower than in gas- or oil-fired boilers, so a greater surface area must be provided.

In addition, coal characteristics have a major impact on the design and operation of a coal-fired boiler. Coals having a low volatile-matter content usually require higher ignition temperatures and those with less than 12 to 14 percent volatile matter may require supplementary fuel to stabilize ignition. Generally, western U.S. coals are more reactive than others and, consequently, easier to ignite, but because of high moisture content they require higher air temperatures to the mills for drying the coal to achieve proper pulverization. Extremely high-ash coal also may present problems in ignition and stabilization. The ash constituents and the quantity of ash will have a decided influence on sizing the furnace. Accordingly, a thorough review of coal characteristics is needed to establish the effect on the design and operation of a boiler.

Superheaters and Reheaters A superheater raises the temperature of the steam generated above the saturation level. An important function is to minimize moisture in the last stages of a turbine to avoid blade erosion. With continued increase of evaporation temperatures and pressures, however, a point is reached at which the available superheat temperature is insufficient to prevent excessive moisture from forming in the low-pressure turbine stages. This condition is resolved by removing the vapor for reheat at constant pressure in the boiler and returning it to the turbine for continued expansion to condenser pressure. The thermodynamic cycle using this modification of the Rankine cycle is called the *reheat cycle*.

Economizers Economizers improve boiler efficiency by extracting heat from the discharged flue gases and transferring it to feedwater, which enters the steam generator at a temperature appreciably lower than the saturation-steam temperature.

Industrial Boilers Industrial boilers are steam generators that provide power, steam, or both to an industrial plant, in contrast to a utility boiler in a steam power plant. A common configuration is a stationary water-tube boiler in which some of the steam is generated in a convection-section tube bank (also termed a *boiler bank*). In the original industrial boilers, in fact, almost all of the boiling occurred in that section, but now many industrial steam generators of 180,000 kg/h (397,000 lb/h) and greater capacity are radiant boilers. The boiler steam pressure and temperature and feedwater temperature determine the fraction of total heat absorbed in the boiler bank. For a typical coal-fired boiler producing about 90,000 kg/h (198,000 lb/h):

% total steam in boiler bank	Boiler pressure		Steam temperature		Feedwater temperature	
	MPa	psia	K	°F	K	°F
45	1.4	200	460	369	389	241
30	4.1	600	672	750	389	241
16	10.3	1500	783	950	450	351
10	12.4	1800	811	1000	450	351

The thicker plate for operation at higher pressures increases the cost of the boiler. As a result, it is normally not economical to use a boiler bank for heat absorption at pressures above 10.7 MPa (1550 psia).

Industrial boilers are employed over a wide range of applications, from large power-generating units with sophisticated control systems, which maximize efficiency, to small low-pressure units for space or process heating, which emphasize simplicity and low capital cost. Although their usual primary function is to provide energy in the form of steam, in some applications steam generation is incidental to a process objective, e.g., a chemical recovery unit in the paper industry,

TABLE 24-14 Solid-Waste Fuels Burned in Industrial Boilers

Waste	HHV, kJ/kg*
Bagasse	8374–11,630
Furfural residue	11,630–13,956
Bark	9304–11,630
General wood wastes	10,467–18,608
Coffee grounds	11,397–15,119
Nut hulls	16,282–18,608
Rich hulls	12,095–15,119
Corncobs	18,608–19,306
Rubber scrap	26,749–45,822
Leather	27,912–45,822
Cork scrap	27,912–30,238
Paraffin	39,077
Cellophane plastics	27,912
Polyvinyl chloride	40,705
Vinyl scrap	40,705
Sludges	4652–27,912
Paper wastes	13,695–18,608

*To convert kilojoules per kilogram to British thermal units per pound, multiply by 4.299×10^{-1} .

a carbon monoxide boiler in an oil refinery, or a gas-cooling waste-heat boiler in an open-hearth furnace. It is not unusual for an industrial boiler to serve a multiplicity of functions. For example, in a paper-pulp mill, the chemical-recovery boiler is used to convert black liquor into useful chemicals and to generate process steam. At the same plant, a bark-burning unit recovers heat from otherwise wasted material and also generates power.

Industrial boilers burn oil, gas, coal, and a wide range of product and/or waste fuels, some of which are shown in Tables 24-4 and 24-14. Natural gas has become the principal fuel of choice, accounting for approximately 80 percent of all the energy fired in industrial boilers across a range of manufacturing industries (Table 24-15). Coal is the second most prevalent fuel, accounting for about 15 percent of the energy fired. Waste fuels, however, are increasing in importance.

An excellent brief exposition of industrial boilers is presented as Chapter 8 of *Combustion—Fossil Power*, Singer (ed.), 4th ed., Combustion Engineering, Windsor, Conn., 1991.

Design Criteria Industrial-boiler designs are tailored to the fuels and firing systems involved. Some of the more important design criteria include:

- Furnace heat-release rates, both W/m^3 and W/m^2 of effective projected radiant surface ($Btu/[h \cdot ft^3]$ and $Btu/[h \cdot ft^2]$)
- Heat release on grates
- Flue-gas velocities through tube banks
- Tube spacings

TABLE 24-16 Typical Design Parameters for Industrial Boilers

Furnace		Heat-release rate, W/m^2 of EPRS†	
Natural gas-fired		630,800	
Oil-fired		551,900–630,800	
Coal: pulverized coal		220,780–378,480	
Spreader stoker		252,320–410,020	
Stoker, coal-fired		Grate heat-release rate, W/m^2	
Continuous-discharge spreader		2,050,000–2,207,800	
Dump-grade spreader		1,419,300–1,734,700	
Overfeed traveling grate		1,261,000–1,734,700	
Flue-gas velocity: type		Baffled	
Fuel-fired	Single-pass Boiler, m/s	Boiler, m/s	Economizer, m/s
Gas or distillate oil	30.5	30.5	30.5
Residual oil	30.5	22.9	30.5
Coal (not lignite)			
Low-ash	19.8–21.3	15.2	15.2–18.3
High-ash	15.2	NA‡	12.2–15.2

*To convert watts per square meter to British thermal units per hour-foot, multiply by 0.317.

†Effective projected radiant surface.

‡Not available.

Table 24-16 gives typical values or ranges of these criteria for gas, oil, and coal. The furnace release rates are important, for they establish maximum local absorption rates within safe limits. They also have a bearing on completeness of combustion and therefore on efficiency and particulate emissions. Limiting heat release on grates (in stoker firing) will minimize carbon loss, control smoke, and avoid excessive fly ash.

Limits on flue-gas velocities for gas- or oil-fired industrial boilers are usually determined by the need to limit draft loss. For coal firing, design gas velocities are established to minimize fouling and plugging of tube banks in high-temperature zones and erosion in low-temperature zones.

Convection tube spacing is important when the fuel is residual oil or coal, especially coal with low ash-fusion or high ash-fouling tendencies. The amount of the ash and, even more important, the characteristics of the ash must be specified for design.

Natural-circulation and convection boiler banks are the basic design features on which a line of standard industrial boilers has been developed to accommodate the diverse steam, water, and fuel requirements of the industrial market.

Figure 24-37 shows the amount of energy available for power by using a fire-tube boiler, an industrial boiler, and subcritical- and

TABLE 24-15 Fuel Consumption in Boilers in Various Industries

Industry	Annual energy consumption (PJ/a)				
	Total	Residual fuel oil	Distillate fuel oil	Natural gas	Coal
Chemicals	539	—	—	451	88
Food	323	8	6	237	72
Paper	212	29	2	143	38
Petroleum and coal products	169	6	2	159	2
Transportation equipment	56	—	1	48	7
Plastics and rubber products	54	5	1	48	—
Primary metals	40	—	—	40	—
Beverage and tobacco products	34	—	—	29	5
Computer and electronic products	29	1	1	27	—
Wood products	18	1	1	15	1
Textile mills	15	—	1	—	14
Total	1,489	50	15	1,197	227

SOURCE: 2002 *Manufacturing Energy Consumption Survey*, Energy Information Administration, U.S. Dept. of Energy.

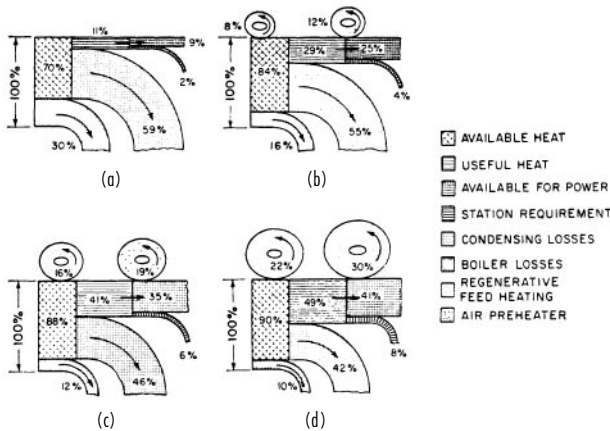


FIG. 24-37 Sankey diagrams for various types of boilers: (a) fire-tube boiler; (b) industrial boiler; (c) subcritical-pressure boiler; (d) supercritical-pressure boiler.

supercritical-pressure boilers. Condensing losses decrease substantially, and regeneration of air and feedwater becomes increasingly important in the most advanced central-station boilers.

The boiler designer must proportion heat-absorbing and heat-recovery surfaces in a way to make the best use of heat released by the fuel. Water walls, superheaters, and reheaters are exposed to convection and radiant heat, whereas convection heat transfer predominates in air preheaters and economizers. The relative amounts of these surfaces vary with the size and operating conditions of the boiler.

Package Boilers In a fire-tube boiler, the hot combustion products flow through tubes immersed in the boiler water, transferring heat to it. In a water-tube boiler, combustion heat is transferred to water flowing through tubes which line the furnace walls and boiler passages. The greater safety of water-tube boilers has long been recognized, and they have generally superseded fire-tube configurations except for small package boiler designs. Fire-tube package boilers range from a few hundred to 18,200 kg/h (40,000 lb/h) steaming capacity. A fire-tube boiler is illustrated in Figs. 24-38 and 24-39. Water-tube package boilers range from a few hundred to 270,000 kg/h (600,000 lb/h) steaming capacity. A water-tube package boiler is illustrated in Fig. 24-40. The majority of water-tube package boilers use natural circulation and are designed for pressurized firing. The most

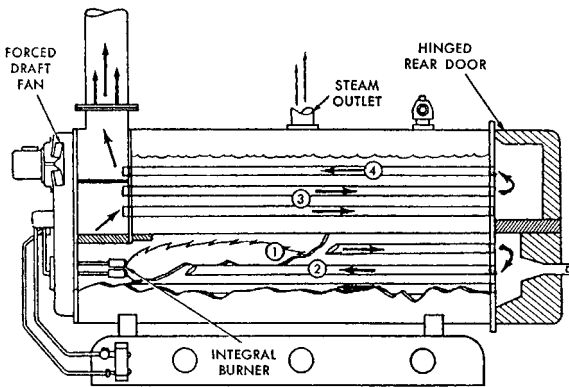


FIG. 24-38 A four-pass packaged fire-tube boiler. Circled numbers indicate passes. (From Cleaver Brooks, Inc. Reproduced from Gas Engineer's Handbook, Industrial Press, New York, 1965, with permission.)

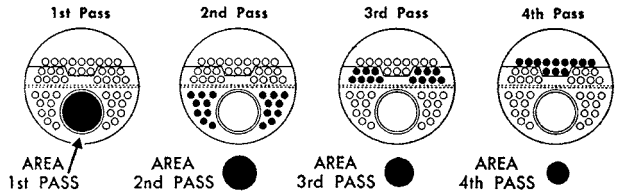


FIG. 24-39 Location and relative size of each of four passes of the flue gas through a fire-tube boiler. (From Cleaver Brooks, Inc. Reproduced from Gas Engineer's Handbook, Industrial Press, New York, 1965, with permission.)

significant advantage of shop-assembled or package boilers is the cost benefit associated with use of standard designs and parts.

Package boilers can be shipped complete with fuel-burning equipment, controls, and boiler trim. It may be necessary to ship the larger units in sections, however, and a shop-assembled boiler with a capacity greater than about 109,000 kg/h (240,000 lb/h) is deliverable only by barge. (For a more detailed discussion of shop-assembled boilers, see Singer, 1991, pp. 8.36–8.42.)

Fluidized-Bed Boilers Although the furnace of a fluid-bed boiler has a unique design, the system as a whole consists mainly of standard equipment items adapted to suit process requirements. The systems for feedstock preparation and feeding (biomass, coal, sorbent, and sand), ash removal, and ash disposal are very similar to those found in PC boiler plants, the main difference being that the top size of the material being handled is greater. The water-wall boiler enclosure and convection pass tubing are also similar to the designs found in PC boilers. The fluidized-bed plant includes particulate removal equipment such as cyclones, baghouses, and ESPs, with designs similar to those found in other solids-handling process plants.

Bubbling FBCs A simplified schematic of a bubbling FBC plant is presented in Fig. 24-41. This design is used primarily for burning biomass, although coal may be cofired to maintain heat release rates when feeding high-moisture feedstocks such as sludges.

The biomass is fed overbed through multiple feed chutes using air jets to help distribute the fuel over the surface of the bed. Variable-speed screw conveyors are usually used to meter the fuel feed rate and control steam output. Feedstocks such as bark and waste wood are chipped to a top size of 25 mm (1 in) to ensure complete combustion. The bed usually consists of sand around 1 m (3 ft) deep. This serves to retain the fuel in the furnace, extending its in-furnace residence time and increasing combustion efficiency. It also provides a heat sink to help maintain bed temperature during periods of fluctuating fuel moisture content.

Biomass fuels, especially forestry products and waste wood, can contain oversized material such as rocks and other debris. If this material is allowed to accumulate, the quality of fluidization deteriorates, resulting in poor fuel mixing and reduced combustion efficiency. To avoid this mal-operation, units typically employ an open-bottom floor design that allows easy solids removal while still ensuring even distribution of the fluidizing air. The fluidizing air (primary combustion air) is fed into large bore pipes extending across the width of the furnace and enters the boiler through a series of nozzles set in the pipes. The pipes are spaced to allow material to drain from all areas of the bed.

The bed temperature control strategies discussed earlier in this section result in the bed operating substoichiometrically. This helps lower the formation of NO_x but increases the amount of CO formed and the amount of unburned fuel leaving the bed. To complete the combustion process, secondary air is introduced through multiple ports above the bed with the upper furnace height designed to achieve 2- to 3-s flue gas residence time. The velocity of the secondary air should be sufficient to penetrate across the furnace and facilitate thorough mixing with the flue gas leaving the surface of the bed. Although the unburned carbon leaving the furnace is low, the CO is still relatively high at 43 to 128 mg/MJ (0.10 to 0.25 lb/MBtu), which may be a problem in nonattainment areas.

Ammonia injected into the upper furnace is used to promote SNCR reactions to reduce NO_x emissions. The optimum temperature for

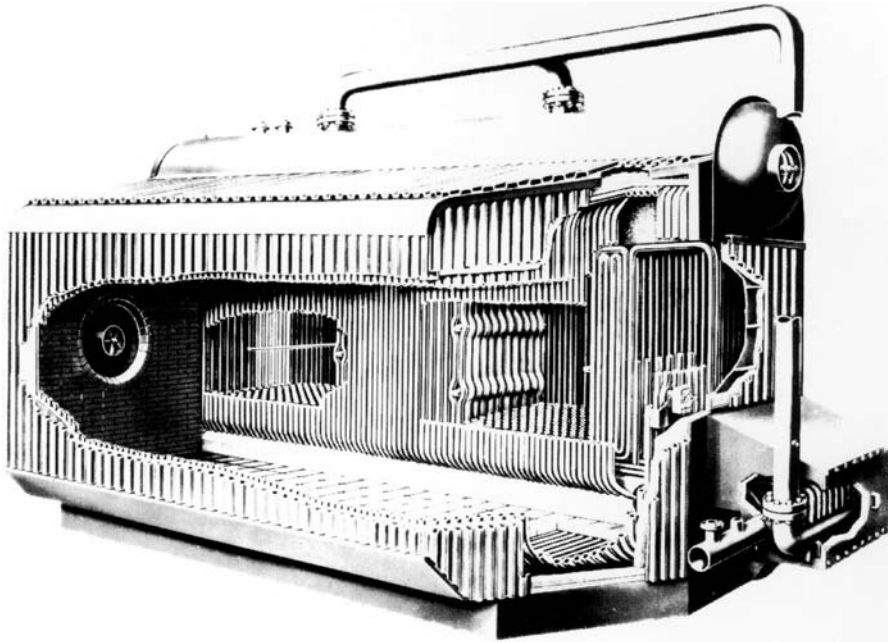


FIG. 24-40 A D-type shop-assembled water-tube boiler. (Combustion Engineering, Inc.)

these reactions is around 830°C (1520°F), but the upper furnace temperature varies depending upon the extent of secondary combustion air usage. To ensure that the ammonia enters into a region at the optimum temperature, multiple levels of injection ports are provided.

Circulating FBCs The circulating FBC is the more widely deployed than the bubbling-bed design and at far larger sizes. A simplified schematic for a design with an external heat exchanger is presented in Fig. 24-42. As of 2005 there were over 20 units in the range of 200 to 320 MWe worldwide, and a similar number were in the planning stages.

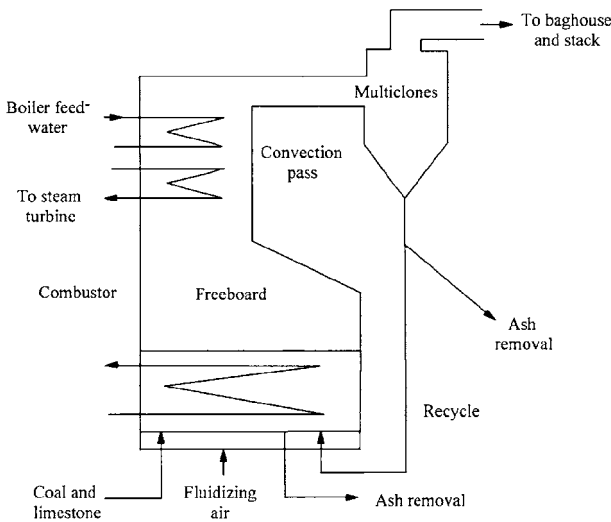


FIG. 24-41 Simplified flow diagram for bubbling AFBC (with underbed feed system).

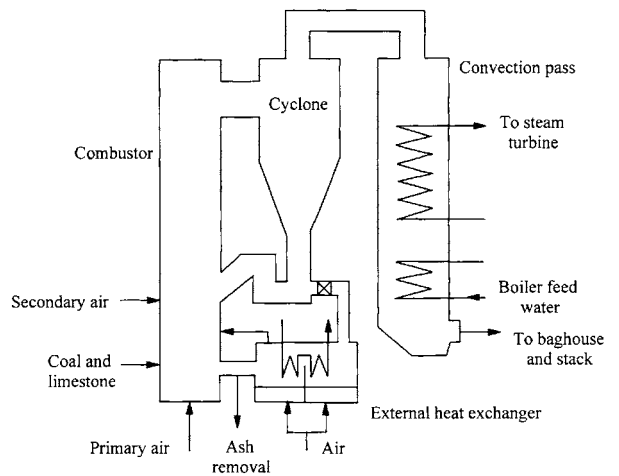


FIG. 24-42 Simplified flow diagram for circulating AFBC (with external heat exchanger).

The most widely used fuels are low-grade coals with high ash and moisture contents, making them unsuitable for use in PC plants. The coal is crushed to a top size of 12 mm (1/2 in), without drying, and fed by gravity into the lower refractory-lined portion of the boiler. The feed points are close to the pressure balance point, and the low backpressure greatly reduces the sealing requirements. In some designs the coal is also introduced into the cyclone ash return lines. The larger units average a feed point for every 23 m² (250 ft²) of freeboard cross section. The highly turbulent bed facilitates good mixing of the coal across the combustor. The sorbent is prepared to a top size of 1 mm (0.04 in) and dried so that it can be pneumatically fed to the combustor also using one feed point for every 23 m² (250 ft²) of freeboard cross section. Load control

is achieved primarily by reducing the coal feed rate, with a corresponding reduction in airflow, to reduce the heat release rate. As the heat-transfer area remains unchanged, the furnace temperature falls.

Almost all the particulate matter leaving the boiler is collected by cyclones and recycled to the base of the unit. The number of cyclones varies in different design concepts, but for the larger units one cyclone is provided for 100 to 130 MWe of generating capacity, providing one recycle point for 210 to 290 m² (720 to 950 ft²) of freeboard cross section. The collected particulate matter is returned against a backpressure of 0.02 MPa (3 psi), through a J-valve. The recycle ratio can be as high as 40:1, corresponding to a relatively long mean particle residence time and accounting for the high performance of circulating units. For bituminous coal combustion, efficiency is close to 99 percent, but like the biomass-fired bubbling beds, CO levels are relatively high at around 43 mg/MJ (0.1 lb/MBtu).

PROCESS HEATING EQUIPMENT

Many major energy-intensive industries depend on direct-fired or indirect-fired equipment for drying, heating, calcining, melting, or chemical processing. This subsection discusses both direct- and indirect-fired equipment, with the greater emphasis on indirect firing for the process industries.

Direct-Fired Equipment Direct-fired combustion equipment transfers heat by bringing the flame and/or the products of combustion into direct contact with the process stream. Common examples are rotary kilns, open-hearth furnaces, and submerged-combustion evaporators. Table 24-17 gives the average energy consumption rates for various industries and processes that use direct heat. Section 12 of this handbook describes and illustrates rotary dryers, rotary kilns, and hearth furnaces. Forging, heat treating, and metal milling furnaces are discussed by Mawhinney (*Marks' Standard Handbook for Mechanical Engineers*, 9th ed., McGraw-Hill, New York, 1987, pp. 7.47-7.52). Other direct-fired furnaces are described later in this section.

Indirect-Fired Equipment (Fired Heaters) Indirect-fired combustion equipment (fired heaters) transfers heat across either a metallic or refractory wall separating the flame and products of combustion from the process stream. Examples are heat exchangers (discussed in Sec. 11), steam boilers, fired heaters, muffle furnaces, and melting pots. Steam boilers have been treated earlier in this section, and a subsequent subsection on industrial furnaces will include muffle furnaces.

TABLE 24-17 Average Energy Consumption for Various Industries Using Direct Heat

Industry	Product/process	Energy consumption per unit of product	
		GJ/Mg	10 ⁶ Btu/US ton
Paper	Kraft process	20.9	18.0
	Integrated plant/paper*	34.2	29.5
	Integrated plant/paperboard*	18.8	16.2
Glass	Flat glass	17.3	14.9
	Container glass	18.1	15.6
	Pressed/blown	31.6	27.2
Clay/ceramics	Portland cement	4.6	4.0
	Lime	5.5	4.7
	Mineral wool	42.7	36.8
Steel	Blast furnace and steel mills	20.7	17.8
Nonferrous metals	Primary copper	34.2	29.5
	Secondary copper	4.6	4.0
	Primary lead	25.1	21.6
	Secondary lead	0.8	0.7
	Primary zinc	69.6	60.0
	Secondary zinc	5.0	4.3
	Primary aluminum	78.9	68.0
Secondary aluminum	5.2	4.5	

SOURCE: *Manufacturing Consumption of Energy*, Energy Information Administration, U.S. Dept. of Energy, 1991.

*Mixture of direct and indirect firing.

Fired heaters differ from other indirect-fired processing equipment in that the process stream is heated by passage through a coil or tubebank enclosed in a furnace. Fired heaters are classified by function and by coil design.

Function Berman [*Chem. Eng.* 85(14):98-104, June 19, 1978] classifies fired heaters into the following six functional categories, providing descriptions that are abstracted here.

Column reboilers heat and partially vaporize a recirculating stream from a fractionating column. The outlet temperature of a reboiler stream is typically 477 to 546 K (400 to 550°F).

Fractionator-feed preheaters partially vaporize charge stock from an upstream unfired preheater en route to a fractionating column. A typical refinery application: a crude feed to an atmospheric column enters the fired heater as a liquid at 505 K (450°F) and leaves at 644 K (700°F), having become 60 percent vaporized.

Reactor-feed-stream preheaters heat the reactant stream(s) for a high-temperature chemical reaction. The stream may be single-phase/single-component [example: steam being superheated from 644 to 1089 K (700 to 1500°F) for styrene-manufacture reactors]; single-phase/multicomponent [example: preheating the feed to a catalytic reformer, a mixture of hydrocarbon vapors and recycle hydrogen, from 700 to 811 K (800 to 1000°F) under pressure as high as 4.1 MPa (600 psia)]; or multiphase/multicomponent [example: a mixture of hydrogen gas and liquid hydrocarbon heated from 644 to 727 K (700 to 850°F) at about 20 MPa (3000 psia) before it enters a hydrocracker].

Heat-transfer-fluid heaters maintain the temperature of a circulating liquid heating medium (e.g., a paraffinic hydrocarbon mixture, a Dowtherm, or a molten salt) at a level that may exceed 673 K (750°F).

Viscous-liquid heaters lower the viscosity of very heavy oils to pumpable levels.

Fired reactors contain tubes or coils in which an endothermic reaction within a stream of reactants occurs. Examples include steam/hydrocarbon reformers, catalyst-filled tubes in a combustion chamber; pyrolyzers, coils in which alkanes (from ethane to gas oil) are cracked to olefins; in both types of reactor the temperature is maintained up to 1172 K (1650°F).

Coil Design Indirect-fired equipment is conventionally classified by tube orientation: vertical and horizontal. Although there are many variations of each of these two principal configurations, they all are embraced within seven major types, as follows.

A *simple vertical cylindrical* heater has vertical tubes arrayed along the walls of a combustion chamber fired vertically from the floor. This type of heater does not include a convection section and is inexpensive. It has a small footprint but low efficiency, and it is usually selected for small-duty applications [0.5 to 21 GJ/h (0.5 to 20 10⁶ Btu/h)].

Vertical cylindrical; cross-tube convection heaters are similar to the preceding type except for a horizontal convective tube bank above the combustion chamber. The design is economical with a high efficiency and is usually selected for higher-duty applications: 11 to 210 GJ/h (10 to 200 10⁶ Btu/h).

The *arbor (wicket)* heater is a substantially vertical design in which the radiant tubes are inverted U's connecting the inlet and outlet terminal manifolds in parallel. An overhead crossflow convection bank is usually included. This type of design is good for heating large gas flows with low pressure drop. Typical duties are 53 to 106 GJ/h (50 to 100 10⁶ Btu/h).

In the *vertical-tube single-row double-fired* heater, a single row of vertical tubes is arrayed along the center plane of the radiant section that is fired from both sides. Usually this type of heater has an overhead horizontal convection bank. Although it is the most expensive of the fired heater designs, it provides the most uniform heat transfer to the tubes. Duties are 21 to 132 GJ/h (20 to 125 10⁶ Btu/h) per cell (twin-cell designs are not unusual).

Horizontal-tube cabin heaters position the tubes of the radiant-section-coil horizontally along the walls and the slanting roof for the length of the cabin-shaped enclosure. The convection tube bank is placed horizontally above the combustion chamber. It may be fired from the floor, the side walls, or the end walls. As in the case of its vertical cylindrical counterpart, its economical design and high efficiency make it the most popular horizontal-tube heater. Duties are 11 to 105 GJ/h (10 to 100 10⁶ Btu).

In the *horizontal-tube box heater with side-mounted convection tube bank*, the radiant-section tubes run horizontally along the walls and the flat roof of the box-shaped heater, but the convection section is placed in a box of its own beside the radiant section. Firing is horizontal from the end walls. The design of this heater results in a relatively expensive unit justified mainly by its ability to burn low-grade high-ash fuel oil. Duties are 53 to 210 GJ/h (50 to 200 10^6 Btu/h).

Vertical cylindrical helical coil heaters are hybrid designs that are classified as vertical heaters, but their in-tube characteristics are like those of horizontal heaters. There is no convection section. In addition to the advantages of simple vertical cylindrical heaters, the helical coil heaters are easy to drain. They are limited to small-duty applications: 5 to 21 GJ/h (5 to 20 10^6 Btu/h).

Schematic elevation sections of a vertical cylindrical, cross-tube convection heater; a horizontal-tube cabin heater; and a vertical cylindrical, helical-coil heater are shown in Fig. 24-43. The seven basic designs and some variations of them are pictured and described in the reference cited above and by R. K. Johnson [*Combustion* 50(5): 10-16, November 1978].

The design of both radiant and convection sections of fired heaters, along with some equipment descriptions and operating suggestions, are discussed by Berman in *Encyclopedia of Chemical Processing and Design* [McKetta (ed.), vol. 22, Marcel Dekker, 1985, pp. 31-69]. He also treats construction materials, mechanical features, and operating points in three other *Chemical Engineering* articles [all in vol. 85 (1978): no. 17, July 31, pp. 87-96; no. 18, August 14, pp. 129-140; and no. 20, Sept. 11, pp. 165-169].

INDUSTRIAL FURNACES

Industrial furnaces serve the manufacturing sector and can be divided into two groups. Boiler furnaces, which are the larger group and are used solely to generate steam, were discussed earlier in the subsection

on industrial boilers. Furnaces of the other group are classified as follows: by (1) source of heat (fuel combustion or electricity), (2) function (heating without change of phase or with melting), (3) process cycle (batch or continuous), (4) mode of heat application (direct or indirect), and (5) atmosphere in furnace (air, protective, or reactive, including vacuum). Each will be discussed briefly.

Source of Heat Industrial furnaces are either fuel-fired or electric, and the first decision that a prospective furnace user must make is between these two. Although electric furnaces are uniquely suited to a few applications in the chemical industry (manufacture of silicon carbide, calcium carbide, and graphite, for example), their principal use is in the metallurgical and metal-treatment industries. In most cases the choice between electric and fuel-fired is economic or custom-dictated, because most tasks that can be done in one can be done equally well in the other. Except for an occasional passing reference, electric furnaces will not be considered further here. The interested reader will find useful reviews of them in *Kirk-Othmer Encyclopedia of Chemical Technology* (4th ed., vol. 12, articles by Cotchen, Sommer, and Walton, pp. 228-265, Wiley, New York, 1994) and in *Marks' Standard Handbook for Mechanical Engineers* (9th ed., article by Lewis, pp. 7.59-7.68, McGraw-Hill, New York, 1987).

Function and Process Cycle Industrial furnaces are enclosures in which process material is heated, dried, melted, and/or reacted. Melting is considered a special category because of the peculiar difficulties that may be associated with a solid feed, a hot liquid product, and a two-phase mixture in between; it is customary, therefore, to classify furnaces as heating or melting.

Melting Furnaces: The Glass Furnace Most melting furnaces, electric or fuel-fired, are found in the metals-processing industry, but a notable exception is the glass furnace. Like most melting furnaces, a glass furnace requires highly radiative flames to promote heat transfer to the feed charge and employs regenerators to conserve heat from the high-temperature process [greater than 1813 K (2300°F)].

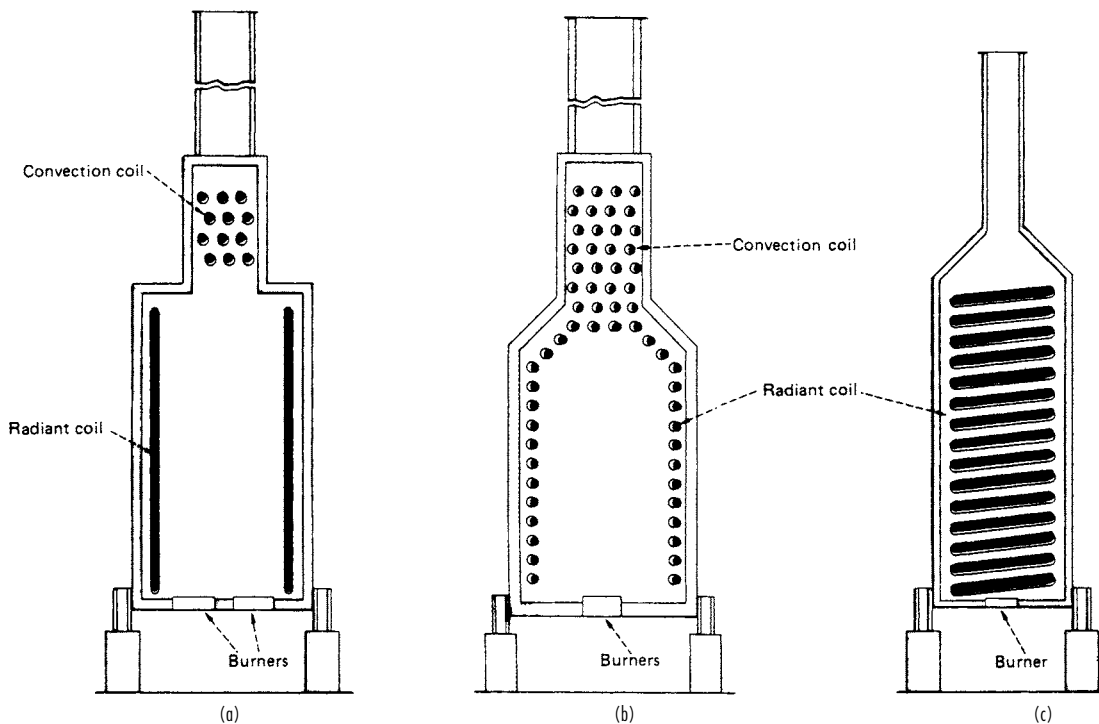


FIG. 24-43 Representative types of fired heaters: (a) vertical-tube cylindrical with cross-flow-convection section; (b) horizontal-tube cabin; (c) vertical cylindrical, helical coil. (From Berman, *Chem. Eng.* 85:98-104, June 19, 1978.)

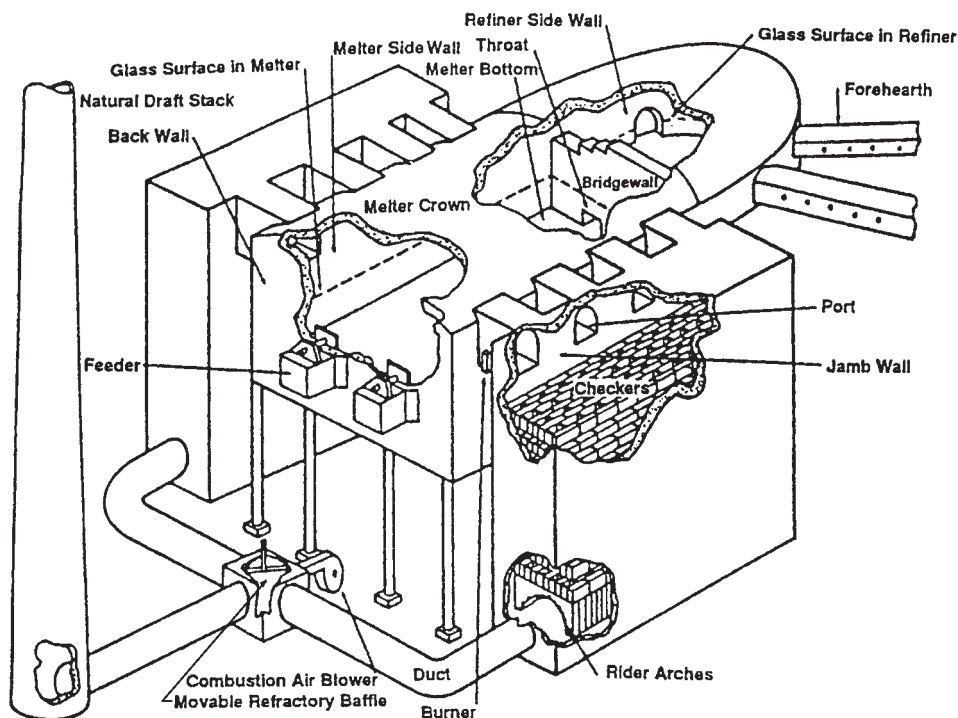


FIG. 24-44 Side-port continuous regenerative glass melting furnace.

A typical side-port continuous regenerative glass melting furnace is shown in Fig. 24-44. Side-port furnaces are used in the flat and container glass industries. The burners are mounted on both sides of the furnace and the sides fire alternately. Refractory-lined flues are used to recover the energy of the hot flue gas. The high temperature of the flue gas leaving the furnace heats a mass of refractory material called a *checker*. After the checker has reached the desired temperature, the gas flow is reversed and the firing switches to the other side of the furnace. The combustion air is then heated by the hot checker and can reach 1533 K (2300°F). The cycle of airflow from one checker to the other is reversed approximately every 15 to 30 min.

The glass melt is generally 1 to 2 m (3 to 6 ft) deep, the depth being limited by the need for proper heat transfer to the melt. Container glass furnaces are typically 6 to 9 m (20 to 30 ft) wide and 6 to 12 m (20 to 40 ft) long. Flat glass furnaces tend to be longer, typically over 30 m (100 ft), because of the need for complete reaction of the batch ingredients and improved quality (fewer bubbles). They typically have a melting capacity of 450 to 630 Mg/day (500 to 750 U.S. ton/d), compared to a maximum of 540 Mg/day (600 U.S. ton/d) for container and pressed/blown glass furnaces.

Though the stoichiometric chemical energy requirement for glass-making is only some 2.3 GJ/Mg (2 10^6 Btu/U.S. ton) of glass, the inherently low thermal efficiency of regenerative furnaces means that, in practice, at least 7 GJ/Mg (6 10^6 Btu/U.S. ton) is required. Of this total, some 40 percent goes to batch heating and the required heat of reactions, 30 percent is lost through the furnace structure, and 30 percent is lost through the stack. The smaller furnaces used in pressed/blown glass melting are less efficient, and energy consumption may be as high as 17.4 TJ/Mg (15 10^6 Btu/U.S. ton).

Industrial furnaces may be operated in batch or continuous mode.

Batch Furnaces This type of furnace is employed mainly for the heat treatment of metals and for the drying and calcination of ceramic articles. In the chemical process industry, batch furnaces may be used for the same purposes as batch-tray and truck dryers when the drying or process temperature exceeds 600 K (620°F). They are employed

also for small-batch calcinations, thermal decompositions, and other chemical reactions which, on a larger scale, are performed in rotary kilns, hearth furnaces, and shaft furnaces.

Continuous Furnaces These furnaces may be used for the same general purposes as are the batch type, but usually not on small scale. The process material may be carried through the furnace by a moving conveyor (chain, belt, roller), or it may be pushed through on idle rollers, the motion being sustained by an external pusher operating on successively entering cars or trays, each pushing the one ahead along the entire length of the furnace and through the exit flame curtains or doors.

Furnace Atmosphere and Mode of Heating

Direct Heating Industrial furnaces may be directly or indirectly heated, and they may be filled with air or a protective atmosphere, or under a vacuum. Direct heating is accomplished by the hot combustion gases being inside the furnace and therefore in direct contact with the process material. Thus, the material is heated by radiation and convection from the hot gas and by reradiation from the heated refractory walls of the chamber. Three styles of direct firing are illustrated in Fig. 24-45. *Simple direct firing* is used increasingly because of its simplicity and because of improved burners. The *overhead* design allows the roof burners to be so placed as to provide optimum temperature distribution in the chamber. *Underfiring* offers the advantage of the charge's being protected from the flame. The maximum temperature in these direct-heated furnaces is limited to about 1255 K (1800°F) to avoid prohibitively shortened life of the refractories in the furnace.

Indirect Heating If the process material cannot tolerate exposure to the combustion gas or if a vacuum or an atmosphere other than air is needed in the furnace chamber, indirect firing must be employed. This is accomplished in a muffle^o furnace or a radiant-tube furnace (tubes carrying the hot combustion gas run through the furnace).

^oA muffle is an impenetrable ceramic or metal barrier between the firing chamber and the interior of the furnace. It heats the process charge by radiation and furnace atmosphere convection.

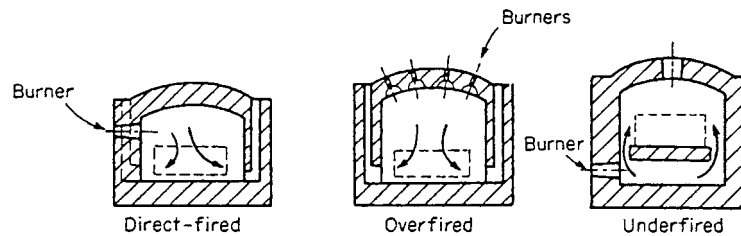


FIG. 24-45 Methods of firing direct-heated furnaces. (From Marks' Standard Handbook for Mechanical Engineers, 9th ed., McGraw-Hill, New York, 1987. Reproduced with permission.)

Atmosphere Protective atmosphere within the furnace chamber may be essential, especially in the heat treatment of metal parts. Mawhinney (in *Marks' Standard Handbook for Mechanical Engineers*, 9th ed., McGraw-Hill, New York, 1987, p. 752) lists pure hydrogen, dissociated ammonia (a hydrogen/nitrogen mixture), and six other protective reducing gases with their compositions (mixtures of hydrogen, nitrogen, carbon monoxide, carbon dioxide, and sometimes methane) that are codified for and by the metals-treatment industry. In general, any other gas or vapor that is compatible with the temperature and the lining material of the furnace can be provided in an indirect-fired furnace, or the furnace can be evacuated.

COGENERATION

Cogeneration is an energy conversion process wherein heat from a fuel is simultaneously converted to useful thermal energy (e.g., process steam) and electric energy. The need for either form can be the primary incentive for cogeneration, but there must be opportunity for economic captive use or sale of the other. In a chemical plant the need for process and other heating steam is likely to be the primary; in a public utility plant, electricity is the usual primary product.

Thus, a cogeneration system is designed from one of two perspectives: it may be sized to meet the process heat and other steam needs of a plant or community of industrial and institutional users, so that the electric power is treated as a by-product which must be either used on site or sold; or it may be sized to meet electric power demand, and the rejected heat used to supply needs at or near the site. The latter approach is the likely one if a utility owns the system; the former if a chemical plant is the owner.

Industrial use of cogeneration leads to small, dispersed electric-power-generation installations—an alternative to complete reliance on large central power plants. Because of the relatively short distances over which thermal energy can be transported, process-heat generation is characteristically an on-site process, with or without cogeneration.

Cogeneration systems will not match the varying power and heat demands at all times for most applications. Thus, an industrial cogeneration system's output frequently must be supplemented by the separate on-site generation of heat or the purchase of utility-supplied

electric power. If the on-site electric power demand is relatively low, an alternative option is to match the cogeneration system to the heat load and contract for the sale of excess electricity to the local utility grid.

Fuel saving is the major incentive for cogeneration. Since all heat-engine-based electric power systems reject heat to the environment, that rejected heat can frequently be used to meet all or part of the local thermal energy needs. Using reject heat usually has no effect on the amount of primary fuel used, yet it leads to a saving of all or part of the fuel that would otherwise be used for the thermal-energy process. Heat engines also require a high-temperature thermal input, usually receiving the working fluid directly from a heating source; but in some situations they can obtain the input thermal energy as the rejected heat from a higher-temperature process. In the former case, the cogeneration process employs a heat-engine topping cycle; in the latter case, a bottoming cycle is used.

The choice of fuel for a cogeneration system is determined by the primary heat-engine cycle. Closed-cycle power systems which are externally fired—the steam turbine, the indirectly fired open-cycle gas turbine, and closed-cycle gas turbine systems—can use virtually any fuel that can be burned in a safe and environmentally acceptable manner: coal, municipal solid waste, biomass, and industrial wastes are burnable with closed power systems. Internal combustion engines, on the other hand, including open-cycle gas turbines, are restricted to fuels that have combustion characteristics compatible with the engine type and that yield combustion products clean enough to pass through the engine without damaging it. In addition to natural gas, butane, and the conventional petroleum-derived liquid fuels, refined liquid and gaseous fuels derived from shale, coal, or biomass are in this category. Direct-coal-fired internal combustion engines have been an experimental reality for decades but are not yet a practical reality technologically or economically.

There are at least three broad classes of application for topping-cycle cogeneration systems:

- Utilities or municipal power systems supplying electric power and low-grade heat (e.g., 422 K [300°F]) for local district heating systems
- Large residential, commercial, or institutional complexes requiring space heat, hot water, and electricity

TABLE 24-18 Cogeneration Characteristics for Heat Engines

Engine type	Size range, MWe/unit	Efficiency at design point	Part-load efficiency	Multifuel capability	Maximum temperature of recoverable heat, °F (°C)*	Recoverable heat, Btu/kWh†	Typical power-to-heat ratio
Steam turbine							
Extraction-condensing type	30–300	0.25–0.30	Fair	Excellent	200 (93)–600 (315)‡	11,000–35,000	0.1–0.3
Backpressure type	20–200	0.20–0.25	Fair	Excellent	200 (93)–600 (315)‡	17,000–70,000	0.05–0.2
Combustion gas turbines	10–100	0.25–0.30	Poor	Poor	1000 (538)–1200 (649)	3000–11,000	0.3–0.45
Indirectly fired gas turbines							
Open-cycle turbines	10–85	0.25–0.30	Poor	Good	700 (371)–900 (482)	3500–8500	0.4–1.0
Closed-cycle turbines	5–350	0.25–0.30	Excellent	Good	700 (371)–900 (482)	3500–8500	0.4–1.0
Diesel engines	0.05–25	0.35–0.40	Good	Fair to poor	500 (260)–700 (371)	4000–6000	0.6–0.85

*°C + 273 = K.

†1 Btu = 1055 J.

‡Saturated steam.

- Large industrial operations with on-site needs for electricity and heat in the form of process steam, direct heat, and/or space heat.

Typical Systems All cogeneration systems involve the operation of a heat engine for the production of mechanical work which, in nearly all cases, is used to drive an electric generator. The commonest heat-engine types appropriate for topping-cycle cogeneration systems are:

- Steam turbines (backpressure and extraction configurations)
- Open-cycle (combustion) gas turbines
- Indirectly fired gas turbines: open cycles and closed cycles
- Diesel engines

Each heat-engine type has unique characteristics, making it better suited for some cogeneration applications than for others. For example, engine types can be characterized by:

- Power-to-heat ratio at design point
- Efficiency at design point
- Capacity range
- Power-to-heat-ratio variability
- Off-design (part-load) efficiency
- Multifuel capability

The major heat-engine types are described in terms of these characteristics in Table 24-18.

ELECTROCHEMICAL ENERGY CONVERSION

Electricity has become as indispensable as heat to the functioning of industrialized society. The source of most of the electricity used is the energy of the fuels discussed earlier in this section: liberated by combustion as heat, it drives heat engines which, in turn, drive electrical generators.

In some instances, however, part of the chemical energy bound in relatively high-enthalpy compounds can be converted directly to electricity as these reactants are converted to products of lower enthalpy (galvanic action). A process in the opposite direction also is possible for some systems: an electric current can be absorbed as the increased chemical energy of the higher-enthalpy compounds (electrolytic action). The devices in which electrochemical energy conversion processes occur are called cells.

Galvanic cells in which stored chemicals can be reacted on demand to produce an electric current are termed *primary cells*. The discharging reaction is irreversible and the contents, once exhausted, must be replaced or the cell discarded. Examples are the dry cells that activate small appliances. In some galvanic cells (called *secondary cells*), however, the reaction is reversible: that is, application of an electrical potential across the electrodes in the opposite direction will restore the reactants to their high-enthalpy state. Examples are rechargeable batteries for household appliances, automobiles, and many industrial applications. Electrolytic cells are the reactors upon which the electrochemical process, electroplating, and electrowinning industries are based.

Detailed treatment of the types of cells discussed above is beyond the scope of this handbook. For information about electrolytic cells, interested readers are referred to Fuller, Newman, Grotheer, and King ("Electrochemical Processing," in *Kirk-Othmer Encyclopedia of Chemical Technology*, 4th ed., vol. 9, Wiley, New York, 1994, pp. 111–197) and for primary and secondary cells, to Crompton (*Battery Reference Book*, 2d ed., Butterworth-Heinemann, Oxford, U.K., 1995). Another type of cell, however, a galvanic cell to which the reactants of an exothermic reaction are fed continuously, in which they react to liberate part of their enthalpy as electrical energy, and from which the products of the reaction are discharged continuously, is called a *fuel cell*. Fuel cell systems for generating electricity in a variety of applications are being commercialized by a number of companies. The rest of this section is devoted to a discussion of fuel cell technology.

FUEL CELLS

GENERAL REFERENCES: W. Vielstich, A. Lamm, H. A. Gasteiger, eds., *Handbook of Fuel Cells*, John Wiley & Sons, 2003. *Fuel Cell Handbook* (Rev. 7), U.S. Department of Energy, DOE/NETL-2004/1206. Appleby and Foulkes, *Fuel Cell Handbook*, Kreger Publishing Co., Molabar, Fla., 1993. Kinoshita and Cairns, "Fuel Cells," in *Kirk-Othmer Encyclopedia of Chemical Technology*, 4th ed., vol. 11, Wiley, New York, 1994, p. 1098. Liebhafsky and Cairns, *Fuel Cells and Fuel Batteries*, Wiley, New York, 1968. Linden (ed.), *Handbook of Batteries and Fuel Cells*, McGraw-Hill, New York, 1984.

Background Energy conversion in fuel cells is direct and simple when compared to the sequence of chemical and mechanical steps in

heat engines. A fuel cell consists of an anode, an electrolyte, and a cathode. On the anode, the fuel is oxidized electrochemically to positively charged ions. On the cathode, oxygen molecules are reduced to oxide or hydroxide ions. The electrolyte serves to transport either the positively charged ions from anode to cathode or the negatively charged ions from cathode to anode. Figure 24-46 is a schematic representation of the reactions in a fuel cell operating on hydrogen and air with a hydrogen-ion-conducting electrolyte. The hydrogen flows over the anode, where the molecules are separated into ions and electrons. The ions migrate through the ionically conducting but electronically insulating electrolyte to the cathode, and the electrons flow through the outer circuit energizing an electric load. The electrons combine eventually with oxygen molecules flowing over the surface of the cathode and hydrogen ions migrating across the electrolyte, forming water, which leaves the fuel cell in the depleted air stream.

A fuel cell has no moving parts. It runs quietly, does not vibrate, and does not generate gaseous pollutants. The idea of the fuel cell is generally credited to Sir William Grove, who lived in the nineteenth century. It took over 100 years for the first practical devices to be built, in the U.S. space program, as the power supply for space capsules and the space shuttle. Commercialization of terrestrial fuel cell systems has only recently begun. Having lower emissions and being more efficient than heat engines, fuel cells may in time become the power source for a broad range of applications, beginning with utility power plants, including civilian and military transportation, and reaching into portable electronic devices.

This slow realization of the concept is due to the very demanding materials requirements for fuel cells. The anodes and cathodes have to be good electronic conductors and must have electrocatalytic properties to facilitate the anodic and cathodic reactions. In addition, the anodes and cathodes must be porous to allow the fuel and oxidant gases to diffuse to the reaction sites, yet they must be mechanically strong enough to support the weight of the fuel cell stacks. The electrolyte must be chemically stable in hydrogen and oxygen, and must

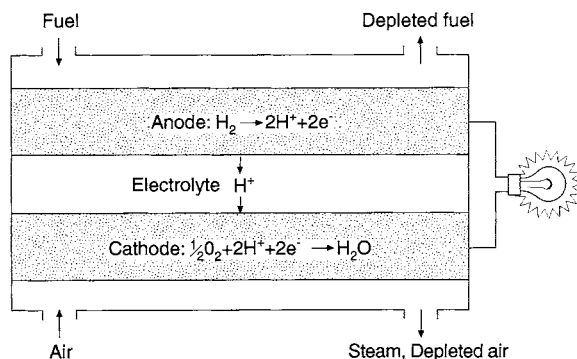


FIG. 24-46 Fuel cell schematic.

have an ionic conductivity of at least 0.1 S/cm. Five classes of electrolytes have been found to meet these requirements: potassium hydroxide, phosphoric acid, perfluorinated sulfonic acid resins, molten carbonates, and oxide-ion-conducting ceramics. Consequently, five types of fuel cell based on these electrolytes have been developed.

Fuel Cell Efficiency The theoretical energy conversion efficiency of a fuel cell ϵ° is given by the ratio of the free energy (Gibbs function) of the cell reaction at the cell's operating temperature ΔG_t to the enthalpy of reaction at the standard state ΔH° , both quantities being based on a mole of fuel:

$$\epsilon^\circ = \frac{\Delta G_t}{\Delta H^\circ} \quad (24-54)$$

The enthalpy of reaction is always taken at a temperature of 298 K (77°F), but the product water can be either liquid or gaseous. If it is liquid, the efficiency is based on the higher heating value (HHV), but if the product is gaseous, the efficiency is based on the lower heating value (LHV). If the fuel cell runs on hydrogen and oxygen at 373 K (212°F), the theoretical conversion efficiency is 91 percent LHV or 83 percent HHV. The theoretical efficiency of fuel cells as given in Eq. (24-54) is equivalent to the Carnot efficiency of heat engines with the working medium absorbing heat at the flame temperature of the fuel and rejecting it at 298 K. Owing to materials and engineering limitations, heat engines cannot operate at the Carnot limit. Fuel cells can run at efficiencies near the theoretical values but only at low power density (power produced per unit of active fuel cell area). At higher power densities, the efficiency of fuel cells is constrained by electrical resistances within the bulk and at the interfaces of the materials, and by gas diffusion losses.

When no net current is flowing, the equilibrium potential of the fuel cell is given by the Nernst equation:

$$E^\circ = \frac{-\Delta G_t}{nF} \quad (24-55)$$

where E° is the electrochemical equilibrium potential, V ; n is the number of electrons transferred in the cell reaction (equivalents), and F is the Faraday constant. If the units of ΔG_t are J/mol, F has the value 96,487 C/mol-equiv. The potential depends on the chemical species of the fuel and the operating temperature. For hydrogen and oxygen, variation of the equilibrium cell potential with temperature is shown in Table 24-19.

When current is flowing, the actual cell operating potential is given by:

$$E = E^\circ - (a_{an} + a_{ca}) - (b_{an} + b_{ca}) \frac{RT}{nF} \ln i - Ai \quad (24-56)$$

where a and b are characteristic constants for the electrochemical reactions at the electrode materials; the subscripts an and ca refer to the anode and the cathode, respectively; R is the gas constant; T is the cell temperature; A is the area-specific resistance of the fuel cell; and i is the current density (current flow per unit of active fuel cell area) in the cell.

Graphs of operating potential versus current density are called *polarization curves*, which reflect the degree of perfection that any particular fuel cell technology has attained. High cell operating potentials are the result of many years of materials optimization. Actual polarization curves will be shown below for several types of fuel cell.

TABLE 24-19 Thermodynamic Values for $H_2 + \frac{1}{2}O_2 = H_2O$ (g)

Temperature, K	Enthalpy of reaction (ΔH°), kJ/mol	Free energy of reaction (ΔG°), kJ/mol	Equilibrium cell potential (E°), V
300	-241.8	-228.4	1.18
500	-243.9	-219.2	1.14
700	-245.6	-208.8	1.06
900	-247.3	-197.9	1.03
1100	-248.5	-187.0	0.97
1300	-249.4	-175.7	0.91

The actual efficiency of an operating fuel cell is given by:

$$\epsilon = \frac{-nFE}{\Delta H^\circ} U_f \quad (24-57)$$

where U_f is the electrochemical fuel utilization (amount of fuel converted divided by amount fed to the cell). For pure hydrogen the fuel utilization can be 1.0, but for gas mixtures it is often 0.85. Equations (24-56) and (24-57) show that the efficiency of fuel cells is not constant, but depends on the current density. The more power that is drawn, the lower the efficiency.

When the fuel gas is not pure hydrogen and air is used instead of pure oxygen, additional adjustment to the calculated cell potential becomes necessary. Since the reactants in the two gas streams practically become depleted between the inlet and exit of the fuel cell, the cell potential is decreased by a term representing the log mean fugacities, and the operating cell efficiency becomes

$$\epsilon_{fc} = \frac{nFU_f}{\Delta H^\circ} \left[E^\circ - \sum a - \sum b \frac{RT}{nF} \ln i - Ai \right] - \frac{RTU_f}{\Delta H^\circ} [v_f \ln(\log \text{mean } \hat{f}_f) + v_{ox} \ln(\log \text{mean } \hat{f}_{ox})] \quad (24-58)$$

The quantities v_f and v_{ox} are the stoichiometric coefficients for the fuel cell reaction, and \hat{f}_f and \hat{f}_{ox} are the fugacities of fuel and oxygen in their respective streams.

Further, as the current density of the fuel cell increases, a point is inevitably reached where the transport of reactants to or products from the surface of the electrode becomes limited by diffusion. A *concentration polarization* is established at the electrode, which diminishes the cell operating potential. The magnitude of this effect depends on many design and operating variables, and its value must be obtained empirically.

Design Principles An individual fuel cell will generate an electrical potential of about 1 V or less, as discussed above, and a current that is proportional to the external load demand. For practical applications, the voltage of an individual fuel cell is obviously too small, and cells are therefore stacked up as shown in Fig. 24-47. Anode/electrolyte/cathode assemblies are electrically connected in series by inserting a bipolar plate between the cathode of one cell and the anode of the next. The bipolar plate must be impervious to the fuel and oxidant gases, chemically stable under reducing and oxidizing conditions, and an excellent electronic conductor. In addition, it is often used to distribute the gases to the anode and cathode surfaces through flow channels cut or molded into it.

The number of fuel cells that are stacked is determined by the desired electrical potential. For 110-V systems it can be about 200 cells. Since a typical fuel cell is about 5 mm (0.2 in) thick, a 200-cell stack assembly (including the end hardware that keeps the unit under compression) is about 2 m (6 ft) tall. The reactant and product gas streams are supplied and removed from the stack by external or internal manifolding. Externally manifolded stacks have shallow trays on each of the four sides to supply the fuel and air and to remove the depleted gases and reaction products. The manifolds are mechanically clamped to the stacks and sealed at the edges. These manifold seals must be gastight, electrically insulating, and able to tolerate thermal expansion mismatches between the stack and the manifold materials as well as dimensional changes due to aging.

Alternatively, reactant and product gases can be distributed to and removed from individual cells through internal pipes in a design analogous to that of filter presses. Care must be exercised to assure an even flow distribution between the entry and exit cells. The seals in internally manifolded stacks are generally not subject to electrical, thermal, and mechanical stresses, but are more numerous than in externally manifolded stacks.

Because fuel cells generate an amount of excess heat consistent with their thermodynamic efficiency, they must be cooled. In low-temperature fuel cells, the cooling medium is generally water or oil, which flows through cooling plates interspaced throughout the stack. In high-temperature cells, heat is removed by the reactant air stream and also by the endothermic fuel reforming reactions in the stack.

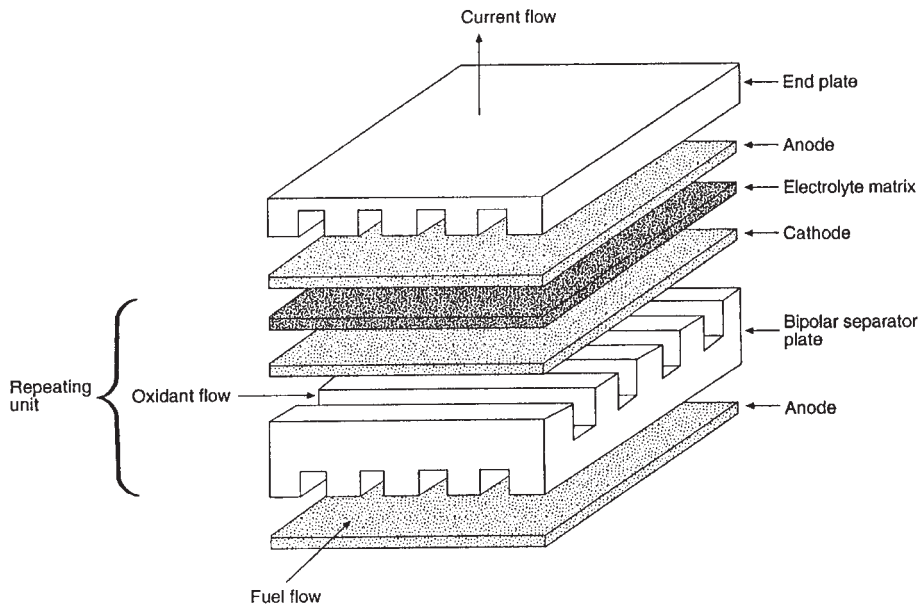


FIG. 24-47 Stacking of individual fuel cells.

Types of Fuel Cells The five major types of fuel cell are listed in Table 24-20. Each has unique chemical features. The *alkaline fuel cell* (AFC) has high power density and has proven itself as a reliable power source in the U.S. space program, but the alkaline electrolyte reacts with carbon dioxide, which is present in reformed hydrocarbon fuels and air. The *polymer electrolyte fuel cell* (PEFC) and the *phosphoric acid fuel cell* (PAFC) are tolerant of carbon dioxide, but both are sensitive to carbon monoxide (PEFC much more so than PAFC), which is adsorbed onto the platinum catalyst and renders it inactive. Therefore, these three types of fuel cell require pure hydrogen as fuel; and if the hydrogen has been obtained by reforming a fuel such as natural gas, the hydrogen-rich fuel stream must be purified before being introduced into the fuel cell. The *molten carbonate fuel cell* (MCFC) and the *solid oxide fuel cell* (SOFC) can tolerate carbon monoxide and carbon dioxide and can operate on hydrocarbon fuels with minimal fuel processing, but they operate at elevated temperatures.

The operating temperature also affects the fuel cell operating potential in more than one way. A high operating temperature accelerates reaction rates but lowers the thermodynamic equilibrium potential. These effects balance one another, and, in practice, the operating point of any fuel cell is usually between 0.7 and 0.8 V. The cell reactions for the five types of fuel cell are summarized in Table 24-21. It is important to note that in cells with acidic electrolytes (PAFC and PEFC) the product water evolves on the air electrode, but in the alkaline ones (AFC, MCFC, and SOFC) it is generated on the fuel electrode. This has consequences for the system design. Whenever water needs to be recovered for generating hydrogen from hydrocarbon fuels, a condenser is required in PAFC and PEFC systems. In others, the depleted fuel can be recycled.

TABLE 24-20 Fuel Cell Characteristics

Type of fuel cell	Electrolyte	Operating temperature		Coolant medium
		K	°C	
Alkaline	KOH	363	90	Water
Polymer	$\text{CF}_3(\text{CF}_2)_n\text{OCF}_2\text{SO}_3^-$	353	80	Water
Phosphoric acid	H_3PO_4	473	200	Steam/water
Molten carbonate	$\text{Li}_2\text{CO}_3\text{-K}_2\text{CO}_3$	923	650	Air
Solid oxide	$\text{Zr}_{0.92}\text{Y}_{0.08}\text{O}_{1.96}$	1273	1000	Air

Following is a summary of the materials, operating characteristics, and mode of construction for each type of fuel cell.

Alkaline Fuel Cell The electrolyte for NASA's space shuttle orbiter fuel cell is 35 percent potassium hydroxide. The cell operates between 353 and 363 K (176 and 194°F) at 0.4 MPa (59 psia) on hydrogen and oxygen. The electrodes contain platinum-palladium and platinum-gold alloy powder catalysts bonded with polytetrafluoroethylene (PTFE) latex and supported on gold-plated nickel screens for current collection and gas distribution. A variety of materials, including asbestos and potassium titanate, are used to form a microporous separator that retains the electrolyte between the electrodes. The cell structural materials, bipolar plates, and external housing are usually nickel-plated to resist corrosion. The complete orbiter fuel cell power plant is shown in Fig. 24-48.

Typical polarization curves for alkaline fuel cells are shown in Fig. 24-49. It is apparent that the alkaline fuel cell can operate at about 0.9 V and 500 mA/cm² current density. This corresponds to an energy

TABLE 24-21 Fuel Cell Reaction Electrochemistry

Type of fuel cell	Conducting ion	Anode reaction	Cathode reaction
Alkaline	OH^-	$\text{H}_2 + 2\text{OH}^- \rightarrow 2\text{H}_2\text{O} + 2\text{e}^-$	$\frac{1}{2}\text{O}_2 + \text{H}_2\text{O} + 2\text{e}^- \rightarrow 2\text{OH}^-$
Polymer	H^+	$\text{H}_2 \rightarrow 2\text{H}^+ + 2\text{e}^-$	$\frac{1}{2}\text{O}_2 + 2\text{H}^+ + 2\text{e}^- \rightarrow \text{H}_2\text{O}$
Phosphoric acid	H^+	$\text{H}_2 \rightarrow 2\text{H}^+ + 2\text{e}^-$	$\frac{1}{2}\text{O}_2 + 2\text{H}^+ + 2\text{e}^- \rightarrow \text{H}_2\text{O}$
Molten carbonate	CO_3^{2-}	$\text{H}_2 + \text{CO}_3^{2-} \rightarrow \text{H}_2\text{O} + \text{CO}_2 + 2\text{e}^-$	$\frac{1}{2}\text{O}_2 + \text{CO}_2 + 2\text{e}^- \rightarrow \text{CO}_3^{2-}$
Solid oxide	O^{2-}	$\text{H}_2 + \text{O}^{2-} \rightarrow \text{H}_2\text{O} + 2\text{e}^-$	$\frac{1}{2}\text{O}_2 + 2\text{e}^- \rightarrow \text{O}^{2-}$

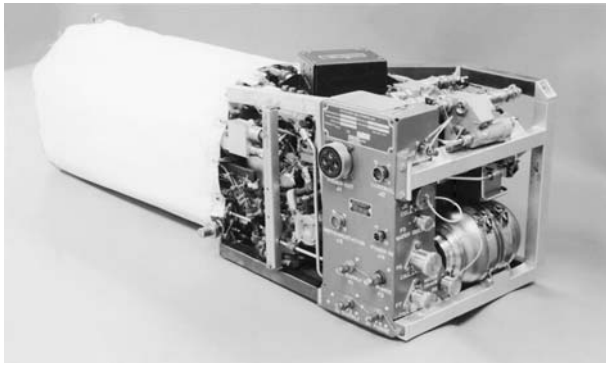


FIG. 24-48 Orbiter power plant. (International Fuel Cells.)

conversion efficiency of about 60 percent HHV. The space shuttle orbiter power module consists of three separate units, each measuring 0.35 by 0.38 by 1 m (14 by 15 by 40 in), weighing 119 kg (262 lb), and generating 15 kW of power. The power density is about 100 W/L and the specific power, 100 W/kg.

Polymer Electrolyte Fuel Cell The PEFC, also known as the *proton-exchange-membrane fuel cell* (PEMFC), is of great interest for transportation applications because it is capable of high power density and it can deliver about 40 percent of its nominal power at room temperature. These features have made the PEFC a candidate to replace internal combustion engines in automobiles. Methanol, ethanol, hydrogen, natural gas, dimethyl ether, and common transportation fuels such as gasoline are being considered as fuel, but hydrogen is currently preferred. The motivation for developing fuel-cell-powered vehicles is a dramatic reduction in environmentally harmful emissions and high fuel economy.

The electrolyte is a perfluorosulfonic acid ionomer, commercially available under the trade name of Nafion™. It is in the form of a membrane about 0.17 mm (0.007 in) thick, and the electrodes are bonded directly onto the surface. The electrodes contain very finely divided platinum or platinum alloys supported on carbon powder or fibers. The bipolar plates are made of graphite-filled polymer or metal.

Typical platinum catalyst loadings needed to support the anodic and cathodic reactions are currently 0.2 to 0.5 mg/cm² of active cell area. Owing to the cost of platinum, substantial efforts have been made to reduce the catalyst loading.

To be ionically conducting, the fluorocarbon ionomer must be “wet”: under equilibrium conditions, it will contain about 20 percent water. The operating temperature of the fuel cell must be

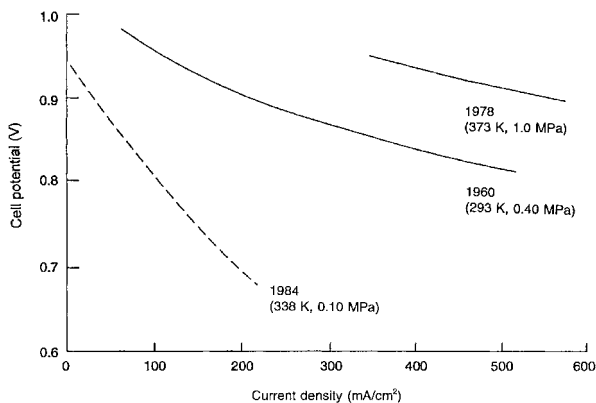


FIG. 24-49 Polarization curves for alkaline fuel cells.

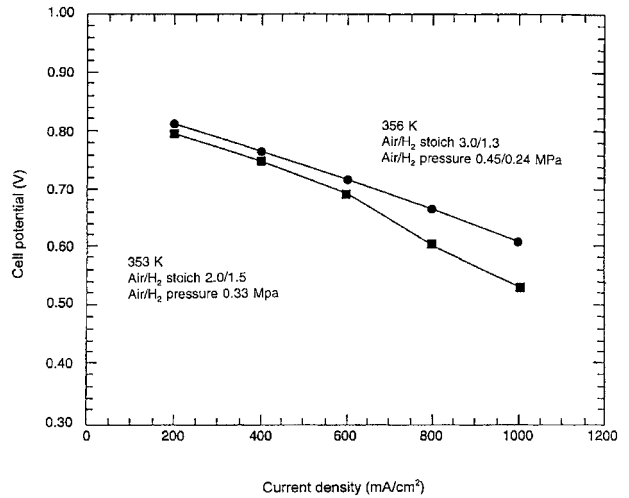


FIG. 24-50 Polarization curves for PEFC stacks.

less than 373 K (212°F), therefore, to prevent the membrane from drying out.

Being acidic, fluorocarbon ionomers can tolerate carbon dioxide in the fuel and air streams; PEFCs, therefore, are compatible with hydrocarbon fuels. However, the platinum catalysts on the fuel and air electrodes are extremely sensitive to carbon monoxide: only a few parts per million are acceptable. Catalysts that are more tolerant to carbon monoxide are being explored. Typical polarization curves for PEFCs are shown in Fig. 24-50.

As mentioned, the primary motivation for the PEFC development was the anticipated applicability in transportation. However, the economics of stationary use are more forgiving, and commercialization of the technology will likely begin as grid-independent power supplies. Figure 24-51 shows a 5-kW PEFC system operating on natural gas.



FIG. 24-51 Natural gas-fueled 5-kW PEFC system. (Courtesy of Plug Power.)

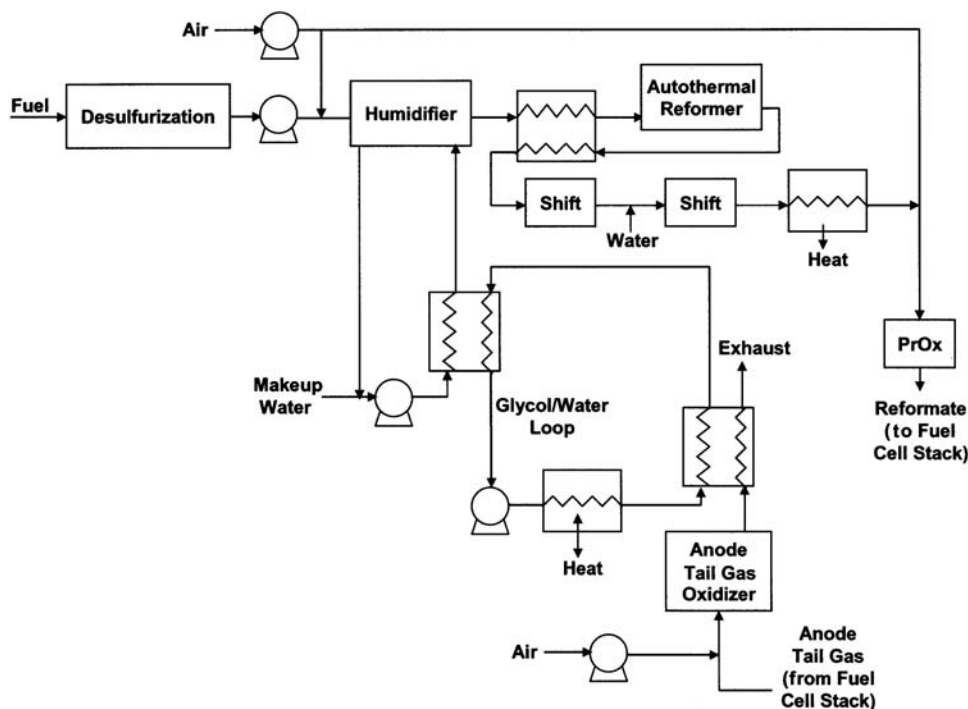


FIG. 24-52 System diagram for reformer-based PEFC system.

The fuel cell stack is visible in the center as a black box, and the fuel processing train is seen on the left. The smaller box on the right contains the power conditioning equipment. Figure 24-52 shows the system diagram for the unit. Natural gas is desulfurized and then mixed with air and steam before entering the autothermal reformer that converts the methane to a mixture of hydrogen, carbon monoxide, and carbon dioxide. Typically this reaction occurs over a catalyst at about 973 K [700°C]. To decrease the carbon monoxide content of this gas, it is cooled to about 623 K [350°C] and reacted with additional water in the so-called shift reactors. Because of the sensitivity of the anode catalyst to carbon monoxide, a preferential oxidation of the remaining carbon monoxide is done before the hydrogen-rich gas is fed to the fuel cell.

About 70 percent of the hydrogen is converted to electricity in the fuel cell stack, and the tail gas is then burned to generate heat which is transferred via a glycol/water loop to the steam generator. The same loop passes through the cooling plates or the fuel cell to remove heat.

A particular version of the PEFC is the **direct methanol fuel cell** (DMFC). As the name implies, an aqueous solution of methanol is used as fuel instead of the hydrogen-rich gas, eliminating the need for reformers and shift reactors. The major challenge for the DMFC is the “crossover” of methanol from the anode compartment into the cathode compartment through the membrane that poisons the electrodes by CO. Consequently, the cell potentials and hence the system efficiencies are still low. Nevertheless, the DMFC offers the prospect of replacing batteries in consumer electronics and has attracted the interest of this industry.

Phosphoric Acid Fuel Cell In this type of fuel cell, the electrolyte is 93 to 98 percent phosphoric acid contained in a matrix of silicon carbide. The electrodes consist of finely divided platinum or platinum alloys supported on carbon black and bonded with PTFE latex. The latter provides enough hydrophobicity to the electrodes to prevent flooding of the structure by the electrolyte. The carbon support of the air electrode is specially formulated for oxidation resistance at 473 K (392°F) in air and positive potentials.

The bipolar plate material of the PAFC is graphite. A portion of it has a carefully controlled porosity that serves as a reservoir for phosphoric

acid and provides flow channels for distribution of the fuel and oxidant. The plates are electronically conductive but impervious to gas crossover.

PAFC systems are commercially available from UTC Power as 200-kW stationary power sources operating on natural gas. The stack cross section is 1 m² (10.8 ft²). It is about 2.5 m (8.2 ft) tall and rated for a 40,000-h life. It is cooled with water/steam in a closed loop with secondary heat exchangers. Fuel processing is similar to that in a PEFC system, but a preferential oxidizer is not needed. These systems are intended for on-site power and heat generation for hospitals, hotels, and small businesses.

Molten Carbonate Fuel Cell The electrolyte in the MCFC is a mixture of lithium/potassium or lithium/sodium carbonates, retained in a ceramic matrix of lithium aluminate. The carbonate salts melt at about 773 K (932°F), allowing the cell to be operated in the 873 to 973 K (1112 to 1292°F) range. Platinum is no longer needed as an electrocatalyst because the reactions are fast at these temperatures. The anode in MCFCs is porous nickel metal with a few percent of chromium or aluminum to improve the mechanical properties. The cathode material is lithium-doped nickel oxide.

The bipolar plates are made from either Type 310 or Type 316 stainless steel, which is coated on the fuel side with nickel and aluminized in the seal area around the edge of the plates. Both internally and externally manifolded stacks have been developed.

In MCFCs, the hydrogen fuel is generated from such common fuels as natural gas or liquid hydrocarbons by steam reforming; the fuel processing function can be integrated into the fuel cell stack because the operating temperature permits reforming using the waste heat. An added complexity in MCFCs is the need to recycle carbon dioxide from the anode side to the cathode side to maintain the desired electrolyte composition. (At the cathode, carbon dioxide reacts with incoming electrons and oxygen in air to regenerate the carbonate ions that are consumed at the anode.) The simplest way is to burn the depleted fuel and mix it with the incoming air. This works well but dilutes the oxygen with the steam generated in the fuel cell. A steam condenser and recuperative heat exchanger can be added to eliminate the steam, but at increased cost.

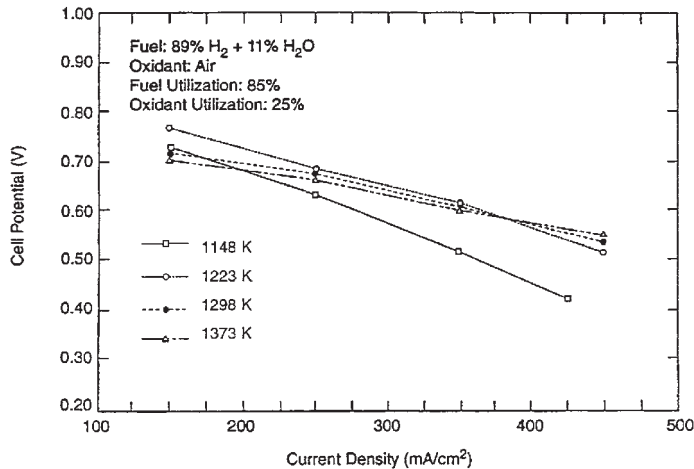


FIG. 24-53 Polarization curves at different temperatures for 50-cm active length thin-wall SOFCs.

The fuel cell must be cooled with either water or air, and the heat can be converted to electricity in a bottoming cycle. The dc electrical output of the stack is usually converted to ac and stepped up or down in voltage, depending on the application. Analogous to PAFCs, MCFC stacks are about 1 m² (10.8 ft²) in plan area and quite tall. A stack generates 200 to 300 kW.

Solid Oxide Fuel Cell In SOFCs the electrolyte is a ceramic oxide ion conductor, such as yttrium-doped zirconium oxide. The conductivity of this material is 0.1 S/cm at 1273 K (1832°F); it decreases to 0.01 S/cm at 1073 K (1472°F), and by another order of magnitude at 773 K (932°F). Because the resistive losses need to be kept below about 50 mV, the operating temperature of the SOFC depends on the thickness of the electrolyte. For a thickness of 100 μm or more, the operating temperature is 1273 K (1832°F) but fuel cells with thin electrolytes can operate between 973 and 1073 K (1292 and 1472°F).

The anode material in SOFCs is a cermet (metal/ceramic composite material) of 30 to 40 percent nickel in zirconia, and the cathode is

lanthanum manganite doped with calcium oxide or strontium oxide. Both of these materials are porous and mixed ionic/electronic conductors. The bipolar separator typically is doped lanthanum chromite, but a metal can be used in cells operating below 1073 K (1472°F). The bipolar plate materials are dense and electronically conductive.

Typical polarization curves for SOFCs are shown in Fig. 24-53. As discussed earlier, the open-circuit potential of SOFCs is less than 1 V because of the high temperature, but the reaction overpotentials are small, yielding almost linear curves with slopes corresponding to the resistance of the components.

SOFCs can have a planar geometry similar to PEFCs, but the leading technology is tubular, as shown in Fig. 24-54. The advantage of the tubular arrangement is the absence of high-temperature seals.

Like MCFCs, SOFCs can integrate fuel reforming within the fuel cell stack. A prereformer converts a substantial amount of the natural gas using waste heat from the fuel cell. Compounds containing sulfur (e.g., thiophene, which is commonly added to natural gas as an odorant)

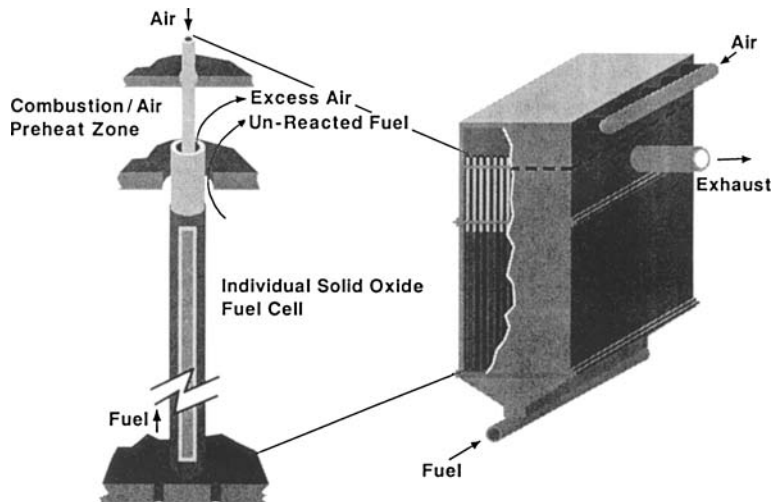


FIG. 24-54 Configuration of the tubular SOFC. (Courtesy of Westinghouse Electric Corporation.)

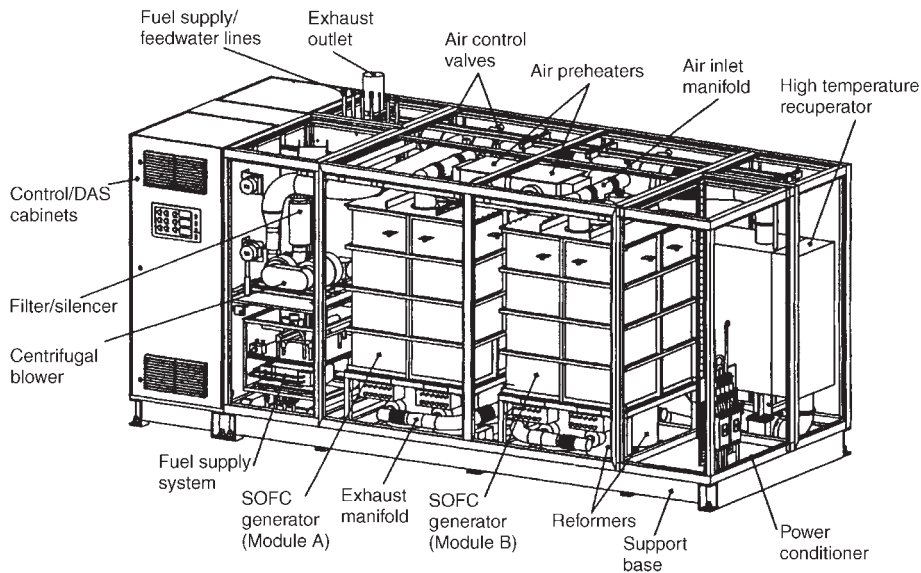


FIG. 24-55 SOFC 25-kW system package. (Courtesy of Westinghouse Electric Corporation.)

must be removed before the reformer. Typically, a hydrodesulfurizer combined with a zinc oxide absorber is used.

The desulfurized natural gas is mixed with the recycled depleted fuel stream containing steam formed in the fuel cell. About 75 percent of the methane is converted to hydrogen and carbon monoxide in the prereformer. The hydrogen-rich fuel is then passed over the

fuel cell anode, where 85 percent is converted to electricity. The balance is burned with depleted air in the combustion zone.

The hot combustion gas preheats the fresh air and the prereformer, and can be used further to generate steam. The system is cooled with 200 to 300 percent excess air. A 25-kW SOFC generator system is shown in Fig. 24-55.

ENERGY RECOVERY

Most processing energy enters and then leaves the process as energy, separate from the product. The energy enters as electricity, steam, fossil fuels, etc. and then leaves, released to the environment as heat, through "coolers," hot combustion flue gases, waste heat, etc. Recovering heat to be used elsewhere in the process is important to increase process efficiency and minimize cost. Minimizing the total annualized costs for this flow of energy through the process is a complex engineering task in itself, separate from classic process design. Since these costs include the costs for getting energy into and out of the process, they should be evaluated together, as elements integrated within a larger system. Such a holistic system evaluation impacts how the overall project will be designed (utilities supply, reaction and separations design, pinch analyses, 3D process layout, plot plan, etc.). Therefore, evaluation and selection of the process energy technology system should be performed at the start of the project design cycle, during **technology selection VIP** (see the subsection "Value-Improving Practices" in Sec. 9), when the **potential to influence project costs exists at its maximum value**.

Following the 1970s energy crisis, enhanced technology systems have been developed which can **significantly reduce the annualized costs for process energy**. Several of these technologies are presented below, because they are broadly applicable, have a rapid payback, and can make a significant reduction in overall annualized energy costs. Wet surface air coolers (WSACs), an evaporative cooling technology, are presented in Sec. 12.

ECONOMIZERS

GENERAL REFERENCES: "Latest Advances in the Understanding of Acid Dew-point Corrosion: Corrosion and Stress Corrosion Cracking in Combustion Gas

Condensates," W.M.M. Huijbregts and R.G.I. Leferink, *Anti-Corrosion Methods and Materials*, vol. 51, no. 3, 2004, pp. 173–188 (<http://www.hbsec.nl/>); "Get Acid Dew Points of Flue Gas," A.G. Okkes, *Hydrocarbon Processing*, July 1987, pp. 53–55.; Lahtvee, T., Schaus, O., *Study of Materials to Resist Corrosion in Condensing Gas-Fired Furnaces*, Final Report to Gas Research Institute, GRI-80/0133, February, 1982; Ball, D., et al., *Condensing Heat Exchanger Systems for Oil-Fired Residential/Commercial Furnaces and Boilers: Phase I and II*, US DOE BNL-51617, 1982; Razgaitis, R., et al., *Condensing Heat Exchanger Systems for Residential/Commercial Furnaces: Phase III*, US DOE BNL-51770, 1984; Razgaitis, R., et al., *Condensing Heat Exchanger Systems for Residential/Commercial Furnaces and Boilers. Phase IV*, BNL-51943, 1985; Butcher, T.A., Park, N., and Litzke, W., "Condensing Economizers: Thermal Performance and Particulate Removal Efficiencies," in *ASME Two Phase Flow and Heat Transfer, HTD*, vol. 197, 1992 (for U.S. DOE reports see: <http://www.osti.gov/energycitations/>).

Economizers improve boiler thermal efficiency by recovering heat from the combustion flue gases exhausted from the steam boiler section. The recovered heat is used to heat colder streams (heat sinks), before ultimate discharge of the waste gas to atmosphere. This recovered heat displaces the need to burn additional fuel to heat these same streams.

Normally, after being heated, these streams are used in the boiler area (deaerator feedwater, cold return condensate, boiler feedwater, RO feedwater) or in the combustion chamber (air preheat). However, economizers can be used to recover and supply heat elsewhere, such as hot process water or hot utility water, especially as used in the food processing and pulp/paper industries. Additionally, recovered flue gas waste heat can be used indirectly; i.e., remote process streams can be heated locally with hot steam condensate, and then the cooled return steam condensate can be reheated in the flue gas economizer. An

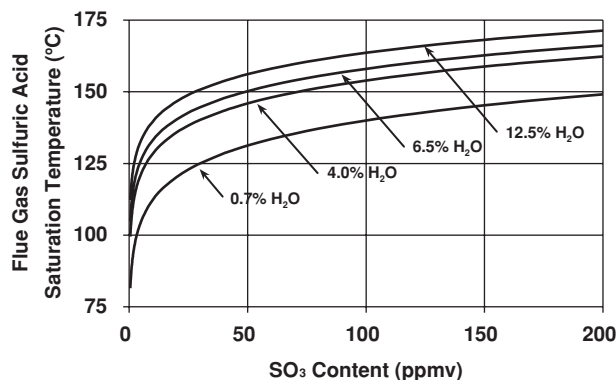


FIG. 24-56 Calculated sulfuric acid dew points, as a function of SO_3 content, for various flue gas water vapor concentrations. (Courtesy W. M. M. Huijbregts, 2004.)

extension of these concepts is provided by the application of using hot water to vaporize LNG: hot-water-based liquid is used to vaporize the process stream [LNG: stored near 122 K (-151°C), returning near 273 K (0°C)] to the hot water heater. Before entering the hot water heater, the cooled stream recovers flue gas waste heat in a condensing economizer.

Acid Dew Point For fossil fuels, the acid dew point temperature is that temperature at which the actual mixed acid vapor pressure equals the mixed acid vapor saturation pressure. The mixed acid dew point can be approximated by the sulfuric acid dew point (Fig. 24-56). It can be described as a function of the SO_3 and water content of the flue gas (Huijbregts). These concentrations result from the sulfur, hydrogen, and free water content of the fuel; the relative humidity of the air; and the amount of excess air used. Using the equation of Verhoff, where T is degrees K and P is mm Hg (see Okkes, A.G.):

$$T_{\text{dew}}(\text{SO}_3) = 1000 / [2.276 - 0.0294 \ln(P_{\text{H}_2\text{O}}) - 0.0858 \ln(P_{\text{SO}_3}) + 0.0062 \ln(P_{\text{H}_2\text{O}} P_{\text{SO}_3})] \quad (24-59)$$

The corrosiveness of flue gas condensate is further complicated by the presence of other components (Cl^- , NO_3^- , etc.). The sources of these components can be either the fuel or the combustion air (salt, ammonia, Freon, chlorine, chlorinated VOCs, etc.), usually producing a more corrosive condensate.

Water Dew Point For flue gas, the water dew point is that temperature at which the actual water vapor pressure equals the water saturation vapor pressure. Cooling the flue gas below this temperature will result in the formation of liquid water [or ice, below 273 K (0°C)]. For example, burning natural gas with 3 percent excess oxygen (15 percent excess air), the flue gas water dew point would be (Fig. 24-57) ~ 330 K (56.7°C).

Boiler Thermal Efficiency Traditionally, boiler thermal efficiency is calculated $Q_{\text{OUT}}/Q_{\text{IN}}$, where Q_{IN} is the LHV (lower heating value) of the fuel. A rule of thumb for economizers is that boiler efficiency increases by ~ 1 percent for every 22°C (40°F) drop in temperature of the dry flue gas. These two statements do not reveal the considerable quantity of **additional heat**, available to be recovered through **condensation of the water vapor** in the flue gas, which is lost to atmosphere with hot flue gas. Based on fuel HHV (higher heating value), the total latent heat loss can be substantial: an additional 9.6 percent (natural gas), 8.0 percent (propane), 6.5 percent (heating oil).

Conventional Economizers Conventional economizers can be constructed from relatively inexpensive materials, such as low-alloy carbon steels, if they will be operated dry on the gas side, with flue gas side metal temperatures above the acid dew point. This practice is done to protect the economizer from corrosion, caused by the acidic flue gas condensate. Conventional economizers can also be con-

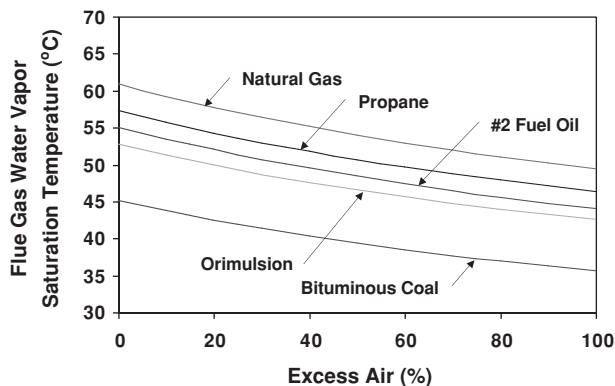


FIG. 24-57 Calculated flue gas water vapor dew points, for different fuel types, as a function of excess air [Orimulsion (28.3% water), Pittsburgh Seam 8 (5% water)]. (Courtesy T. A. Butcher, US DOE; www.bnl.gov.)

structed from more expensive materials, and can be operated below the acid dew point, but above the water dew point. This practice permits greater heat recovery, but with a generally lower payback. A compromise practice for operation below the acid dew point is to use less expensive but less corrosion-resistant materials, accepting an accelerated rate of corrosion, and periodically replacing the damaged heat-transfer surfaces when needed. Nevertheless, when high-sulfur fuel is burned (oil, coal, etc.), typically the water inlet feed to a conventional economizer is preheated to a temperature above the anticipated acid dew point.

Condensing Economizers Flue gas condensing waste heat economizers are designed to operate **below the flue gas water dew point**. This temperature can range from about 316 K (43°C) to 333 K (60°C), depending on the amount of hydrogen and water in the fuel, the amount of excess combustion air used, and the humidity of the air. [Higher flue gas water dew points can be encountered for other industrial applications, such as product driers, fryers (food processing), waste water incinerators, etc.] Such economizers recover **flue gas sensible heat** as well as **water vapor latent heat** from the hot flue gas. Fuel consumption is reduced in proportion to the efficiency increase.

Condensing economizers are constructed from inexpensive, but durable, corrosion-resistant materials. Extensive materials testing has been performed for operation in this service, including for coal combustion (Lahtvee, Ball, Razgaitis, and Butcher). The metallurgy for the tube-side liquid is determined by the liquid chemistry requirements (usually water-based liquid): 304 stainless steel is typical.

For gas-side materials, one available technology employs Teflon-covered metal tubing and Teflon tube sheets. This technology is often operated across both the acid and water dew points, and can accept inlet gas temperatures to 533 K (260°C). Typical applications may achieve a cold-end ΔT below 45°C (80°F), improve the boiler thermal efficiency by ~ 10 percent (LHV basis), and have a simple payback of 2 to 3 years, based on **fuel avoidance** (Figs. 24-58 and 24-59).

A second technology employs metallic finned tubing, extruded over the water tubing. Aluminum 1000 series fins are preferred, for heat-transfer reasons in natural gas applications, but stainless steel (or other material) fins are used for higher temperatures and/or more corrosive flue gas. This second technology both is less expensive and has better heat transfer (per ft^2). Consequently, for the same payback the cold-end approach can be lower, and the water outlet temperature and the boiler efficiency improvement higher. Flue gas condensate from combustion of natural gas typically has a pH of ~ 4.3 , and aluminum fins are suitable. For more acidic (or erosive) flue gas conditions, other metallurgy (Incoloy® 825 and Hastelloy®), or a Hersite or equivalent coating, may be used to prevent corrosion damage (Fig. 24-60).

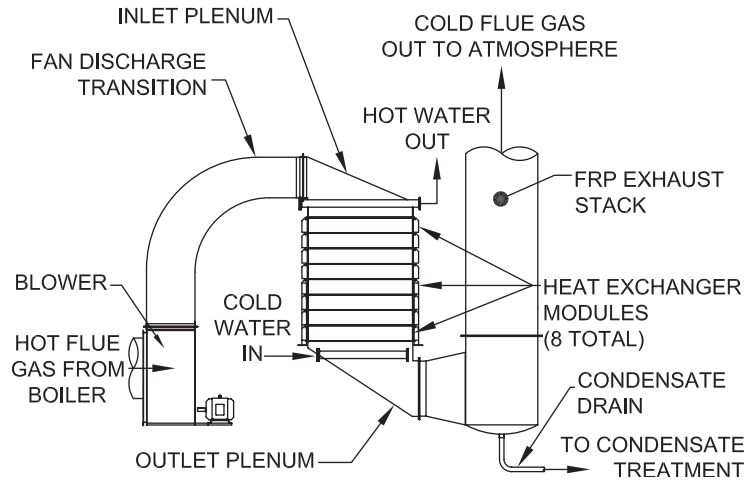


FIG. 24-58 Standard equipment arrangement, flue gas condensing economizer waste heat recovery system (flow: left to right). The ID fan draws hot flue gas from the boiler, propelling it into the top of the condensing economizer. (Courtesy CHX Condensing Heat Exchanger Co.; www.chxheat.com.)

Flue gas condensate at different temperatures, compositions and relative corrosivity condenses and exists at different positions within the condensing economizer. These positions are not fixed in space or time, but move back and forth, in response to changing load conditions

in either stream. Condensing economizers are typically equipped with water spray nozzles for periodic washdown of the flue gas side, to be used (infrequently) for natural gas combustion, but more frequently for services having heavier pollutant loading, such as oil, coal, etc. Over

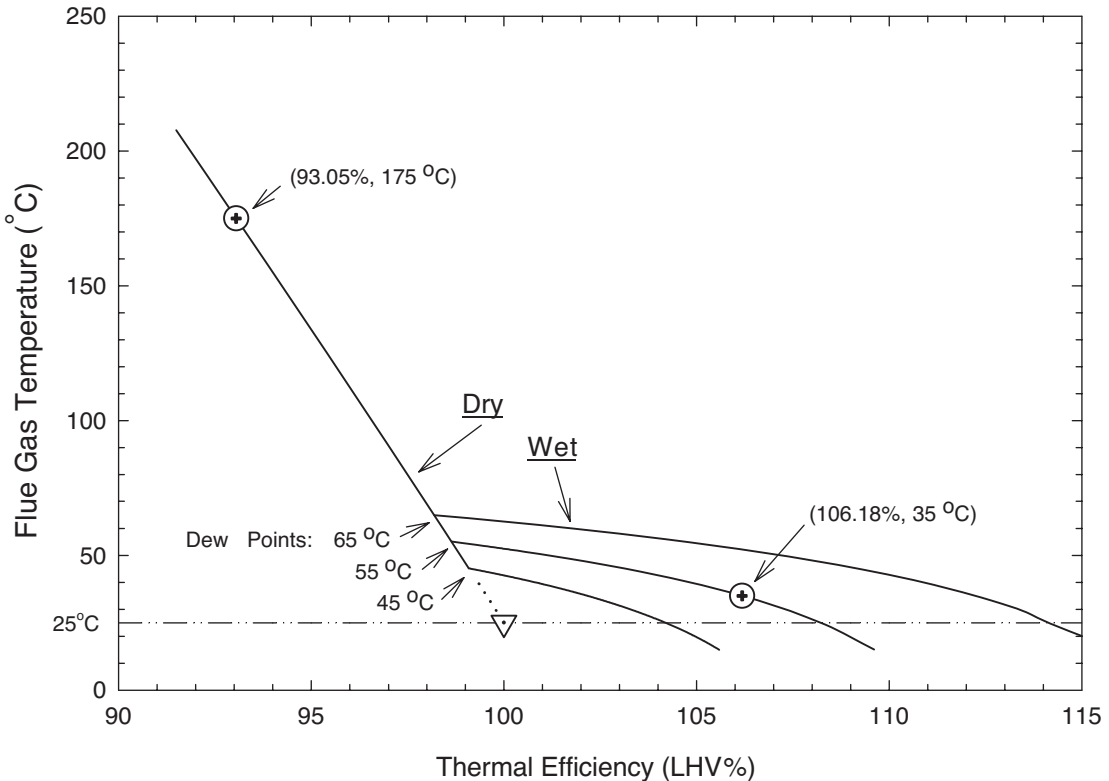


FIG. 24-59 Characteristic curves for boiler thermal efficiency as a function of flue gas effluent temperature and flue gas water dew points. Based on the LHV of a fuel, and stoichiometric reaction, 100 percent efficiency would be achieved if sufficient combustion heat were recovered and removed, so that the temperature of the effluent flue gas was reduced to 25°C. For a flue gas with a 55°C dew point, recovering additional heat via condensation by cooling from 175 to 35°C (as shown) would increase the overall efficiency by more than 13 percent. (Courtesy Combustion & Energy Systems, Ltd.; www.condenergy.com.)

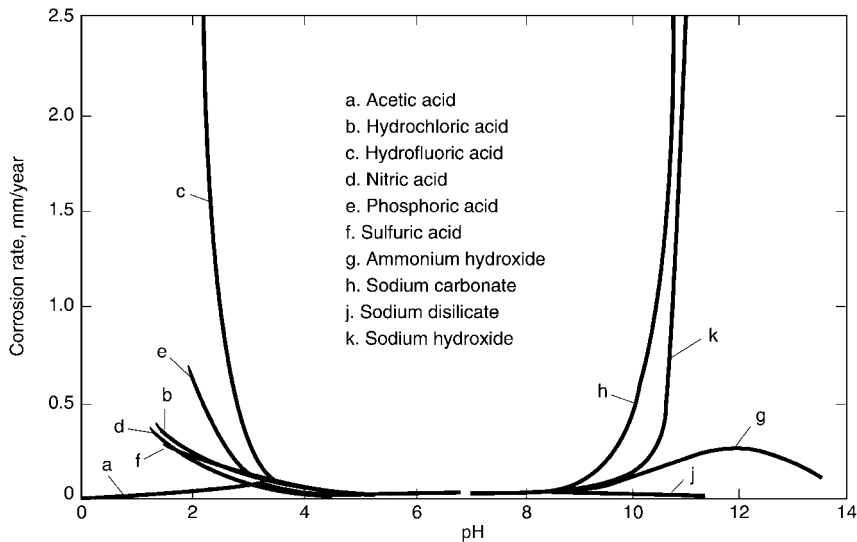


FIG. 24-60 Effect of corrosion on 1100-H14 aluminum alloy by various chemical solutions. Observe the minimal corrosion in the pH range from 4.0 to 9.0. The low corrosion rates in acetic acid, nitric acid, and ammonium hydroxide demonstrate that the nature of the individual ions in solution is more important than the degree of acidity or alkalinity. (With permission from ASM International; www.asminternational.org. Courtesy of Combustion & Energy Systems, Ltd.; www.condenergy.com.)

200 such heat exchangers have been installed, some in service for more than 20 years (2005). This technology is suitable for heat recovery applications of any magnitude.

Several **environmental benefits** are gained through employment of this condensing technology. Burning less fuel proportionally reduces **collateral combustion emissions** (NO_x , SO_x , CO , CO_2 and particulates, including $\text{PM}_{2.5}$). Additionally, **flue gas pollutant removal** occurs in the condensing economizer, as has been extensively investigated, characterized, and modeled by the U.S. DOE (Butcher et al.) including applications burning coal and Orimulsion. Typically, the condensate will contain most (by mass, >90 percent) of the highly dissociated inorganic matter (H_2SO_4 , HCl , HNO_3 , HNO_2 , NH_3 , salts, etc.) and the **larger-diameter particulates** (>10 μm) and a lower but substantial fraction (>60 percent) of the **smaller-diameter particulates** (<5 μm). Such gross pollutant removal can be a cost effective first stage for a traditional air pollution control system, by reducing the volume of the flue gas to be treated (water content and temperature) as well as reducing the concentration of the pollutants in the flue gas to be treated downstream. Unlike spray quenching, such indirect quench-cooling segregates the flue gas pollutants from the cooling system fluid, generating a much smaller, concentrated waste water stream for subsequent waste treatment. Although pollutant removal percentages are high, they are functions of the specific real-time mass- and heat-transfer conditions within the economizer. Condensate treatment from boiler economizers normally is neutralization, often using the boiler blowdown, and release to the sewer and sewage treatment.

REGENERATORS

Storage of heat is a temporary operation since perfect thermal insulators are unknown; thus, heat is absorbed in solids or liquids as sensible or latent heat to be released later at designated times and conditions. The collection and release of heat can be achieved in two modes: on a batch basis, as in the checkerbrick regenerator for blast furnaces, or on a continuous basis, as in the Ljungstrom air heater.

Checkerbrick Regenerators Preheating combustion air in open-hearth furnaces, ingot-soaking pits, glass-melting tanks, by-product coke ovens, heat-treating furnaces, and the like has been universally carried out in regenerators constructed of fireclay, chrome, or silica bricks of various shapes. Although many geometric arrangements have been used in practice, the so-called basketweave design has been adopted in most applications.

Blast-Furnace Stoves Blast-furnace stoves are used to preheat the air that is blown into a blast furnace. A typical blast furnace, producing 1500 Mg (1650 U.S. ton) of pig iron per day, will be blown with 47.2 m^3/s (100,000 std ft^3/min) of atmospheric air preheated to temperatures ranging in normal practice from 755 to 922 K (900 to 1200°F). A set of four stoves is usually provided, each consisting of a vertical steel cylinder 7.3 m (24 ft) in diameter, 33 m (108 ft) high, topped with a spherical dome. Characteristic plan and elevation sections of a stove are shown in Fig. 24-61. The interior comprises three regions: in the cylindrical portion, (1) a side combustion chamber,

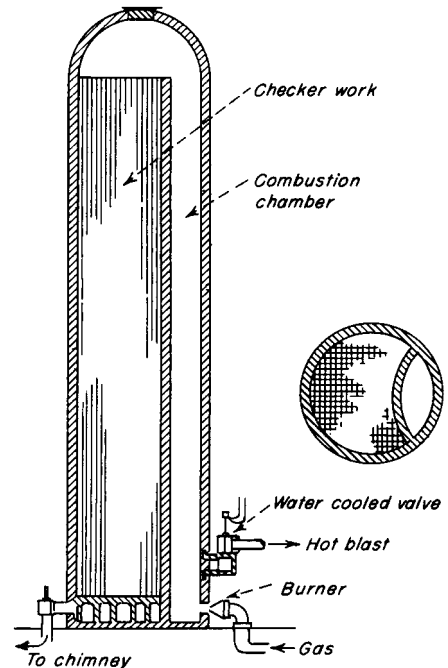


FIG. 24-61 Blast-furnace stove.

lens-shaped in cross section, bounded by a segment of the stove wall and a mirror-image bridgewall separating it from (2) the chamber of the cylinder that is filled with heat-absorbing checkerbrick, and (3) the capping dome, which constitutes the open passage between the two chambers.

The heat-exchanging surface in each stove is just under $11,500 \text{ m}^2$ ($124,000 \text{ ft}^2$). In operation, each stove is carried through a two-step 4-h cycle. In a 3-h *on-gas* step, the checkerbricks in a stove are heated by the combustion of blast-furnace gas. In the alternating *on-wind* 1-h step, they are cooled by the passage of cold air through the stove. At any given time, three stoves are simultaneously on gas, while a single stove is on wind.

At the start of an on-wind step, about one-half of the air, entering at 366 K (200°F), passes through the checkerbricks, the other half being bypassed around the stove through the cold-blast mixer valve. The gas passing through the stove exhausts at 1366 K (2000°F). Mixing this with the unheated air produces a blast temperature of 811 K (1000°F). The temperature of the heated air from the stove falls steadily throughout the on-wind step. The fraction of total air volume bypassed through the mixer valve is continually decreased by progressively closing this valve, its operation being automatically regulated to maintain the exit gas temperature at 811 K . At the end of 1 h of on-wind operation, the cold-blast mixer valve is closed, sending the entire blast through the checkerbricks.

Open-Hearth and Glass-Tank Regenerators These contain checkerbricks that are modified considerably from those used in blast-furnace stoves because of the higher working temperatures, more drastic thermal shock, and dirtier gases encountered. Larger bricks form flue cross sections five times as large as the stove flues, and the percentage of voids in the checkerbricks is 51 percent, in contrast to 32 percent voids in stoves. The vertical height of the flues is limited by the elevation of the furnace above plant level. Short flues from 3 to 4.9 m (10 to 16 ft) are common in contrast to the 26- to 29-m (85- to 95-ft) flue lengths in blast-furnace stoves.

As a result of the larger flues and the restricted surface area per unit of gas passed, regenerators employed with this type of furnace exhibit much lower efficiency than would be realized with smaller flues. In view of the large amount of iron oxide contained in open-hearth exhaust gas and the alkali fume present in glass-tank stack gases, however, smaller checkerbrick dimensions are considered impractical.

Ljungstrom Heaters A familiar continuous regenerative-type air heater is the Ljungstrom heater (Fig. 24-62). The heater assembly consists of a slow-moving rotor embedded between two peripheral housings separated from one another by a central partition. Through one side of the partition a stream of hot gas is being cooled, and, through the other side a stream of cold gas is being heated. Radial and circumferential seals sliding on the rotor limit the leakage between the streams. The rotor is divided into sectors, each of which is tightly packed with metal plates and wires that promote high heat-transfer rates at low pressure drop.

These heaters are available with rotors up to 6 m (20 ft) in diameter. Gas temperatures up to 1255 K (1800°F) can be accommodated. Gas face velocity is usually around 2.5 m/s (500 ft/min). The rotor height depends on service, efficiency, and operating conditions but usually is between 0.2 and 0.91 m (8 and 36 in). Rotors are driven by small motors with rotor speed up to 20 r/min. Heater effectiveness can be as high as 85 to 90 percent heat recovery. Ljungstrom-type heaters are used in power-plant boilers and also in the process industries for heat recovery and for air-conditioning and building heating.

Regenerative Burners In these systems a compact heat storage regenerator (containing ceramic balls, for example) is incorporated into the burner. Operating in pairs, one burner fires while the other exhausts: combustion air is preheated in the regenerator of the firing burner and furnace gas gives up heat to the regenerator in the exhausting burner (see Fig. 24-63). Burner operations are switched periodically. Such systems can yield combustion air preheats between 933 K (1220°F) and 1525 K (2282°F) for furnace temperature between 1073 K (1472°F) and 1723 K (2642°F), respectively.

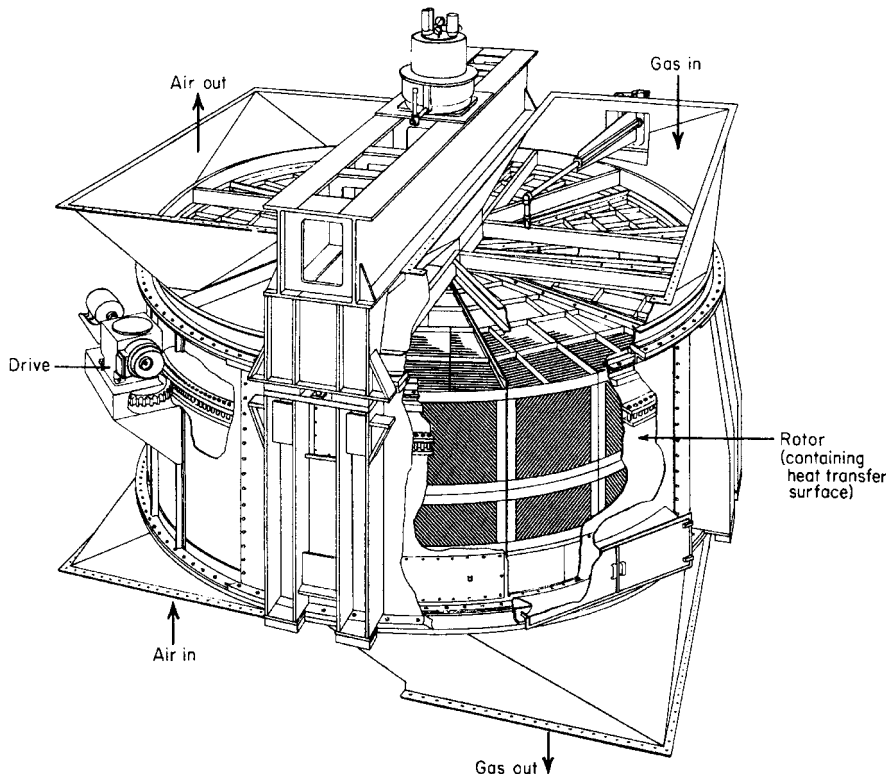


FIG. 24-62 Ljungstrom air heater.

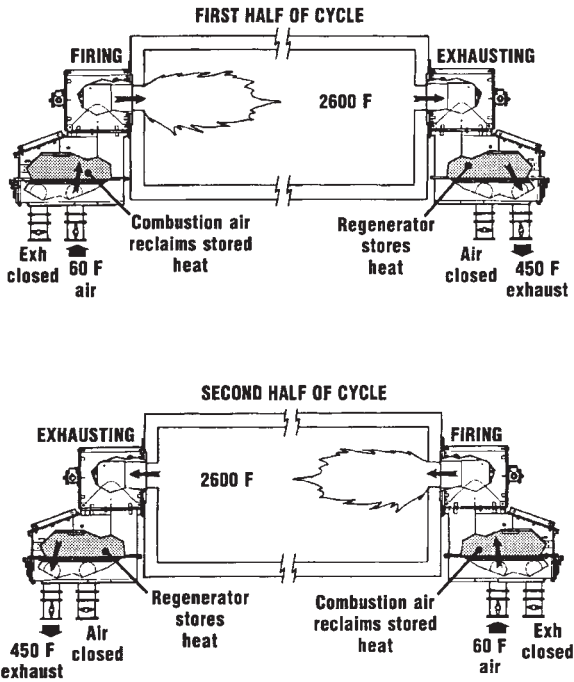


FIG. 24-63 Schematic of a regenerative burner system. (North American Manufacturing Co.)

Corresponding fuel savings compared to cold-air firing will vary approximately from 30 to 70 percent.

Miscellaneous Systems Many other systems have been proposed for transferring heat regeneratively, including the use of high-temperature liquids and fluidized beds for direct contact with gases, but other problems which limit industrial application are encountered. These systems are covered by methods described in Secs. 11 and 12 of this handbook.

RECUPERATORS

Regenerators are by nature intermittent or cycling devices, although, as set forth previously, the Ljungstrom design avoids interruption of the fluid stream by cycling the heat-retrieval reservoir between the hot and cold fluid streams. Truly continuous counterparts of regenerators exist, however, and they are called *recuperators*.

The simplest configuration for a recuperative heat exchanger is the metallic radiation recuperator. An inner tube carries the hot exhaust gases and an outer tube carries the combustion air. The bulk of the heat transfer from the hot gases to the surface of the inner tube is by radiation, whereas that from the inner tube to the cold combustion air is predominantly by convection.

Shell-and-tube heat exchangers (see Sec. 11) may also be used as recuperators; convective heat transfer dominates in these recuperators. For applications involving higher temperatures, ceramic recuperators have been developed. These devices can allow operation at up to 1823 K (2822°F) on the gas side and over 1093 K (1508°F) on the air side. Early ceramic recuperators were built of furnace brick and cement, but the repeated thermal cycling caused cracking and rapid deterioration of the recuperator. Later designs have used various approaches to overcome the problems of leakage and cracking. In one configuration, for example, silicon carbide tubes carry the combustion air through the waste gas, and flexible seals are used in the air headers. In this manner, the seals are maintained at comparatively low temperatures and the leakage rate can be reduced to a few percent of the total flow.

TURBINE INLET (AIR) COOLING

GENERAL REFERENCES: See "Bibliography" at <http://www.turbineinletcooling.org/resources>.

Turbine inlet cooling (TIC) can increase gas turbine (GT) power output on a hot day by 10 to 30 percent, while improving (reducing) the turbine heat rate (kJ/kW_e) by as much as 5 percent. By increasing the air compressor inlet air density, turbine inlet air cooling is the most cost-effective method for increasing turbine gross power output, for fixed-altitude GTs.

GTs are "constant-volume machines," such that a fixed-speed GT air compressor section draws a nearly constant volumetric flow of inlet air, independent of ambient air conditions. Air density drops with increased altitude (reduced barometric pressure), increased ambient temperature, and, to a lesser degree, increased water content (specific humidity).

Increasing the air density increases the GT inlet air mass flow. For a given stoichiometric fuel-to-air-ratio and a given combustion temperature, increased air mass flow allows increased fuel flow, resulting in increased GT power output. Additionally, compressor efficiency increases with decreased air temperatures, resulting in less parasitic compressor shaft work consumed and greater net turbine power output. Therefore, TIC increases net incremental power output faster than incremental fuel consumption, resulting in improved overall fuel efficiency (reduced heat rate); see Fig. 24-64.

Evaporative Technologies These TIC technologies cool the inlet air by vaporizing water in direct contact with the inlet air, using the latent heat of vaporization of water. These technologies either spray water directly into the airstream as a fog or mist or evaporate the water from fixed wetted media placed in the airstream.

Performance of these technologies is typically an 85 percent approach to the ambient wet-bulb temperature (T_{WB}) from the ambient dry-bulb temperature (T_{DB}), limited to a 3°F approach to the ambient T_{WB} . For locations with high T_{DB} and low T_{WB} , the cooling benefit can be significant. For locations with humid conditions, the relative cooling achievable by evaporative technologies can be very limited. Additionally, on a given day, the relative changes in hourly T_{DB} and T_{WB} will result in variable GT peak power output.

Evaporative TIC technologies have the minimum installed and operating costs. The operating electric parasitic load is generally considered insignificant. Water chemistry management is crucial to prevent maintenance problems caused by dissolved or suspended matter in the water, fouling either the evaporation media or the turbines themselves.

Refrigeration Technologies These TIC technologies indirectly cool the inlet air, typically using either chilled water or a vaporizing refrigerant, in a finned coil heat exchanger placed in the incoming airstream. Refrigeration technologies can achieve and maintain much lower air compressor inlet temperatures, largely independent of changing ambient conditions (Fig. 24-65). Best design practices (ice formation / consequent GT damage) have restricted the OEM recommended minimum inlet air cooling temperatures to the 5° to 10°C [41° to 50°F] range. Refrigeration can be supplied by either absorption or mechanical chillers. Absorption chillers employ either LiBr or ammonia absorption. Electrically driven centrifugal packaged chiller systems, using chilled water as a secondary refrigerant, account for the majority of refrigeration machine types. R-123, R-134a, and R-717 are the most common refrigerants offered by vendors. Several installations have used direct refrigeration through R-22 or ammonia (R-717) vaporization in the TIC air coil, with refrigerant condensation in a wet surface air cooler (WSAC) or an air-cooled condenser. Site-specific sources of cooling (the heat sink), such as LNG vaporization, have also been used. The water condensate generated by cooling inlet air below the ambient dew point can be employed as makeup water for a cooling tower or a WSAC.

While refrigeration technologies can provide a near-constant GT inlet air temperature, and thus a nearly constant GT power output, refrigeration TIC systems are significantly more expensive than evaporative systems. However, the incremental net power output from the refrigeration system, when measured on a unit cost basis ($\$/\text{kW}_e$),

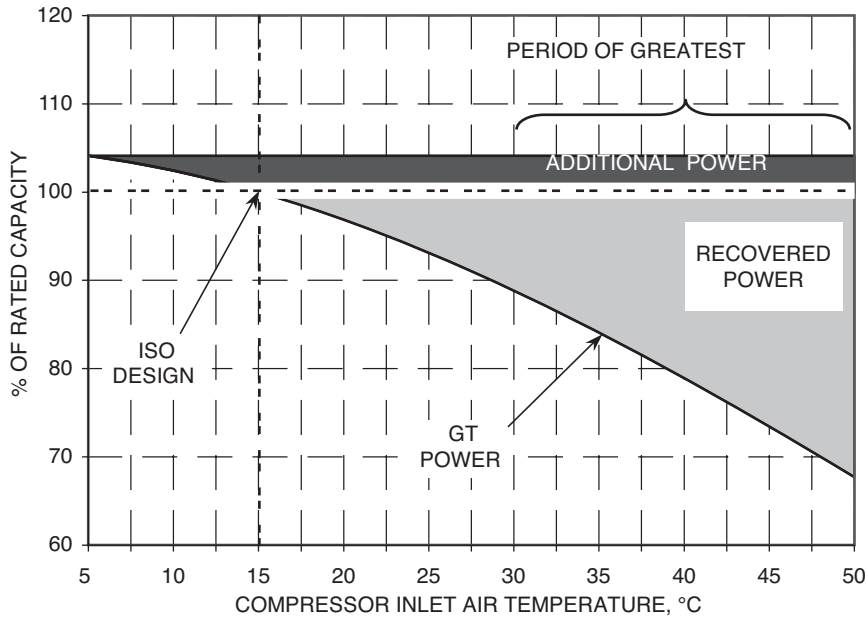


FIG. 24-64 Effect of inlet air ambient temperature on the power output of a typical GT. If ambient air at 95°F (35°C) were cooled to 50°F (10°C), the gross GT power output would be increased by approximately 22 percent, and the gross heat rate improved by 3.7 percent. Operated at its ISO conditions [15°C (59°F) at sea level], GT rated performance is 100 percent. (*Turbine Air Systems; www.tas.com.*)

costs much less than the unit cost of the GT itself, thereby decreasing the overall unit cost of the GT plant. Refrigeration technologies require a significant energy input to operate. In the case of electric-driven chillers, the parasitic electric load can consume 10 percent to 15 percent of the GT gross incremental increase in power. Therefore, the net overall plant incremental output, after allowance for the refrigeration system parasitic load, is used for evaluating the economics of these systems.

Thermal Energy Storage (TES) A TES system consists of an insulated cold storage tank and a chiller, generating ice or chilled water, which is accumulated in the tank. A TES system is typically installed when TIC is required for only a limited number of operating hours per day. The **principal TES benefit** is that the *net* electrical peak output of the power plant is maximized, by shifting the parasitic electric power loss (chiller power demand) from the period of peak demand (midday) to the off-peak hours (night). A **second benefit** is a reduced overall capital cost for a smaller chiller (usually half-sized) because the smaller chiller is operated either continuously (partial storage) or over a nighttime period (full storage). A **third benefit** is

the reduced operating costs, stemming from the ability to use lower-value off-peak power for the chilling load. A **fourth benefit** is that the chiller will typically perform better during the nighttime off-peak period, due to lower ambient temperatures, reducing the energy required for refrigerant compression. A **fifth benefit** is the ability to increase or decrease generation capacity in a short time period, when called upon, to stabilize the transmission system or grid the plant is tied into. However, a TES site footprint may be larger, to include the TES storage tank.

Summary Evaporative technologies have the lowest capital and operating costs, but their benefit is limited by ambient conditions. They are most effective where the peak T_{WB} is lowest, especially at times of peak demand, as are found in hot, arid regions. Refrigeration technologies can achieve and maintain constant lower temperatures, independent of ambient conditions. However, they have higher initial capital and operating costs. Although refrigeration technologies are favored for use in warm, humid regions, where both the peak daytime T_{WB} and air conditioning demand are highest, they have been selected and installed in more northern temperate latitudes (Canada) and arid climates as well. TES and other hybrids, which combine various technologies, are used to minimize the overall annualized costs for TIC systems. The unit costs for TIC technologies are substantially lower than are the unit costs for new GTs. Therefore, the installation of a new TIC technology to an existing GT system may offer the lowest-cost choice for increasing the output capability of that older system. For new installations, the inclusion of an optimal TIC technology with the new GT should result in minimizing the annualized cost for output power. Typical unit costs for TIC options range from \$25 (evaporative) to \$200 (refrigeration) per kW_e of incremental power output, vs. \$300 to \$500 per kW_e for a new single cycle GT. Selection of the most suitable TIC option for any given application (new or retrofit) requires a careful evaluation of (1) the local power requirements and revenues for power generation, (2) the local meteorological conditions, and (3) the capabilities and costs of different TIC technology options, offered by the various TIC vendors (see www.turbineinletcooling.org).

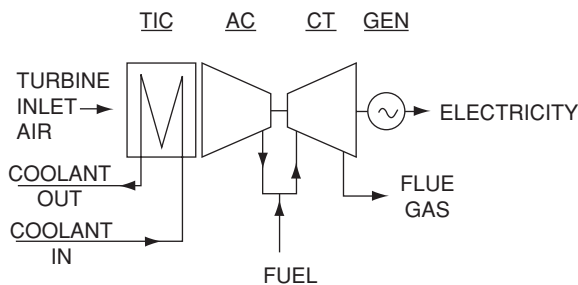


FIG. 24-65 Mechanical refrigeration TIC systems utilizing chilled water for cooling turbine inlet air, and cooling towers to reject the waste heat into the environment, account for the majority of refrigeration TIC systems sold.

SECTION 25

Materials of
Construction

PERRY'S CHEMICAL ENGINEERS' HANDBOOK

8TH EDITION



OLIVER W. SIEBERT, KEVIN M. BROOKS
LAURENCE J. CRAIGIE, F. GALEN HODGE
L. THEODORE HUTTON, THOMAS M. LARONGE
DANIEL H. POPE, SIMON J. SCOTT
JOHN G. STOECKER II

Copyright © 2008, 1997, 1984, 1973, 1963, 1950, 1941, 1934 by The McGraw-Hill Companies, Inc. All rights reserved. Manufactured in the United States of America. Except as permitted under the United States Copyright Act of 1976, no part of this publication may be reproduced or distributed in any form or by any means, or stored in a database or retrieval system, without the prior written permission of the publisher.

0-07-154232-9

The material in this eBook also appears in the print version of this title: 0-07-154207-8.

All trademarks are trademarks of their respective owners. Rather than put a trademark symbol after every occurrence of a trademarked name, we use names in an editorial fashion only, and to the benefit of the trademark owner, with no intention of infringement of the trademark. Where such designations appear in this book, they have been printed with initial caps.

McGraw-Hill eBooks are available at special quantity discounts to use as premiums and sales promotions, or for use in corporate training programs. For more information, please contact George Hoare, Special Sales, at george_hoare@mcgraw-hill.com or (212) 904-4069.

TERMS OF USE

This is a copyrighted work and The McGraw-Hill Companies, Inc. (“McGraw-Hill”) and its licensors reserve all rights in and to the work. Use of this work is subject to these terms. Except as permitted under the Copyright Act of 1976 and the right to store and retrieve one copy of the work, you may not decompile, disassemble, reverse engineer, reproduce, modify, create derivative works based upon, transmit, distribute, disseminate, sell, publish or sublicense the work or any part of it without McGraw-Hill’s prior consent. You may use the work for your own noncommercial and personal use; any other use of the work is strictly prohibited. Your right to use the work may be terminated if you fail to comply with these terms.

THE WORK IS PROVIDED “AS IS.” MCGRAW-HILL AND ITS LICENSORS MAKE NO GUARANTEES OR WARRANTIES AS TO THE ACCURACY, ADEQUACY OR COMPLETENESS OF OR RESULTS TO BE OBTAINED FROM USING THE WORK, INCLUDING ANY INFORMATION THAT CAN BE ACCESSED THROUGH THE WORK VIA HYPERLINK OR OTHERWISE, AND EXPRESSLY DISCLAIM ANY WARRANTY, EXPRESS OR IMPLIED, INCLUDING BUT NOT LIMITED TO IMPLIED WARRANTIES OF MERCHANTABILITY OR FITNESS FOR A PARTICULAR PURPOSE. McGraw-Hill and its licensors do not warrant or guarantee that the functions contained in the work will meet your requirements or that its operation will be uninterrupted or error free. Neither McGraw-Hill nor its licensors shall be liable to you or anyone else for any inaccuracy, error or omission, regardless of cause, in the work or for any damages resulting therefrom. McGraw-Hill has no responsibility for the content of any information accessed through the work. Under no circumstances shall McGraw-Hill and/or its licensors be liable for any indirect, incidental, special, punitive, consequential or similar damages that result from the use of or inability to use the work, even if any of them has been advised of the possibility of such damages. This limitation of liability shall apply to any claim or cause whatsoever whether such claim or cause arises in contract, tort or otherwise.

DOI: 10.1036/0071542078

Materials of Construction*

Oliver W. Siebert, P.E., B.S.M.E. *Affiliate Professor of Chemical Engineering, Washington University, St. Louis, Mo.; Director, North Central Research Institute; President and Principal, Siebert Materials Engineering, Inc.; Registered Professional Engineer (California, Missouri); Fellow, American Institute of Chemical Engineers; Fellow, American Society of Mechanical Engineers (Founding Member and Chairman RTP Corrosion Resistant Equipment Committee; Lifetime Honorary Member RTP Corrosion Resistant Equipment Committee); Fellow, National Association of Corrosion Engineers International (Board of Directors; presented International NACE Conference Plenary Lecture; received NACE Distinguished Service Award); Fellow, American College of Forensic Examiners; Life Member, American Society for Metals International; Life Member, American Welding Society; Life Member, Steel Structures Painting Council; granted three patents for welding processes; Sigma Xi, Pi Tau Sigma, Tau Beta Pi (Section Editor, Corrosion)*

Kevin M. Brooks, P.E., B.S.Ch.E. *Vice President Engineering and Construction, Koch Knight LLC; Registered Professional Engineer (Ohio) (Inorganic Nonmetallics)*

Laurence J. Craigie, B.S.Chem. *Composite Resources, LLC; industry consultant in regulatory, manufacturing, and business needs for the composite industry; Member, American Society of Mechanical Engineers (Chairman RTP Corrosion Resistant Equipment Committee); Member, American Society of Testing and Materials; Member, National Association of Corrosion Engineers International; Member, Composite Fabricators of America (received President's Award) (Reinforced Thermosetting Plastic)*

F. Galen Hodge, Ph.D. (Materials Engineering), P.E. *Associate Director, Materials Technology Institute; Registered Professional Corrosion Engineer (California); Fellow, American Society for Metals International; Fellow, National Association of Corrosion Engineers International (Metals)*

L. Theodore Hutton, B.S.Mech.&Ind.Eng. *Senior Business Development Engineer, ARKEMA, Inc.; Member, American Welding Society [Chairman Committee GIA; Vice Chairman B-2 (Welding Thermoplastics)]; Member, American Society of Mechanical Engineers (Chairman BPE Polymer Subcommittee); Member, National Fire Protection Association; Member, German Welding Society; Member, American Glovebox Society (Chairman Standards Committee); Member, American Rotomolding Society; author, ABC's of PVDF Rotomolding; Editor, Plastics and Composites Welding Handbook; holds patent for specialized Kynar PVDF material for radiation shielding (Organic Thermoplastics)*

Thomas M. Laronge, M.S.Phys.Chem. *Director, Thomas M. Laronge, Inc.; Member, Cooling Technology Institute (Board of Directors; President; Editor-in-Chief, CTI Journal); Member, National Association of Corrosion Engineers International (received NACE International Distinguished Service Award; presented International NACE Conference Plenary Lecture); Phi Kappa Phi (Failure Analysis)*

J. Ian Munro, P.E., B.A.Sc.E.E. *Senior Consultant, Corrosion Probes, Inc.; Registered Professional Engineer (Ontario, Canada); Member, National Association of Corrosion Engineers International; Member, The Electrochemical Society; Member, Technical Association of Pulp & Paper Industry (Anodic Protection)*

Daniel H. Pope, Ph.D. (Microbiology) *President and Owner, Bioindustrial Technologies, Inc.; Member, National Association of Corrosion Engineers International; Sigma Xi (Microbiologically Influenced Corrosion)*

*The contributions of R. B. Norton and O. W. Siebert to material used from the fifth edition; of O. W. Siebert and A. S. Krisher to material used from the sixth edition; and of O. W. Siebert and J. G. Stoecker II to material used from the seventh edition are acknowledged.

Simon J. Scott, B.S.Ch.E. *President and Principal, Scott & Associates; Member, American Society of Mechanical Engineers (Vice Chairman RTP Corrosion Resistant Equipment Committee, Composite Structures); Member, National Association of Corrosion Engineers International; Director, American Composites Manufacturing Association (Organic Plastics)*

John G. Stoecker II, B.S.M.E. *Principal Consultant, Stoecker & Associates; Member, National Association of Corrosion Engineers International; Member, American Society for Metals International; author/editor of two handbooks on microbiologically influenced corrosion published by NACE International (Microbiologically Influenced Corrosion)*

INTRODUCTION

CORROSION AND ITS CONTROL

Introduction	25-3
Fluid Corrosion	25-4
Fluid Corrosion: General	25-4
Introduction	25-4
Metallic Materials	25-4
Nonmetallics	25-4
Fluid Corrosion: Localized	25-4
Pitting Corrosion	25-4
Crevice Corrosion	25-4
Oxygen-Concentration Cell	25-4
Galvanic Corrosion	25-4
Intergranular Corrosion	25-5
Stress-Corrosion Cracking	25-5
Liquid-Metal Corrosion	25-5
Erosion	25-5
Velocity Accelerated Corrosion	25-6
Corrosion Fatigue	25-6
Cavitation	25-6
Fretting Corrosion	25-6
Hydrogen Attack	25-6
Fluid Corrosion: Structural	25-6
Graphitic Corrosion	25-6
Parting, or Dealloying, Corrosion	25-6
Dezincification	25-6
Microbiologically Influenced Corrosion	25-6
Factors Influencing Corrosion	25-8
Solution pH	25-8
Oxidizing Agents	25-8
Temperature	25-9
Velocity	25-9
Films	25-9
Other Effects	25-9
High-Temperature Attack	25-9
Physical Properties	25-9
Mechanical Properties	25-9
Corrosion Resistance	25-9
Combating Corrosion	25-10
Material Selection	25-10
Proper Design	25-10
Altering the Environment	25-10
Inhibitors	25-10
Cathodic Protection	25-10
Anodic Protection	25-10
Coatings and Linings	25-11
Glass-Lined Steel	25-11
Metallic Linings for Severe/Corrosive Environments	25-11
Metallic Linings for Mild Environments	25-12
General Workflow for Minimizing or Controlling Corrosion	25-12
Corrosion-Testing Methods	25-12
Corrosion Testing: Laboratory Tests	25-12
Immersion Test	25-13
Test Piece	25-13
Apparatus	25-14
Temperature of Solution	25-15
Aeration of Solution	25-15
Solution Velocity	25-15
Volume of Solution	25-15
Method of Supporting Specimens	25-15
Duration of Test	25-16
Cleaning Specimens after Test	25-16

Evaluation of Results	25-16
Effect of Variables on Corrosion Tests	25-16
Electrical Resistance	25-17
Linear Polarization	25-18
Potentiodynamic Polarization	25-19
Crevice Corrosion Prediction	25-21
Velocity	25-21
Environmental Cracking	25-22
Electrochemical Impedance Spectroscopy (EIS) and AC Impedance	25-23
Other Electrochemical Test Techniques	25-24
Corrosion Testing: Plant Tests	25-24
Test Specimens	25-24
Test Results	25-25
Electrochemical On-Line Corrosion Monitoring	25-25
Indirect Probes	25-26
Corrosion Rate Measurements	25-27
Other Useful Information Obtained by Probes	25-27
Limitations of Probes and Monitoring Systems	25-28
Potential Problems with Probe Usage	25-28
Economics in Materials Selection	25-28

PROPERTIES OF MATERIALS

Materials Standards and Specifications	25-28
Wrought Materials: Ferrous Metals and Alloys	25-29
Steel	25-29
Low-Alloy Steels	25-30
Stainless Steel	25-30
Wrought Materials: Nonferrous Metals and Alloys	25-32
Nickel and Nickel Alloys	25-32
Aluminum and Alloys	25-33
Copper and Alloys	25-34
Lead and Alloys	25-34
Titanium	25-34
Zirconium	25-34
Tantalum	25-34
Cast Materials	25-34
Cast Irons	25-34
Medium Alloys	25-35
High Alloys	25-35
Casting Specifications of Interest	25-35
Inorganic Nonmetallics	25-36
Glass and Glassed Steel	25-36
Porcelain and Stoneware	25-36
Brick Construction	25-36
Cement and Concrete	25-37
Soil	25-37
Organic Nonmetallics	25-37
Thermoplastics	25-37
Thermosets	25-41
Epoxy (Amine-Cured)	25-44
Epoxy (Anhydride-Cured)	25-44
Epoxy Vinyl Ester	25-44
Bisphenol-A Fumarate Polyester	25-44
Chlorendic Acid Polyester	25-44
Furan	25-44
Isophthalic/Terephthalic Acid Polyester	25-44
Dual-Laminate Construction and Linings	25-44
Rubber and Elastomers	25-44
Asphalt	25-44
Carbon and Graphite	25-44
Wood	25-44

HIGH- AND LOW-TEMPERATURE MATERIALS

Low-Temperature Metals.....	25-45
Stainless Steels.....	25-45
Nickel Steel.....	25-45
Nickel Alloys.....	25-46
Aluminum.....	25-46
Copper and Alloys.....	25-46
High-Temperature Materials.....	25-46

Metals.....	25-46
Hydrogen Atmospheres.....	25-49
Halogens (Hot, Dry, Cl ₂ , HCl).....	25-49
Refractories.....	25-49
Internal Insulation.....	25-49
Refractory Brick.....	25-49
Ceramic-Fiber Insulating Linings.....	25-51
Castable Monolithic Refractories.....	25-51

INTRODUCTION

The selection of materials of construction for the equipment and facilities to produce any and all chemicals is a keystone subject of chemical engineering. The chemical products desired cannot be manufactured without considering the selection of the optimum materials of construction used as the containers for the safe, economical manufacture, and required product quality, i.e., production, handling, transporting, and storage of the products desired. Therefore, within this Section, the selection of materials of construction [for use within the chemical process industries (CPI), and by their consumers] is guided by the general subjects addressed herein,

properties unique to the materials of construction, corrosion of those materials by those chemicals, effect of the products of corrosion upon the product quality, etc. In the cases where specific (and time-sensitive) materials data are needed, that instructive information is to be found in the current reports, technical papers, handbooks (and other texts), etc., of the various other engineering disciplines, e.g., American Society of Metals, ASM; American Society for Testing and Materials, ASTM; American Society of Mechanical Engineers, ASME; National Association Corrosion Engineers, NACE; Society of Plastics Industry, SPI.

CORROSION AND ITS CONTROL

GENERAL REFERENCES: Ailor (ed.), *Handbook on Corrosion Testing and Evaluation*, McGraw-Hill, New York, 1971. Bordes (ed.), *Metals Handbook*, 9th ed., vols. 1, 2, and 3, American Society for Metals, Metals Park, Ohio, 1978–1980; other volumes in preparation. Dillon (ed.), *Process Industries Corrosion*, National Association of Corrosion Engineers, Houston, 1975. Dillon and associates, *Guidelines for Control of Stress Corrosion Cracking of Nickel-Bearing Stainless Steels and Nickel-Base Alloys*, MTI Manual No. 1, Materials Technology Institute of the Chemical Process Industries, Columbus, 1979. Evans, *Metal Corrosion Passivity and Protection*, E. Arnold, London, 1940. Evans, *Corrosion and Oxidation of Metals*, St. Martin's, New York, 1960. Fontana and Greene, *Corrosion Engineering*, 2d ed., McGraw-Hill, New York, 1978. Gackebach, *Materials Selection for Process Plants*, Reinhold, New York, 1960. Hamner (comp.), *Corrosion Data Survey: Metals Section*, National Association of Corrosion Engineers, Houston, 1974. Hamner (comp.), *Corrosion Data Survey: Non-Metals Section*, National Association of Corrosion Engineers, Houston, 1975. Hanson and Parr, *The Engineer's Guide to Steel*, Addison-Wesley, Reading, Mass., 1965. LaQue and Copson, *Corrosion Resistance of Metals and Alloys*, Reinhold, New York, 1963. Lyman (ed.), *Metals Handbook*, 8th ed., vols. 1–11, American Society for Metals, Metals Park, Ohio, 1961–1976. Mantell (ed.), *Engineering Materials Handbook*, McGraw-Hill, New York, 1958. Shreir, *Corrosion*, George Newnes, London, 1963. Speller, *Corrosion—Causes and Prevention*, McGraw-Hill, New York, 1951. Uhlig (ed.), *The Corrosion Handbook*, Wiley, New York, 1948. Uhlig, *Corrosion and Corrosion Control*, 2d ed., Wiley, New York, 1971. Wilson and Oates, *Corrosion and the Maintenance Engineer*, Hart Publishing, New York, 1968. Zapffe, *Stainless Steels*, American Society for Metals, Cleveland, 1949. Kobrin (ed.), *A Practical Manual on Microbiologically Influenced Corrosion*, NACE International, 1993. Stoecker (ed.), *A Practical Manual on Microbiologically Influenced Corrosion*, vol. 2, NACE Press, 2001. *Plus additional references as dictated by manuscript.*

INTRODUCTION*

The metallurgical extraction of the metals from their ore is the noted chemical reaction of removing the metal from its “stable” compound form (as normally found in nature) to become an “unstable,” artificial form (as used by industry to make tools, containers, equipment, etc.). That instability (of those refined metallic compounds) is the desire of

those metals to return to their (original) more stable, natural state. This is, in effect, the (oversimplified) explanation of the corrosion of artificial metallic things. In its simplest form, iron ore exists in nature as one of several iron oxide (or sulfur, etc.) compounds. For example, when refined iron and/or steel is exposed to oxygenated moisture (recall, this is an electrochemical reaction), thus an electrolyte (e.g. water) is required along with oxygen, and what is formed is iron rust (the same compounds as are the stable state/forms of iron in nature). Those (electrochemical) reactions are called *corrosion of metals*; later it is shown that this very necessary distinction is made to fit that electrochemical definition; i.e., only metals *corrode*, whereas nonmetallic materials may deteriorate (or in other ways be destroyed or weakened), but not corroded.

When a metallic material of construction (MOC) is selected to contain, transport, and/or to be exposed to a specific chemical, unless we make a correct, viable, and optimum MOC selection, the life expectancy of those facilities, in a given chemical exposure, can be very short. For the inexperienced in this field, the direct capital costs of the MOC facet of the production of chemicals, the funds spent to maintain these facilities (sometimes several times those initial capital costs), the indirect costs that are associated with outages and loss of production, off-quality product (because of equipment and facility maintenance) as well as from contamination of the product, etc., are many times not even considered, let alone used as one of the major criteria in the selection of that MOC as well as its costs to keep the plant running, i.e., a much overlooked cost figure in the CPI. To emphasize the magnitude and overall economic nature of the direct and indirect (nonproductive) costs/losses that result from the action of corrosion of our metallic facilities, equipment, and the infrastructures, within the United States, Congress has mandated that a survey of the costs of corrosion in the United States be conducted periodically.

The most recent study was conducted by CC Technologies Laboratories, Inc. (circa 1999 to 2001), with support by the Federal Highways Administration and the National Association of Corrosion Engineers, International. The results of the study show that the (estimated) total annual direct costs of corrosion in the United States are \$276 billion, i.e., about 3.1 percent of the U.S. Gross Domestic Product (GDP). That

*Includes information excerpted from papers noted, with the courtesy of ASM, ASTM, and NACE International.

loss to the economy is greater than the GDP of many smaller countries. For example, almost 50 percent of the U.S. steel production is used to compensate for the loss of corroded manufacturing facilities and products; in turn, the petroleum industry spends upward of \$2 million per day due to the corrosion of underground installations, e.g., tanks, piping, and other structures. None of those figures include any indirect costs resulting from corrosion, found to be about as great as the direct costs shown in the study. These indirect costs are difficult to come by because they include losses to the customers and other users and result in a major loss to the overall economy itself due to loss of productivity; at the same time, there are innumerable losses that can only be guessed at. In addition to those economic losses, other factors, e.g., health and safety, are without a method to quantify. The details of this study can be found in the supplement to the July 2002 NACE journal *Materials Performance*, "Corrosion Costs and Preventive Strategies, in the United States," which summarized the FHWA-funded study. It is interesting to note that a similar government-mandated study reported a decade ago in the Seventh Edition of *Perry's Chemical Engineers' Handbook* listed that annual loss at \$300 billion; the earlier evaluation technique was to numerically update (extrapolate) the results of earlier studies, i.e., not nearly so sophisticated as was this 2000 study. A study (similar to the year 2000 U.S. evaluation) was conducted by Dr. Rajan Bhaskaran, of Tamilnadu, India, who has proposed a technique to quantify the global costs of corrosion, both direct and indirect. That global study was published by the American Society for Metals, ASM, in the *ASM Handbook*, vol. 13B, December 2005.

The editors of the "Materials of Construction" section expect that the reader knows little about corrosion; thus, an attempt has been made to present information to engineers of all backgrounds.

A word of caution: Metals, materials in general, chemicals used to study metals in the laboratory, chemicals used for corrosion protection, and essentially any chemicals should be (1) used in compliance with all applicable codes, laws, and regulations; (2) handled by trained and experienced individuals in keeping with workmanlike environmental and safety standards; and (3) disposed only using allowable methods and in allowable quantities.

FLUID CORROSION

In the selection of materials of construction for a particular fluid system, it is important first to take into consideration the **characteristics of the system**, giving special attention to all factors that may influence corrosion. Since these factors would be peculiar to a particular system, it is impractical to attempt to offer a set of hard and fast rules that would cover all situations.

The **materials** from which the system is to be fabricated are the second important consideration; therefore, knowledge of the characteristics and general behavior of materials when exposed to certain environments is essential.

In the absence of factual corrosion information for a particular set of fluid conditions, a reasonably good selection would be possible from data based on the resistance of materials to a very similar environment. These data, however, should be used with considerable reservations. Good practice calls for applying such data for preliminary screening. Materials selected thereby would require further study in the fluid system under consideration.

FLUID CORROSION: GENERAL

Introduction Corrosion is the destructive attack upon a metal by its environment or with sufficient damage to its properties, such that it can no longer meet the design criteria specified. Not all metals and their alloys react in a consistent manner when in contact with corrosive fluids. One of the common intermediate reactions of a metal surface is achieved with oxygen, and those reactions are variable and complex. Oxygen can sometimes function as an electron acceptor and cause cathodic depolarization by removing the "protective" film of hydrogen from the cathodic area. In other cases, oxygen can form protective oxide films. The long-term stability of these films also varies: some are soluble in the environment, others form more stable and inert passive films. Electrochemically, a metal surface is in the *active*

state (the anode), i.e., in which the metal tends to corrode, or is being corroded. When a metal is *passive*, it is in the cathodic state, i.e., the state of a metal when its behavior is much more noble (resists corrosion) than its position in the emf series would predict. Passivity is the phenomenon of an (electrochemically) unstable metal in a given electrolyte remaining observably unchanged for an extended period of time.

Metallic Materials Pure metals and their alloys tend to enter into **chemical** union with the elements of a corrosive medium to form stable compounds similar to those found in nature. When metal loss occurs in this way, the compound formed is referred to as the **corrosion product** and the metal surface is spoken of as being **corroded**.

Corrosion is a complex phenomenon that may take any one or more of several forms. It is usually confined to the metal surface, and this is called **general corrosion**. But it sometimes occurs along defective and/or weak grain boundaries or other lines of weakness because of a difference in resistance to attack or local electrolytic action.

In most aqueous systems, the corrosion reaction is divided into an anodic portion and a cathodic portion, occurring simultaneously at discrete points on metallic surfaces. Flow of electricity from the anodic to the cathodic areas may be generated by local cells set up either on a single metallic surface (because of local point-to-point differences on the surface) or between dissimilar metals.

Nonmetallics As stated, corrosion of metals applies specifically to chemical or electrochemical attack. The deterioration of plastics and other nonmetallic materials, which are susceptible to swelling, crazing, cracking, softening, and so on, is essentially **physiochemical** rather than electrochemical in nature. Nonmetallic materials can either be rapidly deteriorated when exposed to a particular environment or, at the other extreme, be practically unaffected. Under some conditions, a nonmetallic may show evidence of gradual deterioration. However, it is seldom possible to evaluate its chemical resistance by measurements of weight loss alone, as is most generally done for metals.

FLUID CORROSION: LOCALIZED

Pitting Corrosion Pitting is a form of corrosion that develops in highly localized areas on the metal surface. This results in the development of cavities or pits. They may range from deep cavities of small diameter to relatively shallow depressions. Pitting examples: aluminum and stainless alloys in aqueous solutions containing chloride. **Inhibitors** are sometimes helpful in preventing pitting.

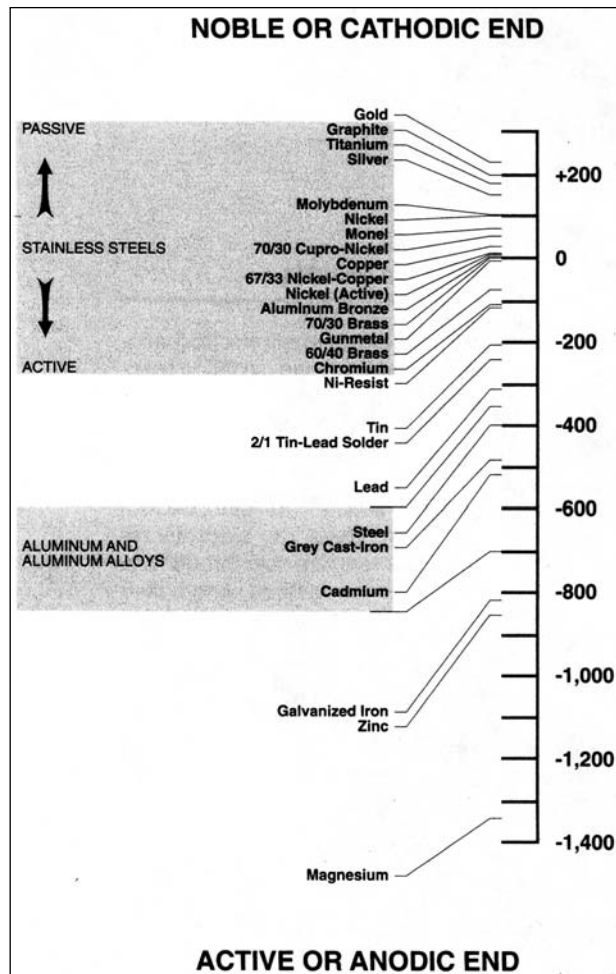
Crevice Corrosion Crevice corrosion occurs within or adjacent to a crevice formed by contact with another piece of the same or another metal or with a nonmetallic material. When this occurs, the intensity of attack is usually more severe than on surrounding areas of the same surface.

This form of corrosion can result because of a deficiency of oxygen in the crevice, acidity changes in the crevice, buildup of ions in the crevice, or depletion of an inhibitor.

Oxygen-Concentration Cell The oxygen-concentration cell is an electrolytic cell in which the driving force to cause corrosion results from a difference in the amount of oxygen in solution at one point as compared with another. Corrosion is accelerated where the oxygen concentration is least, for example, in a stuffing box or under gaskets. This form of corrosion will also occur under solid substances that may be deposited on a metal surface and thus shield it from ready access to oxygen. Redesign or change in mechanical conditions must be used to overcome this situation.

Galvanic Corrosion Galvanic corrosion is the corrosion rate above normal that is associated with the flow of current to a less active metal (cathode) in contact with a more active metal (anode) in the same environment. Table 25-1 shows the **galvanic** series of various metals. It should be used with caution, since exceptions to this series in actual use are possible. However, as a general rule, when dissimilar metals are used in contact with each other and are exposed to an electrically conducting solution, combinations of metals that are as close as possible in the galvanic series should be chosen. Coupling two metals widely separated in this series generally will produce accelerated attack on the more active metal. Often, however, protective oxide films and other effects will tend to reduce galvanic corrosion. Galvanic corrosion can, of course, be prevented by **insulating** the metals from

TABLE 25-1 Practical Galvanic Series of Metals and Alloys



This is a composite galvanic series from a variety of sources and is not necessarily representative of any one particular environment.

each other. For example, when plates are bolted together, specially designed plastic washers can be used.

Potential differences leading to galvanic-type cells can also be set up on a single metal by differences in temperature, velocity, or concentration (see subsection "Crevice Corrosion").

Area effects in galvanic corrosion are very important. An unfavorable area ratio is a large cathode and a small anode. Corrosion of the anode may be 100 to 1,000 times greater than if the two areas were the same. This is the reason why stainless steels are susceptible to rapid pitting in some environments. Steel rivets in a copper plate will corrode much more severely than a steel plate with copper rivets.

Intergranular Corrosion Selective corrosion in the grain boundaries of a metal or alloy without appreciable attack on the grains or crystals themselves is called intergranular corrosion. When severe, this attack causes a loss of strength and ductility out of proportion to the amount of metal actually destroyed by corrosion.

The **austenitic stainless steels** that are not stabilized or that are not of the extra-low-carbon types, when heated in the temperature range of 450 to 843°C (850 to 1,550°F), have chromium-rich compounds (chromium carbides) precipitated in the grain boundaries. This causes grain-boundary impoverishment of chromium and makes the affected metal susceptible to intergranular corrosion in many environments. Hot nitric acid is one environment which causes severe

intergranular corrosion of austenitic stainless steels with grain-boundary precipitation. Austenitic stainless steels stabilized with niobium (columbium) or titanium to decrease carbide formation or containing less than 0.03 percent carbon are normally not susceptible to grain-boundary deterioration when heated in the given temperature range. Unstabilized austenitic stainless steels or types with normal carbon content, to be immune to intergranular corrosion, should be given a solution anneal. This consists of heating to 1,090°C (2,000°F), holding at this temperature for a minimum of 1 h/in of thickness, followed by rapidly quenching in water (or, if impractical because of large size, rapidly cooling with an air-water spray).

Stress-Corrosion Cracking Corrosion can be accelerated by stress, either residual internal stress in the metal or externally applied stress. Residual stresses are produced by deformation during fabrication, by unequal cooling from high temperature, and by internal structural rearrangements involving volume change. Stresses induced by rivets and bolts and by press and shrink fits can also be classified as residual stresses. Tensile stresses at the surface, usually of a magnitude equal to the yield stress, are necessary to produce stress-corrosion cracking. However, failures of this kind have been known to occur at lower stresses.

Virtually every alloy system has its specific environment conditions which will produce stress-corrosion cracking, and the time of exposure required to produce failure will vary from minutes to years. Typical examples include cracking of cold-formed brass in ammonia environments, cracking of austenitic stainless steels in the presence of chlorides, cracking of Monel in hydrofluosilicic acid, and caustic embrittlement cracking of steel in caustic solutions.

This form of corrosion can be prevented in some instances by eliminating high stresses. Stresses developed during fabrication, particularly during welding, are frequently the main source of trouble. Of course, temperature and concentration are also important factors in this type of attack.

Presence of **chlorides** does not generally cause cracking of austenitic stainless steels when temperatures are below about 50°C (120°F). However, when temperatures are high enough to concentrate chlorides on the stainless surface, cracking may occur when the chloride concentration in the surrounding media is a few parts per million. Typical examples are cracking of heat-exchanger tubes at the crevices in rolled joints and under scale formed in the vapor space below the top tube sheet in vertical heat exchangers. The cracking of stainless steel under insulation is caused when chloride-containing water is concentrated on the hot surfaces. The chlorides may be leached from the insulation or may be present in the water when it enters the insulation. Improved design and maintenance of insulation weatherproofing, coating of the metal prior to the installation of insulation, and use of chloride-free insulation are all steps which will help to reduce (but not eliminate) this problem.

Serious stress-corrosion-cracking failures have occurred when chloride-containing hydrotest water was not promptly removed from stainless-steel systems. Use of potable-quality water and complete draining after test comprise the most reliable solution to this problem. Use of chloride-free water is also helpful, especially when prompt drainage is not feasible.

In handling caustic, as-welded steel can be used without developing caustic-embrittlement cracking if the temperature is below 50°C (120°F). If the temperature is higher and particularly if the concentration is above about 30 percent, cracking at and adjacent to non-stress-relieved welds frequently occurs.

Liquid-Metal Corrosion Liquid metals can also cause corrosion failures. The most damaging are liquid metals which penetrate the metal along grain boundaries to cause catastrophic failure. Examples include mercury attack on aluminum alloys and attack of stainless steels by molten zinc or aluminum. A fairly common problem occurs when galvanized-structural-steel attachments are welded to stainless piping or equipment. In such cases it is mandatory to remove the galvanizing completely from the area which will be heated above 260°C (500°F).

Erosion Erosion of metal is the **mechanical** destruction of a metal by abrasion or attrition caused by the flow of liquid or gas (with or without suspended solids); **in no manner is this metal loss an electrochemical corrosion mechanism** (see Velocity Accelerated

Corrosion, below). The use of harder materials and changes in velocity or environment are methods employed to prevent erosion attack.

Velocity Accelerated Corrosion This phenomenon is sometimes (**incorrectly**) referred to as erosion-corrosion or velocity corrosion. It occurs when damage is accelerated by the **fluid exceeding its critical flow velocity at that temperature, in that metal. For that system, this is an undesirable** removal of corrosion products (such as oxides) which would otherwise tend to stifle the corrosion reaction.

Corrosion Fatigue Corrosion fatigue is a reduction by corrosion of the ability of a metal to withstand **cyclic or repeated stresses**. The surface of the metal plays an important role in this form of damage, as it will be the most highly stressed and at the same time subject to attack by the corrosive media. Corrosion of the metal surface will lower fatigue resistance, and stressing of the surface will tend to accelerate corrosion.

Under cyclic or repeated stress conditions, rupture of protective oxide films that prevent corrosion takes place at a greater rate than that at which new protective films can be formed. Such a situation frequently results in formation of anodic areas at the points of rupture; these produce pits that serve as stress-concentration points for the origin of cracks that cause ultimate failure.

Cavitation Formation of transient voids or vacuum bubbles in a liquid stream passing over a surface is called cavitation. This is often encountered around propellers, rudders, and struts and in pumps. When these bubbles collapse on a metal surface, there is a severe impact or explosive effect that can cause considerable mechanical damage, and corrosion can be greatly accelerated because of the destruction of protective films. Redesign or a more resistant metal is generally required to avoid this problem.

Fretting Corrosion This attack occurs when metals slide over each other and cause mechanical damage to one or both. In such a case, frictional heat oxidizes the metal and this oxide then wears away; or the mechanical removal of protective oxides results in exposure of fresh surface for corrosive attack. Fretting corrosion is minimized by using harder materials, minimizing friction (via lubrication), or designing equipment so that no relative movement of parts takes place.

Hydrogen Attack At elevated temperatures and significant hydrogen partial pressures, hydrogen will penetrate carbon steel, reacting with the carbon in the steel to form methane. The pressure generated causes a loss of ductility (hydrogen embrittlement) and failure by cracking or blistering of the steel. The removal of the carbon from the steel (decarburization) results in decreased strength. Resistance to this type of attack is improved by alloying with molybdenum or chromium. Accepted limits for the use of carbon and low-alloy steels are shown in the so-called Nelson curves; see American Petroleum Institute (API) Publication 941, *Steels for Hydrogen Service at Elevated Temperatures and Pressures in Petroleum Refineries and Petrochemical Plants*.

Hydrogen damage can also result from hydrogen generated in electrochemical corrosion reactions. This phenomenon is most commonly observed in solutions of specific weak acids. H₂S and HCN are the most common, although other acids can cause the problem. The atomic hydrogen formed on the metal surface by the corrosion reaction diffuses into the metal and forms molecular hydrogen at microvoids in the metal. The result is failure by embrittlement, cracking, and blistering.

FLUID CORROSION: STRUCTURAL

Graphitic Corrosion Graphitic corrosion usually involves **gray cast iron** in which metallic iron is converted into corrosion products, leaving a residue of intact graphite mixed with iron-corrosion products and other insoluble constituents of cast iron.

When the layer of graphite and corrosion products is impervious to the solution, corrosion will cease or slow down. If the layer is porous, corrosion will progress by galvanic behavior between graphite and iron. The rate of this attack will be approximately that for the maximum penetration of steel by pitting. The layer of graphite formed may also be effective in reducing the galvanic action between cast iron and more noble alloys such as bronze used for valve trim and impellers in pumps.

Low-alloy cast irons frequently demonstrate a superior resistance to graphitic corrosion, apparently because of their denser structure and the development of more compact and more protective graphitic coatings. Highly alloyed **austenitic cast irons** show considerable superiority over gray cast irons to graphitic corrosion because of the more noble potential of the austenitic matrix plus more protective graphitic coatings.

Carbon steels heated for prolonged periods at temperatures above 455°C (850°F) may be subject to the segregation of carbon, which is transformed into graphite. When this occurs, the structural strength of the steel will be affected. Killed steels or low-alloy steels of chromium and molybdenum or chromium and nickel should be considered for elevated-temperature services.

Parting, or Dealloying, Corrosion^o This type of corrosion occurs when only one component of an alloy is selectively removed by corrosion or leaching. The most common type of parting or dealloying is dezincification of a copper zinc brass, i.e., such as the parting of zinc from the brass, leaving a copper residue (see below). Various kinds of selective dissolution have been named after the alloy family that has been affected, usually on the basis of the dissolved metal (except in the case of graphitic corrosion; see "Graphitization" above). Similar selective corrosion also may lead to terms such as *denickelification* and *demolybdenumization*, etc. The element removed is always anodic to the alloy matrix. While the color of the damaged alloy may change, there is no [apparent (macro)] evidence of a loss of metal, shape, or dimensions and generally, even the original surface and contour remains. That said, the affected metal becomes lighter and porous and loses its original mechanical properties.

Dezincification Dezincification is corrosion of a brass alloy containing zinc in which the principal product of corrosion is metallic copper. This may occur as plugs filling pits (plug type) or as continuous layers surrounding an unattacked core of brass (general type). The mechanism may involve overall corrosion of the alloy followed by reposition of the copper from the corrosion products or selective corrosion of zinc or a high-zinc phase to leave copper residue. This form of corrosion is commonly encountered in brasses that contain more than 15 percent zinc and can be either eliminated or reduced by the addition of small amounts of **arsenic, antimony, or phosphorus** to the alloy.

Microbiologically Influenced Corrosion (MIC)^l This brief review is presented from a practical, industrial point of view. Subjects include materials selection, operational, and other considerations that real-world facilities managers and engineers and others charged with preventing and controlling corrosion need to take into account to prevent or minimize potential MIC problems. As a result of active research by investigators worldwide in the last 30 years, MIC is now recognized as a problem in most industries, including the petroleum production and transportation, gas pipeline, water distribution, fire protection, storage tank, nuclear and fossil power, chemical process, and pulp and paper industries.

A seminal summary of the evolutionary study leading to the discovery of a unique type of MIC, the final identification of the mechanism, and its control can be found in Daniel H. Pope, "State-of-the-Art Report on Monitoring, Prevention and Mitigation of Microbiologically Influenced Corrosion in the Natural Gas Industry," Report No. 96-0488, Gas Research Institute.

Microbiologically influenced corrosion is defined by the National Association of Corrosion Engineers as any form of corrosion that is influenced by the presence and/or activities of microorganisms. Although MIC appears to many humans to be a new phenomenon, it is not new to the microbes themselves. Microbial transformation of metals in their elemental and various mineral forms has been an essential part of material cycling on earth for billions of years. Some forms of metals such as reduced iron and manganese serve as energy sources for microbes, while oxidized forms of some metals can substitute for

^oAdditional reference material came from "Dealloying Corrosion Basics," *Materials Performance*, vol. 33, no. 5, p. 62, May 2006, adapted by NACE from *Corrosion Basics—An Introduction*, by L. S. Van Dellinder (ed.), NACE, Houston, Tex., 1984, pp. 105–107.

^lExcerpted from papers by Daniel H. Pope, John G. Stoecker II, and Oliver W. Siebert, courtesy of NACE International and the Gas Research Institute.

oxygen as electron acceptors in microbial metabolism. Other metals are transformed from one physical and chemical state to another as a result of exposure to environments created by microbes performing their normal metabolic activities. Of special importance are microbial activities which create oxidizing, reducing, acidic, or other conditions under which one form of a metal is chemically transformed to another. It is important to understand that the microbes are simply doing "what comes naturally." Unfortunately when microbial communities perform their natural activities on metals and alloys which would rather be in less organized and more natural states (minerals), corrosion often results.

Most microbes in the real world, especially those associated with surfaces, live in communities consisting of many different types of microbes, each of which can perform a variety of biochemical reactions. This allows microbial communities to perform a large variety of different reactions and processes which would be impossible for any single type of microbe to accomplish alone. Thus, e.g., even in overtly aerobic environments, microbial communities and the metal surfaces underlying them can have zones in which little or no oxygen is present. The result is that aerobic, anaerobic, fermentative, and other metabolic-type reactions can *all* occur in various locations within a microbial community. When these conditions are created on an underlying metal surface, then physical, chemical, and electrochemical conditions are created in which a variety of corrosion mechanisms can be induced, inhibited, or changed in their forms or rates. These include oxygen concentration cell corrosion, ion concentration cell corrosion, under-deposit acid attack corrosion, crevice corrosion, and under-deposit pitting corrosion. Note, however, that all these corrosion processes are electrochemical.

Most practicing engineers are not, and do not need to become, experts in the details of MIC. What is needed is to recognize that MIC-type corrosion can affect almost any metal or alloy exposed to MIC-related microbes in untreated waters, and therefore many types of equipment and structures are at risk. It is critical that MIC be properly diagnosed, or else mitigation methods designed to control MIC may be misapplied, resulting in failure to control the corrosion problem, unnecessary cost, and unnecessary concerns about exposure of the environment and personnel to potentially toxic biological control agents. Fortunately better tools are now available for monitoring and detection of MIC (see the later subsections on laboratory and field corrosion testing, both of which address the subject of MIC). Microbiological, chemical, metallurgical, and operational information is all useful in the diagnosis of MIC and should be used if available. All types of information should conform to the diagnosis of MIC—the data should not be in conflict with one another.

Bacteria, as a group, can grow over very wide ranges of pH, temperature, and pressure. They can be obligate aerobes (require oxygen to survive and grow), microaerophiles (require low oxygen concentrations), facultative anaerobes (prefer aerobic conditions but will live under anaerobic conditions), or obligate anaerobes (will grow only under conditions where oxygen is absent). It should be emphasized that most anaerobes will survive aerobic conditions for quite a while, and the same is true for aerobes in anaerobic conditions. Most MIC-related bacteria are heterotrophic and as a group may use as food almost any available organic carbon molecules, from simple alcohols or sugars to phenols and petroleum products, to wood or various other complex polymers. Unfortunately some MIC-related microbial communities can also use some biocides and corrosion inhibitors as food stuffs. Other microbes are autotrophs (fix CO₂, as do plants). Some microbes use inorganic elements or ions (e.g., NH₃, NO₂, CH₃, H₂, S, H₂S, Fe²⁺, Mn²⁺, etc.), as sources of energy. Although microbes can exist in extreme conditions, most require a limited number of organic molecules, moderate temperatures, moist environments, and near-neutral bulk environmental pH.

Buried Structures There has been no dramatic improvement in the protection of buried structures against MIC over the last several decades. Experience has been that coating systems, by themselves, do not provide adequate protection for a buried structure over the years; for best results, a properly designed and maintained cathodic protection (CP) system *must* be used in conjunction with a protective coating (regardless of the quality of the coating, as applied) to control

MIC and other forms of corrosion. Adequate levels of CP (the level of CP required is dependent on local environmental conditions, e.g., soil pH, moisture, presence of sealing chemicals) provide caustic environment protection at the holes (holidays) in the coating that are sure to develop with time due to one cause or another. The elevated pH (>10.0) produced by adequate CP discourages microbial growth and metabolism and tends to neutralize acids which are produced as a result of microbial metabolism and corrosion processes. Proper levels of CP, if applied uniformly to the metal surface, also raise the electrochemical potential of the steel to levels at which it does not want to corrode. Areas of metal surface under disbonded coating, under preexisting deposits (including those formed due to microbial actions), and other materials acting to insulate areas of the pipe and "holidays" from achieving adequate CP will often not be protected and may suffer very rapid under-deposit, crevice, and pitting corrosion. In short, adequate CP must be applied *before* MIC communities have become established under disbonded coating or in holidays. Application of CP after MIC processes and sites have been established may *not* stop MIC from occurring.

The user of cathodic protection must also consider the material being protected with regard to caustic cracking; a cathodic potential driven to the negative extreme of -0.95 V for microbiological protection purposes can cause caustic cracking of a steel structure. The benefits and risks of cathodic protection must be weighed for each material and each application.

Backfilling with limestone or other alkaline material is an added step to protect buried structures from microbiological damage. Providing adequate drainage to produce a dry environment both above and below ground in the area of the buried structure will also reduce the risk of this type of damage.

Corrosion of buried structures has been blamed on the sulfate-reducing bacteria (SRB) for well over a century. It was easy to blame the SRB for the corrosion as they smelled very bad (rotten egg smell). It is now known that SRB are one component of the MIC communities required to get corrosion of most buried structures.

Waters Water is required at a MIC "site" to allow microbial growth and corrosion reactions to occur. Most surfaces exposed to natural or industrial environments have large numbers of potential MIC-related microbes associated with them. Most natural and industrial waters (even "ultrapure," distilled, or condensate waters) contain large numbers of microbes. Since the potential to participate in MIC is a property of a large percentage of known microbes, it is not surprising that the potential for developing MIC is present in most natural and industrial environments on earth. Many industries assumed that they were protected against MIC as they used ultrapure waters, in which they assumed microbes were kept in check by the lack of organic food sources for the microbes. However, as several early cases of MIC in the chemical process industry demonstrated, MIC was capable of causing rapid and severe damage to stainless steel welds which had come into contact only with potable drinking water. Since that time, numerous cases of MIC have been reported in breweries; pharmaceutical, nuclear, and computer chip manufacturing; and other industries using highly purified waters. Many other cases of MIC have been documented in metals in contact with "normally treated" municipal waters.

Hydrostatic Testing Waters Microbes capable of causing MIC are present in most waters (even those treated by water purveyors to kill pathogens) used for hydrostatic (safety) testing of process equipment and for process batch waters. Use of these waters has resulted in a large number of documented cases of MIC in a variety of industries. Guidelines for treatment and use of hydrotest waters have been adopted by several industrial and government organizations in an effort to prevent this damage. Generally, good results have been reported for those who have followed this practice. Unfortunately, this can be an expensive undertaking where the need cannot be totally quantified (and thus justified to management). Cost-cutting practices which either ignore these guidelines or follow an adulteration of proven precautions can lead to major MIC damage to equipment and process facilities.

Untreated natural freshwaters from wells, lakes, or rivers commonly contain high levels of MIC-related microbes. These waters should not be used without appropriate treatment. Most potable

waters are treated sufficiently to prevent humans from having contact with waterborne pathogenic bacteria, but *are not* treated with sufficient disinfectant to kill all MIC-related microbes in the water.

They should not be used for hydrotesting or other such activities without appropriate treatment. Biocide treatment of hydrotest waters should be very carefully chosen to make sure that the chemicals are compatible with the materials in the system to be tested and to prevent water disposal problems (most organic biocides cause disposal problems). Use of inexpensive, effective, and relatively accepted biocides such as chlorine, ozone, hydrogen peroxide and iodine should be considered where compatibility with materials and other considerations permit. (For example, use of relatively low levels of iodine in hydrotest waters might be acceptable in steel pipes while stainless steels are much better tested using waters treated with nonhalogen, but oxidizing biocides such as hydrogen peroxide.) Obviously, chlorine must be used only with great care because of the extensive damage it will cause to the 300-series austenitic stainless steels. In all cases, as soon as the test is over, the water *must be completely* drained and the system thoroughly dried so that no vestiges of water are allowed to be trapped in occluded areas. The literature abounds with instructions as to the proper manner in which to accomplish the necessary and MIC-safe testing procedures. Engineering personnel planning these test operations should avail themselves of that knowledge.

Materials of Construction MIC processes are those processes by which manufactured materials deteriorate through the presence and activities of microbes. These processes can be either direct or indirect. Microbial biodeterioration of a great many materials (including concretes, glasses, metals and their alloys, and plastics) occurs by diverse mechanisms and usually involves a complex community consisting of many different species of microbes.

The corrosion engineers' solution to corrosion problems sometimes includes upgrading the materials of construction. This is a natural approach, and since microbiological corrosion most often results in crevice or under-deposit attack, this option is logical. Unfortunately, with MIC, the use of more materials traditionally thought to be more corrosion-resistant can lead to disastrous consequences. The occurrence and severity of any particular case of MIC are dependent upon the types of microbes involved, the local physical environment (temperature, water flow rates, etc.) and chemical environment (pH, hardness, alkalinity, salinity, etc.) and the type of metals or alloys involved. As an example, an upgrade from type 304 to 316 stainless steel does not always help. Kobrin reported biological corrosion of delta ferrite stringers in weld metal. Obviously, this upgrade was futile; type 316 stainless steel can contain as much as or more delta ferrite than does type 304. Kobrin also reported MIC of nickel, nickel-copper alloy 400, and nickel-molybdenum alloy B heat-exchanger tubes. Although the alloy 400 and alloy B were not pitted as severely as the nickel tubes, the use of higher alloys did not solve the corrosion problem.

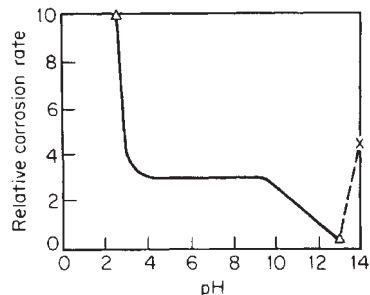
In the past, copper was believed to be toxic to *most* microbiological species. Although this may be true in a test tube under laboratory conditions, it is not generally true in the real world. In this real world, microbial communities excrete slime layers which tend to sequester the copper ions and prevent their contact with the actual microbial cells, thus preventing the copper from killing the microbes. Many cases of MIC in copper and copper alloys have been documented, especially of heat-exchange tubes, potable water, and fire protection system piping.

At this stage of knowledge about MIC, only titanium, zirconium, and tantalum appear to be immune to microbiological damage.

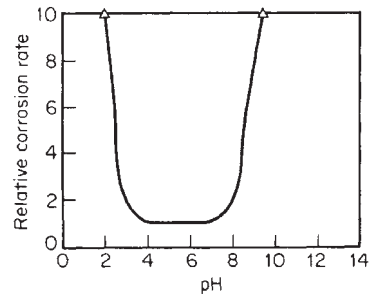
FACTORS INFLUENCING CORROSION

Solution pH The corrosion rate of most metals is affected by pH. The relationship tends to follow one of three general patterns:

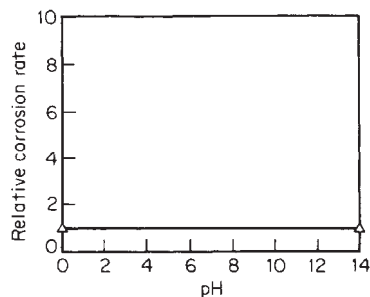
1. Acid-soluble metals such as iron have a relationship as shown in Fig. 25-1a. In the middle pH range (≈ 4 to 10), the corrosion rate is controlled by the rate of transport of oxidizer (usually dissolved O_2) to the metal surface. Iron is weakly amphoteric. At very high temperatures such as those encountered in boilers, the corrosion rate increases with increasing basicity, as shown by the dashed line.



(a)



(b)



(c)

FIG. 25-1 Effect of pH on the corrosion rate. (a) Iron. (b) Amphoteric metals (aluminum, zinc). (c) Noble metals.

2. Amphoteric metals such as aluminum and zinc have a relationship as shown in Fig. 25-1b. These metals dissolve rapidly in either acidic or basic solutions.

3. Noble metals such as gold and platinum are not appreciably affected by pH, as shown in Fig. 25-1c.

Oxidizing Agents In some corrosion processes, such as the solution of zinc in hydrochloric acid, hydrogen may evolve as a gas. In others, such as the relatively slow solution of copper in sodium chloride, the removal of hydrogen, which must occur so that corrosion may proceed, is effected by a reaction between hydrogen and some oxidizing chemical such as oxygen to form water. Because of the high rates of corrosion which usually accompany hydrogen evolution, metals are rarely used in solutions from which they evolve hydrogen at an appreciable rate. As a result, most of the corrosion observed in practice occurs under conditions in which the oxidation of hydrogen to form water is a necessary part of the corrosion process. For this reason, oxidizing agents are often powerful accelerators of corrosion, and in many cases the **oxidizing power of a solution** is its most important single property insofar as corrosion is concerned.

Oxidizing agents that accelerate the corrosion of some materials may also retard corrosion of others through the formation on their surface

of oxides or layers of adsorbed oxygen which make them more resistant to chemical attack. This property of chromium is responsible for the principal corrosion-resisting characteristics of the stainless steels.

It follows, then, that oxidizing substances, such as dissolved air, may accelerate the corrosion of one class of materials and retard the corrosion of another class. In the latter case, the behavior of the material usually represents a balance between the power of oxidizing compounds to preserve a protective film and their tendency to accelerate corrosion when the agencies responsible for protective-film breakdown are able to destroy the films.

Temperature The rate of corrosion tends to increase with rising temperature. Temperature also has a secondary effect through its influence on the solubility of air (oxygen), which is the most common oxidizing substance influencing corrosion. In addition, temperature has specific effects when a temperature change causes phase changes which introduce a corrosive second phase. Examples include condensation systems and systems involving organics saturated with water.

Velocity Most metals and alloys are protected from corrosion, not by *nobility* [a metal's inherent resistance to enter into an electrochemical reaction with that environment, e.g., the (intrinsic) inertness of gold to (almost) everything but aqua regia], but by the formation of a *protective film* on the surface. In the examples of film-forming protective cases, the film has similar, but more limiting, specific assignment of that exemplary-type resistance to the exposed environment (not nearly so broad-based as noted in the case of gold). Velocity-accelerated corrosion is the accelerated or increased rate of deterioration or attack on a metal surface because of relative movement between a corrosive fluid and the metal surface, i.e., the instability (velocity sensitivity) of that protective film.

An increase in the velocity of relative movement between a corrosive solution and a metallic surface frequently tends to accelerate corrosion. This effect is due to the higher rate at which the corrosive chemicals, including oxidizing substances (air), are brought to the corroding surface and to the higher rate at which corrosion products, which might otherwise accumulate and stifle corrosion, are carried away. The higher the velocity, the thinner will be the films which corroding substances must penetrate and through which soluble corrosion products must diffuse.

Whenever corrosion resistance results from the formation of layers of insoluble corrosion products on the metallic surface, the effect of high velocity may be to prevent their normal formation, to remove them after they have been formed, and/or to preclude their reformation. All metals that are protected by a film are sensitive to what is referred to as its *critical velocity*; i.e., the velocity at which those conditions occur is referred to as the *critical velocity* of that chemistry/temperature/velocity environmental corrosion mechanism. When the critical velocity of that specific system is exceeded, that effect allows corrosion to proceed unhindered. This occurs frequently in small-diameter tubes or pipes through which corrosive liquids may be circulated at high velocities (e.g., condenser and evaporator tubes), in the vicinity of bends in pipelines, and on propellers, agitators, and centrifugal pumps. Similar effects are associated with cavitation and mechanical erosion.

Films Once corrosion has started, its further progress very often is controlled by the nature of films, such as passive films, that may form or accumulate on the metallic surface. The classical example is the thin **oxide film** that forms on stainless steels.

Insoluble corrosion products may be completely impervious to the corroding liquid and, therefore, completely protective; or they may be quite permeable and allow local or general corrosion to proceed unhindered. Films that are nonuniform or discontinuous may tend to localize corrosion in particular areas or to induce accelerated corrosion at certain points by initiating electrolytic effects of the concentration-cell type. Films may tend to retain or absorb moisture and thus, by delaying the time of drying, increase the extent of corrosion resulting from exposure to the atmosphere or to corrosive vapors.

It is agreed generally that the characteristics of the **rust films** that form on steels determine their resistance to atmospheric corrosion. The rust films that form on low-alloy steels are more protective than those that form on unalloyed steel.

In addition to films that originate at least in part in the corroding metal, there are others that originate in the corrosive solution. These

include various salts, such as carbonates and sulfates, which may be precipitated from heated solutions, and insoluble compounds, such as "beer stone," which form on metal surfaces in contact with certain specific products. In addition, there are films of oil and grease that may protect a material from direct contact with corrosive substances. Such oil films may be applied intentionally or may occur naturally, as in the case of metals submerged in sewage or equipment used for the processing of oily substances.

Other Effects Stream **concentration** can have important effects on corrosion rates. Unfortunately, corrosion rates are seldom linear with concentration over wide ranges. In equipment such as distillation columns, reactors, and evaporators, concentration can change continuously, making prediction of corrosion rates rather difficult. Concentration is important during plant shutdown; presence of moisture that collects during cooling can turn innocuous chemicals into dangerous corrosives.

As to the effect of time, there is no universal law that governs the reaction for all metals. Some corrosion rates remain constant with time over wide ranges, others slow down with time, and some alloys have increased corrosion rates with respect to time. Situations in which the corrosion rate follows a combination of these paths can develop. Therefore, extrapolation of corrosion data and corrosion rates should be done with utmost caution.

Impurities in a corroder can be good or bad from a corrosion standpoint. An impurity in a stream may act as an inhibitor and actually retard corrosion. However, if this impurity is removed by some process change or improvement, a marked rise in corrosion rates can result. Other impurities, of course, can have very deleterious effects on materials. The chloride ion is a good example; small amounts of chlorides in a process stream can break down the passive oxide film on stainless steels. The effects of impurities are varied and complex. One must be aware of what they are, how much is present, and where they come from before attempting to recommend a particular material of construction.

HIGH-TEMPERATURE ATTACK

Physical Properties The suitability of an alloy for high-temperature service [425 to 1,100°C (800 to 2,000°F)] is dependent upon properties inherent in the alloy composition and upon the conditions of application. Crystal structure, density, thermal conductivity, electrical resistivity, thermal expansivity, structural stability, melting range, and vapor pressure are all physical properties basic to and inherent in individual alloy compositions.

Of usually high relative importance in this group of properties is **expansivity**. A surprisingly large number of metal failures at elevated temperatures are the result of excessive thermal stresses originating from constraint of the metal during heating or cooling. Such constraint in the case of hindered contraction can cause rupturing.

Another important property is alloy **structural stability**. This means freedom from formation of new phases or drastic rearrangement of those originally present within the metal structure as a result of thermal experience. Such changes may have a detrimental effect upon strength or corrosion resistance or both.

Mechanical Properties Mechanical properties of wide interest include creep, rupture, short-time strengths, and various forms of ductility, as well as resistance to impact and fatigue stresses. Creep strength and stress rupture are usually of greatest interest to designers of stationary equipment such as vessels and furnaces.

Corrosion Resistance Possibly of greater importance than physical and mechanical properties is the ability of an alloy's chemical composition to resist the corrosive action of various hot environments. The forms of high-temperature corrosion which have received the greatest attention are **oxidation** and **scaling**.

Chromium is an essential constituent in alloys to be used above 550°C (1,000°F). It provides a tightly adherent oxide film that materially retards the oxidation process. Silicon is a useful element in imparting oxidation resistance to steel. It will enhance the beneficial effects of chromium. Also, for a given level of chromium, experience has shown oxidation resistance to improve as the nickel content increases.

Aluminum is not commonly used as an alloying element in steel to improve oxidation resistance, as the amount required interferes with

both workability and high-temperature-strength properties. However, the development of high-aluminum surface layers by various methods, including spraying, cementation, and dipping, is a feasible means of improving heat resistance of low-alloy steels.

Contaminants in fuels, especially alkali-metal ions, vanadium, and sulfur compounds, tend to react in the combustion zone to form molten fluxes which dissolve the protective oxide film on stainless steels, allowing oxidation to proceed at a rapid rate. This problem is becoming more common as the high cost and short supply of natural gas and distillate fuel oils force increased usage of residual fuel oils and coal.

COMBATING CORROSION

Material Selection The objective is to select the material which will most economically fulfill the process requirements. The best source of data is well-documented experience in an identical process unit. In the absence of such data, other data sources such as experience in pilot units, corrosion-coupon tests in pilot or bench-scale units, laboratory corrosion-coupon tests in actual process fluids, or corrosion-coupon tests in synthetic solutions must be used. The data from such alternative sources (which are listed in decreasing order of reliability) must be properly evaluated, taking into account the degree to which a given test may fail to reproduce actual conditions in an operating unit. Particular emphasis must be placed on possible composition differences between a static laboratory test and a dynamic plant as well as on trace impurities (chlorides in stainless-steel systems, for example) which may greatly change the corrosiveness of the system. The possibility of severe localized attack (pitting, crevice corrosion, or stress-corrosion cracking) must also be considered.

Permissible **corrosion rates** are an important factor and differ with equipment. Appreciable corrosion can be permitted for tanks and lines if anticipated and allowed for in design thickness, but essentially no corrosion can be permitted in fine-mesh wire screens, orifices, and other items in which small changes in dimensions are critical.

In many instances use of **nonmetallic materials** will prove to be attractive from an economic and performance standpoint. These should be considered when their strength, temperature, and design limitations are satisfactory.

Proper Design Design considerations with respect to minimizing corrosion difficulties should include the desirability for free and complete drainage, minimizing crevices, and ease of cleaning and inspection. The installation of baffles, stiffeners, and drain nozzles and the location of valves and pumps should be made so that free drainage will occur and washing can be accomplished without holdup. Means of access for inspection and maintenance should be provided whenever practical. Butt joints should be used whenever possible. If lap joints employing fillet welds are used, the welds should be continuous.

The use of dissimilar metals in contact with each other should generally be minimized, particularly if they are widely separated in their nominal positions in the galvanic series (see Table 28-1a). If they are to be used together, consideration should be given to insulating them from each other or making the anodic material area as large as possible.

Equipment should be supported in such a way that it will not rest in pools of liquid or on damp insulating material. Porous insulation should be weatherproofed or otherwise protected from moisture and spills to avoid contact of the wet material with the equipment. Specifications should be sufficiently comprehensive to ensure that the desired composition or type of material will be used and the right condition of heat treatment and surface finish will be provided. Inspection during fabrication and prior to acceptance is desirable.

Altering the Environment Simple changes in environment may make an appreciable difference in the corrosion of metals and should be considered as a means of combating corrosion. **Oxygen** is an important factor, and its removal or addition may cause marked changes in corrosion. The treatment of boiler feedwater to remove oxygen, for instance, greatly reduces the corrosiveness of the water on steel. Inert-gas purging and blanketing of many solutions, particularly acidic media, generally minimize corrosion of copper and nickel-base alloys by minimizing air or oxygen content. Corrosiveness of acid media to stainless alloys, on the other hand, may be reduced by aeration because of the formation of passive oxide films. Reduction in

temperature will almost always be beneficial with respect to reducing corrosion if no corrosive phase changes (condensation, for example) result. Velocity effects vary with the material and the corrosive system. When pH values can be modified, it will generally be beneficial to hold the acid level to a minimum. When acid additions are made in batch processes, it may be beneficial to add them last so as to obtain maximum dilution and minimum acid concentration and exposure time. Alkaline pH values are less critical than acid values with respect to controlling corrosion. Elimination of moisture can and frequently does minimize, if not prevent, corrosion of metals, and this possibility of environmental alteration should always be considered.

Inhibitors The use of various substances or inhibitors as additives to corrosive environments to decrease corrosion of metals in the environment is an important means of combating corrosion. This is generally most attractive in closed or recirculating systems in which the annual cost of inhibitor is low. However, it has also proved to be economically attractive for many once-through systems, such as those encountered in petroleum-processing operations. Inhibitors are effective as the result of their controlling influence on the cathode- or anode-area reactions.

Typical examples of inhibitors used for minimizing corrosion of iron and steel in aqueous solutions are the chromates, phosphates, and silicates. Organic sulfide and amine materials are frequently effective in minimizing corrosion of iron and steel in acid solution.

The use of inhibitors is not limited to controlling corrosion of iron and steel. They frequently are effective with stainless steel and other alloy materials. The addition of copper sulfate to dilute sulfuric acid will sometimes control corrosion of stainless steels in hot dilute solutions of this acid, whereas the uninhibited acid causes rapid corrosion.

The effectiveness of a given inhibitor generally increases with an increase in **concentration**, but inhibitors considered practical and economically attractive are used in quantities of less than 0.1 percent by weight.

In some instances the amount of inhibitor present is critical in that a deficiency may result in localized or pitting attack, with the overall results being more destructive than when none of the inhibitor is present. Considerations for the use of inhibitors should therefore include review of experience in similar systems or investigation of requirements and limitations in new systems.

Cathodic Protection This electrochemical method of corrosion control has found wide application in the protection of carbon steel underground structures such as pipe lines and tanks from external soil corrosion. It is also widely used in water systems to protect ship hulls, offshore structures, and water-storage tanks.

Two methods of providing cathodic protection for minimizing corrosion of metals are in use today. These are the sacrificial-anode method and the impressed-emf method. Both depend upon making the metal to be protected the cathode in the electrolyte involved.

Examples of the sacrificial-anode method include the use of zinc, magnesium, or aluminum as anodes in electrical contact with the metal to be protected. These may be anodes buried in the ground for protection of underground pipe lines or attachments to the surfaces of equipment such as condenser water boxes or on ship hulls. The current required is generated in this method by corrosion of the sacrificial-anode material. In the case of the impressed emf, the direct current is provided by external sources and is passed through the system by use of essentially nonsacrificial anodes such as carbon, noncorrodible alloys, or platinum buried in the ground or suspended in the electrolyte in the case of aqueous systems.

The requirements with respect to current distribution and anode placement vary with the resistivity of soils or the electrolyte involved.

Anodic Protection* Corrosion of metals, and their alloys, exposed to a given environment requires at least two separate electrochemical (anodic and cathodic) reactions. The corrosion rate is determined at the intersection of these two reactions (see Fig. 25-2a).

Certain metal-electrolyte combinations exhibit active-passive behavior. Carbon steel in concentrated sulfuric acid is a classic example. The surface condition of a metal that has been forced inactive is termed *passive*.

*Citing of these several publications about anodic protection is noted with the courtesy of NACE International.

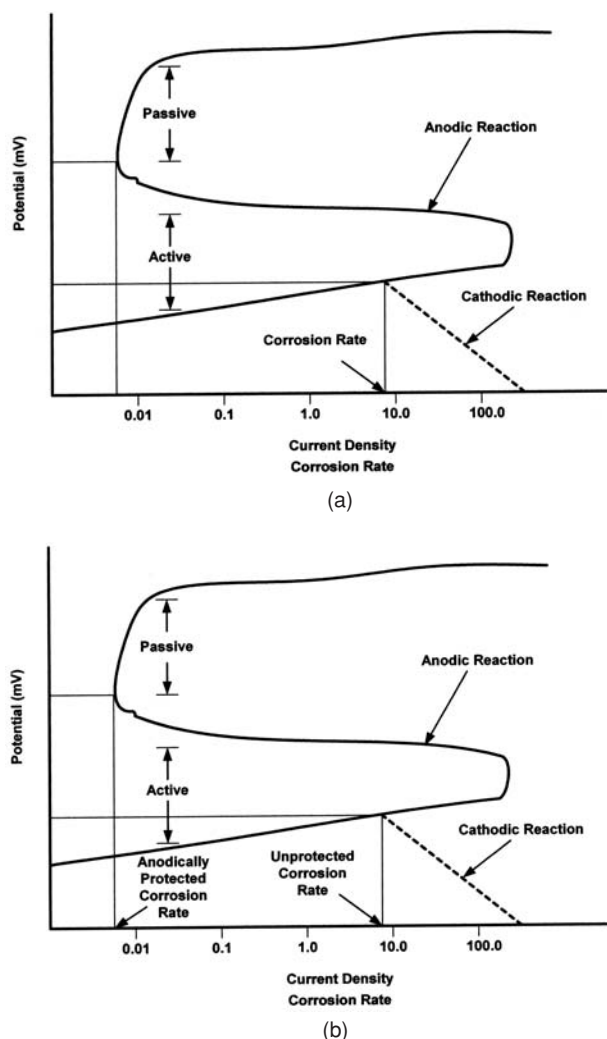


FIG. 25-2 (a) Active-passive behavior. (b) Application of anodic protection.

Anodic protection (AP) is an important method for controlling corrosion when/whereby the corroding (anodic surface) of the metal can be passivated by discharging a current from the surface of that metal, whereby the resulting corrosion product is a protective film. This technique has been known and practiced for nearly 50 years. This electrochemical anodic corrosion protection method relies on an automatic potential controlled current source (potentiostat) to maintain the metal or alloy in a noncorroding (passive) state. See Fig. 25-2b [and Fig. 25-14, the application of the corrosion behavior diagram to select the low-current region (LCR) in the design of an AP system].

The development of improved control instrumentation [e.g., of cathode location (placements), etc.] and many years of proven AP applications in the field have made AP the preferred method of controlling corrosion of uncoated steel equipment handling hot, concentrated sulfuric acid, stainless steel in even hotter exposures, and even steel in nitric acid.

Routinely, AP is used to control corrosion of carbon steel exposed to caustic-sulfide and caustic-aluminate solutions encountered in the pulp and paper and aluminum industries.

With the added benefit of increased product purity (reduced iron contamination), near-zero operational costs speak to AP as the most underapplied corrosion control systems of the ages.

A more recent advancement of AP has come from the application of a controlled cathodic current which can be utilized to shift the corrosion potential back to the passive zone. This (refinement) technique is usually termed the *cathodic potential adjustment protection* (CPAP).

See the NACE Papers: Oliver W. Siebert, "Correlation of Laboratory Electrochemical Investigations with Field Applications of Anodic Protection," *Materials Performance*, vol. 20, no. 2, pp. 38-43, February 1981; "Anodic Protection," *Materials Performance*, vol. 28, no. 11, p. 28, November 1989, adapted by NACE from "Corrosion Basics—An Introduction." (Houston, Tex.: NACE, 1984, pp. 105-107); J. Ian Munro and Winston W. Shim, "Anodic Protection—Its Operation and Applications," vol. 41, no. 5, pp. 22-24, May 2001; and a two-part series, J. Ian Munro, "Anodic Protection of White and Green Kraft Liquor Tankage, Part I, Electrochemistry of Kraft Liquors," and Part II, "Anodic Protection Design and System Operation," *Materials Performance*, vol. 42, no. 2, pp. 22-26, February 2002, and vol. 42, no. 3, pp. 24-28, March 2002.

Coatings and Linings The use of nonmetallic coatings and lining materials in combination with steel or other materials has and will continue to be an important type of construction for combating corrosion.

Organic coatings of many kinds are used as linings in equipment such as tanks, piping, pumping lines, and shipping containers, and they are often an economical means of controlling corrosion, particularly when freedom from metal contamination is the principal objective. One principle that is now generally accepted is that thin nonreinforced paintlike coatings of less than 0.75-mm (0.03-in) thickness should not be used in services for which full protection is required in order to prevent rapid attack of the substrate metal. This is true because most thin coatings contain defects or holidays and can be easily damaged in service, thus leading to early failures due to corrosion of the substrate metal even though the coating material is resistant. Electrical testing for continuity of coating-type linings is always desirable for immersion-service applications in order to detect holiday-type defects in the coating.

The most dependable barrier linings for corrosive services are those which are bonded directly to the substrate and are built up in multiple-layer or laminated effects to thicknesses greater than 2.5 mm (0.10 in). These include flake-glass-reinforced resin systems and elastomeric and plasticized plastic systems. Good surface preparation and thorough inspections of the completed lining, including electrical testing, should be considered as minimum requirements for any lining applications.

Linings of this type are slightly permeable to many liquids. Such permeation, while not damaging to the lining, may cause failure by causing disbonding of the lining owing to pressure buildup between the lining and the steel.

Ceramic or carbon-brick linings are frequently used as facing linings over plastic or membrane linings when surface temperatures exceed those which can be handled by the unprotected materials or when the membrane must be protected from mechanical damage. This type of construction permits processing of materials that are too corrosive to be handled in low-cost metal constructions.

Glass-Lined Steel By proprietary methods, special glasses can be bonded to steel, providing an impervious liner 1.5 to 2.5 mm (0.060 to 0.100 in) thick. Equipment and piping lined in this manner are routinely used in severely corrosive acid services. The glass lining can be mechanically damaged, and careful attention to details of design, inspection, installation, and maintenance is required to achieve good results with this system.

Metallic Linings for Severe/Corrosive Environments The cladding of steel with an alloy is another approach to this problem. There are a number of cladding methods in general use. In one, a sandwich is made of the corrosion-resistant metal and carbon steel by hot rolling to produce a **pressure weld** between the plates.

Another process involves **explosive bonding**. The corrosion-resistant metal is bonded to a steel backing metal by the force generated by properly positioned explosive charges. Relatively thick sections of metal can be bonded by this technique into plates.

In a third process, a **loose liner** is fastened to a carbon steel shell by welds spaced so as to prevent collapse of the liner. A fourth method is **weld overlay**, which involves depositing multiple layers of alloy weld metal to cover the steel surface.

All these methods require careful design and control of fabrication methods to assure success.

Metallic Linings for Mild Environments Zinc coatings applied by various means have good corrosion resistance to many atmospheres. Such coatings have been extensively used on steel. Zinc has the advantage of being anodic to steel and therefore will protect exposed areas of steel by electrochemical action.

Steel coated with tin (**tinplate**) is used to make food containers. Tin is more noble than steel; therefore, well-aerated solutions will galvanically accelerate attack of the steel at exposed areas. The comparative absence of air within food containers aids in preserving the tin as well as the food. Also the reversible potential which the tin-iron couple undergoes in organic acids serves to protect exposed steel in food containers.

Cadmium, being anodic to steel, behaves quite similarly to zinc in providing corrosion protection when applied as a coating on steel. Tests of zinc and cadmium coatings should be conducted when it becomes necessary to determine the most economical selection for a particular environment.

Lead has a good general resistance to various atmospheres. As a coating, it has had its greatest application in the production of terneplate, which is used as a roofing, corncing, and spouting material.

Aluminum coatings on steel will perform in a manner similar to zinc coatings. Aluminum has good resistance to many atmospheres; in addition, being anodic to steel, it will galvanically protect exposed areas. Aluminum-coated steel products are quite serviceable under high-temperature conditions, for which good oxidation resistance is required.

General Workflow for Minimizing or Controlling Corrosion
In general, the process of reducing and controlling corrosion of metals requires the minimization of the progress of electrochemical deterioration. To accomplish this goal without first changing the selection of material(s), the engineer should generate and follow a punchlist of items the goal of which is to remove essentially any material differences/gradients in the environment of the corroding material(s). Since concentration differences/gradients constitute chemical stress or stress risers that tend to drive corrosion reactions, reducing or eliminating such material differences/gradients constitutes reducing or eliminating stress on the corrosion reaction. Removing the chemical stress places the metal "at rest" with respect to the progress of corrosion.

CORROSION-TESTING METHODS*

The primary purpose of materials selection is to provide the optimum equipment for a process application in terms of materials of construction, design, and corrosion-control measures. *Optimum* here means that which comprises the best combination of cost, life, safety, and reliability.

The selection of materials to be used in design dictates a basic understanding of the behavior of materials and the principles that govern such behavior. If proper design of suitable materials of construction is incorporated, the equipment should deteriorate at a uniform and anticipated gradual rate, which will allow scheduled maintenance or replacement at regular intervals. If localized forms of corrosion are characteristic of the combination of materials and environment, the materials engineer should still be able to predict the probable life of equipment, or devise an appropriate inspection schedule to preclude unexpected failures. The concepts of predictive, or at least preventive, maintenance are minimum requirements to proper materials selection. This approach to maintenance is certainly intended to minimize the possibility of unscheduled production shutdowns because of corrosion failures, with their attendant possible financial losses, hazard to personnel and equipment, and resultant environmental pollution.

Chemical processes may involve a complex variety of both inorganic and organic chemicals. Hard and fast rules for selecting the appropriate materials of construction can be given when the composition is known, constant, and free of unsuspected contaminants; when the rel-

evant parameters of temperature, pressure, velocity, and concentration are defined; and when the mechanical and environmental degradation of the material is uniform, that is, free of localized attack. For example, it is relatively simple to select the materials of construction for a regimen of equipment for the storage and handling of cold, concentrated sulfuric acid. On the other hand, the choice of suitable materials for producing phosphoric acid by the digestion of phosphate rock with sulfuric acid is much more difficult because of the diversity in kind and concentration of contaminants, the temperatures of the reactions, and the strength of sulfuric and phosphoric acid used or formed. Probably the best way to approach the study of materials selection is to categorize the types of major chemicals that might be encountered, describe their inherent characteristics, and generalize about the corrosion characteristics of the prominent materials of construction in such environments.

The background information that materials selection is based on is derived from a number of sources. In many cases, information as to the corrosion resistance of a material in a specific environment is not available and must be derived experimentally. It is to this need that the primary remarks of this subsection are addressed.

Unfortunately, there is no standard or preferred way to evaluate an alloy in an environment. While the chemistry of the operating plant environment can sometimes be duplicated in the laboratory, factors of velocity, hot and cold wall effects, crevice, chemical reaction of the fluid during the test, stress levels of the equipment, contamination with products of corrosion, trace impurities, dissolved gases, and so forth also have a controlling effect on the quality of the answer. Then, too, the progress of the corrosion reaction itself varies with time. Notwithstanding, immersion testing remains the most widely used method for selecting materials of construction.

There is no standard or preferred way to carry out a corrosion test; the method must be chosen to suit the purpose of the test. The principal types of tests are, in decreasing order of reliability:

1. Actual operating experience with full-scale plant equipment exposed to the corroding medium.
2. Small-scale plant-equipment experience, under either commercial or pilot-plant conditions.
3. Sample tests in the field. These include coupons, stressed samples, electrical-resistance probes exposed to the plant corroding medium, or samples exposed to the atmosphere, to soils, or to fresh, brackish, or saline waters. Samples for viable microbes involved in MIC must be processed immediately in the field into appropriate growth media.
4. Laboratory tests on samples exposed to "actual" plant liquids or simulated environments should be done only when testing in the actual operating environment cannot be done. When MIC is a factor in the test, microbial communities from the actual environment of interest must be used. Pure cultures of single types of microbes cannot provide conditions present in the actual operating environment.

Plant or field corrosion tests are useful for

1. Selection of the most suitable material to withstand a particular environment and to estimate its probable durability in that environment
2. Study of the effectiveness of means of preventing corrosion

CORROSION TESTING: LABORATORY TESTS

Metals and alloys do not respond alike to all the influences of the many factors that are involved in corrosion. Consequently, it is impractical to establish any universal standard laboratory procedures for corrosion testing except for inspection tests. However, some details of laboratory testing need careful attention in order to achieve useful results.

In the selection of materials for the construction of a chemical plant, resistance to the corroding medium is often the determining factor; otherwise, the choice will fall automatically on the cheapest material mechanically suitable. Laboratory corrosion tests are frequently the quickest and most satisfactory means of arriving at a preliminary selection of the most suitable materials to use. Unfortunately, however, it is not yet within the state of the art of laboratory tests to predict with accuracy the behavior of the selected material under plant-operating conditions. The outstanding difficulty lies not so much in carrying out the test as in interpreting the results and translating

*Includes information from papers by Oliver W. Siebert, John G. Stoecker II, and Ann Van Orden, courtesy of NACE International; Oliver W. Siebert and John R. Scully, courtesy of ASTM; John R. Scully and Robert G. Kelly, courtesy of ASM; and Metal Samples Company, Division of Alabama Specialty Products Company, Munford, Alabama.

them into terms of plant performance. A laboratory test of the conventional type gives mainly one factor—the chemical resistance of the proposed material to the corrosive agent. There are numerous other factors entering into the behavior of the material in the plant, such as dissolved gases, velocity, turbulence, abrasion, crevice conditions, hot-wall effects, cold-wall effects, stress levels of metals, trace impurities in corrodent that act as corrosion inhibitors or accelerators, and variations in composition of corrodent.

Immersion Test One method of determining the chemical-resistance factor, the so-called **total-immersion test**, represents an unaccelerated method that has been found to give reasonably concordant results in approximate agreement with results obtained on the large scale when the other variables are taken into account. Various other tests have been proposed and are in use, such as salt-spray, accelerated electrolytic, alternate-immersion, and aerated-total-immersion; but in view of the numerous complications entering into the translation of laboratory results into plant results the simplest test is considered the most desirable for routine preliminary work, reserving special test methods for special cases. The total-immersion test serves quite well to eliminate materials that obviously cannot be used; further selection among those materials which apparently can be used can be made on the basis of a knowledge of the properties of the materials concerned and the working conditions or by constructing larger-scale equipment of the proposed materials in which the operating conditions can be simulated.

The National Association of Corrosion Engineers (NACE) TMO169-95 "Standard Laboratory Corrosion Testing of Metals for the Process Industries," and ASTM G31 "Recommended Practice for Laboratory Immersion Corrosion Testing of Metals" are the general guides for immersion testing. Small pieces of the candidate metal are exposed to the medium, and the loss of mass of the metal is measured for a given period of time. Immersion testing remains the best method to eliminate from further consideration those materials that obviously cannot be used. This technique is frequently the quickest and most satisfactory method of making a preliminary selection of the best candidate materials.

Probably the most serious disadvantage of this method of corrosion study is the assumed average-time weight loss. The corrosion rate could be high initially and then decrease with time (it could fall to zero). In other cases the rate of corrosion might increase very gradually with time or it could cycle or be some combination of these things.

The description that follows is based on these standards.

Test Piece^o The size and the shape of specimens will vary with the purpose of the test, nature of the material, and apparatus used. A large surface-to-mass ratio and a small ratio of edge area to total area are desirable. These ratios can be achieved through the use of rectangular or circular specimens of minimum thickness. Circular specimens should be cut preferably from sheet and not bar stock to minimize the exposed end grain.

A circular specimen of about 32-mm (1.25-in) diameter is a convenient shape for laboratory corrosion tests. With a thickness of approximately 3 mm (1/8 in) and an 8- or 11-mm- (5/16- or 7/8-in-) diameter hole for mounting, these specimens will readily pass through a 45/50 ground-glass joint of a distillation kettle. The total surface area of a circular specimen is given by the equation:

$$A = \frac{\pi}{2} (D^2 - d^2) + t\pi D + t\pi d$$

where t = thickness, D = diameter of the specimen, and d = diameter of the mounting hole. If the hole is completely covered by the mounting support, the final term ($t\pi d$) in the equation is omitted.

Rectangular coupons [50 by 25 by 1.6 or 3.2 mm (2 by 1 by 1/16 or 1/8 in)] may be preferred as corrosion specimens, particularly if interface or liquid-line effects are to be studied by the laboratory test.

Shapes of typical (commercially available) test coupons are shown in Fig. 25-3: circular in Fig. 25-3a, rectangular in Fig. 25-3b, welded rectangular in Fig. 25-3c, and horseshoe stressed in Fig. 25-3d. Many desired shapes of coupons are also available in various sizes and can be obtained in any size, shape, material of construction, and surface finish

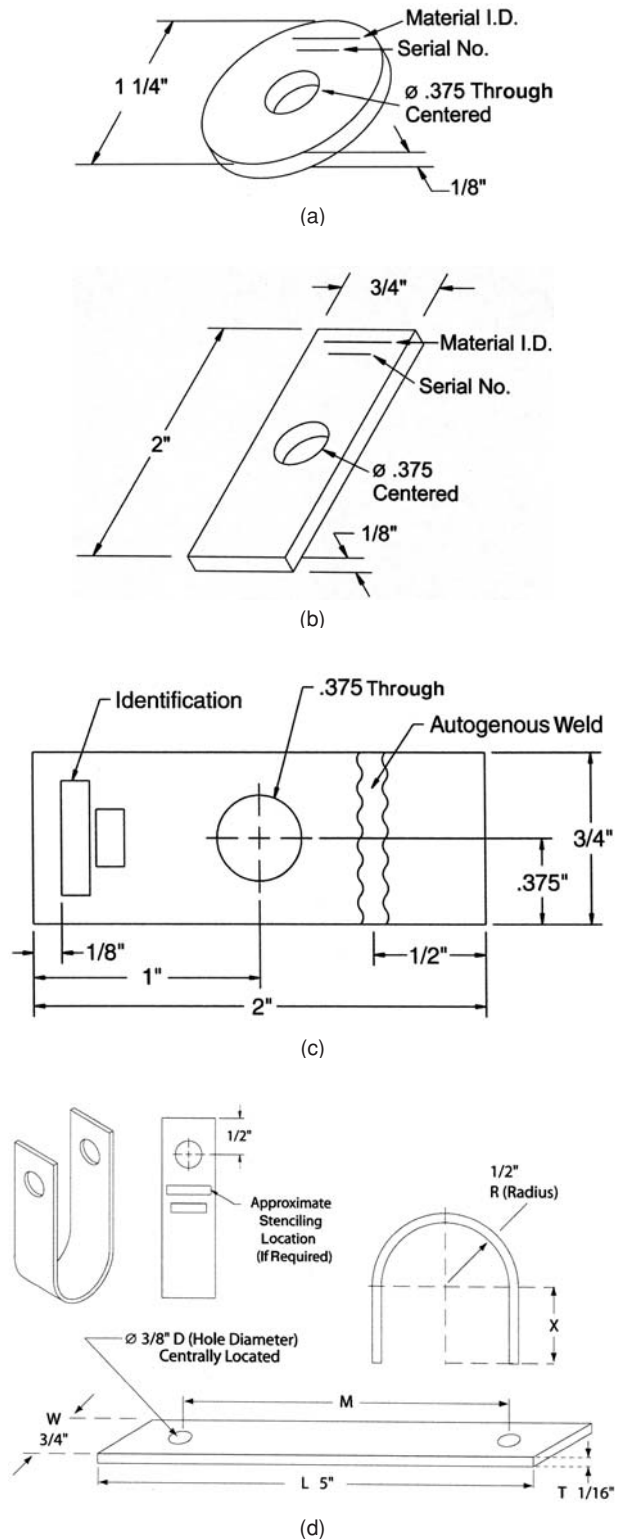


FIG. 25-3 Typical commercially available test coupons: (a) circular; (b) rectangular; (c) welded rectangular; (d) horseshoe stressed.

^oCoupons and racks/holders as well as availability information are courtesy of Metal Samples, Mumfords, Ala.

25-14 MATERIALS OF CONSTRUCTION

required to fit unique laboratory test equipment. There are also a series of somewhat generic racks and holders for mounting corrosion coupons so that they may be installed, exposed, and recovered for examination, after the plant exposures. Several typical pieces of hardware are shown in Fig. 25-4: a pipeline insertion rack in Fig. 25-4a, a spool rack for general equipment exposures in Fig. 25-4b, and a flat bar rack for attachment to accessories within equipment in Fig. 25-4c.

All specimens should be measured carefully to permit accurate calculation of the exposed areas. An area calculation accurate to plus or minus 1 percent is usually adequate.

More uniform results may be expected if a substantial layer of metal is removed from the specimens to eliminate variations in condition of the original metallic surface. This can be done by chemical treatment (pickling), electrolytic removal, or grinding with a coarse abrasive paper or cloth, such as No. 50, using care not to work-harden the surface. At least 2.5×10^{-3} mm (0.0001 in) or 1.5 to 2.3 mg/cm² (10 to

15 mg/in²) should be removed. If clad alloy specimens are to be used, special attention must be given to ensure that excessive metal is not removed. After final preparation of the specimen surface, the specimens should be stored in a desiccator until exposure if they are not used immediately.

Specimens should be finally degreased by scrubbing with bleach-free scouring powder, followed by thorough rinsing in water and in a suitable solvent (such as acetone, methanol, or a mixture of 50 percent methanol and 50 percent ether), and air-dried. For relatively soft metals such as aluminum, magnesium, and copper, scrubbing with abrasive powder is not always needed and can mar the surface of the specimen. The use of towels for drying may introduce an error through contamination of the specimens with grease or lint. The dried specimen should be weighed on an analytic balance.

Apparatus A versatile and convenient apparatus should be used, consisting of a kettle or flask of suitable size (usually 500 to 5,000 mL), a

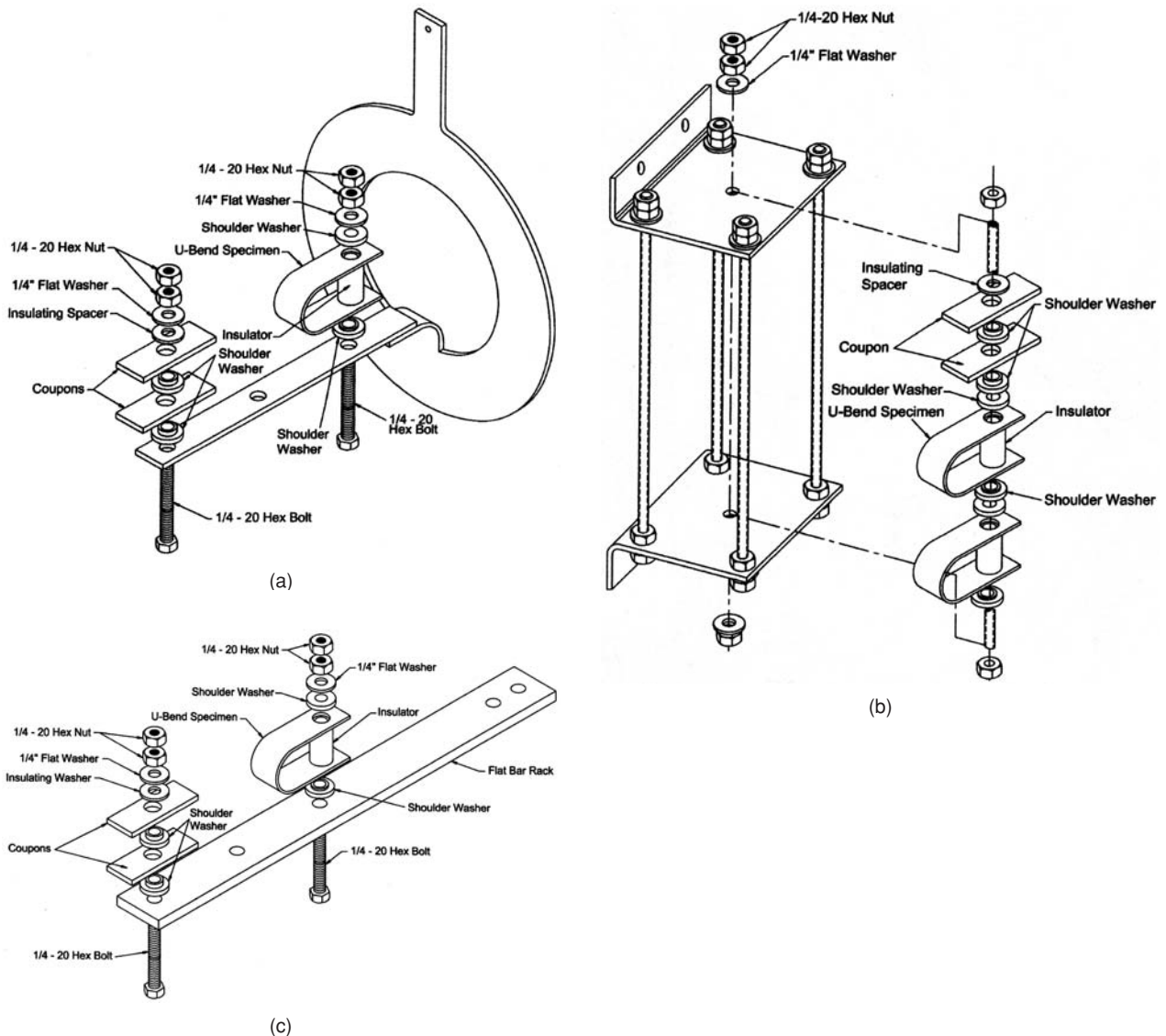


FIG. 25-4 Corrosion racks used to expose corrosion samples in operating production equipment: (a) inside pipes; (b) inside process vessels; (c) to be bolted onto baffles and brackets with process vessels.

reflux condenser with atmospheric seal, a sparger for controlling atmosphere or aeration, a thermowell and temperature-regulating device, a heating device (mantle, hot plate, or bath), and a specimen-support system. If agitation is required the apparatus can be modified to accept a suitable stirring mechanism such as a magnetic stirrer. A typical resin-flask setup for this type of test is shown in Fig. 25-5. Open-beaker tests should *not* be used because of evaporation and contamination.

In more complex tests, provisions might be needed for continuous flow or replenishment of the corrosive liquid while simultaneously maintaining a controlled atmosphere.

Heat flux apparatus for testing materials for heat-transfer applications is shown in Fig. 25-6. Here the sample is at a higher temperature than the bulk solution.

If the test is to be a guide for the selection of a material for a particular purpose, the limits of controlling factors in service must be determined. These factors include oxygen concentration, temperature, rate of flow, pH value, and other important characteristics.

The **composition of the test solution** should be controlled to the fullest extent possible and be described as thoroughly and as accurately as possible when the results are reported. Minor constituents should not be overlooked because they often affect corrosion rates. Chemical content should be reported as percentage by weight of the solution. Molarity and normality are also helpful in defining the concentration of chemicals in the test solution. The composition of the test solution should be checked by analysis at the end of the test to determine the extent of change in composition, such as might result from evaporation.

Temperature of Solution Temperature of the corroding solution should be controlled within $\pm 1^\circ\text{C}$ ($\pm 1.8^\circ\text{F}$) and must be stated in the report of test results.

For tests at ambient temperatures, the tests should be conducted at the highest temperature anticipated for stagnant storage in summer months. This temperature may be as high as 40 to 45°C (104 to 113°F) in some localities. The variation in temperature should be reported also (e.g., $40^\circ\text{C} \pm 2^\circ\text{C}$).

Aeration of Solution Unless specified, the solution should not be aerated. Most tests related to process equipment should be run with the natural atmosphere inherent in the process, such as the vapors of the boiling liquid. If aeration is used, the specimens should not be located in the direct air stream from the sparger. Extraneous effects can be encountered if the air stream impinges on the specimens.

Solution Velocity The effect of velocity is not usually determined in laboratory tests, although specific tests have been designed for this purpose. However, for the sake of reproducibility some velocity control is desirable.

Tests at the boiling point should be conducted with minimum possible heat input, and boiling chips should be used to avoid excessive turbulence and bubble impingement. In tests conducted below the boiling point, thermal convection generally is the only source of liquid velocity. In test solutions of high viscosities, supplemental controlled stirring with a magnetic stirrer is recommended.

Volume of Solution Volume of the test solution should be large enough to avoid any appreciable change in its corrosiveness through either exhaustion of corrosive constituents or accumulation of corrosion products that might affect further corrosion.

A suitable volume-to-area ratio is 20 mL (125 mL) of solution/ cm^2 (in^2) of specimen surface. This corresponds to the recommendation of ASTM Standard A262 for the Huey test. The preferred volume-to-area ratio is $40\text{ mL}/\text{cm}^2$ ($250\text{ mL}/\text{in}^2$) of specimen surface, as stipulated in ASTM Standard G31, Laboratory Immersion Testing of Materials.

Method of Supporting Specimens The supporting device and container should not be affected by or cause contamination of the test solution. The method of supporting specimens will vary with the apparatus used for conducting the test but should be designed to insulate the specimens from each other physically and electrically and to insulate the specimens from any metallic container or supporting device used with the apparatus.

Shape and form of the specimen support should assure free contact of the specimen with the corroding solution, the liquid line, or the vapor phase, as shown in Fig. 25-5. If clad alloys are exposed, special procedures are required to ensure that only the cladding is exposed (unless the purpose is to test the ability of the cladding to protect cut edges in the test solution). Some common supports are glass or

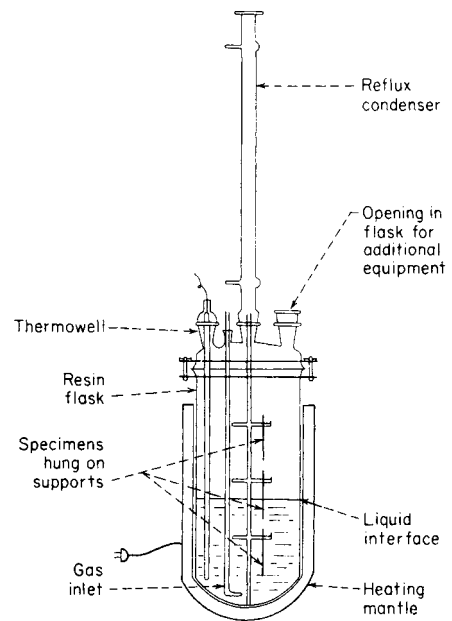


FIG. 25-5 Laboratory-equipment arrangement for corrosion testing. (Based on NACE Standard TMO169-95.)

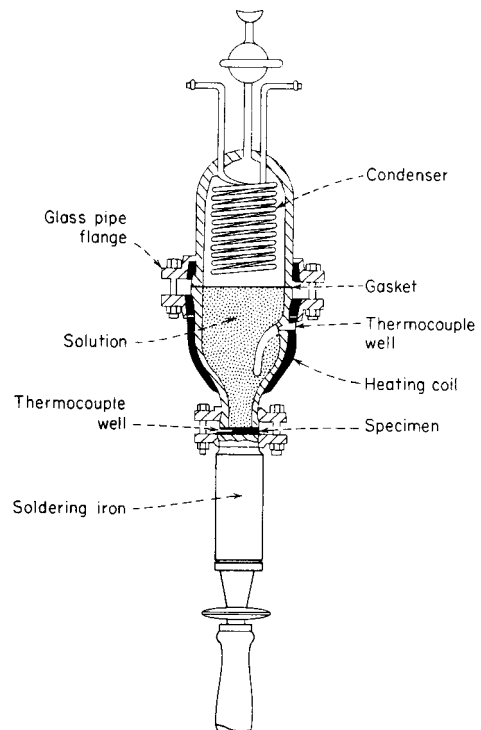


FIG. 25-6 Laboratory setup for the corrosion testing of heat-transfer materials.

ceramic rods, glass saddles, glass hooks, fluorocarbon plastic strings, and various insulated or coated metallic supports.

Duration of Test Although the duration of any test will be determined by the nature and purpose of the test, an excellent procedure for evaluating the effect of time on corrosion of the metal and also on the corrosiveness of the environment in laboratory tests has been presented by Wachter and Treseder [*Chem. Eng. Prog.*, 315-326 (June 1947)]. This technique is called the **planned-interval test**. Other procedures that require the removal of solid corrosion products between exposure periods will not measure accurately the normal changes of corrosion with time.

Materials that experience severe corrosion generally do not need lengthy tests to obtain accurate corrosion rates. Although this assumption is valid in many cases, there are exceptions. For example, lead exposed to sulfuric acid corrodes at an extremely high rate at first while building a protective film; then the rate decreases considerably, so that further corrosion is negligible. The phenomenon of forming a protective film is observed with many corrosion-resistant materials, and therefore short tests on such materials would indicate high corrosion rates and would be completely misleading.

Short-time tests also can give misleading results on alloys that form passive films, such as stainless steels. With borderline conditions, a prolonged test may be needed to permit breakdown of the passive film and subsequently more rapid attack. Consequently, tests run for long periods are considerably more realistic than those conducted for short durations. This statement must be qualified by stating that corrosion should not proceed to the point at which the original specimen size or the exposed area is drastically reduced or the metal is perforated.

If anticipated corrosion rates are moderate or low, the following equation gives a suggested test duration:

$$\begin{aligned} \text{Duration of test, } h &= \frac{78,740}{\text{corrosion rate, mm/y}} \\ &= \frac{2000}{\text{corrosion rate, mils/y}} \end{aligned}$$

Cleaning Specimens after Test Before specimens are cleaned, their appearance should be observed and recorded. Locations of deposits, variations in types of deposits, and variations in corrosion products are extremely important in evaluating localized corrosion such as pitting and concentration-cell attack.

Cleaning specimens after the test is a vital step in the corrosion-test procedure and, if not done properly, can give rise to misleading test results. Generally, the cleaning procedure should remove all corrosion products from specimens with a minimum removal of sound metal. Set rules cannot be applied to cleaning because procedures will vary with the type of metal being cleaned and the degree of adherence of corrosion products.

Mechanical cleaning includes scrubbing, scraping, brushing, mechanical shocking, and ultrasonic procedures. Scrubbing with a bristle brush and a mild abrasive is the most widely used of these methods; the others are used principally as supplements to remove heavily encrusted corrosion products before scrubbing. Care should be used to avoid the removal of sound metal.

Chemical cleaning implies the removal of material from the surface of the specimen by dissolution in an appropriate chemical agent. Solvents such as acetone, carbon tetrachloride, and alcohol are used to remove oil, grease, or resin and are usually applied prior to other methods of cleaning. Various chemicals are chosen for application to specific materials; some of these treatments in general use are outlined in the NACE standard.

Electrolytic cleaning should be preceded by scrubbing to remove loosely adhering corrosion products. One method of electrolytic cleaning that has been found to be useful for many metals and alloys is as follows:

Solution: 5 percent (by weight) H_2SO_4
 Anode: carbon or lead
 Cathode: test specimen
 Cathode current density: 20 A/dm² (129 A/in²)
 Inhibitor: 2 cm³ organic inhibitor per liter
 Temperature: 74°C (165°F)
 Exposure period: 3 min

Precautions must be taken to ensure good electrical contact with the specimen, to avoid contamination of the solution with easily reducible metal ions, and to ensure that inhibitor decomposition has not occurred. Instead of using 2 mL of any proprietary inhibitor, 0.5 g/L of inhibitors such as diorthotolyl thiourea or quinoline ethiodide can be used.

Whatever treatment is used to clean specimens after a corrosion test, its effect in removing metal should be determined, and the weight loss should be corrected accordingly. A "blank" specimen should be weighed before and after exposure to the cleaning procedure to establish this weight loss.

Evaluation of Results After the specimens have been reweighed, they should be examined carefully. Localized attack such as pits, crevice corrosion, stress-accelerated corrosion, cracking, or intergranular corrosion should be measured for depth and area affected.

Depth of localized corrosion should be reported for the actual test period and not interpolated or extrapolated to an annual rate. The rate of initiation or propagation of pits is seldom uniform. The size, shape, and distribution of pits should be noted. A distinction should be made between those occurring underneath the supporting devices (concentration cells) and those on the surfaces that were freely exposed to the test solution. An excellent discussion of pitting corrosion has been published [*Corrosion*, 25t (January 1950)].

The specimen may be subjected to simple bending tests to determine whether any **embrittlement** has occurred.

If it is assumed that localized or internal corrosion is not present or is recorded separately in the report, the **corrosion rate** or penetration can be calculated alternatively as

$$\frac{\text{Weight loss} \times 534}{(\text{Area})(\text{time})(\text{metal density})} = \text{mils/y (mpy)}$$

$$\frac{\text{Weight loss} \times 13.56}{(\text{Area})(\text{time})(\text{metal density})} = \text{mm/y (mmpy)}$$

where weight loss is in mg, area is in in² of metal surface exposed, time is in hours exposed, and density is in g/cm³. Densities for alloys can be obtained from the producers or from various metal handbooks.

The following **checklist** is a recommended guide for reporting all **important information and data**:

- Corrosive media and concentration (changes during test)
- Volume of test solution
- Temperature (maximum, minimum, and average)
- Aeration (describe conditions or technique)
- Agitation (describe conditions or technique)
- Type of apparatus used for test
- Duration of each test (start, finish)
- Chemical composition or trade name of metals tested
- Form and metallurgical conditions of specimens
- Exact size, shape, and area of specimens
- Treatment used to prepare specimens for test
- Number of specimens of each material tested and whether specimens were tested separately or which specimens were tested in the same container

Method used to clean specimens after exposure and the extent of any error expected by this treatment

Actual weight losses for each specimen
 Evaluation of attack if other than general, such as crevice corrosion under support rod, pit depth and distribution, and results of microscopic examination or bend tests

Corrosion rates for each specimen expressed as millimeters (mils) per year

Effect of Variables on Corrosion Tests It is advisable to apply a factor of safety to the results obtained, the factor varying with the degree of confidence in the applicability of the results. Ordinarily, a factor of from 3 to 10 might be considered normal.

Among the more important points that should be considered in attempting to base plant design on laboratory corrosion-rate data are the following.

Galvanic corrosion is a frequent source of trouble on a large scale. Not only is the use of different metals in the same piece of equipment dangerous, but the effect of cold working may be sufficient to establish potential differences of objectionable magnitude between different

parts of the same piece of metal. The mass of metal in chemical apparatus is ordinarily so great and the electrical resistance consequently so low that a very small voltage can cause a very high current. Welding also may leave a weld of a different physical or chemical composition from that of the body of the sheet and cause localized corrosion.

Local variations in temperature and crevices that permit the accumulation of corrosion products are capable of allowing the formation of **concentration cells**, with the result of accelerated local corrosion.

In the laboratory, the **temperature** of the test specimen is that of the liquid in which it is immersed, and the measured temperature is actually that at which the reaction is taking place. In the plant (heat being supplied through the metal to the liquid in many cases), the temperature of the film of (corrosive) liquid on the inside of the vessel may be a number of degrees higher than that registered by the thermometer. As the relation between temperature and corrosion is a logarithmic one, the rate of increase is very rapid. Like other chemical reactions, the speed ordinarily increases twofold to threefold for each 10°C temperature rise, the actual relation being that of the equation $\log K = A + (B/T)$, where K represents the rate of corrosion and T the absolute temperature. This relationship, although expressed mathematically, must be understood to be a qualitative rather than strictly a quantitative one.

Cold walls, as in coolers or condensers, usually have somewhat decreased corrosion rates for the reason just described. However, in some cases, the decrease in temperature may allow the formation of a more corrosive second phase, thereby increasing corrosion.

The effect of **impurities** in either structural material or corrosive material is so marked (while at the same time it may be either accelerating or decelerating) that for reliable results the actual materials which it is proposed to use should be tested and not types of these materials. In other words, it is much more desirable to test the actual plant solution and the actual metal or nonmetal than to rely upon a duplication of either. Since as little as 0.01 percent of certain organic compounds will reduce the rate of solution of steel in sulfuric acid 99.5 percent and 0.05 percent bismuth in lead will increase the rate of corrosion over 1000 percent under certain conditions, it can be seen how difficult it would be to attempt to duplicate here all the significant constituents.

Electrical Resistance The measurement of corrosion by electrical resistance is possible by considering the change in resistance of a thin metallic wire or strip sensing element (probe) as its cross section decreases from a loss of metal. Since small changes in resistance are encountered as corrosion progresses, changes in temperature can cause enough change in the wire resistance to complicate the results. Commercial equipment, such as the Corrosometer®, have a protected reference section of the specimen in the modified electrical Wheatstone bridge (Kelvin) circuit to compensate for these temperature changes. Since changes in the resistance ratio of the probe are not linear with loss of section thickness, compensation for this variable must be included in the circuit. In operation, the specimen probe is exposed to the environment and instrument readings are periodically recorded. The corrosion rate is the loss of metal averaged between any two readings.

The corrosion rate can be studied by this method over very short periods of time, but not instantaneously. The environment does not have to be an electrolyte. Studies can be made in corrosive gas exposures. The main disadvantage of the technique is that local corrosion (pitting, crevice corrosion, galvanic, stress corrosion cracking, fatigue, and so forth) will probably not be progressively identified. If the corrosion product has an electrical conductivity approaching that of the lost metal, little or no corrosion will be indicated. The same problem will result from the formation of conducting deposits on the specimen.

The electrical-resistance measurement has nothing to do with the electrochemistry of the corrosion reaction. It merely measures a bulk property that is dependent upon the specimen's cross-section area. Commercial instruments are available (Fig. 25-7).

Advantages of the electrical-resistance technique are:

1. A corrosion measurement can be made without having to see or remove the test sample.
2. Corrosion measurements can be made quickly—in a few hours or days, or continuously. This enables sudden increases in corrosion rate to be detected. In some cases, it will be possible then to modify the process to decrease the corrosion.

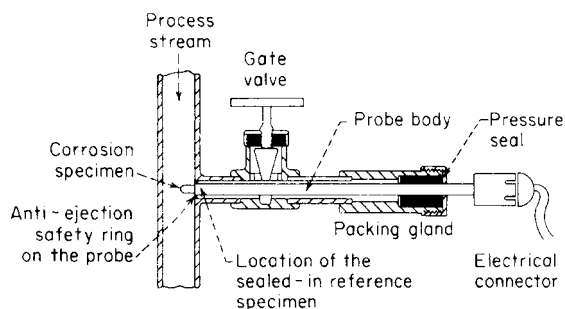


FIG. 25-7 Typical retractable corrosion probe.

3. The method can be used to monitor a process to indicate whether the corrosion rate is dependent on some critical process variable.

4. Corrodent need not be an electrolyte (in fact, need not be a liquid).

5. The method can detect low corrosion rates that would take a long time to detect with weight-loss methods.

Limitations of the technique are:

1. It is usually limited to the measurement of uniform corrosion only and is not generally satisfactory for localized corrosion.

2. The probe design includes provisions to compensate for temperature variations. This feature is not totally successful. The most reliable results are obtained in constant-temperature systems.

EMF versus pH (Pourbaix) Diagrams Potential (EMF) versus pH equilibrium (Pourbaix) diagrams derived from physical property data about the metal and its environment provide a basis for the expression of a great amount of thermodynamic data about the corrosion reaction. These relatively simple diagrams graphically represent the thermodynamics of corrosion in terms of electromotive force, that is, an indication of oxidizing power and pH, or acidity. As an aid in corrosion prediction, their usefulness lies in providing direction for establishing a corrosion study program.

Figure 25-8 is a typical Pourbaix diagram. Generally, the diagrams show regions of immunity (the metal), passivity (the surface film), and corrosion (metallic ions). While of considerable qualitative usefulness, these diagrams have important limitations. Since they are calculated from thermodynamic properties, they represent equilibrium conditions and do not provide kinetic information. Thus, while they show conditions where corrosion will not occur, they do not necessarily indicate under what conditions corrosion will occur. To determine the quantitative value of corrosion, kinetic rate measurement would still be required. Pourbaix diagrams were developed for the study of pure metals. Since few engineering structures are made of pure metals, it is important to extend this technique to include information on the passive behavior of alloys of engineering interest. Values of the open circuit corrosion potential (OCP) or a controlled potential occur, if a steady site potential can be used in conjunction with the solution pH and these diagrams to show what component is stable in the system defined by a given pH and potential. Theoretical diagrams so developed estimate the corrosion product in various regions. The use of computers to construct diagrams for alloy systems provides an opportunity to mathematically overcome many of the limitations inherent in the pure metal system.

A potentiokinetic electrochemical hysteresis method of diagram construction has led to consideration of three-dimensional Pourbaix diagrams for alloy systems useful in alloy development, evaluation of the influence of crevices, prediction of the tendency for dealloying, and the inclusion of kinetic data on the diagram is useful in predicting corrosion rather than just the absence of damage. These diagrams are kinetic, not thermodynamic, expressions. The two should not be confused as being the same reaction, as they are not.

Tafel Extrapolation Corrosion is an electrochemical reaction of a metal and its environment. When corrosion occurs, the current that flows between individual small anodes and cathodes on the metal surface causes the electrode potential for the system to change. While

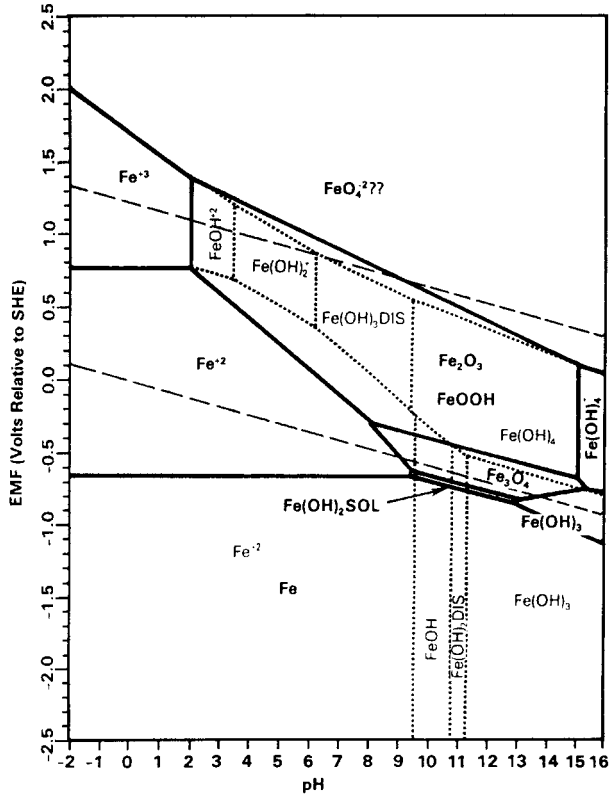


FIG. 25-8 EMF-pH diagram for an iron-water system at 25°C. All ions are at an activity of 10^{-6} .

this current cannot be measured, it can be evaluated indirectly on a metal specimen with an inert electrode and an external electrical circuit. Polarization is described as the extent of the change in potential of an electrode from its equilibrium potential caused by a net current flow to or from the electrode, galvanic or impressed (Fig. 25-9).

Electrochemical techniques have been used for years to study fundamental phenomenological corrosion reactions of metals in corrosive environments. Unfortunately, the learning curve in the reduction of these electrochemical theories to practice has been painfully slow. However, a recent survey has shown that many organizations in the chemical process industries are now adding electrochemical methods to their materials selection techniques. Laboratory electrochemical tests of metal/environment systems are being used to show the degree of compatibility and describe the limitations of those relationships. The general methods being used include electrical resistance, Tafel extrapolation, linear polarization, and both slow and rapid-scan potentiodynamic polarization. Depending upon the study technique used, it has also been possible to indicate the tendency of a given system to suffer local pitting or crevice attack or both. These same tools have been the basis of design protection of less-noble structural metals.

To study the anode reaction of a specimen in an environment, sufficient current is applied to change the freely corroding potential of the metal in a more electropositive direction with respect to the inert electrode (acting as a cathode). The opposite of this so-called anodic polarization is cathodic polarization. Polarization can be studied equally well by varying the potential and measuring the resultant changes in the current. Both of the theoretical (true) polarization curves are straight lines when plotted on a semilog axis. The corrosion current can be measured from the intersection of the corrosion potential and

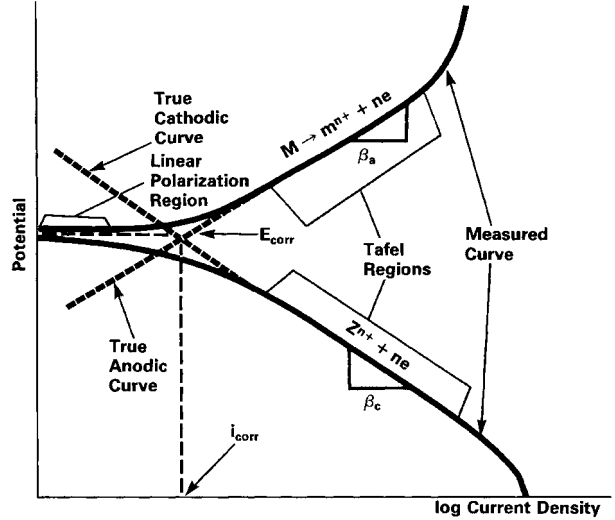


FIG. 25-9 Tafel extrapolation and linear polarization curves.

either the anodic or cathodic curve. The corrosion rate of the system is a function of that corrosion current. Experimentally derived curves are not fully linear because of the interference from the reactions between the anodes and cathodes in the region close to the corrosion potential. IR losses often obscure the Tafel behavior. Away from the corrosion potential, the measured curves match the theoretical (true) curves. The matching region of the measured curves is called the **Tafel region**, and their (Tafel) slopes are constant. Corrosion rates can be calculated from the intersection of the corrosion potential and the extrapolation of the Tafel region. The main advantage of the technique is that it is quick; curves can be generated in about an hour.

The technique is of limited value where more than one cathodic reduction reaction occurs. In most cases it is difficult to identify a sufficient linear segment of the Tafel region to extrapolate accurately. Since currents in the Tafel region are one to two orders of magnitude larger on the log scale than the corrosion current, relatively large currents are required to change the potentials from what they are at the corrosion potential. The environment must be a conductive solution. The Tafel technique does not indicate local attack, only an average, uniform corrosion rate.

The primary use of this laboratory technique today is as a quick check to determine the order of magnitude of a corrosion reaction. Sometimes the calculated rate from an immersion test does not "look" correct when compared to the visual appearance of the metal coupon. While the specific corrosion rate number determined by Tafel extrapolation is seldom accurate, the method remains a good confirmation tool.

Linear Polarization Some of the limitations of the Tafel extrapolation method can be overcome by using the linear-polarization technique to determine the corrosion rate. A relationship exists between the slope of the polarization curves E/I (with units of resistance, linear polarization is sometimes termed *polarization resistance*) and instantaneous corrosion rates of a freely corroding alloy. The polarization resistance is determined by measuring the amount of applied current needed to change the corrosion potential of the freely corroding specimen by about 10-mV deviations. The slope of the curves thus generated is directly related to the corrosion rate by Faraday's law. Several instruments are available that are used in linear polarization work. The main advantage is that each reading on the instrument can be translated directly into a corrosion rate.

As with all electrochemical studies, the environment must be electrically conductive. The corrosion rate is directly dependent on the Tafel slope. The Tafel slope varies quite widely with the particular corroding system and generally with the metal under test. As with the

Tafel extrapolation technique, the Tafel slope generally used is an assumed, more or less average value. Again, as with the Tafel technique, the method is not sensitive to local corrosion.

The amount of externally applied current needed to change the corrosion potential of a freely corroding specimen by a few millivolts (usually 10 mV) is measured. This current is related to the corrosion current, and therefore the corrosion rate, of the sample. If the metal is corroding rapidly, a large external current is needed to change its potential, and vice versa.

The measuring system consists of four basic elements:

1. **Electrodes.** Test and reference electrodes and, in some cases, an auxiliary electrode.
2. **Probe.** It connects the electrodes in the corrodent on the inside of a vessel to the electrical leads.
3. **Electrical leads.** They run from the probe to the current source and instrument panel.
4. **Control system.** Current source (batteries), ammeter, voltmeter, instrument panel, and so on.

Commercial instruments have either two or three electrodes. Also, there are different types of three-electrode systems. The application and limitations of the instruments are largely dependent upon these electrode systems.

Potentiodynamic Polarization Not all metals and alloys react in a consistent manner in contact with corrosive fluids. One of the common intermediate reactions of a metal (surface) is with oxygen, and those reactions are variable and complex. Oxygen can sometimes function as an electron acceptor; that is, oxygen can act as an oxidizing agent, and remove the "protective" film of hydrogen from the cathodic area, **cathodic depolarization.** The activation energy of the oxygen/hydrogen reaction is very large. This reaction does not normally occur at room temperature at any measurable rate. In other cases, oxygen can form protective oxide films. The long-term stability of these oxides also varies; some are soluble in the environment, others form more stable and inert or passive films.

Because corrosion is an electrochemical process, it is possible to evaluate the overall reaction by the use of an external electrical circuit called a **potentiostat.** When corrosion occurs, a potential difference exists between the metal and its ions in solution. It is possible to electrically control this potential; changes in potential cause changes in current (corrosion). Oxidation is a reaction with a loss of electrons (anodic—the reacting electrode is the anode); reduction is a reaction with a gain of electrons (cathodic—the reacting electrode is the cathode). Rather than allowing the electrons being evolved from the corrosion reaction to combine with hydrogen, these electrons can be removed by internal circuitry, and sent through a potentiostat, causing a cathodic (or anodic) reaction to occur at a platinum counter electrode. This is always true for the external polarization method; it is not unique for a potentiostat.

It is now well established that the activity of pitting, crevice corrosion, and stress-corrosion cracking is strongly dependent upon the corrosion potential (i.e., the potential difference between the corroding metal and a suitable reference electrode). By using readily available electronic equipment, the quantity and direction of direct current required to control the corrosion potential in a given solution at a given selected value can be measured. A plot of such values over a range of potentials is called a polarization diagram. By using proper experimental techniques, it is possible to define approximate ranges of corrosion potential in which pitting, crevice corrosion, and stress-corrosion cracking will or will not occur. With properly designed probes, these techniques can be used in the field as well as in the laboratory.

The potentiostat has a three-electrode system: a reference electrode, generally a saturated calomel electrode (SCE); a platinum counter, or auxiliary, electrode through which current flows to complete the circuit; and a working electrode that is a sample of interest (Fig. 25-10). The potentiostat is an instrument that allows control of the potential, either holding constant at a given potential, stepping from potential to potential, or changing the potential anodically or cathodically at some linear rate.

In the study of the anode/cathode polarization behavior of a metal/environment system, the potentiostat provides a plot of the relationship of current changes resulting from changes in potential most often presented as a plot of log current density versus potential, or Evans

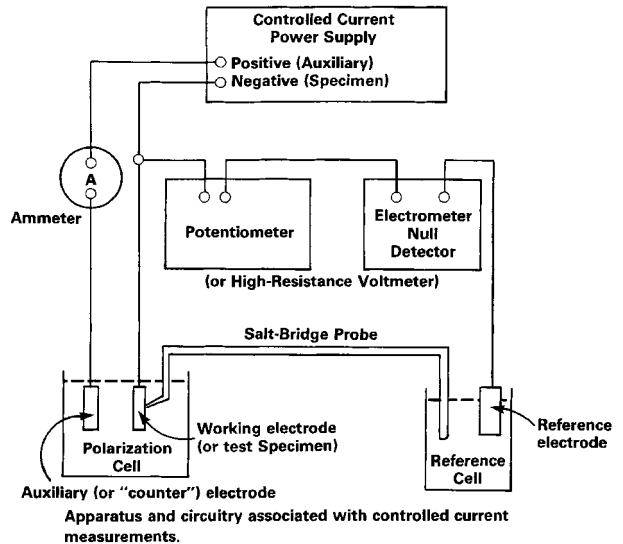


FIG. 25-10 The potentiostat apparatus and circuitry associated with controlled potential measurements of polarization curves.

diagram. A typical active/passive metal anodic polarization curve is seen in Fig. 25-11, generally showing the regions of active corrosion and passivity and a transpassive region.

Scan Rates Sweeping a range of potentials in the anodic (more electropositive) direction of a potentiodynamic polarization curve at a high scan rate of about 60 V/h (high from the perspective of the corrosion engineer, slow from the perspective of a physical chemist) is to indicate regions where intense anodic activity is likely. Second, for otherwise identical conditions, sweeping at a relatively slow rate of

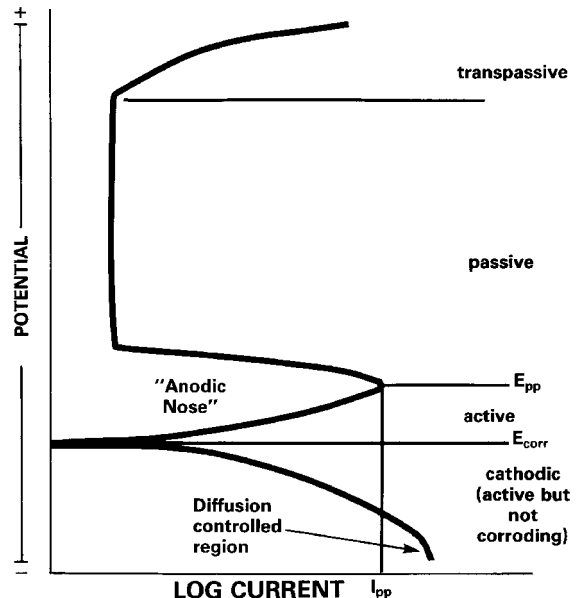


FIG. 25-11 Typical electrochemical polarization curve for an active/passive alloy (with cathodic trace) showing active, passive, and transpassive regions and other important features. (NOTE: E_{pp} = primary passive potential, E_{corr} = freely corroding potential.)

potential change of about 1 V/h will indicate regions wherein relative inactivity is likely. The rapid sweep of the potential range has the object of minimizing film formation, so that the currents observed relate to relatively film-free or thin-film conditions. The object of the slow sweep rate experiment is to allow time for filming to occur. A zero scan rate provides the opportunity for maximum stability of the metal surface, but at high electropositive potentials the environment could be affected or changed. A rapid scan rate compromises the steady-state nature of the metal surface but better maintains the stability of the environment. Whenever possible, corrosion tests should be conducted using as many of the techniques available, potentiodynamic polarization at various scan rates, crevice, stress, velocity, and so forth. An evaluation of these several results, on a holistic basis, can greatly reduce or temper their individual limitations.

Slow-Scan Technique In ASTM G5 "Polarization Practice for Standard Reference Method for Making Potentiostatic and Potentiodynamic Anodic Polarization Measurements," all oxygen in the test solution is purged with hydrogen for a minimum of 0.5 h before introducing the specimen. The test material is then allowed to reach a steady state of equilibrium (open circuit corrosion potential, E_{corr}) with the test medium before the potential scan is conducted. Starting the evaluation of a basically passive alloy that is already in its "stable" condition precludes any detailed study of how the metal reaches that protected state (the normal intersection of the theoretical anodic and cathodic curves is recorded as a zero applied current on the ASTM potentiostatic potential versus applied current diagram). These intersections between the anodic and cathodic polarization curves are the condition where the total oxidation rate equals the total reduction rate (ASTM G3 "Recommended Practice for Conventions Applicable to Electrochemical Measurements in Corrosion Testing").

Three general reaction types compare the activation-control reduction processes. In Fig. 25-12, in Case 1, the single reversible corrosion potential (anode/cathode intersection) is in the active region. A wide range of corrosion rates is possible. In Case 2, the cathodic curve intersects the anodic curve at three potentials, one active and two passive. If the middle active/passive intersection is not stable, the lower and upper

intersections indicate the possibility of very high corrosion rates. In Case 3, corrosion is in the stable, passive region, and the alloys generally passivate spontaneously and exhibit low corrosion rates. Most investigators report that the ASTM method is effective for studying Case 1 systems. An alloy-medium system exhibiting Case 2 and 3 conditions generally cannot be evaluated by this conventional ASTM method.

The potentiodynamic polarization electrochemical technique can be used to study and interpret corrosion phenomena. It may also furnish useful information on film breakdown or repair.

Rapid-Scan Corrosion Behavior Diagram (CBD) Basically, all the same equipment used in the conductance of an ASTM G5 slow-scan polarization study is used for rapid-scan CBDs (that is, a standard test cell, potentiostat, voltmeters, log converters, X-Y recorders, and electronic potential scanning devices). The differences are in technique: the slow scan is run at a potential sweep rate of about 0.6 V/h; the rapid-scan CBDs at about 50 V/h.

Different from the slow-scan technique, which is generally limited to Case 1 alloy/medium systems, the rapid-scan technique allows full anodic polarization study of alloys showing all Case 1, 2, and 3 behavior (Fig. 25-12). In Case 1, the single reversible corrosion potential (the anode/cathode intersection) is in the active region. A wide range of corrosion rates is possible. In Case 2, the cathodic curve intersects the anodic curve at three potentials, one in the active region and two in the passive. Since the middle active/passive intersection is not stable, the intersections indicate the possibility of very high corrosion rates depending on the environment or even slight changes to the exposure/environment system. In Case 3, the curves intersect in the most stable, passive region; the alloys generally passivate spontaneously and exhibit low corrosion rates. Case 2 exhibits the most corrosion, is difficult to study, and presents the most risk for materials of construction selection. Anything that can change the oxygen solubility of the oxidizing agent can alter the corrosion reaction.

The CBD diagram can provide various kinds of information about the performance of an alloy/medium system. The technique can be used for a direct calculation of the corrosion rate as well as for indicating the conditions of passivity and tendency of the metal to suffer local pitting and crevice attack. There are *benefits* from using the rapid-scan technique (the so-called corrosion behavior diagram, Fig. 25-13), and some *limitations* (when compared to the aforementioned slow-scan technique). Since *none* of the electrochemical corrosion test techniques that are currently in vogue, be they the slow-scan, rapid-scan, cyclic potentiodynamic polarization, EIS/AC impedance, or frequency modulation, are, in and of themselves, a true evaluation, measurement, and portrayal of the corrosion reaction being studied; only during the so-called open-circuit potential are we viewing real-life corrosion. Then why are these several electrochemical test methods used? Because (of those various test methods) each provides some valuable information that is more accurate (or not available) than that obtained when using some different test method. The more experienced the electrochemist in understanding these differences, the more closely she or he is able to approach accuracy in her or his corrosion understanding and thus results. For example, in designing an anodic protection system, one of the most critically sensitive parameters is the optimum protection potential at which the corrosion rate of the metal is able to be maintained at its lowest value (the true, lowest anodic protection control is not necessarily the whole length of the passive area of the E versus $\log I$ curve; see Fig. 25-11). Thus (conservatively), the control set point should be selected at the midpoint of the lowest corrosion rate (LCR) of the CBD, i.e., the region of protective oxide formation. If for no other reason than that, the CBD may be a test technique of choice for that anodic protection study. When using electrochemical test methods, many electrochemists try to employ a variety of test methods to arrive at the optimum selection of choice for any MOC study.

Those desiring a more detailed review of the subject of electrochemistry (and/or corrosion testing using electrochemistry) are directed to additional reference material from the following: Perry's *Chemical Engineers' Handbook*, 7th ed., Sec. 28, O. W. Siebert and J. G. Stoecker, "Materials of Construction," pp. 28-11 to 28-20, 1997; J. G. Stoecker, O. W. Siebert, and P. E. Morris, "Practical Applications

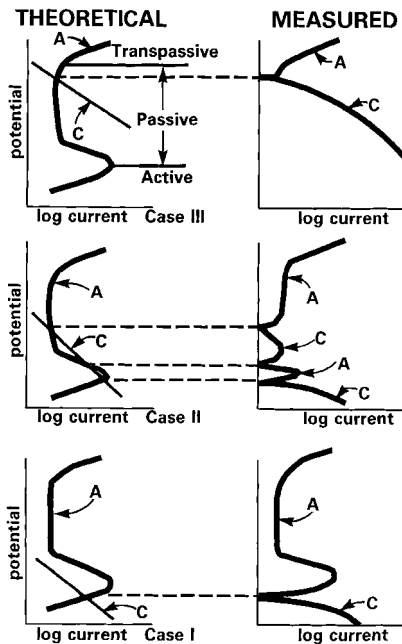


FIG. 25-12 Six possible types of behavior for an active/passive alloy in a corrosive environment.

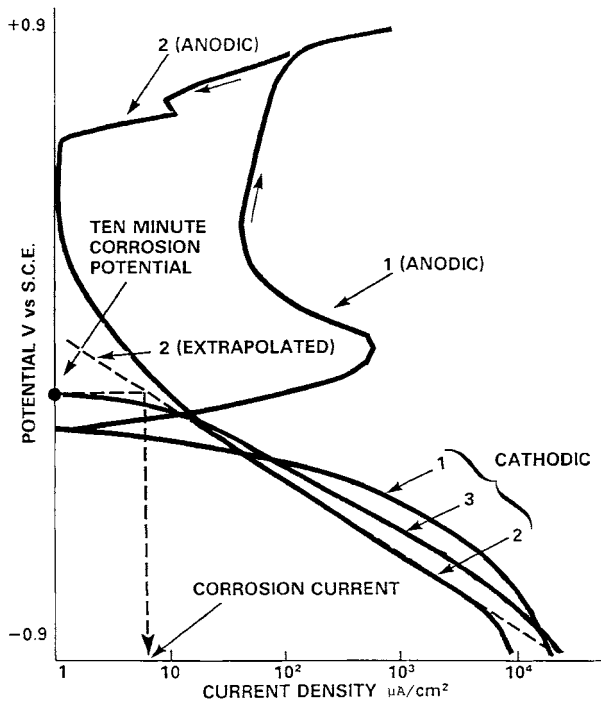


FIG. 25-13 Corrosion behavior diagram (CBD).

of Potentiodynamic Polarization Curves in Materials Selection," *Materials Performance*, vol. 22, no. 11, pp. 13-22, November 1983; O. W. Siebert, "Correlation of Laboratory Electrochemical Investigations with Field Application of Anodic Protection," *Materials Performance*, vol. 20, no. 2, pp. 38-43, February 1981; and the assorted historical literature of Stern, Geary, Evans, Sudbury, Riggs, Pourbaix, and Edeleanu, and other studies referred to in their publications.

Crevice Corrosion Prediction The most common type of localized corrosion is the occluded mode crevice corrosion. Pitting can, in effect, be considered a self-formed crevice. A crevice must be wide enough to permit liquid entry, but sufficiently narrow to maintain a stagnant zone. It is nearly impossible to build equipment without mechanical crevices; on a microlevel, scratches can be sufficient crevices to initiate or propagate corrosion in some metal/environment systems. The conditions in a crevice can, with time, become a different and much more aggressive environment than those on a nearby, clean, open surface. Crevices may also be created by factors foreign to the original system design, such as deposits, corrosion products, and so forth. In many studies, it is important to know or to be able to evaluate the crevice corrosion sensitivity of a metal to a specific environment and to be able to monitor a system for predictive maintenance.

Historically, the immersion test technique involved the use of a crevice created by two metal test specimens clamped together or a metal specimen in contact with an inert plastic or ceramic. The Materials Technology Institute of the Chemical Process Industries, Inc. (MTI) funded a study that resulted in an electrochemical cell to monitor crevice corrosion. It consists of a prepared crevice containing an anode that is connected through a zero-resistance ammeter to a freely exposed cathode. A string bridge provides a solution path that is attached externally to the cell. The electrochemical cell is shown in Fig. 25-14. A continuous, semiquantitative, real-time indication of crevice corrosion is provided by the magnitude of the current flowing between an anode and a cathode, and a qualitative signal is provided by shifts in electrode potential. Both the cell current and electrode potential produced by the test correlate well with the initiation and

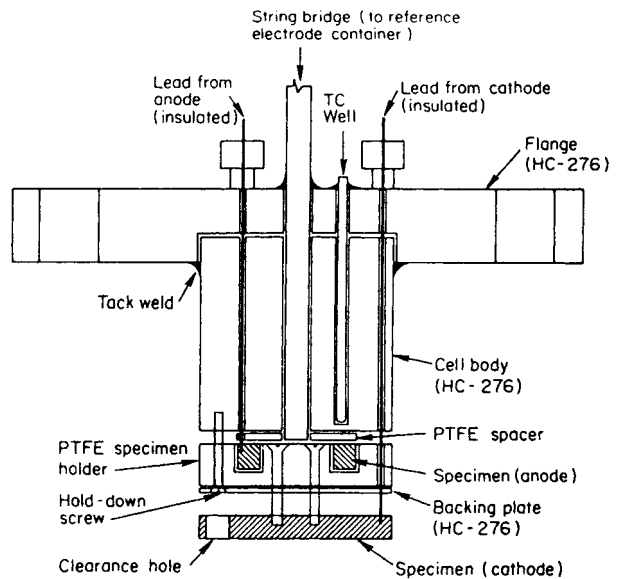


FIG. 25-14 Schematic diagram of the electrochemical cell used for crevice corrosion testing. Not shown are three hold-down screws, gas inlet tube, and external thermocouple tube.

propagation of crevice corrosion. During development of the MTI test technique, results were compared with crevice corrosion produced by a grooved TFE Teflon® plastic disk sandwich-type crevice cell. In nearly every instance, corrosion damage on the anode was similar in severity to that produced by the sandwich-type cell.

Velocity For corrosion to occur, an environment must be brought into contact with the metal surface and the metal atoms or ions must be allowed to be transported away. Therefore, the rate of transport of the environment with respect to a metal surface is a major factor in the corrosion system. Changes in velocity may increase or decrease attack depending on its effect involved. A varying quantity of dissolved gas may be brought in contact with the metal, or velocity changes may alter diffusion or transfer of ions by changing the thickness of the boundary layer at the surface. The boundary layer, which is not stagnant, moves except where it touches the surface. Many metals depend upon the development of a protective surface for their corrosion resistance. This may consist of an oxide film, a corrosion product, an adsorbed film of gas, or other surface phenomena. The removal of these surfaces by effect of the fluid velocity exposes fresh metal, and as a result, the corrosion reaction may proceed at an increasing rate. In these systems, corrosion might be minimal until a so-called **critical velocity** is attained where the protective surface is damaged or removed and the velocity is too high for a stable film to reform. Above this critical velocity, the corrosion may increase rapidly.

The NACE Landrum Wheel velocity test, originally TM0270-72, is typical of several mechanical-action immersion test methods to evaluate the effects of corrosion. Unfortunately, these laboratory simulation techniques did not consider the fluid mechanics of the environment or metal interface, and service experience very seldom supports the test predictions. A rotating cylinder within a cylinder electrode test system has been developed that operates under a defined hydrodynamics relationship (Figs. 25-15 and 25-16). The assumption is that if the rotating electrode operates at a shear stress comparable to that in plant geometry, the mechanism in the plant geometry may be modeled in the laboratory. Once the mechanism is defined, the appropriate relationship between fluid flow rate and corrosion rate in the plant equipment as defined by the mechanism can be used to predict the expected corrosion

*See Review Paper by David C. Silverman, courtesy of NACE International.

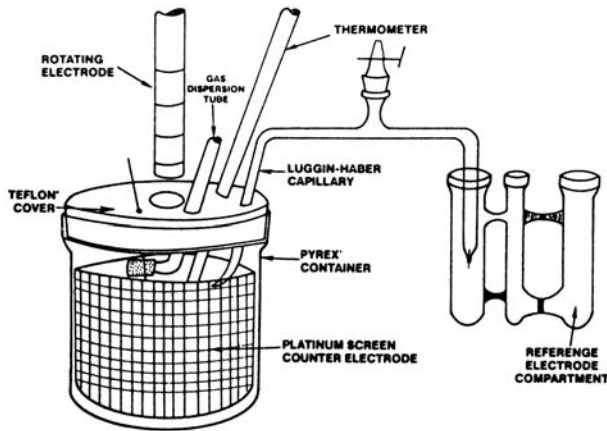


FIG. 25-15 Rotating cylinder electrode apparatus.

rate. If fluid velocity does affect the corrosion rate, the degree of mass transfer control, if that is the controlling mechanism (as opposed to activation control), can be estimated. Conventional potentiodynamic polarization scans are conducted as described previously. In other cases, the corrosion potential can be monitored at a constant velocity until steady state is attained. While the value of the final corrosion potential is virtually independent of velocity, the time to reach steady state may be dependent on velocity. The mass-transfer control of the corrosion potential can be proportional to the velocity raised to its appropriate exponent. The rate of breakdown of a passive film is velocity-sensitive. To review a very detailed and much needed refinement of the information and application of the rotating electrode technique as used for evaluation of the effect of velocity on corrosion, the reader is directed to a recent seminal study by David C. Silverman, "The Rotating Cylinder Electrode for Examining Velocity-Sensitive Corrosion—A Review," *Corrosion*, vol. 60, no. 11, pp. 1003–1023, Nov. 2004.

Environmental Cracking The problem of environmental cracking of metals and their alloys is very important. Of all the failure mechanism tests, the test for stress corrosion cracking (SCC) is the most illusive. Stress corrosion is the acceleration of the rate of corrosion damage by static stress. SCC, the limiting case, is the spontaneous cracking that may result from combined effects of stress and corrosion. It is important to differentiate clearly between **stress corrosion cracking** and **stress accelerated corrosion**. Stress corro-

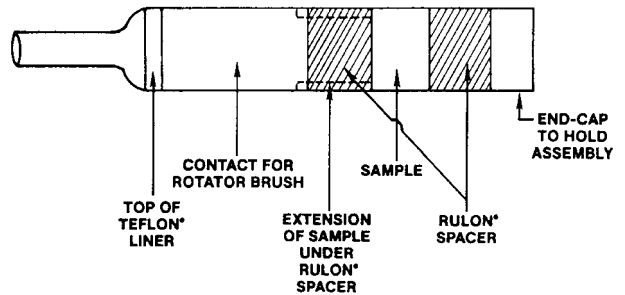


FIG. 25-16 Inner rotating cylinder used in laboratory apparatus of Fig. 25-15.

sion cracking is considered to be limited to cases in which no significant corrosion damage occurs in the absence of a corrosive environment. The material exhibits normal mechanical behavior under the influence of stress; before the development of a stress corrosion crack, there is little deterioration of strength and ductility. Stress corrosion cracking is the case of an interaction between chemical reaction and mechanical forces that results in structural failure that otherwise would not occur. SCC is a type of brittle fracture of a normally ductile material by the interaction between specific environments and mechanical forces, for example, tensile stress. Stress corrosion cracking is an incompletely understood corrosion phenomenon. Much research activity (aimed mostly at mechanisms) plus practical experience has allowed crude empirical guidelines, but these contain a large element of uncertainty. No single chemical, structural, or electrochemical test method has been found to respond with enough consistent reproducibility to known crack-causing environmental/stressed metal systems to justify a high confidence level.

As was cited in the case of immersion testing, most SCC test work is accomplished using mechanical, nonelectrochemical methods. It has been estimated that 90 percent of all SCC testing is handled by one of the following methods: (1) constant strain, (2) constant load, or (3) precracked specimens. Prestressed samples, such as are shown in Fig. 25-17, have been used for laboratory and field SCC testing. The variable observed is "time to failure or visible cracking." Unfortunately, such tests do not provide acceleration of failure.

Since SCC frequently shows a fairly long induction period (months to years), such tests must be conducted for very long periods before reliable conclusions can be drawn.

In the constant-strain method, the specimen is stretched or bent to a fixed position at the start of the test. The most common shape of

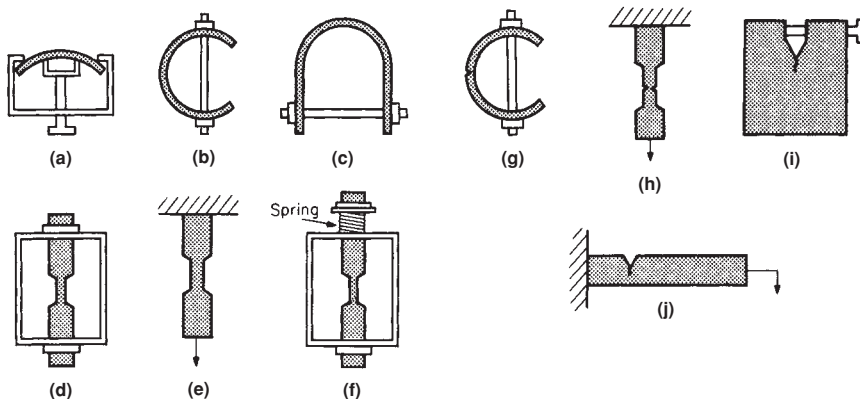


FIG. 25-17 Specimens for stress-corrosion tests. (a) Bent beam. (b) C ring. (c) U bend. (d) Tensile. (e) Tensile. (f) Tensile. (g) Notched C ring. (h) Notched tensile. (i) Precracked, wedge open-loading type. (j) Precracked, cantilever beam. [Chem. Eng., 78, 159 (Sept. 20, 1971).]

the specimens used for constant-strain testing is the U-bend, hair-pin, or horseshoe type. A bolt is placed through holes in the legs of the specimen, and it is loaded by tightening a nut on the bolt. In some cases, the stress may be reduced during the test as a result of creep. In the constant-load test the specimen is supported horizontally at each end and is loaded vertically downward at one or two points and has maximum stress over a substantial length or area of the specimen. The load applied is a predetermined, fixed dead weight. Specimens used in either of these tests may be precracked to assign a stress level or a desired location for fracture to occur or both as is used in fracture mechanics studies. These tensile-stressed specimens are then exposed in situ to the environment of study.

Slow Strain-Rate Test In its present state of development, the results from slow strain-rate tests (SSRT) with electrochemical monitoring are not always completely definitive; but, for a short-term test, they do provide considerable useful SCC information. Work in our laboratory shows that the SSRT with electrochemical monitoring and the U-bend tests are essentially equivalent in sensitivity in finding SCC. The SSRT is more versatile and faster, providing both mechanical and electrochemical feedback during testing.

The SSRT is a test technique where a tension specimen is slowly loaded in a test frame to failure under prescribed test conditions. The normal test extension rates are from 2.54×10^{-7} to 2.54×10^{-10} m/s (10^{-5} to 10^{-8} in/s). Failure times are usually 1 to 10 days. The failure mode will be either SCC or tensile overload, sometimes accelerated by corrosion. An advantage behind the SSRT, compared to constant-strain tests, is that the protective surface film is thought to be ruptured mechanically during the test, thus giving SCC an opportunity to progress. To aid in the selection of the value of the potential at which the metal is most sensitive to SCC that can be applied to accelerate SSRT, potentiodynamic polarization scans are conducted as described previously. It is common for the potential to be monitored during the conduct of the SSRT. The strain rates that generate SCC in various metals are reported in the literature. There are several disadvantages to the SSRT. First, indications of failure are not generally observed until the tension specimen is plastically stressed, sometimes significantly, above the yield strength of the metal. Such high-stressed conditions can be an order of magnitude higher than the intended operating stress conditions. Second, crack initiation must occur fairly rapidly to have sufficient crack growth that can be detected using the SSRT. The occurrence of SCC in metals requiring long initiation times may go undetected.

Modulus Measurements Another SCC test technique is the use of changes of modulus as a measure of the damping capacity of a metal. It is known that a sample of a given test material containing cracks will have a lower effective modulus than does a sample of identical material free of cracks. The technique provides a rapid and reliable evaluation of the susceptibility of a sample material to SCC in a specific environment. The so-called internal friction test concept can also be used to detect and probe nucleation and progress of cracking and the mechanisms controlling it.

The Young's modulus of the specimen is determined by accurately measuring its resonant frequency while driving it in a standing longitudinal wave configuration. A Marx composite piezoelectric oscillator is used to drive the specimen at a resonant frequency. The specimen is designed to permit measurements while undergoing applied stress and while exposed to an environmental test solution. The specimens are three half-wavelengths long; the gripping nodes and solution cup are silver-soldered on at displacement nodes, so they do not interfere with the standing wave. As discussed for SSRT, potentiodynamic polarization scans are conducted to determine the potential that can be applied to accelerate the test procedure. Again, the potential can be monitored during a retest, as is the acoustic emission (AE) as an indicator of nucleation and progress of cracking.

Conjunctive Use of Slow- and Rapid-Scan Polarization The use of the methods discussed in the preceding requires a knowledge of the likely potential range for SCC to occur. Potentiodynamic polarization curves can be used to predict those SCC-sensitive potential ranges. The technique involves conducting both slow- and rapid-scan sweeps in the anodic direction of a range of potentials. Comparison of the two curves will indicate any ranges of potential within which high anodic activity in the film-free condition reduces to insignificant activ-

ity when the time requirements for film formation are met. This should indicate the range of potentials within which SCC is likely. Most of the SCC theories presently in vogue predict these domains of behavior to be between the primary passive potential and the onset of passivity. This technique shortens the search for that SCC potential.

Separated Anode/Cathode Realizing, as noted in the preceding, that localized corrosion is usually active to the surrounding metal surface, a stress specimen with a limited area exposed to the test solution (the anode) is electrically connected to an unstressed specimen (the cathode). A potentiostat, used as a zero-resistance ammeter, is placed between the specimens for monitoring the galvanic current. It is possible to approximately correlate the galvanic current I_g and potential to crack initiation and propagation, and, eventually, catastrophic failure. By this arrangement, the galvanic current I_g is independent of the cathode area. In other words, the potential of the anode follows the corrosion potential of the cathode during the test. The SSRT apparatus discussed previously may be used for tensile loading.

Fracture Mechanics Methods These have proved very useful for defining the minimum stress intensity K_{ISCC} at which stress corrosion cracking of high-strength, low-ductility alloys occurs. They have so far been less successful when applied to high-ductility alloys, which are extensively used in the chemical-process industries.

Work on these and other new techniques continues, and it is hoped that a truly reliable, accelerated test or tests will be defined.

Electrochemical Impedance Spectroscopy (EIS) and AC Impedance* Many direct-current test techniques assess the overall corrosion process occurring at a metal surface, but treat the metal/solution interface as if it were a pure resistor. Problems of accuracy and reproducibility frequently encountered in the application of direct-current methods have led to increasing use of electrochemical impedance spectroscopy (EIS).

Electrode surfaces in electrolytes generally possess a surface charge that is balanced by an ion accumulation in the adjacent solution, thus making the system electrically neutral. The first component is a double layer created by a charge difference between the electrode surface and the adjacent molecular layer in the fluid. Electrode surfaces may behave at any given frequency as a network of resistive and capacitive elements from which an electrical impedance may be measured and analyzed.

The application of an impressed alternating current on a metal specimen can generate information on the state of the surface of the specimen. The corrosion behavior of the surface of an electrode is related to the way in which that surface responds to this electrochemical circuit. The AC impedance technique involves the application of a small sinusoidal voltage across this circuit. The frequency of that alternating signal is varied. The voltage and current response of the system are measured.

The so-called white-noise analysis by the fast Fourier transform technique (FFT) is another viable method. The entire spectrum can be derived from one signal. The impedance components thus generated are plotted on either a Nyquist (real versus imaginary) or Bode (log real versus log frequency plus log phase angle versus log frequency) plot. These data are analyzed by computer; they can be used to determine the polarization resistance and, thus, the corrosion rate if Tafel slopes are known. It is also thought that the technique can be used to monitor corrosion by examining the real resistance at high and low frequency and by assuming the difference is the polarization resistance. This can be done in low- and high-conductivity environments. Systems prone to suffer localized corrosion have been proposed to be analyzed by AC impedance and should aid in determining the optimum scan rate for potentiodynamic scans.

The use of impedance electrochemical techniques to study corrosion mechanisms and to determine corrosion rates is an emerging technology. Electrode impedance measurements have not been widely used, largely because of the sophisticated electrical equipment required to make these measurements. Recent advantages in microelectronics and computers has moved this technique almost overnight from being an academic experimental investigation of the concept

*Excerpted from papers by Oliver W. Siebert, courtesy of NACE International and ASTM.

itself to one of shelf-item commercial hardware and computer software, available to industrial corrosion laboratories.

Other Electrochemical Test Techniques A seminal summary of the present state of electrochemical test techniques can be found in John R. Scully, Chapter 7, "Electrochemical Tests," 2005 *ASTM Manual* 20. Professor Scully performs a praiseworthy job of presenting the theories associated with the mechanisms of corrosion, addressing both the thermodynamics and the kinetics of their electrode reactions. He then follows with a detailed encapsulation of major test methods being used in the academic and industrial research laboratories throughout the world for both basic information as well as to predict the scope and types of metallic corrosion experienced. In addition to some of those methods (already) addressed in *Perry's* above, we have noted several others from his presentation, wherein he has provided a much more thorough review, e.g., concentration polarization effects, frequency modulation methods, electronic noise resistance, methods based upon mixed-potential theory, scratch-repassivation method for local corrosion, and many more. The editors of this section of *Perry's* recommend this timely ASTM review for readers who need a greater treatment of electrochemical corrosion testing than is included in this presentation. In addition, Prof. Scully and his associate at the University of Virginia, Prof. Robert G. Kelly, have coauthored a similar quality presentation, "Methods for Determining Aqueous Corrosion Reaction Rates," in the 2005 *ASM Metals Handbook*, vol. 13.

Use and Limitations of Electrochemical Techniques A major caution must be noted as to the general, indiscriminate use of many electrochemical tests. Corrosion is a surface phenomenon. It must be kept in mind that the only condition present during any type of corrosion test that is a true representation of the real-life circumstance is the so-called open-circuit potential (OCP). The OCP is the electrical circuit that exists on the metal surface during the naturally spontaneous accumulation of the electrical potential that forms on the metal surface when exposed to a liquid environment. Any kind of an electrical current that is *added* to that surface is an artifact that no longer represents the true nature of that corrosion reaction. Is this to say that any form of induced electrical variable makes any corrosion test invalid? Absolutely not. Collectively, we have devised a number of unique electronic instruments that are designated to allow us to test/evaluate the influence of one or more variables present in a given corrosion reaction; for example, the application of anodic protection to control the corrosion of bare steel in concentrated sulfuric acid (see the subsection "Anodic Protection" earlier in Sec. 25). The AP system is designed to introduce an applied electrical current, that is, purposely "making" the steel surface the anode, making it corrode, and then taking advantage of its resultant electrochemical reaction to control that corroding surface into a condition with an extremely low rate of corrosion. We had earlier suggested that those electrochemists very well schooled and experienced in their trade also understand the major limitations of many of these types of techniques in real-life situations. Professor Scully, in the *ASTM Manual* referenced above, included a separate section addressing these limitations. An applicable example is the limitations to the general use of AC and EIS test techniques, for the study of corrosion systems. AC and EIS techniques are applicable for the evaluation of very thin films or deposits that are uniform, constant, and stable—for example, thin-film protective coatings. Sometimes, researchers do not recognize the dynamic nature of some passive films, corrosion products, or deposits from other sources; nor do they even consider the *possibility of a change* in the surface conditions during the course of their experiment. As an example, it is noteworthy that this is a *major* potential problem in the electrochemical evaluation of microbiological corrosion (MIC).

MIC depends on the complex structure of corrosion products and passive films on metal surfaces as well as on the structure of the biofilm. Unfortunately, electrochemical methods have sometimes been used in complex electrolytes, such as microbiological culture media, where the characteristics and properties of passive films and MIC deposits are *quite active* and not fully understood. It must be kept in mind that microbial colonization of passive metals can drastically change their resistance to film breakdown by causing *localized* changes in the type, concentration, and thickness of anions, pH, oxygen gradients, and inhibitor levels at the metal surface during the course of a

normal test; viable single-cell microorganisms divide at an exponential rate. These changes can be expected to result in important modifications in the electrochemical behavior of the metal and, accordingly, in the electrochemical parameter measured in laboratory experiments.

Warnings are noted in the literature to be careful in the *interpretation* of data from electrochemical techniques applied to systems in which complex and often poorly understood effects are derived from surfaces which contain *active* or *viable* organisms, and so forth. Rather, it is even more important to not use such test protocol unless the investigator fully understands both the corrosion mechanism and the test technique being considered—and their interrelationship.

CORROSION TESTING: PLANT TESTS

It is not always practical or convenient to investigate corrosion problems in the laboratory. In many instances, it is difficult to discover just what the conditions of service are and to reproduce them exactly. This is especially true with processes involving changes in the composition and other characteristics of the solutions as the process is carried out, as, for example, in evaporation, distillation, polymerization, sulfonation, or synthesis.

With many natural substances also, the exact nature of the corrosive is uncertain and is subject to changes not readily controlled in the laboratory. In other cases, the corrosiveness of the solution may be influenced greatly by or even may be due principally to a constituent present in such minute proportions that the mass available in the limited volume of corrosive solution that could be used in a laboratory setup would be exhausted by the corrosion reaction early in the test, and consequently the results over a longer period of time would be misleading.

Another difficulty sometimes encountered in laboratory tests is that contamination of the testing solution by corrosion products may change its corrosive nature to an appreciable extent.

In such cases, it is usually preferable to carry out the corrosion-testing program by exposing specimens in operating equipment under **actual conditions of service**. This procedure has the additional advantages that it is possible to test a large number of specimens at the same time and that little technical supervision is required.

In certain cases, it is necessary to choose materials for equipment to be used in a process developed in the laboratory and not yet in operation on a plant scale. Under such circumstances, it is obviously impossible to make plant tests. A good procedure in such cases is to construct a pilot plant, using either the cheapest materials available or some other materials selected on the basis of past experience or of laboratory tests. While the pilot plant is being operated to check on the process itself, specimens can be exposed in the operating equipment as a guide to the choice of materials for the large-scale plant or as a means of confirming the suitability of the materials chosen for the pilot plant.

Test Specimens In carrying out plant tests it is necessary to install the test specimens so that they will not come into contact with other metals and alloys; this avoids having their normal behavior disturbed by galvanic effects. It is also desirable to protect the specimens from possible mechanical damage.

There is no single standard size or shape for corrosion-test coupons. They usually weigh from 10 to 50 g and preferably have a large surface-to-mass ratio. Disks 40 mm (1½ in) in diameter by 3.2 mm (¼ in) thick and similarly dimensioned square and rectangular coupons are the most common. Surface preparation varies with the aim of the test, but machine grinding of surfaces or polishing with a No. 120 grit is common. Samples should not have sheared edges, should be clean (no heat-treatment scale remaining unless this is specifically part of the test), and should be identified by stamping. See Fig. 25-18 for a typical plant test assembly.

The choice of materials from which to make the holder is important. Materials must be durable enough to ensure satisfactory completion of the test. It is good practice to select very resistant materials for the test assembly. Insulating materials used are plastics, porcelain, Teflon, and glass. A phenolic plastic answers most purposes; its principal limitations are unsuitability for use at temperatures over 150°C (300°F) and lack of adequate resistance to concentrated alkalis.

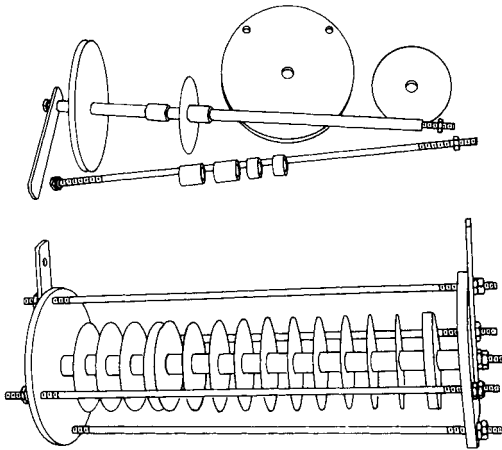


FIG. 25-18 Assembly of a corrosion-test spool and specimens. (Mantell, ed., Engineering Materials Handbook, McGraw-Hill, New York, 1958.)

The method of supporting the specimen holder during the test period is important. The preferred position is with the long axis of the holder horizontal, thus avoiding dripping of corrosion products from one specimen to another. The holder must be located so as to cover the conditions of exposure to be studied. It may have to be submerged, or exposed only to the vapors, or located at liquid level, or holders may be called for at all three locations. Various means have been utilized for supporting the holders in liquids or in vapors. The simplest is to suspend the holder by means of a heavy wire or light metal chain. Holders have been strung between heating coils, clamped to agitator shafts, welded to evaporator tube sheets, and so on. The best method is to use test racks.

In a few special cases, the standard "spool-type" specimen holder is not applicable and a suitable special test method must be devised to apply to the corrosion conditions being studied.

For conducting tests in **pipe lines** of 75-mm (3-in) diameter or larger, a spool holder as shown in Fig. 25-19, which employs the same disk-type specimens used on the standard spool holder, has been used. This frame is so designed that it may be placed in a pipe line in any position without permitting the disk specimens to touch the wall of the pipe. As with the strip-type holder, this assembly does not materially interfere with the fluid through the pipe and permits the study of corrosion effects prevailing in the pipe line.

Another way to study corrosion in pipe lines is to install in the line short sections of pipe of the materials to be tested. These test sections should be insulated from each other and from the rest of the piping

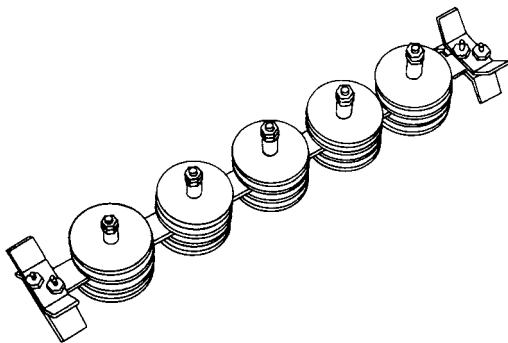


FIG. 25-19 Spool-type specimen holder for use in 3-in-diameter or larger pipe. (Mantell, ed., Engineering Materials Handbook, McGraw-Hill, New York, 1958.)

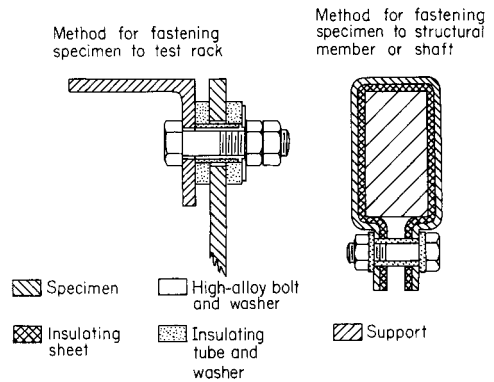


FIG. 25-20 Methods for attaching specimens to test racks and to parts of moving equipment. (Mantell, ed., Engineering Materials Handbook, McGraw-Hill, New York, 1958.)

system by means of nonmetallic couplings. It is also good practice to provide insulating gaskets between the ends of the pipe specimens where they meet inside the couplings. Such joints may be sealed with various types of dope or cement. It is desirable in such cases to paint the outside of the specimens so as to confine corrosion to the inner surface.

It is occasionally desirable to expose corrosion-test specimens in operating equipment without the use of specimen holders of the type described. This can be accomplished by attaching specimens directly to some part of the operating equipment and by providing the necessary insulation against galvanic effects as shown in Fig. 25-20. The suggested method of attaching specimens to racks has been found to be very suitable in connection with the exposure of specimens to corrosion in seawater.

Test Results The methods of cleaning specimens and evaluating results after plant corrosion tests are identical to those described earlier for laboratory tests.

Electrochemical On-Line Corrosion Monitoring* On-line corrosion monitoring is used to evaluate the status of equipment and piping in chemical process industries (CPI) plants. These monitoring methods are based on electrochemical techniques. To use on-line monitoring effectively, the engineer needs to understand the underlying electrochemical test methods to be employed. This section covers many of these test methods and their applications as well as a review of potential problems encountered with such test instruments and how to overcome or avoid these difficulties.

Most Common Types of Probes There are three most common types of corrosion monitoring probes used. Other types of probes are used, but in smaller numbers.

1. **Weight loss probes.** Coupons for measuring weight loss are still the primary type of probe in use. These may be as simple as samples of the process plant materials which have been fitted with electrical connections and readouts to determine intervals for retrieval and weighing, to commercially available coupons of specified material, geometry, stress condition, and other factors, ready to be mounted on specially designed supports at critical points in the process. Coupons can be permanently installed prior to plant start-up or during a shutdown. This type of permanent installation requires a plant shutdown for probe retrieval as well. Shutdown can be avoided by installing the probe in a bypass. Weight loss measurements do not accurately measure the severity of pitting corrosion, including that due to MIC.

2. **Electrical resistance probes.** These probes are the next most common type of corrosion probes after coupons. This type of probe measures changes in the electrical resistance as a thin strip of metal gets

*Excerpted from papers by Oliver W. Siebert, courtesy of NACE International and ASTM.

thinner with ongoing corrosion. As the metal gets thinner, its resistance increases. This technique was developed in the 1950s by Draviniaks and Cataldi and has undergone many improvements since then.

3. Linear polarization resistance probes. LPR probes are more recent in origin, and are steadily gaining in use. These probes work on a principle outlined in an ASTM guide on making polarization resistance measurements, providing instantaneous corrosion rate measurements (G59, "Standard Practice for Conducting Potentiodynamic Polarization Resistance Measurements").

LPR probes measure the electrochemical corrosion mechanism involved in the interaction of the metal with the electrolyte. To measure linear polarization resistance R_p , Ω/cm^2 , the following assumptions must be made:

- The corrosion rate is uniform.
- There is only cathodic and one anodic reaction.
- The corrosion potential is not near the oxidation/reduction potential for either reaction.

When these conditions are met, the current density associated with a small polarization of the metal (less than +10 mV) is directly proportional to the corrosion rate of the metal.

Multiinformational Probes Corrosion probes can provide more information than just corrosion rate. The next three types of probes yield information about the type of corrosion, the kinetics of the corrosion reaction, as well as the local corrosion rate.

Electrochemical impedance spectroscopy, AC probes. EIS, although around since the 1960s, has primarily been a laboratory technique. Commercially available probes and monitoring systems that measure EIS are becoming more widely used, especially in plants that have on-staff corrosion experts to interpret the data or to train plant personnel to do so.

In EIS, a potential is applied across a corroding metal in solution, causing current to flow. The amount of current depends upon the corrosion reaction on the metal surface and the flow of ions in solution. If the potential is applied as a sine wave, it will cause harmonics of the current output. The relationship between the applied potential and current output is the impedance, which is analogous to resistance in a DC circuit.

Since the potential and current are sinusoidal, the impedance has a magnitude and a phase, which can be represented as a vector. A sinusoidal potential or current can be pictured as a rotating vector. For standard AC current, the rotation is at a constant angular velocity of 60 Hz.

The voltage can also be pictured as a rotating vector with its own amplitude and frequency. Both current and potential can be represented as having real (observed) and imaginary (not observed) components.

In making electrochemical impedance measurements, one vector is examined, using the others as the frame of reference. The voltage vector is divided by the current vector, as in Ohm's law. Electrochemical impedance measures the impedance of an electrochemical system and then mathematically models the response using simple circuit elements such as resistors, capacitors, and inductors. In some cases, the circuit elements are used to yield information about the kinetics of the corrosion process.

Polarization probes. Polarization methods other than LPR are also of use in process control and corrosion analysis, but only a few systems are offered commercially. These systems use such polarization techniques as galvanodynamic or potentiodynamic, potentiostatic or galvanostatic, potentiostaircase or galvanostaircase, or cyclic polarization methods. Some systems involving these techniques are, in fact, used regularly in processing plants. These methods are used in situ or in the laboratory to measure corrosion. Polarization probes have been successful in reducing corrosion-related failures in chemical plants.

Polarization probes rely on the relationship of the applied potential to the output current per unit area (current density). The slope of applied potential versus current density, extrapolated through the origin, yields the polarization resistance R_p , which can be related to the corrosion rate.

There are several methods for relating the corrosion current, the applied potential, and the polarization resistance. These methods involve various ways of stepping or ramping either the potential or current. Also, a constant value of potential or current can be applied.

Electrochemical noise monitoring probes. Electrochemical noise monitoring is probably the newest of these methods. The method characterizes the naturally occurring fluctuations in current and potential due to the electrochemical kinetics and the mechanism of

the corroding metal interface. Measurements are taken without perturbing the interface by applying a potential or current to it. In this way, electrochemical processes are not interrupted and the system is measured without being disturbed. Methods including signal processing and mathematical transformation are used to provide information on the reaction kinetics at the surface and the corrosion rate.

This technique, originally discovered in the 1960s, remained a laboratory technique until recently, when some manufacturers began producing commercial devices. There are a few cases where electrochemical noise is being used in process-plant-type environments, and an ASTM committee has been formed to look at standardization of this technique. However, in general it remains a laboratory method with great potential for on-line monitoring. Recent research has demonstrated that electrochemical noise can be used to monitor MIC under laboratory conditions when appropriate probe configurations are used. Tests of these techniques in actual operating environments have been limited.

Indirect Probes Some types of probes do not measure corrosion directly, but yield measurements that also are useful in detecting corrosion. Examples include:

Pressure probes. Pressure monitors or transducers may be of use in corrosion monitoring in environments where buildup of gases such as hydrogen or H_2S may contribute to corrosion.

Gas probes. The hydrogen patch probe allows users to determine the concentration of hydrogen in the system. This is an important measurement since hydrogen can foster corrosion. Detecting production of certain gases may give rise to process changes to eliminate or limit the gaseous effluent and, therefore, lower the possibility of corrosion caused by these gases.

pH probes. Monitoring the pH may also aid in the early detection of corrosion. The acidity or alkalinity of the environment is often one of the controllable parameters in corrosion. Monitoring of the pH can be combined with other corrosion measurements to provide additional data about process conditions and give another level of process control.

Ion probes. Determining the level of ions in solution also helps to control corrosion. An increase in concentration of specific ions can contribute to scale formation, which can lead to a corrosion-related failure. Ion-selective electrode measurements can be included, just as pH measurements can, along with other more typical corrosion measurements. Especially in a complete monitoring system, this can add information about the effect of these ions on the material of interest at the process plant conditions.

Microbially influenced corrosion (MIC) probes. Devices are available which it is claimed can be used to measure the amount of microbial activity in some environments. Most of these "MIC monitoring devices" are limited in their application. The major problem lies in proving that the corrosion being detected is due to MIC. This is an exciting area for development of corrosion probes and monitoring systems.

Use of Corrosion Probes The major use of corrosion monitoring probes is to measure the corrosion rate in the plant or the field. In addition to corrosion-rate measurements, corrosion probes can be used to detect process upsets that may change the corrosion resistance of the equipment of interest. This is usually equally as important a measurement as corrosion rate since a change in the process conditions can lead to dramatic changes in the corrosion rate.

If the upset can be detected and dealt with in short order, the system can be protected. Some of the probes that measure parameters such as pH, ion content, and others are sensitive to process upsets and may give the fastest most complete information about such changes.

Monitoring can also be used to optimize the chemistry and level of corrosion inhibitors used. If too little inhibitor is used, enhanced corrosion can result and failure may follow. If too much is used, costs will increase without providing any additional protection. Optimization of the addition of inhibitor in terms of time, location in the process, and method of addition can also be evaluated through the use of carefully placed probes.

Another area where probes can be used effectively is in monitoring of deposits such as scale. One method of measurement is detecting specific ions that contribute to scale buildup or fouling; another is measuring the actual layers. Scale and fouling often devastate the corrosion resistance of a system, leading to a costly corrosion-related plant shutdown.

A final type of measurement is the detection of localized corrosion, such as pitting or crevice attack. Several corrosion-measuring probes can be used to detect localized corrosion. Some can detect localized corrosion instantaneously and others only its result. These types of corrosion may contribute little to the actual mass loss, but can be devastating to equipment and piping. Detection and measurement of localized corrosion is one of the areas with the greatest potential for the use of some of the newest electrochemically based corrosion monitoring probes.

Corrosion Rate Measurements Determining a corrosion rate from measured parameters (such as mass loss, current, or electrical potential) depends on converting the measurements into a corrosion rate by use of relationships such as Faraday's law.

Information on the process reaction conditions may be important to prolonging the lifetime of process equipment. Techniques such as EIS and potentiodynamic polarization can provide just such information without being tied to a specific corrosion-rate measurement.

This is also the case with methods that yield information on localized corrosion. The overall corrosion rate may be small when localized attack occurs, but failure due to perforation or loss of function may be the consequence of localized attack.

Measuring Corrosion Rate with Coupons Corrosion rate determined with typical coupon tests is an average value, averaged over the entire life of the test. Changes in the conditions under which the coupons are tested are averaged over the time the coupon is exposed. *Uniform attack is assumed to occur.* Converting measured values of loss of mass into an average corrosion rate has been covered extensively by many authors, and standard practices exist for determining corrosion rate.

Corrosion rates may vary during testing. Since the rate obtained from coupon testing is averaged over time, the frequency of sampling is important. Generally, measurements made over longer times are more valid. This is especially true for low corrosion rates, under 1 mil/y, mpy (0.001 in/y). When corrosion rates are this low, longer times should be used.

Factors may throw off these rates—these are outlined in ASTM G31, "Standard Practice for Laboratory Immersion Corrosion Testing of Metals." Coupon-type tests cannot be correlated with changing plant conditions that may dramatically affect process equipment lifetimes. Other methods must be used if more frequent measurements are desired or correlation with plant conditions is necessary.

A plot of mass loss versus time can provide information about changes in the conditions under which the test has been run. One example of such a plot comes from the ASTM Standard G96, "Standard Guide." As mentioned previously, weight loss measurements are appropriate for measurement of localized pitting corrosion, including that caused by MIC.

Heat Flux Tests Removable tube test heat exchangers find an ideal use in the field for monitoring heat flux (corrosion) conditions, NACE TMO286-94 (similar to laboratory test, Fig. 25-6).

The assumption of uniform corrosion is also at the heart of the measurements made by the electrical resistance (ER) probes. Again, ASTM Standard G96 outlines the method for using ER probes in plant equipment. These probes operate on the principle that the electrical resistance of a wire, strip, or tube of metal increases as its cross-sectional area decreases:

$$R = \frac{\rho L}{A}$$

where R = resistance, Ω
 ρ = resistivity, Ω/cm
 L = length, cm
 A = cross-sectional area, cm^2

Usually, in practice, the resistance is measured as a ratio between the actual measuring element and a similar element protected from the corrosive environment (the reference), and is given by R_M/R_R where subscript M is for measured and R is for reference.

Measurements are recorded intermittently or continuously. Changes in the slope of the curve obtained thus yields the corrosion rate.

The initial measurement of electrical resistance must be made after considerable time. Phenomenological information has been determined based on the corrosion rate expected at what period of time to initiate readings of the electrical resistance. Since these values are

based on experiential factors rather than on fundamental (so-called *first*) principles, correlation tables and lists of suggested thicknesses, compositions, and response times for usage of ER-type probes have developed over time, and these have been incorporated into the values read out of monitoring systems using the ER method.

Electrochemical Measurement of Corrosion Rate There is a link between electrochemical parameters and actual corrosion rates. Probes have been specifically designed to yield signals that will provide this information. LPR, ER, and EIS probes can give corrosion rates directly from electrochemical measurements. ASTM G102, "Standard Practice for Calculation of Corrosion Rates and Related Information from Electrochemical Measurements," tells how to obtain corrosion rates directly. Background on the approximations made in making use of the electrochemical measurements has been outlined by several authors.

ASTM G59, "Standard Practice for Conducting Potentiodynamic Polarization Resistance Measurements," provides instructions for the graphical plotting of data (from tests conducted using the above-noted ASTM Standard G103) as the linear potential versus current density, from which the polarization resistance can be found.

Measurements of polarization resistance R_p , given by LPR probes, can lead to measurement of the corrosion rate at a specific instant, since values of R_p are instantaneous.

To obtain the corrosion current I_{corr} from R_p , values for the anodic and cathodic slopes must be known or estimated. ASTM G59 provides an experimental procedure for measuring R_p . A discussion of the factors which may lead to errors in the values for R_p , and cases where R_p technique cannot be used, are covered by Mansfield in "Polarization Resistance Measurements—Today's Status, Electrochemical Techniques for Corrosion Engineers" (NACE International, 1992).

Some data from corrosion-monitoring probes do not measure corrosion rate, but rather give other useful information about the system. For example, suppose conditions change dramatically during a process upset. An experienced corrosion engineer can examine the data and correlate it with the upset conditions. Such analysis can provide insight into the process and help to improve performance and extend equipment lifetime. Changes in simple parameters such as pH, ion content, and temperature may lead to detection of a process upset. Without careful analysis, process upsets can reduce the corrosion lifetime of equipment and even cause a system failure.

Analysis of biological activity is sometimes difficult to correlate to corrosion rates. However, with detection and correlation of microbiological processes, especially those known to be related to corrosion (e.g., respiration rates, amount of acidity being produced) with process conditions, such information may also lead to improvements in the corrosion lifetime of the process equipment.

Evidence of localized corrosion can be obtained from polarization methods such as potentiodynamic polarization, EIS, and electrochemical noise measurements, which are particularly well suited to providing data on localized corrosion. When evidence of localized attack is obtained, the engineer needs to perform a careful analysis of the conditions that may lead to such attack. Correlation with process conditions can provide additional data about the susceptibility of the equipment to localized attack and can potentially help prevent failures due to pitting or crevice corrosion. Since pitting may have a delayed initiation phase, careful consideration of the cause of the localized attack is critical. Laboratory testing and involvement of an experienced corrosion engineer may be needed to understand the initiation of localized corrosion. Theoretical constructs such as Pourbaix diagrams can be useful in interpreting data obtained by on-line monitors.

Combinations of several types of probes can improve the information concerning corrosion of the system. Using only probes that provide corrosion-rate data cannot lead to as complete an analysis of the process and its effect on the equipment as with monitoring probes, which provide additional information.

Other Useful Information Obtained by Probes Both EIS and electrochemical noise probes can be used to determine information about the reactions that affect corrosion. Equivalent circuit analysis, when properly applied by an experienced engineer, can often give insight into the specifics of the corrosion reactions. Information such as corrosion product layer buildup, or inhibitor effectiveness, or coating breakdown can be obtained directly from analysis of the data from EIS or

indirectly from electrochemical noise data. In most cases, this is merely making use of methodology developed in the corrosion laboratory.

Some assumptions must be made to do this, but these assumptions are no different from those made in the laboratory. Recent experience involving in-plant usage of EIS has shown that this technique can be used effectively as a monitoring method and has led to development of several commercial systems.

Making use of the information from monitoring probes, combined with the storage and analysis capabilities of portable computers and microprocessors, seems the best method for understanding corrosion processes. Commercial setups can be assembled from standard probes, cables, readout devices, and storage systems. When these are coupled with analysis by corrosion engineers, the system can lead to a better understanding of in-plant corrosion processes.

Limitations of Probes and Monitoring Systems There are limitations even with the most up-to-date systems. Some of the things which cannot be determined using corrosion probes include:

Specifics on the types and rates of microbiological attack. These must be determined by using other methods such as chemical and microbiological analysis of the solution and materials from the corrosion sites. Consideration must be given to limitations of electrochemical techniques for MIC studies, noted previously under "Corrosion Testing: Laboratory Tests" and subsequent subsections.

Actual lifetime of the plant equipment. Corrosion monitoring provides data, which must then be analyzed with additional input and interpretation. However, only estimates can be made of the lifetime of the equipment of concern. Lifetime predictions are, at best, carefully crafted guesses based on the best available data.

Choices of alternative materials. Corrosion probes are carefully chosen to be as close as possible to the alloy composition, heat treatment, and stress condition of the material that is being monitored. Care must be taken to ensure that the environment at the probe matches the service environment. Choices of other alloys or heat treatments and other conditions must be made by comparison. Laboratory testing or coupon testing in the process stream can be used to examine alternatives to the current material, but the probes and the monitors can only provide information about the conditions which are present during the test exposure and cannot extrapolate beyond those conditions.

Failure analysis. Often, for a corrosion-related failure, data from the probes are examined to look for telltale signs that could have led to detection of the failure. In some cases, evidence can be found that process changes were occurring which led to the failure. This does not mean that the probes should have detected the failure itself. Determination of an imminent corrosion-related failure is not possible, even with the most advanced monitoring system.

The aforementioned limitations are not problems with the probes or the monitoring systems but occur when information is desired that cannot be measured directly or which requires extrapolation. Many of the problems that are encountered with corrosion-monitoring systems and probes are related to the use to which probes are put.

Potential Problems with Probe Usage Understanding the electrochemical principles upon which probes are based helps to eliminate some of the potential problems with probes. However, in some situations, the information desired is not readily available.

For example, consider localized corrosion. Although data from corrosion probes indicate corrosion rate, it is not possible to tell that localized corrosion is the problem. It is certainly not possible to demonstrate the mechanisms responsible for the localized corrosion.

This is an example of measuring the wrong thing. In this case, the probes work adequately, the monitoring system is adequate, as is the monitoring interval, but detection of the type of corrosion cannot be made based on the available data. Different types of probes and testing are required to detect the corrosion problem.

Another problem can arise if the probes and monitors are working properly but the probe is placed improperly (this is very common in natural gas transmission pipelines). Then the probe does not measure the needed conditions and environment. The data obtained by the probe will not tell the whole story and can in fact give very misleading results.

An example of this is in a condenser where the corrosion probe is in a region where the temperature is lower than that at the critical condition of interest. Local scale buildup is another example of this type of situation, as is formation of a crevice at a specific location.

The type of probe, its materials, and method of construction must be carefully considered in designing an effective corrosion-monitoring system. Since different types of probes provide different types of information, it may be necessary to use several types.

Incorrect information can result if the probe is made of the wrong material and is not heat treated in the same way as the process equipment (as well as because of other problems). The probe must be as close as possible to the material from which the equipment of interest is made. Existence of a critical condition, such as weldments or galvanic couples or occluded cells in the equipment of concern, makes the fabrication, placement, and maintenance of the probes and monitoring system of critical importance, if accurate and useful data are to be obtained.

Before electrochemical techniques are used in the evaluation of any situation involving microbes, the test protocol must receive considerable review by personnel quite experienced in *both* electrochemical testing and microbiologically influenced corrosion. It must be demonstrated that the method is capable of detecting and in some cases quantitatively measuring corrosion influenced by microbes.

The data obtained from probes and monitoring systems are most useful when analyzed by a corrosion specialist. Data not taken, analyses not made, or expertise not sought can quickly lead to problems even with the most up-to-date corrosion probes and monitoring system.

ECONOMICS IN MATERIALS SELECTION

In most instances, there will be more than one alternative material which may be considered for a specific application. Calculation of true long-term costs requires estimation of the following:

1. Total cost of fabricated equipment and piping
2. Total installation cost
3. Service life
4. Maintenance costs: amount and timing
5. Time and cost requirements to replace or repair at the end of service life
6. Cost of downtime to replace or repair
7. Cost of inhibitors, extra control facilities, and so on, required to assure achievement of predicted service life
8. Time value of money
9. Factors which impact taxation, such as depreciation and tax rates
10. Inflation rate

Proper economic analysis will allow comparison of alternatives on a sound basis. Detailed calculations are beyond the scope of this section. The reader should review the material in the NACE Publication 3C194, Item No. 24182, "Economics of Corrosion," Sept., 1994.

PROPERTIES OF MATERIALS

MATERIALS STANDARDS AND SPECIFICATIONS

There are obvious benefits to be derived from consensus standards that define the chemistry and properties of specific materials. Such standards allow designers and users of materials to work with confidence that the materials supplied will have the expected minimum

properties. Designers and users can also be confident that comparable materials can be purchased from several suppliers. Producers are confident that materials produced to an accepted standard will find a ready market and therefore can be produced efficiently in large factories.

TABLE 25-2 Unified Alloy Numbering System (UNS)

UNS was established in 1974 by ASTM and SAE to reduce the confusion involved in the labeling of commercial alloys. Metals have been placed into 15 groups, each of which is given a code letter. The specific alloy is identified by a five-digit number following this code letter.

Nonferrous metals and alloys	
A00001–A99999	Aluminum and aluminum alloys
C00001–C99999	Copper and copper alloys
E00001–E99999	Rare-earth and rare-earth-like metals and alloys
L00001–L99999	Low-melting metals and alloys
M00001–M99999	Miscellaneous nonferrous metals and alloys
N00001–N99999	Nickel and nickel alloys
P00001–P99999	Precious metals and alloys
R00001–R99999	Reactive and refractory metals and alloys
Ferrous metals and alloys	
D00001–D99999	Specified-mechanical-properties steels
F00001–F99999	Cast irons and cast steels
G00001–G99999	AISI and SAE carbon and alloy steels
H00001–H99999	AISI H steels
K00001–K99999	Miscellaneous steels and ferrous alloys
S00001–S99999	Heat- and corrosion-resistant (stainless) steels
T00001–T99999	Tool steels

When possible, earlier widely used three- or four-digit alloy numbering systems such as those developed by the Aluminum Association (AA), Copper Development Association (CDA), American Iron and Steel Institute (AISI), etc., have been incorporated by the addition of the appropriate alloy-group code letter plus additional digits. For example:

Alloy description	Former designation		UNS designation
	System	No.	
Aluminum + 1.2% Mn	AA	3003	A93003
Copper, electrolytic tough pitch	CDA	110	C11000
Carbon steel, 0.2% C	AISI	1020	G10200
Stainless steel, 18 Cr, 8 Ni	AISI	304	S30400

Proprietary alloys are assigned numbers by the AA, AISI, CDA, ASTM, and SAE, which maintains master listings at their headquarters. Handbooks describing the system are available. (Cf. ASTM publication DS-56AC.)

SOURCE: ASTM DS-56A. (Courtesy of National Association of Corrosion Engineers.)

While a detailed treatment is beyond the scope of this subsection, a few of the organizations which generate standards of major importance to the chemical-process industries in the United States are listed below. An excellent overview is presented in the *Encyclopedia of Chemical Technology* (5th ed., Wiley, Hoboken, N.J., 2006).

1. **American National Standards Institute (ANSI)**, formerly American Standards Association (ASA). ANSI promulgates the piping codes used in the chemical-process industries.

2. **American Society of Mechanical Engineers (ASME)**. This society generates the Boiler and Pressure Vessel Codes.

3. **American Society for Testing and Materials (ASTM)**. This society generates specifications for most of the materials used in the ANSI Piping Codes and the ASME Boiler and Pressure Vessel Codes.

4. **International Organization for Standardization (ISO)**. This organization is engaged in generating standards for worldwide use. It has 80 member nations.

With only a few noticeable exceptions, metals and their alloys possess a distinct shape. To generate the principal shape, metals are said to be **wrought** or **cast**. Wrought metals receive their shape through deformation steps; cast metals receive their shape through solidification steps. Materials of construction are available in both wrought and cast forms. Each group is discussed separately.

WROUGHT MATERIALS: FERROUS METALS AND ALLOYS

Steel Carbon steel is the most common, least expensive, and most versatile metal used in industry. It has excellent ductility, permitting many cold-forming operations. Steel is also very weldable. The grades of steel most commonly used in the chemical-process industries have tensile strength in the 345- to 485-MPa (50,000 to

TABLE 25-3 Coefficient of Thermal Expansion of Common Alloys*

	UNS	10 ⁻⁶ in/ (in·°F)	10 ⁻⁶ mm/ (mm·°C)	Temperature range, °C
Aluminum alloy AA1100	A91100	13.1	24.	20–100
Aluminum alloy AA5052	A95052	13.2	24.	20–100
Aluminum cast alloy 43	A24430	12.3	22.	20–100
Copper	C11000	9.4	16.9	20–100
Red brass	C23000	10.4	18.7	20–300
Admiralty brass	C44300	11.2	20.	20–300
Muntz Metal	C28000	11.6	21.	20–300
Aluminum bronze D	C61400	9.0	16.2	20–300
Ounce metal	C83600	10.2	18.4	0–100
90-10 copper nickel	C70600	9.5	17.1	20–300
70-30 copper nickel	C71500	9.0	16.2	20–300
Carbon steel, AISI 1020	G10200	6.7	12.1	0–100
Gray cast iron	F10006	6.7	12.1	0–100
4-6 Cr, ½ Mo steel	S50100	7.3	13.1	20–540
Stainless steel, AISI 410	S41000	6.1	11.0	0–100
Stainless steel, AISI 446	S44600	5.8	10.4	0–100
Stainless steel, AISI 304	S30400	9.6	17.3	0–100
Stainless steel, AISI 310	S31000	8.0	14.4	0–100
Stainless steel, ACI HK	J94224	9.4	16.9	20–540
Nickel alloy 200	N02200	7.4	13.3	20–90
Nickel alloy 400	N04400	7.7	13.9	20–90
Nickel alloy 600	N06600	7.4	13.3	20–90
Nickel-molybdenum alloy B-2	N10665	5.6	10.1	20–90
Nickel-molybdenum alloy C-276	N10276	6.3	11.3	20–90
Titanium, commercially pure	R50250	4.8	8.6	0–100
Titanium alloy T1- 6A1-4V	R56400	4.9	8.8	0–100
Magnesium alloy AZ31B	M11311	14.5	26.	20–100
Magnesium alloy AZ91C	M11914	14.5	26.	20–100
Chemical lead		16.4	30.	0–100
50-50 solder	L05500	13.1	24.	0–100
Zinc	Z13001	18.	32.	0–100
Tin	L13002	12.8	23.	0–100
Zirconium	R60702	2.9	5.2	0–100
Molybdenum	R03600	2.7	4.9	20–100
Tantalum	R05200	3.6	6.5	20–100

*Courtesy of National Association of Corrosion Engineers.

70,000 lbf/in²) range, with good ductility. Higher strength levels are achieved by cold work, alloying, and heat treatment.

Carbon steel is easily the most commonly used material in process plants despite its somewhat limited corrosion resistance. It is routinely used for most organic chemicals and neutral or basic aqueous solutions at moderate temperatures. It is also used routinely for the storage of concentrated sulfuric acid and caustic soda [up to 50 percent and 55°C (130°F)]. Because of its availability, low cost, and ease of fabrication, steel is frequently used in services with corrosion rates of 0.13 to 0.5 mm/yr (5 to 20 mils/yr), with added thickness (**corrosion allowance**) to ensure the achievement of desired service life. Product quality requirements must be considered in such cases.

Corrosion under insulation is a major problem with carbon steels and must be taken into consideration in the RBI analysis of any plant to avoid serious failures. Several techniques are available to minimize this attack including painting, spraying with aluminum, and/or wrapping with aluminum foil.

TABLE 25-4 Melting Temperatures of Common Alloys*

	UNS	Melting range	
		°F	°C
Aluminum alloy AA1100	A91100	1190–1215	640–660
Aluminum alloy AA5052	A95052	1125–1200	610–650
Aluminum cast alloy 43	A24430	1065–1170	570–630
Copper	C11000	1980	1083
Red brass	C23000	1810–1880	990–1025
Admiralty brass	C44300	1650–1720	900–935
Muntz Metal	C28000	1650–1660	900–905
Aluminum bronze D	C61400	1910–1940	1045–1060
Ounce metal	C83600	1510–1840	854–1010
Manganese bronze	C86500	1583–1616	862–880
90-10 copper nickel	C70600	2010–2100	1100–1150
70-30 copper nickel	C71500	2140–2260	1170–1240
Carbon steel, AISI 1020	G10200	2760	1520
Gray cast iron	F10006	2100–2200	1150–1200
4-6 Cr, ½ Mo Street	S50100	2700–2800	1480–1540
Stainless steel, AISI 410	S41000	2700–2790	1480–1530
Stainless steel, AISI 446	S44600	2600–2750	1430–1510
Stainless steel, AISI 304	S30400	2550–2650	1400–1450
Stainless steel, AISI 310	S31000	2500–2650	1400–1450
Stainless steel, ACI HK	J94224	2550	1400
Nickel alloy 200	N02200	2615–2635	1440–1450
Nickel alloy 400	N04400	2370–2460	1300–1350
Nickel alloy 600	N06600	2470–2575	1350–1410
Nickel-molybdenum alloy B-2	N10665	2375–2495	1300–1370
Nickel-molybdenum alloy C-276	N10276	2420–2500	1320–1370
Titanium, commercially pure	R50250	3100	1705
Titanium alloy T1-6Al-4V	R56400	2920–3020	1600–1660
Magnesium alloy AZ 31B	M11311	1120–1170	605–632
Magnesium alloy HK 31A	M13310	1092–1204	589–651
Chemical lead		618	326
50-50 solder	L05500	361–421	183–216
Zinc	Z13001	787	420
Tin	Z13002	450	232
Zirconium	R60702	3380	1860
Molybdenum	R03600	4730	2610
Tantalum	R05200	5425	2996

*Courtesy of National Association of Corrosion Engineers.

Low-Alloy Steels Alloy steels contain one or more alloying agents to improve the mechanical and corrosion-resistant properties over those of carbon steel. A typical low-alloy grade [American Iron and Steel Institute (AISI) 4340] contains 0.40 percent C, 0.70 percent Mn, 1.85 percent Ni, 0.80 percent Cr, and 0.25 percent Mo. Many other alloying agents are used to produce a large number of standard AISI and proprietary grades. Nickel increases toughness and improves low-temperature properties and corrosion resistance. Chromium and silicon improve hardness, abrasion resistance, corrosion resistance, and resistance to oxidation. Molybdenum provides strength at elevated temperatures. The addition of small amounts of alloying materials greatly improves corrosion resistance to atmospheric environments but does not have much effect against liquid corrosives. The alloying elements produce a tight, dense, adherent rust film, but in acid or alkaline solutions corrosion is about equivalent to that of carbon steel. However, the greater strength permits thinner walls in process equipment made from low-alloy steel.

Stainless Steel There are more than 70 standard types of stainless steel and many special alloys. These steels are produced in the wrought form (AISI types) and as cast alloys [Alloy Casting Institute (ACI) types]. Generally, all are iron-based, with 12 to 30 percent chromium, 0 to 22 percent nickel, and minor amounts of carbon, niobium (columbium), copper, molybdenum, selenium, tantalum, and titanium. These alloys are very popular in the process industries. They are heat- and corrosion-resistant, noncontaminating, and easily fabricated into complex shapes.

There are four groups of stainless alloys: (1) martensitic, (2) ferritic, (3) austenitic, and (4) duplex.

The **martensitic alloys** contain 12 to 20 percent chromium with controlled amounts of carbon and other additives. Type 410 is a typical member of this group. These alloys can be hardened by heat treatment, which can increase tensile strength from 550 to 1380 MPa (80,000 to 200,000 lbf/in²). Corrosion resistance is inferior to that of austenitic stainless steels, and martensitic steels are generally used in mildly corrosive environments (atmospheric, freshwater, and organic exposures). In the hardened condition, these materials are very susceptible to hydrogen embrittlement.

TABLE 25-5 Carbon and Low-Alloy Steels^a

Steel type	ASTM	UNS	Composition, % ^b	Mechanical properties ^c		
				Yield strength, kip/in ² (MPa)	Tensile strength, kip/in ² (MPa)	Elongation, %
C-Mn	A53B	K03005	0.30 C, 1.20 Mn	35 (241)	60 (415)	
C-Mn	A106B	K03006	0.30 C, 0.29–1.06 Mn, 0.10 min. Si	35 (241)	60 (415)	30
C	A285A	K01700	0.17 C, 0.90 Mn	24 (165)	45–55 (310–380)	30
HSLA	A517F	K11576	0.08–0.22 C, 0.55–1.05 Mn, 0.13–0.37 Si, 0.36–0.79 Cr, 0.67–1.03 Ni, 0.36–0.64 Mo, 0.002–0.006 B, 0.12–0.53 Cu, 0.02–0.09 V	100 (689)	115–135 (795–930)	16
HSLA	A242(1)	K11510	0.15 C, 1.00 Mn, 0.20 min Cu, 0.15 P	42–50 (290–345)	63–70 (435–480)	21
2¼ Cr, 1 Mo	A387(22)	K21590	0.15 C, 0.30–0.60 Mn, 0.5 Si, 2.00–2.50 Cr, 0.90–1.10 Mo	30 (205) ^d 45 (310) ^e	60–85 (415–585) ^d 75–100 (515–690) ^e	18 ^d 18 ^d
4–6 Cr, ½ Mo	A335 (P5)	K41545	0.15 C, 0.30–0.60 Mn, 0.5 Si, 4.00–6.00 Cr, 0.45–0.65 Mo	30 (205)	60 (415)	
9 Cr, 1 Mo	A335 (P9)	K81590	0.15 C, 0.30–0.6 Mn, 0.25–1.00 Si, 8.00–10.00 Cr, 0.90–1.10 Mo	30 (205)	60 (415)	
9 Ni	A333(8), A353(1)	K81340	0.13 C, 0.90 Mn, 0.13–0.32 Si, 8.40–9.60 Ni	75 (515)	100–120 (690–825)	20
	AISI 4130	G41300	0.28–0.33 C, 0.80–1.10 Mn, 0.15–0.3 Si, 0.8–1.10 Cr, 0.15–0.25 Mo	120 (830) ^f	140 (965) ^f	22 ^f
	AISI 4340	G43400	0.38–0.43 C, 0.60–0.80 Mn, 0.15–0.3 Si, 0.70–0.90 Cr, 1.65–2.00 Ni, 0.20–0.30 Mo	125 (860) ^g	148 (1020) ^g	20 ^g

^aCourtesy of National Association of Corrosion Engineers. To convert MPa to lbf/in², multiply by 145.04.

^bSingle values are maximum values unless otherwise noted.

^cRoom-temperature properties. Single values are minimum values.

^dClass 1.

^eClass 2.

^f1-in.-diameter bars water-quenched from 1,575°F (860°C) and tempered at 1,200°F (650°C).

^g1-in.-diameter bars oil-quenched from 1,550°F (845°C) and tempered at 1,200°F (650°C).

TABLE 25-6a Typical Physical Properties of Low-Alloy AISI Steels^a

AISI type	Melting temperature, °F	Thermal conductivity, Btu/(h-ft ²)(°F/ft)] (212°F)	Coefficient of thermal expansion (0-1,200°F) per °F	Specific heat (68-212°F), Btu/(lb-°F)
13XX		27	7.9 × 10 ^{-6b}	0.10-0.11
23XX	2,600-2,620	38.3 ^c	8.0 × 10 ⁻⁶	0.11-0.12
25XX	2,610-2,620	34.5-38.5 ^c	7.8 × 10 ⁻⁶	0.11-0.12
40XX		27	8.3 × 10 ^{-6b}	0.10-0.11
41XX		24.7 ^d		0.11
43XX	2,740-2,750	21.7 ^c	8.1 × 10 ⁻⁶	0.107
46XX		27 ^d	6.3 × 10 ^{-6e}	0.10-0.11
48XX	2,750	26 ^f	8.6 × 10 ⁻⁶	
51XX	2,720-2,760	27-34 ^g	7.4 × 10 ^{-6h}	0.10-0.11
61XX		27	8.1 × 10 ^{-6b}	0.10-0.11
86, 87XX	2,745-2,755	21.7 ^c	8.2 × 10 ⁻⁶	0.107
92, 94XX		27	8.1 × 10 ^{-6b}	0.10-0.12

XX = nominal percent carbon.
^aDensity for all low-alloy steels is about 0.28 lb/in³.
^b68 to 1200°F.
^c120°F.
^d68°F.
^e0 to 200°F.
^f75°F.
^g32 to 212°F.
^h100 to 518°F.

Ferritic stainless steel contains 15 to 30 percent Cr, with low carbon content (0.1 percent). The higher chromium content improves its corrosive resistance. Type 430 is a typical example. The strength of ferritic stainless can be increased by cold working but not by heat treatment. Fairly ductile ferritic grades can be fabricated by all standard methods. They are fairly easy to machine. Welding is not a problem, although it requires skilled operators. Corrosion resistance is rated good, although ferritic alloys are not good against reducing acids such as HCl. But mildly corrosive solutions and oxidizing media are handled without harm. Type 430 is widely used in nitric acid plants. In addition, it is very resistant to scaling and high-temperature oxidation up to 800°C (1500°F).

Austenitic stainless steels are the most corrosion-resistant of the four groups. These steels contain 16 to 26 percent chromium and 6 to 22 percent nickel. Carbon is typically kept low (0.03 percent maximum) to minimize carbide precipitation. These alloys can be work-hardened, but heat treatment will not cause hardening. Tensile strength in the annealed condition is about 585 MPa (85,000 lbf/in²), but work hardening can increase this to 2000 MPa (300,000 lbf/in²) by creating martensite in the matrix. Austenitic stainless steels are tough and ductile. They can be fabricated by all standard methods. But austenitic grades are not easy to machine; they work-harden and gall. Rigid machines, heavy cuts, and low speeds are essential. Welding, however, is readily performed, although welding heat may cause chromium carbide precipitation, which depletes the alloy of some chromium and lowers its corrosion resistance in some specific environments, notably nitric acid. The carbide precipitation can be eliminated by heat treatment (solution annealing). To avoid precipitation, special stainless steels stabilized with titanium, niobium, or tantalum have been developed (types 321 and 347). The addition of molybdenum to the austenitic alloy (types 316, 316L, 317, and 317L) provides generally better corrosion resistance and improved resistance to pitting. Nitrogen additions have also shown benefit in improving localized corrosion resistance. Nitrogen also increases the strength, and materials today are frequently dual-certified, i.e., 304/304L but with a carbon content equal to a 304L.

In the stainless group, nickel greatly improves corrosion resistance over straight chromium stainless. Even so, the chromium-nickel steels, particularly the 18-8 alloys, perform best under **oxidizing conditions**, since resistance depends on an oxide film on the surface of the alloy. Reducing conditions and chloride ions destroy this film and

TABLE 25-6b Typical Mechanical Properties of Low-Alloy AISI Steels^a

AISI type	Tensile strength, 1,000 lbf/in ²	Yield strength (0.2% offset), 1000 lbf/in ²	Elongation (in 2 in), %	Reduction of area, %	Hardness, Brinell	Impact strength (Izod), ft-lbf
1,330 ^b	122	100	19	52	248	
1,335 ^c	126	105	20	59	262	
1,340 ^c	137	118	19	55	285	
2,317 ^c	107	72	27	71	222	84
2,515 ^c	113	94	25	69	233	85
E2,517 ^c	120	100	22	66	244	80
4,023 ^d	120	85	20	53	255	
4,032 ^c	210	182	11	49	415	
4,042 ^f	235	210	10	42	461	
4,053 ^g	250	223	12	40	495	
4,063 ^h	269	231	8	15	534	
4,130 ^j	200	170	16	49	375	25
4,140 ^j	200	170	15	48	385	16
4,150 ^k	230	215	10	40	444	12
4,320 ^l	180	154	15	50	360	32
4,337 ^k	210	140	14	50	435	18
4,340 ^k	220	200	12	48	445	16
4,615 ^d	100	75	18	52	42	42
4,620 ^l	130	95	21	65	68	68
4,640 ^j	185	160	14	52	390	25
4,815 ^d	150	125	18	58	325	44
4,817 ^d		15	52	355	36	
4,820 ^j		13	47	380	28	
5,120 ^m	143	114	13	45	302	6
5,130 ^m	189	175	13	51	380	
5,140 ^m	190	170	13	43	375	16
5,150 ^m	224	208	10	40	444	
6,120 ⁿ	125	94	21	56		28
6,145 ^o	176	169	16	52	429	20
6,150 ^o	187	179	13	42	444	13
8,620 ^p	122	98	21	63	245	76
8,630 ^p	162	142	14	54	325	42
8,640 ^p	208	183	13	43	420	18
8,650 ^p	214	194	12	41	423	
8,720 ^p	122	98	21	63	245	76
8,740 ^p	208	183	13	43	420	18
8,750 ^p	214	194	12	41	423	
9,255 ^q	232 ^r	215	9	21	477	6
9,261 ^r	258 ^r	226	10	30	514	12

^aProperties are for materials hardened and tempered as follows: ^bwater-quenched from 1,525°F, tempered at 1,000°F; ^coil-quenched from 1,525°F, tempered at 1,000°F; ^dpseudocarbonized 8 h at 1700°F, oil-quenched, tempered 1 h at 300°F; ^ewater-quenched from 1,525°F, tempered at 600°F; ^foil-quenched from 1,500°F, tempered at 600°F; ^goil-quenched from 1,475°F, tempered at 600°F; ^hoil-quenched from 1,450°F, tempered at 600°F; ⁱwater-quenched from 1,500 to 1,600°F, tempered at 800°F; ^joil-quenched from 1,550°F, tempered at 800°F; ^koil-quenched from 1,525°F, tempered at 800°F; ^lnormalized at 1,650°F, reheated to 1,475°F, oil-quenched, tempered at 800°F; ^mnormalized at 1,625°F, reheated to 1,550°F, water-quenched, tempered at 800°F; ⁿcarburized 10 h at 1,680°F, pot-cooled, oil-quenched from 1,525°F, tempered at 300°F; ^onormalized at 1,600°F, oil-quenched from 1,575°F, tempered at 1,000°F; ^poil-quenched tempered at 800°F; ^qnormalized at 1,650°F, reheated to 1,625°F, quenched in agitated oil, tempered at 800°F; ^rnormalized at 1,600°F, reheated to 1,575°F, quenched in agitated oil, tempered at 800°F.

NOTE: °C = (°F - 32) × 5/9. To convert Btu/(h-ft²·°F) to W/(m²·°C), multiply by 0.8666; to convert Btu/(lb·°F) to kJ/(kg·°C), multiply by 0.2388; to convert lbf/in² to MPa, multiply by 0.006895; and to convert ft-lbf to J, multiply by 0.7375.

bring on rapid attack. Chloride ions tend to cause pitting and crevice corrosion; when combined with high tensile stresses, they can cause stress-corrosion cracking.

A specialty group of alloys has been created with chromium and molybdenum significantly above the standard stainless grades. Many of these grades are proprietary and contain chromium of 20 percent and molybdenum of 6 to 7 percent, and most also contain nitrogen to

25-32 MATERIALS OF CONSTRUCTION

TABLE 25-7 Cast-Iron Alloys

Alloy	ASTM	UNS	Composition, % †	Condition	Mechanical properties ‡			
					Yield strength, kip/in ² (MPa)	Tensile strength, kip/in ² (MPa)	Elongation, %	Hardness, HB
Gray cast iron	A159 (G3000)	F10006	3.1–3.4 C, 0.6–0.9 Mn, 1.9–2.3 Si	As cast		30 (207)		187–241
Malleable cast iron	A602 (M3210)	F20000	2.2–2.9 C, 0.15–1.25 Mn, 0.9–1.90 Si	Annealed	32 (229)	50 (345)	12	130
Gray cast iron	A436(1)	F41000	3.0 C, 1.5–2.5 Cr, 5.5–7.5 Cu, 0.5–1.5 Mn, 13.5–17.5 Ni, 1.0–2.8 Si	As cast		25 (172)		150
Gray cast iron	A436(2)	F41002	3.0 C, 1.5–2.5 Cr, 0.50 Cu, 0.5–1.5 Mn, 18–22 Ni, 1.0–2.8 Si	As cast		25 (172)		145
Gray cast iron	A436(5)	F41006	2.4 C, 0.1 Cr, 0.5 Cu, 0.5–1.5 Mn, 34–36 Ni, 1.0–2.0 Si	As cast		20 (138)		110
Ductile austenitic cast iron	A439(D-2)	F43000	3.0 C, 1.75–2.75 Cr, 0.7–1.25 Mn, 18–22 Ni, 1.5–3.0 Si	As cast	30 (207)	58 (400)		170
Ductile austenitic cast iron	A439 (D-5)	F43006	2.4 C, 0.1 Cr, 1.0 Mn, 34–36 Ni, 1.0–2.8 Si	As cast	30 (207)	55 (379)		155
Silicon cast iron	A518	F47003	0.7–1.1 C, 0.5 Cr, 0.5 Cu, 1.50 Mn, 0.5 Mo, 14.2–14.75 Si	As cast		16 (110)		520

To convert MPa to lbf/in², multiply by 145.04.

†Single values are maximum values.

‡Typical room-temperature properties.

improve localized corrosion resistance. This family is collectively known as the **6Mo family** and has corrosion resistance intermediate between the standard grades and some of the nickel-based alloys. They also have improved stress corrosion and localized corrosion resistance. Typical of this family are Avesta 254 SMO and Allegheny AL6XN.

Duplex stainless steels were created by adjusting the composition so that approximately equal amounts of the austenitic phase and the ferritic phase are present in the alloy. Three general families of alloys have been developed that contain 18 percent Cr, 22 percent Cr, and 25 percent Cr. As the chromium content increases, so does the general resistance of the alloys. All duplex alloys have better stress-corrosion resistance than the austenitic grades while the general corrosion resistance is not significantly increased. Because the structure is a mixture of ferritic and austenitic grains, the yield strength of this class of materials is significantly higher than that for the austenitic grades. Some of the “super duplex” (25 Cr) alloys have been used in offshore oil platforms because

of their strength and corrosion resistance, and they are finding increasing uses in chemical plants. These alloys suffer from a 474°C (885°F) embrittlement and so have lower maximum-use temperatures than the austenitic alloys. The presence of sigma phase in the microstructure can cause serious corrosion and mechanical problems. ASTM A 923 was developed to assist in determining the presence of sigma phase.

WROUGHT MATERIALS: NONFERROUS METALS AND ALLOYS

Nickel and Nickel Alloys Nickel is available in practically any mill form as well as in castings. It can be machined easily and joined by welding. Generally, oxidizing conditions favor corrosion, while reducing conditions retard attack. Neutral alkaline solutions, seawater, and mild atmospheric conditions do not affect nickel. The metal is widely used for

TABLE 25-8 Standard Wrought Martensitic Stainless Steels

AISI type	UNS	Composition, %*					Mechanical properties †			
		Cr	Ni	Mo	C	Other	Yield strength, kip/in ² (MPa) ‡	Tensile strength, kip/in ² (MPa) ‡	Elongation, %	Hardness, HB
403	S40300	11.5–13.0			0.15		40 (276)	75 (517)	35	155
410	S41000	11.5–13.5			0.15		35 (241)	70 (483)	30	150
414	S41400	11.5–13.5	1.25–2.5		0.15		90 (621)	115 (793)	20	235
416	S41600	12–14		0.6	0.15	0.15S§	40 (276)	75 (517)	30	155
416Se	S41623	12–14			0.15	0.15Se§	40 (276)	75 (517)	30	155
420	S42000	12–14			0.15		50 (345)	95 (655)	20	195
420F	S42020	12–14		0.6	0.15§	0.155§	55 (379)	95 (655)	22	220
422	S42200	11–13	0.5–1.0	0.75–1.25	0.20–0.25	0.15–0.30 V, 0.75–1.25 W	125 (862)	145 (1000)	18	320
431	S43100	15–17	1.25–2.5		0.20		95 (665)	125 (862)	20	260
440A	S44002	16–18		0.75	0.6–0.75		60 (414)	105 (724)	20	210
440B	S44003	16–18.0		0.75	0.75–0.95		62 (427)	107 (738)	18	215
440C	S44004	16–18		0.75	0.95–1.20		65 (448)	110 (758)	14	220
501	S50100	4–6		0.40–0.65	0.10§		30 (207)	70 (483)	28	160
502	S50200	4–6		0.40–0.65	0.10		25 (172)	65 (448)	30	150

*Single values are maximum values unless otherwise noted.

†Typical room-temperature properties of annealed plates.

‡To convert MPa to lbf/in², multiply by 145.04.

§Minimum.

TABLE 25-9 Standard Wrought Ferritic Stainless Steels

AISI type	Composition, %†								Mechanical properties‡			
	UNS	Cr	C	Mn	Si	P	S	Other	Yield strength, kip/in ² (MPa)*	Tensile strength, kip/in ² (MPa)*	Elongation, %	Hardness, HB
405	S40500	11.5–14.5	0.08	1.0	1.0	0.04	0.03	0.1–0.3 Al	40 (276)	65 (448)	30	150
409	S40900	10.5–11.75	0.08	1.0	1.0	0.045	0.045	(6 × C) Ti§	35 (241)	65 (448)	25	137
429	S42900	14–16	0.12	1.0	1.0	0.04	0.03		40 (276)	70 (483)	30	163
430	S43000	16–18	0.12	1.0	1.0	0.04	0.03		40 (276)	75 (517)	30	160
430F	S43020	16–18	0.12	1.25	1.0	0.06	0.15¶	0.6 Mo	55 (379)	80 (552)	25	170
434	S43400	16–18	0.12	1.0	1.0	0.04	0.03	0.75–1.25 Mo	53 (365)	77 (531)	23	160
436	S43600	16–18	0.12	1.0	1.0	0.04	0.03	0.75–1.25 Mo (5 × C)(Cb + Ta)§	53 (365)	77 (531)	23	160
442	S44200	18–23	0.20	1.0	1.0	0.04	0.03		45 (310)	80 (552)	20	185
446	S44600	23–27	0.20	1.5	1.0	0.04	0.03	0.25N	55 (379)	85 (586)	25	160

*To convert MPa to lbf/in², multiply by 145.04.

†Single values are maximum values unless otherwise noted.

‡Typical temperature properties of annealed plates.

§0.70 maximum.

¶Minimum.

handling alkalis, particularly in concentrating, storing, and shipping high-purity caustic soda. Chlorinated solvents and phenol are often refined and stored in nickel to prevent product discoloration and contamination. A large number of nickel-based alloys are commercially available.

One of the best known of these is **Monel 400**, 67 percent Ni and 30 percent Cu. It is available in all standard forms. This nickel-copper alloy is ductile and tough and can be readily fabricated and joined. Its corrosion resistance is generally superior to that of its components, being more resistant than nickel in reducing environments and more resistant than copper in oxidizing environments. The alloy can be used for relatively dilute sulfuric acid (below 80 percent), although aeration will result in increased corrosion. Monel will handle hydrofluoric acid up to 92 percent and 115°C (235°F) although aeration can produce cracking. Alkalies have little effect on this alloy, but it will not stand up against very highly oxidizing or reducing environments.

Another important alloy is a Ni-Mo alloy, **Hastelloy alloy B-3**. This alloy is 74 percent nickel and 26 percent molybdenum. The alloy is resistant to all hydrochloric acid solutions and other strongly reducing acids. The addition of oxidizers such as ferric or cupric ions or oxygen will accelerate corrosion. Work hardening presents some fabrication difficulties, and machining is somewhat more difficult than for 316L stainless.

The addition of chromium forms a family of Ni-Cr-Mo alloys such as **Hastelloy alloys C-276, C-22, and C-2000**. These alloys contain 16 to 22 percent chromium and 13 to 16 percent molybdenum and are very resistant to a wide variety of chemical environments. They are considered resistant to stress-corrosion cracking and very resistant to localized corrosion in chloride-containing environments. These alloys are resistant to strong oxidizing solutions, such as wet chlorine and hypochlorite solutions. They are among only a few alloys that are completely resistant to seawater. The carbon contents are low enough that weld sensitization is not a problem during fabrication. These alloys are also more difficult to machine than stainless steel, but fabrication is essentially the same.

Replacing some of the nickel with iron produces a family of alloys with intermediate corrosion resistance between stainless steels and the Ni-Cr-Mo alloys. Alloys such as **Incoloy 825** and **Hastelloy G-3 and G-30** are in this family. Incoloy 825 has 40 percent Ni, 21 percent Cr, 3 percent Mo, and 2.25 percent Cu. Hastelloy G-3 contains 44 percent Ni, 22 percent Cr, 6.5 percent Mo, and 0.05 percent C maximum. These alloys have extensive applications in sulfuric acid systems. Because of their increased nickel and molybdenum contents they are more tolerant of chloride-ion contamination than are standard stainless steels. The nickel content decreases the risk of stress-corrosion cracking; molybdenum improves resistance to crevice corrosion and pitting. Many of the nickel-based alloys are proprietary and are covered by the following specifications:

1. Sheet and plate: ASTM B 333, B575
2. Bar: ASTM B 335, B 574
3. Forgings: ASTM B 564

4. Welded pipe and tubing: ASTM B 626, B 619

5. Seamless pipe and tubing: ASTM B 622

6. Fittings: ASTM B 366

All the nickel alloys are readily fabricated and welded. Their design strengths allow use to elevated temperatures and with relatively thin wall thicknesses. The Nickel Institute (<http://www.nickelinstitute.org>) has excellent publications available that detail the properties and fabrication requirements for both stainless steels and nickel-based alloys, as does SSINA (<http://www.ssina.com>) and so do many of the manufacturers of these alloys.

Aluminum and Alloys Aluminum and its alloys are made in practically all the forms in which metals are produced, including castings. Thermal conductivity of aluminum is 60 percent of that of pure copper, and unalloyed aluminum is used in many heat-transfer applications. Its high electrical conductivity makes aluminum popular in electrical applications. Aluminum is one of the most workable of metals, and it is usually joined by inert-gas-shielded arc-welding techniques.

Commercially pure aluminum has a tensile strength of 69 MPa (10,000 lbf/in²), but it can be strengthened by cold working. One limitation of aluminum is that strength declines greatly above 150°C (300°F). When strength is important, 200°C (400°F) is usually considered the highest permissible safe temperature for aluminum. However, aluminum has excellent low-temperature properties; it can be used at -250°C (-420°F). Aluminum has high resistance to atmospheric conditions as well as to industrial fumes and vapors and fresh, brackish, or salt waters. Many mineral acids attack aluminum, although the metal can be used with concentrated nitric acid (above 82 percent) and glacial acetic acid. Aluminum cannot be used with strong caustic solutions.

Note that a number of **aluminum alloys** are available (see Table 25-17). Many have improved mechanical properties over pure aluminum. The wrought heat-treatable aluminum alloys have tensile strengths of 90 to 228 MPa (13,000 to 33,000 lbf/in²) as annealed; when they are fully hardened, strengths can go as high as 572 MPa (83,000 lbf/in²). However, aluminum alloys usually have lower corrosion resistance than the pure metal.

The **Alclad** alloys have been developed to overcome this shortcoming. Alclad consists of a pure aluminum layer metallurgically bonded to a core alloy. The corrosion resistance of aluminum and its alloys tends to be very sensitive to trace contamination. Very small amounts of metallic mercury, heavy-metal ions, or chloride ions can frequently cause rapid failure under conditions which otherwise would be fully acceptable. When alloy steels do not give adequate corrosion protection—particularly from sulfidic attack—steel with an **aluminized surface coating** can be used.

A spray coating of aluminum on a steel is not likely to spall or flake, but the coating is usually not continuous and may leave some areas of the steel unprotected. Hot-dipped “aluminized” steel gives a continuous coating and has proved satisfactory in a number of applications,

particularly when sulfur or hydrogen sulfide is present. It is also used to protect thermal insulation and as weather shields for equipment. The coated steel resists fires better than solid aluminum.

Copper and Alloys Copper and its alloys are widely used in chemical processing, particularly when heat and electrical conductivity are important factors. The thermal conductivity of copper is twice that of aluminum and 90 percent that of silver. A large number of copper alloys are available, including brasses (Cu-Zn), bronzes (Cu-Sn), cupronickels (Cu-Ni), and age-hardenable alloys such as copper beryllium (Cu-Be) and copper nickel tin (Cu-Ni-Sn).

Copper has excellent low-temperature properties and is used at $\sim 200^{\circ}\text{C}$ ($\sim 320^{\circ}\text{F}$). Brazing and soldering are common joining methods for copper, although welding, while difficult, is possible. Generally, copper has high resistance to industrial and marine atmospheres, seawater, alkalis, and solvents. Oxidizing acids rapidly corrode copper. However, the alloys have somewhat different properties from those of commercial copper.

Brasses with up to 15 percent Zn are ductile but difficult to machine. Machinability improves with increasing zinc up to 36 percent Zn. Brasses with less than 20 percent Zn have corrosion resistance equivalent to that of copper but with better tensile strengths. Brasses with 20 to 40 percent Zn have lower corrosion resistance and are subject to dezincification and stress-corrosion cracking, especially when ammonia is present.

Bronzes are somewhat similar to brasses in mechanical properties and to high-zinc brasses in corrosion resistance (except that bronzes are not affected by stress cracking).

Aluminum and silicon bronzes are very popular in the process industries because they combine good strength with corrosion resistance. Copper-beryllium alloys offer the greatest strength and excellent corrosion resistance in seawater and are resistant to stress-corrosion cracking in hydrogen sulfide.

Cupronickels (10 to 30 percent Ni) have become very important as copper alloys. They have the highest corrosion resistance of all copper alloys and find application as heat-exchanger tubing. Resistance to seawater is particularly outstanding. Cu-Ni-Sn spinodal strengthened alloys offer higher strength than the cupronickels along with excellent corrosion resistance. These alloys demonstrate very low weight loss in sulfide-containing environments and negligible weight loss in seawater.

The Copper Development Association has excellent references on copper and its alloys at <http://www.copper.org>.

Lead and Alloys Chemical leads of 99.9 percent purity are used primarily in the chemical industry in environments that form thin, insoluble, and self-repairable protective films, e.g., salts such as sulfates, carbonates, or phosphates. More soluble films such as nitrates, acetates, or chlorides offer little protection. Alloys of antimony, tin, and arsenic offer limited improvement in mechanical properties, but the usefulness of lead is limited primarily because of its poor structural qualities. It has a low melting point and tensile stress as low as 1 MPa (145 lbf/in²).

For information on lead and its uses, contact Lead Development Association International at <http://www.leadint.org>.

Titanium Titanium has become increasingly important as a construction material. It is strong and of medium weight. Corrosion resistance is very superior in oxidizing and mild reducing media (Ti-Pd alloys Grade 7 and 11 have superior resistance in reducing environments, as does the Ti-Mo-Ni alloy Grade 12). Titanium alloys with lower amounts of Pd and Ru have been developed to reduce the cost (Grades 16 and 26). Titanium is usually not bothered by impingement attack, crevice corrosion, or pitting attack in seawater. Its general resistance to seawater is excellent. Titanium is resistant to nitric acid at all concentrations except with red fuming nitric. The metal also resists ferric chloride, cupric chloride, and other hot chloride solutions. However, there are a number of disadvantages to titanium which have limited its use. Titanium is not easy to form, it has a high springback and tends to gall, and welding must be carried out in an inert atmosphere.

For complete information on titanium, its properties and uses, contact the International Titanium Association at <http://www.ita.org>.

Zirconium Zirconium was originally developed as a construction material for atomic reactors. Reactor-grade zirconium contains very

little hafnium, which would alter zirconium's neutron-absorbing properties. Commercial-grade zirconium, for chemical-process applications, however, contains 2.5 percent maximum hafnium. Zirconium resembles titanium from a fabrication standpoint. All welding must be done under an inert atmosphere. Zirconium has excellent resistance to reducing environments. Oxidizing agents frequently cause accelerated attack. It resists all chlorides except ferric and cupric. Zirconium alloys should *not* be used in concentrations of sulfuric acid above about 70 percent. There are a number of alloys of titanium and zirconium, with mechanical properties superior to those of the pure metals.

Tantalum The physical properties of tantalum are similar to those of mild steel except that tantalum has a higher melting point. Tantalum is ductile and malleable and can be worked into intricate forms. It can be welded by using inert-gas-shielded techniques. The metal is practically inert to many oxidizing and reducing acids (except fuming sulfuric). It is attacked by hot alkalis and hydrofluoric acid. Its cost generally limits use to heating coils, bayonet heaters, coolers, and condensers operating under severe conditions. When economically justified, larger items of equipment (reactors, tanks, etc.) may be fabricated with tantalum liners, either loose (with proper anchoring) or explosion-bonded-clad. Since tantalum linings are usually very thin, very careful attention to design and fabrication details is required.

CAST MATERIALS

Cast Irons Generally, cast iron is not a particularly strong or tough structural material, although it is one of the most economical and is widely used industrially.

Gray cast iron, low in cost and easy to cast into intricate shapes, contains carbon, silicon, manganese, and iron. Carbon (1.7 to 4.5 percent) is present as combined carbon and graphite; combined carbon is dispersed in the matrix as iron carbide (cementite), while free graphite occurs as thin flakes dispersed throughout the body of the metal. Various strengths of gray iron are produced by varying the size, amount, and distribution of graphite. Gray iron has outstanding damping properties, i.e., ability to absorb vibration, as well as wear resistance. However, gray iron is brittle, with poor resistance to impact and shock. Machinability is excellent. With some important exceptions, gray-iron castings generally have corrosion resistance similar to that of carbon steel. They do resist atmospheric corrosion as well as attack by natural or neutral waters and neutral soils. However, dilute acids and acid-salt solutions will attack this material. Gray iron is resistant to concentrated acids (nitric, sulfuric, phosphoric) as well as to some alkaline and caustic solutions. Caustic fusion pots are usually made from gray cast iron with low silicon content; cast-iron valves, pumps, and piping are common in sulfuric acid plants.

White cast iron is brittle and difficult to machine. It is made by controlling the composition and rate of solidification of the molten iron so that all the carbon is present in the combined form. Very abrasion- and wear-resistant, white cast iron is used as liners and for grinding balls, dies, and pump impellers.

Malleable iron is made from white cast iron. It is cast iron with free carbon as dispersed nodules. This arrangement produces a tough, relatively ductile material. Total carbon is about 2.5 percent. Two types are produced: standard and pearlitic (combined carbon plus nodules). Standard malleable iron is easily machined; pearlitic, less so. Both types will withstand bending and cold working without cracking. Large welded areas are not recommended with fusion welding because welds are brittle. Corrosion resistance is about the same as for gray cast iron.

Ductile cast iron includes a group of materials with good strength, toughness, wear resistance, and machinability. This type of cast iron contains combined carbon and dispersed nodules of carbon. Composition is about the same as that of gray iron, with more carbon (3.7 percent) than malleable iron. The spheroidal graphite reduces the notch effect produced by graphite flakes, making the material more ductile. There are a number of grades of ductile iron; some have maximum toughness and machinability, others have maximum resistance to oxidation. Generally, corrosion resistance is similar to that of gray iron. But ductile iron can be used at higher temperatures—up to 590°C (1100°F) and sometimes even higher.

Alloy Cast Irons Cast iron is not usually considered corrosion-resistant, but this condition can be improved by the use of various cast-iron alloys. A number of such materials are commercially available.

High-silicon cast irons have excellent corrosion resistance. Silicon content is 13 to 16 percent. This material is known as Durion. Adding 4 percent Cr yields a product called Durichlor, which has improved resistance in the presence of oxidizing agents. These alloys are not readily machined or welded. Silicon irons are very resistant to oxidizing and reducing environments, and resistance depends on the formation of a passive film. These irons are widely used in sulfuric acid service, since they are unaffected by sulfuric acid at all strengths, even up to the boiling point. Because they are very hard, silicon irons are good for combined corrosion-erosion service.

Another group of cast-iron alloys is called **Ni-Resist**. These materials are related to gray cast iron in that they have high carbon contents (3 percent), with fine graphite flakes distributed throughout the structure. Nickel contents range from 13.5 to 36 percent, and some have 6.5 percent Cu. Generally, nickel-containing cast irons have superior toughness and impact resistance compared with gray irons. The nickel-alloy castings can be welded and machined. Corrosion resistance of nickel-containing cast-iron alloys is superior to that of cast irons but less than that of pure nickel. There is little attack from neutral or alkaline solutions. Oxidizing acids such as nitric are highly detrimental. Cold, concentrated sulfuric acid can be handled. Ni-Resist has excellent heat resistance, with some grades serviceable up to 800°C (1500°F). Also, a ductile variety is available as well as a hard variety (Ni-Hard).

Cast stainless alloys are widely used in pumps, valves, and fittings. These casting alloys are designated under the ACI system. All corrosion-resistant alloys have the letter C plus a second letter (A to N) denoting increasing nickel content. Numerals indicate maximum carbon. While a rough comparison can be made between ACI and AISI types, compositions are not identical and analyses cannot be used interchangeably. Foundry techniques require a rebalancing of the wrought chemical compositions. However, corrosion resistance is not greatly affected by these composition changes. Typical members of this group are CF8, similar to type 304 stainless, and CF8M, similar to type CD3MWCuN, which represent the 25 Cr duplex stainless grades and have improved resistance to nitric, sulfuric, and phosphoric acids. Other duplex grades are CD3MN and CE3MN.

In addition to the C grades, there is a series of heat-resistant grades of ACI cast alloys, identified similarly to the corrosion-resistant grades, except that the first letter is H rather than C. Mention should also be made of precipitation-hardening (PH) stainless steels, which can be hardened by heat treatments at moderate temperatures. Very strong and hard at high temperatures, these steels have but moderate corrosion resistance. A typical PH steel, CB7Cu-1, containing 17 percent Cr, 7 percent Ni, and 1.1 percent Al, has high strength, good fatigue properties, and good resistance to wear and cavitation corrosion. A large number of these steels with varying compositions are commercially available. Essentially, they contain chromium and nickel with added alloying agents such as copper, aluminum, beryllium, molybdenum, nitrogen, and phosphorus.

Medium Alloys The group of (mostly) proprietary alloys with somewhat better corrosion resistance than stainless steels is called medium alloys. A popular member of this group is the **20 alloy**, made by a number of companies under various trade names. Durimet 20 is a well-known cast version, containing 0.07 percent C, 29 percent Ni, 20 percent Cr, 2 percent Mo, and 3 percent Cu. The ACI designation of this alloy is CN7M. Worthite is another proprietary 20 alloy with about 24 percent Ni and 20 percent Cr. The 20 alloy was originally developed to fill the need for a material with sulfuric acid resistance superior to that of the stainless steels. Also included are the 6Mo alloys such as CK3MCuN, similar to alloy 254SMO, and CN3MN, similar to alloy AL6XN.

Other members of the medium-alloy group do not have ACI designations but are listed in ASTM specifications (refer to ASTM A 494) such as **Incoloy 825 and Hastelloy G-3 and G-30**. Several nickel-based alloys that are normally only wrought have cast equivalents but are not listed in any specifications. Hastelloy G-3 contains 44 percent

Ni, 22 percent Cr, 6.5 percent Mo, and 0.05 percent C maximum while alloy G-30 has 30 percent Cr. These alloys have extensive applications in sulfuric acid systems. Because of their increased nickel and molybdenum contents they are more tolerant of chloride-ion contamination than are standard stainless steels. The nickel content decreases the risk of stress-corrosion cracking; molybdenum improves resistance to crevice corrosion and pitting. **Inconel 600** (80 percent Ni, 16 percent Cr, and 7 percent Fe) should also be mentioned as an intermediate alloy. It contains no molybdenum. The corrosion-resistant grade is recommended for reducing-oxidizing environments, particularly at high temperatures. When heated in air, this alloy resists oxidation up to 1100°C (2000°F). The alloy is outstanding in resisting corrosion by gases when these gases are essentially sulfur-free. The alloy is also used with a number of alkalies.

High Alloys The materials called high alloys all contain relatively large percentages of nickel. **N-12MV** contains 61 percent Ni and 28 percent Mo while **N7-M** has 63 percent Ni and 32 percent Mo. Control of carbon and silicon is better with **N7-M** and is important to receiving quality castings. Work hardening presents some fabrication difficulties, and machining is somewhat more difficult than for type 316 stainless. Conventional welding methods can be used. The alloy has unusually high resistance to all concentrations of hydrochloric acid at all temperatures in the absence of oxidizing agents. Sulfuric acid attack is low for all concentrations at 65°C (150°F), but the rate goes up with temperature. Oxidizing acids and salts rapidly corrode these Ni-Mo cast materials, but alkalies and alkaline solutions cause little damage.

Ni-Cr-Mo castings are covered by **CW-12MW**, which is a nickel-based alloy containing chromium (16 percent), molybdenum (16 percent), and tungsten (3 percent) as major alloying elements. This alloy is a cast modification of Hastelloy alloy C. This alloy is resistant to strong oxidizing chloride solutions, such as wet chlorine and hypochlorite solutions. It is one of the very few alloys which are totally resistant to seawater. **CW-6M** is a similar alloy with improved carbon control. Two improved alloys in this family are **CW-2M** and **CX-2MW**. The lower residuals in **CW-2M** provide for a material with much better thermal stability while the higher chromium of **CX-2MW** provides for better general corrosion resistance than the older grades.

Casting Specifications of Interest Refer to these specifications for the chemical analyses and properties of the various alloys:

1. ASTM A 217/A 217M-04 Standard Specification for Steel Castings, Martensitic Stainless and Alloy, for Pressure-Containing Parts, Suitable for High-Temperature Service (contains CA15)
2. ASTM A 297/A 297M-97(2003) Standard Specification for Steel Castings, Iron-Chromium and Iron-Chromium-Nickel, Heat Resistant, for General Application (contains most of the H grade, e.g., HP, castings)
3. ASTM A 351/A 351M-05 Standard Specification for Castings, Austenitic, Austenitic-Ferritic (Duplex), for Pressure-Containing Parts (contains most of the stainless grades, mostly corrosion, but some high-temperature)
4. ASTM A 494/A 494M-04 Standard Specification for Castings, Nickel and Nickel Alloy (contains many of the corrosion nickel alloy castings)
5. ASTM A 743/A 743M-03 Standard Specification for Castings, Iron-Chromium, Iron-Chromium-Nickel, Corrosion Resistant, for General Application (contains many of the corrosion grades)
6. ASTM A 744/A 744M-00(2004) Standard Specification for Castings, Iron-Chromium-Nickel, Corrosion Resistant, for Severe Service (contains some of the austenitic corrosion grades)
7. ASTM A 747/A 747M-04 Standard Specification for Steel Castings, Stainless, Precipitation Hardening (contains CB7Cu-1 and -2)
8. ASTM A 890/A 890M-99(2003) Standard Specification for Castings, Iron-Chromium-Nickel-Molybdenum Corrosion-Resistant, Duplex (Austenitic/Ferritic) for General Application (contains the major duplex grades)
9. ASTM A 990-05 Standard Specification for Castings, Iron-Nickel-Chromium and Nickel Alloys, Specially Controlled for Pressure Retaining Parts for Corrosive Service [currently contains CW-2M (C-4C) and two others].

TABLE 25-10 Properties of Chemical-Resistant Brick

Property	Red shale	Fireclay	Carbon	Silica
Specific gravity (ASTM C 20)	2.4–2.5	2.2–2.3	1.53	1.8–1.9
Compressive strength, psi (ASTM C 133)	10–30,000	10–30,000	7–10,000	4000–7000
Water absorption, % (ASTM C 20)	1.0–7.0	1.0–7.0	7.0–12.0	6.0–7.0
Apparent porosity, % (ASTM C 20)	4.0–12.0	4.0–12.0	18.0–21.0	12.0–16.0
Coefficient of thermal expansion, per °F (ASTM E 228)	$2.5\text{--}3.0 \times 10^{-6}$	$2.5\text{--}3.0 \times 10^{-6}$	3.5×10^{-6}	$2.2\text{--}2.8 \times 10^{-6}$
Thermal conductivity, Btu/(ft ² ·h·°F) (ASTM C 113)	8–10	8–10	30–40	5–9

INORGANIC NONMETALLICS

Glass and Glassed Steel Glass is an inorganic product of fusion which is cooled to a rigid condition without crystallizing. With unique properties compared with metals, these materials require special considerations in their design and use.

Glass has excellent resistance to all acids except hydrofluoric and hot, concentrated H₃PO₄. It is also subject to attack by hot alkaline solutions. Glass is particularly suitable for piping when transparency is desirable.

The chief drawback of glass is its brittleness, and it is also subject to damage by thermal shock. However, glass armored with epoxy-polyester fiberglass can readily be protected against breakage. On the other hand, glassed steel combines the corrosion resistance of glass with the working strength of steel. Accordingly, **glass linings** are resistant to all concentrations of hydrochloric acid to 120°C (250°F), to dilute concentrations of sulfuric to the boiling point, to concentrated sulfuric to 230°C (450°F), and to all concentrations of nitric acid to the boiling point. Acid-resistant glass with improved alkali resistance (up to 12 pH) is available.

A nucleated crystalline ceramic-metal composite form of glass has superior mechanical properties compared with conventional

glassed steel. Controlled high-temperature firings chemically and physically bond the ceramic to steel, nickel-based alloys, and refractory metals. These materials resist corrosive hydrogen chloride gas, chlorine, or sulfur dioxide at 650°C (1200°F). They resist all acids except HF up to 180°C (350°F). Their impact strength is 18 times that of safety glass; abrasion resistance is superior to that of porcelain enamel. They have 3 to 4 times the thermal-shock resistance of glassed steel.

Porcelain and Stoneware Porcelain and stoneware materials are about as resistant to acids and chemicals as glass, but with greater strength. This is offset by a greater potential for thermal shock. **Porcelain enamels** are used to coat steel, but the enamel has slightly inferior chemical resistance. Some refractory coatings, capable of taking very high temperatures, are also available.

Brick Construction Brick-lined construction can be used for many severely corrosive conditions under which high alloys would fail. Brick linings can be installed over metal, concrete, and fiberglass structures. Acid-resistant bricks are made from carbon, red shale, or acid-resistant refractory materials. Red-shale brick is not used above 175°C (350°F) because of spalling. Acid-resistant refractories can be used up to 870°C (1600°F). See Table 25-10.

TABLE 25-11 Standard Wrought Austenitic Stainless Steels

AISI type	UNS	Composition, %°							Mechanical properties†			
		Cr	Ni	Mo	C	Si	Mn	Other	Yield strength, kip/in ² (MPa)‡	Tensile strength, kip/in ² (MPa)‡	Elongation, %	Hardness, HB
304	S30400	18–20	8–10.5		0.08	1.0	2.0		35 (241)	82 (565)	60	149
304L	S30403	18–20	8–12		0.03	1.0	2.0		33 (228)	79 (545)	60	143
308	S30800	19–21	10–12		0.08	1.0	2.0		30 (207)	85 (586)	55	150
309	S30900	22–24	12–15		0.20	1.0	2.0		40 (276)	95 (655)	45	170
309S	S30908	22–24	12–15		0.08	1.0	2.0		40 (276)	95 (655)	45	170
310	S31000	24–26	19–22		0.25	1.5	2.0		45 (310)	95 (655)	50	170
310S	S31008	24–26	19–22		0.08	1.5	2.0		45 (310)	95 (655)	50	170
316	S31600	16–18	10–14	2.0–3.0	0.08	1.0	2.0		36 (248)	82 (565)	55	149
316L	S31603	16–18	10–14	2.0–3.0	0.03	1.0	2.0		34 (234)	81 (558)	55	146
317	S31700	18–20	11–15	3.0–4.0	0.08	1.0	2.0		40 (276)	85 (586)	50	160
317L	S31703	18–20	11–15	3.0–4.0	0.03	1.0	2.0		35 (241)	85 (586)	55	150
321	S32100	17–19	9–12		0.08	1.0	2.0	(5 × C) Ti§	30 (207)	85 (586)	55	160
347	S34700	17–19	9–13		0.08	1.0	2.0	(10 × C)(Cb + Ta)§ 0.20 Co	35 (241)	90 (621)	50	160

°Single values are maximum values unless otherwise noted.
 †Typical room-temperature properties of solution-annealed plates.
 ‡To convert MPa to lbf/in², multiply by 145.04.
 §Minimum.
 ¶Minimum except Ta = 0.1 maximum.

TABLE 25-12 Standard Wrought Austenitic/Ferritic Duplex Stainless Steels

Alloy	UNS	Composition, %°							Mechanical properties†			
		Cr	Ni	Mo	C	Si	Mn	Other	Yield strength, kip/in ² (MPa)‡	Tensile strength, kip/in ² (MPa)‡	Elongation, %	Hardness, HB
329	S32900	25-30	3-6	1.0-2.0	0.10	1.0	2.0		80 (552)	105 (724)	25	230
3RE60	S31500	18-19	4.25-5.25	2.5-3.0	0.03	1.4-2.0	1.2-2.0	0.05-0.10 N	A789			
2205	S32205	22-23	4.5-6.5	3.0-3.5	0.03	1.0	2.0	0.05-0.20 N	65 (450)	95 (655)	25	293
2304	S32304	21.5-21.5	3.0-5.5	0.5-0.6	0.03	1.0	2.5	0.05-0.25 N 0.05-0.6 Cu	58 (400)	87 (600)	25	290
Ferru- lium	S32550	24-27	4.5-6.0	2.9-3.9	0.04	1.0	1.5	0.10-0.25 N 1.5-2.5 Cu	80 (550)	110 (760)	15	302
44LN	S31200	24-26	5.5-6.5	1.2-2.0	0.03	1.0	2.0	0.14-0.20 N	65 (450)	100 (690)	25	293
DP3	S31260	24-26	5.5-7.5	2.5-3.0	0.03	1.0	0.75	0.10-0.30 N 0.2-0.8 Cu	70 (485)	100 (690)	25	293
2507	S32750	24-26	6.0-8.0	3.0-5.0	0.03	0.8	1.2	0.24-0.32 N	80 (550)	116 (795)	15	310

°Single values are maximum values unless otherwise noted.
 †Typical room-temperature properties of solution-annealed plates.
 ‡To convert MPa to lbf/in², multiply by 145.04.

A number of **cement** materials are used with brick. Standard are polymer resin, silicate, and sulfur-based materials. The most widely used resins are furane, vinyl ester, phenolic, polyester, and epoxies. Carbon-filled furanes and phenolics are good against nonoxidizing acids, salts, and solvents. Silicates and silica-filled resins should not be used in hydrofluoric or fluorosilicic acid applications. Sulfur-based cements are limited to 93°C (200°F), while resins can be used to about 180°C (350°F). Silicate-based cements are available for service temperatures up to 1000°C (1830°F).

Brick porosity, which can be as high as 20 percent, necessitates an intermediate lining of lead, asphalt, rubber, or plastic. This membrane functions as the primary barrier to protect the substrate from corrosion damage. The brick lining provides thermal and mechanical protection for the membrane. The membrane system also allows for the differential thermal expansion between the brick lining and supporting substrate. The design of brick linings exposed to higher operating pressure should take into account chemical expansion in addition to thermal expansion.

Cement and Concrete Concrete is an aggregate of inert reinforcing particles in an amorphous matrix of hardened cement paste. Concrete made of portland cement has limited resistance to acids and bases and will fail mechanically following absorption of crystallizing solutions such as brines and various organics. Concretes made of corrosion-resistant cements (such as calcium aluminate) or polymer resins can be selected for specific chemical exposures.

Soil Clay is the primary construction material for settling basins and waste treatment evaporation ponds. Since there is no single type of clay even within a given geographic area, the shrinkage, porosity, absorption characteristics, and chemical resistance must be checked for each application. Geotextiles can be incorporated into basin and pond clay construction to improve the performance of the structure.

ORGANIC NONMETALLICS

Plastic polymers are materials made from organic compounds that have been joined to form long-chain, large-molecular-weight molecules that can be easily processed. There are two basic families of plastic polymers. Thermoplastics are a family of polymers that can be repeatedly heated, changed in shape, then cooled and solidified. Typical polymers within this family are polyolefins, polyvinyls, and the fluoropolymers. The second family of polymers is the thermosets. Unlike the thermoplastics, these materials crosslink during initial processing and cannot be reheated and reshaped. Upon reheating thermosets will not melt before they reach their decomposition temperature. Thermosets are typically more rigid than the thermoplastic polymers.

Thermoplastics Thermoplastics are used in a number of ways. They may be freestanding vessels, pipe, and other equipment; as linings in metallic vessels or as dual laminates in combination with thermoset

plastics. The processing of the thermoplastic raw materials has a great degree of influence on the final properties of the thermoplastic part. Processing techniques include extrusion, injection molding, compression molding, blow molding, rotational molding, and powder coating. Thermoplastics can be welded using various techniques. For critical applications it is highly recommended that welders be certified by independent, impartial organizations such as the German Welding Society (DVS) or a similar qualified organization. DVS certification is available in North America for the polymers and welding techniques covered within its guidelines. Visual inspection criteria for thermoplastic welds are available from the American Welding Society (AWS), DVS, and American Society of Mechanical Engineers Bio-processing standard (ASME- BPE). See Table 25-18 for typical thermoplastic properties.

The use of plastic polymers is limited to relatively moderate temperatures and pressures; 450°F (230°C) is considered high for polymers. They are also less resistant to mechanical abuse and have high expansion, low strength (thermoplastics), and only fair resistance to solvents. Plastic polymers are lightweight, are good thermal and electrical insulators, and are easy to fabricate and install. The chemical resistance of the thermoplastics is one of the major attributes of these materials. Virtually all chemical resistance tables and purity data are derived from the screen tests that were designed and for short-term environmental damage. Some long-term environmental data are available in the DVS guidelines. Care must be exercised when using these data as the test results are for individual chemicals and not typically mixtures of chemicals.

Polytetrafluoroethylene (Teflon) (PTFE) is the most corrosion-resistant thermoplastic polymer. This polymer is resistant to practically every known chemical or solvent combination and has the highest useful temperature of commercially available polymers. It retains its properties up to 500°F (260°C). Because of its exceedingly high molecular weight PTFE is processed by sintering. The PTFE resin is compressed into shapes under high pressure at room temperature and then heated to 700°F (371°C) to complete the sintering process.

Fluorinated ethylene propylene (Teflon) (FEP) is a fully fluorinated plastic. This polymer was developed to have a combination of unique properties. It combines the desirable properties of PTFE with advantageous melt processing properties.

Perfluoroalkoxy (Teflon) (PFA) was introduced in 1972 and is a fully fluorinated polymer that is melt-processible with better melt flow and molding properties than the FEP. The PFA has excellent resistance to chemicals. It can withstand acids as well as caustic materials. PFA has better mechanical properties than FEP above 300°F (149°C) and can be used up to 500°F (260°C) for some applications. The low physical strength and high cost of this polymer limit use for some applications.

Polyvinylidene fluoride (Kynar) (PVDF) is probably the most widely used fluorinated polymer for chemical applications. It can be melt-processed using virtually all the melt-processible procedures. PVDF components such as pipe fittings, tubing, sheet, shapes, and

TABLE 25-13 Special Stainless Steels

Alloy	UNS	Composition, % ^a							Mechanical properties [†]			
		Cr	Ni	Mo	C	Mn	Si	Other	Yield strength, kip/ in ² (MPa) [‡]	Tensile strength, kip/ in ² (MPa) [‡]	Elongation, %	Hardness, HB
A-286	S66286	13.5–16	24–27	1.0–1.5	0.08	2.0	1.0	1.90–2.35 Ti, 0.1–0.5 V, 0.001–0.01 B, 8 × C–1.0 Cb	100 (690)	140 (970)	20	
20Cb-3	N08020	19–21	32–38	2.0–3.0	0.07	2.0	1.0	3.0–4.0 Cu	53 (365)	98 (676)	33	185
PH13-8Mo	S13800	12.25–13.25	7.5–8.5	2.0–2.5	0.05	0.2	0.1	0.90–1.35 Al	120 (827)	160 (1100)	17	300
PH14-8Mo	S14800	13.75–15.0	7.75–8.75	2.0–3.0	0.05	1.0	1.0	0.75–1.5 Al, 0.15–45 Cb	55–210 (380–1450)	125–230 (860–1540)	2–25	200–450
15-5PH	S15500	14.0–15.5	3.5–5.5		0.07	1.0	1.0	2.5–4.5 Cu	145 (1000)	160 (1100)	15	320
PH15-7Mo	S15700	14.0–16.0	6.5–7.75	2.0–3.0	0.09	1.0	1.0	0.75–1.5 Al, 0.15–0.45 Cb	55–210 (380–1450)	130–220 (900–1520)	2–35	200–450
17-4PH	S17400	15.5–17.5	3.0–5.0		0.07	1.0	1.0	3.0–5.0 Cu, 0.4 Al	145 (1000)	160 (1100)	15	320
17-7PH	S17700	16.0–18.0	6.5–7.75		0.09	1.0	1.0	0.75–1.5 Al	40 (276)	130 (710)	10	185
Nitronic 60	S21800	16.0–18.0	8.0–9.0		0.10	7.0–9.0	3.5–4.5	0.08–0.18 N	60 (410)	103 (710)	62	210
21-6-9	S21900	18.0–21.0	5.0–7.0		0.08	8.0–10.0	1.0	0.15–0.40 N	68 (470)	112 (770)	44	220
AM350	S35000	16.0–17.0	4.0–5.0	2.5–3.25	0.07–0.11	0.5–1.25	0.5	0.07–0.13 N	60–173 (410–1200)	145–206 (1000–1420)	13.5–40	200–400
AM355	S35500	15.0–16.0	4.0–5.0	2.5–3.25	0.10–0.15	0.5–1.25	0.5		182 (1250)	216 (1490)	19	402–477
Stab. 26-1	S44626	25.0–27.0	0.5	0.75–1.50	0.06	0.75	0.75	7 × (C + Ni)–1.0 Ti, 0.15 Cu	50 (345)	70 (480)	30	165
29-4	S44700	28.0–30.0	0.15	3.5–4.2	0.010	0.3	0.2	0.02 N, 0.15 Cu	70 (480)	90 (620)	25	210
29-4-2	S44800	28.0–30.0	2.0–2.5	3.5–4.2	0.010	0.3	0.2	0.02 N, 8 × C Cb min.	85 (590)	95 (650)	25	230
Custom 450	S45000	14.0–16.0	5.0–7.0	0.5–1.0	0.05	1.0	1.0	1.25–1.75 Cu	117–184 (800–1270)	144–196 (990–1350)	14	270–400
Custom 455	S45500	11.0–12.5	7.5–9.5	0.5	0.05	0.5	0.5	1.5–2.5 Cu, 0.8–1.4 Ti	115–220 (790–1500)	140–230 (970–1600)	10–14	290–460
254 SMO	S31254	19.5–20.5	17.5–18.5	6.0–6.5	0.02	1.0	0.8	0.18–0.22 N	45 (310)	95 (655)	35	223
AL6XN	N08367	20.0–22.0	23.5–25.5	6.0–7.0	0.03	2.0	1.0	0.18–0.25 N	45 (310)	95 (655)	30	241
27-7Mo	S31277	20.5–23.0	26.0–28.0	6.5–8.0	0.02	3.0	0.5	0.3–0.4 N 0.5–1.5 Cu	52 (260)	112 (770)	40	168

^aSingle values are maximum values unless otherwise noted.

[†]Typical room-temperature properties.

[‡]To convert MPa to lbf/in², multiply by 145.04.

TABLE 25-14 Standard Cast Heat-Resistant Stainless Steels

ACI	Equivalent AISI	UNS	Composition, % ^a						Mechanical properties at 1600°F				
									Short term		Stress to rupture in 1000 h		
			Cr	Ni	C	Mn	Si	Other	Tensile strength, kip/in ² (MPa) [†]	Elonga- tion, %	kip/in ²	MPa [†]	
HC	446	J92605	26-30	4	0.5	1.0	2.0			23 (159)	18	1.3	9.0
HD	327	J93005	26-30	4-7	0.5	1.5	2.0					7.0	48 [‡]
HE		J93403	26-30	8-11	0.2-0.5	2.0	2.0						
HF	302B	J92603	18-23	9-12	0.2-0.4	2.0	2.0			21 (145)	16	4.4	30
HH		J93503	24-28	11-14	0.2-0.5	2.0	2.0	0.2 N		18.5 (128)	30	3.8	26
HH-30	309	J93513	24-28	11-14	0.2-0.5	2.0	2.0	0.2 N		21.5 (148)	18	3.8	26
HI		J94003	26-30	14-18	0.2-0.5	2.0	2.0			26 (179)	12	4.8	33
HK	310	J94224	24-28	18-22	0.2-0.6	2.0	2.0			23 (159)	16	6.0	41
HL		N08604	28-32	18-22	0.2-0.6	2.0	2.0			30 (207)			
HN		J94213	19-23	23-27	0.2-0.5	2.0	2.0			20 (138)	37	7.4	51
HP		N08705	24-28	33-37	0.35-0.75	2.0	2.5			26 (179)	27	7.5	52
HT	330	N08002	13-17	33-37	0.35-0.75	2.0	2.5			19 (131)	26	5.8	40
HU		N08004	17-21	37-41	0.35-0.75	2.0	2.5			20 (138)	20	5.2	36
HW-50		N08006	10-14	58-62	0.35-0.75	2.0	2.5			19 (131)		4.5	31
HX		N06006	15-19	64-68	0.35-0.75	2.0	2.5			20.5 (141)	48	4.0	28

^aSingle values are maximum values; S and P are 0.04 maximum; Mo is 0.5 maximum.

[†]To convert MPa to lbf/in², multiply by 145.04.

[‡]At 1400°F (760°C).

TABLE 25-15 Standard Cast Corrosion-Resistant Stainless Steels

ACI	Equivalent AISI	UNS	Composition, % ^a							Mechanical properties ^b				
										Yield strength, kip/in ² (MPa) ^c	Tensile strength, kip/in ² (MPa) ^c	Elonga- tion, %	Hardness, HB	
			Cr	Ni	Mo	C	Mn	Si	Other					
CA-15	410	J91150	11.5-14	1.0	0.5	0.15	1.0	1.5			150 (1034) ^d	200 (1379) ^d	7 ^d	390 ^d
CA-15M		J91151	11.5-14	1.0	0.15-1.0	0.15	1.0	1.5			150 (1034) ^d	200 (1379) ^d	7 ^d	390 ^d
CA-6NM		J91540	11.5-14	3.5-4.5	0.4-1.0	0.06	1.0	1.0			100 (690) ^e	120 (827) ^e	4 ^e	269 ^e
CA-40	420	J91153	11.5-14	1.0	0.5	0.20-0.40	1.0	1.5			165 (1138) ^d	220 (1517) ^d	1 ^d	470 ^d
CB-30	431	J91803	18.21	2.0		0.30	1.0	1.5			60 (414) ^f	95 (655) ^f	15 ^f	195 ^f
CC-50	446	J92615	26-30	4.0		0.50	1.0	1.5			65 (448) ^g	97 (669) ^g	18 ^g	210 ^g
CE-30	312	J93423	26-30	8-11		0.30	1.5	2.0			63 (434)	97 (669)	18	190
CB-7Cu ⁻¹	17-4PH	J92180				0.07					165 (1138)		3	418
CB-7Cu ⁻²	15-5PH	J92110	14.0-15.5	4.2-5.5		0.07	0.7	1.0	2.5-3.5 Cu					
CF-3	304L	J92500	17-21	8-12		0.03	1.5	2.0			36 (248)	77 (531)	60	140
CF-8	304	J92600	18-21	8-11		0.08	1.5	2.0			37 (255)	77 (531)	55	140
CF-3M	316L	J92800	17-21	9-13	2.0-3.0	0.03	1.5	1.5			38 (262)	80 (552)	55	150
CF-8M	316	J92900	18-21	9-12	2.0-3.0	0.08	1.5	2.0			42 (290)	80 (552)	50	160
CF-10M	316H	J92901	18-21	9-12	2.0-3.0	0.12	1.5	1.5			42 (290)	80 (552)	50	160
CG-12	317	J93001	18-21	9-13	3.0-4.0	0.08	1.5	1.5			44 (303)	83 (572)	45	170
CG-3M	317L	J92999	18-21	9-13	3.0-4.0	0.03	1.5	1.5			40 (275)	80 (552)	50	150
CF-8C	347	J92710	18-21	9-12		0.08	1.5	2.0	(8 × C) Cb ^h		38 (262)	77 (531)	39	149
CF-16F	303	J92701	18-21	9-12	1.50	0.16	1.5	2.0			40 (276)	77 (531)	52	150
CH-20	309	J93402	22-26	12-15		0.20	1.5	2.0			50 (345)	88 (607)	38	190
CK-20	310	J94202	23-27	19-22		0.20	1.5	2.0			38 (262)	76 (524)	37	144
CN-7M	Alloy20 2205	J95150	19-22	27.5-30.5	2.0-3.0	0.07	1.5	1.5	3-4 Cu		32 (221)	69 (476)	48	130
		J92205	21.0-23.5	4.5-6.5	7.5-3.5	0.03	1.5	1.0	0.1-0.3 N		60 (414)	90 (621)	20	250
CD-4MCu		J93372	25-26.5	4.75-6.0	1.75-2.25	0.04	1.0	1.0	2.75-3.25 Cu		82 (565)	108 (745)	25	253

^aSingle values are maximum values. P and S values are 0.04 maximum.

^bTypical room-temperature properties for solution-annealed material unless otherwise noted.

^cTo convert MPa to lbf/in², multiply by 145.04.

^dFor material air-cooled from 1800°F and tempered at 600°F.

^eFor material air-cooled from 1750°F and tempered at 1100 to 1150°F.

^fFor material annealed at 1450°F, furnace-cooled to 1000°F, then air-cooled.

^gAir-cooled from 1900°F.

^h1.0 maximum.

TABLE 25-16 Nickel and Cobalt Alloys

Alloy	UNS	Composition, % ^o						Mechanical properties [†]				
		Ni or Co	Cr	Fe	Mo	C	Other	Condition	Yield strength, kip/in ² (MPa) [‡]	Tensile strength, kip/in ² (MPa) [‡]	Elongation, %	Hardness, HB
Corrosion Alloys												
200	N02200	99.		0.4		0.15		Annealed	15–30 (103–207)	55–80 (379–552)	55–40	90–120
201	N02201	99.		0.4		0.02		Annealed	10–25 (69–172)	50–60 (345–414)	60–40	75–102
400	N04400	63–70		1.0–2.5		0.3	28–34 Cu	Annealed	25–50 (172–345)	70–90 (483–621)	60–35	110–149
K-500	N05500	63–70		2.0		0.25	2.3–3.15 Al 0.35–0.85 Ti, 30 Cu	Age-hardened Annealed	85–120 (586–827)	130–165 (896–1138)	35–20	250–315
600	N06600	72.	14–17	6–10		0.15		Annealed	30–50 (207–345)	80–100 (552–690)	55–35	120–170
625	N06625	Bal.	20–23	5	8–10	0.10	3.15–4.15 (Cb + Ta)	Annealed	60–95 (414–655)	120–150 (827–1034)	60–30	145–220
825	N08825	38–46	19.5–23.5	Bal.	2.5–3.5	0.05	1.5–3.0 Cu, 0.6–1.2 Ti	Annealed	35–65 (241–448)	85–105 (586–724)	50–30	120–180
B-3	N10665	65.	1.0–3.0	1.0–3.0	27–32	0.010	Ni + Mo = 94.0–98.0	Annealed	76 (524)	139 (958)	53	210
C-276	N10276	Bal.	14.5–16.5	4–7	15–17	0.010	3.0–4.5 W	Annealed	52 (358)	115 (793)	61	194
C-22	N06022	Bal.	20.0–22.5	2–6	12.5–14.5	0.015	2.5–3.5 W	Annealed	52 (358)	115 (793)	61	194
C-2000	N06200	Bal.	22.0–24.0	3	15.0–17.0	0.010	1.3–1.9 Cu	Annealed	52 (358)	115 (793)	61	194
MAT21	N06210	Bal.	18.0–20.0	1.0	18.0–20.0	0.015	1.5–2.2 Ta	Annealed	52 (358)	115 (793)	61	194
686	N06686	Bal.	19.0–23.0	5.0	15.0–17.0	0.010	3.0–4.4 W, 0.02–0.25 Ti	Annealed	52 (358)	115 (793)	61	194
G-3	N06985	Bal.	21.0–23.5	18.0–21.0	6.0–8.0	0.015	Cb + Ta 0.5	Annealed	52 (358)	115 (793)	61	194
G-35	N06035	Bal.	32.3–34.3	2.0	7.6–9.0	0.05		Annealed	52 (358)	115 (793)	61	194
High-Temperature Alloys												
600	N06600	72.	14–17	6–10		0.15		Annealed	30–50 (207–345)	80–100 (552–690)	55–35	120–170
601	N06601	58–63	21–25	Bal.		0.10	1.0–1.7 Al	Annealed	30–60 (207–414)	80–115 (552–793)	70–40	110–150
625	N06625	Bal.	20–23	5	8–10	0.10	3.15–4.15 (Cb + Ta)	Annealed	60–95 (414–655)	120–150 (827–1034)	60–30	145–220
706	N09706	39–44	14.5–17.5	Bal.		0.06		Solution-treated and aged	161 (1110)	193 (1331)	20.	371.
718	N07718	50–55	17–21	Bal.	2.8–3.3	0.08	4.75–5.5 (Cb + Ta)	Special heat treatment	171 (1180)	196 (1351)	17.	382.
X-750	N07750	70	14–17	5–9		0.08	0.65–1.15 Ti, 0.2–0.8 Al 0.7–1.2 (Cb + Ta) 2.25–2.75 Ti, 0.4–1.0 Al	Special heat treatment	115–142 (793–979)	162–193 (1117–1331)	30–15	300–390
800	N08800	30–35	19–23	Bal.		0.10	0.15–0.6 Al, 0.15–0.6 Ti	Annealed	30–60 (207–414)	75–100 (517–690)	60–30	120–184
800H	N08810	30–35	19–23	Bal.		0.05–0.10	0.15–0.6 Al, 0.15–0.6 Ti	Solution-treated	20–50 (138–345)	65–95 (448–655)	50–30	100–184
801	N08801	30–34	19–22	Bal.		0.10	0.75–1.5 Ti	Stabilized	79.5 (548)	129 (889)	29.5	
803	S35045	32–37	25–29	Bal.		0.06–0.10	0.15–0.6 Al, 0.15–0.6 Ti	Annealed				
X	N06002	Bal.	20.5–23	17–20	8–10	0.05–0.15	0.2–1.0 W	Annealed	56 (386)	110 (758)	45	178
HR-120	N08120	35–39	223–27	Bal.	2.5	0.02–0.1		Annealed				
230	N06230	Bal.	20–24	3	1.0–3.0	0.05–0.15	13.15 W, 0.005–0.05 La	Annealed	45 (310)	110 (760)	40	187
617	N06617	44.5	20–24	3	8.0–10.0	0.05–0.15	10–15 Co, 0.8–1.5 Al	Annealed	35 (240)	95 (655)	30	170
HR-160	N12160	Bal.	26–30	3.5	1.0	0.15	27–33 Co, 2.4–3.0 Si	Annealed	35 (240)	90 (670)	40	170
N155R30155		18.2–21	20–22.5	Bal.	2.5–3.5	0.08–0.16	19–21 Ni, 0.75–1.25 Cb 2.0–3.0 W	Annealed	50 (345)	110 (760)	30	192
25R30605		Bal.	19–21	3		0.38–0.48	9–11 Ni, 14–16 W	Annealed	69 (475)	146 (1005)	50	200
188R30188		Bal.	20–24	3		0.05–0.45	20–24 Ni, 13–16 W 0.03–0.15 La	Annealed	69 (475)	142 (985)	55	200

*Single values are maximum unless otherwise noted.

†Typical room-temperature properties.

‡To convert MPa to lbf/in², multiply by 145.04.

§Single values are minima. Those alloys with N UNS numbers are nickel and R numbers are cobalt alloys.

TABLE 25-17 Aluminum Alloys

AA designation	UNS	Composition, %*						Condition†	Mechanical properties†				
		Cr	Cu	Mg	Mn	Si	Other		Yield strength, kip/in ² (MPa)	Tensile strength, kip/in ² (MPa)	Elongation in 2 in, %	Hardness, HB	
Wrought													
1060	A91060							99.6 Al min.	0	4 (28)	10 (69)	43	19
1100	A91100		0.05–0.2					99.0 Al min.	0	5 (34)	13 (90)	45	23
2024	A92024	0.1	3.8–4.9	1.2–1.8	0.3–0.9	0.5			T4	47 (324)	68 (469)	19	120
3003	A93003		0.05–0.2		1.0–1.5	0.6			H14	21 (145)	22 (152)	16	40
5052	A95052	0.15–0.35	0.1	2.2–2.8	0.1				0	13 (90)	2.8 (193)	30	47
5083	A95083	0.05–0.25	0.1	4.0–4.9	0.4–1.0	0.4			0	21 (145)			
5086	A95086	0.05–0.25	0.1	3.5–4.5	0.2–0.7	0.4			0	17 (117)	38 (262)	30	
5154	A95154	0.05–0.35	0.1	3.1–3.9	0.1	0.25			0	17 (117)	35 (241)	27	58
6061	A96061	0.04–0.35	0.15–0.4	0.8–1.2	0.15	0.4–0.8			T6	40 (276)	45 (310)	17	95
6063	A96063	0.1	0.1	0.45–0.9	0.1	0.2–0.6			T6	31 (214)	35 (241)	18	73
7075	A97075	0.18–0.28	1.2–2.0	2.1–2.9	0.3	0.40	5.1–6.1 Zn		T6	73 (503)	63 (572)	11	150
Cast													
242.0	A02420	0.25	3.5–4.5	1.2–1.8	0.35	0.7	1.7–2.3 Ni	S-T571		29 (200)			
295.0	A02950		4.0–5.0	0.03	0.35	0.7–1.5		S-T4		29 (200)		6	
336.0	A03360		0.5–1.5	0.7–1.3	0.35	11–13	2.0–3.0 Ni	P-T551		31 (214)			
B443.0	A24430		0.15	0.05	0.35	4.5–6.0		S-F		17 (117)		3	
514.0	A05140		0.15	3.5–4.5	0.35	0.35		S-F		22 (152)		6	
520.0	A05200		0.25	9.5–10.6	0.15	0.25		S-T4		22 (152)	42 (290)	12	

*Single values are maximum values.
 †Typical room-temperature properties.
 ‡S = sand-cast; P = permanent-mold-cast; other = temper designations.
 SOURCE: Aluminum Association. To convert MPa to lb/in², multiply by 145.04.

other configurations are commercially available. PVDF has a use range from -40 to 302°F (150°C). PVDF has a high tensile strength, flex modulus, and heat deflection temperature. It is easily welded, resists permeation, and offers a high-purity smooth polymer surface. This is the polymer of choice for high-purity applications such as semiconductor, bioprocessing, and pharmaceutical industries.

Ethylene chlorotrifluoroethylene (Halar) (ECTFE) has excellent chemical resistance to most chemicals including caustic. ECTFE can be used from -105°F (-76°C) to 302°F (150°C). To obtain good extrusion characteristics, this polymer is usually compounded with a small amount of extrusion aid.

Ethylene trifluoroethylene (Tefzel) (ETFE) has good mechanical properties from cryogenic levels to 350°F (177°C). It has an upper continuous working temperature limit of 300°F (149°C).

Polyethylene (PE) is one of the lowest-cost polymers. There are various types of polyethylene denoted by their molecular weight. This ranges from low-density polyethylene (LDPE) through ultrahigh-molecular-weight (UHMW) polyethylene. Physical properties, processability, and other characteristics of the polyethylene vary greatly with the molecular weight.

Polypropylene (PP) is a crystalline polymer suitable for low-stress applications up to 225°F (105°C). For piping applications this polymer is not recommended above 212°F (100°C). Polypropylene is shielded, pigmented, or stabilized to protect it from uv light. Polypropylene is often a combination of polyethylene and polypropylene which enhances the ductility of the polymer.

Polyvinyl chloride (PVC) has excellent resistance to weak acids and alkaline materials. PVC is commonly utilized for applications that do not require high-temperature resistance or a high-purity resin. Chlorinated PVC (CPVC or PVC-C) represents more than 80 percent of all the PVC used in North America. PVC contains 56.8 percent chlorine by weight in contrast to about 67 percent for CPVC. Both PVC and CPVC are compounded with ingredients such as heat stabilizers, lubricants, fillers, plasticizers, pigments, and processing aids. The actual amount of polymer may range from 93 to 98 percent. The remaining 2 to 7 percent is filler, pigment, stabilizer, lubricant, and plasticizer.

Other commercial thermoplastics include **acrylonitrile butadiene styrene** (ABS), **cellulose acetate butyrate** (CAB), **polycarbonate** (PC), **nylon** (PA), and **acetals**. These resins are frequently used in consumer applications.

Thermosets* There are several generic types of thermosetting resins used for the manufacture of fiberglass-reinforced plastic (FRP composites) equipment. Unlike thermoplastic polymers, thermosetting polymers are hardened by an irreversible crosslinking cure and are almost exclusively used with fiber reinforcement such as glass or carbon fibers in structural applications. It is important to note that because thermoset resins are used with fiber reinforcements, the properties of the resultant laminate are dependent upon the resin and the type, amount, and orientation of reinforcement fibers. To reduce the number of generally used constructions, ASTM and ASME RTP-1 define several standard corrosion-resistant laminate constructions suitable for most equipment. In addition to new construction, thermoset composites are providing practical solutions to the engineer faced with the challenges of restoring structural integrity, increasing load-bearing capabilities, and/or enhancing the strength and stiffness of aging structures. See Table 25-19 for typical thermoset fiber reinforced laminate properties.

The advantages of composites are inherent in their construction. A variety of resin/fiber systems can yield possible solutions for many types of situations. Depending on the product and application, FRP products for civil and mechanical applications can deliver the following benefits:

- Part design (orientation of the fibers) can be optimized for specific loads.
- Reduced structure dead load can increase load ratings.
- Reduced maintenance costs due to resistance from salts and other corrosive agents.
- Engineered system packaging reduces field installation time.
- Faster installation due to lower weight.
- Enhanced durability and fatigue characteristics—FRP does not rust nor is it chloride susceptible.

Myriad FRP products are available for either the repair or the outright replacement of existing structures. In addition to chemical-process pipes and tanks, FRP composite products include structural shapes, bridge systems, grating, handrail ladders, etc.

*Note: Thermosets are also used in non-fiber-reinforced applications such as gel coats and cast polymer.

TABLE 25-18 Typical Thermoplastic Properties

	Units	PP		PVC	CPVC	PVDF		ECTFE	ETFE	FEP	TFE	PFA
		Homopolymer	Copolymer			Homopolymer	Copolymer					
Density	g/cm ³	0.91	0.88–0.91	1.38	1.5	1.75–1.79	1.76–1.79	1.68	1.70	2.12–2.17	2.2–2.3	2.12–2.17
Melting point (crystalline)	°C	160–175	150–175	—	—	160–170	141–160	220–245	270	275	327	310
	°F	320–347	302–347	—	—	320–340	285–320	460	518	527	621	590
Physical Properties												
Break strength; ASTM D 638	kpsi	4.5–6.0	4.0–5.3	6.0–7.5	—	4.5–7.0	3.5–6.0	6.6–7.8	6.5	2.7–3.1	2.0–2.7	4.0–4.5
Modulus flex @ 73°F; ASTM D 790	MPa	1135–1550	345–1035	—	—	—	—	—	—	—	—	—
	kpsi	165–225	50–150	—	—	165–325	90–180	180–260	200	80–95	190–235	120
Yield strength; ASTM D 638	kpsi	4.5–5.4	1.6–4.0	—	—	5.0–8.0	2.9–5.5	—	7.1	—	—	—
Thermal Properties												
HDT at 0.46 MPa (66 psi); ASTM D 648	°C	107–121	75–89	57	—	132–150	93–110	90	104	70	221	75
	°F	225–250	167–192	135	—	270–300	200–230	194	220	158	250	166
Linear coefficient of expansion; ASTM D 696	in/(in·°C) × 10 ⁻⁵	10	7–9.5	4.4	3.9	7.2–14.4	14.0	8	6	8–11	10	12
Conductivity; ASTM C 177	W/(m·K)	0.1	0.16	—	—	0.17–0.19	0.16	—	—	—	—	—
	Btu/(ft ² ·h· °F/in)	0.7	1.1	—	—	1.18–1.32	1.11	—	—	—	—	—

TABLE 25-19 Typical Thermoset Fiber-Reinforced Laminate Properties

Property →	Glass fiber, %	Specific gravity	Density, lb/in ³	Tensile strength, 10 ³ psi	Tensile modulus, 10 ⁶ psi	Elongation, %	Flexural strength, 10 ³ psi	Flexural modulus, 10 ⁶ psi	Compress. strength, 10 ³ psi	Impact strength, ft-lb/in of notch	Flam-mability	Specific heat, Btu/(lb·°F)	Thermal coeff. of expansion, 10 ⁻⁶ in/(in·°F)	Heat distortion, °F at 264 psi	Thermal conductivity ^a , Btu/h, ft ² /°F/in	Dielectric strength, V/mil.	Water absorption, % in 24 h	Mold shrinkage, in/in
ASTM test method	D 790	D 792		D 638	D 638	D 638	D 790	D 790	D 695	D 256	UL-94		D 696	D 648	C 177	D 149	D 570	D 955
Polyester preform, low profile	24	1.74	0.063	11.5	1.70	2.5	28.5	1.32	20.0	20.8	°	0.30	14.0	400+	1.3	400	.8	0.000
(Compression) general-purpose	25	1.55	0.056	13.5	1.80	2.5	27.0	1.10	25.0	18.0	°	0.30	14.0	350+	1.5	400	.25	0.001
(Compression) high glass	40	1.70	0.061	21.5	2.25	2.5	38.5	1.50	32.0	23.0	°	0.30	14.0	400+	1.5	400	.4	0.0005
Carbon/epoxy fabric				23.0	2.10	1.0	25.0	2.00					°			N/A		
Polyester SMC LP, low profile	30	1.85	0.067	12.0	1.70	<1.0	26.0	1.60	24.0	16.0	°	0.30	12.0	400+	1.5	400	.2	0.001
(Compression) general-purpose	22	1.78	0.064	10.5	1.70	0.4	21.2	1.40	23.0	12.0	°	0.30	12.0	350+	1.5	400	.2	0.001
(Compression) high glass	50	2.00	0.072	23.0	2.27	1.7	45.0	2.00	32.0	19.4	°	0.30	15.0	500	1.5	375	.5	0.0005
Carbon/vinyl ester		1.50		22.0	6.0	0.4	71.0	4.00					°			N/A	.13	
Polyester BMC (compression)	22	1.82	0.066	6.0	1.75	<0.5	12.8	1.58	20.0	4.3	°	0.30	8.0	500	1.5	200	.5	0.001
Polyester BMC (injection)	22	1.82	0.066	4.9	1.53	<0.5	12.7	1.44	—	2.9	°	0.28	4.0	—	1.5	250	.5	—
Polyester (pultruded)	55	1.69	0.061	30.0	2.50	—	30.0	1.60	30.0	25.0	°	0.31	—	400+	1.50	350	.5	0.003
Polyester (spray-up, lay-up)	30	1.37	0.049	12.5	1.00	1.3	28.0	0.75	22.0	14.0	°	—	—	400+	—	300	.5	0.002
Polyester woven roving (lay-up)	50	1.64	0.059	37.0	2.25	1.6	46.0	2.25	27.0	33.0	V-0	0.23		400+	1.92	—	0.50	0.008
Epoxy (filament-wound)	80	2.08	0.075	80.0	4.00	1.6	100.0	5.00	45.0	45.0	V-0	—		—	—	—	—	—
Polyurethane, milled fibers (RRIM)	13	1.07	0.039	2.8	—	140.0	—	0.05	—	—	V-0	—		—	—		—	—
Polyurethane, glass flake (RRIM)	23	1.17	0.042	4.4	—	38.9	—	0.15	—	2.1							—	—

^aPolyester thermosets can be formulated to meet a wide range of flame, smoke, and toxicity specifications.

Epoxy (Amine-Cured) Bisphenol A-based epoxy resins used for composite fabrication are commonly cured with multifunctional primary amines. For optimum chemical resistance these generally require a heat cure or postcure. The cured resin has good chemical resistance, particularly to basic environments, and can have good temperature resistance.

Epoxy (Anhydride-Cured) Epoxy resins may be crosslinked with various anhydrides by using a tertiary amine accelerator and heat. These cured polymers generally have good chemical resistance especially to acids.

Epoxy Vinyl Ester Vinyl ester resins are typified by a highly aromatic Bisphenol-A structure and exhibit a broad range of chemical resistance, particularly to caustic solutions, and are the most resilient of the corrosion-resistant resins, generally resulting in the toughest laminate. Brominated versions have about the same corrosion resistance as other Bisphenol-A vinyl esters plus they offer a degree of fire retardancy. The novolac vinyl ester resins exhibit high-temperature resistance and a broad range of chemical resistance, particularly to solvents, oxidizing media, and strong acids.

Bisphenol-A Fumarate Polyester These resins exhibit a broad range of chemical resistance, particularly to caustic solutions. Brominated versions have about the same corrosion resistance as other Bisphenol-A vinyl esters plus they offer a degree of fire retardancy.

Chlorendic Acid Polyester These resins have excellent resistance to acids, good resistance to oxidizing acid media and high-temperature resistance, and moderate fire resistance.

Furan Furan resins are thermosetting polymers derived from furfuryl alcohol and Furfural. The cure must be carefully controlled to avoid the formation of blisters and delaminations. To obtain optimum strength and corrosion resistance, furan composites must undergo a postcure schedule at carefully selected temperatures depending upon the laminate thickness. Equipment made with furan resins exhibits excellent resistance to solvents and combinations of acids and solvents. These resins are not for use in strong oxidizing environments.

Isophthalic/Terephthalic Acid Polyester Typically, isophthalic acid is reacted in a two-stage process with glycols such as propylene or neopentyl glycol and then with maleic anhydride. The crosslinked, fully cured isophthalic-based composites exhibit good weathering resistance and good corrosion resistance to acid media.

Dual-Laminate Construction and Linings The availability of some of the thermoplastic resins in sheet form with a bondable surface allows them to be utilized in a fashion similar to metal cladding. The sheets can be bonded in place and welded to form a barrier surface. When they are used in conjunction with thermoset resin technology for the fabrication of vessels, the procedure is referred to as *dual-laminate*. This fabrication technique extends the chemical resistance of the thermoset resin and the structural strength of the thermoplastic, providing a strong vessel that is highly chemically resistant internally and externally yet lightweight and easily fabricated. Standards for the fabrication of dual-laminate structures can be found in the ASME RTP-1 standard. See Table 25-20 for dual-laminate construction and lining properties.

Rubber and Elastomers Rubber and elastomers are widely used as lining materials. To meet the demands of the chemical industry, rubber processors are continually improving their products. A number of synthetic rubbers have been developed, and while none has all the properties of natural rubber, they are superior in one or more ways. The isoprene and polybutadiene synthetic rubbers are duplicates of natural.

The ability to bond natural rubber to itself and to steel makes it ideal for lining tanks. Many of the synthetic elastomers, while more chemically resistant than natural rubber, have very poor bonding characteristics and hence are not well suited for lining tanks.

Natural rubber is resistant to dilute mineral acids, alkalis, and salts, but oxidizing media, oils, and most organic solvents will attack it. **Hard rubber** is made by adding 25 percent or more of sulfur to natural or synthetic rubber and, as such, is both hard and strong. **Chloroprene** or **neoprene rubber** is resistant to attack by ozone, sunlight, oils, gasoline, and aromatic or halogenated solvents but is

easily permeated by water, thus limiting its use as a tank lining. **Styrene rubber** has chemical resistance similar to that of natural. **Nitrile rubber** is known for resistance to oils and solvents. **Butyl rubber's** resistance to dilute mineral acids and alkalis is exceptional; resistance to concentrated acids, except nitric and sulfuric, is good. **Silicone rubbers**, also known as polysiloxanes, have outstanding resistance to high and low temperatures as well as against aliphatic solvents, oils, and greases. **Chlorosulfonated polyethylene**, known as **Hypalon**, has outstanding resistance to ozone and oxidizing agents except fuming nitric and sulfuric acids. Oil resistance is good. **Fluoroelastomers (Viton A, Kel-F, Kalrez)** combine excellent chemical and temperature resistance. **Polyvinyl chloride elastomer (Koro seal)** was developed to overcome some of the limitations of natural and synthetic rubbers. It has excellent resistance to mineral acids and petroleum oils.

The **cis-polybutadiene**, **cis-polyisoprene**, and **ethylene-propylene** rubbers are close duplicates of natural rubber. The newer ethylene-propylene rubbers (EPR) have excellent resistance to heat and oxidation.

Asphalt Asphalt is used as a flexible protective coating, as a brick-lining membrane, and as a chemical-resisting floor covering and road surface. Resistant to acids and bases, asphalt is soluble in organic solvents such as ketones, most chlorinated hydrocarbons, and aromatic hydrocarbons.

Carbon and Graphite The chemical resistance of impervious carbon and graphite depends somewhat on the type of resin impregnated used to make the material impervious. Generally, impervious graphite is completely inert to all but the most severe oxidizing conditions. This property, combined with excellent heat transfer, has made impervious carbon and graphite very popular in heat exchangers, as brick lining, and in pipe and pumps. One limitation of these materials is low tensile strength. Threshold oxidation temperatures are 350°C (660°F) for carbon and 400°C (750°F) for graphite.

Several types of resin impregnates are employed in manufacturing impervious graphite. The standard impregnate is a phenolic resin suitable for service in most acids, salt solutions, and organic compounds. A modified phenolic impregnate is recommended for service in alkalis and oxidizing chemicals. Furan and epoxy thermosetting resins are also used to fill structural voids. The chemical resistance of the impervious graphite is controlled by the resin used. However, no type of impervious graphite is recommended for use in over 60 percent hydrofluoric, over 20 percent nitric, and over 96 percent sulfuric acids and in 100 percent bromine, fluorine, or iodine.

Wood While fairly inert chemically, wood is readily dehydrated by concentrated solutions and hence shrinks badly when subjected to the action of such solutions. It is also slowly hydrolyzed by acids and alkalis, especially when hot. In tank construction, if sufficient shrinkage once takes place to allow crystals to form between the staves, it becomes very difficult to make the tank tight again.

A number of manufacturers offer wood impregnated to resist acids or alkalis or the effects of high temperatures.

Wood, one of people's oldest materials, remains an important (and too often, overlooked) *corrosion-resistant* material of construction in the chemical-process industry. Wood tanks and wood piping have long met engineers' requirements for dependable service and excellent performance in industrial applications. A very thorough and detailed treatise can be found in a three-part publication, by Oliver W. Siebert, "Wood—Nature's High-Performance Material," NACE, *Materials Performance*, vol. 31, nos. 1-3, January through March 1992.*

Types of wood and their chemical resistance and physical characteristics are reviewed, including examples showing the manufacture of typical tank and pipe construction. In-service case histories are included. While this coverage takes you from the "Forest" to the plants making acetic acid, that is beyond the need for most users; it is hoped that the reader becomes aware that this product family is the *only* MOC for several CPI applications and is a *competitive* choice over some quite exotic materials, e.g., titanium, in others.

*Reference cited courtesy of NACE International.

TABLE 25-20 Dual-Laminate Construction and Lining Properties

Technology	Materials	Fabrication	Design	Size limit	NDT	Repair
Adhesively bonded	PVDF (60, 90, 118 mils) Synthetic and glassbacked ECTFE (60,90)" "	Contact or thermosetting adhesive	Pressure ok	None	Visual	Possible
	ETFE (60, 90 mils) glass-backed PTFE (80, 120 mils)" FEP (60, 90 mils)" PFA (90, 110 mils)" MFA (60, 90 mils)"	Weld rod and cap strip welds Shop or field	Full vacuum up to 120°F Max. temp. 275°F		Spark	Testing recommended
Rotolining	ETFE PVDF ECTFE All up to 250 mils (normal thickness: 186 mils)	Rotationally molded No seams No primer Shop only	Pressure ok Limited vacuumability	Max size 8' × 22'	Visual Spark	By hot patching Testing recommended
Spray and baked	FEP (10 mils), PFA (10–40 mils and up to 80 mils when reinforced or filled) PVDF (20–40 mils and up to 90 mils when reinforced with carbon cloth)	Primer and multicoat conventional spray equipment Each coat baked Shop only	Pressure ok Vacuum ok	12' × 12' × 37'	Visual Spark	By hot patching Testing recommended
			Pressure ok Vacuum ok	12' × 12' × 37'	Visual Spark	By hot patching Testing recommended
Electrostatic spray	ETFE (up to 50 mils), FEP (10 mils), PFA (25–40 mils) ECTFE (35–90 mils), PVDF (35–125 mils)	Primer and multicoat Each coat baked Shop only				
Loose lining	FEP PFA Modified PTFE All 60, 90, 125, 187 mils	Liner fabricated outside the housing and slipped inside Liner fabricated by hand and machine welding Shop only	No vacuum Pressure ok	Determined by body flange (12') and section height (12')	Visual Spark	Difficult
Dual laminate (fluoropolymer- lined FRP)	Same as adhesively bonded	Fabricate liner first on a mandrel (hand and machine welding) and build FRP laminate over the liner. Use carbon cloth for spark testing Shop and field	Pressure ok (RTP-1 Dual lam. or Section X) Vacuum ok for FRP/fluoro- polymer bond. Design FRP for vacuum	~33' diameter max.	Visual Spark AE CRBBD Needs to be defined	Possible Testing recommended

HIGH- AND LOW-TEMPERATURE MATERIALS

LOW-TEMPERATURE METALS

The low-temperature properties of metals have created some unusual problems in fabricating cryogenic equipment.

Most metals lose their ductility and impact strength at low temperatures, although in many cases yield and tensile strengths increase as the temperature goes down.

Materials selection for low-temperature service is a specialized area. In general, it is necessary to select materials and fabrication methods which will provide adequate toughness at all operating conditions. It is frequently necessary to specify Charpy V-notch (or other appropriate) qualification tests to demonstrate adequate toughness of carbon and low-alloy steels at minimum operating temperatures.

Stainless Steels Chromium-nickel steels are suitable for service at temperatures as low as -250°C (-425°F). Type 304 is the most pop-

ular. The original cost of stainless steel may be higher than that of another metal, but ease of fabrication (no heat treatment) and welding, combined with high strength, offsets the higher initial cost. Sensitization or formation of chromium carbides can occur in several stainless steels during welding, and this will affect impact strength. However, tests have shown that impact properties of types 304 and 304L are not greatly affected by sensitization but that the properties of 302 are impaired at -185°C (-300°F).

Nickel Steel Low-carbon 9 percent nickel steel is a ferritic alloy developed for use in cryogenic equipment operating as low as -195°C (-320°F). ASTM specifications A 300 and A 353 cover low-carbon 9 percent nickel steel (A 300 is the basic specification for low-temperature ferritic steels). Refinements in welding and (ASME code-approved) elimination of postweld thermal treatments make 9 percent steel competitive with many low-cost materials used at low temperatures.

TABLE 25-21 Copper Alloys

Alloy	CDA	UNS	Composition, % ^a						Mechanical properties [†]			
			Cu	Zn	Sn	Al	Ni	Other	Yield strength, kip/in ² (MPa)‡	Tensile strength, kip/in ² (MPa)‡	Elongation in 2 in, %	
Wrought												
Copper	110	C11000	99.90							10 (69)	32 (221)	55
Commercial bronze	220	C22000	89–91	Rem.						10 (69)	37 (255)	50
Red brass	230	C23000	84–86	Rem.						10 (69)	40 (276)	55
Cartridge brass	260	C26000	68.5–71.5	Rem.						11 (76)	44 (303)	66
Yellow brass	270	C27000	63–68.5	Rem.						14 (97)	46 (317)	65
Muntz metal	280	C28000	59–63	Rem.						21 (145)	54 (372)	52
Admiralty brass	443	C44300	70–73	Rem.	0.9–1.2				0.02–0.1 As	18 (124)	48 (331)	65
Admiralty brass	444	C44400	70–73	Rem.	0.9–1.2				0.02–0.1 Sb	18 (124)	48 (331)	65
Admiralty brass	445	C44500	70–73	Rem.	0.9–1.2				0.02–0.1 P	18 (124)	48 (331)	65
Naval brass	464	C46400	59–62	Rem.	0.5–1.0					25 (172)	58 (400)	50
Phosphor bronze	510	C51000	Rem.	0.3	4.2–5.8				0.03–0.35 P	19 (131)	47 (324)	64
Phosphor bronze	524	C52400	Rem.	0.2	9.0–11.0				0.03–0.35 P	28 (193)	66 (455)	70
Aluminum bronze	613	C61300	86.5–93.8		0.2–0.5	6–8	0.5		3.5 Fe	30 (207)	70 (483)	42
Aluminum bronze D	614	C61400	88.0–92.5	0.2		6–8			1.5–3.5 Fe, 1.0 Mn	33 (228)	76 (524)	45
Nickel-aluminum bronze	630	C63000	78–85	0.3	0.2	9–11	4.0–5.5		2.0–4.0 Fe, 1.5 Mn, 0.25 Si	36 (248)	90 (620)	10
High-silicon bronze	655	C65500	94.8	1.5			0.6		0.8 Fe, 0.5–1.3 Mn, 2.8–3.8 Si	21 (145)	56 (386)	63
Manganese bronze	675	C67500	57–60	Rem.	0.5–1.5	0.25			0.05–0.5 Mn, 0.8–2.0 Fe	30 (207)	65 (448)	33
Aluminum brass	687	C68700	76–79	Rem.		1.8–2.5			0.02–0.1 As	27 (186)	60 (414)	55
90-10 copper nickel	706	C70600	86.5	1.0			9.0–11.0		1.0–1.8 Fe, 1.0 Mn	16 (110)	44 (303)	42
70-30 copper nickel	715	C71500	Rem.	1.0			29–33		0.4–1.0 Fe, 1.0 Mn	20 (138)	54 (372)	45
65-18 nickel silver	752	C75200	63–66.5	Rem.			16.5–19.5		0.25 Fe, 0.5 Mn	25 (172)	56 (386)	45
Copper beryllium	172	C17200	Rem.			0.2	0.6		1.80–2.00 Be	28 (193)	60 (413)	65
Copper nickel tin	729	C72900	Rem.		8.0		15			140 (965)§	165 (1140)§	15
										20 (138)	50 (345)	30
										110 (758)¶	125 (861)¶	10
Cast												
Ounce metal	836	C83600	84–86	4–6	4–6	0.005	1.0		4–6 Pb	17 (117)	37 (255)	30
Manganese bronze	865	C86500	55–65	36–42	1.0	0.5–1.5	1.0		0.4–2.0 Fe, 0.1–1.5 Mn	28 (193)	71 (490)	30
G bronze	905	C90500	86–89	1.0–3.0	9–11	0.005	1.0			22 (152)	45 (310)	25
M bronze	922	C92200	86–90	3.0–5.0	5.5–6.5	0.005	1.0		1.0–2.0 Pb	20 (138)	40 (276)	30
Ni-Al-Mn bronze	957	C95700	71			7.0–8.5	1.5–3.0		2.0–4.0 Fe, 11–14 Mn	45 (310)	95 (665)	26
Ni-Al bronze	958	C95800	79			8.5–9.5	4.0–5.0		3.5–4.5 Fe, 0.8–1.5 Mn	38 (262)	95 (655)	25
Copper nickel	964	C96400	65–69				28–32		0.5–1.5 Cb, 0.25–1.5 Fe, 1.5 Mn	37 (255)	68 (469)	28

^aSingle values are maximum values except for Cu, which is minimum.

[†]Typical room-temperature properties of annealed or as-cast material.

[‡]To convert MPa to lbf/in², multiply by 145.04.

[§]Age-hardened condition.

[¶]Spinodal-hardened condition.

Nickel Alloys Alloy C-4 (16 Cr, 16 Mo, Balance Ni) and alloy C-276 (16 Cr, 16 Mo, 3.5 W, 5 Fe, balance Ni) have been used for closure seals on cryogenic gas cylinders because the alloys retain all their ductility down to -327°C (-557°F). The impact strength at liquid nitrogen temperatures is the same as that at room temperature.

Aluminum Aluminum alloys have an unusual ability to maintain strength and shock resistance at temperatures as low as -250°C (-425°F). Good corrosion resistance and relatively low cost make these alloys very popular for low-temperature equipment. For most welded construction the 5000-series aluminum alloys are widely used. These are the aluminum-magnesium and aluminum-magnesium-manganese materials.

Copper and Alloys With few exceptions the tensile strength of copper and its alloys increases quite markedly as the temperature goes

down. However, copper's low structural strength becomes a problem when constructing large-scale equipment. Therefore, alloy must be used. One of the most successful for low temperatures is silicon bronze, which can be used to -195°C (-320°F) with safety.

HIGH-TEMPERATURE MATERIALS*

Metals Successful applications of metals in high-temperature process service depend on an appreciation of certain engineering factors. Among the most important properties are creep, rupture,

*An excellent reference book for the high-temperature corrosion resistance of materials of construction is George Y. Lai, *High-Temperature Corrosion of Engineering Alloys*, ASM International, Metals Park, Ohio, 1990.

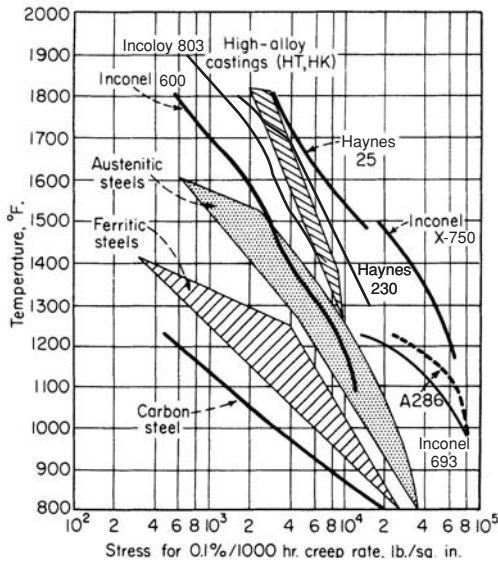


FIG. 25-21 Effect of creep on metals for high-temperature use. $^{\circ}\text{C} = (^{\circ}\text{F} - 32) \times \frac{5}{9}$; to convert lb/in^2 to MPa, multiply by 6.895×10^{-3} . [Chem. Eng., 65, p. 140 (Dec. 15, 1958); modified 2005 using producer data.]

and short-time strengths (see Figs. 25-21 and 25-22). **Creep** relates initially applied stress to rate of plastic flow. **Stress rupture** is another important consideration at high temperatures since it relates stress and time to produce rupture. As the figures show, ferritic alloys are weaker than austenitic compositions, and in both groups molybdenum increases strength. Austenitic castings are much stronger than their wrought counterparts. And higher strengths are available in the nickel- and cobalt-based alloys. Other properties that become important at high temperatures include thermal conductivity,

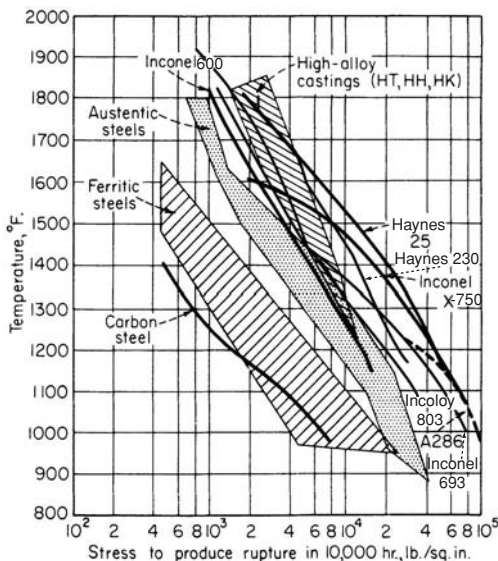


FIG. 25-22 Rupture properties of metals as a function of temperature. $^{\circ}\text{C} = (^{\circ}\text{F} - 32) \times \frac{5}{9}$; to convert lb/in^2 to MPa, multiply by 6.895×10^{-3} . [Chem. Eng., 65, p. 140 (Dec. 15, 1958); modified 2005 using producer data.]

thermal expansion, ductility at temperature, alloy composition, and stability.

Actually, in many cases strength and mechanical properties become of secondary importance in process applications, compared with resistance to the corrosive surroundings. All common heat-resistant alloys form oxides when exposed to hot oxidizing environments. Whether the alloy is resistant depends upon whether the oxide is stable and forms a protective film. Thus, mild steel is seldom used above 480°C (900°F) because of excessive scaling rates. Higher temperatures require chromium. Thus, type 502 steel, with 4 to 6 percent Cr, is acceptable to 620°C (1150°F). A 9 to 12 percent Cr steel will handle 730°C (1350°F). The well-known austenitic stainless steels have excellent oxidation resistance: up to 900°C (1650°F) for 18-8; however, their strength limits their use. Chromium is also important in nickel-based alloys as a very protective chromium-nickel spinel oxide forms at lower temperatures. At temperatures above 1000°C (1832°F) the addition of significant quantities of aluminum or silicon will enhance the oxidation resistance. There is a synergistic effect between silicon or aluminum in the formation of more resistant oxide layers.

Figure 25-23 shows the oxidation resistance of a variety of commercially significant alloys. The penetration shown is a combination of the uniform scaling that occurred during exposure and the internal penetration of oxide into the microstructure. This value of penetration is considered to be conservative but better from a prediction of life basis. The lower curve for alloy 214 shows the beneficial effect of aluminum in reducing oxidation at high temperatures; however, the use of this alloy is limited by its high temperature strength. These curves were generated using a program called ASSET that was developed by Shell Global solutions and is available for purchase. The curves are based on actual data that were generated and then used to calculate a parameter that allows extrapolation to different temperatures. The heavy line is from actual data while the thin line is extrapolated data.

Chromium is the most important material in imparting resistance to sulfidation (formation of sulfidic scales similar to oxide scales). The austenitic alloys are generally used because of their superior mechanical properties and fabrication qualities, despite the fact that nickel in the alloy tends to lessen resistance to sulfidation somewhat.

Aluminum and silicon also improve the resistance of alloys to oxidation as well as sulfidation. But use as an alloying agent is limited because the amount required interferes with the workability and

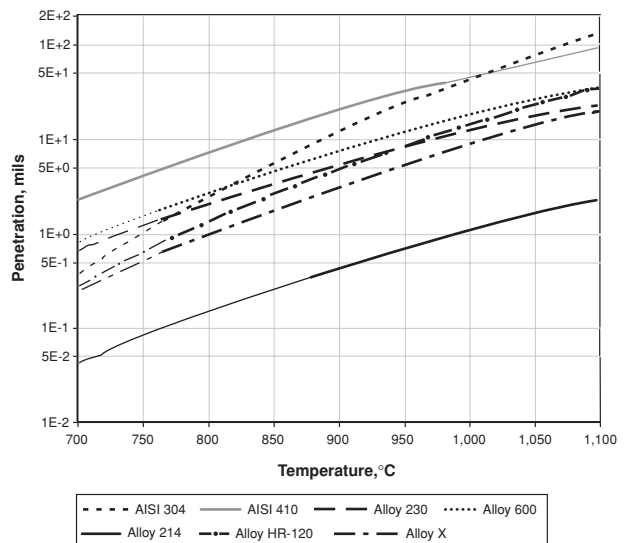


FIG. 25-23 Penetration curves for oxidation in still air of several commercially significant high-temperature alloys.

TABLE 25-22 Miscellaneous Alloys

Alloy	Designation	UNS	Composition, %°	Condition	Mechanical properties†			
					Yield strength, kip/in ² (MPa)‡	Tensile strength, kip/in ² (MPa)‡	Elongation, %	Hardness, HB
Refractory Alloys								
Niobium (columbium)		R04210	99.6 Cb	Annealed	37 (255)	53 (365)	26	80
Molybdenum		R03600	0.01–0.04 C					
Molybdenum, low C		R03650	0.01 C					
Molybdenum alloy		R03630	0.01–0.04 C, 0.40–0.55 Ti, 0.06–0.12 Zn					
Tantalum		R05210	99.8 min. Ta	Annealed		50 (345)	40	45
Tungsten		R07030	99.9 min. W	Annealed		270 (1862)		
Zirconium		R60702	4.5 Hf, 0.2 Fe + Cr, 99.2 Zr + Hf	Annealed	16 (110)	36 (248)	31	77
Precious Metals and Alloys								
Gold		P00020	99.95 min. Au	Annealed		19 (131)	45	25
Silver		P07015	99.95 min. Ag	Annealed	8 (55)	18 (124)	54	27
Sterling silver		P07931	6.50–7.90 Cu, 92.1–93.5 Ag	Annealed	20 (138)	41 (283)	26	65
Platinum		P04955	99.95 min. Pt	Annealed		18 (124)	38	39
Palladium		P03995	99.80 min. Pd	Annealed		25 (172)	27	38
Lead Alloys								
Chemical lead		L50049	99.9 min. Pb	Rolled	1.9 (13)	2.5 (17)	50	5
Antimonial lead			90 Pb, 10 Sb	Rolled		4.1 (28)	47	13
Tellurium lead			99.85 Pb, 0.04 Te, 0.06 Cu	Rolled	2.2 (15)	3 (21)	45	6
50-50 solder		L05500	50 Pb, 50 Sn, 0.12 max. Sb	Cast		6.8 (47)	50	14
Magnesium Alloys								
Extended Shapes	AZ31B	M11311	2.5–3.5 Al, 0.20 min. Mn, 0.6–1.4 Zn	Annealed	15–18 (103–124)	32 (220)	9–12	56
Cast alloy	AZ91C	M11914	8.1–9.3 Al, 0.13 min. Mn, 0.4–1.0 Zn	As cast	11 (76)	23 (159)		60
Cast alloy	EZ33A	M12330	2.0–3.1 Zn, 0.5–1.0 Zr	Aged	14 (97)	20 (138)	2	50
Wrought alloy	LA141A	M14141	1.0–1.5 Al, 13–15 Li	Stress hard-annealed	24–26 (165–179)	33–34 (228–234)	4	57
Titanium Alloys								
Commercial pure	Gr. 1	R50250	0.20 Fe, 0.18 O	Annealed	35 (241)	48 (331)	30	120
Commercial pure	Gr. 2	R50400	0.30 Fe, 0.25 O	Annealed	50 (345)	63 (434)	28	200
Ti-Pd	Gr. 7	R52400	0.30 Fe, 0.25 O, 0.12–0.25 Pd	Annealed	50 (345)	63 (434)	28	200
Ti-6Al-4V	Gr. 5	R56400	5.5–5.6 Al, 0.40 Fe, 0.20 O, 3.5–4.5 V	Annealed	134 (924)	144 (993)	14	330
Low alloy	Gr. 12	R53400	0.2–0.4 Mo, 0.6–0.9 Ni	Annealed	65 (448)	75 (517)	25	
Ti-LowPd	Gr. 16	R52402	0.30 Fe, 0.25 O, 0.04–0.08 Pd	Annealed	50 (345)	63 (434)	28	200
Ti-Ru	Gr. 26	R52404	0.3 Fe, 0.25 O, 0.08–0.14 Ru	Annealed	50 (345)	63 (434)	28	200

°Single values are maximum values unless otherwise noted.

†Typical room-temperature properties.

‡To convert MPa to lbf/in², multiply by 145.04.

TABLE 25-23 Typical Physical Properties of Surface Coatings for Concrete

	Concrete	Polyester		Epoxy		Urethane*
		Isophthalic	Bisphenol	Polyamide	Amine	
Tensile strength (ASTM C307), lbf/in ²	200–400	1200–2500	1200–2500	600–4000	1200–2500	200–1200
MPa	1.4–2.8	8.3–17	8.3–17	4.0–28	8.3–17	1.4–8.3
Thermal coefficient of expansion (ASTM C531)						
Maximum in/(in·°F)	6.5 × 10 ⁶	20 × 10 ⁶	20 × 10 ⁶	40 × 10 ⁶	40 × 10 ⁶	†
Maximum mm/(mm·°C)	11.7 × 10 ⁶	36 × 10 ⁶	36 × 10 ⁶	72 × 10 ⁶	72 × 10 ⁶	†
Compressive strength, (ASTM C579), lbf/in ²	3500	10,000	10,000	4000	6000	†
MPa	24	70	70	28	42	†
Abrasion resistance, Taber abraser—weight loss, mg, 1000-g load/1000 cycles		15–27	15–27	15–27	15–27	†
Shrinkage, ASTM C531, %		2–4	2–4	0.25–0.75	0.25–0.75	0–2
Work life, min		15–45	15–45	30–90	30–90	15–60
Traffic limitations, h after application		16	16	24	24	24
	Light	36	36	48	48	48
	Heavy	48	48	72	72	72
	Ready for service	Poor	Fair	Excellent	Good	Fair
Adhesion characteristics‡		1500	1500	1000	1500	†
Flexural strength (ASTM C580), lbf/in ²		10	10	7	10	
MPa						

NOTE: All physical values depend greatly on reinforcing. Values are for ambient temperatures.

*Type of urethane used is one of three: (1) Type II, moisture-cured; (2) Type IV, two-package catalyst; or (3) Type V, two-package polyol. (Ref. ASTM C16.)

†Urethanes not shown because of great differences in physical properties, depending on formulations. Adhesion characteristics should be related by actual test data. Any system which shows concrete failure when tested for surfacing adhesion should be rated excellent with decreasing rating for systems showing failure in cohesion or adhesion below concrete failure.

‡Adhesion to concrete: primers generally are used under polyesters and urethanes to improve adhesion.

SOURCE: NACE RP-03-76, *Monolithic Organic Corrosion Resistant Floor Surfacing*, 1976. Courtesy of National Association of Corrosion Engineers.

high-temperature strength properties. The formation of Ni₃Al precipitates in a nickel alloy increases the strength but reduces the ductility. The development of high aluminum surface layers by spraying, dipping, and cementation is a feasible means of improving the corrosion resistance of low-alloy steels.

Hydrogen Atmospheres Austenitic stainless steels, by virtue of their structure and high chromium contents, are usually resistant to hydrogen atmospheres. Ferritic alloys are more susceptible to hydrogen embrittlement.

TABLE 25-24 Chemical Resistance of Elastomers

Type of rubber	Features
Butadiene styrene	General-purpose; poor resistance to hydrocarbons, oils, and oxidizing agents
Butyl	General-purpose; relatively impermeable to air; poor resistance to hydrocarbons and oils
Chloroprene	Good resistance to aliphatic solvents; poor resistance to aromatic hydrocarbons and many fuels
Chlorosulfonated polyethylene	Excellent resistance to oxidation, chemicals, and heat; poor resistance to aromatic oils and most fuels
cis-Polybutadiene	General-purpose; poor resistance to hydrocarbons, oils, and oxidizing agents
cis-Polyisoprene	General-purpose; poor resistance to hydrocarbons, oils, and oxidizing agents
Ethylene propylene Fluorinated	Excellent resistance to heat and oxidation
Natural	Excellent resistance to high temperature, oxidizing acids, and oxidation; good resistance to fuels containing up to 30% aromatics
Nitrile (butadiene acrylonitrile)	General-purpose; poor resistance to hydrocarbons, oils, and oxidizing agents
Polysulfide	Excellent resistance to oils, but not resistant to strong oxidizing agents; resistance to oils proportional to acrylonitrile content
Silicone	Good resistance to aromatic solvents; unusually high impermeability to gases; poor compression set and poor resistance to oxidizing acids
Styrene	Excellent resistance over unusually wide temperature range [–100 to 260°C (–150 to 500°F)]; fair oil resistance; poor resistance to aromatic oils, fuels, high-pressure steam, and abrasion
	Synonymous with butadiene-styrene

Halogens (Hot, Dry Cl₂, HCl) Pure nickel and nickel alloys are useful with dry halogen gases. The presence of oxygen with Cl₂ or HCl gas will alter the choice of materials. But even with the best materials, corrosion rates are relatively high at high temperature. There are cases in which equipment for high-temperature halogenation has used platinum-clad nickel-based alloys. These materials have high initial cost but long life. Platinum and gold have excellent resistance to dry HCl even at 1100°C (2000°F).

Refractories Refractories are selected to accomplish four objectives:

1. Resist heat
2. Resist high-temperature chemical attack
3. Resist erosion by gas with fine particles
4. Resist abrasion by gas with large particles

Refractories are available in three general physical forms: solids in the form of brick and monolithic castable ceramics and as ceramic fibers.

The primary method of selection of the type of refractory to be used is by gas velocity:

- <7.5 m/s (25 ft/s): fibers
- 7.5–60 m/s (25–200 ft/s): monolithic castables
- >60 m/s (200 ft/s): brick

Within solids the choice is a tradeoff because, with brick, fine particles in the gas remove the mortar joints and, in the monolithic castables, while there are no joints, the refractory is less dense and less wear-resistant.

Internal Insulation The practice of insulating within the vessel (as opposed to applying insulating materials on the equipment exterior) is accomplished by the use of fiber blankets and lightweight aggregates in ceramic cements. Such construction frequently incorporates a thin, high-alloy shroud (with slip joints to allow for thermal expansion) to protect the ceramic from erosion. In many cases this design is more economical than externally insulated equipment because it allows use of less expensive lower-alloy structural materials.

Refractory Brick Nonmetallic refractory materials are widely used in high-temperature applications in which the service permits the appropriate type of construction. The more important classes are described in the following paragraphs.

Fireclays can be divided into plastic clays and hard flint clays; they may also be classified as to alumina content. **Firebricks** are usually made of a blended mixture of flint clays and plastic clays which is formed, after mixing with water, to the required shape. Some or all of

TABLE 25-25 Properties of Graphite and Silicon Carbide

	Graphite	Impervious graphite	Impervious silicon carbide
Specific gravity	1.4–1.8	1.75	3.10
Tensile strength, lbf/in ² (MPa)	400–1400 (3–10)	2,600 (18)	20,650 (143)
Compressive strength, lbf/in ² (MPa)	2000–6000 (14–42)	10,500 (72)	150,000 (1000)
Flexural strength, lbf/in ² (MPa)	750–3000 (5–21)	4,700 (32)	
Modulus of elasticity ($\times 10^6$), lbf/in ² (MPa)	0.5–1.8 (0.3–12 $\times 10^4$)	2.3 (1.6 $\times 10^4$)	56 (39 $\times 10^4$)
Thermal expansion, in/(in \cdot °F $\times 10^{-6}$) [mm/(mm \cdot °C)]	0.7–2.1 (1.3–3.8)	2.5 (4.5)	1.80 (3.4)
Thermal conductivity, Btu/(h \cdot ft ²)(°F/ft) [(W/(m \cdot K)]	15–97 (85–350)	85 (480)	60 (340)
Maximum working temperature (inert atmosphere), °F (°C)	5000 (2800)	350 (180)	4,200 (2300)
Maximum working temperature (oxidizing atmosphere), °F (°C)	660 (350)	350 (180)	3,000 (1650)

SOURCE: Carborundum Co. Courtesy of National Association of Corrosion Engineers.

the flint clay may be replaced by highly burned or calcined clay, called *grog*. A large proportion of modern brick production is molded by the dry-press or power-press process, in which the forming is carried out under high pressure and with a low water content. Extruded and hand-molded bricks are still made in large quantities.

The dried bricks are burned in either periodic or tunnel kilns at temperatures ranging between 1,200 and 1,500°C (2,200 and 2,700°F). Tunnel kilns give continuous production and a uniform burning temperature.

Fireclay bricks are used in kilns, malleable-iron furnaces, incinerators, and many portions of metallurgical furnaces. They are resistant to spalling and stand up well under many slag conditions but are not generally suitable for use with high-lime slags or fluid-coal-ash slags or under severe load conditions.

High-alumina bricks are manufactured from raw materials rich in alumina, such as diaspore. They are graded into groups with 50, 60, 70, 80, and 90 percent alumina content. When well fired, these bricks contain a large amount of mullite and less of the glassy phase than is present in firebricks. Corundum is also present in many of these bricks. High-alumina bricks are generally used for unusually severe temperature or load conditions. They are employed extensively in lime kilns and rotary cement kilns, in the ports and regenerators of glass tanks, and for slag resistance in some metallurgical furnaces; their price is higher than that of firebrick.

Silica bricks are manufactured from crushed ganister rock containing about 97 to 98 percent silica. A bond consisting of 2 percent lime is used, and the bricks are fired in periodic kilns at temperatures of 1,500 to 1,540°C (2,700 to 2,800°F) for several days until a stable volume is obtained. They are especially valuable when good strength is required at high temperatures. Superduty silica bricks are finding some use in the steel industry. They have a lowered alumina content and often a lowered porosity.

Silica bricks are used extensively in coke ovens, the roofs and walls of open-hearth furnaces, and the roofs and sidewalls of glass tanks and

as linings of acid electric steel furnaces. Although silica brick is readily spalled (cracked by a temperature change) below red heat, it is very stable if the temperature is kept above this range and for this reason stands up well in regenerative furnaces. Any structure of silica brick should be heated up slowly to the working temperature; a large structure often requires 2 weeks or more.

Magnesite bricks are made from crushed magnesium oxide, which is produced by calcining raw magnesite rock to high temperatures. A rock containing several percent of iron oxide is preferable, as this permits the rock to be fired at a lower temperature than if pure materials were used. Magnesite bricks are generally fired at a comparatively high temperature in periodic or tunnel kilns. A large proportion of magnesite brick made in the United States uses raw material extracted from seawater.

Magnesite bricks are basic and are used whenever it is necessary to resist high-lime slags, as in the basic open-hearth steel furnace. They also find use in furnaces for the lead- and copper-refining industries. The highly pressed unburned bricks find extensive use as linings for cement kilns. Magnesite bricks are not so resistant to spalling as fireclay bricks.

Chrome bricks are manufactured in much the same way as magnesite bricks but are made from natural chromite ore. Commercial ores always contain magnesia and alumina. Unburned hydraulically pressed chrome bricks are also available.

Chrome bricks are very resistant to all types of slag. They are used as separators between acid and basic refractories, also in soaking pits and floors of forging furnaces. The unburned hydraulically pressed bricks now find extensive use in the walls of the open-hearth furnace. Chrome bricks are used in sulfite-recovery furnaces and to some extent in the refining of nonferrous metals. Basic bricks combining various properties of magnesite and chromite are now made in large quantities and have advantages over either material alone for some purposes.

The **insulating firebrick** is a class of brick that consists of a highly porous fire clay or kaolin. Such bricks are light in weight (about one-half to one-sixth of the weight of fireclay), low in thermal conductivity, and yet sufficiently resistant to temperature to be used successfully on the hot side of the furnace wall, thus permitting thin walls of low thermal conductivity and low heat content. The **low heat content** is particularly valuable in saving fuel and time on heating up, allows rapid changes in temperature to be made, and permits rapid cooling. These bricks are made in a variety of ways, such as mixing organic matter with the clay and later burning it out to form pores; or a bubble structure can be incorporated in the clay-water mixture which is later preserved in the fired brick. The insulating firebricks are classified into several groups according to the maximum use limit; the ranges are up to 870, 1,100, 1,260, 1,430, and above 1,540°C (1,600, 2,000, 2,300, 2,600, and above 2,800°F).

Insulating refractories are used mainly in the heat-treating industry for furnaces of the periodic type. They are also used extensively in stress-relieving furnaces, chemical-process furnaces, oil stills or heaters, and the combustion chambers of domestic-oil-burner furnaces. They usually have a life equal to that of the heavy brick that they replace. They are particularly suitable for constructing experimental or

TABLE 25-26 Minimum Temperature without Excessive Scaling in Air (Continuous Service)*

Alloy	°F	°C
Carbon steel	1050	565
½Mo steel	1050	565
1Cr ½Mo steel	1100	595
2¼Cr 1Mo steel	1150	620
5Cr ½Mo steel	1200	650
9Cr 1Mo steel	1300	705
AISI 410	1300	705
AISI 304	1600	870
AISI 321	1600	870
AISI 347	1600	870
AISI 316	1600	870
AISI 309	2000	1090
AISI 310	2100	1150

*Courtesy of National Association of Corrosion Engineers.

TABLE 25-27 Important Commercial Alloys for High-Temperature Process Service

	Nominal composition, %			
	Cr	Ni	Fe	Other
Ferritic steels				
Carbon steel			Bal.	
2¼ chrome	2¼		Bal.	Mo
Type 502	5		Bal.	Mo
Type 410	12		Bal.	
Type 430	16		Bal.	
Type 446	27		Bal.	
Austenitic steels				
Type 304	18	8	Bal.	
Type 321	18	10	Bal.	Ti
Type 347	18	11	Bal.	Cb
Type 316	18	12	Bal.	Mo
Type 309	24	12	Bal.	
Type 310	25	20	Bal.	
Type 330	15	35	Bal.	
Nickel-base alloys				
Nickel		Bal.		
Incoloy 800	21	32	Bal.	
Hastelloy B		Bal.	6	Mo
Hastelloy C	16	Bal.	6	W, Mo
60-15	15	Bal.	25	
Inconel 600	15	Bal.	7	
80-20	20	Bal.		
Hastelloy X	22	Bal.	19	Co, Mo
Multimet	21	20	Bal.	Co
Rene 41	19	Bal.	5	Co, Mo, Ti
Cast irons				
Ductile iron			Bal.	C, Si, Mg
Ni-Resist, D-2	2	20	Bal.	Si, C
Ni-Resist, D-4	5	30	Bal.	Si, C
Cast stainless (ACI types)				
HC	28	4	Bal.	
HF	21	11	Bal.	
HH	26	12	Bal.	
HK	15	20	Bal.	
HT	15	35	Bal.	
HW	12	Bal.	28	
Superalloys				
Inconel X	15	Bal.	7	Ti, Al, Cb
A 286	15	25	Bal.	Mo, Ti
Stellite 25	20	10	Co-base	W
Stellite 21 (cast)	27.3	2.8	Co-base	Mo
Stellite 31 (cast)	25.2	10.5	Co-base	W

laboratory furnaces because they can be cut or machined readily to any shape. They are not resistant to fluid slag.

There are a number of types of special brick obtainable from individual producers. **High-burned kaolin refractories** are particularly valuable under conditions of severe temperature and heavy load or severe spalling conditions, as in the case of high-temperature oil-fired boiler settings or piers under enameling furnaces. Another brick for the same uses is a high-fired brick of Missouri aluminous clay.

There are on the market a number of bricks made from **electrically fused materials**, such as fused mullite, fused alumina, and fused magnesite. These bricks, although high in cost, are particularly suitable for certain severe conditions.

Bricks of **silicon carbide**, either recrystallized or clay-bonded, have a high thermal conductivity and find use in muffle walls and as a slag-resisting material.

Other types of refractory that find use are forsterite, zirconia, and zircon. Acid-resisting bricks consisting of a dense body like stoneware are used for lining tanks and conduits in the chemical industry. Carbon blocks are used as linings for the crucibles of blast furnaces, very extensively in a number of countries and to a limited extent in the United States. Fusion-cast bricks of mullite or alumina are largely used to line glass tanks.

Ceramic-Fiber Insulating Linings Ceramic fibers are produced by melting the same alumina-silica china (kaolin) clay used in conventional insulating firebrick and blowing air to form glass fibers. The fibers, 50.8 to 101.6 mm (2 to 4 in) long by 3 µm in diameter, are interlaced into a mat blanket with no binders or chopped into shorter fibers and vacuum-formed into blocks, boards, and other shapes. Ceramic-fiber linings, available for the temperature range of 650 to 1,430°C (1,200 to 2,600°F), are more economical than brick in the 650 to 1,230°C (1,200 to 2,250°F) range. Savings come from reduced first costs, lower installation labor, 90 to 95 percent less weight, and a 25 percent reduction in fuel consumption.

Because of the larger surface area (compared with solid-ceramic refractories) the chemical resistance of fibers is relatively poor. Their acid resistance is good, but they have less alkali resistance than solid materials because of the absence of resistant aggregates. Also, because they have less bulk, fibers have lower gas-velocity resistance. Besides the advantage of lower weight, since they will not hold heat, fibers are more quickly cooled and present no thermal-shock structural problem.

Castable Monolithic Refractories Standard portland cement is made of calcium hydroxide. In exposures above 427°C (800°F) the hydroxyl ion is removed from portland (water removed); below 427°C (800°F), water is added. This cyclic exposure results in spalling. Castables are made of calcium aluminate (rather than portland); without the hydroxide they are not subject to that cyclic spalling failure.

Castable refractories are of three types:

1. *Standard.* 40 percent alumina for most applications at moderate temperatures.

2. *Intermediate purity.* 50 to 55 percent alumina. The anorthite (needle-structure) form is more resistant to the action of steam exposure.

3. *Very pure.* 70 to 80 percent alumina for high temperatures.

Under reducing conditions the iron in the ceramic is controlling, as it acts as a catalyst and converts the CO to CO₂ plus carbon, which results in spalling. The choice among the three types of castables is generally made by economic considerations and the temperature of the application.

Compared with brick, castables are less dense, but this does not really mean that they are less serviceable, as their cements can hydrate and form gels which can fill the voids in castables. Extra-large voids do indicate less strength regardless of filled voids and dictate a lower allowable gas velocity. If of the same density as a given brick, a castable will result in less permeation.

Normally, castables are 25 percent cements and 75 percent aggregates. The aggregate is the more chemically resistant of the two components. The highest-strength materials have 30 percent cement, but too much cement results in too much shrinkage. The standard insulating refractory, 1:2:4 LHV castable, consists of 1 volume of cement, 2 volumes of expanded clay (Haydite), and 4 volumes of vermiculite.

Castables can be modified by a clay addition to keep the mass intact, thus allowing application by air-pressure gunning (gumite). Depending upon the size and geometry of the equipment, many castable linings must be reinforced; wire and expanded metal are commonly used.

Index

- Abinito methods, computational chemistry, **7-38**
absolute humidity, **12-4 to 12-5, 12-26**
absorption, multicomponent systems, **14-18 to 14-19**
absorption, pollutants, **22-38**
absorption with chemical reaction, **14-20 to 14-25**
 applicability of physical design methods, **14-22**
 design strategy, **14-20**
 dominant effects in absorption with chemical reactions, **14-20**
 mass transfer and kinetic models, parameterization of, **14-25**
 rigorous computer-based absorber design, **14-24**
 scaling up from laboratory data, **14-23**
 thermodynamic model for physical and chemical equilibrium, **14-25**
absorptivity, **5-19 to 5-20**
 radiant volume, **5-35**
 water vapor, **5-32**
accounting equation, **9-4**
accumulated depreciation, **9-5**
accumulated retained earnings, **9-6**
acentric factor, **2-473 to 2-475**
acetic acid:
 Antoine vapor pressure, **13-14**
 BIP data, **13-13**
acetic-acid/water separation, **15-8**
acetone:
 absorption in water, **14-17**
 Antoine vapor pressure, **13-14**
 BIP data, **13-13**
 residue curve, **13-90**
 residue map, **13-79**
 thermodynamic properties, **2-209 to 2-210**
 VLE data, **13-7, 13-9**
acetylene, saturated, thermodynamic properties, **2-186, 2-210**
acid catalyzed isomerization, **7-15**
acrylonitrile, **17-17**
activated complex, **7-14**
activation energy, **7-6**
activation overpotential, **7-32**
activity, **12-26, 12-28**
actuator, **8-76 to 8-77, 8-84**
A/D converter, **8-66**
A/D integrating, **8-66**
adaptive control, **8-26**
adiabatic adsorption, breakthrough curves, **16-33 to 16-34**
adiabatic saturation temperature, **12-5**
adjusted propagation velocity, **16-46**
adsorbed-solution theory, **16-15**
adsorbents:
 classification, **16-8**
 physical properties, **16-10**
adsorption:
 equipment:
 adsorber vessel, **16-61 to 16-63**
 cycle control, **16-64**
 design, **16-61**
 hypersorption, **16-66**
 PuraSiv HR vessel, **16-66**
 regeneration, **16-63**
 continuous countercurrent systems, **16-64**
 cross-flow systems, **16-64**
 pollutants, **22-37**
 pressure-swing, **16-50**
 process descriptors, **16-60**
 process selection matrix, **16-60**
 reaction rates, **7-19**
 temperature swing, **16-49**
 UOP nine-bed polybed PSA H2 unit, **16-65**
adsorption and ion exchange:
 adsorbents and ion exchangers, **16-8 to 16-9**
 batch adsorption, **16-27 to 16-30**
 chromatography, **16-38 to 16-48**
 conservation equations, **16-17 to 16-18**
 design concepts, **16-4 to 16-7**
 equipment, **16-61 to 16-67**
 fixed-bed transitions, **16-31 to 16-38**
 process cycles, **16-49 to 16-60**
 rate and dispersion factors, **16-18 to 16-25**
 sorption equilibrium, **16-11 to 16-14**
adsorption cycles:
 energy application, **16-58**
 hybrid recycle systems, **16-58**
 steam regeneration, **16-58**
adsorption equilibrium, **7-16**
adsorption-desorption, rapid, **16-25**
adsorption-rate controlling, reaction kinetics, **7-18**
adsorptive bubble separation methods:
 adsorption:
 factors affecting, **20-31**
 limiting equations, **20-31 to 20-33**
 bubble fractionation, **20-34 to 20-35**
 adsorptive bubble separation methods (*Cont.*):
 definition and classification, **20-30 to 20-31**
 foam-column theory:
 breaking, **20-34**
 coalescence, **20-34**
 drainage and overflow, **20-34**
 equations, **20-32 to 20-33**
 operation, **20-33**
 aerobic, biocatalysis, **7-18**
 aerobic fermentation, **7-30**
 aerodynamic diameter, **17-24**
 affinity laws, **10-36**
 agglomerated materials, fracture properties, **21-103**
 agglomeration processes, **21-82**
 breakage and attrition, **21-100**
 fracture measurements, **21-101**
 fracture properties, **21-101**
 mechanisms of attrition and breakage, **21-102**
 classification, **21-91**
 growth and consolidation, **21-89**
 deformability and interparticle forces, **21-92**
 deformability and wet mass rheology, **21-93**
 granule consolidation and densification, **21-99**
 granule deformability, **21-89**
 high agitation intensity growth, **21-96**
 low agitation intensity, **21-95**
 types of granule growth, **21-90**
 paste extrusion, **21-108**
 compaction in a channel, **21-108**
 drag-induced flow in straight channels, **21-108**
 paste rheology, **21-108**
 powder compaction, **21-103**
 compact density, **21-105**
 compact strength, **21-105**
 compaction cycles, **21-107**
 compaction pressure, **21-105**
 controlling powder compaction, **21-108**
 hiestand tableting indices, **21-107**
 powder feeding, **21-104**
 stress transmission, **21-106**
 wetting, **21-82**
 examples of the impact of wetting, **21-86**
 mechanics of the wetting rate process, **21-82**
 methods of measurement, **21-83**
 nucleation and wetting, regimes, **21-86**
 air, dry, thermodynamic properties, **2-215**

2 INDEX

- air, thermodynamic properties, 2-211 to 2-214
air conditioning:
 equipment, 11-77 to 11-78
 central systems, 11-77
 load calculation, 11-77
 unitary refrigerant-based systems, 11-77
 ventilation, 11-76
air cooler, wet surface, 12-17, 12-22 to 12-25
 application, 12-24
 configuration, 12-23
air pollutants, general, 22-28
 control-equipment selection, 22-36
 effects of air pollutants, 22-31
 estimating emissions from sources, 22-31
 gaseous pollutants, 22-28
 particulate pollutants, 22-29
 source-control-problem strategy, 22-35
air pollutants, hazardous, 22-11 to 22-12
air quality standards, 22-6
air spring effect, 8-86
alarm, rate of change, 8-67
alarms, 8-67
algebra, elementary:
 binomial theorem, 3-8
 operations, 3-8 to 3-9
 permutations, combinations, and probability, 3-10
 progressions, 3-9 to 3-10
 theory of equations, 3-10 to 3-11
 cubic, 3-10
 determinants, 3-11
 factor theorem, 3-10
 fundamental theorem of algebra, 3-10
 linear, 3-10
 quadratic, 3-10
 remainder theorem, 3-10
algebraic inequalities, 3-5 to 3-6
 arithmetic-geometric inequality, 3-5
 Carleman's inequality, 3-5
 Cauchy-Schwarz inequality, 3-5
 Holder's inequality, 3-5
 Lagrange's inequality, 3-5
 Minkowski's inequality, 3-5
alkyl chloride, 17-17
allocated capital, 9-10, 9-17
alphabet, Greek, 1-18
Ambose-Walton modification of Lee-Kesler vapor
 pressure equations, 2-473 to 2-475
ammonia, thermodynamic properties, 2-217
 to 2-219
amortization, 9-22
amplifier network, 8-84
anabolic, 7-31
anaerobic fermentations, 7-18
analog input and output channels, 8-65, 8-72
analog signal transmission, 8-65
analytical geometry, plane:
 asymptotes, 3-12
 conic sections, 3-12
 coordinate systems, 3-11
 parametric equations, 3-13
 straight line, 3-11 to 3-12
analyzer controller, 8-43
angles and sides of triangles relations, 3-17 to 3-18
angular displacement, 8-89
annular liquid separation bed, 16-67
anode, electrochemical reactions, 7-32
Antoine equation, 12-5
API gravity, 13-99
approximation identities, mathematical, 3-43
argon, thermodynamic properties, 2-221 to 2-223
argon-nitrogen-oxygen system, liquid vapor
 equilibrium data, 2-224 to 2-227
aromatic extracting, simplified, 15-9
Arrhenius equation, 7-6
ASME boiler and pressure code section VIII, division 1, quick reference guide, 10-153 to 10-154
ASME B16.5 flanges, dimensions of, 10-83 to 10-86
assets, 9-5
 current assets, 9-5
 accounts receivable, 9-5
 cash, 9-5
 cash equivalents, 9-5
 inventories, 9-5
 marketable securities, 9-5
 prepaid expenses, 9-5
 fixed assets, 9-5
 net property and equipment, 9-5
 total property, plant, and equipment, 9-5
 total assets, 9-5, 9-6
Assman psychrometer, 12-6
asymptotic solution, 16-35
atmosphere, international standard, thermodynamic
 properties, 2-228
atmospheric dust concentrations, 17-52
atomizers, 14-94
autocatalysis, 7-16
autocatalytic reaction, 7-16
autoignition temperature, 2-515 to 2-517
automation, 8-94
automation projects, 8-29
autotune function, 8-26
auto-tuning, 8-69
azeotropic mixtures:
 definition of, 13-6
 heterogenous, 13-6 to 13-7, 13-68
 homogenous, 13-6 to 13-7, 13-68
 maximum boiling, 13-7, 13-68
 minimum boiling, 13-7, 13-68
 reactive, 13-94, 13-95
backpressure, 8-78
baffle towers, 15-80
baffles, trays, 14-35
balance sheet, 9-4, 9-5, 9-6
bancroft point, 13-68
band compression factor, 16-45
BASIC, 8-70
batch dryers, control, 8-46
batch process control, 8-46
batch reactor control, 8-51
batch reactors, 7-34
 electrical or thermal conductivity, 7-31
 light adsorption, 7-34
 polarography, 7-34
 viscosity of polymerization, 7-34
bearings, 10-65 to 10-67
 thrust bearings, 10-66
 plain washer, 10-67
 taper land, 10-67
 temperature characteristics, 10-68
 tilting pad, 10-67
 thrust-bearing power loss, 10-67
 types of bearings, 10-65
 circumferential grooved, 10-65
 comparison of, 10-66
 cylindrical bore, 10-65
 lemon bore or elliptical, 10-66
 offset halves, 10-66
 plain journal, 10-65
 pressure or pressure dam, 10-65
 three-lobe, 10-66
 tilt-pad, 10-66
bed profiles, 16-33
beds of solids, 6-39 to 6-40
 fixed beds of granular solids, 6-39
 fluidized beds, 6-40
 porous media, 6-39 to 6-40
 tower packing, 6-40
bellows element, 8-59
benzene:
 Antoine vapor pressure, 13-14
 thermodynamic properties, 2-229 to 2-230
 Txy diagram, 13-8
 x-y diagram, 13-8
Bernoulli relationship, flow control calculation, 8-80
Bernoulli's equation, 8-9
Bhelousov-Zhabotinsky reaction, 7-39
binary input, digital technology, 8-70
binary signal, pseudo random, 8-12
biocatalysis, 7-18
biochemical reactions, 7-30
 balanced growth, 7-30
 mechanism, 7-31
 yield coefficients, 7-31
biochemical separation processes:
 background, 20-71 to 20-73
 final purification, 20-79 to 20-83
 alternative columns, 20-82
 chromatographic development, 20-81
 to 20-82
 column packings, 20-82
 scale-up of liquid chromatography, 20-83
 schematic, 20-80
 sequencing of chromatographic steps, 20-83
 types of chromatography, 20-79 to 20-81
initial product harvest and concentration, 20-73
 to 20-76
 cell disruption, 20-73 to 20-74
 clarification methods, 20-75 to 20-76
 protein refolding, 20-74 to 20-75
 selection of unit operation, 20-76
initial purification:
 adsorption, 29-78
 liquid-liquid partitioning, 20-76 to 20-78
 membrane ultrafiltration, 20-78
 precipitation, 20-76
 integration of unit operations, 20-84
 product polishing and formulation, 20-83
 drying, 20-83
 lyophilization, 20-83
biological APC technologies, 22-48 to 22-51
 biofilters, 22-50
 biofiltration, 22-48
 bioscrubbers, 22-50
 biotrickling filters, 22-51
biological systems, 7-30
 kinetics, 7-31
 mechanisms, 7-31
 yield coefficients, 7-31
biomass:
 biochemical reactions, 7-30
 See also solid wastes
bioreactors, 7-18, 7-35
 batch, 7-35
 CSTR, 7-35
 chemostat, 7-35
 dilution rate, 7-35
 semibatch, 7-35
Biot number, 16-30
BIPS binary interaction parameters, 13-13
black-body behavior, 8-58
blending:
 chemical reactions, 18-16
 high viscosity systems, 18-15
block diagrams, use in modeling, 8-8
block-diagram analysis, 8-22
blowdown calculation, 12-20
boil up/bottom flow ratio, 8-43
boilers, 24-35 to 24-41
 design issues, 24-36
 circulation and heat transfer, 24-36

- boilers (*Cont.*):
 fluidized-bed:
 bubbling FBCs, 24-39
 circulating FBCs, 24-40 to 24-41
 industrial:
 boiler band, 24-37
 design parameters and criteria, 24-38
 fire-tube boilers, 24-39
 fuel consumption, 24-38
 package boilers, 24-39
 solid-waste fuels burned, 24-38
 utility steam generators:
 economics, 24-37
 fuel characteristics, 24-37
 reheat cycle, 24-37
 steam-generator circulation system, 24-37
 superheaters and reheaters, 24-37
- boiling, 5-14 to 5-15
 coefficients, 5-15
 film boiling, 5-15
 maximum heat flux, 5-15
 nucleate boiling, 5-14 to 5-15
 pool boiling, 5-14
 boiling point:
 curve, 13-101
 initial (IBP), 13-99
 true (TBP), 13-100
 boiling point, normal, 2-471 to 2-476
 calculation methods, 2-471 to 2-473
 Nannoolal method, 2-471 to 2-473
 Pailhes method, 2-472
 group contributions for Nannoolal method, 2-474
 intermolecular interaction corrections, 2-476
 bolometer, detector, 8-62
 bonnets, 8-75
 booster relays, 8-90
 bottom products, 8-42
 boundary layer flows, 6-40 to 6-41
 continuous cylindrical surface, 6-41
 continuous flat surface, 6-41
 cylindrical boundary layer, 6-41
 flat plate, zero angle of incidence, 6-40 to 6-41
 bourdon tube, 8-57, 8-59
 broad-spectrum noise, 8-81
 bromine, saturated, thermodynamic properties, 2-231
 bubble point temperature, def, 13-15
 bubble tube, 8-61
 budget control, 9-10
 burst mode, 8-87
 butanes:
 K-value versus pressure, 13-12
 thermodynamic properties, 2-232 to 2-233
 butanol, 13-86
 Antoine vapor pressure, 13-14
 BIP data, 13-13
 VLE data, 13-9
 butene:
 cis-2:
 thermodynamic properties, 2-236 to 2-237
 thermodynamic properties, 2-234 to 2-235
 Butler-Volmer equation, electrochemical reaction, 7-33
 butyric acid, BIP data, 13-13
 butterfly valve, 8-75
 bypass valve, 8-90
- calcinations, 17-17 to 17-18
 calciner, fluid-bed, 17-18
 calibration of a measurement device, 8-55
 calorimetry, 7-35
 capacitance probes, 8-60
 capillary flow, 12-26
- capital cost estimation, 9-10 to 9-17
 carbon dioxide:
 absorption in NaOH, 14-21
 solubility in MEA, 14-8
 thermodynamic properties, 2-240 to 2-244, 2-200
 carbon $\frac{1}{2}$ Mo steel (group 1.5 materials), pressure-temperature ratings, 10-109
 carbon steel (group 1.1 materials), pressure-temperature ratings for, 10-108
 carbon steel materials, tabular values for minimum temperatures without impact testing for, 10-128 to 10-129
 carbon tetrachloride:
 Antoine vapor pressure, 13-14
 BIP data, 13-13
 saturated:
 thermodynamic properties, 2-245
 carbon tetrafluoride (R14), saturated thermodynamic properties, 2-245
 carbonyl sulfide, thermodynamic properties, 2-246 to 2-247
 cascade control, 8-24
 cascade factor, 12-74
 cash flow, 9-27
 cumulative cash position plot, 9-28
 example of, 9-11, 9-29
 cumulative cash position, 9-27
 example of, 9-25, 9-28
 catabolic pathway, biological reactions, 7-31
 catalysis, 7-9, 8-44
 solid, 7-16
 catalyst deactivation, 7-22
 catalyst poisoning, 7-22
 catalysts, solid, 7-35
 effectiveness, 7-35
 catalytic cracking, 7-16
 catalytic reactions, 7-9
 biocatalysis, 7-18
 fluid-solid, 7-16
 gas-liquid solid, 7-28
 gas-solid, 7-19
 heterogeneous, 7-10
 homogeneous, 7-10
 solid, 7-16
 solid-liquid, 7-18
 catalytic reactors:
 fixed beds, 19-30 to 19-33
 heterogeneous 1D model, 19-32
 heterogeneous 2D model, 19-32 to 19-33
 homogeneous 1D model, 19-31
 homogeneous 2D model, 19-31 to 19-32
 thermal conductivity, 19-32
 wall heat transfer, 19-32
 fluidized beds, 19-33 to 19-36
 monolith catalysts, 19-27 to 19-30
 types of, 19-29
 moving beds, 19-33
 examples, 19-35
 multifunctional reactor, 19-36
 slurry reactors, 19-36
 transport reactors, 19-36
 wire gauzes, 19-27
 cathode, chemical reduction at, 7-32
 cation and anion exchangers, 16-15
 cavitations, pump behavior, 8-82
 centrifugal filtration:
 costs:
 purchase, 18-140
 installation, 18-141
 maintenance, 18-142
 labor, 18-142
- centrifugal filtration (*Cont.*):
 filtering, 18-140
 moisture, residual, 18-139
 rate of filtration, 18-138
 sedimentation, 18-140
 theory, 18-138
 centrifugal force:
 industrial centrifuges, 18-118
 variation w/rpm, 18-119
 centrifugal pump, 8-91
 centrifugal separation, principles diagram, 18-116
 centrifugal separator, 15-92
 centrifuge equipment, photos and sketches:
 bottom unloading vertical basket, 18-130
 bowls, disk stack, 18-123
 cylindrical-conical screen-bowl, 18-126
 disc stack, 18-122
 installation, vertical basket, 18-130
 inverted filter, 18-133 to 18-134
 peeler cross section, 18-131
 pharma peeler, 18-133
 pusher cross section, 18-136
 pusher process steps, 18-137
 pusher product moisture gradient, 18-138
 pusher solids transport representation, 18-137
 scroll screen, 18-135
 sedicanter, 18-125
 siphon peeler cross section, 18-132
 sorticanter, 18-126
 three-phase decanter, 18-125
 top unloading vertical basket, 18-129
 top-suspended, vertical, 18-131
 two-phase decanter, 18-122, 18-124
 centrifuge equipment:
 batch filtering centrifuges, 18-127 to 18-133
 bottom unloading vertical basket centrifuges, 18-128
 horizontal peeler centrifuge, 18-29 to 18-131
 inverting filter centrifuge, 18-133
 pharma peeler centrifuge, 18-132 to 18-133
 pressurized siphon peeler centrifuge, 18-132
 siphon peeler centrifuge, 18-131 to 18-132
 top suspended vertical centrifuges, 18-128 to 18-129
 top unloading vertical basket centrifuges, 18-128
 continuous filtering centrifuges, 18-133
 centrifugal filtration theory, 18-138
 cylindrical or conical pusher centrifuge, 18-138
 multi-stage pusher centrifuges, 18-136
 single-stage pusher centrifuges, 18-136
 costs, 18-140 to 18-142
 expression, 18-143 to 18-146
 filtering centrifuges, 18-127
 introduction, 18-115
 general principles, 18-115 to 18-118
 cake conveyance power, 18-117
 cake dryness, 18-116
 cake liquid saturation, 18-116
 cake porosity, 18-116
 centrifuge rotor stress, 18-117
 centripetal and centrifugal acceleration, 18-115
 clarification, 18-115
 classification, 18-115
 Coriolis acceleration, 18-115
 critical speeds, 18-117
 dewatering or deliquoring, 18-116
 Ekman layers, 18-115
 Ekman number, 18-115
 feed acceleration power, 18-117
 g-acceleration, 18-117
 g-level, 18-115
 momentum transfer, 18-115

4 INDEX

- centrifuge equipment, general principles (*Cont.*):
 - performance criteria, 18-116
 - polymer dosage, 18-116
 - power consumption, 18-16
 - recovery, 18-116
 - Rosby number, 18-115
 - sedimentation and filtering centrifuges, 18-115
 - solids purity, 18-117
 - thickening, 18-115
 - throughput capacity, 18-117
 - vibrational harmonics, 18-117 to 18-118
 - volumetric and solids throughput, 18-117
 - wash ratio, 18-117
 - yield, 18-17
- sedimentation centrifuges, 18-118 to 18-127
 - Ambler's sigma factor, 18-127
 - cake-slurry interface, 18-120
 - centrifugal gravity, 18-118
 - continuous centrifugal sedimentation theory, 18-126 to 18-127
 - decanter centrifuges, 18-121 to 18-125
 - disc nozzle centrifuges, 18-120 to 18-121
 - imperforate bowl test, 18-119 to 18-120
 - knife-discharge centrifugal clarifiers, 18-120 to 18-121
 - liquid-slurry interface, 18-120
 - manual disc stack centrifuges, 18-120
 - multichamber centrifuges, 18-120
 - screenbowl centrifuges, 18-125 to 18-126
 - sedicanter, 18-125
 - self-cleaning disc centrifuges, 18-120
 - solids concentration, 18-120
 - spin-tube tests, 18-118 to 18-119
 - transient centrifugation theory, 18-120
 - tricanter centrifuges, 18-125
 - tubular-bowl centrifuges, 18-120
 - yield stress, 18-119
 - selection, 18-140
- cesium, saturated, thermodynamic properties, 2-248
- chain or tape float gauge, 8-60
- chain reaction mechanism, 7-14
- chain reactions, 7-14
- change of state alarm, 8-67
- charcoal, 24-7
- Chebyshev method, 12-18
- check valves, 8-79
- chemical composition analyzers V, 8-62
- chemical dynamics determination, 7-38
- chemical equilibrium, 7-7
 - gas phase, 7-17
- chemical reaction:
 - bimolecular, 7-5
 - stoichiometry, 4-35
 - trimolecular, 7-5
 - unimolecular, 7-5
- chemical reactors, control of, 8-44
- chemical sensors, 8-63
- chemical systems, 7-30
- chemisorption, 16-4
- chemostat, 7-31
- Chilton-Colburn analogy, 12-6, 12-53
- chlorine:
 - enthalpy-pressure, 2-250
 - saturated:
 - thermodynamic properties, 2-249
- chloroform:
 - Antoine vapor pressure, 13-14
 - residue map, 13-79
 - VLE data, 13-7 to 13-9
 - saturated:
 - thermodynamic properties, 2-251
- choke, 8-80
- chopped light system, 8-62
- chromatographic analyzers, 8-62
- chromatographs, 8-66
- chromatography:
 - displacement development, 16-39
 - elution, 16-38
 - curves, 16-43
 - gradient, 16-38, 16-44
 - isocratic, 16-38, 16-42, 16-47
 - frontal analysis, 16-39
 - Gaussian peak, 16-41 to 16-42
 - ion exchange, 16-45
 - operation, 16-38
 - peak asymmetry factor, 16-41
 - peak skew, 16-41
 - plate models, 16-42
 - resolution, 16-41
 - reversed-phase, 16-45
 - Sanmatsu Kogyo process, 16-58
 - tailing peaks, 16-41
- circular trigonometric functions, 3-16 to 3-17
 - common angle values, 3-16
 - identities, 3-17
 - plane trigonometry, 3-16
 - single angle relations, 3-16 to 3-17
- clarifiers:
 - instrumentation, 18-78
 - types:
 - circular, 18-74
 - clarifer-thickener, 18-74
 - inclined plate, 18-75
 - rectangular, 18-74
 - secondary, industrial waster, 18-74
 - solids contact, 18-75
- closed loop, 8-13
- closed-circuit cooling, 12-24 to 12-25
- closed-loop system, general control system, 8-5
- closed-loop time constant, 8-74
- coal, 24-4 to 24-6
 - classification, 24-4
 - coal-ash:
 - characteristics, 24-5
 - composition, 24-6
 - fouling, 24-6
 - composition, 24-5
 - as-received, 24-5
 - dry, ash-free, 24-5
 - moisture-free, 24-5
 - ultimate analysis, 24-5
 - heating value, 24-5
 - mercury emissions, 24-5
 - origin, 24-4
 - physical properties:
 - bulk density, 24-6
 - free-swelling index, 24-6
 - Hargrove grindability index, 24-6
 - mean specific heat, 24-6
 - size stability, 24-6
 - reserves by region, 24-5
 - sulfur content, 24-5
- coal char, 24-7
- coal conversion, 24-12 to 24-21
 - gasification. *See* coal gasification
 - liquefaction. *See* coal liquefaction
 - production diagram, 24-13
- coal gasification, 24-12 to 24-16
 - background, 24-12
 - chemical reactions, 24-14
 - coal-derived gas compositions, 24-13
 - cost of gasification-based power systems, 24-16
 - current technology, 24-16
 - gasification-based power systems, 24-14 to 24-16
 - gasifier types:
 - entranced bed, 24-14
 - fluidized bed, 24-14
 - moving bed, 24-14
 - temperature profiles, 24-15
 - theoretical considerations, 24-12 to 24-14
- coal liquefaction, 24-16 to 24-21
 - background, 24-16
 - chemicals from syngas, 24-20 to 24-21
 - coal-oil coprocessing, 24-18 to 24-19
 - commercial operations, 24-19, 24-21
 - direct hydrogenation, 24-17
 - direct liquefaction 24-17 to 24-19
 - conditions and product yields, 24-18
 - kinetics, 24-17 to 24-18
 - process diagram, 24-17
 - Exxon donor solvent process, 24-18
- coating flows, 6-42 to 6-43
- cogeneration, 24-44 to 24-45
 - background, 24-44
 - characteristics for heat engines, 24-44
 - choice of fuel, 24-44
 - typical systems, 24-45
- coke, 24-6 to 24-7
 - description, 24-6
 - properties table, 24-6
 - types of:
 - foundry, 24-6
 - high-temperature, 24-6
 - low-temperature, 24-6
 - medium-temperature, 24-6
 - needle, 24-7
 - petroleum, 24-6 to 24-7
 - pitch, 24-6
- collection efficiency, 17-23, 17-27
- collision theory, 7-6
- colorimetric detection selective oxidation, 8-62
- column pressure, 8-43
- columns, tray and packed bed, pollutants, 22-38
- combined wave, 16-32
- combustion, background:
 - available heats, 24-22
 - excess air, 24-22
 - flame speed, 24-23
 - flame temperature, 24-22 to 24-23
 - flammability limits, 24-23
 - products, 24-22
 - theoretical oxygen and air, 24-21 to 24-22
 - various fuel characteristics, 24-23
- combustion, gaseous fuels, 24-32 to 24-35
 - gas burners:
 - fully premixed, 24-33
 - nozzle-mix, 24-33
 - partially premixed, 24-33
 - staged, 24-33
 - system illustrations, 24-33 to 24-35
 - combustion, liquid fuels, 24-31 to 24-32
 - atomizers, 24-31 to 24-32
 - illustrations of different types, 24-31 to 24-32
 - oil burners, 24-32
 - pressure atomizers, 24-31
 - twin-fluid, 24-32
 - dew point vs. sulfur content, 24-31
- combustion, solid fuels:
 - fluidized-bed combustion. *See* fluidized-bed combustion
 - fuel-bed firing. *See* fuel-bed firing
 - suspension firing. *See* suspension firing
- combustion systems, pollutants, 22-38
- commodity plants, control of, 8-47
- comparators, use in control, 8-71
- comparison of alternative investments, 9-35
 - cash flow method, 9-36
 - net present worth method, 9-36
 - uniform annual cost (USC) method, 9-36
- complex reactions. *See* global reactions
- complex variables, 3-27 to 3-29
- compressibilities:
 - composition of selected refrigerant mixtures, 2-143
 - liquids, 2-145, 2-144

- compressibilities (*Cont.*):
 R 407A, compressibility factors, 2-143
 R 407B, compressibility factors, 2-143
 solids, 2-146, 2-144
- compressibility factor, 7-8
- compressible flow, 6-22 to 6-26
 adiabatic flow with friction in a duct of constant cross section, 6-24
 adiabatic frictionless nozzle flow, 6-23 to 6-24
 convergent/divergent nozzles (De Laval nozzles), 6-24 to 6-26
 isothermal gas flow in pipes and channels, 6-22 to 6-23
 Mach number and speed of sound, 6-22
- compression, gas, 10-42
 adiabatic calculations, 10-44
 efficiency curve, 10-45
 polytropic curve, 10-46
 work, 10-45
- compression processes, thermodynamics, 4-16 to 4-17
- compressors, 10-40 to 10-48
 high-pressure, 10-47
 metallic diaphragm, 10-48
 performance characteristics of, 10-45
 reciprocating compressors, 10-45
 clearance unloaders, 10-47
 closed-suction unloaders, 10-47
 control devices, 10-46
 five-step control, 10-47
 nonlubricated cylinders, 10-47
 open inlet-valve unloaders, 10-47
 piston-rod packing, 10-48
 single-stage, double-acting water-cooled compressor, 10-47
 three-step control, 10-47
 valve losses, 10-46
- selection, 10-42
- theory of, 10-42
 adiabatic, 10-42
 isothermal, 10-42
 polytropic, 10-42
- types of, 10-44
- compressors, centrifugal problems, 10-67
 failure, 10-69
 barrel-type compressor, 10-69
 fouling, 10-68
 air compressors, 10-68
 blade coating, 10-68
 prevention techniques, 10-68
- impeller problems, 10-69
- journal bearing failures, 10-70
- rotator thrust problems, 10-69
- seal problems, 10-70
- thrust bearing failures, 10-70
 causes, 10-70
 wear points in the bearing, 10-70
- compressors, continuous-flow, 10-52 to 10-57
 axial-flow, 10-54 to 10-56
 centrifugal, 10-52
 choke or stonewall, 10-52
 compressor map, 10-53
 configurations, 10-53, 10-54
 fabrication techniques, impellers, 10-54
 impeller fabrication, 10-54
 pressure and velocity through, 10-52
 surge, 10-52
- positive-displacement, 10-56
 reciprocating, 10-56
 rotary, 10-56
- rotary, 10-56
 liquid-piston type, 10-56
 screw-type, 10-56
 sliding-vane type, 10-56
 straight-lobe type, 10-56
- computational fluid dynamics, 18-26, 6-47 to 6-49
- computer controllers, 8-72
 personal, 8-69, 8-73
- computerized cost estimation, 9-17
 ASPENTECH ICARUS 2000, 9-17
- computers in process control, 8-5
 concentration types, 7-8
 mole fractions, 7-8
 partial pressures, 7-8
 volumetric concentration, 7-8
- condensation, 5-12 to 5-14
 coefficients, 5-12 to 5-14
 banks of horizontal tubes, 5-14
 horizontal tubes, 5-14
 vapor shear controlling, 5-14
 vertical intube condensation, 5-14
- mechanisms, 5-12 to 5-14
 dropwise, 5-12
 film-type condensation, 5-12, 5-13
 scrubbing, 17-39
 Stefan-flow mechanism, 17-39
- condensers, pollutants, 22-39
- conduction, 5-3 to 5-7
 steady-state, 5-3 to 5-6
 heat source, 5-5
 one-dimensional, 5-3 to 5-4
 resistances, 5-5
 two- and three-dimensional, 5-5 to 5-6
 unsteady-state, 5-6 to 5-7
 one-dimensional, 5-6 to 5-7
 two- and three-dimensional, 5-7
- conductometric analysis, 8-63
- confidence level, 7-37
- conjugate gradient, multivariable optimization, 8-34
- conservation of energy, basis for modeling, 8-6
- conservation of mass, basis for modeling, 8-6, 8-80
- conservation of momentum, basis for modeling, 8-6
- constant-rate period, 12-26
- constants:
 fundamental physical, 1-20
 gas law, values of, 1-17
- constrained optimization, 8-34
- contact discontinuity, 16-32
- continuous measurements, 8-54
- continuous models, use in control, 8-8
- continuous variable approximation method, 7-30
- control alarm, 8-73
- control limits:
 lower and upper, 8-36
 specified, 8-38
- control network, 8-70
- control switches, 8-49
- control systems design and simulation, 8-31
- control valves, 8-74
- controller:
 comparison, 8-16
 design, 8-31
 multiloop, 8-72
 performance, 8-17, 8-73
 reliability and application trends, 8-73
 single-loop, 8-69, 8-72 to 8-73
 tuning, 8-16
- controlling rate factor, determination of, 16-25
- convection, 5-7 to 5-12, 12-26
 forced convection, 5-9 to 5-12
 coiled tubes, 5-10
 external flows, 5-10
 falling films, 5-11
 fin efficiency, 5-11 to 5-12
 finned tubes, 5-11
 horizontal tubes, 5-11 to 5-12
 noncircular ducts, 5-9 to 5-10
 round tubes, 5-9
- convection, forced convection (*Cont.*):
 tube banks, 5-10 to 5-12
 vertical tubes, 5-12
 non-newtonian flows, 5-12
 circular tubes, 5-12
- conversion factors:
 calculations, U.S. customary to SI units, 1-21
 common, alphabetical listing of, 1-14 to 1-16
 factors:
 common, 1-17
 metric, exact numerical multiples of SI units, 1-12 to 1-13
 U.S. customary and commonly used units to SI units, 1-3 to 1-11
- formulas:
 kinematic-viscosity, 1-17
 temperature, 1-18
- SI, 1-2
- conveyor dryers, 8-46
- cooling towers, 12-17 to 12-22
 applications, 12-21
 cooling pond, 12-21
 cooling range, 12-20
 cross-flow tower, 12-19
 counterflow, 12-19
 cycles of concentration, 12-20
 fogging and plume abatement, 12-21
 forced-draft tower, 12-19
 horsepower chart applications, 12-20
 induced-draft tower, 12-19
 mechanical draft tower, 12-19
 natural draft tower 12-21
 new technologies, 12-21
 spray pond, 12-21
 theory, 12-17
 thermal performance, 12-21
 time of contact, 12-19
 tower characteristic, 12-18
 water makeup, 12-20
- copolymerization, 7-29 to 7-30
- Coriolis mass flowmeters, 8-59 to 8-60
- corporate information systems, 8-69
- corrosion:
 anodic protection, 25-10 to 25-11
 cathodic protection, 25-10
 concentration effects, 25-9 to 25-10
 dealloying, 25-6
 design considerations, 25-10
 embrittlement, 25-16
 EMF, 25-17
 fatigue, 25-6
 film, 25-9
 fluid, 25-4 to 25-6
 cavitation, 25-3
 crevice, 25-4
 erosion, 25-5
 fretting, 25-6
 galvanic, 25-4, 25-16
 hydrogen attack, 25-6
 hydrogen embrittlement, 25-6
 intergranular, 25-5
 liquid-metal, 25-5
 oxygen-concentration cell, 25-4
 stress cracking, 25-5
 velocity acceleration, 25-6
- graphitic, 25-6
- high-temperature attack, 25-9 to 25-10
 expansivity, 25-9
 structural stability, 25-9
- inhibitors, 25-10
- laboratory testing, 25-12 to 25-24
 AC impedance, 25-23
 apparatus, 25-14
 cathodic depolarization, 25-19
 CBD, 25-20

6 INDEX

- corrosion, laboratory testing (*Cont.*):
 cleaning, 25-16
 crevice corrosion prediction, 25-20
 EIS, 25-23
 electrical resistance, 25-17
 environmental cracking, 25-22
 Fourier transform technique, 25-23
 immersion, 25-13
 linear polarization, 25-18
 planned interval, 25-16
 potentiodynamic polarization, 25-19
 potentiostat, 25-19
 slow scan, 25-20
 slow-strain rate, 25-23
 solution-composition, 25-15
 stress accelerated corrosion, 25-22
 Tafel region, 25-17
 test piece, 25-13
- linings, 25-11, 25-12
 ceramic, 25-11
 glass-lined, 25-11
 metallic, 25-11
 organic, 25-11
- MIC:
 electrochemical noise monitoring probes, 25-26
 electrical resistance probes, 25-25
 gas probes, 25-26
 heat flux, 25-22
 hydrostatic testing, 25-7 to 25-8
 ion probes, 25-26
 linear polarization resistance probes, 25-26
 MIC probes, 25-26
 multi-informational probes, 25-26
 oxydation, 25-8 to 25-9
 parting, 25-6
 pH, 25-8
 pH probes, 25-26
 plant testing, 25-24 to 25-28
 polarization probes, 25-26
 pressure probes, 25-26
 weight loss probes, 25-25
- cost control, 9-10
cost estimation, 9-10
 classification of 9-10
 battery limits, 9-10
 grass roots, 9-10
 quality of, 9-10
 definitive, 9-10
 detailed, 9-10
 order-of-magnitude, 9-10
 preliminary, 9-10
 study, 9-10
 requirements for, 9-11
- cost of capital, 9-9
costs, fuel and energy, 24-12
countercurrent evaporator, control of, 8-45
critical constants, 2-138 to 2-142
critical moisture content, 12-26
critical properties, 2-468 to 2-471
 calculation methods, 2-468 to 2-471
 Ambrose, 2-468 to 2-470
 Fedors', 2-468 to 2-471
 Joback, 2-468, 2-470
 compressibility factor, 2-468
 pressure, 2-468 to 2-471
 temperature, 2-468 to 2-471
 volume, 2-468 to 2-471
- crushing, performance of jaw crusher, 21-58
crushing and grinding. *See* grinding and crushing
- cryogenic processes, 11-99 to 11-109
 cryogenic fluids, properties of, 11-99
 instrumentation of, 11-108 to 11-109
 flow, 11-109
 liquid level, 11-109
- cryogenic processes, instrumentation of (*Cont.*):
 pressure, 11-109
 temperature, 11-109
 process equipment, 11-103 to 11-104
 expanders, 11-104
 heat exchangers, 11-103
 refrigeration and liquefaction, 11-100
 to 11-103
 expansion types of refrigerators, 11-101
 miniature refrigerators, 11-103
 thermodynamic analyses of cycles, 11-103
 safety, 11-109 to 11-110
 flammability and explosion hazards, 11-110
 high pressure gas hazards, 11-110
 materials and construction hazards, 11-109
 physiological hazards, 11-109
 separation and purification systems, 11-104
 to 11-107
 air-separation systems, 11-105
 gas purification, 11-106
 helium and natural gas systems separation, 11-106
- solids, properties of, 11-99 to 11-100
 electrical properties, 11-100
 structural properties, 11-99
 superconductivity, 11-100
 thermal properties, 11-100
 storage and transfer systems, 11-107 to 11-108
 insulation principles, 11-107
 types of insulation, 11-107
- cryogenic service, 8-76
- crystallization from solution, 18-39 to 18-58
 costs, 18-58
 equipment, 18-50 to 18-57
 Armstrong crystallizer, 18-53
 classified-suspension crystallizer, 18-52
 direct-contact-refrigeration crystallizer, 18-51
 double-pipe scraped-surface crystallizer, 18-52
 to 18-53
 draft-tube-baffle (DTB) evaporator-crystallizer, 18-50 to 18-51
- operation, 18-58
 magma (slurry) density, 18-58
 nuclei formation rate, 18-58
 recovery period, 18-58
- principles of crystallization, 18-39 to 18-50
 coefficient of variation, 18-44
 crystal formation, 18-41 to 18-44
 crystal nucleation and growth, 18-44 to 18-47
 crystallizers with fines removal, 18-48 to 18-50
 crystallography, 18-39
 examples, 18-40 to 18-41, 18-47
 fractional crystallization, 18-41
 geometry of growth, 18-42
 heat effects, 18-40
 product purity, 18-42 to 18-44
 solubility and phase diagrams, 18-39
 to 18-40
 yield, 18-40
 specifications, 18-57 to 18-58
- CSTR:
 modeling, 19-8
 tracers, 19-15 to 19-16
- current density, 7-32
current efficiency, 7-32
current-to-pressure transducer, 8-89
cut diameter, 17-21
cut-power correlation, 17-39
cyclical batch, control of, 8-47
- cyclohexane:
 residue map, 13-70
 thermodynamic properties, 2-252 to 253
- cyclone, uniflow, 17-36
cyclone collectors, pollutants, 22-36
cyclone design alternatives, 17-35
- cyclone separators, 17-28 to 17-31
 axial cyclone, 17-35
 barrel friction, 17-32
 cyclone efficiency, 17-36
 cyclone inlets, 17-34
 cyclone roughness, 17-32
 design factors, 17-32
 exit contraction, 17-32
 gas flow reversal, 17-32
 helical cyclone, 17-35
 inlet contraction, 17-31
 inlet loading, 17-31
 multiclones, 17-35
 particle acceleration, 17-32
 particle collection efficiency curve, 17-30
 proportions, 17-29
 required cyclone length, 17-33, 17-35
 solids loading, 17-34
 spiral cyclone, 17-35
 theoretical particle size, 17-30
 uniflow cyclone, 17-35, 17-36
 cyclone solids-return seal, 17-15
- De Priester charts, 13-8 to 13-11
deactivation, uniform, 7-23
 effectiveness, 7-23
 power rate law, 7-23
dead band, control valve consideration, 8-13, 8-86
dead polymer. *See* product polymer
dead time, in process measurement, 8-55
dead-time dominant, 8-18
dead-time element, 8-10
death rate, catalytic reactions, 7-19
decane, thermodynamic properties, 2-254 to 2-255
decantation, continuous:
 design, 18-81
 equipment, 18-81
decontamination index, 17-21, 17-27
decoupling control system, 8-27
deflagration indices and pressure for selected gases
 and vapors, 23-13
defoamers, types and applications, 14-129
degree of polymerization, 7-30
deionizing system, two-bed, 16-67
densities of aqueous inorganic solutions at 1 atm,
 2-104 to 2-114
densities of aqueous organic solutions:
 acetic acid, 2-115
 ethyl alcohol, 2-117
 ethyl alcohol and water mixtures, 2-113, 2-118
 ethyl alcohol and water mixtures, specific gravity,
 2-119
 formic acid, 2-114
 glycerol, 2-121
 hydrazine, 2-121
 isopropyl alcohol, 2-120
 methyl alcohol, 2-116
 miscellaneous organic compounds, 2-122
 to 2-123
 n-propyl alcohol, 2-120
 oxalic acid, 2-16
densities of miscellaneous materials:
 miscellaneous solids and liquids, specific gravities
 and densities, 2-124 to 2-125
 selected elements as a function of temperature,
 2-125
densities of pure substances:
 inorganic and organic liquids, 2-98 to 2-103
 mercury from 0 to 350°C, 2-97
 saturated liquid water from the triple point to the
 critical point, 2-96
density, 2-497 to 2-504, 8-61
 bulk, 16-9
 gases, 2-497

- density, gases (*Cont.*):
 accentric deviations $Z(1)$ from compressibility factor for a simple fluid, 2-501
 calculation methods, 2-497
 cubic equation of state, 2-499
 cubic equation of state relationships, 2-502
 compressibility factors $Z(0)$ for a simple fluid, 2-500
 Lee-Kesler method, 2-499
 Lee-Kesler method constants for two reference fluids, 2-502
 Peng-Robinson equation of state, 2-502
 Rackett method, 2-503
 Soave equation of state, 2-502
 Tsonopoulos method, 2-498
- liquids, 2-503
 calculation methods, 2-503
 Rackett method, 2-503
- mixtures, 2-503
 calculation methods, 2-503
 cubic equation of state, 2-504
 Spencer-Danner-Li method, 2-504
- solids, 2-503
 calculation methods, 2-503
 Goodman method, 2-503
- density function theory, 7-38
- depletion, 9-22
 IRS publication 535, 9-22
- depreciation, 9-21
 MACRS modified accelerated cost recovery system, 9-21
 depreciation class lives, 9-21
 example of, 9-22
 straight-line, 9-21
- derating factors, 14-41
- derivation, response curve, 8-18
- design, process safety, 23-38 to 23-41
 actions needed for safer and user-friendly plants, 23-39
 attenuation or moderation, 23-38
 ease of control, 23-39
 intensification or minimization, 23-38
 knock-on effects, 23-38
 limitation of effects of failures, 23-38
 low leak rate, 23-39
 making incorrect assembly impossible, 23-39
 making status clear, 23-39
 simplification, 23-38
 software, 23-39
 substitution, 23-38
 tolerance, 23-39
 incident investigation and human error, 23-39
 recommendations for prevention/mitigation, 23-40
- dessicant cooling cycle flow diagram, 16-59
- determinant, 7-9
- detuning, 8-27
- deuterium oxide (heavy water), thermodynamic properties, 2-209, 2-256 to 2-257
- deviation alarms, 8-67
- device-level diagnostics, 8-89
- dew-point method, moisture measurement, 8-63
- dew-point temperature, 12-4, 13-15
- diaphragm elements, 8-59
- dielectric constant, 8-62
- difference equations, 3-34 to 3-36
 factorization, 3-36
 homogeneous, 3-35
 method of undetermined coefficients, 3-35
 method of variation of parameters, 3-35
 nonhomogeneous, 3-35
 reduction of order, 3-36
 Riccati difference equation, 3-36
 substitution, 3-36
 variable coefficients, 3-35
- differential calculus:
 continuity, 3-19
 derivatives, 3-19 to 3-21
 functional notation, 3-18
 limits, 3-18 to 3-19
 differentials, 3-19 to 3-20
 differentiation, 3-19
 L'Hospital's Theorem, 3-20
 operations, 3-19
 partial, 3-20 to 3-21
- differential data analysis, 7-36
- differential gap, 8-13
- differential pressure controller, 8-42
- differential transformer, 8-64
- diffusion, solid, 16-20
- diffusion in porous solids, 5-58 to 5-59
- diffusion limitations, 7-21
- diffusivity, 7-25
 estimation of gas, 5-50 to 5-53
 binary mixtures, 5-50 to 5-52
 correlations, 5-51
 multicomponent mixtures, 5-53
 supercritical mixtures, 5-52
 estimation of liquids, 5-53 to 5-58
 binary mixtures, 5-54 to 5-57
 multicomponent mixtures, 5-57 to 5-58
 interdiffusion coefficient, 5-45
 mass, 5-45
 mutual, 5-45
 self-diffusivity, 5-45, 5-52
 tables, 5-50
 tracer, 5-45
- digital controllers, single station, 8-5
- digital field communications, 8-70, 8-86
- digital hardware in process control, 8-69
- digital systems, 8-65
- digital technology for process control, 8-68
 measurement devices, 8-68
 production controls, 8-68
 real-time optimization, 8-68
 regulatory controls, 8-68
 safety, 8-68
- digital valve controller, 8-87 to 8-88
- digital valves, 8-76
- dimensional analysis, 3-88 to 3-89
- dimensionless concentration variables, 16-13
- dimethylpropane (neopentane), thermodynamic properties, 2-258 to 2-259
- diphenyl, saturated, thermodynamic properties, 2-260
- direct-fired combustion equipment, 24-41
- discharge coefficient, 8-59
- discrete control models, 8-8
- discrete device states, 8-49
- discrete logic, 8-50
- discrete measurements, 8-54
- disperser plate, 15-72
- dispersion, axial:
 breakthrough behavior, 16-35
 in packed beds, 16-22 to 16-23, 16-25
- dispersion fundamentals, liquid-liquid, 15-41 to 15-44
 drop size, 15-42-15-43
 characteristic diameter, 15-42
 Weber number, 15-42
- holdup, 15-41
- interfacial area, 15-41
- liquid-liquid dispersion stability, 15-43
 emulsion breakage, 15-43
 Marangoni instabilities, 15-43 to 15-44
 phase dispersal factors, 15-41 to 15-42
 Sauter-mean diameter, 15-41
 solid-surface wettability, 15-43
 wear-related surface alterations, 15-43
- dispersion units, 16-31
- displacement purge, 16-53
- distance-velocity lag, in control systems, 8-10
- distillation:
 azeotropic, 13-68, 13-81 to 13-87, 13-116
 batch, 13-116
 design, 13-87
 entrainer selection, 13-81 to 13-85
 immiscible liquids, 13-85
 operation, 13-87
 batch, 13-5, 13-109 to 13-116
 azeotropic, 13-116
 binary calculations, 13-11 to 13-14
 constant level, 13-114
 multicomponent calculations, 13-114
 operation, 13-110 to 13-111
 with recification, 13-109 to 13-110
 simple, 13-109
 definition of, 13-4
 degrees of freedom and design variables, 13-55 to 13-58
 analysis, 13-56 to 13-58
 definitions, 13-55
 efficiencies, 13-25, 13-43 to 13-44
 Murphree, 13-25, 13-43 to 13-44
 overall column, 13-43
 Taylor-Baur-Krishna (TBK), 13-43
 equilibrium stage correct, 13-5
 extractive, 13-87 to 13-93
 design/optimization, 13-89 to 13-91
 solvent effects, 13-88 to 13-89
 solvent selection, 13-91 to 13-93
 graphical methods, 13-16 to 13-25
 McCabe-Thiele, 13-6 to 13-25, 13-35 to 13-39
 heat integration, 13-65 to 13-67
 multicomponent methods, 13-25 to 13-55
 continuation methods, 13-35
 Fenske-Underwood-Gilliland (FUG), 13-25 to 13-27
 inside-out method, 13-33
 Kremser method, 13-28 to 13-30
 simultaneous convergence, 13-33
 tearing method, 13-33
 nonequilibrium modeling, 13-46 to 13-55
 Maxwell-Stefan approach, 13-52 to 13-55
 software, 13-55
 petroleum, 13-99 to 13-109
 applications, 13-102
 characterization, 13-97
 design procedures, 13-103 to 13-108
 pitchfork boundary, 13-85
 pressure swing, 13-82 to 13-83
 pseudocritical point, 13-9
 reactive, 13-93 to 13-98
 application, 13-94, 13-96 to 13-97
 design/implementation, 13-95
 modeling, 13-94
 region diagrams, 13-72 to 13-77
 single stage equilibrium flash calculations, 13-15 to 13-16
 adiabatic flash, 13-16
 isothermal flash, 13-15
 specifications, 13-16
 three-phase, 13-16
 systems, 13-58 to 13-67
 direct split, 13-58
 dividing wall columns, 13-59 to 13-64
 indirect split, 13-58
 pretractorator, 13-59
 thermally coupled, 13-59 to 13-64
 thermodynamic data and models, 13-6 to 13-15
 phase equilibrium data, 13-6 to 13-14
 thermodynamic efficiency, 13-65 to 13-67
 tower configurations, 13-61 to 13-63
 tray efficiencies, 13-5
 trays, binary systems, 13-7

8 INDEX

- distillation column, control of, **8-41**
distributed control system, **8-29, 8-50, 8-69, 8-72, 8-86**
distributed database, **8-70**
distributed lags, tuning rule in control, **8-18**
dodecane, thermodynamic properties, **2-261 to 2-262**
dominant lag, tuning rule in control, **8-16, 8-18**
Donnan uptake, **16-14**
double-entry bookkeeping, **9-4**
 credit side, **9-4**
 debit side, **9-4**
dry-basis humidity, **12-4**
dryer, fluosolids, **17-18**
dryer modeling, design and scale-up, **12-50 to 12-56**
 drying time, **12-51**
 falling rate kinetics, **12-51**
 heat/mass balance, **12-50, 12-75**
 scale up effects, **12-51**
 scaling models, **12-52 to 12-54**
 incremental model, **12-52**
drying (solids) equipment selection, **12-48 to 12-50**
drying equipment (solids):
 agitated and rotating batch dryers, **12-56, 12-65 to 12-81**
 calculations of dimensions, **12-70**,
 conical mixer dryer, **12-68**
 heated agitators, **12-67**
 horizontal pan dryer, **12-67 to 12-68**
 tumbler or double-cone dryers, **12-69, 12-73**
 vertical pan dryer, **12-68**
 agitated flash dryers, **12-101 to 12-104**
 batch through-circulation dryers, **12-44, 12-59**
 cascading rotary dryers, **12-56**
 centrifuge dryers, **12-89**
 classification, **12-40**
 continuous agitated dryers, **12-71 to 12-81**
 direct rotary kiln, **12-72**
 direct Roto-Louvre dryer, **12-72, 12-80 to 12-81**
 indirect rotary calciner, **12-72, 12-79 to 12-80**
 indirect steam-tube dryer, **12-72, 12-77**
 paddle dryers, **12-45, 12-71, 12-73**
 continuous sheeting dryers, **12-45**
 continuous through circulation band dryers, **12-44, 12-64 to 12-65, 12-67**
 cylinder dryers, **12-44, 12-89 to 12-90**
 dielectric (RF and microwave) dryers, **12-42, 12-45, 12-105 to 12-106**
 direct rotary dryers, **12-45, 12-46, 12-72, 12-74, 12-77, 12-78**
 dispersion, dryers, **12-42**
 drum dryers, **12-44, 12-87 to 12-89**
 dryer classification, **12-40 to 12-48**
 gas circuit, **12-47**
 gas-solids separations, **12-47**
 heater, **12-47**
 solids feeders, **12-47**
 entrainment dryers, **12-56**
 film dryers, **12-89**
 filterdryers, **12-89**
 fluid-bed dryers, **12-45, 12-56, 12-82**
 batch fluid beds, **12-85**
 continuous backmix beds, **12-86**
 continuous contact fluid beds, **12-86**
 continuous fluid beds, **12-86**
 continuous plug-flow beds, **12-86**
 direct heat vibrating conveyor dryer, **12-82 to 12-87**
 fluid-bed granulators, **12-87**
 fluidization velocity, **12-84**
 freeze dryers, **12-104 to 12-105**
 gas-flow pattern **12-47**
 drying equipment (solids) (*Cont.*):
 gas-flow pattern,
 gravity or moving bed dryers, **12-63**
 infrared dryers, **12-42, 12-45, 12-105 to 12-106**
 layer dryers, **12-42, 12-46**
 pan dryers, **12-43**
 plate dryers, **12-61 to 12-62**
 pneumatic conveying dryers, **12-45, 12-97 to 12-99**
 residence time, **12-54, 12-55, 12-72, 12-74, 12-75**
 ring dryers, **12-99 to 12-103**
 screw conveyor and indirect rotary dryers, **12-43**
 spouted bed dryers, **12-45, 12-82**
 spray dryers, **12-45, 12-87, 12-90 to 12-98**
 rotary atomizer **12-91 to 12-93, 12-97**
 stenters and textile dryers, **12-90**
 tower dryers, **12-63**
 tray and compartment dryers, **12-44, 12-46, 12-54, 12-56 to 12-61**
 tunnel/continuous tray dryers, **12-44, 12-59, 12-63 to 12-64**
 belt conveyor or screen conveyor, **12-63**
 ceramic tunnel kiln, **12-64**
 vacuum freeze dryers, **12-43**
 vacuum horizontal agitated and rotary dryers, **12-43, 12-72**
 vacuum tray/shelf dryers, **12-43, 12-59, 12-60**
 vibrating tray, vacuum band dryers, **12-44**
 drying kinetics, **12-29 to 12-30**
 drying curve, **12-29**
 period of drying, **12-29 to 12-30**
 drying of solids, **12-25 to 12-109**
 drying software, **12-109**
 mass and energy balances, **12-26 to 12-28**
 mathematical modeling, **12-30 to 12-35**
 characteristic drying curve, **12-34**
 characteristic moisture content, **12-34**
 mass balance equations, **12-31**
 moisture transport mechanisms, **12-29**
 relative drying rate, **12-35, 12-53**
 thermodynamics, **12-28 to 12-29**
 drying operations, **8-46**
 Dubinin-Radushkevich equation, **16-14**
 Duhem's theorem, **4-27 to 4-28**
 Dukler theory, **5-14**
 dumb transmitters, conventional transmitter, **8-66**
 dust clouds, combustion data for, **23-14**
 dust collection, **17-28 to 17-63**
 air filters, **17-52 to 17-55**
 air-filter types, **17-54 to 17-55**
 air-filtration theory, **17-52 to 17-54**
 applications of, **17-52**
 cyclone separators, **17-28 to 17-36**
 case of vortex, **17-29**
 commercial equipment and operations, **17-35 to 17-36**
 cyclone design factors, **17-32 to 17-33**
 cyclone efficiency, **17-30 to 17-31**
 fields of applications, **17-29**
 flow pattern, **17-29 to 17-30**
 performance curves, **17-38 to 17-39**
 performance models, **17-37 to 17-39**
 pressure drop, **17-31 to 17-32**
 dry scrubbing, **17-43 to 17-45**
 electrical precipitators, **17-55 to 17-63**
 applications, **17-57**
 charging of particles, **17-56**
 coal combustion fly-ash, **17-59**
 collection efficiency, **17-57**
 conditioning agents, **17-59**
 current flow, **17-56**
 electric wind, **17-56**
 dust collection, electrical precipitators (*Cont.*):
 field strength, **17-55**
 high-pressure, high-temperature EP, **17-57 to 17-59**
 particle mobility, **17-56 to 17-57**
 potential and ionization, **17-55 to 17-56**
 power supply, **17-62**
 rapping, **17-61**
 resistivity issues, **17-59**
 types of, **17-60 to 17-63**
 fabric filters (bag filters with baghouses), **17-46 to 17-51**
 collection efficiency, **17-49 to 17-51**
 filter fabrics, **17-49**
 filter types, **17-47 to 17-49**
 gas pressure drops, **17-46 to 17-47**
 granular-bed filters, **17-51 to 17-52**
 Kozeny-Carman equation, **17-46**
 gravity settling chambers, **17-28**
 impingement separators, **17-28**
 mechanical centrifugal separators, **17-36**
 mechanisms, **17-26 to 17-27**
 sonic or acoustic agglomeration, **17-26**
 Stefan flow, **17-26**
 particulate scrubbers, **17-36 to 17-43**
 performance, **17-27**
 purpose of, **17-24**
 scrubber types:
 cyclone, **17-42**
 ejector venturi, **17-40**
 electronically augmented, **17-43**
 fiber-bed, **17-43**
 mechanical, **17-43**
 mobile-bed, **17-42 to 17-43**
 packed-bed, **17-42**
 plate tower, **17-42**
 self-induced spray, **17-41**
 spray, **17-41 to 17-42**
 venturi, **17-40 to 17-41**
 dust collector design, **17-27**
 polydisperse test dust, **17-27**
 dust separation, **17-14**
 cyclones, **17-14 to 17-16**
 cyclone arrangements, **17-15**
 solids return seals, **17-15**
 dynamic compensation, in control analysis, **8-22**
 dynamic models, use in control, **8-30**
 fitting to experimental data, **8-12**
 simulation, **8-7**
 Eckert pressure-drop correlation, packed towers, **14-58**
 economic journal, **9-4**
 account title, **9-4**
 example of, **9-5**
 invoices, **9-4**
 receipts, **9-4**
 economic project, execution and analysis, **9-41 to 9-53**
 economizers:
 acid dew point, **24-52**
 background, **24-51**
 boiler thermal efficiency, **24-52**
 condensing, **24-52 to 24-54**
 collateral combustion emissions, **24-54**
 efficiency graph, **24-53**
 environmental benefits, **24-54**
 flue gas pollutant removal, **24-54**
 flue gas sensible heat, **24-52**
 fuel avoidance, **24-52**
 technologies, **24-52 to 24-54**
 water vapor latent heat, **24-52**
 conventional, **24-52**
 water dew point, **24-52**

- EFV, equilibrium flash distillation, 13-102
- jectors, 10-57 to 10-58
- condensers, 10-57
 - aftercondenser, 10-57
 - direct-contact (barometric), 10-57
 - performance, 10-57
 - constant-area mixing, 10-57
 - use of, 10-58 to 10-58
- elastic element method, 8-59
- elasticity, modulus of, nonmetals, 10-126
- electric field, separations based on:
- dielectrophoresis, 20-23 to 20-27
 - applications, 20-25 to 20-27
 - field warpage, 20-26
 - limitations, 20-25
 - principle and theory, 20-24
 - electrofiltration, 2-21 to 20-23
 - concepts, 20-21
 - cross-flow, 20-22
 - theory, 20-22
 - electrophoresis, 20-20 to 20-21
 - theory, 20-19 to 20-20
 - permittivity, 20-20
 - zeta potential, 20-20
- electrical efficiency, percent, 8-92
- electrical precipitators, 17-55 to 17-63
- alternating current precipitators, 17-63
 - charging of particles, 17-56
 - collection efficiency, 17-57
 - conditioning agents, 17-59
 - corona, 17-55 to 17-63
 - current flow, 17-56
 - design curves, 17-60
 - electric wind, 17-56
 - electrode insulators, 17-62
 - field strength, 17-55
 - horizontal flow plate precipitator, 17-60
 - ionic mobilities, 17-56
 - particle mobility, 17-56
 - potential and ionization, 17-55
 - power supply, 17-62
 - resistivity problems, 17-59
 - single-stage precipitators, 17-60
 - sparking potential, 17-56
 - two-stage precipitators, 17-62
- electrically augmented scrubbers, 17-43
- electroanalytical instruments, 8-63
- electrochemical measurement, 8-62
- electrochemical reactions, 7-32
- transfer coefficient, 7-33
- electrode reduction potentials, 7-32
- electrodialysis:
- energy requirements, 20-70 to 20-71
 - energy not transporting ions, 20-71
 - pump energy requirements, 20-71
 - equipment and economics, 20-71
 - examples, 20-66 to 20-67
 - membranes, 20-67
 - anion-exchange, 20-67
 - cation-exchange, 20-67
 - efficiency, 20-67
 - process configuration, 20-69 to 20-79
 - diffusion dialysis, 20-70
 - Donnan dialysis, 20-70
 - electrodes, 20-69
 - electrodialysis reversal, 20-69
 - electrodialysis-moderated ion exchange, 20-70
 - peripheral components, 20-69
 - pretreatment, 20-69
 - process flow, 20-69
 - water splitting, 20-69 to 20-70
 - process description, 20-66 to 20-69
 - concentration polarization, 20-68
 - ion transfer, 20-67 to 20-68
 - limiting current density, 20-68 to 20-69
- electrohydraulic actuators, 8-77
- electromagnetic solenoid, 8-78
- electronic digital controllers, 8-72
- electrostatic precipitators, pollutants, 22-37
- Ely-Rideal kinetics, 7-17
- emf-measuring device, 8-56
- emissions measurements, 22-46
- sampling methodologies, 22-55
- emissivity:
- combustion products, 5-31
 - example, 5-32 to 5-33
 - gas, 5-31
 - Hottel emissivity charts, 5-32, 5-34
 - spectral, 5-32
 - table, 5-21 to 5-22, 5-33, 5-34
- emulsion polymerization, 7-29
- emulsions, 18-20
- mixer-settlers, 18-20
- energy balance, 16-18
- energy resources, 24-3 to 24-4
- fossil fuels, 24-3 to 24-4
 - energy content, 24-4
 - reserves in United States, 24-4
 - nonrenewable, 24-3
 - renewable, 24-3
- enhancement factor, mass transfer rate, 7-28
- enterprise resource planning, optimization, 8-35, 8-69
- enthalpy:
- of combustion:
 - inorganic and organic compounds, 2-196 to 2-200
 - of formation, 2-478 to 2-485
 - calculation methods, 2-478
 - standard state thermal properties, 2-479 to 2-484
 - function of T and P or T and V, 4-6 to 4-7
 - of fusion:
 - calculation methods, 2-487
 - Chikos method, 2-487
 - Cs group values for Chickos, 2-488
 - Ct group values for Chickos, 2-488
 - ideal gas state, evaluation of, 4-8 to 4-9
 - postulate definition, 4-4
 - potential difference, 12-17
 - residual from PVT correlations, 4-9 to 4-12
 - of sublimation, 2-488
 - calculation methods, 2-488
 - equation 2-42, 2-488
 - Goodman method, 2-489
 - group contributions and corrections, 2-489
 - of vaporization, 2-486
 - calculation methods, 2-486
 - corresponding states correlation, 2-487
 - vapor pressure correlation, 2-486
 - Vetere method, 2-487
- enthalpy-humidity chart, 12-55
- entrainment separation, 17-40
- entropy, 2-485 to 2-486
- balance for open systems, 4-14 to 4-15
 - calculation methods, 2-485
 - Domalski-Hearing method, 2-485
 - statistical mechanics, 2-485
 - function of T and P or T and V, 4-6 to 4-7
 - ideal gas state, evaluation of, 4-8 to 4-9
 - inorganic and organic compounds, 2-196 to 2-200
 - postulate definition, 4-5
 - residual from PVT correlations, 4-9 to 4-12
- environmental enclosures, 8-91
- environmental issues, plant strategies, 22-5
- environmental regulation in the United States, 22-4
- air quality legislation, U.S., 22-6
- Clean Air Act of 1970, 22-6
 - Clean Air Act of 1990, 22-9
 - controlled-trading program, 22-9
 - nonattainment (NA), 22-9, 22-10
- environmental regulation in the United States, air quality legislation, U.S. (*Cont.*):
- prevention of significant deterioration (PSD), 2-6
 - regulatory direction, 22-12
 - solid waste legislation and regulations, U.S., 22-17, 22-82, 22-96
 - National Environmental Policy Act, 1969, 22-17
 - regulatory direction, 22-17
 - Resource Conservation and Recovery Act, 1976, 22-17
 - Resource Recovery Act, 1970, 22-17
 - Rivers and Harbors Act, 1899, 22-17
 - Solid Waste Disposal Act, 1965, 22-17
 - Toxic Substances Control Act, 1976, 22-17
 - water quality legislation and regulations, U.S., 22-12, 22-58
 - biological criteria, 22-15
 - Bioterrorism Act of 2003, 22-17
 - Clean Water Act of 1977, 22-15
 - control of toxic pollutants, 22-15
 - cooling water intake regulation, 22-17
 - CWA amendments 1987, 22-15
 - Federal Water Pollution Control Act, 22-12
 - metal bioavailability and toxicity, 22-16
 - regulatory direction, 22-17
 - source-based effluent limitations, 22-15
 - total maximum daily load (TMDL), 22-16
 - water quality trading, 22-16
 - water reuse, 22-17
- enzyme kinetic, 7-15
- enzymes, 7-15, 7-30
- expressed, 7-30
 - repressed, 7-30
- equality constraints, 8-33
- equations of state:
- cubic:
 - definition, 4-11 to 4-12
 - parameter assignments, 4-11
 - ideal gas model:
 - definition, 4-7
 - residual properties, 4-7 to 4-8
 - solution thermodynamics, 4-19
 - modified Raoult's law, 4-28 to 4-29
 - Pfizer's generalized correlations, 4-12
 - virial, 4-9 to 4-11
- equilibria, characterization of, 16-5
- equilibrium constant, 7-7
- inverse, 7-16
- equilibrium exchange current, 7-33
- equilibrium moisture content, 12-26
- equilibrium potential, 7-32
- equipment cost, 9-12
- algorithms, 9-12
 - cost-capacity plots, 9-12
 - cost-indices, 9-12
 - example of, 9-13
 - current equipment cost data, 9-12
 - equipment sizing, 9-13
 - inflation, 9-13
 - six-tenths rule, 9-12
- equipment, safety, process design and operation, 23-74
- emergency relief device effluent collection and handling, 23-80
- equipment selection criteria and guidelines, 23-86
- sizing and design of equipment, 23-88
 - types of equipment, 23-80
- flame arresters, 23-92
- deflagration arresters, 23-94
- detonation arresters, 23-95
- testing and standards, 23-96
- key procedures, 2-143
- inspection and testing of protective equipment, 23-110

- equipment, safety, process design and operation,
 key procedures (*Cont.*):
 key performance indicators, 23-110
 preparation of equipment for maintenance,
 23-109
- pressure relief systems, 23-74
 codes, standards, and guidelines, 23-75
 pressure relief devices, 23-76
 reactive systems, 23-77
 relief design scenarios, 23-75
 relief system flow capacity, 23-78
 sizing of pressure relief systems, 23-77
 terminology, 23-74
- safety instrumented systems, 23-102
 definitions, 23-102
 engineering, installation, commissioning, and
 validation (EICV), 23-104
 hazard and risk analysis, 23-103
 operating basis, 23-104
 process and safety requirements specification,
 23-104
- security, 23-104
 countermeasures and security risk management
 concept, 23-108
 defining the risk to be managed, 23-107
 security management system, 23-109
 security strategies, 23-108
 security vulnerability assessment, 23-106
 SVA methodologies, 23-106
 terminology, 23-104
 threats of concern, 23-106
- storage and handling of hazardous materials,
 23-97
 basic design strategies, 23-98
 causes, loss of containment, 23-102
 established practices, 23-98
 maintaining mechanical integrity, containment
 system, 23-102
 release detection and mitigation, 23-102
 site selection, layout and spacing, 23-99
 storage, 23-99
- Ergun equation, 17-44
- error, normally distributed, 7-37
- ethane:
 K-value versus pressure, 13-12
 thermodynamic properties, 2-263 to 2-264
- ethanol:
 activity coefficient plot, 13-14
 Antoine vapor pressure, 13-14
 BIP data, 13-13
 VLE data, 13-7
 thermodynamic properties, 2-265 to 2-266
- ethernet protocols, 8-70
- ethyl alcohol, aqueous, thermodynamic properties,
 2-267
- ethylacetate:
 Antoine vapor pressure, 13-14
 BIP data, 13-13
 VLE data, 13-7 to 13-8
- ethylene, thermodynamic properties,
 2-268 to 269
- ethylene glycol, VLE data, 13-7
- Euler integration method, 8-7
- evaporation, 12-26
 evaporation load, 8-46
 evaporative cooling, 12-17 to 12-25
- evaporators, 8-45, 11-110 to 11-121
 accessories, 11-119 to 11-121
 condensers, 11-119
 salt removal, 11-120
 vent systems, 11-120
 arrangement of, 11-116 to 11-118
 forward-feed, 11-117
 heat recovery systems, 11-117
 mixed feed, 11-117
- evaporators, arrangement of (*Cont.*):
 multiple-effect evaporation, 11-116
 parallel feed, 11-117
 sea water evaporators, 11-117
 single-effect evaporators, 11-116
 thermocompression, 11-116
- calculations, 11-118 to 11-119
 boiling temperature, 11-118
 flash evaporators, 11-118
 multi-effect evaporators, 11-119
 optimization, 11-119
 thermocompression evaporators, 11-118
- co-current:
 control of, 8-45
- evaporator types and applications, 11-111 to
 11-114
 agitated film, 11-114
 disk or cascade, 11-114
 flash, 11-114
 forced circulation, 11-111
 horizontal tube, 11-113
 long-tube vertical, 11-112
 miscellaneous forms of heating surface,
 11-114
 short-tube vertical, 11-112
 submerged combustion, 11-114
 swirl flow, 11-111
- operation of, 11-121
 primary design problems, 11-110 to 11-111
 temperature difference, utilization of,
 11-114
- vapor-liquid separation, 11-114 to 11-116
- event-triggered recording, 8-88
- exchange of sensible heat, heat exchanger control,
 8-41
- execution rate, digital controller, 8-74
- exothermic reactions, 7-6
- expense, manufacturing-operating, 9-18 to
 9-21
 direct, 9-18
 estimation, rapid manufacturing, 9-20
 Holland expression, 9-20
 general overhead, 9-20
 indirect, 9-20
 packaging and shipping, 9-20
 raw material, 9-18
 scale up of, 9-21
 total manufacturing, 9-20
 total operating, 9-20
 total product, 9-20
- expert systems, 8-26
- expression:
 compactable filter cakes, 18-143
 definition, 18-143
- equipment:
 batch, 18-144
 continuous, 18-146
 theory, 18-143
- extent of reaction, 7-7
- external mass transfer, 7-19, 16-21
 correlations, 16-21
 resistance, 7-20
- extinction, 8-44
- extraction:
 acid gas, 15-9
 calculation methods, process fundamentals,
 15-44 to 15-51
 calculation procedures, 15-51 to 15-58
 computer simulations, 15-53 to 15-55
 immiscible solvents, 15-52
 partially miscible solvents with dilute solute,
 15-52 to 15-53
 partially miscible solvents with high solute
 concentration, 15-53
 shortcut calculations, 15-51 to 15-53
- extraction (*Cont.*):
 caprolactam (CPL), separations, 15-15
 counter-current, 15-11
 cross-current, 15-11
 dual-solvent with extract reflux, 15-13
 dual-solvent fractional without reflux, 15-13
 emerging developments, 15-103 to 15-106
 electrically-enhanced extraction, 15-104
 to 15-105
 extraction factor and general performance
 trends, 15-49 to 15-50
 fractional extraction calculations, 15-55
 to 15-56
 single-solvent with extract reflux, 15-56
 to 15-58
 symmetric separation, 15-55 to 15-56
- ionic liquids, 15-105
- membrane-based processes, 15-103 to 15-104
 liquid-based, 15-104
 polymer-based, 15-103 to 15-104
- phase-transition extraction, 15-105
- rate-based calculations, 15-47 to 15-49
 mass-transfer rate, 15-47
 mass-transfer units, 15-48 to 15-49
 overall mass-transfer coefficients, 15-48
 solute diffusion and mass-transfer coefficients,
 15-47
- single-solvent with extract reflux, 15-14
 solute purification and standard extraction:
 potential for, 15-50 to 15-51
 theoretical stage calculations, 15-44 to 15-47
 Kremser-Souder-Brown equation, 15-45
 to 15-46
 McCabe-Thiele, 15-45
 stage efficiency, 15-46 to 15-47
 tunable solvents, 15-105
- extraction, commercial processes, 15-13
 to 15-20
 biodiesel production, 15-17
 extractions, 15-13 to 15-20
 dissociative, 15-15 to 15-16
 fractional, 15-13 to 15-15
 liquid-solid (leaching), 15-19
 pH-swing, 15-16
 reaction-enhanced, 15-16
 reversed micellar, 15-18
 standard, 15-13
 supercritical fluid, 15-19 to 15-20
 temperature-swing, 15-17
 two-phase, aqueous, 15-18
- extractive reaction, 15-16 to 15-17
- hybrid extraction processes, 15-18 to 15-19
- liquid-liquid partitioning, 15-19
 fine solids, 15-19
- toluene nitration, 15-17
- extraction, cross-current, 15-11
- extraction, emerging developments, 15-103 to
 15-106
 electrically-enhanced extraction, 15-104 to
 15-105
 ionic liquids, 15-105
 membrane-based processes, 15-103 to
 15-104
 liquid-based, 15-104
 polymer-based, 15-103 to 15-104
 phase-transition extraction, 15-105
 tunable solvents, 15-105
- extraction cascade, counter-current, 15-45
- extraction operation, 15-20 to 15-21
 design considerations, 15-20 to 15-21
- extractor:
 CMS, 15-90
 static, 15-64
- extraparticle transport and dispersion mechanisms,
 16-19

- fabric filters, **17-46 to 17-57**
 air permeabilities, **17-50**
 cake puncture, **17-51**
 collection efficiency, **17-49**
 filter fabrics, **17-49**
 removal efficiency, **17-55**
 resistance factors, **17-50**
 reverse-flow cleaned, **17-47, 17-49**
 reverse-pulse cleaned, **17-47, 17-49, 17-50**
 shaker cleaned, **17-47, 17-48**
 three-compartment bag filter, **17-48**
- failure logic, in control, **8-50**
- Fair's correlation, entrainment, **14-38**
- falling films, **6-43 to 6-44**
 effect of surface tension, **6-44**
 flooding, **6-44**
 laminar flow, **6-43**
 minimum wetting rate, **6-43**
 turbulent flow, **6-43 to 6-44**
- falling-film crystallization, **20-10 to 20-13**
 equipment and applications, **20-13**
 principles of operation, **20-13**
 process diagrams, **20-10 to 20-12**
 reference list of specific processes, **20-13**
- falling-rate period (hindered drying), **12-26**
- fan horsepower, **12-21**
- fans and blowers, **10-49 to 10-52**
 axial-flow fans, **10-49**
 backward-curved blade blowers, **10-50**
 centrifugal blowers, **10-49**
 fan performance, **10-52**
 forward-curved blade blowers, **10-50**
 scirocco-type fan, **10-52**
- Faraday's law, **7-32**
- fast Fourier transform, **3-59**
- FCC unit, **17-17**
- feed stream, **8-42**
- feedback control, **8-5, 8-21**
- feedback control system, **8-12**
- feedforward control, **8-5, 8-21**
- feedforward dynamic compensator, **8-22**
- fermentation, **7-30**
- fermentative pathways, **7-31**
- fermenter, **7-18**
- fiber mist eliminators, **14-125**
- fiber saturation point, **12-26**
- fiber-bed scrubbers, **17-43**
- fiber-film contactor, **15-91**
- fiber-optic sensors, **8-63**
- Fibonacci search, **8-34**
- Fick's First Law, diffusion, **5-45**
- Fick's law, diffusion, **16-19**
- Fick's 2nd law, diffusion, **12-34**
- fieldbus controller, **8-73**
- fieldbus foundation, **8-70**
- field-sensing devices, **8-73**
- FIFO, first in first out basis, **9-10**
- filament pyrometers, disappearing, **8-58**
- filter, bag, **17-48**
- filter (electric), granular bed, **17-52**
- filter, reverse-pulse fabric, **17-49**
- filter, shaker fabric, **17-49**
- filtering, excessive, effect on signal, **8-73**
- filters:
 aids:
 diatomaceous earth, **18-99**
 perlite, **18-99**
 batch cake filters:
 centrifugal-discharge, **18-104**
 external cake tube, **18-102**
 filter press, **18-99**
 horizontal plate, **18-99**
 internal cake tube, **18-102**
 nutsche, **18-99**
 pressure leaf, **18-103**
- clarifying filters, **18-109**
- continuous cake filters:
 colifilter, **18-106**
 horizontal belt, **18-108**
 horizontal table, **18-108**
 horizontal vacuum, **18-108**
 precoat filters, **18-106**
 pressure filters, **18-106**
 removable media, **18-106**
 roll-discharge, **18-106**
 rotary drum, **18-105**
 scraper discharge, **18-105**
 sing compartment, **18-106**
 string discharge, **18-105**
 tilting pan, **18-108**
- dry, **17-54**
- filter thickeners, **18-109**
- media:
 beds, granular, **18-98**
 characteristics, **18-98**
 fabrics, metal, **18-97**
 fabrics, screens, **18-97**
 fabrics, woven, **18-97**
 felts, **18-98**
 membranes, polymer, **18-98**
 papers, **18-98**
 pollutants, **22-37, 22-40**
 prices, **18-114**
 selection, **18-112**
- filtration:
 classification, **18-82, 18-114**
 filter prices, **18-114**
 selection of filtration equipment, **18-112 to 18-114**
 cake washing, **18-112 to 18-113**
 continuous operation, **18-113**
 equipment-related factors, **18-112**
 filtration rate, **18-113 to 18-114**
 theory, **18-83**
- filtration, batch:
 constant pressure, **18-95**
 constant rate, **18-95**
 pressure tests, **18-96**
 compression-permeability, **18-98**
 leaf, **18-96**
 plate and frame, **18-97**
 variable pressure, rate, **18-96**
- filtration, continuous:
 performance evaluation, **18-95**
 scale-up:
 actual area, **18-94**
 cake discharge, **18-93**
 factor, overall, **18-94**
 sizing, **18-95**
 testing, small scale:
 correlation, data, **18-89**
 factors, **18-83**
 procedure, **18-85**
- financial report, **9-5**
- fire and explosion protection, in control, **8-91**
- fired heaters. *See* indirect-fired combustion equipment
- first order-transfer function, **8-8**
- first-order lag, **8-9**
- Fischer-Tropsch synthesis, **17-17, 7-28**
- fixed capital investment, **9-10**
 detailed estimate method, **9-16**
 code of accounts, **9-15, 9-16**
 estimation, **9-13**
 exponential method, **9-13**
 seven-tenths rule, **9-14**
 methods, **9-15**
 discipline method, **9-15**
 Garrett method, **9-15**
 Guthrie method, **9-15**
- fixed capital investment (*Cont.*):
 order of magnitude methods, **9-13**
 capital ratio, **9-13**
 turnover ratio, **9-13**
 study methods, **9-14**
 Hand method, **9-14**
 Lang method, **9-14**
 step-counting method, **9-15**
 Wroth method, **9-14**
- fixed-bed:
 analysis methods, **16-6**
 behavior, **16-6**
 limiting behavior, **16-7**
 profiles, **16-7**
- fixed-point level, **8-61**
- flammability limits, **2-515 to 2-516**
 calculation methods, **2-515**
 group contributions for inorganic compounds, **2-516**
 group contributions for organic compounds, **2-516**
 Pintar method, **2-515**
- flammable gas, vapors and liquids, measures against ignition by hot surfaces, **23-17**
- flash calculations:
 adiabatic, **13-16**
 isothermal, **13-15**
 specifications, **13-16**
 three phase, **13-16**
- flash point:
 calculation methods, **2-515**
 Thornton method, **2-515**
- flexibility factor k and stress intensification factor i , **10-119 to 10-120**
- flexible batch, processes, control, **8-47**
- float-actuated devices, **8-60**
- flooding, column. *See* tray columns, flooding
- Flory distribution, **7-30**
- flow, orifices, nozzles, and venturis, expansion factor Y , values of, **10-19**
- flow characteristics, valve flow, **8-83**
- flow measurements:
 in control, **8-59**
 pressure, **10-7 to 10-10**
 equalizers and straighteners, **10-10**
 head, **10-8**
 manometer, liquid-column, **10-8**
 mechanical gauges, **10-9**
 multiplying gauges, **10-8**
 perfect fluid, **10-6**
 piezometer ring, **10-11**
 stagnation, **10-6**
 static head, **10-15**
 static pressure, **10-6**
 total pressure, **10-6 to 10-7**
 properties and behavior of, **10-6**
 adiabatic, **10-6**
 flowing fluid, **10-6**
 ideal gas, **10-6**
 isentropic, **10-6**
 isotropic, **10-6**
 perfect fluid, **10-6**
 stagnation, **10-6**
 static pressure, **10-6**
 total pressure, **10-6 to 10-7**
 temperature, **10-7**
 dry- and wet-bulb, **10-7**
 resistive thermal detectors (RTDs), **10-7**
 static, **10-7**
 thermocouples, **10-7**
 total, **10-7**
- velocity, **10-7 to 10-14**
 anemometer, **10-13 to 10-14**
 current meter, **10-21**

12 INDEX

- flow measurements, velocity (*Cont.*):
 - flow disturbances, 10-11
 - kiel probe, 10-11
 - mean, traversing for, 10-13
 - pitometer, 10-13
 - pitot tubes, 10-11
 - pitot-static tube, 10-11 to 10-12
 - pitot-venturi tubes, 10-13
 - point velocities, 10-11
 - profile effects, 10-11
 - pulsating flow, 10-12
 - special pitot tubes, 10-13
 - variables affecting measurement, 10-1
 - flow nonuniformities, 16-21
 - flow reactors, 7-35
 - CSTRs, 7-35
 - PFRs, 7-35
 - flow through orifices, 6-22
 - flow velocity pitot tubes, special, 10-13
 - pitometer, 10-13
 - pitot-venturi, 10-13
 - shielded total-pressure tubes, 10-13
 - flowmeters, differential pressure, 10-15
 - accuracy, 10-20 to 10-21
 - abnormal velocity distribution, 10-20
 - flow pulsation, 10-20
 - minimum Hodgson numbers, 10-21
 - order of reliability for square-edged orifices and venturi tubes, 10-20
 - swirling flow, 10-20
 - elbow meters, 10-20
 - flow nozzles, 10-19
 - critical flow conditions, 10-19
 - critical flow nozzles, 10-19
 - critical pressure ratio, 10-19
 - perfect gas, 10-19
 - permanent pressure loss, 10-19
 - rate of discharge, 10-19
 - orifice meters, 10-16 to 10-18
 - annular, 10-18
 - coefficient of discharge, 10-17
 - critical flow, 10-17
 - eccentric, 10-18
 - permanent pressure loss, 10-17
 - quadrant-edged, 10-16
 - segmented, 10-18
 - sharp-edged, 10-16
 - slotted-edge, 10-16
 - square-edged, 10-16
 - venturi meters, 10-18
 - discharge coefficients, 10-19
 - Herschel-type, 10-19
 - multiventuri systems, 10-19
 - permanent pressure loss, 10-19
 - rate of discharge, 10-19
 - pressure taps, 10-16
 - corner taps, 10-16
 - pipe taps, flange taps, 10-16
 - radius taps, 10-16
 - vena contracta, 10-16
 - flowmeters, general:
 - classes, 10-23
 - classification, 10-14
 - differential pressure meters, 10-14
 - mass meters, 10-14
 - open-channel flow measurement, 10-14
 - variable-area meters, 10-14
 - velocity meters, 10-14
 - volumetric meters, 10-14
 - guidelines and standards, 10-14, 10-16
 - technologies, comparison of, 10-15
 - selection, 10-23
 - weirs, 10-23
- flowmeters, mass, 10-21
 - axial-flow transverse-momentum, 10-21
 - coriolis, 10-22
 - inferential, 10-21
 - flowmeters, two-phase, 10-22
 - gas-liquid mixtures, 10-23
 - gas-solid mixtures, 10-23
 - liquid-solid mixtures, 10-23
 - flowmeters, ultrasonic, 8-59 to 8-60
 - flowmeters, variable-area, 10-22
 - rotometers, 10-22
 - flowmeters, velocity, 10-21
 - anemometer, 10-21
 - vane anemometer, 10-21
 - current, 10-21
 - cup meter, 10-21
 - propeller meter, 10-21
 - turbine, 10-21
 - flowmeters, weirs, 10-23
 - broad-crested, 10-23
 - narrow rectangular notches, 10-24
 - rectangular, 10-24
 - triangular-notch, 10-24
 - sharp-edged, 10-23
 - flue gas desulfurization, 17-44
 - fluid and particle dynamics nomenclature and units, 6-3
 - fluid distribution, 6-32 to 6-34
 - beds of solids, 6-34
 - flow straightening devices, other, 6-34
 - perforated plates and screens, 6-34
 - perforated-pipe distributions, 6-32 to 6-33
 - slot distributions, 6-33
 - turning valves, 6-33 to 6-34
 - fluid dynamics, conservation equations, 6-6 to 6-9
 - Cauchy momentum and Navier-Stokes equations, 6-8
 - fluid statics, 6-8 to 6-9
 - macroscopic and microscopic balances, 6-6
 - macroscopic equations, 6-6
 - mass balance, 6-6
 - mass balance, continuity equation, 6-7
 - mechanical energy balance, Bernoulli equation, 6-7
 - microscopic balance equations, 6-7
 - momentum balance, 6-6 to 6-7
 - stress tensor, 6-7 to 6-8
 - total energy balance, 6-7
 - fluid dynamics, dimensionless groups, 6-49 to 6-51
 - fluid flow, kinematics, 6-5 to 6-6
 - compressive and incompressible flow, 6-5
 - laminar and turbulent flow, Reynold's number, 6-6
 - one-dimensional flow, 6-5
 - rate of deformation tensor, 6-5
 - streamlines, pathlines, and streaklines, 6-5
 - velocity, 6-5
 - vorticity, 6-5 to 6-6
 - fluid flow:
 - thermodynamics:
 - duct flow, 4-15
 - pipe flow, 4-15
 - fluid mixing, 6-34 to 6-36
 - pipeline mixing, 6-36
 - stirred tank agitation, 6-35 to 6-36
 - fluidization vessel, 17-6
 - fluidized beds, uses of, 17-16 to 17-20
 - catalytic reactions, 17-16 to 17-17
 - acrylonitrile production, 17-17
 - chlorination of olefins, 17-17
 - cracking, 17-16
 - Fischer-Tropsch synthesis, 17-17
 - naphthalene oxidation, 17-17
 - polyethylene production, 17-17
- fluidized beds, uses of (*Cont.*):
 - noncatalytic reactions, 17-17 to 17-20
 - calcination, 17-17 to 17-18
 - circulating fluidized-bed combustors, 17-19
 - improved coal combustion, 17-18 to 17-19
 - incineration, 17-19
 - pressurized fluidized-bed combustion (PFBC), 17-19
 - physical contacting, 17-20
 - adsorption-desorption, 17-20
 - coating, 17-20
 - drying, 17-20
 - heat treatment, 17-20
 - fluidized-bed combustion, 24-29 to 24-31
 - bubbling beds, 24-29
 - circulating beds, 24-29 to 24-30
 - fuel flexibility, 24-30
 - mercury emissions, 24-31
 - nitrogen oxide emissions, 24-30
 - particulate emissions, 24-30 to 24-31
 - sulfur emissions, 24-30
 - fluidized-bed seal leg, 17-14
 - fluidized-bed steam generator, 17-18
 - fluidized-bed systems, 17-2 to 17-20
 - adsorption-desorption, 17-20
 - applications, 17-16 to 17-20
 - bed height, nominal, 17-16
 - bed weight, overall, 17-16
 - bubbling or turbulent beds, 17-9
 - catalytic reactions, 17-16 to 17-17
 - circulating fluidized-bed combustors, 17-19
 - circulating or fast fluidized-beds, 17-11
 - coating, 17-20
 - cone valve, 17-13
 - dip leg, 17-15
 - drying, 17-20
 - entrainment, 17-7
 - flow measurements, 17-16
 - fluid-bed status graph, 17-4
 - fluidization regime, 17-4
 - fluidized-bed steam generator, 17-18
 - gas distributor, 17-7 to 17-9
 - gas mixing, 17-12
 - gas-solid systems, 17-2
 - Geldart categorization, 17-2
 - heat transfer, 17-11 to 17-12
 - bed-to-surface heat transfer coefficient, 17-11
 - heat treatment, 17-20
 - heterogeneous reactions, 7-17
 - higher velocity transport regime, 17-5
 - hot windbox, incinerator, 17-20
 - instrumentation, 17-15 to 17-16
 - flow measurement, 17-16
 - pressure measurement, 17-15 to 17-16
 - temperature, 17-15
 - l valve, 17-13, 17-14
 - lower-velocity fast fluidized-bed regime, 17-5
 - materials tar, 17-6
 - multicompartment fluidized-bed, FluoSolids, 17-18
 - phase diagram, 17-3
 - physical contacting, 17-20
 - plenum chamber, 17-9
 - pneumatic conveying regime, 17-5
 - pneumatic conveying systems, 17-11
 - powder classification diagram, 17-2
 - pressurized fluidized-bed combustion, 17-19
 - quench tank, 17-13
 - reactions, noncatalytic, 17-17 to 17-20
 - reactor shell, hot spots, 17-6
 - regime diagram, 17-3
 - rotary valve, 17-13
 - scale-up, 17-9 to 17-16
 - bubble growth, 17-9
 - bubble model, 17-10

- fluidized-bed systems, scale-up (*Cont.*):
 bubbling or turbulent beds, 17-19
 fast fluidized (Circulating) beds, 17-11
 fluoseal, 17-13
 gas mixing, 17-12
 heat transfer surfaces, 17-11
 knife-gate valves, 17-12
 pneumatic conveying, 17-11
 pressure drop, 17-13
 size enlargement, 17-12
 size reduction, 17-12
 solids discharge 17-13
 solids mixing, 12-12
 stand pipe, 17-13
 two-phase model, 17-10
 screw feeder, 17-13
 seal legs, 17-14
 single-stage FluoSolids roaster, 17-18
 size enlargement, onion skinning, 17-12
 size reduction, attrition, 17-12
 slide valve, 17-13
 solids discharge, 17-13
 solids feeders, 17-12
 solids flow control, 17-12
 solids mixing, 17-12
 staging methods, 17-10
 standpipes, 17-12
 table feeder, 17-13
 temperature control, 17-12
 adiabatic, 17-12
 gas circulation, 17-12
 liquid injection, 17-12
 solids circulation, 17-12
 total transport regime, 17-5
 transport disengaging height, 17-7
 two-phase theory of fluidization, 17-2
- fluidized-bed:
 fluosolids, 17-18
 fractionation, 17-20
 noncatalytic 17-6
 systems, 17-5
- fluidizing velocity, minimum, 17-5 to 17-6
- fluids, bulk transport of, 10-149
 marine transportation, 10-151
 container ships, 10-151
 portable tanks, 10-151
 materials of construction for bulk transport, 10-151
 pipe lines, 10-149
 tank cars, 10-150
 tank trucks, 10-151
 portable tanks, drums, or bottles, 10-151
 tanks, 10-149
- fluids, nature of, 6-4 to 6-5
 Bingham plastic, 6-4
 Deborah number, 6-5
 deformation and stress, 6-4
 dilatant, 6-5
 Newtonian, 6-4
 non-Newtonian, 6-4
 rheology, 6-4
 rheoplectic, 6-5
 shear-thinning, 6-4 to 6-5
 time-dependent, 6-5
 viscoelastic, 6-5
 viscosity, 6-4
- fluids, pastes and doughs, viscous, mixing of:
 continuous mixers, 18-34 to 18-37
 AP Conti paste mixer, 18-35
 Ferrel continuous mixer, 18-35
 Holo-Flite processor, 18-35
 Kenics static mixer, 18-36 to 18-37
 miscellaneous continuous mixers, 18-35
 motionless mixers, 18-36
 pug mills, 18-35
- fluids, pastes and doughs, viscous, mixing of, continuous mixers (*Cont.*):
 single-screw extruders, 18-34
 Sulzer static mixer, 18-37
 trough-and-screw mixers 18-35
 twin-screw extruders, 18-34 to 18-35
- equipment selection, 18-38 to 18-39
 heating and cooling mixers, 18-38
 intensive mixers, 18-32 to 18-34
 Banbury mixers, 18-32 to 18-33
 conical mixers, 18-32
 high-intensity mixers, 18-32
 miscellaneous batch mixers, 18-32
 pan mullers, 18-32 to 18-34
 plowshare mixers, 18-32
 ribbon blenders, 18-32
 roll mills, 18-32
- process design considerations, 18-37 to 18-39
 scale-up of batch mixers, 18-37 to 18-38
 scale-up of continuous mixers, 18-38
- fluorine, thermodynamic properties, 2-270 to 2-271
- fluoSeal, type UA, 17-14
- flutec, 2-217, 2-271
- flux expressions, 5-49 to 5-50
 Stefan-Maxwell equation, 5-50
- formal potential, electrochemical reactions, 7-32
- formation and combustion reactions, properties:
 ideal gas sensible enthalpies, 2-201
 ideal gas sensible entropies, 2-202
 inorganic and organic compounds, 2-195 to 2-200
- formic acid:
 Antoine vapor pressure, 13-14
 BIP data, 13-13
- FORTTRAN, 8-70
- Fourier Law, 5-3
 coefficients, 5-6
- Fourier number, 12-34, 12-54
- free moisture content, 12-26
- free radicals, 7-14
- freezing, progressive, 20-4 to 20-5
 applications, 20-5
 component separation, 20-4
 concentration-solidification curve, 20-5
- frequency-shift keying, 8-87
- frictional losses in pipeline elements, 6-16 to 6-20
 contraction and entrance losses, 6-16 to 6-17
 curved pipes and coils, 6-19 to 6-20
 equivalent length and velocity head methods, 6-16
 expansion and exit losses, 6-17
 fittings and valves, 6-17 to 6-19
- front-end loading, 9-41 to 9-48
 characteristics of, 9-42
- fuel cells:
 background, 24-45
 characteristics, 24-47
 design principles, 24-46 to 24-47
 efficiency, 24-46
 polarization curves, 24-48 to 24-50
 reaction electrochemistry, 24-47
 schematics, 24-45 to 24-51
 thermodynamic valves, 24-47
 types:
 alkaline, 24-47
 direct methanol, 24-49
 molten carbonate, 24-49
 phosphoric acid, 24-49
 polymer electrolyte, 24-48 to 24-49
 solid-oxide, 24-50
- fuel fired furnace models, 5-39 to 5-43
 long plug flow furnace, 5-39 to 5-40
 performance parameters, 5-39
- fuel fired furnace models (*Cont.*):
 well-stirred combustion chamber, 5-40 to 5-43
 dimensional approach, 5-40
 dimensionless approach, 5-40 to 5-41
 example, 5-41 to 5-43
- fuel-bed firing, 24-28 to 24-29
 comparison to suspension, 24-29
 overfeed firing stokers:
 cross-feed (mass-burning), 24-28
 spreader, 24-28 to 24-29
 underfeed firing, 24-28
- fugacity:
 coefficient:
 definition, 4-19 to 4-20
 evaluation of, 4-20
 definition, 4-19 to 4-20
- function libraries, 8-50
- funicular state, 12-26
- furnaces, industrial:
 atmosphere, 24-44
 batch furnace, 24-43
 continuous furnace, 24-43
 function and process cycle, 24-42
 heat source, 24-42
 heating mode:
 direct, 24-43, 24-44
 indirect, 24-43
 overhead, 24-43, 24-44
 underfiring, 24-43, 24-44
 melting furnace, 24-42
 muffle furnace, 24-43
 fuzzy logic control, 8-26
- ganging alarm, use in control, 8-68
- gas absorption, heat-effects, 14-15 to 14-17
 classical adiabatic design method, 14-17
 classical isothermal design method, 14-16
 comparison of design methods, 14-17
 equipment considerations, 14-16
 operating variables, 14-16
 rigorous design methods, 14-17
- gas absorption solvent rate, 14-17
- gas blanketing system, use of regulator, 8-92
- gas chromatography, 8-62
- gas diffusivity, 7-20
- gas distributor, multiple-pipe, 17-8
- gas phase reactors, 19-21
- gas phone mass-transfer units, 14-13
- gas pressure drops, 17-46
 resistance coefficients, 17-46
- gas-absorption systems, design of, 14-7 to 14-10
 design diagrams, 14-10
 design of absorber-stripper systems, 14-10
 design procedures, 14-7
 equipment, selection, 14-9
 liquid-to-gas ratio, calculation of 14-9
 scrubbing chlorine from air, 14-11
 selection of solvent and nature of solvents, 14-7
- gaseous emissions, control of, 22-41
 absorption, 22-41
 adsorption, 22-42
 biological APC technologies, 22-48
 combustion, 22-44
 condensation, 22-47
 membrane filtration, 22-51
- gaseous fuels, 24-10 to 24-12
 acetylene, 24-12
 hydrogen, 24-12
 liquefied petroleum gas, 24-12
 miscellaneous, 24-12
 natural gas. *See* natural gas
- gaseous pollutants, sources and significance, 22-30

14 INDEX

- gases, storage of, **10-148**
 - cavern storage, **10-149**
 - gas holders, **10-148**
 - materials, **10-149**
 - differential thermal expansion, **10-149**
 - solution of gases in liquids, **10-148**
 - storage in pressure vessels, bottles and pipe lines, **10-148 to 10-149**
- gas-in-liquid dispersions, **14-98**
 - axial dispersion, **14-111**
 - characteristics of dispersion, **14-102**
 - equipment selection, **14-106**
 - mass transfer, **14-108**
 - methods of gas dispersion, **14-102**
 - theory of bubble and foam formation, **14-100**
- gas-liquid, suspension:
 - dispersion, **18-18**
 - mass transfer, **18-19**
- gas-liquid column costs, **14-85**
 - cost of column, **14-86**
 - cost of internals, **14-85**
- gas-liquid contactors, **14-90**
 - bypassing limits spray tower performance in gas cooling, **14-91**
 - converting liquid mass-transfer data to direct contact heat transfer, **14-91**
 - devolatilizers, **14-91**
 - mass transfer data, **14-91**
 - simple spray towers, **14-91**
 - spray towers as direct contact condensers, **14-91**
 - spray towers in liquid-limited systems-hollow cone atomizing nozzles, **14-91**
 - vertical reverse jet contactor, **14-90**
- gas-liquid phase dispersion, **14-86**
 - basics of interfacial contactors, **14-86**
 - droplet size, **14-88**
 - interfacial area, impact of droplet or bubble size, **14-88**
 - steady-state systems, bubbles and droplets, **14-86**
 - surface tension, effect on stability, **14-88**
 - unstable systems, froths and hollow cone atomizing nozzles, **14-88**
- gas-liquid reactors, **19-38 to 19-41**
 - absorption tables, **19-39**
 - examples, **19-41, 19-45**
- gas-liquid systems, equilibrium data sources, **14-7**
- gas-liquid-solid, suspension, **18-20**
 - loop reactors, **18-21**
- gas-solid, systems, **17-2 to 17-6**
 - air fluidization diagram, **17-2**
 - choking velocity, **17-5**
 - fluidization regime diagram, **17-4**
 - particulate fluidization, **17-6**
 - vibrofluidization, **17-6**
 - pneumatic conveying regime, **17-5**
 - simplified fluid-bed status graph, **17-4**
 - solid types, **17-2**
 - two-phase fluidization theory, **17-2**
 - upward gas flow phase diagram, **17-3**
- gas-solids separation, **17-21 to 17-63**
 - air filters, **17-52 to 17-55**
 - automatic filters, **17-54**
 - classification, **17-55**
 - high efficiency air cleaning, **17-54**
 - high efficiency particulate air, **17-54**
 - isolated fiber efficiency, **17-53**
 - air filtration theory, **17-52**
 - atmospheric pollution measurements, **17-24**
 - cyclone scrubbers, **17-42**
 - dry scrubbing, **17-43 to 17-45**
 - emission control, **17-45**
 - evaporation lifetimes, **17-45**
 - VERT filter list, **17-45**
 - gas-solids separation (*Cont.*):
 - dust collection, **17-24 to 17-28**
 - design, **17-27**
 - diffusional deposition, **17-26, 17-27**
 - electrostatic precipitation, **17-27**
 - flow-line interception, **17-26, 17-27**
 - gravity settling, **17-27, 17-28**
 - inertial deposition, **17-26, 17-27**
 - mechanisms, **17-26 to 17-27**
 - nomenclature of, **17-21 to 17-23**
 - particle deposition, **17-28**
 - performance, **17-27**
 - sonic agglomeration, **17-26**
 - thermal deposition, **17-26, 17-27**
 - gauge, pressure, manometers, **10-8**
 - bourdon-tube gauge, **10-9**
 - closed U tubes, **10-8**
 - mercury barometer, **10-8**
 - compound gauges, **10-9**
 - conditions, **10-9**
 - deadweight gauge for high pressure, **10-9**
 - differential, **10-8**
 - differential U tube, **10-8**
 - draft gauge, **10-9**
 - inclined U tube, **10-9**
 - inverted differential U tube, **10-8**
 - manometric fluid, changes of, **10-9**
 - mechanical, **10-9**
 - diaphragm, **10-9**
 - micrometers, **10-9**
 - multiplying gauges, **10-8 to 10-9**
 - open gauge, **10-8**
 - open U tube, **10-8**
 - pressure transducers with fluid-mounted diaphragms, **10-9**
 - tube size for, **10-8**
 - two-fluid U tube, **10-9**
 - gauges, pressure-measuring, types of, **10-7**
 - electric sensing devices, **10-8**
 - piezoelectric transducers, **10-8**
 - piezoresistive transducers, **10-8**
 - strain gauges, **10-8**
 - gauges based on height of liquid column, **10-7**
 - manometers, **10-7**
 - mechanical pressure gauges, **10-7**
 - Bourdon-tube, **10-7**
 - Gauss-Jordan decomposition, **7-9**
 - Geldart diagram, **12-84**
 - Geldart's classification, aeration behavior, **21-22, 21-23**
 - Geng Wang equation, **12-93**
 - genome, **7-31**
 - Gibbs energy:
 - excess:
 - models, **4-23 to 4-26**
 - fundamental property relations:
 - excess-property relation, **4-22 to 4-23**
 - and related properties, **4-22**
 - residual-property relation, **4-21 to 4-22**
 - partial molar, **4-19**
 - Gibbs energy of formation, **2-486**
 - inorganic and organic compounds, **2-196 to 2-200**
 - Gibbs-Duhem equation:
 - partial molar properties, **4-18**
 - global reactions, **7-5, 7-14**
 - globe and angle, **8-74**
 - glycolysis, **7-31**
 - golden search, **8-34**
 - granular-bed filters, **17-51**
 - cleanable granular bed filters, **17-51**
 - fixed granular bed filters, **17-51**
 - granulation, fluid bed and mixer, operating variable, **21-113 to 21-123**
 - granulation processes, control and design, **21-110**
 - controlling processing in practice, **21-113**
 - controlling breakage in practice, **21-117**
 - controlling growth and consolidation in practice, **21-117**
 - controlling wetting in practice, **21-113**
 - engineering approaches to design, **21-110**
 - scale: granulator vessel, **21-113**
 - scale: granule size and primary feed particles, **21-111**
 - scale: granule volume element, **21-112**
 - scales of analysis, **21-110**
 - granulation processes, modeling, **21-143**
 - modeling individual growth mechanisms, **21-144**
 - attrition, **21-145**
 - coalescence, **21-144**
 - layering, **21-144**
 - nucleation, **21-144**
 - population balance, **21-143**
 - simulation of granulation circuits with recycle, **21-147**
 - solution of the population balance, **21-146**
 - analytical solutions, **21-146**
 - effects of mixing, **21-146**
 - numerical solutions, **21-146**
- graphical implementations, **8-50**
- gravity decanter (horizontal), **15-98**
- gravity sedimentation operations:
 - clarifiers:
 - circular clarifiers, **18-74**
 - clarifier-thickener, **18-74**
 - inclined-plate clarifiers, **18-74**
 - industrial waste secondary clarifiers, **18-74**
 - rectangular clarifiers, **18-74**
 - clarifier and thickener testing, **18-67 to 18-68**
 - coagulant and/or flocculant selection, **18-67 to 18-68**
 - feed characterization, **18-67**
 - sedimentation testing, **18-67**
 - batch bench-scale settling tests, **18-67**
 - continuous piloting, **18-67**
 - semi-continuous bench-scale tests, **18-67**
 - specifications for design and sizing, **18-67**
 - settleable solids and sedimentation, **18-66 to 18-67**
 - types, **18-66 to 18-67**
 - testing for clarification, **18-68**
 - bulk settling, **18-68**
 - detention, **18-68**
 - solids recycle, **18-68**
 - testing for thickening:
 - determination of thickener basin area, **18-69 to 18-70**
 - optimization of flocculation conditions, **18-68 to 18-69**
 - scale-up factors, **18-70**
 - thickener-basin depth, **180-70**
 - torque requirements, **18-70 to 18-71**
 - underflow pump requirements, **18-71**
 - thickeners, **18-71 to 18-74**
 - design features, **18-73**
 - operations, **18-74**
 - types, **18-72 to 18-73**
- grinding, cost, **21-46**
- grinding and crushing, industrial practice, **21-68**
 - biological materials—cell disruption, **21-73**
 - cement, lime, and gypsum, **21-71**
 - dry-process cement, **21-71**
 - finish-grinding of cement clinker, **21-71**
 - gypsum, **21-71**
 - lime, **21-71**
 - portland cement, **21-71**
 - wet-process cement, **21-71**

- grinding and crushing, industrial practice (*Cont.*):
 cereals and other vegetable products, **21-68**
 flour and feed meal, **21-68**
 soybeans, soybean cake and other pressed cakes, **21-68**
 starch and other flours, **21-69**
 chemicals, pigments and soaps, **21-72**
 chemicals, **21-72**
 colors and pigments, **21-72**
 soaps, **21-72**
 coal, coke and other carbon products, **21-71**
 anthracite, **21-71**
 bituminous coal, **21-71**
 coke, **21-71**
 other carbon products, **21-72**
 fertilizers and phosphates, **21-70**
 ores and minerals, **21-69**
 asbestos and mica, **21-70**
 carbonates and sulfites, **21-70**
 clays and kaolins, **21-69**
 crushed stone and aggregate, **21-70**
 metalliferous ores, **21-69**
 nonmetallic minerals, **21-69**
 silica and feldspar, **21-70**
 talc and soapstone, **21-70**
 types of milling circuits, **21-69**
 pharmaceutical materials, **21-73**
 polymers, **21-72**
 gums and resins, **21-72**
 molding powders, **21-72**
 powder coatings, **21-72**
 rubber, **21-72**
 processing waste, **21-72**
 grinding and crushing equipment, **21-56**
 gyratory crushers, **21-57**
 control of crushers, **21-58**
 design and operation, **21-57**
 performance, **21-58**
 hammer mills, **21-59**
 operation, **21-59**
 impact breakers, **21-58**
 cage mills, **21-59**
 hammer crusher, **21-58**
 prebreakers, **21-59**
 jaw crushers, **21-56**
 comparison of crushers, **21-57**
 design and operation, **21-57**
 performance, **21-57**
 pan crushers, **21-61**
 design and operation, **21-61**
 performance, **21-61**
 roll crushers, **21-60**
 roll press, **21-60**
 roll ring-roller mills, **21-60**
 Raymond ring-roller mill, **21-60**
 grinding and crushing equipment, fluid-energy, **21-61**
 design, **21-61**
 types, **21-61**
 opposed jet mill, **21-61**
 other jet mill designs, **21-62**
 spiral jet mill, **21-61**
 grinding and crushing equipment, wet/dry grinding, **21-62**
 disk attrition mills, **21-67**
 dispensers and emulsifiers, **21-68**
 dispersion and colloid mills, **21-68**
 media mills and roll mills, **21-68**
 microfluidizer, **21-68**
 pressure homogenizers, **21-68**
 hicom mill, **21-67**
 media selection, **21-62**
 mill efficiencies, **21-65**
 capacity and power consumption, **21-65**
 overview, **21-62**
 grinding and crushing equipment, wet/dry grinding (*Cont.*):
 performance of bead mills, **21-66**
 residence time distribution, **21-66**
 planetary-ball mills, **21-67**
 stirred media mills, **21-65**
 annular gap mills, **21-66**
 attritors, **21-65**
 design, **21-65**
 horizontal media mills, **21-65**
 manufacturers, **21-66**
 vertical mills, **21-65**
 tumbling mills, **21-63**
 design, **21-63**
 dry vs. wet grinding, **21-64**
 dry-ball milling, **21-64**
 material and ball charges, **21-64**
 multicompartmented mills, **21-63**
 operation, **21-64**
 wet-ball milling, **21-64**
 vibratory mills, **21-66**
 performance, **21-67**
 residence time distribution, **21-67**
 grinding processes, modeling, **21-52**
 batch grinding, **21-53**
 breakage function, **21-53**
 closed-circuit milling, **21-54**
 continuous-mill simulation, **21-53**
 residence time distribution, **21-53**
 solution for continuous milling, **21-54**
 data on behavior of grinding functions, **21-55**
 grinding rate functions, **21-55**
 grinding rate function, **21-53**
 solution of batch-mill equations, **21-53**
 modeling of milling circuits, **21-52**
 scale-up and control of grinding circuits, **21-55**
 parameters for scale-up, **21-55**
 scale-up based on energy, **21-55**
 half-cell reaction, **7-32**
 half-life method, **7-36**
 batch time, **7-36**
 Hall effect sensors, **8-64**
 halon, **2-218, 2-271**
 Hartree Fock, compositional chemistry, **7-38**
 Hatta number, **7-28**
 hazardous materials and conditions, chemical reactivity:
 designing facilities for avoidance of unintended reaction, **23-27**
 identifying potential reactions, **23-28**
 incompatible materials, **23-29**
 oxidizers and organic peroxides, **23-29**
 peroxide formers, **23-28**
 polymerizing, decomposing, and rearranging substances, **23-28**
 self-accelerating decomposition temperature (SADT), **23-28**
 spontaneously combustible and pyrophoric substances, **23-28**
 water-reactive substances, **23-28**
 designing mitigation systems to handle uncontrolled reactions, **23-29**
 depressuring systems, **23-29**
 dump systems, **23-29**
 inhibitor injection, **23-29**
 quench systems, **23-29**
 short-stop system, **23-29**
 designing processes for control of intended chemical reactions, **23-26**
 design of emergency relief and effluent treatment systems, **23-27**
 endothermic compounds, **23-27**
 endothermic reactions, **23-27**
 hazardous materials and conditions, chemical reactivity, designing processes for control of intended chemical reactions (*Cont.*):
 exothermic reactions and runaway reactions, **23-26**
 semibatch reactions, **23-27**
 temperature of no return (T_{NR}), **23-26**
 life-cycle considerations during process development, **23-25**
 considering inherently safer approaches to reactivity hazards, **23-25**
 scale-up considerations, **23-26**
 reactive hazard reviews and process hazard analyses, **23-30**
 hazard and operability (HAZOP), **23-30**
 reactivity testing, **23-30**
 onset temperature, **23-30**
 sources of reactivity data, **23-30**
 accelerating rate calorimetry (ARC), **23-30**
 advanced reactive system screening tool (ARSSTTM), **23-30**
 calculations, **23-30**
 differential thermal analysis (DTA), **23-30**
 mixing cell calorimetry (MCC), **23-30**
 shock sensitivity, **23-30**
 vent sizing package (VSP2TM), **23-30**
 hazardous materials and conditions, flammability:
 boiling-liquid expanding-vapor explosions, **23-13**
 combustion and flammability hazards, **23-8** to **23-11**
 aerosols and mists, **23-10**
 estimating flammability limits, **23-8**
 flammability diagram, **23-9**
 flammability limit dependence on temperature, **23-8**
 flammability limit dependence on pressure, **23-8**
 ignition sources and energy, **23-9, 23-10**
 limiting oxygen concentration, **23-9**
 liquid mixtures, **23-8**
 minimum ignition energy (MEI), **23-10**
 vapor mixtures, **23-8**
 dust explosions, **23-15**
 apparatus for collecting explosion data for dust, **23-12**
 dust explosion device, pressure data from, **23-13**
 terminology, **23-15**
 explosions, **23-11**
 apparatus for collecting explosion data, **23-12**
 boiling-liquid expanding-vapor explosions, **23-13** to **23-14**
 characterizing explosive behavior for vapors and dusts, **23-12**
 confined explosions, **23-11**
 deflagration index, **23-13**
 detonation and deflagration, **23-11**
 vapor cloud explosions, **23-13**
 fire triangle, **23-7**
 flammability limits in pure oxygen, **23-11**
 ignition sensitivity of dusts as a function of protective measures, **23-17**
 relation between flammability properties, **23-8**
 static electricity, **23-22**
 brush discharges, **23-23**
 causes of hazardous discharges with liquids, **23-24**
 charge dissipation, **23-23**
 charge induction, **23-22**
 charge-dissipative materials, **23-23**
 contact electrification, **23-22**

- hazardous materials and conditions, flammability, static electricity (*Cont.*):
 corona, 23-23
 electrostatic charging, 23-22
 electrostatic discharges, 23-23
 external causes of incendive static discharges, 23-24
 mists, 23-22
 personnel and clothing, 23-24
 powders, 23-24
 propagating brush discharges, 23-23
 spark discharges, 23-23
 spray nozzles, 23-22
 terminology, static electricity, 23-22
- hazardous materials and conditions, toxicity:
 data compilation, 23-32
 dosage equation, 23-31
 guidance for the corrosivity of chemical substances, 23-32
 inert hazards, 23-36
 asphyxiation and toxicity hazards, 23-36
 chemical incompatibility hazards, 23-37
 OSHA's respiratory protection standard, 23-36
 physiological effects of reduced carbon dioxide atmospheres, 23-37
 physiological effects of reduced oxygen atmospheres, 23-36
 sources of inerts, 23-36
 ingestion toxicity, 23-32
 inhalation toxicity, 23-31
 Haber equation, 23-31
 overinerting, 23-38
 physical hazards, 23-37
 high and low pressure, 23-37
 high and low temperature, 23-37
 static electricity, 23-22, 23-37
 probit equation, 23-31
 safeguards against toxicity hazards, 23-34
 skin-contact toxicity, 23-32
 vacuum hazards, 23-34
 causes of equipment underpressurization, 23-34
 consequences of vacuum damage, 23-34
 equipment limitations, 23-34
 protective measures for equipment, 23-34
- hazardous waste storage and containers, 22-90
- head devices, level measurement, 8-61
- heat capacity, 7-7, 2-489 to 2-498
 gases, 2-489
 Benson method, 2-490
 calculation methods, 2-489
 ideal gas, 2-490
 ideal gas heat capacity group contributions, 2-491 to 2-495
 statistical mechanics, 2-490
- liquids, 2-490
 calculation methods, 2-495
 liquid heat capacity group parameters, 2-496 to 2-497
 Ruzicka-Domalski method, 2-495
- solids, 2-495
 calculation methods, 2-495
 Element contributions for modified Kopp's rule, 2-498
 Goodman method, 2-495
 group values and nonlinear correction, 2-498
 modified Kopp's rule, 2-497
 terms for Goodman method, 2-498
- heat exchangers:
 air cooled heat exchangers, 11-49 to 11-53
 air flow control, 11-52
 heat exchangers, air cooled heat exchangers (*Cont.*):
 costs, 11-53
 design considerations, 11-53
 fan drivers, 11-51
 fans, 11-51
 humidification chambers, 11-52
 trim coolers, 11-52
 compact and nontubular heat exchangers, 11-55 to 11-60
 atmospheric sections, 11-60
 bayonet-tube exchangers, 11-59
 cascade coolers, 11-59
 graphite heat exchangers, 11-59
 plate and frame exchangers, 11-55, 11-58
 printed-circuit heat exchangers, 11-58
 spiral tube exchangers, 11-59
 control, 8-40
 hairpin/double-pipe, 11-48 to 11-49
 applications, 11-49
 construction, principles of, 11-48
 finned double pipes, 11-48
 multitube hairpins, 11-48
 nonmetallic heat exchangers, 11-60
 ceramic, 11-60
 PDYF, 11-60
 Teflon, 11-60
 solids, heat exchangers for, 11-60 to 11-69
 divided solids, heat-transfer equipment for, 11-64 to 11-69
 fusion of solids, equipment for, 11-63
 sheeted solids, heat-transfer equipment for, 11-63
 solidification, equipment for, 11-60 to 11-63
 TEMA-style shell-and-tube, 11-33 to 11-46
 baffles and tube bundles, 11-43
 bimetallic tubes, 11-45
 characteristics of tubing, table, 11-12
 clad tube sheets, 11-46
 construction, principle types of, 11-36
 corrosion in, 11-45
 costs of, 11-46
 design considerations, 11-35
 fabrication, 11-46
 falling film, 11-40
 features of, table, 11-11
 fixed tube sheet, 11-36
 impervious graphite, 11-46
 internal floating head, 11-40
 material of construction, 11-45
 nonmetallic construction, 11-46
 outside-packed floating-head, 11-40
 packed lantern ring, 11-39
 pull-through floating-head, 11-40
 shell side, construction of, 11-43
 tube side, construction of, 11-41
 U-tube, 11-37
 heat flow controller, 8-41
 heat of formation, 7-6
 heat of reaction, 7-6
 heat pump, 13-66 to 13-67
 heats and free energies of formation, inorganic compounds, 2-186 to 2-195
 heats of combustion, inorganic and organic compounds, 2-196 to 2-200
 heats of solution:
 inorganic compounds in water, 2-203 to 2-205
 organic compounds in water (at infinite dilution and room temperature), 2-206
 heat-transfer coefficient, 12-6, 12-53, 12-57, 12-76, 12-88
 heat-transfer rate, 8-41
 heat-transfer resistances, chemical kinetics, 7-22
 heat-transfer surface fouling, 8-44
 helium, thermodynamic properties, 2-272 to 2-273
 Henry's Law:
 constants:
 estimation of, 22-49
 references, 22-48
 heptane:
 activity coefficient plot, 13-14
 K-value versus residue, 13-12
 residue map, 13-70
 thermodynamic properties, 2-274 to 2-275
 HETP, 16-44
 height equivalent to a theoretical plate, 13-44 to 13-45
 hexane:
 activity coefficient plot, 13-14
 Antoine vapor pressure, 13-14
 BIP data, 13-13
 K-value versus pressure, 13-12
 residue map, 13-70
 thermodynamic properties, 2-276 to 2-277
 Higgins contractor, 16-68
 high-frequency process disturbances, 8-66
 high-level computer language, 8-72
 high/low alarms, 8-67
 high-order lag, 8-11
 high-viscosity process valve, 8-76
 homogeneous catalysis, 7-15
 homopolymerization, 7-29, 7-30
 low conversion, 7-30
 mechanics and kinetics, 7-30
 step growth, 7-30
 h-transformation, 16-45
 HTU, 5-61
 Huckel, 7-38
 humid enthalpy, 12-5
 humid gas density, 12-4, 12-5
 humid heat, 12-5, 12-6
 humid volume, 12-5
 humidity, percentage absolute, 12-4
 humidity measurement, 12-16 to 12-17
 dew point method, 12-16
 electric hygrometer, 12-16
 gravimetric method, 12-17
 mechanical hygrometer, 12-17
 sling or whirling psychrometer, 12-16
 wet-bulb method, 12-16
 hydraulic transients, 6-44 to 6-46
 cavitation, 6-45 to 6-46
 pulsating flow, 6-45
 water hammer, 6-44 to 6-45
 hydrazine, saturated, thermodynamic properties, 2-278
 hydrocyclone flow patterns, 15-102
 hydrogen, para. *See* para-hydrogen
 hydrogen, thermodynamic properties, 2-279 to 2-280
 hydrogen bromide synthesis, 7-15
 hydrogen chloride, aqueous, partial pressures, 2-80
 hydrogen peroxide, thermodynamic properties, 2-282
 hydrogen sulfide, thermodynamic properties, 2-283 to 2-284
 hydrometallurgical PFD example, 15-10
 hygroscopic material, 12-26
 hyperbolic trigonometry, 3-18
 hysteresis effects, 8-86, 12-28
 I/P transducers, 8-87
 ideal reactors:
 continuously stirred tank reactor, 7-10, 7-12

- ideal reactors, continuously stirred tank reactor
(*Cont.*):
liquid phase reaction, 7-12
residence time, 7-12
series, 7-12
steady state, 7-12
plug flow reactor, 7-10, 7-12
constant-density system, 7-12
residence time, 7-12
recycle reactor, 7-12
- impellers:
design:
axial-flow, 18-14
large tanks, 18-14
side-entering, 18-14
top-entering, 18-14
impeller Reynolds number:
fluid characteristics, 18-12
tanks, types:
baffled, 18-11
unbaffled, 18-10
types:
axial flow, 18-9
close-clearance, 18-9
radial flow, 18-9
- implementation of MPC, 8-31
incineration, 17-19
incinerator, hot windbox, 17-20
income statement, 9-6
ammortization, 9-6
bottom line, 9-6
consolidated, 9-4, 9-6
cost of sales, 9-6
depreciation, 9-6
dividends, 9-6
example of, 9-6
expenses, 9-6
administrative, 9-6
general, 9-6
selling, 9-6
gross margin, 9-6
income before extraordinary loss, 9-6
income taxes, 9-6
interest income, 9-6
net income, 9-6
net sales, 9-6
operating income, 9-6
- incompressible flow in pipes and channels, 6-9 to 6-15
drag reduction, 6-14
economic pipe diameter:
laminar flow, 6-15
turbulent flow, 6-14 to 6-15
entrance and exit effects, 6-11
friction factor and Reynolds number, 6-10
laminar and turbulent flow, 6-10 to 6-11
mechanical energy balance, 6-9
molecular flow, 6-15
noncircular channels, 6-12
nonisothermal flow, 6-12 to 6-13
non-Newtonian flow, 6-13 to 6-14
open channel flow, 6-13
residence time distribution, 6-11 to 6-12
slip flow, 6-15 to 6-16
surface roughness values, 6-10
vacuum flow, 6-15
velocity profiles, 6-11
- indirect-fired combustion equipment, 24-41 to 24-42
coil design:
arbor, 24-41
cross-tube convection, 24-41, 24-42
horizontal-tube box with side-mounted convection tube bank, 24-42
horizontal-tube cabin, 24-41, 24-42
- indirect-fired combustion equipment, coil
design (*Cont.*):
simple vertical, cylindrical, 24-41
vertical cylindrical helical, 24-42
vertical-tube, single-row, double-fired heater, 24-41
function:
column reboilers, 24-41
fired reactors, 24-41
fractionator-feed preheater, 24-41
heat-transfer fluid, 24-41
reactor-feed stream, 24-41
viscous-liquid, 24-41
inequality constraints, 8-31, 8-33
inert purge, 16-52
infinite series:
convergence and divergence tests, 3-26
definitions, 3-25
operations, 3-25 to 3-26
partial sums, 3-27
series summation and identities, 3-26 to 3-27
arithmetic progression, 3-26
binomial series, 3-26
exponential series, 3-26
geometric progression, 3-26
harmonic progression, 3-26
logarithmic series, 3-26
Maclaurin's series, 3-26
sums for numbers to integer powers, 3-26
Taylor's series, 3-26
trigonometric series, 3-26 to 3-27
- information technology, 8-69
infrared analyzers, 8-62
in-line blending system, control of, 8-26
input conversion network, 8-84
intangibles, economic, 9-5
goodwill, 9-5, 9-6
intellectual capital, 9-5
licenses, 9-5
particular scrubber, 17-36
patents, 9-5, 9-6
- integral calculus:
definite integral, 3-24 to 3-25
methods of integration, 3-24 to 3-25
properties, 3-24
indefinite integral, 3-22 to 3-23
methods of integration, 3-23
algebraic substitution, 3-23
direct formula, 3-23
partial fractions, 3-23 to 3-24
series expansion, 3-24
trigonometric substitution, 3-23
- integral control, 8-14
integral equations, 3-36 to 3-37
classification, 3-36
methods of solution, 3-37
numerical solution, 3-54
relation to differential equations, 3-36 to 3-37
- integral transforms, 3-37 to 3-40
convolution integral, 3-39
Fourier cosine transform, 3-39 to 3-40
Fourier transform, 3-39
Laplace transform, 3-37 to 3-40
z-transform, 3-39
- integrated absolute error, control, 8-16
intelligent alarm, use in control, 8-68
intelligent field devices, use in control, 8-69
interaction number, 17-22
interest, 9-23
effective rates, 9-25
types of, 9-23
compounding-discounting, 9-23
continuous compounding, 9-23
discrete compounding, 9-23
simple, 9-23
- interfacial mass-transfer rates, 14-89
approach to equilibrium-finite contactor with no bypassing, 14-89
bypassing, 14-90
transfer coefficient-impact of droplet size, 14-90
turbulence, effect of, 14-90
- interlocks, 8-49
intermodal communications, 8-70
internal diffusion, 12-26
internal energy:
function of T and P or T and y, 4-6 to 4-7
postulate definition, 4-4
- interpolation and finite differences, 3-45 to 3-47
central differences, 3-46
divided differences of higher order, 3-45
equally spaced backward differences, 3-46
equally spaced forward differences, 3-45
Lagrange interpolation formulas, 3-46
linear interpolation, 3-45
spline functions, 3-46 to 3-47
- intraparticle diffusion, 7-20
effectiveness factor, 7-20
external mass-transfer resistance, 7-22
gas diffusivity, 7-20
observed order and activation energy, 7-20
reaction networks, 7-21
reaction rate, 7-20
- intraparticle transport mechanisms, 16-18
inventory evaluation and cost control, 9-9
inverse trigonometric functions, 3-17
investment capital, 9-10
ion electrodes, 8-63
ion exchange:
Asahi countercurrent process, 16-69
Himsley continuous system, 16-69
mixed-bed, 16-54
regeneration, 16-54
- ion exchangers:
fixed bed, design data, 16-68
physical properties, 16-9 to 16-11
pore size classification, 16-8
- ionic self-diffusivities, 16-20
irreversible reaction, 7-5
ISA symbols, 8-40
isobutane, thermodynamic properties, 2-286 to 2-287
isobutene, thermodynamic properties, 2-288 to 2-289
isolation, 8-78
isosteric heat of adsorption, 16-12
isotactic pattern, 16-39
- isotherms:
BET, 16-13
constant pattern behavior, 16-34
constant separation factor, 16-35
Freundlich, 16-13
linear, 16-13
Sips, 6-13
square-root spreading, 16-37
Toth, 16-13
- jet behavior, 6-20 to 6-22
Joule-Thomson effect:
approximate inversion-curve locus in reduced coordinates, 2-137
Joule-Thomson coefficient, additional references, 2-137
- Kachford and Kile, 13-5
Karr column, 15-84
kinetic control, electrochemical reactions, 7-32
kinetic models, simplified, 12-32
experimental methods, 12-35 to 12-36
moisture determination, 12-36
sample techniques, 12-36

- kinetic parameters, 7-35
 Arrhenius temperature dependence, 7-35
 kinetic rate equation, complex, 7-37
 kinetics, surface-reaction controlling, 7-17
 Kirchhoff's law, 5-19
 Kister and Gill correlation, structured packing, 14-59
 Kister and Haas spray regime, 14-42
 Knox equation, 16-44
 Kozeny-Carman equation, 17-46
 krypton, thermodynamic properties, 2-290 to 2-291
 Kuhn column, 15-83
 K-values:
 analytical correlations, 13-9 to 13-15
 Ivan Laar, 13-13
 Margules, 13-13
 SKK, 13-12
 Uniquil, 13-13
 Wilson, 13-13
 definition of, 13-7
 graphical correlations, 13-8 to 13-9
 Hadden's method, 13-9
- lab-on-a-chip, 8-63
 ladder diagram, 8-50
 ladder logic, 8-72
 lag phase, 7-19
 Lagrange multipliers, 8-35
 LAN-based, 8-70
 landfill sites, 22-100
 Langmuir-Hinshelwood rate, 7-35
 Laplace transforms, 8-7
 Lapple equation, 17-46
 laser level transmitter, 8-61
 latent heat of evaporation, 12-5, 12-26
 latent heats:
 elements and inorganic compounds, 2-145 to 2-147
 inorganic compounds (J/kmol), 2-155
 miscellaneous materials, 2-147
 organic compounds, 2-148 to 2-149
 law of mass action, 7-6
 leaching, 18-59 to 18-66
 definitions, 18-59 to 18-60
 mechanism, 18-60
 methods of operation, 18-60
 equipment, 18-60 to 18-64
 batch-stirred tanks, 18-62
 BMA diffusion tower, 18-64
 Bollman-type extractor, 18-61
 Bonotto extractor, 18-63
 continuous dispersed-solids leaching, 18-63
 de Smet belt extractor, 18-61
 dispersed-solids leaching, 18-61 to 18-62
 gravity sedimenter, 18-63
 Hildebrandt total-immersion extractor, 18-64
 Kennedy extractor, 18-61
 Lurgi frame belt, 18-61
 Pachuca tanks, 18-62 to 18-63
 percolators, 18-60
 rotocel extractor, 18-61
 screw-conveyor extractors, 18-64
 tray classifier, 18-64
 process selection and/or design, 18-64 to 18-66
 composition diagrams, 18-66
 extractor-sizing calculations, 18-65
 graphical method, 18-66
 leaching cycle and contact method, 18-65
 process and operating conditions, 18-65
 software packages, 18-65
 solvent choice, 18-65 to 18-65
 temperature, 18-65
 terminal stream compositions and quantities, 18-65
 type of reactor, 18-65
- least squares, partial, 8-39
 ledger, economic, 9-4
 closed and balanced, 9-4
 example of, 9-5
 ledger accounts, 9-4
 asset account, 9-4
 expense account, 9-4
 liability account, 9-4
 revenue account, 9-4
 Lefebvre formula, 12-93
 level control, 8-43
 level measurements, 8-60
 liabilities, economic, 9-5
 current liabilities, 9-5
 accounts payable, 9-5
 accrued expenses, 9-5
 current part of long term debt, 9-5
 income taxes payable, 9-5
 notes payable, 9-5
 long-term liabilities:
 bonds and notes, 9-5
 deferred income taxes, 9-5
 total liabilities, 9-5, 9-6
 life-cycle analysis and multimedia analysis, 22-21
 LIFO, last in first out basis, 9-10
 limit switches, 8-91
 limiting current, electrochemical reactions, 7-33
 limiting reactant, reaction kinetics, 7-7
 linear driving force approximation, 16-22
 linear programming, 8-29
 liqui-Cel membrane contactors, 15-103
 liquid chromatography, high-performance, 8-62
 liquid fuels, 24-7 to 24-11
 nonpetroleum:
 characteristics, 24-11
 coal-derived, 24-10
 shale oil, 24-10
 tar sands, 24-10
 petroleum. *See* petroleum fuels
 liquid phase reactors, 19-20 to 19-21
 liquid-column pressure measure, methods, 8-58
 liquid-in-gas dispersions, 14-91
 atomizers, 14-93
 droplet breakup-high turbulence, 14-92
 droplet size distribution, 14-93
 dropwise distribution, 14-98
 effect of physical properties on drop size, 14-93
 effect of pressure drop and nozzle size, 14-93
 entrainment due to gas bubbling/jetting through a liquid, 14-96
 fog condensation-the-other way to make little droplets, 14-97
 growth on foreign nuclei, 14-98
 hydraulic (pressure) nozzles, 14-93
 isolated droplet breakup-in a velocity field, 14-92
 liquid breakup into droplets, 14-91
 liquid-column breakup, 14-92
 liquid-sheet breakup, 14-92
 pipeline contactors, 14-95
 rotary atomizers, 14-95
 spontaneous (homogeneous) nucleation, 14-98
 spray angle, 14-93
 two-fluid (pneumatic) atomizers, 14-94
 "upper limit" flooding vertical tubes, 14-97
 liquid/liquid equilibrium, thermodynamics, 4-35
 liquid-liquid extraction, 15-6 to 15-22
 definitions:
 continuous phase, 15-10
 counter-current cascade, 15-11
 counter-current extraction, 15-11
 cross-current extraction, 15-11
 cross-flow extraction, 15-11
 differential contactor, 15-11
 dilutant, 15-10
 dispersed phase, 15-10
 liquid-liquid extraction, definitions (*Cont.*):
 dispersion, 15-10
 distribution coefficient (k), 15-10
 distribution constant (k), 15-10
 distribution ratio, 15-11
 emulsion, 15-10
 equilibrium stage, 15-10
 extract, 15-10
 extractant, 15-10
 extraction factor, 15-11
 extraction solvent, 15-10
 feed, 15-10
 feed as carrier solvent, 15-10
 flood point, 15-11
 flooding, 15-11
 fractional extraction, 15-11
 interfacial tension, 15-10
 k-value, 15-10
 liquid-liquid extraction, 15-10
 mass-transfer coefficients, 15-11
 mass-transfer units, 15-11
 mixed solvent as solvent blend, 15-10
 modifier, 15-10
 pK_a, 15-15
 partition ratio (k), 15-10
 phase inversion, 15-11
 phase velocity, 15-11
 raffinate, 15-10
 Sauter-mean drop diameter, 15-10
 selectivity, 15-11
 separating agent, 15-10
 separation factor, 15-11
 solutes, 15-10
 solutrope, 15-11
 solvent extraction, 15-10
 staged contactor, 15-11
 standard extraction, 15-11
 theoretical stage, 15-10
 throughput, 15-11
 uses, 15-7 to 15-10
 acetic acid recovery example, 15-8
 antibiotic recovery from fermentation broth, 15-8
 aromatic compound petrochemical separation, 15-8
 distillation impracticalities, 15-8
 hydro metallurgical applications, 15-8
 removal of acid residue from liquefied petroleum gases (LPG), 15-8
 liquid-liquid extraction, equipment, 15-58 to 15-93
 agitated extraction columns, 15-79 to 15-86
 kuhni column, 15-82 to 15-83
 pulsed-liquid columns, 15-85
 raining-bucket contactor, 15-85 to 15-86
 reciprocating-plate columns, 15-83 to 15-84
 rotating-disk contactor, 15-84 to 15-85
 rotating-impeller columns, 15-79 to 15-80
 scheibel extraction column, 15-80 to 15-82
 centrifugal extractors, 15-92 to 15-93
 multistage, 15-92 to 15-93
 single-stage, 15-91 to 15-92
 extractor selection, 15-58 to 15-59
 volumetric efficiency, 15-59
 hydrodynamics of column extractors, 15-59 to 15-63
 axial mixing, 15-60 to 15-62
 computational fluid dynamics (CFD), 15-62 to 15-63
 flooding phenomena, 15-59 to 15-60
 mixer-settler equipment, 15-86 to 15-91
 liquid-liquid mixes design, 15-87 to 15-88
 mass-transfer models, 15-86 to 15-87
 miniplant tests, 15-87
 scale-up, 15-88 to 15-89

- liquid-liquid extraction, equipment, mixer-settler equipment (*Cont.*):
 - specialized equipment, 15-89 to 15-90
 - suspended-fiber contactor, 15-90 to 15-91
- static extraction columns, 15-63 to 15-79
 - baffle tray columns, 15-78 to 15-79
 - features and design concepts, 15-63 to 15-69
 - packed columns, 15-70 to 15-74
 - sieve tray columns, 15-74 to 15-78
 - spray columns, 15-69 to 15-70
- liquid-liquid extraction, thermodynamic basis, 15-22 to 15-32
 - activity coefficients, 15-22 to 15-25
 - extraction factor, 15-22 to 15-23
 - ionizable organic salts and pH, 15-23 to 15-25
 - min and max solvent-to solvent ratios, 15-23
 - salting-out, salting-in and non-ionic solutes, 15-24
 - separation factor, 15-23
 - temperature effect, 15-23 to 15-24
 - data collection equations, 15-27 to 15-32
 - data quality, 15-28 to 15-32
 - thermodynamic models, 15-28
 - tie-line correlations, 15-27 to 15-28
 - experimental methods, 15-27
 - phase diagrams, 15-25 to 15-27
 - plait point, 15-26
 - phase equilibrium data source, 15-32
 - recommended model systems, 15-32
- liquid-liquid phase separation equipment, 15-96 to 15-103
 - feed characteristics, 15-96
 - other separators, 15-101 to 15-102
 - centrifuges, 15-101
 - coalescers, 15-101
 - electrotreaters, 15-102
 - hydrocyclones, 15-101 to 15-102
 - ultrafiltration membranes, 15-102
 - overall process considerations, 15-96
 - settlers, 15-97 to 15-100
 - decanters with coalescing intervals, 15-99
 - design considerations, 15-97 to 15-98
 - sizing methods, 15-99 to 15-100
 - vented decanters, 15-98 to 15-99
- liquid-liquid reactors, 19-41 to 19-42
 - examples, 19-43
 - types of, 19-42 to 19-47
 - agitated stir tanks, 19-42 to 19-44
 - bubble columns, 19-44 to 19-46
 - packed, spray and trayed towers, 19-46 to 19-47
 - tubular reactors, 19-46
- liquids, storage of, 10-140
 - atmospheric tanks, 10-140
 - types of, 10-143
 - pressure tanks:
 - calculation of tank volume, 10-144
 - container materials and safety, 10-145
 - pond and underground cavern storage, 10-146
- shop-fabricated storage tanks, 10-140
- USTs versus ASTs, 10-140
 - aboveground storage tank types and options, 10-142
 - double-wall, 10-142
 - elevated tanks, 10-143
 - environmental regulations, 10-142
 - fire codes, 10-141
 - fixed roofs, 10-143
 - open tanks, 10-143
 - posttensioned concrete, 10-143
 - secondary containment ASTs, 10-142
 - separation distances, 10-144
 - standards, 10-141
 - state and local jurisdictions, 10-142
 - variable-volume tanks, 10-143
 - venting, 10-144
- lithium, saturated, thermodynamic properties, 2-292
- load cells, serial interface, 8-66
- loading ratio correlation, 16-13
- local equilibrium theory, 16-31
- Loeb equation, 17-56
- logical operators, 8-71
- long-term scheduling, 8-48
- low alarms, 8-67
- low level, switch, 8-50
- low-frequency process disturbances, 8-66
- lumping, mechanism reduction, 7-38, 7-39
- magnetic flowmeters, 8-59 to 8-60
- magnetically coupled devices, 8-60
- management information systems, 8-69
- manufacturing expenses, 9-18 to 9-21
- manufacturing resource planning, 8-68
- mass action law, 16-14 to 16-17
- mass flow controllers, 8-60
- mass flow network, 7-30
- mass fraction, 12-4
- mass ratio, 12-4
- mass spectroscopy, 8-63
- mass transfer, 5-43 to 5-83
 - Chilton-Colburn analogy, 5-83
 - coefficients, 5-45, 5-61
 - definitions, 5-61
 - effects of chemical reactions, 5-74, 5-82 to 5-83
 - effects of concentrations, 5-74
 - effects of system physical properties, 5-74, 5-82
 - effects of total pressure, 5-68
 - effects of total temperature, 5-68
 - flow in pipes, 5-66 to 5-68
 - packed two-phase contactors, 5-80 to 5-82
 - particles, drops, and bubbles in agitated systems, 5-75 to 5-76
 - single flat plate, 5-63 to 5-64
 - submerged objects, 5-69 to 5-70
 - volumetric, 5-83
 - constant separation factors, 16-27 to 16-28, 16-30
 - correlations, 5-62 to 5-82
 - drops, bubbles, and bubble columns, 5-75 to 5-76
 - falling films, 5-65
 - fixed and fluidized beds, 5-77 to 5-79
 - external mass-transfer control, 16-27
 - interfacial mass transfer area, 5-83
 - principles, 5-59 to 5-61
 - concentrated systems, 5-60 to 5-61
 - diluted systems, 5-59 to 5-60
 - rate equations in absorbent particles, 16-24
 - solid diffusion control, 16-27
 - theories, 5-61 to 5-62
- mass-transfer coefficients, 12-6, 12-53, 14-24
- mass-transfer controlled, 7-33
- material balance, 5-49, 16-17
- materials:
 - low temperature metals, 25-45 to 25-46
 - high-temperature metals, 25-46 to 25-51
- materials of construction, properties:
 - aluminum and alloys, 25-33
 - brass, 25-34
 - bronze, 25-34
 - cast iron:
 - austenitic, 25-5, 25-31
 - carbon steel, 25-6
 - duplex, 25-32
 - low-alloy, 25-6
 - martensitic alloys, 25-31
 - 6Mo family alloys, 25-32
 - stainless steel, ferritic, 25-31
 - ceramic-fiber insulated linings, 25-51
 - materials of construction, properties (*Cont.*):
 - copper and alloys, 25-34
 - creep, 25-47
 - cupronickel, 25-34
 - firebrick, 25-49
 - Hastelloy alloys, 25-33
 - incoloy, 25-35
 - inorganic, nonmetallics:
 - brick, 25-36
 - cement, concrete, 25-37
 - glass, 25-36
 - glassed steel, 25-36
 - porcelain, 25-36
 - lead and alloys, 25-34
 - Monel 400, 25-33
 - nickel alloys, 25-32 to 25-34
 - organic, nonmetallics, 25-37 to 25-44
 - epoxy, 25-44
 - ethylene chlorotrifluoroethylene, 25-41
 - ethylene trifluoroethylene, 25-41
 - fluorinated ethylene propylene, 25-37
 - furon, 25-44
 - perfluoroalkoxy, 25-37
 - polyethylene, 25-41
 - polytetrafluoroethylene, 25-37
 - polyvinyl chloride, 25-41
 - polyvinylidene fluoride, 25-37
 - rubber, 25-44
 - thermoplastics, 25-41
 - thermosets, 25-37
 - stress rupture, 25-47
 - tantalum, 25-34
 - tinplate, 25-41
 - titanium, 25-34
 - zirconium, 25-34
 - mathematical constants, 3-4
 - mathematical signs, 3-4
 - matrix algebra, 3-40 to 3-41
 - equality of matrices, 3-40
 - matrices, 3-40
 - matrix operations, 3-40 to 3-41
 - matrix calculus, 3-41
 - differentiation, 3-41
 - integration, 3-41
 - matrix computations, 3-41 to 3-43
 - LU factorization, 3-41 to 3-42
 - principal component analysis, 3-42 to 3-43
 - QR factorization, 3-42
 - singular-value decomposition, 3-42
 - McCabe-Thiele method, 13-16 to 13-25
 - construction, 13-19 to 13-22
 - B-line, 13-19 to 13-22
 - feed stage location, 13-22
 - operating line, 13-19 to 13-22
 - optimum reflux ratio, 13-24
 - pinch point, 13-24
 - MCM-41, 16-8
 - measurement, direct mass, 8-61
 - mechanical centrifugal separators, 17-36
 - mechanical deactivation, 7-23
 - mechanical scrubbers, 17-43
 - melt crystallization:
 - comparison of features, 20-3
 - comparison of processes, 20-3
 - from the bulk, 20-6 to 2-10
 - axial dispersion coefficients, 20-8
 - center-fed crystallizers, 20-7 to 20-9
 - end-fed crystallizers, 20-9
 - equipment and applications, 20-9 to 20-10
 - phase diagrams, 20-3, 20-4
 - melting point, normal, 2-471 to 2-472
 - calculation methods, 2-471
 - Constantinov and Gani method, 2-471
 - first-order groups contributions, 2-472
 - second-order groups contributions, 2-472

20 INDEX

- membrane separation processes:
 - background and definitions:
 - applications, **20-36 to 20-37**
 - component transport, **20-38 to 20-39**
 - membrane types, **20-37 to 20-38**
 - membrane systems, modules:
 - NFF, **20-40 to 20-41**
 - process configurations:
 - batch and fed-batch, **20-43 to 20-45**
 - continuous, **20-44 to 20-45**
 - diafiltration, **20-43 to 20-44**
 - single-pass, **20-42, 20-44**
 - TFF, **20-40 to 20-43**
 - commercial modules, **20-43**
 - membranes, gas separation:
 - description, **20-57**
 - economics, **20-61 to 20-63**
 - compression, **20-61**
 - membrane replacement, **20-63**
 - product losses, **20-62**
 - examples:
 - carbon dioxide-methane, **20-57**
 - gas dehydration, **20-58**
 - helium, **20-58**
 - hydrogen, **20-57**
 - oxygen-nitrogen, **20-57**
 - vapor recovery, **20-58**
 - kinetic diameters, **20-57**
 - principles of operation:
 - Barrar conversion factors, **20-58**
 - driving force, **20-58**
 - equations, **20-58**
 - gas permeation units, **20-58**
 - limiting cases, **20-59**
 - plasticization, **20-59**
 - selectivity and permeability, **20-59 to 20-60**
 - high performance polymers, **20-59**
 - polarization, **20-60**
 - temperature effects, **20-60**
 - time effects, **20-60**
 - system design, **20-60 to 20-61**
 - energy requirements, **20-61**
 - fouling, **20-61**
 - modules and housings, **20-61**
 - partial pressure pinch, **20-61**
 - types of:
 - advanced materials, **20-60**
 - catalytic, **20-60**
 - caulked, **20-60**
 - metallic, **20-60**
 - organic, **20-60**
 - membranes, liquid separation:
 - description, **20-57**
 - economics, **20-61 to 20-63**
 - compression, **20-61**
 - membrane replacement, **20-63**
 - product losses, **20-62**
 - examples:
 - carbon dioxide-methane, **20-57**
 - gas dehydration, **20-58**
 - helium, **20-58**
 - hydrogen, **20-57**
 - oxygen-nitrogen, **20-57**
 - vapor recovery, **20-58**
 - kinetic diameters, **20-57**
 - principles of operation:
 - Barrar conversion factors, **20-58**
 - driving force, **20-58**
 - equations, **20-58**
 - gas permeation units, **20-58**
 - limiting cases, **20-59**
 - plasticization, **20-59**
 - selectivity and permeability, **20-59 to 20-60**
 - high performance polymers, **20-59**
 - polarization, **20-60**
 - temperature effects, **20-60**
 - time effects, **20-60**
 - system design, **20-60 to 20-61**
 - energy requirements, **20-61**
 - fouling, **20-61**
 - modules and housings, **20-61**
 - partial pressure pinch, **20-61**
 - types of:
 - advanced materials, **20-60**
 - catalytic, **20-60**
 - caulked, **20-60**
 - metallic, **20-60**
 - organic, **20-60**
 - membranes, membrane separation:
 - description, **20-57**
 - economics, **20-61 to 20-63**
 - compression, **20-61**
 - membrane replacement, **20-63**
 - product losses, **20-62**
 - examples:
 - carbon dioxide-methane, **20-57**
 - gas dehydration, **20-58**
 - helium, **20-58**
 - hydrogen, **20-57**
 - oxygen-nitrogen, **20-57**
 - vapor recovery, **20-58**
 - kinetic diameters, **20-57**
 - principles of operation:
 - Barrar conversion factors, **20-58**
 - driving force, **20-58**
 - equations, **20-58**
 - gas permeation units, **20-58**
 - limiting cases, **20-59**
 - plasticization, **20-59**
 - selectivity and permeability, **20-59 to 20-60**
 - high performance polymers, **20-59**
 - polarization, **20-60**
 - temperature effects, **20-60**
 - time effects, **20-60**
 - system design, **20-60 to 20-61**
 - energy requirements, **20-61**
 - fouling, **20-61**
 - modules and housings, **20-61**
 - partial pressure pinch, **20-61**
 - types of:
 - advanced materials, **20-60**
 - catalytic, **20-60**
 - caulked, **20-60**
 - metallic, **20-60**
 - organic, **20-60**
 - membranes, membrane systems, modules:
 - NFF, **20-40 to 20-41**
 - process configurations:
 - batch and fed-batch, **20-43 to 20-45**
 - continuous, **20-44 to 20-45**
 - diafiltration, **20-43 to 20-44**
 - single-pass, **20-42, 20-44**
 - TFF, **20-40 to 20-43**
 - commercial modules, **20-43**
 - membranes, membrane systems, modules:
 - NFF, **20-40 to 20-41**
 - process configurations:
 - batch and fed-batch, **20-43 to 20-45**
 - continuous, **20-44 to 20-45**
 - diafiltration, **20-43 to 20-44**
 - single-pass, **20-42, 20-44**
 - TFF, **20-40 to 20-43**
 - commercial modules, **20-43**
 - membranes, membrane systems, modules:
 - NFF, **20-40 to 20-41**
 - process configurations:
 - batch and fed-batch, **20-43 to 20-45**
 - continuous, **20-44 to 20-45**
 - diafiltration, **20-43 to 20-44**
 - single-pass, **20-42, 20-44**
 - TFF, **20-40 to 20-43**
 - commercial modules, **20-43**
 - methane (Cont.):
 - K-value versus pressure, **13-12**
 - pressure versus time data obtained from gas explosion apparatus, **23-12**
 - thermodynamic properties, **2-296 to 2-297**
 - methane in air, pressure as a function of volume percent concentration, **23-12**
 - methanol:
 - Antoine vapor pressure, **13-14**
 - BIP data, **13-13**
 - residue curve, **13-90**
 - residue map, **13-79**
 - thermodynamic properties, **2-298 to 2-299**
 - methyl acetate:
 - Antoine vapor pressure, **13-14**
 - BIP data, **13-13**
 - methyl butane (isopentane), thermodynamic properties, **2-300 to 2-301**
 - methyl chloride, saturated, thermodynamic properties, **2-304**
 - methyl ethyl ketone:
 - residue map, **13-70, 13-79**
 - sensitivity of composition and temperature, **13-79 to 13-80**
 - methyl pentane (isohexane), thermodynamic properties, **2-302 to 2-303**
 - microfiltration:
 - applications, **20-56 to 20-57**
 - chemical, **2-57**
 - flow schemes, **20-57**
 - food and dairy, **20-57**
 - pharmaceutical, **20-56**
 - water, **20-57**
 - description, **20-54**
 - economics, **20-57**
 - equipment configuration:
 - cassettes, **20-56**
 - ceramics, **20-56**
 - conventional design, **20-56**
 - examples, **20-54**
 - membranes, **20-54 to 20-56**
 - ceramic, **20-54**
 - characterization and tests, **20-55 to 2-56**
 - from solids, **20-54**
 - inversion, **20-55**
 - stretched polymers, **20-55**
 - track-etched, **20-54**
 - process limitations:
 - fouling, **20-56**
 - polarization, **20-56**
 - microprocessor-based transmitters, **8-66**
 - microscopic reversibility, **7-7**
 - mixed potential principle, **7-33**
 - mixed-feed evaporator, control of, **8-45**
 - mixers-settlers, **15-89**
 - equipment, **18-21**
 - flow, line mixers, **18-21**
 - definition, **18-21**
 - injectors, **18-21**
 - jet mixers, **18-21**
 - line mixer, **18-22**
 - nozzles, **18-21**
 - orifices, **18-21**
 - packed tubes, **18-22**
 - pipe lines, **18-22**
 - pumps, **18-22**
 - valves, **18-22**
 - liquid-liquid extraction, **18-24**
 - purposes, **18-20**
 - vessels, agitated:
 - coalescence, **18-24**
 - dispersion, **18-23**
 - drop size, **18-23**
 - mechanical agitation, **18-23**
 - uniformity, **18-23**
- mixing:
 - maximum mixedness, **19-18 to 19-20**
 - mixing times, **19-20**
 - ratio, **12-4, 12-6**
- mobile-bed scrubbers, **17-42**
- model development, **8-31**
- model predictive control, **8-29**
 - advantages, **8-29**
 - disadvantages, **8-29**
 - moving horizon, **8-31**
- modular field-mounted controllers, **8-69**
- moisture bound, **12-26**
- moisture change, unaccomplished, **12-26**
- moisture content and gradient, **12-26**
- moisture measurement, **8-63**
 - capacitance method, **8-63**
- moisture, unbound, **12-26**
- mole fraction, **12-4**
- mole ratio, **12-4**
- molecular weight distribution, **7-29**
 - number chain length distribution, **7-29**
 - number molecular weight distribution, **7-29**
 - weight chain length distribution, **7-29**
 - weight molecular weight distribution, **7-29**
- moments:
 - method of, **7-30, 16-40**
 - of distribution, polymers, **7-29**
- Monod kinetics, **7-18, 7-31**
 - equation, **7-31**
 - grow rate, **7-31**
 - product inhibition, **7-31**
 - substrate inhibition, **7-31**
- Monte Carlo simulations, **3-54**
- motion conversion, **8-77**
- motorized valves, **8-87**
- moving bed systems, simulated, **16-56**
- MPC, integration of, **8-22**
- multi-input, multi-output systems, **8-12**
- multiphase flow, **6-26 to 6-32**
 - gases and solids, **6-30**
 - liquids and gases, **6-26 to 6-30**
 - solid/liquid or slurry, **6-30 to 6-32**
- multiphase reactors, **19-49 to 19-60**
 - bioreactors, **19-49 to 19-50**
 - CSTRs, **7-35**
 - electrochemical reactors, **19-50 to 19-53**
- types:
 - agitated slurry reactors, **19-53 to 19-56**
 - fluidized GLS reactors, **19-57**
 - slurry bubble column reactors, **19-56 to 19-57**
 - trickle bed reactors, **19-57**
- multiple reactions, **7-33**
- multiple transition system, **16-32**
- multiplexer, **8-65, 8-70**
- multiport, **8-76**
- multivariable calculus and thermodynamics, **3-21 to 3-22**
 - partial derivatives of all thermodynamic functions, **3-22**
 - state functions, **3-21**
 - thermodynamic state functions, **3-21**
- multivariable control, **8-26**
- multivariable optimization, **8-34**
- multivariable statistical techniques, **8-39**
- municipal waste, leachate, **22-103**
- nanofiltration. *See* reverse osmosis
- National Electric Code, **8-91**
- natural gas, **24-10 to 24-12**
 - analysis, **24-11**
 - background, **24-10 to 24-11**
 - liquefied, **24-11 to 24-12**
 - supercompressibility, **24-11**
 - negative feedback loop, **8-5**

- neon, thermodynamic properties, 2-305 to 2-306
 Nernst equation, 7-32
 net worth economic, 9-6
 neutralization-extraction hybrid, 15-19
 Newton's linearization, 7-38
 Newton's method, 8-34
 nitrogen:
 enthalpy-pressure, 2-309
 removal systems, 22-72
 thermodynamic properties, 2-307 to 2-308
 nitrogen oxides, catalytic reduction, 22-54
 nitrogen tetroxide, saturated, thermodynamic properties, 2-240, 2-310
 nitrogen trifluoride, thermodynamic properties, 2-311 to 2-312
 nitrous oxide, 2-313 to 2-315
 nodes, high and low boiling, 13-70
 noise control, 8-81
 noise measurement, 8-66
 nomograph, 12-19
 non self-regulating, 8-19
 nonane, thermodynamic properties, 2-316 to 2-317
 nonharmonic frequency, 8-81
 nonhygroscopic material, 12-26
 nonlinear decouplers, 8-28
 nonlinear equations in one variable, numerical solutions, 3-44 to 3-45
 Descartes rule, 3-44
 methods, 3-44 to 3-45
 false position, 3-44
 method of continuity (homotopy), 3-45
 method of successive substitution, 3-44
 method of Wegstein, 3-44
 methods of perturbation, 3-44
 Newton-Raphson method, 3-45
 Newton-Raphson procedure, 3-44
 successive substitutions, 3-44
 polynomials, 3-44
 nonlinear programming, 8-35
 nonlinear regression, 7-38
 non-self regulating, 8-18
 normal logic, 8-50
 nozzle amplifier, 8-90
 nozzles:
 characteristics, 4-15
 thermodynamics, 4-15 to 4-16
 NTU, 5-61
 Nukiyama and Tanasaws equation, 17-37
 numerical differentiation, 3-47
 first-degree least squares with three points, 3-47
 numerical derivatives, 3-47
 second-degree least squares with five points, 3-47
 smoothing techniques, 3-47
 three-point formulas, 3-47
 numerical integration (quadrature), 3-47 to 3-48
 computer methods, 3-48
 Gaussian quadrature, 3-47
 parabolic rule (Simpson's rule), 3-47
 Romberg's method, 3-48
 singularities, 3-48
 trapezoidal rule, 3-47
 two-dimensional formula, 3-48
 Nusselt number, 12-58
 objective function, 7-37, 8-34
 weighted, 7-37
 occupational safety and health act, 8-81
 O'Connell correlation, column efficiency, 14-15
 octane, thermodynamic properties, 2-318 to 2-319
 offsite capital, 9-10, 9-17
 Ohmic control, 7-33
 on/off control, 8-12
 open systems:
 energy balances:
 open systems, energy balances (*Cont.*):
 general, 4-14
 steady-state, 4-14
 entropy balance, 4-14 to 4-15
 equations of balance, 4-15
 mass, 4-14
 open-loop method, 8-19
 open-loop system, 8-5
 operating curve, absorber, 14-12
 operating expenses, 9-18 to 9-21
 operating margin, economic, 9-6
 operating points, purpose of controller, 8-8
 operation and troubleshooting, 12-106 to 12-109
 opportunity cost, 9-39
 optimization, 3-60 to 3-70
 development of optimization models, 3-70
 global optimization, 3-66 to 3-67
 gradient-based nonlinear programming, 3-60 to 3-64
 mixed integer programming, 3-67 to 3-69
 optimization methods without derivatives, 3-65 to 3-66
 single-variable, 8-34
 unconstrained, 8-34
 ordinary differential equations:
 first order, 3-30
 exact equations, 3-30
 linear equations, 3-30
 separable variables, 3-30
 higher order, 3-30
 complex roots, 3-30
 dependent variable missing, 3-30
 distinct real roots, 3-30
 independent variable missing, 3-30 to 3-31
 linear homogeneous, 3-30
 linear nonhomogeneous, 3-31
 multiple real roots, 3-30
 special differential equations, 3-31 to 3-32
 Bessel's equation, 3-31
 Chebyshev's equation, 3-32
 Euler's equation, 3-31
 Hermite's equation, 3-32
 Laguerre's equation, 3-32
 Legendre's equation, 3-32
 ordinary differential equations, boundary value problems:
 adaptive meshes, 3-53 to 3-54
 finite difference method, 3-52
 spreadsheet solutions, 3-52 to 3-53
 Galerkin finite element method, 3-53
 molecular dynamics, 3-51 to 3-52
 numerical solutions, 3-51 to 3-54
 orthogonal collocation, 3-53
 singular problems and infinite domains, 3-54
 ordinary differential equations, initial value problems:
 computer software, 3-50 to 3-51
 differential-algebraic systems, 3-50
 implicit methods, 3-49 to 3-50
 numerical solution, 3-48 to 3-51
 sensitivity analysis, 3-51
 stability, bifurcations, limit cycles, 3-51
 stiffness, 3-50
 organic pollutants, partial pressures over various substrates, 22-43 to 22-44
 orifice meter, 8-59
 orifices:
 quadrant-edge, discharge coefficients for, 10-18
 sharp-edge, 8-59
 out-of-control situation, 8-27
 overflow, quench tank for, 17-13
 overload conditions, 16-48
 overpressure protection, 8-94
 override control, 8-25
 oxidation, partial, 7-16
 oxidative phosphorylation, 7-31
 oxide sensors, 8-63
 oxygen, thermodynamic properties, 2-320 to 2-322
 oxygen-nitrogen mixture at 1 atm, enthalpy-concentration, 2-323
 ozone conversion to oxygen in presence of chlorine, 7-14
 packed bed height, calculation, 14-11
 packed columns, packing, 14-53
 packing objectives, 14-53
 random packings, 14-54, 14-60
 structured packings, 14-54
 packed-bed scrubbers, 17-42
 packed-column flood and pressure drop, 14-55
 flood and pressure-drop prediction, 14-57
 flood-point definition, 14-56
 pressure drop, 14-59
 packed-tower design, gas-liquid systems, 14-11 to 14-13
 calculation of transfer units, 14-12
 HETP data for absorber design, 14-13
 HTU and K data, 14-13
 mass-transfer-rate expression, 4-11
 operating curve, 4-11
 stripping equations, 4-13
 transfer units, calculation, 14-11
 packed-tower design, scale-up, 14-72
 aging of packing, 14-73
 diameter, 14-72
 distributors, 14-73
 height, 14-72
 high viscosity and surface tension, 14-80
 liquid holdup, 14-76
 loadings, 14-73
 minimum wetting rate, 14-79
 preflooding, 14-73
 two liquid phases, 14-79
 undervetting, 14-73
 wetting, 14-73
 packing efficiency, 14-63
 comparison of various packing efficiencies for absorption and stripping, 14-68
 effect of errors, VLE, 14-68
 effect of pressure, 14-67
 factors affecting HETP, 14-63
 HETP prediction, 14-63
 HETP vs. fundamental mass transfer, 14-63
 implications of maldistribution for packing design practice, 14-70
 maldistribution and its effects on packing efficiency, 14-69
 modeling and prediction, 14-69
 physical properties, effect off, 14-67
 undervetting, 14-67
 para-hydrogen, thermodynamic properties, 2-281 to 2-282
 paramagnetism, 8-62
 parameter estimation, 7-37
 linear model, single reaction, 7-37
 network of reactions, 7-38
 nonlinear models, single reaction, 7-38
 parametric pumping, 16-55
 temperature, 16-55
 partial differential equations, 3-32 to 3-34
 numerical solution, 3-54 to 3-59
 computer software, 3-58
 elliptic equations, 3-56
 finite volume methods, 3-58
 hyperbolic equations, 3-56 to 3-58
 parabolic equations in one dimension, 3-54 to 3-56
 parabolic equations in two or three dimensions, 3-58

22 INDEX

- partial molar properties:
equation of state parameters, 4-18 to 4-19
Gibbs-Duhem equation, 4-18
Gibbs energy, 4-19
- particle density, 16-10
- particle dispersion, 17-24, 21-11
dust, 17-24
fume, 17-24
wet, dry, 21-12
- particle dispersoid properties, 17-24
Stokes' settling diameter, 17-24
- particle dynamics, 6-51 to 6-56
gas bubbles, 6-54 to 6-55
hindered settling, 6-53
liquid drops in gases, 6-55 to 6-56
liquid drops in liquids, 6-55
nonspherical rigid particles, 6-52 to 6-53
spherical particles, 6-51 to 6-52
terminal settling velocity, 6-51 to 6-56
time-dependent motion, 6-53 to 6-54
wall effects, 6-56
- particle measurements, 17-24 to 17-26
atmospheric pollution, 17-24
particle-size analysis, 17-24
process-gas sampling, 17-24
isokinetic sampling, 17-24
- particle Nusselt number, 12-54, 12-76
- particle Reynolds number, 12-53
- particle shape, 21-10
- particle shape factor, 17-23
- particle size analysis, 17-24 to 17-25
methods and equipment, 17-25
- particle-size analysis in the process environment, 21-19
at-line, 21-19
in-line, 21-19
on-line, 21-19
verification, 21-19
- particle-size measurement, 21-12
acoustic methods, 21-14
Brownian motion, 21-14
centrifugal sedimentation methods, 21-17
differential electrical mobility analysis (DMA), 21-18
diffraction patterns, 21-13
dynamic image analysis, 21-13
dynamic light scattering method, 21-14
electrical sensing zone methods, 21-16
focused-beam techniques, 21-15
Fraunhofer theory, 21-12 to 21-13
gas adsorption, 21-18
gravitational photo sedimentation methods, 21-16
gravitational sedimentation methods, 21-16
gravitational x-ray sedimentation methods, 21-17
hydrodynamic diameter, 21-14
image analysis method, 21-13
laser diffraction methods, 21-12
Leeds and Northrup, 21-14
light extinction, 21-15
light scattering, 21-15
Lorenz-Mie theory, 21-12
mercury porosimetry, 21-18
sedimentation balance methods, 21-17
shape factor, 21-12
sieving methods, 21-18
single-particle light interaction methods, 21-15
small-angle x-ray scattering method, 21-15
spectroscopy, photon correlation and cross-correlation, 21-14
static image analysis, 21-13
Stokes' diameter, 21-16
Stokes' law, 21-16
surface area determination, 21-18
ultrafine particle size analyzer, 21-14
ultrasonic attenuation spectroscopy, 21-14
- particle size reduction, principles, 21-45
energy required and scale-up, 21-47
breakage modes and grindability, 21-48
energy laws, 21-47
fine size limit, 21-48
grindability methods, 21-49
industrial uses of grinding, 21-45
operational considerations, 21-50
cryogenic grinding, 21-51
dispersing agents and grinding aids, 21-51
hygroscopicity, 21-51
mill wear, 21-50
temperature stability, 21-51
size reduction combined with other operations, 21-51
liberation, 21-52
other systems involving size reduction, 21-52
size classification, 21-52
size reduction combined with size classification, 21-51
theoretical background, 21-46
single-particle fracture, 21-46
types of grinding, particle fracture vs. deagglomeration, 21-45
typical grinding circuits, 21-46
wet vs. dry grinding, 21-46
- particle sizing, 21-8
data, 21-8
distribution, 21-8 to 21-10
particulates specification, 21-8
- particles, sampling and sample splitting, 21-10
powders, cohesive and free-flowing, 21-11
sampling reliability, 21-11
spinning riffler, 21-11
- particles and particle dispersoids characteristics, 17-25
- particulate emissions, source control, 22-53
- particulate fluidization, 17-6
- particulate formulation, control in flames:
carbon monoxide and unburned hydrocarbons, 24-25
nitrogen oxides, 24-23 to 24-24
air and fuel staging, 24-23
emission control, 24-23
flue gas recirculation, 24-24
fuel, prompt, and thermal NO_x, 24-23
lean premixing, 24-24
- particulates:
cenospheres, 24-24 to 24-25
mineral matter, 24-24
soot, 24-25
sulfate, 24-24
unburned carbon, 24-24
sulfur oxides, 24-24
- particulate scrubber, 17-36
- partition ratio, 16-31
- pattern tests, 8-35
- peak-to-peak amplification, 8-19
- peat, 24-7
- pendular state, 12-26
- pentane:
K-value versus pressure, 13-12
residue map, 13-70
thermodynamic properties, 2-324 to 2-325
- perforate and siphon centrifuge coparison, 18-132
- performance index, 8-30
- permeability, 12-26
- pervaporation:
definitions, 20-64 to 20-65
enrichment factor, 20-65
description, 20-63
examples:
dehydration, 20-65
organic from water, 20-65
pollution control, 20-65
- pervaporation (*Cont.*):
membranes, 20-64 to 20-66
hydrophilic, 20-64
hydrophobic, 20-64
modules, 20-66
operational factors, 20-65
vapor feed, 20-65
- petroleum fuels:
considerations:
commercial, 24-10
safety, 24-10
properties, 24-8 to 24-10
heat capacity, 24-9
heat of combustion, 24-9
kinematic viscosity, 24-9
pour point, 24-9
relative density, 24-9
thermal conductivity, 24-9 to 24-10
thermal expansion, 24-9
ultimate analyses, 24-9
requirements for fuel oils, 24-8
specification, 24-7 to 24-8
- PFBC unit, 17-19
- pH measurement, 8-63
- pH neutralization, 8-26
- phase rule, 4-27
- phase separation, 14-111
gas-phase continuous systems, 1-111
collection equipment, 14-114
collection mechanisms, 14-113
continuous phase uncertain, 14-126
design and selection of collection devices, 14-113
electrically charged collectors, 14-25
electrostatic precipitators, 14-125
energy requirements for inertial-impaction efficiency, 14-123
fiber mist eliminators, 14-125
fine mists, collection of, 14-124
gas sampling, 14-112
mist and spray definitions, 14-112
other collectors, 14-126
particle growth and nucleation, 14-126
particle size analysis, 14-112
- liquid-phase continuous systems, 14-126
automatic foam control, 14-129
chemical defoaming techniques, 14-128
foam prevention, 14-129
physical defoaming techniques, 14-128
separation of foam, 14-127
separations of unstable systems, 14-127
types of gas-in-liquid dispersions, 14-126
- pH-auxostat, 7-35
- phosgene synthesis, 7-14
- photobodies, 8-58
- photoconductors, 8-58
- photoelectric pyrometer, 8-58
- photometric moisture analysis, 8-64
- physical properties:
prediction and correlation, 2-463 to 2-517
density, 2-497 to 2-504
flammability properties, 2-515 to 2-517
heat capacity, 2-489 to 2-497
latent enthalpy, 2-486 to 2-489
physical constants, 2-468 to 2-477
surface tension, 2-513 to 2-515
thermal conductivity, 2-509 to 2-513
thermal properties, 2-478 to 2-486
vapor pressure, 2-477 to 2-478
viscosity, 2-504, 2-509
- physical properties, estimation methods, classification of, 2-467 to 2-468
computational chemistry (CCC), 2-468
corresponding states (CS), 2-467
empirical QSPR correlations, 2-468

- physical properties, estimation methods,
 classification of (*Cont.*):
 group contributions (GC), 2-467 to 2-468
 molecular simulations, 2-468
 theory and empirical extensions, 2-467
- physical properties, pure substances:
 elements and inorganic compounds, 2-7 to 2-27
 organic compounds, 2-28 to 2-46
- physical property specifications, 8-35
- physisorption, 16-4
- PID controllers, 8-5
- piezoelectric crystal, 8-63
- piezoelectric method, 8-63
- piezoelectric transducers, 8-59
- piezoelectric transmitter, 8-61
- piezoresistive transducers, 8-59
- pilot-operated regulator, 8-93
- pipe fittings:
 locations of orifices and nozzles relative to, 10-20
 miter bends, nomenclature for, 10-113
- pipe joining, acceptance criteria for welds and
 examination methods, 10-130 to 10-131
- pipes, properties for, 10-78 to 10-80
- piping and instrumentation diagram, 8-39
- piping materials, cost rankings and cost ratios for,
 10-136
- piping system materials, selection of, 10-74
 bolting, 10-85
 flanged joints, 10-81
 flanged-end fittings, 10-81
 flanged-end pipe, 10-81
 flanges, carbon and alloy steel, types of, 10-82,
 10-86
 ring joint flanges, 10-85
 with conical ends, 10-104
- gates, 10-93
 dimensions of, 10-94 to 10-95
 globe, 10-96
 plug, 10-97, 10-98
 swing check, 10-98
 tilting-disk check valves, 10-98
- general considerations, 10-74
- metallic components, 10-76
 seamless pipe and tubing, 10-76
 tubing, 10-76
 welded pipe and tubing, 10-76
- methods of pipe joining, 10-76
 branch connections, 10-77
 seal weld, 10-81
 socket weld, 10-81
 straight-pipe threads, 10-81
 threaded joints, 10-81
 union joints, 10-81
 welded joints, 10-77
- miscellaneous mechanical joints, 10-87
 bite-type fitting joints, 10-89, 10-90
 compression-fitting joints, 10-89, 10-90
 expanded joints, 10-87
 flared-fitting joint, 10-89
 grooved joints, 10-88
 O-ring seal joints, 10-89, 10-90
 packed-gland joints, 10-87
 poured joints, 10-87
 pressure-seal joints, 10-88, 10-89
 push-on joints, 10-87
 seal ring joints, 10-88
 silver brazed joints, 10-89
 soldered joints, 10-89
 tubing joints, 10-88
 V-clamp joints, 10-88
- pipe, fitting and bends, 10-89
 butt-welding fittings, 10-90, 10-93
 elbow fittings, 10-90
 flanged fittings, dimensions of, 10-91 to
 10-92
- piping system materials, selection of, pipe, fitting
 and bends (*Cont.*):
 malleable-iron threaded fittings, 10-90
 reducing elbow fittings, 10-93
- pipe, thermoplastic, recommended temperature
 limit for, 10-76
 thermoplastic used as linings,
 thermosetting resin pipe, 10-77
- specific material consideration, metals, 10-75
- specific material consideration, nonmetallics,
 10-75
- valves, 10-93
 angle, 10-96
 ball, 10-97
 butterfly, 10-98
 check and lift-check, 10-98
 diaphragm, 10-96
 dual-plate check, 10-98
- piping systems, cast iron, ductile iron, and high-sili-
 con iron, 10-98
 cast iron and ductile iron, 10-98
 ductile-iron pipe, dimension of, 10-100
 hard-drawn copper threadless pipe, 10-103
 high-silicon iron, 10-99
 pipe, 10-100
- piping systems, cost comparison of, 10-135
- piping systems, design of, 10-107
 air condensation effects, 10-108
 category D, 10-107
 category M, 10-107
 classification of fluid services, 10-107
 cyclic effects, 10-108
 design conditions, 10-107
 ambient influences, 10-107
 dynamic effects, 10-108
 pressure, 10-107
 temperature, 10-107
 thermal expansion and contraction effects,
 10-108
 weight effects, 10-108
 design criteria, metallic pipe, 10-108
 effects of support, anchor, and terminal move-
 ments, 10-108
 limits of calculated stresses due to sustained
 loads and displacement strains, 10-111
 pressure design of metallic components, 10-111
 reactions:
 anchors for expansion joints, 10-123
 displacement strains, 10-123
 elastic behavior, 10-123
 expansion joints, 10-121
 maximum reactions for simple systems,
 10-120
 pipe supports and attachments, 10-124
 support fixtures, 10-123
 reduced ductility, 10-108
 safeguarding, 10-107
 test conditions, 10-113
 thermal expansion and flexibility, 10-114
 cold spring, 10-115
 displacement strains, 10-114
 flexibility stress, 10-115
 piping systems, flexibility classification for,
 10-121
 required weld quality assurance, 10-120
 requirements for analysis, 10-115
 total displacement strains, 10-114
 values for reactions, 10-115
- piping systems, fabrication, 10-123
 assembly and erection, 10-126
 bending and forming, 10-126
 joining nonmetallic pipe, 10-126
 preheating and heat treatment, 10-126
 welding, brazing, or soldering, 10-123
 typical weld imperfections, 10-132
- piping systems, forces of piping on process
 machinery and piping vibration, 10-135
 displacement strains, 10-123
 elastic behavior, 10-123
 expansion joints, 10-121
 maximum reactions for complex systems,
 10-121
 maximum reactions for simple systems, 10-120
 pipe supports and attachments, 10-124
 support fixtures, 10-123
- piping systems, heat tracing of, 10-135
 types of heat-tracing systems, 10-137
 electric tracing, types of, 10-139 to 10-140
 fluid-tracing systems, 10-137
 steam tracing versus electric tracing, economics
 of, 10-137
 steam-tracing system, 10-137
- piping systems, metallic with nonmetallic pipe and
 linings, 10-103
 cement-lined carbon-steel pipe, 10-103, 10-104
 concrete pipe, 10-104
 fused silica or fused quartz, 10-105
 glass pipe and fittings, 10-104
 dimensions for glass pipe and flanged joints,
 10-104
 glass-lined steel pipe and fittings, 10-105
 plastic pipe, 10-106
 clamped-insert joint, 10-106
 polyethylene, 10-106
 polypropylene, 10-107
 plastic-lined steel pipe, 10-105
 kynar liners, 10-105
 polypropylene liners, 10-105
 polyvinylidene chloride liners, 10-105
 PTFE and PFA lined steel pipe, 10-105
 reinforced-thermosetting-resin (RTR) pipe,
 10-107
 hanger-spacing ranges for RTR pipe, 10-107
 rubber-lined steel pipe, 10-106
- piping systems, nonferrous metal, 10-99
 aluminum, 10-99
 copper and copper alloys, 10-100
 standard copper water tube sizes, 10-101
 standard dimensions, copper and red-brass
 pipe, 10-102
 standard dimensions for coil lengths, 10-101
 standard dimensions for straight lengths, 10-102
 flexible metal hose, 10-101
 nickel and nickel-bearing alloys, 10-103
 titanium, 10-101
- piping systems, tracing, choosing the best, 10-140
- piston power, 8-77
- Planck's Law, 5-16
- Planck's distribution law, 8-58
- plant capacity, 8-48
- plate towers, 17-42
- plug-flow reactor:
 modeling, 19-8
 tracers, 19-16
- pneumatic amplifier, 8-89
- pneumatic controller, 8-71, 8-86
- pneumatic measurement devices, 8-65
- pneumatic transmission, 8-65
- point alarm, 8-68
- pollutants:
 control techniques, 22-32 to 22-35
 emission statistics, 22-29
- polluting gases, oxidation of, 7-16
- pollution prevention, barriers and incentives, 22-24
 barriers to pollution prevention ("the dirty
 dozen"), 22-24
 economic considerations associated with pollu-
 tion-prevention programs, 22-25
 pollution prevention incentives ("a baker's
 dozen"), 22-24

- pollution prevention, ethical issues, 22-27
 pollution-prevention assessment procedures, 22-22
 assessment phase, 22-22
 assessment phase material balance calculations, 22-23
 feasibility analysis, 22-22
 implementation, 22-23
 industry programs, 22-23
 planning and organization, 22-22
 sources of information, 22-23
 pollution-prevention hierarchy, 22-1
 Polanyi potential theory, 16-14
 Polyani linear approximation, 7-38
 polydispersity, 7-29
 polyethylene, 17-17
 polymer characterization, 7-29
 polymer live. *See* polymer, growing
 polymer, growing, 7-30
 polymerization bread, 7-29
 polymerization chain, 7-15
 polymerization kinetics, 7-29
 polymerization rate, 7-15
 polymerization reactions, 7-29, 19-21 to 19-25
 polymerization, bulk, 7-29
 stirred bulk polymerization, 7-29
 polymers, 7-29
 pore diffusion, 16-19
 pore structure, bidispersed, 16-21 to 16-23
 porosity, internal, 16-10
 positioner application, 8-86
 positioner/actuator stiffness, 8-86
 positive displacement meter, 8-59
 posting, economic, 9-4
 potassium:
 Mollier diagram, 2-17, 2-236
 saturated, thermodynamic properties, 2-326
 powder flow behavior, 21-20
 failure, active vs passive, 21-20
 flowability, 21-20
 yield stress, 21-20
 Powell's method, 8-34
 power-law rate, 7-23
 precipitator:
 blast-furnace pipe, 17-60
 horizontal-flow, 17-60
 vertical-flow, 17-62
 water-film, 17-61
 preforming, 12-64 to 12-65
 pressure, static:
 average, 10-10
 local, 10-10
 specifications for piezometer taps, 10-10
 pressure measurements, 8-58
 pressure relief valves, 8-78
 pressure vessels, 10-151
 additional ASME code considerations, 10-155
 brittle fracture, 10-156
 metal fatigue, 10-156
 ASME code developments, 10-158
 ASME code section VII, divisions 1 and 2, 10-152 to 10-155
 care of pressure vessels, 10-158
 corrosion, 10-159
 mechanical damage, 10-159
 temperature extremes, 10-158
 vacuum, 10-158
 code administration, 10-151
 other regulations and standards, 10-157
 pressure-vessel cost and weight, 10-159
 vessel codes other than ASME, 10-158
 vessel design and construction, 10-158
 vessels with unusual construction, 10-157
 concrete pressure vessels, 10-158
 graphite and ceramic vessels, 10-158
 high-strength steels, 10-157
 pressure vessels, vessels with unusual construction (*Cont.*):
 lined vessels, 10-157
 plastic pressure vessels, 10-158
 pressure-drop correlations:
 packed tower, 14-58
 tray columns, 14-45
 prilling operations, common characteristics, 21-136
 principal component analysis, 8-39
 probability of propagation, 7-30
 process actions, 8-49
 process analyzers, sampling systems, 8-64
 process capability indices and ratios, 8-38
 process control:
 advanced, benefits of, 8-20
 considerations:
 controlled-cycling operation mode, 15-94 to 15-96
 sieve tray column interface control, 15-94
 steady-state process control, 15-93 to 15-94
 empirical models, 8-6
 integrity, 8-95
 failure mode and effect analysis, 8-96
 hazard and operability studies, 8-96
 interlocks, 8-96
 process actions, 8-96
 safety interlocks, 8-96
 languages, 8-70 to 8-71
 linear models, 8-7
 nonlinear models, 8-7
 physical models, 8-6
 plant safety in, 8-94
 hazard, 8-94
 regulatory, 8-94
 risk, 8-94
 technical, 8-94
 safety, 8-95
 statistical, 8-35
 subroutine libraries, 8-50
 testing, 8-96
 valves, solenoid actuated, 8-72
 process dynamics, 8-71
 process gain, 8-7
 process gas sampling, 17-24
 process measurements, 8-54
 accuracy, 8-54
 cost, 8-55
 dynamics, 8-55
 electrical classification, 8-55
 invasive, 8-55
 materials of construction, 8-55
 measurement span, 8-55
 physical access, 8-55
 prior use, 8-55
 range and span, 8-54
 reliability, 8-55
 repeatability, 8-54
 selection criteria, 8-55
 process models, development of, 8-33
 process optimization, real-time, 8-32
 process plant, examination, inspection, and testing, 10-126
 examination and inspection, 10-126
 examination methods, 10-128
 liquid-penetrant examination, 10-129
 magnetic-particle examination, 10-129
 radiographic examination, 10-129
 ultrasonic examination, 10-131
 visual examination, 10-128
 type and extent of required examination, 10-131
 examination—category D fluid service, 10-132
 impact testing, 10-133
 normally required, 10-131
 pressure testing, 10-131
 process plant, examination, inspection, and testing,
 type and extent of required examination (*Cont.*):
 requirements for heat treatment, 10-134
 types of examinations for evaluating imperfections, 10-135
 process plant, piping:
 code contents and scope, 10-74
 codes and standards, 10-73
 government regulations, OSHA, 10-73
 international regulations, 10-74
 national standards, 10-73
 pipe and tubing sizes and ratings, 10-73
 pressure-piping codes, 10-73
 process safety analysis:
 atmospheric dispersion, 23-61 to 23-66
 atmospheric dispersion models, 23-64 to 23-66
 estimation of damage effects, 23-66
 parameters affecting atmospheric dispersion, 23-62
 project review and audit processes, 23-71 to 23-74
 discharge rates from punctured lines and vessels, 23-54
 accuracy of discharge rate predictions, 23-61
 types of discharge, 23-55
 hazard analysis, 23-41 to 23-47
 CCPS preliminary screening for chemical reactivity hazards, 23-43
 definitions, 23-41
 ranking methods, 23-45 to 23-47
 HAZOP guide words associated with time, 23-45
 HAZOP guide words used with process parameters, 23-44
 logic model methods, 23-47
 NFPA 704 system for hazard identification, 23-46
 process drawing and fault tree for explosion of an air receiver, 23-50
 risk analysis, 23-47 to 23-53
 assessment, 23-48
 criteria, 23-53
 decision making, 23-53
 estimation, 23-52
 version of a risk analysis process, 23-49
 process simulation, 3-89 to 3-90
 classification, 3-89
 commercial packages, 3-90
 process modules or blocks, 3-89 to 3-90
 process topology, 3-90
 thermodynamics, 3-89
 process states, 8-49
 process technology, 8-53
 processor-based positioners, 8-86
 product polymer, 7-30
 product quality, 12-38 to 12-40
 biochemical degradation, 12-39
 surface tension, 12-38
 product technology, 8-53
 production limitation, 8-35
 production monitoring, 8-48
 production scheduling, 8-48
 productostat, 7-35
 profit margin, 9-6
 profitability:
 economic balance, 9-39 to 9-40
 factors, 9-21
 amortization, 9-22
 cash flow, 9-27
 depletion, 9-22
 depreciation, 9-21
 taxes, 9-22
 time value of money, 9-23

- profitability (*Cont.*):
 feasibility analysis, 9-34
 qualitative measures, 9-32
 quantitative measures, 9-30 to 9-32
 discounted cash flow (DCFRROR), 9-30
 net present worth (NPW), 9-30
 payout period (POP) plus interest, 9-30
 sensitivity analysis, 9-32 to 9-33
 break-even analysis, 9-32
 relative sensitivity plot, 9-32
 Strauss plot, 9-33
 tornado plot, 9-33
 uncertainty analysis, 9-33 to 9-34
 Monte Carlo technique, 9-34
- programmable logic control, 8-50, 8-69, 8-72
- programming languages, 8-50
- propane:
 K-value versus pressure, 13-12
 thermodynamic properties, 2-327 to 2-328
- propanol:
 Antoine vapor pressure, 13-14
 BIP data, 13-13
- propionil acid, BID data, 13-13
- proportional band, 8-18, 8-74
- proportional control, 8-14
- proportional element, 8-9
- proportional-integral derivative, 8-13
 control, 8-15
- propylene, thermodynamic properties, 2-329 to 2-300
- pseudo-steady-state, reaction kinetics, 7-14
- psychrometer coefficient and equation, 12-6, 12-6
- psychrometric calculations, 12-13 to 12-16
 methods for various humidity parameters, 12-14
- psychrometric charts, 12-6 to 12-15
 Bowen chart, 12-6
 Grosvenor chart, 12-6 to 12-9, 12-11
 Mollier chart, 12-6, 12-10, 12-12, 12-15
 Salen-Soininen, 12-7
- psychrometric ratio, 12-3, 12-6
- psychrometric software, 12-13 to 12-14
- psychrometry, 12-3 to 12-17
 calculation formulas, 12-5
 interconversion formulas, 12-4
- phthalic anhydride, 17-17
- pulse inputs, 8-65
- pulse testing, 8-12
- pulsed liquid columns, 15-85
- pulse-width-modulated combination, 8-92
- pump, adjustable-speed, 8-91 to 8-92
- pumping horsepower, 12-21
- pumps, 10-24 to 10-40
 classification, 10-26
 governing standards, 10-25
 net positive suction head (NPSH), 10-27
 available, NPSH, 10-28
 NPSH calculation, 10-28
 NPSH reductions for pumps handling hydrocarbon liquids and high-temperature water, 10-28
- pump performance curve, 10-36
- selection, 10-27
 range of operation, 10-27
- specifications, 10-28
- terminology, 10-25 to 10-27
 capacity, 10-25
 centrifugal force, 10-25
 displacement, 10-25
 electromagnetic force, 10-25
 friction head, 10-27
 measurement of performance, 10-25
 mechanical impulse, 10-25
 power input and output, 10-27
 static discharge head, 10-26
 static suction head, 10-26
 total dynamic head, 10-26
- pumps, terminology (*Cont.*):
 total static head, 10-26
 total suction head, 10-26
 transfer of momentum, 10-25
 velocity, 10-27
 velocity head, 10-27
 viscosity, 10-27
 work performed in pumping, 10-27
- pumps, centrifugal, 10-32 to 10-37
 action of, 10-33
 canned-motor, 10-36, 10-38
 casings, 10-33
 circular, 10-33
 diffuser-type, 10-33, 10-40
 guide vanes or diffusers, 10-33
 volute, 10-33
 characteristics, 10-33
 affinity laws, 10-34, 10-36
 chemical pump, sealing, 10-35
 close-coupled, 10-35, 10-38
 double-suction single-stage, 10-35
 impeller, 10-33
 double-suction, 10-33, 10-40
 open- or semiopen-type, 10-33
 performance curves, open impeller, 10-35
 shrouded or closed-type, 10-33
 single-suction, 10-33
 multistage, 10-37
 volute-type, 10-39
- process pumps, 10-34
 horizontal and vertical, 10-35, 10-39
 selection, 10-34
- sump pump, 10-37
- system curves, 10-34, 10-36
- vertical pumps, 10-36, 10-39
 dry-pit, 10-36
 vertical process, 10-36
 wet-pit, 10-36
- pumps, electromagnetic, 10-39
- pumps, positive-displacement, 10-29
 diaphragm pumps, 10-29, 10-30, 10-32
 pneumatically actuated diaphragm pumps, 10-31, 10-32
- fluid-displacement, 10-32
 acid egg or blowcase, 10-32
 air lift, 10-32, 10-33
- gear pumps, 10-31, 10-32
 duplex double-acting pumps, 10-30
 exterior-bearing type, 10-32
 interior-bearing type, 10-31
 simplex double-acting pumps, 10-30
- plunger pump, 10-29, 10-30
 duplex single-acting, 10-31
 metering or proportioning pumps, 10-30, 10-31
- power pumps, 10-30, 10-31
- reciprocating pumps, 10-29
 diaphragm pumps, 10-29
 piston pumps, 10-29
 plunger pumps, 10-29
- rotary or reciprocating pumps, 10-29 to 10-32
 flow variations, 10-29
- screw pumps, 10-32 to 10-33
- pumps, problems, 10-43
 capacity-type, 10-43
 cavitating-type, 10-43
 overload, 10-44
- pumps, propeller and turbine:
 axial flow (propeller) pump, 10-37, 10-41
 jet, 10-39
 ejectors, 10-39
 injectors, 10-39
 regenerative pumps, 10-38, 10-41
 turbine, 10-38, 10-41
- pumps, reciprocating, flow variation of, 10-40
- pumps, specific speed variations, types of, 10-37
- pumps, vibration monitoring, 10-71 to 10-72
 machinery faults, frequency range, 10-72
 vibration spectrum, 10-72
- purge/concentration, swing adsorption, 16-52
- PVT systems:
 phase rule, 4-27
 postulate definition, 4-5
 thermodynamics:
 constant-composition, 4-5 to 4-8
 equilibrium criteria, 4-26 to 4-27
 variable composition, 4-17 to 4-26
- pyrometers, 8-56 to 8-58
 accuracy, 8-58
- quadratic programming, 8-29, 8-35
- quality control, 8-35, 8-42
- quantum Monte Carlo, 7-38
- quasi-newtonian methods, 8-34
- radar level transmitters, 8-61
- radiation, 5-15 to 5-43
 augmented black view factors, 5-27
 black body, 5-16 to 5-19
 direct exchange areas, 5-20 to 5-24
 enclosures, 5-24 to 5-30
 from gases, 5-30 to 5-35
 flames and particle clouds, 5-34 to 5-35
 mean beam length, 5-31
 opaque surfaces, 5-19 to 5-20
 radiative equilibrium, 5-26
- radiation pyrometers, 8-58
- radiation-density gauge, 8-61
- radius of gyration, 2-475 to 2-477
 calculation methods, 2-476 to 2-477
 electron density distribution, 2-477
 principle moments of inertia 2-476
- raining-bucket contactor, 15-85
- Raleigh-Jeans Formula, 5-16
- Raman spectroscopy, 8-63
- range resistor, 8-65
- Raoult's law:
 modified, def, 13-15
 negative deviation, 13-68
 positive deviation, 13-68
- rapping, 17-61 to 17-62
- rate factors, 16-18
- rate meter, 8-59
- rate-determining step, reaction kinetics, 7-14
- rate-of-drying, process control, 8-46
- ratio pyrometers, 8-58
- ratios, financial, 9-7
 activity ratios, 9-7
 debt/equity ratio, 9-9
 example of, 9-7
 leverage ratios, 9-7
 liquidity ratios, 9-7
 profitability ratios, 9-7
- RC filter, analog, 8-66
- reactant, gas phase, 7-17
- reaction equilibrium, 7-5
- reaction initiation, 7-14
- reaction initiation efficiency, 7-30
- reaction kinetics:
 adiabatic, 7-6
 homogeneous gas, 7-6
 heterogeneous gas-liquid, 7-6
 heterogeneous gas-liquid-liquid, 7-6
 heterogeneous gas-liquid-solid, 7-6
 heterogeneous gas-solid, 7-6
 homogeneous liquid, 7-6
 heterogeneous liquid-liquid, 7-6
 heterogeneous liquid-solid, 7-6
 heterogeneous solid-solid, 7-6

- reaction kinetics (*Cont.*):
 integral data analysis, 7-36
 BR equation, 7-36
 isothermal constant pressure, 7-6
 isothermal constant volume, 7-6
 temperature-controlled, 7-6
 theoretical methods, 7-38
 chaotic behavior, 7-39
 lumping and mechanism reduction, 7-38
 multiple steady states, 7-39
 oscillations, 7-39
 prediction of mechanisms and kinetics, 7-38
- reaction mechanism, 7-5, 7-16
 nonchain, 7-14
- reaction mechanism discrimination, 7-38
- reaction mechanism reduction, 7-38
- reaction networks, 7-9
 independent reactions, 7-9
 procedure, 7-9
- reaction product, 7-5
- reaction propagation, 7-14
- reaction rate, 7-5
- reaction termination, 7-14
- reaction yield, 7-8
- reaction-diffusion regime, 7-27
 fast reaction regime, 7-27
 mass transfer time, 7-28
 slow reaction regime, 7-27, 7-28
- reactions:
 elementary, 7-5
 endothermic, 7-6
 nonchain, 7-15
 order of, 7-6
- reactions, noncatalytic, 7-9
 gas-liquid reactions, 7-27
 gas-solid noncatalytic reactions, 7-23
 diffusion control, 7-26
 diffusion models, 7-23
 reaction control, 7-26
 sharp interface model, 7-23, 7-25
 volume reaction model, 7-25
- reactions network, 7-5
- reactor (high pressure), polyethylene, 17-17
- reactor case studies, 19-61
- reactor concepts:
 parametric sensitivity, 19-13
 pressure drop, heat and mass transfer, 19-10 to 19-11
 reactor dynamics, 19-11 to 19-13
- reactor modeling:
 batch reactor, 19-8
 semibatch reactor, 19-8
- reactors, 7-10
 batch, 7-10, 7-11
 constant volume, 7-11
 conversion, 7-11
 liquid-phase reactions, 7-11
 residence time, 7-11
- laboratory, 7-33
 batch reactors, 7-34
 bioreactors, 7-35
 catalytic gas-solid, 7-34
 flow reactors, 7-35
 gas-liquid, 7-34
 gas-liquid-solid, 7-34
 homogeneous gas, 7-34
 homogeneous liquid, 7-34
 liquid solid, 7-34
 multiphase reactors, 7-35
 noncatalytic gas-solid, 7-34
 reaction rate, 7-34
 solid catalysis, 7-35
 solid-solid, 7-34
 statistical model, 7-34
- reactors (*Cont.*):
 noncatalytic:
 examples, 19-37
 rotary kilns, 19-36
 vertical kilns, 19-36, 19-38
 semibatch, 7-12
 real-number system, 3-4
 receding horizon approach, 8-30
 recirculation, with batch processing, 8-52
 recuperators, 24-56
 configuration, 24-56
 recycle, 8-44
 recycle ratio, 7-13
 redox neutral, 7-31
 reduction-oxidation, 7-32
 reflux condensers, with batch processing, 8-52
 reflux ratio, 8-43
 external, 13-19 to 13-21
 internal, 13-19 to 13-21
 minimum, 13-26
 total, 13-22
 refractive index, 8-61
- refrigerants:
 gaseous at atmospheric pressure, velocity of sound in, 2-420
 saturated liquid, surface tension, 2-419
 saturated liquid, velocity of sound in, 2-420
 thermodynamic properties, 2-331 to 2-399
- refrigeration:
 capacity control, 11-96
 equipment, 11-82 to 11-90
 centrifugal compressors, 11-85
 compressors, 11-82
 condensers, 11-85
 evaporators, 11-87
 positive displacement compressors, 11-83
 system analysis, 11-87
 other refrigeration systems applied in the industry, 11-90 to 11-96
 ammonia water cycle, 11-92
 lithium bromide cycle, 11-90
 steam-jet (ejector) systems, 11-94
 refrigerants, 11-96 to 11-98
 organic compounds (inhibited glycols), 11-98
 secondary refrigerants (antifreezes or brines), 11-97
 safety in, 11-98
 vapor compression systems, 11-79 to 11-82
 cascade systems, 11-82
 multistage systems, 11-79 to 11-82
- regenerators:
 checkerbrick, 24-54 to 24-55
 blast-furnace stoves, 24-54 to 24-55
 glass-tank, 24-55
 open-hearth, 24-55
 Ljungstrom heaters, 24-55
 miscellaneous systems, 24-56
 regenerative burners, 24-55 to 24-56
 schematic, 24-56
 regulators, 8-92 to 8-94
 relative gain, multivariable control, 8-28
 relative humidity, 12-4, 12-26
 relative volatility:
 definition of, 13-7
 distillation process control, 8-43
 relative-humidity, methods of calculation, 8-63
 remote control units, 8-70
 replacement analysis, 9-36
 residence time:
 conversion, 19-17 to 19-20
 table, 19-5
 residual error, 7-37
 resistance thermometer, 8-56
 response surface analysis, 7-34
 retained earning statements, 9-4
- retention factor, 16-40
 reverse osmosis:
 applications, 20-45 to 20-47
 component transport, 20-48
 osmotic pressure, 20-48
 solute retention, 20-48
 configurations, 20-47 to 20-48
 design considerations (osmotic pinch), 20-49
 diavolumes, 20-46
 economics, 20-49 to 20-50
 membrane types, 20-47
 pretreatment and cleaning, 20-48 to 20-49
 particle and oxidant removal, 20-49
 sanitization, 20-49
- Reynolds number, 17-22
- robbins chart, 13-91 to 13-93
- Robbin's correlation, packed column, 14-65
- Robinson equation, 17-58
- rotameter, flow measurement, 8-60
- rotary dryer, control of, 8-46
- rotor dynamics, 10-70
 amplification factor, 10-71
 response plot, 10-71
- rubidium, saturated, thermodynamic properties, 2-400
- Runge Kutta method, 8-7
- safety restrictions, process optimization, 8-35
- sampling point, process control, 8-64
- saturated air, thermodynamic properties, 12-11
- saturated volume, 12-5
- saturation constant, 7-78
- saturation humidity, 12-4
- saturation temperature, 12-4
- saturation vapor pressure, 12-4, 12-5
- scalable process control systems, 8-69
- Scheibel column, 15-83
- scrubbers, 17-41
 ejector-venturi, 17-40
 fibrous-bed, 17-43
 mechanical, 17-43
 mobile-bed, 17-42
 performance curves, 17-38, 17-39
 pollutants, 22-37
 self-induced spray scrubbers, 17-41
 spray, self-induced, 17-41
 venturi, 17-40
- seawater, saturated, thermodynamic properties, 2-400
- second-order element, process modeling, 8-9
- Securities and Exchange Commission, 9-5
- sedimentation, gravity:
 controls, 18-80
 design criteria, 18-80
 equipment, 18-75
 instrumentation, 18-78
- sedimentation recovery versus g-seconds, 18-119
- selective process control, 8-25
- selectivity, 7-7
- self-diffusion coefficients, 16-21
- self-operated regulators, 8-92, 8-93
- self-tuning, digital hardware, 8-69
- semi-batch, operations, control of, 8-47
- semiclassical method, 7-38
- semiempirical methods, 7-38
- sensible heat, 12-26
- separation factor, 16-14
- separators:
 impingement, 17-28
 mechanical centrifugal, 17-36
- sequence logic, process control, 8-49
- serial interfaces, 8-66
- set point, process control, 8-5, 8-19, 8-26

- shafts, rotating, sealing of, **10-59** to **10-65**
 internal and external seals, **10-64**
 labyrinth seals, **10-59**
 mechanical face seals, **10-63**
 mechanical seal selection, **10-63**
 equipment, **10-63**
 main seal body, **10-63**
 product, **10-63**
 seal arrangement, **10-63**
 seal environment, **10-63**
 seal face combinations, **10-63**
 seal gland plate, **10-63**
 secondary packing, **10-63**
 noncontact seals, **10-59**
 packing seal, **10-62**
 application of, **10-62**
 butt and skive joints, **10-62**
 lubricant, **10-63**
 seal cage or lantern ring, **10-63**
 ring seals, **10-62**
 fixed, **10-62**
 floating, **10-62**
 packing, **10-62**
 throttle bushings, **10-64**
 materials, **10-65**
 shaft sealing elements, types of, **10-64**
- Sherwood chart, **8-36**
 Sherwood number, **12-58**
 signal processing, **8-54**
 simple wave, **16-32**
 simultaneous reactions, **7-5**
 single-input single-output systems, **8-12**
 sintering, **7-23**
- size enlargement, equipment and practice, **21-117**
 centrifugal granulators, **21-134**
 centrifugal designs, **21-134**
 granulation rate processes, **21-135**
 particle motion and scale-up, **21-134**
 fluidized-bed and related granulators, **21-130**
 controlling granulation rate processes, **21-130**
 draft tube designs and spouted beds, **21-133**
 hydrodynamics, **21-130**
 mass and energy balances, **21-130**
 scale-up and operation, **21-133**
 mixer granulators, **21-123**
 controlling granulation rate processes, **21-126**
 high-speed mixers, **21-123**
 low-speed mixers, **21-123**
 powder flow patterns and scaling of mixing, **21-125**
 scale-up and operation, **21-127**
 pressure compaction processes, **21-136**
 pellet mills, **21-139**
 piston and molding presses, **21-137**
 roll presses, **21-137**
 screw and other paste extruders, **21-139**
 tableting presses, **21-137**
 spray processes, **21-135**
 flash drying, **21-136**
 prilling, **21-135**
 spray drying, **21-135**
 thermal processes, **21-142**
 drying and solidification, **21-143**
 sintering and heat hardening, **21-142**
 tumbling granulators, **21-118**
 controlling granulation rate processes, **21-120**
 disc granulators, **21-118**
 drum granulators, **21-119**
 granulator-dryers for layering and coating, **21-122**
 moisture control in tumbling granulation, **21-121**
 scale-up and operation, **21-123**
 size enlargement, methods and application, **21-76**
 size enlargement, principles, **21-73**
 mechanics, **21-74**
 compaction microlevel processes, **21-77**
 granulation rate processes, **21-74**
 key historical investigations, **21-80**
 process vs. formulation design, **21-77**
 product characterization, **21-80**
 flow property tests, **21-82**
 permeability, **21-82**
 physiochemical assessments, **21-82**
 porosity and density, **21-81**
 redispersion test, **21-82**
 size and shape, **21-80**
 strength testing methods, **21-81**
 scope and applications, **21-73**
 skeletal density, **16-10**
 slugging, **17-2**
 slurry reactors, **7-29**
 smart transmitters, **8-66**
 Smith predictor technique, **8-24**
 soda-lime, **17-44**
 sodium:
 Mollier diagram, **2-402**
 saturated, thermodynamic properties, **2-401**
 sodium hydroxide, aqueous solution, enthalpy-concentration, **2-403**
 solenoid valves, **8-91**
 solid analytical geometry:
 coordinate systems, **3-13** to **3-14**
 lines and planes, **3-14**
 space curves, **3-14**
 surfaces, **3-15**
 solid-liquid, suspension:
 dispersion, **18-17**
 extraction, **18-18**
 fluid motion, **18-24**
 pumping, **18-25**
 heat transfer, **18-25**
 leaching, **18-18**
 mass transfer, **18-17**
 separation, equipment selection, **18-149**
 speed for just suspension, **18-16**
 solid-liquid separations, **20-28**
 solid-solid reactors, **19-48** to **19-49**
 SHS, **19-48**
 solid wastes, **24-7**
 sources and types, **22-83**
 solid wastes, characteristics and handling, **22-82**
 generation of, **22-82**
 hazardous waste, **22-83**
 properties of solid wastes, **22-86**
 quantities of solid wastes, **22-86**
 sources of industrial wastes, **22-84**
 types of solid wastes, **22-82**
 on-site handling, storage, and processing, **22-88**
 on-site handling, **22-89**
 on-site processing of solid wastes, **22-90**
 on-site storage, **22-89**
 processing and resource recovery, **22-90**
 concentrations of WTE incinerators, **22-96**
 materials-recovery systems, **22-92**
 processing techniques for solid waste, **22-90**
 recovery of biological conversion products, **22-92**
 thermal processes, **22-92**
 ultimate disposal, **22-98**
 landfilling of solid waste, **22-98**
 solid wastes, price index, **22-100**
 solids, bulk flow properties, **21-23**
 angle of repose, **21-32**
 Beverloo equation, **21-30**
 Carr and Hausner ratios, **21-32**
 coefficient of internal friction, **21-27**
 critical state line, **21-27**
 critically consolidated, **21-25**
 solids, bulk flow properties (*Cont.*):
 direct shear cells, **21-25**
 effective angle of power friction, **21-28**
 effective angle of wall friction, **21-28**
 effective coefficient of powder friction, **21-28**
 effective coefficient of wall friction, **21-28**
 effective yield locus, **21-27**
 flow function, **21-28**
 flow indices and flowability indices, **21-28**
 flow indices, **21-29**
 hopper flow characterization, **21-32**
 internal angle of friction, **21-27**
 isotropic hardening, **21-27**
 mass discharge rates for coarse solids, **21-30**
 methods of flow characterization, **21-31**
 Mohr-Coulomb, **21-27**
 overconsolidated, **21-25**
 pneumatic conveying, **21-24**
 powder flowability, **21-28**
 powder shear cells, **21-26**
 powder yield loci, **21-27**
 shear cell measurements, **21-23**
 shear cell standards validation, **21-29**
 shear plane, **21-23**
 time flow function, **21-28**
 unconfined uniaxial compressive yield stress, **21-28**
 underconsolidated, **21-25**
 wall adhesion, **21-28**
 wall friction measurements, **21-23**
 wall yield locus, **21-28**
 yield behavior of powders, **21-25**
 yield locus, **21-27**
 solids, bulk, permeability and aeration properties, **21-20**
 aerated cohesion, **21-20**
 air-augmented flow, **21-22**
 Darcy's law, **21-21**
 deaeration measurement, **21-22**
 dense-phase conveying, **21-22**
 dilute-phase conveying, **21-22**
 Dixon classification, **21-22**
 Ergun's relation, **21-22**
 excess gas velocity, **21-20**
 fixed-bed, **21-20**
 fluidization measurement, **21-20**
 Geldart's classification, **21-22**
 homogeneous fluidization, **21-20**
 Kozeny-Carman relation, **21-21**
 minimum bubbling velocity, **21-20**
 minimum fluidization velocity, **21-20**
 permeability and deaeration, **21-20**
 permeameters, **21-20**
 solids, mixing principles, **21-33**
 ideal mixtures, **21-36**
 industrial relevance of solids mixing, **21-33**
 measuring the degree of mixing, **21-37**
 mixing mechanisms: dispersive and convective mixing, **21-33**
 mixture quality: the statistical definition of homogeneity, **21-34**
 on-line procedures, **21-38**
 segregation in solids and demixing, **21-34**
 transport segregation, **21-34**
 solids, summary of compaction expressions, **21-105**
 solids drying, *See* drying of solids
 solids metering, **8-76**
 solids mixing, equipment, **21-38**
 bunker and silo mixers, **21-38**
 mixed stockpiles, **21-38**
 mixing by feeding, **21-40**
 rotating mixers or mixers with rotating component, **21-39**

- solids mixing process, design, **21-42**
 batch mixing, **21-43**
 feeding and weighing equipment for a batch mixing process, **21-44**
 goal and task formulation, **21-42**
 mixing with batch or continuous mixers, **21-42**
- solubilities:
 air, **2-131**
 ammonia-water at 10 and 20°C, **2-131**
 carbon dioxide, **2-131**
 carbonyl sulfide, **2-131**
 chlorine, **2-132**
 chlorine dioxide, **2-132**
 gases in water, as function of temperature and Henry's constant at 25°C, **2-130**
 Henry's constant, **2-130, 2-131**
 hydrogen chloride, **2-132**
 hydrogen sulfide, **2-132**
 inorganic compounds in water at various temperatures, **2-126 to 2-129**
 sulfur dioxide over water, partial vapor pressure, **2-133**
- solution:
 thermodynamics:
 binary liquid solutions, behavior of, **4-26**
 excess properties, **4-21**
 fugacity, **4-19 to 4-20**
 ideal gas mixture model, **4-19**
 ideal solution model, **4-20 to 4-21**
 property changes of mixing, **4-21**
 relations connecting property changes of mixing and excess properties, **4-21**
- solution crystallization, definition of, **20-3**
- solution polymerization, **7-29**
- solvent properties, desirable:
 availability and cost, **15-13**
 construction materials, **15-13**
 density difference, **15-12**
 environmental requirements, **15-12**
 freezing point, **15-12**
 industrial hygiene, **15-12**
 interfacial tension, **15-12**
 loading capacity, **15-11**
 multi-use, **15-13**
 mutual solubility, **15-12**
 partition ratio ($K_i + y_i/x_i$), **15-12**
 safety, **15-12**
 solute selectivity, **15-12**
 stability, **15-12**
 viscosity, **15-12**
- solvent screening methods, liquid-liquid extraction, **15-32 to 15-41**
 assessing liquid-liquid miscibility, **15-34 to 15-38**
 design, computer-aided, **15-38 to 15-39**
 high-throughput experimental methods, **15-39 to 15-41**
 Donahue-Bartell collection, **15-40**
 Du Nouy's method, **15-40**
 Fu, Li, and Wang ternary system correlation, **15-41**
 Wilhelmly method, **15-40**
 Robbins' chart, **15-32 to 15-33**
 thermodynamic data, **15-32**
 thermodynamic screening calculations, **15-33 to 15-34**
 Hanson model, **15-34**
 LSER, **15-34**
 MOSCED, **15-34**
 NRTL-SAC, **15-34**
 UNIFAL, **15-33**
 UNIQUAL, **15-33 to 15-34**
- solvents, nonaqueous, **12-36 to 12-38**
- sonic methods, **8-61**
- Sonntag equation, **12-5**
- sorption equilibrium:
 experiments, **16-13**
 heterogeneity, **16-12**
 isotherm classification, **16-12**
 model categorization, **16-12**
 surface excess, **16-12**
- sorption isotherm, **12-28**
- sorptive separations:
 classification of, **16-5**
- sound intensity, **8-81**
- specialty plants, **8-47**
- specific gravity, measurement of, **8-61**
- units conversions, **1-19**
 degrees Baume', **1-19**
 degrees Twaddell, **1-19**
- specific growth rate, **7-18**
- specific heats, aqueous solutions, **2-183 to 2-184**
- specific heats, miscellaneous materials:
 miscellaneous liquids and solids, **2-185**
 oils, **2-185**
- specific heats, pure compounds:
 elements and inorganic compounds, **2-156 to 2-163**
 gases at 1 atm, Cp/Cv ratios, **2-182**
 inorganic and organic compounds, ideal gas state fit to a polynomial Cp, **2-174 to 2-175**
 inorganic and organic compounds, ideal gas state fit to hyperbolic functions Cp, **2-176 to 2-181**
 inorganic and organic liquids, **2-165 to 2-170**
 organic solids, **2-171 to 2-173**
- specific heats, selected elements, **2-164**
- specific humidity, yw, **12-4**
- specific rate constant, **7-6**
- specification limit, lower, **8-38**
- split operator technique, **7-38**
- spray column with two-phase dispersed, **15-71**
- spray nozzles, **14-95**
- spray scrubbers, **17-41 to 17-42**
 flow regime, **17-42**
 nonatomizing reverse-jet froth, **17-41**
- S-shape step response, **8-9**
- stability limit, **8-6, 8-13**
- stack gas emissions, dispersion, **22-37**
 design calculations, **22-38**
 miscellaneous effects, **22-40**
 preliminary design considerations, **22-37**
- stainless steel:
 type 304 (group 2.1 materials), pressure-temperature ratings for, **10-109**
 type 304L and 316L, pressure-temperature rating, **10-110**
 type 316 (group 2.2 materials), pressure-temperature rating, **10-110**
 type 316 (group 2.2 materials), pressure-temperature ratings for, **10-110**
- start-up expenses, **9-10, 9-17**
- static air horsepower, **12-21**
- statistical control, state of, **8-37**
- statistics, **3-70 to 3-88**
 enumeration data and probability distributions, **3-72 to 3-73**
 error analysis of experiments, **3-86**
 factorial design of experiments and analysis of variance, **3-86 to 3-88**
 least squares, **3-84 to 3-86**
 measurement data and sampling densities, **3-73 to 3-78**
 tests of hypothesis, **3-78 to 3-84**
- status alarms, **8-67**
- steady-state multiplicity, **7-39**
- steady-state steady-flow processes, thermodynamic analysis, **4-39 to 4-40**
- steepest descent method, **8-34, 7-38**
- Stefan-Boltzman Law, **5-16**
- step growth, **7-29**
- step response coefficients, **8-30**
- step size, **8-34**
- stirred-tank reactor, **8-44**
- STNS, state-task networks, **13-59**
- stockholders' equity, **9-4, 9-6**
 common stock, **9-6**
 paid in capital, **9-6**
 preferred stock, **9-6**
 retained earnings, **9-6**
- stoichiometric balances, **7-8**
 constant volume, **7-8**
 isothermal constant-pressure ideal gas, **7-9**
- stoichiometric matrix, **7-9**
- stoichiometry, **7-5**
 chemical reaction, **4-35**
- Stokes' law, **17-28, 17-56**
- storage and process vessels, **10-140 to 10-159**
- storage facilities, cost of, **10-149**
- strain gauges, **8-59**
- stroke test, partial, **8-89**
- structured batch logic, **8-53**
- styrene polymerization, **7-30**
- substrates, biochemical reactions, **7-30**
- sulfur dioxide, thermodynamic properties, **2-404 to 2-405**
- sulfur hexafluoride, thermodynamic properties, **2-406 to 2-409**
- sulfuric acid, aqueous solution at 1 atm, enthalpy-concentration, **2-409**
- sum of squares of residual errors, **7-37**
- supercritical conditions, **19-21**
- supercritical fluid separations:
 extraction, **20-16 to 20-17**
 applications, **20-16 to 20-17**
 concepts, **20-16**
 crystallization by reaction, **20-18**
 mass transfer, **20-16**
- phase equilibria:
 cosolvents and complexing agents, **20-15**
 liquid-fluid models, **20-15**
 polymer-fluid and glass transition, **20-15**
 solid-fluid, **20-15**
 surfactants and colloids, **20-15 to 20-16**
- physical properties:
 density-pressure diagram, **20-14**
 thermodynamic, **20-14**
 transport, **20-15**
- supply chain management, **8-35, 8-69**
- suppressed-zero ranges, **8-59**
- surface tension, **2-513 to 2-515**
 calculation methods, **2-513**
 Jasper method, **2-513**
 liquid mixtures, **2-514**
 Brock-Bird method, **2-513**
 calculation methods, **2-514**
 Parachor method, **2-513**
 Parachor group contributions for Knotts method, **2-514**
- suspending agent, **7-29**
- suspension firing, **24-25 to 24-28**
 char oxidation, **24-25**
 cyclone furnaces, **24-27 to 24-28**
 devolatilization, **24-25**
 pulverized coal furnaces, **24-26 to 24-27**
 configurations, **24-26, 24-27**
 fantail vertical firing, **24-26**
 low-NOx burners, **24-26**
 overfire air, **24-26 to 24-27**
 reburn, **24-27**
 tangential firing, **24-26**
- pulverizers, **24-27**
 capacity vs. grindability, **24-27**
 capacity vs. moisture in coal, **24-28**

- suspensions:
 classification, **18-6**
 gas-liquid, **18-18**
 gas-liquid-solid, **18-20**
 solid-liquid, **18-16**
 SUVA AC 9000, **2-302, 2-409**
 synthesis reactions, **7-16**
- t statistics, **7-38**
 taxes, **9-22**
 example of, **9-19, 9-22**
 TCA cycle, **7-31**
 telemetering, **8-65**
 temperature control, **8-41, 8-44**
 temperature measurements, **8-56**
 tetrahydrofuran:
 Antoine vapor pressure, **13-14**
 BIP data, **13-13**
 thermal afterburners, combustion or pollutants, **22-46**
 thermal conductivity, **2-509 to 2-513, 5-3, 8-62**
 gases, **2-510**
 calculation methods, **2-510**
 Chung-Lee-Starling method, **2-510**
 Stiel-Thodos method, **2-510**
 liquid mixtures, **2-512**
 calculation methods, **2-512**
 Filippov correlation, **2-512**
 Li correlation, **2-512**
 liquids, **2-510**
 baroncini method, **2-510**
 calculation methods, **2-510**
 Missenard method, **2-510**
 Sastri-Rao method, **2-511**
 thermal conductivity correlation parameters
 for Baroncini method, **2-511**
 thermal conductivity group contributions for
 Sastri-Rao method, **2-511**
 solids, **2-512**
 thermal deactivation, **7-23**
 thermal decomposition, **19-48**
 thermal design of heat-transfer equipment:
 batch operations:
 applications, **11-18**
 external heat loss or gain, effect of, **11-19**
 heating and cooling vessels, **11-18 to 11-20**
 condensers, design of, **11-11 to 11-13**
 multicomponent, **11-12**
 single-component, **11-11**
 thermal design, **11-12**
 evaporators, design of, **11-13 to 11-18**
 fluid properties, effect of, **11-17**
 forced-circulation, **11-14**
 heat transfer from, **11-16**
 long-tube vertical, **11-14**
 miscellaneous types of **11-16**
 noncondensables, effect of, **11-18**
 short-tube vertical, **11-15**
 extended or finned surfaces, **11-22 to 11-23**
 applications, **11-22**
 high fins, **11-23**
 low fins, **11-23**
 pressure drop, **11-23**
 fouling and scaling, **11-23 to 11-24**
 control of, **11-23**
 deposits, removal of, **11-24**
 transients and operating periods, **11-24**
 heat exchanger design approach, **11-5 to 11-6**
 countercurrent or cocurrent flow, **11-4**
 mean temperature differences, **11-4**
 reversed, mixed or crossflow, **11-5**
 heating and cooling of tanks, **11-21 to 11-22**
 bayonet heaters, **11-22**
 external coils or tracers, **11-22**
 fin tube coils, **11-22**
- thermal design of heat-transfer equipment, heating
 and cooling of tanks (*Cont.*):
 jacketed vessels, **11-22**
 spiral baffles, **11-22**
 Teflon immersion coils, **11-22**
 reboilers, thermal design of, **11-13**
 forced-recirculation, **11-13**
 horizontal thermosiphon reboilers, **11-13**
 kettle reboilers, **11-13**
 vertical thermosiphon, **11-13**
 scraped-surface exchangers, **11-31**
 single-phase heat transfer, **11-5 to 11-11**
 baffled shell-and-tube exchangers, **11-7**
 calculation, **11-7 to 11-11**
 double-pipe heat exchangers, **11-5**
 solids processing, **11-24 to 11-31**
 conductive heat transfer, **11-24**
 contactive heat-transfer, **11-29**
 convective heat-transfer, **11-30**
 cylindrical rotating shell, **11-30**
 drying rate, **11-30**
 emissivity, table, **11-10**
 evaporative cooling, **11-30**
 fluidization, **11-27**
 radiative heat transfer, **11-30**
 solidification, **11-28**
 vibratory devices, **11-29**
 tank coils, thermal design of, **11-20 to 11-21**
 thermal diffusivity, **12-54**
 thermal expansion:
 linear expansion:
 miscellaneous substances, **2-136, 2-135**
 solid elements, **2-135, 2-134**
 volume expansion:
 liquids, **2-137, 2-136**
 solids, **2-138, 2-136**
 thermal expansion coefficients, nonmetal, **10-125**
 thermal inertia, **8-58**
 thermal insulation:
 economic thickness of **11-72 to 11-76**
 installation practice, **11-76**
 insulation materials, **11-70**
 system selection, **11-71**
 thermal mass flowmeters, **8-60**
 thermal regeneration, **16-34**
 thermistors, **8-56**
 thermocompressor, **8-45**
 thermocouples, **8-56**
 thermodynamics:
 analysis of processes, **4-38 to 4-40**
 calculations:
 ideal work, **4-38 to 4-39**
 K values, VLE, and flash, **4-31 to 4-32**
 lost work, **4-39**
 equilibrium:
 chemical reaction **4-35 to 4-38**
 criteria, **4-26 to 4-27**
 laws:
 first law, **4-4**
 second law, **4-5**
 nomenclature and units, **4-3**
 property relations:
 liquid phase, **4-13**
 liquid/vapor phase transition, **4-13 to 4-14**
 mathematical structure of, **4-6**
 thermometers, bimetal, **8-57**
 thermophysical properties, **2-463**
 nonmetallic solid substances, **2-463**
 thickeners, costs:
 equipment, **18-82**
 operating, **18-82**
 Thiele modulus, **7-20**
 three-state controller, **8-13**
 throttling process, thermodynamics, **4-16**
 thrust limit, **8-89**
- time constants, **8-55**
 time-delay compensation, **8-24**
 Tofel empirical equation, **7-33**
 toluene:
 activity coefficient plot, **13-14**
 K-value data, **13-12**
 thermodynamic properties, **2-410 to 2-411**
 Txy diagram, **13-8**
 X-Y diagram, **13-8**
 tortuosity, **7-20**
 toxic materials ERPG values and other toxicity
 values for, **23-33 to 23-34**
 trace solute separations, **16-48**
 trans-2-butene, thermodynamic properties, **2-238**
 to **2-239**
 transcription, biological systems, **7-31**
 transducers, **8-89**
 transfer functions, **8-8**
 process characteristics, **8-9**
 transition state complex, **7-14**
 transition state theory, **7-6**
 translation, biological systems, **7-31**
 transmitter networks, **8-66**
 transmitters, **8-54**
 transport properties:
 diffusivities:
 gases and vapor pairs (1 atm), **2-454 to 2-455**
 liquids (25°C), **2-456 to 2-458**
 selected elements, thermal diffusivity, **2-462**
 gases, transport properties at atmospheric
 pressure, **2-445**
 Prandtl numbers:
 air, **2-451**
 refrigerants, **2-451**
 thermal conductivities:
 alloys at high temperatures, **2-461**
 building and insulating materials, **2-459**
 to **2-460**
 chromium alloys, **2-461**
 insulating materials at high temperatures,
2-461
 insulating materials at low temperatures, **2-462**
 insulating materials at moderate temperatures,
2-462
 liquids, inorganic and organic substances,
2-439 to 2-444
 metals, **2-460**
 organic liquids, **2-450**
 refrigeration and building insulation materials,
2-330, 2-461
 vapor, inorganic and organic substances, **2-433**
 to **2-438**
 thermophysical properties, miscellaneous
 saturated liquids, **2-452 to 2-453**
 viscosities, inorganic and organic substances:
 gases, **2-317, 2-446 to 2-447**
 liquids at 1 atm, **2-427 to 2-432, 2-448 to 2-449**
 sucrose solutions, **2-450**
 vapor, **2-241 to 2-426**
 tray columns, flooding, **14-36**
 derating ("system") factors, **14-40**
 downcomer backup flooding, **14-38**
 downcomer choke flooding, **14-39**
 entrainment (jet) flooding, **14-36**
 spray entrainment flooding prediction, **14-36**
 tray columns, gas-liquid systems, **14-26 to 14-34**
 baffle trays, **14-34**
 bubble-cap trays, **14-34**
 centrifugal force deentrainment, **14-34**
 clearance under the downcomer, **14-31**
 downcomers, **14-29**
 dual flow trays, **14-34**
 flow regimes on trays, **14-17**
 fractional hole area, **14-31**
 hole sozes, **14-31**

30 INDEX

- tray columns, gas-liquid systems (*Cont.*):
 multipass balancing, 14-32
 outlet weir, 14-29
 radial trays, 14-34
 tray area definitions, 14-26
 tray capacity enhancement, 14-32
 tray considerations, 14-29
 tray spacing, 14-29
 truncated downcomers/forward push trays, 14-32
 vapor and liquid-load definitions, 14-27
- tray columns, other hydraulic limits, 14-40
 dumping, 14-46
 entrainment, 14-40
 froth emulsions, 14-48
 loss under downcomer, 14-44
 pressure drop, 14-42
 transition between flow regimes, 14-47
 turndown, 14-47
 valve trays, 14-48
 vapor channeling, 14-47
 weeping, 14-44
- tray efficiencies, 14-48, 14-51, 14-52
 calculation, 14-50
 empirical efficiency production, 14-52
 experience factors, 14-50
 rigorous testing, 14-50
 scale-up from a pilot or bench-scale column, 14-51
 scale-up from an existing commercial column, 14-50
 theoretical efficiency prediction, 14-53
 definitions, 14-48
 factors affecting, 14-49
 fundamentals, 14-48
- tray towers and packed towers, comparison, 14-80
 capacity and efficiency comparison, 14-81
 factors favoring packings, 14-80
 factors favoring trays, 14-80
 trays vs random packings, 14-81
 trays vs structured packings, 14-81
- tray-tower design, gas-liquid systems, 14-14
 to 14-15
 algebraic method for concentrated gases, 14-14
 algebraic method for dilute gases, 14-14
 graphical design procedure, 14-14
 steam stripping, 14-15
 stripping equations, 14-14
 tray efficiencies in tray absorbers and strippers, 14-15
- trend alarm, 8-67
- trip valves, 8-91
- tube banks, 6-36 to 6-39
 laminar region, 6-37 to 6-39
 transition region, 6-37
 turbulent flow, 6-36 to 6-37
- tubular reactor, 19-46
 modeling, 19-9
 tracers, 19-16
- tuning method:
 known process models, 8-18
 process model is unknown, 8-19
- turbidostat, 7-35
- turbine flowmeters, 8-65
- turbine inlet cooling:
 background, 24-56
 schematic, 24-57
 technologies:
 evaporative, 24-56
 refrigeration, 24-56 to 24-57
 temperature effects, 24-57
 thermal energy storage (TES), 24-57
 benefits, 24-57
- turbine meter, 8-60
- turbines, thermodynamics, 4-16
- turbulence, 6-46 to 6-47
 closure models, 6-46 to 6-47
 eddy spectrum, 6-47
 time averaging, 6-46
- ultrafiltration:
 applications, 20-50
 component transport:
 flux behavior, 20-52
 solute flux, 20-53
 solute passage/retention, 20-53
 design considerations:
 continuous, 20-54
 single pass TFF, 20-54
 economics, 20-53 to 20-54
 membranes, 20-50
 properties, 20-50
 modules and systems, 20-50 to 20-51
- ultraviolet and visible radiation analyzer, 8-62
- under damped, dynamic measurements, 8-55
- uniform cycle, 8-19
- unit operations control, 8-39
- units, fluid cracking, 17-16
- units and quantities:
 common, 1-17
 SI:
 base and supplementary, 1-2
 derived, additional common, 1-2
 derived, with special names, 1-2
- UOP cyclesorb process, 16-59
- UOP sorbex process, 16-56
- upper specification limit, 8-38
- uranium, leaching and extraction, 18-18
- vacuum, 8-52
- vacuum systems, 10-58
 diffusion pump, 10-58
 vacuum equipment, 10-58
 vacuum levels attainable with various types of equipment, 10-60
- value, quick opening, 8-83
- value-improving practices, 9-48, 9-52
- valve assemblies, 8-85
- valve control devices, 8-84
- valve design, 8-79
 materials ratings, 8-79
 sizing, 8-79
- valve positioner, 8-84
- valve types, 8-74
- valves for on/off applications, 8-78
- vapor pressure, 2-477 to 2-478, 8-80, 12-4, 12-26
- liquids:
 Antoine equation, 2-477
 calculation methods, 2-477
 Reidel equation, 2-477
 Wagner vapor pressure equation, 2-477
- pure substances:
 inorganic and organic liquids, 2-55 to 2-60
 inorganic compounds, up to 1 atm, 2-65 to 2-79
 water ice from 0 to -40°C, 2-48
 water, liquid from 0 to 100°C, 2-48
 water, supercooled liquid from 0 to -40°C, 2-48
- solids:
 calculation methods, 2-478
 Clausius-Clapeyron equation, 2-478
- solutions:
 acetic acid aqueous solutions, total vapor pressures, 2-89
 HCl over aqueous HCl solutions, partial pressures, 2-80
 HI over aqueous HI solutions at 25°C, partial pressures, 2-89
- vapor pressure, solutions (*Cont.*):
 HNO₃ and water over aqueous HNO₃ solutions, partial pressures, 2-88
 NH₃ over aqueous NH₃ solutions, partial pressures, 2-92
 NH₃ over aqueous NH₃ solutions, total vapor pressure, 2-93
 sulfur trioxide over aqueous sulfuric acid solutions, partial pressures, 2-84 to 2-85
 sulfuric acid over aqueous sulfuric acid solutions, partial pressures, 2-86
 sulfuric acid over aqueous sulfuric acid solutions, total pressure, 2-87
 water and CH₃OH over aqueous methyl alcohol solutions, partial pressures, 2-94
 water and HBr over aqueous HBr solutions at 20 to 55°C, partial pressures, 2-89
 water in saturated air over aqueous H₃PO₄ solutions, weights, 2-81
 water over aqueous HCl solutions, partial pressures, 2-81
 water over aqueous H₃PO₄ solutions, partial pressures, 2-81
 water over aqueous NaOH solutions, partial pressures, 2-94
 water over aqueous NH₃ solutions, mole percentages, 2-91
 water over aqueous NH₃ solutions, partial pressures, 2-90
 water over aqueous sodium carbonate solutions, partial pressures, 2-94
 water over aqueous SO₂ solutions, partial pressures, 2-81
 water over aqueous sulfuric acid solutions, partial pressures, 2-82 to 2-83
 water-sulfuric acid-nitric acid, vapor pressures of the system, 2-89
- vaporization/implosion transitions, 8-82
- vapor/liquid equilibrium:
 calculations:
 K-values, VLE, and flash, 4-31 to 4-32
 data reduction, 4-30 to 4-31
 definition, 4-28
 equation-of-state approach, 4-32 to 4-34
 extrapolation of data with temperature, 4-34 to 4-35
 gamma/phi approach, 4-28
 modified Raoult's law, 4-28 to 4-29
 results for methanol/acetone, 4-35
 solute/solvent systems, 4-31
 thermodynamics, 4-35
 variance-covariance matrix, 7-37
 various liquids, surface tension, 2-309, 2-419
 velocity; abnormal distribution, 10-20
 minimum Hodgson numbers, 10-21
 order of reliability for square-edged orifices and venturi tubes, 10-20
 swirling flow, 10-20
 velocity ratio versus Reynolds number, 10-13
 resistive thermal detectors (RTDs), 10-7
 static, 10-7
 thermocouples, 10-7
- vena contracta condition, valve design, 8-80
- vena contracta region, valve design, 8-82
- venture-scrubber models, 17-37, 17-40 to 17-41
- venturi meter, 8-59
- vessels, agitated, jackets and coils, 18-25
- vibrofluidization, 17-6
- view factors, 5-20 to 5-24
- viscosity, 2-504 to 2-509
 density, and kinematic viscosity of water and air in terms of temperature, 10-6
 gases, 2-504
 calculation methods, 2-505
 Jossi-Stiel-Thodos method, 2-505

- viscosity, gases (*Cont.*):
 Reichenberg group contribution values, 2-505
 Reichenberg method, 2-505
 Yoon-Thodos method, 2-505
- kinematic, 10-7
- liquids, 2-506
 calculation methods, 2-506
 Hsu method, 2-506
 Hsu method group contributions, 2-507 to 2-508
- liquid mixtures, 2-506
 calculation methods, 2-506
 Grunberg-Nissan equation, 2-506
 UNIFAC-VISCO method, 2-508
 UNIFAC-VISCO group interaction parameters, 2-509
- viscous materials, mixing (pastes and doughs):
 anchor, 18-28
 double, triple shaft, 18-31
 helical ribbon, 18-28
 kneading, double arm, 18-31
 planetary, 18-30
- VOCs, removal for air, costs, 22-51
- voidage, total, 16-10
- volumetric growth rate, 7-18
- volumetric humidity, 12-4, 12-5
- von Deemter equation, 16-44
- vortex shedding, 6-41 to 6-42
 flowmeters, 8-60
- waste fuel analysis, 24-7
- wastewater, categories, 22-59
- wastewater, characteristics and treatment, 22-69
 dissolved solids, 22-62
 equalization, 22-63
 grease and oil removal, 22-64
 inorganics, 22-62
 neutralization, 22-63
 nutrients and eutrophication, 22-62
 oil and grease, 22-63
 organics, 22-60
 pH and alkalinity, 22-62
 physical-chemical treatment, 22-76
 adsorption, 22-76
 advanced oxidation process, 22-77
- wastewater, characteristics and treatment,
 physical-chemical treatment (*Cont.*):
 chemical oxidation, 22-77
 concentration: thickening and flotation, 22-79
 industrial reuse, 22-78
 ion exchange, 22-77
 membrane bioreactors (MBRs), 22-78
 membrane processes, 22-78
 objectives, 22-78
 sludge processing, 22-78, 22-80
 stabilization, 22-79
 stripping, 22-77
 pretreatment, 22-63
- primary, treatment, 22-64
 chemical precipitation, 22-65
 gravity sedimentation, 22-64
 grit chambers, 22-64
 screens, 22-64
- priority pollutants, 22-60
- secondary treatment, 22-65
 activated sludge, 22-69
 biological fluidized beds, 22-75
 design of biological treatment systems, 22-66
 determination of kinetic and stoichiometric pseudo constants, 22-68
 fixed-film reactor systems, 22-74
 lagoons, 22-72
 packed-bed fixed-film systems, 22-74
 reactor concepts, 22-67
 rotating biological contactors (RBCs), 22-74
 trickling filters, 22-3
- solids, 22-62
 temperature, 22-62
- toxic substances, 22-64
- wastewater treatment, 22-63
- whole effluent toxicity (WET), 22-63
- water:
 Antoine vapor pressure, 13-14
 BIP data, 13-13
 residue curve, 13-90
 residue maps, 13-70, 13-79
 saturated solid/vapor, thermodynamic properties, 2-412
 sensitivity of composition and temperature, 13-79 to 13-80
- water (*Cont.*):
 thermodynamic properties, 2-413 to 2-415
 VLE data, 13-9, 13-7, 13-9
 water content of air, 2-95
 water substance along the melting line, thermodynamic properties, 2-416
 water treatment ion exchange cycles, 16-54
 wave shape, 16-38
 weighting factor, 8-30
 weights and measures, U.S. customary, 1-18
 western electric rule, 8-37
 wet basis, 12-26
 humidity, 12-4
 wet density, 16-10
 wet-bulb temperature, 12-5, 12-6
 wet-dry cooling, 12-25
 wetted-wall columns, 14-82
 flooding in wetted-wall columns, 14-85
 mass transfer, 14-83
- Wien equation, 5-16
- wood, 24-7
- work:
 ideal, 4-38 to 4-39
 lost, 4-39
- working capital, 9-6, 9-9, 9-10, 9-17
- workstations, process control, 8-70
- Wurster coaters, sizes and capacities, 21-133
- xenon, 2-307, 2-417 to 2-418
- z transform, 7-30, 8-8
- zeolites, 16-8
- Ziegler and Nichols closed-loop method, 8-19
- zone melting, 20-5 to 20-6
 applications, 20-6
 component separation, 20-5
 zone method, 5-24 to 5-27, 5-36 to 5-39
 electrical network analog, 5-27 to 5-28
 examples, 5-28 to 5-29
 matrix formulation, 5-25, 5-36 to 5-37
 methodology, 5-25
 multizone enclosures, 5-27
 two zone enclosure, 5-26